 © 1991 The Chemical Society of Japan Bull. Chem. Soc. Jpn., 64, 1—4 (1991)

Translational Energy Distributions and Emission Cross Sections of the Excited Hydrogen Atom Produced in e-SiH_4 Collisions

Toshiyuki Tsuboi, Keiji Nakashima, and Teiichiro Ogawa*
Department of Molecular Science and Technology, Kyushu University,
Kasuga-shi, Fukuoka 816
(Received August 1, 1990)

The translational energy distributions of H* (n=3, 4) produced in e-SiH_4 collisions were obtained by measuring the Doppler profiles of the Balmer-α and β lines with a Fabry–Perot interferometer. There are three major components in the translational energy distributions of H* (n=3,4). The first component lies in the 0—3 eV region, the second one peaks at 2—3 eV, and the third one lies at above 4 eV. Thus, dissociation of SiH_4 for the formation of H* (n=3,4) should proceed through three different groups of Rydberg states. The emission cross sections were determined separately for H* (n=3,4) with the translational energy of 0—2, 2—4, 4—6, 6—8, and 8—10 eV, respectively.

The study of electron–silane (SiH_4) interaction has received considerable attention due to its importance to plasma diagnostics in semiconductor technology. The mechanism and cross sections of electron-impact dissociation of SiH_4 are needed for understanding and simulating deposition processes of amorphous silicon films.

High resolution spectroscopy on electron–molecule collision processes is a powerful tool for such studies.[1] The translational energy distribution of fragments,[1,2] the emission cross section of certain fragments produced in a specified dissociation process[1,3] and the symmetry of dissociation processes[1,4] have been obtained with this technique. Reactivity of an excited species may depend on the translational energy it has. Thus, the emission cross section of an excited species should be more useful for a simulation of a plasma, if it is determined separately for species with different translational energies.

Perrin et al.[5–8] investigated the dissociation dynamics of SiH_4 and determined the emission cross section of fragments such as H*, Si*, Si$^+$*, SiH*, and SiH$^+$*. The translational energy distributions of H* (n=4) were obtained with the use of a grating spectrometer and three groups of H* (n=4) were found in the translational energy distribution; their peaks lay at about 0.3 eV, 2.5 eV and a higher energy.[7] The excitation functions of H* (n=3,4) were determined and three major thresholds were found for the formation of H* (n=3,4).[6,9,10] Cooper et al.[11] obtained absolute oscillator strengths for photoabsorption, photoionization, and ionic photofragmentation, and photofragmentation branching ratios of silane, and concluded that the $(3a_1)^{-1}$ state is a many-body state and plays an important role for the formation of H^+.

We have measured high-resolution spectra of the Balmer-α and β lines with a Fabry–Perot interferometer and obtained the translational energy distributions of H* (n=3,4). We have also determined the emission cross sections for the excited hydrogen atom of certain translational energy with an expectation that such values are useful for an understanding and simulation of plasma. To our best knowledge, this is the first attempt to determine the emission cross section separately for species with different translational energies.

Experimental

The experimental apparatus was described in detail in the previous papers.[12,13] In brief, the stainless-steel collision chamber has an electron gun and a gas cell. The sample gas (10.1% SiH_4 in He; obtained from Seitetsu Kagaku) was collided with the electron beam. The typical electron-beam current was 10—100 μA and the typical operating pressure was 1—4×10^{-5} Torr (uncorrected, 1 Torr=133.322 Pa) at the wall of the collision chamber.

The optical radiation was measured perpendicularly with the electron beam with a Spex 1269 monochromator when the broad band spectra were obtained. The Doppler profile of the Balmer lines was measured at 55° (magic angle) with respect to the electron beam with a Mizoziri Fabry–Perot interferometer. The optical resolution was 0.010 nm for the Balmer-α line and 0.007 nm for the Balmer-β line. A DIF-C filter ($\Delta\lambda_{1/2}$=1.0 nm: Vac. Opt. Co. Jpn.) was used for separating the Balmer-α line and another DIF-C filter ($\Delta\lambda_{1/2}$= 1.3 nm) for the Balmer-β line. The photons were counted with a Hamamatsu R585 or R649 photomultiplier.

The relative emission cross sections of the excited hydrogen atom with each translational energy were determined from its translational energy distributions, and the summed totals were normalized to those measured by Sato and Goto[9] in order to make the relative values absolute.

Results and Discussion

Doppler Profiles and Translational Energy Distribution. The silane molecule produces lines of H*, Si*, and Si$^+$*, and bands of SiH* and SiH$^+$*.[5,6,9] We have separated the Balmer lines of H* (n=3,4) and measured their Doppler profiles with the use of a high-resolution Fabry–Perot interferometer, as shown in Fig. 1. The electron energy was 25—100 eV; however, no reliable profile of H* (n=3) was obtained at 25 eV due to poor signal-to-noise ratio. The Doppler profiles are dependent on the electron energy. It

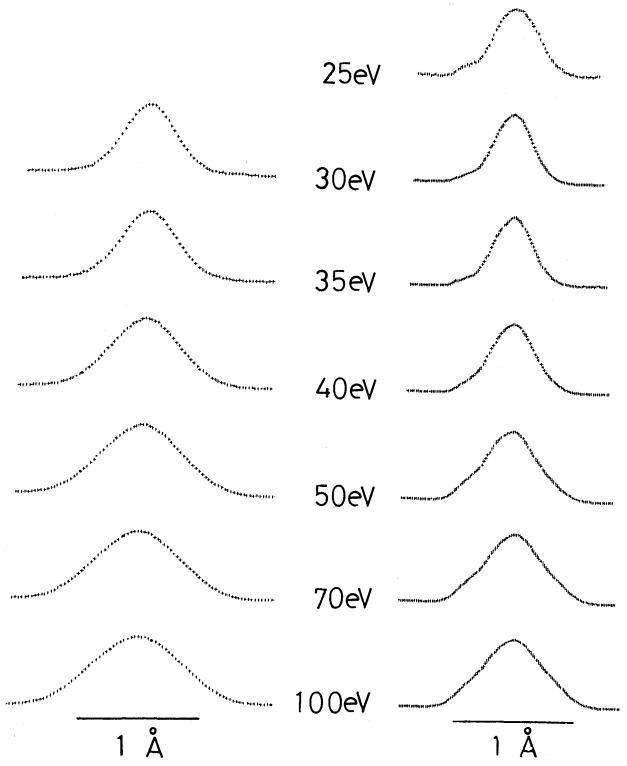

Fig. 1. Doppler profiles of the excited hydrogen atom (n=3, 4) produced in e–SiH_4 collisions. Observation angle: 55° with respect to the electron beam. (left) H*(n=3), (right) H*(n=4).

becomes wider at higher electron energies. There are two helium lines and one unidentified line (probably molecular origin) on the shorter wavelength (left) side of the Balmer-β line; they are clear on the spectrum taken with the Spex monochromator. Thus, the longer wavelength (right) side of the profile was used for the determination of the translational energy distribution of H* (n=4).

The translational enenrgy distribution of an excited species can be obtained by differentiating the Doppler profile obtained at 55° (magic angle),[14] so that any effect due to anisotropy should be negligible. The differentiation was carried out by smoothing the profile curve by a least square procedure using a 5-point cubic convolute.[15] The translational energy distributions of H* (n=3,4) are shown in Figs. 2 and 3. The distribution at 25 eV is noisier due to weak signals.

At incident electron energies of 25 and 30 eV, there is a clear peak in the translational energy distribution at about 0.5 eV, as shown in Figs. 2 and 3. This component is located in the 0—3 eV region and is dominant at electron energies of 25—35 eV. Another component starts to appear on the distribution at an incident energy of 40 eV. This component has a peak at 2—3 eV becomes more intense at higher incident energies. The third one appears on the distribution at

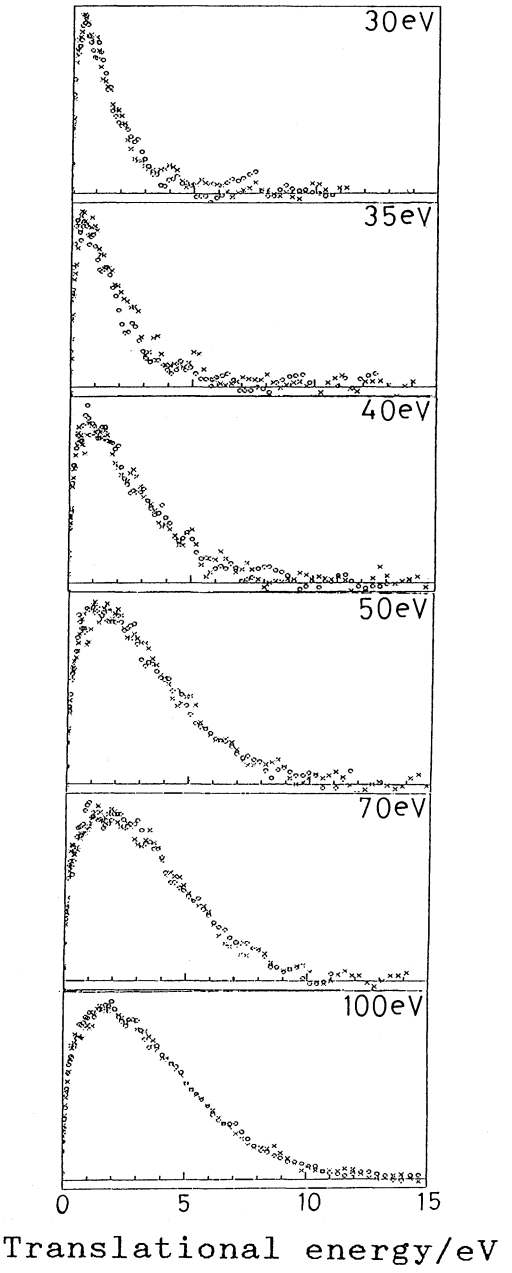

Fig. 2. Translational energy distributions of H*(n=3) produced in e–SiH_4 collisions. The translational energy distribution obtained from the longer wavelength side of the Doppler profile is shown as ○, and that obtained from the shorter wavelength side as ×. The two distributions agree with each other within experimental errors.

above 50 eV; this component lies in the 4—10 eV region of the translational energy. Thus, there are three major components on the translational energy distributions of H* (n=3,4) as Perrin and Schmitt observed.[7] This finding indicates that there should be at least three major dissociation processes for the formation of the excited hydrogen atom from silane.

Both of the translational energy distributions of H*

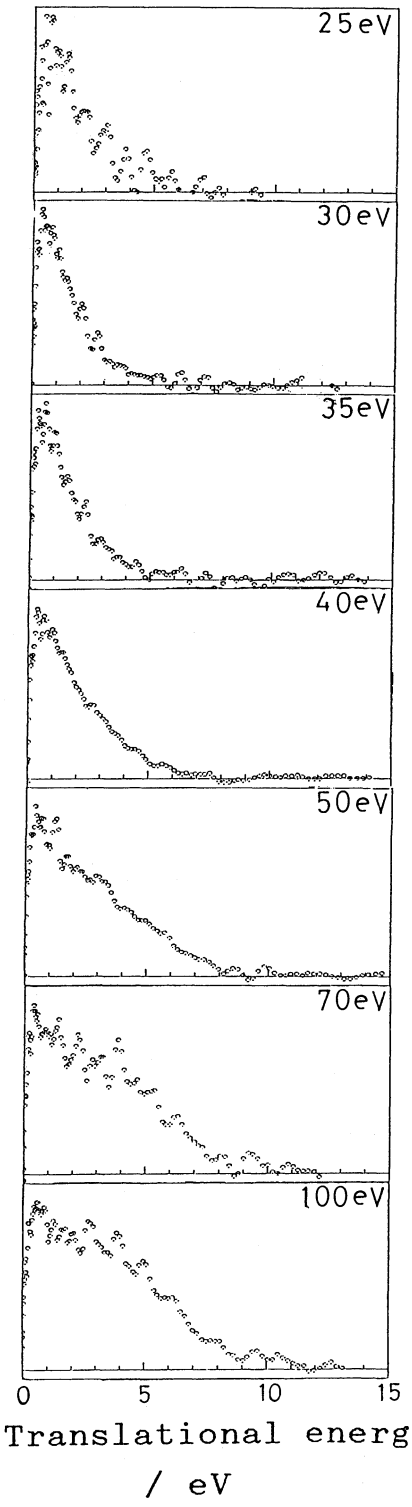

Fig. 3. Translational energy distributions of H*(n=4) produced in e-SiH_4 collisions. The translational energy distribution was obtained from the longer wavelength side of the Doppler profile.

(n=3) and H* (n=4) have three components and they are qualitatively similar. Relative intensity of the three component is, however, different; the second component of H* (n=3) is relatively more intense than that of H* (n=4).

There are three thresholds on the excitation function of H* produced in e-SiH_4 collisions; they lie at about 19 eV, 23 eV, and 35—40 eV.[6,9,10] However, these thresholds and the translational energy distribution do not show one-to-one correspondence. The first and second thresholds can be correlated with the first component of the translational energy distributions. The second component appears at 40 eV and becomes dominant at higher electron energies; the threshold of this component should be slightly below 40 eV. The difference in the relative intensity of the second component of H* (n=3) and H* (n=4) may correspond to the difference of their excitation function; the one for H* (n=3) has a steeper rise at about 40 eV.[9] The threshold of the third component is not clear.

Dissociation Process of Silane. Perrin and Schmitt[7] described that the formation of H* (n=4) proceeds via dissociative superexcited Rydberg states. Importance and contribution of such states were shown on various molecules.[1] The photoelectron spectrum of silane indicated that the $(3a_1)^{-1}$ state lies in the 17—40 eV region.[16] The dipole (e,e) spectrum also indicated that the $(3a_1)^{-1}$ state lies in the 16—40 eV region and that this state consists of the main state (threshold: 18 eV) and a many-body state (threshold: 24 eV); the appearance potential of H^+ was found at 24 eV, and H^+ should be produced through the $(3a_1)^{-1}$ state.[11] The formation of H^+ was correlated specifically with the many-body state of $(3a_1)^{-1}$.[11]

Since there is no onset of H^+ at about 19 eV in the dipole (e,e) spectrum, we can conclude that the threshold of H* (n=3,4) at 19 eV can be correlated with an optically-forbidden minor dissociation process; this process would be a triplet process. The major part of the first component of the translational energy distribution can be correlated with the threshold at 23 eV and the formation of H* (n=3,4) would proceed through Rydberg states converging to the many-body state of the $(3a_1)^{-1}$ state.

The first component has larger translational energy than the second one in the case of methane. The Rydberg state converging to the $(2a_1)^{-1}$ state of methane was correlated with processes leading to the excited hydrogen atom with the translational energy of about 3 eV. While, the second component was slow. The contribution of curve crossing in the excited Rydberg states may be different between methane and silane and such difference can induce the observed difference in the translational energy distributions of H* (n=3,4) produced from the two molecules.

The second component in the translational energy distribution has the threshold at about 35 eV. There may be some doubly-excited Rydberg states such as $(2t_2)^{-2}(nR)^2$ (nR: a Rydberg orbital) in this energy region, which may play important roles for the formation of this component.

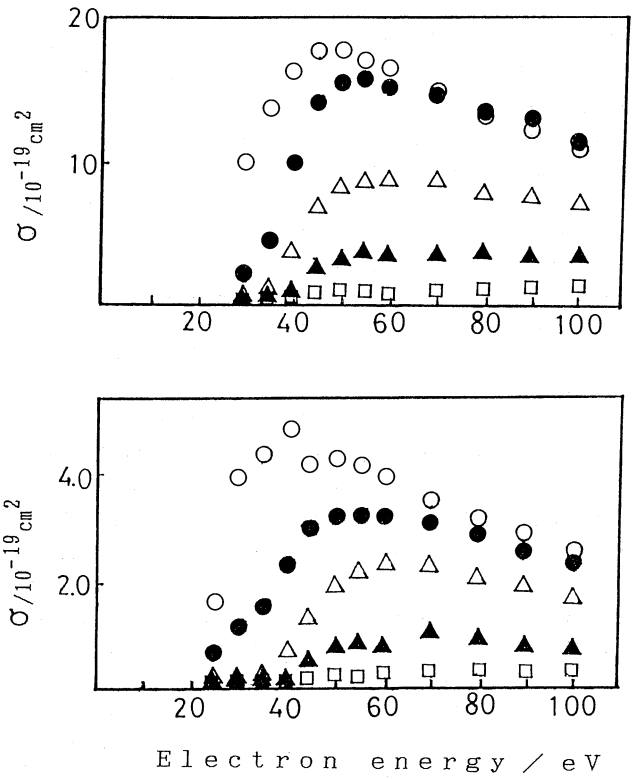

Fig. 4. Emission cross sections of H*(n=3, 4) with certain range of the translational energy distribution. (top) H*(n=3), (bottom) H*(n=4). ○: 0—2 eV, ●: 2—4 eV, △: 4—6 eV, ▲: 6—8 eV, □: 8—10 eV.

Emission Cross Sections. The total emission cross sections of H* (n=3,4) were determined previously.[9] We have determined the emission cross sections of H* (n=3,4) with certain translational energy separately by measuring their relative emission cross sections and by normalizing them to the total. No correction for collection efficiency was carried out, since such correction would be small for the Balmer-α and β lines.[17]

The emission cross sections of H* (n=3,4) of translational energy of 0—2 eV(○), 2—4 eV(●), 4—6 eV(△), 6—8 eV(▲) and 8—10 eV(□) are shown in Fig. 4. The H* (n=3,4) with translational energy above 10 eV is weak and was omitted in this Figure for clarity; its energy dependence is approximately identical with that of 8—10 eV. These results show that the first component is relatively more important for H* (n=4). Whereas the rise of H* (n=3) in the 2—4 eV region is steeper, and this finding indicates that the second component is more important for H* (n=3). The emission cross sections at an electron energy of 100 eV are shown in Table 1.

The chemical reactivity can depend on the translational energy of the species concerned. Such energy dependence is not yet discovered in plasma processing; however the partial emission cross section for each translational energy obtained here may be useful for its simulation.

Table 1. Emission Cross Sections of H* (n=3, 4) Produced in e-SiH_4 Collisions at an Electron Energy of 100 eV

Translational energy/eV	H* (n=3) 10^{-19} cm²	H* (n=4) 10^{-19} cm²
Total[9]	36	7.5
0—2 eV	10.9	2.4
2—4 eV	11.2	2.2
4—6 eV	7.5	1.7
6—8 eV	3.8	0.78
8—10 eV	1.7	0.27
Above 10 eV	1.0	0.15

The present work is partially supported by the Grant-in-Aid for Scientific Research on Priority Areas Nos. 63632519 and 01632517 from the Ministry of Education, Science and Culture.

References

1) T. Ogawa, *Eng. Sci. Repts. Kyushu Univ.*, **7**, 231 (1986).
2) T. Ogawa and M. Higo, *Chem. Phys. Lett.*, **65**, 610 (1979); *Chem. Phys.*, **44**, 279 (1979).
3) M. Higo, S. Kamata, and T. Ogawa, *Chem. Phys.*, **73**, 99 (1982); T. Ogawa and J. Kurawaki, *Chem. Phys. Lett.*, **95**, 274 (1983).
4) K. Nakashima and T. Ogawa, *J. Chem. Phys.*, **83**, 4920 (1985).
5) J. Perrin, J. P. M. Schmitt, G. de Rosny, B. Drevillon, J. Huc, and A. Loret, *Chem. Phys.*, **73**, 383 (1982).
6) J. Perrin and J. F. M. Aarts, *Chem. Phys.*, **80**, 351 (1983).
7) J. Perrin and J. P. M. Schmitt, *Chem. Phys. Lett.*, **112**, 69 (1984).
8) J. P. M. Schmitt, P. Gressier, M. Krishnan, G. de Rosny, and J. Perrin, *Chem. Phys.*, **84**, 281 (1984).
9) T. Sato and T. Goto, *Jpn. J. Appl. Phys.*, **25**, 937 (1986).
10) S. Tsurubuchi, private communication (1990).
11) G. Cooper, T. Ibuki, and C. E. Brion, *Chem. Phys.*, **140**, 133 (1990).
12) T. Ogawa, H. Tomura, K. Nakashima, and H. Kawazumi, *Chem. Phys.*, **113**, 65 (1987).
13) T. Ogawa, H. Tomura, K. Nakashima, J. Kurawaki, and H. Kawazumi, *J. Spectrosc. Soc. Jpn.*, **35**, 303 (1986).
14) T. Ogawa and M. Higo, *Chem. Phys.*, **52**, 55 (1980).
15) A. Savitzky and M. J. E. Golay, *Anal. Chem.*, **36**, 1627 (1964).
16) G. G. B. de Souza, P. Morin, and I. Nenner, *Phys. Rev. Sect. A*, **34**, 4770 (1986).
17) J. M. Marendic, M. D. Tasic, and J. M. Kurepa, *Chem. Phys.*, **91**, 273 (1984).

Temperature Effect on the Adsorption and Micelle Formation of Aqueous Dodecyltrimethylammonium Chloride-Hexane System

Koji ABE,* Ichiro KAJIWARA, Norihiro IKEDA,
Makoto ARATONO, and Kinsi MOTOMURA
Department of Chemistry, Faculty of Science, Kyushu University 33,
Fukuoka 812
(Received August 9, 1990)

The adsorption at water/hexane interface and micelle formation of dodecyltrimethylammonium chloride (DTAC) were studied by measuring its interfacial tension as a function of temperature under atmospheric pressure at various concentrations around the critical micelle concentration (cmc). By applying the thermodynamic equations developed previously, the entropy and energy changes associated with the adsorption from monomeric and micellar states were estimated and compared with those of the DTAC solution-air system. It was found that the entropy and energy of the adsorbed film of DTAC are remarkably depressed by the coexistent hexane phase. This finding explains the positive entropy change associated with the adsorption of DTAC at water/air interface.

The adsorption and micelle formation of surfactants are affected by the oil phase coexisting with its aqueous solution.[1-5] In our series of the thermodynamic studies, we investigated the effect of hexane on the adsorption and micelle formation of dodecylammonium chloride (DAC) and sodium dodecyl sulfate in terms of entropy, volume, and energy.[6,7] Further the pressure dependence of interfacial tension of dodecyltrimethylammonium chloride (DTAC) solution against oil phase was discussed in terms of volume.[8-10] On the other hand, it was found that the entropy change associated with the adsorption of DTAC from the micellar state is positive at water/air interface while that of DAC is negative at both water/air and water/hexane interfaces. It is now required to examine the temperature dependence of the interfacial tension of the DTAC solution-hexane system.

In the present work, the interfacial tension of the aqueous DTAC solution against hexane is measured as a function of temperature at various concentrations around the critical micelle concentration (cmc). By applying the thermodynamics[11] to experimental results, the entropy and energy changes associated with the adsorption and micelle formation are estimated numerically. The thermodynamic quantities obtained of the DTAC solution-hexane system are compared with those of the DTAC solution-air system.[12]

Experimental

Dodecyltrimethylammonium chloride (DTAC) was synthesized and purified by the method described previously.[8] Water was distilled triply from dilute alkaline permanganate solution. Hexane was purified by distillation.

The equilibrium interfacial tension was measured by the pendant drop technique within an experimental error of 0.05 mN m^{-1} under atmospheric pressure.[13] The temperature was kept constant within 0.01 K.

Results and Discussion

The interfacial tension γ of the aqueous DTAC solution against hexane was measured as a function of temperature T at constant molality m_1 of surfactant under atmospheric pressure. Given in Fig. 1a are the γ

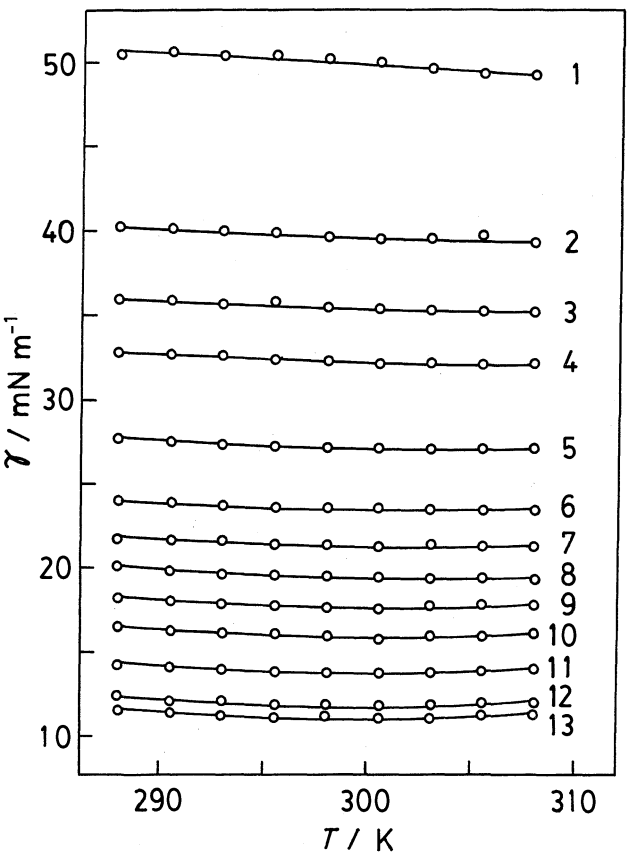

Fig. 1a. Interfacial tension vs. temperature curves at constant molality under atmospheric pressure: (1) m_1=0 mmol kg^{-1}; (2) 1.16; (3) 2.09; (4) 3.02; (5) 5.26; (6) 7.47; (7) 9.08; (8) 10.52; (9) 12.23; (10) 14.10; (11) 16.94; (12) 19.71; (13) 20.62.

vs. T curves at concentrations below the critical micelle concentration (cmc). It is seen that the curve decreases monotonously with increasing temperature at a low concentration while it has the minimum at a higher concentration. In Fig. 1b, a break point is observed on the curve at concentration near the cmc. This finding indicates that micelle formation takes place in the aqueous solution.[11] At a concentration above the cmc, the curve becomes the linear γ vs. T plot with a positive slope.

Picking up the γ values around the cmc at a given temperature from Figs. 1a and 1b, the γ vs. m_1 curves are drawn at constant temperature and illustrated in Fig. 2. It is seen that the curve breaks distinctly at cmc. The values of cmc C are plotted against temperature in Fig. 3; the C vs. T curve shows a shallow minimum and bears a great resemblance in shape to that of the DTAC solution–air (DTAC/A) system.[12] It is noteworthy, however, that the DTAC solution–hexane

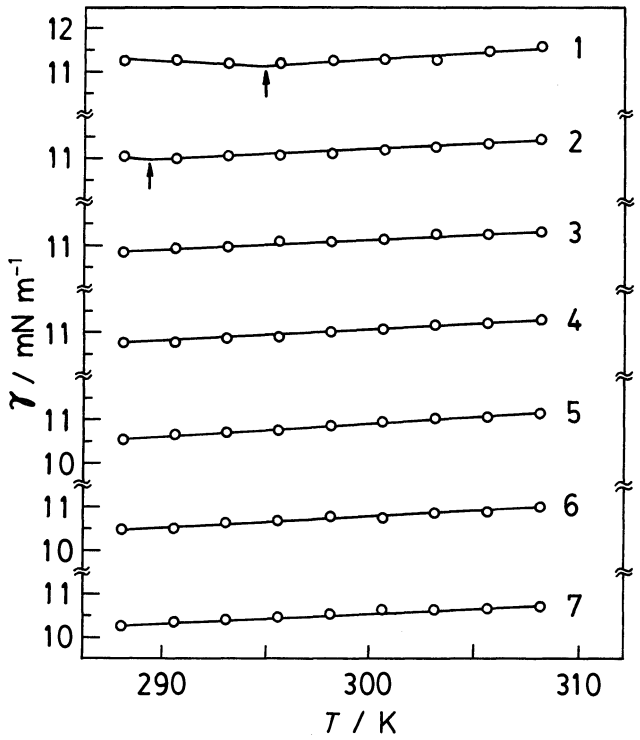

Fig. 1b. Interfacial tension vs. temperature curves at constant molality under atmospheric pressure: (1) m_1=21.32 mmol kg^{-1}; (2) 21.92; (3) 22.92; (4) 25.32; (5) 27.55; (6) 32.02; (7) 43.36.

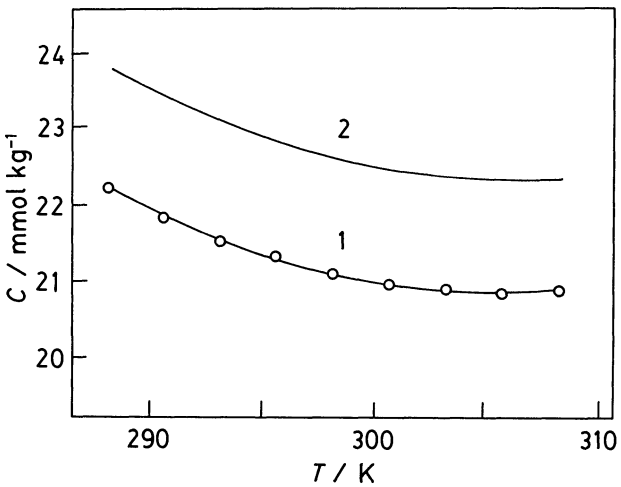

Fig. 3. Critical micelle concentration vs. temperature curves under atmospheric pressure: (1) DTAC/H system; (2) DTAC/A system.

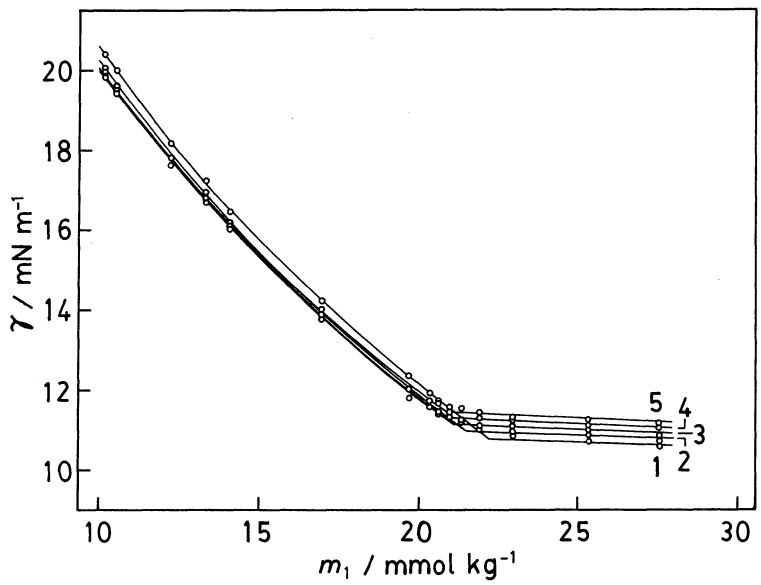

Fig. 2. Interfacial tension vs. molality curves at constant temperature under atmospheric pressure: (1) T=288.15 K; (2) 293.15; (3) 298.15; (4) 303.15; (5) 308.15.

(DTAC/H) system has a C value smaller than the DTAC/A system. The similar observation has been reported on the aqueous surfactant solution–oil systems and explained by the solubilization of oil.[1,3-5]

To examine more closely the influence of hexane on interfacial and micellar properties of the aqueous DTAC solution, let us evaluate the interfacial density and the thermodynamic quantities associated with adsorption and micelle formation of surfactant. Assuming the aqueous solution of DTAC to be a dilute ideal solution, the interfacial density Γ_1^H of surfactant is calculated by applying the relation

$$\Gamma_1^H = -(m_1/2RT)(\partial\gamma/\partial m_1)_{T,p} \quad (1)$$

to the γ vs. m_1 curve and is shown as a function of m_1 at constant T in Fig. 4. The interfacial pressure π vs. area per surfactant molecule A curve is useful to consider the state of adsorbed film. Here π and A are defined by

$$\pi = \gamma^0 - \gamma \quad (2)$$

and

$$A = 1/N_A\Gamma_1^H, \quad (3)$$

where γ^0 is the interfacial tension of the DTAC/A and DTAC/H systems without surfactant and N_A is Avogadro's number. The π vs. A curve is depicted at 298.15 K and compared with corresponding curve of the DTAC/A system in Fig. 5. It is obvious that the adsorbed film of the DTAC/H system is more expanded than that of the DTAC/A system.

It has been demonstrated that the thermodynamic treatment of the adsorption of surfactant from its micellar solution is useful.[6-12,14-16] According to the thermodynamics, the entropy change associated with the adsorption of surfactant from its monomeric state, $\Delta s(1)$, and that from its micellar state, $\Delta s(M)$, are evaluated respectively by the equations

$$\Delta s(1) = \Gamma_1^H(s^H/\Gamma_1^H - s_1^W) \quad (4)$$

$$= -(\partial\gamma/\partial T)_{p,m_1}, \quad m_1 < C \quad (5)$$

and

$$\Delta s(M) = \Gamma_1^H(s^H/\Gamma_1^H - s^M/N_1^M) \quad (6)$$

$$= -(\partial\gamma/\partial T)_{p,m_1}, \quad m_1 \geqq C, \quad (7)$$

where s^H, s^M, s_1^W, and N_1^M are the interfacial excess entropy per unit area, the molar entropy of micelle, the

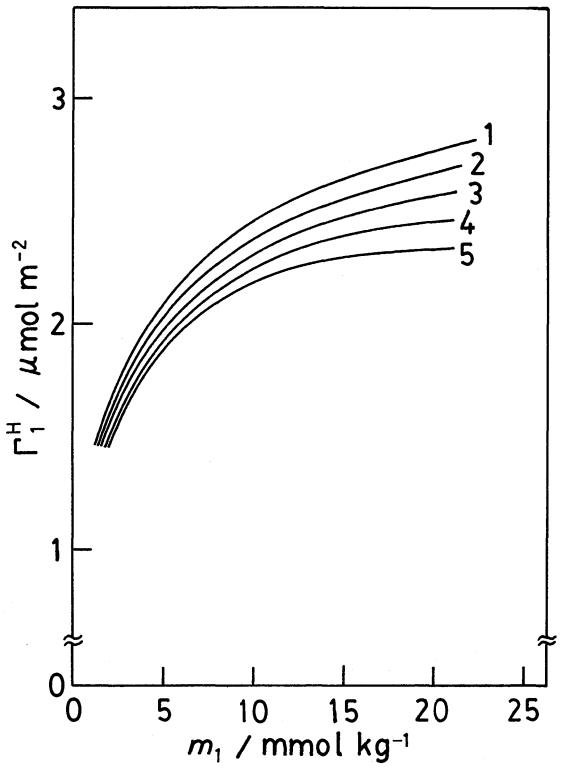

Fig. 4. Interfacial density vs. molality curves at constant temperature under atmospheric pressure: (1) T=288.15 K; (2) 293.15; (3) 298.15; (4) 303.15; (5) 308.15.

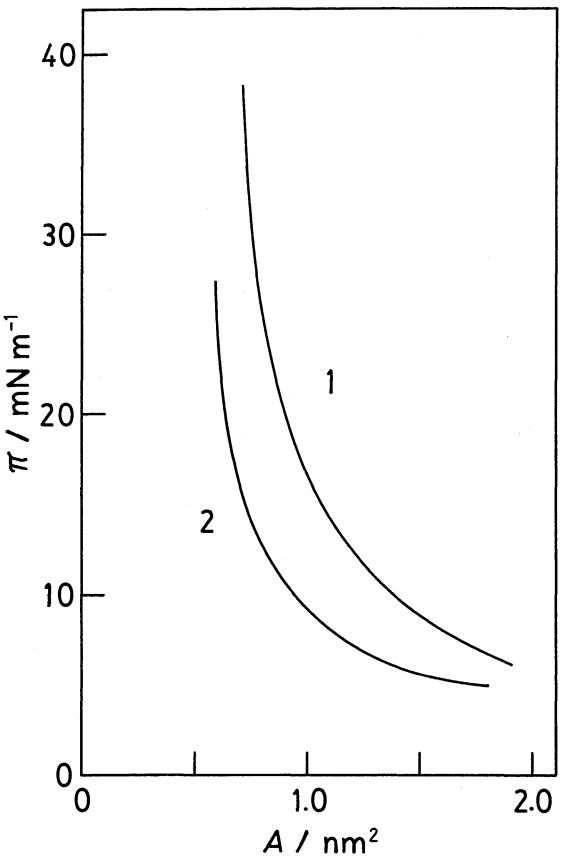

Fig. 5. Interfacial pressure vs. area per molecule curves at 298.15 K under atmospheric pressure: (1) DTAC/H system; (2) DTAC/A system.

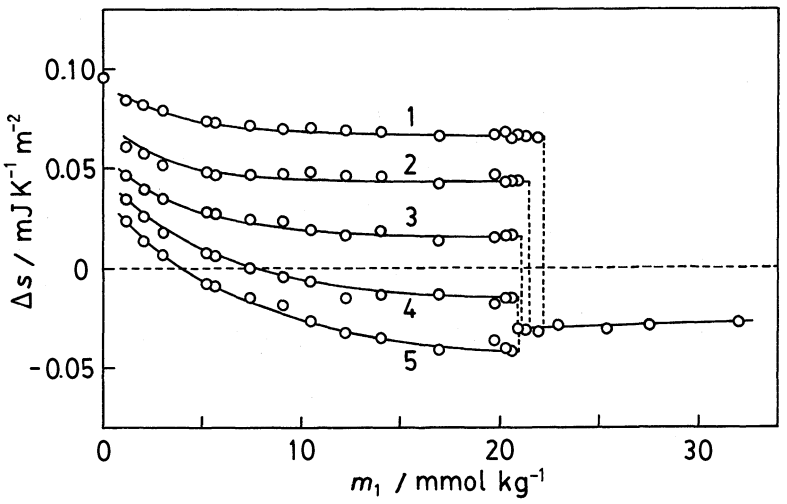

Fig. 6. Entropy change associated with adsorption vs. molality curves at constant temperature under atmospheric pressure: (1) T=288.15 K; (2) 293.15; (3) 298.15; (4) 303.15; (5) 308.15.

partial molar entropy of surfactant in the solution, and the number of surfactant ion in the micelle particle, respectively. Here, Eqs. 6 and 7 were derived on the assumption that the micelle formation can be treated thermodynamically like the appearance of a new macroscopic phase when its thermodynamic quantities are given by the excess thermodynamic quantities similar to those used for the adsorbed film. In Fig. 6, the entropy changes evaluated are plotted against molality at various temperatures. The value of $\Delta s(1)$ is found to decrease with increasing concentration and temperature. On the other hand, the value of $\Delta s(\mathrm{M})$ exhibits little dependence on m_1 and T. These results indicate that the temperature dependence of entropy of the adsorbed film is similar to that of the micelle through markedly different from that of the aqueous solution. Now it is important to note that the $\Delta s(\mathrm{M})$ value of the DTAC/H system is negative while that of the DTAC/A system is positive. In Fig. 7, the $\Delta s/\Gamma_1^{\mathrm{H}}$ vs. m_1 curve is drawn together with that of the DTAC/A system[12] at 298.15 K.

Here, let us consider the difference between the entropies in the solution and micelle at the cmc. The entropy of micelle formation at the cmc is defined by

$$\Delta_{\mathrm{W}}^{\mathrm{M}}s = s^{\mathrm{M}}/N_1^{\mathrm{M}} - s_1^{\mathrm{W}} \tag{8}$$

and evaluated by use of the relation

$$\Delta_{\mathrm{W}}^{\mathrm{M}}s = [\Delta s(1) - \Delta s(\mathrm{M})]/\Gamma_1^{\mathrm{H}}. \tag{9}$$

The $\Delta_{\mathrm{W}}^{\mathrm{M}}s$ value is plotted against T in Fig. 8. It is alternatively evaluated by applying the equation

$$\Delta_{\mathrm{W}}^{\mathrm{M}}s = -(2RT/C)(\partial C/\partial T)_p \tag{10}$$

to the C vs. T curve drawn in Fig. 3. The comparison

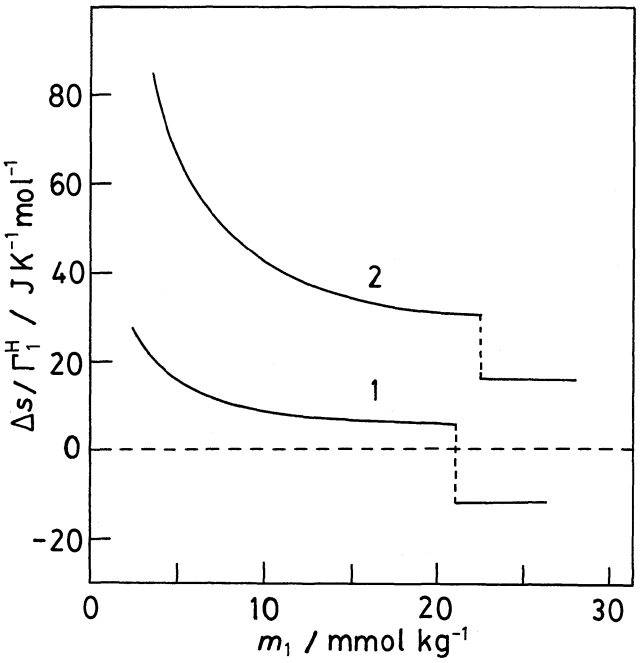

Fig. 7. Entropy change associated with adsorption per mole of surfactant vs. molality curves at 298.15 K under atmospheric pressure: (1) DTAC/H system; (2) DTAC/A system.

between them are also made in Fig. 8; the agreement is satisfactory. This proves that the assumption described above is probable at a concentration near the cmc. Furthermore, the $\Delta_{\mathrm{W}}^{\mathrm{M}}s$ vs. T curve of the DTAC/H system is compared with the curve of the DTAC/A system in Fig. 8. Both the curves seem to be close to each other. Thus, it is found that the micelle formation of DTAC in the DTAC/H system is similar to that in the DTAC/A system. This finding tells us that the difference in $\Delta s(\mathrm{M})$ between the DTAC/H and

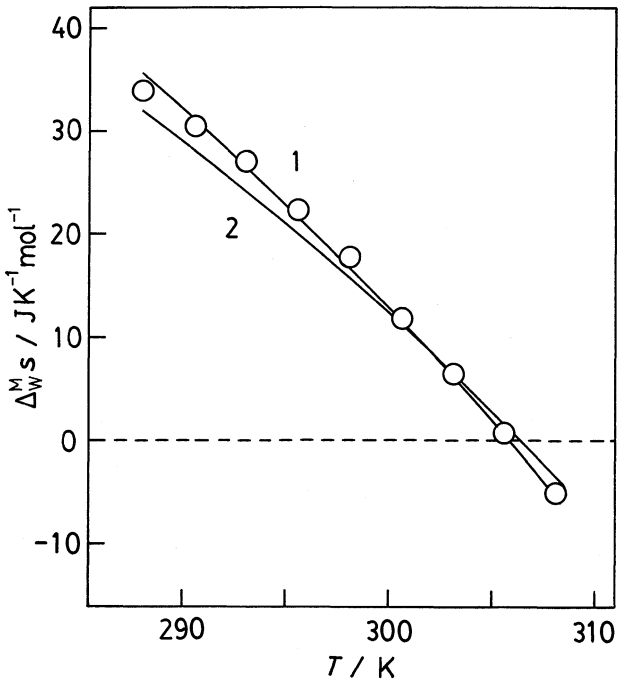

Fig. 8. Entropy of micelle formation vs. temperature curves under atmospheric pressure: (O) Eq. 9; (—) Eq. 10; (1) DTAC/H system; (2) DTAC/A system.

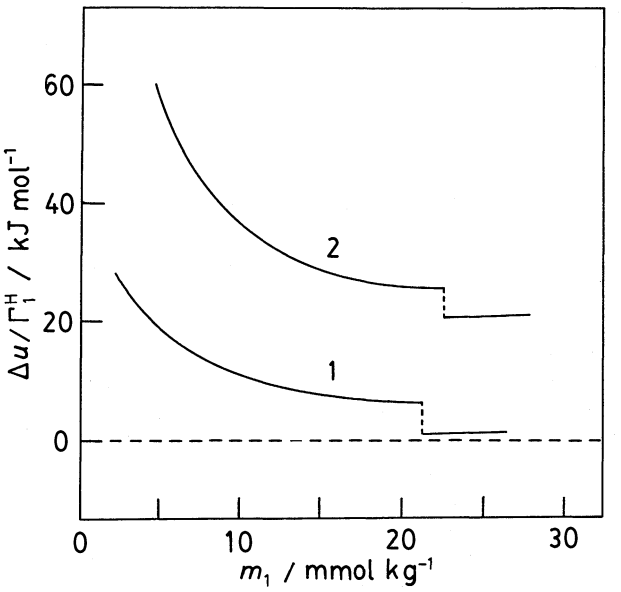

Fig. 9. Energy change associated with adsorption per mole of surfactant vs. molality curves at 298.15 K under atmospheric pressure: (1) DTAC/H system; (2) DTAC/A system.

DTAC/A systems stems from the difference in s^H. Therefore, remembering the results given in Fig. 7, we can conclude that the DTAC molecules adsorbed at water/hexane interface are forced to have a fairly restricted conformation as compared with those at water/air interface. The corresponding results of DAC support this view.[17]

The energy change associated with the adsorption of surfactant from its monomeric state, $\Delta u(1)$, and that from its micellar state, $\Delta u(M)$, are obtained respectively by the equations

$$\Delta u(1) = \gamma + T\Delta s(1) - p\Delta v(1) \quad (11)$$

and

$$\Delta u(M) = \gamma + T\Delta s(M) - p\Delta v(M), \quad (12)$$

where $\Delta v(1)$ and $\Delta v(M)$ are the corresponding volume changes. The Δu value was estimated numerically by making use of γ and Δs values given in Figs. 1 and 6 since the $p\Delta v$ terms are negligibly small compared with other terms under atmospheric pressure.[7-10] The results are shown in the form of $\Delta u/\Gamma_1^H$ vs. m_1 curve at 298.15 K in Fig. 9, where for comparison the curve of the DTAC/A system is also depicted. Further, the plot of the energy of micelle formation $\Delta_W^M u$ defined by a similar equation to Eq. 8 against T are compared between the DTAC/H and DTAC/A systems at the cmc in Fig. 10. Taking into account that the $\Delta_W^M u$ vs. T curves of both systems are quite similar to each other,

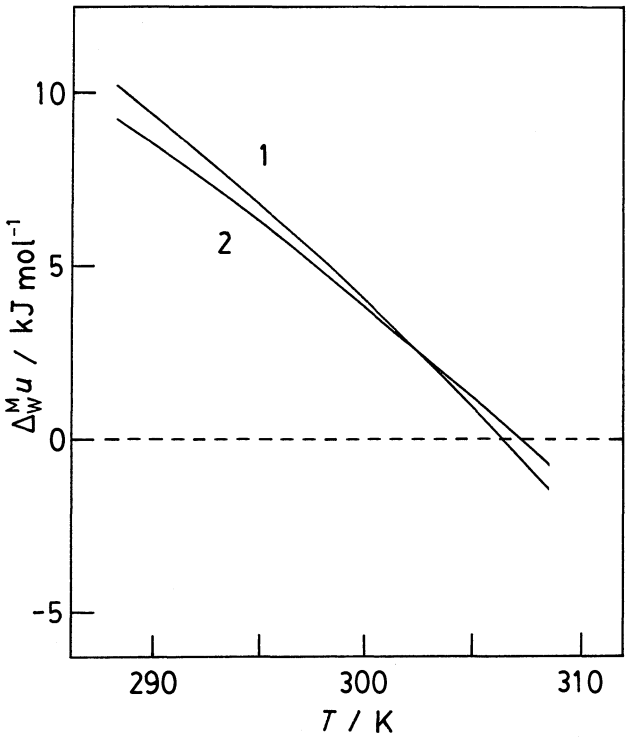

Fig. 10. Energy of micelle formation vs. temperature curves under atmospheric pressure: (1) DTAC/H system; (2) DTAC/A system.

the u^H value of the DTAC/A is said to be significantly larger than that of the DTAC/H system. It is clear that this large u^H value is closely related to the large s^H value cited above. In the case of DAC, an analogous

behavior is obtained. These results indicate that the adsorption of surfactant at the interfaces is remarkably affected by the air phase coexisting with its aqueous solution.

References

1) A. W. Ralston and D. N. Eggenberger, *J. Phys. Chem.*, **70**, 983 (1948).
2) N. D. Weiner, H. C. Parreira, and G. Zografi, *J. Pharm. Sci.*, **55**, 187 (1966).
3) S. J. Rehfeld, *J. Phys. Chem.*, **71**, 739 (1967).
4) B. R. Vijayendran and T. P. Brush, *J. Colloid Interface Sci.*, **68**, 383 (1979).
5) D. S. Murphy and M. J. Rosen, *J. Phys. Chem.*, **92**, 2870 (1988).
6) M. Yamanaka, N. Aratono, H. Iyota, K. Motomura, and R. Matuura, *Bull. Chem. Soc. Jpn.*, **55**, 2744 (1982).
7) M. Yamanaka, H. Iyota, M. Aratono, K. Motomura, and R. Matuura, *J. Colloid Interface Sci.*, **94**, 451 (1983).
8) M. Yamanaka, M. Aratono, K. Motomura, and R. Matuura, *Colloid Polym. Sci.*, **262**, 338 (1984).
9) M. Yamanaka, M. Aratono, and K. Motomura, *Bull. Chem. Soc. Jpn.*, **59**, 2695 (1986).
10) M. Yamanaka, M. Aratono, Y. Hayami, and K. Motomura, *Colloid Polym. Sci.*, **268**, 70 (1990).
11) K. Motomura, S. Iwanaga, M. Yamanaka, M. Aratono, and R. Matuura, *J. Colloid Interface Sci.*, **86**, 151 (1982).
12) M. Aratono, T. Okamoto, and K. Motomura, *Bull. Chem. Soc. Jpn.*, **60**, 2361 (1987).
13) N. Matubayasi, K. Motomura, S. Kaneshina, M. Nakamura, and R. Matuura, *Bull. Chem. Soc. Jpn.*, **50**, 523 (1977).
14) K. Motomura, S. Iwanaga, S. Uryu, H. Matsukiyo, M. Yamanaka, and R. Matuura, *Colloids Surf.*, **9**, 19 (1984).
15) M. Aratono, T. Okamoto, N. Ikeda, and K. Motomura, *Bull. Chem. Soc. Jpn.*, **61**, 2773 (1988).
16) K. Motomura, I. Kajiwara, N. Ikeda, and M. Aratono, *Colloids Surf.*, **38**, 61 (1989).
17) K. Motomura, S. Iwanaga, Y. Hayami, S. Uryu, and R. Matuura, *J. Colloid Interface Sci.*, **80**, 32 (1981).

Crystal Structures of Polymorphic $[Fe_4(\eta^5\text{-}C_5H_5)_4S_4](PF_6)$

Mamoru SHIMOI,* Asako SATOH, and Hiroshi OGINO*
Department of Chemistry, Faculty of Science, Tohoku University,
Aoba-ku, Sendai 980
(Received June 30, 1990)

$[Fe_4(\eta^5\text{-}C_5H_5)_4S_4](PF_6)$ crystals showed polymorphism depending on the recrystallization conditions. Recrystallization from acetonitrile-H_2O solution gave monoclinic crystals: $C2/c$ with lattice constants a=18.555(2), b=7.650(1), c=17.850(3) Å, β=96.81(2)°, and Z=4. Recrystallization from *N*,*N*-dimethylacetamide-ether solution gave tetragonal crystals: $I\bar{4}$ with lattice constants a=12.917(2), c=7.637(1) Å, and Z=2. Molecular structures of both crystal systems are almost the same as each other, if the structure for the latter was analyzed assuming that enantiomeric cations are disordered.

Cubane type metal clusters $[M_4L_4X_4]$ are known for many kinds of metals, terminal ligands L, and bridging ligands X.[1] Among them $[Fe_4(\eta^5\text{-}C_5H_5)_4S_4]^{n+}$ as well as $[Fe_4(\eta^5\text{-}C_5H_5)_4Se_4]^{n+}$ have been studied in relation to the structures of clusters and their oxidation states.[1–6] Molecular orbital calculation showed that $[Fe_4(\eta^5\text{-}C_5H_5)_4S_4]^+$ has a lower symmetry, D_2, than the D_{2d} symmetries of $[Fe_4(\eta^5\text{-}C_5H_5)_4S_4]$ and $[Fe_4(\eta^5\text{-}C_5H_5)_4S_4]^{2+}$ due to a first-order Jahn–Teller effect.[5] In fact, Dahl et al. reported that the Fe_4 core of $[Fe_4(\eta^5\text{-}C_5H_5)_4S_4]$ Br has D_2 symmetry.[4]

In the course of our study for isolation of $[Fe_4(\eta^5\text{-}C_5H_5)_4S_4]^{n+}$ species,[7] we found polymorphism of the hexafluorophosphate of the monocation: monoclinic and tetragonal. As will be shown below, the space group of the tetragonal crystal was determined to be $I\bar{4}$. This space group would impose D_{2d} symmetry on the cation, which contradicts the molecular orbital calculation. To elucidate the origin of this discrepancy, we undertook the X-ray crystal structure analyses for both forms.

Experimental

Materials. $[Fe_4(\eta^5\text{-}C_5H_5)_4S_4]$ (PF_6) was prepared as described in a preceding report.[7]

Crystal Structure Determination of Monoclinic $[Fe_4(\eta^5\text{-}C_5H_5)_4S_4](PF_6)$. An acetonitrile solution of $[Fe_4(\eta^5\text{-}C_5H_5)_4S_4]$ (PF_6) was layered on water in a test tube and allowed to stand for 5 days. The slow diffusion of water into acetonitrile gave black crystals with parallelepiped shape. A crystal with the dimensions 0.1×0.1×0.3 mm was used for the collection of intensity data. The data with $3<2\theta/°<60$ were collected with Mo $K\alpha$ radiation monochromated by graphite, applying ω–2θ scan mode with the use of a Rigaku AFC-6A automated four-circle diffractometer. The unit cell dimensions were determined by the least-squares method with 71 reflection data ($25<2\theta/°<30$). The crystal data are listed in Table 1. The probable space group is either Cc or $C2/c$ according to the systematic absence. The successful

Table 1. Crystal Data of Monoclinic and Tetragonal $[Fe_4(\eta^5\text{-}C_5H_5)_4S_4](PF_6)$

Formula	$C_{20}H_{20}F_6Fe_4PS_4$	$C_{20}H_{20}F_6Fe_4PS_4$
Formula weight	756.99	756.99
Crystal system	Monoclinic	Tetragonal
Space group	$C2/c$	$I\bar{4}$
Systematic absence	$h\ k\ l$: $h+k=2n+1$ $h\ 0\ l$: $l=2n+1$	$h\ k\ l$: $h+k+l=2n+1$
a/Å	18.555 (2)	12.917 (2)
b/Å	7.650 (1)	
c/Å	17.850 (3)	7.637 (1)
β/°	96.81 (2)	
Z	4	2
V/Å^3	2515.9 (7)	1274.2 (3)
D_m/g cm^{-3}	2.00	1.98
D_c/g cm^{-3}	2.00	1.97
μ(Mo $K\alpha$)/cm^{-1}	27.5	27.1
Crystal size/mm	0.1×0.1×0.3	0.1×0.2×0.3
Scan mode	2θ–ω	2θ–ω
$2\theta_{max}$/°	60	60
Reflcns measd	$\pm h, k, l$	h, k, l
No. of reflcns measd	4758	2150
No. of reflcns used ($\lvert F_o\rvert > 3\sigma(F_o)$)	2309	590
R[a]	0.053	0.052
R_w[b]	0.067	0.052

a) $R=\sum\lvert\lvert F_o\rvert-\lvert F_c\rvert\rvert/\sum\lvert F_o\rvert$. b) $R_w=[\sum w(\lvert F_o\rvert-\lvert F_c\rvert)^2/\sum w\lvert F_o\rvert^2]^{1/2}$; $w=[\sigma^2(\lvert F_o\rvert)+aF_o^2]^{-1}$, where a=0.0015 for monoclinic $[Fe_4(\eta^5\text{-}C_5H_5)_4S_4](PF_6)$. Unit weighting scheme was applied for tetragonal $[Fe_4(\eta^5\text{-}C_5H_5)_4S_4](PF_6)$.

refinement justified the choice of the latter centrosymmetric space group. The conventional heavy atom method was used: A Patterson function gave the positions of two iron atoms, two sulfur atoms, and a phosphorus atom. Other non-hydrogen atoms were located by successive block-diagonal least-squares and Fourier syntheses. Anisotropic temperature factors were applied to non-hydrogen atoms. The hydrogen atoms were located from a difference Fourier synthesis and refined with isotropic temperature factors. Convergence was reached at R=0.053 and R_w=0.067. A final difference Fourier synthesis was virtually featureless.

Crystal Structure Determination of Tetragonal [$Fe_4(\eta^5$-$C_5H_5)_4S_4$] (PF_6). Black columnar tetragonal crystals were obtained by slow diffusion of diethyl ether into a *N,N*-dimethylacetamide solution of [$Fe_4(\eta^5$-$C_5H_5)_4S_4$] (PF_6). A crystal with the dimensions 0.1×0.2×0.3 mm was used for the collection of the intensity data. Crystal data is also included in Table 1. Of the possible space groups, $I4$, $I\bar{4}$, and $I4/m$ according to the systematic absence, $I\bar{4}$ was chosen because a four-fold axis cannot be imposed on the cubane cluster. The structure was solved by the heavy atom method: the positions of each one of the iron and sulfur atoms were obtained from a Patterson function, and the positions of carbon, phosphorus, and fluorine atoms were deduced from successive least-squares and Fourier syntheses. However, unrestricted refinement gave quite large thermal parameters. Therefore the crystal was considered to be disordered. Each atom except for the phosphorus atom on a special position was divided into two halves applying 50% occupancy factors for each atom, for the reason mentioned in the discussion. Anisotropic temperature factors were applied for iron, sulfur, and phosphorus atoms and isotropic ones for carbon and fluorine atoms. The final R value was 0.052.

All the calculations were carried out on an NEC ACOS-2000 computer at the computer center of Tohoku University, using Universal Crystallographic Computation Program System UNICS III.[8] The atomic scattering factors were taken from Ref. 9 for non-hydrogen atoms and from Ref. 10 for hydrogen atoms.

Table 2. Final Atomic Parameters for Monoclinic [$Fe_4(\eta^5$-$C_5H_5)_4S_4$](PF_6) (Coordinates are multiplied by 10^4.)

Atom	x	y	z	B_{eq}/Å^2
Fe(1)	168.6 (4)	2296.4 (10)	1610.6 (4)	2.8
Fe(2)	890.3 (4)	−24.9 (9)	2517.4 (4)	2.6
S(1)	−66.6 (7)	−496 (2)	1683.6 (8)	2.8
S(2)	768.1 (7)	2773 (2)	2732.7 (8)	3.1
C(11)	−315 (4)	3831 (10)	712 (4)	4.6
C(12)	263 (4)	4742 (8)	1105 (4)	4.4
C(13)	893 (4)	3766 (10)	1040 (4)	4.6
C(14)	701 (4)	2290 (10)	612 (4)	5.2
C(15)	−54 (4)	2358 (10)	408 (4)	5.3
C(21)	1558 (3)	−1705 (10)	1947 (4)	4.5
C(22)	1431 (3)	−2392 (8)	2654 (5)	4.7
C(23)	1722 (3)	−1236 (10)	3219 (4)	4.9
C(24)	2027 (3)	151 (10)	2864 (5)	5.3
C(25)	1930 (3)	−124 (10)	2093 (4)	4.8
P(1)	2500	2500	5000	4.8
F(1)	2060 (3)	3820 (9)	5450 (3)	8.5
F(2)	2845 (3)	1666 (9)	5770 (3)	8.0
F(3)	1839 (3)	1206 (9)	4970 (4)	9.5

Results and Discussion

Description of the Crystal Structure of Monoclinic [$Fe_4(\eta^5$-$C_5H_5)_4S_4$] (PF_6). The positional and equivalent isotropic temperature factors are listed in Table 2. The bond lengths and angles are listed in Table 3.[11] The structure of the cubane cation is shown in Fig. 1. A crystallographic C_2 axis passes through the centers of the Fe(1)–Fe(1′) and Fe(2)–Fe(2′) bonds. Thus the Fe(1)–Fe(2) bond is equivalent to the Fe(1′)–Fe(2′) bond and the Fe(1)–Fe(2′) bond is equivalent to the Fe(1′)–Fe(2) bond. Furthermore, the interatomic distances of Fe(1)–Fe(1′) and Fe(2)–Fe(2′) are almost the same (3.308 (4) and 3.297 (2) Å). Therefore, the Fe_4 core has approximate D_2 symmetry: opposite bonds of the tetrahedron are equivalent. This feature is compatible with the structure predicted by a molecular orbital calculation.[5] Due to a first-order Jahn–Teller effect, [$Fe_4(\eta^5$-$C_5H_5)_4S_4$]$^+$ should have D_2 symmetry which is lower than the D_{2d} symmetry of [$Fe_4(\eta^5$-$C_5H_5)_4S_4$] and [$Fe_4(\eta^5$-$C_5H_5)_4S_4$]$^{2+}$.[5] Nineteen cluster

Table 3. Selected Bond Lengths (l) and Bond Angles (ϕ) for Monoclinic [$Fe_4(\eta^5$-$C_5H_5)_4S_4$](PF_6)

Bond length	(l/Å)	Bond length	(l/Å)
Fe(1)-Fe(1′)	3.308 (4)	Fe(1)-Fe(2′)	3.188 (2)
Fe(2)-Fe(2′)	3.297 (2)	Fe(1)-Fe(2)	2.656 (2)
Fe(1)-S(1)	2.187 (2)	Fe(2)-S(1)	2.207 (2)
Fe(2)-S(2)	2.191 (2)	Fe(2′)-S(1)	2.240 (3)
Fe(1)-S(2)	2.203 (3)	Fe(1)-S(2′)	2.239 (3)
Bond angle	**(ϕ/°)**	**Bond angle**	**(ϕ/°)**
S(1)-Fe(1)-S(2)	100.97 (11)	S(1)-Fe(2)-S(1′)	81.26 (9)
S(1)-Fe(2)-S(2)	100.73 (8)	S(2)-Fe(2)-S(1′)	87.30 (9)
Fe(1)-S(1)-Fe(2)	74.36 (6)	Fe(1)-S(1)-Fe(2′)	92.11 (8)
Fe(1)-S(2)-Fe(2)	74.36 (9)	Fe(2)-S(1)-Fe(2′)	95.71 (13)
S(1)-Fe(1)-S(2′)	87.43 (8)	Fe(1)-S(2)-Fe(1′)	96.28 (8)
S(2)-Fe(1)-S(2′)	80.60 (12)	Fe(2)-S(2)-Fe(1′)	92.04 (8)
Fe(1′)-Fe(1)-Fe(2)	63.52 (6)	Fe(2′)-Fe(1)-Fe(2)	68.00 (4)
Fe(1′)-Fe(1)-Fe(2′)	48.22 (5)	Fe(1)-Fe(2′)-Fe(2)	48.31 (3)
Fe(1′)-Fe(2′)-Fe(2)	63.69 (3)	Fe(1′)-Fe(2′)-Fe(1)	68.26 (4)

Table 4. Comparison of Bond Lengths (l) and Bond Angles[a] (ϕ) between $[Fe_4(\eta^5\text{-}C_5H_5)_4S_4]Br$ and Monoclinic and Tetragonal $[Fe_4(\eta^5\text{-}C_5H_5)_4S_4](PF_6)$

Bond length[d]	$[Fe_4(\eta^5\text{-}C_5H_5)_4S_4]Br$[b] l/Å	Monoclinic $[Fe_4(\eta^5\text{-}C_5H_5)_4S_4](PF_6)$[c] l/Å	Tetragonal $[Fe_4(\eta^5\text{-}C_5H_5)_4S_4](PF_6)$[c] l/Å
Fe(1)-Fe(1′)	3.319 (3)	3.303 (3)[a]	3.302 (6)[a]
Fe(1)-Fe(2′)	3.188 (3)	3.188 (2)	3.213 (4)
Fe(1)-Fe(2)	2.652 (5)[a]	2.656 (2)	2.631 (4)
Fe(1)-S(1)	2.186 (5)	2.187 (2)	2.178 (6)
Fe(2)-S(1)	2.210 (5)	2.207 (2)	2.147 (6)
Fe(1)-S(2)	2.214 (5)	2.203 (3)	2.238 (6)
Fe(2)-S(2)	2.183 (5)	2.191 (2)	2.211 (6)
Fe(1)-S(2′)	2.245 (5)	2.239 (3)	2.278 (6)
Fe(2′)-S(1)	2.246 (5)	2.240 (3)	2.227 (7)
Bond angle	ϕ/°	ϕ/°	ϕ/°
S(1)-Fe(1)-S(2)	100.9 (2)	100.85 (10)	101.12 (22)
Fe(1)-S(1)-Fe(2)	74.2 (2)	74.36 (8)	73.74 (19)
S(1)-Fe(1)-S(2′)	87.5 (2)	87.37 (9)	86.75 (22)
S(2)-Fe(1)-S(2′)	80.5 (2)	80.93 (11)	81.04 (23)
Fe(1)-S(1)-Fe(2′)	92.1 (2)	92.08 (8)	92.53 (21)
Fe(2)-S(1)-Fe(2′)	96.3 (2)	96.00 (11)	95.98 (24)

a) Average value. b) Ref. 4. c) This work. d) The atomic numbering schemes for the bromide and the tetragonal hexafluorophosphate are made to coincide with monoclinic $[Fe_4(\eta^5\text{-}C_5H_5)_4S_4](PF_6)$.

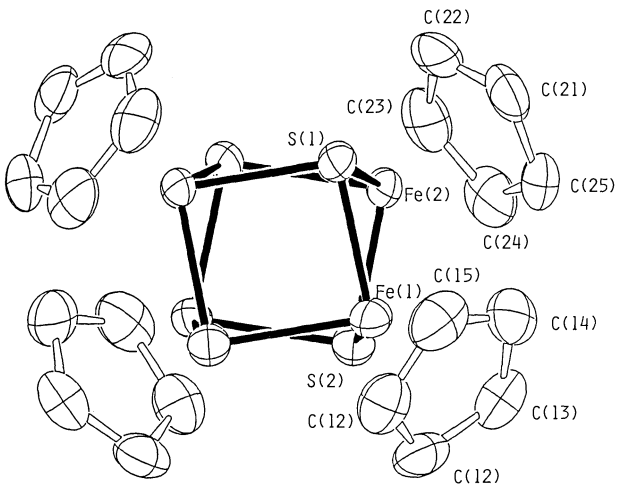

Fig. 1. ORTEP diagram of $[Fe_4(\eta^5\text{-}C_5H_5)_4S_4]^+$ ion in the monoclinic hexafluorophosphate. Hydrogen atoms are omitted for clarity.

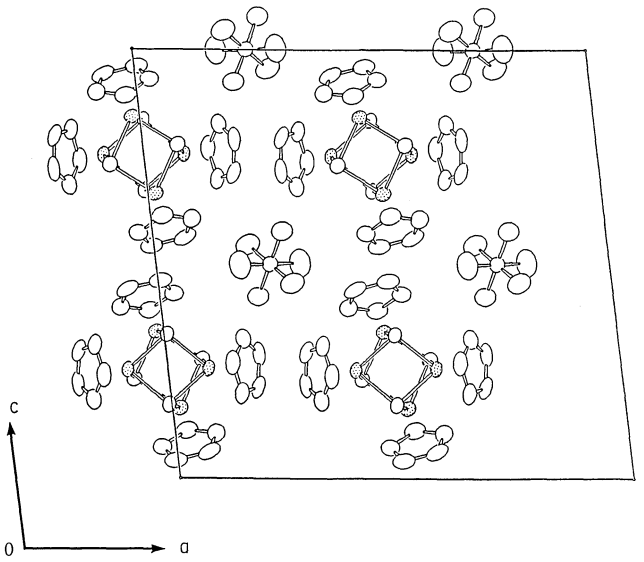

Fig. 2. Packing diagram of monoclinic $[Fe_4(\eta^5\text{-}C_5H_5)_4S_4](PF_6)$.

electrons in $[Fe_4(\eta^5\text{-}C_5H_5)_4S_4]^+$ result in a total Fe–Fe bond order of 2.5 for Fe_4 core. The two shortest Fe–Fe bonds (Fe(1)–Fe(2) and Fe(1′)–Fe(2′) are 2.656 (2) Å) correspond to those with bond order 1; the next shortest Fe–Fe bonds (Fe(1)–Fe(2′) and Fe(1′)–Fe(2) are 3.188 (2) Å) correspond to those with bond order 0.25, and the longest bonds (Fe(1)–Fe(1′) and Fe(2)– Fe(2′)), to those with bond order 0.

The structure is quite similar to that already reported for the monocation complex, $[Fe_4(\eta^5\text{-}C_5H_5)_4S_4]Br$.[4] A comparison of the bond lengths and angles including the tetragonal hexafluorophosphate is shown in Table 4. The only difference between the bromide and the monoclinic hexafluorophosphate is that a crystallographic C_2 axis passes through the shortest Fe–Fe bonds for the former, but passes through the longest ones for the latter.

Figure 2 shows the packing diagram of a unit cell. A cation is surrounded by four anions tetrahedrally and four cations form a square surrounding an anion. This packing mode is similar to those for PdO, PtO, and PtS.[12]

Description of Crystal Structure of Tetragonal $[Fe_4(\eta^5\text{-}C_5H_5)_4S_4](PF_6)$. Atomic parameters are shown in Table 5. The bond lengths and angles are listed in Table 4.[11] Figure 3 shows the ORTEP diagram of the

Table 5. Final Atomic Parameters for Tetragonal $[Fe_4(\eta^5\text{-}C_5H_5)_4S_4](PF_6)$
(Coordinates for Fe, S, and P atoms are multiplied by 10^4 and those for C and F atoms are 10^3.)

Atom	x	y	z	B_{eq}/Å^2
Fe(1A)	948 (2)	870 (2)	1151 (3)	4.0
Fe(1B)	1157 (3)	524 (2)	1181 (4)	5.4
S(1A)	974 (5)	487 (4)	−1626 (6)	5.3
S(1B)	859 (4)	761 (4)	−1642 (5)	4.9
P(1)	0	5000	2500	18.5
Atom	x	y	z	B_{iso}
C(11A)	239 (2)	89 (2)	258 (3)	6.9 (6)
C(11B)	175 (3)	194 (3)	238 (5)	11.4 (11)
C(12A)	152 (2)	134 (2)	360 (3)	6.0 (5)
C(12B)	181 (1)	93 (1)	356 (3)	4.7 (4)
C(13A)	114 (2)	210 (2)	302 (3)	5.7 (5)
C(13B)	245 (2)	31 (2)	279 (4)	8.1 (7)
C(14A)	167 (2)	236 (2)	131 (3)	6.2 (5)
C(14B)	277 (3)	74 (3)	126 (5)	11.5 (10)
C(15A)	259 (1)	135 (1)	92 (3)	4.9 (4)
C(15B)	225 (1)	181 (1)	112 (3)	5.2 (4)
F(1A)	−33 (2)	385 (2)	312 (4)	17.2 (10)
F(1B)	−31 (4)	401 (3)	179 (6)	26.0 (17)
F(2A)	−46 (4)	468 (4)	48 (8)	18.0 (20)
F(2B)	−59 (4)	463 (5)	442 (9)	21.4 (24)

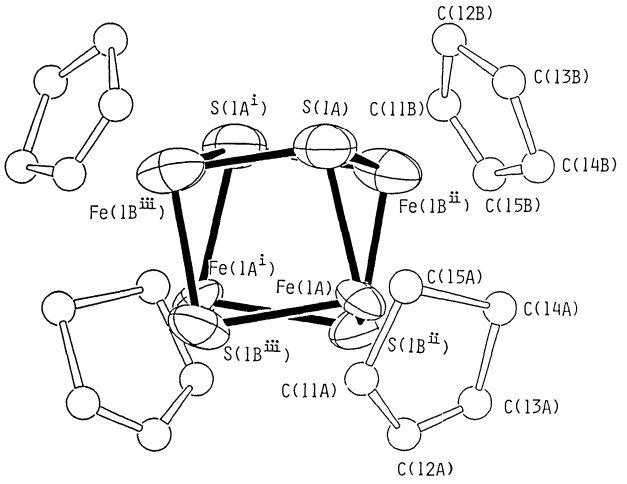

Fig. 3. ORTEP diagram of $[Fe_4(\eta^5\text{-}C_5H_5)_4S_4]^+$ ion in the tetragonal hexafluorophosphate. The atomic numbering scheme corresponds to that in Table 4 as follows: Fe(1A)=Fe(2), Fe(1A^{i})=Fe(1′), Fe(1B^{ii})=Fe(2), Fe(1B^{iii})=Fe(2′), S(1A)=S(1), S(1A^{i})=S(1′), S(1B^{ii})=S(2), S(1B^{iii})=S(2), (Key to the symmetry operation; i, $-x$, $-y$, z; ii, y, $-x$, $-z$; iii, $-y$, x, $-z$).

cation. The conventional analysis applying the space group $I\bar{4}$ gave the cation D_{2d} symmetry which is incompatible with the molecular orbital calculation. Furthermore it gave quite large thermal parameters for the iron, sulfur, and carbon atoms. Therefore we adopted a disordered model by dividing these atoms into two halves, respectively. Thus this model gave a pair of enantiomeric cation structures which has approximate D_2 symmetry, compatible with the molecular orbital calculation. Thermal parameters and reliability factors thus obtained are reasonable. Bond lengths and angles are similar to the monoclinic hexafluorophosphate and the bromide (Table 4). The PF_6 anion showed also a disordered pattern around $\bar{4}$ (S_4) axis.

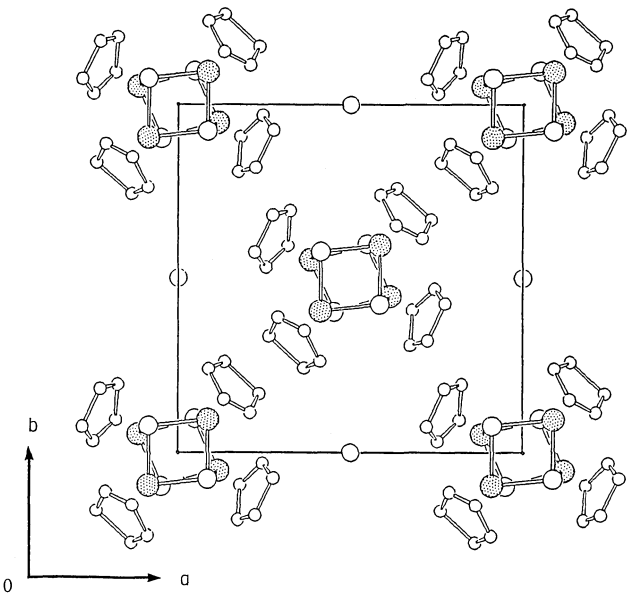

Fig. 4. Packing diagram of tetragonal $[Fe_4(\eta^5\text{-}C_5H_5)_4S_4](PF_6)$. Only one orientation of the disordered pairs of cations is depicted and fluorine atoms are omitted for clarity.

Figure 4 shows the packing diagram, only one orientation of disordered molecules being shown for clarity. A cation is surrounded by four anions tetrahedrally and an anion vice versa, in a deformed zinc blende type packing.[12]

The apparent D_{2d} symmetry for tetragonal $[Fe_4(\eta^5\text{-}C_5H_5)_4S_4](PF_6)$ is derived from the disordered packing of enantiomers with D_2 symmetry. The lower density for the tetragonal crystal reflects the disordered packing.

References

1) S. Harris, *Polyhedron*, **8**, 2843 (1989) and references therein.
2) R. A. Schunn, C. J. Fritchie, Jr., and C. T. Prewitt, *Inorg. Chem.*, **5**, 892 (1966).
3) C. H. Wei, G. R. Wilkes, P. M. Treichel, and L. F. Dahl, *Inorg. Chem.*, **5**, 900 (1966).
4) Trinh-Toan, W. P. Fehlhammer, and L. F. Dahl, *J. Am. Chem. Soc.*, **99**, 402 (1977).
5) Trinh-Toan, B. K. Teo, J. A. Ferguson, T. J. Meyer, and L. F. Dahl, *J. Am. Chem. Soc.*, **99**, 408 (1977).
6) H. Ogino, H. Tobita, K. Yanagisawa, M. Shimoi, and C. Kabuto, *J. Am. Chem. Soc.*, **109**, 5841 (1987).
7) H. Ogino, A. Satoh, and M. Shimoi, *Bull. Chem. Soc. Jpn.*, **63**, 2314 (1990).
8) T. Sakurai and K. Kobayashi, *Rikagaku Kenkyuusho Hokoku*, **55**, 69 (1979).

9) "International Tables for X-Ray Crystallography," Kynoch, Birmingham, England (1974), Vol. IV, Tables 2.2A and 2.3.1.

10) R. F. Stewart, E. R. Davidson, and W. T. Simpson, *J. Chem. Phys.*, **42**, 3175 (1965).

11) Some additional bond lengths and angles, the positional and thermal parameters of hydrogen atoms, the final anisotropic thermal parameters, and F_o-F_c tables are deposited as Document No. 9091 at the Office of the Editor of Bull. Chem. Soc. Jpn.

12) R. C. Evans, "An Introduction to Crystal Chemistry," 2nd ed, Cambridge University Press, Cambridge (1964).

Nucleophilic Substitution Reactions between Diphosphonate and Orthophosphate Characterized by High-Performance Liquid Chromatography and ^{31}P NMR Spectroscopy

Norimasa YOZA,* Miki OKAMATSU, Noriko TOKUSHIGE, Tohru MIYAJIMA, and Yoshinobu BABA†
Department of Chemistry, Faculty of Science, Kyushu University,
Hakozaki, Fukuoka 812
†Kobe Women's College of Pharmacy, Kitamachi, Motoyama,
Higashinada, Kobe 658
(Received July 5, 1990)

Inorganic diphosphonate with phosphorus of an oxidation number +3 was found to react with orthophosphate (oxidation number +5) at 50 °C to give phosphonylated compounds; dimeric isohypophosphate (oxidation numbers +3 and +5) and a novel trimeric compound (oxidation numbers +3 and +5). Orthophosphate ion is considered to act as a ligand with two or three nucleophilic sites that were phosphonylated stepwise by diphosphonate. Kinetic processes of the nucleophilic reactions were monitored by HPLC and ^{31}P NMR. Two products, the dimer having one P–H bond and the trimer with two P–H bonds, were well-resolved by HPLC and their yields, based on orthophosphate applied, were 85% (dimer) and 3% (trimer) when a mixed solution of 0.5 M diphosphonate and 0.1 M orthophosphate was incubated at 50 °C for 21 h. A complicated ^{31}P NMR spectrum that indicated a large coupling constant(J_{PH}=650 Hz) and grew with incubation time is reasonably assigned to the unsymmetrical isohypophosphate composed of both a phosphate group and a phosphonate group. Apparent formation constants of the dimer and trimer were evaluated.

Inorganic diphosphonate,[1,2] $P^{III}P^{III}$, a dimeric form of phosphonate(phosphite), P^{III}, has been characterized to be very reactive as an acceptor in a nucleophilic substitution reaction in Eq. 1 and its wide applicability in phosphonylating various nucleophilic biomolecules and inorganic phosphorus compounds(R) has been demonstrated.[3–11]

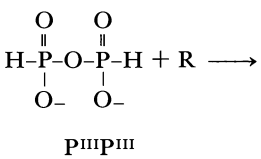

$P^{III}P^{III}$

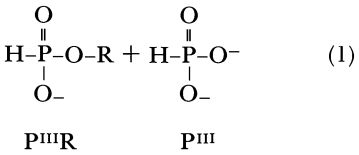

(1)

$P^{III}R$ P^{III}

Each phosphorus compound was expressed by an abbreviated nonation based on the arrangement of structural constituents; phosphonyl group with a P–H bond, P(III), and/or phosphoryl group, P(V), and was shown for convenience in a dissociated form.

In the nucleophilic reaction in Eq. 1 one of phosphonyl groups in diphosphonate transfers to R to form a phosphonylated compound, $P^{III}R$, as exemplified by the phosphonylation of ADP which resulted in the formation of an ATP analogue having a terminal phosphonyl group, $P^{III}P^{V}P^{V}A$.[9] If orthophosphate ion, P^{V}, is used as R, isohypophosphate, $P^{III}P^{V}$, is expected to be formed according to Eq. 2 liberating phosphonate.

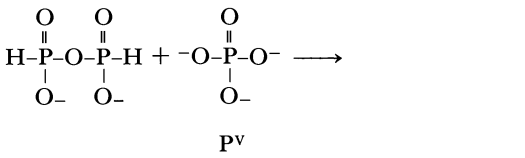

P^{V}

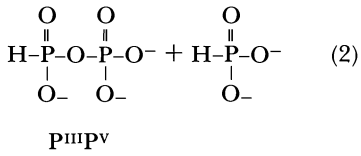

(2)

$P^{III}P^{V}$

Since orthophosphate ion is a ligand with three nucleophilic sites further addition of phosphonyl groups to the $P^{III}P^{V}$ is also expected to produce a trimeric compound in Eq. 3 and, with less probability, a branched compound with three phosphonyl groups, $P^{III}P^{V}(P^{III})P^{III}$.

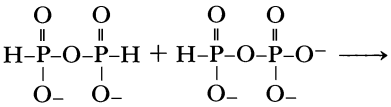

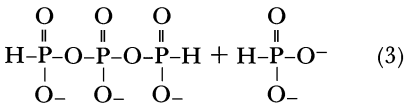

(3)

$P^{III}P^{V}P^{III}$

Attempts to characterize the substitution reactions in Eqs. 2 and 3 by gel chromatography had been made in our laboratory.[3,4] Analytical methodologies had been proposed capable of resolving and identifying such reaction products that were complex in structure and included unknown species. A preliminary experiment

with HPLC[5] and detailed experiments to give theoretical discussion about kinetics and mechanisms of the substitution reactions[6] have been reported. Baba's works[6] with advanced techniques, HPLC and ^{31}P NMR, presented more improved chromatographic resolution and structural diagnosis of reaction products. The present paper was undertaken to examine the usefulness and reliability of HPLC and ^{31}P NMR in practical synthetic experiments with diphosphonate. In accordance with the earlier observations these techniques were confirmed to be valuable for visualizing the reaction processes in Eqs. 2 and 3.

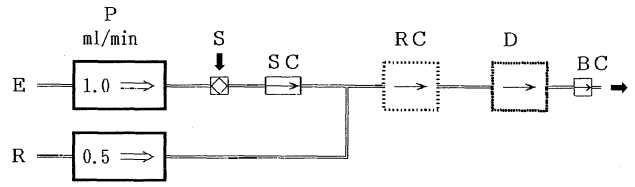

Fig. 1. HPLC system for the selective determination of P(V)-containing compounds. <P> Pump, <S> Sample injector, <SC> Separation column (4 mm I.D.×25 cm, TSK-gel SAX), <RC> Reaction coil (0.5 mm I.D.×20 m, 140 °C), <D> Spectrophotometric detector (820 nm, 650 nm), <BC> Back-pressure coil (0.3 mm I.D.×2 m), <E> Eluent, 0.25 M KCl+0.1% EDTA(4Na), <R> Mo(V)-Mo(VI) reagent.

Experimental

Chemicals. Disodium diphosphonate, $Na_2P_2H_2O_5$, was prepared according to the previous paper.[8] Other chemicals were guaranteed reagents from Wako (Osaka, Japan).

HPLC Measurement. Detailed procedures used for the analysis of phosphorus compounds by employing a high-temperature detection system (Fig. 1) have been shown in the previous papers.[7–11]

NMR Measurement. ^{31}P NMR measurement was made by use of a JEOL JNM-GX-400 (161.8 MHz) spectrometer. Orthophosphoric acid (85%) was used as an external standard.

Results and Discussion

Separation by HPLC. In order to monitor phosphorus compounds in Eqs. 2 and 3 the HPLC system in Fig. 1 was employed. The system consisted of an anion-exchange separation column (TSK-gel SAX) and a post-column detection system using a Mo(V)–Mo(VI) reagent.[7–11] The detection system was able to permit the selective detection of P(V)-units in the presence of P(III)-units. Hence, P^{V} and $P^{III}P^{V}$ in Eq. 2 were detectable, while $P^{III}P^{III}$ and P^{III} did not indicate HPLC peaks.

A mixed solution composed of 0.5 M diphosphonate ($Na_2P_2H_2O_5$, M=mol dm^{-3}) and 0.1 M orthophosphate (Na_2HPO_4) was allowed to stand at 50 °C for 24 h.

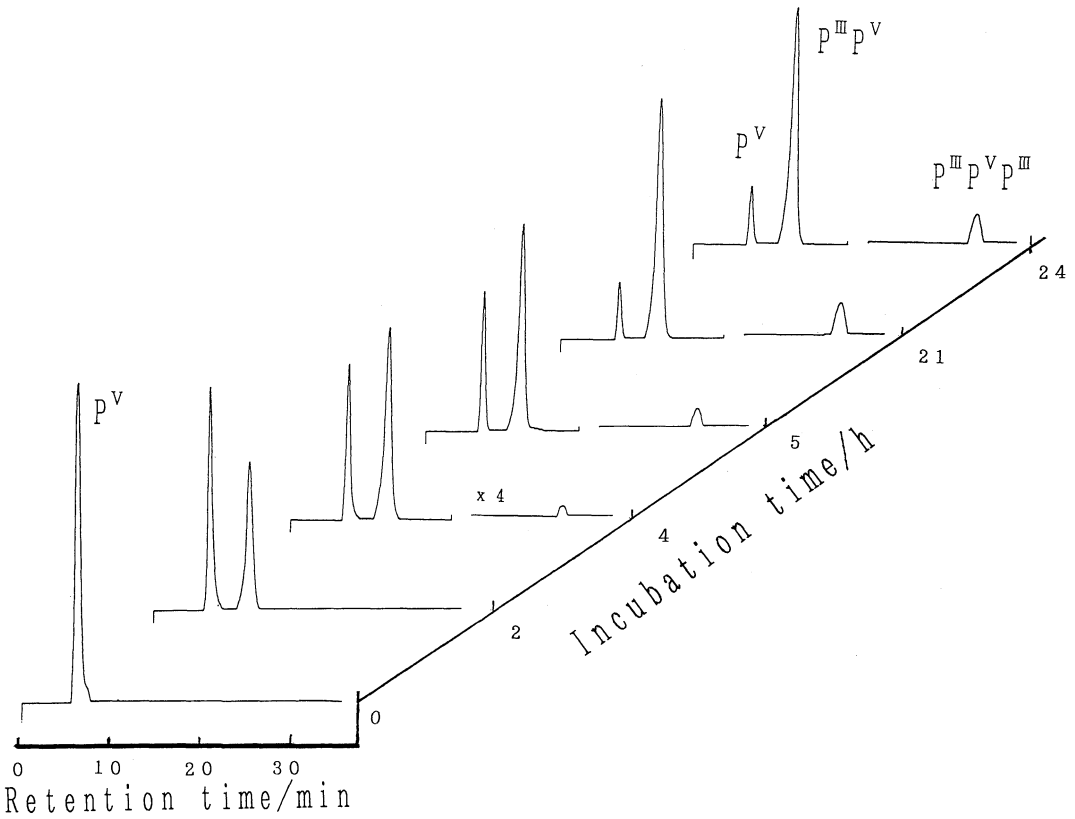

Fig. 2. HPLC profiles indicating progressive phosphonylation of orthophosphate by diphosphonate at 50 °C. <Sample> A mixed solution of 0.1 M P^{V} and 0.5 M $P^{III}P^{III}$.

The pH of the sample solution decreased with the progress of substitution reactions, from initial pH value ca. 7 to final ca. 5.5, because any buffer agents were not used to avoid their side reactions with diphosphonate. Aliquots of the incubated solution were 100-fold diluted and analyzed by HPLC at desired time-intervals to observe the progressive conversion of phosphorus compounds in Eqs. 2 and 3. As shown in Fig. 2 the peak height for $P^{III}P^{V}$ increased with time, in contrast to the decrease of the peak height for the starting material, P^{V}. The peaks for $P^{III}P^{V}P^{III}$ in Eq. 3 were recorded with 4-fold amplification after 4 h incubation. In should be noted that the distributions of P^{III} and $P^{III}P^{III}$ were confirmed by a separate detection method based on the preoxidation of P(III) to P(V) and the chemical compositions of $P^{III}P^{V}$ and $P^{III}P^{V}P^{III}$ were determined by differential analyses of P(III) and P(V) as shown in the previous papers.[3–7]

Since P(III) unit is not to be detected with this spectrophotometric detection method and each species in Fig. 2 includes one detectable P(V) unit per molecule, the relative peak areas of P^{V}, $P^{III}P^{V}$, and $P^{III}P^{V}P^{III}$, calculated by a data processor Shimadzu CR1-B, can be used to represent the relative molar concentrations of the three species. About 50% of the initial P^{V} was phosphonylated at 2 h to form $P^{III}P^{V}$. The relative amounts in molar concentration of P^{V}(12%), $P^{III}P^{V}$(85%), and $P^{III}P^{V}P^{III}$(3%) tended to become unchanged at 21—24 h, suggesting the attainment of equilibrium or steady states[8,9] of the substitution reactions.

The growing rates of the three peaks were dependent on the initial reactant concentrations. With decreased initial sample concentrations, 0.1 M diphosphonate and 0.1 M orthophosphate, the relative amount of $P^{III}P^{V}$ increased more slowly than that in Fig. 2 to attain 42% after 22 h and no peak for $P^{III}P^{V}P^{III}$ was observed. On the other hand, when the initial sample concentrations were increased to 0.25 M orthophosphate and 1.25 M diphosphonate, keeping the same molar ratio of the reactants as in Fig. 2, both peaks of $P^{III}P^{V}$ and $P^{III}P^{V}P^{III}$ appeared as soon as two reactants were mixed. After 3 h the reactions attained to the distribution equilibrium of three species; P^{III}(8%), $P^{III}P^{V}$(78%) and $P^{III}P^{V}P^{III}$(14%).

Characterization by ^{13}P NMR. The NMR spectra to indicate the progress of substitution reactions in Eqs. 2 and 3 are shown in Fig. 3. The sample

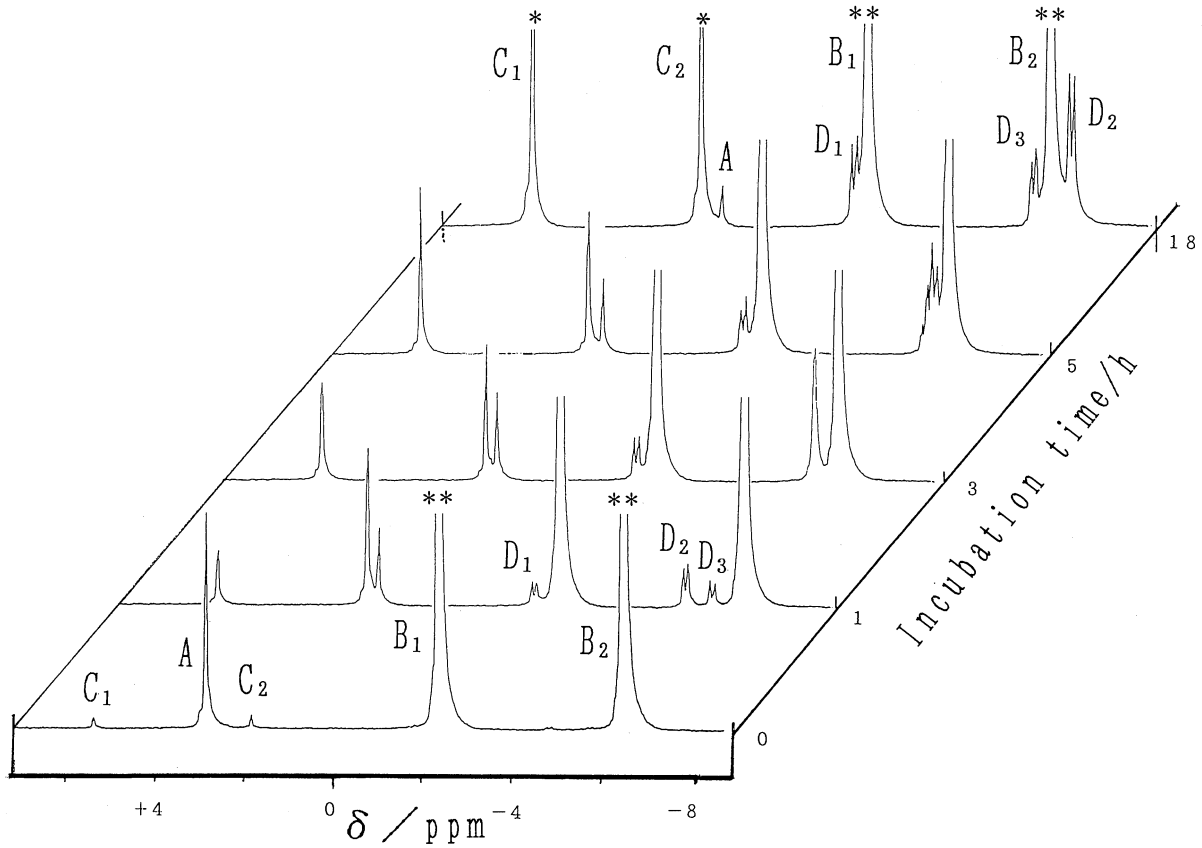

Fig. 3. ^{31}P NMR spectra showing progressive phosphonylation of orthophosphate by diphosphonate at 50 °C. <Sample> A mixed solution of 0.1 M P^{V} and 0.5 M $P^{III}P^{III}$. <Assignment> Signal A for P^{V}; B_1 and B_2 for $P^{III}P^{III}$; C_1 and C_2 for P^{III}; D_1, D_2, and D_3 for $P^{III}P^{V}$. Single asterisk (*) on the cut peaks of P^{III} refers to singlet and double asterisk (**) of $P^{III}P^{III}$ indicates "doublet" that is apparently observed as a doublet, but has been more finely resolved to be a triplet (double triplet for $P^{III}P^{III}$; Refs. 9 and 12).

composition, 0.1 M P^{V} and 0.5 M $P^{III}P^{III}$, was the same as that in Fig. 2. If the reactants and products are composed of P(III) units and/or P(V) units, it is useful in assigning the NMR spectra to keep in mind two general characteristics[2,6-8,11-14] arising from the P–H coupling and the pH dependence of chemical shift: (1) P(V) group gives a singlet signal or a multiplet with small peak splitting, ca. 18 Hz, due to P–P coupling and its chemical shift (δ value) shifts to the high field with decreasing pH, from the initial pH 7 to the final pH 5.5 in Fig. 3 and (2) P(III) group having a P–H bond gives a doublet signal with a coupling constant (J_{PH} value) as large as ca. 600 Hz and its chemical shift is less dependent on pH. Additional small peak splittings due to P–P couplings are also expected to be observed for P(III) groups in polymers.

As shown in Fig. 3 a signal A for P^{V}(δ=2.84 ppm) and a pair of two signals, B_1 and B_2, for $P^{III}P^{III}$ (δ=−4.46 ppm, J_{PH}=670 Hz) were observed as the principal signals when NMR spectra were recorded as soon as P^{V} and $P^{III}P^{III}$ were mixed (ca. pH 7). A pair of small signals C_1 and C_2 are for P^{III}(δ=3.47 ppm, J_{PH}=580 Hz). With increasing incubation time the signal A as well as B_1 and B_2 decreased and the signals C_1 and C_2 increased as could be expected from Eq. 2. Probably due to the decrease in pH to ca. pH 5.5 (final, 18 h), P^{III} indicated small change in δ value (final, 3.2 ppm) and considerable change in J_{PH} value (final, 620 Hz), while both δ value and J_{PH} value for $P^{III}P^{III}$ remained unchanged. The peak A for P^{V} shifted across the signal C_2 to the high field after 3 h and finally appeared at +0.86 ppm.

Three signals, D_1 (doublet: δ=−1.84), D_2 (doublet: δ=−5.25), and D_3 (doublet: δ=−5.85), appeared at 1 h incubation with intensity ratio 1:2:1 (D_1:D_2:D_3), were assigned to $P^{III}P^{V}$. The signal D_2 that shifted remarkably with time, as well as A, to appear finally at the right hand side of B_2 (δ=−6.99) was assigned to the P(V) unit of $P^{III}P^{V}$. The pair of D_1 and D_3 attributable to the P(III) unit of $P^{III}P^{V}$ indicated a large coupling constant (J_{PH}=650 Hz) that was slightly variable with incubation time. The change in δ value from −3.8 ppm to −4.1 ppm (final) was small. The splitting of each D_1, D_2, and D_3, 17.8—18.5 Hz, was ascribed to P–P coupling of unsymmetrical $P^{III}P^{V}$.[2] In addition to the proton-coupled experiments in Fig. 3 proton-decoupled experiments[8,9] were also made. As expected the paired signals of D_1 and D_3 for $P^{III}P^{V}$ in Fig. 3 disappeared to give a signal (doublet) at −3.8 ppm (initial). Similar effects of proton-decoupling were also observed for P^{III} and $P^{III}P^{III}$. Unfortunately, ^{31}P NMR signals for the trimeric $P^{III}P^{V}P^{III}$ could not be recorded, probably due to its low concentration that can be estimated from the chromatographic data in Fig. 2 to be less than 0.003 M.

Equilibrium Constants. In designing synthetic experiments to obtain high yields of products it is convenient to have information about apparent or conditional equilibrium constants of the substitution reactions of interest, even if the constants are based not strictly on thermodynamic consideration. This section deals with the evaluation of such apparent equilibrium constants for Eqs. 2 and 3 on the assumption that no side reactions such as hydrolysis of diphosphonate take place.[6,7]

Equilibrium constants, $K_{III,V}$ and $K_{III,V,III}$, for the formation of $P^{III}P^{V}$ and $P^{III}P^{V}P^{III}$ in Eqs. 2 and 3 are given as follows in terms of molar concentrations of each species at equilibrium conditions.

$$K_{III,V} = \frac{[P^{III}P^{V}][P^{III}]}{[P^{V}][P^{III}P^{III}]}, \quad (4)$$

$$K_{III,V,III} = \frac{[P^{III}P^{V}P^{III}][P^{III}]}{[P^{III}P^{III}][P^{III}P^{V}]}. \quad (5)$$

$[P^{V}]$, $[P^{III}P^{V}]$, and $[P^{III}P^{V}P^{III}]$ can be directly calculated from the relative peak areas in Fig. 2 since the total concentration of three species having P(V) units or the initial concentration of orthophosphate,$[P^{V}]_0$, is known. The initial concentration $[P^{III}P^{III}]_0$ is also known and hence two unknown concentrations are calculated as follows.

$$[P^{III}] = [P^{III}P^{V}] + 2[P^{III}P^{V}P^{III}], \quad (6)$$

$$[P^{III}P^{III}] = [P^{III}P^{III}]_0 - [P^{III}]. \quad (7)$$

The equilibrium constants thus obtained with the sample solution of 0.1 M orthophosphate and 0.5 M diphosphonate in Fig. 2 were; $K_{III,V}$=1.7 and $K_{III,V,III}$=0.008. Higher values, $K_{III,V}$=2.7 and $K_{III,V,III}$=0.05, were obtained for the sample of higher initial concentrations, 0.25 M orthophosphate and 1.25 M diphosphonate, while the sample of lower initial concentrations, 0.1 M orthophosphate and 0.1 M diphosphonate, gave a lower constant, $K_{III,V}$=0.50. The remarkable variation in the equilibrium constant with sample concentrations is not surprising because the experiments were made at high sample concentrations and the variable effects of pH, sodium ion and hydrolysis of diphosphonate[6-10] were not taken into consideration. The equilibrium constants provided by the simple chromatographic procedures are valuable from the practical viewpoint of predicting yields of the reaction products. Extended experiments based on the above prediction are in progress to prepare so much amount of the novel $P^{III}P^{V}P^{III}$ that is enough to do NMR expepriment for its structural characterization.

References

1) D. E. C. Corbridge, "Phosphorus: An Outline of Its Chemistry, Biochemistry, and Technology," Elsevier, Am-

sterdam (1985).

2) M. M. Crutchfield, C. H. Dungan, J. H. Letcher, V. Mark, and J. R. Van Wazer, "P^{31} Nuclear Magnetic Resonance," John-Wiley & Sons, New York (1967).

3) N. Yoza, M Tokuda, T. Inoue, and S. Ohashi, *Inorg. Nucl. Chem. Lett.*, **9**, 385 (1973).

4) N. Yoza, K. Ishibashi, and S. Ohashi, *J. Chromatogr.*, **134**, 497 (1978).

5) N. Yoza, K. Ito, Y. Hirai, and S. Ohashi, *J. Chromatogr.*, **196**, 471 (1980).

6) Y. Baba, D. Sci. Thesis, Kyushu University, Fukuoka, 1986.

7) Y. Yamamoto, M. Sci. Thesis, Kyushu University, Fukuoka, 1986.

8) Y. Yamamoto, Y. Baba, M. Mizokuchi, M. Onoe, T. Sumiyama, M. Tsuhako, N. Yoza, and S. Ohashi, *Bull. Chem. Soc. Jpn.*, **61**, 3217 (1988).

9) Y. Baba, T. Sumiyama, M. Tsuhako, and N. Yoza, *Bull. Chem. Soc. Jpn.*, **62**, 1587 (1989).

10) N. Yoza, N. Tokushige, T. Nakazato, K. Takehara, Y. Ide, and Y. Baba, *Chem. Lett.*, **1990**, 1487.

11) N. Yoza, Y. Sagara, H. Morioka, T. Handa, H. Hirano, Y. Baba, and S. Ohashi, *J. Flow Injection Anal.*, **3**, 37 (1986).

12) R. E. Mesmer and R. L. Carroll, *J. Am. Chem. Soc.*, **88**, 1381 (1966).

13) C. F. Callis, J. R. Van Wazer, J. N. Shoolery, and W. A. Anderson, *J. Am. Chem. Soc.*, **79**, 2719 (1957).

14) E. Schwarzmann and J. R. Van Wazer, *J. Inorg. Nucl. Chem.*, **14**, 296 (1960).

15) J. Emsley and D. Hall, "The Chemistry of Phosphorus," Harper & Row, London (1976).

 © 1991 The Chemical Society of Japan Bull. Chem. Soc. Jpn., 64, 21—28 (1991)

Preparation and Properties of Heteropoly Molybdovanadate(V) Complexes

Sadayuki HIMENO,* Toshiyuki OSAKAI, and Atsuyoshi SAITO
Department of Chemistry, College of Liberal Arts, Kobe University, Kobe 657
(Received July 30, 1990)

Tetrabutylammonium salts of the mixed heteropoly molybdovanadate(V) anions, $[H_{x-1}V(V_xMo_{12-x})O_{40}]^{4-}$ (x=1—3) were prepared from a Mo(VI)–V(V)–CH_3CN system at room temperature. These mixed heteropoly anions were distinguished by their voltammetric behavior; the anions with x=1, 2, and 3 were electroreduced by one-, two-, and three-electrons due to the peripheral V atoms at a glassy carbon electrode. The spectroscopic properties were also reported. Their formation conditions were compared with those of 12-molybdovanadate (V), $[VMo_{12}O_{40}]^{3-}$, especially regarding the concentrations of Mo(VI), V(V), acid, and organic solvents, the nature of organic solvents, and the ionic strength of the system. It should be emphasized that the 12-molybdovanadate(V) and mixed molybdovanadate(V) complexes are not formed in the absence of organic solvents.

We have prepared several heteropolymolybdate complexes, which are formed only in the presence of water-miscible organc solvents such as acetonitrile.[1] In the course of the preparative studies from aqueous–organic media, we have recently isolated tetrabutylammonium (n-Bu_4N^+) salts of 12-molybdovanadate(V), which is considered to be a Keggin anion with a central VO_4 tetrahedron, from an acidic Mo(VI)–V(V) solution admixed with acetonitrile.[2] In the present study, the existence of several vanadium-substituted mixed molybdovanadate(V) complexes was ascertained in the solid state and in aqueous–organic solution.

Fortuitously, a mixed-valence reduced crystal of a mixed molybdovanadate(V) complex, $K_6V(V^{IV}V^{V}Mo_{10})O_{40}\cdot 13H_2O$ has been obtained upon slow crystallization of $K_8V_8Mo_4O_{36}\cdot 12H_2O$, and it has been shown by X-ray diffraction analysis that the mixed complex possesses a Keggin-type structure.[3] According to recent ^{51}V NMR studies,[4] heteropoly molybdovanadate(V) complexes are only supposed to be formed in an aqueous Mo(VI)–V(V) system. On the basis of our results, however, it should be stressed that the presence of organic solvents in concentrations greater than 30% (v/v) is essential for the formation of heteropoly molybdovanadate(V) complexes.

The present study was undertaken to characterize the mixed molybdovanadate(V) complexes and to elucidate their formation conditions in relation to those of 12-molybdovanadate(V). This paper also reports voltammetric evidence for the spontaneous conversion of $[VMo_5O_{19}]^{3-}$ into heteropoly molydovanadate(V) anions in acidified aqueous–organic system.

Experimental

UV-visible absorption spectra were recorded on a Hitachi Model 220-A spectrophotometer using a quartz cell with path length of 1.0 cm. Voltammetric measurements were made with a PARC Model 174-A polarographic analyzer equipped with a Yokogawa Model 3023 X-Y recorder. A working electrode was a glassy carbon (Tokai Carbon, GC-30S) with a surface area of 0.071 cm^2. A platinum wire was used as the counter electrode and a saturated calomel electrode (SCE) as the reference. Unless stated otherwise, voltage scan rate was set at 100 mV s^{-1}. UV-visible spectrophotometric and voltammetric measurements were made at 25±0.1 °C. Controlled potential electrolysis was carried out with a Hokuto Denko Model HA-501 potentiostat. TG-DTA was carried out with a Rigaku Denki 8002-SD thermal analyzer. A Hitachi Model 270-30 spectrophotometer was used to record IR spectra using KBr pellets.

Results and Discussion

Preparation of Molybdovanadate(V) Complexes.

(n-Bu_4N)$_3VMo_{12}O_{40}$: This complex was prepared and purified as described.[2]

(n-Bu_4N)$_4V(VMo_{11})O_{40}$: A solution of 1.17 g (10.0 mmol) NH_4VO_3 in 125 ml of 2 M HCl (1 M=1 mol dm^{-3}) was added to a solution of 6.05 g (25.0 mmol) of $Na_2MoO_4\cdot 2H_2O$ in 75 ml of water. Then, 300 ml of acetonitrile was added with stirring to the mixture. This resulted in a rapid color change from pale-yellow due to vanadate(V) to orange-yellow. After the solution was stirred for 1 h at room temperature, 10 g of n-Bu_4NBr was added to precipitate an orange-yellow salt. The salt was isolated by filtration, and washed with water and ethanol (Yield 5.4 g). The salt was purified by recrystallization from 350 ml of acetonitrile.

Anal. Calcd for (n-Bu_4N)$_4V(VMo_{11})O_{40}$: Mo, 38.14; V, 3.68; C, 27.78; H, 5.25; N, 2.02%. Found: Mo, 37.70; V, 3.82; C, 27.71; H, 5.42; N, 2.08%.

(n-Bu_4N)$_4HV(V_2Mo_{10})O_{40}$: This preparation is similar to that of the preceding salt. A solution of 2.05 g (17.5 mmol) of NH_4VO_3 in 100 ml of 2 M HCl was added to a solution of 6.05 g (25.0 mmol) of $Na_2MoO_4\cdot 2H_2O$ in 100 ml of water. After the addition of 300 ml of acetonitrile, the solution was stirred for 1 h at room temperature. The addition of 10 g of n-Bu_4NBr led to immediate precipitation of an orange salt (Yield 6.3 g), which was subsequently recrystallized from 300 ml of acetonitrile.

Anal. Calcd for (n-Bu_4N)$_4HV(V_2Mo_{10})O_{40}$: Mo,

35.25; V, 5.61; C, 28.24; H, 5.37; N, 2.06%. Found: Mo, 34.89; V, 5.63; C, 27.94; H, 5.20; N, 2.06%.

(n-$Bu_4N)_4H_2V(V_3Mo_9)O_{40}$: This compound was prepared with the use of the procedure described for (n-$Bu_4N)_4HV(V_2Mo_{10})O_{40}$ by substituting 2.98 g (25.0 mmol) of NH_4VO_3 for 2.05 g (Yield 6.8 g).

Anal. Calcd for (n-$Bu_4N)_4H_2V(V_3Mo_9)O_{40}$: Mo, 32.23; V, 7.61; C, 28.69; H, 5.49; N, 2.09%. Found: Mo, 32.58; V, 7.57; C, 28.29; H, 5.50; N, 2.13%.

In the TG-DTA, the evolution of water was not observed up to about 260 °C for the mixed heteropoly molybdovanadate(V) complexes.

The mixed molybdovanadate(V) complexes are not distinguished by their IR spectra because they show the strong absorption bands of the same pattern at 946, 880, and 774 cm^{-1}; the 12-molybdovanadate(V) complex gives the corresponding bands at 958, 887, and 776 cm^{-1}.[2] Despite various attempts , complexes with higher vanadium contents were not successfully prepared.

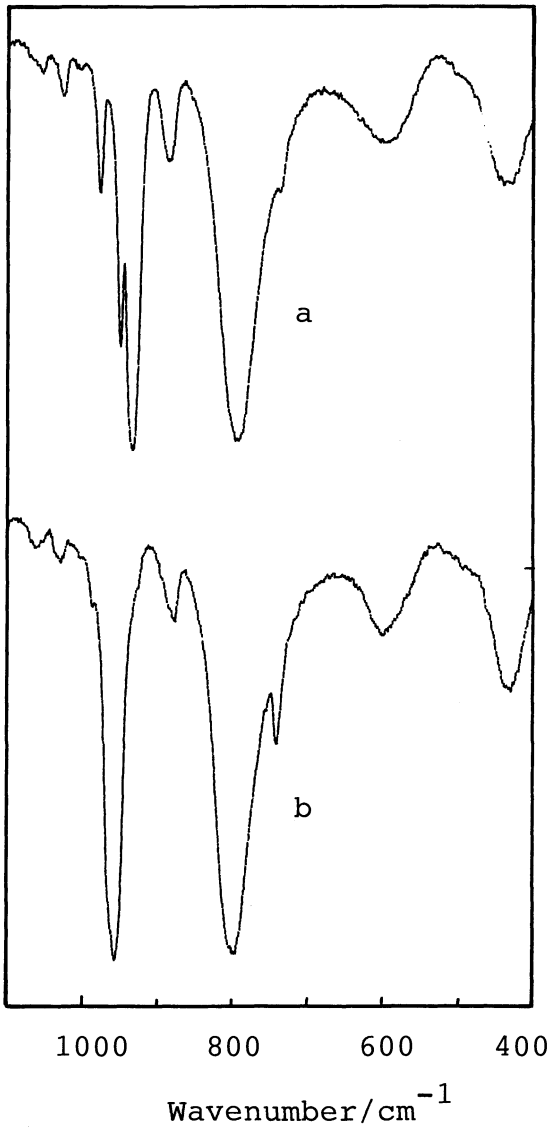

Fig. 1. IR spectra of (a) (n-$Bu_4N)_3VMo_5O_{19}$ and (b) (n-$Bu_4N)_2Mo_6O_{19}$ in the KBr pellets. Numerical data are given in the Text.

In addition, the $[VMo_5O_{19}]^{3-}$ anion was prepared with a view to investigating the possibility of its transformation reaction into hereropoly molybdovanadate(V) anions.[5] According to Flynn, Jr. and Pope,[6] mixed tungstovanadate(V) anions such as $[V(V_2W_{10})O_{40}]^{5-}$ and $[V(V_3W_9)O_{40}]^{6-}$ have been prepared by acidifying the aqueous solution of the mixed Lindqvist anion, $[V_2W_4O_{19}]^{4-}$, although 12-tungstovanadate(V) is still unknown.

(n-$Bu_4N)_3VMo_5O_{19}$: A solution of 0.234 g (2.0 mmol) NH_4VO_3 in 20 ml of 0.15 M NaOH was added to a solution of 2.42 g (10.0 mmol) of $Na_2MoO_4 \cdot 2H_2O$ in 480 ml of water, and the pH of the solution was adjusted to pH 3.2 with HCl.[7] The resulting yellow solution was stirred for 1 h at room temperature. A yellow salt was precipitated by the addition of 5 g of n-Bu_4NBr, being filtered off, washed with water and ethanol, and dried at 40 °C (Yield 2.9 g). The yellow salt was recrystallized from 100 ml of acetonitrile.

Anal. Calcd for (n-$Bu_4N)_3VMo_5O_{19}$; Mo, 30.71; V, 3.26; C, 36.91; H, 6.97; N, 2.69%. Found: Mo, 30.76; V, 3.27; C, 36.76; H, 7.11; N, 2.75%. IR (400—1000 cm^{-1}): 978, 950, 934, 796, 596, 436 cm^{-1} (Fig. 1(a)). For comparison, Fig. 1(b) shows an IR spectrum of (n-$Bu_4N)_2Mo_6O_{19}$ prepared according to the previous procedure.[8] IR (400—1000 cm^{-1}): 956, 798, 598, 436 cm^{-1}.

UV-Visible Spectra. The n-Bu_4N^+ salts of the mixed heteropoly molybdovanadate(V) anions are reasonably soluble in polar aprotic solvents such as

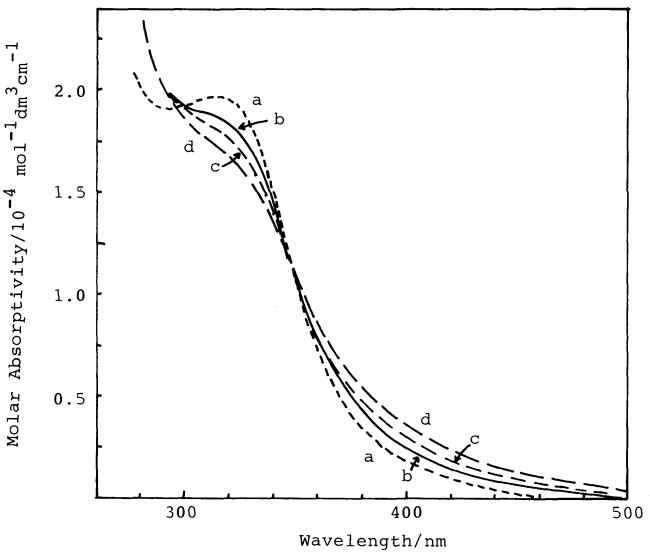

Fig. 2. UV-visible spectra of 0.04 mM $[H_{x-1}V(V_xMo_{12-x})O_{40}]^{4-}$ in neat acetonitrile. (b), x=1; (c), x=2; (d), x=3. The spectrum of 0.04 mM $[VMo_{12}O_{40}]^{3-}$ is included for comparison (curve (a)).

acetonitrile and acetone, and insoluble in water, ethanol, and 1,4-dioxane. Figure 2 shows UV-visible absorption spectra of 0.04 mM (M=mol dm^{-3}) solutions of the $[H_{x-1}V(V_xMo_{12-x})O_{40}]^{4-}$ anions in neat acetonitrile. The solutions obeyed Beer's law in the spectral region studied. As the substituted vanadium content increased, the spectrum appeared like a shoulder and there was a decrease in molar absorptivities at 310 nm (1.90×10^4, 1.82×10^4, and 1.75×10^4 mol^{-1} dm^3 cm^{-1} for the $[H_{x-1}V(V_xMo_{12-x})O_{40}]^{4-}$ anions with x=1, 2, and 3, respectively). These behaviors are similar to those of a series of mixed molybdovanadophosphate(V) complexes with the Keggin-type structure.[9,10]

Voltammetric Characterization of the Heteropoly Molybdovanadate(V) Anions. Figures 3 and 4 show cyclic and normal pulse voltammograms, respectively, of 0.2 mM solutions of the heteropoly molybdovanadate(V) complexes in 95% (v/v) CH_3CN containing 0.1 M $HClO_4$.

The $[VMo_{12}O_{40}]^{3-}$ Anion: Reproducible voltammograms were obtained (curve (a)). As already described,[2] the first reduction wave corresponds to a reversible two-electron transfer. The separation of the cathodic and anodic peaks averages 27—30 mV. The peak-potential (E_p) showed positive shift as the $HClO_4$ concentration was increased in the range of −log

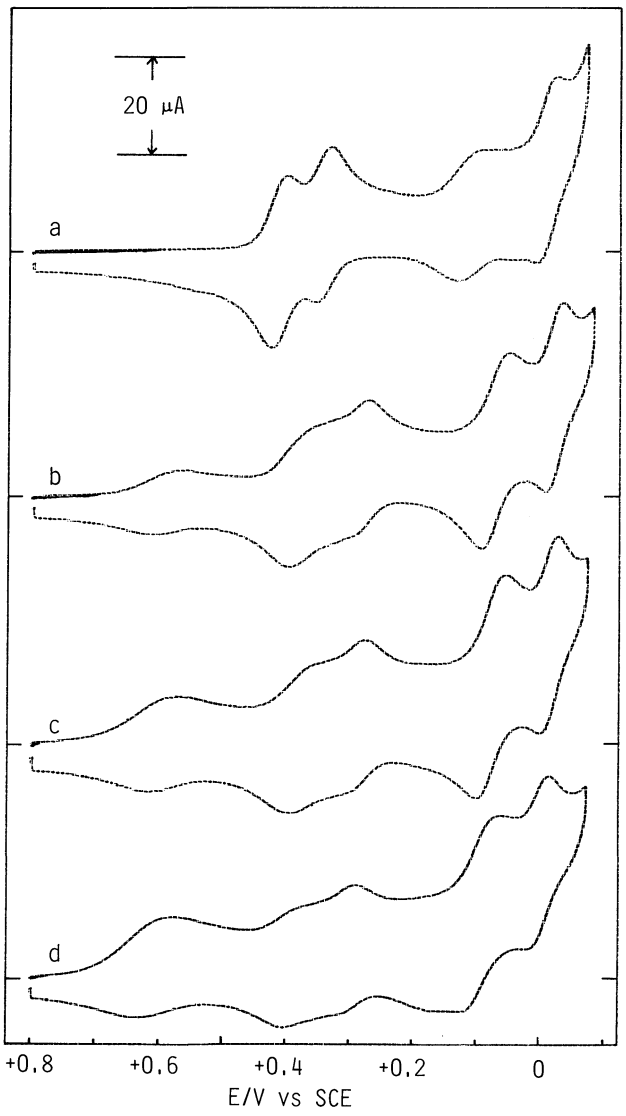

Fig. 3. Cyclic voltammograms of 0.2 mM $[H_{x-1}V(V_xMo_{12-x})O_{40}]^{4-}$ in 95%(v/v) CH_3CN–water containing 0.1 M $HClO_4$. (b) x=1; (c), x=2; (d), x=3. The voltammogram of 0.2 mM $[VMo_{12}O_{40}]^{3-}$ is included for comparison (curve (a)).

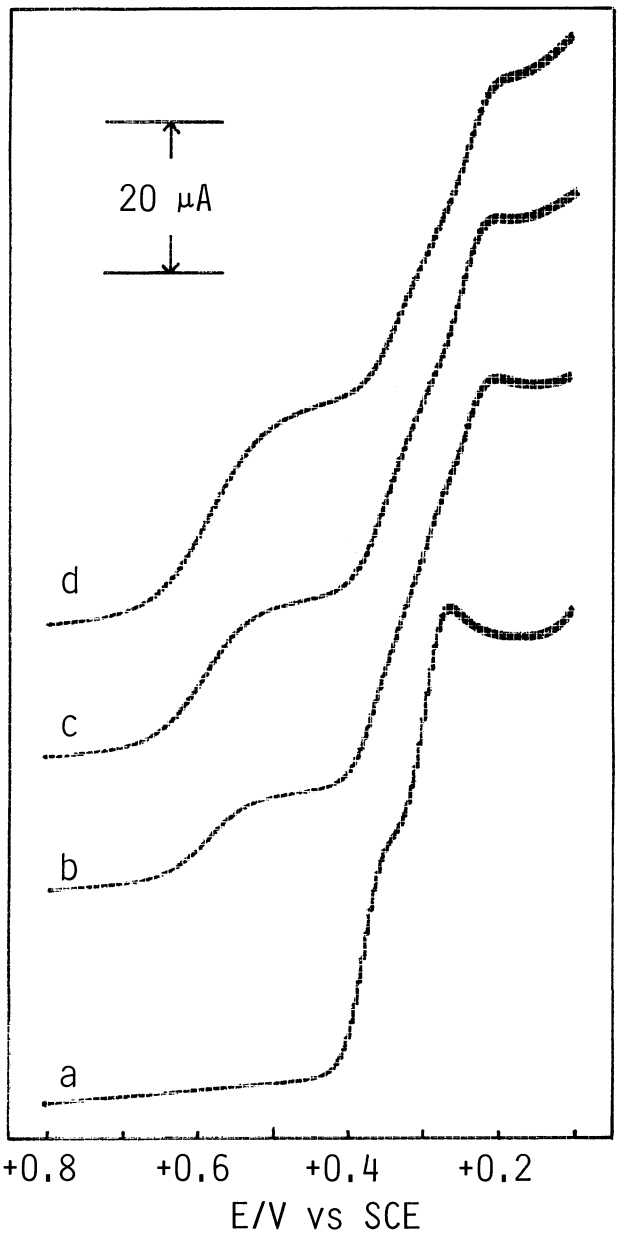

Fig. 4. Normal pulse voltammograms of 0.2 mM $[H_{x-1}V(V_xMo_{12-x})O_{40}]^{4-}$ in 95%(v/v) CH_3CN–water containing 0.1 M $HClO_4$. (b), x=1; (c), x=2; (d), x=3. The voltammogram of 0.2 mM $[VMo_{12}O_{40}]^{3-}$ is included for comparison (curve (a)).

$[H^+]$=2.6—1.0 (I=0.1 M ($NaClO_4$)), where I=ionic strength. The slope of E_p/−log $[H^+]$ was estimated to be 65 mV, indicating that two protons are consumed in the reduction process:

$$[VMo_{12}O_{40}]^{3-} + 2e + 2H^+ = [H_2V(Mo^V_2Mo_{10})O_{40}]^{3-}$$

The $[H_{x-1}V(V_xMo_{12-x})O_{40}]^{3-}$ Anions: The voltammograms recorded 1 h later remained identical under these conditions; however, the solutions examined after 24 h standing gave decayed or distorted voltammograms, indicating the decomposition of the complexes. Therefore, curves (b)—(d) of Figs. 3 and 4 were recorded for freshly prepared solutions.

The voltammograms for the $[H_{x-1}V(V_xMo_{12-x})O_{40}]^{4-}$ anions gave additional reduction waves at about 0.2 V more positive than the first reduction wave of $[VMo_{12}O_{40}]^{3-}$. The currents were dependent on the square root of the voltage scan rate (20—200 mV s^{-1}), indicating that the electrode processes are diffusion-controlled. The additional waves can be ascribed to the reduction of the peripheral V atoms, because the reduction currents are dependent on the vanadium content. This is in line with the previous observations that the V atoms in the peripheral structure are more easily reduced than the Mo or W atoms in vanadium-substituted mixed complexes with P as the central heteroatom, i.e., $[P(V_xMo_{12-x})O_{40}]^{(3+x)-}$ and $[P(V_xW_{12-x})O_{40}]^{(3+x)-}$.[11-14]

As long as the $[V(VMo_{11})O_{40}]^{4-}$ anion is concerned, the voltammetric wave corresponds to a reversible one-electron transfer, because the separation of the cathodic and anodic peaks are 60 mV, being independent of the voltage scan rate (20—200 mV s^{-1}) in cyclic voltammetry. The E_p's for the reduction and oxidation waves were shifted to more positive potentials as the $HClO_4$ concentration was increased in the range of −log $[H^+]$=2.6—1.0 (I=0.1 M ($NaClO_4$)), and the slope was estimated to be 65 mV, which indicates that the electrode process corresponds to the reaction:

$$[V(V^VMo_{11})O_{40}]^{4-} + e + H^+ = [HV(V^{IV}Mo_{11})O_{40}]^{4-}$$

Both cyclic and normal pulse voltammetric reduction currents for the $[HV(V_2Mo_{10})O_{40}]^{4-}$ and $[H_2V(V_3Mo_9)O_{40}]^{4-}$ anions were approximately 2 and 3 times that for the one-electron reduction current of the $[V(VMo_{11})O_{40}]^{4-}$ anion. These results indicate that both reduction processes involve a sequence of 2 and 3 one-electron steps with different standard potentials, E^0, rather than single two- and three-electron reductions, respectively:[15-17] In the case of the reduction of the $[HV(V_2Mo_{10})O_{40}]^{4-}$ anion, for example,

$$[HV(V_2^VMo_{10})O_{40}]^{4-} \underset{E_1^0}{\overset{e}{\rightleftarrows}} [HV(V^{IV}V^VMo_{10})O_{40}]^{5-}$$

$$\underset{E_2^0}{\overset{e}{\rightleftarrows}} [HV(V_2^{IV}Mo_{10})O_{40}]^{6-}$$

When $-90\ mV < \Delta E^0 (= E_2^0 - E_1^0) < 0$ mV, the individual waves merge into one broad wave.[17] This is further substantiated by the fact that in cyclic voltammetry, the E_p values for the cathodic and anodic waves were not affected by the voltage scan rate (20—200 mV s^{-1}) (the separation averaged 60—70 mV). These reduction behaviors suggest that the V atoms are not in the adjacent position in the peripheral structure.[15] It has been shown by X-ray crystallographic structural analysis that the Mo and V atoms are randomly distributed in the peripheral structures of $[V(V^{IV}V^V-Mo_{10})O_{40}]^{6-}$ and $[P(V_xMo_{12-x})O_{40}]^{(3+x)-}$ (x=2 and 3).[3,18] It was found that the E_p values shifted to more positive potentials with an increase of the $HClO_4$ concentration. However, quantitative treatment could not be made owing to the complicated electrode processes.

As shown in curves (b)—(d) of Fig. 3, the voltammetric waves due to the reduction of molybdenum appeared at potentials more negative than +0.4 V, being distorted similar to irreversible waves. However, the distorted waves remained unchanged in position on the potential axis as a function of the voltage scan rate (20—200 mV s^{-1}), which indicates the reversible nature of their electrode processes. At present we are unable to account quantitatively for this electrode behavior; however, a possible explanation can be given in terms of the existence of several isomers in oxidized and/or reduced forms with slightly different E^0.[17]

The distorted waves due to the reduction of molybdenum decreased in height with an increase of the vanadium content in the complexes. These results can be accounted for in terms of the decomposition of the vanadium-substituted complexes as a result of the reduction of the peripheral V atoms. This is confirmed by the following observations: For the $[H_{x-1}V(V_xMo_{12-x})O_{40}]^{4-}$ anions, the solutions changed from orange to blue by controlled potential electrolysis at a reduction potential of the peripheral V atoms; however, colorless solutions resulted at the end of controlled potential electrolysis because of the decomposition of the blue species.

Formation of the Heteropoly Molybdovanadate(V) Anions. Figure 5 shows cyclic voltammograms of a 10 mM Mo(VI)–0.2 M HCl–50%(v/v) CH_3CN system. In the absence of V(V), as shown in curve (a), no voltammetric waves were obtained until a current rise due to the reduction of $[Mo_6O_{19}]^{2-}$ around +0.1 V.[8,19] On the addition of 0.2 mM V(V), a two-step voltammetric wave with an equal height was obtained (curve (b)). The currents were diffusion-controlled. As shown in curve (a) of Fig. 6, the voltammetric currents attained to a constant value around one min

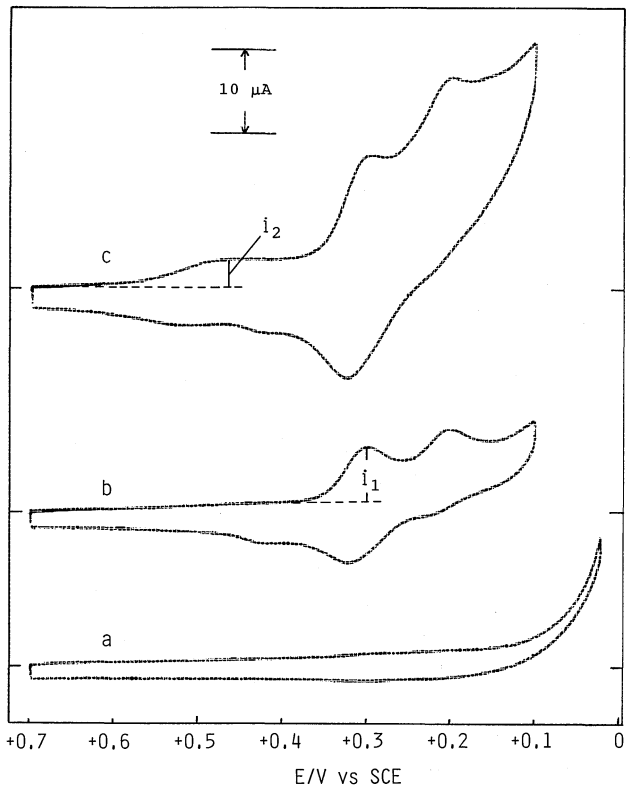

Fig. 5. Cyclic voltammograms of 10 mM Mo(VI)–0.2 M HCl–50%(v/v) CH_3CN systems. [V(V)]/mM, (a) none; (b) 0.2; (c) 1.0.

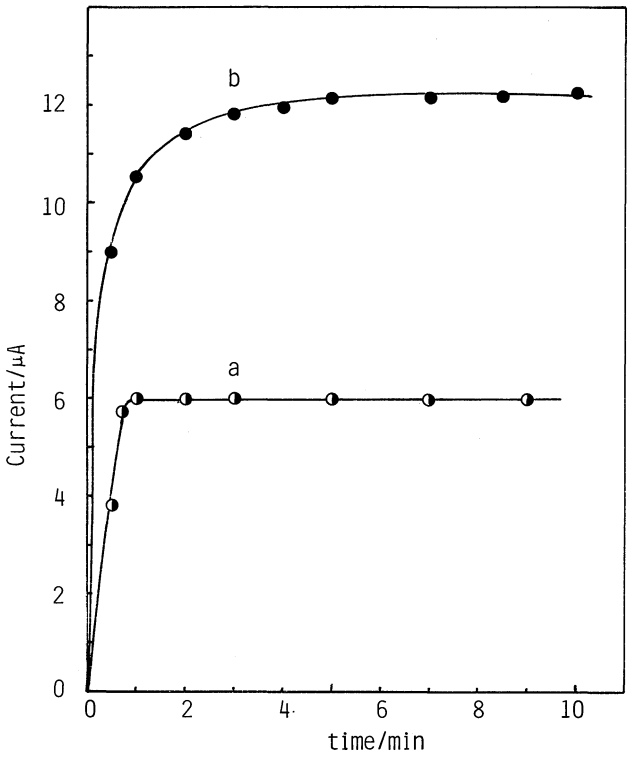

Fig. 6. Current-time profiles for 30 mM Mo(VI)–0.1 M $HClO_4$–50%(v/v) CH_3CN systems. [V(V)]/mM, (a), 0.2 (i_1); (b), 2.0 (i_2).

after the addition of V(V). The $[VMo_{12}O_{40}]^{3-}$ anion is responsible for the voltammetric waves shown in curve (b) of Fig. 5. The first peak current is represented by i_1 in the following.

The increase of the V(V) concentration caused the voltammetric behavior to change significantly. With an increase of the V(V) concentration while other conditions were kept unchanged, the solution turned from yellow to orange. Simultaneously, a new voltammetric wave appeared at more positive potentials than those for the voltammetric wave of $[VMo_{12}O_{40}]^{3-}$ (curve (c) of Fig. 5). The new voltammetric current corresponding to the reduction of the peripheral V atoms attained to a constant value around 5 min after the addition of V(V) as shown in curve (b) of Fig. 6, being denoted as i_2 in the following. This behavior can be ascribed to the formation of vanadium-substituted derivatives of the $[VMo_{12}O_{40}]^{3-}$ anion. After the current-increase periods, both 12-molybdovanadate(V) and vanadium-substituted derivatives are stable under these conditions, as judged by no change of i_1 and i_2.

Figure 7 shows the dependence of i_1 and i_2 on the concentration of V(V) in 10 mM Mo(VI)–0.2 M HCl–50%(v/v) CH_3CN systems. For V(V) concentrations< 0.5 mM, i_2 was hardly detected, which indicates that $[VMo_{12}O_{40}]^{3-}$ is predominant. Both i_1 and i_2 increased as the V(V) concentration was increased from 0.5 to 1 mM. Above 1 mM V(V), i_2 increased further at the expense of i_1.

The formation conditions of 12-molybdovanadate (V) and vanadium-substituted derivatives were inves-

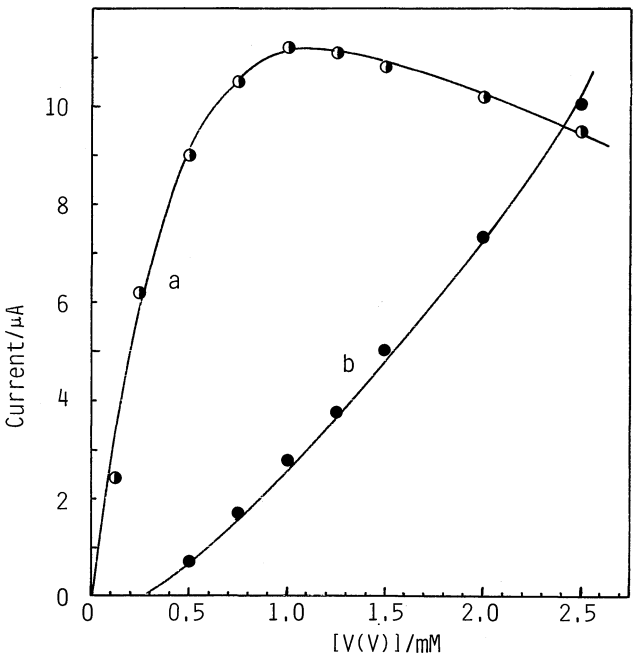

Fig. 7. Dependence of (a) i_1 and (b) i_2 on the concentration of V(V) for 10 mM Mo(VI)–0.2 M HCl–50%(v/v) CH_3CN systems.

tigated by monitoring i_1 and i_2, respectively. Curves (a) and (b) of Fig. 8 show i_1 and i_2 as a function of the $HClO_4$ concentration for 30 mM Mo(VI)–50%(v/v) CH_3CN systems containing 0.1 and 0.5 mM V(V), respectively. The ionic strength was adjusted to be 0.5 M with $NaClO_4$. The 12-molybdovanadate(V) anion is formed in the $HClO_4$ concentration range 0.06—0.6 M while the vanadium-substituted derivative anions are formed in 0.04—0.4 M $HClO_4$. Curve (c) shows absorbance values at 400 nm for 30 mM Mo(VI)–50%(v/v) CH_3CN systems in the absence of V(V) to illustrate the formation conditions of $[Mo_6O_{19}]^{2-}$. The $[VMo_5O_{19}]^{3-}$ ion was not detected in these aqueous–organic solutions; the anion is formed in aqueous solutions of about pH 3,[4,7] or in nonaqueous media.[5]

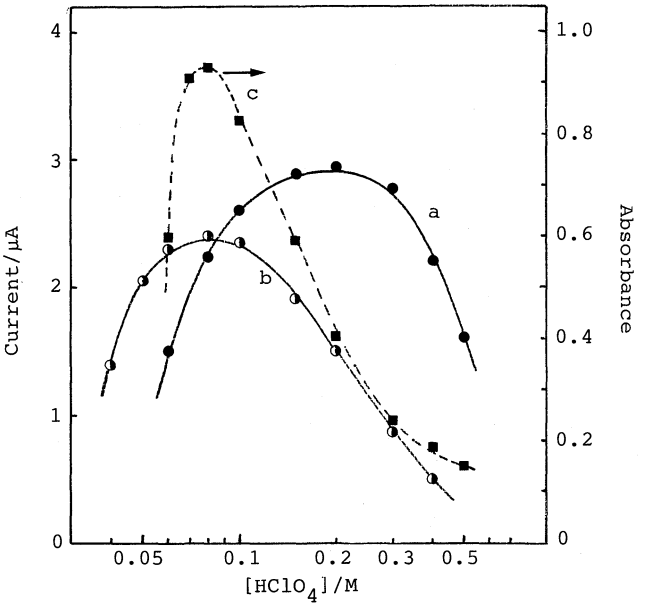

Fig. 8. Formation ranges of (a) $[VMo_{12}O_{40}]^{3-}$, (b), $[H_{x-1}V(V_xMo_{12-x})O_{40}]^{4-}$, and (c) $[Mo_6O_{19}]^{2-}$ for 30 mM Mo(VI)–50%(v/v) CH_3CN systems as a function of the $HClO_4$ concentration (I=0.5 M ($NaClO_4$)). (a), i_1 for [V(V)]=0.1 mM; (b) i_2 for [V(V)]=0.5 mM; (c) absorbances at 400 nm in the absence of V(V).

Figure 9 shows the dependence of i_1 and i_2 on the ionic strength for 30 mM Mo(VI)–0.1 M $HClO_4$–50%-(v/v) CH_3CN systems containing various concentrations of $NaClO_4$ (0—0.4 M). It was found that i_1 decreased while i_2 increased with an increase of the ionic strength from 0.1 to 0.5 M, which means that the increase of the ionic strength of the solution favors the formation of the tetravalent anions rather than the trivalent anion.

The effects of the nature and concentration of organic solvents on the formation of 12-molybdovanadate(V) and vanadium-substituted derivatives were also investigated by measuring i_1 and i_2 in solutions of 30 mM Mo(VI) containing 0.2 and 2.0 mM V(V), respectively. Figures 10 and 11 show the results. It can be concluded that neither of 12-molybdovanadate(V) and vanadium-substituted derivatives is formed in the absence of organic solvents, and the increase of the concentration of organic solvents favors the formation of the heteropoly molybdovanadate(V) complexes.

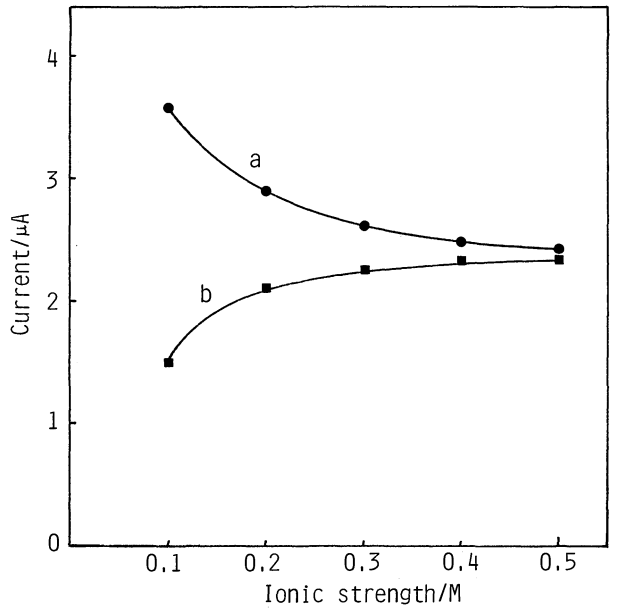

Fig. 9. Effect of ionic strength on (a) i_1 and (b) i_2 for 30 mM Mo(VI)–0.1 M $HClO_4$–50%(v/v) CH_3CN systems containing various concentrations of $NaClO_4$ (0—0.4 M).

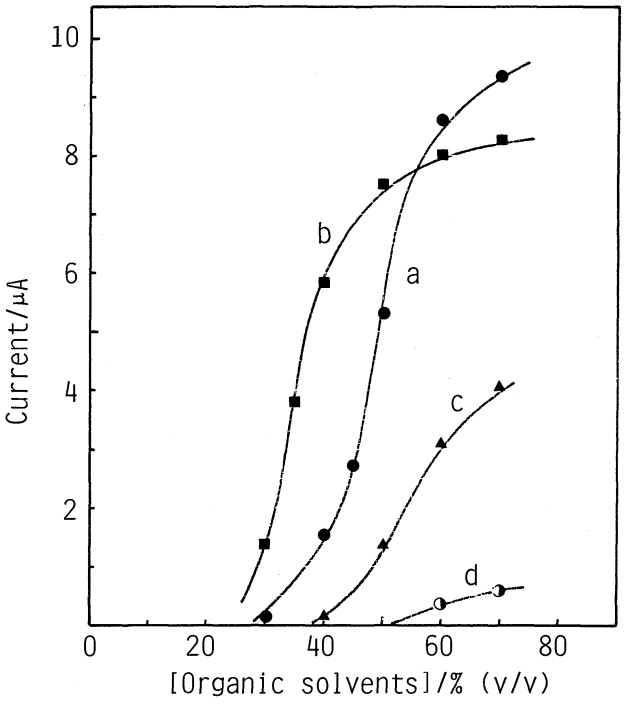

Fig. 10. Effect of concentrations of organic solvents on i_1 for 30 mM Mo(VI)–0.2 mM V(V)–0.3 M $HClO_4$ systems containing (a) acetonitrile; (b), acetone; (c), ethanol; (d), 1,4-dioxane.

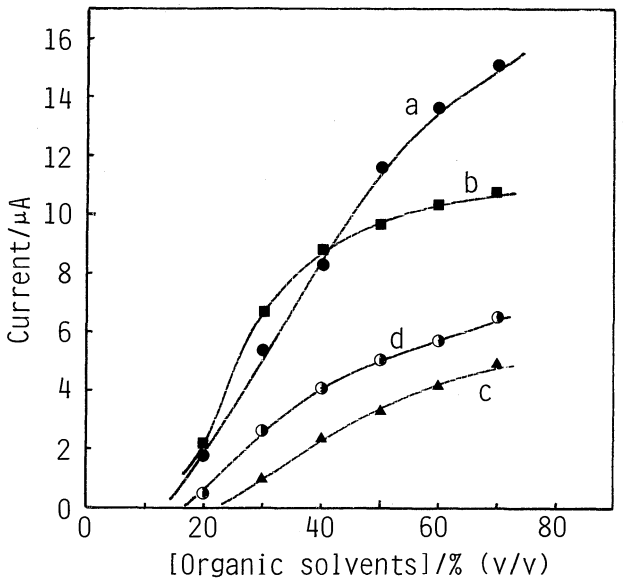

Fig. 11. Effect of concentrations of organic solvents on i_2 for 30 mM Mo(VI)–2.0 mM V(V)–0.05 M $HClO_4$ systems (I=0.1 M ($NaClO_4$)) containing (a), acetonitrile; (b), acetone; (c), ethanol; (d), 1,4-dioxane.

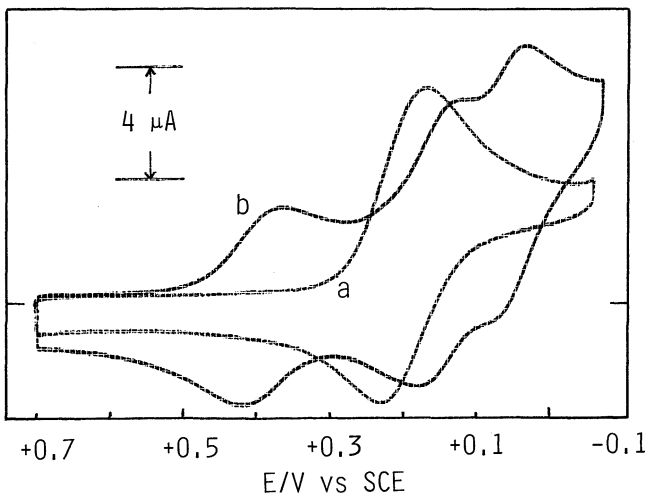

Fig. 12. Cyclic voltammograms of 0.32 mM $[VMo_5O_{19}]^{3-}$ in 90%(v/v) CH_3CN–water containing 0.001 M $HClO_4$ (I=0.1 M ($NaClO_4$)). Recorded (a) immediately after the addition of $[VMo_5O_{19}]^{3-}$; (b) after 60 min.

Conversion of $[VMo_5O_{19}]^{3-}$ into Mixed Heteropoly Molybdovanadate(V) Anions. As shown in curve (a) of Fig. 12, a cyclic voltammogram of 0.32 mM $[VMo_5O_{19}]^{3-}$ showed a couple of reduction and oxidation waves in 90%(v/v) CH_3CN–water containing 0.001 M $HClO_4$ (I=0.1 M ($NaClO_4$)). The waves were diffusion-controlled. The peak-separation for the reduction-oxidation couple was found to be 70 mV, and the E_p values were almost independent of the voltage scan rate (20—100 mV s^{-1}), which indicates that the wave corresponds to the reversible reduction of $[VMo_5O_{19}]^{3-}$ to $[V^{IV}Mo_5O_{19}]^{4-}$. In addition to the reversible wave, an irreversible reduction wave appeared at potentials more negative than −0.1 V. The irreversible wave can be ascribed to the reduction of molybdenum because the four-electron reduction wave of $[Mo_6O_{19}]^{2-}$ appears around the same potentials under these conditions.[19]

As time elapsed, a new reduction wave appeared with an E_p value of +0.37 V; the current increased with time until a constant value was attained in ca. 60 min. The ultimate voltammogram is shown in curve (b). Orange salts were obtained by the addition of tetraethylammonium bromide to the solution, being identified as mixed heteropoly molybdovanadate(V) complexes by the IR spectroscopic measurement. These results clearly show that the $[VMo_5O_{19}]^{3-}$ anion transforms spontaneously into mixed heteropoly molybdovanadate(V) anions under these conditions. Comparison of the reduction currents due to the peripheral V atoms in Fig. 12 with those in Fig. 3 leads to the conclusion that a mixture of $[V(VMo_{11})O_{40}]^{4-}$ and $[HV(V_2Mo_{10})O_{40}]^{4-}$ is formed as a result of the transformation. This conversion reaction was observed for 90%(v/v) CH_3CN–water solutions containing 0.001—0.1 M $HClO_4$ (I=0.1 M); however, it did not occur in the absence of acid. Similar conversion reaction was also observed in acidic solutions containing >60%(v/v) acetone. Flynn, Jr. and Pope have reported similar conversion of $[V_2W_4O_{19}]^{4-}$ into mixed heteropoly tungstovanadate(V) anions in acidified aqueous solutions.[6]

References

1) T. Hori and S. Himeno, *Chem. Lett.*, **1987**, 53; S. Himeno, T. Hori, and A. Saito, *Bull. Chem. Soc. Jpn.*, **62**, 2184 (1989); T. Hori, O. Tamada, and S. Himeno, *J. Chem. Soc., Dalton Trans.*, **1989**, 1491; S. Himeno, A. Saito, and T. Hori, *Bull. Chem. Soc. Jpn.*, **63**, 1602 (1990); S. Himeno, T. Osakai, A. Saito, and T. Hori, *Talanta*, **37**, 1071 (1990).

2) S. Himeno and A. Saito, *Inorg. Chim. Acta*, **171**, 135 (1990).

3) A. Bjornberg and B. Hedman, *Acta Crystallogr., Sect. B*, **36**, 1018 (1980).

4) R. I. Maksimovskaya and N. N. Chumachenko, *Polyhedron*, 6, 1813 (1987).

5) M. Filowitz, R. K. C. Ho, W. G. Klemperer, and W. Shum, *Inorg. Chem.*, **18**, 93 (1979).

6) C. M. Flynn, Jr. and M. T. Pope, *Inorg. Chem.*, **10**, 2745 (1971); **11**, 1950 (1972).

7) G. W. Wallace and M. G. Mellon, *Anal. Chim. Acta*, **23**, 355 (1960).

8) S. Himeno, N. Ishii, M. Hasegawa, A. Saito, and T. Hori, *Inorg. Chim. Acta*, **131**, 11 (1987).

9) P. Courtin, F. Chauveau, and P. Souchay, *C. R. Acad. Sci. (Paris)*, **258**, 1247 (1964).

10) P. Courtin, *Rev. Chim. Miner.*, **8**, 75 (1971).

11) M. P. Courtin, *Bull. Soc. Chim. Fr.*, **1968**, 4799.

12) G. A. Tsigdinos and C. J. Hallada, *J. Less-Common*

Met., **36**, 79 (1974).
13) D. P. Smith and M. T. Pope, *Inorg. Chem.*, **12**, 331 (1973).
14) G. A. Tsigdinos, "Electrochemical Properties of Heteropoly Molybdates," Climax Molybdenum Company Bulletin Cdb-15, 1971.
15) W. F. Sokol, D. H. Evans, K. Niki, and T. Yagi, *J. Electroanal. Chem. Interfacial Electrochem.*, **108**, 107 (1980).
16) A. J. Bard and L. R. Faulkner, "Electrochemical Methods," John Wiley and Sons, New York (1980), Chap. 6.
17) D. S. Polcyn and I. Shain, *Anal. Chem.*, **38**, 370 (1966).
18) V. S. Sergienko, M. A. Porai-Koshits, and E. N. Yurchenko, *J. Struct. Chem. (Eng. Transl.)*, **21**, 87 (1980).
19) T. Osakai, S. Himeno, A. Saito, and T. Hori, *J. Electroanal. Chem. Interfacial Electrochem.*, **258**, 209 (1990).

 © 1991 The Chemical Society of Japan Bull. Chem. Soc. Jpn., 64, 29—34 (1991)

Synthesis and Characterization of Directly Linked Salen-Porphyrin System with Constrained Geometries

Kazuhiro MARUYAMA,* Fumikazu KOBAYASHI, and Atsuhiro OSUKA
Department of Chemistry, Faculty of Science, Kyoto University, Kyoto 606
(Received July 2, 1990)

Novel heterobinucleating porphyrin complexes, in which porphyrin and salen [*N*, *N'*-disalicylideneethylenediamine] subunits were directly linked with restricted geometries, were synthesized. These complexes showed a small change in their UV-vis spectra and oxidation potentials, but the fluorescence of porphyrin was effectively quenched by the linked nickel–salen subunit.

Extensive studies of binuclear metal complexes have been made in recent years as simple chemical models for biological metalloproteins containing bimetallic centers. One of the important aspects for the model complexes is close proximity of two metal centers in a well-defined three dimensional geometry, as such in biological systems.

Recently we have reported the synthesis and spectroscopic investigation of salen-capped porphyrins,[1] in which salen subunits were just held over the porphyrin macrocycle. Electronic interactions between these two metal complexes, which were seen in their absorption and fluorescence spectra, and oxidation potentials, were strongly influenced by mutual geometry of the metal complexes.

Now we have synthesized another set of salen-linked porphyrins **1** and **2** as well as salen-bridged dimeric porphyrins **3** and **4**, in which the salen subunit is directly connected to the *meso* position of the porphyrin macrocycle. Since the 5-aryl group was

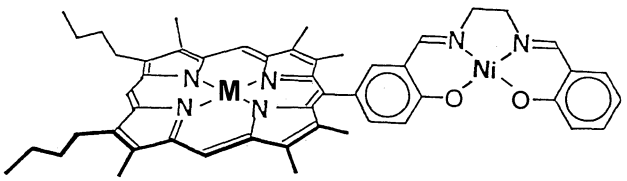

1a M = H_2

1b M = Zn

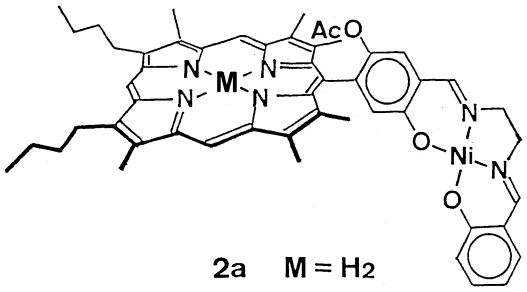

2a M = H_2

2b M = Zn

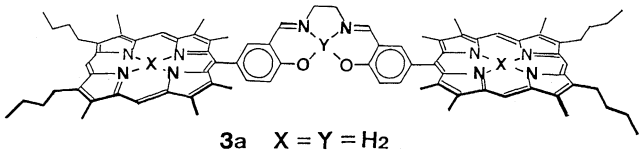

3a X = Y = H_2

3b X = H_2, Y = Ni

3c X = Zn, Y = Ni

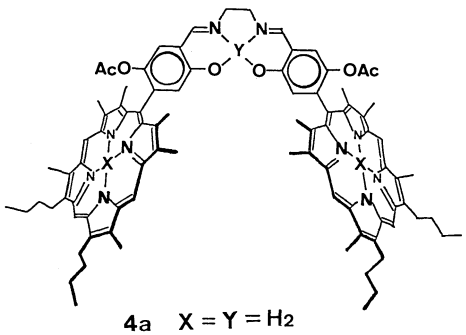

4a X = Y = H_2

4b X = H_2, Y = Ni

4c X = Zn, Y = Ni

forced to be perpendicular to the porphyrin plane due to the steric hindrance against the β-alkyl groups,[2] the geometry between the porphyrin and the salen complex can be considered to be rigidly fixed. On the basis of Corey–Pauling–Koltun (CPK) models, the metal-to-metal distances of the nickel–salen-linked zinc porphyrins **1b** and **2b** are both estimated to be ca. 10Å. In the case of the salen-bridged dimeric porphyrins **3** and **4**, the salen subunit acts as the bridging group as well as the third metal binding site. In the metal-free salen form, two porphyrins are linked only by flexible ethylene chain, while two porphyrins are expected to adopt a rather fixed geometry upon the nickel complexation at the salen site owing to a preferred planar geometry of the nickel–salen complexes.[3] On the basis of CPK models, the center-to center distances and interplane angles of two porphyrins are estimated to be 20 Å and 180° in **3b—3c**, and 13 Å and 60° in **4b—4c**, respectively.

Results and Discussion

Salen-linked porphyrins **1** and **2** were prepared from

salicylaldehyde-linked porphyrins **7** and **12**, respectively. A key porphyrinic intermediate **7** was prepared by the acid-catalyzed condensation of the biladiene-*ac*-21,24-diium dibromide **5**[4] with 4-hydroxy-1,3-benzenedicarbaldehyde (**6**)[5] (HBr/MeOH, 24 h, reflux), which furnished **7** in 28% yield together with **8** (30%).[6] (Scheme 1) Another salicylaldehyde-linked porphyrinic intermediate **12** was prepared as follows:— Condensation of **5** and 2,5-dimethoxy-1,4-benzenedicarbaldehyde (**9**) afforded an acetal porphyrin **10** in 52% yield, which was treated with BBr_3 in CH_2Cl_2 at low temperature to give a deprotected porphyrin **11** in 95% yield. Selective acetylation of **11** was achieved by the reaction with small excess amounts of acetyl chloride in the presence of pyridine in CH_2Cl_2 (Scheme 2).

The salicylaldehyde-linked porphyrins **7** thus pre-

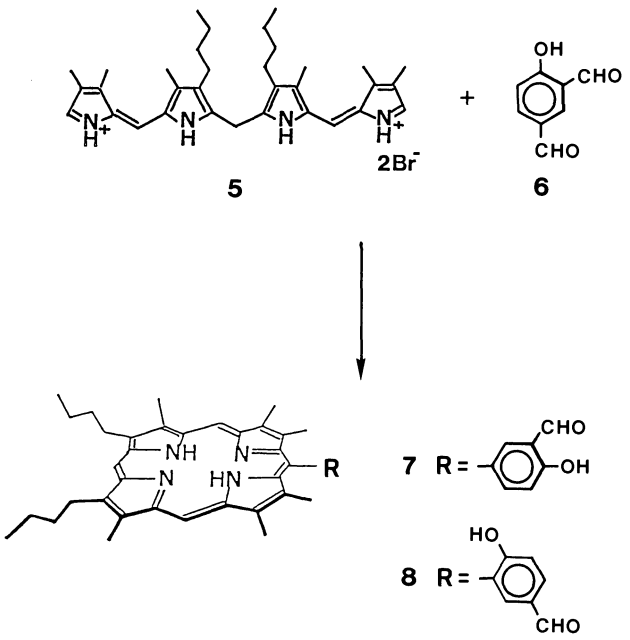

Scheme 1.

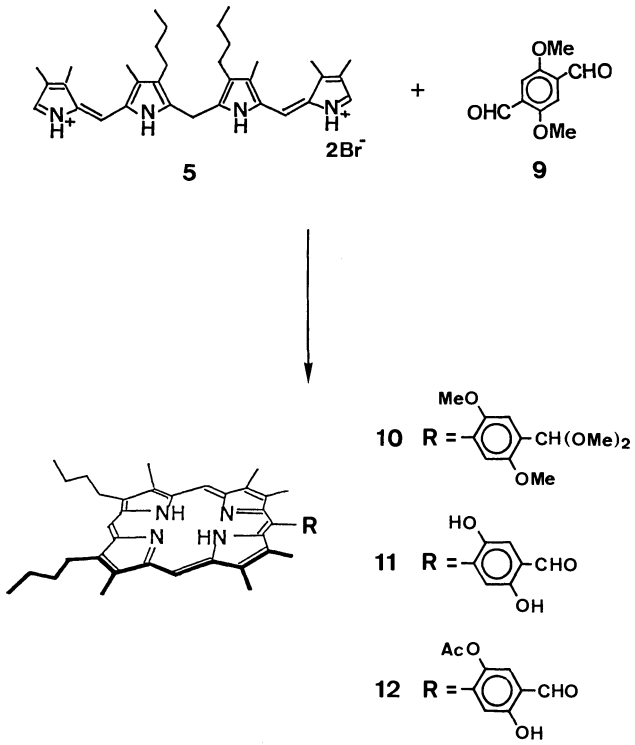

Scheme 2.

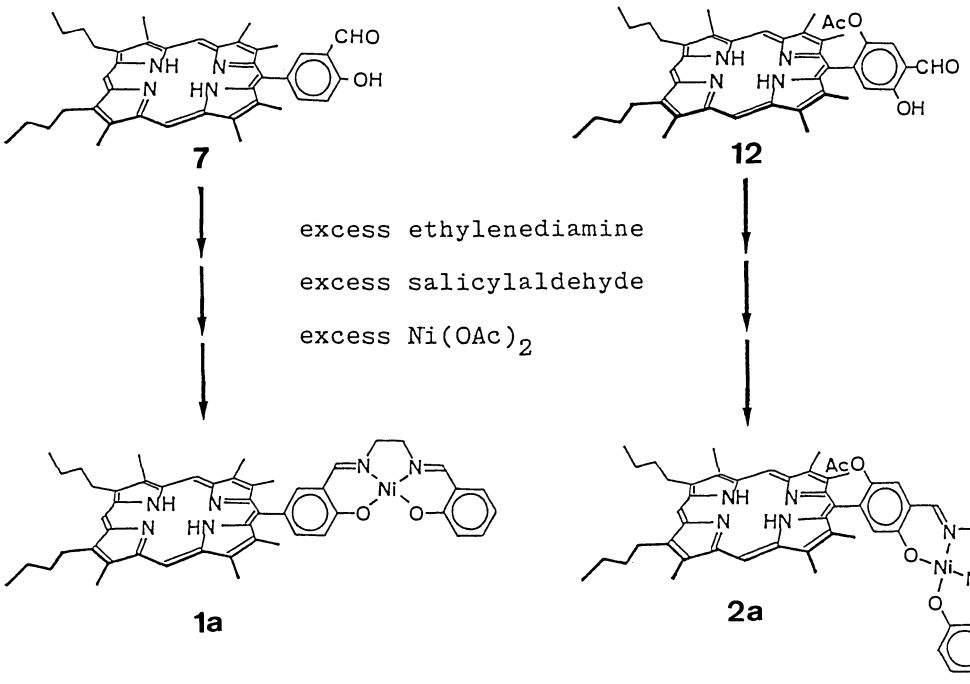

Scheme 3.

pared was dissolved in CH_2Cl_2 and treated with 5 fold excess of ethylenediamine. After 1 h, 7 fold excess of salicylaldehyde was added and the mixture was stirred overnight to yield a crude salen-linked porphyrin. Since a metal free salen moiety was acid-labile, the salen site was converted to the nickel complex by treating with nickel(II) acetate at room temperature. The resulting mixture was separated on silica-gel column eluting with CH_2Cl_2–5% ether (v/v) to yield a nickel–salen-linked porphyrin **1a** in 49% yield. The nickel–salen-linked porphyrin **2a** was prepared in the same manner from the salicylaldehyde-linked porphyrin **12** in 42% yield.

The salen-bridged dimeric porphyrins **3a** and **4a** were prepared by Schiff base condensation of salicylaldehyde-linked porphyrins **7** and **12** with ethylenediamine.[1a] The salicyllaldehyde-linked porphyrins **7** and **12** were treated with 0.5 equimolar amount of ethylenediamine in CH_2Cl_2 at room temperature for 2 weeks to allow a nearly complete transformation into the corresponding salen-bridged dimeric porphyrins **3a** and **4a**, respectively. After recrystallization from CH_2Cl_2–methanol, **3a** and **4a** were obtained in high yields (over 85% yield) in pure form.

In the nickel–salen-linked zinc porphyrin **1b** and **2b**, the absorption of the porphyrin subunit was almost unchanged by covalent linkage with the nickel–salen, but the porphyrin Soret band was slightly broadened and red-shifted (Table 1). The Soret band of dimers were more broadened and red-shifted in **3c** but slightly blue-shifted in **4c**. These additional shifts in the dimers **3c** and **4c** were in agreement with exciton coupling interactions between the two porphyrins in flat and oblique geometries, respectively.[2]

The oxidation potentials of these complexes (**1b**, **2b**, **3c**, and **4c**) were slightly lower than that of the reference zinc porphyrin **13** (Table 2). These results are in contrast to that of the salen-capped porphyrin (**14**) which showed 140 mV lower oxidation potential and red-shifted Soret band.[1b]

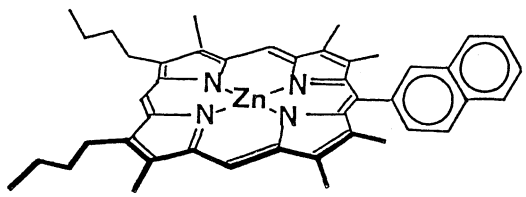

13

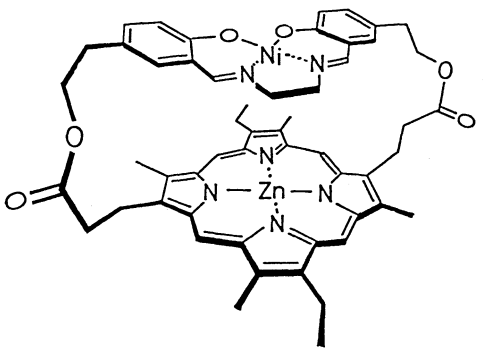

14

Table 1. UV-Vis Spectral Data[a]

Compound	λ_{max}/nm	
	Soret	Q-bands
1b	407 (15)	535 571
2b	407 (15)	535 571
3c	408 (18)	535 571
4c	404 (18)	534 571
13	405 (12)	534 570
14	410 (28)	538 574

a) Measured in CH_2Cl_2 solution. Numbers given in parentheses show full width at half-height of the maximum absorbance of the Soret band (nm).

Table 2. Oxidation Potentials[a]

Compound	$E^{ox}_{1/2}$/mV	
1b	145	380
2b	160	435
3c	140	385
4c	165	420
13	170	415
14	30	460

a) Oxidation potentials (mV vs. ferrocene/ferrocenium, +0.45 V vs. SCE) were measured by cyclic voltammetry at a Pt electrode, in CH_2Cl_2 containing 0.1 M (1 M= 1 mol dm^{-3}) tetrabutylammonium perchlorate at 20 °C; accuracy ±10 mV.

Since it has been well established that porphyrins generally show red-shifted Soret bands and lower oxidation potentials in electron donating solvents or with electron donating axial ligands,[7] these spectral red shift and low oxidation potential of **14** can be ascribed to electron donation from the nickel(II)–salen to the zinc–porphyrin in the ground state, indicating the important role of electron-filled d orbitals (especially

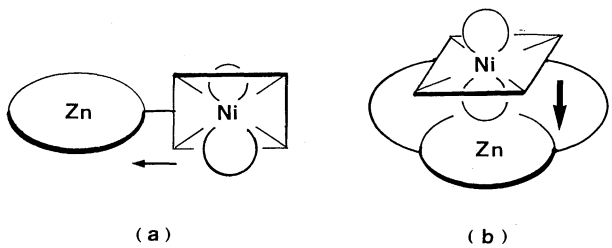

Fig. 1. Schematic representation of molecular geometry and dz^2 orbital of Ni(II) for the salen-linked porphyrin **1b** (a), and the salen-capped porphyrin **14** (b).

dz^2) of nickel(II) to the ground state interactions between zinc porphyrin and nickel-salen moieties (Fig. 1). In contrast, the interactions between the zinc porphyrin and the nickel-salen of **1b**, **2b**, **3c**, and **4c** in their ground states were small. The expected d-orbital interactions shown in Fig. 1b are presumably impossible in the molecules **1b**, **2b**, **3c**, and **4c** (Fig. 1a).

On the other hand, the fluorescence of the zinc porphyrins **1b**, **2b**, **3c**, and **4c** were all strongly quenched by the appended nickel-salen moieties (Table 3). The effective fluorescence quenching and extremely short-lived fluorescence lifetimes of **1b**, **2b**, **3c**, and **4c** suggest the strong interactions between the singlet excited state of the zinc porphyrin and the directly bound nickel-salen. The observed fluorescence lifetimes of **1b**, **2b**, **3c**, and **4c** are much shorter than the salen-capped porphyrins **14**, even though the orbital overlap between the Zn porphyrin π-system and the d-orbitals on Ni(II) seems more favorable in the latter molecule. The fact that a rapid decay of the $S_n \leftarrow S_1$ obsorption observed in the picosecond time-resolved spectra of **14** was followed by no enhancement of the $T_n \leftarrow T_1$ absorption[1b] indicates that the intersystem crossing of the singlet excited state of zinc-porphyrin was not accelerated by the Ni-salen. Although it was difficult to detect clearly the ion pair state presumably due to its rapid charge recombination, the electron transfer mechanism was expected to play a predominant role for the fluorescence quenching in these zinc-porphyrin-nickel-salen linked molecules.

Table 3. Fluorescence Spectral Data[a]

Compd	λ_{em}/nm	Φ_f, rel[b]	τ/ns[c]
1b	577 627	0.01	<0.05
2b	576 626	0.01	0.032 (100%)
3c	574 626	0.04	0.056 (97%)
			1.06 (3%)
4c	576 626	0.03	0.048 (95%)
			1.14 (5%)
13	575 626	1.0	1.5 (100%)
14	569 622	—	0.108 (88%)
			0.710 (12%)

a) Measured in CH_2Cl solution. b) Relative fluorescence intensities of Q(00) bands with respect to **13**; excitation at Soret wavelength. c) Fluorescence lifetime measured by time-correlated single photon counting technique (Ref. 8); excited at 514.5 nm by Ar laser pulse. Numbers in parentheses indicate the normalized pre-exponential factor.

An additional unique character of the salen-bridged dimeric porphyrins **3** and **4** was also observed in their ^{1}H NMR spectra. The changes in the ^{1}H NMR spectra of salen-bridged porphyrin dimers upon complexation of nickel(II) into the salen sites are summarized in Table 4. Nickel(II) complexation can be seen clearly in their up-field shifts of salen protons (CH=N-CH_2). In the metal free salen form, the chemical shifts of the peripheral protons of the porphyrin (*meso*-H, β-CH_3, β-Bu) of **3a** and **4a** were comparable. Upon complexation of nickel(II), these protons were not shifted or slightly downfield shifted in **3b**, but were instead upfield shifted by 0.1 ppm in **4b**, reflecting the ring current effect of the other porphyrin ring in the oblique geometry.

In summary, the directly linked porphyrin-salen system described herein showed only weak interactions in the ground state, while strong interactions were observed in the singlet excited state.

Experimental

The ^{1}H NMR spectra were recorded at 400 MHz on a JEOL JNM-GX-400 spectrometer, with tetramethylsilane or $CHCl_3$ as internal reference. All spectra were measured in $CDCl_3$ solution. Fast atom bombardment mass spectra were recorded on a JEOL JMS-DX-300 (1.5 kV) with *m*-nitrobenzyl alcohol as the matrix. UV-vis spectra were recorded in dichloromethane on a Shimadzu UV-200 and a Shimadzu UV-3000 spectrophotometer. Steady-state fluorescence spectra were recorded by using a Shimadzu RF-502a spectrofluorometer. Fluorescence lifetimes were measured by picosecond time-correlated single photon counting technique.[8] Cyclic Voltammetry was performed with a PAR Model 174.

Flash column chromatography was carried out using Merck Kieselgel 60H Art. 7736.

Unless othewise stated all reactions were performed under an atmosphere of dry nitrogen. All organic extracts were dried over anhydrous sodium sulfate.

5-(3-Formyl-4-hydroxyphenyl)-13,17-dibutyl-2,3,7,8,12,18-hexamethylporphine (7). A suspension of 8,12-dibutyl-2,3,7,13,17,18-hexamethylbiladiene-*ac*-21,24-diium dibromide

Table 4. ^{1}H NMR Data for Salen-Bridged Dimeric Porphyrins

Compd	Chemical shift/ppm										
	meso-H			β-Me			β-Bu			CH=N-CH_2	
3a	10.13	9.96	3.62	3.47	2.56	4.05	2.29	1.78	1.13	8.68	4.17
3b	10.17	9.95	3.65	3.57	2.69	4.05	2.29	1.78	1.14	7.77	3.6
$\Delta\delta$[a]	0.04	−0.01	0.03	0.10	0.13	0	0	0	0.01	−0.91	−0.6
4a	10.15	9.98	3.63	3.52	2.75	4.06	2.27	1.76	1.12	8.84	4.31
4b	10.04	9.85	3.54	3.46	2.73	3.96	2.18	1.67	1.04	7.95	3.78
$\Delta\delta$[a]	−0.11	−0.13	−0.09	−0.06	−0.02	−0.10	−0.09	−0.09	−0.08	−0.89	−0.53

a) Chemical shift changes induced by nickel(II) complexation into the salen site. Negative value shows the upfield shift.

(**5**)[4] (230 mg, 0.35 mmol) and 4-hydroxy-1,3-benzenedicarbaldehyde (**6**)[5] (515 mg, 3.4 mmol) in methanol containing acetic acid (four drops) saturated with hydrogen bromide was heated under reflux for 24 h.[6] The mixture was cooled and poured into water, and extracted with $CHCl_3$. The organic layer was washed with aqueous sodium hydrogencarbonate, with water, and then evaporated. The residue was flash chromatographed on silica gel eluted with CH_2Cl_2–5% ether. The first band eluted was the desired porphyrin **7**. Recrystallization from CH_2Cl_2–methanol gave purple microcrystals (61 mg, 0.097 mmol, 28%).

^1H NMR ($CDCl_3$) δ=11.43 (1H, s, OH), 10.16+9.97 (2H+1H, s+s, *meso*-H), 10.07 (1H, s, CHO), 8.22+7.40 (2H+1H, m+d, ArH), 4.04 (4H, t, Bu), 3.63+3.54+2.52 (6H+6H+6H, s+s+s, β-Me), 2.28+1.77+1.13 (4H+4H+6H, m+m+t, Bu), −3.18+−3.30 (1H+1H, br, NH). MS (FAB) *m/z* 627 ($M+H^+$).

5-(2,5-Dimethoxy-4-(dimethoxymethyl)phenyl)-13,17-dibutyl-2,3,7,8,12,18-hexamethylporphine (10). A suspension of the biladiene-*ac*-21,24-diium dibromide (**5**) (206 mg, 0.31 mmol) and 2,5-dihydroxy-1,4-benzenedicarbaldehyde (**9**) (304 mg, 1.57 mmol) in methanol containing acetic acid (four drops) saturated with hydrogen dromide was heated under reflux for 41 h and the product worked up as in the previous experiment. (116 mg, 0.16 mmol, 52%)

^1H NMR ($CDCl_3$) δ=10.13+9.94 (2H+1H, s+s, *meso*-H), 7.54+7.31 (1H+1H, s+s, ArH), 6.05 (1H, s, C<u>H</u>$(OMe)_2$), 4.04 (4H, t, Bu), 3.78+3.71+3.61 (3H+3H+6H, s+s+s, OMe), 3.63+3.54+2.60 (6H+6H+6H, s+s+s, β-Me), 2.29+1.78+1.13 (4H+4H+6H, m+m+t, Bu), −3.14+−3.29 (1H+1H. br, NH). MS(FAB) *m/z* 717 ($M+H^+$).

5-(2,5-Dihydroxy-4-formylphenyl)-13,17-dibutyl-2,3,7,8,12,18-hexamethylporphine (11). The porphyrin **10** (77 mg, 0.11 mmol) was dissolved in dry CH_2Cl_2 (45 ml) and treated with BBr_3 (0.5 ml) at −78 °C. The mixture was stirred overnight and gradually warmed to room temperature, and then poured into water. The product was extracted with CH_2Cl_2 and the extract was washed with aqueous sodium hydrogencarbonate, with water, and then evaporated. Recrystallization from CH_2Cl_2–hexane gave purple microcrystals (68 mg, 0.11 mmol, 99%).

^1H NMR ($CDCl_3$) δ=10.82 (1H, br, OH), 10.21 (1H, s, CHO), 10.19+10.01 (2H+1H, s+s, *meso*-H), 7.53+7.48 (1H+1H, s+s, ArH), 4.04 (4H, t, Bu), 3.64+3.56+2.70 (6H+6H+6H, s+s+s, β-Me), 2.28+1.77+1.13 (4H+4H+6H, m+m+t, Bu). MS (FAB) *m/z* 643 ($M+H^+$).

5-(2-Acetoxy-4-formyl-5-hydroxyphenyl)-13,17-dibutyl-2,3,7,8,12,18-hexamethylporphine (12). The dihydroxy porphyrin **11** (68 mg, 0.11 mmol) was dissolved in dry CH_2Cl_2 (25 ml) containing pyridine (50 µl) and acetyl chloride (50 µl) in CH_2Cl_2 (10 ml) was added. The mixture was stirred for 2 days and then poured into water. The organic layer was washed with water, dried, and evaporated. The residue was purified by flash column chromatography (CH_2Cl_2). The first band eluted was the desired porphyrin **12**. Recrystallization from CH_2Cl_2–methanol gave purple microcrystals (23 mg, 0.033 mmol, 32%).

^1H NMR ($CDCl_3$) δ=11.20 (1H, br, OH), 10.24 (1H, s, CHO), 10.17+9.99 (2H+1H, s+s, *meso*-H), 7.85+7.79 (1H+1H, s+s, ArH), 4.05 (4H, t, Bu), 3.64+3.55+2.69 (6H+6H+6H, s+s+s, β-Me), 2.28+1.77+1.13 (4H+4H+6H, m+m+t, Bu), 1.03 (3H, s, CH_3CO), −3.20 (2H, br, NH). MS (FAB) *m/z* 685 ($M+H^+$).

Salen-Linked Porphyrin 1a. The salicylaldehyde-linked porphyrin **7** (4.7 mg, 0.007 mmol) was dissolved in CH_2Cl_2 (7 ml) and ethylenediamine (0.15 M solution in methanol, 0.2 ml) was added. After the solution was stirred at room temperature for 1 h, salicylaldehyde (0.1 M solution in CH_2Cl_2, 0.65 ml) was added and stirring was continued overnight. To this solution, a saturated methanolic solution of nickel(II) acetate (ca. 1 ml) was added, and the mixture was stirred for 2 h at room temperature. The solvent was removed, and the residue was purified by flash column chromatography (CH_2Cl_2). Recrystallization from CH_2Cl_2–methanol gave purple crystals (3.0 mg, 0.004 mmol, 49%).

1a: ^1H NMR ($CDCl_3$) δ=10.14+9.94 (2H+1H, s+s, *meso*-H), 7.69+7.61 (1H+1H, s+s, CH=N), 7.90+7.68+7.45+7.30+7.17+6.62 (7H, dd+d+d+d+t+t, Ar-H), 4.04 (4H, t, Bu) 3.62+3.53+2.61 (6H+6H+6H, s+s+s, β-Me), 3.49 (4H, s, NCH_2), 2.28+1.77+1.12 (4H+4H+6H, m+m+t, Bu), −3.3 (2H, br, NH). UV-vis (CH_2Cl_2) 407, 504, 537, 572, and 624 nm. MS (FAB) *m/z* 829 ($M+H^+$).

1b: ^1H NMR ($CDCl_3$) δ=10.14+10.05 (2H+1H, s+s, *meso*-H), 7.69+7.64 (1H+1H, s+s, CH=N), 7.91+7.68+7.45+7.3+7.18+6.62 (7H, dd+d+d+d+m+t, Ar-H), 4.06 (4H, t, Bu), 3.63+3.53+2.62 (6H+10H+6H, s+s+s, β-Me and NCH_2), 2.30+1.80+1.15 (4H+4H+6H, m+m+t, Bu). UV-vis (CH_2Cl_2) 407, 535, and 571 nm.

Salen-Linked Porphyrin 2a. From the salicylaldehyde-linked porphyrin **12** (5.0 mg, 0.007 mmol, in CH_2Cl_2 20 ml), the salen-linked porphyrin **2a** was synthesized by the same procedure as described above to give purple crystals (2.7 mg, 0.003 mmol, 42%).

2a: ^1H NMR ($CDCl_3$) δ=10.14+9.95 (2H+1H, s+s, *meso*-H), 7.86+7.58 (1H+1H, s+s, CH=N), 7.73+7.41+7.13+6.95+6.54 (6H, s+s+m+d+t, Ar-H), 4.04 (4H, t, Bu) 3.63+3.53+2.77 (6H+6H+6H, s+s+s, β-Me), 3.6 (4H, m, NCH_2), 2.26+1.75+1.11 (4H+4H+6H, m+m+t, Bu), 0.94 (3H, s, CH_3CO), −3.30 (2H, br, NH). UV-vis (CH_2Cl_2) 405, 503, 537, 572, and 625 nm.

2b: ^1H NMR ($CDCl_3$) δ=10.14+10.05 (2H+1H, s+s, *meso*-H), 7.88+7.62 (1H+1H, s+s, CH=N), 7.78+7.41+7.13+6.95+6.54 (6H, s+s+m+d+t, Ar-H), 4.06 (4H, t, Bu) 3.63+3.53+2.77 (6H+6H+6H, s+s+s, β-Me), 3.58 (4H, m, NCH_2), 2.28+1.78+1.13 (4H+4H+6H, m+m+t, Bu), 0.80 (3H, s, CH_3CO). UV-vis (CH_2Cl_2) 407, 535, and 571 nm.

Salen-Bridged Dimeric Porphyrin 3a. The salicylaldehyde-linked porphyrin **7** (8.9 mg, 0.014 mmol) was dissolved in CH_2Cl_2 (20 ml) and ethylenediamine (0.15 M solution in methanol, 50 µl) was added. The solution was stirred for 2 weeks. Evaporation of the solvent and subsequent recrystallization (CH_2Cl_2–methanol) gave the porphyrin **3a** as purple crystals (8 mg, 0.006 mmol, 88%).

3a: ^1H NMR ($CDCl_3$) δ=10.13+9.96 (4H+2H, s+s, *meso*-H), 8.68 (2H, s, CH=N), 8.01+7.40 (4H+2H, m+d, Ar-H), 4.17 (4H, s, NCH_2), 4.05 (8H, t, Bu), 3.62+3.47+2.56 (12H+12H+12H, s+s+s, β-Me), 2.29+1.78+1.13 (8H+8H+12H, m+m+t, Bu), −3.2 (4H, br, NH). UV-vis (CH_2Cl_2) 405, 503, 536, 570, and 623 nm. MS (FAB) *m/z* 1278 ($M+H^+$).

3b: ^1H NMR ($CDCl_3$) δ=10.17+9.95 (4H+2H, s+s, *meso*-H), 7.77 (2H, s, CH=N), 7.89+7.76+7.57 (2H+2H+2H, dd+d+d, Ar-H), 4.05 (8H, t, Bu), 3.65+3.57+2.69 (12H+12H+12H, s+s+s, β-Me), 3.6 (4H, br, NCH_2), 2.29+1.78+1.14 (8H+8H+12H, m+m+t, Bu), −3.23 (4H, br, NH). UV-vis

(CH_2Cl_2) 406, 503, 536, 571, and 623 nm. MS (FAB) *m/z* 1333—1338 ($M+H^+$).

3c: UV-vis (CH_2Cl_2) 408, 535, and 571 nm. MS (FAB) *m/z* 1457—1464 ($M+H^+$).

Salen-Bridged Dimeric Porphyrin 4a. The salicylaldehyde-linked porphyrin **12** (8.8 mg, 0.013 mmol) was treated with ethylenediamine (0.15 M solution in methanol, 40 μl) by the same procedure as **3a** to give purple crystals (8 mg, 0.006 mmol, 88%).

4a: ^1H NMR ($CDCl_3$) δ=13.46 (2H, br, OH), 10.15+9.98 (4H+2H, s+s, *meso*-H), 8.84 (2H, s, CH=N), 7.79+7.62 (2H+2H, s+s, Ar-H), 4.31 (4H, s, NCH_2), 4.06 (8H, m, Bu), 3.63+3.52+2.75 (12H+12H+12H, s+s+s, β-Me), 2.27+1.76 +1.12 (8H+8H+12H, m+m+m, Bu), 0.95 (6H, s, CH_3CO), −3.18+−3.33 (4H, br, NH). MS (FAB) *m/z* 1392—1398 (M^+).

4b: ^1H NMR ($CDCl_3$) δ=10.04+9.85 (4H+2H, s+s, *meso*-H), 7.95(2H, s, CH=N), 7.64+7.45 (2H+2H, s+s, Ar-H), 3.96 (8H, m, Bu), 3.78(4H, s, NCH_2), 3.54+3.46+2.73 (12H+12H+ 12H, s+s+s, β-Me), 2.18+1.67+1.04 (8H+8H+12H, m+m+ m, Bu), 0.91 (6H, s, CH_3CO), −3.4 (4H, br, NH). UV-vis (CH_2Cl_2) 404, 503, 537, 572, and 624 nm. MS (FAB) *m/z* 1448—1455 (M^+).

4c: ^1H NMR ($CDCl_3$) δ=10.04+9.97 (4H+2H, s+s, *meso*-H), 7.96 (2H, s, CH=N), 7.65+7.45 (2H+2H, s+s, Ar-H), 3.98 (8H, m, Bu), 3.80 (4H, br, NCH_2), 3.55+3.47+2.74 (12H+12H+ 12H, s+s+s, β-Me), 2.20+1.69+1.06 (8H+8H+12H, m+m+ m, Bu), 0.81 (6H, s, CH_3CO). UV-vis (CH_2Cl_2) 404, 534, and 571 nm. MS (FAB) *m/z* 1572—1580 (M^+).

The work was partially supported by the Grant-in-Aid for Scientific Research No. 01649508 from the Ministry of Education, Science and Culture, Nissan Science Foundation, and the Kurata Research Grant. We thank Professor S. Hirayama of Kyoto Institute of Technology for measurement of picosecond fluorescence lifetimes.

References

1) a) K. Maruyama, F. Kobayashi, and A. Osuka, *Chem. Lett.*, **1987**, 821; b) K. Maruyama, F. Kobayashi, and A. Osuka, *Bull. Chem. Soc. Jpn.*, **63**, 2672 (1990).

2) A. Osuka and K. Maruyama, *J. Am. Chem. Soc.*, **110**, 4454 (1988).

3) L. M. Schol'nikova, E. M. Yumal', E. A. Shugam, and V. A. Voblikova, *J. Struct. Chem. (Engl. Transl.)*, **11**, 819 (1970).

4) The synthesis of this compound was analogous to the fully methylated derivative. A. W. Johnson and I. T. Kay, *J. Chem. Soc.*, **1965**, 1620. *n*-Bu group was introduced in order to increase the solubility of porphyrins.

5) S. J. Angyal, P. S. Morris, J. R. Tetaz, and J. G. Wilson, *J. Chem. Soc.*, **1950**, 2141.

6) D. Harris, A. W. Johnson, and R. Gaete-Holmes, *Bioorg. Chem.*, **9**, 63 (1980).

7) M. Nappa and J. S. Valentine, *J. Am. Chem. Soc.*, **100**, 5075 (1978).

8) S. Hirayama and Y. Shimoto, *J. Chem. Soc., Faraday Trans. 2*, **80**, 941 (1984).

 © 1991 The Chemical Society of Japan Bull. Chem. Soc. Jpn., 64, 35—41 (1991)

Preparation, Stereochemistry, and Antibacterial Activity of Gramicidin S Analogs Containing *N*-Methyl Groups

Masao KAWAI,* Masashi OHYA, Norihito FUKUTA, Yasuo BUTSUGAN, and Kazuki SAITO†
Department of Appliced Chemistry, Nagoya Institute of Technology, Gokiso-cho, Showa-ku, Nagoya 466
†Department of Analytical Chemistry, Faculty of Pharmaceutical Sciences, University of Tokyo, Hongo, Bunkyo-ku, Tokyo 113
(Received August 1, 1990)

The *N*-methylated analogs of gramicidin S, namely [Orn(Me_3^+)$^{2,2'}$]-, [MeOrn$^{2,2'}$, D-MePhe$^{4,4'}$]-, [MeOrn(Me)$^{2,2'}$, D-MePhe$^{4,4'}$]-, and [MeOrn(Me_3^+)$^{2,2'}$, D-MePhe$^{4,4'}$]gramicidin S, were prepared by the use of quaternization reaction of free amino groups with CH_3I–$KHCO_3$ in methanol and/or selective amide-methylation with CH_3I–Ag_2O in DMF. The conformations of these synthetic analogs were shown to be of β-sheet type similar to that of parent gramicidin S by ^1H NMR analysis and CD spectral comparison. The *N*-methyl group-containing analogs exhibited essentially the same antibacterial activity against Gram-positive bacteria as gramicidin S itself.

Gramicidin S (GS) is a cyclic decapeptide with the primary structure cyclo(–Val–Orn–Leu–D-Phe–Pro–)$_2$ showing strong antibacterial activity against Gram-positive bacteria. GS is one of the peptide antibiotics that have been most extensively studied by the synthetic approach.[1] The secondary structure of GS is established as the antiparallel β-sheet conformation having four intramolecular hydrogen bonds between two pairs of Val and Leu residues as shown in Fig. 1. Consequently the twelve nitrogen atoms present in GS are classified into four groups: two free amino groups of Orn side chains, four intramolecularly hydrogen-bonded amide NH's of Val and Leu residues, four solvent-exposed amide NH's of Orn and D-Phe residues, and two secondary amide nitrogens of Pro carrying no hydrogens. This paper deals with preparation of new analogs of GS having methyl groups on different N atoms by the application of two kinds of *N*-methylation reactions to GS or its derivatives. Stereochemistry and antibacterial activity of the *N*-methylated analogs are also described.

Preparation of Analogs

N-Methylation of a free amino group using CH_3I–$KHCO_3$ in methanol to afford a trimethylammonio group was reported by Chen and Benoiton.[2] The quaternization reaction was applied to GS to obtain a new analog of GS.[3] To the solution of GS·2HCl (**1**, 0.1 mmol) in methanol (20 ml) were added CH_3I (32 mmol) and $KHCO_3$ (10 mmol), and the mixture was stirred for 45 h. Workup and purification furnished the desired product [Orn(Me_3^+)$^{2,2'}$]GS·$2I^-$ (**2**),[4] mp 228—231.5 °C, in 75% yield, where Orn(Me_3^+) stands for a side-chain-quaternized Orn residue namely NHCH($CH_2CH_2CH_2N^+Me_3$)CO. The ^1H NMR spectrum of **2** exhibited a singlet peak at δ (DMSO-d_6) 3.11 assignable to the two trimethylammonio groups, and amino acid analysis and elemental analysis were also satisfactory.

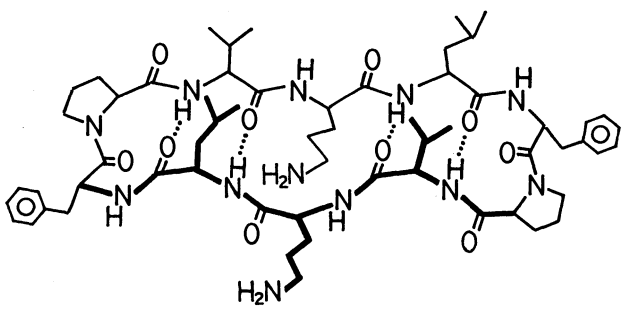

Fig. 1. β-Sheet conformation of GS with four intramolecular hydrogen bonds having C_2-symmetry.

Methylation of amide N atoms of GS was then studied. Kawai and Nagai reported conformational analysis of cyclic peptides in micromolar quantities using selective *N*-methylation with CH_3I and Ag_2O in DMF followed by amino acid analysis of the acid hydrolyzate.[5] In the case of side-chain-protected GS only solvent-exposed amide NH's of Orn and D-Phe residues were methylated while intramolecularly hydrogen-bonded amide NH's of Val and Leu residues being kept intact. The selective methylation of the diphthaloyl derivative, [Orn(Pht)$^{2,2'}$]GS, was carried out in preparative scale to yield a methylated product in 88% yield. Amino acid analysis of the acid hydrolyzate indicated that only the solvent-exposed amide NH's of Orn(Pht) and D-Phe residues had been methylated establishing the structure of the product as the desired tetramethyl derivative, namely [MeOrn-(Pht)$^{2,2'}$, D-MePhe$^{4,4'}$]GS. Removal of the phthaloyl groups with $H_2NNH_2·H_2O$ and column chromatographic purification furnished the tetramethyl analog [MeOrn$^{2,2'}$, D-MePhe$^{4,4'}$]GS·2HCl (**3**),[6] mp 200.5—203 °C, in 58% yield.

The tetramethyl analog **3** was subjected to the quaternization reaction affording a decamethyl analog [MeOrn(Me_3^+)$^{2,2'}$, D-MePhe$^{4,4'}$]GS·$2I^-$ (**4**), mp 226—232.5 °C, in 76% yield. The same compound **4** was also obtained by the application of the selective *N*-

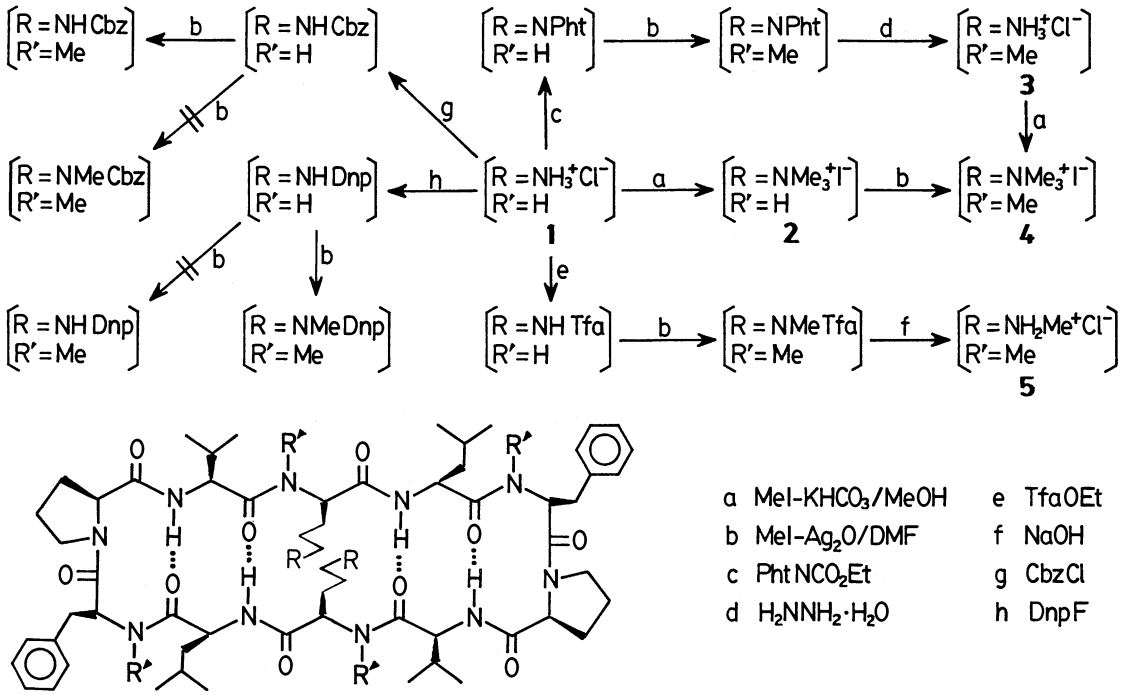

Scheme 1.

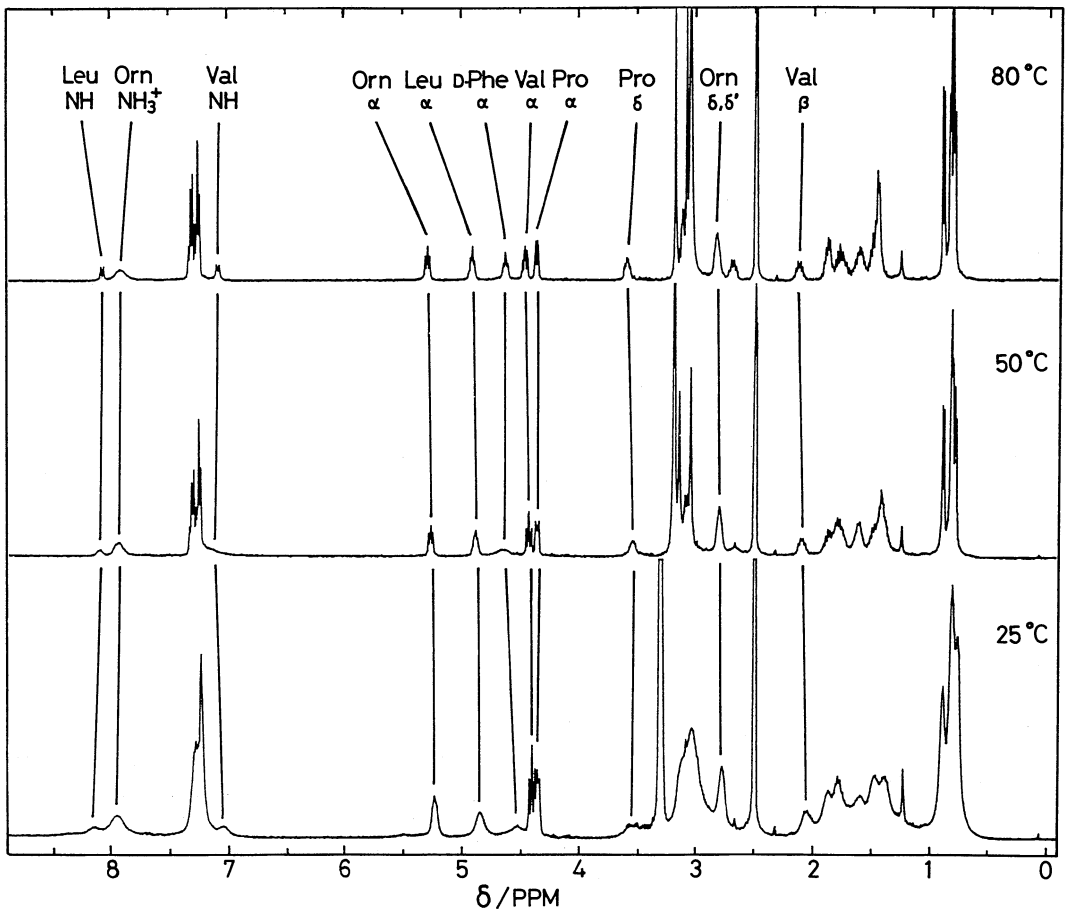

Fig. 2. 400 MHz ^{1}H NMR spectra of [MeOrn$^{2,2'}$,D-MePhe$^{4,4'}$]GS (**3**) measured in DMSO-d_6 at different temperatures.

methylation reaction to the side-chain-quaternized analog **2** in a similar manner to the *N*-methylation of the diphthaloyl derivative.

For the purpose of preparing an analog of GS having monomethylated Orn side chains, namely [MeOrn(Me)$^{2,2'}$, D-MePhe$^{4,4'}$]GS, the selective methylation reaction was applied to the bis(benzyloxycarbonyl) derivative [Orn(Cbz)$^{2,2'}$]GS. Contrary to the expectation no significant methylation at urethane NH of Orn side chain was observed, resulting in the formation of tetramethylated product [MeOrn(Cbz)$^{2,2'}$, D-MePhe$^{4,4'}$]GS. This unexpected resistance to methylation of the protected Orn side chains was noteworthy considering that the bis(2,4-dinitrophenyl) derivative [Orn(Dnp)$^{2,2'}$]GS under the same conditions afforded a hexamethyl derivative [MeOrn(Dnp,Me)$^{2,2'}$, D-MePhe$^{4,4'}$]-GS in good yield in spite of the presence of hydrogen bonding between the NH and *ortho*-NO_2 groups. The bis(trifluoroacetyl) derivative [Orn(Tfa)$^{2,2'}$]GS was found to give a hexamethyl derivative [MeOrn(Me,Tfa)$^{2,2'}$, D-MePhe$^{4,4'}$]GS on selective methylation. Alkaline hydrolysis of the trifluoroacetamido groups furnished the desired hexamethyl analog [MeOrn(Me)$^{2,2'}$, D-MePhe$^{4,4'}$]GS (**5**). Preparation of the methylated analogs **2**—**5** was summarized in Scheme 1.

Conformation of *N*-Methyl Analogs

^{1}H NMR spectral analysis of the synthetic analogs was undertaken to study their stereochemistry. The bis(trimethylammonio) analog **2** exhibited the spectra closely resembling those of GS **1**. The chemical shifts of N$^\alpha$H and coupling constants $J_{N^\alpha H\text{-}C^\alpha H}$ in the ^{1}H NMR spectrum of **2** recorded in DMSO-d_6 at 25 °C (Val δ=ca. 7.2, J=9.5 Hz; Leu δ=8.29, J=9.2 Hz; Orn δ=8.70, J=9.2 Hz; D-Phe δ=9.11, J=4.0 Hz) indicated that **2** adopted a β-sheet conformation with C_2-symmetry closely similar to that of **1**.[7] The ^{1}H NMR spectra of the tetra-*N*-methyl analog **3**, on the other hand, were apparently dissimilar to those of **1** and **2**, showing broad signals indicative of a mixture of slowly interconverting conformers. Varying-temperature study as shown in Fig. 2, however, revealed that **3** also exhibited clearly resolved sharp signals of typical β-sheet conformation at the temperatures higher than 60 °C due to rapid interconvertion of conformers. Thus, it can be assumed that although **3** exists as a comformational mixture at ambient temperature time-averaged conformation of **3** is of β-sheet type with C_2-

Table 1. 400 MHz ^{1}H NMR Spectral Data (δ/ppm) of *N*-Methylated Analogs **2**—**5** Measured in DMSO-d_6 Solutions at 80 °C

Assignments	**2**	**3**	**4**	**5**
Val				
NH[a]	7.17 (9.5)	7.08 (8.5)	7.04 (8.5)	7.18 (7.0)
C$^\alpha$H	ca. 4.40	4.46	4.41	4.47
C$^\beta$H	2.08	2.13	2.10	2.14
(C$^\gamma$H$_3$)$_2$	0.81, 0.85	0.82, 0.89	0.83, 0.92	0.83, 0.91
Orn				
N$^\alpha$H[a] or N$^\alpha$CH$_3$	8.43 (9.2)	ca. 3.17	ca. 3.1 or 3.19	3.08 or 3.18
C$^\alpha$H	4.83	5.29	5.49	5.30
C$^\beta$H$_2$	ca. 1.5, 1.76	1.88	ca. 1.83	ca. 1.76, ca. 1.92
C$^\gamma$H$_2$	ca. 1.7[b]	ca. 1.49	ca. 1.45, 1.61[b]	ca. 1.53
C$^\delta$H$_2$	3.33[b]	2.82	ca. 3.26, ca. 3.39	ca. 2.93
N$^\delta$H$_3^+$ or N$^\delta$CH$_3$	3.13	7.86	3.12	2.55
Leu				
NH[a]	8.15 (8.9)	8.07 (9.8)	8.00 (9.8)	8.09 (9.5)
C$^\alpha$H	4.59	4.91	4.92	4.92
C$^\beta$H$_2$	1.32, 1.43	ca. 1.4	ca. 1.4	ca. 1.4
C$^\gamma$H$_2$	ca. 1.5	ca. 1.4	ca. 1.4	ca. 1.4
(C$^\delta$H$_3$)$_2$	0.83	0.80, 0.83	0.81, 0.85	0.79, 0.82
D-Phe				
NH[a] or N-CH$_3$	8.76 (4.0)	ca. 3.17	ca. 3.1 or 3.19	3.08 or 3.18
C$^\alpha$H	ca. 4.40	4.63	4.56	4.70
C$^\beta$H$_2$	2.82, 2.96	ca. 3.1	ca. 3.1	ca. 3.1
arom-C$_6$H$_5$	ca. 7.25	ca. 7.3	ca. 7.3	ca. 7.3
Pro				
C$^\alpha$H	4.24	4.36	4.22	4.38
C$^\beta$H$_2$	ca. 1.61	ca. 1.77	ca. 1.78	ca. 1.76
C$^\gamma$H$_2$	ca. 1.56, 1.93[b]	ca. 1.60	ca. 1.45	1.61
C$^\delta$H$_2$	2.65, 3.59	2.68, 3.58	2.71, 3.58	2.70, 3.58

a) Coupling constant $J_{NH\text{-}CH}$ (Hz) is given in parentheses. b) Tentative assignment.

symmetry. The analogs **4** and **5** exhibited similar NMR characteristics to **3** showing well-resolved peaks at high temperatures. The ^{1}H NMR spectral data of the analogs **2**—**5** recorded at 80 °C in DMSO-d_6 solutions are summarized in Table 1, which indicates that all these analogs adopt similar conformations to that of parent **1**.

Conformation of the *N*-methyl analogs was also studied by their CD spectra measured in methanol as shown in Fig. 3. The CD spectrum of bis(trimethylammonio)-type analog **2** showing a negative maximum at 206 nm ([θ] −39500) and a shoulder at 215 nm was closely similar to that of **1**,[8] which was also consistent with their conformational similarity established by ^{1}H NMR study. The spectrum of the amide-methylated analog **3**, on the other hand, was of different pattern exhibiting a single negative maximum at the longer wavelength ([θ]$_{221}$ −37500). The difference between the spectra of **1** and **3**, however, did not indicate the conformational dissimilarity but was reasonably assumed to be due to difference of the amide chromophores, -CONH- and -CONMe-. The

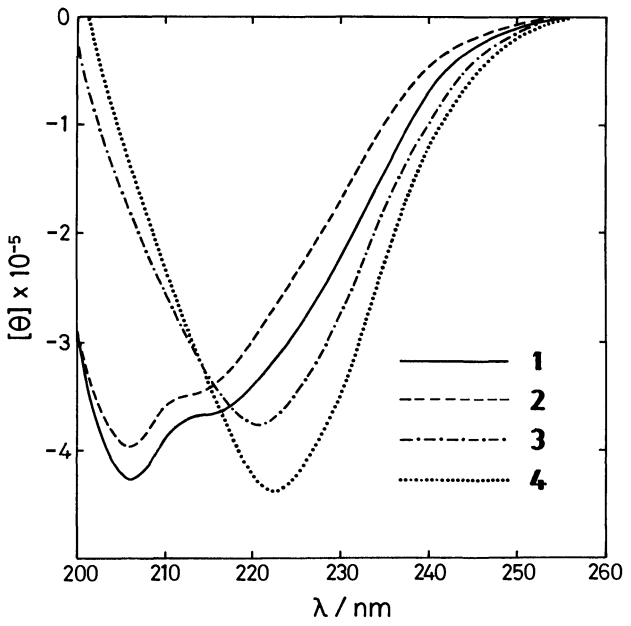

Fig. 3. CD spectra of GS·2HCl (**1**) and the *N*-methyl analogs **2**—**4** measured in MeOH at room temperature.

decamethyl analog **4** possessing also four *N*-methylated amide groups exhibited similar CD spectrum to that of **3** supporting the conformational resemblance of these analogs.

Antibacterial Activities of *N*-Methyl Analogs

Antibacterial activities of the synthetic analogs **2**—**5** were tested against several microorganisms, and minimum inhibitory concentrations of these analogs are summarized in Table 2. As expected from their conformational similarity, the *N*-methylated analogs showed essentially the same antibacterial activity against *Staphylococcus aureus* and *Bacillus subtilis* strains as parent GS **1** itself.

Discussion

Synthesis of analogs containing *N*-methyl group(s) is useful for the study of the structure-activity relationships of biologically active peptides.[9] *N*-Methylamino acid-containing analogs of GS, namely [MeVal^1]GS, [MeVal$^{1,1'}$]GS, [MeLeu^3]GS, and [MeLeu$^{3,3'}$]-GS, were synthesized by Izumiya's group[10] revealing the unexpected antibacterial activities of MeLeu-containing analogs. These analogs were synthesized by the classical methods using protected *N*-methyl-amino acids as building blocks. An alternative way to prepare the *N*-methylated analogs is modification of the parent peptide molecules by the use of selective *N*-methylation reactions. In the present study two kinds of *N*-methylations, quaternization of NH_2 group into NMe_3^+ group and selective methylation of solvent-exposed -CONH- goup into -CONMe- group were employed. Preparation of enkephalin analogs by the application of the *N*-methylation reactions to suitably protected [D-Ala^2, Leu^5]enkephalin derivatives was already reported.[11]

GS derivatives possessing various groups on N^δ atoms of Orn side chains were subjected to amide-methylation and in all cases solvent-exposed N^α atoms of Orn and D-Phe were methylated while Val and Leu residues being kept intact. As an attempt to methylate the N atoms of Val and Leu residues, [Orn(Pht)$^{2,2'}$]GS was subjected to prolonged methylation with larger amount of reagents still resulting in the isolation of only the tetramethyl derivative [MeOrn(Pht)$^{2,2'}$, D-MePhe$^{4,4'}$]GS. These results indicated that the

Table 2. Antibacterial Activities of GS **1** and Its *N*-Methyl Analogs **2**—**5** (Minimum Inhibitory Concentrations in μg cm^{-3})

Microorganism	1	2	3	4	5
Staphylococcus aureus FDA 209 PJC-1	1.56	1.56	1.56	1.56	1.56
Staphylococcus aureus Terajima	3.1	1.56	3.1	3.1	3.1
Bacillus subtilis ATCC 6633	1.56	1.56	1.56	3.1	1.56
Klebsielle pneumoniae PCI-602	12.5	12.5	50.0	>100	50.0
Escherichia coli K 12 C 600	50.0	50.0	50.0	>100	100
Escherichia coli NIHJ-JC-2	50.0	50.0	100	>100	100

intramolecularly hydrogen-bonded β-sheet conformation of GS is very stable regardless of the various modification of Orn side chains and also that the stability of the conformation is maintained during and after the methylation of solvent-exposed amide-N atoms.

It is quite interesting that the side chains of Orn protected with benzyloxycarbonyl groups in GS were intact during the amide-methylation being in contrast to the methylation of [Orn(Tfa)$^{2,2'}$]GS and [Orn(Dnp)$^{2,2'}$]GS, in which N$^{\delta}$ atoms were also methylated in good yield. Model reaction using Ac–Orn(Cbz)–OMe and Ac–Lys(Cbz)–OMe under the same conditions revealed that both urethane NH in the side chain and acetamido groups were methylated without difficulty yielding Ac–MeOrn(Cbz,Me)–OMe and Ac–MeLys(Cbz,Me)–OMe, respectively. The results suggested the presence of some interaction between Orn side chains and the rest of the molecule in [Orn(Cbz)$^{2,2'}$]-GS. Hydrogen bonding of one of the Orn side chains with the CO group of Phe residue was actually observed for GS-urea complex in crystalline state.[12]

NMR and CD spectral studies on conformational characteristics of the synthetic analogs showed the conformational resemblance of the *N*-methyl analogs **2**—**5** and parent GS **1**. ^{1}H NMR spectra of the amide-methylated analogs **3**—**5** measured in DMSO-d_6 solution at 25 °C exhibited broad signals due to slow conformational interconversion. Since sharp signals assignable to β-sheet conformation were observed at higher temperature as a result of rapid interconvertion among conformers, averaged conformation at the low temperature was also considered to resemble the conformation of **1**. In fact ^{1}H NMR spectrum of **3** measured in $CDCl_3$ at 25 °C exhibited well-resolved sharp signals characteristic of GS-type β-sheet conformation. Thus, it can be concluded that all these GS analogs possess essentially the same conformational characteristics as GS and that methyl groups at the solvent-exposed N atoms cause slight decrease in conformational mobility resulting in the slow conformational interchange in strongly solvating DMSO solution. This also suggests that the well-established β-sheet conformation having C_2-symmetry as shown in Fig. 1 of GS and its derivatives can be considered as an averaged structure of the assembly of slightly different conformers in equilibrium.[13]

From the intensive studies on the structure-antibacterial activity relationships of the analogs of GS it is known that both the stable β-sheet conformation of GS and the presence of positively charged side chains are important for the activity. As given in Table 2 the *N*-methylated analogs **2**—**5** showed very similar activity to that of parent **1**, which is consistent with the conformational similarity of all these analogs as described above. As for the Orn side chains the essentially same activity of the trimethylammonio analog **2** as **1** has demonstrared that when these antibiotics bind to bacterial membrane or receptor molecules the function of the charged Orn side chains does not involve interaction through hydrogen bonding but is simply electrostatic in nature. The activity of **3**—**5** has also indicated that the exposed amide NH's of Orn and D-Phe residues do not play any important role in the binding of GS molecules to bacteria and in manifesting the antibactrial activity.

Experimental

GS·2HCl (**1**) was supplied by Nikken Kagaku Ltd. Mp's were determined with a hot-stage apparatus and uncorrected. Silica gel (Merck, #7734) and Sephadex LH-20 were used for column chromatographic separation. Purity of each product was ascertained by TLC, HPLC, and/or ^{1}H NMR spectral analysis. TLC analysis was performed using precoated silica gel plates (Merck, Silica Gel 60 F_{254}) with the solvent systems $CHCl_3$–MeOH, $CHCl_3$–MeOH–AcOH, or 1-butanol–AcOH–H_2O. HPLC was performed using FineSIL 20 (JASCO) with $CHCl_3$–MeOH as eluent or Unisil C18 (Gasukuro Kogyo) with MeOH–$NaClO_4$ aq. ^{1}H NMR spectra were recorded on a JEOL GX-400 or on a Varian XL-200 spectrometer. CD spectra were measured on a JASCO J-40C spectropolarimeter. For amino acid analysis synthetic peptides were hydrolyzed in concd HCl–AcOH (1:1) at 110 °C for 24 h. Proline was taken as an internal standard, and Orn(Me_3^+) and MeOrn were determined by the comparison with the authentic mixture. Antibacterial assay was performed at Research Center, Mitsubishi Kasei Corporation, and elemental analysis was performed at Elemental Analysis Center of Kyoto University.

[Orn(Me_3^+)$^{2,2'}$]GS·2I$^-$ (2). CH_3I (2 cm^3, 32 mmol) and $KHCO_3$ (1.0 g, 10 mmol) were added to the solution of **1** (125 mg, 0.1 mmol) in MeOH (20 cm^3) and the mixture was stirred in the dark for 45 h at room temperature. The solvent was evaporated and the residue was extracted with $CHCl_3$. Sephadex LH-20 column chromatography of the $CHCl_3$ extract using MeOH as eluent and recrystallization from MeOH–H_2O afforded **2** (116 mg, 75%) as colorless needles, mp 228—231.5 °C. Amino acid analysis: Pro (1.00), Val (1.02), Leu (0.97), Phe (1.00), Orn (0.00), Orn (Me_3^+) (1.00).

Found: C, 50.67; H, 7.52; N, 10.89%. Calcd for $C_{66}H_{106}N_{12}O_{10}I_2 \cdot 5H_2O$: C, 50.44; H, 7.44; N, 10.70%.

[MeOrn(Pht)$^{2,2'}$, D-MePhe$^{4,4'}$]GS. [Orn(Pht)$^{2,2'}$]GS (42 mg, 0.03 mmol), prepared from **1** and *N*-(ethoxycarbonyl)phthalimide,[14] was dissolved in DMF (1 cm^3), and CH_3I (2.5 cm^3, 40 mmol) and Ag_2O (232 mg, 1.0 mmol) were added to the solution. After stirring for 4 h at room temperature MeOH (4 cm^3) was added and the precipitate was filtered off. The solvent was evaporated and the residue was extracted with $CHCl_3$. Silica-gel column chromatography of the $CHCl_3$ extract using $CHCl_3$–MeOH as eluent and crystallization from MeOH–H_2O afforded [MeOrn(Pht)$^{2,2'}$, D-MePhe$^{4,4'}$]GS (38.5 mg, 88%), mp 170.5—173.5 °C. ^{1}H NMR ($CDCl_3$) δ=3.21 (6H, s, N-Me) and 3.52 (6H, s, N-Me). Amino acid analysis: Pro (1.00), Val (1.00), Leu (0.95), Phe (0.00), Orn (0.00), MeOrn (1.05).

Found: C, 64.93; H, 7.09; N, 11.56%. Calcd for $C_{80}H_{104}N_{12}O_{14}I_2 \cdot H_2O$: C, 65.11; H, 7.24; N, 11.39%.

[MeOrn$^{2,2'}$, D-MePhe$^{4,4'}$]GS·2HCl (3). $H_2NNH_2 \cdot H_2O$ (5

cm^3) was added dropwise to the solution of [MeOrn(Pht)$^{2,2'}$, D-MePhe$^{4,4'}$]GS (73 mg, 0.05 mmol) in EtOH (2 cm^3) and the mixture was stirred overnight at room temperature. After the addition of H_2O (10 cm^3) precipitate was collected by filtration and was dissolved in EtOH (5 cm^3), to which 1 M (M=mol dm^{-3}) HCl aq (1 cm^3) was added. The solvent was evaporated and the residue was chromatographed with silica gel ($CHCl_3$–MeOH–AcOH) and then with Sephadex LH-20 (MeOH) affording **3** (37 mg, 58%), mp 200.5—203 °C.

Found: C, 55.97; H, 8.37; N, 11.53%. Calcd for $C_{64}H_{100}N_{12}O_{10}\cdot 2HCl\cdot 3CH_3OH\cdot 4H_2O$: C, 55.94; H, 8.55; N, 11.68%.

[MeOrn(Me$_3^+$)$^{2,2'}$, D-MePhe$^{4,4'}$]GS·2I$^-$ (4) Quaternization of **3** (63 mg 0.05 mmol) was undertaken in a similar manner to the preparation of **2** from **1**. Sephadex LH-20 column chromatography (MeOH) of the product and crystallization from MeOH–Et_2O–hexane gave **2** as colorless needles (57 mg, 76%), mp 226—232.5 °C. Amino acid analysis: Pro (1.00), Val (0.99), Leu (1.06), Phe (0.00), Orn (0.00).

Found: C, 52.13; H, 7.24; N, 10.47%. Calcd for $C_{70}H_{114}N_{12}O_{10}I_2\cdot 4H_2O$: C, 52.23; H, 7.64; N, 10.44%.

N-Methylation of **2** in a similar manner to the preparation of [MeOrn(Pht)$^{2,2'}$, D-MePhe$^{4,4'}$]GS from [Orn(Pht)$^{2,2'}$]GS afforded the same compound **4** in 32% yield.

[Orn(Tfa)$^{2,2'}$]GS. Ethyl trifluoroacetate (3 cm^3) was added to the solution of **1** (121 mg, 0.1 mmol) and Et_3N (0.03 cm^3, 0.2 mmol) in MeOH (5 cm^3), and the mixture was stirred overnight at room temperature. The solvent was evaporated and the residue was dissolved in $CHCl_3$ and washed with H_2O. Evaporation of $CHCl_3$ and crystallization of the residue from MeOH–H_2O gave [Orn(Tfa)$^{2,2'}$]GS as colorless prisms (112 mg, 83%), mp 273 °C (decomp).

Found: C, 56.49; H, 6.89; N, 12.40%. Calcd for $C_{64}H_{90}N_{12}F_6O_{12}\cdot 1.5H_2O$: C, 56.50; H, 6.89; N, 12.39%.

[MeOrn(Me,Tfa)$^{2,2'}$, D-MePhe$^{4,4'}$]GS. *N*-Methylation of [Orn(Tfa)$^{2,2'}$]GS (45 mg, 0.033 mmol) was carried out in a similar manner to the preparation of [MeOrn(Pht)$^{2,2'}$, D-MePhe$^{4,4'}$]GS from [Orn(Pht)$^{4,4'}$]GS. Silica-gel column chromatography ($CHCl_3$–MeOH) of the product and crystallization from MeOH–H_2O gave [MeOrn(Me,Tfa)$^{2,2'}$, D-MePhe$^{4,4'}$]GS (39 mg, 83%), mp 125—126.5 °C. ^{1}H NMR ($CDCl_3$) δ=3.14 (6H, s, *N*-Me), 3.25 (6H, s, *N*-Me), and 3.41 (6H, s, *N*-Me). Amino acid analysis: Pro (1.00), Val (0.98), Leu (0.96), Phe (0.00), Orn (0.00).

[MeOrn(Me)$^{2,2'}$, D-MePhe$^{4,4'}$]GS·2HCl (5). To the solution of [MeOrn(Me,Tfa)$^{2,2'}$, D-MePhe$^{4,4'}$]GS (53 mg, 0.043 mmol) in MeOH (3 cm^3) was added 4M NaOH aq (0.7 cm^3) and the mixture was stirred for 2 h at room temperature. The solution was acidified by the addition of 6M HCl aq and was evaporated, and the residue was extracted with $CHCl_3$. Sephadex LH-20 column chromatography (MeOH) of the $CHCl_3$ extract afforded **5** (40 mg, 82%), mp 175—177.5 °C.

Found: C, 56.72; H, 8.21; N, 12.09%. Calcd for $C_{66}H_{104}N_{12}O_{10}\cdot 2HCl\cdot 5.5H_2O$: C, 56.72; H, 8.44; N, 12.03%.

***N*-Methylation of [Orn(Cbz)$^{2,2'}$]GS.** [Orn(Cbz)$^{2,2'}$]GS[15] (127 mg, 0.09 mmol) was subjected to the *N*-methylation reaction in a similar manner to the preparation of [MeOrn(Pht)$^{2,2'}$, D-MePhe$^{4,4'}$]GS from [Orn(Pht)$^{4,4'}$]GS. The crude product showed a prominent single spot on TLC accompanied with some minor spots, and silica-gel column chromatography ($CHCl_3$–MeOH) and crystallization from MeOH–H_2O yielded [MeOrn(Cbz)$^{2,2'}$, D-MePhe$^{4,4'}$]GS (103 mg, 76%), mp 127.5—129.5 °C. Amino acid analysis: Pro (1.00), Val (1.01), Leu (0.93), Phe (0.00), Orn (0.00), MeOrn (1.01).

***N*-Methylation of [Orn(Dnp)$^{2,2'}$]GS.** [Orn(Dnp)$^{2,2'}$]GS[16] (74 mg, 0.05 mmol) was subjected to the *N*-methylation reaction as described above. Silica-gel column chromatography ($CHCl_3$–MeOH) afforded [MeOrn(Me,Dnp)$^{2,2'}$, D-MePhe$^{4,4'}$]GS (73 mg, 95%), mp 135—138 °C. ^{1}H NMR ($CDCl_3$) δ=2.88 (s, 6H, *N*-Me), 3.19 (s, 6H, *N*-Me), and 3.38 (s, 6H, *N*-Me).

Found: C, 58.72; H, 6.85; N, 13.77%. Calcd for $C_{78}H_{108}N_{16}O_{18}\cdot 2H_2O$: C, 58.78; H, 7.08; N, 14.06%.

2,4-Dinitrophenylation of **4** (15 mg, 0.012 mmol) in EtOH (1 cm^3) with DnpF (105 mg, 0.56 mmol) and Et_3N (0.05 cm^3) for 2 h at room temperature also yielded the same compound, mp 135—136 °C, in 87% yield.

The authors are grateful to Mr. Jun'ichi Ohya of Research Center, Mitsubishi Kasei Corporation for the antibacterial assay, to Dr. Showbu Sato of Mitsubishi Kasei Institute of Life Sciences for amino acid analysis, to Dr. Ukon Nagai of the same Institute for helpful discussions, to Professor Tatsuo Miyazawa of The University of Tokyo for ^{1}H NMR analysis, and to Nikken Kagaku Co., Ltd. for the supply of gramicidin S.

References

1) N. Izumiya, T. Kato, H. Aoyagi, M. Waki, and M. Kondo, "Synthetic Aspects of Biologically Active Cyclic Peptides–Gramicidin S and Tyrocidines," Kodansha, Tokyo, and Halsted Press, New York (1979).

2) F. C. M. Chen and N. L. Benoiton, *Can. J. Chem.*, **54**, 3310 (1976).

3) In 1959 Uehara reported preparation and antibacterial activity against *Bacillus subtilis* of side-chain-quaternized analogs of gramicidin J_1, which was later ascertained to be identical with gramicidin S, but the analogs were not characterized by spectroscopic measurements but only by elemental analyses based on the incorrectly assumed molecular structures: cyclo[Val–Orn(Me$_2$,C$_n$H$_{2n+1}^+$)–D-Phe–D-Leu–Phe–Pro–D-Orn(Me$_2$, C$_n$H$_{2n+1}^+$)]·2Br$^-$. T. Uehara, *J. Osaka City Med. Cent. (Osaka Shiritsu Daigaku Igaku Zasshi)*, **8**, 1489 (1959); *Chem. Abstr.*, **54**, 17229h (1960).

4) Preparation of **2** was preliminary reported; M. Kawai, N. Fukuta, N. Ito, M. Ohya, Y. Butsugan, M. Maruyama, and Y. Kudo, *J. Chem. Soc., Chem. Commun.*, **1986**, 955.

5) M. Kawai and U. Nagai, *Chem. Lett.*, **1977**, 1397.

6) Preparation of **3** was preliminary reported; M. Kawai, M. Ohya, Y. Butsugan, K. Saito, and T. Higashijima, *Chem. Lett.*, **1984**, 1835.

7) A. Stern, W. A. Gibbons, and L. C. Craig, *Proc. Natl. Acad. Sci. U.S.A.*, **61**, 734 (1968).

8) M. Kawai and U. Nagai, *Biopolymers*, **17**, 1549 (1978).

9) A. F. Spatola, "Chemistry and Biochemistry of Amino Acids, Peptides and Proteins," ed by B. Weinstein, Marcel Dekker, New York (1983), Vol. 7, p. 267.

10) H. Sugano, H. Abe, M. Miyoshi, T. Kato, and N. Izumiya, *Bull. Chem. Soc. Jpn.*, **47**, 698 (1974); H. Abe, K. Sato, T. Kato, and N. Izumiya, *ibid.*, **49**, 3113 (1976).

11) M. Kawai, N. Fukuta, N. Ito, T. Kagami, Y. Butsugan,

M. Maruyama, and Y. Kudo, *Int. J. Peptide Protein Res.*, **35**, 452 (1990).

12) S. E. Hull, R. Karlsson, P. Main, M. M. Woolfson, and E. J. Dodson, *Nature*, **275**, 206 (1978).

13) Presence of two conformers was observed for [MeOrn-(Pht)$^{2,2'}$, D-MePhe$^{4,4'}$]GS and also for [MeOrn(Dnp,Me)$^{2,2'}$, D-MePhe$^{4,4'}$]GS in the 270 MHz ^{1}H NMR spectra measured at 25 °C in DMSO-d_6 solutions. At 80 °C each compound exhibited well-resolved sharp signals assignable to a single β-sheet conformer.

14) R. Schwyzer and U. Ludescher, *Biochemistry*, **7**, 2519 (1968).

15) M. Waki and N. Izumiya, *Bull. Chem. Soc. Jpn.*, **40**, 1687 (1967).

16) U. Nagai, M. Kurumi, and T. Umemura, *Tetrahedron*, **28**, 4959 (1972).

Aromatic Nucleophilic Substitution of Halobenzenes with Amines under High Pressure

Toshikazu IBATA,* Yasushi ISOGAMI, and Jiro TOYODA
Institute of Chemistry, College of General Education, Osaka University, Toyonaka, Osaka 560
(Received August 15, 1990)

The nucleophilic substitution reactions of aromatic halides having electron-attracting groups on ortho or para position with various primary and secondary amines were accelerated by high pressure to give the corresponding *N*-substituted anilines in high yields. The bulkiness of amines affects its reactivity to lower the yields of the products. Although the secondary amines are usually less reactive than primary amines, cyclic secondary amines such as morpholine, piperidine, and pyrrolidine were found very reactive. 1,4-Diazabicyclo[2.2.2]octane and quinuclidine gave *N*-quaternary ammonium halides in high yields in contrast to the low reactivity of acyclic tertiary amines. Dichloro- and trichloro-nitrobenzenes also react with diethylamine, pyrrolidine, and morpholine to give mono-, di-, and trisubstitution products depending upon the amount of amine and the position of nitro group in these chlorides.

Nucleophilic substitutions of aromatic halides with amines are generally difficult to proceed under ordinary pressure,[1] and are limited to some fluorides or chlorides having a strongly electron-attracting group such as nitro group at ortho or para position. These aromatic nucleophilic substitution (S_NAr) reactions are confirmed to proceed through the Meisenheimer type dipolar intermediate.[2] Because bond formation and charge separation are occurring in the transition state of this reaction, the S_NAr reaction is expected to be accelerated under high pressure.[3] However, no S_NAr reaction of aromatic halides with amines had been reported under high pressure from the synthetic point of view,[3] until our preliminary paper was published.[4] Matsumoto and his co-workers reported the high pressure S_NAr reaction of trifluoromethyl-substituted halobenzenes,[5] halogenopyridines,[6] and halogenothiazoles with amines.[7]

Herein, we describe the S_NAr reaction of substituted monohalobenzenes with various primary and secondary amines under high pressure. We also report the reaction of dichloro- and trichloro-nitrobenzenes with secondary amines such as diethylamine, pyrrolidine, and morpholine under high pressure in order to test the applicability of this reaction for the preparation of polyamino-substituted nitrobenzenes.

The high pressure reactions were carried out in a Teflon capsule using a Hikari Kouatsu High Pressure Reaction Apparatus.[8] When *p*-nitrochlorobenzene (**1a**) was treated with five molar equivalents of propylamine in a freshly distilled tetrahydrofuran (THF) solution at 50 °C under 7.2 kbar# for 20 h, *N*-propyl-*p*-nitroaniline (**3a**) was obtained as yellow crystals in 93% yield along with an almost quantitative amount of propylamine hydrochloride. The products were characterized by the spectroscopic measurement. The reaction did not proceed even at 80 °C under ordinary pressure.

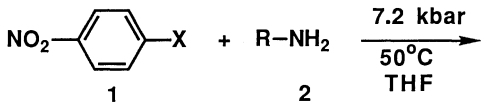

1 2

1a : X=Cl
1b : X=I
1c : X=F
1d : X=Br

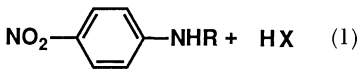

3 (1)

In order to ascertain the acceleration effect on the reaction rate, the yields of the reactions of **1a** with propylamine, morpholine, and pyrrolidine were examined under the variation of pressure in the range of 1/1000—10.0 kbar (Table 1). The reactions of **1a** with propylamine and morpholine are dramatically accelerated at the pressure of 6 kbar. However, 6 kbar is not enough for the completion of these reactions. On the other hand, pyrrolidine is more reactive than these amines and the reaction is completed at 6 kbar.

The reactions of *p*-nitrochlorobenzene (**1a**) with other primary amines under the high pressure of 7.2—12.0 kbar also gave the corresponding secondary *p*-nitroanilines as shown in Table 2. The yields of the reactions are affected strongly by the bulkiness of amines. For example, isopropylamine gave *N*-isopropyl-*p*-nitroaniline (**3c**) only in 26% yield under the same reaction conditions with those of propylamine, despite the basicity of these amines is almost same (pK_a; 10.63 and 10.53).[9] Similar results were also observed in the reactions of four butylamines (Table 2, Runs d—i). In these cases the order of the yields of **3** is the same as the order of the bulkiness of the butyl groups. *p*-Nitroiodobenzene (**1b**) is less reactive than **1a** (Table 2, Runs b, e, and i) in accordance with the usual S_NAr reactions of aromatic halides.[10]

Cyclohexylamine gave *N*-cyclohexyl-*p*-nitroaniline (**3k**) in 18% yield similar to the cases of isopropylamine

1 kbar=0.1 GPa

Table 1. Pressure Effect on the Yields of the Reaction of *p*-Nitrochlorobenzene (**1a**) with Propylamine, Morpholine, and Pyrrolidine[a]

Pressure/kbar	Propylamine		Morpholine		Pyrrolidine	
	3a/%	**1a**/%[b]	**6h**/%	**1a**/%[b]	**6m**/%	**1a**/%[b]
1/1000[c]	0	100	0	100	16.7	81
1.0	0.6	96	0.5	96	43.2	56
2.0	1.7	96	1.4	94	63.5	35
4.0	4.4	94	13.0	81	90.6	5
6.0	28.3	70	36.5	61	100	0
8.0	42.8	53	88.9	10	—	—
10.0	81.1	17	99.7	0	—	—

a) The reactions were carried out in THF solution at 50 °C for 3 h using 1.0 mmol of **1a** and 10.0 mmol of amine. b) Percentage of recovered **1a**. c) Atmospheric pressure.

Table 2. Reaction of *p*-Nitrohalobenzenes with Primary Amines under High Pressure[a]

Run	Halide X	Amine **2**	Pressure kbar	Reaction time/h	Product **3**	Mp θ_m/°C (lit)	Yield[b] %
a	Cl	$PrNH_2$	7.2	20	**3a**	68—69 (63.9—71.1)[c]	93 (0)
b	I	$PrNH_2$	12.0	20	**3a**		28 (0)
c	Cl	*i*-$PrNH_2$	7.2	20	**3c**	68—69 (85.5—85.6)[c]	26 (0)
d	Cl	$BuNH_2$	7.2	20	**3d**	60—61 (56.2—57.2)[c]	76 (0)
e	I	$BuNH_2$	8.0	50	**3d**		35 (0)
f	Cl	*i*-$BuNH_2$	7.2	20	**3f**	76—77 (95.9—96.1)[c]	61 (0)
g	Cl	*s*-$BuNH_2$	7.2	20	**3g**	Oil (40.4)[c]	13 (0)
h	Cl	*t*-$BuNH_2$	7.2	20	**3h**	Oil	2 (0)
i	I	*t*-$BuNH_2$	12.0	50			0 (0)
j	Cl	*Hex*NH_2	7.2	20	**3j**	67—68	65 (0)
k	Cl	*c*-$C_6H_{11}NH_2$	7.2	20	**3k**	104—105 (100.2—100.5)[c]	18 (0)
l	Cl	CH_2=$CHCH_2NH_2$	7.2	20	**3l**	72—73 (68.2—69.2)[c]	67 (0)
m	Cl	*p*-$AnisNH_2$	9.0	50	**3m**	158—159 (152.2)[c]	2 (0)
n	Cl	*p*-$TolNH_2$	9.0	75			0 (0)
o	Cl	$PhNH_2$	9.0	50			0 (0)
p	F	*p*-$AnisNH_2$	9.0	25	**3m**		11 (0)
q	F	*p*-$TolNH_2$	9.0	50	**3q**	145—146 (140—141)[c]	6 (0)
r	F	$PhNH_2$	9.0	50	**3r**	140—142 (136)[c]	7 (0)

a) All reactions listed were carried out in THF solution at 50 °C using 1.0 mmol of **1** and 5.0 mmol of amines. b) Yields in parentheses refer to reactions under 1 atm at 80 °C, for 50 h. c) H. Suhr, *Ann. Chem.*, **687**, 175 (1965).

(26%) and *s*-butylamine (13%). Aromatic primary amines have lower reactivity than that of the aliphatic amines because of their low basicity. For example, *p*-anisidine gave *p*-nitro-*p'*-methoxydiphenylamine (**3m**) only in 2% yield under the forced reaction conditions (9.0 kbar, 50 h). Aniline and *p*-toluidine gave no substitution product under the same reaction conditions. *p*-Nitrofluorobenzene (**1c**) is more reactive than **1a** and gave substitution products in the reactions with aromatic amines in low yields (Table 2, Runs p—r).

Secondary amines exhibit lower reactivities than the corresponding primary amines as shown in Table 3 (compare Runs c, d, and e in Table 3 with Runs a, c, and d in Table 2, respectively). However, cyclic secondary amines such as morpholine, piperidine, and pyrrolidine indicate extremely higher reactivities (Table 3, Runs h—v) than those of acyclic secondary amines such as diethylamine and diisopropylamine. The difference in reactivities of these high pressure S_NAr reactions seems to be attributed to both basicity and bulkiness of amine.

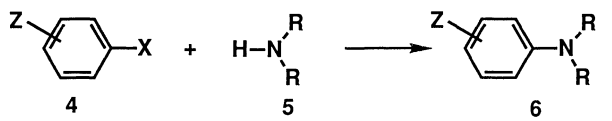

4 **5** **6**

4a : Z=o-NO_2, X=F
4b : Z=o-NO_2, X=Cl
4c : Z=m-NO_2, X=F
4d : Z=m-NO_2, X=Cl
4e : Z=p-CN, X=Cl
4f : Z=p-Ac, X=Cl

+ HX (2)

Although *o*-nitrochlorobenzene (**4b**) showed high reactivity toward pyrrolidine (Table 3, Run q) as that of *p*-nitrochlorobenzene (**1a**), *m*-nitrochlorobenzene (**4d**) was shown to have much less reactivity (Run t).

Table 3. The S_NAr Reaction of Aromatic Halides with Secondary Amines under High Pressure[a]

Run	Aromatic Z	Halide X	Amine	Pressure kbar	Reaction time/h	Product **6**	Mp θ_m/°C (lit)	Yield[b] %
a	*p*-NO_2	Cl	Et_2NH	7.2	20	**6a**	77—78 (73—74)[c]	39 (0)
b	*p*-NO_2	I	Et_2NH	8.0	250	**6a**		49 (0)
c	*p*-NO_2	Cl	Pr_2NH	7.2	20	**6c**	62—63 (59)[d]	24 (0)
d	*p*-NO_2	Cl	*i*-Pr_2NH	7.2	50	**6d**		0 (0)
e	*p*-NO_2	Cl	Bu_2NH	7.2	20	**6e**	Oil	15 (0)
f	*p*-NO_2	Cl	*i*-Bu_2NH	7.2	20	**6f**		Trace (0)
g	*p*-NO_2	I	*i*-Bu_2NH	12.0	72			0 (0)
h	*p*-NO_2	Cl	Morpholine	6.0	20	**6h**	158—159 (149.5—150.0)[c]	100 (3)
i	*p*-NO_2	I	Morpholine	12.0	50	**6h**		100 (2)
j	*p*-NO_2	Cl	Piperidine	6.0	20	**6j**	108—109 (99.5—100)[c]	100 (22)
k	*p*-NO_2	I	Piperidine	12.0	20	**6j**		100 (4)
l	*p*-NO_2	Cl	*N*-Methylpiperazine	6.0	20	**6l**	105—106 (108)[e]	96
m	*p*-NO_2	Cl	Pyrrolidine	6.0	20	**6m**	178—179 (167)[c]	100 (92)
n	*p*-NO_2	Br	Pyrrolidine	8.5	20	**6m**		100 (51)
o	*p*-NO_2	I	Pyrrolidine	12.0	20	**6m**		100 (14)
p	*o*-NO_2	F	Pyrrolidine	7.2	20	**6p**	Oil	100
q	*o*-NO_2	Cl	Pyrrolidine	8.5	20	**6p**		100 (85)
r	*o*-NO_2	Cl	Morpholine	6.0	20	**6r**	Oil	100
s	*m*-NO_2	F	Pyrrolidine	9.0	87	**6s**	98—100	98
t	*m*-NO_2	Cl	Pyrrolidine	9.0	50	**6s**		2 (0)
u	*p*-CN	Cl	Pyrrolidine	6.0	20	**6u**	90—91 (81)[f]	34 (0)
v	*p*-CH_3CO	Cl	Pyrrolidine	7.2	20	**6v**	135—136	18 (0)

a) All reactions listed were carried out in THF solution at 50 °C using 1.0 mmol of **4** and 5.0 mmol of amine. b) Yields in parentheses refer to reactions under 1 atm at 80 °C, for 50 h. c) E. Matsumura, Y. Tohda, and M. Ariga, *Bull. Chem. Soc. Jpn.*, **55**, 2174 (1982). d) N. Nagornow, *J. Russ. Phys-Chem. Soc.*, **29**, 699. e) L. Loewe, H. Mieth, and H. Suschitzky, *J. Chem. Soc.*, **1963**, 1666. f) S. F. Beach, J. D. Hepworth, J. Sawyer, G. Hallas, R. Marsden, M. M. Mitchell, D. A. Ibbitson, A. M. Jones, and G. T. Neal, *J. Chem. Soc., Perkin Trans. 2*, **1984**, 217.

This indicates that the nitro group increases the reactivity of chloride only at ortho or para position. However, *m*-nitrofluorobenzene (**4c**) is exceptionally reactive toward pyrrolidine (Run s). *p*-Nitrobromobenzene (**1d**) and *p*-nitroiodobenzene (**1b**) reacted with pyrrolidine to give **6m** in high yields (Runs n and o). *p*-Cyanochlorobenzene (**4e**) and *p*-chloroacetophenone (**4f**) gave the corresponding *N*-arylpyrrolidines in moderate yields (Runs u and v). These results indicate that cyano and acetyl groups are not so good substituent as nitro group to promote the reaction, and that 9.0 kbar is not enough to accelerate the S_NAr reactions of these chlorides.

In contrast to triethylamine, bicyclic tertiary amines such as 1,4-diazabicyclo[2.2.2]octane (DABCO) and quinuclidine react with *p*-nitrohalobenzenes to give the corresponding quaternary ammonium salts **8**[9] in quantitative yields at 6.0 kbar.

The reaction of 2,3-dichloronitrobenzene (**9**) with diethylamine, pyrrolidine, and morpholine gave ortho substitution product **10** in quantitative yield without affording meta substitution product (Table 4). The structure of **10** was determined by the observation that ^1H NMR signal of aromatic proton H_c changes only a little by the reaction of **9**. This substitution pattern is consistent with the observation that *m*-nitrochlorobenzene has very low reactivity as described above.

Similarly, 2,5-dichloronitrobenzene (**11**) and 3,4-dichloronitrobenzene (**13**) react with these amines at ortho or para position to nitro group, respectively, to

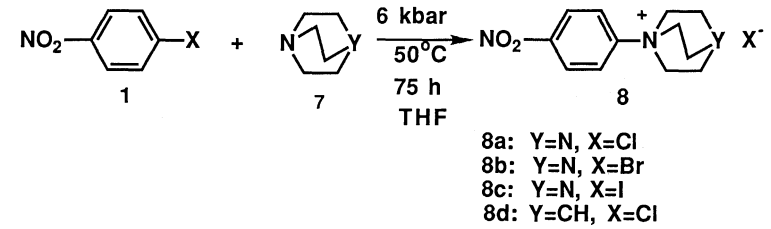

(3)

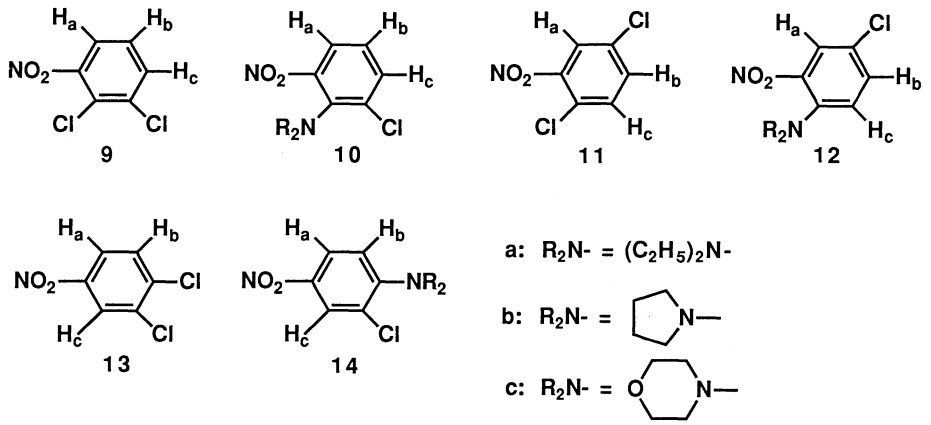

Fig. 1.

Table 4. Reaction of Dichloronitrobenzenes with Secondary Amines,[a] and ^1H NMR Data of the Reaction Products

Halide	R_2NH	Product	Yield %	^1H NMR/δ						
				H_a	H_b	H_c	NCH_2	CH_3	CH_2	OCH_2
9	Diethylamine	**10a**	98	7.47(dd)	7.10(t)	7.39(dd)	3.12	1.03	—	—
9	Pyrrolidine	**10b**	100	7.47(d)	7.01(t)	7.45(d)	3.24	—	1.94	—
9	Morpholine	**10c**	100	7.53(dd)	7.11(t)	7.46(dd)	3.07	—	—	3.77
				(7.70(d)	7.36(dd)	7.70(d))[b]				
11	Diethylamine	**12a**	98	7.61(d)	7.34(dd)	7.06(d)	3.14	1.11	—	—
11	Pyrrolidine	**12b**	97	7.64(d)	7.22(dd)	6.79(d)	3.16	—	1.97	—
11	Morpholine	**12c**	100	7.74(d)	7.43(dd)	7.09(d)	3.03	—	—	3.82
				(7.87(d)	7.50(dd)	7.43(d))[b]				
13	Diethylamine	**14a**	91	7.96(dd)	6.97(d)	8.12(d)	3.35	1.11	—	—
13	Pyrrolidine	**14b**	98	7.82(dd)	6.54(d)	8.01(d)	3.61	—	1.97	—
13	Morpholine	**14c**	98	8.05(dd)	7.03(d)	8.16(d)	3.21	—	—	3.88
				(8.07(dd)	7.61(d)	8.33(d))[b]				

a) The reactions were carried out in the following conditions; 6 kbar, 50 °C, 20 h, in THF. b) The values in the parentheses are the chemical shift of starting dichloronitrobenzenes.

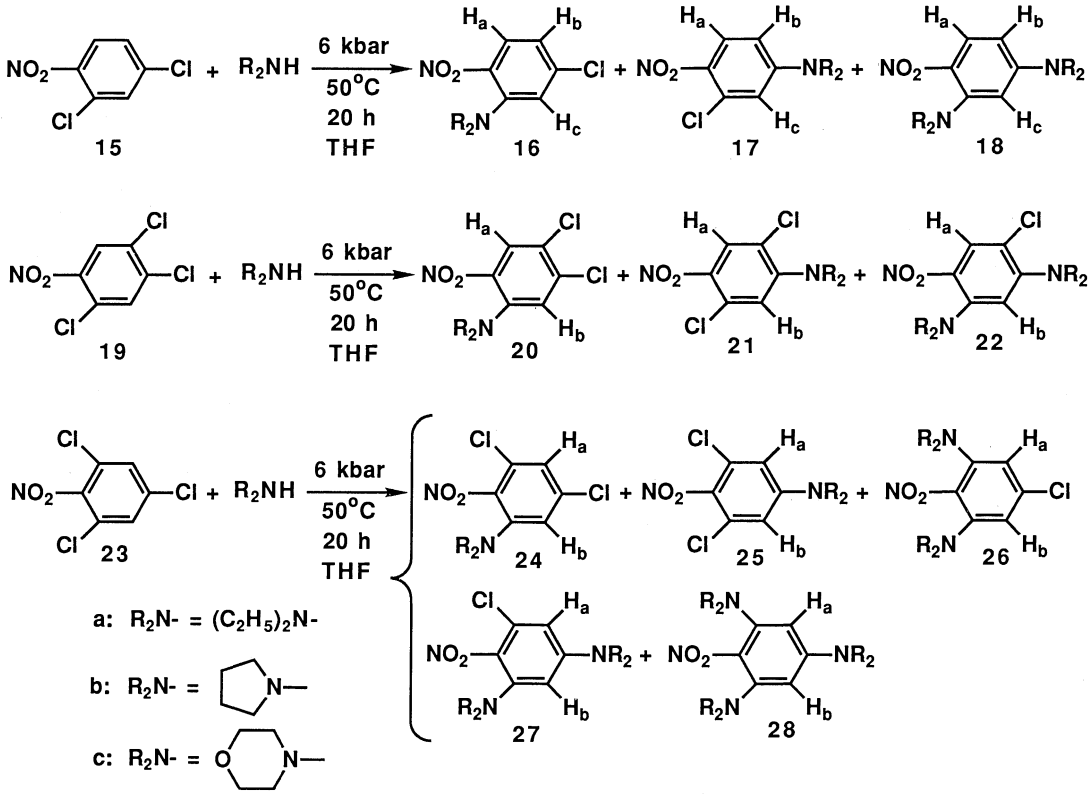

Fig. 2.

give a single product **12** and **14** in quantitative yields (Table 4). The structure of the products was based on the NMR spectra. For example, the fact that only ortho substitution takes place in the reactions of **11**, was concluded by the observation that this reaction caused the largest chemical shift change for H_c in the aromatic protons of **11** (Table 4). These three dichloronitrobezenes were found to be more reactive than monochloronitrobenzenes, and then no difference in the reactivity of amines was observed in these reactions.

2,4-Dichloronitrobenzene (**15**) has ortho and para chlorine atoms which are both reactive. The reactions of **15** gave a mixture of ortho substitution product **16**, para substitution product **17**, and disubstitution product **18**. Yields of these three types of products depend on the reactivity and the amount of the amine used. When five molar equivalents of amine was used, diethylamine gave ortho-mono substitution product in high yield along with a small amount of **18**. On the other hand, pyrrolidine and morpholine gave the disubstitution product **18** as a major product together with a small amount of ortho-mono substitution product **16**. In these cases, isolation of para-mono substitution product was unsuccessful (Table 5). In the case of 1.1 molar equivalent of pyrrolidine or morpholine was used, ortho-mono substitution products became predominant together with a small amount of para-mono and disubstitution products. These results may be explained by the assumption that the para-mono substitution products **17** are more reactive than ortho-mono product **16** in the second substitution. Diethylamine is less reactive than pyrrolidine or morpholine in this second step.

Table 5. Reaction of 2,4-Dichloronitrobenzene (**15**) with Secondary Amines[a]

Amine	Amount of amine[b]	Yield/%		
		16	**17**	**18**
Diethylamine	5.0	90	0	10
Pyrrolidine	5.0	15	0	85
Pyrrolidine	1.1	89	3	2
Morpholine	5.0	36	0	61
Morpholine	1.1	86	2	11

a) The reactions were carried out under the following conditions; 6 kbar, 50 °C, 20 h, in THF. b) Amount of amine was shown in molar equivalent.

In the reactions of 2,4,5-trichloronitrobenzene (**19**), no substitution was observed at meta position and the reaction proceeded in a manner similar to that of 2,4-dichloronitrobenzene (Table 6-1). In these cases, yields of disubstitution products **22** were higher than the case of **15** and even diethylamine gave **22a** as the major product. This means that **19** is more reactive than **15** due to the effect of 5-chlorine atom. When 1.2 molar

equivalent of morpholine was used in the presence of triethylamine to trap hydrogen chloride generated, ortho-mono and disubstitution products were obtained without yielding para-mono product. This is explained by the assumption that the ortho position of para-mono product **21** is more reactive than the para

Table 6. Reaction of Trichloronitrobenzenes with Secondary Amines[a]

(1) Reaction of 2,4,5-Trichloronitrobenzene (**19**)

Amine	Amount of amine[b]	Yield/%		
		20	**21**	**22**
Diethylamine	5.0	37	0	59
Pyrrolidine	5.0	0	0	100
Morpholine	5.0	0	0	94
Morpholine	1.2	53	0	34

(2) Reaction of 2,4,6-Trichloronitrobenzene (**23**)

Amine	Amount of amine[b]	Yield/%				
		24	**25**	**26**	**27**	**28**
Diethylamine	5.0	0	91	0	0	0
Pyrrolidine	5.0	0	0	0	5	93
Pyrrolidine	1.1	0	85	8	2	0
Morpholine	5.0	0	0	80	6	1
Morpholine	1.1	87	3	8	2	0

a) The reactions were carried out under the following conditions; 6 kbar, 50 °C, 20 h, in THF. b) Amount of amine was shown in molar equivalent.

Table 7. ^1H NMR Data of the Reaction Products[a]

Product	H_a	H_b	H_c	NCH_2	CH_3	CH_2	OCH_2
16a	7.59(d)	6.80(dd)	7.04(d)	3.15	1.11	—	—
16b	7.63(d)	6.61(dd)	6.84(d)	3.19	—	1.98	—
16c	7.74(d)	6.77(dd)	7.05(d)	3.04	—	—	3.83
17b	8.03(d)	6.35(dd)	6.49(d)	3.36	—	2.06	—
17c	7.98(d)	6.67(dd)	6.81(d)	3.31	—	—	3.83
18a	7.94(d)	6.10(dd)	6.13(d)	3.17	1.11	—	—
				3.39	1.21		
18b	7.81(d)	5.93(dd)	5.68(d)	3.20	—	1.93	—
				3.31		2.00	
18c	7.98(d)	6.43(dd)	6.31(d)	3.05	—	—	3.83
				3.32			
20a	7.75(s)	7.14(s)	—	3.15	1.13	—	—
20c	7.89(s)	7.17(s)	—	3.03	—	—	3.81
22a	7.86(s)	6.54(s)	—	3.14	1.11	—	—
				3.24	1.13		
22b	7.87(s)	5.94(s)	—	3.19	—	1.97	—
				3.54			
22c	7.98(s)	6.53(s)	—	3.04	—	—	3.83
				3.16			3.87
24c	7.18(d)	7.06(d)	—	2.93	—	—	3.70
25a	7.08(s)	—	—	3.05	1.04	—	—
25b	6.66(s)	—	—	3.25	—	1.98	—
25c	6.78(s)	—	—	3.30	—	—	3.90
26b	6.24(s)	—	—	3.20	—	1.90	—
26c	6.95(s)	—	—	2.93	—	—	3.72
27b	5.97(d)	5.60(d)	—	3.22	—	1.93	—
				3.27		2.00	
27c	6.58(d)	6.44(d)	—	2.97	—	—	3.76
				3.21			3.85
28b	5.12(s)	—	—	3.33	—	1.93	—
				3.40		1.97	
28c	6.36(s)	—	—	2.94	—	—	3.74
				3.17			3.83

a) Chemical shifts were shown in δ.

position of **20**, and that **21** produced by the first substitution of **19** was consumed completely in the second substitution.

Product ratio of the reaction of 2,4,6-trichloronitrobenzene (**23**) is affected by the amine used. When five molar equivalents of amine was used, diethylamine gave para-mono substitution product **25a** as a sole product. Pyrrolidine gave trisubstitution product **28b**, and morpholine gave ortho-ortho disubstitution product **26c** as major products (Table 6-2). These results suggest that the order of reactivity of amines in this reaction is as follows; pyrrolidine>morpholine>diethylamine.

The reaction with 1.1 molar equivalent of amine gave mono substitution product as a major product. Pyrrolidine yielded para-mono product **25b** which was confirmed by the singlet signal of aromatic proton observed at 6.66 in its ^{1}H NMR spectrum. On the other hand, morpholine gave ortho-mono product **24c** which has two doublet signals of aromatic protons at 7.06 and 7.18. The difference in the behavior of these two amines may be attributed mainly to the bulkiness of amines.

Experimental

Melting points were measured with a Yanagimoto Melting Point Apparatus and not corrected. IR spectra were recorded on a Perkin-Elmer model 983. ^{1}H NMR spectra were measured on a Varian EM-390 in a $CDCl_3$ solution using TMS as an internal standard.

Materials. All aromatic halides were purified by recrystallization or distillation of commercial compounds just before use. THF and amines were purified by distillation under an atmosphere of nitrogen after appropriate drying procedure.

General Procedure of the S_NAr Reaction of Aromatic Halides with Primary or Secondary Amines under High Pressure. A THF solution (5 cm^3) of aromatic halide (1.0 mmol) and amine (5.0 mmol) was pressurized in Teflon capsule under the cited reaction conditions using Hikari Kouatsu High Pressure Apparatus.[3] After the removal of solvent under reduced pressure the residue was suspended in benzene, and amine hydrohalide was removed by filtration on glass filter and the solid was washed several times with benzene (10 cm^3). The combined benzene solution was separated by medium pressure column chromatography (silica gel, benzene). Products were characterized by IR and ^{1}H NMR spectra. The characteristic ^{1}H NMR data were listed in Tables 4 and 7. In their IR spectra, absorptions of aromatic NO_2 were observed in the regions of 1480—1520 and 1330—1350 cm^{-1}, and the aromatic absorption near 1600 cm^{-1} was very strong. The results of elemental analysis were shown in Table 8. The reactions with 1.1—1.2 molar equivalent of amines were carried out using 1.0 cm^3 (ca. 7.2 mmol) of triethylamine and treated in the same way.

The Reactions of *p*-Nitrohalobenzenes with DABCO or Quinuclidine under High Pressure. The reaction was carried out in the similar manner under the following reaction conditions; 6.0 kbar, 50 °C, 75 h, in THF. After the reaction was over, the yellow crystals that precipitated in the Teflon capsule were collected by filtration and washed with benzene several times, and dried. The melting points of the salts were higher than 300 °C. The elemental analyses of these products did not give correct results for salts **8**[11] because purification of the salts was difficult due to the low solubility in usual organic solvents.

Table 8. Melting Points and Results of Elemental Analysis of the Products[a]

Product	Mp	Found/%			Calcd/%			Molecular formula
	θ_m/°C	C	H	N	C	H	N	
3j	b)	64.86	8.23	12.53	64.84	8.16	12.60	$C_{12}H_{18}N_2O_2$
10b	76—77	53.05	4.91	12.36	52.99	4.89	12.36	$C_{10}H_{11}N_2O_2Cl$
10c	100—101[c]							
12c	50—51[c]							
14b	101—103	53.05	4.90	12.34	52.99	4.89	12.36	$C_{10}H_{11}N_2O_2Cl$
14c	135—136[c]							
16b	86—87	52.99	4.89	12.33	52.99	4.89	12.36	$C_{10}H_{11}N_2O_2Cl$
16c	75—76[c]							
18b	140—141	64.55	7.37	16.09	64.35	7.33	16.08	$C_{14}H_{19}N_3O_2$
18c	175—176	57.42	6.55	14.21	57.33	6.53	14.33	$C_{14}H_{19}N_3O_4$
22b	160—161	57.11	6.15	14.21	56.88	6.13	14.21	$C_{14}H_{18}N_3O_2Cl$
22c	183—185	51.52	5.61	12.75	51.30	5.54	12.82	$C_{14}H_{18}N_3O_4Cl$
24c	160—161	43.47	3.66	10.11	43.34	3.64	10.11	$C_{10}H_{10}N_2O_3Cl_2$
25b	87—88	46.24	3.90	10.67	46.00	3.86	10.73	$C_{10}H_{10}N_2O_2Cl_2$
25c	143—144	43.34	3.64	10.06	43.34	3.64	10.11	$C_{10}H_{10}N_2O_3Cl_2$
26b	183—184	56.85	6.22	14.11	56.85	6.13	14.21	$C_{14}H_{18}N_3O_2Cl$
26c	137—139	51.53	5.62	12.73	51.30	5.54	12.82	$C_{14}H_{18}N_3O_4Cl$
27b	169—170	56.95	6.16	14.31	56.85	6.13	14.21	$C_{14}H_{18}N_3O_2Cl$
28b	144—145	65.70	7.99	16.75	65.43	7.93	16.96	$C_{18}H_{26}N_4O_2$
28c	234—236	57.40	6.95	14.60	57.13	6.93	14.80	$C_{18}H_{26}N_4O_5$

a) Other products omitted in this Table did not give correct analytical results because of difficulty in purification due to low yields or low melting point of the products. b) Listed in Table 2. c) Melting points reported in literature: **10c** 97 °C; **12c** 45—46 °C; **14c** 130 °C; **16c** 70—71 °C; M. D. Nair and R. Adams, *J. Am. Chem. Soc.*, **83**, 3518 (1961).

References

1) J. F. Bunnett and R. E. Zahler, *Chem. Rev.*, **49**, 273 (1951).

2) J. F. Bunnett, *Quart. Rev. (London)*, **12**, 1 (1958); J. Sauer and R. Huisgen, *Angew. Chem.*, **72**, 294 (1960); S. Ross, *Progr. Phys. Org. Chem.*, **1**, 31 (1963).

3) K. Matsumoto, A. Sera, and T. Uchida, *Synthesis*, **1985**, 1.

4) T. Ibata, Y. Isogami, and J. Toyoda, *Chem. Lett.*, **1987**, 1187.

5) K. Matsumoto, T. Uchida, T. Okamoto, and S. Hashimoto, *Chem. Express*, **2**, 551 (1987).

6) S. Hashimoto, S. Otani, T. Okamoto, and K. Matsumoto, *Heterocycles*, **27**, 319 (1988); K. Matsumoto, T. Uryu, and M. Munakata, *Chem. Express*, **3**, 739 (1988).

7) K. Matsumoto, S. Hashimoto, H. Minatogawa, M. Munakata, and S. Otani, *Chem. Express*, **5**, 473 (1990).

8) T. Ibata, H. Nakawa, Y. Isogami, and K. Matsumoto, *Bull. Chem. Soc. Jpn.*, **59**, 3197 (1986).

9) H. K. Hall, Jr., *J. Am. Chem. Soc.*, **79**, 5441 (1957).

10) S. Isaacs, "Physical Organic Chemistry," Longman Scientific & Technical, New York (1987), p. 454.

11) Although the correct elemental analyses were not obtained, the authors tentatively propose the structure of these salts as **8**.

1,3-Diol Fragmentation Using a Reactive Benzylic Hydroxyl Group as a Nucleofuge. Synthesis of a Tobacco Sesquiterpene

Michiharu KATO,* Youichi TOOYAMA, and Akira YOSHIKOSHI
Chemical Research Institute of Non-Aqueous Solutions, Tohoku University,
Katahira 2-1-1, Aoba-ku, Sendai 980
(Received August 23, 1990)

A benzylic hydroxyl group activated by electron-donative aromatic function was found to be a remarkably reactive nucleofuge for 1,3-diol fragmentation. Thus, treatment of α-(2,6-dimethoxy-4-methylphenyl)-2β-hydroxy-2α,5,5,8aβ-tetramethyl-4aα-decahydro-1β-naphthalenemethanol with pyridinium chloride or pyridinium *p*-toluenesulfonate in dichloromethane underwent the 1,3-diol fragmentation smoothly to produce *r*-1-[(*E*)-2-(2,6-dimethoxy-4-methylphenyl)ethenyl]-*t*-2-(3-oxobutyl)-1,3,3-trimethylcyclohexane (**24**) in quantitative yield. Starting from **24**, a tobacco sesquiterpene, 4-(2,2,6-trimethyl-6-vinylcyclohexyl)-2-butanone, was synthesized in racemic form by seven steps.

As one of C–C bond cleavage reactions, fragmentation reaction has been extensively utilized in structural elucidation and synthetic study in the natural product chemistry.[1] On the C(2)–C(3) bond cleavage in 1,3-diol i by fragmentation reaction, a primary hydroxyl group itself is generally less effective as a nucleofuge,[2] as can be judged from the consideration that the more stable a carbonium ion formed is, the easier the 1,3-diol fragmentation reaction occurs. When the diol i is converted to the corresponding benzyl alcohol ii possessing a phenyl group (Ar) substituted by electron-donative groups at ortho and para positions, the benzylic hydroxyl group in ii eliminates easily to give a stable carbonium ion, and therefore, the fragmentation reaction would proceed, to our expectation, providing the desired product iii.

The above conception was founded on the following observation made earlier in the course of our synthetic study on siccanin,[3] an antibiotic mold metabolite. We examined deprotection of the tetrahydropyranyl(THP) ether **1**. Under mild hydrolytic conditions (AcOH–THF–H_2O), well-known for cleavage of THP ethers,[4] not only deprotection of **1** but also concomitant 1,3-diol fragmentation proceeded smoothly to give olefinic ketone **2** in quantitative yield.[5] Surprisingly, treatment of **1** with pyridinium *p*-toluenesulfonate (PPTS) in ethanol also provided **2** in almost quantitative yield.[5] Moreover, oxidation of benzyl alcohol **3** with pyridinium chlorochromate in dichloromethane (CH_2Cl_2) furnished a ring-opened product **4** as one of the products. The olefin **4** could be accounted for by fragmentation, when presuming that a chromate ester group initially formed at the benzylic position of **3** would act as a nucleofuge.[5] These results indicate that generation of a carbonium ion assisted by electron-donative aromatic function causes the remarkably facile 1,3-diol fragmentation of this type. We wish to describe here results of our studies on the 1,3-diol fragmentation using a reactive benzylic hydroxyl group as a nucleofuge, and its application to the synthesis of (±)-4-(2,2,6-trimethyl-6-vinylcyclohexyl)-2-butanone (**5**),[6] a seco-sesquiterpene isolated from sun-cured Greek tobacco, *Nicotiana tabacum* L.[7]

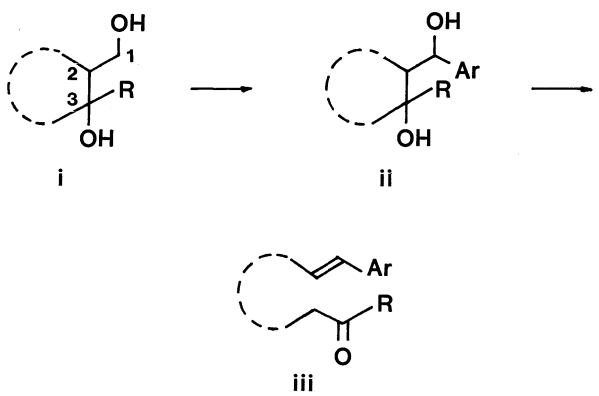

Fig. 1.

Results and Discussion

Our key compound selected for this work was drimane-8β,11-diol (**17**),[8] and its synthesis began with

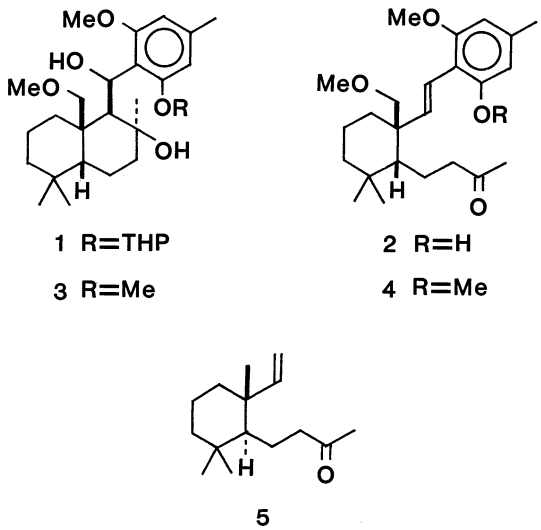

Fig. 2.

protection of the oxo group in the known keto ester **6**[9] (Scheme 1). Acetalization of **6** with ethylene glycol followed by reduction of the resulting ethylenedioxyl ester **7** with lithium aluminium hydride provided crystalline alcohol **8**. Reaction of **8** with PPTS in acetone at 40 °C led to the exclusive formation of hydroxy ketone **9**, whereas treatment of **8** with catalytic *p*-toluenesulfonic acid at room temperature gave a mixture of **9** (45%) and the known enone **18** (32%).[9] Subsequent protection of the hydroxyl group in **9** with 3,4-dihydro-2*H*-pyran gave the THP ether **10** in 73% overall yield from **6**. The compound **10** was also prepared by an alternate route. Hydroxymethylation of the lithium enolate of *trans*-octalone **11**[10] with gaseous formaldehyde under the kinetically controlled conditions occurred stereoselectively from the α-side, affording the α-hydroxymethyl enone **12** in good yield, which was then converted to the corresponding THP ether **13**. Inversion of stereochemistry of the oxygenated side chain in **13** to equatorial configuration was carried out by regioselective deprotonation of **13** with lithium diisopropylamide (LDA) followed by kinetically controlled protonation with 10% citric acid, giving the desired enone **14** and dienone **15** in 45 and 41% yield, respectively. Catalytic hydrogenation of the former **14** afforded **10** in 34% overall yield from **11**. The decalone **10** upon methylation with excess methylmagnesium iodide in ether at −60 °C gave a single alcohol **16**. The stereochemistry of **16** was predicted from the consideration that the Grignard reagent would approach preferentially from the less hindered α face of **10**. This prediction was confirmed as follows. Deprotection of **16** afforded the required diol **17** (mp 133—134 °C) in 86% overall yield from **10**. The physical constants (mp, IR, and ^{1}H NMR) of **17** were identical with those of (±)-drimane-8β,11-diol reported by Pelletier and co-workers.[8]

In order to confirm the consideration mentioned in the beginning, a number of preliminary experiments were undertaken. The diol **17** was treated with pyridinium chloride or PPTS in CH_2Cl_2 at room temperature or under refluxing. However, it was completely recovered unchanged. Hence, **17** was transformed into the tosylate **19**. When **19** was treated with sodium hydride in 1,2-dimethoxyethane (DME) at 60 °C for 15 h, the sole product obtained in 30% yield was the oxetane **20**, and no formation of the fragmentation product, i.e. **5**, was detectable on the careful inspection of the reaction mixture.

At this juncture, we turned our attention to utilization of a reactive benzylic hydroxyl group as a nucleofuge. According to the published procedure,[8] the diol **17** was oxidized by Collins reagent to give the drimanic aldehyde **21** in 47% yield (lit,[8] 42% yield).

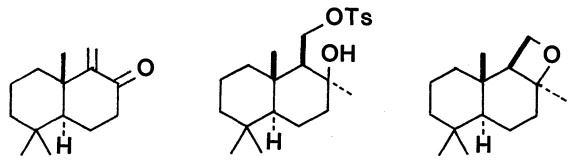

18 19 20

Fig. 3.

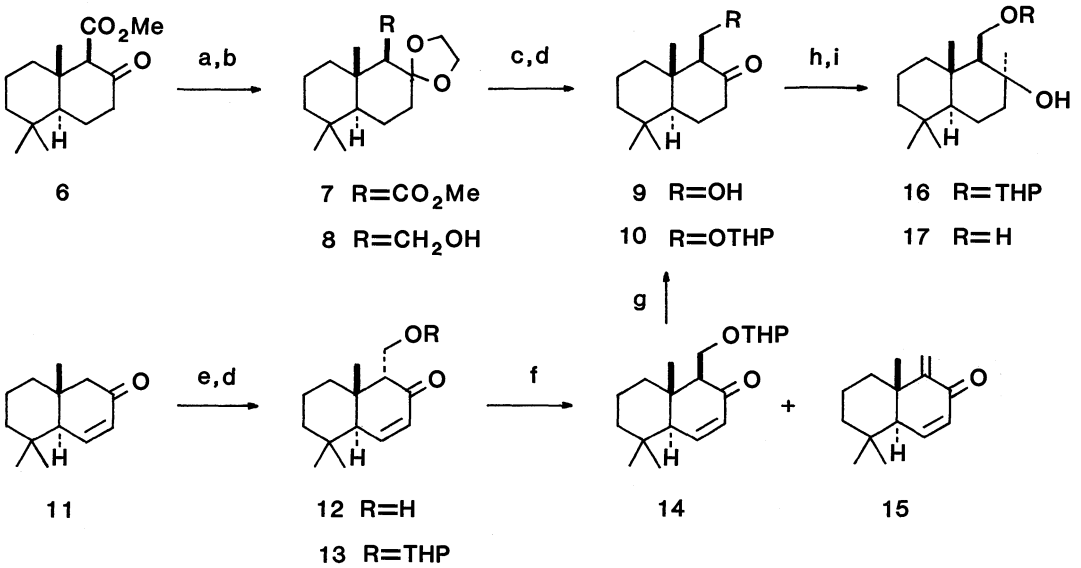

6 7 R=CO_2Me 8 R=CH_2OH 9 R=OH 10 R=OTHP 16 R=THP 17 R=H

11 12 R=H 13 R=THP 14 15

Scheme 1. (a) Ethylene glycol, *p*-TsOH, PhH (99%): (b) $LiAlH_4$, THF (69%): (c) PPTS, acetone (96%): (d) DHP, PPTS (quant): (e) LDA, THF, −78 °C, then CH_2O(g) (78%): (f) LDA, THF, −78 °C, then 10% citric acid (45%): (g) H_2, 10% Pd-C, dioxane (95%): (h) MeMgI, Et_2O, −60 °C (94%): (i) PPTS, MeOH (91%).

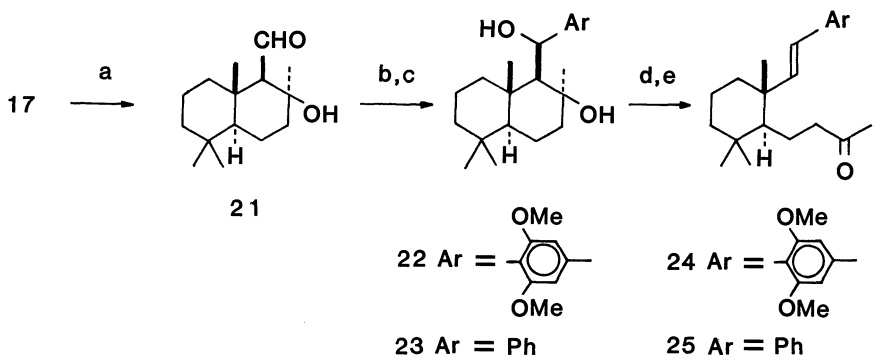

Scheme 2. (a) NCS, Me_2S, toluene (63%): (b) 1,3-dimethoxy-5-methylbenzene (**26**), BuLi, DME (92%): (c) PhLi, DME (90%): (d) Py·HCl or PPTS, CH_2Cl_2, rt, a few minutes (quant): (e) *p*-TsCl, Py, 60 °C, 2d (58%).

After a few attempts to improve the yield of **21**, it was found that oxidation by Corey–Kim method[11] employing *N*-chlorosuccinimide (NCS) and dimethyl sulfide was more effective to provide crystalline **21** in 63% yield (Scheme 2). For the purpose of constructing a reactive benzyl alcohol moiety, the use of 1,3-dimethoxy-5-methylbenzene (**26**)[12] was deemed most favorable, because its precursor, 5-methyl-1,3-benzenediol(orcinol) monohydrate, was commercially available and moderate in price, and readily convertible to **26** with dimethyl sulfate.[12] The lithium salt prepared from **26** with butyllithium in DME was submitted to condensation with **21**, providing **22** as an epimeric mixture with a minor quantity of one epimer regarding the newly formed hydroxyl group, from which a major epimer **22**[13] was obtained as crystals in 92% yield. For comparison, benzyl alcohol **23**,[13] a major epimer of stereoisomers, was prepared in high yield by treatment of **21** with phenyllithium followed by recrystallization of products. On exposure to pyridinium chloride in CH_2Cl_2 at room temperature, **22** underwent the 1,3-diol fragmentation within a few minutes to afford olefinic ketone **24**[14] in almost quantitative yield. In similar fashion, almost conversion of **22** into **24** was detected on treatment with PPTS. In contrast to **22**, benzyl alcohol **23** was recovered unchanged under the same reaction conditions described above. On prolonged heating of **23** with *p*-toluenesulfonyl chloride in pyridine at 60 °C, a fragmentation product **25** was obtained in 58% yield. The stereochemistry of the double bond in **25** was assigned to be E on the basis of a coupling constant (J=16.2 Hz) of two olefinic protons in the ^1H NMR spectrum. Obviously unsubstituited phenyl group as an activator was insufficient to cause the fragmentation under the above mild conditions, and difference in reactivity observed in the above two types of reactions is dependent on liability to generate a carbonium ion. After all, it was found that 2,6-dimethyoxy-4-methylphenyl function remarkably assists elimination of the benzylic hydroxyl group in the 1,3-diol fragmentation even under the mild conditions. The reaction conditions used here would be practically useful, especially when the substrate is an acid-labile compound.

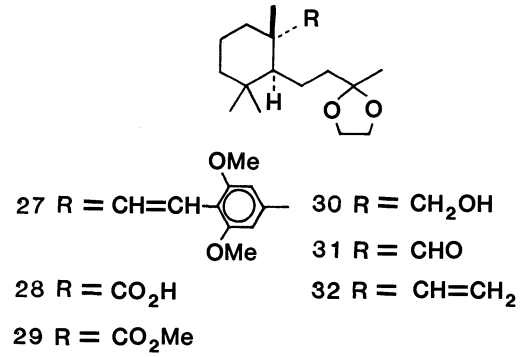

Fig. 4.

As an extension of this study to the natural product synthesis, we envisioned the olefinic ketone **24** to be a resonable intermediate for the synthesis of Tobacco sesquiterpene **5**. Transformation of **24** to **5** was accomplished by a conventional but straightforward sequence of reactions. Acetalization of **24** followed by ozonolysis of the resulting acetal **27** in CH_2Cl_2 directly provided carboxylic acid **28** in 55% overall yield. Esterification of **28** with diazomethane yielded ester **29**. As attempt to reduce the ester **29** with diisobutylaluminium hydride to the corresponding aldehyde **31** failed, **29** was converted to alcohol **30** by lithium aluminium hydride reduction. Collins oxidation of **30** afforded **31** in good yield, and methylenation of the latter with methylenetriphenylphosphorane provided olefin **32**. Finally, deprotection of **32** gave the target molecule (±)-4-(2,2,6-trimethyl-6-vinylcyclohexyl)-2-butanone (**5**), whose physical data (IR and NMR) were identical with those of the natural **5**.[6,15]

Experimental

Melting points are uncorrected. IR spectra were obtained with a JASCO A-3 infrared spectrometer. ^{1}H NMR spectra were recorded on a JEOL FX90Q spectrometer with tetramethylsilane as an internal standard. Dry THF and DME were obtained by distillation over lithium aluminium hydride, and other organic solvents were purified according to the standard procedure. All reactions were carried out under dry N_2 or Ar atmosphere. Extracts obtained on aqueous workup were dried over Na_2SO_4. Column chromatography was performed by using silica gel (Merck, kieselgel 60, 70—230 mesh), and kieselgel GF_{254} was employed for preparative thin-layer chromarography (TLC) as an absorbent. Solvents used for elution are shown in parentheses.

Methyl 2,2-Ethylenedioxy-5,5,8aβ-trimethyl-4aα-decahydro-1β-naphthalenecarboxylate (7). A solution of **6**[9] (1.665 g, 6.61 mmol), ethylene glycol (492 mg, 7.93 mmol), and *p*-toluenesulfonic acid (5 mg) in benzene (70 ml) was refluxed azeotropically for 30 h. After cooling, the mixture was washed successively with aqueous $NaHCO_3$, water, and brine, and dried. Removal of the solvent left a semicrystalline residue, which was filtered through a short silica-gel column with hexane–ether (1:1) to give **7** (1.946 g, 99%) as crystals: Mp 103—104 °C (from hexane–ether); IR (KBr) 1730 cm^{-1}; ^{1}H NMR ($CDCl_3$) δ=0.85 and 0.88 (6H in total, s each $C(CH_3)_2$), 1.22 (3H, s, C–CH_3), 0.9—2.0 (12H, m), 3.63 (3H, s, O–CH_3), 3.7—4.15 (4H, m, $O(CH_2)_2O$).

Found: C, 68.77; H, 9.27%. Calcd for $C_{17}H_{28}O_4$: C, 68.89; H, 9.52%.

2,2-Ethylenedioxy-5,5,8aβ-trimethyl-4aα-decahydro-1β-naphthalenemethanol (8). To a stirred mixture of lithium aluminium hydride (230 mg, 5.97 mmol) in THF (20 ml) wad added a solution of **7** (1.767 g, 5.97 mmol) in THF (2 ml), and the mixture was gently refluxed for 5 h. After cooling, the reaction mixture was quenched by addition of wet ether followed by water, and filtered. The solid was washed with ether, and the combined filtrate and wash were dried. Concentration gave an oil which was chromatographed on silica gel with hexane–ether (1:1) to give **8** (1.103 g, 69%) as crystals: Mp 90—91 °C (from hexane–ether); IR (KBr) 3300 cm^{-1}; ^{1}H NMR ($CDCl_3$) δ=0.81, 0.83, and 0.89 (9H, in total, s each, $C(CH_3)_2$ and C–CH_3), 1.0—2.0 (12H, m), 2.95 (1H, dd, J=7.2 and 3 Hz, OH), 3.5—4.2 (6H, m, CH_2–OH and $O(CH_2)_2O$).

Found: C, 71.44; H, 10.84%. Calcd for $C_{16}H_{28}O_3$: C, 71.60; H, 10.52%.

1β-[(Tetrahydropyranyloxy)methyl]-5,5,8aβ-trimethyl-4aα-octahydro-2(1*H*)-naphthalenone (10). (a) A solution of **8** (890 mg, 3.32 mmol) and PPTS (5 mg) in acetone (15 ml) was warmed with stirring at 40 °C for 15 h. The solvent was mostly taken off under reduced pressure and the residue was dissolved in ether. The ethereal solution was washed with brine and dried. Removal of the solvent left an oil which was filtered through a short silica-gell column with hexane–ether (1:1) to give ketol **9** (714 mg, 96%): IR (film) 3300 cm^{-1}; ^{1}H NMR ($CDCl_3$) δ=0.80, 0.85, and 0.97 (9H in total, s each, $C(CH_3)_2$ and C–CH_3), 1.0—2.6 (13H, m), 3.8—4.1 (2H, m, CH_2–OH). This material was used for the next reaction without further purification. A mixture of **9** (714 mg, 3.18 mmol), 3,4-dihydro-2*H*-pyran (267 mg, 3.18 mmol), PPTS (5 mg), and CH_2Cl_2 (15 ml) was stirred at room temperature for 15 h, and washed with brine, and dried. Evaporation followed by filtration of an oily residue through a short silica-gel column with hexane–ether (3:2) gave **10** (950 mg, 97%): IR (film) 1710 cm^{-1}; ^{1}H NMR ($CDCl_3$) δ=0.75, 0.85, and 0.95 (9H in total, s each, $C(CH_3)_2$ and C–CH_3), 1.1—2.4 (18H, m), 3.3—4.2 (4H, m, CH_2–O–CH–O–CH_2), 4.58 (1H, br s, O–CH–O).

Found: C, 73.90; H, 10.60%. Calcd for $C_{19}H_{32}O_3$: C, 73.98; H, 10.46%.

(b) A mixture of **14** (41 mg, 0.13 mmol), 10% Pd-C (5 mg), and dioxane (1 ml) was stirred at room temperature under H_2 for 20 h, and filtered. Concentration of the filtrate left an oil which was purified by preparative TLC (hexane–ether, 2:1) to give **10** (38 mg, 95%).

1α-Hydroxymethyl-5,5,8aβ-trimethyl-4aα,5,6,7,8,8a-hexahydro-2(1*H*)-naphthalenone (12). To a stirred solution of diisopropylamine (156 mg, 1.10 mmol) in THF (4 ml) was added dropwise at −78 °C a solution of 1.5 M butyllithium in hexane (0.96 ml, 1.43 mmol). The bath was replaced by an ice bath and the mixture was stirred for 30 min, then recooled at −78 °C. A solution of **11**[9] (212 mg, 1.10 mmol) in THF (4 ml) was added dropwise and stirring was continued for an additional 1.5 h. To this solution, Gaseous formaldehyde, generated by heating paraformaldehyde (ca. 3 g) at 160—170 °C, was passed through by means of a stream of dry N_2 for 30 min. The reaction was quenched by addition of aqueous NH_4Cl and the product was extracted with ether. The combined extracts were washed with brine and dried. Evaporation left an oil which was purified by preparative TLC (hexane–ether 1:1) to give **12** (191 mg, 78%) and **11** (15 mg, 7%).

12: a colorless crystals; mp 104—105 °C (from hexane–ether); IR (KBr) 3350 and 1680 cm^{-1}; ^{1}H NMR ($CDCl_3$) δ=0.94, 1.04, and 1.08 (9H in total, s each, $C(CH_3)_2$ and C–CH_3), 1.1—1.8 (6H, m), 2.10 (1H, ddd, J=8.2, 4.8, and 1.0 Hz, CH–CH_2O), 2.28 (1H, br t, J=1.7 Hz, CH–C=C), 2.3 (1H, br, OH), 3.65—4.18 (2H, m, CH_2–O), 6.04 (1H, ddd, J=10.4, 3.2, and 1.0 Hz, C=CH–CO), 6.96 (1H, dd, J=10.4 and 1.8 Hz, CH=C–CO). Upon irradiation at 6.04 ppm, the absorptions at 2.10, 2.28, and 6.96 ppm changed a double doublet (J=8.2, 4.8 Hz), a doublet (J=1.8 Hz), and a doublet (J=1.8 Hz), respectively. ^{1}H NMR ($CDCl_3$–D_2O) δ=3.76 (1H, dd, J=10.8, 8.2 Hz, CHH–O), 4.05 (1H, dd, J=10.8, 4.8 Hz, CHH–O).

Found: C, 75.78; H, 9.80%. Calcd for $C_{14}H_{22}O_2$: C, 75.63; H, 9.97%.

1α-[(Tetrahydropyranyloxy)methyl]-5,5,8aβ-trimethyl-4aα,5,6,7,8,8a-hexahydro-2(1*H*)-naphthalenone (13). A mixture of **12** (50 mg, 0.23 mmol), 3,4-dihydro-2*H*-pyran (29 mg, 0.34 mmol), catalytic amount of PPTS, and CH_2Cl_2 (2 ml) was stirred at room temperature for 6 h, and washed with brine. Removal of the solvent left an oil which was purified by preparative TLC (hexane–ether, 3:2) to give **13** (68 mg, quantitative): IR (film) 1680 cm^{-1}; ^{1}H NMR ($CDCl_3$) δ=0.93, 1.02, and 1.07 (9H in total, s each, $C(CH_3)_2$ and C–CH_3), 1.1—1.9 (12H, m), 2.13 (1H, br t, J=5.4 Hz), 2.57 and 2.68 (1H in total, br t, C=C–CH), 3.3—4.2 (4H, m, CH_2–O–CH–O–CH_2), 4.55 (1H, br s, O–CH–O), 6.02 (1H, dd, with fine splittings, J=10.4 and 3.2 Hz, C=CH–CO), 6.90 (1H, dd, J=10.4 and 1.9 Hz, CH=C–CO).

1β-[(Tetrahydropyranyloxy)methyl]-5,5,8aβ-trimethyl-4aα,

5,6,7,8,8a-hexahydro-2(1*H*)-naphthalenone (14) and dienone 15. By the same procedure described in the preceding experiment, LDA solution was prepared from 1.5 M (1 M=1 mol dm^{-3}) butyllithium in hexane (0.52 ml, 0.76 mmol) and diisopropylamine (93 mg, 0.90 mmol) in THF (3 ml). A solution of **13** (120 mg, 0.46 mmol) in THF (2 ml) was added dropwise to the above solution at −78 °C. After stirring for 10 min, 10% citric acid (1 ml) was added and stirring was continued at −78 °C for an additional 30 min. Water was added, and the product was extracted with ether. Evaporation left an oil which was purified by preparative TLC (hexane–ether, 2:1) to give **14** (54 mg, 45%) and **15** (49 mg, 41%).

14: IR (film) 1680 cm^{-1}; ^1H NMR ($CDCl_3$) δ=0.84, 0.95, and 1.05 (9H in total, s each, $C(CH_3)_2$ and C–CH_3), 1.0—2.0 (12H, m), 2.2—2.4 (2H, m, C=C–CH and CH–CO), 3.4—4.44 (4H, m, $C\underline{H}_2$–O–CH–O–$C\underline{H}_2$), 4.65 (1H, br s, O–CH–O), 6.08 (1H, dd. J=10.2 and 3.0 Hz, C=CH–CO), 6.92 (1H, dd, J=10.2 and 2.2 Hz, CH=C–CO).

Found: C, 74.57; H, 10.13%. Calcd for $C_{19}H_{30}O_3$: C, 74.47; H, 9.87%.

15: IR (film) 1675 and 1620 cm^{-1}; ^1H NMR ($CDCl_3$) δ=0.98, 1.03, and 1.17 (3H, s each, $C(CH_3)_2$ and C–CH_3), 1.1—1.9 (6H, m), 2.22 (1H, br t, C=C–CH), 5.16 and 5.87 (1H s with fine splittings each, $C=CH_2$), 6.20 (1H, dd, J=10.4 and 3.2 Hz, C=CH–CO), 7.01 (1H, dd, J=10.4 and 2.1 Hz, CH=C–CO).

Drimane-8β,11-diol (17). To a stirred solution of **10** (490 mg, 1.59 mmol) in ether (10 ml) was added dropwise at −78 °C a solution of 0.95 M methylmagnesium iodide in ether (7 ml, 4.0 mmol) and stirring was continued for an additional 5 h over a range of −78 to −10 °C. The reaction was quenched by the addition of aqueous NH_4Cl and the product was extracted with ether. Evaporation of the combined extracts gave an oil, which was chromatographed on silica gel with hexane–ether (7:3) to give alcohol **16** (485 mg, 94%): IR (film) 3300 cm^{-1}; ^1H NMR ($CDCl_3$) δ=0.85 (6H, s, $C(CH_3)_2$), 1.15, 1.22, and 1.30 (6H in total, s each, C–CH_3 and O–C–CH_3), 0.9—2.0 (19H, m), 3.2—4.3 (4H, m, $C\underline{H}_2$O–CH–O–$C\underline{H}_2$), 4.35 (1H, br s, O–CH–O). A mixture of **16** (485 mg, 1.50 mmol), PPTS (5 mg), and methanol (7 ml) was stirred at 60 °C for 15 h. The solvent was removed under reduced pressure to give a semicrystalline residue which was chromatographed on silica gel with hexane–ether (3:7), giving **17** (328 mg, 91%) as crystals: Mp 133—134 °C [lit,[8] 133.8—134.5 °C (from hexane–ether)]; IR (KBr) 3280 cm^{-1}; ^1H NMR ($CDCl_3$) δ=0.87 (6H, s, $C(CH_3)_2$), 1.23 (3H, s, C–CH_3), 1.35 (3H, s, O–C–CH_3), 1.0—2.1 (13H, m), 2.94 (1H, br s, OH), 4.06 (2H, d, J=3 Hz, CH_2–O). The physical constants (mp, IR, and ^1H NMR) were identical with those of drimane-8β,11-diol reported by Pelletier.[8]

1β-[(*p*-Tolylsulfonyloxy)methyl]-2α,5,5,8aβ-tetramethyl-4aα-decahydronaphthalen-2β-ol (19). A solution of **17** (60 mg, 0.25 mmol) and *p*-toluenesulfonyl chloride (71 mg, 0.37 mmol) in pyridine (1 ml) was stirred at room temperature for 10 h and diluted with ether. The ethereal solution was washed successively with aqueous copper(II) sulfate, water, and brine, and dried. Evaporation left a solid, which was filtered through a short silica-gel column with hexane–ether (1:1) to give **19** (85 mg, 88%) as crystals: Mp 96—97 °C (from hexane–ether); ^1H NMR ($CDCl_3$) δ=0.80, 0.85, and 0.89 (9H in total, s each, $C(CH_3)_2$ and C–CH_3), 1.12 (3H, s, O–C–CH_3), 0.9—1.8 (13H, m), 2.44 (3H, s, Ar–CH_3), 4.10 (1H, d, J=10.8 and 2.8 Hz, O–C$\underline{H}$H), 4.32 (1H, d, J=10.8 and 3.9 Hz, O–CH$\underline{H}$), 7.32 and 7.78 (1H, dd each, J=8.6 Hz, Ar–H).

Found: C, 66.93; H, 8.79%. Calcd for $C_{22}H_{34}O_4$: C, 66.96; H, 8.63%.

Reaction of 19 with Sodium Hydride. To a stirred mixture of 60% sodium hydride dispersion in mineral oil (6 mg, 0.14 mmol) in DME (1 ml) was added a solution of **19** (50 mg, 0.13 mmol) in DME (1 ml), and the mixture was stirred at 60 °C for 15 h. After cooling, ether was added and the ethereal solution was washed successively with water and brine, and dried. Removal of the solvent left an oil, which was purified by preparative TLC (hexane–ether, 3:1) to give oxetane **20** (10 mg, 30%) and **19** (35 mg, 70%).

20: IR (film) 970 cm^{-1}; ^1H NMR ($CDCl_3$) δ=0.83, 0.95, and 1.17 (3H, s each, $C(CH_3)_2$ and C–CH_3), 1.98 (3H, s, O–C–CH_3), 1.0—2.0 (11H, m), 2.24 (1H, t, J=6.8 Hz, O–CH_2–C$\underline{H}$), 4.55 (2H, d, J=6.8 Hz, O–$C\underline{H}_2$–CH).

Found: C, 86.39; H, 8.45%. Calcd for $C_{22}H_{26}O$: C, 86.23; H, 8.55%.

2β-Hydroxy-2α,5,5,8aβ-tetramethyl-4aα-decahydro-1β-naphthalenecarbaldehyde (21). To a stirred solution of NCS (400 mg, 3.0 mmol) in toluene (10 ml) was added dropwise at 0 °C a solution of dimethyl sulfide (0.3 ml, 4.1 mmol), and stirring was continued for an additional 30 min. The reaction mixture was cooled at −25 °C, and a solution of **17** (480 mg, 2.0 mmol) in toluene (5 ml) was added. After stirring for 3 h, triethylamine (0.5 ml) was added and the whole was stirred for 30 min, and diluted with ether. The ethereal solution was washed successively with 1% HCl, water and brine, and dried. Removal of the solvent gave an oil, which was chromatographed on silica gel with hexane–ether (4:1) to give **21** (295 mg, 63%) and **17** (50 mg).

21: Crystals; mp 72—73 °C (from hexane–ether); IR (KBr) 3400 and 1700 cm^{-1}; ^1H NMR ($CDCl_3$) δ=0.82 and 0.89 (6H in total, s each, $C(CH_3)_2$), 1.15 and 1.18 (6H in total, s each, C–CH_3 and O–C–CH_3), 1.0—2.8 (11H, m), 2.10 (1H, d, J=3.2 Hz, C$\underline{H}$–CHO), 2.90 (1H, br s, OH), 10.1 (1H, d, J=3.2 Hz, CHO).

Found: C, 75.41; H, 10.86%. Calcd for $C_{15}H_{26}O_2$: C, 75.58; H, 11.00%.

α-(2,6-Dimethyoxy-4-methylphenyl)-(2β-hydroxy-2α,5,5,8aβ-tetramethyl-4aα-decahydro-1β-naphthalenemethanol (22). To a stirred solution of 1,3-dimethoxy-5-methylbenzene[12] (1.272 g, 8.37 mmol) in DME (15 ml) was added dropwise at −60 °C a solution of 1.6 M butyllithium in hexane (5.26 ml, 8.37 mmol). The reaction mixture was stirred at −60 °C for 30 min, and at room temperature for 2 h, and recooled at −60 °C. A solution of **21** (249 mg, 1.05 mmol) in DME (2 ml) was added and the whole was allowed to stir for 2 h over a range of −60 to 0 °C, and then at room temperature for 30 min. After cooling at 0 °C, wet ether followed by water were added, and the product was extracted with ether. The combined extracts were washed with brine and dried. Removal of the solvent left a crystalline residue, whose ^1H NMR spectrum indicated that it is a mixture of stereoisomers with regard to a benzylic hydroxyl group. The residue was chromatographed on silica gel with hexane–ether (1:1) to give **22** (378 mg, 92%) as crystals: Mp 131—133 °C (from hexane–ether); IR (KBr) 3300 cm^{-1}; ^1H NMR ($CDCl_3$) δ=0.88 (6H, s, $C(CH_3)_2$), 1.17 (3H, s, C–CH_3), 1.35

(3H, s, O-C-CH_3), 1.0—2.1 (12H, m), 2.32 (3H, s, Ar-CH_3), 3.82 (6H, s, O-CH_3), 4.80 (1H, br s, C-OH), 5.38 (1H, d, J=4.3 Hz, CH-OH), 5.75 (1H, m, CH-OH), 6.35 (2H, s, Ar-H).

Found: C, 73.67; H, 9.85%. Calcd for $C_{24}H_{38}O_4$: C, 73.80; H, 9.81%.

α-Phenyl-2β-hydroxy-2α,5,5,8aβ-tetramethyl-4aα-decahydro-1β-naphthalenemethanol (23). To a stirred solution of **21** (101 mg, 0.42 mmol) in DME (7 ml) was added at −60 °C a solution of 1.8 M phenyllithium in cyclohexane-ether (0.95 ml, 1.69 mmol), and the mixture was stirred for 1 h over a range of −60 to −20 °C, and then at 0 °C for 1 h. The reaction was quenched by addition of aqueous NH_4Cl and the product was extracted with ether. The combined extracts were washed with brine and dried. Evaporation followed by purification of the oily residue by preparative TLC (hexane-ether, 3:1) gave **23** (126 mg, 94%), which crystallized on standing. The ^1H NMR spectrum indicated that it is a mixture of stereoisomers regarding a benzylic hydroxyl group. Recrystallization of the crystals from hexane-ether (5:1) gave analytically pure sample: Mp 155—156 °C; IR (KBr) 3300 cm^{-1}; ^1H NMR ($CDCl_3$) δ=0.91 (6H s, $C(CH_3)_2$), 1.01 (3H, s, C-CH_3), 1.35 (3H, s, O-C-CH_3), 1.0—2.0 (11H, m), 2.98 (1H, s, C-OH), 4.23 (1H, d, J=3.6 Hz, CH-OH), 5.35 (1H, br d, J=4 Hz, CH-OH), 7.2—7.58 (5H, Ar-H).

Found: C, 79.82; H, 10.43%. Calcd for $C_{21}H_{32}O_2$: C, 79.70; H, 10.19%.

***r*-1-[(*E*)-2-(2,6-Dimethoxy-4-methylphenyl)ethenyl]-*t*-2-(3-oxobutyl)-1,3,3-trimethylcyclohexane (24).** (a) A solution of **22** (483 mg, 1.24 mmol) and pyridinium chloride (71 mg, 0.62 mmol) in CH_2Cl_2 (10 ml) was stirred at room temperature for 10 min, and washed with brine, and dried. Removal of the solvent gave an oil, which was chromatographed on silica gel with hexane-ether (3:1) to give **24** (459 mg, quantitative) as crystals: Mp 102—103 °C (from hexane-ether); IR (KBr) 1710 cm^{-1}; ^1H NMR ($CDCl_3$) δ=0.90 and 0.95 (6H in total, s each, $C(CH_3)_2$), 1.15 (3H, s, C-CH_3), 1.2—1.7 (7H, m), 1.98 (3H, s, CO-CH_3), 2.33 (3H, s, Ar-CH_3), 2.4—2.6 (2H, m, CH_2-CO), 3.90 (6H, s, O-CH_3), 6.37 (4H, br s, CH=CH and Ar-H).

Found: C, 77.37; H, 9.53%. Calcd for $C_{24}H_{36}O_3$: C, 77.37; H, 9.74%.

(b) A solution of **22** (91 mg, 0.23 mmol) and PPTS (5 mg) in CH_2Cl_2 (2 ml) was stirred at room temperature for 20 min. The solvent was removed and a crystalline residue was purified by preparative TLC (hexane-ether, 1:1) to give **24** (83 mg, 97%).

***t*-2-(3-Oxobutyl)-1,3,3-trimethyl-*r*-1-[(*E*)-styryl]cyclohexane (25).** A solution of **23** (34 mg, 0.11 mmol) and *p*-toluenesulfonyl chloride (31 mg, 0.2 mmol) in pyridine (1 ml) was stirred at 60 °C for 2 d. After cooling, water was added and the product was extracted with ether. The combined extracts were washed successively with aqueous copper(II) sulfate, water, and brine and dried. Evaporation left an oil, which was purified by preparative TLC (hexane-ether, 2:3) to give **25** (18 mg, 58%): IR (film) 1710 and 1605 cm^{-1}; ^1H NMR ($CDCl_3$) δ=0.90 and 0.94 (6H in total, s each, $C(CH_3)_2$), 1.14 (3H, s, C-CH_3), 1.95 (3H, s, CO-CH_3), 1.0—2.3 (11H, m), 5.95 and 6.23 (2H in total, d each, J=16.2 Hz, CH=CH), 7.3 (5H, br s, Ar-H).

Found: C, 84.45; H, 10.05%. Calcd for $C_{21}H_{30}O$: C, 84.51; H, 10.13%.

Methyl *t*-2-[3,3-(Ethylenedioxy)butyl]-1,3,3-trimethyl-*r*-1-cyclohexanecarboxylate (29). A mixture of **24** (83 mg, 0.22 mmol), ethylene glycol (28 mg, 0.44 mmol), *p*-toluenesulfonic acid (5 mg) and benzene (10 ml) was refluxed azeotropically for 5 h. After cooling, aqueous $NaHCO_3$ was added and the product was extracted with ether. The combined extracts were washed with brine and dried. The oily residue obtained by evaporation was filtered through a short silica-gel column with hexane-ether (1:1) to give acetal **27** (84 mg, 91%) as crystals: Mp 107—108 °C (from hexane-ether); ^1H NMR ($CDCl_3$) δ=0.94 and 0.97 (6H in total, s each, $C(CH_3)_2$), 1.13 (3H, s, C-CH_3), 1.22 (3H, s, O-CH_3), 1.0—1.8 (11H, m), 2.32 (3H, s, Ar-CH_3), 3.80 (4H, s, O-$(CH_2)_2$-O), 6.38 and 6.40 (4H in total, s each, CH=CH and Ar-H).

To a stirred solution of **27** (143 mg, 0.35 mmol) in CH_2Cl_2 (20 ml) was passed ozone at −78 °C for 20 min. After the excess ozone was removed by bubbling through with N_2, dimethyl sulfide (0.5 ml) was added, and the mixture was stirred at −78 °C for 1 h and at room temperature for 30 min. Evaporation left an oil, which was chromatographed on silica gel with hexane-ether (1:2) to give **28** (46 mg, 52%): IR (film) 3300—2800, 1700, and 1050 cm^{-1}; ^1H NMR ($CDCl_3$) δ=0.90 and 0.92 (6H in total, s each, $C(CH_3)_2$), 1.18 (3H, s, C-CH_3), 2.09 (3H, s, O-C-CH_3), 1.0—1.8 (11H, m), 3.90 (4H, s, O-$(CH_2)_2$-O), 7.7 (1H, br, CO_2H).

To a stirred solution of **28** (40 mg, 0.15 mmol) in ether (5 ml) was added at 0 °C a solution of diazomethane in ether. Evaporation and purification of the oily residue by preparative TLC (hexane-ether, 3:1) gave **29** (41 mg, quntitative): IR (film) 1730 cm^{-1}; ^1H NMR ($CDCl_3$) δ=0.90 and 0.93 (6H in total, s each, $C(CH_3)_2$), 1.18 (3H, s, C-CH_3), 1.28 (3H, s, O-C-CH_3), 1.0—2.0 (11H, m), 3.63 (3H, s, O-CH_3), 3.91 (4H, s, O-$(CH_2)_2$-O).

Found: C, 68.40; H, 10.29%. Calcd for $C_{17}H_{30}O_4$: C, 68.42; H, 10.13%.

4-(2,2,6-Trimethyl-*t*-6-vinylcyclohex-*r*-1-yl)-2-butanone Ethylene Acetal (32). To a stirred mixture of lithium aluminium hydride (14 mg, 0.36 mmol) in THF (4 ml) was added at 0 °C a solution of **29** (54 mg, 0.18 mmol) in THF (1 ml), and the reaction mixture was stirred at room temperature for 7 h, and quenched by addition of wet ether. A solid was filtered and washed with ether. The combined filtrate and wash were dried and evaporated to give an oil. Filtration through a short silica-gel column with hexane-ether (1:1) gave **30** (48 mg, quantitative): IR (film) 3300 cm^{-1}; ^1H NMR ($CDCl_3$) δ=0.80 and 0.89 (9H in total, s each, $C(CH_3)_2$ and C-CH_3), 1.0—1.9 (12H, m), 1.33 (3H, s, O-C-CH_3), 3.0—3.3 (2H, m, CH_2-OH), 3.96 (4H, s, O-$(CH_2)_2$-O).

Chromium(VI) oxide (118 mg) was added at 0 °C to a stirred solution of pyridine (0.2 ml) in CH_2Cl_2 (4 ml). After stirring for 1 h, Celite 545 (400 mg) followed by a solution of **30** (32 mg, 0.12 mmol) in CH_2Cl_2 (2 ml) was added. After stirring for 10 min, sodium hydrogensulfate monohydrate (400 mg) was added and the whole was stirred for 10 min. Filtration followed by evaporation of the filtrate left an oil, which was purified by preparative TLC (hexane-ether, 3:1) to give **31** (30 mg, quantitative): IR (film) 1705 cm^{-1}; ^1H NMR ($CDCl_3$) δ=0.90 and 0.97 (6H in total, s each, $C(CH_3)_2$), 1.10 (3H, s, C-CH_3), 1.28 (3H, s, O-C-CH_3), 1.0—1.8 (11H, m), 3.90 (4H, s, O-$(CH_2)_2$-O), 9.30 (1H, s, CHO).

To a stirred suspension of 60% sodium hydride dispersion in mineral oil (10 mg, 0.25 mmol) in toluene (0.5 ml) was added a solution of 1-pentanol (23 mg) in toluene (0.5 ml), and the mixture was stirred at 60 °C for 1 h. After cooling, methyltriphenylphosphonium bromide (98 mg, 0.27 mmol) was added, and the resulting mixture was stirred at room temperature for 1 h. To a yellow suspension obtained, a solution of **31** (32 mg, 0.12 mmol) in toluene (0.5 ml) was added, and the whole was allowed to stir for 10 h, and then quenched by addition of wet ether. The ethereal solution was washed successively with water and brine, and dried. Removal of the solvent gave an oil, which was purified by preparative TLC (hexane–ether, 2:1) to give **32** (24 mg, 77%): IR (film) 3060, 1630, and 910 cm^{-1}; ^1H NMR ($CDCl_3$) δ=0.90 (6H, s, $C(CH_3)_2$), 1.08 (3H, s, $C-CH_3$), 1.38 (3H, s, $O-C-CH_3$), 1.0—1.8 (11H, m), 3.98 (4H, s, $O-(CH_2)_2-O$), 4.90, 5.02, and 5.77 (3H in total, ABX system, J=18, 9, and 1.8 Hz, $CH=CH_2$).

4-(2,2,6-Trimethyl-*t*-6-vinylcyclohex-*r*-1-yl)-2-butanone (5). A solution of **32** (20 mg, 0.08 mmol) and PPTS (5 mg) in acetone (2 ml) was stirred at 40 °C for 5 h. Removal of the solvent left an oil, whose purification by preparative TLC (hexane–ether, 4:1) gave **5** (18 mg, quantitative). The physical data (IR and ^1H NMR) were identical of those of natural **5** reported by Enzell.[6]

References

1) C. A. Grob and P. W. Schiess, *Angew. Chem. Int. Ed. Engl.*, **6**, 1 (1967).

2) For the use of the term nucleofuge instead of the term leaving group; see Ref. 1.

3) M. Kato, Y. Matsumura, K. Heima, N. Fukamiya, C. Kabuto, and A. Yoshikoshi, *Tetrahedron*, **43**, 711 (1987).

4) T. W. Greene, "Protective Groups in Organic Synthesis," John Wiley & Sons, New York (1981).

5) M. Kato and A. Yoshikoshi, unpublished results.

6) J. R. Hlubucek, A. J. Aasen, B. Kimland, and C. R. Enzell, *Phytochemistry*, **12**, 2553 (1973).

7) Part of this work has been published as preliminary communications: M. Kato, Y. Tooyama, and A. Yoshikoshi, *Chem. Lett.*, **1989**, 61.

8) S. W. Pelletier, S. Lajsic, Y. Ohtsuka, and Z. Djarmati, *J. Org. Chem.*, **40**, 1602 (1975).

9) J. D. White, R. W. Skeen, and G. L. Trammell, *J. Org. Chem.*, **50**, 1939 (1985).

10) M. Kato and A. Yoshikoshi, submitted to *J. Chem. Soc., Perkin Trans. 1*, **1990**.

11) E. J. Corey and C. U. Kim, *J. Am. Chem. Soc.*, **94**, 7586 (1972).

12) R. Adam, H. Wolff, C. K. Cain, and J. H. Clark, *J. Am. Chem. Soc.*, **62**, 1779 (1940).

13) The stereochemistry of the benzylic hydroxyl group is unknown.

14) Although no informative data were obtained from the ^1H NMR spectrum for assignment of the double bond geometry (see Experimental), E geometry was deduced in connection with the result obtained by the fragmentation reaction of **23**, as mentioned later.

15) (Other syntheses) J. R. Hlubuck, A. J. Aasen, S-O. Almqvist, and C. R. Enzell, *Acta Chem. Scand., Ser. B*, **28**, 18 (1974); E. J. Corey and R. R. Sauers, *J. Am. Chem. Soc.*, **81**, 1734 (1959).

Conversion of Hydroxyl Groups in Alcohols to Other Functional Groups with *N*-Hydroxy-2-thiopyridone, and Its Application to Dialkylamines and Thiols

Hideo Togo,* Misa Fujii, and Masataka Yokoyama*
Department of Chemistry, Faculty of Science, Chiba University, Yayoi-cho 260
(Received August 23, 1990)

The radical decarboxylation reaction of *N*-alkoxyoxalyloxy-2-thiopyridone which was prepared by the reaction of alcohol, oxalyl chloride, and *N*-hydroxy-2-thiopyridone was studied both in the absence and presence of olefinic compounds. The same reactions with olefinic and acetylenic alcohols gave the corresponding lactone derivatives. On the other hand the unsymmetrical alkyl 2-pyridyl disulfides were obtained by the same reaction with aliphatic thiols.

Recently, free radical reactions have been used in organic synthesis extensively and their high functional abilities have been recognized.[1] In those reactions, Barton's method which is the radical decarboxylation reaction of thiohydroxamic esters (*O*-acyl derivatives of *N*-hydroxy-2-thiopyridone) prepared from carboxylic acid chlorides and *N*-hydroxy-2-thiopyridone, is very attractive because both the reaction procedure and the purification of the reaction products are simple.[2] We studied this reaction for intermolecular carbon–carbon bond formation with olefinic compounds previously.[3] On the other hand a few reports on the same radical decarboxylative reaction with alcohols instead of carboxylic acids have been known.[4] But in those reports, the reactions only with tertiary alcohols were studied and detailed study was not carried out.

As the applications of this decarboxylation reaction to other functional groups instead of carboxylic acids, herein we report the reactions with alcohols, amines, and thiols.

Table 1. Decarboxylative Reaction of Alcohols **1** to Sulfide **4** and S-2-Pyridyl Thiocarbonate **5**[a]

	ROH	Solvent	Reaction time/min	Yield **4**/%	Yield **5**/%
1a	$CH_3(CH_2)_7$–OH	Benzene	60	<3	60
		Toluene	30	8	65
		Chlorobenzene	10	12	34
1b	*c*-C_6H_{11}–OH	Benzene	60	11	48
1c	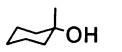	Benzene	60	41	4
1d	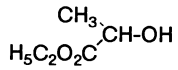	Benzene	60	47	—
1e	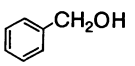	Toluene	30	50	0
1f	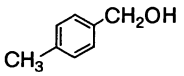	Benzene	60	54	0
1g	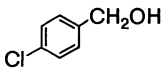	Benzene	60	53	0
1h	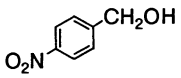	Benzene	60	68	0
1i	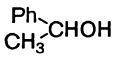	Toluene	30	47	0
1j	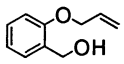	Benzene	90	58	0
1k	CH_3CH_2OH	Benzene	60	0	59[b]
		Dichloromethane[c]	40	0	75

a) The reaction was carried out in refluxing conditions. b) Diethyl oxalate and 2,2′-dipyridyl disulfide were obtained in 26 and 34% yields, respectively. c) The reaction was carried out under irradiation conditions (500 W tungsten lamp) at −16—−18 °C.

Results and Discussion

I). The Reaction with Saturated Alcohols. At first, when the reaction was carried out with 1-octanol we obtained both compounds; **4a** as a minor product and **5a** as a major product. The mixed diester **3**, which is prepared in situ from the corresponding alcohol, oxalyl chloride, and *N*-hydroxy-2-thiopyridone, is so unstable that it is hydrolyzed on silica gel TLC plate easily and completely. But **3** can be observed both by NMR and IR measurements as a crude state. Thus **3k** which was prepared from ethyl chloroglyoxylate with *N*-hydroxy-2-thiopyridone at 0 °C was obtained as a yellow oil, which was unstable on TLC, sunlight, and heat. The compound (**3k**) had two characteristic carbonyl absorptions in its IR spectrum and gave ethyl *S*-2-pyridyl thiocarbonate (**5k**) by heating in benzene. The same reaction was carried out with some primary, secondary, tertiary, and benzylic alcohols as shown in Table 1.

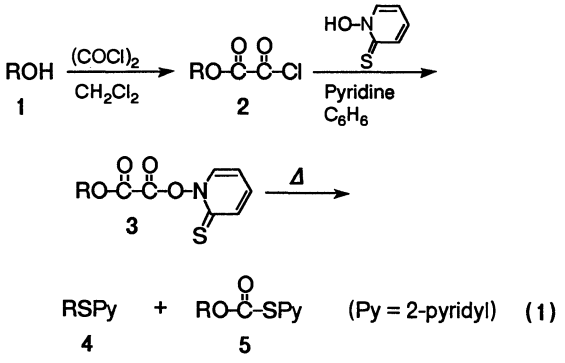

The reaction probably proceeds as follows: Cleavage of N–O bond[2] of ester (**3**) followed by decarboxylation gives alkoxycarbonyl radical (**II**). In the case of primary and secondary alcohols, the dissociation energies of C–O bond are large as compared with those of tertiary and benzylic alcohols.[5] Thus the major product of the former two compounds is a *S*-2-pyridyl thiocarbonate, while that of the latter two compounds is a 2-pyridylthio compound. Especially in both benzylic alcohols and α-hydroxyester, the corresponding 2-pyridylthio compounds **4** were formed dominantly. The result in the reaction with **3j** suggests that the formed benzylic radical does not cyclize to give chroman derivative because of the high stability of benzylic radical.

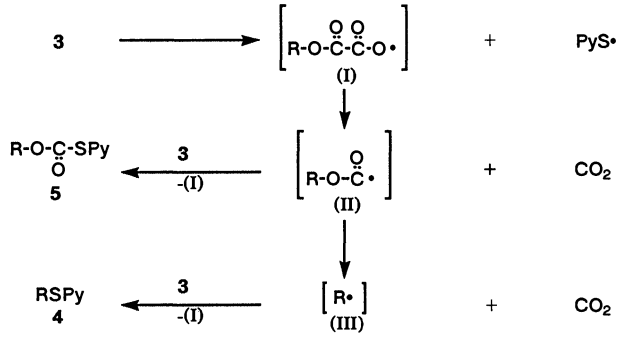

Scheme 1.

II). Inter- and Intramolecular Carbon–Carbon Bond Formations. Then, we attempted carbon–carbon bond formation starting from alcohol via alkoxycarbonyl radical (**II**) or alkyl radical (**III**) in the presence of phenyl vinyl sulfone. The reaction was carried out by dropping of the prepared chloroglyoxylic ester (**2**) to the mixture of sodium salt of *N*-hydroxy-2-thiopyridone and phenyl vinyl sulfone in refluxing benzene. The results were shown in Table 2.

In the case of cyclohexanol, the major product was **7**, which was formed by the reaction of decarboxylated radical (**II**) with phenyl vinyl sulfone. While the activated alcohol like benzyl alcohol gave **6** as a major product by the reaction of double decarboxylated radical (**III**) with phenyl vinyl sulfone. But, in *p*-nitrobenzyl alcohol (**1h**), *p*-nitrobenzyl 2-pyridyl sulfide was obtained as a sole product. The reason is that the addition reaction of (**IIIh**) onto phenyl vinyl sulfone is reversible as shown in Eq. 3 and its equilibrium declines to left-hand side probably because the high stability of (**IIIh**) as compared with the adduct radical (**IVh**). Next we tried to trap the formed benzyloxycarbonyl radical with 5-*exo* cyclization method starting from **1I**. But the 5-*exo*-trig cyclized lactone derivative (**9I**) was not obtained (Eq. 4). This result suggests that the rate of decarboxylation reaction of (**II**) to (**III**) in benzylic alcohols is perhaps over $>10^5\ s^{-1}$.[6]

Table 2. Intermolecular Carbon–Carbon Bond Formation[a]

	R–OH	Yield **6**/%	Yield **4**/%	Yield **7**/%
1b	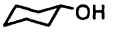	18	0	>80[b]
1e	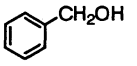	45	9	0
1f	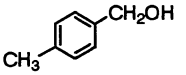	58	—	0
1g	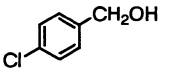	60	13	0
1h	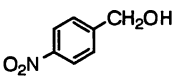	0	>95	0
1i	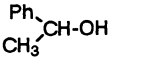	44	12	0

a) The yields were determined by NMR. b) Without H_2NNH_2 treatment.

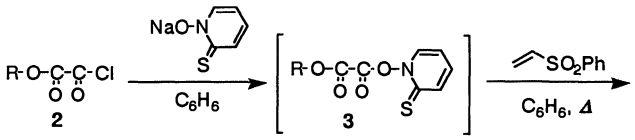

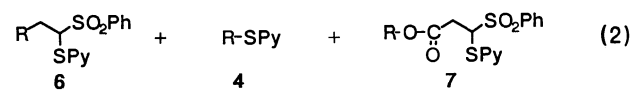

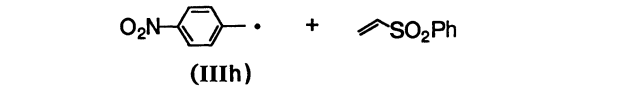

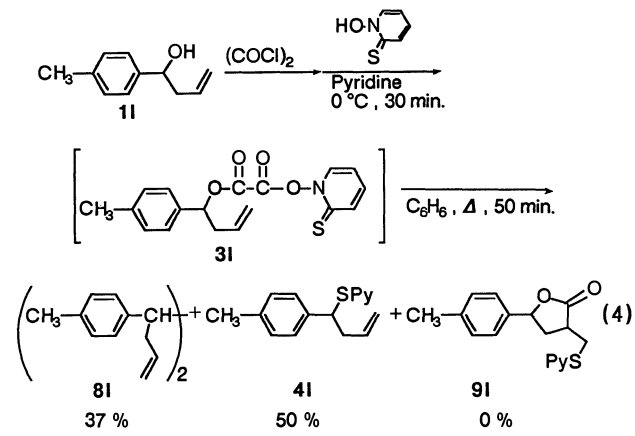

Adduct (**6e**) in Table 2 was converted to the other useful compounds as shown in Eq. 5. Particularly the conversion to carboxylic acid (**11e**) is equivalent to the preparation of C_2-gained carboxylic acid from alcohol.

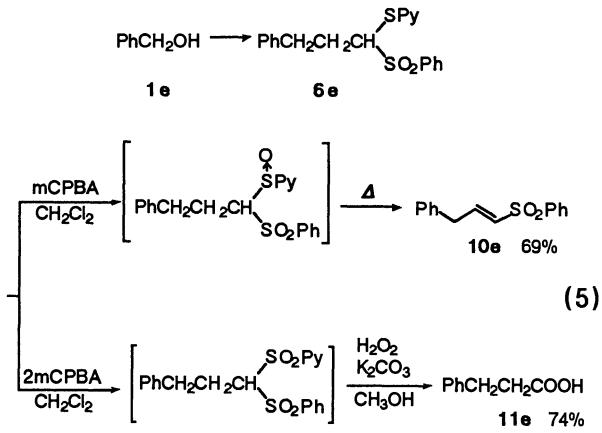

As mentioned above, the alkoxycarbonyl radical (**II**) formed from non-activated alcohol like primary and secondary alcohols does not decarboxylate to give (**III**). This result suggests that the formed alkoxycarbonyl radical (**II**) can be captured by olefinic groups via intra- and intermolecular carbon-carbon bond formation. Thus, when we carried out this reaction with 3-buten-1-ol (**1m**),[7] the γ-butyrolactone derivative (**12m**), which was a very important component for the synthesis of natural products,[8] was obtained in a moderate yield via intramolecular radical cyclization (5-*exo*-trig) as shown in Table 3 and Scheme 2.

A similar kind of reaction, which was the formation of α-methylene-γ-butyrolactone derivatives by the

Table 3. Reactions of Mediated Alkenyloxycarbonyl Radicals[a]

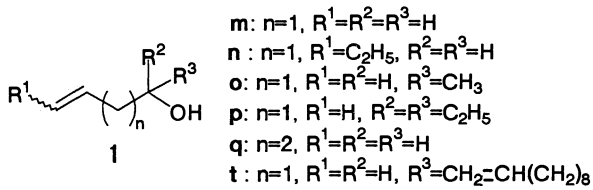

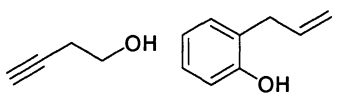

Substrate (2 mmol)	$(COCl)_2$/ml	Lactone **12**/%	S-2-Pyridyl thiocarbonate **5**/%
1m	0.8	42	1
1m	1.0	51	5
1m	1.5	46	4
1n-*trans*	1.0	71 (*RS*,*SR*):(*RR*,*SS*)=29:71	7
1n-*cis*	1.0	74 (*RS*,*SR*):(*RR*,*SS*)=29:71	6
1o	1.0	51 (ratio=34:66)	4
1p	1.0	43	—
1q	1.0	0	48
1q	1.0[b]	18	23
1r	1.0	40 (cis)	8
1s	1.0	41	—
1t	1.0	69 (ratio=34:66)	4

a) The reactions were carried out in benzene for 1 h. b) Dropping procedure of chloroglyoxylic ester of **1** into the sodium salt of *N*-hydroxy-2-thiopyridone over 4 h was used.

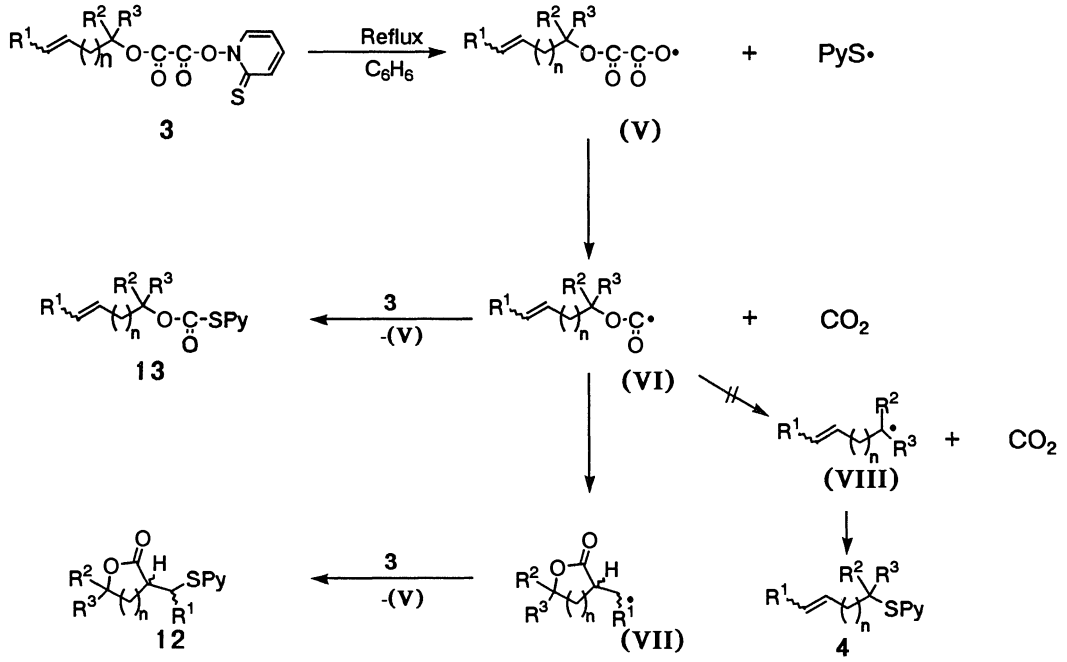

Scheme 2. Reaction Pathway (n=1, 2)

reaction of chloroformates, *Se*-phenyl selenocarbonates, and *S*-methyl dithiocarbonates of homopropargylic alcohol derivatives with Bu_3SnH[9] and Bu_3SnH/Et_3B[10], was reported recently. But in our system, γ-butyrolactone derivatives can be obtained in one pot reaction from olefinic and acetylenic alcohols, and further this reaction does not require the toxic organotin compounds. γ-Butyrolactone derivatives (**12o** and **12p**) could be also obtained in moderate yields from sec- and tert-alcohols (**1o** and **1p**), respectively. Then, the obtained lactone (**12m**) was oxidized with mCPBA (1.1 equiv) and the sulfoxide thus formed was heated at about 100 °C under reduced pressure to give α-methylene-γ-butyrolactone in 49% yield, which was tulipalin A isolated from tulip bulbs.[11] Both *trans* and *cis* isomers of 3-hexen-1-ol (**1n**) gave **12n** in good yields and the ratios of the formed diastereomers of **12n** in both reactions were same. This result suggests that both reactions proceed via the same intermediate (**VIIn**) to give **12n**. While, the use of 4-penten-1-ol (**1q**) yielded *S*-2-pyridyl thiocarbonate (**5q**) as a sole product. This result can be explained by the big difference in the cyclization rates between 3-butenoxycarbonyl radical (**VIm**) and 4-pentenoxycarbonyl radical (**VIq**). Thus, the difference is deduced from the cyclization rates of 5-hexenyl radical (k=2.3×10^5 s^{-1} at 25 °C) and 6-heptenyl radical (k=5.4×10^3 s^{-1} at 25 °C), respectively.[12] However, the formation of δ-valerolactone could be accelerated by adding dropwise a chloroglyoxylic ester (**2q**) (chloroglyoxylic ester of **1q**) to the sodium salt of *N*-hydroxy-2-thiopyridone in benzene. By this procedure, δ-valerolactone was obtained in 18% yield. While 3-propanolide could not be obtained from allyl alcohol.

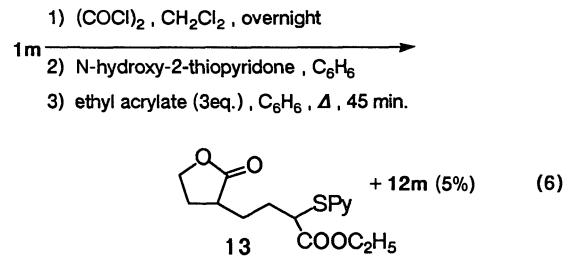

Further, the present reaction was carried out in the presence of ethyl acrylate to give an ester (**13**) in 40% yield, which was formed via both intra- and intermolecular radical reactions, along with **12m**. Finally α-pyridylthiomethylene-γ-butyrolactone was obtained in 40% yield from 3-butyn-1-ol (**1r**) by this system.

The formations of **12o** and **12p** mean that the formed carbonyl radicals (**VIo**) and (**VIp**) cyclize before the decarboxylation to alkenyl radicals (**VIIIo**) and (**VIIIP**), and therefore the sulfides (**4**) were not formed. While, in these reactions the small amount (≤10%) of dialkenyl oxalates were observed after the reaction. Most of these products were formed by radical coupling reaction[13] of alkenoxycarbonyl radicals (**VI**) because they were not formed during the preparation of **3**. The same reaction was carried out with diethylamine and *N*-(3-butenyl)aniline. In the former reaction, **15**, an *N*-analogue compound of **5**, was obtained in good yield in the presence of triethylamine. While the latter amine gave the cyclized

Table 4. Reactions of Mediated Carbamoyl Radicals[a)]

	RR'NH **14**	Base	RR'N-C(=O)-SPy **15**/%	γ-Lactam **16**/%
a	Et_2NH (2 mmol)	—	20	—
	Et_2NH (4 mmol)	C_5H_5N (2 mmol)	39	—
	Et_2NH (6 mmol)	C_5H_5N (2 mmol)	53	—
	Et_2NH (3 mmol)	Et_3N (5 mmol)	80	—
b	PhMeNH (6 mmol)	—	71	—
c	NHPh (6 mmol)	—	39	12
	NHPh (6 mmol)	Dropping procedure[b)]	35	20

a) The reactions were carried out in benzene for 1 h and the yields were calculated based on 2 mmol of *N*-hydroxy-2-thiopyridone. b) Dropping procedure of diethylamidooxalyl chloride into the sodium salt of *N*-hydroxy-2-thiopyridone over 4.5 h was used.

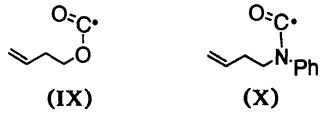

(IX) (X)

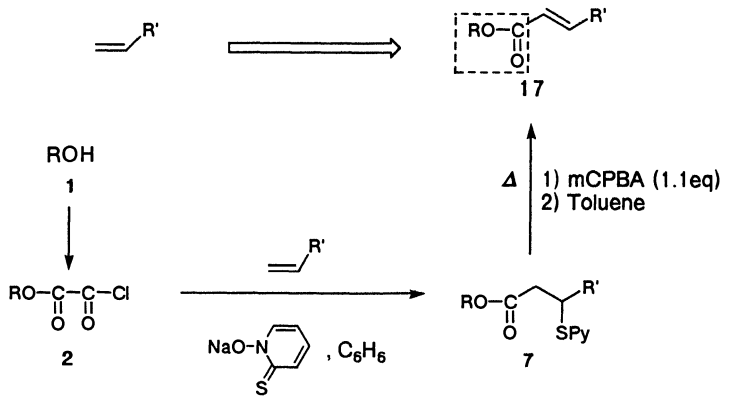

Scheme 3. Intermolecular Radical Reaction with Olefins

Table 5. Reactions of Mediated Alkoxycarbonyl Radical with Olefin[a)]

	ROH **1**	(or ≡–R')		RO-C(=O)-C(R')=C(SPy)-R' **7** (%)	RO-C(=O)-SPy **5** (%)	RO-C(=O)-CH=CH-R' **17** (%)
a	n-$C_8H_{17}OH$	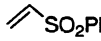	(3 equiv)	70	0	92
b	c-$C_6H_{11}OH$	▪	(5 equiv)	80	—	66
k	C_2H_5OH	i) ▪	(3 equiv)	70	0	84
		▪	(3 equiv)	42[b)]	42	—
		ii)	(3 equiv)	40	—	70
		▪	(3 equiv)	35[b)]	41	—
		iii)	(3 equiv)	34	27	49
		iv)	(3 equiv)	31	36	68
		v) $HC{\equiv}C-(CH_2)_4CH_3$	(3 equiv)	3	51	—
		vi) HC≡C–Ph	(3 equiv)	11	34	—

a) Dropping procedure of chloroglyoxylic ester of **1** into the sodium salt of *N*-hydroxy-2-thiopyridone over 1 h was used. b) $h\nu$/0°C.

product (**16**), a γ-lactam derivative, but the yield was low. Even when the dropping procedure of dialkylamidooxalyl chloride to *N*-hydroxy-2-thiopyridone in benzene was employed, the major product was **15**. So, we believe that the cyclization rate of (**IX**) is larger than that of (**X**).

Then we carried out this reaction in the presence of olefinic compound. If the adduct compound (**7**) could be obtained, it would be easily converted to α,β-unsaturated ester (**17**) as shown in Scheme 3. Practically, the alkoxycarbonyl radical (**II**) formed from alcohol (Scheme 1), reacted with some olefinic compounds to give the corresponding adducts (**7**) in good to moderate yields depending upon the olefinic compounds via intermolecular radical addition reaction.

The results in Table 5 suggests that the alkoxycarbonyl radical is nucleophilic. Therefore the yield of addition product with phenyl vinyl sulfone was high, while that with 1-dodecene was lower. These obtained compounds (**7**) were oxidized by mCPBA to give the corresponding sulfoxides which were then heated in benzene to give α,β-unsaturated esters (**17**) in good yields.

III). The Reaction with Thiols. We also studied the radical decarboxylative reaction with thiols. Phenylmethanethiol (**18e**) gave benzyl 2-pyridyl sulfide (**4e**) as a main product like benzyl alcohol. While, cyclohexanethiol (**18b**) and methyl 3-mercaptopropionate (**18t**) gave the corresponding unsymmetrical disulfides (**19b** and **19t**) which disproportionated slowly to two symmetrical disulfides respectively.

This result suggests that the formed alkylthiocarbonyl radical easily decomposes to give alkylthio radical (**XIII**) and carbon monooxide. Even when the reaction was carried out with 3-hexene-1-thiol, the major product was the corresponding unsymmetrical disulfide (**19n**). Therefore, the fragmentation reaction of (**XII**) to (**XIII**) should be extremely fast.

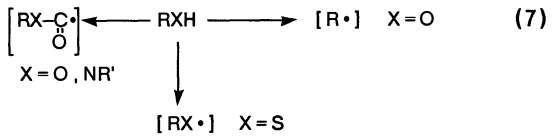

(7)

Table 6. Decarboxylative Reactions of Thiols

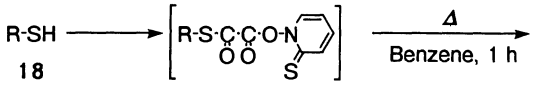

R-SPy + R-S-S-Py
4 19

	18 R-	4	19
b		—	40[a]
e	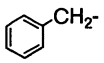	25	5
n	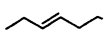	—	50[a]
t	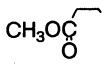	—	38[a]

a) RSSR was obtained ca. 10%.

In conclusion, the radical decarboxylative reactions of *N*-alkoxyoxalyloxy-2-thiopyridones which were prepared from activated alcohols, oxalyl chloride, and *N*-hydroxy-2-thiopyridone gave the corresponding sulfides or C–C bonded compounds in the presence of olefinic compounds. On the other hand those reactions with general prim-, sec-, tert-alcohols, and dialkylamines gave the corresponding *S*-2-pyridyl thiocarbonates and thiocarbamates respectively, and the cyclized products, γ-lactones and γ-lactams were obtained starting from 3-olefinic alcohols or amines in one-pot reaction via intramolecular radical cycliza-

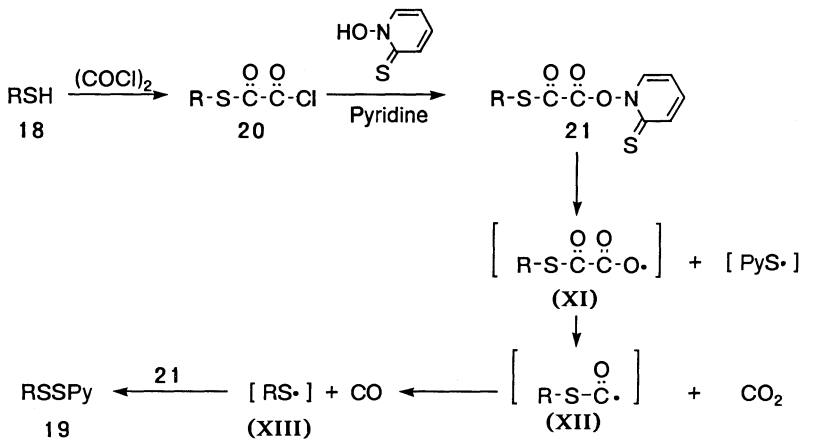

Schme 4.

tion. And further the intermolecular radical addition reactions with alcohols onto olefins gave the adducts which were easily converted to the α,β-unsaturated esters. On the other hand, the reactions with thiols gave the unsymmetrical disulfides via alkylthio radical.

Experimental

Microanalyses were performed with a Perkin-Elmer 240 elemental analyser at the Chemical Analysis Center of Chiba University. IR and ^{1}H NMR spectra were measured with Hitachi 215, JEOL-MH-100, JEOL-JNM-FX270, and JEOL-GSX-500 spectrometers, respectively. Wakogel C-200 was used for column chromatography, Kieselgel 60 F_{254} (Merck) was used for TLC, and Wakogel B-5F was used for preparative TLC (pTLC).

N-hydroxy-2-thiopyridone is commercially available as aqueous solution of sodium salt (sodium omadine). This solution (100 ml) was treated with concd HCl at pH 2, and the formed precipitates were separated by filtration and recrystallized from methanol. Sodium salt of *N*-hydroxy-2-thiopyridone was prepared as follows. To the ice-cold solution of *N*-hydroxy-2-thiopyridone (50 mmol) in methanol (100 ml) was added the ice-cold solution of sodium hydroxide (50 mmol) in methanol (100 ml). Then solvent was removed and the residue was washed with benzene and dried with vacuum pump.

1) The Preparation of *N*-Ethoxyoxalyloxy-2-thiopyridone 3k. To ethyl chloroglyoxylate (3.2 mmol) in benzene (7 ml) were added *N*-hydroxy-2-thiopyridone (3 mmol) and pyridine (4 mmol) dissolved in benzene (3 ml) under cooling by ice bath. Then the reaction mixture was stirred at 0 °C for 30 min. During this reaction, the reaction vessel was wrapped with aluminium foil tightly. Then, the reaction mixture was filtered quickly and the filtrate was evaporated to give **3k** as a yellow oil in quantitative yield.

3k: Oil; ^{1}H NMR ($CDCl_3$) δ=1.40 (t, 3H, J=6.7 Hz, $-CH_3$), 4.40 (q, 2H, J=6.7 Hz, $-CH_2-$), 7.00—7.30 (m, 2H, aromatic-4, 5H), 7.72 (dd, 1H, J=7.6, 2.7 Hz, aromatic-3H), 8.10 (dd, 1H, J=6.1, 2.7 Hz, aromatic-6H); IR (NaCl) 1810, 1730—1760 cm^{-1}.

2) General Procedure for the Conversion of Alcohol to 2-Pyridyl Sulfide. A solution of alcohol (2 mmol) in dichloromethane (2 ml) was added to a mixture of oxalyl chloride (1 ml, 11 mmol) and dichloromethane (3 ml). After keeping at room temperature overnight, the excess chloride and solvent were removed by evaporation. Then, the reaction vessel was wrapped with aluminium foil tightly, and benzene (3 ml), *N*-hydroxy-2-thiopyridone (2.1 mmol), and pyridine (3 mmol) in benzene (2 ml) were added successively at 0 °C. After stirring at 0 °C for 30 min, the obtained yellow solution was refluxed for one hour. Then the solvent was removed and the residue was washed with water and purified by pTLC. (eluent; $CHCl_3$). The reaction with thiols was carried out by using the same procedure.

4a: Oil; ^{1}H NMR (CCl_4) δ=0.85 (t, 3H, J=6.1 Hz, $-CH_3$), 1.20—1.80 (m, 12H, $-(CH_2)_2-$), 3.10 (t, 2H, J=7.6 Hz, $-CH_2S$), 6.70—7.40 (m, 3H, Py-3, 4, 5H), 8.30 (d, 1H, J=6.1 Hz, Py-6H); IR (NaCl) 2900, 2840, 1575, 1553 cm^{-1}.

Found: C, 69.40; H, 9.41; N, 5.76%. Calcd for $C_{13}H_{21}NS$: C, 69.90; H, 9.48; N, 6.27%.

4d: Oil; ^{1}H NMR (CCl_4) δ=1.19 (t, 3H, J=6.6 Hz, $-CH_3$), 1.58 (d, 3H, J=7.5 Hz, $-CH_3$), 4.06 (q, 2H, J=6.6 Hz, $-CH_2$), 4.55 (q, 1H, J=7.5 Hz, -CH), 6.76—7.14 (m, 2H, Py-4, 5H), 7.25—7.46 (m, 1H, Py-3H), 8.22 (b, 1H, Py-6H); IR (NaCl) 1725, 1580, 1417, 1260, 1165, 1130 cm^{-1}.

Found: C, 56.73; H, 6.17; N, 6.58%. Calcd for $C_{10}H_{13}NO_2S$: C, 56.84; H, 6.20; N, 6.63%.

4g: Oil; ^{1}H NMR (CCl_4) δ=4.56 (s, 2H, $-CH_2$), 6.70—7.36 (m, 8H, aromatic), 8.24 (d, 1H, J=4.5 Hz, Py-6H); IR (NaCl) 1570, 1488, 1410, 1120 cm^{-1}.

Found: C, 61.06; H, 4.30; N, 5.87%. Calcd for $C_{12}H_{10}ClNS$: C, 61.14; H, 4.28; N, 5.94%.

4h: Mp 61—63 °C; ^{1}H NMR (CCl_4) δ=4.37 (s, 2H, $-CH_2$), 6.74—7.04 (m, 2H, Py-4, 5H), 7.20—7.50 (m, 3H, aromatic), 7.90 (d, 2H, J=9.0 Hz, aromatic), 8.24 (d, 1H, J=5.4 Hz, Py-6H); IR (KBr) 1575, 1515, 1415, 1350, 1130 cm^{-1}.

Found: C, 58.66; H, 4.15; N, 11.18%. Calcd for $C_{12}H_{10}N_2O_2S$: C, 58.52; H, 4.09; N, 11.38%.

4i: Oil; ^{1}H NMR (CCl_4) δ=1.68 (d, 3H, J=7.5 Hz, $-CH_3$), 5.06 (q, 1H, J=7.5 Hz, -CH), 6.68—7.52 (m, 8H, aromatic), 8.26 (d, 1H, J=4.1 Hz, Py-6H); IR (NaCl) 1575, 1552, 1412, 1123 cm^{-1}.

Found: C, 72.49; H, 6.11; N, 6.26%. Calcd for $C_{13}H_{13}NS$: C, 72.52; H, 6.09; N, 6.51%.

4j: Oil; ^{1}H NMR (CCl_4) δ=4.38 (s, 2H, $-CH_2$), 4.48 (d, 2H, J=3.6 Hz, OCH_2), 5.24 (m, 2H, $=CH_2$), 5.74—6.08 (m, 1H, -CH=), 6.58—7.38 (m, 7H, aromatic), 8.28 (d, 1H, J=4.6 Hz, Py-6H); IR (NaCl) 1595, 1575, 1552, 1490, 1412, 1250, 1125 cm^{-1}.

Found: C, 69.52; H, 6.00; N, 4.18%. Calcd for $C_{15}H_{15}NOS$: C, 70.01; H, 5.88; N, 5.44%.

5a: Oil; ^{1}H NMR (CCl_4) δ=0.90 (t, 3H, J=6.1 Hz, $-CH_3$), 1.16—1.45 (m, 10H, $-(CH_2)_5-$), 1.45—1.80 (m, 2H, $-CH_2-$), 4.20 (t, 2H, J=6.1 Hz, $-OCH_2-$), 7.10 (t, 1H, J=6.2 Hz, Py-5H), 7.40—7.75 (m, 2H, Py-3, 4H), 8.40 (d, 1H, J=5.5 Hz, Py-6H); IR (NaCl) 2900, 2840, 1720, 1160, 1115 cm^{-1}.

Found: C, 62.68; H, 7.84; N, 5.16%. Calcd for $C_{14}H_{21}NO_2S$: C, 62.89; H, 7.92; N, 5.24%.

5b: Oil; ^{1}H NMR (CCl_4) δ=1.04—2.04 (m, 10H, $-(CH_2)_5-$), 4.72 (b, 1H, -CH), 6.90—7.18 (m, 1H, Py-5H), 7.38—7.77 (m, 2H, Py-3, 4H), 8.38 (d, 1H, J=4.5 Hz, Py-6H); IR (NaCl) 1570, 1560, 1420, 1170, 1112 cm^{-1}.

Found: C, 61.02; H, 6.44; N, 5.84%. Calcd for $C_{12}H_{15}NO_2S$: C, 60.73; H, 6.37; N, 5.90%.

5c: Oil; ^{1}H NMR (CCl_4) δ=1.04—1.74 (m, 11H, $-CH_3$ and cyclohexyl), 1.99—2.30 (m, 2H, cyclohexyl), 6.92—7.10 (m, 1H, Py-5H), 7.34—7.70 (m, 2H, Py-3, 4H), 8.26 (d, 1H, J=4.5 Hz, Py-6H); IR (NaCl) 1720, 1572, 1560, 1422, 1182, 1115 cm^{-1}.

5k: Oil; ^{1}H NMR ($CDCl_3$) δ=1.25 (t, 3H, J=7.6 Hz, $-CH_3$), 4.28 (q, 2H, J=7.6 Hz, $-CH_2-$), 7.10—7.30 (m, 1H, Py-5H), 7.72—7.60 (m, 2H, Py-3, 4H), 7.50 (d, 1H, J=6.1 Hz, Py-6H); IR (NaCl) 1720, 1150, 1115 cm^{-1}.

Found: C, 52.08; H, 5.00; N, 7.52%. Calcd for $C_8H_9NSO_2$: C, 52.44; H, 4.95; N, 7.64%.

19b: Oil; ^{1}H NMR (CCl_4) δ=1.08—2.12 (m, 10H, $-(CH_2)_5-$), 2.60—2.98 (br, 1H, CH), 6.77—7.02 (m, 1H, Py-5H), 7.30—7.70 (m, 2H, Py-3, 4H), 8.22 (d, 1H, J=4.5 Hz, Py-6H); IR (NaCl) 1570, 1560, 1418, 1122 cm^{-1}.

Found: C, 58.57; H, 6.74; N, 6.20%. Calcd for $C_{11}H_{15}NS_2$: C, 58.62; H, 6.71; N, 6.22%.

19e: Oil; ^{1}H NMR (CCl_4) δ=3.92 (s, 2H, $-CH_2$), 6.72—7.34 (m, 8H, Ph, Py-3, 4, 5H), 8.20 (d, 1H, J=4.5 Hz, Py-6H);

IR (NaCl) 1560, 1392, 1412, 1115 cm^{-1}.

19t: Oil; ^1H NMR (CCl_4) δ=2.55—3.06 (m, 4H, $-CH_2CH_2-$), 3.60 (s, 3H, $-CH_3$), 6.76—6.96 (m, 1H, Py-5H), 7.34—7.60 (m, 2H, Py-3, 4H), 8.26 (d, 1H, J=4.5 Hz, Py-6H); IR (NaCl) 1732, 1570, 1560, 1418, 1360, 1250, 1150, 1120 cm^{-1}.

Found: C, 47.00; H, 4.88; N, 6.04%. Calcd for $C_9H_{11}NO_2S_2$: C, 47.13; H, 4.83; N, 6.11%.

19n: Oil; ^1H NMR ($CDCl_3$) δ=0.95 (t, 3H, J=7.6 Hz, $-CH_3$), 1.80—2.10 (m, 2H, $-CH_2-$), 2.20—2.50 (m, 2H, $-CH_2-$), 2.85 (t, 2H, J=7.6 Hz, $-SCH_2-$), 5.35—5.60 (m, 2H, -CH=CH-), 6.90—7.20 (m, 1H, Py-5H), 7.40—7.80 (m, 2H, Py-3, 4H), 8.50 (d, 1H, J=4.5 Hz, Py-6H); IR (NaCl) 1560, 1442, 1416, 1120 cm^{-1}.

Found: C, 59.24; H, 7.09; N, 5.51%. Calcd for $C_{11}H_{15}NS_2$: C, 58.62; H, 6.71; N, 6.22%.

3) Typical Procedure for the C-C Bond Formation. A solution of a chloroglyoxylic ester (**2**) (2 mmol) prepared as described above in benzene (8 ml) was added dropwise to the refluxing solution of sodium salt of *N*-hydroxyl-2-thiopyridone (2.1 mmol) and phenyl vinyl sulfone (10 mmol) in benzene (4 ml) over one hour. After the addition, refluxing was continued for one hour. Then the solvent was removed and the residue was diluted with THF (16 ml) and hydrazine (1.6 g) was added at 0 °C. After the addition, the ice bath was removed and the solution was stirred at room temperature for 10 min. Then the solvent was removed by evaporation and the residue was chromatographed on silica gel (eluent; CH_2Cl_2:Et_2O=9:1).

6b: Mp 78.2—79.5 °C; ^1H NMR (CCl_4) δ=0.64—2.34 (m, 13H, cyclohexyl), 5.53 (dd, 1H, J=12.0, 3.6 Hz, CH), 6.62—6.91 (m, 3H, aromatic), 7.03—7.34 (m, 5H, aromatic), 7.60—7.84 (m, 2H, aromatic), 8.06 (d, 1H, J=4.5 Hz, Py-6H); IR (Nujol) 1575, 1555, 1420, 1380, 1310, 1300, 1155 cm^{-1}.

6e: Mp 85.0—86.0 °C; ^1H NMR (CCl_4) δ=1.78—3.06 (m, 4H, $-CH_2CH_2-$), 5.50 (dd, 1H, J=10.5, 3.6 Hz, CH), 6.58—7.32 (m, 11H, aromatic), 7.58—7.80 (m, 2H, aromatic), 7.84—8.06 (m, 1H, Py-6H); IR (KBr) 1570, 1415, 1305, 1290, 1145, 1125 cm^{-1}.

Found: C, 64.97; H, 5.20; N, 3.80%. Calcd for $C_{20}H_{19}NO_2S_2$: C, 65.01; H, 5.18; N, 3.79%.

6f: Mp 88.2—89.5 °C; ^1H NMR (CCl_4) δ=2.22 (s, 3H, $-CH_3$), 2.34—3.02 (m, 4H, $-CH_2CH_2-$), 5.50 (dd, 1H, J=10.5, 3.0 Hz, CH), 6.58—7.43 (m, 10H, aromatic), 7.36—7.77 (m, 2H, $PhSO_2$-2, 6H), 7.95 (d, 1H, J=4.5 Hz, Py-6H); IR (KBr) 1570, 1560, 1515, 1415, 1305, 1290, 1150, 1120 cm^{-1}.

Found: C, 65.64; H, 5.51; N, 3.60%. Calcd for $C_{21}H_{21}NO_2S_2$: C, 65.75; H, 5.52; N, 3.65%.

6g: Mp 90.7—91.5 °C; ^1H NMR (CCl_4) δ=1.88—3.08 (m, 4H, $-CH_2CH_2-$), 5.42 (dd, 1H, J=10.5, 3.6 Hz, CH), 6.62—7.38 (m, 11H, aromatic), 7.60—7.82 (m, 2H, $PhSO_2$-2, 6H), 7.96 (d, 1H, J=4.5 Hz, Py-6H); IR (NaCl) 1575, 1560, 1495, 1417, 1310, 1155, 1128 cm^{-1}.

Found: C, 59.39; H, 4.55; N, 3.47%. Calcd for $C_{19}H_{18}NO_2S_2Cl$: C, 59.39; H, 4.63; N, 3.57%.

6i: Oil (diastereomeric mixture); ^1H NMR (CCl_4) δ=1.27 (d, 3H, J=6.0 Hz, CH_3), 1.80—2.20 (m, 1H, CH), 2.36—2.77 (m, 1H, CH), 3.03 (bs, 1H, CH), 5.14 (dd, 1/2H, J=12.0, 3.3 Hz, $CHSO_2$), 6.64 (dd, 1/2H, J=10.5, 3.3 Hz, $CHSO_2$), 6.54—7.40 (m, 11H, aromatic), 7.31—7.84 (m, 2H, $PhSO_2$-2, 6H), 7.97 (d, 1H, J=3.6 Hz, Py-6H); IR (NaCl) 1578, 1560, 1500, 1420, 1320, 1310, 1150, 1122 cm^{-1}.

Found: C, 65.66; H, 5.51; N, 3.59%. Calcd for $C_{21}H_{21}NO_2S_2$: C, 65.76; H, 5.52; N, 3.65%.

4) Conversion of Compound 6e to Vinyl Sulfone 10e. To **6e** (0.28 g, 0.77 mmol) in dichloromethane (8 ml) at 0 °C was added *m*-chloroperbenzoic acid (0.21 g, 1.1equiv). Then, ice bath was removed and the reaction mixture was stirred at room temperature for one hour. The reaction mixture was washed with sat. aq $NaHCO_3$ and water. The organic layer was dried over Na_2SO_4, filtered, and the solvent was removed. 1 M-HCl (10 ml 1 M=1 mol dm^{-3}) was added to the residue and the mixture was heated at 100 °C for 2 h. The organic components were extracted with ethyl acetate, and dried over Na_2SO_4. After the purification by pTLC. (eluent; $CHCl_3$:AcOEt=40:1), 0.14 g of **10e** was obtained (69% yield).

10e: Mp 107—109 °C (Et_2O/hexane); ^1H NMR (CCl_4, $CDCl_3$) δ=7.84—6.82 (m, 11H, aromatic and -CH=), 6.11 (d, 1H, J=13.5 Hz, -CH=), 3.40 (d, 2H, J=6.0 Hz, $-CH_2-$); IR (KBr) 1310, 1150 cm^{-1}.

Found: C, 69.55; H, 5.51%. Calcd for $C_{15}H_{14}O_2S$: C, 69.74; H, 5.46%.

5) Conversion of 6e to Dihydrocinnamic Acid 11e. To **6e** (0.28 g, 0.76 mmol) in dichloromethane (6 ml) was added mCPBA (0.56 g, 3 equiv) under cooling by ice bath. Then, the reaction mixture was stirred at room temperature for 5 h. The reaction mixture was poured into ether, wased with sat. aq $NaHCO_3$, and dried over Na_2SO_4 to give disulfone as a crude state. The formed disulfone was dissolved in methanol containing K_2CO_3 (8 mmol). Hydrogen peroxide (30%) was added dropwise to the solution under refluxing conditions for 3 h. After the reaction was completed, the solvent was removed and the residue was acidified with concd. HCl and then extracted with ether to give dihydrocinnamic acid in 74% yield which was identified with authentic commercial compound.

6) General Procedure for the Preparation of γ-Lactones 12. Dichloromethane solution containing olefinic alcohol (2 mmol) were added to a stirred oxalyl chloride (0.8—1.5 ml) at room temperature and the mixture was stirred overnight. After the evaporation of solvent and excess oxalyl chloride, *N*-hydroxy-2-thiopyridone (2.1 mmol) and 4 ml of dry benzene solution of pyridine (3 mmol) were added to the mixture and the resulting solution was stirred at 0 °C for 30 min under nitrogen atmosphere. Then the reaction mixture was refluxed for 60 min. After the removal of solvent, compounds (**5** and **12**) were separated by column chromatography on silica gel.

12m: Oil; ^1H NMR ($CDCl_3$, 500 MHz) δ=2.10—2.18 (m, 1H, $-CH_2-$), 2.38—2.45 (m, 1H, $-CH_2-$), 3.05 (dtd, 1H, J=10.5, 8.4, 4.5 Hz, -CHCO-), 3.25 (dd, 1H, J=14.0, 8.4 Hz, $-SCH_2-$), 3.84 (dd, 1H, J=14.0, 4.5 Hz, $-SCH_2-$), 4.16 (td, 1H, J=8.8, 6.6 Hz, $-OCH_2-$), 4.34 (td, 1H, J=8.8, 2.5 Hz, $-OCH_2-$), 6.98 (ddd, 1H, J=7.9, 5.0, 1.0 Hz, Py-5H), 7.17 (dt, 1H, J=7.9, 10 Hz, Py-3H), 7.47 (td, 1H, J=7.9, 2.0 Hz, Py-4H), 8.40 (m, 1H, Py-6H); IR (NaCl) 1765, 1150, 1025 cm^{-1}.

Found: C, 57.22; H, 5.34; N, 6.64%. Calcd for $C_{10}H_{11}NSO_2$: C, 57.39; H, 5.30; N, 6.69%.

5m: Oil; ^1H NMR ($CDCl_3$) δ=2.40 (t, 2H, J=7.6 Hz, $-CH_2-$), 4.23 (t, 2H, J=7.6 Hz, $-OCH_2-$), 4.90—5.20 (m, 2H, $=CH_2$), 5.45—6.00 (m, 1H, =CH-), 7.10—7.20 (m, 1H, Py-5H), 7.55—7.70 (m, 2H, Py-3, 4H), 8.50 (d, 1H, J=6.1 Hz, Py-6H); IR (NaCl) 1720, 1150, 1110 cm^{-1}.

Found: C, 57.72; H, 5.43; N, 6.55%. Calcd for $C_{10}H_{11}NSO_2$:

C, 57.39; H, 5.30; N, 6.69%.

Next, the obtained lactone (**12m**) was oxidized with mCPBA (1.1 equiv) and the sulfoxide thus formed was heated at about 100 °C under reduced pressure to give in 49% yield α-methylene-γ-butyrolactone, which was identified with commercial compound.

13: Oil; ^{1}H NMR ($CDCl_3$, 500 MHz) δ=8.37—8.40 (m, 1H, Py-6H), 7.48—7.51 (m, 1H, Py-3, 4H), 7.19—7.21 (m, 1H, Py-3, 4H), 6.99—7.02 (m, 1H, Py-5H), 4.32—4.38 (m, 1H, $-OCH_2$), 4.14—4.24 (m, 3H, $-OCH_2$), 2.55—2.63 (m, 1H, CHCO), 2.41—2.45 (m, 1H, CHCO), 1.93—2.18 (m, 4H, $-CH_2-$), 1.58—1.69 (m, 2H, $-CH_2-$), 1.22—1.29 (m, 3H, $-CH_3$); IR (NaCl) 1760, 1725, 1245, 1180, 1150, 1025 cm^{-1}.

Found: C, 58.25; H, 6.31; N, 4.26%. Calcd for $C_{15}H_{19}NSO_4$: C, 58.23; H, 6.19; N, 4.53%.

12r: Mp 111—112 °C (AcOEt/Hexane); cis; ^{1}H NMR ($CDCl_3$) δ=2.88 (td, 2H, *J*=7.5, 3.0 Hz, $-CH_2C=$), 4.40 (t, 2H, *J*=7.5 Hz, $-OCH_2-$), 7.00—7.30 (m, 2H, Py), 7.40—7.60 (m, 1H, Py), 8.40—8.55 (m, 2H, Py-6H); IR (NaCl) 1725, 1185 cm^{-1}.

Found: C, 57.98; H, 4.39; N, 6.73%. Calcd for $C_{10}H_9NSO_2$: C, 57.95; H, 4.38; N, 6.76%.

5q: Oil; ^{1}H NMR ($CDCl_3$) δ=1.75 (q, 2H, *J*=6.4 Hz, $-CH_2-$), 2.00—2.25 (m, 2H, $-CH_2-$), 4.20 (t, 2H, *J*=6.8 Hz, $-OCH_2-$), 4.85—5.10 (m, 2H, $CH_2=$), 5.50—6.00 (m, 1H, =CH–), 7.10—7.30 (m, 1H, Py-5H), 7.60—7.70 (m, 2H, Py-3, 4H), 8.50 (d, 1H, *J*=6.1 Hz, Py-6H); IR (NaCl) 1710, 1150, 1110 cm^{-1}.

Found: C, 60.67; H, 6.35; N, 5.87%. Calcd for $C_{11}H_{13}NSO_2$: C, 60.73; H, 6.37; N, 5.90%.

12q: Oil; ^{1}H NMR ($CDCl_3$, 500 MHz) δ=1.64—1.72 (m, 1H, $-CH_2-$), 1.86—1.98 (m, 2H, $-CH_2-$), 2.28—2.35 (m, 1H, $-CH_2-$), 2.91—2.97 (m, 1H, –CH–), 3.33 (dd, 1H, *J*=14.0, 7.40 Hz, $-CH_2-S-$), 3.81 (dd, 1H, *J*=14.0, 5.0 Hz, $-CH_2-S-$), 4.30 (t, 2H, *J*=5.9 Hz, $-OCH_2-$), 6.98 (ddd, 1H, *J*=7.1, 5.0, 1.0 Hz, Py-5H), 7.19 (dt, 1H, *J*=8.3, 1.1 Hz, Py-3H), 7.47 (ddd, 1H, *J*=8.3, 7.1, 1.9 Hz, Py-4H), 8.41 (ddd, 1H, *J*=5.0, 1.9, 1.1 Hz,, Py-6H); IR (NaCl) 1730, 1150, 1130 cm^{-1}.

Found: C, 59.23; H, 5.96; N, 6.13%. Calcd for $C_{11}H_{13}NSO_2$: C, 59.17; H, 5.87; N, 6.27%.

12n: Oil; (mixture of two diastereomers); ^{1}H NMR ($CDCl_3$, 500 MHz) Less polar (minor amount) δ=1.10 (t, 3H, *J*=7.4 Hz, $-CH_3$), 1.74—1.84 (m, 2H, $-CH_2-$), 2.22—2.30 (m, 1H, $-CH_2-$), 2.33—2.39 (m, 1H, $-CH_2-$), 3.30 (ddd, 1H, *J*=10.7, 9.3, 3.3 Hz, –CHCO–), 4.17 (td, 1H, *J*=9.3, 7.1 Hz, CH–S–), 4.36—4.31 (m, 2H, $-O-CH_2-$), 6.99 (ddd, 1H, *J*=7.7, 5.0, 0.8 Hz, Py-5H), 7.19 (dt, 1H, *J*=7.7, 0.8 Hz, Py-3H), 7.48 (td, 1H, *J*=7.7, 1.9 Hz, Py-4H), 8.41 (ddd, 1H, *J*=5.0, 1.9, 0.8 Hz, Py-6H); Polar (major amount) δ=1.08 (t, 3H, *J*=7.1 Hz, $-CH_3$), 1.82—1.97 (m, 2H, $-CH_2-$), 2.25—2.33 (m, 1H, $-CH_2-$), 2.45—2.38 (m, 1H, $-CH_2-$), 3.03 (td, 1H, *J*=9.0, 5.2 Hz, –CHCO–), 4.21 (td, 1H, *J*=9.0, 7.4 Hz, –CH–S–), 4.38—4.44 (m, 2H, $-O-CH_2-$), 6.98 (ddd, 1H, *J*=7.7, 5.0, 0.8 Hz, Py-5H), 7.20 (dt, 1H, *J*=7.7, 0.8 Hz, Py-3H), 7.46 (td, 1H, *J*=7.7, 1.9 Hz, Py-4H), 8.42 (ddd, 1H, *J*=5.0, 1.9, 0.8 Hz, Py-6H); IR (NaCl) 1760, 1160, 1122, 1022 cm^{-1}.

Found: C, 59.15; H, 5.92; N, 6.21%. Calcd for $C_{12}H_{15}NSO_2$: C, 59.17; H, 5.87; N, 6.27%.

The assignment of two diastereomers (29:71) was carried out by the NMR measurement of α-propylidene-γ-lactones [32(cis):68(trans)] which were obtained by the treatment of **12n** with mCPBA (1.1 equiv) followed by heating at 70 °C for 50 min.

12o: Oil; [mixture of two diastereomers: A and B (34:66)] ^{1}H NMR ($CDCl_3$, 500 MHz)

A 1.36 (d, 3H, *J*=6.68 Hz, $-CH_3$),
B 1.41 (d, 3H, *J*=6.1 Hz, $-CH_3$),
B 1.70 (td, 1H, *J*=12.1, 10.4 Hz, $-CH_2-$),
A 2.06 (ddd, 1H, *J*=13.2, 9.1, 4.1 Hz, $-CH_2-$),
A 2.32 (dt, 1H, *J*=13.2, 8.0 Hz, $-CH_2-$),
B 2.54 (ddd, 1H, *J*=12.1, 8.2, 5.5 Hz, $-CH_2-$),
A,B 3.12—3.20 (m, 1H, –CHCO–),
B 3.23 (dd, 1H, *J*=13.7, 8.5 Hz, $-CH_2S-$),
A 3.31 (dd, 1H, *J*=13.7, 8.7 Hz, $-CH_2S-$),
A 3.80 (dd, 1H, *J*=13.7, 4.7 Hz, $-CH_2S-$),
B 3.87 (dd, 1H, *J*=13.7, 4.4 Hz, $-CH_2S-$),
B 4.45—4.51 (m, 1H, –O–CH–),
A 4.70—4.74 (m, 1H, O–CH–),
A,B 6.98—7.01 (m, 1H, Py-5H),
A,B 7.18—7.20 (m, 1H, Py-3H),
A,B 7.47—7.50 (m, 1H, Py-4H),
A,B 8.41—8.43 (m, 1H, Py-6H),
IR (NaCl) 1760, 1185, 1125 cm^{-1}.

Found: C, 58.88; H, 5.89; N, 6.18%. Calcd for $C_{11}H_{13}NSO_2$: C, 59.17; H, 5.87; N, 6.27%.

12t: Oil; [mixture of two diastereomers: A and B (34:66)] ^{1}H NMR ($CDCl_3$, 270 MHz)

A,B 1.40—1.80 [m, 14H, $-(CH_2)_7-$],
A,B 1.95—2.55 (m, 4H, $2-CH_2-$),
A,B 3.05—3.35 (m, 2H, –SCH–CHCO–),
A 3.80 (dd, 1H, *J*=13.8, 4.9 Hz, –SCH–),
A 3.85 (dd, 1H, *J*=13.0, 4.1 Hz, –SCH–),
B 4.34 (dtd, 1H, *J*=10.8, 7.3, 5.4 Hz, –OCH–),
A 4.54 (tt, 1H, *J*=7.8, 5.4 Hz, –OCH–),
A,B 4.90—5.04 (m, 2H, $CH_2=$),
A,B 5.72—5.90 (m, 1H, –CH=),
A,B 6.98—7.04 (m, 1H, Py-5H),
A,B 7.20 (d, 1H, *J*=8.1 Hz, Py-3H),
A,B 7.44—7.55 (m, 1H, Py-4H),
A,B 8.41 (d, 1H, *J*=4.6 Hz, Py-6H);
IR (NaCl) 1760, 1175 cm^{-1}.

Found: C, 68.89; H, 8.69; N, 4.13%.Calcd for $C_{20}H_{29}NSO_2$: C, 69.12; H, 8.41; N, 4.03%.

5n: Oil; ^{1}H NMR ($CDCl_3$, 500 MHz)

Trans isomer δ=0.97 (t, 3H, *J*=7.4 Hz, $-CH_3$), 1.99—2.04 (m, 2H, $-CH_2-$), 2.35—2.40 (m, 2H, $-CH_2-$), 4.27 (t, 2H, *J*=6.8 Hz, $-OCH_2-$), 5.38—5.32 (m, 1H, –CH=), 5.55—5.60 (m, 1H, –CH=), 7.29—7.26 (m, 1H, Py-5H), 7.75—7.70 (m, 2H, Py-3, 4H), 8.60—8.59 (m, 1H, Py-6H);

Cis isomer δ=0.98 (t, 3H, *J*=7.5 Hz, $-CH_3$), 2.01—2.09 (m, 2H, $-CH_2-$), 2.42—2.47 (m, 2H, $-CH_2-$), 4.26 (t, 2H, *J*=7.0 Hz, $-OCH_2-$), 5.32—5.29 (m, 1H, –CH=), 5.51—5.55 (m, 1H, –CH=), 7.26—7.29 (m, 1H, Py-5H), 7.70—7.75 (m, 2H, Py-3, 4H), 8.60—8.59 (m, 1H, Py-6H); IR (NaCl) 1720, 1150, 1115 cm^{-1}.

Found: C, 60.26; H, 6.35; N, 5.77%. Calcd for $C_{12}H_{15}NSO_2$: C, 60.73; H, 6.37; N, 5.90%.

12p: Oil; ^{1}H NMR ($CDCl_3$) δ=0.90 (t, 6H, *J*=7.6 Hz, $-CH_3\times2$), 1.65 (q, 4H, *J*=7.6 Hz, $-CH_2-\times2$), 1.80—2.40 (m, 2H, $-CH_2-$), 3.00—3.40 (m, 2H, $-CH_2S-$, –CHCO–), 3.70—4.00 (m, 1H, $-CH_2S-$), 6.80—7.00 (m, 1H, Py-5H), 7.00—7.20 (m, 1H, Py-3H), 7.30—7.50 (m, 1H, Py-4H), 8.35 (d, 1H, *J*=6.1 Hz, Py-6H); IR (NaCl) 1760, 1125, 1220 cm^{-1}.

Found: C, 63.18; H, 7.21; N, 5.17%. Calcd for $C_{14}H_{19}NSO_2$:

C, 63.36; H, 7.22; N, 5.28%.

12s: Oil; ^{1}H NMR ($CDCl_3$) δ=2.80—3.40 (m, 4H, $-CH_2-\times2$), 3.60—4.05 (m, 1H, -CH-), 6.70—7.45 (m, 7H, Py-3, 4, 5H, aromatic), 8.30 (d, 1H, J=6.1 Hz, Py-6H); IR (NaCl) 1760, 1575, 1125 cm^{-1}.

Found: C, 66.93; H, 4.98; N, 4.82%. Calcd for $C_{15}H_{13}NSO_2$: C, 66.40; H, 4.83; N, 5.16%.

4l: Oil; ^{1}H NMR ($CDCl_3$) δ=2.25 (s, 3H, $-CH_3$), 2.85—2.65 (m, 3H, $-CH_2-$), 4.90—5.05 (m, 2H, $CH_2=$), 5.50—5.90 (m, 1H, -CH=), 6.80—7.40 (m, 3H, Py-3, 4, 5H), 7.00 (d, 2H, J=7.6 Hz, aromatic), 7.22 (d, 2H, J=7.6 Hz, aromatic), 8.35 (d, 1H, J=6.1 Hz, Py-6H); IR (NaCl) 1570, 1410, 1125 cm^{-1}.

Found: C, 75.22; H, 6.78; N, 5.39%. Calcd for $C_{16}H_{17}NS$: C, 75.25; H, 6.71; N, 5.49%.

7ki: Mp 90—91 °C; ^{1}H NMR ($CDCl_3$) δ=1.17 (t, 3H, J=7.1 Hz, $-CH_3$), 2.85 (dd, 1H, J=16.7, 10.6 Hz, $-CH_2-$), 3.45 (dd, 1H, J=16.7, 4.5 Hz, $-CH_2-$), 4.12 (q, 2H, J=7.1 Hz, $-O-CH_2-$), 6.24 (dd, 1H, J=10.6, 4.5 Hz, $-CH-SO_2-$), 6.80—7.00 (m, 2H, Py), 7.25—7.50 (m, 4H, $PhSO_2$-3, 4, 5H and Py), 7.94 (dd, 2H, J=9.1, 3.0 Hz, $PhSO_2$-2, 6H), 8.22 (d, 1H, J=5.1 Hz, Py-6H); IR (Nujol) 1740, 1455, 1314, 1222, 1150 cm^{-1}.

Found: C, 54.73; H, 4.89; N, 3.94%. Calcd for $C_{16}H_{17}NS_2O_4$: C, 54.68; H, 4.88; N, 3.99%.

17ki: Oil; ^{1}H NMR ($CDCl_3$) δ=1.30 (t, 3H, J=7.6 Hz, $-CH_3$), 4.26 (q, 2H, J=7.6 Hz, $-CH_2-$), 6.82 (d, 1H, J=13.9 Hz, -CH=), 7.36 (d, 1H, J=13.9 Hz, -CH=), 7.50—7.70 (m, 3H, $PhSO_2$-3, 4, 5H), 7.90—8.00 (dd, 2H, J=9.1, 3.0 Hz, $PhSO_2$-2, 6H); IR (NaCl) 1712, 1295, 1145 cm^{-1}.

Found: C, 55.15; H, 5.01%. Calcd for $C_{11}H_{12}SO_4$: C, 54.99; H, 5.03%.

15a: Oil; ^{1}H NMR ($CDCl_3$) δ=1.20 (t, 6H, J=7.6 Hz, $-CH_3\times2$), 3.35 (q, 4H, J=7.6 Hz, $-CH_2-\times2$), 6.90—7.10 (m, 1H, Py-5H), 7.35—7.65 (m, 2H, Py-3, 4H), 8.35 (d, 1H, J=5.1 Hz, Py-6H); IR (NaCl) 1650, 1400, 1250, 1112 cm^{-1}.

Found: C, 56.90; H, 6.71; N, 13.19%. Calcd for $C_{10}H_{14}N_2SO$: C, 57.12; H, 6.91; N, 13.32%.

15b: Mp 80—82 °C; ^{1}H NMR ($CDCl_3$) δ=3.50 (s, 3H, $-CH_3$), 7.10—7.20 (m, 1H, Py-5H), 7.30 (s, 5H, Ph), 7.50—7.70 (m, 2H, Py-3, 4H), 8.45 (d, 1H, J=5.1 Hz, Py-6H); IR (KBr) 1660, 1340, 1268, 1108 cm^{-1}.

Found: C, 63.74; H, 4.94; N, 11.45%. Calcd for $C_{13}H_{12}N_2SO$: C, 63.91; H, 4.95; N, 11.47%.

15c: Mp 54—56 °C; ^{1}H NMR ($CDCl_3$) δ=2.30 (q, 2H, J=7.9 Hz, $-CH_2-$), 3.85 (t, 2H, J=7.9 Hz, $-NCH_2-$), 4.90—5.10 (m, 2H, $CH_2=$), 5.40—5.90 (m, 1H, -CH=), 7.00—7.20 (m, 1H, Py-5H), 7.30 (s, 5H, Ph), 7.50—7.60 (m, 2H, Py-3, 4H), 8.40 (d, 1H, J=5.1 Hz, Py-6H); IR (KBr) 1660, 1360, 1250, 1115 cm^{-1}.

Found: C, 67.57; H, 5.72; N, 9.89%. Calcd for $C_{16}H_{16}N_2S_2O$: C, 67.58; H, 5.69; N, 9.85%.

16c: Mp 63—65 °C; ^{1}H NMR ($CDCl_3$, 500 MHz) δ=2.01 (m, 1H, β-H), 2.35 (m, 1H, β-H), 3.07 (ddd, 1H, J=17.5, 9.4, 3.8 Hz, α-H), 3.34 (dd, 1H, J=13.1, 9.4 Hz, $-CH_2S-$), 3.76 (dd, 1H, J=9.4, 2.2 Hz, γ-H), 3.77 (d, 1H, J=9.4 Hz, γ-H), 3.88 (dd, 1H, J=13.1, 3.8 Hz, $-CH_2S-$), 6.96 (dd, 1H, J=7.8, 5.0 Hz, Py-4H), 7.12 (t, 1H, J=7.8 Hz, Ph-4H), 7.19 (dd, 1H, J=7.8, 0.8 Hz, Py-3H), 7.34 (t, 2H, J=7.8 Hz, Ph-3, 5H), 7.46 (td, 1H, J=7.8, 2.5 Hz, Py-4H), 7.62 (d, 2H, J=7.8 Hz, Ph-2, 6H), 8.40 (ddd, 1H, J=5.0, 2.5, 0.8 Hz, Py-6H); IR (KBr) 1678, 1400 cm^{-1}.

Found: C, 67.35; H, 5.67; N, 9.79%. Calcd for $C_{16}H_{16}N_2S_2O$: C, 67.58; H, 5.67; N, 9.85%.

8l: Oil; ^{1}H NMR ($CDCl_3$, mixture of two diastereomers) δ=2.25 (s, 6H, $-CH_3\times2$), 2.30 (s, 6H, $-CH_3\times2$), 2.00—3.00 (m, 12H, $-CH_2CH-\times4$), 4.50—5.00 (m, 8H, $CH_2=\times4$), 4.10—4.70 (m, 4H, $-CH=\times4$), 6.65 (d, 4H, J=9.1 Hz, aromatic), 6.90 (4H, J=9.1 Hz, aromatic), 6.90—7.30 (m, 8H, aromatic); IR (NaCl) 1635, 1510, 920, 825 cm^{-1}.

Found: C, 90.90; H, 9.08%. Calcd for $C_{22}H_{26}$: C, 90.98; H, 9.02%.

7a: Melt at room temperature (25 °C); ^{1}H NMR ($CDCl_3$) δ=0.60 (m, 3H, $-CH_3$), 1.20—1.90 (bs, 12H, $-(CH_2)_6-$), 2.90 (dd, 1H, J=16.4, 10.6 Hz, $-CH_2CO-$), 3.42 (dd, 1H, J=16.4, 5.2 Hz, $-CH_2CO-$), 4.04 (t, 2H, J=12.1, $-OCH_2-$), 6.15 (dd, 1H, J=10.6, 5.2 Hz, -CH-), 6.80—7.10 (m, 1H, Py-5H), 7.20—7.60 (m, 5H, Ph-3, 4, 5H, Py-3, 4H), 7.90 (d, 2H, J=6.1 Hz, Ph-2, 6H), 8.20 (d, 1H, J=5.1 Hz, Py-6H); IR (NaCl) 1740, 1320, 1153, 1087 cm^{-1}.

Found: C, 60.91; H, 6.77; N, 3.17%. Calcd for $C_{22}H_{29}NS_2O_4$: C, 60.66; H, 6.71; N, 3.22%.

7b: Mp 102.5—103.5 °C; ^{1}H NMR (CCl_4) δ=1.03—2.02 (m, 10H, $-(CH_2)_5-$), 2.73 (dd, 1H, J=19.4, 10.5 Hz, CH_2CO), 3.31 (dd, 1H, J=19.4, 4.5 Hz, CH_2CO), 2.62 (br, 1H, CH-O-), 5.93 (dd, 1H, J=10.5, 4.5 Hz, $-SO_2CH-$), 6.66—7.43 (m, 6H, aromatic), 7.62—7.90 (m, 2H, aromatic), 8.04 (d, 1H, J=4.5 Hz, Py-6H); IR (KBr), 1740, 1710, 1570, 1412, 1375, 1310, 1150, 1120 cm^{-1}.

Found: C, 59.38; H, 5.71; N, 3.39%. Calcd for $C_{20}H_{23}NO_2S_2$: C, 59.23; H, 5.72; N, 3.45%.

17a: Mp 38—39 °C; ^{1}H NMR ($CDCl_3$) δ=0.90 (m, 3H, $-CH_3$), 1.30 (br s, 10H, $-(CH_2)_5-$), 1.50—1.80 (m, 2H, $-CH_2-$), 4.16 (t, 2H, J=6.4 Hz, $-OCH_2-$), 6.80 (d, 1H, J=15.2 Hz, -CH=), 7.30 (d, 1H, J=15.2 Hz, -CH=), 7.45—7.65 (m, 3H, Ph-3, 4, 5H), 7.87 (d, 2H, J=7.6 Hz, Ph-2, 6H); IR (NaCl) 1714, 1460, 1300, 1150 cm^{-1}.

Found: C, 63.41; H, 7.51%. Calcd for $C_{17}H_{24}SO_4$: C, 62.93; H, 7.46%.

17b: Oil; ^{1}H NMR ($CDCl_3$) δ=1.08—2.18 (m, 10H, $-(CH_2)_5-$), 4.80 (br s, 1H, CHO), 6.70 (d, 1H, J=15.0 Hz, CH=), 7.22 (d, 1H, J=15 Hz, CH=), 7.36—7.72 (m, 3H, Ph-3, 4, 5H), 7.86 (d, 2H, J=7.8 Hz, Ph-2, 6H); IR (NaCl) 1715, 1320, 1290, 1225, 1145, 965 cm^{-1}.

Found: C, 61.39; H, 6.16%. Calcd for $C_{15}H_{18}O_4S$: C, 61.20; H, 6.16%.

7kii: Oil; ^{1}H NMR ($CDCl_3$) δ=1.20 (t, 3H, J=7.6 Hz, $-CH_3$), 1.22 (t, 3H, J=7.6 Hz, $-CH_3$), 2.90—3.10 (m, 2H, $-CH_2-$), 4.10 (q, 2H, J=7.6 Hz, $-OCH_2-$), 4.13 (q, 2H, J=7.6 Hz, OCH_2-), 4.86 (dd, 1H, J=7.9, 6.1 Hz, -CH-), 6.90—7.00 (m, 1H, Py-5H), 7.00—7.20 (m, 1H, Py-3H), 7.30—7.50 (m, 1H, Py-4H), 8.28 (d, 1H, J=5.1 Hz, Py-6H); IR (NaCl) 1730, 1575, 1150—1260 (broad), 1030 cm^{-1}.

Found: C, 55.26; H, 6.16; N, 4.79%. Calcd for $C_{13}H_{17}NSO_4$: C, 55.11; H, 6.05; N, 4.94%.

7kiv: Oil; ^{1}H NMR ($CDCl_3$) δ=0.85 (m, 3H, $-CH_3$), 2.24 (m, 21H, $-(CH_2)_9-$, $-CH_3$), 1.50—2.00 (m, 2H, $-CH_2CO-$), 2.70 (m, 1H, PySCH-), 4.06 (q, 2H, J=6.7 Hz, $-OCH_2-$), 6.80—7.40 (m, 3H, Py-3, 4, 5H), 8.30 (d, 1H, J=5.1 Hz, Py-6H); IR (NaCl) 2910, 1740, 1580, 1170 cm^{-1}.

Found: C, 68.33; H, 9.45; N, 3.89%. Calcd for $C_{20}H_{33}NSO_2$: C, 68.33; H, 9.46; N, 3.98%.

7kvi: Oil; ^{1}H NMR ($CDCl_3$) δ= 1.02 (t, 3H, J=6.4 Hz, $-CH_3$), 3.90 (q, 2H, J=6.4 Hz, $-OCH_2-$), 6.00 (s, 1H, -CH=), 6.90—7.56 (m, 8H, Ph, Py-3, 4, 5H), 8.40 (d, 1H, J=5.1 Hz,

Py-6H); IR (NaCl) 1692, 1266, 1194, 1152, 1030 cm^{-1}.

Found: C, 67.33; H, 5.38; N, 4.82%. Calcd for $C_{16}H_{15}NSO_2$: C, 67.34; H, 5.30; N, 4.91%.

References

1) B. Giese, "Tetrahedron Symposia-In-Print," *Tetrahedron*, **41**, 3887 (1985); M. Ramiah, *ibid.*, **43**, 3541 (1987); B. Giese, "Radical in Organic Synthesis; Formation of Carbon–Carbon Bonds," Pergamon Press, Oxford (1986); D. P. Curran, *Synthesis*, **1988**, 417, 489.

2) D. H. R. Barton, D. Crich, and W. B. Motherwell, *J. Chem. Soc., Chem. Commun.*, **1983**, 939; *idem., Tetrahedron*, **41**, 3901 (1985); D. H. R. Barton and S. Z. Zard, *Pure Appl. Chem.*, **58**, 675 (1986); H. Togo, M. Fujii, and M. Yokoyama, *Yuki Gosei Kagaku Kyokai Shi*, **48**, 641 (1990).

3) D. H. R. Barton, H. Togo, and S. Z. Zard, *Tetrahedron*, **23**, 5507 (1985); *idem., Tetrahedron Lett.*, **26**, 6349 (1985); D. H. R. Barton, B. Garcia, H. Togo, and S. Z. Zard, *ibid.*, **27**, 1327 (1986).

4) D. H. R. Barton and D. Crich, *J. Chem. Soc., Chem. Commun.*, **1984**, 774; D. H. R. Barton and D. Crich, *Tetrahedron Lett.*, **26**, 757 (1985); D. Crich and S. M. Fortt, *Synthesis*, **1987**, 35.

5) T. L. Cottrell, "The Strength of Chemical Bonds," Academic Press, New York (1954).

6) A. L. J. Beckwith and C. H. Schiesser, *Tetrahedron*, **41**, 3925 (1985); A. L. J. Beckwith, C. J. Easton, T. Lawrence, and A. K. Serelis, *Aust. J. Chem.*, **36**, 545 (1983).

7) Preliminary report; H. Togo and M. Yokoyama, *Heterocycles*, **31**, 437 (1990).

8) Y. Asakawa and T. Takemoto, *Heterocycles*, **8**, 563 (1977); Y. S. Rao, *Chem. Rev.*, **76**, 625 (1976); H. Wamhoff and F. Korte, *Synthesis*, **1972**, 151; P. A. Grieco, *ibid.*, **1975**, 67.

9) M. D. Bachi and E. Bosch, *Tetrahedron Lett.*, **27**, 641 (1986); **29**, 2581 (1988); M. Yamamoto, T. Uruma, S. Iwasa, S. Kohmoto, and K. Yamada, *J. Chem. Soc., Chem. Commun.*, **1989**, 1265.

10) K. Nozaki, K. Ohsima, and K. Utimoto, *Tetrahedron Lett.*, **29**, 6127 (1988).

11) R. Tschesche, F. -J. Kammerer, and G. Wulff, *Chem. Ber.*, **102**, 2057 (1969); U. W. Brongersma-Oosterhoff, *Recl. Trav. Chim. Pays-Bas*, **86**, 705 (1967).

12) A. L. J. Beckwith and C. H. Schiesser, *Tetrahedron*, **41**, 3925 (1985); C. Chatgilialoglu, K. U. Ingold, and J. C. Sciano, *J. Am. Chem. Soc.*, **103**, 7739 (1981); A. L. J. Beckwith and G. Moad, *J. Chem. Soc., Chem. Commun.*, **1974**, 472.

13) S. Goldstein, G. Czapski, H. Cohen, and D. Meyerstein, *J. Am. Chem. Soc.*, **110**, 3903 (1988).

Sulfur Nitride in Organic Chemistry. Part 19.[1] Selective Formation of Benzo- and Benzobis[1,2,5]thiadiazole Skeleton in the Reaction of Tetrasulfur Tetranitride with Naphthalenols and Related Compounds

Shuntaro MATAKA,* Kazufumi TAKAHASHI,† Youji IKEZAKI,†† Taizo HATTA,††
Akiyoshi TORI-I,† and Masashi TASHIRO
Institute of Advanced Material Study, 86, Kyushu University,
6-1 Kasuga-koh-en, Kasuga-shi, Fukuoka 816
† Kurume College of Technology, 1232, Komorino,
Kurume-shi, Fukuoka 830
†† Department of Molecular Science and Technology, Graduate
School of Engineering Sciences, 39, Kyushu University,
6-1 Kasuga-koh-en, Kasuga-shi, Fukuoka 816
(Received July 21, 1990)

Tetrasulfur tetranitride (N_4S_4) reacted with 2-naphthols to afford naphtho [1,2-*c*][1,2,5] thiadiazoles (**13**) in high yields, while 1-naphthaols gave naphtho[1,2-*c*:3,4-*c'*]bis[1,2,5]thiadiazoles as a major product, together with a small amount of **13**. In the reactions with naphthalenediols such as 1,5-, 2,6-, 2,7-, 1,6-, and 1,7-diol, naphtho[1,2-*c*:5,6-*c'*]- or naphtho[1,2-*c*:7,8-*c'*]bis[1,2,5]thiadiazoles were obtained in varying yields. In some cases, naphtho[1,2-*c*:3,4-*c'*:5,6-*c''*]tris[1,2,5]thiadiazole was formed as a by-product. In reactions with 5-isoquinolinol, 8-quinolinoles, 9*H*-carbazol-2-ol, and dibenzofuran-2-ol, one and/or two 1,2,5-thiadiazole-ring-fused heteroaromatic compounds were obtained.

Recently, it was reported that the reaction of tetrasulfur tetranitride (N_4S_4) (**1**) with phenols and polyhydroxybenzenes afforded benzo-,[2] benzobis-,[1] and benzotris[1,2,5]thiadiazoles.[1] These 1,2,5-thiadiazoles were converted to polyaminobenzenes[1,2] such as benzenediamine, -tetramine, and -hexamine.

It was already reported that the reaction of **1** with benzyl ketone derivatives afforded 4-substituted 3-aryl-1,2,5-thiadiazoles in good yields.[3–5]

As an extention of the above, we investigated the reaction of **1** with naphthalenols from the following viewpoints; in a reaction with 2-naphthol, **1** was expected to attack the benzylic position of tautomer **A**, giving naphtho[1,2-*c*][1,2,5]thiadiazole, while both naphtho[1,2-*c*][1,2,5]thiadiazole and naphtho[1,2-*c*:3,4-*c'*]bis[1,2,5]thiadiazole might be formed in a reaction with 1-naphthol by an attack of **1** on the two tautomers, **B** and **C** (Scheme 1).

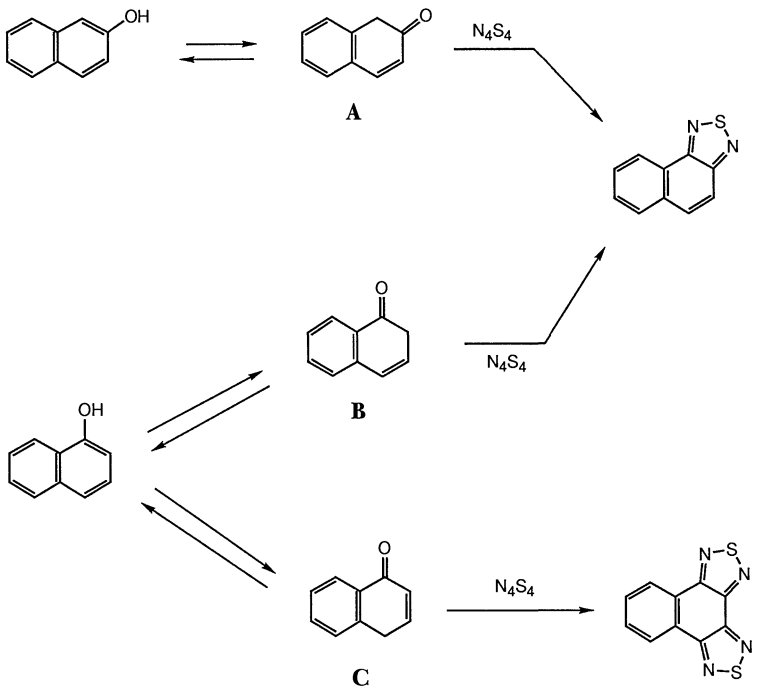

Scheme 1.

The present paper describes the reactions of **1** with naphthalenols and some related hydroxy-substituted benzoheterocycles.

Results and Discussion

All reactions of **1** with naphthalenols and hydroxy-substituted benzoheterocycles were carried out in refluxing toluene for 48 h; the results are summarized in Table 1 and Scheme 2.

The reaction of **1** with 1-naphthol (**2a**) afforded naphtho[1,2-*c*][1,2,5]thiadiazole (**13a**) and naphtho-[1,2-*c*:3,4-*c'*]bis[1,2,5]thiadiazole (**14a**) in 9 and 14% yield, respectively. Compound **14a** was obtained from halogenated 1-naphthols, such as 2,4-dichloro-1-naphthol (**2b**) and 2,4-dibromo derivative (**2c**), in better yields than **2a**; the reactions with **2b** and **2c** afforded **14a** in 19 and 27% yield, respectively. In the reaction with **2b**, *N,N'*-thiobis[1,4-naphtoquinone monoimine] (**15**) and 5-chloronaphtho[1,2-*c*][1,2,5]thiadiazole (**13b**) were formed as a side product (3 and 1% yield, respectively).

On the contrary, the reaction with 2-naphthol (**3a**) afforded **13a** as the sole product in fair yield (84%). Similarly, 6-bromo-2-naphthol (**3b**) gave 7-bromo-

Table 1. Reaction of Tetrasulfur Tetranitride (**1**) with Naphthalenols

	Naphthalenols	N_4S_4 (**1**)/substrate[a]	Product/mol %[b]
2a	1-OH	2	**13a** (9), **14a** (14)
2b	1-OH 2,4-Cl_2	2	**13b** (1), **14a** (19), **15** (3)
2c	1-OH 2,4-Br_2	2	**14a** (27)
3a	2-OH	2	**13a** (84)
3b	2-OH 6-Br	2	**13c** (96)
3c	2-OH 1-Br	4	**13a** (51)
4a	1,5-$(OH)_2$	2	**16a** (5), **17** (+)[c]
4b	1,5-$(OH)_2$ 2,6-Br_2	3	**16a** (35), **17** (11)
4c	1,5-$(OH)_2$ 2,4-Br_2	4	**14b** (9), **17** (4)
5a	2,6-$(OH)_2$	2	**16a** (43)
5b	2.6-$(OH)_2$ 1,5-Br_2	3	**16a** (88)
5c	2,6-$(OH)_2$ 1,3,5,7-Br_4	4	**16b** (61)
6a	2,7-$(OH)_2$	2	**18a** (5)
6b	2,7-$(OH)_2$ 1,3,6-Br_3	4	**18b** (61)
7	1,6-$(OH)_2$	2	**16a** (5)
8a	1,7-$(OH)_2$	2	**13d** (+),[c] **18a** (2)
8b	1,7-$(OH)_2$ 2,6,8-Br_3	4	**17** (8)

a) Molar ratio. b) Isolated yield; calculated on the basis of the substrate used. c) Plus sign means that the yield is less than 1%.

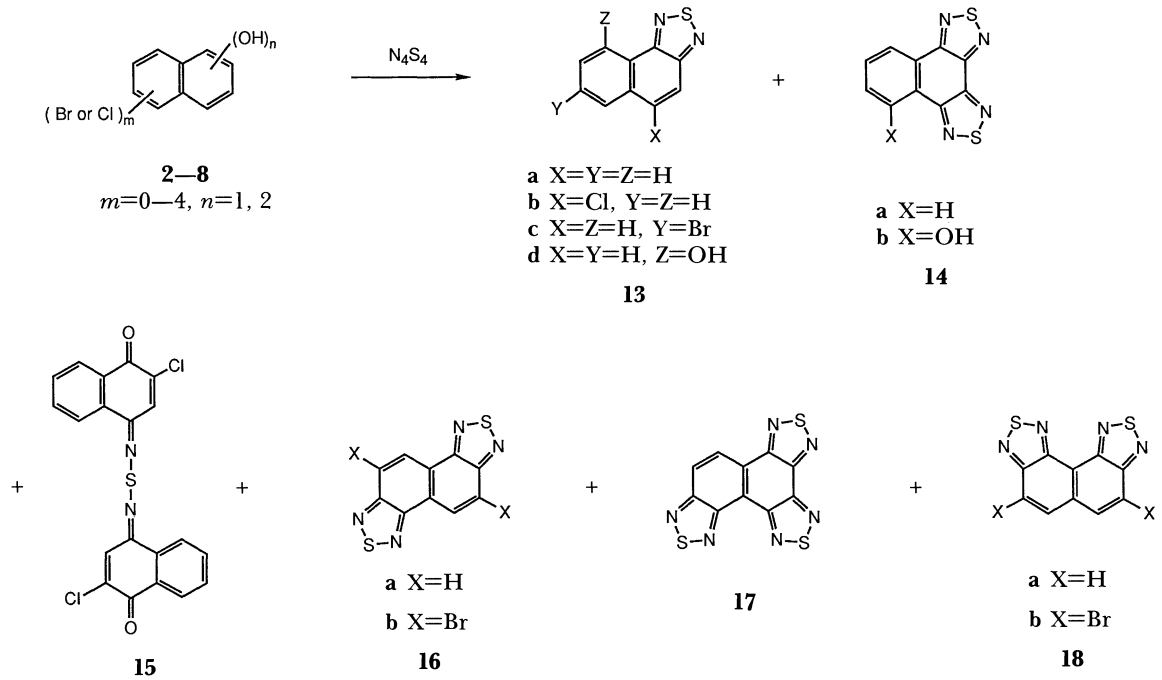

Scheme 2.

[1,2-*c*][1,2,5]thiadiazole (**13c**) in an almost quantitative yield. Also, 1-bromo-2-naphthol (**3c**) gave the expected **13a** in modest yield (51%).

The above-mentioned results demonstrated the selective construction of the naphthobis[1,2,5]thiadiazole and naphtho[1,2,5]thiadiazole skeleton by a reaction of **1** with 1-naphthol (**2**) and 2-naphthol (**3**), respectively.

Next, the reaction of **1** with naphthalenediols and their halogenated derivatives, which have one hydroxyl group in each benzene ring, was investigated. Since 1,5-naphthalenediol (**4a**) has two hydroxyl groups at the α-positions in each benzene ring, the formation of naphthotetrakis[1,2,5]thiadiazole was expected. The reaction with **4a** afforded naphtho[1,2-*c*:5,6-*c'*]bis[1,2,5]thiadiazole (**16a**) in only 5% yield, accompanied with a trace amount of naphtho[1,2-*c*:3,4-*c*:5,6-*c''*]tris[1,2,5]thiadiazole (**17**). The yields of **16a** and **17** increased to 35 and 11%, respectively, in the reaction with 2,6-dibromo derivative **4b**. In contrast with this result, the 2,4-dibromo derivative **4c** gave naphtho[1,2-*c*:3,4-*c*]bis[1,2,5]thiadiazol-7-ol (**14b**) (9%) as a main product, accompanied by **17** (4%). Finally, a reaction with the 2,4,6,8-tetrabromo derivative **4d** only gave a complex mixture of unidentified products.

Naphthalenes having two hydroxyl groups on the β-positions gave the expected naphthobis[1,2,5]thiadiazoles in a reaction with **1**, generally in good yield. The reaction with 2,6-naphthalenediol (**5a**) afforded naphtho[1,2-*c*;5,6-*c*]bis[1,2,5]thiadiazole (**16a**) in 43% yield. The yield of **16a** was increased up to 88% in a reaction with the 1,5-dibromo derivative **5b**. As expected, the 1,3,5,7-tetrabromo derivative **5c** gave 4,9-dibromo compound **16b** in 61% yield. On the other hand, another β,β'-dihydroxy type, 2,7-naphthalenediol (**6a**), afforded naphtho[1,2-*c*:7,8-*c'*]bis[1,2,5]thiadiazole (**18a**) in only 5% yield, though the reaction with 1,3,6-tribromo derivative **6b** gave 4,7-dibromo compound **18b** in 61% yield.

Since the unsubstituted compound **18a** was obtained only in poor yield, the hydrodebromination of **18b** was carried out by using $NaBH_4$ in refluxing ethanol, giving **18a** in 58% yield (Scheme 3). Compound **18a** became accessible via **18b** in moderate yield. Compound **16b** was sparingly soluble in any organic solvents and could not be reduced to **16a**.

The reaction of naphthalenediols bearing two hydroxyl groups each on the α and β positions gave poor results: **16a** and **18a** were obtained from **7** and **8** in 5 and 2% yield, respectively. In the reaction with **8**, a trace amount of naphtho[1,2-*c*][1,2,5]thiadiazol-9-ol (**13d**) was formed. The 2,6,8-tribromo derivative (**8b**)

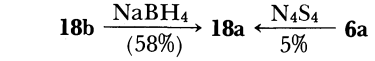

Scheme 3.

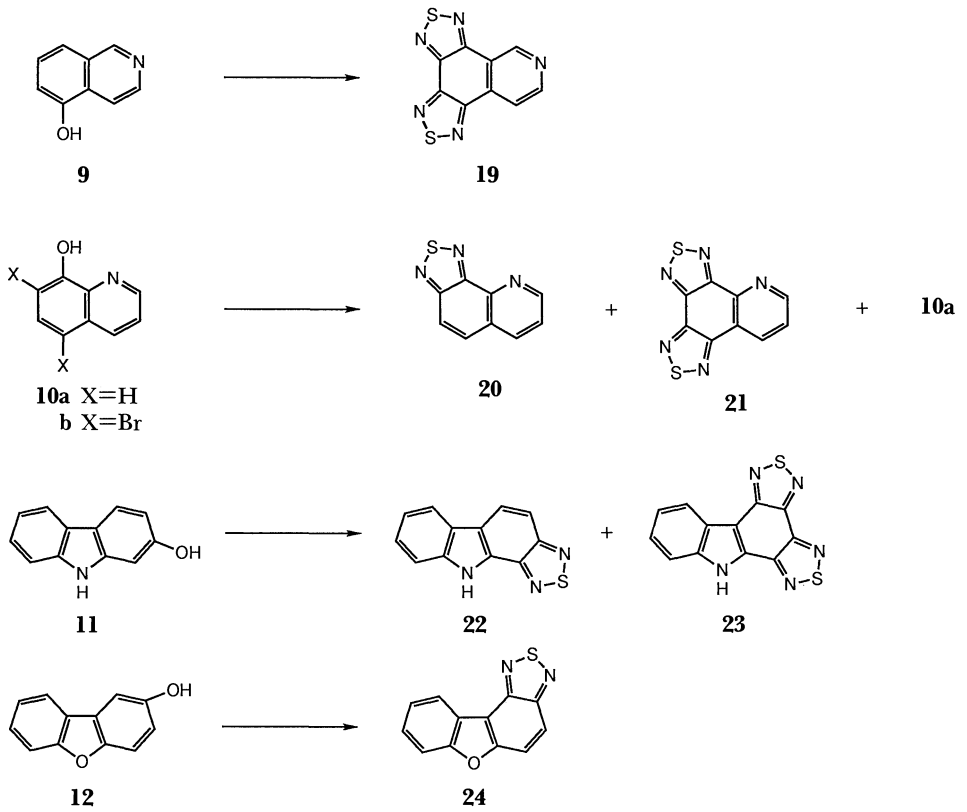

Scheme 4.

Table 2. Reaction of Tetrasulfur Tetranitride (**1**) with Hydroxy-Substituted Benzoheterocycles

Hydroxy-substituted benzoheterocycle[a]	Products/mole %[b]
9	**19** (18)
10a	**20** (25), **21** (7), **10a** (4)
10b	**21** (27)
11	**22** (26), **23** (6)
12	**24** (97)

a) Molar ratio of N_4S_4 (**1**): substrate=2:1. b) Isolated yield; calculated on the basis of the substrate used.

afforded **17** in 8% yield.

The selective construction of mono- and bis[1,2,5]-thiadiazole-fused skeleton was also observed in the reaction of **1** with hydroxy-substituted benzoheterocycles (Table 2 and Scheme 4), though not so remarkable as in the case of the naphthalenols. The reaction of **1** with 5-isoquinolinol (**9**) afforded only bis[1,2,5]thiadiazolo[3,4-*f*:3′,4′-*h*]isoquinoline (**19**) in 18% yield. Unexpectedly, 8-quinolinol (**10a**) afforded [1,2,5]thiadiazolo[3,4-*h*]quinoline (**20**) in 25% yield and bis[1,2,5]-thiadiazolo[3,4-*f*:3′,4′-*h*]quinoline (**21**) in 7% yield with a 4% yield of recovered **10a**. Only **21** was obtained in 27% yield in a reaction with 5,7-dibromo derivative **10b**. The reaction with 9*H*-carbazol-2-ol (**11**) afforded predominantly [1,2,5]thiadiazolo[3,4-*a*]carbazole (**22**) in 20% yield, with bis[1,2,5]thiadiazolo[3,4-*a*:3′,4′-*c*]carbazole (**23**) as a by-product.

As previously reported,[6] tetra-*t*-butylated dibenzofuran-1-ol reacted with **1**, gave tri-*t*-butylbenzofuro-[3,2-*e*][2,1,3]benzothiadiazole in 61% yield. The reaction with dibenzofuran-2-ol (**12**) afforded benzofurobenzothiadiazole (**24**) in an almost quantitative yield (97%).

The product selectivity observed in the reaction of **1** with **2**—**12** seems to be correlated with the difference in the mode of keto–enol tautomerism of 1-hydroxy derivatives and 2-hydroxy ones, as stated in the introductory part, though the detailed mechanism of the above-mentioned reactions is not known.

Experimental

General. All melting points were determined on a Mitamurariken MELT THERMO and are uncorrected. The IR spectra were measured as KBr pellets on a Nippon-Bunko A-102. The NMR spectra were recorded at 270 MHz with a JEOL GSX-270 using Me_4Si as an internal standard in $CDCl_3$, unless otherwise stated. Mass spectra were obtained on a JEOL JMS-O1SG-2 mass spectrometer at 75 eV using a direct inlet system. UV and VS spectra were measured on a Hitachi 220A spectrophotometer. Column chromatography was carried out on silica gel (Wako gel, C-300).

Materials. Compounds **2c**,[7] **4b**,[8,9] **4c**,[9] **4d**,[8] and **5b**[10] were prepared by the reported methods.

2,4-Dibromo-1-naphthol (2c): Colorless needles (ethanol); mp 98—101 °C (lit,[7] mp 105 °C). Found: C, 40.09; H, 2.11%.

2,6-Dibromo-1,5-naphthalenediol (4b): Gray needles (AcOH); mp >350 °C (it became colored around 200 °C) [lit,[8] mp >300 °C (darkened at 200 °C) and lit,[9] mp 224 °C (decomp)]. Found: C, 37.89; H, 2.02%.

2,4-Dibromo-1,5-naphthalenediol (4c): Colorless needles (hexane); mp 147—149 °C (lit,[9] mp 147.5 °C); ^{1}H NMR δ=6.00 (1H, s, D_2O-exchanged), 7.11 (1H, dd, J=8 and 1 Hz), 7.45 (1H, dd, J=8 and 8 Hz), 7.65 (1H, s), 7.88 (1H, dd, J=8 and 1 Hz), and 7.95 (1H, s, D_2O-exchanged).

2,4,6,8-Tetrabromo-1,5-naphthalenediol (4d): Yellowish white plates (toluene); mp 220—223 °C (lit,[8] mp >300 °C); IR 3460, 3320 cm^{-1}; MS m/z 480 (M^+), 478 (M^+), 476 (M^+), 474 (M^+), and 472 (M^+). Found: C, 25.55; H, 1.11%.

1,5-Dibromo-2,6-naphthalenediol (5b): Colorless prisms (dioxane), mp 209—213 °C (lit,[10] mp >223 °C); ^{1}H NMR (CD_3OD) δ=7.22 (2H, d, J=9 Hz) and 8.00 (2H, d, J=9 Hz). Found: C, 37.98; H, 1.87%.

1,3,5,7-Tetrabromo-2,6-naphthalenediol (5c). A mixture of **5a** (9.1 g, 57 mmol) and bromine (12 ml, 233 mmol) in AcOH (400 ml) was refluxed for 2 h. After it cooled, the mixture was poured into water and the precipitates were filtered, washed well with acetone, and filtered to give **5c** (0.97 g, 4%): Colorless needles; mp 279—282 °C (decomp); IR 3480 and 3350 cm^{-1}; ^{1}H NMR (CD_3OD) δ=8.32 (s); MS m/z 480 (M^+), 478 (M^+), 476 (M^+), 474 (M^+), and 472 (M^+). Found: C, 25.45; H, 0.92%. Calcd for $C_{10}H_4Br_4O_2$:C, 25.25; H, 0.85%.

1,3,6-Tribromo-2,7-naphthalenediol (6b). To a mixture of **6a** (4.0 g, 25 mmol) in AcOH (100 ml), bromine (5.2 ml, 101 mmol) in AcOH (20 ml) was added dropwise. During the addition, the temperature of the mixture was increased to about 40 °C. The mixture was refluxed for 2 h. After it cooled, precipitated **6b** (7.29 g, 74%) was collected by filtration: Colorless powder; mp 183—197 °C; IR 3490 and 3420 cm^{-1}; ^{1}H NMR (CD_3COCD_3) δ=7.57 (1H, s), 8.04 (1H, s), 8.05 (1H, s), 8.69 (1H, s, D_2O-exchanged), 9.57 (1H, s, D_2O-exchanged); MS m/z 400 (M^+), 398 (M^+), 396 (M^+), and 394 (M^+). Found: C, 30.44; H, 1.42%. Calcd for $C_{10}H_5Br_3O_2$:C, 30.26; H, 1.27%.

2,6,8-Tribromo-1,7-naphthalenediol (8b). A mixture of bromine (5 ml, 97 mmol) in AcOH (15 ml) was added dropwise to a mixture of **8a** (5.0 g, 31 mmol) in AcOH (80 ml) at room temperature; the reaction mixture was then stirred for 30 min. The precipitated **8b** (7.56 g, 61%) was collected by filtration and recrystallized from carbon tetrachloride, giving **8b** as grayish blue needles: Mp >300 °C; IR 3500 cm^{-1}; ^{1}H NMR (CD_3COCD_3) δ=7.44 (1H, d, J=9 Hz), 7.81 (1H, s), and 8.09 (1H, d, J=9 Hz); MS m/z 400 (M^+), 398 (M^+), 396 (M^+), and 394 (M^+). Found: C, 30.50; H, 1.69%. Calcd for $C_{10}H_5Br_3O_2$: C, 30.27; H, 1.27%.

5,7-Dibromo-8-quinolinol (10b). A mixture of **10a** (5.0 g, 34 mmol) and bromine (1.8 ml, 35 mmol) in AcOH (120 ml) was stirred at room temperature. Compound **10b** gradually precipitated; after one night it was colllected by filtration (2.02 g, 19%): Yellow needles (AcOH); mp 218—220 °C; IR 3300—2400 cm^{-1}; MS m/z 305 (M^+), 303 (M^+), and 301 (M^+). Found : C, 35.52; H, 2.13; N, 4.52%. Calcd for $C_9H_5Br_2NO$: C, 35.68; H, 1.66; N, 4.62%.

General Procedure for the Reaction of 1 with Naphthalenols (2—8) and Hydroxy-Substituted Benzoheterocycles (9—12). After a mixture of **1** and an appropriate amount of

naphthalenols or hydroxy-substituted benzoheterocycles in toluene (100 ml) was heated under reflux for 48 h, it was cooled to room temperature. An insoluble material containing unidentified inorganic compounds was filtered off and the filtrate was concentrated to 30 ml; the condensate was then chromatographed. Sulfur was first eluted with hexane and unreacted N_4S_4 with a mixture of hexane and benzene. Then, products **10a**, **13a**[11]—**13d**, **14a**—**b**, **16a**, **17**, **18a**—**b**, **19**, **20**, **21**, **22**, and **24** were obtained from the fraction eluted with benzene. Products **15** and **23** were eluted with chloroform.

Compound **16b** was obtained as precipitates during the reaction and washed successively with benzene, chloroform, and then ethanol. An analytical sample of **16b** was obtained by recrystallization from dioxane. The physical properties of the new compounds obtained in this study are shown below.

5-Chloronaphtho[1,2-*c*][1,2,5]thiadiazole (13b): Colorless needles (ethanol); mp 121—123 °C; MS *m/z* 222 (M^+) and 220 (M^+). Found: C, 54.54; H, 2.17; N, 12.49%. Calcd for $C_{10}H_5ClN_2S$: C, 54.43; H, 2.28; N, 12.69%.

7-Bromonaphtho[1,2-*c*][1,2,5]thiadiazole (13c): Colorless plates (ethanol); mp 157—160 °C; ^{1}H NMR δ=7.60—7.85 (3H, m), 7.96 (1H, d, *J*=2 Hz), and 8.51 (1H, d, *J*=8 Hz); ^{13}C NMR δ=121.1, 123.7, 125.6, 127.0, 131.0, 131.1, 131.6, 134.5, 153.7, and 154.3; MS *m/z* 266 (M^+) and 264 (M^+). Found: C, 45.39; H, 1.78; N, 10.73%. Calcd for $C_{10}H_5BrN_2S$: C, 45.30; H, 1.90; N, 10.57%.

Naphtho[1,2-*c*][1,2,5]thiadiazol-9-ol (13d): Pale yellow needles (ethanol); mp 113—116 °C; IR 3300 cm^{-1}; ^{1}H NMR δ=7.32 (1H, d, *J*=8 Hz), 7.44 (1H, d, *J*=7 Hz), 7.65 (1H, dd, *J*=7 and 8 Hz), 7.77 (1H, d, *J*=9 Hz), 7.86 (1H, d, *J*=9 Hz), and 10.26 (1H, s); MS *m/z* 202 (M^+). Found: C, 59.16; H, 2.69; N, 13.63%. Calcd for $C_{10}H_6N_2OS$: C, 59.39; H, 2.99; N, 13.85%.

Naphtho[1,2-*c*:3,4-*c*] bis [1,2,5]thiadiazole (14a): Straw colored needles (ethanol); mp 203—208 °C; UV (MeOH) 331 (ε 17000), 315 (18600), 300 (17400), 263 (16600), and 239 nm (34700); ^{1}H NMR δ=7.78—7.81 (2H, m) and 8.64—8.67 (2H, m); ^{13}C NMR δ=126.4, 127.1, 130.9, 148.2, and 156.4; MS *m/z* 244 (M^+). Found: C, 49.33; H, 1.58; N, 22.53%. Calcd for $C_{10}H_4N_4S_2$: C, 49.17; H, 1.65; N, 22.93%.

Naphtho[1,2-*c*;3,4-*c*]bis[1,2,5]thiadiazol-7-ol (14b): Pale pink needles (ethanol); mp 236—239 °C (it changed to prisms around 175 °C); IR 3255 cm^{-1}; ^{1}H NMR δ=7.37 (1H, dd, *J*=8 and 1 Hz), 7.71 (1H, dd, *J*=8 and 8 Hz), 8.19 (1H, dd, *J*=8 and 1 Hz), and 10.38 (1H, s, D_2O-exchanged); MS *m/z* 260 (M^+). Found: C, 45.64; H, 1.89; N, 21.17%. Calcd for $C_{10}H_4N_4OS_2$: C, 46.14; H, 1.55; N, 21.52%.

***N,N'*-Thiobis[3-chloro-1,4-naphthoquinone 1-imine] (15):** Red needles (ethanol); mp 260—264 °C (decomp); IR 1660 cm^{-1}; ^{1}H NMR δ=7.65—7.69 (2H, m), 7.75—7.78 (2H, m), 7.98 (2H, s), 8.24 (2H, dd, *J*=9 and 1 Hz), and 8.35 (2H, dd, *J*=8 and 2 Hz); MS *m/z* 416 (M^+), 414 (M^+), and 412 (M^+). Found: C, 57.79; H, 2.12; N, 6.86%. Calcd for $C_{20}H_{10}Cl_2N_2O_2S$: C, 58.13; H, 2.44; N, 6.78%.

Naphtho[1,2-*c*:5,6-*c*]bis[1,2,5]thiadiazole (16a): Straw colored needles (ethanol); mp 203—208 °C; UV (MeOH) 331 (ε 16700), 315 (18600), 300 (17400), 263 (16600), and 239 nm (34700); ^{1}H NMR δ=7.78—7.81 (2H, m), 8.64—8.67 (2H, m); ^{13}C NMR δ=126.4, 127.1, 130.9, 148.2, and 156.4; MS *m/z* 244 (M^+). Found: C, 49.33; H, 1.58; N, 22.53%. Calcd for $C_{10}H_4N_4S_2$: C, 49.17; H, 1.65; N, 22.93%.

4,9-Dibromonaphtho[1,2-*c*:5,6-*c'*]bis[1,2,5]thiadiazole (16b): Yellow needles (dioxane); mp >350 °C; MS *m/z* 494 (M^+), 492 (M^+), and 490 (M^+). Found: C, 30.13; H, 0.91; N, 13.75%. Calcd for $C_{10}H_2Br_2N_4S_2$: C, 29.87; H, 0.50; N, 13.93%.

Naphtho[1,2-*c*:3,4-*c'*:5,6-*c''*]tris[1,2,5]thiadiazole (17): Pale yellow needles (ethanol); mp 311—313 °C; ^{1}H NMR δ=8.37 (1H, d, *J*=9 Hz) and 8.97 (1H, d, *J*=9 Hz); MS *m/z* 302 (M^+). Found: C, 39.57; H, 0.53; N, 27.47%. Calcd for $C_{10}H_2N_6S_3$: C, 39.72; H, 0.67; N, 27.79%.

Naphtho[1,2-*c*:7,8-*c'*]bis[1,2,5]thiadiazole (18a): Yellow needles (ethanol); mp 244—248 °C; UV (MeOH) 373 (ε 12300), 356 (14450), 345 (22400), 330 (15850), 255 (46770), and 250 nm (46770); ^{1}H NMR δ=8.14 (2H, *J*=8 Hz), 8.88 (2H, d, *J*=8 Hz); ^{13}C NMR δ=121.6 and 127.5; MS *m/z* 244 (M^+). Found: C, 49.27; H, 1.52; N, 22.73%. Calcd for $C_{10}H_4N_4S_2$: C, 49.17; H, 1.65; N, 22.93%.

4,7-Dibromonaphtho[1,2-*c*:7,8-*c'*]bis[1,2,5]thiadiazole (18b): Pale yellow plates (benzene); mp 298—316 °C; ^{1}H NMR δ=8.27 (s); MS *m/z* 404 (M^+), 402 (M^+), and 400 (M^+). Found: C, 29.98; H, 0.85; N, 13.69%. Calcd for $C_{10}H_2Br_2N_4S_2$: C, 29.87; H, 0.50; N, 13.93%.

Bis[1,2,5]thiadiazolo[3,4-*f*:3',4'-*h*]isoquinoline (19): Pink needles (ethanol); mp 220—221 °C; ^{1}H NMR δ=8.48 (1H, d, *J*=5 Hz), 9.03 (1H, d, *J*=5 Hz), and 9.99 (1H, s); ^{13}C NMR δ=118.8, 121.2, 131.9, 148.4, 148.8, 149.2, 150.7, 154.2, and 154.3; MS *m/z* 245 (M^+). Found: C, 43.87; H, 1.08; N, 28.42%. Calcd for $C_9H_3N_5S_2$: C, 44.07; H, 1.23; N, 28.55%.

[1,2,5]Thiadiazolo[3,4-*h*]quinoline (20): Colorless needles (methanol); mp 139—141 °C; ^{1}H NMR δ=7.65 (1H, dd, *J*=8 and 4 Hz), 7.83 (1H, d, *J*=9 Hz), 7.94 (1H, d, *J*=9 Hz), 8.24 (1H, dd, *J*=8 and 2 Hz), and 9.09 (1H, dd, *J*=4 and 2 Hz); ^{13}C NMR δ=121.0, 124.0, 128.7, 130.7, 136.5, 143.1, 150.8, 153.8, and 156.1; MS *m/z* 187 (M^+). Found: C, 57.50; H, 2.37; N, 22.81%. Calcd for $C_9H_5N_3S$: C, 57.74; H, 2.69; N, 22.44%.

Bis[1,2,5]thiadiazolo[3,4-*f*:3'4'-*h*]quinoline (21): Pale purple needles (ethanol); mp 257—259 °C; ^{1}H NMR δ=7.72 (1H, dd, *J*=8 and 4 Hz), 8.96 (1H, dd, *J*=8 and 1 Hz), and 9.11 (1H, dd, *J*=4 and 1 Hz); ^{13}C NMR δ=123.5, 125.2, 134.4, 144.0, 148.0, 149.1, 152.7, 154.9, and 155.5; MS *m/z* 244 (M^+). Found: C, 44.10; H, 1.11; N, 28.19%. Calcd for $C_{12}H_7N_3S$: C, 44.07; H, 1.23; N, 28.55%.

[1,2,5]Thiadiazolo[3,4-*a*]carbazole (22): Bright yellow needles (purified by sublimation); mp 256—258 °C; IR 3302 cm^{-1}; ^{1}H NMR δ=7.35 (1H, dd, *J*=7 and 7 Hz), 7.48 (1H, dd, *J*=7 and 7 Hz), 7.62 (1H, d, *J*=8 Hz), 7.75 (1H, d, *J*=9 Hz), 8.10 (1H, d, *J*=8 Hz), 8.24 (1H, d, *J*=9 Hz) and 9.33 (1H, br s); MS *m/z* 225 (M^+). Found: C, 64.09; H, 2.73; N, 18.65%. Calcd for $C_{12}H_7N_3S$: C, 63.98; H, 3.13; N, 18.65%.

Bis[1,2,5]thiadiazolo[3,4-*a*:3',4'-*c*]carbazole (23): Green needles (benzene); mp 308—314 °C; IR 3295 cm; ^{1}H NMR (CD_3SOCD_3) δ=7.35—7.51 (2H, m), 7.72 (1H, d, *J*=9 Hz), 8.41 (1H, d, *J*=8 Hz), and 12.86 (1H, br s); MS *m/z* 283 (M^+). Found: C, 51.08; H, 1.41; N, 24.35%. Calcd for $C_{12}H_5N_5S_2$: C, 50.87; H, 1.78; N, 24.72%.

Benzofuro[3,2-*e*][2,1,3]benzothiadiazole (24): Pale yellow needles (ethanol); mp 115—116 °C; ^{1}H NMR δ=7.46—7.50 (2H, m), 7.59—7.66 (1H, m), 7.84 (1H, d, *J*=9 Hz), 7.95 (1H, d, *J*=9 Hz), and 8.34—8.38 (1H, m); ^{13}C NMR δ=112.1, 114.0, 117.7, 119.9, 122.5, 123.7, 124.3, 127.1, 150.0, 153.3, 156.2, and 156.3; MS *m/z* 226 (M^+). Found: C, 63.47; H, 2.43; N, 12.25%. Calcd for $C_{12}H_6N_2OS$: C, 63.70; H, 2.67; N, 12.38%.

Hydrodebromination of 18b. A mixture of **18b** (100 mg, 0.25 mmol) and sodium borohydride (500 mg, 13 mmol) in ethanol (50 ml) was refluxed for 5 min, cooled to room temperature, and filtered to give **18a** (35 mg, 58%).

References

1) Part18, S. Mataka, H. Eguchi, K. Takahashi, T. Hatta, and M. Tashiro, *Bull. Chem. Soc. Jpn.*, **62**, 3127 (1989).

2) S. Mataka, K. Takahashi, S. Shiwaku, and M. Tashiro, *J. Chem. Res., Symop.*, **1985** 345; *Miniprint*, 3649.

3) S. Mataka, K. Takahashi, A. Hosoki, and M. Tashiro, *Synthesis*, **1979**, 524.

4) S. Mataka, K. Takahashi, A. Hosoki, and M. Tashiro, *J. Heterocycl. Chem.*, **17**, 1681 (1980).

5) S. Mataka, K. Takahashi, A. Hosoki, and M. Tashiro, *Synthesis*, **1982**, 976.

6) K. Takahashi, H. Eguchi, S. Shiwaku, T. Hatta, E. Kyoya, T. Yonemitsu, S. Mataka, and M. Tashiro, *J. Chem. Soc., Perkin Trans. 1*, **1988**, 1869.

7) J. Krynski, *Rocz. Chem.*, **8**, 71 (1892); *Chem. Abstr.*, **22**, 4119 (1928).

8) A. S. Wheeler and D. R. Ergle, *J. Am. Chem. Soc.*, **52**, 4872 (1930).

9) A. H. Carter, E. Race, and F. M. Rowe, *J. Chem. Soc.*, **1942**, 236.

10) S. N. Chakravart and V. Pasupati, *J. Chem. Soc.*, **1937**, 1859.

11) V. Bertini, A. D. Munno, and A. Marraccini, *J. Org. Chem.*, **37**, 676 (1972).

 © 1991 The Chemical Society of Japan Bull. Chem. Soc. Jpn., 64, 74—80 (1991) [Vol. 64, No. 1

Hydrolytic Metalloenzyme Models. Micellar Effects on the Activation of the Hydroxyl Groups of *N*-Alkyl-2-(hydroxymethyl)-imidazole Ligands by Cu^{2+} in the Transacylation of *p*-Nitrophenyl Picolinate

Waichiro TAGAKI,* Kenji OGINO, Osamu TANAKA, Koji MACHIYA,
Nobuyuki KASHIHARA, and Toshiharu YOSHIDA
Department of Bioapplied Chemistry, Faculty of Engineering, Osaka City University,
Sugimoto-3, Sumiyoshi-ku, Osaka 558
(Received August 24, 1990)

The activation of the hydroxyl groups of two *N*-methyl/dodecyl-2-(hydroxymethyl)imidazole ligands by complexation with Cu^{2+} was investigated kinetically by observing the rates of the release of *p*-nitrophenol in the transacylation of *p*-nitrophenyl picolinate (**PNPP**). The kinetics were carried out in aqueous buffers of pH ranging from 4.5 to 8.0 at 25 °C in the absence of surfactant micelles for a hydrophilic *N*-methyl ligand, and in the presence of micelles for a lipophilic *N*-dodecyl ligand. The kinetic analyses indicated that the 1:1 and 2:1 complexes of the ligand and Cu^{2+} are active nucleophiles with the *N*-methyl and *N*-dodecyl ligand, respectively. The pK_a's of the hydroxyl groups of these complexes were determined to be 7.00 in water and 6.41 in aqueous **CTABr** micelles, respectively, by analyses of the pH-rate profiles. The rate constants, which show the nucleophilic reactivities of ionized hydroxyl anions of complexes toward **PNPP**, were determined to be k_N=1.11×10^4 and 1.25×10^6 mol^{-1} dm^3 s^{-1} with *N*-methyl and *N*-dodecyl ligands, respectively, indicating that the latter micellar complex is 100-times more active than the former non-micellar counterpart.

One of the roles of metal ions in hydrolytic metalloenzymes such as carboxypeptidase A,[1] carbonic anhydrase,[2] or alkaline phosphatase[3] is to activate the substrate as an electrophilic catalysts, stabilizing the negative charges that are formed during the reaction.[4] Another important function of a metal ion is to act as a source of hydroxide ions at neutral pH.[4] It is not uncommon that a metal-bound water molecule ionizes with a pK_a near 7, about 9 units below that of free water, yielding a high fraction of hydroxide ions at neutral pH. Here, a remarkable feature is that such a metal-bound hydroxide ion is a potent nucleophile retaining most of the reactivity of free hydroxide ion.[5,6]

The above-mentioned metal ion functions are quite attractive for designing artificial hydrolytic metalloenzymes. Thus, early in 1972, Sigman and Jorgensen showed that the hydroxyl group of *N*-(2-hydroxyethyl)-ethylenediamine is remarkably activated for the transacylation of *p*-nitrophenyl picolinate (**PNPP**) when complexed with Zn^{2+}.[7] This complex showed the pK_a of the hydroxyl group to be 8.4, much lower than that of the free ligand. More recently, Brown et al. reported that a basic form of the aqua complex of tris(imidazolyl)phosphine and Co^{3+} with pK_a 7.6—7.8 is the active species for the hydrolysis of **PNPP**.[8] Breslow et al. reported that a Zn^{2+} complex of tetraaza-macrocycle is active in the form of hydroxide with a pK_a of 8.7 in the hydrolysis of aryl phosphates.[9] The high reactivities of metal-bound hydroxyl groups with low pK's have also been observed in other recent model studies.[10]

On the other hand, we have been interested in designing micellar models of hydrolytic metalloenzymes.[11] Our search for active ligands has led us to find *N*-alkyl-2-(hydroxymethyl)imidazoles. They were highly active when complexed with bivalent metal ions in the hydrolysis of **PNPP**.[12] Interestingly, the activation was much larger for lipophilic ligands under micellar conditions than for hydrophilic ligands under non-micellar conditions.[13] Recently, there have been an increasing number of studies on the micellar models of hydrolytic metalloenzymes.[13–19] However, most of them were investigated under a particular pH, without dealing with the ionization of a ligand hydroxyl group.

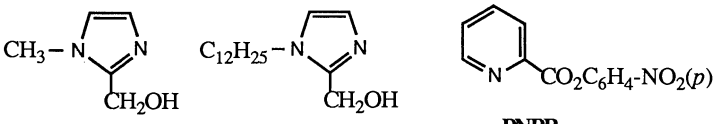

1 **2** **PNPP**

$CH_3(CH_2)_{15}N^+Me_3Br^-$ **CTABr**

$CH_3(CH_2)_{11}OSO_3^-Na^+$ **SDS**

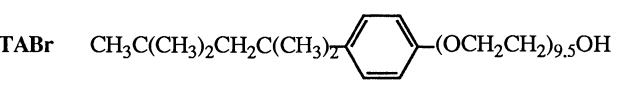

Triton X-100

We wish to report herein the micellar effects on the ionization and reactivity of the hydroxyl group of a Cu^{2+} complex of *N*-dodecyl-2-(hydroxymethyl)imidazole (**2**) ligand, as compared to a non-micellar *N*-methyl counterpart (**1**) in the transacylation of **PNPP**. The surfactants used for micellization were cationic hexadecyltrimethylammonium bromide(**CTABr**), anionic sodium dodecyl sulfate(**SDS**), and non-ionic **Triton X-100**. The ionization of the hydroxyl group of **2** was examined in **CTABr** micelles.

Results

A Survey of Rates at pH 7.03. Ligand **1** was water-soluble, while ligand **2** was hardly soluble in water but, rather, was solubilized by surfactant micelles, so that the kinetics were carried out in plain buffers for the former and in buffered micelles with the latter ligand. The rates of hydrolysis were determined by monitoring the release of *p*-nitrophenol from the substrate **PNPP** spectrophotometrically by using a UV-VIS or a stopped-flow spectrophotometer. In Table 1 are shown the pseudo-first-order rate constants (k_{obsd}) obtained under the conditions of an excess ligand and Cu^{2+} over the substrate at pH 7.03 and 25 °C.

Table 1. Pseudo-First-Order Rate Constants (k_{obsd}) for the Release of *p*-Nitrophenol from **PNPP** at pH 7.03, 25 °C[a)]

Run	System	$k_{obsd}\times10^2/s^{-1}$
1	None	0.00167
2	Cu^{2+}	1.98
3	**1**	0.068
4	**1**+Cu^{2+}	13.8
5	**CTABr**	0.00193
6	**CTABr**+**2**	0.192
7	**CTABr**+Cu^{2+}	3.78
8	**CTABr**+**2**+Cu^{2+}	491

a) In 0.1 mol dm^{-3} 2,6-lutidine–HNO_3 buffer; μ=0.2 (KNO_3), [ligand]=[Cu^{2+}]=1×10^{-4} mol dm^{-3}, [**PNPP**]=5×10^{-5} mol dm^{-3}, [**CTABr**]=1×10^{-2} mol dm^{-3}.

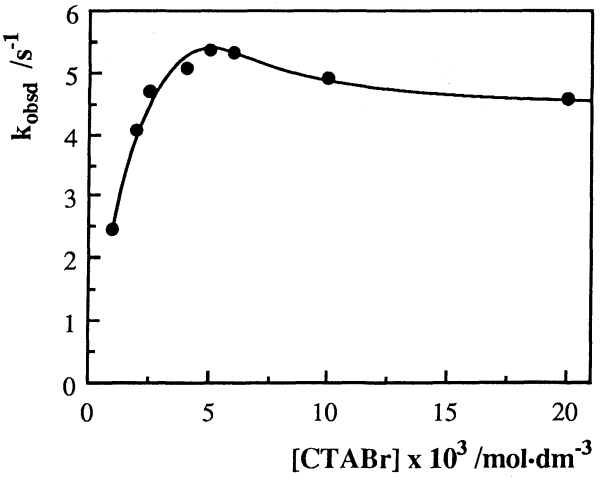

Fig. 1. Effect of **CTABr** concentration on the pseudo-first-order rate constants for the transacylation of **PNPP** at 25 °C, pH 7.03; [**2**]=[Cu^{2+}]=1×10^{-4} mol dm^{-3}, [**PNPP**]=5×10^{-5} mol dm^{-3}.

As indicated, a cationic surfactant **CTABr**, itself, showed almost no rate-enhancing effect (Run 1 vs. 5), although the concentration (1×10^{-2} mol dm^{-3}) used was sufficient to form micelles, i.e larger than the CMC value of about 10^{-3} mol dm^{-3} under the kinetic conditions (see also Fig. 1). The rate enhancement by the ligand alone was also small in each case of **1** under non-micellar (Run 3) and **2** under micellar conditions (Run, 6), as compared to the other cases involving Cu^{2+}. A large rate enhancement of more than 10^3-fold was observed by the addition of 1×10^{-4} mol dm^{-3} of Cu^{2+} (Runs 2 and 7). Even a more remarkable rate acceleration was observed in the coexistence of the ligand and Cu^{2+} (Runs 4 and 8). Thus, a rate enhancement of 4.5×10^5 fold was attained in the presence of 1×10^{-4} mol dm^{-3} each of **2** and Cu^{2+} in **CTABr** micelles (Run 8). As described below, these rate enhancements are dependent on the concentrations of the ligand, Cu^{2+}, and the surfactant, as well as the pH.

Effects of CTABr Concentrations. As shown in Fig. 1, saturation kinetics was observed, i.e. the rates (k_{obsd}) increased with increasing the **CTABr** concentration up to the saturation level. A breaking point in the curve near CMC, usually observed for a micellar reaction,[20,21] could not be detected, simply because of the hardly soluble nature of lipophilic **2** at a low surfactant concentration. The rate saturation of this type can be accounted for as being the saturation of substrate incorporation into the micelles.[20,21] It can be seen that 1×10^{-2} mol dm^{-3} of **CTABr** (Table 1) has sufficient concentration for saturation, and is appropriate as a standard concentration for subsequent experiments.

Reaction Scheme and the Rate Equations. It seems helpful to first explain the reaction schemes and the rate equations used for the analyses of the experimentally observed rates in generalized forms.

As described in the next sections, the rates could be analyzed by assuming a reaction Scheme 1 involving Eqs. 1—3, which is essentially the same as that

$$M + nL \underset{}{\overset{K_M}{\rightleftharpoons}} M\text{-}L_n;\ K_M = [M\text{-}L_n]/[M][L]^n \quad (1)$$

$$S + M\text{-}L_n \xrightarrow{k_N'} P \quad (2)$$

$$S \xrightarrow{k_o'} P \quad (3)$$

Scheme 1.

proposed for the Zn^{2+}-catalyzed reactions.[11-13] The scheme indicates that a metal ion (M) forms a complex (M-L_n) with n ligands (L) with an association constant (K_M) (Eq. 1), and that the complex reacts with the substrate (S) bimolecularly in the rate-limiting step with an apparent second-order rate constant (k_N') to afford the products (P) (Eq. 2). The products are also formed through k_o' process without involving an M-L_n complex (Eq. 3). The scheme leads to rate Eqs. 4-11,

$$k_o' = k_o + k_L[L]_T + k_M[M]_T \quad (4)$$

$$\text{Rate} = k_{obsd}[S] = (k_o' + k_N'[M\text{-}L_n]_T)[S] \quad (5)$$

$$n = 1 \qquad k_{obsd} = k_o' + \frac{k_N'K_M[L]_T[M]_T}{1 + K_M([L]_T + [M]_T)} \quad (6)$$

$$\frac{1}{(k_{obsd} - k_o')} = \frac{1}{k_N'[L]_T} + \frac{1 + K_M[L]_T}{k_N'K_M[L]_T} \cdot \frac{1}{[M]_T} \quad (7)$$

$$n = 2 \qquad k_{obsd} = k_o' + \frac{k_N'K_M[L]_T^2[M]_T}{1 + K_M[L]_T^2 + 4K_M[L]_T[M]_T} \quad (8)$$

$$\frac{1}{(k_{obsd} - k_o')} = \frac{4}{k_N'[L]_T} + \left(\frac{1}{k_N'} + \frac{1}{k_N'K[L]_T^2}\right) \cdot \frac{1}{[M]_T} \quad (9)$$

$$k_N' = \frac{k_NK_a}{K_a + [H^+]} \quad (10)$$

$$\frac{1}{k_N'} = \frac{1}{k_N} + \frac{1}{k_NK_a} \cdot [H^+] \quad (11)$$

where k_L and k_M are the second-order rate constants due to the ligand and Cu^{2+} alone, and $[L]_T$ and $[M]_T$ are the total concentrations of the ligand and Cu^{2+}, respectively.

An alternative scheme involving a ternary complex, S·M·L_n, may well be considered. The choice of Eq. 2 in Scheme 1 instead of such a ternary complex is simply due to the consideration that the substrate pyridine moiety should be weak as a ligand base in the ground state in aqueous buffers, although it becomes effective upon the formation of an intermediate (see below).

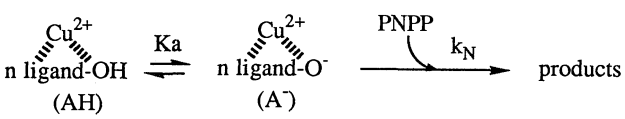

$$[M\text{-}L_n]_T = [AH] + [A^-]$$

Scheme 2.

Eqs. 6 and 8 are approximate equations for 1:1 (n=1) and 2:1 (n=2) complexes of the ligand and metal ion. The validities of these approximations can be confirmed from linear plots of Eqs. 7 and 9. Then, the k_N' and K_M values can be obtained by analyzing the intercepts and slopes. They should be pH-dependent if the active nucleophile is a dissociated complex anion (A^-) as illustrated in Scheme 3. The k_N for the fully dissociated hydroxyl group of the complex and its acid dissociation constants K_a can be obtained based on the relationship between Eqs. 10 and 11.

The Determination of n, k_N, and K_M Values for the Ligands 1 and 2. (a) Job Plots: A convenient method to estimate the above n values is the kinetic version of Job plots,[22] in which the rate constants are plotted as a function of the mole fraction of a ligand or metal ion, keeping their total concentration being constant. The results are shown in Fig. 2. Figure 2 indicates the necessity of the coexistence of the ligand and Cu^{2+} to attain higher rates (k_{obsd}). It also indicates the existence of an optimum γ value to attain a maximum rate. For ligand **1**, the maximum rate is seen at γ=0.5, indicating that the 1:1 complex (n=1) is the active species. For ligand **2**, the rate maxima of three plots are all seen at γ=0.67, indicating that the 2:1 complex (n=2) is the active species in all three kinds of micelles, although the reactivities are variable

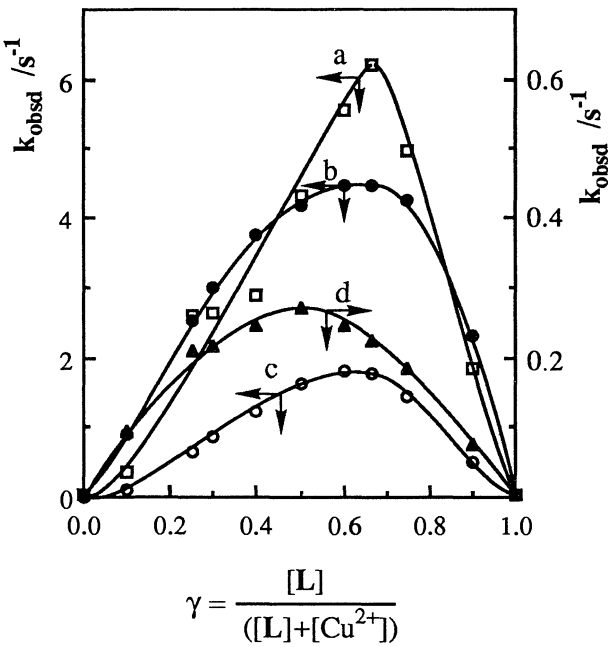

Fig. 2. Job plots for the ligand and Cu^{2+} ion complexation as measured by the rates of transacylation of **PNPP** at 25 °C, pH 7.0: a □, **2**, in [**Triton X-100**]=2×10^{-3} mol dm^{-3}; b ●, **2** in [**CTABr**]=1×10^{-2} mol dm^{-3}; c ○, **2** in [**SDS**]=3×10^{-2} mol dm^{-3}; ([**2**]+[Cu^{2+}])=1×10^{-4} mol dm^{-3}, d ▲, **1** in aqueous buffer, ([**1**]+[Cu^{2+}]=2×10^{-4} mol dm^{-3}, [**PNPP**]=1×10^{-5} mol dm^{-3}.

depending on the micelles.

(b) Saturation Kinetics: As shown in Figs. 3 (**1**) and 4 (**2**), the k_{obsd} values obtained with a constant $[L]_T$ and pH were plotted against Cu^{2+} concentrations ($[M]_T$) to give a saturation curve for each pH. Figures 3 and 4 indicate that the reactivities of **2** under micellar conditions are much higher than those of **1** under non-micellar conditions. Plots of $1/(k_{obsd}-k_o')$ vs. $1/[M]_T$ gave thus straight lines, as shown in Figs. 5 and 6, confirming the relationship between Eqs. 6 and 7 for the ligand **1** (n=1), and Eqs. 8 and 9 for the ligand **2** (n=2). Here, the k_o' values (Eq. 4) were one or two orders smaller than the k_{obsd} values (compare the Runs 2 and 4, or 7 and 8 in Table 1). The intercepts and the slopes of these straight lines allowed us to obtain the k_N' and the K_M values as listed in Tables 2 and 3. The solid lines in Figs. 3 and 4 were calculated by using these k_N' and K_M values and according to Eqs. 6 and 8, again confirming their relationships. The fitting between these calculated solid lines and the experimental k_{obsd} values seems to be satisfactory for most of the pH's

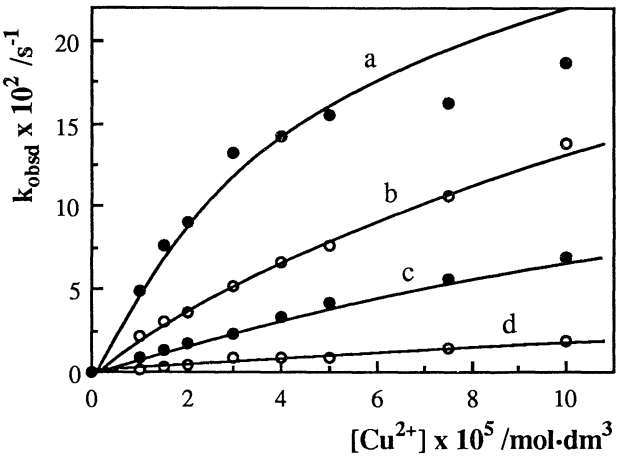

Fig. 3. Pseudo-first-order rate constants for the transacylation of **PNPP** in aqueous buffer at 25 °C as the function of Cu^{2+} concentration: pH's were 7.50(a), 7.00(b), 6.50(c), and 6.00(d); [**1**]=5×10^{-5} mol dm^3, [**PNPP**]=1×10^{-5} mol dm^3.

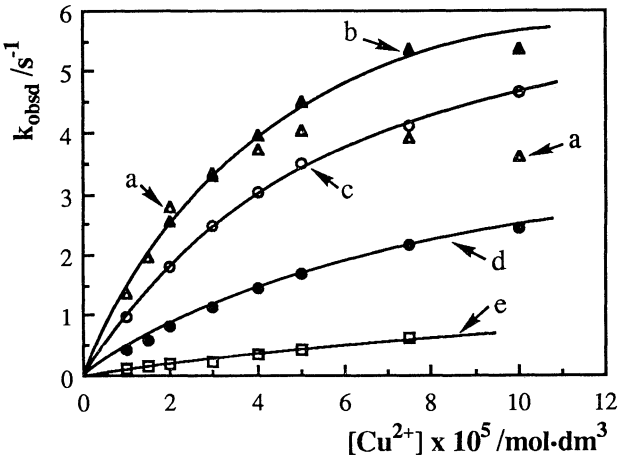

Fig. 4. Pseudo-first-order rate constants for the transacylation of **PNPP** in **CTABr** micelles at 25 °C as the function of Cu^{2+} concentration: pH's were 7.49(a), 7.03(b), 6.50(c), 6.01(d), and 5.51(e); [**2**]= 5×10^{-5} mol dm^3, [**PNPP**]=1×10^{-5} mol dm^3, [**CTABr**]=1×10^{-2} mol dm^3.

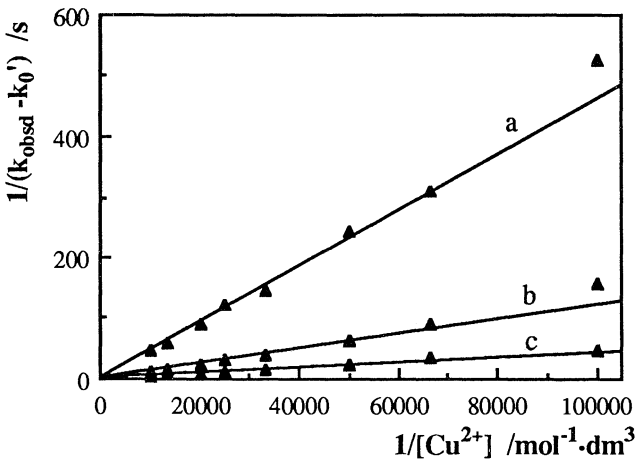

Fig. 5. Plots of $1/(k_{obsd}-k_o')$ vs. $1/[Cu^{2+}]$ for **1-PNPP**: a, pH 6.00; b, pH 6.50; c, pH 7.00.

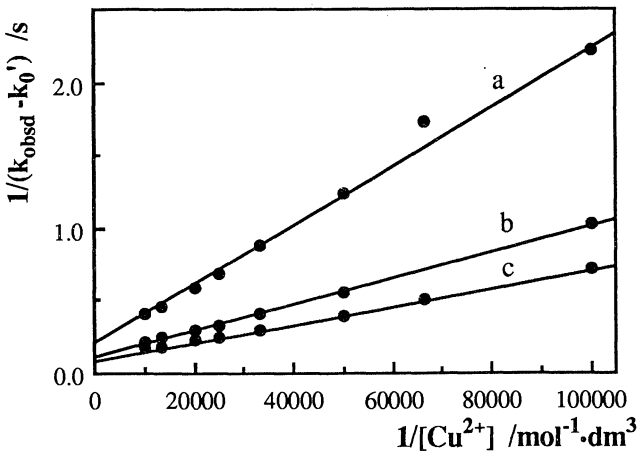

Fig. 6. Plots of $1/(k_{obsd}-k_o')$ vs. $1/[Cu^{2+}]$ for **2-PNPP**: in **CTABr** micelles: a, pH 6.01; b, pH 6.50; c, pH 7.03.

Table 2. pH Dependencies of k_N' and K_M of **1**-Cu^{2+} Complex under Non-micellar Conditions, 25 °C

pH	k_N'/mol^{-1} dm^3 s^{-1}	K_M/mol^{-2} dm^3
4.97	1.05×10^2	2.00×10^3
5.50	3.33×10^2	4.34×10^3
6.00	1.00×10^3	2.16×10^3
6.50	3.16×10^3	4.47×10^3
7.00	7.69×10^3	7.03×10^3
7.50	1.00×10^4	2.07×10^4
8.00	8.85×10^3	2.22×10^4

Table 3. pH Dependencies of k_N' and K_M of **2**-Cu^{2+} Complex under Micellar Conditions, of **CTABr**, 25 °C

pH	k_N'/mol^{-1} dm^3 s^{-1}	K_M/mol^{-2} dm^6
4.46	1.36×10^4	6.46×10^6
4.97	4.46×10^4	6.42×10^6
5.51	1.33×10^5	3.61×10^7
6.01	4.00×10^5	5.75×10^7
6.50	7.62×10^5	6.87×10^7
7.03	8.60×10^5	9.29×10^7
7.49	8.70×10^5	9.09×10^7
8.00	4.04×10^5	5.23×10^7

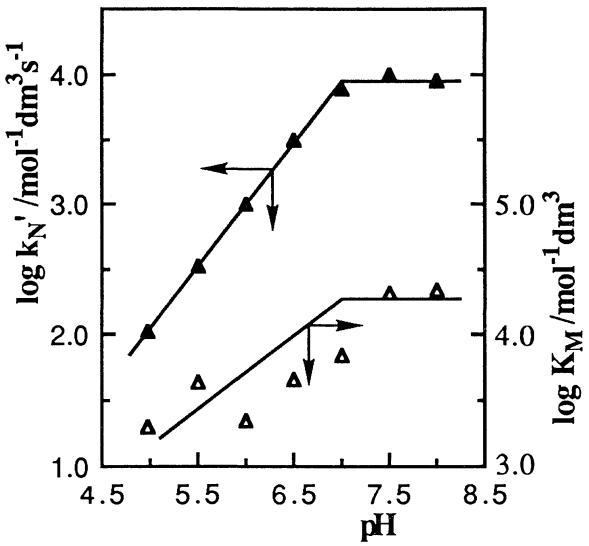

Fig. 7. Plots for log k_N' and log K_M vs. pH for **1**-Cu^{2+} in aqueous buffer.

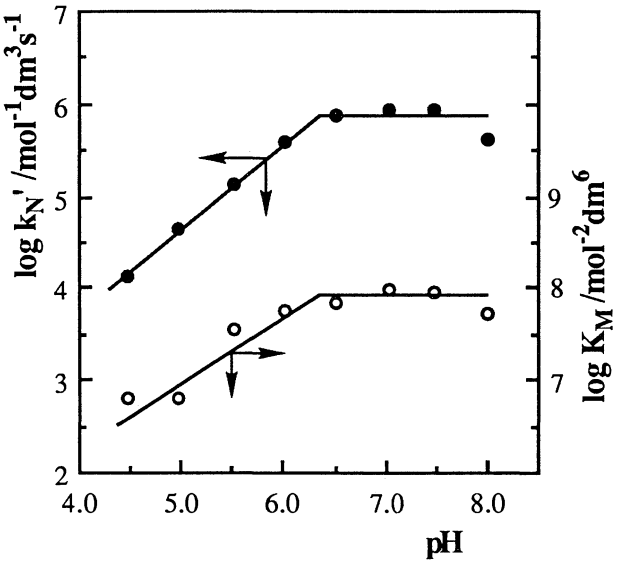

Fig. 8. Plots for log k_N' and log K_M vs. pH for **2**-Cu^{2+} in **CTABr** micelles.

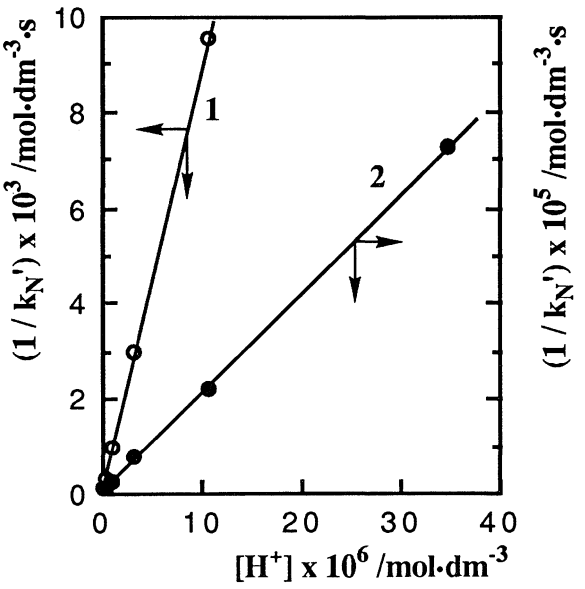

Fig. 9. Plots of $1/k_N'$ vs. $[H^+]$ for the reaction of **PNPP** with Cu^{2+} complexes of **1** and **2**.

examined. However, as can be seen in Figs. 3 and 4, such fitting tends to deviate at higher pH and higher Cu^{2+} concentration, presumably due to the decomposition of active complexes by hydroxide ion as well as the change in the n value.

(c) pH-Rate Profiles: The above k_N' and K_M values were both pH-dependent. As shown in Figs. 7 and 8, the log k_N' values increased linearly with a slope of 1 with increasing pH; they then become pH independent at higher pH. These pH-rate profiles can be accounted for by assuming that the dissociated complex anions (A^- in Scheme 2) are much more active than undissociated complexes (AH). Then, the pK_a's of AH and the k_N values of A^- could be calculated from the plots of $1/k_N'$ vs. $[H^+]$ shown in Fig. 9 (Eq. 11). The results obtained are: $k_N=1.11\times10^4$ mol^{-1} dm^3 s^{-1} and $pK_a=7.00$ for **1**, and 1.25×10^6 mol^{-1} dm^3 s^{-1} and 6.41 for **2**, respectively. The effects of pH on the log K_M values are qualitatively similar to those on the log k_N' values, i.e. the values increase and then level off with increasing pH. It is reasonable that complexation with a metal ion is stronger with dissociated A^- than with undissociated AH.

Discussion

It has already been established that a bivalent metal-ion catalyzed reaction of an *N*-alkyl-2-(hydroxymethyl)-imidazole with **PNPP** occurs through a two-step process involving the acylation of the 2-hydroxymethyl group, followed by deacylation, although the reaction conditions examined were limited in most cases to those at a particular pH near 7.[11-13] Of these two-steps, the above-mentioned kinetics focused on the acylation step (K_a and k_N in Scheme 2), by carrying

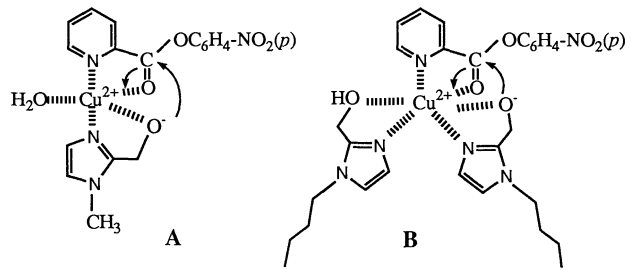

Fig. 10. Proposed structures of ternary complexes of **1** or **2**-Cu^{2+}·**PNPP**.

them out under conditions of excess ligand over the substrate.[23]

These results indicate the following differences between the reactions of non-micellar **1**-Cu^{2+} and micellar **2**-Cu^{2+} complexes: 1) the stoichiometries of complexation, 2) the pK_a's of ligand hydroxyl groups, and 3) the k_N values.

The observed stoichiometry was 1:1 for the former **1**-Cu^{2+}, while 2:1 for the latter **2**-Cu^{2+} complex. Thus, such structures as **A** and **B** are conceivable for the transition states of the two reaction systems, as illustrated in Fig. 10. In both cases, the complexation of **PNPP** with Cu^{2+} involving pyridine nitrogen is presumed to be unimportant at the ground state, but becomes important at the rate-determining step of attacking a ligand-oxido anion nucleophile on the substrate carbonyl carbon to form an addition intermediate.[11,13] The reason for forming a 1:1 complex in a non-micellar system, but a 2:1 complex in a micellar system is not clear. Presumably, the hydration of Cu^{2+} is sufficiently strong to stabilize a 1:1 complex with a hydrophilic ligand in the non-micellar aqueous phase, but not in the micellar phase for a lipophilic ligand; instead, the 2:1 complex becomes more stable. The charge on the micellar surface does not seem to be critical in determining the complex stoichiometry, since the same 2:1 ratio was observed in three different micelles (i.e. anionic, cationic, and non-ionic, Fig. 2).

The pK_a's of the complexes were found to be 7.0 and 6.41 for **1** and **2**, respectively. Thus, for both ligands, a remarkable lowering of pK_a occurred upon complexation with Cu^{2+}, as expected from the previous information.[4] One may notice that the pK_a of **2**-Cu^{2+} is about 0.6 as small as that of **1**-Cu^{2+}. The electron-donating effect as well as the hydrophobic nature to increase pK_a must be larger with the dodecyl than with the methyl group, contrary to observation. However, this reversal of pK_a is not unusual in view of the micellar effect, since it is known that the pK_a of a weak acid, such as phenol, is lowered by 1-2 units when solubilized in cationic micelles, like **CTABr**.[23]

Finally, it is interesting to compare the nucleophilic reactivities of the two systems. At a lower pH, when $[H^+] \gg K_a$, the apparent reactivity is $k_N' = k_N K_a/[H^+]$ (Eq 10). Then, a comparison of the above-mentioned two sets of $k_N K_a$ values indicate that the micellar complex is 428-times more reactive than the non-micellar complex. At a higher pH, when $K_a \gg [H^+]$, k_N' becomes pH independent k_N, that of the dissociated anion (A^-). The ratio of two k_N values indicates that the micellar complex is still 100-times more active than the non-micellar complex. It may be necessary to divide this ratio by a statistical factor of 2 for a fair comparison, since the 2:1 complex has two hydroxyl groups, instead of one in the 1:1 complex. A further correction may be required, since in the micellar reaction the reactants are concentrated in the micellar pseudo-phase so as to enhance the rate of a bimolecular reaction. Bunton et al. proposed a correction factor 0.14 to be multiplied to the experimentally observed second-order rate constant so as to obtain a real micellar rate constant.[20] These two corrections reduce the above 100 to 7. Thus, an apparent large rate enhancement in a micellar system as compared to a non-micellar one seems to be mainly due to a different mode (stoichiometry) of metal ion-ligand complexation as well as to the concentration effect to bring the reactants together in a relatively small volume of a micellar pseudo-phase. However, it should be pointed out that these rate comparisons are still tentative, since the above correction factor (0.14) may not be applied to the present system. The reason is the observation in Fig. 1 that a rate reduction after the maximum is small, as compared to a sharp rate reduction commonly observed for a bimolecular nucleophilic reaction, which requires a correction factor of 0.14 to calculate a real rate constant.

In summary, it has been shown that the Cu^{2+} enhances the apparent reactivity of a coordinated hydroxyl group to a remarkable extent in the neutral pH region by lowering its pK_a. It was further demonstrated that such activation of the hydroxyl group by Cu^{2+} was more pronounced in a micellar system. The obtained information is valuable for any further design of artificial hydrolytic metalloenzymes.

Experimental

Materials. The water used for kinetics was obtained by distilling deionized water twice. Acetonitrile was purified by distillation over P_2O_{10}. Commercially available, 2,6-lutidine, *N*-ethylmorpholine, and acetic acid were purified prior to use by distillation. Commercially available extra-pure $Cu(NO_3)_2 \cdot 6H_2O$ was used without further purification. Other inorganic salts used for buffer preparation were also commercial extra-pure reagents. Hexadecyltrimethylammonium bromide(**CTABr**) and sodium dodecyl sulfate(**SDS**) were recrystallized from acetonitrile before use. Poly(oxyethylene)(9.5) *p*-(1,1,3,3-tetramethylbutyl)phenol (**Triton X-100**, Kishida Chemicals) was used without further purification. The buffers were CH_3COOH–CH_3COONa (pH 4.46—4.97), 2,6-lutidine–HNO_3 (pH 5.50—6.50), and *N*-

ethylmorpholine-HNO_3 (pH 7.03—8.00), and the ionic strength was maintained at 0.2 mol dm^{-3} with NaCl (pH 4.46—4.97) or with KNO_3 (pH 5.50—8.00). *p*-Nitrophenyl picolinate(**PNPP**),[7] *N*-methyl-2-(hydroxymethyl)imidazole,[12b] and *N*-dodecyl-2-(hydroxymethyl)imidazole[13] were prepared and purified according to previous methods. **PNPP** stock solutions for kinetics were prepared in acetonitrile.

Kinetics. Kinetics were carried out according to essentially the same method as reported previously.[11-14] A Hitachi-Horiba pH meter F-8 was used for the pH determination and control. The kinetic runs for slow rates were conducted by using either a Hitachi 220 or 220A spectrophotometer equipped with a thermostated cell compartment. They were initiated by introducing a 10 μl of the **PNPP** stock solution into a 3 ml of a buffer solution containing the desired reagents. Kinetic runs for fast rates were conducted by using an Union Giken RA-401 stopped-flow spectrophotometer equipped with an RA-454 thermobath and an RA-451 computer. The **PNPP** stock solution was diluted by a buffer before use. The reactions were initiated by mixing an equal volume of **PNPP** buffer and the desired reagent solutions. In both slow and fast reactions, the rates were followed by monitoring the release of *p*-nitrophenol at 400 nm (pH 6.5—8.0) or at 320 nm (pH 4.5—6.0). The kinetic runs used for the calculation of rate constants obeyed the pseudo-first-order kinetics for at least 3 half-lives. The absorbance at infinite time (OD_∞) was recorded for each run, and the pseudo-first-order rate constants were obtained by using $k_{obsd}=(2.30/t)\log[(OD_\infty-OD_0)/(OD_\infty-OD_t)]$. The graphical methods for the analyses of these k_{obsd} to obtained k_N', K_M, k_N, and K_a are described in the text (Eqs. 7, 9, and 11).

This research was supported in part by a Grant-in-Aid for Scientific Research No. B 60470097 from the Ministry of Education, Science and Culture.

References

1) W. N. Lipscomb, *Acc. Chem. Res.*, **3**, 81 (1970); D. W. Christianson and W. N. Lipscomb, *ibid.*, **22**, 62 (1989).

2) S. Lindskog, "Adv. Inorg. Biochem.," ed by G. L. Eichhorn and L. G. Marzilli, Elsevier, New York (1982), Vol. 4, Chap. 4, pp. 115—170, S. Lindskog, *Prog. Inorg. Biochem. Biophys.*, **1**, 307 (1986).

3) J. E. Coleman and J. F. Chlebowski, "Adv. Inorg. Biochem.," ed by G. L. Eichhorn and L. G. Marzilli, Elsevier, New York (1979), Vol. 1, Chap. 1, pp. 1—66.

4) A. Fersh, "Enzyme Structure and Mechanism," 2nd ed, W. H. Freeman, New York (1985).

5) R. B. Martin, *J. Inorg. Chem.*, **38**, 511 (1976).

6) L. M. Sayre, *J. Am. Chem. Soc.*, **108**, 1632 (1986) and references therein.

7) D. S. Sigman and C. T. Jorgensen, *J. Am. Chem. Soc.*, **94**, 1724 (1972).

8) R. S. Brown, M. Zamkanei, and J. L. Cocho, *J. Am. Chem. Soc.*, **106**, 5222 (1984).

9) S. H. Gelman, R. Petter, and R. Breslow, *J. Am. Chem. Soc.*, **108**, 2388 (1986).

10) J. T. Groves and R. R. Chambers, Jr., *J. Am. Chem. Soc.*, **106**, 630 (1984); T. H. Fife and T. J. Przystas, *ibid.*, **107**, 1041 (1985); J. Suh, A. Han, and B. Chang, *ibid.*, **108**, 1839 (1986); D. R. Jones, L. F. Lindoy, and A. M. Sargeson, *ibid.*, **105**, 7327 (1983); Y. Pocker and N. Janjic, *ibid.*, **111**, 731 (1989).

11) W. Tagaki and K. Ogino, *Top. Curr. Chem.*, **128**, 143 (1985).

12) a) T. Eiki, S. Kawada, K. Matsushima, and M. Mori, and W. Tagaki, *Chem. Lett.*, **1980**, 997; b) K. Ogino, K. Shindo, T. Minami, W. Tagaki, and T. Eiki, *Bull. Chem. Soc. Jpn.*, **56**, 1101 (1983).

13) T. Eiki, M. Mori, S. Kawada, K. Matsushima, and W. Tagaki, *Chem. Lett.*, **1980**, 1431.

14) a) K. Ogino, N. Kashihara, T. Fujita, T. Ueda, T. Isaka, and W. Tagaki, *Chem. Lett.*, **1987**, 1303; b) T. Fujita, H. Minami, K. Ogino, and W. Tagaki, *ibid.*, **1987**, 2289; c) T. Fujita, K. Ogino, and W. Tagaki, *ibid.*, **1988**, 981; d) T. Fujita, Y. Inaba, K. Ogino, and W. Tagaki, *Bull. Chem. Soc. Jpn.*, **61**, 1661 (1988).

15) R. Fornasier, D. Milani, P. Scrimin, and U. Tonellato, *J. Chem. Soc., Perkin Trans. 2*, **1986**, 223; R. Fornasier, P. Scrimin, P. Tecilla, and U. Tonellato, *J. Am. Chem. Soc.*, **111**, 224 (1989).

16) T. Kuwamura, Y. Yano, S. Inokuma, Y. Takenouchi, and H. Tokue, *Chem. Lett.*, **1986**, 1519.

17) F. M. Menger, L. H. Gan, E. Johnson, and D. H. Durst, *J. Am. Chem. Soc.*, **109**, 2800 (1987).

18) L. L. Melhado and C. D. Gutsche, *J. Am. Chem. Soc.*, **100**, 1850 (1978); H.-P. Lau and C. D. Gutsche, *ibid.*, **100**, 1857 (1978); C. D. Gutsche and G. C. Mei, *ibid.*, **107**, 7964 (1985).

19) S. H. Gillman, R. Petter, and R. Breslow, *J. Am. Chem. Soc.*, **108**, 2388 (1986).

20) C. A. Bunton and L. S. Romsted, "The Chemistry of Acid Derivatives," ed by S. Patai, John Wiley & Sons, New York (1977), Part II, Chap. IV.

21) J. H. Fendler, "Membrane Mimetic Chemistry," John Wiley & Sons, New York (1982).

22) A. Martell and S. Chabarek, "Organic Sequestering Agents," Wiley, New York (1989).

23) Preliminary experiments on burst kinetics to use an excess substrate over the ligand indicated that the deacylation step is slow, so that the reaction is not catalytically efficient under the present reaction conditions.

 © 1991 The Chemical Society of Japan Bull. Chem. Soc. Jpn., 64, 81—86 (1991)

NAD(P)H-NAD(P)+ Models. 73. Structure-Stereochemistry Relationship in the Reaction of NAD Analog

Atsuyoshi OHNO,* Yuji MIKATA, Mutsuo GOTO, Takeshi KASHIWAGI,
Takanori TANAKA,† and Masami SAWADA†
Institute for Chemical Research, Kyoto University, Uji, Kyoto 611
†Material Analysis Center, The Institute of Scientific
and Industrial Research, Osaka University,
Ibaraki, Osaka 567
(Received August 31, 1990)

Four different NAD(P)H analogs have been oxidized by various substituted and unsubstituted 1,4-benzoquinones in the presence or absence of magnesium ion. The stereospecificity of the reaction depends not only on the reactivity of quinone but also on that of the analogs as well as on the presence or absence of magnesium ion. The results are discussed from the viewpoint of reaction mechanism for the transfer of a (net) hydride ion.

The central chirality at the C_4-position in 3-(*N*-methyl-*N*-α-methylbenzylcarbamoyl)-1,2,4-trimethyl-1,4-dihydroquinoline (Me_3MQPH) is converted into the axial chirality with respect to the C_3–$C_{carbonyl}$ bond in 3-(*N*-methyl-*N*-α-methylbenzylcarbamoyl)-1,2,4-trimethylquinolinium ion (Me_3MQP^+) on oxidation.[1] Stereospecificity of the chirality-transformation depends on the reactivity of the oxidizing reagent.[2,3] It is also known that the reverse reaction proceeds with high stereospecificity under appropriate reaction conditions.[4] However, the structure–stereochemistry, or the reactivity–stereochemistry, relationship in the compounds that undergo the chirality-transformation has not yet been studied, because the compound available for the investigation is limited.

Recently, we found that the axial chirality in 3-(*N*-methyl-*N*-α-methylbenzylcarbamoyl)-1-propyl-2,4-dimethylpyridinium ion (Me_3PNP^+) in a nonpolar solvent is reasonably stable at room temperature and the stereospecific conversion of the central chirality in 3-(*N*-methyl-*N*-α-methylbenzylcarbamoyl)-1-propyl-2,4-dimethyl-1,4-dihydropyridine (Me_3PNPH) into the corresponding axial chirality in Me_3PNP^+ can be studied by means of ^1H NMR spectroscopy. 4-Deuteriated Me_3MQPH and Me_3PNPH (Me_3MQPD and Me_3PNPD, respectively) are other substrates to be studied. Having four substrates in hand, we thus studied the stereospecificity associated with the chirality-transformation from the viewpoint of the structure–stereochemistry, or the reactivity–stereochemistry, relationship. The results will be discussed in relation to the mechanism of the (net) hydride transfer.

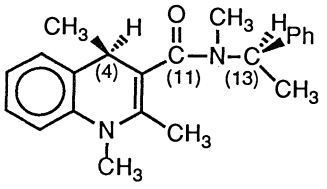

(4*R*,13*R*)-Me_3MQPH

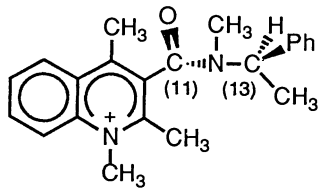

(11*R*,13*R*)-Me_3MQP^+

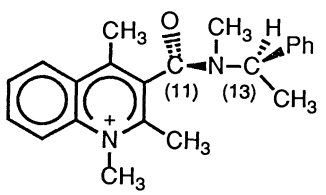

(11*S*,13*R*)-Me_3MQP^+

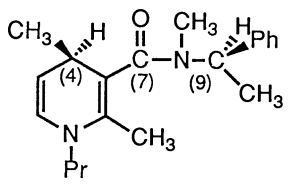

(4*R*,9*R*)-Me_3PNPH

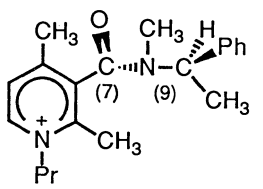

(7*R*,9*R*)-Me_3PNP^+

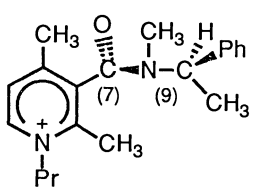

(7*S*,9*R*)-Me_3PNP^+

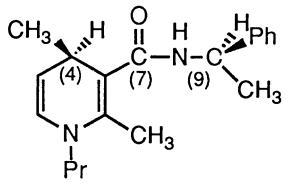

(4*R*,9*R*)-Me_2PNPH

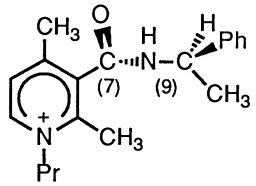

(7*R*,9*R*)-Me_2PNP^+

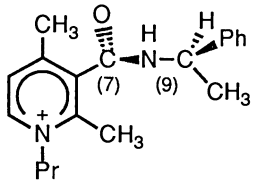

(7*S*,9*R*)-Me_2PNP^+

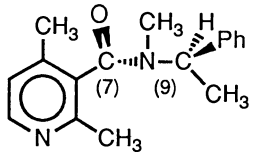

(7*R*,9*R*)-Me_3PyP

Results

Absolute Configuration and Alkylation of 3-(*N*-methyl-*N*-α-methylbenzylcarbamoyl)-2,4-dimethylpyridine. In order to study the chirality-transformation, it is neccessary to elucidate the absolute configuration at chiral centers. The absolute configuration with respect to the central chirality in Me_3PNPH has been established by the X-ray analysis on a similar compound, 3-(*N*-α-methylbenzylcarbamoyl)-1-propyl-2,4-dimethyl-1,4-dihydropyridine (Me_2PNPH).[5,6] The axial chirality in Me_3PNP^+, however, has not been studied yet. Since this onium salt is highly hygroscopic and did not afford a single crystal suitable for the X-ray crystallography, a crystal of 3-(*N*-methyl-*N*-(*R*)-α-methylbenzylcarbamoyl)-2,4-dimethylpyridine ((9*R*)-Me_3PyP) was employed for the structure analysis. Since it can be confirmed that a diastereoisomer which exerts the C_2-methyl signal at a lower field and $N_{carbamoyl}$-methyl signal at a higher field than the corresponding methyl signals from the other diastereoisomer in the ^{1}H NMR spectrum of racemic Me_3PyP corresponds to the diastereoisomer of Me_3PNP^+ which exerts the C_2-methyl signal at a lower field and $N_{carbamoyl}$-methyl signal at a higher field, the absolute configuration of Me_3PNP^+ can be correlated directly to that of Me_3PyP.

The ORTEP drawing for the diastereoisomer which exerts the C_2-methyl signal at a lower field is shown in Fig. 1. Thus, the absolute configuration of this compound is (7*R*,9*R*). The plane of pyridine-ring and that of the carbonyl group in this isomer are set close to perpendicular each other, or the C_2–C_3–C_7–O_{12} dihedral angle is −89.3°. In addition, the atoms O_{12}–C_7–N_8–C_{13} are set in the same plane. That is, it is the $N_{carbamoyl}$-methyl group that produces the axial chiralities in Me_3PyP and its derivatives. Indeed, the axial chiralities in 3-(*N*-(*R*)-α-methylbenzylcarbamoyl)-

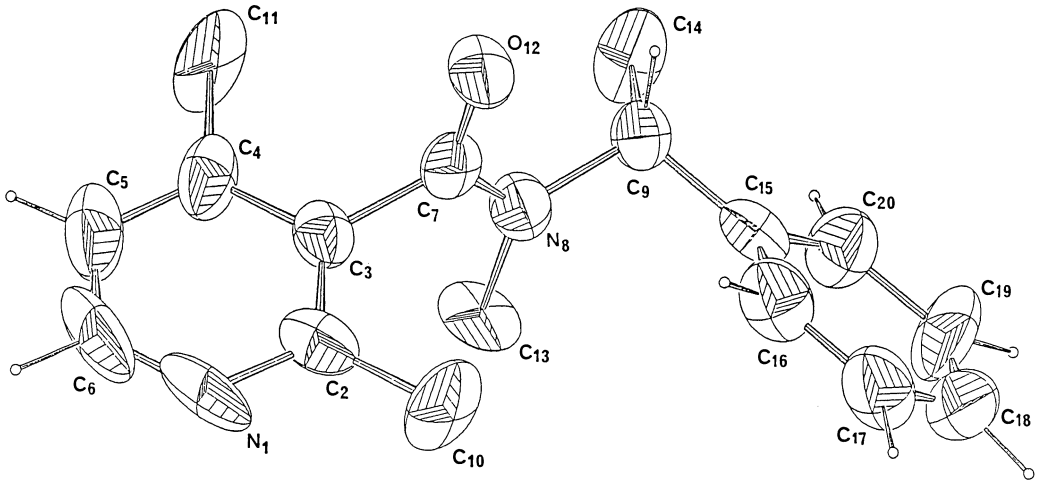

Fig. 1. ORTEP representation of (7*R*,9*R*)-Me_2PyP.

Table 1. Stereospecificity in the Oxidation in the Presence of Magnesium Ion

1,4-Benzoquinone	$E°$/V (vs. SCE)[a]	R/S Ratio (Chemical yield/%)			
		Me_3MQPH	Me_3MQPD	Me_3PNPH	Me_3PNPD
Unsubstituted	−0.50	1.0/4.9 (100)	1.0/5.6 (100)	1.0/3.9 (74)	—
Chloro-	−0.34	1.0/2.1 (100)	1.0/2.1 (92)	1.0/4.6 (90)	(49)[b]
2,5-Dichloro-	−0.18	1.0/1.3 (100)	1.0/1.4 (86)	1.0/4.7 (79)	(57)[b]
2,6-Dichloro-	−0.18	1.0/1.2 (77)	1.0/1.2 (89)	1.0/4.2 (90)	(53)[b]
Trichloro-	−0.13[c]	1.2/1.0 (100)	1.0/1.4 (71)	1.0/4.1 (73)	(64)[b]
Tetrachloro-	−0.08	1.5/1.0 (94)	1.0/1.3 (95)	1.0/4.0 (68)	(88)[b]
2,3-Dichloro-5,6-dicyano-	+0.51	1.1/1.0 (74)	1.0/1.8 (62)	1.0/4.2 (100)	(94)[b]

a) Ref. 19. b) The R/S ratio could not be determined. See Experimental for the detail. c) The mean of the values for 2,6-dichloro- and tetrachloro-1,4-benzoquinones.

Table 2. Stereospecificity in the Oxidation in the Absence of Magnesium Ion

1,4-Benzoquinone	$E°$/V (vs. SCE)[a]	R/S Ratio (Chemical yield/%)			
		Me_3MQPH	Me_3MQPD	Me_3PNPH	Me_3PNPD
Unsubstituted	−0.50	b)	b)	b)	b)
Chloro-	−0.34	1.3/1.0 (7)	1.0/1.0 (22)	1.0/2.3 (36)	1.0/2.9 (43)
2,5-Dichloro-	−0.18	1.3/1.0 (9)	1.2/1.0 (45)	1.0/1.2 (47)	1.0/1.0 (67)
2,6-Dichloro-	−0.18	1.1/1.0 (36)	1.2/1.0 (22)	1.0/2.4 (51)	1.0/2.3 (65)
Trichloro-	−0.13[c]	2.0/1.0 (62)	1.7/1.0 (100)	1.0/1.5 (76)	1.6/1.0 (76)
Tetrachloro-	−0.08	1.3/1.0 (85)	1.2/1.0 (75)	2.4/1.0 (68)	2.4/1.0 (93)
2,3-Dichloro-5,6-dicyano-	+0.51	1.0/1.0 (92)	1.0/1.5 (100)	1.0/1.2 (68)	(72)[d]

a) Ref. 19. b) No reaction. c) The mean of the values for 2,6-dichloro- and tetrachloro-1,4-benzoquinones. d) The R/S ratio could not be determined. See Experimental for the detail.

2,4-dimethylpyridine (Me_2PyP), the compound which has no methyl group on the carbamoyl-nitrogen, and its derivatives are too unstable to be fixed at room temperature, and their diastereoisomers are unable to be separated each other.

For the transformation of Me_3PyP into Me_3PNP+ by the Menschutkin N-alkylation, it is neccessary, however, to run the reaction at low temperature in order to avoid undesirable racemization. Since the reaction of Me_3PyP with propyl bromide under an atmospheric pressure requires as high temperature as to reflux the solution, the alkylation was carried out at room temperature under a high pressure (10000 kg cm^{-2}) for 25 days, and Me_3PNP+ thus obtained was recrystallized from chloroform. It was found that the propylation of (7*S*,9*R*)-Me_3PyP with propyl bromide yields a racemic mixture of (9*R*)-Me_3PNP+, whereas (7*R*,9*R*)-Me_3PyP affords a 3:1 mixture of (7*R*,9*R*)- and (7*S*,9*R*)-Me_3PNP+. On the other hand, methylation of (7*S*,9*R*)- and (7*R*,9*R*)-Me_3PyP with methyl iodide afforded the corresponding N_{ring}-methylated onium salt with 100% retention of the configuration.

Stereochemistry of the Reaction.[7] Oxidations of Me_3MQPH, Me_3MQPD, Me_3PNPH, and Me_3PNPD with various substituted and unsubstituted 1,4-benzoquinones in the presence or absence of magnesium ion in acetonitrile were run and the R/S ratios with respect to the axial chirality in the corresponding onium salts were measured on ^{1}H NMR spectrometer. The results are summarized in Tables 1 and 2.

Discussion

First of all, it is recognizable that the R/S ratio in Me_3MQP+ obtained from the reactions of Me_3MQPH without magnesium ion is not affected appreciably by the oxidation potentials of the quinones employed. However, in the presence of magnesium ion, the value of log (R/S) changes linearly from negative to positive as the oxidation potential of the quinone becomes larger. On the other hand, the R/S ratio in Me_3PNP+ obtained from the oxidations of Me_3PNPH in the absence of magnesium ion is affected by the oxidation potentials of the quinone, whereas the ratio stays at a constant value of 1/4—1/5 when magnesium ion exists in the reaction mixture.

In a previous paper where we reported the amine-catalyzed stereochemistry, we proposed that earliness and lateness of the transition state in the major process (with the highest activation energy, but not necessarily be the rate-determining step) of the reaction determine the syn/anti configurational preference[8] at the transition state: the early transition state prefers entropically favorable anti-conformation, but the late transition state prefers enthalpically favorable syn-conformation.[9] It was also proposed that the proton-transfer step is involved in the rate-determining step of the reaction of

Me_3MQPH, although the initial electron-transfer step requires larger activation energy than the proton-transfer step in the reaction with non-DDQ quinones.[9]

It is anticipated that the dihydroquinoline ring (a bicyclic system) will resist more strongly than the dihydropyridine ring (a monocyclic system) against the ring-deformation associated with their one-electron oxidation. Therefore, the former may require higher energy for oxidation (with less C_4–H bond deformation) than the latter. In other words, it is reasonable to expect that the transition-state in the stereo-determining step of the reaction with Me_3MQPH comes earlier than that with Me_3PNPH.[10] Since the proton on the C_4-position is not dissociated enough in an early transition state, the reacting quinone has to come close to the substrate.

At the same time, Me_3MQPH is sterically larger than Me_3PNPH. Both electronic and steric effects make the entropically favorable anti-configuration lower in Gibbs energy than enthalpically favored syn-configuration at the transition-state of the reaction with Me_3MQPH as illustrated in Fig. 2.[9]

Magnesium ion is known to interact with both the electron-donor and -acceptor to make the two reacting components in closer approach as an ES-complex in an enzymatic reaction.[11,12] Since the oxidizing and reducing reagents face against each other by sandwiching a magnesium ion between them, steric tightness is less important here than in the reaction without magnesium ion, and the transition state in the reaction with magnesium ion feels no (or little) stress to assume enthalpically favored but entropically disfavored syn-configuration provided the reactivity of the quinone is low enough. The statement is equivalent to say that the presence of magnesium ion retards the abstraction of a proton to set the transition state late, because the coordination of the positively charged magnesium ion makes the radical anion of quinone less reactive toward the proton-abstraction.

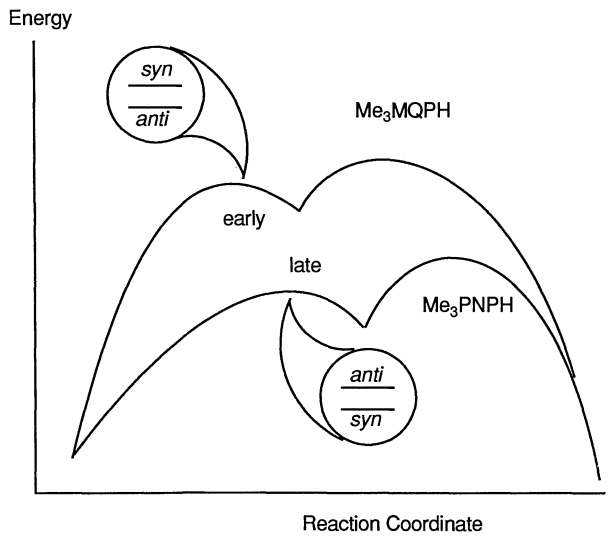

Fig. 2. Energy diagrams for the early and late transition states.

On the other hand, the transition state of the reaction with Me_3PNPH is always later than that with Me_3MQPH (with more C_4–H bond deformation) regardless the reactivity of the quinone,[9] and always passes through the syn-transition state even in the absence of magnesium ion. Of course, the presence of magnesium ion in this reaction shifts the specificity further toward the syn-preferency.

When the C_4-hydrogen in Me_3MQPH is substituted by a deuterium, the energy barrier for the proton-transfer process becomes higher due to kinetic isotope effect, then the *R*/*S* ratio, or the stereospecificity of the reaction, may be the subject of the isotope effect.[13] It is seen in Table 1 that the stereospecificity is reversed by going from Me_3MQPH (anti-preferency) to Me_3MQPD (syn-preferency) in the reactions with the quinones of high reduction potentials such as DDQ, chloranil, and trichloro-1,4-benzoquinone in the presence of magnesium ion. The isotopic difference is not so significant in the absence of magnesium ion.

The results can also be interpreted in terms of tight and loose transition states: in the reaction with Me_3MQPH(D), the proton-migrating step is affected by the isotopic substitution more sensitively than the initial electron-transfer step, and total energy barrier in the reaction of Me_3MQPD becomes higher than that of Me_3MQPH. Thus, the formation of the electron-transfer intermediate is followed by the rate-determining second step in the reaction of the deuteriated compound. Under such a circumstance, the transition state for Me_3MQPD is later and looser than that for Me_3MQPH and the formation of (11*S*,13*R*)-Me_3MQP$^+$ is more preferred by the former than the latter. As the reactivity of the quinone decreases (or in the absence of magnesium ion as well), the energy barrier for the initial electron-transfer process becomes higher, and, consequently, relative importance of the difference in energy barrier for the proton-transfer process becomes less and the isotope effect becomes smaller.

Experimental

Instruments. ^{1}H NMR spectra were recorded at 200 MHz and 400 MHz on a Varian VXR 200 FT-NMR and a JEOL JNM-GX400 FT-NMR spectrometers, respectively. ^{2}H NMR spectra were recorded at 31 MHz on a Varian VXR 200 FT-NMR spectrometer. UV spectra were obtained on a Hitachi U-3210 spectrophotometer with a Hitachi SDR-30 temperature controller. Elemental analyses were performed with a Yanaco MT-3 elemental analyzer.

Materials. Anhydrous solvents were prepared in the following way before the use: benzene, tetrahydrofuran (THF), and ether were distilled over sodium diphenyl ketyl. Acetonitrile was distilled over calcium hydride. Magnesium perchlorate was powdered, dried at 100 °C under reduced

pressure in the presence of diphosphorus pentaoxide, and placed in a sealed tube.

3-(*N*-(*R*)-α-methylbenzylcarbamoyl)-1,2,4-trimethylquinolinium iodide ($Me_2MQP^+I^-$),[14] (4*R*)-3-(*N*-(*R*)-α-methylbenzylcarbamoyl)-1,2,4-trimethyl-1,4-dihydroquinoline (Me_2MQPH)[14], 3-(*N*-(*R*)-α-methylbenzylcarbamoyl)-1-propyl-2,4-dimethylpyridinium bromide ($Me_2PNP^+Br^-$),[15] (4*R*)-3-(*N*-(*R*)-α-methylbenzylcarbamoyl)-1-propyl-2,4-dimethyl-1,4-dihydropyridine (Me_2PNPH),[15] and 3-(*N*-methyl-*N*-(*R*)-α-methylbenzylcarbamoyl)-1-propyl-2,4-dimethylpyridinium iodide ($Me_3PNP^+I^-$),[1] were prepared according to the literature procedures. Trichloro-1,4-benzoquinone was prepared according to the literature procedure.[16]

Preparation of (4*R*)-3-(*N*-Methyl-*N*-(*R*)-α-methylbenzylcarbamoyl)-1,2,4-trimethyl-1,4-dihydroquinoline (Me_3-MQPH). In a 20 ml round-bottomed flask equipped with a magnetic stirrer and sealed with a serum cap, 128 mg (0.40 mmol) of Me_2MQPH and 227 mg (2.0 mmol) of potassium *t*-butoxide were placed. Then, the atmosphere inside the flask was replaced with nitrogen and 20 ml of anhydrous THF was injected into it through a syringe. The mixture was stirred for a while. The color turned pale yellow. Therein, 0.125 ml (2.0 mmol) of methyl iodide was injected dropwise with continuous stirring. An exothermic reaction occurred and white precipitates were formed. The mixture was stirred for an hour at room temperature in the dark under an atmosphere of nitrogen. The precipitates were filtered off and the filtrate was concentrated by evaporation of the solvent under reduced pressure. The residue was dissolved into dichloromethane. The solution was washed twice with water, dried over sodium sulfate, passed through a silica pad, and the solvent was evaporated under reduced pressure. Me_3MQPH was obtained in 120 mg (0.35 mmol) as a slightly yellow oil in 87% yield. Spectral data were the same as those reported.[1] The 4-deuteriated compound was prepared similarly.

Preparation of (4*R*)-3-(*N*-Methyl-*N*-(*R*)-α-methylbenzylcarbamoyl)-1-propyl-2,4-dimethyl-1,4-dihydropyridine (Me_3-PNPH). Me_2PNPH was methylated at the carbamoylnitrogen in 84% yield with the same procedure as described above. The 4-deuteriated compound was prepared similarly. It was recognized that all the six hydrogens in the C_2- and C_4-methyl groups exchanged with deuteriums during the 4-deuteration.

Although Me_3PNPH is reasonably stable in a solution to be reacted with quinones and other oxidizing reagents, it decomposes immediately into unidentified product(s) when the solvent is evaporated completely under reduced pressure at room temperature or below, and elemental analysis of this compound does not give satisfactory results.

^1H NMR ($CDCl_3$): δ^{TMS}=0.89 (t, 3H), 1.11 (m, 3H), 1.53 (br.d, 3H), 1.84 (s, 3H), 2.73 (s, 3H), 2.8—3.3 (m, 3H), 4.45 (br.s, 1H), 6.18 (br.s, 1H), and 7.3—7.4 (m, 5H).

Preparation of 3-(*N*-Methyl-*N*-(*R*)-α-methylbenzylcarbamoyl)-2,4-dimethylpyridine ((9*R*)-Me_3PyP). In a 200 ml three-necked round-bottomed flask equipped with a magnetic stirrer and a reflux condenser protected with a calcium chloride tube, were placed 5 g (27 mmol) of 2,4-dimethylpyridine-3-carboxylic acid hydrochloride[15] and 28 ml (0.38 mol) of thionyl chloride. The solution was refluxed for 40 min. The color of the solution turned red. After excess thionyl chloride was removed by distillation under reduced pressure, the brown residue was obtained. Onto the residue, 13 ml of triethylamine dissolved in 20 ml of dichloromethane was added dropwise with stirring and cooling in an ice-salt bath. A brown solid precipitated. Subsequently, 3.7 g (30 mmol) of *N*-methyl-(*R*)-α-methylbenzylamine dissolved in 20 ml of dichloromethane was added to the solution over an hour with cooling in an ice-salt bath. The reaction mixture was stirred overnight at room temperature. After evaporation of the solvent keeping the temperature below 40 °C under reduced pressure, a brown residue was obtained. To the residue, 25 ml of concd hydrochloric acid and 100 ml of water were added and the solution was treated three times with activated charcoal. Thus obtained yellow solution was neutralized with sodium carbonate to obtain white precipitates. The reaction mixture was extracted with dichloromethane. The combined organic layer was washed with aqueous sodium hydrogencarbonate and two portions of water, and dried over sodium sulfate. Removal of the solvent under reduced pressure gave a white solid, which was washed with ether to give 2.11 g (8.2 mmol) of Me_3PyP in 30.4% yield. This is a mixture of two diastereomers with respect to the carbamoyl rotation.

Each diastereomers were partially separated by silica-gel column chromatography with a 1:1 mixture of acetone and hexane as an eluent. The crystals were recrystallized from a solution of chloroform in a refrigerator to obtain a single crystal of (7*R*,9*R*)-Me_3PyP; mp (uncorrected) 104—105 ° C for the (7*R*,9*R*)-isomer: 80—81 °C for the (7*S*,9*R*)-isomer.

Anal. Calcd for $C_{17}H_{20}N_2O$ (a 3/1 7*R*/7*S* mixture): C, 76.09; H, 7.51; N, 10.44%. Found: C, 75.98; H, 7.58; N, 10.35%.

^1H NMR ($CDCl_3$): (7*R*,9*R*)-Me_3PyP (earlier eluent); δ^{TMS}= 1.64 (d, 3H), 2.31 (s, 3H), 2.44 (s, 3H), 2.47 (s, 3H), 6.32 (q, 1H), 7.02 (d, 1H), 7.30—7.48 (m, 5H), and 8.37 (d, 1H). (7*S*,9*R*)-Me_3PyP (later eluent); δ^{TMS}=1.64 (d, 3H), 2.25 (s, 3H), 2.43 (s, 3H), 2.52 (s, 3H), 6.32 (q, 1H), 6.98 (d, 2H), 7.30—7.48 (m, 5H), and 8.36 (d, 1H).

Preparation of 3-(*N*-Methyl-*N*-(*R*)-α-methylbenzylcarbamoyl)-1-propyl-2,4-dimethyl-1,4-dihydropyridinium Bromide ($Me_3PNP^+Br^-$). Into a Teflon tube, 106 mg (0.41 mmol) of Me_3PyP and 3.4 g (27 mmol) of propyl bromide in 2 ml of ethanol were placed. The tube was placed in an autoclave under high pressure (10000 kg cm^{-2}) for 25 days at room temperature to undergo the reactions. After the evaporation of the ethanol under reduced pressure, the residue obtained in quantitative yield was washed with ether and subjected to ^1H NMR spectroscopy. The $Me_3PNP^+Br^-$ obtained from (7*R*,9*R*)-Me_3PyP was diastereomerically purer than that obtained from (7*S*,9*R*)-Me_3PyP, which was an equivalent mixture of the two diastereoisomers. This compound is too hygroscopic to obtain satisfactory results from elemental analysis.

^1H NMR ($CDCl_3$): $Me_3PNP^+Br^-$ from (7*R*,9*R*)-Me_3PyP; δ^{TMS}=1.00 (m, 3H), 1.15 (d, 3H), 1.85 (m, 2H), 2.52 (s, 3H), 2.53 (s, 3H), 2.61 (s, 3H), 4.56 (q, 2H), 6.08 (q, 1H), 7.3—7.5 (m, 5H), 7.88 (d, 1H), and 8.98 (d, 1H). $Me_3PNP^+Br^-$ from (7*S*,9*R*)-Me_3PyP; in addition to the signals listed above δ^{TMS}=2.40 (s, 3H), 2.51 (s, 3H), and 2.71 (s, 3H).

X-Ray Analysis. Crystal data of Me_3PyP are as follows: MW=268.36. Orthorhombic. Space group $P2_12_12_1$. a= 14.471(1), b=14.483(2), c=7.387(1) Å. V=1548.2(0.7) Å^3, Z=4 molecules/cell, and D_c=1.156 g cm^{-3}.

A piece of crystal (size 0.4×0.4×0.5 mm^3) was used for the

data collection. Cell dimensions were determined by least squares calculations with 2θ values of 25 reflections measured on a Rigaku AFC-5FOS four-circle diffractometer by using graphite-monochromated Mo-$K\alpha$ radiation (λ= 0.7107 Å). Intensity data of 1537 reflections with $2\theta \leq 55°$ were collected by the use of the θ-2θ mode with a scanning rate of 16° min^{-1} in 2θ. The reflection data were not corrected for absorption.

All of the reflections were used for solution. The structure was solved by means of MULTAN 84.[17] Block-diagonal least squares refinement with anisotropic temperature factors for non-hydrogen atoms converged successfully to R=0.067. Eight hydrogen atoms were included in computation. Calculations were performed on FACOM S3500 superminicomputer in TASMAC, ISIR, Osaka University.

Selected torsional angles are as follows: $\angle C_4$-C_3-C_7-O_{12}= 82.5°, $\angle C_4$-C_3-C_7-N_8=−95.9°, $\angle C_2$-C_3-C_7-O_{12}=−89.3°, $\angle C_2$-C_3-C_7-N_8=92.3°, $\angle C_{11}$-C_4-C_3-C_7=9.0°, $\angle O_{12}$-C_7-N_8-C_9=0.3°, $\angle O_{12}$-C_7-N_8-C_{13}=−177.8°.

The complete F_o−F_c data are deposited as Document No. 9092 at the Office of the Editor of Bull. Chem. Soc. Jpn.

Reaction. In a 50 ml round-bottomed flask equipped with a magnetic stirrer and sealed with a serum cap, 0.03 mmol of a 1,4-benzoquinone derivative was placed. Then, the atmosphere inside the flask was replaced with argon and 28 ml of anhydrous acetonitrile was injected through a syringe. To the solution, 2 ml of acetonitrile solution containing 10 mg (0.03 mmol) of Me_3MQPH (and 6.7 mg (0.03 mmol) of magnesium perchlorate, if necessary) was injected through a syringe. Then, the mixture was stirred for 24 h at room temperature in the dark. After evaporation of the solvent below 40 °C under reduced pressure, the residue was washed twice with ether and the crude Me_3MQP^+ was dissolved in CD_3CN and subjected to ^1H NMR spectroscopy to elucidate the diastereomer ratio and the yield of the product. The ^1H NMR spectrum of Me_3MQP^+ thus obtained was the same as that reported.[1] The R/S ratio was measured by means of the N_{ring}-methyl signals (for Me_3MQP^+) or the C_2- and C_4-methyl signals (For Me_3PNP^+). Therefore, in principle, the ratio in Me_3PNP^+ produced from Me_3PNPD (i.e. $(CD_3)_2MePNP^+$) could not be measured. However, the deuteriums in $(CD_3)_2MePNP^+$ again exchanged with hydrogens during the reaction without magnesium ion, probably due to the presence of trace amount of water in the solvent. Magnesium perchlorate is a well-known drying agent.[18] No doubt that the hydrogen-deuterium exchange does not affect the stereochemistry.[13]

It was confirmed, using 1:1 and 3:1 mixtures of the diastereoisomers, that the conformation of Me_3MQP^+ is sufficiently stable during the reaction, work-up and the spectroscopy.

The stereospecificities in the reactions with other compounds were determined similarly.

We thank financial support for this research by Japanese Ministry of Education, Science and Culture under the Grant-in-Aid Nos. 01470022, 01303007, 02303004, and 02740265.

References

1) A. Ohno, M. Kashiwagi, Y. Ishihara, S. Ushida, and S. Oka, *Tetrahedron*, **42**, 961 (1986).

2) A. Ohno, M. Ohara, and S. Oka, *J. Am. Chem. Soc.*, **108**, 6438 (1986).

3) A. Ohno, M. Ogawa, and S. Oka, *Tetrahedron Lett.*, **29**, 3079 (1988).

4) A. Ohno, M. Ogawa, and S. Oka, *Tetrahedron Lett.*, **29**, 1951 (1988).

5) H. J. G. van Hooff, P. M. van Lier, L. A. M. Bastiaansen, and H. M. Buck, *Rec. Trav. Chim. Pays-Bas*, **101**, 191 (1982).

6) P. M. van Lier, M. C. A. Donkersloot, A. S. Koster, H. J. G. van Hooff, and H. M. Buck, *Rec. Trav. Chim. Pays-Bas*, **101**, 119 (1982).

7) In the present research, the compounds we employed always have the R-configuration at the α-methylbenzyl group on the amide-nitrogen. At the same time, the configuration at the C_4-position in $Me_3MQPH(D)$ or $Me_3PNPH(D)$ is always R. Therefore, we will neglect hereafter, for simplicity of the discussion, the signs to indicate the chirality at these positions in these compounds, unless neccessary. With this understanding, we can only deal with the axial chiralities in Me_3MQP^+ or Me_3PNP^+, which will be indicated by R or S without specifying the position. Stereospecificity of the reaction has been confirmed using other diastereoisomers of Me_3MQPH and Me_3PNPH.[2]

8) The *anti*-transition state is the one in which the C_4–H and C=O bonds in Me_3MQPH or Me_3PNPH point the opposite face of the molecular plane each other, whereas these bonds point the same face in the *syn*-transition state.

Recently, we obtained thermodynamic parameters for the *syn*- and *anti*-transition states to support our proposal on their relative stabilities. The results will be published elsewhere in near future.

9) A. Ohno, M. Ogawa, Y. Mikata, and M. Goto, *Bull. Chem. Soc. Jpn.*, **63**, 813 (1990).

10) The earliness and lateness of transition state, which may be substituted by the term "molecular polarizability", have been witnessed kinetically: A. Ohno, M. Goto, Y. Mikata, T. Kashiwagi, and T. Maruyama, *Bull. Chem. Soc. Jpn.*, **64**, 87 (1991). (The succeding paper)

11) A. Ohno, T. Kimura, H. Yamamoto, S. G. Kim, S. Oka, and Y. Ohnishi, *Bull. Chem. Soc. Jpn.*, **50**, 1535 (1977).

12) A. Ohno, J. Nakai, K. Nakamura, T. Goto, and S. Oka, *Bull. Chem. Soc. Jpn.*, **54**, 3482 (1981).

13) The secondary kinetic deuterium isotope effect has been found to be 1.01.[10]

14) A. Ohno, Y. Ishihara, S. Ushida, and S. Oka, *Tetrahedron Lett.*, **23**, 3185 (1982).

15) A. Ohno, M. Ikeguchi, T. Kimura, and S. Oka, *J. Am. Chem. Soc.*, **101**, 7036 (1979).

16) H. Biltz and W. Giese, *Chem. Ber.*, **37**, 4010 (1904).

17) P. Main, G. Germain, and M. M. Woolfson, MULTAN 84, a computer program for the automatic solution of crystal structures from X-ray diffraction data, University of York, York, England (1984).

18) Cf. M. F. Powell and T. C. Bruice, *J. Am. Chem. Soc.*, **104**, 5834 (1982); A. Ohno, H. Kobayashi, and S. Oka, *Tetrahedron Lett.*, **24**, 1263 (1983).

19) S. Fukuzumi, N. Nishizawa, and T. Tanaka, *J. Org. Chem.*, **49**, 3571 (1984).

 © 1991 The Chemical Society of Japan Bull. Chem. Soc. Jpn., 64, 87—90 (1991)

NAD(P)H-NAD(P)+ Models. 74. Entropy-Controlled Kinetics, Stereochemistry, and Tunneling Effect

Atsuyoshi OHNO,* Mutsuo GOTO, Yuji MIKATA,
Takeshi KASHIWAGI, and Tetsushi MARUYAMA
Institute for Chemical Research, Kyoto University, Uji, Kyoto 611
(Received August 31, 1990)

Kinetics have been studied for the reactions of three NAD(P)H analogs and their 4-deuteriated compounds with 2,6-dichloro- and tetrachloro-1,4-benzoquinones. It has been elucidated that the entropy term occupies 50—90% of the Gibbs energy of activation at 298 K. Thus, the reaction is almost entropy-controlled. For certain combinations of the reducing and oxidizing reagents, quantum mechanical tunneling effect plays a large role to determine the reaction rate. The tunneling effect may be another measure of the stereochemistry.

Stereochemistry in the oxidation of 3-(*N*-methyl-*N*-α-methylbenzylcarbamoyl)-1,2,4-trimethyl-1, 4-dihydroquinoline (Me_3MQPH) or 3-(*N*-methyl-*N*-α-methylbenzylcarbamoyl)-1-propyl-2,4-dimethyl-1,4-dihydropyridine (Me_3PNPH) exert free-energy structure–reactivity–stereochemistry relationship; that is, the stereospecificity associated with the transfer of the central chirality in Me_3MQPH or Me_3PNPH into the axial chirality in their corresponding oxidized forms (Me_3MQP^+ or Me_3PNP^+, respectively) depends on the oxidation and reduction potentials of the reducing and oxidizing reagents.[1,2] The reactive pair prefers the anti-transition state while the less reactive pair prefers the syn-transition state.[3] Based on the stereochemical results, it was concluded that the syn/anti preferency in the transition state stems from the earliness or lateness of the transition state.[1,2]

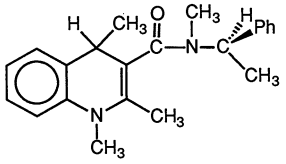

Me_3MQPH

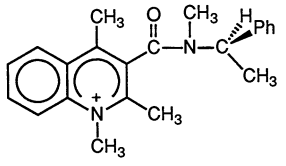

Me_3MQP^+

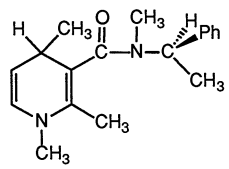

Me_3PNPH

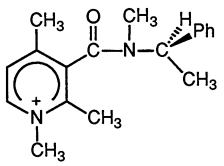

Me_3PNP^+

In order to obtain further evidence for the proposed structure of transition state of the reaction, we studied kinetics and elucidated kinetic parameters. Since kinetics become very much complicated in the presence of magnesium ion,[4] the reaction without magnesium ion was studied. 2,6-Dichloro-1,4-benzoquinone (**2Q**) and tetrachloro-1,4-benzoquinone (chloranil, **4Q**) were chosen as the least and most reactive oxidizing reagents, hence, corresponding to the latest and earliest transition states, respectively, under the reaction conditions employed.[5] Although there are many contributions on the kinetics and kinetic isotope effects to discuss on the reaction mechanism of NAD(P)H analogs,[4,6–18] kinetic parameters have scarcely been studied and discussed.[11]

Results

Since the present study does not require to deal with stereochemistry, it is not neccessary to use a compound with a stable axial chirality. Therefore, we employed 3-(*N*-α-methylbenzylcarbamoyl)-1,2,4-trimethyl-1,4-dihydroquinoline (Me_2MQPH) and 3-(*N*-α-methylbenzylcarbamoyl)-1-propyl-2,4-dimethyl-1,4-dihydropyridine (Me_2PNPH) in place of Me_3MQPH and Me_3PNPH.

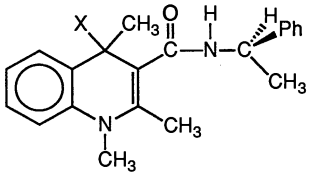

X=H : Me_2MQPH
X=D : Me_2MQPD

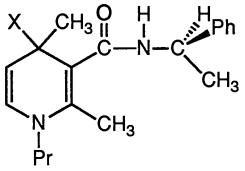

X=H : Me_2PNPH
X=D : Me_2PNPD

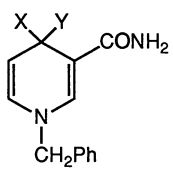

X=H,Y=H : BNAH
X=H,Y=D : BNAD
X=D,Y=D : $BNAD_2$

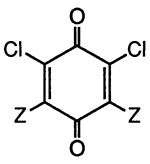

Z=H : 2Q
Z=Cl : 4Q

In addition to Me_2MQPH and Me_2PNPH, and their 4-deuteriated derivatives (Me_2MQPD and Me_2PNPD, respectively), *N*-benzyl-1,4-dihydronicotinamide (BNAH) and its 4-deuteriated and 4,4-dideuteriated derivatives (BNAD and $BNAD_2$, respectively) were also studied to convince of the results from the former compounds. BNAH is a compound which has been studied most

extensively.

When an acetonitrile solution of Me_2PNPH was mixed with that of **4Q** under argon atmosphere, a yellow color appeared immediately. This strong absorption band at λ_{max}=449 nm (ε=8,000 M^{-1}) was identified to that of the radical anion from **4Q**.[19] **2Q** behaved similarly (λ_{max}=448 nm). The ESR spectrum of each solution exhibited a signal from the radical anion of the quinone.[19-21] The radical anions thus produced were stable in the presence of excess amount of the quinones, but disappeared gradually at room temperature when the NAD(P)H analog existed in excess amount. The kinetics of the reaction of BNAH with quinones have been studied extensively by Fukuzumi and his co-workers,[11] and we employed the reaction scheme proposed by them.

The observed pseudo-first-order rate constants (with more than 10-fold excess of a reagent), calculated by following the increase in absorbances at the absorption maxima of the corresponding radical anions, are plotted against the concentrations of the analog and of the quinone, respectively, indicating that the reaction is first-order in both the analog and the quinone. Temperatures employed for the measurements ranged from 273 to 323 K with 5 to 15 K intervals. The second-order rate constants, primary and secondary kinetic deuterium isotope effects, and kinetic parameters are summarized in Tables 1 and 2. Primary kinetic deuterium isotope effects in the BNAH systems are in good agreement with those reported.[12]

Discussion

It is apparent that the overall reaction is controlled by the entropy; at 298 K, the entropy term amounts about 10 kcal mol^{-1}, which is about 50—90% of the Gibbs energy of activation. This is a brand-new and important observation because there has ever appeared no discussion on the reaction mechanism of the

Table 1. Kinetic Parameters, Isotope Effects, and Stereochemistry of the Oxidation of NAD(P)H Analogs with Chloranil[a]

	Me_2MQPD		Me_2MQPH	$BNAD_2$	BNAD	BNAH	Me_2PNPD		Me_2PNPH
$k_2/M^{-1}\,s^{-1}$	27.8		130	233	716	1210	19600		45000
$(k_H/k_D)_{obsd}$		4.68			5.14			2.30	
$(k_H/k_D)_{calcd}$[b]		4.30			8.90			3.22	
$(k_H/k_D)_{second}$[c]					1.01				
$\Delta G^{\neq}$/kcal mol^{-1}	15.5		14.6	14.2	13.6	13.2	11.6		11.1
$\Delta H^{\neq}$/kcal mol^{-1}	5.84		4.98	4.29	3.07	3.00	1.16		0.47
$-\Delta S^{\neq}$/cal mol^{-1} deg^{-1}	32.3		32.7	33.4	35.2	34.3	35.0		35.6
δE_a[d]/kcal mol^{-1}		−0.86			−1.29			−0.69	
A_H/A_D		1.15			0.62			0.72	
Mechanism[e]		Classic			Tunnel			Classic	
R/S Ratio[f]		1.2—1.3/1			—			2.4/1	

a) The values listed in the Table are those at 298 K. Errors in rate constants and kinetic isotope effects are estimated to be ±3 and ±5%, respectively. Those for parameters of activation are less than ±10%. The deuterium content in $BNAD_2$ was 97%, which was corrected to obtain the observed rate constant. b) Calculated from the enthalpy of activation assuming no difference in entropy of activation for protiated and deuteriated compounds. c) Calculated according to the Powell and Bruice's equation; Ref. 28. d) $\delta=X_H-X_D$. e) Ref. 24. f) Ref. 1.

Table 2. Kinetic Parameters, Isotope Effects, and Stereochemistry of the Oxidation of NAD(P)H Analogs with 2,6-Dichloro-1,4-benzoquinone[a]

	Me_2MQPD		Me_2MQPH	$BNAD_2$	BNAD	BNAH	Me_2PNPD		Me_2PNPH
$k_2/M^{-1}\,s^{-1}$	6.89		25.9	13.9	62.0	84.4	1990		6030
$(k_H/k_D)_{obsd}$		3.75			6.01			3.03	
$(k_H/k_D)_{calcd}$[b]		5.35			11.48			7.39	
$(k_H/k_D)_{second}$[c]					1.01				
$\Delta G^{\neq}$/kcal mol^{-1}	16.3		15.6	15.9	15.1	14.8	13.0		12.3
$\Delta H^{\neq}$/kcal mol^{-1}	7.98		6.99	6.67	5.50	5.23	2.01		0.829
$-\Delta S^{\neq}$/cal mol^{-1} deg^{-1}	28.0		28.8	30.9	32.2	32.2	36.9		38.4
δE_a[d]/kcal mol^{-1}		−1.00			−1.43			−1.18	
A_H/A_D		0.67			0.54			0.47	
Mechanism[e]		Classic			Tunnel			Tunnel	
R/S Ratio[f]		1.2—1.1/1			—			1/2.3—2.4	

a) The values listed in the Table are those at 298 K. Errors in rate constants and kinetic isotope effects are estimated to be ±3 and ±5%, respectively. Those for parameters of activation are less than ±10%. The deuterium content in $BNAD_2$ was 97%, which was corrected to obtain the observed rate constant. b) Calculated from the enthalpy of activation assuming no difference in entropy of activation for protiated and deuteriated compounds. c) Calculated according to the Powell and Bruice's equation; Ref. 28. d) $\delta=X_H-X_D$. e) Ref. 24. f) Ref. 1.

NAD(P)H analog from the viewpoint of entropy.

The entropy of activation changes most evidently on changing Me_2PNPH to Me_2PNPD in the reaction with **2Q**, where the syn-transition state is preferred: That is, the primary kinetic deuterium isotope effect calculated on the basis of enthalpy of activation (7.39) is more than twice as large as that observed (3.03). The result strongly suggests that the quantum mechanical tunneling effect plays a major role in differentiating the reactivities of protiated and deuteriated compounds.[22,23] The importance of the tunneling effect can also be recognized by Kwart's diagnosis.[24] Although a part of Kwart's proposal has been claimed,[25,26] the reaction with a large difference in E_a (ca. 1.5—6 kcal mol^{-1}) and very small A_H/A_D value (<0.6) can safely be attributed to a tunneling transition state. With this criterion, the reaction of Me_2PNPH with **2Q** as well as the reactions of BNAH with both **2Q** and **4Q** is believed to pass through the tunneling transition state.[14–18] This is not true for the reaction with Me_2MQPH which passes through the anti-transition state preferentially.

Namely, although the changes in Gibbs energy of activation at 298 K on deuteriation are the same for the Me_2MQPH and the Me_2PNPH systems in the reaction with **2Q** ($\delta\Delta G^{\neq}=-0.7$ kcal mol^{-1}), the changes in enthalpy and entropy of activation for the Me_2MQPH system ($\delta\Delta H^{\neq}=-0.99$ kcal mol^{-1}; $\delta\Delta S^{\neq}=-0.8$ cal mol^{-1} deg^{-1}) are largely different from those for the Me_2PNPH system ($\delta\Delta H^{\neq}=-1.18$ kcal mol^{-1}; $\delta\Delta S^{\neq}=-1.5$ cal mol^{-1}deg^{-1}) in accord with the proposal of classical transition state for Me_2MQPH and quantum mechanical tunneling effect for Me_2PNPH.

In the reactions with **4Q**, the tunneling effect is smaller (or even negligible) than that in the reaction with **2Q**, which reveals that the proton (or hydrogen atom)-transfer process in a reaction with the former quinone requires larger movement of the nucleus than that in a reaction with the latter quinone. Since the reactivity of **4Q** for the electron-transfer process is much larger than that of **2Q**, the electron-transfer takes place at the early stage of the ring-deformation, or the C_4–H bond in the NADH analog is less elongated, and the C_4-proton (or hydrogen atom) of the NADH analog in the reaction with **4Q** has to migrate longer distance than that in the reaction with **2Q** in the succeding proton (or hydrogen atom)-transfer process.[1)]

The present result again supports the multi-step reaction mechanism for the transfer of a (net) hydride by proving that when the electron-transfer process is associated with a low activation energy and proceeds fast, the succeeding proton (or hydrogen atom)-transfer process becomes slow due to a high activation energy.[7,8)]

The oxidation potentials of Me_2MQPH, Me_2PNPH, and BNAH measured by the scanning rate method[6,13)] are +0.83, +0.62, and +0.59 (lit,[12)] 0.57) V (vs. SCE), respectively, which means that the rate of the initial electron-transfer increases in this order. Taking into consideration the discussion mentioned above for the proton (or hydrogen atom)-transfer process, the energy diagrams along the total reaction coordinate may be those that are represented in Fig. 1.[1)]

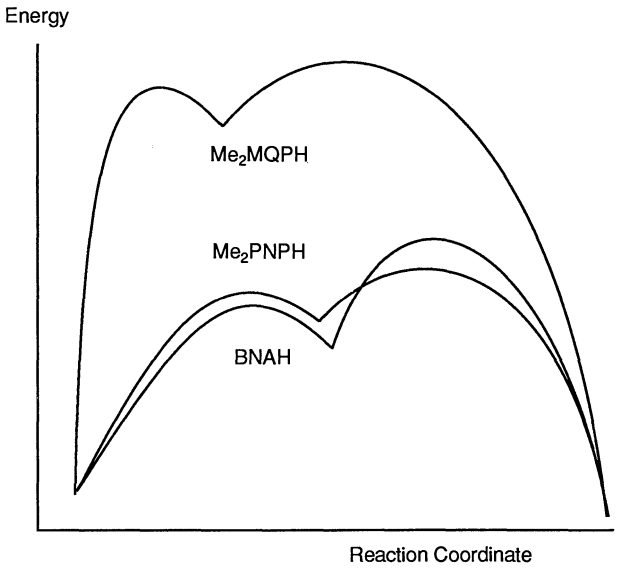

Fig. 1. Energy diagram along the reaction coordinate in the reactions of Me_2MQPH, Me_2PNPH, and BNAH.

The present conclusion is in good agreement with the idea proposed previously that the syn-configuration is favored enthalpically in a late transition state but the anti-configuration is favored entropically in an early transition state.[1,2)] That is, the NAD(P)H analog in a reaction which has to pass through a hindered transition state as a result of strong interaction between two reacting reagents prefers to assume entropically favorable anti-conformation to make the transition state less hindered and entropically favorable, whereas that in another reaction which is accompanied by less small entropy of activation can assume enthalpically favored syn-conformation at the transition state.

It is thus interesting to point out that, although the syn/anti selection is controlled by the electronic effect from the reagent(s), or there holds a linear free-energy reactivity-stereochemistry relationship,[1,2)] the essential of the effect stems from the entropic (or steric) effect instead of the enthalpic effect. That is, the electronic effect controls molecular assembly at the intermediate and/or transition state, and the molecular assembly is the subject of entropy-control, at the same time. Consequently, the electronic effect is related to the entropic effect, then to stereospecificity. In this sense, the electronic effect discussed in this paper is entirely

different from the stereoelectronic effect proposed and developed by Delongchamps and other researchers.[27]

A careful inspection of Tables 1 and 2 suggests that the classical (which corresponds to the early or anti-configurational) or quantum mechanical tunneling (which corresponds to the late or syn-configurational) transition state may be another measure of the stereochemistry of the reaction. We need more data before concluding the stereochemistry–transition-state structure relationship.

Experimental

Instruments. ^{1}H NMR spectra were recorded at 200 and 400 MHz on a Varian VXR 200 FT-NMR and a JEOL JNM-GX400 FT-NMR spectrometers, respectively. ^{2}H NMR spectra were recorded at 31 MHz on a Varian VXR 200 FT-NMR spectrometer. UV spectra were obtained on a Hitachi U-3210 spectrometer with a Hitachi SDR-30 temperature controller. ESR spectra were recorded on a JEOL JES-RE 2XG spectrometer. Kinetic measurements were performed with a Union Giken RA-401 Rapid Reaction Analyzer equipped with a Union Giken K2R temperature controller and a Union Giken System 77 or a NEC PC9801 microcomputer system. Elemental analyses were performed with a Yanako MT-3 elemental analyzer.

Cyclic voltammetry and controlled potential macro-electrolysis were performed with a Hokuto Denko HAB-151 potentiostat/galvanostat. Cyclic voltammograms were recorded on a Riken Denshi F-35 X-Y recorder. A platinum electrode sealed in heat-shrinkable Teflon was employed as the working electrode. A platinum wire and an Ag/AgCl electrodes were used as the counter and reference electrodes, respectively.

Materials. Detailed procedures for the preparation and purification of reagents employed for the present study were described in the previous report.[1]

Kinetics. Kinetics measurements were carried out by using a stopped-flow apparatus from 273 to 323 K with 5 to 15 K intervals under argon atmosphere. Reaction rate was followed by observing the increase in absorbance at the absorption maxima of the anion radical of quinones in acetonitrile under pseudo-first-order conditions by using more than 10-fold excess quinone. Pseudo-first-order rate constants and kinetic parameters were calculated by the least-squares curve-fit, using a personal computer.

Oxidation Potential. The oxidation peak potentials of Me_2MQPH, Me_2PNPH, and BNAH were measured with cyclic voltammetry at 298 K in 10 ml acetonitrile containing 0.1 M (M=mol dm^{-3}) tetraethylammonium perchlorate and 2 mM NADH analog by changing the scan rate in the range 20—2,000 mV/s. The error in observation was estimated to be ±0.005 mV. The detailed procedure has been described in a literacture.[12] The observed potential against Ag/AgCl electrode was corrected for the potential against SCE by subtracting a value of 0.042 V.

We thank financial support for this research by Japanese Ministry of Education, Science and Culture under the Grant-in-Aid Nos. 01470022, 01303007, 02303004, and 02740265. We also wish to thank Professor R. L. Schowen, the University of Kansas, for his valuable advice.

References

1) A. Ohno, Y. Mikata, M. Goto, T. Kashiwagi, T. Tanaka, and M. Sawada, *Bull. Chem. Soc. Jpn.*, **64**, 81 (1991). (The preceding paper)

2) A. Ohno, M. Ogawa, Y. Mikata, and M. Goto, *Bull. Chem. Soc. Jpn.*, **63**, 813 (1990) and references cited therein.

3) The syn-transition state is the one in which the C_4–H and C=O bonds in Me_3MQPH or Me_3PNPH point the same face of the molecular plane, whereas these bonds point the opposite face in the anti-transition state.

4) A. Ohno, H. Yamamoto, T. Okamoto, S. Oka, and Y. Ohnishi, *Bull. Chem. Soc. Jpn.*, **50**, 2385 (1977).

5) DDQ is more reactive quinone than chloranil. However, DDQ is different in reactivity from other quinones and cannot be appointed as a representative of quinones.[6]

6) L. L. Miller and J. R. Valentine, *J. Am. Chem. Soc.*, **110**, 3982 (1988).

7) A. Ohno, H. Yamamoto, and S. Oka, *J. Am. Chem. Soc.*, **103**, 2041 (1981).

8) A. Ohno, T. Shio, H. Yamamoto, and S. Oka, *J. Am. Chem. Soc.*, **103**, 2045 (1981).

9) T. Okamoto, A. Ohno, and S. Oka, *J. Chem. Soc., Chem. Commun.*, **1977**, 181.

10) S. Fukuzumi and T. Tanaka, *Chem. Lett.*, **1982**, 1513.

11) S. Fukuzumi, N. Nishizawa, and T. Tanaka, *J. Org. Chem.*, **49**, 3571 (1984).

12) S. Fukuzumi, N. Nishizawa, and T. Tanaka, *J. Chem. Soc., Perkin Trans. 2*, **1985**, 371.

13) S. Fukuzumi, S. Koumitsu, K. Hironaka, and T. Tanaka, *J. Am. Chem. Soc.*, **109**, 305 (1987).

14) M. M. Kreevoy, D. Ostovic, and D. G. Truhlar, *J. Phys. Chem.*, **90**, 3766 (1986).

15) M. M. Kreevoy, D. Ostovic, I-S. H. Lee, D. A. Binder, and G. W. King, *J. Am. Chem. Soc.*, **110**, 524 (1988).

16) I-S. H. Lee, D. Ostovic, and M. M. Kreevoy, *J. Am. Chem. Soc.*, **110**, 3989 (1988).

17) M. M. Kreevoy and A. T. Kotchevar, *J. Am. Chem. Soc.*, **112**, 3579 (1990).

18) W. P. Huskey and R. L. Schowen, *J. Am. Chem. Soc.*, **105**, 5704 (1983).

19) Y. Iida, *Bull. Chem. Soc. Jpn.*, **43**, 2772 (1970).

20) Y. Harada and H. Inokuchi, *Mol. Phys.*, **1966**, 265.

21) K. B. Patsl and R. L. Willson, *J. Chem. Soc., Faraday Trans. 1*, **69**, 814 (1973).

22) D. K. Fong, *Acc. Chem. Res.*, **9**, 433 (1976).

23) W. Siebrand, T. A. Wildman, and M. Z. Zgierski, *J. Am. Chem. Soc.*, **106**, 4083 (1984).

24) H. Kwart, *Acc. Chem. Res.*, **15**, 401 (1982).

25) R. A. Marcus and N. Sutin, *Biochim. Biophys. Acta*, **811**, 265 (1985).

26) N. S. Isaacs, K. Javaid, and E. Rannala, *J. Chem. Soc., Perkin Trans. 2*, **1978**, 709.

27) For a recent review: M. L. Sinnott, *Adv. Phys. Org. Chem.*, **24**, 113 (1988).

28) M. F. Powell and T. C. Bruice, *J. Am. Chem. Soc.*, **105**, 7139 (1983).

 © 1991 The Chemical Society of Japan Bull. Chem. Soc. Jpn., 64, 91—98 (1991)

NMR Spectra of Organogermanium Compounds. X.[1] Syntheses, ^{13}C and ^{73}Ge NMR Spectra and Molecular Mechanics Calculations of Germacyclopentanes and Germacyclopentenes

Yoshito TAKEUCHI,* Katsumi TANAKA, and Toshie HARAZONO
Department of Chemistry, The College of Arts and Sciences,
The University of Tokyo, Komaba, Meguro-ku, Tokyo 153
(Received June 22, 1990)

Germacyclopentane, its 1-methyl, and 1,1-dimethyl derivatives together with some germacyclopentenes were prepared and their ^{13}C and ^{73}Ge NMR spectra were determined. Molecular mechanics calculations of germacyclopentanes indicate that the symmetric twist form is the most stable in contrast to cyclopentane where the envelop and twist forms have much the same energy. Though both ^{13}C and ^{73}Ge chemical shifts are less sensitive to the stereochemistry of the methyl group as compared with the corresponding germacyclohexanes, the spectroscopic results can be explained in terms of the structures as depicted by molecular mechanics calculations.

In the previous communications we have reported the preparation and structural study of 1-methyl-[2], 1-phenyl-[3] and 1-*t*-butyl-germacyclohexanes[1] (**GC**) based on ^{13}C and ^{73}Ge chemical shifts, molecular mechanics calculations (MM2) and molecular orbital calculations (MNDO). It was found that the conformational energy of a methyl or a phenyl group bonded to germanium is essentially zero while that of a *t*-butyl group is ca. 1.3 kcal mol^{-1} in a sharp contrast with the case of corresponding cyclohexanes (**C**).

This very small conformational energy is due to the flattening of **GC** ring around germanium atom as well as the extended C–Ge bond length, both of which will reduce the repulsion between the axial substituent on germanium and the C-3, 5 methylene moieties.[2] In this connection it will be interesting to see the structural features of germacyclopentanes (**GP**) which have hitherto never been described.

It is well established that cyclopentane (**1CP**) is a free pseudorotator and the an envelop (hereafter abbreviated as **E**) and a twist-boat (hereafter abbreviated as **T**) form have an identical energy.[4] Alkylcyclopentanes are not any more a free pseudorotator, and in the case of methylcyclopentane (**2CP**) the most stable form is the one with the methyl group at the tip of envelop. The energy difference between **E** and **T** is, however, essentially zero.

This feature of cyclopentanes (**CP**) will make the stereochemical significance of equatorial and axial orientations of the substituent nearly identical. This can most simply be exemplified by the ^{13}C chemical shifts of *trans*-1,3-dimethylcyclohexane and -cyclopentane. In both compounds one of the two methyl groups is necessarily axial (or pseudo-axial), which will be expected to make averaged chemical shifts to highfield than those of corresponding 1,3-*cis* isomers. In the case of dimethylcyclopentanes the chemical shifts difference between *trans*- and *cis*-isomers is only 0.3 ppm (the former is in the higher field)[5] while the similar difference of dimethylcyclohexanes amounts to 2.35 ppm with the *trans*-isomer in the higher field.[6]

Hence three questions have arisen concerning the stereochemistry of **GP**. One is the determination of the most stable structure of germacyclopentane (**1GP**) or **GP** in general. The second one is to determine the extent of difference between (pseudo)equatorial and (pseudo)axial orientations of the methyl group on germanium in **GP**. The second question is interesting in relation to our previous finding that the two conformers (equatorial and axial) of 1-methylgermacyclohexane (**2GC**) have essentially similar MM2 steric energy with a slight preference to the axial isomer (by ca. 0.2 kcal mol^{-1}).[2] The third one is the possibility that a methyl group or any other substituent bonded to the ring carbon might alter the most stable structure from **T** to something else.

With these in mind we prepared **1GP**, 1-methylgermacyclopentane (**2GP**), and 1,1-dimethylgermacyclopentane (**3GP**). We also attempted to prepare 1,1,3-trimethylgermacyclopentane (**4GP**) and 1,1,3,4-tetramethylgermacyclopentane (**5GP**) without success. Instead, 1,1-dimethyl-3,4-epoxygermacyclopentane (**10GP**) and 1,1-dimethylgermacyclopentan-3-ol (**11GP**) were prepared . Compounds **4GP**, **5GP**, **10GP**, and **11GP** were selected because in these compounds the stereochemical environment of two methyl groups bonded to germanium can be different.

Four germacyclopentenes, 1,1-dimethylgermacyclopent-3-ene (**6GP**), 1,1,3-trimethylgermacyclopent-3-ene (**7GP**), 1,1-diethyl-3-methylgermacyclopent-3-ene (**8GP**), and 1,1,3,4-tetramethylgermacyclopent-3-ene (**9GP**) were prepared. Compounds **7GP** and **9GP** were expected to be the precursor for **4GP** and **5GP**, respectively. The compound **8GP** was chosen to assess the effect of an ethyl group bonded to germanium upon chemical shifts.

We deteremined the ^{13}C and ^{73}Ge NMR spectra of the compounds prepared, and carried out molecular mechanics calculations of **1GP—4GP**. For other compounds molecular mechanics calculations were

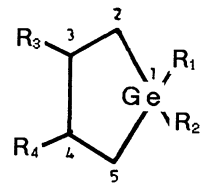

	R_1	R_2	R_3	R_4
1	H	H	H	H
2	Me	H	H	H
3	Me	Me	H	H
4	Me	Me	Me	H
5	Me	Me	Me	Me
10	Me	Me	OH	H
11	Me	Me	—O—	

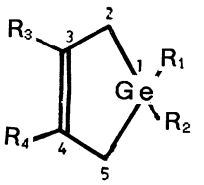

	R_1	R_2	R_3	R_4
6	Me	Me	H	H
7	Me	Me	Me	H
8	Et	Et	Me	H
9	Me	Me	Me	Me

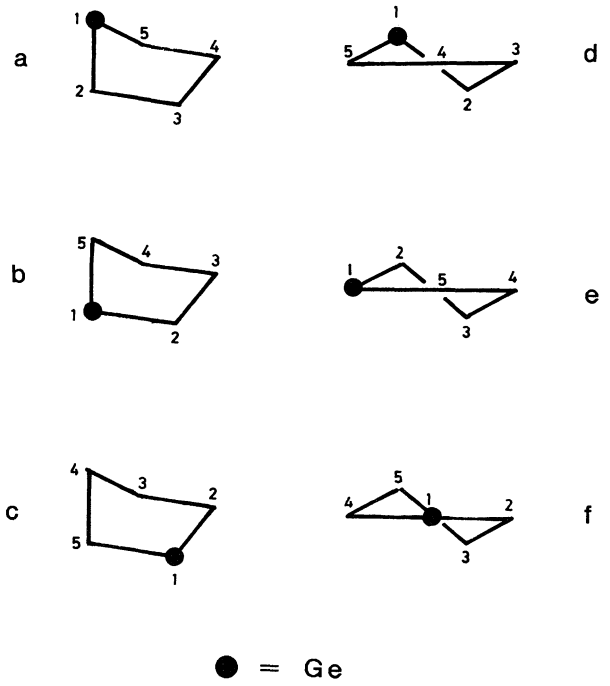

Fig. 1. Input structures for MM2 calculation of germacyclopentane.

impossible because of the lack of parameters.

Results and Discussion

Molecular Mechanics Calculations. Molecular mechanics calculations were carried out for germacyclopentanes **1GP—4GP** with the aid of MM2 program[7] to which parameters for germanium as reported by Ouellette[8] were incorporated. The appropriateness of this combination together with the reason why the new germanium parameters reported by Allinger et al.[9] was not employed has already been discussed in our previous paper.[1]

For the input structures for MM2 calculations, **GP** can either be an envelop or a twist and in each structure the germanium atom can have three different positions (a, b, and c for an envelop, and d, e, and f for a twist). In other words, there are six possible input structures for **1GP** (Fig. 1). A similar situation should be involved in the case of **3GP**. In the case of **2GP** the situation is more complicated since for each of the structures a—e, there are two orientations, equatorial (abbreviated as **eq-2GP**) and axial (**ax-2GP**), of the methyl group. For the input structure f, the equatorial and axial structures are degenerated, and hence for **2GP** altogether eleven input structures were considered. For **4GP**, the situation is the same with the case of **2GP**, and eleven input structures were calculated.

The steric energy and its components for each optimized structure are given in Table 1. In MM2 calculations, total steric energies (E_s) are the sum of compression energy (E_c), bending energy (E_b), stretch-bend energy (E_{sb}), torsional energy (E_t) and van der Waals energy which is subdivided into the energy associated with 1,4-interaction ($E_{1,4}$) and that with other interactions (E_{other}). The geometrical parameters for each optimized structures are given in Table 2.

1GP: It is interesting to notice that the input structure **1GP-a** was optimized to an envelop, **E(1GP)**, while the input structure **1GP-b** and **1GP-c** were optimized to a symmetric (in the sence that the germanium nucleus is on the C_2 axis) twist **T(1GP)**. The latter is by ca. 2 kcal mol^{-1} more stable than the former. When the input structure was a twist form, the situation is considerably different, and both **1GP-e** and **1GP-f** were optimized to the same **T**. The input structure **1GP-d** was, however, optimized to a different structure, an unsymmetrical twist **A(1GP)**.

The difference between **T** and **A** is clear when the dihedral angle was compared. In **T** there are two paris of nearly equal dihedral angles while in **A** all five are more or less different. Otherwise, the steric energy of this unsymmetrical species is nearly the same with that of **E(1GP)**.

2GP: The situation is very similar for the case of **1GP**. The most stable structure is again **T(2GP)**, a symmetrical twist. There are two cases (**eq-2GP-a** and **ax-2GP-a**) where the input structures are optimized to **E**. Both envelops have a steric energy about 2 kcal mol^{-1} higher than **T**. The small energy difference between **E** from **eq-2GP-a** and that from **ax-2GP-a** (0.26 kcal mol^{-1}) in favor of the latter is a reminiscence of the situation for equatorial- and axial-1-methylgermacyclohexane (**2GC**).[2]

Two input structures **eq-2GP-c** and **ax-2GP-d** are

Table 1. MM2 Component Steric Energies[a] of Germacyclopentanes and Corresponding Cyclopentanes (in kcal mol^{-1}: 1 cal=4.18 J)

Compound[b]	Input[c]	Output[d]	E_s	E_c	E_b	E_{sb}	E_t	$E_{1,4}$	E_{other}
1GP	a	E	15.58	0.62	7.43	0.11	6.43	1.41	−0.44
	b,c,e,f	T	13.57	0.40	5.10	−0.01	7.31	1.13	−0.37
	d	A	15.58	0.60	7.21	0.11	6.66	1.44	−0.44
eq-2GP	a	E	14.98	0.65	7.38	0.12	6.68	1.01	−0.86
	b,c,e,f	T	12.80	0.41	5.06	0.00	7.47	0.75	−0.89
	d	A	14.99	0.64	7.21	0.12	6.85	1.04	−0.86
ax-2GP	a	E	14.72	0.65	7.34	0.12	6.70	1.02	−1.12
	b,c,e,f	T	12.80	0.41	5.06	0.00	7.47	0.75	−0.89
	d	A	14.72	0.65	7.31	0.12	6.74	1.02	−1.11
3GP	a	E	13.91	0.68	7.28	0.13	6.92	0.64	−1.74
	b,c,e,f	T	11.81	0.43	5.01	0.00	7.60	0.38	−1.61
	d	A	13.93	0.68	7.18	0.13	7.03	0.65	−1.73
eq-4GP	a,c,d,e,f	eq-T	11.89	0.55	5.11	0.02	7.53	0.94	−2.25
	b	ax-T	13.02	0.62	5.07	0.06	8.58	0.90	−2.21
ax-4GP	b,d	eq-T	11.89	0.55	5.11	0.02	7.53	0.94	−2.25
	c,e,f	ax-T	13.02	0.62	5.07	0.06	8.58	0.90	−2.21
	a	A	14.25	0.82	7.28	0.16	7.00	1.33	−2.34
1CP	a	E	11.41	0.33	2.19	−0.10	6.33	3.16	−0.51
	d	T	11.40	0.33	2.20	−0.10	6.33	3.16	−0.51
eq-2CP	a	E	11.56	0.37	2.43	−0.08	6.23	3.58	−0.98
	b,c	A	11.58	0.38	2.42	−0.07	6.23	3.59	−0.97
ax-2CP	a	E	12.76	0.41	2.19	−0.06	7.43	3.78	−0.98
	b,c	A	11.58	0.38	2.42	−0.07	6.23	3.59	−0.97
3CP	a,b	E	13.00	0.57	2.29	−0.03	7.38	4.13	−1.34
	c	A	12.93	0.68	2.52	−0.05	6.83	4.30	−1.34

a) For difinition of each component steric energies, see text. b) For definition of structures of compounds, see text. c) Input structure: see Fig. 1 for definition. d) Output structure: for definition see text.

optimized to an unsymmetrical twist **A**. These two as well as the optimized structure from an envelop **E(2GP)** have a similar steric energy.

It is interesting to see the conformation of the methyl group bonded to germanium. For optimized **E** structure for **eq-2GP** (which is not the energy minium) the dihedral angles Me–Ge-1–C-2–C-3 (and Me–Ge-1–C-5–C-4) is ca. 155°, which corresponds to 163° for the value of **eq-2CP** (dihedral angle Me–C-1–C-2–C-3). The dihedral angle for optimized *E* structure of **ax-2GP** are 74° while for **ax-2CP** the corresponding values are ca. 82°. Thus, the dihedral angles for **2GP** are generally smaller than those for **2CP**.

The corresponding values for **eq-2GC** (Me–Ge-1–C-2–C-3) and **eq-2C** (Me–C-1–C-2–C-3) are 167° and 180°, respectively, while the corresponding values for **ax-2GC** and **ax-2C** are ca. 69° and 73°, respectively. There is, however, no comparing since both *E* forms of **eq-** and **ax-2GP** are not energy minima. The two dihedral angles for **T** form of **2GP**, 129° and 100°, clearly indicates there is no butane-gauche type interaction between the methyl group and C-3/C-4 methylene moieties in the optimized **T** form.

3GP: An essentially identical situation with the previous case was observed for **3GP**. The most stable structure is a symmetric twist **T(3GP)**. The envelop **E(3GP)**, which is from the input structure **3GP-a**, is 1.8 kcal mol^{-1} higher in energy than **T(3GP)**. An unsymmetrical twist **A(3GP)**, from **3GP-d**, has a similar steric energy with that of **E(3GP)**.

4GP: In order to prove that the most stable structure is in fact **T**, an examination of NMR spectra of such a compound as **4GP** will be helpful. In **T** form the two Ge-1 methyl group remain nearly equivalent regardless of the presence of C-3 methyl group. On the other hand, if **GP** is in **E**, the presence of C-3 methyl will restrain the ring reversal and/or pseudorotation to avoid one of Ge-1 methyl and C-3 methyl will become 1, 3-diaxial. The net effect is that the **GP** ring will remain in **E** in which two Ge-1 methyl groups can be differentiated.

The most stable structure is again **T(4GP)** with an

Table 2. Structures of Germacyclopentanes and Cyclopentanes[a)]

Compound		$r_{1,2}$	$r_{2,3}$	$r_{3,4}$	$r_{4,5}$	$r_{5,1}$	θ_1	θ_2	θ_3	θ_4	θ_5	$\psi_{1,2}$	$\psi_{2,3}$	$\psi_{3,4}$	$\psi_{4,5}$	$\psi_{5,1}$
		nm	nm	nm	nm	nm	°	°	°	°	°	°	°	°	°	°
1GP	E	0.1936	0.1541	0.1555	0.1542	0.1936	88.8	103.8	111.8	112.1	104.1	−38.9	29.7	−1.4	−27.7	38.7
	T	0.1944	0.1541	0.1547	0.1541	0.1945	92.7	104.4	108.1	108.1	104.5	−14.0	38.7	−52.4	38.3	−13.5
	A	0.1936	0.1539	0.1554	0.1544	0.1937	89.2	102.9	111.2	112.5	105.2	−40.2	36.9	−12.7	−18.1	33.6
eq-2GP	E	0.1935	0.1542	0.1556	0.1542	0.1934	89.2	103.6	112.0	112.2	103.9	−38.7	29.6	−1.6	−27.3	37.9
	T	0.1943	0.1541	0.1547	0.1541	0.1944	93.1	104.1	108.1	108.3	104.3	−14.7	39.1	−52.4	37.7	−12.8
	A	0.1935	0.1540	0.1555	0.1544	0.1935	89.5	102.9	111.5	112.6	104.8	−40.0	35.6	−11.0	−19.4	34.2
ax-2GP	E	0.1935	0.1542	0.1555	0.1542	0.1935	89.1	103.7	112.0	112.2	103.8	−38.5	29.0	−0.8	−27.9	38.0
	T	0.1944	0.1541	0.1547	0.1541	0.1943	93.1	104.3	108.2	108.1	104.2	−13.4	38.2	−52.4	38.6	−14.0
	A	0.1935	0.1541	0.1555	0.1543	0.1935	89.2	103.4	111.7	112.3	104.2	−39.1	31.4	−4.2	−25.2	36.9
3GP	E	0.1934	0.1542	0.1556	0.1543	0.1933	89.5	103.5	111.2	112.4	103.7	−38.4	29.4	−1.4	27.1	−37.6
	T	0.1942	0.1541	0.1548	0.1542	0.1942	93.4	104.0	108.2	108.3	104.1	−14.1	38.6	−52.4	38.0	−13.3
	A	0.1934	0.1544	0.1556	0.1544	0.1934	89.7	103.0	111.8	112.6	104.3	−39.3	33.2	−7.5	−22.2	35.4
eq-4GP	eq-T	0.1942	0.1544	0.1550	0.1541	0.1941	93.3	104.4	107.9	108.4	103.9	−13.0	37.3	−52.3	39.0	−14.5
ax-4GP	ax-T	0.1942	0.1545	0.1552	0.1541	0.1941	93.5	105.0	107.8	109.8	104.0	−13.0	36.1	−49.9	37.0	−13.2
	A	0.1934	0.1543	0.1559	0.1544	0.1933	89.7	103.1	111.1	112.6	104.6	−39.7	34.9	−10.3	−19.7	34.2
1CP	E	0.1534	0.1537	0.1541	0.1537	0.1534	102.3	103.9	105.9	106.4	103.9	−40.5	25.1	0.0	−25.1	40.5
	T	0.1540	0.1535	0.1534	0.1535	0.1540	106.3	105.2	102.7	102.8	105.2	−13.4	34.6	−42.6	34.4	−13.0
eq-2CP	E	0.1535	0.1537	0.1541	0.1537	0.1535	102.1	103.9	106.0	106.0	103.9	−40.8	25.5	−0.2	−25.1	40.7
	A	0.1535	0.1534	0.1539	0.1540	0.1537	102.8	102.6	104.8	106.3	105.5	−42.6	36.9	−17.0	−9.4	32.1
ax-2CP	E	0.1537	0.1537	0.1540	0.1537	0.1537	102.0	104.9	106.0	106.1	104.9	−38.8	24.6	−0.6	−23.6	38.4
	A	0.1537	0.1540	0.1539	0.1534	0.1535	102.8	105.6	106.3	104.8	102.6	−42.5	36.9	−17.1	−9.3	32.0
3CP	E	0.1540	0.1537	0.1540	0.1537	0.1540	101.5	105.2	105.9	106.0	105.2	−38.7	24.7	−0.6	−23.7	38.3
	T	0.1547	0.1534	0.1532	0.1535	0.1548	105.1	105.4	102.3	102.8	106.0	−16.9	37.2	−43.0	32.8	−9.9

a) The definition of the structure parameters are as follows: $r_{1,2}$ is the distance between Ge and C-2 in nm, θ_1 is the bond angle C5–Ge–C2 in degrees and $\psi_{1,2}$ is the torsion angle in degrees defined by the C5–Ge–C2–C3. The other parameters are defined analogously.

equatorial methyl at C-3, similar to previous examples. It must be pointed out that **T(4GP)** with an axial C-3 methyl group can be an energy minimum though the steric energy is by more than 1 kcal mol^{-1} larger than the former. The asymmetric twist **A(4GP)** has much higher energy and cannot contribute to the structure.

The values of component energies indicate that the stability of **T** form is to be ascribed to the low E_b term, which is ca. 2.2 kcal mol^{-1} smaller as compared with **E** or **A**. The E_t term of **T** is generally slightly larger than these for **E** and **A**. The E_c and $E_{1,4}$ terms of **T** are slightly but consistently smaller than those for **E** and **A**; the sum is, however, smaller than the gain in E_b.

The difference in steric energy between **E** and **T** may be reflected in the geometrical parameters given in Table 2. Firstly, in the high energy structure (**E** and **A**) of **GP**, the bond angle θ_1 (C5–Ge–C2)(ca. 89°) is always by ca. 4° smaller than that of low energy structures (**T**:93°). This smaller bond angle in **E** and **A** seems to couple with a very small (0.001 nm) but consistent decrease of bond length $r_{1,2}$ and $r_{5,1}$. These two effects associated with germanium in **E** should cause an increase in the E_b term. It must be pointed out such a difference in bond angle also exists for **E** and **T** forms of **CP**.

Another point to be considered is the average flattening. The sum of five dihedral angle is a measure of ring flattening. In **GP** the sum for **E** is less than that for **T** by more than 20° while for **CP** the difference is only ca. 7°. Excessive flattening should increase the steric energy of the system and for this reason the **T** form is the most stable among possible conformers.

Preparation of Germacyclopentanes. The preparation of **1GP—3GP** was carried out in a similar manner that used in the preparation of corresponding germacyclohexanes.[10]

The preparation of **4GP** and **5GP** was attemped, starting from isoprene (2-methyl-1,3-butadiene) and 2,3-dimethyl-1,3-butadiene, respectively, and germanium(II) iodide (GeI_2). 1,1-Diiodo-3-methyl- and 1,1-diiodo-3,4-dimethylgermacyclopent-3-ene initially formed were converted to **7GP** and **9GP**, respectively with the aid of methylmagnesium iodide (MeMgI). **7GP** and **9GP** were hydrogenated with H_2/Ni (50 atm) but the desired **4GP** and **5GP** could not be isolated.

Instead we decided to prepare **10GP** and **11GP** because the possible precursor **6GP** can relatively easily be obtained from butadiene and trichlorogermane ($HGeCl_3$), and a subsequent treatment with MeMgI. **6GP** was treated with *m*-perbenzoic acid to give **10GP** which was treated with lithium aluminum hydride (LAH) to afford **11GP**.

^{73}Ge Chemical Shifts. In Table 3, ^{13}C and ^{73}Ge chemical shifts of germacylopentanes and germacyclopentenes are listed. The values in parentheses are those of the corresponding **GC**.

The chemical shifts of three compounds **1GP—3GP** indicate that the effect of a methyl group is similar in magnitude as that in **GC**. Thus the span is ca. 140 ppm for **GP** and ca. 120 ppm for **GC**. In **GP**, however, the resonances are considerably in lower

Table 3. ^{73}Ge[a] and ^{13}C[b] NMR Chemical Shifts of Germacyclopentanes, Germacyclopentenes, and Germacyclohexanes[c]

Compounds	Ge-1	C-2	C-3	C-4	C-5	Me-1	Me-3
1GP	−101.1 (−130.3)	13.22 (9.32)	29.20 (26.78)	29.20 (26.78)	13.22 (9.32)		
2GP	−27.4 (−65.6)	11.86 (12.61)	28.60 (26.09)	28.60 (26.09)	11.86 (12.61)	−5.20 (−6.55)	
3GP	40.0 (−11.3)	14.45 (15.33)	28.65 (28.65)	28.65 (25.90)	14.45 (15.33)	−2.38 (−3.77)	
6GP	37.0	21.78	134.03	134.03	21.78	0.27	
7GP	44.6	23.88	139.76	125.67	20.41	−2.16	22.63
8GP	70.9	20.77	141.12	127.04	17.30	7.20 (CH_2) 10.19 (Me)	23.67
9GP	9.7	27.08	130.71	130.71	27.08	−2.38	19.59
10GP		16.96	58.01	58.01	16.96	−0.22 −1.89	
11GP		24.22	74.44	36.13	10.89	−1.44 −1.84	

a) In ppm relative to external $GeMe_4$ (δ=0). b) In ppm relative to internal $SiMe_4$ (δ=0). c) Values in pharentheses are corresponding germacyclohexanes. Data taken from Ref. 2.

field. This low field shift is most likely due to the reduced bond angle θ_1. A similar effect was reported for ^{29}Si chemical shifts of 1,1-dimethylsilacyclohexane (−1.0 ppm) and 1,1-dimethylsilacyclopentane (16.8 ppm).[11]

The correlation between ^{73}Ge chemical shifts and those of ^{29}Si was reported as below.[12]

$$\delta(^{73}\text{Ge}) = 3.32\delta(^{29}\text{Si}) + 39.9$$

Thus, the ^{73}Ge shift difference between **3GP** and **3GC** is expected to be about 59 ppm based on the above correlation. The observed difference, 51.3 ppm, is not very far from the prediction, indicating that the correlation is, though empirical, quite general.

^{73}Ge chemical shifts of **GP** (**6GP—9GP**) are puzzling. In view of a very small chemical shift difference between 1,1-dimethylgermacyclohexane (**3GC**; −11.3 ppm) and 1,1,3-trimethylgermacyclohexane (**4GC**; −12.2 ppm), similarly small differences are expected for the chemical shifts of three compounds, **6GP**, **7GP**, and **9GP** since the effect of a pseudo-equatorial methyl group at C-3 should not be large. In fact, the difference between **6GP** and **7GP** is 7.6 ppm, a rather unexpectedly large value. Furthermore, the shift for **9GP** is considerably in high field.

The only possible explanation is the change of most stable structure in **9GP**. According to molecular mechanics calculations, the most stable conformation of cyclopentene is an envelop with nearly planar double bond moiety.[13,14] The *cis*-dimethyl substituents will suffer from a strong repulsion, and the deviation from the planarity will be increased. One of the methyl group will be bent to the direction opposite to the flap while the other to direction of flap. The latter methyl is expected to induce a substantial high field shift induced by the steric interaction with 1,1-dimethyl moiety. Lack of the relevant parameters inhibit us from carrying out molecular mechanics calculations to prove this explanation.

^{73}Ge chemical shift of **8GP** is also puzzling. Since the shift for tetraethylgermane is 17.8 ppm relative to tetramethylgermane (δ=0), a large difference of 26.3 ppm between **7GP** and **8GP** is unexpected. Here the deviation of germanium from tetrahedral structure seem to be involved though more extensive data should be accumulated before a concrete conclusion can be drawn.

^{13}C Chemical Shifts. The assignment of ^{13}C signals is more or less straightforward, based on the comparison with the data for **GC** and on the number of attached proton(s) as indicated by the INEPT experiment.

There is one anomaly in ^{13}C chemical shifts of C-2, 5. In **GC** C-2 exhibits a low field shift as the number of methyl group bonded to germanium increases. This is also the case with methylcyclohexanes.[6] In **GP**, however, the resonance of C-2 of **2GP** is in the highest field among three compounds investigated. We do not have any explanation for this anomaly.

The chemical shift difference between two methyls of **10GP** and **11GP** is informative. In **11GP** the difference is very small even compared with that of 1,1,3-trimethylgermacyclohexane (2.30 ppm).[15] This is consistent with a symmetric twist **T** structure where the effect of pseudo-equatorial substituent to two methyl groups on germanium is very similar. The fact that the epoxide **10GP** shows a larger difference (1.66 ppm) might indicate that in the particular compound the germacyclopentane ring is not **T**. On the other hand, the epoxide ring cannot be coplanar with the ring, to make the stereochemical enviroment of two methyls somewhat different.

In conclusion, it can be assumed that the optimized structure of the germacyclopentane ring is a symmetric twist **T** regardless of the number and orientation of methyl group(s) bonded to germanium. This makes a sharp contrast to the cyclopentane ring, essentially a free rotator, where an envelop and a twist boat has much the same steric energy.

Most of the ^{73}Ge and ^{13}C NMR data are accounted for in terms of the symmetric twist structure of **GP**. How to explain some anomaly remains, however, to be solved in future.

Experimental

Infrared spectra were obtained with a JASCO A102 grating infrared spectrophotometer as a liquid film. The ^{1}H NMR spectra were recorded with a Varian EM-390 spectrometer as $CDCl_3$ solution containing a small amount of tetramethylsilane (TMS) as the internal standard.

The ^{73}Ge NMR spectra were recorded as solutions in $CDCl_3$ (1:1 v/v) on a JEOL FX-90Q spectrometer equipped with an NM-IT 10LF low-frequency insert, operating at 3.10 MHz, in a 10 mm tube at 30 °C. Typical measurement conditions were as follows: pulse width, 150 μs (90°); spectral width, 2000 Hz; number of scans, 5000; pulse delay, 100 ms; data points, 4096. The ^{13}C NMR spectra were determined for the same solutions on the same instrument at 22.50 MHz. Typical measurement conditions were as follows: pulse width, 13 μs (40°); spectral width, 2000 Hz; number of scans, 500; pulse delay, 1 s; data points, 4096. The combined results are given in Table 3.

Molecular Mechanics Calculations. The program used was Allinger's MM2(85).[7] Since in MM2(85) the parameters for germanium are not available, we installed the parameters reported by Ouellette[8] in MM2(85). For the sake of comparison, calculations were also carried out for the corresponding cyclopentanes (**1CP—4CP**) and the results were also included in Tables 1 and 2.

Preparation of Germacyclopentane and Germacyclopentane Derivatives (1GP—11GP). Some of organogermanium compounds are sensitive to air and moisture, and elemental analyses are not necessarily feasible. The purity was in most cases monitored by a combination of gas chromatography, mass and NMR spectra.

Preparation of **1GP—3GP** was carried out, with some modification, according to the literature.[10] Thus, the reaction between the bis-Grignard reagent of 1,4-dibromobutane and tetrachlorogermane afforded 1,1-dichlorogermacyclopentane, which was treated with LAH to give **1GP** and with methylmagnesium iodide (MeMgI) to give **3GP**.

1-Methylgermacyclopentane (2GP): 1,1-Dichlorogermacyclopentane was treated with phenylmagnesium bromide to give 1,1-diphenylgermacyclopentane, which was monobrominated, and treated with methylmagnesium bromide. The resultant 1-methyl-1-phenylgermacyclopentane was successively treated with bromine and LAH to afford the desired **2GP**.

1,1-Dimethylgermacyclopent-3-ene (6GP): An ether solution of trichlorogermane (25.1 g, 0.10 mol) was cooled to −78 °C, to which butadiene (30 ml) was added in one portion. The mixture was stirred for 14 h while the temperature was gradually raised to the room temperature. By usual work-up, 1,1-dichlorogermacyclopent-3-ene (11.6 g, 42%) was obtained, bp 65 °C/15 mmHg (1 mmHg=133.322 Pa). The dichloro compound was treated with MeMgI to afford 1,1-dimethylgermacyclopent-3-ene (**6GP**) (4.87 g, 53%), bp 113 °C/766 mmHg. IR (neat) 1607 (C=C).

1,1,3-Trimethylgermacyclopent-3-ene (7GP): GeI_2 (20.0 g, 61.2 mmol) and isoprene (4.5 g, 66.2 mmol) were placed in a sealed tube, which was heated at 60 °C for 4 h. to give viscous, orange-colored 1, 1-diiodo-3-methylgermacyclopent-3-ene. Since this unsaturated compound was found unstable and hence employed in the next step without isolation nor purification. MeMgI was prepared from MeI (52.1 g; 367 mmol) and Mg (8.92 g, 367 mmol) in diethyl ether (200 ml) under argon. The ether solution of the Grignard reagent was cooled to −45 °C to which the diiodide solution (70 ml) was added and the mixture was gradually brought to room temperature. Under ice-cooling the mixture was treated with HCl (2 mol dm^{-3}), and the organic layer was separated, dried with $CaCl_2$. The ether layer was removed and the residue was distilled under a reduced pressure to give 1,1,3-trimethylgermacyclopent-3-ene (**7GP**) (6.51 g, 62%), bp 70—72 °C/35 mmHg (lit,[16] bp 139 °C/741 mmHg).

Found: C, 49.42; H, 8.09%. Calcd for $C_7H_{14}Ge$; C, 49.23; H, 8.26%.

1,1-Diethyl-3-methylgermacyclopent-3-ene (8GP): GeI_2 (5.88 g, 18 mmol) and isoprene (3.12 g, 46 mmol) were placed in a sealed tube, which was heated at 60 °C for 3 h. to give viscous, orange-colored 1,1-diiodo-3-methylgermacyclopent-3-ene. Ethylmagnesium iodide (150 mmol) was prepared in ether (150 ml) was prepared to which the ether solution (70 ml) of above diiodide was dropwise added at −30 °C, stirred for 2 h and kept at room temperature overnight. Under ice-cooling the mixture was treated with saturated aqueous solution of NH_4Cl, and the organic layer was separated, dried with $CaCl_2$. The ether layer was removed and the residue was distilled under a reduced pressure to give **8GP** (2.42 g, 68%), bp 82 °C/58 mmHg. IR (neat) 1635 (C=C).

1,1,3,4-Tetramethylgermacycloent-3-ene (9GP): GeI_2 (16.6 g, 50.8 mmol) and 2,3-dimethylbutadiene (4.3 g, 52.4 mmol) were mixed and gradually heated under a steam of Ar to 50 °C when the reaction was initiated to give an yellow solution. The mixture was further kept at 110 °C for 2 h to complete the reaction. The crude diiodide was dissolved in ether (100 ml), to which MeMgI (200 mmol) in ether (150 ml) was dropwise added under reflux. Refluxing was further continued for 2 h and hydrolyzed with aqueous saturated NH_4Cl solution under ice cooling. The ether layer was washed with water, dried over $CaCl_2$, and the ether was removed. The residue was distilled in vacuo to afford **9GP** (6.93 g, 74%), bp 88 °C/45 mmHg.

1,1-Dimethyl-3,4-epoxygermacyclopentane (10GP): 6GP (18.9 g, 0.12 mol) was treated with *m*-chloroperbenzoic acid (22.9 g, 0.13 mol) in dichloromethane under ice cooling. Stirring was continued for 2.5 h, and *m*-chlorobenzoic acid was filtered off. The organic layer was successively treated with aqueous sodium hydrogensulfite, sodium carbonate, and ammonium chloride, and dried with magnesium sulfate. By distillation, **10GP** was obtained (13.8 g, 66%), bp 68—70 °C/45 mmHg.

1,1-Dimethylgermacyclopentan-3-ol (11GP): 10GP (118 g, 68 mmol) was dropwise added to LAH (1.3 g, 34 mmol) in diethyl ether (100 ml) in a stream of argon. After refluxed for 3 h, the mixture was decomposed with aqueous HCl (2 mol dm^{-3}) under ice cooling. The organic layer was washed, dried with magnesium sulfate, and distilled to afford **11GP** (9.6 g, 81%), bp 83 °C/15 mmHg. IR (neat) 3330 (O–H).

Attempted Preparation of 1,1,3-Trimethylgermacyclopentane (4GP): 7GP (5.39 g, 31.6 mmol) was dissolved in absolute ethanol (100 ml) to which Raney Ni (W-1) (2.0 g) was added and hydrogenated (110 °C, H_2 pressure 50 kg cm^{-2}) for 5 h. After the completion of reaction, the solvent was removed and the residue was distilled in vacuo, preparative gas chromatography. The NMR spectrum indicated that the sample contains at least three inseparable components.

The authors thank the Ministry of Education, Science and Culture, Japanese Government for Grant-in-Aid for Scientific Research on Priority Areas No. 02230108, the Japan Society for the Promotion of Science, and the ASAI Germanium Research Institute for financial support.

References

1) Part IX. Y. Takeuchi, K. Tanaka, T. Harazono, and S. Yoshimura, *Bull. Chem. Soc. Jpn.*, **63**, 708 (1990).
2) Y. Takeuchi, M. Shimoda, K. Tanaka, S. Tomoda, K. Ogawa, and H. Suzuki, *J. Chem. Soc., Perkin Trans. 2*, **1988**, 7.
3) Y. Takeuchi, K. Tanaka, T. Harazono, K. Ogawa, and S. Yoshimura, *Tetrahedron*, **44**, 7531 (1988).
4) N. L. Allinger, *J. Am. Chem. Soc.*, **99**, 8127 (1977).
5) M. Christl, H. J. Reich, and J. D. Roberts, *J. Am. Chem. Soc.*, **93**, 3463 (1971).
6) D. K. Dalling and D. M. Grant, *J. Am. Chem. Soc.*, **89**, 6612 (1967).
7) N. L. Allinger and Y. H. Yuh, *QCPE*, MM2(85) (1985).
8) R. J. Ouellette, *J. Am. Chem. Soc.*, **94**, 7674 (1972).
9) N. L. Allinger, M. I. Quinn, K. Chen, R. Thompson, and M. R. Freierson, *J. Mol. Struct.*, **194**, 1 (1989).
10) P. Mazerolles, *Bull. Soc. Chem. Fr.*, **1962**, 1907.
11) M. L. Filleux-Blanchard, Nguyen-Din-An, and G. Manuel, *Org. Magn. Reson.*, **11**, 150 (1978).
12) O. J. Watkinson and K. M. Mackay, *J. Organomet.*

Chem., **275**, 39 (1984).
13) N. L. Allinger and J. T. Sprague, *J. Am. Chem. Soc.*, **94**, 5734 (1972).
14) U. Burkert, *Angew. Chem., Int. Ed. Engl.*, **20**, 572 (1981).
15) Y. Takeuchi, Y. Ichikawa, K. Tanaka, and N. Kakimoto, *Bull. Chem. Soc. Jpn.*, **61**, 2875 (1988).
16) P. Mazerolles, unpublished result.
17) O. M. Nefedov, S. P. Kolesnikov, and V. I. Scheichenko, *Angew. Chem.*, **76**, 498 (1964).
18) G. Manuel, P. Mazerolles, and J. C. Florence, *C. R. Acad. Sci., Ser. C*, **269**, 1553 (1969).

Thermal Reactions of 6-Methyl-5-[(substituted hydrazono)methyl]-2,4(1*H*,3*H*)-pyrimidinediones with Electron-Deficient Olefins and Acetylene[1)]

Michihiko NOGUCHI,* Yasutoshi KIRIKI, Takashi TSURUOKA, Takahiro MIZUI, and Shoji KAJIGAESHI
Department of Industrial Chemistry, Faculty of Engineering, Yamaguchi University, Tokiwadai, Ube 755
(Received July 20, 1990)

The thermal reactions of some 6-methyl-5-[(substituted hydrazino)methyl]-2,4(1*H*,3*H*)-pyrimidinediones (**1**) were investigated. The 1,5-hydrogen shift in **1** gave 5,6-dihydro-5,6-bis(methylene)-2,4(1*H*,3*H*)-pyrimidinedione intermediates, while the 1,2-hydrogen shift in **1** gave azomethine imine intermediates. These reaction profiles depend on the substituents of hydrazone moieties.

Much attention has been paid for the heterocyclic compounds containing pyrimidine nuclei, since the ring systems are widely found in biologically active compounds.[2)]

Some 5,6-dihydro-5,6-bis(methylene)-2,4(1*H*,3*H*)-pyrimidinediones (**B**) have been reported as being useful intermediates for the synthesis of fused pyrimidine derivatives.[3)] Intermediates **B** could be formed by a 1,5-hydrogen shift of the corresponding precursors **A**. Recently, intermediate **2a** from 1,3,6-trimethyl-5-[(dimethylhydrazono)methyl]-2,4(1*H*,3*H*)-pyrimidinedione (**1a**; R^1=R^2=Me) was confirmed by a [4+2]cycloaddition reaction with *N*-methylmaleimide (**3**), giving a pyrrolo[3,4-*g*]quinazoline derivative **4a**.[3d)]

In order to obtain a better understanding of the reaction profiles, the thermal reactions of some 6-methyl-5-[(substituted hydrazono)methyl]-2,4(1*H*,3*H*)-pyrimidinediones and their pyrimidine analogs were investigated.

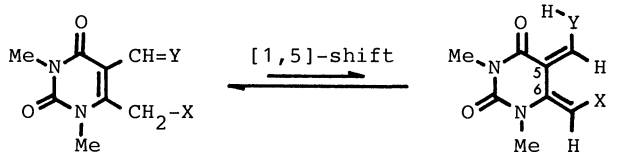

A **B**

Results and Discussion

Heating of 5-(disubstituted hydrazono)methyl derivatives **1b** (R^1,R^2=$-(CH_2)_5-$) and **1c** (R^1,R^2=$-(CH_2)_2-O-(CH_2)_2-$) and **3** in dioxane under reflux gave the

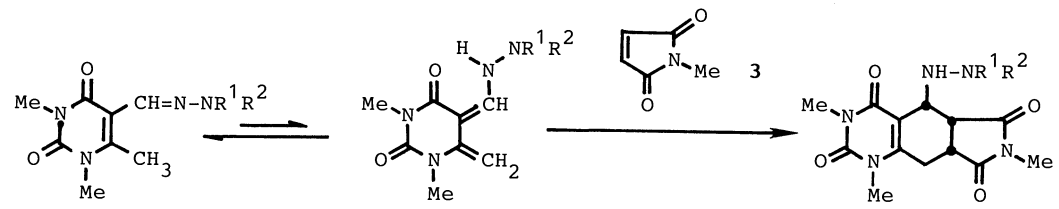

1a: R^1= R^2= Me
1b: R^1, R^2= $-(CH_2)_5-$
1c: R^1, R^2= $-(CH_2)_2-O-(CH_2)_2-$

2a–c **4a–c**

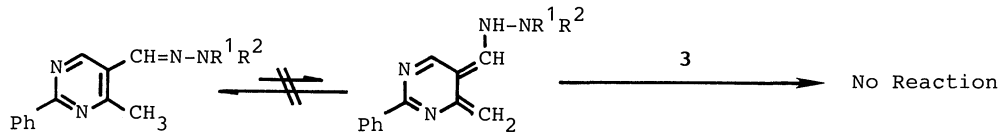

5a: R^1= R^2= Me
5b: R^1, R^2= $-(CH_2)_5-$
5c: R^1, R^2= $-(CH_2)_2-O-(CH_2)_2-$

6a–c

Scheme 1.

expected 5-(2,2-disubstituted hydrazino)pyrrolo[3,4-*g*]-quinazolines **4b**, **c** in good yields (Scheme 1). The synthetic usefulness of the 5,6-dihydro-5,6-bis(methylene)-2,4(1*H*,3*H*)-pyrimidinedione intermediate **2a** leading to quinazoline derivatives was briefly described in a preliminary paper.[3d]

However, a similar reaction of 4-methyl-2-phenyl-5-[(disubstituted hydrazono)methyl]pyrimidines **5a** (R^1=R^2=Me), **5b** (R^1,R^2=$-(CH_2)_5-$), and **5c** (R^1,R^2=$-(CH_2)_2-O-(CH_2)_2-$) with **3** did not give any adducts. This means that a 1,5-hydrogen shift in **5a**—**c** leading to diene-intermediates **6** would be unfavorable because of a loss of the aromaticity of the pyrimidine ring (Scheme 1).

The effect of the N-substituent of the hydrazone moiety on the reaction profiles was also investigated. Heating of 1,3,6-trimethyl-5-[(methylhydrazono)-methyl]-2,4(1*H*,3*H*)-pyrimidinedione (**1d**) and **3** in dioxane under reflux gave two products, **7d** and **8d**, in 86% total yield. Their molecular formula indicate that **7d** is a 1:1 adduct of **1d** and **3**, while **8d** is a dehydrogenated product from **7d**. The pyrrolo[3,4-*c*]-pyrazole structures of **7d** and **8d** were determined by their spectral data; their ^{1}H NMR spectra showed the existence of a 1,2,3,4-tetrahydro-1,3,6-trimethyl-2,4-dioxo-5-pyrimidinyl moiety. The five signals in the ^{13}C NMR spectrum of **7d**, δ=51.2(3a-C), 60.7(6a-C), 69.7(3-C), 174.7, 175.6(4- and 6-C), were assignable to carbons of the pyrrolo[3,4-*c*]pyrazole moiety. On the other hand, the ^{13}C NMR spectrum of **8d** showed two sp^3-carbon signals, δ=55.0(3a-C) and 65.0(6a-C), and three sp^2 signals, δ=152.5(3-C), 172.3, 173.4(4- and 6-C), for the pyrrolo[3,4-*c*]pyrazole moiety. The ratio of products **7d** and **8d** depended on both the reaction conditions and the procedures, while the combined yield of **7d** and **8d** was almost constant. The initially formed product **7d** was easily converted to **8d** during the work-up.

In order to elucidate the reaction profiles, **1d** was allowed to react with methyl fumarate (**9**) and ethyl acrylate (**10**). The pyrazolidine **11** and 2-pyrazoline derivatives **12** and **13** were obtained, respectively. The

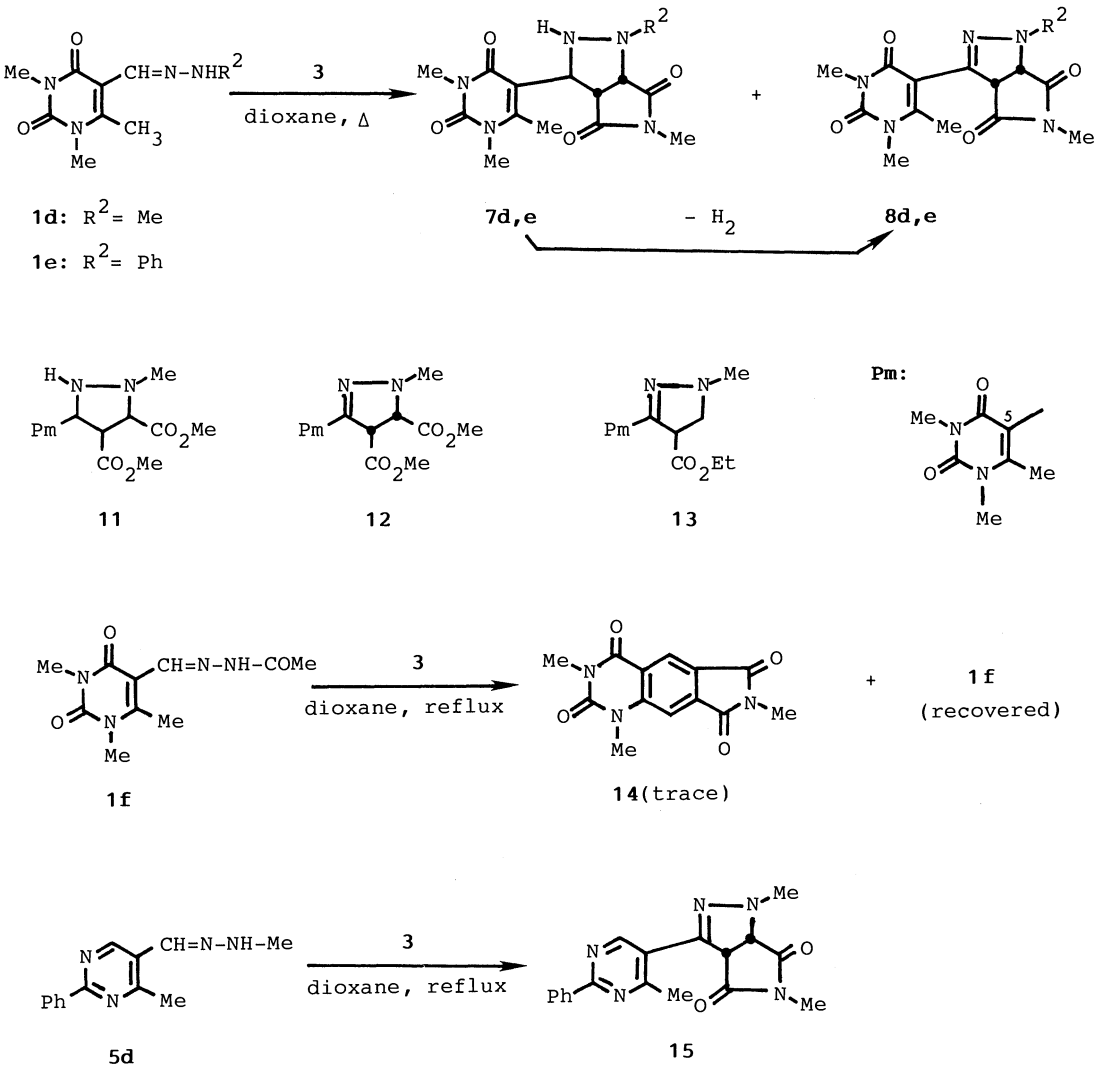

Scheme 2.

reaction of 5-(phenylhydrazono)methyl derivative **1e** with **3** gave pyrrolopyrazoles **7e** and **8e** in good total yield. On the other hand, the reaction of 5-(acetylhydrazono)methyl derivative **1f** with **3** gave a trace of pyrrolo[3,4-g]quinazoline **14**[3d] (in 3% yield) with a recovery of the starting materials. A similar reaction of 4-methyl-5-[(methylhydrazono)methyl]-2-phenylpyrimidine (**5d**) with **3** in refluxing dioxane gave a pyrrolo[3,4-*c*]pyrazole-4,6(1*H*,5*H*)-dione **15** in 75% yield (Scheme 2).

These pyrrolopyrazole preparations are explainable by the intermediacy of azomethine imine 1,3-dipole (**D**), which could be formed via a 1,2-hydrogen shift in hydrazone **C**, as demonstrated by Grigg et al.[4] The 1,3-dipolar cycloaddition of **D** with **3** gave tetrahydropyrrolo[3,4-*c*]pyrazole-4,6(1*H*,5*H*)-dione **E**, which was dehydrogenated to 3a,6a-dihydropyrrolo[3,4-*c*]pyrazole-4,6(1*H*,5*H*)-dione **F** (Scheme 3).

The differences on the reaction profiles between 5-(monosubstituted hydrazono)methyl derivatives and 5-(disubstituted hydrazono)methyl ones were found in the reaction with dimethyl acetylenedicarboxylate (**16**). Heating of **1a** and **16** in dioxane under reflux gave 5-cyano-1,3,6-trimethyl-2,4(1*H*,3*H*)-pyrimidinedione (**17**) in 58% yield. The same type of product **18** was obtained by the reaction of **5a** with **16**.

A nucleophilic attack of hydrazone nitrogen to acetylenic carbon would initially take place to give a betaine **G**, which is converted to the cyano compounds, **17** and **18**, with the elimination of 2-(dimethylamino), maleate **19** (Scheme 4). Recently, a similar reaction pathway was proposed for the formation of 2-cyanothiophene by the reaction of 2-[(dimethylhydrazono)methyl]thiophene with **16**.[5]

Heating of **1d** and **16** in dioxane under reflux gave 2-pyrazoline **12**, the same product from the reaction of

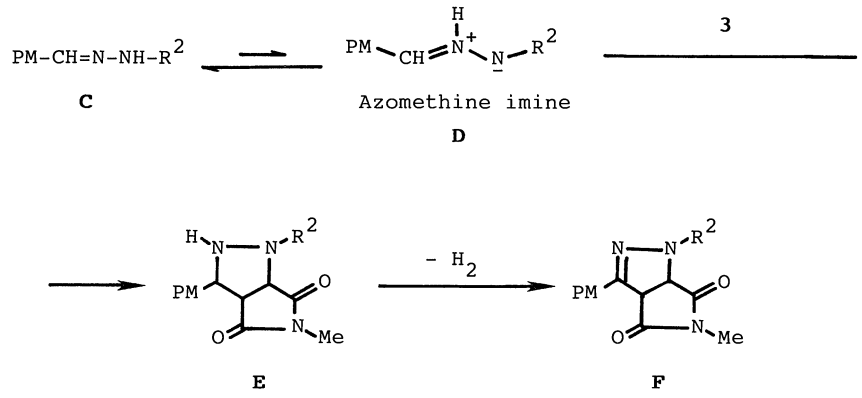

PM: 1,2,3,4-Tetrahydro-1,3,6-trimethyl-2,4-dioxo-5-pyrimidinyl; 4-Methyl-2-phenyl-5-pyrimidinyl

Scheme 3.

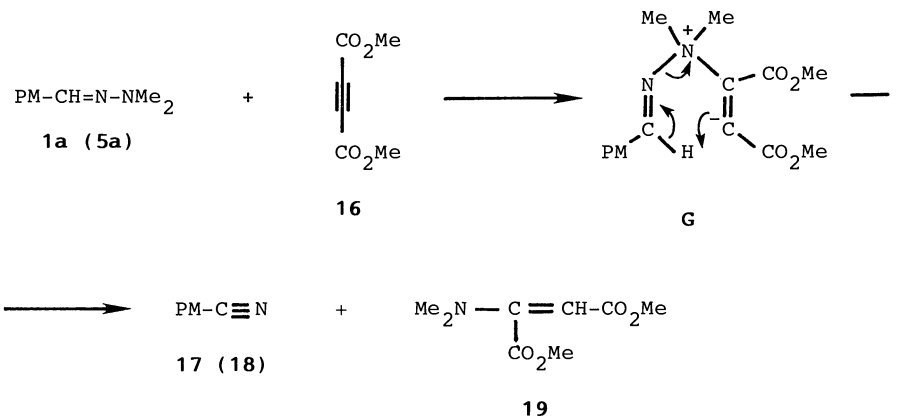

PM: 1,2,3,4-Tetrahydro-1,3,6-trimetyl-2,4-dioxo-5-pyrimydinyl; 4-Methyl-2-phenyl-5-pyrimidinyl

Scheme 4.

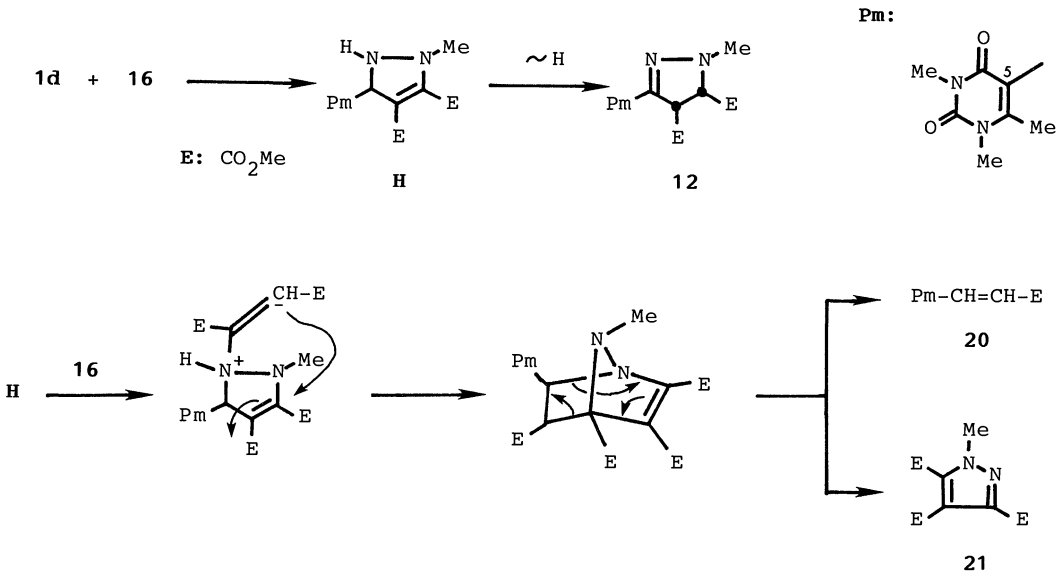

Scheme 5.

1d with dimethyl fumarate (**9**), methyl 2-(1,2,3,4-tetrahydro-1,3,6-trimethyl-2,4-dioxo-5-pyrimidinyl)-acrylate (**20**), and 3,4,5-tris(methoxycarbonyl)-1-methyl-1*H*-pyrazole (**21**). In this reaction a thermal 1,2-hydrogen shift in **1d** gave the 1,3-dipole, which underwent a cycloaddition reaction with **16** to give a 3-pyrazoline derivative **H**. Its isomerization gave 2-pyrazoline derivative **12** with 4,5-cis configuration. A plausible pathway for the formation of **20** and **21** via **H** is demostrated in Scheme 5, which is based on the result of the reaction of benzaldehyde phenylhydrazone with **16**.[6]

In conclusion, the reaction profiles of 6-methyl-5-[(substituted hydrazono)methyl]-2,4(1*H*,3*H*)-pyrimidinediones **1** and their pyrimidine analogs **5** depended not only upon the nature of the pyrimidine rings, but also upon the substituents of the hydrazone moieties. The thermal reaction of 6-methyl-5-[(disubstituted hydrazono)methyl]-2,4(1*H*,3*H*)-pyrimidinediones **1a—c** gave 5,6-dihydro-5,6-bis(methylene)-2,4(1*H*,3*H*)-pyrimidinedione intermediates (**B**) via the 1,5-hydrogen shift, while that of 6-methyl-5-[(monosubstituted hydrazono)methyl]-2,4(1*H*,3*H*)-pyrimidinediones **1d, e** and their pyrimidine analog **5d** gave azomethine imine intermediates (**D**) via the 1,2-hydrogen shift. The cycloaddition reaction using these intermediates, **B** and **D**, gave a useful synthetic tool for the heterocycles containing pyrimidine nuclei.

Experimental

General. All melting points are uncorrected. The IR spectra were measured on a JASCO IR-Report-100 spectrophotometer. The ^1H NMR spectra were obtained on JEOL GSX-400, 270, and/or JMN-MH-100 spectrometers. The chemical shifts are expressed in parts per million downfield from internal tetramethylsilane. Splitting patterns are indicated as s, singlet; d, doublet; t, triplet; q, quartet; m, multiplet; br, broad signal; and ov, overlapping with each other. The ^{13}C NMR spectra were obtained on a JEOL GSX-400 or 270 spectrometer. The mass spectra were determined with a JEOL JMS-012G-2 or JMS-D spectrometer at an ionization energy of 75 eV. Elemental analyses were performed on a Hitachi 026 CHN analyzer. All nonaqueous reactions were run under a positive pressure of argon. All solvents were dried by standard methods before use. The progress of most reactions was monitored by thin-layer chromatography (Silica Gel 60F-254, Merck). Visualization was made ultraviolet light (254 and 365 nm). Chromatographic purification was performed with Wakogel C-200 (100—200 mesh, Wako Pure Chemical Industries) and/or Silica Gel 60 (230—400 mesh, Merck).

Unknown hydrazones **1b—d,f** and **5a—d** were prepared by usual methods.

1,3,6-Trimethyl-5-[(1-piperidinyl)iminomethyl]-2,4-(1*H*,3*H*)-pyrimidinedione (1b): Colorless prisms (ethanol); mp 138—140 °C. Calcd for $C_{13}H_{20}N_4O_2$: C, 59.07; H, 7.63; N, 21.20%. Found: C, 59.21; H, 7.64; N, 21.35%.

1,3,6-Trimethyl-5-[(morpholinoimino)methyl]-2,4(1*H*,3*H*)-pyrimidinedione (1c): Colorless prisms (ethanol); mp 180—181 °C. Calcd for $C_{12}H_{18}N_4O_3$: C, 54.12; H, 6.81; N, 21.04%. Found: C, 53.93; H, 6.92; N, 21.17%.

1,3,6-Trimethyl-5-[(methylhydrazono)methyl]-2,4(1*H*,3*H*)-pyrimidinedione (1d): Colorless prisms (ethanol); mp 108—110 °C. Calcd for $C_9H_{14}N_4O_2$: C, 51.42; H, 6.71; N, 26.65%. Found: C, 51.76; H, 6.80; N, 26.74%.

5-[(Acetylhydrazono)methyl]-1,3,6-trimethyl-2,4(1*H*,3*H*)-pyrimidinedione (1f): Colorless prisms (ethanol); mp 268—271 °C. Calcd for $C_{10}H_{14}N_4O_3$: C, 50.42; H, 5.92; N, 23.52%. Found: C, 50.44; H, 6.00; N, 23.40%.

6-Methyl-5-[(dimethylhydrazono)methyl]-2-phenylpyrimidine (5a): Yellow prisms (hexane); mp 98—99 °C. Calcd

for $C_{14}H_{16}N_4$: C, 69.97; H, 6.71; N, 23.31%. Found: C, 70.02; H, 6.73; N, 23.22%.

6-Methyl-5-[(1-piperidinyl)iminomethyl]-2-phenylpyrimidine (5b): Pale yellow prisms (ethanol); mp 98—100 °C. Calcd for $C_{17}H_{20}N_4$: C, 72.82; H, 7.19; N, 19.99%. Found: C, 72.75; H, 7.38; N, 19.90%.

6-Methyl-5-[(morpholinomethyl)methyl]-2-phenylpyrimidine (5c): Pale yellow plates (ethanol); mp 134—136 °C. Calcd for $C_{16}H_{18}N_4O$: C, 68.06; H, 6.43; N, 19.85%. Found: C, 68.25; H, 6.46; N, 19.80%.

6-Methyl-5-[(methylhydrazono)methyl]-2-phenylpyrimidine (5d): Pale yellow needles (ethanol); mp 108—112 °C. Calcd for $C_{13}H_{14}N_4$: C, 69.00; H, 6.24; N, 24.76%. Found: C, 68.93; H, 6.00; N, 24.45%.

Reaction of 6-Methyl-5-[(disubstituted hydrazono)methyl]-2,4(1*H*,3*H*)-pyrimidinediones with *N*-Methylmaleimide (3). General Procedure: A solution of **1b** (264 mg, 1.0 mmol) and **3** (122 mg, 1.1 mmol) in dioxane (5 ml) was heated under reflux for 2 days. The reaction mixture was evaporated under reduced pressure to give a residue, which was subjected to column chromatography on silica gel to afford **4b** (339 mg, 90%) as an eluate of hexane/ethyl acetate (1/5).

5a,8a-Dihydro-1,3,7-trimethyl-5-[(1-piperidinyl)amino]-1*H*-pyrrolo[3,4-*g*]quinazoline-2,4,6,8(3*H*,5*H*,7*H*,9*H*)-tetrone (4b): Colorless prisms (ethanol); mp 208—209 °C; IR(KBr) 3200 (NH), 1770, 1700, 1650(CO) cm^{-1}; ^1H NMR ($CDCl_3$) δ=1.72 (1H, br s, NH), 1.27, 1.50, 2.08, 2.55—2.75 (total 10H, 4m, piperidinyl methylene), 2.82 (1H, dd, 5a-H, J_{5-5a}=3.9 and J_{5a-8a}=8.8 Hz), 3.05 (3H, s, $-CH_3$), 3.1—3.2 (total 2H, ov, 8a- and 9-H), 3.31(1H, dd, 9-H, J_{8a-9}=5.9 and J_{gem}=15.6 Hz), 3.36, 3.49 (each 3H, 2s, $-CH_3$), 5.02 (1H, d, 5-H, J_{5-5a}=3.9 Hz); ^{13}C NMR ($CDCl_3$) δ=23.0 (9-C), 25.0, 28.4, 31.7 ($-CH_3$), 38.0 (8a-C), 44.8 (5a-C), 48.0 (5-C), 24.0, 25.8, 56.8 (piperidinyl methylene-C), 108.1 (4a-C), 151.6 (9a-C), 151.9 (2-C), 160.8 (4-C), 176.3, 179.2 (6- and 8-C); MS *m/z* 376 (M^+). Calcd for $C_{18}H_{25}N_5O_4$: C, 57.58; H, 6.71; N, 18.66%. Found: C, 57.85; H, 6.69; N, 18.38%.

5a,8a-Dihydro-1,3,7-trimethyl-5-morpholinomethyl-1*H*-pyrrolo[3,4-*g*]quinazoline-2,4,6,8(3*H*,5*H*,7*H*,9*H*)-tetrone (4c): Yield 92%; colorless prisms (hexane–dichloromethane); mp 251—252 °C; IR(KBr) 3200 (NH), 1770, 1700, 1650 (CO) cm^{-1}; ^1H NMR (DMSO-d_6) δ=2.15, 2.35, 2.66 (total 4H, 3m, morpholino methylene), 2.82 (1H, dd, 5a-H, J_{5-5a}=3.9 and J_{5a-8a}=8.3 Hz), 2.96 (3H, s, $-CH_3$), 3.17 (1H, br s, NH), 3.2—3.4 (total 3H, ov, 8a- and 9-H), 3.28, 3.47 (each 3H, 2s, $-CH_3$), 3.6 (4H, m, morpholino methylene), 4.87 (1H, d, 5-H, J_{5-5a}=3.9 Hz); ^{13}C NMR (DMSO-d_6) δ=21.3 (9-C), 23.2, 26.7, 30.0 ($-CH_3$), 30.1 (8a-C), 43.3 (5a-C), 46.1 (5-C), 54.1, 65.0 (morpholino methylene-C), 105.9 (4a-C), 150.2 (9a-C), 150.7 (2-C), 159.2 (4-C), 175.0, 177.8 (6- and 8-C); MS *m/z* 377 (M^+). Calcd for $C_{17}H_{23}N_5O_5$: C, 54.10; H, 6.14; N, 18.56%. Found: C, 54.25; H, 6.11; N, 18.40%.

Reaction of 6-Methyl-5-[(monosubstituted hydrazono)-methyl]-2,4(1*H*,3*H*)-pyrimidinediones with 3. General Procedure: A solution of **1d** (1.0 mmol) and **3** (1.1 mmol) in dioxane (5 ml) was heated under reflux for 20 h. The reaction mixture was evaporated under reduced pressure to give a residue, which was subjected to column chromatography on silica gel to afford **7d** (137 mg, 43%) (hexane/ethyl acetate=1/3) and **8d** (138 mg, 43%) (ethyl acetate). The ratio of **7d** and **8d** varied according to the reaction conditions; prolonged heating (for 36 h) gave **7d** (19%) and **8d** (60%). A treatment of the reaction mixture (under reflux for 20 h) with flash chromatography on silica gel (hexane/ethyl acetate= 1/2—1/4) gave **7d** (55%) and **8d** (29%).

Tetrahydro-3-(1,2,3,4-tetrahydro-1,3,6-trimethyl-2,4-dioxo-5-pyrimidinyl)-1,5-dimethylpyrrolo[3,4-*c*]pyrazole-4,6(1*H*,5*H*)-dione (7d): Colorless crystals; mp 110—113 °C; IR(KBr) 3300(NH), 1770, 1710, 1630(CO) cm^{-1}; ^1H NMR ($CDCl_3$) δ=2.40 (3H, s, 6′-CH_3), 2.76, 2.95, 3.22, 3.50 (each 3H, 4s, N-CH_3), 3.4 (1H, ov, 3a-H), 4.10 (1H, dd, 3-H, J_{2-3}=7.7 and J_{3-4a}=9.0 Hz), 4.65 (1H, d, 6a-H, J_{3a-6a}=7.1 Hz), 5.8 (1H, br d, NH, J_{2-3}=7.7 Hz); ^{13}C NMR ($CDCl_3$) δ=16.8 (6′-CH_3), 25.1, 28.0, 32.4, 41.7 (N-CH_3), 51.2 (3a-C), 60.7 (6a-C), 69.7 (3-C), 104.8 (5′-C), 151.0, 153.0 (2′- and 6′-C), 160.8 (4′-C), 172.3, 173.4 (4- and 6-C). Calcd for $C_{14}H_{19}N_5O_4$: C, 52.33; H, 5.96; N, 21.80%. Found: C, 52.70; H, 5.77; N, 22.12%.

1,3a-Dihydro-3-(1,2,3,4-tetrahydro-1,3,6-trimethyl-2,4-dioxo-5-pyrimidinyl)-1,5-dimethylpyrrolo[3,4-*c*]pyrazole-4,6(1*H*,5*H*)-dione (8d): Colorless prisms (benzene); mp 144—146 °C; IR(KBr) 1780, 1700, 1630(CO)cm^{-1}; ^1H NMR ($CDCl_3$) δ=2.31 (3H, s, 6′-CH_3), 2.99, 3.12, 3.38, 3.47 (each 3H, 4s, N-CH_3), 4.27 (1H, d, 3a-H, J_{3a-6a}=10.7 Hz), 5.16 (1H, d, 6a-H, J_{3a-6a}=10.7 Hz); ^{13}C NMR ($CDCl_3$) δ=17.9 (6′-CH_3), 25.1, 28.3, 32.5, 42.6 (N-CH_3), 55.7 (3a-C), 69.8 (6a-C), 104.2 (5′-C), 140.8 (3-C), 151.5, 152.4 (2′- and 6′-C), 161.4 (4′-C), 173.2, 174.3 (4- and 6-C); MS *m/z* 320 (M^+). Calcd for $C_{14}H_{17}N_5O_4$: C, 52.66; H, 5.37; N, 21.93%. Found: C, 52.90; H, 5.37; N, 22.00%.

A similar reaction of **1e** with **3** gave **7e** and **8e** in a total yield of 98%.

Tetrahydro-3-(1,2,3,4-tetrahydro-1,3,6-trimethyl-2,4-dioxo-5-pyrimidinyl)-5-methyl-1-phenylpyrrolo[3,4-*c*]pyrazole-4,6-(1*H*,5*H*)-dione (7e): Colorless prisms (ethyl acetate); mp 190—193 °C; IR(KBr) 3290 (NH), 1790, 1700, 1630 (CO) cm^{-1}; ^1H NMR ($CDCl_3$) δ=2.31 (3H, s, 6′-CH_3), 3.00, 3.27, 3.48 (each 3H, 3s, N-CH_3), 3.40(1H, dd, 3a-H, J_{3-3a}=9.0 and J_{3a-6a}=7.7 Hz), 4.30 (1H, dd, 3-H, J_{2-3}=12.3 and J_{3-3a}=9.0 Hz), 4.82 (1H, d, 6a-H, J_{3a-6a}=7.7 Hz), 6.15 (1H, d, NH, J_{2-3}=12.3 Hz), 6.8—7.0, 7.2—7.4 (total 5H, 2m, phenyl); ^{13}C NMR ($CDCl_3$) δ=16.6 (6′-CH_3), 25.2, 28.0, 32.6 (N-CH_3), 51.2 (3a-C), 60.7 (6a-C), 69.7 (3-C), 102.7 (5′-C), 114.4, 120.8, 129.3, 150.4 (phenyl-C), 150.8, 151.4 (2′- and 6′-C), 163.0 (4′-C), 174.7, 175.6 (4- and 6-C); MS *m/z* 383 (M^+). Calcd for $C_{19}H_{21}N_5O_4$: C, 59.52; H, 5.52; N, 18.27%. Found: C, 59.22; H, 5.71; N, 18.62%.

3a,6a-Dihydro-3-(1,2,3,4-tetrahydro-1,3,6-trimethyl-2,4-dioxo-5-pyrimidinyl)-5-methyl-1-phenylpyrrolo[3,4-*c*]pyrazole-4,6(1*H*,5*H*)-dione (8e): Colorless prisms (benzene), mp 313—316 °C; IR(KBr) 1790, 1710, 1640(CO) cm^{-1}; ^1H NMR ($CDCl_3$) δ=2.38 (3H, s, 6′-CH_3), 3.02, 3.40, 3.50 (each 3H, 3s, N-CH_3), 5.08 (1H, d, 3a-H, J_{3a-6a}=11.0 Hz), 5.46 (1H, d, 6a-H, J_{3a-6a}=11.0 Hz), 6.9—7.0, 7.2—7.5 (total 5H, 2m, phenyl); ^{13}C NMR ($CDCl_3$) δ=18.0 (6′-CH_3), 25.4, 28.3, 32.6 (N-CH_3), 55.0 (3a-C), 65.0 (6a-C), 103.9 (5′-C), 114.4, 121.6, 129.2, 140.3 (phenyl-C), 144.6 (6′-C), 151.5, 152.5 (3- and 2′-C), 161.3 (4′-C), 172.3, 173.4 (4- and 6-C); MS *m/z* 381 (M^+). Calcd for $C_{19}H_{19}N_5O_4$: C, 59.83; H, 5.02; N, 18.36%. Found: C, 59.98; H, 5.16; N, 18.40%.

1,3,7-Trimethyl-1*H*-pyrrolo[3,4-*g*]quinazoline-2,4,6,8(3*H*,7*H*)-tetrone (14): Yellow prisms (benzene–ethanol); mp 253—238 °C; IR(KBr) 1700, 1650(CO) cm^{-1}; ^1H NMR ($CDCl_3$) δ=2.69 (1H, dd, 9-H, J_{gem}=17.6 and J_{8a-9}=17.1 Hz), 3.10, 3.39, 3.57 (each 3H, 3s, N-CH_3), 3.43 (1H, dd, 9-H, J_{gem}=17.6 and

J_{8a-9}=8.3 Hz), 3.62 (1H, ddd, 8a-H, J_{5-8a}=2.9 and J_{8a-9}=17.1 and 8.3 Hz), 7.56 (1H, d, J_{5-8a}=2.9 Hz); ^{13}C NMR ($CDCl_3$) δ=24.8 (9-C), 25.6, 28.5, 32.3 (N-CH_3), 37.9 (8a-C), 107.6 (4a-C), 120.2, 124.9 (5- and 5a-C), 151.3, 151.5 (2- and 9a-C), 160.0 (4-C), 166.8, 174.1 (6- adn 8-C); MS *m/z* 275 (M^+). Calcd for $C_{13}H_{13}N_3O_4$: C, 56.72; H, 4.76; N, 15.27%. Found: C, 56.85; H, 4.75; N, 15.04%.

The reaction of **1d** with dimethyl fumarate (**9**) gave **11** and **12** in a total yield of 59%. It is too difficult to isolate each other from the mixture as pure forms. The mixture of **11** and **12** in dioxane was heated under reflux in the presence of palladium/charcoal for 5 h to give only product **12**.

3-(1,2,3,4-Tetrahydro-1,3,6-trimethyl-2,4-dioxo-5-pyrimidinyl)-4,5-bis(methoxycarbonyl)-1-methylpyrazolidine (11): ^{1}H NMR ($CDCl_3$) δ=2.44 (3H, s, 6′-CH_3), 3.37, 3.53 (each 3H, 2s, N-CH_3), 3.80, 3.91 (each 3H, 2s, O-CH_3), 3.4—3.5, 3.5—3.6 (each 1H, ov, 5- and 6-H).

3-(1,2,3,4-Tetrahydro-1,3,6-trimethyl-2,4-dioxo-5-pyrimidinyl)-4,5-bis(methoxycarbonyl)-1-methyl-2-pyrazoline (12): Colorless needles (benzene); mp 124—126 °C; IR(KBr) 1750, 1730, 1700, 1650(CO) cm^{-1}; ^{1}H NMR ($CDCl_3$) δ=2.36 (3H, s, 6′-CH_3), 3.04, 3.33, 3.47 (each 3H, 3s, N-CH_3), 3.68, 3.82 (each 3H, 2s, O-CH_3), 4.18 (1H, d, 4-H, J_{4-5}=12.5 Hz), 4.57 (1H, d, 5-H, J_{4-5}=12.5 Hz); ^{13}C NMR ($CDCl_3$) δ=17.9 (6′-CH_3), 28.1, 32.5, 42.7 (N-CH_3), 52.7, 52.8 (O-CH_3), 57.7 (4-C), 71.9 (5-C), 104.9 (5′-C), 142.6 (3-C), 151.7, 151.9 (2′- and 6′-C), 161.3 (4′-C), 169.4, 169.8 (COO); MS *m/z* 353 (M^+). Calcd for $C_{15}H_{20}N_4O_6$: C, 51.13; H, 5.72; N, 15.90%. Found: C, 51.14; H, 5.72; N, 15.55%.

The cis configuration between 4- and 5-position of **12** was confirmed by a NOE measurement; the 7.0% enhancement of signal area of 5-H was observed on irradiation at 4-H. Compound **12** was also obtained in the reaction of **1d** and dimethyl acetylenedicarboxylate (**16**). This implies that **12** with the 4,5-cis configuration is more stable than the 4,5-trans isomer. A similar reaction of **1d** with dimethyl maleate gave only an unseparable mixture of products. We therefore proposed the formation of **12** as follows: the 1,3-dipolar cycloaddition of the azomethine imine to fumarate **9** would proceed stereoselectively to give a trans-adduct (*trans*-**11**), as known from many examples.[7] Isomerization to the 4,5-cis configuration should occur during the dehydrogenation process of **11** to **12**, but the mechanism has not been clear.

4-Ethoxycarbonyl-3-(1,2,3,4-tetrahydro-1,3,6-trimethyl-2,4-dioxo-5-pyrimidinyl)-1-methyl-2-pyrazoline (13): Yield 20%; pale yellow oil; ^{1}H NMR ($CDCl_3$) δ=1.20 (3H, t, -CH_3, J=6.5 Hz), 2.46 (3H, s, 6′-CH_3), 2.90, 3.36, 3.50 (each 3H, 3s, N-CH_3), 3.3—3.5 (1H, ov, 5-H), 3.63 (1H, dd, 5-H, J_{gem}=9.8 and J_{4-5}=5.9 Hz) 4.12 (2H, q, -CH_2-, J=6.5 Hz), 4.57 (1H, dd, 4-H, J_{4-5}=5.9 and J_{4-5}=10.8 Hz); ^{13}C NMR ($CDCl_3$) δ=14.2 (-CH_2-CH_3), 18.0 (6′-CH_3), 28.1, 32.5 (1′- and 3′-CH_3), 43.0 (1-CH_3), 53.2 (4-C), 59.4 (5-C), 61.4 (O-CH_4-), 105.9 (5′-C), 145.4 (3-C), 151.7, 151.9 (2′- and 6′-C), 161.6 (4′-C), 170.8 (COO); MS *m/z* 309 (M^+). This compound could not be isolated as a pure form and did not give satisfactory analytical data.

3a,6a-Dihydro-1,5-dimethyl-3-(4-methyl-2-phenyl-5-pyrimidinyl)pyrrolo[3,4-*c*]pyrazole-4,6(1*H*,5*H*)-dione (15): Colorless prisms (ethanol); mp 199—200 °C; IR(KBr) 1780, 1690(CO) cm^{-1}; ^{1}H NMR ($CDCl_3$) δ=2.82 (3H, s, 4′-CH_3), 3.02, 3.24 (each 3H, 2s, N-CH_3), 4.33 (1H, d, 3a-H, J_{3a-6a}=10.7 Hz), 4.78 (1H, d, 6a-H, J_{3a-6a}=10.7 Hz), 7.4—7.5, 8.4—8.5 (total 5H, 2m, phenyl), 9.14 (1H, s, 6′-H); ^{13}C NMR ($CDCl_3$) δ=25.4 (4′-CH_3), 26.7, 41.9 (N-CH_3), 54.6 (3a-C), 68.9 (6a-C), 121.5 (5′-C), 128.4, 128.6, 130.8, 137.3 (phenyl-C), 138.8 (3-C), 156.3 (6′-C), 162.1 (4′-C), 165.9 (2′-C), 172.4, 173.2 (4- and 6-C); MS *m/z* 336 (M^+). Calcd for $C_{18}H_{17}N_5O_2$: C, 64.46; H, 5.11; N, 20.89%. Found: C, 64.68; H, 5.10; N, 21.22%.

Reaction of 1a with Dimethyl Acetylenedicarboxylate (16). General Procedure: A solution of **1a** (100 mg, 0.45 mmol) and **16** (71 mg, 0.50 mmol) in dioxane (2 ml) was heated under reflux for 2 d. The reaction mixture was evaporated to dryness, and then subjected to column chromatography on silica gel to give **17** (47 mg, 58%), and dimethyl 2-(dimethylamino)maleate (**19**; 37%) was obtained as eluate of hexane/ethyl acetate (5/1).

5-Cyano-1,3,6-trimethyl-2,4(1*H*,3*H*)-pyrimidinedione (17): Colorless needles (hexane); mp 149—151 °C; IR(KBr) 2220 (CN), 1650(CO) cm^{-1}; ^{1}H NMR ($CDCl_3$) δ=2.58 (3H, s, 6-CH_3), 3.32, 3.51 (each 3H, 2s, N-CH_3); MS *m/z* 179 (M^+). Calcd for $C_8H_9N_3O_2$: C, 53.62; H, 5.06; N, 23.45%. Found: C, 53.75; H, 4.98; N, 23.59%.

Dimethyl 2-(Dimethylamino)maleate (19): ^{1}H NMR ($CDCl_3$) δ=2.86 (6H, s, N-CH_3), 3.60, 3.90 (each 3H, 2s., O-CH_3), 4.56 (1H, s, -CH_3); MS *m/z* 187 (M^+).

5-Cyano-4-methyl-2-phenylpyrimidine (18): Yield 66%; pale yellow needles (ethanol); mp 171—173 °C; IR(KBr) 2210(CN) cm^{-1}; ^{1}H NMR ($CDCl_3$) δ=2.92 (3H, s, -CH_3), 7.7—7.9, 8.7—8.9 (total 5H, 2m, phenyl), 9.22 (1H, s, 6-H); MS *m/z* 195 (M^+). Calcd for $C_{12}H_9N_3$: C, 73.83; H, 4.65; N, 21.53%. Found: C, 73.43; H, 4.55; N, 21.20%.

Reaction of 1d with 16. A solution of **1d** (210 mg, 1.0 mmol) and **16** (0.18 ml, 1.4 mmol) in dioxane (5 ml) was heated under reflux for 8 h. The reaction mixture was evaporated to dryness and subjected to column chromatography on silicagel to afford **21** (100 mg, 39%) (hexane/ethyl acetate=3/1), **20** (86 mg, 36%) (2/1), and **12** (79 mg, 23%) (1/1).

Methyl 3-(1,2,3,4-Tetrahydro-1,3,6-trimethyl-2,4-dioxo-5-pyrimidinyl)acrylate (20): This was obtained as *E*/*Z* (= 10/9) mixture.

(*E*)-20: Colorless needles (ethanol); mp 181—183 °C; IR(KBr) 1720, 1700, 1640(CO) cm^{-1}; ^{1}H NMR ($CDCl_3$) δ=2.48 (3H, s, 6′-CH_3), 3.39, 3.54 (each 3H, 2s, N-CH_3), 3.78 (3H, s, O-CH_3), 7.12 (1H, d, 2-H, J=15.6 Hz), 7.58 (1H, d, 3-H, J=15.6 Hz); ^{13}C NMR ($CDCl_3$) δ=17.0 (6′-CH_3), 28.4, 32.8 (N-CH_3), 51.6 (O-CH_3), 107.1 (5′-C), 120.8 (2-C), 135.7 (2-C), 149.7 (6′-C), 151.8 (4′-C), 161.1 (2′-C), 165.8 (1-C); MS *m/z* 239 (M^+). Calcd for $C_{11}H_{14}N_2O_4$: C, 55.45; H., 5.92; N, 11.76%. Found: C, 55.38; H, 6.03; N, 12.02%.

(*Z*)-20: Colorless plates (ethanol); mp 116—117 °C; IR (KBr) 1720, 1700, 1640(CO) cm^{-1}; ^{1}H NMR ($CDCl_3$) δ=2.24 (3H, s, 6′-CH_3), 3.36, 3.48 (each 3H, 2s, N-CH_3), 3.69 (3H, s, O-CH_3), 6.15 (1H, d, 2-H, J_{1-2}=11.7 Hz), 6.79 (1H, d, 1-H, J_{1-2}=11.7 Hz); ^{13}C NMR ($CDCl_3$) δ=18.2 (6′-CH_3), 28.3, 32.3 (N-CH_3), 51.5 (O-CH_3), 108.1 (5′-C), 123.5 (2-C), 137.0 (3-C), 149.7 (6′-C), 151.8 (4′-C), 161.1 (2′-C), 165.8 (1-C); MS *m/z* 239 (M^+). Calcd for $C_{11}H_{14}N_2O_4$: C, 55.45; H, 5.92; N, 11.76%. Found: C, 55.38; H, 6.03; N, 12.02%.

3,4,5-Tris(methoxycarbonyl)-1-methyl-1*H*-pyrazole (21): Colorless primsms (ethanol); mp 96—97 °C; IR(KBr) 1740, 1720(CO) cm^{-1}; ^{1}H NMR ($CDCl_3$) δ=4.00 (total 6H, s, O-CH_3), 4.30 (3H, s, N-CH_3); ^{13}C NMR ($CDCl_3$) δ(off

resonance)=40.7 (q, N-CH_3), 52.5, 52.8, 52.9 (each q, O-CH_3), 121.6 (s, 4-C), 131.6 (s, 5-C), 138.8 (s, 3-C), 158.4, 160.7, 163.6 (each s, COO); MS *m/z* 256(M^+). Calcd for $C_{10}H_{12}N_2O_6$: C, 46.88; H, 4.72; N, 10.93%. Found: C, 46.93; H, 4.72; N, 10.67%.

The authors wish to thank UBE Scientific Analysis Laboratory for the help of the structural analyses using NMR spectrometers at 270 and/or 400 MHz.

References

1) Studies on Fused Pyrimidine Derivatives. Part IX. Part IIIV in this series: M. Noguchi, Y. Kiriki, T. Ushijima, and S. Kajigaeshi, *Bull. Chem. Soc. Jpn.*, **63**, 2938 (1990).

2) D. J. Brown and S. F. Mason, "The Chemistry of Heterocyclic Compounds. The Pyrimidines," ed by A. Weissberger, Interscience, New York (1962); D. J. Brown, R. F. Evans, and T. J. Batterham, "The Chemistry of Heterocyclic Compounds. The Pyrimidines Supplement I," ed by A. Weissberger and E. C. Taylor, Wiley-Interscience, New York (1970); J. H. Lister, "Heterocyclic Compounds Fused Pyrimidines Part II; Purines," ed by A. Weissberger and E. C. Taylor, Wiley-Interscience, New York (1871). G. Maury, "Special Topics in Heterocyclic Chemistry," ed by A. Weissberger and E. C. Taylor, Wiley-Interscience, New York (1977), p. 179.

3) a) S. Senda, T. Asao, I. Sugiyama, and K. Hirota, *Tetrahedron Lett.*, **21**, 531 (1980); b) M. Noguchi, K. Sakamoto, S. Nagata, and S. Kajigaeshi, *J. Heterocycl. Chem.*, **25**, 205 (1988); c) M. Noguchi, Y. Kiriki, and S. Kajigaeshi, *Bull. Chem. Soc. Jpn.*, **62**, 3043 (1989); d) M. Noguchi, K. Doi, Y. Kiriki, and S. Kajigaeshi, *Chem. Lett.*, **1989**, 2115.

4) R. Grigg, J. Kemp, and N. Thompson, *Tetrahedron Lett.*, **1978**, 2827.

5) M. E. Gonzalez, P. Sancho, C. Soriano, R. Ballesteros, B. Abarca, and J. Sepulveda, *Heterocycles*, **27**, 1227 (1988).

6) H. Ogura, K. Kubo, Y. Watanabe, and T. Itoh, *Chem. Pharm. Bull.*, **21**, 2026 (1973).

7) R. Grashey, "1,3-Dipolar Cycloaddition Chemistry. Azomethine Imines", ed by A. Padwa, Wiley-Interscience, New York (1984), p. 733.

Reactions of Benzocyclopropene with Sulfonyl Isocyanates and Nitrones:[1] Cycloadditions through C–C σ-Bond Rupture of Three-Membered Ring

Shinzo KAGABU,* Katsuhiro SAITO,† Hiroyuki WATANABE,†
Kensuke TAKAHASHI,† and Katsuaki WADA††
Department of Chemistry, Faculty of Education, Gifu University,
Yanagido, Gifu 501-11
† Department of Applied Chemistry, Nagoya Institute of Technology,
Gokiso-cho, Showa-ku, Nagoya 466
†† Yuki Research Center, Nihon Tokushu Noyaku Seizo and Co.,
Nishihanjozuka, Yuki, Ibaragi 307
(Received July 26, 1990)

Alkane- and arenesulfonyl isocyanates were added to benzocyclopropene across the C–C σ-bond of the three-membered ring, giving 2-sulfonyl-1-isoindolinones. The reaction with *C,N*-diphenylnitrone afforded a similar cyclization product, 3,4-dihydro-3,4-diphenyl-1*H*-2,3-benzoxazine. These reactions are considered to proceed through zwitterionic intermediates formed by the fission of the C–C σ-bond of the three-membered ring by the electrophiles.

Highly strained benzocyclopropene (**1**) has recently attracted much interest of chemists.[2] A fusion of the two rings results in a considerable deformation of the benzene ring and, consequently in a reduction of the aromatic stabilization. Of particular note concerning to the unusual molecular geometry has been a solution to the question of bond fixation[3] and the cleavage mechanism of the three-membered ring in the reaction with electrophiles. Recently, Apeloig and Arad[4] depicted a suggestive FMO picture using a 3-21G method, showing that the HOMO has a higher energy than does the benzene, and is localized at both the fused bond C_1–C_6 and the C_3–C_4 bond.

According to FMO theory, an electrophilic attack should, therefore, occur preferably at the fused bond and more readily than on benzene. Some cycloaddition experiments agree with this argument: **1** reacts smoothly with electron-defficient (hetero)dienes in a concerted [2σs+4πs] fashion to give 1,6-methano[10]-annulenes and the hetero analogues.[5,6] Bond localization was also advocated by its almost quantitative reaction with dihalocarbenes.[7] On the other hand, halogenes, acids, and alcohols with metal ion catalysts provoke the reaction in another way: dissociating the σ-bond of the cyclopropene moiety exclusively to form the benzyl cation intermediates.[8]

The dependence of the different cleavage course on the types of electrophiles prompted us to examine the reactions with electrophilic polar double bonds or charge-separated organic species. To date, there have been only a couple of examples reported in this context; thus with arenecarbonitrile oxides[9] and mesoions,[10] and in both cases, the reaction apparently proceeded in a concerted manner to give the cycloaddition products across the fused bond.[11]

We have examined the reaction with other polar electrophiles to find a contrasting result regarding the yield of [2σ+4π]-type products with some isocyanates and nitrones. These cycloadditions are considered to proceed through an internal coupling of the intermediary zwitterions.

Results

The reaction of benzocyclopropene (**1**) with an equimolar amount of the sulfonyl isocyanate (**2**) was monitored by thin-layer chromatography and NMR spectroscopy. The reactions with methyl and phenyl isocyanates were quite sluggish. The mixture showed practically no change at room temperature over a period of one week.[12] In contrast, the reaction of **1** with *p*-toluenesulfonyl isocyanate (**2d**) proceeded smoothly at 60 °C; the peak at 3.17 ppm of the methylene protons disappeared completely within 40 h. The reaction mixture was subjected to thin-layer chromatography on silica gel to give colorless crystalline 2-*p*-tolylsulfonyl-1-isoindolinone (**3d**) and 1-isoindolinone (**4**) in 39 and 4% yields, respectively. 1-Isoindolinone (**4**) is obviously a secondary product from **3d**, since the isolated **3d** slowly decomposed to **4** in chloroform, and rapidly upon adding a few drops of ammonia water to it.

Similarly, warming a mixture of 1 and benzenesulfonyl isocyanate (**2c**) at 60 °C for 30 h afforded *N*-benzenesulfonyl derivative (**3c**) in 36% yield along with a small quantity of **4**. The cycloadditions with methanesulfonyl isocyanate (**2a**) and 1-butanesulfonyl isocyanate (**2b**) proceeded rather readily even at room temperature, to afford the corresponding 2-alkylsulfonyl-1-isoindolinones (**3a** and **3b**) in more than 20% yields after 3 days.

On the other hand, in reactions with 1,3-dipoles, such as methyl azidoformate and ethyl diazoacetate, we could not detect the corresponding adducts in any case at 60 °C after 4—6 days. In contrast, electrophilic *C,N*-diphenylnitrone (**5**) was sufficiently reactive toward **1** to produce the cycloadduct, 3,4-dihydro-3,4-diphenyl

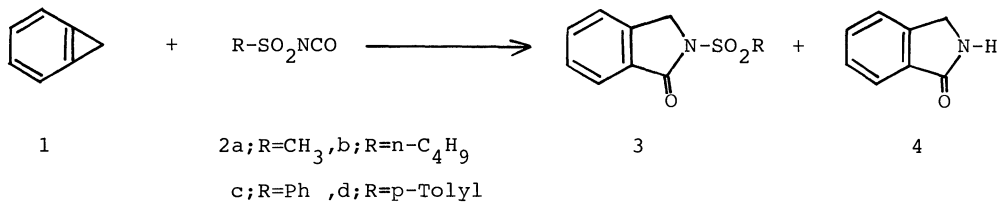

1 2a;R=CH3,b;R=n-C4H9 3 4
c;R=Ph ,d;R=p-Tolyl

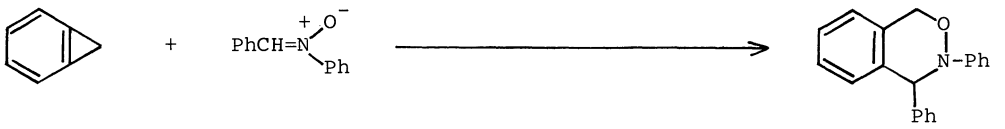

1 5 6

Fig. 1.

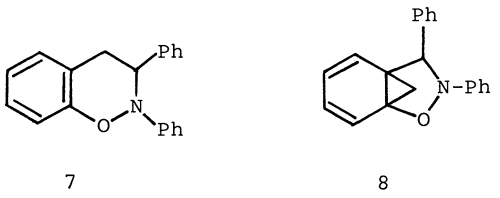

7 8

Fig. 2.

9 10

Fig. 3.

1*H*-2,3-benzoxazine (**6**), in 54% yield.

The structures of **3** were confirmed by IR, ^{1}H NMR, ^{13}C NMR, and mass spectroscopic studies. In ^{1}H NMR spectra the chemical shifts of the methylene protons (around 4.9 ppm) was close to 4.38 ppm of 1-isoindolinone, itself, rather than to 3.50 ppm of the methylene peak of the possible regional isomer, 2-indolinone (**9**). Their ^{13}C NMR spectra indicated carbonyl carbons at between 166 and 167 ppm near to the corresponding value of 158.2 ppm of *N*-methylsaccharin (**10**), composing of the partial structure of $-SO_2NRCO-$.[13] In IR spectra the higher shift of carbonyl absorptions of **3** (around 1720 cm^{-1}) from that of 1-isoindolinone (1680 cm^{-1}) indicated the presence of an electronegative substituent at the nitrogen atom.

In EI mass spectroscopy, the 2-arylsulfonyl-1-isoindolinones (**3c, d**) showed no molecular ion peaks; instead, SO_2-eliminated ions appeared as their parent peaks, which is in contrast with the *N*-alkylsulfonyl derivatives whose parent peaks are 1-oxoisoindolin-2-ylium ion arising from a fragmentation of the alkylsulfonyl radicals. A similar SO_2 extrusion has been observed in *N*-arylsulfonylcarbamates, and the mechanism (not simple cheletropic) has been variously discussed.[14] On the other hand, a milder ionization method (CIMS) using isobutane displayed M$^+$+1 peaks with a distinctively strong intensity.

The structure of the oxazine (**6**) is determined spectroscopically, especially by NMR study. A singlet peak at 5.63 ppm and two doublet peaks at 5.19 and 5.29 ppm with a large geminal coupling constant (J=14 Hz) in ^{1}H NMR as well as the existence of only two aliphatic signals at 67.9 and 70.3 ppm in ^{13}C NMR support the structure (**6**). The formation of a possible regional isomer (**7**) and a norcaradiene derivative (**8**) are excluded.

Discussion

The smooth reaction of **1** with strongly electrophilic sulfonyl isocyanates reflects well the electron-donating nature of **1**. One explanation for the product is that the reaction proceeds in the fashion of an electrophilic aromatic substitution in which an electrophile attacks the HOMO-π-system located at C_1 to form the annelated cyclopropylium ion (**11**). A subsequent ring opening with a relief of strain energy forms a zwitterionic intermediate (**13**), which then recloses to give **3**. However, considering the enormously high strain energy (290 kJ mol^{-1}) of **1**, owing to the fused cyclopropene construction, it is not deniable that at first a σ-bond rupture on the three-membered ring occurs through an intermediate **12**, leading to the zwitterion (**13**). The preferable path between the π-

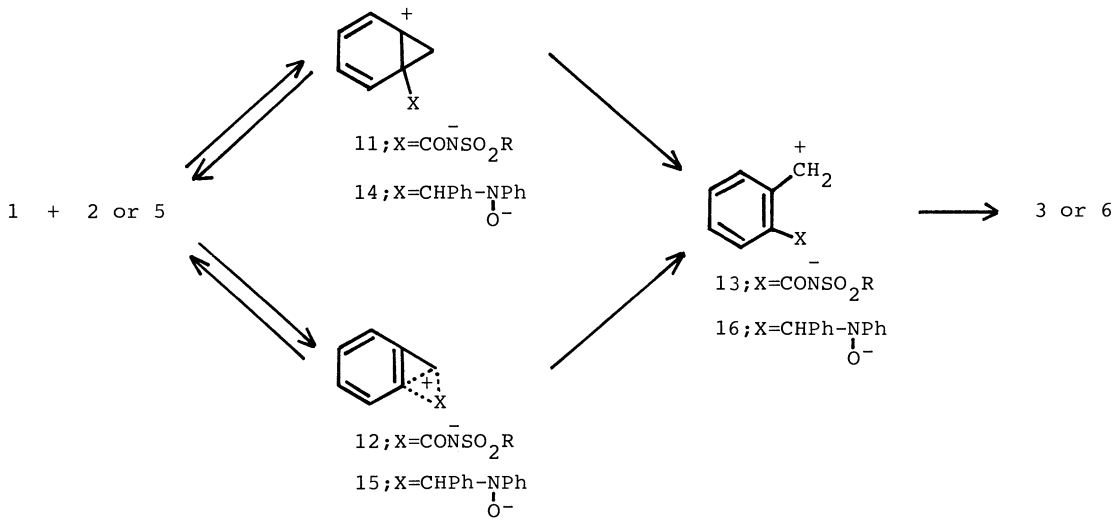

Fig. 4.

and σ-route has not yet been decided at the present stage, due to a lack of information regarding the stability of the intermediates.

Cycloaddition reactions of 1,3-dipoles have been highly studied over the past 20 years by Huisgen and others.[15] Houk et al. have discussed the reactivity and regioselectivity in synchronous dipolar additions in terms of FMO theory.[16] Among various types of 1,3-dipoles, nitrones and nitrile oxides having lower LUMO energies are expected to exert a considerable orbital interaction with the HOMO of **1**, especially when they are perturbated by the phenyl substituent.

The finding by Nitta and his co-workers is in accord with the theoretical prediction; they isolated a bridged norcaradiene, stable up to 120 °C, by a reaction with aromatic nitrile oxides.[9] In our study with diphenyl nitrone (**5**), however, we could not detect the formation of the tricyclic system (**8**); also, the possibility of a [1,3] sigmatropic shift of **8** to **6** is unrealistic under the reaction conditions.

It is most likely that the formation of **6** involved a stepwise process through a zwitterionic intermediate (**16**), which was derived via **14** or **15**. The regioselectivity of the addition is rationally accounted for by a CNDO/2 calculation on **5**, estimating that the LUMO coefficient on the carbon atom is greater than that on the oxygen atoms.[16] Thus, the orbital overlapping between the carbon atom of the nitrone and the π- or σ-bond of the three-membered ring develops as they approach to form the zwitterion (**16**), which leads to the product (**6**) by the resulting internal coupling. However, despite having a close LUMO energy level to that of nitrle oxide, why the nitrone does not add across the fused bond of **1** is still unclear.

As described above regarding the reaction with sulfonyl isocyanates and nitrones, the adjoining σ-bond to the benzene ring of **1** is formally replaced by a new σ-bond supplied from the entering electrophiles. Such an exceptional facile leaving of C–C bond from the aromatic ring is obviously ascribed to a highly strained cyclic system.

Experimental

The melting points were recorded on a Yanagimoto micro melting point apparatus and were uncorreced. The IR spectra were determined on a JASCO A-100 or a JASCO A-102 spectrometers. The NMR spectra were recorded by using a JNM GX-270 or a Varian XL-200 spectrometers in $CDCl_3$ solution with tetramethylsilane as an internal standard. Low- and high-resolution mass spectra were measured using a Shimadzu 9020-DF or a JMX DX-300 spectrometers. The UV spectra were recorded on a Hitachi 210 spectrometer. The solvents used were purified according to the standard procedures.[17] Methyl and phenyl isocyanates and benzene- and *p*-toluenesulfonyl isocyanates were commercially available. Methane- and 1-butanesulfonyl isocyanates were prepared by a method described in the literature.[18] Plates for preparative thin-layer chromatography were prepared with Merck Silica gel PF-254 or Wako gel B5-F.

General Procedure for the Reaction of Sulfonyl Isocyanates with 1. A solution of **1** (1.0 mmol) in chloroform (2.0 ml) was added to an ice-cold solution of sulfonyl isocyanate (**2**) (1.0 mmol) in the same solvent (3.0 ml). The combined solution was gently bubbled with dry nitrogen gas for ten min and allowed to stand at room temperature, or warmed. After the solvent was evaporated, the residual crude reaction mixture was chromatographed on TLC plates using chloroform–ethyl acetate–hexane (2:1:3) as a developing solvent to give crystalline products, which were further purified by recrystallization from 2-propanol. The yields were determined when the sample showed a single spot on TLC and contained practically no contaminates on the NMR spectra. 1-Isoindolinone (**4**) was identified by a comparison of TLC (R_f=0.1) and the melting point of 151—153 °C (Lit,[19] 155—156 °C) with an authentic sample.[19]

2-Methylsulfonyl-1-isoindolinone (3a): Yield: 21%. Colorless needles, mp 162 °C, R_f=0.3. Found: C, 51.17; H, 4.33; N, 6.67; S, 15.32%. Calcd for $C_9H_9NO_3S$: C, 51.17; H, 4.30; N, 6.63; S, 15.18%. EIMS *m/z* (rel intensity) 211 (M^+, 24), 133 (30), 132 (100), 105 (23), 104 (38), 77 (39). CIMS (isobutane) *m/z* (rel intensity) 212 (M^++1, 78), 134 (79), 57 (C_4H_9+1, 100). IR (KBr) 1720, 1340, 1142, 1130, 1092 cm^{-1}. ^1H NMR ($CDCl_3$) δ=3.42 (s, 3H), 4.89 (s, 2H), 7.2—7.6 (m, 2H), 7.71 (dd, 1H, *J*=7.3 and 7.3 Hz), 7.92 (d, 1H, *J*=7.7 Hz). ^{13}C NMR ($CDCl_3$) δ=41.1 (q), 49.2 (t), 123.5 (d), 125.2 (d), 129.0 (d), 130.0 (s), 134.2 (d), 141.2 (s), 167.2 (s).

2-Butylsulfonyl-1-isoindolinone (3b): Yield 26%. Calorless needles, mp 102.5 °C, R_f=0.7. Found: C, 56.70; H, 5.93; N, 5.60; S, 12.71%. Calcd for $C_{12}H_{15}NO_3S$: C, 56.89; H, 5.97; N, 5.53; S, 12.66%. EIMS *m/z* (rel intensity) 253 (M^+, 21), 134 (51), 133 (100), 132 (70), 105 (24), 104 (23), 77 (46). CIMS (isobutane) *m/z* (rel intensity) 254 (M^++1, 49), 134 (79), 57 ($C_4H_9^+$, 100). IR (KBr) 1720, 1340, 1320, 1155, 1105 cm^{-1}. ^1H NMR ($CDCl_3$) δ=0.94 (t, 3H, *J*=7.3 Hz), 1.48 (m, 2H), 1.83 (m, 2H), 3.61 (t, 2H, *J*=8.1 Hz), 4.88 (s, 2H), 7.5—7.6 (m, 2H), 7.70 (dd, 1H, *J*=6.6 and 6.6 Hz), 7.92 (d, *J*=7.3 Hz). ^{13}C NMR ($CDCl_3$) δ=13.5 (q), 21.4 (t), 24.9 (t), 49.7 (t), 53.2 (t), 123.5 (d), 125.2 (d), 129.0 (d), 130.1 (s), 134.1 (d), 141.3 (s), 167.1 (s).

2-Phenylsulfonyl-1-isoindolinone (3c): The reaction was carried out in benzene. Yield: 36% (1-isoindolinine (**4**) was by-produced in 4% yield). Colorless needles, mp 193.5 °C, R_f=0.5. Found: C, 61.58; H, 3.97; N, 5.08; S, 11.53%. Calcd for $C_{14}H_{11}NO_3S$: C, 61.52; H, 4.06; N, 5.15; S, 11.53%. EIMS *m/z* (rel intensity) 209 (M^+-SO_2, 68), 208 (100), 132 (25), 77 45). CIMS (isobutane) *m/z* (rel intensity) 274 (M^++1, 76), 134 (79), 57 ($C_4H_9^+$, 100). IR (KBr) 1722, 1360, 1182, 1175, 1100 cm^{-1}. ^1H NMR ($CDCl_3$) δ=4.92 (s, 2H), 7.4—7.7 (m, 6H), 7.82 (d, 1H, *J*=8.1 Hz), 8.16 (m, 2H). ^{13}C NMR ($CDCl_3$) δ=49.9 (t), 123.4 (d), 125.1 (d), 128.1 (d), 128.9 (d), 129.1 (d), 130.1 (s), 133.9 (d), 134.1 (d), 138.4 (s), 141.0 (s), 166.1 (s).

2-*p*-Tolylsulfonyl-1-isoindolinone (3d): Yield: 39% (1-isoindolinone (**4**) was by-produced in 4% yield). Colorless needles, mp 218 °C, R_f=0.6. Found: C, 62.63; H, 4.60; N, 4.94; S, 11.15%. Calcd for $C_{15}H_{13}NO_3S$: C, 62.67; H, 4.56; N, 4.88; S, 11.16%. EIMS *m/z* (rel intensity) 223 (M^+-SO_2, 100), 222 (62), 132 (22), 91 (36). CIMS (isobutane) *m/z* (rel intensity) 288 (M^++1, 81), 134 (67), 57 ($C_4H_9^+$, 100). IR (KBr) 1720, 1340, 1142, 1130, 1092 cm^{-1}. ^1H NMR ($CDCl_3$) δ=2.41 (s, 3H), 4.91 (s, 2H), 7.33 (d, 2H, *J*=8.4 Hz), 7.4—7.5 (m, 2H), 7.63 (ddd, 1H, *J*=1.1, 7.0, and 9.0 Hz), 7.80 (dd, 1H, *J*=1.1 and 8.1 Hz), 8.03 (d, 2H, *J*=8.4 Hz). ^{13}C NMR ($CDCl_3$) δ=21.7 (q), 49.8 (t), 123.3 (d), 125.0 (d), 128.2 (d), 128.8 (d), 129.8 (d), 130.2 (s), 133.8 (d), 135.5 (s), 141.0 (s), 145.2 (s), 166.1 (s).

Reaction of 1 with 5. A solution of **1** (33 mg, 0.37 mmol) and **5** (145 mg, 0.74 mmol) in deuteriochloroform (0.5 ml) was heated at 60 °C for 70 h. After evaporation of the solvent the resluting mixture was subjected to this-layer chromatography on silica gel using hexane–ethyl acetate (7:3) as a developing solvent to give colorless crystals **6** (57 mg, 54%, R_f=0.74).

6: Mp 104 °C. HRMS *m/z* 287.1309. Calcd for $C_{20}H_{17}NO$ *m/z* 287.1309. EIMS *m/z* (rel intensity) 287 (M^+, 100), 269 (50), 180 (90), 165 (42). IR (KBr) 3050, 3010, 1600, 1500, 760 cm^{-1}. UV (MeOH) 245 nm (log ε, 3.97). ^1H NMR ($CDCl_3$) δ=5.19 (d, 1H, *J*=14.0 Hz), 5.29 (d, 1H, *J*=14.0 Hz), 5.63 (s, 1H), 7.26 (bs, 14H). ^{13}C NMR ($CDCl_3$) δ=67.9, 70.3, 118.3, 122.8, 124.0, 126.6, 127.7, 128.1, 128.4, 129.9, 133.6, 135.9, 139.3, 148.6.

References

1) A preliminary communication on part of this work has appeared: S. Kagabu and T. Inoue, *Chem. Lett.*, **1989**, 2181.

2) a) B. Halton, *Chem. Rev.*, **73**, 113 (1973); b) W. E. Billups, *Acc. Chem. Res.*, **11**, 245 (1978); c) B. Halton, *Ind. Eng. Chem. Prod. Res. Dev.*, **19**, 349 (1980); d) B. Halton and M. C. Banwell, "Cyclopropenes," in "The Chemistry of Functional Groups," ed by Z. Rappoport, Wiley, Chichester (1987), pp. 1223—1340; e) B. Halton, *Chem. Rev.*, **89**, 1161 (1989).

3) The semiempirical calculations support bond fixation favoring the structure **1a**, while the ab initio calculations imply bond fixation in the opposite direction to **1b**, see P. C. Hiberty, G. Ohanessian, and F. Delbecq, *J. Am. Chem. Soc.*, **107**, 3095 (1985); C. Wentrup, C. Mayor, J. Becker, and H. J. Linder, *Tetrahedron*, **41**, 1601 (1985).

1a 1b

Fig. 5.

4) Y. Apeloig and D. Arad, *J. Am. Chem. Soc.*, **108**, 3241 (1986); According to the photoelectron measurement by Heilbronner et al, the orbital energy of HOMO of **1** is −8.82 eV relative to −9.25 eV of benzene; F. Brogli, E. Giovannini, E. Heilbronner, and R. Schurter, *Chem. Ber.*, **106**, 961 (1973).

5) E. Vogel, J. Ippen, and V. Buch, *Angew. Chem. Int. Ed. Engl.*, **14**, 566 (1975); M. L. Maddox, J. C. Martin, and J. M. Muchowski, *Tetrahedron Lett.*, **27**, 7 (1980); J. C. Martin and J. M. Muchowski, *J. Org. Chem.*, **49**, 1040 (1984); R. Neidlein L. Tadesse, *Helv. Chim. Acta*, **71**, 249 (1988); The mechanistic argument about the reaction with electron-rich dienes, see Ref. 6.

6) K. Saito, H. Ishihara, and S. Kagabu, *Bull. Chem. Soc. Jpn.*, **60**, 4141 (1987); S. Korte, Ph. D. Thesis, University Köln, 1968.

7) S. Kagabu and K. Saito, *Tetrahedron Lett.*, **29**, 675 (1988).

8) However, iodination ocurrs across the fused bond in dark as well as by irradiation; E. Vogel, W. Grimme, and S. Korte, *Tetrahedron Lett.*, **1965**, 3625; R. Okazaki, M. O-oka, N. Tokitoh, and N. Inamoto, *J. Org. Chem.*, **50**, 180 (1985).

9) M. Nitta, S. Sogo, and T. Nakayama, *Chem. Lett.*, **1979**, 1431.

10) H. Kato and S. Toda, *J. Chem. Soc., Chem. Commun.*, **1982**, 510; H. Kato, Y. Arikawa, Y. Hashimoto, and M. Masuzawa, *ibid.*, **1983**, 938.

11) Attempted cycloadditions of **1** with *p*-toluenesulfonyl and *p*-nitrophenyl azides and diphenylnitrile imine as well as ethyl diazoacetate have not thus far recorded; unpublished results cited in Ref. 2c.

12) After the subsequent warming at 70 °C for more than

ten hours **1** disappeared on TLC and NMR spectra. However, the viscous brown liquid remained proved to be intractable and nospectroscopic data could be obtained after TLC.

13) ^{13}C NMR data for the analogous compounds; see for example, E. Breitmaier and W. Voelter, "Carbon-13 NMR Spectroscopy," 3rd ed, VCH, Weinheim (1987); H. O. Kalinowski, S. Berger, and S. Braun, "Carbon-13 NMR Spectroscopy," Wiley, Chichester (1988); ^{13}C NMR data for *N*-methylsaccharin by our own measurement are δ=23.0 (q), 121.4 (d), 124.8 (d), 126.6 (s), 134.9 (d), 135.4 (d), 136.7 (q), 158.2 (s).

14) W. H. Daly and C. W. Heurtevant, *Org. Mass Spectrom.*, **4**, 165 (1970); Further discussion on the SO_2 fragmentation in organic compounds; see, H. Nakata, *Synth. Org. Chem. Jpn.*, **30**, 228 (1972).

15) J. J. Tuffariello, "1,3-Dipolar Cycloaddition Chemistry," Wiley, New York (1984); P. Confalone and E. M. Huie, *Org. React.*, **36**, 1 (1988).

16) K. N. Houk, "Application of Frontier Orbital Theory to Pericyclic Reactions," in "Pericyclic Reactions," ed by A. P. Marchand and R. E. Lehr, Academic Press, New York (1977), Vol. 2, Chap. 4; K. N. Houk, J. Sims, R. F. Duke, Jr., R. W. Strozier, and J. K. George, *J. Am. Chem. Soc.*, **95**, 7387 (1973); K. N. Houk, J. Sims, C. R. Watts, and L. J. Luskus, *ibid.*, **95**, 7301 (1973); R. Huisgen, R. Sustmann, and K. Bunge,*Chem. Ber.*, **105**, 1324 (1972).

17) T. Wieland and W. Sucrow, "Die Praxis des Organischen Chemikers," 43rd ed, Walte de Gruyter, Berlin (1982), pp. 110—117.

18) W. H. Daly and H. J. Holle, *J. Org. Chem.*, **39**, 1597 (1974).

19) S. Danishefsky, T. A. Bryson, and J. Puthenpurayil, *J. Org. Chem.*, **40**, 796 (1975).

 © 1991 The Chemical Society of Japan Bull. Chem. Soc. Jpn., 64, 111—117 (1991)

Polypeptide Synthesis Using the *S*-Alkyl Thioester of a Partially Protected Peptide Segment. Synthesis of the DNA-Binding Domain of *c*-Myb Protein (142—193)-NH_2

Hironobu Hojo and Saburo Aimoto*
Institute for Protein Research, Osaka University, 3-2 Yamadaoka, Suita, Osaka 565
(Received August 23, 1990)

A method for polypeptide synthesis using *S*-alkyl thioester of a partially protected peptide segment has been developed. The DNA-binding domain of *c*-Myb protein (142—193) was synthesized by this method to estimate its usefulness. The partially protected peptide segments, Boc-[Lys(Boc)^{143,144,160}]-*c*-Myb protein(142—163)-$SCH_2CH_2CONH_2$ and [Lys(Boc)^{171,182,192}]-*c*-Myb protein(164—193)-NH_2, were highly purified from peptides obtained by a solid-phase method. The thioester in the carboxyl component of the peptide segment was converted to the corresponding *p*-nitrophenyl ester in the presence of silver ions and *p*-nitrophenol and then the two segments were condensed. The coupling reaction proceeded almost completely yielding a highly-purified product after removal of Boc groups.

In our preceding paper,[1] we reported the synthesis of bovine pancreatic trypsin inhibitor (BPTI) consisting of 58 amino acid residues, using partially protected peptide segments prepared from peptides obtained by a solid-phase method. This method was proven to be very effective in reducing the time required for chemical synthesis of polypeptide and to give a highly pure product.

However in this method, it was necessary to protect the side-chain carboxyl groups in peptide segments for selective activation of the terminal carboxyl group. Moreover peptide segments containing side-chain carboxyl groups could be prepared only by the solid-phase method using N^{α}-3-nitro-2-pyridinesulfenyl-amino acids (Npys-amino acids) developed by Matsueda et al.[2]

There arose two problems. The first was that of peptide segment solubility during purification by reversed-phase high-performance liquid chromatography (RPHPLC). Generally, an increase in the number of hydrophobic protecting groups decreases the solubility of a paptide segment in a solvent such as aq acetonitrile. Consequently, the purification of such a peptide by RPHPLC becomes difficult and the recovery yield is usually low. If the number of the protecting groups on a peptide segment can be reduced, the solubility will increase and its purification will be facilitated. The second issue was the complexity of the method for segment preparation. We had to change the procedure for peptide segment preparation depending on the presence or absence of a side-chain carboxyl group. In polypeptide synthesis, it is very important to normalize the procedure for the preparation of a peptide segment.

To overcome these problems, we designed a simpler method based upon our previous protocol and the thiocarboxyl segment strategy, by which Blake et al. achieved perfectly-selective activation of the terminal carboxyl group,[3] and synthesized several proteins.[4,5]

In the new method, the *S*-alkyl thioester of a partially protected peptide segment is used as a building block for polypeptide synthesis. The thioester group should be activated by silver ions. If so, the terminal thioester group will be selectively activated. Furthermore the thioester group does not have such a nucleophilic character as the thiocarboxyl group. Hence, various kinds of protecting groups can be introduced into the side-chain amino groups using a protective reagent such as *N*-(*t*-butoxycarbonyloxy)-succinimide (Boc-ONSu). If an *S*-alkyl thioester of a peptide segment could be synthesized by a solid-phase method with a high yield, a very promising method for polypeptide synthesis would be developed.

To examine the efficiency of this strategy, we attempted to synthesize the DNA-binding domain of *c*-Myb protein consisting of 52 amino acid residues, which is similar in size to BPTI.

In this paper, we describe the preparation of Boc-Gly-SCH_2CH_2CONH-resin, the synthesis of the *S*-alkyl thioester of a partially protected peptide segment, its chemical characteristics and the coupling of the segments and discuss the efficiency of this method.

Results and Discussion

The amino acid sequence of an oncogene product of *c*-Myb protein was deduced from cDNA clones of murine *c-myb* mRNA.[6] This protein binds to DNA at a domain near the N-terminal region.[7] The binding domain was found to have a 3-time tandem repeat of an analogous primary structure.[6] The peptide we synthesized was the third part of the repeat corresponding to the amino acids from 142 to 193. The amino acid sequence is shown in Fig. 1. Two partially protected peptide segments **1** and **2** were prepared and segment coupling of the peptides was carried out at the site indicated by an arrow (Fig. 1) according to the scheme shown in Fig. 2.

Preparation of Boc-Gly-SCH_2CH_2CONH-Resin. Crystalline Boc-Gly-SCH_2CH_2COOH was prepared from Boc-Gly-ONp and $HSCH_2CH_2COOH$. This

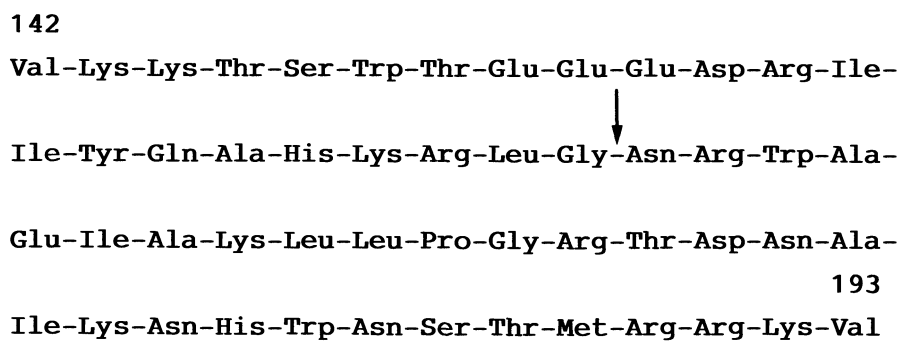

Fig. 1. Primary sequence of *c*-Myb protein(142—193) deduced from cDNA clone of murine *c-myb* mRNA.[6] Arrow indicates the site of segment coupling.

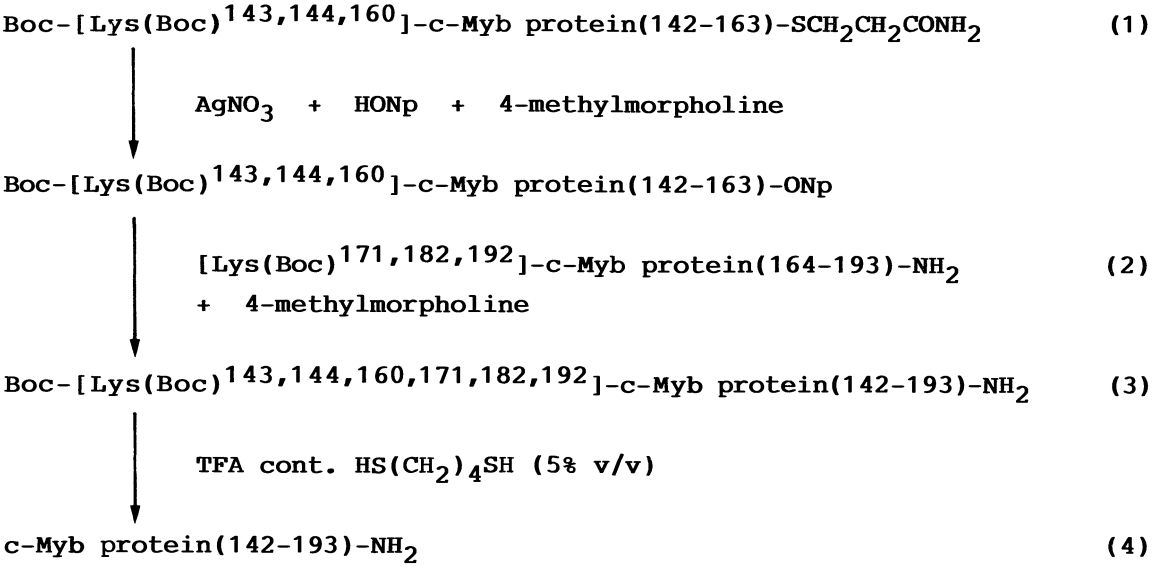

Fig. 2. Synthetic route leading to *c*-Myb protein(142—193)-NH_2 (**4**) by segment coupling.

compound was introduced to a *p*-methylbenzhydrylamine resin (MBHA resin) (NH_2–Resin) by a routine procedure similar to the introduction of Boc–amino acids to an MBHA resin. The resulting thioester resin was stable enough to withstand assemblage of the peptide chain corresponding to *c*-Myb protein(142—163).

Preparation of Boc-[Lys(Boc)^{143,144,160}]-*c*-Myb Protein (142—163)-$SCH_2CH_2CONH_2$ (1). Peptide **1** was prepared according to the route shown in Fig. 3. Starting from Boc–Gly–SCH_2CH_2CONH–resin (Gly 0.33 mmol g^{-1}, 1.5 g), a protected *c*-Myb protein (142—163)–SCH_2CH_2CONH–resin was prepared according to the protocol of the system software version 1.40 NMP/HOBt *t*-Boc without any modifications. End capping by acetic anhydride was carried out after each amino-acid introduction reaction. The resin weight increased by 1.4 g. This resin (500 mg from 2.9 g) was treated by anhydrous HF in the presence of *p*-cresol and 1,4-butanedithiol at 0 °C for 90 min. Judging from the elution profile of the crude product by RPHPLC, the thioester was stable under HF-treatment. The crude peptide was purified by RPHPLC to yield 40 mg (14.4 μmol) of highly pure peptide **5**. The yield was 16.7% based on the glycine in the starting resin. The yield of peptide **5** was about one-half that of peptide amide **6** (29.6%) synthesized on the MBHA resin as described later. This could be mainly due to partial aminolysis or hydrolysis of the thioester bond during the chain elongation reaction. The yield of peptide **5** was acceptable at the present stage, but further investigation of the chemical design as well as the preparation method of the thioester anchoring group is still required to increase the peptide thioester yield. But the thioester in peptide **5** was quite stable during purification on RPHPLC or during prolonged storage at 4 °C. The introduction reaction of Boc groups to peptide **5** proceeded almost quantitatively and did not accompany any side-reaction when

Fig. 3. Synthetic scheme of Boc-[Lys(Boc)^{143,144,160}]-*c*-Myb protein(142—163)-$SCH_2CH_2CONH_2$.

Boc–ONSu was used as the protective reagent. The yield of peptide **1** was practically quantitative.

Preparation of [Lys(Boc)^{171,182,192}]-*c*-Myb Protein(164—193)-NH_2 (2). The preparation of peptide amide **2** was carried out according to the scheme shown in Fig. 4. This procedure functions well in the synthesis of BPTI.[1] A peptide chain of *c*-Myb protein (164—193) was assembled on 0.78 g of MBHA resin (NH_2 0.64 mmol g^{-1}) according to the same protocol described for the synthesis of peptide **1**. After the completion of chain assembly, a 2,2,2-trichloroethoxycarbonyl (Troc) group was introduced to protect the terminal amino group using *N*-(2,2,2-trichloroethoxycarbonyloxy)-succinimide (Troc–ONSu). The final weight of the protected peptide resin was 3.2 g. An aliquot of the resin (0.8 g) was treated with HF in the presence of *p*-cresol and 1,4-butanedithiol at 0 °C for 90 min to yield a crude product (580 mg), which was purified on RPHPLC to give 140 mg of highly purified peptide amide **6**. The yield was 29.6% based on the amino group in the starting MBHA resin. Boc groups were introduced to peptide amide **6** according to the conditions described for the preparation of peptide **1**. The reaction proceeded completely to result in peptide amide **7** at a yield of 82%. The Troc group of peptide amide **7** was removed by zinc dust treatment in 50% aq acetic acid under nitrogen with mild sonication at room temperature for 1 h. Peptide amide **2** was obtained at a yield of 65% without any serious side reactions. But it must be noted that the almost total decomposition of peptide amide **7** was occurred when the peptide solution was sonicated for 4 h under insufficient replacement by nitrogen gas.

Preparation of *c*-Myb Protein(142—193)-NH_2 (4). As shown in Fig. 2 the thioester group in peptide **1** was converted to the corresponding active ester in the presence of *p*-nitrophenol (HONp) and $AgNO_3$ in dimethyl sulfoxide (DMSO). To the DMSO solution, peptide amide **2** and 4-methylmorpholine (NMM) were added and the solution was stirred. The

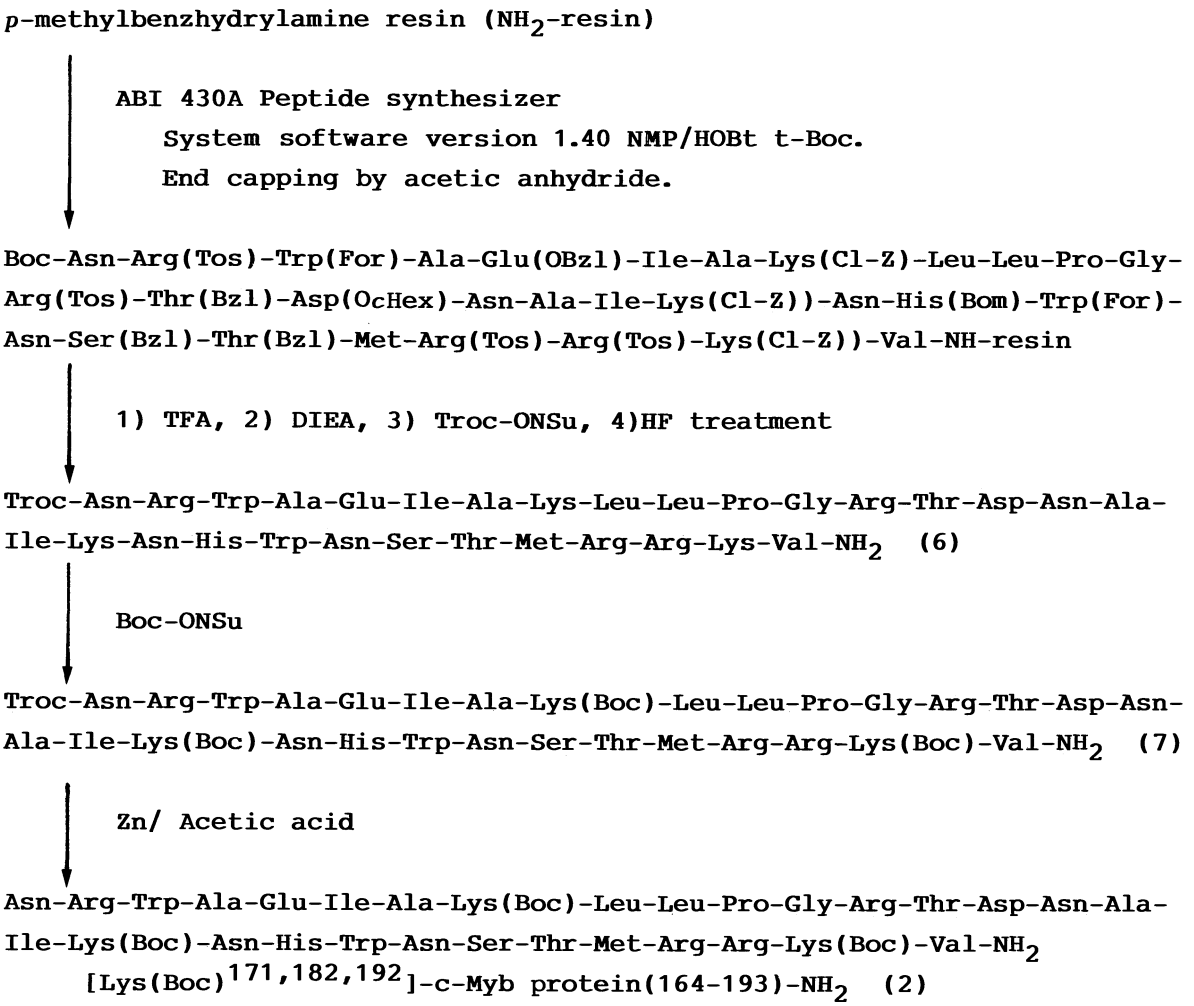

Fig. 4. Synthetic scheme of [Lys(Boc)^{171,182,192}]-*c*-Myb protein(164—193)-NH_2.

concentrations of peptides **1** and **2** were 16 mM# and 10 mM, respectively. The coupling reaction was monitored by RPHPLC. After 3 d, condensation reaction was almost complete (Fig. 5). Silver ions were removed as AgCl. The product was precipitated by adding ethyl acetate, collected by centrifugation, suspended in dioxane and freeze-dried. The powder was treated with TFA containing 1,4-butanedithiol at room temperature for 10 min. After removal of TFA, a product was isolated by RPHPLC (Fig. 6). The yield was 1.1 μmol, 50%. This yield is quite high, if the nonspecific adsorption of peptide amide **4** during the isolation process is taken into account. *N*-Hydroxysuccinimide ester corresponding to peptide **1** gave results as good as those of *p*-nitrophenyl ester with regard to the segment condensation reaction between peptides **1** and **2**. However in this experiment, we employed *p*-nitrophenyl ester, which was mild in reactivity but considerably more stable in the presence of moisture. Methionine was not damaged by silver ions. No serious side reaction was observed during segment coupling under this minimum protection strategy.

Confirmation of Synthetic *c*-Myb Protein(142—193)-NH_2 (4). The amino acid composition of the purified peptide amide **4** obtained from RPHPLC is shown in Table 1. Peptide amide **4** was eluted as a symmetrical peak by ion-exchange chromatography (Fig. 7). These data suggest that highly pure peptide amide **4** was obtained from this synthesis. Two-dimensional NMR spectroscopy of peptide amide **4** also confirmed the purity of this peptide.[8]

Evaluation of the Newly-Developed Method. Partially protected peptide segments **1** and **2** were successfully prepared and all the peptide segments were well characterized by amino acid analysis and fast atom bombardment mass spectrometry. The thioester group of peptide **1** was activated by silver ions and converted to the corresponding active ester. The terminal carbonyl group was selectively activated by a thioester strategy exactly the same as the thiocarboxyl

1 M=1 mol dm^{-3}

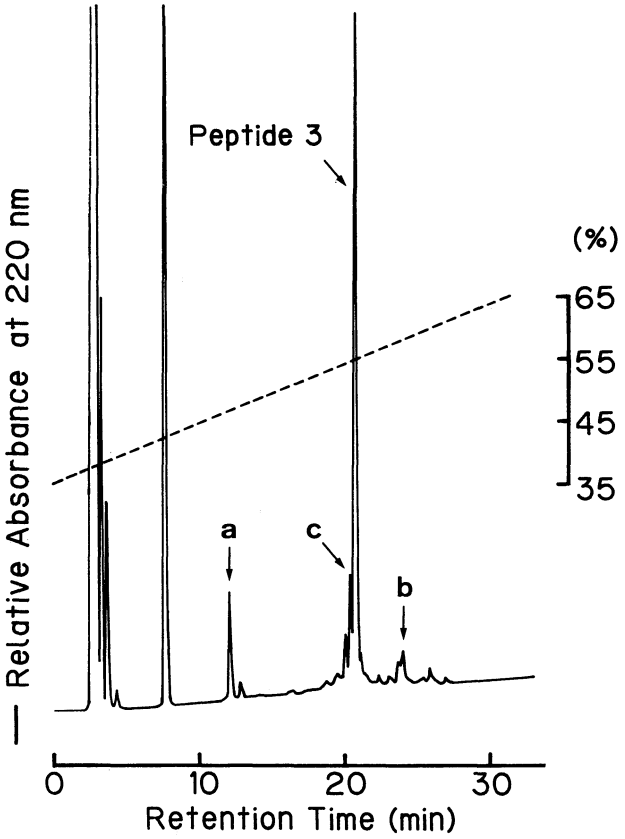

Fig. 5. HPLC profile of the reaction mixture of peptide amide **3** after 3-day reaction. Chromatography was carried out on Cosmosil 5C18 at a flow rate of 1 ml min^{-1} at 40°C. Broken line indicates the acetonitrile concentration in 0.1% aq TFA solution. Arrow **a** indicates the elution position of peptide amide **2**. Arrow **b** indicates the elution position of the active ester of peptide **1**. Arrow **c** indicates the elution position of the hydrolyzed product of peptide **1**.

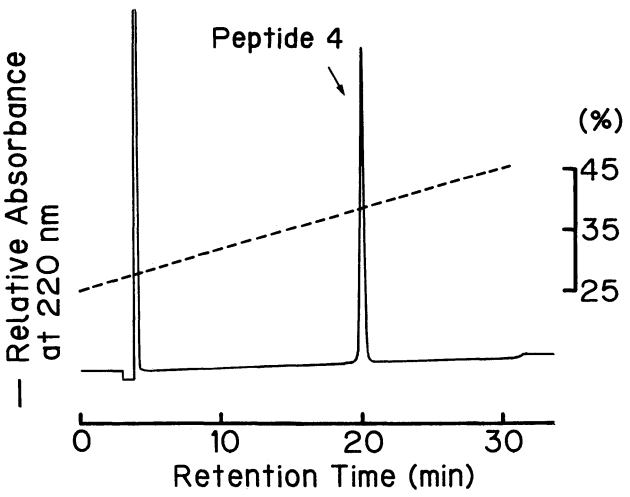

Fig. 6. HPLC profile of synthetic *c*-Myb protein-(142—193)-NH_2 (**4**) after preparative RPHPLC purification. Chromatography was carried out on Cosmosil 5C18 at a flow rate of 1 ml min^{-1} at 40°C. Broken line indicates the acetonitrile concentration in 0.1% aq TFA solution.

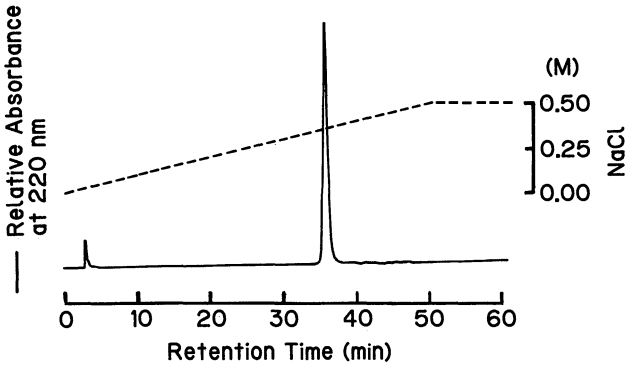

Fig. 7. Ion-exchange chromatogram of synthetic *c*-Myb protein(142—193)-NH_2 on TSK gel CM-5PW. Broken line indicates the concentration of NaCl in buffer.

Table 1. Amino Acid Composition of c-Myb Protein(142—193)-NH_2

	Peptide **4**	Expected
Asp	6.08	6
Thr	3.93	4
Ser	1.78	2
Glu	5.13	5
Pro	0.93	1
Gly	2.15	2
Ala	4	4
Val	2.05	2
Met	1.09	1
Ile	3.19	4
Leu	3.03	3
Tyr	1.01	1
His	2.16	2
Lys	6.11	6
Trp	2.34	3
Arg	6.07	6

strategy. As a result, protection of the side-chain carboxyl groups was unnecessary. Only the functional groups that required protection were amino groups in this synthesis. The thioester group did not react with Boc-ONSu though the thiol of the thiocarboxyl group was modified. If a peptide thioester is employed, various kinds of protecting groups may be introduced to the side chain, as well as α-amino groups after purification of a peptide segment on RPHPLC. Protecting groups such as the Boc group enhance the solubility of a partially protected peptide segment in DMSO or *N*,*N*-dimethylformamide (DMF) more than the citraconoyl group. In the thiocarboxyl segment strategy, side-chain amino groups were protected by citraconoyl groups.[4,5]

Only one protecting group existed on peptide **5** or **6** when purified on RPHPLC. Consequently, purification was much simpler compared with BPTI synthesis.[1] Therefore long peptide segments were easily prepared. The yield of segment coupling was also satisfactory.

In conclusion, the partially protected peptide

thioester is a promising building block for polypeptide synthesis.

Materials and Methods

MBHA resin hydrochloride and Boc-amino acid derivatives were purchased from the Peptide Institute Inc. (Minoh, Osaka). Solvents and reagents used for solid-phase peptide synthesis were purchased from Applied Biosystems Japan (Tokyo). Dimethyl sulfoxide used for segment coupling was silylation grade (Pierce, Rockford, IL). Analytical RPHPLC was performed on Cosmosil 5C18 (4.6×250 mm) (Nacalai Tesque, Kyoto) and preparative RPHPLC was on YMC-Gel ODS S-5 AM-type (10×250 mm or 20×250 mm) (YMC, Kyoto). Amino acids were analyzed on an L-8500 amino acid analyzer (Hitachi Ltd., Tokyo) after hydrolysis by 4 M methanesulfonic acid at 110 °C for 24 h in an evacuated sealed tube. Peptide mass number was determined by fast atom bombardment mass spectrometry using a JMS-HX100 (Jeol Ltd., Tokyo) equipped with a JMA-3100 mass data system. Peptide weight was calculated based upon the amino acid analysis data. Ultrasonication was carried out using a Branson Model B-220.

Synthesis

Peptide Chain Elongation on a Solid-Support. Solid-phase synthesis of a peptide segment was carried out on a peptide synthesizer 430A (Applied Biosystems Inc., Foster City, CA.) employing the 0.5 mmol scale standard protocol of the benzotriazole active ester method of the system software version 1.40 NMP/HOBt *t*-Boc. End capping by acetic anhydride was performed after each amino-acid introduction reaction. The side-chain protecting groups of Boc-amino acids used were *o*-chlorobenzyloxycarbonyl (Cl-Z) for the N^{ε} of Lys, *o*-bromobenzyloxycarbonyl (Br-Z) for the phenolic OH of Tyr, benzyl (Bzl) for the alcoholic OH of Thr and Ser, cyclohexyl ester (O*c*Hex) for the β-carboxyl group of Asp, benzyl ester (OBzl) for the γ-carboxyl group of Glu, benzyloxymethyl (Bom) for the N^{π} of imidazole of His, tosyl (Tos) for the N^{g} of Arg and formyl (For) for the N^{i} of Trp.

Preparation of Boc-Gly-SCH_2CH_2COOH. To a solution of Boc-Gly-ONp (1.5 g, 5 mmol) dissolved in DMF (50 ml), 3-mercaptopropionic acid (0.5 g, 5 mmol) and *N,N*-diisopropylethylamine (DIEA) (1.0 g, 7.5 mmol) were added with stirring at room temperature for 15 h. After evaporation of the solvent under reduced pressure, the product was dissolved in ethyl acetate. The ethyl acetate layer was washed with 0.1 M HCl (2×) and water saturated with NaCl (5×) and dried over sodium sulfate. The ethyl acetate solution was concentrated. An oil obtained was dissolved in ether. To the ethereal solution cyclohexylamine (CHA) (450 mg, 4.5 mmol) was added to give crystals, which were recrystallized from hot ethyl acetate: Boc-Gly-$SCH_2CH_2COOH \cdot$CHA; 1.70 g, 94.0%, mp 112.5—123.2 °C. This CHA salt (1.66 g) was suspended in ethyl acetate and CHA was extracted by dilute aq citric acid. The organic layer was washed with water saturated with NaCl (3×) and dried over sodium sulfate. After concentration of the solution, hexane was added to give Boc-Gly-SCH_2CH_2COOH (1.11 g, 91.6%), mp 104—106 °C. Found: H, 6.60; C, 45.49; N, 5.40%. Calcd for $C_{10}H_{17}O_5NS$: H, 6.51; C, 45.61; N, 5.32%.

Preparation of Boc-Gly-SCH_2CH_2CONH-Resin. MBHA resin hydrochloride (NH_2 0.47 mequiv g^{-1}, 3.4 g) was washed with 5% DIEA/dichloromethane (DCM) (2×5 min) and DCM (3×1 min), successively. Boc-Gly-SCH_2CH_2COOH (718 mg, 2.74 mmol) dissolved in 20 ml of DCM and a 0.5 M solution of dicyclohexylcarbodiimide (DCC) in DCM (4 ml) were successively added to the reaction vessel, which was shaken overnight. The resin obtained was treated with 5% acetic anhydride in DCM (2×5 min) and dried after washing the resin with 2-propanol (3×2 min) and DCM (3×1 min) to give 3.77 g of a resin (Gly: 0.33 mmol g^{-1}).

***c*-Myb Protein (142—163)-$SCH_2CH_2CONH_2$ (5).** Starting from Boc-Gly-SCH_2CH_2CONH-resin (1.5 g), peptide chain elongation was carried out by a 430A peptide synthesizer to give 2.9 g of a protected peptide resin. An aliquot of the resin (500 mg) was treated with anhydrous HF (11 ml) containing *p*-cresol (0.5 ml) and 1,4-butanedithiol (1.7 ml) at 0 °C for 90 min. After evaporation of HF, the residual solid was washed with ether (3×). Crude peptide was extracted with 10% aq acetic acid and freeze-dried to give a powder (192 mg). This crude product was purified on RPHPLC to give peptide **5** (40 mg, 14.4 μmol, 16.7%). Found *m/z* 2774.9 $(M+H)^+$. Calcd *m/z* 2774.6 $(M+H)^+$. Amino acid analysis of peptide **5**: $Asp_{1.04}Thr_{1.94}Ser_{0.92}Glu_{4.27}Gly_{1.04}Ala_1Val_{1.02}Ile_{1.23}Leu_{0.97}Tyr_{0.92}His_{1.08}Lys_{2.85}Trp_{0.65}Arg_{1.89}$.

Boc-[Lys(Boc)^{143,144,160}]-*c*-Myb Protein(142—163)-$SCH_2CH_2CONH_2$ (1). Peptide **5** (25 mg, 9.0 μmol) was dissolved in DMSO (0.4 ml) containing triethylamine (TEA) (9.6 μl). Boc-ONSu (15 mg, 72 μ mol) was added to the solution and stirred at room temperature for 2.5 h, after which ethyl acetate and ether were added. The precipitate was washed with ethyl acetate and lyophilized from a dioxane suspension to give peptide **1** (25.8 mg, 90%). Found *m/z* 3174.8 $(M+H)^+$. Calcd *m/z* 3174.8 $(M+H)^+$. Amino acid analysis of peptide **1**: $Asp_{1.00}Thr_{1.98}Ser_{0.90}Glu_{4.39}Gly_{1.07}Ala_1Val_{0.97}Ile_{1.25}Leu_{0.97}Tyr_{0.93}His_{1.08}Lys_{2.82}Trp_{0.63}Arg_{1.84}$.

Troc-*c*-Myb Protein(164—193)-NH_2 (6). Starting from MBHA resin hydrochloride (NH_2 0.64 mequiv g^{-1}, 0.78 g), chain elongation reaction was carried out. After completion of a peptide chain elongation cycle, the peptide resin was treated with 55% trifluoroacetic acid (TFA) in DCM for 5 and then 15 min, followed by neutralization with 5% DIEA in DCM for 5 min twice. Troc-ONSu (440 mg, 1.5 mmol) was allowed to react with the terminal amino group at room temperature for 15 h. The peptide resin thus obtained was 3.2 g. An aliquot of the resin (0.8 g) was treated with anhydrous HF (17.2 ml) containing *p*-cresol (0.8 ml) and 1,4-butanedithiol (2.7 ml) at 0 °C for 90 min. After evaporation of HF, the residual solid was washed with ethyl acetate (3×) and with ether (3×). The peptide amide was extracted with 5% aq acetic acid and lyophilized to give a crude product (580 mg). This peptide was purified on RPHPLC to obtain peptide amide **6** (140 mg, 37 μmol, yield 29.6%). Found *m/z* 3749.3 $(M+H)^+$. Calcd *m/z* 3749.1 $(M+H)^+$. Amino acid analysis of peptide amide **6**: $Asp_{5.10}Thr_{1.93}Ser_{0.79}Glu_{1.29}Pro_{0.75}Gly_{1.12}Ala_3Val_{1.10}Met_{1.01}Ile_{1.94}Leu_{1.94}His_{1.07}Lys_{3.06}Trp_{1.75}Arg_{3.78}$.

Troc-[Lys(Boc)^{171,182,192}]-*c*-Myb Protein(164—193)-NH_2 (7). Peptide amide **6** (24 mg, 6.5 μmol) was dissolved in DMSO (200 μl) containing TEA (7.8 μl) and Boc-ONSu (13 mg, 60 μmol) and stirred for 2.5 h. Peptide amide **7** was obtained according to the procedure of the preparation of peptide **1**: Yield 21 mg, 5.2 μmol, 80%. Found *m/z* 4050.0

$(M+H)^+$. Calcd m/z 4049.3 $(M+H)^+$. Amino acid analysis of peptide amide **7**: $Asp_{5.16}Thr_{1.93}Ser_{0.87}Glu_{1.15}Pro_{0.91}Gly_{1.09}Ala_3Val_{1.03}Met_{1.12}Ile_{2.01}Leu_{1.97}His_{1.07}Lys_{2.85}Trp_{1.30}Arg_{3.81}$.

[Lys(Boc)^{171,182,192}]-*c*-Myb Protein(164—193)-NH_2 (2). Peptide amide **7** (40 mg) was dissolved in a mixture of acetic acid (1 ml) and water (1 ml). Zinc (100 mg) was added under a nitrogen atmosphere and the solution was sonicated for 1 h at room temperature. After centrifugation of the reaction mixture, the supernatant was applied to an ODS column. The isolated product was freeze-dried to give peptide amide **2**: Yield 25 mg, 6.4 μmol, 65%. Found m/z 3875.5 $(M+H)^+$. Calcd m/z 3875.3 $(M+H)^+$. Amino acid analysis of peptide amide **2**: $Asp_{5.23}Thr_{1.95}Ser_{0.90}Glu_{1.37}Pro_{0.78}Gly_{1.25}Ala_3Val_{1.06}Met_{1.15}Ile_{2.05}Leu_{1.99}His_{1.12}Lys_{3.00}Trp_{1.39}Arg_{3.82}$.

***c*-Myb Protein(142—193)-NH_2 (4).** Peptide **1** (11.5 mg, 3.6 μmol) was dissolved in DMSO (220 μl) containing HONp (6.5 mg, 47 μmol) and NMM (0.3 μl, 2.7 μmol). $AgNO_3$ (2.4 mg, 14 μmol) was added and the solution was stirred at room temperature in the dark. After 2 h, peptide amide **2** (8.6 mg, 2.2 μmol) and NMM (0.6 μl, 5.5 μmol) were added. After stirring overnight, NMM (0.3 μl, 2.7 μmol) was added and the solution was stirred for 3 d. To the solution, solid NaCl (1.2 mg) was added. The precipitate formed was removed by centrifugation. Ethyl acetate was added to the supernatant. The precipitate formed was collected by centrifugation and washed with ethyl acetate. The peptide obtained was suspended in dioxane and freeze-dried to give a crude product of peptide amide **3**, which was treated with TFA (200 μl) containing 1,4-butanedithiol (10 μl) at room temperature for 10 min. TFA was removed by N_2 air flush. The residual solid was washed with dry ether (2×) and isolated by RPHPLC to give peptide amide **4** (6.9 mg, 1.1 μmol); yield: 50% based on peptide amide **2** used for coupling reaction. Amino acid analysis of peptide amide **4**: $Asp_{6.08}Thr_{3.93}Ser_{1.78}Glu_{5.13}Pro_{0.93}Gly_{2.15}Ala_4Val_{2.05}Met_{1.09}Ile_{3.19}Leu_{3.03}Tyr_{1.01}His_{2.16}Lys_{6.11}Trp_{2.34}Arg_{6.07}$.

Purity Check by Ion-Exchange Chromatography. Peptide amide **4** purified on RPHPLC was subjected to a TSK gel CM-5PW column (TOSO, Tokyo) (7.5 mm×75 mm) equilibriated with 0.05 M sodium phosphate buffer (pH 8.0) and chromatographed by a linear 0—0.5 M NaCl gradient in buffer over 50 min at a flow rate of 1 ml min^{-1}.

The authors wish to express their thanks to professor Yasutsugu Shimonishi of the Institute for Protein Research, Osaka University for allowing the use of the facilities for mass spectra measurement and professor Yoshifumi Nishimura of Yokohama City University for his valuable comments on *c*-Myb protein. Their thanks also extended to Ms. Shoko Yoshimura for solid-phase synthesis of peptides and Ms. Chieko Maegawa for amino acid analysis. This research was partly supported by grants-in-aid for Scientific Research No. 62540407, No. 01740322, and No. 02263101 from the Ministry of Education, Science and Culture.

References

1) S. Aimoto, N. Mizoguchi, H. Hojo, and S. Yoshimura, *Bull. Chem. Soc. Jpn.*, **62**, 524 (1989).
2) R. Matsueda and R. Walter, *Int. J. Pept. Protein Res.*, **16**, 392 (1980).
3) J. Blake, *Int. J. Pept. Protein Res.*, **17**, 273 (1981).
4) J. Blake, *Int. J. Pept. Protein Res.*, **27**, 191 (1986).
5) J. Blake, D. Yamashiro, K. Ramasharma, and C. H. Li, *Int. J. Pept. Protein Res.*, **28**, 468 (1986).
6) T. J. Gonda, N. M. Gough, A. R. Dunn, and J. de Blaquiere, *EMBO J.*, **4**, 2003 (1985).
7) K-H. Klempnauer and A. E. Sippel, *EMBO J.*, **6**, 2719 (1987).
8) The NMR study on the solution structure of synthetic *c*-Myb protein(142—193) will be reported elsewhere by Y. Nishimura et al.

Redox Reaction of Aromatic Aldehydes with $Fe_3(CO)_{12}$

Keiji ITOH,† Saburo NAKANISHI, and Yoshio OTSUJI*
Department of Applied Chemistry, College of Engineering,
University of Osaka Prefecture, Mozu-Umemachi,
Sakai, Osaka 591
† Department of Industrial Chemistry, Osaka Prefectural College
of Technology, Saiwaicho, Neyagawa, Osaka 572
(Received August 31, 1990)

Aromatic aldehydes react with $Fe_3(CO)_{12}$ in refluxing benzene ultimately to give arylmethyl alcohols and 1,2-diaryl-1,2-ethanedione in a 1:1 ratio. In some cases, small amounts of 2,4,5-triaryl-1,3-dioxolanes are formed as minor products. Dinuclear iron complex (1,2-diphenyl-1,2-ethanedioxido)$Fe_2(CO)_7$ has been isolated as an intermediate in the reaction of benzaldehyde with $Fe_3(CO)_{12}$. The mechanism of this redox reaction of aromatic aldehydes are discussed on the basis of the kinetic study of the reaction and also of the reactivity of the isolated dinuclear iron complex.

Iron carbonyl complexes induce a variety of organic transformations.[1] However, no systematic information is yet available, especially about the chemical properties of polynuclear iron complexes. Previously, we reported that a trinuclear iron complex $Fe_3(CO)_{12}$ has a strong reducing ability toward oxygen-containing compounds and induces the reductive deoxygenation of 1,2-oxazines to give pyrroles.[2] We now report the reactivity features of $Fe_3(CO)_{12}$ toward aromatic aldehydes.

Takegami and co-workers have reported that aromatic aldehydes undergo a Tishchenko type reaction to give esters upon treating with $Na_2Fe(CO)_4$.[3] In this reaction, the ferrate complex acts as both of base and hydride-transfer agent. However, neutral iron complexes such as $Fe(CO)_5$ and $Fe_2(CO)_9$ exhibit no or little reactivity toward aromatic aldehydes in less polar solvents under ordinary conditions. We now report that $Fe_3(CO)_{12}$ gives rise to the redox reaction of aromatic aldehydes in benzene to afford arylmethyl alcohols and 1,2-diaryl-1,2-ethanediones as major products. We also discuss the mechanistic features of this reaction on the basis of the reactivity of a dinuclear iron complex isolated from the reaction mixture and also of the kinetic study of the reaction.

Results and Discussion

Reaction of Aromatic Aldehydes with $Fe_3(CO)_{12}$. The reaction of benzaldehyde (**1a**) with one tenth molar equiv of $Fe_3(CO)_{12}$ in refluxing benzene for 20 h, followed by acidification of the reaction mixture with an aqueous HCl, gave benzyl alcohol (**2a**) and 1,2-diphenyl-1,2-ethanedione (**3a**) approximately in a 1:1 ratio, along with a small amount of 2,4,5-triphenyl-1,3-dioxolane (**4a**). These products, except **2a**, were formed only after treating the reaction mixture with an aqueous HCl. Other aromatic aldehydes (**1b—e**) reacted similarly with $Fe_3(CO)_{12}$, giving arylmethyl alcohols (**2b—e**) and 1,2-diaryl-1,2-ethanediones (**3b—e**) as major products. In some cases, 1,3-dioxolanes were obtained as minor products. The results are given in Table 1. For this reaction, $Fe(CO)_5$ was

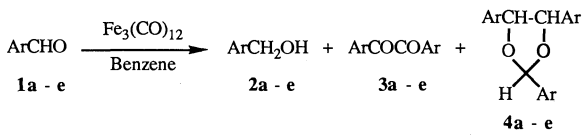

a: Ar=C_6H_5 **b**: Ar=p-$CH_3C_6H_4$ **c**: Ar=p-$CH_3OC_6H_4$ **d**: Ar=p-ClC_6H_4 **e**: Ar=2-Furyl

Table 1. Reaction of Aromatic Aldehydes with Iron Carbonyls[a]

ArCHO	Iron carbonyl	Products[b] (yield/%[c])		
		Alcohol	Diketone	1,3-Dioxolane
1a: Ar=C_6H_5	$Fe(CO)_5$	**2a** (Trace)	**3a** (Trace)	**4a** (Trace)
1a:	$Fe_2(CO)_9$	**2a** (3.0)	**3a** (4.5)	**4a** (Trace)
1a:	$Fe_3(CO)_{12}$	**2a** (56)	**3a** (56)	**4a** (4.0)
1b: Ar=*p*-$CH_3C_6H_4$	$Fe_3(CO)_{12}$	**2b** (60)	**3b** (65)	**4b** (3.0)
1c: Ar=*p*-$CH_3OC_6H_4$	$Fe_3(CO)_{12}$	**2c** (38)	**3c** (38)	**4c** (Trace)
1d: Ar=*p*-ClC_6H_4	$Fe_3(CO)_{12}$	**2d** (60)	**3d** (64)	**4d** (Trace)
1e: Ar=Furyl	$Fe_3(CO)_{12}$	**2e** (18)	**3e** (18)	—

a) The reaction was carried out in refluxing benzene for 20 h by using an excess aldehyde (20 mmol) and an iron complex ($Fe(CO)_5$: 6.0 mmol, $Fe_2(CO)_9$: 3.0 mmol, $Fe_3(CO)_{12}$: 2.0 mmol). b) The products **3a—e** and **4a—d** were isolated after acidification of the reaction mixtures with an aqueous HCl. c) Isolated yields based on iron carbonyls used.

ineffective, and $Fe_2(CO)_9$ was effective but its efficiency was extremely low as compared with that of $Fe_3(CO)_{12}$.

To elucidate the reaction pathways, kinetic study for the reaction of **1a** with $Fe_3(CO)_{12}$ was carried out under the same conditions as those of the preparative reaction. The reaction was followed by analyzing products produced at appropriate time intervals. The result is shown in Fig. 1. This result suggests that the reaction proceeds via the pathways outlined in Scheme 1. An important feature of this reaction is that **3a**, **5a**, and **6a** exist in the reaction mixture as their iron complexes which can be hydrolyzed with HCl. In the actual reaction, the iron complex of 1,2-diphenyl-1,2-ethanediol (**5a**) is produced at the initial stage. This is converted to final products **2a** and **3a** via the iron complex of 2-hydroxy-1,2-diphenylethanone (**6a**). A separate experiment indicated that in the conversion of the iron complexes of **5a** to **3a**, **1a** acts as a hydrogen acceptor; hence **2a** and **3a** are produced in a 1:1 molar ratio (see later). The acid hydrolysis of the iron complexes gives **3a**, **5a**, and **6a**. Compound **4a** can be formed by the acid-catalyzed condensation of **5a** with **1a**.

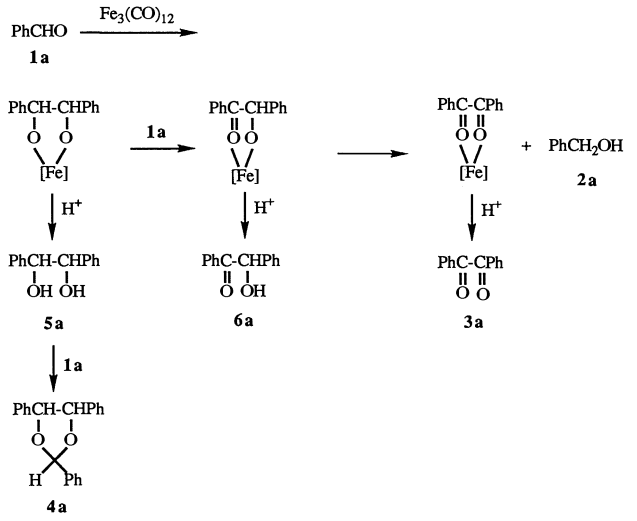

Scheme 1.

Isolation Intermediary Iron Complex. Compound **1a** was allowed to react with $Fe_3(CO)_{12}$ in benzene at 80 °C for 30 min. Careful work-up of the reaction mixture gave (1,2-diphenyl-1,2-ethanedioxido)$Fe_2(CO)_7$ (**7**) in a 46% yield. The same iron complex was also obtained by treating **5a** with $Fe_3(CO)_{12}$ in benzene. The structural formula of this complex was assigned from its spectral data and elemental analysis. The elemental analysis was consistent with the assigned structural formula. In the mass spectrum, the parent peak (M^+, m/z 520) was not observed. However, several fragment peaks that support the assigned structural formula were observed. The peaks appeared at m/z 518 (M^+-H_2) and 504 (M^+-16) that are assignable to $[(PhCOCOPh)Fe_2(CO)_7]^+$ and $[(PhCH{=}C(OH)Ph)Fe_2(CO)_7]^+$ or $[(PhCH_2COPh)Fe_2(CO)_7]^+$, re-

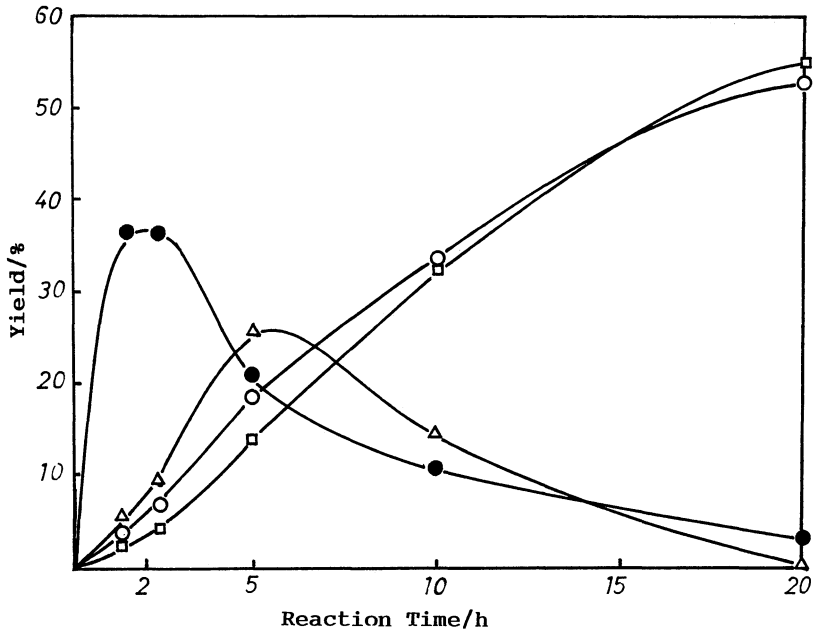

Fig. 1. Kinetic study of the reaction of **1a** with $Fe_3(CO)_{12}$ (**1a**: 20 mmol, $Fe_3(CO)_{12}$: 2.0 mmol, benzene: 15 cm^3. Reaction temperature: 80 °C). ○: Benzyl alcohol (**2a**), □: 1,2-Diphenyl-1,2-ethanedione (**3a**), ●: 1,2-Diphenyl-1,2-ethanediol (**5a**)+2,4,5-triphenyl-1,3-dioxolane (**4a**), △: 2-Hydroxy-1,2-diphenylethanone (**6a**). Compounds **3a**, **4a**, **5a**, and **6a** were isolated after acidification of the reaction mixture with an aqueous HCl.

spectively. Organic fragments were also observed at *m/z* 214, 210, 196, and 107 which can be assigned to [PhCH(OH)CH(OH)Ph]$^+$, [PhCOCOPh]$^+$, [$PhCH_2$-COPh]$^+$, and [PhCHOH]$^+$, respectively. Similar fragmentation pattern was observed in the mass spectrometry of **5a** which is the organic ligand of the complex.[4] The IR spectrum in a KBr disk showed complex absorptions due to the CO ligands attached to Fe at 2035, 1990, 1980, 1965, 1950, 1930, and 1815 cm^{-1}. The lowest absorption suggests the existence of one bridging CO ligand. The ^1H NMR spectrum in $CDCl_3$ exhibited two broad signals at δ=4.88 and 7.28 in the relative intensities of 1:5. These signals can apparently be assigned to the methylidyne and phenyl groups, respectively. The ^{13}C NMR spectrum in $CDCl_3$ at room temperature showed only one broad signal for the CO carbon atom at δ=211.9 where is the region of terminal CO ligands in binuclear iron complexes.[5] This implies that all seven CO groups are scrambled rapidly over two Fe atoms on the NMR time scale at room temperature in a $CDCl_3$ solution. This result indicates that the complex is a sort of a fluxional molecule in the sense that bridging and terminal CO groups are interchanging with each other. This kind of fluxionality in CO ligands has been found also in the other binuclear Fe complexes such as (Ph_2PCH_2-PPh_2)$Fe_2(CO)_7$[5] and (1,2-diazine)$Fe_2(CO)_7$.[6] The other feature in the ^{13}C NMR spectrum was that the CH carbon signal in the organic ligand initially appeared at δ=78, but this signal gradually disappeared. This suggests that [PhCH(O)CH(O)Ph]$Fe_2(CO)_7$ is converted to (PhCOCOPh)$Fe_2(CO)_7$ during the NMR measurement. The instability and the limited solubility at lower temperatures of this complex have prevented us from obtaining more detailed information about the structure of the complex. However, from the above results, we propose **8** as a tentative structure of complex **7** by reference to the established structures of dinuclear Fe complexes of the type $XYFe_2(CO)_7$;[5,6] in this structure, the formal 18 electron configuration is attained at each Fe atom.

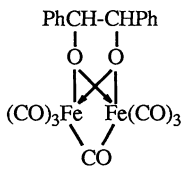

8

Reaction of Intermediary Iron Complex. Treatment of **7** with excess *p*-methylbenzaldeyde (**1b**) in benzene at 80 °C for 15 h afforded *p*-methylbenzyl alcohol (**2b**) and **3a** in a 1:1 molar ratio in good yields. These products were formed after acidification of the reaction mixture with an aqueous HCl. The results are summarized in Scheme 2.

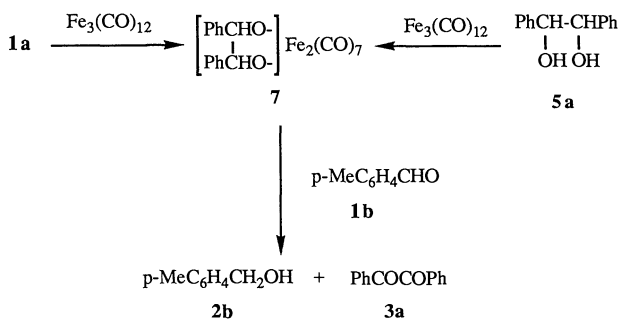

Scheme 2.

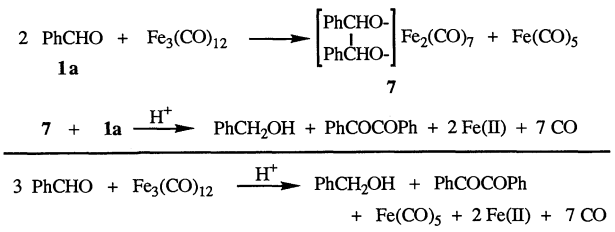

Scheme 3.

Stoichiometry. The reaction of **1a** with one tenth molar equiv of $Fe_3(CO)_{12}$ in benzene was carried out in a sealed vessel. This enabled measurement of the volume of a gas evolved during the reaction. The reaction was started by heating the system at 80 °C. The gas evolution started after 3 h, and ceased after 20 h. A comparison of this result with that of Fig. 1 indicates that CO starts to evolve after **1a** is converted to **7**. The GLC analysis of the evolved gas showed that approximately seven molar equiv of CO are evolved from one molar equiv of $Fe_3(CO)_{12}$ at the end of the reacion.

In a separate experiment, a volatile material produced from the reaction of **1a** with $Fe_3(CO)_{12}$ was collected in a cooled vessel. The collected liquid was identified as $Fe(CO)_5$ from its characteristic IR spectrum. Furthermore, the quantitative analysis of this liquid after converting it to Fe(II) ion by oxidizing with nitric acid indicated that one molar equiv of $Fe(CO)_5$ is produced from one molar equiv of $Fe_3(CO)_{12}$. In this reaction, the production of $Fe(CO)_5$ ceased within 1.5 h. This result indicates that $Fe(CO)_5$ is formed only at the initial stage of the reaction. All of the above results can be explained in terms of the stoichiometric equations shown in Scheme 3.

The initial step is the formation of the diiron complex **7** by the reaction of **1a** with $Fe_3(CO)_{12}$, accompanied with elimination of $Fe(CO)_5$. At the second step, the iron complex reacts further with **1a** to give **2a** and the iron complex of **3a** with evolution of CO, probably accompanying production of Fe(II) ion. During this reaction, hydride migration occurs from **7**

to **1a**. This reaction may be assisted by an intramolecular electron transfer from $[Fe_2(CO)_7]$ to the 1,2-diphenyl-1,2-ethanedioxido ligand in **7**.

Experimental

General. ^1H and ^{13}C NMR spectra were recorded on HITACHI R-24B and JEOL FT-270 spectrometers using TMS as an internal standard. The IR, UV, and MS spectra were taken with Shimadzu IR 27G, Hitachi 228, and JEOL JMS-DX300 spectrometers, respectively. GLC analyses were performed on a Shimadzu GC 4CPF chromatograph using a column packed with SE 30 (10%) (3 mm×1 m). Aromatic aldehydes were all commercial products and purified by distillation prior to use. Benzene was purified by a standard procedure and stored under an argon atmosphere. 1,2-Diphenyl-1,2-ethanediol was prepared from 2-hydroxy-1,2-diphenylethanone.[7] Pentacarbonyliron (0) was a commercial product and used without further purification. Nonacarbonyldiiron (0)[8] and dodecacarbonyltriiron (0)[9] were prepared from $Fe(CO)_5$.

General Procedure for the Reaction of Aromatic Aldehydes with Iron Carbonyls. A mixture of benzaldehyde (20 mmol) and $Fe_3(CO)_{12}$ (2.0 mmol) in benzene (15 cm^3) was heated with stirring at 80 °C for 20 h under N_2 atmosphere, and then acidified with 6 M HCl (10 cm^3, 1 M=1 mol dm^{-3}) at room temperature. The mixture was extracted with ether (30 cm^3). The extract was washed with water, dried (Na_2SO_4) and concentrated under reduced pressure. Chromatography of the residue on silica gel successively with benzene, benzene/ether (9/1), and hexane gave 1,2-diphenyl-1,2-ethanedione, benzyl alcohol, and 2,4,5-triphenyl-1,3-dioxolane in 56%, 56%, and 4% yields, respectively. The reactions of other aldehydes with $Fe_3(CO)_{12}$ were carried out in a similar manner. The results are summarized in Table 1. The products were identified by comparison of their IR and NMR spectra with those of authentic specimens. In all cases, when GLC analyses of the reaction mixtures were carried out before acidification with HCl, only benzyl alcohols were detected. Spectral data of the products were as follows.

2a: Bp 205.0—206.0 °C; IR(neat) 3300, 1036, 1022, 736, 696 cm^{-1}; ^1H NMR ($CDCl_3$) δ=2.81 (s, 1H), 4.68 (s, 2H), 7.24 (m, 5H).

2b: Mp 59.5—60.2 °C; IR(neat) 3400, 1035, 812 cm^{-1}; ^1H NMR ($CDCl_3$) δ=1.88 (s, 1H), 2.36 (s, 3H), 4.60 (s, 2H), 7.17 (m, 4H).

2c: Mp 23.2—24.0 °C; IR(neat) 3400, 1030, 815 cm^{-1}; ^1H NMR ($CDCl_3$) δ=1.93 (s, 1H), 3.80 (s, 3H), 4.55 (s, 2H), 6.83 (d, J=4.12 Hz, 2H), 7.24 (d, J=4.12 Hz, 2H).

2d: Mp 72.4—73.2 °C; IR(neat) 3400, 1030, 830 cm^{-1}; ^1H NMR ($CDCl_3$) δ=2.10 (s, 1H), 4.59 (s, 2H), 7.26 (s, 4H).

2e: Bp 168—170 °C; IR(neat) 3380, 1145, 1020, 740 cm^{-1}; ^1H NMR ($CDCl_3$) δ=2.70 (s, 1H), 4.50 (s, 2H), 6.15 (m, 2H), 7.32 (m, 1H).

3a: Mp 94.5—94.9 °C; IR (KBr) 1655, 1592, 1210, 716 cm^{-1}; ^1H NMR δ=7.21—7.65 (m, 6H), 7.67—8.02 (m, 4H).

3b: Mp 104—105 °C; IR(KBr) 3060, 2920, 1665, 1600, 1210, 1165 cm^{-1}; ^1H NMR ($CDCl_3$) δ=2.38 (s, 6H), 7.16 (d, J=4.10 Hz, 4H), 7.76 (d, J=4.10 Hz, 4H).

3c: Mp 132—133 °C; IR(KBr) 3030, 1660, 1600, 1210 cm^{-1}; ^1H NMR ($CDCl_3$) δ=3.83 (s, 6H), 6.89 (d, J=4.12 Hz, 4H), 7.86 (d, J=4.12 Hz, 4H).

3d: Mp 195—196 °C; IR(KBr) 3030, 1665, 1600, 1165 cm^{-1}; ^1H NMR ($CDCl_3$) δ=7.36 (d, J=4.12 Hz, 4H), 7.89 (d, J=4.12 Hz, 4H).

3e: Mp 163—165 °C; IR(KBr) 2835, 1645, 1450, 751 cm^{-1}; ^1H NMR ($CDCl_3$) δ=6.59 (dd, J=1.80, 3.53 Hz, 2H), 7.58 (d, J=3.53 Hz, 2H), 7.73 (d, J=1.80 Hz, 2H).

4a: Mp 83—84 °C; IR(KBr) 3030, 2840, 1606, 1100, 1065, 1015, 1000, 690 cm^{-1}; ^1H NMR ($CDCl_3$) δ=4.68 (s, 2H), 6.18 (s, 1H), 7.08—7.26 (m, 15H).

4b: Mp 87—89 °C; IR(KBr) 3030, 2920, 1610, 1120, 1080, 1035, 1020, 810 cm^{-1}; ^1H NMR ($CDCl_3$) δ=2.23 (s, 9H), 4.58 (s, 2H), 6.12 (s, 1H), 6.88—7.34 (m, 12H).

4c: Mp 102—103 °C; IR(KBr) 3030, 2930, 1605, 1230, 1080, 1035, 1020, 805 cm^{-1}; ^1H NMR δ=3.73 (s, 9H), 4.67 (s, 2H), 6.18 (s, 1H), 6.55—7.56 (m, 12H).

4d: Mp 97—98 °C; IR(KBr) 3030, 2940, 1610, 1120, 1085, 1035, 835, 810 cm^{-1}; ^1H NMR ($CDCl_3$) δ=4.60 (s, 2H), 6.15 (s, 1H), 7.06—7.70 (m, 12H).

Kinetic Study of Reaction of 1a with $Fe_3(CO)_{12}$. A solution of **1a** (20 mmol) and $Fe_3(CO)_{12}$ (2.0 mmol) in benzene (15 cm^3) was heated under N_2 at 80 °C for a given period of time. The mixture was acidified with aqueous 6M HCl (10 cm^3). The benzene solution was washed with water, dried, and analyzed by GLC using pyrene as an internal standard. The product analyses were performed in a similar manner by changing reaction time. The results are shown in Fig. 1.

5a: Mp 116.2—119.0 °C; IR(KBr) 3630, 3520, 3380, 3060, 2980, 1190, 1038, 770, 698 cm^{-1}; ^1H NMR ($CDCl_3$) δ=4.43 (s, 2H), 4.53 (s, 2H), 7.10 (m, 10H).

6a: Mp 132—134 °C; IR(KBr) 3450, 3050, 2980, 1680, 1600, 1283, 1260, 1085, 1068, 978, 680 cm^{-1}; ^1H NMR ($CDCl_3$) δ=4.50 (br d, 1H), 5.89 (br d, 1H), 7.26—7.40 (m, 8H), 7.73—7.92 (m, 2H).

Isolation of Iron Carbonyl Complex Produced from Reaction of 1a with $Fe_3(CO)_{12}$. A solution of benzaldehyde (20 mmol) and $Fe_3(CO)_{12}$ (2.0 mmol) in benzene (15 cm^3) was heated at 80 °C under N_2 for 30 min. The solvent was evaporated and the residue was washed with ether and then with petroleum ether until excess of benzaldehyde and $Fe_3(CO)_{12}$ were completely removed. The residual solid was dissolved in THF (10 cm^3) and filtered. Concentration of the filtrate gave 480 mg of a dark brown solid. The IR spectral data of the solid were identical in all respects with those of the complex which was prepared from 1,2-diphenyl-1,2-ethanediol (see below).

Preparation of (1,2-Diphenyl-1,2-ethanedioxido)$Fe_2(CO)_7$. All operations were performed under argon. A solution of 1,2-diphenyl-1,2-ethanediol (1.0 mmol) and $Fe_3(CO)_{12}$ (1.0 mmol) in benzene (10 cm^3) was heated at 80 °C for 3 h. The resulting mixture was evaporated to dryness under reduced pressure, and the residue was washed several times with petroleum ether. The residue was taken up in THF (10 cm^3) and filtered. Evaporation of the filtrate gave 260 mg of (1,2-diphenyl-1,2-ethanedioxido)$Fe_2(CO)_7$ as a dark brown solid. IR(KBr) 2035 (s), 1990 (s), 1980 (s), 1965 (sh), 1950 (m), 1930 (sh), 1815 cm^{-1} (m). ^1H NMR ($CDCl_3$) δ=4.88 (br s, 2H), 7.28 (br s, 10H). ^{13}C NMR ($CDCl_3$) δ=78.0, 127.3, 128.2, 128.3, 211.9. Found: C, 48.02; H, 2.56; Fe, 21.50%. Calcd for $C_{21}H_{12}O_9Fe_2$: C, 48.50; H, 2.33; Fe, 21.48%. FD-MS (rel intensity) m/z 518 (0.7), 392 (3), 214 (100), 210 (12), 196 (12),

107 (145) under rapidly increasing emitter current intensities, and *m/z* 504 (2.5), 214 (37), 210 (100), 197 (7), 107 (147 under slowly increasing current intensities.

Reaction of (1,2-Diphenyl-1,2-ethanedioxido)$Fe_2(CO)_7$ with *p*-Methylbenzaldehyde. A solution of benzaldehyde (2 mmol) and $Fe_3(CO)_{12}$ (2.0 mmol) in benzene (15 cm^3) was heated at 80 °C under N_2 for 1.5 h. *p*-Tolualdhyde (**1b**) (15 mmol) was then added to the mixture. The resulting mixture was heated at 80 °C for 15 h, and acidified with 6 M HCl (10 cm^3). The products were isolated as described above. Compounds **3a** and **2b** were obtained in 62% and 58% yields, respectively.

A mixture of 1,2-diphenyl-1,2-ethanediol (1.3 mmol) and $Fe_3(CO)_{12}$ (1.5 mmol) in benzene (10 cm^3) was heated at 80 °C under N_2 for 2 h. Compound **1b** (15 mmol) was added. The resulting mixture was heated at 80 °C for 15 h and acidified with 6 M HCl (10 cm^3). The products were isolated as described above. Compounds **3a** and **2b** were obtained in 56% and 56% yields, respectively.

Quantitative Determination of Evolved CO. A solution of **1a** (10 mmol) and $Fe_3(CO)_{12}$ (1.0 mmol) in benzene (6 cm^3) was placed in a sealed vessel which was connected with a gas burette. The mixture was heated at 80 °C under N_2 atmosphere. At the initial stage, no gas evolution was observed. The gas evolution started after heating for 3 h, but the rate of the gas evolution was moderate. The gas evolution ceased after heating for 20 h. The evolved gas was analyzed by GLC. The analysis showed that the evolved gas contained 6.77 mmol of CO and 0.03 mmol of H_2. The molar ratios of these gases to $Fe_3(CO)_{12}$, which was used initially, were 6.77 for CO and 0.03 for H_2, respectively.

Quantitative Determination of Evolved $Fe(CO)_5$. A solution of **1a** (10 mmol) and $Fe_3(CO)_{12}$ (1.0 mmol) in benzene (5 cm^3) was placed in a flask equipped with a gas trap which was immersed in a Dry Ice-acetone bath. The mixture was heated at 80 °C under N_2 atmosphere for several hours. Benzene and volatile materials were collected in the trapping flask at reduced pressure. The IR spectrum of the trapped material showed that it contained $Fe(CO)_5$. The trapped material was oxidized by adding 4 M HNO_3 (10 cm^3) at room temperature. The resulting aqueous solution was subjected to a Fe(II) ion analysis. The analysis was accomplished by a standard 1,10-phenanthroline method.[10]

This work was partially supported by a Grant-in Aid for Scientific Research No. 02640403 from the Ministry of Education, Science and Culture.

References

1) H. Alper, "Transition metal organometallics in organic synthesis," Academic Press, New York (1976), Vol. 1. I. Wender and P. Pino, "Organic Synthesis via Metal Carbonyls," John Wiley and Sons, Inc., New York (1977), Vol. 2. J. P. Collmann, *Acc. Chem. Res.*, **9**, 209 (1976).

2) S. Nakanishi, Y. Shirai, K. Takahashi, and Y. Otsuji, *Chem. Lett.*, **1981**, 861. S. Nakanishi, T. Hirano, Y. Otsuji, and K. Itoh, *Chem. Lett.*, **1987**, 2167.

3) M. Yamashita, Y. Watanabe, T. Mitsudo, and Y. Takegami, *Bull. Chem. Soc. Jpn.*, **49**, 3597 (1976).

4) H. Budzikiewicz, C. Djerassi, and D. H. Williams, "Mass Spectrometry of Organic Compounds," Holden-Day, Inc., San Francisco (1967).

5) F. A. Cotton and J. M. Troup, *J. Am. Chem. Soc.*, **96**, 4422 (1974).

6) F. A. Cotton, B. E. Hanson, J. D. Jamerson, and B. R. Stults, *J. Am. Chem. Soc.*, **99**, 3293 (1977) and references therein.

7) "Jikkenn Kagaku Koza," Nippon Kagaku Kai, Maruzen (1956), Vol. 17, p. 11.

8) R. B. King, "Organometallic Syntheses," Academic Press (1965), Vol. 1, p. 93.

9) R. B. King, "Organometallic Syntheses," Academic Press (1965), Vol. 1, p. 95.

10) "Kougyou Bunseki Kagaku," ed by T. Takeuchi, Gakujutsu Tosho Shuppan Sha (1968), Vol. 1, p. 272.

 © 1991 The Chemical Society of Japan Bull. Chem. Soc. Jpn., 64, 123—127 (1991)

Product Selectivity Affected by Cationic Species in Electrochemical Reduction of CO_2 and CO at a Cu Electrode[1)]

Akira MURATA and Yoshio HORI*
Department of Applied Chemistry, Faculty of Engineering,
Chiba University, Yayoi-cho, Chiba 260
(Received May 21, 1990)

Electroreduction of CO_2 and CO was studied with a copper electrode in hydrogencarbonate solutions of various cations. Product selectivity was greatly affected by cationic species as well as HCO_3^- concentration. H_2 evolution prevailed over CO_2 reduction in Li^+ electrolyte, whereas CO_2 reduction was favorable in Na^+, K^+, and Cs^+ solutions. C_2H_4 formation became greater than CH_4 with increase of the cation size, i.e. with sequence of Li^+, Na^+, K^+, Cs^+. The variation of the product selectivity caused by cationic species is rationalized by the difference of outer Helmholtz plane (OHP) potential. The OHP potential will vary with cationic species in accordance with the degree of specific adsorption. The concentration of H^+ at the electrode will depend upon the OHP potential, since H^+ is a charged species. This difference of pH at the electrode will lead to the variation of product selectivity.

Metallic copper is an effective electrocatalyst for reduction of CO and CO_2 to CH_4, C_2H_4, and alcohols as firstly reported by the present authors.[2-5)] Other investigators also confirmed the formation of hydrocarbons and alcohols at Cu electrodes.[6-10)] The electroreduction of CO_2 at Cu proceeds with intermediate formation of CO adsorbed on the electrode as reported in the previous paper.[5,11)] In the course of this study, we found that the product selectivity is significantly affected by cationic species of aqueous electrolyte. The present paper reports the experimental results, discussing the model.

Experimental

A copper electrode (99.999%, 2 cm×2 cm) was electropolished in concentrated phosphoric acid. Aqueous 0.1 M hydrogencarbonate solutions of Li, Na, K, and Cs were employed as the electrolytes, prepared with doubly distilled deionized water. $LiHCO_3$ and $CsHCO_3$ solutions were prepared by dissolving the respective carbonate and saturating with CO_2. The solubility of Li_2CO_3 is 1.31 g in 100 g of saturated solution, or 0.18 M at 20 °C.[12)] The upper limit of concentration of $LiHCO_3$ is thus 0.36 M (1 M=1 mol dm^{-3}). The electrolytes were purified by pre-electrolysis with a Pt black cathode. Coulometric measurements were conducted in a three compartment cell in which two anode compartment faced each side of the cathode. The cathode compartment was separated from two anodes with sheets of cation-exchange membrane. Electrolysis was carried out at 18.5 °C with controlled current densities. The cathode potential was measured with respect to an Ag/AgCl reference electrode, corrected for the IR drop by a potentiostat equipped with a positive feedback electronic circuit. Effluent gas from the cell was analyzed by gas chromatographs. Alcohols and formate ion dissolved in the electrolyte were analyzed by a gas chromatograph and an ion chromatograph after electrolysis. Other experimental details were described elsewhere.[11)]

Results

Some measurements were carried out for 1 h. The concentration of gaseous products remained nearly constant during coulometric measurements. Thus most of the works were conducted for 30 min. Table 1 presents average faradaic efficiencies of products in electroreduction of CO_2 in 0.1 M various hydrogencarbonate solutions with constant current density 5.0 mA cm^{-2}. The sums of the faradaic efficiencies are close to 100%; the tabulated substances will be the major products of this reaction. H_2 evolution is favorable with the sequence of $Li^+ > Na^+ > Cs^+ > K^+$. The faradaic efficiencies of CH_4 and C_2H_4 depend greatly upon cationic species. The highest value of methane formation takes place in Na^+ electrolyte. C_2H_4 formation is the most favorable in Cs^+ electrolyte. CH_4/C_2H_4 faradaic efficiency ratio C_1/C_2 increases in the order of $Cs^+ < K^+ < Na^+ < Li^+$. C_2H_5OH and n-C_3H_7OH are fairly produced in K^+ and Cs^+ electrolytes.

Table 1. Current Efficiencies of the Products in Electrochemical Reduction of CO_2 in 0.1 M Hydrogencarbonate Solutions[a)]

Cation	Potential	Current efficiency/%								C_1/C_2
	V/SHE	CH_4	C_2H_4	CO	EtOH	PrOH	$HCOO^-$	H_2	Total	
Li^+	−1.45	32.2	5.2	Tr	1.6	Tr	4.7	60.5	104.2	6.19
Na^+	−1.45	55.1	12.9	1.0	4.2	0.6	7.0	25.1	105.9	4.27
K^+	−1.39	32.0	30.3	0.5	10.9	1.6	8.3	14.5	98.1	1.06
Cs^+	−1.38	16.3	30.5	2.4	7.2	4.4	15.8	24.4	101.0	0.534

a) Current density: 5.0 mA cm^{-2}. Temperature: 18.5 °C. pH value at the electrode is estimated to be 9.5 under the experimental conditions (See text).

Table 2. Current Efficiencies of the Products in Electrochemical Reduction of CO in 0.1 M Hydrogencarbonate Solutions[a)]

Cation	Potential	Current efficiency/%						C_1/C_2
	V/SHE	CH_4	C_2H_4	EtOH	PrOH	H_2	Total	
Li^+	−1.40	26.0	13.4	0.4	Tr	61.1	100.9	1.94
Na^+	−1.43	21.6	15.8	1.4	1.1	59.9	99.6	1.37
K^+	−1.37	8.9	25.7	3.1	2.2	54.7	94.6	0.346
Cs^+	−1.31	2.0	15.9	1.7	1.3	76.8	97.7	0.126

a) Current density: 1.5 mA cm^{-2}. Temperature: 18.5 °C. pH value at the electrode is estimated to be 9.1 under the experimental conditions.

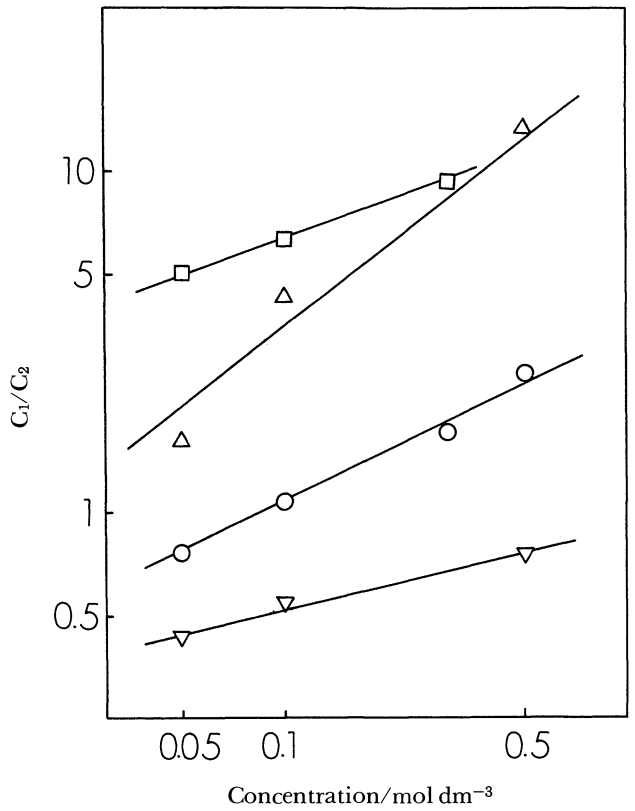

Fig. 1. Variation of the C_1/C_2 in the electroreduction of CO_2 in hydrogencarbonate solutions of various concentration. Current density: 5.0 mA cm^{-2}. Temperature: 18.5 °C. Cationic species; □, Li; △, Na; ○, K; ▽, Cs. Estimated pH values ranged between 8.9 in 0.5 M solution and 10.1 in 0.05 M solution (See text).

CO formation is very low. $HCOO^-$ increases in the order of $Li^+<Na^+<K^+<Cs^+$. C_2H_6 and CH_3OH were not detected at all.

Figure 1 illustrates variation of C_1/C_2 in various electrolytes at the current density 5.0 mA cm^{-2}. C_1/C_2 rises linearly with logarithm of electrolyte concentration, and falls in the order of $Li^+>Na^+>K^+>Cs^+$, identical with the order of cation size. C_2H_4 formation becomes favorable with decrease of HCO_3^- concentration and increase of cation size.

Table 2 presents faradaic efficiencies of products in the electroreduction of CO in 0.1 M hydrogencarbonate solutions at a constant current density 1.5 mA cm^{-2}. The current efficiency of H_2 formation, not much different with one another, is relatively low in Na^+ and K^+ electrolytes, and takes the highest value in Cs^+ electrolyte. These values are higher than those obtained in CO_2 reduction. The solubility of CO is ca. 1/40 that of CO_2.[12] The electrolysis current 1.5 mA cm^{-2} may exceed the limiting current governed by CO diffusion to the electrode, and the H_2 may be evolved more easily. CH_4, C_2H_4, C_2H_5OH, and n-C_3H_7OH are produced in the electroreduction of CO as well. C_1/C_2, ranging to a similar extent with CO_2 reduction, increases with the sequence of $Cs^+<K^+<Na^+<Li^+$.

Discussion

Product Selectivity Affected by Concentration of HCO_3^-. Cathodic reduction of CO_2, CO, and H_2O releases an OH^- per one electron.

$$CO_2 + 6H_2O + 8e^- = CH_4 + 8OH^- \quad (1)$$

$$CO + 5H_2O + 6e^- = CH_4 + 6OH^- \quad (2)$$

$$2H_2O + 2e^- = H_2 + 2OH^- \quad (3)$$

In the case of $HCOO^-$ production, one OH^- is formed per two electrons.

$$CO_2 + H_2O + 2e^- = HCOO^- + OH^- \quad (4)$$

The rate of OH^- formation is thus determined by the current density and the product distribution.

OH^- produced at the electrode will be instantaneously neutralized by HCO_3^- in the diffusion layer.

$$OH^- + HCO_3^- = CO_3^{2-} + H_2O \quad (5)$$

In dilute hydrogencarbonate solutions, the transport of HCO_3^- may be short of neutralization of OH^-; pH value will rise in the neighborhood of the electrode. A simple model may clarify the situation. H_2O is reduced to H_2 at a plane electrode in 0.1 M $KHCO_3$ solution without CO_2. Released OH^- reacts with HCO_3^-, giving CO_3^{2-}. pH value can easily be

Table 3. Current Efficiencies of the Products in Electrochemical Reduction of CO_2 in Various Concentration of KCl Solutions[a)]

Concn	Potential	Current efficiency/%								C_1/C_2
M	V/SHE	CH_4	C_2H_4	EtOH	PrOH	CO	$HCOO^-$	H_2	Total	
0.05	−1.59	14.2	44.5	18.9	2.7	2.4	7.5	11.3	101.5	0.342
0.1	−1.44	11.5	47.8	21.9	3.6	2.5	6.6	5.9	99.8	0.241
0.3	−1.49	14.2	40.8	16.0	2.1	2.1	11.3	10.9	97.4	0.348
1.0	−1.42	8.7	42.2	15.5	1.8	3.3	9.6	15.8	96.9	0.206

a) Current density: 5.0 mA cm^{-2}. Temperature: 18.5 °C. The values were obtained at 15 min after the start of electrolysis. pH value at the electrode is estimated to be 10.6 under the experimental conditions.

calculated in this case as a simple steady state diffusion problem. With assumption of the diffusion layer thickness 0.0030 cm, pH at the electrode is ca. 9.1 and 9.7 for the current density of 1.5 and 5.0 mA cm^{-2} respectively.[13)] pH at the electrode becomes higher in dilute hydrogencarbonate solution due to low buffer capacity in Eq. 5. The pH values at the electrode during CO reduction will be equal to those calculated in this manner. The details of the procedure were described in the previous paper.[11)]

In CO_2 saturated solution, pH at the electrode may differ from the values obtained by the method described above since OH^- will be partially neutralized by CO_2. However, the rate of neutralization of CO_2 by OH^- is very low as is well-known.[14)] CO_2 will thus be present under non-equilibrium situations at the electrode in spite of high pH value.[11)] We have strictly treated the diffusion problem accompanied with simultaneous neutralization of CO_2 by CO_3^{2-} (or OH^-) and the electroreduction of CO_2 in a mathematical procedure. pH values at the electrode surface have been obtained for hydrogencarbonate solutions saturated with CO_2. The procedure and the results were partially reported[15)] and the details will be published in near future. The pH values at the electrode calculated in this manner ranged between 8.9 in 0.5 M solution and 10.1 in 0.05 M solution as shown in Fig. 1, Tables 1 and 3. However, the calculation was carried out without taking into consideration of the cation effect described below.

CO_2 is reduced to CH_4 and C_2H_4 with CO intermediately produced. In CO electroreduction, C_2H_4 formation relatively increases with pH of the bulk solution.[5,11)] It is thus reasonable that C_1/C_2 tends to smaller value in more dilute hydrogencarbonate solution, in which pH becomes higher at the electrode.

Variation of the Potential at Outer Helmholz Plane with Cationic Species and Its Effects on CO_2 Reduction and Hydrogen Evolution. We previously reported electroreduction of CO_2 to $HCOO^-$ at a Hg pool electrode in various hydrogencarbonate solutions, referring to the effect of cationic species.[16)] The electrode potential at a constant partial current of $HCOO^-$ formation shifts to the positive direction with the sequence of Li^+, Na^+, K^+. We discussed the results in connection with the variation of potential at the outer Helmholz plane (OHP) E_2.

Variation of the product selectivity with cationic species indicated in Tables 1 and 2 can be rationalized in terms of the potential distribution at the electrode surface. If ions are strongly hydrated, they will not be specifically adsorbed on the electrode. The hydration number of Li^+ is the largest, and that of Cs^+ is the smallest among alkali metal ions.[17)] The potential of zero charge (pzc) of Cu is −0.3 to −0.7 V vs. SHE in neutral electrolytes.[18)] The electrode potentials during the electrolysis are far more negative than the pzc, nevertheless there may be some differences with regard to the degree of the cationic adsorptions. The extent of specific adsorption of Li^+ would be the least on the electrode, and that of Cs^+ the greatest. Specific adsorption of cation will shift E_2 to the positive direction. Thus, the value of E_2 would be more positive in the sequence of $Cs^+ > K^+ > Na^+ > Li^+$.

The cation specific adsorption and its effect on H_2 evolution were partly substantiated by Maznichenko et al.[19)] They measured the overvoltages of H^+ reduction at constant current and discussed the relation with E_2. The overvoltages measured in mixtures of HCl and alkali halide aqueous solution are greater in the sequence of $Cs^+ > K^+ > Na^+ > Li^+$.

The effect of E_2 on the rate of an electrode reaction is twofold, according to Frumkin.[20)] First, the concentration of the ions at OHP undergoing an electrode reaction is changed as compared to the bulk concentration in the solution. Second, the effective potential difference which determines the charge transfer current density is $|E-E_2|$, where E is the electrode potential. If E_2 become more positive, E at constant current density will naturally be more positive as well. The situations are depicted in Fig. 2. The potential variations in Tables 1 and 2 confirm the validity of this model.

CO_2 is not electrically charged, and the concentration of CO_2 at OHP will not be changed from that of the bulk of the solution, if we neglect the concentration gradient due to transport process. However, H^+ is positively charged, and the concentration at OHP $[H^+]_s$ will be given as follows.[20)]

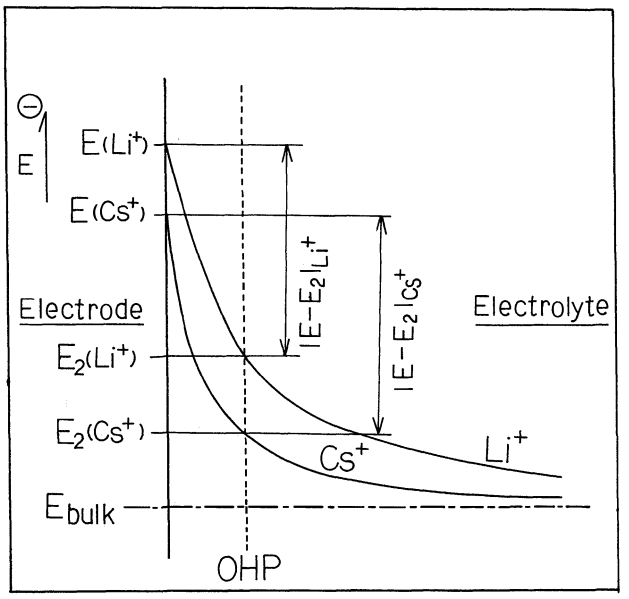

Fig. 2. Potential distribution in the neighborhood of the electrode.

$$[H^+]_s = [H^+] \exp(-FE_2/RT) \quad (6)$$

The more negative E_2 is, the more concentrated H^+ will be. pH at the electrode surface will be lower in the sequence of $Cs^+ > K^+ > Na^+ < Li^+$. During the electrolysis, the rate of OH^- release at the electrode is approximately constant at constant current density. Thus, pH at OHP will be relatively lower in Li^+ solution, and higher in Cs^+ solution. The H_2 evolution will most favorably proceed in Li^+ solution, as is confirmed by Table 1. One would expect that the current efficiency of H_2 would be the least in Cs^+ solution in accordance with the present model. But Cs^+ solution is more advantageous for H_2 evolution than K^+ and Na^+ solutions, especially in the CO electroreduction. The reason is unknown at present.

Ito et al. carried out the electrochemical reduction of CO_2 at an indium electrode in various alkali carbonate solutions.[21] Alkali carbonate solutions must have been converted to hydrogencarbonate ones since the solutions were saturated with CO_2. According to their report, the current efficiency of $HCOO^-$ increases in the sequence of $Rb^+ < K^+ < Na^+ < Li^+$. This result does not agree with ours obtained with a Hg pool electrode.[16] The discrepancy may be caused by the difference of experimental conditions such as the preparation and the treatment of the electrode surface. Additionally, CO_2 reduction is sensitive to contamination of the electrode surface, but Ito et al. did not give any remarks to this point. It is impossible to discuss this problem more extensively.

Product Ratio of CH_4 and C_2H_4. C_1/C_2 significantly decreases with decrease of HCO_3^- concentration (Fig. 1) or increase of pH at the electrode surface; C_2H_4 formation is favorable in high pH conditions. pH at the electrode will be in the order of $Li^+ < Na^+ < K^+ < Cs^+$ as discussed above. Thus C_1/C_2 will decrease in the order of increasing pH at OHP, $Li^+ > Na^+ > K^+ > Cs^+$, as shown in Tables 1, 2 and Fig. 1.

It is remarkable that the variation of cations affects similarly the product distribution of both CO and CO_2 reduction. This fact indicates the validity of the specific adsorption/ OHP potential model. It can also confirm the intermediate formation of CO in the course of CO_2 reduction.

According to Tables 1 and 2, C_1/C_2 takes higher values in CO_2 reduction than CO reduction. pH at the electrode is 9.5 in CO_2 reduction at 5.0 mA cm^{-2}, whereas 9.1 in CO reduction at 1.5 mA cm^{-2}.[22] These facts do not appear compatible with the model described above that high pH value leads to low C_1/C_2. This apparent contradiction may be rationalized as below. The current efficiency of CH_4 exceeds that of C_2H_4 as the electrode potential tends negatively as revealed by the potentiostatic electroreduction of CO_2 in 0.1 M $KHCO_3$ solution.[11] Thus C_1/C_2 is enhanced with increase of negative potential. As shown in Tables 1 and 2, the potential in CO_2 reduction is more negative than in CO reduction, C_1/C_2 becoming higher in CO_2 reduction. We undertook identical experiments under potentiostatic conditions. Potentiostatic electrolysis measurements are accompanied with change of the current density during the measurements probably due to the change of surface condition of the electrode. pH at the electrode will vary if the current is not kept constant in accordance with the model of electrogenerated OH^- mentioned above. However, C_1/C_2 value similarly depended on the cationic species as demonstrated in Tables 1 and 2 obtained in constant current electrolyses.

Table 3 shows the results obtained in CO_2 electroreduction in KCl solutions of various concentrations. C_1/C_2 does not vary to a great extent as those in hydrogencarbonate solutions illustrated in Fig. 1. It is evident that the product distribution does not depend upon concentration of cation and anion which do not neutralize OH^-. The invariant C_1/C_2 values in Table 3 may suggest that the amount of specifically adsorbed cations does not depend upon the concentration; the specific adsorption would be saturated at the electrode in 0.1 M KCl solution. It is also remarkable that C_1/C_2 assumes smaller values since pH at the electrode would be much higher in KCl solutions than in $KHCO_3$ ones.

References

1) The content of this article was briefly reported by Y. Hori and A. Murata in the 58th Meeting of the Chemical Society of Japan, Kyoto, April 1989, Abstr., No. 2IB38.

2) Y. Hori, K. Kikuchi, and S. Suzuki, *Chem. Lett.*, **1985**, 1685.

3) Y. Hori, K. Kikuchi, A. Murata, and S. Suzuki, *Chem. Lett.*, **1986**, 897.

4) Y. Hori, A. Murata, R. Takahashi, and S. Suzuki, *J. Chem. Soc., Chem. Commun.*, **1988**, 17.

5) Y. Hori, A. Murata, R. Takahashi, and S. Suzuki, *J. Am. Chem. Soc.*, **109**, 5022 (1987).

6) R. L. Cook, R. C. MacDuff, and A. F. Sammels, *J. Electrchem. Soc.*, **134**, 1873 (1987).

7) R. L. Cook, R. C. MacDuff, and A. F. Sammels, *J. Electrochem. Soc.*, **134**, 2375 (1987).

8) J. J. Kim, D. P. Summers, and K. W. Frese, Jr., *J. Electroanal. Chem.*, **245**, 233 (1988).

9) H. Noda, S. Ikeda, Y. Oda, and K. Ito, *Chem. Lett.*, **1989**, 289.

10) D. W. Dewulf, T. Jin, and A. J. Bard, *J. Electrochem. Soc.*, **136**, 1686 (1989).

11) Y. Hori, A. Murata, and R. Takahashi, *J. Chem. Soc., Faraday Trans. 1*, **85**, 2309 (1989).

12) J. A. Dean, "Lange's Handbook of Chemistry," 12th ed, McGraw-Hill, New York (1979).

13) The diffusion layer thickness was assumed to be 0.01 cm as a probable value in the previous paper.[11] In the present experimental conditions, the diffusion layer thickness was estimated to be 0.0030 cm from measurements of limiting current densities of anodic oxidation of $Fe(CN)_6^{4-}$ at a Pt electrode with equivalent hydraulic conditions.

14) B. R. W. Pinsent, L. Pearson, and F. J. W. Roughton, *Trans. Faraday Soc.*, **52**, 1512 (1956).

15) Y. Hori, Y. Yoshinami, and H. Kawarada, 41th Meeting of International Society of Electrochemistry, Praha, August 1990, Abstr., No. Mo.-110.

16) Y. Hori and S. Suzuki, *Bull. Chem. Soc. Jpn.*, **55**, 660 (1982).

17) J. O'M. Bockris and A. K. N. Reddy, "Modern Electrochemistry," Plenum Press, New York (1970), Vol. 1.

18) G. J. Clark, T. N. Andersen, R. S. Valentine, and H. Eyring, *J. Electrochem. Soc.*, **121**, 618 (1974). Cited from R. S. Perkins, Ph. D. Thesis, University of Utah, U. S. A., 1967.

19) P. Delahay, "Double Layer and Electrode Kinetics," Wiley, London (1965). Maznichenko et al.'s work was relevantly mentioned. Originally, E. A. Maznichenko, B. B. Damaskin, and Z. A. Iofa, *Dokl. Akad. Nauk SSSR*, **138**, 1377 (1961).

20) K. J. Vetter, "Electrochemical Kinetics," Academic Press, New York (1967). Frumkin's theory was relevantly mentioned and discussed. Originally, A. N. Frumkin, *Z. Phys. Chem., Abt. A*, **164**, 121 (1933).

21) K. Ito, T. Murata, and S. Ikeda, *Bull. Nagoya Inst. Techn.*, **27**, 209 (1975).

22) The product distribution of CO_2 reduction may be preferably compared with that of CO reduction at the same current density. However, it is impossible due to the reason below. The CO_2 reduction does not proceed effectively at 1.5 mA cm^{-2} with Li^+ and Cs^+ electrolytes, yielding only H_2 with slight amount of CH_4 and C_2H_4. CO must be adsorbed at the electrode surface for formation of CH_4 and C_2H_4 from CO_2. Under the conditions of 1.5 mA cm^{-2}, H_2 evolution preferentially proceeds, and little CO is formed from CO_2 on the Cu electrode surface.

On the other hand, the solubility of CO in aqueous solution is low, and the current density of 5 mA cm^{-2} will be far beyond the limiting current.

Broadening of the Proton Magnetic Resonance Spectra of Sulfonate Anions by Ion Pairing with Paramagnetic Chromium(III) Complexes

Masayasu IIDA* and Haruhiko YOKOYAMA†
Department of Chemistry, Faculty of Science, Nara Women's University, Kita-uoya-nishi-machi, Nara 630
† Department of Chemistry, Yokohama City University, Seto, Kanazawa-ku, Yokohama 236
(Received May 28, 1990)

The paramagnetic line broadening of both the ^1H spectra of $CH_3SO_3^-$ and $(CH_2SO_3)_2^{2-}$ was observed in aqueous solutions including chromium(III) complexes such as $[Cr(en)_3]^{3+}$ (en=ethylenediamine), $[Cr(phen)_3]^{3+}$ (phen=1,10-phenanthroline), and *lel,lel,lel*-$[Cr(chxn)_3]^{3+}$ (chxn=*trans*-1,2-cyclohexanediamine). The dependence of the line broadening on the concentration of chromium(III) complexes was attributed to contact ion-pair formation. The distances between the Cr atom and the H atoms of the anions in contact ion pairs were derived in order to discuss their configurations. The anions were considered to be in contact with the complex ions through one or two sulfonate groups directed toward the Cr atom in the open space along the C_3-axis of the complex or in hollow regions between the ligands.

The formation of ion pairs between the metal complex cations and the various anions was previously studied using conductivity measurements.[1] The differences between the experimental and theoretical ion-pair formation constants were attributed to the presence of such interactions as the hydrophobic type and hydrogen bonding between the metal complex cations and the anions.

Nuclear magnetic resonance spectroscopy has provided a powerful tool for studying the microdynamic behavior of ions in solution.[2,3] If one of the ions in an ion pair is paramagnetic, the diamagnetic counterions will experience a magnetic field caused by that paramagnetic ion. This paramagnetism on the counterion produces an NMR spectrum that is either a resonance shift, line broadening, or both. From such a spectrum we can obtain configurational information concerning the ion pair.[4] Paramagnetic line-broadening of the diamagnetic ion is related to the dynamic behavior of the ion pair. In the simplest case of isotropic reorientational motion, the dipolar contribution of a paramagnetic ion to the line width, $(\Delta\nu_{1/2})_{IP}$ in Hz, or the transverse relaxation time, T_2, for the proton is expressed as[4,5]

$$\pi(\Delta\nu_{1/2})_{IP} = (T_2^{-1})_{IP} = J\tau_C r_{CrH}^{-6}[7 + 13/(1 + \omega_S^2\tau_C^2)]/15. \quad (1)$$

For the present system, τ_C is the dipolar correlation time, ω_S the electron spin resonance frequency, and r_{CrH} the electron-nuclear distance corresponding to the distance between the chromium(III) atom of the complex and the hydrogen atoms of the anion within the ion pair.

The parameter J is given by

$$J = S(S + 1)\gamma_H^2 g^2\beta^2, \quad (2)$$

where S is the total electron spin of Cr(III), γ_H is the nuclear gyromagnetic ratio of proton, and g and β are the g-factor for the magnetic moment and the Bohr magneton of electron spin in Cr(III), respectively. In the present study, the paramagnetic line-broadening of the hydrogen atoms of $CH_3SO_3^-$ or $(CH_2SO_3)_2^{2-}$ was observed in the presence of chromium(III) complex cations and was analyzed by considering their ion-pair formations. The values of r_{CrH} given in Eq. 1 were estimated through $(\Delta\nu_{1/2})_{IP}$ based on some assumptions; the configurations of the ion pairs are discussed.

Experimental

The ^1H NMR measurements were performed using a JEOL GX-270 Fourier-transform spectrometer operating at 270.0 MHz with 5-mm (diameter) tubes at 27 °C on aqueous solutions of sodium salt of $CH_3SO_3^-$ or $(CH_2SO_3)_2^{2-}$ of 0.0100 mol dm^{-3} in the presence of chlorides of the Cr(III) complexes while changing their concentrations from 0.00600 to 0.0200 mol dm^{-3}. The preparation of the salts used was proviously described.[1]

Results and Discussion

The ^1H NMR spectra of both the $CH_3SO_3^-$ and $(CH_2SO_3)_2^{2-}$ ions were single lines with widths less than 1 Hz; they were assigned to the methyl and the methylene protons, respectively. The observed half widths, $(\nu_{1/2})_{obsd}$, depended on the concentrations of the chromium(III) complexes, while the chemical shifts did not. The concentration dependence of the half width can be attributed to the ion-pair formation of the anions with chromium(III) complexes.[4] In the present study we assumed that a formed ion pair could be classified into a solvent-separated ion pair and a contact type in a similar manner as before.[6] The equilibria for the ion-pair formations are expressed by

$$M+A \rightleftharpoons MA(sep) \rightleftharpoons MA(con), \quad (3)$$

where M is the free complex ion, A the free anion, MA(sep) the solvent-separated ion pair, and MA(con) the contact ion pair. Since the relaxation time for the exchange of anions between free and ion-pairing types

is sufficiently shorter than T_2, the observed half width change, $(\Delta\nu_{1/2})_{obsd}$, can be written as

$$\begin{aligned}(\Delta\nu_{1/2})_{obsd} &= (\nu_{1/2})_{obsd} - (\nu_{1/2})_0 \\ &= [P_A(T_2^{-1})_A + P_{MA(sep)}(T_2^{-1})_{MA(sep)} \\ &\quad + P_{MA(con)}(T_2^{-1})_{MA(con)}]/\pi, \end{aligned} \quad (4)$$

where $(\nu_{1/2})_0$ is the half width in a sodium sulfonate solution having no complex ion and P is the fraction of each species in solution. Since terms including $(T_2^{-1})_A$ and $(T_2^{-1})_{MA(sep)}$ are presumed to be negligible, since the distance between the Cr(III) atom of the complex and the H atoms of the free anions or of the anions in the solvent-separated ion-pair should be considerably larger than that in the contact ion pair ($r_{MA(con)}$), we approximate Eq. 4 as

$$\begin{aligned}(\Delta\nu_{1/2})_{obsd} &= P_{MA(con)}(T_2^{-1})_{MA(con)}/\pi \\ &= P_{MA(con)}(\Delta\nu_{1/2})_{MA(con)} \\ &= (1 - P_A)x_{MA(con)}(\Delta\nu_{1/2})_{MA(con)}, \end{aligned} \quad (5)$$

where the fact that $1-P_A$ is identical to $P_{MA(sep)}+P_{MA(con)}$, and $x_{MA(con)}$ means that the fraction of contact ion pairs out of the total number of ion pairs, which is equivalent to [MA(con)]/{[MA(sep)]+[MA(con)]} or $P_{MA(con)}/(1-P_A)$.

The values of P_A for each solution can be evaluated by using the ion-pair formation constant (K) obtained on the basis of the usual thermodynamic methods. For the present ion-pair systems, the concentration equilibrium constants (K_c),

$$K_c = ([MA(sep)] + [MA(con)])/([M][A]), \quad (6)$$

were determined from conductivity measurements under an ionic strength (I) of 0.01 at 25 °C;[1] the values of K_c are summarized in Table 1. Although the present study was carried out at 27 °C, these K_c values were used without any correction. The P_A values, however, were calculated by correcting K_c for the difference in the ionic strength with the Debye–Hückel equation[1,7] for the activity coefficients of ions and also by considering the effect of ion-pair formation of the complex ion with coexisting chloride ions. The values of P_A, thus obtained, are shown in Table 2, together with those of $(\Delta\nu_{1/2})_{obsd}$.

Using the concentration equilibrium constant for the solvent-separated ion-pair formation,

$$K_{c(sep)} = [MA(sep)]/([M][A]), \quad (7)$$

we can express $x_{MA(con)}$ in Eq. 5 as

$$x_{MA(con)} = 1 - K_{c(sep)}/K_c. \quad (8)$$

The $K_{c(sep)}$ can be estimated by using a theoretical equation for ion association,[1,7,8] since the formation of a solvent-separated ion pair is presumed to be governed by such a simple electrostatic interaction as that explained by theory. The inter-ionic distance for a solvent-separated ion pair, which is included in the theoretical equation, was taken as being the sum of $\sum r_{ef}$ and $2r(H_2O)$, where $2r(H_2O)$ is the diameter of a water molecule and was regarded as being 0.28 nm; $\sum r_{ef}$ is the sum of the effective ionic radii of the cation and the anion, the values of which were regarded as being 0.362 nm for $[Cr(en)_3]^{3+}$, 0.445 nm for *lel*$_3$-$[Cr(chxn)_3]^{3+}$ (*lel*$_3$=*lel,lel,lel*), 0.498 nm for $[Cr(phen)_3]^{3+}$, 0.257 nm for $CH_3SO_3^-$, and 0.315 nm for $(CH_2SO_3)_2^{2-}$.[1] The values of $x_{MA(con)}$, $\sum r_{ef}$, and $K_{c(sep)}$ are summarized in Table 1 and those of $(\Delta\nu_{1/2})_{MA(con)}$ obtained are shown in Table 2.

The theoretical expression for $(\Delta\nu_{1/2})_{MA(con)}$ is given by Eq. 1, where $(\Delta\nu_{1/2})_{IP}$ should be replaced by $(\Delta\nu_{1/2})_{MA(con)}$ and the second term in the brackets can be neglected since $\omega_S^2\tau_C^2 \gg 1$, where ω_S is 1.12×10^{12} s^{-1} and τ_C is larger than 10^{-11} s; the latter condition is demonstrated below. If we assume that the sulfonate anion is tightly bound to the complex ion in the ion pair and that the two ions rotate together, by keeping their configurations we can express the dipolar correlation time (τ_C) by

$$\tau_C^{-1} = \tau_R^{-1} + \tau_{MA(con)}^{-1} + \tau_S^{-1}, \quad (9)$$

where τ_R and $\tau_{MA(con)}$ are the rotational correlation time and the lifetime of the contact ion pair, respectively, and τ_S is the electron spin-lattice relaxation time. In the present systems, the contributions of $\tau_{MA(con)}^{-1}$ and τ_S^{-1} to τ_C^{-1} were neglected, since these are relatively small compared with that of τ_R^{-1}, as described later. A value of 5×10^{-9} s has been reported for $\tau_{MA(con)}$ for the

Table 1. Values of $\sum r_{ef}$, $\log K_c$, $\log K_{c(sep)}$, and $x_{MA(con)}$ for Each Ion Pair

Ion pair	$\sum r_{ef}$/nm	$\log K_c$[a]	$\log K_{c(sep)}$[c]	$x_{MA(con)}$
$[Cr(en)_3]^{3+}CH_3SO_3^-$	0.619	1.26±0.05	0.95	0.51±0.06
$[Cr(en)_3]^{3+}(CH_2SO_3)_2^{2-}$	0.677	2.35±0.02	1.96	0.60±0.03
lel$_3$-$[Cr(chxn)_3]^{3+}CH_3SO_3^-$	0.702	1.26±0.05	0.91	0.55±0.05
lel$_3$-$[Cr(chxn)_3]^{3+}(CH_2SO_3)_2^{2-}$	0.760	2.43±0.01	1.91	0.70±0.01
$[Cr(phen)_3]^{3+}CH_3SO_3^-$	0.755	1.04[b]	0.89	0.3
$[Cr(phen)_3]^{3+}(CH_2SO_3)_2^{2-}$	0.813	2.13±0.01	1.89	0.42±0.02

a) Experimental values at I=0.01 (25 °C).[1] b) Theoretical value at I=0.01 where the inter-ionic distance used in the calculation is the sum of the effective ionic radii of the cation and the anion (25 °C).[1,8] c) Theoretical values at I=0.01 (25 °C).[8]

Table 2. Values of $(\Delta\nu_{1/2})_{obsd}$, P_A, and $x_{MA(con)}(\Delta\nu_{1/2})_{MA(con)}$

Complex	(1) $CH_3SO_3^-$			
	c(complex)	$(\Delta\nu_{1/2})_{obsd}$	P_A	$x_{MA(con)}(\Delta\nu_{1/2})_{MA(con)}$
	10^{-2} mol dm^{-3}	Hz		Hz
$[Cr(en)_3]^{3+}$	0.600	7.5	0.942	129
	0.800	9.1	0.929	128
	1.00	11.2	0.918	137
	1.50	14.7	0.895	140
	2.00	16.8	0.876	135
lel$_3$-$[Cr(chxn)_3]^{3+}$	0.600	16.5	0.940	277
	0.800	20.3	0.927	279
	1.00	24.6	0.915	290
	1.50	33.5	0.890	305
	2.00	39.6	0.869	302
$[Cr(phen)_3]^{3+}$	0.600	5.7	0.961	147
	0.800	6.8	0.952	143
	1.00	8.5	0.944	153
	1.50	11.4	0.927	156
	2.00	13.3	0.912	151
Complex	(2) $(CH_2SO_3)_2^{2-}$			
	c(complex)	$(\Delta\nu_{1/2})_{obsd}$	P_A	$x_{MA(con)}(\Delta\nu_{1/2})_{MA(con)}$
	10^{-2} mol dm^{-3}	Hz		Hz
$[Cr(en)_3]^{3+}$	0.600	35.6	0.786	166
	0.800	48.4	0.746	191
	1.00	55.7	0.714	195
	1.50	74.9	0.658	219
	2.00	79.0	0.621	208
lel$_3$-$[Cr(chxn)_3]^{3+}$	0.600	88.9	0.755	363
	0.800	110.5	0.707	377
	1.00	122.8	0.669	371
	1.50	150.4	0.600	376
	2.00	170.0	0.555	382
$[Cr(phen)_3]^{3+}$	0.600	34.3	0.830	202
	0.800	41.5	0.796	203
	1.00	48.8	0.769	211
	1.50	57.6	0.717	204
	2.00	67.0	0.680	209

ion pair $[Co(en)_3]^{3+}SO_4^{2-}$ from an ultrasonic absorption measurement;[9] the value of τ_S for the aqua chromium(III) complex is around 5×10^{-10} s,[10] although those for the chromium(III) complexes used here are not available (we assume that the τ_S values are close to that for the aqua complex). On the other hand, the values of τ_R for the ion pairs of $[Co(en)_3]^{3+}$ with some monovalent and divalent anions are 3.2 to 8.7×10^{-11} s at 33 °C; that for the ion pair of $[Co(phen)_3]^{3+}$ with a sulfate ion is 1.2×10^{-10} s at the same temperature.[2]

The values of τ_R for unpaired $[Co(en)_3]^{3+}$ and $[Co(phen)_3]^{3+}$ are 3.2×10^{-11} and 1.0×10^{-10} s at 33 °C, respectively, and are well represented by assuming nearly sticking hydrodynamic boundary conditions on the Stokes-Einstein-Debye relation:[2]

$$\tau_R = CV_R\eta/kT, \tag{10}$$

where V_R is the volume of rotating molecule, η the viscosity of the solution, and C a dimensionless parameter related to the shape of the rotating molecule and the hydrodynamic boundary condition. We used this equation in order to estimate the possible range of τ_R by assuming a sticking boundary condition with the following two extreme cases: In case 1, the ion pair could be regarded as being a sphere having a volume equal to the sum of the van der Waals' volumes of the cation and the anion; this corresponds to the assumption that $V_R=\sum 4\pi r_{ef}^3/3$ and $C=1$ and gives the smallest τ_R. In case 2, the ion pair could be regarded as being a rotational ellipsoid of prolate shape having major and minor axes lengths of $2a=2\sum r_{ef}$ and $2b=2r_{ef(complex)}$, respectively, and a volume of $V_R=4\pi ab^2/3$. The rotation of the major axis gives the largest τ_R, where C can be calculated as a function of the ratio a/b from the relation $(\xi^*/8)\cdot(a/b)^2$, where ξ^* is a dimensionless friction coefficient defined by Hu and Zwanzig;[11] its values for the sticking boundary condition have been given.[11,12] The values of V_R in both cases and those of C in Case 2 are shown in Table 3.

Table 3. Values of $(\Delta\nu_{1/2})_{MA(con)}$, τ_R/r_{CrH}^6, C, V_R, and r_{CrH} for Each Ion Pair

Ion pair	$(\Delta\nu_{1/2})_{MA(con)}$[a]	τ_R/r_{CrH}^6	Case 1[b]		Case 2[b]		
			V_R	r_{CrH}	C	V_R	r_{CrH}
	Hz	10^{-9} s nm^{-6}	nm^3	nm		nm^3	nm
$[Cr(en)_3]^{3+}CH_3SO_3^-$	260±40	1.90±0.30	0.270	0.56±0.02	1.31	0.340	0.60±0.02
$[Cr(en)_3]^{3+}(CH_2SO_3)_2^{2-}$	320±50	2.34±0.37	0.330	0.56±0.02	1.42	0.372	0.60±0.02
lel$_3$-$[Cr(chxn)_3]^{3+}CH_3SO_3^-$	520±60	3.80±0.44	0.440	0.54±0.02	1.24	0.582	0.58±0.02
lel$_3$-$[Cr(chxn)_3]^{3+}(CH_2SO_3)_2^{2-}$	520±20	3.80±0.15	0.500	0.55±0.01	1.31	0.630	0.60±0.01
$[Cr(phen)_3]^{3+}CH_3SO_3^-$	490±60	3.58±0.44	0.588	0.57±0.02	1.21	0.784	0.62±0.02
$[Cr(phen)_3]^{3+}(CH_2SO_3)_2^{2-}$	470±30	3.43±0.22	0.648	0.58±0.01	1.27	0.845	0.63±0.01

a) After the viscosity correction. b) See text.

From Eqs. 1, 9, and 10 and the above-mentioned considerations,

$$(\Delta\nu_{1/2})_{MA(con)} = (7J/15\pi)\tau_R/r_{CrH}^6 = (7J\eta/15\pi kT)(CV_R/r_{CrH}^6). \quad (11)$$

Here, J is 9.2×10^{-43} s^{-2} m^6, which was obtained from Eq. 2 by taking $S=3/2$, $\gamma_H=2.675\times10^8$ s^{-1} T^{-1}, $g=2.00$, and $\beta=9.27\times10^{-24}$ JT^{-1}.[5] The viscosities of solutions, η, in Eq. 11 were estimated by using the following approximated expression for the Jones–Dole's equation[13] on a mixed electrolyte solution:

$$\eta = \eta_0(1 + \sum B_i c_i), \quad (12)$$

where η_0 is the viscosity of water at 27 °C (being equal to 8.51×10^{-4} Pa s[14]) c_i is the salt concentration, and B_i is the so-called B coefficient of the salt; the $A\sqrt{c_i}$ term in the Jones–Dole equation was ignored. The following values of B in dm^3 mol^{-1} at 25 °C were used for the present calculations: 0.198 for CH_3SO_3Na,[15] 0.403 for $(CH_2SO_3Na)_2$,[16] 0.53 for $[Cr(en)_3]Cl_3$,[17] and 1.52 for $[Cr(phen)_3]Cl_3$ and *lel*$_3$-$[Cr(chxn)_3]Cl_3$.[18] The difference between η and η_0 were within 3% under the present conditions and led to only small differences within 10 Hz in $(\Delta\nu_{1/2})_{MA(con)}$. The averaged values of $(\Delta\nu_{1/2})_{MA(con)}$ after the viscosity correction were used for the calculation of τ_R/r_{CrH}^6 by the use of Eq. 11.

The values of $(\Delta\nu_{1/2})_{MA(con)}$ and τ_R/r_{CrH}^6 and the resulting ones of r_{CrH} estimated for Case 1 and Case 2 are summarized in Table 3. The differences in r_{CrH} between the two cases were about 0.04—0.05 nm. When r_{CrH} is compared with $\sum r_{ef}$ in Case 1 or Case 2, we can say follows: the differences in r_{CrH} between the contact ion pairs of $CH_3SO_3^-$ and $(CH_2SO_3)_2^{2-}$ for the same complex are very small, in spite of the fact that the anions have a difference of 5.8×10^{-2} nm with $\sum r_{ef}$; the differences in r_{CrH} between different complexes for the same anion are also significantly smaller than those in $\sum r_{ef}$; the absolute values of r_{CrH} are smaller than those of $\sum r_{ef}$. It should be noted that $\sum r_{ef}$ corresponds to a kind of averaged contact distance between the center of the complex ion and that of the anion, since the r_{ef} values of the ions were derived from their van der Waals' volumes by regarding them as spherical.[1] The complex ions, *lel*$_3$-$[Cr(chxn)_3]^{3+}$ and $[Cr(phen)_3]^{3+}$, have open spaces along the C_3-axis and hollows between the ligands, which can receive an anion. When an anion comes into contact with a complex in such a location, their contact distance becomes shorter than $\sum r_{ef}$. However, the distance between the Cr(III) atom of the complex and the H atoms of the anion (r_{CrH}) depends on the stereochemical configuration of the contact ion pair.

The values of r_{CrH} obtained for the ion pairs of $CH_3SO_3^-$ are in a range 0.54 to 0.62 nm (Table 3), in agreement with the configuration of the ion pair that the sulfonate group of the anion is directed toward the Cr(III) atom in the open spaces along the C_3-axis of the complex or in the hollows between the ligands: the Cr–H distances presumed for such configurations from the Stuart-type molecular models are around 0.6 nm for the ion pair of $[Cr(en)_3]^{3+}$ or $[Cr(chxn)_3]^{3+}$ and about 0.6—0.7 nm for that of $[Cr(phen)_3]^{3+}$; if the methyl group of $CH_3SO_3^-$ is directed toward the Cr(III) atom in the same positions around the complex (as stated above), the Cr–H distances are presumed to be around 0.35 nm for an ion pair of $[Cr(en)_3]^{3+}$ or $[Cr(chxn)_3]^{3+}$ and around 0.4 nm for that of $[Cr(phen)_3]^{3+}$. For the last two ion pairs, however, we cannot completely exclude the configuration that the methyl group is directed to the Cr(III) atom across one chxn or phen ligand, since it gives about 0.5—0.7 nm for the Cr(III)–H distance.

The $(CH_2SO_3)_2^{2-}$ ion could stereochemically have two types of conformations (trans and gauche forms) with the two sulfonate groups. The values of r_{CrH} obtained for the ion pairs of $(CH_2SO_3)_2^{2-}$ are in the range 0.55 to 0.63 nm, suggesting the following probable configurations of the contact ion pairs: when the conformation is gauche, one or two sulfonate groups are directed toward the Cr(III) atom in the space along the C_3-axis or in the hollows between the ligands; when the conformation is trans, one sulfonate group is directed toward the Cr(III) atom in the same positions. However, we could not decide which conformation of the $(CH_2SO_3)_2^{2-}$ ion is dominant in the contact ion pairs. The Cr(III)–H distances presumed from the molecular models are as follows: in

the case of the gauche form of the anion, it is about 0.5—0.7 nm for the ion pairs of $[Cr(en)_3]^{3+}$ or $[Cr(chxn)_3]^{3+}$ and about 0.6—0.8 nm for that of $[Cr(phen)_3]^{3+}$; in the case of the trans form, similar distances are estimated for the ion pairs of $CH_3SO_3^-$. The possibility of other configurations is similar, as described for the ion pairs of $CH_3SO_3^-$.

The results obtained for r_{CrH} are consistent with the predictions from the molecular models (as described above). This suggests that the several assumptions made in the present study are reasonable, especially that the lifetimes of detected contact ion pairs having a given configuration are longer than τ_R. Such tight configurations may be maintained by the short-range interactions between the sulfonate group of the anions and the amino groups of $[Cr(en)_3]^{3+}$ or $[Cr(chxn)_3]^{3+}$, and also by a partial separation of anions from the atmosphere of the solvent into the hollows of the complex.

The values of $\log K_c$ or $\log K_{c(con)}$ for ion-pair formation of *lel*$_3$-$[Cr(chxn)_3]^{3+}$ with anions are similar to or slightly larger than those of $[Cr(en)_3]^{3+}$, in spite of the former complex ion having a relatively large ionic size. This may be due to the difference in the hydration of the complex ions and/or to the presence of some specific interactions, such as a hydrophobic type, due to the chxn ligand in the formation of *lel*$_3$-$[Cr(chxn)_3]^{3+}(CH_2SO_3)_2^{2-}$. In either case, not only the positively charged sites, such as the hydrogen atoms of the amino group in the ligand, but also the hollows among the ligands which can receive the anion may contribute to the formation of a contact ion pair. These considerations are supported by the r_{CrH} values obtained in the present study, which give the information concerning the major position of the hydrogen atoms of the anion around the complex ion in the contact ion pair.

The present work was partially supported by a Grant-in-Aid for Scientific Research No. 62124039 from the Ministry of Education, Science and Culture. The authors would like to acknowledge Associate Professor Yuichi Masuda of Ochanomizu University for his helpful discussion.

References

1) M. Iida, M. Iwaki, Y. Matsuno, and H. Yokoyama, *Bull. Chem. Soc. Jpn.*, **63**, 993 (1990).
2) Y. Masuda and H. Yamatera, *J. Phys. Chem.*, **87**, 5339 (1983); *ibid.*, **88**, 3425 (1984).
3) Y. Masuda, M. Sano, and H. Yamatera, *J. Phys. Chem.*, **89**, 3086 (1985); *J. Chem. Soc., Faraday Trans. 1*, **81**, 127 (1985).
4) G. N. La Mar, "NMR of Paramagnetic Molecules," ed by G. N. La Mar, W. D. Horrocks, and R. H. Holm, Academic Press, New York (1973), Chap. 10.
5) A. Carrington and A. D. McLachlan, "Introduction to Magnetic Resonance," Harper & Row, New York (1967).
6) M. Yudasaka, T. Sugawara, H. Iwamura, and T. Fujiyama, *Bull. Chem. Soc. Jpn.*, **54**, 1933 (1981).
7) R. A. Robinson and R. H. Stokes, "Electrolyte Solutions," 2nd ed, Butterworths, London (1959), Chap. 9, p. 229.
8) H. Yokoyama and H. Yamatera, *Bull. Chem. Soc. Jpn.*, **48**, 2708 (1975); *ibid.*, **54**, 2286 (1981).
9) A. Elder and S. Petrucci, *Inorg. Chem.*, **9**, 19 (1970).
10) The τ_S value is cited from the following book: H. G. Hertz, "Water," ed by F. Franks, Plenum Press (1973), Vol. 3, Chap. 7. If we use this value for $[Cr(phen)_3]^{3+}$ (having the smallest τ_R^{-1} value among the three kinds of the complexes), the τ_S^{-1} value is about 20% of the τ_R^{-1} one as stated in the text. This magnitude results, however, in only 3% contribution to the r_{CrH} value and so the contribution of τ_S^{-1} will be negligible. This assumption is also used, for example, in the following paper: R. A. Marusak and A. G. Lappin, *J. Phys. Chem.*, **93**, 6856 (1989).
11) C. -M. Hu and R. Zwanzig, *J. Chem. Phys.*, **60**, 4354 (1974).
12) F. Perrin, *J. Phys. Radium*, **5**, 33 (1934); **7**, 1 (1936).
13) G. Jones and M. Dole, *J. Am. Chem. Soc.*, **51**, 1950 (1929).
14) Ref. 7, Appendix 1. 1, p. 457.
15) K. Tamaki, Y. Ohara, M. Inabe, T. Mori, and F. Numata, *Bull. Chem. Soc. Jpn.*, **56**, 1930 (1983).
16) K. Tamaki, private communication, 1990.
17) K. Kurotaki and S. Kawamura, *J. Chem. Soc., Faraday Trans. 1*, **77**, 217 (1981).
18) The *B* coefficients for these complex salts are approximated to that for $[Co(phen)_3]Cl_3$ reported in M. Yasuda, *Bull. Chem. Soc. Jpn.*, **41**, 139 (1968).

Acidic Property of Rh and Ru Complexes

Yuan KOU,† Nobuo YAMADA, Susumu AKUTAGAWA,* Geng ZHANG,†† and Kozo TANABE*,††
Takasago Research Institute, Inc., 5-38-31, Kamata, Ohta-ku, Tokyo 144
† Lanzoh Institute of Chemical Physics, Lanzoh, China
†† Department of Chemistry, Hokkaido University, Sapporo 060
(Received July 30, 1990)

The acidic property of [Rh(nbd)(dppb)]ClO_4, [Ru(binap)]$(BF_4)_2$, and [Ru(dmso)$_6$]$(ClO_4)_2$ was measured by using the acetalization of cyclohexanone as a test reaction and the temperature-programmed desorption [TPD] of pyridine. The acid strengths were estimated to be $H_0=-2.1$ for [Ru(dmso)$_6$]$(ClO_4)_2$ and $H_0=-2.2$ for [Ru(binap)]$(BF_4)_2$ and [Rh(nbd)(dppb)]ClO_4 by the test reaction method. The TPD method gave consistent results.

Metal complexes are known to be active and highly selective as catalysts for diversified reactions. For the hydroformylation of camphene, rhodium phosphine complexes, such as $RhCl(PPh_3)_3$ and $RhCl(CO)(PPh_3)_2$, have been reported to be active as catalysts,[1,2] the latter being highly selective in the formation of the aldehyde. We recently found that [1,4-bis(diphenylphosphino)butane](η^4-norbornadiene)rhodium perchlorate[3] (abbreviated to [Rh(nbd)(dppb)]ClO_4), [2,2′-bis[bis(4-methylphenyl)phosphino]-1,1′-binaphthyl]-ruthenium bis(tetrafluoroborate)[4] (abbreviated to [Ru(binap)]$(BF_4)_2$), and hexakis(dimethyl sulfoxide)ruthenium diperchlorate[5] (abbreviated to [Ru(dmso)$_6$]$(ClO_4)_2$) showed high catalytic activities for the hydroformylation reaction, the selectivity being different depending on the metal complexes.[6] In order to elucidate the role of the acidic property of the metal complexes regarding catalytic activity and selectivity, the present work was initiated.

Since no study has been made concerning the acidic property of Rh and Ru complexes, a measurement of the acidic property was attempted in the present work. Acidity measurements involving the indicator method, which was applied to uncolored samples;[7] the IR method, which was applied to metal halides by Cook;[8] and the NMR method, which was applied to boron compounds by Pasto and Balasubramaniyan,[9] were found to be unsuccessful in our catalyst system. Therefore, a kinetic method using acetalization of cyclohexanone which is known to be catalyzed by acids and the TPD method were employed in the present research.

Experimental

[Rh(nbd)(dppd)]ClO_4, [Ru(binap)]$(BF_4)_2$, and [Ru(dmso)$_6$]$(ClO_4)_2$ were prepared according to methods described in literature.[3–5] Cyclohexanone and methanol were purified by distillation. Organic acids used as reference catalysts, bases used in the TPD measurement, and indicators used for measuring the acid strength were commercially available and of guaranteed reagent grade. A SiO_2 used as a reference substance in the TPD experiment was Fuji-Davison Type ID.

The acetalization of 37.4 mmol of cyclohexanone in 50 ml of methanol was carried out at 40 °C under a dry nitrogen atmosphere with rapid stirring after 0.01 mmol of the catalyst was added. The products were analyzed by gas chromatography (Shimadzu GC-9A).

The tempeprature-programmed desorption (TPD) experiment was performed as follows. The metal complex catalyst was transferred to an adsorption tube in a dry nitrogen stream and evacuated at room temperature to 1.33×10^{-2} Pa, and then subjected to a TPD run. The TPD background of the sample, itself, was measured at a temperature-increase rate of 5 °C min^{-1}. The relative amounts of desorbed gases were determined as the peak height relative to that of Ar as an internal standard.

The TPD profiles of adsorbed ammonia, pyridine, and triethylamine were obtained by adsorbing ammonia (6.66×10^3 Pa) for 15 min, pyridine (1.33×10^3 Pa) for 10 min, and triethylamine (2.67×10^3 Pa) for 15 min at room temperature on a new sample, respectively, evacuating them at room temperature and desorbing at elevated temperatures at a temperature-increase rate of 5 °C min^{-1}. In the case of an SiO_2 sample evacuated at 600 °C for 2 h, TPD of pyridine was obtained similarly to that mentioned above.

The acid strength of SiO_2 used as a reference substance was estimated by observing the color change of a Hammett indicator adsorbed on the solid sample.[4] The indicators used were *p*-dimethylaminobenzene ($pK_a=+3.3$) and 4-(phenylazo)diphenylamine ($pK_a=+1.5$).

Results and Discussion

Acidic Property by Acetalization. The negative values of the logarithm (pk) of the first-order rate constant (k) with respect to the concentration of cyclohexanone for acetalization of cyclohexanone with methanol were plotted against the pK_a values[10] of various organic acids used as catalysts. As shown in Fig. 1, an almost straight line was obtained between the pk values and the pK_a values. Since the pk values obtained in cases of [Ru(dmso)$_6$]$(ClO_4)_2$, [Ru(binap)]$(BF_4)_2$, and [Rh(nbd)(dppb)]ClO_4 are 4.67, 4.70, and 4.70, respepctively, the acid strengths ($H_0\simeq pK_a$) of the metal complexes are estimated to be −2.1, −2.2, and −2.2 from the straight line.

Acidic Property by TPD. Fig. 2 shows some main peaks of the TPD profile of Rh[(nbd)(dppb)]ClO_4, itself, as background. The fact that the desorption

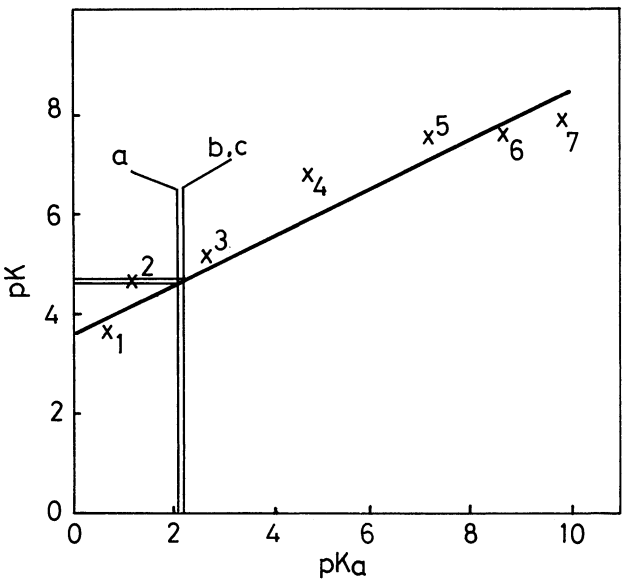

Fig. 1. Relation between the first-order rate constants (pk) for acetalization of cyclohexanone in organic acids and their acid strengths (pK_a). (1) trichloroacetic acid; (2) dichloroacetic acid; (3) bromoacetic acid; (4) acetic acid; (5) *o*-nitrophenol; (6) *p*-chlorophenol; (7) phenol; (a) $[Ru(dmso)_6](ClO_4)_2$; (b) [Rh(nbd)(dppb)]-ClO_4; (c) $[Ru(binap)](BF_4)_2$.

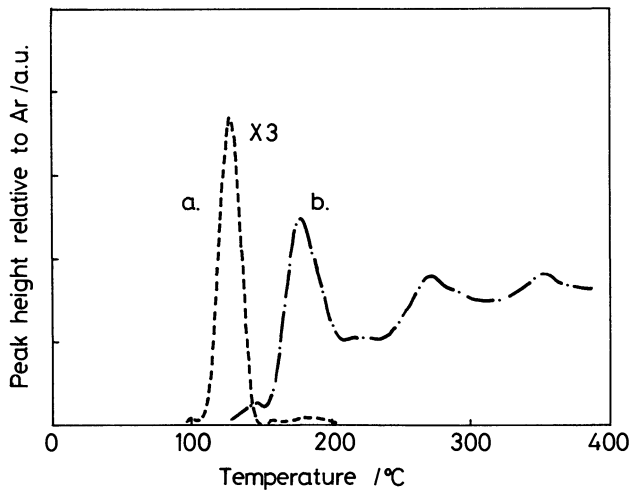

Fig. 2. Temperature programmed decomposition of [Rh(nbd)(dppb)]ClO_4. (a) m/z=42; (b) m/z=78.

peak of m/z=42 appeared at 129 °C is considered to be due to a fragment, cyclopropylium ion, formed by the decomposition of dppb, while the peak of m/z=78 appearing at 189 °C seems to be fragments ($C_6H_6^+$) formd by the decomposition of nbd.

The TPD profile of pyridine adsorbed on Rh[(nbd)-(dppb)]ClO_4 is shown in Fig. 3. A peak of m/z=79 which did not appear in the background profile, attributed to pyridine was observed at 93 °C. When pyridine was adsorbed, the peak at m/z=42 (the fragments of DPPB) shifted to a lower desorption

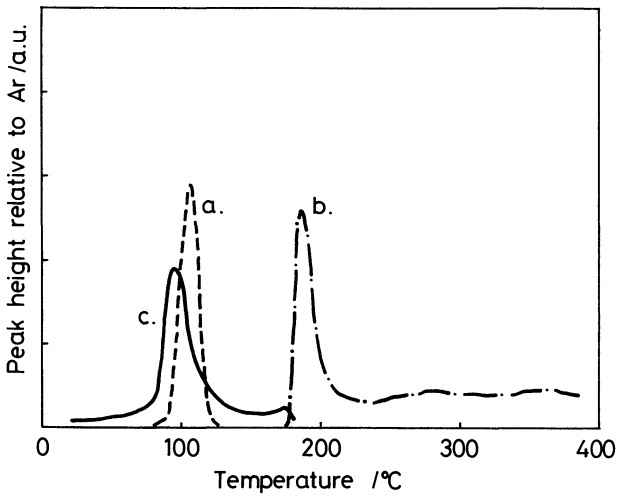

Fig. 3. Temperature programmed desorption of pyridine from [Rh(nbd)(dppb)]ClO_4 and temperature programmed decomposition of [Rh(nbd)(dppb)]ClO_4 after adsorption of pyridine at room temperature. (a) m/z=42; (b) m/z=78; (c) m/z=79.

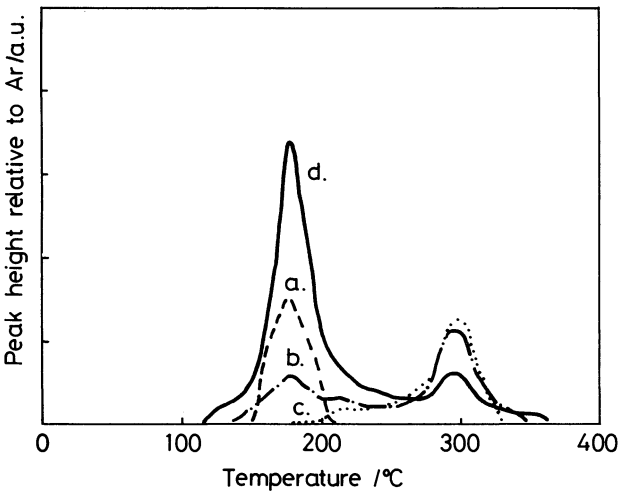

Fig. 4. Temperature programmed decomposition of $[Ru(dmso)_6](ClO_4)_2$. (a) m/z=63; (b) m/z=35; (c) m/z=52; (d) m/z=79.

temperature by 20 °C. This indicates that the bond between dppb and Rh is weakened by pyridine adsorption. In the case of ammonia TOD, no desorption peak was observed as long as the Rh complex did not decompose, probably due to the adsorption of small-size ammonia at strong acid sites where pyridine can not approach. Triethylamine whose acid strength is higher than ammonia did not adsorb on the Rh complex, probably because of its larger steric hindrance.

The main peaks of the TPD profile of $[Ru(dmso)_6]$-$(ClO_4)_2$, itself a background, are shown by a, b, c, and d in Fig. 4. The peak of m/z=63 at 177 °C is considered due to the fragment (CH_3SO^+) formed by decomposition

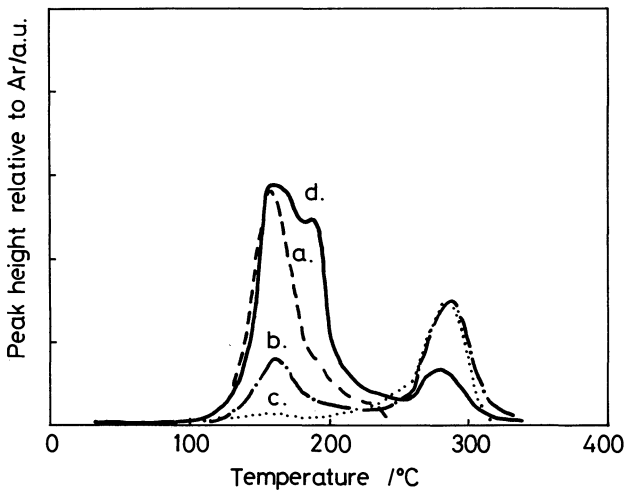

Fig. 5. Temperature programmed desorption of pyridine from $[Ru(dmso)_6](ClO_4)_2$ and temperature programmed decomposition of $[Ru(dmso)_6](ClO_4)_2$ after adsorption of pyridine at room temperature. (a) m/z=63; (b) m/z=35; (c) m/z=52; (d) m/z=79.

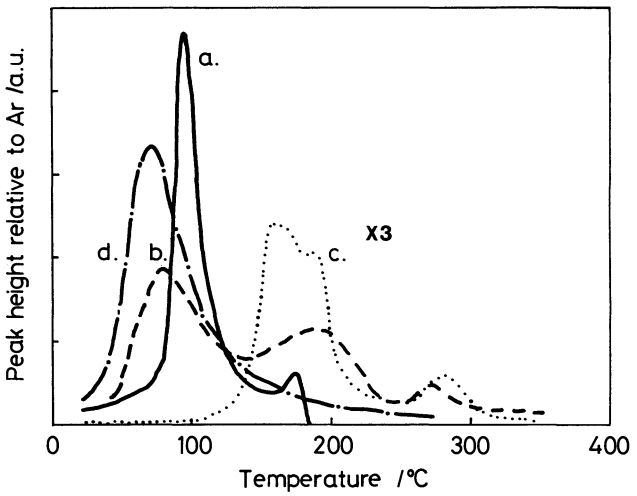

Fig. 6. Temperature programmed desorption of pyridine from (a) $[Rh(nbd)(dppb)]ClO_4$; (b) $[Ru(binap)](BF_4)_2$; (c) $[Ru(dmso)_6](ClO_4)_2$; (d) SiO_2.

of dmso. At 293 °C, the Ru complex is considered to completely decompose, since the peaks of m/z=35 due to the Cl^+ fragment and m/z=52 due to the $HClO^+$ fragment appear. A peak at m/z=79 was also observed in the background. When pyridine was adsorbed on $[Ru(dmso)_6](ClO_4)_2$, a new peak at m/z=79 was observed at 162 °C (Fig. 5); it was assigned to desorbed pyridine by a comparison of Fig. 5 with Fig. 4.

The desorption peak of pyridine (m/z=79) from $[Ru(binap)](BF_4)_2$ appeared at 78, 190, and 268 °C. The decomposition of the complex started at the same temperature, though the TPD profiles are not shown here.

Fig. 6 shows the desorption peaks (a, b, c, and d) of pyridine (m/z=79) adsorbed on $[Rh(nbd)(dppb)]ClO_4$, $[Ru(dmso)_6](ClO_4)_2$, $[Ru(binap)](BF_4)_2$, and SiO_2, respectively. In the temperature range of 70—100 °C, there is no peak of pyridine for $[Ru(dmso)_6](ClO_4)_2$. On the other hand, there is no peak of pyridine for SiO_2 and a relatively small peak was observed for $[Rh(nbd)(dppb)]ClO_4$ in the range of 150—200 °C. In a higher temperature range of 270—300 °C, pyridine desorption peaks were observed only for the Ru complex. Since a material having a higher acid strength shows a higher desorption temperature of pyridine, the order of the acid strength of the metal complexes and SiO_2 is as follows:

$$[Ru(dmso)_6](ClO_4)_2 \simeq [Ru(binap)](BF_4)_2 > [Ru(nbd)(dppb)]ClO_4 \gg SiO_2$$

The highest acid strength of SiO_2 measured by the indicator method was in the range $1.5 < H_0 < 3.3$. Therefore, the fact that the acid strengths of Ru and Rh complexes estimated by TPD method are much stronger than that of SiO_2 is consistent with the result measured by the acetalization method.

The authors thank Dr. H. Kumobayashi for his valuable discussion and Mr. N. Sayo for his preparation of some metal complexes.

References

1) W. O. Haag and D. D. Whitehurst, U. S. Patent 4098727; *Chem. Abstr.*, **82**, 1990v (1979).
2) J. Hagen and K. Bruns, Ger. Offen 2849742; *Chem. Abstr.*, **83**, 1866/3a (1980).
3) M. D. Fryzuk and B. Bosnich, *J. Am. Chem. Soc.*, **100**, 5491 (1978).
4) H. Takaya, T. Ohta, R. Noyori, N. Sayo, H. Kumobayashi, and S. Akutagawa, Japan Patent Kokai, 61-184651 (1986).
5) P. Evans, A. Spencer, and G. Wilkinson, *J. Chem. Soc., Dalton Trans.*, **1973**, 204.
6) T. Kou, et al. unpublished results.
7) K. Tanabe, "Solid Acids and Bases," Academic Press, New York and London (1970), pp. 5—7.
8) D. Cook, *Can. J. Chem.*, **41**, 522 (1963).
9) D. J. Pasto and P. Balasubramaniyan, *J. Am. Chem. Soc.*, **89**, 295 (1967).
10) "CRC Handbook of Chemistry and Physics," ed by R. C. Weast, CRC Press, Inc. Boca Raton (1985).

Spectroelectrochemistry of New Prussian Blue Films Prepared by a Cast Method

Ru-Jang LIN and Naoki TOSHIMA*
Department of Industrial Chemistry, Faculty of Engineering, The University of Tokyo, Hongo, Bunkyo-ku, Tokyo 113
(Received July 31, 1990)

New Prussian Blue (PB) films were prepared by being cast from colloidal PB dispersions in an organic solvent containing cationic surfactants. The electrochromic behaviors of the cast PB films are similar to those of electrodeposited PB films. However, the cyclic voltammetries of both the PB films were quite different from each other. To make the difference clear, scanning electron microscopy (SEM), energy dispersive X-ray analysis (EDX), and X-ray photospectroscopy (XPS) were used in measurements of these films grown on Pt and indium tin oxide electrodes. The EDX results for fresh PB films indicated that cast films contain K^+ ions, suggesting a soluble-form PB, $KFe[Fe(CN)_6]$, while electrodeposited films do not, suggesting an insoluble-form PB, $Fe_4[Fe(CN)_6]_3$. The transient spectral observations indicated the participation of a unique electrochemically active iron(III) site in the reductive cycles of a cast film, although the participation of a plural electrochemically active iron(III) sites was proposed for an electrodeposited film. After a repeated cyclic scan a cast PB film maintained its unique active site, while an electrodeposited film had plural sites comprising both a soluble and an insoluble form of PB.

Prussian Blue (PB, iron(III) hexacyanoferrate(II), Fe(III/II)) is a well-known colorant used extensively in the formulation of paints, lacqures, and painting inks. Recently, Neff devised a chemical method to deposit thin films of this material onto platium and gold electrodes,[1] and were the first to investigate the electrochemistry of these films.[2,3] Neff's preparation method was modified by Itaya et al., who reported on the spectroscopies and electrochemical properties of these films prepared electrochemically on a number of substrates;[4,5] they then applied this knowledge to construct an electrochromic display.[6] For such a device to be practically useful, however, the preparation method must be modified to allow deposits on a large area and to also allow long-term stability. It is not very easy to manufacture a uniform PB film of large area by the above-mentioned methods. Though the casting of PB colloids in a nonaqueous solvent is considered to be effective to overcome this problem, such a cast film has not yet been developed.

We have found that PB colloids can be extracted from an aqueous solution by an organic solvent containing some cationic surfactants.[7,8] A PB composite film was prepared onto a transparent electrode by casting an extracted PB solution. This novel method is unique in that it enables the preparation of uniform PB films of large area. The cast PB film can be electrochemically reduced or oxidized, demonstrating a stable electrochromism, as observed in electrodeposited PB films. In this paper we describe the results of electrochemical, analytical, and spectroelectrochemical studies of a cast PB film and compare them with those of electrodeposited PB film in order to clarify the difference between the two PB films.

Experimental

Materials. Potassium hexacyanoferrate(II), $K_4[Fe(CN)_6]$, and iron(III) chloride, $FeCl_3 \cdot 6H_2O$ were the purest grade commercially available. Cationic surfactants, such as hexadecyltrimethylammonium chloride (HTAC), were purified by the standard procedures.

Preparation of Cast PB Films. The colloidal dispersions of PB were prepared by rapid mixing of aqueous solutions of both $K_4[Fe(CN)_6]$ and $FeCl_3 \cdot 6H_2O$ at an equimolar ratio. The colloidal solution, thus prepared at the concentration of 20 mmol dm^{-3} (or less), was continuously stirred before extraction in order to prevent any aggregation of the colloids; the colloidal PB was then extracted from the solution within 1 d. The extraction was carried out by using a chloroform solution containing two- or three-fold moles of a cationic surfactant.[8] The extracted chloroform solution of PB (hereafter denoted as PB-surfactant) was dried over anhydrous magnesium sulfate. To form a cast PB-surfactant film, the solution of PB-surfactant was cast onto an indium tin oxide electrode (ITO, 1 cm×1 cm, 10 Ω/□) for spectroelectrochemical studies, and onto a Pt electrode for elemental analysis by EDX.

It was found that, in general, a treatment that involved one H_2O-immersing and air-drying of the as-cast film substantially enhanced the adhesion of the cast film on the electrode. To obtain stable voltammograms, all of the cast films were finally immersed in pure H_2O and dried in a desiccator before performing a voltammetric scan.

Preparation of Electrodeposited PB Film. The electrodeposited PB films were prepared by using essentially the same method proposed by Itaya et al.[4,5] The PB was deposited galvanostatically (10 μA cm^{-2}) for 8 min onto the same ITO electrode (1 cm×1 cm, 10Ω/□) from an aqueous solution containing $K_3[Fe(CN)_6]$ (20 mmol dm^{-3}), $FeCl_3 \cdot 6H_2O$ (20 mmol dm^{-3}), KCl (0.01 mol dm^{-3}), and HCl (0.01 mol dm^{-3}).

Voltammetric and Spectroelectrochemical Measurement. Voltammograms were obtained with a Toho Technical Research model PS-2000 potentiostat equipped with a model FG-02 function generator and a model 3320 digital coulometer. A small KCl-saturated Ag–AgCl electrode was used as a reference. The cell used for spectroelectrochemical measurements was almost the same as that designed by Hoang et al.[9] and was purged with pure nitrogen gas. In

order to measure the transient spectral change during the electrochemical process, rapid scanning multichannel photodiode array spectrometers (Otsuka Electronics Co., MCPD-100A and IMUC-7000S) were used with an ITO working electrode. The MCPD coupled with Toho's model FG-02 function generator was triggered and operated by an NEC model 9801-VX personal computer. The transient absorption spectra were recorded at a 12.5 s interval with slow scanning (2 mV s^{-1}) of the ITO potential, and at a 0.08 s interval with stepping of the ITO potential. All potential values cited in this paper refer to Ag/AgCl.

Surface Analyses. A Hitachi S-430 scanning electron microscope (SEM) and a KEVEX-7000 energy-dispersive X-ray analyzer (EDX) were used to examine the alteration in the surface morphology as well as the chemical composition of the films on the surface both before and after immersing into the electrolyte, as well as subsequent voltammetric scanning in an electrolyte of 0.1 mol dm^{-3} $KClO_4$ at pH 4.0.

Results and Discussion

Chemical Composition of the PB in the Extracted Solution and in the Cast Film. We have shown that PB colloids can be extracted by an organic solution containing cationic surfactants.[7,8] The fact that only cationic surfantants can extract the PB colloids from the aqueous solution suggests the formation of composite micelles between the cationic surfactant molecules and negatively charged PB colloids having $Fe^{III}[Fe^{II}(CN)_6]^-$ units.

In general, PBs prepared in various ways can be devided into two formulations (a "soluble" form, $KFe^{III}[Fe^{II}(CN)_6]$, and an "insoluble" form, $Fe^{III}_4[Fe^{II}(CN)_6]_3 \cdot 6H_2O$) depending on the specific preparation conditions.[10] The PB, which was recrystallized[11] or electrodeposited,[4,5] was reported to have the composition of $Fe^{III}_4[Fe^{II}(CN)_6]_3 \cdot 6H_2O$, the "insoluble" form. For PB prepared by mixing $K_4[Fe(CN)_6]$ and $FeCl_3$, Wilde et al. proposed that when an excess of $K_4[Fe(CN)_6]$ to $FeCl_3$ is used a "soluble" PB is formed, while an excess of $FeCl_3$ to $K_4[Fe(CN)_6]$ gives an "insoluble" PB.[12] In fact, the composition of PB as a colloidal form in an aqueous solution was reported by Kaneko et al. as $KFe^{III}[Fe^{II}(CN)_6]$, the "soluble" form.[13]

In order to clarify the relation between the preparation conditions and the extractability by surfactants, an extraction of PB was carried out by an organic solution containing such cationic surfactants as HTAC (hexadecyltrimethylammonium chloride) from various aqueous PB solutions which were prepared by altering the molar ratio between potassium hexacyanoferrate(II) and iron(III) chloride. It was then found that the extraction of PB is effective only when the ratio of $Fe^{II}/(Fe^{II}+Fe^{III})$ is larger than 0.5.[8] This fact strongly suggests that only the "soluble" form PB can be extracted by an organic solution containing cationic surfactants.

The extracted PB solution was cast onto an ITO electrode or a Pt electrode to form a cast PB-surfactant film. Among the cationic surfactants examined, cationic surfactants with a longer alkyl chain than C_{14} were effective to form a stable cast PB film.

The chemical composition of PB in the cast film was measured by energy-dispersive X-ray analysis (EDX), which showed that cast PB film is still composed of the "soluble" form PB.[8] Details are discussed later in the present paper.

Electrochromic Behaviors of the Cast Films. The electrochromic behaviors of the cast PB-surfactant films were investigated by in-situ UV-vis spectroscopy, as mentioned briefly in a preliminary communication.[7] Figure 1(a) shows the absorption spectral changes of the PB-HTAC film measured under voltammetric scanning between −0.3 V and +1.4 V vs. Ag/AgCl with a scan rate of 50 mV s^{-1}. The color changes of the PB-HTAC film are not so large, compared with those of the electrodeposited PB film (Fig. 1(c)), for which the so-called Berlin Brown (BB, Fe(III/III), at +1.4 V vs. Ag/AgCl), and Prussian White (PW, Fe(II/II), at −0.3 V vs. Ag/AgCl) are well-known.[5] This small change in color may be due to the low ionic conductivity of the PB-HTAC film. To improve the conductivity of the PB-HTAC film,

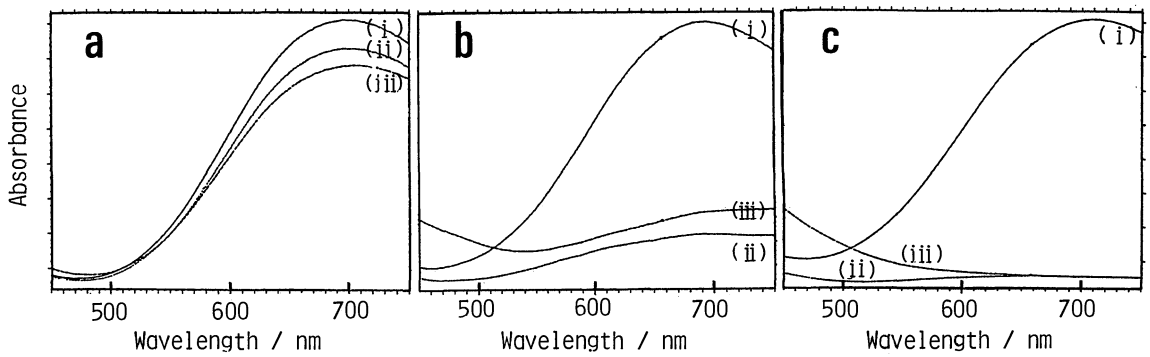

Fig. 1. Absorption spectral changes of the cast PB films, (a) PB-HTAC and (b) PB-HTAC-$LiClO_4$, and (c) the electrodeposited PB film measured under repeated voltammetric scanning. The curves show spectra at (i) +0.5 V, (ii) −0.3 V, and (iii) +1.4 V.

lithium perchlorate $LiClO_4$ in acetone was added to the extracted PB–HTAC solution in chloroform as a promoter for ionic conductivity.[14] The mixed solution was cast to form a PB–HTAC–$LiClO_4$ film. The UV-vis spectra of the PB–HTAC–$LiClO_4$ film at the oxidized and reduced states show a clear and rapid electrochromic behavior, as shown in Fig. 1(b). The oxidized and reduced films are yellow and colorless at +1.4 V and −0.3 V, respectively. The transient spectral changes of the PB–HTAC–$LiClO_4$ film are similar to those of an electrodeposited PB film dipped in an aqueous electrolyte (Fig. 1(c)).

Figure 2 illustrates the change of the absorbance at 700 nm (λ_{max} of PB) in the PB–HTAC, PB–HTAC–$LiClO_4$ and electrodeposited PB films, for which the potential is stepped between +0.5 V and +1.4 V. The electrochromic response of the PB–HTAC–$LiClO_4$ film (b) is remarkably more rapid than that of the PB–HTAC film (a), and close to that of the electrodeposited PB film (c). This would be due to the higher ionic conductivity of the PB–HTAC–$LiClO_4$ film than PB–HTAC. A similar behavior in the electrochromic response of these films was also observed in a reduction by potential stepping between +0.5 and −0.3 V.

The reproducibility of the electrochromic response is one of the most important factors for the practical utilization of the films. The electrodeposited PB film is known to be well reproducible in the reduction and

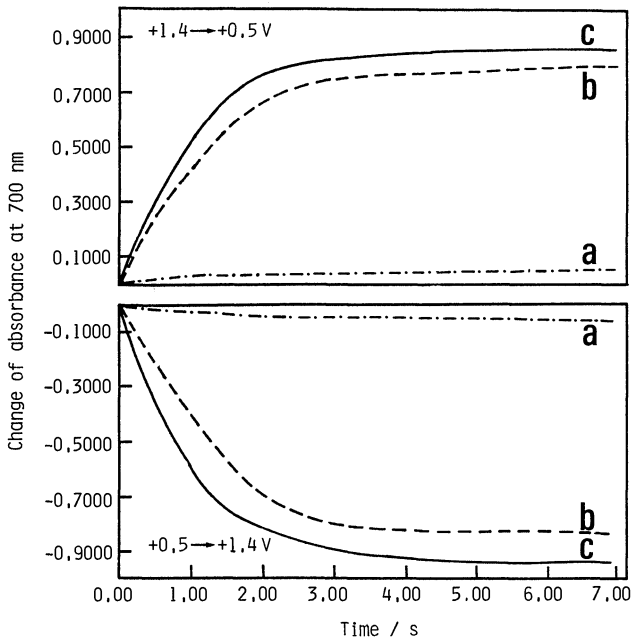

Fig. 2. Absorbance changes at 700 nm with time for (a) PB–HTAC, (b) PB–HTAC–$LiClO_4$, and (c) electrodeposited PB films when the potentials are stepped from +0.5 V to 1.4 V (lower parts) and from +1.4 V to +0.5 V (upper parts) in 0.1 mol dm^{-3} $KClO_4$.

reoxidation of PB. With respect to a cast PB film, on the negative potential step, the electrochromic response of a cast PB–HTAC–$LiClO_4$ film is as stable as that of the electrodeposited PB film during repeated potential steps. On the positive potential step, furthermore, the electrochromic response of the cast PB–HTAC–$LiClO_4$ film is more stable than that of the electrodeposited PB film. This behavior may be due to a higher stability of the oxidized form of PB in a cast film than in an electrodeposited film. More detailed discussions regarding this behavior is given later in terms of a cyclic voltammogram and spectroelectrochemistry.

Voltammetry of PB–HTAC–$LiClO_4$ Films. Cyclic voltammograms (CV) of the cast PB–HTAC–$LiClO_4$ films were taken in a 0.1 mol dm^{-3} $KClO_4$ electrolyte at a scanning rate of 20 mV s^{-1}. An example is shown in Fig. 3(a), as well as the CV of the electrodeposited PB film in Fig. 3(b).

In the region of a negative potential scan (between +0.5 V and −0.3 V), which causes a reduction of PB to PW, the CV curves of both the cast and the electrodeposited PB film are similar to each other regarding fundamental features. However, a precise comparison of both CV curves makes the differences clear. To make the difference more clear, the CVs of both films were measured at a slow scanning rate of 2 mV s^{-1} as well. The results are shown in Figs. 4(a) and (b), which are quite different each other.

The CV curve of the cast film is both sharper and simpler than that of the electrodeposited film, which has a complex curve comprising a sharp peak centered at 0.18 V and broad shoulders at ca. 0.0 V and 0.3 V. In successive scans, the CV peak feature of the cast film remains without any large change, even though the peak current at 0.18 V increases slightly. In contrast, on an electrodeposited film, the broader shoulder observed in the first reductive scan gradually diminishes during repeated scans and becomes sharp; this is rather similar to the simple wave observed for a cast film. This sharp spike was earlier noted by Ellis et al.[2] for a PB-modified gold electrode. Itaya et al.[5] assumed that uncoordinated $[Fe(CN)_6]^{4-/3-}$ and $Fe^{2+/3+}$ ions seem to be reason for the current spike. However, we have found that the sharp spike could not be observed on an electrodeposited PB film voltammetrically scanned in an aqueous KCl solution.[15] On the other hand, such sharp spikes were frequently observed on polymer-modified electrodes,[16,17] for which a structural change was proposed as a possible reason for the spikes, since the structures of polymers are strongly affected by the redox reaction. In the present case, repeated scans caused a structural change of the electrodeposited PB to a new one which has a similar structure to that of cast PB, even though some part of the virgin form of the electrodeposited PB remained. The structural change of the electrodeposited PB is discussed again later on the basis of spectroelectrochemical measure-

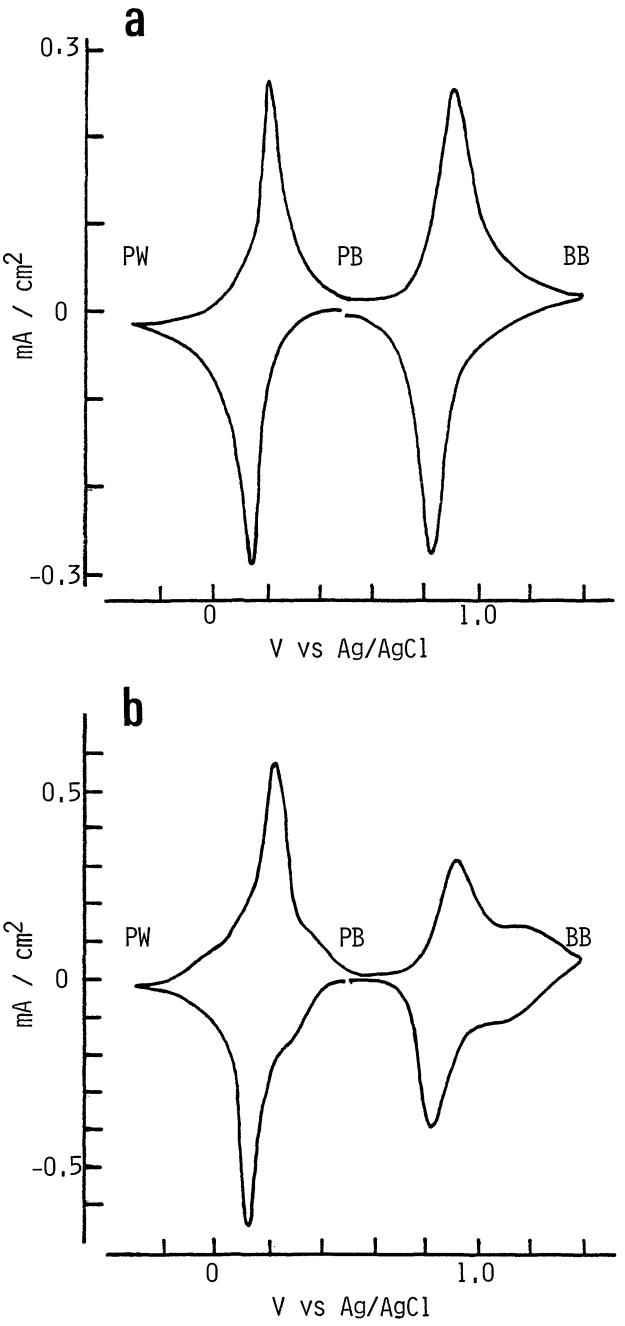

Fig. 3. Cyclic voltammograms of (a) PB–HTAC–$LiClO_4$ and (b) electrodeposited PB films on ITO electrodes in 0.1 mol dm^{-3} $KClO_4$. Scan speed= 20 mV s^{-1}. Only the stable voltammograms are presented.

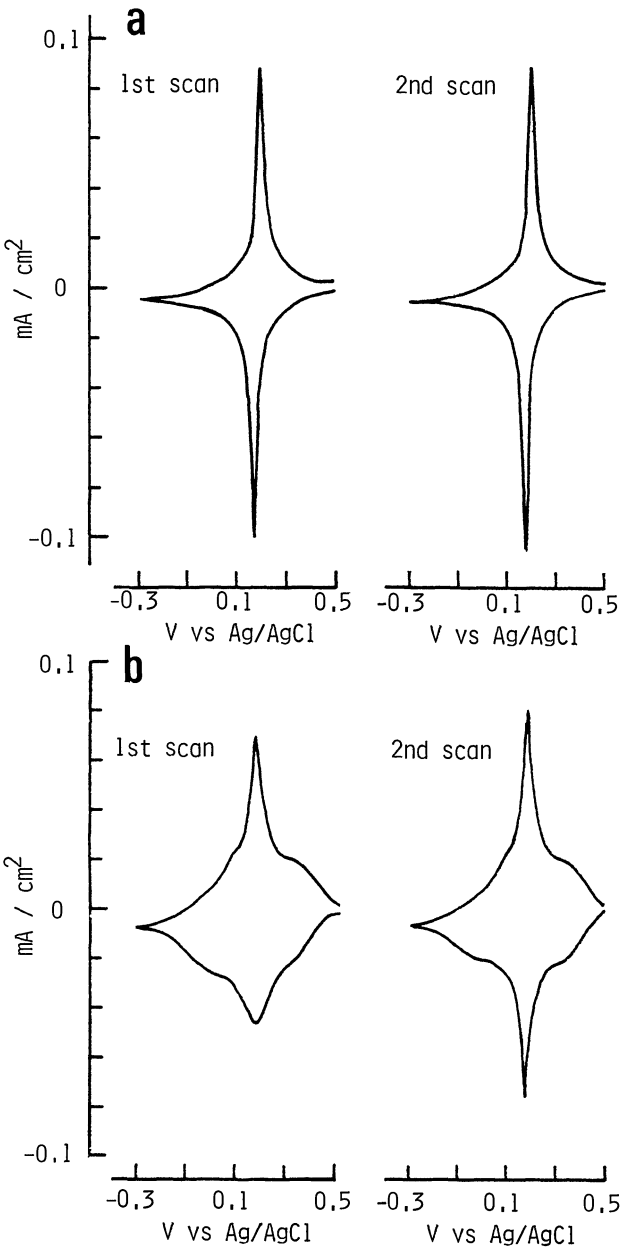

Fig. 4. Cyclic voltammograms of (a) PB–HTAC–$LiClO_4$ and (b) electrodeposited PB films on ITO electrodes in 0.1 mol dm^{-3} $KClO_4$. Scan speed= 2 mV s^{-1}. The first and second reductions are presented, respectively.

ments.

On the other hand, the oxidation of PB in a positive potential scan has been reported to correspond to a partial of full oxidation of the hexacyanoferrate(II) sites to Berlin Green (BG) or Berlin Brown, depending on the positive extent of the potential scan.[4,5] A positive potential scan (between +0.5 V and +1.4 V) causes an oxidation of PB to BB. If the voltammetric scanning started directly from Fe(III/II) to Fe(III/III) for a cyclic electrochemical oxidation of PB, a small loss of the peak current occurred for the cast film in successive scans, while a considerable decay of the peak current was observed for the electrodeposited PB film. It is possible that a cast film can be oxidized to a fully oxidized form with considerable stability, as proposed above. However, a cast film is highly stable if it is pretreated by a reductive cycle from Fe(III/II) to Fe(II/II) before the oxidative scan, as was reported for electrodeposited films.[5]

In an oxidative scan of a pretreated PB film, the CV

curve of a cast PB film is much sharper and simpler than that of an electrodeposited film, as well as in the reductive curve. A symmetrical single redox peak was observed for a cast film in a positive potential scan, while two separate waves were observed for an electrodeposited PB film at electrode potentials higher than +1.0 V in addition to the main redox peak at +0.92 V, as previously reported.[4,5] This indicates that the oxidation of a cast film is also much simpler than that of an electrodeposited film.

These voltammetric differences suggest that electrochromism occur under different reactions in both cast and electrodeposited films. The electric charge used for the oxidation wave is about 70% of that for the reduction wave in an electrodeposited PB film. The ratio was reported to give fairly accurate proof for the formula of the electrodeposited PB, proposing the redox reactions according to the Eqs. 1 and 2:[4,5]

$$Fe^{III}_4[Fe^{II}(CN)_6]_3 + 4K^+ + 4e^- = K_4Fe^{II}_4[Fe^{II}(CN)_6]_3 \quad (1)$$

and

$$Fe^{III}_4[Fe^{II}(CN)_6]_3 + 3X^- - 3e^- = Fe^{III}_4[Fe^{III}(CN)_6]X_3. \quad (2)$$

On the basis of the above considerations, the ratio of the charges for the cast film was measured. The ratio shown in Fig. 3(a) is about 1.05, rather than 0.7 for an electrodeposited film. This result gives the first fairly consistent proof that the formula of cast PB is the "soluble" form, $KFe[Fe(CN)_6]$, which had been proposed due to the result of extractability, as mentioned above. On the basis of the results of coulometry and the EDX (vide infra), the possible electrochemical reactions of the "soluble" PB in the cast film can be proposed as follows:

$$KFe[Fe(CN)_6] + K^+ + e^- = K_2Fe[Fe(CN)_6] \quad (3)$$

and

$$KFe[Fe(CN)_6] - K^+ - e^- = Fe[Fe(CN)_6]. \quad (4)$$

SEM and Analytical Studies. SEM photographs of cast PB–HTAC–$LiClO_4$ films and electrodeposited PB films are shown in Figs. 5 and 6, respectively. Included in these Figures for a comparison are SEM photographs of the electrodes (a) before and (b) after treatment by immersing or voltammetric scanning in aqueous $KClO_4$. No morphological change was observed for the electrodeposited PB film after immersing or voltammetric scanning. On the contrary, the integrity of the cast PB–HTAC–$LiClO_4$ film, which has been kept after immersing in pure H_2O, became breached in places after immersing in aqueous $KClO_4$, and the porous substructure became visible. The typical rough, porous surface was retained and no decomposition of the film was observed during repeated voltammetric scanning. A similar morphological change was also observed for cast PB–HTAC films during the same treatments. These results suggest that though a morphological change is rarely brought

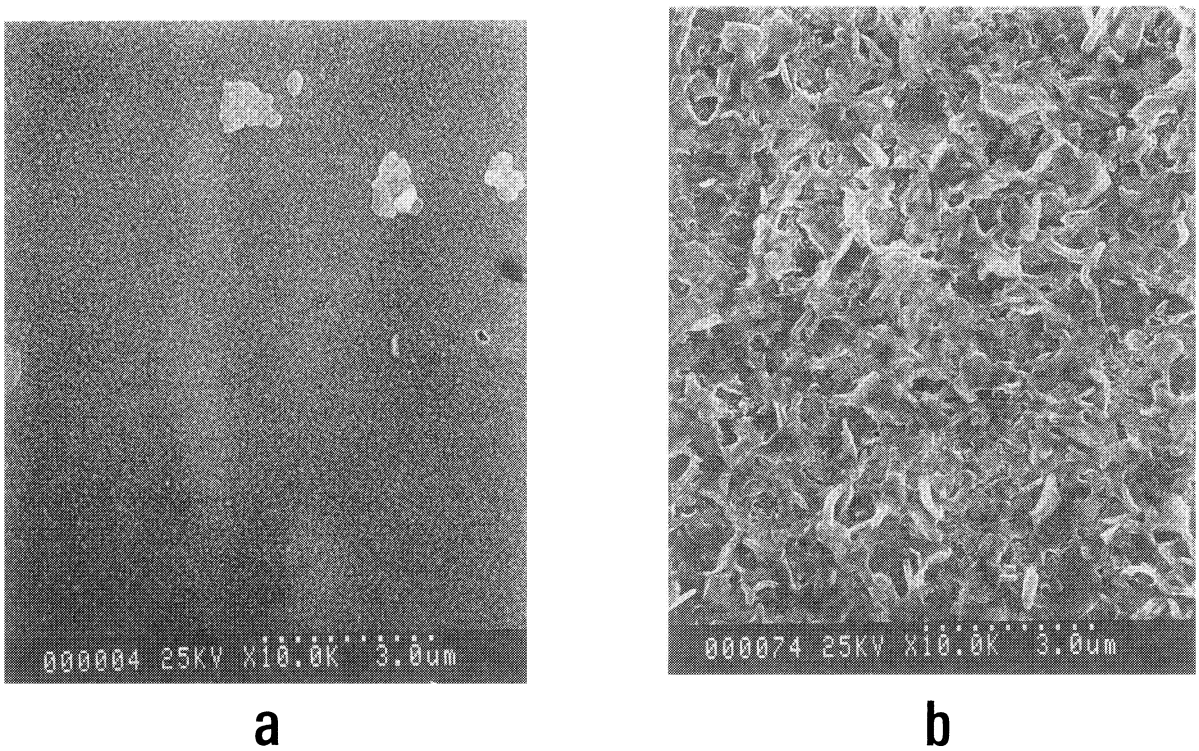

Fig. 5. Scanning electron micrographs of the cast PB–HTAC–$LiClO_4$ film (a) before and (b) after the treatment of immersing or voltammetric scanning in 0.1 mol dm^{-3} $KClO_4$. Mag.$\times 10^4$.

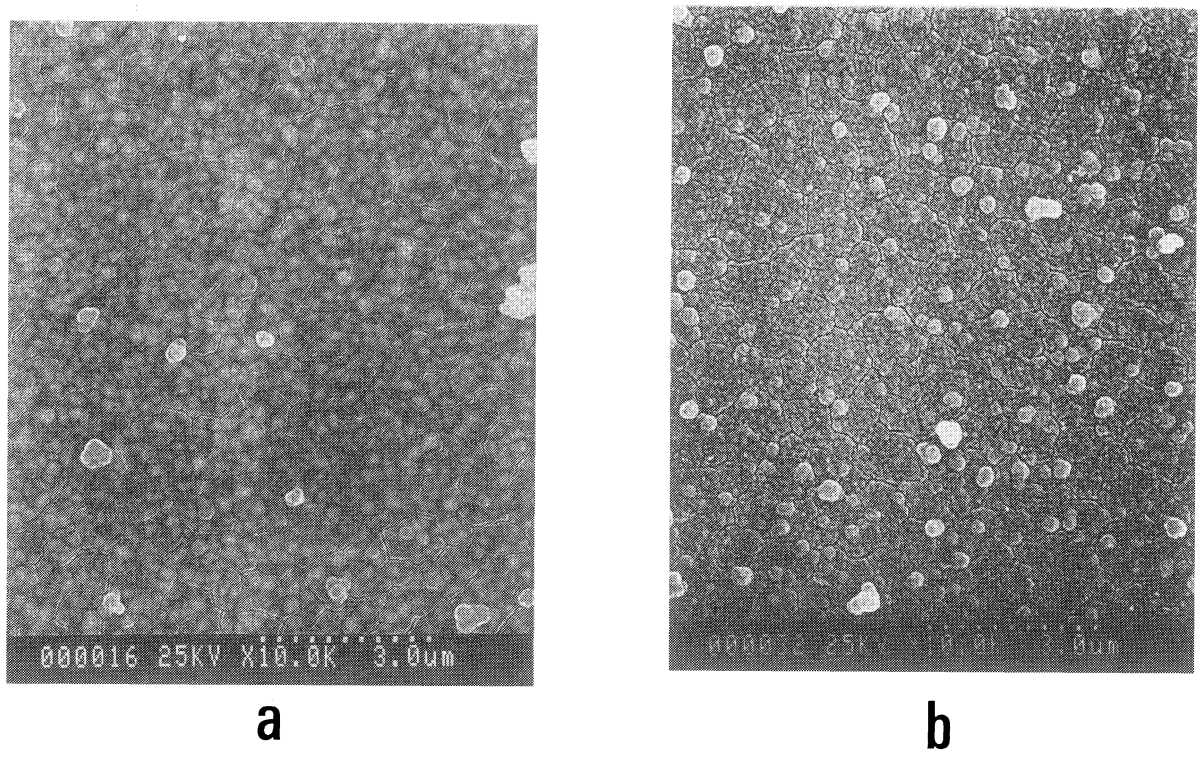

Fig. 6. Scanning electron micrographs of the electrodeposited PB film (a) before and (b) after the treatment of immersing or voltammetric scanning in 0.1 mol dm^{-3} $KClO_4$. Mag.$\times 10^4$.

about by an electrochemical reaction, it is probably due to a rearrangement of the surface structures of a film composed of PB and surfactants. In other words an "improvement" of the conductivity of the cast film by the addition of $LiClO_4$ is a probable reason for accelerating the electrochromic and voltammetric response, as mentioned above.

Since the uncertainty in composition of PB has hampered any interpretation of electrochemical studies concerning PB films, studies on the chemical composition are considered to give key knowledge on such films. In particular, the K^+ content of the films should reflect which form (soluble or insoluble) of mixed-valence complex is present. A series of the cast PB–HTAC–$LiClO_4$ films were analyzed by EDX and XPS in order to explore this problem; the EDX results were compared with those of electroposited PB films, as shown in Figs. 7 and 8.

The EDX (and some XPS) measurements reveal the presence of the K^+ ions on the cast PB–HTAC–$LiClO_4$ films, although K^+ is absent on the electrodeposited PB film in the as-deposited state, as previously reported.[18] The EDX data support the idea that a cast PB film comprises the "soluble" form, $KFe[(CN)_6]$, as proposed above.

The changes in the chemical composition of these films with a subsequent treatment were traced by EDX measurements. The K^+ ions appear in the electrodeposited PB film (Fig. 8(b)) as a result of simply immersing an as-deposited film in 0.1 mol dm^{-3} $KClO_4$ (at open circuit), while the K^+ content of the cast PB–HTAC–$LiClO_4$ film (Fig. 7(b)) is kept constant after immersion. On the contrary, the Cl^- content of a cast PB–HTAC–$LiClO_4$ film (Fig. 7(b)) increases in quantity, while the Cl^- peak of an electrodeposited PB film (Fig. 8(b)) scarcely changes after immersion. Since the chlorine atoms in different species can be distinguished by the peak position in XPS, i.e., chlorine atoms in a HTAC surfactant, PB and perchlorate appear at 198, 199, and 208 eV, respectively, the XPS measurements of the cast film clearly indicated the origin of the chlorine atoms. Based on the results of XPS measurements, the incease in the Cl^- content of the cast film by simple immersion in $KClO_4$ can be accounted for by the incorporation of ClO_4^- into the cast film by an exchange with Cl^- in the reverse micelles.

When the iron(III) states are reduced at −0.3 V in a 0.1 mol dm^{-3} $KClO_4$ solution at pH 4.0, the K^+ peak of the cast PB–HTAC–$LiClO_4$ films in the EDX spectra increases, as shown in Fig. 7(c), indicating the incorporation of a large quantity of K^+ ions into the cast films. As for the oxidation of the hexacyanoferrate(II) states of the cast films in which the iron(III) states have been reductively cycled in advance, the oxidation of the hexacyanoferrate(II) sites at +1.0 V in $KClO_4$ drives all of the K^+ ions from the cast film, as shown in Fig. 7(d). This oxidation reaction can be

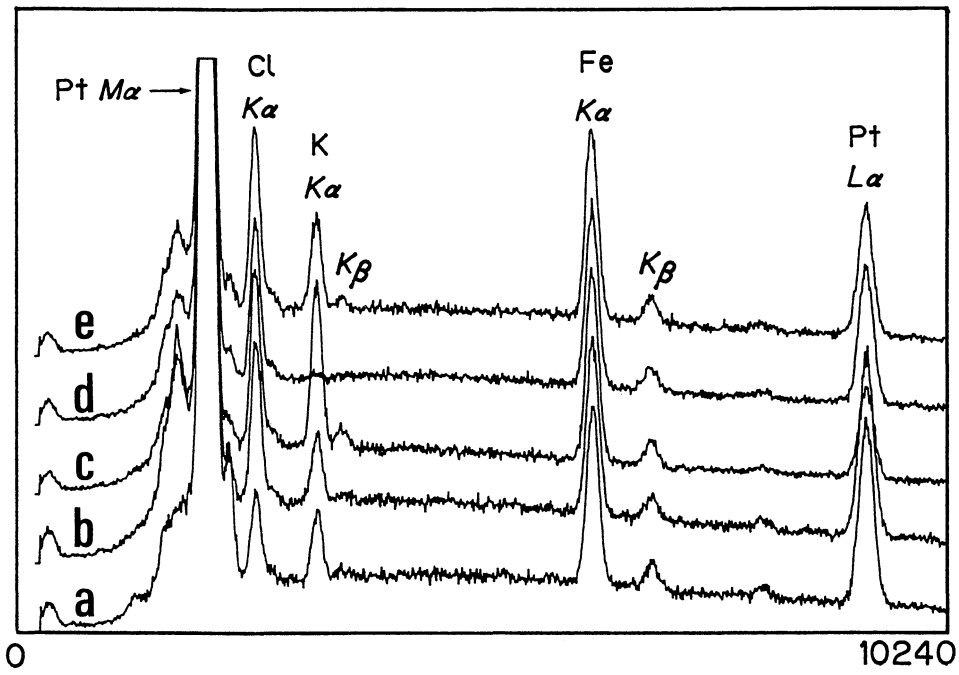

Fig. 7. EDX spectra of the cast PB–HTAC–$LiClO_4$ films on Pt electrodes: (a) as-cast, (b) immersed in 0.1 mol dm^{-3} $KClO_4$, (c) reduced in 0.1 mol dm^{-3} $KClO_4$ three times, (d) oxidized at 1.0 V in 0.1 mol dm^{-3} $KClO_4$, and (e) oxidized at 1.0 V and then re-reduced to Fe(III/II) in 0.1 mol dm^{-3} $KClO_4$. Accelerating voltage=10 kV.

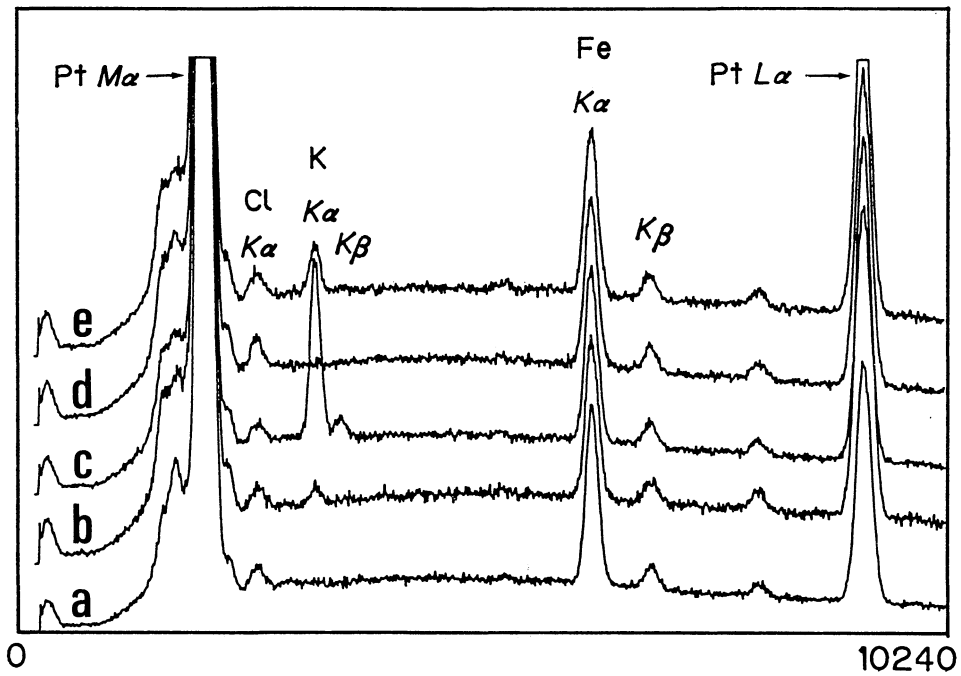

Fig. 8. EDX spectra of the electrodeposited PB films on Pt electrodes: (a) as-grown, (b) immersed in 0.1 mol dm^{-3} $KClO_4$, (c) reduced in 0.1 mol dm^{-3} $KClO_4$ three times, (d) oxidized at 1.0 V in 0.1 mol dm^{-3} $KClO_4$, and (e) oxidized at +1.0 V and then re-reduced to Fe(III/II) in 0.1 mol dm^{-3} $KClO_4$. Accelerating voltage=10 kV.

represented by Eq. 4. Re-reduction back to the Fe (III/II) state reproduces the original K^+ content, as shown in Fig. 7(e). However, the Cl^- content of the cast film is little changed by cyclic electrochemical redox between the Fe(II/II) and Fe(III/III) states.

In a similar investigation concerning an electrodeposited film (Fig. 8(c)—(e)) the contents of both K^+ and Cl^- ions change during the redox cycle in the same manner as for a cast film, as previously reported for 0.5 mol dm^{-3} KCl.[18]

These results have clarified several points concerning the change in the chemical composition of a cast PB–HTAC–$LiClO_4$ film as well as an electrodeposited PB film during the electrochemical reaction: (a) The K^+ content of the as-cast state of a cast PB film is consistent with the "soluble" form of PB, while an electrodeposited PB film does not contain K^+, suggesting an "insoluble" form of PB. (b) The ion exchange between ClO_4^- of the supporting electrolyte and Cl^- of the surfactant probably leads to the micelle swelling and morphological change observed in the SEM micrograph. (c) The fact that ClO_4^- enters into a

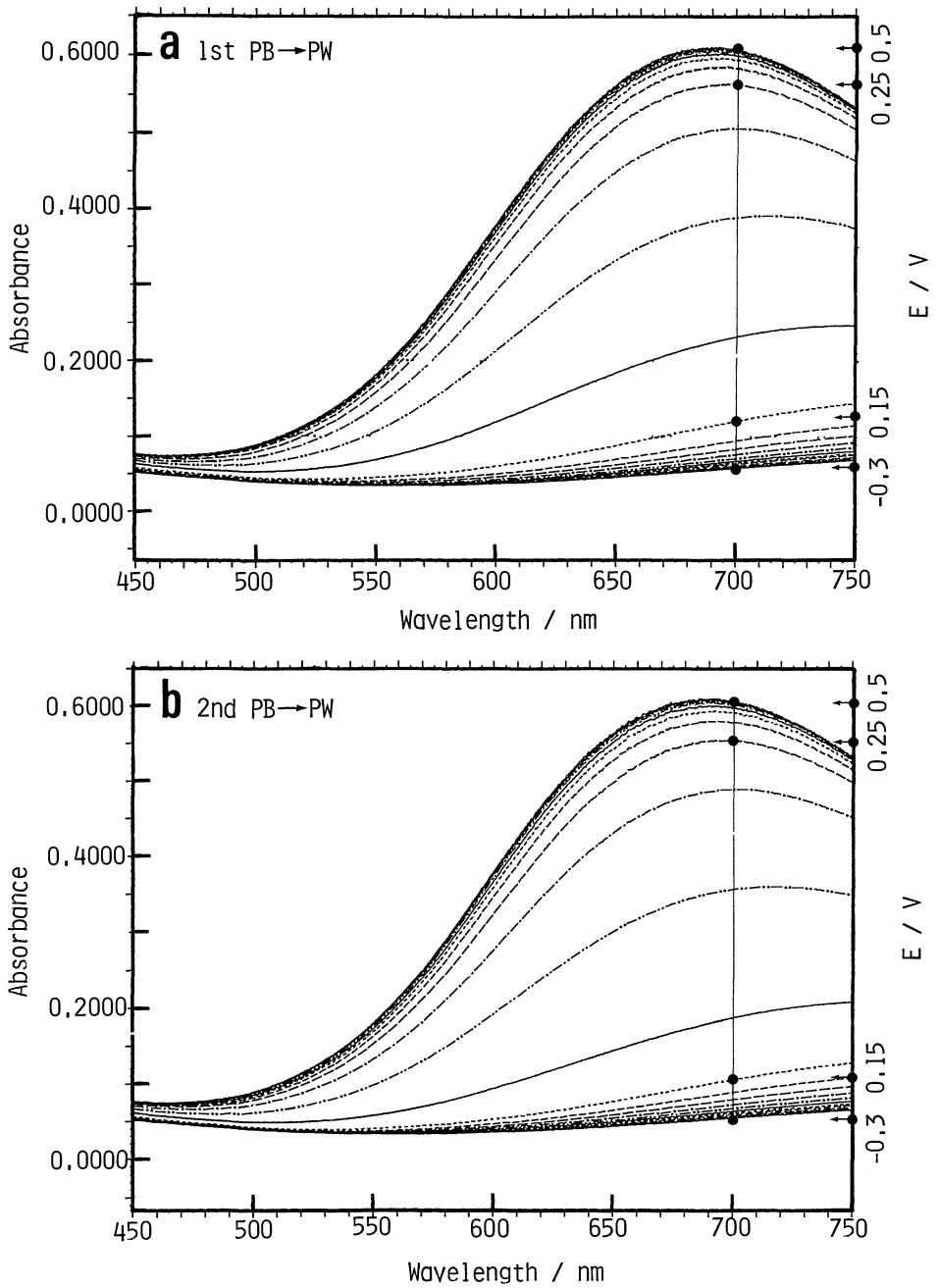

Fig. 9. Visible absorption spectra of the PB–HTAC–$LiClO_4$ film cast on an ITO electrode during the reduction in 0.1 mol dm^{-3} $KClO_4$; (a) the first and (b) the second reduction of PB to PW. Scan speed=2 mV s^{-1}. Spectra were recorded in 25-mV intervals.

reversed micelle upon immersion in a 0.1 mol dm^{-3} $KClO_4$ solution may be accounted for both in terms of a delocalization of the electric charge of ClO_4^-, based on the large molecular size and (probably more importantly) the hydrophobic affinity of the ClO_4^- to the reversed micelle. (d) The absence of a K^+ exchange, observed for a cast PB–HTAC–$LiClO_4$ film during immersion in 0.1 mol dm^{-3} $KClO_4$, may be accounted for by a repulsive force between the strong ionic property of small K^+ ions and a reversed micelle having a hydrophobic environment.

Spectroelectrochemistry. The transient visible spectra of a cast PB–HTAC–$LiClO_4$ film and an electrodeposited PB film on ITO electrodes were taken at closely spaced potential intervals during a negative potential scan from +0.5 to −0.3 V in 0.1 mol dm^{-3} $KClO_4$. The spectra of the cast and electrodeposited films are shown in Figs. 9 and 10, respentively.

Both spectra of the as-cast PB–HTAC–$LiClO_4$ film and the as-deposited PB film are similar to each other, but differ regarding some points. The major difference is in the wavelengths of the maximum absorbance

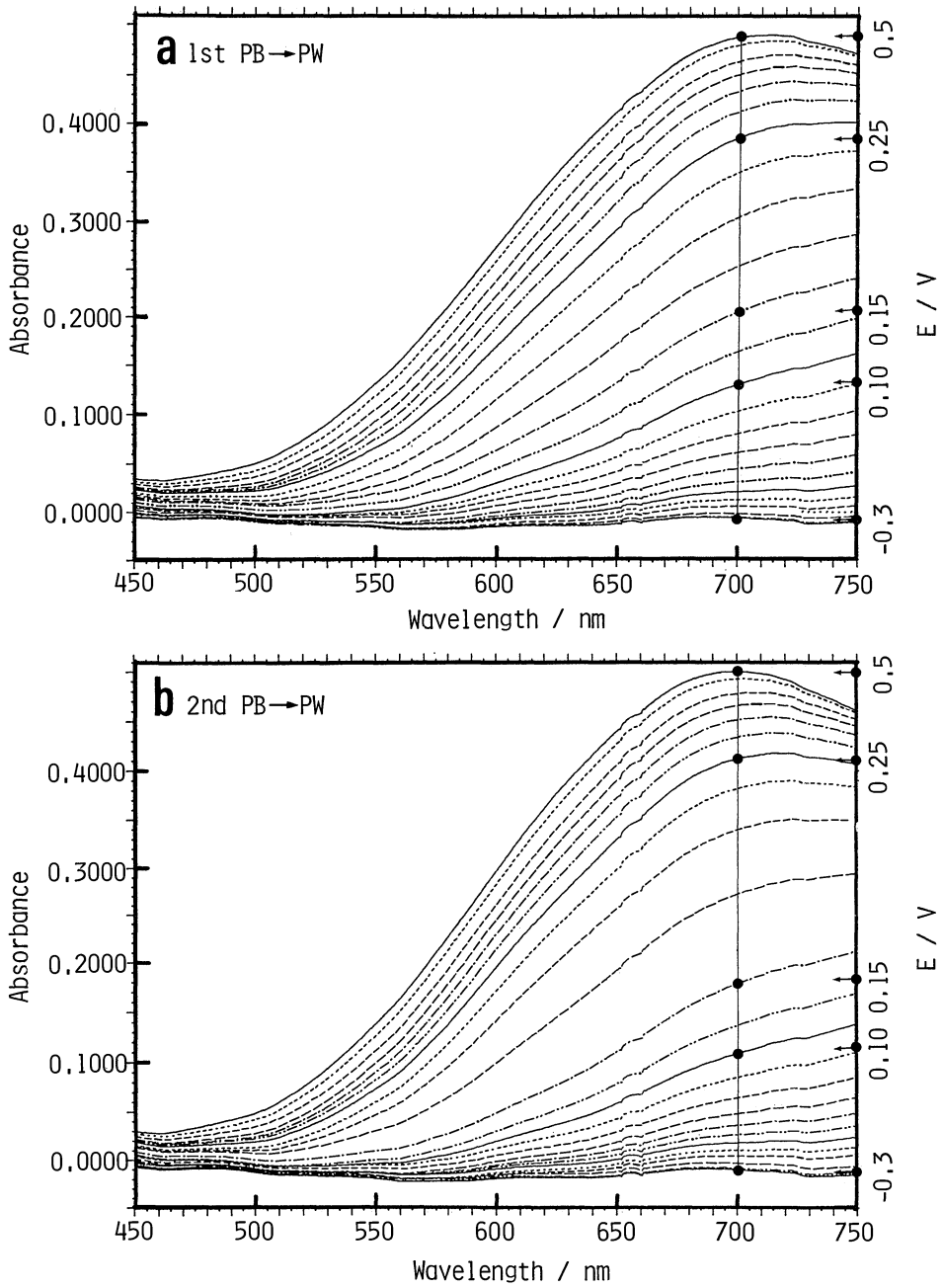

Fig. 10. Visible absorption spectra of the electrodeposited PB film on an ITO electrode during the reduction in 0.1 mol dm^{-3} $KClO_4$; (a) the first and (b) the second reduction of PB to PW. Scan speed= 2 mV s^{-1}. Spectra were recorded in 25-mV intervals.

(λ_{max}), which are in the 690 and 715 nm regions for the cast and electrodeposited films, respectively. The λ_{max} of the cast PB–HTAC–$LiClO_4$ film remained unchanged after voltammetric scanning (compare the first (a) and second (b) scans in Fig. 9). On the contrary, the λ_{max} of the electrodeposited film shifts from about 715 nm to a lower wavelength of about 695 nm after initial reduction cycle (compare (a) and (b) in Fig. 10). This is consistent with the spectroelectrochemical data of Mortimer and Rosseinsky[19] who showed a shift in the spectra of an electrodeposited PB film after the first reduction cycle. The spectral shift was proposed to be due to a partial conversion of an "insoluble" PB into a "soluble" PB. The absence of a λ_{max} shift for the cast PB film directly supports the idea that cast films comprise only "soluble" PB, as mentioned above.

Figures 11 and 12 show how the 600, 645, 701, and 745 nm absorbances change with a reductive applied potential in a $KClO_4$ electrolyte for a cast PB–HTAC–$LiClO_4$ film and an electrodeposited PB film, respectively. The absorbances are normalized to the highest initial value for ease of comparison. In the case of a cast film, the absorbance–potential response (Fig. 11) is the same at each wavelength and remains unchanged during subsequent scans in a $KClO_4$ electrolyte (compare (a) and (b) in Fig. 11). Each absorbance change is very sharp and centered at +0.18 V, agreeing with the sharp central peak in the voltammogram in a $KClO_4$ electrolyte (Fig. 4a). In the case of an electrodeposited film, the initial absorbance–potential response (Fig. 12a) is different at each wavelength centered at between +0.4 and −0.1 V, agreeing with the broad peak in the initial voltammogram shown in Fig. 4b. Upon a subsequent scan (Fig. 12b), the absorbance change at each wavelength was slightly sharper than the first scan and centered at +0.17 V, but still tailed between +0.1 V and −0.1 V. This feature is clearly associated with the +0.17 V sharp central peak and the 0.0 V shoulder in the voltammetry in $KClO_4$ shown in Fig. 4b, the 2nd scan.

The results of Figs. 11 and 12 are consistent with the voltammetric and compositional results mentioned above, i.e., cast films maintain a soluble form structure, even after a reduction cycle. On the contrary, in electrodeposited films, some parts of the PBs in the insoluble form probably change to a soluble form structure after the reduction cycle; other parts, however, retain their insoluble form. The consistency of the absorbance–potential response with the voltammetric result suggests that a cast PB–HTAC–$LiClO_4$ film contains single species in which a unique electrochemical iron(III) site participates in the cyclic electrochemical reduction. In contrast, plural species are suggested in an electrodeposited PB film as a

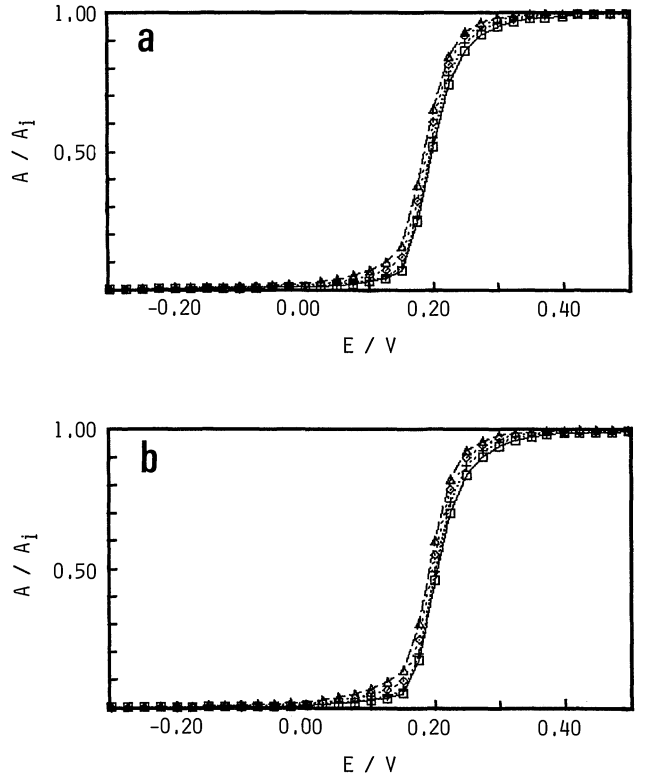

Fig. 11. Normalized absorption vs. potential curves of the cast PB–HTAC–$LiClO_4$ film in 0.1 mol dm^{-3} $KClO_4$ at (□) 600, (+) 645, (◇) 701, and (△) 745 nm: (a) The first and (b) the second reduction.

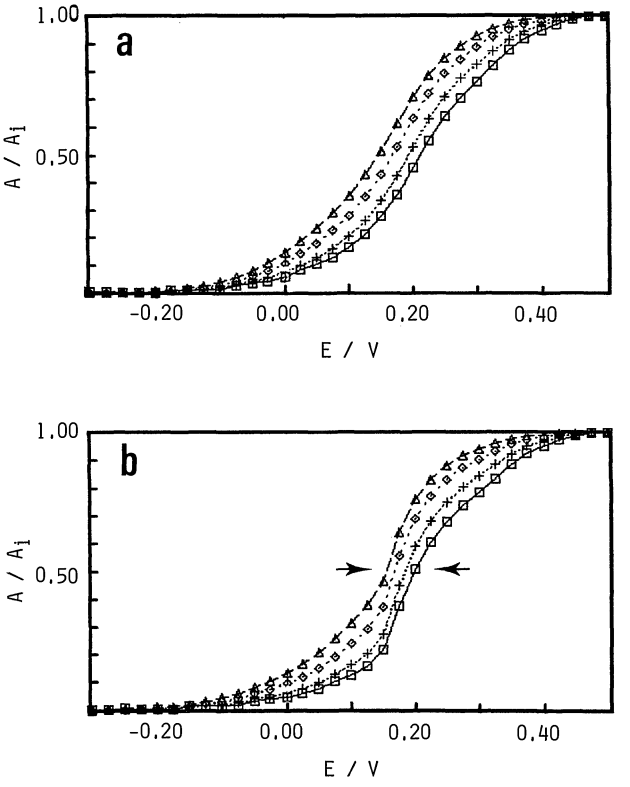

Fig. 12. Normalized absorption vs. potential curves of the electrodeposited PB film in 0.1 mol dm^{-3} $KClO_4$ at (□) 600, (+) 645, (◇) 701, and (△) 745 nm: (a) The first and (b) the second reduction.

mixture of nonequivalent electrochemical iron(III) sites. This somewhat complicated behavior appears to be attractive, but difficult to explain.

The spectral changes for the oxidation of cast PB–HTAC–$LiClO_4$ and the electrodeposited PB films in $KClO_4$ are illustrated in Figs. 13 and 14, respectively. The absorbance–potential response for the oxidation are plotted at 600, 645, 701, and 745 nm in Figs. 15 and 16 in a similar way to that in Figs. 11 and 12 for the reduction. The difference in patterns between Figs. 15 and 16 for the oxidation is less distinct than that between Figs. 11 and 12 for the reduction. Nevertheless, the absorbance response of the cast PB–HTAC–$LiClO_4$ film in Fig. 15 is quick and singly centered at about

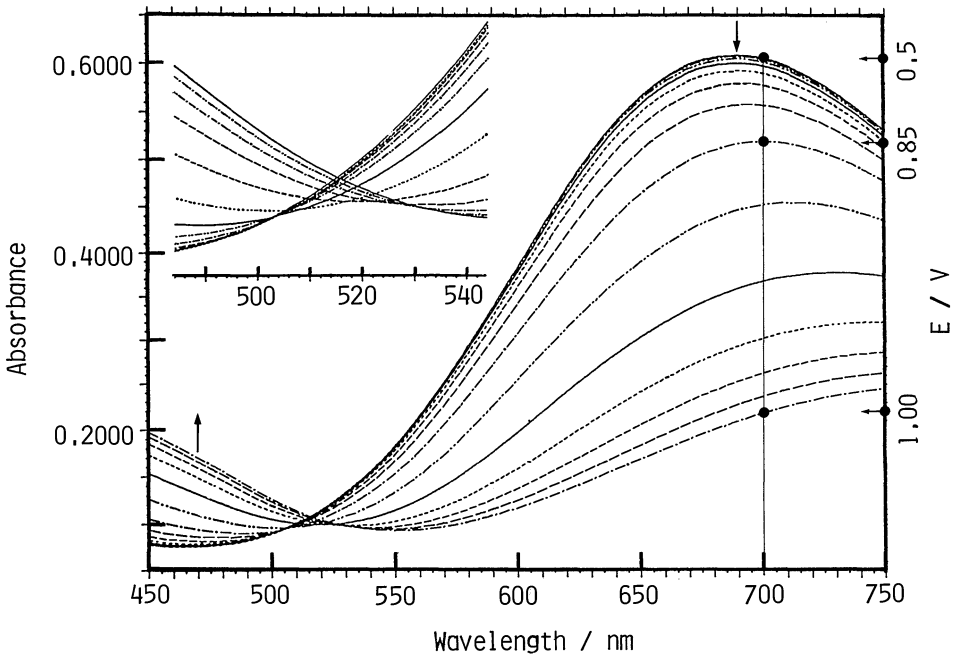

Fig. 13. Visible absorption spectra of the PB–HTAC–$LiClO_4$ film cast on an ITO electrode during the oxidation from PB to BG in 0.1 mol dm^{-3} $KClO_4$. Scan speed=2 mV s^{-1}. Spectra were recorded in 25-mV intervals.

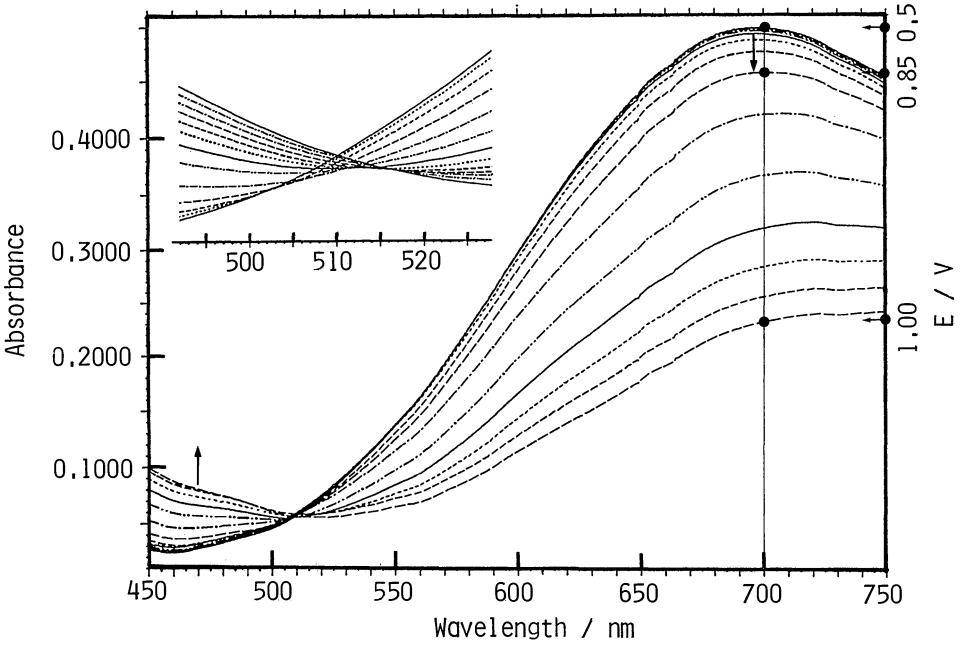

Fig. 14. Visible absorption spectra of the electrodeposited PB film on an ITO electrode during the oxidation from PB to BG in 0.1 mol dm^{-3} $KClO_4$. Scan speed=2 mV s^{-1}. Spectra were recorded in 25-mV intervals.

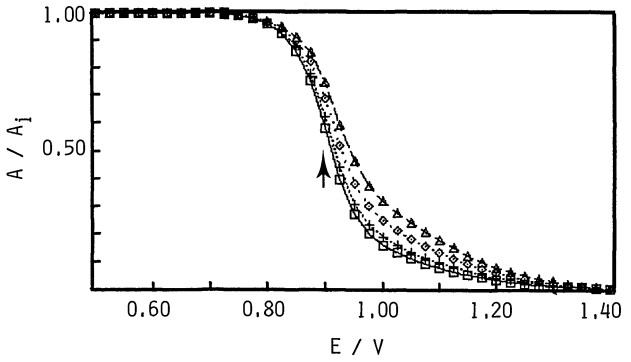

Fig. 15. Normalized absorption vs. potential curves of the cast PB-HTAC-$LiClO_4$ film in 0.1 mol dm^{-3} $KClO_4$ at (□) 600, (+) 645, (◇) 701, and (△) 745 nm for oxidation.

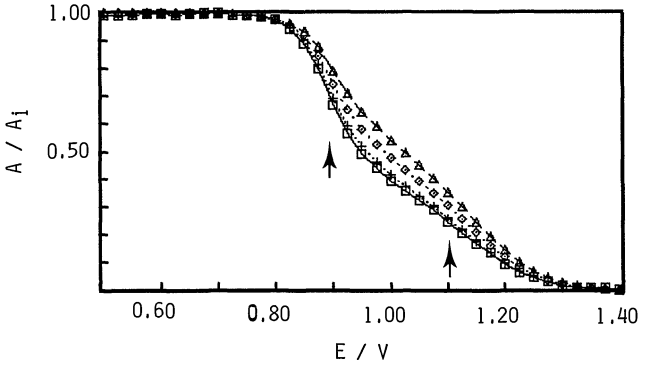

Fig. 16. Normalized absorption vs. potential curves of the electrodeposited PB film in 0.1 mol dm^{-3} $KClO_4$ at (□) 600, (+) 645, (◇) 701, and (△) 745 nm for oxidation.

+0.89 V, while the electrodeposited PB film in Fig. 16 shows an additional change centered at about +1.1 V in addition to the main change at about +0.89 V.

On the other hand, the spectrum of the fully oxidized form of the cast film at +1.4 V was different from that of the electrodeposited film. The spectral change with the application of a potential in the cast film (Fig. 13) is also faster than in the electrodeposited film (Fig. 14). The extent of the oxidation between +0.5 and +1.0 V is about 80% of the full oxidation for the cast film, while the electrodeposited film is oxidized by about 50%. Although a reasonable explanation for the oxidation has not been yet offered, the inset of Fig. 13, as well as the inset of Fig. 14, indicates that spectral changes with the application of the oxidative potential give two isosbestic points, as previously reported,[18,20] and that the transition from one isosbestic point to the other occurs at +0.89 V of the applied potential. The spectral changes giving the two isosbestic points are common to both the cast (Fig. 13) and electrodeposited (Fig. 14) films, and the applied potential giving the two isosbestic points (+0.89 V) is consistent with the main oxidation peaks from PB to BB in the cyclic voltammograms (Fig. 3) of both the cast and electrodeposited films. Although the reason for two isosbestic points is not clear yet, the common spectral change suggests that the change arises from the oxidation of a soluble form of PB both in the cast and the electrodeposited films. The oxidation shoulder wave of the electrodeposited film at +1.1 V observed in Fig. 3b may be attributed to the peculiar oxidation of the insoluble form of PB in the electrodeposited film. Though this specific change in oxidative voltammetry can not be readily resolved, some unknown species (nonequivalent complicated iron sites) probably exist only in the electrodeposited PB film. It is so hard for the species to be oxidized that the potential required for full oxidation is more positive than that for the simple species in the cast PB-HTAC-$LiClO_4$ film.

Conclusion

For the practical usage of the PB films, a simplified method of preparing a uniform film with large area and long-term stability is required. The casting of a colloidal PB dispersion in an organic solution provides an effective answer to this request.

According to the present experiments concerning the extraction of colloid PB dispersion, only cationic surfactants can extract PB colloids from an aqueous solution. PB composite films can be prepared onto ITO and Pt electrodes with a novel, simplified casting method by using an extracted PB solution. Particularly, when the ratio of $Fe^{II}/(Fe^{II}+Fe^{III})$ is larger than 0.5, the extraction of PB is considerably effective. This extraction result suggests that only the "soluble" form of PB can be extracted by an organic solution containing cationic surfactants.

The electrochemical behavior of cast films was compared with those of electrodeposited films. Some new facts found in the present investigation are listed:

1) The electrochromism of a cast film was observed to be similar to that of an electrodeposited PB film in a $KClO_4$ solution. The electrochromic response was improved by the addition of $LiClO_4$ to the cast film.

2) Cyclic voltammograms of a cast PB-HTAC-$LiClO_4$ film measured in a $KClO_4$ solution was simpler and more symmetrical than that of an electrodeposited PB film.

3) EDX (and some XPS) measurements show that as-cast films contain K^+ ions, which suggests a "soluble" form of PB, while electrodeposited films do not contain K^+ ions, which suggests an "insoluble" form of PB.

4) The λ_{max} of a cast film remains unchanged, even after successive scans, while that of an electrodeposited film shifts to lower wavelength after the first reduction cycle.

Although some points are not readily resolved in oxidative voltammetry, the present method provides a promising prospect for preparing a simple, stable, and

useful PB cast film.

The authors wish to express their sincere thanks to Dr. Masao Kaneko in Riken for his helpful discussion, as well as Dr. Masanori Owari at Institute of Industrial Science, The University of Tokyo (EDX) and Dr. Mitsuhiro Adachi at Engineering Research Institute, The University of Tokyo (SEM) for their technical assistance. This work was supported by the Grant-in Aid for Scientific Research on Priority Area of "Macromolecular Complexes" Nos. 62612002, 63612003, and 01612002 from the Ministry of Education, Science and Culture.

References

1) V. D. Neff, *J. Electrochem. Soc.*, **125**, 886 (1978).
2) D. Ellis, M. Eckhoff, and V. D. Neff, *J. Phys. Chem.*, **85**, 1225 (1981).
3) K. P. Rajan and V. D. Neff, *J. Phys. Chem.*, **86**, 4361 (1982).
4) K. Itaya, H. Akahoshi, and S. Toshima, *J. Electrochem. Soc.*, **129**, 1498 (1982).
5) K. Itaya, A. Tatsuaki, and S. Toshima, *J. Am. Chem. Soc.*, **104**, 4767 (1982).
6) K. Itaya, K. Shibayama, H. Akahoshi, and S. Toshima, *J. Appl. Phys.*, **53**, 804 (1982).
7) N. Toshima, R.-J. Lin, and M. Kaneko, *Chem. Lett.*, **1990**, 485.
8) R.-J. Lin and N. Toshima, *Kobunshi Rombunshu*, **47**, 825 (1990).
9) P. M. Hoang, S. Holdcraft, and B. L. Funt, *J. Electrochem. Soc.*, **132**, 2129 (1985).
10) K. Itaya, I. Uchida, and V. D. Neff, *Acc. Chem. Res.*, **19**, 162 (1986).
11) H. J. Buser, D. Schwarzenbach, W. Petter, and A. Ludi, *Inorg. Chem.*, **16**, 2704 (1977).
12) R. E. Wilde, S. N. Ghosh, and B. J. Marshall, *Inorg. Chem.*, **9**, 2512 (1970).
13) M. Kaneko, X.-H. Hou, and A. Yamada, *J. Chem. Soc., Faraday Trans. 1*, **82**, 1637 (1986).
14) M. Armand, *Solid State Ionics*, **9/10**, 745 (1983).
15) R.-J. Lin and N. Toshima, unpublished results.
16) P. J. Peerce and A. J. Bard, *J. Electroanal. Chem. Interfacial Electrochem.*, **114**, 89 (1980).
17) E. Laviron and L. Roullier, *J. Electroanal. Chem. Interfacial Electrochem.*, **115**, 65 (1980).
18) C. A. Lundgren and R. W. Murray, *Inorg. Chem.*, **27**, 933 (1988).
19) R. J. Mortimer and D. R. Rosseinsky, *J. Chem. Soc., Dalton Trans.*, **1984**, 2059.
20) N. Toshima, R.-J. Lin, and M. Kaneko, *Chem. Lett.*, **1989**, 1099.

 © 1991 The Chemical Society of Japan Bull. Chem. Soc. Jpn., 64, 149—153 (1991)

Crystal and Molecular Structure of [2-(2-Benzoxazolyl)phenolatotetrachloroplatinum]·[2-(2-Benzoxazolyl)phenol]·Ethanol, $[PtCl_4(C_{13}H_8O_2N)]\cdot(C_{13}H_9O_2N)\cdot C_2H_5OH$: Possibly a Stable New Pentavalent Platinum Complex

Akiko FURUHASHI,* Isao ONO, Akira OUCHI,† and Akira YAMASAKI††
Department of Chemistry, Aoyama Gakuin University, 1-1, Morinosato-Aoyama, Atsugi-shi, Kanagawa 243-01
† Department of Chemistry, College of Arts and Sciences, The University of Tokyo, Komaba, Meguro-ku, Tokyo 153
†† Department of Applied Chemistry and Physics, The University of Electro-Communications, 1-5-1, Chofugaoka, Chofu-shi, Tokyo 182
(Received May 31, 1990)

The crystal and the molecular structures of the title complex were determined by means of the single-crystal X-ray diffraction method. The crystal of $PtC_{28}H_{23}O_5N_2Cl_4$, F. W. 804.40, (black-violet in color) is monoclinic, with the space group of $P2_1/a$, a=18.293(4), b=9.682(2), c=15.797(3) Å, β=96.55(2)°, U=2779.6(9) Å^3, Z=4, D_m=1.90, D_x=1.92 g cm^{-3}, and μ (Mo $K\alpha$)=57.37 cm^{-1}. The platinum atom is in a hexa-coordinated octahedral geometry, where one 2-(2-benzoxazolyl)phenolate (bxp^-) ion is chelated with its N and phenolato O atoms. The bxp^- ligand as well as the free Hbxp molecule are both approximately planar, and their planes are approximately in parallel: They are arranged alternately and are laid roughly along the a-axis. Although the overlappling areas of the neighboring rings are only 23 and 13% respectively of the whole ring area, the interplane distances are 3.42 and 3.49 Å.

The 2-(2-benzoxazolyl)phenol (Hbxp) is known to make chelates with many kinds of metal ions, where the ligand acts as the uninegative ion, bxp^-. Among these, the structures of its copper(II),[1] cadmium(II),[1] and iron(III),[2] chelates have already been elucidated. In these complexes, the benzoxazolyl (bxz) and the phenolate (pho) rings of the chelating ligand are approximately on the same plane. In the iron(III) complex, the bxp^- rings of the neighboring complexes are approximately in parallel and they are partly overlapped with each other, so some π–π interaction between them is expected.[2] On the other hand, the platinum(II) cmplex, $[PtCl_2(Hbxp)_2]\cdot C_2H_5OH$ (**2**), on which the present authors recently reported, has unidentate non-charged Hbxp ligands, and the bxz and Hpho planes of each ligand are not in parallel.[3,4] During the process of synthesizing this platinum(II) complex, it was found unexpectedly that the title complex crystals, black-violet in color, were deposited together with the yellow platinum(II) crystals from the mother liquor, and in some cases they also precipitated from the filtrate of the main product. Although efforts to synthesize this complex separately have not yet been successful, its crystals have a characteristic color and shape different from the yellow platinum(II) complex **2**, so they can easily be separated by hand. Its crystal and molecular structures have been determined by the single crystal X-ray diffraction method.

Experimental

Growth of the Crystals of the Title Complex. The mother liquor used to obtain the title complex, [2-(2-benzoxazolyl)phenolatotetrachloroplatinum]·[2-(2-benzoxazolyl)phenol]·ethanol (**1**), has the same composition as that used to synthesize the Pt(II) complex **2**:[3,4] A solution of platinum(IV) chloride pentahydrate (1 g, 2 mmol in 15 cm^3 of ethanol) was mixed with a solution of Hbxp (1.5 g, 7 mmol in 300 cm^3 of ethanol), and the mixture was stirred, and left standing at room temperature for one month or longer. By this procedure, the yellow platinum(II) complex **2** crystals[3,4] can be reliably obtained, but the black-violet crystals of the title complex have appeared only in a few cases, always coprecipitated as a minor component with **2**. All attempts to precipitate only the black-violet crystals including addtion of some oxydizing agents, or changing the composition of the mother liquor, have ended in failure so far. In the best results to date, the amount of the obtained title complex, which appeared as the minor component of the bivalent complex, is approximately 0.02 g (1.1%) from the starting materials of the above mentioned quantities. Found: C, 40.87; H, 2.76; N, 3.39%. Calcd for $PtC_{28}H_{23}O_5N_2Cl_4$: C, 41.79; H, 2.88; N, 3.48 %.

X-Ray Crystal Structure Analysis. The black-violet crystal used for the structure determination was shaped into a sphere (ϕ=0.31 mm). The intensities of the range of $3<2\theta<55°$ (2θ) were collected on a Rigaku AFC-6A automated four-circle X-ray differactiometer using graphite-monochromated Mo $K\alpha$ radiation (λ=0.71073 Å), by means of ω–2θ scan technique (scan speed, 4° min^{-1} (ω), scan width, 1.14+0.35 tan θ (ω/°)). The intensities were corrected for Lorentz and polarization factors, as well as for absorption. Of 6817 indenpendent intensities collected, 4217 with $|F_o|>3\sigma(|F_o|)$ were used for the structure calculation.

All the calculations were carried out on a HITAC M-682H computer at the Computer Centre of the University of Tokyo using a local version of UNICS program.[5] The scattering factors were taken from Ref. 6.

The structure was solved by the heavy-atom method. The positional and thermal parameters were refined by a block-diagonal least-squares method. At the final stage, all the non-hydrogen atoms were found and were refined anisotropically. All the hydrogen atoms were excluded from the

structure calculations. The final R and R_w values obtained were reduced to 0.057 and 0.064, respectively.[7]

The proton nmr spectra were recorded using JEOL JNM-GX270 FT NMR Spectrometer.

Results and Discussion

The selected bond lengths and bond angles are tabulated in Table 1, the perspective view of the complex together with the numbering scheme of the atoms is shown in Fig. 1, the projection of the unit cell along b-axis in Fig. 2, and the projection of the atoms of the bxp$^-$ ring on both sides to a mean square plane of one Hbxp ring in Fig. 3.[8]

As shown in Fig. 1, the central platinum atom is in a 4Cl, N, O-hexa-coordinated octahedral geometry, where the bxp$^-$ ligand acts as a bidentate ligand forming a

Table 1. Selected Bond Lengths and Bond Angles of the Complex with Their Standard Deviations in Parentheses

Bond length	(l/Å)	Bond length	(l/Å)
Pt–Cl(1)	2.302(6)	Pt–Cl(2)	2.331(6)
Pt–Cl(3)	2.310(4)	Pt–Cl(4)	2.301(3)
Pt–O(1)	2.005(9)	Pt–N(1)	2.008(7)
O(2)–C(9)	1.352(18)	N(1)–C(1)	1.458(19)
N(1)–C(7)	1.327(16)	O(4)–C(29)	1.34(2)
N(2)–C(21)	1.47(2)	N(2)–C(27)	1.34(2)
O(4)···O(5)	2.501(19)		
Bond angle	**(ϕ/°)**	**Bond angle**	**(ϕ/°)**
Cl(1)–Pt–Cl(2)	177.4(2)	Cl(1)–Pt–Cl(3)	89.69(17)
Cl(1)–Pt–Cl(4)	90.59(17)	Cl(1)–Pt–O(2)	90.3(3)
Cl(1)–Pt–N(1)	88.8(3)	Cl(2)–Pt–Cl(3)	92.37(17)
Cl(2)–Pt–Cl(4)	91.04(16)	Cl(2)–Pt–O(2)	87.9(3)
Cl(2)–Pt–N(1)	89.4(3)	Cl(3)–Pt–Cl(4)	87.64(12)
Cl(3)–Pt–O(2)	173.7(3)	Cl(3)–Pt–N(1)	96.4(2)
Cl(4)–Pt–O(2)	86.1(3)	Cl(4)–Pt–N(1)	175.9(2)
O(2)–Pt–N(1)	89.9(3)	Pt–O(2)–C(9)	122.6(8)
Pt–N(1)–C(1)	133.4(8)	Pt–N(1)–C(7)	123.1(9)
O(2)–C(9)–C(8)	125.8(14)	O(2)–C(9)–C(10)	115.0(11)
O(4)–C(29)–C(28)	117.5(15)	O(4)–C(29)–C(30)	120.9(14)
C(1)–N(1)–C(7)	103.5(10)	C(21)–N(2)–C(27)	106.9(12)

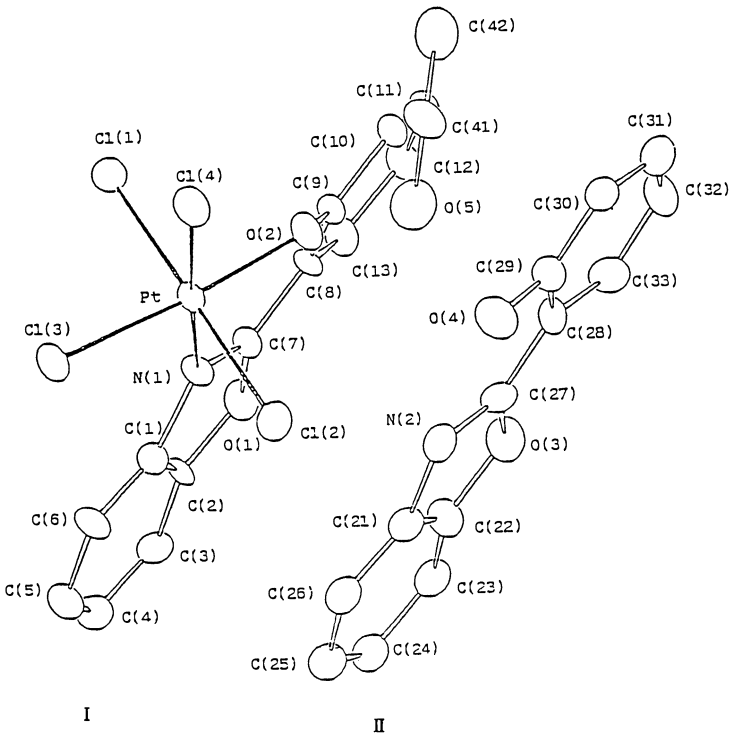

I II

Fig. 1. Perspective drawing of the complex with the numbering scheme of the atoms.

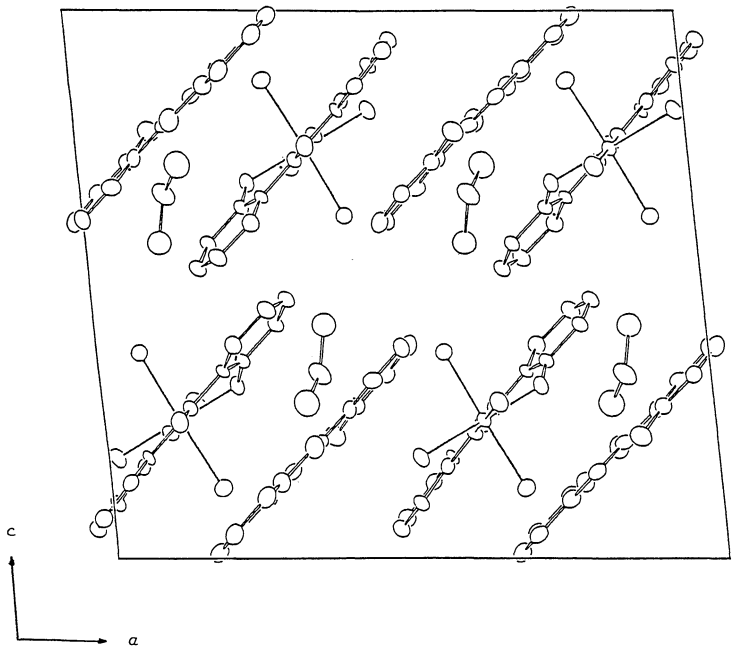

Fig. 2. A projection of the unit cell along c-axis. (i, 0.5+x, 1.5−y, z).

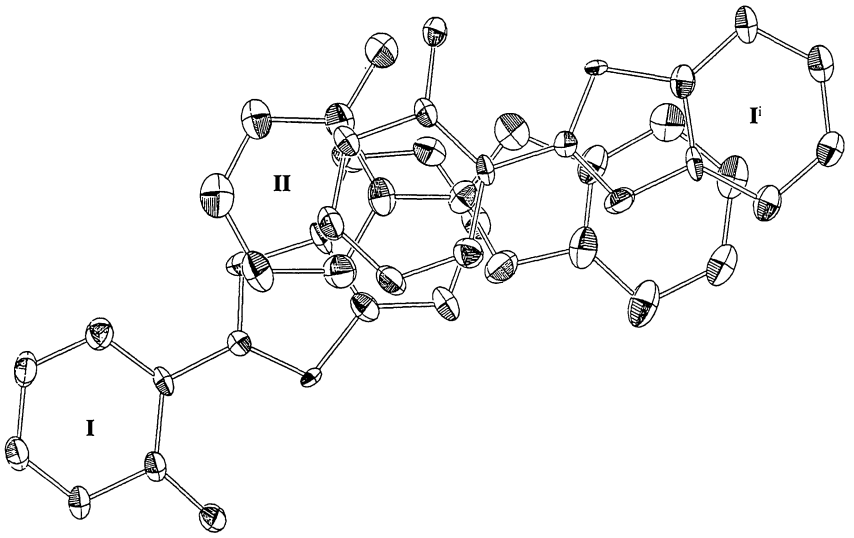

Fig. 3. A projection of the chelated ligand rings on the mean square plane of the non-coordinated Hbxp ring. (i, 0.5+x, 1.5−y, z).

five-membered ring chelate. The coordination geometry is not much deformed from the typical octahedron. As shown in Table 1, the average Pt–Cl, and Pt–N(1), and Pt–O(2) bond lengths are, 2.311 on the average (2.301(3)—2.331(6)), 2.008(7), and 2.005(9) Å, respectively.

The oxidation state of the central platinum seems to be somewhat peculiar, because the 2-(2-benzoxazolyl)-phenol ligand acts as a uninegative bxp$^-$ ion in these complexes. Considering the stoichiometry as well as the characteristically intense color of the crystals, the oxidation number of the central platinum can be expected to be +5. As the bond lengths are usually affected by the valence and coordination number of the bonding atoms, the bond lengths around the platinum atom were compared with the sum of the Shannon's ionic radii.[9] In the hexa-coordinated octahedral complexes, Pt–Cl, Pt–N, and Pt–O bond lengths estimated from the Shannon's ionic radii show clearly different values for Pt(V) and Pt(IV). For Pt(V) complexes, Pt–Cl, Pt–N, and Pt–O bond lengths are: 2.435, 2.085, and 1.975 Å, and for Pt(IV) complexes,

Table 1a. Positional Parameters ($\times 10^3$)

Atom	x	y	z	B_{eq}/Å^2
Pt	1258.3(2)	3870.8(4)	2516.8(3)	2.44
Cl(1)	718 (2)	4113 (3)	3755 (2)	3.70
Cl(2)	1837 (2)	3715 (3)	1280 (2)	3.89
Cl(3)	150 (2)	3108 (4)	1827 (2)	4.03
Cl(4)	1534 (2)	1601 (3)	2845 (2)	3.95
O(1)	1249 (4)	8100 (7)	2484 (5)	3.53
O(2)	2244 (4)	4316 (8)	3148 (5)	3.17
O(3)	3386 (5)	8498 (9)	2021 (6)	4.56
O(4)	3751 (5)	4369 (10)	2222 (6)	4.92
N(1)	1082 (5)	5890 (7)	2286 (5)	2.29
N(2)	2991 (6)	6465 (12)	1576 (6)	4.21
C(1)	581 (6)	6648 (12)	1669 (7)	3.06
C(2)	680 (6)	7999 (13)	1834 (7)	2.86
C(3)	322 (7)	9070 (13)	1383 (8)	3.57
C(4)	−195 (7)	8642 (13)	722 (8)	3.82
C(5)	−309 (7)	7251 (14)	530 (8)	3.98
C(6)	74 (6)	6168 (14)	998 (7)	3.73
C(7)	1446 (6)	6881 (11)	2737 (7)	2.60
C(8)	2034 (5)	6771 (12)	3409 (6)	2.53
C(9)	2376 (6)	5495 (12)	3598 (7)	2.78
C(10)	2974 (6)	5428 (13)	4259 (7)	3.15
C(11)	3182 (6)	6596 (14)	4718 (7)	3.53
C(12)	2847 (7)	7862 (14)	4520 (8)	3.83
C(13)	2248 (7)	7935 (13)	3886 (8)	3.62
C(21)	2539 (7)	7495 (13)	1074 (8)	4.03
C(22)	2789 (7)	8719 (15)	1383 (9)	4.54
C(23)	2520 (7)	9969 (16)	1113 (9)	5.21
C(24)	1928 (7)	9854 (14)	439 (9)	4.51
C(25)	1660 (7)	8563 (15)	100 (9)	4.59
C(26)	1953 (7)	7303 (15)	424 (8)	4.22
C(27)	3478 (7)	7165 (13)	2111 (7)	3.36
C(28)	4035 (6)	6635 (15)	2705 (8)	3.76
C(29)	4161 (7)	5187 (14)	2771 (8)	3.79
C(30)	4716 (7)	4641 (15)	3347 (8)	4.18
C(31)	5133 (7)	5577 (17)	3871 (9)	5.09
C(32)	5009 (7)	7005 (17)	3831 (9)	4.78
C(33)	4472 (8)	7517 (13)	3239 (8)	4.15
C(41)	3601 (8)	1045 (15)	3359 (10)	5.28
C(42)	3752 (10)	1502 (21)	4248 (11)	7.49
O(5)	3335 (7)	2152 (12)	2824 (8)	7.53

2.38, 2.03, and 1.92 Å respectively. However, the observed bond lengths of Pt–Cl and Pt–N for our complex **1** were much shorter than those of these Pt(V) and Pt(IV) complexes, and Pt–O bond length was a little longer than the Shannon's values. Therefore, it cannot be decided whether the valence of the platinum ion in **1** is +5 or +4 from X-ray analysis. The relatively large covalent character of the Pt–Cl bond of **1** may decrease the bond length, and the steric effect of the large bxp$^-$ ligand may also affect the bond lengths of Pt–N and Pt–O.

Although there is a possibility that the chelating ligand is a non-changed Hbxp and that the central metal platinum ion has the oxidation number of +4, such type chelate ring of the bxp ligand has not yet been found in any metal complexes.

The benzoxazolyl (bxz) ring and the phenol (Hpho) or phenolato (pho) ring of a bxp$^-$ as well as of Hbxp in **1** are approximately planar: The average of the deviation of all the atomic positions from their respective ring planes (mean square planes of the bxz or the pho ring atoms) is only 0.016 Å (0.0018—0.0503 Å). The dihedral angles between the mean square planes of the whole ring atoms and the respective mean square planes of the bxz and pho or Hpho ring atoms are bxp$^-$=12.3°, and Hbxp=3.2°. This is much different from what was found in **2**, where the Hbxp act as unidentate ligands where the dihedral angle between the two ring planes in each ligand is much larger.[3,4] The dihedral angle between the mean square plane of the Hbxp(II) ring atoms and the bxp$^-$ ring atoms neighboring on both sides of the former plane (I, and I^i; i, 0.5+x, 1.5−y, z) are 3.7° and 4.5° respectively. As a result, in the crystal of **1**, bxp$^-$ and Hbxp rings are arranged approximately in parallel and are laid alternately along a-axis. The interplanar distances between the neighboring bxp$^-$

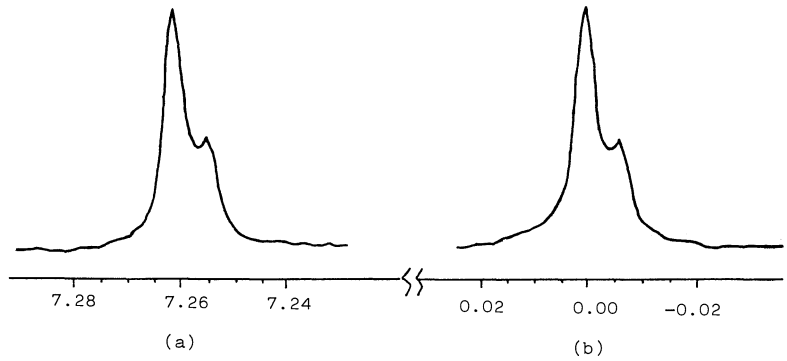

Fig. 4. 270 MHz proton NMR spectra of TMS-containing deuteriochloroform with centrally placed black-violet platinum complex (2.0 mg inserted in coaxially placed capillary of 1.0 mm outer diameter) in the ordinary 5 mm sample tube. (a) $CHCl_3$ (impurity in $CDCl_3$) (b) TMS. Paramagnetically shifted signals are clearly shown in both species.

(I) plane and a Hbxp (II) plane (calculated by the average distance between the bxp^- ring atom positions and the mean square plane of the Hbxp) is 3.42 Å, while that of the Hbxp (II) and the other neighboring bxp^- (I^i) ring is 3.49 Å. The overlapping of the rings II and I or I^i are calculated from the overlapping areas between the rings of II and the projection of the ring I or I^i on it as show in Fig. 3: They were 23% (I–II) and 13% (II–I^i) respectively. Consequently, the π-electron clouds of the neighboring bxp^- and Hbxp rings are thought to be interacting by overlapping each other.

If the platinum ion has an oxidation number of +5, it must have unpaired electrons and should show clear paramagnetism due to these unpaired electrons.[10] Unfortunately the small quantity of the obtained sample prevented us from measuring the magnetic susceptibility by ordinary methods such as Gouy balances. Moreover, this complex is not readily soluble in appropriate solvents, or decomposes gradually by the reaction with solvents.

An attempt to detect paramagnetism with the highly sensitive customary NMR technique,[11–13] was carried out with slight modification.[14] A capillary containing about 2 mg of the sample was coaxially placed in an NMR tube filled with deuterio-chloroform with TMS as a standard of chemical shift. The two proton signals due to $CHCl_3$ (impurity in $CDCl_3$) and TMS were recorded by the usual procedure. The two chemical shift values of the main peak (bulk liquid) remained unchanged, and the smaller components of both signals showed a clear upfield shift (Fig. 4) which showed that the closely neighboring nuclei surrounding the capillary tube are affected by the paramagnetism.

As this signal splitting was observed only when the sample in the capillary is paramagnetic,[14] it may be safely concluded that the present complex is paramagnetic.

These rather queer characteristics of complex **1** suggest that there is some possibility of the existence of apparently pentavalent platinum in this complex.

Although more detailed studies would be needed to elucidate this peculiar oxidation state, it seems quite interesting to compare our complex with the other already-known Pt(V) complexes. Some Pt(V) complexes, mainly its fluoro complexes, have been already reported: For example, $XePt(V)F_6$,[15] and $(O_2)Pt(V)F_6$.[16] However, these compounds are not stable and are easily reduced. On the other hand, the obtained complex is stable in open air.

Probably the electrons of the complex are diffused, not only in the ligated bxp^- ligand, but also all throughout the lined up complexes and Hbxp molecules via overlapping π-electron clouds. This delocalization of the electrons may be the cause of the extraordinary apparent valence of the metal ion in this complex.

References

1) P. Stenson, *Acta Chem. Scand.*, **23**, 1514 (1969).

2) A. Furuhashi, T. Inayoshi, and A. Ouchi, *Bull. Chem. Soc. Jpn.*, **60**, 3207 (1987).

3) A. Furuhashi, K. Endo, A. Ouchi, and Y. Saito, *Chem. Lett.*, **1988**, 1479.

4) A. Furuhashi, K. Endo, Y. Kondo, A. Ouchi, and Y. Saito, *Croat. Chem. Acta*, **62**, 141 (1989).

5) T. Sakurai, "The Universal Crystallographic Computation Program System (UNICS)," Tokyo (1967).

6) "International Tables for X-Ray Crystallography," Kynoch Press, Birmingham (1974), Vol. IV, pp. 72, 150.

7) $R=\Sigma||F_o|-|F_c||/\Sigma|F_o|$; $R_w=[\Sigma w(|F_o|-|F_c|)^2/\Sigma wF_o^2]^{1/2}$ and $w=1/[\sigma(|F_o|)^2+(F_w\times F_o)^2]$, where $F_w=0.2$ was adopted.

8) The final atomic positional as well as anisotropic thermal parameters, the structure factor table, and some additional bond lengths and bond angles of the complex are deposited as Document No. 9095 at the Office of the Editor of Bull. Chem. Soc. Jpn.

9) R. D. Shannon, *Acta Crystallogr., Sect. A*, **32**, 751 (1976). According to this report, the ionic radii are as follows; Pt (valence, +2, coord. no. 6), 0.80; (valence, +4, coord. no. 6), 0.625; (valence, +5, coord. no. 6), 0.75; O (valence, −2, coord. no. 2), 1.35 Å: N (valence, −3, coord. no. 4), 1.46: Cl (valence, −1, coord. no. 6), 1.81 Å.

10) S. E. Livingstone, "Comprehensive Inorganic Chemistry," ed by J. C. Bailar, Jr., H. J. Emeléus, Sir Ronald Nyholm, and A. F. Trotman-Dickenson, Pergamon Press, Oxford (1973), Vol. 3, p. 1365.

11) J. Q. Adams, *Rev. Sci. Instrum.*, **38**, 1099 (1966).

12) J. Löliger and R. Scheffold, *J. Chem. Educ.*, **49**, 646 (1972).

13) D. F. Evans, *Proc. Chem. Soc.*, **1958**, 115; *J. Chem. Soc.*, **1959**, 2003.

14) A. Furuhashi, I. Ono, and A. Yamasaki, *Anal. Sci.*, Submitted for Publication.

15) N. Bartlett, F. Einstein, D. F. Stewart, and J. Trotter, *Chem. Commun.*, **1966**, 550.

16) N. Bartlett and D. H. Lohmann, *J. Chem. Soc.*, **1964**, 619.

Local Structure, T_g, and IR Transparency of Potassium Titanate Glasses and the Local Structure of Calcium Titanate Ceramics

Tetsuaki NISHIDA,* Yasuharu YAMAGUCHI, Miho YAMADA, and Yoshimasa TAKASHIMA
Department of Chemistry, Faculty of Science, Kyushu University,
Hakozaki, Higashiku, Fukuoka 812
(Received June 16, 1990)

The Mössbauer spectrum of xK$_2$O·(95−x)TiO$_2$·5Fe$_2$O$_3$ glasses (x=35—60), consisting of a paramagnetic doublet peak due to tetrahedral Fe^{3+}, suggests that the Fe^{3+} is substituted for the tetrahedral Ti^{4+}. The isomer shift (δ=0.20—0.23 mm s^{-1}) and the quadrupole splitting (Δ=0.72—0.81 mm s^{-1}) decrease linearly with the increasing K$_2$O content. The glass transition temperature (T_g) decreases similarly as the Δ does, supporting the "T_g–Δ rule" discovered by Nishida et al., i.e., the T_g of oxide glasses is expressed by $T_g=a\Delta+b$. (The slope "a" is 680 °C mm^{-1} s.) The IR absorption spectra show two peaks at 880 and 640 cm^{-1} corresponding to the Ti(Fe)O$_4$ and TiO$_6$ units, respectively. The relative absorption intensity of the Ti(Fe)O$_4$ units becomes higher when the K$_2$O content increases. The potassium titanate glasses (plate) show IR transparency, having the transmission edge of 5.4 μm. The Mössbauer spectrum of xCaO·(95−x)TiO$_2$·5Fe$_2$O$_3$ ceramics (x=5—50) consists of two doublet peaks due to Fe^{3+} and Fe^{2+}. Both the δ and Δ of the Fe^{3+} are constant irrespective of the CaO content, whereas the fraction (relative absorption area) of the Fe^{3+} decreases linearly from 94 to 75% when the CaO content is increased from 5 to 50 mol%.

It is known that TiO$_2$-based (titanate) crystals such as BaTiO$_3$ and CaTiO$_3$ are excellent dielectric compounds. Titanate glasses are also known to have high dielectric constants and low thermal expansion coefficients. Structural study of the titanate glasses carried out by some groups revealed that Ti^{4+} ions are four- and six-fold coordinated with oxygen atoms.[1–3] In the IR and PAS (photoacoustic spectroscopy) study, Yoshimaru et al.[1] elucidated that the coordination number of Ti^{4+} depends on the basicity of the glass. Greegor et al.[4] reported that the coordination number of Ti^{4+} was four in the TiO$_2$–SiO$_2$ glass system, in which the TiO$_2$ content was several mol%.

The Mössbauer spectroscopy is useful for the structural study of oxide glasses, because the Mössbauer ions (e. g. Fe^{3+}) are easily substituted for the network forming ions (NWF) such as Al^{3+}, Ga^{3+}, Te^{4+}, and V^{5+}.[5–12] The present Mössbauer study was carried out in order to elucidate the coordination number of Fe^{3+} and Ti^{4+} in the K$_2$O–TiO$_2$ glasses and that in the CaO–TiO$_2$ ceramics. Five mol% of Fe$_2$O$_3$ is incorporated in these samples for the Mössbauer measurement. IR absorption measurement was carried out in order to elucidate the coordination number of Ti^{4+} and Fe^{3+} and also to confirm whether the Fe^{3+} is substituted for the Ti^{4+}, as was done for the Al^{3+} in the study of calcium aluminate glass.[6] The IR transparency of the K$_2$O–Ti(Fe)O$_2$ glasses was found by measuring the IR spectrum of a piece of block (plate) sample. The other aim of this study is to confirm whether the "T_g–Δ rule", discovered by Nishida et al.[5] for several oxide glasses, holds for the titanate glasses.

Experimental

Potassium titanate glasses denoted by xK$_2$O·(95−x)TiO$_2$·5Fe$_2$O$_3$ were prepared by melting individual mixtures (1 g) of commercially available K$_2$CO$_3$, TiO$_2$, and Fe$_2$O$_3$ of guaranteed reagent grade. Each mixture in a platinum crucible was melted at 1400 °C for 2 h by use of an electric muffle furnace. After the fusion in air, each melt was quenched by quickly immersing the bottom of the platinum crucible into ice-cold water. As the result, brown glass samples could be obtained when the x was 35—60. Calcium titanate ceramics denoted by xCaO·(95−x)TiO$_2$·5Fe$_2$O$_3$ were prepared by fusing individual mixtures (1 g) composed of CaCO$_3$, TiO$_2$, and Fe$_2$O$_3$ at 1400 °C for 30 min. After the fusion, the melt was gradually cooled down to 150 °C. As the result, ceramic samples of reddish brown to gray color were obtained, depending on the CaO content. In the xCaO·(95−x)TiO$_2$·5Fe$_2$O$_3$ system, no glass sample was prepared by the quenching procedure described above.

Mössbauer measurement was made on pulverized samples at room temperature by a constant acceleration method. Ten mCi (3.7×10^8 Bq) of cobalt-57 diffused into a palladium foil was used as the Mössbauer source. As the reference of the isomer shift (δ), a piece of metallic iron foil was used. The iron was also used for calibrating the velocity scale of the spectrometer. Each Mössbauer spectrum of the xK$_2$O·(95−x)TiO$_2$·5Fe$_2$O$_3$ glasses was analyzed into a doublet peak having an equal linewidth by a least-squares method. In the case of xCaO·(95−x)TiO$_2$·5Fe$_2$O$_3$ ceramic system, the Mössbauer spectrum was analyzed into two doublet peaks. DTA was conducted at the heating rate of 5 °C min^{-1}, ranging from room temperature to 900 °C. Alpha-Al$_2$O$_3$ powder was used as the standard in the DTA measurements. IR absorption measurement was performed by the conventional KBr disk method, whereas the IR transmission measurement was made on the untreated xK$_2$O·(95−x)TiO$_2$·5Fe$_2$O$_3$ glasses by use of a small block (plate) sample.

Results and Discussion

Potassium Titanate Glasses. The Mössbauer spectrum of potassium titanate glasses consists of a paramagnetic quadrupole doublet, as is illustrated in Fig. 1a. The quadrupole doublet indicates the presence of paramagnetic Fe^{3+} ions homogeneously

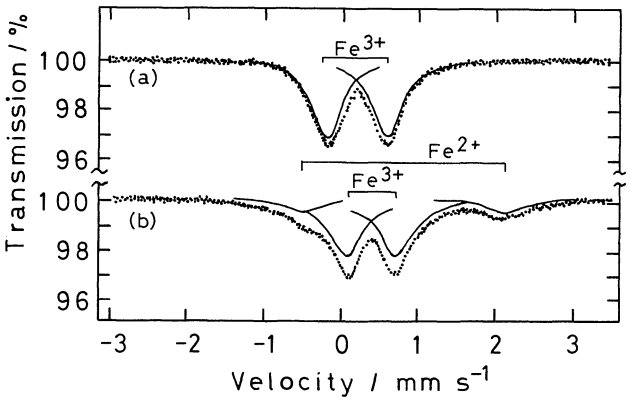

Fig. 1. The Mössbauer spectra of (a) $45K_2O \cdot 50TiO_2 \cdot 5Fe_2O_3$ glass and (b) $45CaO \cdot 50TiO_2 \cdot 5Fe_2O_3$ ceramic, measured at room temperature.

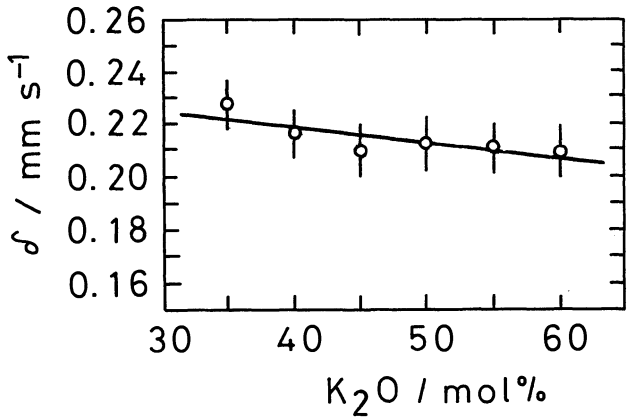

Fig. 2. The isomer shift (δ) for the $xK_2O \cdot (95-x)TiO_2 \cdot 5Fe_2O_3$ glasses plotted against the K_2O content.

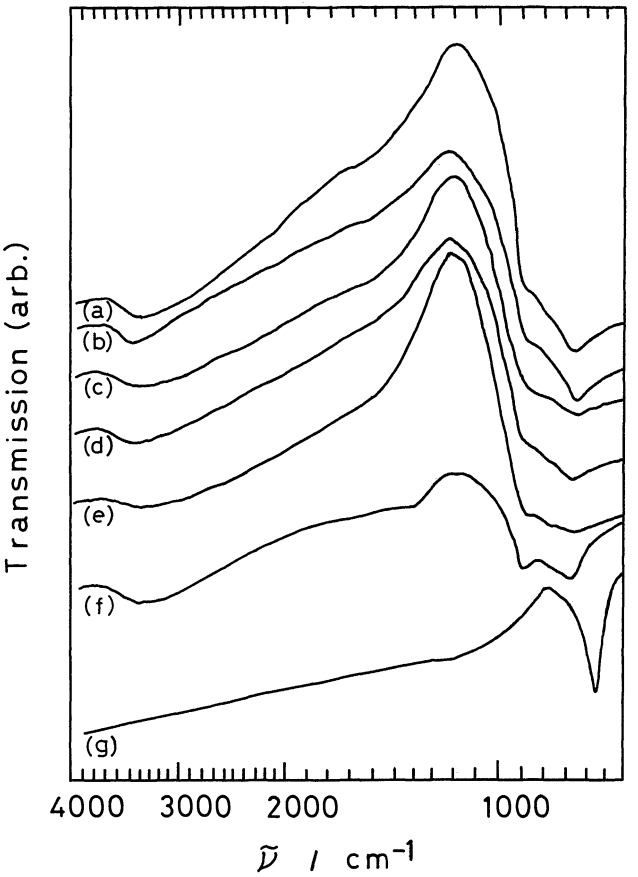

Fig. 3. The IR absorption spectra of $xK_2O \cdot (95-x)TiO_2 \cdot 5Fe_2O_3$ glasses; (a): $x=35$, (b): $x=40$, (c): $x=45$, (d): $x=50$, (e): $x=55$, (f): $x=60$. (g): The IR spectrum of Fe_2O_3.

distributed in the glass matrix; no magnetic species due to iron or iron oxide is observed. The isomer shift (δ), ranging from 0.20 to 0.23 mm s^{-1}, indicates the presence of tetrahedrally coordinated Fe^{3+} ions with oxygen atoms, as was observed for several oxide glasses.[5-10] The experimental error of the δ is estimated to be ± 0.01 mm s^{-1}. The relatively small δ values reflect that the Fe^{3+}–O bond is fairly covalent. The compositional dependence of the δ is illustrated in Fig. 2, which shows a slight decrease when the K_2O content is increased from 35 to 60 mol%. A similar phenomenon has recently been observed in the Mössbauer studies of aluminate,[5] gallate,[5,7] and vanadate[8-10] glasses; the formation of nonbridging oxygen (NBO) causes the decrease of δ, corresponding to the increase of 4s-electron density at the nuclear site of iron, because the bond length of the Fe^{3+}–NBO bond is smaller than that of the Fe^{3+}–BO (bridging oxygen) bond. The coordination number of network former (NWF), i.e. Ti^{4+} in this study, can easily be known from the IR spectra.[13] Tarte reported that tetrahedrally and octahedrally coordinated Ti^{4+} have the IR absorption bands at 690—800 cm^{-1} and 500—650 cm^{-1}, respectively. The IR absorption spectra of the $xK_2O \cdot (95-x)TiO_2 \cdot 5Fe_2O_3$ glasses studied in this paper are shown in Fig. 3, together with the IR spectrum of α-Fe_2O_3 (Fig. 3g) used for the sample preparation. According to Tarte,[13] the absorption peaks observed at 880 and 640 cm^{-1} in Figs. 3a—f are ascribed to the tetrahedral and octahedral Ti^{4+}, respectively. Figures 3a—f shows a systematic change, i.e., the relative absorption intensity A_{tet}/A_{oct} increases with the increasing K_2O content. (The subscript "tet" and "oct" refer to the tetrahedral and octahedral Ti^{4+}, respectively.) Figure 3 indicates that the $xK_2O \cdot (95-x)TiO_2 \cdot 5Fe_2O_3$ glasses are composed of only the TiO_4 tetrahedra and the TiO_6 octahedra, and that no absorption peak due to Fe–O bond is observed. It is seen from Fig. 3 that the fraction of TiO_4 tetrahedra is increased at the expense of TiO_6 octahedra when the K_2O content is increased, as was observed in the case of iron-free titanate glasses.[1] These results suggest that the structural change occurring at the Fe^{3+} site is essentially the same as that occurring at the tetrahedral Ti^{4+} site, and that small amount (5 mol%) of Fe_2O_3 itself brings about no specific structural change in the

K_2O–TiO_2 glasses. (We can obtain the structural information on the tetrahedral Ti^{4+} from the Mössbauer measurements.)

It is the characteristic feature of Figs. 3a—f that the Fe–O stretching vibration is not observed, whereas it was originally observed at 542 cm^{-1} in the IR spectrum of α-Fe_2O_3 (Fig. 3g). The absence of the Fe–O vibration suggests that no aggregate or precipitate of iron (Fe^{3+}) oxide is present in the $xK_2O\cdot(95-x)TiO_2\cdot 5Fe_2O_3$ glasses, and that the Fe^{3+} is vibrating at the substitutional site of the Ti^{4+}. In other words, the Fe^{3+} in the potassium titanate glasses seems to behave as if it were Ti^{4+} from the lattice vibrational point of view. It is noted that the Ti^{4+}/Fe^{3+} ratio is large, being in the range of 7—12 when the K_2O content is 35—60 mol%. The atomic substitution of Fe^{3+} for the NWF has also been confirmed in the case of Al^{3+}, which constitutes the network structure of calcium aluminate glass,[6] i.e., only the stretching vibration due to the Al^{3+}–O bond was observed in the original aluminate glass having 5 mol% of Fe_2O_3. No characteristic vibration due to the Fe^{3+}–O bond was observed in the aluminate glass,[6] whereas the corresponding vibration appeared as the crystallization (precipitation of $12CaO\cdot 7Al_2O_3$ phase) proceeded. In the present study, it is concluded that the Fe^{3+} ions are forming FeO_4 tetrahedra at the substitutional site of the TiO_4 tetrahedra, and therefore it is considered that the bond length of the Fe^{3+}–O bond is essentially the same as that of the Ti^{4+}–O bond. (The ionic radius of the Fe^{3+} (0.64 Å) is reported to be almost identical with that of the Ti^{4+} (0.68 Å).[14])

The quadrupole splitting (Δ), corresponding to the difference in the energy level of nucleus (I=3/2) at the excited state, is expressed by

$$\Delta = (e^2qQ/2)\times(1+\eta^2/3)^{1/2}, \quad (1)$$

where eq and Q are the electric field gradient tensor (=V_{zz}) along the z-axis and the nuclear quadrupole moment, respectively.[15] The η is an asymmetry parameter of the electric field gradient tensor, i.e., $(V_{xx}-V_{yy})/V_{zz}$.[15] We can obtain useful information on the local distortion in the glasses, i.e., a deviation from the cubic symmetry of the NWF-oxygen polyhedra, since the Mössbauer ions (Fe^{3+} in this paper) are substituted for the NWF. Figure 4 demonstrates the compositional dependence of the Δ for Fe^{3+} in the $xK_2O\cdot(95-x)TiO_2\cdot 5Fe_2O_3$ glasses. The experimental error is estimated to be ± 0.02 mm s^{-1}. The Δ shows a linear decrease with the increasing K_2O content, suggesting that the symmetry of FeO_4 tetrahedra becomes higher. This is also the case for the TiO_4 tetrahedra, because the FeO_4 tetrahedra are substituted for the TiO_4 tetrahedra, as described above. The decrease of the Δ (i.e. an increase of the symmetry) is ascribed to the formation of NBO in the $Ti(Fe)O_4$ tetrahedra, as was observed for the $V(Fe)O_4$ tetrahedra

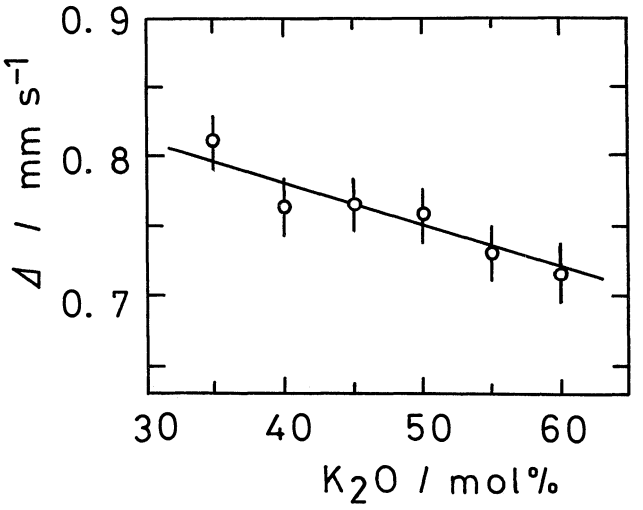

Fig. 4. The quadrupole splitting (Δ) for the $xK_2O\cdot(95-x)TiO_2\cdot 5Fe_2O_3$ glasses plotted against the K_2O content.

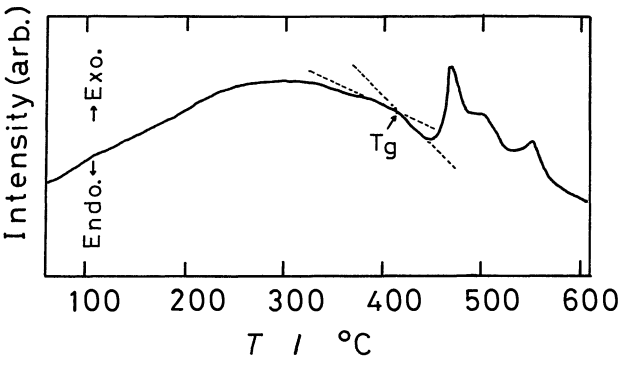

Fig. 5. A DTA curve of the $45K_2O\cdot 50TiO_2\cdot 5Fe_2O_3$ glass.

in the vanadate glasses.[8–10] The formation of NBO in the present titanate glasses indicates the destruction of three-dimensional network structure composed of TiO_4 and TiO_6 octahedra.

One of the DTA curve is shown in Fig. 5, in which the T_g is observed at about 415 °C. The compositional change of the T_g is illustrated in Fig. 6. The experimental error for the T_g is estimated to be ± 1 °C. A linear decrease of the T_g from 436 to 398 °C, observed when the K_2O content is increased from 35 to 60 mol%, is consistent with the decrease of δ (Fig. 2) and that of Δ (Fig. 4), from which the formation of NBO was deduced. The decrease of the T_g ascribed to the formation of NBO suggests that the rotation of oxygen atoms becomes frequently at lower temperatures. The less complicated structure of the titanate glasses will be directly concerned with the lowering of the T_g.

The T_g obtained for the $xK_2O\cdot(95-x)TiO_2\cdot 5Fe_2O_3$ glasses is plotted against the Δ of Fe^{3+} (Fig. 7). It is seen from Fig. 7 that a linear relationship exists. The linear relationship ("T_g–Δ rule") has recently been discovered by Nishida et al.[5] for several oxide glasses,

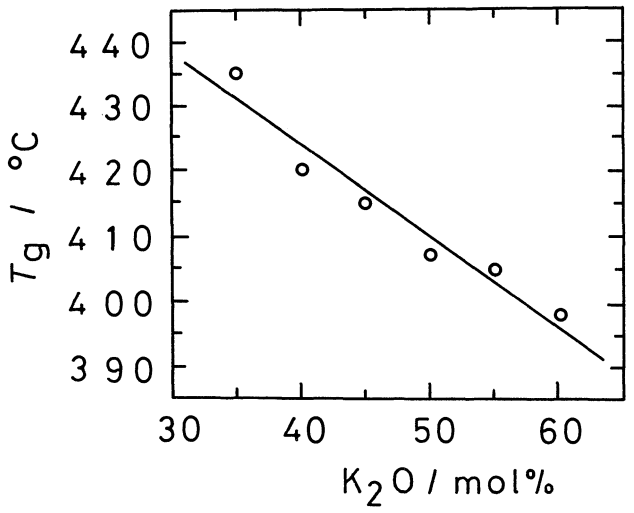

Fig. 6. The glass transition temperature (T_g) of xK$_2$O·(95−x)TiO$_2$·5Fe$_2$O$_3$ glasses plotted against the K$_2$O content.

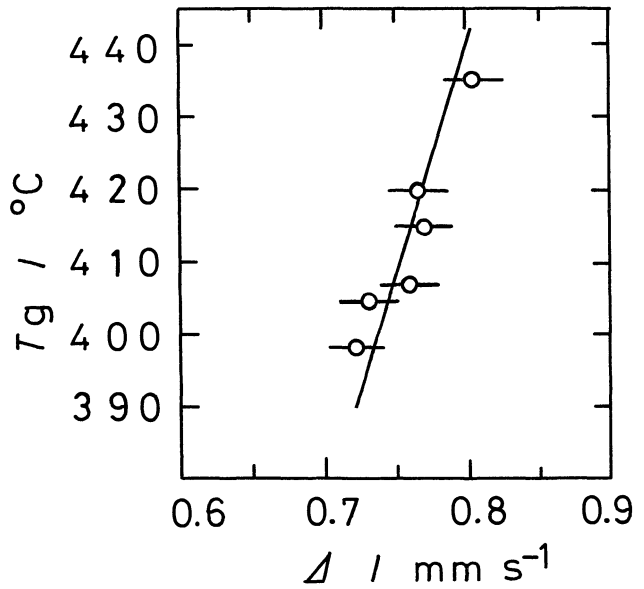

Fig. 7. The T_g-Δ plot for the xK$_2$O·(95−x)TiO$_2$·5Fe$_2$O$_3$ glasses.

i.e., the T_g (°C) and the Δ (mm s^{-1}) can be expressed by the following equation,

$$T_g = a\Delta + b, \quad (2)$$

where "a" is 680 °C mm^{-1} s and "b" is −180 °C (±100 °C) when the Fe^{3+} is present at the substitutional site of the NWF. The slope "a" of the straight line shown in Fig. 7 is estimated to be 680 °C mm^{-1} s and the intercept "b" is −100 °C, which is identical to that obtained for several oxide glasses, i.e. −180 °C,[5] if we take account of the experimental error of ±100 °C. The "T_g-Δ rule" indicates that the T_g is closely concerned with the Δ, being proportional to the asymmetry of NWF (Ti^{4+} in this study)-oxygen polyhedra, i.e., to the local distortion of the network structure. It should be noted that the T_g is little related to the binding energy of the NWF–oxygen bond, as was discussed in Ref. 5.

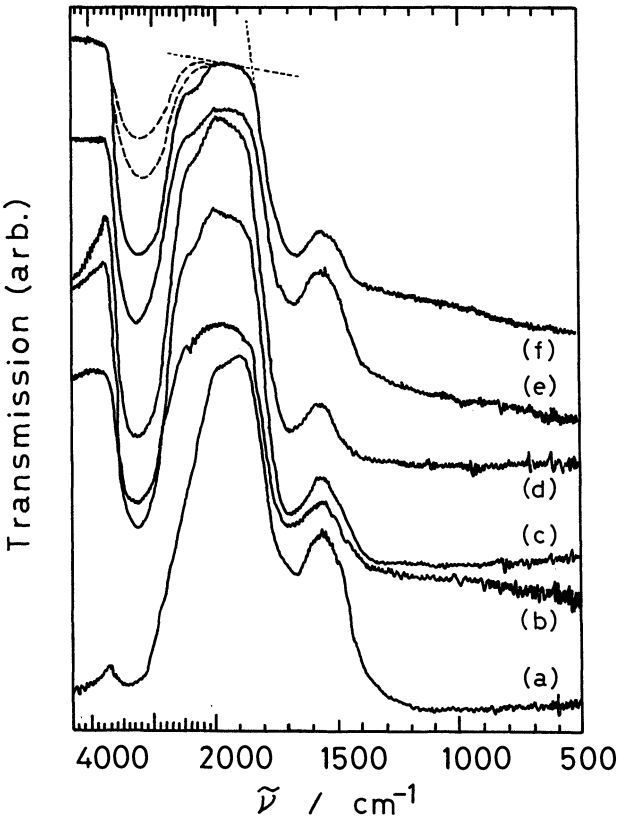

Fig. 8. The IR transmission spectra of the xK$_2$O·(95−x)TiO$_2$·5Fe$_2$O$_3$ glasses; (a): x=35, (b): x=40, (c): x=45, (d): x=50, (e): x=55, (f): x=60. The transmission edge is indicated by the intersection point of two straight lines (dotted line).

A small block (plate) of the xK$_2$O·(95−x)TiO$_2$·5Fe$_2$O$_3$ glasses shows IR transparency, as is illustrated in Fig. 8. All the titanate glasses have the identical transmission edge of 5.4 μm (1850 cm^{-1}). The absorption edge is estimated to be about 7 μm (1400 cm^{-1}). The IR transparency, having the similar transmission edge as the present titanate glasses, is reported in the case of aluminate glasses with[16] and without[17] TiO$_2$ as well as gallate and tellurite glasses.[5] It seems that the highly optical transparency of the titanate glasses in the IR region is closely concerned with the noticeable local distortion and the large number of NBO atoms, similarly to the case of aluminate, gallate, and tellurite glasses.[5] The optical transparency in the IR region indicates that the titanate glasses can be a good candidate for the "optical memory" in the field of optoelectronics, in analogy with the aluminate, gallate, and tellurite glasses. We can utilize a change (usually a decrease) of the IR transmittance caused by the crystallization of the IR-transmitting glasses.

Figure 8 demonstrates an intense absorption due to the OH group around the wave number of 3 μm (3300 cm^{-1}). The absorption intensity due to the OH group is little changed by the heat treatment at 110 °C for 2 h, whereas it is reduced to ca. 63 and 45% by the treatment at 200 °C for 2 and 17 h, respectively. This is shown with broken lines in Fig. 8. These experimental results suggest that the OH group is not physically adsorbed on the surface of the glass sample, but is chemically bonded to the Ti^{4+} or Fe^{3+} constituting the network structure.

Calcium Titanate Ceramics. The Mössbauer spectrum of $45CaO \cdot 50TiO_2 \cdot 5Fe_2O_3$ ceramic is shown in Fig. 1b, which consists of a quadrupole doublet due to Fe^{3+} and a weak doublet due to Fe^{2+}. (Mössbauer measurements were performed in the velocity range of ±5.0 mm s^{-1}, and no magnetic species was observed.) All the Mössbauer spectra of $xCaO \cdot (95-x)TiO_2 \cdot 5Fe_2O_3$ ceramics consist of the two kinds of doublet peaks. The linewidth (Γ) of the doublet peaks is in the range of 0.36—0.60 mm s^{-1}, being almost comparable to that of several oxide glasses such as aluminate,[5,6] gallate,[5,7] vanadate,[8–10] and tellurite[11,12] glasses. It is seen from Fig. 1a and 1b that the Γ of $xCaO \cdot (95-x)TiO_2 \cdot 5Fe_2O_3$ ceramics is comparable to that of $xK_2O \cdot (95-x)TiO_2 \cdot 5Fe_2O_3$ glasses. This means that both the Fe^{3+} and Fe^{2+} are present in the glassy phase of the $xCaO \cdot (95-x)TiO_2 \cdot 5Fe_2O_3$ ceramics. They should be called glass-ceramics rather than ceramics. The formation of crystalline phase in the glass-ceramics was confirmed from the X-ray diffraction measurements. Figure 9 indicates the presence of TiO_2 phase precipitated in all the $xCaO \cdot (95-x)TiO_2 \cdot 5Fe_2O_3$ ceramic samples. Each diffraction peak corresponding to the TiO_2 phase is marked with an open circle in Fig. 9a.

The isomer shift (δ) of the Fe^{3+} falls in the range of 0.37—0.40 mm s^{-1}, irrespective of the CaO content, and the average is 0.38 mm s^{-1} (Fig. 10a). The δ indicates the tetrahedral Fe^{3+}–O bond in the glassy phase of the $xCaO \cdot (95-x)TiO_2 \cdot 5Fe_2O_3$ glass-ceramics, since the δ of tetrahedral Fe^{3+} is reported to be equal to or less than 0.4 mm s^{-1}.[5–10] Almost identical δ values have been obtained in the case of $V(Fe)O_4$ tetrahedra constituting several vanadate glasses.[8–10] The δ of the octahedral Fe^{3+} is reported to be more than 0.42 mm s^{-1}, as was observed in the case of phosphate glasses.[18] Recently, Menil reported that the δ of tetrahedral Fe^{3+} is less than 0.30 mm s^{-1} (with respect to metallic iron (α-Fe)) in the case of several crystalline compounds, and that the δ of octahedral Fe^{3+} is more than 0.30 mm s^{-1}.[19] It is noted that the δ (0.30 mm s^{-1}), criterion between the octahedral and tetrahedral Fe^{3+} in crystals, is smaller than the corresponding δ (0.40 mm s^{-1}) reported for glasses.[5–10,18] The difference of the δ (0.40—0.30=0.10 mm s^{-1}) is ascribed to the difference of the mean Fe^{3+}–O bond

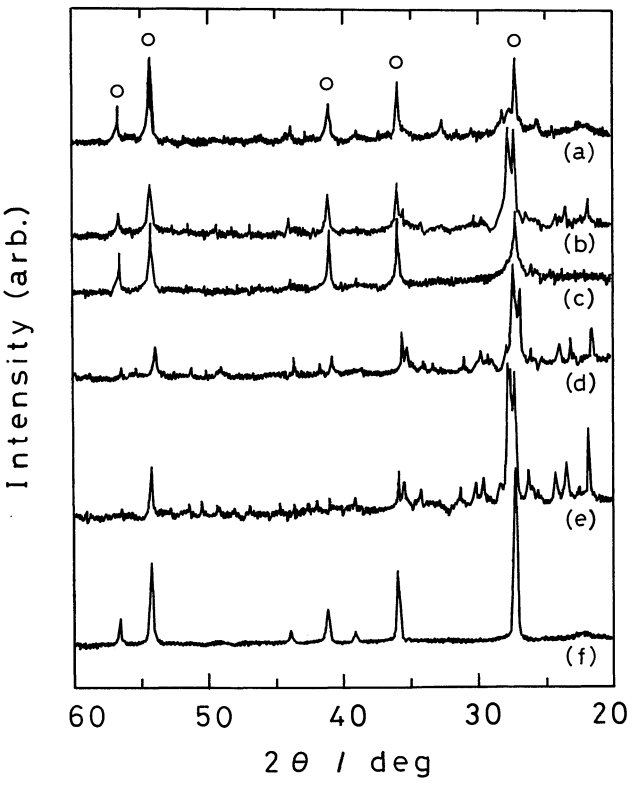

Fig. 9. The X-ray diffraction patterns of $xCaO \cdot (95-x)TiO_2 \cdot 5Fe_2O_3$ ceramics; (a): x=10, (b): x=20, (c): x=30, (d): x=40, (e): x=50. (f): The X-ray diffraction pattern due to TiO_2.

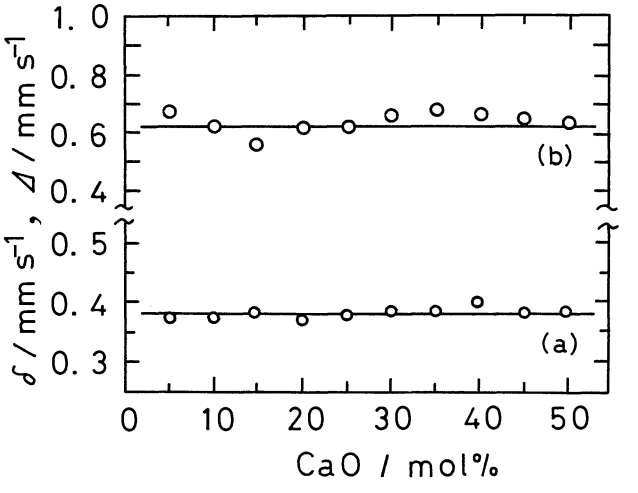

Fig. 10. The compositional dependence of (a): the isomer shift (δ) of the Fe^{3+} and (b): the quadrupole splitting (Δ) of the Fe^{3+} for the $xCaO \cdot (95-x)TiO_2 \cdot 5Fe_2O_3$ ceramics.

length; the longer Fe^{3+}–O bond length will cause the larger δ values for the glasses. (It is well known that the molar volume of "glass" is larger than that of "crystal." This is also the case for each the bond length.) The δ of Fe^{3+} obtained for the $xCaO \cdot (95-x)TiO_2 \cdot 5Fe_2O_3$ ceramics (Fig. 10a) is much larger than that of the $xK_2O \cdot (95-x)TiO_2 \cdot 5Fe_2O_3$ glasses

(δ=0.20—0.23 mm s^{-1}) illustrated in Fig. 2, indicating the highly ionic character of the Fe^{3+}–O bond. The constant δ (Fig. 10a) suggests that a change of the CaO content results in little structural change in the $Ti(Fe)O_4$ tetrahedra. This is consistent with the compositional dependence of the Δ of Fe^{3+} obtained for the xCaO·(95−x)TiO_2·5Fe_2O_3 ceramics (Fig. 10b); the Δ is almost constant irrespective of the CaO content, having an average value of 0.63 mm s^{-1}. This means that the symmetry of TiO_4 and FeO_4 tetrahedra is little changed when the chemical composition is changed. The DTA curve of the xCaO·(95−x)TiO_2·5Fe_2O_3 ceramics comprises a broad exothermic curve, of which maximum is observed at the identical temperature of 384±1 °C. No endothermic peak corresponding to the T_g is observed in the DTA curve. The experimental results shown in Fig. 10 are quite different from those obtained for the $x$$K_2O$·(95−$x$)$TiO_2$·5$Fe_2O_3$ glasses (Figs. 2 and 4), in which the increase of K_2O content resulted in the decrease both of the δ and Δ owing to the formation of NBO in the $Ti(Fe)O_4$ tetrahedra.

The distinct change brought about in the xCaO·(95−x)TiO_2·5Fe_2O_3 ceramics is reflected in the relative absorption area of Fe^{3+} and Fe^{2+}, as is shown in Fig. 11. The relative absorption area (A) of the Fe^{3+} (fraction of the Fe^{3+}) decreases linearly from 94 to 75%, while that of the Fe^{2+} increases from 6 to 25% when the CaO content is stepwise increased from 5 to 50 mol%. A similar phenomenon was observed in the case of potassium phosphate glasses,[18] in which the electron transfer from the neighboring oxygen atom to the Fe^{3+} was speculated on the basis of the ESR measurements of the PO_4^{2-} radicals produced by the γ-ray irradiation. Figures 10 and 11 suggest that the introduction of CaO into the TiO_2 matrix results in the reduction of Fe^{3+} into Fe^{2+}, without changing the δ and Δ of the Fe^{3+}.

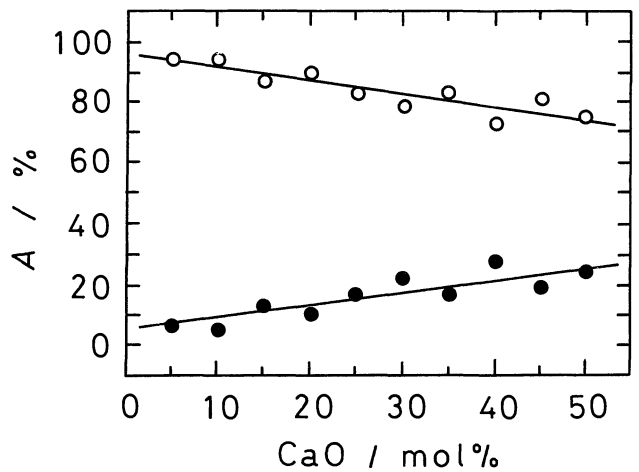

Fig. 11. Relative absorption area (fraction) of the Fe^{3+} (○) and that of the Fe^{2+} (●) obtained from the Mössbauer spectra of the xCaO·(95−x)TiO_2·5Fe_2O_3 ceramics.

The δ of Fe^{2+} falls in the range of 0.70—0.83 mm s^{-1}, having the average of 0.76 mm s^{-1}. These δ values indicate the presence of four-fold coordinated Fe^{2+} species.[15,19] (It is known that the δ of octahedral Fe^{2+} species is larger than 1.0 mm s^{-1}).[15,19] The δ values are almost constant irrespective of the CaO content, similarly to the case of the δ obtained for Fe^{3+} (Fig. 10a). The small δ for the Fe^{2+} (ca. 0.76 mm s^{-1}) indicates a strong covalency, reflecting a much shorter Fe^{2+}–O bond length. (It is considered that the short bond length was favorable for the electron transfer from oxygen to Fe^{3+}.) The Δ of Fe^{2+} falls in the range of 2.13—2.60 mm s^{-1}, being increased with an increasing CaO content. It is considered that the mixed valence state of Fe^{2+} and Fe^{3+} causes the decrease of the symmetry of Fe^{2+} O_4 tetrahedra.

Conclusion

1) In the K_2O–TiO_2–Fe_2O_3 glasses, the Fe^{3+} is substituted for the tetrahedral Ti^{4+}. This is confirmed from the Mössbauer and IR measurements. The Fe^{3+} plays a role of NWF.

2) The TiO_4 tetrahedra/TiO_6 octahedra ratio becomes higher in the K_2O–TiO_2 glasses when the K_2O content is increased.

3) The fraction of NBO in the TiO_4 tetrahedra also increases when the K_2O content is increased.

4) The K_2O–TiO_2–Fe_2O_3 glasses have the IR transparency. The transmission edge and the absorption edge are 5.4 and 7 μm, respectively.

5) A TiO_2 phase is precipitated in the matrix of the CaO–TiO_2–Fe_2O_3 ceramics.

6) Reduction of the Fe^{3+} into Fe^{2+} is observed in the CaO–TiO_2–Fe_2O_3 ceramics. This becomes noticeable with the increasing CaO content.

The authors are grateful to Prof. Yasukuni Matsumoto (Kinki University in Kyushu) for the help in the X-ray diffraction measurements. On of the authors, Tetsuaki Nishida, is indebted to the Japan Securities Scholarship Foundation for the financial support.

References

1) T. Yoshimaru, Y. Ueda, K. Morinaga, and T. Yanagase, *Yogyo Kyokai Shi*, **92**, 481 (1984).

2) T. Hanada, T. Aikawa, and N. Soga, *J. Am. Ceram. Soc.*, **67**, 52 (1984).

3) K. Kamiya, T. Yoko, and S. Sakka, *J. Mater. Sci.*, **20**, 906 (1985).

4) R. B. Greegor and F. W. Lytle, *J. Non-Cryst. Solids*, **55**, 27 (1983).

5) T. Nishida, H. Ide, and Y. Takashima, *Bull. Chem. Soc. Jpn.*, **63**, 548 (1990).

6) T. Nishida, H. Ide, T. Shinmyozu, Y. Takashima, and Y. Matsumoto, *Jpn. J. Appl. Phys.*, **29**, 1293 (1990).

7) T. Nishida, S. Saruwatari, and Y. Takashima, *Bull.*

Chem. Soc. Jpn., **61**, 2347 (1988).
8) T. Nishida, M. Ogata, and Y. Takashima, Proc. VI Int. Conf. Phys. Non-Cryst. Solids, Kyoto, 1987; *J. Non-Cryst. Solids*, **95/96**, 241 (1987).
9) T. Nishida, S. Saruwatari, and Y. Takashima, *Bull. Chem. Soc. Jpn.*, **61**, 2343 (1988).
10) T. Nishida, H. Ide, Y. Takashima, T. Yagi, S. Tomariguchi, T. Ishizuka, and A. Sakai, *J. Mater. Sci.*, **24**, 1687 (1989).
11) T. Nishida, S. Saruwatari, and Y. Takashima, *Bull. Chem. Soc. Jpn.*, **61**, 4093 (1988).
12) T. Nishida, M. Yamada, H. Ide, and Y. Takashima, *J. Mater. Sci.*, **25**, 3546 (1990).
13) P. Tarte, *Spectrochim. Acta*, **18**, 467 (1962).
14) L. Pauling, "The Nature of the Chemical Bond," Cornell Univ. Press, New York (1960), Chap. 13.
15) N. N. Greenwood and T. C. Gibb, "Mössbauer Spectroscopy," Chapman and Hall, London (1971), Chaps. 3 and 5.
16) T. Kokubo, M. Nishimura, and M. Tashiro, *J. Non-Cryst. Solids*, **22**, 125 (1976).
17) H. C. Hafner, N. J. Kreidl, and R. A. Weidel, *J. Am. Ceram. Soc.*, **41**, 315 (1958).
18) T. Nishida, T. Shiotsuki, and Y. Takashima, *J. Non-Cryst. Solids*, **43**, 115 (1981).
19) F. Menil, *J. Phys. Chem. Solids*, **46**, 763 (1985).

Formation of $Na_{0.9}Mo_6O_{17}$ in a Solid-Phase Process. Transformations of a Hydrated Sodium Molybdenum Bronze, $Na_{0.23}(H_2O)_{0.78}MoO_3$, with Heat Treatments in a Nitrogen Atmosphere

Kazuo EDA,* Kouichi FURUSAWA,† Fumikazu HATAYAMA,††
Sadao TAKAGI,† and Noriyuki SOTANI
College of Liberal Arts, Kobe University, Tsurukabuto,
Nada, Kobe 657
† Department of Chemistry, Faculty of Science and Technology,
Kinki University, Kowakae, Higashi-Osaka 577
†† School of Allied Medical Sciences, Kobe University,
Tomogaoka, Suma, Kobe 654-01
(Received August 22, 1990)

The transformations of hydrated sodium molybdenum bronze, $Na_{0.23}(H_2O)_{0.78}MoO_3$, with heat treatments in a nitrogen atmosphere are as follows: $Na_{0.23}(H_2O)_{0.78}MoO_3$ (AD) $\xrightarrow{\text{at 330 K}}$ $Na_{0.23}(H_2O)_{0.5}MoO_3$ (VD) $\xrightarrow{\text{at 457 K}}$ $Na_{0.23}MoO_3$ (with VD structure) $\xrightarrow{\text{at 583 K}}$ $Na_{0.9}Mo_6O_{17}$ + a small amount of other materials $\xrightarrow{\text{at 800 and 900 K}}$ melt. This indicates a new and variable formation process of alkali metal molybdenum bronzes. In this process, $Na_{0.9}Mo_6O_{17}$ was formed in the solid phase without the formation of any intermediate products. Its formation temperature was about 600 K, which was less than those of the usual preparation methods by about 200 K.

It is well-known that alkali metal molybdenum bronzes exhibit low-dimensional electronic properties.[1-3] They are semiconductors and most of them show a semiconductor-metal transition.[4-7] In particular, $Li_{0.9}Mo_6O_{17}$ is known to exhibit superconductivity.[8] They have been extensively studied because of interest in these properties.[1-11] On the other hand, hydrated alkali molybdenum bronzes, $A_x(H_2O)_yMoO_3$, have been synthesized by Schöllhorn et al.[12] These bronzes are apparently different regarding their Mo–O frameworks from the metal bronzes; i.e., hydrated bronzes possess a Mo–O framework based on the MoO_3 structure, while the metal bronzes possess different Mo–O frameworks.[13] However, their compositions are similar to each other, excluding the hydration water. We have thus been interested in the structural changes of hydrated molybdenum bronzes after removing the hydration water. We therefore investigated the structural changes of a hydrated sodium molybdenum bronze with heat treatments in a nitrogen atmosphere and found that $Na_{0.9}Mo_6O_{17}$ is formed from the hydrated bronze. Alkali metal molybdenum bronzes have usually been synthesized by an electrolytic reduction of A_2MoO_4–MoO_3 melts and by heating stoichiometric mixtures of A_2MoO_4, MoO_3, and MoO_2 in a vacuum.[1-11] In these syntheses, the formations of the bronzes proceed in a liquid phase above 800 K. The formation of $Na_{0.9}Mo_6O_{17}$ from a hydrated bronze proceeds at about 600 K in the solid phase without the formation of any intermediate products. This fact not only suggests that the formation proceeds by way of a new mechanism, but also provides a new and variable synthesis method of alkali metal molybdenum bronzes. This paper describes them in full detail.

Experimental Procedure and Results

Preparation. Hydrated sodium molybdenum bronze was prepared by Thomas and McCarron, III's method.[13] The composition of the hydrated bronze was $Na_{0.23}(H_2O)_{0.78}MoO_3$.

Differential Thermal Analysis. TG-DTA was carried out in a nitrogen atmosphere on a MAC SCIENCE TG-DTA 2000. A TG-DTA heating curve was obtained at a heating rate of 10 K min^{-1}, while a cooling curve was gotten by cooling naturally.

The TG-DTA curve of hydrated sodium molybdenum bronze is shown in Fig. 1. Four endothermic (at 330, 457, 800, and 927 K) and two exothermic peaks (at 583 and 633 K) can be seen. The endothermic peaks at 330 and 457 K are

Table 1. The Results of Analysis

Treatment condition	H_2O wt%[a]	Mo wt%	Na wt%	Mo^{5+}/total Mo
As-prepared	8.7	59.4 (65.1)	3.3 (3.6)	0.23
420 K	5.7	62.1 (65.9)	3.5 (3.7)	0.21
520 K	4.3[b]	62.2 (65.0)	3.5 (3.7)	0.21
600 K	0	65.8 (65.8)	3.5 (3.5)	0.22
650 K	0	64.8 (64.8)	3.6 (3.6)	0.23
840 K	0	64.8 (64.8)	3.6 (3.6)	0.22

a) This value is given by TG analysis. b) This value means the re-hydration water on cooling. Values in parentheses are calculated by excluding water contents.

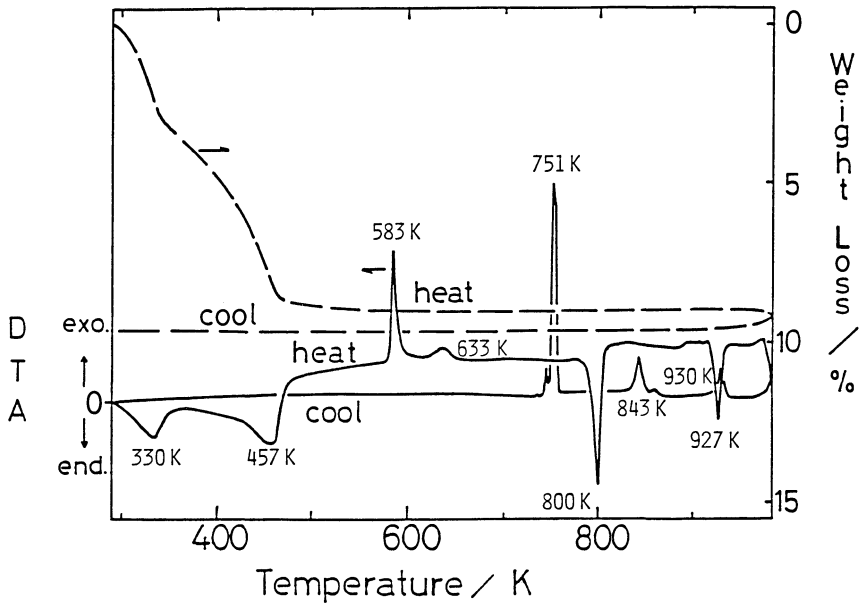

Fig. 1. TG–DTA curve of the hydrated sodium molybdenum bronze in a nitrogen atmosphere on heating and on cooling.

accompanied by a large weight loss, while the other peaks are not. The peaks at 330, 457, 583, and 633 K disappear upon cooling, and arise from irreversible phase transformations, while the peaks at 800 and 927 K are reversible transformations. The peaks at 330 and 457 K are attributed to the release of hydration water, due to the large weight losses.

Investigation of Phase Transformations. The samples heated both before and after each DTA peak temperature were investigated in detail using chemical analysis and an X-ray diffraction (XRD) method. Samples heated below 520 K were dark blue in color and those heated above 600 K were dark red. Sintering of the sample occurred above 800 K. The Na and Mo contents in the samples were measured by using a HITACHI 180-80 atomic absorption spectrophotometer with the 3302.3 Å line of Na and the 3132.6 Å line of Mo. The Mo^{5+} contents of the samples were determined chemically by Choain and Marion's method.[14] XRD patterns were obtained by using a RIGAKUDENKI GEIGER D-1 FLEX diffractometer with Cu $K\alpha$ radiation. Samples for the measurements were mixed with an internal standard (ca. 5 wt% Si).

The analytical results are summarized in Table 1. The quantity of Mo^{5+} remains constant. Upon heat treatments, as increase in the heating temperature, the H_2O content of the sample decreases. Samples heated below 520 K contain H_2O and those heated above 600 K do not. According to a differential thermal analysis, a sample after an endotherm at 457 K should contain no hydration water. Nevertheless, a sample heated at 520 K contains 4.3 wt% of water. When the sample was cooled to room temperature, the weight gain was observed by TG measurements. Therefore, the water in the sample is re-hydration water. The composition of a sample heated above 600 K is $Na_{0.23}MoO_3$, while that of a sample heated at 420 K is $Na_{0.23}(H_2O)_{0.5}MoO_3$. The real composition of a sample at 520 K is $Na_{0.23}MoO_3$. The XRD patterns of the

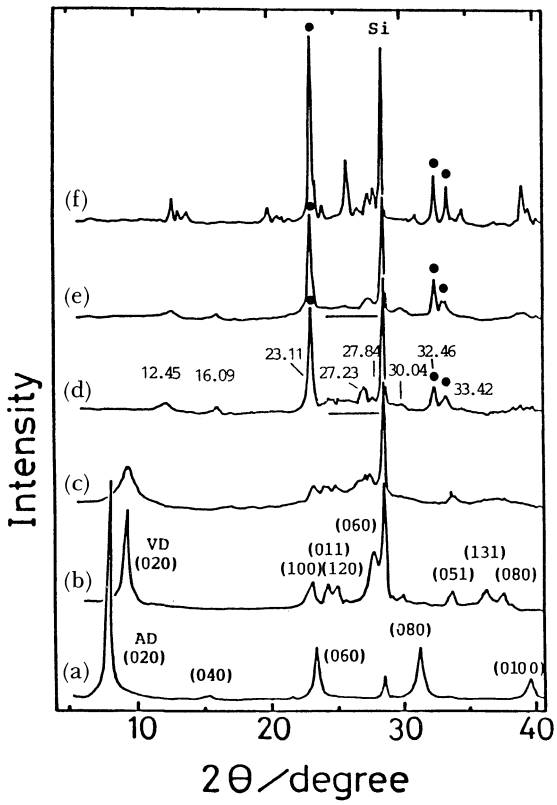

Fig. 2. Changes in X-ray diffraction patterns of the hydrated sodium molybdenum bronze by heat treatments in a nitrogen atmosphere. (a) as-prepared, and heated (b) at 420 K, (c) at 520 K, (d) at 600 K, (e) at 650 K, and (f) at 840 K.

samples are shown in Fig. 2. An as-prepared sample and a sample heated at 420 K are identical with an air-dried

hydrated sodium molybdenum bronze (denoted as AD), $[Na(H_2O)_x]_{0.25}MoO_3$ ($2<x\leqslant 6$), and an vacuum-dried hydrated sodium molybdenum bronze (denoted as VD), $[Na(H_2O)_2]_{0.25}MoO_3$, of Thomas and McCarron, III, respectively.[13] A sample heated at 520 K still maintains its VD structure, although the diffraction peaks become rather broad. By heating at 600 K, the diffraction peaks of VD disappear and new peaks appear at 12.45, 16.09, 23.11, 27.23, 27.84, 30.04, 32.46, and 33.42°. The peaks marked by the symbol ● are attributed to $Na_{0.9}Mo_6O_{17}$.[10] Others show the formation of a small amount of MoO_3 and $Na_2Mo_2O_7$. A sample heated at 650 K gives nearly the same diffraction pattern as that at 600 K, except for minor differences in the range 24—28°. For a sample heated at 840 K, the diffraction peaks of $Na_{0.9}Mo_6O_{17}$ remain, though many other peaks also appear. These peaks are attributed to MoO_3 and a solid solution of $Na_2Mo_4O_{13}$+ MoO_3.[15]

Discussion

Transformations in a Nitrogen Atmosphere. The first release of hydration water gives rise to a transformation from AD to VD. After the second release of hydration water, i.e., the complete removal of the hydration water, the sample still retains the VD structure up to 583 K. This sample can incorporate water molecules from the atmosphere. The broadening in the XRD pattern of this sample (Fig. 2(c)) may be due to inadequate hydration.[16] The main product of a sample heated at 600 K was $Na_{0.9}Mo_6O_{17}$. The DTA peak at 583 K is, therefore, attributed to a transformation from VD to $Na_{0.9}Mo_6O_{17}$. According to the X-ray results, though the sample before and after the DTA peak at 633 K give no characteristic change, a minor difference appears in the range 24—28°. A differential thermal analysis of the hydrated bronze with lower Na content[17] revealed that the peak at 633 K is also correlated to the formation of $Na_{0.9}Mo_6O_{17}$. The DTA endothermic peaks at 800 and 927 K are reversible. Appreciable sintering of the sample took place above 800 K, as mentioned above. Thus, these peaks are due to melting of the sample. Compared with the phase diagram of Na_2MoO_4 and MoO_3,[15] we presume that the peaks at 800 and 927 K arise from transformations to an equilibrium mixture of the solid and solution and to solution, respectively. According to chemical analyses, the compositions of the samples heated above 583 K are $Na_{0.23}MoO_3$. On the other hand, the composition of the dominant product is $Na_{0.9}Mo_6O_{17}$. The appearance of a few materials other than $Na_{0.9}Mo_6O_{17}$ in samples heated above 600 K may result from a deviation of the compositions of the samples from $Na_{0.9}Mo_6O_{17}$. Transformations of the hydrated bronze with heat treatments in a nitrogen atmosphere are formulated as follows:

$$\underset{(Na_{0.23}(H_2O)_{0.78}MoO_3)}{\overset{\text{AD}}{}} \xrightarrow[\text{end. peak at 330 K}]{\uparrow H_2O}$$

$$\underset{(Na_{0.23}(H_2O)_{0.50}MoO_3)}{\overset{\text{VD}}{}} \xrightarrow[\text{end. peak at 457 K}]{\uparrow H_2O}$$

$$\underset{(Na_{0.23}MoO_3^{\#})}{\overset{\text{VD structure}}{}} \xrightarrow[\text{exo. peak at 583 K}]{} Na_{0.9}Mo_6O_{17} + \text{other} \xrightarrow[\text{exo. peak at 633 K}]{}$$

$$Na_{0.9}Mo_6O_{17} + \text{other}^{\dagger} \xrightarrow[\text{end. peaks at 800 K and 927 K}]{} \text{melt}$$

#When cooled in the presence of water vapor, this sample with a VD structure can easily contain re-hydration water. †Other materials, which are identical with MoO_3 and $Na_2Mo_2O_7$, are contained in small amounts.

Formation Mechanism of $Na_{0.9}Mo_6O_{17}$. $Na_{0.9}Mo_6O_{17}$ was formed at 583 K from a hydrated sodium molybdenum bronze. The sample has a VD structure just before the formation of $Na_{0.9}Mo_6O_{17}$. The formation temperature is lower than the melting points of the sample by at least 200 K. These facts indicate that the formation proceeds directly from VD in the solid-phase process. This formation mechanism is different from those by usual methods. By the usual methods, the formation proceeds in the liquid phase and via intermediate products with similar structures.[7,10] The formation of $Na_{0.9}Mo_6O_{17}$ from VD is a structural phase transition. Formation at a lower temperature (based on the phase transition) may arise from the fact that the hydrated bronze possesses Na atoms already inserted in the Mo–O framework. The structures of $Na_{0.9}Mo_6O_{17}$ and VD have already been reported,[11,13] as shown in Fig. 3. These structures can be described as being slabs connected by Na atoms. The slab of $Na_{0.9}Mo_6O_{17}$ is build up of 4 layers of Mo octahedra and 2 layers of tetrahedra sharing corners, while that of VD contains 2 layers of Mo octahedra sharing edges. An inspection of these two structures suggests that the direct formation of $Na_{0.9}Mo_6O_{17}$ from VD is possible through the following steps, as shown in Fig. 3(b): (i) passing of Na atoms through the slabs, (ii) linkage of each two slabs, and (iii) reformation of the Mo–O framework. The radius of a sphere which can pass through an open space in the slabs of VD may be smaller than 0.3 Å. This value is obtained from well established atomic positions of $D_{0.36}MoO_3$,[18] of which the Mo–O framework is comparable to that of VD. (An ion radius of O atom, 1.4 Å, was used.[19]) The ion radius of Na atoms is 1.12 Å[20] and is too large to pass through the open space. However, the chemical bonds in the bronze are expected to be rather loose at 600 K, which corresponds to a few hundred degree below its melting point. The loose bonds may permit Na atoms to pass through the slabs.

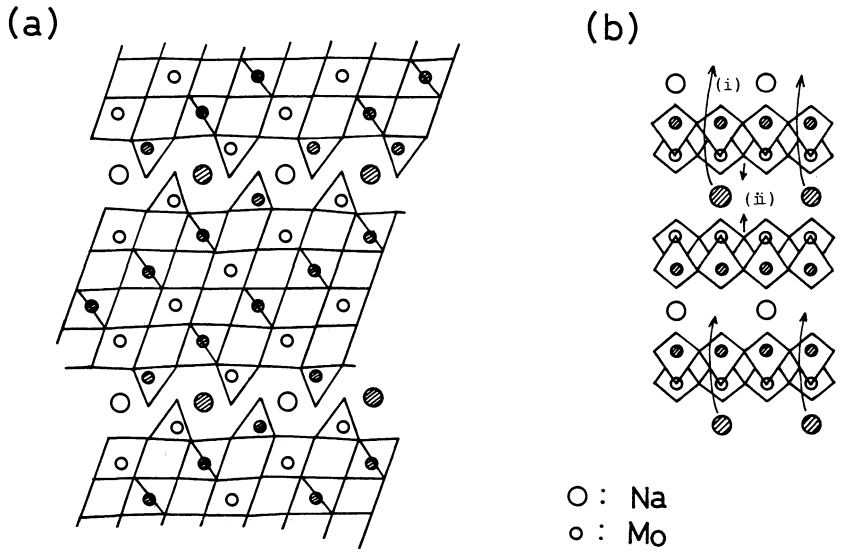

Fig. 3. Crystal structures of (a) $Na_{0.9}Mo_6O_{17}$ and (b) VD. Open and hatched circles indicate atomic positions at $Z=0$ and $1/2$, respectively.

The formation of $Na_{0.9}Mo_6O_{17}$ from VD is a new formation process, which stimulates not only great interest in the physical phenomenon, but also merits for applications. The preparation of alkali metal molybdenum bronzes from hydrated alkali molybdenum bronzes can be performed at a lower temperature than by the usual fused methods. The preparation of bronzes in a thin film or a complex form is also possible, since the formation of bronzes proceeds in a solid-phase process without any formation of melts. In this work, the formation of $Na_{0.9}Mo_6O_{17}$ was accompanied by the coexistence of a small amount of other materials. This prevents a realization of the above applications. To prepare bronzes without such a coexistence, the composition of the hydrated sodium molybdenum bronze must be controlled. Methods to control the composition are now being studied. Moreover, an investigation regarding other hydrated alkali molybdenum bronzes is also in progress.

References

1) M. Greenblatt, *Chem. Rev.*, **88**, 31 (1988).
2) D. S. Perloff, M. Vlasse, and A. Wold, *J. Phys. Chem. Solids, Suppl.*, **1**, 361 (1967).
3) M. H. Whangbo and L. F. Schneemeyer, *Inorg. Chem.*, **25**, 2424 (1986).
4) A. Wold, W. Kunnmann, R. J. Arnott, and A. Fekrretti, *Inorg. Chem.*, **3**, 545 (1964).
5) A. Wold, *Bull. Soc. Chim. Fr.*, **1965**, 1059.
6) G. H. Bouchard, J. Perlstein, and M. J. Sienko, *Inorg. Chem.*, **6**, 1682 (1967).
7) P. Strobel and M. Greenblatt, *J. Solid State Chem.*, **36**, 331 (1981).
8) M. Greenblatt, W. H. McCarroll, R. Neifeld, M. Croft, and J. V. Waszczak, *Solid State Commun.*, **51**, 671 (1984).
9) J. M. Reau, C. Fouassier, C. Gleitzer, and M. Parmentier, *Bull. Soc. Chim. Fr.*, **1970**, 479.
10) K. V. Ramanujachary, M. Greenblatt, and W. H. McCarroll, *J. Cryst. Growth*, **70**, 476 (1984).
11) B. M. Gatehouse, D. J. Lloyd, and B. K. Miskin, "Solid State Chemistry," NBS Special Publication 364, ed by R. S. Roth and S. J. Schneider, V. S. Dept. of Commerce, Washington, D. C.(1972), p. 15.
12) R. Schöllhorn, R. Kuhlmann, and J. O. Besenhard, *Mater. Res. Bull.*, **11**, 83 (1976).
13) D. M. Thomas and E. M. McCarron, III, *Mater. Res. Bull.*, **21**, 945 (1986).
14) C. Choain and F. Marion, *Bull. Soc. Chim. Fr.*, **1963**, 212.
15) P. Caillet, *Bull. Soc. Chim. Fr.*, **1967**, 4750.
16) Sodium atoms in original VD are octahedrally coordinated by two oxygen atoms of hydration water molecules and four terminal oxygen atoms of MoO_3.[13] However, some of sodium atoms in this sample are not octahedrally coordinated, because of the lack of hydration water. This generates distortions of the lattice and gives rises to the broadening.
17) Thermal differential analysis was carried out for the hydrated sodium bronze of which Na content was reduced by a treatment with an acidic solution, i.e., Na^+–H^+ ion-exchange. As Na content decreased, the exothermic peak at 583 K shifted to a higher temperature side and finally overlapped with the peak at 633 K. For the bronze with Na/Mo=0.16, which showed only one exothermic peak at 633 K, $Na_{0.9}Mo_6O_{17}$ was formed at the peak temperature.
18) P. G. Dickens, J. J. Birtill, and C. J. Wright, *J. Solid State Chem.*, **28**, 185 (1979).
19) R. B. Heslop and K. Jones, "Inorganic Chemistry," Elsevier Scientific Publishing Co., Amsterdam (1976).
20) F. A. Cotton and G. Wilkinson, "Advanced Inorganic Chemistry," 5th Edition, John Wiley & Sons, New York (1988).

 © 1991 The Chemical Society of Japan Bull. Chem. Soc. Jpn., 64, 165—174 (1991)

Physical and Chemical Properties of Mononuclear Cobalt Dioxygen Complexes with Tetraimidazolyl-Substituted Pyridine Chelates

Seizo TAMAGAKI, Yutaka KANAMARU, Masanori UENO, and Waichiro TAGAKI*
Department of Bioapplied Chemistry, Faculty of Engineering, Osaka City University, Sugimoto 3, Sumiyoshi-ku, Osaka 558
(Received May 7, 1990)

A new calss of mononuclear superoxocobalt complexs containing four equal imidazolyl-donors and one pyridyl-donor per cobalt(II) ion was prepared and their chemical and physical properties were compared with those of cobalt(II) Schiff-base type dioxygen complexes.

Since the first recoginition of oxygen fixation by the Co^{II} complex of a synthetic chelate, *N,N'*-disalicylideneethylenediamine (salen),[1] reversible oxygenations with mononuclear peroxo complexes of low valent transition metals such as Ir^{I}, Rh^{I}, Co^{I}, and Ni^{0} have been reported, in which the two oxygen atoms are equidistant from the metal.[2,3] Meanwhile, a wide variety of binuclear μ-peroxo complexes have been synthesized[2,4] and it has been found that in the presence of pyridine and imidazole reversible dioxygenation is possible with analogs of Co^{II} (salen) complexes such as Co^{II} (3-methoxysalen)[5,6] and Co^{II} (acacen), [*N,N'*-ethylenebis(4-imino-2-pentanonato)]-cobalt(II)),[7] forming the corresponding dioxygen complexes, whose structures were characterized as paramagnetic mononuclear superoxocobalt(III) complexes being in equilibrium with the corresponding μ-peroxo complexes;

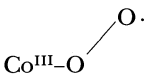

Metal dioxygen complexes are important for (1) a better understanding of the role of hemoglobin and myoglobin in biological systems;[8] (2) development of efficient catalysts for oxygenation of organic substrates;[9] (3) use in separating dioxygen from air or removing traces of dioxygen from inert gases.[10] In this work we have synthesized a new class of imidazolylmethyl-substituted pyridine chelates (hereinafter this will be referred to as tip) and have studied the physical and chemical properties of their cobalt dioxygen complexes as well as their utility for oxygenations of phenols to fully characterize them.

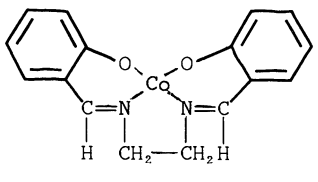

Co(salen)

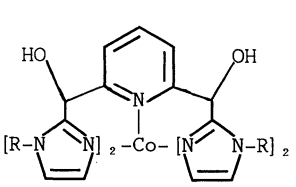

[Co(tip(a—e))]$^{2+}$;
R: CH_3 (tip(a))
n-C_4H_9 (tip(b))
n-C_8H_{17} (tip(c))
CH_3OCH_2 (tip(d))
CH_3CH_2 (tip(e))

Experimental

Materials. Solvents used in this study were purified via standard procedures by distillation, and only the central fraction was used. Special grade cobalt nitrate and perchlorate as the hydrates were purchased from Kishida Chemical Co. and used without further purification. Tetraimidazolylmethyl-substituted pyridine ligands, tip (tip-(a)—tip(d)), were prepared by the procedure previously described with minor modifications:[11] A 500 mL flask was flame-dried. After cooling it with a stream of nitrogen, 200 mL of freshly distilled, dry THF containing 0.1 mol of *N*-alkylimidazole was added with cooling to Dry Ice/acetone temperature (−78 °C) under nitrogen. Sixty-three mL of a 1.6 M solution of butyllithium in hexane (M=mol dm^{-3}) was injected dropwise to that solution using a glass syringe. To assure the completion of the reaction, the reaction temperature was maintained at the same temperature for additional one hour. To the solution diethyl 2,6-pyridinedicarboxylate (5.6 g, 0.024 mol) in 50 mL of THF was added dropwise. The reaction temperature was then allowed to rise to room temperatue. After the mixture was stirred for 4 h, water was added and the organic solvent was stripped off. Continuous extraction of the water layer with ethyl acetate gave a white crystalline solid, tip(a), which was recrystallized from $CHCl_3$–hexane.

Tip(a): Yield 54.3%; mp 181—184 °C; NMR ($CDCl_3$) δ=3.09 (16H, s, CH_3), 6.10 (2H, s, OH), 6.68 (4H, s, Im-2H), 6.89 (4H, s, Im-3H), 7.13 (1H, m, py-4H), 7.52 (2H, m, py-3,5H).

Tip(b) was purified by recrystallization from benzene–hexane after evaporation of the THF, extraction with $CHCl_3$ and evaporation of the $CHCl_3$.

Tip(b): Yield 48.7%; mp 164—166 °C; NMR ($CDCl_3$) δ=0.7—1.6 (28H, m, $(CH_2)_2CH_3$), 3.58 (8H, t, N-CH_2), 6.04 (2H, s, OH), 6.79 (8H, s, Im-CH=CH), 7.23—7.70 (3H, m, py-3,4,5H).

With tip(c) and tip(d), the $CHCl_3$ extracts were subjected to preparative TLC and the solids obtained were recrystallized from hexane (yield 34.7% mp 107—108 °C) and from benzene–hexane (yield 45.1%; mp 178—179 °C), respectively.

Tip(d): 2.92 (12H, s, OCH_3), 6.60 (2H, s, OH), 6.78, 6.91 (8H, d, CH=CH), 7.1—7.8 (3H, m, py-3,4,5H).

Isolation of [Co(tip) $(O_2)]^{2+}$ and Its Reaction Product. Tip(a) (0.1 mmol) was mixed at −30 °C with an equimolar amount of $Co(NO_3)_2 \cdot 6H_2O$ in 25 mL of nitromethane, and tip(b) or tip(c) in 25 mL of CH_2Cl_2, and bubbling of oxygen gave immediately dark-red solutions of $[Co(tip)(O_2)]^{2+}$ complexes, which were entirely stable to a further reaction at such a low temperature in solution. Evaporation of the solvent below −30 °C under a reduced pressure of 1 mmHg (1 mmHg=133.322 Pa) afforded dark-red colored solids. [Co(tip(a)) $(O_2)]^{2+}$ salt: yield 98%. Meanwhile, when tip(a) (0.1 mmol) was added with stirring to $Co(NO_3)_2 \cdot 6H_2O$ (0.1 mmol) in 10 mL of acetone at room temperature under oxygen, dark-red solids began to precipitate. (The $[Co(tip)]^{2+}$ complex itself did not precipitate out under nitrogen.) After 1 h, the precipitates were filtered, washed with acetone, and dried under vacuum, affording an analytical sample.

$[Co(tip(a))(O_2)](NO_3)_2(H_2O)_2$: Yield 91%; decomp 140—143 °C.

Anal. Calcd for $C_{23}H_{29}N_{11}O_{12}Co$: C, 38.88; H, 4.11; N, 21.69%. Found: C, 39.11; H, 4.43; N, 21.27%.

When tip(a) (0.2 mmol) was mixed with $Co(NO_3)_2 \cdot 6H_2O$ (0.2 mmol) in 25 mL of acetonitrile under oxygen at room temperature, complete bleaching of the solution was effected in 2 days. The solution was then evaporated to dryness and the residue was washed thoroughly with acetonitrile. Yield 90% in weight; decomp. 187—190 °C. Because of its tendency to decompose when subjection to recrystallization or precipitation, it is not possible to obtain the product in the pure form. The elemental analysis of this product gave no constant value within analytical accuracy with samples taken from different runs, but most likely agrees with a dimeric complex $[Co_2(tip(a))_2(O_2)](NO_3)_4$.

Isolation of [Co(tip(a))(base)]$^{2+}$ Complexes. To stoichiometric amounts of tip(a) and $Co(NO_3)_2 \cdot 6H_2O$ (0.3 mmol each) was added a large excess of a desired base, for example, *N*-methylimidazole (Meim) under nitrogen in 25 mL of nitromethane. Rotary evaporation of the solvent provided slightly pink powders in 96% yield, which were precipitated from nitromethane/CH_2Cl_2/benzene in the presence of excess 1-methylimidazole.

[Co(tip(a)) (Meim)] $(NO_3)_2(H_2O)_2$: decomp. 245—250 °C. Anal. Calcd for $C_{27}H_{35}N_{13}O_{10}Co$: C, 42.65; H, 4.61; N, 23.95%. Found: C, 42.33; H, 4.8; N, 24.45%.

Oxygen Uptake Experiment. The amount of oxygen absorbed by $[Co((tip(a))]^{2+}$ was determined at 20 °C according to the Warburg's manometry.[12] K_{O_2} is the equilibrium constant defined according to the equation below:

$$LCo^{2+} + O_2 \rightleftharpoons LCoO_2^{2+} \qquad K_{O_2} = \frac{[LCoO_2^{2+}]}{[LCo^{2+}] \times P_{O_2}}$$

where P_{O_2} is the oxygen pressure in mmHg. The full equilibriation was presumed to be quickly attained.

Kinetic Procedure for Disappearance of the Superoxocobalt Complexes. All experiments have been done at 25 °C under 1 atm oxygen pressure. The progress of disappearance of a cobalt oxygen complex was followed by monitoring the disappearance of absorption at 505 nm. As the superoxo complex is formed in relatively fast equiliblium, its disappearance reaction was monitored soon after injecting a needed volume of acetonitrile solution of $Co(NO_3)_2$ into 3 mL of a tip acetonitrile (0.5 mM each) in a 1 cm UV-cell capped with a rubber septum.

Electrochemistry. Cyclic voltammetric measurements were performed under nitrogen using a NP-IR 1000 potentiostat/galvanostat. Special grade acetonitrile was distilled from P_4O_{10}. Tetrabutylammonium perchlorate was used as the supporting electrolyte. To 20 mL of an acetonitrile solution containing 3 mM tip(b) and 0.1M Bu_4NClO_4 was added 100 μL of 0.6 M $Co(ClO_4)_2$ under nitrogen. The measurements utilized a platina wire working electrode, a platina wire auxiliary electrode, and an Ag/AgCl reference electrode in a one-compartment cell. The cyclic voltammograph of $[Co(tip(b))]^{2+}$ thus obtained is given in Fig. 1a. Figure 1b shows a cyclic voltammograph in the presence of 5-fold excess of pyridine. The $E_{1/2}$ values were estimated from cyclic voltammograms using the expression $E_{1/2}=(E_P+E_{p/2})/2$ where E_p is the peak potential and $E_{p/2}$ is the half peak potential.

ESR Spectrum. The solid cobalt–oxygen complex was placed in an ESR tube, after which the tube was degassed. The ESR signals were recorded at −196 °C on a JES-ME-3X spectrometer with an X-band microwave unit and 100 KHz field modulation.

Oxygenation of 2,4-Di-*t*-butylphenol. To a red solution of an equimolar mixture of $Co(ClO_4)_2 \cdot 6H_2O$ (9.15 mg, 0.025 mmol, 0.5 M) and tip(b) (15.68 mg) in 50 ml of various solvents was added 1.0 mmol (206 mg) of 2,4-di-*t*-butylphenol. The reaction was allowed to proceed under oxygen at room temperature for 44 h. For determination of product yields, the solvent was rotary evaporated at room temperature, and then the residue was subjected to thin-layer chromatography with Kiesel gel G/$CHCl_3$, affording 3,5-di-*t*-butyl-*o*-benzoquinone and 3,3′,5,5′-tetra-*t*-butyl-1,1′-biphenyl-2,2′-diol (hereafter designated as biphenyl-2,2′-diol): Mp 193—195 °C; NMR ($CDCl_3$) δ=1.3 (36H, d, *t*-butyl), 5.08 (2H, s, Ar-O<u>H</u>), 6.94—7.21 (4H, m, Ar-<u>H</u>); MS (70 eV) *m/z* (rel intensity) 410 (M^+; 100), 395(52), 339(20), 283(15), and 190(48). Determination of the quinone yield was made spectrophotometrically at 400 nm (δ=1704) in MeCN within experimental error of ±3%.[13] The yields in various solvents are collected in Table 2.

Oxygenation of 2,6-Di-*t*-butylphenol. To a solution of 0.05 mmol each of tip(b) and $Co(NO_3)_2 \cdot 6H_2O$ in 25 ml solvents was added 2,6-*t*-butylphenol (103 mg, 0.5 mmol). The reaction was continued with gentle stirring at room temperature under oxygen. After 24 h, the solvent was stripped off under reduced pressure at room temperature and the residue was subjected to preparative thin-layer chromatography using benzene–hexane (1:1) as eluant giving two products. The yields were determined spectrophotometrically. 2,6-Di-*t*-butyl-*p*-benzoquinone (*p*-BQ): 450 nm (ε=39)[14] and a diphenoquinone (DPQ): 260 nm (ε=4056).[15]

Kinetic Method for Oxygenation. Reactions were performed under the conditions specified in Fig. 8. Unless otherwise noted, the concentration of 3,5-di-*t*-butylphenol was in 10-fold excess over the catalyst. In a typical experiment, a septum-capped flask containing pure O_2-saturated acetone solution of $Co(NO_3)_2$ and tip(b) was maintained at 25 °C. Reactions were initiated by injecting the phenol dissolved in acetone. A 75 μL aliquot of the reaction mixture was then transferred by a microsyringe into a UV cell containing 3 mL of acetonitrile. The increasing absorbance at 400 nm characteristic of the product quinone

was monitored every 30 minutes.

Instrumentals. NMR, IR, and UV spectra were obtained on a Hitachi R-24B, a Nihon Bunko A-202 infrared spectrometer, and a Hitachi 220 spectrophotometer, respectively.

Results and Discussion

Physical Properties of $[Co(tips)]^{2+}$ and Their Oxygen Complexes. In cyclic voltammograms of oxygen-free $[Co(tip(b))]^{2+}$ and $[Co(tip(b))(base)]^{2+}$ complexes a single quasi-reversible redox wave associated with cobalt(II/III) couples appears at negative potentials. (Fig. 1a and 1b). The redox-potentials are summarized in Table 1. There is no distinct correlation between

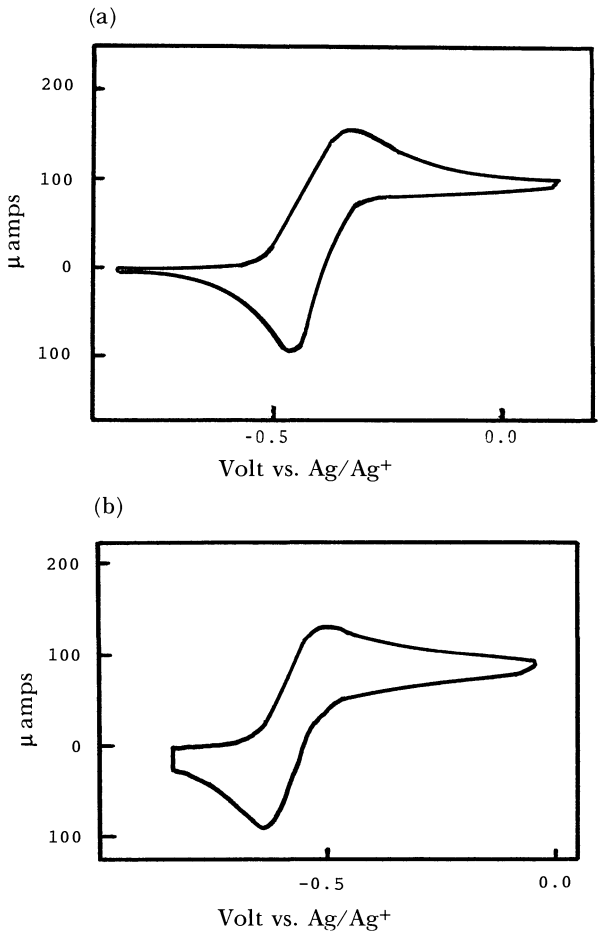

Fig. 1. Cyclic voltammograph of a) $[Co(tip(b))]^{2+}$ and b) $[Co(tip(b)(py)]^{2+}$. Scan rate 50 mV^{-1}. E versus Ag/Ag^+. Counter anion: ClO_4^- in MeCN.

Table 1. Redox Potentials of $[Co(tip(b))(base)]^{2+}$ Complexes[a)]

Base	pK_a	$E_{1/2}$/V vs. Ag/AgCl
Pyridine	5.27	−0.51
Piperidine	11.3	−0.54
1-Methylimidazole	7.25	−0.65
Butylamine	10.61	−0.66

a) Conditions: $[tip(b)]=[Co(ClO_4)_2]=3$ mM; [Base]= 15 mM; $[Bu_4NClO_4]=0.1$ M in MeCN at 27 °C.

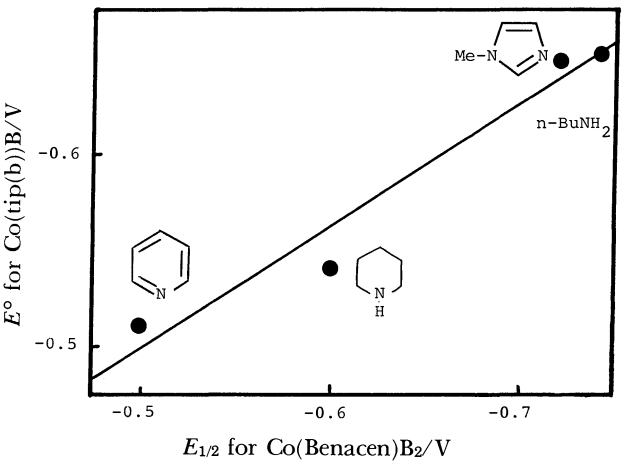

Fig. 2. Correlation of $E_{1/2}$ for $[Co(tip(b))(B)]^{2+}$ with that for $Co(benacen)B_2$. $[Co(tip(b))^{2+}]=3$ mM; [B]= 15 mM; $[Bu_4NClO]_4=0.1$ M in MeCN at 27 °C.

$E_{1/2}$ values and pK_a values of bases, probably because piperidine, a secondary cyclic amine, is sterically hindered and N-methylimidazole is a good π-electron donating base. In Fig. 2 is shown a plot of the redox potentials of $[Co(tip(b))]^{2+}$ vs. those of Co(benacen) complex, [N,N'-ethylenebis(3-imino-1-phenyl-1-butanonato)]cobalt(II), in the presence of various bases.[16] The $E_{1/2}$ values of $[Co(tip(b))(B)]^{2+}$ (B=base) are linearly related to those of $Co(benacen)(B)_2$ with a

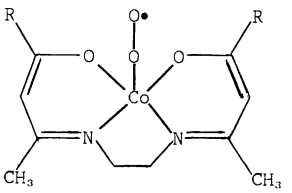

R = Ph: $Co(benacen)(O_2)$

R = Me: $Co(acacen)(O_2)$

slope of 0.66. The slope close to 0.5 is simply interpreted by considering that the latter has one more additional base than the former. Figure 3 shows a plot of the absorbance against cobalt nitrate concentrations under an atmosphere of dioxygen gas in acetonitrile, keeping the concentration of tip(b) fixed. A nearly linear correlation up to a 1:1 molar ratio of cobalt nitrate to the chelate demonstrates that the chelate and cobalt ion form a 1:1 complex.

In our preliminary report, it was established that addition of dioxygen to $[Co(tip(a))]^{2+}$ in acetonitrile is apparently reversible since a stream of nitrogen bubbling into the solution at ambident temperature resulted in the disappearance of its original red color characteristic of the $[Co(tip(O_2)]^{2+}$ complex.[11] Subsequent bubbling of oxygen through the solution restored the red color and, hence, the complex was formulated as a mononuclear superoxocobalt(III) complex. The elemantal analysis for $[Co(tip(a)(O_2)]^{2+}\cdot 2NO_3^-$ supports the validity of the proposed

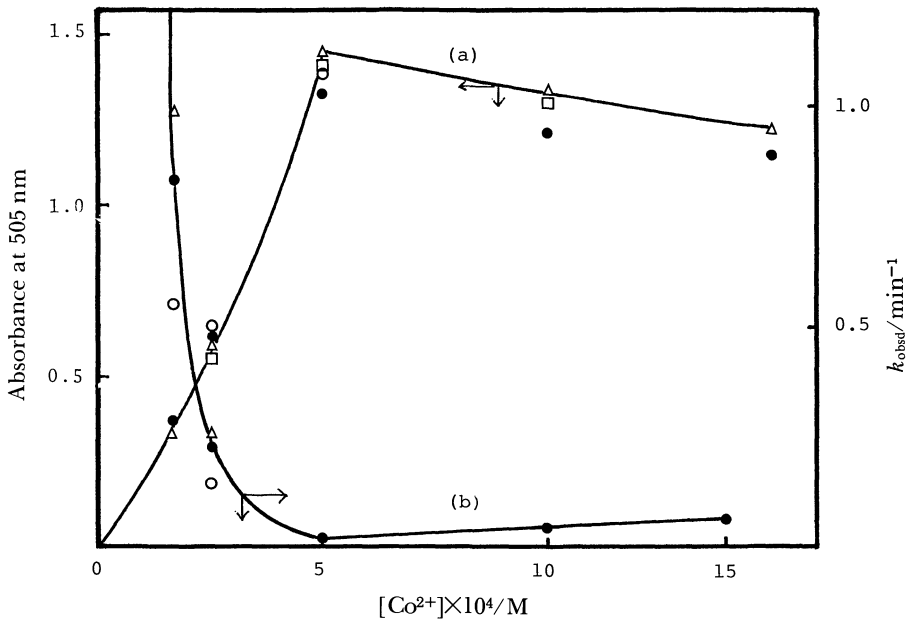

Fig. 3. Effects of altering concentrations of $Co(NO_3)_2$ on the formation (a) and disappearance (b) of $[Co(tip)(O_2)]^{2+}$ complexes under oxygen in $MeNO_2$ at 25 °C, the tip concentration being fixed constant at 0.5 mM. ○: tip(a); △: tip(b); □: tip(c); ●: tip(e).

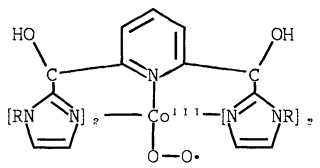

$[Co(tip)(O_2)]^{2+}$

structure.

The apparent extinction coefficient at 505 nm of the superoxocobalt complex thus formed is ε=1.4×10^3 and 1.9×10^3 M^{-1} cm^{-1} in acetonitrile and water, respectively, but the observed small reversible oxygen binding constant (log K_{O_2} mm^{-1}=−4.1, −4.0, and −3.9 in water, acetonitrile, and nitromethane, respectively, at 20 °C) indicates that only a portion of $[Co(tip(b))]^{2+}$ is oxygenated in solution; hence, the real extinction coefficient is ε=2.5×10^4 in water. The K_{O_2} value is roughly the same in magnitude as that of Co(benacen) (py) in toluene (log K_{O_2}=−1.36 mm^{-1} at −31 °C; −4.4 at 20 °C (extrapolated))[16] and nearly 3-order of magnitude smaller than that of Co(salen) (py) (log K_{O_2}=−1.05, 20 °C).[17] The comparable oxygen-binding stabilities for $[Co(tip)]^{2+}$ and Co(benacen) (py) reflect a similarity in their reducing ability; $E_{1/2}$=−0.51 V for $[Co(tip)(py)]^{2+}$ and −0.50 V (vs. SCE) for Co(benacen) $(py)_2$.[18]

The immediate formation of the superoxocobalt complex was observed as soon as $Co(NO_3)_2$ was added to an oxygen-saturated solution of a tip ligand, then followed by its slow disappearance. In Fig. 3 a plot of rate constants for the disappearance of absorbance at 505 nm in nitromethane is also displayed, showing that the rate is significantly dependent on changing

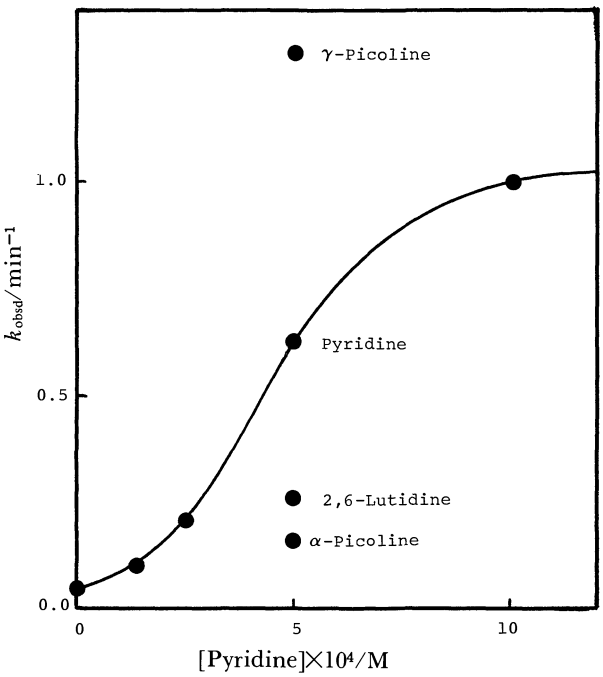

Fig. 4. Effect of changing concentrations of pyridine bases on the rate of disappearance of $[Co(tip(c))(O_2)]^{2+}$ under oxygen in $MeNO_2$ at 25 °C. [tip(c)]=[$Co(NO_3)_2$]= 0.5 mM.

concentrations of the metal ion. In particular, the use of a large excess of the chelate vs. metal ion causes rapid loss of the superoxocobalt complex. This is interpreted as due to interception of $[Co(tip(b))]^{2+}$ by free imidazolyl chelate (tip(b)) to make a new stable

$[Co(tip(b))]^{2+}$–tip(b) adduct. In fact, as one can see in Fig. 4, a simple base, pyridine or *N*-methylimidazole (Meim), was also found to bring about facile disappearance of the superoxo complex to form the $[Co(tip)]^{2+}$–base complex. In order to confirm this interpretation, we performed product analysis using tip(a) as the ligand under two extreme conditions; without added pyridine (or 1-methylimidazole) the reaction produced a slightly pink-colored solid, which evolved gas when heated to >150 °C (140 °C) in a capilary tube, while, addition of a large excess of pyridine (Meim) afforded a white solid which melted out at 258—265 °C (235—240 °C) without gas evolution and, when dissolved in solvents, exhibited at 505 nm an absorption band characteristic of the superoxo complex. These observations strongly support that the former is the dimer $[Co_2(tip(a))_2(O)_2]^{4+}$ and the latter is the adduct [Co(tip(a)) (B)]$^{2+}$. When the former was reacted with excess pyridine or when the latter was dissolved in nitromethane under oxygen, the $[Co(tip)]^{2+}$ was present as a mixture of $[Co_2(tip)_2(O_2)]^{4+}$ and [Co(tip) (B)]$^{2+}$ in either case. Thus, they are interconvertible with each other. However, the equilibrium below lies so far to the left.

$$[Co_2(tip)_2(O_2)]^{4+} + 2B \rightleftharpoons 2[Co(tip)(B)]^{2+} + O_2$$

The rate of disappearance of the superoxocobalt complex itself is strongly solvent-dependent, and the kinetic orders with regard to the complex concentrations are changing from zero-order in THF to first-order in acetone, dichloromethane, nitromethane, and *t*-butyl alcohol (the rate increases along this solvent series), and to second-order in ethyl acetate, chlorobenzene, benzene, *o*-tolunitrile, nitrobenzene, benzonitrile, acetonitrile, and 1,2-dimethoxyethane (the rate increases in this order) (Fig. 5). As can be seen in, for example, Fig. 6, we could find no simple relationship between initial rates and any solvent properties like dielectric constant, steric bulkiness, polarity, donor number, and degree of oxygen saturation etc., which we could not determine. The irregularlity might be due to involvement of several comparable equilibria, which contribute to the overall rate in a complicated way. However, in contrast to the suggestion by Martell and co-wokers that Co(benacen) and Co(porphyrin) superoxo complexes are more favored in nonpolar solvents such as toluene, the $[Co(tip)]^{2+}$ and O_2 1:1 complex is destabilized either in low or highly polar solvents. Furthermore, this $[Co(tip)]^{2+}$–O_2 system is very interesting, since it can exist even in an aqueous solvent; to date, no superoxocobalt(III) complexes in aqueous solution at room temperature have been reported in the literature.[2,19]

In the meantime, the superoxo complex [(Co(tip(a)) $(O_2)]^{2+}$ in the solid state was dark-red and so stable toward deoxygenation at room temperature even

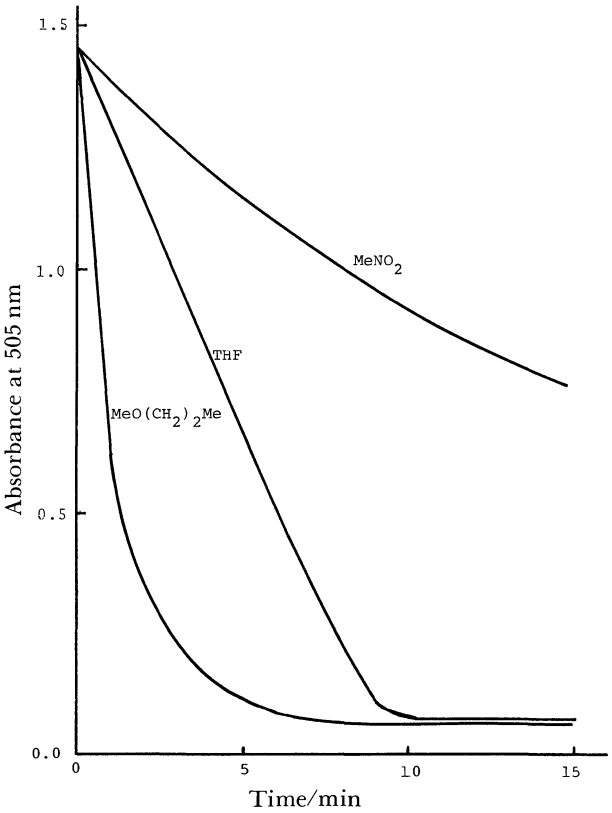

Fig. 5. Time courses of disappearance of absorption due to $[Co(tip(c))(O_2)]^{2+}$ in various solvents. [tip(c)]= $[Co(NO_3)_2]$=0.5 mM.

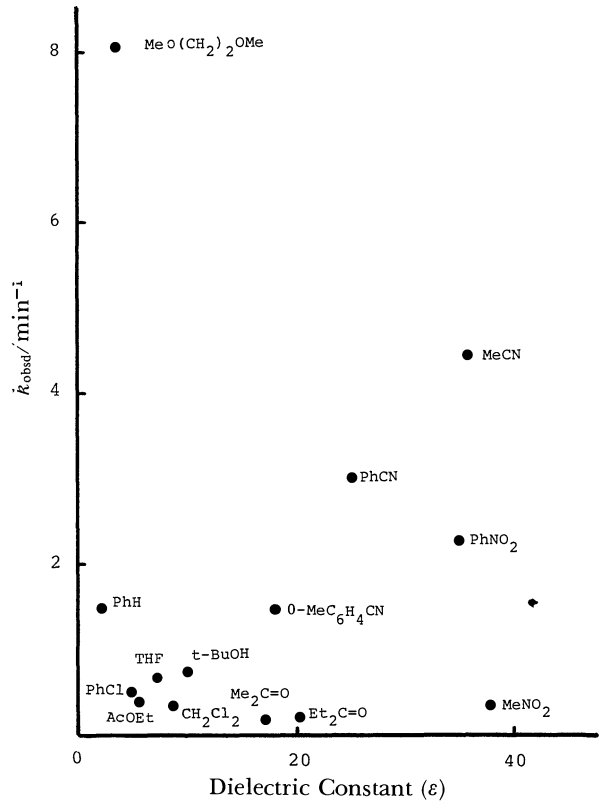

Fig. 6. Influence of solvent change on rate of disappearance of $[Co(tip(c))(O_2)]^{2+}$. Counter anion: NO_3^-.

under a reduced pressure (1 mmHg). However, heating it for one hour at 140 °C in vacuo results in loss of the color. Upon its exposure to air at room temperature for one day the decolorized complex takes up dioxygen and the original red color is restored. Thus, addition of oxygen to the cobalt-tip(a) complex is apparently reversible. In the reported case of brown-colored oxygenated Co(salen),[20] heating it at 100 °C forms red solids. As is revealed by Table 2, the shorter the ligand alkyl-chain length, the higher is the decolorization temperature and the melting point of the superoxo complex. This follows the same order as the melting points of the ligands themselves. The extent of recovery of $[Co(tip(a))(O_2)]^{2+}$ complex was measured at 505 nm to be 54% on each deoxygenation–oxygenation cycle. This recovery extent is almost the same both in the solid and liquid states.

Figure 7 displays the ESR spectrum of $[Co(tip(a))(O_2)](NO_3)_2$ in the solid state at liquid nitrogen temperature, where eight equivalent hyperfine-splitting signals with low intensity due to ^{59}Co (I=7/2) can be observed. Just analogous spectral patterns were reported for Co(acacen) (py) (O_2)[21] in a toluene matrix at −58 °C and $[Co(CN)_5(O_2)]^{3-}$.[22] $Co(NO_3)_2$ and $[Co(tip(a))(py)]NO_3)_2$ exhibited no ESR signals owing probably to their electron configurations of high spin states.

Table 2. Decolorization Temperatures and Melting Points of $[Co(tip)(O_2)]^{2+}$ Complexes[a]

Substituent on imidazolyl group	Decolorization temperature[b]/°C	Melting point °C
CH_3	140	236—254
n-C_4H_9	100	160—165
n-C_8H_{17}	<100	110—125

a) Counter anion: NO_3^-. b) Under 1 mmHg.

Oxygenations of Phenols. There are a number of reports on the oxygenations of sterically hindered

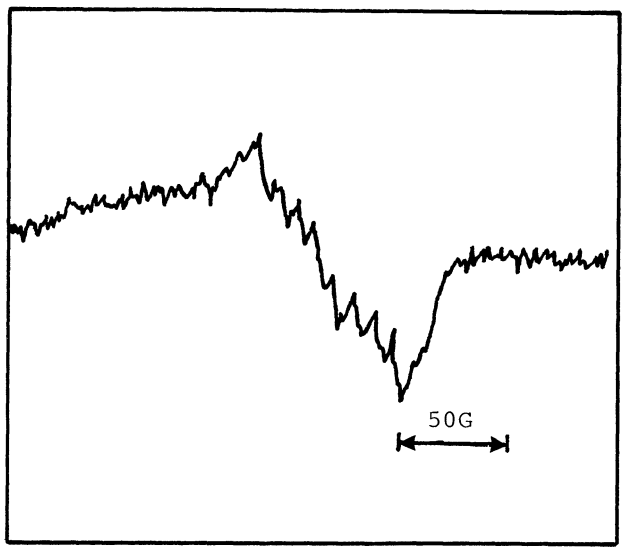

Fig. 7. ESR spectrum of $[Co(tip(a))(O_2)]^{2+}$ in the solid state at −196 °C. Counter anion: NO_3^-.

Table 3. Product Yields for Oxygenation of 2,4-Di-t-butylphenol with in situ Generated $[Co(tip(b))]^{2+}$ Catalyst

Catalyst	Solvent	Quinone yield/% (±3%) 44 h[a]	Quinone yield/% (±3%) 24 h[b]	Biphenyl-2,2′-diol yield/% (±2%) 24 h	Recovered[d] yield/% 24 h
$[Co(tip(b))]^{2+}$	$MeNO_2$	39			
			89		
	$Me_2C=O$		85	6	3
			82[c]	11	Trace
	MeCN	38			
			63	7	15
			66[c]	4	15
	CH_2Cl_2	16			
			23	10	50
	t-BuOH		42		
	DMF	14			
			6.9		
	MeOH	8.6			
			6.0	11	77
	$CHCl_3$		5.5	10	66
	$MeO(CH_2)_2OMe$		0		
$[Co_2(tip(b))_2(O)_2]^{4+}$	MeCN		34[c]	2	58
			3.2[e]	8.3	72
	MeOH		10.4		
Co (salen)	CH_2Cl_2[24]			100	
Co (NMesalpr)	CH_2Cl_2[24]		>85		

Conditions: 2,4-di-t-butylphenol 1 mmol; solvent 50mL; under O_2 at room temperature. a) tip(b) 0.025 mmol; $Co(ClO_4)_2$ 0.025 mmol. b) tip(b) 0.1 mmol; $Co(ClO_4)_2$ 0.1 mmol. c) $Co(NO_3)_2$ was used. d) A blank denotes that a yield was not determined. e) tip(b) 0.2 mmol; $Co(NO_3)_2$ 0.2 mmol; the phenol 1 mmol under N_2.

phenols; for instance, 2,4-di-*t*-butylphenol was selectively oxidized with Co(salen) catalyst to the corresponding quinone in DMF and to 3,3′,5,5′-tetra-*t*-butyl-1,1′-biphenyl-2,2′-diol (biphenyl-2,2′-diol) in dichloromethane or methanol.[23,24] In the present study the $[Co(tip(b))]^{2+}$ complex was tested as catalyst for oxygenations of two typical phenols.

The reaction of 2,4-di-*t*-butylphenol catalytically gave rise to 3,5-di-*t*-butyl-*o*-benzoquinone (*o*-BQ) together with biphenyl-2,2′-diol, irrespective of the nature of used solvents (Table 3), without accompanying oxidative cleavage of the aromatic ring as with $MnCl_2$.[25] However, the yield was largely dependent on the solvent employed; generally, nonpolar solvents

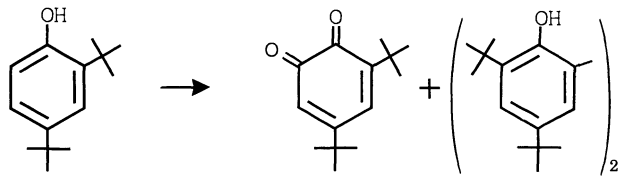

are least effective. Highly polar solvents such as methanol or *N*,*N*-dimethylformamide led to poorer yields than moderately polar solvents such as nitromethane, acetone, or acetonitrile This seems to reflect an absolutely low concentration of the reaction-triggering superoxocobalt complexes in those solvents, probably because a $[Co(tip(b))]^{2+}$–solvent adduct rather than the superoxo complex predominantly exists, such as was observed when basic pyridines were added. As a result, a poorer yield of the *o*-BQ was obtained.

$$[Co(tip(b))(O_2)]^{2+} \underset{+B}{\overset{+O_2}{\rightleftharpoons}} [Co(tip(b))B]^{2+}$$

B: base

As is demonstrated in the same table or Fig. 8, the dimeric μ-peroxo complex retains considerable activity under the identical conditions although it is less effective than the in situ generated oxygen complex. This is because, even if the μ-peroxo species itself is inactive, the active superoxo species is produced from it according to the back-reaction of the equilibrium below.

$$[Co(tip(b))(O_2)]^{2+} + [Co(tip(b))(S)]^{2+} \rightleftharpoons [Co_2(tip(b))_2(O_2)]^{4+} + S$$

S: solvent

The following tentative mechanism, being consistent with the above observations and reported literature results, completes the sequence of events, where LCo denotes chelated cobalts, H-PH a di-*t*-butylphenol, and PH· and PH^- a phenoxyl radical and phenolate ion, respectively.

$$LCo^{II} + O_2 \rightleftharpoons \underset{[I]}{LCo^{III}O_2^-} \rightleftharpoons LCo^{III}\text{-}OO\text{-}Co^{III}L \quad (1)$$

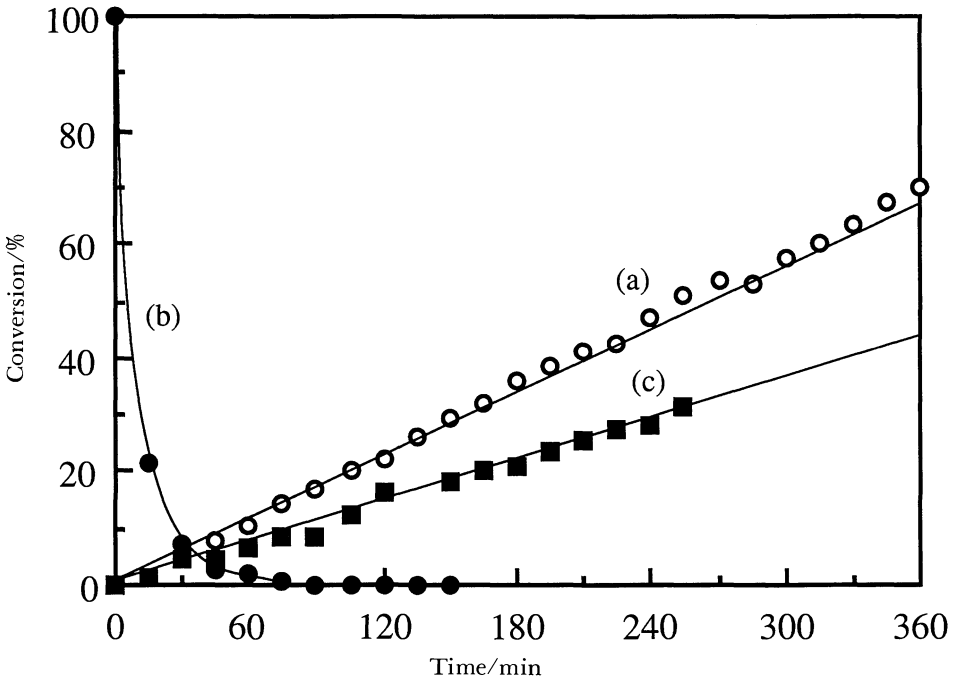

Fig. 8. Time-%conversion profiles for increasing quinone in oxygenation of 2,4-di-*t*-butylphenol using (a) in situ generated $[Co(tip(b))(O_2)]^{2+}$ and (c) $[Co_2(tip(b))^2(O_2)]^{4+}$ and for (b) decreasing $[Co(tip(b))(O_2)]^{2+}$ in Me_2CO under oxygen. $[Co(NO_3)_2]=[(tip(b))]=2.0\times10^{-3}$ M, $[phenol]=2.0\times10^{-2}$ M.

slow

$$I + H\text{-}PH \longrightarrow LCo^{III}O_2H^- + \cdot PH \quad (2)$$

$$LCo^{III}O_2H^- \longrightarrow LCo^{III}OH^- + 1/2\ O_2 \quad (3)$$

$$LCo^{III}OH^- + H\text{-}PH \rightleftharpoons LCo^{III}PH^- + H_2O \quad (4)$$

[II]

$$\cdot PH + LCo^{II} \rightleftharpoons II\ [LCo^{III}PH^- \leftrightarrow LCo^{II}PH\cdot] \quad (5)$$

[II_i] [II_r]

$II_i + O_2 \longrightarrow$ 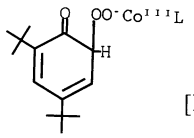 (6)

[III]

III $\xrightarrow{\text{slow}}$ 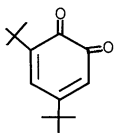 $+ LCo^{III}OH^-$ (7)

$2\cdot PH \longrightarrow$ 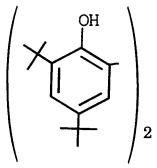 (8)

At first, the reaction sequence appears to be triggered by abstraction of the hydrogen atom of the phenol by the superoxocobalt complex yielding the hydrogenperoxocobalt complex (Eq. 2), which decomposes to yield a hydroxocobalt complex and oxygen (Eq. 3). Then, the hydroxo complex abstracts the proton from the phenol to form the phenolato LCo^{III} complex (II) with resonance forms II_r and II_i (Eqs. 4 and 5); the ionic form (II_i) would be favored in polar solvents such as acetonitrile and acetone to eventually produce *o*-BQ by reacting with molecular oxygen in its ortho-position (Eq. 6 followed by Eq. 7), while the radicalish form (II_r), which is expected to be favored in nonpolar solvents, is thought to be in equilibrium with the phenoxyl free radical (Eq. 5). The increasing stability of the phenolato complex in a polar solvent, accordingly, resulted in a higher proportion of the quinone vs. the radical coupling product, biphenyl-2,2′-diol, and vice versa in nonpolar solvents, as was observed. A similar metal–phenolate interaction has been proposed by Nishinaga[26] and Que[27] for an explanation of quinone formations.

Nishinaga et al. have kinetically studied the closely related oxidation in detail using 4-substituted 2,6-di-*t*-butylphenol and Co(salpr) and have proposed a similar mechanism which involves a fast superoxo complex formation followed by the rate-determining phenolic hydrogen atom abstraction (Eqs. 1 and 2).[23] A comparison of kinetic curves (a) and (b) in Fig. 8 shows, however, that the conversion of 2,4-di-*t*-butylphenol to *o*-BQ continued to increase linearly with time up to 80% completion, while the superoxo-

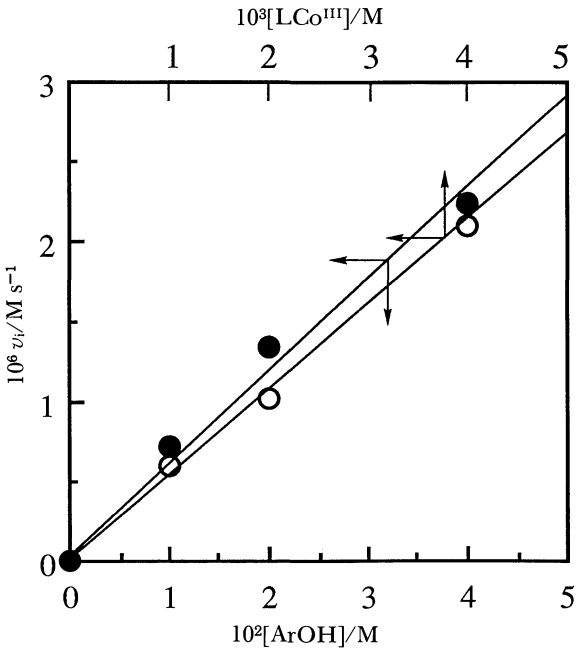

Fig. 9. Plots of initial rates (v_i) vs. initial concentrations of $[Co(tip(b))]^{2+}$ and 2,4-di-*t*-butylphenol (ArOH) concentrations with constant concentrations of the phenol (2.0×10^{-2} M) and $[Co(tip(b))]^{2+}$ (2.0×10^{-3} M) in Me_2CO under oxygen.

cobalt had completely disappeared early in the course of the reaction. It is evident that the present reaction does not involve hydrogen atom abstraction by the superoxide as rate-determining. Meanwhile, as Fig. 9 shows, the initial rates, which were calculated from a slope at time zero in an absorbance–time profile, were proportional to the added catalyst and phenol concentrations and dependent on the exerted oxygen pressure over the solution. Because of the complexity of the present system, no quantitative description of the concentration-dependency of the rate is attempted. In order to explain these results only qualitatively, therefore, we presents two assumptions that (1) the decomposition of III to *o*-BQ is virtually rate-determining and (2) the hydroxocobalt complex ($LCoOH^-$) plays an important role as a limiting intermediate species in a catalytic cycle (Eqs. 4, 5, 6, and 7); the aforementioned finding that the amount of produced *o*-BQ increased linearly with reaction time evidences that the steady state is reached and thus the steady-state concentrations of the hydroxo complex and III must be kept constant during the course of the reaction. Since catalytic levels of III as well as the hydroxo complex or its precursor would rise with the increasing concentrations of the phenol, metal catalyst, and dissolved oxygen, the overall rate would increase accordingly, as was observed.

Meanwhile, product analysis for the catalytic oxygenation of 2,6-di-*t*-butylphenol,[28] yielding 2,6-di-*t*-butyl-*p*-benzoquinone (*p*-BQ) and a diphenoquinone

Table 4. Oxygenation of 2,6-Di-*t*-butylphenol (±2% error in yield)[a)]

Catalyst	Solvent	Reaction time/h	Conversion/% (±3%)	*p*-BQ/DPQ
$[Co(tip(b))]^{2+}$	$MeNO_2$	24	70	94/6
	$Me_2C=O$	24	67	96/4
	MeCN	24	51	93/7
	MeOH	24	49	86/14
	CH_2Cl_2	24	10	78/22
	$CHCl_3$	24	6	61/39
$[Co(tip(d))]^{2+}$	MeCN	24	12	86/14
$[Co_2(tip(b))_2(O_2)]^{4+}$	MeCN	24	21	81/19
Co(NMesalpr)	MeCN	1	100	100/0[32)]
	Toluene	6	100	100/0[32)]
Co(salpn)	$CHCl_3$-py	24	40	80/20[32)]

a) Conditions: substrate 0.5 mmol; catalyst 0.05 mmol in 25 ml solvent under an oxygen atmosphere at room temperature. NMesalpr: *N*,*N*′-disalicylidene-4-methyl-4-azaheptane-1,7-diamine; Salpn: *N*,*N*′-disalicylidene-1,3-propanediamine.

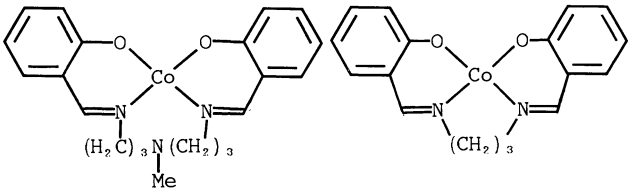

(DPQ),[29)] is somewhat instructive to implicate the reaction mechanism. The results obtained in this work are compared with reported literature data, which are also included in Table 4. Complete interpretation for these results is still rather difficult owing to a lack of available data. However, the mechanism analogous to that for 2,4-di-*t*-butylphenol seems most plausible; the reaction proceeds either via a radical pathway including a phenoxyl radical or via an ionic pathway involving the phenolato LCo^{III} complex.[30)] Several points about Table 4 are noteworthy; as with the case of 2,4-di-*t*-butylphenol, generally, use of polar solvents such as nitromethane and acetonitrile gave rise to better total yields and

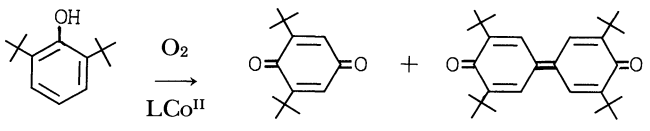

(*p*-BQ) (DPQ)

preferred formation of *p*-BQ over DPQ, since polar solvents would enhance the production of the metal-complexed phenolate [II_i] and hence would increase the contribution of the ionic process. Replacement of the alkyl group in the imidazolyl ligand with an electron-withdrawing methoxymethyl group diminishes the reducing ability of the central Co^{II} toward a phenoxyl radical, resulting in a higher yield of DPQ vs. *p*-BQ.[31)]

In conclusion, the pyridyl ligand symmetrically substituted with four imidazolyl groups stoichiometrically binds Co^{2+} ion at a 1:1 ratio to form $[Co(tip)]^{2+}$, which then immediately takes up molecular oxygen to form the cobalt-dioxygen complex entirely stable in the solid state and enough stable below −30 °C in solution. As is visualized by the CPK space filling molecular model, $[Co(tip)]^{2+}$ adopts a loose square-pyramidal geometry; ineffective interaction between the four equivalent imidazolyl nitrogen lone-pairs and the central metal cation causes elongation of the Co–N(py) bond to reduce the fifth coordination of the pyridyl nitrogen to the metal ion, which coordination appears to be a necessary prerequisite of oxygen fixation. In accord with this inference, the catalytic behavior of $[Co(tip)]^{2+}$ differs greatly from those of tetra-coordinated Co(salen) in non-coordinating solvents and penta-coordinate Co(salpr), which selectively afford biphenyl-2,2′-diol and the *o*-quinone, respectively (Table 3). Thus, the catalytic behavior of $[Co(tip)]^{2+}$ becomes intermediate between them. The present cobalt oxygen complex is unique in structure among oxygen complexes because it possesses four equal imidazolyl groups as peripheral ligands. However, it should be born in mind that our structural assignment is based on an only limited data. The O–O streching frequencies of cobalt oxygen adduct has been the focus of recent studies since it is a measure of electron donating ability of the chelate. Therefore, resonance Raman or IR studies are under investigation for a detailed characterization of the Co–O and O–O bonding. The results will be published in the near future.

References

1) T. Tumaki, *Bull. Chem. Soc. Jpn.*, **13**, 252 (1938).
2) L. Vaska, *Science*, **140**, 809 (1963); L. H. Vogt, H. M. Faigenbaum, and S. E. Wiberley, *Chem. Rev.*, **63**, 269 (1963); M. M. Taqui Khan and A. E. Martell, "Homogeneous Catalysis by Metal Complexes," Academic Press, New York (1974); E. C. Niederhoffer, J. H. Timmons, and A. E. Martell, *Chem. Rev.*, **84**, 137 (1984).
3) A. B. P. Lever and H. B. Gray, *Acc. Chem. Res.*, **11**, 348 (1978).
4) F. Basolo, B. M. Hoffman, and J. A. Ibers, *Acc. Chem. Res.*, **8**, 384 (1975); D. A. Summervile and F. Basolo, *Chem. Rev.*, **79**, 139 (1979); R. S. Drago, J. Gaul, A. Zombeck, and D. K. Straub, *J. Am. Chem. Soc.*, **102**, 1033 (1980); M. Suzuki, H. Kinatomi, and I. Murase, *Bull. Chem. Soc. Jpn.*, **57**, 36 (1984); A. E. Martell and R. J. Motekaitis, *J. Am. Chem. Soc.*, **110**, 8059 (1988).
5) M. Calligaris, G. Nardin, L. Randaccio, and A. Ripamonti, *J. Chem. Soc. A*, **1970**, 1069.
6) C. Floriani and F. Calderazzo, *J. Chem. Soc. A*, **1969**, 946.
7) A. L. Crumbliss and F. Basolo, *J. Am. Chem. Soc.*, **92**, 55 (1970); G. A. Rodley and W. T. Robinson, *Nature (London)*, **235**, 438 (1972).
8) J. H. Wang, *J. Am. Chem. Soc.*, **80**, 3168 (1958); J. P. Collman, R. R. Gagne, C. A. Reed, T. R. Halbert, G. Lang, and W. T. Robinson, *J. Am. Chem. Soc.*, **97**, 1427 (1975).
9) R. A. Sheldon and J. K. Kochi, "Metal-Catalyzed Oxidations of Organic Compounds," Academic Press, New York (1981), Chap. 4; W. K. Seok and T. J. Meyer, *J. Am. Chem. Soc.*, **110**, 7358 (1988).
10) M. J. Barnes, R. S. Drago, and K. J. Balkus, Jr., *J. Am. Chem. Soc.*, **110**, 6780 (1988). R. J. Motekaitis and A. E. Martell, *ibid.*, **110**, 7715 (1988).
11) S. Takano, Y. Yano, and W. Tagaki, *Chem. Lett.*, **1981**, 1177.
12) Y. Sasagawa, "Wargburg's Manometric Method," Jikken Kagaku Koza, Maruzen, Tokyo (1958), Vol. 24, p. 86.
13) K. Ley and E. Müller, *Chem. Ber.*, **89**, 1402 (1956).
14) E. Müller and K. Ley, *Chem. Ber.*, **88**, 601 (1955).
15) M. S. Kharasch and B. S. Joshi, *J. Org. Chem.*, **22**, 1439 (1957).
16) M. J. Carter, D. P. Rillema, and F. Basolo, *J. Am. Chem. Soc.*, **96**, 392 (1974).
17) G. Tauzher, G. Amiconi, E. Antonini, M. Brunori, G. Antonini, and G. Costa, *Nature (London)*, **241**, 222 (1973).
18) J. C. Stevens and D. H. Busch, *J. Am. Chem. Soc.*, **102**, 3285 (1980).
19) A. E. Martell, *Acc. Chem. Rec.*, **15**, 155 (1982).
20) M. S. Calvin, R. H. Bailes, and W. K. Wilmarth, *J. Am. Chem. Soc.*, **68**, 2254 (1946).
21) B. M. Hoffman, D. L. Diemente, and F. Basolo, *J. Am. Chem. Soc.*, **92**, 61 (1970).
22) G. McLendon, S. R. Pickens, and A. E. Martell, *Inorg. Chem.*, **16**, 1551 (1977).
23) A. Nishinaga and H. Tomita, *J. Mol. Catal.*, **7**, 179 (1970).
24) A. Nishinaga, H. Tomita, K. Nishizawa, and T. Matsuura, *J. Chem. Soc., Dalton Trams.*, **1981**, 1506.
25) R. R. Grinstead, *Biochemistry*, **3**, 1308 (1964); C. R. H. I. de Jonge, "Organic Syntheses by Oxidation with Metal Compounds," ed by W. J. Mils and C. R. H. I. de Jonge, Plenum Press, New York (1986), p. 473.
26) A. Nishinaga, H. Iwasaki, T. Kondo, and T. Matsuura, *Chem. Lett.*, **1985**, 5; A. Nishinaga, H. Tomita, and T. Matsuura, *ibid.*, **1979**, 2893.
27) D. D. Cox and L. Que, Jr., *J. Am. Chem. Soc.*, **110**, 8085 (1988).
28) V. Kothari and J. J. Tazuma, *J. Catal.*, **41**, 180 (1976); H. M. van Dort and H. J. Geursen, *Recl. Trav. Chim. Pay-Bas*, **86**, 520 (1967).
29) L. H. Vogt, J. G. Wirth, and H. L. Finkbeiner, *J. Org. Chem.*, **34**, 273 (1969); A. S. Hay, *ibid.*, **34**, 1160 (1969).
30) D. L. Tomaja, L. H. Vogt, and J. G. Wirth, *J. Org. Chem.*, **35**, 2029 (1970); A. Nishinaga, H. Tomita, K. Nishizawa, and T. Matsuura, *J. Chem. Soc., Dalton Trans.*, **1981**, 1504.
31) D. L. Tomaja, H. L. Vogt, and J. G. Wirth, *J. Org. Chem.*, **35**, 2029 (1970).
32) M. Frostin-Rio, D. Pujol, C. Bied-Charreton, M. Perrée-Fauvet, and A. Gaudemer, *J. Chem. Soc., Perkin Trans. 1*, **1984**, 1971.

Synthesis of a Chiral α-(Aminooxy)arylacetic Ester. II.[1] A Route through a Chiral 2-Hydroxy-2-phenylacetic Acid Derivative

Hisao IWAGAMI,* Masanobu YATAGAI, Masakazu NAKAZAWA, Haruo ORITA, Yutaka HONDA, Takashi OHNUKI, and Toshihide YUKAWA
Central Research Laboratories, Ajinomoto Co., Inc., 1-1, Suzuki-cho, Kawasaki-ku, Kawasaki 210
(Received June 21, 1990)

A simple and practical synthetic route has been developed for the synthesis of a chiral α-(aminooxy) ester (*S*)-**16**, which is a synthetic intermediate for a potent antipseudomonal cephalosporin antibiotic M-14659. In this synthetic route, the key intermediate is α-hydroxy acid (*R*)-**7** (100%ee), which is prepared by an asymmetric reduction of α-keto ester with $NaBH_4$-(*R*,*R*)-tartaric acid followed by a hydrolysis and an optical resolution using L-Leu-$NHNH_2$. (*S*)-**16** is obtained stereoselectively through 3 steps from (*R*)-**7**. HPLC analyses and NMR studies have proved that the (*S*)-**16** thus prepared is completely optically pure.

Although α-(aminooxy) acid derivatives **1** are regarded as analogues of α-amino acids, there have been very few studies concerning the synthesis of optically active **1**[2]. α-(Aminooxy) esters of structure **2** were required as synthetic intermediates for M-14659 (**3**),[3] which is a potent antipseudomonal cephalosporin antibiotic. In the preceding report[1] we have shown that optically active α-(aminooxy) ester (*S*)-**4** can be prepared from α-(phthalimidooxy) acid (*S*)-**5** which is obtained by optical resolution.

In search for a simpler and more practical synthetic route to α-(aminooxy) esters of structure **2**, we turned our attention to the following facts found in the course of investigations previously reported:[1] (1) α-hydroxy acid (*R*)-**7** in nearly 100%ee is obtainable by an optical resolution using L-Leu-$NHNH_2$ (Eq. 1), and accordingly, we can use (*R*)-**7** as a chiral starting material; (2) although, as previously described, attempts to obtain optically active 2-halo derivatives (*R*)-**6** were unsuccessful due to the presence of an electron-donating group at the para position, an S_N2 reaction itself at the benzylic position proceeds with virtually complete inversion of configuration (Eq. 2).

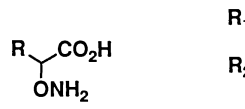

1

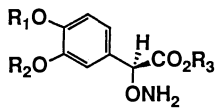

2

R_1, R_2, R_3: protective group

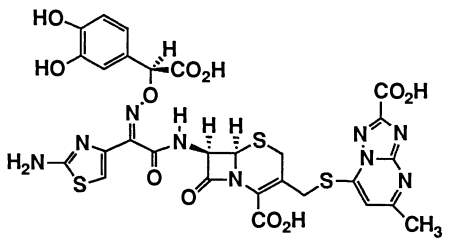

3

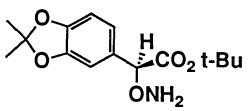

(*S*)-4

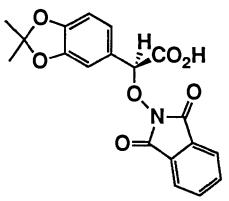

(*S*)-5

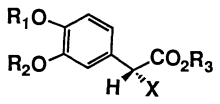

(*R*)-6

X= halogen

R_1, R_2, R_3 : protective group

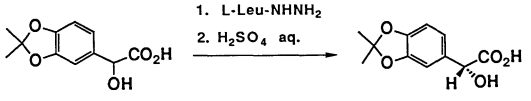

(1)

7 (*R*)-7 (96%ee)

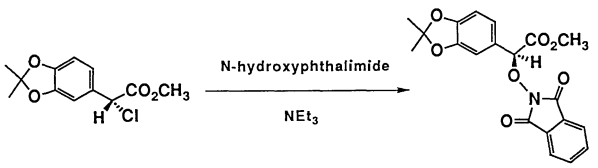

(2)

(*R*)-8 (50%ee) (*S*)-9 (48%ee) 80% yield

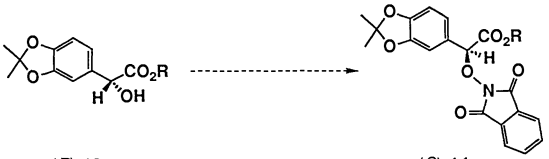

(3)

(*R*)-10 (*S*)-11

R: a protecting group

Namely, it appeared to us that α-(phthalimidooxy) ester (*S*)-**11** could be prepared from α-hydroxy acid (*R*)-**10** with a steric inversion under appropriate conditions (Eq. 3). In addition, tedious operations involved in the recovery of the undesired enantiomer and its racemization might be omitted in this approach. In this paper, we report some details of this synthetic strategy.

Results and Discussion

We have already shown two synthetic sequences to racemic **7** starting from catechol[1] and, as described above, (*R*)-**7** is obtainable by optical resolution of racemic **7**.[1] On the other hand, however, one of the most convenient methods for the preparation of optically active α-hydroxy esters is asymmetric reduction of their corresponding α-keto esters. Consequently, an asymmetric reduction of α-keto ester **13a** was first explored in order to obtain ethyl (*R*)-2-(3,4-isopropylidenedioxyphenyl)-2-hydroxyacetate [(*R*)-**14a**] (Scheme 1). Starting material **13a** was prepared by the method shown in Scheme 1.

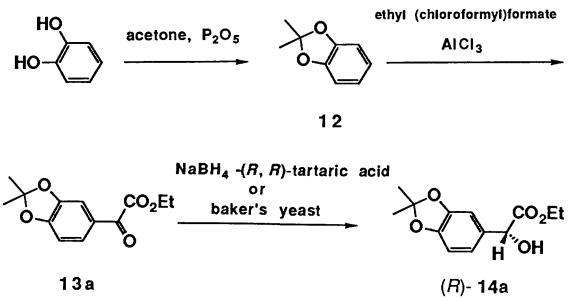

Scheme 1.

An isopropylidenation of catechol in toluene by using acetone in the presence of phosphorus pentaoxide gave 1,2-isopropylidenedioxybenzene (**12**) in 70% yield. α-Keto ester **13a** was prepared by the Friedel–Crafts acylation[4] of **12** with ethyl (chloroformyl)formate in 86% yield without cleavage of isopropylidene protection.[5]

Asymmetric reduction of α-keto esters has been widely studied. One of them utilizes chiral reducing agents[6] and another is a catalytic hydrogenation in the presence of chiral ligands.[7] Although high optical purities are obtained in these cases, neither the chiral reducing agents nor hydrogenation catalysts are necessarily easily accessible. Also, diastereoselective reductions of chiral α-keto amides or α-keto esters with metal hydrides have been well documented.[8] However, because these methods are of multi-step process, they do not fill our requirements for the practical preparation of (*R*)-**14a**. On the other hand, asymmetric reductions of prochiral ketones and cyclic imines with chiral $NaBH_4$ derived systems which are prepared by a reaction of $NaBH_4$ with a monosaccharide[9] or with an α-amino acid derivative (especially L-Pro derivative),[10] have been investigated actively. Although these methods result in moderate optical purities, their simple systems seem applicable to our needs which aim at a more efficient and economical synthetic method for (*R*)-**14a**. Accordingly, we focused

Table 1. Asymmetric Reduction of **13a** with Modified Reagents Prepared from $NaBH_4$ and Various Chiral Compounds[a]

Run	Chiral compound	**14a** Chemical yield/%	**14a** Optical yield/%ee[d]
1	L-Pro	80	53 (*R*)
2	(*R*,*R*)-Tartaric acid	96	70 (*R*)
3	Benzyloxycarbonyl-L-Pro	75	17 (*R*)
4		c)	29 (*R*)
5	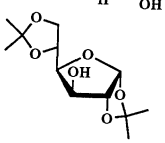 +$ZnCl_2$[b]	c)	9 (*S*)
6	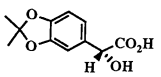	c)	8 (*R*)
7	(*S*)-Mandelic acid	c)	5 (*R*)
8	(*S*)-Malic acid	c)	0
9	*O*,*O*-Dibenzoyl-(*R*,*R*)-tartaric acid	c)	0
10	(*R*,*R*)-Diethyl tartarate	c)	0

a) Reaction conditions: A solution of **13a** (1.0 mmol) in THF (5 ml) was added at 0 °C to a stirred suspension of chiral reducing agent prepared from $NaBH_4$ (1.0 mmol) and a chiral compound (1.0 mmol) in THF (5 ml) at room temperature for 3 h; the whole was then stirred at 0 °C for 1 d. b) See Ref. 10(e). c) Not estimated. d) Assayed by HPLC analysis using a chiral column. See Experimental Section.

on the asymmetric reduction of **13a** by using chiral $NaBH_4$ derived systems prepared in situ. Reductions of **13a** with reagents prepared in situ from $NaBH_4$ (1.0 equiv) and various chiral compounds (1.0 equiv) were carried out in THF at 0 °C (Table 1).

As can be seen in Table 1, the system derived from $NaBH_4$ and (*R*,*R*)-tartaric acid provided (*R*)-**14a** with an enantiomeric excess as high as 70% (Run 2, Table 1). The optical purity in this system was enhanced to 78%ee by using 1.5 equiv of (*R*,*R*)-tartaric acid and lowering the reaction temperature to −20 °C.[11] The chiral reducing agents derived from L-Pro (Run 1, Table 1) and its derivatives (Runs 3 and 4, Table 1) were found to be less effective. The asymmetric reduction of propiophenone with the reagent prepared from $NaBH_4$ and (*S*,*S*)-tartaric acid has already been reported, which, however, gives (*S*)-1-phenyl-1-propanol in only 10% optical yield.[12] Interestingly, the systems using other chiral α-hydroxy acids were found to be much less effective (Runs 6, 7, and 8, Table 1). Also, in the case where either a hydroxyl group or a carboxyl group of (*R*,*R*)-tartaric acid was protected, the stereoselectivities were completely out of operation (Runs 9 and 10, Table 1). Presumably, the steric configuration in the chelation between $NaBH_4$ and bidentate (*R*,*R*)-tartaric acid exerts and effect on the course of the hydride-transfer step in the transition state.

Asymmetric reductions of keto esters to hydroxy esters by microbial transformation have also been widely studied.[13] Consequently, we undertook a study aiming at an asymmetric reduction of **13a** by using a yeast. A reduction of **13a** with baker's yeast in water containing sucrose gave (*R*)-**14a** in 94%ee optical yield (65% chemical yield). The absolute configuration of the product obtained by reduction of a carbonyl group containing a large group and a small group to an alcohol is known to be determined by application of Prelog's rule.[14] Because 3,4-isopropylidenedioxyphenyl group is larger than ethoxycarbonyl group in bulkiness, the absolute configuration of **14a** obtained by yeast reduction is expected to be an (*R*)-configuration. Furthermore, **14a** obtained by yeast reduction showed a Cotton effect $[\theta]_{241}=-14900$ ($c=2.64\times10^{-4}$ M, 17 °C) (1 M=1 mol dm^{-3}). It has been reported that the sign of Cotton effect in the low-wavelength region is negative for the aromatic chromophere of (*R*)-mandelic acid esters.[15] Therefore, it is concluded that **14a** obtained by yeast reduction has an (*R*)-configuration. The absolute configuration of the products in Table 1 was determined by a comparison with (*R*)-**14a** obtained by yeast reduction in HPLC analysis using a chiral column.

A treatment of (*R*)-**14a** (78%ee) with NaOH in aq MeOH gave (*R*)-**7** quantitatively (Scheme 2). The optical purity of the obtained (*R*)-**7** proved that none of (*R*)-**7** racemized in the course of the alkaline hydrolysis. The obtained (*R*)-**7** was treated with L-Leu–$NHNH_2$ in aq MeOH and subjected to a pH adjustment with H_2SO_4 aq to give a diastereomer salt, which was recrystallized by pH adjustment to afford a purified diastereomer salt [100%ee as (*R*)-**7**]. Subsequently acidification of the diastereomer salt followed by crystallization gave (*R*)-**7** (100%ee) in 75% chemical yield from (*R*)-**14a** (Scheme 2).[16] The optical purity of (*R*)-**7** was confirmed by HPLC analysis of a diastereomer prepared from (*R*)-**7** and L-Leu-OMe. Thus, (*R*)-**7** was coupled with L-Leu-OMe by using 1-(3-dimethylaminopropyl)-3-ethylcarbodiimide hydrochloride (WSC·HCl) and 1-hydroxybenzotriazole (HOBt) to give *N*-[2-(3,4-isopropylidenedioxyphenyl)-2-hydroxyacetyl]-L-Leu-OMe. The optical purity determined by the diastereomer was in accord with that determined by the assay of the enantiomer.

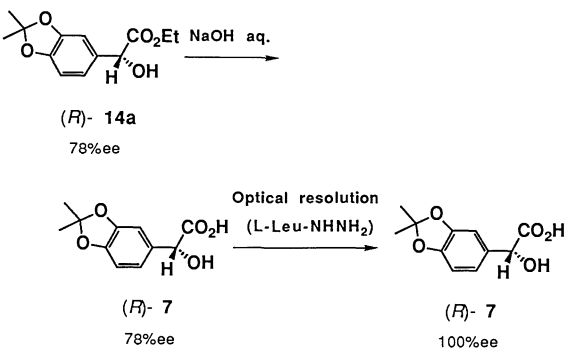

Scheme 2.

As previously described, the protective group R_3 in a compound of structure **2** should be removable under conditions in which β-lactam ring is stable. Although *t*-butyl group seemed to be suitable for R_3, attempts to obtain α-hydroxy *t*-butyl ester (*R*)-**14b** in both chemically and optically high yield were unsuccessful. Namely, an initial attempt to treat (*R*)-**7** with *O*-*t*-butyl-*N*,*N*′-dicyclohexylisourea[17] gave (*R*)-**14b** in 72% yield even in using 5.0 equiv of the alkylating agent (Scheme 3a). Also, an asymmetric reduction of *t*-butyl

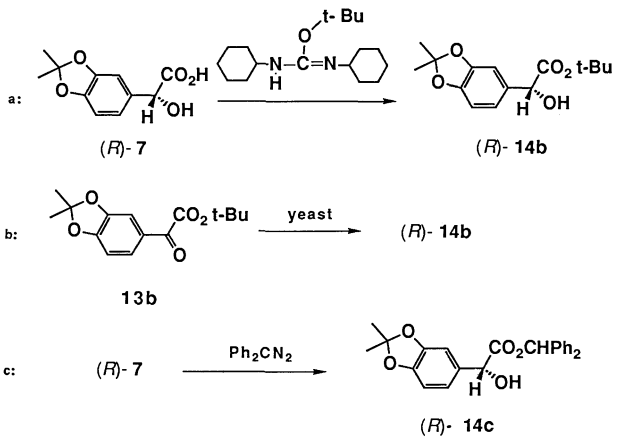

Scheme 3.

ester of α-keto acid **13b** by using baker's yeast gave (*R*)-**14b** in 87%ee (Scheme 3b).[18] Consequently, we chose a diphenylmethyl group as the protective group R_3. A treatment of (*R*)-**7** with Ph_2CN_2 in AcOEt gave diphenylmethyl ester of α-hydroxy acid (*R*)-**14c** quantitatively (Scheme 3c). No decrease in optical purity was observed in this esterification.

The Mitsunobu reaction has proven to be a useful and practical method for conversion of alcohols to various derivatives.[19] Especially it is known that the reaction proceeds with virtually complete inversion of configuration.[20] Accordingly, we made a study on an application of the Mitsunobu reaction to the conversion of (*R*)-**14c** into α-(phthalimidooxy) ester (*S*)-**15**. The reaction of alcohols with *N*-hydroxyphthalimide under the Mitsunobu conditions has been known.[21] An initial attempt to obtain (*S*)-**15** from (*R*)-**14c** (100%ee) by the treatment with *N*-hydroxyphthalimide in the presence of triphenylphosphine and diethyl azodicarboxylate in AcOEt at room temperature, gave (*S*)-**15** in only 30%ee optical purity and in 46% chemical yield. However, both the optical purity and chemical yield were enhanced to 99.4%ee and 95%, respectively, by carrying out the reaction at −20 °C and by minimizing the H_2O content in the reaction solution (Scheme 4). Because the pK_a value of *N*-hydroxyphthalimide is 6.91 in aqueous medium,[22] the rate-determining step of the whole Mitsunobu process may be the S_N2 step rather than the alcohol activation step.[20d] Actually the reaction followed the S_N2 kinetics, being first order in each of (*R*)-**14c** and *N*-hydroxyphthalimide. Attempts to detect phosphorus-containing intermediates, phosphoranes[23] or alkoxyphosphonium salts,[20d,24] by using HPLC analyses or ^{31}P NMR studies were unsuccessful.[25] A recrystallization of (*S*)-**15** (99.4%ee) from MeOH gave (*S*)-**15** (100%ee) as white crystals (isolated yield 86% from (*R*)-**14c**). It is important to run the Mitsunobu reaction under controlled conditions in order to obtain (*S*)-**15** (100%ee).

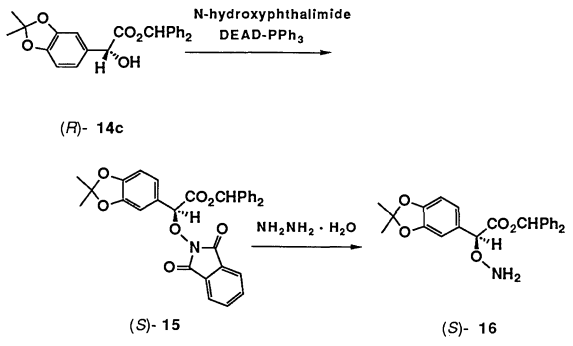

Scheme 4.

Finally, the removal of the phthalimido group by using hydrazine hydrate in CH_2Cl_2 gave (*S*)-**16** (100%ee) in 97% chemical yield (Scheme 4). Furthermore, it was confirmed by an HPLC analysis of the diastereomer prepared from (*S*)-**16** and (+)-10-camphorsulfonyl chloride. Thus, the obtained (*S*)-**16** was treated with (+)-10-camphorsulfonyl chloride in CH_3CN containing NEt_3 to give sulfoneamide (*S*)-**17**. The optical purity of the diastereomer was in accord with the enantiomer. It was also reconfirmed by ^1H NMR spectra of (*S*)-**17** and (+)-3,3,3-trifluoro-2-methoxy-2-phenylpropionamide[26] ((*S*)-**18**) that the obtained (*S*)-**16** was completely free from (*R*)-enantiomer. The signals of the methylene proton at position 10 in (*S*)-**17** and the methyl proton of methoxyl group in (*S*)-**18** were usable to detect the (*R*)-enantiomer.

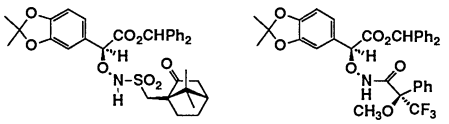

(*S*)-17 (*S*)-18

In conclusion, a simpler and more practical synthetic route for the chiral α-(aminooxy) ester (*S*)-**16** (100%ee) has been established. In this synthetic route, (*S*)-**16** was prepared through 3 steps from α-hydroxy acid (*R*)-**7** (100%ee), which was obtained by the asymmetric reduction of α-keto ester **13a** with $NaBH_4$-(*R*,*R*)-tartaric acid followed by a hydrolysis and an optical resolution using L-Leu-$NHNH_2$. The procedures described here have been used to prepare multikilogram batches of (*S*)-**16**, which is in turn converted to M-14659, a potent antipseudomonal cephalosporin antibiotic.

Experimental

General. All reactions except optical resolution were carried out under nitrogen atmosphere. Unless otherwise noted, materials were obtained from commercial suppliers and used without further purification. Melting points were determined using a Büchi 510 apparatus and are uncorrected. ^1H NMR spectra were obtained on a Varian VXR-300 (300 MHz) spectrometer with tetramethylsilane as the internal standard. IR spectra were obtained on a JASCO IR-800

Table 2. HPLC Analyses of the Synthetic Intermediates[a]

Compound	Retention time/min
12	11.3
13a	12.1
14a	7.1
7	3.2
14c	15.6
15	35.4
16	17.6

a) HPLC conditions: column NUCLEOSIL-ODS (5 μm) 6 mm×200 mm, eluent CH_3CN–H_2O (6:4, v/v), flow 1.0 ml min^{-1}, 50 °C, and λ 290 nm.

Table 3. HPLC Analyses of the Optical Isomers

Compound	Column	Eluent	Flow	Column temperature	UV detection	Retention time/min	
			ml min^{-1}	°C	nm	(*R*)-	(*S*)-
14a	Daicel CHIRALPAK OT(+) 4.6 mm×250 mm	MeOH	0.50	−2	290	8.2	13.0
7	Daicel CHIRALPAK WH 6.4 mm×250 mm	0.25 M $CuSO_4$ aq	1.0	50	238	31	25
7-L-Leu-OMe	NUCLEOSIL-5NH_2 6 mm×200 mm	Hexane–*i*-PrOH (92.5:7.5)[a]	1.0	20	288	29.6	22.7
14c	Daicel CHIRALPAK OT(+) 4.6 mm×250 mm	MeOH–H_2O (92:8)[a]	0.50	−2	290	18.5	22.5
15	Daicel CHIRALCEL OA 4.6 mm×250 mm	Hexane–EtOH–*i*-PrOH–H_2O (100:10:5:0.5)[a]	0.50	20	290	32.1	37.1
16	Daicel CHIRALCEL OD 4.6 mm×250 mm	Hexane–EtOH–*i*-PrOH (100:10:10)[a]	0.50	20	290	18.3	23.1
17	NUCLEOSIL 7.2 mm×250 mm	CH_3CN–H_2O (6:4)[a]	1.0	20	290	47	40

a) Volume ratio.

or a Perkin–Elmer 1640 spectrometer in the indicated phase. Mass spectra were measured on a JEOL DX-300 mass spectrometer. Optical rotations were recorded on a JEOL DIP-140 polarimeter. Analytical thin-layer chromatography (TLC) was performed on Merck silica gel 60 F_{254} glass-backed plates. Column chromatography was done using Merck silica gel 60 (70—230 mesh). Chemical purities of the synthetic intermediates (accordingly, yields in each step) were determined by HPLC analysis. All compounds were assayed under the same conditions. The HPLC conditions and the retention times of all intermediates were tabulated in Table 2. Optical purities of enantiomeric intermediates were also determined by HPLC analysis using a chiral column. Some of optically active intermediates were converted to diastereomers whose optical purities were determined. The conditions were summarized in Table 3.

1,2-Isopropylidenedioxybenzene (12). A mixture of catechol (110 g, 1.0 mol) and P_2O_5 (28.4 g, 0.20 mol) in toluene (500 ml) was heated at 75 °C. To the suspension was added dropwise acetone (147 ml, 2.0 mol) over 3 h. After the addition had been started, four portions of P_2O_5 (28.4 g, 0.20 mol) were added to the reaction mixture every 30 min. Totally 142 g of P_2O_5 was used. After the addition of acetone, the mixture was stirred at 75 °C for further 1 h. After removing the oily compound (the lower layer), 150 ml of 25% NaOH was added. The organic layer was separated, washed with H_2O and concentrated in vacuo to give an oil, from which **12** was obtained by distillation as a colorless liquid: Yield 105 g (70%); bp 75—78 °C/23.5 mmHg (1 mmHg=133.322 Pa); ^{1}H NMR ($CDCl_3$) δ=1.65 (s, 6H) and 6.7—6.8 (m, 4H).

Ethyl 2-(3,4-Isopropylidenedioxyphenyl)-2-oxoacetate (13a). To a suspension of $AlCl_3$ (5.0 g, 37.5 mmol) in CH_2Cl_2 (30 ml) cooled to 5 °C was added slowly ethyl (chloroformyl)formate (3.41 g, 25.0 mmol) and the resulting solution was stirred for 15 min at 5 °C. To the solution was added **12** (3.75 g, 25.0 mmol) over 5 min. After the addition the mixture was stirred at room temperature for 1 h. The reaction mixture cooled to 5 °C was poured slowly into 25 ml of H_2O cooled to 5 °C. The organic layer was separated, washed (satd. $NaHCO_3$ and then H_2O), dried ($MgSO_4$), filtered and concentrated in vacuo to give a wine-red liquid, from which **13a** was obtained by distillation as a yellowish liquid: Yield 5.38 g (86%); bp 129—131 °C/0.65 mmHg; ^{1}H NMR ($CDCl_3$) δ=1.40 (t, 3H), 1.68 (s, 6H), 4.42 (q, 2H), 6.69 (d, 1H, *J*=11), 7.38 (d, 1H, *J*=2.5), and 7.55 (dd, 1H, *J*=11, 2.5); MS (FD) *m/z* 250 (M^+).

Ethyl (*R*)-2-(3,4-Isopropylidenedioxyphenyl)-2-hydroxyacetate [(*R*)-14a]. Reduction by $NaBH_4$-(*R*, *R*)-Tartaric Acid. $NaBH_4$ (1.26 g, purity 90%, 30.0 mmol) and (*R*,*R*)-tartaric acid (4.50 g, 30.0 mmol) were suspended in THF (100 ml) and the resulting suspension was heated at 70 °C for 4 h. The suspension cooled to −20 °C was added dropwise **13a** (5.0 g, 20.0 mmol) in 10 ml of THF over 5 min. After the addition, the reaction mixture was stirred at −20 °C for 15 h. To the mixture were added 50 ml of AcOEt and 25 ml of 1M (1 M=1 mol dm^{-3}) HCl at −20 °C. The organic layer was separated, washed (satd. $NaHCO_3$), dried ($MgSO_4$), filtered and concentrated in vacuo to give a pale yellow oil. Chromatographic separation on silica gel (30 g, hexane–AcOEt, 6:1 v/v) gave **14a** as an oil: Yield 4.74 g (94%, optical purity 78%ee); ^{1}H NMR ($CDCl_3$) δ=1.25 (t, 3H), 1.65 (s, 6H), 3.25 (b, 1H), 4.22 (m, 2H), 5.03 (s, 1H), 6.68 (d, 1H, *J*=10), 6.79 (d, 1H, *J*=2.5), and 6.82 (dd, 1H, *J*=10, 2.5); MS (FD) *m/z* 252 (M^+).

Reduction by $NaBH_4$-L-Pro. $NaBH_4$ (5.04 g, 90% purity, 120 mmol) and L-Pro (13.8 g, 120 mmol) were suspended in 240 ml of THF and the resulting suspension was stirred at room temperature for 3.5 h. To the resulting clear solution cooled to 0 °C was added **13a** (30.0 g, 120 mmol) in 30 ml of THF over 10 min and the mixture was stirred at 0 °C for 17.5 h. The solvent of the reaction mixture was removed in vacuo. The obtained oil was dissolved in toluene (120 ml) and H_2O (120 ml). The organic layer was separated, washed (H_2O), dried ($MgSO_4$), filtered and concentrated in vacuo to give **14a** as an oil: Yield 29.5 g (86% chemical purity, 84% yield, 52%ee). The NMR spectra were identical with those of **14a** prepared above.

Reduction by Yeast. A mixture of sucrose (15 g) and baker's yeast[27] (14 g) in 100 ml of distilled water was stirred

at 30 °C for 1 h. To the mixture was added **13a** (7.84 g, 31.4 mmol) and the fermenting suspension was stirred at 30 °C for another 22 h. The mixture was worked up by adding 3 g of Celite and filtering. The Celite was washed with 50 ml of AcOEt and then with 50 ml of H_2O. The washings were combined with the filtrate. The organic layer was separated and the aquesous layer was washed with AcOEt (30 ml×3). The combined AcOEt extracts were washed (brine), dried ($MgSO_4$), filtered and concentrated in vacuo to give an oil. Chlomatographic separation on silica gel (30 g, hexane–AcOEt, 6:1 v/v) gave **14a** as a pale yellow oil: Yield 5.14 g (65%, 94%ee). The NMR spectra were identical with those of **14a** prepared above.

(*R*)-2-(3,4-Isopropylidenedioxyphenyl)-2-hydroxyacetic Acid [(*R*)-7]. α-Hydroxy ester **14a** [56.3 g, chemical purity 88%, optical purity 76%ee, 173 mmol as (*R*)-**14a**] was dissolved in a mixture of MeOH (150 ml) and 48% NaOH (17 ml). The mixture was stirred at 30 °C for 1.5 h. To the mixture was added L-Leu-$NHNH_2$ (28.6 g, 197 mmol) in 150 ml of MeOH. An adjustment of pH to 6.8 with 95% H_2SO_4 followed by a crystallization with stirring at 28 °C for 2 h gave white crystals, which were recrystallized by a pH adjustment to give a diastereomer salt [58.7 g, 100%ee, 92% from (*R*)-**14a**]. The obtained salt was suspended in 300 ml of H_2O and the pH of the mixture was adjusted to 2.0 with 95% H_2SO_4. A crystallization with stirring at 33 °C for 3.5 h gave (*R*)-**7** as a white powder: Yield 30.7 g [optical purity 100%ee, 79% from (*R*)-**14a**]; mp 132—133 °C; $[\alpha]_D^{24}$ −88.7° (*c*=1.36, MeOH); ^1H NMR (Me_2SO-d_6) δ=1.61 (s, 6H), 3.3 (b, 1H), 4.85 (s, 1H), and 6.73—6.88 (m, 3H); IR(KBr) 1702 cm^{-1} (C=O). Found: C, 58.80; H, 5.63%. Calcd for $C_{11}H_{12}O_5$: C, 58.92; H, 5.40%.

Optical Purity Determination of (*R*)-7 by HPLC Analysis of a Diastereomer Prepared from (*R*)-7 and L-Leu-OMe. A sample of (*R*)-**7** (0.224 g, 1.0 mmol) and L-Leu-OMe·HCl (0.272 g, 1.50 mmol) were suspended in 7 ml of CH_3CN containing NEt_3 (0.21 ml, 1.50 mmol). To the obtained clear solution cooled to 0 °C were added 1-hydroxybenzotriazole (0.177 g, 1.0 mmol) and 1-(3-dimethylaminopropyl)-3-ethylcarbodiimide hydrochloride (0.211 g, 1.10 mmol) and the reaction mixture was stirred at room temperature for another 2 h. Et_2O (15 ml) was added to the reaction mixture. The organic layer was separated and washed with 1 M HCl and then with saturated $NaHCO_3$. After dilution with an eluent, the organic layer was analyzed by HPLC under the conditions which are shown in Table 3.

Diphenylmethyl (*R*)-2-(3,4-Isopropylidenedioxyphenyl)-2-hydroxyacetate [(*R*)-14c]. α-Hydroxy acid (*R*)-**7** (22.4 g, 100 mmol, 100%ee) was suspended in 120 ml of AcOEt and to the suspension was added dropwise Ph_2CN_2 (20.4 g, 105 mmol) in 15 ml of CH_2Cl_2 over 1 h. During the addition the inner temperature was kept below 35 °C. After the addition, the reaction was stirred for another 1 h. After quenching the excess Ph_2CN_2 with AcOH, the reaction mixture was washed with saturated $NaHCO_3$. The organic layer was separated and concentrated in vacuo to give a white powder, which was recrystallized from EtOH to give (*R*)-**14c** as a white powder: Yield 35.9 g (92%, 100%ee); mp 136—136.5 °C; $[\alpha]_D^{22}$ −34.7° (*c*=0.944, $CHCl_3$); ^1H NMR ($CDCl_3$) δ=1.65 (s, 6H), 5.15 (s, 1H), 6.84 (d, 1H, *J*=10), 6.88 (d, 1H, *J*=2.4), 6.92 (dd, 1H, *J*=10, 2.4), 6.94 (s, 1H), 6.99 (m, 2H), and 7.15—7.4 (m, 8H); IR(KBr) 1731 cm^{-1} (C=O); MS (FD) *m/z* 390 (M^+). Found: C, 73.79; H, 5.74%. Calcd for $C_{24}H_{22}O_5$: C, 73.83; H, 5.68%.

Diphenylmethyl (*S*)-2-(3,4-Isopropylidenedioxyphenyl)-2-(phthalimidooxy)acetate [(*S*)-15]. To a solution of (*R*)-**14c** (19.5 g, 50.0 mmol, 100%ee) in 200 ml of AcOEt were added triphenylphosphine (17.6 g, 67.0 mmol) and *N*-hydroxyphthalimide (9.79 g, 60.0 mmol). To the obtained suspension cooled to −20 °C was added diethyl azodicarboxylate (11.7 g, 67.0 mmol) in one mass. The reaction mixture was stirred at −20 °C for 1 h. The solvent was removed in vacuo. A recrystallization from 160 ml of MeOH at 5 °C gave (*S*)-**15a** as white crystals: Yield 23.0 g (86%, 100%ee); mp 117.5—118 °C; $[\alpha]_D^{22}$ +116.7° (*c*=1.30, $CHCl_3$); ^1H NMR ($CDCl_3$) δ=1.65 (s, 6H), 5.29 (s, 1H), 6.66 (d, 1H, *J*=10), 6.92 (d, 1H, *J*=2.4), 6.97 (dd, 1H, *J*=10, 2.4), 6.99 (s, 1H), 7.1—7.35 (m, 10H), and 7.65—7.8 (m, 4H); IR(KBr) 1793, 1752, and 1734 cm^{-1} (C=O). Found: C, 71.49; H, 4.94; N, 2.51%. Calcd for $C_{32}H_{25}NO_7$: C, 71.76; H, 4.71; N, 2.62%.

Diphenylmethyl (*S*)-2-(3,4-Isopropylidenedioxyphenyl)-2-(aminooxy)acetate [(*S*)-16]. To a solution of (*S*)-**15** (16.1 g, 30.0 mmol, 100%ee) in 60 ml of CH_2Cl_2 was added NH_2NH_2·H_2O (3.60 g, 72.0 mmol). The mixture was stirred at room temperature for 1 h. H_2O (150 ml) was added to the reaction mixture and the resulting precipitates were removed by filtration. The organic layer of the filtrate was separated, washed (H_2O), dried ($MgSO_4$), filtered and concentrated in vacuo to give a white solid. A recrystallization from MeOH gave (*S*)-**16** as a white powder: Yield 11.8 g (97%, 100%ee); mp 96—97 °C; $[\alpha]_D^{24}$ +24.5° (*c*=0.669, $CHCl_3$); ^1H NMR ($CDCl_3$) δ=1.66 (s, 6H), 5.22 (s, 1H), 6.66 (d, 1H, *J*=10), 6.75 (d, 1H, *J*=2.4), 6.81 (dd, 1H, *J*=10, 2.4), 6.92 (s, 1H), 7.07—7.11 (m, 2H), and 7.20—7.32 (m, 10H); IR(KBr) 1730 cm^{-1} (C=O); Found: C, 70.89; H, 5.60; N, 3.40%. Calcd for $C_{24}H_{23}NO_5$: C, 71.10; H, 5.72; N, 3.45%.

Diphenylmethyl (*S*)-2-(3,4-Isopropylidenedioxyphenyl)-2-[[(+)-10-camphorsulfonyl]aminooxy]acetate [(*S*)-17]. To a solution of (*S*)-**16** (81 mg, 0.20 mmol, 92.0%ee by HPLC analysis using a chiral column) in 2 ml of CH_3CN were added NEt_3 (0.056 ml, 0.40 mmol) and (+)-10-camphorsulfonyl chloride (100 mg, 0.40 mmol). The reaction mixture was stirred at room temperature for 1 h. The solvent was removed in vacuo to give an oil, which was dissolved in 20 ml of AcOEt. After washed with 1 M HCl aq, saturated $NaHCO_3$ and brine in this order, the organic layer was assayed by HPLC under the conditions which are shown in Table 3 to result in 92.3%ee. Racemic **16** was converted to racemic **17** by the method shown above. Each of (*S*)-**17** and (*R*)-**17** was isolated by preparative HPLC under the conditions shown in Table 3. (*S*)-**17**: ^1H NMR ($CDCl_3$) δ=0.94 (s, 3H), 1.00 (s, 3H), 1.67 (s, 3H), 1.68 (s, 3H), 1.87—2.14 (m, 6H), 2.41 (m, 1H), 2.89, 2.94, 3.81, and 3.86 (ABq, 2H, methylene proton at position 10), 5.58 (s, 1H), 6.68 (d, 1H, *J*=10), 6.77 (d, 1H, *J*=2.4), 6.84 (dd, 1H, *J*=10, 2.4), 6.88 (s, 1H), 7.07—7.11 (m, 2H), 7.18—7.30 (m, 8H), and 8.43 (s, 1H). (*R*)-**17**: ^1H NMR ($CDCl_3$) δ=0.90 (s, 3H), 0.95 (s, 3H), 1.665 (s, 3H), 1.662 (s, 3H), 1.90—2.20 (m, 6H), 2.41 (m, 1H), 2.79, 2.84, 3.70, and 3.75 (ABq, 2H, methylene proton at position 10), 5.61 (s, 1H), 6.63 (d, 1H, *J*=10), 6.76(d, 1H, *J*=2.4), 6.80 (dd, 1H, *J*=10, 2.4), 6.95 (s, 1H), 7.13—7.33 (m, 10H), and 9.12 (s, 1H).

Diphenylmethyl (*S*)-2-(3,4-Isopropylidenedioxyphenyl)-2-[[(2*R*)-3,3,3-trifluoro-2-methoxy-2-phenylpropionyl]aminooxy]acetate [(*S*)-18]. To a solution of (*S*)-**16** (203 mg, 0.50 mmol, 100%ee) in 5 ml of CH_3CN containing NEt_3 (0.075 ml, 0.60 mmol) was added (*R*)-(+)-3,3,3-trifluoro-2-methoxy-2-phenylpropionyl chloride[29] (0.150 mg, 0.60 mmol). The reaction mixture was stirred at room temperature for 1 h. The solvent was removed in vacuo and the obtained oil was dissolved in 20 ml of Et_2O. The Et_2O solution was washed with 1 M HCl, saturated $NaHCO_3$ and brine in this order and then concentrated in vacuo to give an oil, which was analyzed by NMR: ^1H NMR ($CDCl_3$) δ=1.66 (s, 6H), 3.25 (s, 3H, methyl proton in methoxyl group), 5.53 (s, 1H), 6.68 (d, 1H, J=10), 6.79 (s, 1H, J=2.4), 6.82 (dd, 1H, J=10, 2.4), 6.88 (s, 1H), 7.03—7.48 (m, 15H), and 9.52 (s, 1H). On the other hand, racemic **18** showed two peaks at δ=3.25 and 3.18 corresponding to methyl proton in methoxyl group.

The anthors wish to thank Drs. Kazuo Kato and Kimihiro Murakami, Fuji Central Research Laboratory, Mochida Pharmaceutical Co., Ltd for their helpful discussions.

References

1) Part I: H. Iwagami, M. Nakazawa, M. Yatagai, T. Hijiya, Y. Honda, H. Naora, T. Ohnuki, and T. Yukawa, *Bull. Chem. Soc. Jpn.*, **63**, 3073 (1990).

2) a) Brit. Patent 1394170 (1975); *Chem. Abstr.*, **83**, 96439 (1975); b) K. Undheim, P. Bamberg, and B. Sjoberg, *Acta Chem. Scand.*, **19**, 317 (1965); c) E. Testa, B. J. R. Nicolaus, L. Mariani, and G. Pagani, *Helv. Chim. Acta*, **85**, 766 (1963); d) T. Kolasa and A. Chimiak, *Rocz. Chem.*, **50**, 367 (1976); e) T. Kolasa and M. J. Miller, *J. Org. Chem.*, **51**, 3055 (1986); f) H. Schweer, *J. Chromatogr.*, **243**, 149 (1982).

3) a) H. Mochizuki, Y. Oikawa, H. Yamada, S. Kusakabe, T. Shiihara, K. Murakami, K. Kato, J. Ishiguro, and H. Kosuzume, *J. Antibiot.*, **41**, 377 (1988); b) H. Mochizuki, H. Inaba, M. Mizota, K. Kato, H. Kosuzume, H. Tajima, H. Onishi, and E. Mochida, 25th Intersci. Conf. on Antimicro. Agents Chemother., Minneapolis, Sept 29—Oct. 2, 1985, Abstr., No. 356, p. 156; c) K. Kato, K. Murakami, I. Yamamoto, M. Ohashi, A. Tomiguchi, and H. Mochizuki, 26th Intersci. Conf. on Antimicro. Agents Chemother., New Orleans, Sept. 28—Oct. 1, 1986, Abstr, No. 1303, p. 332: d) H. Mochizuki, Y. Oikawa, H. Inaba, K. Kato, K. Murakami, and E. Mochida, *ibid.*, No. 1304, p. 332.

4) a) O. Itoh, T. Nagata, I. Nomura, T. Takanaga, T. Sugita, and K. Ichikawa, *Bull. Chem. Soc. Jpn.*, **57**, 810 (1984); b) T. Sohda, K. Mizuno, E. Imamiya, H. Tawada, K. Meguro, Y. Kawamatsu, and Y. Yamamoto., *Chem. Pharm. Bull.*, **30**, 3601 (1982).

5) It has been reported that **13a** is prepared from 4-bromo-1,2-isopropylidenedioxybenzene, butyllithium, and diethyl oxalate. However, no details concerning the preparation of **13a** were presented. Furthermore, 4-bromo-1,2-benzenediol is not easily accessible as an industrial material. See: W. J. Middieton and E. M. Bingham, *J. Org. Chem.*, **45**, 2883 (1980).

6) For example: a) H. C. Brown, B. T. Cho, and W. S. Park, *J. Org. Chem.*, **51**, 3396 (1986); b) H. C. Brown and G. G. Pai, *ibid.*, **50**, 1394 (1985); c) T. Mukaiyama, K. Tomimori, and T. Oriyama, *Chem. Lett.*, **1985**, 813.

7) For example: H. Takahashi, T. Morimoto, and K. Achiwa, *Chem. Lett.*, **1987**, 855.

8) For example: a) R. Kinishi, Y. Nakajima, J. Oda, and Y. Inouye, *Agric. Biol. Chem.*, **42**, 869 (1978); b) T. Munegumi and K. Harada, *Bull. Chem. Soc. Jpn.*, **56**, 298 (1983); c) K. Soai, K. Komiya, Y. Shigematsu, H. Hasegawa, and A. Ookawa, *J. Chem. Soc., Chem. Commun.*, **1982**, 1282; d) K. Soai, T. Isoda, H. Hasegawa, and M. Ishizaki, *Chem. Lett.*, **1986**, 1897.

9) a) J. D. Morrison, E. R. Grandbois, and S. I. Howard, *J. Org. Chem.*, **45**, 4229 (1980); b) A. Hirao, S. Nakahama, D. Mochizuki, S. Itsuno, M. Oohwa, and N. Yamazaki, *J. Chem. Soc., Chem. Commun.*, **1979**, 807; c) A. Hirao, H. Mochizuki, S. Nakahama, and N. Yamazaki, *J. Org. Chem.*, **44**, 1720 (1979); d) A. Hirao, S. Nakahama, H. Mochizuki, S. Itsuno, and N. Yamazaki, *ibid.*, **45**, 4231 (1980); e) A. Hirao, M. Ohwa, S. Itsuno, H. Mochizuki, S. Nakahama, and N. Yamazaki, *Bull. Chem. Soc. Jpn.*, **54**, 1424 (1981); f) A. Hirao, S. Itsuno, M. Ohwa, S. Nagami, H. Mochizuki, H. H. A. Zoorov, S. Nakahama, and N. Yamazaki, *J. Chem. Soc., Perkin Trans. 1*, **1981**, 900.

10) a) N. Umino, T. Iwakuma, and N. Itoh, *Chem. Pharm. Bull.*, **27**, 1479 (1979); b) K. Yamada, M. Takeda, and T. Iwakuma, *Tetrahedron Lett.*, **22**, 3869 (1981); c) Z. Kilic and N. Grunduz, *Tetrahedron*, **42**, 1 (1986); d) K. Yamada, M. Takeda, and T. Iwakuma, *J. Chem. Soc., Perkin Trans. 1*, **1983**, 265; e) M. F. Grundon, D. G. MaCleery, and J. W. Wilson, *ibid.*, **1981**, 231.

11) For a general application of this system to an asymmetric reduction, see M. Yatagai and T. Ohnuki, *J. Chem. Soc., Perkin Trans. 1*, in press.

12) A. Hirao, H. Mochizuki, H. H. A. Zoorov, I. Igarashi, S. Itsuno, and M. Ohwa, *Agric. Biol. Chem.*, **45**, 693 (1981).

13) a) S. S. Deol, D. D. Ridley, and G. W. Simpson, *Aust. J. Chem.*, **29**, 2459 (1976); b) D. D. Ridley and M. Stlalow, *J. Chem. Soc., Chem. Commun.*, **1975**, 400; c) D. Seebach, M. A. Sutter, R. H. Weber, and M. F. Zuger, *Org. Synth.*, **63**, 1, (1985) and references cited therein.

14) a) V. Prelog, *Pure Appl. Chem.*, **9**, 119 (1964); b) R. Macleod, H. Prosser, L. Fikentscher, J. Lanyi, and H. S. Mosher, *Biochemistry*, **3**, 838 (1964).

15) O. Korver, *Tetrahedron*, **26**, 5507 (1970).

16) (*R*)-(−)-2-(4-Methoxyphenyl)-2-hydroxyacetic acid and (*R*)-(−)-2-(3,4-methylenedioxyphenyl)-2-hydroxyacetic acid have been prepared by optical resolution using (+)-α-methylbenzylamine and (−)-ephedrine, respectively. However, details concerning the procedure and yield are not clear. See J. R. E. Hoover, G. L. Dunn, D. R. Jakas, L. L. Lam, J. J. Taggart, J. R. Guarin, and L. Phillips, *J. Med. Chem.*, **17**, 34 (1974).

17) E. Vowinkel, *Chem. Ber.*, **99**, 1479 (1966).

18) The yeast reduction of **13b** proceeded very slowly, which gave (*R*)-**14b** in 14.5% chemical yield after stirring at 30 °C for 3 d.

19) O. Mitsunobu, *Synthesis*, **1981**, 1.

20) For example: a) O. Mitsunobu, M. Wada, and T. Sano, *J. Am. Chem. Soc.*, **94**, 679 (1972); b) M. Wada, T. Sano, and O. Mitsunobu, *Bull. Chem. Soc. Jpn.*, **46**, 2833 (1973); c) D. G. Mellio, I. Shinkai, T. Liu, K. Ryan, and M. Sletzinger, *Tetrahedron Lett.*, **21**, 2783 (1980): d) D. L. Hughes, R. A. Reaman, J. J. Bergan, and E. J. J. Grabowski, *J. Am. Chem.*

Soc., **110**, 6487 (1988).

21) a)E. Grochowski and J. Jurczak, *Synthesis*, **1976**, 682; b) E. Grochowski, E. M. Nashed, and J. Jurczak, *Bull. Acad. Pol. Sci., Ser Sci. Chem.*, **35**, 255 (1987).

22) A. A. Harfoush, K. A. Idriss, and A. El-kholy, *Curr. Sci.*, **55**, 93 (1986).

23) a) E. Grochowski, B. D. Hilton, R. J. Kupper, and C. J. Michejda, *J. Am. Chem. Soc.*, **104**, 6876 (1982); b) W. Adam, N. Narita, and Y. Nishizawa, *ibid.*, **106**, 1843 (1984); c) M. von Itzstein and I. D. Jenkins, *Aust. J. Chem.*, **36**, 557 (1983); d) R. D. Guthrie and I. D. Jenkins, *ibid.*, **35**, 767 (1982).

24) M. Varasi, A. M. Walker, and M. L. Maddox, *J. Org. Chem.*, **52**, 4235 (1987).

25) In the absence of *N*-hydroxyphthalimide, there were three major peaks, one at +30.8 ppm (positive chemical shifts are in ppm downfield of PPh_3 as an internal standard) corresponding to $Ph_3P=O$, another at +50.5 ppm corresponding to the betaine prepared from DEAD and triphenylphosphine, and the other at −43.7 ppm consistent with the pentavalent phosphorane, in the ^{31}P NMR spectra of the reaction mixture. The addition of *N*-hydroxyphthalimide to the above reaction mixture resulted in the complete disappearance of the peak at −43.7 ppm. However, in the presence of *N*-hydroxyphthalimide, the observed peaks in ^{31}P NMR spectra of the reaction mixture were only those corresponding to $Ph_3P=O$ and the remaining Ph_3P.

26) J. A. Dale, D. L. Dull, and H. S. Mosher, *J. Org. Chem.*, **34**, 2543 (1969).

27) Commercially available baker's yeast was used.

28) Bp 83—85 °C/15 mmHg. See Ref. 26.

 © 1991 The Chemical Society of Japan Bull. Chem. Soc. Jpn., 64, 183—190 (1991)

Palladium-Catalyzed Vinylation of Haloazulenes and Halotropolones with Olefins. Utility of the Heck Reaction in the Conjugated Carbon Chain Preparation[1,2]

Hiroshi Horino,* Toyonobu Asao, and Naoto Inoue
Department of Chemistry, College of General Education, Tohoku University, Kawauchi, Aoba-ku, Sendai 980
(Received July 18, 1990)

The reactions of 3-iodotropolone with styrenes (styrene, *p*-methoxystyrene, and 2-vinylpyridine), methyl acrylate, and allylic compounds (methyl 3-butenoate, 3-butenenitrile, 1-allyl-3,4-dimethoxybenzene, and 1-allyl-3,4-methylenedioxybenzene) were carried out, according to the modified Heck's procedure, to give 3-styryl-, 3-(2-carboxyvinyl)-, and 3-(3-substituted 1-propenyl)tropolones, respectively. Similarly, 4-bromo- or 5-bromotropolone was made to react with these olefins to yield 4-styryltropolone or the corresponding 5-(2-substituted vinyl)- and 5-(3-substituted 1-propenyl)tropolones. Substitution of 2-chlorotropone by styrenes produced 2-styryltropones. Extension of the vinylation to 2-amino-6-bromoazulenes, ethyl 3-bromo-1-azulenecarboxylate, and diethyl 2-chloro-1,3-azulenedicarboxylate resulted in a similar substitution.

Many investigations have been undertaken on the chemical and spectroscopic properties of the conjugated or cross-conjugated compounds including azulenes and tropolones. For example, the absorption spectra of azulenes are known to be strongly influenced by the degree of conjugation of the carbon chain substituents as well as their positions.[3d] Such a study needs the synthetic methods for elongation or introduction of a conjugated carbon chain to these compounds. Although many efforts have been devoted, the hitherto-known methods making a carbon–carbon double bond on azulene nuclei or tropolone rings are limited.[3] However, the recent development of the carbon–carbon coupling reactions by transition metal complexes is providing us short-step syntheses of new nonbenzenoid aromatic compounds by coupling the common azulenes or tropolones with easily accessible reagents. Since we reported the palladium-catalyzed vinylation of halotropolones and halotropones about a decade ago,[4] the palladium-catalyzed cross-coupling reactions such as carbonylative coupling[5] as well as alkenyl, alkyl, and aryl coupling with organostannanes,[6] aryl coupling with organoboranes,[7] and aryl coupling with organozinc compounds[8] have been published successively. Nickel-assisted coupling of halotropones or haloazulene to synthesize bitropones and bitropolones[9a,c] or biazulene[9b] has also reported. The benzidine-type rearrangement of 2-(2-arylhydrazino)tropones to 2-amino-5-(4-aminoaryl)tropones,[10] and the base-catalyzed[11] or homolytic rearrangement[12] of 2-benzyloxytropones to 3-arylmethyltropolones have recently been reported as another category of carbon–carbon bond formation. Extension of the metal-assisted or catalyzed coupling reactions to the azulene chemistry is still unsatisfactory except for the copper-promoted coupling of haloazulenes and acetylene moieties.[13] Application of the Heck's vinylation to halotropolones and haloazulenes aiming to conjugated carbon substituents seems promising, because the halogen atoms of easily available halotropolones or haloazulenes are replaced regioselectively by the vinyl groups of commercially available olefins to give a variety of substituted vinyl compounds in one step under mild conditions. In this paper, we describe the details of the vinylic substitution of halotropolones with various olefins catalyzed by palladium complexes and its extension to haloazulenes.

Results and Discussion

The reactions of 3-iodotropolone **1a** with styrene, *p*-methoxystyrene, 2-vinylpyridine, and methyl acrylate were carried out in sealed tubes by heating the THF solutions of the mixtures in the presence of triethylamine and tetrakis(triphenylphosphine)palladium, $Pd(PPh_3)_4$. The change of the reaction products to their sodium salts to remove the catalyst and excess base, and the subsequent acidification gave 3-styryl- **2a**, 3-[2-(*p*-methoxyphenyl)vinyl]- **2b**, 3-[2-(2-pyridyl)-vinyl]tropolone **2c**, and 3-(2-carboxylvinyl)tropolone **2d**, respectively, in moderate yields. Methyl 3-butenoate and other allylic compounds were made to react similarly to produce the corresponding 3-(3-substituted 1-propenyl)tropolones **2e—2h**, as listed in Table 1. The allylic products **2e—2f** having electron-withdrawing groups were the mixtures of allylic double bond isomers from their NMR spectra. An allylic isomerization appears to have produced the thermodynamically stable products during the vinylation as described by Heck[14] or during the treatment of the products with alkaline solutions. An extension of the reaction to 4-bromotropolone **1b** afforded 4-styryltropolone **2i** in the same procedure. All of the olefins used in the reaction of **1a** could be applied to the reaction with 5-bromotropolone **1c**, which produced 5-(2-substituted vinyl)tropolones **2j—2m** and 5-(3-substituted 1-propenyl)tropolones **2n—2o** in good yields. Nozoe et al. proposed and partially succeeded in the synthetic pathway directed toward colchicine, a tricyclic alkaloid including tropolone ring, which consisted of intra-

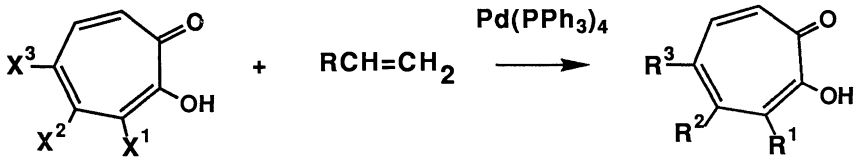

1a: X^1=I, X^2=X^3=H
b: X^2=Br, X^1=X^3=H
c: X^3=Br, X^1=X^2=H
d: X^3=I, X^1=X^2=H
e: X^3=Cl, X^1=X^2=H
4: X^2=Ph, X^3=Br, X^1=H

2a: R^1=PhCH=CH, R^2=R^3=H
b: R^1=p-$MeOC_6H_4CH$=CH, R^2=R^3=H
c: R^1=2-PyCH=CH, R^2=R^3=H
d: R^1=HO_2CCH=CH, R^2=R^3=H
e: R^1=HO_2CCH_2CH=CH, R^2=R^3=H
f: R^1=$NCCH_2CH$=CH, R^2=R^3=H
g: R^1=3,4-$(MeO)_2C_6H_3CH_2CH$=CH, R^2=R^3=H
h: R^1=3,4-$(CH_2O_2)C_6H_3CH_2CH$=CH, R^2=R^3=H
i: R^2=PhCH=CH, R^1=R^3=H
j: R^3=PhCH=CH, R^1=R^2=H
k: R^3=p-$MeOC_6H_4CH$=CH, R^1=R^2=H
l: R^3=2-PyCH=CH, R^1=R^2=H
m: R^3=HO_2CCH=CH, R^1=R^2=H
n: R^3=3,4-$(MeO)_2C_6H_3CH_2CH$=CH, R^1=R^2=H
o: R^3=3,4-$(CH_2O_2)C_6H_3CH_2CH$=CH, R^1=R^2=H
5a: R^2=Ph, R^3=PhCH=CH, R^1=H
b: R^2=Ph, R^3=HO_2CCH=CH, R_1=H

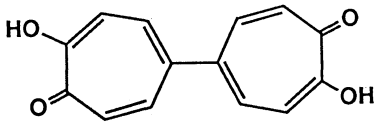

3

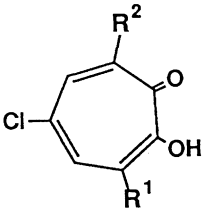

6: R^1=R^2=Br
7: R^1=R^2=PhCH=CH

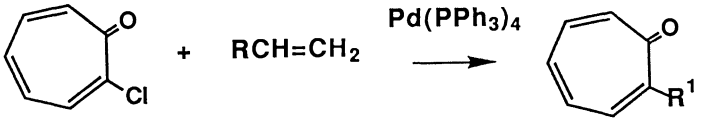

8

9a: R^1=PhCH=CH
b: R^1=p-$MeOC_6H_4CH$=CH
c: R^1=2-PyCH=CH

Scheme 1.

molecular cyclization of 4-(3-arylpropyl)tropolone derivatives.[15] Then, 3-substituted tropolones **2g** and **2h** and 5-substituted products **2n** and **2o** are regarded as the model compounds approaching to the synthetic precursor for colchicine.

Although aryl iodides are usually more reactive than the corresponding aryl bromides,[14] the yields of **2a**—**2h** from 3-iodotropolone **1a** are lower than those of **2j**—**2o** from 5-bromotropolone **1c**. Surprisingly, the reaction of 5-iodotropolone **1d** with styrene or *p*-methoxystyrene gave mainly unexpected bitropolone **3**, accompanied by a small amount of **2j** as shown in

Table 1. Vinylic Substitution of Halotropolones (**1**, **4**, **6**), and 2-Chlorotropone **8**[a]

Entry	Halotropolone	Olefin	Product	Yield (%)[b]
1	**1a**	Styrene	**2a**	(39)
2	**1a**	*p*-Methoxystyrene	**2b**	(51)
3	**1a**	2-Vinylpyridine	**2c**	(43)
4	**1a**	Methyl acrylate	**2d**	(50)
5	**1a**	Methyl 3-butenoate[c]	**2e**	(51)
6	**1a**	3-Butenenitrile[d]	**2f**	(36)
7	**1a**	1-Allyl-3,4-dimethoxybenzene	**2g**	(67)
8	**1a**	1-Allyl-3,4-methylenedioxybenzene	**2h**	(34)
9	**1b**	Styrene	**2i**	(33)
10	**1c**	Styrene	**2j**	(83)
11	**1c**	Styrene	**2j**	(75)[e]
12	**1c**	Styrene	**2j**	(83)[f]
13	**1c**	Styrene	**2j**	(69)[g]
14	**1c**	Styrene	**2j**	(59)[h]
15	**1c**	*p*-Methoxystyrene	**2k**	(65)
16	**1c**	2-Vinylpyridine	**2l**	(80)
17	**1c**	Methyl acrylate	**2m**	(70)
18	**1c**	1-Allyl-3,4-dimethoxybenzene	**2n**	(55)
19	**1c**	1-Allyl-3,4-methylenedioxybenzene	**2o**	(83)
20	**1d**	Styrene	**2j**	(9)
			3	(44)
21	**1d**	*p*-Methoxystyrene	**2j**	(5)
			3	(66)
22	**4**	Styrene	**5a**	(24)
23	**4**	Methyl acrylate	**5b**	(18)
24	**6**	Styrene	**7**	(26)
25	**8**	Styrene	**9a**	(25)
26	**8**	*p*-Methoxystyrene	**9b**	(49)
27	**8**	2-Vinylpyridine	**9c**	(36)[i]

a) Carried out by heating the mixture of halotropolone (2 mmol), olefin (6 mmol), triethylamine (0.7 cm^3), and $Pd(PPh_3)_4$ (0.1 mmol) in THF (10 cm^3) at 100—110 °C for 18—20 h. b) Isolated yields based on halotropolones and 2-chlorotropone. c) A 1:1 mixture of allylic double bond isomers. d) A mixture of 3-(3-cyano-1-propenyl)- and 3-(3-cyano-2-propenyl)tropolones by a ratio of 1:2. e) $Pd_2(dba)_3 \cdot CHCl_3$ (0.1 mmol) was used as the catalyst. f) The mixture of $Pd_2(dba)_3 \cdot CHCl_3$ (0.1 mmol) and PPh_3 (0.4 mmol) as the catalyst. g) The mixture of $Pd_2Cl_4(PPh_3)_2$[18] (0.1 mmol) and PPh_3 (0.4 mmol) was used as the catalyst. h) The mixture of $Pd(OAc)_2$ (0.1 mmol) and PPh_3 (0.4 mmol) was used as the catalyst. i) Purified yield through picrate formation.

Entries 20 and 21. The structure of **3** was determined by the comparison with the authentic sample, which was previously synthesized by the nickel-catalyzed homocoupling of 5-bromo-2-diethylaminotropone and the following hydrolysis.[9c] The dimerization of organic iodides is known to occur when the unreactive olefins such as trisubstituted compounds are used.[14] Therefore, it is remarkable that **1d** dimerizes in preference to vinylic substitution with the reactive styrene. The reactivity of halogen at the 3-position of the tropolone ring may be retarded sterically by the neighboring carbonyl or hydroxyl group, which prevents from the homocoupling of **1a**. The steric effect by the neighboring group was also examined by the reaction of 5-bromo-4-phenyltropolone **4** with styrene and methyl acrylate. The yields of the reaction products **5a** and **5b** (Entries 22 and 23) were considerably lower than those of **2j** and **2m** (Entries 10 and 17), in accordance with the reported results for sterically hindered halides.[14]

The reaction of 5-chlorotropolone **1e** with styrene did not occur even in a more prolonged reaction period (40 h). The difference in the reactivity of the halogen can be utilized for selective vinylation at a desired halogen position of polyhalotropolones. Divinylation of 3,7-dibromo-5-chlorotropolone **6** was carried out by the reaction with styrene to produce 5-chloro-3,7-distyryltropolone **7**. Such a selective dialkenylation at the iodinated carbons of polyhaloarenes in preference to the brominated carbons had reported recently.[16] It is noteworthy that 2-chlorotropone **8** reacted with styrenes to give 2-styryltropones **9a—9c**, though the yields were relatively low, probably by the steric factor found in the behavior of **1a**.

When both of the cis- and trans-isomers are produced in the vinylation products, the thermodynamically stable olefin is known to be favored.[14] The coupling constants of the vinylic protons (about 16 Hz) in the NMR spectra illustrate that most vinylated products are trans-isomers. However, some unresolved signals of aromatic and vinylic protons have been observed by superposition upon each other,

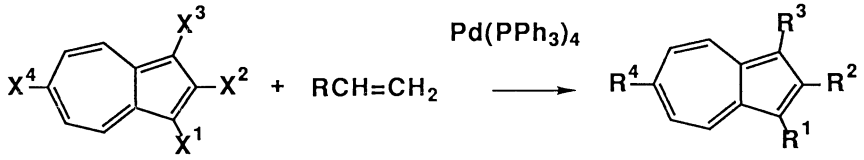

10a: $X^1=X^3=CO_2Et$, $X^2=NH_2$, $X^4=Br$
b: $X^1=X^3=H$, $X^2=NHAc$, $X^4=Br$
12: $X^1=Br$, $X^2=X^4=H$, $X^3=CO_2Et$
14a: $X^1=X^3=CO_2Et$, $X^2=Cl$, $X^4=H$
b: $X^1=X^3=X^4=H$, $X^2=I$

11a: $R^1=R^3=CO_2Et$, $R^2=NH_2$, $R^4=PhCH=CH$
b: $R^1=R^3=CO_2Et$, $R^2=NH_2$, $R^4=2\text{-}PyCH=CH$
c: $R^1=R^3=CO_2Et$, $R^2=NH_2$, $R^4=MeO_2CCH=CH$
d: $R^1=R^3=H$, $R^2=NHAc$, $R^4=PhCH=CH$
13a: $R^1=CO_2Et$, $R^2=R^4=H$, $R^3=PhCH=CH$
b: $R^1=CO_2Et$, $R^2=R^4=H$, $R^3=MeO_2CCH=CH$
15a: $R^1=R^3=CO_2Et$, $R^2=PhCH=CH$, $R^4=H$
b: $R^1=R^3=CO_2Et$, $R^2=2\text{-}PyCH=CH$, $R^4=H$
c: $R^1=R^3=CO_2Et$, $R^2=MeO_2CCH=CH$, $R^4=H$
d: $R^1=R^3=R^4=H$, $R^2=PhCH=CH$

Scheme 2.

and a further investigation should be done before determining which product is cis- or trans-isomer. Some kinds of palladium complexes are effective for the vinylation of **1c** with styrene (Entries 11 to 14). Tris(dibenzylideneacetone)dipalladium(0), $Pd_2(dba)_3\cdot CHCl_3$[17] was used as the reaction catalyst. Addition of triphenylphosphine to the system somewhat improved the yield, so that phosphine complexes appear to be favorable for the vinylic substitution. Divalent palladium complex $Pd_2Cl_4(PPh_3)_2$[18] as well as $Pd(OAc)_2$ can be used as the catalyst without interference of the tropolone moiety for chelation.

The vinylic substitution with olefins was then extended to azulene derivatives, using easily available 1-, 2-, and 6-haloazulenes[3d] as the starting materials. These results are listed in Table 2. Diethyl 2-amino-6-bromo-1,3-azulenedicarboxylate **10a** was made to react with styrene, 2-vinylpyridine, and methyl acrylate in a similar way to the vinylation of halotropolones to afford the corresponding 6-styryl- **11a**, 6-[2-(2-pyridyl)-vinyl]- **11b**, and 6-[2-(methoxycarbonyl)vinyl]azulene **11c** in fairly good yields. Similarly, 2-acetamido-6-bromoazulene **10b** gave 2-acetamido-6-styrylazulene **11d**. The bromine atom at the 1-position of **12** was easily replaced by the vinyl groups of styrene and methyl acrylate to give the corresponding vinylated azulenes **13a** and **13b**. It is remarkable that diethyl 2-chloro-1,3-azulenedicarboxylate **14a** reacted with all kinds of used olefins at the sterically crowded 2-position, and the corresponding 2-substituted azulenes **15a—15c** were obtained in moderate yields. Activation

Table 2. Vinylic Substitution of Haloazulenes (**10**, **12**, and **14**)[a]

Entry	Haloazulene	Olefin	Product	Yield (%)[b]
1	**10a**	Styrene	**11a**	(70)
2	**10a**	2-Vinylpyridine	**11b**	(89)
3	**10a**	Methyl acrylate	**11c**	(99)
4	**10b**	Styrene	**11d**	(85)
5	**12**	Styrene	**13a**	(66)
6	**12**	Methyl acrylate	**13b**	(88)
7	**14a**	Styrene	**15a**	(21)
8	**14a**	2-Vinylpyridine	**15b**	(52)
9	**14a**	Methyl acrylate	**15c**	(57)
10	**14b**	Styrene	**15d**	(30)

a) The reactions were carried out in the same manner as in Table 1. b) Isolated yields based on haloazulenes after purification by column chromatography.

of the chlorine atom at the 2-position may be attributed to the electron-withdrawing character of the neighboring ethoxycarbonyl groups. A similar phenomenon was reported in the reaction of **14a** with copper(I) phenylacetylide.[13] As for the synthesis of unsubstituted azulenes except for the unsaturated carbon chain in question, the reaction of 2-iodoazulene **14b** with styrene was carried out to give 2-styrylazulene **15d**, which had previously been synthesized by partial hydrogenation of the corresponding ethynyl compound[13] or by condensation of 2-methylazulene with benzaldehyde.[19] The results mentioned above show that the vinylation reaction catalyzed by palladium complexes can be effectively applied to most of azulenes, tropolones, and related compounds, and that the reaction will be a handy tool for preparing a conjugated carbon chain at the desired halogen position on the nonbenzenoid aromatic compounds.

Experimental

Melting points were obtained by a Yanaco Micro-melting point apparatus and are uncorrected. The IR spectra were recorded on a Hitachi 215 using KBr disk. Most of the ^{1}H NMR spectra were measured on a Hitachi R-22 spectrometer (90 MHz) using TMS as the internal standard, and some spectra were obtained by a Hitachi 90H FT-NMR spectrometer (90 MHz). The UV-visible spectra were recorded on a Hitachi 340 spectrophotometer. Elemental analyses were performed by the Instrumental Analysis Center for Chemistry, Faculty of Science, Tohoku University. Solvents used for the reactions were distilled over sodium, and stored under an inert atmosphere. Chromatography was done on a 300 mesh silica gel (Wako C-300). Palladium complexes, $Pd(PPh_3)_4$,[20] and $Pd_2(dba)_3 \cdot CHCl_3$ (dba=dibenzylideneacetone),[17] were prepared according to the literatures. The following haloazulenes and halotropolones were also prepared according to the literatures: 3-iodotropolones **1a**,[21] 4-bromotropolone **1b**,[22] 5-bromo- **1c**,[23] 5-chloro- **1e**,[23] and 5-iodotropolone **1d**,[23] 2-chlorotropone **8**,[24] diethyl 2-amino-6-bromo-1,3-azulenedicarboxylate **9a**,[25] 2-acetamido-6-bromoazulene **9b**,[26] ethyl 3-bromo-1-azulenecarboxylate **12**,[27] diethyl 2-chloro-1,3-azulenedicarboxylate **14a**,[25] and 2-iodoazulene **14b**.[25]

As the typical procedures, the reactions of **1a**, **1d**, **8**, and **10a** with styrene are given as follows.

3-Styryltropolone 2a: The ampoule (60 cm^3) was purged with nitrogen, and **1a** (545 mg, 2 mmol) and $Pd(PPh_3)_4$ (120 mg, 0.1 mmol) were placed successively. The mixture was dissolved in deaerated THF (10 cm^3), and styrene (0.7 cm^3, 6.1 mmol) and triethylamine (0.7 cm^3) were added as rapidly as possible. The ampoule was sealed, and heated in an oil bath at 100—110 °C for 20 h. The reaction mixture was transferred into a flask equipped with a rotatory evaporator, and concentrated under reduced pressure. The residue was dissolved in benzene (30 cm^3), and extracted with 5% NaOH solution (50 cm^3×3). Acidification of the solution with 6 M HCl (M=mol dm^{-3}) gave a white turbid solution, which was then extracted with ethyl acetate. After the solution was dried (Na_2SO_4) and concentrated under reduced pressure, the yellow oil (298 mg) obtained was chromatographed on silica gel (9.0 g) using benzene as an eluent, to give yellow crystals of **2a** (173 mg, 39%), mp 58—62 °C. Recrystallization from ethanol raised the melting point of **2a** up to 73—75 °C. (lit,[28] mp 111.5—112.5 °C; Discrepancy between the melting points of **2a** and the authentic sample is unexplainable yet, but the following spectra of **2a** are consistent with the strucure of 3-styryltropolone). IR (KBr) 3160 (OH), 1650, 1550 (CO, C=C), 685 (Ph) cm^{-1}; ^{1}H NMR ($CDCl_3$) δ=6.95—7.65 (10H, m), 7.83 (1H, d, J=6 Hz). Found: C, 80.23; H, 5.63%. Calcd for $C_{15}H_{12}O_2$: C, 80.33; H, 5.39%.

3-[2-(*p*-Methoxyphenyl)vinyl]tropolone 2b: Mp 134—136 °C (benzene); IR (KBr) 3170 (OH), 1605, 1580 (C=C, CO), 1250 (C–O) cm^{-1}; ^{1}H NMR ($CDCl_3$) δ=3.78 (3H, s), 6.82 (1H, d, J=12 Hz), 7.29 (2H, d, J=11 Hz), 7.32 (2H, d, J=12 Hz), 6.90—7.65 (8H, m), 7.77 (1H, d, J=10 Hz). Found: C, 75.73; H, 5.44%. Calcd for $C_{16}H_{14}O_3$: C, 75.57; H, 5.55%.

3-[2-(2-Pyridyl)vinyl]tropolone 2c: Mp 96—97.5 °C (benzene–cyclohexane); IR (KBr) 3230 (OH), 1585, 1530 (CO, C=N) cm^{-1}; ^{1}H NMR ($CDCl_3$) δ=6.95—8.25 (10H, m), 8.58 (1H, d, J=6 Hz). Found: C, 74.93; H, 4.84; N, 6.16%. Calcd for $C_{14}H_{11}O_2N$: C, 74.65; H, 4.92; N, 6.22%.

3-(2-Carboxyvinyl)tropolone 2d: Mp 224 °C (decomp) (EtOH) (lit,[29] mp 233—235 °C). IR (KBr) 3180—2300, 1685 (carboxyl), 1620, 1600 (CO, C=C) cm^{-1}.

3-(3-Carboxy-1-propenyl)tropolone 2e: Mp 155 °C (EtOH); IR (KBr) 3180 (OH), 3100—2550 (carboxyl), 1720—1690 (CO) cm^{-1}; ^{1}H NMR ($CDCl_3$) δ=3.73 (2H, d, J=7 Hz), 6.48 (1H, d, J=16 Hz), 6.9—7.3 (4H, m), 7.69 (1H, d, J=11 Hz). Found: C, 63.89; H, 4.88%. Calcd for $C_{11}H_{10}O_4$: C, 64.07; H, 4.89%.

3-(3-Cyano-1-propenyl)tropolone 2f: Mp 74—75 °C (benzene–hexane); ^{1}H NMR ($CDCl_3$) δ=3.48 (2H, d, J=6 Hz), 6.48 (1H, d, J=16 Hz), 6.9—7.5 (4H, m), 7.61 (1H, d, J=11 Hz). Found: C, 70.53; H, 4.86; N, 7.42%. Calcd for $C_{11}H_9O_2N$: C, 70.58; H, 4.85; N, 7.48%.

3-[3-(3,4-Dimethoxyphenyl)-1-propenyl]tropolone 2g: Mp 80—81 °C (benzene–EtOH); IR (KBr) 3200 (OH), 1605, 1550 (C=C, C=O), 1240 (C–O) cm^{-1}; ^{1}H NMR (CCl_4) δ=3.61 (2H, d, J=6 Hz), 3.72 (3H, s), 3.75 (3H, s), 6.30 (1H, d, J=14 Hz), 6.53—6.95 (5H, m), 7.14—7.15 (2H, m), 7.45 (1H, d, J=11 Hz). Found: C, 72.40; H, 6.13%. Calcd for $C_{18}H_{18}O_4$: C, 72.46; H, 6.08%.

3-[3-(3,4-Methylenedioxyphenyl)-1-propenyl]tropolone 2h: Mp 106—107.5 °C (EtOH); IR (KBr) 3170 (OH), 1620, 1560 (CO, C=C), 1260 (C–O) cm^{-1}; ^{1}H NMR ($CDCl_3$) δ=3.69 (2H, d, J=6 Hz), 5.85 (2H, s), 6.10—6.30 (2H, m), 6.50—7.30 (6H, m), 7.45 (1H, d, J=11 Hz). Found: C, 72.23; H, 4.97%. Calcd for $C_{17}H_{14}O_2$: C, 72.33; H, 5.00%.

4-Styryltropolone 2i: Mp 85—87 °C (lit,[30] mp 90—91 °C). IR (KBr) 3200 (OH), 1590, 1530, (CO, C=C), 690 (Ph) cm^{-1}; ^{1}H NMR ($CDCl_3$) δ=6.63 (1H, d, J=11 Hz), 6.85—7.65 (10H, m).

5-Styryltropolone 2j: Mp 133—135 °C (lit,[31] mp 131—132 °C); IR (KBr) 3220 (OH), 1615, 1530 (CO, C=C), 690 (Ph) cm^{-1}; ^{1}H NMR ($CDCl_3$) δ=7.25—7.52 (9H, m), 7.60 (2H, d, J=7 Hz).

5-[2-(*p*-Methoxyphenyl)vinyl]tropolone 2k: Mp 194—195 °C (EtOH) (lit,[31] mp 195 °C); IR (KBr) 3150 (OH), 1610, 1550 (CO, C=C), 1275, 1255, 1180 (C–O) cm^{-1}; ^{1}H NMR ($CDCl_3$) δ=3.82 (3H, s), 6.95 (3H, m), 7.25—7.65 (7H, m).

5-[2-(2-Pyridyl)vinyl]tropolone 2l: Mp 140.5—141.5 °C

(EtOH); IR (KBr) 3240, (OH), 1620, 1590, 1555 (C=C, CO, C=N) cm^{-1}; ^1H NMR ($CDCl_3$) δ=6.95—7.80 (10H, m), 8.59 (1H, d, J=7 Hz). Found: C, 74.46; H, 4.85; N, 6.13%. Calcd for $C_{14}H_{11}O_2N$: C, 74.65; H, 4.92; N, 6.22%.

5-(2-Carboxyvinyl)tropolone 2m: Mp 238—239 °C (decomp) (EtOH) [lit,[29] mp 239 °C (decomp)]; IR (KBr) 3200—2500, 1700 (carboxyl), 1615, 1565 (CO, C=C) cm^{-1}; ^1H NMR (DMSO-d_6) δ=6.42 (1H, d, J=16 Hz), 7.12 (2H, d, J=11 Hz), 7.50 (2H, d, J=16 Hz), 7.70 (2H, d, J=11 Hz).

5-[3-(3,4-Dimethoxyphenyl)-1-propenyl]tropolone 2n: Mp 140.5—142 °C (EtOH); IR (KBr) 3200 (OH), 1610, 1550 (C=C, C=O), 1270, 1215, 1140 (C-O) cm^{-1}; ^1H NMR ($CDCl_3$) δ=3.50 (2H, d, J=7 Hz), 3.88 (6H, s), 6.32 (1H, m), 6.75—6.95 (3H, m), 7.30 (5H, s), 7.32 (1H, s). Found: C, 72.21; H, 6.17%. Calcd for $C_{18}H_{18}O_4$: C, 72.46; H, 6.08%.

5-[3-(3,4-Methylenedioxyphenyl)-1-propenyl]tropolone 2o: Mp 123—124 °C (EtOH); IR (KBr) 3230 (OH), 1620, 1550 (C=C, CO), 1260, 1210 (C-O) cm^{-1}; ^1H NMR ($CDCl_3$) δ=3.52 (2H, d, J=7 Hz), 5.92 (2H, s), 6.32 (1H, m), 6.78 (3H, m), 7.30 (4H, s), 7.96 (1H, s). Found: C, 72.38; H, 5.03%. Calcd for $C_{17}H_{14}O_4$: C, 72.33; H, 5.00%.

Formation of 5,5′-Bitropolone 3: A mixture of **1d** (545 mg, 2.0 mmol), styrene (0.6 cm^3), $Pd(PPh_3)_4$ (120 mg, 0.1 mmol), triethylamine (0.8 cm^3) in THF (10 cm^3) was heated at 115—120 °C for 21 h, and the resulting mixture was treated similarly. Acidification of the alkaline solution with 6 M HCl yielded brownish yellow precipitates, which were collected by filtration, and washed with ethyl acetate (50 cm^3) to give 106 mg (0.44 mmol, 44%) of **3**; mp 255 °C (decomp), which was identical with the authentic sample[9c] by the comparison of their IR spectra [lit,[9c] 260 °C (decomp)]; IR (KBr) 3460 (OH), 1620, 1552 (C=C, CO) cm^{-1}; ^1H NMR (DMSO-d_6) δ=7.52 (4H, d, J=12 Hz), 7.84 (4H, d, J=12 Hz). The filtrate was extracted with ethyl acetate, which was combined with the solvent used for washing the precipitates, and dried over Na_2SO_4. Concentrating the solution followed by extracting the residue with ethanol gave 38 mg (0.17 mmol, 8.5%) of **2j**.

5-Bromo-4-phenyltropolone 4: To a solution of 5-amino-4-phenyltropolone[32] (1.28 g, 6.0 mmol) in dioxane (10 cm^3) and water (6 cm^3), concd H_2SO_4 (1.0 cm^3) and then a solution of sodium nitrite (0.50 g, 7.2 mmol) in water (2 cm^3) were added at 0—5 °C in 15 min. After the successive addition of copper(I) bromide (2.20 g, 15.3 mmol) and 48% HBr (8 cm^3) during 15 min, the solution was stirred for 1 h, until the temperature reached to room temperature. Then the solution was heated at 60 °C for 10 min, and poured into water (60 cm^3). The produced precipitates (1.60 g) were dissolved in dichloromethane (100 cm^3), and treated with a flow of hydrogen sulfide. After evaporating the solvent, crystallization from ethanol gave yellow crystals of **3** (1.25 g, 75%). Mp 188—189 °C ($CHCl_3$–EtOH); IR (KBr) 3230 (OH), 1600, 1550 (C=C, C=O) 700 (Ph) cm^{-1}; ^1H NMR ($CDCl_3$) δ=7.07 (1H, d, J=12 Hz), 7.21 (1H, s), 7.22—7.43 (5H, m), 7.80 (1H, d, J=12 Hz). Found: C, 56.58; H, 3.45%. Calcd for $C_{13}H_9O_2Br$: C, 56.34; H, 3.27%.

4-Phenyl-5-styryltropolone 5a: Mp 95—96 °C (EtOH); IR (KBr) 3200 (OH), 1600, 1530 (C=C, C=O), 700 (Ph) cm^{-1}; ^1H NMR ($CDCl_3$) δ=6.86 (1H, d, J=11 Hz), 7.0—7.7 (13H, m), 7.88 (1H, d, J=11 Hz). Found: C, 79.00; H, 5.13%. Calcd for $C_{21}H_{16}O_2$: C, 79.02; H, 5.00%.

5-(2-Carboxyvinyl)-4-phenyltropolone 5b: Mp 242—243 °C (THF); IR (KBr) 3150 (OH), 3050—2550 (carboxyl), 1590, 1560 (C=C, C=O), 695 (Ph) cm^{-1}; ^1H NMR (THF-d_8) δ=6.25 (1H, d, J=16 Hz), 7.10—7.45 (7H, m), 7.20 (1H, d, J=16 Hz), 7.85 (1H, d, J=11 Hz). Found: C, 71.18; H, 4.68%. Calcd for $C_{16}H_{12}O_4$: C, 71.68; H, 4.51%.

5-Chloro-3,7-distyryltropolone 7: Mp 185 °C ($CHCl_3$–EtOH); IR (KBr) 3050 (OH), 1625, 1550 (C=C, C=O), 690 (Ph) cm^{-1}; ^1H NMR ($CDCl_3$) δ=7.15—7.20 (1H, t, J=5 Hz), 7.20—7.40 (7H, m), 7.45—7.60 (6H, m), 7.70—7.90 (3H, m). Found: C, 76.28; H, 4.87%. Calcd for $C_{23}H_{17}O_2Cl$: C, 76.55; H, 4.75%.

2-Styryltropone 9a: A mixture of **8** (280 mg, 2.0 mmol), styrene (310 mg, 3.0 mmol), and triethylamine (0.4 cm^3) in THF (15 cm^3) was heated at 120 °C for 18 h in the presence of $Pd(PPh_3)_4$ (120 mg, 0.1 mmol) in a sealed tube. After filtration of palladium that had been deposited during the reaction, the filtrate was concentrated, and the residue was chromatographed on silica gel (10 g) using benzene–ethyl acetate (1 : 0—1 : 1). Evaporation of the benzene–ethyl acetate (10 : 1) eluent gave yellow crystals of **9a** (102 mg, 49.0%), which were recrystallized from carbon tetrachloride: Mp 91—92 °C (CCl_4) (lit,[33] mp 94—95 °C); IR (KBr) 1620, 1565 (C=C, C=O) cm^{-1}; ^1H NMR ($CDCl_3$) δ=6.85—7.10 (4H, m), 7.20—7.65 (8H, m).

2-[2-(*p*-Methoxyphenyl)vinyl]tropone 9b: Mp 93—95 °C (benzene) (lit,[33] mp 98 °C); IR (neat) 1625, 1580 (C=C, C=O) cm^{-1}. (Found: C, 79.57; H, 5.94%).

2-[2-(2-Pyridyl)vinyl]tropone 9c: Mp 90—91.5 °C (benzene–cyclohexane); picrate, mp 202—204 °C (decomp); IR (KBr) 1625, 1570 (C=C, CO, C=N), 770 cm^{-1}; ^1H NMR ($CDCl_3$) δ=6.75—7.10 (4H, m), 7.30—7.70 (6H, m). Found: C, 80.27; H, 5.22; N, 6.62%. Calcd for $C_{14}H_{11}ON$: C, 80.36; H, 5.30; N, 6.69%.

Diethyl 2-Amino-6-styryl-1,3-azulenedicarboxylate 11a: A THF solution (10 cm^3) of **10a** (735 mg, 2 mmol), $Pd(PPh_3)_4$ (120 mg, 0.1 mmol), styrene (1.2 cm^3, 10.5 mmol), and triethylamine (1.5 cm^3) was sealed in an ampoule (60 cm^3). After heating in an oil bath at 110—120 °C for 18 h, the mixture was concentrated under reduced pressure, and then the residue was chromatographed on silica gel (10 g). Elution with a mixture of benzene and ethyl acetate (1 : 1) gave reddish-orange crystals of **11a** (551 mg, 70%). Mp 148—149 °C (EtOH) (lit,[34] mp 147.5—148 °C); IR (KBr) 3450, 3350 (NH_2), 1680 (ester), 990 (Ph) cm^{-1}. (Found: C, 74.32; H, 5.92; N, 3.54%).

Diethyl 2-Amino-6-[2-(2-pyridyl)vinyl]-1,3-azulenedicarboxylate 11b: Mp 146—148 °C (benzene); IR (KBr) 3480, 3340 (NH_2), 1680 (ester) cm^{-1}; ^1H NMR ($CDCl_3$) δ=1.47 (6H, t, J=7 Hz), 4.46 (4H, q, J=7 Hz), 7.04—7.35 (4H, m), 7.55—7.82 (5H, m), 8.54 (1H, d, J=5 Hz), 8.98 (2H, d, J=11 Hz); UV (MeOH) 250 (log ε 4.53), 349 (4.75), 454 nm (4.49). Found: C, 71.04; H, 5.38; N, 6.92%. Calcd for $C_{23}H_{22}O_4N_2$: C, 70.75; H, 5.18; N, 7.18%.

Diethyl 2-Amino-6-[2-(methoxycarbonyl)vinyl]-1,3-azulenedicarboxylate 11c: Mp 197—198 °C (THF); IR (KBr) 3490, 3350 (NH_2), 1705, 1685, 1650 (ester) cm^{-1}; ^1H NMR ($CDCl_3$) δ=1.50 (6H, t, J=7 Hz), 3.80 (3H, s), 4.46 (4H, q, J=7 Hz), 6.47 (1H, d, J=16 Hz), 7.50—7.90 (5H, m), 9.01 (2H, d, J=11 Hz); UV (EtOH) 248 (log ε 4.29), 340 (4.61), 447 nm (4.19). Found: C, 64.66; H, 5.74; N, 3.71%. Calcd for $C_{20}H_{21}O_6N$: C, 64.68; H, 5.70; N, 3.77%.

2-Acetamido-6-styrylazulene 11d: Mp 257 °C (THF); IR (KBr) 3290 (NH), 1600, 1595, 1570, 1530 (amide) cm^{-1};

^{1}H NMR (DMSO-d_6) δ=3.10 (3H, s), 7.10—7.70 (11H, m), 8.35 (2H, d, J=16 Hz), 11.50 (1H, s); UV (MeOH) 224 (log ε 4.50), 313 (4.70), 325 (4.70), 411 (4.58), 432 (4.59), 559 nm (2.72). Found: C, 78.14; H, 6.00; N, 4.45%. Calcd for $C_{20}H_{17}ON \cdot H_2O$: C, 78.66; H, 6.27; N, 4.59%.

Ethyl 3-Styryl-1-azulenecarboxylate 13a: Mp 80—82 °C (EtOH); IR (KBr) 1690 (ester), 1215—1205 (C-O), 690 (Ph) cm^{-1}; ^{1}H NMR ($CDCl_3$) δ=1.49 (3H, t, J=7 Hz), 4.47 (2H, q, J=7 Hz), 7.10—7.70 (10H, m), 8.54 (1H, d, J=9 Hz), 8.67 (1H, s), 9.48 (1H, d, J=9 Hz); UV (MeOH) 237 (log ε 4.22), 277 (4.28), 316 (4.60), 395 (4.44), 409 (3.94), 597 nm (2.70). Found: C, 83.52; H, 6.02%. Calcd for $C_{21}H_{18}O_2$: C, 83.42; H, 6.00%.

Ethyl 3-[2-(Methoxycarbonyl)vinyl]-1-azulenecarboxylate 13b: Mp 114—115.5 °C (benzene); IR (KBr) 1690, 1620 (ester), 1220, 1160 (C-O) cm^{-1}; ^{1}H NMR ($CDCl_3$) δ=1.45 (3H, t, J=7 Hz), 3.80 (3H, s), 4.45 (2H, q, J=7 Hz), 6.45 (1H, d, J=16 Hz), 7.40—7.85 (3H, m), 8.20 (1H, d, J=16 Hz), 8.85—8.70 (2H, m), 9.58 (1H, d, J=11 Hz); UV (MeOH) 247 (log ε 4.37), 306 (4.65), 346 (sh, 4.31), 387 (4.19), 551 nm (2.95). Found: C, 71.59; H, 5.63%. Calcd for $C_{17}H_{16}O_4$: C, 71.82; H, 5.67%.

Diethyl 2-Styryl-1,3-azulenedicarboxylate 15a: Mp 79—81 °C (EtOH); IR (KBr) 1670 (ester), 1200, 1170 (C-O), 990 (Ph) cm^{-1}; ^{1}H NMR ($CDCl_3$) δ=1.23 (6H, t, J=7 Hz), 4.44 (2H, q, J=7 Hz), 6.82 (1H, d, J=16 Hz), 7.22—7.80 (10H, m), 8.04 (1H, d, J=16 Hz); UV (MeOH) 230 (log ε 4.24), 292 (4.34), 335 (4.48), 397 (3.89), 527 nm (2.54).

Diethyl 2-[2-(2-Pyridyl)vinyl]-1,3-azulenedicarboxylate 15b: Mp 95—97.5 °C (EtOH); IR (KBr) 1670 (ester), 1200, 1175 (C-O) cm^{-1}; ^{1}H NMR ($CDCl_3$) δ=1.37 (6H, t, J=7 Hz), 4.47 (4H, q, J=7 Hz), 6.92 (1H, d, J=17 Hz), 7.05—7.85 (7H, m), 8.48 (1H, d, J=17 Hz), 9.35 (2H, d, J=12 Hz); UV (MeOH) 230 (log ε 4.33), 330 (4.67), 392 (sh, 4.00), 530 nm (3.19). Found: C, 73.83; H, 5.71; N, 3.62%. Calcd for $C_{23}H_{21}O_4N$: C, 73.58; H, 5.64; N, 3.73%.

Diethyl 2-[2-(Methoxycarbonyl)vinyl]-1,3-azulenedicarboxylate 15c: Mp 93—94 °C; IR (KBr) 1720, 1685 (ester), 1190, 1180 (C-O) cm^{-1}; ^{1}H NMR ($CDCl_3$) δ=1.88 (6H, t, J=7 Hz), 3.80 (3H, s), 4.40 (4H, q, J=7 Hz), 6.06 (1H, d, J=18 Hz), 7.68 (2H, d, J=11 Hz), 7.79 (1H, t, J=11 Hz), 8.47 (1H, d, J=18 Hz), 9.40 (2H, d, J=11 Hz); UV (MeOH) 236 (log ε 4.34), 306 (4.72), 355 (3.91), 529 nm (2.78). Found: C, 67.18; H, 5.77%. Calcd for $C_{20}H_{20}O_6$: C, 67.40; H, 5.66%.

2-Styrylazulene 15d: Mp 207—208 °C (benzene) (lit,[19] mp 207—208 °C). The IR spectrum of **15d** was identical with the authentic sample.[19]

The authors wish to express their thanks to Emeritus Professor Tetsuo Nozoe of Tohoku University and Professor Takashi Toda of Utsunomiya University for their encouragement throughout this work. We are grateful to Professor Masafumi Yasunami and Dr. Tadayoshi Morita of Tohoku University for a gift of some halotropolones, and for a kind guidance of preparing 3-iodotropolone and some azulene derivatives. We also wish to thank Professor Masaji Oda of Osaka University for the comparison of the IR spectra of 5,5′-bitropolone. The present work was partially supported by Grant-in-Aid for Scientific Reserach No. 57540270 from the Ministry of Education, Science and Culture.

References

1) Dedicated to the Emeritus Professor Tetsuo Nozoe of Tohoku University on the occasion of his 88th birthday.

2) A part of this work was presented at the 14th symposium of nonbenzenoid aromatic chemistry, The Chemical Society of Japan, Okayama, October 1981, Abstr., No. 1X20.

3) a) T. Nozoe, K. Takase, H. Matsumura, T. Asao, K. Kikuchi, and S. Ito, "Dai Yuki Kagaku (Comprehensive Organic Chemistry," ed by M. Kotake, Asakura, Tokyo (1960), Vol. 13. b) F. Pietra, *Chem. Rev.*, **73**, 293 (1973). c) D. Lloyd, "Nonbenzenoid Conjugated Carbocyclic Compounds," Elsevier, Amsterdam (1984). d) K.-P. Zeller, "Carbocyclische pai-Elecronen-Systeme," Houben-Weyl, ed by E. Müllen, Georg Thieme, Stuttgart (1985), Vol. V, Part 2c, p. 127.

4) H. Horino, N. Inoue, and T. Asao, *Tetrahedron Lett.*, **22**, 741 (1981).

5) A. M. Echavarren and J. K. Stille, *J. Am. Chem. Soc.*, **110**, 1557 (1988).

6) M. G. Banwell, M. P. Collis, G. T. Crisp, J. N. Lambert, M. E. Reum, and J. A. Scoble, *J. Chem. Soc., Chem. Commun.*, **1989**, 616.

7) V. Nair, D. W. Dawell, and S. W. Smi, *Synth. Commun.*, **17**, 1897 (1987).

8) R. M. Keenan and L. I. Kruse, *Synth. Commun.*, **19**, 5 (1989).

9) a) M. Iyoda, K. Sato, and M. Oda, *J. Chem. Soc., Chem. Commun.*, **1985**, 1547. b) M. Iyoda, K. Sato, and M. Oda, *Tetrahedron Lett.*, **26**, 3829 (1985). c) M. Iyoda, K. Sato, and M. Oda, *ibid.*, **28**, 625 (1987).

10) T. Nozoe, K. Takase, M. Yasunami, M. Ando, H. Saito, K. Imafuku, B.-Z. Yin, M. Honda, Y. Goto, T. Hanaya, Y. Hara, and H. Yamamoto, *Bull. Chem. Soc. Jpn.*, **62**, 128 (1989).

11) H. Takeshita, A. Mori, and H. Suizu, *Bull. Chem. Soc. Jpn.*, **60**, 1429 (1987).

12) a) H. Takeshita, H. Mametsuka, A. Chisaka, and N. Matsuo, *Chem. Lett.*, **1981**, 73. b) H. Takeshita and H. Mametsuka, *Heterocycles*, **22**, 663 (1984). c) H. Takeshita, A. Mori, and Y. Goto, *Bull. Chem. Soc. Jpn.*, **59**, 1125 (1986).

13) T. Morita, T. Nakadate, and K. Takase, *Sci. Rept. Tohoku Univ.*, **I**, **71**, 1 (1988).

14) R. F. Heck, "Organic Reactions," ed by W. G. Dauben, John Wiley & Sons, New York (1982), Vol. 27, Chap. 2, p. 345.

15) a) T. Nozoe, K. Takase, N. Kawabe, T. Asao, and H. Yamamoto, *Bull. Chem. Soc. Jpn.*, **56**, 3099 (1983). b) H. Yamamoto, A. Hara, S. Inokawa, and T. Nozoe, *ibid.*, **56**, 3106 (1983), and the references cited therein.

16) W. Tao, S. Nesbitt, and R. F. Heck, *J. Org. Chem.*, **55**, 63 (1990), and the references cited therein.

17) T. Ukai, H. Kawazure, Y. Ishii, J. J. Bonnet, and J. A. Ibers, *J. Organomet. Chem.*, **65**, 253 (1974).

18) The formula $Pd_2Cl_4(PPh_3)_2$ is tentative. The complex was prepared by stirring a methanolic solution of equimolecular amounts of lithium tetrachloropalladate(II) and triphenylphosphine at room temperature. An analogous complex $Pd_2Cl_4(PMe_2Ph)_2$ was reported in J. M. Jenkins and B. L. Shaw, *J. Chem. Soc. A*, **1966**, 770.

19) M. Saito, T. Morita, and K. Takase, *Bull. Chem. Soc. Jpn.*, **53**, 3276 (1980).

20) D. R. Coulson, *Inorg. Synth.*, **13**, 121 (1972).
21) Y. Kitahara and T. Arai, *Proc. Jpn. Acad.*, **27**, 423 (1951).
22) T. Sato, *Nippon Kagaku Zasshi*, **80**, 1171 (1959).
23) T. Nozoe, S. Seto, S. Ebine, and S. Ito, *J. Am. Chem. Soc.*, **73**, 1895 (1951).
24) B. J. Abadir, J. W. Cook, J. D. Loudon, and D. K. V. Steel, *J. Chem. Soc.*, **1952**, 2350.
25) T. Nozoe, S. Seto, and S. Matsumura, *Bull. Chem. Soc. Jpn.*, **35**, 1990 (1962).
26) S. Matsumura, *Chem. Pharm. Bull.*, **10**, 1024 (1962).
27) T. Morita and K. Takase, *Sci. Rept. Tohoku Univ.*, **I**, **62**, 83 (1980).
28) H. Matsumura, *Nippon Kagaku Zasshi*, **82**, 774 (1961).
29) E. Sebe and S. Matsumoto, *Sci. Rept. Tohoku Univ.*, **I**, **38**, 308 (1954).
30) D. S. Tarbell, K. I. H. Williams, and E. J. Sehm, *J. Am. Chem. Soc.*, **81**, 3443 (1959).
31) H. Higashi, H. Kurosawa, and H. Matsumoto, *Bull. Chem. Soc. Jpn.*, **43**, 3236 (1970).
32) H. Horino, *Nippon Kagaku Zasshi*, **90**, 85 (1969).
33) I. Kawamoto, Y. Sugimura, and Y. Kishida, *Tetrahedron Lett.*, **1973**, 877.
34) H. Matsumura, *Nippon Kagaku Zasshi*, **85**, 901 (1964).

Asymmetric Transformation of (*RS*)-2-Phenylglycine via Formation of Salt with (1*S*)-10-Camphorsulfonic Acid

Tadashi SHIRAIWA,* Shinji SAKATA, Keiko FUJISHIMA, and Hidemoto KUROKAWA
Faculty of Engineering, Kansai University, Yamate-cho, Suita, Osaka 564
(Received July 20, 1990)

An asymmetric transformation of (*RS*)-2-phenylglycine [(*RS*)-Phg] was carried out via formation of a salt with (1*S*)-10-camphorsulfonic acid [(*S*)-CS] in acetic acid, propanoic acid, or butanoic acid by heating at 100 °C without using any catalysts such as aldehydes. The rate of epimerization of a more soluble salt of (*S*)-Phg with (*S*)-CS was estimated to be lowest in acetic acid and highest in butanoic acid. The asymmetric transformation in propanoic acid, however, was achieved successfully to give the salt of (*R*)-Phg with (*S*)-CS with 100% optical purity in 82% yield. Optically pure (*R*)-Phg was obtained from the salt in 80% yield based on the (*RS*)-Phg used as the starting material.

(*R*)-2-Phenylglycine [abbreviated as (*R*)-Phg] as a useful material for ampicillin has been obtained from synthetic (*RS*)-Phg by optical resolution[1–6] because (*R*)-Phg is not found in natural amino acids. (*S*)-Phg, however, is also given by optical resolution but is not of value as a material for ampicillin. Asymmetric transformation is carried out by combination of selective crystallization of a less soluble diastereomeric salt with epimerization of a more soluble salt, and has a possibility of converting a racemate solely into a desirable enantiomer. (1*S*)-10-Camphorsulfonic acid [(*S*)-CS] is a good resolving agent for the optical resolution of (*RS*)-Phg because (*S*)-CS is easily available and forms a salt with (*R*)-Phg as a less soluble diastereomeric salt without coverting (*RS*)-Phg into any derivatives such as ester. The asymmetric transformation of (*RS*)-Phg has been attempted via formation of the salt with (*S*)-CS in acetic acid in the presence of salicylaldehyde as a catalyst for epimerization.[7] Since the presence of aldehyde, such as salicylaldehyde, in the reaction system raises the solubility of the less soluble salt, the yield of the salt of (*R*)-Phg with (*S*)-CS [(*R*)·(S) salt] seems not to be so high.[7]

Optically active (*R*)- and (*S*)-Phg were apt to racemize on heating in carboxylic acid. We, therefore, tried asymmetric transformations of (*RS*)-Phg by heating in acetic acid, propanoic acid, or butanoic acid without using any catalyst, such as aldehyde, to establish a more efficient method for obtaining (*R*)-Phg. In addition, rates of racemization of (*R*)-Phg and (*R*)-2-(4-hydroxyphenyl)glycine [(*R*)-Hpg] were examined in these carboxylic acids to estimate the rate of epimerization of the more soluble salt of (*S*)-Phg with (*S*)-CS [(*S*)·(S) salt].

Experimental

Materials. (*RS*)- and (*R*)-Phg, (*R*)-Hpg, and (*RS*)- and (*S*)-CS were purchased from Wako Pure Chemicals Ind.

Asymmetric Transformation. A mixture of 20.0 mmol (3.02 g) of (*RS*)-Phg and 18.0 (4.18 g), 19.0 (4.41 g), or 20.0 (4.64 g) mmol of (*S*)-CS in 10 cm^3 of acetic acid, propanoic acid, or butanoic acid was stirred for 1—10 h at 100 °C. After further adding 1.00 mmol (0.232 g) and 2.00 mmol (0.464 g) of (*S*)-CS to the mixture at 60 °C in the reaction consuming 19.0 and 18.0 mmol of (*S*)-CS, respectively, the mixture was stirred for 5 min at 60 °C and successively for 20 min in an ice bath. The formed (*R*)·(*S*) salt was filtered off, washed with diethyl ether, and dried. The optical purity of the obtained salt was determined on the basis of the specific rotations of the salts of Phg with (*S*)-CS: (*R*)·(S) salt, $[\alpha]_D^{25}$ −49.7° (*c* 2, 1 mol dm^{-3} HCl);[7] the salt of (*RS*)-Phg with (*S*)-CS, $[\alpha]_D^{25}$ +13.6° (*c* 2, 1 mol dm^{-3} HCl).[7] The degrees of crystallization of the (*R*)·(*S*) and (*S*)·(*S*) salts ($DC_{(R)}$ and $DC_{(S)}$/%) were calculated by

$$DC_{(S)}/\% = (1/2)[\text{Yield}/\% \times (100 - \text{Optical purity}/\%)]/100, \quad (1)$$

$$DC_{(R)}/\% = [\text{Yield}/\% \times \text{Optical purity}/\%] + DC_{(S)}/\%. \quad (2)$$

The obtained salt was dissolved in methanol (10 cm^3 g^{-1}) at room temperature. After adding an equivalent of triethylamine to the solution, the mixture was stirred for 0.5 h in an ice bath. The precipitated (*R*)-Phg was filtered off, washed with methanol, and dried. The optical purity of the obtained (*R*)-Phg was determined on the basis of the specific rotation ($[\alpha]_D^{20}$ −157.8° (dil HCl))[8] of authentic (*R*)-Phg.

Rate Constant for Racemization. (*R*)-Phg (0.151 g, 1.00 mmol) or (*R*)-Hpg (0.167 g, 1.00 mmol) and (*RS*)-CS (0.220 g, 0.950 mmol or 0.232 g, 1.00 mmol) were immediately dissolved in 30 cm^3 of acetic acid, propanoic acid, or butanoic acid or in a mixture of 30 cm^3 of the carboxylic acid and 3 cm^3 of water at 100 °C, respectively. Portions of the solution were pipetted out at appropriate time intervals and the optical rotation was measured. The rate constant (k_R/s^{-1}) for racemization was calculated by the least-squares method from

$$\ln \alpha_0/\alpha_t = k_R \cdot t, \quad (3)$$

where α_t is the optical rotation at time t and α_0 that extrapolated to zero time. The half-life period ($t_{1/2}$/s) was calculated on the basis of the obtained k_R value.

Measurement. Optical and specific rotations at 589 nm were measured with a Union Giken PM-101 digital

polarimeter equipped with a quartz cell of 0.100 or 0.500 dm path length.

A mixture of (*RS*)-Phg (20.0 mmol) and (*RS*)-CS (20.0 mmol) in 20 cm^3 of acetic acid, propanoic acid, or butanoic acid was stirred for 2 h at 100 °C and successively for 5 h at 10 °C. The formed salt of (*RS*)-Phg with (*RS*)-CS [(*RS*)·(*RS*) salt] was rapidly filtered off, washed with diethyl ether, and thoroughly dried. The solubilities of the (*RS*)·(*RS*) salt in acetic acid, propanoic acid, or butanoic acid at 10 °C were estimated on the basis of the weight of the (*RS*)·(*RS*) salt and those of the (*RS*)-Phg and (*RS*)-CS used as the starting materials.

Results and Discussion

Racemization of (*R*)-2-Phenylglycine and (*R*)-2-(4-Hydroxyphenyl)glycine. One of the major problems in asymmetric transformation is the rate of epimerization of a more soluble diastereomeric salt, that is, the racemization of optically active substances. (*R*)-Phg was racemized by heating in carboxylic acid; for example, (*R*)-Phg (20.0 mmol) was stirred for 3 h at 100 °C in 10 cm^3 of acetic acid and successively for 20 min in an ice bath to give approximately racemic Phg ($[\alpha]_D^{20}$ −3.6° (*c* 1.00, 1 mol dm^{-3} HCl)) in 97.7% (2.95 g) yield. The rates of racemization of (*R*)-Phg and (*R*)-Hpg, therefore, were measured in acetic acid, propanoic acid, or butanoic acid in the presence of (*RS*)-CS at 100 °C, as described in the experimental section. The rates of (*R*)-Hpg in propanoic acid or butanoic acid were measured in mixtures of 30 cm^3 of the carboxylic acid and 3 cm^3 of water because (*R*)-Hpg did not dissolve completely in these carboxylic acids. Since the racemization of (*R*)-Phg and (*R*)-Hpg in the carboxylic acids is an acid-catalyzed reaction, the rates depend upon the concentration of (*R*)-Phg or (*R*)-Hpg and the carboxylic acid. The racemization, however, could be regarded as a pseudo first-order reaction because the carboxylic acids existed in large excess in the reaction system and linear relationships were found between $\ln \alpha_0/\alpha_t$ and time *t*. The rate constant of racemization (k_R/s^{-1}) and the half-life period ($t_{1/2}/s$) are listed in Table 1.

The racemization involves protonation of the carbonyl oxygen atom in the carboxyl group, followed by the loss of α-hydrogen atom by formation of the enol; these steps are reversible.[9] (*RS*)-CS acts as an extremely stronger proton donor for the amino groups in (*R*)-Phg and (*R*)-Hpg than the carboxylic acids. The presence of the positively charged nitrogen atom resulting from such a protonation hinders the second protonation of the carbonyl oxygen atom.[9] The rate of racemization in the presence of free (*R*)-Phg or (*R*)-Hpg, therefore, is more speeded up than in the presence of equimolar amounts of (*R*)-Phg or (*R*)-Hpg and (*RS*)-CS. The ammonium ion in (*R*)-Hpg is estimated to be more stable by the presence of the hydroxyl group on the aromatic ring than in (*R*)-Phg. The rate of racemization of (*R*)-Hpg, therefore, is slower than that of (*R*)-Phg.

Since the rate-determining step is the formation of

Table 1. Rate Constant and Half-Life Period for Racemization[a]

(*R*)-Amino acid	Conditions			k_R[d]	$t^{1/2}$
	Carboxylic acid[b]	Water / cm^3	(*RS*)-CS[c] / mmol	10^{-4} s^{-1}	10^2 s
(*R*)-Phg	AcA	0	0.95	4.63	15.0
		3	0.95	2.11	32.9
		0	1.00	4.14	16.7
		3	1.00	1.17	59.2
	PrA	0	0.95	14.0	4.95
		3	0.95	3.63	19.1
		0	1.00	8.23	8.42
		3	1.00	2.59	26.8
	BuA	0	0.95	80.0	0.866
		3	0.95	4.23	16.4
		0	1.00	44.7	1.55
		3	1.00	2.77	25.0
(*R*)-Hpg	AcA	0	0.95	1.24	55.9
		3	0.95	0.476	146
		0	1.00	0.508	136
		3	1.00	0.238	291
	PrA	3	0.95	0.810	85.6
		3	1.00	0.486	143
	BuA	3	0.95	0.920	75.3
		3	1.00	0.555	125

a) Conditions: (*R*)-2-phenylglycine [(*R*)-Phg] 1.00 mmol; (*R*)-2-(4-hydroxyphenyl)glycine [(*R*)-Hpg] 1.00 mmol; carboxylic acid 30 cm^3; temperature 100 °C. b) AcA=acetic acid; PrA=propanoic acid; BuA=butanoic acid. c) (*RS*)-CS: (1*RS*,4*SR*)-10-Camphorsulfonic acid. d) k_R: Rate constant for racemization. e) $t_{1/2}$: Half-life period.

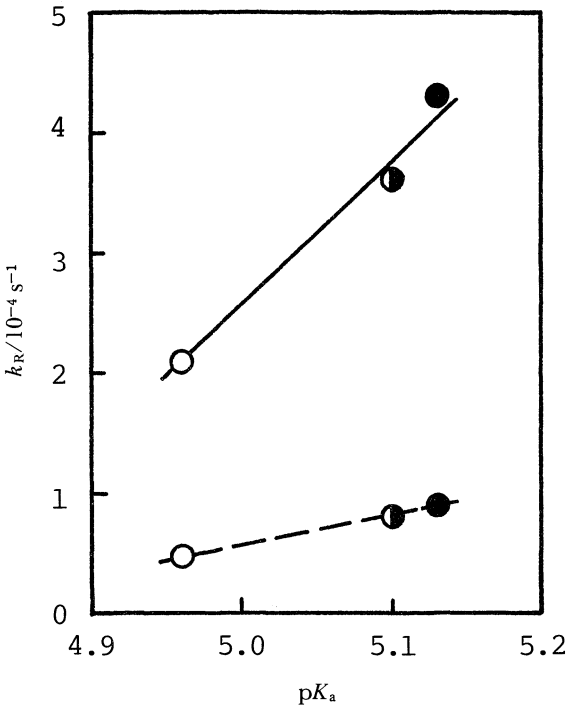

Fig. 1. Rate constant for racemization in carboxylic acids. pK_a: The value at 100 °C was estimated from data 0—60 °C. —: (*R*)-2-Phenylglycine (1.00 mmol). ---: (*R*)-2-(4-Hydroxyphenyl)glycine (1.00 mmol). (1*RS*,4*SR*)-10-Camphorsulfonic acid: 0.95 mmol. Temperature: 100 °C. Solvent: Mixture of 30 cm^3 of carboxylic acid and 3 cm^3 of water. k_R: Rate constant for racemization. Carboxylic acid: ○ Acetic acid; ◑ propanoic acid; ● butanoic acid.

the enol by abstract of the α-hydrogen atom by the carboxylate anion, the rates of racemization of (*R*)-Phg and (*R*)-Hpg seem to be dependent of the basicity of the carboxylate anions, that is, the acidity of the carboxylic acids employed as the solvent. The acidity constants at 100 °C of the carboxylic acids were estimated from data at 0—60 °C;[10] the pK_a values of acetic acid, propanoic acid, and butanoic acid were calculated to be 4.96, 5.10, and 5.13,[10] respectively. The relationship between the k_R and pK_a values is shown in Fig. 1.

The k_R value increased with increase in the pK_a value; k_R values obtained under other conditions, in Table 1, had a tendency to change similar to that shown in Fig. 1. The acidity constant suggests that the order of proton abstraction at 100 °C should be butanoate anion>propanoate anion>acetate anion, and hence the racemization of (*R*)-Phg and (*R*)-Hpg are speeded up in this order. The epimerization of the more soluble (*S*)·(*S*) salt, therefore, is estimated to be most rapid in butanoic acid and to be slowest in acetic acid.

Asymmetric Transformation of (*RS*)-2-Phenylglycine. Influence of Reaction Amount of (1*S*)-10-Camphorsulfonic Acid: The preceding result suggests that

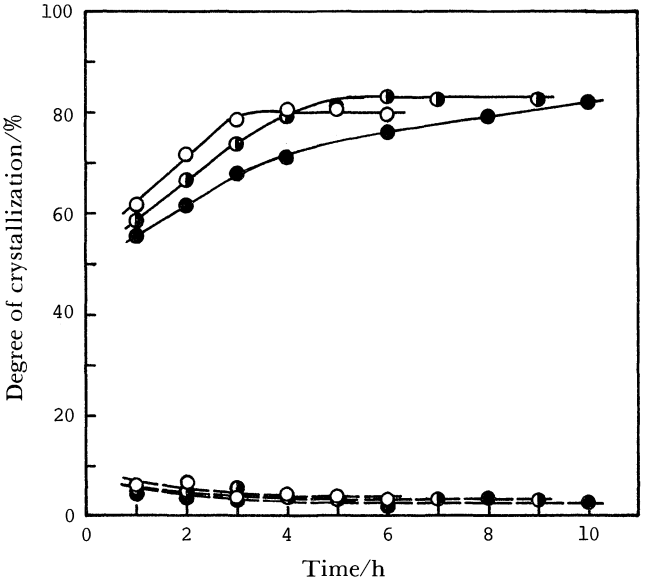

Fig. 2. Influence of amount of (1*S*)-10-camphorsulfonic acid on asymmetric transformation. (*RS*)-2-Phenylglycine [(*RS*)-Phg]: 20.0 mmol. (1*S*)-10-Camphorsulfonic acid [(*S*)-CS]: ○ 18.0 mmol; ◑ 19.0 mmol; ● 20.0 mmol. Solvent: 10 cm^3 of butanoic acid. Temperature: 100 °C. —: Salt of (*R*)-Phg with (*S*)-CS. ---: Salt of (*S*)-Phg with (*S*)-CS.

the rate of epimerization of the more soluble (*S*)·(*S*) salt is most rapid in butanoic acid and is increased in the presence of free (*RS*)-Phg. The asymmetric transformation of (*RS*)-Phg was tried in butanoic acid by consuming 20.0 mmol of (*RS*)-Phg and 18.0, 19.0, or 20.0 mmol of (*S*)-CS. The relationship between the degree of crystallization of the (*R*)·(*S*) and (*S*)·(*S*) salts and reaction time is shown in Fig. 2. Although the asymmetric transformation of (*RS*)-Hpg was attempted similarly to that of (*RS*)-Phg, the formed salt could not be obtained because the salt was strongly hygroscopic.

As shown in Fig. 2, after a rapid crystallization of the (*R*)·(*S*) salt in a short time period, the degree of crystallization of the (*R*)·(*S*) salt reached a maximal value and subsequently became constant in spite of elapse of time; when 20.0 mmol of (*S*)-CS was consumed, the degree of crystallization seemed to increase gradually even at 10 h. The epimerization of the (*S*)·(*S*) salt seems to be most rapid when 18.0 mmol of (*S*)-CS was consumed, as shown in Fig. 2. This result agreed with the estimate from the racemization of (*R*)-Phg. The asymmetric transformation consuming 18.0 mmol of (*S*)-CS, however, requires the addition of 2.00 mmol of (*S*)-CS after reaction at 100 °C and the formed salt should be the salt of (*RS*)-Phg with (*S*)-CS. The optical purity of the obtained (*R*)·(*S*) salt, therefore, was lower than those obtained by consuming 19.0 and 20.0 mmol of (*S*)-CS. Although the asymmetric transformation consuming 20.0 mmol of (*S*)-CS may give the (*R*)·(*S*) salt

with higher optical purity in higher yield, acquisition of such (*R*)·(*S*) salt requires extremely long time. The asymmetric transformation consuming 19.0 mmol of (*S*)-CS gave the (*R*)·(*S*) salt with 92% optical purity in 86% yield after reaction for 6 h. These results suggest that the favorable amount of (*S*)-CS is 19.0 mmol for 20.0 mmol of (*RS*)-Phg.

Influence of Carboxylic Acid Used as Solvent: The asymmetric transformation was carried out by reacting 20.0 mmol of (*RS*)-Phg and 19.0 mmol of (*S*)-CS at 100 °C in acetic acid, propanoic acid, or butanoic acid. These results are listed in Table 2 and shown in Fig. 3.

The solubilities of the salt of (*RS*)-Phg with (*RS*)-CS [(*RS*)·(*RS*) salt] at 10 °C in acetic acid, propanoic acid, and butanoic acid were 6.97, 4.19, and 2.61 g/(100 cm^3 of carboxylic acid), respectively; the (*RS*)·(*RS*) salt is estimated to consist of equimolar amounts of the (*R*)·(*S*) salt and its enantiomer. The order of solubilities of the (*R*)·(*S*) and (*S*)·(*S*) salts are estimated to be equal to that of the (*RS*)·(*RS*) salt. The asymmetric transformation in propanoic acid and butanoic acid gave the (*R*)·(*S*) salt with over 90% optical purity in over 80% yield by reaction for 5—9 h. Although the (*R*)·(*S*) salt obtained by a reaction for 1—5 h in acetic acid had 92—95% optical purity, the yield was low (55—60%) because the (*R*)·(*S*) and (*S*)·(*S*) salts are more soluble in acetic acid than in propanoic acid or butanoic acid. In addition, the epimerization of the (*S*)·(*S*) salt in acetic acid seems to be extremely slower than those in propanoic acid or

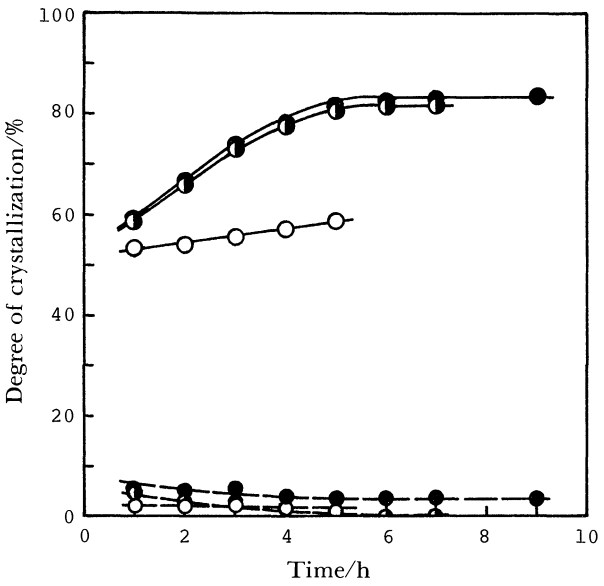

Fig. 3. Influence of carboxylic acid used as solvent on asymmetric transformation. (*RS*)-2-Phenylglycine [(*RS*)-Phg]: 20.0 mmol. (1*S*)-10-Camphorsulfonic acid [(*S*)-CS]: 19.0 mmol. Solvent: ○ Acetic acid; ◑ propanoic acid; ● butanoic acid. Temperature: 100 °C. —: Salt of (*R*)-Phg with (*S*)-CS. ---: Salt of (*S*)-Phg with (*S*)-CS.

Table 2. Asymmetric Transformation of (*RS*)-2-Phenylglycine[a]

Carboxylic acid[b]	Reaction time	(*R*)·(*S*) Salt[c]		(*R*)-Phg	
		Yield	Optical purity	Yield[e]	Optical purity
	h	g [%[d]]	%	%	%
AcA	1	4.22 [55.0]	92.4	54.4	92.1
	2	4.27 [55.7]	93.0	54.6	93.1
	3	4.43 [57.6]	93.0	57.0	92.8
	4	4.50 [58.7]	94.9	57.5	94.7
	5	4.60 [60.0]	94.9	59.1	95.0
PrA	1	4.82 [62.8]	86.3	61.4	86.1
	2	5.28 [68.8]	91.0	67.4	90.5
	3	5.77 [75.2]	93.4	73.5	94.3
	4	6.07 [79.1]	95.9	77.4	94.9
	5	6.22 [81.1]	98.3	79.6	98.2
	6	6.26 [81.6]	100	80.4	100
	7	6.27 [81.8]	100	80.6	100
BuA	1	4.90 [63.9]	83.4	62.8	84.2
	2	5.48 [71.4]	85.9	69.8	86.0
	3	6.05 [78.9]	85.7	77.2	85.7
	4	6.36 [82.9]	90.2	80.1	89.2
	5	6.52 [85.0]	92.0	83.5	91.9
	6	6.63 [86.4]	92.1	84.8	92.0
	7	6.64 [86.6]	92.0	84.9	92.0
	9	6.66 [86.8]	91.8	85.2	91.8

a) Conditions: (*RS*)-2-Phenylglycine [(*RS*)-Phg] 20.0 mmol; (1*S*)-10-(camphorsulfonic acid [(*S*)-CS] 19.0 mmol; carboxylic acid 10 cm^3; temperature 100 °C. b) AcA=Acetic acid; PrA=propanoic acid; BuA=butanoic acid. c) (*R*)·(*S*) Salt: Salt of (*R*)-Phg with (*S*)-CS. d) The yield was calculated on the basis of 20.0 mmol (7.67 g) of the (*R*)·(*S*) salt. The yield was calculated on the basis of 20.0 mmol (3.02 g) of (*R*)-Phg.

butanoic acid, as shown in Fig. 3, and is estimated from the racemization of (*R*)-Phg. Acetic acid, therefore, is not favorable as the solvent for the asymmetric transformation of (*RS*)-Phg.

The epimerization of the (*S*)·(*S*) salt in butanoic acid seems to be a little faster than in propanoic acid. Although the asymmetric transformation in butanoic acid gave the (*R*)·(*S*) salt with 92% optical purity in over 86% yield, recrystallization of the salt from water lowers the yield extremely.[7]

The (*R*)·(*S*) salt with 100% optical purity was obtained in 82% yield by the asymmetric transformation in propanoic acid. Isolation of (*R*)-Phg from the optically pure salt was carried out almost quantitatively by treatment of the methanol solution of the salt with triethylamine to obtain optically pure (*R*)-Phg in 80% yield based on the (*RS*)-Phg used as the starting material.

The above results show that the asymmetric transformation of (*RS*)-Phg is possible by heating in the carboxylic acids without using any catalysts such as aldehydes and gives optically pure (*R*)-Phg efficiently.

References

1) J. Santhanam, British Patent 1210495 (1967); *Chem. Abstr.*, **74**, 42618 (1971).

2) T. Watanabe, S. Hayashi, S. Ouchi, and S. Senoo, Japan Patent 78137 (1973); *Chem. Abstr.*, **80**, 71099 (1974).

3) K. Murakami, N. Katsuta, K. Takano, Y. Yamamoto, T. Kakegawa, K. Saigo, and H. Nohira, *Nippon Kagaku Kaishi*, **1979**, 765.

4) T. Shiraiwa, Y. Ohmichi, K. Iwafuji, and H. Kurokawa, *Nippon Kagaku Kaishi*, **1983**, 1070.

5) T. Shiraiwa, H. Miyazaki, S. Konishi, and H. Kurokawa, *Nippon Kagaku Kaishi*, **1985**, 1577.

6) T. Shiraiwa, H. Miyazaki, T. Imai, M. Sunami, and H. Kurokawa, *Bull. Chem. Soc. Jpn.*, **60**, 661 (1987).

7) C. Hongo, R. Yoshioka, M. Tohyama, S. Yamada, and I. Chibata, *Bull. Chem. Soc. Jpn.*, **56**, 3744 (1983).

8) J. S. Davies, "Amino Acids and Peptides," Chapman and Hall, London and New York (1985), p. 65.

9) M. Bodanszky, "Peptide Chemistry," Springer-Verlag, Berlin, Heidelberg, New York, London, Paris, and Tokyo (1988), pp. 115—116.

10) H. Ootaki, "Youeki Kagaku," Shoukabou, Tokyo (1985), pp. 184—186.

Aryliminodimagnesium Reagents. XIX.[1] Effects of Miscellaneous Metal Halides on Oxidative Self-Coupling of the Reagent, and on Its Condensation with Nitrobenzene. A New Preparative Route to *o,o'*-Dihydroxyazobenzene

Masao Ōkubo* and Haruko Shiku
Department of Chemistry, Faculty of Science and Engineering, Saga University, Honjo-machi, Saga 840
(Received August 1, 1990)

Fourteen metal halides (MX_n) were each added to the solutions of aryliminodimagnesium (*p*-$RC_6H_4N(MgBr)_2$, IDMg) in tetrahydrofuran, and the effect of MX_n on relative yields of products was examined in the following three IDMg reactions: (A) oxidative coupling leading to symmetrical azobenzene, (B) condensation with nitrobenzene, and (C) condensation with *o*-hydroxy-substituted (*o*-HO) nitrobenzene. Reaction A was promoted by addition of $CuCl_2$, and the yield of azoxybenzenes in reaction B was improved by addition of $NiCl_2$ or $CdCl_2$. Reaction C was similarly modified by addition of $CdCl_2$ so as to improve the yield of *o*-HO-azoxybenzenes. Their acetyl derivatives underwent a facile photoinduced migration of azoxy oxygen and were successively hydrolyzed to afford bidentate chelating agents, *o,o'*-$(HO)_2$-azobenzenes.

Modification of the reaction mode and reactivity of Grignard reagents by addition of miscellaneous metal halides was studied early by Kharasch[2] and later by Kochi[3] and their co-workers. The studies have contributed to the development of the vast and fascinating field of organometallic chemistry.

The nitrogenating ability of N–Mg reagent, aryliminodimagnesium ($RC_6H_4N(MgBr)_2$, IDMg) derived from anilines, via condensation with aromatic carbonyl and nitro compounds has been established.[4] The utility of the IDMg procedure is thus desired to be developed, and the effect of addition of each of fourteen metal halides on typical IDMg reactions was examined. The reactions selected are oxidative coupling to give symmetrical (*sym*-) azobenzenes[5] and condensation with nitrobenzenes to give unsymmetrical (*unsym*-) azoxy- and azobenzenes[4b,c] (Scheme 1: A and B). Reaction A was sufficiently promoted solely by $CuCl_2$ of the metal halides examined, whereas reaction B was modified by $NiCl_2$ or $CdCl_2$ to improve the yield of *unsym*-azoxybenzenes. The latter result was applied to condensation with *o*-hydroxy-substituted (*o*-HO) nitrobenzene (reaction C),[6a] and the obtained *o*-HO-azoxybenzene in improved yield was converted into a bidentate chelating agent, *o,o'*-$(HO)_2$-azobenzene. The results will be summarized and reported in this paper.

Results and Discussion

The metal halides examined are listed below according to their atomic numbers given in brackets: $TiCl_3$[22], $CrCl_3$[24], $MnCl_2$[25], $FeCl_3$[26], $CoCl_2$[27], $NiCl_2$[28], Cu(I)Cl[29], Cu(II)X_2[29], (X=Cl, Br), $ZrCl_4$[40], $MoCl_5$[42], AgCl[47], $CdCl_2$[48], Sn(II)Cl_2[50], Sn(IV)Cl_4[50], $HgCl_2$[80], and $BiCl_3$[83].

Relative yields of products will be discussed in terms of reported governing factors. The principal factor of reactions of IDMg and ArMgBr is the relative efficiency of single electron transfer (SET) regardless of the normal condensation and addition modes; the combination of electron-donating and -accepting abilities (EDA and EAA) was evaluated by the difference (ΔE) between oxidation and reduction potentials of reactants.[7] Owing to the weaker EDA of

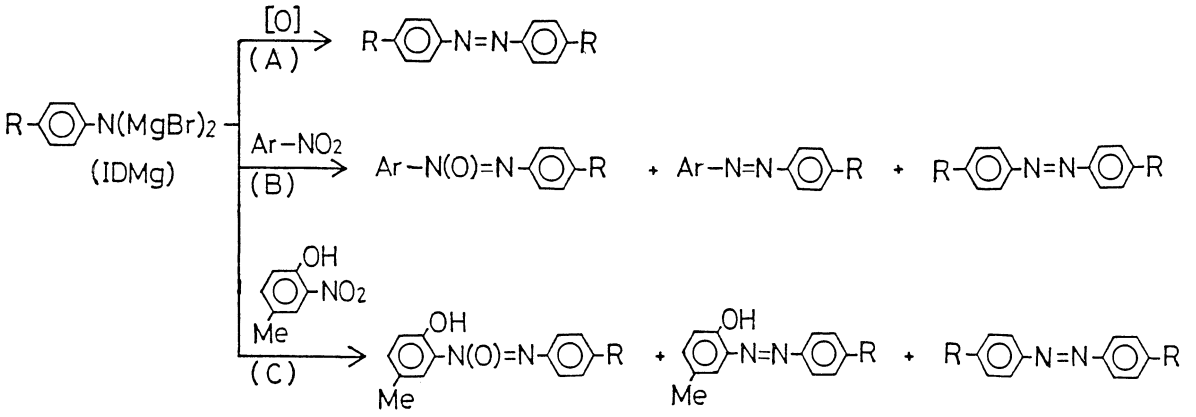

Scheme 1.

IDMg than that of ArMgBr,[6] a second factor originating from aggregation of IDMg molecules was disclosed.[6]

(A) Effect of Added $CuCl_2$ on Oxidative Coupling of IDMg. Concerning the formation of *sym*-azobenzenes from anilines, air oxidation in the presence of Cu(I)Cl and pyridine[9] and oxidative coupling of IDMg[5] by use of I_2, $C_6H_5IO_2$, and OsO_4 in tetrahydrofuran (THF) were reported. The use of Cu(II)Cl_2 for reaction A leads to higher yield than that in a previous study,[5] and is available for *sym*-azobenzene preparation. The coupling took place only by use of CuX_2 (X=Cl, Br) or $FeCl_3$, the latter giving poor yield. The use of $CuBr_2$ led to lower conversion probably due to its larger redox potential than that of $CuCl_2$.

Figure 1a illustrates the effect of substituents (R) of IDMg on its conversion by use of two molar equivalents of $CuCl_2$ under fixed conditions: R=*p*-Me and H are more favorable than R=*p*-MeO and *p*-Cl, whereas R=*o*-Me and *o*-MeO give poor yields due to steric hindrance. Figure 1b illustrating effects of reaction conditions shows that *p*-Me reagent is sufficiently converted by use of $CuCl_2$ in two molar equivalents. The maximum yield, 75%, however, was not further improved by adding $CuCl_2$ at −20 or 0 °C. Neither addition at lower temperatures (−40 and −78 °C) nor use of greater amounts of $CuCl_2$ was effective. Mechanistic reasons why the retained 25% is not overcome and the *p*-MeO and *p*-Cl groups are less favorable, remain to be examined.

(B) Moderating Effect of $NiCl_2$ and $CdCl_2$ on the Condensation with Nitrobenzene. The condensation

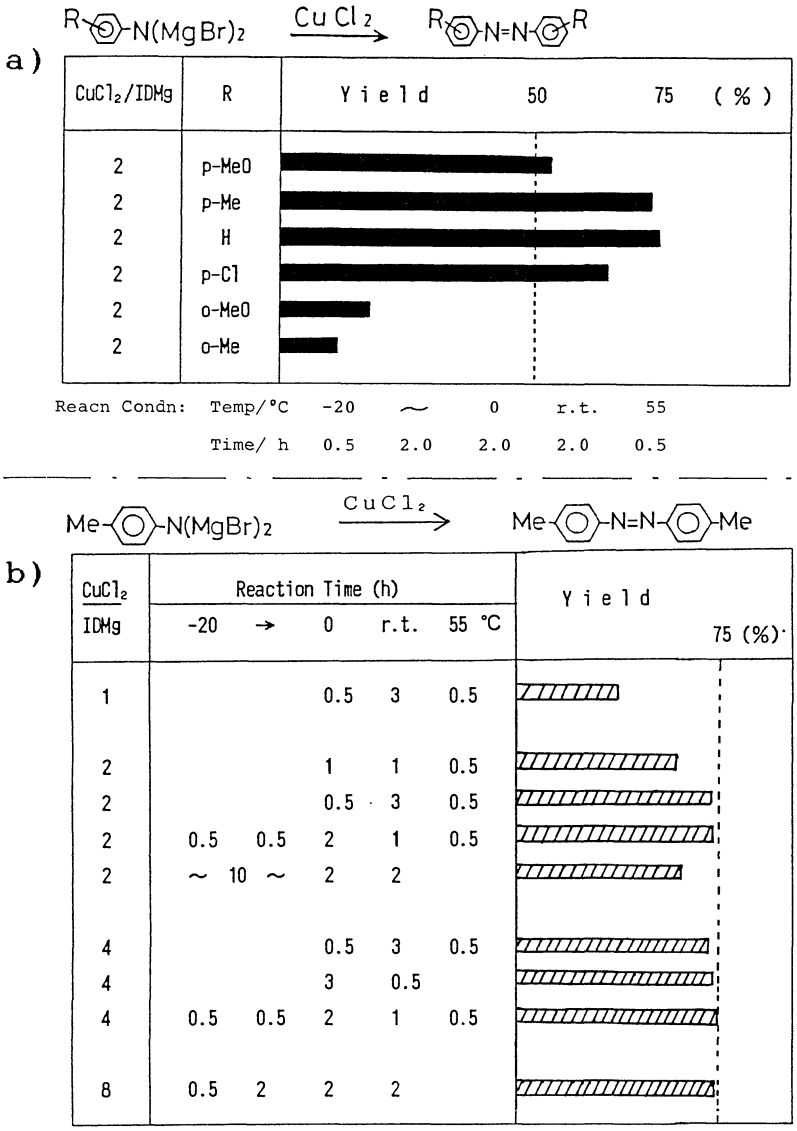

Fig. 1. Effect of $CuCl_2$ addition on the oxidative coupling of IDMg reagents (reaction A). a): Substituent effect on the yield of azobenzene under fixed conditions of reaction. b): Effect of reaction conditions on the oxidative coupling of *p*-MeC_6H_4-IDMg.

with nitrobenzene (Scheme 1B) is composed of two normal successive processes, I (condesation) and II (deoxygenation), both being favored by aggregation of IDMg.[6a,b] Of reactions of IDMg, reaction B is most important not only because this provides a new method for independent preparation of ONN and NNO isomers of *unsym*-azoxybenzenes by exchange of substituents of the nitro- and aminobenzenes[4c] but also because this and the Grignard addition to Ar_2CO are "SET-controlled" reactions having comparable ΔE values.[7] Thus, preparation of azoxybenzene (**1**) from combination of R=MeO and Ar=*p*-ClC_6H_4 (Scheme 2) encounters difficulties under ordinary conditions: High SET efficiency (small ΔE) is responsible not only for rapid I and II but also for oxidative and reductive couplings of IDMg and $ArNO_2$, respectively, to give **2**,

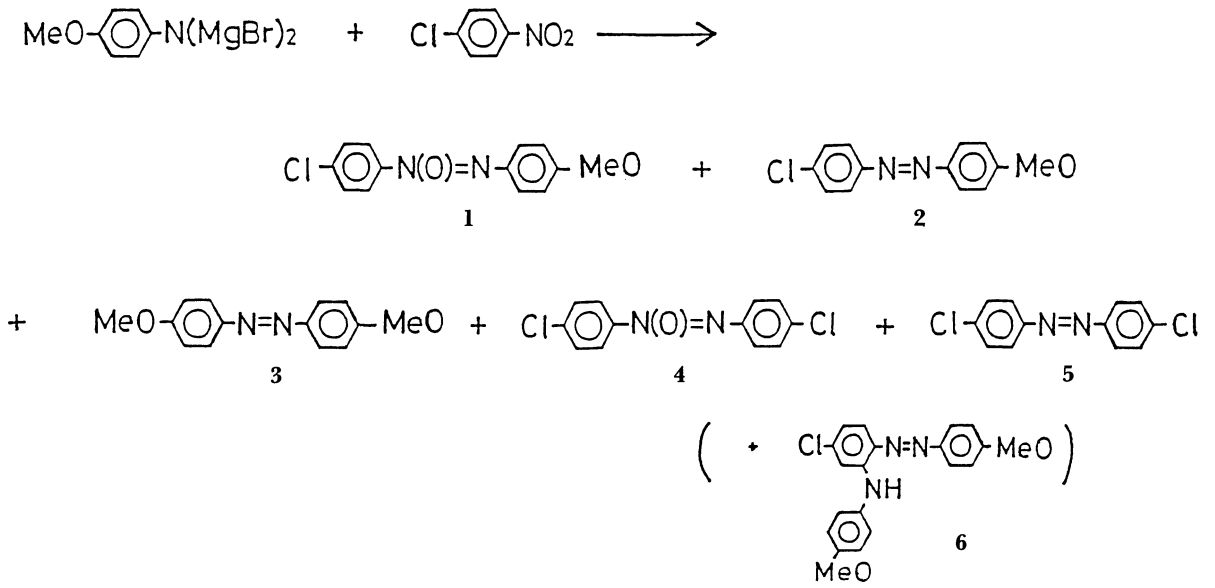

Scheme 2.

Table 1. Yields of Products **1**—**5** Affected by MX_n Addition in the Condensation Reaction B (See Scheme 2)

MX_n M^n	Atom No.	Yield[a]/%						
		1	2	3	4	5	Recov.	Overall
—	—	41	15	18	24	0	0	98
(Type **a**)								
Cr(III)	[24]	35	32	30	0	0	0	97
Mn(II)	[25]	43	21	25	10	Trace	0	99
Ni(II)	[28]	58	20	17	5	0	0	100
Cu(I)	[29]	24	10	28	38	0	0	100
Zr(IV)	[40]	15	44[b]	23	0	0	0	82
Ag(I)	[47]	51	12	30	7	Trace	0	100
Cd(II)	[48]	65	13	16	0	0	0	94
Sn(IV)	[50]	51	30	17	2	0	0	100
Ni[c]	—	56	20	18	6	0	0	100
Cd[d]	—	63	17	20	0	0	0	100
(Type **b**)								
Ti(III)	[22]	0	27	10	0	0	0	37
Fe(III)	[26]	0	19	39	0	0	0	58
Sn(II)	[50]	20	6	0	12	10	0	42
(Type **c**)								
Co(II)	[27]	45	5	12	0	0	34	97
Mo(V)	[42]	0	0	46	0	0	49	95
Hg(II)	[80]	27	21	21	0	0	31	100
Bi(III)	[83]	20	2	6	0	0	52	90

a) Yields obtained at the ratio [IDMg]:[$ArNO_2$]:[MX_n]=4:1:4 unless otherwise noted. b) Yield of **2** in cludes that of **6** (see text). c) [IDMg]:[$ArNO_2$]:[MX_n]=4:1:1. d) [IDMg]:[$ArNO_2$]:[MX_n]=4:1:0.5.

3, and **4**. The dimeric abnormal products, **3** and **4**, are formed via SET taking place from aggregated IDMg due to "pre-interaction[7b] between reactants having small ΔE." With use of this combination, "moderating effect" caused by $NiCl_2$ or $CdCl_2$ to improve the yield of **1** was disclosed.

By comparison with the yields of **1**—**5** without use of MX_n (Table 1), characteristic variation in the yields caused by an equimolar amount of MX_n was surveyed, and manners of variation were classified into three types **a**—**c**. Type **a**: no recovery and improved combined yield of **1** plus **2** with two exceptional cases; **b**: no recovery and poor overall yield; **c**: appreciable recovery and fairly good overall yields.

In type **a**, i.e., improved efficiency of the reaction indicated by no recovery, effects of MX_n on the relative yields of **1** and **2** are classified into four kinds: (i) Improved effciency of I at the expense of **4** by addition of Ni, Ag, Cd, or Sn(IV) chloride; (ii) improved efficiency of II by addition of $CrCl_3$; (iii) the combined yield of **1** and **2** is not improved due to reductive coupling to give **4** by addition of Mn(II) or Cu(I) chloride; (iv) the highest yield of azo products, including **2** and an *o*-anilino-substituted one **6**, indicating a very rapid SET,[10] by addition of $ZrCl_4$.

According to the EDA-EAA concept, type **b**, poor efficiency of I and II and no recovery, implies that $ArNO_2$ is decomposed via a much accelerated SET. Type **c**, depression of the reaction itself indicated by recovery of $ArNO_2$, implies that the SET is retarded. The peculiar effect caused by $MoCl_5$ is noted; only **3** was formed due to oxidative coupling of IDMg in the presence of $ArNO_2$ but not formed in the absence.

Even from the preliminary results obtained under unoptimized conditions, the effect of MX_n on IDMg reactions is distinct from that on Grignard reactions. Whereas Grignard reagent is oxidatively coupled by Co(II) and Ag(I) salts,[2b,3b] IDMg is unaffected (see Reaction A). The formation of mild C–Cd reagent by addition of Cd(II) salt to Grignard solution[11] seems different from a "catalytic" effect suggested from the comparable yields obtained by use of $NiCl_2$ and $CdCl_2$ in 1/1 and 1/4 or 1/8 molar amounts (see Table 1); no evidence for N–Cd bond formation is obtained.

The effect of $NiCl_2$ and $CdCl_2$, i.e., improved yield of **1** at the expense of **4** (Table 1), is noted. The EDA-EAA concept claims that[7,8] this originates from moderate SET, modified EDA being suggested. Moreover, a modified state of IDMg aggregation[6] is also suggested from the almost completely reduced yield of **4** contrary to the difficultly reduced yield of **3**. The modifications must arise from interaction of IDMg with d-orbitals of metal ions, remaining to be studied in detail. Nevertheless, the "catalytic moderating effect" is applied to preparation of *unsym-o*-HO-azoxybenzenes described below.

(C)-Synthetic Use of $CdCl_2$: Preparation of *o*-HO-Azoxybenzene and Conversion into *o,o'*-$(HO)_2$-Azobenzene. *sym-o,o'*-$(HO)_2$-Azobenzenes, utilizable as chelating agents, have so far been prepared by coupling of appropriate aryldiazonium salt by use of hydroxylamine–$CuSO_4$.[12] *unsym-p'*-Methyl- and *p'*-octyl-*o*-HO-azobenzenes, also utilized for selective solvent extraction of Ag(I) and Cu(II) ions,[13] are prepared by coupling of the cooresponding arenediazonium salt with phenols. An alternative prepara-

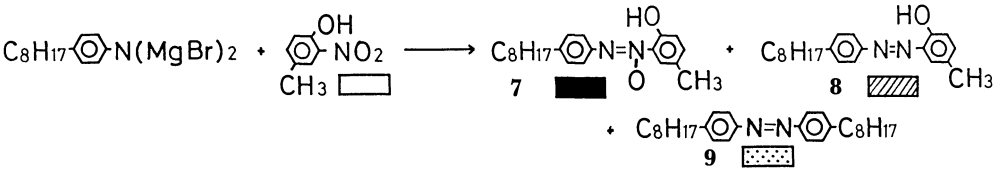

Entry No.	MXn	M:R:S	Reaction Time (h) add. (°C)	45°C	55°C	yield (%) 50
1	—	4:1	45	1		
2	—	4:1	0		3	
3	$NiCl_2$	5:5:1	0		3	
4	—	8:1	45	1		
5	—	8:1	0		3	
6	—	8:1	0		1	
7	$NiCl_2$	4:8:1	0		1	
8	$CdCl_2$	4:8:1	0		1	

M:R:S = $[MX_n]:[IDMg]:[ArNO_2]$

Fig. 2. Effect of addition of $NiCl_2$ and $CdCl_2$ on the condensation of *p*-octyl-C_6H_4–IDMg with 2-HO-5-Me-nitrobenzene (reaction C).

tion of *unsym-o*-HO-azo compounds by use of IDMg (Scheme 1C) was reported,[6a] and modified by addition of $CdCl_2$ to provide a synthetic route to *unsym-o,o'*-$(HO)_2$-azo compounds.

Reaction C using 2-HO-5-Me-nitrobenzene and 4.0 or 8.0 molar equivalents of *p*-octyl-C_6H_4-IDMg was carried out in the absence and presence of $NiCl_2$ or $CdCl_2$. Figure 2 illustrates the effect of reaction conditions on the yields of *o*-HO-azoxybenzene (**7**), *o*-HO-azobenzene (**8**), *sym*-azobenzene (**9**), and the amount of recovery. In accord with previous results obtained by use of *p*-Me-C_6H_4-IDMg,[6a] the use of four molar equivalents of *p*-octyl-C_6H_4-IDMg (both in the absence and in the presence of $NiCl_2$) led to a combined yield of **7** plus **8** lower than 50%, i.e., insufficient efficiency of condensation. Though the combined yield was improved so as to exceed 70% by the use of eight molar equivalents of IDMg, the yield of **7** was still lower than 45% in the absence of $NiCl_2$ or $CdCl_2$.[6a] However, in the presence of the latter, the yield of **7** was improved to more than 60%.

Direct photoconversion of the *o*-HO-azoxy compound **7** (R=Me) into *o,o'*-$(HO)_2$-azo product by Wallach-type azoxy-ortho migration of oxygen[14] is quite sluggish due to intramolecular hydrogen bonding, and instead, deoxygenation predominates after a longer time of irradiation (see Table 2). However, evoking the behavior of some *o*-MeO- and *o*-halo-azoxybenzenes,[14] the *o*-acetyl-azoxy compound derived from **7** was easily photoconverted into *o*-acetyl-*o'*-HO-azo product, which was successively hydrolyzed to give the desired *o,o'*-$(HO)_2$-azo compound (Scheme 3). The *p'*-octyl derivative of **7** (R=octyl) behaves similarly.

For the use of bidentate *o,o'*-$(HO)_2$-azobenzenes for solvent extraction, the facile and complete recovery of *p'*-octyl derivative from the binary solvent system due to reduced solubility in water is of greater advantage than for *p'*-methyl derivative.

Experimental

Materials and Procedures. Guaranteed grade anhydrous metal halides were commercially available and used without further purification. The IDMg reagents were prepared on a 6—8 mmol scale in 50 ml THF by treatment of the corresponding anilines with two molar equivalents of EtMgBr.[4b,8] For reaction A, a calculated amount of $CuCl_2$ was added to the IDMg solution in THF at −20 or 0 °C, and the mixture was stirred under the time and temperature conditions indicated in Figs. 1a and 1b. The mixture was quenched with aqueous ammonium chloride, and the azobenzene was chromatographically separated on silica gel (Wako Gel FC-40).

For reaction B (see Scheme 2), a calculated amount of MX_n was added at 0 °C to the THF solution of IDMg with subsequent addition of the nitrobenzene. The resulting mixture was stirred at room temperature for 3 h and at 55 °C for 0.5 h. Product mixtures were similarly separated. The yields of products **1—6** are given in Table 1. Reaction C was similarly carried out, and molar ratios of reagent versus substrate, reaction temperatures and times, and yields of products **7—9** are shown in Fig. 2. The distinctive behavior of *o*-HO- and o-acetoxy-azoxy compounds under photo-irradiation using the given concentration in ethanol[14] (see Scheme 3) is shown by the product yields given in Table 2.

All the products are known, and the structures were determined by ^1H NMR spectra: The signals appearing at δ=8.1—8.3 and δ=7.7—7.9 were assigned to the ortho protons of azoxy and azo products, respectively.[4c] The

Table 2. Behavior of *o*-RO-Substituted (R=H, CH_3CO) Azoxybenzenes under Photoirradiation in Ethanol (0.002 mol dm^{-3}) (See Scheme 3)

Azoxy R	Irradn. time/h	Yield/%		Recov.	Overall
		o-RO-*o'*-HO	*o*-RO		
H(**7**)	0.5	6	15(**8**)	77	98
H(**7**)	3.0	17	47(**8**)	15	79
CH_3CO	0.5	51	0	23	74

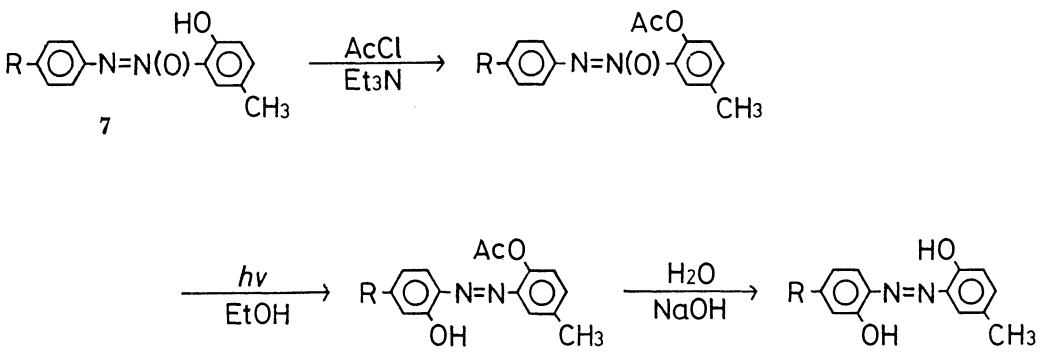

Scheme 3.

signal of the HO protons of 7 appearing at δ=11.92 indicates intramolecular hydrogen bonding.

The financial support by a Grant-in-Aid for Scientific Research No. 01540435 from the Ministry of Education, Science and Culture is acknowledged. The authors wish to thank Dr. Yoshinari Baba, the Joint Research and Development Center, Saga University for his discussion and experiments on the function of *o*-HO-azo compounds in solvent extraction.

References

1) Part XVIII: M. Ōkubo, M. Tanaka, and K. Matsuo, *Chem. Lett.*, **1990**, 1005.

2) a) M. S. Kharasch and O. Reinmuth, "Grignard Reactions of Nonmetallic Substances," Prentice-Hall, Inc., New York (1954), Chap. 5; b) M. S. Kharasch and E. K. Fields, *J. Am. Chem. Soc.*, **63**, 2316 (1941).

3) a) J. K. Kochi, "Free Radicals," John Wiley & Sons, New York (1973), Vol. 1, Chap. 11; b) M. Tamura and J. K. Kochi, *Bull. Chem. Soc. Jpn.*, **45**, 1120 (1971) and literatures cited therein.

4) a) M. Ōkubo, *Bull. Chem. Soc. Jpn.*, **58**, 3108 (1985); b) M. Ōkubo, T. Takahashi, and K. Koga, *ibid.*, **56**, 199 (1983); c) M. Ōkubo and K. Koga, *ibid.*, **56**, 203 (1983).

5) M. Ōkubo, S. Yoshida, Y. Egami, K. Matsuo, and S. Nagase, *Bull. Chem. Soc. Jpn.*, **60**, 1741 (1987).

6) M. Ōkubo, T. Nakashima, and H. Shiku, *Bull. Chem. Soc. Jpn.*, **62**, 1621 (1989); b) M. Ōkubo, K. Matsuo, and A. Yamauchi, *ibid.*, **62**, 915 (1989).

7) a) M. Ōkubo, T. Tsutsumi, and K. Matsuo, *Bull. Chem. Soc. Jpn.*, **60**, 2085 (1987); b) M. Ōkubo, Y. Fukuyama, M. Sato, K. Matsuo, T. Kitahara, and M. Nakashima, *J. Phys. Org. Chem.*, **3**, 379 (1990).

8) M. Ōkubo, T. Tsutsumi, A. Ichimura, and T. Kitagawa, *Bull. Chem. Soc. Jpn.*, **57**, 2679 (1984).

9) K. Kinoshita, *Bull. Chem. Soc. Jpn.*, **32**, 777 (1959).

10) M. Ōkubo, C. Sugimori, M. Tokisada, and K. Matsuo, *Bull. Chem. Soc. Jpn.*, **59**, 1644 (1986).

11) D. A. Shirley, *Org. React.*, **8**, 28 (1954).

12) D. C. Freeman and C. E. White, *J. Org. Chem.*, **21**, 379 (1956); *J. Am. Chem. Soc.*, **78**, 2678 (1956).

13) Y. Baba, H. Shiku, and M. Ōkubo, The 51st Conference of Analytical Chemistry of Japan, Saga, May 1990.

14) M. Ōkubo, H. Hyakutake, and N. Taniguchi, *Bull. Chem. Soc. Jpn.*, **61**, 3005 (1988).

Thermally Irreversible Photochromic Systems. Photoreaction of Diarylethene Derivatives with Imidazo[1,2-*a*]pyridine Rings

Yasuhide NAKAYAMA, Koichiro HAYASHI, and Masahiro IRIE*,†
The Institute of Scientific and Industrial Research, Osaka University,
Mihogaoka 8-1, Ibaraki, Osaka 567
† Institute of Advanced Material Study, Kyushu University,
Kasuga-Koen 6-1, Kasuga, Fukuoka 816
(Received September 13, 1990)

A non-symmetrical diarylethene with imidazo[1,2-*a*]pyridine ring on one end and thiophene ring on the other end, 1,2-dicyano-1-(2-methylimidazo[1,2-*a*]pyridin-3-yl)-2-(2,4,5-trimetyl-3-thienyl)ethene **2Z** underwent a hexatriene-cyclohexadiene type reversible ring-closure reaction by photoirradiation, while an only *Z*–*E* isomerization was observed for a symmetrical diarylenthene with two imidazo[1,2-*a*]pyridine rings, 1,2-dicyano-1,2-bis(2-methylimidazo[1,2-*a*]pyridin-3-yl)ethene **1Z**. The ring-closure reaction was not discerned. The photogenerated closed-ring form **2C** had the absorption band at 535 nm, which is 23 nm longer wavelengths than that of the corresponding dithienylethene, and kept the absorption intensity constant for more than 24 h at 80 °C. The quantum yield close to unity was observed for the photochemical ring-opening reaction of **2C** with 546 nm light.

Recently, a new type of thermally stable photochromic systems, diarylethene derivatives with heterocyclic rings, has been developed, such as 1,2-dicyano-1,2-bis(2,4,5-trimethyl-3-thienyl)ethene and 2,3-bis-(2,4,5-trimethyl-3-thienyl)maleic anhydride.[1] The compounds have no thermochromic property even at 300 °C and the closed-ring forms are stable for more than 3 months at 80 °C.[2,3] In addition, no appreciable fatigue was observed for the diarylethenes with benzothiophene rings even after 8×10^3 ring closure/opening cycles.[2]

Although these compounds have promising properties for optical data storage media,[4–6] they still lack several indispensable conditions, such as diode laser sensitivity and non-destructive read out capability. The absorption edges of the closed-ring forms are less than 700 nm. Replacement of the thiophene rings with indole ones, which have high electron-donating ability, shifted the absorption maximum of the closed-ring form as much as 60 nm, and the absorption edge of the acid anhydride derivative reached 800 nm.[7] Although the compound has the sensitivity at the diode laser wavelength ($780<\lambda<830$ nm), the conversion of the open-ring to the closed-ring form in the photostationary state under irradiation with 474 nm light is less than a few percent, and the thermal stability of the closed-ring form is insufficient.

In the present study, we synthesized a symmetrical diarylethene derivative with two imidazo[1,2-*a*]pyridine rings, which have higher electron-donating ability than indole ring, and a non-symmetrical one with imidazo[1,2-*a*]pyridine ring on one end and thiophene ring on the other end in attempting to shift the absorption bands to longer wavelengths.

Results and Discussion

A Symmetrical Diarylethene Derivative with Two Imidazo[1,2-*a*]pyridine Rings. A diarylethene derivative with two imidazo[1,2-*a*]pyridine rings was prepared by a self-coupling reaction[1] of two 3-(cyanomethyl)-2-methylimidazo[1,2-*a*]pyridine. The mixture of *Z* and *E* forms was dissolved in benzene and exposed to 490 nm light to convert the *E* form to the *Z* form. The *Z* form was separated from the mixture of *Z* and *E* forms by HPLC and purified by crystallization from a hexane–ether mixture.

The *Z* form, **1Z**, was irradiated in benzene (6.8×10^{-5} mol dm^{-3}) in the presence of air with 475 nm light, and the reaction was followed by absorption and HPLC measurements (silica-gel column, 1:1 chloroform–acetone). Figure 1 shows the spectra of **1Z** before and after photoirradiation with 475 nm light in the

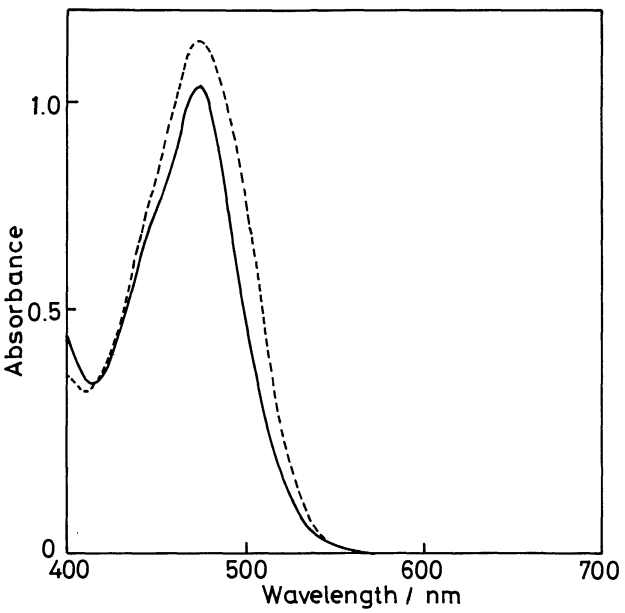

Fig. 1. Absorption spectra of **1Z** (6.8×10^{-5} mol dm^{-3}) (—) before photoirradiation and (---) in the photostationary state under irradiation with 475 nm light.

dilute benzene solution. The absorption maximum of **1Z** was observed at 475 nm and the molar absorption coefficient was 15,000 $dm^3\,mol^{-1}\,cm^{-1}$. The absorption maximum shifts to a longer wavelength as much as 40 nm in comparison with *Z* form of 1,2-dicyano-1,2-bis(1,2-dimethyl-3-indolyl)ethene.[7] Upon irradiation with 475 nm light, the intensity of the absorption in 420—550 nm region increases. Any new absorption was not observed at longer wavelengths. It was inferred from the NMR measurement that the absorption intensity change is due to the *Z*–*E* isomerization from **1Z** to **1E** (see below). Under the photostationary state, the *Z* to *E* ratio was estimated by HPLC to be **1E**/**1Z**=33/67. A ring-closure reaction was not discerned even after prolonged irradiation with lights of 420—550 nm wavelengths.

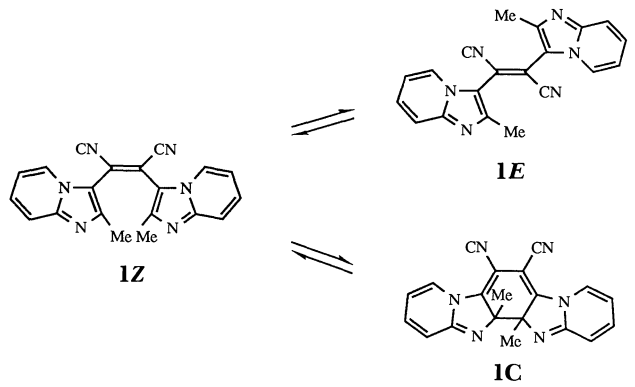

Scheme 1.

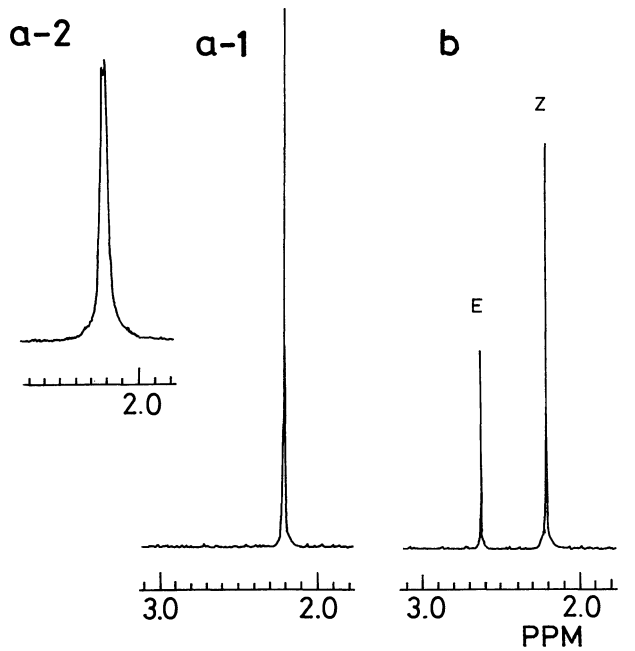

Fig. 2. ^1H NMR spectra (270-MHz) of **1E** in $CDCl_3$: (a-1) before irradiation at room temperature; (a-2) at −25 °C; (b) after irradiation with 475 nm light.

Figure 2 a-1 and b show the 270-MHz ^1H NMR spectra of methyl protons of **1Z** in $CDCl_3$ before and after photoirradiation with 475 nm light in benzene solution, respectively. Figure 2 a-2 shows the signals of methyl protons of **1Z** in $CDCl_3$ at −25 °C. At this temperature, the sharp singlet splits into two peaks at 2.19 and 2.21 ppm. The two methyl protons indicate the existence of two atropisomers in the compound **1Z**. A similar line-shape change was reported for dibenzothiophene derivatives.[8] One conformer has two imidazo[1,2-*a*]pyridine rings in mirror symmetry (in parallel orientation) and the other C_2 symmetry (in anti-parallel orientation).

After photoirradiation a new signal appeared at 2.63 ppm (Fig. 2). The absence of other signals except the one line indicates that the signal is ascribable to the *E* form and the ring-closure reaction is negligible. The assignment was further confirmed by the ^{13}C NMR measurement. Any signal ascribable to sp^3 carbons was not discerned after photoirradiation.

A Non-symmetrical Diarylethene Derivative with Imidazo[1,2-*a*]pyridine and Thiophene Rings. A diarylethene derivative with imidazo[1,2-*a*]pyridine ring on one end and thiophene ring on the other end was prepared by a cross-coupling reaction[2] of 3-(cyanomethyl)-2-methylimidazo[1,2-*a*]pyridine[9] and 4-(cyanomethyl)-2,3,5-trimethylthiophene.[1] The mixture of *E* and *Z* forms was dissolved in benzene and exposed to the light longer than 450 nm. The

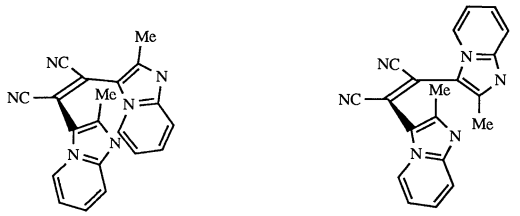

Scheme 2.

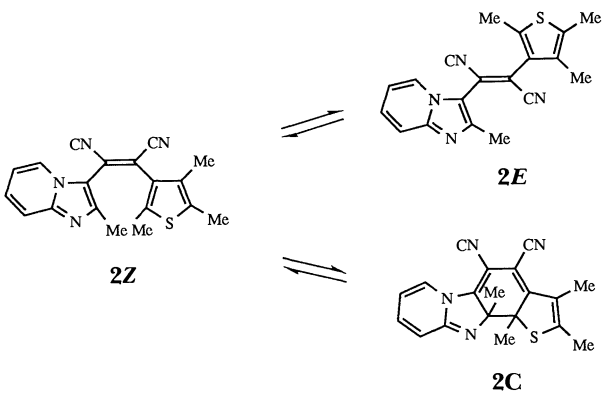

Scheme 3.

irradiation is expected to convert the *E* form to the *Z* form. The *Z* form was separated by HPLC and purified by crystallization from a hexane–ether mixture.

The *Z* form, **2Z**, was irradiated in benzene (1.25×10^{-4} mol dm^{-3}) in the presence of air with 450 nm light, and the reaction was followed by absorption and HPLC measurement (silica-gel column, chloroform). Figure 3 shows the spectra of **2Z** before and after photoirradiation with 450 nm light. Irradiation of the yellow benzene solution with 450 nm light led to the formation of a red solution, in which a visible absorption was observed at 535 nm and a shoulder at 580 nm. The visible absorption was ascribed to the closed-ring form, **2C**, from the NMR measurement (see below).

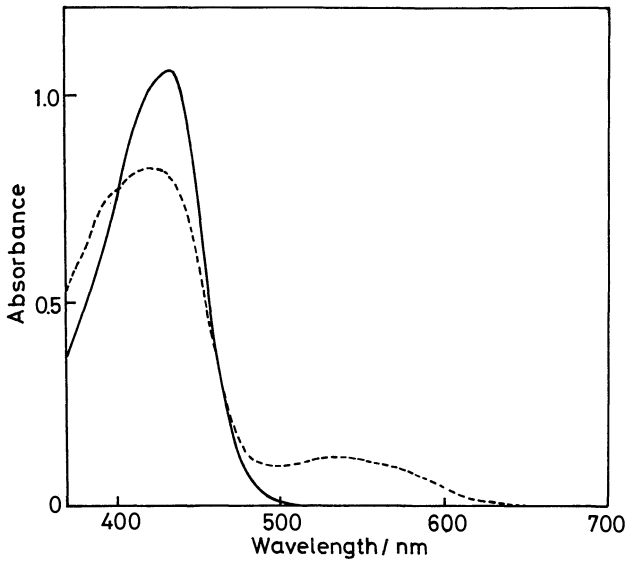

Fig. 3. Absorption spectra of **2*E*** (1.25×10^{-4} mol dm^{-3}) (—) before photoirradiation and (---) in the photostationary state under irradiation with 450 nm light.

The replacement of one of imidazo[1,2-*a*]pyridine rings with a thiophene ring enables the diarylethene to undergo the ring-closure reaction. The absorption maximum wavelength is 23 nm longer than that of the dithienylethene derivative.[1] The conversion from **2Z** to **2C** in the photostationary state under irradiation with 450 nm light was estimated to be 30% by HPLC analysis.

The irradiation was also accompanied with a *Z–E* isomerization from **2Z** to **2*E***. In the photostationary state, the contents of each isomer were estimated by HPLC as **2Z** (40%), **2C** (30%), and **2*E*** (30%). The yield of the closed-ring form depended on the irradiation wavelength. When the solution was irradiated with 425 nm light, the conversion was decreased to less than 15%.

The ^{1}H NMR spectra (360-MHz) of **2Z** in C_6D_6 before photoirradiation and after irradiation with 450 nm light are shown in Fig. 4 a and b. Before photoirradiation, 4 lines were observed at 1.41, 1.50, 1.62, and 1.96 ppm, which are assigned to the **2Z** form.

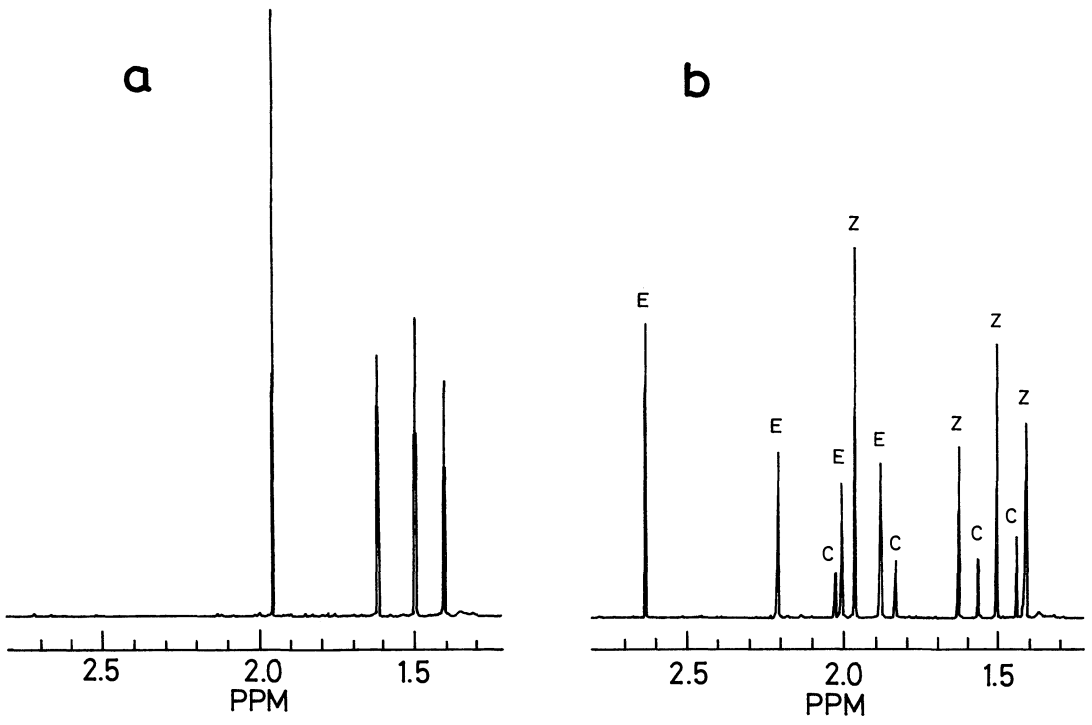

Fig. 4. ^{1}H NMR spectra (360-MHz) of **2Z** in C_6D_6: (a) before irradiation (b) after irradiation with 450 nm light.

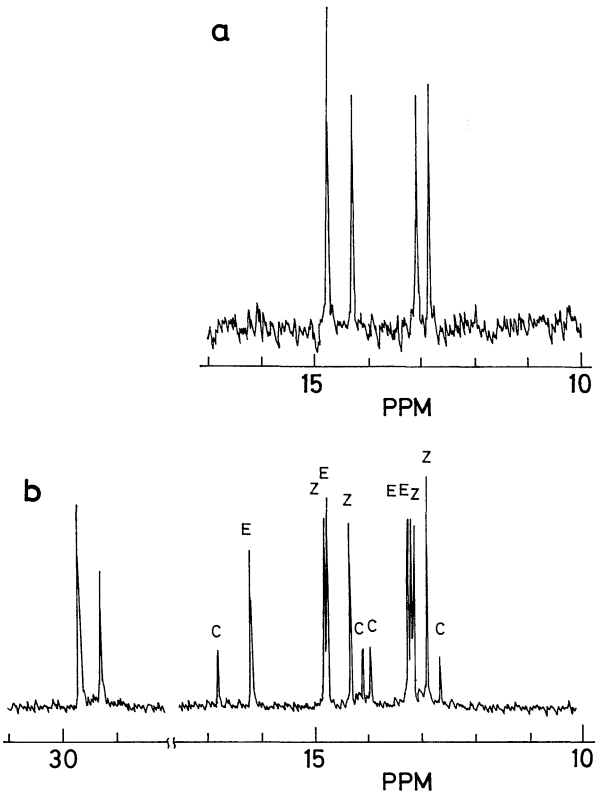

Fig. 5. ^{13}C NMR spectra (68-MHz) of **2Z** in $CDCl_3$: (a) before irradiation (b) after irradiation with 450 nm light.

Upon irradiation with 450 nm light, new 8 lines appeared at 1.43, 1.56, 1.83, 1.87, 2.00, 2.02, 2.20, and 2.62 ppm along with a decrease of the intensity of the 4 lines. The eight lines observed after photoirradiation indicate the co-existence of three isomers, **2Z**, **2C**, and **2*E***. The assignments are shown in the figure.

Figure 5 a and b show the 68-MHz ^{13}C NMR spectra of methyl carbon of **2** in $CDCl_3$ before photoirradiation and after irradiation with 450 nm light, respectively. Before photoirradiation, 4 lines were observed at 12.86, 13.09, 14.32, and 14.77 ppm, which are due to **2Z** form. Upon irradiation, new 8 lines appeared at 12.57, 13.12, 13.19, 13.92, 14.11, 14.74, 16.17, and 17.01. These 8 lines may be classified into two groups (13.12, 13.19, 14.74, and 16.17 ppm) and (12.57, 13.92, 14.11, and 17.01 ppm). The former is assigned to the *E* form, **2*E***, and the latter to the closed-ring form, **2C**. The other two lines at 29.29 and 29.69 ppm observed after photoirradiation indicate the existence of sp^3 carbon after photoirradiation. This result confirms that closed-ring form, **2C**, was formed by photoirradiation.

The photogenerated closed-ring form, **2C** was thermally stable. Any changes of the absorption intensity at 535 nm was not observed even at 80 °C. The absorption intensity remained constant for more than 24 h, at 80 °C.

Table 1. Quantum Yields for Ring-Closure and Ring-Opening Reactions in Benzene Solution

Reaction	Excitation wavelength / nm	Quantum yield
2Z→**2C**	405	0.06
2C→**2Z**	546	1.00

Quantum yields for the cyclization and the ring-opening reactions of **2** were determined in benzene solution in the presence of air at 25 °C. Table 1 summarized the results. The cyclization quantum yield of the imidazo[1,2-*a*]pyridine-thiophene derivative **2Z** at 405 nm was 0.06, which is similar value observed for 1,2-dicyano-1,2-bis(1,2-dimethyl-3-indolyl)-ethene[7] and 2,3-bis(2,4,5-trimethyl-3-thienyl)maleic anhydride.[1] The quantum yield of the ring-opening reaction at 546 nm was obtained to be close to unity. The value is 8 times larger than that observed for dithienylethene derivative.[1] The large value is possibly due to the steric strain of the closed-ring form, especially the strain of the imidazo[1,2-*a*]pyridine ring.[7,8]

Summary

Diarylethene derivatives with imidazo[1,2-*a*]pyridine rings were synthesized. The symmetric diarylethene derivative with two imidazo[1,2-*a*]pyridine rings underwent only the *Z*–*E* photoisomerization. The ring-closure reaction was not observed. On the other hand, the non-symmetrical diarylethene derivative with imidazo[1,2-*a*]pyridine ring on one end and thiophene ring on the other end underwent both the *Z*–*E* isomerization and the ring-closure reaction. The absorption maximum showed a bathochromic shift as much as 23 nm in comparison with that of dithienylethene derivative. A quantum yield close to unity was observed for the ring-opening reaction of **2C**.

Experimental

General Method. IR spectra were measured with a Perkin Elmer Model 1618 spectrophotometer using KBr disks. ^1H NMR spectra (360 MHz) were recorded with a Bruker WN-360 spectrometer. Samples were measured in C_6D_6 or $CDCl_3$ using the tetramethylsilane (0 ppm) as an internal standard. ^{13}C NMR spectra (68 MHz) were recorded on JOEL JNM-GSX-270 spectrometer using $CDCl_3$ as the solvent with tetramethylsilane as an internal standard. Mass spectra and elemental analyses were performed in the Material Analysis Center of Osaka University. Melting points were determined by using a Gallenkamp melting point apparatus (MP-41). HPLC analysis was carried out on a JASCO 800 system. Stainless-steel columns (length, 250 mm; i.d., 4.6 mm, for analytical purposes, length, 250 mm; i.d., 10.0 mm, for preparative purposes) were slurry packed using silica gel (Fine SIL-5). Absorption spectra were measured with a Shimadzu MPS-200 instrument.

Photoirradiation was carried out with a EWIG XC-500 Xenon lamp. The wavelength of light was selected by passing the light through a monochrometer (Jobin Yvon H10-UV). Quantum yields were determined by measuring the rate of isomerization in the initial stage of the reaction at low concentration (absorbance at the irradiation wavelength <0.2) and the light intensity was measured with a photometer (International Light IL1700).

Materials. 1,2-Dicyano-1,2-bis(2-methylimidazo[1,2-*a*]-pyridin-3-yl)ethene and 1,2-dicyano-1-(2-methylimidazo[1,2-*a*]pyridin-3-yl)-2-(2,4,5-trimethyl-3-thienyl)ethene were synthesized as follows.

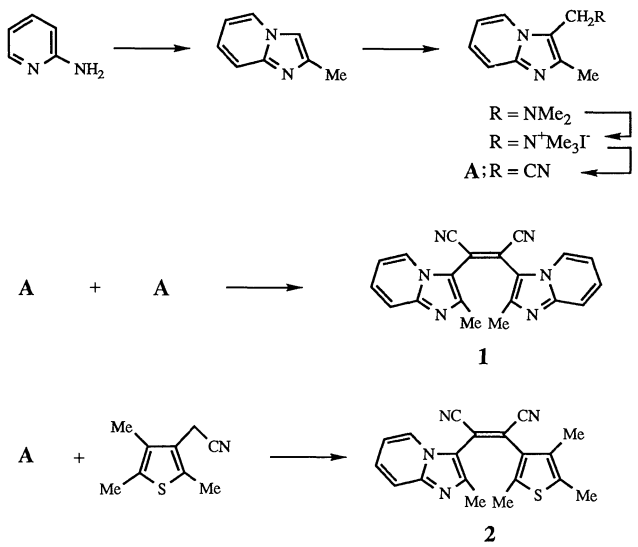

2-Methylimidazo[1,2-*a*]pyridine.[9] A mixture of 11.3 g (0.12 mol) of 2-aminopyridine and 11.1 g (0.12 mol) of chloroacetone in 120 mL of ethanol was heated under reflux for 20 h. The ethanol was removed by evaporation, and the residual material was dissolved in 100 mL of water. The aqueous solution was extracted with dichloromethane (4×20 mL). The dichloromethane extracts were washed with water (20 mL). The aqueous solutions were combined, and adjusted to pH 11.5—12 by the addition of 50% sodium hydroxide (ca. 12 mL). The basic aqueous solution was extracted with dichloromethane (3×20 mL). The dichloromethane extracts were combined and washed with water (20 mL). The aqueous solution was cooled with ice and was adjusted to pH 7 by the addition of 6 M hydrochloric acid (ca. 20 mL, M=mol dm^{-3}). After the solution was allowed to stand overnight, the solid that precipitated was isolated by filtration, washed with water and dried. Recrystallization from dichloromethane–methanol gave 5.6 g (0.042 mol) (35%) of 2-methylimidazo[1,2-*a*]pyridine. bp 120 °C/0.35 mmHg (1 mmHg=133.322 Pa). ^{1}H NMR ($CDCl_3$), δ=2.45 (s, 3H), 7.00 (dt, J=1.1 and 6.8 Hz, 1H), 7.09 (ddd, J=1.4, 6.8, and 9.4 Hz, 1H), 7.32 (s, 1H), 7.49 (d, J=9.4 Hz, 1H), 8.01 (dt, J=6.5 and 1.1 Hz, 1H).

3-[(Dimethylamino)methyl]-2-methylimidazo[1,2-*a*]pyridine.[9] A mixture of 5.6 g (0.042 mol) of 2-methylimidazo-[1,2-*a*]pyridine, 4.45 g (0.055 mol) of dimethylamine hydrochloride and 1.64 g (0.055 mol) of paraformaldehyde in 40 mL of methanol was heated under reflux for 1.5 h with stirring. Thereafter, the mixture was evaporated. Upon cooling to ambient temperature, the reaction mixture was acidified by the addition of concentrated hydrochloric acid (ca. 4 mL) and stirred for 18 h. The solid was isolated by filtration and washed with methanol and finally ether. After drying the solid was dissolved in 52 mL of hot water. The aqueous solution was adjusted to pH 11—12 by adding 50% sodium hydroxide. The mixture was cooled to 0 °C and extracted with dichloromethane (3×20 mL). The extracts were combined and washed with aqueous NaCl solution (20 mL). The dichloromethane was removed under reduced pressure to give an oil 3-[(dimethylamino)methyl]-2-methylimidazo[1,2-*a*]pyridine 7.9 g (0.042 mol) (100%). This material was used without further purification. ^{1}H NMR ($CDCl_3$), δ=2.22 (s, 6H), 2.44 (s, 3H), 3.65 (s, 2H), 6.75 (td, J=7.0 and 1.1 Hz, 1H), 7.13 (ddd, J=1.1, 6.8, and 9.0 Hz, 1H), 7.49 (d, J=9.0 Hz, 1H), 8.17 (d, J=7.2 Hz, 1H).

2-Methyl-3-[(trimethylammonio)methyl]imidazo[1,2-*a*]pyridine Iodide.[9] 3-[(Dimethylamino)methyl]-2-methylimidazo-[1,2-*a*]pyridine 7.9 g (0.042 mol) was dissolved in 58 mL of ethanol. To the ethanol solution at 0 °C was added dropwise with stirring 6.6 g (0.047 mol) of methyl iodide. The reaction mixture was stirred at ambient temperature overnight. The solid that formed was isolated by filtration and washed with ethanol (10 mL) and finally ether (35 mL). After drying, 14.0 g (0.042 mol) (100%) of 2-methyl-3-[(trimethylammonio)methyl]imidazo[1,2-*a*]pyridine iodide was obtained.

3-(Cyanomethyl)-2-methylimidazo[1,2-*a*]pyridine.[9] A mixture of 14.0 g (0.042 mol) of 2-methyl-3-[(trimethylammonio)-methyl]imidazo[1,2-*a*]pyridine iodide and 2.16 g (0.044 mol) of sodium cyanide in 120 mL of *N*,*N*-dimethylformamide was heated on a steam bath for 1 h with stirring. The mixture was poured into ice/water (360 mL) and stirred for 1 h. The solid was isolated by filtration, washed with water, and dried. Recrystallization from acetonitrile gave 2.4 g (0.014 mol) (33%) of 3-(cyanomethyl)-2-methylimidazo[1,2-*a*]pyridine. IR(KBr) 2246 cm^{-1}; MS (EI) *m*/*z* (rel intensity), 171 (M^+, 100), 156 (M^+—Me, 29), 145 (M^+—CN, 37); ^{1}H NMR ($CDCl_3$), δ=2.47 (s, 3H), 3.98 (s, 2H), 6.91 (t, J=6.8 Hz, 1H), 7.24 (t, J=7.9 Hz, 1H), 7.57 (d, J=9.0 Hz, 1H), 7.94 (d, J=6.8 Hz, 1H); mp 157—9 °C; Found: C, 70.31; H, 5.23; N, 24.46%. Calcd for $C_{10}H_9N_3$: C, 70.16; H, 5.30; N, 24.54%.

1,2-Dicyano-1,2-bis(2-methylimidazo[1,2-*a*]pyridin-3-yl)-ethene 1*Z*. This was prepared by a self-coupling reaction of 3-(cyanomethyl)-2-methylimidazo[1,2-*a*]pyridines by the method of Irie et al.[1] To 1.1 mL of 50% NaOH aqueous solution containing tetrabutylammonium bromide (0.07 g, 0.2 mmol) was added over a period 0.5 h a mixture of 3-(cyanomethyl)-2-methylimidazo[1,2-*a*]pyridine (462 mg, 2.7 mmol) and carbon tetrachloride (0.79 mL, 8 mmol), benzene 0.79 mL and acetone 1.0 mL at 40 °C. The solution was stirred for 3 h at 45 °C. Then the reaction mixture was poured into water. The aqueous solution was extracted with $CHCl_3$ and the organic phase was dried over $MgSO_4$. After the solvent was removed, the mixture of *Z* and *E* form was obtained in 79% yield by column chromatography on silica gel. The mixture of *Z* and *E* forms was dissolved in benzene and then exposed to 490 nm light. The *Z* form was separated from the solution by HPLC and then purified by recrystallization from a hexane–ether mixture. Mp 250—2 °C; IR(KBr) 2211 cm^{-1}; ^{1}H NMR[10] ($CDCl_3$), δ=2.21 (s, 6H), 6.75

(td, J=6.8 and 1.3 Hz, 2H), 7.27 (ddd, J=1.4, 6.5, and 8.3 Hz, 2H), 7.53 (d, J=9.7 Hz, 2H), 7.54 (d, J=6.8 Hz, 2H); ^{1}H NMR (C_6D_6), δ=2.02 (s, 6H), 5.77 (td, J=6.8 and 1.4 Hz, 2H), 6.31 (ddd, J=8.6, 7.2, and 1.4 Hz, 2H), 6.71 (d, J=6.8 Hz, 2H), 7.07 (d, J=8.6 Hz, 2H); MS (EI) m/z (rel intensity) 338 (M^+, 100) 323 (M^+−Me, 8); Found: C, 70.93; H, 3.98; N, 24.83%. Calcd for $C_{20}H_{14}N_6$: C, 70.99; H, 4.17; N, 24.84%.

1,2-Dicyano-1-(2-methylimidazo[1,2-*a*]pyridin-3-yl)-2-(2,3,5-trimethyl-3-thienyl)ethene 2*Z*.[2] This was prepared by a cross-coupling reaction of 3-(cyanomethyl)-2-methylimidazo-[1,2-*a*]pyridine and 4-(cyanomethyl)-2,3,5-trimethylthiophene[1] and isolated in 18% yield, mp>300 °C; IR(KBr) 2215 cm^{-1}; ^{1}H NMR[11] ($CDCl_3$), δ=1.79 (s, 6H), 2.00 (s, 6H), 2.12 (s, 6H), 2.18 (s, 6H), 6.88 (td, J=6.8 and 1.4 Hz, 2H), 7.39 (ddd, J=1.4, 6.8, and 9.0 Hz, 2H), 7.58 (d, J=8.6 Hz, 2H), 7.87 (td, J=6.8 and 1.1 Hz, 2H); ^{1}H NMR (C_6D_6) δ=1.41 (s, 6H), 1.50 (s, 6H), 1.62 (s, 6H), 1.96 (s, 6H), 6.05 (td, J=6.8 and 1.1 Hz, 2H), 6.49 (ddd, J=7.6, 6.8, and 1.1 Hz, 2H), 7.22 (d, J=7.6 Hz, 2H), 7.33 (d, J=6.8 Hz, 2H); ^{13}C NMR ($CDCl_3$), δ=12.86, 13.09, 14.32, 14.77, 113.00, 113.75, 114.383, 114.529, 116.01, 117.38, 119.59, 124.08, 127.15, 128.85, 130.26, 132.55, 137.69, 146.88, 147.95; MS (EI) m/z (rel intensity), 332 (M^+, 100), 317 (M^+−Me, 63); Found: C, 68.58; H, 4.96; N, 16.71%. Calcd for $C_{19}H_{16}N_4S_1$: C, 68.65; H, 4.85; N, 16.85%.

We thank Mr. Masato Sekiguchi (Osaka Univ.) for his helps in NMR measurements.

References

1) M. Irie and M. Mohri, *J. Org. Chem.*, **53**, 803 (1988).
2) M. Irie, *Jpn. J. Appl. Phys.*, **28-23**, 215 (1989).
3) M. Irie, "Polymers in Information Storage Technology," ed by K. L. Mittaled, Plenum, New York (1989), p. 105.
4) A. P. Glaze, S. A. Harris, H. G. Heller, W. Johncock, S. N. Oliver, P. J. Strydom, and J. Whittal, *J. Chem. Soc., Perkin Trans. 1*, **1985**, 957.
5) Y. Yokoyama, H. Hayata, H. Ito, and Y. Kurita, *Bull. Chem. Soc. Jpn.*, **63**, 1607 (1990).
6) H. Suzuki, A. Tomoda, M. Ishizuka, A. Kaneko, M. Furui, and R. Matsushima, *Bull. Chem. Soc. Jpn.*, **62**, 3968 (1989).
7) Y. Nakayama, K. Hayashi, and M. Irie, *J. Org. Chem.*, **55**, 2592 (1990).
8) K. Uchida, Y. Nakayama, and M. Irie, *Bull. Chem. Soc. Jpn.*, **63**, 1311 (1990).
9) J. J. Kaminski, J. A. Bristol, S. Puchalski, R. G. Lovey, A. J. Elliott, H. Guzik, D. M. Solomon, D. J. Conn, M. S. Domalski, S. Wong, E. H. Gold, J. F. Long, P. J. S. Chiu, M. Steinberg, and A. T. Mcphail, *J. Med. Chem.*, **28**, 876 (1985).
10) **1*E*** form: ^{1}H NMR ($CDCl_3$) δ=2.63 (s, 6H), 7.07 (td, J=6.8 and 1.1 Hz, 2H), 7.46 (ddd, J=1.4, 6.8, and 9.0 Hz, 2H), 7.72 (d, J=9.0 Hz, 2H), 8.30 (d, J=6.5 Hz, 2H); ^{1}H NMR (C_6D_6) δ=2.56 (s, 6H), 6.10 (td, J=1.4 and 6.8 Hz, 2H), 6.55 (ddd, J=1.4, 7.0, and 8.8 Hz, 2H), 7.33 (d, J=8.6 Hz, 2H), 7.79 (d, J=7.2 Hz, 2H).
11) **2*E*** form: ^{1}H NMR ($CDCl_3$) δ=2.21 (s, 3H), 2.35 (s, 3H), 2.52 (s, 3H), 7.05 (td, J=6.8 and 1.1 Hz, 1H), 7.43 (ddd, J=10.1, 6.8 and 1.1 Hz, 1H), 7.69 (d, J=10.1 Hz, 1H), 8.20 (d, J=6.8 Hz, 1H); ^{1}H NMR (C_6D_6) δ=1.87 (s, 3H), 2.00 (s, 2H), 2.20 (s, 2H), 2.62 (s, 2H), 6.08 (td, J=7.2 and 1.4 Hz, 2H), 6.54 (ddd, J=7.9, 7.2, and 1.4 Hz, 2H), 7.33 (d, J=7.2 Hz, 2H), 7.71 (d, J=7.9 Hz, 2H).

Synthetic Photochemistry. LVI.[1] Photorearrangement of Dimethyl 2-Oxohomobarrelene-6,7-dicarboxylates

Akira MORI, Yasuhiro NUKII,† Akihiro ENDO,† and Hitoshi TAKESHITA*
Institute of Advanced Material Study, 86, Kyushu University,
Kasuga-koen, Kasuga, Fukuoka 816
† Graduate School of Engineering Sciences, 39, Kyushu University,
Kasuga-koen, Kasuga, Fukuoka 816
(Received September 25, 1990)

The direct irradiation of dimethyl 2-oxohomobarrelene-6,7-dicarboxylates in chloroform gave indanone derivatives. A benzophenone-sensitized reaction gave a new tricyclic compound, dimethyl 5-oxotricyclo-[4.3.0.0^{2,9}]nona-3,7-diene-1,2-dicarboxylate, the formation of which was quenched by isoprene.

Bicyclo[3.2.2]nona-3,6,8-trien-2-ones (homobarrelenones) are interesting molecules with regard to the photochemical reactivity, since they have a transannular conjugated tri-π-methane chromophore, in which one of the double bonds is conjugated with a carbonyl group. The photochemical reactivity of these transannularly delocalized π-systems has attracted much attention and, indeed, the photochemical reactions for parent homobarrelenone[2] and benzo and dibenzo derivatives[3,4] as well as 2-methylenehomobarrelenes[5] have already been investigated. However, the reactions of the homobarrelenones with substituents were limited, since their preparation was somewhat difficult.

We recently developed a new synthetic method for producing homobarrelenones, the Diels–Alder cycloaddition of tropones to dimethyl 7-oxabicyclo[2.2.1]hepta-2,5-diene-2,3-dicarboxylate and subsequent fragmentation.[6] Furthermore, we could synthesize quinone-fused homobarrelenones, e.g., tricyclo[6.3.2.0^{2,7}]trideca-2(7),4,10,12-tetraene-3,6,9-trione (**1**) via a high-pressure Diels–Alder reaction of tropone with *p*-benzoquinone followed by dehydrogenation. We have verified that **1**, upon UV-irradiation, exclusively gave tetracyclo-[6.5.0.0^{1,9}.0^{5,9}]trideca-2,6,11-triene-4,10,13-trione (**2**).[7] This photochemical reaction of **1** has been shown to be different with regard to the product distribution to that of the parent homobarrelenone. It is therefore worth investigating other homobarrelenone derivatives having different chromophores. Herein, we describe the photorearrangement of dimethyl 2-oxohomobarrelene-6,7-dicarboxylate (**3**) with some mechanistic aspects.

When dimethyl 2-oxohomobarrelene-6,7-dicarboxylate (**3a**)[8] was irradiated in chloroform by means of a 100-W high-pressure mercury lamp, four products (**4a**, **5**, **6a**, **7**) were obtained in 24, 2.3, 16, and 3.8% yields, respectively. The major product, **4a**, was identified as dimethyl 7-oxobicyclo[4.3.0]nona-2,4,8-triene-1,6-dicarboxylate by an ^{1}H NMR spectral comparison with an authentic sample, which has already been isolated from the thermal reaction of **3a**.[8] While the minor product, **5**, could not be separated completely from **3a**, its ^{1}H NMR spectrum was identical with that of authentic dimethyl 1-oxoindan-4,5-dicarboxylate.[8] The structure of **6a** was determined to be isomeric dimethyl 1-oxoindan-5,6-dicarboxylate, since aromatic proton signals appeared separately at δ=7.74 and 8.19 as singlets. Compound **7** had an ethoxycarbonyl group instead of the ketonic carbonyl group in the ^{13}C NMR spectrum, and its UV spectrum indicated a cycloheptatriene derivative. Since the signals for four olefinic protons and six olefinic carbons were recognized, **7** was deduced to be ethyl 3,4-bis(methoxycarbonyl)-2,4,6-cycloheptatrienylacetate. Evidently, **7** was formed via a ketene intermediate.

The irradiation of **3a** in chloroform in the presence of benzophenone afforded five products, four of which were the same as those characterized by direct irradiation. The structure of a new tricyclic compound (**8**) was determined as depicted on the basis of ^{1}H and ^{13}C NMR spectral analyses; the NMR spectral data for a common unsaturated ring moiety of **8** and **2**[7] were almost superimposable on each other.

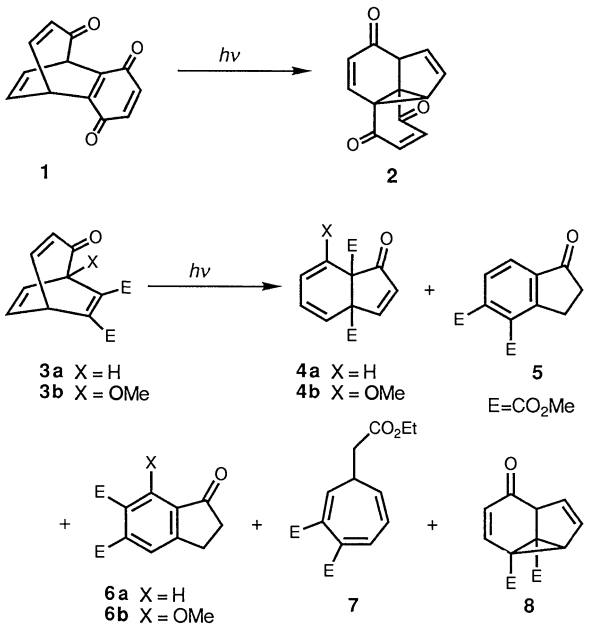

Scheme 1.

On the other hand, dimethyl 1-methoxy-2-oxohomobarrelene-6,7-dicarboxylate (**3b**) was irradiated under similar conditions; two products (**4b** and **6b**) were obtained in 41 and 42.4% yields, respectively.

The structure of **4b** was elucidated to be dimethyl 5-methoxy-7-oxobicyclo[4.3.0]nona-2,4,8-triene-1,6-dicarboxylate according to the NMR spectral similarity with **4a**. **6b** was identified to be dimethyl 7-methoxy-1-oxoindan-5,6-dicarboxylate, since no NOE was observed between the aromatic proton signal and the methoxyl signal. The irradiation of **3b** in the presence of benzophenone resulted in the formation of the same products (**4b** and **6b**) as those produced by direct irradiation.

When the benzophenone-sensitized photoreaction of **3a** was monitored by the ^{1}H NMR spectra, as shown in Fig. 1, the consumption of **3a** was accelerated and the ratios of **3a**/**4a** increased.

In parallel, a quenching effect of the photoreaction of **3a** was analyzed by using isoprene. As shown in Table 1, compound **8** was undetectable and the product distribution was similar to that produced by direct irradiation. These results clearly show that **8** was formed via the triplet excited state and that the other products (indanones and **7**) were formed via singlet excited state, as illustrated in Scheme 2. The pathway to **8** can be explained in terms of di-π-methane rearrangements[2] of the diradical, **A**, which must be more stable than the alternative diradical, **B**, since both radical moieties of **A** were stabilized by the adjacent carbonyl groups.

Ketene intermediates, **C** and **D**, as has already been proposed regarding indanone formation in the thermal reaction of **3a**,[8,9] would be involved in photorear-

Table 1. Product Distributions of Photoreactions of **3a**

Solvent (Additive)	Yield/% 4a	5	6a	7	8	Recovered 3a
Chloroform	24	2.3	16	3.8	0	21
Chloroform (Benzophenone)	16	4.3	7.5	2.4	13	10
Chloroform (Isoprene)	28	1.9	13	3.7	0	24

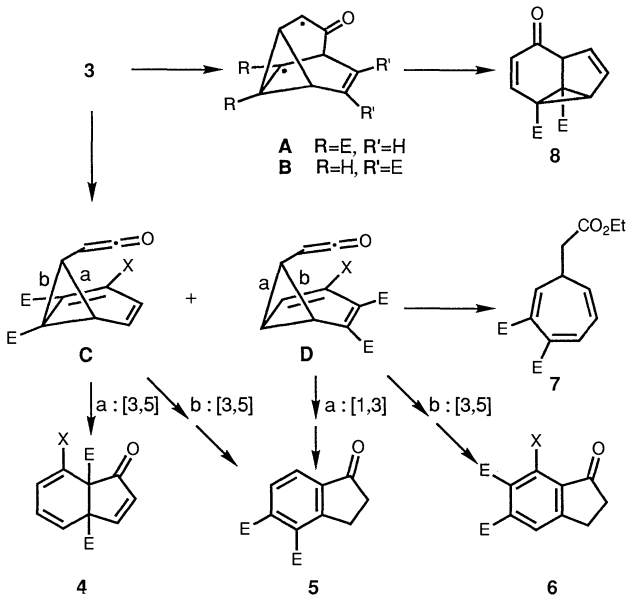

Scheme 2.

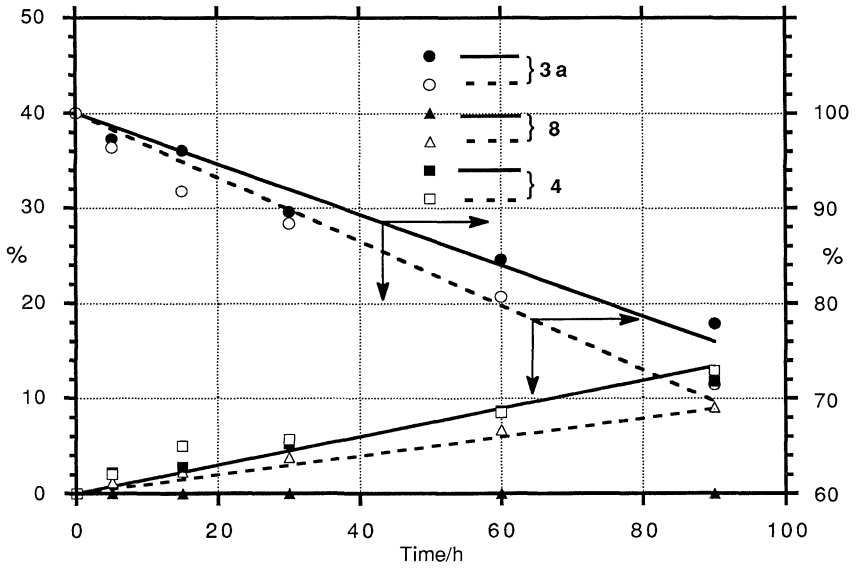

Fig. 1. Time-course of benzophenone-sensitized photorearrangement of **3a**. —: in $CDCl_3$, -----: with benzophenone in $CDCl_3$. ● and ○: **3a**, ▲ and △: **8**, ■ and □: **4**.

rangements of **3**. The [3,5] shifts of bond a in **C** and bond b in **D** give **4** and **6**, respectively. Two paths, [3,5] shift of bond b in **C** and [1,3] shift of bond a in **D**, were equally possible to give **5** and were undistinguishable. In **3b**, the methoxyl group at C-1 assisted the [3,5] shifts of bond a in **C** and bond b in **D** to give **4b** and **6b**. The selective bridging between the enone part and the ethene part with substituents in the thermal reaction of **3** could be explained by a molecular orbital consideration.[9] However, according to the present photoreaction of **3**, both ketene intermediates were equally reactive and no selectivity of the bridging was observed.

In conclusion, the present study confirmed that the photoreaction of homobarrelenones having electron-withdrawing substituents, **3**, was different from the other electron-withdrawing homobarrelenone, **1**. Though the photoisomerization of **1** exclusively gave **2**, **3** afforded various products. The different product distributions between these two fundamental derivatives may be attributable to a difference in the primary excitation part; **3** absorbs light at the α,β-unsaturated keto group, while **1** does so at the ene-dione chromophore.

Experimental

Elemental analyses were performed by Miss S. Hirashima and Miss T. Mizoguchi of the Institute of Advanced Material Study, Kyushu University. The NMR spectra were measured by means of a JEOL FX 100 Model and JEOL GSX 270 H Model spectrometer in a $CDCl_3$ solution (unless otherwise specified); The chemical shifts are expressed in units of δ. The mass spectra were measured with a JEOL O1SG-2 spectrometer. The IR spectra were taken as KBr disks or as a liquid film inserted between NaCl plates using a JASCO IR-A 102 spectrometer. The UV spectra were measured by using a Hitachi U-3200 spectrophotometer.

Irradiation of 3a. a) A $CHCl_3$ solution (3 cm^3) of **3a** (101 mg) in a Pyrex vessel was irradiated by means of a 100-W high-pressure mercury lamp for 5 h. The solvent was removed and the mixture was purified by silica-gel column chromatography and HPLC to give 18.8 mg (24%) of **4a**, 1.8 mg (2.3%) of **5**, 12.5 mg (16%) of **6a**, and 3.4 mg (3.8%) of **7** together with 21.6 mg (21%) of recovered **3a**.

4: Colorless crystals, mp 78.5—79.0 °C (lit,[8] mp 79.5—80.5 °C); ^1H NMR δ=3.70 (3H, s), 3.71 (3H, s), 5.65 (1H, dt, J=9.2, 1.1 Hz), 6.02 (1H, ddd, J=9.2, 5.5, 1.1 Hz), 6.09 (1H, ddd, J=9.5, 5.5, 1.1 Hz), 6.18 (1H, dt, J=9.5, 1.1 Hz), 6.55 (1H, d, J=5.8 Hz), and 7.95 (1H, d, J=5.8 Hz).

5: Not isolated as a pure form (lit,[8] mp 114—115 °C); ^1H NMR δ=2.7—2.8 (2H, m), 3.2 (2H, m), 3.94 (3H, s), 3.97 (3H, s), 7.86 (1H, d, J=7.7 Hz), and 7.89 (1H, d, J=7.7 Hz).

6a: Colorless crystals, mp 59—60 °C; ^1H NMR δ=2.7—2.8 (2H, m), 3.2 (2H, m), 3.93 (3H, s), 3.95 (3H, s), 7.74 (1H, s), and 8.19 (1H, s); ^{13}C NMR δ=26.0, 36.5, 52.6, 53.0, 125.1, 127.0, 129.9, 130.3, 138.5, 157.9, 166.5, 168.1, and 205.1; IR(KBr) 2956, 1741, 1714, 1618, 1274, 1201, and 1074 cm^{-1}; MS m/z (%) 248 (M^+, 26), 217 (100), and 189 (8).

Found: m/z 248.0684 (M^+). Calcd for $C_{13}H_{12}O_5$: 248.0684 (M).

7: A pale yellow oil; ^1H NMR δ=1.27 (3H, t, J=7.0 Hz), 2.3—2.4 (1H, m), 2.78 (2H, dd, J=7.0, 1.1 Hz), 3.72 (3H, s), 3.80 (3H, s), 4.20 (2H, q, J=7.0 Hz), 5.67 (1H, dd, J=9.8, 5.1 Hz), 6.31 (1H, d, J=6.6 Hz), 6.31 (1H, ddd, J=9.8, 6.6, 1.5 Hz), and 7.69 (1H, dd, J=5.9, 1.1 Hz); ^{13}C NMR δ=14.2, 35.4, 37.0, 52.3 (2C), 60.8, 125.8, 128.0, 132.5, 133.7, 136.6, 138.0, 166.8, 167.4, and 171.3; IR (oil) 2984, 2952, 1729, 1260, 1208, and 742 cm^{-1}; UV (MeOH) 220 nm (ε: 12800 sh) and 270 (4900); MS m/z (%) 294 (M^+, 8), 262 (100), 248 (18), and 189 (39).

Found: m/z 294.1101 (M^+). Calcd for $C_{15}H_{18}O_6$:1 294.1102 (M).

b) A $CHCl_3$ solution (3 cm^3) of **3a** (97.5 mg) and benzophenone (72.8 mg) was irradiated as mentioned above for 5 h to give 14.2 mg (16%) of **4a**, 3.8 mg (4.3%) of **5**, 6.6 mg (7.5%) of **6a**, 2.5 mg (2.4%) of **7**, and 11.5 mg (13%) of **8** together with 9.9 mg (10%) of recovered **3a**.

8: A colorless oil; ^1H NMR δ=3.71 (3H, s), 3.81 (3H, s), 3.9 (1H, m), 3.98 (1H, d, J=2.2 Hz), 5.73 (1H, dd, J=5.5, 2.2 Hz), 5.92 (1H, ddd, J=5.5, 2.2, 1.1 Hz), 6.22 (1H, dd, J=10.3, 0.7 Hz), and 6.69 (1H, d, J=10.3 Hz); ^{13}C NMR δ=39.5, 51.5, 52.7, 53.2, 55.1, 59.4, 129.7, 130.1, 134.7, 137.6, 168.4, 168.9, and 195.8; IR(oil) 3454, 2956, 1732, 1695 and 1268 cm^{-1}; UV (MeOH) 214 nm (ε: 9100), 251 (4100), 303 (1500 sh), and 336 (1100 sh); MS m/z (%) 248 (M^+, 46), 220 (38), 216 (100), and 188 (34).

Found; m/z 248.0685 (M^+). Calcd for $C_{13}H_{12}O_5$: 248.0684 (M).

c) A $CHCl_3$ solution (3 cm^3) of **3a** (102 mg) was irradiated as mentioned above for 5 h in the presence of isoprene (47.8 mg) to give 22.1 mg (28%) of **4a**, 1.5 mg (1.9%) of **5**, 10.2 mg (13%) of **6a**, and 3.4 mg (3.7%) of **7** together with 24.3 mg (24%) of **3a**.

d) A $CHCl_3$ solution (3 cm^3) of **3a** (134.5 mg) and benzophenone (100 mg) was irradiated by means of 400 W high-pressure lamp for 5 h to give 14.7 mg (11%) of **4a**, 3.3 mg (2%) of **6a**, 40.5 mg (22%) of **7**, and 14 mg (10%) of **8**.

Irradiation of 3b. a) A $CHCl_3$ solution (2 cm^3) of **3b** (50 mg) was irradiated for 5 h under similar conditions. The solvent was removed and the mixture was purified by a silica-gel column chromatography and HPLC to give 20.5 mg (41%) of **4b** and 21.2 mg (42.4%) of **6b**.

4b: Colorless needles, mp 128—130 °C; ^1H NMR δ=3.69 (6H, s), 3.70 (3H, s), 5.27 (1H, d, J=6.6 Hz), 5.53 (1H, J=9.5 Hz), 6.12 (1H, dd, J=9.5, 6.6 Hz), 6.58 (1H, d, J=5.9 Hz), and 7.47 (1H, J=5.9 Hz); ^{13}C NMR δ=52.9, 53.2, 56.1, 62.8, 94.1, 115.4, 123.0, 123.3, 133.9, 151.8, 159.3, 167.8, 170.7, and 197.8; IR(KBr) 1746, 1732, 1592, 1436, 1263, 1231, 1189, and 1049 cm^{-1}; UV (MeOH) 211 nm (ε: 13380) and 282 (4770); MS m/z (%) 278 (M^+, 38), 219 (100), 191 (66), 175 (67), 160 (25), and 132 (28).

Found: m/z 278.0789. Calcd for $C_{14}H_{14}O_6$: 278.0789 (M).

6b: Colorless needles, mp 148—149 °C; ^1H NMR δ=2.76 (2H, m), 3.17 (2H, m), 3.92 (3H, s), 3.95 (3H, s), 4.03 (3H, s), and 7.80 (1H, s); ^{13}C NMR δ=25.8, 37.1, 52.8, 53.0, 63.5, 123.0, 129.0, 131.7, 134.2, 155.4, 158.0, 165.1, 167.0, and 202.8; IR(KBr) 1743, 1711, 1453, 1302, 1272, 1231, 1194, 1150, and 1078 cm^{-1}; UV (MeOH) 206 nm (ε: 24360), 258 (12200), and 316 (2730); MS m/z (%) 278 (M^+, 54), 247 (100), 233 (54), and 160 (68).

Found: C, 60.40; H, 5.41%. Calcd for $C_{14}H_{14}O_6$: C, 60.46; H, 5.04%.

b) A $CHCl_3$ solution (2 cm^3) of **3b** (150 mg) and

benzophenone (100 mg) was irradiated for 3 h. A similar work-up gave 51.5 mg (34.3%) of **4b** and 50.3 mg (33.5%) of **6b**.

Kinetics. A $CDCl_3$ solution (0.6 cm^3) of **3a** (72.6 mg) and a $CDCl_3$ solution (0.6 cm^3) of **3a** (73.7 mg) and benzophenone (51.2 mg) were irradiated using a "Merry-Go-Round" apparatus. The reaction was monitored by means of the ^1H NMR spectra. The results are summarized in Fig. 1.

The authors wish to express their thanks to Dr. Tadao Uyehara of Tohoku University for providing the spectral data of **4a** and **5**.

References

1) Part LV. A. Mori, T. Kubota, Y. Ikeda, and H. Takeshita, *Bull. Chem. Soc. Jpn.*, **63**, 2264 (1990).

2) A. S. Kende and Z. Goldschmidt, *Tetrahedron Lett.*, **1970**, 783.

3) J. Ciabattoni, J. E. Crowley, and A. S. Kende, *J. Am. Chem. Soc.*, **89**, 2778 (1967); O. L. Chapman, M. Kane, J. D. Lassila, R. L. Loeschen, and H. E. Wright, *ibid.*, **91**, 6856 (1969); A. S. Kende, Z. Goldschmidt, and P. T. Izzo, *ibid.*, **91**, 6858 (1969).

4) I. Murata and Y. Sugihara, *Tetrahedron Lett.*, **1972**, 625.

5) G. R. Tian, S. Sugiyama, A. Mori, and H. Takeshita, *Bull. Chem. Soc. Jpn.*, **61**, 4397 (1988); **62**, 614 (1989); G. R. Tian, A. Mori, H. Takeshita, M. Higashi, and H. Yamaguchi, *Bull. Chem. Soc. Jpn.*, **62**, 1567 (1989).

6) H. Takeshita, A. Mori, and G. R. Tian, *Yuki Gosei Kagaku Kyokai Shi*, **48**, 132 (1990), and references cited therein.

7) A. Mori, Z.-H. Li, H. Nakashima, and H. Takeshita, *Bull. Chem. Soc. Jpn.*, **63**, 1636 (1990).

8) T. Uyehara, M. Funamizu, and Y. Kitahara, *Chem. Ind.*, **1970**, 1500. The photorearrangement of **3a** was carried out in a preliminary account (Private communication from Dr. Uyehara).

9) T. Uyehara, S. Miyakoshi, and Y. Kitahara, *Bull. Chem. Soc. Jpn.*, **52**, 2023 (1979).

Crystal Structure of the Organic Metal $(DMET)_2BF_4$ with Two Columns along Two Crystallographic Axes

Yoshimitsu ISHIKAWA,† Kazuya SAITO, Koichi KIKUCHI, Keiji KOBAYASHI,†† and Isao IKEMOTO*
Department of Chemistry, Faculty of Science, Tokyo Metropolitan University, Fukuzawa, Setagaya-ku, Tokyo 158
†† Department of Chemistry, College of Arts and Sciences, The University of Tokyo, Komaba, Meguro-ku, Tokyo 153
(Received June 19, 1990)

The crystal structure of $(DMET)_2BF_4$: 5,6-dihydro-2-(4,5-dimethyl-1,3-diselenol-2-ylidene)dithiolo[4,5-*b*][1,4]dithiinium tetrafluoroborate (2:1), $(C_{10}H_{10}S_4Se_2)_2BF_4$, is determined. Crystal data: M_r=919.49, triclinic, $P\bar{1}$, a=7.032(2), b=7.812(3), c=27.502(11) Å, α=90.87(2), β=90.28(2), γ=106.22(2)°, V=1450.5(15) Å^3, Z=2, D_x=2.11 Mg m^{-3}, λ(Mo $K\alpha$)=0.71068 Å, μ=5.60 mm^{-1}, $F(000)$=890, T=297 K, R=0.077 for 4600 reflections. Two crystallographically independent DMET molecules separately form columns along nearly perpendicular directions, and ordered BF_4 anions are located between the DMET columns.

In recent years, radical salts of DMET, which is a hybrid donor between TMTSF and BEDT-TTF, with some monovalent anions have been studied.[1–5] In the course of the study, seven superconductors have been discovered. The DMET salts, in addition to superconductivity, exhibit a variety of electronic properties; metal, semiconductor, and spin density wave (SDW) transition.[3,5] The DMET salts were classified into five Groups on the basis of temperature dependence of conductivity and the shape of counter anions. The salts of Group 2, which is with tetrahedral anions, show metallic behavior at room temperature under the normal pressure. A metal-insulator transition occurs at low temperature.

Besides these attractive electronic properties, crystal structures of DMET salts are interesting from the point of view of the asymmetry of donor molecule. The crystal structure has been determined for PF_6,[6] ReO_4,[7] $Au(CN)_2$,[8] AuI_2,[9] $AuBr_2$,[10] $AuCl_2$,[11] IBr_2,[12] and I_3[13] salts. In these salts, except for the $AuBr_2$ salt of Group 5, DMET molecules are stacked with an alternate molecular orientation and form one-dimensional columns. Within the columns some short intermolecular contacts exist and some salts additionally have intermolecular contacts between the columns. These intra- and intercolumnar contacts highten the dimensionality of the salt.

The title compound show the room temperature conductivity of about 130 S cm^{-1}.[6] On cooling, the metallic character continues down to about 40 K, where the temperature dependence of the conductivity changes to that of insulator. These behaviors are characteristic to the salts of Group 2.[1] The EPR study revealed that an SDW transition occurred at 20 K. Although the transition temperature is a little lower than the temperature of the conductivity maximum, the metal-insulator transition is probably due to the formation of SDW.

† Present address: Tokyo Research Center, TOSOH Corp., Hayakawa, Ayase, Kanagawa 252.

The shape of $(DMET)_2BF_4$ crystals is not needle-like as seen in other DMET salts, but rhombus-like. It is suggested that $(DMET)_2BF_4$ has two-dimensionality. This conjecture was supported by the fact that the anisotropy of steady[14] and optical[15] conductivity of $(DMET)_2BF_4$ crystal was about 1 to 4, and was confirmed through the crystal structure determination reported preliminarily.[4] In this paper, the molecular structure and crystal structure of $(DMET)_2BF_4$ are reported in detail.

Experimental

Crystals of $(DMET)_2BF_4$ were prepared by electrochemical oxidation of DMET in 1,1,2-trichloroethane solution in the presence of $(n\text{-}Bu_4N)\cdot BF_4$ at a constant current (1 μA). D_m was not determined. The crystal used for the data collection was black and rhombus-like: 0.35×0.25×0.13 mm^3. The data collection was performed with the Rigaku AFC-M automated four-circle diffractometer with graphite monochromated Mo $K\alpha$ radiation (λ=0.71068 Å). Unit-cell dimensions were determined from 38 selected reflections ($16°<2\theta<28°$). The intensity data were collected using the ω-scan technique ($2\theta<30°$) and the ω–2θ scan technique ($2\theta>30°$) with a scan rate 3.75° min^{-1} ($\Delta\omega=1.55°+0.50°\cdot\tan\theta$) in ω to $(\sin\theta)/\lambda$= 0.65 Å^{-1} ($0\leq h\leq 8$, $-9\leq k\leq 9$, $-35\leq l\leq 35$). Two standard reflections (measured at an interval of 100 reflections) showed small (<0.6%) random variations. The data were corrected for absorption effect using a Gaussian integration procedure; T_{min}=0.26, T_{max}=0.50. 6516 independent reflections were collected and 4600 reflections ($|F_o|>3\sigma(|F_o|)$) were used in the structure refinement. Intensity statistics indicated space group $P\bar{1}$ rather than $P1$ and this choice was later confirmed by the successful structure solution and least-squares refinement. The Se and S atoms were located by the Patterson method and the structure was solved by successive Fourier synthesis and refined by the block-diagonal least-squares method. The atomic and anomalous scattering factors were taken from International Tables for X-ray Crystallography.[16] All computations were carried out using UNICS III program.[17] No hydrogen atoms were located. $\sum w\cdot(|F_o|-|F_c|)^2$ was minimized, where $w=\sigma^{-2}(|F_o|)$, with σ ($|F_o|$) based on counting statistics. The maximum value of Δ/σ was 0.01 for B_{23} of C(8A) in the final least-squares cycle.

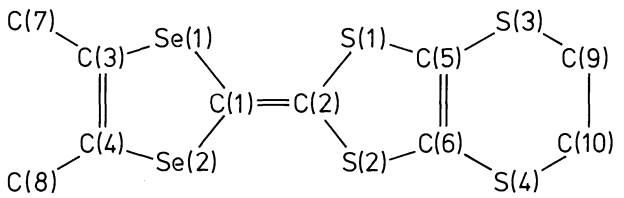

It resulted in the agreement factors R=0.077, wR=0.047 and S=8.32. No correction was made for the secondary extinction. A difference synthesis based on the structure factors derived from the final parameter values showed some peaks of density (−1.4 to 1.3 $e \cdot Å^{-3}$). The temperature factor of the ethylene group in one DMET molecule was anomalously large. Although a difference synthesis using all parameters showed no significant peak around the C(10A) atom, the difference synthesis using the final parameters except those for C(10A) showed double peaks (3.7 and 2.0 $e \cdot Å^{-3}$). The parameters reported for the C(10A) atom are, therefore, averaged ones in some way. ORTEP II[18] was used to produce crystal structure illustrations.

Results and Discussion

The final positional and thermal parameters are tabulated in Table 1.[19] The bond lengths and angles are given in Tables 2 and 3, respectively. The geometry of the DMET molecule A, which consists in the column along the a axis, is in reasonable agreement with those observed in other DMET salts[7-9,11,12] except ethylenedithio moiety (-S-CH_2-CH_2-S-). The apparent bond length of C(9A)-C(10A), given in the table, is shorter than those in other salts (ca. 1.51 Å) owing to the positional disorder of C(10A).

Table 1. Fractional Atomic Coordinates and the Equivalent Isotropic Temperature Factors of $(DMET)_2BF_4$

Atom	$10^4 \cdot x$	$10^4 \cdot y$	$10^4 \cdot z$	B_{eq}[a]/Å^2	Atom	$10^4 \cdot x$	$10^4 \cdot y$	$10^4 \cdot z$	B_{eq}/Å^2
Molecule A					Molecule B				
Se(1)	2034(2)	−1303(2)	−576.5(4)	2.79(4)	Se(1)	−2727(2)	2599(2)	4586.3(4)	2.69(4)
Se(2)	3195(2)	2466(2)	−45.6(4)	2.67(4)	Se(2)	1877(2)	3737(2)	4381.2(4)	2.73(4)
S(1)	1645(4)	−3175(4)	496 (1)	2.7 (1)	S(1)	−1694(4)	1218(4)	5669 (1)	2.7 (1)
S(2)	2785(4)	279(4)	1008 (1)	2.6 (1)	S(2)	2575(4)	2256(4)	5471 (1)	3.1 (1)
S(3)	1122(5)	−5345(4)	1371 (1)	4.1 (1)	S(3)	−1357(5)	81(4)	6672 (1)	3.3 (1)
S(4)	2447(5)	−1231(4)	1993 (1)	3.7 (1)	S(4)	3778(4)	1298(5)	6437 (1)	3.7 (1)
C(1)	2516(15)	−27(14)	12 (4)	2.3 (3)	C(1)	−135(14)	2734(14)	4800 (4)	2.5 (3)
C(2)	2329(15)	−849(13)	440 (3)	2.1 (3)	C(2)	184(14)	2136(14)	5259 (3)	2.1 (3)
C(3)	2579(14)	783(14)	−964 (3)	2.3 (3)	C(3)	−1824(15)	3589(13)	3970 (4)	2.9 (4)
C(4)	3061(14)	2413(15)	−741 (4)	2.9 (4)	C(4)	138(15)	4099(14)	3873 (4)	2.8 (4)
C(5)	1703(14)	−3223(14)	1125 (4)	2.8 (4)	C(5)	−108(14)	999(13)	6147 (4)	2.3 (3)
C(6)	2248(14)	−1616(14)	1353 (4)	2.6 (4)	C(6)	1806(15)	1449(15)	6050 (4)	2.8 (4)
C(7)	2390(15)	440(16)	−1517 (4)	3.6 (4)	C(7)	−3487(16)	3757(16)	3640 (4)	3.2 (4)
C(8)	3537(16)	4220(15)	−976 (5)	4.1 (4)	C(8)	1154(16)	4917(14)	3413 (4)	3.0 (4)
C(9)	1150(23)	−4918(18)	2024 (4)	6.8 (6)	C)9)	620(16)	−406(16)	7040 (4)	4.0 (4)
C(10)	2010(35)	−3407(20)	2213 (5)	14.9 (11)	C(10)	2551(17)	1094(16)	7027 (4)	3.8 (4)
BF_4									
B(1)	5581(21)	3362(19)	2314 (5)	3.6 (5)					
F(1)	6417(11)	5124(10)	2369 (3)	7.4 (3)					
F(2)	6878(12)	2428(11)	2449 (3)	7.6 (4)					
F(3)	3933(11)	2829(11)	2591 (3)	6.9 (3)					
F(4)	5102(11)	2975(10)	1834 (2)	6.2 (3)					

a) $B_{eq}=(4/3)\cdot(B_{11}\boldsymbol{a}\cdot\boldsymbol{a}+B_{12}\boldsymbol{a}\cdot\boldsymbol{b}+B_{13}\boldsymbol{a}\cdot\boldsymbol{c}+\cdots)$.

Table 2. Bond Lengths (l)

Bond	l/Å	l/Å	Bond	l/Å	l/Å
DMET	Molecule A	Molecule B		Molecule A	Molecule B
Se(1)-C(1)	1.868(10)	1.886(10)	S(3)-C(9)	1.822(13)	1.842(13)
Se(1)-C(3)	1.909(11)	1.909(11)	S(4)-C(6)	1.778(11)	1.775(11)
Se(2)-C(1)	1.881(11)	1.834(10)	S(4)-C(10)	1.758(16)	1.830(12)
Se(2)-C(4)	1.913(10)	1.929(11)	C(1)-C(2)	1.339(14)	1.391(14)
S(1)-C(2)	1.755(10)	1.745(10)	C(3)-C(4)	1.359(15)	1.354(15)
S(1)-C(5)	1.730(11)	1.759(11)	C(3)-C(7)	1.539(14)	1.513(16)
S(2)-C(2)	1.764(10)	1.754(11)	C(4)-C(8)	1.513(17)	1.515(14)
S(2)-C(6)	1.723(11)	1.752(11)	C(5)-C(6)	1.350(15)	1.322(14)
S(3)-C(5)	1.741(11)	1.751(10)	C(9)-C(10)	1.268(19)	1.527(15)
BF_4					
B(1)-F(1)	1.343(16)		B(1)-F(3)	1.358(15)	
B(1)-F(2)	1.370(19)		B(1)-F(4)	1.370(15)	

Table 3. Bond Angles (θ)

Angle	θ/°	θ/°	Angle	θ/°	θ/°
DMET	Molecule A	Molecule B		Molecule A	Molecule B
C(1)–Se(1)–C(3)	94.2(4)	92.5(5)	Se(1)–C(3)–C(7)	115.4(8)	113.1(7)
C(1)–Se(2)–C(4)	94.7(5)	94.5(4)	C(4)–C(3)–C(7)	125.4(10)	126.8(10)
C(2)–S(1)–C(5)	97.2(5)	95.8(5)	Se(2)–C(4)–C(3)	117.0(8)	116.2(8)
C(2)–S(2)–C(6)	95.8(5)	94.9(5)	Se(2)–C(4)–C(8)	115.2(8)	115.4(7)
C(5)–S(3)–C(9)	103.6(6)	102.8(5)	C(3)–C(4)–C(8)	127.8(10)	128.4(10)
C(6)–S(4)–C(10)	101.9(6)	100.3(5)	S(1)–C(5)–S(3)	115.0(6)	113.7(5)
Se(1)–C(1)–Se(2)	114.9(5)	116.6(6)	S(1)–C(5)–C(6)	115.6(8)	116.3(8)
Se(1)–C(1)–C(2)	121.8(8)	120.3(7)	S(3)–C(5)–C(6)	129.3(9)	129.9(9)
Se(2)–C(1)–C(2)	123.3(8)	123.2(7)	S(2)–C(6)–S(4)	115.1(6)	113.7(6)
S(1)–C(2)–S(2)	112.6(5)	114.3(6)	S(2)–C(6)–C(5)	118.8(8)	118.5(8)
S(1)–C(2)–C(1)	123.4(8)	124.2(8)	S(4)–C(6)–C(5)	126.2(9)	127.8(8)
S(2)–C(2)–C(1)	124.0(8)	121.5(7)	S(3)–C(9)–C(10)	122.3(11)	112.4(9)
Se(1)–C(3)–C(4)	119.2(7)	120.1(8)	S(4)–C(10)–C(9)	131.9(14)	113.5(8)
BF_4					
F(1)–B(1)–F(2)	110.7(10)		F(2)–B(1)–F(3)	108.6(11)	
F(1)–B(1)–F(3)	110.6(12)		F(2)–B(1)–F(4)	107.8(12)	
F(1)–B(1)–F(4)	109.0(11)		F(3)–B(1)–F(4)	110.0(10)	

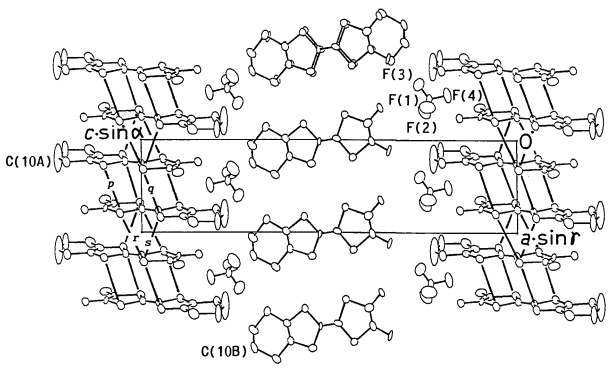

Fig. 1. Crystal structure of $(DMET)_2BF_4$ viewed along the b axis. Thermal ellipsoids indicate the region of 50% probability. Thin solid lines show the shorter intermolecular contacts than the sum of van der Waals radii. Their distances; p=3.771(3) Å, q=3.735(3) Å, r=3.939(2) Å and s=3.803(3) Å.

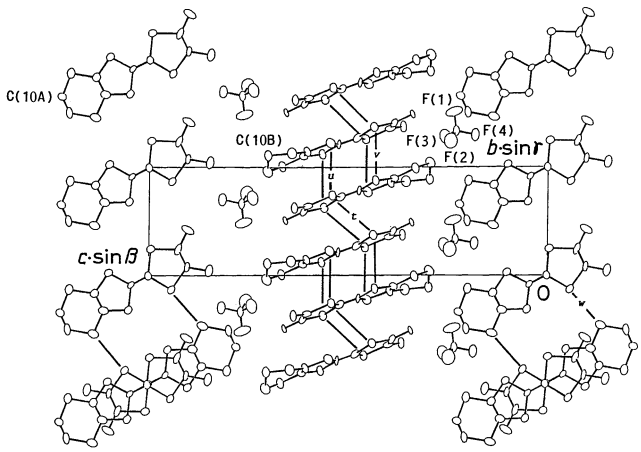

Fig. 2. Crystal structure of $(DMET)_2BF_4$ viewed along the a axis. Thermal ellipsoids indicate the region of 50% probability. Thin solid lines show the shorter intermolecular contacts than the sum of van der Waals radii. Their distances; t=3.924(2) Å, u=3.825(4) Å, v=3.837(4) Å and w=3.618(4) Å.

The DMET molecule A is almost planar except for the "averaged" C(10A) atom. The other atoms are within about 0.07 Å from the molecular plane determined by the Se(1A), Se(2A), S(1A), S(2A), C(1A), and C(2A) atoms.

The geometry of the molecule B, which consists in the column along the b axis, is slightly different from those observed in other salts. In the molecule B the bond length of C(1B)–C(2B) is longer and that of C(5B)–C(6B) is shorter than the corresponding lengths in other DMET salts. The molecule B is almost planar except for the C(10B) atom. It is about 0.8 Å apart from the molecular plane determined as molecule A; the other atoms are within about 0.2 Å from the plane. Such magnitude of the deviation from the planality has been reported for other DMET salts.

As seen in Fig. 1, there exist two types of DMET columns along the a and the b axes. A similar structure was reported for $(DIMET)_2ClO_4$;[20] DIMET ($C_{10}H_{10}S_6$) is a 2-(4,5-dimethyl-1,3-dithiol-2-yliden) analog of DMET. In both types of columns A and B, DMET molecules stack with an alternate orientation related by an inversion center. The BF_4 anion is located in between two types of columns (a crystallographic general point), and no orientational disorder is detected.

In the column A, the molecular plane determined with two Se, two inner S and two central C atoms is almost normal to the a axis (87.4°). The angle between the normal to the plane and the stacking axis (2.6°) is very small as compared with those in other $(DMET)_2X$ (typically ca. 20°).[7–9,11,12] Although two interplanar distances are almost equal (3.51 and 3.52 Å) to each other, two intermolecular contact patterns between the neighboring molecules in the columns are different.

One type of overlap has four Se–S contacts (refered as *p* and *q* in the Figure) shorter than the sum of the van der Waals radii, the other has two Se–Se (*r*) and two Se–S (*s*) ones. It is noted that the ethylenedithio moiety is not responsible for shorter contacts. There also exist short intermolecular contacts between the adjacent two columns A as seen in Fig. 2, where the interatomic (two Se–S) contacts (*w*) indicated are shorter than the sum of the van der Waals radii. These contacts lie between the molecules related by an inversion. The pattern of the intermolecular contacts within and between columns A has not been seen in other DMET salts and is different from that of the column B of this salt. This stacking mode, however, resemble that of TMTSF salts.[21]

In the column B, the normal to the molecular plane is tilted by 23.7° from the *b* axis. The DMET molecules are stacked with an alternate molecular orientation related by an inversion center as in the column A. Two interplanar distances are not equal (3.56 and 3.59 Å) to each other. One type of overlap has four shorter Se–S contacts (*u* and *v*), and the other has two shorter Se–Se contacts (*t*) and four slightly longer Se–S ones. This stacking mode has widely been observed in other DMET salts.[6–13] As shown in Fig. 1, there is no short intermolecular contact between the columns B. It is noted that the ethylenedithio moiety is not responsible for shorter contacts in both types of overlap of DMET molecules within the columns A and B.

Between the column A and the column B there is no short intermolecular contact. The BF_4 anions exist between the columns A and B, and are ordered. They are surrounded by four DMET molecules, and each BF_4 anion contacts with four methyl groups and two ethylene groups.

The little dimerization of DMET molecules within the one-dimensional columns seems responsible for metallic behavior at room temperature under the normal pressure. The same conjecture will apply to $(DMET)_2BF_4$. Comparing the structure of the column with those in other DMET salts, the structure of the column B resembles those of $(DMET)_2[Au(CN)_2]$[8] and $(DMET)_2[AuCl_2]$.[11] Interatomic distances of $(DMET)_2BF_4$ within the column are, however, slightly longer than those of the $Au(CN)_2$ and the $AuCl_2$ salts. Accordingly, the interaction within the column is weak in the BF_4 salt. The lower conductivity at room temperature than $Au(CN)_2$ and $AuCl_2$ salts is probably due to these differences in the interatomic distances and interaction.

Although ReO_4 is the same in shape, i.e., tetrahedral, the crystal structure of $(DMET)_2[ReO_4]$ is very different from that of $(DMET)_2BF_4$ probably because of the larger anion size.[7] In this respect, crystal structures of other tetrahedral anions are interesting, and the result will be published shortly.[12,22]

This work was supported in part by Grant-in-Aid for Specially Promoted Research No. 63060004 from the Ministry of Education, Science and Culture.

References

1) K. Murata, K. Kikuchi, T. Takahashi, K. Kobayashi, Y. Honda, K. Saito, K. Kanoda, T. Tokiwa, H. Anzai, T. Ishiguro, and I. Ikemoto, *J. Mol. Electron.*, **4**, 173 (1988).

2) K. Kikuchi, K. Saito, I. Ikemoto, K. Murata, T. Ishiguro, and K. Kobayashi, *Synth. Met.*, **27**, B269 (1988).

3) K. Kanoda, T. Takahashi, K. Kikuchi, K. Saito, I. Ikemoto, and K. Kobayashi, *Synth. Met.*, **27**, B385 (1988).

4) K. Kikuchi, Y. Ishikawa, K. Saito, I. Ikemoto, and K. Kobayashi, *Synth. Met.*, **27**, B391 (1988).

5) K. Kanoda, T. Takahashi, K. Kikuchi, K. Saito, Y. Honda, I. Ikemoto, and K. Kobayashi, *Phys. Rev. B*, **39**, 3996 (1989).

6) K. Kikuchi, I. Ikemoto, and K. Kobayashi, *Synth. Met.*, **19**, 551 (1987).

7) K. Saito, Y. Ishikawa, M. Ishibashi, K. Kikuchi, K. Kobayashi, and I. Ikemoto, *Bull. Chem. Soc. Jpn.*, **63**, 1865 (1990).

8) K. Kikuchi, Y. Ishikawa, K. Saito, I. Ikemoto, and K. Kobayashi, *Acta Crystallogr., Sect. C*, **44**, 466 (1988).

9) Y. Ishikawa, K. Kikuchi, K. Saito, I. Ikemoto, and K. Kobayashi, *Acta Crystallogr., Sect. C*, **45**, 572 (1989).

10) K. Kikuchi, Y. Honda, Y. Ishikawa, K. Saito, I. Ikemoto, K. Murata, H. Anzai, T. Ishiguro, and K. Kobayashi, *Solid State Commun.*, **66**, 405 (1988).

11) Y. Ishikawa, K. Saito, K. Kikuchi, I. Ikemoto, K. Kobayashi, and H. Anzai, *Acta Crystallogr., Sect. C*, **46**, 1652 (1990).

12) Y. Ishikawa, H. Saitoh, K. Kikuchi, K. Saito, K. Kobayashi, and I. Ikemoto, in preparation.

13) M. Z. Aldoshina, L. O. Atovmyan, L. M. Gol'denberg, O. N. Krasochka, R. N. Lyubovskaya, R. B. Lyubovskii, and M. L. Khidekel', *Dokl. Akad. Nauk SSSR*, **289**, 1140 (1986).

14) Y. Honda, K. Kikuchi, K. Saito, K. Kobayashi, and I. Ikemoto, unpublished.

15) K. Miyazaki, K. Kikuchi, K. Saito, K. Kobayashi, and I. Ikemoto, in preparation.

16) "International Tables for X-ray Crystallography," ed by J. A. Ibers and W. C. Hamilton, Kynoch Press, Birmingham (1974), Vol. IV.

17) T. Sakurai and K. Kobayashi, UNICS III, *Rep. Inst. Phys. Chem. Res. (Jpn.)*, **55**, 69 (1979).

18) C. K. Johnson, ORTEP II, Report ORNL-3794, Oak Ridge National Laboratory, Tennessee (1974).

19) Tables of anisotropic temperature factors and $|F_o|-|F_c|$ data are deposited as Document No. 9098 at the Office of the Editor of Bull. Chem. Soc. Jpn.

20) H. Endres, R. Heid, H. J. Keller, I. Heinen, and D. Schweitzer, *Acta Crystallogr., Sect. C*, **43**, 115 (1987).

21) D. Jerome, A. Mazaud, M. Ribault, and K. Bechgaard, *J. Phys. (Paris), Lett.*, **41**, L-95 (1980).

22) T. G. Takhirov, O. N. Krasochka, O. A. D'Yachenko, L. O. Atovmyan, M. L. Petrov, I. K. Pubtsova, and R. N. Lyubovskaya, *Zh. Strukt. Khim.*, **30**, 114 (1989).

Behavior of the Excited Cis Singlet State of a One-Way Isomerizing Olefin. Further Insight into Potential Energy Surfaces of 1-(3,3-Dimethyl-1-butenyl)pyrene

Hiroaki Okamoto, Tatsuo Arai,* Hirochika Sakuragi, Katsumi Tokumaru,* and Yuji Kawanishi†
Department of Chemistry, University of Tsukuba, Tsukuba, Ibaraki 305
† Research Institute for Polymers and Textiles, Tsukuba, Ibaraki 305
(Received July 20, 1990)

The decay processes of the excited singlet state and potential energy surfaces of 1-(3,3-dimethyl-1-butenyl)pyrene (BP) were investigated. A long-lived fluorescence from the cis isomer and involvement of a quantum chain process for one-way isomerization suggest that the isomerization on direct excitation proceeds in the triplet manifold after intersystem crossing at the cis conformation.

On direct excitation, olefins can undergo photoisomerization in the singlet manifold, triplet manifold, or both depending on the properties of substituents on the ethylenic carbons. In the case of stilbene, cis-trans two-way isomerization occurs mutually between the both isomers in the singlet manifold.[1] However, 2-anthrylethylenes undergo cis-to-trans one-way isomerization in the triplet manifold even on direct irradiation; the initially produced singlet excited state does not undergo isomerization at all, but undergoes efficiently intersystem crossing to the triplet state.[2-4]

We reported previously that 1-(3,3-dimethyl-1-butenyl)-pyrene (BP) undergoes cis-to-trans one-way isomerization on triplet sensitization.[5] In this paper we elucidate the mechanism of its photoisomerization on direct irradiation, which is now revealed to proceed in the triplet state after intersystem crossing of the singlet excited state. In addition, on the basis of fluorescence studies and differential scanning calorimetry we propose the potential energy surfaces of the ground and excited singlet states of BP.

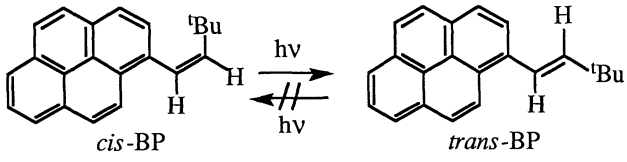

Experimental

Materials. Preparation of *cis*- and *trans*-1-(3,3-dimethyl-1-butenyl)pyrene (BP)[5] and purification of benzil and solvent benzene were done as described previously.[3]

Fluorescence Studies. Fluorescence spectra were measured on a Hitachi F-4000 spectrofluorimeter, and fluorecsence lifetimes were determined using a single photon counting apparatus, Horiba NAES-1100.

Steady Irradiations. Photostationary state isomer ratios and isomerization quantum yields were measured by irradiating degassed benzene solutions of BP with 366-nm light from a 400-W high-pressure mercury lamp through a band pass filter (Corning 7-60, 0-52). The isomer ratio was determined by HPLC (Waters 600 Multisolvent Delivery System) equipped with an LC spectrophotometer (Waters 490 Programmable Multiwavelength Detector) using 1,3-bis(bromomethyl)benzene as an internal standard. Light intensity was determined by potassium tris(oxalato)ferrate(III) actinometry.

Laser Flash Photolyses. Laser flash photolyses were performed with 308-nm (XeCl, 10-ns fwhm) and 435-nm laser pulses (Stilbene 3, 10-ns fwhm) from an excimer laser (Lambda Physik EMG-101) and an excimer laser-pumped dye laser (Lambda Physik FL-3002), respectively, and with a pulsed xenon arc (Wacom KXL-151, 150 W) as a monitoring light source. The detailed laser photolysis set-up was described previously.[3,5] Sample solutions containing BP (1.2×10^{-4} M, M=mol dm^{-3}) were deaerated by three freeze-pump-thaw cycles or by bubbling with argon for 30 min.

Differential Scanning Calorimetry. Energy difference between the ground-state trans (^{0}t) and cis isomer (^{0}c) was obtained by using differential scanning calorimetry (DSC). A Seiko Electric DSC-200/SSC5000 was used at the laboratory of Research Institute for Polymers and Textiles after calibration.[6] Approximately 2 mg of samples were scanned at 2—7.5 °C min^{-1}.

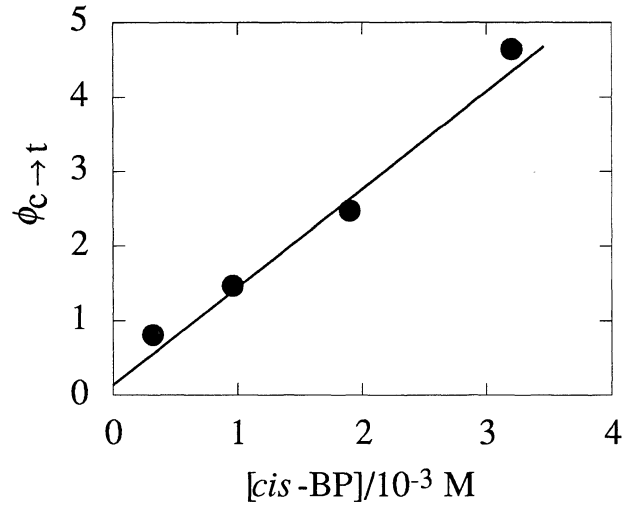

Fig. 1. Plot of quantum yields for cis→trans isomerization of BP ($\phi_{c\rightarrow t}$) in benzene as a function of *cis*-BP concentration on direct irradiation.

Results

Photostationary State Isomer Ratios and Isomerization Quantum Yields. Direct irradiation of BP ($0.16-1.6\times10^{-3}$ M) with 366-nm light in degassed benzene resulted in 100% of the trans isomer on starting from either cis or trans isomer as observed on triplet sensitized irradiation.[3] The quantum yield for cis→trans isomerization ($\phi_{c\to t}$) increased almost linearly with increasing cis isomer concentration ($0.32-3.2\times10^{-3}$ M), attaining 4.6 at the highest *cis*-BP concentration employed (Fig. 1).

Fluorescence Studies. A freshly prepared sample of *cis*-BP in benzene gave a fluorescence (Fig. 2a) different from that of *trans*-BP (Fig. 2b) at room temperature, while the spectrum was changed gradually to that of *trans*-BP at every scanning (Fig. 3). This is attributed to the photoexcitation of the trans isomer accumulated by photoisomerization of the cis isomer under excitation beam in the spectrometer during the measurement. At 77 K, each isomer showed a fluorescence spectrum (Figs. 2c and 2d) slightly more sharp than that observed at room temperature, without spectral change during the measurement.

The singlet excitation energies were estimated from the 0–0 band of the fluorescence spectrum (378 and 392 nm) to be 76 and 73 kcal mol^{-1} (1 cal=4.184 J) for *cis*- and *trans*-BP, respectively (Fig. 2). The quantum yields (ϕ_f) of fluorescence emission of *trans*- and *cis*-BP (3×10^{-6} M) were determined in benzene as 0.64 and 0.43, respectively, by using pyrene (ϕ_f=0.58)[7] and phenanthrene (ϕ_f=0.11)[7] as standards.

The fluorescence lifetime of *trans*-BP was measured in benzene at room temperature as 65 ns by single photon counting (SPC) technique. It is clear that the excited singlet state of *cis*-BP has a sufficient lifetime to emit its own fluorescence; however, its gradual isomerization to the trans isomer at room temperature during SPC measurements prevented to determine its lifetime directly.

The fluorescence spectra of *cis*- and *trans*-BP were efficiently quenched by oxygen without changing the spectral profile. The Stern–Volmer constants, $K_{SV}=k_q\tau_s$, for fluorescence quenching with oxygen were determined as 1760 and 1170 M^{-1} for *trans*- and *cis*-BP, respectively. By use of the lifetime of singlet excited *trans*-BP (τ_s=65 ns) the quenching rate constant for *trans*-BP was determined as $k_q=2.7\times10^{10}$ M^{-1} s^{-1}. If

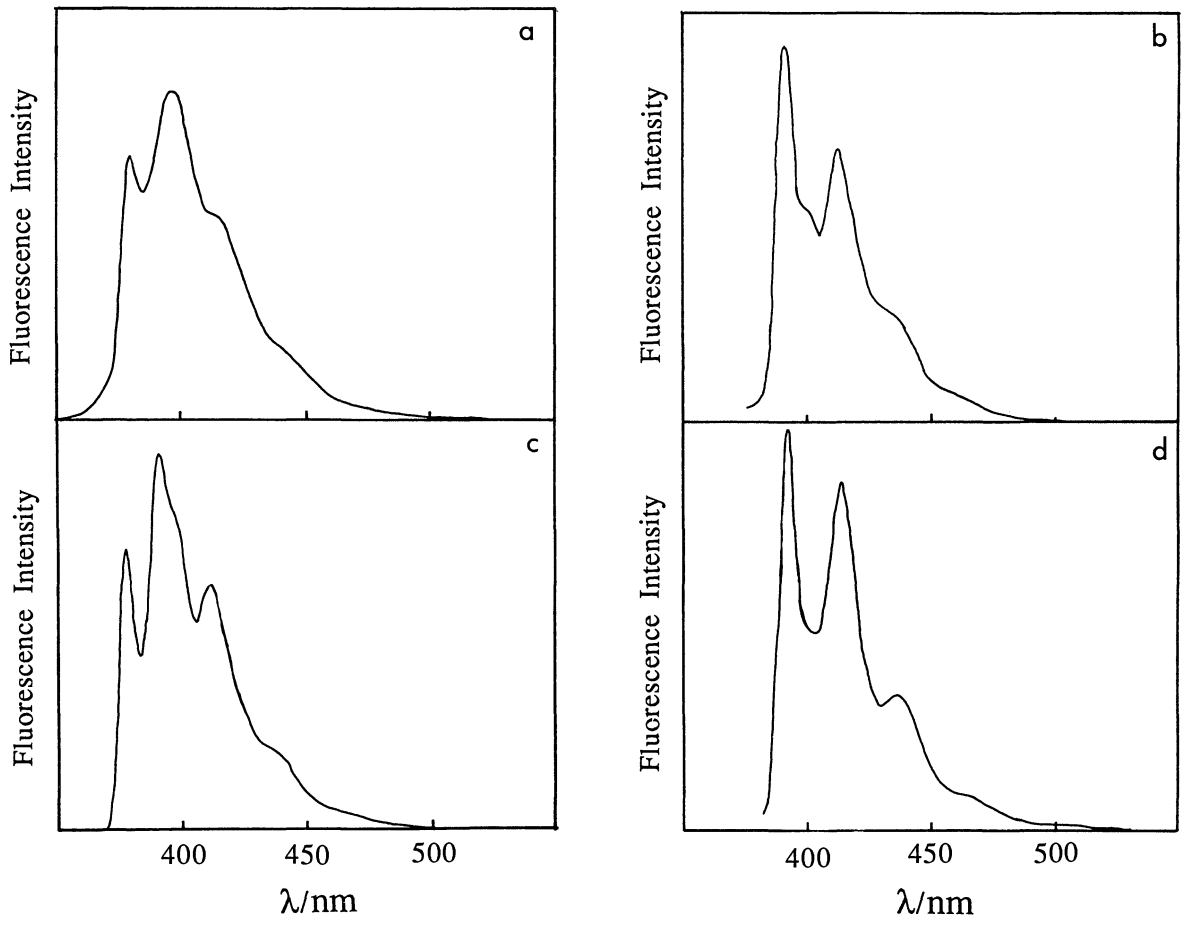

Fig. 2. Fluorescence spectra of *cis*- (a) and *trans*-BP (b) in benzene at room temperature and of *cis*- (c) and *trans*-BP (d) in EPA at 77 K.

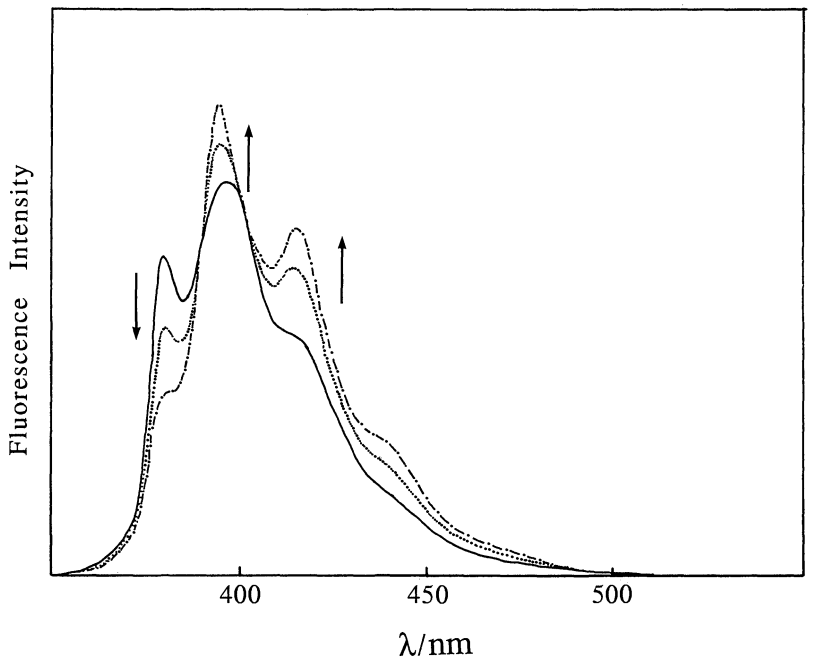

Fig. 3. Fluorescence spectrum change of *cis*-BP in benzene at room temperature.

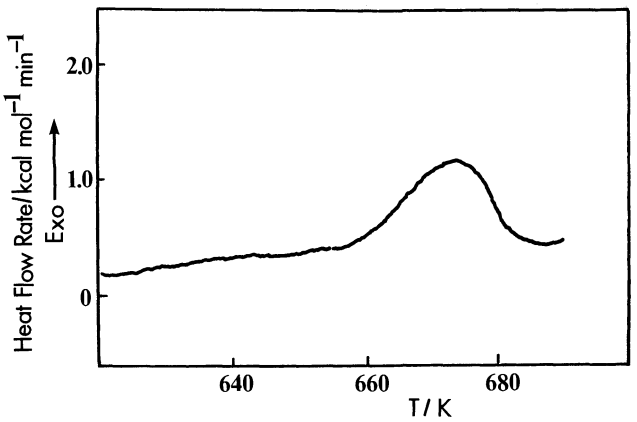

Fig. 4. DSC thermogram obtained for *cis*-BP at a rising rate of temperature of 2.5 °C min^{-1}.

singlet excited *cis*-BP is assumed to be quenched by oxygen with the same rate constant as *trans*-BP, its lifetime is estimated as 43 ns.

Quantum Yields for Intersystem Crossing. Solutions of anthracene and *cis*-BP optically matched at 308 nm (in the absence of benzil) or at 435 nm (in the presence of benzil as a sensitizer) were irradiated with 308-nm or 435-nm laser pulses and the initial T-T absorption intensities (ΔOD_0) were estimated by extrapolating the decay curve to time zero. These ΔOD_0 values combined with the quantum yield for intersystem crossing of anthracene, ϕ_{isc}(An) (=0.75[7]), give ϕ_{isc}(*cis*-BP) of 0.21. This value is almost identical to that of *trans*-BP (0.23).[5]

Energy Difference between Ground-State Cis (^{0}c) and Trans (^{0}t) Isomers. Energy difference between *cis*-BP (^{0}c) and *trans*-BP (^{0}t) in the ground state was obtained from the DSC thermogram (Fig. 4) as 4.9±0.3 kcal mol^{-1} at different rising rates of temperature (2—7.5 °C min^{-1}).

Discussion

Isomerization Mechanism on Direct Excitation. Stilbene isomerizes in a two-way mode in the excited singlet state as well as in the triplet state through a decay at the perpendicular conformation, resulting in a photostationary state mixture of a finite isomer ratio, $([t]/[c])_s$.[1] In contrast to stilbene, BP undergoes cis-to-trans one-way isomerization with a quantum chain process not only on triplet sensitization but on direct excitation, as evidenced by the photostationary state isomer ratios and isomerization quantum yields. For the one-way isomerization of BP observed on direct irradiation, the following mechanisms can be considered: i) an adiabatic cis-to-trans conversion in the singlet manifold involving a quantum chain process, ii) an isomerization through a decay from the perpendicular conformation on a stilbene-like excited singlet energy surface, and iii) an isomerization on the triplet energy surface after intersystem crossing at the cis conformation. The isomerization mechanism similar to that proposed for the stilbene singlet (mechanism ii) is ruled out since the decay at the perpendicular conformation to the ground state should afford a finite photostationary state isomer

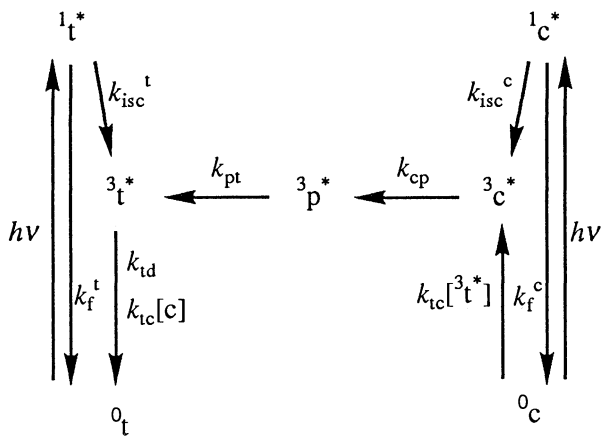

Scheme 1.

ratio instead of 100/0 and also cannot account for the chain process.

cis-BP and *trans*-BP exhibit the fluorescence spectra different from each other. Both spectra were efficiently quenched by oxygen, while the spectral profile of each isomer was essentially unchanged under oxygenated atmosphere. If an adiabatic cis-to-trans conversion in the singlet manifold efficiently took place, the fluorescence spectrum observed for *cis*-BP might consist of those emitted by the cis singlets and the resulting trans singlets, and under oxygenated atmosphere that of *cis*-BP might be more sustained compared to *trans*-BP fluorescence. However, the above results indicate that the *cis*-BP excited singlet is not converted to the *trans*-BP excited singlet, but emits fluorescence or intersystem crosses to the cis triplet. These facts indicate that the *cis*-BP excited singlet is located at an energy minimum, and exclude the possibility of the first mechanism.

Therefore, it is reasonable to propose that the isomerization of *cis*-BP on direct excitation proceeds in the triplet manifold after intersystem crossing of the cis singlet state as depicted in Scheme 1, where k's are the rate constants for the corresponding processes. According to Scheme 1, the quantum yield under direct irradiation is expressed by the following equation, Eq 1,[5,8] where ϕ_{isc}, k_{tc}, and τ_T denote the quantum yield for intersystem crossing of the cis singlet, the rate constant for energy transfer from the resulting trans triplet to the cis isomer, a key step for the quantum chain process, and the lifetime of the trans triplet state, respectively.

$$\phi_{c\to t}=\phi_{isc}(1+k_{tc}\tau_T[cis\text{-BP}]). \quad (1)$$

The linear dependence of $\phi_{c\to t}$ on [*cis*-BP] in Fig. 1 affords $\phi_{isc}=0.27$ and $\phi_{isc}k_{tc}\tau_T=1.3\times10^3\ M^{-1}$ as the intercept and the slope, respectively. Use of the values reported previously,[5] $\tau_T=1/k_{td}=54\ \mu s$ and $k_{tc}=1.2\times10^8\ M^{-1}\ s^{-1}$, gives $\phi_{isc}=0.25$. The value for ϕ_{isc} is in good agreement with the aforementioned value obtained by laser photolysis (0.21). This result strongly supports that the isomerization takes place at the triplet surface and eliminates a possibility of participation of the singlet state to the isomerization.

The following consideration also supports the mechanism iii. In Fig. 1 the ratio of slope/intercept ($1.3\times10^3\ M^{-1}/0.27=5\times10^3\ M^{-1}$) corresponds to the quenching constant ($k_q\tau$) of the excited state responsible for the quantum chain process. In the singlet state this magnitude of quenching constant could be achieved only when the quenching rate constant is larger than the diffusion-controlled value, because the singlet lifetime of *trans*-BP is 65 ns; thus, k_q should be $7.7\times10^{10}\ M^{-1}\ s^{-1}$. However, energy transfer from $^1t^*$ to *cis*-BP, if it occurs, should take place as an endothermic process with a rate constant much lower than the diffusion controlled, since the singlet excitation energy of *cis*-BP is 3 kcal mol^{-1} higher than that of *trans*-BP. This is contrasted with a reasonable value for k_{tc} in the triplet state.

Potential Energy Surfaces of BP. The energy difference (ΔH) between ^0c and ^0t was obtained as 4.9 kcal mol^{-1} from DSC experiments. This value is very similar to the most reliable value for stilbene (4.6 kcal mol^{-1}).[9] Thus, the energy differences between ^0c and ^0t for diarylethylenes and arylalkylethylenes seem to be similar (ca. 5 kcal mol^{-1}) as we usually assume.

As mentioned above, the cis and trans conformations of the excited singlet state are located at the energy minima with the excitation energies of 76 and 73 kcal mol^{-1}, respectively. The aforementioned failure of isomerization in the excited singlet state indicates the presence of a considerably high energy barrier which prevents the isomerization of $^1c^*$ on the singlet excited energy surface at room temperature. A rough estimation of the cis-to-trans conversion rate (k_{isom}) might be less than 1/100 of the total decay rate ($1/\tau_s=1.5\times10^7\ s^{-1}$). This corresponds to an activation energy higher than at least ca. 7 kcal mol^{-1}, when a range of 10^{11}—$10^{12}\ s^{-1}$ is assumed as the frequency factor, A, in Eq 2.

$$k_{isom}=A\exp(-E_a/RT). \quad (2)$$

Taking into account the energy barrier for twisting, the top of the energy surface of the singlet excited state must be located at the energy of 88 kcal mol^{-1} higher than ground-state *trans*-BP. There is still no evidence clarifying whether the energy barrier exists at the perpendicular conformation ($^1p^*$) or between $^1c^*$ (or $^1t^*$) and $^1p^*$. However, it is likely that the latter is the case because the energy of $^1p^*$ is usually assumed to be less than 80 kcal mol^{-1} over ^0t.[1]

Previously, we proposed the energy surface of the triplet state of BP undergoing cis-to-trans one-way isomerization by way of an adiabatic process; the

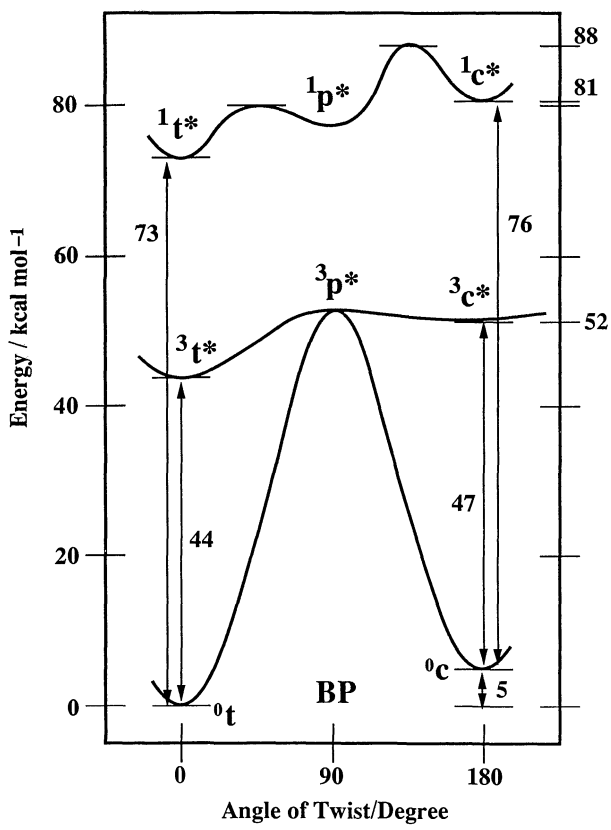

Fig. 5. Potential energy surfaces of cis-trans isomerization of BP.

initially resulting $^3c^*$ is converted to $^3t^*$, which either undergoes unimolecular deactivation to trans or transfers energy to cis to give trans and to regenerate $^3c^*$.

The present experimental results provide us sound basis to depict the potential energy surfaces of BP as shown in Fig. 5.

The authors thank to Drs. Takashi Tamaki, Tatsuko Hatakeyama, and Masako Sakuragi, Research Institute for Polymers and Textiles, for their help and discussions on DSC experiments. We also thank to the Ministry of Education, Science and Culture for partial support of this work by Grant-in-Aid for Special Project Research Nos. 61123001, 62113001, and 63104001 (K. T.) and by Grant-in-Aid for Scientific Research Nos. 61740242 and 01740255 (T. A.).

References

1) a) J. Saltiel., J. D'Agostino, E. D. Megarity, L. Metts, K. R. Neuberger, M. Wrighton, and O. C. Zafiriou, in "Organic Photochemistry," Vol. 3, ed by O. L. Chapman, Marcel Dekker, New York (1973), p. 1; b) J. Saltiel and J. L. Charlton, in "Rearrangement in Ground and Excited States," Vol. 3, ed by P. de Mayo, Academic Press, New York (1980), p. 25.

2) a) T. Arai, T. Karatsu, H. Sakuragi, and K. Tokumaru, *Tetrahedron Lett.*, **24**, 2873 (1983); b) T. Karatsu, T. Arai, H. Sakuragi, and K. Tokumaru, *Chem. Phys. Lett.*, **115**, 9 (1985); c) H. Hamaguchi, M. Tasumi, T. Karatsu, T. Arai, and K. Tokumaru, *J. Am. Chem. Soc.*, **108**, 1698 (1986).

3) a) T. Arai, T. Karatsu, M. Tsuchiya, H. Sakuragi, and K. Tokumaru, *Chem. Phys. Lett.*, **149**, 161 (1988); b) T. Karatsu, M. Tsuchiya, T. Arai, H. Sakuragi, and K. Tokumaru, *Chem. Phys. Lett.*, **169**, 36 (1990).

4) T. Arai, T. Karatsu, H. Misawa, Y. Kuriyama, H. Okamoto, T. Hiresaki, H. Furuuchi, H. Zeng, H. Sakuragi, and K. Tokumaru, *Pure Appl. Chem.*, **60**, 989 (1988), and references cited therein.

5) a) T. Arai, H. Okamoto, H. Sakuragi, and K. Tokumaru, *Chem. Phys. Lett.*, **157**, 46 (1989); b) H. Okamoto, T. Arai, H. Sakuragi, and K. Tokumaru, *Bull. Chem. Soc. Jpn.*, **63**, 2881 (1990).

6) T. Seki and K. Ichimura, *Macromolecules*, **23**, 31 (1990).

7) S. L. Murov, "Handbook of Photochemistry," Marcel Dekker, New York (1973), p. 5.

8) a) T. Arai, Y. Kuriyama, T. Karatsu, H. Sakuragi, K. Tokumaru, and S. Oishi, *J. Photochem.*, **36**, 125 (1987); b) H. Furuuchi, T. Arai, Y. Kuriyama, H. Sakuragi, and K. Tokumaru, *Chem. Phys. Lett.*, **162**, 211 (1989).

9) J. Saltiel, S. Ganapathy, and C. Werking, *J. Phys. Chem.*, **91**, 2755 (1987).

 © 1991 The Chemical Society of Japan Bull. Chem. Soc. Jpn., 64, 221—226 (1991)

Isotope Effects on the Reorientational Motion of Hydrated H_2O Molecules in Alkali Metal Bromide Dilute Aqueous Solutions Studied by NMR Spectroscopy

Akio SHIMIZU and Yoshihiro TANIGUCHI*
Department of Chemistry, Faculty of Science and Engineering, Ritsumeikan University, Kita-ku, Kyoto 603
(Received July 21, 1990)

The spin-lattice relaxation times of ^1H and ^{17}O nuclei of hydrated H_2O molecules in alkali metal bromide (LiBr, NaBr, KBr, and CsBr) dilute aqueous solutions in the concentration range from 0.2 to 1.0 mol kg^{-1} at 25 °C were measured by NMR spectroscopy. The reorientational correlation times for the intramolecular ^1H–^1H (τ_{HH}^{+}) and ^1H–^{17}O (τ_{OH}^{+}) axes, as well as the perpendicular axis (^{17}O nuclei, $\tau_{\perp O}^{+}$) to the molecular plane of a hydrated H_2O molecule were determied. The two reorientational correlation times (τ_{HH}^{+} and τ_{OH}^{+}) of pure H_2O and hydrated H_2O molecules in Li^+, Na^+, K^+, and Cs^+ ions were equal, respectively. Comparing previous data for hydrated D_2O molecules with that calculated by using correction values (r_{HH}, r_{OH}, and quadrupolar constant) for H_2O molecules, the ratios of $\tau_D^{+}(D_2O)/\tau_{OH}^{+}(H_2O)$ and $\tau_{\perp O}^{+}(D_2O)/\tau_{\perp O}^{+}(H_2O)$ were found to be of the same order as $\eta(D_2O)/\eta(H_2O)$, except for the $\tau_{\perp O}^{+}(D_2O)/\tau_{\perp O}^{+}(H_2O)$ value for the Li^+ ion.

To comprehend the complete picture regarding the dynamic properties of ionic hydration in water it is necessary to consider both macro- and microdynamic approaches. Regarding aqueous solutions, studies have accumulated many precise limiting values at infinite dilution regarding both the thermodynamic and transport properties.[1] On the other hand, our understanding concerning electrolyte solutions and the microdynamic properties of hydrated H_2O molecules of ions in water studied by NMR spectroscopy is very poor due to a lack of fundamental research concerning the concentration dependence, except for studies of Hertz et al.[2–5] and Leyte et al.[6–10] They have provided limiting values of the reorientational relaxation rates of hydrated water molecules of ions at infinite dilution by using a polynominal expression of the relaxation rates as a function of high concentrations, including both ion–ion and ion–water interactions.

Presently, the NMR technique that was developed is preferable for studying the reorientational motion of hydrated water molecules at lower concentrations, due to the ion–water interaction, to any other available experimental techniques. A study of the spin–lattice relaxation rates (R_1) of the ^1H, ^2D, and ^{17}O nuclei of water molecules in electrolyte solutions provides information about the reorientational motion of water molecules. The ^2D and ^{17}O relaxations are determined intramolecularly by quadrupole interactions, due to a rotational motion for the reorientation of the ^2D and ^{17}O electric field gradient tensor. The proton R_1 however, is governed by both intra and intermolecular ^1H–^1H dipolar interactions due to the reorientational and translational motions. The intra and intermolecular contributions to proton R_1 can be divided and determined from each theoretical expression by applying the extreme narrowing limit as well as measurements of the self-diffusion coefficient of water molecules by the spin–echo method;[2] it is also possible to study the ^1H relaxation in ^{17}O enriched water.[6]

From a previous study concerning the concentration dependence on the nuclear relaxation rates of the ^2D and ^{17}O nuclei of hydrated D_2O molecules of ions in dilute electrolyte solutions,[11] we found the both rates can be represented by linear functions against the concentrations of electrolyte solutions. The relationship between R_1 and the salt concentration is important for determining the limiting value, exclusively, due to the ion–water interaction on the base of the two-state model, i.e., hydrated water molecules and water molecules having a bulk water structure. By analysing these results, the reorientational motion along the O–D axis of the D_2O molecule was found to be 10% faster than those perpendicular to the D_2O molecular plane for the structure-making ions of Li^+ and Na^+ ions; for the structure-breaking ions of K^+ and Cs^+ ions, the tendency was inversed. This significant anisotropy regarding the reorientational motion of hydrated D_2O molecules in salt solutions comes from a local dynamic structure induced by a difference in the intermolecular interactions among ions, hydrated water molecules, and water molecules having a bulk water structure.

The local dynamic structure of hydrated water molecules in the vicinity of ions is strongly controlled by the solvent viscosity, which can be changed by various factors: i.e., temperature, pressure, solvent, and isotope effects. Though the isotope effect is a unique factor among them, no systematic study has been carried out by the NMR method. The dielectric properties of H_2O and D_2O are almost identical as most the other macroscopic properties.[12] The largest difference in the properties of pure water is its viscosity, which is 23% higher in D_2O than in H_2O at

25 °C.[13] Such differences as the thermodynamic properties of liquid H_2O and D_2O are consistent due to the O–D···O hydrogen bond being somewhat stronger than the O–H···O hydrogen bond. Therefore, in addition to the earlier study concerning the D_2O molecule,[11] NMR studies of the reorientational motion of H_2O molecules in dilute alkali metal bromide (LiBr, NaBr, KBr, CsBr) solutions have usefully helped to reach definite conclusions about both the hydration and anisotropy of the reorientational motion of hydrated water molecules of alkali metal ions in an H_2O system.

Experimental

Samples. Alkali metal bromide (LiBr, NaBr, KBr, CsBr) salts from Nakarai Tesque. Inc (extra-pure grade) were recrystallized from either water or ethanol. Deionized water was destilled with the addition of a small amount potassium permanganate. Sample preparation before an NMR measurement was reported previously.[11]

NMR Measurement. The ^1H relaxation times were measured on a JEOL GX-270 pulsed spectrometer operating at 270.0 MHz. Samples were kept in 4 mm diameter glass tubes and then inserted in 5 mm diameter glass tubes containing neat D_2O. The spin–lattice relaxation times (T_1) were measured by inversion-recovery methods, using a pulse sequence of 180°—t—90° pulses; The T_1 values were determined for each sample at 16 different time intervals (t), and the pulse delay time (PD) was more than $10T_1$. The frequency was 700 Hz for the ^1H nucleus. The free indicational decay of the ^1H nucleus was accumulated 4 times for all concentrations. Measurements of the ^{17}O nucleus relaxation times were carried out under the same condition which were reported previously.[11] The temperature was controlled to 25±0.1 °C by means of gas-thermostating.

Results and Discussion

Concentration Dependence of R_1 of H_2O Molecules in Aqueous Bromide Solutions. The relation between the spin–lattice relaxation rates ($R_1=1/T_1$) of the ^1H and ^{17}O nuclei of H_2O molecules and their concentrations in bromide solutions at 25 °C is shown in Figs. 1 and 2 and Table 1 along with data concerning the ^1H nucleus at 1 mol kg^{-1}, studied by Endom et al.[2] Our relaxation rates for the ^1H nucleus at 1 mol kg^{-1} agree with those of Endom et al.[2] within the experimental error. The ratios (R_1/R_1^0) vary linearly with increasing concentration up to 1.0 mol kg^{-1}. The R_1/R_1^0 (R_1^0 for pure H_2O) values are expressed as a linear function of the concentration, up to 1.0 mol kg^{-1}. Their values of ^1H and ^{17}O nuclei at a certain concentration are in the order LiBr>NaBr>KBr>CsBr. The structure-making salts of Li and Na increase the R_1/R_1^0 values of ^1H and ^{17}O of H_2O. On the other hand, the structure-breaking salts of K and Cs decrease the R_1/R_1^0 value of H_2O.

For ^1H and ^{17}O nuclei the concentration dependence of R_1 is given by linear equations at a concentration below 1.0 mol kg^{-1}, as follows:

$$R_1 = (1 + Bm)R_1^0, \quad (1)$$

where R_1 and R_1^0 are the spin–lattice relaxation rates at an electrolyte concentration of m and for pure H_2O, respectively. The B_H, $B_{^{17}O}$, and B_H–$B_{^{17}O}$ values are shown in Table 2 along with those of the D_2O system. From these results, the structure-making effect of Li and Na salts and the structure-breaking effect of K and Cs salts predominantly affect the B coefficient of the ^1H nucleus, rather than those of the ^{17}O nucleus of the

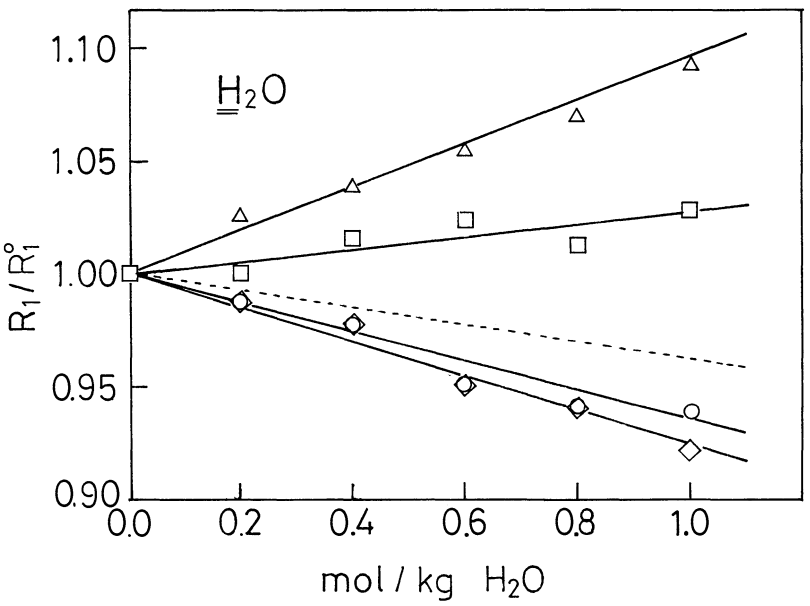

Fig. 1. Plots of H relxation rates (R_1/R_1^0) of a H_2O molecule in alkali metal bromide solutions at 25 °C. △: LiBr, □: NaBr, ○: KBr, ◇: CsBr, ---: KCl.

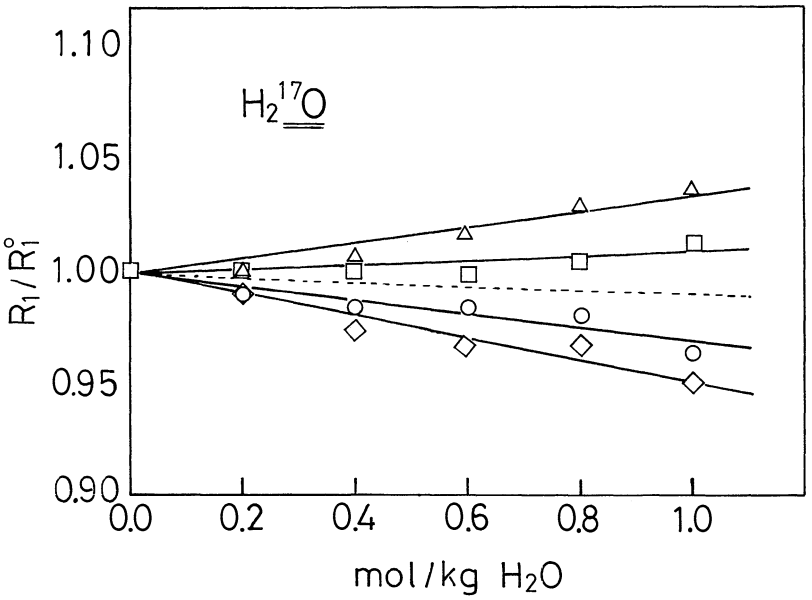

Fig. 2. Plots of ^{17}O relxation rates (R_1/R_1^0) of a H_2O molecule in alkali metal bromide solutions at 25 °C. △: LiBr, □: NaBr, ○: KBr, ◇: CsBr, ---: KCl.

Table 1. The ^1H and ^{17}O Spin-Lattice Relaxation Rates $R_1(s^{-1})$ of a H_2O Molecule at 25 °C[a]

Salt	H_2O/mol kg^{-1}									
	0.2		0.4		0.6		0.8		1.0	
	^1H	^{17}O	^1H	^{17}O	^1H	^{17}O	^1H	^{17}O	^1H	^{17}O
LiBr	0.289	138	0.292	139	0.297	140	0.301	142	0.307 (0.304)	143
NaBr	0.281	138	0.286	138	0.290	138	0.283	139	0.289 (0.290)	140
KBr	0.278	136	0.276	136	0.267	136	0.264	136	0.264 (0.265)	133
CsBr	0.278	137	0.277	134	0.269	133	0.265	134	0.259 (0.260)	131
KCl	0.278	138	0.274	137	0.273	137	0.277	137	0.273 (0.273)	137

a) For pure H_2O, the R_1 value of ^1H and ^{17}O are 0.281 and 138 s^{-1}, respectively. ( ) are data of Endom et al.[2]

Table 2. The B_H, $B_{^{17}O}$, $B_H-B_{^{17}O}$, and B-Coefficient of Viscosity for Various Alkaline Metal Aqueous Solutions at 25 °C

Salt	B_H	$B_{^{17}O}$	$B_H-B_{^{17}O}$	B-coefficient[a]
LiBr	0.096 (0.065)	0.031 (0.058)	0.065 (0.007)	0.108
NaBr	0.029 (0.010)	0.004 (0.010)	0.025 (0.000)	0.044
KBr	−0.066 (−0.060)	−0.034 (−0.032)	−0.032 (−0.028)	−0.049
CsBr	−0.073 (−0.074)	−0.053 (−0.047)	−0.020 (−0.027)	−0.087
KCl	−0.034	−0.011	−0.023	−0.014

a) Ref. 14. ( ) is D_2O systems in Ref. 11.

hydrated H_2O molecules of ions. There are no differences between the effect of the structure-breaking salts of K and Cs on the B coefficients of the both nuclei in H_2O and D_2O systems. However, the effect of the structure-making salts of Li and Na on the B coefficients of the ^1H nucleus in H_2O is enhanced more than those of the ^2D nucleus in D_2O; its effect on the B coefficient of the ^{17}O nucleus is vice versa to that in H_2O and D_2O systems. The correlation factors of the B coefficients between the NMR and viscosity of solutions are ca. 1.0 for B_H and ca. 0.4 for $B_{^{17}O}$.

Reorientational Motion of Hydrated H_2O Molecules. A linear relation between the relaxation rates and the salt concentration shown in Figs. 1 and 2 has been established in dilute salt solutions below 1.0 mol kg^{-1}. We can therefore consider that the ion–ion interaction is eliminated in this system and that each observed relaxation can be expressed as a weighted sum of the limiting relaxation rates in infinite dilution on the

base of two state model, as follows:

$$(R_1)_X = (1 - x^+ - x^-)(R_1)_X^0 + x^+(R_1)_X^+ + x^-(R_1)_X^- \quad (2)$$

and

$$(R_1)_X/(R_1)_X^0 = 1 + x^+\{(R_1)_X^+/(R_1)_X^0 - 1\} + x^-\{(R_1)_X^-/(R_1)_X^0 - 1\}, \quad (3)$$

where $(R_1)_X^0$, $(R_1)_X^+$, $(R_1)_X^-$, x^+, and x^- are the spin-lattice relaxation rates of pure water, cation and anion hydrated water, and the mole fraction of the cation and anion, respectively. The subscript X can be ^{17}O, HH, or OH when the relaxation path is, respectively, ^{17}O quadrupolar, an intramolecular ^1H–^1H dipolar interaction, or an intramolecular ^1H–^{17}O dipolar interaction.

By defining a coordination number, $n^\pm$, the mole fraction $x^\pm$ can be expressed in terms of the molarlity m of the solution,

$$x^\pm = n^\pm \times m/55.5. \quad (4)$$

The observed proton, R_1, in H_2O molecules is given by intra and intermolecular ^1H–^1H interactions, as follows:

$$(R_1)_H = (R_1)_{HH}^{intra} + (R_1)_{HH}^{inter}. \quad (5)$$

As compared to $(R_1)_H$=0.281 s^{-1} at 25 °C, Hertz[13] obtained the $(R_1)_{HH}^{inter}$=0.106 s^{-1} using experimental data of the self-diffusion coefficients of water as well as the theoretical jumping model of translational motion. If we arbitrarily take this value, $(R_1)_{HH}^{intra}$ contributes 62% of $(R_1)_H$. Later, Lankhorst et al.[6] measured the ^1H relaxation rates in ^{17}O-enriched water as a function of the ^{17}O mole fraction, $\chi(^{17}O)$. In view of the observed lineality, they obtained

$$(R_1)_H = (R_1)_{HH} + \chi(^{17}O)R_{OH}. \quad (6)$$

Of course, the R_{OH} value is the sum of the intra- and intermolecular ^1H–^{17}O dipolar interactions. For various salt solutions and pure water, they observed that the average ratios, $(R_1)_H/(R_1)_{HH}$ and $(R_1)_H/(R_1)_{OH}$ (^{17}O is a natural abundance), for various salts are 1.00±0.02 and 1.03±0.10, respectively.[9,10] The intramolecular contribution to $(R_1)_{HH}$ is 57%, and the intermolecular contribution to $(R_1)_{OH}$ is 2%.[9,10] The ^{17}O nucleus relaxes intramolecularly by quadrupole interactions, and the observed relaxation rates are directly correlated to the intramolecular term. Assuming that $R_1^+(K^+)=R_1^-(Cl^-)$ is satisfied for a KCl solution, in the case of an equal splitting of the B-coefficient into an ionic component[11,14] in Eq. 3, the $(R_1)_{HH}^{+,intra}$ $(R_1)_{OH}^{+,intra}$, $(R_1)_{^{17}O}^{\pm}$ values for various cations are determined from the both relations of the 57% intramolecular contribution to $(R_1)_{HH}$ and the 2% intermolecular contribution to $(R_1)_{OH}$. Table 3 shows the calculated R_1^+ values of ^1H and ^{17}O nuclei, and the $(R_1)_{HH}^{+,intra}$ and $(R_1)_{OH}^{+,intra}$ relaxation rates of intramolecular ^1H–^1H and ^1H–^{17}O dipolar interactions of hydrated H_2O molecules of the alkali metal ions. It was concluded that the intramoleculer contribution of ca. 62% to $(R_1)_{HH}^{+,intra}$ determined by Hertz et al.[15,16] is considerably overestimated.[10] Comparing the relaxation rates of the intramolecular ^1H–^1H dipolar interaction, the intramolecular ^1H–^{17}O dipolar interaction, and the ^{17}O quadrupolar interaction of hydrated H_2O molecules with those of pure H_2O molecules, the ^1H nucleus relative relaxation rate ($(R_1)_{HH}^{+,intra}/(R_1)_{HH}^{0,intra}$= $(R_1)_{OH}^{+,intra}/(R_1)_{OH}^{0,intra}$=$(R_1)_H^+/(R_1)_H^0$) are almost of the same order as the ^{17}O nucleus relative relaxation rates ($(R_1)_{^{17}O}^+/(R_1)_{^{17}O}^0$) for the structure-breaking ions of K^+ and Cs^+ ions. On the other hand, the structure-making effect of Li^+ and K^+ ions on the ^1H nucleus relaxation rates are larger than those of the ^{17}O nucleus.

Under extra narrowing conditions the intramolecular term of the spin-lattice relaxation rate, $(R_1)_X^{\pm,intra}$, of hydrated water molecules is the product of an interaction constant, $C_X^\pm$, and a reorientational correlation time, $\tau_X^\pm$:

$$(R_1)_X^{\pm,intra} = C_X^\pm \times \tau_X^\pm. \quad (7)$$

The intramolecular ^1H–^1H dipolar interaction is given by

$$(R_1)_{HH}^{\pm,intra} = \frac{3\gamma_H^4\hbar^2}{2r_{HH}^6}\tau_{HH}^\pm, \quad (8)$$

Table 3. The Relaxation Rates of a Hydrated H_2O Molecule in Alkali Metal Ions at 25 °C

Ion	$(R_1)_{^{17}O}^+/(R_1)_{^{17}O}^0$	$(R_1)_{^{17}O}^+$ / s^{-1}	$(R_1)_H^+/(R_1)_H^{0a)}$	$(R_1)_H^+$ / s^{-1}	$(R_1)_{HH}^{+,intra b)}$ / s^{-1}	$(R_1)_{HH}^{+,intra c)}$ / s^{-1}	$(R_1)_{OH}^{+,intra d)}$ / s^{-1}
Li^+	1.55	214	2.34	0.658	0.408	0.283	0.626
Na^+	1.30	179	1.72	0.484	0.300	0.208	0.460
K^+	0.949	131	0.843	0.237	0.147	0.102	0.225
Cs^+	0.775	107	0.779	0.219	0.136	0.094	0.209
Pure water		138		0.281	0.174	0.121	0.267

a) $(R_1)_H^+/(R_1)_H^0$=$(R_1)_{HH}^{+,intra}/(R_1)_{HH}^{0,intra}$=$(R_1)_{OH}^{+,intra}/(R_1)_{OH}^{0,intra}$. b) The calculated values by using 0.62×$(R_1)_H^+$ in Ref. 4. c) The calculated values by using 0.43×$(R_1)_H^+$ in Refs. 6 and 10. d) The calculated values by using 0.95×$(R_1)_H^+$ in Refs. 6 and 10.

where γ_H is the proton gyromagnetic ratio, $\hbar$ Planck's constant divided by 2π, r_{HH} the intraproton distance of the water molecule, and $\tau^{\pm}_{HH}$ the reorientational correlation time for the intramolecular ^1H–^1H axis.

The intramolecular contribution of the ^1H–^{17}O dipolar interaction is given by

$$(R_1)^{\pm,\mathrm{intra}}_{OH} = \frac{35}{3}\frac{\gamma_H^2\gamma_{^{17}O}^2\hbar^2}{r_{OH}^6}\tau^{\pm}_{OH}, \quad (9)$$

where $\gamma_{^{17}O}$ is the oxygen gyromagnetic ratio, r_{OH} the interdistance between the oxygen and the proton of the water molecule, and $\tau^{\pm}_{OH}$ the reorientational correlation time for the intramolecular ^1H–^{17}O axis. The ^{17}O (I=5/2) relaxation is determined intramolecularly by quadrupolar interactions; the rate is give by

$$(R_1)_{^{17}O} = \frac{3}{135}\left(\frac{e^2qQ}{\hbar}\right)^2\left(1+\frac{\eta^2}{3}\right)\tau_{^{17}O}, \quad (10)$$

where e^2q is the electric field gradient at the nucleus, Q the electric quadrupole moment of the nucleus, η the asymmetry parameter, and $\tau_{^{17}O}$ the correlation time for the reorientational of the oxygen electric field gradient tensor (perpendicular axis to the H_2O molecular plane). From Eqs. 3 and 10, the following relation is derived:

$$\frac{(R_1)_{^{17}O}}{(R_1)^0_{^{17}O}} = 1 + \left\{x^+\left(k^+\frac{\tau^+_{^{17}O}}{\tau^0_{^{17}O}} - 1\right) + x^-\left(k^-\frac{\tau^-_{^{17}O}}{\tau^0_{^{17}O}} - 1\right)\right\} \quad (11)$$

and

$$k^{\pm} = \{(e^2qQ/\hbar)^{\pm}/(e^2qQ/\hbar)^0\}^2, \quad (12)$$

where $\tau^0_{^{17}O}$, $\tau^+_{^{17}O}$, and $\tau^-_{^{17}O}$, are the correlation times of pure H_2O and H_2O in the hydration sphere of a cation and an anion, respectively. Here, k=1 is for the case when the e^2qQ of hydrated water molecules in cations equals that of pure water molecules; and k=0.82 is the correction value reported by van der Maarel et al.,[9] i.e., the e^2qQ value is about 10% smaller than that of pure water molecules. Table 4 shows the three reorientational correlation times of pure and hydrated H_2O molecules for alkali metal ions calculated by two assumptions at 25 °C. One is that the three parameters (r_{HH}, r_{OH}, and k) of hydratd water molecules equal that of pure H_2O molecules; the other equals the correction values reported by van der Maarel et al.[9] From those results, it is clarified that the reorientational correlation time (τ^+_{HH}=τ^+_{OH}) for two parallel axes to the H_2O molecular plane is the same values for each cation within the experimental error. Therefore, the reorientational motion of these two axes is isotropic.

Table 5 shows the anisotropy ($\tau^+_{HH}/\tau^+_{^{17}O}$ or $\tau^+_{OH}/\tau^+_{^{17}O}$) and the solvent isotope effects for the reorientational motion of hydrated H_2O molecules for alkali metal ions in a dilute aqueous solution. The τ^+_{OH} and τ^+_D values are the reorientational correlation times for the intramolecular ^1H–^{17}O axis and O–D axis, respectively. Consequently, these two reorientational correlation times give information concerning the reorientational motion of the similar axis (^1H–^{17}O axis and O–D axis). The reorientational motion of a hydrated H_2O molecule in alkali metal bromide solutions is anisotropic, similar to the tendency of a hydrated D_2O molecule. That is, for a hydrated H_2O molecule of positive hydration of Li^+ and Na^+ ions, the reorientational motion of the perpendicular axis to the H_2O molecular plane ($\tau^+_{^{17}O}$) is faster than the reorientational

Table 4. Reorientational Correlation Times of a Hydrated H_2O Molecule and Pure Water at 25 °C[a]

Ion	τ^+_{HH}[b]		τ^+_{OH}[b]		$\tau^+_{^{17}O}(H_2O)$	
	ps		ps		ps	
Li^+	4.53	4.83	4.54	4.81	2.90	3.54
Na^+	3.36	3.58	3.34	3.54	2.43	2.96
K^+	1.64	1.75	1.63	1.73	1.77	2.16
Cs^+	1.52	1.62	1.50	1.59	1.45	1.77
Pure water	1.96		1.93		1.87	

a) The values of left sides are the calculated by using the parameters (r_{HH}=0.1549 nm, r_{OH}=0.098 nm, and k=1.00) of pure water molecule. The values of right sides are calculated values by using the parameters (r_{HH}=0.1566 nm, r_{OH}=0.099 nm, and k=0.82). b) Calculated from $(R_1)^+_{HH}$[b] and $(R_1)^+_{OH}$[c] values in Table 3.

Table 5. Reorientational Anisotropy and Solvent Isotope Effect on the Reorientational Correlation Time of a Hydrated H_2O Molecule and Pure Water at 25 °C[a]

Ion	$\tau^+_{OH}/\tau^+_{^{17}O}$		$\tau^+_D/\tau^+_{^{17}O}$[b]	$\tau^+_D(D_2O)/\tau^+_{OH}(H_2O)$[b]		$\tau^+_{^{17}O}(D_2O)/\tau^+_{^{17}O}(H_2O)$[b]	$\frac{\tau^+_{OH}/\tau^+_{^{17}O}}{\tau^+_D/\tau^+_{^{17}O}}$	
Li^+	1.57	1.36	1.12	1.04	1.20	1.45	0.72	0.82
Na^+	1.37	1.20	1.13	1.04	1.23	1.27	0.82	0.97
K^+	0.92	0.80	0.89	1.20	1.38	1.24	0.96	1.11
Cs^+	1.03	0.90	0.92	1.11	1.28	1.24	0.89	1.03
Pure water	1.03		1.00	1.23		1.27	0.97	

a) The values of left sides are calculated by using the parameters (r_{HH}=0.1549 nm, r_{OH}=0.098 nm, and k=1.00) of pure water molecule. The values of right sides are calculated by using the parameters (r_{HH}=0.1566 nm, r_{OH}=0.099 nm, and k=0.82). The $\tau^+_D/\tau^+_{^{17}O}$ and $\tau^+_{^{17}O}(D_2O)/\tau^+_{^{17}O}(H_2O)$ values are the same for each k. b) D_2O data are from Ref. 11.

motion of the intramolecular ^1H–^1H and ^1H–^{17}O axes. The reorientational anisotropies for the negative hydration of K^+ and Cs^+ ions are vice versa. The reorientational anisotropy of a H_2O molecule around the positive hydration ions, especially for the Li^+ ion, is larger than that of a D_2O molecule, in spite of the anisotropy of H_2O molecules around the negative hydration ions is almost the same order of a D_2O molecule.

As shown the last column in Table 5, we can observe the large solvent isotope effect on the reorientational anisotropy of a water molecule in the Li^+ hydration sphere. The reasons may be explained by comparing the solvent isotope effect on the reorientational correlation times within the hydration sphere with the effect on the correlation times in water molecules having a bulk water structure. Our results for the ^2D and ^{17}O isotope effects on the reorientational correlation times of a pure water molecule ($\tau_D^+(D_2O)/\tau_{OH}^+(H_2O)=1.23$ and $\tau_{^{17}O}^+(D_2O)/\tau_{^{17}O}^+(H_2O)=1.27$) are in good agreement with the ^2D isotope effect on the reorientational correlation time obtained by Lankhorst et al. ($\tau(D_2O)/\tau(H_2O)=1.28$)[6] and some related dynamical properties, such as the self-diffusion ($(D(H_2O)/D(D_2O)=1.23$)[17] and viscosity ($\eta(D_2O)/\eta(H_2O)=1.23$).[13] The solvent isotope effects on the reorientational correlation times in negative hydration water molecules (calculated assuming pure water parameters (r_{HH}, r_{OH}, and e^2qQ)), are almost of the same order as that of the isotope effects on the reorientational correlation times in pure water molecules. The solvent isotope effects on the reorientational correlation time of ^1H and ^{17}O nuclei in the positive hydration water of Li^+ ion are remarkable compared with those of a hydration water molecule in the nagetive hydration sphere of another cation and a pure water molecule in water. This isotope effect on the reorientational correlation time of the intermolecular ^1H–^{17}O and ^1H–^1H dipolar interactions is smaller than that of a pure water molecule, and the effect of the ^{17}O nucleus of the hydration water molecule of the Li^+ ion is larger. On the other hand, the solvent isotope effect on the reorientational correlation time of the negative and positive hydration water molecule calculated by using the correction values are of the same order in pure water, except for that of ^{17}O nucleus. The solvent isotope effect on the ^{17}O nucleus of the hydrated water molecule of the Li^+ ion is enhanced to be 1.45. It is natural that the ^1H–^1H, ^1H–^{17}O distance, and the quadrupole coupling constant of water molecules in the hydration sphere change with respect to pure water.[9] Therefore, the solvent isotope effect by using the correction values may give a true value; thus, the ^{17}O nuclei of the hydrated water molecule of the Li^+ ion only shows a different large solvent isotope effect against that of a pure water molecule. The hydrated water molecule of the Li^+ cation is orientated with their oxygen atom pointing towards the ion, and the Li^+ ion has the largest surface charge density among the univalent cations. Consequently, H_2O molecules around the Li^+ ion are strongly hydrated, so that the largest solvent isotope effect is observed on the ^{17}O nucleus of a hydrated water molecule of the Li^+ ion.

References

1) For example, F. Frank, "Water," Plenum Press, New York (1973), Vol. 3. R. A. Horn, "Water and Aqueous Solutions," John Wiely & Sons, Inc., New York (1972), Chap. 12—15.

2) L. Endom, H. G. Hertz, B. Thull, and M. D. Zeidler, *Ber. Bunsenges. Phys. Chem.*, **71**, 1008 (1967).

3) F. Fister and H. G. Hertz, *Ber. Bunsenges. Phys. Chem.*, **71**, 1032 (1967).

4) G. Engel and H. G. Hertz, *Ber. Bunsenges. Phys. Chem.*, **72**, 808 (1968).

5) H. G. Hertz, R. Tutsch, and H. Versmid, *Ber. Bunsenges. Phys. Chem.*, **75**, 1177 (1971).

6) D. Lankhorst, J. Schriever, and J. C. Leyte, *J. Phys. Chem.*, **86**, 215 (1982).

7) C. W. R. Mulder, J. Schriever, W. J. Jesse, and J. C. Leyte, *J. Phys. Chem.*, **87**, 2336 (1983).

8) C. W. R. Mulder, J. Schriever, W. J. Jesse, and J. C. Leyte, *J. Phys. Chem.*, **87**, 2342 (1983).

9) J. R. C. van der Maarel, D. Lankhorst, J. de Bleijster, and J. C. Leyte, *J. Phys. Chem.*, **90**, 1470 (1986).

10) R. P. W. J. Struis, J. de Bleijster, and J. C. Leyte, *J. Phys. Chem.*, **91**, 1639 (1987).

11) A. Shimizu and Y. Taniguchi, *Bull. Chem. Soc. Jpn.*, **63**, 1572 (1990).

12) G. S. Kell, "Thermodynamic and Transport Properties of Fluid Water," ed by F. Franks, Prenum Press, New York (1973), Vol. 1, Chap. 10.

13) F. J. Millero, R. Dexter, and E. Hoff, *J. Chem. Eng. Data*, **16**, 85 (1971).

14) M. Kaminsky, *Discuss. Faraday Soc.*, **24**, 171 (1957).

15) H. G. Herzt, "Theorie der Elektrolyte," Herzel Verlag, Leipzig (1971).

16) K. Krynicki, *Physica*, **32**, 167 (1966).

 © 1991 The Chemical Society of Japan Bull. Chem. Soc. Jpn., 64, 227—235 (1991)

Pillared Tetrasilicic Mica Catalysts Having Fixed Interlayer Ca Ions. Comparison with Other Clays

Hiroaki SAKURAI,† Kazuo URABE,* and Yusuke IZUMI*
Department of Synthetic Chemistry, Faculty of Engineering, Nagoya University, Furo-cho, Chikusa-ku, Nagoya 464
(Received July 30, 1990)

Three kinds of Ca^{2+}-modified pillared clays (TSM, taeniolite, and montmorillonite) were prepared from Ca^{2+}-exchanged clays. The cumene cracking activity over the TSM-based catalyst was greatly dependent on the calcination temperature before pillaring, and gave a maximum at 300—400 °C. In contrast, no appreciable increase in the activity with the calcination temperature before pillaring was observed in montmorillonite- and taeniolite-based catalysts. The amount of residual Ca in the modified pillared TSM was increased with a rise in the calcination temperature before pillaring, whereas the amount of Al incorporated through pillaring was decreased, showing the progress of Ca^{2+} fixation during the stage of thermal treatment of Ca^{2+}-exchanged unpillared TSM. Thus, the cracking activity was greatly enhanced by the fixation of Ca^{2+}. The cracking activity, however, dropped due to a pretreatment above 400 °C, since the Al-pillars which prop silicate layers are reduced while causing a decline in the surface area of the resulting pillared TSM; also, the strong acid sites were decreased due to excessive packing of Ca^{2+} fixed over the surface of silicate layers. In the cases of montmorillonite and taeniolite, the remaining amounts of Ca and Al were almost constant, irrespective of the calcination temperature before pillaring. This indicates that Ca^{2+} fixation does not occur in these clays.

Since pillared clay as a heat-stable porous material was synthesized by Brindley and Sempels in 1977,[1] clay minerals have attracted attention as potential catalytic materials, since pillared clays have both acidity and a molecular sieve ability. Pillared clay can be regarded as being an intercalated compound comprising a host silicate and guest oxide pillars. An aluminum hydroxy cluster cation, $[Al_{13}O_4(OH)_{24}(H_2O)_{12}]^{7+}$, with a diameter of ca. 9 Å is most widely employed as a precursor of a pillar. To intercalate such a large cation between layers, the host clay, which has a free-swelling property in an aqueous medium, must be employed. Besides smectite clays (such as montmorillonite, hectorite, and saponite), the sodium form of fluor-tetrasilicic mica (TSM) fulfills the above-mentioned requisites; the clay is also swellable and cation exchangeable, and can form a porous pillared variant. Though the resulted pillared TSM (PTSM) had few acidic sites and was unattractive as an acidic catalyst, the acidity of the PTSM can be greatly enhanced by the fixation of interlayer cations onto the silicate layer of pillared TSM.[2] The fixation mode was classified into five types according to the valence and size of the cation to be fixed.[3] In these studies, TSM was employed as a host layer silicate. Since cation fixation into or onto a layered structure is due to an electrostatic force between dehydrated positive cations and negatively charged silicate layers, the ease of fixation might be affected not only by the nature of the cation, but also by the structure of the silicate layer.

The migration of small cations (such as Li^+, Al^{3+}, and Mg^{2+}) into a layer structure is known as the Hofmann–Klemen effect,[4–6] and occurs only in dioctahedral and octahedrally substituted clay minerals.[7] This principle, therefore, has been applied to the diagnostic method for montmorillonite.[7,8] It was found that the TSM layer with octahedral vacancies also gave rise to this type of migration-fixation.[3] The fixation of monovalent and fairly large cations (such as K^+ and Cs^+) has also been investigated in detail, and some factors that contribute to this type of fixation have already been reviewed in connection with both the interlayer cations and the silicate layer.[9,10]

On the other hand, the detailed controlling factors concerning the silicate layer are not yet known regarding the fixation of polyvalent and large cations. Only a few examples of La^{3+} and Ca^{2+} fixation by montmorillonite can be found in the literature.[11–13] No notable improving effect on the catalytic activity of pillared clay by the fixation of these cations has been ascertained in the case of clays other than TSM.

In this study, a similar modification of pillared clay was applied to other two clays, montmorillonite and taeniolite. Although the highest catalytic activity was exhibited by La^{3+}–PTSM among various cation modified catalysts, Ca^{2+} was employed here as a modifier, because Ca^{2+} is less susceptible to hydrolysis than is La^{3+}; a more quantitative discussion may be possible concerning fixation. Three kinds of pillared clays (Ca^{2+}–PTSM, Ca^{2+}–PM, and Ca^{2+}–PT) were compared with respect to their cracking activity. The residual cations (Ca^{2+}, Na^+) and the incorporated Al as a pillar component were determined. We also discuss here the relationship between cation-fixation and the change in the catalytic activity. Moreover, the distribution of Ca on the silicate surface was calculated based on a random distribution modes as a function of the amount of fixed Ca and is discussed in connection with the catalytic activity.

† Present address: Government Industrial Research Institute of Osaka, Midorigaoka 1, Ikeda 563.

Experimental

Material Clay. Both the sodium form of fluor-tetrasilicic mica and the lithium form of taeniolite were supplied from Topy Ind. These samples were refined by means of a conventional sedimentation technique, and a <5 μm fraction was collected. The refined TSM contained only small amounts of impurities, such as α-cristobalite. Reportedly, the composition of TSM by chemical analysis is[14,15] $Na_{1.00}(Mg_{2.63})^{oct}(Si_{3.94}Al_{0.05}Mg_{0.01})^{tet}O_{10.19}F_{1.81}$.

Refined natural montmorillonite (Kunipia F) with high purity was supplied by Kunimine Ind., and used without further purification. The chemical formula of this montmorillonite is[15] $(K_{0.01}Na_{0.43}Mg_{0.01})(Al_{1.57}Fe^{3+}_{0.08}Fe^{2+}_{0.02}Mg_{0.34})^{oct}(Si_{3.88}Al_{0.12})^{tet}O_{10}(OH)_2$.

These clays were Ca^{2+}-exchanged by the use of either aqueous calcium nitrate or calcium chloride. In the case of TSM and taeniolite, an in situ cation exchange was performed during the sedimentation stage; that is, aqueous calcium chloride was added to an aqueous dispersion of clay containing a <5 μm fraction of TSM or taeniolite particles. Ca^{2+}-exchanged clays were washed repeatedly with deionized water until salt free; they were then dried at 60°C.

Catalyst Preparation. Ca^{2+}-modified pillared clays (Ca^{2+}-PTSM, TSM; Ca^{2+}-PM, montmorillonite; Ca^{2+}-PT, taeniolite) were prepared according to a previously reported method.[2] The preparative procedure is as follows. Ca^{2+}-exchanged clays (Ca^{2+}-TSM, Ca^{2+}-M, and Ca^{2+}-T) were first calcined at 60—700°C for 3 h (procedure of calc. 1). The calcined clays were dispersed in a mixed solution of acetone and water; an aluminum cluster cation solution (OH/Al=2.0)[2] was then added as a pillaring agent and stirred for 12 h. After air-drying at 60°C, the clay samples were finally calcined at 300°C for 3 h. The second calcination operation is referred to as calc. 2.

Reaction Procedure and Analysis. Cumene cracking was carried out using a conventional continuous-flow system under atmospheric pressure. All of the liquid products were collected in an ice trap and were analyzed by GLC using Bentone 34 and DNP column (4 m).

Characterization. X-Ray diffraction (XRD) analysis was carried out employing oriented clay films formed on glass slides.

The nitrogen adsorption over the catalyst was measured at 78 K after evacuation at 300°C for 1 h; its surface area was calculated by either BET or Langmuir equation according to the type of adsorption isotherm. The pore-size distribution was computed from the isotherm according to the Cranston-Inkley method.[16]

The solid acidity of various catalysts was examined by the temperature-programmed desorption (TPD) of the adsorbed ammonia. The experimental conditions have already been described in a previous paper.[3]

The IR spectra of adsorbed pyridine were recorded on a JASCO IR-810 spectrophotometer according to a method described in a previous paper.[2]

Quantitative measurements of Ca, Al, and Na were carried out by use of an X-ray fluorescence spectrometer, VF-310 (Shimadzu Co., Ltd.). The clay sample (0.3 g) was fused with $Li_2B_4O_7$ (5.0 g) at 1100°C, cooled in air, and a glass bead sample was obtained for the measurement.

Results and Discussion

Catalytic Activity Change. Figure 1 and Table 1 show the cumene cracking activity as a function of the calc. 1 temperature over a Ca^{2+}-modified pillared TSM catalyst (Ca^{2+}-PTSM). When the catalyst was dried at 60°C as calc. 1, the cumene conversion (0.21%) was almost the same as that of nonmodified PTSM (0.18%). Beyond 200°C, the activity drastically increased with a rise in temperature, and reached a maximum at 300—400°C; it then decreased monotonously. The maximum conversion was 4.2%, which was about half the conversion on La^{3+}-PTSM (max. 7.6% at 300°C).[2] While La^{3+}-PTSM became almost inactive at 500°C (0.1% conversion) due to an interlayer collapse, Ca^{2+}-PTSM maintained a >1.5% conversion, even at 700°C.

In the case of the other two clays Ca^{2+}-PM, montmorillonite; Ca^{2+}-PT, taeniolite), both catalysts dried at 60°C already had a >10% conversion (Table 1). The conversion of Ca^{2+}-PM (13.3%) was about the

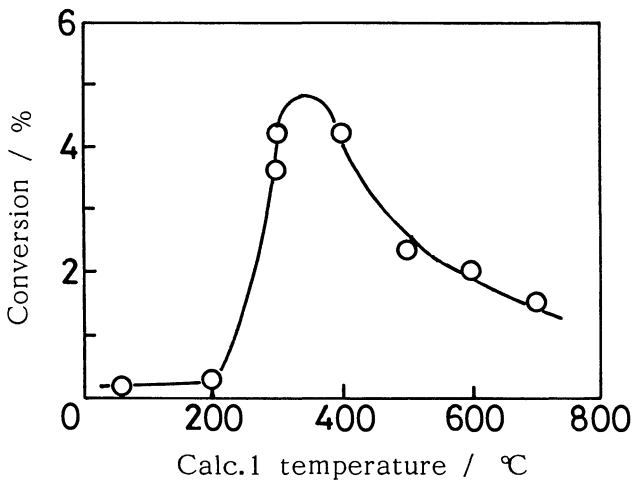

Fig. 1. Effect of the temperature of calc. 1 on cumene cracking activity of Ca^{2+}-PTSM. Reaction temp 300°C, W/F=33 g h mol^{-1}, flow rate of N_2 carrier gas 600 ml h^{-1}.

Table 1. Cumene Cracking Activity of Ca^{2+}-Modified Pillared Clays[a]

Calc. 1 Temp	Conversion over each catalyst/%		
°C	Ca^{2+}-PTSM	Ca^{2+}-PM	Ca^{2+}-PT
60	0.21	13.3	11.9
200	0.30	—	—
300	4.2	15.4	9.4
400	4.2	—	—
500	2.3	—	—
600	2.0	—	—
700	1.5	—	—

a) Reaction temp 300°C, W/F=33 g-cat. h mol^{-1} (W= weight of catalyst, F=feed rate of reactant), flow rate of N_2 carrier gas 600 ml h^{-1}, averaged initial activity for 1 h after feeding of reactant.

same level as that of nonmodified conventional pillared montmorillonite (PM; 14.3% conversion). No outstanding increase in the activity with a rise in the calc. 1 temperature until 300°C was found in these clays, which was the most significant difference from the case of TSM.

The Amount of Ca Fixed in Pillared Clay. Figure 2 shows the residual amounts of Ca in Ca^{2+}–PTSM, Ca^{2+}–PM, and Ca^{2+}–PT after calc. 2 at 300°C. The amount of Ca is expressed for convenience as the mole ratio of Ca to Si when taking 4.00 for Si, because TSM ideally has a half unit cell formula, $Na^{+}(Mg_{5/2})^{oct.}(Si_4)^{tet.}O_{10}F_2$.

The Ca^{2+}-exchanged TSM before pillaring (Ca^{2+}–TSM) had a Ca amount of 1.03 (left side of Fig. 2), which corresponded to about twice the amount (0.50) calculated from the theoretical CEC (Cation Exchange Capacity) of TSM. Though the reason for this discrepancy is not clear, it is possibly due to an unavoidable hydrolysis of Ca^{2+} to form $Ca(OH)_2$. Reportedly, in cation-exchange process on H^{+}-montmorillonite with Cu^{2+}, Zn^{2+},[17] and La^{3+},[18] montmorillonite can retain these polyvalent cations beyond the CEC under a certain condition (pH, concentration, and the kind of coexisting anions), which is considered to be due to hydroxide precipitation.[17,18] Ca^{2+}-exchanged taeniolite (Ca^{2+}–T) also had excess Ca (0.80), as shown in Fig. 2. Under the present experimental conditions, however, Ca^{2+}-montmorillonite (Ca^{2+}–M) had a nearly equivalent amount (0.20) to the theoretical value (0.23) corresponding to the CEC which was calculated from the chemical formula shown above. Thus, the extensive hydrolysis of Ca^{2+} appears to be related to the layer charge of the clay.

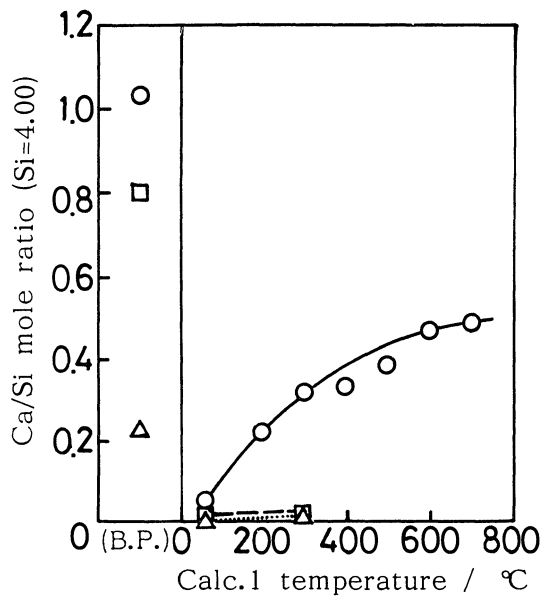

Fig. 2. Effect of the temperature of calc. 1 on the residual amount of Ca in Ca^{2+}-modified pillared clays. (○) TSM, (△) montmorillonite, (□) taeniolite. (B.P.) Ca^{2+}-exchanged clay before pillaring.

When calc. 1 was carried out at 60°C, most parts of both the exchangeable Ca^{2+} and the above-mentioned excess of Ca incorporated in these clays were released after pillaring manipulation, being replaced by aluminum hydroxy cluster cations. Fortunately, under such circumstances, thermally fixed Ca is clearly quantitatively distinguishable from other types of Ca at higher temperatures of calc. 1. Indeed, the residual amount of Ca in Ca^{2+}–PTSM progressively increased with increasing calc. 1 temperature and reached 0.48 at 700°C, coming near to a critical amount (0.50) limited by the CEC. This result is direct evidence of thermally induced Ca^{2+} fixation by the TSM layers. On the contrary, the residual Ca^{2+} did not increase at 300°C at all in montmorillonite and taeniolite, suggesting that fixation did not occur in these clays. The fixation phenomenon well accounts for the change in catalytic activity shown in Fig. 1; that is, the activity of TSM is greatly enhanced with the progress of fixation, though no noticeable changes in the activity (see Table 1) are found in montmorillonite and taeniolite because of the absence of fixation.

The Ca^{2+} fixation by bentonite or montmorillonite, which brings about a reduction of CEC by a heat treatment, was reported by Hofmann and Endell[12] and Kondo.[13] Nevertheless, the fixation of Ca^{2+} by montmorillonite was not observed in the present study. The CEC of clay minerals is usually measured by the use of an aqueous salt solution under neutral conditions,[19] while in this study, the heated Ca^{2+}-montmorillonite was dispersed in a mixed solvent of acetone and water and then Ca^{2+} ions were subjected to exchange with an aqueous solution of aluminum hydroxy cluster cations (pH=4.0). The use of acetone and an acidic cation-exchange condition is possibly related to the difficulty of Ca^{2+} fixation onto the layer surface of montmorillonite. The large dipole moment of the acetone molecule facilitates the solvation of interlayer cations of charge-reduced montmorillonite.[20]

The most important question is what factor influence the ease of Ca^{2+} fixation in the three different clays. For an explanation, some of the known factors[9,10] controlling K^{+} fixation in soils and clay minerals are applicable, since both K^{+} and Ca^{2+} fix onto a silicate-layer surface, partly lodging in the hexagonal holes in a similar way.[3] These factors involve a layer charge as well as a substitution of F for OH in the octahedral sheet.[10] TSM has a much larger layer charge than dose montmorillonite, and can hold any fixed cations firmly. When a clay has an OH at the bottom of a hexagonal hole, the K^{+} ion receives an electrostatic repulsion force from the protonic part of the OH group. The substitution of F for OH removes this repulsion effect and facillitates the fixation of K^{+}.[10] Therefore, the F substitution in TSM must further facilitate the fixation of Ca^{2+} in addition

to the effect of a large layer charge. However, these factors cannot account for the difference between TSM and taeniolite. The octahedral vacancies which exist in TSM must play an important role. In the case of K^+ fixation, it is also known that dioctahedral minerals hold K^+ ions more tightly than do trioctahedral minerals.[9] The Ca^{2+} fixation observed in TSM thus suggests the dioctahedral-like character of TSM.

The Amount of Al Incorporated by Pillaring. Figure 3 shows the amount of Al in the three catalysts after calc. 2. These clays had different amounts of Al before pillaring. The amounts of Al in TSM (0.05) and montmorillonite (1.61) determined by the present study agreed very well with the reported values[14,15] shown in the experimental section.

After pillaring, each clay increased in Al amount by intercalation of aluminum hydroxy cluster cations. When the calc. 1 procedure was performed at 60°C, the amount that increased from the value before pillaring corresponded to the amount of Al incorporated by pillaring in the absence of Ca^{2+} fixation. These amounts of Al in TSM (1.06) and taeniolite (0.95) were greater than that of montmorillonite (0.79), reflecting a difference in the layer charge of native calys. The average positive charge per Al atom incorporated (Q_{Al}) was calculated using the following equation for both montmorillonite and TSM:

$$Q_{Al} = (Q_{layer} - M_{Na} - 2M_{Ca})/M_{Al},$$

where Q_{layer} denotes the layer charge of montmorillonite (0.46) or TSM (1.00) after Ref. 15; M_{Na} and M_{Ca} are the amounts of Na and Ca, respectively, remaining after pillaring, and M_{Al} is the amount of incorporated Al. The calculated values of Q_{Al} for TSM (0.56) and montmorillonite (0.57) were not only in fair agreement with a reported value on montmorillonite (0.56),[21] but were also very close to the Al charge (0.54) calculated from the formula of aluminum hydroxy cluster cation, $[Al_{13}O_4(OH)_{24}(H_2O)_{12}]^{7+}$. This indicates that a direct exchange of Al_{13} cations occurred in these two clays.

The amount of incorporated Al monotonously decreased with increasing calc. 1 temperature in TSM. The decline curve was just upside-down to the rising curve of the Ca^{2+} amount in Fig. 2, suggesting that the layer charge reduction caused by Ca^{2+} fixation led to the decrease in the uptake of Al_{13} polycations. In contrast, no decrease in the Al amount was observed in montmorillonite and taeniolite, which is in harmony with the result that these clays do not fix Ca^{2+} ions.

Residual Amount of Na. The residual amount of Na in Ca^{2+}–PTSM is also plotted in Fig. 4 as a function of the calc. 1 temperature.

Ca^{2+}-exchanged TSM before pillaring had a considerable amount of residual Na (0.41; not shown in Fig. 4). Goto et al. reported that the cation exchange ratio of Na^+–TSM by divalent cations (Ca^{2+}, Mg^{2+}, and Ba^{2+}) was ca. 75%.[14] Ohtsuka et al. also described that 60—80% of Na^+ in TSM could be exchanged by Ni^{2+},[22] Co^{2+},[23] or Fe^{2+}.[24] Moreover, Kitajima et al. stated that 50—65% of the Li^+ ions in Li^+-taeniolite was exchangeable by monovalent cations and 70—85% by divalent cations.[25] The low exchange ratio in these expandable micas must be related to their high layer charges, since Na-type fluor-hectorite with a low layer

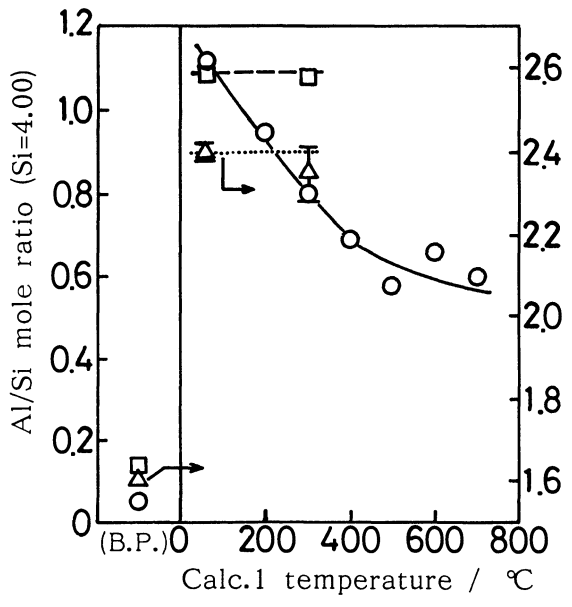

Fig. 3. Effect of the temperature of calc. 1 on the amount of Al in Ca^{2+}-modified pillared clays. (○) TSM, (△) montmorillonite, (□) taeniolite. (B.P.) Ca^{2+}-exchanged clay before pillaring.

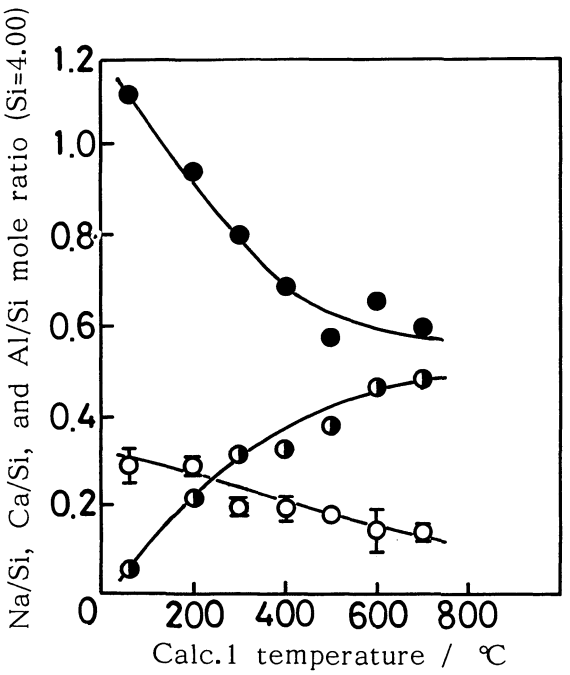

Fig. 4. Effect of the temperature of calc. 1 on the residual amount of Na, Ca, and Al in Ca^{2+}–PTSM. (○) Na, (◑) Ca, (●) Al.

Table 2. Basal Spacing of Each Catalyst

Calc. 1 temp	Basal spacing d_{001}/Å				
	Ca^{2+}-PTSM			Ca^{2+}-PM	Ca^{2+}-PT
	After calc. 1	After pillaring	After calc. 2	After calc. 2	After calc. 2
60	15.4	17.5	17.7	17.8	17.0
200	15.2	17.7	17.8	—	—
300	12.5	17.5	17.8	17.8	17.0
400	12.5	17.7	17.8	—	—
500	12.4/9.6	17.3	17.8	—	—
600	12.5/9.7	17.3	18.4	—	—
700	12.4	17.8	18.4	—	—

charge (1/3 per half unit cell) can exchange cations in a higher ratio than does taeniolite (90—95% of Na^+ are exchangeable by monovalent cations and 95—98% by divalent cations).[25]

The residual Na was decreased from 0.41 ro 0.29 due to a subsequent cation exchange with Al hydroxy cluster cations in a pillaring procedure when calc. 1 was performed at 60°C. Quite different from the case of Ca, the Na amount was further decreased with a rise in temperature at calc. 1. This implies that a thermally induced fixation of Na never occurs, supporting the classification of the fixation mode already discussed in a preceding paper.[3]

Change in Basal Spacing and Surface Area. Table 2 shows the change in the basal spacing with the temperature in the calc. 1 procedure. Ca^{2+}-exchanged TSM after calc. 1 at 60 or 200°C had a double-layer hydrated form (d_{001}=15.2—15.4 Å). The spacing decreased to 12.5 Å at 300—400°C, where the clay is a single-layer hydrated form. In addition to the appearance of an anhydrous phase at 500—600°C (d_{001}=9.6—9.7 Å), Ca^{2+}-TSM still maintained the single-layer hydrated form, even above 500°C. This feature was very different from that of La^{3+}-TSM, since only an anhydrous form was observed at 400°C or above in La^{3+}-TSM. An expansion of the basal spacing to 17—18 Å by pillaring was observed throughout the temperature range 60—700°C; this spacing was maintained after calc. 2 at 300°C. The Ca^{2+}-PTSM, thereby, showed a >1.5% cumene cracking conversion, even when the temperature of calc. 1 exceeded 500°C, whereas La^{3+}-PTSM was almost inactive in toluene alkylation due to a collapsed basal spacing (d=9.7 Å) when treated at 500°C in calc. 1. This structural difference beween Ca^{2+}-PTSM and La^{3+}-PTSM is possibly ascribed to a difference in the charge of the modification cations. The higher charge of La^{3+} can neutralize the negative charge of TSM layers more effectively than Ca^{2+}, as revealed from the ^{29}Si-MASNMR data.[3] The highly charge-reduced La^{3+} exchanged TSM (above 500°C of calc. 1 temperature) is too much decreased in swellability to uptake Al polycations between layers in a pillaring manipulation.[2]

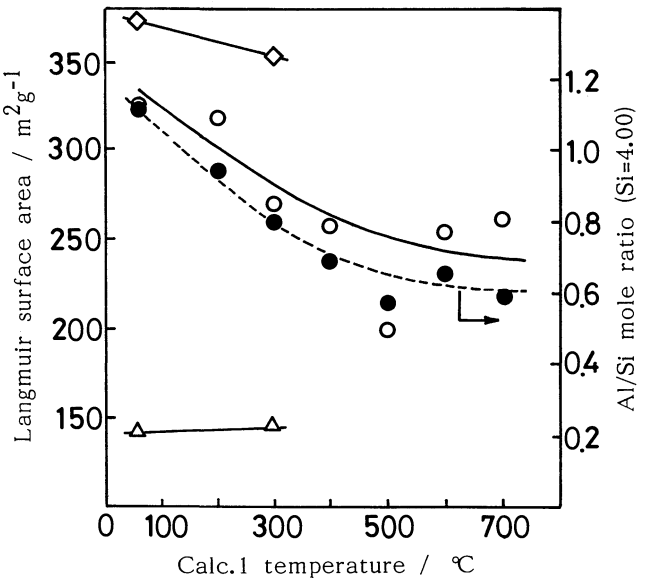

Fig. 5. Effect of the temperature of calc. 1 on the surface area of catalysts. (○) TSM, (◇) montmorillonite, (△) taeniolite. (●) The amount of Al in Ca^{2+}-PTSM.

Table 3. Surface Area of Ca^{2+}-PTSM

		Calc. 1 at 60°C	Calc. 1 at 300°C
Surface area[a] / $m^2 g^{-1}$	S_{all}	324	270
	S_{ext}	37.0	41.8
	S_{int}	287	228

a) S_{all}: Total Langmuir surface area, S_{ext}: external surface area, S_{int}: internal surface area.

The formation of a pillared structure with a basal spacing of 17—18 Å was also confirmed both in Ca^{2+}-PM and in Ca^{2+}-PT. No difference in the basal spacing was found when each of them was subjected to a thermal treatment in calc. 1 at temperature of 60 and 300°C.

Figure 5 shows the change in the surface area. Ca^{2+}-PTSM diminished its surface area with a rise in the calc. 1 temperature. The decreasing curve was similar to that of the change (Fig. 3) in the amount of

Al remaining in the catalyst. On the basis of a pore-size distribution analysis, the surface areas belonging to both the internal micropore (S_{int}) and the exteranl mesopore (S_{ext}) were calculated (Table 3). S_{int} is a measure of the micropores formed between silicate layers by pillaring.[26] When S_{int} and S_{ext} are compared after thermal treatments at between 60 and 300°C, it is noticed that the reduction of the total surface area (S_{all}) is ascribed to a decrease in the internal micropore surface area (S_{int}). The reduction in the surface area is, thus, based on a reduction in the amount of the Al-pillar, which prop silicate layers according to the progress of Ca^{2+} fixation.

In Ca^{2+}-PT, however, the surface area did not decrease. Though the surface area decreased by 20 $m^2 g^{-1}$ between 60 and 300°C in Ca^{2+}-PM, the decreasing ratio (5%) was much smaller than that of Ca^{2+}-PTSM (17%). From these data it is concluded that the structural change is little in catalyst systems where cation fixation does not occur.

Change in Acidic Property. Figure 6 shows the IR spectra of the pyridine adsorbed on Ca^{2+}-PTSM treated at 300°C on the calc. 1 procedure, which exhibited the highest conversion (4.2%) in cumene cracking. The features of the spectra were similar to that of La^{3+}-PTSM, as a whole. This similarity is reasonable, since both cations (Ca^{2+} and La^{3+}) belong to the same group according to the classification given in the preceding paper.[3] After pyridine adsorption at 150°C, followed by evacuation, both a strong band at 1450 and a weaker band at 1490 cm^{-1} were observed, indicating the Lewis acidic nature of the catalyst. The 1450 cm^{-1} band remained constant, even after successive evacuation at 450°C. When water adsorbed on this catalyst 200°C followed by evacuation, the 1550 cm^{-1} band appeared silightly and the genesis of Brønsted acidity was suggested. It is well-known that cumene cracking is catalyzed by Brønsted acidity.[27] The active sites of Ca^{2+}-PTSM must be situated close to fixed Ca, and they must exist as the Brønsted acid sites formed by the reaction of residual water and Ca^{2+}, as already reported.[2]

The above-mentioned Ca^{2+}-PTSM (calc. 1 temp 300°C), most active for cumene cracking, had an acid amount of 222 μmol g^{-1}, which was estimated from the amount of desorbed ammonia in the TPD spectra shown in Fig. 7. The acid amount slightly increased at 400°C, and then decreased above this temperature. The change in the acid amount exhibited a good

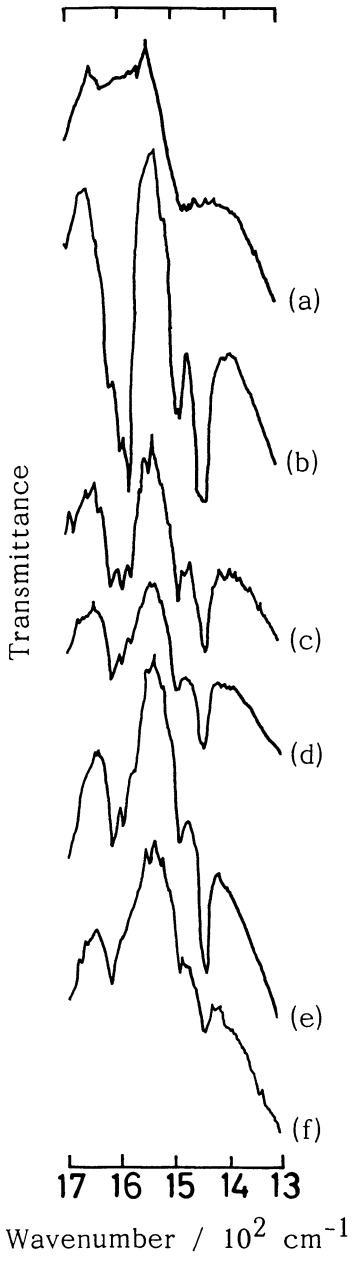

Fig. 6. IR spectra of pyridine adsorbed on Ca^{2+}-PTSM (both calc. 1 and calc. 2 at 300°C). (a) Back ground spectra, (b) after pyridine adsorption followed by evacuation at 150°C, (c—e) followed by successive evacuation at 250°C (c), 350°C (d) and at 450°C (e), (f) followed by water vapor adsorption and evacuation at 200°C.

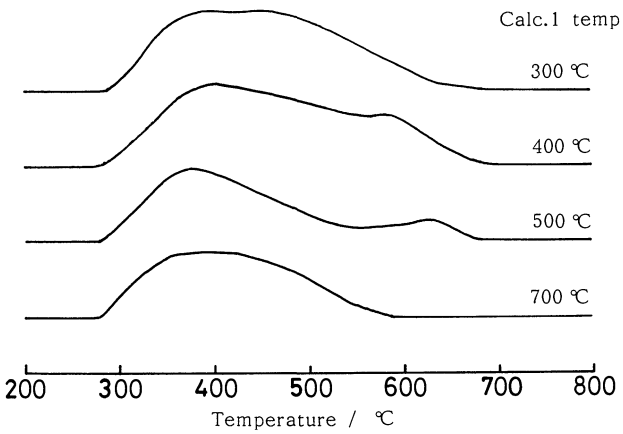

Fig. 7. TPD spectra of adsorbed ammonia on Ca^{2+}-PTSM.

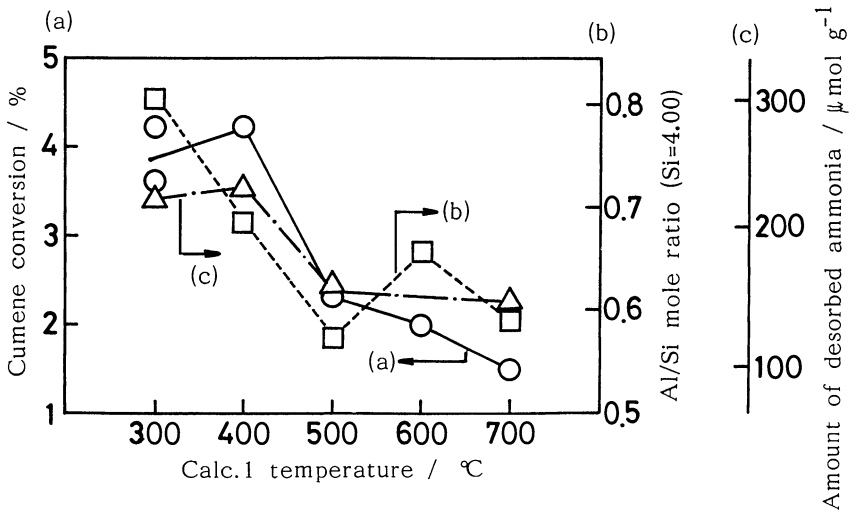

Fig. 8. Cumene cracking activity of Ca^{2+}–PTSM (a), the amount of Al (b), and the amount of desorbed ammonia in TPD (c) as a function of calc. 1 temperature.

correlation with the change in the cracking activity (Fig. 8). A similar relationship between cumene cracking activity, or the measure of Brønsted acidity, and the acid amount estimated from TPD has been ascertained for various-cation fixed pillared TSM catalysts.[3)]

The acid amount further correlated with the residual amount of Al at 400°C or above, which may be associated with the fact that the precursor of pillar (Al hydroxy cluster cation) functions as a proton source, since it releases protons upon calcination. The released protons migrate onto the silicate layers and can form acidic sites near the Ca-fixed sites.

In connection with the acid strength, a decrease in the number of strong acidic sites was observed with an increase in the calc. 1 temperature, which is indicated in Fig. 8 by the gradual decrease in the amount of ammonia desorbed between 400 and 650°C.

Distribution of Fixed Ca Ion on the Surface of Silicate Layer. Figure 9 depicts the basal oxygen plane of the silicate layer of TSM. The open circles represnt the center of hexagonal holes, or the possible sites of fixed Ca ions. When one of these sites is analyzed, it can be seen that there are six nearest-neighbor sites around it. When a fixed Ca is surrounded by several nearest-neighbor Ca ions (k in number), the Ca is called a "type nk calcium." Thus, seven types of Ca (n0, n1, .., n6) are distinguishable. The proportion of each type, which depends on the total occupancy of hexagonal holes by Ca, can be calculated based on the two following assumptions.

1. Fixed Ca ions are distributed in a completely random fashion.

2. The fixed ions are divided into halves on both surfaces of silicate layers when Al-pillars are inserted between them.

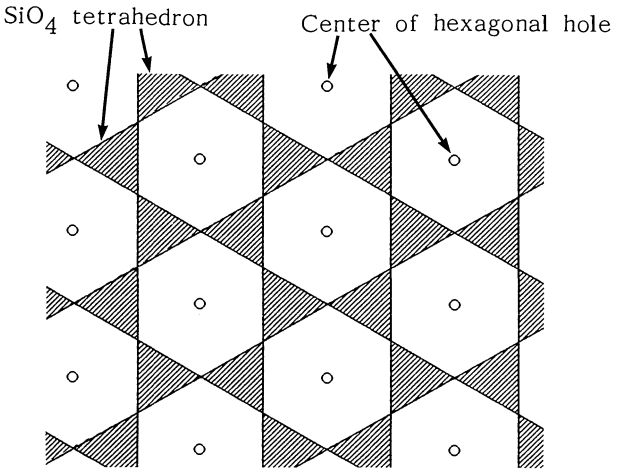

Fig. 9. Basal oxygen plane of layer silicate.

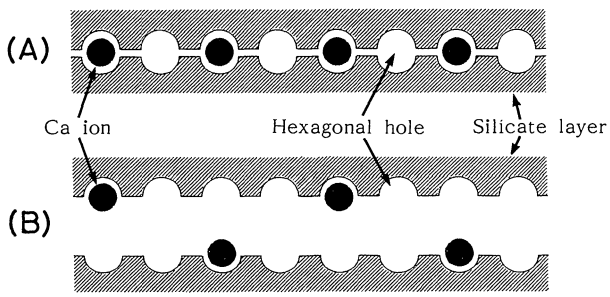

Fig. 10. Schematic diagram of Ca distribution on layer surface. (A) Before pillaring (Ca exchange rate of 100%). (B) After pillaring.

The first assumption is reasonable from the result of ^{29}Si-MASNMR, since the Q^3(0Al) signal in Ca^{2+}–TSM is markedly broadened upon heating, and such broadening is reasonably understood by Ca fixation in

a random fashion.[3] Fig. 10 illustrates the situation regarding the second assumption. At a maximum cation-exchange ratio of 100%, the exchanged Ca^{2+} ions should occupy half the hexagonal holes of TSM, which has a layers charge of 1.00 per Si_4O_{10} unit. Since these Ca ions are divided into halves after pillaring, the occupancy of hexagonal holes by Ca becomes 25% if all of the Ca ions are fixed and remain on the silicate surface.

The distributions were then calculated according to the following binominal equations, which are similar to the equation employed for the calculation of the siting of Si and Al atoms in the faujasite-type zeolite lattice:[28]

$$F_{nk} = \frac{6!}{k!(6-k)!} x^k(1-x)^{6-k}$$

and

$$N_{nk} = \frac{6!}{k!(6-k)!} x^{k+1}(1-x)^{6-k}.$$

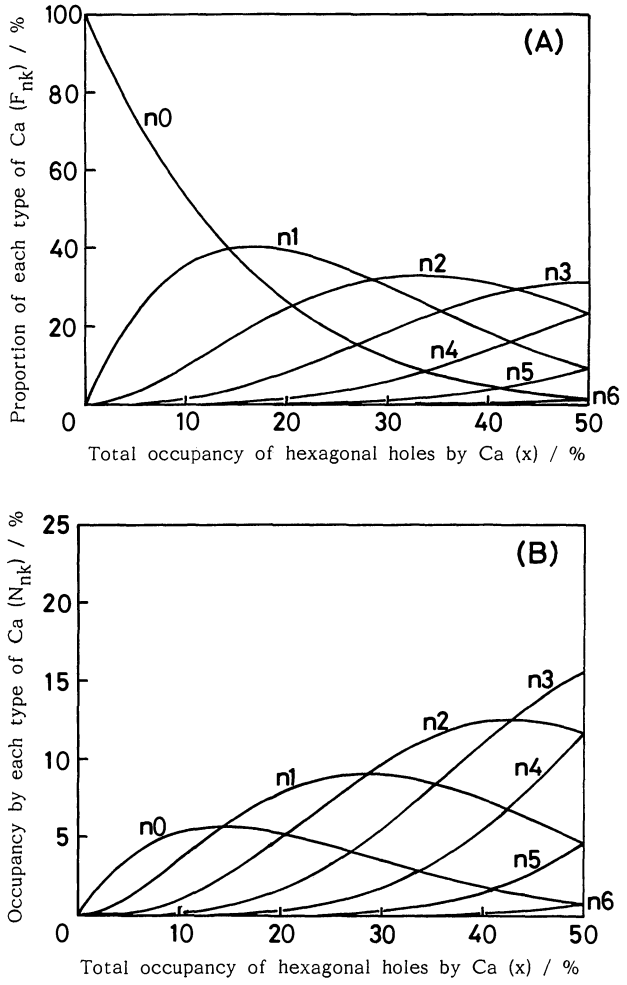

Fig. 11. Distribution of types of Ca atoms in Ca^{2+}–PTSM. (A) Proportion of each type of Ca. (B) Occupancy of hexagonal holes by each type of Ca.

Here, x is the occupancy of hexagonal holes by all types of Ca, F_{nk} the proportion of each type of Ca (type nk, k=0..6), and N_{nk} the occupancy of hexagonal holes by each types of Ca. The result of computing is shown in Figs. 11 (A) and (B). These curves of the Ca distribution are similar to that of Al in the framework of faujasite-type zeolites.[29–31] Since in zeolites two Al ions can not occupy adjacent tetrahedral sites (Loewenstein's rule), the next nearest-neighbor sites are considered for the calculations. Since zeolite acidity arises from an isomorphous substitution of Al for Si, the distribution state of Al sensitively influences the catalytic activity. Only isolated Al, which has no next nearest-neighbor Al, generates strong acidity.[32] The catalyst which has such sites in maximum number shows the highest activity in reactions which require strong acidity, such as cracking.[32,33]

In the case of the Ca^{2+}–PTSM catalysts, the acid strength must depend entirely on the distribution of the fixed Ca. Because neither silicate layers, themselves, nor pillars have acidic sites, the acidic sites are formed on silicate layers by Ca fixation. The obtained Ca distribution on a TSM layer, then, is discussed in connection with the cracking activity. When Ca^{2+}–PTSM is most active for cumene cracking, or when the catalyst is treated at 300—400°C on calc. 1 procedure (Fig. 1), the fixed amount of Ca is 0.31—0.33 per Si=4 (Fig. 2). This amount corresponds to a total occupancy of 16% under the above-mentioned second assumption. Fig. 11 indicates that the isolated Ca (type n0) is predominant until this Ca content. Moreover, the number of type n0 calcium becomes maximum near this total occupancy (according to the above equation, N_{n0} gives a maximum value at x=0.143), showing good agreement with the maximum catalytic activity. This agreement strongly supports the fixation model in the present study: that the Ca cations fix onto the silicate-layers while lodging in the hexagonal holes and taking charge of the genesis of acidic sites.

Concluding Remarks

When the same procedure for the preparation of Ca^{2+}-modified pillared clays were applied to three different clays (TSM, montmorillonite, and taeniolite), only Ca^{2+}–PTSM showed a notable acidity enhancement by Ca^{2+} fixation. Ca^{2+} was not fixed by the other two clays under the same preparation conditions. The ease of Ca fixation onto the TSM layer must come from the structural characteristics of TSM: a high layer charge and the existence of an octahedral vacancy. The dependence of the catalytic activity of Ca^{2+}–PTSM on the calcination temperature before pillaring was successfully interpreted in terms of the random distribution model for Ca^{2+} fixed on the surface of the TSM layer.

We thank the Iwatani Memorial Foundation for financial support of this work, JGC Co., Ltd. for permitting us to use the X-ray fluorescence spectrometer, Mr. Kenichiro Sugimori (Chemical Div., Topy Ind.) for supplying the synthetic TSM and taeniolite samples, and Prof. Kunio Kitajima (Dept. Chemistry and Material Engineering, Shinshu Univ.) for his helpful discussions.

References

1) G. W. Brindley and R. E. Sempels, *Clay Miner.*, **12**, 229 (1977).
2) H. Sakurai, K. Urabe, and Y. Izumi, *Bull. Chem. Soc. Jpn.*, **62**, 3221 (1989).
3) H. Sakurai, K. Urabe, and Y. Izumi, *Bull. Chem. Soc. Jpn.*, **63**, 1389 (1990).
4) U. Hofmann and R. Klemen, *Z. Anorg. Allg. Chem.*, **262**, 95 (1950).
5) W. F. Jaynes and J. M. Bigham, *Clays Clay Miner.*, **35**, 440 (1987).
6) G. W. Brindley and J. Lemaitre, "Chemistry of Clays and Clay Minerals," ed by A. C. D. Newman, Mineralogical Society (1987), p. 319.
7) R. Green-Kelly, *Nature*, **170**, 1130 (1952).
8) R. Green-Kelly, *J. Soil Sci.*, **4**, 233 (1953).
9) B. L. Sawhney, *Clays Clay Miner.*, **20**, 93 (1972).
10) K. W. T. Goulding, *Adv. Agron.*, **36**, 215 (1983).
11) T. Mozas, S. Bruque, and A. Rodriguez, *Clay Miner.*, **15**, 421 (1980).
12) U. Hofmann and J. Endell, *Angew. Chem.*, **52**, 708 (1939).
13) M. Kondo, *Nendo Kagaku*, **21**, 1 (1981).
14) S. Goto, K. Sugimori, T. Hayashi, and R. Kondo, *Nendo Kagaku*, **17**, 18 (1977).
15) T. Hayashi, C. T. Song, A. Nishida, S. Goto, M. Daimon, R. Kondo, and K. Sugimori, *Nendo Kagaku*, **20**, 21 (1980).
16) R. W. Cranston and F. A. Inkley, *Adv. Catal.*, **9**, 143 (1957).
17) F. T. Bingham, A. L. Page, and J. R. Sims, *Soil Sci. Soc. Am. Proc.*, **28**, 351 (1964).
18) S. Bruque, T. Mozas, and A. Rodriguez, *Clay Miner.*, **15**, 413 (1980).
19) T. Sudo, "Nendo Koubutsugaku," Iwanami Shoten, Tokyo (1974), p. 231.
20) G. W. Brindley and G. Ertem, *Clays Clay Miner.*, **19**, 399 (1971).
21) H. Kodama and S. S. Singh, *Solid State Ionics*, **32/33**, 363 (1989).
22) K. Ohtsuka, M. Suda, M. Ono, M. Takahashi, M. Sano, and S. Ishio, *Bull. Chem. Soc. Jpn.*, **60**, 871 (1987).
23) K. Ohtsuka, J. Koga, M. Suda, M. Ono, and T. Takahashi, *Bull. Chem. Soc. Jpn.*, **60**, 2843 (1987).
24) K. Ohtsuka, M. Suda, and M. Ono, *Bull. Chem. Soc. Jpn.*, **61**, 815 (1988).
25) K. Kitajima, N. Daimon, and R. Kondo, *Nippon Kagaku Kaishi*, **1976**, 597.
26) K. Urabe, H. Sakurai, and Y. Izumi, "Proc. 9th Int. Cong. Catal.," ed by M. J. Phillips et al., The Chemical Institute of Canada, Ottawa (1988), Vol. 4, p. 1858.
27) K. Tanabe, "Solid Acids and Bases — Their Catalytic Properties," Kodansha, Tokyo; Academic Press, New York and London (1970), p. 125.
28) R. J. Mikovsky, *Zeolites*, **3**, 90 (1983).
29) L. A. Pine, P. J. Maher, and W. A. Wachter, *J. Catal.*, **85**, 466 (1984).
30) R. J. Mikovsky and J. F. Marshall, *J. Catal.*, **44**, 170 (1976).
31) B. Beagley, J. Dwyer, F. R. Fitch, R. Mann, and J. Walters, *J. Phys. Chem.*, **88**, 1744 (1984).
32) D. Barthomeuf, *Mat. Chem. Phys.*, **17**, 49 (1987).
33) J. R. Sohn, S. J. DeCanio, P. O. Fritz, and J. H. Lunsford, *J. Phys. Chem.*, **90**, 4847 (1986).

Effect of ZnO Addition on Cobalt-Alumina Interaction Species

Yasuaki Okamoto,* Toshinori Adachi, Akinori Maezawa,† and Toshinobu Imanaka
Department of Chemical Engineering, Faculty of Engineering Science, Osaka University, Toyonaka, Osaka 560
(Received August 10, 1990)

The effect of ZnO addition on cobalt–alumina interaction modes was studied using TPR and XPS. It was found that the addition of 2 wt% ZnO markedly affects the distribution of the cobalt species in CoO/Al_2O_3 (5 wt% CoO): cobalt–alumina surface interaction species are removed and migration of cobalt into an alumina subsurface phase is promoted by ZnO. A formation of Co–Zn–O mixed oxide is proposed for $ZnO–CoO/Al_2O_3$ at high ZnO content. The dispersion and distribution of ZnO on Al_2O_3 are also strongly modified by the presence of cobalt.

In connection with $CoO–MoO_3/Al_2O_3$ hydrodesulfurization (HDS) catalyst systems, CoO/Al_2O_3 catalysts have been extensively studied using various physicochemical techniques.[1–12] It has been shown that several $CoO–Al_2O_3$ interaction species are formed on CoO/Al_2O_3 catalysts and that the interaction mode depends on the CoO content and calcination temperature. At usual calcination temperatures (670—870 K), (sub)surface cobalt species in tetrahedral configurations (aluminate like species) are selectively formed at an initial dose of cobalt.[2,4,6–9] Formation of surface cobalt species in octahedral symmetries are also proposed on the basis of XPS and ISS studies coupled with H_2-reduction.[8] A crystalline Co_3O_4 phase appears above about 2 wt% CoO and increases precipitously in the amount with a further increase of cobalt content.[2,6,8,10] With CoO/Al_2O_3 systems calcined at various temperatures, a detailed characterization of cobalt species was conducted by Arnoldy and Moulijn[11,12] using temperature-programmed reduction (TPR) techniques. The formations of surface Co^{3+} and Co^{2+} species, $Co^{3+}–Al^{3+}$ mixed oxide, and subsurface Co^{2+} are proposed in addition to Co_3O_4 and aluminate-like species.

The cobalt–alumina interaction modes are expected to be strongly modified by adding metal oxide which interacts with Al_2O_3, such as ZnO. The additive effects on the cobalt–alumina interactions are, accordingly, considered to provide more detailed information of the interaction species. Furthermore, doping of a small amount of a second promoter, such as ZnO, NiO, or MgO, is often claimed to improve the HDS activity and stability of $CoO–MoO_3/Al_2O_3$ catalysts.[13] However, only a few fundamental investigations have been made to reveal the additive effect on cobalt–alumina interaction modes and the beneficial effects of the second promoter.[14–20]

It has been demonstrated in our previous study[21] using XPS that molybdenum oxide–alumina interaction modes are not appreciably affected on the addition of ZnO. This may suggest that ZnO alters the cobalt oxide–alumina or cobalt oxide–molybdenum oxide interaction modes. With $ZnO–CoO/Al_2O_3$ at varying CoO contents and 1 wt% Zn, Chin and Hercules[15] have actually shown by XPS and ISS that the presence of ZnO enhances the formation of cobalt "surface spinel" at $\leqslant$8 wt% Co, while at higher Co loadings the addition of 1% Zn drastically increases the dispersion of cobalt oxide. No further detailed information on $ZnO–CoO/Al_2O_3$ systems has been reported. A more detailed study on $ZnO–CoO/Al_2O_3$ might provide information about the role of the second promoter in $CoO–MoO_3/Al_2O_3$ catalysts as well as cobalt–alumina interaction modes.

In the present study, the effect of ZnO addition was investigated on the cobalt–alumina interaction modes in CoO/Al_2O_3 using TPR and XPS. It was found that the addition of a small amount of ZnO remarkably altered the distribution of cobalt–alumina interaction species.

Experimental

Supported cobalt catalysts were prepared by impregnating γ-Al_2O_3 with an aqueous solution of cobalt salt. γ-Al_2O_3 (pore volume: 0.66 $cm^3\,g^{-1}$, 163 $m^2\,g^{-1}$) was supplied by the Catalysis Society of Japan as a reference catalyst (JRC-ALO-4).[22] The amount of the aqueous solution of cobalt nitrate was adjusted to be 1.3 cm^3 per g-Al_2O_3 to prepare CoO/Al_2O_3 containing 5 wt% CoO. The supported amount of CoO is represented with respect to the support. After the catalyst precursor was dried at 383 K for 16 h, it was calcined at 673, 823, or 1073 K for 5 h in air by using an electric furnace. $ZnO–CoO/Al_2O_3$ samples containing 5 wt% CoO and varying amounts of ZnO were prepared by simultaneous impregnation of appropriate amounts of cobalt and zinc nitrates.

In TPR studies, the cobalt catalyst (0.2 g) was reduced in a 5% H_2/Ar stream (72 cm^3 STP min^{-1}), which was purified by passing through a deoxygenation catalyst layer, followed by a zeolite trap cooled at a methanol–Dry Ice temperature. After evacuation at 623 K for 1 h, the reduction temperature was raised from 300 to ca. 920 K at an uniform heating rate (β) of 2.5 K min^{-1}. The H_2 concentration in the effluent gas was analyzed by a TCD cell at 303 K after removing water vapor by a cold trap at a methanol–Dry Ice temperature.

† Present address; Shizuoka University, Shirokita, Hamamatsu 432.

The XPS measurements were made on a Hitachi 507 photoelectron spectrometer using Al $K\alpha_{1,2}$ radiation (1486.6 eV). The anode was operated at 9 kV and 50 mA. Assuming linear backgrounds, XPS intensity ratios were obtained by using the planimetered peak areas of the Co 2p, Al 2p, Zn 2p, and Zn($L_3M_{4,5}M_{4,5}$) levels. Binding energies were referenced to the Al 2p level (74.3 eV) of the support, which had been separately determined by using the C 1s band at 285.0 eV due to adventitious carbon.

Results

The TPR profiles for $ZnO-CoO/Al_2O_3$ are shown in Fig. 1 as a function of ZnO content and calcination temperature (673 and 823 K). The profiles for CoO/Al_2O_3 consisted of several distinctly different reduction peaks as reported by Arnoldy and Moulijn.[11] The cobalt species are characterized by the reduction temperatures of 503—553 K (Co-I), 633—643 K (Co-IIA), 693 K (Co-IIB), 753—773 K (Co-III), and 853—873 K (Co-IV) in the present study. The reduction temperatures depended on the calcination temperature and loading level of CoO. Since the rate of temperature increase, flow rate of H_2/Ar, and H_2-concentration are different, the reduction temperatures in Fig. 1 cannot be directly compared with the values reported by Arnoldy and Moulijn.[11] The present

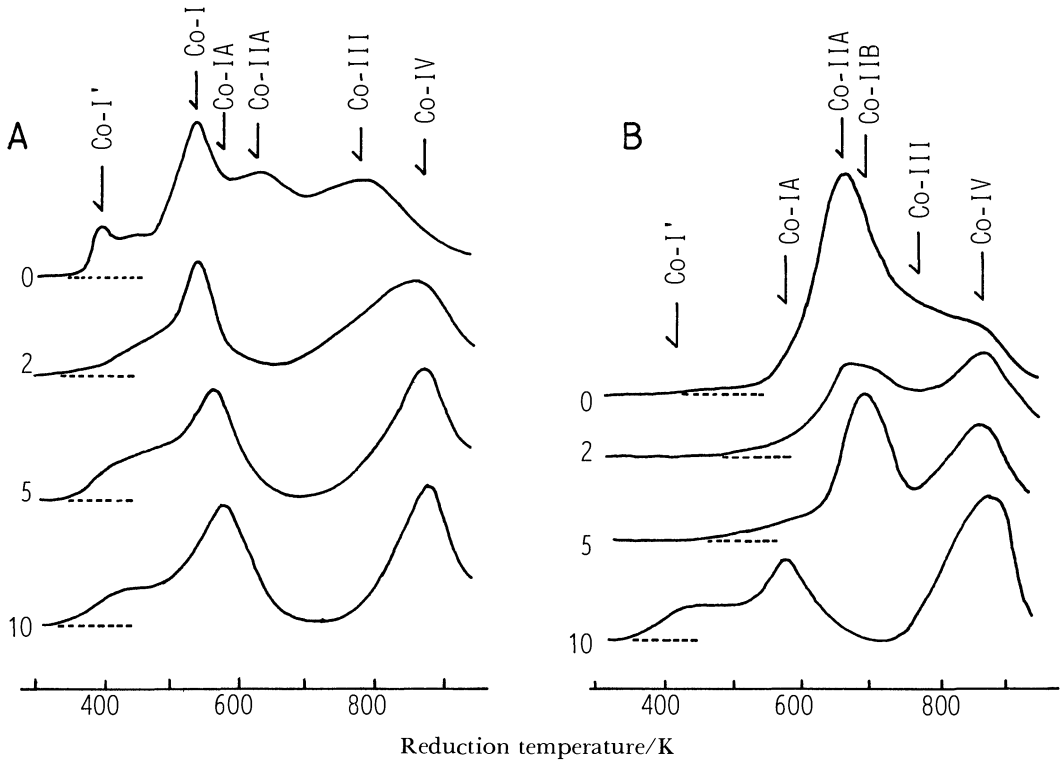

Fig. 1. TPR profiles of $ZnO-CoO/Al_2O_3$ (CoO; 5 wt%) as a function of ZnO content and calcination temperature. (A): calcined at 673 K and (B): 823 K. Numbers in the figure denote ZnO content (wt%). Dotted lines show backgrounds after vertical replacements. β=2.5 K min^{-1}.

Table 1. TPR Results on CoO/Al_2O_3

Cobalt species	Reduction temperature/K		Assignments[a]
	Moulijn et al.[a]	This work[b]	
Co-I'	—	400—450	Amorphous Co-oxide[c]
Co-I	600	503—553	Crystalline Co_3O_4
Co-IA	—	580	Co-Zn-O[b]
Co-IIA	750	633—643	Surface Co^{3+}
Co-IIB	750	693	Co^{3+}-Al^{3+}-oxide
Co-III	900	753—773	Surface Co^{2+}
Co-IV	1130—1240	853—873	(Sub)surface Co^{2+}
Co-V[d]	1150—1230	>920	$Co_xAl_{(8/3-2x/3)}O_4$ $CoAl_2O_4$

a) Refs. 11 and 12, β=10 K min^{-1}. b) β=2.5 K min^{-1}, this work. c) Ref. 26. d) Co-IVC and IVD in Refs. 11 and 12.

reduction temperatures of cobalt species are compared in Table 1 with those in Ref. 11. A good parallel correlation in Table 1 indicates that the cobalt species detected here correspond well to those observed by Arnoldy and Moulijn.[11] The reduction peaks are denoted as in Table 1 according to Arnoldy et at.[11,12] in the order of the reduction temperature. Co-IVC and Co-IVD observed at 1150—1230 K by Arnoldy and Moulijn[11] are supposed to be detected at >920 K in the present study. Hydrogen consumptions at >920 K in the TPR profiles in Fig. 1 indicate the presence of these reduction peaks (denoted Co-V here). In addition to Co-I—V peaks, Co-I′ appeared at 400—450 K in the present study.

The TPR profile of Co_3O_4 consisted of a slightly asymmetric single peak. The reduction temperature depended on the particle size of Co_3O_4 and the samples with the particle diameter of 50 and 1200 nm (SEM observations) showed the TPR peaks at 570 and 590 K, respectively.

The addition of ZnO into CoO/Al_2O_3 was found to strongly affect the TPR profiles. As shown in Fig. 1, the addition of 2 wt% ZnO into 5 wt% CoO/Al_2O_3 catalyst (673 K) removed almost completely Co-IIA and most of Co-III. Further additions of ZnO completely eliminated Co-III. Although the TPR intensity of Co-I was not signicantly altered by the addition of 5 and 10 wt% ZnO, the reduction temperature of Co-I (538 K) increased by 20 K at 5 wt% ZnO and additionally augmented by 20 K, reaching 580 K at 10 wt% ZnO. Co-I species could not be found at such a high temperature of 580 K for supported CoO systems, for instance, CoO/Al_2O_3 and CoO/SiO_2 containing up to 20 wt% CoO. No appreciable change in the crystallite size of Co_3O_4 was observed by means of XRD on the addition of ZnO. Accordingly, the reduction peak at 580 K is concluded to be ascribed to a new cobalt phase and denoted Co-IA here.

With $ZnO–CoO/Al_2O_3$ calcined at 823 K, the intensities of Co-IIA and III were significantly decreased by the addition of 2 wt% ZnO as observed with the sample calcined at 673 K. The presence of Co-IIB became clearly observable by the elimination of Co-IIA. Co-IIB remaind intact on the addition of 5 wt% ZnO. On the other hand, the addition of 10 wt% ZnO removed Co-IIB and brought about the formations of Co-IA and I′. The intensity of Co-IV increased at 2 wt% ZnO but was not strongly affected by a further addition of ZnO, irrespective of the calcination temperature. As for ZnO/Al_2O_3 systems (below 10 wt% ZnO), no reduction peaks were observed below 900 K under the present TPR conditions.

The intensity of TPR profile was found to depend on the ZnO content. The total TPR areas between room temperature and 920 K are shown in Fig. 2 as a function of ZnO content. It was found that the addition of ZnO also strongly affected the TPR

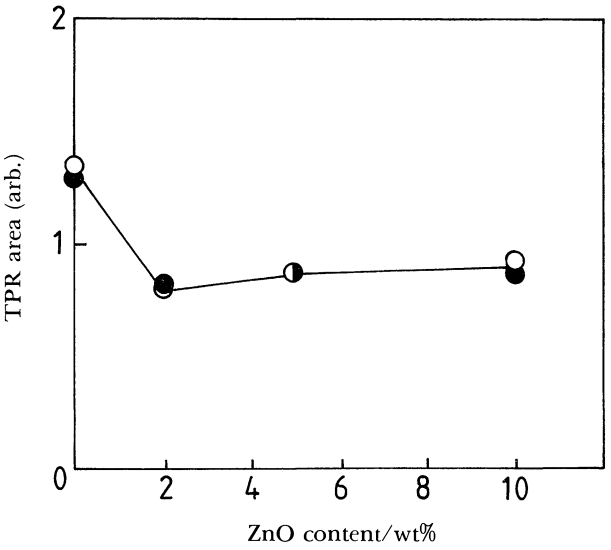

Fig. 2. Variations of the TPR area intensity with ZnO content (wt%) for $ZnO–CoO/Al_2O_3$ catalysts (5 wt% CoO) calcined at 673 K (○) and at 823 K (●).

intensity of CoO/Al_2O_3 (5 wt% CoO). The TPR areas decreased by 40% at 2 wt% ZnO and were almost invariant on a further addition of ZnO at the calcination temperatures of 673 and 823 K. On the basis of the XPS study of CoO/Al_2O_3 (8 wt% Co) calcined at 673 K, Chin and Hercules[15] have reported that the fraction of cobalt which is H_2-reducible at 623 K decreases from 20 to 15% (by 25% decrease) on the addition of 1% Zn. The TPR results in Fig. 2 are in line with their XPS observations.

XPS characterization of the $ZnO–CoO/Al_2O_3$ systems was carried out as a function of ZnO loading. The BE values of Co $2p_{3/2}$ band for 5 wt% CoO/Al_2O_3 calcined at 673 and 823 K were 780.3 and 781.2 eV, respectively. They are in between those for $CoAl_2O_4$ (781.3—782.2 eV)[4,6–8] and Co_3O_4 (779.6—779.8 eV).[6,7] When CoO/Al_2O_3 was calcined at 1073 K, the BE of Co $2p_{3/2}$ band (781.5 eV) was very close to that of $CoAl_2O_4$. The Co $2p_{3/2}$ BE was not influenced by the addition of ZnO within experimental accuracy (±0.2 eV). The BE of Zn 2p level and the kinetic energy (KE) of Zn($L_3M_{4,5}M_{4,5}$) Auger band were independent of ZnO and CoO contents and calcination temperature and were 1021.8 and 987.5 eV, respectively. These BE and KE values for Zn indicate that Zn^{2+} cations are in an aluminate-like phase.[21,23]

The Co 2p/Al 2p or Zn 2p/Al 2p XPS intensity ratio depends on both dispersion and surface concentration of Co or Zn. A higher XPS intensity ratio is expected for higher dispersion and/or higher surface concentration of Co or Zn.[24] The effect of ZnO addition on the Co 2p/Al 2p ratio for CoO/Al_2O_3 is shown in Fig. 3 as a function of ZnO content. When $ZnO–CoO/Al_2O_3$ was calcined at 673 or 823 K, no appreciable change in

the Co 2p/Al 2p ratio was detected, except for the 2 wt% ZnO sample calcined at 673 K, while the ratio for $ZnO-CoO/Al_2O_3$ calcined at 1073 K decreased gradually with increasing ZnO content. A small decrease in the Co 2p/Al 2p ratio for 2 wt% CoO/Al_2O_3 calcined at 673 K is consistent with the observations by Chin and Hercules.[15]

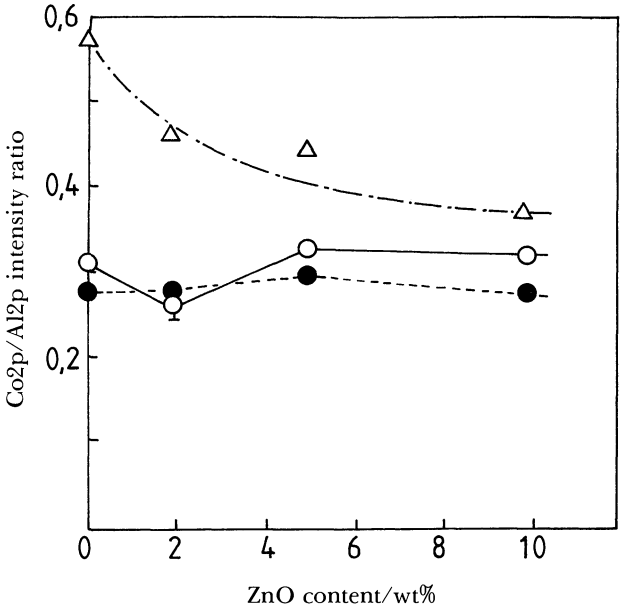

Fig. 3. Dependencies of the Co 2p/Al 2p XPS intensity ratio on ZnO content (wt%) for $ZnO-CoO/Al_2O_3$ (CoO; 5 wt%) calcined at 673 K (○), 823 K (●), and 1073 K (△).

Figure 4 depicts the Zn 2p/Al 2p (A) and Zn(LMM)/Zn 2p (B) intensity ratios to estimate the dispersion and depth profile of Zn^{2+} cations in $ZnO-CoO/Al_2O_3$ samples containing 5 wt% CoO. According to Penn,[25] the escape depths of the photo- and Auger-electrons are estimated to be 0.8 and 1.5 nm, respectively. The Zn-Auger/Zn 2p ratio for pure ZnO was 1.2 for the present spectrometer.[21]

The Zn 2p/Al 2p ratio for $ZnO-CoO/Al_2O_3$ decreased with increasing calcination temperature, whereas the Zn Auger/Zn 2p ratio increased. These behaviors are analogous to those for ZnO/Al_2O_3 samples[21] as presented in Fig. 4. However, it was found that when $ZnO-CoO/Al_2O_3$ is calcined at 673 or 823 K the coimpregnation of CoO significantly decreases the Zn 2p/Al 2p intensity ratios compared to those for ZnO/Al_2O_3, whereas the presence of CoO increases the Zn(LMM)/Zn 2p ratio. Both ratios for the samples calcined at 1073 K were not affected by the presence of CoO (5 wt%).

Discussion

The TPR and XPS studies of $ZnO-CoO/Al_2O_3$ catalysts with varying ZnO contents were carried out to reveal the effect of ZnO addition on the cobalt-alumina interaction species. In the present study, it has been definitely demonstrated for the first time that the addition of a small amount of ZnO greatly affects the cobalt-alumina interaction modes and the distribution of cobalt species.

In the TPR experiments, it is assumed that the respective reduction peaks correspond to distinct

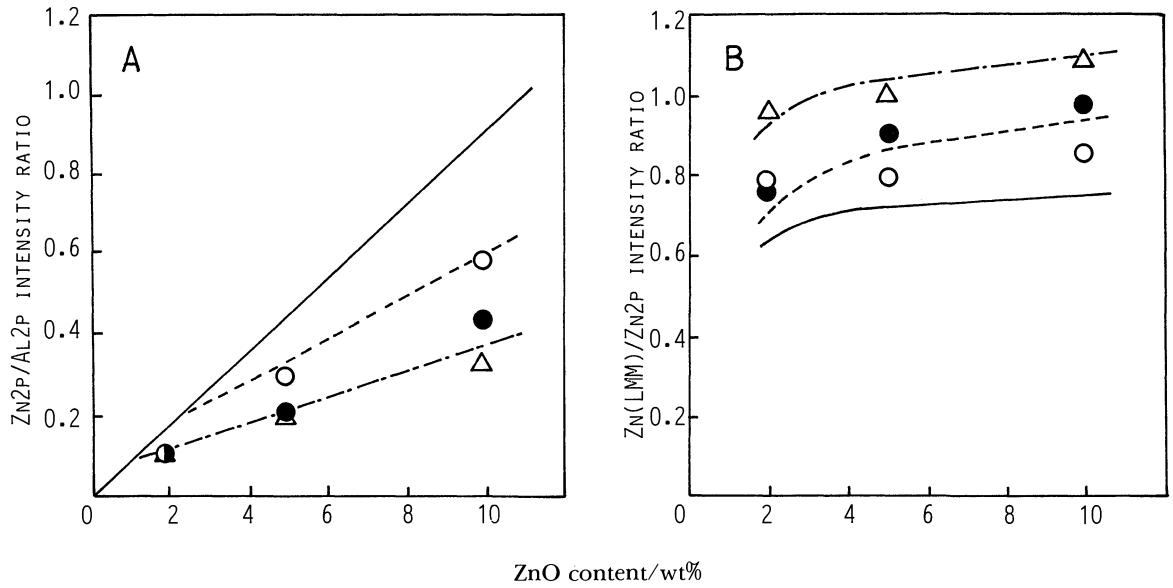

Fig. 4. Zn 2p/Al 2p XPS intensity ratio (A) and Zn(LMM)/Al 2p intensity ratio (B) vs. ZnO content (wt%) for $ZnO-CoO/Al_2O_3$ (CoO; 5 wt%). ○: calcined at 673 K, ●: 823 K, and △: 1073 K. Solid line: ZnO/Al_2O_3 calcined at 673 K, dotted line: 823 K, and dashed line: 1073 K.[21]

cobalt species in different oxidation states and/or different chemical environments, since the reduction of Co_3O_4 showed only a relatively narrow peak with slight shoulder and since the peak separations among Co-I—IV seem to be too large to assign them to successive reduction processes of cobalt, e.g. Co^{3+} to Co^{2+} and Co^{2+} to Co metal. The TPR peaks for CoO/Al_2O_3 have been assigned by Moulijn et al.[11,12] as summarized in Table 1 on the basis of XRD and the amount of H_2-consumption. A combined TPR and XPS study[26] on CoO/Al_2O_3 with varying CoO loadings essentially support their assignments in Table 1.

It is demonstrated from the TPR spectra in Fig. 1 that dramatic alterations in cobalt–alumina interaction modes in CoO/Al_2O_3 are brought about by the addition of ZnO. The addition of 2 wt% ZnO effectively eliminates surface cobalt–alumina interaction species (Co-IIA and III) and enhances a formation of (sub)surface spinel species, while the amount of bulk Co_3O_4 phase is not affected in the presence of ZnO. On the base of XPS and ISS studies on ZnO–CoO/Al_2O_3, Chin and Hercules[15] suggested that the formation of cobalt "surface spinel" is enhanced by the addition of 1 or 2% Zn at $\leqslant$8 wt% Co. The TPR results in Figs. 1 and 2 definitely support their conclusions and provide more convincing and detailed information on the effect of ZnO on $CoO–Al_2O_3$ interaction modes.

The changes in cobalt species on the addition of ZnO are considered to result from competitive occupations of limited numbers of surface and bulk sites of Al_2O_3 by Co^{2+}, Co^{3+}, Al^{3+}, and Zn^{2+} cations. The structure of γ-Al_2O_3 is described as a defect spinel[27] and these cations occupy octahedral and/or tetrahedral sites of Al_2O_3 on solid state reactions during calcination.[1,2,28–30] Before discussing the cobalt species in ZnO–CoO/Al_2O_3, it is considered first how the distribution and dispersion of Zn^{2+} cations in ZnO/Al_2O_3 are affected by the cobalt addition.

The escape depth of the Zn(LMM) Auger band is higher than that of the Zn 2p band. Since the Zn(LMM)/Zn 2p ratios for ZnO/Al_2O_3 (673 K) are significantly lower than that of pure ZnO, in which zinc is expected to be homogeneously distributed in depth, it is concluded that Zn^{2+} cations are segregated in the surface layer of ZnO/Al_2O_3 at 673 K.[21] The intensity ratio of Zn(LMM)/Zn 2p can be expressed as follows for Al_2O_3 with a zinc–aluminate surface layer of thickness, d.

$$[\mathrm{Zn(LMM)/Zn\ 2p}] = [\mathrm{Zn(LMM)/Zn\ 2p}]_0 \times [1 - \exp(-d/\lambda_{\mathrm{Zn(LMM)}})]/[1 - \exp(-d/\lambda_{\mathrm{Zn\,2p}})] \quad (1)$$

where $[\mathrm{Zn(LMM)/Zn\ 2p}]_0$ indicates the intensity ratio for an infinitely thick, homogeneous Zn-layer and is observed to be 1.2 for ZnO.[21] $\lambda_{\mathrm{Zn(LMM)}}$ and $\lambda_{\mathrm{Zn\,2p}}$ denote the escape depths of the Zn(LMM) Auger- and Zn 2p photo-electrons and are 1.5 and 0.8 nm, respectively. The intensity ratios are calculated to be 0.68, 0.82, 0.96, and 1.13 from Eq. 1 for Zn-containing layers of thickness of 0.2 (monolayer), 1, 2, and 4 nm, respectively. A comparison with the results in Fig. 4-B implies that Zn^{2+} cations preferentially occupy surface sites forming a monolayer in ZnO/Al_2O_3 calcinated at 673 K and containing less than about 6 wt% ZnO.

The increase in the Zn(LMM)/Zn 2p ratio with increasing calcination temperature indicates the diffusion of Zn^{2+} cations into the Al_2O_3 bulk (1—2 nm at 823 K and 2—5 nm at 1073 K). The increase in the thickness of Zn layer is obviously observed as ZnO content increases. These findings are a consequence of enhanced diffusivity of Zn^{2+} cations at a higher temperature and limited surface sites for Zn^{2+} cations. These behaviors of Zn^{2+} cations in ZnO/Al_2O_3 were qualitatively confirmed by Ar^+ sputtering techniques.[21]

With the ZnO–CoO/Al_2O_3 systems calcined at 673 and 823 K, the Zn(LMM)/Zn 2p intensity ratios increased on the addition of CoO, indicating that the cobalt addition enhances the diffusion of Zn^{2+} cations into the Al_2O_3 bulk phase. This is also supported by the decrease in the Zn 2p/Al 2p XPS intensity ratios on the addition of CoO. On the other hand, it should be noted that the Zn(LMM)/Zn 2p ratios for ZnO–CoO/Al_2O_3 are still far below the ratio for pure ZnO and, in consequence, that a considerable proportion of Zn^{2+} cations occupies surface sites in ZnO–CoO/Al_2O_3 calcined at 673 or 823 K. A significant depletion of Zn^{2+} at surface would lead to the ratio Zn(LMM)/Zn 2p$>$1.2, which is contrary to the experimental observations.

The differences in the site preference between Zn^{2+}, Co^{2+}, Co^{3+}, and Al^{3+} cations are considered to determine the site distributions of cations in the ZnO–CoO/Al_2O_3 systems. Surface Zn^{2+} cations are expected to occupy tetrahedral sites of Al_2O_3 because of low stability in octahedral sites (octahedral preference energy: +7.6 kcal mol^{-1}) as compared to Al^{3+} (−10.6 kcal mol^{-1}).[31] This was confirmed by the BE of Zn 2p band and KE of Zn(LMM) level for ZnO/Al_2O_3 and ZnO–CoO/Al_2O_3. Divalent cobalt cations are also anticipated to be present mainly in tetrahedral sites (95% in $CoAl_2O_4$ spinel structure) (+3 kcal mol^{-1}). On the other hand, it is suggested by Arnoldy and Moulijn[11] using a ligand field theory that Co^{3+} shows a tendency to occupy octahedral sites in an Al_2O_3 lattice. The order of tetrahedral site preference in spinel structures is, accordingly, estimated to be $Zn^{2+}>Co^{2+}>Al^{3+}>Co^{3+}$.

As aforementioned, the Zn^{2+} cations in ZnO–CoO/Al_2O_3 occupy preferentially surface tetrahedral sites of Al_2O_3 at a low ZnO content. This eventually results in an occupation of octahedral sites with Al^{3+} cations as in $ZnAl_2O_4$. It is deduced that the preferential incor-

poration of Zn^{2+} cations in surface tetrahedral sites significantly retards formations of both surface Co^{2+} (Co-IIA) and Co^{3+} (Co-III) species in octahedral and tetrahedral sites, respectively, in conformity with the TPR profiles in Fig. 1. The cobalt cations expelled from the surface sites are expected to be incorporated into tetrahedral sites in an Al_2O_3 lattice as long as these sites are available because of higher thermodynamic stability of cobalt aluminate formation. The enhanced diffusions of Zn^{2+} and Co^{2+} cations into subsurface layer of Al_2O_3 result from competitive occupations of surface and bulk sites.

The ratio of bulk oxide (Co-I and IIB) and (sub)-surface cobalt species may depend on the calcination temperature and ZnO content, but actually it was almost invariant at 673 and 823 K (Fig. 2). The bulk oxide species are conjectured to be produced via oxidation of Co^{2+} to Co^{3+} during calcination.[26] The proportion of Co^{3+} depends strongly on the starting salt but weakly on the calcination temperature ($\leqslant$823 K) and ZnO content. This is because the calcination temperature of 673 or 823 K is too low for the cations to attain equilibrium distributions in an Al_2O_3 lattice (Tammann temperature: ca. 1140 K) as suggested by Burggraf et al.[9] On the contrary, diffusions of Co^{2+} and Zn^{2+} are significantly enhanced at 1073 K because of competitive site occupation and elevated calcination temperature which facilitates bulk diffusion to attain equilibrium distribution.

The formation of Co-IA was observed at high ZnO content. It is proposed that the high reduction temperature of Co-IA as compared to that of Co_3O_4 is attributed to the dissolution of Zn^{2+} into Co_3O_4 phase. The Zn^{2+} cations are expected to occupy tetrahedral sites in Co_3O_4 as in $ZnCo_2O_4$ (normal spinel structure).[30] The amount of Co-IA is very close to Co_3O_4 (Co-I) at 673 K, indicating no formation of Co_3O_4 is promoted by the addition of ZnO at this temperature. On the other hand, when 10 wt% $ZnO–CoO/Al_2O_3$ was calcined at 823 K, Co-IA was produced in spite of the absence of precursor Co_3O_4 (Fig. 1-B). This finding is interpreted in terms of an extensive occupation of tetrahedral sites of an Al_2O_3 lattice with Zn^{2+} cations due to an enhanced diffusivity at 823 K and a large number of Zn^{2+} cations doped.

Mixed oxide formation between dispersed Co_3O_4 particles and the support constituent increases the reduction temperature of cobalt as a consequence of enhanced polarization of Co–O bondings.[11] The incorporation of Al^{3+} into octahedral interstices of Co_3O_4 (Co-IIB) significantly increase the reduction temperature (ca. 150 K) of Co_3O_4. Formation of $Si^{4+}{}_{x/2}Co^{2+}{}_{1-x}Co^{3+}{}_2O_4$ with spinel structure is proposed for CoO/SiO_2 and the reduction temperature increases by 55 K compared with Co_3O_4.[32] The effect of cation incorporation is in the order $Al^{3+} \gg Si^{4+} > Zn^{2+}$ as might be expected, taking into account a cation charge and a low concentration of Si^{4+} in the lattice.

Analogously to the enhanced bulk diffusion of Zn^{2+} in the presence of Co^{2+}, the diffusion of Co^{2+} cations into the bulk phase is promoted by a simultaneous impregnation of ZnO as evidenced by a considerable decrease in the TPR area in Fig. 2. This is partly substantiated by the decrease in the Co 2p/Al 2p XPS intensity ratio at 2 wt% ZnO in Fig. 3 for $ZnO–CoO/Al_2O_3$ (673 K) in line with the observations by Chin and Hercules.[15] With $ZnO–CoO/Al_2O_3$ at high ZnO or calcined at 823 K, however, the Co 2p/Al 2p XPS intensity ratios are not appreciably affected by the addition of ZnO in spite of the bulk diffusion of cobalt species. This may be interpreted in terms of compensating effects on the XPS intensity ratio, that is, diffusion of the surface cobalt species into a bulk phase deeper than the sampling depth of XPS (2—3 nm) and the increase in cobalt dispersion due to the reactions with Al_2O_3 (formations of Co-IV and V at the expense of Co-IIB).

In summary, it was found that the addition of 2 wt% ZnO markedly affected the cobalt–alumina interaction modes. The distribution of the cobalt species in CoO/Al_2O_3 was greatly altered: cobalt–alumina surface interaction species were removed and migration of cobalt into alumina subsurface phase was promoted by ZnO. A formation of Co–Zn–O mixed oxide is proposed for $ZnO–CoO/Al_2O_3$ at high ZnO contents (5—10 wt%).

We gratefully acknowledge Messrs. K. Inamura and T. Takyu in Central Research Laboratory, Idemitsu Kosan Co., Ltd. for helpful discussions and the TPR (TPRS-200) and SEM measurements of Co_3O_4 and CoO/Al_2O_3.

References

1) F. E. Massoth, *Adv. Catal.*, **27**, 265 (1978).
2) M. Lo Jacono, A. Cimino, and G. C. A. Schuit, *Gazz. Chim. Ital.*, **103**, 1281 (1973).
3) Y. Okamoto, H. Nakano, T. Imanaka, and S. Teranishi, *Bull. Chem. Soc. Jpn.*, **48**, 1163 (1975).
4) J. Grimblot, J. P. Bonnelle, and J. P. Beaufils, *J. Electron Spectrosc. Relat. Phenom.*, **8**, 437 (1976). J. P. Bonnelle, J. Grimblot, and A. D'Huysser, *J. Electron Spectrosc. Relat. Phenom.*, **7**, 151 (1975).
5) R. I. Declerck-Grimee, P. Canesson, R. M. Friedman, and J. J. Fripiat, *J. Phys. Chem.*, **82**, 885 (1978).
6) K. S. Chung and F. E. Massoth, *J. Catal.*, **64**, 320 (1980); **64**, 332 (1980).
7) Y. Okamoto, T. Imanaka, and S. Teranishi, *J. Catal.*, **65**, 448 (1980).
8) R. L. Chin and D. M. Hercules, *J. Phys. Chem.*, **86**, 360 (1982).
9) L. W. Burggraf, D. E. Leyden, R. L. Chin, and D. M. Hercules, *J. Catal.*, **78**, 360 (1982).
10) C. Wivel, B. S. Clausen, R. Candia, S. Mørup, and H. Topsøe, *J. Catal.*, **87**, 497 (1984).

11) P. Arnoldy and J. A. Moulijn, *J. Catal.*, **93**, 38 (1985).
12) P. Arnoldy, J. L. de Brooys, B. Scheffer, and J. A. Moulijn, *J. Catal.*, **96**, 122 (1985).
13) "Molybdenum Catalyst Bibliography," Climax Molybdenum Co., Michigan (1964—1981), No. 1—8.
14) P. Porta and A. Anichini, *J. Chem. Soc., Faraday Trans. 1*, **76**, 2448 (1980).
15) R. L. Chin and D. M. Hercules, *J. Catal.*, **74**, 121 (1982).
16) J. F. Patzer, W. L. Kehl, and H. E. Swift, *J. Catal.*, **62**, 211 (1980).
17) N. P. Martinez and P. C. H. Mitchell, "Proc. Climax Third Inter. Conf. Chemistry and Uses of Molybdenum," ed by H. F. Barry and P. C. H. Mitchell, Climax Molybdenum Comp., Ann Arbor, Michigan (1982), p. 105.
18) F. L. Gil Llambias, J. L. G. Fierro, J. M. Tascon, and A. Lopez Agudo, "Proc. Climax Fourth Inter. Conf. Chemistry and Uses of Molybdenum," ed by H. F. Barry and P. C. H. Mitchell, Climax Molybdenum Comp., Ann Arbor, Michigan (1982), p. 361.
19) J. G. L. Fierro, A. Lopez Agudo, P. Grange, and B. Delmon, "Proc. 8th Inter. Congr. Catal.," Verlag Chemie, Weinheim, Berlin (1984), Vol. 2, p. 363.
20) A. Lycoughitis, C. Defosse, F. Delannay, J. Lemaitre, and B. Delmon, *J. Chem. Soc., Faraday Trans. 1*, **76**, 1677 (1980).
21) A. Maezawa, Y. Okamoto, and T. Imanaka, *J. Chem. Soc., Faraday Trans. 1*, **83**, 665 (1987).
22) T. Uchijima, "Proc. First Tokyo Conf. Advanced Catal. Sci. Tech.," Tokyo, July 1990, Abstr., I-31.
23) B. R. Strohmeier and D. M. Hercules, *J. Catal.*, **86**, 266 (1984).
24) F. P. J. M. Kerkhof and J. A. Moulijn, *J. Phys. Chem.*, **83**, 1612 (1979).
25) D. R. Penn, *J. Electron Spectrosc. Relat. Phenom.*, **9**, 29 (1976).
26) Y. Okamoto, T. Adachi, K. Nagata, M. Odawara, and T. Imanaka, to be submitted.
27) H. Knözinger and P. Ratnasamy, *Catal. Rev. -Sci. Eng.*, **17**, 31 (1978).
28) M. Lo Jacono, M. Schiavello, and A. Cimino, *J. Phys. Chem.*, **75**, 1044 (1971).
29) A. Cimino, M. Lo Jacono, and M. Schiavello, *J. Phys. Chem.*, **79**, 243 (1975).
30) R. J. Hill, J. R. Craig, and G. V. Gibbs, *Phys. Chem. Miner.*, **4**, 317 (1979).
31) A. Navrotsky and O. J. Kleppa, *J. Inorg. Nucl. Chem.*, **29**, 2701 (1967).
32) Y. Okamoto, K. Nagata, T. Adachi, T. Imanaka, K. Inamura, and T. Takyu, *J. Phys. Chem.*, in press.

 © 1991 The Chemical Society of Japan Bull. Chem. Soc. Jpn., 64, 243—247 (1991)

Catalysis by Heteropoly Compounds. XVIII.† Oxidation of Methacrylaldehyde over 12-Molybdophosphoric Acid and Its Alkali Salts

Noritaka MIZUNO,†† Tetsuji WATANABE,††† and Makoto MISONO*
Department of Synthetic Chemistry, Faculty of Engineering,
The University of Tokyo, Hongo, Bunkyo-ku, Tokyo 113
(Received September 6, 1990)

The reaction scheme for the methacrylaldehyde oxidation over heteropoly compounds proposed previously (M. Misono et al., Proc. 7th Intl. Congr. Catal., 1980) was confirmed by ^{18}O tracer experiments using the Pulse-MS method (combination of pulse reactor/mass spectrometer). The occurrence of direct and rapid oxygen exchange between methacrylaldehyde and the polyanion of $M_xH_{3-x}PMo_{12}O_{40}$ (M=Na, Cs, x=0—3.15) was verified under the reaction conditions. The results also suggested that this reaction is catalyzed by Brønsted acid sites of the catalysts via such intermediates as (**I**) and/or (**II**) in scheme 1. It was shown that the methacrylaldehyde oxidation is a surface-tyepe reaction and the catalytic activity is controlled by the oxidizing ability of the catalyst surface.

The selective oxidation of methacrylaldehyde to methacrylic acid has recently been industrialized by utilizing 12-molybdovanadophosphates,[1] although improvements in the selectivity and durability are still desirable. As for the reaction mechanism, we previously proposed the following scheme.[2]

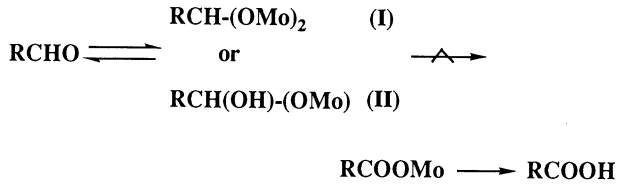

Scheme 1.

We also showed that the oxygen atoms of the polyanion and/or water are directly incorporated into the products in accordance with the scheme, and that the oxygen in the feed gas reoxidizes the reduced polyanion (i.e., a redox mechanism). In this mechanism, such intermediates as (**I**) and (**II**), having C–O–Mo bonds, are assumed to exist. Isopoly compounds having partial structures similar to (**I**) and (**II**) have been synthesized,[3] and it was suggested that they are the intermediates in the oxidation of aldehydes.[3,4] If (**I**) and (**II**) are indeed the intermediates and the first step of Scheme 1 is rapid, direct exchange of oxygen must proceed rapidly between 12-molybdophosphoric acid and aldehyde. We actually found rapid oxygen isotopic exchange among aldehyde, water, and the catalyst in the case of acrylaldehyde oxidation over 12-molybdophosphoric acid.[2] However, in that case it was not clear whether the exchange proceeds directly between the catalyst and aldehyde, or via oxygen exchange with water.

A direct exchange would be good evidence for the existence of (**I**) or (**II**). In view of this, we investigated in the present work the oxygen exchange between methacrylaldehyde and 12-molybdophosphates. The factors controlling each step of Scheme 1 have also been examined. If the second step is rate-limiting, the oxidizing ability of catalysts should control the overall rate. Further, attempts were made to clarify whether the methacrylaldehyde oxidation belongs to a bulk (**II**)-type or surface-type reaction.[5,6]

Experimental

Catalysts and Reagents. 12-Molybdophosphoric acid ($H_3PMo_{12}O_{40}\cdot 27.4H_2O$, abbreviated as PMo_{12}) was commercially obtained. The Na and Cs salts ($M_xH_{3-x}PMo_{12}O_{40}$, M=Na, Cs, x=0—3.15) were prepared with Na_2CO_3 and Cs_2CO_3 by a method described previously.[6] The surface areas of catalysts were measured by the BET method based on N_2 adsorption after the same pretreatments as those for the reactions.

Methacrylaldehyde (MAL) from Aldrich Chem. Co., Inc. was distilled and stored at ca. 253 K. No impurity was detected in it by gas chromatography. Pyridine (Py) was used after removing water as impurity with Molecular Sieve 3A. $H_2{}^{18}O$ (^{18}O content; 98—99%, Japan Radioisotope Association) was used for the ^{18}O exchange reaction.

Reactions. ^{18}O exchange reactions were carried out at 473 K with a pulse reactor directly connected to a mass spectrometer (NEVA NAG 531) (Pulse-MS method, Figure 1). The path from the injection port at the top of the reactor up to the inlet of mass spectrometer, was heated at 423 K to suppress isotopic contamination by oxygen exchange with water adsorbed on the wall. The influence of the adsorbed water was minimized by pretreating the system properly as detailed in Results and Discussion. The ^{18}O content in each reactant was measured with the mass spectrometer directly connected to the outlet of the reactor. The weight of catalysts used was 100 mg. After exposing the catalysts to a He stream (30 $cm^3\ min^{-1}$) at 473 K for 1.5 h, water, MAL, or Py was injected at the top of the reactor at 473 K. No

† Part XVII: H. Mori, N. Mizuno, and M. Misono, *J. Catal.*, submitted.

†† Present address: Catalysis Research Center, Hokkaido University, Sapporo 060.

††† Present address: Central Technical Research Lab., Nippon Oil Co., Ltd., Yokohama 231.

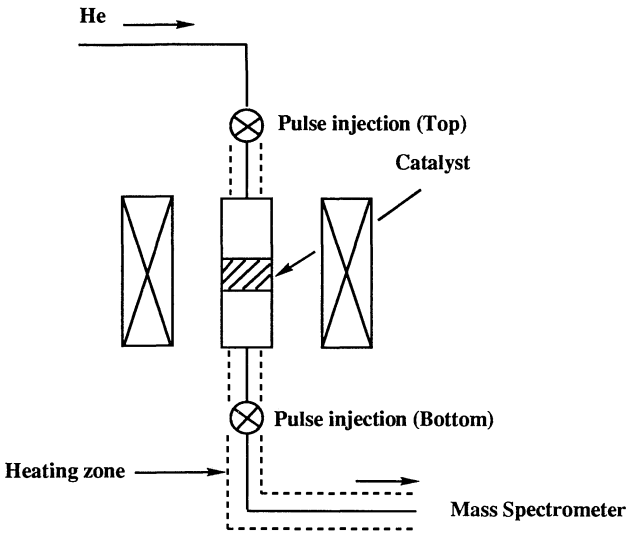

Fig. 1. Pulse-MS apparatus for the ^{18}O exchange reaction.

methacrylic acid formation took place when MAL was injected at the outlet of the reactor.

The oxidation of MAL was carried out with a conventional flow reactor as described previously.[2] The conditions were as follows; temperature, 573 K; weight of catalyst, 0.5 g; flow rate, 32.5 $cm^3\ min^{-1}$; MAL, 2%; O_2, 12%; N_2, balance.

Results and Discussion

Direct Oxygen Isotopic Exchange between MAL and PMo_{12}. Table 1 summarizes the results of the ^{18}O exchange reaction among PMo_{12}, MAL, and water. Different run numbers denote separate experiments carried out with fresh catalysts. PMo_{12} and M_xPMo_{12}, to which 3 μl of $H_2{}^{18}O$ was injected 10—14 times, are denoted as ^{18}O-PMo_{12} and ^{18}O-M_xPMo_{12}, respectively. After $H_2{}^{18}O$ was injected 10—14 times, the ^{18}O content in water at the outlet of the reactor reached a constant value in a range of 90—100%. The amount of ^{18}O incorporated into the catalyst corresponded to approximately three quarters the amount of oxide ions in the whole polyanions. Therefore, the whole bulk was nearly equilibrated with $H_2{}^{18}O$; the ^{18}O content in the polyanions not only on the surface but also in the large portion of the bulk is close to 90—100%. The oxygen isotopic exchange between the polyanion and water has already been reported.[7,8]

The agreements of the ^{18}O contents in water and MAL between Runs No. 1 and 2 and among Runs No. 3—5 in Table 1 ensure a high reproducibility of the experiments. In Runs No. 2′ and 5′, the reactants were injected at the outlet of the reactor. The results were also highly reproducible. These experiments were carried out to estimate the oxygen exchange between the reactants injected and water adsorbed on the wall from the outlet of the reactor to the detector of the mass spectrometer. The ^{18}O contents in MAL in Runs No. 2′ and 5′ were less than 1%. The low ^{18}O content in MAL ($\leqslant$1%) indicates that the oxygen exchange of MAL proceeded to a small extent in the absence of the catalysts. Oxygen exchange between water and the wall proceeded to some extent.

The occurrence of direct isotopic exchange between MAL and PMo_{12} can be concluded from the results of Runs No. 1, 2, and 2′, as follows. The ^{18}O content in MAL (40—44%) was greater than that in water (35—37%) in Runs No. 1 and 2, which were carried out after the system was equilibrated with $H_2{}^{18}O$. This difference is meaningful, because the isotopic exchange with water adsorbed on the wall was much slower for MAL than for water (No. 2′). Hence ^{18}O was incorporated into MAL not only from water but also directly from PMo_{12}, because the ^{18}O content in MAL will never exceed that in water if a direct exchange is absent.

The following explanation based on Fig. 2, which illustrates the results of Runs No. 1, 2 (top), and 3—5 (bottom), would make clearer the occurrence of direct oxygen exchange between MAL and PMo_{12}. The ^{18}O content in MAL at the outlet in Runs No. 3—5 (23—

Table 1. Oxygen Isotopic Exchange among Methacrylaldehyde, Water, and $H_3PMo_{12}O_{40}$ at 473 K (Pulse-MS Method)

Run	Catalyst	Reactants injected	^{18}O content in water	^{18}O content in MAL
			%	
1	^{18}O-PMo_{12}[a]	$H_2{}^{16}O$(0.5)+MAL(3)[b]	37	44
2	^{18}O-PMo_{12}[a]	$H_2{}^{16}O$(0.5)+MAL(3)[b]	35	40
2′[c]	^{18}O-PMo_{12}[a]	$H_2{}^{16}O$(0.5)+MAL(3)[b]	8	<1
3	PMo_{12}	$H_2{}^{18}O$(3)+MAL(3)	34	26
4	PMo_{12}	$H_2{}^{18}O$(3)+MAL(3)	32	23
5	PMo_{12}	$H_2{}^{18}O$(3)+MAL(3)	35	25
5′[c]	PMo_{12}	$H_2{}^{18}O$(3)+MAL(3)	86	1
6	^{18}O-PMo_{12}[a]	$H_2{}^{18}O$(3)+MAL(3)	78	70
7	Py-^{18}O-PMo_{12}[a]	$H_2{}^{18}O$(3)+MAL(3)[b]	75	17
8	Py-^{18}O-PMo_{12}[a]	Py(2)+$H_2{}^{18}O$(3)+MAL(3)	79	3

a) Oxide ions of polyanion were fully exchanged (equilibrated) with ^{18}O of water prior to pulse. b) The value in parenthesis is the amount (μl) of reactant injected. c) Reactants were injected at the outlet of reactor.

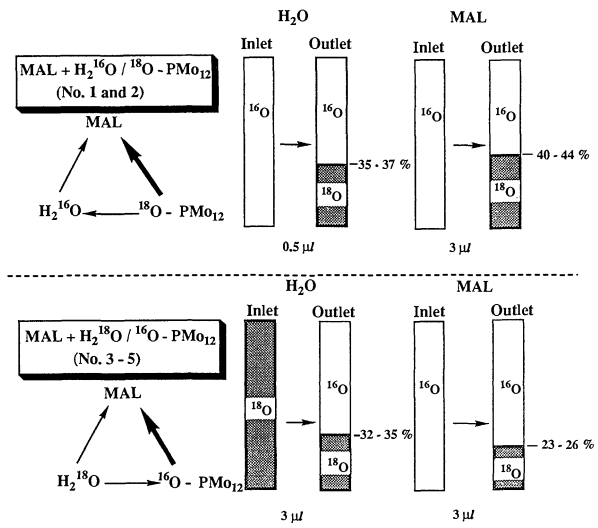

Fig. 2. Explanation of the presence of the direct ^{18}O exchange between methacrylaldehyde and $H_3PMo_{12}O_{40}$. Arrows indicate the flow of ^{18}O. Solid; indirect path, bold; direct path.

26%) was lower than those for Runs No. 1 and 2 (40, 44%), although the ^{18}O content in water which was in contact with MAL during the passage of the pulse through the catalyst bed was much greater for Runs No. 3—5 (100% at the inlet to ca. 35% at the outlet, bottom in Fig. 2) than for Runs No. 1 and 2 (0 to ca. 35%, top in Fig. 2). If the oxygen of MAL was exchanged with that of PMo_{12} only via water (absence of the direct path, bold arrows in Fig. 2), the ^{18}O content in MAL should be higher for Runs No. 3—5 than that for Runs No. 1 and 2. However, the experimental observations were definitely opposite. In addition, this would favor a conclusion that the amount of water injected in Runs No. 3—5 was larger than that in Runs No. 1 and 2. Therefore, these findings evidence the occurrence of "direct" oxygen exchange between MAL and the polyanion of PMo_{12}.

The occurrence of direct oxygen exchange demonstrates the formation of such intermediates as (**I**) and (**II**), which possess direct bonds between PMo_{12} and MAL (i.e., C–O–Mo bond), and supports the mechanism of Scheme 1.

Roles of Water Vapor and Acidity in Isotopic Exchange. The quantity of MAL pulsed in the present study was 3 μl (36 μmol). This corresponds to ca. three times and 2%, respectively, of those of surface and bulk oxide ions of PMo_{12} (12 μmol surface oxide ions and 1.7 mmol bulk oxide ions for 0.1 g of PMo_{12} ($3.8\ m^2\ g^{-1}$)). If the oxygen exchange between MAL (^{16}O) and ^{18}O–PMo_{12} proceeds only on the surface of PMo_{12}, the ^{18}O content in MAL at the isotopic equilibrium would never exceed 25%. Therefore, the ^{18}O content greater than 25% in the presence of $H_2{}^{16}O$ (in Runs No. 1 and 2) demonstrates that the oxide ion of the polyanion in the catalyst bulk was transferred to MAL. The acceleration of the ^{18}O incorporation into MAL by water (^{16}O) (No. 1 and 2) may be due to the promotion of oxide ion diffusion from the bulk in the form of water molecules or hydroxide ions, as was suggested previously.[2,5,6]

On the other hand, when MAL (^{16}O, 3 μl) was injected without water onto ^{18}O–M_xPMo_{12}, the ^{18}O content in MAL at the outlet was only 8—10%. Therefore, the exchange of oxygen between MAL and PMo_{12} in the absence of water probably proceeds on the surface alone. This is consistent with a view that aldehyde oxidation is a surface-type reaction.

The results from Runs No. 6—8 show the effects of Py poisoning on the oxygen isotopic exchange. ^{18}O–PMo_{12}, to which 2 μl of Py was injected 7 times, is denoted as Py–^{18}O–PMo_{12}. The amount of Py absorbed corresponded to 2.7 molecules·anion^{-1}. The extent of ^{18}O exchange of MAL decreased from 70% (No. 6) to 17% (No. 7) when Py was pre-absorbed. Further, the ^{18}O content in MAL dramatically decreased to 3% when Py was co-pulsed with MAL over Py–^{18}O–PMo_{12} (No. 8). The inhibition of ^{18}O exchange by Py suggests that the oxygen exchange between MAL and the polyanion directly (first step in Scheme 1) and/or indirectly via water is catalyzed by Brønsted acid sites as was previously suggested.[2] This is probably not due to a decrease in the absorptivity of water or MAL by the salt formation of PMo_{12} with Py.

The following observations are also in line with a view that the first step in Scheme 1 is catalyzed by a Brønsted acid. When MAL was injected to ^{18}O–M_x-PMo_{12} at the inlet of the reactor, the ^{18}O content in MAL divided by the surface area of catalyst decreased with x as seen in Fig. 3. Since the amount of water

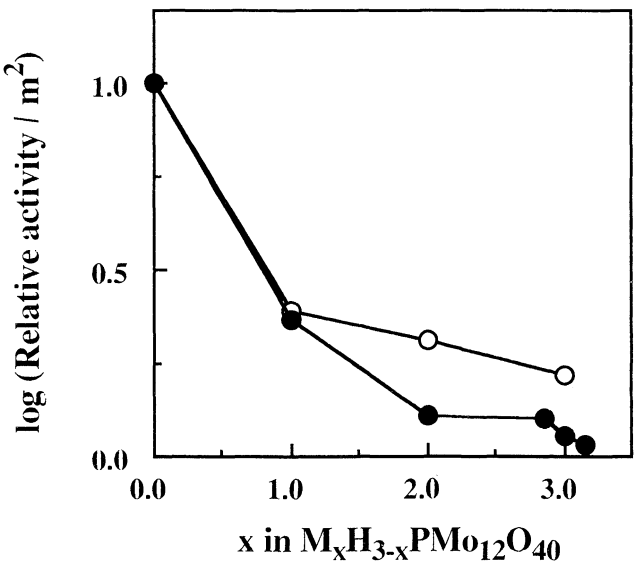

Fig. 3. Effect of alkali content on the ^{18}O exchange between methacrylaldehyde and $M_xH_{3-x}PMo_{12}O_{40}$. ●: $Cs_xH_{3-x}PMo_{12}O_{40}$. ○: $Na_xH_{3-x}PMo_{12}O_{40}$. The activity of $H_3PMo_{12}O_{40}$ was taken as unity.

evolved was only 0.04—0.05 μl, the ^{18}O exchange between water evolved and MAL could be ignored in this case and the ^{18}O content in MAL may be considered as a measure of the catalytic activity for direct oxygen exchange between MAL and the polyanion. A similar dependence of the amount of Brønsted acid sites on the Na or Cs content was observed.[3]

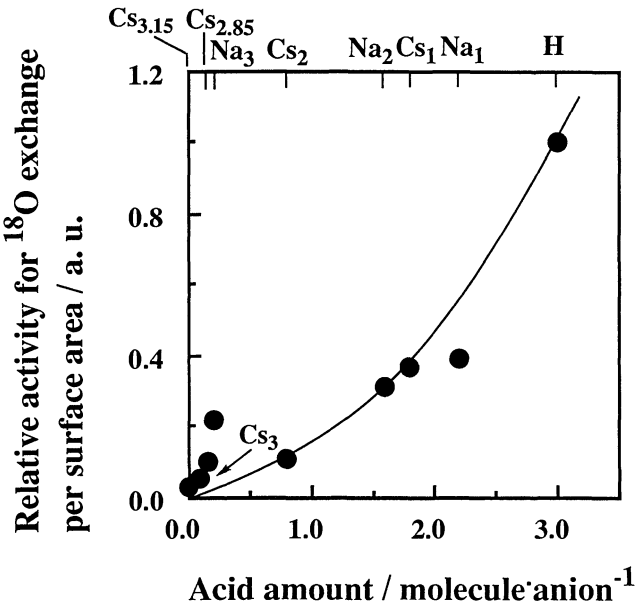

Fig. 4. Dependency of the catalytic activity for the ^{18}O exchange on the amount of Brønsted acid measured by the amount of pyridine absorbed or adsorbed. H and M_x denote $H_3PMo_{12}O_{40}$ and $M_xH_{3-x}PMo_{12}O_{40}$, respectively. The relative activity for the ^{18}O exchange per surface area of $H_3PMo_{12}O_{40}$ was taken as unity.

Figure 4 shows the correlation between the amount of Brønsted acid sites of 12-molybdophosphates measured by Py uptake (taken from Ref. 9) and their relative activity for oxygen exchange between MAL and the polyanion. The relative activity increased with an increase in the amount of Brønsted acid sites. This result would indicate that direct oxygen exchange between MAL and the polyanion, namely the first step in scheme 1 is catalyzed by a Brønsted acid.

Type of Catalysis and Factors Controlling the Rate. We previously reported that there are two different groups of reactions as classified by the dependency of the rate of non-catalytic reduction of 12-molybdophosphates on the specific surface area.[6,9] One is the oxidative dehydrogenation reaction, for which the rate per unit weight of catalyst does not depend on the specific surface area. H_2, isobutyric acid, and cyclohexene are typical reactants. In this case, rapid migration of protons and electrons leads to reduction of the whole solid.

The other is the oxygen-addition reaction, for which the rate is proportional to the surface area, presumably because the redox carrier is oxide ion with slow diffusion.

We also reported that the catalyst oxidizing ability as assayed with CO (a surface-type reductant) represents the oxidizing ability of catalyst surface, and is correlated with such surface-type catalysis as oxidations of acetaldehyde and CO.[5,6] Here, we will extend this

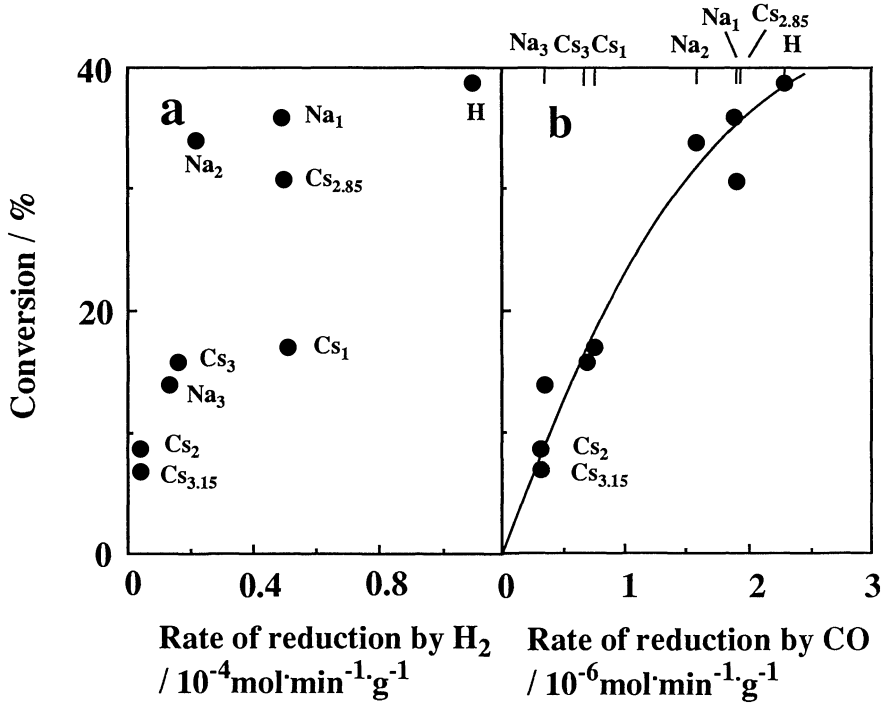

Fig. 5. Correlations between the conversion of methacrylaldehyde and the rate of reduction of catalyst by H_2 (a) or CO (b).

classification to the catalytic oxidation of MAL.

The main products of the oxidation of MAL over M_xPMo_{12} were methacrylic acid, acetic acid, CO, and CO_2. Since they all are oxygenated products, the reaction would belong to the surface-type.[5,10] The selectivities to methacrylic acid, acetic acid, and CO_x ($CO+CO_2$) are slightly different among the M_xPMo_{12} catalysts.

Figure 5 shows a correlation between the % conversion of MAL and the rates of non-catalytic reduction of catalysts by H_2 or CO. In Fig. 5, the results of oxidation reactions in the absence of water vapor are displayed, because the presence of water would make a surface-type reaction behave like a bulk-type reaction.[5] A good correlation exists between the catalytic activity (conversion of MAL) and the rate of catalyst reduction by CO (Fig. 5b), while the correlation is poor between the catalytic activity and the rate of catalyst reduction by H_2 (Fig. 5a).

These results are very similar to those observed for other surface-type reactions such as the oxidation of acetaldehyde and CO.[5,6] The good correlation noted in Fig. 5b not only confirms that the oxidation of MAL (in the absence of water vapor) is a surface-type reaction, but also indicates that the catalytic activity is controlled by the oxidizing ability of catalysts. The formation of methacrylate by oxidative dehydrogenation in scheme 1 is most probably the rate-determining step.

This study has been supported in part by a Grant-in-Aid for Scientific Research from the Ministry of Education, Science and Culture of Japan.

References

1) M. Ueshima, H. Tsuneki, and N. Shimizu, *Hyomen*, **24**, 582 (1986); M. Wada, *Shokubai (Catalyst)*, **32**, 223 (1990).

2) M. Misono, K. Sakata, Y. Yoneda, and W. Y. Lee, in "Proc. 7th Intl. Congr. Catal., Tokyo, 1980," Kodansha-(Tokyo)-Elsevier(Amsterdam), 1981, p. 1047; Y. Konishi, K. Sakata, M. Misono, and Y. Yoneda, *J. Catal.*, **77**, 169 (1982).

3) E. M. McCarron III and R. L. Harlow, *J. Am. Chem. Soc.*, **105**, 6179 (1985); V. W. Day, M. F. Frederic, W. G. Klemperer, and R-S. Liu, *ibid.*, **101**, 491 (1979); R. D. Adams, W. G. Klemperer, and R-S. Liu, *J. Chem. Soc., Chem. Commun.*, **1979**, 256.

4) E. M. Serwicka, J. B. Black, and J. B. Goodenough, *J. Catal.*, **106**, 23 (1987).

5) N. Mizuno, T. Watanabe, H. Mori, and M. Misono, *J. Catal.*, **123**, 157 (1990).

6) N. Mizuno, T. Watanabe, and M. Misono, *J. Phys. Chem.*, **94**, 890 (1990); *ibid.*, **89**, 80 (1985).

7) K. Sakata, M. Misono, and Y. Yoneda, *Chem. Lett.*, **1980**, 151.

8) N. Mizuno, K. Katamura, Y. Yoneda, and M. Misono, *J. Catal.*, **83**, 384 (1983).

9) T. Koyama and M. Misono, *Chem. Lett.*, **1983**, 1177.

10) M. Misono, *Catal. Rev.-Relat. Subj.*, **29**, 269 (1987).

Molecular and Crystal Structure of Azobenzene-Containing Amphiphile, $C_6AzoC_{10}N^+Br^-$

Guiqing Xu, Kenji Okuyama,* and Masatsugu Shimomura
Faculty of Technology, Tokyo University of Agriculture and Technology, Koganei, Tokyo 184
(Received May 1, 1990)

A totally synthetic azobenzene-containing amphiphile $C_{32}H_{52}N_3O_3Br$ ($C_6AzoC_{10}N^+Br^-$) was crystallized from its solution in trichloromethane and ethanol. The crystal is triclinic with space group $P\bar{1}$; Z=2; a=24.317(5), b=8.632(1), and c=8.043(2) Å; and α=91.41(2), β=80.62(2), and γ=99.01(1)°. The structure was solved by the direct method and refined by the full-matrix least-squares method: R=0.038 for 4305 observed reflections ($2\theta<120°$, Cu $K\alpha$, λ=1.5418 Å). Two molecules in a unit cell are related by a center of symmetry and pack tail-to-tail in a bilayer structure. The plane of the azobenzene chromophore is almost perpendicular to the layer surface and is overlapped with that of the azobenzene chromophore along its long axis with a separation of 3.55 Å. Different from other homologous compounds, this molecule bends almost 90° at the neck of the hydrophilic head group.

Totally synthetic azobenzene-containing amphiphiles with a single alkyl chain, $C_nAzoC_mN^+Br^-$, show several types of azobenzene chromophore aggregation states, depending on the number of carbon atoms in the tail part (n) and the spacer part (m).[1] The J-like aggregation between adjacent chromophores was found in single crystals, casted films, and aqueous dispersions of $C_nAzoC_5N^+Br^-$ (n=6, 8, 10, and 12). Their detailed crystal structures were determined by X-ray single crystal structure analyses and bore out the J-like aggregation of azobenzene chromophores at an atomic level.[2-4] Compared with $C_nAzoC_5N^+Br^-$, the title amphiphile, $C_6AzoC_{10}N^+Br^-$, shows several different properties, such as thermal properties, spectroscopic properties, and shapes of single crystals.

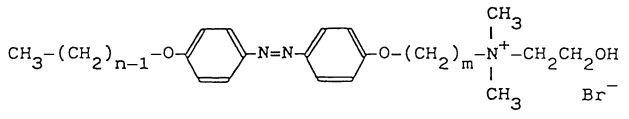

Scheme 1.

In this paper, we discuss the detailed molecular and crystal structure of this compound for understanding the relationship between its structure and physical properties.

Experimental and Structure Determination

4-(Hexyloxy)-4′-[ω-(dimethylethanolammonio)-decyloxy]-azobenzenebromide (abbreviated as $C_6AzoC_{10}N^+Br^-$) (30 mg) was dissolved in a solution (3 ml) of trichloromethane and ethanol (trichloromethane/ethanol=1/5 by volume). Yellow, plate-like crystals with dimensions of 0.5×0.2×0.1 mm³ were obtained by keeping the solution at room temperature for about a week. The density was measured by the flotation method in a solution of hexane and tetrachloromethane.

Lattice parameters and diffraction intensities were

Table 1. Fractional Coordinates and Equivalent Isotropic Temperature Factor for Non-Hydrogen Atoms of $C_6AzoC_{10}N^+Br^-$ with Estimated Standard Deviations in Parentheses
$B_{eq}=4/3(B_{11}a^2+B_{22}b^2+B_{33}c^2+2(B_{12}ab+B_{23}bc+B_{31}ca))$

Atom	x	y	z	B_{eq}/Å²	Atom	x	y	z	B_{eq}/Å²
Br	0.90450(2)	0.17892(3)	0.41310(3)	4.73(2)	C(14)	0.7369(1)	−1.2428(4)	1.2603(4)	4.84(10)
O(1)	1.0123(1)	−0.2066(3)	−0.0595(3)	7.05(10)	C(15)	0.7364(1)	−1.4968(3)	1.3821(4)	4.25(9)
O(2)	0.76664(9)	−1.3649(2)	1.3028(3)	5.13(7)	C(16)	0.7679(1)	−1.6134(4)	1.4109(4)	4.54(10)
O(3)	0.57875(9)	−2.5666(3)	1.9741(3)	6.15(8)	C(17)	0.7424(1)	−1.7493(3)	1.4923(4)	4.41(10)
N(1)	0.95978(9)	−0.2780(3)	0.3007(3)	3.88(7)	C(18)	0.6787(1)	−1.5192(4)	1.4345(4)	4.93(11)
N(2)	0.6536(1)	−1.9116(3)	1.6309(3)	4.87(9)	C(19)	0.6534(1)	−1.6588(4)	1.5164(4)	5.09(11)
N(3)	0.6842(1)	−2.0107(3)	1.6570(3)	4.78(8)	C(20)	0.6845(1)	−1.7728(3)	1.5459(4)	4.27(9)
C(1)	1.0420(2)	−0.1563(5)	0.0765(6)	5.71(13)	C(21)	0.6548(1)	−2.1503(3)	1.7385(4)	4.35(10)
C(2)	1.0027(1)	−0.1372(4)	0.2381(4)	4.76(10)	C(22)	0.6879(1)	−2.2545(4)	1.7797(4)	4.92(10)
C(3)	0.9121(2)	−0.2922(6)	0.2022(4)	9.73(24)	C(23)	0.6649(1)	−2.3956(4)	1.8591(4)	4.87(10)
C(4)	0.9886(2)	−0.4203(4)	0.2913(4)	6.75(15)	C(24)	0.5963(1)	−2.1879(4)	1.7761(4)	5.19(11)
C(5)	0.9369(1)	−0.2451(3)	0.4844(4)	4.02(9)	C(25)	0.5728(1)	−2.3278(4)	1.8548(4)	5.54(12)
C(6)	0.8871(1)	−0.3638(4)	0.5616(4)	4.46(10)	C(26)	0.6069(1)	−2.4318(4)	1.8971(4)	4.64(10)
C(7)	0.8681(1)	−0.3237(4)	0.7458(4)	4.99(11)	C(27)	0.6105(1)	−2.6778(4)	2.0256(4)	5.52(12)
C(8)	0.8173(1)	−0.4435(4)	0.8240(4)	5.33(12)	C(28)	0.5683(2)	−2.8086(4)	2.1149(5)	6.38(14)
C(9)	0.8328(1)	−0.6006(4)	0.8672(4)	4.94(11)	C(29)	0.5961(2)	−2.9380(4)	2.1723(4)	5.85(13)
C(10)	0.7822(1)	−0.7145(4)	0.9545(4)	4.66(10)	C(30)	0.5523(2)	−3.0736(4)	2.2539(5)	6.84(15)
C(11)	0.8018(1)	−0.8614(4)	1.0122(4)	4.90(11)	C(31)	0.5789(2)	−3.2044(4)	2.3102(5)	6.92(15)
C(12)	0.7558(1)	−0.9817(4)	1.1051(4)	4.49(10)	C(32)	0.5369(2)	−3.3432(5)	2.3824(6)	9.16(22)
C(13)	0.7806(1)	−1.1147(4)	1.1735(4)	4.88(10)					

measured on a Rigaku four circle diffractometer (RASA-5RII) with graphite monochromatized Cu $K\alpha$ radiation (λ=1.5418 Å). The lattice parameters were refined by the least-squares fit using 21 reflections ($40.0° \leqslant 2\theta \leqslant 60.0°$). By using the ω–2θ scan mode with a scan rate of 6° min^{-1}, intensities of 4725 reflections were measured up to 120° in 2θ. The scan width was $\Delta\omega=(1.3+0.14\tan\theta)°$. Three reflections monitored every 100 reflections showed no significant intensity deterioration. Corrections were made for the Lorentz and polarization factors, but not for absorption effect. A total of 4305 reflections with $|F_o|>3\sigma(F)$ was used for the calculation.

Crystal Data: $C_{32}H_{52}N_3O_3Br$; F.W.=606.7; triclinic; space group $P\bar{1}$; Z=2; a=24.317(5), b=8.632(1), and c=8.043(2) Å; α=91.41(2), β=80.62(2), and γ=99.01(1)°; μ(calcd)=17.5 cm^{-1}; V=1645.2(6) Å^3; D_X=1.225 and D_m=1.23 g cm^{-3}.

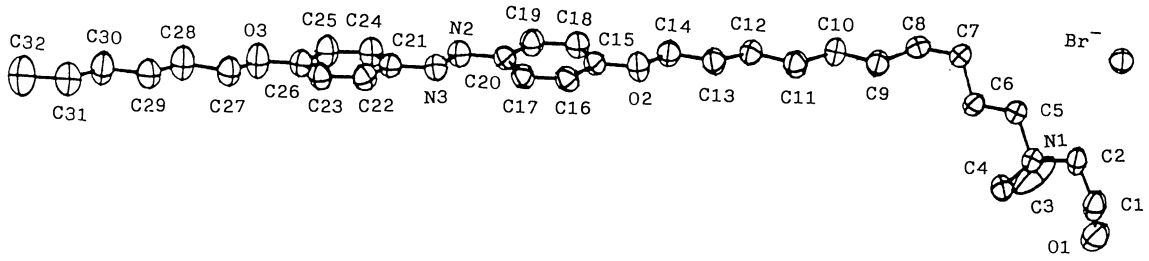

Fig. 1. Molecular structure and atomic numbering scheme for $C_6AzoC_{10}N^+Br^-$. Thermal ellipsoids are drawn at the 50% probability level (ORTEP[11]) drawing).

Table 2. Intramolecular Bond Distances (l) and Bond Angles (θ) with Estimated Standard Deviations in Parentheses

Bond distances	l/Å		l/Å		l/Å
O1–C1	1.429(2)	C13–C14	1.506(4)	C22–C23	1.383(4)
C1–C2	1.504(3)	C14–O2	1.445(4)	C23–C26	1.381(4)
C2–N1	1.510(3)	C15–O2	1.365(3)	C24–C25	1.374(4)
C3–N1	1.496(5)	C15–C16	1.401(5)	C25–C26	1.395(5)
C4–N1	1.500(4)	C15–C18	1.384(4)	C26–O3	1.362(4)
C5–N1	1.528(3)	C16–C17	1.366(4)	C27–O3	1.430(4)
C5–C6	1.517(4)	C17–C20	1.389(4)	C27–C28	1.510(4)
C6–C7	1.527(4)	C18–C19	1.392(4)	C28–C29	1.509(5)
C7–C8	1.539(4)	C19–C20	1.377(5)	C29–C30	1.534(5)
C8–C9	1.526(5)	C20–N2	1.434(4)	C30–C31	1.499(6)
C9–C10	1.533(4)	N2–N3	1.259(4)	C31–C32	1.507(5)
C10–C11	1.530(5)	C21–N3	1.417(4)		
C11–C12	1.513(4)	C21–C22	1.376(5)		
C12–C13	1.532(5)	C21–C24	1.393(4)		

Bond angles	θ/°		θ/°
O1–C1–C2	112.3(2)	C16–C15–C18	120.0(3)
C1–C2–N1	117.0(2)	C15–C18–C19	118.3(3)
C2–N1–C3	109.0(3)	C18–C19–C20	121.7(3)
C2–N1–C4	109.1(2)	C19–C20–N2	116.5(3)
C2–N1–C5	106.7(2)	C17–C20–N2	124.0(3)
C3–N1–C4	113.9(3)	C20–N2–N3	113.8(3)
C3–N1–C5	108.3(2)	N2–N3–C21	115.1(3)
C4–N1–C5	109.6(2)	N3–C21–C22	115.9(3)
N1–C5–C6	114.2(2)	N3–C21–C24	124.8(3)
C5–C6–C7	110.5(2)	C21–C22–C23	122.0(3)
C6–C7–C8	110.5(2)	C22–C23–C26	118.4(3)
C7–C8–C9	113.9(3)	C23–C26–C25	120.2(3)
C8–C9–C10	113.0(3)	C22–C21–C24	119.3(3)
C9–C10–C11	110.2(3)	C21–C24–C25	119.3(3)
C10–C11–C12	115.4(3)	C24–C25–C26	120.8(3)
C11–C12–C13	111.1(3)	C23–C26–O3	124.4(3)
C12–C13–C14	113.8(3)	C25–C26–O3	115.4(3)
C13–C14–O2	107.0(3)	C26–O3–C27	118.9(2)
C14–O2–C15	118.9(2)	O3–C27–C28	106.7(3)
O2–C15–C16	115.6(3)	C27–C28–C29	112.6(3)
O2–C15–C18	124.4(3)	C28–C29–C30	111.6(3)
C15–C16–C17	120.9(3)	C29–C30–C31	112.6(3)
C16–C17–C20	119.6(3)	C30–C31–C32	113.8(3)
C17–C20–C19	119.6(3)		

The structure was solved by the direct method using the program SAPI-85.[5] All the non-hydrogen atoms were found on the E-map. After several cycles of full-matrix least-squares refinements, positions of hydrogen atoms were obtained from the D-Fourier map. The final refinement with the anisotropic parameters for all non-hydrogen atoms and isotropic ones for 49 hydrogen atoms gave finally R=0.038 and R_W=0.037. The quantity minimized in the refinement was $\sum w(|F_o|-|F_c|)^2$ with $w=1/[\sigma^2(F_o)+(0.005\times F_o)^2]$. The final atomic parameters for non-hydrogen atoms are

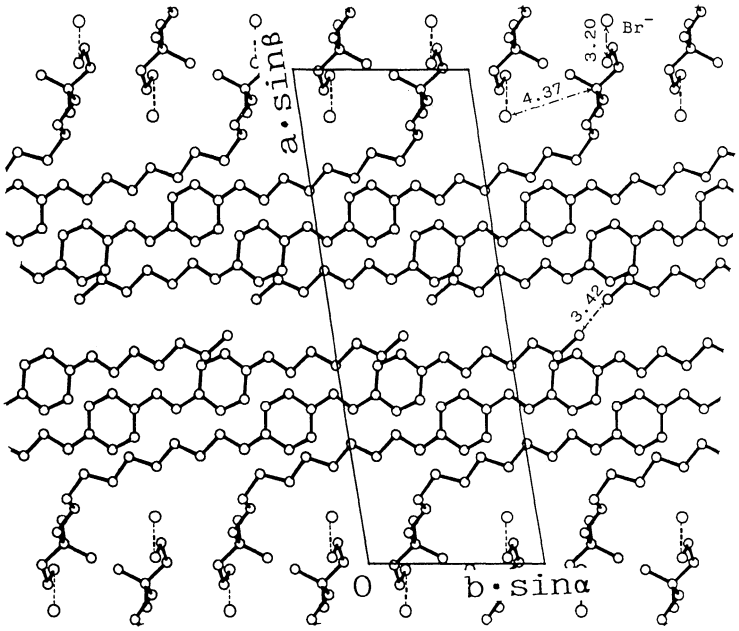

Fig. 2. Packing of $C_6AzoC_{10}N^+Br^-$ projected along the c axis. Hydrogen bonds between bromide anions and hydroxyl groups are indicated by broken lines. Some short interatomic distances (l/Å) are shown (ORTEP[11]).

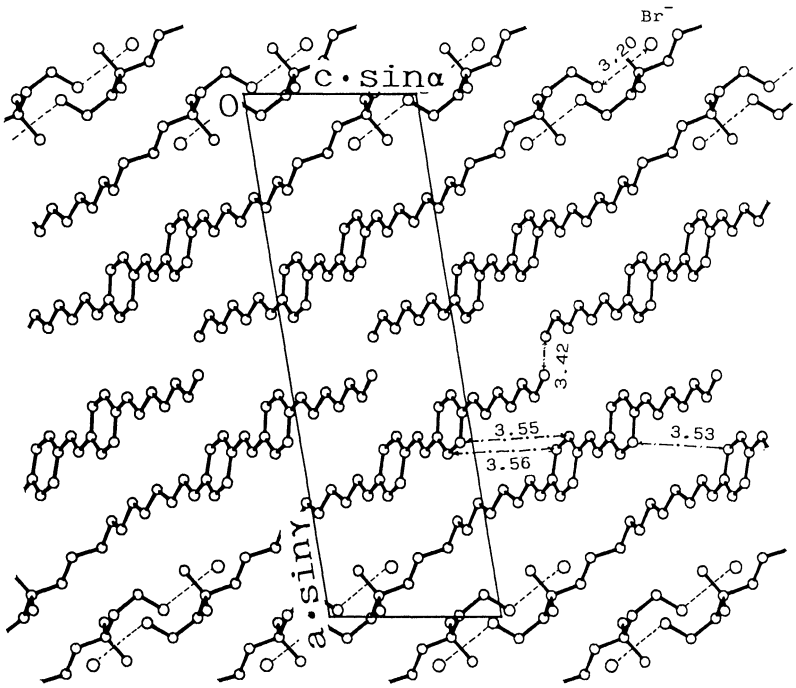

Fig. 3. Packing of $C_6AzoC_{10}N^+Br^-$ projected along the b axis (ORTEP[11]).

given in Table 1.[6]

The atomic scattering factors were taken from International Tables for X-Ray Crystallography.[7] All calculations have been performed on an A-70 minicomputer with the aid of the CRYSTAN program in RASA5R-II system (Rigaku Denki).

Results and Discussion

Molecular Structure of $C_6AzoC_{10}N^+Br^-$. The molecular structure and the atom numbering scheme are given in Fig. 1. Bond distances and angles are shown in Table 2. The average C–C bond distance and C–C–C bond angle in the alkyl spacer and tail parts are 1.520(5) Å and 112.4(3)°, respectively. They are in good agreement with values previously found in other amphiphilic compounds with long hydrocarbon chains.[2–4,8,9]

The main difference in molecular conformation between $C_nAzoC_5N^+Br^-$ and $C_6AzoC_{10}N^+Br^-$ is the dihedral angle of C(6)–C(7)–C(8)–C(9). That is, in the former it is *trans*, while in the latter it is *gauche*, which makes the section (70 Å^2=bc sin α) of the hydrophilic part larger than that of $C_nAzoC_5N^+Br^-$ by about 20 Å^2.

Crystal Structure of $C_6AzoC_{10}N^+Br^-$. The packing arrangement viewd along the c- and b-axis are shown in Figs. 2 and 3, respectively. The crystal structure can be considered as an alternation of the hydrophobic and hydrophilic layers stacked along the a axis. In the hydrophobic layer, two molecules are related by the inversion symmetry in the tail-to-tail fashion with the shortest distance of 3.42(1) Å. The alkyl chains and azobenzene moieties are stabilized by the van der Waals interaction. In the hydrophilic layer, the bromide anion is linked to the hydroxyl group of the adjacent molecule by a hydrogen bond with a distance of 3.200(2) Å. Through the hydrogen bonds between the bromide anions and hydroxyl groups, the hydrophilic head groups of amphiphiles are interdigitate mutually in adjacent bilayers. In addition to the electrostatic interaction between the cationic ammonium nitrogens and bromide anions, this interdigitated orientation stabilizes the crystal.

In the case of $C_nAzoC_5N^+Br^-$ crystals, the ammonium cations and bromide anions have almost the same values of x fractional coordinates,[2–4] so they make the common plane parallel to the layer surface. In this crystal, however, the ammonium cation is separated from the bromide anion about 1.34 Å along the a-direction (Table 1).

The azobenzene chromophores in the $C_6AzoC_{10}N^+Br^-$ crystal show an absorption maximum (λ_{max}) at 365 nm. On the other hand, those in the typical J-aggregates, $C_nAzoC_5N^+Br^-$, show λ_{max} at 375 nm.[10] The difference in λ_{max} must be due to the difference of the chromophore orientations in the crystals. In the case of $C_6AzoC_{10}N^+Br^-$, the adjacent azobenzenes are overlapped with each other along their long axes with a separation of about 3.55 Å. On the other hand, in the case of $C_nAzoC_5N^+Br^-$, the adjacent azobenzenes are overlapped in a similar way, but the overlapped region is small and the interplanar spacing is large (about 3.62 Å).

References

1) M. Shimomura, R. Audo, and T. Kunitake, *Ber. Bunsen-Ges. Phys. Chem.*, **87**, 1134 (1983).

2) K. Okuyama, H. Watanabe, M. Shimomura, K. Hirabayashi, T. Kunitake, T. Kajiyama, and N. Yasuoka, *Bull. Chem. Soc. Jpn.*, **59**, 3351 (1986).

3) H. Watanabe, K. Okuyama, Y. Ozawa, K. Hirabayashi, M. Shimomura, T. Kunitake, and N. Yasuoka, *Nippon Kagaku Kaishi*, **1987**, 550.

4) K. Okuyama, C. Mizuguchi, G. Xu, and M. Shimomura, *Bull. Chem. Soc. Jpn.*, **62**, 3211 (1989).

5) J. Yao, C. Zheng, J. Qian, F. Han, Y. Gu, and H. Fan, SAPI-85. "A System of Computer Programs for the Automatic Solution of Crystal Structures from X-ray diffraction Data," Academia Sinica, Beijing, China (1985).

6) Tables of anisotropic thermal parameters, coordinates of hydrogen atoms, and observed and calculated structure factors are deposited as Document No. 9097 at the Office of the Editor of Bull. Chem. Soc. Jpn.

7) "International Tables for X-ray Crystallography," Kynoch Press, Birmingham (1974), Vol. IV, p. 71.

8) S. Abrahamson, B. Dahlen, and I. Pascher, *Acta Crystallogr., Sect. B*, **33**, 2008 (1977).

9) I. Pascher and S. Sundell, *Chem. Phys. Lipids*, **20**, 175 (1977).

10) K. Okuyama, *Hyōmen*, **27**, 989 (1989).

11) C. K. Johnson, ORTEP II, Report ORNL-5138, Oak Ridge National Laboratory, Tennessee (1976).

Studies on Mixed Chelates. XIX. 5-Coordinate Nickel(II) Complexes with *N,N,N′N″,N″*-Pentamethyldiethylenetriamine and β-Diketonates[1)]

Noriko SHINTANI, Kozo SONE,* Yutaka FUKUDA,* and Yuji OHASHI†
Department of Chemistry, Faculty of Science, Ochanomizu University, Otsuka, Bunkyo-ku, Tokyo 112
† Department of Chemistry, Faculty of Science, Tokyo Institute of Technology, Ookayama, Meguro-ku, Tokyo 152
(Received June 2, 1990)

Mixed Ni(II) chelates with *N,N,N′,N″,N″*-pentamethyldiethylenetriamine (pmdt) and a β-diketonate (dike) such as acetylacetonate(acac), dipivaloylmethanate(dipm), pivaloyltrifluoroacetonate(pfac), trifluoroacetylacetonate(tfac) or hexafluoroacetylacetonate(hfac) were prepared, and their structure and properites were studied. X-Ray crystal analysis confirmed that [Ni(acac)(pmdt)]ClO_4 is a distorted square pyramidal complex, and the solid reflection spectra of the remaining chelates indicated that most of them are also essentially square pyramidal. This structure is retained in a nonpolar solvent like 1,2-dichloroethane, but in strong donor solvents like DMSO or DMF it is converted into a 6-coordinated structure, [Ni(dike)(pmdt)(Solvent)]$^+$, containing a solvent molecule. The formation of this species is favored by increasing donor number(DN) of the solvent, and in the following order of dike:dipm<acac≪tfac, pfac≪hfac, which is almost opposite to the order of their pK_a values.

In the foregoing papers of this series[2–4)], it was reported that the 4-coordinate Ni(II) chelates with *N,N,N′,N′*-tetramethylethylenediamine(tmen; $Me_2N(CH_2)_2NMe_2$) and a β-diketonate (dike), [Ni(dike)(tmen)]X (X=ClO_4^- or BPh_4^-) are soluble in various organic solvents, and are strongly solvatochromic, changing from red(square planar form) in 1,2-dichloroethane(DCE) to green (octahedral disolvated form) in dimethyl sulfoxide(DMSO) or *N,N*-dimethylformamide(DMF). The equilibrium between these two forms depends upon the donor properties of the solvent:

$$[Ni(acac)(tmen)]^+ + 2Solvent \rightleftharpoons [Ni(acac)(tmen)(Solvent)_2]^+$$

4-coordinate(red) 6-coordinate(green)

It shifts extremely to the left hand side in a weak donor solvent like DCE, and vice versa in a strong donor solvent like DMSO.

In order to compare with them, we have now prepared the corresponding mixed Ni(II) chelates with *N,N,N′,N″,N″*-pentamethyldiethylenetriamine(pmdt; $Me_2N(CH_2)_2NMe(CH_2)_2NMe_2$) and a dike, and studied their structure and solvatochromic changes. Pmdt is a bulky tridentate ligand which, like tmen, cannot form bis-type chelates with the metal ions of the first transition series, and has a marked tendency of forming 5-coordinate complex species with them. After the pioneering work of Ciampolini and Speroni,[5)] a large amount of works has been published on its complexes (cf., e.g., the series of Hendrickson et al.[6)] on its characteristic dimeric complexes with Cu(II)). As to its Ni(II) complexes, the species such as [NiX_2(pmdt)],[5)] [NiX(NH_3)(pmdt)]X·nH_2O(X$^-$=Cl^-, Br^- or I^-),[7)] and [Ni(NH_3)$_2$(pmdt)](ClO_4)$_2$[7)] have been studied; all of them are typically 5-coordinate, evidently owning to the bulkiness of pmdt which hinders the coordination of the 6th ligand.

As can be expected, most of the newly obtained mixed chelate were also found to be 5-coordinate, and they show a new kind of solvatochromism which will be discussed in this paper.

Experimental

Materials. The ligands used are pmdt, acetylacetone(Hacac), dipivaloylmethane(Hdipm), pivaloyltrifluoroacetone(Hpfac), trifluoroacetylacetone(Htfac) and hexafluoroacetylacetone(Hhfac). These and other reagents used are of the best commercial grade, and were used without further purification. Solvents used for spectral measurements are "Spectro-grade"; if necessary, they were purified by distillation.

Syntheses of the Chelates, [Ni(dike)(pmdt)]ClO_4. 10 mmol of Ni(ClO_4)$_2$·6H_2O were dissolved in 30 ml of methanol (MeOH), and 10 mmol of pmdt were added to it with stirring. Then a solution containing a diketone (Hdike) and KOH (10 mmol each) in 30 ml of MeOH was added to the mixture with heating and stirring. The resultant solution was filtered, and let stand for a few days. Crude green crystals which precipitated were recrystallized from DCE.

The analytical data, colors, and magnetic moments of the obtained chelates are shown in Table 1. The pfac and hfac chelates were found to be monohydrates; TG-DTA data show that they lose their water at about 70 °C in static air.

Measurements of Electronic Spectra. Electronic spectra of solutions were obtained with a Hitachi 340 recording spectrophotometer using 10 mm quartz cells at room temperature (ca. 20 °C). The electronic spectral data ($\tilde{\nu}_{max}$ and ε_{max}) in various organic solvents are deposited as Document No. 9099 (Table A) at the Office of the Editor of Bull. Chem. Soc. Jpn. Powder reflection spectra were recorded with the same instrument equipped with an

Table 1. Analytical Data, Color, Magnetic Moments, and K Values of the New Chelates

	C%[a]	H%[a]	N%[a]	Color	μ_{eff}/B.M.	K[b]
[Ni(dipm)(pmdt)]ClO_4	45.87 (46.76)	8.03 (8.04)	8.08 (8.18)	Green	3.25	1.5
[Ni(acac)(pmdt)]ClO_4	39.04 (39.05)	6.78 (7.02)	9.84 (9.76)	Green	3.22	3.2
[Ni(pfac)(pmdt)(H_2O)]ClO_4	37.35 (37.63)	6.07 (6.13)	7.76 (7.74)	Green	3.23	25[c]
[Ni(tfac)(pmdt)]ClO_4	34.62 (34.62)	5.43 (5.62)	8.67 (8.67)	Green	3.24	19.4
[Ni(hfac)(pmdt)(H_2O)]ClO_4	30.38 (30.22)	4.14 (4.50)	7.78 (7.55)	Light green	2.78[d]	88[c]

a) Calculated values are in parentheses. b) See text. c) Measured with dehydrated chelates. d) The reason for this smaller value is an open question.

integrating sphere, using $BaSO_4$ as the reference. The determination of the equilibrium constants(K) of the equilibrium(1) (see text) was made with a JASCO Ubest-30 spectrophotometer. A series of DCE solutions containing 10 mM (M=mol·dm^{-3}) of the 5-coordinate species and various amounts (between 0.2 M and 1.5 M) of DMSO was prepared with each chelate, and their spectra between 500 and 850 nm were measured at 25±0.5 °C, using the DCE solution (10 mM) of the same chelate with no DMSO as the reference. The values of K were then calculated from the obtained absorbances by means of the Benesi-Hildebrand plots.[8]

Other Physical Measurements. Infrared spectra (400—5000 cm^{-1}) were measured in Nujol mulls with a JASCO IR-A3 Grating Spectrophotometer. Magnetic susceptibility measurements were performed with a Shimadzu Torsion Magnetometer MB-100 at room temperature. Thermogravimetry-differential thermal analysis (TG-DTA) measurements were performed with a Differential Thermal Analyser TGD-3000M (Shinku-Riko) under static air with the heating rate of 3 °C min^{-1} or 1 °C min^{-1}.

Crystal Structure Analysis of [Ni(acac)(pmdt)]ClO_4. Green plate crystals were grown from a DCE solution. Crystals of approximate dimensions 0.3×0.3×0.4 mm^3 were used. The unit cell dimensions and space group were determined from oscillation and Weissenberg photographs. Accurate cell parameters were determined by a least-squares fit for 18 reflections within the range $18°<2\theta<28°$ measured on a Rigaku AFC-4 diffractometer with Mo $K\alpha$ radiation (λ= 0.71069 Å) monochromated by graphite.

Crystal Data: Mr=430.57, $NiC_{14}ClH_{30}N_3O_6$, monoclinic, $P2_1$, a=8.8285(8), b=13.467(1), c=8.590(1) Å, β=92.25(2), V=1020.5(2) Å^3, Z=2, d=1.401 g cm^{-3}, μ=10.49 cm^{-1}, $F(000)$= 456.

Reflection data were collected on a 2θ-ω scan mode, up to 2θ=55° with scan widths of $\Delta\omega=(1.0+0.35\tan\theta)$. Backgrounds were counted for 5 s at both ends of scan. Three standard reflections were recorded after every 50 reflections. This crystal was slowly decomposed probably due to deliquescence, of which intensity data decreased by 10%. The data were corrected using standard reflections. A total of 2447 reflections were collected at the rate of 8° (2θ) min^{-1}, of which 2203 were treated as significant ($|F_o|>3\sigma(|F_o|)$). The structure was solved by the direct method by using the program MALTAN78[9] and was refined by full matrix least-squares with SHELX76.[10] The quantity minimized was $\sum\omega(|F_o|-|F_c|)^2$, where $\omega=(\sigma(F_o)^2+0.004|F_o|^2)^{-1}$. Atomic scattering factors were taken from the International Tables for X-ray Crystallography.[11] All the non-hydrogen atoms were refined anisotropically. Hydrogen atoms found in the difference Fourier maps and derived geometrically were refined isotropically. Max. Δ/ρ and max. $\Delta\rho$ in the final difference map were 0.30 and 0.55 e Å^{-3} (within 1 Å from Nickel). Final R (and R_w) was 0.053 (0.059). The final coordinates of non-hydrogen atoms are given in Table 2. Computations were carried out on IBM 4381-R24 computer at the Computer Center of Ochanomizu University. The tables for the anisotropic temperature factors for non-hydrogen atoms (Table B), the F_o—F_c list (Table C), the atomic parameters for the H atoms (Table D) and remaining bond distances and angles (Table E) are deposited as Document No. 9099 at the Office of the Editor of Bull.

Table 2. Final Atomic Coordinates with Their Estimated Standard Deviations, Multiplied by 10^4 for All the Atoms

Atom	x	y	z	B(eq)
Ni	7731(1)	3485	4983(1)	2.9
N(1)	9740(7)	3090(5)	3875(8)	3.9
N(2)	8312(9)	2327(5)	6504(7)	4.3
N(3)	6443(8)	4017(5)	6807(7)	4.2
O(1)	7507(6)	4739(4)	3819(6)	3.8
O(2)	6178(6)	2781(4)	3733(6)	3.8
O(3)	2892(11)	5562(10)	9545(14)	9.5
O(4)	382(11)	5347(10)	10119(12)	9.7
O(5)	1889(18)	3998(9)	9350(18)	12.0
O(6)	1161(13)	5160(11)	7597(8)	9.6
C(1)	9472(11)	2903(9)	2188(10)	5.4
C(2)	10827(10)	3913(8)	4104(13)	5.3
C(3)	10293(11)	2165(7)	4612(12)	5.3
C(4)	9966(13)	2148(8)	6337(13)	5.5
C(5)	7442(12)	1411(6)	6160(11)	4.8
C(6)	7988(15)	2717(8)	8077(9)	6.1
C(7)	6484(14)	3222(7)	8012(10)	5.7
C(8)	7197(17)	4909(8)	7462(13)	6.7
C(9)	4866(13)	4261(15)	6344(16)	8.3
C(10)	6536(9)	4864(6)	2683(8)	3.8
C(11)	6549(12)	5863(7)	1899(12)	5.2
C(12)	5527(9)	4143(6)	2088(9)	3.8
C(13)	5425(9)	3158(6)	2636(9)	3.8
C(14)	4334(11)	2481(7)	1765(11)	4.9
Cl	1579(2)	5019(2)	9185(2)	4.5

Chem. Soc. Jpn.

Results and Discussion

Structure of Crystalline Chelates. As can be seen from Table 1, we obtained five new chelates of two types, one formulated as $[Ni(dike)(pmdt)]ClO_4$ and the other as $[Ni(dike)(pmdt)(H_2O)]ClO_4$. They are all green high-spin d^8 chelates, with magnetic moments corresponding to two unpaired electrons.

Table 3. Bond Lengths (Å) and Angles (°)

		N(1)-Ni-N(2)	84.5(3)
Ni-N(1)	2.114(7)	N(1)-Ni-N(3)	155.7(3)
Ni-N(2)	2.086(7)	N(1)-Ni-O(1)	93.2(2)
Ni-N(3)	2.098(6)	N(1)-Ni-O(2)	102.3(2)
Ni-O(1)	1.968(5)	N(2)-Ni-N(3)	85.1(3)
Ni-O(2)	1.954(6)	N(2)-Ni-O(1)	167.7(3)
N(1)-C(1)	1.481(14)	N(2)-Ni-O(2)	97.6(3)
N(1)-C(2)	1.474(13)	N(3)-Ni-O(1)	92.3(2)
N(1)-C(3)	1.472(12)	N(3)-Ni-O(2)	100.8(3)
N(2)-C(4)	1.492(14)	O(1)-Ni-O(2)	94.8(2)
N(2)-C(5)	1.477(14)	Ni-N(1)-C(1)	112.2(5)
N(2)-C(6)	1.488(15)	Ni-N(1)-C(2)	107.7(5)
N(3)-C(7)	1.488(14)	Ni-N(1)-C(3)	106.8(5)
N(3)-C(8)	1.474(16)	C(1)-N(1)-C(2)	109.7(8)
N(3)-C(9)	1.470(22)	C(1)-N(1)-C(3)	108.3(8)
O(1)-C(10)	1.284(10)	C(2)-N(1)-C(3)	112.1(7)
O(2)-C(13)	1.240(10)	Ni-N(2)-C(4)	106.1(5)
O(3)-Cl	1.396(13)	Ni-N(2)-C(5)	112.6(5)
O(4)-Cl	1.422(14)	Ni-N(2)-C(6)	104.7(5)
O(5)-Cl	1.408(16)	C(4)-N(2)-C(5)	110.4(8)
O(6)-Cl	1.411(14)	C(4)-N(2)-C(6)	111.6(8)
C(3)-C(4)	1.521(15)	C(5)-N(2)-C(6)	111.1(8)
C(6)-C(7)	1.491(18)	Ni-N(3)-C(7)	105.9(5)
C(10)-C(11)	1.505(14)	Ni-N(3)-C(8)	108.3(6)
C(10)-C(12)	1.401(12)	C(7)-N(3)-C(8)	108.8(9)
C(12)-C(13)	1.412(12)	C(7)-N(3)-C(9)	110.3(10)
C(13)-C(14)	1.503(13)	C(8)-N(3)-C(9)	109.2(11)
		Ni-O(1)-C(10)	123.3(5)
		Ni-O(2)-C(13)	124.2(5)
		N(1)-C(3)-C(4)	111.0(8)
		N(2)-C(4)-C(3)	108.4(9)
		N(2)-C(6)-C(7)	109.2(10)
		N(3)-C(7)-C(6)	110.6(10)
		O(1)-C(10)-C(11)	116.2(7)
		O(1)-C(10)-C(12)	125.6(7)
		C(11)-C(10)-C(12)	118.2(8)
		C(10)-C(12)-C(13)	125.3(8)
		O(2)-C(13)-C(12)	126.8(8)
		O(2)-C(13)-C(14)	116.4(8)
		C(12)-C(13)-C(14)	116.8(8)
		O(3)-Cl-O(4)	110.0(8)
		O(3)-Cl-O(5)	109.4(8)
		O(3)-Cl-O(6)	109.1(8)
		O(4)-Cl-O(5)	113.1(9)
		O(4)-Cl-O(6)	109.4(8)
		O(5)-Cl-O(6)	105.7(9)

The structure of $[Ni(acac)(pmdt)]ClO_4$ with the atomic numbering is presented in Fig. 1, and its selected bond lengths and angles are shown in Table 3. The atoms in the first coordination sphere form a distorted square pyramid, a typical 5-coordinate structure; the three N atoms of pmdt (N1, N2, N3) and one O atom of acac (O1) form a distorted square around Ni(II), which is capped by another O of acac (O2). The four atoms forming the distorted square are not exactly coplanar; two (N1, N3) are below and two (N2, O1) are above, each ca. 0.1 Å away from the mean plane. The central Ni(II), on the other hand, lies at 0.31 Å above it. It is also noted that an O(O6) of ClO_4^- is located at the opposite side of the cap, seemingly occupying the 6th coordination site. But the Ni-O6 distance is so long (4.33 Å) that no significant bonding is expected along it. The bond lengths between the nickel(II) ion and five donor atoms are nearly the same as those reported for another distorted square pyramidal nickel(II) complex $[Ni\{5\text{-Cl-SALen-N}(C_2H_5)_2\}_2]$,[12] and

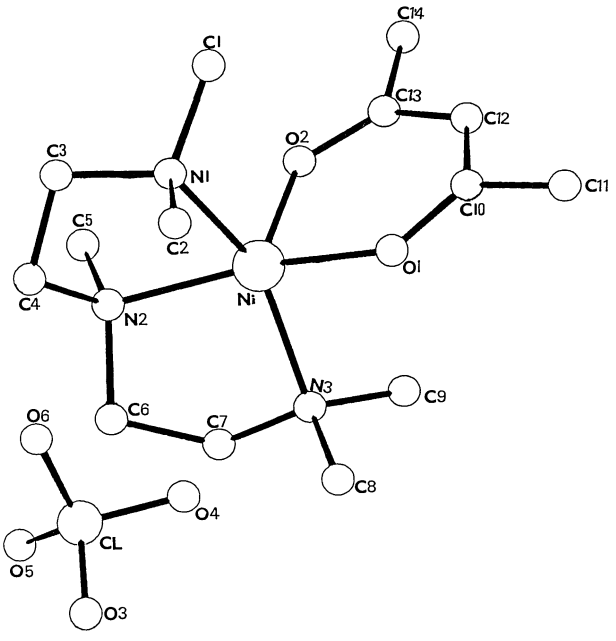

Fig. 1. Structure of $[Ni(acac)(pmdt)]ClO_4$.

Table 4. Band Maxima of the Powder Reflection Spectra

Chelate	$\tilde{\nu}_{max}/10^3$ cm^{-1}			
$[Ni(dipm)(pmdt)]ClO_4$	10.79	13.33	16.26	27.06
$[Ni(acac)(pmdt)]ClO_4$	10.98	12.90	16.36	26.78(sh)[b]
$[Ni(pfac)(pmdt)(H_2O)]ClO_4$	10.12	16.29		
$[Ni(pfac)(pmdt)]ClO_4$[a]	10.80	13.16	16.44	26.5(sh)[b]
$[Ni(tfac)(pmdt)]ClO_4$	11.05	13.07	16.45	26.5(sh)[b]
$[Ni(hfac)(pmdt)(H_2O)]ClO_4$	10.53	16.28		

a) Measured after dehydration of the hydrated chelate (see text). b) sh=shoulder.

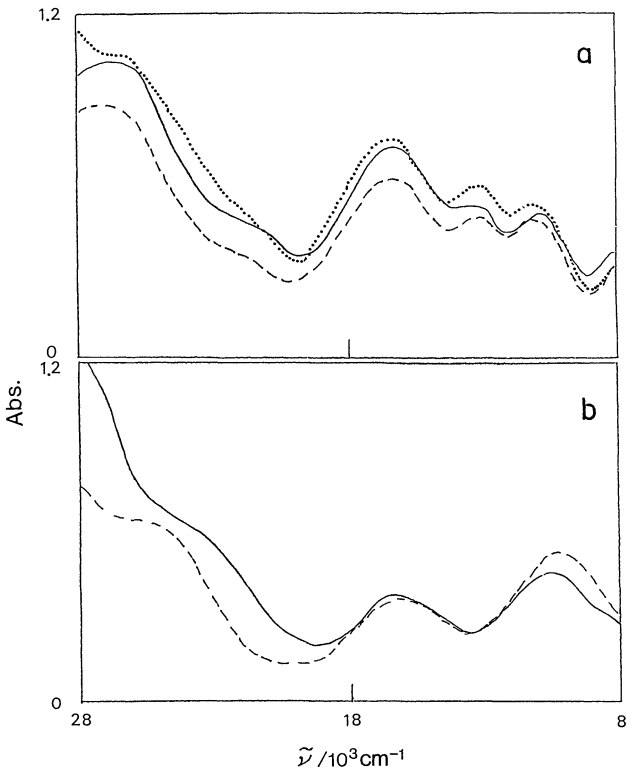

Fig. 2. Powder reflection spectra of the new 5-coordinate chelates [Ni(dike)(pmdt)]ClO_4 (a) and 6-coordinate hydrates [Ni(dike)(pmdt)(H_2O)]ClO_4 (b). The dike's in (a) are dipm (—), acac (----), and tfac (·····); those in (b) are hfac (—) and pfac (----).

for the related octahedral Ni(II) complexes.[13]

The solid reflection spectra of the dipm, acac, and tfac chelates are now very similar (cf. Fig. 2a), showing 4 bands at ca. 11×10^3 cm^{-1}, 13×10^3 cm^{-1}, 16×10^3 cm^{-1} and 27×10^3 cm^{-1}. This fact indicates that all these chelates are stereochemically similar, i.e., are 5-coordinated square pyramidal chelates; in fact the positions of these bands are not very different from those of the square pyramidal Ni(II) chelate mentioned above, the spectrum of which was explained with a crystal field model.[12,14] Although the angular overlap model shows that such a Ni(II) complex should be unstable in comparison with the 6-coordinate octahedral one,[15] the obtained complexes are apparently very stable, probably owing to the steric hindrance of the bulky groups on pmdt.

On the other hand, the hydrated pfac and hfac chelates show spectra of a different type, with only two bands at ca. 10×10^3 cm^{-1} and 16×10^3 cm^{-1}, which is characteristic to Ni(II) chelates of 6-coordinate structure (Fig. 2b). This indicates that these chelates should be formulated as [Ni(dike)(pmdt)(H_2O)]ClO_4 with an H_2O molecule at the 6th coordination site. When the hydrated pfac chelate is heated at 60 °C in vacuum, a remarkable spectral change takes place, until the spectrum becomes quite similar to those in Fig. 2a. The ν_{OH} band in its IR spectrum is lost at the same time. These changes show that the chelate become 5-coordinated by dehydration.

The reflection and IR spectra of the hydrated hfac chelate, however, were found to change only little by such a treatment, although TG-DTA data show that it is dehydrated nearly as easily as the hydrated pfac chelate. Here it seems that the dehydrated chelate absorbs atmospheric water so readily, that most of it reverts to the hydrated state in the course of spectral measurements. Thus the spectrum of the dehydrated hfac chelate in solid state has not yet been obtained.

Solvatochromism in Organic Solvents. When these chelates are dissolved in DCE, they form green solutions. The spectra of the solutions of the acac, dipm, tfac chelates show strong bands at ca. 16×10^3 cm^{-1} and 26×10^3 cm^{-1}, and weaker bands (or shoulders) at ca. 11×10^3 cm^{-1} and 13×10^3 cm^{-1}. The spectra thus resemble those of their solids (in the case of the pfac chelate, that of the dehydrated one), indicating that the 5-coordinate structure in the solid state is retained in DCE solution.

In the case of the dipm and acac chelates, similar spectra are observed also in a number of other solvents, i.e., nitromethane(NM), methanol(MeOH), ethanol(EtOH), acetone, and acetonitrile(MeCN). However, the solutions in DMF and DMSO show different spectra with two peaks at ca. 9×10^3 cm^{-1} and 16×10^3 cm^{-1}, which are similar to the solid spectra of hydrated chelates of pfac and hfac. This spectral change indicates that, in these solvents of very high DN (Gutmann's donor number),[16] a solvent molecule combines with the 5-coordinated chelate, and converts it into a 6-coordinate species, [Ni(dike)(pmdt)(Solvent)]$^+$.

A closer look at these spectral data, some of which are shown in Figs. 3a—3c, reveals further that, in the case of the acac chelate, the ε values of the two strong bands of the 5-coordinated species gradually decrease in the order of

$$DCE>NM>Acetone>EtOH>MeOH$$

with the increase of the DN of the solvent, indicating that the equilibrium

$$[Ni(dike)(pmdt)]^+ + Solvent \rightleftharpoons [Ni(dike)(pmdt)(Solvent)]^+ \quad (1)$$

established in these solutions is shifted to the right hand side with the increase of solvent DN. In the case of the dipm chelate, on the other hand, the ε values in these solvents are mostly not very different from each other, showing that the 5-coordinated species predominates in them. (A notable exception from these general tendencies is the case of MeCN; while its DN lies between those of NM and acetone, the ε values of the bands of the 5-coordinate species in it are lower than

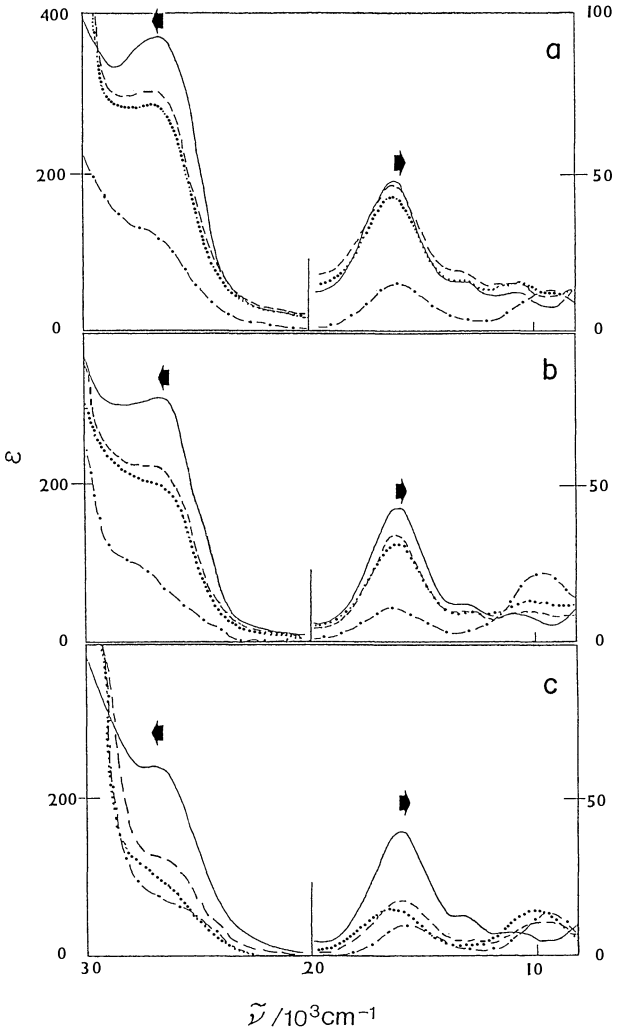

Fig. 3. Electronic spectra of [Ni(dipm)(pmdt)]ClO_4 (a), [Ni(acac)(pmdt)]ClO_4 (b), and [Ni(tfac)(pmdt)]-ClO_4 (c) in DCE (—), MeOH (----), MeCN (·····), and DMSO (-·-·-). Concn: ca. 1.0×10^{-3} M (M= mol dm^{-3}).

those in methanol, suggesting that the rod-like (and π-electron rich) molecule of MeCN can get into the sterically hindered 6th coordination site of Ni(II) more easily than alcohols and acetone, as was observed also in other cases[17]).

In the case of the tfac chelate, the ε values of the bands of the 5-coordinate species in acetone (e.g., 31 at 16.13×10^3 cm^{-1}) are notably lower than those in DCE(40) and NM(37), and the spectra in alcohols and MeCN are nearly those of the 6-coordinate species. Similar trends are observed also with the pfac chelate; here the coordinated H_2O molecule in the solid hydrate readily dissociates from Ni in an organic solvent, so that the spectra of the hydrated and dehydrated chelates in it are nearly the same. In the case of the hydrated hfac chelate, the spectra show that the 6-coordinate species exist predominantly in all solvents, even in DCE; comparison of their $\tilde{\nu}_{max}$ values

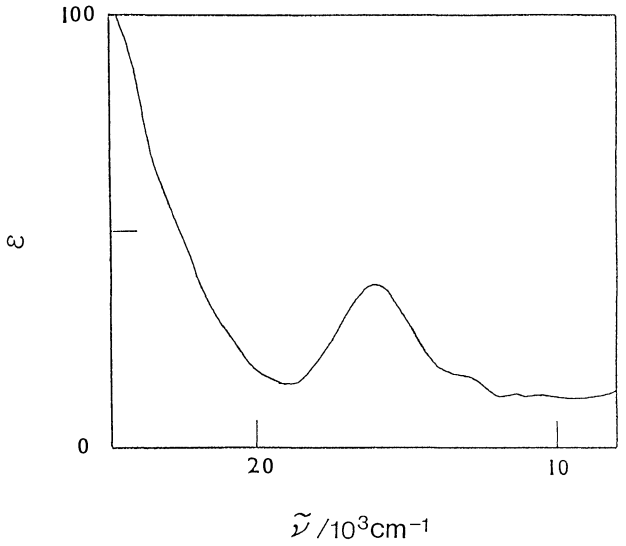

Fig. 4. Electronic spectrum of a DCE solution containing [Ni(hfac)(pmdt)]ClO_4 (see text). Concn: ca. 1.0×10^{-3} M.

(e.g., 10.4 and 16.1 in DCE, 9.8 and 16.0 in Me_2CO and 9.4 and 15.7 in DMSO, in 10^3 cm^{-1}) with those of the solid (10.5 and 16.3) shows that the 6th ligand is water in solvents of low DN, but it is substituted by a solvent molecule in more polar solvents.

Comparison of all these spectra thus leads to the conclusion that the equilibrium (1) is shifted to the right hand side with the increase of solvent DN (except MeCN; see above), and in the following order of the dike ligands:

$$\text{dipm} < \text{acac} \ll \text{tfac},\ \text{pfac} \ll \text{hfac} \qquad (2)$$

That is to say, the hfac chelate tends to be 6-coordinate in all solvents, combining with water when the coordination ability of the solvent is too low. The tfac and pfac chelates are 5-coordinate in DCE, but are converted to the 6-coordinate species even in solvents of relatively low DN. On the other hand, the dipm chelate is 5-coordinate (or mainly so) in most solvents tried, and gets 6-coordinate only in solvents of very high DN, and the acac chelate comes between these extremes.

A quantitative support to this view was obtained by the determination of K of the equilibrium(1) for each chelate, using DMSO as the coordinating solvent and studying the equilibrium in DCE. In the case of the hfac chelate, special care was taken to remove water from the system; using freshly dehydrated materials, a DCE solution which shows a typical spectrum of a 5-coordinate species (i.e., which contains the 5-coordinate chelate $[Ni(hfac)(pmdt)]^+$; cf. Fig. 4) was obtained and used for study. The obtained K values (Table 1) increase in the order of (2), or with the decrease of the pK_a of the dike ligand (cf. Fig. 5);[18–20] since the latter values can be taken as the measures of the ligand field strengths of the dike ligands, these

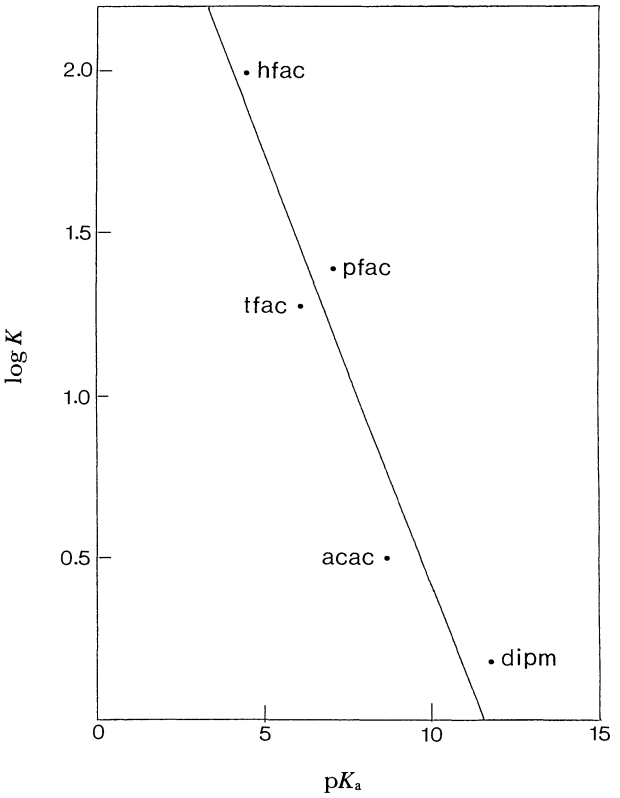

Fig. 5. Relation between pK_a of dike[19,20] and $\log K$ for the formation of [Ni(dike)(pmdt)(DMSO)]ClO_4 in DCE.

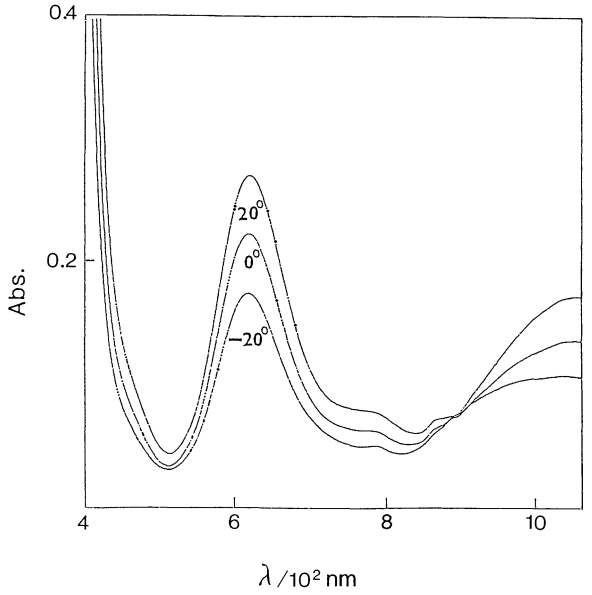

Fig. 6. Temperature dependence of the spectrum of [Ni(acac)(pmdt)]ClO_4 in a DCE–DMSO solution. Concn of the chelate: 9.88×10^{-3} M; concn of DMSO: 2.26×10^{-1} M.

results lead to the reasonable conclusion that the tendency of a $[Ni(dike)(pmdt)]^+$ type chelate to combine with solvent (i.e., its Lewis acidity) increases with the decrease of the ligand field strength (i.e., Lewis basicity) of dike.

It was also found that the DCE solutions of the dipm, acac, tfac, and pfac chelates containing DMSO are thermochromic; the data of the acac chelate are in Fig. 6. The band at 16×10^3 cm^{-1} becomes stronger and that at 10×10^3 cm^{-1} weaker, with the rise of temperature, forming an isosbestic point, and showing that the equilibrium(1) is shifted to the left hand side by heating. Similar but smaller spectral changes were also obtained with the dipm, tfac, and pfac chelates; in these cases, the equilibrium (1) is shifted more strongly to the left (dipm) or right (tfac, pfac) hand side than acac, so that the systems seem to be more insensitive to the temperature change.

We are grateful to Ms. Yuko Kojima (Ochanomizu Univ.) and Ms. Akiko Sekine (Tokyo Institute of Technology) for their technical assistance in the crystal structure analysis. This work was partially supported by a Grant-in-Aid for Scientific Research No. 02453038 from the Ministry of Education, Science and Culture.

References

1) Part XVIII: Y. Fukuda, Y. Akutagawa, Y. Ihara, and K. Sone, *Synth. React. Inorg. Met. Org. Chem.*, in press (1991).
2) Y. Fukuda and K. Sone, *Bull. Chem. Soc. Jpn.*, **43**, 2282 (1970).
3) Y. Fukuda and K. Sone, *J. Inorg. Nucl. Chem.*, **34**, 2315 (1972); **37**, 455 (1975).
4) K. Sone and Y. Fukuda, "Inorganic Thermochromism," Springer, Heidelberg (1987).
5) M. Ciampolini and G. P. Speroni, *Inorg. Chem.*, **5**, 45 (1966).
6) M. S. Haddad, E. N. Duesler, and D. N. Hendrickson, *Inorg. Chem.*, **18**, 141 (1979), and foregoing papers of the same series.
7) A. Uehara, M. Shimizu, E. Kyuno, and R. Tsuchiya, *Thermochim. Acta*, **105**, 127 (1986).
8) H. A. Benesi and J. H. Hildebrand, *J. Am. Chem. Soc.*, **71**, 2703 (1949).
9) P. Main, S. E. Hull, L. Lessinger, G. Germain, J. P. Declercq, and M. M. Woolfson, MULTAN 78. A System of Computer Programs for the Automatic Solution of X-ray Diffraction Data, Univs. of York, England and Louvain, Belgium (1978).
10) G. M. Sheldrick, SHELX76. A Program for Crystal Structure Determination, Univ. of Cambridge (1976).
11) "International Tables for X-Ray Crystallography," Kynoch Press, Brimingham (1974), Vol. IV.
12) L. Sacconi, P. L. Orioli, and M. Di. Vaira, *J. Am. Chem. Soc.*, **87**, 2059 (1965).
13) Y. Fukuda, C. Fujita, H. Miyamae, H. Nakagawa, and K. Sone, *Bull. Chem. Soc. Jpn.*, **62**, 745 (1989).
14) M. Ciampolini, *Inorg. Chem.*, **5**, 35 (1966).
15) Cf., e.g., K. F. Purcell and J. C. Kotz, "Inorganic Chemistry," Saunders, Philadelphia (1977).
16) V. Gutmann, "The Donor-Acceptor Approach to

Molecular Interactions," Plenum, New York (1978).
17) Cf., e.g., Y. Fukuda, M. Cho, and K. Sone, *Bull. Chem. Soc. Jpn.*, **62**, 51 (1989).
18) L. G. Sillen and A. E. Martell, "Stability Constants," the Chemical Society, London (1971).
19) T. Sekine, Y. Hasegawa, and N. Ihara, *J. Inorg. Nucl. Chem.*, **35**, 3968 (1973).
20) E. B. Sandell and H. Onishi, "Photometric Determination of Traces of Metals," 4th ed, Wiley, New York (1978).

 © 1991 The Chemical Society of Japan Bull. Chem. Soc. Jpn., 64, 259—265 (1991)

Substituent Effects in the Decomposition of *t*-Alkyl *t*-Butyl Peroxides

Kazuo MATSUYAMA* and Yoshiki HIGUCHI
Chemicals & Explosives Research Laboratory, Nippon Oil & Fats Co., Ltd.,
Taketoyo-cho, Chita-gun, Aichi 470-23
(Received August 2, 1990)

The decomposition rates and products of various *t*-alkyl *t*-butyl peroxides were examined in cumene at several temperatures. The decomposition of these peroxides took place homolytically, depending on the structure of the *t*-alkoxyl moieties ($RC(CH_3)_2$–O), and was retarded in the order: $R=(CH_3)_3CCH_2>(CH_3)_2CH>CH_3CH_2CH_2>PhCH_2>CH_3CH_2>ClCH_2>CH_3$. The rate constants for the electron-donating alkyl substitutents at 150 °C are correlated very well to a Taft equation ($\log k_d=-10.93\,\Sigma\sigma^*-6.61$ (correlation coefficient of 0.9501)), which is fairly different from the equation $\log k_d=-0.131\,\Sigma\sigma^*-3.422$ for electorn-withdrawing polar substituents. From this correlation and a product analysis, the nature of the polar character at the transition state of the decomposition is discussed.

Dialkyl peroxides have received considerable attention as clean sources of alkoxyl radicals and important intermediates in the oxidation or combustion of hydrocarbons. So far, many studies concerning the decomposition of dialkyl peroxides have been carried out.[1] The decomposition of di-*t*-butyl peroxide, which is probably one of the best-studied reaction in chemical kinetics, is accompanied by a slight radical-induced decomposition in most cases. However, the substituent effect correlation on the decomposition of dialkyl peroxides has not yet been made sufficiently clear, though it is believed that the decomposition rates are accelerated by electron-donating alkyl substituents.

Richardson et al. found a linear free-energy correlation concerning the decomposition of di-*t*-alkyl peroxides (*t*-alkyl denotes 1,1-dimethylalkyl through this paper) having electron-withdrawing polar substituents, where there was a very small change in the rates (ca. 1.5 times with 1.0 σ^* unit variation of the substituents studied).[2] On the other hand, the substituent effect correlation regarding the decomposition of dialkyl peroxides having electron-donating alkyl substituents was unsuccessful, because they contained primary and secondary dialkyl peroxides. Probably, the decomposition rates of bis(primary and secondary alkyl) peroxides were somewhat enhanced by an induced decomposition (Eq. 1) and a concerted decomposition (Eq. 2):[1b]

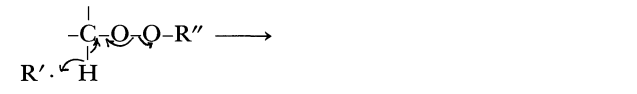

$$R'H + \rangle C{=}O + \cdot OR'' \qquad (1)$$

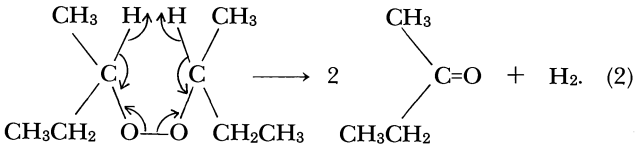

(2)

Di-*t*-alkyl peroxides, having a smaller possibility for induced decomposition, are most suitable for studying the substituent effect on O–O bond homolysis. In this work we studied the decomposition rates and products in the homolytic decomposition of *t*-alkyl *t*-butyl peroxides (**1**) in cumene in order to clearify the substituent effect. Cumene is a good solvent for investigating the homolytic reaction due to the formation of simple decomposition products:

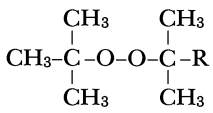

(**1**$_a$; R=CH_3, **1**$_b$; R=CH_3CH_2, **1**$_c$; R=$CH_3CH_2CH_2$, **1**$_d$; R=$(CH_3)_3CCH_2$, **1**$_e$; R=$(CH_3)_2CH$, **1**$_f$; R=$PhCH_2$, **1**$_g$; R=$ClCH_2$)

Results

The di-*t*-alkyl peroxides **1** were prepared mainly by the reaction of *t*-butyl hydroperoxide with the corresponding alcohols or olefins in the presence of sulfuric acid. The rates and products for the decomposition of **1** in cumene were determined with gas–liquid chromatography (GC) using alkanes as internal standards. Good first-order rate constants were obtained over 10—80% conversion in all cases. Decomposition rates and products data are given in Tables 1 and 2, respectively, together with calculated activation parameters. The rate constants had no appreciable change for a 10-fold increase in the concentration, thus seeming rule out any induced decomposition.

An isokinetic relationship was obtained for the decomposition of **1** in cumene (Fig. 1). Here, the steric interaction in the ground state was not important, since the values of the activation entropy decreased with those of the activation enthalpy.

Table 1 also includes a sum of the substituent constant for each peroxide. Where substituent constants were not reported, they were calculated by

Table 1. Rate Constants and Activation Parameters for Decomposition of *t*-Alkyl *t*-Butyl Peroxides in Cumene[a]

R in Peroxide, **1**	Temp	Conc	Rate const.	Activation parameter		$\Sigma\sigma^*$[b]
	°C	mol dm^{-3}	$10^6\ k_d$/s^{-1}	ΔH^*/kJ mol^{-1}	ΔS^*/J K^{-1} mol^{-1}	
CH_3[c]	125		16	154.3	48.5	−0.600
(**1a**)	135		52			
	145		156			
CH_3CH_2	110	0.05	3.86±0.04	154.1±0.8	51.5±4.2	−0.615
(**1b**)	120	0.02	12.87±0.14			
		0.05	13.20±0.10			
		0.20	14.48±0.18			
	130	0.05	43.0 ±0.4			
	140	0.05	140.6 ±1.3			
$CH_3CH_2CH_2$	110	0.05	4.38±0.04	152.9±0.1	49.4±0.8	−0.630
(**1c**)	120	0.02	15.37±0.07			
		0.05	15.37±0.19			
		0.20	15.67±0.15			
	130	0.05	49.9 ±0.4			
	140	0.05	154.4 ±1.0			
$(CH_3)_3CCH_2$	110	0.05	10.85±0.05	147.6±0.3	43.1±1.7	−0.644
(**1d**)	120	0.02	37.3 ±0.5			
		0.05	37.0 ±0.5			
		0.20	36.7 ±0.2			
	130	0.05	114.1 ±1.1			
	140	0.05	340 ±2			
$(CH_3)_2CH$	110	0.05	7.07±0.08	149.7±0.1	45.2±0.4	−0.640
(**1e**)	120	0.02	23.74±0.21			
		0.05	23.80±0.10			
		0.20	23.92±0.12			
	130	0.05	76.2 ±0.4			
	140	0.05	230.8 ±2.5			
$PhCH_2$	110	0.05	4.35±0.01	151.7±0.3	46.0±1.3	−0.420
(**1f**)	120	0.02	14.58±0.15			
		0.05	14.63±0.06			
		0.20	14.76±0.09			
	130	0.05	47.0 ±0.3			
	140	0.05	146.3 ±0.7			
$ClCH_2$	120	0.05	8.82±0.05	155.9±0.3	52.3±1.3	−0.115
(**1g**)	130	0.02	28.0 ±0.6			
		0.05	29.0 ±0.2			
		0.20	29.9 ±0.6			
	140	0.05	92.6 ±0.6			
	150	0.05	278 ±4			

a) Rate constants and their standard deviations were calculated by the method of least squares. b) See Ref. 2. c) See Ref. 1e.

Table 2. Decomposition Products of *t*-Alkyl *t*-Butyl Peroxides (**1**) in Cumene at 130°C

Substituent, R in **1**	Decomposition products[a]/mol mol^{-1}				Ratio[b]
	$[(CH_3)_3COH]$	$[CH_3COCH_3]$	$[RC(CH_3)_2OH]$	$[(PhC(CH_3)_2)_2]$	
CH_3	1.57	0.39	—	0.99	0.25
CH_3CH_2	0.78	0.95	0.13	0.91	5.77
$CH_3CH_2CH_2$	0.83	0.86	0.29	0.96	2.28
$(CH_3)_3CCH_2$	0.77	1.02	0.12	0.94	6.83
$(CH_3)_2CH$	0.84	1.16	Not detected	0.89	Infinite
$PhCH_2$	0.73	1.11	Not detected	0.53[c]	Infinite

a) The amount of decomposition products formed per the decomposed peroxide, **1**. b) The ratio of yield of acetone against that of the corresponding alcohol formed from a *t*-alkoxyl moiety. c) In addition to this compound, toluene (0.45), 1,2-diphenylethane (0.05), and 1,2-diphenyl-2-methylpropane (0.23) were detected by GC.

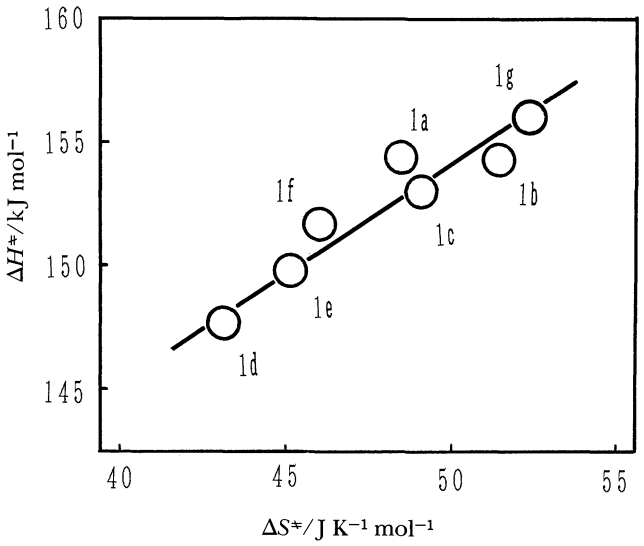

Fig. 1. An isokinetic relationship in the decomposition of *t*-alkyl *t*-butyl peroxides in cumene.

Table 3. Results of Taft Equation in Decomposition of *t*-Alkyl *t*-Butyl Peroxides[a]

Temp	ρ^* Value	Intercept	Correlation coefficient
110	−12.57	−13.16	0.9434
120	−12.28	−12.44	0.9441
130	−11.74	−11.60	0.9474
140	−11.16	−10.74	0.9453
150[b]	−10.99	−6.61	0.9501

a) The data were calculated by the method of least squares. b) The values were estimated by extrapolation using Arrhenius equation.

the known method.[2] With the exception of $\mathbf{1}_f$ and $\mathbf{1}_g$, the data in Table 1 satisfy the Taft equation as follows:

$$\log k_d = \rho^*\Sigma\sigma^* + c \quad (3)$$

Here, k_d is the rate constant for the decomposition of **1**, $\Sigma\sigma^*$ is the sum of the substituent constants by Taft, ρ^* is a reaction constant and c is an intercept, respectively. The calculated ρ^* values are shown in Table 3, together with the intercepts and correlation coefficients.

The yields of acetone and alcohols formed from **1**, and 2,3-dimethyl-2, 3-diphenylbutane (**2**) from cumene are given in Table 2, respectively. The alcohols corresponding to the *t*-alkoxyl moieties were not detected for $\mathbf{1}_e$ and $\mathbf{1}_f$. The yields of **2** were over ca. 90 %, with the exception of $\mathbf{1}_f$. The decomposition of $\mathbf{1}_f$ gave, in addition to **2** (53%), 2-methyl-2-propanol (73%), acetone (111%), toluene (45%), 1,2-diphenylethane (5%), and 1,2-diphenyl-2-methylpropane (23%). The products from the benzyl segment of $\mathbf{1}_f$ were detected in 78% yield. All of these products were formed by radical reactions. These facts suggest that **1** decomposes homolytically to follow a radical reaction outside of the solvent cage. The yield of the β-scission product, acetone from the *t*-butoxyl moiety for each peroxide of $\mathbf{1}_b$—$\mathbf{1}_f$, is equal to half that for $\mathbf{1}_a$. The acetone is obtained indpendently from the *t*-alkoxyl ($RC(CH_3)_2$-O) and *t*-butoxyl ($C(CH_3)_3$-O) moieties in each peroxide, respectively. Accordingly, the yield of the acetone from a *t*-alkoxyl moiety can be estimated by subtracting 0.39/2 (cf. $\mathbf{1}_a$) from the total acetone obtained by the decomposition of each peroxide. The ratio of the yield of the acetone against that of the corresponding alcohol formed from the *t*-alkoxyl moiety is shown in Table 2.[2]

Discussion

The effects of electron-withdrawing polar substituents on the decomposition were reported to be small. For example, Richardson et al. found the following Taft equation:

$$\log k_d = -0.131\Sigma\sigma^* - 3.422 \quad (4)$$

This equation is for the decomposition of the di-*t*-alkyl peroxides with polar substituents in chlorobenzene at 150 °C.[2] Similarly, kinetic data regarding the decomposition of bis(trifluoromethyl) peroxide in the gas phase were within the experiment error of those measured for $\mathbf{1}_a$, and the expected inductive effect of the electronegatively substituted fluorine atoms ($\Sigma\sigma^* > +2.65$) was not found.[3]

However, the electron-donating alkyl substituents considerably accelerated the decomposition of **1** in this work. Table 4 shows the relative rates (k_d/k_{d0}) of **1** against $\mathbf{1}_a$ at 150 °C, together with the data of Richardson et al. A plot of $\log(k_d/k_{d0})$ vs. $\Sigma\sigma^*$ consists of two straight lines intersecting each other at the point of $\mathbf{1}_a$ (Fig. 2). One is for the electron-donating alkyl substituents with a large slop of $\rho^* = -10.99$; the other is for the electron-withdrawing polar substituents with a small slope of $\rho^* = -0.131$. The considerable rate acceleration by the electron-donating alkyl substituents suggests that the polar character of an activation complex seems to stabilize the transition state much more. Huyser and Van Scoy investigated the effects of solvents on the unimolecular decomposition of $\mathbf{1}_a$, and indicated the dipolar character in the C–O bond of the *t*-butoxyl moiety at the transition state.[4] Similarly, the polar character of the *t*-alkoxyl moiety at the transition state was pointed out in the decomposition of *t*-alkyl 2,2-dimethylperoxypropionates,[5] which showed a similar substituent effect as that of **1**, though not sufficiently correlated with $\Sigma\sigma^*$ (correlation coefficient of 0.3890 in Table 4).

The O–O bond may be polarized when stretched at the transition state of the decomposition. That is to say, the activation complexes of **3** and **4** are stabilized by the electron-donating alkyl and electron-with-

Table 4. Influence of Substituents on Rates in Decomposition of Di-*t*-Alkyl Peroxides and Peroxy Esters in Cumene[a]

Substituent, R	Relative rate	
	$RC(CH_3)_2OOC(CH_3)_3$ at 150°C[b]	$C(CH_3)_3CO_3C(CH_3)_2R$ at 60°C[c]
CH_3	1.00	1.00
CH_3CH_2	1.52	1.19
$CH_3CH_2CH_2$	1.69	1.14
$(CH_3)_3CCH_2$	3.59	2.10
$(CH_3)_2CH$	2.46	1.74
ρ^* Value	−10.99	−6.55
Correlation coefficient	0.9051	0.3890
$PhCH_2$	1.58	2.34
$BrCH_2$[d]	(0.82)[e]	—
$ClCH_2$	1.03 (0.93)[e]	—
ρ^* Value	−0.25	—
Correlation coefficient	0.4876	—

a) The values in the table show the relative rates against R=CH_3 for decomposition rates of di-*t*-alkyl peroxides and peroxy esters. b) The extrapolated values to 150°C in this work. c) See Ref. 5. d) The sum of the substituent constant is −0.133. e) The values in parentheses is the data in chlorobenzene of Ref. 2.

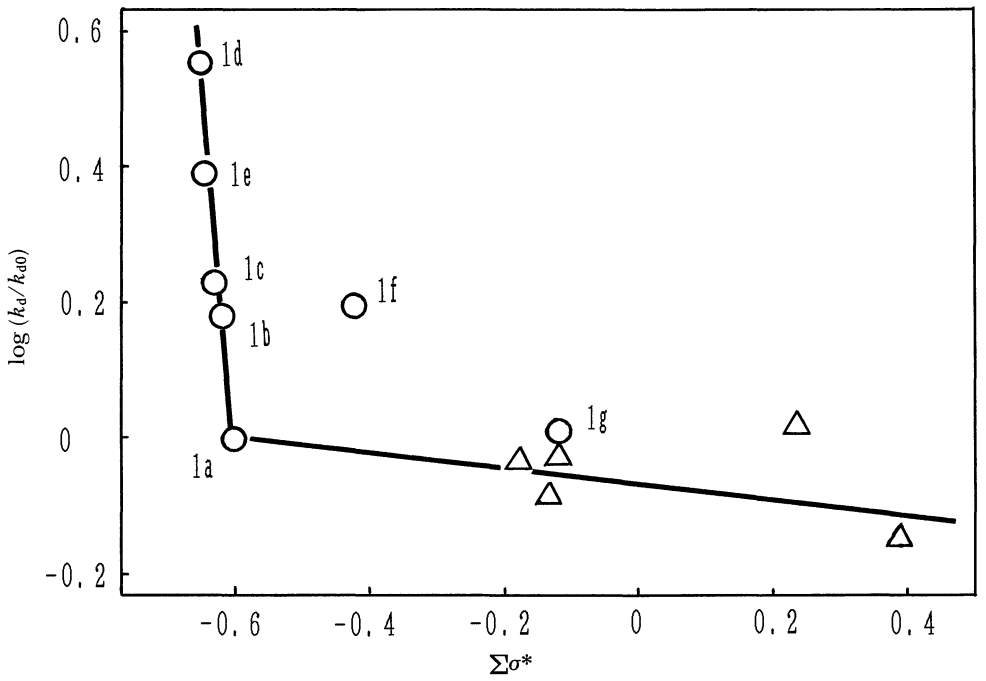

Fig. 2. A plot of log (k_d/k_{d0}) vs. $\Sigma\sigma^*$ in the decomposition of dialkyl peroxides at 150°C; ○, this work; △, the data of Richardson et al.[2]

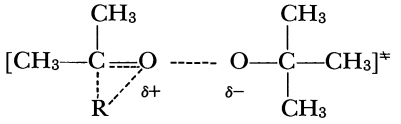

(3)

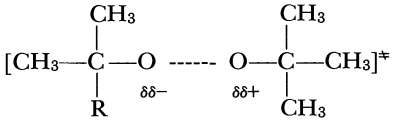

(4)

drawing polar substituents, respectively. The substituent effects of **3** and **4** are expepcted to be $\rho^*<0$ and $\rho^*>0$, respectively, but the absolute value of ρ^* in the former seems to be much larger than that in the later, by considering the difficulty that the *t*-butoxyl group is hardly able to stabilize the positive charge in **4**. On the other hand, the substituent effect in the ground state is expected to be $\rho^*<0$ on account of the stabilization by electron-withdrawing polar substituent.[2,6] Consequently, the experimental results in Fig. 2 can be understood in terms of the fact that

Table 5. Influence of Substituents on β-Scission Product Formation from *t*-Alkoxyl Moieties in Decomposition of Di-*t*-alkyl Peroxides, Peroxy Esters and Hypochlorites[a]

Substituent, R	Relative rate		
	$RC(CH_3)_2OOC(CH_3)_3$ at 130 °C	$C(CH_3)_3CO_3C(CH_3)_2R$ at 60 °C[b]	RR′R″COCl at 40 °C[c]
CH_3	0.037	0	0.01[d]
CH_3CH_2	1.00	1.00	1.00
$CH_3CH_2CH_2$	0.33	0.52	0.78[d]
$(CH_3)_3CCH_2$	1.01	1.74	0.44[d]
$(CH_3)_2CH$	Infinite	3.38	27.1[e]
$PhCH_2$	Infinite	3.19	2.72[e]
$ClCH_2$	0.057[f]	—	0.35[e]

a) The values in the table show the relative rates against R=CH_3CH_2. b) See Ref. 5. c) The data of β-scission for *t*-alkyl hypochlorites with dirrect competition method. d) See Ref. 7b. e) See Ref. 7a. f) The data of Ref. 2 at 150 °C.

negatively large ρ^* value is due to an overlap of the substituent effects at the transition and ground states in the same direction, and that the negatively small ρ^* value is a compensation of those in the opposite direction.

The substituent effect on β-scission products from the *t*-alkoxyl moiety in the decomposition of **1** is shown in Table 5 as the relative rates of **1** against $\mathbf{1_b}$ on the formation ratios of acetone against the corresponding alcohols and compared with those of *t*-alkyl 2,2-dimethylperoxypropinates[5] and *t*-alkyl hypochlorites.[7] The β-scission from **1** in this work was a non-chain decomposition, and reactions between radical pairs within a solvent cage were very few, as shown by high yields of **2**. The relative rate of **1** against $\mathbf{1_b}$ on acetone formation decreased in the following order: $R=(CH_3)_2CH\approx PhCH_2\gg CH_3CH_2>CH_3CH_2CH_2>ClCH_2\approx CH_3$. These results seem to approximately correspond to those of the peroxy esters, through the both are a little different because acetone formation in the later was suppressed by disproportionation between the *t*-butyl and the *t*-alkoxyl radicals within a solvent cage. The difference from the hypochlorites (particularly, R=$PhCH_2$ and $(CH_3)_3CCH_2$) suggests that the acetone from **1** may be formed by β-scission within a solvent cage or directly from the activation complex at the transition state.

Based on these facts, it is speculated that the C_α–C_β bond neighbouring the peroxyl oxygen atom in the di-*t*-alkyl peroxides may be slightly stretched, together with the homolytic scission of the O–O bond at the transition state.[8] Consequently, the decomposition of **1** proceeds mainly as follows:

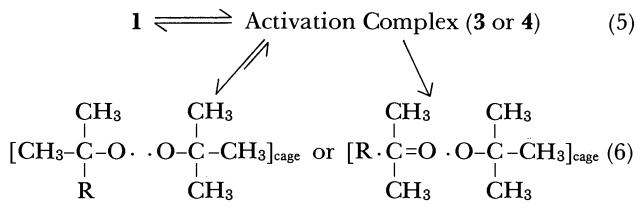

(Radical Pairs)

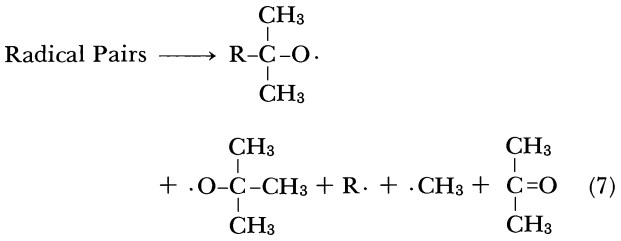

The β-scission of *t*-alkoxyl radicals out of a solvent cage competes with hydrogen abstraction from cumene. The various radicals produced in these ways easily abstract the hydrogen of cumene to form the 1-methyl-1-phenylethyl radical which couples mainly with each other to give **2**.

A positively charged partner, **5**, of the activation complex, **3**, may be written as a resonance hybrid of the following limiting formulas:

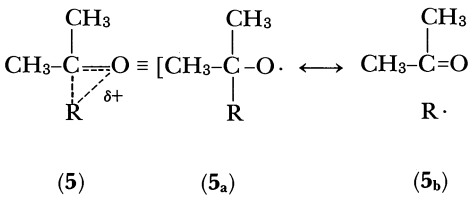

(**5**) (**5**$_a$) (**5**$_b$)

and

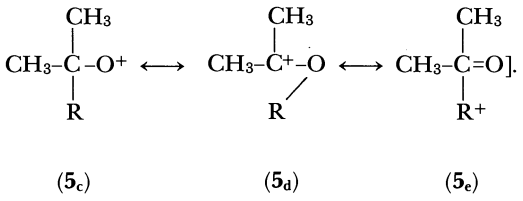

(**5**$_c$) (**5**$_d$) (**5**$_e$)

It can well explain the substituent effects on the decomposition rates and products of **1**. These structures are supported by data regarding the *t*-butoxyl radical optimalized energetically by the MINDO/3-RHF method using the MOPAC program to give both atomic charges and bond orders as follows:

Atomic charge:

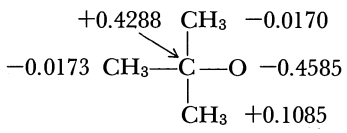

and

Bond order:

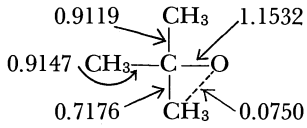

The deviation from the Taft equation and the formation of an additional β-scission product for $\mathbf{1_f}$ may be understood in terms of stabilization by a resonance effect of the $PhCH_2$ radical ($\mathbf{5_b}$).

Experimental

IR, NMR and UV spectra were recorded on JASCO A-3, JEOL JNM-MH-100 and Shimadzu UV-200S spectrometers, respectively. GC-MS spectra were recorded on a JEOL JMS-D 300 mass spectrometer. GC analysis was carried out using Shimadzu GC-2D gas chromatography with columns: SE-30 (5%) and PEG-20M (25%) on Shimalite W (QW-DMCS). A LC analysis was carried out using a JASCO TRIROTAR-V with a column: JASCO Finepak SIL C_{18} and an eluent ($MeOH:H_2O=9:1$). A TLC analysis was carried out using columns with a Merck Kieselgel 60 F_{254} and a Kieselgel 60. The products were purified by flash chromatography on a Merck Kieselgel (40 and 60). The purities of the dialkyl peroxides were determined by GC.

Materials. *t*-Butyl, 1,1-dimethylbutyl, and 1,1,3,3-tetramethylbutyl hydroperoxides were the products of Nippon Oil & Fats Co., Ltd. 2-Methyl-2-butanol, 2-methyl-1-pentene, 2-methyl-2-pentanol, 2-methyl-1-phenyl-2-propanol, and 2-methyl-2-propanol were the products of Wako Pure Chemical Ind., Co. Cumene was stirred for several hours with concentrated sulfuric acid, washed with 10% NaOH aqueous solution and distilled H_2O, dried with drying agents and distilled through a 24-in Vigreaux column.

Preparation of Di-*t*-Alkyl Peroxides. Di-*t*-butyl peroxide ($\mathbf{1_a}$) was purified to 99.2% by distillation (62—63 °C/58 mmHg, 1 mmHg=133.322 Pa) of a commercial product of Nippon Oil & Fats Co., Ltd.

***t*-Butyl *t*-Pentyl Peroxide ($\mathbf{1_b}$).** To an aquous solution of 80% H_2SO_4 (59.0 g, 0.48 mol) there was added dropwise 2-methyl-2-butanol (35.5 g, 0.40 mol) below 10 °C. Then, the solution was kept at 0 °C for 15 min, added dropwise for 5 min by 70% *t*-butyl hydroperoxide (53.0 g, 0.41 mol), and stirred for 2 h at 20 °C to complete the reaction. The oil layer was separated from the reaction mixture, washed with 10% NaOH and H_2O, dried with anhydrous $MgSO_4$ and distilled at reduced pressure (62—63 °C/58 mmHg) to give $\mathbf{1_b}$ of 53.7 g (purity 95.5%, yield 80.0%). IR ν_{O-O} 880 cm^{-1}; ^1H NMR δ=0.99 [3H, t, $-CH_2CH_3$], 1.44 [6H, s, $-OO-C(CH_3)_2-CH_2-$], 1.21 [9H, s, $-OO-C(CH_3)_2$], and 1.53 [2H, q, $-CH_2-CH_3$]; MS (m/z) 160 [M^+].

***t*-Butyl 1,1-Dimethylbutyl Peroxide ($\mathbf{1_c}$).** To an aquous solution of 65% H_2SO_4 (90.6 g, 0.60 mol) there was added dropwise 2-methyl-1-penten (42.1 g, 0.50 mol) below 10 °C. Then, the solution was kept for 10 min at 0 °C, added dropwise for 5 min by 70% *t*-butyl hydroperoxide (64.4 g, 0.50 mol), and stirred for 2 hr at 20 °C to complete the reaction. The oil layer was separated from the reaction mixture, washed with 10% NaOH and H_2O, dried with anhydrous $MgSO_4$ and distilled at reduced pressure (75—76 °C/57 mmHg) to give $\mathbf{1_c}$ of 69.5 g (purity 96.9%, yield 77.3%). IR ν_{O-O} 880 cm^{-1}; ^1H NMR δ=0.98 [3H, t, $-CH_2-CH_3$], 1.16 [6H, s, $-OO-C(CH_3)_2-CH_2-$], 1.20 [9H, m, $-OO-C(CH_3)_3$], and 1.3—1.5 [4H, m, $-(CH_2)_2-CH_3$]; MS(m/z) 174 [M^+].

***t*-Butyl 1,1,3,3-Tetramethylbutyl Peroxide ($\mathbf{1_d}$).** To an aqueous solution of 80% H_2SO_4 (14.8 g, 0.12 mol) there was added dropwise 2-methyl-2-propanol (22.2 g, 0.30 mol) below 10 °C. Then, the solution was kept at 0 °C for 20 min, added dropwise for 10 min by 1,1,3,3-tetramethylbutyl hydroperoxide (15.0 g, 0.10 mol), stirred for 2 h at 25 °C to complete the reaction. The oil layer was separated from the reaction mixture, added with hexane and H_2O, washed with 10% NaOH and H_2O, dried with anhydrous $MgSO_4$, and distilled at reduced pressure (57—58 °C/6 mmHg) to give $\mathbf{1_d}$ of 17.8 g (purity 95.7%, yield 60.5%). IR ν_{O-O} 880 cm^{-1}; ^1H NMR δ=1.02 [9H, s, $-CH_2-C(CH_3)_3$], 1.22 [6H, s, $-OO-C(CH_3)_3$], 1.28 [6H, s, $-OO-C(CH_3)_2-CH_2-$] and 1.54 [2H, s, $-CH_2-$]; MS (m/z) 202 [M^+].

***t*-Butyl 1,1,2-Trimethylpropyl Peroxide ($\mathbf{1_e}$).** To an aqueous solution of 80% H_2SO_4 (33.7 g, 0.275 mol) there was added dropwise 2,3-dimethyl-2-butanol (25.5 g, 0.25 mol) below 10 °C. Then, the solution was kept at 0 °C for 10 min, added dropwise for 15 min by 70% *t*-butyl hydroperoxide (36.3 g, 0.25 mol), and stirred for 2 h at 20 °C to complete the reaction. The oil layer was separated from the reaction mixture, washed with 10% NaOH and H_2O, dried with anhydrous $MgSO_4$ and distilled at reduced pressure (73—75 °C/47 mmHg) to give $\mathbf{1_e}$ of 10.6 g (purity 95.6%, yield 23.2%). IR ν_{O-O} 865 cm^{-1}; ^1H NMR δ=0.89 ppm [6H, d, $-CH(CH_3)_3$], 1.12 [6H, s, $-OO-C(CH_3)_2-$], 1.21 [9H, s, $-OO-C(CH_3)_3$], and 1.91 [1H, m, $-CH(CH_3)_2$]; MS (m/z) 174 [M^+].

***t*-Butyl 1,1-Dimethyl-2-phenylethyl Peroxide ($\mathbf{1_f}$).** To an aqueous solution of 80% H_2SO_4 (4.54 g, 37 mmol) there was added dropwise 2-methyl-2-propanol (7.41 g, 100 mmol) below 10 °C. Then, the solution was kept at 0 °C for 20 min, added dropwise for 5 min by a solution of diethyl ether (3 cm^3) and 1,1-dimethyl-2-phenylethyl hydroperoxide (4.73 g, 28.5 mmol) which was prepared by reaction of the corresponding alcohol with 50% H_2O_2 in the presence of 72% H_2SO_4 at 40 °C in THF,[5] and stirred for 2 h at 20 °C to complete the reaction. The oil layer was separated from the reaction mixture, washed with 10% NaOH and H_2O, and dried with anhydrous $MgSO_4$. The crude product (5.2 g) after evaporation of solvent was purified by flash chromatography to give $\mathbf{1_f}$ of 3.68 g (purity 99.5%, yield 57.8%). IR ν_{O-O} 880 cm^{-1}; ^1H NMR δ=1.15 [6H, s, $-C(CH_3)_2-CH_2-$], 1.22 [9H, s, $-OO-C(CH_3)_3$], 1.28 [6H, s, $-CH_2-Ph$] and 1.54 [2H, s, $-Ph$]; MS (m/z) 222 [M^+].

***t*-Butyl 2-Chloro-1,1-dimethylethyl Peroxide ($\mathbf{1_g}$)** was prepared by the method of Richardson et al.[2] and purified to

95.2% by distillation (54—55 °C/20 mmHg) of the crude reaction product.

Kinetic Procedure. A dilute solution of dialkyl peroxide in cumene was placed in sealed tubes (content of 7.5 cm^3) under vacuum and heated in a constant-temperature bath (±0.2 °C). The remaining amount of dialkyl peroxide was determined by GC with a column of SE-30 (5%) using unternal standards. The reaction was followed up to 70—80% decomposition and exhibited first-order kinetics.

Decomposition Products. Di-*t*-alkyl peroxide at the concentration of 0.05 mol dm^{-3} in cumene was decomposed completely at 130 °C and the solution was analyzed by GC using internal standards. The yields of acetone and 2-methyl-2-propanol were determined with columns of PEG-20M (25%), and the others, SE-30 (5%).

References

1) a) S. W. Benson and R. Shaw, "Organic Peroxides," ed by D. Swern, Wiley-Interscience (1970), Vol. I, Chap. II; b) R. Hiatt, "Organic Peroxides," ed by D. Swern, Wiley-Interscience (1972), Vol. III, Chap. I; c) R. A. Sheldon, "The chemistry of peroxides," ed by S. Patai, John Wiley & Sons (1983), Chap. 6; d) L. F. Martin, "Organic Peroxide Technology," Noyes Data Corporation, New Jersey (1973); e) J. H. Raley, F. F. Rust, and W. E. Vanghan, *J. Am. Chem. Soc.*, **70**, 88 (1948).

2) W. H. Richardson, M. B. Yelvingtion, A. H. Andrist, E. W. Ertlev, R. S. Smith, and T. D. Johnson, *J. Org. Chem.*, **38**, 4219 (1973); The sum of the substituent constants, $\Sigma\sigma^*$, for $RC(CH_3)_2$ group was obtained by adding each substituent constant of RCH_2 and two CH_3CH_2.

3) R. Ireton, A. S. Gordon, and D. C. Tardy, *Int. J. Chem. Kinet.*, **9**, 769 (1977).

4) E. S. Huyser and R. M. VanScoy, *J. Org. Chem.*, **33**, 3524 (1968).

5) T. Komai, K. Matsuyama, and M. Matsushima, *Bull. Chem. Soc. Jpn.*, **61**, 1641 (1988).

6) D. Cremer, "The Chemistry of Peroxides," ed by S. Patai, Wiley & Sons (1983), Chap. 1.

7) a) C. Walling and A. Padwa, *J. Am. Chem. Soc.*, **85**, 1593 (1963); b) J. D. Bacha and J. K. Kochi, *J. Org. Chem.*, **30**, 3272 (1965).

8) Decomposition of peroxides has been generally clasified to non-concerted (stepwise) and concerted ones. However, there is a borderline decomposition which can not be distinguished from the both ones. See, for example, T. Koenig, "Fee Radicals," ed by J. K. Kochi, Wiley-Interscience (1973), Vol. I, Chap. 3.

Effect of Oxidants on the Oxidative Coupling of Methane over a Lead Oxide Catalyst

Kenji ASAMI,† Tsutomu SHIKADA,†† and Kaoru FUJIMOTO*
Department of Synthetic Chemistry, Faculty of Engineering, The University of Tokyo, Hongo 7-3-1, Bunkyo-ku, Tokyo 113
(Received July 3, 1990)

Oxidative coupling of methane was studied over a PbO/MgO catalyst using a variety of oxidants such as N_2O, NO, CO_2, and SO_2. While N_2O showed both high activity and selectivity for the title reaction, NO produced CO_2, exclusively. The coupling reaction was assumed to proceed via the redox cycle of Pb and PbO on each oxidant mentioned above. Carbon dioxide produced small amounts of C_2 hydrocarbons and CO, while SO_2, was inactive for the reaction. Oxygen, N_2O, CO_2 could oxidize the Pb/MgO which had been formed by the reaction of PbO/MgO with methane at 1023 K. Thus-prepared PbO/MgO produced C_2 hydrocarbons from methane. Even NO, which gave no C_2 hydrocarbons in the CH_4–NO cofeed reaction, converted the Pb/MgO to PbO/MgO and the PbO/MgO gave C_2 hydrocarbons exclusively upon reacting with CH_4. NO seems to oxidize the methyl radical, which is an intermediate of the coupling reaction to CO_2. The ineffectiveness of SO_2 as an oxidant was attributed to the formation of PbS, which is inactive in the methane activation.

Since the pioneering work by Keller and Bashin,[1] a great number of catalysts have been found to be effective for the title reaction. The reaction systems reported so far are classified into 4 groups:

(A) Metal oxides, which exhibit abilities to change the oxidation state easily under reaction conditions, such as PbO,[2,3] MnO,[5] Bi_2O_3,[6] NiO,[7] and Tl_2O_3.[8]

(B) Alkaline earth metal oxides, such as MgO and CaO, which are undoped[9,10] or doped with Li^+,[11–14] Na^+,[15] K^+,[16] alkaline earth metal halide[17,18] or rare earth oxides.[19]

(C) Rare earth oxides, which are undoped[20] or doped with alkali metal compounds.[21]

(D) Noncatalyzed gas-phase reaction.[22,23]

Active oxygen species for the catalysts which belong to group (A) have been claimed to be bulk oxygen in metal oxides,[7,24] while the surface oxide ion or adsorbed oxygen has been proposed for the catalysts of group (B) and group (C).[12,25,26]

Oxidants other than O_2, such as N_2O or CO_2, have been applied to the methane coupling reaction. Ito et al. compared the reactivity of dinitrogen monoxide to methane with O_2 over a lithium promoted magnesium oxide catalyst and concluded that dinitrogen monoxide is not a preferable oxidant.[12] Otsuka et al. studied the effect of N_2O oxidation over a series of rare earth oxides and confirmed that N_2O gave a lower conversion of methane but a higher selectivity for C_2 hydrocarbons than O_2.[27] Meng et al. examined methane activation by N_2O over lead oxide catalysts supported on γ-Al_2O_3 and NaY zeolite to find that C_2 hydrocarbons were formed with a selectivity of 40%.[28] Hutching et al. found that on a Li/MgO catalyst N_2O promoted CH_4 coupling but NO inhibited the reaction while giving CO_2, exclusively and claimed the presence of two oxidizing species on the catalyst.[29] We have reported that in the noncatalyzed gas-phase system N_2O gave a higher selectivity than O_2 for the formation of C_2 hydrocarbons from CH_4, whereas NO was inactive for the reaction.[22] We also reported that methane reacted with CO_2 to form C_2 hydrocarbons and CO over a PbO/MgO catalyst.[30] Aika and Nishiyama also reported a promotional effect of added CO_2 on the CH_4–O_2 cofeed reaction over PbO/MgO.[31]

In this study the effects of a series of oxidants such as O_2, N_2O, NO, SO_2 and CO_2 were examined systematically over a PbO/MgO catalyst in order to clarify how each oxidant activates methane and the active oxygen species for the coupling reaction.

Experimental

The catalyst used was 20 wt%-PbO/MgO, prepared by impregnating commercially available magnesium with lead(2) nitrate from aqueous solution and then calcining it at 800 °C.[10] Methane oxidation reactions were conducted with a fixed-bed flow-type reaction apparatus under atmospheric pressure; the catalyst charge was 1 g. The reactor was a quartz tube with an inner diameter of 10 mm, in which another quqartz tube (6 mm o. d.) was inserted as a thermocouple holder. Methane conversions were performed according to the following two procedures: One was a CH_4–oxidant cofeed reaction and another was a periodic oxidation–reduction reaction. The reaction conditions of the cofeed reaction were 650—800 °C, W/F=1 g h mol^{-1}, $P(CH_4)$=14 kPa, P(oxidant)=1—4 kPa, and helium balance. In the case of CO_2, the composition of the reactant was CH_4: CO_2=1:1 and W/F was 5 g h mol^{-1}.

A periodic reaction was conducted along the following flow module: Air oxidation⟶N_2 purge(5 min)⟶CH_4 reaction(20 min) N_2 purge(20 min)⟶Oxidation(10 min). The cycle of the CH_4 reaction and oxidation was repeated at least 2 times. The procedure of the periodic reaction has

Present address:
† Coal Chemistry Laboratory, Chemical Research Institute of Non-Aqueous Solutions, Tohoku University, Katahira 2-1-1, Aoba-ku, Sendai 980.
†† Technical Research Center, NKK Corporation, 1-1 Minamiwa, Kawasaki-ku, Kawasaki 210.

been described elsewhere.[24] However, the first activation of the catalyst was performed by oxygen (air); then the second and the third activations were performed by each oxidant. All of the reactions and products were analyzed by gas chromatography. The separation columns used were Porapak R for dinitrogen monoxide and sulfur dioxide and MS-13 X for nitrogen monoxide, respectively. The analysis methods for other reactants and produucts have been described elsewhere.[24] A Toshiba-Beckmann 951 NO/NO_x meter was also used for the analysis of nitrogen monoxide. X-Ray diffraction (XRD) measurements of the catalysts were recorded with a Rigaku Denki Ru-200 diffractometer with Ni-filtered Cu-K radiation.

Results and Discussion

Thermodynamic Consideration. The free-energy changes of ethane formation from methane with these oxidants are shown in Table 1. From a thermodynamic perspective, oxygen and nitrogen oxides are favorable oxidants for a coupling reaction ($G°_f<0$), whereas sulfur dioxide and carbon dioxide are unfavorable ($G°_f>0$). However, the equilibrium conversion of methane by CO_2 oxidation is about 10% under the conditions of 750 °C, $CH_4/CO_2=1$, and normal pressure.

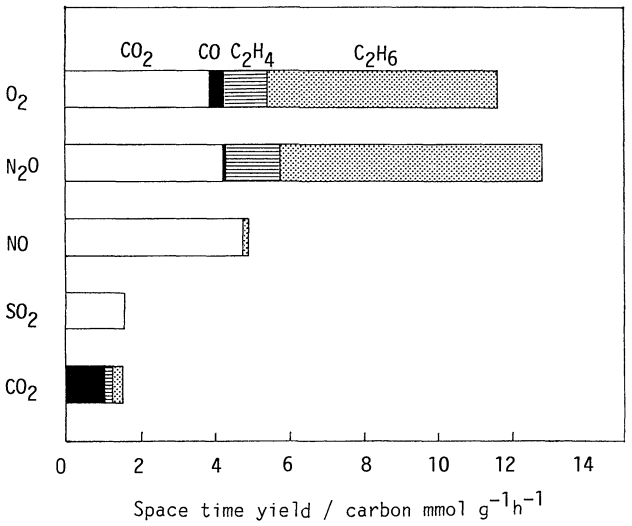

Fig. 1. Effect of oxidant on oxidative coupling of methane. Cat.; 20 wt%-PbO/MgO, 750 °C, W/F= 1.0 g h mol^{-1}, $P(CH_4)$=14 kPa, P(oxidant)=1.6 kPa (for O_2, N_2O, NO, SO_2), W/F=5.0 g h mol^{-1}, $P(CH_4)$= 5 kPa, $P(CO_2)$=5 kPa, (for CO_2).

CH_4-Oxidant Cofeed Reaction. In Fig. 1 are shown the space-time yields (STY) of the reaction products obtained by various cofeed reactions at 750 °C over a 20 wt%-PbO/MgO catalyst. The partial pressure of dinitrogen monoxide and nitrogen monoxide in the feed gas was set to be about twice that of oxygen in order to adjust the CH_4–O stoichiometry. In the case of the CH_4–CO_2 reaction, $P(CO_2)$ and the modified residence time (W/F) were 50 kPa and 5 g h mol^{-1}, respepctively, because of the low reaction rate.

(a) N_2O. Dinitrogen monoxide gave a similar STY of CH_4 oxidation (12.8 mmol $g^{-1}h^{-1}$) to that obtained by O_2 (11.6 mmol g^{-1} h^{-1}), the values of which correspond to CH_4 conversions of 8.5 and 8.1%, respepctively (Fig. 1). The product distribution was also similar to that of the CH_4–O_2 reaction, except for the lack of CO. The temperature dependence of the reaction using N_2O revealed that a higher temperature is favored for making C_2 hydrocarbons (Fig. 2), which is also similar to the case of O_2 oxidation.[10] We have reported that N_2O is effective to make C_2 hydrocarbons in a noncatalyzed system[22] while giving a higher selectivity (88%). However, the production rate was lower by about two orders of magnitude than that in the

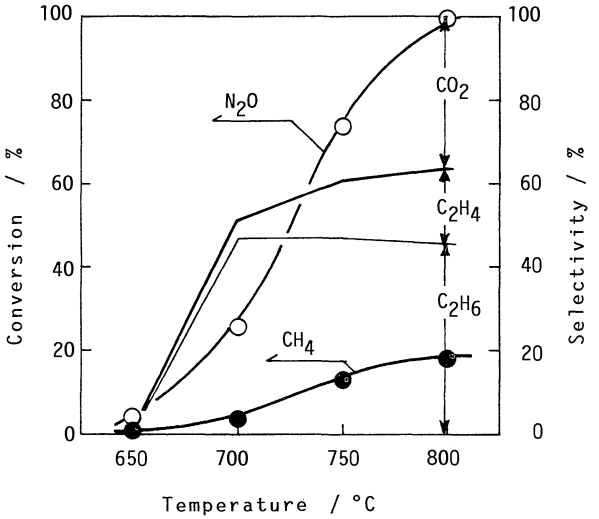

Fig. 2. Effect of temperature on the oxidative coupling of methane with N_2O as oxidant. Cat.; 20 wt%-PbO/MgO, 1.0 g h mol^{-1}, CH_4: N_2O: He= 10:4:86.

Table 1. Changes in Gibbs Free Energy in Oxidative Coupling of Methane with Various Oxidants

Reaction		$\Delta G_f°$/kcal mol^{-1}		
		700 °C	750 °C	800 °C
$2CH_4+1/2O_2 \rightarrow C_2H_6+H_2O$	(1)	−28.9	−28.1	−27.3
$2CH_4+N_2O \rightarrow C_2H_6+H_2O+N_2$	(2)	−66.2	−66.5	−66.7
$2CH_4+1/2NO \rightarrow C_2H_6+H_2O+1/2N_2$	(3)	−47.7	−46.8	−45.9
$2CH_4+1/2SO_2 \rightarrow C_2H_6+H_2O+S$	(4)	7.2	7.9	8.7
$2CH_4+1/3SO_2 \rightarrow C_2H_6+2/3H_2O+1/3H_2S$	(5)	6.2	6.6	7.0
$2CH_4+CO_2 \rightarrow C_2H_6+H_2O+CO$	(6)	17.8	17.4	16.9

present case, indicating that the reaction in the present system proceeds mainly on the catalyst surface.

The oxidative coupling of CH_4 over PbO/MgO has been clarified to be consist of a redox cycle between Pb and PbO; that is, a methane conversion into C_2 hydrocarbons by PbO (Eq. 7) and a reoxidation of metallic Pb with dioxygen (Eq. 8):

$$2\,CH_4 + PbO \longrightarrow C_2H_6 + H_2O + Pb, \quad (7)$$

and

$$Pb + 1/2O_2 \longrightarrow PbO. \quad (8)$$

The Gibbs free energy changes for the oxidation of Pb by N_2O oxidants shows as listed in Table 2 that the N_2O reaction with PbO (Eq. 9) is also thermodynamically favorable, as well as O_2. Therefore, the mechanism for the formation of C_2 hydrocarbons by N_2O is believed to be the same as that by O_2; namely, the reaction of CH_4 with PbO (Eq. 7) and the reoxidation reaction of reduced lead by N_2O (Eq. 9). We have confirmed that N_2O was completely decomposed to N_2 and O_2 on the PbO/MgO catalyst at 750 °C. Therefore, it is not clear whether N_2O reacts directly with Pb or after being converted to O_2.

(b) NO. Although a methane oxidation with NO is thermodynamically favorable (Table 1), the yield of C_2 hydrocarbons in the CH_4–NO reaction was much lower than those in the O_2–or N_2O– oxidation on the PbO/MgO catalyst, as indicated in Fig. 1. As shown in Table 3, CO_2 was formed exclusively (selectivity; >97%) under all reaction conditions. However, NO exhibited a strong oxidative ability of Pb; the oxidized Pb by NO gave C_2 hydrocarbons as well as N_2O or O_2 (Table 4). Therefore, the extremely low selectivity of C_2 hydrocarbons in a cofeed reaction might be interpreted in terms of the two possible reasons given below.

[1] surface oxygen species derived from NO is active only for a complete oxidation of methane. The species would be an adsorbed one on PbO ($PbO\text{–}O_x$), since such a species derived from O_2 is considered to be active regarding the formation of carbon oxides.[24]

[2] NO inhibits a coupling reaction; thus molecular NO attacks the methyl radical, which is formed by the reaction of CH_4 with PbO, in the gas phase to form CH_3NO. It is then finally decomposed to CO_2. It is well-known that nitrogen monoxide is a radical inhibitor.[32] The fact that NO oxidized Pb to PbO and PbO oxidized CH_4 to C_2H_6 by periodic oxidation (Table 4 and Fig. 4) suggests that concept [2] is more plausible.

(c) SO_2. When sulfur dioxide was used as an oxidant, CO_2 was produced exclusively, as shown in Fig. 1. Though other by-products (not shown) were carbonyl sulfide and elemental sulfur, neither hydrogen sulfide nor methane thiol was formed. Further consideration is presented later.

(d) CO_2. It is noticeable that the oxidative coupling of methane proceeded to some extent by utilizing CO_2 as an oxidant (Fig. 1). The product distribution is explained by assuming the following reaction stoichiometry (Eq. 14—16):

$$CO_2 \longrightarrow CO + (O), \quad (14)$$

$$2\,CH_4 + (O) \longrightarrow C_2H_6 + H_2O, \quad (15)$$

Table 2. Changes in Gibbs Free Energy in Oxidation of Lead with Various Oxidants

Reaction		$\Delta G_f°$/kcal mol^{-1} 700 °C	750 °C	800 °C
$Pb+1/2O_2 \rightarrow PbO$	(8)	−29.6	−28.5	−27.4
$Pb+N_2O \rightarrow PbO+N_2$	(9)	−67.0	−66.9	−66.8
$Pb+NO \rightarrow PbO+1/2N_2$	(10)	−48.4	−47.2	−46.0
$Pb+1/2SO_2 \rightarrow PbO+1/2S$	(11)	6.4	7.5	8.6
$Pb+CO_2 \rightarrow PbO+CO$	(12)	17.0	16.9	16.8
$Pb+S \rightarrow PbS$	(13)	−22.5	−22.4	−22.4

Table 3. Methane Conversion by NO over 20 wt%-PbO/MgO Catalyst. W/F=1.0 g h mol^{-1}, He Balance

	Concentration/mol%				
CH_4	11.5	16.0	12.1	13.1	12.7
NO	1.5	3.7	7.5	3.7	3.7
Temperature/°C	750	750	750	800	700
Conversion/mol%					
CH_4	2.0	3.3	4.0	5.6	2.1
NO	6.3	7.2	19.4	24.5	3.5
Selectivity/C-mol%					
C_2H_6	1.7	1.0	0	2.5	0
CO_2	98.3	98.9	100	97.5	100

Table 4. Characterization of PbO Catalyst by XRD.[a] Same Experiments Shown in Figs. 3 to 6

	Oxidant	XRD peak PbO	Pb	PbS
After oxidation	O_2	VS	—	—
	N_2O	VS	—	—
	NO	VS	—	—
	SO_2	W	—	S
	CO_2	VS	—	—
After CH_4 conversion	O_2	VW	VS	—
	N_2O	VW	VS	—
	NO	VW	VS	—
	SO_2	—	W	S
	CO_2	VW	VS	—

a) Peak intensity: VS; very strong, S; strong, W; weak, VW; very weak, —; not detected.

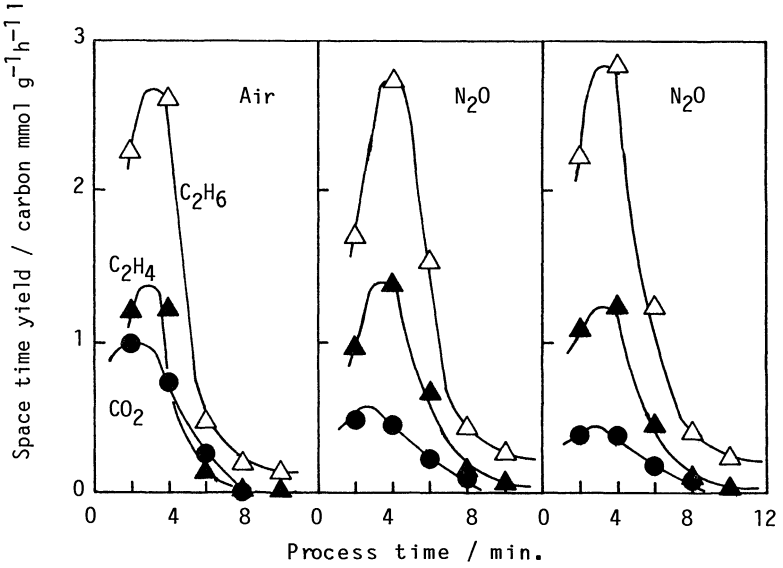

Fig. 3. Transient response of periodic CH_4 conversion: Effect of N_2O reoxidation. Cat.; 20 wt%-PbO/MgO, 750 °C, 4.3 g h mol^{-1}.

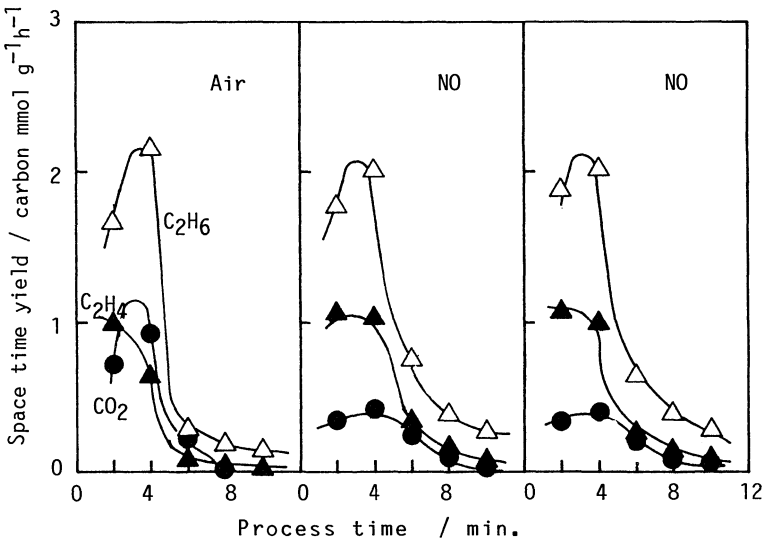

Fig. 4. Transient response of periodic CH_4 conversion: Effect of NO reoxidation. Cat.; 20 wt%-PbO/MgO, 750 °C, 4.3 g h mol^{-1}.

and

$$2\,CH_4 + 2\,(O) \longrightarrow C_2H_4 + 2H_2O. \quad (16)$$

Carbon dioxide is dissociated to carbon monoxide and a reactive surface oxygen species (O) (Eq. 14), which may react with methane to form ethane (Eq. 15) and ethylene (Eq. 16). In fact, CO_2 oxidized Pb to PbO and PbO oxidized CH_4 to C_2H_6 (Table 4 and Fig. 5). However, the amount of CO formed was larger than the amount calculated from reactions (14)—(16). Thus, reaction (17) should be accounted for. Reactions (14) and (17) are converted to the reaction stoichiometry shown in Eq. 18, which means that one fourth of the CO was formed from CH_4.

$$CH_4 + 3\,(O) \longrightarrow CO + 2\,H_2O \quad (17)$$

$$C^*H_4 + 3\,CO_2 \longrightarrow C^*O + 3\,CO + 2\,H_2O \quad (18)$$

The product distribution is shown as Fig. 1. Even at 800 °C the selectivity of C_2 hydrocarbons was not high. Thus low selectivity might be attributed to the formation of surface $MgCO_3$, which is not a favorable

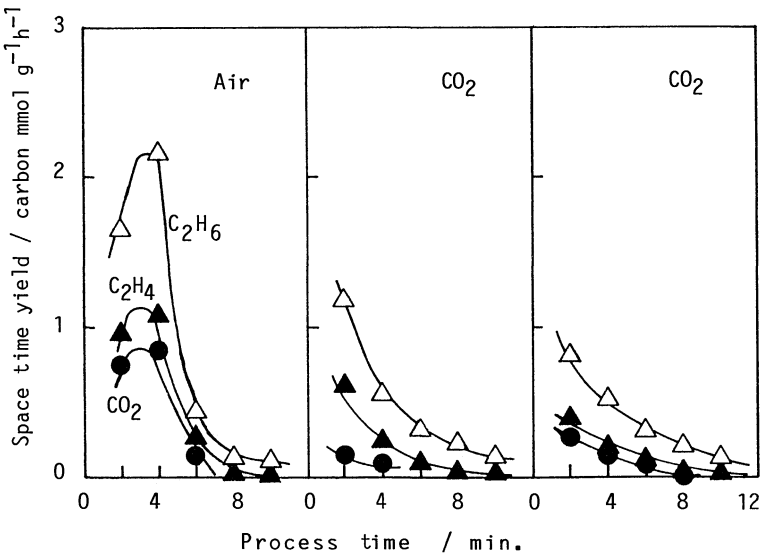

Fig. 5. Transient response of periodic CH_4 conversion: Effect of CO_2 reoxidation. Cat.; 20 wt%-PbO/MgO, 750 °C, 4.3 g h mol^{-1}.

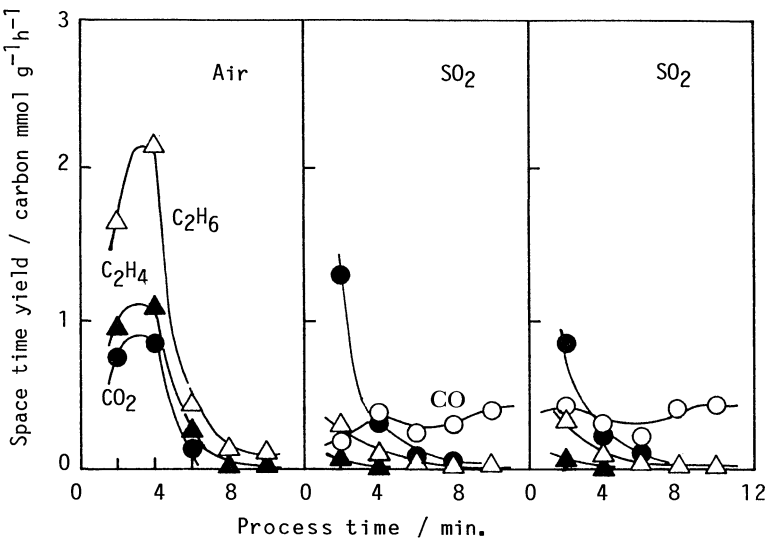

Fig. 6. Transient response of periodic CH_4 conversion: Effect of SO_2 reoxidation. Cat.; 20 wt%-PbO/MgO, 750 °C, 4.3 g h mol^{-1}.

support material. This subject will be discussed later.

Periodic Oxidation-Reduction Reaction. In the case of the CH_4–oxidant cofeed reaction, O_2 and N_2O exhibited excellent performance in the formation of C_2 hydrocarbons, similar to that of O_2, whereas other oxidants (NO, SO_2, and CO_2) did not produce the desired products selectively (as described above). However, a periodic oxidation–reduction reaction gave different results, as shown in Figs. 3 to 6. Also, the lead species identified after each reaction are shown in Table 4.

(a) N_2O, NO, and CO_2. Dinitrogen monoxide gave a similar result to that of the cofeed reaction containing O_2. Also, the periodic reaction gave C_2H_6 selectively over a catalyst which was oxidized by N_2O as demonstrated in Fig. 3. These facts correspond to that regarding O_2, which suggests that the oxidation state of lead oxidized by N_2O is similar to that oxidized by O_2 (Table 2).

Although little C_2 hydrocarbons were formed in a cofeed reaction containing NO (Fig. 1), they were formed with high selectivity in the CH_4–NO periodic reaction (Fig. 4). It was also clarified that NO has an ability to oxidize metallic Pb to PbO, and PbO gave C_2

hydrocarbons upon a reaction with CH_4, as demonstrated in Table 4. This means that although the redox cycle is possible in the CH_4–NO cofeed reaction system, NO inhibits the coupling reaction, probably because it reacts with the methyl radical to form CO_2. C_2 hydrocarbons were formed selectively at a comparable rate in a periodic CH_4–CO_2 operation (Fig. 5), while the rate of C_2 formation in a cofeed reaction was much lower than that in the O_2-containing cofeed reaction (Fig. 1). However, the amount of C_2 hydrocarbons formed in the second treatment was slightly smaller and the amount of CO formed was slightly larger than that obtained in the first treatment. This observation might be attributed to the formation of a surface carbonate species of carrier material of the catalyst (MgO) which is unfavorable for the coupling reaction.[24]

(b) SO_2. When sulfur dioxide was used as an oxidant, a small amount of C_2 hydrocarbons was formed in the periodic reaction (Fig. 6), although no C_2 hydrocarbons were formed at all in the cofeed reaction. The low CH_4 selectivity even in a periodic reaction, should be attribuuted to the formation of PbS according to Eqs. 11 and 13 during a reaction with SO_2 (Table 4), since PbS is never reduced by a reaction with CH_4. It is thus concluded that the redox cycle expressed as reactions (7) and (11) is inhibited by the formation of PbS.

Conclusion

Methane activation with a MgO-supported PbO catalyst was studied by using a variety of oxidants such as O_2, N_2O, NO, SO_2, and CO_2 resulting in the following conclusion:

1) In a CH_4–oxidant cofeed reaction, N_2O exhibited excellent activity and selectivity for the formation of C_2 hydrocarbons as well as O_2, whereas NO and CO_2 gave only small amounts of the desired product and SO_2 made no C_2 hydrocarbons.

2) Not only O_2 and N_2O, but also NO and CO_2, showed high selectivity for the formation of C_2 hydrocarbons in a periodic oxidation–reduction operation. This was because of the formation of PbO, which gave C_2 hydrocarbons upon a reaction with CH_4, with the reaction of a reduced catalyst and these oxidants as well as O_2 and N_2O. However, NO or CO_2 seems to have some inhibiting effect on the coupling reaction.

3) When SO_2 was used as an oxidant for methane conversion, lead sulfide was formed, which impeded the coupling reaction in either the cofeed reaction or the periodic reaction.

We thank Professor H. Tominaga for his discussion.

References

1) G. E. Keller and M. M. Bhasin, *J. Catal.*, **73**, 9 (1982).
2) W. Hinsen, W. Bytyn, and M. Baerns, *Proc. ICC, 8th*, **3**, 581 (1984).
3) K. Asami, S. Hashimoto, T. Shikada, K. Fujimoto, and H. Tomonaga, *Chem. Lett.*, **1986**, 1233.
4) G. Wendt, C. -D. Meinecke, and W. Schmitz, *Appl. Catal.*, **45**, 209 (1988).
5) J. A. Sofranko, J. J. Leonard, and C. A. Jones, *J. Catal.*, **103**, 311 (1987).
6) I. T. Ali Emesh and Y. Amenomiya, *J. Phys. Chem.*, **90**, 4785 (1986).
7) K. Otsuka, Q. Liu, M. Hatano, and A. Morikawa, *Chem. Lett.*, **1986**, 353.
8) K. Fujimoto and K. Asami, unpublished.
9) T. Mori, N. Takasaki, E. Iwamatsu, and K. Aika, *Chem. Lett.*, **1986**, 1165.
10) N. Yamagata, K. Tanaka, S. Sasaki, and S. Okazaki, *Chem. Lett.*, **1987**, 81.
11) T. Ito and L. Lunsford, *Nature*, **314**, 721 (1985).
12) T. Ito, J. -X. Wang, C. -H. Lin, and J. H. Lunsford, *J. Am. Chem. Soc.*, **107**, 5062 (1985).
13) S. J. Korf, J. A. Roos, N. A. deBruijn, J. G. Van Ommen, and J. R. H. Ross, *Catal. Today*, **2**, 535 (1988).
14) V. T. Amorebieta and A. J. Colussi, *J. Chem. Phys.*, **92**, 4576 (1988).
15) E. Iwamatsu, T. Moriyama, N. Takasaki, and K. Aika, *J. Catal.*, **113**, 25 (1988).
16) J. A. S. P. Carreiro and M. Baerns, *J. Catal.*, **117**, 396 (1989).
17) K. Fujimoto, S. Hashimoto, K. Asami, and H. Tominaga, *Chem. Lett.*, **1987**, 2157.
18) K. Fujimoto, S. Hashimoto, K. Asami, and H. Tominaga, *Appl. Catal.*, **50**, 223 (1989).
19) V. R. Choudhary, S. T. Chaudhari, A. M. Rajput, and V. H. Rane, *J. Chem. Soc., Chem. Commun.*, **1989**, 555.
20) K. Otsuka, Q. Liu, M. Hatano, and A. Morikawa, *Chem. Lett.*, **1986**, 467.
21) K. Otsuka, K. Jinno, and A. Morikawa, *Chem. Lett.*, **1985**, 499.
22) K. Asami, K. Omata, K. Fujimoto, and H. Tominaga, *Energy Fuels*, **2**, 574 (1988).
23) G. S. Lane and E. E. Wolf, *J. Catal.*, **113**, 144 (1988).
24) K. Asami, T. Shikada, K. Fujimoto, and H. Tominaga, *Ind. Eng. Chem. Res.*, **26**, 2348 (1987).
25) N. W. Cant, C. A. Lukey, P. F. Nelson, and R. J. Tyler, *J. Chem. Soc., Chem. Commun.*, **1988**, 766.
26) K. Otsuka, A. A. Said, K. Jinno, and T. Komatsu, *Chem. Lett.*, **1987**, 77.
27) K. Otsuka and T. Nakajima, *J. Chem. Soc., Faraday Trans. 1*, **83**, 1315 (1987).
28) H. Meng and R. D. Sanger, *Appl. Catal.*, **32**, 347 (1987).
29) G. J. Hutching, M. S. Scurrell, and J. R. Woodhouse, *J. Chem. Commun.*, **1989**, 765.
30) K. Asami, T. Shikada, K. Fujimoto, and H. Tominaga, Annual Meeting of the Chemical Society of Japan, Kyoto (1986).
31) K. Aika and T. Nishiyama, *J. Chem. Soc., Chem. Commun.*, **1988**, 70.
32) P. G. Ashmore, "Catalysis and Indibition of Chemical Reactions," Butterworths, London (1963).

Characteristics of Suspended Ru/Carbon Catalyst for 2-Propanol Dehydrogenation Applicable to Chemical Heat Pump

Masaru YAMASHITA,* Tokiji KAWAMURA, Minoru SUZUKI, and Yasukazu SAITO
Department of Industrial Chemistry, Faculty of Engineering, The University of Tokyo, 7-3-1 Hongo, Bunkyo-ku, Tokyo 113
(Received July 19, 1990)

Liquid-phase dehydrogenation of $(CH_3)_2CHOH$, $(CH_3)_2CHOD$ and $(CH_3)_2CDOH$ was performed at 82.4 °C with high activity and selectivity under refluxing conditions by heating the suspended solution at 100 °C with a carbon-supported ruthenium catalyst. Since the mixture of $(CH_3)_2CHOH$ and $(CD_3)_2CO$(10 vol%) gave 2-propan-1,1,1,3,3,3-d_6-ol at a rate 7.15-times higher than that of hydrogen evolution, hydrogen transfer from 2-propanol to acetone ought to proceed simultaneously with dehydrogenation. Relatively small kinetic isotope effects of 1.69 and 1.57, obtained from $(CH_3)_2CHOD$ and $(CH_3)_2CDOH$, respectively, on the Ru/carbon catalyst for dehydrogenation, suggests that the slowest step is not a splitting of the methine C–H bond but, rather, the formation of molecular hydrogen from surface hydrogen species. Further improvements regarding easy desorption of both acetone and hydrogen are necessary for the catalyst most suitable for 2-propanol dehydrogenation in a chemical heat pump system.

The utilization of solar and geothermal heat as well as waste heat in factories has recently attracted considerable attention. Chemical heat pumps are important from this viewpoint.[1] Aiming at large temperature rises, high thermal efficiencies and the functions of energy storage and transport, a new chemical heat pump system has been proposed in which an endothermic reaction at low temperature was coupled with its exothermic reverse reaction at high temperature.[2,3] Among the three processes shown in Eqs. 1—3, 2-propanol dehydrogenation in the liquid phase is the most difficult, but essential, reaction, since the endothermic reaction at low temperature converts thermal energy of low quality into chemical energy.

$$(CH_3)_2CHOH(l) \longrightarrow (CH_3)_2CO(g) + H_2(g), \quad (1)$$

$$(CH_3)_2CO(g) + H_2(g) \longrightarrow (CH_3)_2CHOH(g), \quad (2)$$

$$(CH_3)_2CHOH(g) \longrightarrow (CH_3)_2CHOH(l). \quad (3)$$

In spite of the thermodynamic disadvantage, the liquid-phase dehydrogenation of 2-propanol takes place catalytically under boiling conditions, where the product hydrogen is expelled from the reaction medium immediately. On the other hand, acetone hydrogenation is favorable below 202 °C at atmospheric pressure,[4] which is much higher than the boiling temperature of the 2-propanol/acetone mixed solution(82.4—56.3 °C). The role of a coolant at ambient temperature is also to be noted, because the separation of 2-propanol from the gaseous mixture makes it possible to raise the temperature from 80 °C to 200 °C in one effort.

As for the present chemical heat pump system, the development of excellent catalysts is indispensable for both gaseous hydrogenation of acetone and 2-propanol dehydrogenation in the liquid phase.

Hydrogenation of geseous acetone was widely investigated using various metal catalysts,[5] whereas Raney nickel,[6] nickel boride,[7] and fine-particle nickel,[8,9] prepared by a gas-evaporation technique,[10] were both active and selective for 2-propanol dehydrogenation. Homogeneous catalysts comprising rhodium,[11] ruthenium,[12] and iridium complexes[13] were useful for this reaction as well.

High thermal efficiency in the present heat pump system is attainable with high endothermic reaction rates in low temperature regions. A ruthenium catalyst supported on carbon (abbreviated hereafter as Ru/carbon) was recently found to be superior for 2-propanol dehydrogenation in a well-dispersed state.[14]

In the present paper, an elucidation of the characteristics has been attempted for a suspended Ru/carbon catalyst with deuterium-substituted 2-propanol and acetone for the purpose of designing the most suitable catalyst for a chemical heat pump system.

Experimental

Dehydrogenation of unlabled 2-propanol(hereinafter described as propanol-d_0) and its deuterio-isomers, i.e., $(CH_3)_2CHOD$ and $(CH_3)_2CDOH$ (Division of Merck, Frost, Inc.), as well as $(CH_3)_2CHOH$ including 10 vol% $(CH_3)_2CO$ or $(CD_3)_2CO$ were performed under boiling and refluxing conditions at atmospheric pressure. An appropriate amount (200 mg) of a Ru(5 wt%)/carbon powder catalyst (supplied by N. E. Chemcat Co.) and 5 ml of reactant 2-propanol were placed at room temperature in a Schlenk flask(20 ml), through which nitrogen was passed in order to remove both water and oxygen in sufficient amounts.

After the Ru/carbon catalyst was dispersed ultrasonically (Kaijyo Denki Co., Sona 50a) in 2-propanol, the suspension was agitated vigorously by a magnetic stirrer (500 rpm) and heated with an oil bath kept at 100 °C. The product gas was collected in a gas burette (250 ml) through a refluxing condenser cooled to 20 °C.

A gas-chromatographic analysis for gaseous and liquid-phase products was performed with active carbon and PEG

20M columns, respectively. The deuterium distribution in product dihydrogen was determined every fifteen or thirty minutes using a quadrupole-type mass spectrometer(NEC Anelva Co., AQA 360), whereas the ^2H NMR spectra of the solution were taken after appropriate reaction periods in order analyze how the substituted deuterium atoms were transferred among the liquid-phase components using an FT-NMR spectrometer(JEOL Co, GX-400).

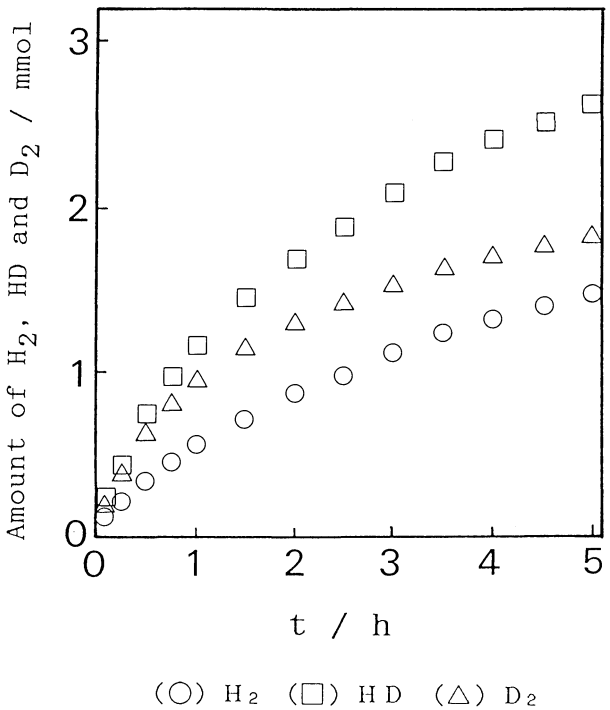

Fig. 1. Accumulation of H_2, HD, and D_2 evolved at 82.4°C from $(CH_3)_2CHOD$ under refluxing conditions (heat at 100°C) with Ru(5 wt%)/carbon catalyst.

Results

Dehydrogenation of 2-Propanol-*d*. The Ru/carbon catalyst suspended in $(CH_3)_2CHOD$ under boiling and refluxing conditions gave acetone and gaseous hydrogen as a mixture of H_2, HD, and D_2:

$$(CH_3)_2CHOD(l) \longrightarrow (CH_3)_2CO(l) + H_2, HD, D_2. \quad (4)$$

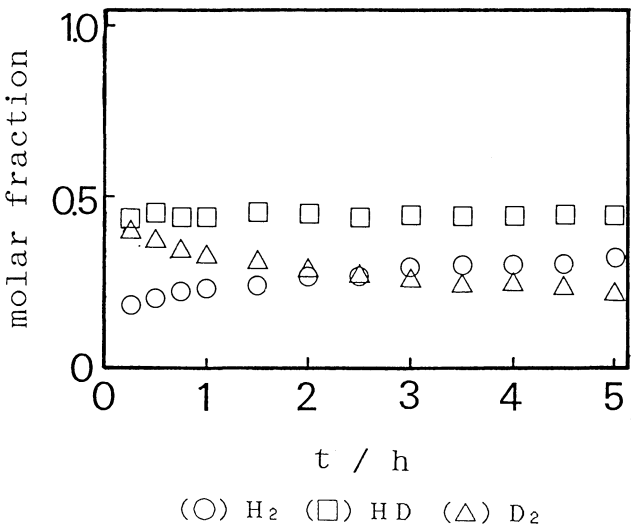

Fig. 2. Deuterium distribution among gaseous hydrogen at the time of evolution from $(CH_3)_2CHOD$ at 82.4°C under refluxing conditions (heat at 100°C) with Ru(5 wt%)/carbon catalyst.

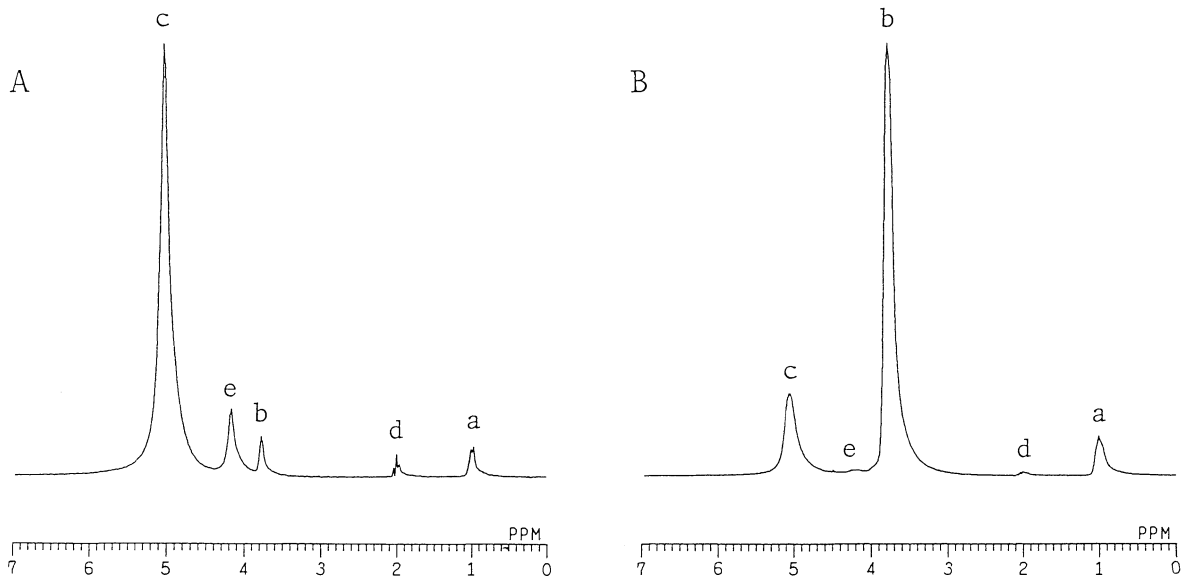

Fig. 3. ^2H NMR spectra of $(CH_3)_2CHOD$ (A) and $(CH_3)_2CDOH$ (B) solutions after 5-h reaction at 82.4°C under refluxing conditions (heat at 100°C) with Ru(5 wt%)/carbon catalyst. Peaks identified as 2-propanol methyl (a), methine (b) and hydroxyl (c) groups, acetone (d), and water (e).

A kinetic isotope effect of 1.69 was obtained from the initial dehydrogenation rates of $(CH_3)_2CHOH$ and $(CH_3)_2CHOD$. The amounts of H_2, HD, and D_2 produced from $(CH_3)_2CHOD$ are shown in Fig. 1 as a function of time.

The H/D ratio of gaseous hydrogen was smaller than unity (0.65) during the initial stage (15 min). The constitution of evolving hydrogen, however, changed with time, as represented in the variation of H_2, HD, and D_2 (Fig. 2). After 5 h from the start of the reaction, the H/D ratio of hydrogen newly-evolved increased to 1.22 at a conversion of 8.5%.

The deuterium distribution among the liquid-phase components after the 5-h reaction can be seen in the ^2H NMR spectrum (Fig. 3A). A part of the hydrogen atoms in the methine and methyl groups of $(CH_3)_2$-CHOD, as well as in the methyl group of $(CH_3)_2CO$, was exchanged with the deuterium supplied from the OD group of the reactant. In addition, a new peak due to HDO appeared, since water exuded from the carbon support was contaminated with deuterium.

The total amount of deuterium remaining in the solution was 58.27 mg-atom, as calculated from the $(CH_3)_2CHOD$ charged (64.51 mmol) and gaseous deuterium evolved (6.24 mg-atom). The deuterium distribution among the liquid-phase components is summarized in Table 1.

Dehydrogenation of 2-Propan-2-*d*-ol. The dehydrogenation products of $(CH_3)_2CDOH$ were acetone and the mixture of H_2, HD, and D_2:

$$(CH_3)_2CDOH(l) \longrightarrow (CH_3)_2CO(l) + H_2, HD, D_2. \quad (5)$$

The amounts of H_2, HD, and D_2 produced from $(CH_3)_2CDOH$ are shown in Fig. 4 as a function of time. Figure 5 depicts the variation in the molar fractions of H_2, HD, and D_2 produced at the reaction time concerned. As for $(CH_3)_2CDOH$, the H/D ratio of newly-evolved hydrogen changed from 1.7 to 6.9 during a 5-h reaction. In contrast to slight deuterium transfer to the methyl groups of 2-propanol and acetone, an H–D exchange at the hydroxyl group

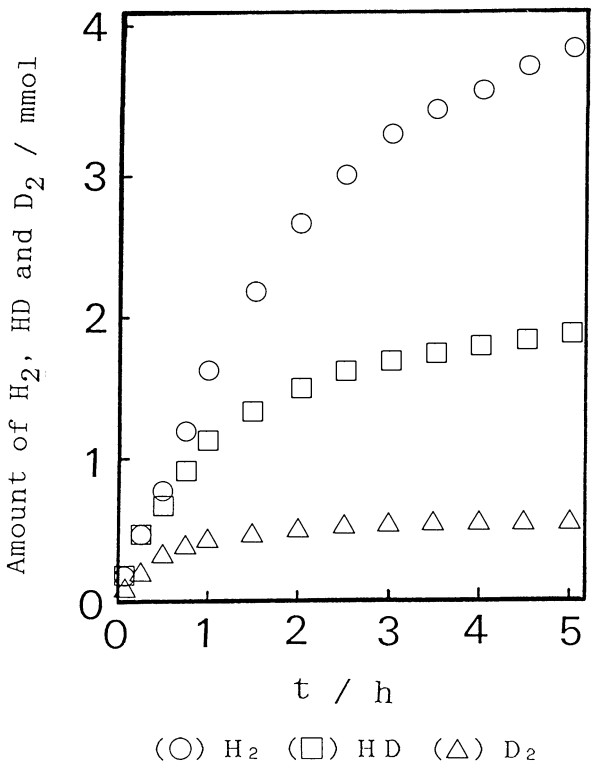

Fig. 4. Accumulation of H_2, HD, and D_2 evolved at 82.4°C from $(CH_3)_2CDOH$ under refluxing conditions (heat at 100°C) with Ru(5 wt%)/carbon catalyst.

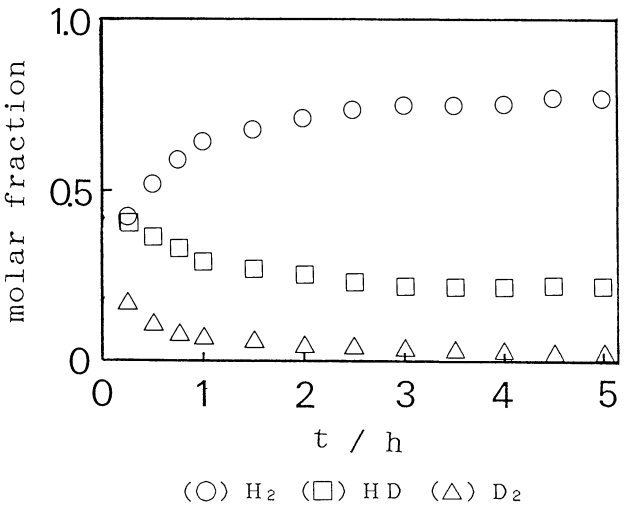

Fig. 5. Deuterium distribution among gaseous hydrogen at the time of evolution at 82.4°C from $(CH_3)_2CDOH$ under refluxing conditions (heat at 100°C) with Ru(5 wt%)/carbon catalyst.

Table 1. Deuterium Distribution in Liquid-Phase Components Obtained from $(CH_3)_2CHOD$ or $(CH_3)_2CDOH$ after 5-h Reaction under Refluxing Conditions (100°C) with Ru(5 wt%)/Carbon Catalyst

Reactant	Deuterium amount in solution	Deuterium distribution/%				
	mmol	2-Propanol			Acetone	Water
		Methyl	Methine	Hydroxyl		
$(CH_3)_2CHOD$	58.27	2.97	3.17	83.54	1.19	9.12
$(CH_3)_2CDOH$	61.61	6.16	74.48	17.62	1.17	0.47

amounted to an extent as large as 17.6% (Fig. 3B and Table 1).

The initial dehydrogenation rates of $(CH_3)_2CHOH$ and $(CH_3)_2CDOH$ gave a k_H/k_D of 1.57.

Dehydrogenation of the Mixture of 2-Propanol-d_0 and Acetone-d_6. As previously reported for a nickel fine-particle catalyst,[8] the initial rate of 2-propanol dehydrogenation on the Ru/carbon catalyst was suppressed 1/2.95 times by adding acetone (10 vol%). A mixture of $(CH_3)_2CHOH$ and $(CD_3)_2CO$ (10 vol%) gave gaseous hydrogen as mainly H_2, the molar ratios of HD/H_2 and D_2/H_2 being 0.03 and 0.02, respectively.

Most of the hydroxyl and methine groups of 2-propanol remained intact after the 1-h reaction, since the extents of deuterium exchange shown in the ^2H NMR spectrum (Fig. 6A) were only 0.78 and 0.49% of all the deuterium species in the solution, respectively. On the contrary, 75.2% of the deuterium atoms in acetone-d_6 changed to the methyl group of 2-propanol within 1 h.

The extent of hydrogen transfer from 2-propanol-d_0 to acetone-d_6, yielding 2-propan-1,1,1,3,3,3-d_6-ol within 1 h, was estimated to be 4.65 mmol from the deuterium peaks due to the two kinds of methyl groups, which was 7.15-times larger than that of hydrogen evolution (0.65 mmol).

After a reaction for 5 h, 88% of the added acetone-d_6 changed into 2-propanol (Fig. 6B and Table 2).

Effects of Gaseous Hydrogen and Hydrogen Surface Species on Deuterium Distribution. In order to ascertain the possibility of a reverse reaction between gaseous hydrogen and acetone under the dehydrogenation conditions of 2-propanol, a suspended Ru/carbon catalyst was heated in $(CH_3)_2CHOH$ as well as in $(CH_3)_2CHOH$ including $(CH_3)_2CO$ (10 vol%) under a deuterium atmosphere. After the solution was boiled for 5 h, a ^2H NMR analysis was performed at room temperature.

The amount of hydrogen evolved from the mixture of 2-propanol and acetone (10 vol%) under refluxing conditions for 5 h (2.33 mmol) was much larger than that of deuterium incorporated from the gas phase to the liquid components (0.17 mmol). The extents of H–D exchange between gaseous deuterium and the

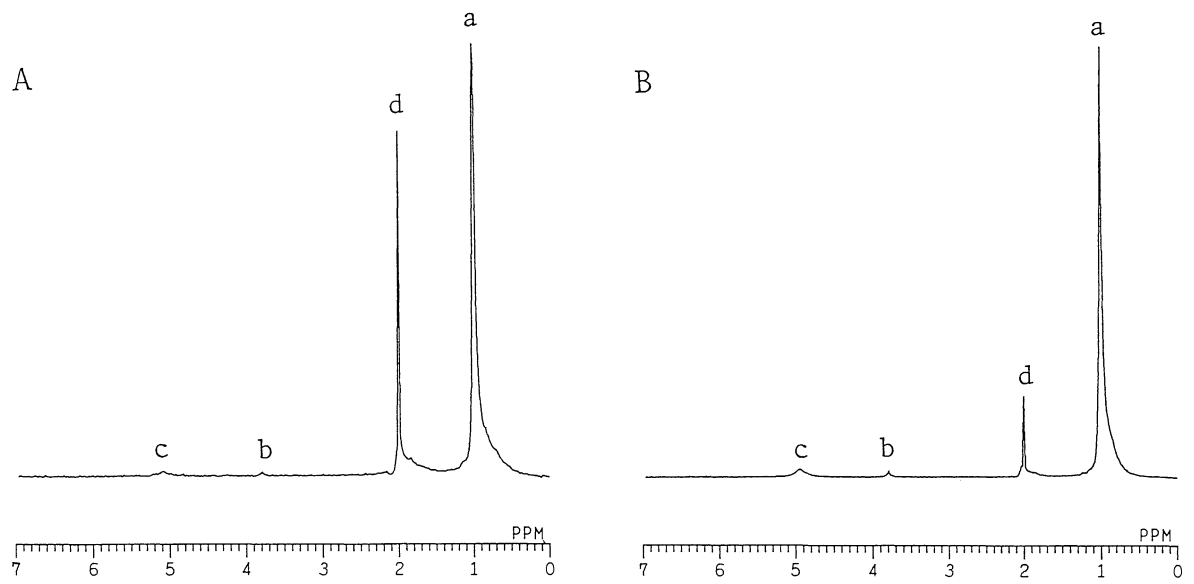

Fig. 6. ^2H NMR spectra of the mixed solution of $(CH_3)_2CHOH$ and $(CD_3)_2CO$ (10 vol%) after 1-h (A) or 5-h (B) reaction at 77.0°C under refluxing conditions (heat at 100°C) with Ru(5 wt%)/carbon catalyst. Peaks identified as 2-propanol methyl (a), methine (b) and hydroxyl (c) groups, and acetone (d).

Table 2. Deuterium Distribution in Liquid-Phase Components Obtained from the Mixture of $(CH_3)_2CHOH$ and $(CD_3)_2CO$ (10 vol%) after 1-h or 5-h Reaction at 77°C under Refluxing Conditions (100°C) with Ru(5wt%)/Carbon Catalyst

Reaction time/h	Deuterium distribution/%			
	2-Propanol			Acetone
	Methyl	Methine	Hydroxyl	
0	0.00	0.00	0.00	100.00
1	75.24	0.49	0.78	23.50
5	88.07	0.76	1.22	9.94

Table 3. Incorporation and Distribution of Deuterium from Gaseous Phase or Pre-Adsorbed State into Liquid-Phase Components as the Mixture of $(CH_3)_2CHOH$ and $(CH_3)_2CO$ (10 vol%) during the Reaction at 77.0 °C for 5 h under Refluxing Conditions (100 °C) with Ru(5 wt%)/Carbon Catalyst

Deuterium origin	Deuterium incorporated into solution	Deuterium distribution/mmol			
		2-Propanol			Acetone
	ppt	Methyl	Methine	Hydroxyl	
Gas phase	33.0	94.1	34.4	39.8	1.3
Pre-adsorbed at 130 °C	32.7	94.1	26.1	47.0	1.7

hydrogen atoms in 2-propanol or acetone were extremely small with no predominance to the methine and hydroxyl groups of 2-propanol (Table 3). The distribution and extent of deuterium incorporation in the solution of 2-propanol alone were similar to those obtained in a mixed solution of 2-propanol and acetone.

The effect of deuterium pre-adsorption on the catalyst was examined for a mixture of 2-propanol and acetone (10 vol%) at either 80 °C or 130 °C (Table 3). An extremely small amount of deuterium (0.17 mmol) was incorporated into the liquid components, irrespective of the pre-adsorption temperatures (80 °C and 130 °C) of gaseous deuterium.

Discussion

Surface Species Formed on the Ru/Carbon Catalyst during 2-Propanol Dehydrogenation. The reaction mechanism previously proposed for 2-propanol dehydrogenation (Eqs. 6—9)[7] seems to be responsible for the Ru/carbon catalyst as well.

$$(CH_3)_2CHOH \longrightarrow (CH_3)_2CHO_{ads} + H_{ads}, \quad (6)$$

$$(CH_3)_2CHO_{ads} \longrightarrow (CH_3)_2CO_{ads} + H_{ads}, \quad (7)$$

$$(CH_3)_2CO_{ads} \longrightarrow (CH_3)_2CO, \quad (8)$$

$$H_{ads} + H_{ads} \longrightarrow H_2. \quad (9)$$

As is apparent from the constitutions of the product hydrogen as the mixture of H_2, HD, and D_2, hydrogen molecules are formed irrespective of the groups to which the hydrogen atoms previously belonged.

The H/D ratio of gaseous hydrogen produced from $(CH_3)_2CHOD$ was slightly smaller than unity during the initial stage, whereas the H/D ratio from $(CH_3)_2CDOH$ exceeded unity to some extent. It is therefore conceivable that the hydroxyl group of 2-propanol is dissociated more easily than its methine group, while supplying an excess amount of isopropoxyl and hydrogen species adsorbed on the catalyst surface. A gradual increase in the H/D ratio of gaseous hydrogen indicates that the methyl and methine hydrogen atoms of either $(CH_3)_2CHOD$ or $(CH_3)_2CDOH$ exchange with the surface deuterium species directly, but slowly.

The low extent of H–D exchange between the surface hydrogen species and acetone was also confirmed by the fact that most of the gaseous hydrogen which evolved from the $(CH_3)_2CHOH/(CD_3)_2CO$ (90/10 mixed by volume) solution was H_2. The possibility of acetone adsorption in its enol form[15] is therefore unlikely on a Ru/carbon catalyst.

Hydrogen Transfer from 2-Propanol to Acetone. Acetone hydrogenation is thermodynamically more favorable than 2-propanol dehydrogenation in temperature regions as low as the boiling point of 2-propanol (82.4 °C).[4] Under boiling conditions, however, hydrogen evolution took place catalytically, even at 77.0 °C, from the 2-propanol/acetone (90/10 mixed by volume) solution.

The small extents of deuterium incorporation from pre-adsorbed deuterium or from gaseous deuterium under the reaction conditions indicate that either an intermediation of pre-adsorbed hydrogen or a dissolution and adsorption of gaseous hydrogen are insignificant for the reaction. Once expelled from the reaction medium to the gas phase, the product hydrogen becomes indifferent to the catalysis under refluxing conditions. The observed rate retardation due to acetone (1/2.95 times in the 90/10 mixed solution) would be ascribed to the following two factors: (i) occupation of sites active for 2-propanol dehydrogenation and (ii) consumption of surface hydrogen by adsorbed acetone through hydrogen transfer from 2-propanol.

As for the 2-propanol/acetone-d_6 (90/10) mixed solution, hydrogen transfer from 2-propanol to acetone is described as

$$(CH_3)_2CHOH(l) + (CD_3)_2CO_{ads} \longrightarrow (CD_3)_2CHOH(l) + (CH_3)_2CO_{ads}. \quad (10)$$

The surface hydrogen species supplied from 2-propanol is consumed not only by evolving gaseous hydrogen, but also by converting $(CD_3)_2CO$ into $(CD_3)_2CHOH$ (Eqs. 11—14):

$$(CH_3)_2CHOH \longrightarrow (CH_3)_2CO_{ads} + 2H_{ads}, \quad (11)$$

$$(CD_3)_2CO \longrightarrow (CD_3)_2CO_{ads}, \quad (12)$$

$$(CD_3)_2CO_{ads} + 2H_{ads} \longrightarrow (CD_3)_2CHOH, \quad (13)$$

and

$$(CH_3)_2CO_{ads} \longrightarrow (CH_3)_2CO. \quad (14)$$

Eq. 13 is eventually the reverse process of 2-propanol dehydrogenation(Eqs. 6 and 7).

Even through hydrogen transfer proceeded rapidly from $(CH_3)_2CHOH$ to $(CD_3)_2CO$, deuterium was incorporated into the methine and hydroxyl groups infinitesimally. As is evident from the ^2H NMR spectra shown in Fig. 6, $(CH_3)_2CO$ and $(CD_3)_2CHOH$ were yielded predominantly during the dehydrogenation of $(CH_3)_2CHOH$ in the presence of $(CD_3)_2CO$.

After the reaction of 2-propanol-d for 5 h, deuterium in the methine and methyl groups of 2-propanol-*d* amounted to 3.17 and 2.97%, respectively (Table 1). H–D exchange of the methine group proceeded more extensively than that of the methyl group per hydrogen atom (3.17/1 vs. 2.97/6), which strongly suggests that the surface deuterium species is incorporated through a transfer reaction to acetone (Eq. 15) more efficiently than through an exchange reaction with methyl hydrogen (Eq. 16):

$$(CH_3)_2CO_{ads} + 2D_{ads} \longrightarrow (CH_3)_2CDOD, \quad (15)$$

and

$$(CH_3)_2CHOD + D_{ads} \longrightarrow (CH_3)(CH_2D)CHOD + H_{ads}. \quad (16)$$

The reactions of hydrogen transfer and hydrogen evolution ought to proceed simultaneously, since the rate of either Eq. 13 or Eq. 15 is large.

Reaction Mechanism of 2-Propanol Dehydrogenation on the Ru/Carbon Catalyst. The isotope effects for hydrogen evolution from 2-propan-2-*d*-ol and 2-propanol-*d* with a suspended Ru/carbon catalyst were obtained during the initial stage as 1.57 and 1.69, respectively.

It should not be assumed that splitting the methine C–H bond is difficult, since the magnitude (1.57) is rather small as a primary isotope effect for the elimination of β-hydrogen[16] and is preceded by the magnitude obtained from 2-propanol-*d*.

Provided that the formation of molecular hydrogen from the surface hydrogen species is the slowest step, these magnitudes and tendency of the isotope effects become conceivable. More abundant deuterium species were supplied from $(CH_3)_2CHOD$ than from $(CH_3)_2CDOH$ on the catalyst surface, as indicated by the difference between 0.65 and 1.7 in the H/D ratios of molecular hydrogen formed during the initial stage. It should also be noted that the magnitudes of the k_H/k_D obtained from $(CH_3)_2CDOH$ and $(CH_3)_2CHOD$ are comparable to those for the formation of molecular hydrogen from metal hydride complexes, i. e., $Co(H)_2P(OCH_3)_3]_4^+$ (k_H/k_D=1.51 at 23 °C)[17] and $[Ir(H)_2(CO)_2(PMePh_2)_2]^+$(2.1 at 20 °C).[18]

As $(CH_3)_2CDOH$ changed appreciably into $(CH_3)_2CHOD$ on the catalyst (Table 1), the dissociation and formation processes of the methine C–H bond were facile. These distinctive characteristics of the Ru/carbon catalyst would be the reason for its superiority regarding the activity of 2-propanol dehydrogenation.[14] The splitting process of the methine C–H bond has been considered to be the most difficult step for catalytic 2-propanol dehydrogenation.[19]

New abilities for easy desorption of both acetone and hydrogen should be added to the Ru/carbon catalyst from the viewpoint of designing a catalyst most suitable for 2-propanol dehydrogenation in a chemical heat pump system.

Conclusive Remarks

The suspended Ru/carbon catalyst exhibited the following characteristics for 2-propanol dehydrogenation: i) highly selective and active performance under boiling conditions, ii) relatively small isotope effects, being larger for $(CH_3)_2CHOD$ than $(CH_3)_2CDOH$, iii) simultaneous occurrence of hydrogen evolution and hydrogen transfer from 2-propanol to acetone on the catalyst surface, and iv) the slowest step presumed not to be the splitting process of the methine C–H bond but to be the formation of molecular hydrogen from the surface hydrogen species.

Further improvements of the Ru/carbon catalyst are necessary, especially regarding easy desorption of both acetone and hydrogen.

The present work was supported by a Grant-in Aid on Priority-Area Research No. 63603007 from the Ministry of Education, Science and Culture.

References

1) S. Fujii, H. Kameyama, K. Yoshida, and D. Kunii, *J. Chem. Eng. Jpn.*, **10**, 224 (1977); W. M. Raldow and W. E. Wentworth, *Sol. Energy*, **23**, 75 (1979).

2) M. Noda, S. Shinoda, and Y. Saito, *Nippon Kagaku Kaishi*, 1017 (**1984**).

3) Y. Saito, H. Kameyama, and K. Yoshida, *Int. J. Energy Res.*, **11**, 594 (1987).

4) D. R. Stull, E. F. Westrum, Jr., and G. C. Sinke, "The Chemical Thermodynamics of Organic Compounds," John Willey and Sons, New York (1969), pp. 649—651.

5) C. H. T. Stoddart and C. Kemball, *J. Colloid Sci.*, **11**, 532 (1956); F. Velasco, *Chim. Ind.*, **81**, 521 (1959); T. Kato, N. Nakagawa, and H. Kameyama, *Kagaku-Kogaku*, **5**, 714 (1987).

6) F. Claes and J. C. Jungers, *Bull. Soc. Chim. Fr., Ser. 5*, **25**, 1167 (1958).

7) D. E. Mears and M. Boudart, *AIChE J.*, **12**, 313 (1966).
8) M. Noda, S. Shinoda, and Y. Saito, *Bull. Chem. Soc. Jpn.*, **61**, 961 (1988).
9) M. Noda, S. Shinoda, and Y. Saito, *Bull. Chem. Soc. Jpn.*, **61**, 3421 (1988).
10) S. Kasyu, M. Nagase, C. Hayashi, R. Uyeda, N. Wada, and N. Kamijo, *Jpn. J. Appl. Phys.*, **24**, L3 (1985).
11) H. B. Charman, *J. Chem. Soc. B*, **1970**, 584; S. Shinoda, Y. Tokushige, T. Kojima, and Y. Saito, *J. Mol. Catal.*, **17**, 81 (1982); S. Shinoda, T. Kojima, and Y. Saito, *J. Mol. Catal.*, **18**, 99 (1983).
12) A. Dobson and S. D. Robinson, *Inorg. Chem.*, **16**, 137 (1977); W. K. Ryabck and J. J. Ziolkowski, *J. Mol. Catal.*, **11**, 367 (1981).
13) T. Yamakawa, H. Miyake, H. Moriyama, S. Shinoda, and Y. Saito, *J. Chem. Soc., Chem. Commun.*, **1986**, 326.
14) Y. Saito, M. Yamashita, and E. Ito, 8th World Hydrogen Energy Conference, Honolulu, July 1990, Abstr., B1-6.
15) H. Miyata, M. Wakamiya, Y. Kubokawa, *J. Catal.*, **34**, 117 (1974); K. Nagai, K. Tanaka, and K. Miyahara, *Bull. Chem. Soc. Jpn.*, **47**, 2847 (1974).
16) The primary isotope effect of β-hydrogen elimination from alkyl groups on an aluminium film was obtained as 2.6 at 520 K: B. E. Bent, R. G. Nuzzo, and L. H. Dubois, *J. Am. Chem. Soc.*, **111**, 1634 (1989).
17) E. L. Muetterties and P. L. Watson, *J. Am. Chem. Soc.*, **100**, 6978 (1978).
18) M. J. Mays, R. N. F. Simpson, and F. P. Stefanini, *J. Chem. Soc. A*, **1970**, 300.
19) O. V. Krylov, "Catalysis by Nonmetals," Academic Press, London (**1970**).

High-Resolution Solid-State Cross-Polarization Magic-Angle Spinning ^{13}C NMR of Metal-Free Phthalocyanines

Toshio ENOKIDA,* Ryo HIROHASHI,† and Nobuo MOROHASHI††
Graduate School of Science and Technology, Chiba University, 1-33 Yayoi-cho, Chiba 260
† Faculty of Engineering, Chiba University, 1-33 Yayoi-cho, Chiba 260
†† Tsukuba Research Laboratory, Toyo Ink Mfg. Co., Ltd., 27 Wadai, Tsukuba, Ibaraki 305-42
(Received December 27, 1989)

Synopsis. The high-resolution solid-state cross-polarization magic-angle spinning ^{13}C NMR spectra of α, β, τ and X-form metal-free phthalocyanines (H_2pc) were investigated. Chemical shifts differed according to crystal forms. As a result of the temperature dependence of chemical shifts, we could observe the change in the spectra because of the inner protons.

Phthalocyanines are a very interesting class of organic compounds owing to their highly functional properties. In particular, metal-free phthlocyanines (H_2pcs) have specific phenomena. The H_2pc molecule has two inner protons; their locations are somewhat controversial. Cross-polarization magic-angle spinning (CP-MAS) ^{13}C nuclear magnetic resonance (NMR) has been developed as an effective method to investigate the state of a solid and its morphology. Thus, many researchers have been investigating the relationship between inner protons and phthalocyanine rings.[1,2] An especially, important theme is whether the two inner protons are directly bonded with a diagonally opposed pair of nitrogens (bonded type) or are shared by four equivalent pyrrole nitrogens (bridged type). The proton dynamics in an α-form H_2pc were observed using a two-dimensional chemical exchange in the solid-state by Meier et al.[1] They demonstrated the utility of two-dimensional exchange spectroscopy, and proposed that the way to obtain kinetic information about this system is through difficult isotope labeling. Toscano studied electrically conductive metallo-macrocyclic assemblies.[2]

This paper describes ^{13}C NMR spectroscopy that can be applied to detect and identify the difference in crystal forms of H_2pc (α, β, X, and τ-forms). Moreover, the ^{13}C NMR spectra change between -100 °C and room temperature; a peak shift, disappearance and reappearance can be found in the exchange reaction of two inner protons between the two tautomeric positions, depending upon the temperature.

Experimental

Samples. The β-H_2pc used in this work was prepared from crude H_2pc by vacuum sublimation in a zone furnace at 470 °C under a pressure of 10^{-5} Torr (1 Torr=133.322 Pa) for 8 h. Acid pasting of this β-H_2pc gave a fine powder of α-H_2pc. The X-H_2pc was prepared as previously described.[3,4] Conversion to the τ-form was achieved by a wet milling method.[5] All samples were purified by a solvent-extraction technique with methyl ethyl ketone and methanol. The individual crystal forms were checked by their powder X-ray diffraction patterns as well as infrared absorption spectra.

Spectroscopy. High-resolution CP-MAS ^{13}C NMR spectra were obtained on a JOEL GSX-270W spectrometer at a frequency of 67.5 MHz with accessories. The techniques of magic-angle spinning, cross-polarization and dipole dephasing delay were employed in order to enhance the single-to-noise ratio as well as the spectral resolution. The resolution was within 5 Hz at a spinning speed of 4.5 kHz within the temperature range used. Admantane was used for measurements of the resolution. The temperature was measured with a thermocouple positioned close to the spinner in the range the -100—25 °C. The repetition time was within 10 seconds. The ^{13}C chemical shifts were determined by using liquid tetramethyl silane (TMS) as an external reference.

Results and Discussion

H_2pc has four representative polymorphic forms: the β-form is thermodynamically stable and the α-form is metastable, while the X- and τ-forms are quite differently packed in the middle energy states between the α- and β- forms. The differences in the crystal forms found by crystallographic, spectroscopic, and photoconducting methods are attributable to a distinct stacking of phthalocyanine molecules and to the state of the inner protons.

Chemical Shifts of H_2pc at Room Temperature. The CP-MAS ^{13}C NMR spectra of H_2pcs measured at room temperature are shown in Fig. 1. The chemical shifts and their assignments are summarized in Table 1. In order to assign the quaternary carbons, the dipole dephasing delay method was used. The assignments followed the described methods by Meier et al.[5]

In the case of α-H_2pc having four equivalent central nitrogens, one resonance line comprises a contribution from four equivalent carbons (Scheme 1), due to a fast hydrogen exchange rate between the inner nitrogens. These broad lines suggest a lower regularity and a wide distribution of the crystalline structure, compar-

Table 1. Chemical Shifts and Assignments of ^{13}C NMR Spectra with Metal-Free Phthalocyanines at Room Temperature (ppm)[a]

α	β	τ	X
	119.6 (4,4′)	118.6 (4′)	118.7 (4′)
122.1 (4,4′)	121.9	122.9 (4)	
	124.5 (3,3′)	125.8 (3′)	126.2 (3,3′,4)
128.2 (3,3′)	126.8	128.9 (3)	
	130.6	131.6 (2′)	131.2 (2′)
132.6 (2,2′)	133.8 (2,2′)	137.2 (2)	137.3 (2)
	136.7		
145.6 (1,1′)	142.8	145.1 (1′)	144.9 (1′)
	146.3 (1,1′)	150.6 (1)	150.4 (1)
	149.8		

a) Numerals in parentheses present the assignment of carbon atoms which exhibit in Scheme 1.

ed with the other three forms. We have observed four broad resonance lines of oxo(phthalocyaninato)titanium (IV) ([TiO(pc)] in CP-MAS ^{13}C spectra.[6] It is known that metallophthalocyanines possess four central nitrogen atoms equivalently bonded to the hydrogen atoms.[7,8] This result may support the fact that four resonance lines appear for α-H_2pc. The β-H_2pc actually has a much more complicated tautomerism, and the molecules tend to be packed as close as their geometry allows. Thus, the β-H_2pc have a number of chemical shifts, possibly due to the diversity of carbon atoms in the molecules. The τ-H_2pc are assigned to the eight well-split carbon atoms. The chemical shifts of the same numerals differ by approximately 5.5 ppm in relation to whether the bridge nitrogens are bonded with the inner hydrogens or not. The resonance lines, which bond with hydrogen-bonded nitrogen, appear in the lower magnetic field. Since two inner protons of τ-H_2pc are directly bonded with a diagonally opposed pair of nitrogens in a molecule, the N–H bonds may further weaken the overlapping of the π-electrons and induce differences in their chemical shifts. Though X-H_2pc has relatively similar shifts compared to the τ-form above 140 ppm, a broad shift can be seen from 120 to 130 ppm. The structures of the crystal packing of τ-H_2pc may be stable, and the distances of each molecule are in suppose to be longer than those of X-H_2pc.

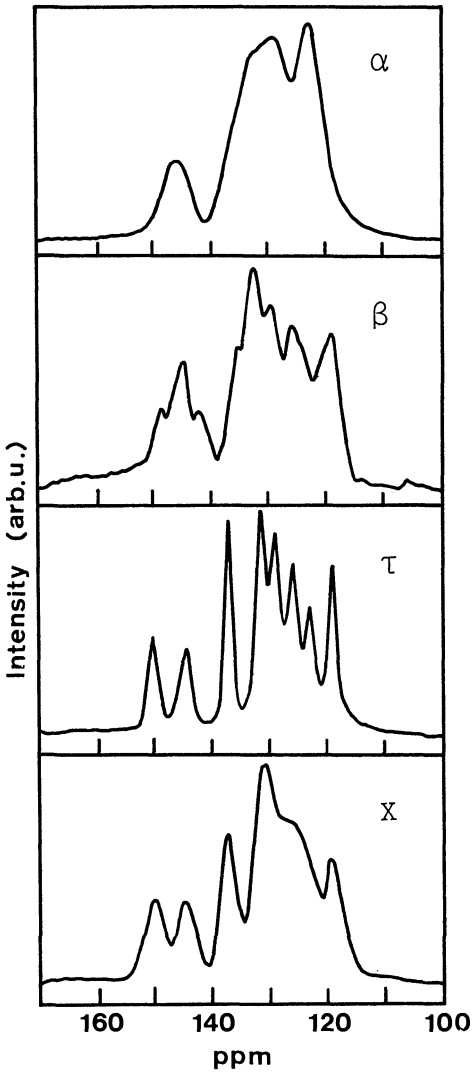

Fig. 1. Solid-state ^{13}C NMR spectra of four kinds of metal-free phthalocyanines using the CP-MAS method at 27 °C.

Variation of the Chemical Shifts as a Function of the Temperature. The temperature dependences of the CP-MAS ^{13}C NMR spectra with H_2pcs are given in Fig. 2. These shifts are attributable to a change in the

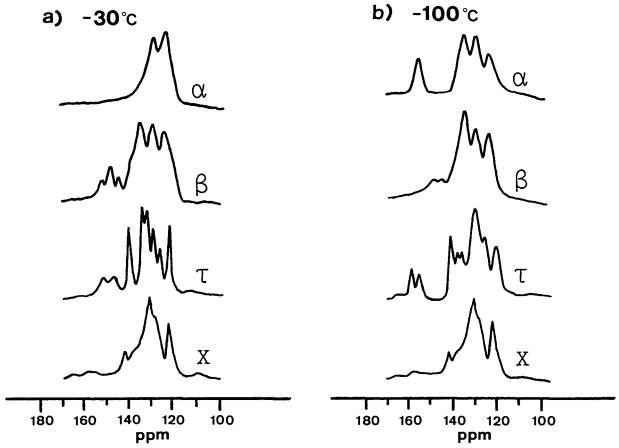

Fig. 2. Solid-state ^{13}C NMR spectra of four kinds of metal-free phthalocyanines using the CP-MAS method. a) −30 °C, b) −100 °C.

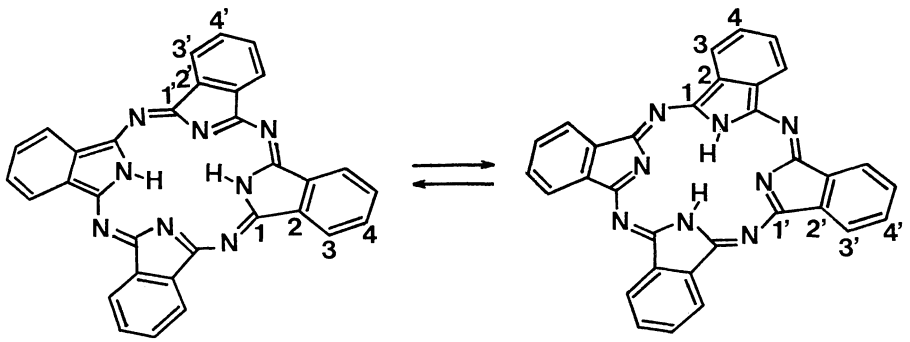

Scheme 1.

exchange limits between −30 °C and −100 °C. The chemical shifts from 130 to 150 ppm of α-H_2pc progressively decrease from room temperature to −30 °C, because of a decreasing intermolecular interaction, while the intermolecular interaction increases. Below −30 °C, these shifts increase with decreasing temperature under a smaller magnetic field (151 ppm). The temperature dependence of β-H_2pc is rather low until −100 °C. It can be concluded that a proton exchange reaction with an intramolecular interaction will occur at the same time in β-H_2pc, due to these complicated spectra. The change in the shifts of τ-H_2pc accompanied by temperature differences is remarkable. Two lines assigned to two kinds of carbons, which bond with nitrogens, shift downfield as for α-H_2pc; they disappear at −40 °C, but appear again below −60 °C. The distance of the two shifts varied at −30 °C (6.2 ppm) and −100 °C (3.0 ppm), resulting from the proton exchange velosity. The narrow distance of two equivalent spins suggests a faster exchange regime. Below −60 °C, the intermolecular interaction becomes greater due to the weakened forces of the intermolecular interaction. The influence is larger than other H_2pcs due to the high sensitivity of τ-H_2pc to the nuclear magnetic moments. Moreover, the chemical shifts of carbon in resonating benzene rings are well separated in this temperature region. The chemical shifts of resonating carbon atoms are not well separated compared with those of τ-H_2pc, and the distances of chemical shifts with carbon 2 and 2′ are 5.0 ppm at −30 °C and 4.2 ppm at −100 °C. The energy stage of X-H_2pc may be located near that of τ-H_2pc. However, the lines of the inner carbons cannot separate like those of τ-H_2pc, probably at −100 °C, because of inperfections in crystal packing.

Though the α, X and τ-H_2pcs show a changed limit at a temperature of approximately −30 °C, we can not observe this situation for the β-H_2pc. This result may be because the strong interaction of molecular packing prevents the formation of intramolecular N–H bonding, instead of the intermolecular N–H bonding with neighbor molecules.

We thank Toyo Ink Mfg. Co., Ltd. for assistance in the measurements of the NMR spectra. We also thank Mr. Deguchi, of JOEL Ltd., for his helpful discussions concerning the NMR study.

References

1) B. H. Meier, C. B. Storm, and W. L. Earl, *J. Am. Chem. Soc.*, **108**, 6074 (1986).
2) P. J. Toscano and T. J. Marks, *J. Am. Chem. Soc.*, **108**, 437 (1986).
3) J. H. Sharp and M. Lardon, *J. Phys. Chem.*, **72**, 3230 (1968).
4) J. F. Byrne and P. F. Kurz, U. S. Patent 3357989 (1967).
5) S. Takano, T. Enokida, A. Kakuta, and Y. Mori, *Chem. Lett.*, **1984**, 2037.
6) T. Enokida and R. Hirohashi, *Nippon Kagaku Kaishi*, **1990**, 211.
7) Z. Berkovitch-Yellin and D. E. Ellis, *J. Am. Chem. Soc.*, **103**, 6066 (1986).
8) B. Wehrle, H. Zimmermann, and H. H. Limbach, *J. Am. Chem. Soc.*, **110**, 7014 (1988).

High-Pressure Fourier Transform Infrared Spectroscopy Study of the Diels-Alder Reaction of Isoprene and Maleic Anhydride in Supercritical Carbon Dioxide

Yutaka IKUSHIMA,* Norio SAITO, and Masahiko ARAI†
Government Industrial Research Institute, Tohoku, Nigatake 4-chome, Miyagino-ku, Sendai 983
† Chemical Research Institute of Non-Aqueous Solutions, Tohoku University, Katahira, Aoba-ku, Sendai 980
(Received July 23, 1990)

Synopsis. A high-pressure FTIR spectroscopy was used to make an in situ study on the Diels-Alder reaction of isoprene and maleic anhydride catalyzed with aluminum chloride in supercritical carbon dioxide at 306 K and 7.45 and 7.85 MPa, suggesting a two-step mechanism and showing a pressure effect.

Considerable attension has recently been focused on the highly compressible properties of supercritical fluids (SCFs) in the near-critical region from scientific and industrial points of view.[1-5] The solvent strength varies widely with both the pressure and temperature in that region; this sensitivity can be applied to the control of chemical reaction processes. A few studies have shown that the use of SCFs as reaction media leads to significant increases in the reaction rates and the variation in product distributions.[1,2,6-8] However, detailed studies have rarely been made to examine the elementary processes involved in reactions in SCFs.[9] This is mainly because it is difficult to follow reactions in situ under supercritical conditions.

In the present work, high-pressure Fourier transform infrared (FTIR) spectroscopy was applied to a study of a chemical reaction in supercritical carbon dioxide. The reaction that we conducted was a Diels-Alder reaction of isoprene and maleic anhydride catalyzed with aluminum chloride. It was followed by examining changes in the absorption intensities for some functional groups characteristics to both the reactants and product. The present note presents information concerning the mechanism of the reaction under supercritical conditions and demonstrates that the FTIR technique used in this work is promising for the study of chemical reactions in SCFs.

Details of the experimental system used, including a high-pressure cell that can withstand high pressures and temperatures such as 50 MPa and 373 K, was described elsewhere.[10] A 2.94 g (0.03 mol) of maleic anhydride with 0.40 g (0.003 mol) of aluminum chloride was dissolved in 20 ml of benzene. A 0.35 μL portion of this solution and 0.15 μL of isoprene were simultaneously injected into the system from two injection valves. The reactants reached the high-pressure flow cell immediately after injection by stopping the flow. The reaction was conducted at 306±0.1 K and at 7.45 and 7.85 MPa. During the reaction, FTIR measurements were made at certain time intervals. Interferrograms were accumulated at a rate of 1 scan per 1.2 s and 4—5 scans were made for each measurement. A spectrum of supercritical carbon dioxide alone was used to provide the background spectrum.

Figure 1 shows the changes in the intensities of the absorption bands at 1597, 1784, and 1798 cm^{-1} during the reaction. The bands at 1597 and 1784 cm^{-1} can be

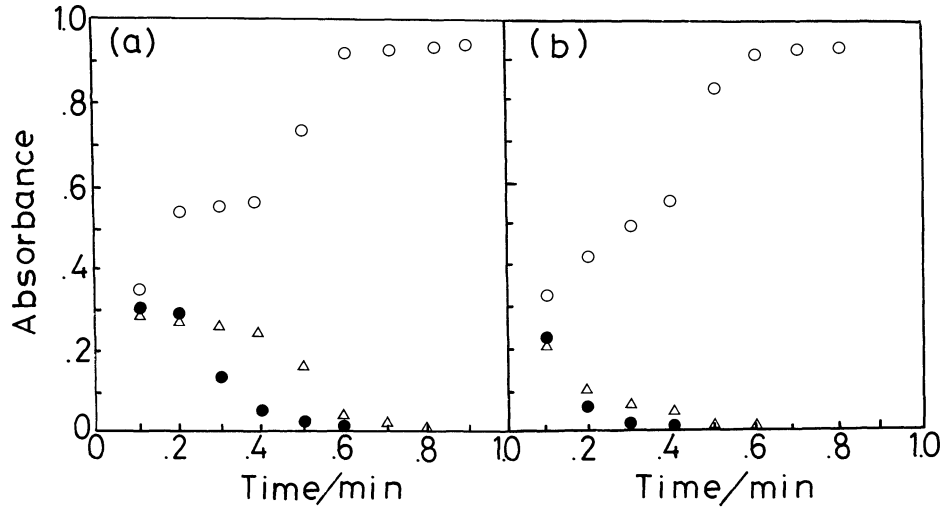

Fig. 1. Changes of the intensities of the absorption bands at 1597 (●), 1798 (○), and 1784 cm^{-1} (△) with time on the Diels-Alder reaction of maleic anhydride and isoprene catalyzed with aluminum chloride in supercritical carbon dioxide at 306 K. Pressure: (a) 7.45 MPa; (b) 7.85 MPa.

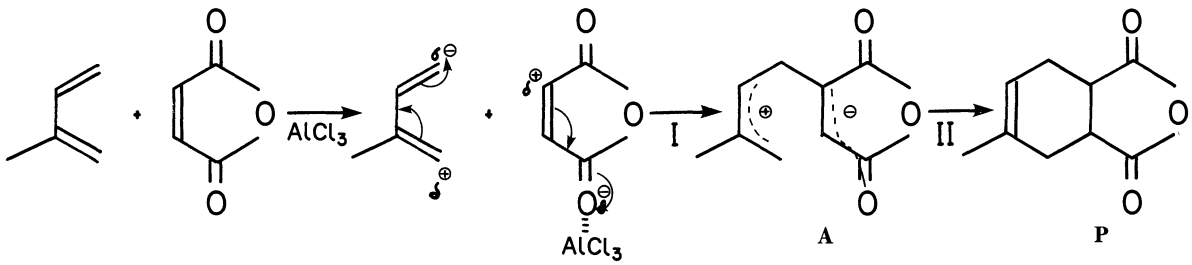

Scheme 1.

assigned to a C=C stretching of the isoprene and a C=O stretching of the maleic anhydride, respectively. From a NMR measurement, compound (**P**) shown in Scheme 1 was proved to be the only product in the present cycloaddition. The absorption at 1798 cm^{-1} is assigned to C=O stretching of this product. The formation of a cyclic adduct increases the frequency of the C=O stretching absorption band as a result of conjugation. Figure 1(a) indicates that the absorbance at 1597 cm^{-1} decreased and disappeared at about 0.6 min and that at 1784 cm^{-1} gradually decreased during a period of 0.2—0.4 min and then decreased more rapidly, disappering after about 0.6 min. The absorbance at 1798 cm^{-1} increased until 0.2 min, remained almost unchanged during the period from 0.2—0.4 min, and then increased again, reaching a constant value. The results at a higher pressure of 7.85 MPa are given in Fig. 1(b), showing some pressure effect; the absorbance at 1597 and 1784 cm^{-1} disappeared within a shorter time, and that at 1798 cm^{-1} increased throughout the reaction until about 0.5 min and attained the same constant value within a shorter time as compared with the reaction at 7.45 MPa. It follows that the overall reaction rate was enhanced by increasing the pressure from 7.45 to 7.85 MPa.

It is commonly said that Diels-Alder reactions proceed via a one-step, concerted mechanism under ordinary conditions.[11] However, the results shown in Fig. 1 strongly suggest a two-step mechanism for the present Diels–Alder reaction in carbon dioxide under supercritical conditions. The step-wise increase in the intensity of the 1798 cm^{-1} absorption during the reaction would be indirect evidence for the presence of some intermediate. One possible explanation for the changes in the absorbance shown in Fig. 1 is that the reaction proceeds via the two steps shown in Scheme 1: the formation of one σ-bond giving an intermediate (**A**), followed by a ring closure, yielding the cycloadduct (**P**). The observed step-wise increase of the 1798 cm^{-1} absorption is believed to correspond to the formation of two σ-bonds in the two steps. A gradual decrease in the C=O absorbance at 1784 cm^{-1} of maleic anhydride, as observed more clearly at 7.45 MPa, also suggests that the intermediate has two C=O bonds, similar to those of maleic anhydride and the product. One might expect that the IR carbonyl stretching frequency and band intensity for (**A**) are different from those for (**P**). The present FTIR measurements, however, did not support this idea.

In a few cases of Lewis-acid catalyzed cycloadditions, the mechanism of a [2+2] addition followed by a rearrangement, giving a [2+4] adduct, was reported in the literature.[12] Such a mechanism might be possible for the present Diels–Alder reaction. However, the intermediate that can be expected from this mechanism could not well support the FTIR results of Fig. 1. Also, the present reaction takes place with thermal energy; it is therefore natural to believe that it proceeds through a [2+4] addition mechanism. We presently believe that Scheme 1 is a possible tentative mechanism for the Diels–Alder reaction in supercritical carbon dioxide; further work is required to obtain a definite conclusion. Since the reaction is carried out under unordinary conditions, we should consider the solvent properties of carbon dioxide at supercritical conditions.

Regarding the influence of increasing pressure, the results in Fig. 1 show an enhancement in the overall reaction rate. If one can adopt the mechanism shown in Scheme 1, it is speculated that the second step depends more strongly on the pressure than does the first step, since the change of the 1798 cm^{-1} absorbance during the initial stage of the reaction seems to be little influenced by the pressure. It is a current subject of study to examine the effects of the pressure of SCFs on the reactions and to clarify the key physical/chemical properties governing the effects.

References

1) M. E. Paulaitis, J. M. L. Penninger, R. D. Gray, Jr., and P. Davison, "Chemical Engineering at Supercritical Fluid Conditions," Ann Arbor Science, Ann Arbor, MI (1983).

2) M. A. McHugh and V. J. Krukonis, "Supercritical Fluid Extraction, Principles and Practice," Butterworths, Stoneham, MA (1986).

3) K. Sunwook and K. P. Johnston, *Ind. Eng. Chem. Res.*, **26**, 1206 (1987).

4) J. F. Brennecke and C. A. Eckert, *AIChE J.*, **35**, 1409 (1989).

5) B. Subramanian and M. A. McHugh, *Ind. Eng. Chem. Process Des. Dev.*, **25**, 1 (1986).

6) M. E. Paulaitis and G.C. Alexander, *Pure Appl. Chem.*, **59**, 61 (1987).

7) T. G. Squires, C. G. Venier, and T. Aida, *Fluid Phase Equilib.*, **10**, 261 (1983).

8) S. Kim and K. P. Johnston, *Chem. Eng. Commun.*, **63**, 49 (1988).

9) S. V. Olesik, S. B. French, and M. Novotny, *Anal. Chem.*, **58**, 2256 (1986).

10) Y. Ikushima, N. Saito, H. Hatakeda, S. Ito, and T. Goto, *Chem. Lett.*, **1989**, 1707.
11) J. Sauer and R. Sustmann, *Angew. Chem., Int. Ed. Engl.*, **19**, 779 (1980).
12) F. Kataoka, N. Shimizu, and S. Nishida, *J. Am. Chem. Soc.*, **102**, 711 (1980).

^{17}O NMR Study of Aqueous Electrolyte Solutions; Effect of KCl and NaCl on the ^{17}O NMR Parameters of Water

Akira HIGASHIYAMA, Yasuhiko YAMAMOTO, and Riichirō CHŪJŌ*
Department of Biomolecular Engineering, Tokyo Institute of Technology, O-okayama 2-chome, Meguro-ku, Tokyo 152
(Received August 1, 1990)

Synopsis. The aqueous solutions containing KCl or NaCl at various concentrations have been studied by ^{17}O NMR. The line width of the signal increases and decreases with an addition of KCl above and below 55 °C, respectivly, and these results indicate that the effect of KCl on the water structure depends on temperature.

The chemical shift changes induced on the ^{17}O NMR signal of water by an addition of salts such as KCl and NaCl have been used to study interaction between H_2O and solute molecules.[1,2] Hydrogen bonding network among water molecules and motion of water molecule have been investigated from the line width of its ^1H or ^{17}O NMR signal[3,4] and their spin-lattice (T_1) or/and spin-spin relaxation time (T_2), respectively.[5–11]

In this report, we have studied the effects of KCl and NaCl on the ^{17}O NMR parameters of water. The line width decreases with an addition of KCl below 55 °C. On the contrary, above this temperature, it increases with an addition of KCl. These results indicate that KCl acts as water structure breaking and forming salt, below and above 55 °C, respectively.

Experimental

Materials. H_2O was prepared by distillation of deionized water. D_2O was purchased from MSD Isotopes and used as received. KCl and NaCl were obtained from Sigma Chemical Co. and they were dried under reduced pressure at 150 °C for 24 h before use.

NMR Measurement. All ^{17}O NMR experiments were carried out using JEOL GSX-270 spectrometer operating at the resonance freaqency of 36.6 MHz. The spectra were recorded with proton decoupling, and the signal to noise ratio of the spectra was improved by apodization which introduced 10 Hz line broadening. The chemical shifts are given in parts per million (ppm) and the ^{17}O NMR signal of D_2O at 35 °C was used as a reference (0 ppm). T_1 values were determined by using a saturation recovery method[12] and T_2 was calculated from the line width of the signal.

Results and Discussion

Chemical Shifts. The chemical shift change for the ^{17}O NMR signal of water is plotted against the concentration of salt at 35 °C in Fig. 1. The plots for KCl and NaCl exhibit straight lines, over the salt concentration range examined, with the slope [∂(ppm)/∂(mol dm^{-3})] of 0.80 and 0.45, respectively. The ^{17}O NMR signal moves toward downfield with the addition of salt. Since K^+ and Na^+ are known to shift the signal upfield, the observed downfield shift of the signal is attributed to the large downfield shift effect of Cl^-.[1,2] Hence, the smaller slope of the plot for NaCl, compared with that for KCl, indicates that the upfield effect of Na^+ is larger than that of K^+.

Relaxation Times. Relaxation parameters measured under various conditions are summarized in Table 1. T_1 of ^{17}O NMR signal of H_2O was determined to be

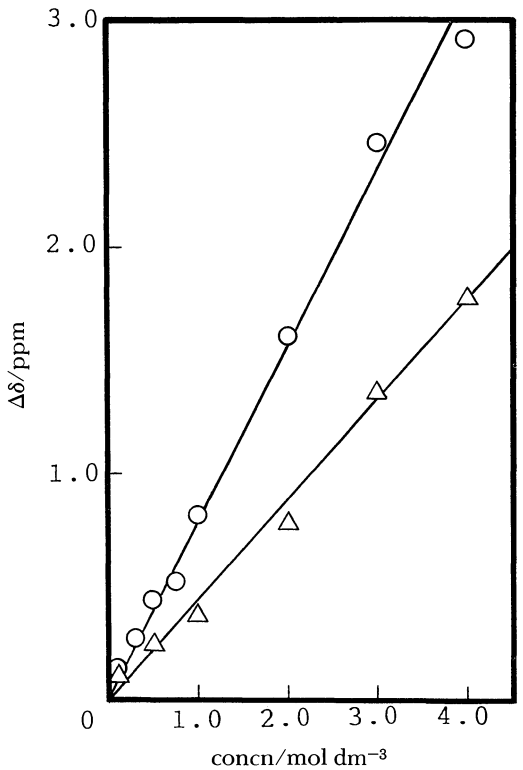

Fig. 1. Plot of observed chemical shift for the ^{17}O NMR signal of D_2O against the concentration of salt added at 35 °C. KCl (○), and NaCl (△).

Table 1. T_1, T_2*[a], and τ_c[b] of the ^{17}O NMR of Water

	H_2O	D_2O		D_2O/1.0 mol dm^{-3} KCl	
	35 °C	35 °C	75 °C	35 °C	75 °C
T_1/ms	6.2±1.0	7.9±1.0	14.3±0.7	8.2±1.0	12.1±0.7
T_2*/ms	6.1±0.3	4.8±0.2	9.1±0.6	5.3±0.3	8.2±0.5
τ_c/ps	2.9±0.5	2.3±0.3	1.2±0.1	2.2±0.3	1.5±0.1

a) Calculated from the observed line width. b) Estimated from the determined T_1 value with $e^2qQ/\hbar$=7.7 MHz.[7]

6.2±1.0 ms at 35 °C. This value is almost comparable to the previously reported value.[5] The apparent spin-spin relaxation time (T_2*) was calculated to be 6.1±0.3 ms from the line width of 52.5 Hz at 35 °C. Hence, T_2 is nearly equal to T_1 at this temperature. When $T_1=T_2$, i.e., a rapid motional limit, T_1^{-1} (T_2^{-1}) of ^{17}O nucleus is given by[13]

$$T_1^{-1} = T_2^{-1} = (3/125)(1 + \eta^2/3)(e^2qQ/\hbar)^2\tau_c$$

where η is an asymetric parameter of the electrical field gradient around ^{17}O nucleus and is known to be negligibly small for bulk water molecule.[14] $e^2qQ/\hbar$ is the quadrupole coupling constant of ^{17}O nucleus and τ_c is the correlation time of water molecule. The $e^2qQ/\hbar$ value for both H_2O and D_2O have been reported to be 7.7±0.1 MHz at temperature from 5 to 95 °C.[6,7] Since the $e^2qQ/\hbar$ is expected to be independent of the salt concentration, change in relaxation times is attributed to alteration of τ_c. T_1 is larger than T_2* for D_2O samples and this may be attributed to the D–O scalar coupling, although its magnitude is modulated by the dynamic process of deuterium exchange.

Effect of Salt Concentration on the Line Width. The line width of ^{17}O NMR signal of D_2O is plotted against KCl concentration in Fig. 2. At 55 °C, the line width is independent of KCl concentration. At lower temperature (35 °C), the line width decreases with increasing KCl concentration and reaches a steady-state value (ca. 59 Hz). On the contrary, at higher temperature (75 °C), the line width increases with KCl concentration and reaches another steady-state value

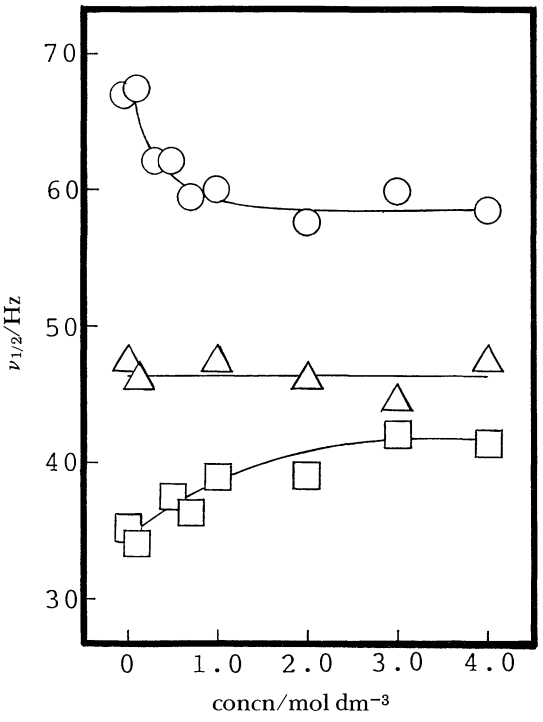

Fig. 2. Plot of the observed line width for the ^{17}O NMR resonance of D_2O against the concentration of KCl. 35 °C (○), 55 °C (△), and 75 °C (□).

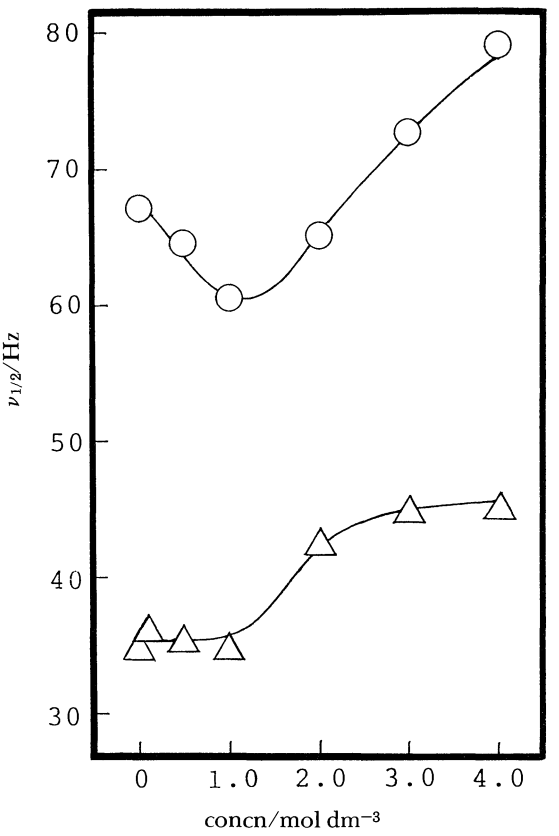

Fig. 3. Plot of the observed line width for the ^{17}O NMR resonance of D_2O against the concentration of NaCl. 35 °C (○), and 75 °C (△).

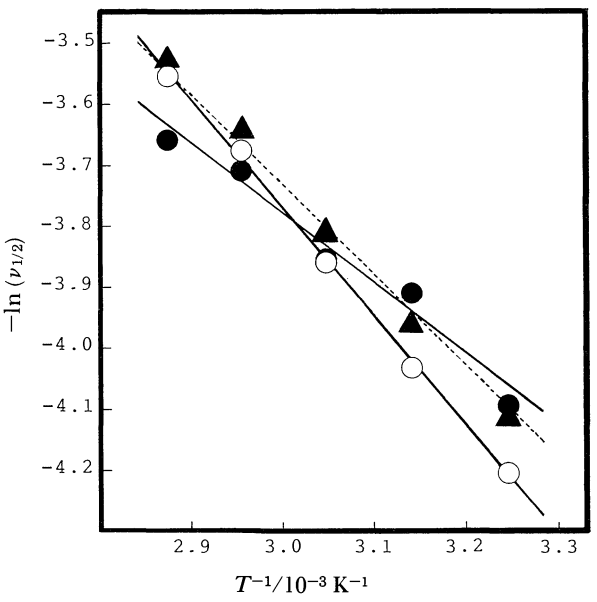

Fig. 4. Arrhenius plots for the observed line width of the ^{17}O NMR resonance of D_2O (○), D_2O containing 1.0 mol dm^{-3} of KCl (●), and NaCl (▲). The $\Delta E^{\neq}$ values determined from these plots are 10 (D_2O without salt), 15 (D_2O containing KCl), and 12 kJ mol^{-1} (D_2O containing NaCl).

(ca. 40 Hz). A similar plot for the D_2O solution containing NaCl is shown in Fig. 3. The line width of the signal at 75 °C seems to be independent of NaCl concentration below 1.0 mol dm^{-3}. But an anomalous behavior is observed above 1.0 mol dm^{-3}.

Effect of Temperature on the Line Width. Figure 4 shows the Arrhenius plots of the line width of the ^{17}O NMR signal for D_2O with and without salts in the temperature range from 35 to 75 °C. The Arrhenius plot for T_1 of ^{17}O NMR signal of water (from −14 to 180 °C) has shown to deviate from a straight line.[8] However, the plots in Fig. 4 exhibit straight lines in the temperature range studied. These two lines in Fig. 4 cross with each other at $3.0\times10^{-3}K^{-1}$ (ca. 55 °C), indicating that the line width decreases and increases below and above 55 °C, respectively, as discussed above. This result also confirms the KCl concentration independency of the line width at 55 °C. It has been reported from the ^1H NMR studies that K^+, Na^+, and Cl^- in H_2O act as water structure breaking ions at room temperature.[15] In Fig. 2, such an effect of KCl is clearly observed below 55 °C. On the contrary, above 55 °C, the increase of the line width by an addition of KCl is interpreted as an increase of τ_c, indicating that the added ions inhibit molecular motion of water, i.e., KCl acts as a water structure forming salt above 55 °C.

For NaCl solution, similar experiments were performed. The temperature where the Arrhenius plot for D_2O solution containing 1.0 mol dm^{-3} of NaCl crosses with that for D_2O is 2.9×10^{-3} K^{-1} (ca. 75 °C), reflecting that the line width is independent of NaCl concentration up to 1.0 mol dm^{-3}.

We are indebted to the central laboratry of Rengo Co., Ltd. for leaving A. Higashiyama to Tokyo Institute of Technology for this study.

References

1) Z. Luz and G. Yagil, *J.Phys.Chem.*, **70**, 554 (1966).
2) F. Fister and H. G. Hertz, *Ber. Bunsen-Ges. Phys. Chem.*, **71**, 1032 (1967).
3) S. Horike, H. Ohkuma, H. Tamai, and R. Akahosi, *Nippon Nogei Kagaku Kaishi*, **1982**, 13.
4) T. Tamaki, K. Matushita, K. Hioka, and Y. Takamiya, *Nippon Nogei Kagaku Kaishi*, **1986**, 191.
5) J. C. Hindman, A. Svirmikas, and M. Wood, *J. Phys. Chem.*, **74**, 1266 (1970).
6) B. B. Garrett, A. B. Denison, and S. W. Rabideau, *J. Phys. Chem.*, **71**, 2606 (1967).
7) M. J. Tait, A. Suggett, F. Franks, S. Ablett, and P. A. Quickenden, *J. Solution Chem.*, **1**, 131 (1972).
8) J. C. Hindman, A. J. Zielen, A. Svirmickas, and M. Wood, *J. Chem. Phys.*, **54**, 621 (1971).
9) H. Uedaira, M. Ikura, and H. Uedaira, *Bull. Chem. Soc. Jpn.*, **62**, 1 (1989).
10) E. W. Lang and H. D. Ludemann, *Ber. Bunsen-Ges. Phys. Chem.*, **85**, 603 (1981).
11) J. A. Glasel, *Proc. N. A. S.*, **58**, 28 (1967).
12) J. R. Lyerla and G. C. Levy, "Topics in Carbon-13 NMR Spectroscopy," Wiley Interscience, New York(1974), Chap. 3.
13) H. G. Hertz, "Progress in NMR Spectroscopy," Pergamon Press, London (1967), Vol. 3.
14) H.G.Hertz, "Water," Plenum Press, New York(1973), Vol. 7.
15) J. C. Hindman, *J. Chem. Phys.*,**36**, 1000 (1962).

Hydration of Cyclic Oligo(oxyethylene) Compounds. Ultrasonic Velocities and Compressibilities of Binary Systems of Water with 12-Crown-4, 15-Crown-5, and 18-Crown-6

Yoshio MIYAZAKI and Hiroatsu MATSUURA*,†
Faculty of Engineering, Toyo University, Kujirai, Kawagoe, Saitama 350
†Department of Chemistry, Faculty of Science, Hiroshima University, Higashisenda-machi, Naka-ku, Hiroshima 730††
(Received August 8, 1990)

Synopsis. Ultrasonic velocities of binary systems of water with 12-crown-4, 15-crown-5, and 18-crown-6 were measured and the adiabatic compressibilities were evaluated therefrom. The results indicate that the most compacted hydration structure is formed at the mole ratio, approximately 2:1, of water to oxyethylene monomer unit and that the poly(oxyethylene) chain enhances structuring of the liquid water network.

Structure of aqueous solutions of poly(oxyethylene) (POE) chains, $(-OCH_2CH_2-)_m$, is one of the important subjects in the fields not only of polymer chemistry but also of surface and colloid science, since the structural aspect of this chain is closely related to the size and shape of the micelles and the phase behavior of a number of nonionic surfactants that contain the POE chain as a hydrophilic moiety.[1] Kjellander and Florin[2] have previously discussed possible structure models for POE–water systems and indicated that water molecules form a highly linked network allowing the hydrocarbon groups to be reasonably encaged. In such a water network, hydrogen bonding between water molecules and ether oxygens of the POE chain plays an important role in forming the stable structure. Thus the hydration of the POE chain is a fundamental factor for understanding the network structure and its stability.

In an earlier study,[3] we have investigated the hydration of short model compounds of POE, namely $CH_3(OCH_2CH_2)_mOCH_3$ (m=1—4) and $CH_3(OCH_2CH_2)_m$-OH (m=2 and 3), by measuring hypersonic velocities in aqueous solutions of these compounds. This study showed that a specific hydration complex of approximately $2(H_2O):1(OCH_2CH_2)$ is formed, in agreement with the results by different experimental methods.[2,4] In the present work, we have extended the hydration study of the POE chain to cyclic oligo(oxyethylene) compounds, i.e., 1,4,7,10-tetraoxacyclododecane (12-crown-4), 1,4,7,10,13-pentaoxacyclopentadecane (15-crown-5), and 1,4,7,10,13,16-hexaoxacyclooctadecane (18-crown-6). In evaluating extent of hydration of the POE chain, the complexity arising from an effect of terminal groups is absent in these cyclic compounds, though there may be a possible steric effect associated with the limited conformational freedom of the ring molecules.

Experimental

The ultrasonic velocities in binary systems of water with 12-crown-4, 15-crown-5, and 18-crown-6 with various compositions were measured at 20.0±0.01 °C by the sing-around method with a model UVM-2 of Choompa Kogyo Co. at a frequency of 2 MHz. The densities of the solutions were also measured in order to evaluate the adiabatic compressibilities.

Results and Discussion

The adiabatic compressibilities, κ_S, were obtained by the relation

$$\kappa_S = 1/(\rho v^2), \quad (1)$$

where ρ is the density and v is the sound velocity in the binary mixtures. The adiabatic compressibilities obtained this way for the systems of water with the three crown ethers are shown in Fig. 1. The deviations, to be denoted by $\Delta\kappa_S$, of the observed κ_S values of the mixtures from the values based on the mole-fraction mixture law are given by

$$\Delta\kappa_S = \kappa_S - (x_1\kappa_{S1} + x_2\kappa_{S2}), \quad (2)$$

where κ_S is the observed adiabatic compressibility of the binary mixture, x_1 and x_2 are the mole fractions of the components 1 and 2 in the mixture, and κ_{S1} and κ_{S2} are the adiabatic compressibilities of the two pure components.

According to Fig. 1, the deviations $\Delta\kappa_S$ are always negative for the three systems, indicating that specific interactions exist between water molecules and POE chains. It is therefore highly suggestive of the formation of the intermolecular complexes between the crown ethers and water. The POE chain thus promotes structuring of the water network by forming hydrogen bonds between the ether oxygens and water. This implies that the ether oxygens of the POE chain are constituents of the structured water network. The close fit of the POE chain into the water lattice is geometrically favorable, since the closest oxygen–oxygen distance (0.28—0.30 nm) of POE[5] and 18-crown-6[6] with the gauche($O-CH_2-CH_2-O$) conformation is coincident with the oxygen–oxygen distance (0.285 nm) of liquid water at 25 °C.[7] Our conformational studies of POE[8] and 18-crown-6[9] have in fact indicated that these molecules in aqueous solutions much more prefer the gauche($O-CH_2-CH_2-O$) conformation with more dilution with water than the trans conformation. This consideration strongly suggests the effective incorporation of the ether oxygens of the POE chain into the structured water network around the chain. The hydrophobic CH_2CH_2 groups of the POE chain then fill out the interstitial voids of the

†† Address after October 1991: Department of Chemistry, Faculty of Science, Hiroshima University, Kagamiyama, Higashi-Hiroshima 724.

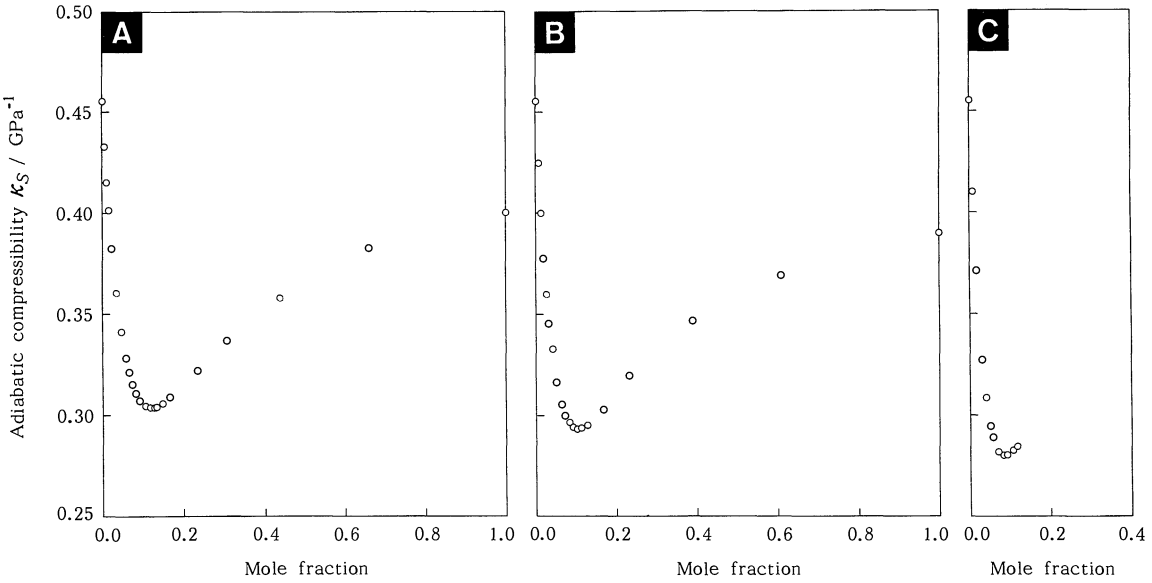

Fig. 1. Adiabatic compressibilities of the binary systems; A: water–12-crown-4, B: water–15-crown-5, and C: water–18-crown-6. Mole fraction for abscissa implies that of the crown ether. Since the water–18-crown-6 system with a large fraction of 18-crown-6 is solid at 20°C, no measurements were possible of the compressibilities in the liquid state for high concentrations.

water network, resulting in the formation of more compacted structure than the liquid structure of pure water or of the oxyethylene compounds. The observed negative values of $\Delta\kappa_S$ are thus elucidated by a model of the structured water network with the hydrophobic groups encaged.[2]

Figure 1 indicates that the absolute values of $\Delta\kappa_S$ are the largest at mole fractions of 0.113 for 12-crown-4, 0.095 for 15-crown-5, and 0.082 for 18-crown-6; the corresponding mole ratios of water to crown ether and those converted to water to oxyethylene monomer unit are shown in Table 1. The present experimental findings indicate that the most compacted hydration structure is formed at the mole ratio of approximately $2(H_2O):1(OCH_2CH_2)$ between water and the POE chain. For the compositions with more water molecules than this, the compressibility of the whole liquid mixture is increased owing to the structure of the excess bulk water, which contains a large fraction of interstitial space.[7] In more concentrated solutions than the mole ratio 2:1, on the other hand, the highly structured water network is partially broken with insufficient proton donors available to the ether oxygens of the POE chain.[2] The number of water molecules per oxyethylene unit for the most compacted hydration structure is essentially the same for the three crown ethers irrespective of the size of the POE ring. It is suggested therefore that a possible steric effect on the hydration arising from the limited conformational freedom of the ring molecule is substantially negligible.

The present work has indicated that the interstitial space of the water network is filled completely with the hydrophobic group of the POE chain with two water molecules per oxyethylene monomer unit. This result is consistent with the generally accepted hydration structure of the POE chain with two water molecules per oxyethylene unit.[2–4] A previous NMR study[10] showed, however, that three molecules of water were required for the hydration of each oxyethylene unit, but a later reexamination[4] has pointed out that the number of water molecules per oxyethylene unit is actually close to two instead of three. A recent infrared study[11] has indicated the presence of three different hydration complexes with water to oxyethylene mole ratios of 4:1, 2:1, and 1:1. The present and previous[3] studies on the cyclic and open-chain oligo(oxyethylene) compounds have demonstrated that, of these possible complexes, the 2:1 complex gives rise to the least compressible or the most elastic structure with the oxyethylene ether oxygens incorporated into the water lattice. In conclusion, the POE chain, whether it is cyclic or open-chain, enhances structuring of the liquid water network.

Table 1. Mole Ratios, at Which the Absolute Values of $\Delta\kappa_S$ are the Largest, for the Binary Systems of Water with 12-Crown-4, 15-Crown-5, and 18-Crown-6

Binary system	Mole ratios	
	H_2O:Crown ether	H_2O:OCH_2CH_2[a]
Water–12-crown-4	7.8:1	1.96:1
Water–15-crown-5	9.5:1	1.91:1
Water–18-crown-6	11.2:1	1.87:1

a) The estimated uncertainty in the number of water molecules per oxyethylene unit is ±0.1.

References

1) "Nonionic Surfactants: Physical Chemistry," ed by M. J. Schick, Marcel Dekker, New York (1987).
2) R. Kjellander and E. Florin, *J. Chem. Soc., Faraday Trans. 1*, **77**, 2053 (1981).
3) H. Matsuura and K. Fukuhara, *Bull. Chem. Soc. Jpn.*, **59**, 763 (1986).
4) P. Molyneux, "Synthetic Polymers," in "Water: A Comprehensive Treatise," ed by F. Franks, Plenum, New York (1975), Vol. 4, Chap. 7, pp. 569—757.
5) Y. Takahashi and H. Tadokoro, *Macromolecules*, **6**, 672 (1973).
6) P. Seiler, M. Dobler, and J. D. Dunitz, *Acta Crystallogr., Sect. B*, **30**, 2744 (1974).
7) A. H. Narten, *J. Chem. Phys.*, **56**, 5681 (1972).
8) H. Matsuura and K. Fukuhara, *J. Mol. Struct.*, **126**, 251 (1985).
9) K. Fukuhara and H. Matsuura, to be published.
10) K.-J. Liu and J. L. Parsons, *Macromolecules*, **2**, 529 (1969).
11) A. M. Dwivedi and D. S. Jayasuriya, *Polym. Mater. Sci. Eng.*, **54**, 392 (1986).

Surface Active Properties of Heptyl β-D-Xyloside Synthesized by Utilizing the Transxylosyl Activity of β-Xylosidase

Hirofumi SHINOYAMA,*,† Yasuo GAMA, Hisae NAKAHARA, Yutaka ISHIGAMI, and Tsuneo YASUI††
National Chemical Laboratory for Industry, Tsukuba, Ibaraki 305
†† Institute of Applied Biochemistry, University of Tsukuba, Tsukuba, Ibaraki 305
(Received August 27, 1990)

Synopsis. The surface-active properties of heptyl β-D-xyloside were investigated. The critical micelle concentration of this surfactant was determined to be 30 mM (M=mol dm^{-3}). The corresponding molecular area at saturation adsorption, the micellar weight and the aggregation number were 43 Å, 20700 and 78, respectively. This surfactant was found to have a surface activity similar to that of octyl β-D-glucoside.

The nonionic surfactants, octyl β-D-glucoside (octyl glucoside), heptyl β-D-thioglucoside (heptyl thioglucoside), sucrose monodecanoate, etc., are being increasingly utilized for solubilization, reconstitution of biological membranes and the preparation of lipid vesicles.[1–7] Based on a similar point of view, we have developed a new enzymatic process to synthesize alkyl β-D-xyloside homologues by utilizing the transxylosyl activity of *Aspergillus niger* β-xylosidase.[8,9] In the present studies, the authors have tried clarify the relation between the surface activity and the hydrophile-lipophile balance of alkyl β-D-xyloside molecules, such as heptyl β-D-xyloside (heptyl xyloside). The results were compared with other detergents, such as octyl glucoside and heptyl β-D-glucoside (heptyl glucoside).

The homologues of heptyl xyloside[9] were synthesized as previously described. All other chemicals used were of the highest grade commercially available. Two typical methods were employed to determine the critical micelle concentration (cmc) of heptyl xyloside. In the first procedure the effect of the detergent concentration on the fluorescence intensity of solubilized ANS (8-anilino-1-naphthalenesulfonic acid) was measured at 50 °C. In the second procedure, cmc was determined from a break in the surface tension vs. concentration curve, as measured by Shimadzu Surface Tensiometer ST-1 at 50 °C. Light-scattering measurements were also carried out in order to estimate the micellar size at 40 °C with a wavelength of 633 nm, using a light-scattering photometer (Ootsuka Photoelectric Co. DLS-700). Scattered light was observed at 90 degrees relative to the incident beam.

Figure 1(A) shows a sudden rise of the fluorescence intensity of solubilized ANS at concentrations of heptyl xyloside higher than 30 mM, while a break appeared at 22 mM for octyl glucoside and 67 mM for heptyl glucoside. Surface tension-log concentration curves are shown in Fig. 1(B). The inflection (30 mM) in the curve corresponds to the cmc of the surfactant.[10] Thus, the two results agreed very well, and the cmc of heptyl xyloside was determined to be 30 mM. This value was higher than those obtained for sucrose monodecanoate, triton X-100 and SDS, and was similar to that for octyl glucoside (Table 1).

From the slope of the curve in Fig. 1(B), the surface

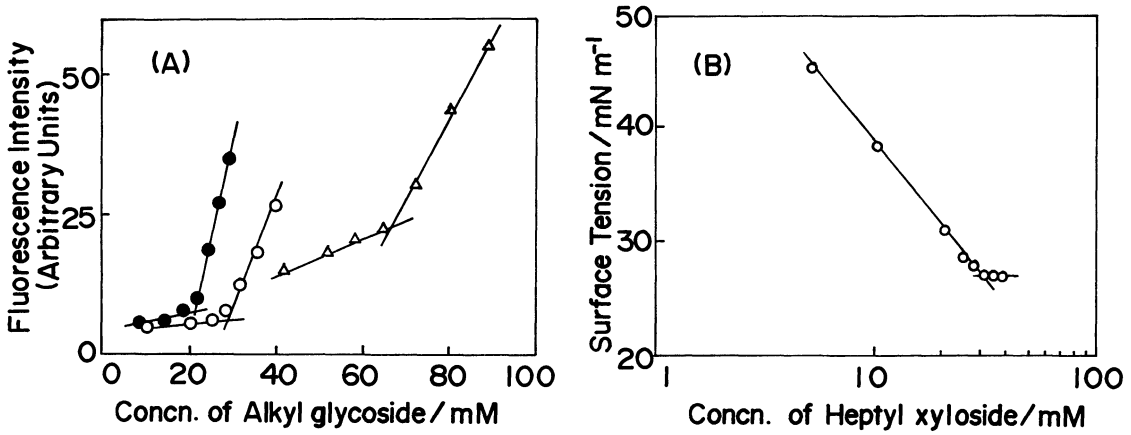

Fig. 1. Determination of cmc of heptyl xyloside. (A): Assay mixture (2.0 ml) contained 10 μM ANS and various concentrations of surfactants. Fluorescence intensity of ANS was measured at excitation wavelength of 345 nm and emission wavelength of 480 nm. (○), heptyl xyloside; (△), heptyl glucoside; (●), octyl glucoside. (B): The surface tension-log concentration curve of heptyl xyloside.

† Present address: Department of Agricultural Chemistry, Chiba University, 648, Matsudo-shi, Chiba 271.

Table 1. Surface Active Properties of Alkyl Glycosides and Some Other Surfactants

Surfactants	cmc/mM	A/Å	Micellar wt. (Agg. Numbr.)
Heptyl xyloside	30	43	20700 (78)
Octyl glucoside	22	41**[10]	25800**[11] (87)
Sucrose monodecanoate	2.52**[5]	—	10500**[5] (22)
Triton X-100	0.25**[12]	52.4**[12]	63000**[12] (100)
SDS	8.1**[13]	45**[13]	23000**[14] (80)

**, From literatures.

excess (Γ) at saturation adsorption and the corresponding molecular area (A) were calculated by applying Gibbs adsorption isotherm, $\Gamma=-(1/RT)(\partial\gamma/\partial \ln C)_T$, where the notations used have their usual meanings. The obtained results are listed in Table 1. The A values of heptyl xyloside and octyl glucoside are almost the same. The micellar weight and the aggregation number, as obtained from light-scattering measurements for heptyl xyloside, are 20,700 and 78, respectively, which are comparable to the values for octyl glucoside (Table 1). This suggests that these compounds are similar in nature.

Among the surfactants currently used in membrane biochemistry, octyl glucoside is an excellent one[1] and has been used for the extraction and purification of the lactose carrier of *Escherichia coli*,[2] as well as for the preparation of lipid vesicles.[7] The above-mentioned applicability of heptyl xyloside to membrane biochemistry will be tested in a follow-up study. The xylose group of alkyl xyloside seems to show a fundamental difference in its properties from that of glucose in alkyl glucoside. Namely, heptyl xyloside has a Krafft point of 33.7 °C, whereas the heptyl glucoside does not show a Krafft temperature phenomena. The difference in the hydration of these compounds may cause these characteristics. A further comparison should also be made regarding the xylose and glucose groups in various glycoside.

This work was supported in part by a Grant-in-Aid for Encouragement of Young Scientists No. 01790450 from the Ministry of Education, Science and Culture.

References

1) C. Baron and T. E. Thompson, *Biochim. Biophys. Acta*, **382**, 276 (1975).
2) M. J. Newman, D. L. Foster, T. H. Wilson, and H. R. Kaback, *J. Biol. Chem.*, **256**, 11804 (1981).
3) T. Tsuchiya and S. Saito, *J. Biochem.*, **96**, 1593 (1984).
4) T. Shimamoto, S. Saito, and T. Tsuchiya, *J. Biochem.*, **97**, 1807 (1985).
5) S. Makino, S. Ogimoto, and S. Koga, *Agric. Biol. Chem.*, **47**, 319 (1983).
6) S. Matsui, M. Seidou, S. Horiuchi, I. Uchiyama, and Y. Kito, *J. Gen. Physiol.*, **92**, 55 (1988).
7) R. A. Parente, M. Hochli, and B. R. Lentz, *Biochim. Biophys. Acta*, **812**, 493 (1985).
8) H. Shinoyama, Y. Kamiyama, and T. Yasui, *Agric. Biol. Chem.*, **52**, 2197 (1988).
9) H. Shinoyama, Y. Kamiyama, and T. Yasui, *Nippon Nōgeikagaku Kaishi*, **63**, 1479 (1989).
10) K. Shinoda, T. Yamanaka, and K. Kinoshita, *J. Phys. Chem.*, **63**, 648 (1959).
11) K. Kameyama and T. Takagi, The Special Meeting on Colloid and Interfacial Chemistry, Surfactants —Solution Properties, Functions, Applications—, 1988, Abstr., p. 9.
12) Y. Ishii, "The Nonionic Detergents," Seibundoshinkosha, Tokyo (1962), p. 123.
13) K. Tajima, M. Muramatsu, and T. Sasaki, *Bull. Chem. Soc. Jpn.*, **43**, 1991 (1970).
14) L. I. Osipow, "Surface Chemistry," Reinhold Publishing Co., New York (1962), Chap. 9, p. 180.

Oxidative Dimerization of 1-Propyne on a 2-Pyridylethyl Copper Complex Fixed Silica Catalyst

Yuji UKISU,*,†† Akio KAZUSAKA,*,††† and Masaharu NOMURA†
Catalysis Research Center, Hokkaido University, Supporo 060
† Photon Factory, National Laboratory for High Energy Physics, Tsukuba, Ibaraki 305
(Received August 29, 1990)

Synopsis. A 2-pyridylethyl copper complex fixed silica catalyst was applied to an oxidative-coupling dimerization reaction of 1-propyne to 2,4-hexadiyne at 100 °C, which is a typical test reaction for Cu–(N base)-complex catalyst in the homogeneous phase. It was found to be highly catalytically active for this reaction compared with a conventional CuO/SiO_2 catalyst. The reaction was deduced to proceed through a redox cycle of copper ions coordinated with the pyridine derivative.

In the presence of pyridine, CuCl has proved to be catalytically active for homogeneous oxidative-coupling reactions of acetylenes,[1] aromatic amines,[2] or phenols.[3] In a previous paper we reported the preparation and spectroscopic characterization of a novel silica-fixed copper catalyst, in which each copper ion is coordinated with four pyridine moietyies of 2-pyridylethyl group fixed on silica as:

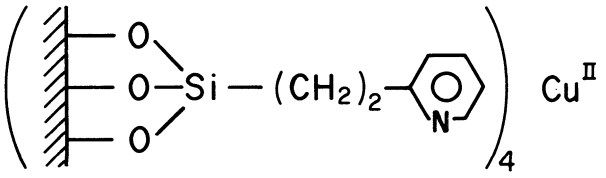

and which was denoted as Cu–Py–SiO_2. Such copper ions were also subject to an easy reversible redox reaction under vacuum at 200 °C or with molecular oxygen.[4]

The present paper is concerned with the application of this catalyst to a heterogeneous oxidative-coupling reaction of 1-propyne, which is a typical test reaction for a Cu–(N base)-complex catalyst in the homogeneous phase, and gives a comparison of its catalytic nature with that of a conventional CuO/SiO_2 catalyst.

Experimental

The Cu–Py–SiO_2 catalyst (1.3 wt% of Cu) was prepared and characterized spectroscopically as described in a previous paper.[4] It was used after outgassing at 200 °C for 1 h and successive activation under an O_2 atmosphere at room temperature for 24 h. For a comparison, a conventional silica-supported copper catalyst (2.6 wt% of Cu) was used, which was prepared from a tetraamminecopper complex ($[Cu^{II}(NH_3)_4]$) by an ion-exchange method, and calcined with O_2 at 300 °C.[5]

A conventional closed recirculating reactor (0.7 l volume) was employed for the catalytic oxidative-coupling reaction of 1-propyne. The partial pressure of 1-propyne, O_2 or CO_2 was monitored with an on-line gas chromatograph. Analysis of the reaction product, 2,4-hexadiyne, was carried out with a Hitachi RMU-6 mass spectrometer.

The states of copper ions were monitored using an ESR or XANES (X-Ray Absorption Near-Edge Structure) spectroscopic technique. ESR spectra were obtained with a Varian E-4 spectrometer at a frequency of 9 GHz. The g-values were calculated relative to DPPH as a standard (g=2.0036). XANES spectra were measured in the transmission mode at the BL10B station of the photon Factory using sychrotron radiation from the 2.5 GeV electron storage ring.[6]

The O_2 or 1-propyne gas was of high-purity grade from Takachiho Kagaku Kogyo and was used without further purification.

Results and Discussion

Figure 1A shows the time course of the reaction between 1-propyne and O_2 on Cu–Py–SiO_2 at 100 °C. Each reactant decreased monotonously at a ratio of 4–1, respectively, indicating that this reaction proceeded catalytically within the reaction times. The 2,4-hexadiyne has found by mass spectroscopy to be

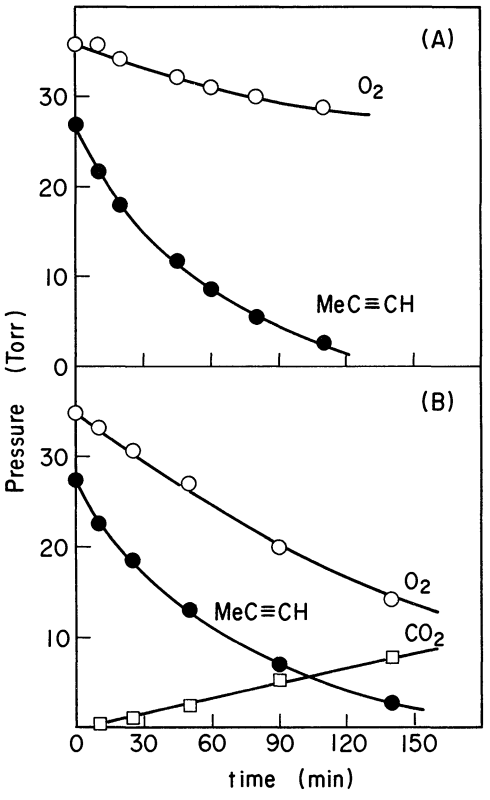

Fig. 1. Time course of reaction between 1-propyne and oxygen. (A) Cu–Py–SiO_2 at 100 °C; (●): 1-propyne; (○): O_2, (B) CuO/SiO_2 at 200 °C; (●): 1-propyne; (○): O_2; (□): CO_2.

†† Present address: Institute for Molecular Science, Myodaiji, Okazaki 444.

††† Present address: Faculty of Veterinary Medicine, Hokkaido University, Sappro 060.

the main product derived from the dimerization of 1-propyne, though its amount could not be followed quantitatively because of its low vapor pressure. Neither CO_2 nor CO was detected. Therefore, the following reaction stoichiometry can be proposed:

$$2\ CH_3\text{-}C{\equiv}C\text{-}H + 1/2\ O_2 \longrightarrow CH_3\text{-}C{\equiv}C\text{-}C{\equiv}C\text{-}CH_3 + H_2O. \quad (1)$$

The activity of the CuO/SiO_2 catalyst, on the other hand, was too low to follow the reaction at 100 °C, indicating that Cu–Py–SiO_2 is specifically effective for this reaction. Fig. 1B shows the time course at 200 °C on CuO/SiO_2. As can be seen from these results, the kinetic behavior was different from that on Cu–Py–SiO_2. CO_2 was detected as one of the reaction products in addition to 2,4-hexadiyne, showing that a complete oxidation of 1-propyne proceeded other than by dimerization as:

$$CH_3\text{-}C{\equiv}C\text{-}H + 4\ O_2 \longrightarrow 3\ CO_2 + 2\ H_2O. \quad (2)$$

The Cu–Py–SiO_2 catalyst activated under an O_2 atmosphere had a dark-green color, and exhibited an ESR signal with parameters of $g_{//}$=2.24, $g_{\perp}$=2.04, $A_{//}$=170 G and A_N=15 G (Fig.2a); these are characteristic of Cu(II) ions. When the sample was exposed to 100 Torr of 1-propyne at 100 °C for 3 h (1 Torr= 133.322 Pa), it turned to a gray color and the ESR signal showed a considerably weakened intensity (Fig. 2B), indicating that 1-propyne reduced a large part of the Cu(II) ions on the catalyst. When the sample was exposed again to 100 Torr of O_2 at 50 °C after outgassing at room temperature, it turned back to a dark-green color and restored the ESR signal completely in its intensity (Fig. 2C). The copper ions were oxidized again under these conditions. This redox cycle was confirmed to be reversible by repeating the above-mentioned experiment several times.

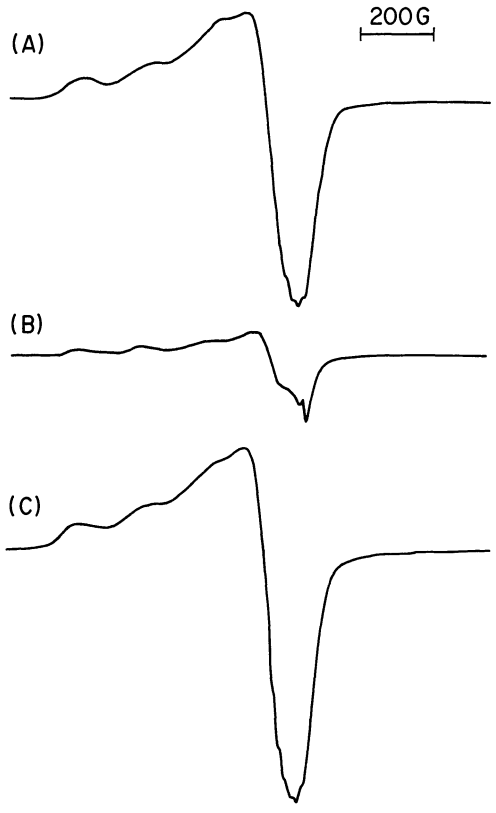

Fig. 2. ESR spectra of Cu–Py–SiO_2. (A) after activation under O_2 atmosphere, (B) after exposure to 100 Torr of 1-propyne at 100 °C for 3 h, (C) after exposure to 100 Torr of O_2 at 50 °C overnight after outgassing at room temperature. Spectra were observed at room temperature.

Such an easy reversible redox behavior was not observed for CuO/SiO_2 upon exposure to either 1-propyne or O_2. Therefore, this must be related to the low catalytic activity of CuO/SiO_2 for the above-mentioned reaction.

The following reaction mechanism has been suggested for the oxidative-coupling reaction of acetylenes in an aqueous alkaline solution,[1]

$$2\ R\text{-}C{\equiv}C\text{-}H \longrightarrow 2\ R\text{-}C{\equiv}C^- + 2\ H^+ \quad (3)$$

$$2\ R\text{-}C{\equiv}C^- + 2\ Cu^{2+} \longrightarrow 2\ R\text{-}C{\equiv}C\cdot + 2\ Cu^+ \quad (4)$$

and

$$2\ R\text{-}C{\equiv}C\cdot \longrightarrow R\text{-}C{\equiv}C\text{-}C{\equiv}C\text{-}R, \quad (5)$$

and from (3) + (4) + (5)

$$2\ R\text{-}C{\equiv}C\text{-}H + 2\ Cu^{2+} \longrightarrow R\text{-}C{\equiv}C\text{-}C{\equiv}C\text{-}R + 2\ H^+ + 2\ Cu^+. \quad (6)$$

Here, the first step consists of the ionization of acetylenic compounds, the second one is a single-electron transfer from ethynyl anions to Cu(II) ions to lead the formation of ethynyl radicals, and the last one is the dimerization of ethynyl radicals.

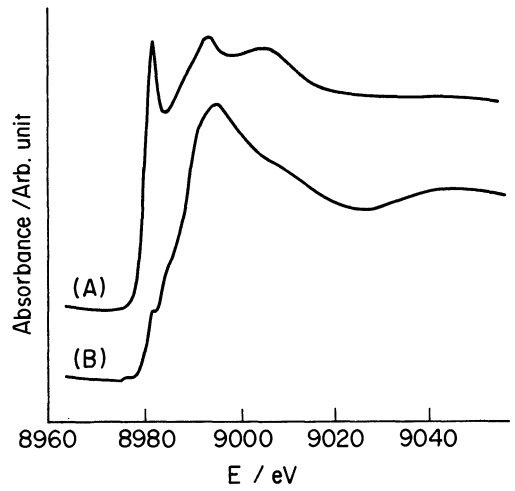

Fig. 3. XANES spectra of Cu–Py–SiO_2. (A) reduction by outgassing at 200 °C for 1 h, (B) exposure to 100 Torr of O_2 at room temperature for 24 h after observing spectrum (B).

The copper ions in Cu–Py–SiO_2 were found to be easily reduced with 1-propyne or to be oxidized with O_2, as described previously. Furthermore 1-propyne and O_2 were found to be decreased at a 4–1 ratio, as previously expressed by the stoichiometry of (1). These facts seem to indicate that the above reaction mechanism is also operative on the Cu–Py–SiO_2 catalyst, even though ethynyl radicals could not be detected by ESR spectroscopy.

Thus, the copper–pyridine derivative complex fixed on silica was proved to be active for the catalytic oxidative-coupling reaction of 1-propyne, in which the redox cycle of copper ions plays an important role.

Finally, the redox process of Cu–Py–SiO_2 was studied using XANES spectroscopy, which is usefull in distinguishing the oxidation state of copper ions; Cu(0), Cu(I) or Cu(II). In Fig.3 are shown the Cu–K edge XANES spectra of the sample. In its oxidized form, a small peak was observed around 8976 eV, which is due to the 1s→3d transition and is characteristic of Cu(II) ions. The sample which was outgassed at 200 °C, on the other hand, exhibited a quite different spectrum: the 8976 eV peak disappeared and a more intense one was observed around 8982 eV, which is due to 1s→4pπ transition and is characteristic of Cu(I) complex with a small coordination number.[7]

This work was partially supported by a Grant-in-Aid for Scientific Research No.63550589 from the Ministry of Education, Science and Culture.

References

1) G. Eglinton and W. McCrae, *Adv. Org. Chem., Methods and Results*, **4**, 225 (1963).
2) K. Kinosita, *Bull. Chem. Soc. Jpn.*, **32**, 777, 780 (1959).
3) G. F. Endres, A. S. Hay, and J. W. Eustance, *J. Org. Chem.*, **28**, 1300 (1963).
4) Y. Ukisu and A. Kazusaka, *J. Mol. Catal.*, **43**, 31 (1987).
5) N. Kakuta, A. Kazusaka, A. Yamazaki, and K. Miyahara, *J. Chem. Soc., Faraday Trans. 1*, **80**, 3245 (1984).
6) M. Nomura, A. Kazusaka, N. Kakuta, Y. Ukisu, and K. Miyahara, *J. Chem. Soc., Faraday Trans. 1*, **83**, 1227 (1987).
7) L. S. Kau, D. J. Spira-Solomon, J. E. Penner-Hahn, K. O. Hodgson, and E. I. Solomon, *J. Am. Chem. Soc.*, **109**, 6433 (1987).

Effects of Lateral Substituents on the Mesomorphic Properties of *N*-[4-(4-Methoxybenzoyloxy)benzylidene]aniline and Its Isomeric Compound

Hiroyuki HASEGAWA, Yoshio MATSUNAGA,* and Nobuhiko MIYAJIMA
Department of Chemistry, Faculty of Science, Hokkaido University, Sapporo 060
(Received September 27, 1990)

Synopsis. The nematic phases exhibited by the title compounds carrying a hydroxyl or cyano group at the 2-position of the aniline moiety are thermally more stable than expected on the basis of the relationship between the nematic–isotropic transition temperature of the corresponding halogeno derivatives and the van der Waals volume of the substituents.

The effects of lateral substituents on the mesomorphic properties have been the subject of extensive studies by many workers.[1] For example, Gray et al. examined the thermal behavior of 4-[(4-alkoxybenzylidene)amino]biphenyls and 4,4′-bis[(4-alkoxybenzylidene)amino]biphenyls with methyl or halogeno-substituents in the 2-position of the biphenyl core, and showed that both the smectic–nematic and the nematic–isotropic transition temperatures decrease smoothly with increasing the molecular breadth.[2,3] Moreover, Osman's recent work on 1,4-bis(4-*trans*-pentylcyclohexyl)benzenes revealed that all of the nematic–isotropic transition temperatures lie on a smooth curve when the temperature is plotted against the van der Waals volume of the lateral substituent.[4] The substituents employed by the latter author were halogens and methyl as well as cyano groups.

However, experience has shown that the effects of a substituent on the mesomorphic properties vary with the type of parent system, and also that a steric factor cannot account for all of the observed effects regarding terminal substituents; therefore, the above-mentioned relationship may not hold for other types of compounds. Indeed, we found that the nematic–isotropic transition temperatures of *N*-[4-(4-methoxybenzoyloxy)-benzylidene]-2-hydroxy and 2-cyanoanilines (**1**) deviate appreciably from a smooth curve constructed by those of the corresponding halogeno derivatives. Similarly, marked deviations were also observed with a series of isomeric compounds, 4-methoxyphenyl 4-[4-(2-substituted phenyliminomethyl)]benzoates (**2**).

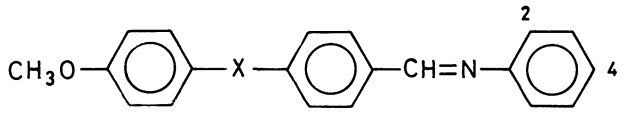

(**1**) X = -CO-O- (**2**) X = -O-CO-.

Experimental

The Schiff bases were prepared and then esterification was carried out, following the procedure of Hassner and Alexanian, to obtain the desired compounds.[5] Microscopic and calorimetric examinations were made, as described in a previous paper.[6]

Results and Discussion

The van der Waals volumes of substituents at the 2- or 4-position of the aniline moiety, the transition temperatures, and the associated enthalpy changes of compounds **1** and **2** are presented in Tables 1 and 2, respectively. For a comparison, the corresponding 4-substituted compounds were included in our examination. All of the van der Waals volumes of the substituents were taken from Bondi's work, except for that of the hydrogen atom (0.7 $cm^3\ mol^{-1}$), which was calculated concerning the basis of a van der Waals radius of hydrogen of 0.100 nm, a C–H bond length of 0.110 nm, and a van der Waals radius of carbon of 0.170 nm.[7] Here, K, N, and I stand for the crystalline, nematic, and isotropic liquid phases, respectively.

As is shown in Fig. 1, plots of the N–I transition temperature of the parent compounds and their 2-halogeno derivatives against the van der Waals volume of the substituent give smooth curves. The curve for series 1 is slightly concave upwards, whereas the curve for series 2 is slightly convex upwards. Contrary to what has been reported for the above-mentioned cases, the transition temperatures of the hydroxy and cyano derivatives in the present series deviate markedly from a smooth relationship.

In the case of *N*-(2-hydroxy-4-methoxybenzylidene)-4-butylaniline, the hydroxyl group does not exert its

Table 1. Van der Waals Volume ($cm^3\ mol^{-1}$) of Substituent,[a] and Transition Temperatures (°C) and Enthalpy Changes ($kJ\ mol^{-1}$) of Compounds **1**[b]

Substituent	V	K	N	I
H[c]	0.7	. 129 (31)	. 177 (0.4)	.
2-F[c]	5.8	. 135 (39)	. 145 (0.3)	.
2-OH	8.0	. 140 (35)	. 153 (0.3)	.
2-Cl[c]	12.0	. 129 (34)	[. 118 (0.3)]	.
2-CH_3[c]	13.7	. 150 (41)	[. 121 (0.2)]	.
2-CN	14.7	. 162 (39)	[. 144 (0.5)]	.
2-Br[c]	15.1	. 140 (34)	[. 105 (0.2)]	.
2-I[c]	19.6	. 133 (36)	[. 81 (0.2)]	.
4-F[c]	5.8	. 131 (32)	. 255 (0.8)	.
4-OH	8.0	. 202 (35)	. 305[d]	.
4-Cl[c]	12.0	. 172 (27)	. 285 (1.6)	.
4-CH_3[c]	13.7	. 129 (28)	. 278 (1.1)	.
4-CN	14.7	. 180 (38)	. 324 (0.8)	.
4-Br[c]	15.1	. 187 (38)	. 280 (0.9)	.
4-I[c]	19.6	. 202 (21)	. 274 (0.4)	.

a) Taken from Ref. 7. b) The last values are in parentheses. The braced quantities represent monotropic transitions. c) Taken from Ref. 8. d) Approximate decomposition temperature.

Table 2. Van der Waals Volume ($cm^3\ mol^{-1}$) of Substituent,[a] and Transition Temperatures (°C) and Enthalpy Changes ($kJ\ mol^{-1}$) of Compounds **2**[b]

Substituent	V	K		N		I
H[c]	0.7	.	151 (40)	.	173 (0.3)	.
2-F	5.8	.	118 (31)	.	152 (0.3)	.
2-OH	8.0	.	174 (43)	[.	161 (0.2)]	.
2-Cl[c]	12.0	.	129 (35)	.	132 (0.3)	.
$2\text{-}CH_3$	13.7	.	142 (41)	[.	129 (0.2)]	.
2-CN	14.7	.	171 (44)	[.	149 (0.5)]	.
2-Br	15.1	.	143 (38)	[.	119 (0.3)]	.
2-I	19.6	.	146 (38)	[.	97 (0.2)]	.
4-F	5.8	.	146 (36)	.	251 (0.8)	.
4-OH	8.0	.	226 (56)	.	330[d]	.
4-Cl	12.0	.	168 (39)	.	284 (0.8)	.
$4\text{-}CH_3$	13.7	.	149 (36)	.	275 (0.9)	.
4-CN	14.7	.	204 (36)	.	276 (0.6)	.
4-Br	15.1	.	169 (42)	.	280 (0.7)	.
4-I	19.6	.	193 (46)	.	274 (0.5)	.

a) Taken from Ref. 7. b) The last values are in parentheses. The braced quantities represent monotropic transitions. c) Taken from Ref. 6. d) Approximate decomposition temperature.

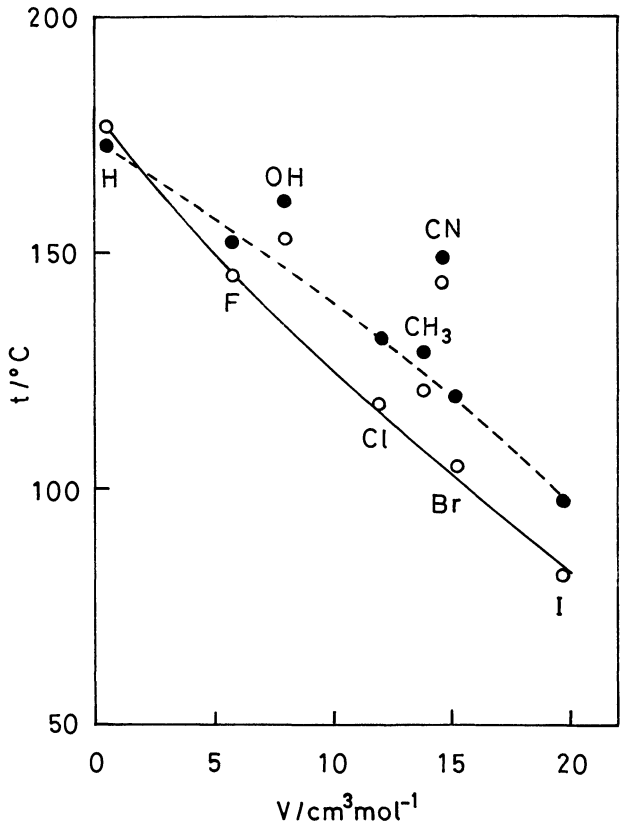

Fig. 1. Plots of the N–I transition temperature of compounds **1** (○) and of compounds **2** (●) against the van der Waals volume of substituents at the 2-position.

full breadth effect, and gives rise to an enhancement of the N–I transition temperature because it is held in the *cis*-position through intramolecular hydrogen bonding.[9] Similarly, we found that the transition temperatures of 4-(2-hydroxybenzylideneamino)phenyl 4-methoxybenzoate (193 °C) and 4-methoxyphenyl 4-(2-hydroxybenzylideneamino)benzoate (181 °C), which are isomeric with compounds **1** and **2**, are higher than those of their parent compounds (171 °C and 159 °C, respectively). For the 2-hydroxy derivatives of the present series too, an intramolecular hydrogen bonding is conceivable but stabilization of the nematic phase is clearly less significant. The same group at the 4-position is subject to intermolecular hydrogen bonding and gives rise to a promotion of the mesophase if the structural criteria for liquid crystallinity are satisfied.[10,11] The present 4-hydroxy derivative gives the highest, or the second-highest, N–I transition temperature in each series.

The terminal cyano group is well-known to give rise to an antiparallel correlation of molecular dipoles, which often results in higher N–I transition temperatures than with a comparable nonpolar substituent. As a matter of fact, the 4-cyano derivative gives the highest clearing point among compounds **1**, but the fourth among compounds **2**. The deviation of the N–I transition temperature from a smooth curve suggests that dipolar attractive forces due to a lateral cyano group cannot be ignored compared with dispersive forces in influencing the nematic thermal stability of our compounds.

A relatively small deviation of the N–I transition temperature of the methyl derivative in series 1 from a smooth curve cannot be ascribed to dipolar attractive forces and remains to be clarified.

The effects of terminal substituents on the mesomorphic behavior are certainly not simple. For example, even in the case of halogeno derivatives the nematic thermal stability increases in the order F, I, Br, Cl and cannot be explained in terms of either molecular length or van der Waals volume. It is likely that all of the factors applicable to the terminal substituents should, more or less, be considered for the lateral substituents. Apparently, the simple relationship reported by previous authors does not provide a general interpretation of the effects of lateral substituents on the N–I transition temperatures.

References

1) K. J. Toyne, "Thermotropic Liquid Crystals," ed by G. W. Gray, John Wiley, Chichester (1987), pp. 47—57.
2) D. J. Byron, G. W. Gray, A. Ibbotson, and B. M. Worrall, *J. Chem. Soc.*, **1963**, 2246.
3) S. J. Branch, D. J. Byron, G. W. Gray, A. Ibbotson, and B. M. Worrall, *J. Chem. Soc.*, **1964**, 3279.
4) M. A. Osman, *Mol. Cryst. Liq. Cryst.*, **128**, 45 (1985).
5) A. Hassner and V. Alexanian, *Tetrahedron Lett.*, **1978**, 4475.
6) Y. Matsunaga and K. Yasuhara, *Mol. Cryst. Liq. Cryst.*, in press.
7) A. Bondi, *J. Phys. Chem.*, **68**, 441 (1964).
8) H. Hasegawa, T. Masuda, Y. Matsunaga, S. Seo, and K. Yasuhara, *Bull. Chem. Soc. Jpn.*, **62**, 2875 (1989).
9) I. Teucher, C. M. Paleos, and M. M. Labes, *Mol. Cryst. Liq. Cryst.*, **11**, 187 (1970).
10) D. C. Schroeder and J. P. Schroeder, *J. Org. Chem.*, **41**, 2566 (1976).
11) H. Takeda, Y. Sakurai, S. Takenaka, H. Miyake, T. Doi, and S. Kusabayashi, *Chem. Lett.*, **1989**, 1335.

Synthesis and Reaction of *trans*-Dichlorobis(*o*-phenylenediamine)rhodium(III) Perchlorate with Some Oxidizing Agents

Akiko FURUHASHI,* Kunihiko ENDO, Shiro TAKAGI, and Yukichi YOSHINO
Department of Chemistry, Aoyama Gakuin University, 1-1 Morinosato-Aoyama, Atsugi 243-01
(Received May 18, 1990)

Synopsis. A new rhodium(III) complex with *o*-phenylenediamine, *trans*-$[RhCl_2\{C_6H_4(NH_2)_2\}_2]ClO_4$ was synthesized and the reaction with oxidizing agents studied. Due to coordination with the rhodium(III) ion the *o*-phenylenediamine (opd) was greatly stabilized against oxidation and the complex was oxidized slowly by periodate via intermediate radical complex to bis(*o*-benzoquinone diimine)-dichlororhodium(III) complex which decomposed to the final products.

A number of kinetic studies on the acid or base hydrolysis of various cationic rhodium(III)–amine complexes have been reported.[1–5] Even though *o*-phenylenediamine has the same bidentate function (–N–C–C–N–) as such compounds as ethylenediamine, there has been no report either on the synthesis or on the reactions of rhodium(III) complexes with *o*-phenylenediamine. The reason for this may be that the diamine possibly is oxidized by some oxidizing agents or even by the air and forms 2,4-hexadienedinitrile in the presence of some metal ions which can act as a catalyst for the oxidation reaction.[6–8] In other cases, synthesized metal complexes contain the oxidized state of the amine, *o*-benzoquinonediimine.[9,10] However, many stable complexes of bivalent metal ions such as nickel, cobalt, and so on, with opd have been reported.[11,12]

The authors tried to react rhodium(III) ion with opd in an atmosphere of nitrogen gas, and obtained the new title complex, then the oxidation process of the complex was investigated by means of spectrophotometry. Analysis of the reaction mechanism proved to be extremely difficult in the higher pH region (above 6.5) owing to the rapid and simultaneous oxidation of the coordinated diamine and the base hydrolysis of the complex. For this reason the reaction of the complex with oxidizing agents in the pH region from 5.4 to 6.2 have been focused upon.

In the pH range, reactions appeared to proceed via three steps. These may be looked upon as oxidation of the coordinated opd in the first two steps, then decomposition of the complex in the third step.

Experimental

Synthesis of The Complex. Rhodium(III) chloride trihydrate (1.5 g, 5.7 mmol) and opd (1.8 g, 17 mmol) were dissolved into hot water which had been deaerated by boiling (50 ml). The solution was then refluxed for 5 h under nitrogen gas flow. At the initial step, whitish yellow precipitate formed, but it disappeared with continuing reflux and the solution became clear and yellowish red in color. Then by adding about 5 ml of 70% perchloric acid into the hot solution, yellow crystals were obtained. The collected crystals were recrystallized repeatedly using minimal amounts of hot water.

Analysis. Found: C, 29.14; H, 3.27; N, 11.44; Cl, 21.74%. Calcd for $RhC_{12}H_{16}O_4N_4Cl_3$; C, 29.44; H, 3.29; N, 11.45; Cl, 21.73%.

Reaction Studies. The reactions were studied by measuring absorbance changes in the electronic spectra in the range from 200 to 700 nm using a Shimadzu UV-240 spectrophotometer on solutions containing 10^{-4} mol dm^{-3} of the complex in the presence of 2.12—7.1-fold excess of potassium periodate (KIO_4) as an oxidizing agent. The pH values were adjusted with acetic acid–sodium acetate buffer solutions in the range from pH 5.4 to 6.2, and the ionic strength was set at 0.3 mol dm^{-3} by using sodium perchlorate. The temperature of the solutions was controlled with an electric thermocontroller in the range of ±0.1 °C.

Results and Discussion

The spectra of the complex in aqueous solution showed a peak at 403 nm ($\log \varepsilon$=2.17) which is typical of the dichlorobis(diamine) type complex ion in a trans form.[1–5]

The spectral change of the complex solution containing potassium periodate at pH 5.85 at 50 °C is shown in Fig. 1. The increase in the absorbance at 420 nm is first order with respect to Rh(III)–opd complex in the first stage, and this may be due to oxidation of the coordinated opd when compared with the spectral change of the solution containing free opd and potassium periodate. The increase in the absorbance could be stopped by addition of hydroxylamine hydrochloride. When free opd was oxidized, formation of the radical was proved by measurements of the ESR spectra for the same solution as was used for the spectral measurements. In this case ESR spectra showed the presence of the radical and the signal disappeared with time. This change in the same as the change of the spectra at 420 nm: At 420 nm, the absorbance increased with time to a maximum, after which it steadily declined.

On the other hand, the increase in the absorbance with time at 420 nm for the complex solution with KIO_4 was much slower than that for the solution containing free opd and KIO_4, indicating the opd must be much resist to oxidation by coordination to the rhodium (k_{obsd} for opd is times greater than that for Rh–opd complex). In this case, ESR spectra did not show the presence of the radical even though the pattern of the spectral change at 420 nm was the same as opd oxidation.

It is assumed that the reaction of Rh(III)–opd with KIO_4 is initiated by a slow loss of an electron from the nitrogen atom of an opd ligand yielding an intermediate short-lived radical complex, $[RhCl_2(opd)(opd^+)]^{2+}$.[13,14] This may be followed by a rapid

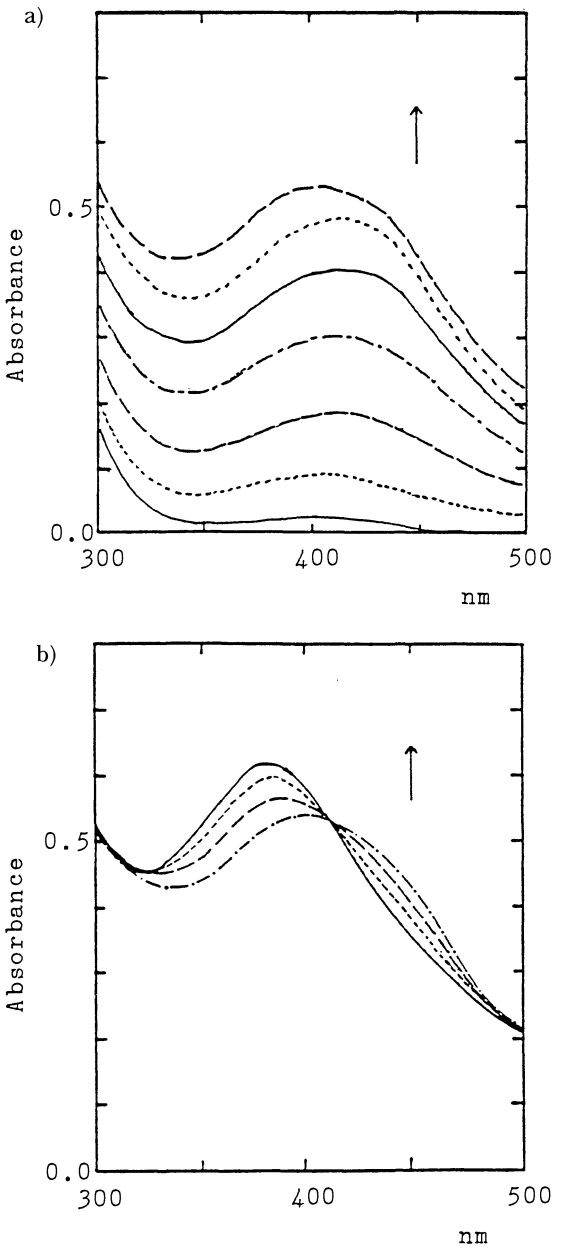

Fig. 1. The spectral change of the complex solution (1.23×10^{-4} M) containing potassium periodate (8.73×10^{-4} M) at pH 5.85 and 50 °C. (M=mol dm^{-3}). (a) From the start (bottom), curves show 20 min. intervals up to 120 min. b) From 130 min. to 180 min. 130 min. 140 min. 150 min. 180 min.

electron loss at another opd ligand in trans position thus forming $[RhCl_2(opd^+)_2]^{3+}$ (420 nm). In this intermediate radical complex, there may be two spin-coupled opd^+ radical ions coordinated to Rh(III) in trans-position, forming a diamagnetic complex as in the case of oxidation of the $Ni(opd)_2$ complex ion.[15]

As seen in Fig. 1, after the absorbance at 420 nm approached maximum, the spectra changed showing a new peak at 387 nm with an isosbestic point at 412 nm. In this stage, the color of the solution remained yellow. This step is assumed to be caused by the change of the coordinated opd radical. And this change was zeroth-order with respect to Rh(III)–opd complex. During these oxidation reactions, there may not be significant hydrolysis of the complex itself because the complex solution without the oxidizing agent showed only slight change in this pH region. This second peak at 387 nm, did not appear when free opd was oxidized. That means the second step of oxidation of opd produce a stable state only when opd is coordinated to the rhodium ion. At the last stage, the color of the solution gradually changed from yellow to dark red, implying the formation of *o*-benzoquinonediimine.[9,10,13,15,16] Then the absorbance at 387 nm decreased slowly, and finally an almost black precipitate was formed. The precipitate is thought to be a decomposed and polymerized form of the complex.

The process depends on the pH of the solution. The lower the pH, the slower the reaction rate. However, at pH 6.76, the spectral change is too complicated to analyze, indicating that overlapping of steps must occur at the same time, along with hydrolysis. In such higher pH ranges the absorbance of the peak at 420 nm decreased soon after it reached the maximum without the peak at 387 nm which was seen in the lower pH region.

The processes of the spectral change can be tentatively put as Rh–opd→A (step 1), A→B (step 2), and B→decomposed products (step 3). The examination of the effect of mole ratio of KIO_4 to the complex in the solution revealed that the higher the mole ratio KIO_4/Rh(III)–opd was, the faster the absorbance at 420 nm increased; however, the mole ratio did not much affect the rate of the step-2 change.

The absorption peak at 387 nm also can be observed with an aqueous solution of the complex which contains no other materials (buffer, $NaClO_4$ for adjusting of ionic strength, and KIO_4), although the change is too slow to follow the process quantitatively (it takes one month or more). Being such a slow process, the complex is undoubtedly oxidized even by the air.

Plots of log [A] vs. time in the step 1 change and plots of [B] vs. time in step 2 result in straight lines. From the slopes, pseudo-first-order rate constant, k^A_{obsd}, and zeroth-order rate constant, k^B_{obsd}, were evaluated. And from the Arrhenous plots, activation energies were also obtained for three different pH values. The results are shown in Table 1, and dependence of the observed rate constants on the concentration of periodate at 60 °C are given in Table 2.

The effects of other oxidizing reagents were investigated. In the case of NaClO, the previously mentioned two peaks at 420 and 387 nm could be observed, but there was no equilibrium between step 1 and step 2. $KMnO_4$ was also examined, but no fruitful results were obtained. At this time, only KIO_4 has given such quantitative results.

The same experiments were done with other Rh(III) complexes with diamines such as ethylenediamine and *cis*-1,2-cyclohexanediamine. However, similar spectral

Table 1. Temperature Dependence of the Rates of Reaction of $[RhCl_2(opd)_2]^+$ with $[KIO_4]$
$[RhCl_2(opd)_2]^+=1.23\times10^{-4}$ M, $[KIO_4]=8.37\times10^{-4}$ M, $I=0.3(NaClO_4)$ M dm^{-3}

Temp/°C	pH=6.17		pH=5.85		pH=5.41	
	$k^A_{obsd}\times10^3/s^{-1}$	$k^B_{obsd}\times10^8/Ms^{-1}$	$k^A_{obsd}\times10^3/s^{-1}$	$k^B_{obsd}\times10^8/Ms^{-1}$	$k^A_{obsd}\times10^3/s^{-1}$	$k^B_{obsd}\times10^8/Ms^{-1}$
50	1.32	7.83	1.23	3.0	0.57	1.30
55	2.30	9.17	1.87	4.0	0.73	1.83
60	3.57	11.2	2.23	5.67	0.86	3.00
E_a/kJ mol^{-1}	89.2	31.7	53.2	56.9	38.3	74.8

Table 2. Dependence of the Observed Rate Constants on the Concentration of Periodate at pH 6.17 and 60 °C, $[RhCl_2(opd)_2^+]=1.23\times10^{-4}$ M, $I=0.3(NaClO_4)$ M dm^{-3}

$KIO_4/[RhCl_2(opd)_2^+]$	$k^A_{obsd}\times10^3/s^{-1}$	$k^B_{obsd}\times10^8/Ms^{-1}$
2.1	0.90	1.08
3.2	1.12	1.13
5.0	2.67	0.95
7.1	3.57	0.98

changes for the Rh(III)–opd could not be observed.

From our experimental results, it can be concluded that the reaction of the Rh(III)–opd complex with KIO_4 is initiated by the formation of a radical of opd coordinated to Rh(III). After the formation of the opd radical complex, $[Rh^{III}Cl_2\{opd^+\}_2]^{3+}$ is completed, it easily changes to the stable state over time regardless of its concentration (step 2). The opd radical complex is apt to be oxidized by molecular oxygen to benzoquinone diimine complex, $[RhCl_2\{C_6H_4(NH)_2\}_2]^+$,[16] which eventually forms decomposed products.

The authors would like to express their gratitude to Professors Yuzo Nishida and Tatsuji Nisoku of Yamagata University for their arduous work in the ESR measurements.

References

1) A. Poë and C. Vuik, *J. Chem. Soc., Dalton Trans.*, **1976**, 661.
2) M. P. Hancock, *Acta Chem. Scand., Ser. A*, **31**, 678 (1977).
3) M. P. Hancock and B. T. Heaton, *J. Chem. Soc., Dalton Trans.*, **1979**, 761.
4) A. J. Poe and M. V. Twigg, *Can. J. Chem.*, **50**, 1089 (1972).
5) M. P. Hancock, *Acta Chem. Scand., Ser. A*, **29**, 468 (1975).
6) F. Ullmann and F. Mauthner, *Ber.*, **35**, 4302 (1902).
7) K. Nakagawa and H. Onoue, *Chem. Commun.*, **1965**, 396.
8) H. Takahashi, T. Kajimoto, and J. Tsuji, *Synth. Commun.*, **2**, 181 (1972).
9) A. L. Balch and R. H. Holm, *J. Am. Chem. Soc.*, **88**, 5201 (1966).
10) L. F. Warren, *Inorg. Chem.*, **16**, 2814 (1977).
11) D. R. Marks, D. J. Phillips, and J. P. Redfern, *J. Chem. Soc. A*, **1967**, 1464.
12) E. J. Duff, *J. Chem. Soc. A*, **1968**, 434.
13) K. Wüthrich and S. Fallab, *Helv. Chim. Acta*, **47**, 1440 (1964).
14) T. Hoshi, J. Okubo, M. Yanamoto, and S. Tanabe, *Ber. Bunsen-Ges. Phys. Chem.*, **91**, 1069 (1987).
15) G. G. Christoph and V. L. Goedken, *J. Am. Chem. Soc.*, **95**, 3869 (1973).
16) Y. Yoshino, M. Kasahara, and M. Saito, *Polyhedron*, **4**, 1019 (1985).

Preparation and Magnetic Properties of the Copper(II) Mixed Carboxylates with Haloacetate and Ammonioacetate

Shuji EMORI* and Kayoko YOSHIDZU
Department of Chemistry, Faculty of Science and Engineering, Saga University, Honjo-machi, Saga 840
(Received August 28, 1990)

Synopsis. Copper(II) mixed carboxylate compounds, $CuX(X'CH_2COO)(R_3NCH_2COO)\cdot mH_2O$ (X=Cl, Br; X'=F, Cl; R=H, CH_3), were prepared, and then characterized by means of magnetic susceptibility and IR-spectroscopy. The mixed carboxylates with betaine have the copper(II) acetate-type dinuclear structures. The amount of spin-exchange coupling through betaine bridges was estimated.

A study of the ligand displacement reactions of copper(II) acetate with some carboxylate dinucleating ligands, such as the chloroacetate,[1,2] myristate,[3] and 2,6-dimethoxybenzoate anions[4] has shown that these reactions yield mixed carboxylates; an X-ray structure determination[2,4] has shown that these mixed carboxylates retain the copper(II) acetate-type[5,6] dinuclear structures with the bridging ligands of both the acetate and substituent anions. Although some carboxylic acids tend to separate the copper(II) salts characterized by weak spin-exchange couplings, their mixed carboxylates may adopt the copper(II) acetate-type dinuclear structures. We can then estimate the amounts of spin-exchange coupling through such carboxylates acting as bidentate bridging ligands. We, thus, investigated the reactions between copper(II) ammonioacetate compounds and copper(II) haloacetates, and measured the room-temperature magnetic susceptibilities and IR spectra of the obtained compounds. The effective magnetic moments were evaluated from the magnetic susceptibilities, which were corrected for the diamagnetic contribution using the Pascal constants[7] and for temperature-independent paramagnetism using the value of 60×10^{-6} emu mol^{-1} (1 emu=$4\pi\times10^{-6}$ m^3). The IR spectra of the solid compounds were recorded using nujol mulls in the 4000—600 cm^{-1} range.

The ammonioacetate compounds with copper(II) halide, $CuX_2(R_3NCH_2COO)_2\cdot nH_2O$ (X=Cl, Br; R=H, CH_3), were prepared in a way similar to that for the corresponding ω-ammoniocarboxylate compounds.[8] From the reaction mixtures of the bromides, copper(I) species were removed upon recrystallization from 0.1 mol dm^{-3} hydrobromic acid solutions. Their magnetic moments (μ_{eff}=1.75 and 1.81 BM for the betaine and glycine compounds, respectively)[9] are similar to those for the mononuclear copper(II) compounds (μ_{eff}=1.8—2.0 BM), indicating weak spin-exchange couplings between copper(II) ions. These copper(II) ammonioacetate compounds were dissolved in aqueous solutions of copper(II) haloacetates, $Cu(X'CH_2COO)_2\cdot H_2O$ (X'=F, Cl), which are well known to have the copper(II) acetate-type dinuclear structures (μ_{eff}=1.32[10,11] and 1.43[12] BM at room temperature for X'=F and Cl, respectively), in a 1:1.2 molar ratio. The resulting solutions were allowed to stand in a refrigerator until fine green crystals separated. A chemical analysis indicates that the products are mixed carboxylates, $CuX(X'CH_2COO)(R_3NCH_2COO)\cdot mH_2O$ (X=Cl, Br; R=H, CH_3; X'=F, Cl). The products are not equimolar mixtures of the reactants, since their magnetic moments differ entirely from the average of those for the reactants (Table 1).

There is a remarkable difference in the magnetic moments between the mixed carboxylates with glycine and with betaine. The former are characterized by weak spin-exchange couplings (μ_{eff}=1.73 and 1.85 BM), while the latter are characterized by strong antiferromagnetic couplings between copper(II) ions (μ_{eff}= 1.34—1.42 BM). Furthermore, the IR spectra of the latter show bands as 1605—1630 and 1410—1420 cm^{-1} characteristic of bridging carboxylate due to unsymmetric and symmetric carboxyl stretching vibrations,[13] while the bands arising from two kinds of carboxylate groups lie too close together to enable the groupings to be readily differentiated. The temperature dependence

Table 1. Analytical Data and Effective Magnetic Moments at 20°C

Compound	Found (Calcd)/%					μ_{eff}/BM
	Cu	C	H	N	Cl^-Br^-	
$CuCl(FCH_2COO)[(CH_3)_3NCH_2COO]$	21.65 (21.67)	28.65 (28.68)	4.43 (4.47)	4.79 (4.78)	12.15 (12.09)	1.35
$CuBr(FCH_2COO)[(CH_3)_3NCH_2COO]$	18.77 (18.82)	24.78 (24.90)	3.78 (3.88)	4.17 (4.15)	23.53 (23.67)	1.34
$CuCl(ClCH_2COO)[(CH_3)_3NCH_2COO]$	20.32 (20.52)	27.03 (27.15)	4.16 (4.23)	4.56 (4.52)	11.65 (11.45)	1.42
$CuBr(ClCH_2COO)[(CH_3)_3NCH_2COO]\cdot H_2O$	16.97 (17.08)	22.54 (22.60)	3.97 (4.06)	3.86 (3.76)	21.59 (21.47)	1.41
$CuCl(ClCH_2COO)(H_3NCH_2COO)\cdot H_2O$	22.42 (22.25)	16.76 (16.82)	3.04 (3.18)	4.74 (4.90)	12.67 (12.42)	1.85
$CuBr(ClCH_2COO)(H_3NCH_2COO)\cdot 3H_2O$	17.56 (17.36)	13.03 (13.12)	3.45 (3.58)	3.84 (3.83)	21.79 (21.83)	1.73

of the susceptibilities for $CuCl(X'CH_2COO)[(CH_3)_3NCH_2COO]$ (X'=F, Cl) shows the Bleaney-Bowers behavior[14] with parameters $2J=-311\ cm^{-1}$ and $g=2.18$ for X'=F and $2J=-270\ cm^{-1}$ and $g=2.19$ for X'=Cl. The magnetic and IR spectral data indicate that the mixed carboxylates with betaine have bridged dinuclear structures, similar to that of copper(II) acetate monohydrate.[5,6] The crystals may consist of a repetition of the identical dinuclear units with 2:2 mixed bridges, which are seen in copper(II) acetate 2,6-dimethoxybenzoate monohydrate,[4] or may comprise a composite of the dinuclear units with variously mixed bridges, which are seen in the copper(II) acetate chloroacetate adduct with urea.[2]

In either case, because of the additive property of spin-exchange couplings, the magnetic moment for dinuclear mixed carboxylate can be adequately approximated by the average of those for the dinuclear salts of its constituent carboxylic acids. We can thereby estimate the magnetic property of the hypothetical dinuclear betaine compound, $CuCl_2[(CH_3)_3NCH_2COO]_2$, from those for the present mixed carboxylate, chloroacetate (μ_{eff}=1.38—1.40 BM and $2J=-278\ cm^{-1}$), [15] and fluoroacetate (μ_{eff}=1.26—1.28 BM and $2J=-359\ cm^{-1}$)[16] compounds. The estimated values, μ_{eff}=1.44 BM and $2J=-262\ cm^{-1}$ are a little larger than those of the copper(II) chloroacetate compounds. This fact is consistent with the well known correlation between the magnetic properties of a series of dinuclear copper(II) (substituted acetate)s and the acidities of their parent acids,[19] since betaine is a stronger acid than chloroacetic acid (pK_a=1.8 and 2.68 for betaine and chloroacetic acid, respectively).

References

1) Yu. V. Jablokov, V. V. Gavrilov, L. N. Milkova, and A. V. Ablov, *Dokl. Akad. Nauk SSSR*, **199**, 159 (1971).
2) V. I. Ivanov, Yu. A. Simonov, A. V. Ablov, and L. N. Milkova, *Dokl. Akad. Nauk SSSR*, **220**, 365 (1975).
3) B. P. Baranwal, G. K. Parashar, and R. C. Mehrotra, *J. Indian Chem. Soc.*, **61**, 923 (1984).
4) L. S. Erre, G. Micera, P. Piu, F. Cariati, and G. Ciani, *Inorg. Chem.*, **24**, 2297 (1985).
5) J. N. von Niekerk and F. R. L. Schoening, *Acta Crystallogr.*, **6**, 227 (1953).
6) G. M. Brown and R. Chidambaram, *Acta Crystallogr., Sect. B*, **29**, 2393 (1973).
7) G. Foex, "Constants Sélectioneés, Diamagnétisme et Paramagnétisme," Masson, Paris (1957).
8) S. Emori, T. Noguchi, and Y. Muto, *Bull. Chem. Soc. Jpn.*, **58**, 2733 (1985).
9) M. Castillo and E. Ramirez, *Transition Met. Chem.*, **9**, 268 (1984).
10) K. S. Patel and J. A. Faniran, *J. Inorg. Nucl. Chem.*, **38**, 1001 (1976).
11) M. Melnik, *Finn. Chem. Lett.*, **1978**, 255.
12) M. Melnik, *Coord. Chem. Rev.*, **36**, 1 (1981).
13) L. J. Bellamy, "The Infrared Spectra of Complex Molecules," 3rd ed, Chapman and Hall, London (1975).
14) B. Bleaney and K. D. Bowers, *Proc. R. Soc. London, Ser. A*, **214**, 451 (1952).
15) S. Emori, N. Haramaki, and Y. Muto, *Bull. Chem. Soc. Jpn.*, **58**, 761 (1985).
16) S. Emori, N. Morishita, and Y. Muto, *Bull. Chem. Soc. Jpn.*, **60**, 1913 (1987).

Complex Formation of Poly(Acrylic Acid) with Lead(II) Ion

Hiromichi HAYASHI* and Tsuyoshi KOMATSU†
Government Industrial Research Institute, Tohoku, Miyaginoku, Sendai, Miyagi 983
† Department of Polymer Science, Faculty of Science, Hokkaido University, Kitaku, Sapporo, Hokkaido 060
(Received September 10, 1990)

Synopsis. The equilibrium constants of Poly(acrylic acid)-Pb(II) complex formation reactions were evaluated from stoichiometric equations by means of pH titration with a Pb(II) ion selective electrode. The thermodynamic parameters were obtained from the temperature dependence of the equilibrium constants. The Poly(acrylic acid)-Pb(II) complexes seem to be stable due to an exothermic process.

There are many investigations on the interaction between divalent metal ions and polyelectrolytes.[1–4] Many workers have extensively discussed the stability of polyelectrolyte complexes from the equilibrium constants of complex formation reactions. Gregor and co-workers have shown that the Bjerrum method of pH titration for the evaluation of formation constants of complexes may be applied to the divalent metal–polyelectrolyte complex systems.[1]

On the other hand, the amount of complexed metal ions in aqueous solution can be evaluated from the amount of free metal ions. However, it is not so easy to determine this amount, although several methods have been proposed. Yamashita et al. showed that the potentiometric titration by use of a copper(II) ion selective electrode(Cu–ISE) is useful to investigate the complex formation in the copper(II) ion–polycarboxylic acid system. Cu–ISE is able to detect free metal ion alone. The values of equilibrium constants of complex formation reactions were evaluated from stoichiometric equations.[4]

In this paper, the complex formation in the lead(II)–poly(acrylic acid) system was investigated potentiometrically. On the basis of the data from pH titration by a lead(II) ion selective electrode(Pb–ISE), stability constants were evaluated from stoichiometric equations. Thermodynamic parameters were evaluated from the temperature dependence of stability constants for complex formation reactions.

Experimental

Materials. Poly(sodium acrylate)(PAANa) was purchased from Nakarai Chemical Co. PAANa was dissolved in distilled water and transformed to poly(acrylic acid)(PAA) by addition of excess hydrochloric acid. The aqueous solution of PAA was refined by dialysis. The molecular weight of PAA was 5.2×10^5 by viscometric measurement.[5] The other chemicals and lead(II) perchlorate used were of guaranteed reagent grade. The concentration of lead perchlorate stock solution was determined by chelatemetric titration with Xylenol Orange(XO) as the indicator.

Potentiometric Titration. The pH measurements were carried out in a nitrogen atmosphere at 15.0, 25.0, and 35.0 (±0.1)°C and ionic strength of 0.1 mol dm^{-3} $NaClO_4$ by use of a digital ion meter (Orion 801A) with glass and calomel electrodes. The activity measurements of lead(II) ion were performed with a digital ion meter (Orion Model 801A) with lead selective (Orion 948200) and calomel electrodes.

Double junction salt bridges of 1.0 mol dm^{-3} with sodium perchlorate agar and ammonium chloride-saturated agar were used between a glass (or Pb–ISE) and a reference calomel electrode in order to avoid the formation of Pb(II) chloride complex. The concentration of lead(II) ions was determined with the calibration curve obtained for the system without any polymer. The limit of detection for Pb–ISE was 10^{-6} mol dm^{-3}.

The lead perchlorate solution was added to the PAA solutions neutralized with a sodium hydroxide solution in order to avoid the precipitation. The potentiometric titration was thus carried out with a perchloric acid solution.

Results and Discussion

The average coordination number($\bar{n}$) obtained from the pH titration curve is given as follows:

$$\bar{n} = \Sigma i[PbA_i]/[Pb], \quad (1)$$

where [Pb] and [PbA_i] represent the total concentrations of lead ion and 1:i lead-carboxylate complex, respectively. Calculation of $\bar{n}$ was done by the method of reference plot contrived by Mandel et al.[2] $\bar{n}$ and the fraction of free lead ion determined with Pb–ISE are shown in Fig. 1 as two functions of the degree of dissociation of carboxyl group (α). $\bar{n}$ increased with α and reached nearly 1.8 in contrast to the decrease in fraction of free lead ion. An almost complete binding occurred above 0.3 of α. At α=0.1, 70% of lead ions was

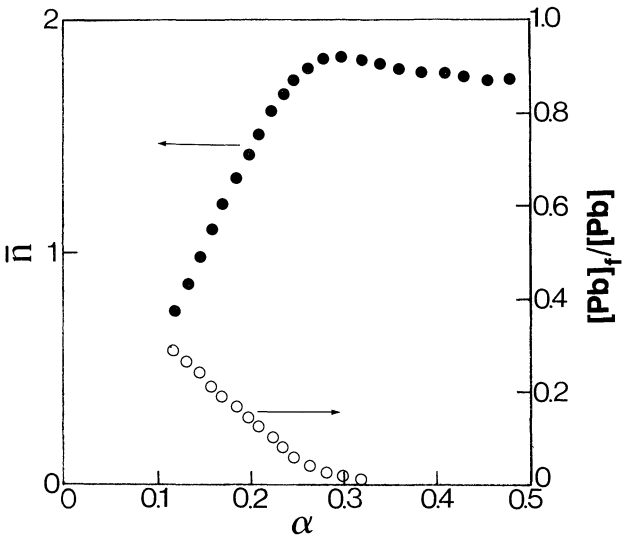

Fig. 1. Formation curve of PAA–Pb(II) complex at 25°C: ●; $\bar{n}$ (average coordination number), ○; $[Pb]_f/[Pb]$ (fraction of free lead ion). [PAA]= 1.00×10^{-2} mol dm^{-3} [Pb]=1.01×10^{-3} mol dm^{-3}.

already bound to polymer, indicating that Pb(II)–PAA complex is stable. Below 0.1 of α, the precipitation occurred.

As is shown in Fig. 1, $\bar{n}$ does not exceed 2; it indicates that 2 is the maximum number of carboxylate groups bound to a lead ion. Assuming that both monocarboxylate (1:1) and dicarboxylate complexes (1:2) are formed, the following equation holds:

$$[\mathrm{Pb}] = [\mathrm{Pb}]_f + [\mathrm{PbA}] + [\mathrm{PbA_2}], \quad (2)$$

where $[\mathrm{Pb}]_f$, [PbA], and $[\mathrm{PbA_2}]$ represent the concentrations of free lead ion, monocarboxylate complex, and dicarboxylate complex, respectively. In the present study, the concentration of free lead ion can be determined by Pb–ISE, and Eq. 1 can be rewritten as

$$\bar{n}\,[\mathrm{Pb}] = [\mathrm{PbA}] + 2[\mathrm{PbA_2}]. \quad (3)$$

The simultaneous Eqs. 2 and 3 purposely gave the concentrations of two species [PbA] and $[\mathrm{PbA_2}]$.

The fractions of PbA and $\mathrm{PbA_2}$ are shown as two functions of α in Fig. 2. The fraction of $\mathrm{PbA_2}$ increased with α in contrast to a decrease in the fraction of PbA, suggesting that each of complex formation reactions is stepwise as is in the case of the monomeric ligand. In a low α region, monocarboxylate complex predominated over dicarboxylate complex. As α increased, monocarboxylate complex changed to dicarboxylate complex under increasing carboxylate group concentration.

The stability constants of monocarboxylate and dicarboxylate Pb(II) complexes, K_1 and K_2 are given by

$$K_1 = [\mathrm{PbA}]/[\mathrm{Pb}]_f\,[\mathrm{A}] \quad (4)$$

and

$$K_2 = [\mathrm{PbA_2}]/[\mathrm{PbA}]\,[\mathrm{A}], \quad (5)$$

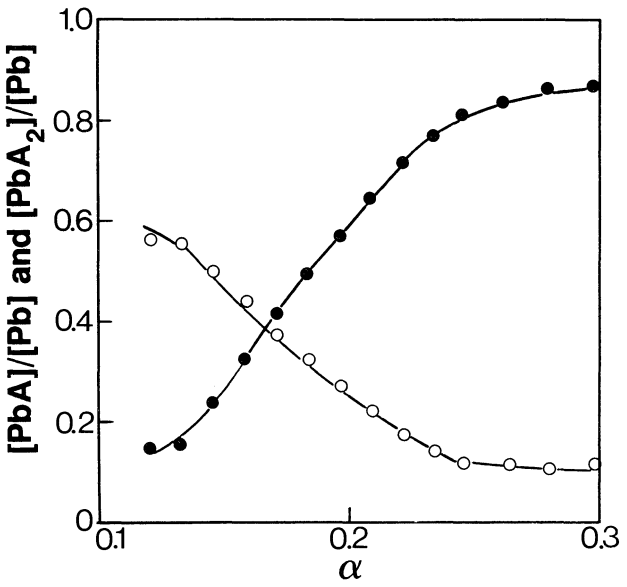

Fig. 2. Fractions of monocarboxylate and dicarboxylate Pb(II) complexes, [PbA]/[Pb] (○) and $[\mathrm{PbA_2}]$/[Pb] (●) as two functions of α.

where [A] represents the concentration of nonchelating carboxylate group determined by reference plot method proposed by Mandel and Leyte.[2] The values of K_1, K_2 calculated by the above equations in the α range of 0.1 to 0.3 are plotted in Fig. 3. The value of K_1 was nearly constant, whereas, the values of K_2 depended on α. K_2 increased with α and saturated at 0.25 of α. The behavior of K_2 is attributed to the change in negative charge density on each polymer chain, because the negative charge of carboxylate group adjacent to dicarboxylate complex raises the stability constant K_2. The stability constants of K_1 and K_2 at 0.15 of α ($\bar{n}$=1.0 in Fig. 1) were $10^{3.64}$ and $10^{3.11}$ $\mathrm{dm^3\,mol^{-1}}$, respectively.

In order to determine the change in enthalpy and entropy of the complex formation, the temperature dependence of stability constants was measured. The gross stability constant of the dicarboxylate Pb(II) complex, β_2 is given by

$$\beta_2 = K_1K_2. \quad (6)$$

The logarithmic values of β_2 were 6.86, 6.75, and 6.66 at 15, 25, and 35 °C under the conditions of 0.15 of α,

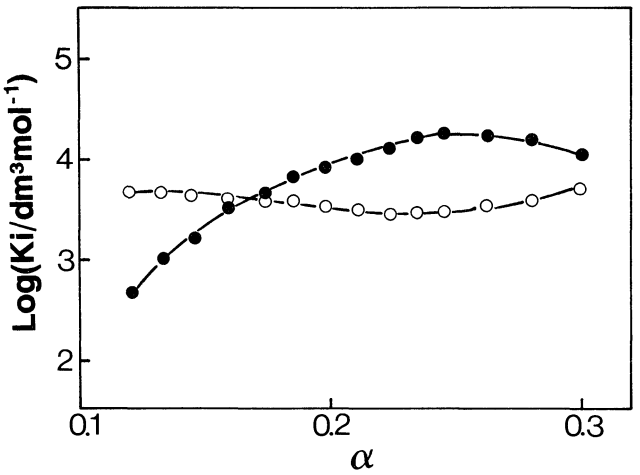

Fig. 3. Stability constants of monocarboxylate and dicarboxylate Pb(II) complexes, K_1 (○) and K_2 (●) as two functions of α.

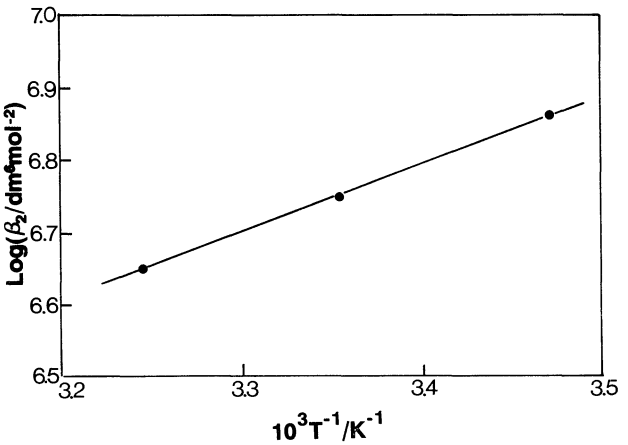

Fig. 4. Plots of log β_2 vs. T^{-1}.

Table 1. Gross Stability Constants and Thermodynamic Parameters

Metal ion	Ligand	β_2	$\Delta G^\ominus$	$\Delta H^\ominus$	$\Delta S^\ominus$
		$dm^6\ mol^{-2}$	$kJ\ mol^{-1}$	$kJ\ mol^{-1}$	$J\ mol^{-1}\ K^{-1}$
Pb^{2+}	PAA	$10^{6.75}$	−38.5	−18.0	67
Pb^{2+} [a]	Acetic acid	$10^{3.62}$	−20.5	−0.6	67
Cu^{2+} [b]	PAA	$10^{5.86}$	−33.5	2.1	117

a) Data taken from Ref. 6. b) Data taken from Ref. 7.

respectively. Figure 4 gives the plot of $\log \beta_2$ vs. T^{-1}. Log β_2 values were on the straight line between 15 and 35 °C, indicating that the enthalpy change is constant. The standard enthalpy change (ΔH) was obtained from Eq. 7:

$$\Delta H = -2.303\ R\ \mathrm{d}(\log \beta_2 / T^{-1}), \quad (7)$$

where T is the absolute temperature, and R is the gas constant. The free energy change (ΔG) obtained from the value of $\log \beta_2$ at 25 °C and the entropy change (ΔS) was calculated by $(\Delta H - \Delta G)/T$. Gross stability constants and the thermodynamic parameters obtained by the present analysis are summarized in Table 1, together with the literature values for the corresponding lead acetate,[6] and copper–PAA[7] as a comparison. The dicarboxylate complex is 10^3 times as stable as the Pb(II) acetate complex. Standard enthalpy changes for Pb(II)–PAA complex and Pb(II) acetate complex were negative, indicating that the formation of a chelate between one lead ion and two carboxylate groups is an exthothermic process. The absolute value of enthalpy change was favorable of the formation of Pb(II)–PAA complex. In the polymer–metal system, the standard enthalpy change is more negative than that in the monomeric analogue–metal ion system, so that the metal ions are more tighly bound to the polymer than to the monomeric analogue.[8]

The standard entropy change for Pb(II)–PAA complex is smaller than that for Cu(II)–PAA complex which is the most stable one among divalent metal–PAA complexes investigated, the entropy change was favorable of Cu(II)–PAA complex, whereas the enthalpy change for the former is larger than that for the latter. It is known that enthalpy change for transition divalent metal–polycarboxylate complexes are positive.[9] These comparisons show that the lead–PAA complex must be stabilized by a highly exthothermic process. It is concluded that Pb(II)–PAA complex is the most stable one of the divalent metal ion–PAA complexes which have been investigated in accord with the order of magnitude of stability constant for the divalent metal ion–monomeric carboxylate complex, that is Pb>Cu>Cd.[10]

References

1) H. P. Gregor, L. B. Luttinger, and E. M. Loebl, *J. Phys. Chem.*, **59**, 34 (1955).
2) M. Mandel and J. C. Leyte, *J. Polym. Sci., Part A*, **2**, 2883 (1964).
3) C. Travers and J. A. Marinsky, *J. Polym. Sci., Polym. Symp.*, **47**, 285 (1974).
4) F. Yamashita, T. Komatsu, and T. Nakagawa, *Bull. Chem. Soc. Jpn.*, **49**, 2073 (1973).
5) R. Sakamoto and K. Imabori, *Nippon Kagaku Kaishi*, **83**, 389 (1962).
6) Gerning P., *Acta Chem. Scand.*, **21**, 2015 (1967).
7) E. M. Loebl, L. B. Luttinger, and H. P. Gregor, *J. Phys. Chem.*, **59**, 559 (1955).
8) B. J. Felber and N. Purdie, *J. Phys. Chem.*, **75** (8), 1136 (1971).
9) M. Morcellet, *J. Polym. Sci., Polym. Lett. Ed.*, **23**, 99 (1985).
10) M. Yasuda, K. Yamasaki, and H. Ohtaki, *Bull. Chem. Soc. Jpn.*, **33**, 1067 (1960).

Conjugate Reduction of 2-Butene-1,4-diones with $LiAlH_4$-$SbCl_3$

Shinsei SAYAMA* and Yutaka INAMURA
Department of Chemistry, Fukushima Medical College, Hikarigaoka, Fukushima 960-12
(Received June 15, 1990)

Synopsis. The reagent $LiAlH_4$-$SbCl_3$ was found to be more effective for a conjugate reduction of 2-butene-1,4-diones in comparison with the reagent $LiAlH_4$-other metal halides.

The effect of the addition of $AlCl_3$ to $LiAlH_4$ was to produce more mild and specific reagents for reducing epoxides and halo ketones.[1] Therefore, a chemoselective reduction of polyfunctional compounds with $LiAlH_4$ in the presence of various other metal halides has been the subject of much study.[2] It was reported that the reduction of α,β-unsaturated ketones with $LiAlH_4$-Cu_2I_2 or $LiAlH_4$-metal halides (e.g., Cu_2Br_2, Cu_2Cl_2, $TiCl_3$, $FeCl_3$) gave the corresponding ketones arising from a conjugate reduction.[3,4] Since γ-keto-α,β-unsaturated ketones, such as 2-butene-1,4-diones, afforded 1,2-reduction products predominantly with $LiAlH_4$ or $NaBH_4$, there has been much interest in mild, convenient methods for a conjugate reduction of γ-keto-α,β-unsaturated ketones. The reduction of γ-keto-α,β-unsaturated ketones with $LiAlH_4$-metal halides, however, has not been carried out.[1-7] Moreover, $SbCl_3$ has not been used as a metal halide in a conjugate reduction of α,β-unsaturated ketones and γ-keto-α,β-unsaturated ketones. Since antimony is one of the representative elements which possess both metallic and nonmetallic properties and Sb^{3+} is a borderline acid in the classification of hard and soft acids,[2a,6,7] it can be expected that the reduction of carbonyl compounds with $LiAlH_4$-$SbCl_3$ has a new reactivity in comparison with $LiAlH_4$-transition metal halides. We would like to report on the results of studies concerning the selective conjugate reduction of γ-keto-α,β-unsaturated ketones, such as 2-butene-1,4-diones, with $LiAlH_4$-$SbCl_3$.

The reduction of *trans*-1-phenyl-2-pentene-1,4-dione (**1**), chosen as a representative 2-butene-1,4-dione for this study, with $LiAlH_4$ (LAH)-$SbCl_3$ in various stoichiometric ratios was carried out. The results are summarized in Table 1. At the ratio of enedione **1**, LAH, and $SbCl_3$ (1:1:1, 1:1:3, or 1:3:1), a mixture of 4-hydroxy-1-phenyl-1-pentanone, 1-phenyl-2-pentene-1,4-diol and 1-phenylpentane-1,4-diol and **1** was mainly obtained, accompanied by a small amount of 1-phenylpentane-1,4-dione (**1a**). At a stoichiometric ratio of 1:3:3 or 1:3:4, enedione **1** was reduced to give a conjugate reduction product **1a** in nearly quantitative yield. The optimum conditions for the conjugate reduction of **1** with LAH-$SbCl_3$ found in the present experiments are as follows: i) $SbCl_3$ is essential for effecting a regioselective conjugate reduction. ii) There is need to use either an equal or excess molar equivalent of $SbCl_3$ over LAH in order to suppress the reaction of 1,2-reduction with LAH. iii) There is need to use more than two molar equivalents of LAH and $SbCl_3$ over **1** for obtaining conjugate reduction products in high yield.

The results of a LAH-$SbCl_3$ reduction of other 2-butene-1,4-diones are shown in Table 2. The reductions of *trans*-3-decene-2,5-dione (**2**), ethyl 3-benzoylacrylate (**3**), *trans*- and *cis*-1,4-diphenyl-2-butene-1,4-diones (**5** and **6**), even diethyl azodicarboxylate (**4**) and 3-benzoyl-1-phenyl-2-pentene-1,4-dione (**7**) with LAH-$SbCl_3$ took place to give the corresponding conjugate reduction products in good yields.

The results of a LAH-$SbCl_3$ reduction of α,β-unsaturated carbonyl compounds are shown in Table 3. The reduction of α,β-unsaturated ketones (**9** and **10**) was not selective, as shown. Only the formyl group of **8** was reduced to a hydroxyl group in 92% yield. The chemoselective reduction of aldehydes in the presence of ketones with this reagent was also examined in the following competition experiments. Equimolar amounts of 3,7-dimethyl-6-octenal and ethyl levulinate were

Table 1. Reduction of *trans*-1-Phenyl-2-pentene-1,4-dione **1** with $LiAlH_4$-$SbCl_3$ in THF at 0 °C for 4 h[a]

Entry	Molar ratio			Products, yield/%[b]			
	Enedione **1**	$LiAlH_4$	$SbCl_3$	1-Phenylpentane-1,4-dione **1a**	Hydroxy compound		Recovered enedione **1**
					Hydroxy ketone **1b**	Diol **1c**	
1	1	2	0	—	56[c]	38[d]	—
2	1	1	1	32	30[e]	—	33
3	1	1	3	23	—	—	76
4	1	2	2	60	10[c]	—	21
5	1	3	3	84	6[c]	—	—
6	1	3	1	14	42[e]	43[f]	—
7	1	3	9	87	—	—	—
8	1	3	4	93	—	—	—
9	1	0	3	—	—	—	99

a) LAH; 1.0—3.0 mmol; Solvent; 10—15 ml. b) Yield is based on enedione **1** used. c) 4-Hydroxy-1-phenyl-1-pentanone. d) 1-Phenyl-2-pentene-1,4-diol. e) Mixture of **1b** and **1c**. f) Mixture of enediol and saturated diol.

Table 2. Reduction of 2-Butene-1,4-dione with $LiAlH_4$–$SbCl_3$ in THF at 0 °C for 4 h[a]

Substrate	(S)	Molar ratio S : LAH : $SbCl_3$	Products	Yield/%[b]
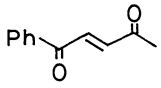	**1**	1 : 3 : 3	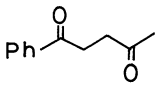	**1a**[8] 84
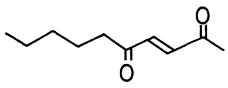	**2**	1 : 3 : 3	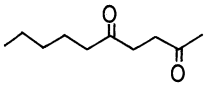	**2a**[8,9] 94
$PhCOCH{=}CHCO_2Et$	**3**	1 : 3 : 3	$PhCOCH_2CH_2CO_2Et$	**3a**[8] 86
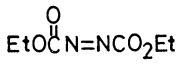	**4**	1 : 3 : 3	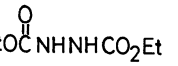	**4a** 81
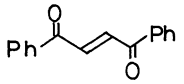	**5**	1 : 3 : 3	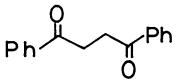	**5a**[12,13] 78
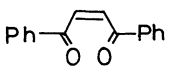	**6**	1 : 3 : 3	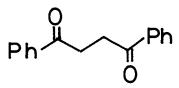	**5a**[12,13] 81
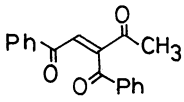	**7**	1 : 2.5 : 2.5	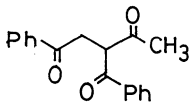	**7a** 64

a) LAH; 1.0—3.0 mmol; Solvent; 10—15 ml. b) Yield is based on 2-butene-1,4-dione used.

Table 3. Reduction of Carbonyl Compounds with $LiAlH_4$–$SbCl_3$ in THF at 0 °C for 4 h[a]

Substrate	(S)	Molar ratio S : LAH : $SbCl_3$	Products	Yield[b]/%
$C_6H_5CH{=}CHCHO$	**8**	1 : 2 : 2	$C_6H_5CH{=}CHCH_2OH$ **8a** 92 $C_6H_5CH_2CH_2CH_2OH$ **8b** 7	
$C_6H_5CH{=}CHCOCH_3$	**9**	1 : 3 : 3	$C_6H_5CH_2CH_2COCH_3$ **9a** 12 $C_6H_5CH{=}CHCH(OH)CH_3$ **9b** 44 Recovered **9** 42	
$C_6H_5CH{=}CHCOC_6H_5$	**10**	1 : 3 : 3	$C_6H_5CH_2CH_2COC_6H_5$ **10a** 16 Recovered **10** 50	

a) LAH; 1.0—3.0 mmol; Solvent; 10—15 ml. b) Yield is based on the carbonyl compounds used.

allowed to compete for the reduction with three molar equivalents of LAH–$SbCl_3$. 3,7-Dimethyl-6-octenal was selectively reduced to 3,7-dimethyl-6-octene-1-ol in 70% yield and ethyl levulinate was recovered unchanged. In addition, carbonyl groups of 1-phenylbutane-1,3-dione and 1-phenylpentane-1,4-dione and ester, nitrile, and acetal groups in ethyl levulinate and 4-phenyl-4,4-ethylenedioxybutanenitrile were not affected under the above-mentioned reduction conditions.

On the other hand, the reduction of enedione **1** with LAH–other metal halides such as Cu_2I_2, $CuCl_2$, $AlCl_3$, $FeCl_3$, and $TiCl_4$ gave no 1,4-reduction products, and complex mixture of hydroxy derivatives were obtained under various ratios of LAH and metal halides.

Thus, the reagent LAH–$SbCl_3$ provides a new convenient method for a mild, selective conjugate reduction of 2-butene-1,4-diones. Further application of reduction with LAH–$SbCl_3$ to aldehyde and other functional groups is now in progress.

Experimental

IR spectra were recorded on a JASCO A-100 spectrometer. ^1H NMR spectra were taken on a Hitachi R-24B spectrometer with TMS as an internal standard. The products were identified by spectroscopic data.

General Procedure. To a suspension of LAH (113 mg, 3 mmol) in THF (8 ml) at 0 °C was added $SbCl_3$ (684 mg, 3 mmol) dissolved in THF (2 ml). The resulting mixture was stirred for 5 min at 0 °C, and then 2-butene-1,4-dione (1 mmol) in THF (2 ml) was added. After stirring for 4 h at 0—18 °C, the reaction mixture was treated with 1 M aq Na_2CO_3 and extracted with ethyl acetate. The organic layer was washed by 0.5 M aq HCl and successively saturated aq

NaCl and dried by $MgSO_4$. After removal of the solvent in vacuo, the residue was purified by column chromatography on silica gel (Wakogel C-300) with CCl_4 and $CHCl_3$ (3:1). Conjugate reduction products **1a—7a** were obtained in 64—94% yield.

2-Butene-1,4-diones were prepared according to a procedure from the literature.

trans-1-Phenyl-2-pentene-1,4-dione (**1**)[11] and *trans*-3-decene-2,5-dione (**2**) were prepared by pyridinium chlorochromate (PCC) oxidation of the corresponding 2,5-dialkylfuran derivatives.[10]

trans-1,4-Diphenyl-2-butene-1,4-dione (**5**)[11,12] was prepared by Friedel–Crafts acylation of benzene with fumaryl chloride.[14] *cis*-1,4-Diphenyl-2-butene-1,4-dione (**6**)[11,12] and 3-benzoyl-1-phenyl-2-pentene-1,4-dione (**7**) were prepared by oxidation of corresponding furan derivatives with HNO_3 in acetic acid.[15]

3-Benzoyl-1-phenylpentane-1,4-dione (7a): Mp 83—84°C (from CCl_4); IR (KBr) 1720, 1690, and 1675 cm^{-1}; ^1H NMR ($CDCl_3$) δ=2.22 (3H, s), 3.70 (2H, m), 5.30 (1H, t, J=6.0), 7.26—8.26 (10H, m).

***trans*-3-Decene-2,5-dione (2):** Mp 46—47°C (from hexane); IR (KBr) 1670 cm^{-1}; ^1H NMR ($CDCl_3$) δ=0.85 (3H, t, J=7.0), 1.13—2.00 (6H, m), 2.33 (3H, s), 2.47—2.83 (2H, m), 6.70 (2H, s).

3-Benzoyl-1-phenyl-2-pentene-1,4-dione (7): Mp 112—113°C (from ethanol); IR (KBr) 1685 and 1660 cm^{-1}; ^1H NMR ($CDCl_3$) δ=2.35 (3H, s), 7.20—8.10 (11H, m).

References

1) a) H. O. House, "Modern Synthetic Reactions," W. A. Benjamin, Inc., Menlo Park, California (1972), p. 45; b) E. C. Ashby and B. Cooke, *J. Am. Chem. Soc.*,**90**, 1625 (1968).

2) a) T. Imamoto, T. Takeyama, and T. Kusumoto, *Chem. Lett.*, **1985**, 1491; b) E. C. Ashby and J. J. Lin, *Tetrahedron Lett.*, **1977**, 4481.

3) E. C. Ashby, J. J. Lin, and R. Kover, *J. Org. Chem.*, **41**, 1939 (1976), and references cited therein.

4) T. Tsuda, T. Fujii, K. Kawasaki, and T. Saegusa, *J. Chem. Soc., Chem. Commun.*, **1980**, 1013.

5) a) M. Fieser and L. F. Fieser, "Reagents for Organic Synthesis," John Wiley & Sons,Inc., New York, Vol. 1—13; b) S. S. Pizey, "Synthetic Reagents," John Wiley & Sons,Inc., New York (1974), Vol. 1, p. 101.

6) T.-L. Ho, "Hard and Soft Acids and Bases Principle in Organic Chemisty," Academic Press, New York (1977), p. 93.

7) J. Bottin, O. Eisenstein, C. Minot, and N. T. Anh, *Tetrahedron Lett.*, **1972**, 3015.

8) H. Stetter, *Angew. Chem., Int. Ed. Engl.*, **15**, 639 (1976).

9) H. Stetter and H. Kuhlmann, *Tetrahedron Lett.*, **1974**, 4505.

10) G. Piancatelli, A. Scettri, and M. D'Auria, *Tetrahedron*, **36**, 661 (1980).

11) C.-S. Chien, T. Kawasaki, M. Sakamoto, Y. Tamura, and Y. Kita, *Chem. Pharm. Bull.*, **33**, 2743 (1985).

12) Y. Inamura and Y. Inamura, *Nippon Kagaku Kaishi*, **1985**, 134.

13) Y. Kobayashi, T. Taguchi, T. Morikawa, E. Tokuno, and S. Sekiguchi, *Chem. Pharm. Bull.*, **28**, 262 (1980).

14) R. E. Lutz, "Organic Syntheses," John Wily & Sons, Inc., New York (1955), Coll. Vol. III, p. 248.

15) a) R. E. Lutz and R. J. Rowlett, Jr., *J. Am. Chem. Soc.*, **70**, 1359 (1948); b) R. E. Lutz and F. N. Wilder, *ibid.*, **56**, 978 (1934).

Synthesis of 5′-[1-(Methoxycarbonyl)-2-(*p*-methoxyphenyl)ethyl]- and 5′-[2-(Methoxycarbonyl)-1-(*p*-methoxyphenyl)ethyl]-2′,3′,4,4′,6′-pentamethoxychalcone

Heitaro OBARA,* Jun-ichi ONODERA, Mitsuhiro TSUCHIYA, Hiroyuki MATSUEDA, Shingo SATO, and Shigeru MATSUBA
Department of Materials Science and Engineering, Faculty of Engineering, Yamagata University, Yonezawa 992
(Received July 27, 1990)

Synopsis. 5′-[1-(Methoxycarbonyl)-2-(*p*-methoxyphenyl)-ethyl]- and 5′-[2-(methoxycarbonyl)-1-(*p*-methoxypheny)-ethyl]-2′,3′,4,4′,6′-pentamethoxychalcone were synthesized. The latter compound was completely identical with the methylated derivative of aglycone of safflomin C, a constituent of safflower (*Carthamus tinctorius L*).

Recently, we isolated a yellow pigment, safflomin C, from safflower yellow, the water soluble yellow constituent of safflower (*Carthamus tinctorius L*), and proposed the structure, **1** or **2**, for this new pigment from its spectral data and the behavior of its derivatives.[1,2]

Safflomin C was hydrolyzed with dilute phosphoric acid and methylated with dimethyl sulfate–potassium carbonate in acetone to give the methylated derivative of its aglycone which seems to have the structure **3** or **4**,[1,2] (Scheme 1).

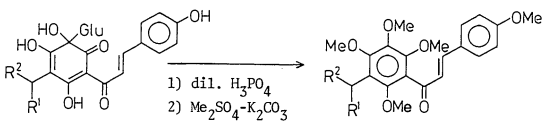

1 R^1=CH_2CO_2H, R^2=C_6H_4OH (*p*) 3 R^1=CO_2Me, R^2=$CH_2C_6H_4OMe$ (*p*)
2 R^1=CO_2H, R^2=$CH_2C_6H_4OH$ (*p*) 4 R^1=CH_2CO_2Me, R^2=C_6H_4OMe (*p*)

Scheme 1.

In this paper, we will report the synthesis of 5′-[1-(methoxycarbonyl)-2-(*p*-methoxyphenyl)ethyl]- and 5′-[2-(methoxycarbonyl)-1-(*p*-methoxyphenyl)ethyl]-2′,3′,4,4′,6′-pentamethoxychalcone (**3** and **4**) and compare these synthetic chalcones with a natural derivative.

First, compound **3** was synthesized by the following method (Scheme 2).

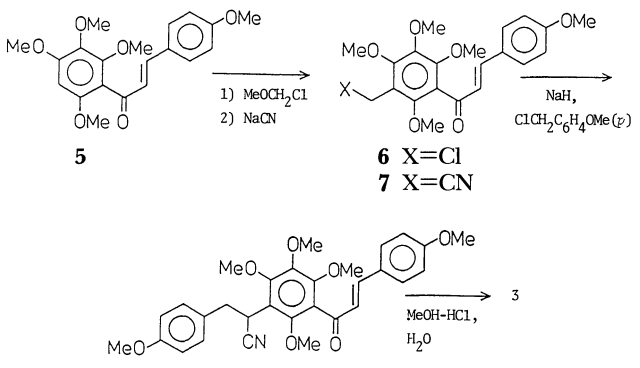

5 6 X=Cl 7 X=CN 8

Scheme 2.

Chloromethylation of 2′,3′,4,4′,6′-pentamethoxychalcone (**5**)[3] with chloromethyl methyl ether in acetic acid gave 5′-chloromethyl-2′,3′,4,4′,6′-pentamethoxychalcone (**6**) in 15% yield. Compound **6** was converted into (cyanomethyl)chalcone (**7**) in 37% yield by treating **6** with sodium cyanide in dimethyl sulfoxide. 5′-[1-Cyano-2-(*p*-methoxyphenyl)ethyl]-2′,3′,4,4′,6′-pentamethoxychalcone (**8**) was obtained by benzylation of **7** with *p*-methoxybenzyl chloride in the presence of sodium hydride in dimethyl sulfoxide in 37% yield. Treatment of **8** with hydrogen chloride in cold methanol followed by the hydrolysis of the resulted imidate hydrochloride gave chalcone **3** in 27% yield.

On the other hand, methoxychalcone **4** was obtained by the following method (Scheme 3).

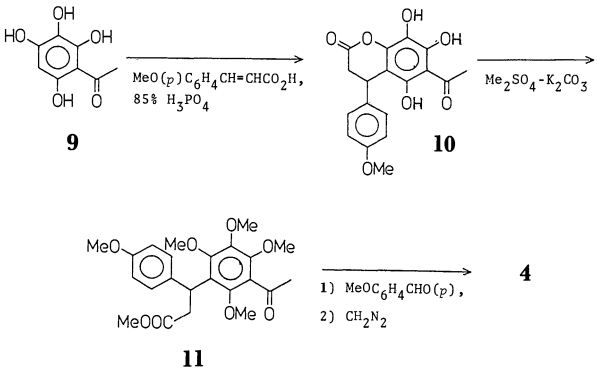

Scheme 3.

5-[2-(Methoxycarbonyl)-1-(*p*-methoxyphenyl)ethyl]-2,3,4,6-tetramethoxyacetophenone (**11**) was obtained by methylation of dihydrocoumarin(**10**) prepared by the Friedel–Crafts reaction of 2,3,4,6-tetrahydroxyacetophenone (**9**) with *p*-methoxycinnamic acid in 85% phosphoric acid in 81% yield.

Condensation of **11** with *p*-methoxybenzaldehyde in the presence of 50% aqueous sodium hydroxide solution in methanol gave 5′-[2-carboxy-1-(*p*-methoxyphenyl)ethyl]-2′,3′,4,4′,6′-pentamethoxychalcone (**12**) which was methylated with diazomethane to give chalcone methyl ester **4** in 90% yield. The IR, ^{1}H- and ^{13}C NMR spectra of **4** were completely identical with those of a natural derivative so that the structure **1** for safflomin C was strongly supported.

Experimental

All the melting points were uncorrected. The IR spectra were recorded by a Hitachi 100-50 spectrometer. The ^{1}H-

and ^{13}C NMR spectra were measured by a Hitachi R-600 and Varian Gemini 200 spectrometer using tetramethylsilane as an internal standard, respectively. The mass spectra were obtained on a Hitachi RMU-6M mass spectrometer.

5′-Chloromethyl-2′,3′,4,4′,6′-pentamethoxychalcone (6). To a solution of 2′,3′,4,4′,6′-pentamethoxychalcone (**5**)[3] (3.0 g) in acetic acid (10 ml) was added dropwise a solution of chloromethyl methyl ether (1.5 g) in acetic acid (2 ml) with stirring under cooling with ice-water. The reaction mixture was allowed to stand for 3 days at room temperature; the mixture then poured into cold water and extracted with ethyl acetate. The extract was chromatographed on silica gel with benzene–ethyl acetate (15:1) to give **6** (0.51 g, 15%) as pale yellow crystals. Mp 82—83 °C, MS *m/z* 407 (M^+), ^1H NMR ($CDCl_3$) δ=3.80 (6H,s), 3.83, 3.92, and 4.01 (each 3H, s), 4.66 (2H, s), 6.83 and 7.34 (each 1H, d, *J*=16.0 Hz), 6.84, and 7.47 (each 2H, d, *J*=8.0 Hz), ^{13}C NMR ($CDCl_3$) δ=35.7 (t), 55.3, 60.7, 61.6, 61.7, and 63.6 (each q), 114.3 (d), 121.0, and 124.6 (each s), 126.0 (d), 127.6 (s) 130.2 (d), 142.7 (s), 145.5 (d), 151.7, 152.6, 153.9, 161.7, and 192.8 (each s). Found: C, 62.08; H, 5.74%. Calcd for $C_{21}H_{23}O_6Cl$: C, 61.99; H, 5.70%.

5′-Cyanomethyl-2′,3′,4,4′,6′-pentamethoxychalcone (7). A mixed solution of **6** (1.0 g) and sodium cyanide (0.13 g) in anhydrous dimethyl sulfoxide (40 ml) was stirred for 1 h at 35 °C. The reaction mixture was poured into cold water (250 ml) and neutralized with 10% hydrochloric acid and extracted with ethyl acetate. The extract was chromatographed on silica gel with benzene–ethyl acetate (10:1) to give **7** (0.36 g, 37%) as pale yellow crystals. Mp 102—103 °C; MS *m/z* 397 (M^+); ^1H NMR ($CDCl_3$) δ=3.63 (2H, s), 3.73, 3.78, 3.83, 3.85, and 4.03 (each 3H, s), 6.79 and 7.31 (each 1H, d, *J*=16.0 Hz), 6.83 and 7.46 (each 2H, d, *J*=8.0 Hz); ^{13}C NMR ($CDCl_3$) δ=12.5 (t), 55.3, 60.8, 61.1, 61.8, and 63.0 (each q), 113.6 (s), 114.4 (d), 118.2, and 124.2 (each s), 125.9 (d), 126.9 (s), 130.3 (d), 142.4 (s), 145.7 (d), 150.7, 151.6, 152.5, 161.8, and 192.6 (each s). Found: C, 66.56; H, 5.86; N, 3.54%. Calcd for $C_{22}H_{23}O_6N$: C, 66.49; H, 5.83; N, 3.52%.

5′-[1-Cyano-2-(*p*-methoxyphenyl)ethyl]-2′,3′,4,4′,6′-pentamethoxychalcone (8). To a reaction mixture of **7** (0.21 g) and sodium hydride (0.018 g) in anhydrous dimethyl sulfoxide (3 ml) was added *p*-methoxybenzyl chloride (0.11 g) in anhydrous dimethyl sulfoxide (1 ml) under cooling with ice-water; the mixture was then stirred for 2 h at room temperature. The reaction mixture was poured into cold dilute hydrochloric acid and extracted with ethyl acetate. The extract was chromatographed on silica gel with benezene–ethyl acetate (15:1) and with petroleum ether–ethyl acetate (4:1) to give **8** (0.092 g, 34%) as pale yellow viscous oil. MS *m/z* 517 (M^+); ^1H NMR ($CDCl_3$) δ=3.09 (1H, dd, *J*=13.4 and 7.3 Hz), 3.33 (1H, dd, *J*=8.2 and 13.4 Hz), 3.61, 3.75, 3.84, 3.85, 3.87, and 4.02 (each 3H, s), 4.34 (1H, dd, *J*=7.3 and 8.2 Hz), 6.87 and 8.27 (each 1H, d, *J*=16.1 Hz), 6.82 and 7.50 (each 2H, d, *J*=8.8 Hz), 6.91 and 7.11 (each 2H, d, *J*=8.8 Hz); ^{13}C NMR ($CDCl_3$) δ=29.5 (d), 38.0 (t), 55.3, 55.4, 60.8, 61.1, 61.9, and 63.0 (each q), 114.0 and 114.5 (each d), 118.1, 121.1, and 123.9 (each s), 126.0 (d), 127.1, and 129.6 (each s), 130.2 and 130.4 (each d), 142.6 (s), 145.9 (d), 150.9, 151.8, 153.3, 158.8, 162.0, and 193.1 (each s). Found: C, 69.38; H, 6.18; N, 2.55%. Calcd for $C_{30}H_{31}O_7N$: C, 69.63; H, 5.99; N, 2.71%.

5′-[1-(Methoxycarbonyl)-2-(*p*-methoxyphenyl)ethyl]-2′,3′,4,4′,6′-pentamethoxychalcone (3). To a solution of **8** (34 mg) in anhydrous methanol (10 ml), dry hydrogen chloride gas was passed under cooling with an ice-salt bath. The reaction mixture was allowed to stand for 3 days in a refrigerator; the solvent was then evaporated in vacuo. To the resulting residue was added dilute hydrochloric acid (10 ml) and allowed to stand overnight at room temperature and extracted with ethyl acetate. The extract was chromatographed on silica gel with benzene–ethyl acetate (10:1) to give **3** (10 mg, 28%) as pale yellow viscous oil. MS *m/z* 550 (M^+); ^1H NMR ($CDCl_3$) δ=3.03 (1H, dd, *J*=13.8 and 9.0 Hz), 3.45 (1H, dd, *J*=6.2 and 13.8 Hz), 3.50 (3H, s), 3.69 (6H, s), 3.79 (3H, s), 3.83 (6H, s), 3.85 (3H, s), 4.21 (1H, dd, *J*=6.2 and 9.0 Hz); 6.72 and 7.00 (each 2H, d, *J*=8.5 Hz), 6.81and 7.18 (each 1H, d, *J*=16.0 Hz), 6.91 and 7.46 (each 2H, d, *J*=8.8 Hz); ^{13}C NMR ($CDCl_3$) δ=35.9 (t), 43.3 (d), 51.8, 55.1, 55.4, 60.5, 60.7, 61.9, and 62.6 (each q), 113.4 and 114.4 (each d), 122.4 and 123.6 (each s), 126.2 (d), 127.2 (s), 130.2 and 130.4 (each d), 132.1 and 142.3 (each s), 145.8 (d), 150.5, 151.1, 153.1, 157.9, 161.8, 174.0, and 195.8 (each s). Found: C, 67.38; H, 6.05%. Calcd for $C_{31}H_{34}O_9$: C, 67.62; H, 6.22%.

6-Acetyl-3,4-dihydro-5,7,8-trihydroxy-4-(*p*-methoxyphenyl)-coumarin (10). A mixed solution of 2,3,4,6-tetrahydroxyacetophenone (**9**)[4] (1.84 g) and *p*-methoxycinnamic acid (1.78 g) in 85% phosphoric acid (60 ml) was stirred for 4 days at room temperature. The reaction mixture was poured into 5% hydrochloric acid and extracted with ethyl acetate. The ethyl acetate layer was washed with water and dried over anhydrous sodium sulfate and evaporated to give **10** (2.8 g, 81%) as pale yellow crystals. Mp 185—186 °C; MS *m/z* 344 (M^+); ^1H NMR ($CDCl_3$–DMSO-d_6) δ=2.78 (3H, s), 3.04 (2H, d, *J*=4.8 Hz), 3.77 (3H, s), 4.65 (1H, t, *J*=4.8 Hz), 6.80 (2H, d, *J*=8.0 Hz), 7.10 (2H, d, *J*=8.0 Hz), 13.58 (1H, s); ^{13}C NMR (DMSO-d_6) δ=32.5 and 33.0 (each q), 36.4 (t), 54.9 (d), 103.4 and 104.9 (each s), 113.9 and 127.5 (each d), 128.5, 132.9, 145.8, 149.1, 151.6, 157.9, 166.5, and 202.3 (each s). Found: C, 62.63; H, 4.61%. Calcd for $C_{18}H_{16}O_7$: C, 62.79; H, 4.68%.

5-[2-(Methoxycarbonyl)-1-(*p*-methoxyphenyl)ethyl]-2,3,4,6-tetramethoxyacetophenone (11). A mixed solution of **10** (1.72 g), dimethyl sulfate (12.0 g), and potassium carbonate (21.0 g) in acetone containing a small amount of water was refluxed for 30 h. The reaction mixture was filtered; the filtrate was evaporated in vacuo and the residue was poured into water (90 ml) and stirred for 6 h at room temperature and extracted with ethyl acetate. The ethyl acetate layer was washed with 10% aqueous sodium carbonate solution and with water, dried over anhydrous sodium sulfate, and then evaporated in vacuo. The residue was chromatographed on silica gel with benzene–ethyl acetate (10:1) to give **11** (1.19 g, 55%) as pale yellow viscous oil. MS *m/z* 432 (M+); ^1H NMR ($CDCl_3$) δ=2.51 (3H, s), 3.26 (2H, d, *J*=8.0 Hz), 3.58 (3H, s), 3.61 (6H, s), 3.76, 3.82, and 3.86 (each 3H, s), 4.99 (1H, t, *J*=8.0 Hz), 6.80 and 7.21 (each 2H, d, *J*=9.0 Hz); ^{13}C NMR ($CDCl_3$) δ=32.5 and 36.2 (each q), 37.8 (t), 51.5 (q), 55.2 (d), 60.5, 61.8, and 63.2 (each q), 75.3 and 77.3 (each s), 113.5 (d), 127.0 (s), 128.3 (d), 128.6, 135.2, 150.3, 153.6, 157.7, 172.9, and 201.5 (each s). Found: C, 64.06; H, 6.64%. Calcd for $C_{23}H_{28}O_8$: C, 63.88; H, 6.53%.

5′-[2-(Methoxycarbonyl)-1-(*p*-methoxyphenyl)ethyl]-2′,3′,4,4′,6′-pentamethoxychalcone (4). To a mixed solution of **11** (2.4 g) and *p*-anisaldehyde (0.78 g) in methanol (11 ml) was added 50% aqueous sodium hydroxide solution (4.8 g) and the mixed solution was allowed to stand for 4 days at room temperature. The reaction mixture was poured into 6 M (M=mol dm^{-3}) hydrochloric acid and extracted with ethyl acetate. The ethyl acetate layer was washed with water and dried over anhydrous sodium sulfate. The ethyl acetate was evaporated in vacuo to give 5′-[2-carboxy-1-(*p*-methoxyphenyl)ethyl]-2′,3′,4,4′,6′-pentamethoxychalcone (**12**) (2.62 g, 90%) as pale yellow crystals. Mp 134—135 °C; MS *m/z* 536 (M^+); IR (KBr) ν 3450 (br.), 1705, 1624, and 1600 cm^{-1}; ^1H NMR ($CDCl_3$) δ=3.25 (2H, m), 3.48, 3.67, and 3.77 (each 3H, s), 3.82, (9H, s), 5.06 (1H, t, *J*=6.0 Hz), 6.80 and 7.52 (each 2H, d, *J*=8.5 Hz), 6.85 and 7.34 (each 1H, d, *J*=16.0 Hz), 6.90 and 7.23 (each 2H, d, *J*=8.0 Hz). To a solution of **12** in ether was added a solution of diazomethane in ether with stirring at room temperature. By evaporating

ether in vacuo **4** was obtained as pale yellow viscous oil in quantitative yield. MS *m/z* 550 (M^+); IR (CCl_4) ν 1740, 1645, and 1600 cm^{-1}; ^1H NMR ($CDCl_3$) δ=3,24 (2H, m), 3.52, 3.62, 3.66, 3.77, 3.83, 3.84, and 3.85 (each 3H, s), 5.02 (1H, t, J=7.9 Hz), 6.83 and 6.90 (each 2H, d, J=9.0 Hz), 6.89 and 7.32 (each 1H, d, J=16.2 Hz), 7.22 and 7.51 (each 2H, d, J=8.5 Hz); ^{13}C NMR ($CDCl_3$) δ=36.3 (d), 37.8 (t), 51.8, 55.4, 55.6, 60.8, 62.0, and 63.1 (each q), 113.8 and 114.7 (each d), 124.6 (s), 126.4 (d), 127.1 and 127.7 (each s), 128.7 and 130.8 (each d), 132.8 and 135.8 (each s), 143.4 (d), 146.5, 150.6, 151.6, 154.1, 158.3, 162.3, 173.7, and 194.7 (each s). Found: C, 67.50; H, 6.09%. Calcd for $C_{31}H_{34}O_9$: C, 67.62; H, 6.22%.

The IR, ^1H-, and ^{13}C NMR spectra of this compound were completely identical with those of natural derivative **4**.

The authors express their thanks to Dr. Masanobu Suzuki of Nippon Kayaku Co., Ltd., for the measurement of ^1H- and ^{13}C NMR spectra. We are also grateful to Mr. Kazuaki Sato for elemental analyses.

References

1) J. Onodera, N. Yokoyama, and H. Obara, The 25th Symposium on the Chemistry of Natural Products, 1982, Symposium papers, pp. 368—373.

2) J. Onodera, H. Obara, R. Hirose, S. Matsuba, N. Sato, S. Sato, and M. Suzuki, *Chem. Lett.*, **1989**, 1571.

3) C. Kuroda, *Nippon Kagaku Zasshi*, **51**, 237 (1930).

4) H. Obara, J. Onodera, Y. Kurihara, and F. Yamamoto, *Bull. Chem. Soc. Jpn.*, **51**, 3627 (1978).

Oxidation of Primary Alcohols over Hydrous Zirconium(IV) Oxide

Hideyuki KUNO,* Makoto SHIBAGAKI, Kyoko TAKAHASHI, and Hajime MATSUSHITA
Life Science Research Laboratory, Japan Tobacco Inc., 6-2 Umegaoka, Midori-ku, Yokohama, Kanagawa 227
(Received July 31, 1990)

Synopsis. The oxidation of primary alcohols with quinone or benzophenone was carried out by catalysis with hydrous zirconium(IV) oxide in both batch and flow reaction systems. As a result, it was elucidated that a lot of primary alcohols can be efficiently oxidized over hydrous zirconium(IV) oxide.

In the oxidation of alcohols with carbonyl compounds by catalysis with metal alkoxide, which is known as an Oppenauer-type oxidation, it has been difficult to apply primary alcohols as the reactants. This is because an aldol condensation easily occurs between an aldehyde of the product and a carbonyl compound of the hydrogen acceptor. Recently, the oxidation of some primary alcohols was reported to proceed efficiently using bis(cyclopentadienyl)zirconium(IV) dihydride as a complex catalyst.[1] However, the oxidation of the primary alcohol over a solid catalyst has never been achieved.

In a previous paper,[2] we reported that the Oppenauer-type oxidation of secondary alcohols with ketones proceeded efficiently over hydrous zirconium(IV) oxide. Several ketones, for example, acetone, diethyl ketone, and cyclohexanone, could be used as a hydrogen acceptor. However, primary alcohols were not efficiently converted to the corresponding aldehydes. As reported in our previous paper,[3] the ability of primary alcohols to provide a hydrogen donor is less than that of secondary alcohols. Further, the aldehydes produced from primary alcohols were easily condensed with ketones when the ketones which have a hydrogen atom at the α-position of the carbonyl group were used as the hydrogen acceptor. Thus, compounds which could not undergo the aldol condensation were used as the hydrogen acceptor for the oxidation.

In this paper we report that the Oppenauer oxidation of primary alcohols proceeds efficiently using *p*-benzoquinone or benzophenone as the hydrogen acceptor over hydrous zirconium(IV) oxide. The Oppenauer oxidation is the best method for the preparation of aldehydes from primary alcohols, since further oxidation of the aldehydes does not theoretically occur. Furthermore, the following advantages are expected in our method; (1) easy product isolation, (2) a lack of the need to maintain water-free conditions, (3) reusability of the catalyst, and (4) durability of the catalytic activity. These oxidations could be carried out in both batch and flow reaction systems.

Experimental

Catalyst and Materials. Hydrous zirconium(IV) oxide was prepared in the manner described in a previous paper.[3] The calcination of the catalyst was performed at 300°C for 5 h. Comercial reagents were used for the reaction without any further purification.

General Procedure in the Batch Reaction System. The following were placed in a 20 cm^3 round-bottomed flask equipped with a reflux condenser: hydrous zirconium oxide (24—60 mesh; 0.1 or 0.3 g), an alcohol (0.1 or 0.25 mmol), a ketone (20 mmol) or *p*-benzoquinone (1.5 mmol), and a hydrocarbon as an internal standard. The contents were then heated under gentle reflux. The reaction mixture was collected at an appropriate time after refluxing, and the products were analyzed by GLC (a capillary column PEG 20 M 30 m or OV101 30 m) and GC-MS (Shimadzu QP1000).

General Procedure in the Flow Reaction System. Catalytic oxidation was carried out in a glass-flow reactor (6.5 mm in diameter) with a fixed-bed catalyst: flow rate of nitrogen=60 $cm^3\ min^{-1}$; catalyst=1.5—2.0 g, 24—60 mesh; reaction temperature=200°C; A xylene solution (10 mmol cm^{-3}) of an alcohol, a ketone (2 mol cm^{-3}), and a hydrocarbon as an internal standard was fed into the reactor (5 $cm^3\ h^{-1}$) by means of a microfeeder. The yields of the products were analyzed in a similar manner to that described above after a steady state condition had been reached.

Results and Discussion

Oxidation of Alcohols with *p*-Benzoquinone. By using *p*-benzoquinone as the hydrogen acceptor, oxida-

Table 1. Oxidation of Primary Alcohols with *p*-Benzoquinone in the Batch Reaction System[a)]

Reactant	Time/h	Yield/%
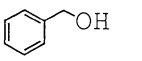	4.0	85.8
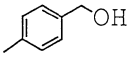	4.0	31.4
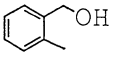	4.0	35.9
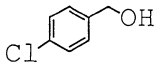	4.0	47.8
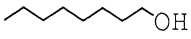	4.0	29.7
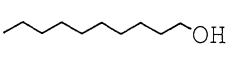	4.0	9.8
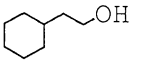	8.0	46.2
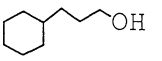	8.0	27.9
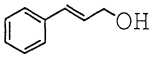	4.0	46.8

a) Catalyst: 0.3 g, alcohol: 0.25 mmol, *p*-benzoquinone: 1.5 mmol, xylene: 10 cm^3, reflux temperature.

Table 2. Oxidation of Primary Alcohols with Benzophenone in the Batch Reaction System[a)]

Reactant	Time/h	Yield/%
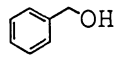	2.0	81.0
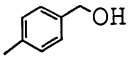	4.0	65.4
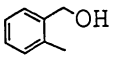	4.0	63.3
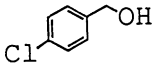	4.0	45.8
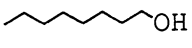	2.0	35.4
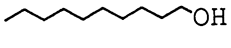	2.0	10.3
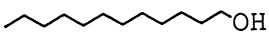	2.0	6.4
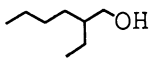	2.0	25.5
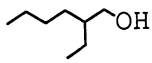	8.0	50.9
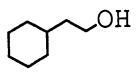	8.0	46.2
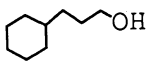	8.0	27.9
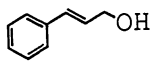	4.0	46.8

a) Catalyst: 0.1 g, alcohol: 0.1 mmol, benzophenone: 20 mmol, xylene: 10 cm^3, reflux temperature.

Table 3. Oxidation of Primary Alcohols with Benzophenone in the Flow Reaction System[a)]

Reactant	Catalyst/g	Yield/%
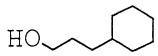	1.5	63.3
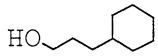	2.0	48.7
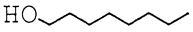	1.5	62.4
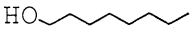	2.0	74.3
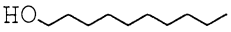	1.5	50.0
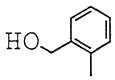	2.0	69.0

Alcohol: 0.05 mmol h^{-1}, benzophenone: 10 mmol h^{-1}, xylene: 5 cm^3 h^{-1}, temperature: 200 °C.

tion of the alcohols was carried out in the batch reaction system. The results are listed in Table 1. Benzyl alcohol was efficiently oxidized to give benzaldehyde in high yield; most of the alcohols were converted to the corresponding aldehydes without aldol condensations, even though the yields were relatively low. The low reactivity in these systems can be explained as being due to the catalyst being inactivated by the strong adsorption of *p*-benzoquinone.

Oxidation of Alcohols with Several Ketones. The oxidation of benzyl alcohol and 1-octanol with several ketones was carried out in the batch reaction system. In the case of acetone, both benzyl alcohol and 1-octanol could not be converted to the corresponding aldehyde. The aldol condensation of the compound produced from the primary alcohol occured with acetone. Since the oxidizing ability of diisopropyl ketone is much smaller than that of acetone,[2)] the oxidation of the primary alcohol does not occur. Compared with these ketones, benzophenone has a high ability for oxidizing the alcohols and resisting aldol condensation. Accordingly, it was elucidated that benzophenone is the best hydrogen acceptor for the oxidation of the primary alcohol among these ketones.

Oxidation of Alcohols with Benzophenone in the Batch Reaction System. All of the alcohols could be oxidized in this system, as shown in Table 2. These yields were almost the same as those when using *p*-benzoquinone as the hydrogen acceptor. Compared with benzyl alcohol and its derivative, the other alcohols were never efficiently convereted to the corresponding aldehydes. The Oppenauer oxidation was believed to proceed via a hydride transfer from the alcohol to ketone, and the reactivity of alcohol was affected by the electron density of the hydrogen on the α-carbon of the hydroxyl group. Compared with aliphatic alcohols, the derivertives of benzyl alcohol had a high ability to provide a hydrogen donor, because of a π-electron donation from the phenyl group.

Oxidation of Alcohols with Benzophenone in the Flow Reaction System. The results of the oxidation of primary alcohols in the flow reaction system are listed in Table 3. Most of the alcohols were efficiently converted to the coresonding aldehydes. In particular, it was noteworthy that the aliphatic alcohols were efficiently oxidized in comparison with the batch reaction system.

In conclusion, it was elucidated that the oxidation of primary alcohols with benzophenone in a flow reaction system proceeds efficiently by catalysis with hydrous zirconium(IV) oxide.

References

1) Y. Ishii, T. Nakano, A. Inada, Y. Kishigami, K. Sakurai, and M. Ogawa, *J. Org. Chem.*, **51**, 240 (1986).

2) H. Kuno, K. Takahashi, M. Shibagaki, and H. Matsushita, *Bull. Chem. Soc. Jpn.*, **63**, 1943 (1990).

3) M. Shibagaki, K. Takahashi, and H. Matsushita, *Bull. Chem. Soc. Jpn.*, **61**, 3283 (1988).

Synthesis and Reaction of Triaminosulfoxonium Salts

Kentaro OKUMA,* Hiroshi TAKEUCHI, Hiroshi OHTA, Haruo MATSUYAMA,†
Nobumasa KAMIGATA,† and Michio KOBAYASHI†
Department of Chemistry, Faculty of Science, Fukuoka University,
Jonan-ku, Fukuoka 814-01
†Department of Chemistry, Faculty of Science, Tokyo Metropolitan University,
Setagaya-ku, Tokyo 158
(Received August 2, 1990)

Synopsis. Triaminosulfoxonium salts were synthesized by the oxidation of triaminosulfonium salts with sodium perbenzoate. The reaction of these salts with nucleophiles was carried out.

Heteroatom substituted sulfoxonium salts are interesting compounds for their anomalous reactivity.[1] Monoaminosulfoxonium salts were prepared by Johnson and Schroek, which acted as good methylene transfer agents.[2] Previously, we synthesized diaminosulfoxonium salts and examined their reactivities.[3] However, to our knowledge, there is no report on the synthesis of triaminosulfoxonium salts (CA Index name; (triamide)-oxosulfur(1+) salts). Recently, we proposed an excellent method for the preparation of sulfoxonium salts from the corresponding sulfonium salts.[4] We also described the general synthesis of triaminosulfonium salts (**1**) by the reaction of thiobisamines with *N*-chlorobenzotriazole followed by the addition of secondary amines.[5] These findings prompted us to investigate the direct formation of triaminosulfoxonium salts (**2**) from **1** by oxidation reaction. In this paper, we would like to report a convenient synthesis of **2**.

Results and Discussion

Triaminosulfonium salts were prepared from 4,4′-thiodimorpholine with *N*-chlorobenzotriazole followed by the addition of secondary amines as mentioned before.[5] Treatment of trimorpholinosulfonium chlorides (CA Index name; tris(morpholino-N⁴)sulfur(1+) chloride) with 3 equiv of sodium perbenzoate in water afforded a pale yellow solution of trimorpholinosulfoxonium chloride (**2a**). Other triaminosulfonium chlorides (**1b—f**) were also oxidized under similar conditions. The triaminosulfoxonium chlorides obtained from **1b—f** were very hygroscopic, which were, therefore, isolated by transferring into the corresponding tetraphenylborates (**2b—f**). These results are summarized in Table 1. When equal amount of sodium perbenzoate was used, only 30 % of **1** were oxidized. Generally, more than 3 equiv of perbenzoate was required for improving the yields of **2**. However, dimethylaminodimorpholinosulfonium chloride (**1g**) could not be oxidized under these conditions. Even if 10 equiv of sodium perbenzoate was used, **1g** could not be oxidized. It is interesting that relatively hindered sulfonium salts (**1a**, **1b**, and **1e**) could be easily oxidized under these conditions.

The ^{1}H NMR spectra of **2** clearly show that sulfur bears a high degree of positive charge which significantly deshields the *N*-methylene protons, thereby shifting the signals downfield to 3.5 ppm around. The *N*-methylene protons of ethyldimorpholinosulfonium tetrafluoroborate were observed at 3.2 ppm.[6] The downfield shift of *N*-methylene protons is characteristic of triaminosulfoxonium salts compared to triaminosulfonium salts. The ^{13}C NMR spectrum of **2c** also shows that the *N*-methylene carbons are shifted to downfields (**1c**; 46.4 and 49.3 ppm→**2c**; 46.9 and 49.8 ppm).

Previously, Noyori and co-workers reported the formation and reaction of tris(diethylamino)sulfonium difluorotrimethylsiliconate with enol silyl ethers to give the corresponding sulfonium enolates and which

Table 1. Preparation of Aminodimorpholinosulfoxonium Salts (**2**)

Aminodimorpholinosulfonium Salt **1**		Aminodimorpholinosulfoxonium Salt **2**			
		2	Yield/%	X^-	Mp/°C
1a	R,R=$-CH_2CH_2OCH_2CH_2-$	**2a**	63	Cl	91—93
1b	R,R=$-CH_2(CH_2)_3CH_2-$	**2b**	66	BPh_4	212—213
1c	R,R=$-CH_2(CH_2)_2CH_2-$	**2c**	58	BPh_4	196—197
1d	R,R=Et	**2d**	54	BPh_4	185—186
1e	R,R=$(CH_3)_2CH-$	**2e**	58	BPh_4	185—187

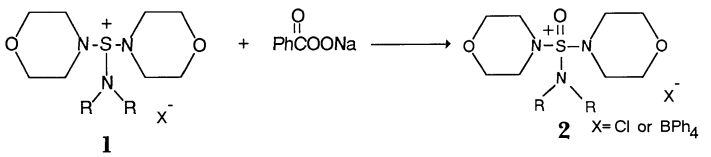

1 **2**

Scheme 1.

Table 2. NMR Methylene Signals of Salts **1** and **2**

	Sulfonium Salt **1**				Sulfoxonium Salt **2**		
	Solvent	N-CH_2	O-CH_2		Solvent	N-CH_2	O-CH_2
1a	D_2O	3.16—3.42	3.63—3.90	**2a**	D_2O	3.37—3.61	3.67—3.88
1a	CD_3COCD_3	3.25—3.49	3.63—3.90	**2a**	CD_3COCD_3	3.60—3.80	3.80—4.00
1a	CD_3SOCD_3	3.20—3.49	3.60—3.87	**2a**	CD_3SOCD_3	3.48—3.55	3.73—3.80
1b	CD_3SOCD_3	3.13—3.35	3.65—3.74	**2b**	CD_3SOCD_3	3.45—3.54	3.72—3.80
1c	CD_3SOCD_3	3.20—3.44	3.62—3.74	**2c**	CD_3SOCD_3	3.50—3.58	3.70—3.77
1d	CD_3SOCD_3	3.10—3.23	3.66—3.78	**2d**	CD_3SOCD_3	3.40—3.52	3.67—3.80

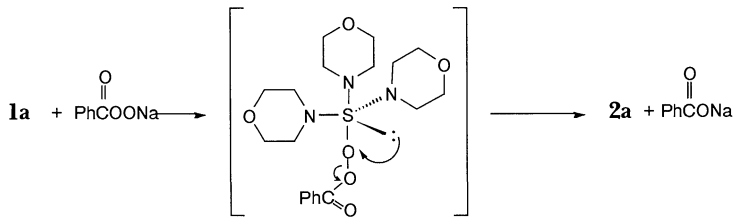

Scheme 2.

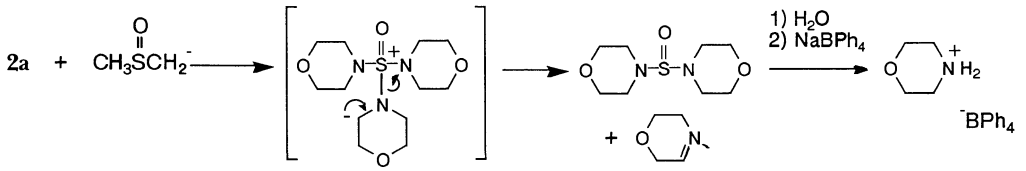

Scheme 3.

did not form covalent sulfuranes.[7] In contrast to their results, we found that triaminosulfonium salts were easily oxidized by attack of the perbenzoate anion. The difference in the reactivity might be owing to the leaving ability of the benzoate anion. The oxidation of sulfonium salt with sodium perbenzoate in aqueous solution may proceed via an S-O sulfurane intermediate to afford a sulfoxonium salt by nucleophilic attack of perbenzoate anion on the cationic sulfur atom of the sulfonium salt as show in Sheme 2.

Then, we studied the reactivity of these sulfoxonium salts. We first tried the reaction of sulfoxonium chloride **2a** with 1-cyclohexenyl silyl ether in THF. However, no reaction was observed and **2a** was recovered almost quantitatively. The reaction of **2a** with other nucleophiles such as butyllithium (room temperature), sodium phenoxide (60 °C), and CH_3SOCH_2Na (120 °C) also gave the same results. We then compared the reactivity of sulfoxonium salts with those of sulfonium salts. The reaction of **1a** with CH_3SOCH_2Na at 100 °C recovered the starting salts in 85% yield. A similar result was obtained by use of **2a**. However, treatment of **2a** with CH_3SOCH_2Na followed by the addition of sodium tetraphenylborate at 150 °C gave morpholinium tetraphenylborate in 66% yield. The reaction is accounted for by the abstraction of α-proton of morpholino group with CH_3SOCH_2Na to afford 5,6-dihydro-2*H*-1,4-oxazine and 4,4′-sulfinyldimorpholine which degradates into morpholinium salt as shown in scheme 3. A similar result is reported by Richards and Tarbel in the reaction of ethyldimorpholinosulfonium salt with butyllithium.[6]

Another heteroatom-substituted sulfoxonium salts, aryloxysulfoxonium salts, have different reactivity toward nucleophiles. Whiting reported that the reaction of aminodiaryloxysulfoxonium salts with primary amines afforded the corresponding sulfoximides in good yields.[8] Still also reported that aryloxydimethylsulfoxonium salts reacted with $NaBH_4$ to afford dimethyl sulfoxide.[9] We also tried the reaction of **2a** with $NaBH_4$ in methanol. However, starting **2a** was recovered almost quantitatively. Thus, triaminosulfoxonium salts were found to react only under drastic conditions as mentioned above and to be quite stable compounds.

In conclusion, triaminosulfoxonium salts were prepared by oxidation of corresponding triaminosulfonium salts. These salts are very stable toward nucleophiles.

Experimental

Melting points were determined on a Shibata-Büchi Model 510 and uncorrected. ^1H NMR spectra were measured on a JEOL PMX 60 spectrometer using TMS as internal standard.

Preparation of Trimorpholinosulfoxonium Chloride (2a). To a solution of sodium perbenzoate (4.8 g, 30 mmol) in water (50 cm^3) was added a solution of trimorpholinosulfonium chloride (**1a**) (3.3 g, 10 mm ol) in water (25 cm^3) at room temperature. After stirring for 12 h, the resulting

suspension was filtered off. The water of filtrate was evaporated to give pale yellow crystals, which were recrystallized from methanol to give trimorpholinosulfoxonium chloride (**2a**) (1.9 g, 5.6 mmol) in 56% yield; mp 91—93 °C. Elemental analysis was carried out after converting this chloride salt into the corresponding tetraphenylborate salt. Anal. Calcd for $C_{36}H_{44}BN_3O_4S$: C, 69.11; H, 7.09; N, 6.71%. Found: C, 68.68; H, 7.14; N, 6.52%.

Preparation of 2b. To a solution of sodium perbenzoate (4.8 g, 30 mmol) in water (50 ml) was added a solution of dimorpholinopiperidinosulfonium chloride (3.3 g, 10 mmol) in water (25 cm^3) at room temperature. After stirring for 12 h, the resulting suspension was filtered off. To this filtrate was added a solution of sodium tetraphenylborate (3.4 g, 10 mmol) in water (25 cm^3). Immediately, colorless fine crystals of **2b** were precipitated. Crude **2b** was collected by filtration and recrystallized from methanol to give colorless crystals (4.2 g, 6.6 mmol, 66%); Anal. Calcd for $C_{37}H_{46}BN_3O_3S$: C, 71.26; H, 7.43; N, 6.77%. Found: C, 71.75; H, 7.01; N, 6.95%.

Compounds **2c**, **2d**, and **2e** were prepared in a similar manner.

2c; (3.5 g, 5.8 mmol, 58%); Anal. Calcd for $C_{36}H_{44}BN_3O_3S$: C, 70.93; H, 7.27; N, 6.89%. Found: C; 70.63; H, 7.51; N, 6.59%.

2d; (3.4 g, 5.4 mmol, 54%); mp 207—208 °C; Anal. Calcd for $C_{36}H_{44}BN_4O_3S$: C, 69.33; H, 7.11%. Found: C, 69.47; H, 7.28%.

2e; (3.8 g, 5.8 mmol, 58%); mp 228—229 °C; Anal. Calcd for $C_{38}H_{52}BN_3O_4S$: C, 69.39; H, 7.97; N, 6.39%. Found: C, 69.05; H, 7.65; N, 6.62%.

Reaction of Trimorpholinosulfonium Chloride (1a) with CH_3SOCH_2Na. Sodium hydride (0.50 g, 5.3 mmol, 50% dispersion) was washed with dry hexane (10 cm^3) for three times. Dimethyl sulfoxide (10 cm^3) was added at 60 °C for 1 h and trimorpholinosulfonium chloride (**1a**) (1.6 g, 5 mmol) was added in one portion to this solution. After stirring at 160 °C for 16 h, the reaction mixture was poured into water (100 cm^3) and a solution of sodium tetraphenylborate (1.7 g, 5 mmol) was added to this solution. Pale yellow crystals were precipitated and collected by filtration. Recrystallization from MeOH/ether afforded colorless crystals of morpholinium salts (1.2 g, 3 mmol, 60%); mp 159—161 °C.

Reaction of Trimorpholinosulfoxonium Chloride (2a) with CH_3SOCH_2Na. Sodium hydride (0.50 g, 5.3 mmol, 50% dispersion) was washed with dry hexane (10 cm^3) for three times. Dimethyl sulfoxide (10 cm^3) was added and warmed up to 60 °C for 1 h. Trimorpholinosulfoxonium chloride (**2a**) (1.7 g, 5 mmol) was added in one portion to this solution. After stirring at 150 °C for 16 h, the reaction mixture was poured into water (100 cm^3) and a solution of sodium tetraphenylborate (1.7 g, 5 mmol) was added to this solution. Pale yellow crystals were precipitated and collected by filtration. Recrystallization from MeOH/ether afforded colorless crystals of morpholinium salts (1.3 g, 3.3 mmol, 66%); mp 159—161 °C.

References

1) G. R. Chalkley, D. J. Snodin, G. Stevens, and M. C. Whiting, *J. Chem. Soc., Perkin Trans. 1*, **1978**, 1580. J. Casanova and R. A. Loewe, *J. Org. Chem.*, **36**, 2891 (1971). For a review, see "The Chemistry of the Sulphonium Group," ed by C. J. M. Stirring, Wiley, New York (1981), Chap. 15.

2) C. R. Johnson and C. W. Schroek, *J. Am. Chem. Soc.*, **95**, 7418 and 7424 (1973).

3) K. Okuma, N. Higuchi, H. Ohta, and M. Kobayashi, *Chem. Lett.*, **1980**, 1503. K. Okuma, N. Higuchi, S. Kaji, H. Takeuchi, H. Ohta, H. Matsuyama, N. Kamigata, and M. Kobayashi, *Bull. Chem. Soc. Jpn.*, **63**, 3223 (1990).

4) M. Mori, H. Takeuchi, H. Minato, M. Kobayashi, M. Yoshida, H. Matsuyama, and N. Kamigata, *Phosphorus Sulfur*, **47**, 157 (1990).

5) H. Minato, K. Okuma, and M. Kobayashi, *J. Chem. Soc., Chem. Commun.*, **1975**, 868. H. Minato, K. Okuma, and M. Kobayashi, *J. Org. Chem.*, **43**, 652 (1978).

6) J. L. Richards and D. S. Tarbell, *J. Org Chem.*, **35**, 2079 (1970).

7) R. Noyori, I. Nishida, J. Sakata, and M. Nishizawa, *J. Am. Chem. Soc.*, **102**, 1223 (1980). R. Noyori, I. Nishida, and J. Sakata, *ibid.*, **105**, 1598 (1983).

8) G. R. Chalkley, D. J. Snodin, G. Stevens, and M. C. Whiting, *J. Chem. Soc., Chem. Commun.*, **1970**, 682. *idem.*, *J. Chem. Soc., Perkin Trans. 1*, **1978**, 1580.

9) I. W. J. Still and S. Szilagyi, *Synth. Commun.*, **9**, 923 (1979). I. W. J. Still and F. J. Ablenas, *J. Org. Chem.*, **48**, 1617 (1983).

O-Ethoxycarbonyl Hydroximoyl Chloride as Nitrile Oxide Precursor

Tomio SHIMIZU,* Yoshiyuki HAYASHI, Nobuhiro FURUKAWA, and Kazuhiro TERAMURA
Department of Chemistry and Materials Technology, Faculty of Engineering and Design,
Kyoto Institute of Technology, Matsugasaki, Sakyo-ku, Kyoto 606
(Received August 20, 1990)

Synopsis. *O*-Ethoxycarbonyl hydroximoyl chloride serves as a stable precursor for nitrile oxide and is converted into the 1, 3-dipole when heated under reflux in pyridine.

2-Isoxazoline and isoxazole derivatives show various biological activities,[1] and are often found in natural products.[2] They are synthetically versatile heterocycles since they are readily converted into γ-amino alcohols and β-hydroxy ketones by reductive cleavage of the ring.[3,4] The most general synthetic approach to these heterocycles is the cycloaddition of olefins or acetylenes with nitrile oxides which have been generated by a variety of methods.[5,6] Of these the most widely used method is the dehydrochlorination of hydroximoyl chloride with base. Recently, an *O*-substituted hydroximoyl chloride has been employed as nitrile oxide precursor, i. e., *O*-(trimethylsilyl)acetohydroximoyl chloride (**1**) undergoes the thermolysis in refluxing toluene to generate acetonitrile oxide.[7]

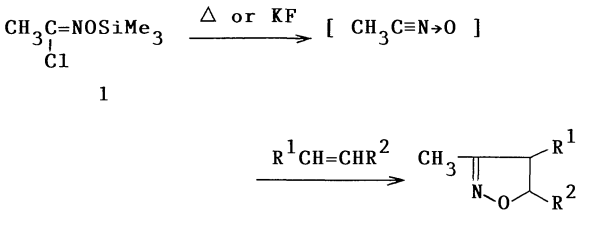

We report here a unique method for the generation of benzonitrile oxide from *O*-ethoxycarbonyl hydroximoyl chloride, *O*-ethoxycarbonylbenzohydroximoyl chloride (**2**), that can be prepared in high yield (81%) by the reaction of (nitromethyl)benzene with ethyl chloroformate in the presence of triethylamine.[8]

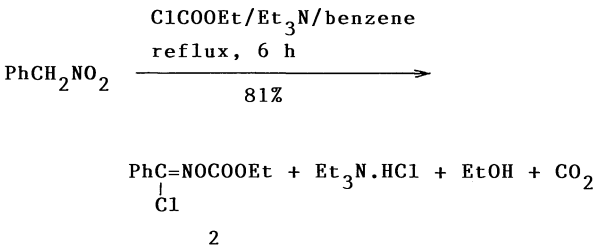

Results and Discussion

The thermal decomposition of **2** was carried out in pyridine at the refluxing temperature for 3 h in the presence of olefin. 2-Isoxazolines (**6a—i**) were isolated from the reaction mixture in good yields as shown in Table 1. During the reaction, evolution of carbon dioxide and ethyl chloride was observed. From these evidences, a probable mechanism of the formation of the cycloadducts may be as follows (see Scheme 1); i) the formation of pyridinium chloride (**3**), ii) the nucleophilic substitution at the carbon atom of carbonate group by chloride ion giving the betaine (**4**), iii) the generation of benzonitrile oxide (**5**) and pyridine in an equiliblium with **4**, and iv) 1,3-dipolar cycloaddition reaction of the nitrile oxide with olefins would give 2-isoxazolines (**6**). This mechanism is in accoord with that reported on the generation of nitrile oxides by the reaction of *O*-unsubstituted hydroximoyl chloride with tertiary amines.[14] It is known that **4** attains an equiliblium with **5** and pyridine.[15]

It is known that ethyl chloroformate decomposes to carbon dioxide and ethyl chloride on refluxing in pyridine.[16] Trapping of carbon dioxode and ethyl chloride in our reaction suggests the formation of ethyl chloroformate.

Another mechanism involving direct formation of **5** from **3** by E2 type elimination shown below would also be supposed.

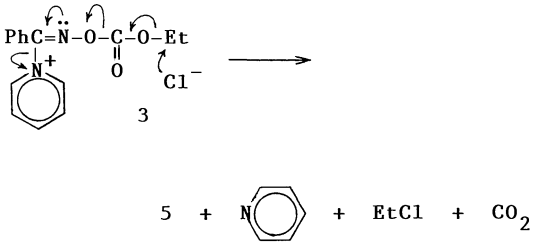

We also investigated the reaction of **2** with pyridine in the absence of dipolarophile and obtained ethyl *N*-phenylcarbamate and benzonitrile in 17% and 20% yields, respectively. These yields were not so varied when the reaction was carried out in the presence of a small amont of water or ethanol. The formation of benzonitrile may be ascribed to the thermal fragmentation[17] of 3,6-diphenyl-1,4,2,5-dioxadiazine (**7**) from (**3**+**3**) head-to-tail dimerization[18] in the presence of pyridine. Although we have no definite evidences for a plausible mechanism of the formation of the carbamate, Beckmann rearrangement of **2** may be involved in the formation during which benzonitrile may be formed as a side product.

Using phenylacetylene as a dipolarophile, 3,5-diphenylisoxazole was obtained in 62% yield.

3-Methoxycarbonylisoxazolines (**9**) were obtained in poor yields (5—30%) from the similar reaction using methyl 2-chloro-2-(ethoxycarbonyloxyimino)acetate (**8**) instead of **2**. On the other hand, no cycloadducts were

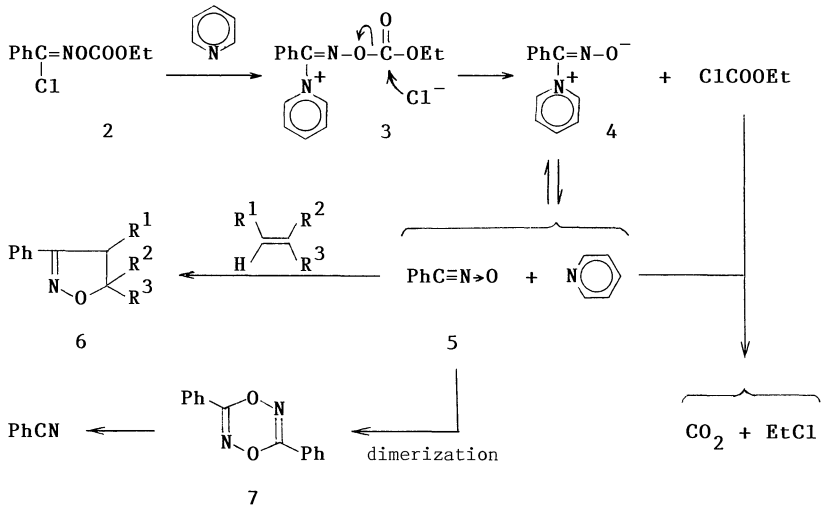

Scheme 1.

Table 1. Yields and Melting (or Boiling) Points of 2-Isoxazolines (**6**)

Compd	R^1	R^2	R^3	Yield[a] %	Mp(θ_m/°C) [Bp(θ_m/°C)/mmHg]	Lit, Mp(θ_m/°C) [Bp(θ_m/°C)/mmHg][b]
6a	H	$C_{12}H_{25}$-*n*	H	75	72—73	72—73[9]
6b	H	CH_2Ph	H	37	63—64	64—65[9]
6c	H	$CH_2OC_6H_4NO_2$-*p*	H	77	151—153	152—153[9]
6d	H	C_6H_5	H	60	72—74	75—76[10]
6e	H	CN	H	51	64—66	66—67[11]
6f	H	$OCOCH_3$	H	42	97—98	90—91[12]
6g	H	OC_4H_9-*n*	H	68	[155/1.5]	[141/1.0][8]
6h	-CON(Ph CO-		H	95	168—171	170—172[9]
6i	H	$COOCH_3$	CH_3	63	[145/1.3]	60[13]

a) Yields of the isolated products based on **2**. b) 1 mmHg=133.322 Pa.

obtained by the reaction using *O*-benzoyl derivative (**10**) of benzohydroximoyl chloride as the nitrile oxide precursor.

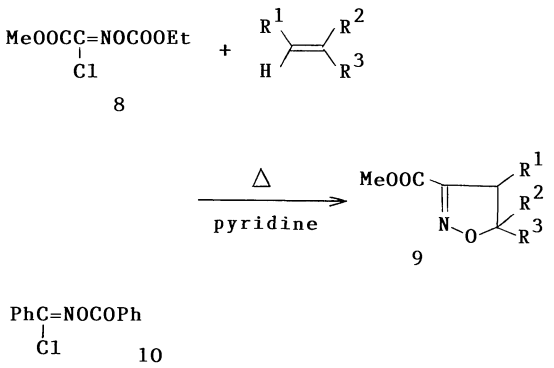

Compared with conventional nitrile oxide precursors, hydroximoyl chlorides [RC(Cl)=NOH] and their *O*-trimethylsilyl derivatives (**1**), our new precursor (**2**) gave more satisfactory results from the standpoints of simple preparative method and the stability of the precursor [in fact, this reagent is so stable to be distilled in vacuo (115°C/0.3 mmHg, 1 mmHg=133.322 Pa) and is stable during the storage for a long time at ambient temperature even in the presence of moisture].

Experimental

Measurements and Materials. All melting and boiling points are uncorrected. *O*-Ethoxycarbonylbenzohydroximoyl chloride (**2**) was prepared similarly according to the method in literature[8] except for the usage of the substrates, (nitromethyl)benzene, ethyl chloroformate, and triethylamine, in 1:3:3 molar ratio [the yield of **2** was improved to 81% yield based on (nitromethyl)benzene by this modification]. Methyl 2-chloro-2-(ethoxycarbonyloxyimino)acetate (**8**) was prepared according to the method in literature.[8] The other reagents were of commercial origin and were used without further purification.

Preparation of 3-Phenyl-2-isoxazolines (6) and 3, 5-Diphenylisoxazole: General Procedure: An equimolar mixture of **2** (1.14 g, 5 mmol) and olefin (5 mmol) in pyridine (30 ml) was heated to reflux for 3 h. Gradual evolution of carbon dioxide (trapped as $CaCO_3$) and ethyl chloride (captured by a chilled trap and identified by ^1H NMR spectral analysis) was observed in the course of the reaction. After evaporation of pyridine, the residue was treated with water and extracted with chloroform. The chloroform layer was dried over anhydrous sodium sulfate and the solvent was evaporated to give crude products. Crystalline crude products were recrystallized from appropriate solvent to give pure cycloadducts (**6a—f** and **6h**) in yields shown in Table 1. 3,5-Diphenylisoxazole was ob-

tained in crystalline state from the reaction of **2** with phenylacetylene; yield; 600 mg (62%); mp 139—141 °C (methanol) (lit,[19] mp 141—142 °C). Oily products obtained from the reaction using butyl vinyl ether or methyl methacrylate as dipolarophile were distilled in vacuo to give pure isoxazolines (**6g** and **6i**) in yields shown in Table 1. All the melting and boiling points of the cycloadducts are well agreed with those appeared in literatures.[8–13,19] ^{1}H NMR spectra of **6a—c**,[9] **6d—f**,[20] **6g**,[8] **6h**,[9] and **6i**[20] appeared in literatures are fully agreed with those of specimens prepared here.

Thermal Treatment of 2 in Pyridine. A solution of **2** (1.14 g, 5 mmol) in pyridine was heated to reflux for 3 h. The reaction mixture was treated according to the procedure described above. Oily residue, thus obtained, was distilled in vacuo to give two fractions, bp 75 °C/15 mmHg and 110 °C/2 mmHg. The former fraction was found to be benzonitrile (0.20 g, 20% yield) and the latter one found to be ethyl phenylcarbamate (0.28 g, 17% yield) by comparison with authentic specimens.

References

1) S. A. Lang, Jr. and Y.-i Lin, "Isoxazole and Their benzo Derivatives," in "Comprehensive Heterocyclic Chemistry," ed by A. R. Katritzky and C. W. Rees, Pergamon Press Ltd., New York (1984), Vol. 6, pp. 1—130.

2) J. B. Wakefield and D. J. Wright, *Adv. Heterocycl. Chem.*, **25**, 147 (1979).

3) A. P. Kozikowski and Y. Y. Chen, *J. Org. Chem.*, **46**, 5248 (1981).

4) D. P. Curran, *J. Am. Chem. Soc.*, **104**, 4024 (1982).

5) C. Grundmann and P. Grünanger, "The Nitrile Oxides," Springer Verlag, New York (1971).

6) P. Caramella and P. Grünanger, in "1,3-Dipolar Cycloaddition Chemistry," ed by A. Padwa, John Wiley & Sons, New York (1984), Vol. 1, Chap. 3, pp. 291—392.

7) R. F. Cunico and L. Bedell, *J. Org. Chem.*, **48**, 2780 (1983).

8) T. Shimizu, Y. Hayashi, H. Shibafuchi, and K. Teramura, *Bull. Chem. Soc. Jpn.*, **59**, 2827 (1986).

9) T. Shimizu, Y. Hayashi, and K. Teramura, *Bull. Chem. Soc. Jpn.*, **57**, 2531 (1984).

10) G. Stagno d'Alcontres and P. Grünanger, *Gazz. Chim. Ital.*, **80**, 831 (1950).

11) G. Stagno d'Alcontres and P. Grünanger, *Gazz. Chim. Ital.*, **80**, 741 (1950).

12) R. Paul and S. Tchelitcheff, *Bull. Soc. Chim. Fr.*, **1962**, 2215.

13) A. Quilico, Stagno d'Alcontres, and P. Grünanger, *Gazz. Chim. Ital.*, **80**, 479 (1950).

14) See Ref. 5, p.167

15) A. Corsaro, G. Perrini, P. Caramella, M. M-Albini, and T. Bandiera, *Tetrahedron Lett.*, **27**, 1517 (1986).

16) T. Hopkins, *J. Chem. Soc.*, **117**, 278 (1938).

17) W. R. Mitchell and R. M. Paton, *J. Chem. Res., Synop.*, **1984**, 58.

18) F. De Sarlo, *J. Chem. Soc., Perkin Trans. 1*, **1974**, 1951.

19) K. Harada, E. Kaji, and S. Zen, *Chem. Pharm. Bull.*, **28**, 3296 (1980).

20) R. Sustmann, R. Huisgen, and H. Huber, *Chem. Ber.*, **100**, 1802 (1967).

Redox Photochromism of Arylviologen Crystals

Hiroyoshi KAMOGAWA* and Shigeki SATO
Department of Applied Chemistry, Yamanashi University, Takeda 4, Kofu 400
(Received September 4, 1990)

Synopsis. Reversible color development induced by near UV light (photochromism) was observed for some crystalline powder of 1,1′-diaryl-4,4′-bipyridinium bis(*p*-toluenesulfonate). Redox mechanism by the electron transfer from the sulfonate anion to viologen dication is claimed.

In previous papers,[1,2] we have reported for the first time that some 1,1′-disubstituted 4,4′-bipyridinium salts (4,4′-viologens), in the crystalline solid state without any additives, exhibit reversible intense *blue or pink* color development with irradiation of near-UV light (photochromism).

In the present study, we wish to report another class of 4,4′-viologens, some members of which are also susceptible to near-UV light in the crystalline state to exhibit reversible *green* color development.

The viologens synthesized and investigated for photochromic behavior in this study were 1,1′-diaryl-4,4′-bipyridinium bis(*p*-toluenesulfonate) (to be abbreviated below as "arylviologen"), as shown in Table 1.

Results and Discussion

Arylviologens (**V**) were prepared by the anion-exchange reaction of the corresponding viologens having the chloride counter ion (**IV**) with *p*-toluenesulfonate anion (PTS^-), using an anion-exchange resin loaded with PTS^-. Compounds **IV** were synthesized, in its turn, starting with 4,4′-bipyridine (**I**) via its diquaternary pyridinium salt (**III**) with 2,4-dinitrochlorobenzene (**II**), followed by the amine-exchange reaction of **III**, as is indicated in Eq. 1.[3]

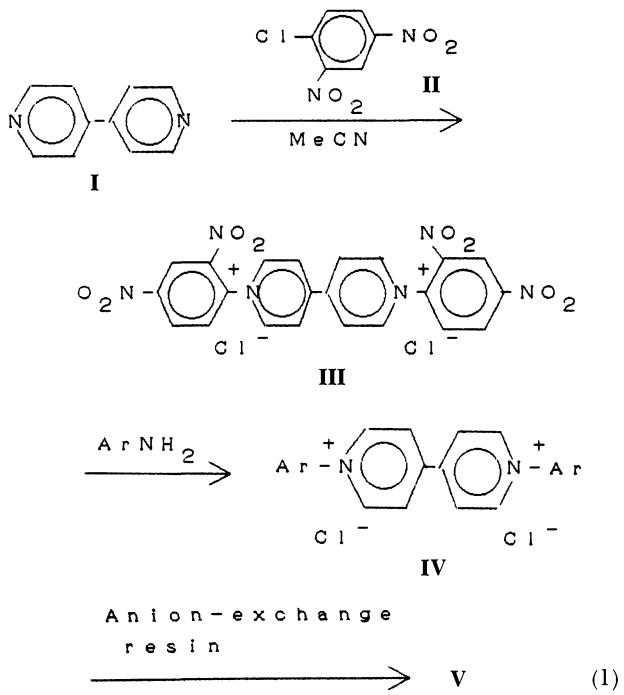

(1)

Table 1. Arylviologens Employed in the Present Study

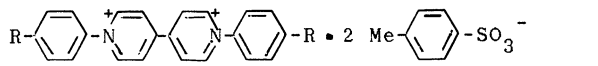

Viologen	R	Viologen	R
IV-1	H[a]	**V-3**	MeO
V-1	H	**V-4**	F
V-2	Me	**V-5**	Cl

a) 1,1′-Diphenyl-4,4′-bipyridinium dichloride.

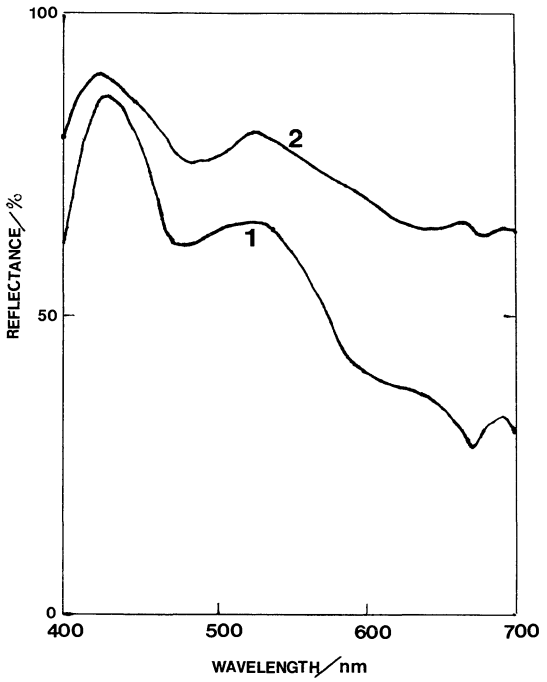

Fig. 1. Typical visible reflection spectra of the colors developed on viologen crystals with irradiation of near-UV light. Ordinate indicates values against those for the unirradiated sample. Curve 1: immediately after 10 s irradiation in air; curve 2: 10 min standing in the dark after irrad., each for 1,1′-bis(*p*-methylphenyl)-4,4′-bipyridinium bis(*p*-toluenesulfonate)(viologen No. **V-2**).

Fig. 1 indicates typical reflectance changes for crystalline powder of arylviologens upon irradiation and subsequent standing in dark.

Thus, with irradiation of light including the near-UV region, reflectances particularly at 600—700 nm decreased rapidly with simultaneous decrease of those at 400—500 nm. Since the viologen crystalline powder before irradiation showed some absorptions at 400—500 nm, the visual color was deep green for the sample during and immediately after the irradiation (curve 1).

It can be also recognized from this Figure that

Table 2. Photochromic Behavior of Viologen Crystals

Viologen No.	Reflectance[a] in air			Abs.[b] peak/nm	Color[c]	Reflectance[a] under vacuum			Abs.[b] peak/nm	Color[c]
	0	10	30			0	10	30		
IV-1	100	100	100	d)	Pale Yellow	100	100	100	d)	Pale Yellow
V-1	76	88	89	660	Green	60	60	61	660	Green
V-2	28	64	66	670	Green	22	24	26	670	Green
V-3	79	81	87	660	Green	60	62	63	660	Green
V-4	63	81	84	630	Green	56	58	63	630	Green
V-5	90	94	100	660	Greenish Yellow	75	80	83	660	Green

a) % Values (based on those for unirradiated viologens) in 0, 10, and 30 min after 10 s irradiation. b) Absorption peak newly developed above 600 nm as a result of irradiation. Reflectance was measured at this wavelength. c) Visual color developed upon irradiation. d) No new peak. The reflectances indicated are those throughout the whole visible range.

reflectance for the irradiated sample was recovered significantly on standing for 10 min in dark (curve 2) [Photochromism].

Table 2 also summarizes the results obtained for the crystalline powder of various arylviologens irradiated and let stand in air or under vacuum.

It can be known from this Table that, in the case of arylviologen, all samples investigated are susceptible to near-UV light, except viologen No. IV-1 bearing the chloride counter anion. This behavior differs notably from that in the previous study,[2] in which only limited numbers of viologens with sulfonate anions showed photochromism in crystals.

The fact that the arylviologens bearing the PTS^- counter anion in the present study exhibit photochromic behavior generally might indicate that the electron transfer to viologen dication from the counter anion induced by light and vice versa in dark (redox photochromism) are allowed in the crystal lattice.

The generation of the radical cation from the viologen dication as a result of photoreduction was demonstrated by the EPR change corresponding to reflectance change. This electron transfer to viologen dication from the sulfonate counter anion has also been observed on the transparent and isotropic films made singly of viologens bearing a long alkyl group in the counter anion part.[4]

In the present case, however, the dication part of the arylviologen molecule is wholly conjugated, so that the whole part of it might participate in radical cation formation, as exemplified in Eq. 2.

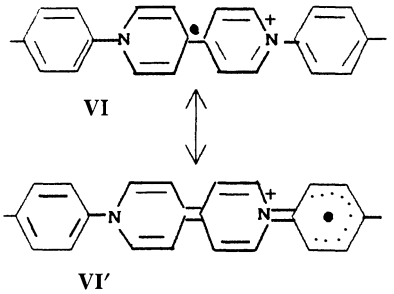

(2)

This whole conjugation may be the cause of a remarkable red shift of a reflectance peak around 600 nm for the radical cations derived from the conventional viologens[1,2] to that at 660 nm or so in this case, with simultaneous shift of that around 400 nm to a yellow region (blue→green color).

High photosensitivities observed in the present type of viologen crystals might also be caused, to some extents, by this extension of conjugation, which might lower the potential barrier of this photoinduced redox reaction.

Table 2 also indicates that the presence of air oxygen promotes the bleaching of the color developed by light considerably due to oxidation of the radical cation (**VI**-VI') back to original dication. Bleachings become very slow mostly at intermediate stages even in air, presumably because some or the major part of the radical cations (VI–VI') within crystal lattices are untouchable with air oxygen.

The stability of VI-VI' confined in crystal lattices may be dependent on temperature and other factors including the kind of the counter anion. Bleaching was complete when crystals were heated above 100°C for 10 min or so, indicating that the back reaction took place by the application of heat energy.

Judging from the results so far obtained, including those in previous studies,[1,2] it can be said safely that the 4,4'-viologens bearing the sulfonate counter anion should exhibit redox photochromism in the solid crystalline state, in case various requisites, especially as the occurrence of the electron transfer within the crystal lattice, are satisfied.

Experimental

Infrared (IR), ^1H NMR, and elemental analyses were conducted using a Hitachi 215 spectrophotometer, a JNM-PMX 60 spectrometer, and a Perkin–Elmer 240 instrument, respectively. Visible reflectance and EPR were taken with a Hitachi C-1020 color sensor and a JES-FE1XG spectrometer, respectively.

1,1'-Bis(2,4-dinitrophenyl)-4,4'-bipyridinium Dichloride (III). A solution of 4,4'-bipyridine (1.6 g, 10 mmol) and 2,4-dinitrochlorobenzene (7.0 g, 35 mmol) in anhydrous acetonitrile (30 mL) was refluxed for 72 h with exclusion of moisture. The reaction mixture was diluted with acetonitrile (30 mL) to afford yellowish precipitate in 95% yield.

Found: C, 47.17; H, 2.71; N, 14.67%. Calcd for

$C_{22}H_{14}N_6O_8C_{12}$: C, 46.91; H, 2.50; N, 14.92%. IR (KBr) 1510, 1330 (NO_2) cm^{-1}.

1,1′-Diphenyl-4,4′-bipyridinium Dichloride (IV-1). Compound **III** (1.1 g, 2 mmol) was dissolved in 50% ethanol (40 mL) by the application of heat. To the stirred resulting solution was then added dropwise a solution of aniline (0.9 mL, 9 mmol) in ethanol (50 mL), followed by stirring at 20°C for 24 h. The red solution was evaporated to dryness on a rotary evaporator, followed by stirring the residue in ether (100 mL) for 30 min. The resulting residue was stirred in water (50 mL) at 100°C for 24 h. Upon cooling, the mixture was filtered and the filtrate was freeze dried to provide crude product, which was recrystallized from ethanol–ethyl acetate (yield, 86%).

Found: C, 69.08; H, 4.82; N, 7.05%. Calcd for $C_{22}H_{18}N_2Cl_2$: C, 68.94; H, 4.73; N, 7.31%. NMR (D_2O) δ=7.9 (s, 10H, 2 phenyl), 8.8 (d, 4H, pyridinium), 9.5 (d, 4H, pyridinium).

1,1′-Diphenyl-4,4′-bipyrdinium Bis(*p*-toluenesulfonate) (V-1). An anion-exchange resin (Diaion SA 10A; 20 g) loaded with *p*-toluenesulfonate anion in the conventional manner was added to a solution of **V** (1.0 g) in water (50 mL). The mixture was stirred gently overnight, filtered, and the filtrate was freeze dried to provide crude product, which was recrystallized from methanol–ether (yield, 60%).

IR (KBr) 1190 (SO_3^-) cm^{-1}. NMR (D_2O) δ=2.3 (s, 6H, 2Me), 7.1—8.0 (18H, Aryl), 8.8 (d, 4H, Pyridinium), 9.1 (d, 4H, Pyridinium).

V-2, **V-3**, and **V-5** were prepared in the same manner as that for **V-1**, except that, in the **III—IV** step, *p*-toluidine, *p*-anisidine, and *p*-chloroaniline were employed instead of aniline, respectively. In the case of **V-4**, stirring with *p*-fluoroaniline at 80°C for 24 h was effected at the first stage of the **III—IV** step, instead of stirring with aniline at 20°C for 24 h, other procedures being equal to those for **V-1**. Analytical results for these viologens synthesized were also satisfactory.

Measurement of Reflection Spectra. Viologen crystals finely powdered (0.2 g) were packed tightly in a glass tube for 5 mL use, which, if necessary, was evacuated carefully under 0.1 mmHg for 30 min and sealed off. The tube was then subjected to the light reflectance measurement using a color sensor covering 400 to 700 nm in approximately one second. Light irradiation to the tube was carried out at a distance of 10 cm from a 75W high-pressure Hg lamp (Toshiba SHLUV-2) for 10 s.

References

1) H. Kamogawa and T. Suzuki, *J. Chem. Soc., Chem. Commun.*, **1985**, 525.

2) H. Kamogawa and T. Suzuki, *Bull. Chem. Soc. Jpn.*, **60**, 794 (1987).

3) H. Kamogawa and S. Sato, *J. Polym. Sci., Part A: Polym. Chem.*, **26**, 653 (1988).

4) T. Ono and H. Kamogawa, 59th Spring Annual Meeting of Chem. Soc. Jpn., Yokohama, April 1990, Abstr., No. 4E104.

Synthesis of 2,6-Dihydronaphth[1,2,3-*cd*]indol-6-ones[1)]

Sadao Arai,* Sigeaki Yamauchi, Takamichi Yamagishi, and Mitsuhiko Hida*
Department of Industrial Chemistry, Faculty of Technology,
Tokyo Metropolitan University, Fukazawa, Setagaya-ku, Tokyo 158
(Received September 10, 1990)

Synopsis. The reaction of 1-aminoanthraquinone with benzyl chloride in KOH–DMSO system afforded 3,11b-dibenzyl-2-phenyl-2,3,7,11b-tetrahydroanthra[1,9-*de*][1,3]-oxazin-7-one (**5**; 78% yield), whose structure was determined by single-crystal X-ray diffraction. The reaction of compound **5** with aluminium chloride gave 1-phenyl-2,6-dihydronaphth[1,2,3-*cd*]indol-6-one (52% yield) having strong fluorescence.

In our previous paper we reported that amide ions were formed by the loss of a proton from the amino group of aminoanthraquinones in the presence of powdered potassium hydroxide (KOH) in dimethyl sulfoxide (DMSO).[1,2)] The amide ion of 1-aminoanthraquinone (**1a**) reacted with excess alkyl halides such as 1-iodobutane and 1-bromohexadecane to yield red 1-alkylaminoanthraquinones, while the *N*-alkylation of 2-aminoanthraquinone (**2a**) afforded 2-dialkylaminoanthraquinones in good yields.[2)] The reaction of **1a** with benzyl chloride, however, produced not a predicted red 1-benzylaminoanthraquinone (**3**) but yellow product together with a trace amount of highly fluorescent compound. These unexpected results prompted us to examine the reaction of aminoanthraquinones with benzyl chloride in KOH–DMSO system. In this paper we will report a new method for the preparation of 2,6-dihydronaphth[1,2,3-*cd*]indol-6-ones having strong fluorescence.

Results and Discussion

Reaction of Aminoanthraquinone (1a or 2a) with Benzyl Chloride in KOH–DMSO System. The compound **1a** or **2a** was first converted to its amide ion by treating it with powdered KOH in DMSO. Then excess benzyl chloride was added to the green amide ion solution (**1b** or **2b**). In the reaction of **2a**, 2-dibenzylaminoanthraquinone (**4**) was obtained in 93% yield. The reaction of **1a**, however, unexpectedly afforded a yellow product with a trace amount of strongly fluorescing compound.

The yellow product shows an M^+ ion at m/z 493. Its IR spectrum shows the presence of carbonyl group but no N–H group. The ^1H NMR shows two remarkable features: AB quartet at around 3.46 and 4.32 ppm, and a singlet at 6.28 ppm. The quartets wre assigned to two sets of benzylic protons caused by restricted rotation. From these results and analytical data we have given this yellow product an oxirane structure (**7**), 1-dibenzylamino-3′-phenylspiro[anthracene-9(10*H*), 2′-oxiran]-10-one in our previous communication.[1)] However, after further examination, we came to a view that 1,3-dihydrooxazine structure (**5**) was more plausible than the previously-proposed **7**. The ^{13}C NMR spectrum displays two benzyl methylene carbons at 49.3 and 51.6 ppm, and

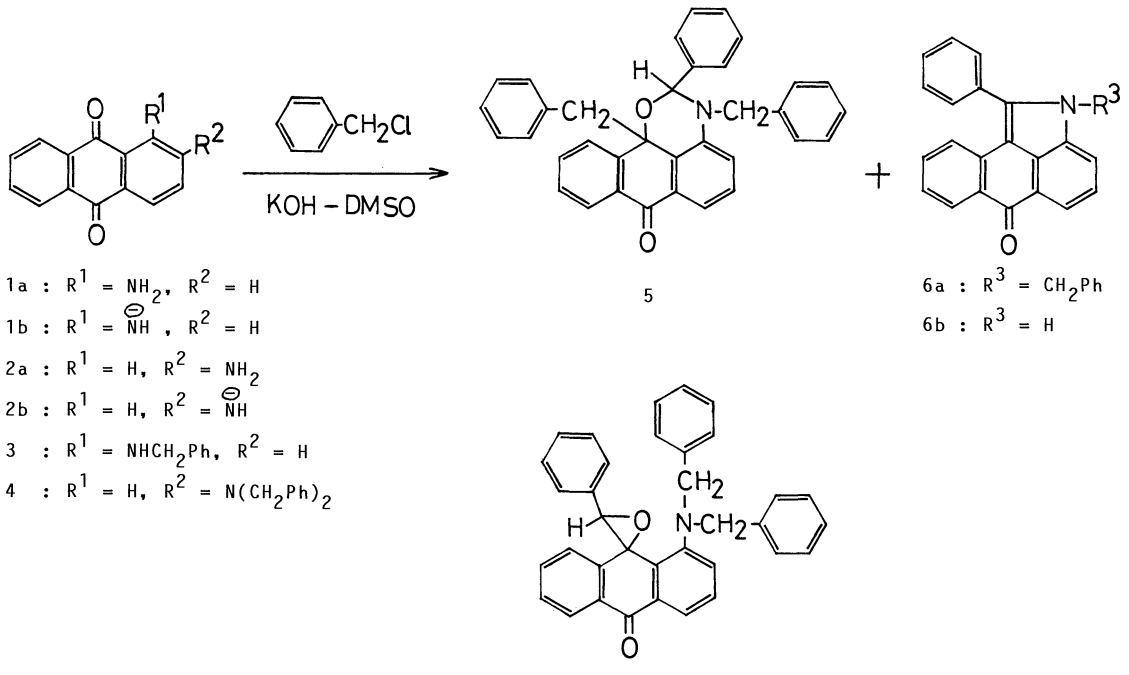

Scheme 1.

carbonyl carbon at 184.0 ppm. These results indicate that two benzyl groups are placed at different positions. Since spiro[anthracene-9(10*H*), 2′-oxiran]-10-one was reported to easily react with boron trifluoride to yield 10-formyl-10-phenylanthrone,[3] oxirane **7** would be expected to afford a formyl compound. In the reaction of the yellow product with excess boron trifluoride in diethyl ether, however, the starting compound was recovered and no formyl compound was observed. These results suggest that the yellow product would not be oxirane **7**. The molecular structure was finally established by X-ray crystal analysis, and the Oak Ridge Thermal Ellipsoid Program (ORTEP) drawing is illustrated in Fig. 1. Figure 1 unequivocally shows that the yellow product is not oxirane **7** but 3,11b-dibenzyl-2-phenyl-2,3,7,11b-tetrahydroanthra[1,9-*de*][1,3]oxazin-7-one (**5**). Figure 1 also suggests that the rotation of the benzyl group is restricted mainly by the steric hindrance in the structure.

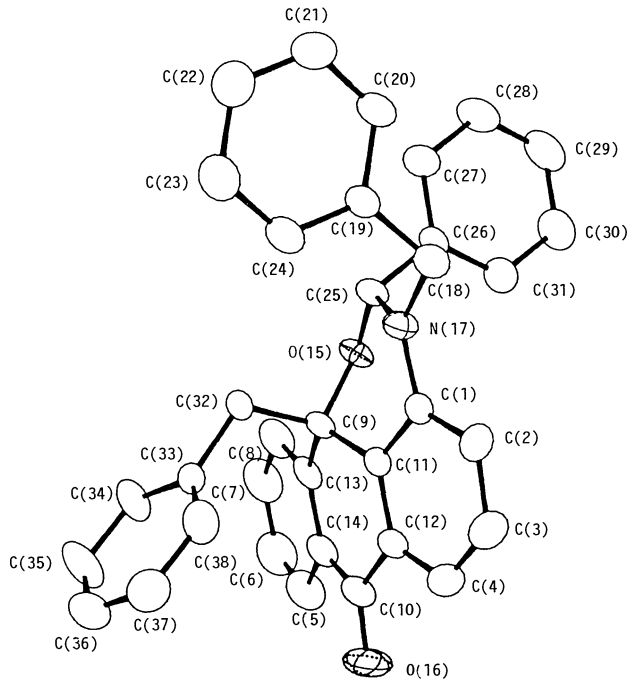

Fig. 1. ORTEP drawing of **5** showing 50% probability ellipsoids for all nonhydrogen atoms.

The structure of the strongly fluorescing compound was determined from both spectroscopic and analytical data to be 2-benzyl-1-phenyl-2, 6-dihydronaphth[1,2,3-*cd*]indol-6-one (**6a**).

Synthesis of 2,6-Dihydronaphth[1,2,3-*cd*]indol-6-ones. The compound **6a** was formed in a trace amount by the reaction of **1a** with benzyl chloride in KOH–DMSO system as described above. In fact the treatment of **5** with KOH in DMSO gave **6a** in very low yield (3%) and **5** was recovered in 85% yield. It was found that **5** was transformed more easily into **6** under acidic conditions. Table 1 shows that both Brønsted and Lewis acids were effective for the transformation. It is interesting to note that in the reaction of **5** with aluminium chloride compound **6b** was obtained together with **6a** and the total yield of **6** was increased, while other Lewis acids ($ZnCl_2$, $FeCl_3$, and $TiCl_4$) did not afford **6b**. The compound **6b** would be obtained by debenzylation of **6a**, because **6b** was obtained in 84% yield by the treatment of **6a** with $AlCl_3$ (see Table 2). The ratio of $AlCl_3$ to **5** was found to be important for the conversion of **5** to **6b**. In the case of 1:1 ratio, **6a** was obtained in 44% yield and **6b** was not formed. The best result (**6b**; 73% and **6a**; 11%) was obtained by the successive addition of $AlCl_3$: the reaction mixture was refluxed at 4:1 ratio for 1 h, then at 6:1 ratio for 2 h. The dealkylation was examined for **6a** and alkylaminoanthraquinones. Table 2 demonstrats that $AlCl_3$ was effective for the debenzylation, though **1a** was obtained in 14% yield in the case of 1-cyclohexyl-

Table 1. The Conversion of **5** into **6**

Reagent	Solvent	Temp/°C	Time/h	Yield/% **6a**	**6b**
KOH[a]	DMSO	30	3	3	0
concd HCl	EtOH	Reflux	3	51	0
concd HCl	PhH	Reflux	3	8	0
CH_3CO_2H	—	Reflux	1	20	0
H_3BO_3[b]	EtOH	Reflux	3	0	0
$ZnCl_2$[b]	PhH–EtOH	Reflux	23	14	0
$FeCl_3$[b]	PhH	RT	10	53	0
$FeCl_3$[b]	PhH	Reflux	1	60	0
$AlCl_3$[b]	PhH	Reflux	1	21	52
$TiCl_4$[b]	PhH	RT	3	45	0

a) Molar ratio. 5: KOH=1: 10. b) Molar ratio. 5: acid= 1: 5.

Table 2. Dealkylation of **6a** and Alkylaminoanthraquinones[a]

Substrate	Acid	Solvent	Time/h	Product	Yield/%
6a	concd HCl	EtOH	7	**6b**	8
6a	$AlCl_3$	PhH	3	**6b**	84
1-$PhCH_2NHAQ$	concd HCl	EtOH	3	—	0
1-$PhCH_2NHAQ$	$AlCl_3$	PhH	0.5	**1a**	94
1-CH_3NHAQ	$AlCl_3$	PhH	2.5	—	0
1-*n*-C_4H_9NHAQ	$AlCl_3$	PhH	3	—	0
1-⟨H⟩-NHAQ	$AlCl_3$	PhH	5	**1a**	14
2-$(PhCH_2)_2NAQ$	$AlCl_3$	PhH	3	**2a**	88

a) The reactions were run at reflux temperature. Molar ratio. Substrate: acid=1: 5.

aminoathraquinone.

Dihydronaphthindolones have been known to be good fluorophores[4] and our procedure is a facial and useful one for the preparation of 2,6-dihydronaphth-[1,2,3-*cd*]indol-6-ones, though some synthetic methods have been reported.[5]

Experimental

Materials. All commercial compounds were reagent grade and used without further purification. Dimethyl sulfoxide was distilled twice under reduced pressure and stored under a nitrogen atmosphere. Benzyl chloride was distilled under a nitrogen atmosphere. Aminoanthraquinones were purified as described previously.[2]

Instruments. Melting points were obtained on a Yamato melting point apparatus MP-21 and are uncorrected. UV and visible spectra were recorded with a Hitachi 220A spectrometer. ^{1}H and ^{13}C NMR data were recorded on a Hitachi R-24 (60 MHz) or JEOL FX90Q (90 MHz) spectrometers using Me_4Si as internal standard. IR spectra were measured on a JASCO IRA-1 spectrometer. Mass spectra were recorded with a JEOL JMS-DX 300 spectrometer by the electron impact (EI) ionizing technique at 70 eV. Elemental analyses were performed on a Yanaco MT2 CHN corder.

Reaction of Aminoanthraquinone with Benzyl Chloride in KOH–DMSO System. A typical procedure is described for the reaction with 1-aminoanthraquinone (**1a**). The compound **1a** (446 mg, 2 mmol) was treated with powdered KOH (1.12 g, 20 mmol) in DMSO (60 cm^3) for 30 min at 30°C and the mixture rapidly turned from red to green. Then, benzyl chloride (2.53 g, 20 mmol) was added and the solution was stirred for 1 h at 30°C. The resulting brown solution was poured into water (1000 cm^3) and then extracted with benzene. After evaporation of the extract, the residue was chromatographed on a silica-gel column with benzene eluent. The yellow fractions (R_f=0.49 by SiO_2 TLC, benzene as eluent) together with a trace amount of orange fractions (R_f=0.23) fluorescing in intense yellowish green were isolated. The yellow fractions were concentrated, and recrystallized from ethanol to afford 3,11b-dibenzyl-2-phenyl-2,3,7,11b-tetrahydroanthra[1,9-*de*][1,3]oxazin-7-one (**5**) (769 mg, 78%) as yellow crystals: Mp 202.0—202.8°C; UV (C_2H_5OH) 259 (log ε 4.32), 275 (sh), and 394 nm (3.17); IR (KBr) 1670 (C=O), 1245, 1150, 830, and 820 cm^{-1}; ^{1}H NMR ($CDCl_3$) δ=3.46 (2H, ABq, J=12 Hz, CH_2), 4.32 (2H, ABq, J=16 Hz, CH_2), 5.9—6.2 (2H, m, ArH), 6.28 (1H, s, CH), and 6.7—8.0 (20H, m, ArH); ^{13}C NMR ($CDCl_3$) δ=49.3, 51.6, 87.5, 115.5, 116.5, 126.4—144.6, and 184.0.

Found: C, 85.13; H, 5.42; N, 2.85%; *m/z* 493.2054. Calcd for $C_{35}H_{27}NO_2$: C, 85.16; H, 5.51; N, 2.83%; M, 493.2042.

The fluorescing fractions were concentrated and recrystallized from ethanol to give 2-benzyl-1-phenyl-2,6-dihydronaphth[1,2,3-*cd*]indol-6-one (**6a**) (23 mg, 3%) as orange crystals: Mp 228.5—230.0°C; UV (C_2H_5OH) 245 (log ε 4.42), 276 (4.23), 306 (4.09), 356 (3.61), and 426 nm (4.16); IR (KBr) 1630, 1610, 1595, 1550, 1180, and 970 cm^{-1}; ^{1}H NMR ($CDCl_3$) δ=5.20 (2H, s, CH_2) and 6.8—8.6 (17H, m, ArH); ^{13}C NMR ($CDCl_3$) δ=47.8, 107.9, 115.4—141.8, 184.0.

MS *m/z* 358 (M^+); Found: C, 87.25; H, 4.69; N, 3.41%. Calcd for $C_{28}H_{19}NO$: C, 87.25; H, 4.97; N, 3.63%.

2-(Dibenzylamino)anthraquinone (4): Mp 144.5—145.5°C; IR (KBr) 3075, 3040, 1670, 1590, 1405, 1300, 943, and 700 cm^{-1}; ^{1}H NMR ($CDCl_3$) δ=4.82 (4H, s, CH_2) and 6.9—8.4 (17H, m, ArH).

MS *m/z* 403 (M^+); Found: C, 83.57; H, 5.18; N, 3.37%. Calcd for $C_{28}H_{21}NO_2$: C, 83.35; H, 5.25; N, 3.47%.

The Conversion of 5 into 6. A typical procedure is described for the reaction of **5** with concd HCl. A mixture of **5** (200 mg, 0.4 mmol) and concd HCl (5 cm^3) in ethanol (35 cm^3) was refluxed for 3 h. The mixture was concentrated and chromatographed on silica gel column with benzene as eluent to afford **6a** (81 mg, 51%).

Dealkylation. A typical procedure is described for the debenzylation of compound **6a.** A mixture of compound **6a** (62 mg, 0.16 mmol) and $AlCl_3$ (106 mg, 0.80 mmol) in benzene was refluxed for 3 h. The mixture was poured into ice-water. The benzene extract was evaporated and chromatographed on a silica-gel column with benzene as eluent to afford 1-phenyl-2,6-dihydronaphth[1,2,3-*cd*]indol-6-one (**6b**) (40 mg, 84%): Mp 321—322°C; UV (C_2H_5OH) 248 (log ε 4.45), 277 (4.12), 305 (4.03), 359 (3.63), and 430 nm (4.08); IR (KBr) 3260, 3050, and 1630 (C=O) cm^{-1}; ^{1}H NMR (DMSO-d_6) δ=7.3—8.5 (12H, m, ArH) and 12.3 (1H, s, NH); ^{13}C NMR (DMSO-d_6) δ=105—141 and 182.4 (C=O).

MS *m/z* 295 (M^+); Found: C, 85.51; H, 4.32; N, 4.67%. Calcd for $C_{21}H_{13}NO$, C, 85.40; H, 4.44; N, 4.74%.

X-Ray Crystallographic Analysis of 5. A large, well-shaped triclinic crystal of **5** was obtained by slow evaporation of an ethanol solution: $C_{35}H_{27}NO_2$=493.2; space group $P\bar{1}$; a=10.043(5), b=15.665(9), c=8.454(4) Å; β=83.02(4)°; V=1270.1 Å^3; Z=2. Lattice constants and intensity data of **5** were measured by using graphite-monochromated Cu$K\alpha$ radiation on a Rigaku AFC-5 diffractometer. A total of 4202 unique reflections with $F_o > 4\sigma(F_o)$ were obtained by using the ω–2θ scanning method with a 2θ scan speed of 4° min^{-1} to 2θ=145°. The structure was solved by the RASA-II system (Rigaku Corp.) on the basis of the direct method and refined to a final R value of 0.073. Further crystallographic details were deposited as Document No. 9094 at the Office of the Editor of Bull. Chem. Soc. Jpn.

The authors wish to express their thanks to Dr. Keiichi Yamaguchi and Professor Masataka Yokoyama of Chiba University for measurement of single-crystal X-ray diffraction.

References

1) S. Arai, T. Yamagishi, and M. Hida, *Chem. Lett.*, **1981**, 1789.

2) S. Arai, S. Kato, and M. Hida, *Bull. Chem. Soc. Jpn.*, **58**, 1458 (1985).

3) G. L. Buchanan and D. B. Jhaveri, *J. Org. Chem.*, **26**, 4295 (1961).

4) J. Houben, "Das Authracen und die Anthrachinone," Georg Thieme, Verlag (1929), pp. 615—617.

5) G. Kranzlein, A. Wolfram, and W. Broeker, Ger. Patent 594168 (1934); *Chem. Abstr.*, **28**, 3418g (1934). b) M. V. Kazankov, N. Makshanova, and E. G. Kuznetsova, *Khim. Geterotsikl. Soedin.*, **1977**, 103; *Chem. Abstr.*, **88**, 22576m (1978).

Flash Vacuum Pyrolysis of 5-Diazodibenzo[*ad*]cycloheptene. Some Insights into Aromatic Carbene-Arylcarbene Rearrangement

Hideo Tomioka* and Noriyuki Kobayashi
Department of Industrial Chemistry, Faculty of Engineering,
Mie University, Tsu, Mie 514
(Received September 14, 1990)

Synopsis. Flash vacuum pyrolysis of the title diazo compound gives 4*H*-cyclopenta[*def*]phenanthrene, which is interpreted as indicating that dibenzo[*ad*]cycloheptatrienylidene (**13**) undergoes the carbene–carbene rearrangement to generate 4-phenanthrylcarbene. The reactivities of **13** are compared with those of other benzoannulated cycloheptatrienylidenes and discussed in terms of the effect of the benzo ring to the activation energy for the rearrangement.

Interconversion of aromatic carbenes (e.g., cycloheptatrienylidene, **1**) and arylcarbenes (e.g., phenylcarbene, **3**) had been attracting continued attention since its discovery not only from the synthetic viewpoint but also from the standpoint of mechanism.[1,2] The rearrangement has permitted the straightforward synthesis of many useful organic compounds which are otherwise not readily obtained, and the mechanism of rearrangement still continues to plague organic chemists.

Although phenylcarbene and cycloheptatrienylidene rapidly interconvert in the gas phase at moderate to high temperatures, this is not a typical reaction of these carbenes in solution. The mechanism involves initial closure of a singlet carbene onto the π system of the aromatic ring to give a cyclopropene intermediate

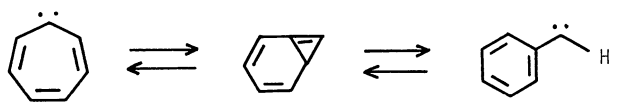

1 2 3

(**2**) that then opens to the new carbene (**3**). It is apparent that the interconversion of aromatic and arylcarbenes should be favored by perturbations that reduce the activation energy for the rearrangement presumably by accelerating closure to **2**. This is supported by the findings[3] that 7*H*-benzocyclohepten-

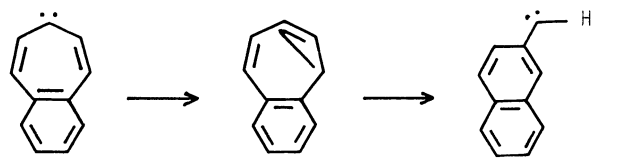

4 5 6

7-ylidene (**4**) gives the products expepcted from the rearranged carbene (**6**) even in solution at −30°C, suggesting that the benzannelation reduces the loss of aromaticity when the ring closes to the nonaromatic tricyclo[5.4.0.0^{4,6}]undeca-2,4,7(1),8,10-pentane **5**. More interestingly, dibenzo[*ac*]cyclohepten-5-ylidene (**7**) also rearranges in solution but only products from 9-phenanthrylcarbene (**9**) are formed and no trace of those expepcted from 1-phenanthrylcarbene (**11**) are

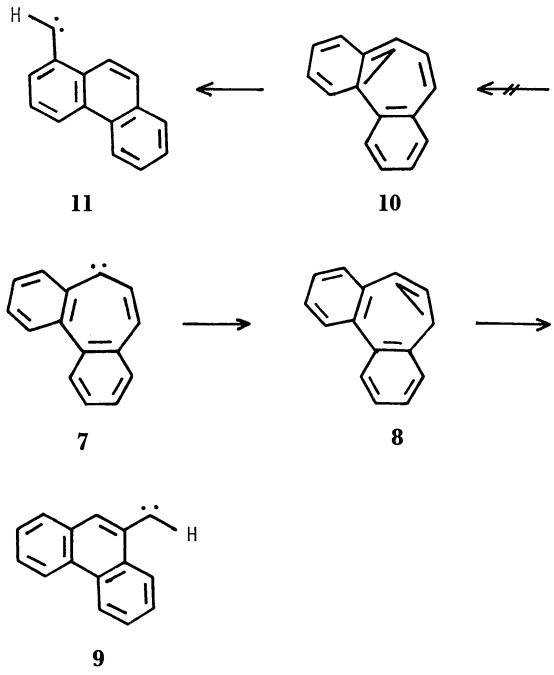

11 10

7 8

9

detected.[4] This is reasonably understood as indicating that the ring closure onto the 2, 3 π system forming **10** and then **11** will result in the destruction of aromaticity of one of the benzocyclic systems. In order to ascertain the mechanism of the rearrangement, we examined the reactivities of dibenzo[*ad*]cyclohepten-5-ylidene (**13**), whose rearrangement will be forced to cause the loss of aromaticity of either of the benzene rings and therefore is expected to be highly unfavorable.

Results and Discussion

Flash vacuum pyrolysis (450°C/10^{-5} Torr, 1Torr= 133.322 Pa) of 5-diazodibenzo[*ad*]cycloheptene (**12**) produced 4*H*-cyclopenta[*def*]phenanthrene (**16**) as a main volatile product in 17% yield along with dibenzo[*ad*]cyclohepten-5-one and dibenzo[*ad*]cycloheptene. The formation of **16** is interpreted as indicating that 4-phenanthrylcarbene (**15**) must be generated presumably by the rearrangement of the carbene (**13**) through tetracyclo intermediate (**14**), since it has been reported[5] that 9-phenanthrylcarbene (**9**) generated by FVP (590°C/0.1Torr) also produces **16**

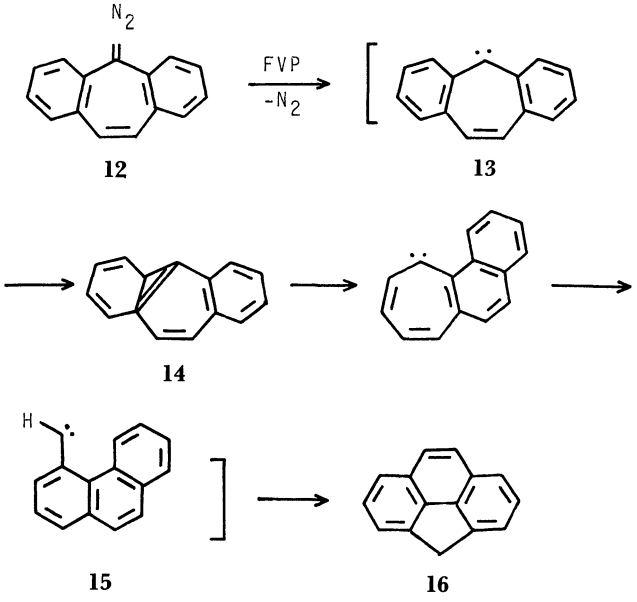

via **15** generated through the repeated carbene rearrangements. The reaction is very similar to that of 10,11-dihydrodibenzo[*ad*]cyclohepten-5-ylidene (**17**), a dihydro analogue of **13**. Thus **17** generated in the gas phase produces 8,9-dihydro-4*H*-cyclopenta[*def*]phenanthrene (**18**) along with two $C_{15}H_{12}$ hydrocarbons (**19**, **20**).[5] The formation of **18** is explicable in terms of the

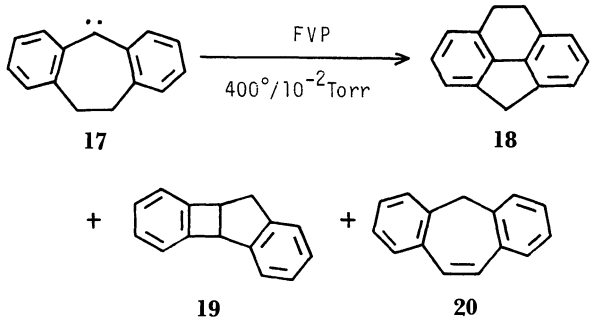

rearrangement forming 1-(9,10-dihydrophenanthryl)carbene, while **19** and **20** can be formed by the transannular insertion reaction in **17**. Apparently, transannular interaction is not feasible in **13** due to the increased strain.

The reactions of **13** in fluid solution or in rigid matrix have been investigated[6,7] to show that it is trapped by trapping reagents before it undergoes the rearrangement. For example, photolysis of **12** in the presence of alkenes at room temperature results in the formation of spirocyclopropanes by the addition of **13** to the alkenes.[6a] This is in a marked contrast with that observed[4] for the isomeric dibenzocycloheptenylidenes (i.e., **7**) which undergoes the rerrangement leading to arylcarbenes (i.e., **9**) in solution even at −60°C. The contrasting difference in the behavior between these two isomeric dibenzannulated aromatic carbenes (i.e., **7** and **13**) can be ascribed to the difference in the activation energy for the rearrangement as advanced above.

The present results coupled with those reported by the others suggest that, although the rearrangement of dibenzo[*ad*]cycloheptenylidene is not observed at low temperature obviously due to the introduction of benzo ring in an improper position, it does undergo the rearrangement at much higher temperature in spite of the destruction of aromaticity of one of the benzocyclic systems during the rearrangement. It is very interesting then to know to what extent the rearrangement will be disfavored by these two benzocyclic groups. The simplest way to estimate this is to determine roughly the lowest temperature at which the rearrangement products form. Thus, we decomposed **12** at various temperatures from 450 to 150°C at 50°C intervals in the gas phase and estimated the lowest temperature required for the rearrangement to be 250°C. For comparison purposes, similar experiments were done with cycloheptatrienylidene (**1**) which produces stilbenes and heptafulvalene, the former being formed as a result of cycloheptatrienylidene–phenylcarbene rearrangement. Stilbenes were not detected when the pyrolysis was carried out at <250°C.

Table 1. Effect of Benzannulation on Carbene–Carbene Rearrangement

Carbenes	Temp/°C[a]	Conditions	Ref.
1	300	Δ at 10^{-4} Torr	This work
4	−30	*hν* in PhH	3)
7	−60	*hν* in THF	4)
13	250	Δ at 10^{-4} Torr	This work

a) The lowest temperature required for rearrangement.

In Table 1, we summarize the lowest temperature required for carbene-carbene rearrangement for a series of isomeric mono-(**4**) and dibenzocycloheptenylidene (**7**, and **13**) as well as the parent carbene (**1**). The results suggest that, although the rearrangement in **13** is highly unfavorable compared to that in **4** and **7**, it is not unduly disfavored compared with that of **1**. Presumably, carbenes generated in the gas phase are forced to undergo multiple rearrangements if possible until they are quenched by a proximate reactive center leading to stable final products. It is very interesting to note here in this connection that tolylmethylenes generated photolytically in the vaper phase produce benzocyclobutene and styrene as a result of rearrangement even at 30°C.[8]

Experimental

Instrumentation. The IR spectra were determined with a JASCO A-100 spectrometer, while the ^{1}H NMR spectra were measured on a JEOL JNM-MH-100 and JNM-GX-400 spectrometer with Me_4Si as the internal reference. The mass spectra were recorded on a Shimadzu QP-1000 mass spectrometer. The GC analyses were performed on a Yanagimoto instrument, Model G-80. The GC column A was prepared from 5% SE-30 on Diasolid L (5.0 mm×2.0 m): column B consisted of 5% PEG-20M on Diazolid L (5.5 mm× 1.0 m).

Materials. The diazo compound (**12**) was prepared according to the methods described.[6]

Flash Vacuum Pyrolysis. The apparatus used for the FVP consisted of a quartz tube (30 mm i.d.×35 cm long)

maintained at the desired temperature by resistance wire. The tube was fitted with a loose plug of quartz wool 10 cm below the top of the heated zone. At the top of the tube, provision was made for the introduction of solid reactants via a solid addition tube. The lower end of the tube was fitted with consecutive U-tubes which were immersed in liquid nitrogen. The pyrolysis tube was bent near the bottom such that the pyrolysis zone was angled about 35° from the vertical.

The carbene precursor was introduced into the hot tube either by subliming at 10^{-4} Torr or by adding the precursor coated on inert support such as powdered quartz. Solvent-assisted sublimation recently advanced by Fowler[9] was also used especially for non-volatile precursors. Products were collected in the U-tubes at −196°C and analysed by MS and NMR.

FVP of 12. In a typical experiment, 50 mg of **12** was dissolved in pentane, quartz powder (ca. 1 ml) was added and the pentane was removed under reduced pressure leaving the diazoalkene coated on the support. The sample was continuously added from the top of the tube at an operating pressure of 10^{-5} Torr. The volatile products were collected in a trap cooled with liquid nitrogen and chromatographed on the preparative TLC over Merck Kiselgel 60 PF_{254} eluting with pet. ether to give a white solid (mp 114—115°C), with NMR and MS spectra identical with those of an authentic sample[10] of 4*H*-cyclopenta[*def*]phenanthrene (**16**).

We thank Professor M. Minabe of Utsunomiya University for the supply of the authentic phenanthrene (**16**). This work was supported by the Grant-in-Aid for Scientific Research from the Ministry of Education, Science and Culture, which is gratefully asknowledged.

References

1) See for pertinent reviews, a) P. P. Gaspar, J.-P. Hus, S. Chari, and M. Jones, Jr., *Tetrahedron*, **41**, 1479 (1985); b) F. R. G. Brown, "Pyrolytic Methods in Organic Chemistry," Academic Press, New York (1980), p. 115; c) C. Wentrup in "Reactive Intermediates," ed by R. A. Abramovitch, Plenum, New York (1980), Vol. 1, p. 263; d) W. M. Jones, in "Rearrangements in Ground and Excited States," ed by P. de Mayo, Academic Press, New York (1980), Vol. 1, p. 95.

2) W. M. Jones, *Acc. Chem. Res.*, **10**, 353 (1977).

3) K. E. Krajca, T. Mitsuhashi, and W. M. Jones, *J. Am. Chem. Soc.*, **94**, 3661 (1972).

4) T. T. Coburn and W. M. Jones, *J. Am. Chem. Soc.*, **96**, 5218 (1974).

5) C. Wentrup, C. Mayor, J. Becker, and H. J. Lindner, *Tetrahedron*, **41**, 1601 (1985).

6) a) S.-I. Murahashi, I. Moritani, and M. Nishino, *J. Am. Chem. Soc.*, **89**, 1257 (1967); b) I. Moritani, S.-I. Murahashi, M. Nishino, Y. Yamamoto, K. Itoh, and N. Masago, *ibid.*, **89**, 1257 (1967); c) S.-I. Murahashi, I. Moritani, and M. Nishino, *Tetrahedron*, **27**, 5131 (1971); d) Y. Yamamoto, I. Moritani, Y. Maeda, and S. Murahashi, *ibid.*, **26**, 251 (1970); e) Y. Yamamoto, S.-I. Murahashi, and I. Moritani, *Tetrahedron Lett.*, **1973**, 589.

7) a) B. B. Wright and M. S. Platz, *J. Am. Chem. Soc.*, **106**, 4175 (1984); b) L. M. Hadel, M. S. Platz, B. B. Wright, and J. C. Scaino, *Chem. Phys. Lett.*, **105**, 539 (1984).

8) W. M. Jones,R. C. Joines, J. A. Myers, T. Mitsuhashi, K. E. Krajca, E. E. Waali, T. L. Davis, and A. B. Turner, *J. Am. Chem. Soc.*, **95**, 826 (1973).

9) J. Magrath and F. W. Fowler, *Tetrahedron Lett.*, **29**, 2171 (1988).

10) M. Minabe, M. Yoshida, and T. Takayanagi, *Bull. Chem. Soc. Jpn.*, **61**, 995 (1988); see for a review, M. Minabe and K. Suzuki, *Yuki Gosei Kagaku Kyokaishi*, **44**, 421 (1986).

The Effect of Hydrogen Sulfide on Acridine Hydrodenitrogenation on a Sulfided NiMo/Al_2O_3 Catalyst

Masatoshi NAGAI
Department of Chemical Engineering, Tokyo University of Agriculture and Technology, Koganei, Tokyo 184
(Received June 14, 1990)

Synopsis. The effect of hydrogen sulfide on acridine hydrodenitrogenation over a sulfided NiMo/Al_2O_3 catalyst at 280—380 °C and 10.1 MPa total pressure was studied. The result showed that the presence of H_2S depressed the total C–N hydrogenolysis at a low P_{H_2S}/P_{H_2} ratio of 1.1—79×10^{-5}, but that it rarely affected the C–N hydrogenolysis at a ratio above 0.003.

Previous studies[1,2] have shown that the presence of various sulfur compounds depressed the C–N hydrogenolysis reactions in the hydrodenitrogenation of acridine and carbazole on the Mo/Al_2O_3 catalysts at 10.1 MPa total pressure. Satterfield *et al.*[3,4] reported, however, that the presence of hydrogen sulfide increased the overall rate of hydrodenitrogenation of pyridine or quinoline on sulfided NiMo/Al_2O_3 catalysts. Recently, Yan *et al.*[5] reported the promoting effect on quinoline hydrodenitrogenation over a sulfided CoMo/Al_2O_3 catalyst. Nickel- or cobalt-promoted molybdenum catalysts might be more active for the C–N hydrogenolysis of nitrogen compounds in the presence of H_2S, as well as the C–S hydrogenolysis. Moreover, the presence of H_2S at a high H_2S/H_2 ratio not only changed the sulfided state of the catalyst's surface[6] but also caused the reduction of organic compounds on MoS_2.[7] In the present work, the effect of the presence of H_2S on acridine hydrodenitrogenation on a sulfided NiMo/Al_2O_3 catalyst is discussed on basis of changes in the ratio of P_{H_2S}/P_{H_2} and the reaction temperature.

Experimental

The study was carried out in a continuous-flow fixed-bed reactor, using the NiMo/Al_2O_3 catalyst and procedures described previously.[1] The catalyst was preheated in air at 450 °C in the reactor before pretreatment. Sulfiding was accomplished *in situ* in a flowing 10 vol% H_2S/H_2 atmosphere (6 $dm^3\ h^{-1}$) at 400 °C for 3 h after the oxidized catalyst was reduced at 400 °C and 10.1 MPa pressure for 3 h. The experiment was performed at 280—380 °C and 10.1 MPa total pressure. A solution of xylene containing 0.25 wt% acridine was fed at a rate of 20 $cm^3\ h^{-1}$ into the reactor with flowing hydrogen at 30 $dm^3\ h^{-1}$. Ethanethiol (0.1 kPa) was added to the feed in order to maintain the sulfided state of the catalyst during the reaction. Ethanethiol was readily decomposable to form H_2S at 10.1 MPa total pressure. No ethanethiol was observed in the reaction products. The reaction reached a steady state in about 3 h. The liquid reaction products were analyzed by FID gas chromatography.

Results and Discussion

The major denitrogenated product was dicyclohexylmethane with a small amount of benzylcyclohexane. Acridine was completely hydrogenated to yield perhydroacridine through *cis*- and *trans*-1,2,3,4,4a,9,9a,10-octahydroacridines, even at 280 °C, while 1,2,3,4,5,6,7,8-octahydroacridine was formed preferentially rather than the 1,2,3,4,4a,9,9a,10-octahydro compounds above 300 °C.

The effect of H_2S on acridine hydrodenitrogenation on the sulfided catalyst at 330 °C is shown in Fig. 1. The presence of H_2S decreased the concentration of dicyclohexylmethane and increased those of octahydroacridine and perhydroacridine. This result showed that the presence of H_2S depressed the C–N hydrogenolysis of perhydroacridine to dicyclohexylmethane at 330 °C. The concentration of dicyclohexylmethane was decreased to 0.18 wt% from 0.2 wt% by the addition of P_{H_2S} of 7.0 kPa from 0.10 kPa at 330 °C, which corresponded to a ratio of P_{H_2S}/P_{H_2} varying from 7.9×10^{-4} to 1.1×10^{-5}. Figure 2 shows, however, that at 280 °C the presence of H_2S decreased the concentrations of perhydroacridine and dicyclohexylmethane and increased that of octahydroacridine. The presence of H_2S depressed the hydrogenation of octahydroacridine to perhydroacridine and resulted in a reduced

Table 1. The Effects of H_2S on Hydrodenitrogenation

Compound	Catalyst	Reaction temperature °C	H_2S pressure kPa	H_2S/H_2 ratio	Effect[a]	Reference
Acridine	Mo/Al_2O_3	280—380	0.3	0.0008	−	1
Carbazole	Mo/Al_2O_3	280—360	0.3	0.0003	−	2
Acridine	NiMo/Al_2O_3	280—340	0.1—7	1.1—79×10^{-5}	−	Present work
Acridine	NiMo/Al_2O_3	300—380	17.8	0.003	+−	Present work
Quinoline	NiMo/Al_2O_3	350—390	13.8—110	2—16×10^{-2}	+−	3,4
Quinoline	NiMo/Al_2O_3	400	0.25	0.052	+	5
SCRII	CoMo/Al_2O_3	400	0.84	0.1	+	7
Benzophenone	MoS_2	200	7.5	1	++	8

a) +, promoting effect; −, depressing effect; +−, a slightly promoting or depressing effect depends on reaction temperature.

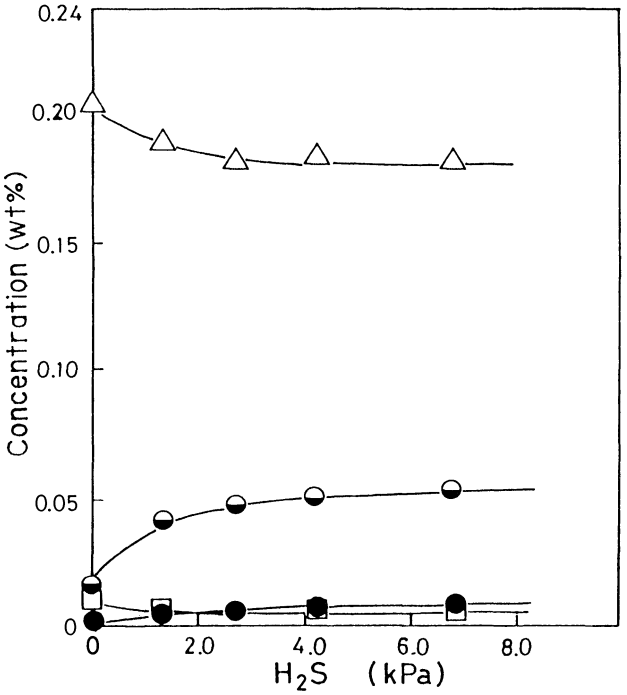

Fig. 1. The effect of H_2S on acridine hydrodenitrogenation on the sulfided $NiMo/Al_2O_3$ catalyst at 330°C and 10.1 MPa total pressure. ●, 1,2,3,4,5,6,7,8-octahydroacridine; ◒, perhydroacridine; △, dicyclohexylmethane; □, benzylcyclohexane.

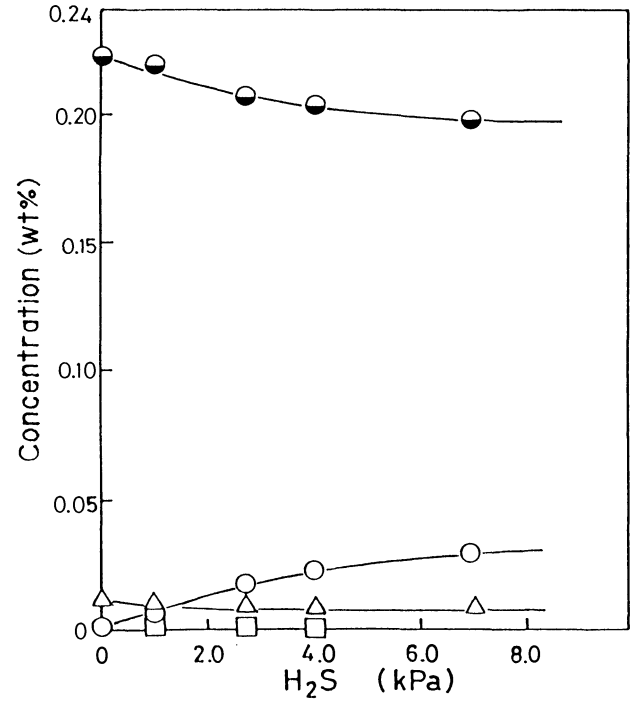

Fig. 2. The effect of H_2S on acridine hydrodenitrogenation on the sulfided $NiMo/Al_2O_3$ catalyst at 280°C and 10.1 MPa total pressure. ○, *cis*- and *trans*-1,2,3,4,4a,9,9a,10-octahydroacridines; See Fig. 1 for other symbols.

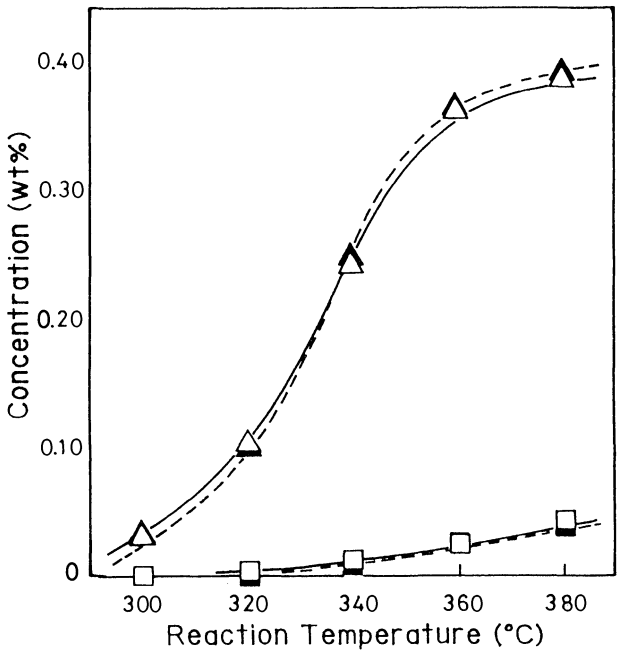

Fig. 3. The hydrodenitrogenation of acridine on the sulfided $NiMo/Al_2O_3$ catalyst at 10.1 MPa total pressure when 0.3 kPa (3×10^{-5} P_{H_2S}/P_{H_2}) (---) and 17.8 kPa (0.003 P_{H_2S}/P_{H_2} ratio) (—) of H_2S were added to the feed; See Fig. 1 for symbols.

C–N hydrogenolysis at lower temperature. These results suggest that the stability of the surface of the sulfided catalyst is probably changed at the reaction temperature.

In order to determine the effect of H_2S on C–N hydrogenolysis at a high ratio of P_{H_2S}/P_{H_2}, the study was carried out at 10.1 MPa total pressure and an H_2S/H_2 ratio of 0.003. The concentration of dicyclohexylmethane was slightly increased at 380°C and remained unchanged up to 360°C. In this case, the presence of H_2S slightly increased the C–N hydrogenolysis at high temperature, but remained unchanged at low temperature. This observation is in agreement with the results obtained by Satterfield and coworkers[3,4] in studies of the hydrodenitrogenation of pyridine and quinoline at 6.9 MPa total pressure and the P_{H_2S}/P_{H_2} ratio of 0.002. Yan et al.[5] reported the promoting effect of H_2S on quinoline hydrodenitrogenation at a H_2S/H_2 ratio of 0.052. Hirschon and Lain[8] also reported the promoting effect on SRCII hydroliquefaction over a $CoMo/Al_2O_3$ catalyst at a H_2S/H_2 ratio of 0.1. Moreover, Itabashi et al.[7] found that the presence of H_2S extremely enhanced the reduction of carbonyl compounds to hydrocarbons over a MoS_2 catalyst at 200°C and about 7.5 MPa H_2S pressure. The promoting effect on the hydrodenitrogenation was carried out at a high ratio of H_2S/H_2 (above 0.003). Consequently, the presence of H_2S depressed the C–N hydrogenolysis at a low P_{H_2S}/P_{H_2} ratio of below 7.9×10^{-4}, but promoted C–N hydrogenolysis at a higher ratio. The total C–N hydrogenolysis remains unchanged at a ratio of about 0.003,

though the effect of H_2S depends on the reaction temperature. The stability of the sulfided catalyst is probably changed thermodynamically in an H_2S/H_2 atmosphere and at the reaction temperature.

References

1) M. Nagai, T. Masunaga, and N. Hanaoka, *J. Catal.*, **101**, 284 (1986).
2) M. Nagai, T. Masunaga, and N. Hanaoka, *Energy Fuel*, **2**, 645 (1988).
3) C. N. Satterfield, M. Modell, and J. A. Wilkens, *Ind. Eng. Chem. Process Des. Dev.*, **19**, 154 (1980).
4) S. H. Yang and C. N. Satterfield, *Ind. Eng. Chem. Process Des. Dev.*, **23**, 20 (1984).
5) J. W. Yan, T. Wakatsuki, T. Obara, and M. Yamada, *Sekiyu Gakkaishi*, **32**, 129 (1989).
6) Y. Yoshimura, S. Yoshitomi, K. Ooishi, T. Sato, H. Shimada, N. Matsubayashi, and A Nishijima, *Preprints of TOCAT*, **1**, 201 (1990).
7) T. Takido, Y. Yamane, and K. Itabashi, *Yukigousei Kyoukai Shi*, **33**, 694 (1975).
8) A. S. Hirschon and R. M. Laine, *Fuel*, **64**, 868 (1985).

Preparation of Ultrafine Particles of Copper by Reduction in a W/O Emulsion System

Hiroyuki ITOH,*,† Moto-o MIURA, Reoki OKAMOTO, and Eiichi KIKUCHI
Department of Applied Chemistry, School of Science and Engineering,
Waseda University, 3-4-1 Okubo, Shinjuku-ku, Tokyo 169
(Received August 20, 1990)

Synopsis. Ultrafine particles (UFP) of Cu were prepared by reduction in a w/o emulsion system, in which Cu(II) ions dissolved in aqueous droplets were reduced by a reducing agent. This method gave a very narrow particle size distribution. Moreover, the average size of UFP could be controlled by choosing the concentration of Cu ions.

Many studies to prepare metallic UFP have been carried out. Although a liquid-phase reduction method[1–3] in which metal ions dissolved in a solution are reduced by a reducing agent is one of these techniques, the conventional liquid-phase reduction method often produces nonreproducible results. The primary objective of this study was to develop a method to prepare UFP having a narrow distribution of particle size. A w/o (water-in-oil) type emulsion system is applied to the conventional liquid-phase reduction method, in which metal ions are dissolved in aqueous droplets in the emulsion.

Experimental

Cu UFP were prepared by reducing Cu(II) ions in an emulsion system. A mixture of a predetermined amount of a $CuCl_2$ aqueous solution, toluene and glycerol monooleate as an emulsifier was vigorously shaken by hand to make an emulsion. The Cu(II) ions were dissolved in water in a w/o-type emulsion as droplets. An excess amount of a $NaBH_4$ aqueous solution was added to the emulsion. A dark-brown "solution" was obtained and then stirred for 1 h. After dilution of the precipitate in the solution with methanol for convenience of subsequent handling, the precipitate was filtered and washed with methanol. The resulting particles were dried in vacuo.

The UFP of Cu were also prepared differently by a conventional liquid-phase reduction method for a comparison. An aqueous solution of $NaBH_4$ was added to the aqueous solution of $CuCl_2$. After being well stirred, the resulting precipitate was first washed with water and then with methanol. The precipitate was dried in vacuo.

All of the procedures were carried out in a nitrogen atmosphere in order to prevent the product from being oxidized.

The average size of aqueous droplets in the emulsion was measured using an optical microscope. The obtained UFP were analyzed by inductively coupled plasma emission spectrometry regarding the chemical composition and by X-ray diffraction method regarding the crystal structure and crystallite size. The particle size distribution was determined by the use of a transmission electron microscope. The size of the UFP was obtained according to a method of Feret,[4] which is one of the methods used to measure the size of irregularly shaped particles. The particle size was defined as being the perpendicular distance between parallel tangents touching opposite sides of the profile.

Results and Discussion

Emulsions. The emulsion prepared by the above-mentioned procedure remained stable upon standing for several hours. An optical micrograph of a typical emulsion is shown in Fig. 1. The sizes of droplets in the emulsion were distributed widely. It is obvious from Fig. 1 that the droplets of the aqueous phase stuck together. The droplet size distributions for emulsions containing the $CuCl_2$ aqueous solution in various concentrations are shown in Fig. 2. It was found that the size of the droplets in the emulsion was independent of the $CuCl_2$ concentration. The mean volumetric diameters of the droplets were determined to be about 15 μm for all of the emulsions used in this study.

Particles. The results of the chemical analysis and the X-ray diffraction analysis are given in Table 1 and Fig. 3, respectively. These results show that the powders obtained in this work were composed of metallic copper and a small amount of Cu_2O. It is not apparent whether the oxide was formed in the course of preparation or during subsequent handling.

Transmission electron micrographs of the UFP prepared in the emulsion system showed sphere-shaped particles, as can be seen in Fig. 4. Similar shaped particles were also observed on the UFP obtained by the conventional method. Figure 5(B) gives the particle size distribution, the mean volumetric diameter (D_v) and the standard deviation of the particle size (SD) of Cu powder prepared in the emulsion system. The particles had a size range from 5 to 40 nm, with a maximum at around 20 nm. The

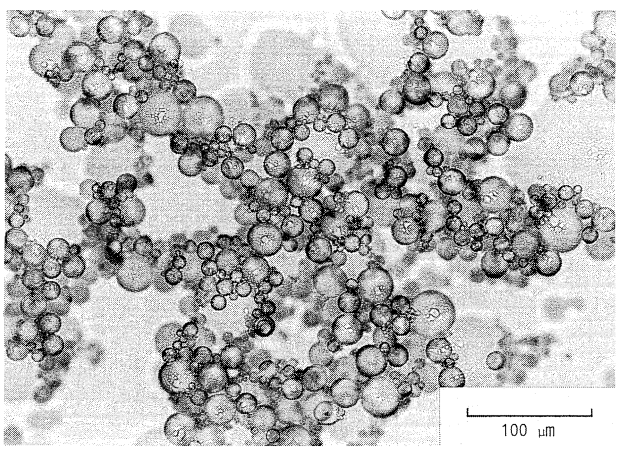

Fig. 1. Optical micrograph of emulsion.

† Present address: Department of Mineral Resources Engineering, School of Science and Engineering, Waseda University, 3-4-1 Okubo, Shinjuku-ku, Tokyo 169.

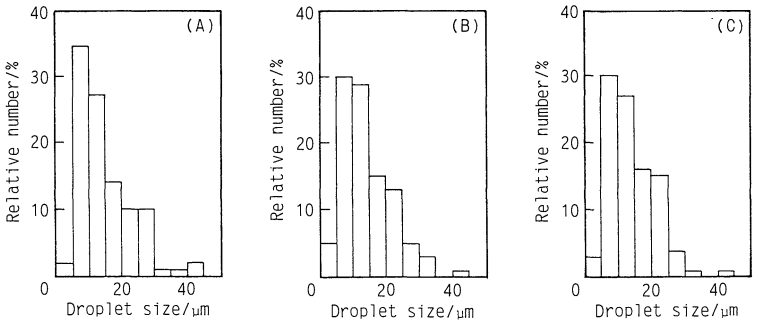

Fig. 2. Effect of $CuCl_2$ concentration in aqueous droplets on distribution of droplet size in emulsions. $CuCl_2$ concentration: A, 0.1; B, 0.5; C, 1 mol dm^{-3}.

Table 1. Composition of Cu UFP Prepared in Emulsion System[a)]

Sample	Composition/wt%			
	Cu	B	Na	Others
A	91.5	Trace	Trace	8.5
B	88.6	Trace	0.2	11.2
C	96.3	Trace	Trace	3.7
D	94.0	Trace	Trace	6.0

a) $CuCl_2$ concentration: A, 1; B, 0.5; C, 0.25; D, 0.1 mol dm^{-3}.

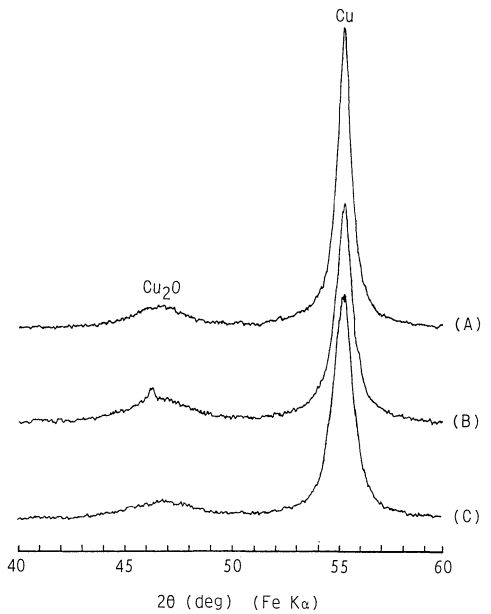

Fig. 3. X-Ray diffraction patterns for Cu UFP prepared in the emulsion system. $CuCl_2$ concentration: A, 1; B, 0.5; C, 0.1 mol dm^{-3}.

size distribution of the particles obtained according to this method was very narrow, when compared with that obtained by the conventional method (Fig. 5(A)).

The formation of particles in the emulsion system was followed by an optical microscope observation, which suggested that the formation of particles or the reduction of Cu ions proceeded according to the following steps, as shown in Fig. 6: (1) initiation of reduction in aqueous droplets, (2) evolution of

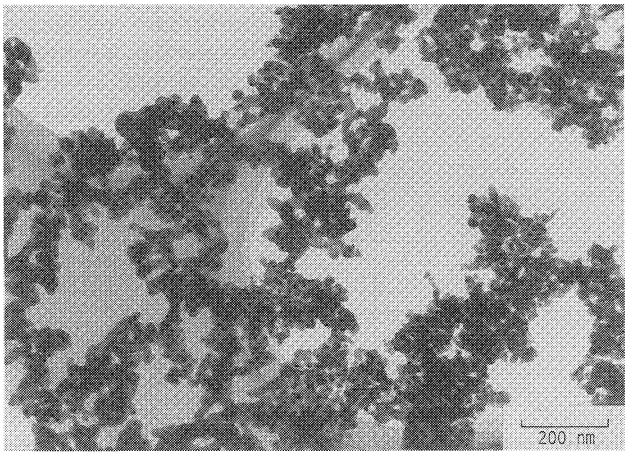

Fig. 4. Transmission electron micrograph of Cu UFP prepared in the emulsion system.

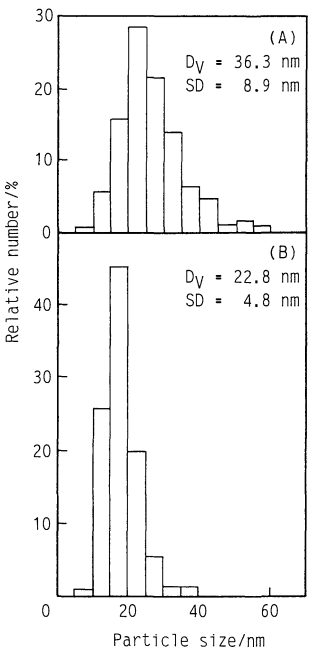

Fig. 5. Particle size distributions, mean volumetric diameters and standard deviations of particle size of Cu UFP obtained by a conventional method (A) and using emulsion system (B).

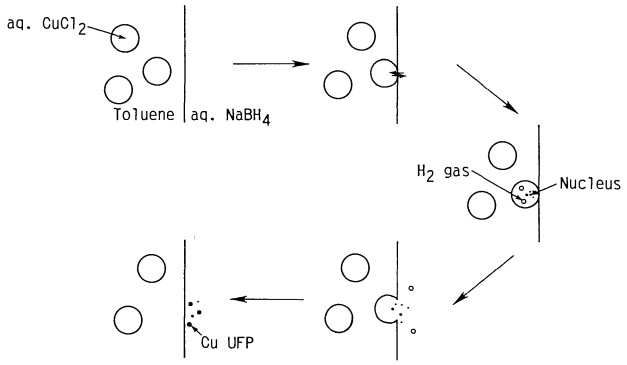

Fig. 6. Model for particle formation in emulsion system.

hydrogen and rupture of the droplets, (3) mixing of the content in droplets with the bulk of the solution of the reducing agent resulting in a further reduction to completion.

From these presumptions, the difference between the powder prepared in the emulsion system and that prepared by the conventional method regarding their particle size distribution is interpreted as being due to a homogeneous reduction of Cu ions: In the case of the conventional method, Cu ions were immediately reduced when the reducing agent was added. Consequently, a local inhomogeneity was unavoidable. On the other hand, in the case of preparation using the emulsion system, the reduction of Cu ions was retarded by toluene, which prevented the Cu ions dissolved in the aqueous droplets from the action of reducing agent. As the aqueous droplets ruptured, reduction took place independently at every droplet. Therefore, homogeneous reduction leading to a narrow particle size distribution was achieved by the use of the emulsion system.

Figure 7 summarizes the effect of the concentration of Cu ions dissolved in aqueous droplets in the emulsion. It is obvious from Fig. 7 that the average particle size was reduced, and that the particle size distribution became narrow with decreasing concentration of Cu ions.

The results presented in this study show that the preparation method using the emulsion system produces UFP having a narrow size distribution. Moreover, the average size of UFP could be controlled by the concentration of Cu ions. It is expected that this method can be used for preparing UFP composed of other materials.

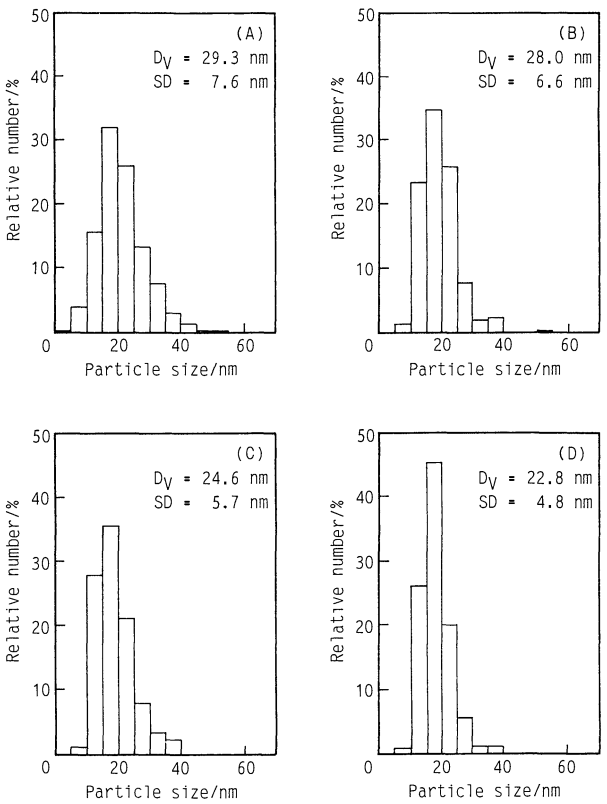

Fig. 7. Effect of $CuCl_2$ concentration in aqueous droplets on particle size distribution, mean volumetric diameter and standard deviation of particle size of Cu UFP. $CuCl_2$ concentration: A, 1; B, 0.5; C, 0.25; D, 0.1 mol dm^{-3}.

References

1) J. van Wonterghem, S. Mørup, C. J. W. Koch, S. W. Charles, and S. Wells, *Nature (London)*, **322**, 622 (1986).

2) A. Corrias, G. Ennas, G. Licheri, G. Marongiu, A. Musinu, G. Paschina, G. Piccaluga, G. Pinna, and M. Magini, *J. Mater. Sci. Lett.*, **7**, 407 (1988).

3) A. Inoue, J. Saida, and T. Masumoto, *Metall. Trans. A*, **19**, 2315 (1988).

4) L. R. Feret, *Assoc. Int. Essai Mater., Congr. Zurich*, **1931**, Vol. 2, Group D (1932).

Oxidation Using Quaternary Ammonium Polyhalides. VIII.[1] Oxidation of 1,4-Benzenediols with Benzyltrimethylammonium Tribromide

Shoji KAJIGAESHI,* Yukihiro MORIKAWA, Shizuo FUJISAKI, Takaaki KAKINAMI,† and Keigo NISHIHIRA††
Department of Industrial Chemistry, Faculty of Engineering,
Yamaguchi University, Tokiwadai, Ube 755
† Department of Chemical and Biological Engineering,
Ube Technical College, Tokiwadai, Ube 755
†† Ube Chemical Factory, Ube Industries Ltd.,
Kogushi, Ube 755
(Received August 31, 1990)

Synopsis. The reaction of 1,4-benzenediols with 1.1 equiv of benzyltrimethylammonium tribromide in dichloromethane in the presence of aqueous sodium acetate at room temperature gave 2,5-cyclohexadiene-1,4-diones in good yields. On the other hand, the reaction of 1,4-benzenediols with a large excess of the reagent in aqueous acetic acid at 40—60°C gave polybromo-substituted 2,5-cyclohexadiene-1,4-diones in good yields.

In general, 1,2- and 1,4-benzenediols are easily oxidized to 3,5-cyclohexadiene-1,2-diones (*o*-benzoquinone derivatives) and 2,5-cyclohexadiene-1,4-diones (*p*-benzoquinone derivatives), respectively. Either or both hydroxyl groups can be replaced by amino groups to give the same quinones. A number of oxidizing agents such as sodium dichromate–sulfuric acid,[2] manganese dioxide,[3] nitrous acid,[4] nitric acid,[5] iron(III) chloride,[6] lead dioxide,[7] nitrosodisulfonate,[8] (diacetoxyiodo)benzene,[9] and salcomin–oxygen[10] have been used. Halogens or their compounds, such as chlorine–hydrochloric acid,[11] bromine–pyridine,[12] chlorine–sodium hypochlorite,[13] sodium hypochlorite,[14] sodium chlorate–vanadium oxide–sulfuric acid,[15] and *N*-bromosuccinimide–water,[16] have also been used.

In previous papers, we have reported that the reaction of 1,4-benzenediol (**1a**) with BTMA Br_3 (2 equiv) in dichloromethane–methanol gave 2,5-dibromo-1,4-benzenediol, electrophilic substitution product, in good yield.[17] In our further investigation regarding the synthetic utility of quaternary ammonium polyhalides, we have now found that benzyltrimethylammonium tribromide (BTMA Br_3) is a useful oxidizing agent.[18] In this paper we wish to report on the oxidation of 1,4-benzenediols (hydroquinone derivatives) (**1**) to 2,5-cyclohexadiene-1,4-diones (**2**) by the use of BTMA Br_3.

Results and Discussion

The reaction of **1** with 1.1 equiv of BTMA Br_3 in dichloromethane in the presence of aqueous sodium acetate at room temperature gave **2** in good yields. The results are summarized in Table (Procedure **A**). The reaction scheme can be represented as follows:

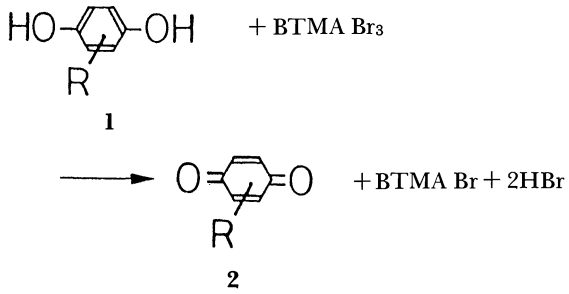

Scheme 1.

Generated hydrogen bromide should be removed with sodium acetate. Otherwise, disodium hydrogenphosphate (equimolar amount for BTMA Br_3) was also used insead of sodium acetate. When aqueous sodium hydroxide was used, a black oil was obtained and the desired benzoquinone derivatives could not be isolated. The end point of the reaction was detected by a decolorization of the initial orange color of the reagent.

Incidentally, when the quantity of the reagent used was less than equivalent weight for **1**, a mixture of **2** and quinhydrone derivatives, dark green needles, was obtained.

The reaction of **1** with BTMA Br_3 (1.1 equiv) in aqueous acetic acid at room temperature also gave **2** in good yields (Table: Procedure **B**). When the reaction of **1** was carried out with a large excess (4.0—7.5 equiv) of the reagent at 40—60°C, polybromo-substituted 2,5-cyclohexadiene-1,4-diones (**3**) were obtained in good yields (Table: Procedure **B**). Products **3** might be derived from **1** through the sequential reactions shown in Scheme 2.

The reaction of 2,5-di-*t*-butyl-1,4-benzenediol (**1b**) with 4—5 equiv of BTMA Br_3 gave only 2,5-di-*t*-butyl-2,5-cyclohexadiene-1,4-dione (**2b**). It can be assumed that 1,4-addition of hydrogen bromide to **2b** does not occur because of the steric hindrance of the bulky *t*-butyl group.

Attempts to prepare 3,5-cyclohexadiene-1,2-diones by the oxidation of 1,2-benzenediols (catechol derivatives) with BTMA Br_3 failed.

We believe that, although many other procedures for the oxidation of **1** to **2** or **3** have been reported, our methods using BTMA Br_3 are characterized by simple operation, mild conditions, and good product yields.

Table 1. Oxidation of 1,4-Benzenediols with BTMA Br_3

Substrate **1**	Procedure A[a] or B[b]	Molar ratio BTMA Br_3/**1**	Reaction conditions Temp/°C	Reaction conditions Time	Product[c] **2** or **3**	Yield[d] %
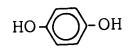 (**1a**)	A	1.1	R.t.	2 h	**2a**	Quant.
	B	1.1	R.t.	5 min	**2a**	Quant.
	B	7.5	60	5 h	**3a**	88
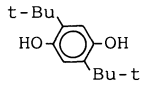 (**1b**)	A	1.1	R.t.	5 h	**2b**	Quant.
	B	1.1	R.t.	10 min	**2b**	Quant.
	B	4.5	60	24 h	**2b**	94
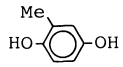 (**1c**)	A	1.1	R.t.	2 h	**2c**	Quant.
	B	1.1	R.t.	10 min	**2c**	96
	B	6.0	60	5 h	**3c**	94
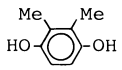 (**1d**)	A	1.1	R.t.	2 h	**2d**	Quant.
	B	1.1	R.t.	10 min	**2d**	Quant.
	B	4.5	60	5 h	**3d**	Quant.
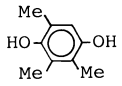 (**1e**)	A	1.1	R.t.	2 h	**2e**	Quant.
	B	1.1	R.t.	10 min	**2e**	93
	B	4.0	40	5 h	**3e**	Quant.
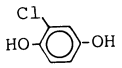 (**1f**)	A	1.1	R.t.	10 h	**2f**	90

a) **A**: Oxidation was carried out in CH_3COONa aq/CH_2Cl_2. b) **B**: Oxidation was carried out in CH_3COOH aq. c) Prodcuts were characterized by comparing ^1H NMR spectra and mp with those of authentic samples or reported data. d) Yield of isolated product.

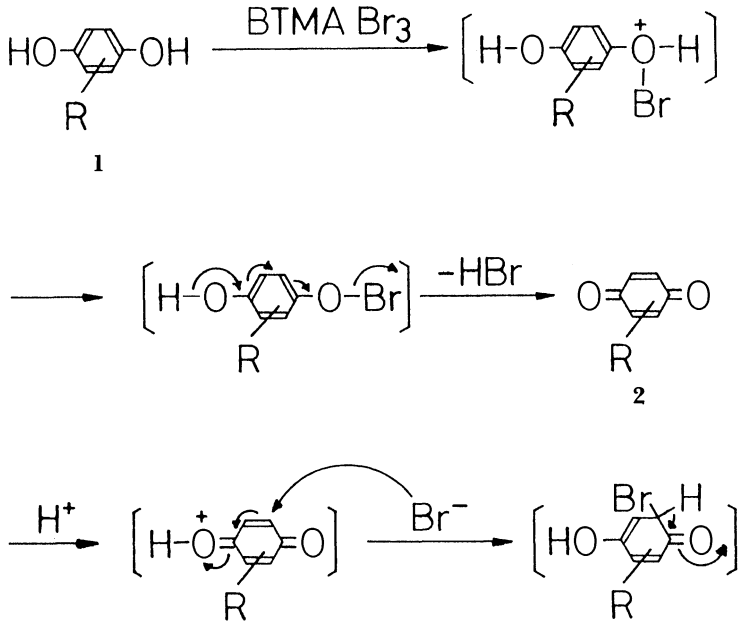

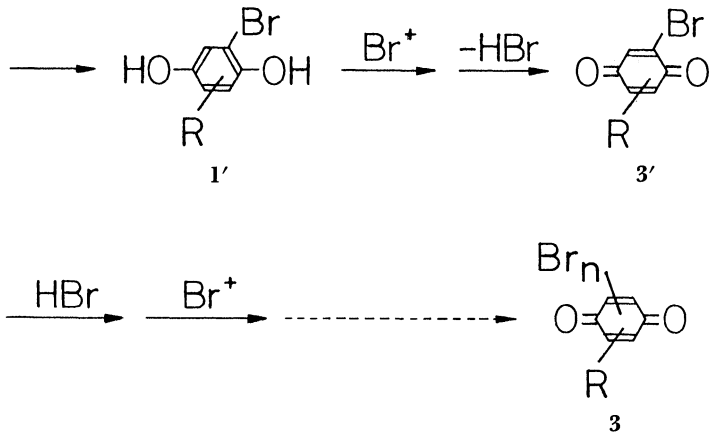

Scheme 2.

Experimental

Oxidation of 1,4-Benzenediol (1a) with BTMA Br_3-CH_3COONa aq. Representative procedures are as follows. To a solution of sodium acetate hydrate ($CH_3COONa \cdot 3H_2O$) (0.82 g, 6 mmol) in water (20 ml) was added **1a** (0.22 g, 2 mmol) and a solution of BTMA Br_3 (0.86 g, 2.2 mmol) in dichloromethane (10 ml). The mixture was stirred at room temperature for only 2 min until the initial orange color faded. Then, the water layer was filtered through wet filter paper. The separated organic layer was washed with water and dried over $MgSO_4$, filtered, and evaporated in vacuo give 2,5-cyclohexadiene-1,4-dione (*p*-benzooquinone) (**2a**) as a yellow needles; yield 0.22 g (quant.); mp 113—115 °C (lit,[19] mp 114.6—115.6 °).

Oxidation of 2,5-Di-*t*-buty-1,4-benzenediol (1b) with BTMA Br_3-AcOH aq. BTMA Br_3 (0.86 g, 2.2 mmol) was added into a solution of **1b** (0.44 g, 2 mmol) in acetic acid (5 ml)-water (10 ml). The mixture was stirred at room temperature for 10 min until the initial orange red color faded. The reaction mixture was extracted with dichloromethane (10 ml×3) and the organic layer was washed with water and dried over $MgSO_4$, filtered, and evaporated in vacuo to give 2,5-di-*t*-butyl-2,5-cyclohexadine-1,4-dione (**2b**) as yellow needles; yield 0.44 g (quant.) mp 153—154 °C (lit,[20] mp 153 °C).

Preparation of 3,5,6-Tribromo-2-methyl-2,5-cyclohexadiene-1,4-dione (3c). BTMA Br_3 (4.68 g, 12 mmol) was added into a solution of 2-methyl-1,4-benzenediol (**1c**) (0.25 g, 2 mmol) in acetic acid (5 ml)-water (10 ml). The mixture was stirred at 60 °C for 5 h, and then allowed to stand at room temperature. Water (100 ml) was added into the reaction mixture and the mixture was cooled in an ice bath. Deposited yellow solids were filtered and washed with water. The filtrate and washings were combined and extracted with ether (20 ml). The ether solution was evaporated in vacuo to give **3c** as yellow plates; yield 0.68 g (94%); mp 243—245 °C (lit,[21] mp 233 °C).

References

1) Part VII of this series: A. Nishida, N. Kohro, S. Fujisaki, and S. Kajigaeshi, *Tech. Rep. Yamaguchi Univ.*, **4**, 309 (1990).
2) E. B. Vliet, *Org. Synth.*, Coll. Vol. I, 482 (1956); L. F. Fieser, *ibid.*, Coll. Vol. I, 383 (1956).
3) K. R. Bharucha, *J. Chem. Soc.*, **1956**, 2446.
4) E. Kremers, N. Wakeman, and R. M. Hixon., *Org. Synth.*, Coll. Vol. I, 511 (1956).
5) E. L. Martin and L. F. Fieser, *Org. Synth.*, Coll. Vol. III, 633 (1955).
6) L. F. Fieser, *Org. Synth.*, Coll. Voll. II, 430 (1950); L. I. Smith, *ibid.*, Coll. Vol. II, 254 (1950).
7) A. R. Surrey, *Org. Synth.*, Coll. Vol. III, 753 (1955).
8) H. Teuber and W. Rau, *Chem. Ber.*, **86**, 1036 (1953).
9) A. Pelter and S. Elgendy, *Tetrahedron Lett.*, **29**, 677 (1988); G. B. Barlin and N. V. Riggs, *J. Chem. Soc.*, **1954**, 3125.
10) C. R. H. I. De Jonge, H. I. Hageman, G. Hoentjen, and W. J. Mijs, *Org. Synth.*, **57**, 78 (1977).
11) R. Schluloff and R. Polak, *Chem.-Ztg.*, **56**, 569 (1932).
12) E. deB. Barnett and M. A. Mattews, *J. Chem. Soc.*, **123**, 380 (1923).
13) B. P. Fedorov and V. A. Semenova, *J. Appl. Chem.*, **13**, 1076 (1941).
14) R. Willstätter and E. Mayer, *Ber.*, **37**, 1494 (1904).
15) H. W. Underwood, Jr. and W. L. Walsh, *Org. Synth.*, Coll. Vol. II, 553 (1966).
16) M. Z. Barakat, M. F. A. El-Wahab, and M. M. El-Sadr, *J. Am. Chem. Soc.*, **77**, 1670 (1955).
17) S. Kajigaeshi, T. Kakinami, H. Tokiyama, T. Hirakawa, and T. Okamoto, *Chem. Lett.*, **1987**, 627.
18) S. Kajigaeshi, K. Asano, S. Fujisaki, T. Kakinami, and T. Okamoto, *Chem. Lett.*, **1989**, 463; S. Kajigaeshi, T. Kakinami, T. Yamaguchi, T. Uesugi, and T. Okamoto, *Chem. Express*, **4**, 177 (1989); S. Kajigaeshi, H. Kawamukai, and S. Fujisaki, *Bull. Chem. Soc. Jpn.*, **62**, 2585 (1989); S. Kajigaeshi, K. Murakawa, K. Asano, S. Fujisaki, T. Kakinami, and T. Okamoto, *J. Chem. Soc., Perkin Trans. 1*, **1989**, 1702; S. Kajigaeshi, K. Murakawa, S. Fujisaki, and T. Kakinami, *Bull. Chem. Soc. Jpn.*, **62**, 3376 (1989); T. Okamoto, T. Uesugi, T. Kakinami, T. Utsunomiya, and S. Kajigaeshi, *Bull. Chem. Soc. Jpn.*, **62**, 3748 (1989).
19) R. E. Harman and J. Cason, *J. Org. Chem.*, **17**, 1058 (1952).
20) F. J. L. Aparicio and W. A. Waters, *J. Chem. Soc.*, **1952**, 4666.
21) J. M. Audrews, D. H. Marrian, and D. R. Maxwell, *J. Chem. Soc.*, **1956**, 1844.

Temperature- or Pressure-Induced Structure Changes of a Spin Crossover Fe(II) Complex; $[Fe(bpy)_2(NCS)_2]$

Michiko KONNO* and Mami MIKAMI-KIDO†
Department of Chemistry, Faculty of Science, Ochanomizu University, Ohtsuka, Bunkyo-ku, Tokyo 112
†Faculty of Liberal Arts, Information Science, Tohokugakuin University, Ichinazaka, Izumi-ku, Sendai, Miyagi 980
(Received April 16, 1990)

The crystal structures of polymorph II of diisothiocyanatobis(2,2′-bipyridine)iron(II), $[Fe(bpy)_2(NCS)_2]$, in the high- (298 K) and low-spin states (175, 110 K) were determined by an X-ray diffraction method. The crystal is orthorhombic, space group *Pcnb* and $Z=4$ over the entire temperature range. At 298 K, $a=13.2044$ (6), $b=16.4820$ (7), $c=10.1086$ (7) Å, $U=2200.0$ (2) Å^3, $D_c=1.462$ g cm^{-3} and at 110 K, $a=12.9842$ (9), $b=16.1067$ (12), $c=9.8938$ (8) Å, $U=2069.1$ (3) Å^3, $D_c=1.555$ g cm^{-3}. The structures were refined to $R=0.047$, 0.044, and 0.042 at 298, 175, and 110 K, respectively. The difference in the average Fe-N bond lengths between high- and low-spin states is 0.17 Å. The pressure dependence of the absorption spectra was also measured up to 8.5 GPa using a diamond anvil cell. These results indicate that with increasing pressure the high-spin state at 1 atm starts to change to the low-spin state at 0.3 GPa and that its low-spin state reverts again to the high-spin state at around 3.3 GPa.

Some iron(II) and iron(III) complexes exhibit spin transitions induced by temperature or pressure between different spin multiplicities.[1-4] Especially in iron(II) complexes, a drastic change was observed in the metal-ligand bond distance between high- and low-spin states[5-12] It is interesting to study the ligand field as well as the mechanism of spin transitions, since changes of ligand substituents, counter anions, solvent molecules, complex geometries, crystal forms, and states (solid or solution) cause various types of conversions between different spin states. Several theoretical models, a cooperative Jahn-Teller interaction,[13,14] the coupling to lattice vibrations[15] and the elastic interaction between high- and low-spin ions via an image pressure,[16] have been introduced in order to lead to a cooperative nature of the spin transitions. In order to understand the nature and the mechanism of spin transitions, it is necessary to investigate the difference among molecular geometries and molecular interactions between low- and high-spin states. The $[Fe(\alpha\text{-pic})_3]^{2+}$ system (α-pic=α-picolylamine) is one of the interesting ionic spin crossover complexes, since the effective magnetic moments depend on the nature of the counter anions or solvent molecules.[17-21] We determined the crystal structures of the $[Fe(\alpha\text{-pic})_3]Cl_2 \cdot EtOH$ compound at 298, 150, and 90 K and found that the average bond distance contracted by 0.18 Å upon making a transition from the high- to the low-spin state.[6,7] On the other hand, $[Fe(phen)_2(NCS)_2]$ (phen=1,10-phenanthroline) and $[Fe(bpy)_2(NCS)_2]$ complexes without solvent molecules are typical molecular spin crossover complexes showing discontinuous spin transitions; they have been investigated in detail by various means.[22-28] König et al.[24] reported on the magnetic susceptibility and Mössbauer spectra for three polymorphs of the $[Fe(bpy)_2(NCS)_2]$ complex as well as the preliminary results of the crystal structure ($R=0.19$—0.20) of polymorph II determined by a photographic method.[5] The difference in the Fe-N bond lengths (0.12 Å) between the high- and low-spin states observed by them appears to be small compared with those observed in other iron(II) spin crossover complexes.[6,7,11] We redetermined the crystal structures of the polymorph II of $[Fe(bpy)_2(NCS)_2]$ at 298, 175, and 110 K by a diffractometer method in order to gain more accurate information and to interpret the nature of the phase transitions and different magnetic behaviors between polymorphs I and II in the temperature range from 273 to 220 K. The change in the absorption spectra was also measured with increasing pressure up to 8.5 GPa in order to investigate the pressure effects for spin states.

Experimental

X-Ray Structure Analysis. Crystals were deep red and thin hexagonal (0 1 0) plates. The crystal specimens used for X-ray data collection were sealed in Lindemann-glass capillaries, since they are rather sensitive to air exposure. Oscillation and Weissenberg photographs taken at room temperature showed the crystal to be polymorph II. The crystal was cooled in a cold N_2 gas flow and kept constant at 175±1 and 110±1 K. The unit cell dimensions were refined by least-squares methods based on the values of 31, 19, and 16 reflections at 298, 175, and 110 K, respectively. The intensities were measured on an automated four-circle diffractometer with Mo$K\alpha$ radiation ($\lambda=0.71069$ Å) monochromated by graphite plate. Three standard reflections were recorded every fifty reflections. Though Lorentz and polarization corrections were applied, no correction was made for either absorption or extinction. Crystal data are summarized in Table 1.

The structure was solved by the conventional heavy-atom method. After several refinement cycles, difference syntheses showed an orientational disorder of an S atom on the

Table 1. Crystal Data of $[Fe(bpy)_2(NCS)_2]$

$[Fe^{II}(C_{10}H_8N_2)_2(NCS)_2]$, M.W. 484.38			
Orthorhombic, Space group *Pcnb*, $Z=4$			
	High-spin state	Low-spin state	
T/K	298	175	110
a/Å	13.2044(6)	13.0101(7)	12.9842(9)
b/Å	16.4820(7)	16.1384(11)	16.1067(12)
c/Å	10.1086(7)	9.9340(7)	9.8938(8)
U/Å^3	2200.0(2)	2085.8(2)	2069.1(3)
D_c/g cm^{-3}	1.462	1.543	1.555
μ(Mo $K\alpha$)/mm^{-1}	0.91	0.96	0.96
Crystal size/mm	0.40×0.35×0.18	0.33×0.27×0.15	
Scan method	ω-2θ	ω	ω
$2\theta_{max}$/°	60	55	55
Maximum repeating number	3	1	1
Independent reflections			
$[\|F_o\|\geq 3\sigma(\|F_o\|)]$	1379	1790	1835
R[a)]	0.047	0.044	0.042
R_2[a)]	0.055	0.052	0.053

a) $R=\sum\||F_o|-|F_c|\|/\sum|F_o|$. $R_2=\{\sum(|F_o|-|F_c|)^2/\sum|F_o|^2\}^{1/2}$.

NCS ligand at room temperature. Full-matrix least-squares refinements including a population of this disordered S atom were carried out by using a program called RADIEL.[29] In the low-spin state (175 and 110 K) the NCS group takes a regular position. Anisotropic thermal parameters were applied, except for H atoms and disordered S atom with a low population. Scatterring factors for Fe^{2+}, S, N, and C atoms were taken from International Tables for X-ray Crystallography[30] and for H atom from Stewart, Davidson, and Simpson.[31] The unit weight was used for all of the reflections. The final refinements for reflections corresponding to $|F_o|\geq 3\sigma(|F_o|)$ led to convergences of R=0.047, 0.044, and 0.042 at 298, 175, and 110 K, respectively. Final atomic parameters are given in Tables 2, 3, and 4.[32]

Table 2. Positional Parameters for Non-Hydrogen Atoms (×10^4, for Fe ×10^5, for S(2)×10^3) in the High-Spin State (298 K)

Atom	x	y	z	10^3U_{eq}[b)]/Å^2
Fe	0	25000	11320(9)	57 (0)
S(1)	−1129 (3)	1027 (5)	4934 (8)	87 (1)
N(1)	−557 (4)	1729 (3)	2551 (5)	85 (2)
N(2)	−240 (3)	1568 (2)	−367 (3)	55 (1)
N(3)	1476 (3)	1965 (2)	795 (4)	61 (1)
C(1)	−809 (4)	1433 (3)	3515 (5)	61 (2)
C(2)	−1143 (4)	1350 (3)	−858 (5)	68 (2)
C(3)	−1287 (5)	692 (4)	−1682 (5)	76 (2)
C(4)	−467 (5)	238 (4)	−2021 (6)	80 (2)
C(5)	466 (5)	443 (3)	−1529 (5)	71 (2)
C(6)	561 (3)	1108 (3)	−693 (4)	55 (2)
C(7)	1531 (3)	1354 (3)	−89 (5)	59 (2)
C(8)	2450 (4)	974 (4)	−381 (7)	89 (2)
C(9)	3312 (5)	1248 (5)	236 (8)	104 (3)
C(10)	3273 (5)	1856 (4)	1105 (8)	95 (3)
C(11)	2341 (5)	2202 (4)	1375 (7)	87 (2)
S(2)	−129 (2)	80 (2)	448 (3)	87 (6)[a)]

The populations for disordered atoms S are S(1)= 0.87(2) and S(2)=0.13(2).
a) Isotropic thermal parameter is given for S(2).
b) $U_{eq}=1/3\sum_i\sum_j U_{ij}a_i^*a_j^*\boldsymbol{a}_i\cdot\boldsymbol{a}_j$.

Table 3. Positional Prameters for Non-Hydrogen Atoms (×10^4, for Fe, S ×10^5) in the Low-Spin State (175 K)

Atom	x	y	z	10^3U_{eq}[b)]/Å^2
Fe	0	25000	9180(7)	21 (0)
S	−10576(8)	10402(7)	47729(11)	37 (0)
N(1)	−413 (3)	1740 (2)	2342 (3)	29 (1)
N(2)	−303 (2)	1635 (2)	−421 (3)	21 (1)
N(3)	1376 (2)	1994 (2)	812 (3)	23 (1)
C(1)	−679 (3)	1456 (2)	3347 (4)	24 (1)
C(2)	−1227 (3)	1454 (2)	−949 (4)	26 (1)
C(3)	−1392 (3)	783 (2)	−1789 (4)	29 (1)
C(4)	−579 (3)	272 (2)	−2107 (4)	30 (1)
C(5)	372 (3)	442 (2)	−1571 (4)	29 (1)
C(6)	491 (3)	1119 (2)	−712 (3)	22 (1)
C(7)	1460 (3)	1340 (2)	−49 (4)	23 (1)
C(8)	2385 (3)	934 (3)	−241 (5)	35 (1)
C(9)	3259 (3)	1207 (3)	412 (5)	37 (1)
C(10)	3177 (3)	1868 (3)	1273 (4)	35 (1)
C(11)	2227 (3)	2242 (2)	1463 (4)	31 (1)

Table 4. Positional Prameters for Non-Hydrogen Atoms (×10^4, for Fe, S ×10^5) in the Low-Spin State (110 K)

Atom	x	y	z	10^3U_{eq}[b)]/Å^2
Fe	0	25000	9032(6)	15 (0)
S	−10539(7)	10520(6)	47886(9)	26 (0)
N(1)	−415 (2)	1743 (2)	2335 (3)	21 (1)
N(2)	−306 (2)	1631 (2)	−430 (3)	15 (1)
N(3)	1376 (2)	1991 (2)	795 (3)	17 (1)
C(1)	−677 (3)	1462 (2)	3355 (3)	18 (1)
C(2)	−1236 (2)	1455 (2)	−962 (3)	19 (1)
C(3)	−1406 (3)	776 (2)	−1799 (3)	22 (1)
C(4)	−593 (3)	260 (2)	−2118 (3)	22 (1)
C(5)	364 (3)	426 (2)	−1573 (3)	20 (1)
C(6)	487 (2)	1113 (2)	−727 (3)	16 (1)
C(7)	1459 (2)	1334 (2)	−53 (3)	17 (1)
C(8)	2384 (3)	915 (2)	−244 (4)	24 (1)
C(9)	3255 (3)	1184 (2)	423 (4)	26 (1)
C(10)	3179 (3)	1864 (2)	1273 (4)	25 (1)
C(11)	2236 (3)	2238 (2)	1449 (4)	23 (1)

Absorption Spectra Measurements at High Pressures. The absorption spectra of a single crystal of $[Fe(bpy)_2(NCS)_2]$ were measured under high pressure up to 8.5 GPa in the wavelength region 450—800 nm. A diamond anvil cell was used to generate high pressure.[33] Measurements were carried out by using a microscopic optical measurement system comprising a Nikon G250 spectrometer. A mixed solvent of pentane and isopentyl alcohol (1 : 1) was used for the pressure medium, since crystals are soluble to methyl or ethyl alcohol. A pressure calibration was made based on a shift of the ruby luminescence peaks. A He-Cd laser was employed for ruby excitation; its beam was 10 μm in diameter. Changes in the crystals were visually observed under the microscope and a TV monitor.

Results and Discussion

Crystal Structure. A projection of the crystal structure along the c-axis in the high-spin state is given in Fig. 1 and those along b-axis in both spin states are shown in Figs. 2(a) and (b). An iron atom of $[Fe(bpy)_2(NCS)_2]$ molecule lies on a crystallographic two-fold axis along the c-axis and is octahedrally coordinated by two N atoms of isothiocyanate ligands in the cis-configuration and four N atoms of bidentate bipyridine ligands. The molecular symmetry of the structure remains the same in both high- and low-spin states. The general feature of the structure is the same as that reported by König and Watson.[5] However, remarkable structural changes according to the electronic configuration of two spin states including some orientational disorder of the NCS ligand were revealed from the present results. No crystallographic change was observed in the temperature range from 175 to 110 K, although a thermal anomaly at 145 K was observed in the heat-capacity measurements by Takahashi et al.,[34] besides a thermal anomaly at 213 K associated with the spin transition. The bond lengths and angles at 175 and 110 K are in good agreement within twice the esd's. They are listed in Table 5 together with those at 298 K. The average Fe-N value is 2.133 Å (298 K) in the high-spin state, while 1.962 (3) Å (175 K) and 1.959 (3) Å (110 K) in the low-spin state. The Fe-N bond difference of 0.17 Å between low- and high-spin states is consistent with that (0.18 Å) observed in $[Fe(\alpha\text{-pic})_3]Cl_2 \cdot EtOH$[6,7] and that (0.20 Å) observed between bis[hydrotris-(1-pyrazolyl)borato]iron(II) in the low-spin state and bis[hydrotris(3,5-dimethyl-1-pyrazolyl)borato]iron(II) in the high-spin state.[11] When looked into with more detail, the Fe-N bond distances were found to shorten by 0.207 Å for the bipyridine ligand and by 0.106 Å for the NCS ligand upon transition from the high- to low-spin state. The considerable $Fe\text{-}N_{(bpy)}$ shortening in the low-spin state appears to show large increase of back-donation of the $d\pi$ electron of the Fe atom to an empty π^* orbital of the bipyridine ligand, as was observed in $Fe\text{-}N_{(py)}$ of $[Fe(\alpha\text{-pic})_3]Cl_2 \cdot EtOH$ compound.[6,7]

The distortion on the FeN_6 core from an octahedron is smaller in the low-spin state than in the high-spin state. The twist angle between two triangles, which are defined by three N atoms on the planes perpendicular to the pseudo three-fold axis, is 45° in the high-spin state and 49° in the low-spin state. The tilt angle between two triangular faces is 8.2° at 298 K and 1.1° at 110 K. The N(1)-Fe-N(3) angle decreases from 100.4(2)° to 91.6(1)° upon going from the high- to the low-spin state, while N(1)-Fe-N(2′) and N(3)-Fe-N(3′) became closer to a linear configuration. Though the increases of the angle in N(2)-Fe-N(2′) and N(2)-Fe-N(3′) are in opposite directions, it seems to be related to a relative detachment of two bipyridine ligands with respect to each other in the low-spin state. This possibly occurs through a repulsion

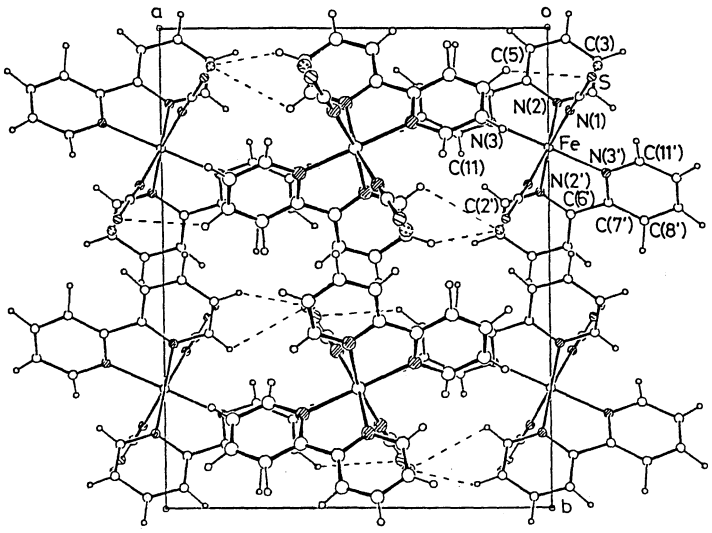

Fig. 1. A projection of $[Fe(bpy)_2(NCS)_2]$ in the high-spin state (298 K) along c-axis.

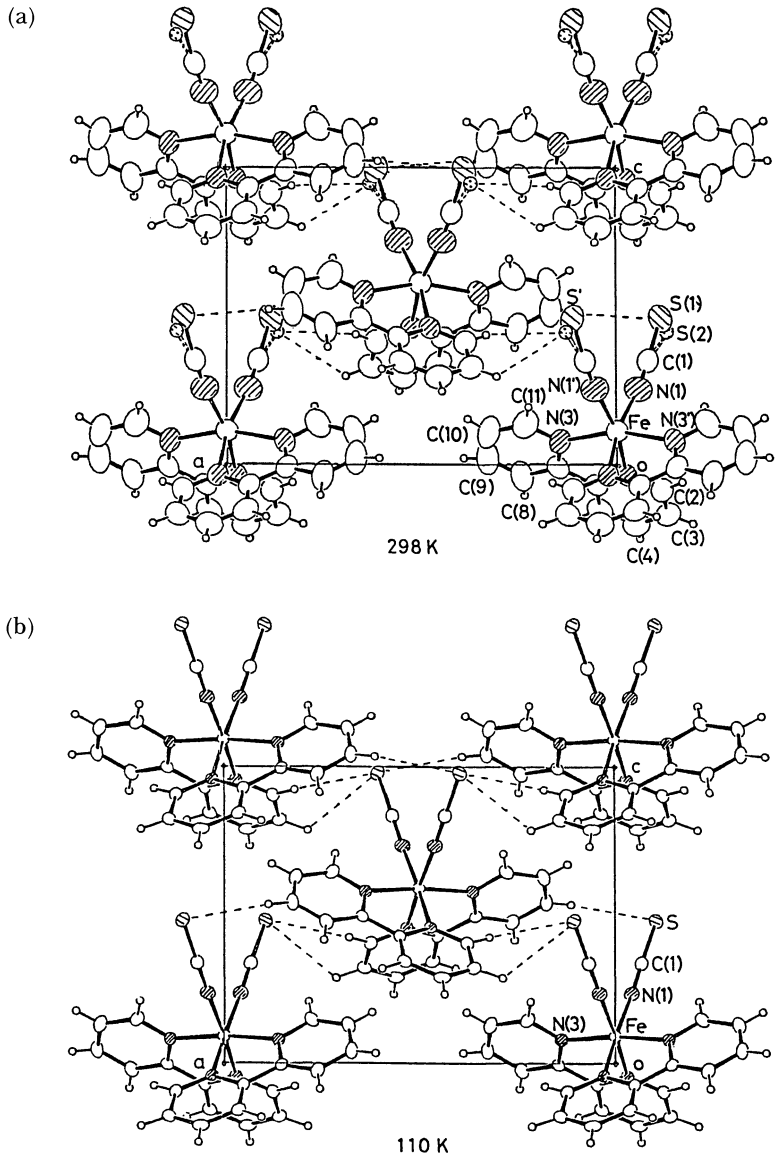

Fig. 2. Projections of $[Fe(bpy)_2(NCS)_2]$ along b-axis. (a) in the high-spin state (298 K), (b) in the low-spin state (110 K). Broken lines show short contacts between S and H atoms.

between an anti-bonding π^* orbital of bipyridine ligands, which has increased occupancy in the low-spin state due to the back-donation.

In the high-spin state the NCS ligands exhibit an orientational disorder of the S atoms at two sites with a population ratio ca. 7 : 1; in the low-spin state the NCS ligand takes a regular position. The S atom with a lower population contacts to H(3) with a short distance of 2.80(6) Å, indicating a weak hydrogen-bond between them. The interatomic distance between the S atom with a higher population and H(9) is 2.95(6) Å. On the other hand, in the low-spin state the NCS ligand takes the same arrangement as that of higher occupancy in the high-spin structure. A short contact between adjacent molecules is found between the S and H(9) with an interatomic distance of 2.89 (4) Å.

The bond distances and angles of the NCS ligand show that it resonates between the $Fe\text{-}N^-\text{=}C\text{=}S$ and $Fe\text{-}N\text{-}C\equiv S^-$ structures. The N(1)-C(1) bond distance is 1.139 (7) and 1.153 (4) Å at 298 and 110 K, respectively, indicating that the bond order is almost triple. The C(1)-S(1) bond length appears to be constant in both the high- and low-spin states and the average value of 1.638 Å seems to suggest that the bond order is between double and single, being much closer to the former. The larger occupation in the $Fe\text{-}N^-\text{=}C\text{=}S$ configuration brings about a larger deviation from 180° regarding the Fe-N-C bond angle owing to the sp^2 configuration of the N atom. The Fe-N(1)-C(1) angle is

Table 5. Bond Lengths and Bond Angles with esd's in Parentheses[a)]

T/K	298	175	110
(a) Bod lengths (l/Å)			
Fe-N(1)	2.053(5)	1.947(3)	1.945(3)
Fe-N(2)	2.181(4)	1.969(3)	1.964(2)
Fe-N(3)	2.166(4)	1.970(3)	1.969(3)
N(1)-C(1)	1.139(7)	1.152(5)	1.157(4)
C(1)-S	1.638(9)	1.642(4)	1.639(3)
N(2)-C(2)	1.341(6)	1.343(5)	1.348(4)
N(2)-C(6)	1.343(6)	1.357(4)	1.357(4)
N(3)-C(7)	1.349(6)	1.363(4)	1.355(4)
N(3)-C(11)	1.341(8)	1.343(5)	1.350(4)
C(2)-C(3)	1.380(8)	1.384(5)	1.389(5)
C(3)-C(4)	1.360(9)	1.379(6)	1.379(5)
C(4)-C(5)	1.371(9)	1.375(6)	1.381(5)
C(5)-C(6)	1.390(7)	1.395(5)	1.396(4)
C(6)-C(7)	1.475(6)	1.466(5)	1.471(4)
C(7)-C(8)	1.397(8)	1.384(5)	1.390(5)
C(8)-C(9)	1.374(9)	1.381(6)	1.380(5)
C(9)-C(10)	1.335(11)	1.375(6)	1.385(5)
C(10)-C(11)	1.383(9)	1.388(6)	1.376(5)
(b) Bond angles (ϕ/°)			
N(1)-Fe-N(2)	89.9(2)	89.4(1)	89.2(1)
N(1)-Fe-N(3)	100.4(2)	91.6(1)	91.7(1)
N(2)-Fe-N(3)	74.6(1)	81.5(1)	81.4(1)
N(1)-Fe-N(1′)	91.4(2)	86.8(1)	86.5(1)
N(1)-Fe-N(2′)	166.9(2)	173.1(1)	172.7(1)
N(1)-Fe-N(3′)	92.3(2)	92.8(1)	92.8(1)
N(2)-Fe-N(2′)	92.0(1)	95.0(1)	95.6(1)
N(2)-Fe-N(3′)	92.7(1)	94.3(1)	94.4(1)
N(3)-Fe-N(3′)	161.9(2)	173.9(1)	173.8(1)
Fe-N(1)-C(1)	165.3(4)	164.4(3)	164.4(3)
Fe-N(2)-C(2)	125.1(3)	126.7(2)	126.4(2)
Fe-N(2)-C(6)	117.0(3)	115.2(2)	115.5(2)
Fe-N(3)-C(7)	117.1(3)	115.3(2)	115.5(2)
Fe-N(3)-C(11)	125.4(4)	126.9(3)	127.0(2)
N(1)-C(1)-S	177.4(6)	179.3(4)	179.2(3)
C(6)-N(2)-C(2)	117.3(4)	117.7(3)	117.8(3)
N(2)-C(2)-C(3)	123.8(5)	123.0(3)	122.7(3)
C(2)-C(3)-C(4)	118.3(6)	119.1(4)	119.3(3)
C(3)-C(4)-C(5)	119.2(6)	118.8(4)	118.8(3)
C(4)-C(5)-C(6)	119.8(6)	119.5(4)	119.4(3)
C(5)-C(6)-N(2)	121.5(4)	121.7(3)	122.0(3)
N(2)-C(6)-C(7)	115.3(4)	114.2(3)	113.8(3)
C(11)-N(3)-C(7)	117.5(4)	117.8(3)	117.5(3)
N(3)-C(7)-C(8)	121.4(5)	121.5(3)	122.1(3)
C(7)-C(8)-C(9)	118.4(6)	120.0(4)	119.4(3)
C(8)-C(9)-C(10)	120.9(7)	118.5(4)	118.7(3)
C(9)-C(10)-C(11)	118.3(7)	119.3(4)	119.1(3)
C(10)-C(11)-N(3)	123.5(6)	122.8(4)	123.1(3)
N(3)-C(7)-C(6)	115.7(4)	113.6(3)	113.7(3)

a) Primed and unprimed atoms are related by a two-fold axis along the c-axis through the iron atom of the molecule.

165.3 (4)° at 298 K and 164.4 (3)° at 110 K, both of them shifting from linear coordination. A deviation of the M-N-C angle from 180° is usually found in octahedral coordination of the NCS ligand;[35,36] in tetrahedrally coordinated complex, however, $Co(NCS)_4Hg$, Co-N-C was observed to be linear.[37]

Two pyridine rings within a bipyridine ligand are slightly bent with respect to a five-membered ring in the opposite direction. As shown in Fig. 1, two pyridine rings of neighboring complexes related by a symmetry center are parallel and overlap each other with an interplanar distance of 3.503 Å (298 K) in the high-spin state and 3.495 Å (175 K) and 3.457 Å (110 K) in the low-spin state. There seems to be a charge-transfer interaction between these rings. The change of the interplanar distance upon a spin transition is small compared to the value expected from thermal expansion, suggesting that the occupation of the π^* orbital of the bipyridine ligand due to a back-donation in the low-spin state weakens the π-π^* charge transfer interaction between them.

Absorption Spectra at High Pressure. The absorption maximum was observed around 540 nm for the spectra of $[Fe(bpy)_2(NCS)_2]$ in the high-spin state at 1 atm; this was in good agreement with the results reported by Takahashi et al.[38] When the crystal was pressed to 0.4 GPa, the color darkened from deep red to dark red and the spectra exhibited a fine structure with two maxima at 545 and 570 nm. This indicates that the spin state had started to change from the high-spin to the low-spin state at 0.3 GPa, since the low-spin state spectra at 77 K/1 atm has two maxima at 538 and 595 nm.[38] The absorption edge of the spectra showed a remarkable red shift with increasing pressure and intensity saturation was observed in the wavelength region less than 600 nm. The intense visible absorption band around 600 nm can be assigned to a charge-transfer transition of t_{2g} to the π^* orbital in

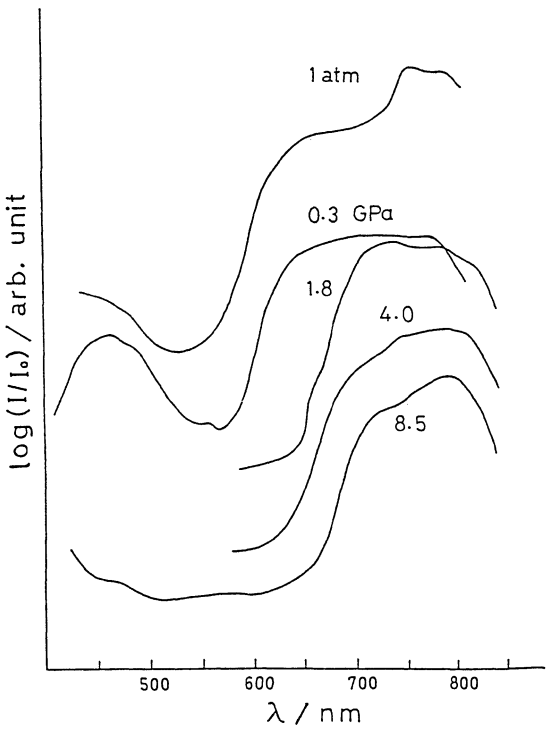

Fig. 3. Absorption spectra of $[Fe(bpy)_2(NCS)_2]$ under high pressure.

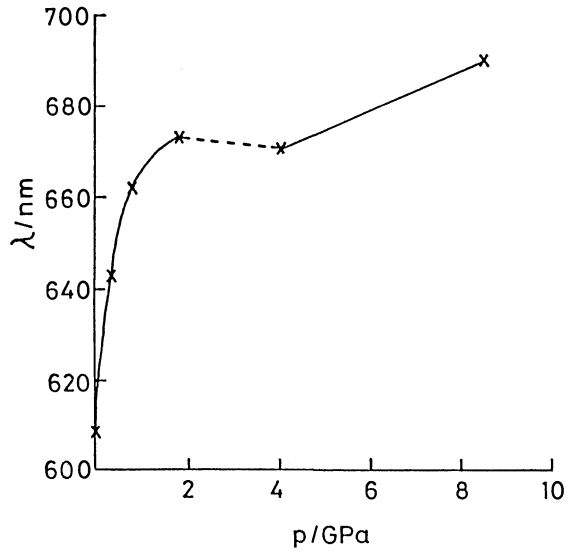

Fig. 4. Variation of absorption edge of $[Fe(bpy)_2(NCS)_2]$ under high pressure.

analogy with the case of $[Fe(phen)_2(NCS)_2]$.[23] At a pressure of 3.3 GPa a microscope observation showed that the crystal made a drastic change, displaying net-like boundaries on the surface, changing at every momemt, which seems to reflect something like a domain structure. Such movement continued for a few minutes; when it settled, the crystal color had lightened and once again became uniform. At that time, the absorption edge shifted back to a shorter wavelength region, as illustrated in Fig. 4. The iron(II) spin crossover complexes are known to exhibit pressure-induced spin transitions of the high- to the low-spin state under rather low pressure (up to ca. 2 GPa) and inversion of the low- to the high-spin state in the higher pressure range based on a ligand field calculation of the electronic states of both spin states.[3] The change around 3.3 GPa can be interpreted as being a latter conversion of the low- to the high-spin state. At 8.5 GPa, however, the spectra showed an entirely different feature from that of either the high- or the low-spin states. When the pressure was slowly reduced to 1 atm, the position of the small absorption maxima was slightly shifted by about 10 nm from the original position. One interpretation for this phenomenon is that the crystals changed from polymorph II to polymorph I by imposing pressure, since polymorph I has a larger density compared to polymorph II, their specific gravity being 1.482 and 1.462 $g\,cm^{-3}$, respectively. This can be understood structurally as being a small rotation of complex molecules, just like propellers facing in a certain direction systematically.

The authors are grateful to Professor Keisuke Suzuki and Jun Takahashi at the Faculty of Science of Kwansei Gakuin Univesity for the single crystals. Thanks are also due to Professor Takehiko Yagi of Institute for Solid State Physics, the University of Tokyo for all the facilities made available for measurements of the absorption spectra under high pressure. This work was carried out under the joint research in the Institute for Solid State Physics, the University of Tokyo.

References

1) H. A. Goodwin, *Coord. Chem. Rev.*, **18**, 293 (1976).
2) P. Gütlich, *Struct. Bonding*, **44**, 83 (1981).
3) D. C. Fisher and H. G. Drickamer, *J. Chem. Phys.*, **54**, 4825 (1971).
4) E. König, G. Ritter, W. Irler, and H. A. Goodwin, *J. Am. Chem. Soc.*, **102**, 4681 (1980).
5) E. König and K. J. Watson, *Chem. Phys. Lett.*, **6**, 457 (1970).
6) M. Mikami, M. Konno, and Y. Saito, *Chem. Phys. Lett.*, **63**, 566 (1979).
7) M. Mikami, M. Konno, and Y. Saito, *Acta Crystallogr, Sect. B*, **36**, 275 (1980).
8) A. M. Greenaway and E. Sinn, *J. Am. Chem. Soc.*, **100**, 8080 (1978).
9) A. M. Greenaway, C. J. O'Connor, A. Schrock, and E. Sinn, *Inorg. Chem.*, **18**, 2692 (1979).
10) B. A. Katz and C. E. Strouse, *J. Am. Chem. Soc.*, **101**, 6214 (1979).
11) J. D. Oliver, D. F. Mullica, B. B. Hutchinson, and W. O. Milligan, *Inorg. Chem.*, **19**, 165 (1980).
12) F. Cecconi, M. D. Vaira, S. Midollini, A. Orlandini, and L. Sacconi, *Inorg. Chem.*, **20**, 3423 (1981).
13) T. Kambara, *J. Chem. Phys.*, **70**, 4199 (1979).
14) T. Kambara, *J. Phys. Soc. Jpn.*, **49**, 1806 (1980).
15) R. Zimmermann and E. König, *J. Phys. Solids*, **38**, 779 (1977).
16) S. Ohnishi and S. Sugano, *J. Phys. C*, **14**, 39 (1981).
17) G. A. Renovitch and W. A. Baker, Jr., *J. Am. Chem. Soc.*, **89**, 6377 (1967).
18) M. Sorai, J. Ensling, and P. Gütlich, *Chem. Phys.*, **18**, 199 (1976).
19) M. Sorai, J. Ensling, K. M. Hasselbach, and P. Gütlich, *Chem. Phys.*, **20**, 197 (1977).
20) H. Koppen, E. W. Muller, C. P. Kohler, H. Spiering, E. Meissner, and P. Gütlich, *Chem. Phys. Lett.*, **91**, 348 (1982).
21) L. Wiehl, G. Kiel, C. P. Köhler, H. Spiering, and P. Gütlich, *Inorg. Chem.*, **25**, 1565 (1986).
22) W. A. Baker, Jr. and H. M. Bobonich, *Inorg. Chem.*, **3**, 1184 (1964).
23) E. König and K. Madeja, *Inorg. Chem.*, **6**, 48 (1967).
24) E. König, K. Madeja, and K. J. Watson, *J. Am. Chem. Soc.*, **90**, 1146 (1968).
25) J. H. Takemoto and B. Hutchinson, *Inorg. Chem.*, **12**, 705 (1973).
26) M. Sorai and S. Seki, *J. Phys. Chem. Solids*, **35**, 555 (1974).
27) P. G. Ganguli, P. Gütlich, E. W. Muller, and W. Irler, *J. Chem. Soc., Dalton Trans.*, **1981**, 441.
28) E. W. Muller, H. Spiering, and P. Gütlich, *Chem. Phys. Lett.*, **93**, 567 (1982).
29) P. Coppens, T. N. Guru-Row, P. Leung, E. D.

Stevens, P. J. Becker, and Y. W. Yang, *Acta Crystallogr., Sect. A*, **35**, 63 (1979).

30) "International Tables for X-Ray Crystallography," Kynoch Press, Birmingham (1974), Vol. IV, pp. 73—78.

31) R. F. Stewart, E. R. Davidson, and W. T. Simpson, *J. Chem. Phys.*, **42**, 3175 (1965).

32) Lists of structure factors, anisotropic thermal parameters for non-hydrogen atoms and positional parameters for hydrogen atoms are deposited as Document No. 9096 at the Office of the Editior of Bull. Chem. Soc. Jpn.

33) H. K. Mao and P. M. Bell, *Carnegie Inst. Washington, Year Book*, **77**, 904 (1978).

34) J. Takahashi, K. Suzuki, K. Tsuji, and S. Aeki, Molecular Structure Symposium of Japan, Kyoto, October 1981, Abstr., p. 470.

35) A. L. Beauchamp, L. Pazdernik, and R. Rivest, *Acta Crystallogr., Sect. B*, **32**, 650 (1976).

36) R. J. Restivo, J. Horney, and G. Ferguson, *J. Chem. Soc., Dalton Trans.*, **1976**, 514.

37) J. W. Jeffery and K. M. Rose, *Acta Crystallogr., Sect. B*, **24**, 653 (1968).

38) J. Takahashi, Y. Moriyama, K. Kashiwai, and K. Suzuki, The 43rd Annual Meeting of Chemical Society of Japan, Tokyo, April 1981, Abstr., Vol. I, p. 499.

Ion Pairing of Radical Ions of Aromatic Alkenes and Alkynes Studied by Pulse Radiolysis

Satoshi YAMAMOTO, Yukio YAMAMOTO,* and Koichiro HAYASHI
The Institute of Scientific and Industrial Research, Osaka University, 8-1 Mihogaoka, Ibaraki, Osaka 567
(Received June 28, 1990)

Pulse radiolysis of 1,2-dichloroethane solutions of *trans,trans*-1,4-bis(2-phenylethenyl)benzene and 1,4-bis(2-phenylethynyl)benzene was undertaken in the presence of Bu_4NPF_6 (Bu=butyl) to investigate the effect of ion pairing of the solute radical cations with PF_6^-. It was also undertaken for the tetrahydrofuran solutions of the above compounds in the presence of Bu_4NPF_6 and $NaBPh_4$, where the solute radical anions are generated and form ion pairs with Bu_4N^+ and Na^+. The decay of the radical ions, which is due to neutralization, is retarded by the ion pairing. The rate constants for the neutralization reactions in the free-ion and ion-paired states were determined. Also presented are the data for the radical ions of *trans*-stilbene, diphenylacetylene, *trans,trans*-1,4-diphenyl-1,3-butadiene, and diphenylbutadiyne. The radical ions of the aromatic alkynes are less stabilized by the ion pairing than those of the aromatic alkenes having the same carbon skeletons probably because of more extensive charge delocalization of the former radical ions. Spectral shifts to shorter wavelengths caused by the ion pairing are appreciable for the radical anions. Dependence of the spectral shifts on the size of the radical anions is described.

Extensive spectrophotometric studies of ion pairing have been undertaken for aromatic radical anions formed by alkali-metal reduction.[1,2] The absorption maxima of the anionic species are shifted to shorter wavelengths when they form contact ion pairs with the alkali-metal cations. The magnitude of the spectral shifts decreases as the interionic separation, or the radius of the cations, increases. Thus, the absorption maxima of solvent-separated ion pairs are essentially the same as those of free anions. The effect of ion pairing has also been studied for negatively charged species generated by pulse radiolysis. The rate constants for the reactions of solvated electrons, aromatic radical anions, and carbanions have been determined for the free-ion and ion-paired states.[3-7]

We have previously reported pulse radiolysis studies of salt effects for aromatic radical cations and anions, which are formed in 1,2-dichloroethane and tetrahydrofuran (THF) solutions, respectively.[8-12] In the solutions containing Bu_4NPF_6 (Bu=butyl) and $NaBPh_4$ (Ph=phenyl) the radical ions form ion pairs with the counter ions derived from the salts, such as PF_6^-, Bu_4N^+, and Na^+. The decay of the radical ions, which is due to neutralization, was retarded by the ion pairing. Spectral shifts to shorter wavelengths by the ion pairing were appreciable for the radical anions. For the radical anions of all-*trans* α,ω-diphenyl-substituted polyenes, $Ph(CH{=}CH)_nPh$ (n=1—4), the magnitude of the spectral shifts varied with the value of n depending on the kind of the counter ions, Bu_4N^+ and Na^+.[12] As the value of n increased, the magnitude of the spectral shift increased for the ion pairs with Bu_4N^+ and decreased for the ion pairs with Na^+. Small spectral shifts were also observed for the radical cations of $Ph(CH{=}CH)_nPh$, when paired with PF_6^-.[11] We are interested in the ion pairing of the radical ions having long conjugated π-electron systems.

The present pulse radiolysis study has been undertaken for the radical ions of *trans,trans*-1,4-bis(2-phenylethenyl)benzene (DStBz) and 1,4-bis(2-phenylethynyl)benzene (DPEBz). Also presented are the data for the radical ions of other aromatic alkenes

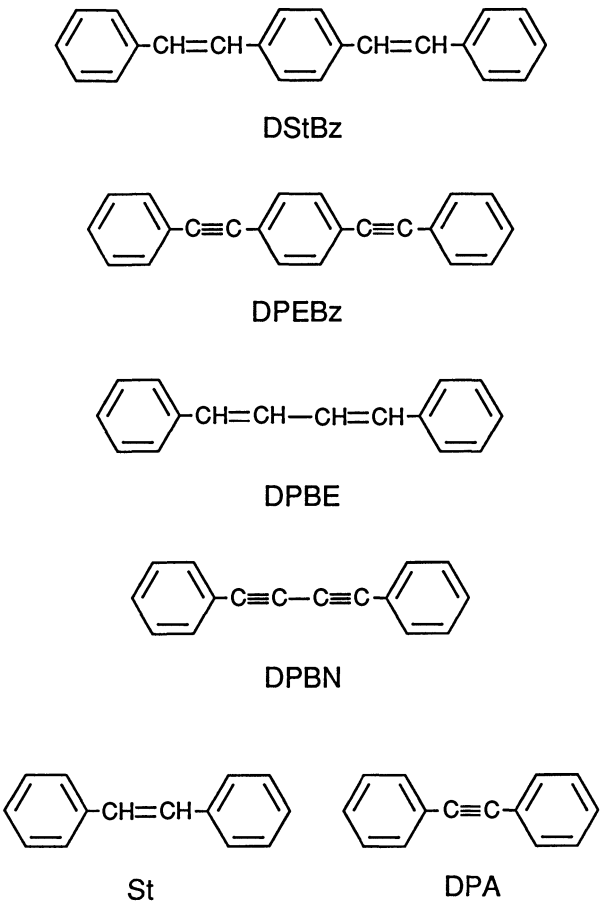

Fig. 1. Structures of the aromatic alkenes and alkynes.

and alkynes such as *trans*-stilbene (St), diphenylacetylene (DPA), *trans,trans*-1,4-diphenyl-1,3-butadiene (DPBE), and 1,4-diphenylbutadiyne (DPBN). The structures of these compounds are shown in Fig. 1. The second-order rate constants for the neutralization reactions of the radical ions were determined in the absence and presence of the salts. The effect of the ion pairing is compared between the radical ions of the aromatic alkenes and alkynes having the same carbon skeletons. The results of the previous studies on the ion pairing of the various aromatic radical ions are summarized in the present paper.

Experimental

1,2-Dichloroethane, THF, Bu_4NPF_6, and $NaBPh_4$ were the same as those used in the previous studies.[8-12] DStBz and DPEBz were prepared by literature procedures[13,14] and recrystallized from benzene and a benzene-hexane mixture, respectively. DPA (Tokyo Kasei) and DPBN (Aldrich) were purified by recrystallization from hexane. The experimental procedures and the techniques of pulse radiolysis have been described in the previous paper.[8] The pulse radiolysis experiments were carried out by using 8 ns electron pulses and at room temperature. The molar extinction coefficients of the radical ions were determined by comparing the absorption intensities based on the values of the St radical ions as in the previous studies.[8-12]

Results

The pulse radiolysis of 1,2-dichloroethane solutions of the aromatic alkenes and alkynes was carried out at a solute concentration of 3×10^{-3} mol dm^{-3} in the presence of 6×10^{-2} mol dm^{-3} biphenyl as in the previous studies.[8-12] The solute radical cations are produced by charge transfer from the biphenyl radical cation initially formed. The decay of the radical cations, $S^{+\cdot}$, is due to neutralization with Cl^-, a product of electron attachment to the solvent.

$$S^{+\cdot} + Cl^- \longrightarrow \text{neutral product}, \quad (1)$$

where S denotes the aromatic solute.

Figures 2 and 3 show the transient absorption spectra measured for the solutions of DStBz and DPEBz, respectively, in the absence of the salt. The absorption spectra did not change during the decay, and all observed peaks are assigned to $DStBz^{+\cdot}$ and $DPEBz^{+\cdot}$. When 6×10^{-3} mol dm^{-3} Bu_4NPF_6 was added, the peaks of the absorption spectra were slightly shifted to shorter wavelengths, and the decay of the absorption was retarded. The absorption spectra measured in the absence and presence of the salt are those of the free-radical cations and their ion pairs with PF_6^-, respectively.

The pulse radiolysis was also carried out for the solutions of DPA and DPBN. The absorption spectra of $DPA^{+\cdot}$ and $DPBN^{+\cdot}$ agreed with those reported in literature.[15] The absorption maxima of the radical cations and the magnitudes of the spectral shifts caused by the ion pairing are listed in Table 1 together with those of $St^{+\cdot}$ and $DPBE^{+\cdot}$ measured in the previous studies.[10,11]

The decay of the absorption of the radical cations obeyed second-order kinetics, suggesting that it is due exclusively to the neutralization. The rate constants, k_1 and k_2, for the neutralization reactions were determined in the absence and presence of the salt, respectively. The data are listed in Table 2. In the presence of the salt the neutralization reactions occur

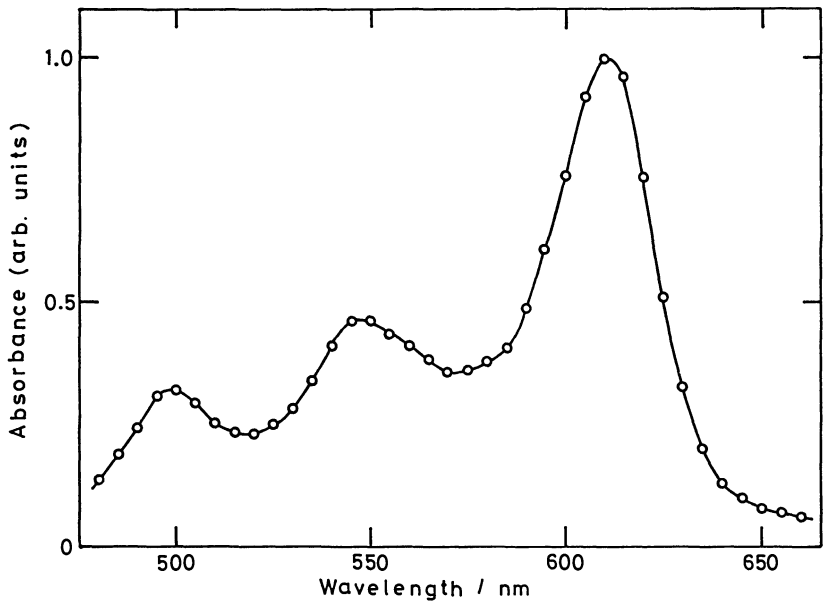

Fig. 2. Transient absorption spectrum of $DStBz^{+\cdot}$ in 1,2-dichloroethane (at 400 ns).

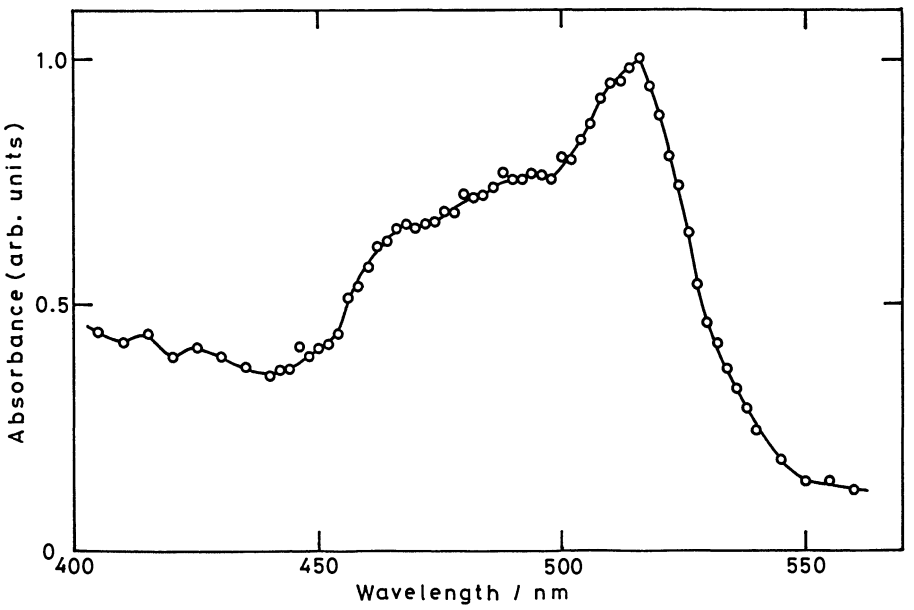

Fig. 3. Transient absorption spectrum of $DPEBz^{+\cdot}$ in 1,2-dichloroethane (at 400 ns).

Table 1. Positions of Absorption Maxima of the Free-Radical Cations and Spectral Shifts Caused by Ion Pairing with PF_6^-

Cation	λ_{max}	$\Delta\lambda$	ε_{max}
	nm	nm	$dm^3\,mol^{-1}\,cm^{-1}$
$St^{+\cdot}$	480	<2	6.5×10^4
$DPBE^{+\cdot}$	546	4	1.2×10^5
$DStBz^{+\cdot}$	610	2	1.1×10^5
$DPA^{+\cdot}$	422	0	3.9×10^4
$DPBN^{+\cdot}$	482	0	1.7×10^4
$DPEBz^{+\cdot}$	515	3	7.1×10^4

Table 2. Rate Constants for the Neutralization Reactions of the Radical Cations in the Free-Ion (k_1) and Ion-Paired (k_2) States

Cation	Rate constant/$dm^3\,mol^{-1}\,s^{-1}$		k_1/k_2
	k_1	k_2	
$St^{+\cdot}$	$(1.6\pm0.2)\times10^{11}$	$(3.3\pm0.2)\times10^{10}$	5.0
$DPBE^{+\cdot}$	$(1.6\pm0.1)\times10^{11}$	$(2.9\pm0.1)\times10^{10}$	5.5
$DStBz^{+\cdot}$	$(8.9\pm0.7)\times10^{10}$	$(1.7\pm0.2)\times10^{10}$	5.2
$DPA^{+\cdot}$	$(1.2\pm0.2)\times10^{11}$	$(4.4\pm0.5)\times10^{10}$	2.7
$DPBN^{+\cdot}$	$(1.5\pm0.2)\times10^{11}$	$(6.4\pm0.4)\times10^{10}$	2.3
$DPEBz^{+\cdot}$	$(1.4\pm0.1)\times10^{11}$	$(4.3\pm0.2)\times10^{10}$	3.3

between the ion pairs.

$$S^{+\cdot}/PF_6^- + Bu_4N^+/Cl^- \longrightarrow \text{neutral product.} \quad (2)$$

The k_1/k_2 ratios are presented as a measure of the salt effect. It can be seen that the k_1/k_2 ratios of the radical cations of the aromatic alkynes are small compared with those of the aromatic alkenes having the same carbon skeletons.

Table 3. Positions of Absorption Maxima of the Free-Radical Anions and Spectral Shifts Caused by the Ion Pairing with Bu_4N^+ and Na^+

Anion	λ_{max}	$\Delta\lambda$/nm ($\Delta\bar{\nu}/10^2\,cm^{-1}$) Counter ions		ε_{max}
	nm	Bu_4N^+	Na^+	$dm^3\,mol^{-1}\,cm^{-1}$
$St^{-\cdot}$	500	5 (2)	20 (8)	6.1×10^4
$DPBE^{-\cdot}$	573	9 (3)	18 (6)	1.1×10^5
$DStBz^{-\cdot}$	634	14 (4)	6 (2)	1.5×10^5
$DPA^{-\cdot}$	449	5 (3)	13 (7)	5.6×10^4
$DPBN^{-\cdot}$	494	6 (2)	14 (6)	1.1×10^5
$DPEBz^{-\cdot}$	519	7 (3)	3 (1)	1.1×10^5

Similar experiments were carried out for the THF solutions of DStBz and DPEBz containing 6×10^{-2} mol dm^{-3} biphenyl, where the solute radical anions are produced by electron transfer from the biphenyl radical anion and are neutralized by the solvent cation.

$$S^{-\cdot} + THF(H^+) \longrightarrow \text{neutral product.} \quad (3)$$

When 6×10^{-3} mol dm^{-3} Bu_4NPF_6 and $NaBPh_4$ were added, the absorption maxima of the radical anions were appreciably shifted to shorter wavelengths. Figures 4 and 5 show the transient absorption spectra measured for the solutions of DStBz and DPEBz, respectively, in the absence and presence of Bu_4NPF_6. The absorption spectra did not change during the decay. The pulse radiolysis was also carried out for the solutions of DPA and DPBN. The absorption spectra of $DPA^{-\cdot}$ and $DPBN^{-\cdot}$ in the absence of the salts agreed with those reported in literature.[15] The absorption maxima of the radical anions are listed in

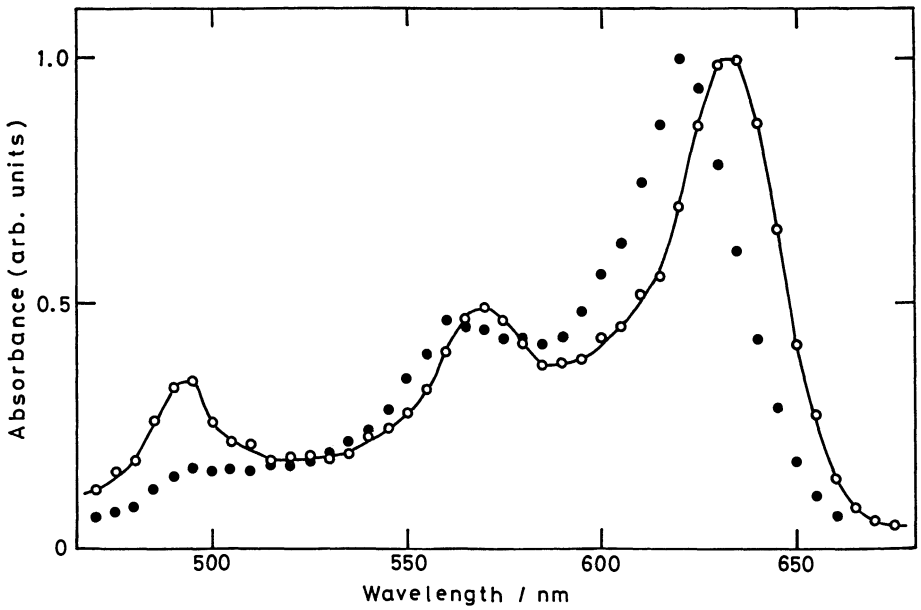

Fig. 4. Transient absorption spectra of DStBz$^{-\cdot}$ in the absence (○) and presence (●) of 6×10^{-3} mol dm^{-3} Bu_4NPF_6 (at 400 ns).

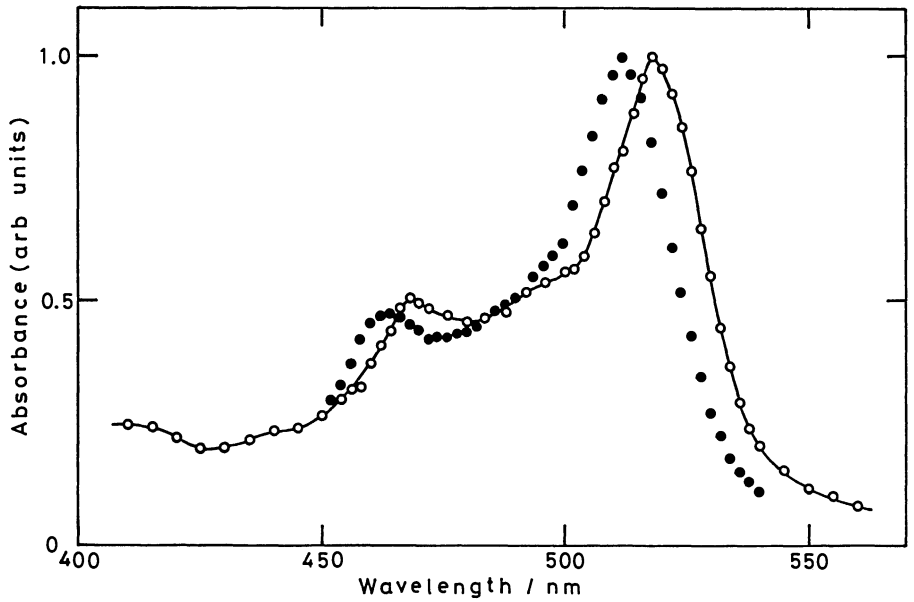

Fig. 5. Transient absorption spectra of DPEBz$^{-\cdot}$ in the absence (○) and presence (●) of 6×10^{-3} mol dm^{-3} Bu_4NPF_6 (at 400 ns).

Table 3 together with those of St$^{-\cdot}$ and DPBE$^{-\cdot}$ measured in the previous studies.[9,12]

The rate constants for the neutralization reactions of the radical anions are listed in Table 4. The k_3 and k_4 values were determined in the absence and presence of 6×10^{-3} mol dm^{-3} Bu_4NPF_6, respectively. The k_4 values are the rate constants for the reactions between the ion pairs.

$$S^{-\cdot}/Bu_4N^+ + THF(H^+)/PF_6^- \longrightarrow \text{neutral product.} \quad (4)$$

Table 4. Rate Constants for the Neutralization Reactions of the Radical Anions

Anion	Rate constant/dm^{-3} mol^{-1} s^{-1}		k_3/k_4
	k_3	k_4	
St$^{-\cdot}$	$(4.0\pm0.3)\times10^{11}$	$(8.2\pm0.3)\times10^{9}$	49
DPBE$^{-\cdot}$	$(3.4\pm0.2)\times10^{11}$	$(9.0\pm0.4)\times10^{9}$	38
DStBz$^{-\cdot}$	$(2.5\pm0.1)\times10^{11}$	$(5.4\pm0.2)\times10^{9}$	47
DPA$^{-\cdot}$	$(2.9\pm0.1)\times10^{11}$	$(7.9\pm0.2)\times10^{9}$	37
DPBN$^{-\cdot}$	$(3.3\pm0.1)\times10^{11}$	$(1.0\pm0.1)\times10^{10}$	33
DPEBz$^{-\cdot}$	$(1.7\pm0.1)\times10^{11}$	$(5.3\pm0.2)\times10^{9}$	32

The k_3/k_4 ratios of the radical anions are much larger than the k_1/k_2 ratios of the radical cations. The rate constants determined in the presence of $NaBPh_4$ were intermediate between the k_3 and k_4 values.

It can be seen for the absorption spectra of $DStBz^{-\cdot}$ that the peak at 495 nm becomes smaller in the presence of Bu_4NPF_6 (Fig. 3). This was also observed in the case of $NaBPh_4$. Furthermore, the intensity of the 500-nm band of $DStBz^{+\cdot}$ was decreased by 20% in the presence of Bu_4NPF_6. However, the extinction coefficients of $DStBz^{+\cdot}$ and $DStBz^{-\cdot}$ at the main absorption peaks were not affected by the addition of the salts.

Discussion

The interaction between oppositely charged species of ion pairs, or the magnitude of spectral shifts caused by the ion pairing, decreases as the ion size increases.[1,2] The charge distribution of the large aromatic radical ions is considered to be responsible for the effect of the ion pairing rather than the apparent size of the charged species. The retardation of the neutralization reactions and the spectral shifts caused by the ion pairing are considered to be the measure of the interaction between the radical ions and the counter ions derived from the salts. Here the ion pairing of the radical ions of the aromatic alkenes and alkynes is discussed by considering the charge distribution and the length of the conjugated π-electron systems.

Radical Cations. The neutralization reactions of the radical cations of the aromatic alkenes and alkynes with Cl^- in the free-ion state are considered to be diffusion controlled and be accelerated by Coulombic attraction between the oppositely charged reactants. This is similar to the case of the radical cations of biphenyl, anthracene, triphenylethylene, and $Ph(CH{=}CH)_nPh$ (n=1—4).[10,11] The rate constants, k_1, of these radical cations are close to each other, lying in the range $(8.6—19)\times10^{10}$ $dm^3\,mol^{-1}\,s^{-1}$. In general, k_1 decreases as the ion size increases because of the slow rate of diffusion of the large radical cations.[10,11] A similar trend is observed for k_3 of the radical anions.[9,12]

In the presence of the Bu_4NPF_6, the rate constants of the radical cations of the aromatic alkenes decrease by a factor of about 5: the k_1/k_2 ratios are in the range 5.0—5.5. On the other hand, the k_1/k_2 ratios of the radical cations of the aromatic alkynes are in the range 2.7—3.3. It is suggested that the alkyne radical cations are less stabilized by the ion pairing with PF_6^- than the alkene radical cations having the same carbon skeletons. This can be explained as follows. The positive charge of the alkyne radical cations is cylindrically distributed around the triple bonds, whereas the charge distribution of the alkene radical cations is restricted to the direction perpendicular to the molecular planes. The charge of the alkyne radical cations may be spread over the aromatic rings more extensively than that of the alkene radical cations, for which the aromatic rings and the olefinic moieties are not completely coplanar. The charge delocalization of the alkyne radical cations results in a lowering of the interaction with PF_6^-.

As reported previously,[10,11] the neutralization reactions of the radical cations of pyrene, perylene, and tetraphenylethylene in the free-ion state are not diffusion controlled: the k_1 values are 9.4×10^9, 7.2×10^9, and 2.8×10^9 $dm^3\,mol^{-1}\,s^{-1}$, respectively, and are one order of magnitude smaller than those of the other radical cations. Furthermore, the salt effect is negligibly small for these radical cations: the k_1/k_2 ratios are nearly unity.[10,11] It can be said that these radical cations have smaller reactivities or interactions with the anions, Cl^- and PF_6^-, than the other radical cations. The result for the tetraphenylethylene radical cation has been interpreted in terms of steric crowding of the phenyl groups, which surround the positive charged center located on the olefinic double bond. For the radical cations of pyrene and perylene the charge delocalization over the large condensed-ring aromatics may be responsible for the small reactivities or interactions with the anions. Formation of a complex has been proposed for the slow neutralization reactions of the radical cations of pyrene and perylene, $P^{+\cdot}$.[10,11]

$$P^{+\cdot} + Cl^- \underset{k_d}{\overset{k_c}{\rightleftarrows}} P^{+\cdot}/Cl^- \xrightarrow{k_n} \text{neutral product.} \qquad (5)$$

The k_1 values correspond to k_nk_c/k_d.

Although both the radical cations and Cl^- are paired with the counter ions from the salt, the retardation of the neutralization is due largely to the ion pairing of the radical cations as reported previously.[10,11] This is based on the result that the k_1/k_2 ratios depend on the kind of the radical cations and are close to unity for the radical cations of pyrene, perylene, and tetraphenylethylene.

Spectral shifts by the ion pairing are observed only for the radical cations having long π-electron systems, such as $DStBz^{+\cdot}$, $DPEBz^{+\cdot}$, and $Ph(CH{=}CH)_nPh^{+\cdot}$ (n=2—4), although very small spectral shifts, <2 nm, are also observed for $St^{+\cdot}$ and the triphenylethylene radical cation.[10,11] An explanation for the spectral shifts of these large radical cations may be the charge localization induced by PF_6^- in the long π-electron systems, resulting in formation of contact ion pairs.[11] It is also possible that the absorption spectra of the radical cations having long π-electron systems are sensitive to the counter ion and are shifted without forming contact ion pairs.

Radical Anions. The appreciable spectral shift by the ion pairing is characteristic of the radical anions. The magnitude depends on the size of the radical anions and on the kind of the counter ions. A

dependence of the spectral shift on the size of the radical anions, similar to that for $Ph(CH=CH)_n$-$Ph^{-\cdot}$,[12] can be seen in Table 3, although the trend is not clear when the magnitude is small. It is suggested that a large radical anion has a strong interaction with a large counter ion while a small one does with a small counter ion. This may be particular to the radical anions having long π-electron systems.

The neutralization reactions of the radical anions with $THF(H^+)$ in the free-ion state are considered to be diffusion controlled. The rate constants, k_3, are in the range $(1.7—4.0)\times10^{11}$ $dm^3\,mol^{-1}\,s^{-1}$, including k_3 of the radical anions of biphenyl, anthracene, pyrene, perylene, triphenylethylene, and $Ph(CH=CH)_nPh$ (n=1—4).[9,12] They are larger than k_1 for the diffusion controlled reactions of the radical cations in 1,2-dichloroethane. This is due mainly to the difference in the solvent viscosity as reported previously.[10] The viscosities of 1,2-dichloroethane and THF at 22 °C are 0.0081 and 0.0048 Pa s, respectively. Corrected for the solvent viscosities, k_1 and k_3 become almost the same.

Contrary to the radical cations, the radical anions of pyrene and perylene have k_3 comparable to those of the other radical anions.[9,12] It has been suggested that the neutralization reactions of the radical anions with $THF(H^+)$ are less selective than those of the radical cations with Cl^- because of the strong electrophilicity of $THF(H^+)$, which is essentially a proton.

The neutralization reactions of the radical anions are significantly affected by the addition of Bu_4NPF_6. The k_3/k_4 ratios are one order of magnitude larger than the k_1/k_2 ratios of the radical cations. It has already been demonstrated that the salt effect on the neutralization reactions is due mainly to the ion pairing of $THF(H^+)$ with PF_6^- rather than to that of the radical anions with Bu_4N^+.[8] Therefore, the large retarding effect for the radical anions can be attributed to the strong interaction of the charge-localized $THF(H^+)$ with PF_6^-.

The k_3/k_4 ratios of the radical anions of the aromatic alkynes are slightly smaller than those of the aromatic alkenes having the same carbon skeletons. This shows that the alkyne radical anions are less stabilized by the ion pairing than the alkene radical anions. This is similar to the radical cations paired with PF_6^-. The dependence of k_4 on the kind of the radical anions suggests that the ion pairing of the radical anions with Bu_4N^+ is partly responsible for the retardation of the neutralization reactions but to a less extent compared to the ion pairing of $THF(H^+)$ with PF_6^-.

We thank the members of the Radiation Laboratory of this Institute for help with the pulse radiolysis experiments and Professor S. Takahashi of this Institute for useful suggestions for the synthesis of DPEBz.

References

1) J. Smid, "Ion and Ion Pairs in Organic Reactions," ed by M. Szwarc, Wiley-Interscience, New York (1972), Vol. 1, p. 85.
2) M. A. Fox, *Chem. Rev.*, **79**, 253 (1979).
3) B. Bockrath and L. M. Dorfman, *J. Phys. Chem.*, **77**, 1002 (1973).
4) B. Bockrath and L. M. Dorfman, *J. Phys. Chem.*, **77**, 2618 (1973).
5) B. Bockrath and L. M. Dorfman, *J. Am. Chem. Soc.*, **96**, 5708 (1974).
6) J. R. Langan and G. A. Salmon, *J. Chem. Soc., Faraday Trans. 1*, **78**, 3645 (1982).
7) J. R. Langan and G. A. Salmon, *J. Chem. Soc., Faraday Trans. 1*, **79**, 589 (1983).
8) Y. Yamamoto, S. Nishida, K. Yabe, K. Hayashi, S. Takeda, and K. Tsumori, *J. Phys. Chem.*, **88**, 2368 (1984).
9) Y. Yamamoto, S. Nishida, X.-H. Ma, and K. Hayashi, *J. Phys. Chem.*, **90**, 1921 (1986).
10) Y. Yamamoto, S. Nishida, and K. Hayashi, *J. Chem. Soc., Faraday Trans. 1*, **83**, 1795 (1987).
11) Y. Yamamoto, T. Aoyama, and K. Hayashi, *J. Chem. Soc., Faraday Trans. 1*, **84**, 2209 (1988).
12) T. Aoyama, Y. Yamamoto, and K. Hayashi, *J. Chem. Soc., Faraday Trans. 1*, **85**, 3353 (1989).
13) K. Sonogashira, Y. Tohda, and N. Hagihara, *Tetrahedron Lett.*, **1975**, 4467.
14) T. W. Campbell and R. N. McDonald, *J. Org. Chem.*, **24**, 1246 (1959).
15) T. Shida and W. H. Hamill, *J. Chem. Phys.*, **44**, 4372 (1966).

Photoelectron Emission Study of Iron(II) and Cobalt(II) Complexes in Aqueous Solution. Reorganization Energies

Iwao WATANABE,* Kaori ONO, and Shigero IKEDA†
Department of Chemistry, Faculty of Science, Osaka University, Toyonaka, Osaka 560
†Faculty of Science and Technology, Ryukoku University, Otsu, Shiga 520-21
(Received July 11, 1990)

The photoelectron emission threshold energies of Fe^{II} and Co^{II} complexes in aqueous solutions have been determined. The values could be successfully used for obtaining the reorganization energies in the one-electron oxidation reaction of these complexes. The obtained reorganization energies were found to be correlated with the rate constants of the electron-self-exchange reactions of Fe^{II}/Fe^{III} and Co^{II}/Co^{III}.

A new spectroscopic technique, Photoelectron Emission Spectroscopy (PEES) of solution,[1-5] provides the photoelectron emission threshold energies, E_t, of molecules or ions in solution. The E_t values for organic molecules in solutions have been found to be linearly correlated with their ionization potentials, I_p, in the gas phase or the oxidation potentials, E_{ox}, in solutions.[4,5] The E_{ox} values used, however, are not of the equilibrium values but the peak potentials in cyclic voltammetry. Since E_{ox} is thermodynamically less meaningful than the standard redox potential, E°, it is essential to measure the E_t values of any samples for which the E° values are accurately known in order to study the correlation between E_t and E°. Iron(II) and cobalt(II) with various ligands or chelates are suitable for this purpose since it is easy to find a variety of E° values from these complexes.

The E_t and E° for a one-electron redox reaction pertain to the energy changes of the following reactions:

$$X^{nz} \rightarrow {}^*X^{nz+1} + e^-(\text{vacuum}) \qquad E_t \quad (1)$$

$$X^{nz} \rightarrow X^{nz+1} + e^-(\text{electrode at the potential of NHE})^{6)} \qquad E^\circ \quad (2)$$

Since the $^*X^{nz+1}$ in Eq. 1 is the product of an optical process (the Franck-Condon transition), the $^*X^{nz+1}$ has a geometrical structure which is exactly the same as that of the X^{nz} with respect to the geometries both in the inner- and the outer-sphere regions, and is in a vibrationally excited state. The vibrational relaxation energy of the $^*X^{nz+1}$, or the reorganization energy, ΔG_r, in the one-electron oxidation reaction of X^{nz}, is defined by

$$^*X^{nz+1} \rightarrow X^{nz+1} \qquad \Delta G_r \quad (3)$$

and given as follows:

$$\Delta G_r = (E^\circ + \Delta G_H) - E_t \qquad (4)$$

where $\Delta G_H (\approx 4.5\text{eV})$[7] is the potential energy of the vacuum level with respect to NHE.

In the Marcus theory for outer-sphere electron transfer reactions, the ΔG_r is a key parameter closely related to the activation energy.[8] Its evaluation is thus essential for the study of the kinetics. Considering the importance of ΔG_r, the potentiality of the PEES of solution providing the ΔG_r value must be fully explored.

Only a few studies have taken place in which ΔG_r values have been obtained from PEES experiments,[9-11] or the values so obtained treated in discussions concerning electron transfer kinetics.[12-16] In the present study, the experimentally obtained ΔG_r values for iron(II)/(III)[17] and cobalt(II)/(III) complexes are compared with the values calculated with the following equations, which are considered to be the only practical method for estimating the ΔG_r values:

$$\Delta G_r = \Delta G_r(\text{in}) + \Delta G_r(\text{out}), \qquad (5)$$

$$\Delta G_r^{calc}(\text{in}) = -(1/2) N f_o (\Delta r)^2, \qquad (6)$$

and

$$\Delta G_r^{calc}(\text{out}) = -(e^2/2a)(\varepsilon_{op}^{-1} - \varepsilon_s^{-1}), \qquad (7)$$

where ΔG_r(in) and ΔG_r(out) are the inner- and outer-sphere components of the reorganization energy, respectively; N is the coordination number of the complex (6 in this study), f_o the force constant for the bond between the central metal and its coordinating atom for the oxidized species (X^{nz+1}), Δr the difference in the coordination bond distances for the X^{nz} and X^{nz+1}, a the mean radius of the assumed boundaries between the inner- and outer-sphere regions for the X^{nz} and X^{nz+1}, and ε_{op} and ε_s the optical and the static dielectric constants of water.

Experimental

Photoelectron Emission Spectrometer for Solution. Details concerning the spectrometer have been described elsewhere.[3,4] Since this technique is extremely sensitive to any surface contamination of a sample solution, a surface scratcher was newly provided to the rotating glass disk. The scratcher is made of a thin plastic film and presses the glass surface very lightly at a few millimeters above the sample solution; it thus prevents organic contaminants floating on the surface of the solution from entering the photoionization region. This greatly improved the cleanliness of the observing surface. Therefore, the slower rotation rate of the glass disk could be utilized, resulting in

smaller capacitive noise currents and better S/N ratios.

Samples. The reagents used to prepare the solutions were of guaranteed reagent grade and were used without further purification. The abbreviations used in this paper are: edta=*N,N,N',N'*-ethylenediaminetetraacetate, pdta=1,2-diaminopropane-*N,N,N',N'*-tetraacetate, cydta=1,2-cyclohexanediamine-*N,N,N',N'*-tetraacetate, bpy=2,2'-bipyridine, dmbpy=4,4'-dimethyl-2,2'-bipyridine, phen=1,10-phenanthroline, tmp=3,4,7,8-tetramethyl-1,10-phenanthroline, Cl-phen=5-chloro-1,10-phenanthroline, tpy=2,2':6',2''-terpyridine, N4=1,4,8,11-tetraazacyclotetradecane.

The constituents of the solutions measured were: $[Fe(H_2O)_6]^{2+}$; 2M(M=mol dm^{-3}), 1M, 0.5M in 3M H_2SO_4, $[Fe(edta)]^{2-}$; 0.2M, 0.1M, 0.05M, $[Fe(CN)_6]^{4-}$; 0.2M in 0.1M KOH, $[Fe(bpy)_3]^{2+}$; 0.8M, 0.4M, 0.2M, $[Fe(dmbpy)_3]^{2+}$; 0.05M, 0.025M, $[Fe(phen)_3]^{2+}$; 0.8M, 0.4M, 0.2M, $[Fe(tmp)_3]^{2+}$; 0.05M, 0.025M, $[Fe(tpy)_2]^{2+}$; 0.05M, 0.025M, $[Co(H_2O)_6]^{2+}$; 0.2M in 2M H_2SO_4, $[Co(NH_3)_6]^{2+}$; saturation in 4M ammonia water, $[Co(edta)]^{2-}$; 0.2M, 0.1M, $[Co(pdta)]^{2-}$; 0.2M, 0.1M, $[Co(cydta)]^{2-}$; 0.2M, 0.1M, $[Co(bpy)_3]^{2+}$; 0.2M, 0.1M 0.02M, $[Co(dmbpy)_3]^{2+}$; 0.2M, 0.1M, $[Co(phen)_3]^{2+}$; 0.2M, 0.1M, 0.04M, $[Co(Cl\text{-}phen)_3]^{2+}$; 0.05M, 0.01M, $[Co(tpy)_2]^{2+}$; 0.025M, 0.0125M, $[Co(N4)]^{2+}$; 0.1M.

The solutions containing edta or its analogues were prepared from $FeSO_4\cdot 7H_2O$, or $CoSO_4\cdot 7H_2O$, and $Na_2H_2edta\cdot 2H_2O$, H_4pdta, or H_4cydta, and the acidities were adjusted to pH ca. 7 with $NaHCO_3$. The solutions containing the bpy, phen, N4 or their analogues were prepared by adding excess amounts of the metal ions so that the free ligands would not exist in the solutions. If a ligand exists in excess of the metal ion, it is possible that the free ligand molecules can coagulate on the solution surface, while perturbing photoelectron emission from the solute.

The $[Co(NH_3)_6]^{2+}$, $[Fe(edta)]^{2-}$ and some others are extremely sensitive to oxidation by air. These samples were therefore prepared under a nitrogen gas atmosphere.

The solutions were cooled to around +1 °C, except for aqueous ammonia solutions, which were cooled to −15 °C since the vapor pressure of ammonia was too high at +1 °C.

Determination of E_t Values. The photoelectron emission yield Y is a function of the exciting photon quantum energy $h\nu$ and the E_t as follows:[1)]

$$Y=A(h\nu-E_t)^n, \tag{8}$$

where A is a proportional constant and n is known to be either 2 or 2.5. A plot of $Y^{1/n}$ gives a straight line and its extrapolation to $Y=0$ gives the E_t value. In this study, after testing both n values, that which gave better statistics to be fitted on a straight line was chosen. Consequently, a value of 2 was used for $[Fe(dmbpy)_3]^{2+}$, $[Co(bpy)_3]^{2+}$, $[Co(phen)_3]^{2+}$, and $[Co(tpy)_2]^{2+}$, and 2.5 was used for the other samples. The E_t values obtained with this extrapolation method are considered to correspond to the energy change of the reaction given in Eq. 1.

The E_t values were reproducible within 0.1 eV or less, irrespective of the concentrations of the metal complexes.

Results and Discussion

The E_t values obtained are listed in Table 1 together with the E° values for the X^{nz}/X^{nz+1} couples. Since both the E_t and E° values pertain to the energy necessary for removing an electron from X^{nz} (cf. Eqs. 1 and 2), one may well expect that they are related with each other. No correlation, however, was observed between them. This is because the complexes presently studied had quite different ΔG_r values. This is in contrast with the results concerning the organic molecules which have been reported.[4,5)]

The ΔG_r values determined by the PEES technique with Eq. 4 are plotted as ΔG_r^{exp} in Fig. 1 against the ΔG_r^{calc} values given by Eqs. 5—7.

The values of Δr in Eq. 6 were collected from reports concerning the X-ray diffraction and EXAFS (Extended X-ray Absorption Fine Structure). The values of a in Eq. 7 are determined according to

$$a=d_{X-L}+r_L, \tag{9}$$

where d_{X-L} is the distance between the central metal atom X and an atom L in the ligand at the most distant position from X, and r_L is the van der Waals radius of L. The values of Δr and a are included in Table 1.

As shown in Fig. 1, the experimental ΔG_r values are in excellent agreement with the calculated ones. The line in the figure indicates the position where both values are the same. It should be noted that both ΔG_r values are the result of a number of approximations and simplifications, as follows. In the derivation of Eq. 6, (1) only the bond length between the metal and the atom directly coordinating to the metal is taken into account; thus, the other differences in geometries of the X^{nz} and X^{nz+1} are neglected. (2) A harmonic potential is adopted for the bond deformation. (3) In Eq. 7, the outer-sphere component is calculated by using the Born model, i.e. the spherical conductor of radius a in a continuous medium with dielectric constants of ε_{op} and ε_s. In the derivation of Eq. 4, there exists (4) the uncertainty in ΔG_H, and (5) the double layer potential or the surface potential at the solution/gas interface is neglected. In Eq. 8, there is (6) the uncertainty in the value of n, and (7) the density of states for the ion solvated is represented by a delta function; thus, the concept of adiabatic and vertical ionization energies is abandoned.[18)] However, considering the excellent agreement between the experimental and calculated ΔG_r values, it seems that the approximations used here are adoptable within the present experimental accuracy.

Due to a spin-state change during the oxidation process for many of the cobalt complexes, i.e. the high-spin state for Co^{II} to the low-spin state for Co^{III}, these complexes have the large bond differences, Δr, and thus large ΔG_r values compared to the iron complexes whose spin states remain high. It is now important to note that the electronic state of cobalt complexes just after photoionization is not of the low-spin cobalt(III)(^1A: t_{2g}^6, e_g^0) but of a ^3T state as expressed by

Table 1. Standard Redox Potentials $E°$, Photoelectron Emission Threshold Energies E_t of M^{II}, Parameters to Calculate Reorganization Energies ΔG_r^{calc}, and Experimentally Determined Reorganization Energies ΔG_r^{exp} for Iron and Cobalt Complexes in Aqueous Solutions

	Complex	$E°$	E_t	a	Δr	$-\Delta G_r^{calc}$ (in)	$-\Delta G_r^{calc}$ (out)	$-\Delta G_r^{calc}$	$-\Delta G_r^{exp}$
		V	eV	pm	pm	eV	eV	eV	eV
1	$[Fe(H_2O)_6]^{2+/3+}$	0.77	7.09	390	13	0.81	1.01	1.82	1.82
2	$[Fe(edta)]^{2-/-}$	0.117	7.06	(547)[a]			(0.72)[a]		2.44
3	$[Fe(CN)_6]^{4-/3-}$	0.36	5.60	456	1	0.01	0.86	0.87	0.74
4	$[Fe(bpy)_3]^{2+/3+}$	1.085	6.15	697	0	0	0.57	0.57	0.57
5	$[Fe(dmbpy)_3]^{2+/3+}$	0.905	6.12	729	0	0	0.54	0.54	0.72
6	$[Fe(phen)_3]^{2+/3+}$	1.056	6.14	735	0	0	0.54	0.54	0.58
7	$[Fe(tmp)_3]^{2+/3+}$	0.832	5.73	838	0	0	0.47	0.47	0.40
8	$[Fe(tpy)_2]^{2+/3+}$	1.062	6.05	591	0	0	0.64	0.64	0.49
9	$[Co(H_2O)_6]^{2+/3+}$	1.82	8.04	374	21	2.06	1.06	3.12	1.72
10	$[Co(edta)]^{2-/-}$	0.40	7.18	548	22	1.84	0.72	2.56	2.28
11	$[Co(pdta)]^{2-/-}$	0.33	7.34	548	22	1.84	0.72	2.56	2.51
12	$[Co(cydta)]^{2-/-}$	0.31	7.57	548	22	1.84	0.72	2.56	2.76
13	$[Co(bpy)_3]^{2+/3+}$	0.315	6.25	708	20	1.83	0.56	2.39	1.44
14	$[Co(dmbpy)_3]^{2+/3+}$	0.239	7.15	740	20	1.83	0.54	2.37	2.41
15	$[Co(phen)_3]^{2+/3+}$	0.37	7.48	741	20	1.83	0.53	2.36	2.61
16	$[Co(Cl\text{-}phen)_3]^{2+/3+}$	0.43	7.26	740	20	1.83	0.54	2.37	2.33
17	$[Co(tpy)_2]^{2+/3+}$	0.31	5.89	706	14	0.93	0.53	1.46	1.08
18	$[Co(N4)(H_2O)_2]^{2+/3+}$	0.421	7.12	524[b]	0	0	0.76	1.44	2.20
				374[c]	22	0.68	1.00	1.68	
19	$[Co(NH_3)_6]^{2+/3+}$	0.058	7.58	380	22	2.21	1.04	3.25	3.02

The structural information is collected from the following reports for each sample. Some of the parameters are estimated from the data for the samples having similar structure. (1) Ref. 22; J. K. Beattie, S. P. Best, B. W. Skelton, and A. H. White, *J. Chem. Soc., Dalton Trans.*, **1981**, 2105; J. Strouse,S. W. Layten, and C. E. Strouse, *J. Am. Chem. Soc.*, **99**, 562 (1977). (2) M. D. Lind, M. J. Hamor, T. A. Hamor, and J. L. Hoard, *Inorg. Chem.*, **3**, 34 (1964). (3) Ref. 22; B. I. Swanson, S. I. Hamburg, and R. R. Ryan, *Inorg. Chem.*, **13**, 1685 (1974); K. Yanagi, Y. Ohashi, Y. Sasada, Y. Kaizu, and H. Kobayashi, *Bull. Chem. Soc. Jpn.*, **54**, 118 (1981). (4) M. E. G. Posse, M. A. Juri, P. J. Aymonino, O. E. Piro, H. A. Negri, and E. E. Catellano, *Inorg. Chem.*, **23**, 948 (1984). (5) Estimated. (6) Ref. 22; A. Zalkin, D. H. Templeton, and T. Ueki, *Inorg. Chem.*, **12**, 1641 (1973); J. Baker, L. M. Engelhardt, B. N. Figgis, and A. H. White, *J. Chem. Soc., Dalton Trans.*, **1975**, 530. (7) Estimated. (8) A. T. Baker and H. A. Goodwin, *Aust. J. Chem.*, **38**, 207 (1985). (9) The Refs. for sample (1); S. Ray, A. Zalkin, and D. H. Templeton, *Acta Crystallogr., Sect. B*, **29**, 2741 (1973); T. B. Vance, Jr., E. M. Holt, C. G. Rierpont, and S. L. Holt, *Acta Crystallogr., Sect. B*, **36**, 150 (1980); A. F. K. McCandish, T. K. Michael, J. A. Neal, E. C. Lingafelter, and N. J. Rose, *Inorg. Chem.*, **17**, 1383 (1978). (10) H. A. Weakliem and J. L. Hoard, *J. Am. Chem. Soc.*, **81**, 549 (1959). (11) Estimated. (12) Estimated. (13) The Refs. for sample (3); D. J. Szalda, C. Creutz, D. Mahajan, and N. Sutin, *Inorg. Chem.*, **22**, 2372 (1983). (14) Estimated. (15) Ref. 22. (16) Estimated. (17) C. L. Raston and A. H. White, *J. Chem. Soc., Dalton Trans.*, **1976**, 7; B. N. Figgis, E. S. Kucharski, and A. H. White, *Aust. J. Chem.*, **36**, 1537 (1983); B. N. Figgis, E. S. Kucharski, and A. H. White, *Aust. J. Chem.*, **36**, 1527 (1983), and B. N. Figgis, E. S. Kucharski, and A. H. White, *Aust. J. Chem.*, **36**, 1563 (1983). (18) J. F. Endicott, B. Durham, M. D. Glick, T. J. Anderson, J. M. Kuszaj, W. G. Schmonsees, and K. P. Balakrishnan, *J. Am. Chem. Soc.*, **103**, 1431 (1981); J. F. Endicott, J. Lilie, J. M. Kuszaj, B. S. Ramaswamy, W. G. Schmonsees, M. G. Simic, M. D. Glick, and D. P. Rillema, *J. Am. Chem. Soc.*, **99**, 429 (1977). (19) Ref. 22. The force constants are collected from K. Nakamoto, "Infrared and Raman Spectra of Inorganic and Coordination Compounds," 3rd ed, Wiley-Interscience, New York (1978), and J. T. Hupp and M. J. Weaver, *J. Phys. Chem.*, **89**, 2795 (1985). Some are estimated from the data for the complexes having similar structure. a) Estimated from the data for $[Fe(edta)]^-$. b) The parameters for equatorial bonds, and c) for axial bonds.

$$Co(II)(^4T: t_{2g}^5, e_g^2) \rightarrow {}^*Co(III)(^3T: t_{2g}^5, e_g^1) + e^-(vacuum). \quad (10)$$

Therefore, the ΔG_r^{exp} value for this process must be expressed as

$$\Delta G_r^{exp} = -(1/2)Nf_o(\Delta r)^2 - (e^2/2a)(\varepsilon_{op}^{-1} - \varepsilon_s^{-1}) + \Delta E_{spin}, \quad (11)$$

where ΔE_{spin} is the energy difference between the two spin states as follows and is regarded as having a positive value:

$${}^*Co^{III}(^3T: t_{2g}^5, e_g^1) \rightarrow {}^*Co^{III}(^1A: t_{2g}^6, e_g^0). \quad \Delta E_{spin} \quad (12)$$

The structure of the product with * in Eq. 12 still remains the same as that of Co^{II}. The present study

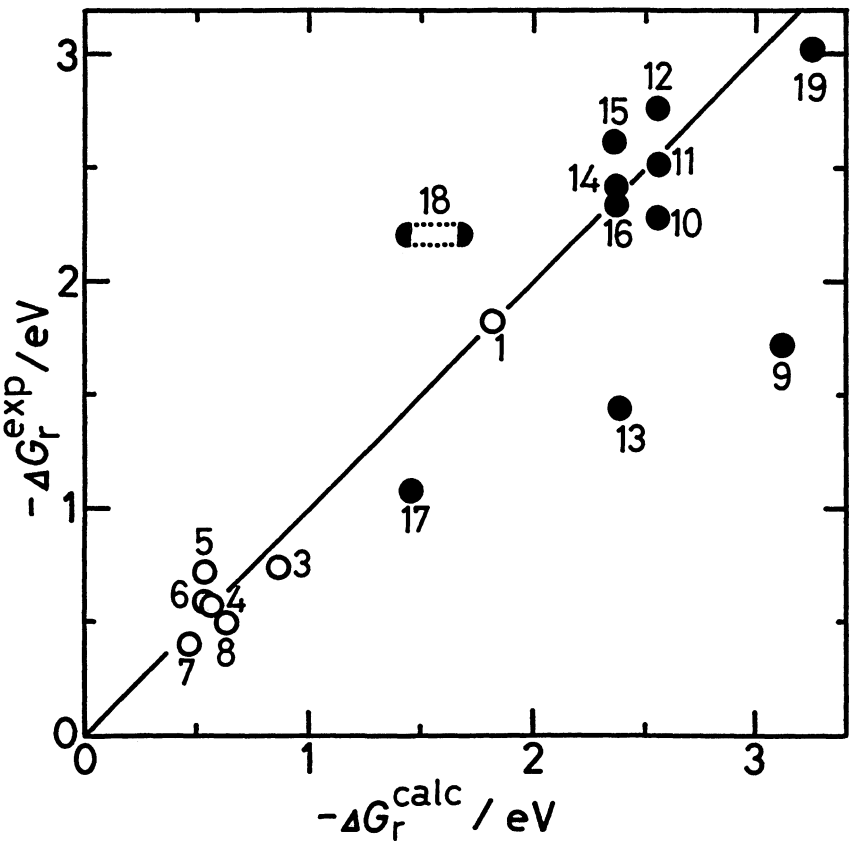

Fig. 1. Plot of the reorganization energies ΔG_r^{exp} determined by the photoelectron emission technique against the ΔG_r^{calc} values calculated by using Eqs. 5—7 for iron (○) and cobalt (●) complexes. The numbers are the same as those in Table 1.

provides the value of ΔE_{spin} as the difference of $(\Delta G_r^{exp} - \Delta G_r^{calc})$. The results shown in Fig. 1 indicate that the ΔE_{spin} values are rather small for most of the cobalt complexes studied here. One exception is $[Co(H_2O)_6]^{2+/3+}$ the value of which is very large (ca. 1.6 eV). The abnormal behavior of this couple concerning the rate of the electron-self-exchange reaction (which has been known for long time[19]) will be studied elsewhere by taking into account their spin states.

The other two samples for which the ΔG_r values do not agree are $[Co(bpy)_3]^{2+/3+}$ and $[Co(N4)(H_2O)_2]^{2+/3+}$. The disagreement for the case of $[Co(bpy)_3]^{2+/3+}$ is not understandable since other complexes which are quite similar to this one give excellent agreement. For the case of $[Co(N4)(H_2O)_2]^{2+/3+}$, the shape of the complex is not spherical since ligand N4 is a flat ring molecule. The equatorial a value used for the calculation of ΔG_r may be too large and the Δr value used here too small, which is regarded as being the same as that of the $[Co(H_2O)_6]^{2+/3+}$.

The relatively small ΔG_r values for $[Co(tpy)_2]^{2+/3+}$ are in accordance with the fact that both ionic states of this complex have a low-spin electron configuration.[20]

It is almost impossible to estimate the ΔG_r value for $[Fe(edta)]^{2-/-}$. The $[Fe(edta)]^-$ is considered to take the heptacoordinate structure of $[Fe(edta)(H_2O)]^-$ in aqueous solution[21] and is too complex to be handled with Eq. 6 (all the metal-ligand atom bond lengths are different in crystals[22]). In addition, the structure in solution is not known for $[Fe(edta)]^{2-}$. In any case, it should be noted that the ΔG_r value (=2.44 eV) for this complex is the largest among the iron complexes. The fact that the $[Fe(edta)]^{2-}$ is an extremely stronger reductant than the $[Fe(H_2O)_6]^{2+}$ (cf. E°=0.117 and 0.77 V, respectively) can be understood as being caused by a large stabilization free energy (2.44 eV) gained after (vertical) one-electron oxidation. This is concluded from the experimental fact that removing an electron vertically from $[Fe(edta)]^{2-}$ requires the same enegy as that from $[Fe(H_2O)_6]^{2+}$ (E_t=7.09 and 7.06 eV, respectively).

It is interesting to compare the ΔG_r^{exp} values obtained by the PEES technique with the rate constants, k_{exch}, of electron-self-exchange reactions in solution. According to the Marcus-Hush theory, the ΔG_r value is closely related to the activation energy, ΔG^*, for the thermal electron-exchange reaction and, thus, to its rate constant. In the simplest model,

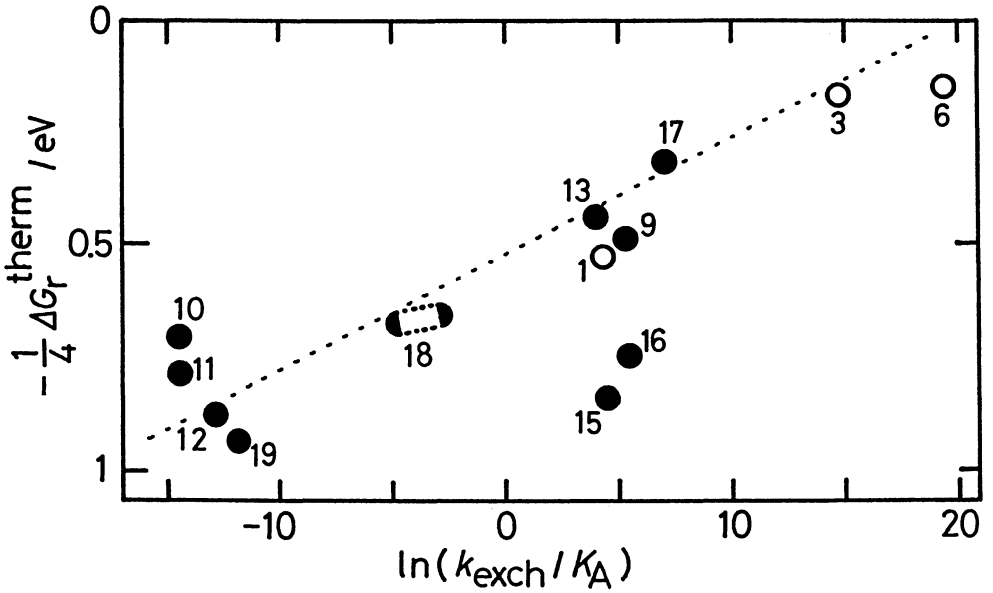

Fig. 2. Correlation between the logarithm of the rate constant k_{exch} for the electron-self-exchange reaction corrected for the formation constant K_A of the precursor complex and a quarter of the thermal reorganization energy ΔG_r^{therm} derived from the ΔG_r^{exp} determined by the photoelectron emission technique for iron (○) and cobalt (●) complexes. The numbers are the same as those in Table 1. The dotted line indicates the slope of RT(=25.7 meV). The k_{exch} and K_A values are collected from Ref. 23.

$\Delta G_r = -4\Delta G^{\ddagger}$. By using many transition metal(II)/(III) couples, Brunschwig and co-workers showed a linear correlation between $(\Delta r)^2$ and ΔG_r(in), as determined by the following equation:[23]

$$\Delta G_r(\text{in}) = 4RT \ln(k_{exch}/K_A) - \Delta G_r^{calc}(\text{out}), \quad (13)$$

where K_A is the equilibrium constant for the formation of the precursor complex for the electron exchange reaction and the ΔG_r^{calc}(out) was obtained by using Eq. 7. Their results support the classical model for evaluating the ΔG_r(in) from Δr, as described in Eq. 6.

The ΔG_r^{exp} determined in the present work is of the optical transition and is different from the ΔG_r^{therm} for the thermal one, like an electron-transfer reaction in solution. For the calculation of ΔG_r in an optical transition, only the force constant, f_o, for X^{nz+1} is used as in Eq. 6, while the f for ΔG_r^{therm} must be evaluated by using the mean value of f_o and f_r for X^{nz}.

According to the Delahay's treatment,[24,1]

$$\Delta G_r^{therm} = \Delta G_r^{opt} + \Delta G_r^{opt}(\text{in}) \cdot [(3f_r - f_o)/(f_r + f_o)], \quad (14)$$

where ΔG_r^{opt} is the reorganization energy pertaining to the optical electron-transfer reaction, i.e. the ΔG_r^{exp} determined by the PEES technique. It is then possible to evaluate ΔG_r^{therm} using $\Delta G_r^{opt}(\text{in}) = \Delta G_r^{exp} - \Delta G_r^{calc}(\text{out})$. The values of the term $(3f_r - f_o)/(f_r + f_o)$ were calculated and found to be almost constant (0.37) for the complexes studied here.

The ΔG_r^{therm}, thus obtained, is obviously related to the k_{exch} corrected for the K_A, as shown in Fig. 2, with an expected slope of RT, which is indicated by the dotted line.

It is worth noting that the anomalous behavior of the $[Co(H_2O)_6]^{2+/3+}$ observed by Brunschwig and co-workers that the experimental k_{exch} value is several orders greater than the predicted value from the classical model,[23] now disappears in the k_{exch} vs. ΔG_r^{exp} relation (the point 9 in Fig. 2). The present results indicate that the thermal electron-transfer reaction proceeds not via the $Co^{III}(^1A)$ state, but via a state which is optically accessible and lies fairly below the $Co^{III}(^1A)$ state when the $[Co(H_2O)_6]^{2+}$ complex deforms its geometry in order to transfer its electron.

This work was supported by Mitsubishi Foundation and by a Grant-in-Aid for Scientific Research No. 01540399 from the Ministry of Education, Science and Culture.

References

1) P. Delahay, "Electron Spectroscopy: Theory, Techniques and Applications," ed by C. R. Brundle and A. D. Baker, Academic Press, London (1984), Vol. 5, pp. 123—196.
2) P. Delahay, *Acc. Chem. Res.*, **15**, 40 (1982).
3) I. Watanabe, J. B. Flanagan, and P. Delahay, *J. Chem. Phys.*, **73**, 2057, (1980).
4) I. Watanabe, K. Maya, Y. Yabuhara, and S. Ikeda, *Bull. Chem. Soc. Jpn.*, **59**, 907 (1986).
5) T. Nakayama, I. Watanabe, and S. Ikeda, *Bull. Chem.*

Soc. Jpn., **61**, 673 (1988).

6) The E° is commonly defined as the potential of an electrode in equilibrium with equi-activity X^{nz} and X^{nz+1} ions with respect to NHE (Normal Hydrogen Electrode). This means that the free energy of X^{nz} in solution is the same as that of the system consisting of X^{nz+1} in solution plus e^- in the electrode having the potential of E°, and that no energy is necessary to transfer an electron from X^{nz} to the electrode at E°. Thus, the transfer of the electron from X^{nz} to NHE requires the energy of $-eE^\circ$, where e is the charge of an electron. Equation 2 is the expression for this process.

7) R. Parsons, "Standard Potentials in Aqueous Solution," ed by A. J. Bard, R. Parsons, and J. Jordan, Marcel Dekker, New York (1985), pp. 13—37.

8) R. A. Marcus and N. Sutin, *Biochim. Biophys. Acta*, **811**, 265 (1985), and other references therein.

9) P. Delahay and A. Dziedzic, *J. Chem. Phys.*, **80**, 5793 (1984).

10) P. Delahay, *Chem. Phys. Lett.*, **90**, 425 (1982).

11) P. Delahay, K. von Burg, and A. Dziedzic, *Chem. Phys. Lett.*, **79**, 157 (1981).

12) S.U.M. Khan and J.O'M. Bockris, *J. Phys. Chem.*, **87**, 4012 (1983).

13) S.U.M. Khan and J.O'M. Bockris, *Chem. Phys. Lett.*, **99**, 83 (1983).

14) P. Delahay and A. Dziedzic, *J. Chem. Phys.*, **80**, 5793 (1984).

15) P. Delahay, *Chem. Phys. Lett.*, **96**, 613 (1983).

16) P. Delahay, *Chem. Phys. Lett.*, **87**, 607 (1982).

17) K. Ono, I. Watanabe, and S. Ikeda, *Chem. Phys. Lett.*, **128**, 287 (1986).

18) If the difference between the values of the vertical I_p and the adiabatic one is large, the E_t values obtained from the present method can be somewhere between the values of the vertical E_t and the adiabatic one: See, K. Maya, I. Watanabe, and S. Ikeda, *J. Electron Spectrosc. Relat. Phenom.*, **40**, 307 (1986).

19) J. F. Endicott, B. Durham, and K. Kumar, *Inorg. Chem.*, **21**, 2437 (1982).

20) R. Farina and R. G. Wilkins, *Inorg. Chem.*, **7**, 514 (1968).

21) K. Kanamori, H. Dohniwa, N. Ukita, I. Kanesaka, and K. Kawai, *Bull. Chem. Soc. Jpn.*, **63**, 1447 (1990).

22) M. D. Lind, M. J. Hamor, T. A. Hamor, and J. L. Hoard, *Inorg. Chem.*, **3**, 34 (1964). See also the references in Ref. 21.

23) B. S. Brunschwig, C. Creutz, D. H. Macartney, T-K. Sham, and N. Sutin, *Faraday Discuss. Chem. Soc.*, **74**, 113 (1982).

24) P. Delahay and A. Dziedzic, *J. Chem. Phys.*, **80**, 5793 (1984).

Hydrates of Organic Compounds. XV. The Formation of Clathrate-Like Hydrates of Tetraisopentylammonium Alkanoates and Alkanedioates

Haruo NAKAYAMA,* Kayoko NAKAMURA, Yukio HAGA, and Yōji SUGIURA
Division of Materials Science and Chemical Engineering, Faculty of Engineering, Yokohama National University, Tokiwadai, Hodogaya-ku, Yokohama 240
(Received September 26, 1990)

The solid–liquid phase diagrams of binary mixtures of water with tetraisopentylammonium alkanoates, $[(i\text{-}C_5H_{11})_4N]C_nH_{2n+1}COO$ (n=0—9), and with bis(tetraisopentylammonium) alkanedioates, $[(i\text{-}C_5H_{11})_4N]_2[OOC(CH_2)_nCOO]$ (n=0—10), were examined in order to confirm the formation of clathrate-like hydrates. The results are summarized as follows: (1) For all the compounds examined the formation of a clathrate-like hydrate is newly confirmed; (2) the melting points of these hydrates are fairly high (lie between 10 and 28 °C); (3) typical hydrates formed by the alkanoates have hydration numbers around 38 and those formed by the alkanedioates around 80; and (4) hydrates with hydration numbers around 14 and larger than 40 are also found for the alkanoate hydrates and around 30 and larger than 80 for the alkanedioate hydrates. The effects of the alkyl chain length of the alkanoate anion and of the methylene chain length of the alkanedioate anion on the stability of the hydrates are not marked, suggesting that a hydrogen-bonded framework of water molecules around a $(i\text{-}C_5H_{11})_4N^+$ cation is fairly stable.

Since the formation of unusual hydrates of tetrabutylammonium alkanoates and aromatic carboxylate like formate, acetate, propionate, and benzoate, which have a large number of water molecules per one ammonium ion (hydration numbers), was reported by Kraus et al.[1] in 1940, the formation of similar kind of alkanoate hydrates has extensively been studied.[2-5]

A single-crystal X-ray examination by Jeffrey and his co-workers on these hydrates[2-3] showed that they were clathrate-like hydrates similar to the so-called gas hydrates:[6] The water structure is a hydrogen-bonded framework and is essentially a regular arrangement of polyhedra-like pentagonal dodecahedra; tetrakaidecahedra and oxygen atoms of the carboxylate anion are incorporated into the water lattice, making an anionic host structure.

Recently, in our phase-diagrammatic studies[7-12] it was concluded that tetrabutylammonium alkanoates or alkanedioates having various alkyl chains or methylene chains could also form a clathrate-like hydrate. Judging from the hydration numbers and melting points of these hydrates, it was assumed that their crystal structure is isostructural with that of a well known $(n\text{-}C_4H_9)_4NF\cdot 30H_2O$ hydrate[13] and that the alkyl group of the alkanoate anions and a methylene chain of the alkanedioate anions is accommodated in a vacant pentagonal dodecahedra.

On the other hand, although some tetraisopentylammonium salts, such as $(i\text{-}C_5H_{11})_4NF$ and $(i\text{-}C_5H_{11})_4NCl$, are known to form similar type hydrates,[2,14,15] no information concerning the formation of a clathrate-like hydrate of tetraisopentylammonium alkanoates or alkanedioates has been reported, except for formate[1] and benzoate.[4] Thus, in this work, phase-diagrammatic studies regarding binary mixtures of tetraisopentylammonium alkanoates or alkanedioates with water were carried out in order to confirm the formation of clathrate-like hydrates. Tetraisopentylammonium alkanoates and alkanedioates are expected to form more stable hydrates than those of tetrabutylammonium alkanoates or alkanedioates since (1) the water frameworks surrounding a $(i\text{-}C_5H_{11})_4N^+$ cation are, in general, more stable than those surrounding a $(n\text{-}C_4H_9)_4N^+$ cation[16] and (2) in a $(i\text{-}C_5H_{11})_4NF$ hydrate,[14] there exists an extended layer structure of connected pentagonal dodecahedra which are suitable to accommodate either an alkyl chain of an alkanoate anion or a methylene chain of an alkanedioate anion.

Experimental

Aqueous solutions of tetraisopentylammonium alkanoates, except for formate and acetate, were prepared by a reaction between tetraisopentylammonium iodide and the corresponding silver alkanoates in water, followed by filtration of silver iodide precipitate. Tetraisopentylammonium iodide was synthesized by allowing a reaction of triisopentylamine with isopentyl iodide in ethyl acetate and purified by repeated recrystallization from ethyl acetate. Each silver alkanoate was obtained as a precipitate by mixing an aqueous solution of silver nitrate with an aqueous solution of sodium alkanoate, followed by repeated washing with water in order to remove the resultant sodium nitrate. Aqueous solutions of tetraisopentylammonium formate, acetate and of all the bis(tetraisopentylammonium) alkanedioates, were obtained by neutralization of tetraisopentylammonium hydroxide solution with the corresponding acids. The hydroxide solution was obtained by treating tetraisopentylammonium iodide with freshly prepared silver(I) oxide in water. The wet silver(I) oxide was prepared by reacting a silver nitrate solution with a sodium hydroxide solution, followed by filtration and repeated washing with water. Triisopentylamine, isopentyl iodide and all the carboxylic acids and some of the dicarboxylic acids were reagent grade commercial materials and used without further purification. Seven dicarboxylic acids, $HOOC(CH_2)_nCOOH$ with n=3—8 and 10, which were purchased from Tokyo Kasei Kogyo Co., Ltd., were recrystallized from water.

The solid-liquid phase diagrams of the binary tetraisopentylammonium alkanoate (or alkanedioate)-water systems were determined in the following manner. A sample solution (about 1.0—1.5 g) of known concentration was prepared by weighing out water and a concentrated mother solution of each alkanoate (or alkanedioate), and was sealed in a small glass ampoule. The concentration of the mother solution was determined by a titration method using a sodium tetraphenylborate solution.[9] Each ampoule was gradually cooled until the solid phase appeared and was annealed for at least 24 h at a temperature several degrees lower than the temperature at which the solid phase completely disssolved. After that, the ampoule was slowly warmed (at the rate of about 0.3—0.5 °C per hour) with shaking in a constant temperature bath and the temperature at which the solid phase completely dissolved was accurately determined.

Results and Discussion

(1) The Formation of Hydrates of Tetraisopentylammonium Alkanoates. The solid-liquid phase diagrams for the binary systems, water-[(i-C_5H_{11})$_4$N]n-$C_nH_{2n+1}COO$, where n=2—5, are shown in Fig. 1. The logarithm of the concentration expressed as the mole fraction, X, is plotted against the reciprocal of the absolute temperature. The temperature expressed in ordinary Celsius units is shown on the upper side of the figure. The phase diagrams of two binary systems, water-[(i-C_5H_{11})$_4$N]HCOO and water-[(i-C_5H_{11})$_4$N]CH_3COO, are not shown in Fig. 1 since the phase diagram of the former system resembles the one of the water-[(i-C_5H_{11})$_4$N]C_2H_5COO system and the latter system the one of the water-[(i-C_5H_{11})$_4$N]n-C_3H_7COO system. The phase diagrams of these systems exhibit congruent melting points at concentrations near X=0.025—0.026, indicating that these carboxylates form a hydrate with hydration numbers around 38. It is interesting to note that (1) these hydrates are fairly stable: the melting points are 22—28 °C; and (2) they can be in equilibrium with very dilute solutions: For

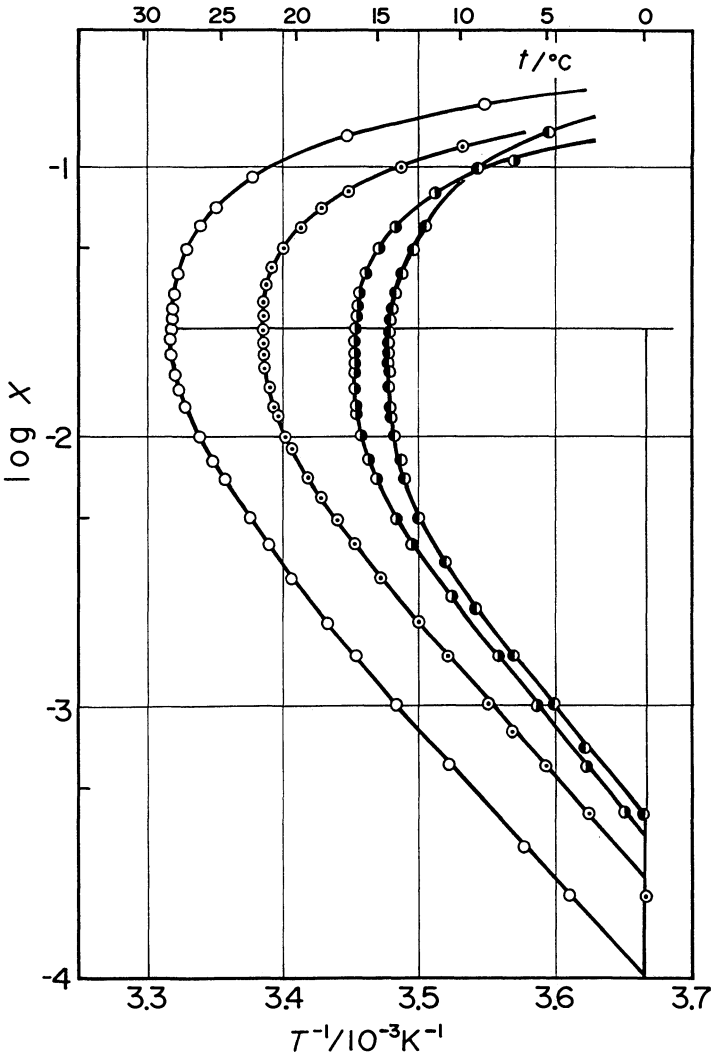

Fig. 1. Solid-liquid phase diagrams for the [(i-C_5H_{11})$_4$N]-RCOO-water systems. ○: R=C_2H_5; ⊙: R=n-C_3H_7; ◑: R=n-C_4H_9; ◐: R=n-C_5H_{11}.

example, the most stable $[(i\text{-}C_5H_{11})_4N]C_2H_5COO$ hydrate is formed in such a dilute solution as $X=1\times10^{-4}$ (0.206 wt%).

The phase diagrams of the two systems with $n=4$ and $n=5$ also exhibit congruent melting points at about 15 °C. However, all the solid phases which are formed in the solutions in the concentration range between $X=0.020$ and $X=0.024$ for $n=4$ salt and between $X=0.018$ and 0.024 for $n=5$ salt dissolve at very narrow temperature range: Between a maximum dissolution temperature and the one only 0.1 °C lower than that. Therefore, exact hydration numbers cannot be determined for these hydrates. A probable reason for this behavior is that some hydrates with different hydration numbers between 40 and 55 are formed simultaneously, depending upon the concentration of the solution. The fact that the slope $-\partial \log X/\partial(1/T)$ in dilute solutions, $X=0.001$ for example, for the above-mentioned two systems, is slightly steeper than that of the systems of $n=2$ and $n=3$ indicates that salts with $n=4$ and $n=5$ form a hydrate with hydration numbers larger than those of $n=2$ and 3 hydrates (around 38), since it has been verified that the slope $-\partial \log X/\partial(1/T)$ is approximately proportional to the hydration numbers of a hydrate.[16]

The solid-liquid phase diagrams for binary systems water-$[(i\text{-}C_5H_{11})_4N]n\text{-}C_nH_{2n+1}COO$ with long alkyl chains as $n=6$ and 9 are shown in Fig. 2. For a comparison, Fig. 2 includes the phase diagram of the $n=2$ system shown in Fig. 1. The phase diagram of a system with $n=7$ is omitted because of the similarity in the data with those of the $n=6$ system. This figure shows the existence of congruent melting points near $X=0.026$, just as in the case of $n=2$, indicating that salts with such long alkyl chains as $n=6$, 7, and 9 can also form a hydrate with hydration numbers around 38, although their melting points (11—16 °C) are

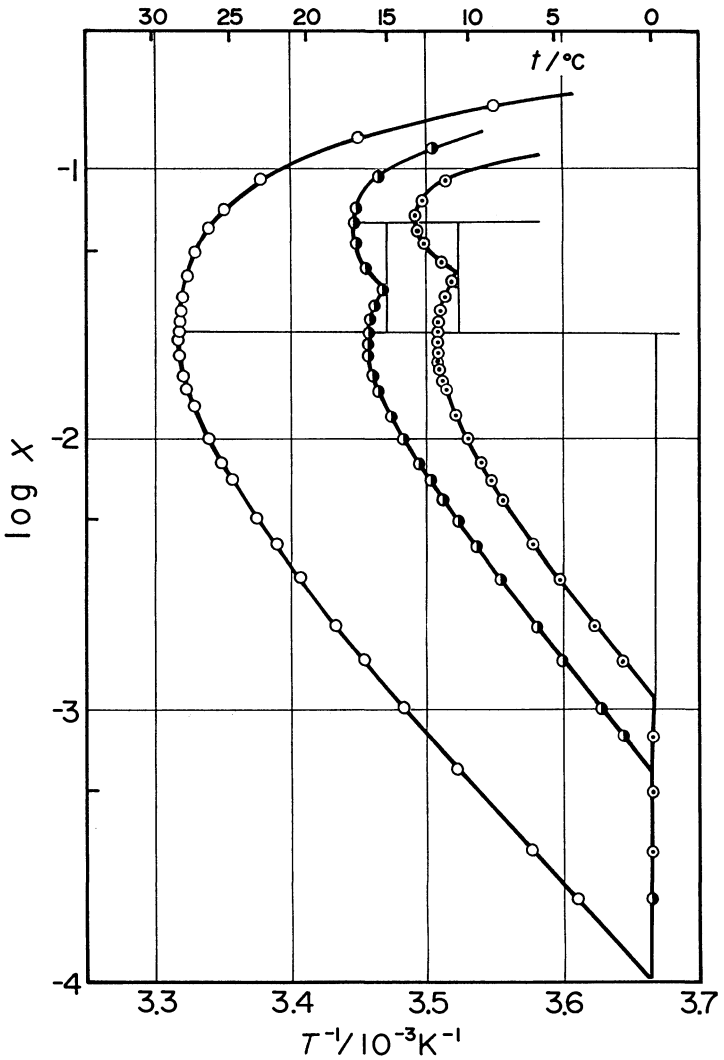

Fig. 2. Solid-liquid phase diagrams for the $[(i\text{-}C_5H_{11})_4N]$-RCOO-water systems. ○: R=C_2H_5; ⊙: R=n-C_6H_{13}; ◑: R=n-C_9H_{19}.

lower than those of the salts with short alkyl chains like n=0—3 (Fig. 1). Furthermore, Fig. 2 indicates that systems with n=6, 9 (and n=7) have another congruent melting point around X=0.067. This means the formation of hydrate with hydration numbers around 14. It is interesting to note that these hydrates have slightly higher melting points than those with hydration numbers around 38.

All of the melting points and hydration numbers, determined from each congruent melting point and congruent composition, are summarized in Table 1.

Table 1. Melting Points and Hydration Numbers of the Clathrate-Like Hydrates Formed by a Series of Tetraisopentylammonium Alkanoates, $[(i\text{-}C_5H_{11})_4N]RCOO$

R	Melting point t_m/ °C	Hydration numbers
H	22.4	37±3
CH_3	24.5	37±2
C_2H_5	28.3	39±2
n-C_3H_7	22.3	39±2
n-C_4H_9	16.5	40—50
n-C_5H_{11}	14.3	40—55
n-C_6H_{13}	11.9	40±2
	13.4	14±1
n-C_7H_{15}	10.7	37±2
	13.1	14±2
n-C_9H_{19}	16.1	37±3
	17.1	15±2

The existence of these hydrates, except for the formate hydrate, has been newly confirmed in this study. However, the melting point 15—20 °C and hydration numbers 50 of the formate hydrate reported by Kraus et al.[1] are fairly different from our values. From Table 1 it is clear that the most typical hydrate is one with hydration numbers around 38. This hydrate is formed regardless of the chain length of the alkyl group in the alkanoate anion and the effect of the chain length of the $C_nH_{2n+1}COO^-$ anion on the melting points of the hydrates is not so marked. Judging from the values of the hydration numbers and the melting points, these hydrates seem to be isostructural clathrate-like hydrates with a well known $(i\text{-}C_5H_{11})_4NF \cdot 39H_2O$ hydrate.[14] Other hydrates found in Table 1 are the ones with hydration numbers larger than 40 and around 14. The former is formed for the salts of n=4 and 5 and the latter for the salts with a longer alkanoate than n=6. Although there is no information concerning the structure of these hydrates, it seems probable that one of the former hydrates has some connection with a tetraisopentylammonium benzoate hydrate, $[(i\text{-}C_5H_{11})_4N]C_6H_5COO \cdot (48\pm2)H_2O$, which was found in a preliminary experiment. This hydrate is fairly unstable with a melting point of about 6.3 °C.

In Fig. 3 the relationship between the melting points of the hydrates and the number of carbon atoms of the alkyl group in the carboxylate anion (n) is shown for the two series of salts, $[(i\text{-}C_5H_{11})_4N]$-$n$-$C_nH_{2n+1}COO$ and $[(n\text{-}C_4H_9)_4N]n$-$C_nH_{2n+1}COO$.[7]

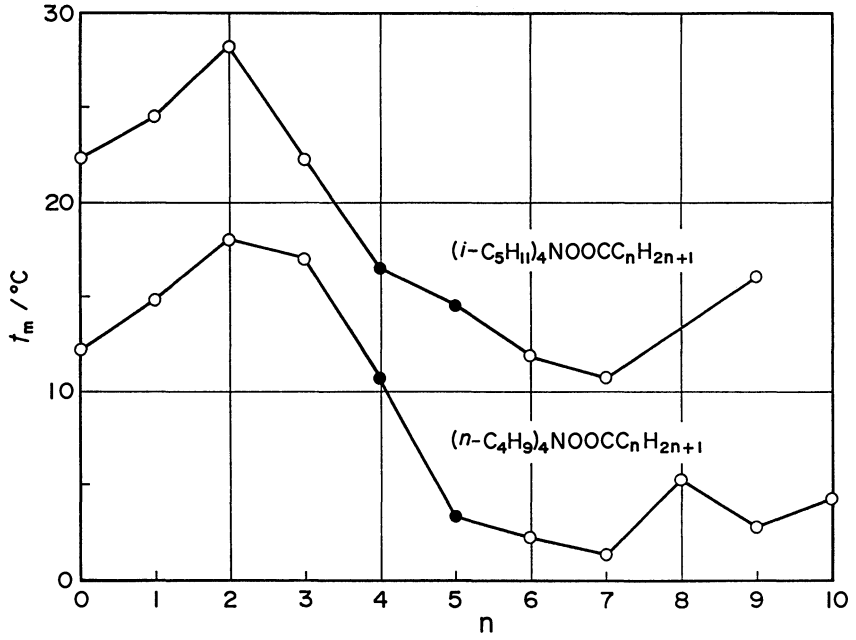

Fig. 3. Relationships between the melting points, t_m, of the tetrabutylammonium and of the tetraisopentylammonium alkanoate hydrates and the chain length of the alkanoate anion. Filled circle indicates a hydrate with somewhat larger hydration numbers as compared with the other hydrates shown by open circles.

The latter series form hydrates with hydration numbers around 30 and only when n=4 and 5, just as in the case of the former salt hydrates, hydrates with hydration numbers larger than 30 are formed.[7] It is interesting to note that both series of hydrates behave almost in a similar manner, except that the melting points of a series of $[(i\text{-}C_5H_{11})_4N]n\text{-}C_nH_{2n+1}COO$ hydrates are about 10 °C higher than those of a series of $[(n\text{-}C_4H_9)_4N]n\text{-}C_nH_{2n+1}COO$ hydrates irrespective of the values of n, coinciding with a general trend that the water frameworks surrounding a $(i\text{-}C_5H_{11})_4N^+$ cation are more stable than those surrounding a $(n\text{-}C_4H_9)_4N^+$ cation.[12,16] The similar behavior of the two series of hydrates leads the conclusion that the same arguement can be applied regarding the way to accommodate an alkyl group, $n\text{-}C_nH_{2n+1}$, of the alkanoate anion within the $[(i\text{-}C_5H_{11})_4N]n\text{-}C_nH_{2n+1}COO$ hydrates as in the $[(n\text{-}C_4H_9)_4N]n\text{-}C_nH_{2n+1}COO$ hydrates:[7-10] (1) Such short alkyl groups as CH_3, C_2H_5, and $n\text{-}C_3H_7$ are encaged in a vacant pentagonal dodecahedron, which exists in a gap between the arrangement of larger polyhedra (tetrakaidecahedra and/or pentakaidecahedra) filled by one of the isopentyl group of a tetraisopentylammonium cation and the highest melting point of the propionate hydrate coincide with the best fitness of the $CH_3CH_2COO^-$ anion to a pentagonal dodecahedron; (2) long alkyl chains like $n\text{-}C_4H_9$—$n\text{-}C_9H_{19}$ penetrate through two (or three) vacant pentagonal dodecahedra forming a hydrogen-bonded anionic host structure with water.

(2) The Formation of Hydrates of Bis(tetraisopentylammonium) Alkanedioates. The solid-liquid phase diagrams for the binary systems, water-$[(i\text{-}C_5H_{11})_4N]_2OOC(CH_2)_nCOO$, where n=0—2 are shown in Fig. 4 in the same manner as in Figs. 1 and 2. All three systems exhibit congruent melting points (20—25 °C) at concentrations around X=0.0125, indicating

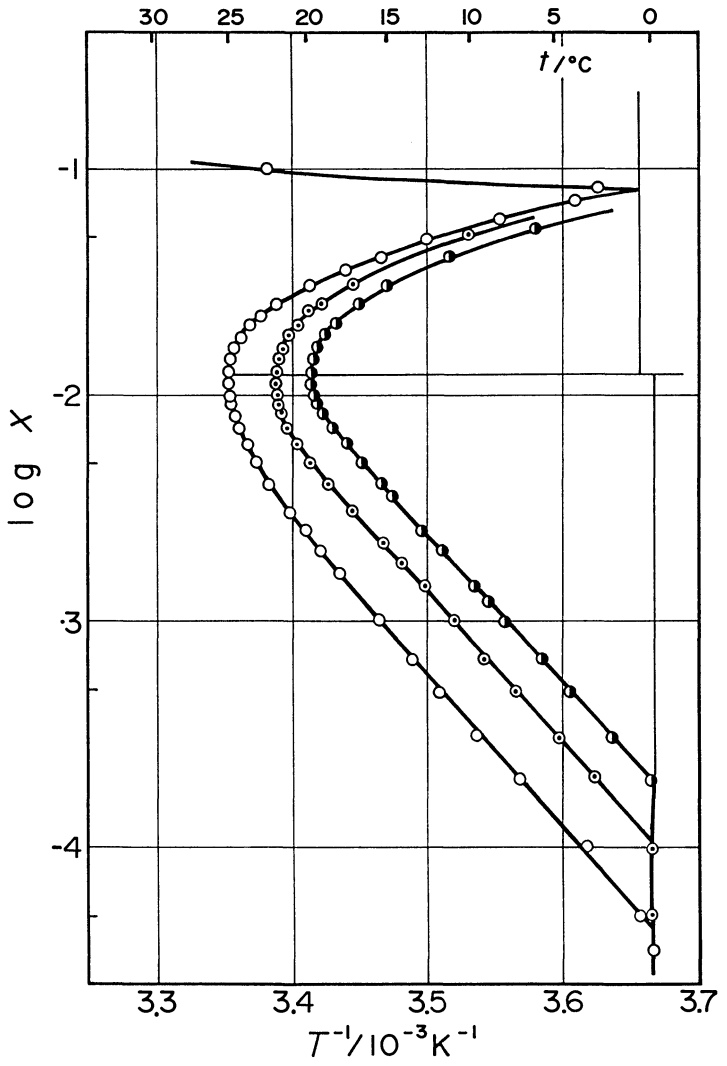

Fig. 4. Solid-liquid phase diagrams for the water-$[(i\text{-}C_5H_{11})_4N]_2OCC(CH_2)_nCOO$ systems. ○: n=0; ⊙: n=1; ◑: n=2.

that these salts form a fairly stable hydrate with hydration numbers of about 80. The melting points of the hydrates decrease with increasing the number of n. The solid-liquid phase diagrams for the other three systems with n=3—5 show similar behaviors as shown in Fig. 4, except that the most stable hydrate is formed by the salt of n=4; its melting point is 27.5 °C.

On the other hand, the solid-liquid phase diagrams, which are shown in Fig. 5, for the binary systems, water-[(i-C_5H_{11})$_4$N]$_2$OOC(CH_2)$_n$COO, where n=6—10, exhibit a somewhat complicated behavior, as compared with the case of n=0—5. The characteristic features of Fig. 5 are summarized as follows: (1) Although there is a maximum dissolution temperature around X=0.0125 for the salts of n=6—8, solid phases formed from the solutions in the concentration range of X=0.012—0.013 for the n=6 salt, X=0.012—0.014 for n=7, and X=0.010—0.0125 for n=8, dissolve at very narrow temperature range around the maximum dissolution temperatures just as in the case of the alkanoate hydrates with n=4 and n=5 (Fig. 2). This indicates that exact hydration numbers of the hydrates cannot be determined. (2) There are incongruent melting points about 1 °C below the maximum dissolution temperature. These temperatures are 18.3 °C for the n=6 salt, 17.2 °C for the n=7 salt and two or three incongruent melting points between 17 and 19 °C for the n=10 salt. The existence of incongruent compositions smaller than X=0.012 clearly indicates the formation of hydrates with hydration numbers larger than 80. (3) For the systems of n=8 and n=10, another congruent melting point is found around X=0.032; this means the formation of a hydrate with hydration numbers around 30.

The melting points and hydration numbers found for the hydrates of a series of bis(tetraisopentylammonium) alkanedioate are summarized in Table 2. All of these hydrates were newly confirmed in this study.

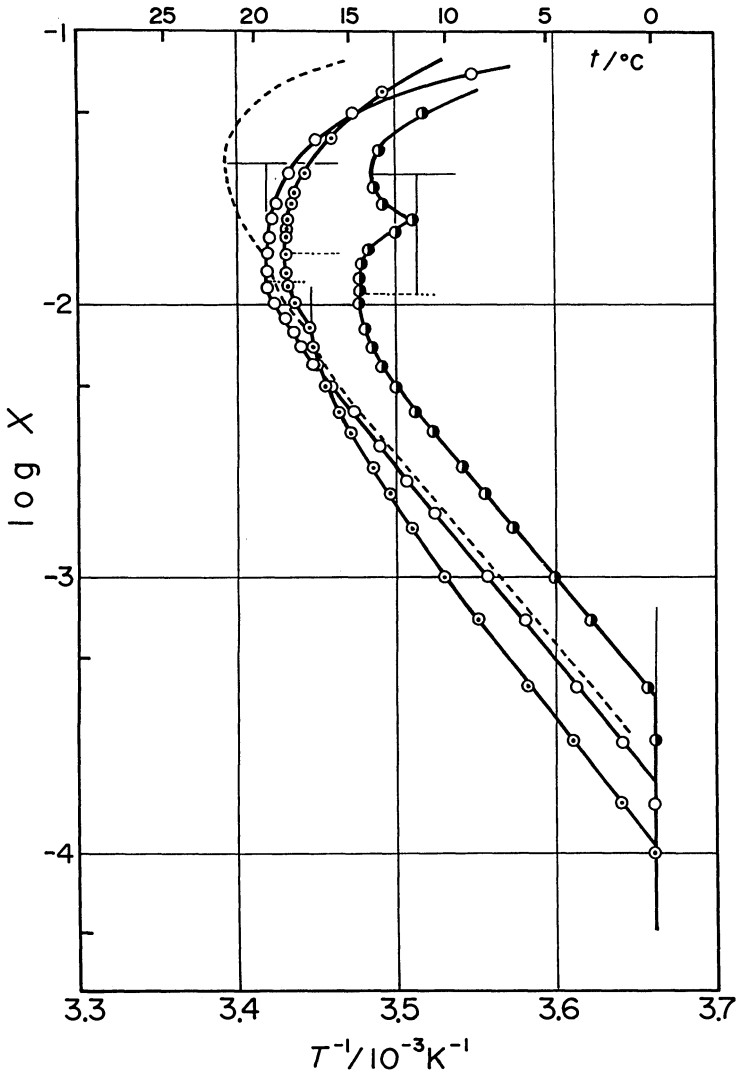

Fig. 5 Solid-liquid phase diagrams for the water-[(i-C_5H_{11})$_4$N]$_2$ OOC(CH_2)$_n$COO systems. ○: n=6; ⊙: n=7; ◑: n=8; broken line: n=10.

As can be seen in Table 2, the most typical hydrate is one with a hydration number around 80. This hydrate is considered to be isostructural with the alkanoate hydrates of hydration numbers around 38 (Table 1), since the hydration number, 80, is about twice of 38. Other hydrates are those with hydration numbers around 30 and larger than 80. As mentioned above, the exact hydration numbers of the latter hydrates cannot be determined owing to the complexity of the phase diagrams. It is not certain whether there is any structural relation between these hydrates and the alkanoate hydrates having hydration numbers larger than 40 (Table 1). The hydrate of the hydration numbers around 30 is formed for alkanedioates with n larger than 8 and, eventually, its hydration numbers are almost twice that (14—15, Table 1) of the alkanoate hydrates which are formed by the alkanoates with n larger than 6. Both hydrates seem to be isostructural with each other.

Table 2. Melting Points and Hydration Numbers of the Clathrate-Like Hydrates Formed by a Series of Bis(tetraisopentylammonium) Alkanedioates, $[(i\text{-}C_5H_{11})_4N]_2OOC(CH_2)_nCOO$

n	Melting point t_m/ °C	Hydration numbers
0	25.1	80±2
1	22.1	80±2
2	19.8	82±2
3	23.7	79±3
4	27.5	80±3
5	19.8	80±3
6	19.4	75—85
	18.3 (incong.)	
7	18.4	70—85
	17.2 (incong.)	
8	14.5	80—100
	13.9	32±3
10	21.5	30±5

The relationship between the melting points, t_m, of the alkanedioate hydrates and the methylene chain length, n, of the alkanedioate anions is shown in Fig. 6 for two series of alkanedioates, $[(i\text{-}C_5H_{11})_4N]_2OOC(CH_2)_nCOO$ and $[(n\text{-}C_4H_9)_4N]_2OOC(CH_2)_nCOO$.[11] In general, the t_m's vary with n in a similar manner for both series of hydrates. Just as in the case of alkanoate hydrates (Fig. 3), the melting points of the tetraisopentylammonium dicarboxylate hydrates are about 10 °C higher than those of the tetrabutylammonium alkanedioate hydrates, though this difference becomes larger when n is larger than 6. The maximum t_m is found in the case n=4 for the bis(tetraisopentylammonium) alkanedioate hydrates whereas n=3 for the bis(tetrabutylammonium) alkanedioate hydrates. This discrepancy will not be essential since the melting point of the hydrate of bis(tetrabutylammonium) alkanedioate with n=4 is also fairly high.

It is interesting to note that the melting points initially decrease with increasing n from 0 to 2 then increase with increasing n from 2 to 4. This can be explained by the fact that the hydrates of salts with such small n as 0—2 are constructed with two kinds of units, $[[(i\text{-}C_5H_{11})_4N]OOC(CH_2)_nCOO]^-$ and (*i*-

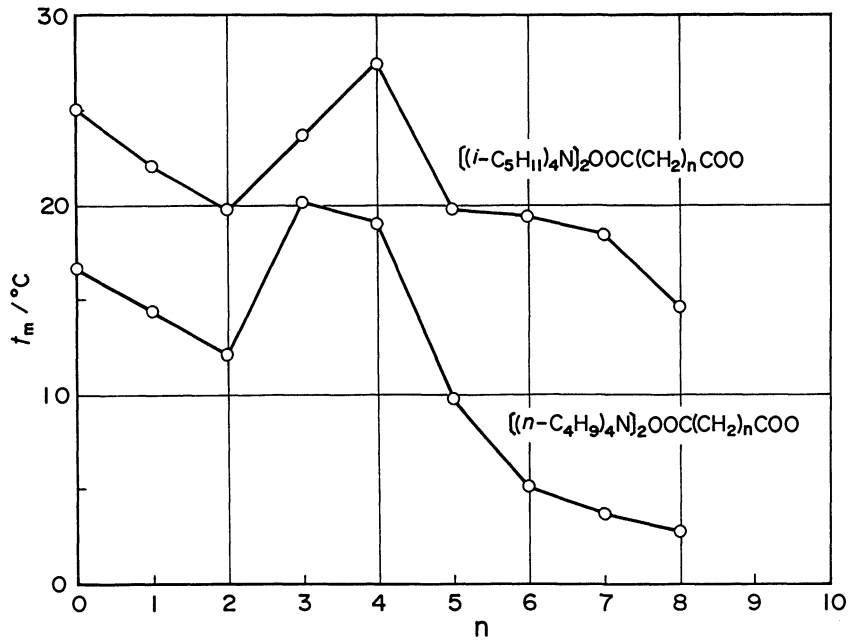

Fig. 6. Relationships between the melting points, t_m, of the bis(tetrabutylammonium) and of the bis(tetraisopentylammonium) alkanedioate hydrates and of the chain length of the methylene chain in the alkanedioate anion.

$C_5H_{11})_4N^+$; then, the distortion effect of the $^-OOC(CH_2)_nCOO^-$ anion on the hydrogen-bonded water network surrounding a $(i\text{-}C_5H_{11})_4N^+$ cation increases with increasing n, leading to a lowering of the melting points of the hydrates. On the other hand, the hydrates of the salts with n larger than 3 can be considered to be constructed by a sequence of $(i\text{-}C_5H_{11})_4N^+ \cdots {}^-OOC(CH_2)_nCOO^- \cdots (i\text{-}C_5H_{11})_4N^+$; the central $^-OOC(CH_2)_nCOO^-$ anion is surrounded by vacant pentagonal dodecahedron or connected pentagonal dodecahedra, leading to the formation of fairly stable hydrate, as is found in the case of tetraisopentylammonium alkanoate hydrates.

References

1) D. L. Fowler, W. V. Loebenstein, D. B. Pall, and C. A. Kraus, *J. Am. Chem. Soc.*, **62**, 1140 (1940).

2) R. McMullan and G. A. Jeffrey, *J. Chem. Phys.*, **31**, 1231 (1959).

3) M. Bonamico, G. A. Jeffrey, and R. K. McMullan, *J. Chem. Phys.*, **37**, 2219 (1962).

4) G. Beurskens, G. A. Jeffrey, and R. K. McMullan, *J. Chem. Phys.*, **39**, 3311 (1963).

5) Yu. A. Dyadin, L. S. Aladko, L. A. Gaponenko, and T. M. Polyanskaya, *Izv. Sib. Otd. Akad. Nauk SSSR, Ser. Khim. Nauk*, **1981**, (**9**), 19.

6) W. F. Clausen, *J. Chem. Phys.*, **19**, 259, 662 (1951). M. von Stackelberg and H. R. Muller, *ibid.*, **19**, 1319 (1951). L. Pauling and R. E. Marsh, *Proc. Natl. Acad. Sci. U.S.A.*, **38**, 112 (1952).

7) H. Nakayama and S. Torigata, *Bull. Chem. Soc. Jpn.*, **57**, 171 (1984).

8) H. Nakayama and H. Usui, *J. Inclusion Phenom.*, **2**, 249 (1984).

9) H. Nakayama, T. Saitoh, and H. Uchida, *J. Inclusion Phenom.*, **8**, 177 (1990).

10) H. Nakayama, H. Usui, and H. Matsui, *Bull. Chem. Soc. Jpn.*, **60**, 4459 (1987).

11) H. Nakayama and K. Watanabe, *Bull. Chem. Soc. Jpn.*, **51**, 2518 (1978).

12) H. Nakayama, *Bull. Chem. Soc. Jpn.*, **60**, 2319 (1987).

13) R. K. McMullan, M. Bonamico, and G. A. Jeffrey, *J. Chem. Phys.*, **39**, 3295 (1963).

14) D. Feil and G. A. Jeffrey, *J. Chem. Phys.*, **35**, 1863 (1961).

15) H. Nakayama, *Bull. Chem. Soc. Jpn.*, **54**, 3717 (1981).

16) H. Nakayama, *Bull. Chem. Soc. Jpn.*, **55**, 389 (1982).

Photoinduced Nucleophilic Addition of Ammonia and Alkylamines to Aryl-Substituted Alkenes in the Presence of *p*-Dicyanobenzene

Toshiaki YAMASHITA,* Koichiro SHIOMORI,† Masahide YASUDA,*,† and Kensuke SHIMA†
Department of Industrial Chemistry, Miyakonojo National College of Technology, Miyakonojo, Miyazaki 885
†Department of Industrial Chemistry, Faculty of Engineering, Miyazaki University,
Gakuen-Kibanadai, Miyazaki 889-21
(Received June 20, 1990)

The photoamination of 1,1-diphenylpropene (**1a**) with ammonia and some primary alkylamines in the presence of *p*-dicyanobenzene gave the corresponding *N*-substituted 2-amino-1,1-diphenylpropane (**2a—e**) along with the formation of 3-methyl-4,4-diphenylbutanenitrile (**3a**), 1,1-diphenylpropane (**4a**), 3,3-diphenylpropene (**5**), and diphenylmethane (**6**). In the case of 1,1-diphenylethene (**1b**), *N*-substituted 1-amino-2,2-diphenylethane (**2f—h**), 4,4-diphenylbutanenitrile (**3b**), and 1,1-diphenylethane (**4b**) were produced. In photoamination with *t*-butylamine in acetonitrile, **3a** and **3b** were mainly formed as a consequence of the incorporation of acetonitrile to **1a** and **1b**. The photoamination of 1-phenyl-3,4-dihydronaphthalene (**1c**) with isopropylamine or *t*-butylamine gave *cis*- and *trans*-*N*-substituted 1-phenyl-2-amino-1,2,3,4-tetrahydronaphthalenes (**15** and **16**) in a ratio of ca. 8:2. The mechanism of photoamination is discussed in terms of a photochemical electron transfer of **1** to *p*-dicyanobenzene followed by a nucleophilic addition of the amine to the cation radical of **1**.

Photoinduced nucleophilic additions in the presence of electron acceptors have been investigated for a variety of electron-donating substances (D) involving aryl-substituted alkenes, strained compounds, and arenes from mechanistic and synthetic points of view.[1] In general, a key pathway for photoinduced nucleophilic additions is the addition of nucleophiles (NuH) to the cation radicals of D ($D^{+\cdot}$) generated from a photochemical electron transfer from D to electron acceptors (A), as shown in Scheme 1. While extensive studies on photoadditions using alcohols, water, and cyanide ion as nucleophiles have accumulated, little is known about the photoaddition of ammonia and amines, except for our reports on the photoamination of arenes with ammonia and alkylamines.[2] Since amines serve as both a nucleophile and a base, their photoaddition is expected to show different features from other nucleophiles. Herein we wish to report on the photoaddition of ammonia and alkylamines to aryl-substituted alkenes (**1**) using *p*-

Table 1. Photoamination of Diphenylalkene (**1**) with Ammonia and Alkylamines in the Presence of *p*-Dicyanobenzene[a]

Run	1	RNH_2	Products (Yield/%)[b]					Conv. of 1/%	Recov. of DCNB/%
1	**1a**	NH_3	**2a** (44)	**3a** (7)		**5** (5)	**6** (23)	76	78
2	**1a**	*i*-$PrNH_2$	**2b** (65)	**3a** (3)	**4a** (2)	**5** (8)	**6** (6)	81	92
			2a (21)						
3	**1a**	*t*-$BuNH_2$		**3a** (72)				100	83
4[c]	**1a**	*t*-$BuNH_2$	**2c** (46)		**4a** (2)	**5** (9)	**6** (12)	59	90
5	**1a**	$MeO(CH_2)_2NH_2$	**2d** (55)	**3a** (tr)	**4a** (4)	**5** (10)	**6** (7)	74	89
6	**1a**	$HO(CH_2)_2NH_2$	**2e** (58)	**3a** (7)	**4a** (1)	**5** (3)	**6** (2)	69	87
7[d]	**1b**	NH_3	**2f** (18)	**3b** (15)	**4b** (tr)	**7** (41)		70	96
8	**1b**	*i*-$PrNH_2$	**2g** (48)	**3b** (27)	**4b** (12)			28	100
			2f (8)						
9	**1b**	*t*-$BuNH_2$	**2h** (22)	**3b** (60)				66	98
10	**1b**	$MeO(CH_2)_2NH_2$	**2i** (19)	**3b** (6)	**4b** (3)	**8** (20)		80	93
11[e]	**1b**	*i*-$PrNH_2$		**3b** (7)	**4b** (17)	**9** (32)		84	—
12[f]	**1b**	*i*-$PrNH_2$			**4b** (12)	**10** (48)	**11** (13)	76	3
						12a(28)	**12b**(7)		
13[g]	**1b**	*i*-$PrNH_2$	**2g** (68)	**3b** (21)	**4b** (9)			22	94
14[h]	**1b**	*i*-$PrNH_2$	**2g** (36)	**3b** (15)	**4b** (19)			39	86

a) For deaerated acetonitrile solutions (150 ml) containing **1** (5.6 mmol), DCNB (16 mmol) and the amine (73 mmol). b) Isolated yields based on consumed **1**. c) For propanenitrile solution. d) For MeCN-H_2O (9:1) solution. e) In the absence of DCNB. f) For DMF solution. g) Redox-photosensitization by phenanthrene; after the photoreaction, 13% of phenanthrene was recovered. *N*-Isopropyl-9-amino-9,10-dihydrophenanthrene (**13**) was isolated in 44% yield based on phenanthrene used. h) Redox-photosensitization by triphenylene; 13% of triphenylene was recoverd after the photoreaction.

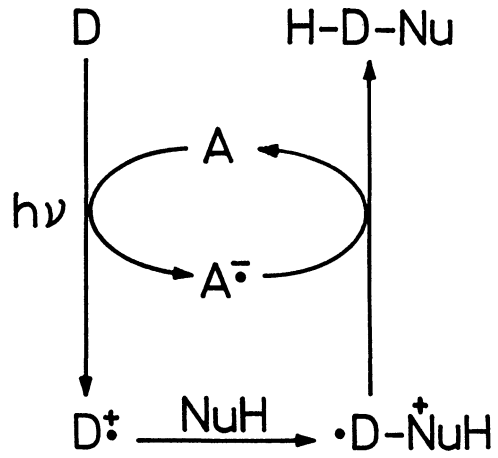

Scheme 1.

dicyanobenzene (DCNB) as A.

Results

The photoamination of diphenylalkene (**1**) was carried out by irradiating a deaerated acetonitrile solution of **1**, DCNB, and ammonia or alkylamines through a Pyrex filter with a high-pressure mercury lamp; incident light was absorbed by both **1** and DCNB under these conditions. The results are summarized in Table 1 and Scheme 2. The photoamination of 1,1-diphenylpropene (**1a**) with ammonia, isopropylamine, 2-methoxyethylamine, and 2-aminoethanol gave the *N*-substituted 2-amino-1,1-diphenylpropanes (**2a—e**) accompanied by the formation of considerable amounts of 3-methyl-4,4-diphenylbutanenitrile (**3a**), 1,1-diphenylpropane (**4a**), 3,3-diphenylpropene (**5**), and diphenylmethane (**6**). Similarly, *N*-substituted 1-amino-2,2-diphenylethanes (**2f—h**), 4,4-diphenylbutanenitrile (**3b**), and 1,1-diphenylethane (**4b**) were formed from the photoamination of 1,1-diphenylethene (**1b**) with ammonia, isopropylamine, and *t*-butylamine. The photoamination of **1b** with 2-methoxyethylamine gave *N*-(2-methoxyethyl)-2,2-diphenylethylamine (**2i**) along with the formation of 1-(2-aminoethoxy)-3,3-diphenylpropane (**8**), **3b**, and **4b** (Scheme 3). In all cases, DCNB was mostly

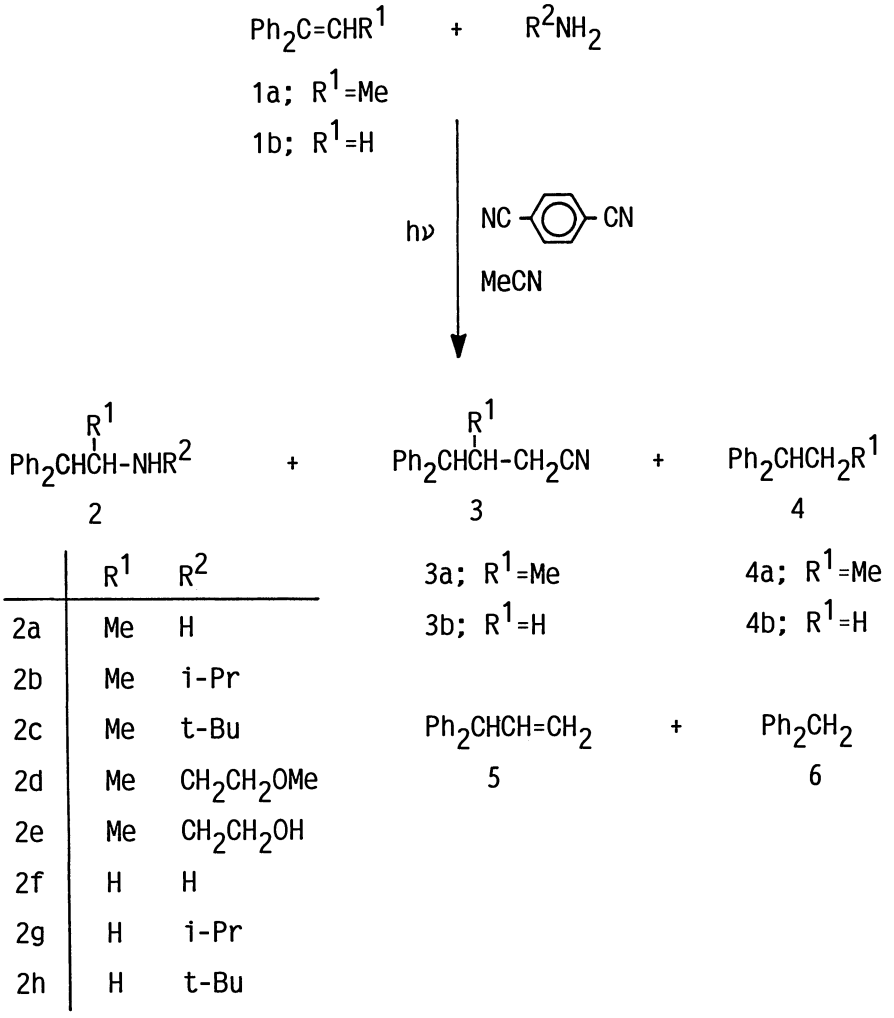

	R^1	R^2
2a	Me	H
2b	Me	i-Pr
2c	Me	t-Bu
2d	Me	CH_2CH_2OMe
2e	Me	CH_2CH_2OH
2f	H	H
2g	H	i-Pr
2h	H	t-Bu

Scheme 2.

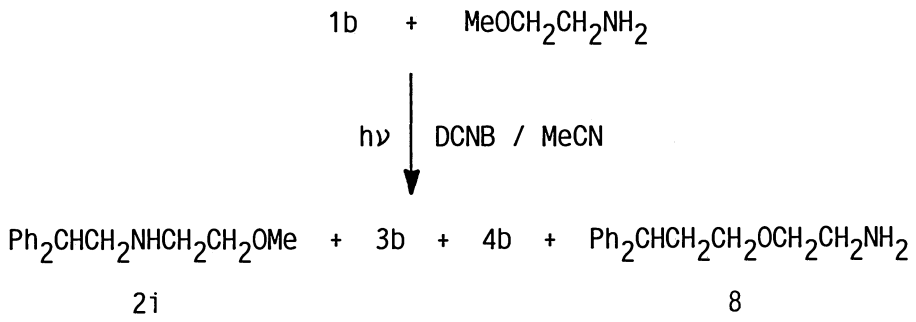

Scheme 3.

Scheme 4.

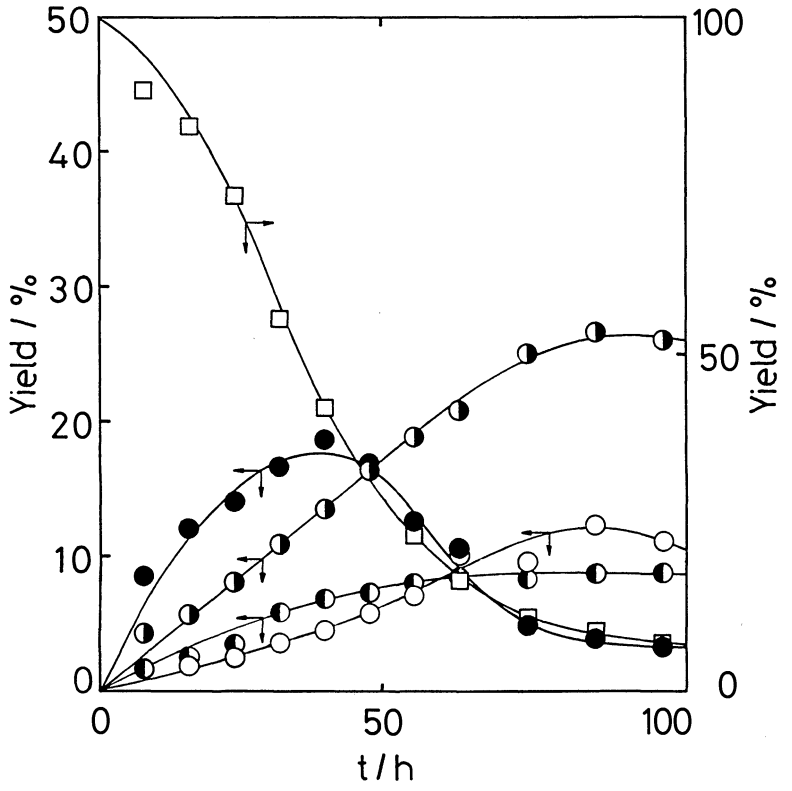

Fig. 1. Time-conversion plots for the disappearance of **1b** (—□—) and for the formation of **2f** (—○—), **2g** (—●—), **3b** (—◑—), and **4b** (—◐—) for the photoamination of **1b** with *i*-$PrNH_2$.

recovered after photoamination. It was confirmed that the photoamination which takes place to afford the aminated products (**2**) does not occur in the absence of an electron acceptor; e.g. the photoreaction of **1b** with isopropylamine in the absence of DCNB gave **3b**, **4b**, and 1,1-dimethyl-3,3-diphenylpropylamine (**9**) (Scheme 4).

Photoamination with isopropylamine gave both **2a** and **2b** from **1a**, and **2f** and **2g** from **1b** in addition to other products. Figure 1 shows plots of the yields of **2f**, **2g**, **3b**, and **4b** vs. the irradiation time for the photoamination of **1b** with isopropylamine; the yields of **3b** and **4b** increased with an increase in the conversion of **1b**, whereas the yield of **2f** gradually increased

at the expense of **2g**.

Although acetonitrile has been found to be an excellent solvent for the photoamination of arenes,[2] the photoamination of **1a** and **1b** in acetonitrile gave considerable amounts of acetonitrile-incorporated products (**3a,b**). It is noteworthy that the photoamination of **1a** and **1b** with *t*-butylamine gave **3a,b** as the major product. It was also found that the photoamination of **1a** with *t*-butylamine occurred in propanenitrile to give **2c** without photoreaction with the nitrile group of the solvent. No photoamination of **1b** occurred in *N,N*-dimethylformamide (DMF), 1,2-dimethoxyethane, or benzene; the photoreaction of **1b** in DMF gave adducts (**10**, **11**, and **12a,b**) of DMF with either **1b** or DCNB (Scheme 5).[3] In the photoamination of **1b** with ammonia in acetonitrile–water (9 : 1), 2,2-diphenylethanol (**7**) was produced in consequence to the photoaddition of water to **1b** along with the formation of **2f**.

Since electron-transfer photosensitization by 9,10-dicyanoanthracene (DCA)[4,5] and 1-naphthonitrile (CNN)[6] or redox-photosensitization[7] by aromatic hydrocarbons have provided useful tools for the photoaddition of alcohols to a variety of aryl-substituted alkenes, these methods were attempted in the present photoamination. However, no photoamination of **1b** with isopropylamine occurred by DCA- or CNN-photosensitization. The redox-photosensitized reaction of **1b** with isopropylamine in the presence of DCNB using phenanthrene as a sensitizer gave **2g**, **3b**, and **4b** accompanied by the formation of *N*-isopropyl-9-amino-9,10-dihydrophenanthrene (**13**). When triphenylene was used as a sensitizer, the photoamination proceeded along with the consumption of triphenylene. Thus, the redox-photosensitized amination of **1b** using phenanthrene or triphenylene are inefficient because of the consumption of sensitizers.

In order to elucidate the stereochemistry of the addition of amines, the photoamination of 1-phenyl-3,4-dihydronaphthalene (**1c**) was performed. The photoamination of **1c** with ammonia, isopropylamine, and *t*-butylamine gave the corresponding *cis*- and *trans*-*N*-substituted 1-phenyl-2-amino-1,2,3,4-tetrahydronaphthalene (**14**, **15**, and **16**) (Scheme 6). The stereochemistries of **14**, **15**, and **16** were determined by their ^{1}H NMR spectra. The signal for the methine proton (H_A) on the C_1 of trans isomers appeared at 0.35—0.50 ppm higher in field than that of cis isomers. The upfield shift of H_A of trans isomers may be due to a shielding effect of lone-pair electrons on the adjacent nitrogen atom. Further support is that the vicinal coupling constants (J=5.0—5.5 Hz) between H_A and H_B in cis isomers were smaller than those in trans isomers (J=7.7—9.0 Hz). Though the ratio of the trans to cis isomer was dependent on the bulkiness of amine, the cis isomers (**15a** and **16a**) were

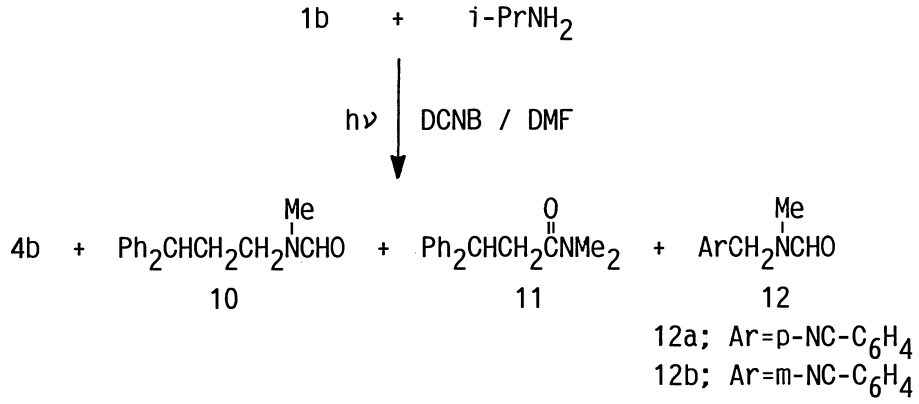

Scheme 5.

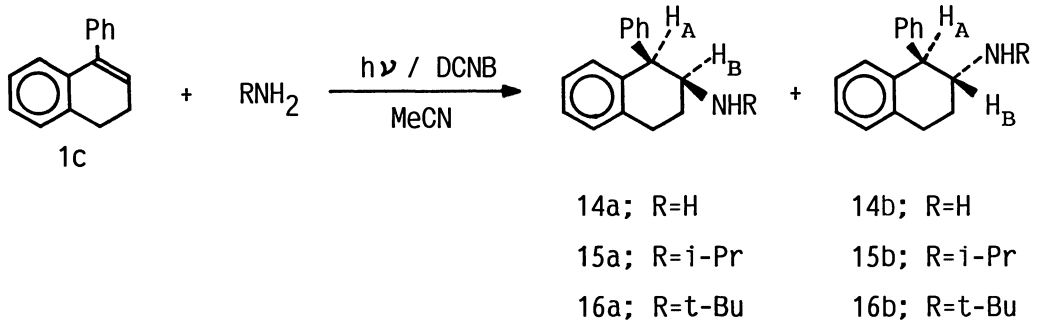

Scheme 6.

Table 2. Photoamination of 1-Phenyl-3,4-dihydronaphthalene (**1c**) with Ammonia and Alkylamines

Run	RNH_2	Products (**a** : **b**)[b]	Yield[a]	Conv. of **1**/%	Recov. of DCNB/%
15[c]	NH_3	**14** (49 : 51)	33	71	86
16	*i*-$PrNH_2$	**15** (75 : 25)	22	64	100
17	*t*-$BuNH_2$	**16** (79 : 21)	28	70	100

a) Isolated yields based on consumed **1c**. b) Isomer ratio of **a** to **b**. c) For MeCN-H_2O (9 : 1) solution.

mainly produced in the cases of photoamination with isopropylamine and *t*-butylamine (Table 2).

Discussion

The photochemical electron transfer reaction from electron-rich substances to aromatic nitriles has been well known to occur in polar solvents.[1] It is proposed that such photoamination is initiated by a photochemical electron transfer from **1** to DCNB, since no photoamination of **1** occurred in the absence of A (Eq. 1). The cation radicals of **1**, thus formed, react with RNH_2 to give aminated cation radicals which are reduced with the anion radical of DCNB and then protonated to afford **2** (Eq. 2).

In the case of **1c**, the resulting aminated anion (**17**) takes both **17a** and **17b** conformations, depending on the bulkiness of the amine, as shown in Scheme 7.

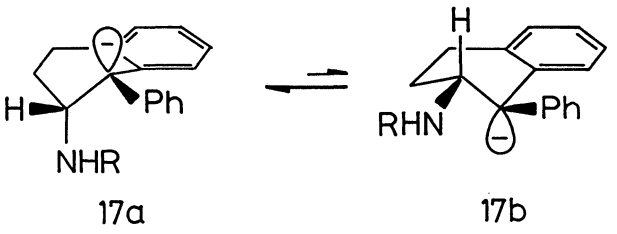

Scheme 7.

The electron pair of **17** may exist in the axial position, which is favorable for a maximum orbital overlap of the electron pair with the aromatic ring. When an amino group has a bulky alkyl group, a steric interaction between the amino group on C-2 and the phenyl group on C-1 may be expected to favor **17a**, in which the amino group is axial and phenyl group is equatorial. Therefore, the protonation of **17** affords mainly the cis isomer (**15a** and **16a**) in the photoamination of **1c** with isopropylamine or *t*-butylamine. This result is in accord with the results reported for the photoaddition of methanol to **1c**.[5]

The fact that 4,4-diphenyl-2,2-dideuterio-1-butanenitrile was formed from the photoamination of **1b** in acetonitrile-d_3 reveals that the cyanomethyl group of **3** can undoubtedly be attributed to acetonitrile. Figure 1 shows that **3b** is the primary product from the photoreaction of **1b**. On the other hand, it has been reported that **3** was not formed at all from the photoaddition of water and alcohols to **1a** or **1b** in the

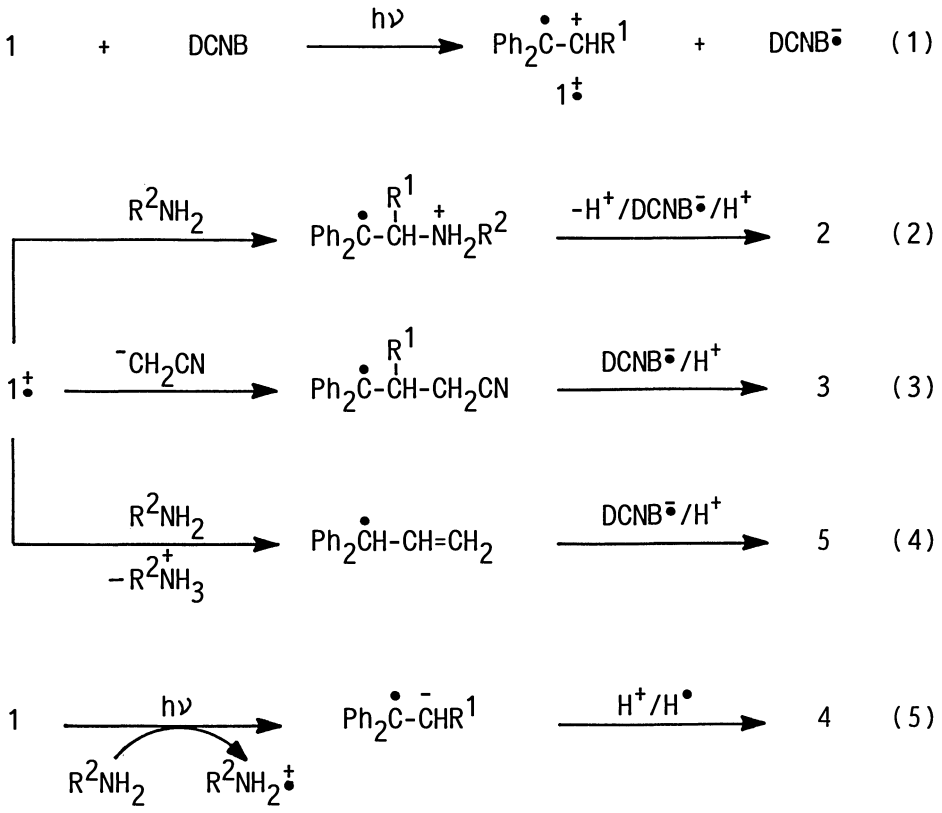

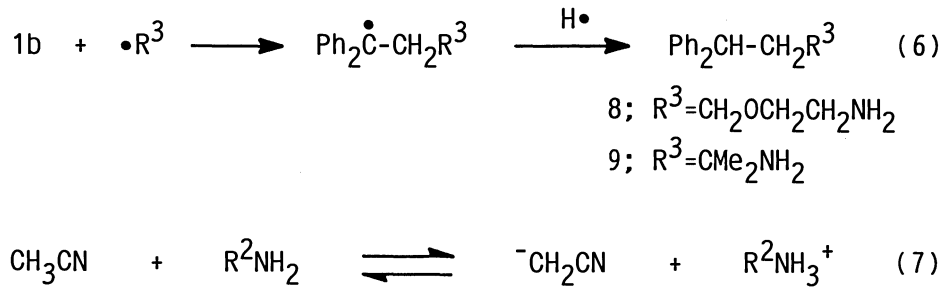

Equation 1—7.

presence of electron acceptors.[5,6] Indeed, when DCNB was used as an electron acceptor, the photoaddition of water to **1b** in the absence of amines in acetonitrile gave only **7** in 41% yield without the formation of **3b**. This fact shows that the presence of amines is requisite for the formation of **3b**. These observations, therefore, suggest that $\mathbf{1}^{+\cdot}$ reacts with the cyanomethyl anion which is generated from the deprotonation of acetonitrile by the amine. The reduction of cyanomethylated radicals by the anion radical of DCNB gives **3** after protonation (Eqs. 3 and 7). Thus, $\mathbf{1}^{+\cdot}$ can undergo Eq. 3 competitively with Eq. 2, depending on the nature of RNH_2. *t*-Butylamine operates more effectively for the formation of **3** compared with other primary alkylamines since the bulky substituent may slow down the nucleophilic addition and/or the strong basicity may facilitate the deprotonation of acetonitrile. Also, amines operate as a base for the isomerization of **1a** to **5**, which proceeds by deprotonation from $\mathbf{1a}^{+\cdot}$ with RNH_2 according to Eq. 4.

The photoreaction of **1b** with isopropylamine in the absence of DCNB would be initiated by a photochemical electron transfer from isopropylamine to **1b** to give a cation radical of the amine and the anion radical of **1b**, as discussed in previous reports.[8,9,11] The protonation of the anion radical of **1b** and the subsequent hydrogen abstraction from such hydrogen sources as isopropylamine gave **4b** (Eq. 5). Equation 5 would take place to some extents, even for photoamination in the presence of DCNB, since a considerable amount of **4b** was produced.

The formation of **9** would occur by the reaction of **1b** with the 2-amino-2-propyl radical which is generated by deprotonation from the cation radical of isopropylamine or by hydrogen abstraction from isopropylamine with a radical species, as shown in Eq. 6. Similarly, the formation of **8** would occur by the reaction of **1b** with the 2-aminoethoxymethyl radical formed by hydrogen abstraction from 2-methoxyethylamine (Eq. 6). The formation of **3b** from the photoreaction in the absence of DCNB would occur by the reaction of **1b** with the cyanomethyl radical formed by hydrogen abstraction from acetonitrile by a radical species in reaction systems; this mechanism is in accord with that for photochemical incorporation of acetonitrile to norbornene.[11]

Degradation of secondary amines (**2b** and **2g**) to primary amines (**2a** and **2f**) can be attributed to be the consequence of secondary reactions, as is shown in Fig. 1. It was confirmed that the photoreaction of isolated **2g** with DCNB gave **2f**. Degradation would occur through an electron transfer reaction from **2b** or **2g** to the excited singlet state of DCNB.[9] Also, the formation of **6** occurred as a secondary reaction which proceeds by C-C bond cleavage of the cation radicals of **2a—e** generated by a photochemical electron transfer to DCNB. This is in agreement with a mechanism which has been reported for the cleavage of tertiary amines[12] and 2,2-diphenylethyl alkyl ethers.[13]

Neither DCA- nor CNN-photosensitization was a useful method for the photoamination of **1**. From the fluorescence quenching of DCA or CNN with **1** or amines, it was found that the excited singlet state of DCA or CNN was efficiently quenched by ammonia and primary amines, as well as by **1**. No occurrence of the DCA- or CNN-sensitized photoamination is caused by the more efficient quenching of the excited singlet state of DCA or CNN by RNH_2 than that by **1** under the reaction conditions.

Experimental

^1H and ^{13}C NMR spectra were taken on a Bruker AC 250P for $CDCl_3$ solutions with tetramethylsilane used as an internal standard. The fluorescence and IR spectra were taken on a Hitachi MPF-4 and a JASCO A-302, respectively. A JEOL JMS-D300S was used for analyzing the mass spectra. GLC analysis was carried out on a Shimadzu GC-14A or a Hitachi 163 with flame-ionization detectors using a capillary column (CBP1-M25-025) or a 50 cm×4 mm column of 2% silicone OV-17 on Chromosorb WAW DMCS.

Spectral grade acetonitrile was distilled from P_2O_5 and then from CaH_2. 1,1-Diphenylethene, *p*-dicyanobenzene, and amines were commercially available. 1,1-Diphenylpropene was prepared from the acid-fragmentation of 2,2-diphenyl-3-methyloxetane prepared from the photoaddition of benzophenone with 2-butene.[14] 1-Phenyl-3,4-dihydronaphthalene was prepared according to a method described in the literature.[15]

Photoamination of 1a,b with Amines. Into a pyrex vessel was introduced an acetonitrile solution (150 ml) containing **1** (5.6 mmol) and DCNB (16 mmol). The amine (73

mmol) was added to the solution after argon bubbling for 50 min, whereas an ammonia solution was obtained by dissolving gaseous ammonia into the solution. The solutions were irradiated for 8—50 h with an Eikosha PIH-300 high-pressure mercury lamp through Pyrex. After evaporation of the solvent, cool methanol was added to the residue and then unreacted DCNB was filtered off. The filtrate was chromatographed on silica gel with hexane to give **1**, **4**, **5**, and **6**. Further elution with hexane-benzene (4:1) gave **3**. The aminated products (**2a—i**) were obtained by elution with benzene-ethyl acetate (4:1) or acetone. Purification was carried out by either recrystallization from hexane-benzene or vacuum distillation. The recrystallization of **2c** and **2h**, however, could not be achieved owing to a failure regarding their acetylation. The structures of **2b**, **2d**, and **2e** were determined by comparisons of the ^{1}H and ^{13}C NMR spectra with authentic samples prepared from the reaction of 1,1-diphenyl-3-propanone with the corresponding amines in the presence of sodium cyanoborohydride.[16] The structures of **4a**, **4b**, **5**,[17] **6**, **7**, and **13**[2a] were determined by direct comparisons with authentic samples.

1-Methyl-2,2-diphenylethylamine (2a). The acetamide: Mp 113.0—113.5 °C; ^{1}H NMR δ=1.12 (3H, d, J=6.4 Hz), 1.80 (3H, s), 3.84 (1H, d, J=10.0 Hz), 4.83—4.93 (1H, m), 5.28 (1H, br d, J=8.5 Hz), and 7.16—7.29 (10H, m); ^{13}C NMR δ=20.4, 23.4, 47.4, 58.0, 126.72, 126.65, 128.1, 128.2, 128.6, 128.7, 141.8, 142.2, and 169.4; MS m/z 253 (M^+); IR ($CHCl_3$) 3430 and 1660 cm^{-1}; Found: C, 80.48; H, 7.29; N, 5.77%. Calcd for $C_{17}H_{19}NO$: C, 80.57; H, 7.56; N, 5.53%.

***N*-Isopropyl-(1-methyl-2,2-diphenylethyl)amine (2b):** ^{1}H NMR δ=0.98 (3H, d J=9.9 Hz), 1.00 (6H, d, J=10.0 Hz), 2.71 (1H, br s), 2.82—2.92 (1H, m), 3.54—3.65 (1H, m), 3.80 (1H, d, J=10.2 Hz), and 7.12—7.39 (10H, m); ^{13}C NMR J=18.7, 21.7, 24.2, 45.9, 53.2, 59.1, 126.4, 126.7, 128.3, 128.5, 128.8, 142.4, and 143.1; MS m/z 253 (M^+). The acetamide: Mp 161.5—162.0 °C; Found: C, 81.58; H, 8.46; N, 4.61%. Calcd for $C_{20}H_{25}NO$: C, 81.31 ; H, 8.53; N, 4.74%.

***N*-*t*-Butyl-(1-methyl-2,2-diphenylethyl)amine (2c):** ^{1}H NMR δ=0.96 (9H, s), 1.08 (3H, d, J=5.8 Hz), 3.54—3.65 (1H, m), 3.70 (1H, d, J=10.2 Hz), and 7.13—7.39 (10H, m); ^{13}C NMR δ=22.5, 29.9, 51.1, 60.3, 126.3, 126.8, 128.5, 128.6, 142.6, and 143.0; MS m/z 267 (M^+).

***N*-(2-Methoxyethyl)-(1-methyl-2,2-diphenylethyl)amine (2d):** ^{1}H NMR δ=1.00 (3H, d, J=6.1 Hz), 2.61—2.70 (1H, m), 2.78—2.88 (1H, m), 3.17 (3H, s), 3.27—3.39 (2H, m), 3.40—3.51 (1H, m), 3.76 (1H, d, J=10.2 Hz), and 7.09—7.38 (10H, m); ^{13}C NMR δ=18.5, 46.6, 55.8, 58.4, 59.3, 71.7, 126.3, 126.6, 128.1, 128.2, 128.5, 128.7, 142.4, and 143.3; MS m/z 269 (M^+).

***N*-(2-Hydroxyethyl)-(1-methyl-2,2-diphenylethyl)amine (2e):** Mp 83.5—84.0 °C; ^{1}H NMR δ=1.05 (3H, d, J=6.1 Hz), 2.63—2.72 (1H, m), 2.74—2.89 (3H, m), 3.46—3.57 (3H, m), 3.78 (1H, d, J=10.3 Hz), and 7.13—7.38 (10H, m); ^{13}C NMR δ=18.5, 48.1, 55.9, 59.0, 60.6, 126.5, 126.8, 128.0, 128.1, 128.6, 128.9, 142.2, and 142.8; MS m/z 255 (M^+).

2,2-Diphenylethylamine (2f). The acetamide: Mp 89.5—90.0 °C; ^{1}H NMR δ=1.82 (3H, s), 3.84 (1H, d, J=7.9 Hz), 3.86 (1H, d, J=7.9 Hz), 4.17 (1H, d, J=7.9 Hz), 5.67 (1H, br s), and 7.16—7.33 (10H, m); ^{13}C NMR δ=23.2 43.9, 50.5, 126.8, 128.0, 128.7, 141.9, and 170.2; MS m/z 239 (M^+). The acetamide of **2f** was unambiguously identified by a direct comparison with an authentic sample.

***N*-Isopropyl-2,2-diphenylethylamine (2g).** The acetamide: Mp 104.5—105.0 °C; ^{1}H NMR δ=0.78 and 1.18 (6H, d J=6.8 and 6.9 Hz), 1.58 and 2.10 (3H, s), 3.78 and 3.87 (2H, d, J=7.5 and 7.0 Hz), 3.74—3.82 and 4.11—4.20 (1H, m), 4.14 and 4.69 (1H, t, J=7.0 and 7.5 Hz), and 7.13—7.39 (10H, m); ^{13}C NMR δ=20.3 and 20.9, 22.3 and 22.6, 47.3 and 49.1, 48.4 and 51.6, 49.6 and 52.5, 126.3 and 126.9, 128.2 and 128.7, 128.6 and 132.7, 142.3 and 143.1, and 171.2; MS m/z 281 (M^+); IR ($CHCl_3$) 1620 cm^{-1}; Found: C, 80.79; H, 8.51; N, 5.07%. Calcd for $C_{19}H_{23}O$: C, 81.10; H, 8.24; N, 4.98%.

***N*-*t*-Butyl-2,2-diphenylethylamine (2h):** ^{1}H NMR δ=1.14 (9H, s), 3.28 (2H, d, J=8.0 Hz), 4.30 (1H, t, J=8.0 Hz), 4.70 (1H, br s), and 7.19—7.35 (10H, m); ^{13}C NMR δ=27.4, 46.9, 50.5, 52.1, 126.8, 128.0, 128.7, and 142.0; MS m/z 253 (M^+).

***N*-(2-Methoxyethyl)-2,2-diphenylethylamine (2i):** A colorless oil, ^{1}H NMR δ=2.81 (2H, t, J=5.3 Hz), 3.25 (2H, d, J=7.7 Hz), 3.30 (3H, s), 3.42 (2H, t, J=5.3 Hz), 4.21 (1H, t, J=7.7 H), and 7.14—7.38 (10H, m); ^{13}C NMR δ=49.1, 51.1, 54.5, 58.6, 71.7, 126.5, 127.9, 128.6, and 142.8; MS m/z 255 (M^+). The acetamide: Found: C, 76.98; H, 7.58; N, 4.98%. Calcd for $C_{19}H_{23}NO_2$: C, 76.73; H, 7.80; N, 4.71%.

3-Methyl-4,4-diphenylbutanenitrile (3a): Mp 55.0—55.5 °C; ^{1}H NMR δ=1.07 (3H, d, J=6.5 Hz), 2.10 (1H, dd, J=16.7 and 7.0 Hz), 2.33 (1H, dd, J=16.7 and 3.8 Hz), 2.62—2.79 (1H, m), 3.65 (1H, d, J=11.4 Hz), and 7.12—7.31 (10H, m); ^{13}C NMR δ=18.3, 23.5, 34.2, 57.6, 118.5, 126.6, 126.9, 127.6, 127.8, 128.7, 129.0, 142.5, and 142.6; MS m/z 235 (M^+); IR ($CHCl_3$) 2220 cm^{-1}.

4,4-Diphenylbutanenitrile (3b): ^{1}H NMR δ=2.20 (2H, t, J=7.5 Hz), 2.30—2.45 (2H, m), 4.03 (1H, t, J=7.9 Hz), and 7.10—7.31 (10H, m); ^{13}C NMR δ=15.7, 31.0, 49.8, 119.3, 126.8,127.7, 128.8, and 142.8; MS m/z 221 (M^+); IR ($CHCl_3$) 2190 cm^{-1}. The structure of **3b** was determined by a comparison with an authentic sample prepared from the cyanation of 3,3-diphenyl-1-propanol according to a reported method.[18]

1-(2-Aminoethoxy)-3,3-diphenylpropane (8). The acetamide: Mp 64.5—65.0 °C (from hexane-benzene); ^{1}H NMR δ=1.95 (3H, s), 2.28—2.36 (2H, m), 3.34—3.39 (6H, m), 4.09 (1H, t, J=7.9 Hz), 5.89 (1H, br s), and 7.15—7.37 (10H, m); ^{13}C NMR δ=23.2, 35.2, 39.3, 47.5, 69.1, 69.3, 126.3, 127.8, 128.5, 144.4, and 170.1; MS m/z 297 (M^+); IR ($CHCl_3$) 3440 and 1660 cm^{-1}; Found: C, 76.73; H, 7.63; N, 4.66%. Calcd for $C_{19}H_{23}NO_2$: C, 76.73; H, 7.80; N, 4.71%.

1,1-Dimethyl-3,3-diphenylpropylamine (9). The acetamide: Mp 120.5-121.0 °C (from hexane-benzene); ^{1}H MMR δ=1.29 (6H, s), 1.44 (3H, s), 2.53 (2H, d, J=7.1 Hz), 4.05 (1H, t, J=7.0 Hz), 5.38 (1H, br s), and 7.18—7.29 (10H, m); ^{13}C NMR δ=23.4, 27.3, 44.1, 47.2, 53.2, 125.6, 126.7, 128.1, 145.0, and 169.1; MS m/z 255 (M^+). IR ($CHCl_3$) 3440 and 1660 cm^{-1}; Found: C, 81.26; H, 8.46; N, 4.82%. Calcd for $C_{19}H_{23}NO$: C, 81.10; H, 8.24; N, 4.98%.

Photoreaction of 1b in *N,N*-Dimethylformamide. After irradiation, the photolysates were dissolved in 150 ml of benzene; then, *N,N*-dimethylformamide was extracted with six 50 ml portions of water. After evaporation of benzene, the residue was chromatographed on silica gel with hexane to give **1b** and **4b**. Further elution with benzene gave **10** and **11**. **12a** and **12b** were obtained by elution with benzene-ethyl acetate (8:1). **11** and **12b** could not be purified from the mixture of either **10** and **11** or **12a** and **12b**.

***N*-(3,3-Diphenylpropyl)-*N*-methylformamide (10):** Mp 60.0—61.0 °C (from hexane-benzene); ^{1}H NMR δ=2.30 and 2.33 (2H, m), 2.85 and 2.86 (3H, s), 3.17 and 3.28 (2H, t,

J=6.9 and 7.7 Hz), 3.86 and 3.94 (1H, t, J=7.9 and 7.8 Hz), 7.14—7.33 (10H, m), 7.60 and 7.98 (1H, s); ^{13}C NMR δ=29.4 and 32.5, 33.5 and 34.7, 43.5 and 47.6, 48.0 and 49.1, 126.4 and 126.7, 127.6 and 127.7, 128.6 and 128.8, 143.5 and 144.1, 162.4 and 162.8; MS m/z 253 (M^+); IR ($CHCl_3$) 1665 cm^{-1}; Found: C, 80.65; H, 7.53; N, 5.79%. Calcd for $C_{17}H_{19}NO$: C, 80.57; H, 7.56; N, 5.53%.

***N,N*-Dimethyl-3,3-diphenylpropanamide (11):** ^{1}H NMR δ=2.86 (6H, s), 3.04 (2H, d, J=7.5 Hz), 4.68 (1H, t, J=7.4 Hz), and 7.13—7.32 (10H, m); ^{13}C NMR δ=35.5, 37.2, 39.3, 47.2, 126.3, 127.8, 128.8, 144.3, and 171.2; MS m/z 253 (M^+); IR ($CHCl_3$) 1645 cm^{-1}.

***N*-(4-Cyanobenzyl)-*N*-methylformamide (12a):** A colorless oil, ^{1}H NMR δ=2.80 and 2.91 (3H, s), 4.49 and 4.58 (2H, s), 7.35—7.38 (2H, d, J=8.0 Hz), 7.64—7.69 (2H, d, J=8.0 Hz), 8.20 and 8.26 (1H, s); ^{13}C NMR δ=29.7 and 34.3, 47.6 and 53.0, 111.6 and 112.2, 118.3 and 118.6, 128.0 and 128.7, 132.5 and 132.8, 141.5 and 141.7, 162.78 and 162.82; MS m/z 174 (M^+); IR ($CHCl_3$) 2230 and 1660 cm^{-1}; Found: C, 68.84; H, 5.89; N, 16.26%. Calcd for $C_{10}H_{10}N_2O$: C, 68.94; H, 5.79; N, 16.08%.

***N*-(3-Cyanobenzyl)-*N*-methylformamide (12b):** ^{1}H NMR δ=2.83 and 2.96 (3H, s), 4.64 and 4.77 (2H, s), 7.27—7.50 (2H, m), 7.57—7.74 (2H, m), 8.20 and 8.34 (1H, s); ^{13}C NMR δ=29.6 and 34.5, 45.8 and 51.4, 112.1 and 112.3, 116.9 and 117.4, 128.3 and 128.8, 128.9 and 132.6, 132.8 and 133.4, 139.5 and 139.9, 162.9 and 163.0; MS m/z 174 (M^+); IR ($CHCl_3$) 2230 and 1660 cm^{-1}.

Photoamination of 1c. In a similar manner to the case of **1a**, the photoamination of **1c** was performed for an acetonitrile solution (50 ml) containing **1c** (2.5 mmol), DCNB (2.5 mmol), and the amine (25 mmol). After irradiation, aminated products were obtained by extraction with dilute hydrochloric acid. The acidic aqueous layer was basified with saturated $NaHCO_3$ followed by extraction with diethyl ether. Evaporation of the ether left crude aminated products. **1c** and DCNB were recovered from benzene solutions and were chromatographed on silica gel with hexane and benzene. A mixture of **14a** and **14b** was acetylated with Ac_2O, and recystallized from hexane-benzene to give the acetamide of **14a**. Also, **15a** was obtained in the same way, though the acetamide of **16** was not purified by recrystallization.

***cis*-2-Amino-1-phenyl-1,2,3,4-tetrahydronaphthalene (14a):** ^{1}H NMR δ=1.62 (2H, br s), 2.03—2.15 (2H, m), 2.88—3.12 (2H, m), 3.32 (1H, ddd, J=8.1, 5.4, and 5.2 Hz), 4.22 (1H, d, J=5.2 Hz), and 6.68—7.40 (9H, m); ^{13}C NMR δ=28.3, 31.0, 51.7, 56.1, 125.9, 126.3, 126.5, 127.9, 128.5, 130.6, 130.8, 136.3, 138.3, and 141.7.

***trans*-2-Amino-1-phenyl-1,2,3,4-tetrahydronaphthalene (14b):** ^{1}H NMR δ=1.62 (2H, br s), 1.72—1.85 (2H, m), 2.88—3.12 (2H, m) 3.20 (1H, ddd, J=10.4, 9.0, and 3.0 Hz), 3.73 (1H, d, J=9.0 Hz), and 6.68—7.40 (9H, m); ^{13}C NMR δ=28.0, 28.5, 50.5, 54.5, 125.9, 126.0, 126.7, 128.6, 128.7, 129.6, 130.2, 136.3, 138.8, and 144.4. The acetamide: Mp 196.5—198.0 °C; Found: C, 81.41; H, 7.32; N, 5.16%. Calcd for $C_{18}H_{19}NO$: C, 81.48; H, 7.22; N, 5.28%.

***cis*-*N*-Isopropyl-2-amino-1-phenyl-1,2,3,4-tetrahydronaphthalene (15a):** ^{1}H NMR δ=1.00 (3H, d, J=6.0 Hz), 1.03 (3H, d, J=6.0 Hz), 1.26 (1H, br s), 1.57—1.83 (2H, m), 3.00—3.05 (2H, m), 3.12 (1H, q, J=6.0 Hz), 3,21 (1H, ddd, J=11.7, 5.0, and 3.3 Hz), 4.36 (1H, d, J=5.0 Hz), and 6.92—7.37 (8H, m); ^{13}C NMR δ=23.0, 23.1, 25.0, 28.9, 44.4, 48.5, 53.3, 125.8, 126.3, 127.8, 128.6, 130.5, 130.8, 136.6, 139.0, and 141.9.

***trans*-*N*-Isopropyl-2-amino-1-phenyl-1,2,3,4-tetrahydronaphthalene (15b):** ^{1}H NMR δ=0.82 (3H, d, J=6.2 Hz), 1.01 (3H, d, J=6.2 Hz), 1.26 (1H, br s), 2.05—2.14 (2H, m), 2.80—2.92 (2H, m), 3.00—3.05 (1H, m), 3,06—3.09 (1H, m), 3.91 (1H, d, J=7.7 Hz), 6.74 (1H, d, J=7.7 Hz), and 6.92—7.37 (8H, m); ^{13}C NMR δ=22.4, 24.2, 26.9, 27.3, 45.6, 52.6, 57.4, 125.9, 126.0, 126.5, 128.4, 128.5, 129.4, 130.7,136.6, 138.4, and 144.7. The acetamide: Mp 143.5—145.0 °C; Found: C, 82.24; H, 7.93; N, 4.61%. Calcd for $C_{21}H_{25}NO$: C, 82.04; H, 8.20; N, 4.56%.

***cis*-*N*-*t*-Butyl-2-amino-1-phenyl-1,2,3,4-tetrahydronaphthalene (16a):** ^{1}H NMR δ=1.09 (9H, s), 1.40 (1H, br s), 1.61—1.91 (2H, m), 2.99—3.05 (2H, m), 3.20 (1H, ddd, J=11.6, 5.5, and 3.5 Hz), 4.12 (1H, d, J=5.5 Hz), 6.91 (1H, d, J=7.7 Hz), and 7.03—7.36 (8H, m); ^{13}C NMR δ=28.6, 29.1, 30.0, 50.8, 51.0, 51.5, 125.7, 126.2, 126.2, 127.6, 128.6, 130.8, 131.0, 136.5, 139.5, and 142.5.

***trans*-*N*-*t*-Butyl-2-amino-1-phenyl-1,2.3,4-tetrahydronaphthalene (16b):** ^{1}H NMR δ=0.87 (9H, s), 1.40 (1H, br s), 2.13—2.24 (2H, m), 2.93 (2H, t, J=5.0 Hz), 2.99—3.05 (1H, m), 3.77 (1H, d, J=9.0 Hz), 6.73 (1H, d, J=7.5 Hz), and 7.03—7.36 (8H, m); ^{13}C NMR δ=28.3, 29.8, 30.0, 51.0, 54.2, 55.4, 125.7, 126.0, 126.6, 127.7, 128.4, 129.8, 130.9, 137.0, 139.2, and 144.7.

The present work was partially supported by a Grant-in-Aid for Scientific Research No. 02640400 from the Ministry of Education, Science and Culture.

References

1) F. D. Lewis, "Photoinduced Electron Transfer," ed by M. A. Fox and M. Chanon, Elsevier, Amsterdam (1988), Part C, p. 1.

2) a) M. Yasuda, T. Yamashita, K. Shima, and C. Pac, *J. Org. Chem.*, **54**, 753 (1987); b) M. Yasuda, Y. Matsuzaki, K. Shima, and C. Pac, *J. Chem. Soc., Perkin Trans. 2*, **1988**, 745.

3) Y. Tsujimoto, M. Hayashi, Y. Nishimura, T. Miyamoto, and Y. Odaira, *Chem. Lett.*, **1977**, 677; T. Miyamoto, Y. Tsujimoto, T. Tsuchinaga, Y. Nishimura, and Y. Odaira, *Tetrahedron Lett.*, **1978**, 2155.

4) J. Eriksen and C. S. Foote, *J. Am. Chem. Soc.*, **102**, 6083 (1980).

5) K. Mizuno, I. Nakanishi, N. Ichinose, and Y. Otsuji, *Chem. Lett.*, **1989**, 1095.

6) Y. Shigemitsu and D. R. Arnold, *J. Chem. Soc., Chem. Commun.*, **1975**, 407; A. J. Maroulis, Y. Shigemitsu, and D. R. Arnold, *J. Am. Chem. Soc.*, **100**, 535 (1978); A. J. Maroulis and D. R. Arnold, *Synthesis*, **1979**, 819; M. Yasuda, C. Pac, and H. Sakurai, *Bull. Chem. Soc. Jpn.*, **53**, 502 (1980).

7) C. Pac, A. Nakanose, and H. Sakurai, *J. Am. Chem. Soc.*, **99**, 5806 (1977); T. Majima, C. Pac, A. Nakanose, and H. Sakurai, *ibid.*, **103**, 4499 (1981).

8) M. Ohashi, K. Miyake, and K. Tsujimoto, *Bull. Chem. Soc. Jpn.*, **53**, 1683 (1980).

9) D. R. Arnold and A. J. Maroulis, *J. Am. Chem. Soc.*, **99**, 7355 (1977).

10) F. D. Lewis, *Acc. Chem. Res.*, **19**, 401 (1986).

11) J. W. Bruno, T. J. Marks, and F. D. Lewis, *J. Am. Chem. Soc.*, **104**, 5580 (1982).

12) L. Y. C. Lee, X. Ci, C. Giannotti, and D. G. Whitten, *J. Am. Chem. Soc.*, **108**, 175 (1986).
13) D. R. Arnold and A. J. Maroulis, *J. Am. Chem. Soc.*, **98**, 5931 (1976).
14) K. Nakabayashi, J. Kojima, K. Tanabe, M. Yasuda, and K. Shima, *Bull. Chem. Soc. Jpn.*, **62**, 96 (1989).
15) R. Weiss, *Org. Synth.*, Coll. Vol. III, 729 (1955).
16) R. F. Borch, M. D. Bernstein, and H. D. Durst, *J. Am. Chem. Soc.*, **93**, 2897 (1971).
17) C. L. Bumgardner, *J. Am. Chem. Soc.*, **83**, 4423 (1961).
18) D. Brett, I. M. Downie, and J. B. Lee, *J. Org. Chem.*, **32**, 855 (1967).

Synthesis of Substituted Pyridines by a Cycloaddition Route Using Nitrile Oxides and Homoallyl Alcohols

Shuji KANEMASA,* Yoshihiko ASAI,† and Junji TANAKA
Institute of Advanced Material Study, Kyushu University, Kasugakoen, Kasuga 816
†Department of Molecular Science and Technology, Interdisciplinary Graduate School of Engineering Sciences, Kyushu University, Kasugakoen, Kasuga 816
(Received August 13, 1990)

Cycloadditions of nitrile oxides with unprotected homoallyl alcohols, followed by Swern oxidations, lead to 5-(2-oxoalkyl)-2-isoxazolines. Subsequent Raney Ni reduction of the resulting heterocycles in ethanol in the presence of excess tetrafluoroboric acid affords substituted pyridine derivatives.

Cycloadditions of nitrile oxides with terminal olefins take place readily and regioselectively to produce 5-substituted 2-isoxazolines in high yields;[1] the nitrogen-oxygen bond of cycloadducts is reductively cleaved to lead to β-imino alcohol intermediates, which are further hydrolyzed into β-hydroxy ketones and related functionalities.[2] Since the synthetic application of β-imino alcohol functionality is quite limited, we planned to open a new entry to the synthesis of pyridine nuclei by utilizing this unusual functional group.

Our synthetic plan of pyridine synthesis consists of the combination of β-imino alcohol and carbonyl functionalities. Dehydrative cyclization of β-hydroxy-δ-imino ketones would offer a convenient construction route of pyridine skeletons, and the shortest access to the requisite β-hydroxy-δ-imino ketone functionality would be the nitrile oxide cycloaddition with β,γ-unsaturated ketones. However, the availability of β,γ-unsaturated ketones is quite narrow due to their susceptibility toward double bond migration.[3,4] Accordingly, we examined the nitrile oxide cycloadditions with homoallyl alcohols.

Nitrile oxides **2a—e** were found to react smoothly with a variety of homoallyl alcohols **1a—f** without protecting the hydroxyl group to give 5-(2-hydroxyalkyl)-2-isoxazolines **3a—m** in satisfactory yields (Scheme 1 and Table 1). These reactions make a striking contrast with the nitrile oxide cycloadditions with allyl alcohols where the use of unprotected dipolarophiles gave cycloadducts in poor yields.[5] Since homoallyl alcohols **1a—f** can be prepared in high yields by the reactions of readily available allyl bromides with aldehydes according to the Akiba's method,[6] this cycloaddition route is synthetically useful to construct pyridine skeletons.

Nitrile oxides **2a—c** and **2e** were generated from the corresponding hydroximoyl halides by dehydrohalogenation with triethylamine, and ethanenitrile oxide (**2d**) was generated from nitroethane and benzenesulfonyl chloride/triethylamine (Scheme 2).[7] An effective generation method of **2d** by the Mukaiyama procedure[8] could not be successfully employed since phenyl isocyanate reacted with **1**.

Although the cycloaddition of **2d**, generated by the Mukaiyama's procedure, with the tetrahydropyranyl (THP) ether of **1a** produced the corresponding cycloadduct **6** in 76% yield, one further deprotection step (73%) was required; the overall yield of **3k** being 55%.

The secondary hydroxyl group of **3a—m** was oxidized according to the Swern oxidation procedure[9] to give ketones **4a—m** in almost quantitative yields (Table 1).

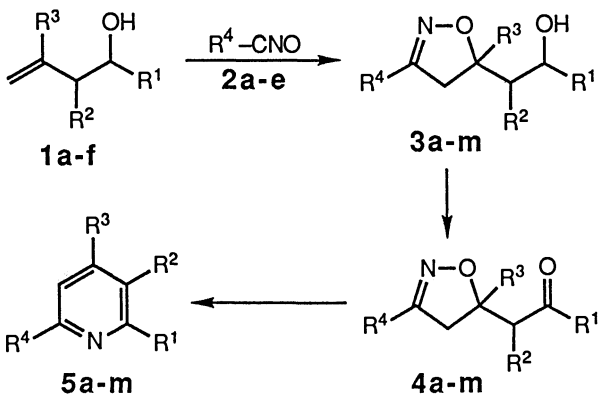

Scheme 1.

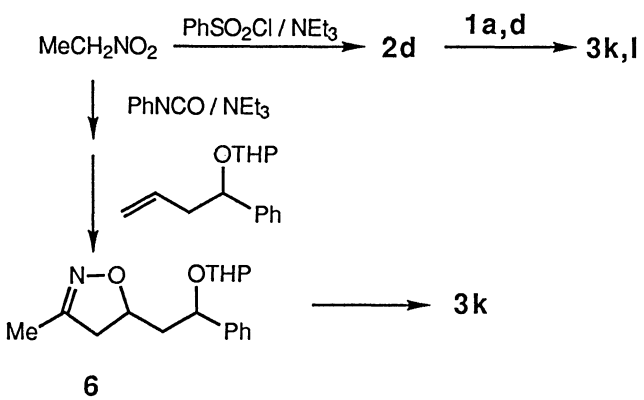

Scheme 2.

Reductive cleavage of the nitrogen-oxygen bond of 5-(2-oxoalkyl)-2-isoxazolines **4a—m** was carried out by use of Raney Ni (W-2). The Raney-Ni reduction of **4a** in the presence of boric acid in aqueous ethanol (ethanol/water=6 : 1 v/v)[10] gave the expected pyridine **5a** in only 19% yield (Scheme 3 and Table 2). In this case, a complex mixture of unidentified products was accompanied.[11]

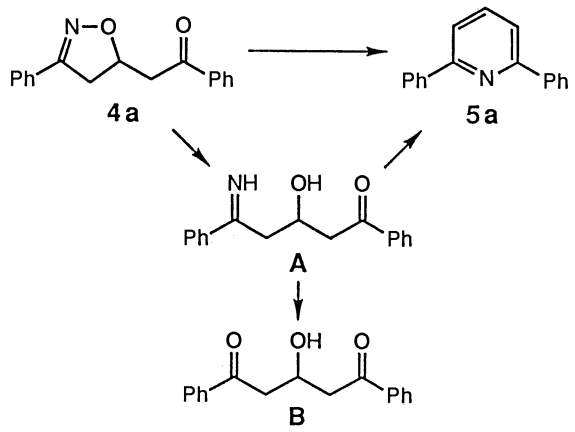

Scheme 3.

It is likely that β-hydroxy-δ-imino ketone intermediate **A** undergoes either dehydrative cyclization to give pyridine **5a** or hydrolysis leading to 3-hydroxy-1,5-diphenyl-1,5-pentanedione (**B**) (Scheme 3). An acid would catalyze both the reactions, and presence of water is not favored for the pyridine formation. Several reaction conditions were examined on these basis, and we found that the Raney Ni reduction of **4a** in ethanol in the presence of tetrafluoroboric acid (42% aqueous solution) took place very cleanly to provide a satisfactory yield of **5a** (82%). Amount of tetrafluoroboric acid is not so important.

Under these reaction conditions, other 5-(2-oxoalkyl)-2-isoxazolines **4a—m** were reduced with Raney Ni to give pyridines **5a—m** (Scheme 1 and Table 1). The very poor yield of pyridine **5e** is in part due to its ready chelate formation with Raney Ni.[12]

In conclusion, substituted pyridines are synthesized by a sequence of the cycloaddition of nitrile oxides with homoallyl alcohols, Swern oxidation, and Raney Ni reduction. Since a variety of nitrile oxides and homoallyl alcohols are readily accessible, this method becomes a useful synthetic method of substituted pyridine derivatives.

Table 1. Pyridine Synthesis by Nitrile Oxide Cycloaddition Route

Entry	Cycloaddition reaction[a]									Swern oxidation[b]		Pyridine cyclization[c]	
	R^4CNO **2a—e**			Homoallyl alcohol **1a—f**				Product	Yield[d]/%	Product	Yield[d]/%	Product	Yield[d]/%
		R^4	Method		R^1	R^2	R^3						
1	**2a**	Ph	A	**1a**	Ph	H	H	**3a**	67	**4a**	98	**5a**	82
2	**2a**	Ph	A	**1b**	Ph	H	Me	**3b**	68	**4b**	100	**5b**	99
3	**2a**	Ph	A	**1c**	Ph	Me	H	**3c**	70	**4c**	97	**5c**	55
4	**2a**	Ph	A	**1d**	Et	H	H	**3d**	69	**4d**	100	**5d**	49
5	**2a**	Ph	A	**1e**	2-Py	H	H	**3e**	84	**4e**	98	**5e**	13
6	**2a**	Ph	A	**1f**	3-Py	H	H	**3f**	84	**4f**	81	**5f**	64
7	**2b**	*p*-$MeOC_6H_4$	A	**1a**	Ph	H	H	**3g**	91	**4g**	100	**5g**	60
8	**2b**	*p*-$MeOC_6H_4$	A	**1d**	Et	H	H	**3h**	72	**4h**	89	**5h**	72
9	**2c**	COOEt	B	**1a**	Ph	H	H	**3i**	87	**4i**	100	**5i**	53
10	**2c**	COOEt	B	**1d**	Et	H	H	**3j**	55	**4j**	100	**5j**	60
11	**2d**	Me	C	**1a**	Ph	H	H	**3k**	40	**4k**	100	**5k**	48
12	**2d**	Me	C	**1d**	Et	H	H	**3l**	30	**4l**	99	**5l**	40
13	**2e**	$(EtO)_2P(O)CH_2$	D	**1a**	Ph	H	H	**3m**	70	**4m**	84	**5m**	83

a) The reactions were carried out according to either of methods A to D (See the experimental section). b) The reaction conditions: $(COCl)_2$ (1.1 equiv), DMSO (2.2 equiv), and NEt_3 (5 equiv) in dichloromethane at −78 °C for 20 min and then at room temperature for 10 min. c) The reaction conditions: Raney Ni (W2) in ethanol containing aqueous HBF_4 (42%, 5 equiv) at room temperature under hydrogen (1 atm) for 14—16 h. d) Yield of isolated product.

Table 2. Reductive Cleavage of Nitrogen-Oxygen Bond of **4a**

Acid (equivalent)	Solvent	Reaction conditions	Yield of **5a**/%
$B(OH)_3$ (2)	$EtOH/H_2O$ (6 : 1 v/v)	Rt, 16 h	19
None	EtOH	Rt, 16 h	56
AcOH (2)	EtOH	Rt, 15 h	63
aq HBF_4 (5)	EtOH	Rt, 16 h	82
aq HBF_4 (10)	EtOH	Rt, 15 h	76

Experimental

Melting points were recorded on a Yanagimoto melting point apparatus and are uncorrected. IR spectra were taken with a JASCO IRA-1 or an A-702 spectrometer. ^{1}H and ^{13}C NMR spectra were measured on a Hitachi R-40 (^{1}H NMR: 90 MHz) or a JEOL GSX-270 (270 MHz for ^{1}H NMR and 67.94 MHz for ^{13}C NMR) instrument. Chemical shifts are expressed in parts per million downfield from tetramethylsilane as an internal standard. Mass spectra and high-resolution mass spectra (HRMS) were taken with a JEOL-01SG-2 spectrometer where the ionization energy of 70 eV was employed unless otherwise stated. Elemental analyses were performed on a Hitachi 026 CHN analyzer. For preparative column chromatography, Wakogel C-200, C-300 (Wako), and Silica gel 60 (Merck) were employed.

General Procedure for Cycloadditions of Homoallyl Alcohols 1a—f with Nitrile Oxides 2a—e Leading to 3a—m. Some typical procedures employing methods A—D for the nitrile oxide generation are described:

Method A: Triethylamine (0.404 g, 4 mmol) was added dropwise to a solution of benzohydroximoyl chloride (0.6 g, 3.85 mmol) and **1a** (0.57 g, 3.85 mmol) in dry diethyl ether (20 ml), and the mixture was stirred at room temperature for 15 h. The triethylammonium chloride was filtered off and the filtrate was evaporated in vacuo. The residue was chromatographed on silica gel by using hexane-ethyl acetate (4:1 v/v) to give **3a** (0.693 g, 67%).

Method B: Triethylamine (1.01 g, 10 mmol) in diethyl ether (14 ml) was added, at 0 °C in a period of 2 h, to a solution of ethyl chloro(hydroxyimino)acetate (1.212 g, 8 mmol) and **1a** (0.592 g, 4 mmol) in diethyl ether (20 ml), and the mixture was stirred at room temperature for 15 h. Similar workup mentioned above and subsequent column chromatography on silica gel using hexane-ethyl acetate (4:1 v/v) gave **3i** (0.92 g, 87%).

Method C: Benzenesulfonyl chloride (1.77 g, 10 mmol) was added dropwise to a solution of nitroethane (0.375 g, 5 mmol), **1a** (0.74 g, 5 mmol), and triethylamine (1.01 g, 10 mmol) in chloroform (25 ml), and the mixture was stirred at room temperature for 17 h. Water (30 ml) was added and the mixture was extracted with dichloromethane (30 ml×3). The combined extract was washed with water (20 ml×3), dried over magnesium sulfate, and the solvent was evaporated in vacuo. The residue was chromatographed on silica gel with hexane-ethyl acetate (2:1 v/v) to give **3k** (0.407 g, 40%).

Method D: To a solution of (diethoxyphosphinyl)acetaldehyde oxime (0.975 g, 5 mmol) in dry *N*,*N*-dimethylformamide (DMF, 10 ml) was added dropwise at −20 °C a DMF solution (10 ml) of *N*-bromosuccinimide (NBS, 2.1 g, 10 mmol). The mixture was stirred at −20 °C for 1 h and then at 0 °C for 30 min. Diethyl ether (10 ml), triethylamine (0.505 g, 5 mmol), and an ether solution (10 ml) of **1a** (1.48 g, 10 mmol) were added dropwise in this order, and the mixture was stirred overnight at room temperature. Water (50 ml) was added and the mixture was extracted with dichloromethane (30 ml×3). The combined extract was washed with water (30 ml×3), dried over magnesium sulfate, and the solvent was evaporated in vacuo. The residue was chromatographed on silica gel with ethyl acetate to give **3m** (1.2 g, 70%). Products **3a—m** were submitted to the Swern oxidation procedure. Spectral data for some of these compounds are given as follows and yields are summarized in Table 1:

3a: Solid (a 3:2 diastereomeric mixture (^{1}H NMR)); ^{13}C NMR ($CDCl_3$) δ=40.62, 40.64 (each C-4), 44.48, 44.62 (each 5-CH_2), 71.14, 72.47 (each C-5), 78.40, 79.67 (each CH(OH)Ph), 125.58, 125.96, 126.68, 126.71, 127.61, 128.58, 128.71, 128.74, 130.09, 130.16, 143.78, 144.36 (each Ph), 156.90, and 156.93 (each C-3). MS *m*/*z* (rel intensity) 267 (M^+, 12), 148 (9), 146 (10), 120 (9), 119 (28), 105 (18), and 104 (100).

3c: Solid (a roughly 1:1 diastereomeric mixture (^{1}H NMR)); IR (KBr) 3320, 1440, 1350, 750, and 690 cm^{-1}; ^{13}C NMR ($CDCl_3$) δ=8.22, 9.16 (each Me), 38.10, 38.21 (each C-4), 44.58, 44.87 (each 5-CH), 73.32, 75.40 (each C-5), 83.24 (CH(OH)Ph), 125.96, 126.22, 126.62, 127.02, 127.31, 128.12, 128.25, 128.66, 129.57, 129.97, 130.05, 143.02, 143.26 (each Ph), 156.73, and 157.04 (each C-3).

3d: Solid (a 1:1 diastereomeric mixture (^{13}C NMR)); IR (KBr) 3380, 1440, 1350, 890, 755, and 690 cm^{-1}; ^{13}C NMR ($CDCl_3$) δ=9.78, 9.85 (each Et), 30.34, 30.74 (each Et), 40.59, 40.65 (each C-4), 41.74, 42.26 (each 5-CH_2), 69.92, 71.24 (each each C-5), 78.77, 80.34 (each CH(OH)Ph), 126.65, 126.68, 128.68, 129.53, 129.67, 130.02, 130.10 (each Ph), 156.96, and 157.08 (each C-3). MS *m*/*z* (rel intensity) 219 (M^+, 27), 147 (10), 146 (100), 145 (23), 144 (13), and 118 (11).

3g: Solid (a 1:1 diastereomeric mixture (^{13}C NMR)); IR (KBr) 3280, 1600, 1240, 1010, 890, and 820 cm^{-1}; ^{13}C NMR ($CDCl_3$) δ=40.81, 40.85 (each 5-CH_2), 44.43, 44.58 (each C-4), 55.32 (MeO), 71.06, 72.41 (each C-5), 78.10, 79.35 (each CH(OH)Ph), 114.11, 114.14, 122.04, 122.17, 125.58, 125.96, 127.50, 127.68, 128.19, 128.22, 128.51, 143.85, 144.44 (Ph and Ar), 156.50, 156.52 (each C-3), 161.03, and 161.09 (each Ar).

3h: Solid (a 1:1 diastereomeric mixture (^{13}C NMR)); IR (KBr) 3320, 1600, 1240, 1015, 890, and 820 cm^{-1}; ^{13}C NMR ($CDCl_3$) δ=9.81, 9.88 (each Et), 30.35, 30.78 (each Et), 40.86, 40.89 (each 5-CH_2), 41.76, 42.27 (each C-4), 55.32 (MeO), 69.95, 71.26 (each C-5), 78.53, 80.08 (each CH(OH)Et), 114.11, 114.14, 122.11, 122.29, 128.17, 128.22 (each Ar), 156.54, 156.65 (each C-3), 161.00, and 161.07 (each Ar).

3i: Oil (a 1:1 diastereomeric mixture (^{13}C NMR)); IR (neat) 3400, 1715, 1250, 930, and 760 cm^{-1}; ^{13}C NMR ($CDCl_3$) δ=14.11 (COOEt), 38.93, 39.08 (each 5-CH_2), 43.99, 44.62 (each C-4), 62.06 (COOEt), 70.73, 71.75 (each C-5), 81.02, 81.90 (each CH(OH)Ph), 125.53, 125.90, 127.79, 127.97, 128.64, 128.66, 143.48, 144.13 (Ph), 151.77, 151.80 (each C-3), and 160.76 (COOEt); MS *m*/*z* (rel intensity) 263 (M^+, 9), 190 (26), 172 (19), 157 (44), 129 (31), 115 (23), 111 (27), 108 (13), 107 (100), 105 (52), 104 (54), and 79 (26).

3j: Oil (a 1:1 diastereomeric mixture (^{13}C NMR)); IR (neat) 3420, 1720, 1590, 1250, 1130, and 930 cm^{-1}; ^{13}C NMR ($CDCl_3$) δ=9.75 (Et), 14.13 (COOEt), 30.44, 30.81 (each Et), 38.96, 39.21 (each 5-CH_2), 41.58, 42.27 (each C-4), 62.06, 62.10 (each COOEt), 69.66, 70.68 (each C-5) , 81.44, 82.72 (each CH(OH)Et), 151.79, 151.92 (each C-3), 160.83, and 160.86 (each COOEt); MS *m*/*z* (rel intensity) 215 (M^+, 12), 186 (11), 183 (12), 157 (20), 142 (100), 129 (12), 124 (12), 114 (47), 111 (14), 96 (10), and 59 (11).

3k: Oil (a 1:1 diastereomeric mixture (^{13}C NMR)); IR (neat) 3380, 1435, 1325, 1040, 760, and 700 cm^{-1}; ^{13}C NMR ($CDCl_3$) δ=13.12, 13.16 (each Me), 44.28, 44.35, 44.42, 44.52 (C-4 and 5-CH_2), 70.87, 72.31 (each C-5), 77.28, 78.60 (each CH(OH)Ph), 125.57, 125.93, 127.38, 127.58, 128.43, 143.94,

144.57 (each Ph), and 155.85 (C-3); MS *m/z* (rel intensity) 205 (M^+, 5), 120 (12), 107 (23), 105 (20), 104 (100), 99 (25), 79 (11), and 57 (29).

3l: Oil (a 1 : 1 diastereomeric mixture (^{13}C NMR)); IR (neat) 3420, 1440, 1335, and 870 cm^{-1}; ^{13}C NMR ($CDCl_3$) δ=9.73, 9.86 (each Et), 13.22, 13.29 (each 3-Me), 30.32, 30.68 (each Et), 41.80, 41.97 (each 5-CH_2), 44.42, 44.65 (each C-4), 70.06, 71.66 (each C-5), 77.69, 79.67 (each CH(OH)Et), 155.79, and 155.91 (each C-3).

General Procedure for the Swern Oxidation of 3a—m Leading to 4a—m. The oxidation of **3a** is described as a typical example. To a solution of oxalyl dichloride (0.14 ml, 1.5 mmol) in dry dichloromethane (3.5 ml) was added dropwise, at −78 °C under nitrogen, a dichloromethane (3 ml) solution of dimethyl sulfoxide (0.24 ml, 3 mmol). After 5 min, a solution of **3a** (0.36 g, 1.35 mmol) in dichloromethane (3 ml) was added, and the stirring was continued for 20 min. Triethylamine (0.682 g, 6.8 mmol) was added. After 10 min, the mixture was warmed to room temperature, and poured into water (50 ml). The mixture was extracted with dichloromethane (30 ml×2). The combined extract was washed with saturated aqueous sodium chloride (30 ml×3), dried over magnesium sulfate, and the solvent was evaporated in vacuo. The residue was chromatographed on silica gel by using hexane–ethyl acetate (1 : 1 v/v) to give **4a** (0.351 g, 98%).

Results are summarized in Table 1.

5-(2-Oxo-2-phenylethyl)-3-phenyl-2-isoxazoline (4a): Colorless needles (ethyl acetate–hexane); mp 141—143 °C; IR (KBr) 1670, 1430, 1205, 910, 760, and 685 cm^{-1}; ^1H NMR ($CDCl_3$) δ=3.08 (1H, dd, J_{gem}=16.9 and $J_{4,5}$=7.7 Hz, one of H-4), 3.26 (1H, dd, J_{gem}=17.4 and $J_{CH,5}$=8.5 Hz, one of 5-CH_2), 3.66 (1H, dd, J_{gem}=17.4 and $J_{CH,5}$=4.6 Hz, the other of 5-CH_2), 3.67 (1H, dd, J_{gem}=16.9 and $J_{4,5}$=10.3 Hz, the other of H-4), 5.25 (1H, dddd, $J_{4,5}$=10.3, 7.7, $J_{5,CH}$=8.5, and 4.6 Hz, H-5), 7.4—7.7 (8H, m, Ph), and 7.9—8.0 (2H, m, Ph); ^{13}C NMR ($CDCl_3$) δ=40.73 (C-4), 43.87 (5-CH_2), 77.46 (C-5), 126.69, 128.09, 128.71, 128.74, 129.53, 130.10, 133.57, 136.51 (each Ph), 156.93 (C-3), and 197.36 (CO); MS *m/z* (rel intensity) 265 (M^+, 12), 160 (11), 147 (11), 146 (100), and 120 (26). Found: C, 77.01; H, 5.92; N, 5.34%. Calcd for $C_{17}H_{15}NO_2$: C, 76.96; H, 5.70; N, 5.28%.

5-(2-Oxo-2-phenylethyl)-5-methyl-3-phenyl-2-isoxazoline (4b): Pale yellow prisms (diethyl ether–hexane); mp 68—70 °C; IR (KBr) 1780, 1450, 1360, 920, 760, and 690 cm^{-1}; ^1H NMR ($CDCl_3$) δ=1.60 (3H, s, 5-Me), 3.32, 3.48 (each 1H, d, J_{gem}=17.2 Hz, H-4), 3.44, 3.59 (each 1H, J_{gem}=16.9 Hz, 5-CH_2), and 7.2—8.0 (10H, m, Ph); ^{13}C NMR ($CDCl_3$) δ=25.92 (5-Me), 45.44 (C-4), 47.69 (5-CH_2), 85.63 (C-5), 126.59, 128.16, 128.68, 128.71, 129.92, 129.97, 133.52, 136.99 (each Ph), 157.26 (C-3), and 197.46 (CO); MS *m/z* (rel intensity) 279 (M^+, 6), 161 (12), 160 (100), and 120 (9). Found: C, 77.77; H, 6.16; N, 4.88%. Calcd for $C_{18}H_{17}NO_2$: C, 77.40; H, 6.13; N, 5.01%.

5-(2-Oxo-1-methyl-2-phenylethyl)-3-phenyl-2-isoxazoline (4c): Obtained as a 1 : 1 mixture of diastereomers (^1H NMR); pale yellow liquid; IR (neat) 1670, 1440, 1215, 890, 760, and 690 cm^{-1}; ^1H NMR ($CDCl_3$) δ=1.23, 1.43 (each 1/2×3H, d, J=7.0 Hz, Me), 2.99, 3.26 (each 1/2H, dd, J_{gem}=17.2 and $J_{4,5}$=8.1 Hz, one of H-4), 3.42, 3.52 (each 1/2H, dd, J_{gem}=17.2 and $J_{4,5}$=11.3 Hz, the other of H-4), 3.77 (1/2H, dq, $J_{CH,Me}$=7.0 and $J_{CH,5}$=6.6 Hz, 5-CH), 3.95 (1/2H, quint, $J_{CH,Me}$=$J_{CH,5}$=7.0 Hz, 5-CH), 5.02 (1/2H, dt, $J_{5,4}$=11.3 and $J_{5,4}$=$J_{5,CH}$=8.1 Hz, H-5), 5.13 (1/2H, ddd, $J_{5,4}$=11.3, 8.1, and $J_{5,CH}$=6.6 Hz, H-5), 7.3—7.7 (8H, m, PH), and 7.9—8.0 (2H, m, Ph); ^{13}C NMR ($CDCl_3$) δ=12.30, 15.93 (each Me), 36.85, 39.42 (each C-4), 44.35, 46.09 (each 5-CH), 82.01, 82.89 (each C-5), 128.45, 128.56, 128.66, 128.71, 128.76, 128.79, 129.48, 130.05, 130.09, 133.37, 133.49, 136.08, 136.27 (each Ph), 156.64, 156.99 (each C-3), 201.43, and 202.46 (each CO); MS *m/z* (rel intensity) 279 (M^+, 5), 146 (47), and 134 (100). Found: C, 77.49; H, 5.95; N, 5.20%. Calcd for $C_{18}H_{17}NO_2$: C, 77.38; H, 6.14; N, 5.02%.

5-(2-Oxobutyl)-3-phenyl-2-isoxazoline (4d): Colorless needles (diethyl ether–hexane); mp 81—82.5 °C; IR (KBr) 1700, 1435, 910, 750, and 690 cm^{-1}; ^1H NMR ($CDCl_3$) δ=1.08 (3H, t, J=7.3 Hz, Et), 2.50, 2.52 (2H, each q, J=7.3 Hz, Et), 2.71 (1H, dd, J_{gem}=16.5 and $J_{CH,5}$=7.5 Hz, one of 5-CH_2), 2.99 (1H, dd, J_{gem}=16.7 and $J_{4,5}$=8.1 Hz, one of H-4), 3.04 (1H, dd, J_{gem}=16.5 and $J_{CH,5}$=5.7 Hz, the other of 5-CH_2), 3.56 (1H, dd, J_{gem}=16.7 and $J_{4,5}$=10.3 Hz, the other of H-4), 5.0—5.1 (1H, dddd, $J_{5,4}$=10.3, 8.1, $J_{5,CH}$=7.5, and 5.7 Hz, H-5), 7.3—7.4 (3H, m, Ph), and 7.6—7.7 (2H, m, Ph); ^{13}C NMR ($CDCl_3$) δ=7.56, 36.84 (each Et), 40.47 (C-4), 47.32 (5-CH_2), 77.07 (C-5), 126.69, 128.72, 129.50, 130.15 (each Ph), 156.78 (C-3), and 208.68 (CO); MS *m/z* (rel intensity) 217 (M^+, 11), 147 (10), 146 (100), and 57 (15). Found: C, 71.98; H, 7.10; N, 6.32%. Calcd for $C_{13}H_{15}NO_2$: C, 71.87; H, 6.96; N, 6.45%.

5-[2-Oxo-2-(2-pyridyl)ethyl]-3-phenyl-2-isoxazoline (4e): Colorless needles (diethyl ether–hexane); mp 81—83 °C; IR (KBr) 1690, 1435, 910, and 760 cm^{-1}; ^1H NMR ($CDCl_3$) δ=3.13 (1H, dd, J_{gem}=16.5 and $J_{4,5}$=7.3 Hz, one of H-4), 3.52 (1H, dd, J_{gem}=17.6 and $J_{CH,5}$=7.7 Hz, one of 5-CH_2), 3.62 (1H, dd, J_{gem}=16.5 and $J_{4,5}$=10.2 Hz, the other of H-4), 3.91 (1H, dd, J_{gem}=17.6 and $J_{CH,5}$=5.9 Hz, the other of 5-CH_2), 5.33 (1H, dddd, $J_{4,5}$=10.2, 7.3, $J_{5,CH}$=7.7, and 5.9 Hz, H-5), 7.3—7.4, 7.6—7.7 (3H and 2H, m, Ph), 7.55, 7.84, 8.05, and 8.68 (each 1H, m, Py); ^{13}C NMR ($CDCl_3$) δ=40.52 (C-4), 43.44 (5-CH_2), 77.41 (C-5), 121.78, 126.71, 127.48, 128.69, 129.69, 130.03, 136.97 (Ph and Py), 149.11, 152.95 (C-2 and C-6 of Py), 156.68 (C-3), and 198.97 (CO); MS *m/z* (rel intensity) 266 (M^+, 2), 163 (10), 122 (9), 121 (100), 93 (14), and 79 (11). Found: C, 72.31; H, 5.45; N, 10.44%. Calcd for $C_{16}H_{14}N_2O_2$: C, 72.17; H, 5.30; N, 10.52%.

5-[2-Oxo-2-(3-pyridyl)ethyl]-3-phenyl-2-isoxazoline (4f): Colorless needles (ethyl acetate–hexane); mp 138.5—139 °C; IR (KBr) 1675, 1570, 1210, 890, 790, and 755 cm^{-1}; ^1H NMR ($CDCl_3$) δ=3.12 (1H, dd, J_{gem}=17.2 and $J_{CH,5}$=7.7 Hz, one of 5-CH_2), 3.28 (1H, dd, J_{gem}=17.6 and $J_{4,5}$=8.1 Hz, one of H-4), 3.68 (1H, dd, J_{gem}=17.2 and $J_{CH,5}$=5.1 Hz, the other of 5-CH_2), 3.71 (1H, dd, J_{gem}=17.6 and $J_{4,5}$=9.9 Hz, the other of H-4), 5.29 (1H, dddd, $J_{5,4}$=9.9, 8.1, $J_{5,CH}$=7.7, and 5.1 Hz, H-5), 7.4—7.5, 7.6—7.7 (3H and 2H, m, Ph), 7.45, 8.25, 8.81, and 9.18 (each 1H, m, Py); ^{13}C NMR ($CDCl_3$) δ=40.72 (C-4), 44.12 (5-CH_2), 76.99 (C-5), 123.74, 126.73, 128.76, 129.31, 130.28, 131.77, 135.42 (Ph and Py), 149.69, 153.96 (C-2 and C-6 of Py), 156.93 (C-3), and 196.35 (CO); MS *m/z* (rel intensity) 266 (M^+, 18), 160 (9), 146 (54), 121 (100), and 106 (18). Found: C, 72.36; H, 5.49; N, 10.65%. Calcd for $C_{16}H_{14}N_2O_2$: C, 72.17; H, 5.30; N, 10.52%.

5-(2-Oxo-2-phenylethyl)-3-(4-methoxyphenyl)-2-isoxazoline (4g): Colorless needles (ethyl acetate–hexane); mp 146—147 °C; IR (KBr) 1670, 1600, 1255, and 890 cm^{-1}; ^1H NMR ($CDCl_3$) δ=3.05 (1H, dd, J_{gem}=16.8 and $J_{4,5}$=9.6 Hz, one of H-4), 3.25 (1H, dd, J_{gem}=17.6 and $J_{CH,5}$=8.5 Hz, one of 5-CH_2), 3.65 (1H, dd, J_{gem}=16.8 and $J_{4,5}$=10.3 Hz, the other of

H-4), 3.68 (1H, dd, J_{gem}=17.6 and $J_{CH,5}$=4.7 Hz, the other of 5-CH_2), 3.82 (3H, s, OMe), 5.23 (1H, dddd, $J_{5,4}$=10.3, 9.6, $J_{5,CH}$=8.5, and 4.7 Hz, H-5), and 6.9—7.9 (9H, m, Ph and Ar); ^{13}C NMR ($CDCl_3$) δ=41.02 (C-4), 43.93 (5-CH_2), 55.35 (MeO), 77.18 (C-5), 114.15, 122.10, 128.12, 128.25, 128.75, 133.57, 136.57 (Ph and Ar), 156.52 (C-3), 161.12 (Ar), and 197.50 (CO); MS *m/z* (rel intensity) 295 (M^+, 19), 177 (11), 176 (100), 175 (65), 147 (10), 120 (14), 105 (38), and 77 (29). Found: C, 73.48; H, 5.89; N, 4.42%. Calcd for $C_{18}H_{17}NO_3$: C, 73.19; H, 5.81; N, 4.74%.

5-(2-Oxobutyl)-3-(4-methoxyphenyl)-2-isoxazoline (4h): Colorless leaflets (diethyl ether-hexane); mp 111—112.5 °C; IR (KBr) 1690, 1595, 1380, 1240, 880, and 815 cm^{-1}; ^{1}H NMR ($CDCl_3$) δ=1.06 (3H, t, J=7.3 Hz, Et), 2.49 (2H, q, J=7.3 Hz, Et), 2.69 (1H, dd, J_{gem}=16.5 and $J_{4,5}$=8.0 Hz, one of H-4), 2.95 (1H, dd, J_{gem}=16.5 and $J_{CH,5}$=7.8 Hz, one of 5-CH_2), 3.02 (1H, dd, J_{gem}=16.5 and $J_{CH,5}$=6.5 Hz, the other of 5-CH_2), 3.51 (1H, dd, J_{gem}=16.5 and $J_{4,5}$=10.5 Hz, the other of H-4), 3.81 (3H, s, MeO), 5.03 (1H, dddd, $J_{5,4}$=10.5, 8.0, $J_{5,CH}$=7.8, and 6.5 Hz, H-5), 6.89, and 7.56 (each 2H, d, J=7.8 Hz, Ar); ^{13}C NMR ($CDCl_3$) δ=7.53, 36.74 (each Et), 40.63 (C-4), 47.31 (5-CH_2), 55.32 (MeO), 76.76 (C-5), 114.12, 122.06, 128.19 (each Ar), 156.32 (C-3), 161.09 (Ar), and 208.73 (CO); Found: C, 68.22; H, 6.95; N, 5.56%. Calcd for $C_{14}H_{17}NO_3$: C, 67.99; H, 6.93; N, 5.66%.

Ethyl 5-(2-Oxo-2-phenylethyl)-2-isoxazoline-3-carboxylate (4i): Colorless prisms (diethyl ether-hexane); mp 74—75.5 °C; IR (KBr) 1710, 1680, 1215, 935, and 755 cm^{-1}; ^{1}H NMR ($CDCl_3$) δ=1.36 (3H, t, J=7.3 Hz, EtO), 2.96 (1H, dd, J_{gem}=18.0 and $J_{4,5}$=8.4 Hz, one of H-4), 3.26 (1H, dd, J_{gem}=17.5 and $J_{CH,5}$=8.0 Hz, one of 5-CH_2), 3.53 (1H, dd, J_{gem}=18.0 and $J_{4,5}$=11.0 Hz, the other of H-4), 3.65 (1H, dd, J_{gem}=18.0 and $J_{CH,5}$=7.1 Hz, the other of 5-CH_2), 4.34 (2H, q, J=7.3 Hz, EtO), 5.33 (1H, dddd, $J_{5,4}$=11.0, 8.4, $J_{5,CH}$=8.0, and 7.1 Hz, H-5), and 7.4—8.0 (5H, m, Ph); ^{13}C NMR ($CDCl_3$) δ=14.11 (EtO), 39.32 (C-4), 43.57 (5-CH_2), 62.03 (EtO), 79.93 (C-5), 128.07, 128.79, 133.80, 136.32 (each Ar), 151.96 (C-3), 160.57 (COOEt), and 196.52 (CO); MS *m/z* (rel intensity) 262 (M^++1, 2), 188 (23), 162 (13), 120 (97), and 105 (100). Found: 64.57; H, 5.84; N, 5.02%. Calcd for $C_{14}H_{15}NO_4$: C, 64.36; H, 5.79; N, 5.36%.

Ethyl 5-(2-Oxobutyl)-2-isoxazoline-3-carboxylate (4j): Pale yellow liquid; IR (neat) 1710, 1250, 1115, and 925 cm^{-1}; ^{1}H NMR ($CDCl_3$) δ=1.07 (3H, t, J=7.3 Hz, Et), 1.36 (3H, t, J=7.1 Hz, EtO), 2.49 (2H, q, J=7.3 Hz, Et), 2.73 (1H, dd, J_{gem}=17.2 and $J_{CH,5}$=7.0 Hz, one of 5-CH_2), 2.88 (1H, dd, J_{gem}=17.6 and $J_{4,5}$=8.2 Hz, one of H-4), 3.03 (1H, dd, J_{gem}=17.2 and $J_{CH,5}$=5.9 Hz, the other of 5-CH_2), 3.43 (1H, dd, J_{gem}=17.6 and $J_{4,5}$=11.0 Hz, the other of H-4), 4.33 (2H, q, J=7.1 Hz, OEt), and 5.16 (1H, m, H-5); ^{13}C NMR ($CDCl_3$) δ=7.47 (Et), 14.11 (EtO), 36.69 (Et), 38.97 (C-4) , 46.91 (5-CH_2), 62.03 (EtO), 79.54 (C-5), 151.80 (C-3), 160.53 (COOEt), and 207.84 (CO); MS *m/z* (rel intensity) 214 (M^++1, 3), 205 (9), 184 (23), 169 (18), 168 (9), 157 (9), 142 (98), 140 (45), 114 (65), 96 (12), 84 (15), 72 (23), and 57 (100). Found: C, 56.20; H, 6.91; N, 6.48%. Calcd for $C_{10}H_{15}NO_4$: C, 56.32; H, 7.09; N, 6.57%.

5-(2-Oxo-2-phenylethyl)-3-methyl-2-isoxazoline (4k): Colorless needles (diethyl ether-hexane); mp 97—98 °C; IR (KBr) 1670, 1435, 1380, 1320, and 1210 cm^{-1}; ^{1}H NMR ($CDCl_3$) δ=2.00 (3H, s, 3-Me), 2.68 (1H, br dd, J_{gem}=17.2 and $J_{4,5}$=7.7 Hz, one of H-4), 3.17 (1H, dd, J_{gem}=17.2 and $J_{CH,5}$=8.0 Hz, one of 5-CH_2), 3.25 (1H, br dd, J_{gem}=17.2 and $J_{4,5}$=9.9 Hz, the other of H-4), 3.58 (1H, dd, J_{gem}=17.2 and $J_{CH,5}$=5.1 Hz, the other of 5-CH_2), 5.07 (1H, m, H-5), and 7.4—8.0 (5H, m, Ph); ^{13}C NMR ($CDCl_3$) δ=13.22 (3-Me), 43.86, 44.42 (C-4 and 5-CH_2), 76.40 (C-5), 128.09, 128.74, 133.55, 136.55 (each Ph), 155.82 (C-3), and 197.49 (CO); MS *m/z* (rel intensity) 203 (M^+, 1), 162 (7), 121 (9), 120 (100), 105 (84), and 84 (67). Found: C, 70.62; H, 6.51; N, 6.86%. Calcd for $C_{12}H_{13}NO_2$: C, 70.90; H, 6.45, N, 6.89%.

5-(2-Oxobutyl)-3-methyl-2-isoxazoline (4l): Colorless liquid; bp 115 °C/27 Pa (bulb-to-bulb); IR (neat) 1695, 1375, 1115, and 850 cm^{-1}; ^{1}H NMR ($CDCl_3$) δ=1.06 (3H, t, J=7.3 Hz, Et), 1.99 (3H, s, 3-Me), 2.49 (2H, q, J=7.3 Hz, Et), 2.60 (1H, dd, J_{gem}=17.2 and $J_{4,5}$=9.6 Hz, one of H-4), 2.63 (1H, dd, J_{gem}=16.9 and $J_{CH,5}$=7.0 Hz, one of 5-CH_2), 2.94 (1H, dd, J_{gem}=16.9 and $J_{CH,5}$=5.9 Hz, the other of 5-CH_2), 3.15 (1H, dd, J_{gem}=17.2 and $J_{4,5}$=10.2 Hz, the other of H-4), and 4.90 (1H, dddd, $J_{5,4}$=10.2, 9.6, $J_{5,CH}$=7.0, and 5.9 Hz, H-5); ^{13}C NMR ($CDCl_3$) δ=7.53 (Et), 13.16 (3-Me), 36.86 (Et), 44.13 (C-4), 47.30 (5-CH_2), 76.05 (C-5), 155.61 (C-3), and 208.85 (CO); MS *m/z* (rel intensity) 155 (M^+, 5), 126 (12), 84 (100), 72 (11), 57 (34), and 43 (10). HRMS Found: *m/z* 155.0944. Calcd for $C_8H_{13}NO_2$: M, 155.0946.

3-[(Diethoxyphosphinyl)methyl]-5-(2-oxo-2-phenylethyl)-2-isoxazoline (4m): Pale yellow liquid; IR (neat) 1670, 1230, 1015, and 950 cm^{-1}; ^{1}H NMR ($CDCl_3$) δ=1.34 (6H, dd, J=7.2 and J_{HP}=4.0 Hz, OEt), 2.86 (1H, ddd, J_{gem}=17.6, $J_{4,5}$=7.3, and J_{HP}=3.7 Hz, one of H-4), 2.98 (2H, d, J_{HP}=22.4 Hz, CH_2P), 3.19 (1H, dd, J_{gem}=17.2 and $J_{CH,5}$=7.8 Hz, one of 5-CH_2), 3.40 (1H, ddd, J_{gem}=17.6, $J_{4,5}$=10.3, and J_{HP}=3.7 Hz, the other of H-4), 3.58 (1H, dd, J_{gem}=17.2 and $J_{CH,5}$=5.1 Hz, the other of 5-CH_2), 4.15 (4H, dq, J=7.2 and J_{HP}=7.0 Hz, OEt), 5.16 (1H, dddd, $J_{5,4}$=10.3, 7.3, $J_{5,CH}$=7.8, and 5.1 Hz, H-5), and 7.4—8.0 (5H, m, Ph); ^{13}C NMR ($CDCl_3$) δ=16.39 (d, J_{CP}=5.9 Hz, OEt), 26.31 d, J_{CP}=141.8 Hz, CH_2P), 42.97 (C-4), 43.64 (5-CH_2), 62.54 (d, J_{CP}=6.8 Hz, OEt), 77.22 (C-5), 128.06, 128.72, 133.56, 136.51 (each Ph), 151.93 (C-3), and 197.17 (CO); MS *m/z* (rel intensity) 339 (M^+, 1), 221 (9), 220 (100), and 192 (10). HRMS Found: *m/z* 339.1233. Calcd for $C_{16}H_{22}NO_5P$: M, 339.1235.

General Procedure for the Reductive N-O Bond Cleavage of 4a—m Leading to Pyridines 5a—m. The conversion of **4a** into **5a** is described as a typical example. To a solution of **4a** (0.068 g, 0.26 mmol) in ethanol (12 ml) were added tetrafluoroboric acid (42% aqueous solution, 0.269 g, 1.29 mmol) and Raney Ni (W-2 in ethanol, 0.8 ml). The mixture was stirred under a hydrogen atmosphere (1 atm) at room temperature for 16 h. The catalyst was removed by filteration and an aqueous solution of sodium hydroxide was added to the filtrate which was then extracted with dichloromethane (30 ml×3). The combined extract was dried over magnesium sulfate and the solvent was evaporated in vacuo. The residue was chromatographed on silica gel by using hexane-ethyl acetate (5 : 1 v/v) to give **5a** (0.049 g, 82%). Mp 82 °C (lit,[13] mp 81—82 °C).

In the case of **5e**, the filtrate from which the catalyst had been filtered off was evaporated in vacuo. The residue was treated with aqueous ethylenediaminetetraacetic acid, extracted with dichloromethane (30 ml×3), and the purification procedure was continued.

Yields of **5a—m** are summarized in Table 1. The following pyridines are all known: 2,6-diphenylpyridine (**5a**);[13,15] 4-methyl-2,6-diphenylpyridine (**5b**);[13] 3-methyl-2,6-diphenylpyridine (**5c**);[14] 2-phenyl-6-(2-pyridyl)pyridine (**5e**);[15] 2-(4-

methoxyphenyl)-6-phenylpyridine (**5g**);[16] 2-methyl-6-phenylpyridine (**5k**);[17] 2-ethyl-6-methylpyridine (**5l**).[18]

2-Ethyl-6-phenylpyridine (5d): Colorless liquid; IR (neat) 1565, 1440, and 760 cm^{-1}; ^1H NMR ($CDCl_3$) δ=1.36 (3H, t, J=7.7 Hz, 2-Et), 2.88 (2H, q, J=7.7 Hz, 2-Et), and 7.0—8.0 (8H, m, Ph and Py); ^{13}C NMR ($CDCl_3$) δ=13.85, 31.56 (each 2-Et), 117.65, 120.31, 126.98, 128.64, 136.90, 139.88, 156.73 (Ph and Py), and 163.36 (C-2 and C-6 of Py); MS m/z (rel intensity) 184 (M^++1, 12), 183 (M^+, 90), 182 (100), 155 (20), 154 (22), 127 (13), and 77 (18). HRMS Found: m/z 183.1047. Calcd for $C_{13}H_{13}N$: M, 183.1047.

2-Phenyl-6-(3-pyridyl)pyridine (5f): Pale yellow liquid; IR (neat) 3000, 1550, 1430, and 750 cm^{-1}; ^1H NMR ($CDCl_3$) δ=7.3—8.7 (11H, m, Ph and Py) and 9.30 (1H, br s, Py); ^{13}C NMR ($CDCl_3$) δ=118.66, 119.35, 123.57, 126.95, 128.76, 129.24, 134.41, 137.75, 139.03 (Ph and Py), 148.35, 149.87, 154.26, and 157.26 (Py); MS m/z (rel intensity) 232 (M^+, 100), 231 (42), 206 (8), 204 (8), and 77 (8). HRMS Found: m/z 232.1002. Calcd for $C_{16}H_{12}N_2$: M, 232.1000.

2-Ethyl-6-(4-methoxyphenyl)pyridine (5h): Colorless liquid; IR (neat) 1570, 1445, 1250, 1035, and 845 cm^{-1}; ^1H NMR ($CDCl_3$) δ=1.36 (3H, t, J=7.8 Hz, Et), 2.86 (2H, q, J=7.8 Hz, Et), 3.82 (3H, s, MeO), 6.93 (2H, d, J=9.2 Hz, Ar), 7.0—7.6 (3H, m, Py), and 7.95 (2H, d, J=9.2 Hz, Ar); ^{13}C NMR ($CDCl_3$) δ=13.82, 31.53 (each Et), 55.25 (MeO), 114.01, 116.83, 119.58, 128.48, 136.80, 156.31, 160.28, and 163.15 (Ar and Py); MS m/z (rel intensity) 214 (M^++1, 16), 213 (M^+, 100), 212 (84), 185 (10), and 170 (12). HRMS Found: m/z 213.1150. Calcd for $C_{14}H_{15}NO$: M, 213.1154.

Ethyl 6-Phenyl-2-pyridinecarboxylate (5i): Pale yellow needles; mp 44—45 °C; IR (KBr) 1720, 1580, 1435, 1280, 1225, 1160, and 740 cm^{-1}; ^1H NMR ($CDCl_3$) δ=1.46 (3H, t, J=7.2 Hz, COOEt), 4.47 (2H, q, J=7.2 Hz, COOEt), and 7.3—8.1 (8H, m, Ph and Py); ^{13}C NMR ($CDCl_3$) δ=14.31, 61.78 (each COOEt), 123.25, 123.42, 127.18, 128.79, 129.41, 137.62, 138.50, 148.36 (Ph and Py), 157.60 (C-5 of Py), and 165.47 (COOEt); MS m/z (rel intensity) 227 (M^+, 14), 156 (13), 155 (100), 154 (29), 127 (18), and 77 (10). Found: C, 74.25; H, 5.83; N, 6.18%. Calcd for $C_{14}H_{13}NO_2$: C, 73.98; H, 5.77; N, 6.17%.

Ethyl 6-Ethyl-2-pyridinecarboxylate (5j): Pale yellow liquid; IR (neat) 1715, 1460, 1300, 1175, and 760 cm^{-1}; ^1H NMR ($CDCl_3$) δ=1.34 (3H, t, J=7.7 Hz, 5-Et), 1.43 (3H, t, J=7.0 Hz, COOEt), 2.94 (2H, q, J=7.7 Hz, 5-Et), 4.47 (3H, q, J=7.0 Hz, COOEt), 7.36 (1H, br d, J=7.7 Hz, H-5 of Py), 7.74 (1H, t, J=7.7 Hz, H-4 of Py), and 7.94 (1H, br d, J=7.7 Hz, H-3 of Py); ^{13}C NMR ($CDCl_3$) δ=14.04 (5-Et), 14.33 (COOEt), 31.43 (5-Et), 61.78 (COOEt), 122.46, 125.31, 137.17, 147.79, 164.18 (each Py), and 165.52 (COOEt); MS m/z (rel intensity) 180 (M^++1, 15), 179 (M^+, 100), 178 (11), 133 (19), 107 (85), 106 (33), 105 (75), 104 (26), 79 (27), 78 (13), and 77 (25). HRMS Found: m/z 179.0946. Calcd for $C_{10}H_{13}NO_2$: M, 179.0946.

2-[(Diethoxyphosphinyl)methyl]-6-phenylpyridine (5m): Pale yellow liquid; IR (neat) 1570, 1450, 1240, and 1020 cm^{-1}; ^1H NMR ($CDCl_3$) δ=1.26 (6H, t, J=7.2 Hz, EtO), 3.51 (2H, d, J_{HP}=21.6 Hz, CH_2P), 4.11 (4H, dq, J_{HP}=7.7 and J=7.2 Hz, EtO), and 7.3—8.0 (8H, m, Ph and Py); ^{13}C NMR ($CDCl_3$) δ=16.34 (d, J_{CP}=6.8 Hz, OEt), 36.68 (d, J_{CP}=134.0 Hz, CH_2P), 62.22 (d, J_{CP}=6.8 Hz, OEt), 118.50, 118.54, 122.56, 122.63, 126.86, 128.68, 128.97, 137.29, 139.12, 152.46, and 156.96 (Py and Ph); MS m/z (rel intensity) 306 (M^++1, 10), 305 (M^+, 48), 256 (12), 181 (11), 170 (14), and 169 (100). HRMS Found: m/z 305.1185. Calcd for $C_{16}H_{20}NO_3P$: M, 305.1181.

References

1) P. Caramella and P. Grünanger, "Nitrile Oxides and Imines in 1,3-Dipolar Cycloaddition Chemistry," ed by A. Padwa, John Wiley & Sons, New York (1984), Vol. 1, Chap. 3, pp. 291—392; D. P. Curran, "Advances in Cycloaddition," ed by D. P. Curran, JAI Press, Greenwich (1988), Vol. 1, pp. 129—189; S. Kanemasa and O. Tsuge, *Heterocycles*, **30**, 719 (1990).

2) G. Jones, "Pyridines and Their Benzo Derivatives: (V) Synthesis in Comprehensive Heterocyclic Chemistry," ed by A. R. Katritzky and C. W. Rees, Pergamon Press, Oxford (1984), Vol. 2, pp. 395—510.

3) M. D'Auria, A. D. Mico, F. D'Onofrio, and A. Scettri, *Synthesis*, **1985**, 988.

4) Oxidation of 1-phenyl-3-buten-1-ol with pyridinium dichromate (PDC) gives a mixture of 1-phenyl-3-buten-1-one (34%) and 1-phenyl-2-buten-1-one (28%).

5) In the nitrile oxide cycloadditions with O-unprotected allyl alcohols, 1 : 2 cycloadducts are often formed. This would be responsible for the low yield formation of 1 : 1 cycloadducts. For the reaction examples with O-protected allyl alcohols, see O. Tsuge, S. Kanemasa, and H. Suga, *Bull. Chem. Soc. Jpn.*, **61**, 2133 (1988).

6) M. Wada, H. Ohki, and K. Akiba, *Tetrahedron Lett.*, **27**, 4771 (1986).

7) T. Shimizu, Y. Hayashi, H. Shibafuchi, and K. Teramura, *Bull. Chem. Soc. Jpn.*, **59**, 2827 (1986).

8) T. Mukaiyama and T. Hoshino, *J. Am. Chem. Soc.*, **82**, 5339 (1960).

9) A. J. Mancuso, S.-L. Huang, and D. Swern, *J. Org. Chem.*, **43**, 2480 (1978).

10) D. P. Curran, *J. Am. Chem. Soc.*, **104**, 4024 (1982); **105**, 5826 (1983).

11) This mixture shows strong and broad signals in the methylene region in ^1H NMR spectrum, indicating the formation of overreduction products.

12) It was necessary to treat the crude product with aqueous ethylenediaminetetraacetic acid in order to liberate **5e** from the complex.

13) E. Wenkert, J. M. Hanna, Jr., M. H. Leftin, E. L. Michelotti, K. T. Potts, and D. Usifer, *J. Org. Chem.*, **50**, 1125 (1985).

14) M. Scholtz, *Ber.*, **32**, 1935 (1899).

15) F. Kroehnke, *Synthesis*, **1976**, 1.

16) M. Scholtz and W. Meyer, *Ber.*, **43**, 1861 (1910).

17) J. Meisenheimer, E. Stratmann, and W. Theilacker, *Ber.*, **65**, 418 (1932).

18) K. Loeffler and F. Thiel, *Ber.*, **42**, 132 (1909).

New Syntheses and Physical Properties of *p*-Alkylcalix[*n*]arenes

Seiji SHINKAI,* Takeshi NAGASAKI, Koji IWAMOTO, Atsushi IKEDA, G.-X. HE, Tsutomu MATSUDA, and Masakazu IWAMOTO†

Department of Organic Synthesis, Faculty of Engineering, Kyushu University, Fukuoka 812
†Department of Industrial Chemistry, Faculty of Engineering, Miyazaki University, Miyazaki 889-21

(Received September 12, 1990)

Calix[*n*]arenes (n=4, 6, and 8) bearing long *p*-alkyl groups (R=hexyl and dodecyl) have been synthesized by "direct" acylation of the *p*-position followed by silane reduction. The method is convenient and the yields are higher than those reported so far. Among them, *p*-hexanoylcalix[4]arene showed a curious phase transition behavior; with raising the temperature it changed as crystal A→liquid→crystal B→liquid. It was found on the basis of the solid ^{13}C NMR spectra that this behavior is ascribed to a conformational change from "cone" (crystal A) to "partial cone" (crystal B).

Calix[*n*]arenes having long aliphatic chains at *p*-position have been of increasing concern in host-guest chemistry and Langmuir monolayer formations.[1-3] They are synthesized by two different methods: (i) one-step synthesis by condensation of *p*-alkylphenols with formaldehyde[1,2,4,5] and (ii) three-step synthesis going from O-acylation of calix[*n*]arenes ($\mathbf{1}_n$) to the Fries rearrangement[6,7] followed by the Wolff-Kishner reduction[3] (Eq. 1). Method (i) is a convenient one-step synthesis, but one has to optimize the reaction conditions by himself so that one can obtain desired *n*-meric *p*-alkylcalix[*n*]arenes: that is, one has to look for the appropriate solvent, temperature, and separation conditions. Furthermore, attempts to synthesize *p*-alkylcalix[4]arenes failed.[3,5] In contrast, method (ii) involves three steps, but one can use well-characterized $\mathbf{1}_n$ as starting materials. Thus, these two methods have both merit and demerit.

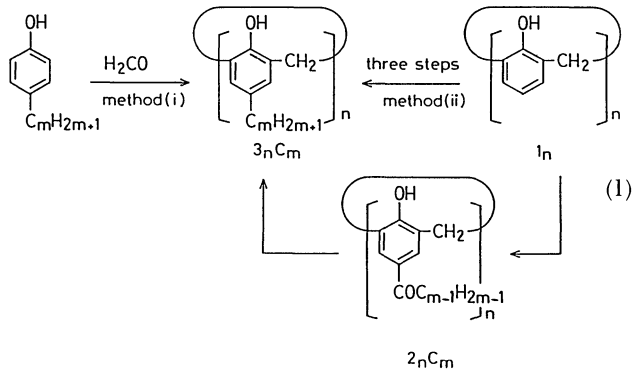

(1)

It occurred to us that if the acyl group could be "directly" introduced into the *p*-position of $\mathbf{1}_n$, one could shorten the reaction route for method (ii). In this paper we report "direct" acylation of $\mathbf{1}_n$ (n=4, 6, and 8) to *p*-acylcalix[*n*]arenes ($\mathbf{2}_n\mathrm{C}_m$) followed by reduction with triethylsilane to *p*-alkylcalix[*n*]arenes ($\mathbf{3}_n\mathrm{C}_m$). In addition, we found that some of these calix[*n*]arenes show very interesting solid and solution properties.

Experimental

Materials. Preparations of $\mathbf{1}_n$ were described previously.[8,9] We studied the Friedel-Crafts reaction of $\mathbf{1}_n$ with $\mathrm{C}_{m-1}\mathrm{H}_{2m-1}\mathrm{COCl}$ (m=6 and 12).

***p*-Hexanoylcalix[4]arene ($\mathbf{2}_4\mathrm{C}_6$).** Hexanoyl chloride (1.4 g; 10 mmol) and $AlCl_3$ (1.4 g; 10 mmol) was mixed in 30 ml of nitrobenzene, and after stirring for 30 min at room temperature under a nitrogen stream $\mathbf{1}_4$ (1.1 g; 2.5 mmol) was added. The reaction mixture was stirred at 50 °C for 10 h and then at 70 °C for 3 h. This operation afforded a homogeneous, brown solution. After cooling, the solution was poured into a 0.1 M# HCl solution (200 ml) and extracted with chloroform (200 ml). The organic layer was separated, washed with 1 M NaCl solution and dried over $MgSO_4$. The solution was concentrated to dryness, the resultant solid being reprecipitated from chloroform to methanol. Finally, the yellow solid product was recrystallized twice from benzene: white powder, mp 94—98 °C, yield 80%; IR (Nujol) ν_{OH} 3600—2500 cm^{-1}, $\nu_{C=O}$ 1680 cm^{-1}; ^{1}H NMR ($CDCl_3$, 30 °C) δ_H=0.6—2.0 (9H, C_4H_9), 2.6—3.0 (2H, CH_2CO), 3.7—4.2 (2H, broad, $ArCH_2Ar$), 7.70 (2H, ArH), 9.5—10.5 (1H, broad, OH).

Other $\mathbf{2}_n\mathrm{C}_m$'s were synthesized in a manner similar to that for $\mathbf{2}_4\mathrm{C}_6$. The reaction conditions, yields, and mp's are summarized in Table 1. The elemental analysis data are recorded in Table 2.

***p*-Hexylcalix[4]arene ($\mathbf{3}_4\mathrm{C}_6$).** Compound $\mathbf{2}_4\mathrm{C}_6$ (0.50 g; 0.60 mmol) was dissolved in 20 ml of trifluoroacetic acid, and triethylsilane (0.70 g; 6.0 mmol) was added dropwise to this solution. The exothermic reaction was initiated immediately after the addition of triethylsilane. After stirring for 10 h at room temperature, the solution was concentrated in vacuo. The residue was dissolved in chloroform and the solution was washed with aqueous $NaHCO_3$. The organic layer was separated and dried over Na_2SO_4. The chloroform solution was concentrated to dryness, the residue being recrystallized from ethanol: white plates, mp 108—109 °C, yield 66%; IR (Nujol) ν_{OH} 3500—2500 cm^{-1}, no $\nu_{C=O}$; ^{1}H NMR ($CDCl_3$, 30 °C) δ_H=0.6—1.9 (11H, C_5H_{11}), 2.2—2.6 (2H, CH_2Ar), 3.2—3.4 (2H, broad, $ArCH_2Ar$), 6.80 (2H, ArH), 10.10 (1H, OH).

1 M=1 mol dm^{-3}.

Other $\mathbf{3}_n\mathrm{C}_m$'s were synthesized in a manner similar to that for $\mathbf{3}_4\mathrm{C}_6$. Compounds $\mathbf{2}_n\mathrm{C}_{12}$ were less reactive than $\mathbf{2}_n\mathrm{C}_6$ and required the more drastic reaction conditions (e.g., reflux for 100 h). The reaction conditions, yields, and mp's are summarlzed in Table 3. The products were recrystallized either from ethanol or ethanol-$CHCl_3$ (or CCl_4). The elemental analysis data are recorded in Table 4.

25,26,27,28-Tetrapropoxy-*p*-hexanoylcalix[4]arene (with a Partial Cone Conformation: $\mathbf{4}_4\mathrm{C}_6$). Compound $\mathbf{2}_4\mathrm{C}_6$ (200 mg; 0.245 mmol) and propyl bromide (1.21 g; 9.81 mmol) were dissolved in 30 ml of DMF and the solution was stirred at 50 °C for 6 h in the presence of Cs_2CO_3 (3.47 g; 9.81 mmol). The HPLC analysis showed that the product contains 90% of partial-cone-$\mathbf{4}_4\mathrm{C}_6$ and 10% of another isomer (probably, cone-$\mathbf{4}_4\mathrm{C}_6$). The solution was filtered, the filtrate being diluted with water. The aqueous solution was extracted with chloroform. The chloroform solution was concentrated to dryness. The residue was viscous oil. This was subjected to preparative TLC separation (silica gel, chloroform-hexane): caramel-like solid (an attempt to crystallize this solid failed), yield 50%, single peak on HPLC; ^{1}H NMR ($CDCl_3$, 30 °C) δ=0.9—1.2 (56H, m, CH_3CH_2 in *n*-Pr and $CH_3(CH_2)_3$), 3.02, 3.61, 3.81 (4H, 2H, 2N (respectively), q each, OCH_2), 2.26, 2.54, 3.87 (2H, 4H, 2H (respectively), t each, $COCH_2$), 3.19, 3.73, 3.78, 4.07 (2H each, d each, $ArCH_2Ar$), 6.84, 7.60, 7.81, 7.94 (2H each, d, d, s, s (respectively), ArH). Found: C, 77.53; H, 9.01%. Calcd for $(C_{16}H_{22}O_2)_4$: C, 78.00; H, 9.00%.

A partial cone conformation results in three different phenol units. The situation is reflected by OCH_2 and $COCH_2$ which appear as three peaks in an integral intensity ratio of 2:1:1. The $ArCH_2Ar$ protons in a partial cone conformation feature two pairs of doublets:[10] one pair with the large chemical shift difference (3.19 and 4.07 ppm in $\mathbf{4}_4\mathrm{C}_6$) is ascribed to those flanked by two syn phenol units (H_{exo} and H_{endo}, respectively) and another pair with the small chemical shift difference (3.73 and 3.78 ppm in $\mathbf{4}_4\mathrm{C}_6$) is ascribed to those flanked by two anti phenol units. These results consistently support the partial cone conformation. The peaks for OCH_2 appear as quartets. This is probably due to the rotational restriction of the OCH_2 group.

^{13}C NMR Spectra. The solid-state ^{13}C NMR spectra were measured with a Bruker PC-250. The ^{13}C cross polarization-magic angle spinning NMR spectra were recorded at 30 °C with a CP-MAS method: the crystalline powder sample was contained in a bullet-type rotor and spun at 3.5 kHz. Contact time was 3 ms and repetition time was 5 s. The ^{13}C chemical shifts were calibrated indirectly through external TMS.

Results and Discussion

As mentioned in Introduction, *p*-alkylcalix[4]arenes cannot be synthesized from formaldehyde and *p*-alkylphenols.[3,5] Thus, they have been synthesized through three steps: that is, tetra-O-acylation, Fries rearrangement, and reduction. According to Gutsche and Lin,[10] acetylation and benzoylation of $\mathbf{1}_n$ occur in 23—38% yields. We could enhance the yields for acylation (using hexanoyl chloride and 2-methylbutanoyl chloride) up to 50—51%.[7] On the other hand, Fries rearrangement occurs in 29—64% yields.[6,7] This means that the total yields of these two steps are at most 30%. As shown in Table 1, on the other hand, "direct" acylation of the *p*-position results in $\mathbf{2}_n\mathrm{C}_m$ in 30—88% yields. Thus, the present method is much superior to the previous method.

It is known that O-acylation of $\mathbf{1}_n$ can be effected even at 0 °C whereas Fries rearrangement proceeds at 70—100 °C.[6,7,10] In the present "direct" acylation method, the products were yielded when the solution was heated at 70 °C. When the reaction temperature was not raised, the product gave the $\nu_{C=O}$ band at 1760 cm^{-1} which is assigned to the ester group. This suggests that the present "direct" acylation actually occurs via O-acylation followed by Fries rearrangement. These two steps proceed in one pot.

According to Nakamoto et al.,[3] $\mathbf{2}_4\mathrm{C}_8$ could be reduced to $\mathbf{3}_4\mathrm{C}_8$ by the Wolff-Kishner method in 70% yield. We found, however, that this method is troublesome because in the reducetion of $\mathbf{2}_4\mathrm{C}_m$ the solution foamed over in the flask. As an alternate

Table 2. Elemental Analysis Data for $\mathbf{2}_n\mathrm{C}_m$

$\mathbf{2}_n\mathrm{C}_m$		Found/%		Calcd/%		
n	*m*	C	H	for	C	H
4	6	76.69	7.85[a]	$(C_{13}H_{16}O_2)_4$	76.44	7.89
4	12	79.26	9.26	$(C_{19}H_{28}O_2)_4$	79.12	9.78
6	6	75.61	7.76	$(C_{13}H_{16}O_2)_6 \cdot 0.1\ CCl_4$	75.59	7.80
6	12	79.10	9.68	$(C_{19}H_{28}O_2)_6$	79.12	9.78
8	6	73.87	7.58	$(C_{13}H_{16}O_2)_8 \cdot 0.4\ CCl_4$	73.95	7.61
8	12	77.81	9.39	$(C_{19}H_{28}O_2)_8 \cdot 0.8\ CHCl_3$	78.07	9.65

a) Recrystallized from benzene.

Table 1. Reaction Conditions for the Synthesis of $\mathbf{2}_n\mathrm{C}_m$

$\mathbf{1}_n$		$C_{m-1}H_{2m-1}COCl$		$AlCl_3$	Yield of $\mathbf{2}_n\mathrm{C}_m$	Mp of $\mathbf{2}_n\mathrm{C}_m$
n	Concn/mmol	*m*	Concn/mmol	mmol	%	°C
4	2.5	6	10	10	80	94—98
6	2.5	6	15	15	52	>310
8	2.5	6	20	20	88	310
4	2.5	12	10	10	60	130—133
6	2.5	12	15	15	62	>310
8	2.5	12	20	20	30	>310

Table 3. Reaction Conditions for the Synthesis of $\mathbf{3}_n\mathrm{C}_m$

$\mathbf{2}_n\mathrm{C}_m$			Et_3SiH	CF_3COOH	Yield of $\mathbf{3}_n\mathrm{C}_m$	Mp of $\mathbf{3}_n\mathrm{C}_m$
n	*m*	Concn/mmol	mmol	ml	%	°C
4	6	0.60	6.0	20	66	108—109
4	12	0.50	10	20	55	98—100
6	6	0.25	10	20[a)]	54	249—250
6	12	0.60	20	30[b)]	52	168—169
8	6	0.70	20	30	50	>300
8	12	0.28	10	20[a)]	81	>300

a) CCl_4 (20 ml) was added. b) CCl_4 (30 ml) was added.

Table 4. Elemental Analysis Data for $\mathbf{3}_n\mathrm{C}_m$

$\mathbf{3}_n\mathrm{C}_m$		Found/%		Calcd/%		
n	*m*	C	H	for	C	H
4	6	81.74	9.57	$(C_{13}H_{18}O)_4 \cdot 0.1$ EtOH	81.88	9.56
4	12	82.73	11.14	$(C_{19}H_{30}O)_4$	83.15	11.02
6	6	80.23	9.31	$(C_{13}H_{18}O)_6 \cdot 0.2\ CCl_4$	80.10	9.28
6	12	83.05	10.92	$(C_{19}H_{30}O)_6$	83.15	11.02
8	6	81.06	9.30	$(C_{13}H_{18}O)_8 \cdot 0.6\ CHCl_3$	80.98	9.39
8	12	81.58	10.57	$(C_{19}H_{30}O)_8 \cdot 0.3\ CCl_4$	81.60	10.79

method, we employed the silane reduction method. Although the yields (55—81%) are not significantly higher than those for the Wolff-Kisher method, the operation is very simple and convenient.

$\mathbf{2}_n\mathrm{C}_m$ and $\mathbf{3}_n\mathrm{C}_m$ thus synthesized showed several interesting physical properties. First, $\mathbf{2}_8\mathrm{C}_{12}$ gellated when recrystallized from benzene, toluene, hexane, heptane, etc.: that is, the solution was apparently solidified. Thus, this compound was recrystallized from ethanol-chloroform (3 : 1 v/v). Such gelation was not found for other $\mathbf{2}_n\mathrm{C}_m$.

More interesting is a phase transition phenomenon of $\mathbf{2}_4\mathrm{C}_6$. As shown in Scheme 1, crystal A (K_A) obtained by recrystallization from benzene melts at 95 °C. From the isotropic liquid phase (I_1) new crystals (K_B) grow up rapidly, which finally melt at 194 °C. When the final isotropic liquid (I_2) is cooled, crystal B results. Only when crystal B is recrystallized from benzene, crystal A is reproduced.

Figure 1 shows a DSC thermogram of $\mathbf{2}_4\mathrm{C}_6$. It is

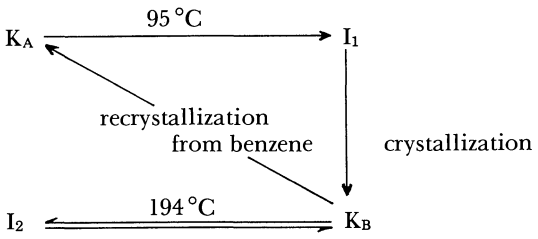

Scheme 1.

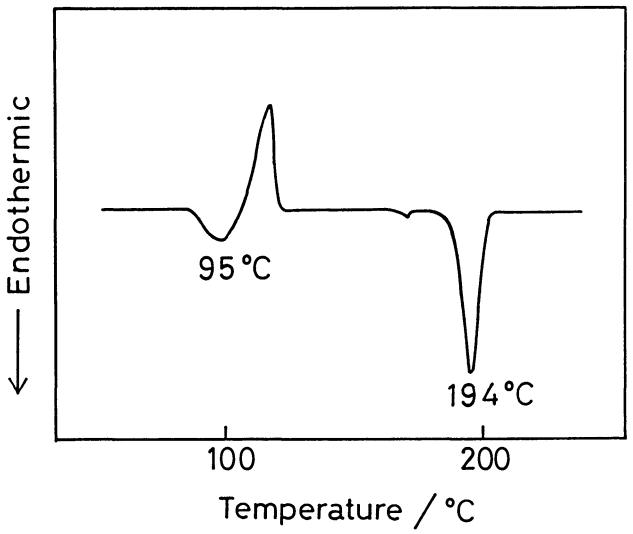

Fig. 1. DSC thermogram of $\mathbf{2}_4\mathrm{C}_6$.

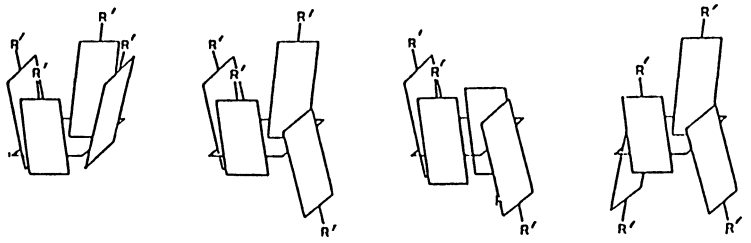

Cone Partial cone 1,2-Alternate 1,3-Alternate

Fig. 2. Four conformational isomers possible for calix[4]-arenes.

seen from Fig. 1 that an endothermic change occurs at 95 °C, which is immediately followed by an exothermic change. These changes correspond to melting of K_A at 95 °C followed by recrystallization to K_B. An endothermic peak at 194 °C corresponds to melting of K_B to I_2. We attempted the preparation of single crystals for X-ray analysis from K_A and K_B but failed. We thus evaluated the structures of these crystals using the solid-state ^{13}C NMR spectroscopy.

Basically, calix[4]arenes can exist in four different conformations; they are cone, partial cone, 1,2-alternate, and 1,3-alternate (Fig. 2). X-ray studies of *p-t*-butylcalix[4]arene and some clathrates show the calixarene moiety to be present in a cone conformation with C_{4v} symmetry.[11-13] Since each phenol unit is equivalent around a 4-fold axis, the CP-MAS ^{13}C NMR should result in a single set of ^{13}C peaks for the phenol unit. Other three conformations have never been found for unmodified calix[4]arenes not only in solution but also in the solid state.[14] One can predict on the basis of their symmetry that partial cone, 1,2-alternate, and 1,3-alternate should give three sets, a single set (but two sets for the $ArCH_2Ar$ methylene carbons), and a single set (including the $ArCH_2Ar$ methylene carbons) of ^{13}C peaks for four phenol units, respectively. To test this hypothesis, we prepared tetra-O-propyl derivative ($\mathbf{4}_4C_6$) with a partial cone conformation from $\mathbf{2}_4C_6$ (Eq. 2).[14] It has been established that being different from unmodified calix[4]-arenes, the propyl group is bulky enough to suppress the oxygen-through-the-annulus rotation and thus tetra-O-propylated calix[4]arene results in conformationally-immobile isomers.[15] As shown in Fig. 3, the ^{13}C NMR spectrum for partial-cone-$\mathbf{4}_4C_6$ is very complex. It is clearly seen from Fig. 3, however, that there appear three peaks for CO (C-6 in Fig. 3) and O-C (in phenyl: C-10 in Fig. 3). This establishes that as predicted from its symmetry, ^{13}C NMR for the partial

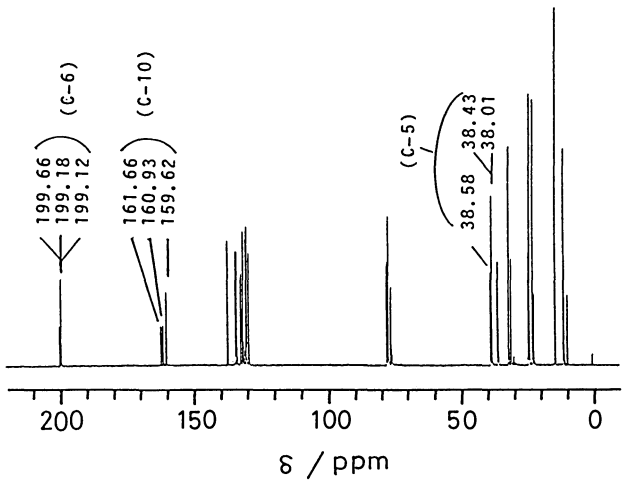

Fig. 3. ^{13}C NMR spectrum of partial-cone-$\mathbf{4}_4C_6$ ($CDCl_3$, 30 °C).

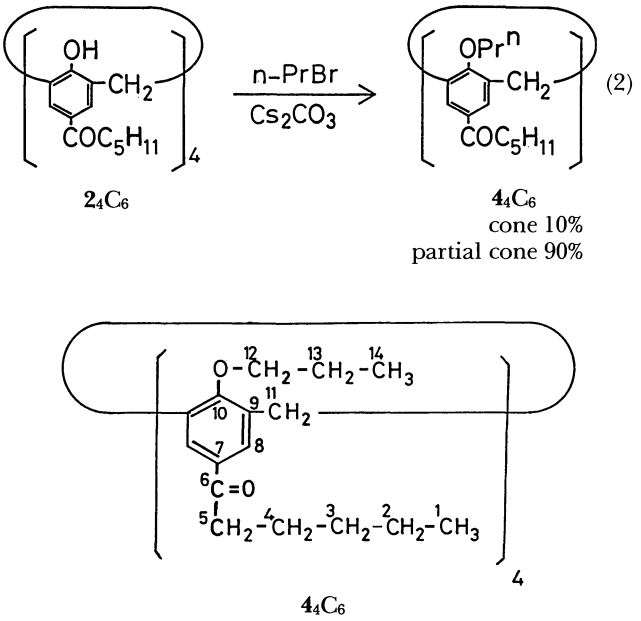

$\mathbf{4}_4C_6$

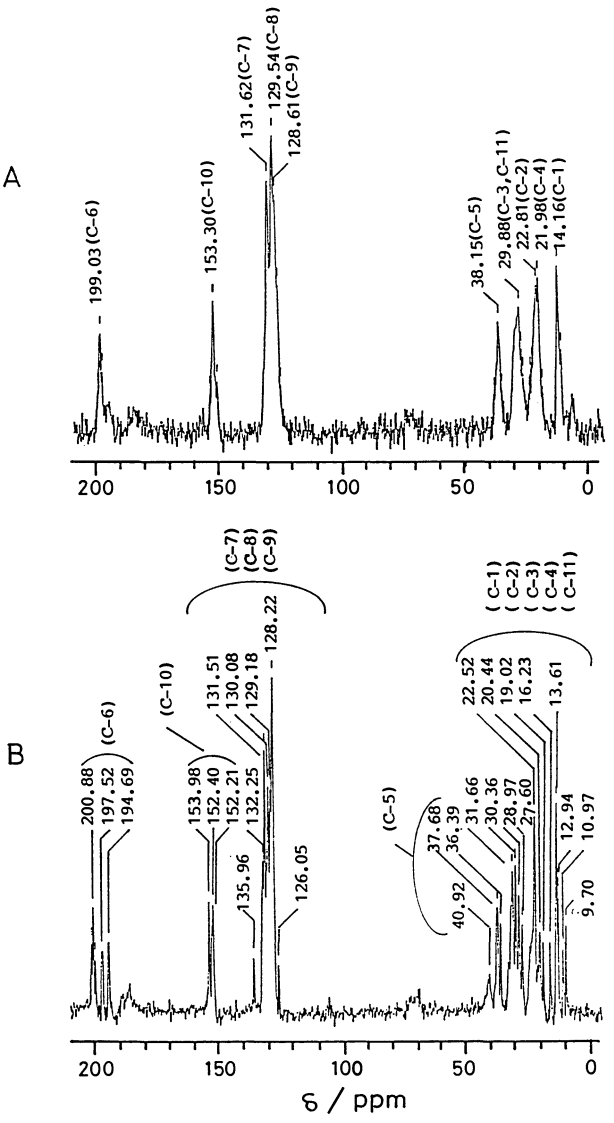

Fig. 4. CP-MAS ^{13}C NMR spectra of (A) crystal A and (B) crystal B. The numbering system is the same as that in Fig. 3.

cone isomer features three sets of ^{13}C peaks.

In Fig. 4, CP-MAS ^{13}C NMR spectra for crystals A and B are illustrated. As expected, crystal A, crystallized from benzene solution, gave a single set of ^{13}C peaks for C-6 and C-10. This provides evidence that crystal A adopts a cone conformation. In contrast, crystal B, which crystallized above 95 °C, gave three sets of ^{13}C peaks for C-6 and C-10. This split pattern is basically commensurate with a partial cone conformation. In the solid state, however, one has to take the presence of noncongruent molecules into consideration: for example, the asymmetry in the solid-state ^{13}C NMR spectra may result from noncongruence in the crystal lattice or from slight distortion of the calix[4]arene ring.[16] Thus, we further confirmed the difference between crystals A and B through IR measurements which possibly reflect the intramolecular structural difference rather than the intermolecular one. Unmodified calix[4]arenes (that is, those having four OH groups) adopt a cone conformation not only in solution but also in the solid state.[10-13,17-19] The exception against this conclusion has never been found. This is due to a large stabilization effect brought forth by intramolecular hydrogen-bonding interactions among OH groups. Hence, compounds $\mathbf{2}_4C_n$ should adopt a cone conformation in the solid state. The FT-IR spectra (KBr, at room temperature) of these compounds showed only one $\nu_{C=O}$ band at around 1680 cm^{-1}: for instance, the $\nu_{C=O}$ for crystal A appeared at 1675 cm^{-1}. In contrast, crystal B showed three $\nu_{C=O}$ bands at 1670, 1679, and 1684 cm^{-1}. This indicates that compound $\mathbf{2}_4C_6$ in crystal B has three different C=O groups which are commensurate with a partial cone conformation. Partial-cone-$\mathbf{4}_4C_6$, synthesized as a reference compound for crystal B also showed three $\nu_{C=O}$ bands at 1671, 1679, and 1689 cm^{-1}. The results, together with those of the ^{13}C NMR spectra, consistently support the view that $\mathbf{2}_4C_6$ in crystal B is a partial-cone conformer.

As described above, calix[4]arenes favorably adopt a cone conformation because of strong intramolecular hydrogen-bonding interactions.[10,17-19] This view is supported not only by X-ray studies[11-13] but also by recent computational studies.[20] To isomerize to other conformers, one or two hydrogen bonds must be cleaved, which causes destabilization of the calix[4]arene ring.[20] Above 95 °C the stabilization effect through hydrogen bonds becomes less important because of a vigorous molecular motion and a cone isomer can isomerize to a partial cone isomer. In the partial cone isomer, one phenol unit is inversed and the hydrogen-bonding interaction with this OH group is disrupted. Instead, the partial cone isomer acquires a flexible seesaw motion around the inversed phenol unit. Probably, this motional freedom is more important than the stabilization by hydrogen bonds above 95 °C. According to the molecular mechanics calculations about *p*-*t*-butylcalix[4]arene, total E values for the cone isomer and the partial cone isomer are -2.0 and 5.7 kcal mol^{-1}, respectively.[20] This supports the view that the concentration of the partial cone isomer increases with raising the temperature. Anyhow, this is the first example for a partial cone isomer of unmodified calix[4]arenes found in the solid state.

In conclusion, the present paper demonstrated new syntheses of *p*-alkylcalix[4]arenes and their interesting physical properties. In particular, the finding of partial-cone-$\mathbf{2}_4C_6$ in the solid state is noteworthy. Further applications of these calixarenes to T_1 measurements, monolayer formations, etc. are currently investigated in these laboratories.

This research was supported by the Grant-in-Aid from the Ministry of Education, Science and Culture.

References

1) S. Shinkai, H. Kawabata, T. Arimura, T. Matsuda, H. Satoh, and O. Manabe, *J. Chem. Soc., Perkin Trans. 1*, **1989**, 1073.

2) S. Shinkai, T. Arimura, K. Araki, H. Kawabata, H. Satoh, T. Tsubaki, O. Manabe, and J. Sunamoto, *J. Chem. Soc., Perkin Trans. 1*, **1989**, 2039.

3) Y. Nakamoto, G. Kallinowski, V. Böhmer, and W. Vogt, *Langmuir*, **5**, 1116 (1989).

4) Y. Nakamoto, T. Ozu, S. Ohya, and S. Ishida, *Netsu Kohkasei Jushi*, **6**, 51 (1985).

5) Z. Asfai and J. Vicens, *Tetrahedron Lett.*, **29**, 2659 (1988).

6) K. No, Y. Noh, and Y. Kim, *Bull. Korean Chem. Soc.*, **7**, 442 (1986).

7) T. Arimura, S. Shinkai, T. Matsuda, Y. Hirata, H. Satoh, and O. Manabe, *Bull. Chem. Soc. Jpn.*, **61**, 3733 (1988).

8) S. Shinkai, S. Mori, H. Koreishi, T. Tsubaki, and O. Manabe, *J. Am. Chem. Soc.*, **108**, 2409 (1986).

9) S. Shinkai, K. Araki, T. Arimura, and O. Manabe, *J. Chem. Soc., Perkin Trans. 1*, **1987**, 2297.

10) C. D. Gutsche and L.-G. Lin, *Tetrahedron*, **42**, 1633 (1986).

11) C. D. Andreetti, R. Ungaro, and A. Pochini, *J. Chem. Soc., Chem. Commun.*, **1979**, 1005.

12) G. D. Andreetti, A. Pochini, and R. Ungaro, *J. Chem. Soc., Perkin Trans. 2*, **1983**, 1773.

13) R. Ungaro, A. Pochini, G. D. Andreetti, and P. Domiani, *J. Chem. Soc., Perkin Trans. 2*, **1985**, 197.

14) When bulky substituents are introduced into the OH groups, calix[4]arenes provide conformational isomers because of inhibition of the oxygen-through-the-annulus rotation. However, the conformation other than cone has never been found for unmodified calix[4]arene. For the synthesis and characterization of conformatinally-immobile calix[4]arenes with tetra-O-substituents see Refs. 15—18.

15) K. Araki, K. Iwamoto, S. Shinkai, and T. Matsuda, *Chem. Lett.*, **1989**, 1747.

16) This possibility was raised by the referee of this paper. Although the presence of non-congruent molecules is not ruled out "completely", the ^{13}C NMR and FT-IR data both

support the view that the asymmetry observed for crystal B is explicable on the basis of a partial cone conformation.

17) C. D. Gutsche, *Acc. Chem. Res.*, **16**, 161 (1983).

18) C. D. Gutsche and L. J. Bauer, *J. Am. Chem. Soc.*, **107**, 6052, 6059 (1985).

19) S. Shinkai, *Pure Appl. Chem.*, **58**, 1523 (1986).

20) P. D. Grootenhuis, P. A. Kollman, L. C. Groenen, D. N. Reinhoudt, G. J. van Hummel, F. Ugozzoli, and G. D. Andreetti, *J. Am. Chem. Soc.*, **112**, 4165 (1990).

 © 1991 The Chemical Society of Japan Bull. Chem. Soc. Jpn., 64, 387—391 (1991)

Asymmetric Diels-Alder Reactions of an Acrylic Acid Derivative Using a Chiral Titanium Catalyst

Koichi NARASAKA,* Hiroko TANAKA, and Fumihiko KANAI
Department of Chemistry, Faculty of Science, The University of Tokyo, Hongo, Bunkyo-ku, Tokyo 113
(Received September 26, 1990)

Asymmetric Diels-Alder reactions of an acrylic acid derivative using a catalytic amount of a chiral titanium reagent were performed with several dienes. The titanium catalyst was prepared by the alkoxy exchange between dichlorodiisopropoxytitanium(IV) and a chiral 1,4-diol derived from (2*R*,3*R*)-tartrate. By the use of the titanium catalyst, the reaction between 3-acryloyl-1,3-oxazolidin-2-one and dienes proceeded in a toluene-petroleum ether mixture in the presence of Molecular Sieves 4A to afford the Diels-Alder adducts in 72—100% yields and 88—>96% enantioselectivity. This reaction can be applied to a diene containing a hetero atom such as 2-ethylthio-1,3-butadiene, which affords the Diels-Alder adduct in a high optical purity. In this paper are also described the methods for determining the optical purities of the obtained 4-substituted 3-cyclohexenecarboxylic acid derivatives.

Diels-Alder reaction is one of the most important reaction for the formation of carbon frameworks in a variety of organic compounds, and has been widely used as a key step in the synthesis of many kinds of natural products. Development of asymmetric Diels-Alder reaction has been in active research,[1] however, the catalytic reaction with a wide applicability and a high enantioselectivity is scarce.

In our laboratory, the exploration of asymmetric reactions, including asymmetric Diels-Alder reaction, has been investigated using a chiral titanium catalyst prepared by an alkoxy exchange between a tartrate derived 1,4-diol (**1**) and dichlorodiisopropoxytitanium(IV) (Eq. 1).[2]

1 2 (1)

We have already found that when 3-(2-alkenoyl)-1,3-oxazolidinone derivatives were used as dienophiles, the reaction with several dienes proceeded in a toluene-petroleum ether (P.E.) mixture in the presence of a catalytic amount of the titanium catalyst and Molecular Sieves (MS) 4A to yield the Diels-Alder adducts in more than 90% enantiomeric excess (ee).[3]

The Diels-Alder adducts of acrylic acid derivatives constitute an important class of compounds as key intermediates for the total synthesis of a variety of natural products.[4] The catalytic asymmetric Diels-Alder reaction was also performed with 3-acryloyl-1,3-oxazolidin-2-one (**3**). However, the only result obtained so far was the reaction carried out in toluene, which afforded the Diels-Alder adduct **4** with cyclopentadiene in only 65% ee[5] and the reaction had never been carried out in the mixed solvent (toluene-petroleum ether (P.E.)) which has been found to be the most suitable solvent in the reaction of other α,β-unsaturated carboxylic acid derivatives.[3] Therefore some modifications in the reaction conditions have to be made to obtain synthetically useful 4-substituted 3-cyclohexenecarboxylic acid derivatives in high optical purities.

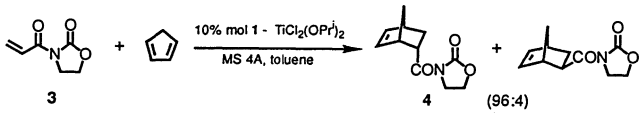

3 4 (96:4) 65% ee (2)

At the same time there arose a need for the development of a method for determining the accurate optical purities of the obtained Diels-Alder adducts, the 4-substituted 3-cyclohexenecarboxylic acid derivatives, since the method for the determination of the optical purities of these products was limited to transforming them to some compounds whose optical rotations are known.[6,7] Such a method lacks in accuracy especially when the enantioselectivities are very high.

In this paper, the reaction conditions using an acrylic acid derivative **3** were optimized to give the Diels-Alder adducts in good to high enantioselectivity, and the method for determining accurate optical purities of the adducts has been developed.

First, the reactions of **3** and several dienes were performed in a mixed solvent of toluene or xylene and P.E. in the presence of MS 4A. (Eq. 3) The results are

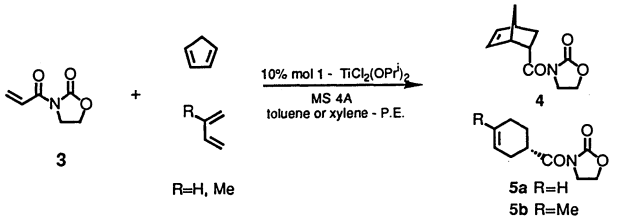

3 R=H, Me 4 5a R=H 5b R=Me (3)

Table 1. Diels-Alder Reaction Using a Catalytic Amount of **1**

Diene	Solvent	Temp, θ/°C	Time	Yield/%	Opt. purity/%ee
Cyclopentadiene	Toluene-P.E.(1 : 1)	−23	24 h	81(12)[a]	88
	p-Xylene-P.E.(1 : 1)	0	3 h	96	75
	m-Xylene-P.E.(1 : 1)	0	12 h	Quant	82
Isoprene	Toluene-P.E.(1 : 1)	0	24 h	89	>96
	p-Xylene-P.E.(1 : 1)	0	12 h	93	>96
	m-Xylene-P.E.(1 : 1)	0	12 h	90	>96
Butadiene	Toluene-P.E.(1 : 1)[b]	RT	6 d	31(46)	88
	p-Xylene-P.E.(1 : 1)[c]	RT	24 h	81	93
	m-Xylene-P.E.(1 : 1)[c]	RT	2 d	67	89

a) Amount of the recovered **3** is shown in ( ). b) 10 mol% catalyst was used. c) 20 mol% catalyst was used.

listed in Table 1.

By the use of a mixed solvent, toluene-P.E. (1 : 1), the reaction of **3** with cyclopentadiene proceeded at −23 °C in the presence of 10% mol of the chiral titanium reagent and MS 4A to give the cycloadduct **4**. Only the endo isomer **4** was obtained and the optical purity of the obtained adduct was found to be greatly enhanced from 65 to 88% ee. In the reaction with 1,3-butadiene, the best result was observed when the reaction was carried out at room temperature in a *p*-xylene-P.E. (1 : 1) mixed solvent using 20% mol of the chiral catalyst, and the optical purity of the adduct **5a** was 93% ee. The reaction with isoprene proceeded at 0 °C using 10% mol of the chiral catalyst and the optical purity of the adduct **5b** was over 96% ee in either toluene-P.E. or xylene-P.E. mixed solvent. In this case too, the obtained cycloadduct consisted of a single isomer and none of the other regio-isomer could be detected. After all, the use of toluene or xylene in the mixed solvent made little or no influence on the optical purity of the obtained product. When 2 molar amounts of the chiral titanium catalyst were used, the reaction proceeded at lower temperatures, but that does not alter the enantioselectivity to a great extent. Next, to obtain a masked cyclohexanone derivative, which is an important synthetic intermediate, the reactions of dienes with a hetero atom were examined. 2-*t*-Butyldimethylsiloxy-1,3-butadiene (**6a**)[8] and 2-methoxy-1,3-butadiene (**6b**)[9] were employed as dienes, but the reaction did not proceed well. With **6a**, the titanium seemed to exchange with the silyl part of the diene and therefore the reaction did not proceed. With **6b**, decomposition of the diene took place prior to the Diels-Alder reaction. 2-Ethylthio-1,3-butadiene (**6c**)[10] containing a sulfur atom instead of an oxygen atom was then examined. With **6c**, the acryloyloxazolidinone **3** reacted smoothly at 0 °C within 2 h in a toluene-P.E. (1 : 1) mixed solvent to afford the adduct **7** in 72% yield and in 91% optical purity along with cyclobutanes **8a** and **8b** (Eq. 4). The *trans* **8a** and *cis* **8b** isomers of the cyclobutane were obtained in 15 and 6% yields, respectively,

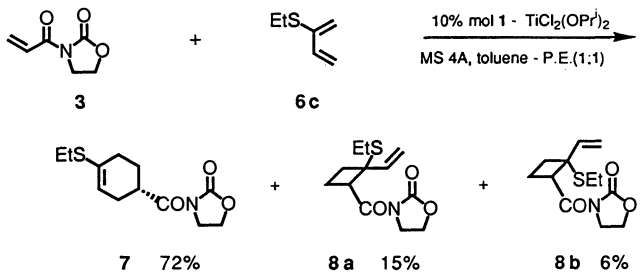

(4)

which are the [2+2] cycloaddition products as we have already reported in the cycloaddition reaction between α,β-unsaturated carbonyl compounds and a ketene dithioacetal, an alkenyl sulfide and an alkynyl sulfide.[11] The obtained Diels-Alder adduct **7** has a vinyl sulfide group, which is easily transformed to some other functional groups.

As mentioned in the beginning, the precise optical purity of the obtained Diels-Alder products, 4-substituted 3-cyclohexenecarboxylic acid derivatives, had never been determined. The optical purities of the cyclohexenecarboxylic acid derivatives **5a** and **5b** prepared above were determined after transformation to the epoxy derivative **12** based on the following Scheme 1.

First the adducts **5a** and **5b** were hydrolyzed to the corresponding carboxylic acids after they were transformed into their methyl esters. The iodolactonization of the carboxylic acids followed by the treatment with sodium methoxide gave the corresponding *cis*-epoxy carboxylic esters (**12a,b**). The optical purities were determined by adding a chiral shift reagent Eu(hfc)$_3$[12] and analyzing their NMR. The methoxyl

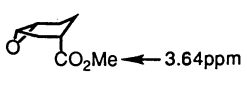

12a

Fig. 1.

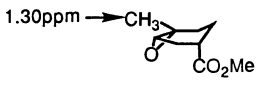

12b

Fig. 2.

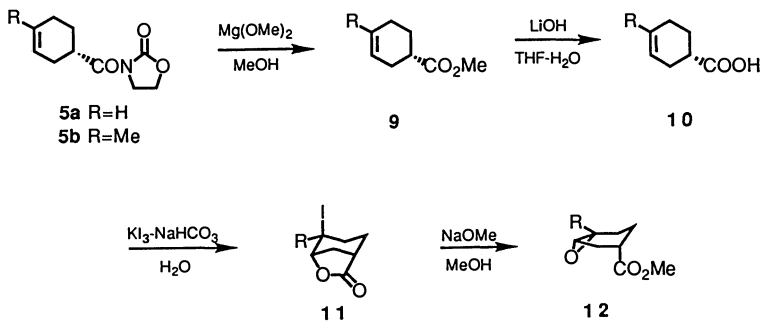

Scheme 1.

peak (δ=3.64) of **12a** (Fig. 1), and the methyl peak (δ=1.30) of **12b** (Fig. 2) were used to determine the optical purities.

The optical purity of the norbornene derivative **4**, was determined by the Mosher's method[13] after the adduct was esterified and reduced with $LiAlH_4$.

In the case of **7**, the product was first transformed into its (+)-trifluoromethylmethoxyphenylacetic acid (MTPA) ester and then the sulfide **13** was oxidized to the sulfone **14** by hydrogen peroxide and $(NH_4)_6Mo_7O_{24}$ catalyst (Eq. 5).[14] Its optical purity was determined by measuring the ^{13}C NMR spectrum. The peak of the chiral center of the cyclohexene ring (δ=32)[15] separated completely.

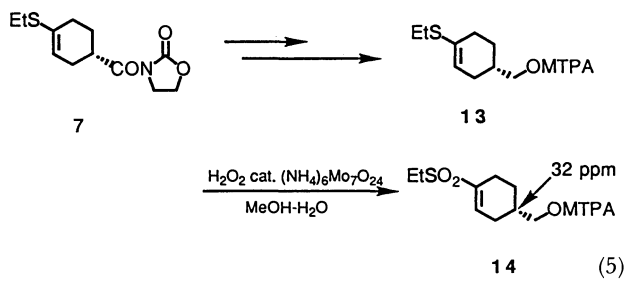

(5)

The absolute configuration of the norbornene derivative **4** was determined by the comparison of its optical rotation with those of the literatures.[3] For the cyclohexene derivatives **5a** and **5b** the obtained adducts were transformed to their benzyl (in the case of **5a**) or methyl (in the case of **5b**) esters and their optical rotations were measured and compared with those of the literatures.[6,7]

Combined with the results of the previous paper,[3] the absolute stereoselection of the Diels-Alder reaction is predictable without any exceptions according to the transition model as depicted in Fig. 3. The chiral titanium species is thought to form a six-membered chelate with 3-acyl-1,3-oxazolidin-2-one, which exists in a pseudo C_2 symmetrical twist chair conformation. The axial phenyl groups in the seven-membered ring orient to the reaction site and restrict the approach of a diene. Therefore, *re*-face of the α-carbon of the unsaturated acid moiety is attacked preferentially in both of the possible transition states shown in Fig. 3, when the (2*R*,3*R*)-1,4-diol is employed as a chiral auxiliary.

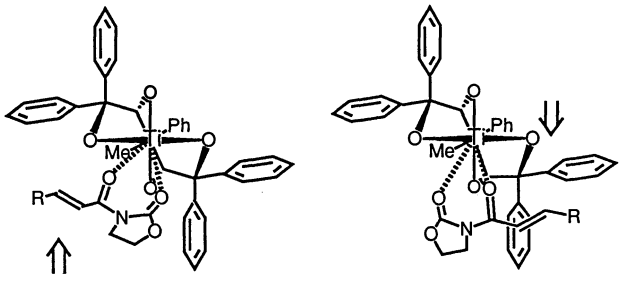

Fig. 3.

In summary, the Diels-Alder reaction of acrylic acid derivative using a catalytic amount of the chiral titanium reagent proceeded to produce the adducts in good yields and in good enantioselectivities. The reaction was carried out in a toluene-P.E.(1 : 1) mixed solvent in the presence of MS 4A. This catalytic asymmetric Diels-Alder reaction totally offers a practical and a convenient method for the preparation of variously substituted 3-cyclohexenecarboxylic acids via 3-alkenoyl-1,3-oxazolidin-2-one in general.

Experimental

General. NMR spectra were recorded on a Hitachi R24B or Bruker AM 500 spectrometer using tetramethylsilane as the internal standard. IR spectra were recorded on a Horiba FT-300S. Optical rotation was measured with a Nippon Bunko DIP-370. Mass spectra were obtained with a JEOL JMS-D300 mass spectrometer.

Dichlorodiisopropoxytitanium was prepared from titanium(IV) chloride and titanium(IV) isopropoxide according to the literature method.[16] Toluene was distilled and dried over MS 4A. Xylenes were distilled from CaH_2 and stored over MS 4A. Tetrahydrofuran was freshly distilled from sodium diphenylketyl.

(2*R*,3*R*)-1,1,4,4-tetraphenyl-2,3-*O*-(1-phenylethylidene)-1,2,3,4-butanetetrol (**1**) and 3-acryloyl-1,3-oxazolidin-2-one (**3**) were prepared according to the literature procedures.[3,7]

Preparation of 2-Ethylthio-1,3-butadiene (6c). 2-Ethylthio-1,3-butadiene was synthesized according to the literature procedure.[10] The crude product was purified by

column chromatography using pentane as an eluent (37% yield). ^{1}H NMR ($CDCl_3$) δ=1.31 (t, 3H, J=7.4 Hz), 2.77 (q, 2H, J=7.4 Hz), 5.02 (s, 1H), 5.17 (d, 1H, J=10.0 Hz), 5.33 (s, 1H), 5.54 (d, 1H, J=17.2 Hz), and 6.44 (dd, 1H, J=10.0, 17.2 Hz).

Asymmetric Diels-Alder Reaction. General Procedure for the Reaction Using a Catalytic Amount of the Titanium Reagent. The reaction of 3-acryloyl-1,3-oxazolidin-2-one (**3**) with isoprene is outlined. To a toluene (4 ml) solution of dichlorodiisopropoxytitanium (145 mg, 0.611 mmol) was added the chiral diol **1**, (325 mg, 0.615 mmol) at room temperature under an argon atmosphere and the mixture was stirred for 1 h. This toluene solution of the chiral titanium catalyst (1 ml, 0.153 mmol) was added to powdered MS 4A under an argon atmosphere, and the mixture was cooled to −78 °C. A toluene (4 ml) solution of 3-acryloyl-1,3-oxazolidin-2-one (**3**) (216 mg, 1.53 mmol) was added to the mixture. Then P.E. (5 ml) and isoprene (1.5 ml) were added. The mixture was stirred overnight at 0 °C, and then pH 7 buffer was added to the mixture. The organic materials were extracted with ethyl acetate and the combined extracts were dried over anhydrous Na_2SO_4. After the evaporation of the solvent, the crude product was purified by thin-layer chromatography (silica gel, AcOEt : hexane=1 : 1) to give the pure product **5b** in 89% yield.

By the same procedure described above, the cycloaddition products **4**, **5a**, and **5b** were obtained.

Spectral data and physical properties of the cycloadducts are as follows:

3-[(1*S*,2*S*,4*S*)-Bicyclo[2.2.1]hept-5-en-2-ylcarbonyl]-1,3-oxazolidin-2-one (4). ^{1}H NMR and IR spectra agreed with those of the literatures.[2] $[\alpha]_D^{25}$ −132.5° (*c* 0.898, CH_2Cl_2), 88% ee, lit, $[\alpha]_D$ −65° (*c* 1.5, CH_2Cl_2), 38% ee.[3]

3-[(1*R*)-3-Cyclohexen-1-ylcarbonyl]-1,3-oxazolidin-2-one (5a). IR (KBr) 1776, 1695 cm^{-1}; ^{1}H NMR ($CDCl_3$) δ=1.14—2.74 (m, 6H), 3.45—4.61 (m, 5H), and 5.65 (s, 2H); $[\alpha]_D^{23}$ −20.2° (*c* 1.75, CH_2Cl_2), 89% ee. HRMS Found: *m/z* 195.0890. Calcd for $C_{10}H_{13}NO_3$: M, 195.0896.

3-[(1*R*)-4-Methyl-3-cyclohexen-1-ylcarbonyl]-1,3-oxazolidin-2-one (5b). IR (KBr) 1776, 1689 cm^{-1}; ^{1}H NMR ($CDCl_3$) δ=1.68 (s, 3H), 1.75—2.40 (m, 6H), 3.72—4.95 (m, 5H), and 5.36 (br, 1H); $[\alpha]_D^{23}$ −38.8° (*c* 2.55, CH_2Cl_2), 96% ee. Anal. Calcd for $C_{11}H_{15}NO_3$: C, 63.14; H, 7.23; N, 6.69%. Found: C, 63.15; H, 7.18; N, 6.71%.

3-[(1*R*)-4-Ethylthio-3-cyclohexen-1-ylcarbonyl]-1,3-oxazolidin-2-one (7). IR (KBr) 1776, 1695 cm^{-1}; ^{1}H NMR ($CDCl_3$) δ=1.26 (t, 3H, J=7.5 Hz), 1.77 (ddd, 1H, J=24.0, 11.0, 5.7 Hz), 2.01—2.06 (m, 1H), 2.20—2.25 (m, 1H), 2.30—2.39 (m, 3H), 2.68 (dq, 1H, J=12.5, 7.2 Hz), 2.71 (dq, 1H, J=12.5, 7.2 Hz), 3.73 (dddd, 1H, J=2.7, 5.8, 9.0, 15.0 Hz), 4.03 (t, 2H, J=8.3 Hz), 4.42 (t, 2H, J=8.3 Hz), and 5.61—5.63 (br, 1H); $[\alpha]_D^{26}$ −44.3° (*c* 0.859, CH_2Cl_2), 91% ee. HRMS Found: *m/z* 255.0902. Calcd for $C_{12}H_{17}NO_3S$: M, 255.0930.

Transformation of 5a and 5b into Their Epoxy Derivatives 12a and 12b. Formation of the Methyl Ester 9b. A few drops of carbon tetrachloride was added to magnesium (80.1 mg, 3.30 mmol). Then dry methanol (6.6 ml) was added under an argon atmosphere at 0 °C to generate magnesium methoxide. When all the magnesium dissolved, an ether (5 ml) solution of the Diels-Alder adduct **5b** (263 mg, 1.26 mmol) was added. The reaction was immediately quenched with saturated ammonium chloride and the methyl ester was extracted with ether. The organic layers were washed with brine and dried over anhydrous sodium sulfate. After the evaporation of the solvent, the crude product **9b** was directly used for further transformations.

Hydrolysis of 9b to the Carboxylic Acid 10b. A THF-water (10 : 1) mixture was added to the methyl ester **9b** (93.1 mg, 0.603 mmol) at room temperature until the ester completely dissolved. Then 2.5 equiv of lithium hydroxide monohydrate (62.9 mg, 1.50 mmol) was added to this solution at room temperature and the mixture was stirred for 8 h. After the evaporation of the solvent, 1M sodium hydroxide solution was added and the water layer was washed with ether. The water layer was made acidic with concd hydrochloric acid, and extracted with ether. The combined organic layers were dried over anhydrous sodium sulfate. After the evaporation of the solvent, the crude carboxylic acid was directly used for further transformations.

Iodolactone 11b. The carboxylic acid **10b** (40.0 mg, 0.285 mmol) was dissolved in 0.5M sodium hydrogencarbonate solution (1.7 ml). To this, an aqueous solution (4 ml) of iodine (148.0 mg, 0.583 mmol) and potassium iodide (285.0 mg, 1.72 mmol) was added and the mixture was stirred overnight at room temperature in the dark. The reaction mixture was diluted with water. Then aqueous $Na_2S_2O_3$ was added and the organic compounds were extracted with CH_2Cl_2. The combined organic layers were washed with saturated sodium hydrogencarbonate solution and dried over anhydrous sodium sulfate. After the evaporation of the solvent, the crude product (**11b**) (76.1 mg) was directly used for obtaining the epoxy derivative **12b**.

Epoxy Derivative 12b. NaOMe (17.1 mg, 0.317 mmol) was dissolved in dry methanol (3 ml) at 0 °C under an argon atmosphere. To this, a THF (3 ml) solution of the iodolactone **11b** (69.6 mg, crude) was added and the mixture was stirred overnight. The reaction mixture was quenched with a pH 7 phosphate buffer after the evaporation of methanol. The epoxy compound was extracted with ether and the combined organic layers were washed with water and brine successively, and dried over anhydrous sodium sulfate. After the evaporation of the solvent, the epoxy derivative **12b** was purified by TLC (hexane : AcOEt=4 : 1). (23.0 mg, 52% yield). The epoxy compound was analyzed by NMR with the addition of a chiral shift reagent, (Eu(hfc)$_3$).[12]

Spectral data of the epoxy compounds are as follows.

Methyl 3,4-Epoxycyclohexane-1-carboxylate (12a). **5a** was transformed to its epoxy derivative **12a** in the same manner. ^{1}H NMR ($CDCl_3$) δ=1.52—1.62 (m, 2H), 1.70—1.77 (m, 2H), 2.10—2.12 (m, 2H), 2.15—2.22 (m, 2H), 3.08 (s, 1H), and 3.64 (s, 3H).

Methyl 4-Methyl-3,4-epoxycyclohexane-1-carboxylate (12b). ^{1}H NMR ($CDCl_3$) δ=1.30 (s, 3H), 1.54—1.71 (m, 4H), 2.02—2.25 (m, 3H), 2.96 (d, 1H), and 3.64 (s, 3H).

Preparation of the MTPA Ester 13. The Diels-Alder adduct **4** was transformed to its benzyl ester by the literature method.[7] To reduce the benzyl ester to the corresponding alcohol, the THF (3 ml) solution of the benzyl ester was added to the mixture containing THF (1 ml) and $LiAlH_4$ (13.8 mg, 0.364 mmol) at 0 °C under an argon atmosphere. After 1 h, the reaction was quenched with saturated aqueous sodium sulfate and the organic materials were extracted with ether by decantation, and dried over anhydrous sodium sulfate. Filtration and evaporation of the solvent afforded the crude product, which was purified by thin layer chromatography (benzene : ether=2 : 1, ×2) to give the pure product

(84% yield). The obtained alcohol was transformed to its MTPA ester **13** by the Mosher's method.[13]

Oxidation of the MTPA Ester to 14.[14] Methanol was added to (1*S*)-4-ethylthio-3-cyclohexen-1-ylmethyl (+)-trifluoromethylmethoxyphenylacetate (**13**) (9.2 mg, 0.024 mmol) until all of **13** had dissolved at 0 °C. Then 30% hydrogen peroxide (1 ml) and $(NH_4)_6Mo_7O_{24}$ (10 mg) were added and the mixture was stirred for 3.5 h. The sulfone (**14**) was extracted with CH_2Cl_2 and the combined organic layers were washed with brine and dried over anhydrous sodium sulfate. After the evaporation of the solvent, the crude product (10.1 mg) was analyzed by ^{13}C NMR without further purification. ^1H NMR ($CDCl_3$) δ=1.25 (t, 3H), 1.26—1.37 (m, 1H), 1.89—2.09 (m, 2H), 2.24—2.50 (m, 3H), 2.89 (dq, 1H), 2.91 (dq, 1H), 3.51 (s, 3H), 4.16 (dd, 1H), 4.30 (dd, 1H), 6.72—6.76 (br, 1H), 7.37—7.43 (m, 3H), and 7.47—7.50 (m, 2H); ^{13}C NMR ($CDCl_3$) δ=7, 23, 25, 28, 30, 31, 32, 47, 56, 69, 122, 128, 129, 130, 139, and 167.

References

1) L. A. Paquette, "Asymmetric Synthesis," ed by J. D. Morrison, Academic Press, Inc., Orlando (1984), Vol. 3, p. 455; G. Helmchen, R. Karge, and J. Weetman, "Modern Synthetic Methods," ed by R. Scheffold, Springer-Verlag, Berlin (1986), Vol. 4, p. 262; W. Oppolzer, *Angew. Chem., Int. Ed. Engl.*, **23**, 876 (1984); D. A. Evans, K. T. Chapman, and J. Bisaha, *J. Am. Chem. Soc.*, **106**, 4261 (1984); S. Masamune, L. A. Reed, J. T. Davis, and W. Choy, *J. Org. Chem.*, **48**, 4441 (1983); T. R. Kelly, A. Whiting, and N. S. Chandrakumar, *J. Am. Chem. Soc.*, **108**, 3510 (1986); E. J. Corey, R. Imwinkelried, S. Pikul, and Y. B. Xiang, *ibid.*, **111**, 5493 (1989); K. Kishikawa, M. Yamamoto, S. Kohmoto, and K. Yamada, *J. Org. Chem.*, **54**, 2488 (1989); K. Maruoka, and H. Yamamoto, *J. Am. Chem. Soc.*, **111**, 789 (1989); K. Furuta, S. Shimizu, Y. Miwa, and H. Yamamoto, *J. Org. Chem.*, **54**, 1481 (1989).

2) N. Iwasawa, Y. Hayashi, H. Sakurai, and K. Narasaka, *Chem. Lett.*, **1989**, 1581.

3) K. Narasaka, N. Iwasawa, M. Inoue, T. Yamada, M. Nakashima, and J. Sugimori, *J. Am. Chem. Soc.*, **111**, 5340 (1989).

4) E. J. Corey, N. M. Weinshenker, T. K. Schaaf, and W. Huber, *J. Am. Chem. Soc.*, **91**, 5675 (1969); E. J. Corey and H. E. Ensley, *ibid.*, **97**, 6908 (1975); R. K. Boeckman, Jr., P. C. Naegely, and S. D. Arthur, *J. Org. Chem.*, **45**, 754 (1980); O. Ceder and H. G. Nilsson, *Acta Chem. Scand. B*, **30**, 908 (1976); E. E. Smissman, J. T. Suh, M. Oxman, and R. Daniels, *J. Am. Chem. Soc.*, **84**, 1040 (1962).

5) The optical purity was determined by converting the product into its benzyl ester and measuring its optical rotation.

6) H. M. Schwartz, W. Wu, P. W. Marr, and J. B. Jones, *J. Am. Chem. Soc.*, **100**, 5199 (1978).

7) D. A. Evans, K. T. Chapman, and J. Bisaha, *J. Am. Chem. Soc.*, **110**, 1238 (1988); J. Colonge and J. Crabalona, *Bull. Chim. Soc. Fr.*, **1960**, 102; H. B. Henbest and R. S. McElhinney, *J. Chem. Soc.*, **1959**, 1834.

8) E. Vedejs, T. H. Eberlein, D. J. Mazur, C. K. McClure, D. A. Perry, R. Ruggeri, E. Schwartz, J. S. Stults, D. L. Varie, R. G. Wilde, and S. Wittenberger, *J. Org. Chem.*, **51**, 1556 (1986).

9) L. J. Dolby and K. S. Marshall, *Org. Prep. Proced.*, **1** (**4**), 229 (1969); *Chem. Abstr.*, **72**, 344 (1970).

10) E. Negishi and F. T. Luo, *J. Org. Chem.*, **48**, 1562 (1983).

11) Y. Hayashi and K. Narasaka, *Chem. Lett.*, **1989**, 793; **1990**, 1295.

12) Eu(hfc)$_3$: tris[3-(heptafluoropropylhydroxymethylene)-*d*-camphorato]europium(III).

13) J. A. Dale, D. L. Dull, and H. S. Mosher, *J. Org. Chem.*, **34**, 2543 (1969).

14) M. Joaquina and S. A. Amaral, *J. Chem. Soc. C*, **1969**, 2495.

15) The peak assignment of the chiral center was done by measurement of DEPT. The chemical shifts of the two separated peaks were δ=31.76 and 31.82. The intensities of the two signals were equal in the racemic compound of **14**.

16) C. Dijkgraaf and J. P. G. Rousseau, *Spectrochim. Acta, Part A*, **24**, 1213 (1968).

On the Reaction of *N*-(Diphenylphosphinyl)-1-phenylethanimine with Aromatic Aldehydes Giving 4-Aryl-2,6-diphenylpyridine Derivatives

Tomoshige KOBAYASHI,* Hidetaka KAKIUCHI, and Hiroshi KATO*
Department of Chemistry, Faculty of Science, Shinshu University, Matsumoto 390
(Received October 1, 1990)

N-(Diphenylphosphinyl)-2-phenyl-1-azaallyl anion (**1**), generated from *N*-(diphenylphosphinyl)-1-phenylethanimine, reacted with aromatic aldehydes in a 2 : 1 molar ratio to give 4-aryl-2,6-diphenylpyridines in moderate yields. The intervention of *N*-phosphinyl-1-azadiene intermediates is proposed on the basis of the independent synthesis of an *N*-phosphinyl-1-azadiene and its conversion into a pyridine by the reaction with **1**.

In the previous paper, we described a novel route to phenyl-substituted pyridines by the reaction of α,β-unsaturated carbonyl compounds with *N*-phosphinyl-1-azaallyl anions, which are easily generated from the corresponding *N*-phosphinylimine and enamine.[1] The *N*-phosphinyl-1-azaallyl anions have shown bidentate reactivity at the β-carbon and the nitrogen atoms to behave as a synthetic equivalent of primary vinylamines, which are labile even at low temperature.[2] The primary vinylamines[2] and their synthetic equivalents such as an *N*, *N*-bis(trimethylsilyl) enamine,[3] 1-amino-2-hydroxyalkylsilanes,[4] and *N*-vinyliminophosphoranes[5] have been reported to provide 2-azadienes upon treatment with aldehydes. Our attention, therefore, turned to the reaction of the *N*-phosphinyl-1-azaallyl anion **1** with aromatic aldehydes **3** to investigate the chemo-selectivity of **1** towards simple carbonyl compounds with the result that the unexpected formations of 4-aryl-2,6-diphenylpyridines was observed.

Results and Discussion

In a preliminary study, *N*-(diphenylphosphinyl)-1-phenylethanimine (**2**)[1,6] was treated with an equimolar amount of benzaldehyde **3a** in the presence of potassium *t*-butoxide to afford 2,4,6-triphenylpyridine **4a** in 8% yield, instead of the presumed 2-azadiene (**2-AD**, Scheme 2). Since the two phenyl groups at the 2- and 6-positions of **4a** seemed to arise from two molecules of **2**, the reaction of **2** and **3a** in a 2 : 1 molar ratio in the presence of potassium *t*-butoxide at ambient temperature was investigated to give the pyridine **4a** in 52% yield along with diphenylphosphinic acid (**5**) and diphenylphosphinic amide (**6**) in 58 and 18% yield, respectively. Similarly, the reactions of the imine **2** with substituted benzaldehydes **3b—h** as well as 2-thiophenecarbaldehyde **3i** also resulted in the regioselective formation of pyridine derivatives **4b—i** in which the aryl groups derived from the aldehydes are located exclusively at the 4-position of the pyridine ring. The use of ortho-substituted benzaldehydes **3g** and **3h** obviously decreases the yields of the pyridines **4g** and **4h**. All the pyridines except **4i** have been reported. Pyridines **4a—f** were characterized by comparison of their spectral data and melting points with those described in the literatures for **4a—f**, and **4g** and **4h** were identified by independent syntheses.

The present reaction can be best explained as shown in Scheme 2. Upon treatment with an aromatic aldehyde **3**, the 1-azaally anion **1** undergoes the condensation reaction on the β-carbon atom to give *N*-phosphinyl-1-azadiene **7**. The 1-azadiene **7** further reacts with **1** to lead to a dihydropyridine **9** via elimination of the phosphinic amide **6** from **8**. Since the phosphinic acid **5** was isolated from the reaction of **2** and **3a**, a route involving release of the phosphinic acid **5** from **9**, followed by dehydrogenation is likely for the formation of the pyridine **4**. However, an alternative route through direct elimination of diphenylphosphine oxide (**11**) from **9** can not be excluded, as **11** was easily converted to the phosphinic acid **5**

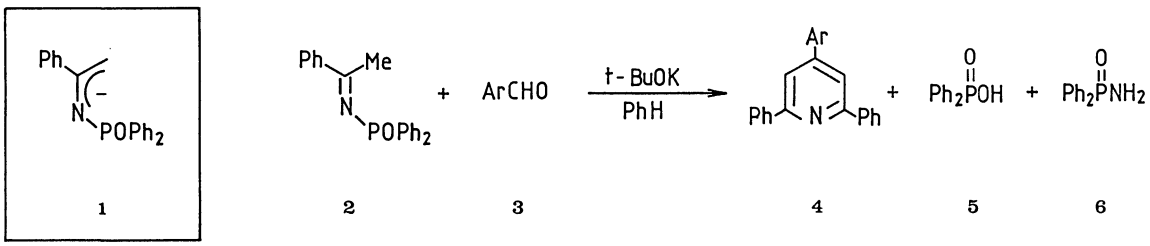

a: Ar=C_6H_5, **b**: Ar=*p*-MeC_6H_4, **c**: Ar=*p*-ClC_6H_4, **d**: Ar=*p*-$O_2NC_6H_4$, **e**: Ar=*p*-$MeOC_6H_4$, **f**: Ar=*p*-$Me_2NC_6H_4$, **g**: Ar=*o*-MeC_6H_4, **h**: Ar=*o*-ClC_6H_4, **i**: Ar=2-Thienyl

Scheme 1.

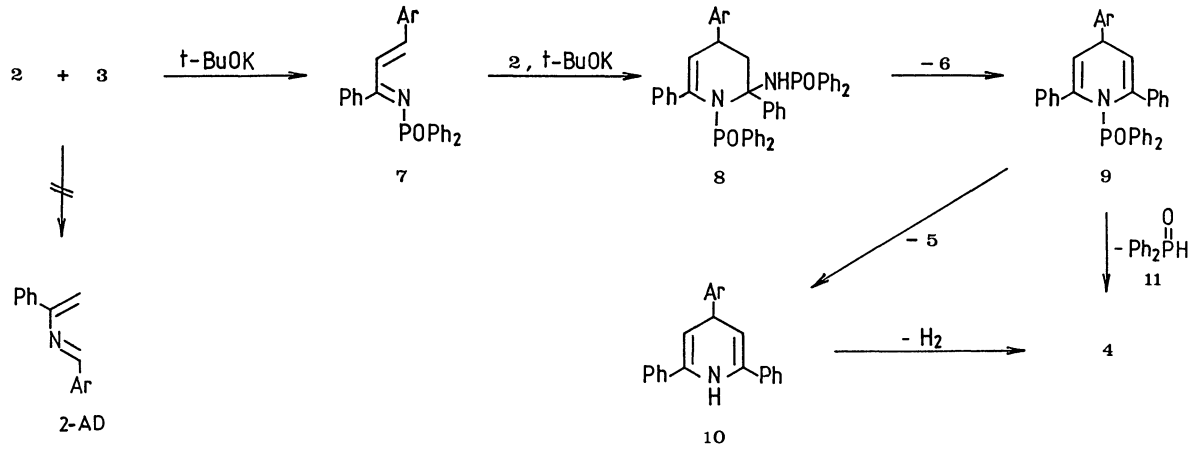

Scheme 2.

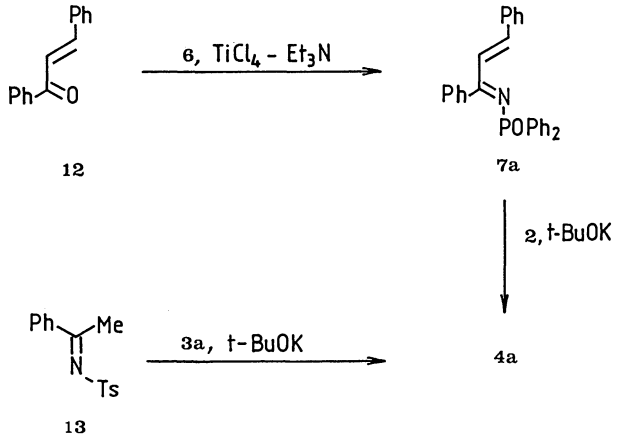

Scheme 3.

under the reaction conditions (see Experimental).

Some efforts were devoted to the isolation and capture of the *N*-phosphinyl-1-azadiene intermediate **7**. The azadiene **7a** could not be formed among the products of the reaction of the imine **2** with two fold excess amount of benzaldehyde **3a**, while the reaction gave the pyridine **4a** in 7% yield. Further, the reaction of **2** and **3a** in the presence of 1-(1-pyrrolidinyl)-1-cyclohexene, 1-trimethylsiloxy-1-cyclohexene, or ethyl vinyl ether did not afford the expected adducts.[7] Thus, an independent synthesis of the azadiene **7a** was performed in 78% yield by treatment of 1,3-diphenyl-2-propen-1-one (**12**) with the phosphinic amide **6** in the presence of titanium tetrachloride and triethylamine in refluxing toluene.[8] Upon treatment with **2** and potassium *t*-butoxide in benzene at ambient temperature, the propenimine **7a** provided the pyridine **4a** in 52% yield, and this outcome agrees with the mechanism shown in Scheme 2 including both an intervention of the 1-azadiene intermediate **7** and its sequential reaction with **1**.

Finally, it should be noted that the phosphinyl group seems to be essential for the present transformation, because a similar reaction of benzaldehyde **3a** with *N*-(*p*-tolylsulfonyl)-1-phenylethanimine (**13**)[9] gave only a trace amount of the pyridine **4a**.

In conclusion, the reaction of *N*-phosphinyl-2-phenyl-1-azaallyl anion **1** with aromatic aldehydes has been found to give 4-aryl-2,6-diphenylpyridines probably via *N*-phosphinyl-1-azadiene intermediate. It is surprising to observe nucleophilic attack exclusively by the anionic carbon of the 1-azaallyl anion **1**. This result sharply contrasts with the behavior of primary vinylamines and their synthetic equivalents known so far.[2-5] Although the yields of the pyridines are modest, the present reaction has shown a novel reactivity of the azaallyl anion **1**.

Experimental[10]

General Procedure for the Reaction of N-(Diphenylphosphinyl)phenylethanimine (2) and Aromatic Aldehydes (3) (2:1 molar ratio). To a solution of the imine **2**[1,6] (160 mg, 0.5 mmol) in anhydrous benzene (5 ml) was added potassium *t*-butoxide (56 mg, 0.5 mmol). The mixture was stirred at ambient temperature for 10 min, and a solution of aromatic aldehyde **3** (0.25 mmol) in anhydrous benzene (3 ml) was added to the mixture. Stirring was continued for 2 h at the same temperature. The mixture was washed with water, dried over Na_2SO_4, and concentrated. The residue was purified on TLC (silica gel, benzene) to give the pyridine **4**. In the reaction of **2** and **3a**, the base line portion on the TLC plate was developed again with benzene–methanol (3:1) to yield diphenylphosphinic amide **6** in 18% yield, and acidification of the aqueous phase with hydrochloric acid provided diphenylphosphinic acid **5** in 58% yield. The yields of the pyridine derivatives **4** are based on the amount of aromatic aldehydes. The spectra of the pyridines **4a**, **4b**, **4c**, and **4e** were previously described.[1] The reactions of the imine **2** and benzaldehyde **3a** in molar ratios of 1:1 and 1:2 were carried out in similar manners.

2,4,6-Triphenylpyridine (4a): 52%; mp and mixed mp 134—135 °C (methanol) (lit,[11] mp 137 °C).

4-(*p*-Methylphenyl)-2,6-diphenylpyridine (4b): 57%; mp

and mixed mp 124.5—125 °C (methanol) (lit,[12] mp 118—119 °C.

4-(*p*-Chlorophenyl)-2,6-diphenylpyridine (4c): 41%; mp and mixed mp 129—130 °C (methanol) (lit,[13] mp 129—130 °C).

4-(*p*-Nitrophenyl)-2,6-diphenylpyridine (4d): 37%; mp 202—203 °C (benzene–hexane=1 : 1) (lit,[14] mp 188 °C); IR ($CHCl_3$) 1590, 1540, 1380, 1350, 1100 cm^{-1}; ^1H NMR ($CDCl_3$) δ=7.20—7.66 (6H, m), 7.85 (2H, s), 7.87 (2H, d, J=9.0 Hz), 8.08—8.25 (4H, m), 8.36 (2H, d, J=9.0 Hz); MS m/z (rel intensity) 352 (M^+, 100), 322 (14), 306 (37). Found: C, 77.95; H, 4.46; N, 7.63%. Calcd for $C_{23}H_{16}N_2O_2$: C, 78.34; H, 4.58; N, 7.95%.

4-(*p*-Methoxyphenyl)-2,6-diphenylpyridine (4e): 34%; mp and mixed mp 99—100 °C (methanol) (lit,[12] mp 99—100 °C).

4-[*p*-(Dimethylamino)phenyl]-2,6-diphenylpyridine(4f): 28%; mp 142—143 °C (methanol) (lit,[14] mp 138 °C); IR ($CHCl_3$) 1590, 1520, 1360, 1180, 1120 cm^{-1}; ^1H NMR ($CDCl_3$) δ=2.99 (6H, s), 6.80 (2H, d, J=8.7 Hz), 7.20—7.60 (6H, m), 7.66 (2H, d, J=8.7 Hz), 7.84 (2H, s), 8.14—8.24 (4H, m); MS m/z (rel intensity) 350 (M^+, 100), 333 (5), 306 (6).

4-(*o*-Methylphenyl)-2,6-diphenylpyridine (4g): 7%; mp and mixed mp 122—123 °C (methanol) (lit,[15] mp 116-117 °C); IR (KBr) 1610, 1580, 1536, 1490, 1400 cm^{-1}; ^1H NMR ($CDCl_3$) δ=2.36 (3H, s), 7.20—7.60 (10H, m), 7.66 (2H, s), 8.12—8.28 (4H, m); MS m/z (rel intensity) 321 (M^+, 75), 320 (100). Found: C, 89.39; H, 5.95; N, 4.44%. Calcd for $C_{24}H_{19}N$: C, 89.68; H, 5.96; N, 4.36%.

4-(*o*-Chlorophenyl)-2,6-diphenylpyridine (4h): 11%; mp and mixed mp 114—115 °C (methanol) (lit,[12] mp 112—113 °C); IR (KBr) 1600, 1551, 1478, 1405 cm^{-1}; ^1H NMR ($CDCl_3$) δ=7.20—7.64 (10H, m), 7.76 (2H, s), 8.08—8.28 (4H, m); MS m/z (rel intensity) 343 (M^++2, 31), 341 (M^+, 100), 306 (51). Found: C, 80.48; H, 4.75; N, 3.81%. Calcd for $C_{23}H_{16}NCl$: C, 80.81; H, 4.72; N, 4.10%.

2,6-Diphenyl-4-(2-thienyl)pyridine (4i): 31%; mp 165—166 °C (methanol); IR (KBr) 1600, 1580, 1560, 1500, 1410, 1250, 1080, 1040 cm^{-1}; ^1H NMR ($CDCl_3$) δ=7.00—7.62 (9H, m), 7.83 (2H, s), 8.02—8.25 (4H, m); MS m/z (rel intensity) 313 (M^+ 100); HR-MS Found: 313.0928. Calcd for $C_{21}H_{15}NS$: 313.0925. Found: C, 80.38; H, 4.75; N, 4.32%. Calcd for $C_{21}H_{15}NS$: C, 80.48; H, 4.82; N, 4.47%.

Diphenyphosphinic Acid (5): Mp and mixed mp 196—198 °C (lit,[16] mp 190—192 °C); IR (KBr) 3450, 1421, 1180, 1138 cm^{-1}.

Diphenylphosphinic Amide (6): Mp and mixed mp 170—171 °C (lit,[17] mp 168 °C); IR (KBr) 3250, 1440, 1190, 1126 cm^{-1}.

Independent Synthesis of the Pyridine 4g.[18] A mixture of 3-(*o*-methylphenyl)-1-phenyl-2-propen-1-one[19] (2.123 g, 9.5 mmol), acetophenone (0.916 g, 7.6 mmol), and $BF_3 \cdot OEt_2$ (3.336 g, 22.8 mmol) was heated at 115 °C for 7 h. The solution was cooled to room temperature, and the product was crystallized from benzene to give 4-(*o*-methylphenyl)-2,6-diphenylpyrylium tetrafluoroborate (1.142 g, 37%) as yellow powders: Mp 113—115 °C (decomp). Found C, 70.58; H, 4.78%. Calcd for $C_{24}H_{19}OBF_4$: C, 70.27; H, 4.67%.

To a suspension of the pyrylium salt (1.076 g, 2.6 mmol) in ethanol (3 ml) was added 25% aq NH_3 (5 ml) and stirring was continued for 24 h at ambient temperature. The product was extracted with dichloromethane prior to drying over Na_2SO_4. After removal of the solvent, recrystallization of the resulting solid from methanol gave the pyridine **4g** (515 mg, 62%).

Independent Synthesis of the Pyridine 4h.[18] By a similar procedure for **4g**, a mixture of 3-(*o*-chlorophenyl)-1-phenyl-2-propen-1-one[19](3.191 g, 13.1 mmol), acetophenone (1.221 g, 10 mmol), and $BF_3 \cdot OEt_2$ (4.346 g, 30 mmol) was heated at 115 °C for 7 h to afford 4-(*o*-chlorophenyl)-2,6-diphenylpyrylium tetrafluoroborate (1.102 g, 26%) as yellow powders: Mp 114—116 °C (decomp). Found: C, 64.15; H, 3.74%. Calcd for $C_{23}H_{16}OClBF_4$: C, 63.63; H, 3.75%. The pyrylium salt was used without further purification.

A similar treatment of the pyrylium salt (1.028 g, 2.4 mmol) gave the pyridine **4h** (610 mg, 67%).

Reaction of Diphenylphosphine Oxide (11) under Basic Conditions.[20] A mixture of the phosphine oxide **11** (89 mg, 0.44 mmol) and potassium *t*-butoxide (62 mg, 0.55 mmol) in benzene was stirred for 3 h at ambient temperature under nitrogen atmosphere. The organic phase was washed with aq $NaHCO_3$, and the aqueous phase was acidified with hydrochloric acid. The product was extracted with dichloromethane prior to drying over $MgSO_4$. Removal of the solvent gave the phosphinic acid **5** (57 mg, 59%).

Independent Synthesis of (2*E*)-*N*-(Diphenylphosphinyl)-1,3-diphenyl-2-propenimine (7a). A mixture of the propenone **12** (2.083 g, 10 mmol), the phosphinic amide **6** (2.384 g, 11 mmol), and triethylamine (3.03 g, 30 mmol) in toluene (20 ml) was heated at 70 °C. To this mixture was slowly added $TiCl_4$ (0.60 ml, 5.5 mmol), and the mixture was heated under reflux for 6 h. Insoluble material was removed by filtration and the filtrate was concentrated. The residue was chromatographed on silica gel using benzene–ethyl acetate (1 : 1) as an eluent to give an oily product, which was crystallized from ether to give **7a** (3.17 g, 78 %) as colorless powders: Mp 120—121 °C; IR (KBr) 3090, 1610, 1590, 1560, 1430, 1300, 1180, 1120, 1100, 1020, 990, 980, 910 cm^{-1}; ^1H NMR ($CDCl_3$) δ=6.99 (1H, d, J=16.4 Hz), 7.21—8.11 (20H, m), 8.28 (1H, dd, J=16.4, 1.4 Hz); ^{13}C NMR ($CDCl_3$) δ=124.2—146.4, 180.3 (J_{P-C}=8.5 Hz, C=N); ^{31}P NMR ($CDCl_3$) δ=19.0; MS m/z (rel intensity) 407 (M^+, 60), 206 (86), 77 (100); HR-MS Found: 407.1426. Calcd for $C_{27}H_{22}NOP$: 407.1439. Found: C, 79.74; H, 5.51; N, 3.33%. Calcd for $C_{27}H_{22}NOP$: C, 79.59; H, 5.44; N, 3.44%.

Reaction of the Ethanimine 2 and the Propenimine 7a. A mixture of the ethanimine **2** (191 mg, 0.6 mmol), the propenimine **7a** (204 mg, 0.5 mmol), and potassium *t*-butoxide (67 mg, 0.6 mmol) in benzene (5 ml) was stirred for 4 h at ambient temperature. The mixture was washed with aq $NaHCO_3$ and water, then dried over Na_2SO_4. Purification on TLC (silica gel, benzene) gave 2,4,6-triphenylpyridine **4a** (80 mg, 52%): Mp and mixed mp 139—140 °C.

Synthesis of *N*-(*p*-Tolylsulfonyl)-1-phenylethanimine (13).[9] To a cooled solution (−35 °C) of acetophenone oxime (16.23 g, 0.12 mol) and triethylamine (12.14 g, 0.12 mol) in petroleum ether–dichloromethane (160 ml, 1 : 1) was added *p*-toluenesulfinyl chloride[21] (20.96 g, 0.12 mol). The mixture was warmed up to room temperature and stirring was continued for 1 h. Insoluble material was filtered and the filtrate was concentrated. The residue was crystallized from ether to give **13** (4.048 g, 12%): Mp 71.5—73.5 °C; IR (KBr) 1605, 1600, 1570, 1313, 1301, 1280 cm^{-1}; ^1H NMR ($CDCl_3$) δ=2.42 (3H, s), 2.96 (3H, s), 7.12—7.58 (5H, m), 7.80—8.00 (4H, m); ^{13}C NMR ($CDCl_3$) δ=21.1 (q), 21.5 (q), 127.1, 128.2, 128.6, 129.4, 133.1, 137.5, 138.8, 143.5, 179.8 (s); MS m/z (rel intensity) 273 (M^+, 26), 209 (24), 155 (95), 91

(100). HR-MS Found: 273.0809. Calcd for $C_{15}H_{15}O_2S$: 273.0823.

Reaction of the *N*-Sulfonylimine (13) with Benzaldehyde (3a). A solution of the *N*-sulfonylimine **13**[9] (547 mg, 2 mmol) and potassium *t*-butoxide (226 mg, 2 mmol) in benzene (5 ml) was stirred at ambient temperature for 10 min. To the mixture was added benzaldehyde **3a** (106 mg, 1 mmol) and stirring was continued for 24 h. The mixture was washed with aq $NaHCO_3$ and dried over $MgSO_4$. Separation on TLC (silica gel, benzene) afforded only a trace amount of the pyridine **4a**, which was detectable only by the ^1H NMR spectrum.

Financial support for T. K. by Grant-in-Aid for Encouragement of Young Scientist (No. 01740303, 1989—1990) from the Ministry of Education, Science and Culture is acknowledged.

References

1) T. Kobayashi, H. Kawate, H. Kakiuchi, and H. Kato, *Bull. Chem. Soc. Jpn.*, **63**, 1937 (1990).

2) J. L. Ripoll, H. Lebrun, and A. Thuillier, *Tetrahedron*, **36**, 2497 (1980).

3) R. J. P. Corriu, V. Huynh, J. J. E. Moreau, and M. Pataud-Sat, *Tetrahedron Lett.*, **23**, 3257 (1982); R. J. P. Corriu, J. J. E. Moreau, and M. Pataud-Sat, *J. Org. Chem.*, **55**, 2878 (1990).

4) S. Tomoda, Y. Matsumoto, Y. Takeuchi, and Y. Nomura, *Chem. Lett.*, **1986**, 1193.

5) J. Barluenga, M. Ferrero, and F. Palacios, *Tetrahedron Lett.*, **29**, 4863 (1988); *idem.*, *J. Chem. Soc., Perkin Trans. 1*, **1990**, 2193.

6) B. Krzyzanowska and W. J. Stec, *Synthesis*, **1982**, 270.

7) The Diels-Alder reaction of an *N*-phosphinyl-1-azadiene with vinyl ethers under high pressure conditions has been reported: D. L. Boger and A. M. Kasper, *J. Am. Chem. Soc.*, **111**, 1517 (1989).

8) W. B. Jennings and C. J. Lovely, *Tetrahedron Lett.*, **29**, 3725 (1988).

9) C. Brown, R. F. Hudson, and K. A. F. Record, *J. Chem. Soc., Perkin Trans. 2*, **1978**, 822.

10) Instruments used in this work and general conditions are described in Ref. 1.

11) A. R. Katritzky, D. E. Leaby, A. Maguestiau, and R. Hamming, *J. Chem. Soc., Perkin Trans. 1*, **1983**, 45.

12) R. Lombard and J.-P. Stephan, *Bull. Soc. Chim. Fr.*, **1958**, 1458.

13) R. L. Frank and R. P. Seven, *J. Am. Chem. Soc.*, **71**, 2629 (1949).

14) G. N. Dorofeenko and S. V. Krivum, *Zh. Obshch. Khim.*, **34**, 105 (1964).

15) N. S. Prostakov, G. A. Vasilev, V. P. Zvolinskü, A. V. Vorlanov, A. A. Savina, O. I. Sorolin, and N. D. Lopatina, *Khim. Geterotsikl. Soedin.*, **1975**, 1112.

16) W. A. Higgins, P. W. Vogel, and W. G. Craig, *J. Am. Chem. Soc.*, **77**, 1864 (1955).

17) N. Kreutzkamp and H. Schindler, *Arch. Pharm. (Weinheim)*, **293**, 296 (1960).

18) A. R. Katritzky, A. M. El-Mowafy, G. Musumarra, K. Sakizadeh, C. Sana-Ullah, S. M. M. El-Shafie, and S. S. Thind, *J. Org. Chem.*, **46**, 3823 (1981).

19) K. T. Potts and R. Robinson, *J. Chem. Soc.*, **1955**, 2466.

20) For the preparation of the phosphine oxide **11** and its conversion to the phosphinic acid **5** under basic conditions, see: R. C. Miller, *J. Org. Chem.*, **24**, 2013 (1959).

21) F. Kurzer, *Org. Synth.*, Coll. Vol. IV, 937 (1963).

Association Characteristics of Amphiphilic α-Helices Connected by Flexible Links

Hisayuki MORII,* Shinya HONDA, Kunihiro ICHIMURA, and Hatsuho UEDAIRA
Research Institute for Polymers and Textiles, 1-1-4 Higashi, Tsukuba, Ibaraki 305
(Received October 2, 1990)

Amphiphilic helical peptides interlinked with sequences bearing a flexible mobility were designed and synthesized. The sequences containing glycine and/or cystine were adopted for the linkage parts. The secondary structure of the peptides was investigated by circular dichroism(CD) and the super-secondary structure was estimated. The CD spectra and their pH dependence show that the peptides have almost the same α-helix contents as designed and that the helices associate to be "coiled-coil" at neutral pH. The apparent helix contents increase at low pH and some of helices are subject to denaturation at high pH. The denaturation of α-helix bundles by guanidine hydrochloride is contemplated to be three-state transition. It is proposed that the peptides construct α-helix bundles with both loose and tight contacts between helices. Two kinds of folded structure constructed with 2 or more helices are also suggested.

The construction of artificial proteins is a very attractive field. Several new designs[1-5] of proteins have been presented in the last several years.

In nature there exist "coiled-coil"[6] and "4-helix bundle"[7] structures which are formed by 2 and 4 α-helices, respectively. Amphiphilicity of cylindrical helices is characteristic of these structures. The contact faces of associated helices are rich in hydrophobic residues and the opposite faces are often hydrophilic. Nishino et al.[8] investigated the association of amphiphilic helices by means of a size exclusion chromatography (SEC). They tested the effect of hydrophobic and hydrophilic amino acids in helices on the association. DeGrado et al.[9,10] revealed an association free energy and the number of association by measuring the concentration dependence of CD intensity. Mutter et al.[11] proposed a new design of peptides and the structure was analyzed with CD and SEC. In these studies the linked helices were found to form more stable aggregates than single helices.

In this work, we designed and synthesized several amphiphilic helical peptides interlinked with flexible connections. The important characteristic of our designed peptides is flexible linkage of amphiphilic helices. The flexible links are expected to play an important role in arranging helices in a stable packing. Moreover, the peptides may be useful as "induced fitting" host molecules. The formation of a bundle structure by amphiphilic helices is already known, however, the folding course and the influence of temperature and pH on a folded structure are not investigated well. In order to make clear the super-secondary structure as well as the folding behavior of linked α-helices the CD spectra were analyzed in detail.

Experimental

Materials. *t*-Butoxycarbonyl-protected amino acids and 4-(bromomethyl)phenylacetic acid were purchased from Kokusan Chemical Works and used without further purification. The other reagents were trifluoroacetic acid (TFA), dicyclohexylcarbodiimide (DCC), ninhydrin, diethyl phosphorocyanidate (DEPC), triethylamine (Et_3N), cesium carbonate (Cs_2CO_3), trifluoromethanesulfonic acid (TFMSA), dichloromethane, *N*,*N*-dimethylformamide (DMF) distilled over CaH_2, and dimethyl sulfoxide (DMSO), which were purchased from Wako Pure Chemical. The solvents were dried over molecular sieve 4A.

Peptide Synthesis and Purification. The peptides P2, P3, P4x, P4w and P6, of which the sequences are shown in Fig. 1 with one letter abbreviations,[12] were synthesized manually by a solid-phase method. The initial Boc-protected amino acid was anchored onto copoly(styrene-1%-divinylbenzene) (Bio-beads S-X1, Bio-Rad) intermediated with 4-(hydroxymethyl)phenylacetamidomethyl group by the method of Mitchell et al.[13] The second and the third residues from C-terminus were introduced in one time with DEPC-Et_3N[14] in order to be free from 2,5-piperazinedione formation.[15] The subsequent residues were coupled stepwise. The side-chain-protecting groups used were Glu(OBzl), Lys(ClZ), and Cys(Acm)[16] (Bzl, benzyl; ClZ, 2-chlorobenzyloxycarbonyl; Acm, acetamidomethyl). The double couplings were carried out for each step by means of DEPC-Et_3N and symmetrical carboxylic anhydride methods.[17] Finally the peptide was deprotected and cleaved from the resin by TFMSA-Me_2S-*m*-cresol system[18] at 0 °C for 28h. For the peptides P4x, P4w, and P6, Cys(Acm) was deprotected and oxidized to be cystine with 0.01 M (1 M=1 mol dm^{-3}) iodine in water-acetic acid (1 : 4) at 20 °C for 1 h.

Each crude peptide was desalted by gel filtration with Sephadex G-15 using 0.1 M acetic acid. The crude yields of the peptides P2, P3, P4x, P4w, and P6 were 24, 17, 29, 30, and 17%, respectively. The collected peptide solution was then applied to a column of CM-Sephadex C-25(1.7 cm by 70 cm) and eluted with a linear gradient 0.01 to 0.60 M ammonium acetate, pH 6.5, using a total volume of 1000 ml (Fig. 2). Two peaks were obtained for peptide P2, however they were found to be the same composition by means of amino acid analysis. The later peak seems to correspond to a dimer. Reversed-phase HPLC's with columns of octadecyl or 2-cyanoethyl silica gel were attempted but resulted in strong adsorption to column packings. The adsorption also occurred in the chromatography with CM-Toyopearl

(P2) AGELKKLLEELKKLLEEAKGKPGGLKKLEELLKKLEELLG

(P3) GELKKLLEELKKLLEGKPGGELKKLLEELKKLLEEAKGKPGGLKKLEELLKKLEELLG

(P4x) GELKKLLEELKKLLEECKGKPGGLKKLEELLKKLEELLG
GELKKLLEELKKLLEECKGKPGGLKKLEELLKKLEELLG

(P4w) CGELKKLLEELKKLLEEAKGKPGGLKKLEELLKKLEELLG
CGELKKLLEELKKLLEEAKGKPGGLKKLEELLKKLEELLG

(P6) CGGELKKLLEELKKLLEGKPGGELKKLLEELKKLLEEAKGKPGGLKKLEELLKKLEELLG
CGGELKKLLEELKKLLEGKPGGELKKLLEELKKLLEEAKGKPGGLKKLEELLKKLEELLG

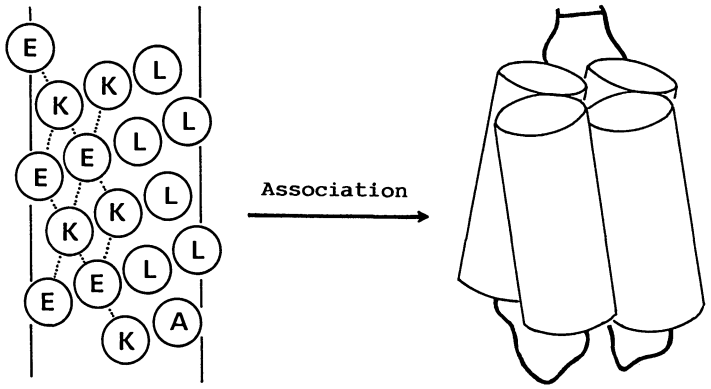

Fig. 1. Primary structures of the peptides represented with one letter abbreviations (upper) and drawing of a helical part to form bundle structure (lower). The peptides were named P2, P3, P4x, P4w, and P6 as shown in parentheses. The underlined sequences are α-helix parts predicted with the method of Chou and Fasman.[28] Cystine bonds are indicated with vertical line segments.

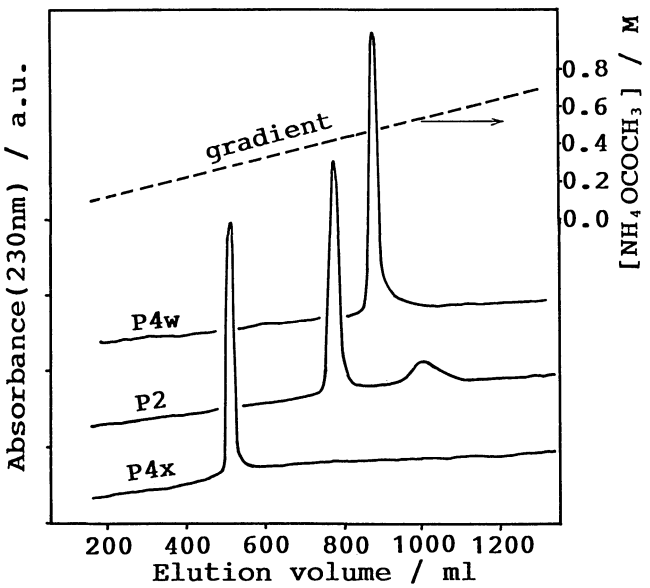

Fig. 2. Ion-exchange chromatography on CM-Sephadex C-25 with linear gradient.

650M and TSKgel G3000PW, and delayed elution was observed. Finally, the peptide was desalted by gel filtration and lyophilized to a fluffy powder.

The formation of a cystine linkage was confirmed by means of iodine titration[19] and quantitation of cysteine with di-(2-pyridyl) disulfide.[20] The amino acid compositions are listed in Table 1. The observed values have good agreements with the theoretical ones.

Table 1. Amino Acid Analyses of the Peptides[a]

Amino acid	P2	P3	P4x /2	P4w /2	P6 /2
Glu	8.91(9)	13.34(13)	8.97(9)	9.03(9)	13.38(13)
Gly	5.09(5)	7.35(8)	4.71(5)	4.82(5)	8.29(9)
Ala	1.75(2)	1.21(1)	(0)	1.00(1)	1.13(1)
Leu	13.26(13)	19.10(19)	13.31(13)	13.16(13)	19.20(19)
Lys	9.80(10)	14.32(15)	9.00(10)	9.33(10)	14.36(15)
Pro	0.93(1)	1.69(2)	0.86(1)	0.90(1)	1.81(2)

a) The values for peptides P4x, P4w, and P6 are related to their half-peptides. The values in parentheses are theoretical.

Measurement. Amino acid analyses were performed on a Hitachi 835 amino acid analyzer. Quantities of peptides were determined from amino acid analyses after hydrolysis[21] in 10 M HCl-TFA mixture (2:1, v/v) for 50 min at 165 °C. The total of the molar ratios of accurately measurable amino acids was used to calculate the peptide concentrations.

CD spectra from 195—205 nm to 260 nm were recorded using a JASCO J600 spectropolarimeter with 10 mm path length cells at a controlled temperature. Peptide concentrations were 6.0×10^{-4} M (for residue) for the measurements

of temperature and pH dependence. The denaturation with guanidine hydrochloride (GuHCl) was measured for 1.2×10^{-3} M (for residue) solution in a 1 mm cell. Mean residue molar ellipticity($[\theta]$) were reproducible within 3%. Sodium phosphate buffer (0.015 M) containing 0.15 M NaCl was used in the pH range from 2.00 to 11.00 where the pH values were adjusted with HCl or NaOH. For the solutions with pH 1.30 and pH 11.50, HCl-NaCl and NaOH-NaCl buffer were used, respectively. GuHCl solutions were prepared with stock buffer solutions of 0.015 M 3-morpholino-1-propanesulfonic acid with and without 8.0 M GuHCl. Each solution of 0—8.0 M GuHCl was adjusted to pH 7.00.

Results and Discussion

Design of Peptides. The peptides were designed to fold in helix-bundle structures (Fig. 1). The peptides P2, P3, P4x, P4w, and P6 contain 2, 3, 4, 4, and 6 helical parts, respectively. P4x and P4w are respectively cross-linked at different positions with disulfide bonds.

The principles for constructing the helical parts are proper choice of residues which tend to form α-helix and arrangement of hydrophobic and hydrophilic residues on opposite sides of a helix cylinder. The hydrophilic residues, Glu and Lys, were arranged to form a salt-bridge between positions i and $i+3$ or $i+4$ which is favored in nature.[22] The sequences of α-helical region are aligned in the order of Lys-Lys-Leu-Glu-Glu-Leu-Leu or Glu-Glu-Leu-Lys-Lys-Leu-Leu. Each helical part contains 14—17 residues and is possible to form a helix winding 4—5 times.

A loop with 5 residues or a cystine bond were used as the linkage part connecting two α-helical parts. The former is -Gly-Lys-Pro-Gly-Gly- and the latter is -Cys-Lys-, Cys-Gly- or Cys-Gly-Gly- coupled by disulfide bond. Glycine residue was chosen because it tends to form turn structures and has flexible mobility compared with α-substituted amino acid. Proline was chosen because of its specific tendency to terminate α-helix chain.[23] These residues widely occur in loop regions. As a loop region seemed to be exposed to water, lysine was added to the sequence as a hydrophilic residue.

The possible conformations of these peptides were examined with computer graphics, which showed us that the helices could associate and form a bundle structure with only a small distortion energy at a loop region. The stable association of the helices may be possible because their linkage parts have high flexibility.

CD Spectra of Peptides. The CD spectra of the peptides are shown in Fig. 3. A typical pattern of α-helix was observed for each peptide. In this condition the peptides seem to undergo little denaturation as shown later (Fig. 5). Generally, three classes, i.e. α-helix, β-sheet, and remainder, are most often used for secondary structures. However, it was pointed out that more splitted classes[24] of β-sheet are necessary

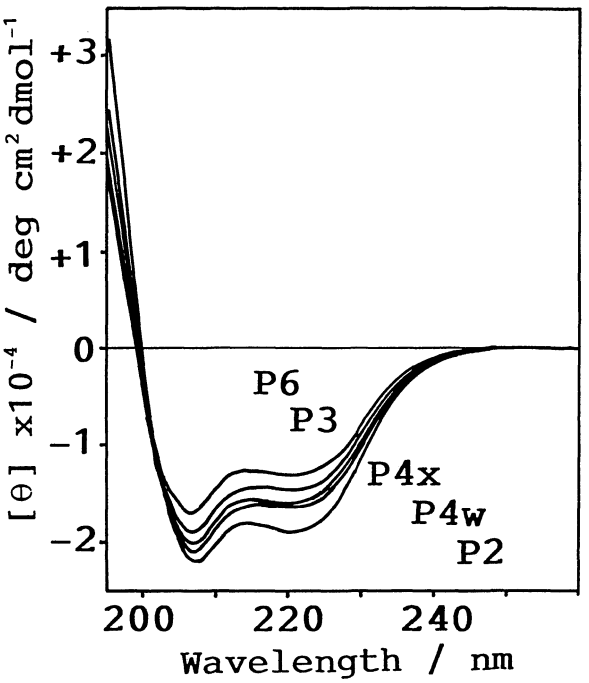

Fig. 3. CD spectra of the peptides in sodium phosphate buffer, pH 7.00, at 20 °C.

in order to obtain an improved accuracy in the analysis of CD spectra. In addition, the CD spectra of poly(amino acid)'s forming β-sheet were related to no single reference spectrum.[25] From these results, the CD analysis of β-sheet seems to be somewhat vague. The remainder structure is also vague because it has no defined structures. On the other hand, α-helix contents appears to be determinable more quantitatively than the other structures.

Chen et al.[26] introduced an empirical chain length dependent factor for a helix and obtained a good agreement with theoretical CD intensity. In Chen's equation, $[\theta]_H=[\theta]_H^\circ\cdot(1-k/n)$, mean residue ellipticity of a helix is a function of chain length, n. The parameters, $[\theta]_H^\circ$ and k, are listed in the literature.[26] According to this equation, the number, n, was calculated on the assumption that $[\theta]_{222}$ for nonhelical residues are from 1000 to 5000 deg cm^2 dmol^{-1} which are the values reported for remainder structures.[27] This leads to the results that the numbers n are smaller by about 3 to 5 per helix than the numbers predicted with the method of Chou and Fasman.[28] The helix contents with this method, which is named here "method-A", are almost consistent with the values obtained with CONTIN program[29] as listed in Table 2. The stabilization of helices with hydrophobic interaction between helices is so significant that it is difficult to interpret these reduced helix contents.

Then, we applied another method which is named "method-B" to determine helix contents. As reference data the method-B adopts the $[\theta]$ values of tropomyosin and its model peptide[30] which form "coiled-

Table 2. The Helix Contents Calculated with Various Methods

Peptide	Designed[a]	CONTIN[b]	Method-A[c]	Method-B[c]
	%	%	%	%
P2	78	60	63	82
P3	78	48	54	69
P4x	74	50	56	73
P4w	78	56	57	74
P6	75	38	49	63

a) The values were calculated with the prediction method of Chou and Fasman.[28] b) The program version 2DP(1984) of CONTIN[29] was used. c) The helix contents were determined with the method described in the text on the assumption that $[\theta]$ values for nonhelical structures were 3000 deg cm^2 dmol^{-1} at 222 nm.

coil", while the method-A and CONTIN are based on the data of familiar globular proteins. The reference $[\theta]_H^\circ$ values for method-B are −1.52, −2.45, −2.57, −2.46, −2.54, −2.67, −2.77, −2.68, −2.11, −1.38, −0.93, −0.56, −0.29, and -0.09×10^4 deg cm^2 dmol^{-1} at every 3 nm from 204 to 243 nm. In a similar manner as above, the differences between the number n and the designed number are estimated to be about −1 to 2 per helix. Thus, the helix contents with method-B are almost consistent with the designed helix contents as listed in Table 2.

Consequently, it may be concluded that the helices of our peptides are coiled-coil structure rather than "general" α-helix found in globular proteins. The peptides containing more than two helices, P3—P6, would have certain helix bundle structures constructed with coiled-coil structural units. These structures are discussed precisely in following sections. The coiled-coil structure has small distortion in comparison with "general" α-helix. This seems to cause the difference in $[\theta]_H^\circ$ values between coiled-coil and "general" α-helix.

In order to estimate the secondary structures of nonhelical parts the calculated spectra for helical regions were subtracted from the observed spectra. The subtracted spectra are converted to mean residue ellipticity and shown in Fig. 4. The spectra have large negative CD peaks at less than 205 nm and resemble the spectra of random-coiled poly(amino acid)'s which have negative peaks with the intensity about −5.0 to -2.5×10^4 deg cm^2 dmol^{-1} at 196—202 nm.[31] As the β-sheet shows positive $[\theta]$ value at this wavelength region, the nonhelical parts of our peptides are considered to have not a β-sheet but a remainder structure which is specific for our designed sequences.

Thermal Transition of the Peptides. The temperature dependence of $[\theta]_{222}$ is shown in Fig. 5. Each peptide undergoes gradual thermal transition. The slope of transition curves is not steep compared with CM-tropomyosin but similar to that of Hodges' peptide.[30] The helices of the peptides are not fully denatured even at 90 °C. The peptide P2 is the most stable and its transition curve is different from the others. It is suggested that the peptide with two amphiphilic helices make a stable folded structure while more than two helices results in somewhat different folded structure containing a helix associated by weaker interac-

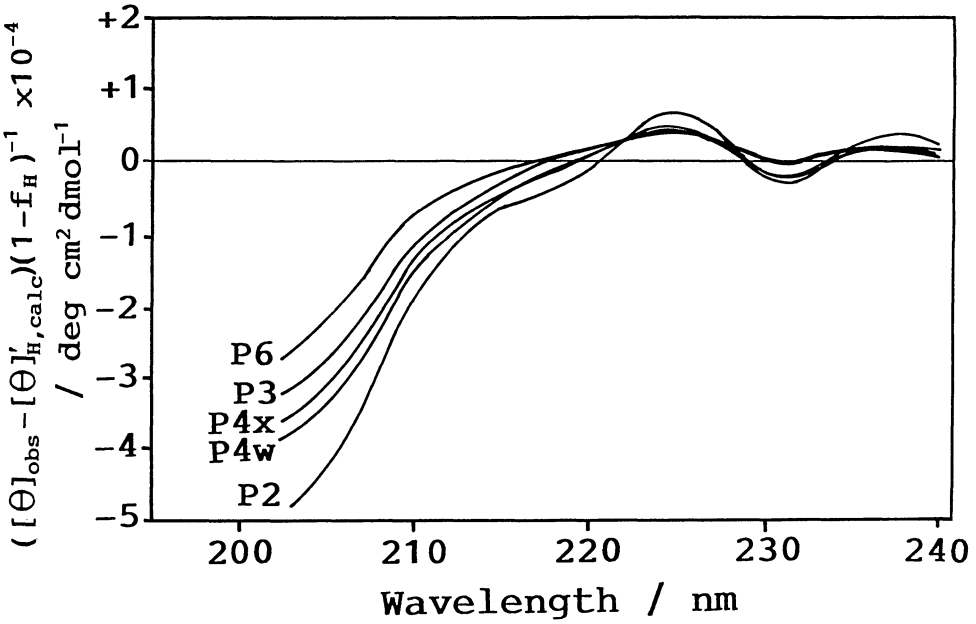

Fig. 4. Remained CD spectra after subtracting those of α-helical parts. $[\theta]_{obs}$, $[\theta]_{H,calc}$ are mean residue ellipticities which are observed and calculated for helical parts, respectively and f_H is a mole fraction of helical residue.

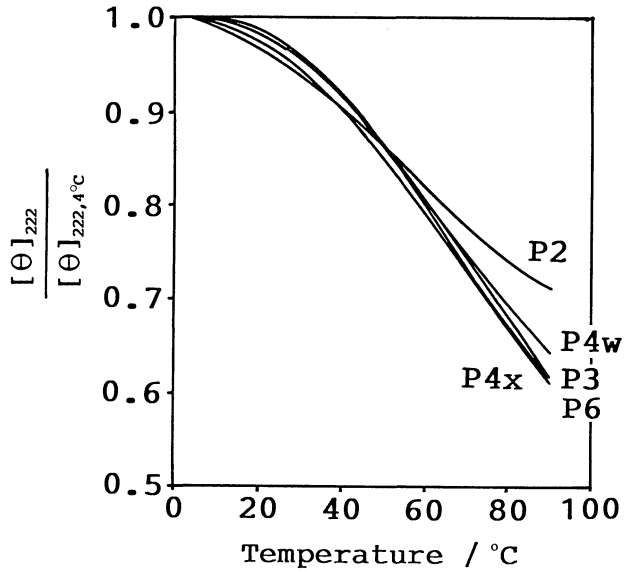

Fig. 5. Temperature dependence of mean residue ellipticity at 222 nm in phosphate buffer, pH 7.00. The values of $[\theta]_{222}$ are normalized at 4 °C.

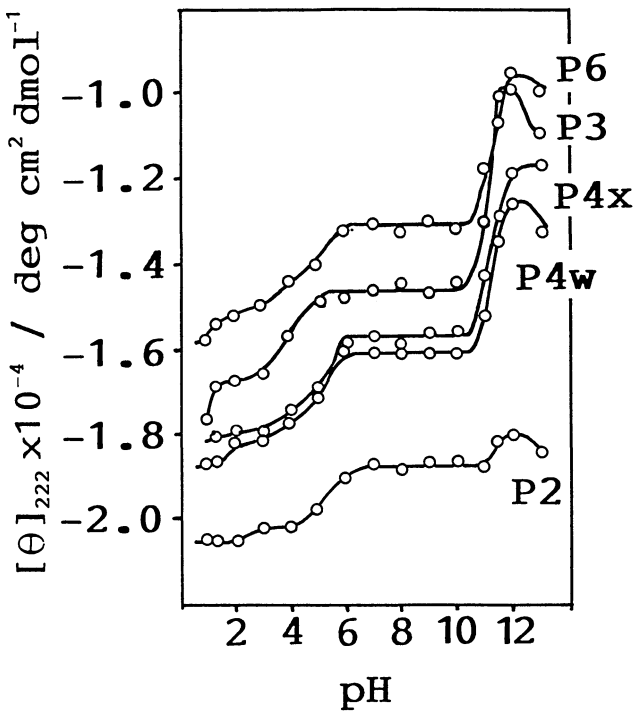

Fig. 6. The pH dependence of mean residue ellipticity at 222 nm.

tion. The disulfide bond does not appear to make a major contribution to the stability.

pH Dependence. The pH dependence of $[\theta]_{222}$ are shown in Fig. 6. For each peptide the intensity at 222 nm is constant at pH 6 to 11. These five peptides have a common tendency that the negative intensity increases in acidic conditions and decreases in basic conditions. The pH regions of the both transitions are consistent with pK_a of Glu and Lys side chains. At pH 12 the spectra are characteristic pattern of α-helix. Though only Glu side chains dissociate in this basic conditions, the denaturation of helices is restricted to some extent. Some denaturation may be attributed to weakened amphiphilicity because the Glu residues exist only at every two turns of helix.

In contrast to the basic conditions, the acidic ones cause a negative shift of $[\theta]_{222}$. The intensity increases by about 20%. If this is due to the increase of a helix content, the linkage region of the peptide will be shortened and become difficult to make a helix bundle. Therefore, it is reasonable to consider that the helix contents are constant but the type of helix changes from coiled-coil to otherwise "general" helix found in globular proteins. This change seems to result in the increase of the intensity of $[\theta]_H^0$ as discussed in the previous section.

As mentioned by Eisenberg et al.,[32] apolar carbon atoms of hydrophilic residues such as Lys and Glu have significant contributions to the stability of the folded structure of proteins. So, even if hydrophilicity is reduced in acidic or basic solutions, where either Lys or Glu is ionized, the helices of these peptides may not be necessarily denatured. The experimental results suggest that the helices of these peptides are susceptible to denaturation only at basic pH. As Lys has a long methylene side chain, non-protonated Lys at basic pH play a role as more hydrophobic residue

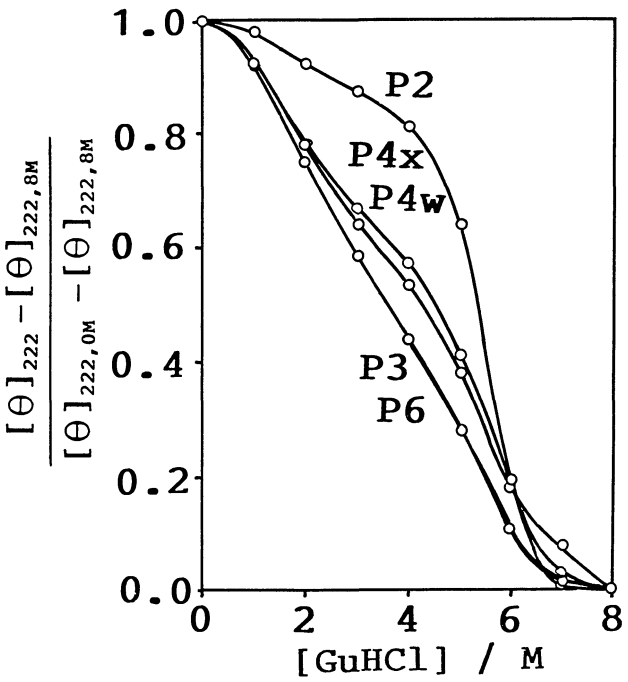

Fig. 7. Guanidine denaturation curves. The values of $[\theta]_{222}$ are normalized to be 1.0 in 0 M GuHCl and 0.0 in 8 M GuHCl. The ellipticities of these peptides in 8 M GuHCl were about 500—900 deg cm^2 dmol^{-1}.

than Glu at acidic pH, which is exposed to water and make α-helix unstable. Insufficient amphiphilicity would cause partial denaturation of helices in basic solutions. Thus, amphiphilicity is important in stabilizing α-helices.

Denaturation with Guanidine Hydrochloride. The helix structures were denatured with the increase of GuHCl concentration and $[\theta]_{222}$ values became about 1000 deg cm^2 dmol^{-1} in 8 M GuHCl. The relative changes of $[\theta]_{222}$ are shown in Fig. 7. The denaturation of P2 is a very steep transition in comparison with those of the other peptides. The midpoint of denaturation for P2 was shifted to a little higher GuHCl concentration when the peptide concentration was increased. This means that intermolecular association occurs in addition to intramolecular association of helices.

Each denaturation curve shows the fine structure that the first transition occurs at 2—3 M of GuHCl and the second at 5—6 M. For the peptide P2 the second transition is a major one, however for the other peptides almost the half of helices is subject to the first transition. It is reported that the peptide containing single amphiphilic α-helical strand takes α-helix form in associating with each other but that it can not form α-helix when isolated in a dilute solution.[9] Therefore, in our conditions no isolated α-helices exist. As all helices are not destroyed in the first denaturation step, the association of helices would exist even up to the second denaturation. So, both transitions relate to changes in association forms. These two types of transition can be explained by two types of interaction constructing a bundle structure. One of these interactions is relatively weak attractive force and the combined helices are susceptible to denaturation.

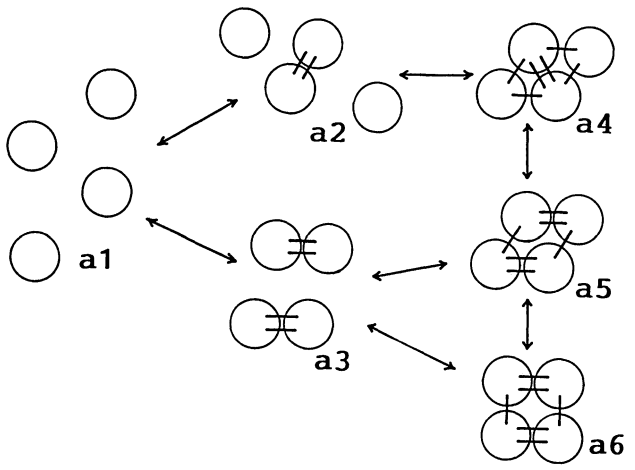

Fig. 8. Probable folded structures and defolding course. An example of 4-helix bundle is illustrated. Each circle represents α-helix as an axial view. Loose and tight contacts are represented with single (-) and double (=) line segments, respectively.

Another interaction brings about close contact of helices like coiled-coil structures.

Defolding Model of Linked Helices. In summarizing the results of denaturation experiments we can assume preliminary model for defolding as drawn in Fig. 8. It is considered that the association of helices is constructed with both loose and tight contacts. Most of P2 molecules take a folded structure with a tight contact, whereas some helices of the other peptides make a loose contact.

The experimental results of GuHCl denaturation are interpreted as follows. As described in the previous section, P2 takes an associated form such as $(P2)_2$. Most of P2 molecules take structures of **a5** or **a6** and turn to **a3** through the first denaturation point at 2—3 M GuHCl. In this course the helices are not subjected to deformation. On the other hand, not a minor molecules of P4x and P4w seem to take structures of **a4**. Through the first denaturation point they turn to **a2** and two helices among four undergo a denaturation, so that the total helix content decreases. The second denaturation point at about 6 M GuHCl is assumed to be related to a destruction of tight contact of helices like **a3** which results in entire transition to random coils. The denaturation of P3 and P6 is explained similarly to P4x and P4w but the number of associated helices could not be determined by only these experiments. It is interesting that the fractions corresponding to the first transition of P3 and P6 are a little larger than those of P4x and P4w. P3 and P6 may have more complicated association forms with loose contact.

The denaturation in basic solution can be explained by a similar consideration. As shown in Fig. 6, $[\theta]_{222}$ of P2 does not change largely in comparison with the others in a condition from neutral to basic. This course is assumed to be a denaturation of a loose contact. As most of P2 is related to a tight contact, the change of $[\theta]_{222}$ seems to result in a small change.

Richmond[33] gave the geometrical data for a packing of helices, that is, the inter-axial distance between helices is 1.05 nm and the outermost surface of leucine residue is 0.74 nm apart from a helix axis. These data lead to a consideration that on the average almost one residue contained in a winding pitch of α-helix contributes to hydrophobic interaction between two helices. As our helices contain -Leu- and -Leu-Leu- alternately in winding pitches, one of serial Leu residues may participate in a loose contact of helices.

It is interesting that our peptide P4w and peptide α4 designed by DeGrado et al.[1] show different GuHCl denaturation curves from each other nevertheless both are made of 4 helical parts. This means that the linkage parts play a significant role to array helices. The flexible mobility of our linkage parts results in two steps of denaturation. The design of linkage parts will be important for specific functions of artificial proteins.

References

1) W. F. DeGrado, Z. R. Wasserman, and J. D. Lear, *Science*, **243**, 622 (1989).
2) M. Mutter and S. Vuilleumier, *Angew. Chem., Int. Ed. Engl.*, **28**, 535 (1989).
3) F. R. Carbone and S. J. Leach, *Int. J. Pept. Protein Res.*, **26**, 225 (1985).
4) E. T. Kaiser and F. J. Kézdy, *Science*, **223**, 249 (1984).
5) R. Moser, S. Frey, K. Münger, T. Hehlgans, S. Klauser, H. Langen, E.-L. Winnacker, R. Mertz, and B. Gutte, *Protein Eng.*, **1**, 339 (1987).
6) F. H. C. Crick, *Acta Crystallogr.*, **6**, 689 (1953).
7) P. C. Weber and F. R. Salemme, *Nature*, **287**, 82 (1980).
8) N. Nishino, Y. Sugita, T. Yamamoto, and T. Fujimoto, *Rep. Asahi Glass Found. Ind. Technol.*, **48**, 149 (1986).
9) S. P. Ho and W. F. DeGrado, *J. Am. Chem. Soc.*, **109**, 6751 (1987).
10) L. Regan and W. F. DeGrado, *Science*, **241**, 976 (1988).
11) M. Mutter and G. Tuchscherer, *Makromol. Chem. Rapid Commun.*, **9**, 437 (1988).
12) IUPAC-IUB Comm. Biochem. Nomencl., *Arch. Biochem. Biophys.*, **125**, i—v (1968).
13) A. R. Mitchell, S. B. H. Kent, M. Engelhard, and R. B. Merrifield, *J. Org. Chem.*, **43**, 2845 (1978).
14) N. Ikota, T. Shioiri, S. Yamada, and S. Tachibana, *Chem. Pharm. Bull.*, **28**, 3347 (1980).
15) B. F. Gisin and R. B. Merrifield, *J. Am. Chem. Soc.*, **94**, 3102 (1972).
16) D. F. Veber, J. D. Milkowski, S. L. Varga, R. G. Denkewalter, and R. Hirschmann, *J. Am. Chem. Soc.*, **94**, 5456 (1972).
17) H. Morii and K. Ichimura, *Bull. Chem. Soc. Jpn.*, **62**, 2730 (1989).
18) J. P. Tam, W. F. Heath, and R. B. Merrifield, *J. Am. Chem. Soc.*, **108**, 5242 (1986).
19) M. J. F. Diez, D. T. Osuga, and R. E. Feenay, *Arch. Biochem. Biophys.*, **107**, 449 (1964).
20) D. R. Grassetti and J. F. Murray, *Arch. Biochem. Biophys.*, **119**, 41 (1967).
21) A. Tsugita and J.-J. Scheffler, *Proc. Jpn. Acad., Ser. B*, **58**, 1 (1982).
22) M. Sundaralingam, Y. C. Sekharudu, N. Yathindra, and V. Ravichandran, *Proteins*, **2**, 64 (1987).
23) P. J. Flory, "Statistical Mechanics of Chain Molecules," John Wiley & Sons, New York (1969), Chap. 7.
24) I. A. Bolotina, V. O. Chekhov, and V. Y. Lugauskas, *Int. J. Quantum Chem.*, **16**, 819 (1979).
25) P. K. Sarkar and P. Doty, *Proc. Natl. Acad. Sci. U.S.A.*, **55**, 981 (1966).
26) Y.-H. Chen, J. T. Yang, and K. H. Chau, *Biochemistry*, **13**, 3350 (1974).
27) K. Hamaguchi and H. Takesada, "Tanpakushitu No Senkousei," Gakkai Syuppan Center, Tokyo (1971), Chap. 3.
28) P. Y. Chou and G. D. Fasman, *Biochemistry*, **13**, 222 (1974).
29) S. W. Provencher and J. Glockner, *Biochemistry*, **20**, 33 (1981).
30) R. S. Hodges, A. K. Saund, P. C. S. Chong, S. A. St.-Oierre, and R. E. Reid, *J. Biol. Chem.*, **10**, 1214 (1981).
31) A. J. Adler, R. Hoving, J. Potter, M. Wells, and G. D. Fasman, *J. Am. Chem. Soc.*, **90**, 4736 (1968).
32) D. Eisenberg and A. D. McLachlan, *Nature*, **319**, 199 (1986).
33) T. J. Richmond and F. M. Richards, *J. Mol. Biol.*, **119**, 537 (1978).

Trialkylborane as an Initiator and Terminator of Free Radical Reactions. Facile Routes to Boron Enolates via α-Carbonyl Radicals and Aldol Reaction of Boron Enolates

Kyoko NOZAKI, Koichiro OSHIMA,* and Kiitiro UTIMOTO*
Department of Industrial Chemistry, Faculty of Engineering, Kyoto University, Sakyo-ku, Kyoto 606
(Received August 29, 1990)

A variety of trialkylborane-induced reactions were examined for the preparation of the α-carbonyl radicals: (1) addition of alkyl radical to methyl vinyl ketone, (2) reduction of α-halo ketone, and (3) intramolecular radical addition to α,β-unsaturated carbonyl moiety. Trialkylborane reacted with α-carbonyl radicals to give boron enolates. The resulting boron enolates were efficiently trapped by carbonyl compounds to give β-hydroxy ketones in good yields.

For the past two decades, there have been much effort to develop the utility of organoborane compounds in organic synthesis. Radical reaction is one of the most important synthetic methods in organoborane chemistry.[1] The 1,4-addition of R_3B to α,β-unsaturated carbonyl compounds was reported by Suzuki et al. in 1967.[2] Generally, trialkylboranes react with neither carbonyl compounds nor carbon-carbon unsaturated bonds. The unusual reactivity of α,β-unsaturated carbonyl compounds was originally explained by six-membered ring transition state. Further investigation by Suzuki and Brown[3] proved this reaction to proceed via radical mechanism by the fact that 5 mol% of galvinoxyl free radical (2,6-di-*t*-butyl-α-(3,5-di-*t*-butyl-4-oxo-2,5-cyclohexadien-1-ylidene)-*p*-tolyloxyl free radical) completely interrupted the reaction (Scheme 1).[4]

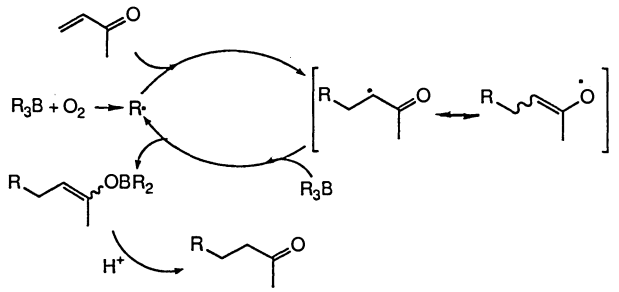

Scheme 1.

The structure of the intermediate boron enolate was confirmed with ^1H NMR by Köster et al.[5,6] We came to be interested in this radical trapping step where α-carbonyl radical reacted with trialkylborane to give boron enolate. In this paper we would like to report radical reactions in which trialkylborane acts as an initiator of radical reactions and, at the same time, works as a terminator to trap the α-carbonyl radical.[7]

First, addition of other radicals than R group of trialkylborane (R_3B) to α,β-unsaturated carbonyl compounds was investigated as a method to obtain α-carbonyl radicals. It is known that trialkylborane reduces active halides, such as benzyl bromide, via radical mechanism. Alkyl radical generated by the reaction of trialkylborane with oxygen abstracts the bromine atom of benzyl bromide to give benzyl radical.[1] We treated *t*-butyl iodide with triethylborane in the hope that *t*-butyl radical would be formed by the action of ethyl radical and that *t*-butyl radical would react with α,β-unsaturated carbonyl compound prior to ethyl radical. In fact, treatment of *t*-butyl iodide (3.0 mmol) with triethylborane[8] (1.0 mmol) in benzene in the presence of methyl vinyl ketone (1.0 mmol) and benzaldehyde (1.0 mmol) gave the three component coupling product **4a** (63% yield as a 66/34 diastereomeric mixture) along with the compound **4e** (2% yield) derived from the reaction of ethyl radical instead

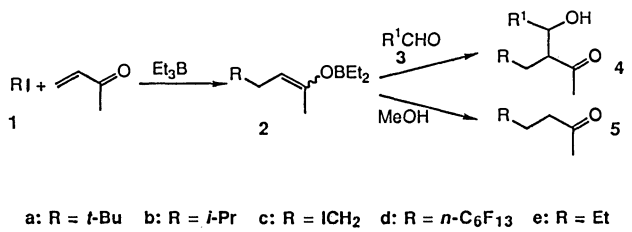

a: R = *t*-Bu b: R = *i*-Pr c: R = ICH_2 d: R = *n*-C_6F_{13} e: R = Et

Scheme 2.

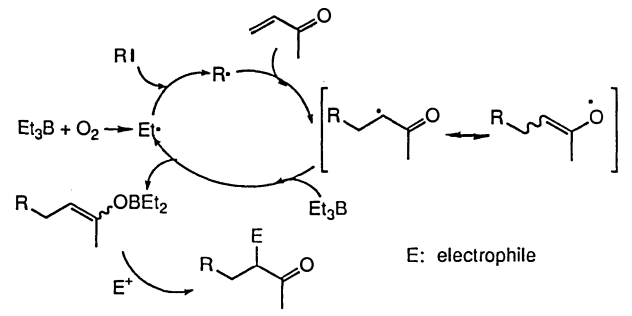

Scheme 3.

of *t*-butyl radical (Scheme 2). We are tempted to assume the following radical cycle reaction mechanism (Scheme 3).

The success of the reaction is ascribed to the characteristics of Et_3B which plays critical two roles: (1) initiation of the radical reaction generating *t*-butyl radical from *t*-butyl iodide and (2) trapping the formed α-carbonyl radical as a boron enolate. Primary iodide such as methyl iodide did not give satisfactory results because ethyl radical from triethylborane competed with primary alkyl radical from alkyl iodide and a mixture of two products were obtained. Not only secondary or tertiary alkyl iodide but also diiodide or perfluoroalkyl iodide such as diiodomethane, perfluorohexyl iodide gave the corresponding adducts in good yield. In the case of Suzuki-Brown's or Köster's work, the nature of the alkyl radicals adding to methyl vinyl ketone are limited because they have to be attached on boron atom directly and therefore hydroboration was mainly used for the preparation of radical sources as trialkylboranes. Meanwhile, in our method, variety of radicals can be used for this purpose taking advantage of the reductive nature of trialkylborane. Methanol worked as an electrophile so efficient as aldehydes affording β-alkylated ketones. The results are summarized in Table 1. In the reaction of diiodomethane, methyl vinyl ketone, and methanol, the use of trioctylborane instead of Et_3B gave octyl iodide indicating the reduction of diiodomethane by octyl radical.

Second, one-electron reduction of α-halo ketones with Ph_3Sn radical was employed to produce α-carbonyl radicals. Recently we have shown that Et_3B is an effective initiator to give triaryltin or triarylgermanium radical from their corresponding hydride in the presence of trace amount of oxygen,[9,10] and that the new system, R_3SnH-Et_3B, enabled us to provide highly selective free radical reactions at lower temperature, e.g. −78 °C.[10,11] Here, this R_3SnH-Et_3B system was utilized for the reductive enolization of α-halo ketones.[12]

The Reformatsky type reaction was carried out as follows. Triethylborane (1.1 mmol) was added to a solution of α-bromo ketone (1.0 mmol) and aldehyde (1.0 mmol) in benzene at 25 °C under an argon atmosphere. To this mixture was slowly added Ph_3SnH (1.0 mmol) to afford β-hydroxy ketone in good yield. In this reaction Et_3B worked as (1) an initiator of the radical reaction generating triphenyltin radical and (2) a terminator trapping the α-carbonyl radical as a boron enolate. The representative results are shown in Table 2. The reaction proceeded chemoselectively so that only formyl group reacted in the presence of ketone (Entries 2 and 14 in Table 2). Whereas the reaction of 7-bromo-6-dodecanone with benzaldehyde gave a mixture of *erythro*- and *threo*-β-hydroxy carbonyl compound (Entry 12 in Table 2), α-bromocyclopentanone or α-bromocyclohexanone provided *threo* adducts with high stereoselectivities.[13] The presence of 5 mol% of galvinoxyl effectively stopped the reaction of α-bromoacetophenone and benzaldehyde. This reaction can be explained by the following radical cycle (Scheme 4).

The reaction of α-iodo ketones with carbonyl compounds proceeded without Ph_3SnH. For instance, an addition of Et_3B to a solution of α-iodoacetophenone and benzaldehyde in benzene gave 1,3-diphenyl-3-hydroxy-1-propanone in 86% yield.[14] The results are also shown in Table 2. The *erythro/threo* ratios of the products were exactly the same as those obtained from the reaction of α-bromo ketones. In this reaction Et_3B also worked as (1) an initiator of the radical reaction generating α-carbonyl radical from α-iodo ketone and (2) a terminator trapping this radical as a boron enolate. The presence of 5 mol% of galvinoxyl also interrupted the reaction of α-iodoacetophenone and benzaldehyde effectively.

Table 1. Coupling Reaction of Alkyl Iodide, Methyl Vinyl Ketone, and Electrophiles

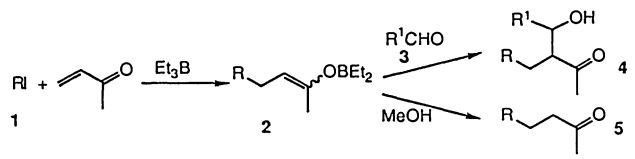

a: R = *t*-Bu b: R = *i*-Pr c: R = ICH_2 d: R = *n*-C_6F_{13} e: R = Et

Entry	RI	R^1CHO or MeOH	Product yield (%) *erythro/threo*
1	*t*-BuI	MeOH	**5a** (79), **5e** (5)
2	*t*-BuI	PhCHO	**4a** (63, 66/34), **4e** (4)
3	*i*-PrI	MeOH	**5b** (79), **5e** (15)
4	*i*-PrI	PhCHO	**4b** (58, 71/29), **4e** (21)
5	*i*-PrI	*n*-$C_6H_{13}CHO$	**4b** (56, 73/27), **4e** (18)
6	CH_2I_2	MeOH	**5c** (69)
7	CH_2I_2	PhCHO	**4c** (74, 61/39)
8	*n*-$C_6F_{13}I$	MeOH	**5d** (62), **5e** (2)
9	*n*-$C_6F_{13}I$	PhCHO	**4d** (31, 77/23), **4e** (2)

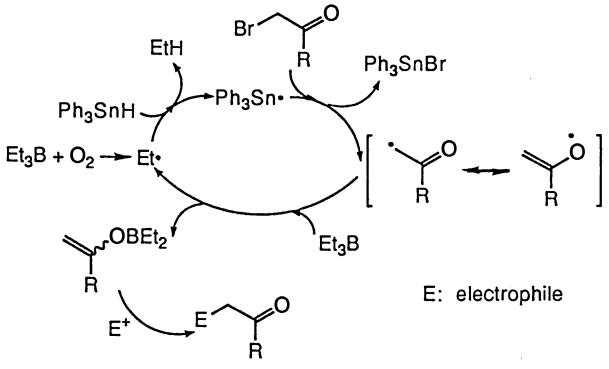

Scheme 4.

Table 2. Reformatsky Type Reaction Mediated by Triethylborane

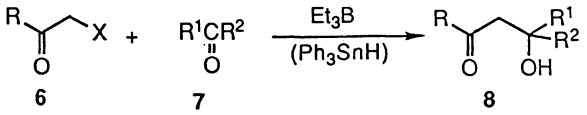

Entry	α-Halo ketone **6**	Carbonyl compound **7**	Product **8**		
				Yield/%	*erythro/threo*
1	α-Bromoacetophenone	PhCHO	**8a**	88	—
2		$CH_3C(O)(CH_2)_8CHO$	**8b**	78	—
3		cyclohexanone	**8c**	81	—
4	2-Bromocyclopentanone	PhCHO	**8d**	92	15/85
5		n-$C_6H_{13}CHO$	**8e**	77	8/92
6		i-PrCHO	**8f**	73	3/97
7		t-BuCHO	**8g**	83	0/100
8	2-Bromocyclohexanone	PhCHO	**8h**	74	22/78
9		n-$C_6H_{13}CHO$	**8i**	82	2/98
10		i-PrCHO	**8j**	76	9/91
11		t-BuCHO	**8k**	82	0/100
12	7-Bromo-6-dodecanone	PhCHO	**8l**	80	65/35
13	α-Iodoacetophenone	PhCHO	**8a**	86	—
14		$CH_3C(O)(CH_2)_8CHO$	**8b**	76	—
15		cyclohexanone	**8c**	77	—
16	2-Iodocyclopentanone	n-$C_6H_{13}CHO$	**8e**	64	6/94
17		i-PrCHO	**8f**	75	3/97
18		t-BuCHO	**8g**	70	0/100
19	2-Iodocyclohexanone	PhCHO	**8h**	83	20/80
20		i-PrCHO	**8j**	68	6/94
21		t-BuCHO	**8k**	72	0/100

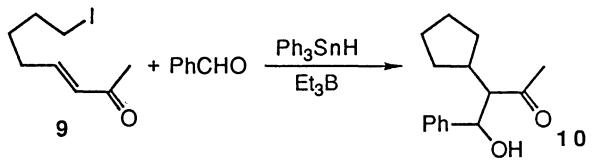

Third, we synthesized 8-iodo-3-octen-2-one (**9**) expecting the intramolecular cyclization under reductive conditions to give an α-carbonyl radical. Treatment of **9** and benzaldehyde with Ph_3SnH-Et_3B gave the cyclized aldol adduct (**10**) in 70% (a mixture of *erythro/threo* or *threo/erythro*=63/37).

To the best of our knowledge, there had been no practical method for this one step cyclization-aldol condensation reaction. 8-Iodo-3-octen-2-one was synthesized from 5-iodopentanal by Horner-Wadsworth-Emmons reaction.[15]

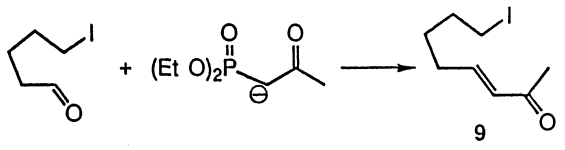

Experimental

Distillation of the products was performed by the use of Kugelrohr (Büchi), and boiling points are indicated by an air bath temperature without correction. All melting points were obtained on a Yanaco MP-50929 melting points apparatus and are uncorrected. The IR spectra were determined on a JASCO IR-810 spectrometer, the mass spectra on a Hitachi M-80 machine, the ^1H and ^{13}C NMR spectra on a Varian XL-200 spectrometer. The chemical shifts of the ^1H NMR are given in δ with Me_4Si as an internal standard, and those of the ^{13}C NMR are given in δ with $CDCl_3$. The analyses were carried out by the staff at the Elemental Analyses Center of Kyoto University. Tetrahydrofuran was freshly distilled from sodium benzophenone ketyls. Purification of products was performed by column chromatography or preparative thin-layer chromatography (TLC) on silica gel.

General Procedure for Three Component Coupling Reaction of Alkyl Iodide, Methyl Vinyl Ketone, and Carbonyl Compound. The reaction of t-BuI and methyl vinyl ketone with benzaldehyde is representative. A benzene solution of methyl vinyl ketone (70 mg, 1.0 mmol) was added to a solution of t-butyl iodide (0.55 g, 3.0 mmol), Et_3B (1.0 M hexane solution, 1 M=1 mol dm^{-3}, 1.0 ml, 1.0 mmol), and benzaldehyde (0.11 g, 1.0 mmol) in benzene at 25 °C under an argon atmosphere. After stirring for 5 min, concentration of the resulting mixture in vacuo followed by purification by preparative TLC gave 3-(α-hydroxybenzyl)-5,5-dimethyl-2-hexanone (**4a**, 0.15 g) in 63% yield (*erythro/threo*=71/29) along with 3-(α-hydroxybenzyl)-2-hexanone (**4e**, 5 mg, 2%, *erythro/threo*=70/30). Assignment of the stereochemistry of *erythro*- and *threo*- isomers was based on the chemical shift and coupling constant of the carbinol proton (PhCH (OH)R). Heathcock et al. have reported that *threo*-isomers exhibited signals of larger coupling

constant at higher field than those for protons in *erythro*-isomers for the aldol type adduct PhCH(OH)CH(Me)C(=O)R.[16]

erythro-3-(α-Hydroxybenzyl)-5,5-dimethyl-2-hexanone (*erythro*-**4a**): Mp 87.8—88.0 °C (hexane); R_f=0.38 (hexane/ethyl acetate=3/1); IR (neat, before crystallization) 3426, 3024, 2934, 1686, 1466, 1390, 1364, 1055, 743, 699 cm^{-1}; ^{1}H NMR δ=0.74 (s, 9H), 1.60 (dd, *J*=1.4, 14.1 Hz, 1H), 1.87 (dd, *J*=9.7, 14.1 Hz, 1H), 2.02 (s, 3H), 2.42 (d, *J*=2.6 Hz, 1H, -OH), 2.95 (ddd, *J*=1.4, 5.5, 9.7 Hz, 1H, RCHC(=O)Me), 4.75 (dd, *J*=2.6, 5.5 Hz, 1H, PhCH(OH)R), 7.37 (bs, 5H). Found: C, 76.88; H, 9.46%. Calcd for $C_{15}H_{22}O_2$: C, 76.87; H, 9.68%.

threo-3-(α-Hydroxybenzyl)-5,5-dimethyl-2-hexanone (*threo*-**4a**): Bp 150 °C (bath temp, 1.0 Torr, 1 Torr=133.322 Pa); R_f=0.31 (hexane/ethyl acetate=3/1); IR (neat) 3404, 3028, 2954, 2864, 1701, 1474, 1365, 1156, 699 cm^{-1}; ^{1}H NMR δ=0.77 (s, 9H), 1.20 (dd, *J*=2.2, 14.2 Hz, 1H), 1.79 (dd, *J*=9.4, 14.2 Hz, 1H), 2.15 (s, 3H), 2.68 (bs, 1H, -OH), 3.05 (ddd, *J*=2.2, 7.4, 9.4 Hz, 1H, RCHC(=O)Me), 4.62 (bd, *J*=7.4 Hz, 1H, PhCH(OH)R). Found: C, 76.60; H, 9.46%. Calcd for $C_{15}H_{22}O_2$: C, 76.88; H, 9.46%.

erythro-3-(α-Hydroxybenzyl)-2-hexanone (*erythro*-**4e**): R_f=0.42 (hexane/ethyl acetate=3/1); IR (neat) 3340, 2956, 2928, 2870, 1701, 1458, 1356, 700 cm^{-1}; ^{1}H NMR δ=0.85 (t, *J*=7.2 Hz, 3H), 1.10—1.40 (m, 2H), 1.55—1.80 (m, 2H), 2.00 (s, 3H), 2.74 (d, *J*=2.5 Hz, 1H, -OH), 2.90 (m, 1H), 4.88 (dd, *J*=2.5, 5.8 Hz, 1H, PhCH(OH)R), 7.40 (s, 5H). Found (for a mixture of *erythro*/*threo*=70/30): C, 75.56; H, 8.88%. Calcd for $C_{13}H_{18}O_2$: C, 75.69; H, 8.79%.

threo-3-(α-Hydroxybenzyl)-2-hexanone(*threo*-**4e**): R_f=0.35 (hexane/ethyl acetate=3/1); IR (neat) 3362, 2956, 2930, 2870, 1702, 1453, 1357, 760, 699 cm^{-1}; ^{1}H NMR δ=0.82 (t, *J*=6.8 Hz, 3H), 1.15—1.40 (m, 3H), 1.45—1.70 (m, 2H), 2.15 (s, 3H), 2.94 (dt, *J*=3.4, 7.8 Hz, 1H), 4.77 (d, *J*=7.8 Hz, 1H, PhCH(OH)R), 7.40 (bs, 5H).

***erythro*-4-Hydroxy-3-(2-methylpropyl)-2-decanone (*erythro*-4b):** Bp 140 °C (bath temp, 1.0 Torr, for a mixture of *erythro*/*threo*=73/27); R_f=0.36 (hexane/ethyl acetate=5/1); IR (neat, for a mixture of *erythro*/*threo*=73/27) 3428, 2952, 2928, 2858, 1701, 1467, 1355 cm^{-1}; ^{1}H NMR δ=0.85—1.03 (m, 9H), 1.20—1.82 (m, 14H), 2.21 (s, 3H), 2.70 (m, 1H, RCHC(=O)Me), 3.81 (m, 1H, R^1R^2CHOH). Found (for a mixture of *erythro*/*threo*=73/27): C, 73.35; H, 12.48%. Calcd for $C_{14}H_{28}O_2$: C, 73.63; H, 12.36%.

***threo*-4-Hydroxy-3-(2-methylpropyl)-2-decanone (*threo*-4b):** R_f=0.36 (hexane/ethyl acetate=5/1); ^{1}H NMR δ=0.85—1.03 (m, 9H), 1.20—1.82 (m, 14H), 2.22 (s, 3H), 2.65 (m, 1H, RCHC(=O)Me), 3.70 (m, 1H, R^1R^2CHOH).

***erythro*-3-(α-Hydroxybenzyl)-5-iodo-2-pentanone (*erythro*-4c):** The title compound quickly decomposed at room temperature under air. R_f=0.27 (hexane/ethyl acetate=3/1); IR (neat, for a mixtire of *erythro*/*threo*=61/39) 3382, 2920, 1702, 1492, 1453, 1356, 1175, 1051, 1025, 762, 700 cm^{-1}; ^{1}H NMR δ=2.08 (s, 3H), 2.15 (m, 1H), 2.45 (m, 1H, -OH), 3.00 (m, 2H), 4.98 (d, *J*=5.6 Hz, 1H, PhRCHOH), 7.35 (bs, 5H).

***threo*-3-(α-Hydroxybenzyl)-5-iodo-2-pentanone (*threo*-4c):** The title compound also quickly decomposed at room-temperature under air. R_f=0.27 (hexane/ethyl acetate=3/1); ^{1}H NMR δ=2.20 (s, 3H), 2.15 (m, 1H), 2.45 (m, 1H, -OH), 3.00 (m, 2H), 4.79 (d, *J*=7.3 Hz, 1H, PhRCHOH), 7.35 (bs, 5H).

The structures of *erythro*- and *threo*-3-(α-hydroxybenzyl)-5-iodo-2-pentanones were confirmed by the reduction of the compounds with *n*-Bu_3SnH–Et_3B to give the corresponding aldol adduct. Tributyltin hydride (0.26 g, 0.90 mmol) and Et_3B (1.0 M in hexane, 0.10 ml, 0.10 mmol) were added to a mixture of *erythro*-**4c**/*threo*-**4c** (161 mg, 0.51 mmol/104 mg, 0.32 mmol) in benzene at 25 °C under an argon atmosphere. After stirring for 1 day to this mixture were added KF (100 mg) and water (1.0 ml). The resulting heterogeneous mixture was stirred vigorously. Filtration, concentration of the organic layer, and purification by silica-gel column chromatography gave 76 mg (0.48 mmol) of *erythro*-3-(α-hydroxybenzyl)-2-pentanone (78% yield) and 48 mg of its *threo*-isomer (78% yield).

erythro-3-(α-Hydroxybenzyl)-2-pentanone: Bp 100 °C (1.0 Torr, bath temp); R_f=0.40 (hexane/ethyl acetate=3/1); IR (neat) 3402, 2964, 2876, 1702, 1456, 1359, 1026, 764, 701 cm^{-1}; ^{1}H NMR δ=0.86 (t, *J*=7.5 Hz, 3H), 1.60—1.85 (m, 2H), 2.02 (s, 3H), 2.75 (bs, 1H, -OH), 2.84 (m, 1H), 4.90 (d, *J*=6.0 Hz, 1H, RPhCHOH), 7.35 (bs, 5H). Found: C, 74.97; H, 8.46%. Calcd for $C_{12}H_{16}O_2$: C, 74.97; H, 8.39%.

threo-3-(α-Hydroxybenzyl)-2-pentanone: Bp 100 °C (1.0 Torr, bath temp); R_f=0.40 (hexane/ethyl acetate=3/1); IR (neat) 3412, 2964, 2932, 2876, 1703, 1455, 1358, 1213, 1169, 767, 701 cm^{-1}; ^{1}H NMR δ=0.83 (t, *J*=7.5 Hz, 3H), 1.30—1.75 (m, 2H), 2.16 (s, 3H), 2.78 (bs, 1H, -OH), 2.87 (m, 1H), 4.80 (d, *J*=7.9 Hz, RPhCHOH), 7.35 (bs, 5H). Found: C, 74.75; H, 8.56%. Calcd for $C_{12}H_{16}O_2$: C, 74.97; H, 8.39%.

***erythro*-5,5,6,6,7,7,8,8,9,9,10,10,10-Tridecafluoro-3-(α-hydroxybenzyl)-2-decanone (*erythro*-4d):** R_f=0.47 (hexane/ethyl acetate=3/1); white solid; IR (neat before crystallization, for a mixture of *erythro*/*threo*=77/23) 3406, 1714, 1364, 1240, 1194, 1145, 1107, 1044, 766, 731, 701 cm^{-1}; ^{1}H NMR δ=2.17 (s, 3H), 2.64 (d, *J*=5.5 Hz, 1H, -OH), 2.75 (m, 2H), 2.70 (m, 1H, R^1R^2CHC(=O)Me), 4.76 (dd, *J*=5.5, 7.2 Hz, 1H, PhCH(OH)R), 7.33 (m, 5H). Found (for a mixture of *erythro*/*threo*=77/23): C, 41.11; H, 2.61%. Calcd for $C_{17}H_{13}O_2F_{13}$: C, 41.14; H, 2.64%.

***threo*-5,5,6,6,7,7,8,8,9,9,10,10,10-Tridecafluoro-3-(α-hydroxybenzyl)-2-decanone (*threo*-4d):** R_f=0.47 (hexane/ethyl acetate=3/1); ^{1}H NMR δ=1.89 (s, 3H), 2.40 (d, *J*=2.5 Hz, 1H, -OH), 2.70 (m, 2H), 3.29 (m, 1H, R^1R^2CHC(=O)Me), 4.75 (dd, *J*=2.5, 7.0 Hz, 1H, PhCH(OH)R), 7.36 (m, 5H).

Methanol Quenching of the Boron Enolates Generated by the Radical Addition of Alkyl Iodide to Methyl Vinyl Ketone in the Presence of Triethylborane. The reaction of *t*-BuI and methyl vinyl ketone is representative. A benzene solution of methyl vinyl ketone (70 mg, 1.0 mmol) was added to a solution of *t*-butyl iodide (0,55 g, 3.0 mmol), Et_3B (1.0 M hexane solution, 1.0 ml, 1.0 mmol), and methanol (0.08 ml, 2.0 mmol) in benzene at 25 °C under an argon atmosphere. After stirring for 5 min, concentration of the resulting mixture and purification by preparative TLC gave 5,5-dimethyl-2-hexanone[17] (**5a**, 0.10 g, 79% yield) along with 2-hexanone (**5e**, 5 mg, 5%).

5-Methyl-2-hexanone (5b): The compound was identical with the sample purchased from Aldrich Chemical Co.[18]

5-Iodo-2-pentanone (5e): The compound slowly decomposed under air at room temperature. R_f=0.47 (hexane/ethyl acetate=5/1); IR (neat) 2956, 1711, 1453, 1420, 1364, 1221, 1176, 701 cm^{-1}; ^{1}H NMR δ=2.07 (tt, *J*=6.7, 7.0 Hz, 2H), 2.17 (s, 3H), 2.60 (t, *J*=7.0 Hz, 2H), 3.23 (t, *J*=6.7 Hz, 2H).

Found: C, 28.49; H, 4.45%. Calcd for C_5H_9OI: C, 28.32; H, 4.28%.

5,5,6,6,7,7,8,8,9,9,10,10,10-Tridecafluoro-2-decanone (5d): Bp 83 °C (bath temp, 20 Torr), R_f=0.53 (hexane/ethyl acetate=5/1); IR (neat) 2922, 2852, 1723, 1364, 1238, 1194, 1144, 1020 cm^{-1}; ^1H NMR δ=2.23 (s, 3H), 2.42 (m, 2H), 2.78 (t, J=7.5 Hz, 2H). Found: C, 30.55; H, 1.81%. Calcd for $C_{10}H_7OF_{13}$: C, 30.79; H, 1.81%.

Methanol Quenching of the Boron Enolates Generated by the Radical Addition of Diiodomethane to Methyl Vinyl Ketone in the Presence of Trioctylborane. A benzene solution of methyl vinyl ketone (70 mg, 1.0 mmol) was added to a solution of diiodomethane (0.80 g, 3.0 mmol), Oct_3B (1.0 M THF solution, 1.0 ml, 1.0 mmol), and methanol (0.08 ml, 2.0 mmol) in benzene at 25 ° under an argon atmosphere. After stirring for 5 min, concentration of the resulting mixture and purification by preparative TLC gave 5-iodo-2-pentanone (**5a**, 0.11 g, 54% yield) and 0.11 g (48%) of octyl iodide.

Triethylborane Mediated Reformatsky Type Reaction of α-Bromo Ketones[19] (or α-Iodo Ketones[20]) and Carbonyl Compounds. The reaction of α-bromoacetophenone and benzaldehyde is representative. A hexane solution of Et_3B (1.0 M, 1.1 ml, 1.1 mmol) was added to a solution of α-bromoacetophenone (0.20 g, 1.0 mmol) and benzaldehyde (0.11 g, 1.0 mmol) in benzene (3.0 ml) at 25 °C under an argon atmosphere. To the mixture was added slowly a benzene solution of Ph_3SnH (0.2 M, 5.0 ml, 1.0 mmol) and the resulting mixture was stirred for 5 min at 25 °C. Then 100 mg of KF and 1.0 ml of water were added and the mixture was stirred vigorously. Filtration and purification by preparative TLC on silica gel gave 1,3-diphenyl-3-hydroxy-1-propanone (**8a**, 0.20 g, 88% yield).[21] In the case of α-iodoacetophenone, the reaction proceeded without an addition of Ph_3SnH.

3-Hydroxy-1-phenyl-1,12-tridecanedione (8b): Mp 50.2—50.5 °C (hexane); R_f=0.29 (hexane/ethyl acetate 5/1); IR (neat, before crystallization) 3400, 2910, 2846, 1706, 1681, 1449, 1379, 1270, 1166, 1079, 752, 688 cm^{-1}; ^1H NMR δ=1.25—1.70 (m, 16H), 2.14 (s, 3H), 3.03 (dd, J= 8.6, 17.7 Hz, 1H), 3.20 (dd, J=3.1, 17.7 Hz, 1H), 3.24 (bs, 1H, -OH), 4.20—4.35 (m, 1H, R^1R^2CHOH), 7.50—7.70 (m, 3H), 8.00—8.03 (m, 2H). Found: C, 74.78, H, 9.27%. Calcd for $C_{19}H_{28}O_3$: C, 74.96; H, 9.27%.

1-(2-Oxo-2-phenylethyl)cyclohexanol (8c): Mp 77.0—77.2 °C (hexane); R_f=0.70 (hexane/ethyl acetate=3/1); IR (neat, before crystallization) 3510, 3050, 2934, 2854, 1675, 1448, 1380, 749, 687 cm^{-1}; ^1H NMR δ=1.25—1.90 (m, 10H), 3.12 (s, 2H), 4.00 (s, 1H, -OH), 7.45—7.75 (m, 3H), 7.96—8.07 (m, 2H). Found: C, 77.02; H, 8.32%. Calcd for $C_{14}H_{18}O_2$: C, 77.03; H, 8.31%.

***erythro*-2-(α-Hydroxybenzyl)cyclopentanone (*erythro* 8d),**[22]

***threo*-2-(α-Hydroxybenzyl)cyclopentanone (*threo* 8d),**[21]

***erythro*-2-(1-Hydroxy-2-methylpropyl)cyclopentanone (*erythro* 8f),**[23]

***threo*-2-(1-Hydroxy-2-methylpropyl)cyclopentanone (*threo* 8f),**[22]

***erythro*-2-(1-Hydroxy-2,2-dimethylpropyl)cyclopentanone (*erythro* 8g),**[22]

***erythro*-2-(α-Hydroxybenzyl)cyclohexanone (*erythro* 8f),**[21]

***threo*-2-(α-Hydroxybenzyl)cyclohexanone (*threo* 8h),**[21]

***erythro*-2-(1-Hydroxy-2-methylpropyl)cyclohexanone (*erythro* 8j),**[21]

***threo*-2-(1-Hydroxy-2-methylpropyl)cyclopentanone (*threo* 8j),**[21]

***erythro*-2-(1-Hydroxy-2,2-dimethylpropyl)cyclohexanone (*erythro* 8k).**[21]

The spectral data of these compounds were identical with those described in the literature.

***erythro*-2-(1-Hydroxyheptyl)cyclopentanone (*erythro* 8e):** R_f=0.54 (hexane/ethyl acetate=5/1); IR (neat) 3400, 2922, 2854, 1735, 1458, 1376, 1272, 1156 cm^{-1}; ^1H NMR δ=0.84 (t, J=6.9 Hz, 3H), 1.15—2.45 (m, 18H), 4.25 (m, 1H); Found: C, 72.80; H, 11.28%. Calcd for $C_{12}H_{22}O_2$: C, 72.68; H, 11.18%.

***threo*-2-(1-Hydroxyheptyl)cyclopentanone (*threo* 8e):** R_f=0.63 (hexane/ethyl acetate=5/1); IR (neat) 3400, 2922, 2854, 1735, 1458, 1376, 1272, 1156 cm^{-1}; ^1H NMR δ=0.84 (t, J=6.9 Hz, 3H), 1.15—2.45 (m, 18H), 3.73 (m, 1H). Found: C, 72.80; H, 11.28%. Calcd for $C_{12}H_{22}O_2$: C, 72.68; H, 11.18%.

***erythro*-2-(1-Hydroxyheptyl)cyclohexanone (*erythro* 8i):** R_f=0.48 (hexane/ethyl acetate=5/1); IR (neat, for a mixture of *erythro*/*threo*=2/98) 3446, 2930, 2856, 1701, 1451, 1312, 1131 cm^{-1}; ^1H NMR δ=0.84 (t, J=6.9 Hz, 3H), 1.15—2.45 (m, 19H), 3.90 (m, 1H), 4.12 (m, 1H); Found (for a mixture of *erythro*/*threo*=2/98): C, 73.32; H, 11.56%. Calcd for $C_{13}H_{24}O_2$: C, 73.54; H, 11.39%.

***threo*-2-(1-Hydroxyheptyl)cyclohexanone (*threo* 8i):** R_f=0.48 (hexane/ethyl acetate=5/1); ^1H NMR δ=0.84 (t, J=6.9 Hz, 3H), 1.15—2.45 (m, 20H), 3.73 (m, 1H).

***erythro*-7-(Hydroxyphenylmethyl)-6-dodecanone (*erythro*-8l):** R_f=0.55 (hexane/ethyl acetate=5/1); IR (for a mixture of *erythro*/*threo*=65/35) 3340, 2922, 2852, 1702, 1458, 1376, 699 cm^{-1}; ^1H NMR δ=0.75—0.95 (m, 6H), 1.05—1.80 (m, 14H), 2.08—2.48 (m, 2H), 2.78—3.06 (m, 2H), 4.88 (dd, J=2.5, 6.0 Hz, 1H), 7.35 (bs, 5H). Found (for a mixture of *erythro*/*threo*=65/35): C, 78.35; H, 10.67%. Calcd for $C_{19}H_{30}O_2$: C, 78.57; H, 10.41%.

***threo*-7-(α-Hydroxybenzyl)-6-dodecanone (*threo*-8l):** ^1H NMR δ=0.75—0.95 (m, 6H), 1.05—1.80 (m, 14H), 2.08—2.48 (m, 2H), 2.78—3.06 (m, 2H), 4.80 (d, J=6.9 Hz, 1H), 7.45—7.60 (m, 3H), 7.68—7.77 (m, 2H).

Triethylborane-Mediated Reformatsky Type Reaction of α-Bromoacetophenones and Benzaldehyde in the Presence of Garvinoxyl. A hexane solution of Et_3B (1.0 M, 1.1 ml, 1.1 mmol) was added to a solution of α-bromoacetophenone (0.20 g, 1.0 mmol), benzaldehyde (0.11 g, 1.0 mmol), and Garvinoxyl (42 mg, 0.10 mmol) in benzene (3.0 ml) at 25 °C under an argon atmosphere. To the mixture was added slowly a benzene solution of Ph_3SnH (0.2 M, 5.0 ml, 1.0 mmol) and the resulting mixture was stirred for 5 min at 25 °C. Then 100 mg of KF and 1.0 ml of water were added and the mixture was stirred vigorously. Filtration and purification by preparative TLC on silica gel gave 1,3-diphenyl-3-hydroxy-1-propanone (**8a**, 80 mg, 36% yield) and complex mixture.

Preparation of 8-Iodo-3-octen-2-one. 5-Iodo-1-pentanol (0.80 g, 3.7 mmol) was added dropwise to a dispersion of PDC (pyridinium dichromate, 2.0 g, 5.3 mmol) in CH_2Cl_2 (40 ml) at room temperature under air. After stirring for 1 h, the liquid phase of the resulting mixture was filtered through silica gel. The precipitate was washed with ether (10 ml, twice) and poured on the silica gel. The combined organic layers were concentrated and purified by silica-gel column chromatography to give 0.38 g (1.8 mmol) of 5-iodopentanal in 48% yield. This aldehyde was quite unsta-

ble under air at room tempareture and it was required to carry out the next step immediately. (Diethyloxyphosphinyl)acetone (0.37 g, 1.9 mmol) was added to a generally prepared THF solution of LDA (lithium diisopropylamide, 0.5 M, 3.8 ml, 1.9 mmol) at 0 °C under an argon atmosphere. After stirring for 1 h at 0 °C this yellow brown mixture was transferred into a THF solution of 5-iodopentanal (0.5 M, 3.6 ml, 1.8 mmol) by syringe. The resulting mixture was stirred for 15 min at 0 °C, 15 min at room temperature, and 30 min at THF reflux. After cooling, the reaction mixture was poured into water and extracted by ethyl acetate (10 ml, twice). The combined organic layers were washed with brine. Concentration and purification by silica-gel column chromatography gave 0.20 g (0.77 mmol, 43%) of 8-iodo-3-octen-2-one (**9**): R_f=0.29 (hexane/ethyl acetate=5/1); IR (neat) 2930, 2854, 1697, 1672, 1626, 1426, 1361, 1254, 1206, 1180, 976 cm^{-1}; ^1H NMR δ=1.52—1.75 (m, 2H), 1.78—1.97 (m, 2H), 2.22—2.36 (m, 2H), 2.25 (s, 3H), 3.20 (t, J=6.7 Hz, 2H), 6.10 (d, J=15.9 Hz, 1H), 6.79 (dt, J=15.9, 6.8 Hz, 1H). Found: C, 38.25; H, 5.23%. Calcd for $C_8H_{13}OI$: C, 38.12; H, 5.20%.

Cyclization-Aldol Condensation of 8-Iodo-3-octen-2-one and Benzaldehyde. A benzene solution of Ph_3SnH (0.18 M, 3 ml, 0.55 mmol) was added dropwise to a mixture of 8-iodo-3-octen-2-one (0.13 g, 0.50 mmol), benzaldehyde (58 mg, 0.55 mmol), and Et_3B (1.0 M in hexane, 0.55 ml, 0.55 mmol) in benzene (7 ml) at room temperature under an argon atmosphere. After stirring for 30 min at room temperature, 50 mg of KF and 2 ml of water were added and stirred vigorously. The resulting mixture was filtered through Celite 545 and washed with brine. The aqueous layer was extracted by ethyl acetate (10 ml, twice). Combined organic layers were concentrated and purified by preparative TLC. 81 mg of 3-cyclopentyl-4-hydroxy-4-phenyl-2-butanone (**10**, 0.35 mmol, 70% yield, *erythro/threo* or *threo/erythro*=55/45) was obtained. **10**: R_f=0.37 (hexane/ethyl acetate=5/1); IR (neat, for a mixture of *erythro/threo* or *threo/erythro*=63/37) 3424, 2950, 2868, 1701, 1453, 1353, 760, 731, 700 cm^{-1}; ^1H NMR (for major) δ=1.07—1.40 (m, 2H), 1.40—2.07 (m, 6H), 1.94 (s, 3H), 2.08—2.40 (m, 1H), 2.68 (bs, 1H, -OH), 2.98 (dd, J=6.5, 8.3 Hz, 1H, R^1R^2CHC(=O)Me), 4.97 (m, 1H, PhRCHOH), 7.35 (m, 5H); ^1H NMR (for minor) δ=1.07—1.40 (m, 2H), 1.40—2.07 (m, 6H), 1.86 (s, 3H), 2.08—2.40 (m, 1H), 2.81 (dd, J=4.4, 9.9 Hz, 1H, R^1R^2CHC(=O)Me), 3.92 (bs, 1H, -OH), 4,97 (m, 1H, PhRCHOH), 7.35 (m, 5H). Found (for a mixture of *erythro/threo* or *threo/erythro*=63/37): C, 77.26; N, 8.68%. Calcd for $C_{15}H_{20}O_2$: C, 77.55; H, 8.68%.

Financial support by the Ministry of Education, Science and Culture of Japan (Grant-in-Aid for Scientific Research No. 63470074) is acknowledged. One of the author (K. O.) wishes to thank Ciba-Geigy Foundation for the Promotion of Science for financial assistance.

References

1) H. C. Brown and M. M. Midland, *Angew. Chem., Int. Ed. Engl.*, **11**, 692 (1972).

2) A. Suzuki, A. Arase, H. Matsumoto, and M. Itoh, *J. Am. Chem. Soc.*, **89**, 5708 (1967).

3) G. W. Kabalka, H. C. Brown, A. Suzuki, S. Honma, A. Arase, and M. Itoh, *J. Am. Chem. Soc.*, **92**, 710 (1970).

4) Many reports have been published concerning to the initiating step (the reaction of trialkylborane and oxygen). No clear conclusion has been suggested, yet. See A. Suzuki, *Yuuki Gosei Kagaku Kyoukai Shi*, **29**, 995 (1971), and references therein.

5) W. Fenzl, R. Köster, and H.-J. Zimmermann, *Liebigs Ann. Chem.*, **1975**, 2201.

6) Köster and Mukaiyama have reported the aldol reaction with the boron enolates derived from the 1,4-addition of trialkylborane to α,β-unsaturated aldehydes or ketones. See a) Ref. 4. b) T. Mukaiyama, K. Inomata, and M. Muraki, *J. Am. Chem Soc.*, **95**, 967 (1973).

7) A part of this work was reported in a communication form. K. Nozaki, K. Oshima, and K. Utimoto, *Tetrahedron Lett.*, **29**, 1041 (1988).

8) We are grateful to Tosoh Akzo Co. for the gift of Et_3B.

9) K. Nozaki, K. Oshima, and K. Utimoto, *J. Am. Chem. Soc.*, **109**, 2547 (1987), *idem.*, *Tetrahedron*, **45**, 923 (1989).

10) Y. Ichinose, K. Wakamatsu, K. Nozaki, K. Oshima, and K. Utimoto, *Tetrahedron Lett.*, **28**, 3709 (1987); K. Nozaki, Y. Ichinose, K. Wakamatsu, K. Oshima, and K. Utimoto, *Bull. Chem. Soc. Jpn.*, **63**, 2268 (1990).

11) K. Nozaki, K. Oshima, and K. Utimoto, *Tetrahedron Lett.*, **29**, 6127 (1988).

12) We have reported the Reformatsky type reaction of α-haloketone with Sn-Al. a) S. Matsubara, N. Tsuboniwa, Y. Morizawa, K. Oshima, and H. Nozaki, *Bull. Chem. Soc. Jpn.*, **57**, 3242 (1984). b) K. Maruoka, S. Hashimoto, Y. Kitagawa, H. Yamamoto, and H, Nozaki, *ibid.*, **53**, 3301 (1980).

13) These findings suggested that the reaction proceeded via boron enolates. (*E*)-Boron enolates have been reported to give *threo* aldol adducts. a) M. Hirama and S. Masamune, *Tetrahedron Lett.*, **1979**, 2225. b) D. E. V. Horn and S. Masamune, *ibid.*, **1979**, 2229. c) D. A. Evans, E. Vogel, and J. V. Nelson, *J. Am. Chem. Soc.*, **101**, 6120 (1979). The low stereoselectivity of *erythro/threo* for 7-bromo-6-dodecanone might be ascribed to the low selectivity of *E/Z* in forming the intermediate boron enolate, although the stereochemistry of the enolate was not determined.

14) Treatment of a solution of α-bromoacetophenone and benzaldehyde in benzene with triethylborane in the absence of Ph_3SnH gave the corresponding β-hydroxyketone in only 25% yield along with the recovered α-bromoacetophenone and unidentified complex by-product after prolonged reaction time (3 h).

15) J. Boutagy and R. Thomas, *Chem. Rev.*, **74**, 87 (1974).

16) Spectra of *erythro*- and *threo*-1-hydroxy-1-phenyl-2,4,4-trimethyl-3-pentanone and *erythro*- and *threo*-3-hydroxy-2-methyl-1,3-diphenyl-1-propanone were reported by Heathcock et al. C. H. Heathcock, C. T. Buse, N. A. Kleschick, M. C. Pirrung, J. E. Sohn, and J. Lampe, *J. Org. Chem.*, **45**, 1066 (1980). Spectra for *erythro*- and *threo*-5-hydroxy-4-methyl-3-octanone were reported by Evans et al. D. A. Evans, J. V. Nelson, E. Vogel, and T. R. Taber, *J. Am. Chem. Soc.*, **103**, 3107 (1981).

17) D. W. K. Yeung and J. Warkentin, *Can. J. Chem.*, **54**, 1345 (1976).

18) Commercially available by Aldrich.

19) α-Bromo ketones were prepared by DMSO oxidation according to the reported procedure. "Reagents for Organic Synthesis," Vol. 2, p. 41.

20) α-Iodo ketones were prepared according to the reported procedure. See Shin Jikken Kagaku Koza, Vol. 14-1, p. 423.
21) For physical data see, H. O. House, D. S. Crumrine, A. Y. Teranishi, and H. D. Olmstead, *J. Am. Chem. Soc.*, **95**, 3310 (1973).
22) For physical data see, T. Mukaiyama, K. Banno, and K. Narasaka, *Chem. Lett.*, **1974**, 7503.
23) For physical data see, J. E. Dubois and M. Dubois, *Bull. Soc. Chim. Fr.*, **1969**, 3553.

Micellar Accelerated Reduction of Ethylenediaminetetraacetatocobaltate(III) by 1-Benzyl-1,4-dihydronicotinamide

Kohichi YAMASHITA, Masahiro CHIBA, Hitoshi ISHIDA, and Katsutoshi OHKUBO*
Department of Applied Chemistry, Faculty of Engineering, Kumamoto University, Kumamoto 860
(Received October 8, 1990)

The electrostatic and hydrophobic effects of ionic micelles on the reduction of ethylenediaminetetraacetato cobaltate(III) ([Co(edta)]$^-$) by 1-benzyl-1,4-dihydronicotinamide (BNAH) were investigated with dodecyltrimethylammonium chloride (DTAC) and/or sodium dodecyl sulfate (SDS). Cationic DTAC accelerated the reduction of [Co(edta)]$^-$, while anionic SDS retarded the reaction. The micellar effects of DTAC on the present reaction at 30 °C were kinetically analyzed by using the ion-exchange model and the Berezin's approach: the evaluated rate constant, $(1.0\pm0.1—1.1\pm0.4)\times10^{-4}$ mol^{-1} dm^3 s^{-1}, for the micellar-phase reaction was ten times smaller than that, 1.46×10^{-3} mol^{-1} dm^3 s^{-1}, for the aqueous-phase one. This fact was well-explained by the electron-transfer rate constant calculated with the experimentally determined redox potentials of BNAH and [Co(edta)]$^-$. The cationic DTAC micelles, however, resulted in considerably larger value (3.58×10^{-3} mol^{-1} dm^3 s^{-1}) of overall reaction rate constant than that (1.46×10^{-3} mol^{-1} dm^3 s^{-1}) of nonmicellar one, because the apparent concentrations of the reactants in the micellar phase increased remarkably by condensation of BNAH and [Co(edta)]$^-$ to the micelles through the hydrophobic interaction and the electrostatic interaction, respectively.

The hydride-transfer reactions from a reduced nicotinamideadenine dinucleotide (NAD(P)H) and its model compounds have been shown to proceed through the sequential electron-proton-electron transfer.[1,2] Since the first electron-transfer step plays a significant role in the reaction of NADH model compounds,[1,2] the reduction of one-electron oxidants such as transition metal complexes by NADH model compounds is useful to evaluate the reactivity of NADH model compounds.[3-9]

Although biochemical processes involving NAD(P)H proceed in a microheterogeneous system composed of an aqueous phase and a lipophilic phase, less attention has been paid to the study of microenvironmental effects on the reaction of NADH model compounds. Since the micellar systems represent a convenient simple model of enzymes to provide important information about the microenvironmental effects on the reaction,[10,11] it is of interest to study the micellar effects on the redox reactions of NADH model compounds.

In a previous paper,[12] we investigated the effects of ionic surfactants on the reduction of hydrophobic and nonionic tris(acetylacetonato)cobalt(III) by 1-benzyl-1,4-dihydronicotinamide (BNAH). The micelles retarded the reaction rates by incorporation of the reactants through the hydrophobic interaction because low polar environments in the micellar phase destabilized the transition states of the reaction.

The reduction of hydrophilic and ionic substrates like ethylenediaminetetraacetatocobaltate(III) ([Co(edta)$^-$] by BNAH might give further information about the micellar effects on the reaction of NADH model compounds, since the ionic micelles can concentrate the ionic substrate by electrostatic interaction.

In this paper, we describe the micellar promoted reduction of [Co(edta)]$^-$ by BNAH in the presence of cationic dodecyltrimethylammonium chloride (DTAC) and anionic sodium dodecyl sulfate (SDS).

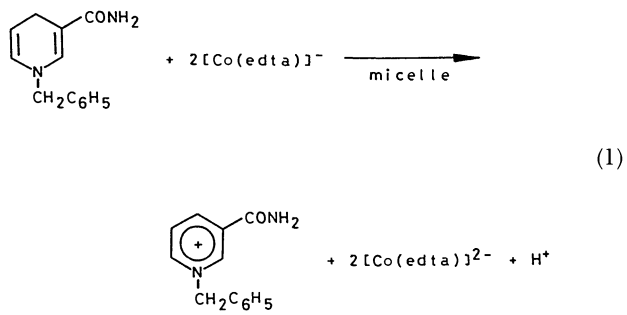

(1)

Experimental

The materials and the procedure of reaction were the same as used in the previous work,[12] except that potassium ethylenediaminetetraacetatocobaltate(III) (K[Co(edta)]·2H$_2$O) were prepared according to the literature.[13] The cyclic voltammetry measurements were performed on a Hokuto Denko HA-301 potentiostat/galvanostat by using a glassy carbon working electrode and a saturated calomel reference electrode. The ion-exchange constant for the equilibrium between [Co(edta)]$^-$ and the surfactant counter ion (Cl$^-$) was determined by employing a molecular sieve filtration on Sephadex G-15.[14] A column (diameter=3 cm and bed-height=30 cm) was maintained at 30±0.1 °C with an outer jacket by circulating water. The void volume (V_o) of the packed column was estimated to be 29.0 cm^3 by using Blue Dextran 2000. Before run the column was equilibrated with 1000 cm^3 of 4%(v/v)methanol-borate buffer (pH 9.0, μ=0.02 mol dm^{-3}) containing the surfactants (0—9.0×10^{-2} mol dm^{-3}). The each run was started by the addition of 1.0 cm^3 of 2×10^{-3}mol dm^{-3} K[Co(edta)]·2H$_2$O. Elution with the appropriate eluent was followed at a rate of 1.0 cm^3 min^{-1}. Fractions (0.5—1.0 cm^3) were collected employing an automatic fraction collector and were monitored at 275

nm spectrophotometrically. The elution volume was given by the total volume of the eluent until the fraction gave the maximum absorbance peak of [Co(edta)]$^-$.

Results and Discussion

When BNAH (5.0×10^{-4} mol dm^{-3}) and [Co(edta)]$^-$ (1.0×10^{-3} mol dm^{-3}) were thermally reacted in 4%(v/v)methanol-0.02 mol dm^{-3} H_3BO_3-NaOH buffer (pH 9.0, μ=0.02 mol dm^{-3} with KCl) containing the surfactants of DTAC or SDS (0—6.0×10^{-2} mol dm^{-3}), both absorptions of BNAH (λ_{max}=360 nm) and [Co(edta)]$^-$ (λ_{max}=540 nm) decreased with time. The spectral changes indicated that 2 moles of [Co(edta)]$^-$ were consumed by 1 mole of BNAH. All the present reactions followed by monitoring the absorbance change of [Co(edta)]$^-$ at 540 nm were found to obey the second-order rate law (Eq. 2).

$$-\frac{d[[Co(edta)]^-]}{dt}=2k_{obsd}[BNAH][[Co(edta)]^-]. \quad (2)$$

Therefore, the following mechanism (Eqs. 3a—c) seems appropriate for the reduction of [Co(edta)]$^-$ by BNAH as reported in other systems.[3,12]

$$BNAH+[Co(edta)]^- \longrightarrow BNAH^{\cdot+}+[Co(edta)]^{2-}, \quad (3a)$$

$$BNAH^{\cdot+} \longrightarrow BNA^{\cdot}+H^+, \quad (3b)$$

$$BNA^{\cdot}+[Co(edta)]^- \longrightarrow BNA^+ +[Co(edta)]^{2-}. \quad (3c)$$

Since the reduction potential (E_{red}^0) of [Co(edta)]$^-$ and the oxidation potential (E_{ox}^0) of BNAH in 4%(v/v)methanol-borate buffer were estimated to be -0.53 ± 0.1 and -0.01 ± 0.1 V vs. SCE, respectively, the first electron-transfer reaction (Eq. 3a) is endothermic. The subsequent deprotonation (Eq. 3b) and the second electron-transfer reaction (Eq. 3c) might proceed very quickly as can be seen from the pK_a value of BNAH$^{\cdot+}$ (3.6)[2] and the oxidation potential of BNA$^{\cdot}$ (-1.08 V vs. SCE).[2] Therefore, the first-electron-transfer step (Eq. 3a) may be a rate-determining step, which might suffer micellar effects.

Figure 1 depicts the micellar effects of SDS and DTAC on the second-order rate constant (k_{obsd}) observed for the reduction of [Co(edta)]$^-$ by BNAH under [surfactant]>cmc. The reaction rate was enhanced remarkably by cationic DTAC and was maximized at [DTAC]=4.0×10^{-2} mol dm^{-3}, while anionic SDS retarded the reaction rate. (The broken line in Fig. 1 will be discussed later.)

Since these micellar effects could result from distribution of the reactants between a micellar phase and an aqueous phase,[10,11] the incorporation of BNAH and [Co(edta)]$^-$ into the micelles were evaluated by using the binding constants and the ion-exchange constants, respectively.[15] The binding constants (K_{BNAH}) of BNAH to SDS and DTAC in 4%(v/v)methanol-borate buffer (pH 9.0, μ=0.02 mol dm^{-3}) at 30 °C were determined to be 236 ± 15 and 102 ± 13 mol^{-1} dm^3, respectively, in our previous work.[12]

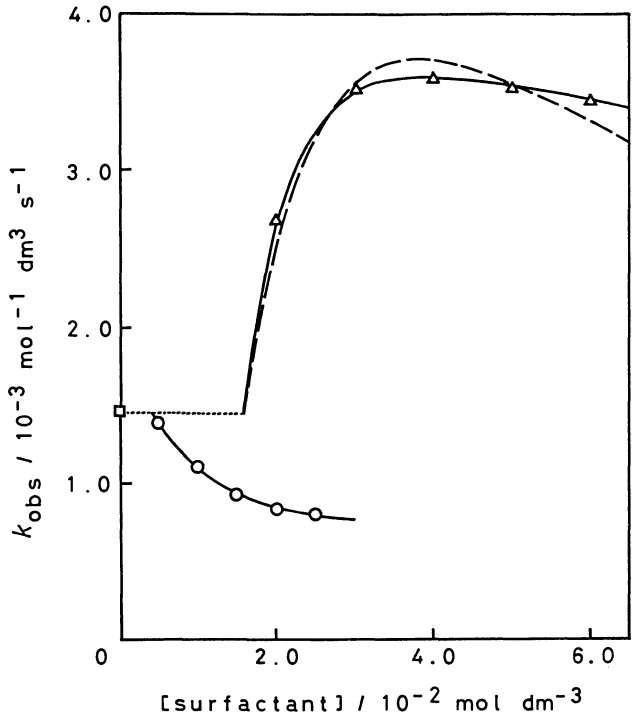

Fig. 1. Micellar effects on second-order rate constants obtained for thermal reduction of [Co(edta)]$^-$ by BNAH with SDS (○) or DTAC (△). The broken line represents the rate constants calculated by Eq. 10.

The ion-exchange constant for the equilibrium between [Co(edta)]$^-$ and the surfactant counter ion was estimated by using a gel filtration chromatography.[14,15] The elution volume (V_e) and the ion-exchange constant (K_1) are related as follows;

$$\frac{1}{V_e-V_o}=\frac{1}{V_i k' K_D}\left(1+K_1\frac{[\overline{Cl^-}]_m}{[\overline{Cl^-}]_w}\right)(1-C_m v), \quad (4)$$

$$k'=(kV_g+V_i)/V_i$$

where V_o and V_i are the void volume and the imbibed (stationary) volume, respectively, V_g is the total volume of a gel matrix, v is the partial molar volume of a surfactant molecule in the micelles, K_D is the molecular sieving constant, C_m, (C_m=[surfactant]—cmc) is the concentration of micelles, k is the constant of proportionality between [Co(edta)]$^-$ absorbed per unit volume of a gel matrix and the equilibrium concentration of [Co(edta)]$^-$ in a liquid phase, $[\overline{Cl^-}]$ is the stoichiometric (bulk) concentration of Cl$^-$, and subscripts w and m refer to an aqueous phase and a micellar phase, respectively.

The concentrations of Cl$^-$ in the micellar phase and in the aqueous phase are calculated by the following equations.[15]

$$[\overline{Cl^-}]_m=(1-\alpha)C_m-[\overline{[Co(edta)]^-}]_m-[\overline{H_2BO_3^-}]_m, \quad (5)$$

$$[\overline{Cl^-}]_w=\alpha C_m+cmc+[\overline{[Co(edta)]^-}]_m+[\overline{H_2BO_3^-}]_m+[\overline{Cl^-}]_{add}, \quad (6)$$

$$K_1=\frac{[\overline{[Co(edta)]^-}]_m\,[\overline{Cl^-}]_w}{[\overline{[Co(edta)]^-}]_w\,[\overline{Cl^-}]_m}, \tag{7}$$

$$K_2=\frac{[\overline{[Co(edta)]^-}]_m\,[\overline{H_2BO_3^-}]_w}{[\overline{[Co(edta)]^-}]_w\,[\overline{H_2BO_3^-}]_m}, \tag{8}$$

$$A\,[\overline{[Co(edta)]^-}]_m^3+B\,[\overline{[Co(edta)]^-}]_m^2+C\,[\overline{[Co(edta)]^-}]_m+D=0, \tag{9}$$

$$A=(1-K_1)(1-K_2),$$

$$B=E(1-K_2)+(K_1[[Co(edta)]^-]_t+[H_2BO_3^-]_t)(1-K_1),$$

$$C=[EK_1+K_1\{[[Co(edta)]^-]_t-(1-\alpha)C_m(1-K_1)\}][[Co(edta)]^-]_t,$$

$$D=-(1-\alpha)C_mK_1K_2[[Co(edta)]^-]_t^2,$$

$$E=\alpha C_m+\mathrm{cmc}+[\overline{Cl^-}]_{add}+K_1[[Co(edta)]^-]_t+(1-\alpha)C_mK_1,$$

where α is the degree of ionization of the micelle, $[\overline{[Co(edta)]^-}]$ and $[\overline{H_2BO_3^-}]$ are the stoichiometric (bulk) concentrations of $[Co(edta)]^-$ and $H_2BO_3^-$, $[\overline{Cl^-}]_{add}$ is the concentration of Cl^- added as KCl, and the subscript t refer to the total concentration. Thus, the $(V_e-V_o)^{-1}$ value is calculated at a given C_m value by using Eqs. 4—9.

When the values of $\alpha=0.2$ and $v=0.256$ mol^{-1}dm^3 were used,[15,16] the data experimentally obtained for the gel filtration chromatography with DTAC were quite adequately simulated by Eq. 4 with values of $K_1=1.2\pm0.1$ and $K_2=0.2\pm0.1$ as shown by the broken line in Fig. 2. On the other hand, the $(V_e-V_o)^{-1}$ values decreased with increasing the SDS micellar concentration. The fact indicates that $[Co(edta)]^-$ is not distributed to the SDS micellar phase due to the electrostatic repulsion between $[Co(edta)]^-$ and anionic SDS. Thus, the anionic SDS micelles retarded the reaction rates by suppressing the reaction of BNAH in the micellar phase with $[Co(edta)]^-$ in the aqueous phase. The K_{BNAH}, K_1, and K_2 values are summarized in Table 1.

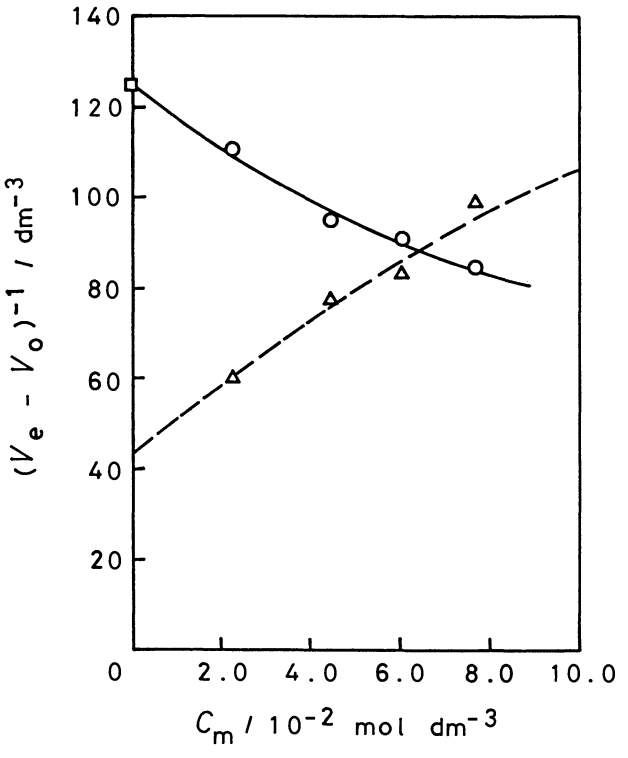

Fig. 2. Plots of $(V_e-V_o)^{-1}$ vs. C_m for elution of $[Co(edta)]^-$ on column of Sephadex G-15 in the presence of SDS (○) or DTAC (△) at 30 °C. The broken line represents the $(V_e-V_o)^{-1}$ values calculated by Eq. 4.

The following reaction scheme can be depicted for the reduction of $[Co(edta)]^-$ by BNAH in the presence of DTAC micelles.[15]

$$\begin{array}{ccc} BNAH_m+[Co(edta)]^-_m & \longrightarrow & \text{products} \\ \uparrow\downarrow K_{BNAH} \quad\quad \uparrow\downarrow K_1 & & \\ BNAH_w+[Co(edta)]^-_w & \longrightarrow & \text{products} \end{array}$$

According to the ion-exchange model, the observed second-order rate constants (k_{obsd}) can be given by Eq. 10.[15]

$$k_{obsd}=\frac{(k^m/v)K_{BNAH}K_1\dfrac{[\overline{Cl^-}]_m}{[\overline{Cl^-}]_w}+k^w}{(1+K_{BNAH}C_m)\left(1+K_1\dfrac{[\overline{Cl^-}]_m}{[\overline{Cl^-}]_w}\right)}, \tag{10}$$

where k^m and k^w are the rate constants of reactions in the micellar phase and the aqueous phase, respectively. The broken line depicted in Fig. 1 shows the second-order rate constants calculated from Eqs. 5—10 by using the above mentioned values of $K_1=1.2\pm0.1$ and $K_2=0.2\pm0.1$, and $\alpha=0.2$. Thus, the rate constants (k^m) of the reaction in the DTAC micellar phase was evaluated to be $(1.0\pm0.1)\times10^{-4}$ mol^{-1}dm^{3}s^{-1} as listed in Table 1. The k^m value obtained by the ion-exchange model was confirmed by comparing with that ($k^m=(1.1\pm0.4)\times10^{-4}$ mol^{-1}dm^{3}s^{-1}) estimated by using the following equations of Berezin's approach in stead of Eqs. 4 and 10.[17]

Table 1. Binding Constants of BNAH to DTAC and SDS (K_{BNAH}), Ion-Exchange Constants for $[Co(edta)]^-$ (K_1 and K_2), and Second-Order Rate Constants (k^w for the Aqueous Phase and k^m for the DTAC Micellar Phase) in 4%(v/v)Methanol-Borate Buffer (pH 9.0) at 30 °C

Surfactant	K_{BNAH}[a] / mol^{-1}dm^3	K_1	K_2	k^w or k^m / 10^{-4} mol^{-1}dm^{3}s^{-1}
None				14.6±0.6
DTAC	102±13	1.2±0.1	0.2±0.1	1.0±0.1
SDS	236±15			

a) Ref. 12.

$$\frac{1}{V_e-V_o}=\frac{K_{Co}}{V_i k' K_D}C_m+\frac{1}{V_i k' K_D}, \quad (11)$$

$$k_{obsd}=\frac{(k^m/v)K_{BNAH}K_{Co}C_m+k^w}{(1+K_{BNAH}C_m)(1+K_{Co}C_m)}, \quad (12)$$

where K_{Co} (=15.3±2.8 mol^{-1}dm^3) is the binding constant of [Co(edta)]$^-$ to the micelles.

The second-order rate constant (k^m) in the DTAC micellar phase was ten times as small as that (k^w=(1.46±0.06)×10^{-3} mol^{-1}dm^{3}s^{-1}) in the aqueous phase. This fact suggests that the reactivities of BNAH and [Co(edta)]$^-$ were affected by the microenvironments in the micellar phase. In this regard, the present micellar system including BNAH was not so effective for the formation of substrate-micelle complex and the activation of the substrate as compared with the native enzymatic system including NADH, because the former excludes the functional parts such as histidine, cysteine, and metal ions.

To elucidate the microenvironmental effects of the micelles on the reactivity of BNAH, the oxidation potential (E_{ox}^0) of BNAH and the reduction potential (E_{red}^0) of [Co(edta)]$^-$ were determined with or without DTAC by cyclic voltammetry measurements.[18] The oxidation and reduction peak potentials (E^p) of BNAH and [Co(edta)]$^-$ are related to the transfer coefficient (β) as Eqs. 13—15 based on Rehm-Weller, Marcus, and Marcus-Levine free energy relationships, respectively.[18]

$$E^p=E^0+\frac{1-2\beta}{[\beta(1-\beta)]^{1/2}}\Delta G_0^{\neq}, \quad (13)$$

$$E^p=E^0+4(1-2\beta)\Delta G_0^{\neq}, \quad (14)$$

$$E^p=E^0+\frac{\ln(\beta^{-1}-1)}{\ln 2}\Delta G_0^{\neq}. \quad (15)$$

The transfer coefficient (β) is calculated from Eq. 16 by using the width of the wave ($|E^p-E^{p/2}|$).

$$\beta=\frac{1.857RT}{F|E^p-E^{p/2}|}. \quad (16)$$

Figure 3 depicted the plots according to Eqs. 13—15 for BNAH oxidation with or without 5.0×10^{-2} mol dm^{-3} DTAC in 4%(v/v)methanol-borate buffer. The E_{ox}^0 values of BNAH in the aqueous solution and micellar solution were estimated to be −0.01±0.1 and 0.14±0.1 V vs. SCE, respectively, from the intercepts of the linear plots.[19] On the other hand, the cyclic voltammetry for [Co(edta)]$^-$ in the presence of DTAC was complicated probably due to the electrostatic interaction between [Co(edta)]$^-$ and DTAC. Therefore, the reduction potentials of [Co(edta)]$^-$ were determined in 4%(v/v) and 30%(v/v)methanol-borate buffer (Fig. 4) because the reaction circumstances in the micellar phase have been reported to be akin to those in solution of 30—50%(v/v)methanol-borate buffer.[12] The E_{red}^0 value (−0.44±0.1 V vs. SCE) obtained for [Co(edta)]$^-$ in 30%(v/v)methanol-borate

Table 2. Oxidation Potentials (E_{ox}^0) of BNAH and Reduction Potentials (E_{red}^0) of [Co(edta)]$^-$ with or without 5.0×10^{-2} mol dm^{-3} DTAC in 4%(v/v)Methanol-Borate Buffer (pH 9.0) at 30 °C

[DTAC]	E_{ox}^0	E_{red}^0
10^{-2} mol dm^{-3}	V vs. SCE	V vs. SCE
0	−0.01±0.1	−0.53±0.1
5.0	0.14±0.1	−0.44±0.1[a]

a) Determined in 30%(v/v)methanol-borate buffer without DTAC.

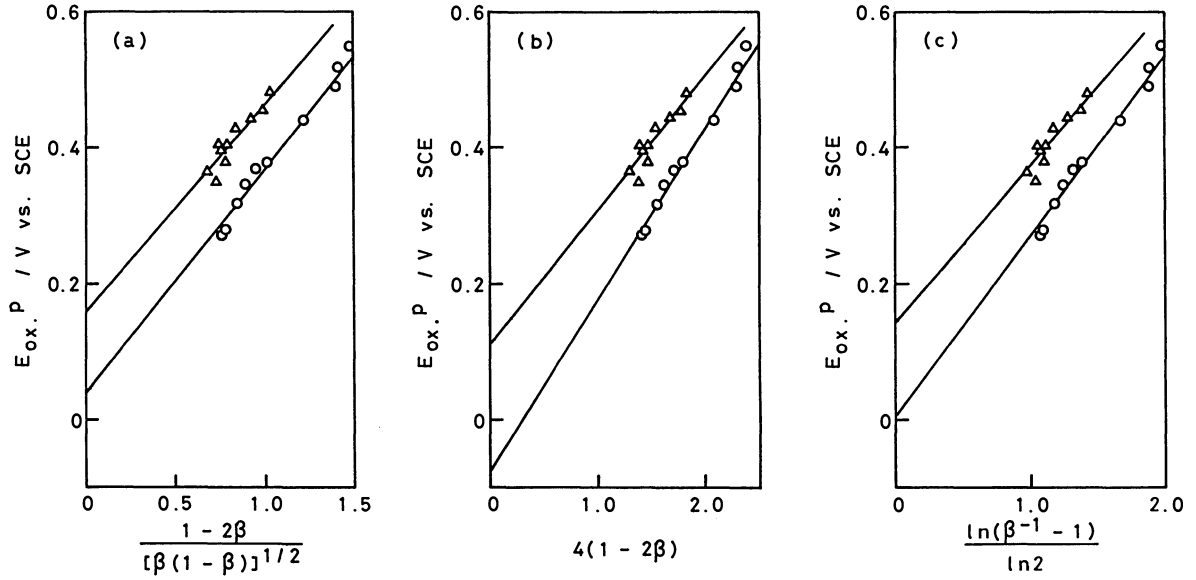

Fig. 3. Plots of E_{ox}^p vs. (a) $(1-2\beta)/[\beta(1-\beta)]^{1/2}$, (b) $4(1-2\beta)$, and (c) $\ln(\beta^{-1}-1)/\ln 2$ for BNAH without surfactants (○) or with 5.0×10^{-2} mol dm^{-3} DTAC (△) in 4% (v/v) methanol-borate buffer.

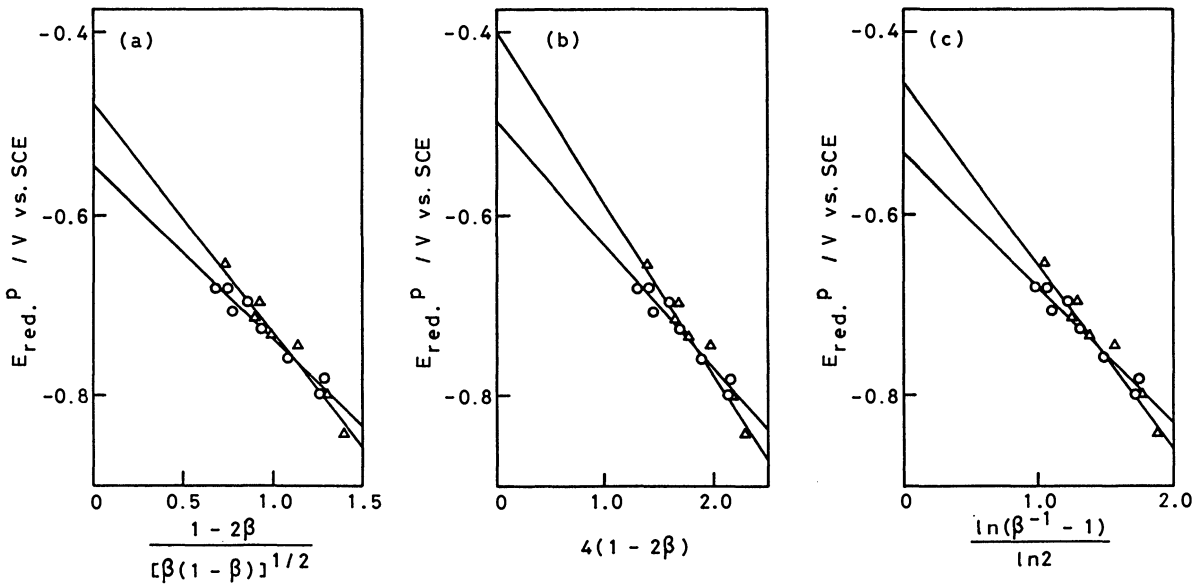

Fig. 4. Plots of E_{red}^{p} vs. (a) $(1-2\beta)/[\beta(1-\beta)]^{1/2}$, (b) $4(1-2\beta)$, and (c) $\ln(\beta^{-1}-1)/\ln 2$ for $[Co(edta)]^-$ in 4% (v/v)- (○) and 30% (v/v) methanol-borate buffer (△).

buffer was slightly positive than that (−0.53±0.1 V) obtained in 4%(v/v)methanol-borate buffer. The E_{ox}^{0} and E_{red}^{0} values were summarized in Table 2.

According to Marcus theory, the rate constant (k_e) of the electron transfer from BNAH to $[Co(edta)]^-$ is related to the E_{red}^{0} and E_{ox}^{0} values by Eq. 17.[21,22]

$$RT \ln k_e = RT \ln K_e k_d + (E_{red}^{0} - E_{ox}^{0}) - (w_p - w_r), \quad (17)$$

where K_e is the equilibrium constant for the formation and the dissociation of the encounter complex ([BNAH $Co(edta)^-$]), k_d is the rate constant for the dissociation of the successor complex ([$BNAH^+$ $Co(edta)^{2-}$]) to $BNAH^{\cdot+}$ and $[Co(edta)]^{2-}$, and w_r and w_p are the work terms required to bring together the reactants and the products, respectively. When the $K_e k_d$ and $(w_p - w_r)$ values were assumed to be constant both in the micellar phase and in the aqueous phase, the k_e value in the micellar phase was calculated to be $k_e = 1.5\times10^{-4}$ $mol^{-1}dm^3s^{-1}$ from Eq. 17 by using the above-mentioned E_{red}^{0}, E_{ox}^{0}, and k^w values. Since the rate constant (k_e) estimated for the reaction between BNAH and $[Co(edta)]^-$ in the micellar phase were very close to that ($k^m = (1.0\pm0.1 — 1.1\pm0.4)\times10^{-4}$ $mol^{-1}dm^3$ s^{-1}) obtained experimentally, the small k^m value in the micellar phase compared with the k^w value in the aqueous phase was attributable to weak reducing ability of BNAH in the micellar phase. That is, low polar microenvironments in the micellar phase are unfavorable for production of ionic species such as $BNAH^{\cdot+}$ and BNA^+. Furthermore, the cationic charge of the DTAC micellar surface suppresses the formation of a positive charge on the nicotinamide ring of BNAH (or BNA·) and the charge separation of produced $[Co(edta)]^{2-}$. Thus, the electron-transfer reaction from BNAH to $[Co(edta)]^-$ was retarded in the DTAC micellar phase. However, the total reaction rate was accelerated by DTAC micelles because $[Co(edta)]^-$ and BNAH were considerably concentrated to the DTAC micellar phase through the electrostatic force and the hydrophobic force, respectively.

This work was partially supported by a Grant-in-Aid for Scientific Research No. 02953035 from the Ministry of Education, Science and Culture.

References

1) L. L. Miller and J. R. Valentine, *J. Am. Chem. Soc.*, **110**, 3982 (1988).
2) S. Fukuzumi, S. Koumitsu, K. Hironaka, and T. Tanaka, *J. Am. Chem. Soc.*, **109**, 305 (1987).
3) T. Okamoto, A. Ohno, and S. Oka, *Bull. Chem. Soc. Jpn.*, **53**, 330 (1980); **52**, 3745 (1979); *J. Chem. Soc., Chem. Commun.*, **1977**, 181; **1977**, 784.
4) S. Fukuzumi, Y. Kondo, and T. Tanaka, *J. Chem. Soc., Perkin Trans. 2*, **1984**, 673.
5) M. F. Powell, J. C. Wu, and T. C. Bruice, *J. Am. Chem. Soc.*, **106**, 3850 (1984); A. Sinha and T. C. Bruice, *ibid.*, **106**, 7291 (1984).
6) B. W. Carlson, L. L. Miller, P. Neta, and J. Grodkowski, *J. Am. Chem. Soc.*, **106**, 7233 (1984); B. W. Carlson and L. L. Miller, *ibid.*, **105**, 7453 (1983).
7) J. Grodkowski, P. Neta, B. W. Carlson, and L. L. Miller, *J. Phys. Chem.*, **87**, 3135 (1983).
8) E. J. Land and A. J. Swallow, *Biochim. Biophys. Acta*, **590**, 273 (1980).
9) B. Czochralska and L. Lindqvist, *Chem. Phys. Lett.*, **101**, 297 (1983).
10) J. H. Fendler and E. J. Fendler, "Catalysis in Micellar and Macromolecular Systems," Academic Press, New York (1977).
11) J. H. Fendler, "Membrane Mimetic Chemistry," Aca-

demic Press, New York (1982).
12) K. Yamashita, H. Ishida, and K. Ohkubo, *J. Chem. Soc., Perkin Trans. 2*, **1989**, 2091.
13) F. P. Dwyer, E. Gyarfas, and D. Mellor, *J. Phys. Chem.*, **59**, 296 (1955).
14) D. G. Herries, W. Bishop, and F. M. Richards, *J. Phys. Chem.*, **66**, 1842 (1964).
15) F. H. Quina and H. Chaimovich, *J. Phys. Chem.*, **83**, 1844 (1979); H. Chaimovich, J. B. S. Bonilha, M. J. Politi, and F. H. Quina, *ibid.*, **83**, 1851 (1979); J. B. S. Bonilha, H. Chaimovich, V. G. Toscano, and F. H. Quina, *ibid.*, **83**, 2463 (1979); F. H. Quina, M. J. Politi, I. M. Caccovia, E. Baumgarten, S. M. Martins-Franchetti, and H. Chaimovich, *ibid.*, **84**, 361 (1980).
16) C. Tanford, Y. Nozaki, J. A. Reynolds, and S. Makino, *Biochemistry*, **13**, 2369 (1974).
17) I. V. Berezin, K. Martinek, and A. K. Yatsimirskii, *Russ. Chem. Rev. (Engl. Transl.)*, **42**, 787 (1973).
18) S. Fukuzumi, K. Hironaka, N. Nishizawa, and T. Tanaka, *Bull. Chem. Soc. Jpn.*, **56**, 2220 (1983).
19) The E_{ox}^0 values of BNAH were observed to be more negative than those of NADH[6,20] measured in the different analytical conditions and analytical methods. The E_{ox}^0 value measured for nonionic BNAH or ionic NADH in aqueous solution might be also affected by their ionic character. Anyhow, the k_e value in the micellar phase calculated from Eq. 19 is considered to be reliable since the k_e value was estimated by using the difference of the E^0 values determined under the same measurement conditions.
20) T. Matsue, M. Suda, I. Uchida, T. Kato, U. Akiba, and T. Osa, *J. Electroanal. Chem.*, **234**, 163 (1987).
21) R. A. Marcus, *J. Chem. Phys.*, **24**, 966 (1956); **43**, 679 (1965); R. A. Marcus and N. Sutin, *Inorg. Chem.*, **14**, 213 (1975).
22) C. R. Bock, J. A. Connor, A. R. Gutierrez, T. J. Meyer, D. G. Whitten, B. P. Sullivan, and J. K. Nagle, *J. Am. Chem. Soc.*, **101**, 4815 (1979).

Oxidative Cleavage of Diselenide by *m*-Nitrobenzenesulfonyl Peroxide. Novel Method for the Electrophilic Benzeneselenenylations of Olefins and Aromatic Rings

Masato YOSHIDA,* Shuichi SASAGE, Kyoko KAWAMURA, Takashi SUZUKI, and Nobumasa KAMIGATA
Department of Chemistry, Faculty of Science, Tokyo Metropolitan University, Fukazawa, Setagaya-ku, Tokyo 158
(Received October 23, 1990)

Diphenyl diselenide was found to be readily converted into benzeneselenenyl *m*-nitrobenzenesulfonate ($PhSeOSO_2C_6H_4NO_2$-*m*) by treating with *m*-nitrobenzenesulfonyl peroxide. When the selenenyl sulfonate thus formed was allowed to react in situ with olefins, such as cyclohexene, 1-octene, or styrene, in the presence of various nucleophiles, the adducts of benzeneselenenyl group and a nucleophile were obtained. As the nucleophiles water, methanol, acetic acid, phenol, and anisole could be employed; oxyselenenylated (PhSe-C-C-OR: R=H, Me, Ac, and Ph) and arylselenenylated (PhSe-C-C-C_6H_4OR: R=H and Me) adducts were afforded. Phenol gave oxyselenenylated products in cyclohexene or 1-octene and arylselenenylated products in styrene. Efficient intramolecular cyclizations of unsaturated alcohols and carboxylic acids were similarly performed by the selenenyl sulfonate to afford corresponding benzeneselenenylated cyclic ethers and lactones. The selenenyl sulfonate was also found to be a highly reactive benzeneselenenylating reagent for aromatic rings, such as anisole, phenol, acetanilide, toluene, and benzene.

Organoselenium reagents can be used as nucleophiles, electrophiles, and radicals according to the conditions. Electrophilic selenenylating reagents are usually prepared from oxidative cleavage of diselenide, which is stable and easy to prepare and handle, by halogens,[1] metal ions,[2] electrolytic oxidation,[3] and photoelectron transfer.[4] We are currently interested in the conversion of stable substrates into electrophilic reagents using nitrobenzenesulfonyl peroxides (NBSP).[5] In the course of the study, we found that diphenyl diselenide could be readily converted into electrophilic selenenylating reagent by treating with *m*-nitrobenzenesulfonyl peroxide (*m*-NBSP), and a preliminary communication has appeared.[6] Since we further investigated the electrophilic selenenylations of olefins and aromatic rings using a combination of diphenyl diselenide with *m*-NBSP in detail under various conditions, we report the results as full account.

Results and Discussion

Diphenyl diselenide (0.5 mmol) was treated with *m*-NBSP (0.5 mmol) in 20 ml acetonitrile at 0 °C, and then to the resulting solution cyclohexene (1.1 mmol) in 5 ml methanol was added. The anti-adduct of benzeneselenenyl and methoxyl groups to cyclohexene was obtained in 92% yield.

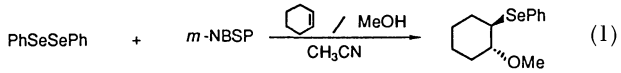

(1)

A plausible mechanism is shown in Scheme 1. Methoxyselenenylations are well-known to occur by the reactions of electrophilic selenenylating reagents with olefins in the presence of methanol,[7] so the formation of cationic benzeneselenenyl species is suggested in the reaction of diphenyl diselenide with *m*-NBSP. We propose benzeneselenenyl *m*-nitrobenzenesulfonate (**1**) as the electrophilic intermediate as shown in Scheme 1. The lone pair on the selenium atom of the diselenide attacks the O-O bond of *m*-NBSP to produce the selenonium salt, and then the cleavage of Se-Se bond gives two moles of benzenesele-

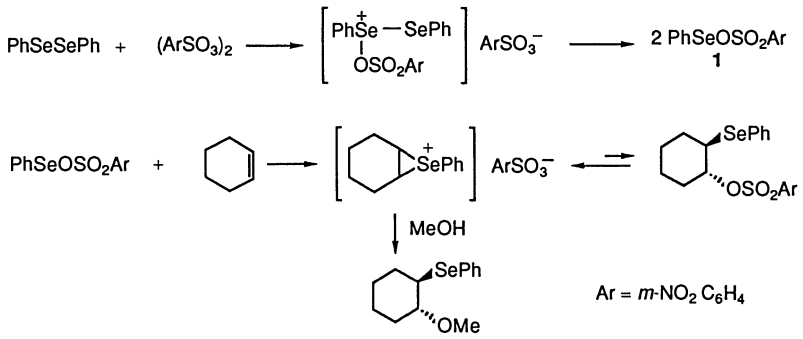

Scheme 1.

nenyl sulfonate.[8] *m*-NBSP is known to behave as a good electrophile in the presence of π- and n-electron donors.[9]

The formation of selenenyl sulfonate **1** was confirmed by ^{13}C NMR studies. Diphenyl diselenide was treated with *m*-NBSP or *p*-NBSP in chloroform-*d*, and ^{13}C NMR was measured to compare with those of benzeneselenenyl trifluoromethanesulfonate. The chemical shifts of the benzeneselenenyl group in benzeneselenenyl *m*-nitrobenzenesulfonate were 130.7, 130.7, 132.5, and 135.8 ppm from internal TMS, and those of bezeneselenenyl *p*-nitrobenzenesulfonate were 130.8, 130.8, 133.2, and 135.6 ppm. The observed chemical shifts were quite similar to those in benzeneselenenyl trifluoromethanesulfonate reported in the literature.[10] Benzeneselenenyl trifluoromethanesulfonate has been prepared from benzeneselenenyl chloride with silver trifluoromethanesulfonate[10,11] or trifluoromethanesulfonic acid.[11]

Electrophilic benzeneselenenylating reagents are known to react with olefins to give episelenonium salts.[7] Although episelenonium salts usually exists in equilibrium with their adducts,[7] the episelenonium nitrobenzenesulfonate did not give adduct, probably because the counter anion, *m*-nitrobenzenesulfonate, is a very stable and weak nucleophile. Therefore, when methanol exists in the reaction system of olefin with **1**, the episelenonium salt thus formed reacts with the methanol to give the adduct of benzeneselenenyl and methoxyl groups (Scheme 1). The anti addition observed in methoxyselenenylation of cyclohexene supports the formation of episelenonium ion. Selenenyl chlorides and bromides have been most widely used for electrophilic selenenylation, however the halide anions act as nucleophiles and often cause an addition of halogen.[7] If it is desired to favor introduction of methanol, the counter anion of episelenonium salt is preferable to be as weak nucleophile as possible. For this purpose it was attempted that selenenyl halides were converted into other selenenylating reagents possessing weak nucleophilic counter anions, such as *N*-phenylselenophthalimide or succinimide.[12] Benzeneselenenyl sulfonates are also expected to be good reagents for oxyselenenylations due to the weak nucleophilicity of sulfonate.[13]

So we investigated the various benzeneselenenylations of styrene, cyclohexene, and 1-octene with **1** in the presence of oxygen nucleophile such as methanol, acetic acid, water, or phenol. Diphenyl diselenide (0.5 mmol) was reacted with *m*-NBSP (0.5 mmol) in a freshly distilled solvent (20 ml), such as dichloromethane, acetonitrile, or nitromethane, and olefin and then nucleophile were added. The results are sum-

Table 1. Reactions of Selenenyl Sulfonate **1** with Olefins in the Presence of Oxygen Nucleophiles

Olefin	Nucleophile		Solvent	Products (Yield/%)[a]
Styrene	MeOH	(5 ml)	CH_3CN	**2** (98)[b]
Cyclohexene	MeOH	(5 ml)	CH_3CN	**3** (92)[b]
1-Octene	MeOH	(5 ml)	CH_3CN	**4a**+**4b** (83)[b,c]
Cyclohexene	MeOH	(5 ml)	CH_2Cl_2	**3** (81)
Cyclohexene	AcOH	(5 ml)	CH_2Cl_2	**6** (trace)
Cyclohexene	AcOH	(5 ml)	CH_3CN	**6** (25)
Cyclohexene	AcOH	(5 ml)	CH_3NO_2	**6** (70)
Styrene	AcOH	(5 ml)	CH_3NO_2	**5** (11)
1-Octene	AcOH	(5 ml)	CH_3NO_2	**7** (73)
Styrene	H_2O	(5 ml)	CH_3CN	**8** (99)
Cyclohexene	H_2O	(5 ml)	CH_3CN	**9** (77), **12** (16)
1-Octene	H_2O	(5 ml)	CH_3CN	**13a**+**13b** (22)[d]
Styrene	H_2O	(5 mmol)	CH_3CN	**8** (61), **11** (Trace)
Cyclohexene	H_2O	(5 mmol)	CH_3CN	**9** (33), **12** (64)
1-Octene	H_2O	(5 mmol)	CH_3CN	**10a** (43),[e] **13a**+**13b** (54)[f]
Styrene	H_2O	(5 ml)	CH_3NO_2	**8** (77)
Cyclohexene	H_2O	(5 ml)	CH_3NO_2	**9** (72)
1-Octene	H_2O	(5 ml)	CH_3NO_2	None
Styrene	PhOH	(10 mmol)	CH_3CN	**16** (78)[b]
Cyclohexene	PhOH	(10 mmol)	CH_3CN	**14** (38)[b]
1-Octene	PhOH	(10 mmol)	CH_3CN	**15** (25)[b]
Styrene	PhOH	(10 mmol)	CH_3NO_2	**16** (82)
Cyclohexene	PhOH	(10 mmol)	CH_3NO_2	**14** (64)
1-Octene	PhOH	(10 mmol)	CH_3NO_2	**15** (62)

a) Products were isolated and the yields were determined based on **1** evaluated from diselenide. b) Data from Ref. 6. c) The products were obtained as a mixture of **4a** and **4b** (80 : 20 by NMR). d) The products were obtained as a mixture of **13a** and **13b** (88 : 12 by NMR). e) A small amount of regioisomer **10b** was contained. f) The products were obtained as a mixture of **16a** and **16b** (84 : 16 by NMR).

marized in Table 1. Methoxyselenenylation (Eq. 2) proceeded in good to excellent yields regardless of olefins and solvents employed.

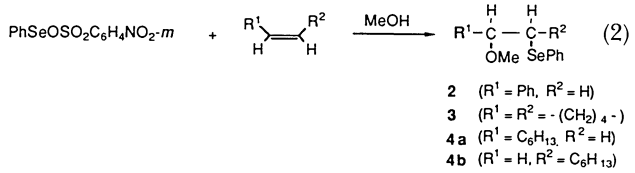

On the other hand, the yields of acetoxyselenenylation (Eq. 3) depended on both solvents and olefins employed. Acetoxyselenenylation of cyclohexene proceeded in nitromethane in good yield, however, in dichloromethane the reaction proceeded only to a small extent. The results mean that selenenyl sulfonate **1** is formed in dichloromethane, acetonitrile, and nitromethane, but the acetoxyselenenylation with **1** is extremely influenced by solvents. Thus, acetoxyselenenylations of styrene and 1-octene were examined in nitromethane; although 1-octene afforded **7** in good yield, the yield of acetoxyselnenylated product of styrene (**5**) was only 11%.

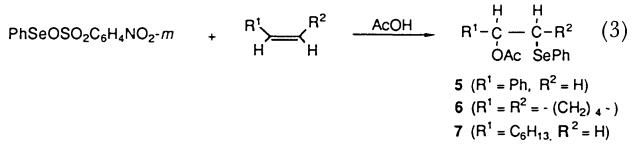

When excess of water (5 ml) was added in acetonitrile, hydroxyselenenylation occurred in good to excellent yields in styrene and cyclohexene to afford **8** and **9**. Hydroxyselenenylation of 1-octene did not occur under similar conditions, but amidoselenenylated product (**13**) was obtained in 22% yield. On the other hand, when small amount of water (5 mmol) was used in acetonitrile, amidoselenenylation of cyclohexene and 1-octene occurred prior to hydroxyselenenylation, but amidoselenenylation of styrene proceeded only in a small yield.

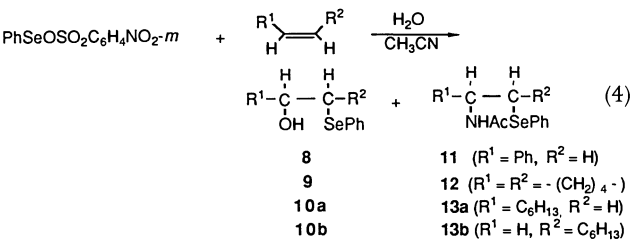

The amidoselenenylation is explained by the reaction of episelenonium ion with acetonitrile as shown in Scheme 2. Amidoselenenylations of olefins have been known to proceed in the reaction of electrophilic benzeneselenenylating reagents with olefin in acetonitrile in the presence of trifluoromethanesulfonic acid and water.[14,15] By the use of nitromethane as a solvent hydroxyselenenylated products of styrene **8** and cyclohexene **9** could be obtained selectively in good yields, however, hydroxyselenenylation of 1-octene did not occur.

Since the nucleophilicity of nitrobenzenesulfonate is very weak, the oxyselenenylation is expected to occur even in the presence of weak oxygen nucleophiles, which are inapplicable with benzeneselenenyl halides. Thus, we investigated the reaction of **1** with olefins in the presence of phenol. Phenoxyselenenylation of cyclohexene and 1-octene occurred in moderate yields in acetonitrile and in good yields in nitromethane (Eq. 5). An unexpected product (**16**) was obtained in the reaction of styrene as shown in Eq. 6. The episelenonium ion produced from the reaction of styrene with **1** electrophilically attacked on the aromatic ring of phenol, whereas those from cyclohexene and 1-octene reacted at oxygen atom of phenol.

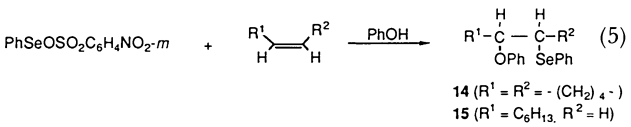

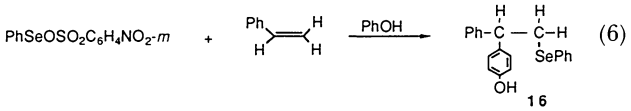

The arylselenenylation is interesting as Friedel-Crafts type C-C bond formation. The electrophilic aromatic substitutions of the episelenonium ion with

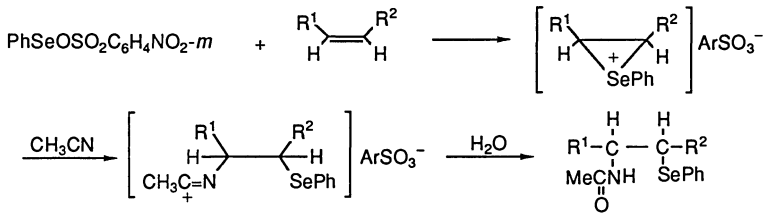

Scheme 2.

anisole were also observed.[6] When anisole was added to the reaction mixture of diselenide with *m*-NBSP and olefin, the adduct of benzeneselenenyl group and anisole to styrene was obtained in excellent yield in acetonitrile (Eq. 7). *p*-Methoxyphenylselenenylations of cyclohexene and 1-octene also occurred in moderate yields in nitromethane (Eq. 7), but not in acetonitrile. Acetonitrile reacted as nucleophile prior to anisole to give amidoselenenylated products **12** and **13** in 51% and 43% yields, respectively. The aromatic substitutions of the episelenonium ion did not occur in benzene and toluene under similar conditions.

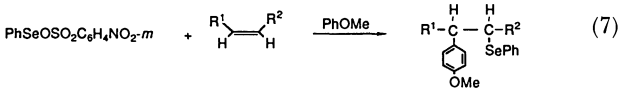

(7)

17 (R^1 = Ph, R^2 = H), 96% in CH_3CN
18 (R^1 = R^2 = -$(CH_2)_4$-), 33% in CH_3NO_2
19 (R^1 = C_6H_{13}, R^2 = H), 53% in CH_3NO_2

Intramolecular ring closure by electrophilic activation of an unsaturated alcohol or carboxylic acid is a useful synthetic methodology for the synthesis of complex natural products. The reagents composed of reactive electrophiles and weak nucleophiles are expected to have the particular advantage of being applicable for cyclofunctionalization, and benzeneselenenyl sulfonates were shown to be good reagents for cycloselenenylations.[10,16,17] We have also examined cyclizations of 4-penten-1-ol, 5-hexen-1-ol, 4-pentenoic acid, and 5-hexenoic acid using our method for preparation of selenenyl sulfonate. To the resulting solution of diphenyl diselenide (0.5 mmol) with *m*-NBSP (0.5 mmol) in acetonitrile (20 ml) 4-penten-1-ol was added at −40 °C, and the solution was further allowed to react at −40 °C for 2 h to give cyclic ether **20** almost quantitatively. When the reaction was carried out at 0 °C, small amoumt of the isomer **21** was obtained in addition to **20**. On the other hand, the cyclic ether **22** was obtained as a sole product at 0 °C from 5-hexen-1-ol.

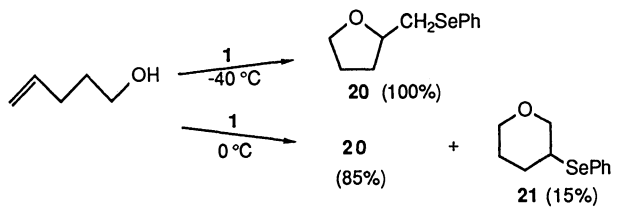

(8)

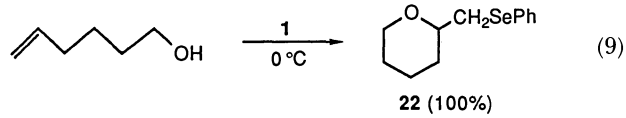

(9)

Similary, lactones **23** and **24** were obtained from 4-pentenoic acid and 5-hexenoic acid in excellent yields, respectively (Eq. 10).

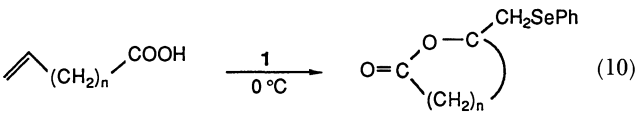

(10)

23 : n = 2 (93%)
24 : n = 3 (96%)

Although electrophilic selenenylating reagents easily react with olefins, electrophilic aromatic substitutions by benzeneselenenyl group have been scarecely reported in the literature. Most methods for the introduction of areneselenenyl group into aromatic rings were nucleophilic displacement of selenium reagents on halobenzenes bearing an electron-withdrawing group.[18–20] Benzeneselenenyl chloride reacted with electron-rich benzenes as a reagent for chlorination rather than selenenylation.[21] Benzeneselenenyl chloride was converted in situ into benzeneselenenyl hexafluorophosphate, which reacted with anisole to give *p*-methoxyphenyl phenyl selenide and bis(*p*-methoxyphenyl)phenylselenonium hexafluorophosphate.[22] Dimethyl(phenylseleno)sulfonium tetrafluoroborate formed from benzeneselenenyl bromide was reported to be a highly reactive selenenylating reagent for electron-rich aromatic compounds, however, aromatic rings were limited to aromatic amines, phenols, and aromatic ethers.[23] Selenenyl sulfonate **1** also electrophilically reacted with aromatic rings to afford aryl phenyl selenides. To the resulting solution of diphenyl diselenide (0.5 mmol) with *m*-NBSP (0.5 mmol) in dichloromethane or acetonitrile, substituted benzene was added, and the solution was allowed to react at room temperature for 1 h and then refluxed for 2 h. Benzeneselenenyl group was introduced into aromatic rings, and the results are summarized in Table 2.

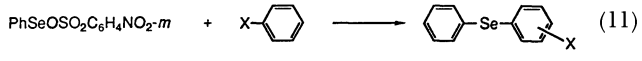

(11)

The electrophilic aromatic substitutions with **1** described herein proceeded in good to excellent yields for electron-rich benzenes such as anisole, phenol, and acetanilide, selectively at the *p*-position, and also could be applied to even toluene and benzene. Thus, benzeneselenenyl group in **1** was found to act as very reactive electrophile to react not only with olefins but also with aromatic rings.

In conclusion, diphenyl diselenide could be readily converted into very reactive electrophilic selenenylating reagents, benzeneselenenyl arenesulfonate, by the oxidative cleavage of Se-Se bond with *m*-NBSP.

Table 2. Benzeneselenenylation of Aromatic Rings with Selenenyl Sulfonate **1**

ArH/mmol		Solvent	Yield[a)]	Isomer ratio para/ortho[a)]
PhOMe	1.1	CH_2Cl_2	94	98/ 2
PhOMe	1.1	CH_3CN	75	99/ 1
PhOH	1.1	CH_2Cl_2	51	88/12
PhOH	1.1	CH_3CN	53	94/ 6
$PhNHCOCH_3$	5.0	CH_2Cl_2	84	100/ 0
$PhNHCOCH_3$	1.1	CH_2Cl_2	18	100/ 0
$PhNHCOCH_3$	5.0	CH_3CN	83	100/ 0
$PhNHCOCH_3$	1.1	CH_3CN	60	100/ 0
$PhCH_3$	5.0	CH_2Cl_2	50	72/28
$PhCH_3$	5.0	CH_3CN	45	68/32
PhH	5.0	CH_2Cl_2	21	
PhH	5.0	CH_3CN	12	
PhCl	5.0	CH_2Cl_2	0	
PhCl	5.0	CH_3CN	0	

a) Yields and isomer ratio were determined by GC.

m-NBSP is readily synthesized from *m*-nitrobenzenesulfonyl chloride with 30% hydrogen peroxide and relatively stable for handling and storage.[24] Thus, the method for electophilic benzeneselenenylation described in this paper is expected to be very attractive and potentially useful in general organic synthesis.

Experimental

^1H NMR spectra were taken with a JEOL JNM PMX 60SI (60 MHz) spectrometer. ^{13}C NMR spectra were taken with a JEOL JNM FX90Q FTNMR spectrometer. IR spectra were recorded on a Hitachi 260-10 spectrometer. Gas chromatography was performed by a Hitachi 263-30 gas chromatograph with SE-30 (10%) 2-m stainless steel column. Gel-permeation chromatography was performed by means of a JAI Model LC-08 liquid chromatograph equipped with two JAIGEL-1H columns (20ϕ×600 mm) with chloroform as eluent. Mass spectra were obtained with a JEOL JMS DX-300 spectrometer by an electron-impact (EI) ionization technique at 70 eV.

Materials. Diphenyl diselenide was obtained from Nacalai Tesque and recrystallized prior to use. *m*-Nitrobenzenesulfonyl peroxide was synthesized from *m*-nitrobenzenesulfonyl chloride and 30% hydrogen peroxide according to the method described in the literature[24] (mp 107 °C (decomp) lit, 112 °C (decomp)). Dichloromethane and acetonitrile were refluxed over calcium hydride and distilled prior to use. Nitromethane was dried over phosphorus pentaoxide and distilled prior to use.

General Procedure for the Preparation of Selenenyl Sulfonate 1. Diphenyl diselenide (0.5 mmol) was dissolved in freshly distilled solvent (20 ml), and solid *m*-NBSP (0.5 mmol) was added to the solution in small portions at 0 °C. The color of the solution turned reddish brown at once, and the resulting solution was further allowed to stir for 10 min at 0 °C and used for reactions in situ.

The Reactions of 1 with Olefins in the Presence of Methanol. Olefin (1.1 mmol) dissolved in methanol (5 ml) was added to the solution of **1** prepared in acetonitrile, and the reaction mixture was allowed to stir at room temperature for 3 h. Ether (20 ml) was added to the reaction mixture, and the solution was washed twice with 20 ml of water, 5% aqueous solution of sodium hydrogencarbonate (20 ml) and then water (20 ml). The separated organic layer from aqueous layer was dried over anhydrous magnesium sulfate, and the solvent was evaporated to give yellow oil, which was subjected to column chromatography on silica gel (Wakogel C-60) to give methoxyselenenylated products (hexane–ethyl acetate 5:1 as eluent). 2-Methoxy-2-phenylethyl phenyl selenide (**2**), 2-methoxycyclohexyl phenyl selenide (**3**) was isolated as pure forms, but 2-methoxyoctyl phenyl selenide (**4a**) could not be separated from a small amount of its regioisomer (**4b**), and these products were identified by comparison of the spectral data with those described in the literature.[25]

The Reaction of 1 with Olefins in the Presence of Acetic Acid. Olefin (1.1 mmol) dissolved in nitromethane and then acetic acid (1 ml) was added to the solution of **1** prepared in nitromethane, and the reaction mixture was allowed to stir for 3 h at room temperature. Ether (20 ml) was added to the reaction mixture, and the solution was washed with 5% aqueous solution of sodium hydrogencarbonate (100 ml) and water (100 ml) twice in order to remove acetic acid and *m*-nitrobenzenesulfonic acid. The organic layer was separated from the aqueous layer and dried over anhydrous magnesium sulfate. The reactions in acetonitrile were similarly performed. When dichloromethane was used as solvent, the reaction mixture was washed with aqueous solution of sodium hydrogencarbonate and water without addition of ether. The evaporation of the solvent left a yellow oil which was subjected column chromatography on Wakogel C-60 to give diphenyl diselenide (hexane as eluent) and acetoxyselenenylated product (hexane–ethyl acetate 5:1). 2-Acetoxy-2-phenylethyl phenyl selenide (**5**), 2-acetoxycyclohexyl phenyl selenide (**6**), and 2-acetoxyoctyl phenyl selenide (**7**) were isolated as almost pure forms and identified by comparison of the spectral data with those described in the literature.[2]

Reactions of 1 with Olefins in the Presence of Water. To the solution of **1** prepared in acetonitrile, olefin (1.1 mmol) and then water (5 mmol) dissolved in acetonitrile was added, and the solution was allowed to react at room temperature for 3 h. After working up the products were separated by column chromatography on Wakogel C-60 using hexane and hexane–ethyl acetate (5:1) as eluent. Amidoselenenylated products (**11**, **12**, **13**)[14] and hydroxyselenenylated products (**8**, **9**, **10**)[26] were identified by comparison of the spectral data with those described in literatures. The reactions in the presence of water (5 ml) in nitromethane and acetonitrile were similarly performed.

The Reaction of 1 with Olefins in the Presence of Phenol. To the solution of **1** prepared in nitromethane or acetonitrile, olefin (1.1 mmol) and then phenol (10 mmol) were added. The reaction mixture was allowed to stir for 3 h at room temperature and worked up as in the case of acetoxyselenenylations. Column chromatography on Wakogel C-60 afforded pure products (hexane–ethyl acetate 5:1 as eluent).

2-(4-Hydroxyphenyl)-2-phenylethyl phenyl selenide (**16**): Yellow oil; ^1H NMR ($CDCl_3$) δ=3.40 (d, J=7.9 Hz, 2H), 4.25 (t, J=7.9 Hz, 1H), 4.63 (s, 1H), 6.44 and 6.88 (ABq, J=9.6 Hz, 4H), and 6.9—7.3 (m, 10H); ^{13}C NMR ($CDCl_3$) δ=34.1, 50.8,

115.5, 126.7, 126.9, 127.8, 128.6, 129.1, 129.1, 129.2, 132.8, 136.0, 144.0, and 154.2; IR (neat) 3340 cm^{-1} (OH); MS *m/z* 354 (M^+); Exact MS 354.0523 (Calcd for $C_{29}H_{18}OSe$: 354.0570).

2-Phenoxycyclohexyl phenyl selenide (**14**): Yellow oil; ^1H NMR ($CDCl_3$) δ=1.0—2.5 (m, 8H), 3.3 (m, 1H), 4.2 (m, 1H), and 6.6—7.7 (m, 10H); ^{13}C NMR ($CDCl_3$) δ=22.9, 25.3, 30.2, 31.2, 46.4, 78.4, 116.3, 121.0, 127.6, 128.4, 128.9, 129.5, 135.4, and 157.7; MS *m/z* 332 (M^+); Exact MS 332.0671 (Calcd for $C_{18}H_{20}OSe$: 332.0678).

2-Phenoxyoctyl phenyl selenide (**15**): Yellow oil; ^1H NMR ($CDCl_3$) δ=0.6—2.3 (m, 13H), 3.05 (d, *J*=6.0 Hz, 1H), 3.10 (d, *J*=3.6 Hz, 1H), 4.27 (m, 1H), and 6.5—7.6 (m, 10H); ^{13}C NMR ($CDCl_3$) δ=14.0, 22.5, 25.3, 29.2, 31.7, 31.8, 34.0, 77.5, 116.1, 120.9, 127.2, 129.0, 129.4, 130.0, 133.3, and 158.0; MS *m/z* 362 (M^+), Exact MS 362.1159 (Calcd for $C_{20}H_{26}OSe$: 362.1158).

The Reaction of 1 with Olefins in the Presence of Anisole. To the solution of **1** prepared in acetonitrile, styrene (1.1 mol) dissolved in anisole (5 ml) was added. The reaction mixture was allowed to stir at room temperature for 3 h, and worked up according to the same procedure described in the case of methoxyselenenylations. The solvent and excess anisole was distilled off in vacuo, and the residue was almost pure 2-(*p*-methoxyphenyl)-2-phenylethyl phenyl selenide (**17**), which was further purified by column chromatography on Wakogel C-60; yellow oil; ^1H NMR ($CDCl_3$) δ=3.49 (d, *J*=7.9 Hz, 2H), 3.70 (s, 3H), 4.25 (t, *J*=7.9 Hz, 1H), 6.74 and 7.05 (ABq, *J*=7.8 Hz, 4H), and 7.1 (m, 10H); ^{13}C NMR ($CDCl_3$) δ=34.1, 50.8, 55.3, 113.9, 126.6, 126.9, 127.7, 128.6, 128.8, 129.1, 130.9, 132.8, 133.0, 135.7, 144.0, and 158.4; MS *m/z* 368 (M^+); Exact MS 368.0679 (Calcd for $C_{21}H_{20}OSe$: 368.0694). Cyclohexene or 1-octene was also allowed to react in nitromethane and worked up as in the case of styrene. The products were separated by preparative layer chromatography (Merck Silica Gel 60 PF) using hexane–chloroform (5 : 1) as eluent. 2-(*p*-Methoxyphenyl)cyclohexyl phenyl selenide (**18**) and 2-(*p*-methoxyphenyl)octyl phenyl selenide (**19**) were further purified by medium-pressure column chromatography (Kusano Kagakukikai Co. CIG Pre-Packed Column CPS-HS-221-05).

2-(*p*-Methoxyphenyl)cyclohexyl phenyl selenide: Mp 136—138 °C (from hexane); ^1H NMR ($CDCl_3$) δ=1.0—2.5 (m, 8H), 2.8 (m, 1H), 3.3 (m, 1H), 3.76 (s, 3H), and 6.8—7.6 (m, 9H), coupling constant between H^1 and H^2 of cyclohexyl group was determined to be 10.0 Hz by spin decoupling technique; ^{13}C NMR ($CDCl_3$) δ=26.5, 27.6, 35.7, 37.1, 49.1, 50.4, 55.2, 113.8, 127.3, 128.2, 128.6, 129.2, 135.7, 137.6, and 158.2; MS *m/z* 346 (M^+); Exact MS 346.0801 (Calcd for $C_{19}H_{22}SeO$: 346.0836).

2-(*p*-Methoxyphenyl)octyl phenyl selenide: Yellow oil; ^1H NMR ($CDCl_3$) δ=0.7—2.1 (m, 13H), 2.5—3.5 (m, 3H), 3.76 (s, 3H), 6.7—7.7 (m, 9H); ^{13}C NMR ($CDCl_3$) δ=14.0, 22.6, 27.5, 29.2, 31.7, 35.9, 36.4, 45.5, 55.2, 113.9, 126.6, 128.4, 128.9, 132.5, 132.7, 136.5, and 158.3; MS *m/z* 376 (M^+); Exact MS 376.1333 (Calcd for $C_{21}H_{28}OSe$: 376.1306).

Reactions of 1 with Unsaturated Alcohols or Carboxylic Acids. To the solution of **1** prepared in acetonitrile 4-penten-1-ol (1.1 mmol) was added at 0 °C or −40 °C. The reaction mixture was allowed to stir at 0 °C for 2 h or −40 °C for 2.5 h and worked up as in the case of methoxyselenenylations. The separated organic layer was dried over anhydrous magnesium sulfate, and the solvent was evaporated. Almost pure tetrahydro-2-(phenylselenomethyl)furan (**20**) was obtained from the reaction mixture at −40 °C. The furan (**20**)[27] was further purified by GPC and identified on the basis of the spectral data. Tetrahydro-3-(phenylseleno)-pyran (**21**),[28] which was obtained from the reaction at 0 °C, could not be separated as pure form. Similarly, the reactions of 5-hexen-1-ol, 4-pentenoic acid, and 5-hexenoic acid were carried out. Tetrahydro-2-(phenylselenomethyl)-pyran (**22**),[27] dihydro-5-(phenylselenomethyl)-2-furanone (**23**),[29] and tetrahydro-6-(phenylselenomethyl)-2-pyranone (**24**)[29] were identified on the basis of spectral data.

Reactions of 1 with Substituted Benzenes. Substituted benzene dissolved in dichloromethane was added to the solution of **1** prepared in dichloromethane, and the solution was allowed to stir at room temperature for 1 h and then refluxed for 2 h. The reaction mixture was washed with 5% aqueous solution of sodium hydrogencarbonate and water, and the organic layer was dried over magnesium sulfate. The products were analyzed by GC-MS and the yields were determined by GC using diphenyl sulfide as an internal standard. The aryl phenyl selenides were isolated by column chromatograpy on Wakogel C-60 and Gel-permeation chromatography. 4-Methoxyphenyl phenyl-selenide,[17] 4-hydroxyphenyl phenyl selenide,[23] 2-hydroxyphenyl phenyl selenide,[23] 4-acetamidophenyl phenyl selenide,[21] 4-methylphenyl phenyl selenide,[20] and diphenyl selenide[30] were identified by their ^1H NMR, ^{13}C NMR, and MS.

References

1) C. Paulmier, "Selenium Reagents and Intermediates in Organic Synthesis," Pergamon Press, Oxford (1986), Chap. 2.

2) N. Miyoshi, Y. Takai, S. Murai, and N. Sonoda, *Bull. Chem. Soc. Jpn.*, **51**, 1265 (1978); N. Miyoshi, Y. Ohno, K. Kondo, S. Murai, and N. Sonoda, *Chem. Lett.*, **1979**, 1309.

3) S. Torii, K. Uneyama, and M. Ono, *Tetrahedron Lett.*, **21**, 2741 (1980); S. Torii, K. Uneyama, M. Ono, and T. Bannou, *J. Am. Chem. Soc.*, **103**, 4606 (1981).

4) G. Pandey, V. J. Rao, and U. T. Bhalero, *J. Chem. Soc., Chem. Commun.*, **1989**, 416.

5) M. Yoshida, H. Mochizuki, and N. Kamigata, *Chem. Lett.*, **1988**, 2017.

6) M. Yoshida, N. Satoh, and N. Kamigata, *Chem. Lett.*, **1989**, 1433.

7) K. B. Sharpless and R. F. Lauer, *J. Org. Chem.*, **39**, 429 (1974); C. Paulmier, "Selenium Reagents and Intermediates in Organic Synthesis," Pergamon Press, Oxford (1986), Chap. 7; A. Toshimitsu and S. Uemura, *Yuki Gosei Kyokai Shi*, **39**, 1201 (1981).

8) Recently, oxidative cleavage of diphenyl diselenide with ammonium peroxydisulfate was reported; M. Tiecco, L. Testaferri, M. Tingoli, D. Chianelli, and D. Bartoli, *Tetrahedron Lett.*, **30**, 1417 (1989).

9) R. V. Hoffman, "The Chemistry of Peroxides," ed by S. Patai, John Wiley & Sons, New York (1983), Chap. 9; R. V. Hoffman, *Org. Prep. Proced. Int.*, **18**, 181 (1986).

10) S. Murata and T. Suzuki, *Chem. Lett.*, **1987**, 849.

11) R. Okazaki and Y. Itoh, *Chem. Lett.*, **1987**, 1575.

12) K. C. Nicolaou, D. A. Claremon, W. E. Barnette, and S. P. Seitz, *J. Am. Chem. Soc.*, **101**, 3704 (1979); K. C. Nicolaou, *Tetrahedron*, **37**, 4097 (1981); K. C. Nicolaou, N.

A. Petasis, and D. A. Claremon, *Tetrahedron*, **41**, 4835 (1985).
13) Recently, electrophilic additions of benzeneselenenyl *p*-toluenesulfonate to acetylenes were reported; T. G. Back and K. R. Muralidharan, *Tetrahedron Lett.*, **31**, 1957 (1990).
14) A. Toshimitsu, T. Aoai, H. Ogawa, S. Uemura, and M. Okano, *J. Org. Chem.*, **46**, 4727 (1981).
15) M. Tiecco, L. Testaferri, M. Tingoli, and D. Bartoli, *Tetrahedron*, **45**, 6819 (1989).
16) S. Murata and T. Suzuki, *Tetrahedron Lett.*, **28**, 4297, 4415 (1987).
17) M. Tiecco, L. Testaferri, M. Tingoli, D. Bartoli, and R. Balducci, *J. Org. Chem.*, **55**, 429 (1990).
18) L. M. Litvinenko and R. S. Chshko, *Zh. Obshch. Kim.*, **30**, 3682 (1960).
19) A. B. Pierini and R. A. Rossi, *J. Organomet. Chem.*, **144**, C12 (1978).
20) H. Suzuki, H. Abe, and A. Osuka, *Chem. Lett.*, **1981**, 151; A. Osuka, H. Ohmasa, and H. Suzuki, *Synthesis*, **1982**, 857.
21) F. D. Ayorinde, *Tetrahedron Lett.*, **24**, 2077 (1983).
22) G. Lindgren and G. H. Schmid, *Chem. Scr.*, **23**, 98 (1984).
23) P. G. Gassman, A. Miura, and T. Miura, *J. Org. Chem.*, **47**, 951 (1982).
24) R. L. Dannley, J. E. Gagen, and O. J. Stewart, *J. Org. Chem.*, **35**, 3076 (1970).
25) A. Toshimitsu, T. Aoai, S. Uemura, and M. Okano, *J. Org. Chem.*, **45**, 1953 (1980).
26) A. Toshimitsu, T. Aoai, H. Owada, S. Uemura, and M. Okano, *Tetrahedron*, **41**, 5301 (1985).
27) K. C. Nicolaou, R. L. Magolda, W. J. Sipio, W. E. Barnette, Z. Lysenko, and M. M. Joullie, *J. Am. Chem. Soc.*, **102**, 3784 (1980).
28) A. Anciaux, A. Eman, W. Dumont, D. Van Ende, and A. Krief, *Tetrahedron Lett.*, **19**, 1613 (1975).
29) K. C. Nicolaou, S. P. Seita, W. J. Sipio, and J. F. Blount, *J. Am. Chem. Soc.*, **101**, 3884 (1979).
30) G. Llabres, M. Baiwir, L. Christianes, and J.-L. Piette, *Can. J. Chem.*, **57**, 2967 (1979).

 © 1991 The Chemical Society of Japan Bull. Chem. Soc. Jpn., 64, 423—430 (1991)

Time Courses of the Numbers of Spins from a Single or Two Organic Compounds on a Decationated Y-Type Zeolite

Hiroshi KASHIWAGI
Faculty of Pharmaceutical Sciences, Toyama Medical and Pharmaceutical University, Sugitani, Toyama 930-01
(Received July 30, 1990)

The time courses of the number of organic radicals produced on the surface of a decationated Y-type zeolite (HY) were followed with electron paramagnetic resonance spectroscopy after the removal of heptane (a solvent). Regardless of the presence of the heptane, the relationship between the amount of adsorption and the number of spins for a binary system of HY and a single organic compound was linear and reversible, suggesting the significance of the presence of an adsorption equilibrium. On the surface of HY, there are two kinds of active sites possessing different times required for attaining constant numbers of spins. Cation radicals from a strong donor (perylene) adsorbed in advance on HY were gradually replaced by those from a weak donor (naphthalene), while a small number of cation radicals from naphthalene adsorbed in advance on HY remained after contact with a sufficiently large quantity of perylene. The coexistence of both donor and acceptor molecules on HY increased the number of both cations and anion radicals, which were significantly dependent on the order of adsorption.

The charge-transfer interaction, resulting in the formation of either cation radicals on solid acid sites or anion radicals on solid base sites on the surfaces of zeolites, was frequently studied using electron paramagnetic resonance (EPR) spectroscopy up to the early 1970's.[1-4] The majority of EPR spectroscopic investigations on the charge-transfer interaction between zeolites and organic compounds were carried out at adsorption equilibrium.[1] These results have been applied, for example, to an evaluation of the activity of zeolites as solid acid or base catalysts and to the construction of a model of active sites.[1]

In general, the content of an organic compound adopted in a mechanistic study of a contact reaction is usually much smaller than that employed in a practical catalytic synthesis. Provided that the spectroscopic studies were carried out with multicomponent systems comprising an aluminosilicate and relatively large quantities of adsorbate molecules, it was observed that some new phenomena occurred only in a complicated system, but disappeared in a simple system. These results might be applicable, for example, to a quantitative evaluation of the activity of practical catalysts.

The time courses of the number of spins induced in a binary system comprising silica-alumina and a large quantity (10%) of glycolic acid after the removal of a solvent were considered quantitatively from both pharmaceutical and mechanochemical points of view.[5] In this case, the number of spins (NOS) was initially small, gradually increased, attained a constant number of spins (CNS), and then decreased from CNS during the final stage.[5] The values of CNS and the duration of CNS (a measure of the oxidation rate or polymerization of glycolic acid) were dependent on the calcination temperature of silica-alumina, on the mechanical energy (shaking or compressing) applied during or after mixing, on the conditions for storing the mixed systems (temperature, atmosphere, or humidity), and on the time interval between mixing and ultraviolet irradiation.[5]

From the viewpoint of surface or catalytic chemistry, we attempted to follow by EPR spectroscopy the time courses of the number of radicals produced from a single or two organic compounds (0.1—10 times the maximal amount of adsorbate molecules/g-HY (A_{max})) adsorbed on the surface of a decationated Y-type zeolite (HY). Since the formation of radicals on HY is attributable to a charge-transfer interaction,[1] the behaviors of radicals from perylene (PE) as a strong donor (ionization potential=6.90 eV),[6] naphthalene (NA) as a weak donor (ionization potential=8.13 eV),[6] tetracyanoethylene (TCNE) as a strong acceptor (electron affinity=2.3 eV),[7] or 1,3-dinitrobenzene (DNB) as a weak acceptor (electron affinity $<$0.7 eV) on HY were compared.

A long time was required for a Hammett indicator adsorbed on an aluminosilicate to attain equilibrium.[8] In the case of HY, the time courses of NOS have not been paid much attention. However, it took a long time for the NOS of an HY-organic system to attain a constant value, suggesting the significance of the presence of nonequilibrium states when HY is applied, for example, to practical contact reactions.

Regardless of the presence of a solvent, the dependence of NOS on the amount of adsorption was found to be linear and reversible in the case of a binary system of HY and a single organic compound, suggesting the significance of adsorption equilibrium. Qualitatively, however, rapid heating or vigorous stirring of this HY-organic system in contact with heptane resulted in an irreversible dependence of NOS on the amount of adsorption. However, the NOS values of ternary systems comprising HY and two organic compounds after the removal of the solvent were suitable for quantitative considerations on this irreversibility. Eventually, cation radicals from a strong donor (PE) adsorbed in advance were gradually replaced by

those from a weak donor (NA), while cation radicals from NA adsorbed in advance remained even after subsequent contact with PE. Further, the coexistence of donor and acceptor molecules on HY increased the number of both the cation and anion radicals, which were considerably dependent on the order of adsorption. Thus, the NOS values of binary (HY-organic) systems behave like being in equilibrium, while those of some ternary (HY-two organic) systems were dependent on the adsorption processes.

The main object of this report is to describe the time courses of NOS with zeolite-organic systems after removing the solvent and to try to search for some new factors necessary for considering NOS of slightly complicated systems, both quantitatively and reproducibly. The obtained results may be available, at least, for improving the reproducibility of some physicochemical data of slightly complicated systems. They may be expected in the future to provide a technique for supplying an HY possessing constant and the desired efficiency or a model of active sites.

Experimental

Materials. An HY was obtained by calcining an NH_4^+-exchanged Y-type zeolite (Si/Al=4.8) at 400 or 650 °C. PE or DNB was recrystallized from toluene or 1/1 (v/v) ethanol/water, respectively. NA and TCNE were purified by sublimation. Freshly distilled heptane was used as a solvent.

Procedure. A binary system of HY and a single organic compound was obtained by impregnating HY with a given volume of a heptane solution (0.1 mol dm^{-3}) of PE, NA, TCNE, or DNB (containing the A_{max} of the organic compound), followed by drying under reduced pressure (ca. 300Pa).

A ternary system of HY and two electron donors or HY and two electron acceptors was obtained by impregnating HY with a given volume of a heptane solution (0.01 mol dm^{-3}) of the first organic compound (containing therein 0.1 times the A_{max} of the organic compound), followed by drying under reduced pressure, soaking again with a given volume of a heptane solution (0.1 mol dm^{-3}) of the second organic compound (containing therein 10 times the A_{max} of the organic compound), and drying again in vacuo. A ternary system arranged in the order HY-TCNE or DNB (A_{max})-PE or NA (A_{max}) or HY-PE or NA (A_{max})-TCNE or DNB (A_{max}) was prepared similarly.

Determination of the Number of Molecules Adsorbed on HY from Heptane Solutions. The number of organic molecules adsorbed when HY (20—50 mg) was brought in contact with a heptane solution (1.0×10^{-4}—3.0×10^{-1} mol dm^{-3}) of an organic compound for a given time of contact (0—72 h) at 25 °C was determined spectrophotometrically.

EPR Measurement. The EPR spectra of the binary and ternary systems were obtained in dry nitrogen at 25 °C with a JEOL JES-FE3X type spectrometer (X band, 100 kHz modulation) at a microwave power of 0.2 mW and a modulation amplitude of 3.2×10^{-3} mT. The NOS values, expressed as spins per gram of dry HY, were estimated by a comparison with standard carbon samples which had previously been calibrated with solutions of 2,2-diphenyl-1-picrylhydrazyl in benzene.[3] The experimental errors in NOS and the amount of organic molecules adsorbed/g-HY were less than 10%.

Results and Discussion

EPR Spectra of Radicals on HY. A fairly well-resolved hyperfine structure was obtained in the EPR spectrum of the PE or NA cation radical or of the DNB anion radical, whereas the spectrum of the TCNE anion radical was unresolved. The EPR spectra of PE, NA, TCNE, and DNB adsorbed on HY were analogous to those reported by Stamires and Turkevich,[2] Flockhart et al.,[3] Hirota et al.,[4] and so on.

An EPR spectrum of a ternary system of HY and two organic compounds was almost the superposition of the spectra of two binary (HY-organic) systems. In addition, one or more band(s) was observed separately from the spectrum of each ion radical. Therefore, the NOS values of two radical species on HY could be determined independently.

Adsorption Equilibrium for Binary Systems during Contact with Heptane Solutions. The adsorption isotherm of PE or TCNE from heptane solutions at 25 °C is shown in Fig. 1. In the low-concentration region of the isotherm, the amount of adsorption is proportional to the number of PE or TCNE molecules in contact with HY, decreasing its increase, and

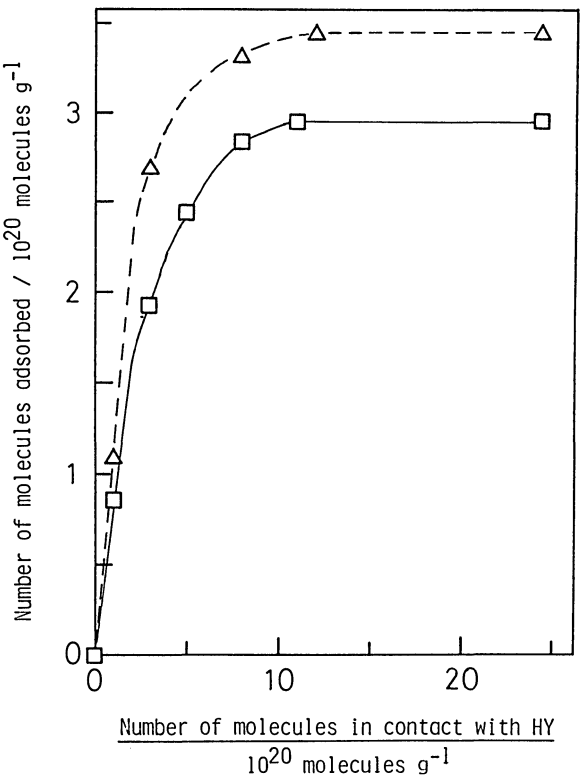

Fig. 1. Room temperature isotherm of PE (□) or TCNE (△) adsorption from heptane solutions on HY calcined at 650 °C.

finally reaching a plateau. Similar results were obtained for the adsorption of NA or DNB.

Figure 2 shows the dependence of the amount of adsorption on the contact time from immediately after bringing HY into contact with heptane solutions (0.1 mol dm^{-3}). During the initial stage, the amount of molecules adsorbed increased linearly with the contact time, decreasing its increase, and finally reaching a plateau. Similar results were confirmed at a PE or TCNE concentration from 0.001 to 0.3 mol dm^{-3} or with the adsorption of NA or DNB. Independent of the calcination temperature of HY (T_{ca}), the time required for reaching the plateau for PE, NA, TCNE, or DNB was ca. 45, 60, 50, or 50 h, respectively.

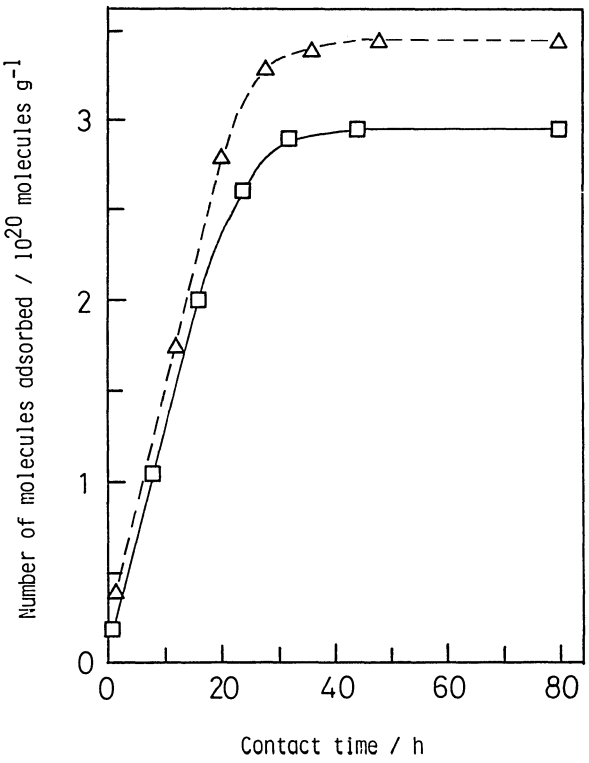

Fig. 2. Time courses of the numbers of PE (□) or TCNE (△) molecules adsorbed on HY calcined at 650 °C from heptane solutions (0.1 mol dm^{-3}) at 25 °C.

Figure 3 illustrates the increase of NOS obtained at the plateau with the adsorption of PE or TCNE from heptane. In agreement with the results of Stamires and Turkevich,[2] NOS increases linearly with an increase in the amount of adsorption, finally reaching the maximal number of spins (g-HY)$^{-1}$ (MNS) at the amount of adsorption of A_{max}. Similar results were obtained with the adsorption of NA or DNB on HY.

The values of A_{max} and MNS as well as g are summarized in Table 1. As shown from Table 1, A_{max} and g are independent of T_{ca}, while MNS is significantly dependent on T_{ca}.

It can be seen from Fig. 3 that the ratio of NOS to the amount of adsorption is independent of the concentrations of the solutions. This suggests the absence of specific parts of HY surfaces advantageous either for the adsorption or for radical formation. That is, both adsorption and radical formation occur

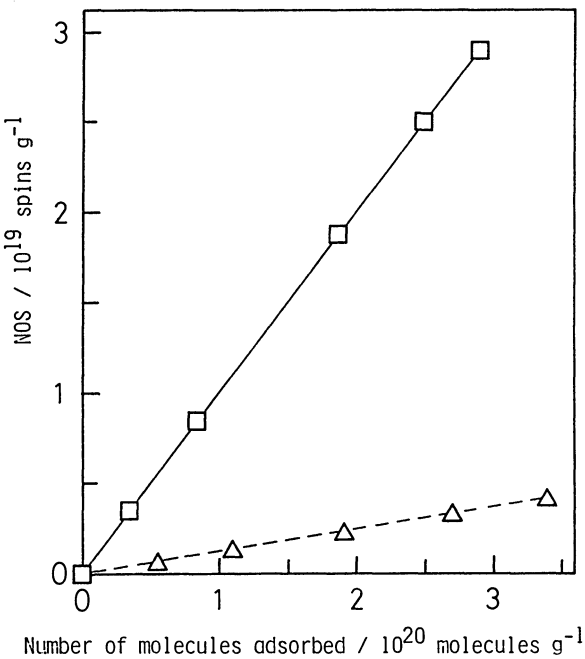

Fig. 3. Increase in NOS with adsorption of PE (□) or TCNE (△) from heptane solutions on HY calcined at 650 °C.

Table 1. Values of g, A_{max}, and MNS for PE, NA, TCNE, or DNB Adsorbed on the Surface of HY

Organic compound	T_{ca} / °C	g	A_{max} / 10^{20} molecules g^{-1}	MNS / 10^{18} spins g^{-1}
PE	650	2.0026	2.9	29
	400	2.0026	2.9	4.1
NA	650	2.0024	6.0	5.4
	400	2.0024	6.0	1.1
TCNE	650	2.0027	3.4	4.2
	400	2.0027	3.4	0.85
DNB	650	2.0041	2.1	2.9
	400	2.0041	2.1	0.26

uniformly on the surface of HY.

When PE or TCNE was desorbed with a large excess of heptane, NOS decreased with a decrease in the number of molecules adsorbed along the same straight line shown in Fig. 3. This reversible relation between NOS and the amount of adsorption may indicate the significance of the presence of an equilibrium upon the adsorption of PE or TCNE on HY from heptane solutions. Though qualitatively, this linear and reversible relationship disappeared when the HY-organic systems were stirred vigorously or heated rapidly during contact with heptane.

Time Courses of NOS for Binary (HY-Organic) Systems Free from Heptane. Figure 4 depicts the time courses of NOS for PE, NA, TCNE, or DNB on HY from immediately after the removal of heptane. NOS is initially small, increases with the passage of time, and finally reached a constant number of spins. CNS increased with an increase in the amount of organic molecules in contact with HY up to A_{max} along the same straight line shown in Fig. 3. The values of CNS were almost identical with those of MNS given in Table 1.

The EPR spectra of these binary systems were unchanged after attaining CNS. A considerable amount of adsorbate molecules were recovered unchanged by desorbing them with a large excess of heptane. CNS decreased with a decrease in the number of adsorbate molecules along the same straight line shown in Fig. 3. This linear and reversible dependence of CNS on the amount of adsorption may support the importance of adsorption equilibrium, even in a heptane-free binary system. Since HY is composed of abundant but relatively weak active sites,[1] radicals produced on HY can possibly remain unchanged for a long time.

The time required for attaining CNS (t_{CNS}) for the HY-organic system in contact with heptane was 45—60 h. The t_{CNS} for a heptane-free system, however, ranges from 1 h (PE on HY calcined at 650 °C) to 140 h (DNB on HY calcined at 400 °C). The rapid diffusion of PE or TCNE molecules may be due to the heat of radical formation on the surface of HY, which might be effectively removed by solvent molecules. CNS increases, while t_{CNS} decreases when a weak donor (NA), weak acceptor (DNB), or HY calcined at a low temperature (400 °C) was employed.

Table 2 shows the dependence of t_{CNS} on the amount of adsorption from 0.1 to 1.0 times A_{max}. The t_{CNS} value for PE or TCNE is independent of the amount of adsorption over the entire region examined. Whereas, the value of t_{CNS} for NA or DNB is near to that for PE or TCNE, respectively, at an adequately decreased amount of adsorption, it increases stepwise, and then remains unchanged at a further increased amount of adsorption. This suggests the coexistence of both an active site possessing a large t_{CNS} and one having a small t_{CNS} on the HY surface. The former may correspond to a weak active site, because a weak donor or acceptor is related to its occurrence.

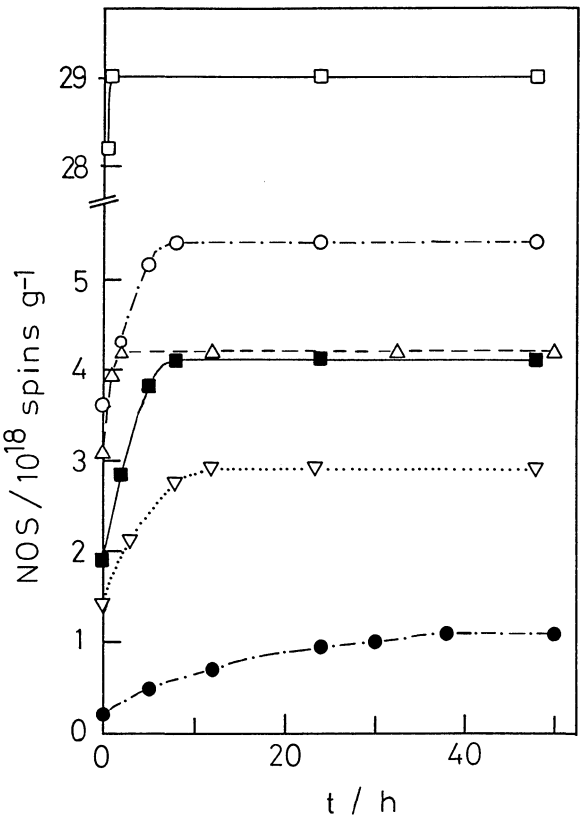

Fig. 4. Time course of the number of PE cation radicals on HY calcined at 650 (□) or 400 (■) °C, of NA cation radicals on HY calcined at 650 (○) or 400 (●) °C, or of TCNE (△) or DNB (▽) anion radicals on HY calcined at 650 °C from immediately after drying HY having been impregnated with a heptane solution (containing A_{max} of the organic compound) under reduced pressure.

Table 2. Dependence of t_{CNS} on the Amount of Adsorption

Organic compound	T_{ca}	t_{CNS}/h				
	°C	A[a)]=0.1	A=0.2	A=0.3	A=0.5	A=1.0
PE	650	1	1	1	1	1
	400	8	8	8	8	8
NA	650	1	1	8	8	8
	400	10	10	40	40	40
TCNE	650	2	2	2	2	2
	400	12	12	12	12	12
DNB	650	2	10	10	10	10
	400	12	120	120	120	120

a) Amount of organic molecules adsorbed divided by A_{max}.

Time Courses of NOS for Two Electron Donors Coexisting on HY. Figure 5 demonstrates a decrease in the number of PE cation radicals and an increase in that of NA cation radicals up to their CNS values, when HY was first adsorbed by PE (0.1 times A_{max}) and

then by NA (10 times A_{max}). The CNS value of the NA cation radicals is almost identical with MNS (shown in Table 1), while that of the PE cation radicals is considerably small.

If a base is gradually added to an aqueous solution containing several acids, the base reacts preferentially with one particular acid possessing the strongest acidity until it is exhausted; it then reacts with another acid having the second strongest acidity. In the case of two donors on HY, however, even cation radicals from a strong electron donor (PE) adsorbed in advance were mostly replaced by those from a weak donor (NA), eventually reaching a new equilibrium. The coexistence of two cation radicals, however, were also qualitatively observed when HY was impregnated with a heptane solution containing both PE and NA.

The t_{CNS} value of PE or NA for this ternary system is considerably greater than that obtained with the corresponding binary system (Fig. 4). CNS for each cation radical increases, while t_{CNS} decreases with an increase in T_{ca}.

A decrease in the number of NA cation radicals and an increase in that of PE cation radicals up to their CNS was obtained with a ternary system adsorbed in the order HY (T_{ca}=650 or 400 °C)-NA (0.1 times A_{max})-PE (10 times A_{max}). Table 3 summarizes CNS and t_{CNS} for two coexisting radical species for this order of adsorption. The CNS value for PE is identical with MNS (Table 1), while a small amount of NA cation radicals remains on HY, even during the final stage.

Different from an acid or base dissolved in a solution, a significant amount of radicals from a weak donor (NA) adsorbed in advance remained at a stationary state attained after subsequent contact with a sufficient quantity of a strong donor (PE).

The t_{CNS} value for NA or PE for this ternary system is much greater than that for the binary system (Fig. 4). CNS increases, while t_{CNS} decreases with an increase in T_{ca}.

Time Courses of NOS for Two Electron Acceptors Coexisting on HY. Figure 6 depicts one curve showing the decrease in the number of TCNE anion radicals and another the increase in the number of DNB anion radicals with a ternary system adsorbed in the HY-TCNE (0.1 times A_{max})-DNB (10 times A_{max})

Table 3. Values of CNS and t_{CNS} for Each Cation Radical[a)]

T_{ca} / °C	Cation radical	CNS / 10^{18} spins g^{-1}	t_{CNS} / h
650	NA	0.06	30
	PE	29	22
400	NA	0.014	95
	PE	4.1	120

a) Order of adsorption: HY (calcined at 650 or 400 °C)-NA (0.1 times the A_{max})-PE (10 times the A_{max}).

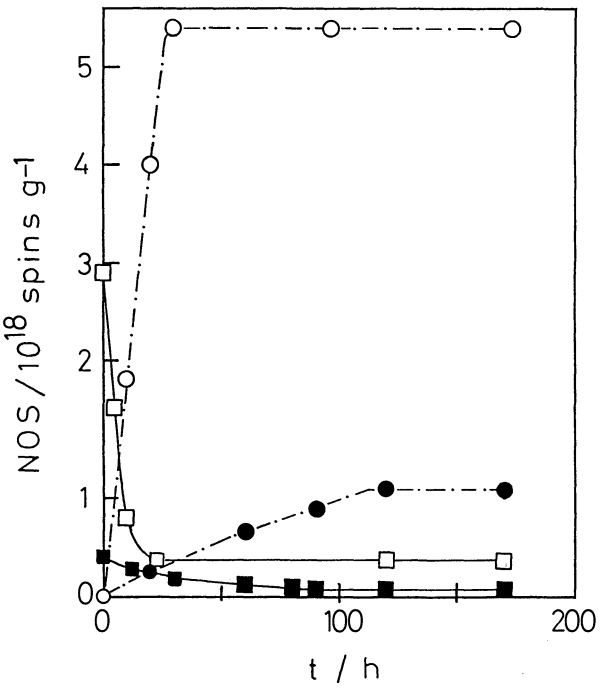

Fig. 5. Time courses of the numbers of PE (□) and NA (○) cation radicals on HY calcined at 650 °C and of PE (■) and NA (●) cation radicals on HY calcined at 400 °C. Order of adsorption: HY-PE (0.1 times the A_{max})-NA (10 times the A_{max}).

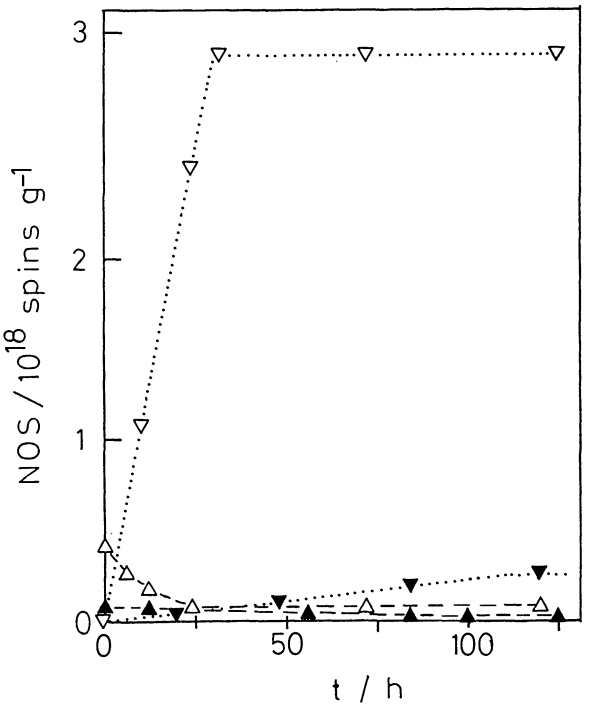

Fig. 6. Time courses of the numbers of TCNE (△) and DNB (▽) anion radicals on HY calcined at 650 °C and of TCNE (▲) and DNB (▼) anion radicals on HY calcined at 400 °C. Order of adsorption: HY-TCNE (0.1 times the A_{max})-DNB (10 times the A_{max}).

Table 4. Values of CNS and t_{CNS} for Each Anion Radical[a)]

T_{ca} °C	Anion radical	CNS 10^{18} spins g^{-1}	t_{CNS} h
650	DNB	0.040	32
	TCNE	4.2	24
400	DNB	0.012	120
	TCNE	0.85	100

a) Order of adsorption: HY (calcined at 650 or 400 °C)-DNB (0.1 times the A_{max})-TCNE (10 times the A_{max}).

Table 5. Values of CNS and t_{CNS} for Coexisting Cation and Anion Radicals on HY[a)]

Order of adsorption	Ion radical	CNS 10^{18} spins g^{-1}	t_{CNS} h
HY-PE-DNB	PE	31.5	6
	DNB	8.0	6
HY-NA-DNB	NA	7.9	10
	DNB	6.4	10

a) Order of adsorption: HY (calcined at 650 °C)-PE or NA (A_{max})-DNB (A_{max}).

order. Table 4 lists the CNS and t_{CNS} of coexisting DNB and TCNE anion radicals in the case of the order of adsorption of HY (T_{ca}=650 or 400 °C)-DNB (0.1 times A_{max})-TCNE (10 times A_{max}). In these cases, anion radicals from a strong acceptor (TCNE) adsorbed in advance were replaced by those from a weak acceptor (DNB), while anion radicals from DNB adsorbed in advance remained even after subsequent contact with a sufficiently large quantity of TCNE.

Time Courses of NOS for Both Donor and Acceptor Molecules Coexisting on HY. Figure 7 shows the time courses of the number of both DNB anions and either PE or NA cation radicals with a ternary system adsorbed in the order HY-DNB-PE or NA. The number of both anions and cation radicals increase with the passage of time up to their CNS. The values of CNS for both anions and cation radicals are much greater than those of MNS shown in Table 1. The ratio of CNS (Fig. 7) to MNS (Table 1) was significant when a weak donor (NA), weak acceptor (DNB), or HY calcined at 400 °C was employed. For example, the ratios for coexisting DNB (A_{max}) and NA (A_{max}) on HY calcined at 400 °C were 3.7 and 4.6, respectively, while those for coexisting DNB (A_{max}) and PE (A_{max}) on HY calcined at 650 °C were 2.4 or 1.1, respectively. Apparently, an increase in the number of solid base sites gives rise to an increase in the number of coexisting solid acid sites, or vice versa.

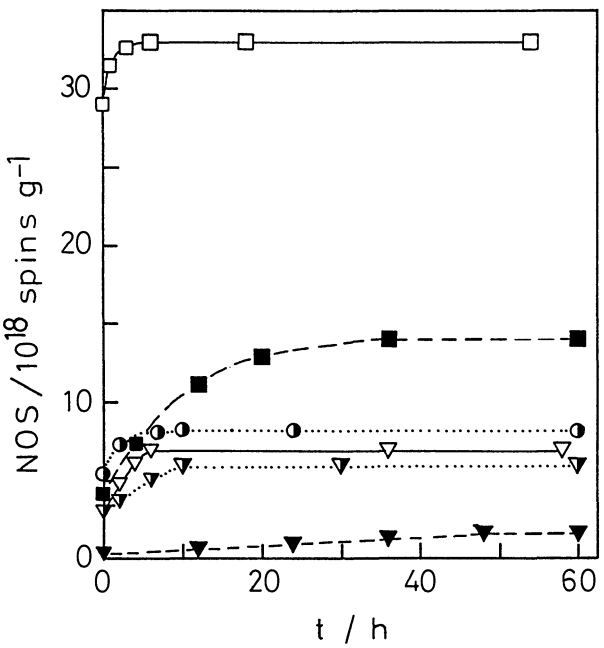

Fig. 7. Time courses of NOS for DNB (▽) and PE (□) on HY calcined at 650 °C, for DNB (▼) and NA (◑) on HY calcined at 650 °C, and for DNB (▼) and PE (●) on HY calcined at 400 °C. Order of adsorption: HY-DNB (A_{max})-PE or NA (A_{max}).

Comparing the time courses of NOS shown in Fig. 7 with those shown in Fig. 4, t_{CNS} for PE or NA in the ternary system increases, while the corresponding t_{CNS} for DNB decreases remarkably. In the neighborhood of CNS, NOS increases rather steeply in the case of DNB, while it increases slowly in the case of coexisting PE or NA. A similar tendency was observed with a ternary system adsorbed in the order HY-TCNE (A_{max})-PE or NA (A_{max}).

Similar time courses of NOS were obtained with a ternary system adsorbed in the order HY (T_{ca}=650 °C)-PE or NA (A_{max})-DNB (A_{max}). Table 5 summarizes CNS and t_{CNS} for two coexisting radical species for this adsorption order.

Dependence of CNS on the Order of Adsorption. In general, a physicochemical property obtained at an equilibrium is independent of the process for reaching equilibrium. Actually, the relationship between CNS and the amount of adsorption for a binary (HY-organic) system was linear and reversible, supporting the importance of equilibrium. As can be seen from Fig. 7 and Table 5, however, the CNS values of a ternary system comprising HY (T_{ca}=650 °C), DNB (A_{max}), and either PE or NA (A_{max}) are significantly dependent on the order of adsorption. On the other hand, the CNS values of this ternary system in contact with heptane were dependent only on the concentrations of two organic compounds, but independent of the order of adsorption.

The dependence on the adsorption order was pronounced for solvent-free systems. The results described above may be applicable to practical catalytic reactions in the solid or gaseous phase. Although it was difficult to observe quantitatively, it occurred in complicated solutions.

The NOS value of a binary system comprising glycolic acid and silica-alumina without a solvent depended on the method of applying mechanical energy (shaking or compressing) or on the time interval between mixing and ultraviolet irradiation.[5] Chemical modifications of the surface energy[9] and mechanochemical transformation of the surface structure or surface property[10] have already been investigated. Then, the dependence of NOS on the order of adsorption may result from either the heat of adsorption or the heat of radical formations.[5] Though this heat may be effectively removed from the surface of HY to the solvent molecules, it may cause a local augmentation in surface energy or a local variation in the surface property in the absence of a solvent.[5,9,10] Other causes of the dependences on the adsorption order will be presented in a subsequent publication.

Interaction between Cation and Anion Radicals Coexisting on HY. Very little radical formation in a mixture of PE and DNB without HY suggests the formation of radicals only on HY. In the case of a ternary system adsorbed in the HY-DNB-PE order at a constant DNB content (A_{max}), CNS for the DNB anion radical increased with an increase in the PE content from 0 (2.9×10^{18} spins/g) to 0.23 times the A_{max} (6.9×10^{18} spins/g), and became unchanged at a further increased PE content. However, CNS for PE (0, 11, or 33×10^{18} spins/g, respectively, at a PE content of 0, 0.23, or 1.0 times the A_{max}) increased, even in the region where CNS for DNB was independent of the PE content. In addition, an observation of the superimposed spectra of the DNB anion and the PE cation radicals suggests little interaction between the anion and cation radicals on HY. Therefore, the formation of anions and cation radicals may occur at different sites.

Practical Application. Probably the most important factor necessary for a quantitative, reproducible consideration concerning the physicochemical properties of slightly complicated systems may be t_{CNS}. A great t_{CNS} usually obtained with an HY-organic system suggests a significant role of nonequilibrium states when HY is used as a practical catalyst. As shown in Fig. 4, the t_{CNS} of PE or TCNE is much smaller than that of NA or DNB. Then, the difference in the spin-generating ability between PE and NA or between TCNE and DNB determined soon after adsorption may be considerably greater than the corresponding difference obtained at equilibrium.

The second factor may be the order of adsorption. Thermodynamically, a physicochemical property obtained at equilibrium is independent of the process to reach equilibrium. Regardless of the presence of heptane, the dependence of CNS of a binary (HY-organic) system on the amount of adsorption was linear and reversible, suggesting the significance of equilibrium. The CNS values of the ternary systems of HY and two organic compounds in contact with heptane was independent of (while those of the ternary system without heptane were dependent on) the adsorption order. The dependence became pronounced when the number of components or the amount of adsorption increased.

The cation radicals formed from two donors or anion radicals from two acceptors on HY exhibited peculiar acid-base characteristics. Further, the CNS of a donor was enhanced by the coexistence of an acceptor. At least, a quantitative consideration of this enhanced radical formation would prompt an improvement in controlling the reproducibility of some physicochemical properties (e. g., the activities of HY as a practical catalyst) of complicated zeolite-organic systems. In the future, a technique for forcing HY to exhibit a constant, desired efficiency might be obtained.

A few results which are probably available for constructing a model of active sites were obtained. As shown in Table 2, there coexist two kinds of active sites on the surface of HY. These exhibit different t_{CNS}. An active site having a small t_{CNS} may correspond to a strong active site, since the PE cation or the TCNE anion radicals on HY calcined at 650 °C is concerned. An active site possessing a large t_{CNS}, however, may correspond to a weak active site, since a weak donor (NA) or acceptor (DNB) on HY calcined at 400 °C is concerned for its occurrence. The latter may play a role in enhanced radical formation in the presence of both a donor and an acceptor or in the dependence on the adsorption order.

Spin-generating sites of HY have been attributed to Lewis acid or base sites, which are known to be produced from Brönsted acid or base sites at a T_{ca} greater than 500 °C.[1,2] However, radicals were produced on HY calcined at 400 °C, especially when HY was in contact with both donor and acceptor molecules. Apparently, an increase in the number of anion radical-generating sites gives rise to an increase in the number of coexisting cation radical-generating sites, or vice versa. Other results necessary for constructing a model of active sites will be described in a subsequent publication.

References

1) K. Tsutsumi and H. Takahashi, "Zeoraito," ed by N. Hara and H. Takahashi, Kodansha Scientific Publishers, Tokyo (1975), pp. 72—78, and references therein.

2) D. N. Stamires and J. Turkevich, *J. Am. Chem. Soc.*, **86**, 749 (1964).

3) B. D. Flockhart, L. McLoughlin, and R. C. Pink, *J. Catal.*, **25**, 305 (1972).

4) K. Hirota, K. Kuwata, and Y. Akagi, *Bull. Chem. Soc. Jpn.*, **38**, 2209 (1965).

5) H. Kashiwagi and S. Enomoto, *Chem. Pharm. Bull.*, **30**, 17 (1982); H. Kashiwagi, M. Inoue, and S. Enomoto, *ibid.*, **37**, 3102 (1989); H. Kashiwagi, S. Enomoto, and M. Inoue, *ibid.*, **37**, 3181 (1989); H. Kashiwagi and M. Inoue,

Bull. Chem. Soc. Jpn., **63**, 891 (1990).

6) "Kagaku Binran, Kisohen," 3rd ed, ed by Nippon Kagakukai, Maruzen, Tokyo (1984), p. II-581.

7) "Kagaku Binran, Kisohen," 3rd ed, ed by Nippon Kagakukai, Maruzen, Tokyo (1984), p. II-588.

8) H. A. Benesi, *J. Phys. Chem.*, **61**, 970 (1957); "Shokubai Jikken Handobukku," ed by Catalysis Society of Japan, Kodansha Scientific Publishers, Tokyo (1986), pp. 170—172.

9) "Kagaku Sousetsu 44, Hyoumen no Kaishitsu," ed by the Chemical Society of Japan, Gakkai Shuppan Senta, Tokyo (1984), pp. 7—52.

10) T. Kubo, "Mekanokemisutorii Gairon," 2nd ed, Kagakudoujin, Tokyo (1978); T. Kubo, "Yuukibutsu no Mekanokemisutorii," Sougou Gijutsu Shuppan, Tokyo (1985).

Exciplex Formation between Perylene and *N,N*-Dimethylaniline in a Ternary Inclusion Compound with γ-Cyclodextrin in H_2O-Ethanol (7:3) Mixture

Sanyo HAMAI
Department of Physics, Miyazaki Medical College, Kiyotake, Miyazaki 889-16
(Received August 1, 1990)

Inclusion compounds in the system of γ-cyclodextrin (γ-CD)-*N,N*-dimethylaniline (DMA)-perylene (Pe) have been studied in an H_2O-ethanol (7:3) mixture by means of absorption and fluorescence spectral measurements. A ternary 1:1:1 inclusion compound of γ-CD-ethanol-Pe is formed by the addition of γ-CD to an H_2O-ethanol solution of Pe. In the presence of γ-CD, a further addition of DMA results in the formation of a γ-CD-DMA-Pe inclusion compound followed by association with a 1:1 γ-CD-DMA inclusion compound to form a ternary 2:2:1 inclusion compound of γ-CD-DMA-Pe. The exciplex fluorescence of Pe-DMA within the γ-CD cavity has been observed from the ternary inclusion compound. Equilibrium constants for the formation of these inclusion compounds have been evaluated.

Cyclodextrins (CDs) are cyclic oligosaccharides consisting of at least six glucose residues which are joined by α-(1→4) linkages. Commercially available α-, β-, and γ-CD have six, seven, and eight glucose units, respectively, and are shaped like a truncated cone having a narrower and a wider end, which has the cavity capable of accommodating many kinds of organic and inorganic substances in aqueous solutions.[1] Among these CDs, γ-CD possessing the largest cavity has been suggested to form 1:2 and 2:2 host-guest inclusion compounds,[2-8] and ternary inclusion compounds.[9-15]

From an induced circular dichroism study, an inclusion of two chlorpromazine molecules entering the single γ-CD cavity has been pointed out.[16] Pyrene and sodium 1-naphthylacetate excimer emissions have been observed in γ-CD aqueous solutions.[7,8,11,17] The 1-naphthylacetate excimer emission has been ascribed to an excimer arising from a ground-state dimer of the guest within the single γ-CD cavity. For the pyrene excimer, however, it has been revealed that the ground-state dimer of pyrene is formed within two γ-CD cavities associating with each other.[8] Owing to the ground-state dimer formation of substrates, themselves, within the γ-CD cavity, it is difficult to investigate the interaction of substrates with other kinds of organic substances within the γ-CD cavity. Until now, there have been few studies on the interaction between different kinds of organic substances bound to the γ-CD cavity in solutions. Thus, as a guest molecule, we selected perylene (Pe), which seems to be too large to form a ground-state dimer within the cavity of a single γ-CD molecule. Because Pe is insoluble in water, an H_2O-ethanol (7:3) mixture was used as the solvent. Although, in general, the formation of inclusion compounds of CDs is unfavored in organic solvents, an alcohol molecule in water associates with 1:1 inclusion complexes of β-CD with pyrene, acenaphthene, fluorene, and 1-naphthonitrile to produce ternary 1:1:1 inclusion compounds.[12,13,15,18-21] In addition, for aromatics such as pyrene, an alcohol molecule included in the β-CD cavity promotes the formation of ternary inclusion compounds formed among β-CD, alcohol, and aromatics. With γ-CD, 1-butanol enables a ground-state pyrene dimer that is positioned inside the γ-CD cavity to dissociate, resulting in the formation of a γ-CD-1-butanol-pyrene inclusion compound.[11] The formation of ternary inclusion compounds of γ-CD-pyrene-alcohol (including ethanol) has also been confirmed.[12-15] Consequently, ethanol as a solvent is anticipated to inhibit the formation of the ground-state Pe dimer within the γ-CD cavity. In this respect, the use of a mixture containing ethanol simplifies the investigation of the interaction between different kinds of guests entering the γ-CD cavity.

Experimental

Perylene (Pe) was purchased from Aldrich and purified by column chromatography. γ-CD (Nakarai) and ethanol (Wako) were used as received. Benzene (Wako) was distilled. Aniline (Wako), *N,N*-Dimethylaniline (Tokyo Kasei), and *N,N*-diethylaniline (Tokyo Kasei) were distilled under reduced pressure.

The absorption spectra were recorded on a Shimadzu 260 spectrophotometer with which spectral data accumulation was repeated 20 times. The fluorescence spectra were obtained with a Shimadzu RF-501 spectrofluorometer equipped with a cooled Hamamatsu R-943 photomultiplier, and were corrected for the wavelength dependence of the sensitivity of the fluorometer. Aerated sample solutions were employed throughout this study, and measured at 25±0.1 °C. A water-ethanol (7:3) mixture was used as the solvent. The concentration of Pe was 3.0×10^{-7} mol dm^{-3}, unless otherwise stated.

Results and Discussion

Inclusion Compound of γ-CD with Pe. Figure 1 shows the absorption spectra of Pe solutions contain-

ing various concentrations of γ-CD. The absorption peaks are red shifted and sharpened accompanied by isosbestic points at 392, 397, 413, 423, and 437 nm, indicating the formation of an inclusion compound consisting of at least γ-CD and Pe. The red shift of the 0-0 band peak from 435 to 445 nm amounts to an energy gap of 520 cm^{-1}, which is comparable to those of 440 and 640 cm^{-1} for the absorption peaks between 1 : 1 : 1 inclusion compounds of β-CD-alcohol-pyrene and -fluorene and free pyrene and fluorene in water, respectively.[18,20] The red shifts are only 90 and 200 cm^{-1} for the peaks of 1 : 1 inclusion compounds of pyrene and fluorene, respectively. In contrast to 1 : 1 inclusion compounds of these aromatics, sharp vibronic bands are characteristic of ternary inclusion compounds containing alcohol, except for a β-CD-alcohol-acenaphthene inclusion compound. This is the case of the inclusion compound of Pe. Furthermore, considerable quantities of ethanol exist in the solvent used in this work. Consequently, the most plausible species responsible for the absorption spectral change shown in Fig. 1 is a ternary inclusion compound comprising γ-CD, ethanol, and Pe. Figure 2 exhibits the absorption spectra of Pe solutions with a fixed concentration of γ-CD (1.0×10^{-3} mol dm^{-3}) and varying amounts of cyclohexane. The addition of cyclohexane results in an enhancement of the 445-nm band at the expense of the 435-nm band. This spectral change resembles that shown in Fig. 1 where the γ-CD concentration is increased. In Fig. 2, cyclohexane acts as if it is γ-CD in Fig. 1. For pyrene solutions with β-CD, cyclohexane or hexane was found to induce an absorption spectral change similar to those observed for the addition of alcohols, indicating the formation of a 1 : 1 : 1 inclusion complex of β-CD with cyclohexane (hexane) and pyrene. Since cyclohexane is much more hydrophobic than ethanol, cyclohexane is expected to readily associate with γ-CD, thereby forming a γ-CD-cyclohexane-Pe inclusion compound analogous to the γ-CD-ethanol-Pe inclusion compound. This explains the effect of added cyclohexane on the absorption spectrum of Pe shown in Fig. 2. The finding of the effect of cyclohexane provides additional evidence for the ternary inclusion compound of γ-CD-ethanol-Pe. As revealed for the β-CD-alcohol-pyrene,[18] -acenaphthene,[19] -fluorene,[20] and -1-naphthonitrile systems,[21] it is most likely that the γ-CD-ethanol-Pe inclusion compound (PEC) comprises a single γ-CD, a single ethanol, and a single Pe molecule:

$$\mathrm{Pe} + \mathrm{EtOH} + \gamma\text{-CD} \overset{K_1}{\rightleftarrows} \mathrm{PEC}, \qquad (1)$$

where EtOH is ethanol, and K_1 is an equilibrium constant for the formation of PEC.

Figure 3 depicts the fluorescence spectra of Pe in the absence and presence of γ-CD. When γ-CD is added to a Pe solution, the fluorescence maxima are red shifted, and isoemissive points are observed at 445, 473, 494, and 506 nm. The spectral change in the fluorescence by the addition of γ-CD is also due to the 1 : 1 : 1 inclusion compound of γ-CD-ethanol-Pe.

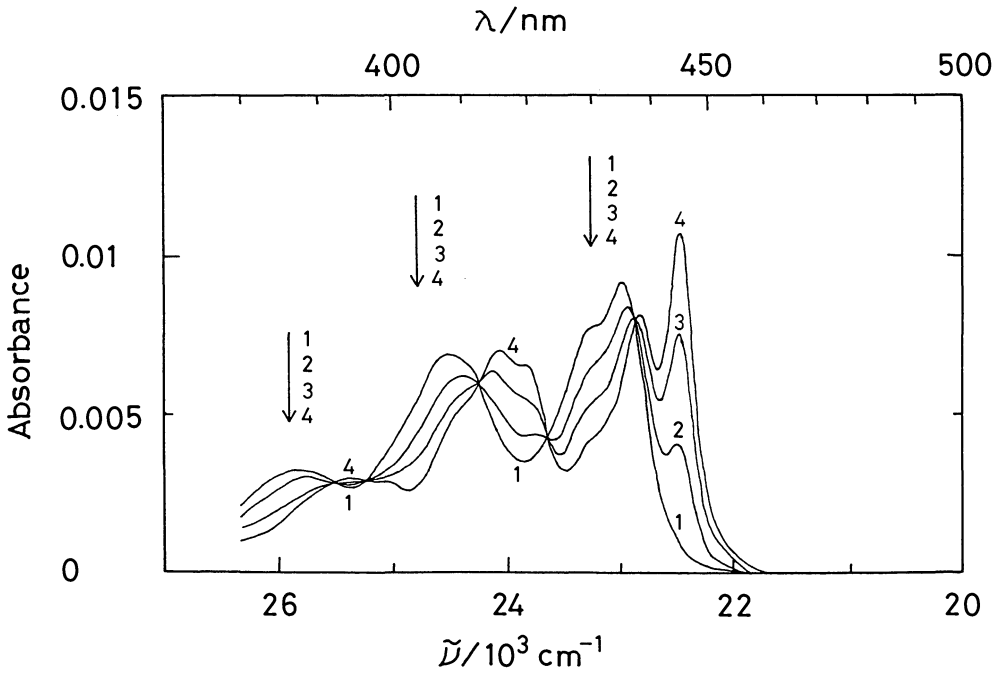

Fig. 1. Absorption spectra of Pe (3.0×10^{-7} mol dm^{-3}) in H_2O-ethanol (7 : 3) containing varying concentrations of γ-CD. Concentration of γ-CD: (1) 0, (2) 1.0×10^{-3}, (3) 2.0×10^{-3}, and (4) 4.0×10^{-3} mol dm^{-3}.

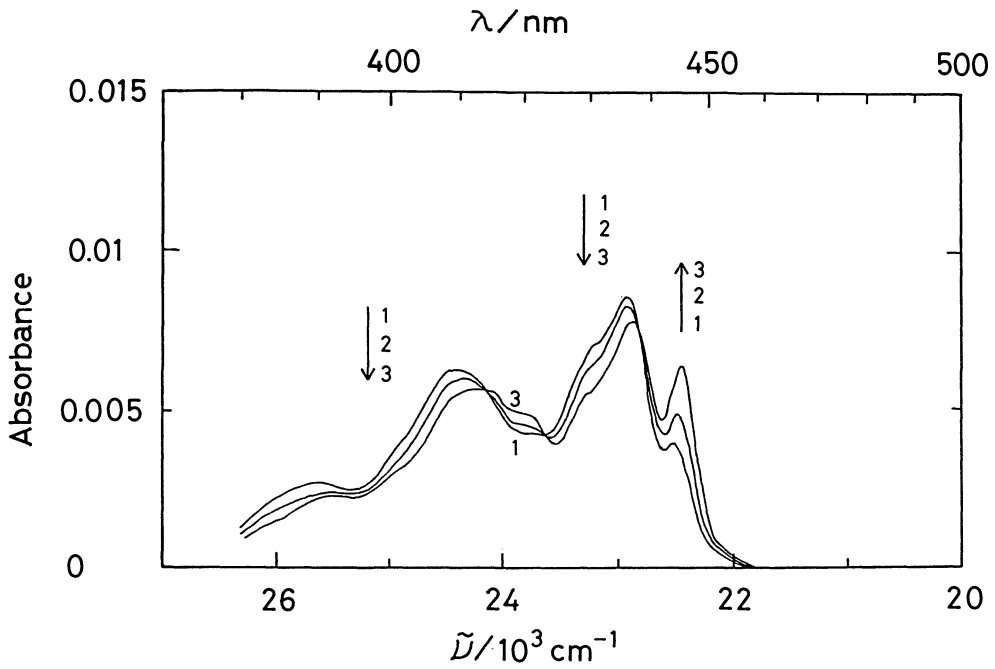

Fig. 2. Absorption spectra of Pe (3.0×10^{-7} mol dm^{-3}) in H_2O–ethanol (7 : 3) containing a fixed concentration of γ-CD (1.0×10^{-3} mol dm^{-3}) and varying concentrations of cyclohexane. Concentration of cyclohexane: (1) 0, (2) 1.85×10^{-3}, and (3) 4.63×10^{-3} mol dm^{-3}.

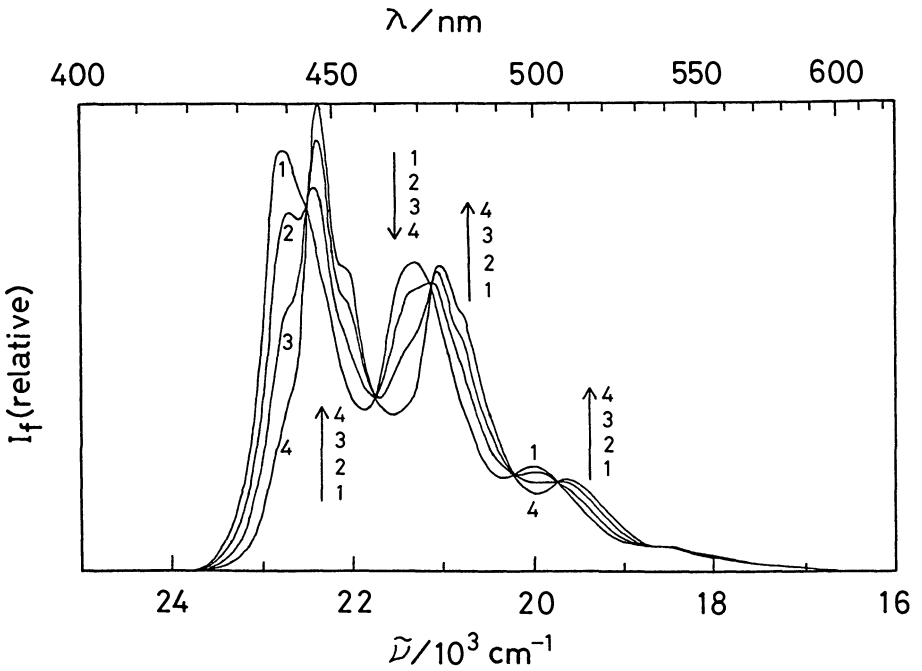

Fig. 3. Fluorescence spectra of Pe (3.0×10^{-7} mol dm^{-3}) in H_2O–ethanol (7 : 3) containing varying concentrations of γ-CD. Concentration of γ-CD: (1) 0, (2) 1.0×10^{-3}, (3) 2.0×10^{-3}, and (4) 4.0×10^{-3} mol dm^{-3}. λ_{ex}=413 nm.

For the equilibrium represented by Eq. 1, the following equation holds:

$$1/\Delta I_f = 1/a + 1/aK_1[\mathrm{EtOH}]_0[\gamma\text{-CD}]_0, \quad (2)$$

where ΔI_f is the difference in the integrated fluorescence intensity between a Pe solution with γ-CD and that without γ-CD, a is a constant, subscript 0 stands for the initial concentration, and $[EtOH]_0$ is 5.11 mol dm^{-3}. According to Eq. 2, K_1 was evaluated to be 37 ± 10 mol^{-2}dm^6. Upon the addition of cyclohexane

to a γ-CD solution of Pe, the Pe fluorescence spectrum shows a change similar to that shown in Fig. 3 where γ-CD is added to a Pe solution without cyclohexane. This spectral change for the fluorescence upon adding cyclohexane corresponds to that for the absorption change shown in Fig. 2.

Inclusion Compound of γ-CD with *N,N*-Dimethylaniline (DMA). DMA was confirmed to form an inclusion compound with γ-CD from the absorption and fluorescence spectral changes. Although there is a possibility that a ternary inclusion compound of γ-CD-ethanol-DMA is formed, we could not obtain evidence for its existence from spectroscopic measurements. Therefore, it is most likely that the spectral change is due to a 1 : 1 inclusion compound of γ-CD-DMA (DC) which is formed according to the equation

$$\text{DMA} + \gamma\text{-CD} \overset{K_2}{\rightleftarrows} \text{DC}, \tag{3}$$

where K_2 is an equilibrium constant for the formation of DC. A fluorometric method was used to determine K_2:

$$1/\Delta I_f = 1/b + 1/bK_2[\gamma\text{-CD}]_0, \tag{4}$$

where b is a constant. From an analysis based on Eq. 4, 27±14 $mol^{-1}dm^3$ was obtained as K_2.

Inclusion Compound of γ-CD with *N,N*-Dimethylaniline (DMA) and Pe. In the DMA concentration range below ca. 1×10^{-3} mol dm^{-3}, addition of DMA to a γ-CD (4.0×10^{-3} mol dm^{-3}) solution of Pe results in red shifts of the absorption maxima accompanied by isosbestic points at 421, 429, and 447 nm (Fig. 4). The absorption change can be attributed to the formation of an inclusion compound consisting of γ-CD, DMA, and Pe. It is most likely that the spectral change at low DMA concentrations is caused by the formation of a 1 : 1 : 1 inclusion compound of γ-CD-DMA-Pe. Above ca. 1×10^{-3} mol dm^{-3} of DMA, however, isosbestic points disappear with further red shifts of the absorption maxima. The absorption bands are broadened as the DMA concentration is raised. Because, as is described later, any benzene that cannot form an electron donor-acceptor complex with Pe causes an absorption spectral change similar to that produced by DMA, this change in the absorption is not due to a charge-transfer interaction between Pe and DMA but, rather, due to a kind of microscopic solvent effect exerted by neighboring DMA. Figure 5 illustrates the fluorescence spectrum of a Pe solution containing γ-CD (4.0×10^{-3} mol dm^{-3}) and DMA (3.16×10^{-3} mol dm^{-3}). Upon the addition of DMA, the Pe monomer band (447-nm band) is quenched. At the same time, a broad emission that is located at longer wavelengths appears with a maximum at 599 nm. For the Pe solution with γ-CD and DMA, the excitation spectrum observed at 580 nm was almost identical to the absorption spectrum. This broad emission is assigned to an exciplex fluorescence of Pe and DMA which enter the γ-CD cavity. If a Pe ground-state dimer within the γ-CD cavity exists in

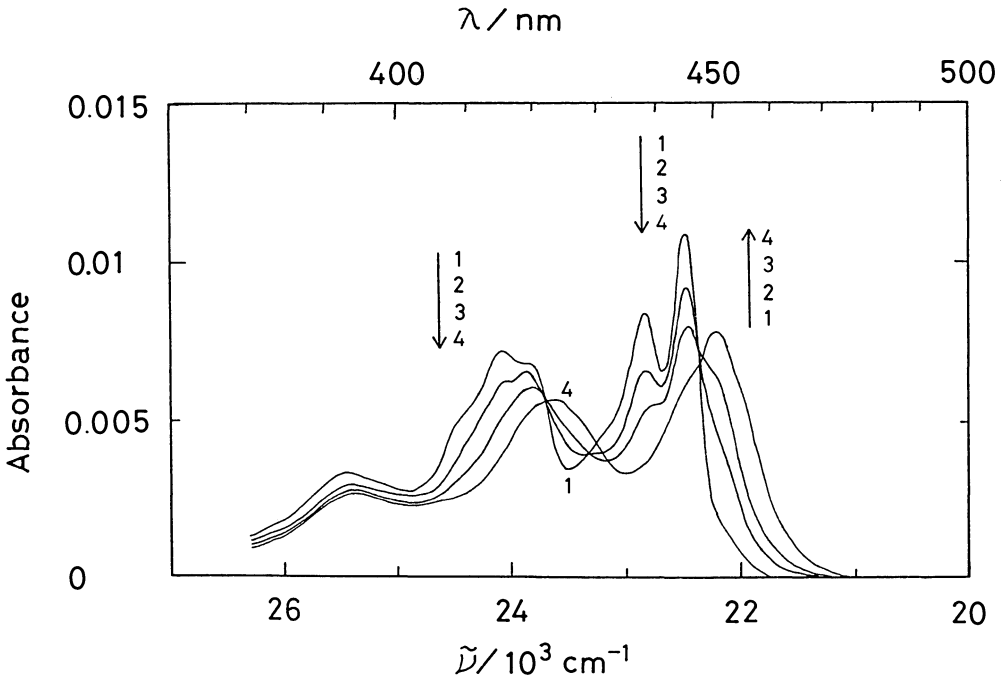

Fig. 4. Absorption spectra of Pe (3.0×10^{-7} mol dm^{-3}) in H_2O-ethanol (7 : 3) containing a fixed concentration of γ-CD (4.0×10^{-3} mol dm^{-3}) and varying concentrations of DMA. Concentration of DMA: (1) 0, (2) 3.16×10^{-4}, (3) 7.89×10^{-4}, and (4) 3.16×10^{-3} mol dm^{-3}.

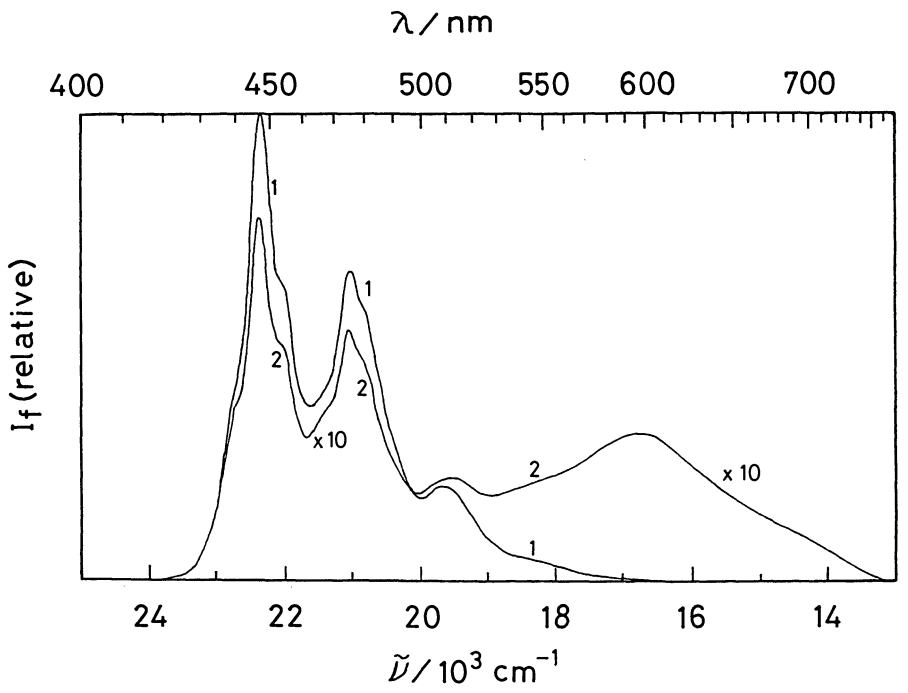

Fig. 5. Fluorescence spectra of Pe (3.0×10^{-7} mol dm^{-3}) in H_2O-ethanol (7 : 3) containing γ-CD (4.0×10^{-3} mol dm^{-3}) in the absence (Spectrum 1) and presence (Spectrum 2) of DMA (3.16×10^{-3} mol dm^{-3}). The fluorescence intensity of a Pe solution with DMA is multiplied by 10. λ_{ex}=402 nm.

H_2O-ethanol (7 : 3), it might be responsible for the broad emission. However, this possibility is excluded due to the following result. Nitrobenzene, which has been found to form an inclusion compound similar to that for DMA, only quenches the Pe monomer band, and does not induce the longer-wavelength emission, as does DMA.

For a Pe solution with both γ-CD (4.0×10^{-3} mol dm^{-3}) and DMA (3.16×10^{-3} mol dm^{-3}), an experiment on the concentration dependence of Pe was performed. The normalized absorption spectrum for 3.0×10^{-7} mol dm^{-3} Pe was identical to that for 1.0×10^{-7} mol dm^{-3} Pe, indicating that only one Pe molecule is included in the inclusion compound responsible for the exciplex fluorescence. A continuous variation plot of the absorbance at 437 nm, which is an isosbestic point for γ-CD-Pe solutions without DMA, against the molar fraction of γ-CD ($[\gamma\text{-CD}]_0/([\gamma\text{-CD}]_0+[\text{DMA}]_0)$) was made in order to identify the relevant inclusion compound under the condition of $[\gamma\text{-CD}]_0+[\text{DMA}]_0=2.0\times10^{-3}$ mol dm^{-3}. The result that the absorbance passes through a minimum at a molar fraction of 0.5 (not shown) revealed that the inclusion compound has a 1 : 1 stoichiometry concerning γ-CD and DMA. Combined with no concentration effect of Pe on the absorption spectrum, both the absorption change shown in Fig. 4 and the exciplex fluorescence in Fig. 5 are evidently due to a complex that includes a single Pe molecule, with a 1 : 1 stoichiometry of γ-CD and DMA. Therefore, as candidates responsible for the exciplex fluorescence, there are a 1 : 1 : 1 inclusion compound of γ-CD-DMA-Pe (PDC) and an inclusion compound (PDC · DC) formed by the association between PDC and DC:

$$\text{PEC}+\text{DMA}\overset{K_3}{\rightleftarrows}\text{PDC}+\text{EtOH}, \quad (5)$$

and

$$\text{PDC}+\text{DC}\overset{K_4}{\rightleftarrows}\text{PDC}\cdot\text{DC}, \quad (6)$$

where K_3 and K_4 are equilibrium constants for the formation of PDC and PDC · DC, respectively. Because the exciplex fluorescence intensity is proportional to the concentration of the emitting species under our experimental conditions, the exciplex fluorescence intensities which are a function of DMA concentration were compared with the concentration curves of the candidates in order to clarify the inclusion compound emitting the exciplex fluorescence. The concentrations of PDC and PDC · DC were calculated from the following equations:

$$[\text{PDC}]=K_1K_3[\text{DMA}][\gamma\text{-CD}]_0[\text{Pe}]_0/(1+K_1[\gamma\text{-CD}]_0([\text{EtOH}]_0+K_3[\text{DMA}])), \quad (7)$$

with $[\text{DMA}]=[\text{DMA}]_0/(1+K_2[\gamma\text{-CD}]_0)$

and

$$[\text{PDC}\cdot\text{DC}]=K_1K_2K_3K_4[\text{DMA}]^2[\gamma\text{-CD}]_0^2[\text{Pe}]_0/(1+K_1[\gamma\text{-CD}]_0([\text{EtOH}]_0+K_3[\text{DMA}]+K_2K_3K_4[\text{DMA}]^2[\gamma\text{-CD}]_0)). \quad (8)$$

The results are given in Fig. 6 together with the

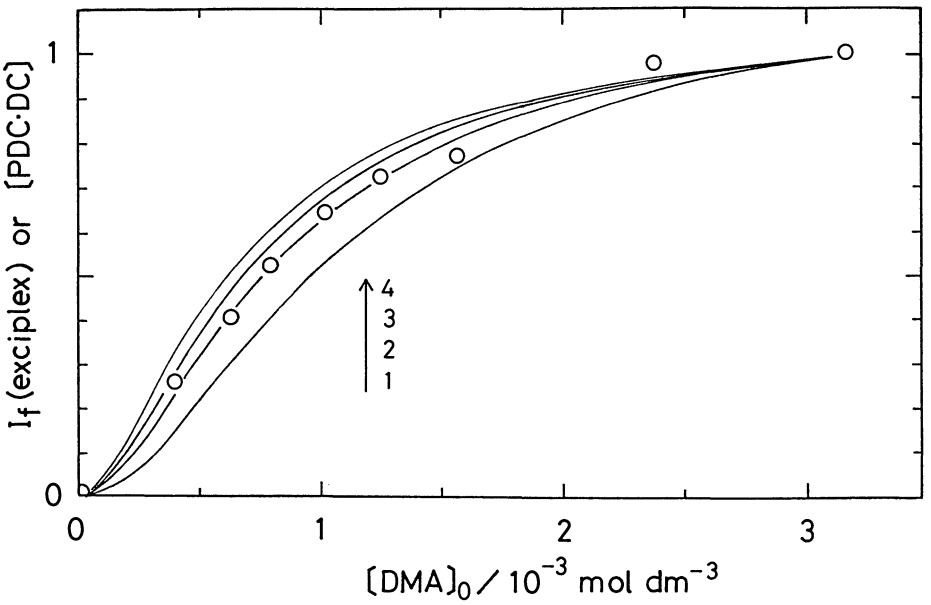

Fig. 6. Comparison of intensities of the Pe-DMA exciplex fluorescence in H_2O-Ethanol (7:3) containing both γ-CD (4.0×10^{-3} mol dm^{-3}) and DMA with calculated curves which are obtained with assumed K_3 and K_4 (20000 mol^{-1} dm^3). The exciplex fluorescence intensities and the curves are normalized to unity at the highest DMA concentration, respectively. Assumed K_3 value: (1) 10000, (2) 20000, (3) 30000, and (4) 40000. $[Pe]_0=3.0\times10^{-7}$ mol dm^{-3}. λ_{ex}=402 nm.

observed intensities of the exciplex fluorescence as a function of DMA concentration. Under the condition that $[\gamma\text{-CD}]_0=4.0\times10^{-3}$ mol dm^{-3}, a calculated curve for PDC·DC with assumed values of K_3=20000 and K_4=20000 mol^{-1} dm^3 was in good agreement with the observed data points, whereas a best-fit curve for PDC afforded K_3=10000. Because these comparisons could not identify the relevant inclusion compound, we next compared the data with calculated curves as a function of γ-CD concentration, keeping the initial DMA concentration at 3.16×10^{-3} mol dm^{-3}. The fitting procedure for PDC·DC gave K_3=20000 and K_4=15000 mol^{-1} dm^3 (not shown), which well agreed with the values evaluated from the previous simulation as a function of DMA concentration. From a similar procedure for PDC, on the other hand, K_3 was estimated to be 2000, which was in disagreement with the K_3 value obtained above for the mechanism of PDC formation. Therefore, we conclude that the exciplex fluorescence is due to PDC·DC. Upon diluting the initial concentration of DMA from 3.16×10^{-3} to 7.89×10^{-4} mol dm^{-3}, the same simulation method for PDC·DC in which comparisons were made as a function of γ-CD concentration afforded K_3=20000 and K_4=20000 mol^{-1} dm^3, which were in excellent agreement with the values already obtained, while the procedure for PDC could not give any K_3 value. These results provide additional evidence that PDC·DC is responsible for the exciplex fluorescence.

The inclusion compound PDC·DC closely resembles in form an association complex of a β-CD-aniline-sodium 1-pyrenesulfonate (or -pyrene) 1:1:1 inclusion compound with a β-CD-aniline 1:1 inclusion compound in the system of β-CD-aniline-sodium 1-pyrenesulfonate (or -pyrene), although a different CD (β-CD) is used.[22] In addition, the charge-transfer fluorescence of sodium 1-pyrenesulfonate- or pyrene-aniline has been observed from the β-CD association complexes. At low DMA concentrations (below ca. 1×10^{-3} mol dm^{-3}), PDC may exist predominantly in a Pe solution with γ-CD, since, as stated previously, there are isosbestic points in the low DMA concentration range. Inclusion compounds similar in form to PDC have also been suggested for the systems of β-CD-aniline-sodium 1-pyrenesulfonate and -pyrene.[22] In contrast to 2:2:1 inclusion compounds, such as PDC·DC, exciplex or charge-transfer emissions are not detected for the 1:1:1 inclusion compounds, such as PDC, probably because the polarity around an excited species within the CD cavity is very high, owing to the smaller degree of shielding from the aqueous phase, compared with the 2:2:1 inclusion compounds including two CD molecules.

Effects of Benzene, Aniline, and *N,N*-Diethylaniline on the Absorption and Fluorescence Spectra of Pe Solutions with γ-CD. When benzene was added to a Pe solution containing γ-CD, the Pe absorption spectrum changed in a fashion similar to that for DMA. This finding shows the formation of an inclusion compound, being of the PDC·DC type, which con-

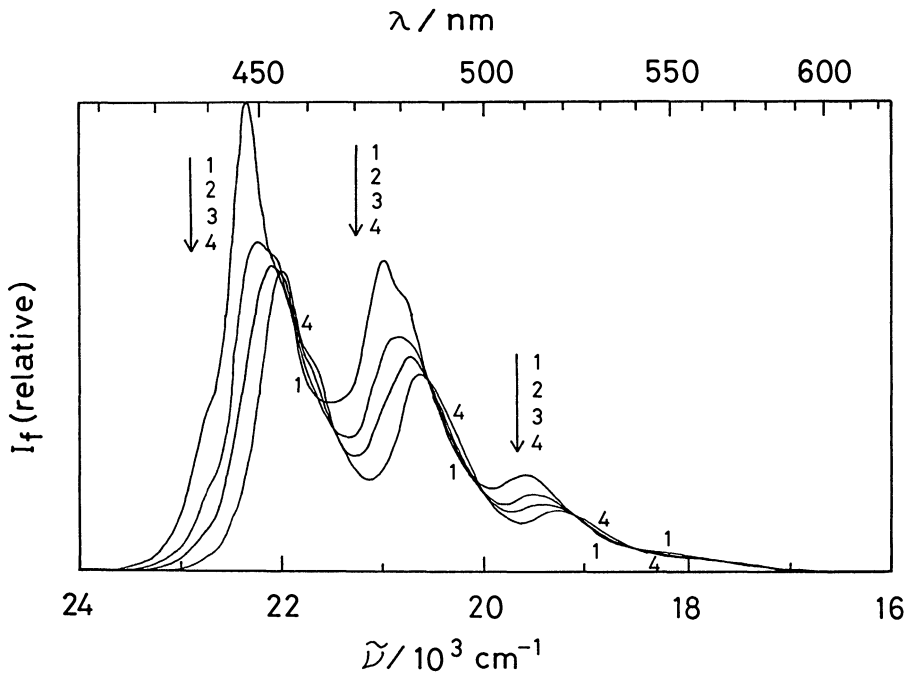

Fig. 7. Fluorescence spectra of Pe (3.0×10^{-7} mol dm^{-3}) in H_2O-ethanol (7 : 3) containing a fixed concentration of γ-CD (4.0×10^{-3} mol dm^{-3}) and varying concentrations of benzene. Concentration of benzene: (1) 0, (2) 5.63×10^{-3}, (3) 1.13×10^{-2}, and (4) 2.25×10^{-2} mol dm^{-3}. λ_{ex}=413 nm.

tains benzene instead of DMA. As the benzene concentration is increased, the fluorescence spectrum exhibits red shifts of peaks accompanied by a slight broadening of bands (Fig. 7). No appearance of long-wavelength emission is observed. In this case, benzene within the γ-CD cavity accommodating Pe exerts microscopic solvent effects, in which, depending on the strength of the interaction with Pe, a microscopic medium (neighboring benzene) influences the band position and band width, etc. Aniline as well as benzene showed similar effects on the absorption and fluorescence spectra, although the Pe monomer fluorescence was relatively efficiently quenched. For aniline, the exciplex fluorescence of Pe was not observed in 1-propanol and ethyl acetate. Consequently, no observation of the Pe-aniline exciplex fluorescence is reasonable for an inclusion compound including Pe and aniline. However, the behavior of *N,N*-diethylaniline towards the Pe fluorescence is intermediate between that of aniline and DMA. That is, both spectral shifts of the Pe monomer fluorescence and the weak exciplex fluorescence of Pe-*N,N*-diethylaniline are observed. In this case, owing to a bulkier diethylamino group in *N,N*-diethylaniline than a dimethylamino group in DMA, a smooth reorientation within the lifetime of excited Pe may be sterically hindered for Pe and *N,N*-diethylaniline molecules inside the γ-CD cavities, resulting in both the exertion of a kind of microscopic solvent effect (the spectral shifts of the monomer fluorescence bands, etc.) and the appearance of the weak exciplex fluorescence.

Polarity of the Interior of the γ-CD Cavities. In order to investigate the polarity within the γ-CD cavities, the exciplex fluorescence maximum (599 nm) was compared with the maxima of the Pe-DMA exciplex fluorescence in organic solvents. This examination has revealed that the dielectric constant around the Pe-DMA exciplex within the γ-CD cavities is close to that of 1-pentanol (ε=13.9), in which the exciplex fluorescence is centered at 600 nm. This value is rather greater than the dielectric constants obtained previously from charge-transfer emissions of a 2-methoxynaphthalene-phthalonitrile complex within the β-CD cavities and 1-pyrenesulfonate- and pyrene-aniline complexes within the β-CD cavities,[22,23] but less than that from a 1-naphthonitrile-anisole exciplex emission in the β-CD-anisole-1-naphthonitrile system.[21] Such differences are, of course, unlikely to be attributed to the differences in property between β- and γ-CD. There have been several studies concerning the polarity of the interior of the CD cavity:[21,22-29] The dielectric constants experienced by fluorescent probes have been reported to be in the very wide range from 2.2 to 55. These results imply that the intrinsic dielectric constant of the CD cavity interior is close to that of 1,4-dioxane (ε=2.2). As pointed out by Cox et al.,[25] the location of a probe molecule inside the cavity is quite critical for the evaluation of the dielectric constants of CDs. A probe molecule does not neces-

sarily totally enter the cavity, since the interior of the CD cavity is not so wide and deep for probes usually used. The polarity sensed by a probe molecule varies from point to point within the cavity. Consequently, the polarity determined from such a probe technique conversely indicates the location of a probe incorporated into the cavity.[21] If the estimated dielectric constant is large, the probe molecule inside the cavity seems to reside near the aqueous phase or to be in contact with water.

The author thanks Professor Fumio Hirayama for his valuable discussion.

References

1) W. Saenger, *Angew. Chem., Int. Ed. Engl.*, **19**, 344 (1980).
2) H. Hirai, N. Toshima, and S. Uenoyama, *Polym. J.*, **13**, 607 (1981).
3) A. Harada and S. Nozakura, *Polym. Bull.*, **8**, 141 (1982).
4) R. J. Clarke, J. H. Coates, and S. F. Lincoln, *Carbohydr. Res.*, **127**, 181 (1984).
5) R. L. Schiller, S. F. Lincoln, and J. H. Coates, *J. Chem. Soc., Faraday Trans. 1*, **83**, 3237 (1987).
6) W. G. Herkstroeter, P. A. Martic, and S. Farid, *J. Chem. Soc., Perkin Trans. 2*, **1984**, 1453.
7) N. Kobayashi, R. Saito, H. Hino, Y. Hino, A. Ueno, and T. Osa, *J. Chem. Soc., Perkin Trans. 2*, **1983**, 1031.
8) S. Hamai, *J. Phys. Chem.*, **93**, 6527 (1989).
9) A. Ueno, K. Takahashi, and T. Osa, *J. Chem. Soc., Chem. Commun.*, **1981**, 194.
10) N. Kobayashi, A. Ueno, and T. Osa, *J. Chem. Soc., Chem. Commun.*, **1981**, 340.
11) K. Kano, I. Takenoshita, and T. Ogawa, *Chem. Lett.*, **1982**, 321.
12) G. Patonay, K. Fowler, A. Shapira, G. Nelson, and I. M. Warner, *J. Inclusion Phenom.*, **5**, 717 (1987).
13) G. Nelson, G. Patonay, and I. M. Warner, *J. Inclusion Phenom.*, **6**, 277 (1988).
14) G. Nelson, G. Patonay, and I. M. Warner, *Anal. Chem.*, **60**, 274 (1988).
15) G. Nelson and I. M. Warner, *J. Phys. Chem.*, **94**, 576 (1990).
16) K. Takamura, S. Inoue, and F. Kusu, *Chem. Lett.*, **1983**, 233.
17) A. Ueno, K. Takahashi, and T. Osa, *J. Chem. Soc., Chem. Commun.*, **1980**, 921.
18) S. Hamai, *J. Phys. Chem.*, **93**, 2074 (1989).
19) S. Hamai, *J. Am. Chem. Soc.*, **111**, 3954 (1989).
20) S. Hamai, *Bull. Chem. Soc. Jpn.*, **62**, 2763 (1989).
21) S. Hamai, *J. Phys. Chem.*, **94**, 2595 (1990).
22) S. Hamai, *J. Phys. Chem.*, **92**, 6140 (1988).
23) S. Hamai, *Bull. Chem. Soc. Jpn.*, **55**, 2721 (1982).
24) R. L. VanEtten, J. F. Sebastian, G. A. Clowes, and M. L. Bender, *J. Am. Chem. Soc.*, **89**, 3242 (1967).
25) G. S. Cox, N. J. Turro, N. C. Yang, and M. Chen, *J. Am. Chem. Soc.*, **106**, 422 (1984).
26) G. S. Cox, P. J. Hauptman, and N. J. Turro, *Photochem. Photobiol.*, **39**, 597 (1984).
27) A. Heredia, G. Requena, and F. G. Sanchez, *J. Chem. Soc., Chem. Commun.*, **1985**, 1814.
28) K. W. Street, Jr., *J. Liq. Chromatogr.*, **10**, 655 (1987).
29) K. W. Street, Jr. and W. E. Acree, Jr., *Appl. Spectrosc.*, **42**, 1315 (1988).

Anisochrony in Rotatable Ligands and Symmetry Non-Equivalence Characterized by Subduction of Coset Representations

Shinsaku FUJITA
Research Laboratories, Ashigara, Fuji Photo Film Co., Ltd., Minami-Ashigara, Kanagawa 250-01
(Received September 27, 1990)

A general method of characterizing symmetry equivalence and non-equivalence in a molecule is developed on the basis of the one-one correspondence between an orbit and a coset representation. This method provides us with a theoretical foundation to understand anisochrony in rotatable ligands. A given molecule is regarded as a combination of a three-dimensional skeleton and ligands. The ligand is referred to as a segment or a fragment according to its environment. Thus, the fragment is defined as a ligand-in-isolation; and the segment denotes a ligand built into a molecule. The symmetry of the ligand as a fragment is restricted to the local symmetry. This restriction is examined by using methyl and methylene ligands as examples. A methyl fragment has a homospheric $\mathbf{C}_{3v}(/\mathbf{C}_s)$ orbit that consists of three hydrogen atoms. On the other hand, a methylene fragment has an enantiospheric $\mathbf{C}_s(/\mathbf{C}_1)$ orbit that contains two hydrogen atoms. Such an orbit is incorporated into various molecules to afford restricted orbits, which are characterized by subduction of coset representations. The restricted orbits are discussed in terms of global and local orbits. This discussion provides a general approach to rationalize various types of anisochronies.

Relationship between global and local symmetries in a molecule has been investigated in order to clarify stereochemical behaviors of the molecule.[1] In particular, chemical shift equivalence (isochrony) and non-equivalence (anisochrony) of nuclei have been discussed in the light of such stereochemical relationships.[2,3]

Anisochrony of methyl protons has been observed in several molecules at low temperatures. Nakamura et al.[4] reported that the bridgehead methyl segment of 1,2,3,4-tetrachloro-5,8,9-trimethyltriptycene (**1**) exhibited three chemical shifts at −90 °C. Anderson and Rawson[5] observed split methyl signals (2:1) in the NMR spectrum of **2** at −141 °C.

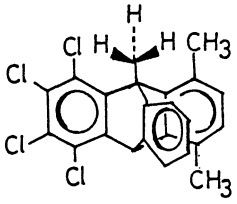

1

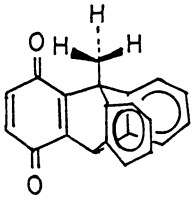

2

On the other hand, anisochrony of geminal groups in an appropriate intramolecular environment was observed independent of temperature.[6] One of such anisochronies was observed in molecules having the general formula ($XYC(CU_2R)_2$). According to Jenning's review,[7] this type of anisochronies can be rationalized by combining the prochirality concept of Hanson[8] with the topic relationships of Mislow and Raban.[2] Eliel reviewed nuclear magnetic resonances with reference to prochiralities.[9] However, since the conventional prochirality concept is not based on a mathematical formulation, rather tedious procedures are required for judging such anisochronies.

Flanzen and Binsch[10] pointed out two general possibilities for realizing another type of anisochrony of geminal groups: Class A is characterized by the general formula $RU_2C\text{-}CX_3^*$, with X* being a chiral substituent; Class B conforms to the general formula $(RU_2C)_3C\text{-}CXYZ$. Reisse et al.[11] added another class $(RU_2C)_3C\text{-}CX_3^*$ to this classification. These phenomena were also analyzed in terms of topic relationships.[1,2] Reisse et al.[11] concluded that anisochronies of diastereotopic and constitutional heterotopic groups stemmed from a single source: symmetry non-equivalence of nuclei. However, such symmetry non-equivalence has been investigated by applying Newmann's projections or other diagrams to every molecule; and there has appeared no comprehensive understanding on this issue.

We recently discussed several applications of coset representations (CRs) and of their subductions.[12-14] These applications are based on the one-one correspondence between a CR and a set (an orbit) of equivalent atoms (or objects). We have clarified that such topic relationships should be used subsidiarily to sphericities (chirality fittingnesses) of such CRs, since diastereotopic and heterotopic relations cannot provide equivalence classes from a mathematical point of view.[14] In other words, the terms "diastereotopic" and "heterotopic" indicate that two objects are different; but are incapable of clarifying how different they are. On the other hand, the chirality fittingness characterizes an orbit as being *homospheric, enantiospheric,* or *hemispheric.* This classification clarifies how different (or how equivalent) such two objects are. In the present paper, we deal with another application of such CRs, which aims at providing a general approach to symmetry (non-)equivalence as well as at rationalizing various types of anisochronies.

1. Orbits of Ligands

An orbit is an equivalence class whose members can be any kind of objects. For discussing stereochemical relationships, such objects may be atoms, bonds, or faces. Moreover, a ligand, which is a set of one or more atoms, can also be such an object. Thereby, a set of equivalent ligands is regarded as an orbit.[15]

The term "ligand" has been used in various meanings, which depend upon how to manipulate the three-dimensional (3D) structure of the ligand. This fact has attracted little attention of organic chemists, inasmuch as such different usages have provided no confusion in most cases. For the purpose of discussing stereochemical relationships in detail, however, we should use this term in a stricter fashion. There are at least three ways to treat the 3D structure of a ligand according to the fact that the ligand has three kinds of attributes: (1) chirality/achirality, (2) a point group, and (3) an internal 3D structure, in ascending order of concreteness. In order to make our discussion clearcut, we here introduce a new term "proligand"; this takes account of the chirality/achirality. The term "ligand" is used for discussing (2) and (3).

A Set of Equivalent Proligands as an Orbit. The molecule **1** (or **2**) is regarded as a combination of a triptycene skeleton and a methyl ligand.[16] These examples contain only one methyl ligand to be examined. However, we should discuss a more general case in which two or more equivalent ligands are taken into consideration.

Before we manipulate such ligands directly, we begin with equivalence and non-equivalence of proligands. A *proligand* is defined as a point ligand that is structureless but has chirality; such a proligand is either chiral or achiral. The term proligand has been introduced in order to explicate a logical standpoint that primarily takes neither the point group nor the internal structure of ligand into consideration. In the present discussion, the proligand concept is coupled with the concept of local symmetry. Although several predecessors of the present cencept (proligand) have been reported for discussing stereochemistry,[8,17] they pay little attention on such implications that are revealed by the proligand term. For simplicity's sake, we here deal with achiral proligands, which apparently behave like atoms. A more general approach will be discussed elsewhere.[18]

We then define a *promolecule* as a three-dimensional (3D) object that consists of a skeleton and proligands. We differentiate such promolecules from molecules, since this differentiation simplifies discussions on stereochemical relationships.

A set of equivalent proligands is regarded as an *orbit*, which is characterized by a coset representation (CR). For illustrating this relationship, we depict several promolecules derived from adamantane skeletons (Fig. 1). Each A is an achiral proligand; the remaining part of each promolecule is regarded as a skeleton without losing generality.[19] Table 1 indicates properties of each orbit concerning the proligands (A's), where other orbits are not taken into account.

Let **G** be the symmetry of a promolecule, which is referred to as a *global symmetry*. Then, a CR for an orbit is represented by $\mathbf{G}(/\mathbf{G}_i)$, where $\mathbf{G}_i$ is an appropriate subgroup of **G**. This CR indicates that $\mathbf{G}_i$ is the *local symmetry* for each member of the orbits.[14] The number of the members is equal to the length of the orbit, which is calculated to be $|\mathbf{G}|/|\mathbf{G}_i|$, where $|\mathbf{G}|$ and $|\mathbf{G}_i|$ denote the orders of **G** and $\mathbf{G}_i$, respectively. For example, the orbit of four equivalent A's of **3** is assigned to the CR, $\mathbf{T}_d(/\mathbf{C}_{3v})$.[20] This assignment is accomplished by using a table of marks for $\mathbf{T}_d$ point group.[13,14] In terms of the CR ($\mathbf{T}_d(/\mathbf{C}_{3v})$), the local symmetry of each A in this molecule is concluded to be $\mathbf{C}_{3v}$, which appears in the parentheses of the symbol of the CR. The achiral proligand (A) is presumed implicitly to have $\mathbf{C}_{\infty v}$ symmetry in isolation; but is restricted to the $\mathbf{C}_{3v}$ local symmetry in this promolecule. The local symmetries in the other promolecules are listed in Table 1, in which they are placed by

Table 1. Coset Representations for Orbits of Proligands

Promolecule	Member(s) of an orbit	Local symmetry	Coset representation	Chirality fittingness (Sphericity)
3	A_4	$\mathbf{C}_{3v}$	$\mathbf{T}_d(/\mathbf{C}_{3v})$	Homospheric
4	A_4	$\mathbf{C}_s$	$\mathbf{D}_{2d}(/\mathbf{C}_s)$	Homospheric
5	A	$\mathbf{C}_{3v}$	$\mathbf{C}_{3v}(/\mathbf{C}_{3v})$	Homospheric
6	A_3	$\mathbf{C}_s$	$\mathbf{C}_{3v}(/\mathbf{C}_s)$	Homospheric
7	A_6	$\mathbf{C}_1$	$\mathbf{C}_{3v}(/\mathbf{C}_1)$	Enantiospheic
8	A_4	$\mathbf{C}_1$	$\mathbf{D}_2(/\mathbf{C}_1)$	Hemispheric
9	A_2	$\mathbf{C}_s$	$\mathbf{C}_{2v}(/\mathbf{C}_s)$	Homospheric
10	A_4	$\mathbf{C}_1$	$\mathbf{S}_4(/\mathbf{C}_1)$	Enantiospheric
11	A	$\mathbf{C}_3$	$\mathbf{C}_3(/\mathbf{C}_3)$	Hemispheric
12	A_3	$\mathbf{C}_1$	$\mathbf{C}_3(/\mathbf{C}_1)$	Hemispheric
13	A	$\mathbf{C}_s$	$\mathbf{C}_s(/\mathbf{C}_s)$	Homospheric
14	A_2	$\mathbf{C}_1$	$\mathbf{C}_s(/\mathbf{C}_1)$	Enantiospheric
15	A_2	$\mathbf{C}_1$	$\mathbf{C}_2(/\mathbf{C}_1)$	Hemispheric

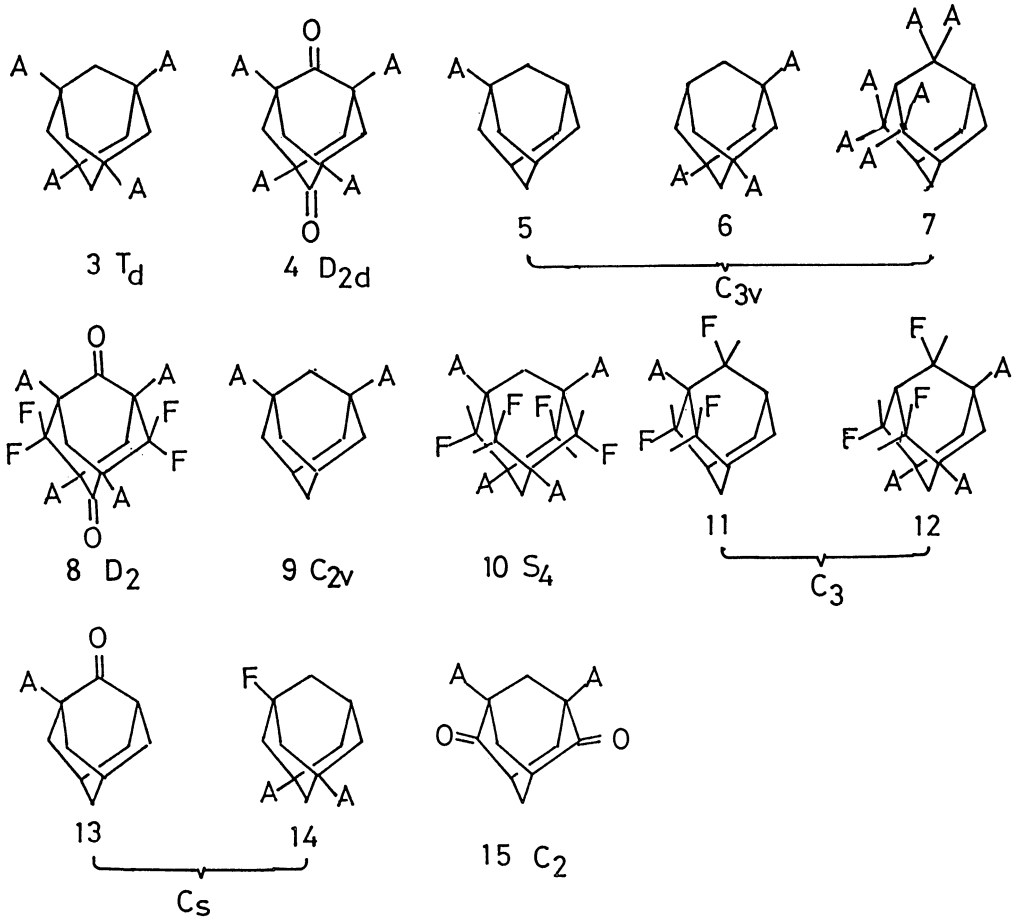

Fig. 1. Promolecules based on adamantane skeletons.
Capital A's in each promolecule denote achiral proligands. The remaining part of the promolecule is regarded as a skeleton. A capital F denotes a fluorine atom, which is here considered to be a component of a skeleton.

the sides of the corresponding CRs.

A proligand in a promolecule is called a *segment* and a proligand in isolation is referred to as a *fragment*. The segment may be different from the corresponding fragment in their symmetries. The promolecules (**5** to **7**) belong to the same C_{3v} symmetry; however, they have different types of orbits concerning A's (Table 1). Thus, one A of **5** constructs a $C_{3v}(/C_{3v})$ orbit; three A's of **6** belong to a $C_{3v}(/C_s)$ orbit; and six A's of **7** build a $C_{3v}(/C_1)$ orbit. The respective local symmetries are C_{3v}, C_s and C_1, as found in the parentheses of the symbols.

A Set of Equivalent Ligands as an Orbit. We now discuss symmetry changes that take place when proligands are replaced by achiral ligands having a 3D structure. The treatment described in this section is concerned with the symmetries of the ligands to such a limited extent that only their point groups are taken into consideration; but without considering their internal structures. Suppose that the achiral proligand (A) in the promolecule (**5**) of C_{3v} symmetry is replaced by a methyl ligand. The resulting molecule (**22**) retains the global C_{3v} symmetry, because the C_{3v} symmetry of the methyl fragment is equal to the local C_{3v} symmetry due to the $C_{3v}(/C_{3v})$ CR (Table 1). Thereby, the methyl segment has the same C_{3v} symmetry as the fragment. Thus, this operation gives rise to no restriction of the fragment symmetry. We also use the terms *segment* and *fragment* for discussing properties of ligands.[21]

In the case of the promolecule (**6**), the replacement of each A by a methyl ligand produces a molecule (**23**) that has a global C_{3v} symmetry equal to that of **6**. However, this conservation of the global symmetry is different from that of **22** described above, because the C_{3v} point group (for the methyl as a fragment) involves the C_s point group (for the local symmetry) as a subgroup. In contrast with the global symmetry, each of the resulting methyl segments has a C_s local symmetry, to which the original C_{3v} symmetry of the methyl ligand (as a fragment) is restricted.

These facts can be generalized as follows: If the symmetry of a fragment is equal to or involves the local symmetry of a promolecule, the resulting molecule has the same symmetry (point group) as does the promolecule; and the segment derived from the frag-

ment is restricted so as to have the symmetry equal to the local symmetry.

Chirality Fittingness of an Orbit. In order to discuss the chirality/achirality of a molecule (or a promolecule), we have introduced the concept "chirality fittingness" (sphericity) in a previous paper.[14] Thus, any $\mathbf{G}(/\mathbf{G}_i)$ orbit is classified into one of the three categories according to $\mathbf{G}$ vs. $\mathbf{G}_i$.

Global symmetry	Local symmetry	Chirality fittingness	Number of orbits	
$\mathbf{G}$	$\mathbf{G}_i$	(Sphericity)	$\downarrow\mathbf{G}$	$\downarrow\mathbf{G}^{max}$
Achiral	Achiral	Homospheric	1	1
Achiral	Chiral	Enantiospheric	1	2
Chiral	Chiral	Hemispheric	1	1

Table 1 collects coset representations and chirality fittingness. For illustrating the chirality fittingness, let us examine homospheric and enantiospheric orbits. For example, the two proligands (A_2) in the promolecule (**9**) (or equivalently the two hydrogen atoms in difluoromethane (CH_2F_2) construct a $\mathbf{C}_{2v}(/\mathbf{C}_s)$ orbit, which is homospheric because both of the $\mathbf{C}_{2v}$ and $\mathbf{C}_s$ point groups are achiral. The two members (A_2) of the orbit are interchangeable by the proper rotations (I and C_2) and the improper rotations ($\sigma_{v(1)}$ and $\sigma_{v(2)}$) contained in the $\mathbf{C}_{2v}$ group. In other words, the homospheric orbit remains unchanged even if we restrict the $\mathbf{C}_{2v}$ into $\mathbf{C}_2=\{I, C_2\}$. As a result, the number of orbits is 1 under the action of $\mathbf{C}_{2v}$ (no restriction) and is unchanged to be 1 under the action of $\mathbf{C}_2$ (restriction denoted by $\downarrow\mathbf{C}_2$). Let $\mathbf{G}^{max}$ be such a subgroup of $\mathbf{G}$ that is composed of all of the proper rotations of $\mathbf{G}$. Then, this case can be generalized as follows. The restriction to the $\mathbf{G}^{max}$ (denoted by $\downarrow\mathbf{G}^{max}$) produces no division of a homospheric $\mathbf{G}(/\mathbf{G}_i)$ orbit.

On the other hand, the two proligands (A_2) in the promolecule (**14**) (or equivalently the two hydrogen atoms in chlorofluoromethane (CH_2ClF)) belong to a $\mathbf{C}_s(/\mathbf{C}_1)$ orbit. This orbit is enantiospheric, because the $\mathbf{C}_s$ is achiral and the $\mathbf{C}_1$ is chiral. The two members (A_2) of the orbit are interchangeable by the improper rotation (σ) but not interchangeable by the proper rotation (I) contained in the $\mathbf{C}_s$ group. As a result, the number of orbits is 1 under the action of $\mathbf{C}_s$ (no restriction) but the orbit is divided into two orbits under the action of $\mathbf{C}_1$ (restriction denoted by $\downarrow\mathbf{C}_1$). This case can be generalized as follows. The restriction to the $\mathbf{G}^{max}$ (denoted by $\downarrow\mathbf{G}^{max}$) divides an enantiospheric $\mathbf{G}(/\mathbf{G}_i)$ orbit into two parts.

Enantiospheric Orbit under a Chiral Environment. Several symmetrical properties of a segment can be discussed in terms of coset representations and chirality fittingnesses (sphericities) collected in Table 1; thus, these determine behaviors of the segment (A) under chiral environments (such as actions of chiral shift reagents and of chiral solvents). The following general theorem is important throughout the present discussions:

Theorem 1 (Fujita[14]). An enantiospheric orbit is capable of separating into two hemispheric orbits of the same length under a chiral environment, whether the change is reversible or irreversible.

This general theorem stems from the difference in the behavior of the enantiospheric orbit toward $\mathbf{G}$ and $\mathbf{G}^{max}$. The theorem can be applied to the orbits of proligands and of ligands. For example, since the six A's (or achiral ligands) of **7** belong to an enantiospheric orbit governed by $\mathbf{C}_{3v}(/\mathbf{C}_1)$, Theorem 1 predicts that they are divided into two sets of three equivalent (hemispheric) segments if **7** is placed under an external chiral environment (e.g, by the action of a chiral shift reagent). If the resulting anisochrony is large enough to determine, there emerge two sets of signals of equal intensities for A's. Similar predictions are obtained with respect to **10** and **14**, since they have an enantiospheric orbit (Table 1). To the best of our knowledge, no example has been reported for such splittings that concern four or more ligands, although several anisochronies concerning two ligands have been observed by the actions of chiral solvents.[22]

Each of the other promolecules (or the corresponding molecules) collected in Table 1 has a homospheric (or hemispheric) orbit only; such an anisochronous effect is predicted not to be observed.

2. Local Orbits and Global Orbits

In the preceding section, we have discussed an orbit of ligands, where we took no account of the internal structure of each ligand. The latter issue is a matter we aim at in this section. Figure 2 illustrates the fundamental principle of formulating a ligand that has an internal 3D structure. Suppose that a ligand-in-isolation (fragment) belongs to **F**-point group. It consists of several atoms, which construct its own orbits. The orbits in the fragment are referred to as *infraorbits*. Each of the infraorbits are govorned by a coset representation ($\mathbf{F}(/\mathbf{F}_p)$), where $\mathbf{F}_p$ is an appropriate subgroup of $\mathbf{F}$. Each $\mathbf{F}(/\mathbf{F}_p)$ infraorbit has the length of $|\mathbf{F}|/|\mathbf{F}_p|$, where $|\mathbf{F}|$ and $|\mathbf{F}_p|$ are the orders of $\mathbf{F}$ and $\mathbf{F}_p$ respectively.

Let us next incorporate this fragment into a molecule. Just as the fragment symmetry ($\mathbf{F}$) of the ligand is restricted into a local symmetry ($\mathbf{F}_q$) when incorporated as a segment, so the infraorbits ($\mathbf{F}(/\mathbf{F}_p)$'s) are restricted to the same local symmetry. The resulting orbits are called *local orbits*. The generation of the local orbits is controlled by the subduction, $\mathbf{F}(/\mathbf{F}_p)\downarrow\mathbf{F}_q$.[12] If we now inspect the whole molecule, we find that an appropriate set of such local orbits, each of which belongs to a segment, constructs an orbit of the molecule. We call the latter orbit a *global orbit*.

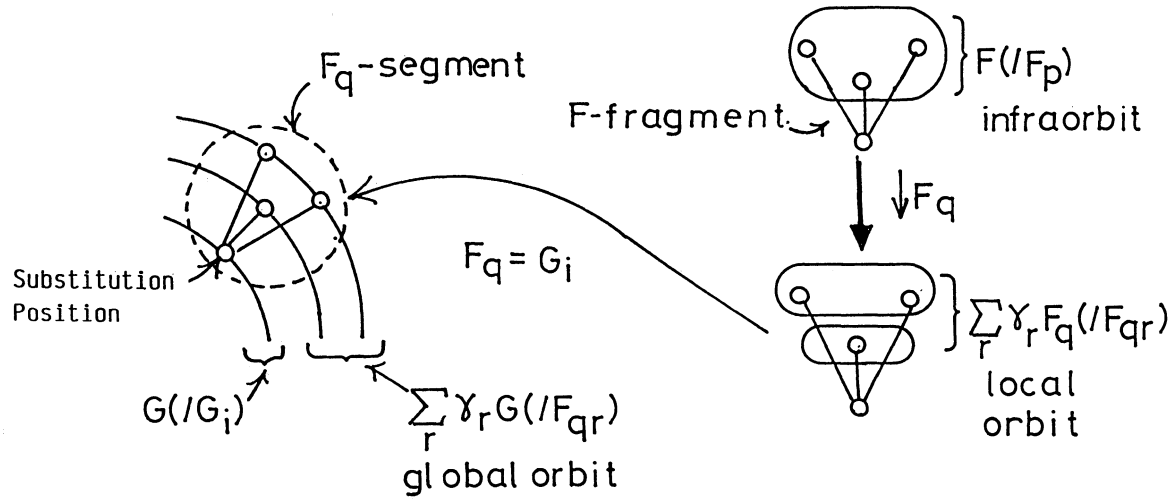

Fig. 2. Infraorbits, local orbits, and global orbits.

Since global orbits and local orbits characterize the same objects from different points of view, there is a close relationship between them.

This relationship is described by means of the following theorems, which can be proved by a slight modification of a mathematical treatment reported elsewhere.[15]

Theorem 2. Suppose that a promolecule has a $\mathbf{G}(/\mathbf{G}_i)$ orbit with $|\mathbf{G}|/|\mathbf{G}_i|$ achiral proligands; and that each of the achiral proligands in the orbit is replaced by an achiral ligand having an $\mathbf{F}(/\mathbf{F}_p)$ infraorbit ($\mathbf{F} \not\geqslant \mathbf{G}_i$). Then, the resulting molecule belongs to $\mathbf{G}$ symmetry. The $|\mathbf{F}|/|\mathbf{F}_p|$-membered infraorbit is divided according to $\mathbf{F}(/\mathbf{F}_p)\downarrow\mathbf{F}_q$, where $\mathbf{G}_i=\mathbf{F}_q$.

The resulting local and global orbits are represented by

Theorem 3. a) If the infraorbit ($\mathbf{F}(/\mathbf{F}_p)$) is restricted in the light of Theorem 2, the restriction is represented by

$$\mathbf{F}(/\mathbf{F}_p)\downarrow\mathbf{F}_q = \sum_{r=1}^{c_q} \gamma_r \mathbf{F}_q(/\mathbf{F}_{qr}), \tag{1}$$

wherein each $\mathbf{F}_{qr}$ is a subgroup of $\mathbf{F}_q$; c_q is the number of representative subgroups; and γ_r is the multiplicity of the $\mathbf{F}_{qr}$ subgroup. The resulting orbits ($\mathbf{F}_q(/\mathbf{F}_{qr})$'s) in the right-hand side are local orbits. Each $\mathbf{F}_q(/\mathbf{F}_{qr})$ orbit has the length of $|\mathbf{F}_q|/|\mathbf{F}_{qr}|$.

b) The corresponding global orbits are represented by

$$\sum_{r=1}^{c_q} \gamma_r \mathbf{G}(/\mathbf{F}_{qr}), \tag{2}$$

wherein c_q is the number of representatives of conjugate subgroups appearing in $\mathbf{F}_q$. Each $\mathbf{G}(/\mathbf{F}_{qr})$ orbit has the length of $|\mathbf{G}|/|\mathbf{F}_{qr}|$. Note that

$$\frac{|\mathbf{G}|}{|\mathbf{G}_i|} \times \left(\sum_{r=1}^{c_q} \frac{\gamma_r |\mathbf{F}_q|}{|\mathbf{F}_{qr}|} \right) = \sum_{r=1}^{c_q} \frac{\gamma_r |\mathbf{G}|}{|\mathbf{F}_{qr}|}, \tag{3}$$

since $\mathbf{G}_i$ is identical with $\mathbf{F}_q$.

It should be noted that Theorems 2 and 3 concern the highest attainable symmetry. These theorems determine symmetry equivalence and non-equivalence in a general fashion. Theorems 2 and 3 are true for any cases; but we hereafter bear special cases in mind: each ligand has an additional $\mathbf{F}(/\mathbf{F})$ orbit at which the ligand is linked to a member of the $\mathbf{G}(/\mathbf{G}_i)$ orbit, so that a free bond rotation at the linking position is allowed.

Comparison between Eqs. 1 and 2 indicates no increase in the number of orbits. In addition, Eqs. 1 and 2 afford a splitting ratio:

$$\begin{aligned}
&\underbrace{\frac{|\mathbf{F}_q|}{|\mathbf{F}_{q1}|}}_{\gamma_1} : \cdots : \underbrace{\frac{|\mathbf{F}_q|}{|\mathbf{F}_{q2}|}}_{\gamma_2} : \cdots : \cdots : \underbrace{\frac{|\mathbf{F}_q|}{|\mathbf{F}_{qc_q}|}}_{\gamma_{c_q}} : \cdots \\
&= \underbrace{\frac{|\mathbf{G}|}{|\mathbf{F}_{q1}|}}_{\gamma_1} : \cdots : \underbrace{\frac{|\mathbf{G}|}{|\mathbf{F}_{q2}|}}_{\gamma_2} : \cdots : \cdots : \underbrace{\frac{|\mathbf{G}|}{|\mathbf{F}_{qc_q}|}}_{\gamma_{c_q}} : \cdots \\
&= \underbrace{\frac{1}{|\mathbf{F}_{q1}|}}_{\gamma_1} : \cdots : \underbrace{\frac{1}{|\mathbf{F}_{q2}|}}_{\gamma_2} : \cdots : \cdots : \underbrace{\frac{1}{|\mathbf{F}_{qc_q}|}}_{\gamma_{c_q}} : \cdots
\end{aligned}$$

These facts mean that non-equivalence can be discussed in terms not only of global orbits but also of local orbits. When two atoms belong to the same global (or local) orbit, they are symmetrically equivalent; otherwise, they are symmetrically non-equivalent. Moreover, such expressions as Eq. 1 can be preestimated in the form of tables of subduction (see below), which simplify our discussions on symmetry equivalence to a great extent. The present methodology, obviously, does not require terms concerning topic

relationships, such as enantiotopic and diastereotopic. In the subsequent sections, we will apply these theorems to several cases and reveal merits of the present approach.

3. Methyl Segments in Various Molecules

Global and Local Orbits for Methyl Segments. Figure 3 illustrates the same concepts as shown in Fig. 2 more concretely by using a D_{2d} skeleton and methyl ligands. In this case, we start from the skeleton (**16**) of D_{2d} symmetry. For simplicity's sake, we use a schematic top view (right) in place of a usual structural diagram (left). Each position of **16** (belonging to $D_{2d}(/C_s)$) is replaced by an achiral proligand (A) to produce the promolecule (**4**). Then the replacement of A's of **4** by methyl ligands produces the molecule (**17**), which has D_{2d} symmetry in a conformation of the highest attainable symmetry. In this conformation, the twelve hydrogen atoms in **17** are split into two orbits (H_4^a and H_8^b), which are governed by $D_{2d}(/C_s)$ and $D_{2d}(/C_1)$, respectively. These orbits are global orbits concerning these twelve hydrogens.

Let us now focus our attention on one of the four methyl ligands in **17**. Each of these methyl ligands is decided to be a C_s segment on the basis of the local symmetry determined by the $D_{2d}(/C_s)$ CR concerning the A_4 of **4**. This C_s segment contains atoms (H^a and H_2^b), which are subject to $C_s(/C_s)$ and $C_s(/C_1)$ if the labeling with a and b is taken into account. These orbits are local orbits concerning the methyl segment.

It should be noted that an object can exhibit simultaneous memberships of several distinct orbits that are presumed from different points of view. Thus, H^a is

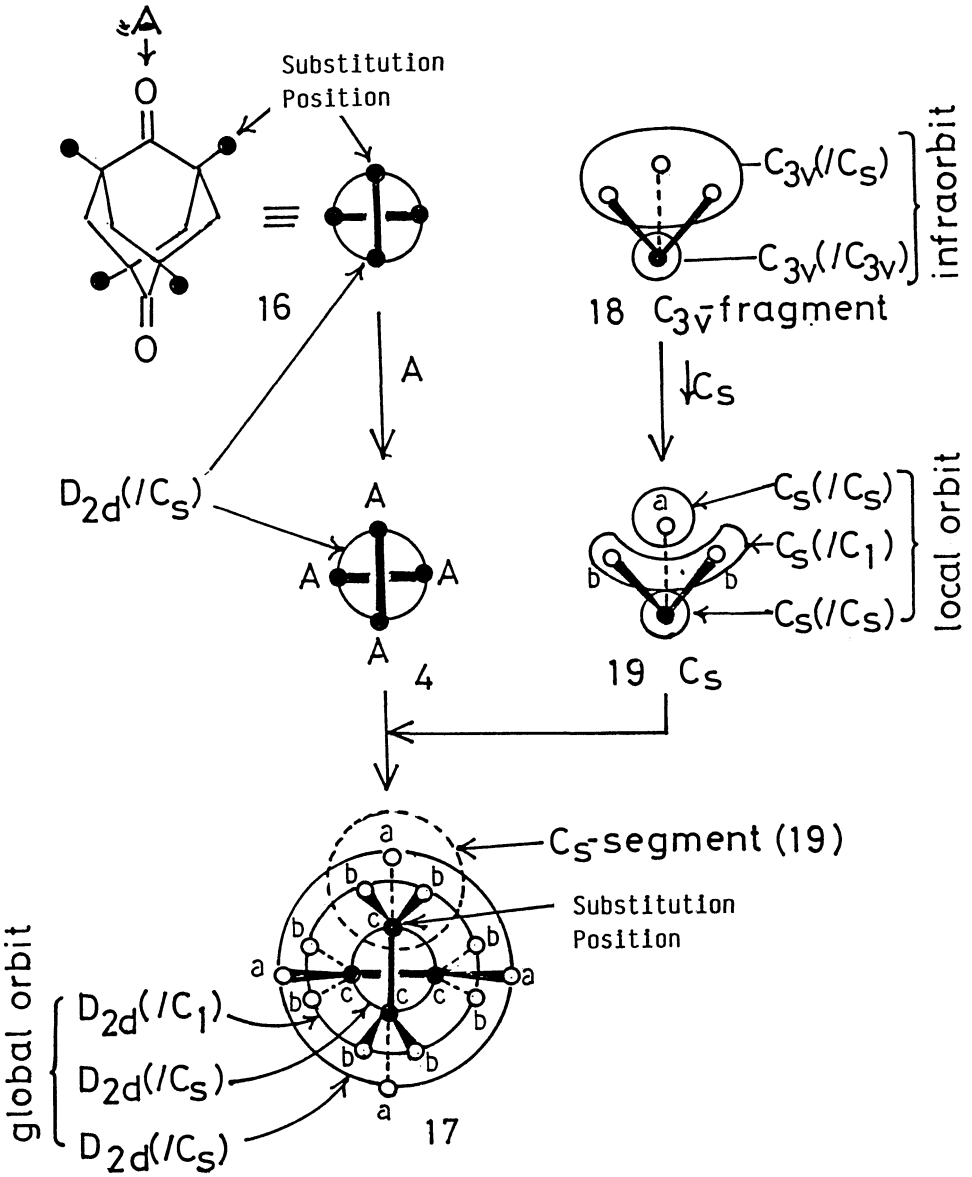

Fig. 3. Infraorbits, local orbits, and global orbits in **17**.

a member of the 4-membered global orbit denoted by $\mathbf{D}_{2d}(/\mathbf{C}_s)$, and, at the same time, belongs to the one-membered local orbit governed by $\mathbf{C}_s(/\mathbf{C}_s)$. Similarly, H^b belongs to the 8-membered $\mathbf{D}_{2d}(/\mathbf{C}_1)$ global orbit and to the 2-membered $\mathbf{C}_s(/\mathbf{C}_1)$ local orbit. The global orbit and the local orbit are linked with each other through the CR $\mathbf{D}_{2d}(/\mathbf{C}_s)$ of the substitution positions.

The local orbit concerning a methyl segment can be interpreted otherwise. This treatment is a direct application of Theorem 3. Let us begin with a methyl ligand in isolation (fragment). The methyl fragment (**18**) has an infraorbit of three hydrogen atoms that is subject to the CR, $\mathbf{C}_{3v}(/\mathbf{C}_s)$. Since this infraorbit is homospheric, it coincides with itself by the rotations and rotoreflections of the $\mathbf{C}_{3v}$ point group. When the methyl ligand is incorporated into **4** in place of A, its infraorbit is restricted to the $\mathbf{C}_s$ local symmetry. This restriction producing **19** is represented by the symbol, $\mathbf{C}_{3v}(/\mathbf{C}_s)\downarrow\mathbf{C}_s$, which is referred to as a *subduced representation* (SR) of the CR. Such a subduced representation is intransitive and can be further reduced into a set of CRs for $\mathbf{C}_s$ point group. For the purpose of such reduction, it is important to prepare a table of subduction of CRs.[12] Table 2 lists the subduction of CRs for $\mathbf{C}_{3v}$ point group. From this table, we obtain an expression:

$$\mathbf{C}_{3v}(/\mathbf{C}_s)\downarrow\mathbf{C}_s = \mathbf{C}_s(/\mathbf{C}_1) + \mathbf{C}_s(/\mathbf{C}_s), \quad (4)$$

which is an explicit form of Eq. 1 denoting this case. Equation 4 indicates that there emerge two orbits; the one (H_2^b) is a two-membered orbit subject to $\mathbf{C}_s(/\mathbf{C}_1)$ and the other (H^a) is a one-membered orbit subject to $\mathbf{C}_s(/\mathbf{C}_s)$. This splitting corresponds to the local orbits depicted in Fig. 3. Theorem 3 indicates that the sum $(\mathbf{C}_s(/\mathbf{C}_1)+\mathbf{C}_s(/\mathbf{C}_s))$ in the right-hand side of Eq. 4 corresponds to the sum $(\mathbf{D}_{2d}(/\mathbf{C}_1)+\mathbf{D}_{2d}(/\mathbf{C}_s))$. This fact agrees with the global orbits described above.

In general, local orbits are deduced from subduction of an infraorbit. Furthermore, global orbits are deduced form the local orbits in terms of Theorem 3. Table 3 lists local and global orbits that are created by the subduction of $\mathbf{C}_{3v}(/\mathbf{C}_s)$ infraorbit of a methyl ligand incorporated in **3** to **15**. These data are easily obtained from Table 2 by restricting $\mathbf{C}_{3v}(/\mathbf{C}_s)$ into the respective local symmetries that are listed in Table 1 and in the CR-for-ligand column of Table 3.

Anisochrony in Methyl Ligands. Symmetry equivalence is ascribed to the membership of the same orbit (local and global); and symmetry non-equivalence stems from the membership of distinct orbits. Then, we ascribe anisochrony to such symmetry non-equivalence. This criterion is mathematically stricter than that of Reisse et al.,[11] in which anisochrony is ascribed to diastereotopism by external or internal comparison.

According to the local-orbit column of Table 3, we can predict isochronies for the methyl segments of **21**, **22**, and **28**, since there appears no splitting of the 3-membered infraorbits. However, the former two (**21** and **22**) are different from **28** in their behaviors. In the cases of **21** (from **3**) and **22** (from **5**), the local symmetry of $\mathbf{C}_{3v}$ provides no restriction to the methyl group. On the other hand, the $\mathbf{C}_3(/\mathbf{C}_3)$ CR restricts the proligand (A) of the promolecule (**11**) so as to

Table 2. Subduction of Coset Representations for $\mathbf{C}_{3v}$ Group

Coset representation	Subduction			
	$\downarrow\mathbf{C}_1$	$\downarrow\mathbf{C}_s$	$\downarrow\mathbf{C}_3$	$\downarrow\mathbf{C}_{3v}$
$\mathbf{C}_{3v}(/\mathbf{C}_1)$	$6\mathbf{C}_1(/\mathbf{C}_1)$	$3\mathbf{C}_s(/\mathbf{C}_1)$	$2\mathbf{C}_3(/\mathbf{C}_1)$	$\mathbf{C}_{3v}(/\mathbf{C}_1)$
$\mathbf{C}_{3v}(/\mathbf{C}_s)$	$3\mathbf{C}_1(/\mathbf{C}_1)$	$\mathbf{C}_s(/\mathbf{C}_1)+\mathbf{C}_s(/\mathbf{C}_s)$	$\mathbf{C}_3(/\mathbf{C}_1)$	$\mathbf{C}_{3v}(/\mathbf{C}_s)$
$\mathbf{C}_{3v}(/\mathbf{C}_3)$	$2\mathbf{C}_1(/\mathbf{C}_1)$	$\mathbf{C}_s(/\mathbf{C}_1)$	$2\mathbf{C}_3(/\mathbf{C}_3)$	$\mathbf{C}_{3v}(/\mathbf{C}_3)$
$\mathbf{C}_{3v}(/\mathbf{C}_{3v})$	$\mathbf{C}_1(/\mathbf{C}_1)$	$\mathbf{C}_s(/\mathbf{C}_s)$	$\mathbf{C}_3(/\mathbf{C}_3)$	$\mathbf{C}_{3v}(/\mathbf{C}_{3v})$

Table 3. Local Orbits and Global Orbits in **3**—**15** Substituted by Methyl Ligands

Molecule	Structure	CR for ligands	Local orbits	Global orbits
21	**3** (A=CH_3)	$\mathbf{T}_d(/\mathbf{C}_{3v})$	$\mathbf{C}_{3v}(/\mathbf{C}_s)$	$\mathbf{T}_d(/\mathbf{C}_s)$
17	**4** (A=CH_3)	$\mathbf{D}_{2d}(/\mathbf{C}_s)$	$\mathbf{C}_s(/\mathbf{C}_1)+\mathbf{C}_s(/\mathbf{C}_s)$	$\mathbf{D}_{2d}(/\mathbf{C}_1)+\mathbf{D}_{2d}(/\mathbf{C}_s)$
22	**5** (A=CH_3)	$\mathbf{C}_{3v}(/\mathbf{C}_{3v})$	$\mathbf{C}_{3v}(/\mathbf{C}_s)$	$\mathbf{C}_{3v}(/\mathbf{C}_s)$
23	**6** (A=CH_3)	$\mathbf{C}_{3v}(/\mathbf{C}_s)$	$\mathbf{C}_s(/\mathbf{C}_1)+\mathbf{C}_s(/\mathbf{C}_s)$	$\mathbf{C}_{3v}(/\mathbf{C}_1)+\mathbf{C}_{3v}(/\mathbf{C}_s)$
24	**7** (A=CH_3)	$\mathbf{C}_{3v}(/\mathbf{C}_1)$	$3\mathbf{C}_1(/\mathbf{C}_1)$	$3\mathbf{C}_{3v}(/\mathbf{C}_1)$
25	**8** (A=CH_3)	$\mathbf{D}_2(/\mathbf{C}_1)$	$3\mathbf{C}_1(/\mathbf{C}_1)$	$3\mathbf{D}_2(/\mathbf{C}_1)$
26	**9** (A=CH_3)	$\mathbf{C}_{2v}(/\mathbf{C}_s)$	$\mathbf{C}_s(/\mathbf{C}_1)+\mathbf{C}_s(/\mathbf{C}_s)$	$\mathbf{C}_{2v}(/\mathbf{C}_1)+\mathbf{C}_{2v}(/\mathbf{C}_s)$
27	**10** (A=CH_3)	$\mathbf{S}_4(/\mathbf{C}_1)$	$3\mathbf{C}_1(/\mathbf{C}_1)$	$3\mathbf{S}_4(/\mathbf{C}_1)$
28	**11** (A=CH_3)	$\mathbf{C}_3(/\mathbf{C}_3)$	$\mathbf{C}_3(/\mathbf{C}_1)$	$\mathbf{C}_3(/\mathbf{C}_1)$
29	**12** (A=CH_3)	$\mathbf{C}_3(/\mathbf{C}_1)$	$3\mathbf{C}_1(/\mathbf{C}_1)$	$3\mathbf{C}_3(/\mathbf{C}_1)$
30	**13** (A=CH_3)	$\mathbf{C}_s(/\mathbf{C}_s)$	$\mathbf{C}_s(/\mathbf{C}_1)+\mathbf{C}_s(/\mathbf{C}_s)$	$\mathbf{C}_s(/\mathbf{C}_1)+\mathbf{C}_s(/\mathbf{C}_s)$
31	**14** (A=CH_3)	$\mathbf{C}_s(/\mathbf{C}_1)$	$3\mathbf{C}_1(/\mathbf{C}_1)$	$3\mathbf{C}_s(/\mathbf{C}_1)$
32	**15** (A=CH_3)	$\mathbf{C}_2(/\mathbf{C}_1)$	$3\mathbf{C}_1(/\mathbf{C}_1)$	$3\mathbf{C}_2(/\mathbf{C}_1)$

belong to C_3 local symmetry. When a methyl ligand is incorporated in **11** to afford **28**, this restriction to the local symmetry results in a subduction: $C_{3v}(/C_s)\downarrow C_3=C_3(/C_1)$. Although this equation indicates no discrimination between three methyl protons of **28**, the methyl ligand is restricted to the C_3 symmetry.

The other molecules collected in Table 3 exhibit a division of the infraorbit of each methyl fragment, which stems from a restriction to the corresponding local symmetry. This division causes an anisochrony of three protons of each methyl ligand. The present restriction is concerned with a conformation having the highest attainable symmetry, which is possible to exist when a sufficient energy barrier is realized under an appropriate condition (e.g., at low temperature). Otherwise, we should take account of bond rotations concerning the methyl segment. The CR ($C_{3v}(/C_s)$) in the left-hand side of Eq. 4 predicts that a free rotation equalizes three methyl protons in **17**. On the other hand, the right-hand side indicates that, if the rotation is slow on the NMR time scale, two anisochronous methyl proton signals (intensity ratio 2:1) can be observed. Note that $|C_s|/|C_1|$ is equal to 2 and $|C_s|/|C_s|$ is equal to 1. Among the molecules listed in Table 3, **23** (from **6**), **26** (from **9**), and **30** (from **13**) involve A's of the same situation as does **17** (from **4**). Thereby, the same prediction can be made for each of these molecules.

The equalization of the methyl protons under free bond rotation can be explained more logically. This process is equivalent to considering CH_3B, where the symbol B denotes an achiral proligand. This hypothetical promolecule belongs to C_{3v} symmetry. Hence, the carbon atom of the CH_3B constructs a $C_{3v}(/C_{3v})$ orbit. By using the C_{3v} local symmetry in place of C_s, we have $C_{3v}(/C_s)\downarrow C_{3v}=C_{3v}(/C_s)$ for the three protons. This equation indicates the equivalence of the methyl protons under free bond rotation.

The methyl protons of **2** are characterized in a similar way. The corresponding promolecule can be obtained by substituting an achiral proligand (A) for the methyl group of **2**. It belongs to C_s symmetry; the A constructs a one-membered orbit governed by C_s ($/C_s$). Since the local symmetry is determined to be C_s, the methyl segment in **2** is also restricted according to Eq. 4. Therefore, the same prediction as above can be obtained, although **4** has D_{2d} and **2** has C_s, as their global symmetries. Since $|C_s|/|C_1|=2$ and $|C_s|/|C_s|=1$, splitting of 2:1 intensity ratio is predicted to be observed in its low-temperature NMR spectrum. This prediction has already been verified experimentally.[5]

Each methyl segment in **24** (from **7**) is restricted to C_1 local symmetry. The subduction represented by $C_{3v}(/C_s)\downarrow C_1=3C_1(/C_1)$ (Table 2) indicates the symmetry non-equivalence of the three methyl protons in a conformation of the highest attainable symmetry. Hence, the three protons can be anisochronous if a bond rotation about a methyl segment is slow on the NMR time scale. If the rotation is fast, an average chemical shift is predicted to be observed because of the CR ($C_{3v}(/C_s)$). This example contains six methyl ligands and indicates an advantage of the present method over conventional ones which use Newmann's projections. In the cases in which so many ligands participate, it would be very tedious task to determine sterochemical non-equivalence in terms of Newmann's projections.

The same prediction is obtained with respect to **27** (from **10**) and **31** (from **14**), which are also characterized by C_1 local symmetry, although the global symmetry of the three molecules are different from each other. It should be noted that the global symmetries of these molecules are achiral (i.e., contain proper and improper rotations); but the local symmetries are chiral (i.e., contain proper rotations only).

A local symmetry of a chiral molecule is always chiral. Since the local symmetry of the ligand (A) in **8** is C_1 the corresponding subduction is represented by $C_{3v}(/C_s)\downarrow C_1=3C_1(/C_1)$. Hence, we can predict non-equivalence of three methyl protons in **25** (from **8**). We can obtain the same prediction about **29** (from **12**) and **32** (from **15**) in the same line, since they have C_1 local symmetries. Note that this type of anisochrony is observed only in a fixed conformation; the free rotation of a methyl ligand equalizes the three methyl protons. Anisochrony observed in the molecule (**1**) is rationalized in a similar way.[4]

The equalization under free bond rotation is equivalent to considering CH_3* where * denotes a chiral proligand. This hypothetical promolecule belongs to C_3 symmetry. Hence, the carbon atom constructs a $C_3(/C_3)$ orbit. By using the C_3 local symmetry in place of the C_1, we have $C_{3v}(/C_s)\downarrow C_3=C_3(/C_1)$ for the three protons. This equation means the equality of the three protons under free bond rotation.

4. CH_2X Segments in Various Molecules

Global Orbits and Local Orbits for CH_2X Segments. Suppose that A's of **3** to **15** are replaced by CH_2X ligands in place of methyl ligands described in the preceding section. The two protons of the CH_2X ligand construct an infraorbit governed by $C_s(/C_1)$. Table 4 collects the results of applying Theorems 2 and 3 to the present cases, where only orbits of the two protons are listed.

Table 5 lists the subduction of CRs for C_s point group. These data control restrictions of ligand symmetries, as collected in the local-orbit column of Table 4. The resulting global orbits are also collected in Table 4.

The case of **33** should be mentioned in contrast with **21**.[23] Although they are derived from the same promolecule (**3**), they are different in their resulting symmetries. Since the condition $\mathbf{F} \gtrdot \mathbf{G}_i$ is true for the case of the methyl ligands applied to **3**, Theorem 2

Table 4. Local Orbits and Global Orbits in **3**—**15** Substituted by CH_2X Ligands

Molecule	Structure	CR for ligands[a]	Local orbits	Global orbits
33	**3** (A=CH_2X)	$\mathbf{D}_{2d}(/\mathbf{C}_s)$*	$\mathbf{C}_s(/\mathbf{C}_1)$	$\mathbf{D}_{2d}(/\mathbf{C}_1)$
34	**4** (A=CH_2X)	$\mathbf{D}_{2d}(/\mathbf{C}_s)$	$\mathbf{C}_s(/\mathbf{C}_1)$	$\mathbf{D}_{2d}(/\mathbf{C}_1)$
35	**5** (A=CH_2X)	$\mathbf{C}_s(/\mathbf{C}_s)$*	$\mathbf{C}_s(/\mathbf{C}_1)$	$\mathbf{C}_s(/\mathbf{C}_1)$
36	**6** (A=CH_2X)	$\mathbf{C}_{3v}(/\mathbf{C}_s)$	$\mathbf{C}_s(/\mathbf{C}_1)$	$\mathbf{C}_{3v}(/\mathbf{C}_1)$
37	**7** (A=CH_2X)	$\mathbf{C}_{3v}(/\mathbf{C}_1)$	$2\mathbf{C}_1(/\mathbf{C}_1)$	$2\mathbf{C}_{3v}(/\mathbf{C}_1)$
38	**8** (A=CH_2X)	$\mathbf{D}_2(/\mathbf{C}_1)$	$2\mathbf{C}_1(/\mathbf{C}_1)$	$2\mathbf{D}_2(/\mathbf{C}_1)$
39	**9** (A=CH_2X)	$\mathbf{C}_{2v}(/\mathbf{C}_s)$	$\mathbf{C}_s(/\mathbf{C}_1)$	$\mathbf{C}_{2v}(/\mathbf{C}_1)$
40	**10** (A=CH_2X)	$\mathbf{S}_4(/\mathbf{C}_1)$	$2\mathbf{C}_1(/\mathbf{C}_1)$	$2\mathbf{S}_4(/\mathbf{C}_1)$
41	**11** (A=CH_2X)	$\mathbf{C}_1(/\mathbf{C}_1)$*	$2\mathbf{C}_1(/\mathbf{C}_1)$	$2\mathbf{C}_1(/\mathbf{C}_1)$
42	**12** (A=CH_2X)	$\mathbf{C}_3(/\mathbf{C}_1)$	$2\mathbf{C}_1(/\mathbf{C}_1)$	$2\mathbf{C}_3(/\mathbf{C}_1)$
43	**13** (A=CH_2X)	$\mathbf{C}_s(/\mathbf{C}_s)$	$\mathbf{C}_s(/\mathbf{C}_1)$	$\mathbf{C}_s(/\mathbf{C}_1)$
44	**14** (A=CH_2X)	$\mathbf{C}_s(/\mathbf{C}_1)$	$2\mathbf{C}_1(/\mathbf{C}_1)$	$2\mathbf{C}_s(/\mathbf{C}_1)$
45	**15** (A=CH_2X)	$\mathbf{C}_2(/\mathbf{C}_1)$	$2\mathbf{C}_1(/\mathbf{C}_1)$	$2\mathbf{C}_2(/\mathbf{C}_1)$

a) The structure marked by an asterisk is desymmetrized in a mismatched fashion.

Table 5. Subduction of Coset Representations $\mathbf{C}_s$ Group

Coset representation	Subduction	
	$\downarrow\mathbf{C}_1$	$\downarrow\mathbf{C}_s$
$\mathbf{C}_s(/\mathbf{C}_1)$	$2\mathbf{C}_1(/\mathbf{C}_1)$	$\mathbf{C}_s(/\mathbf{C}_1)$
$\mathbf{C}_s(/\mathbf{C}_s)$	$\mathbf{C}_1(/\mathbf{C}_1)$	$\mathbf{C}_s(/\mathbf{C}_s)$

indicates that the symmetry ($\mathbf{T}_d$) of **3** retains in **21**. On the other hand, the condition is not satisfied in the substitution of CH_2X ($\mathbf{C}_s$ symmetry), since $\mathbf{F}=\mathbf{C}_s$ and $\mathbf{G}_i=\mathbf{C}_{3v}$. Hence, the symmetry of **3** is restricted into $\mathbf{D}_{2d}$ so as to satisfy the conditions $\mathbf{F} \gtrdot \mathbf{G}_i$ (i.e., $\mathbf{F}=\mathbf{G}_i=\mathbf{C}_s$).[24] This restriction produces **33** of $\mathbf{D}_{2d}$ symmetry, for which Theorem 2 holds. The cases of **35** and **41** (marked with an asterisk in Table 4) are explained in a similar way.

Anisochrony in CH_2X Ligands. Two methylene protons in a CH_2X ligand (fragment) construct a $\mathbf{C}_s(/\mathbf{C}_1)$ orbit. Since this infraorbit is enantiospheric, the two protons are equivalent in isolation; they coincide with each other by improper rotations only, not by proper rotations. Under *any* chiral environment, they are split to construct two hemispheric orbits in terms of Theorem 1. The chiral environment required in Theorem 1 may come from a local symmetry. From the data of Table 4 (the CR-for-ligand column), we can select **37**, **38**, **40**, **41**, **42**, **44**, and **45** as examples of such chiral local symmetries. Note that **37**, **40**, and **44** are achiral; on the other hand, **38**, **41**, **42**, and **45** are chiral. The restriction of such a CH_2X ligand is expressed by the subduction,

$$\mathbf{C}_s(/\mathbf{C}_1)\downarrow\mathbf{C}_1 = 2\mathbf{C}_1(/\mathbf{C}_1), \quad (5)$$

which is selected from Table 5. The two members of the $\mathbf{C}_s(/\mathbf{C}_1)$ orbit are presumed to coincide with each other only by a reflection concerning a mirror plane, if they are isolated hypothetically. However, since they are restricted to the $\mathbf{C}_1$ local symmetry in terms of Eq. 5, they are not superposed even if a free rotation is permitted. Thus, these molecules are predicted to show anisochronies of the geminal protons.

Anisochrony of $XYC(CU_2R)_2$ is obviously ascribed to the same effect as operating in **44**; $RU_2C\text{-}CX_3^*$ is explained in the same line as **41**; and anisochrony of $(RU_2C)_3C\text{-}CXYZ$ is equivalent to that of **42**. Other cases can be rationalized by the same rule. Some of these examples have once been discussed in terms of "intrinsic assymetry".[9] However, Reisse et al.[11] have concluded that continued use of the term is no longer justified. The present analysis strengthens their conclusion; but has an advantage over their method. While the Reisse method requires internal and external comparison for determining diastereotopism, the present method does not require such operations that are based on stereoisomerism; in other words, stereochemical non-equivalence (diastereotopism) is ascribed to membership of distinct orbits.

To the best of our knowledge, such anisochrony has never been reported that concerns four or more CH_2X ligands, probably because there have existed no methods effective to design complicated cases. The present method is capable of predicting anisochronies of such complicated compounds. Experimental verification will be challenging and is open to further investigation.

5. Criteria for Judging Symmetry Equivalence and Non-Equivalence

Our principal idea is here restated as follows: When a fragment is incorporated in a molecule, the CR of its infraorbit is restricted to the corresponding local symmetry; the restriction is represented by a subduction of the CR to the local symmetry. This idea has been exemplified by the discussions in the preceding sections. Thereby, it is generalized in the form of the following criteria.

a) Suppose that, in Theorem 3, the $\mathbf{F}(/\mathbf{F}_p)$ infraorbit is homospheric (for example, in a methyl ligand). The local symmetry $\mathbf{F}_q$ may be achiral or chiral.

- If $\mathbf{F}(/\mathbf{F}_p)\downarrow\mathbf{F}_q$ produces a subdivision of the $\mathbf{F}(/\mathbf{F}_p)$ in terms of Eq. 1, the nuclei in the $\mathbf{F}(/\mathbf{F}_p)$ infraorbit are capable of exhibiting anisochrony due to $\mathbf{F}(/\mathbf{F}_p)\downarrow\mathbf{F}_q$. This anisochrony is observed at such a low temparature as affording slow bond rotations on the NMR time scale; otherwise, it exhibits an average chemical shift.
- If $\mathbf{F}(/\mathbf{F}_p)\downarrow\mathbf{F}_q$ provides no subdivision, there emerges no anisochronies.

b) Suppose that, in Theorem 3, an $\mathbf{F}(/\mathbf{F}_p)$ infraorbit is enantiospheric (for example, in a CH_2X ligand) and that the local symmetry $\mathbf{F}_q$ is achiral. The conclusion for the case a) holds for this case.

c) Suppose that, in Theorem 3, an $\mathbf{F}(/\mathbf{F}_p)$ infraorbit is enantiospheric (for example, in a CH_2X ligand) and

that the local symmetry $\mathbf{F}_q$ is chiral. Equation 1 provides the splitting of the enantiospheric orbit so as to yield two hemispheric orbits. Since this splitting is inherent, split signals can be observed with no respect to the NMR time scale.

These criteria indicate guidelines for determining anisochronies of nuclei; more detailed discussions should be based on concrete forms of SRs. In order to show the scope of these criteria, we examine more complicated molecules (**47**—**49**). The corresponding promolecule (**46**) has a $\mathbf{T}_h(/\mathbf{C}_3)$ orbit that consists of A_8. Since this orbit is enantiospheric, these eight A's are capable of splitting into two 4-membered hemispheric orbits (A_4^a and A_4^b) under an external chiral condition (Theorem 1).

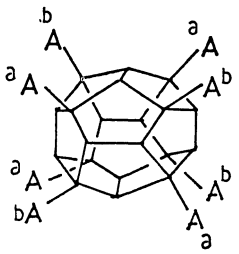

46 A=proligand
47 A=CH_3
48 A= 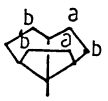
49 A=CH_2OH $\mathbf{D}_{2h}$

The local symmetry of the proligands (A's) is $\mathbf{C}_3$ (chiral) in **46**. The $\mathbf{C}_3$ point group is a subgroup of the $\mathbf{C}_{3v}$ group of a methyl fragment. Hence, when each A is replaced by a methyl ligand, the resulting molecule (**47**) retains $\mathbf{T}_h$ symmetry. The incorporated methyl segment is restricted to the local symmetry in terms of

$$\mathbf{C}_{3v}(/\mathbf{C}_s)\downarrow\mathbf{C}_3=\mathbf{C}_3(/\mathbf{C}_1). \tag{6}$$

This equation indicates that, under any condition, there occurs no splitting of three protons in each methyl segment. In contrast with this, the methyl symmetry is lowered from $\mathbf{C}_{3v}$ to $\mathbf{C}_3$. This effect results in splitting of 8 methyl segments into two sets of equivalent methyl segments (A_4^a and A_4^b in **47**; A=CH_3) under an external chiral condition (e,g., by the action of a chiral shift reagent).

When a ligand has an enantiospheric $\mathbf{C}_{3v}(/\mathbf{C}_1)$ infraorbit as shown in **48**, the criterion c) is satisfied. Thus, we obtain

$$\mathbf{C}_{3v}(/\mathbf{C}_1)\downarrow\mathbf{C}_3=2\mathbf{C}_3(/\mathbf{C}_1). \tag{7}$$

This equation is selected from the $\mathbf{C}_{3v}(/\mathbf{C}_1)$ row of Table 2. Equation 7 means that we can observe two ^{13}C signals for methylene carbons (C_3^a and C_3^b) independent of temperature, if this splitting provides chemical shifts different enough to determine. Experimental verification regarding such a general type of anisochronies predicted here is open to further investigation.

When the same ligand as for **48** is incorporated in **3** ($\mathbf{T}_d$ symmetry), the resulting molecule exhibits a different nature. Since the local symmetry is $\mathbf{C}_{3v}$ (Table 1), the ligand suffers no restriction, i.e., $\mathbf{C}_{3v}(/\mathbf{C}_1)\downarrow\mathbf{C}_{3v}=\mathbf{C}_{3v}(/\mathbf{C}_1)$. Hence, there emerges no anisochrony. If this ligand is applied to any one of the promolecules listed in Fig. 1, its respective behavior can be explained by the $\mathbf{C}_{3v}(/\mathbf{C}_1)$ row of Table 2.

The criterion c) determines the fate of enantiospheric infraorbits incorporated into a chiral local symmetry in any case. When the achiral proligand (A) is substituted by CH_2X, the resulting molecule (**49**) no longer retains $\mathbf{T}_h$ symmetry; but is restricted to $\mathbf{D}_{2h}$ symmetry. Since the $\mathbf{C}_s$ symmetry of CH_2X is incompatible with the local symmetry ($\mathbf{C}_3$) of **46**, this desymmetrization occurs so that the local symmetry is created by $\mathbf{C}_3\cap\mathbf{C}_s=\mathbf{C}_1$. According to this restriction, the original $\mathbf{T}_h(/\mathbf{C}_3)$ orbit is converted into $\mathbf{D}_{2h}(/\mathbf{C}_1)$ orbit.[25] Note that the length of the $\mathbf{T}_h(/\mathbf{C}_3)$ orbit ($|\mathbf{T}_h|/|\mathbf{C}_3|=24/3=8$) is equal to that of the $\mathbf{D}_{2h}(/\mathbf{C}_1)$ orbit ($|\mathbf{D}_{2h}|/|\mathbf{C}_1|=8/1=8$). As a result, the resulting molecule (**49**) of the $\mathbf{D}_{2h}$ global symmetry exibits a $\mathbf{C}_1$ local symmetry at the $\mathbf{D}_{2h}(/\mathbf{C}_1)$ orbit. Thereby, the CH_2X ligand is controlled by

$$\mathbf{C}_s(/\mathbf{C}_1)\downarrow\mathbf{C}_1=2\mathbf{C}_1(/\mathbf{C}_1), \tag{8}$$

which is selected from the $\mathbf{C}_s(/\mathbf{C}_1)$ row of Table 5. This equation satisfies the criterion c); hence, the two protons of the CH_2X in **49** show anisochrony independent of NMR time scale. The corresponding global orbits are concluded to be $2\mathbf{D}_{2h}(/\mathbf{C}_1)$ in terms of Theorem 3. It is important to recognize that such an enantiosphericity of an infraorbit is by no means referred to as "prochirality". The prochirality should concern the enantiosphericity of a global orbit or of its equivalents.

6. Conclusion

A ligand is chracterized as a fragment when isolated and as a segment when incorporated in a molecule. The symmetry of the ligand-in-isolation (fragment) is restricted into the symmetry of the ligand-in-molecule (segment) in accord with the local symmetry of the molecule. As a result, any orbit in the ligand (an infraorbit) is restricted into local orbits. The relationship between such local orbits and global orbits is discussed in terms of subduction of coset representations. This discussion provides a general approach to rationalize various types of anisochronism.

References

1) K. Mislow and J. Siegel, *J. Am. Chem. Soc.*, **106**, 3319 (1984).

2) K. Mislow and M. Raban, *Top. Stereochem.*, **1**, 1 (1967).

3) Convensional usages of the terms "isochrony" and "anisochrony" have been criticized by Fulea.[26] However, his criticism proves to be simply based on the difference between his definition and the convensional one. According to his

definition, the terms are used to refer to a relationship between *states* of two nuclei; hence, any nuclei can be isochronous under one condition and anisochronous under another condition. On the other hand, the terms are conventionally used to refer to a relationship between *properties* (attributes) of two nuclei, though this standpoint has never been mentioned explicitly. Our usage in the present paper restates such an convensional usage more explicitly: Isochronous (chemical-shift equivalent) nuclei are defined as the ones that exhibit equal chemical shifts independent of any environments; anisochronous (chemical-shift non-equivalent) nuclei are defined as the ones that exhibit different chemical shifts but are capable of showing equal chemical shifts under an appropriate condition.

4) M. Nakamura, M. Ōki, H. Nakanishi, and O. Yamamoto, *Bull. Chem. Soc. Jpn.*, **47**, 2415 (1974).

5) J. E. Anderson and D. I. Rawson, *J. Chem. Soc., Chem. Commun.*, **1973**, 830.

6) a) R. M. Silverstein, G. C. Bassler, and T. C. Morrill, "Spectrometric Identification of Organic Compounds," 4th ed, John-Wiley & Sons, New York (1981), p. 201; b) A. Raman, "Nuclear Magnetic Resonance," Springer-Verlag, New York-Berlin-Heidelbelg (1986); c) T. H. Siddall and W. E. Stewart, *Prog. Nucl. Magn. Reson. Spectros.*, **5**, 33 (1969).

7) W. B. Jenning, *Chem. Rev.*, **75**, 307 (1975).

8) K. R. Hanson, *J. Am. Chem. Soc.*, **88**, 2731 (1966).

9) E. L. Eliel, *Top. Curr. Chem.*, **105**, 1 (1982).

10) G. R. Franzen and G. Binsch, *J. Am. Chem. Soc.*, **95**, 175 (1973).

11) J. Reisse, R. Ottinger, P. Bickart, and K. Mislow, *J. Am. Chem. Soc.*, **100**, 911 (1978).

12) a) S. Fujita, *Theor. Chim. Acta*, **76**, 247 (1989); b) S. Fujita, *Bull. Chem. Soc. Jpn.*, **62**, 3771 (1989); c) S. Fujita, *Bull. Chem. Soc. Jpn.*, **63**, 203 (1990); d) S. Fujita, *Tetrahedron*, **46**, 365 (1990); e) S. Fujita, *J. Math. Chem.*, **5**, 99 (1990); f) S. Fujita, *Bull. Chem. Soc. Jpn.*, **63**, 1876 (1990); g) S. Fujita, *Bull. Chem. Soc. Jpn.*, **63**, 2033 (1990).

13) S. Fujita, *Bull. Chem. Soc. Jpn.*, **63**, 315 (1990).

14) S. Fujita, *J. Am. Chem. Soc.*, **112**, 3390 (1990).

15) S. Fujita, *Theor. Chim. Acta*, **77**, 307 (1990).

16) We here use the term "ligand" in place of "group", since the latter chemical term may be confused with the mathematical "group" of group theory.

17) V. Prelog, *Science*, **193**, 17 (1976).

18) S. Fujita, *Tetrahedron*, **47**, 31 (1991).

19) The selection of a skeleton depends upon the purpose of our discussion. For example, adamantane ($C_{10}H_{16}$) itself can be selected to generate a skeleton, $C_{10}\pi_{16}$, where π denotes a substitution position. Thereby, the promolecule (**10**) is produced as a result of an $H_8F_4A_4$ substitution; on the other hand, the promolecule (**14**) comes from an $H_{13}FA_2$ substitution. In these processes, the original symmetry ($\mathbf{T}_d$) of the skeleton is restricted to $\mathbf{S}_4$ for **10** and to $\mathbf{C}_s$ for **14**. When we further replace the A's by ligands, we can start from such proligands as having $\mathbf{S}_4$ and $\mathbf{C}_s$ symmetries. If we do not introduce the concept of promolecule, we should go back to the original $\mathbf{T}_d$ symmetry in every examination. This is the reason for introducting the concept of promolecule in additon to the concept of skeleton.

20) For a concrete form of the CR, see Ref. 12.

21) The term "(imprimitive) block" used Ref. 14 denotes a geometical object that meets mathematical requirements only; hence, such a block is not always equivalent to a ligand. On the other hand, the term "segment" used in this paper designates a ligand-in-molecule, which has a chemical meaning as well as a mathematical one. In other words, a segment is a set of blocks selected so as to possess a chemical meaning.

22) W. H. Pirkle, S. D. Beare, and R. L. Muntz, *J. Am. Chem. Soc.*, **91**, 4575 (1969).

23) The molecules with an asterisk are called mismatched molecules, since the condition $\mathbf{F} \geqslant \mathbf{G}_i$ is not true for these cases. On the other hand, molecules satisfying this condition are called matched molecules. More detailed discussions is reported in Ref. 18.

24) This desymmetrization can be discussed in terms of a subduction table of $\mathbf{T}_d$.[14] It corresponds to the subduction: $\mathbf{T}_d(/\mathbf{C}_{3v})\downarrow\mathbf{D}_{2d}=\mathbf{D}_{2d}(/\mathbf{C}_s)$.

25) This desymmetrization can be expressed by $\mathbf{T}_h(/\mathbf{C}_3)\downarrow\mathbf{D}_{2h}=\mathbf{D}_{2h}(/\mathbf{C}_1)$. A subduction table for $\mathbf{T}_h$ will be reported elsewhere.

26) A. O. Fulea, *Rev. Roum. Chim.* **33**, 39 (1988).

Ion-Exchange Reaction on Cubic Ammonium Molybdate in Acidic and Alkaline Media—Exchange of Structural NH_4^+

Abdul Jabbar KHAN, Mitsuo ABE,* Yasushi KANZAKI, and Masamichi TSUJI
Department of Chemistry, Faculty of Science, Tokyo Institute of Technology,
2-12-1 Ookayama, Meguro-ku, Tokyo 152
(Received July 6, 1990)

The alkali metal ion exchange reaction on cubic ammonium molybdate (CAM) cation exchanger was studied in acidic as well as alkaline media. The ion-exchange reaction and TPD-Mass thermogram of CAM indicated the presence of structural NH_4^+ as interstitial solid solution. The stuctural NH_4^+ in the H^+ form of CAM (H-CAM) was efficiently exchanged with K^+ as compared with other alkali metal ions in the equilibrated solutions. The exchanger was observed to be stable in acid medium, however structural transformations were observed at high pH. The presence of K^+ and Cs^+ at high pH could act as "Structure Building Ions" for CAM or H-CAM.

The ammonium or alkali metal tungstates have been reported by different authors.[1,2] Such type of materials are of interest because of their conductor properties with high ionic mobility due to existence of atomic sized tunnels within their crystal structure. The ionic mobility of NH_4^+ in ammonium tungstate investigated through NMR study, has been reported by Clark et al.[3] The existence of alkali metal ions (e.g. Rb^+) in tunnel structures of niobium and tantalum oxides have been discussed by Fallon and Gatehouse.[4]

The isopolymolybdates contain zigzag rows of MoO_6 octahedra which share corners in two directions forming MoO_4^{2-} layers.[5,6] The interstices of these layers provide channels for transport of cations (monovalent ions). These cations exist as solid solution in metal oxide structure.[7] The displacement of NH_4^+ or exchange of alkali ions (especially K^+) with NH_4^+ in heteropolyacid salts has been extensively reviewed by Amphlett[8] and Clearfield et al.[9] However less interest has been devoted to the study of mobility or transport of cations (e.g. NH_4^+) in the tunnel structure of molybdenum oxides, particularly through ion-exchange investigations.

The synthesis, characterization, and ion-exchange behavior of CAM along with the chromatographic separations of alkali metal ions have already been reported.[10,11] The present work was carried out to investigate the ion-exchange process of structural NH_4^+ in H-CAM through the maximum exchange capacity for alkali metal ions with respect to the crystal system of H-CAM. Ion-exchange equilibria, thermal analyses and X-ray diffractometry were employed for these investigations.

Experimental

Reagents. All the reagents used were analytical grade chemicals of Wako Pure Chemical Ind., Japan. Rubidium hydroxide and cesium hydroxide solutions were prepared through anion-exchange reaction by eluting the corresponding metal chloride solution through a column of Dowex 2-X8 anion exchanger in OH^- form. The N_2 gas was incorporated to avoid the CO_2 contamination in the resulting solutions.

Preparation of CAM and Conversion to H-CAM and A-CAM The cubic ammonium molybdate (CAM) $[(NH_4)_{0.78}(NH_4)_2]O_{1.39}\cdot 14.16MoO_3\cdot 6.08H_2O$ cation exchanger was prepared by the reaction of hexaammonium heptamolybdate and HNO_3 at 60 ±0.5 °C following the previously reported procedure.[10] CAM was converted to its H^+ form (H-CAM) $[(H)_{0.68}(NH_4)_2]O_{1.34}\cdot 14.16MoO_3\cdot 6.92H_2O$ by conditioning with 0.5 mol dm^{-3} HNO_3, using a column. H-CAM (100—200 mesh) was used throughout this work unless otherwise stated. The H-CAM when conditioned with 0.5 mol dm^{-3} NH_4NO_3 solution was converted to NH_4^+-form (A-CAM) $[(NH_4)_{0.68}(NH_4)_2]O_{1.34}\cdot 14.16MoO_3\cdot 5.26H_2O$.

X-Ray Diffractions. X-ray diffractions were taken with a JEOL JDX-7E and a Rigaku Denki Co. (Japan), model CN-5320 A-1/CN-2155 D-5 X-ray diffractometers. The crystal structures were deduced by using SANDMAN computer programs.[12—14]

Thermal Analyses and TPD-Mass Spectra. A Rigaku Denki Thermoflex, model 8001, was used for thermogravimetry (TG) and differential thermal analysis (DTA) at a heating rate of 10 °C min^{-1} using α-Al_2O_3 as a reference material.

The Temperature Programmed Desorption-Mass (TPD-Mass) spectrometry for investigating the desorption of structural ammonia and water in H-CAM was performed on a Quadrupole Mass Analyser MSQ-300 ULVAC. The sample was heated in an evacuated tube in the heating system provided with the said analyzer, at the same heating rate mentioned above. Each component was determined under an appropriate mass number. An adequate quantity of NH_3-gas was used as a reference for the investigation of ammonia in H-CAM.

Ion Selectivity, Maximum Exchange Capacity, and pH Titration. The distribution coefficients (K_d) were determined batchwise by equilibrating H-CAM (0.1 g) with 10 cm^3 solutions of 10^{-4} mol dm^{-3} alkali metal ions in different concentrations of HNO_3 at 30±0.5 °C with intermittent shaking.

The maximum exchange capacity for alkali metal ions on H-CAM was determined by batch experiment using 0.1 mol dm^{-3} MNO_3 (M=Li^+, Na^+, K^+, Rb^+, or Cs^+) solution in

10^{-4} mol dm^{-3} HNO_3. H-CAM (0.25 g) was equilibrated at 30±0.5 °C by the successive addition of each 25 cm^3 of the above solution, till no further uptake of respective metal ion. Similarly the topotactic K^+/NH_4^+ exchange was investigated by equilibrating A-CAM with KNO_3 solution.

The pH titration experiments were conducted by equilibrating H-CAM (0.1 g) with 10 cm^3 solution of a constant ionic strength of 0.1, containing different ratios of MNO_3/MOH or NH_4NO_3/NH_3 aq, at 30±0.5 °C with intermittent shaking.

The pH of the supernatant solutions were determined by a Toa Dempa HM-5B pH meter, the metal ion concentrations by an atomic absorption spectrophotometer, NH_4^+ by Nessler's method and the Mo(VI) cocentration by an Inductively Coupled Plasma (ICP) Spectrometer SPS-7000, Seiko Instruments, Japan.

Results and Discussion

Characteristics of CAM. The X-ray diffraction patterns, IR-spectra, and thermal analysis for CAM and H-CAM or A-CAM were observed to be the same as reported.[10] A-CAM was observed to possess two types of NH_4^+, the H^+-exchangeable NH_4^+ (EA-NH_4^+) and structural NH_4^+ (SA-NH_4^+). A reversible NH_4^+/H^+ exchange reaction was also studied on H-CAM.[10] However the present study showed that beside EA-NH_4^+, H-CAM was capable of exchanging SA-NH_4^+ too, with different selectivity for alkali metal ions. Hence A-CAM showed to possess two types of exchange sites i.e. H^+-exchangeable NH_4^+-site (EA-site) and structural NH_4^+-site (SA-site).

Selectivity of Alkali Metal Ions. The log-log plot (Fig. 1) of K_d vs. [HNO_3] was linear with a slope of −1 indicating an ideal ion-exchange reaction for all alkali metal ions except K^+. The selectivity sequence was observed to be $Cs^+>Rb^+>K^+>Na^+>Li^+$, in proportion to the increasing order of ionic radii (Table 1). The slope for K^+ was >−1 showing greater uptake irrespective of increase in HNO_3 concentration. These observations indicated that even though the exchange reaction for alkali metal ions at low metal ion concentration (i.e. 10^{-4} mol dm^{-3}) was preferred at EA-site, K^+ was more selective for SA-site (the release of NH_4^+ to the equilibrated solution by the uptake of K^+ was the experimental evidence for the exchange reaction).

TPD-Mass Spectroscopy. The TPD-Mass analysis (Fig. 2) showed two step loss of ammonia (solid-line peaks) and water (dashed-line peaks). The peaks around 120 °C indicated the loss of adsorbed ammonia and water on H-CAM, whereas the peaks at 200—350 °C corresponded to the presence of structural NH_4^+ and H_2O. Two peaks for structural H_2O were

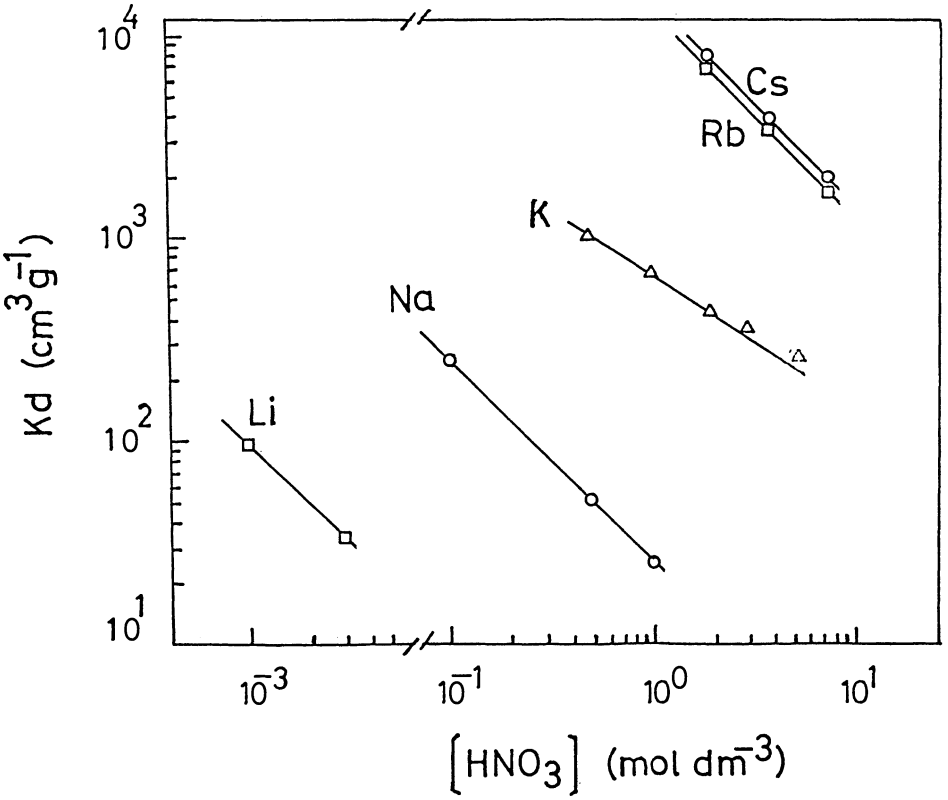

Fig. 1. Distribution coefficients for alkali metal ions on H-CAM as a function of HNO_3 concentration.
H-CAM: 0.10 g, Init. [M^+]: 10^{-4} mol dm^{-3}, Soln. Vol.: 10 cm^3, Temp.: 30 ±0.5 °C.

Table 1. Maximum Ion-Exchange Capacity of Alkali Metal Ions Equilibrated at pH<4 and the Lattice Constant (a) of H-CAM (a=12.94 Å) after Metal Ions Uptake

Ions	r_{eff}[a]	r_{hyd}[c]	Max capacity	Lattice const (a)
	Å	Å	±0.005 mequiv g^{-1}	Å
Li^+	0.59	3.7	0.15	12.939
Na^+	0.99	3.3	0.70	12.965
K^+	1.37	2.5	1.21	12.915
Rb^+	1.52	>2.4	1.05	12.920
Cs^+	1.67	2.4	0.95	12.950
NH_4^+	1.61[b]	2.5	0.31	—
H_3O^+	1.45[c]	2.85	—	—

a) Ref. 18. b) Ref. 19. c) From Stokes radii or Ref. 20.

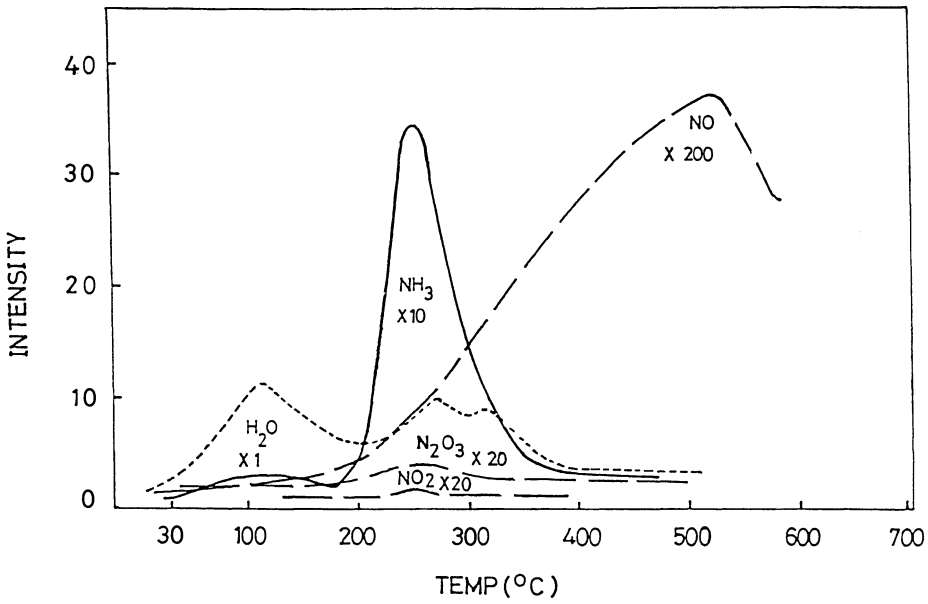

Fig. 2. The TPD-Mass thermogram of H-CAM.
H-CAM: 0.0053 g; Heating: 10 °C min^{-1}; B. K. Press: 4×10^{-7} Torr (1 Torr =133.322 Pa); Init. Intensity: 20×10^{-8} (NH_3 m/z=17), 20×10^{-7} (H_2O m/z=18), 10×10^{-9} (NO m/z=30 and NO_2 m/z=46), 10×10^{-8} (N_2O_3 m/z=76); Heating atm.: vacuum.

observed at temperature >250 °C. The former peak indicated the loss of structural H_2O whereas the latter one stood for the H_2O formed as a result of oxidation of structural NH_4^+ by MoO_3 into NO_x (broken-line peaks). This fact was supported by change in color of the product to black by heating H-CAM upto 600 °C in TPD-Mass experiment. The increase in the NO-peak with the rise of temperature may be attributed to the desorption of the adsorbed nitrogen oxide on molybdenum oxide, in accordance with the observations of Schiavello et al, on WO_3.[15]

The coexistence of structural NH_4^+ and H_2O, made it clear that structural NH_4^+ might stay as an interstitial solid solution in H-CAM lattice. The structural H_2O is probably the water molecules coordinated to Mo(VI) within the layers as noticed by Kerbs,[16] forming the adsorption centers (exchange sites) for NH_4^+ (or K^+ etc.). These observations signified the probability of SA-site being active for K^+ uptake. The presence of intervening NH_4^+ and H_2O molecules have also been reported by Matsumoto et al.[17] in ammonium pentamolybdodisulfate trihydrate.

Ion Exchange Capacity and Thermal Analysis. The maximum ion exchange capacity on H-CAM for all alkali metal ions in HNO_3 medium, ionic radii, and lattice constants of metal ion-exchanged forms of H-CAM i.e. M-CAM (M=Li, Na, K, Rb, or Cs) are given in Table 1. The maximum exchange capacity of H-CAM was observed to be in the order $Li^+<Na^+<Cs^+<Rb^+<K^+$. The equivalents of NH_4^+ released were equal to the equivalents of metal ions uptaken. In the view of experimental maximum

exchange capacity for K^+, the theoretical capacity of H-CAM could be calculated equal to 1.2 mequiv g^{-1}.

The change in the lattice constant of H-CAM after metal ions uptake is shown in Table 1. Almost no change was indicated with the uptake of Li^+. An increase in the lattice constant (a) of H-CAM was observed in Na^+ and Cs^+ exchanged forms ($a_{Na} > a_{Cs} > a_{H\text{-}CAM}$), whereas decrease in lattice constant was indicated by the uptake of K^+ and Rb^+ ($a_K \leqslant a_{Rb} < a_{H\text{-}CAM}$). However no transformation of H-CAM was observed in acid medium. The ion-exchange reaction on H-CAM especially at SA-site

Table 2. Percent Water Contents of H-CAM and Its Metal Ions Exchanged Forms (M-CAM). Data Calculated from Thermogravimetric (TG) Analyses

Samples	H_2O Contents
	%
H-CAM	5.30
Li-CAM	5.58
Na-CAM	6.45
K-CAM	5.53
Rb-CAM	4.66
Cs-CAM	4.47

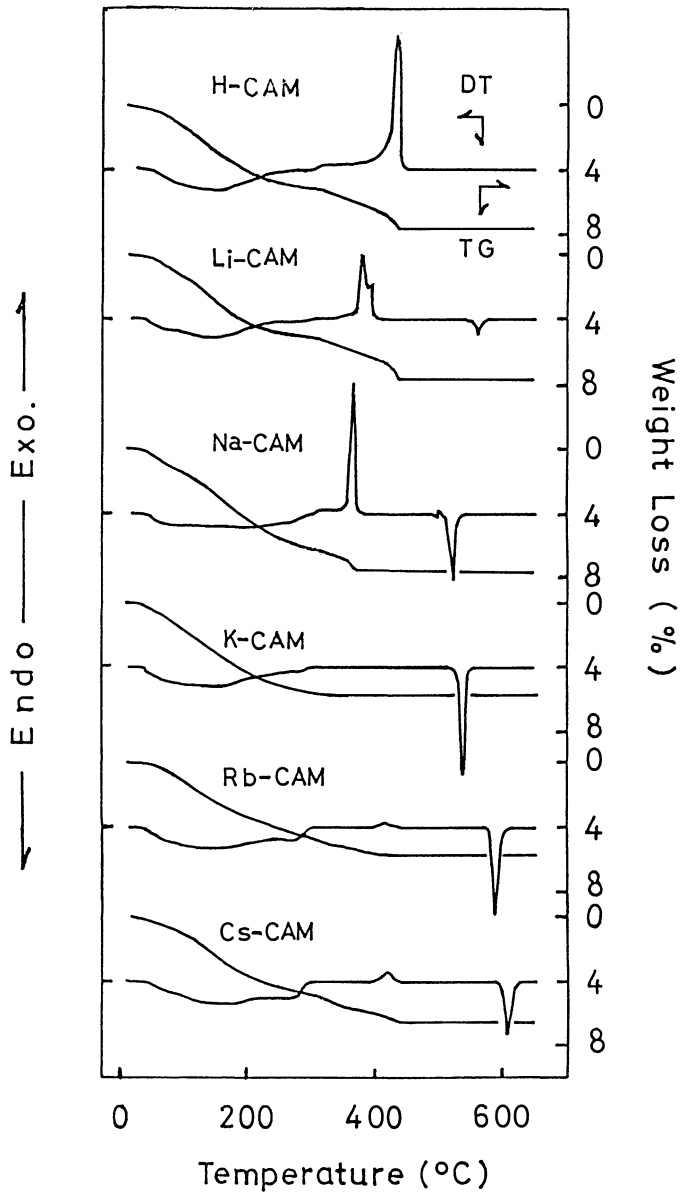

Fig. 3. The differential thermal (DT) and thermogravimetric (TG) curves of H-CAM and alkali metal ion-exchanged forms (M-CAM).
H-CAM or M-CAM: 0.0482 g; Heating: 10 °C min^{-1}; Heating atm.: ordinary.

seemed to be dependent on hydration of M^+ ions. The change in lattice with the uptake of M^+ ions may be attributed to the arrangement or size of hydration sphere (water molecules) around the respective ion in the tetrahedral layers (exchange sites). According to Diamond and Whitney,[21] the arrangement or size of the hydration sphere (water molecules) in the exchanger depends on the kind of metal ions.

Table 2 indicates the percent water contents of H-CAM and M-CAM samples. The water contents were observed to decrease in Rb and Cs forms (Cs-CAM<Rb-CAM<H-CAM) whereas increased in Li, Na, and K forms (Na-CAM>Li-CAM>K-CAM>H-CAM). The alteration (or arrangement) in the water contents brings alteration in the hydration sphere causing free energy (or entropy) changes which results in lattice change of the exchanger. The changes in water contents of M-CAM samples (Table 2) may correspond to the changes in water molecules of hydration sphere (at exchange site) brought about by the uptake of alkali metal ions on H-CAM. Greater free energy change caused by greater disturbance of hydration sphere resulted in greater change of lattice constants (e.g. a_{Na} and a_{Cs}).

The TG/DTA curves of H-CAM and M-CAM are shown in Fig. 3. The rise in DTA curve of H-CAM at >300 °C ending in a sharp exothermic peak at >430 °C indicated the existence of structural ammonia and

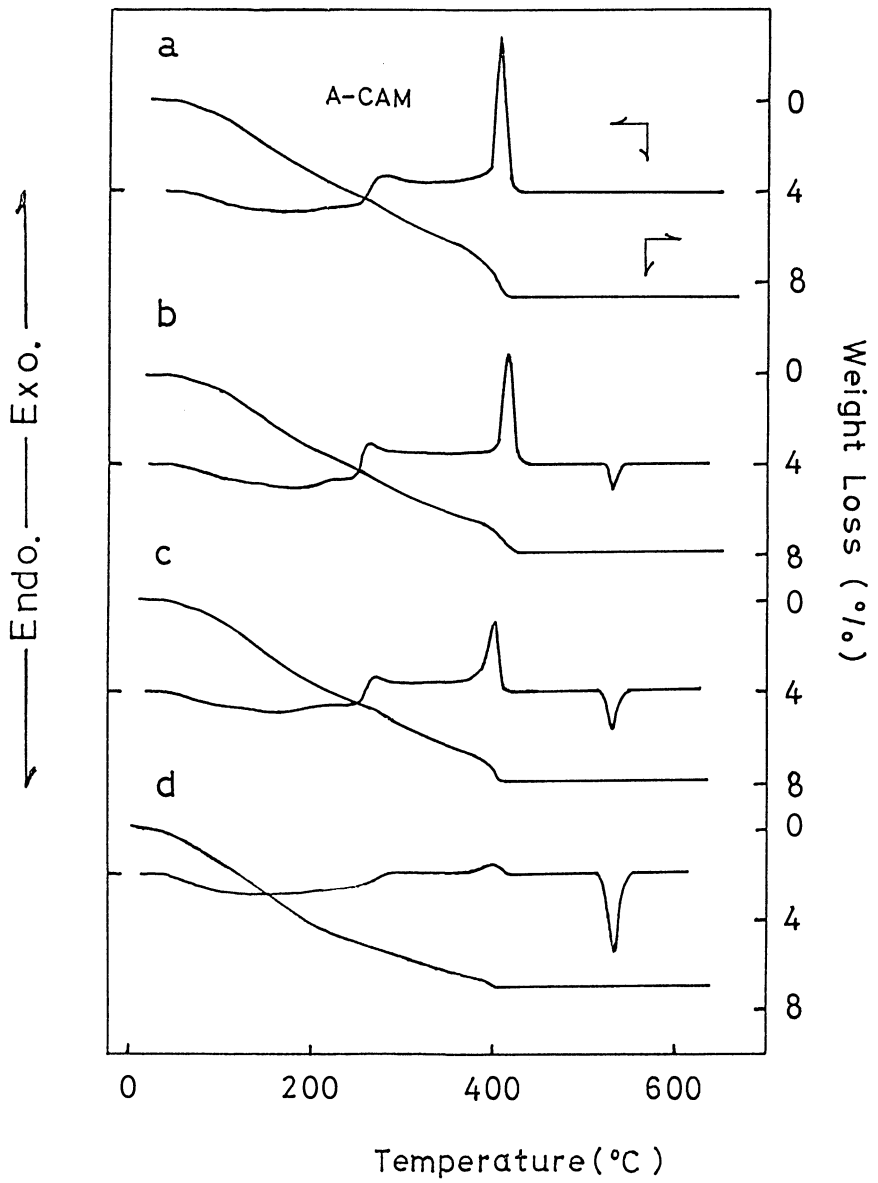

Fig. 4. The differential thermal (DT) and thermogravimetric (TG) curves of A-CAM (a) and K^+-exchanged forms (b—d) at different loadings. A-CAM: 0.0482 g K^+ mequiv g^{-1}: 0.2224 (b), 0.370 (c), 0.9760 (d); Heating: 10 °C min^{-1}; Heating atm.: ordinary.

water.[10] The DTA curves showed the presence of almost same ammonia contents of H-CAM in Li-CAM and Na-CAM indicating almost no exchange of structural ammonia (SA-NH_4^+) for Li^+ and Na^+ might be due to their selectivity preference for H^+-site or EA-site. In case of K^+ no exothermic peak due to structural ammonia was observed i.e. K^+ had replaced all the SA-NH_4^+ in H-CAM. This preference of K^+/NH_4^+ exchange was consistent with the selectivity of K^+ for SA-site in H-CAM. All of the NH_4^+ in H-CAM was not exchanged with Rb^+ and Cs^+ because of steric effect for their larger ionic radii. The very small exothermic peaks in DTA of Rb and Cs-CAM indicated the presence of unexchanged or remaining ammonia in H-CAM. The TG curves of the respective M-CAM were in accordance with the changes in DTA curves. The endothermic peaks in DTA curves at 500—620 °C indicated the fusion of M-CAM samples in the presence of alkali metal ions. No change in the TG curves was indicated at temperature >500 °C.

Exchange Sites and Metal Ion Uptake. The experimental results from K_d, maximum exchange capacity of alkali ions, and thermal analysis of M-CAM were in consistency for the exchange reaction at EA and SA-sites. Li^+ and Na^+ exchange reaction was favored at EA-site and K^+, Rb^+, and Cs^+ at SA-site in H-CAM. However to investigate the exchange reaction of K^+-Cs^+ at EA-site, the topotactic uptake of K^+ versus the apparent change in ammonia at EA/SA-sites was studied on A-CAM with different loadings of K^+. Figure 4a indicates the TG/DTA of A-CAM. The exothermic peaks at around 270 and 400 °C correspond to the loss of NH_4^+ at EA and SA-sites, respectively. Figure 4b,c indicated that the decrease in SA-NH_4^+ was proportional to the loading of K^+ at SA-site. However near the completion of K^+ uptake (maximum capacity), the exchange at both EA and SA-sites was favored (Fig. 4d). These results also provided an evidence for the discrepancy from slope −1 of K_d values for K^+. The cubic structure of both H-CAM and A-CAM was strictly retained after exchange of metal ions.

pH Titrations. The pH titration of H-CAM for alkali metal ions indicated apparently a monobasic acid, showing a large difference in blank and sample titration curves (Fig. 5). However dissolution of H-CAM occurred at pH >4.0 with a sharp increase in pH in NH_4NO_3/NH_3 aq medium. The equilibrium uptake of Li^+, Na^+, and NH_4^+ was observed to increase with increase in pH upto pH>4.0, whereas K^+, Rb^+, and Cs^+ showed a maximum uptake around

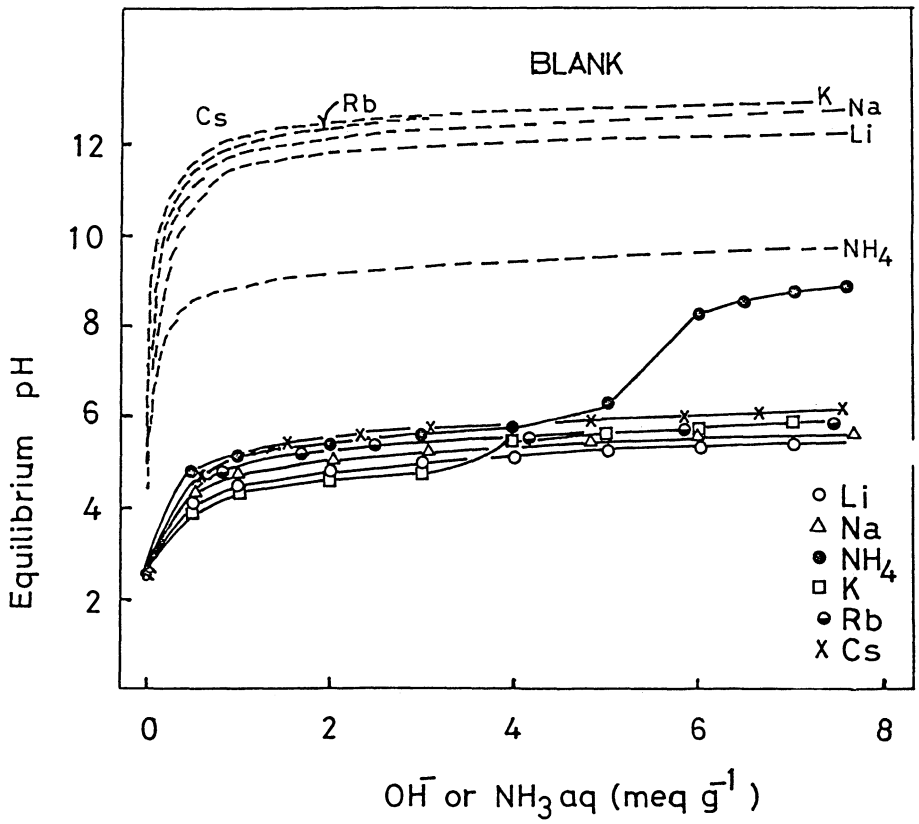

Fig. 5. pH titration curves of H-CAM.
H-CAM: 0.10 g; Soln vol.: 10.0 cm^3; Concn: 0.10 mol dm^{-3} (MCl+MOH) or (NH_4NO_3+NH_3 aq); Temp: 30±0.5 °C.

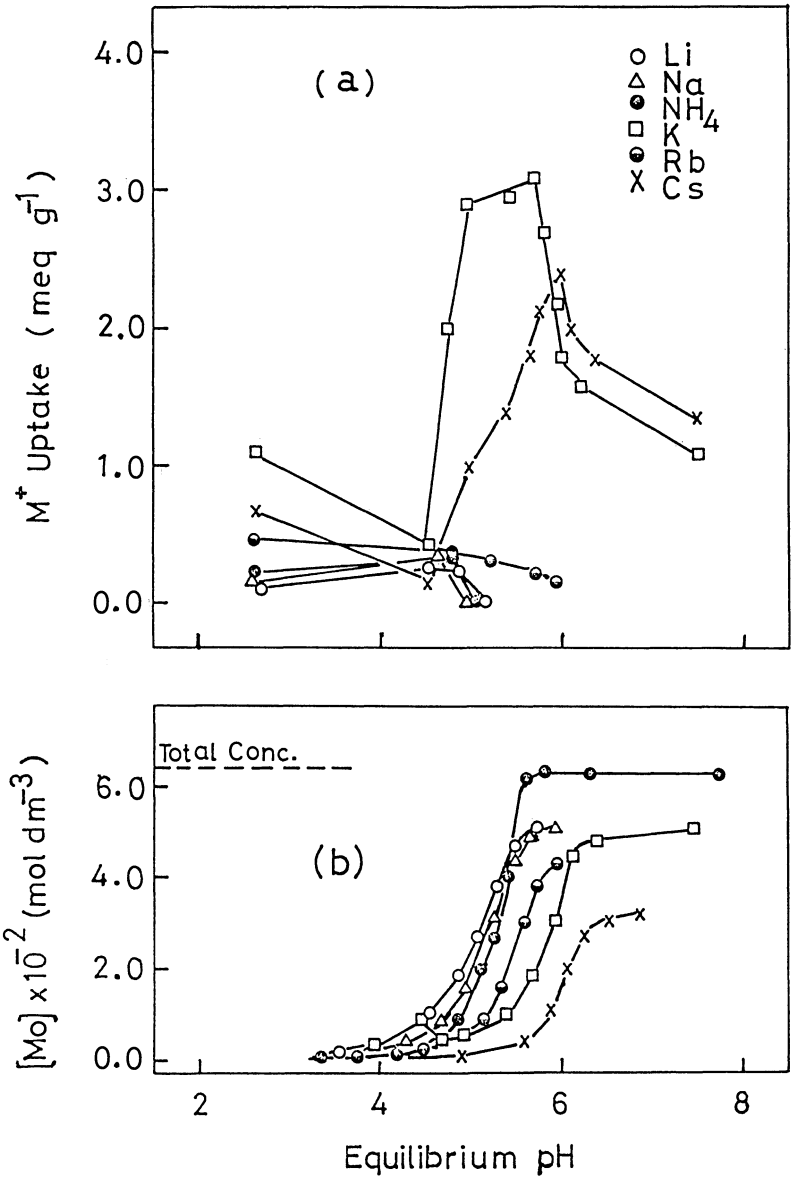

Fig. 6. Uptake of monovalent ions vs. equilibrium pH (a) and [Mo] in the supernatant solutions (b), after pH determination. H-CAM: 0.10 g; Soln vol: 10.0 cm^3; Concn: 0.10 mol dm^{-3} (MCl+MOH) or (NH_4NO_3+NH_3 aq); Temp: 30±0.5 °C.

pH 3 and decreased with increase in pH (Fig. 6a). The increase in the K^+ and Cs^+ uptake curves at pH>4.5 did not correspond to the uptake of these ions by H-CAM through ion-exchange reaction. Figure 6b indicates the dissolved amount of H-CAM {as [Mo(VI)]} in supernatant solutions at higher pH. The K^+ uptake (Fig. 6a) and [Mo(VI)] in the supernatant solutions (Fig. 6b) showed irregular curves with a break point around pH>4.5. The decrease in the K^+ uptake was due to the dissolution of H-CAM at high pH, however further increase in the uptake curve and an inflexion in the [Mo(VI)] curve at pH>4.5 indicated the complexation of K^+ with the dissolved H-CAM. The X-ray diffractions of the precipitates formed indicated the phase transformation of H-CAM to orthorhombic crystal system (with a totally different composition from H-CAM or K-CAM) at pH around 6.0 (Fig. 7). Almost similar observations were noticed for Cs^+ with a complete structural change to a triclinic form at pH around 6.17. The increase in amount (mequiv g^{-1}) of K^+ and Cs^+ (Fig. 6a) at pH>4.5 indicated the amount of these ions complexed with dissolved H-CAM (i.e. Mo(VI)) at higher pH. In the case of Li^+, Na^+, and Rb^+, no structural transformation or recomplexation was observed, though a slight change in the crystal lattice of H-CAM occurred after the uptake of metal ions, with no much difference in case of Rb^+ due to its

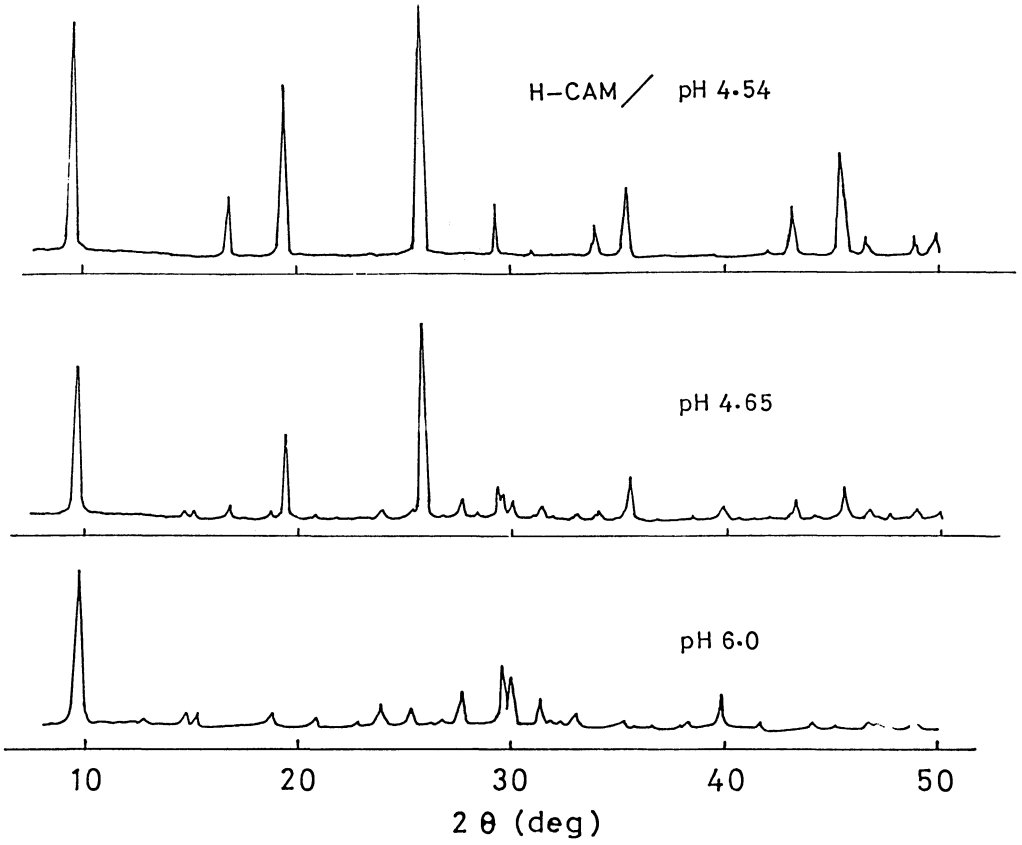

Fig. 7. X-Ray diffraction patterns indicating the pH dependent transformation of H-CAM to orthorhombic K-molybdenum oxide hydrate (KMO) formed (at pH 6.0) during the pH-titration of H-CAM.

nearly similar ionic radius as of NH_4^+.[18,19]

Conclusion

The cubic ammonium molybdate (CAM) cation exchanger possesses two different exchange sites, EA and SA-sites. Both sites were active for exchange of alkali metal ions with different selectivities. The order of selectivity at SA-site and maximum exchange capacity on H-CAM or A-CAM was $K^+ > Rb^+ > Cs^+$. The exchange of these ions for the structural NH_4^+ indicated that the NH_4^+ at SA-sites were mobile (i.e. not fixed up or trapped in the structure), however not accessible for the hydrated H^+ or H_3O^+ to be exchanged with. No change in cubic structure of CAM even with the loss of NH_4^+ indicated that the NH_4^+ seems to be existing in the atomic sized tunnels or layers within the crystal structure and is easy to exchange with ions of greater ionic radii without any alteration in the crystal structure. At high pH, the transformation of CAM or H-CAM to orthorhombic and triclinic-forms of molybdenum oxide in the presence of K^+ and Cs^+ respectively, lead to new concept—"The stucture building of metal oxides by metal ions," for preparation of new inorganic ion-exchange materials.

The help of Mr. K. Honda (a member of our group) in computer programs for X-ray diffraction analyses is hereby acknowledged.

References

1) P. G. Dickens, A. C. Halliwell, D. J. Murphy, and M. S. Whittingham, *Trans. Faraday Soc.*, **67**, 794 (1971).
2) M. S. Whittingham and L. D. Clark, *J. Chem. Phys.*, **53**, 4114 (1970).
3) L. D. Clark, M. S. Whittingham, and R. A. Higgins, *J. Solid State Chem.*, **5**, 487 (1972).
4) G. D. Fallon and B. M. Gatehouse, *J. Solid State Chem.*, **34**, 193 (1980).
5) I. Lindqvist, *Acta Chem. Scand.*, **4**, 650 (1950).
6) C. Gleitzer, *J. Less-Common Met.*, **51**, 215 (1977).
7) E. Banks and A. Goldstein, *Inorg. Chem.*, **7**, 966 (1968).
8) C. B. Amphlett, "Inorganic Ion Exchangers," Elsevier Pub. Co., N. Y. (1964).
9) A. Clearfield, G. H. Nancollas, and R. H. Blessing, in "Ion Exchange and Solvent Extraction," ed by J. A. Marinsky and Y. Marcus, Vol. 5, 1973.
10) A. J. Khan, M. Tsuji, and M. Abe, *Bull. Chem. Soc. Jpn.*, **62**, 3457 (1989).
11) A. J. Khan, M. Abe, M. Tsuji, and Y. Kanzaki, *Bull. Chem. Soc. Jpn.*, in press.

12) T. Ito, "X-Ray Study on Polymorphism," Maruzen Pub. Co., Tokyo (1950).
13) J. W. Visser, *J. Appl. Crystallogr.*, **2**, 89 (1969).
14) W. H. Schreiner, C. Surdukowski, and R. Jenkins, *J. Appl. Crystallogr.*, **15**, 513, 524 (1982).
15) M. Schiavello, R. J. D. Tilley, S. De Rossi, and E. Iguchi, *Z. Physik. Chem. Neue Folge*, **104**, 165 (1977).
16) B. Krebs, *Chem. Commun.*, 50 (1970).
17) K. Y. Matsumoto, M. Kato, and Y. Sasaki, *Bull. Chem. Soc. Jpn.*, **49**, 106 (1976).
18) R. D. Shannon, *Acta Crystallogr., Sect. A*, **32**, 751 (1976).
19) A. A. Khan and W. Baur, *Acta Crystallogr., Sect. B*, **28**, 683 (1972).
20) Y. Kanzaki, M. Konuma, and O. Matsumoto, *J. Phys. Chem. Solids*, **41**, 525 (1980).
21) R. M. Diamond and D. C. Whitney, in "Ion Exchange," ed by J. A. Marinsky, Marcel Dekker Inc., N. Y. (1966), p. 281.

 © 1991 The Chemical Society of Japan Bull. Chem. Soc. Jpn., 64, 459—463 (1991)

Metal Complexes of Peptides. V. Cobalt(III) Complexes with *N*-β-Alanyl-(*S*)-aspartate

Tomoharu AMA,* Ritsuko MAKI, Hiroshi KAWAGUCHI, and Takaji YASUI
Department of Chemistry, Faculty of Science, Kochi University, Akebono-cho, Kochi 780
(Received August 10, 1990)

Three cobalt(III) complexes containing *N*-β-alanyl-(*S*)-aspartic acid (H_3L), [Co(L)(en)] (en: ethylenediamine), [Co(L)(dien)] (dien: diethylenetriamine), and $[Co(HL)(dien)]^+$, were newly prepared and characterized on the basis of their ^{13}C NMR, UV-visible absorption, and circular dichroism spectra. The dipeptide L functions as a quadridentate ligand in [Co(L)(en)] and as terdentate ligands in [Co(L)(dien)] and $[Co(HL)(dien)]^+$. The structures of these complexes are discussed in connection with those of $[Co((S)\text{-asp})(dien)]^+$ (H_2(*S*)-asp: (*S*)-aspartic acid) and $[Co(edma)(dien)]^{2+}$ (Hedma: ethylenediamine-*N*-acetic acid).

Many reports on the preparation and characterization of the cobalt(III) complexes containing dipeptides have been published.[1-17] In most of these complexes, the coordinated dipeptides function as terdentates in a meridional form with respect to the peptide backbones. In the previous paper,[1,2] we reported the novel coordination mode of dipeptide in $[Co(Hcar)(en)(OH_2)]^{2+}$ (H_2car: H_2β-ala-(*S*)-his, carnosine, or *N*-β-alanyl-(*S*)-histidine; en: ethylenediamine), where the carnosine coordinates to cobalt(III) as a facial terdentate with an uncoordinated amino group. This complex was prepared from $[Co(CO_3)_2(en)]^-$ and H_2car in an acidic aqueous solution. On the other hand, $[Co(car)(en)]^+$ complex containing a quadridentate dipeptide was prepared from the same materials in a basic aqueous solution.[1]

Replacement of the imidazolyl group in carnosine with a carboxyl group gives *N*-β-alanyl-(*S*)-aspartic acid (H_3L or H_3β-ala-(*S*)-asp), and it is expected that the latter exhibits similar coordination behavior to that of the former. In the present paper, the preparations of some cobalt(III) complexes with the ligand L will be described, and the coordination modes of the peptide will be discussed in detail on the basis of spectroscopic data of the complexes.

Experimental

Preparation of the Complexes. [Co(L)(en)] (Abbreviation: AA1): $K[Co(CO_3)_2(en)]\cdot H_2O$[18] (1.3 g) was dissolved in 30 cm^3 of water, and the pH of the solution was adjusted to 3 with 1 M (M=mol dm^{-3}) $HClO_4$. After the solution was stirred at room temperature for about 30 min, a solution containing 1.0 g of H_3L in 20 cm^3 of water was added to the solution. The pH of the combined solution was adjusted to 9 with 1 M NaOH, and then the solution was stirred at 65 °C for 8 h. The resultant solution was filtered and poured on an SP-Sephadex column (K^+ form, 4.7 cm×90 cm), and the adsorbed band was developed with water. The red band separated was eluted out, and the solution was concentrated to about 10 cm^3. The concentrated solution was again chromatographed on a QAE-Sephadex column (Cl^- form, 4.7 cm×90 cm). The adsorbed band was separated into pink and red parts by recycle-development with water on the same column. The solution eluted from the red band was concentrated under reduced pressure to a few milliliters, and methanol was added to the concentrated solution to obtain a crude complex. The crude complex was recrystallized from water by addition of methanol. Found: C, 32.94; H, 5.70; N, 16.94%. Calcd for $[Co(L)(en)]\cdot 0.5H_2O=C_9H_{18}N_4O_{5.5}Co$: C, 32.84; H, 5.51; N, 17.02%.

[Co(HL)(dien)]Br (AA2): The pH of a solution containing $[CoCl_3(dien)]$ (1.0 g)[19] (dien: diethylenetriamine) and H_3L (0.83 g) in 65 cm^3 of water was adjusted to 5 with 1 M NaOH. This solution was stirred for 48 h at 60 °C, keeping the pH of the solution to about 5. The reactant solution was cooled to room temperature, filtered, and then charged on an SP-Sephadex column (K^+ form). After the column was swept with 0.5 dm^3 of water, the adsorbed band was developed with 0.2 M KCl to separate a dark-orange band. The solution eluted from dark-orange band was concentrated to small volume under reduced pressure at 35—40 °C. Methanol was added to the concentrated solution, and potassium chloride deposited was removed by filtration. The filtrate was concentrated to about 10 cm^3 and treated with a QAE-Sephadex column (Br^- form). The treated solution was concentrated to small volume. A crude complex was obtained by addition of ethanol to the concentrate, which was recrystallized from water-ethanol solution. Found: C, 27.57; H, 5.88; N, 14.43%. Calcd for $[Co(HL)(dien)]Br\cdot 2H_2O=C_{11}H_{37}N_5O_7CoBr$: C, 27.51; H, 5.67; N, 14.58%.

[Co(L)(dien)] (AA3): A solution containing H_3L (0.83 g) in 15 cm^3 of water was added to the solution of $[CoCl_3(dien)]$ (1.0 g) in 50 cm^3 of warm water. After the pH of the solution was adjusted to 9 with 1 M NaOH, the solution was stirred for 24 h at 60 °C. The reactant solution was cooled to room temperature and filtered. The filtrate was poured onto an SP-Sephadex (K^+ form) column. The orange solution which was eluted with water was concentrated to ca. 20 cm^3 and loaded on a QAE-Sephadex column. Developing with water, the adsorbed band was separated into two parts; an earlier-eluted orange band and a later-eluted red band. The solution eluted from the later-eluted band was concentrated by using a vacuum evaporator and filtered. Crude complex obtained by addition of ethanol to the filtrate was recrystallized from water-ethanol solution. Found: C, 33.17; H, 6.64; N, 17.58%. Calcd for $[Co(L)(dien)]\cdot 2H_2O=C_{11}H_{26}N_5O_7Co$: C, 33.09; H, 6.56; N, 17.54%.

Isomers of [Co((*S*)-asp)(dien)]Cl and [Co(edma)(dien)]Cl_2: The geometrical isomers of $[Co((S)\text{-asp})(dien)]Cl$ (H_2(*S*)-asp: (*S*)-aspartic acid) and $[Co(edma)(dien)]Cl_2$ (Hedma: ethylenediamine-*N*-acetic acid) were obtained according to the

methods described in the previous papers.[20-21]

Absorption and Circular Dichroism Spectral Changes with pH. **AA1** (100 mg) was dissolved in 2 cm^3 of water, and 2 cm^3 of the solution was placed in a measuring flask (10 cm^3). A prescribed volume of 2 M HCl was added to the solution. The volume of the acidic solution was adjusted to 10 cm^3 with water. By the same procedure, nine solutions were prepared at different pH's (0.5—6.0). Absorption and CD spectra and pH of each solution were recorded at room temperature. In the same manner, the spectral changes with pH's were examined for **AA2** and **AA3**.

Measurements. The absorption and CD spectra were measured by a Hitachi 557 spectrophotometer and a JASCO J-22 spectropolarimeter, respectively. The ^{13}CNMR spectra were recorded on a Hitachi R-90H spectrometer. The chemical shifts in ^{13}CNMR were measured relative to internal dioxane (δ=67.40).

Results and Discussion

Structural Assignments of the Complexes. [Co(L)(en)] (AA1): Figure 1 shows the ^{13}CNMR shift patterns of free (uncoordinated) L and its complexes, together with those of the related compounds. The numbering of the carbons in L is also given in Fig. 1.

The carbon resonances of the free ligand L show a considerable difference in chemical shift with the

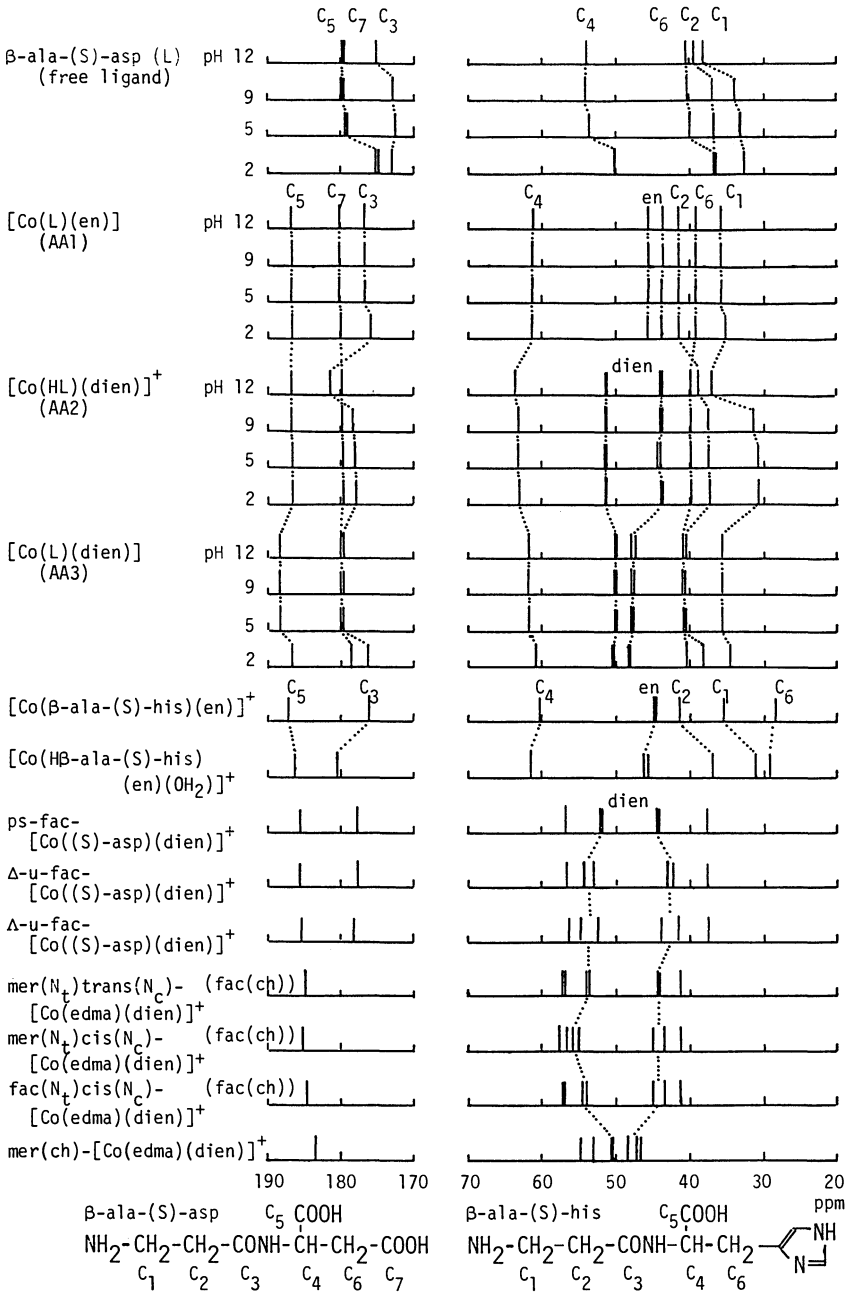

Fig. 1. ^{13}CNMR spectral patterns of β-ala-(*S*)-asp and the cobalt(III) complexes at various pH.

change of pH (12 to 2). The down-field shifts observed for the C_1, C_2, and C_3 carbons at pH 12 are due to the deprotonation of the terminal amino group ($-NH_3^+$). On the other hand, the up-field shifts of the C_4, C_5, C_6, and C_7 carbon resonances at pH 2 are due to the protonation to the α- and β-carboxylate anions. However, such the shift changes with pH as observed in the free ligand L are not observed in the ^{13}C shift pattern of **AA1**. This result suggests that the amino and two carboxyl groups of the peptide L in **AA1** coordinate to cobalt(III).

The chemical shifts of C_1, C_2, C_3, C_4, and C_5 in **AA1** are almost equal to those of the corresponding carbons of β-ala-(*S*)-his in [Co(β-ala-(*S*)-his)(en)]$^+$ at pH 5, in which the β-ala-(*S*)-his coordinates to cobalt(III) as a quadridentate.[1] This result suggests that the coordination mode of L in **AA1** is similar to that of β-ala-(*S*)-his in [Co(β-ala-(*S*)-his)(en)]$^+$. Accordingly, we propose that the ligand L in **AA1** coordinates to cobalt(III) in the quadridentate mode (Fig. 2(A)).

[Co(HL)(dien)]$^+$(AA2): The ^{13}C chemical shift behavior of the (*S*)-asp moiety (C_5, C_6, and C_7) in **AA2** resembles well to that in **AA1**. On the other hand, the shift behavior of the β-ala moiety (C_1 and C_2) in **AA2** is much different from that in **AA1**, but similar to that in [Co(Hβ-ala-(*S*)-his)(en)(OH_2)]$^+$ where Hβ-ala-(*S*)-his coordinates to cobalt(III) as a facial terdentate with free $-NH_3^+$ group.[1,2] These results suggest that L in **AA2** coordinates to cobalt(III) in the coordination mode similar to that of β-ala-(*S*)-his in [Co(Hβ-ala-(*S*)-his)(en)(OH_2)]$^+$; the ligand L coordinates with amide-N and two carboxyl-O's, and amino group is free. The down-field shifts of the β-ala moiety carbons (C_1 and C_2) at pH 12 compared with the shifts at pH 5 are due to the deprotonation from uncoordinated $-NH_3^+$.

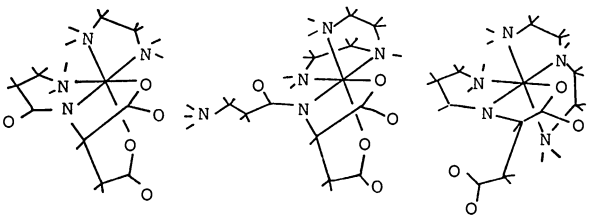

Fig. 2. Proposed structures of the cobalt(III) complexes containing β-ala-(*S*)-asp.

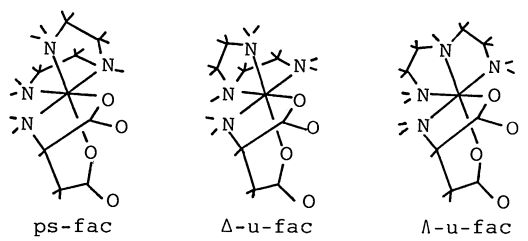

Fig. 3. Structures of the isomers of [Co((*S*)-asp)(dien)]$^+$.

Although the coordination mode of the HL in **AA2** is clarified as mentioned above, three geometries are possible for the structures of **AA2** in the same manner as shown for [Co((*S*)-asp)(dien)]$^+$ in Fig. 3. The geometrical structure of the isolated **AA2** can be assigned in comparison with its ^{13}C NMR spectrum with those of the [Co((*S*)-asp)(dien)]$^+$ isomers; the ^{13}C NMR signals of dien in **AA2** appear in shift pattern similar to that in ps-*fac*-[Co((*S*)-asp)(dien)]$^+$, but not in *Δ*-u-*fac* or *Λ*-u-*fac* (Fig. 3). On the basis of the above mentioned recognition, we propose the structure shown in Fig. 2 (B) for **AA2**.

Whereas the ps-*fac* type isomer of [Co(HL)(dien)]$^+$ was isolated in the preparation of **AA2**, the yields of *Δ*- and *Λ*-u-*fac* type isomers were so little that we did not succeeded to isolate them. The steric repulsion between β-ala moiety in HL and dien $-CH_2-$ may decrease the yields of the *Δ*- and *Λ*-u-*fac* type isomers.

[Co(L)(dien)] (AA3): The ^{13}C NMR signal of **AA3** shows the shift pattern characteristic to the complexes containing meridionally coordinated dien,[22,23] such as mer(ch)-[Co(edma)(dien)]$^{2+}$ (Fig. 1), and it obviously differs from those of the facial isomers of [Co((*S*)-asp)(dien)]$^+$ and of [Co(edma)(dien)]$^{2+}$. This observation suggests that dien in **AA3** coordinates to cobalt(III) in meridional form as a terdentate, and that the ligand L occupies the remaining meridional coordination sites.

The shift behavior of the β-ala moiety (C_1 and C_2) in **AA3** is similar to those in **AA1** at pH 5—12. Such a shift behavior suggests that the $-NH_2$ group of the β-ala moiety in **AA3** coordinates to cobalt(III). In addition, the chemical shifts of β-carbon (C_6) and β-carboxyl-carbon (C_7) in the (*S*)-asp moiety are in up-field at pH 2 compared with its chemical shifts at pH 5. These up-field shifts arise from protonation on the free β-carboxyl group. From these results we propose the structure shown in Fig. 2(C) for **AA3**.

The Absorption and CD Spectral Changes with pH: The absorption and CD spectra of **AA1**, **AA2**, and **AA3** in the neutral aqueous solutions are shown in Fig. 4. All of these complexes exhibited the absorption and CD spectral changes with pH in an aqueous solution. Figure 5 shows the CD spectral change of **AA2** over the pH range 0.63 to 6.08. The iso-circular dichroism points (iso-CD points) appear at 402, 498, and 529 nm, and the isosbestic points in the absorption spectra were observed at 429 and 494 nm. The pK_a value estimated from these changes was ca. 0.7. This value indicates that the spectral changes are related to the protonation on the coordinating amide group of L.[1,4,24] Similar spectral changes were also observed for **AA1** over the pH range 1.10 to 5.67 (iso-CD point: 414 nm; isosbestic point: 432 nm; pK_a value: ca. 0.9).

AA3, which has two proton acceptable groups

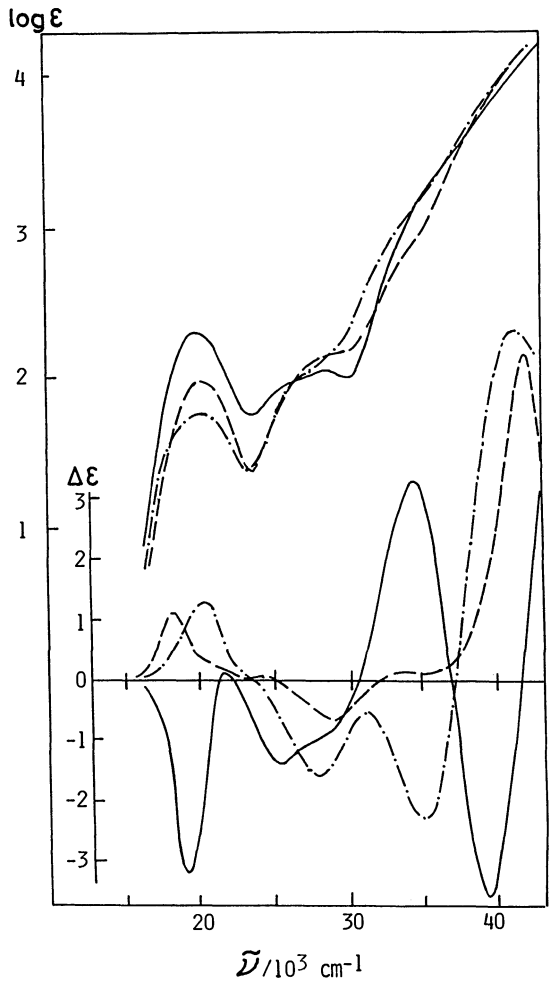

Fig. 4. Absorption and circular dichroism spectra of the complexes containing β-ala-(*S*)-asp: **AA1** (— · —), **AA2** (----), and **AA3** (——). ε and Δε values are given in $mol^{-1}dm^3cm^{-1}$.

(amide and free β-carboxyl), exhibited more complicated CD spectral change in the pH range 6.48—0.88 compared with those of **AA1** and **AA2**. That is, there was no iso-CD point over the pH range 6.48 to 2.0. However, the pK_a value for the amide group was calculated to ca. 1.5 from the CD spectral change in the pH range 2.0—0.88, where iso-CD points appeared at 433 and 507 nm.

Comparing the pK_a values of the coordinating amide groups in **AA1**, **AA2**, and **AA3**, the following result is noteworthy; the pK_a value of **AA3**, in which the peptide backbone is flat and free from the strain caused by the coordination of the β-carboxyl group of L-asp moiety, is larger than those of **AA1** and **AA2**, in which the peptide backbones are bended and strained by the coordination of the β-carboxyl groups in (*S*)-asp moieties.

AA1 did not show obvious spectral changes with time in the pH range 6.0—1.0, but it showed slowly spectral change with time in a strong acidic (2 M HCl) solution, accompanying with lower energy shifts and intensity decreases of the first and second absorption bands. This spectral change with time may be attributed to the fission of the β-carboxyl-cobalt(III) bond.

AA2 showed slowly spectral change with time in a strong acidic (2 M HCl) solution similarly to **AA1**. On the other hand, **AA3**, in which the β-carboxyl group of L does not coordinate to cobalt(III), did not show obvious spectral change with time in 2 M HCl solution. Such a fission of the β-carboxyl-cobalt bond occurring in **AA1** and **AA2** can be attributed to the strained coordination of the β-carboxyl group with six-membered chelate ring.[25]

The pH of the Reaction Solution Controlling the Coordination Mode of Peptide: The reaction between

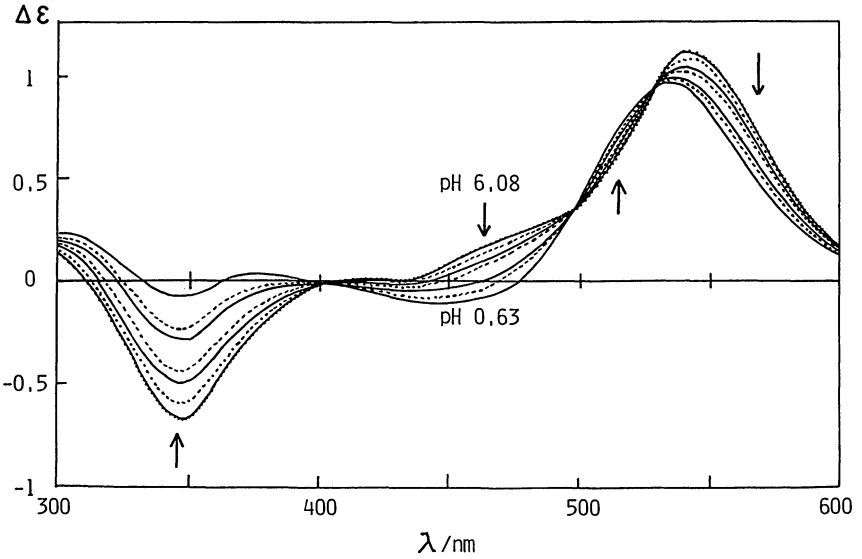

Fig. 5. CD spectral change with pH for the **AA2** complex. pH 6.08, 2.07, 1.60, 1.31, 1.18, 0.95, 0.85, and 0.63. Δε values are given in mol^{-1} dm^3cm^{-1}.

[$CoCl_3$(dien)] and H_3L yielded mainly **AA3** (the peptide functions as a meridional terdentate with uncoordinated β-carboxyl group) in a weakly basic aqueous solution (pH 9) and **AA2** (the peptide functions as a facial terdentate with uncoordinated amino group) in a weakly acidic aqueous solution (pH 5). These results suggest that the coordination modes of peptides can be controlled by the pH of the reaction solution. That is, the amino group on the peptide can not easily coordinate to cobalt(III) in a weakly acidic solution because of the protonation on the amino group, but the carboxyl group can easily coordinate in the weakly acidic solution. Accordingly, the β-ala-(*S*)-asp ligand coordinates to cobalt(III) with the α-carboxyl O, β-carboxyl O, and amide N in the facial terdentate mode (**AA2**; the meridional terdentate mode with α-carboxyl O, β-carboxyl O, and amide N is sterically impossible). However, in a basic aqueous solution, the amino group on the β-ala-(*S*)-asp can be coordinated to cobalt(III) more easily than in an acidic solution. Consequently, when the β-ala-(*S*)-asp is forced into terdentates in the basic solution, the β-ala-(*S*)-asp ligand coordinates to cobalt(III) in the meridional terdentate mode with amino N, α-carboxyl O, and amide N (**AA3**), which is preferable to the facial mode for dipeptides.[1,4,5]

One of the important subjects in bioinorganic chemistry is to control the coordination modes of a peptide on a metal ion. The present results provide useful clues for this subject in the manner different from those obtaind for labile complexes such as copper(II) ones.[26,27] Though the coordination modes of a dipeptide in the labile complexes are controlled by the stability (thermodynamics) rather than by the reaction rates (kinetics) of the ligands in the labile complexes, those in the present cobalt(III) complexes are controlled by the reaction rate of the amino group on the dipeptide. The present cobalt(III) complexes are stable and do not show the structural changes in the skeltons in the wide pH range 1—11 for several hours, even though deprotonation or protonation on the coordinated dipeptide is observed.

References

1) T. Ama, H. Kawaguchi, M. Uchijima, N. Koine, and T. Yasui, *Bull. Chem. Soc. Jpn.*, **62**, 3464 (1989).
2) K. Okamoto, T. Yasui, H. Kawaguchi, T. Ama, and J. Hidaka, *Chem. Lett.*, **1988**, 335.
3) H. Kawaguchi, K. Maeda, T. Ama, and T. Yasui, *Chem. Lett.*, **1979**, 1105.
4) H. Kawaguchi, M. Kanekiyo, T. Ama, and T. Yasui, *Bull. Chem. Soc. Jpn.*, **53**, 3208 (1980).
5) T. Yasui, H. Kawaguchi, and T. Ama, *Bull. Chem. Soc. Jpn.*, **54**, 2918 (1981).
6) H. Kawaguchi, M. Ishii, T. Ama, and T. Yasui, *Bull. Chem. Soc. Jpn.*, **55**, 3750 (1982).
7) J. P. Collman and E. Kimura, *J. Am. Chem. Soc.*, **89**, 6096 (1967).
8) E. Kimura, S. Young, and J. P. Collman, *Inorg. Chem.*, **9**, 1183 (1970).
9) R. D. Gillard and D. A. Phipps, *J. Chem. Soc. A*, **1971**, 1074.
10) Y. Wu and D. H. Busch, *J. Am. Chem. Soc.*, **94**, 4115 (1972).
11) G. G. Smith, A. Khatib, and G. S. Reddy, *J. Am. Chem. Soc.*, **105**, 293 (1983).
12) E. J. Evans, J. E. Grice, C. J. Hawkins, and M. R. Heard, *Inorg. Chem.*, **19**, 3496 (1980).
13) E. J. Evans, C. J. Hawkins, J. Rodgers, and M. R. Snow, *Inorg. Chem.*, **22**, 34 (1983).
14) C. J. Hawkins and J. Martin, *Inorg. Chem.*, **25**, 2146 (1986).
15) L. R. Solujc, R. Herak, B. Prelesnik, and M. B. Celap, *Inorg. Chem.*, **24**, 32 (1985).
16) R. W. Hay, V. M. C. Reid, and D. P. Piplani, *Transition Met. Chem.*, **11**, 302 (1986).
17) N. Mensi and S. S. Isied, *Inorg. Chem.*, **25**, 147 (1986).
18) M. Shibata, *Nippon Kagaku Zasshi*, **87**, 771 (1966).
19) P. H. Crayton, *Inorg. Synth.*, **7**, 207 (1963).
20) J. I. Legg and W. Cooke, *J. Am. Chem. Soc.*, **89**, 6854 (1967).
21) T. Yasui, T. Shikiji, N. Koine, T. Ama, and H. Kawaguchi, *Bull. Chem. Soc. Jpn.*, **60**, 595 (1987).
22) T. Yasui, K. Okamato, J. Hidaka, T. Ama, and H. Kawaguchi, *Bull. Chem. Soc. Jpn.*, **60**, 2573 (1987).
23) G. H. Searle, F. R. Keene, and S. F. Lincoln, *Inorg. Chem.*, **17**, 2362 (1978).
24) L. V. Boas, C. A. Evans, R. D. Gillard, P. R. Mitchell, and D. A. Phipps, *J. Chem. Soc., Dalton Trans.*, **1979**, 582.
25) J. A. McClarin, L. A. Dressel, and J. I. Legg, *J. Am. Chem. Soc.*, **98**, 4150 (1976).
26) E. Farkas, I. Sovago, and A. Gergely, *J. Chem. Soc., Dalton Trans.*, **1983**, 1545.
27) B. D. Reverend, F. Liman, C. Livera, L. D. Pettit, S. Pyburn, and H. Kozlowski, *J. Chem. Soc., Dalton Trans.*, **1988**, 887.

Extraordinary Coordination of Acetonitrile to Square-Planar, 1,4,8,11-Tetraazacyclotetradecanenickel(II) and (1*R*,4*R*,8*S*,11*S*)-1,4,8,11-Tetramethyl-1,4,8,11-tetraazacyclotetradecanenickel(II) Cations

Takashi YOKOYAMA, Etsuro IWAMOTO, and Takahiro KUMAMARU*
Department of Chemistry, Faculty of Science, Hiroshima University,
Higashisenda-machi, Naka-ku, Hiroshima 730
(Received August 22, 1990)

Coordination of dipolar aprotic solvents to the square-planar complexes of nickel(II) was investigated in nitrobenzene (NB) spectrophotometrically. Compared with *N*,*N*-dimethylformamide (DMF) and dimethyl sulfoxide (DMSO), it was observed that acetonitrile (AN) was strongly coordinated to $[NiL]^{2+}$ (L=1,4,8,11-tetramethyl-1,4,8,11-tetraazacyclotetradecane). The stepwise coordination constants K_{NiS1} and K_{NiS2} (mol^{-1} dm^3) for (1*R*,4*R*,8*S*,11*S*)-$[NiL]^{2+}$ were found to be (1.6, 0.5), (1.0, 0.1), (3.4, 6.7), and (0.4, 1.9) for DMSO, DMF, AN, and benzonitrile, respectively. The K_{NiS2} values for nitriles are larger than the K_{NiS1} values, showing that nitriles are coordinated to the metal ion through π-back donation.

$[NiL]^{2+}$ (L=1,4,8,11-tetramethyl-1,4,8,11-tetraazacyclotetradecane) has two stable isomer of 1*R*,4*R*,8*S*,11*S*-nitrogen and 1*R*,4*S*,8*R*,11*S*-nitrogen configuration.[1-9] [Ni(cyclam)]$^{2+}$ (cyclam=1,4,8,11-tetraazacyclotetradecane), (1*R*,4*R*,8*S*,11*S*)-$[NiL]^{2+}$ and (1*R*,4*S*,8*R*,11*S*)-$[NiL]^{2+}$ are described in Scheme (1). (1*R*,4*R*,8*S*,11*S*)-$[NiL]^{2+}$ and [Ni(cyclam)]$^{2+}$ form the six-coordinated complexes where two solvent molecules are attached to the central nickel.[9,10] However, (1*R*,4*S*,8*R*,11*S*)-$[NiL]^{2+}$ forms the five-coordinated complex where only one solvent molecule is attached to the nickel.[7] The rate constants for exchange reaction of the coordinated solvent have been reported in H_2O, acetonitrile(AN), and *N*,*N*-dimethylformamide (DMF).[11-14] Accordingly, the observed values of enthalpy of activation for (1*R*,4*R*,8*S*,11*S*)-$[NiL]^{2+}$ were about twice as large as those for (1*R*,4*S*,8*R*,11*S*)-$[NiL]^{2+}$. It was also found that the coordination of the AN molecule to both isomers of $[NiL]^{2+}$ is stronger than that of other basic solvents.[14]

The axial coordination constants for (1*R*,4*S*,8*R*,11*S*)-$[NiL]^{2+}$ in various binary mixed solvents using nitrobenzene (NB) as a diluent were reported previously,[15] and the values obtained were decreased in the order DMF (5.4 mol^{-1} dm^3)>dimethyl sulfoxide (DMSO) (3.8)>AN (3.1)>benzonitrile (BzN) (0.4), while in pure solvents, the order was AN (13.4)>DMF (10.8)>DMSO (3.5)>BzN (2.4)>H_2O (1.8).[16] In these cases, the coordination constant of AN molecules is larger than that expected from Gutmann's donor number (DN), because DN of the solvents is decreased in the order DMSO>DMF>H_2O>AN>BzN, thus suggesting π-back donation.[15] The first and second coordination constants (K_{NiS1} and K_{NiS2}) for (1*R*,4*R*,8*S*,11*S*)-$[NiL]^{2+}$ have not been reported yet. An investigation of K_{NiS1} and K_{NiS2} might help in understanding the strong coordination of AN. Therefore, the stepwise coordination constants for (1*R*,4*R*,8*S*,11*S*)-$[NiL]^{2+}$ and a comparison with the results for (1*R*,4*S*,8*R*,11*S*)-$[NiL]^{2+}$ and [Ni(cyclam)]$^{2+}$ in NB mixtures are reported.

Experimental

NB, DMF, DMSO, AN, and BzN were purified as described previously.[15,17] $[Ni(cyclam)](ClO_4)_2$, $[Ni(cyclam)](BPh_4)_2$ (BPh_4=tetraphenylborate) and (1*R*,4*R*,8*S*,11*S*)-$[NiL](ClO_4)_2$ were prepared according to the published methods.[7-9,15,18] The purities were confirmed by the elemental analyses of the respective complexes. The instrumentation and procedure used for measurements of conductances and spectra are as reported previously.[15,18,19]

Results and Discussion

NB was selected as the diluent for the donor solvents

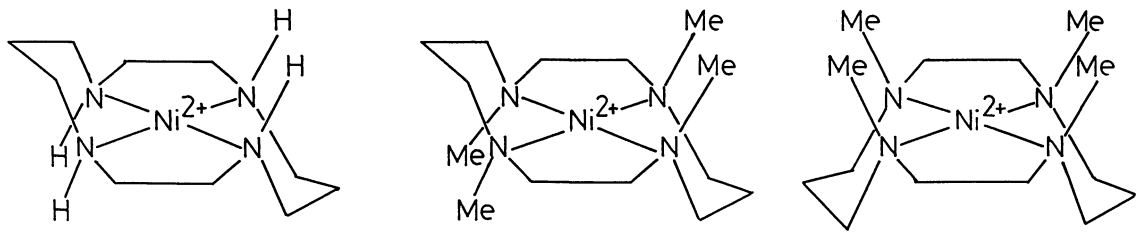

(a) [Ni(cyclam)]$^{2+}$ (b) (1R,4R,8S,11S)-[NiL]$^{2+}$ (c) (1R,4S,8R,11S)-[NiL]$^{2+}$

Scheme 1.

because polar NB dissolves (1*R*,4*R*,8*S*,11*S*)-[NiL]$(ClO_4)_2$ enough to permit measurements of the molar absorptivities spectrophotometrically. As NB has a weak basicity, NB is not coordinated to both (1*R*,4*R*,8*S*,11*S*)-[NiL]$^{2+}$ and [Ni(cyclam)]$^{2+}$, and furthermore larger coordination constants of donor solvents were obtained in NB rather than in nitromethane and propylene carbonate.[15,17] Figures 1 (A) and (B) show variations of the visible spectra for (1*R*,4*R*,8*S*,11*S*)-[NiL]$^{2+}$ and [Ni(cyclam)]$^{2+}$ with AN concentration in NB. The wavelength of absorption maximum is 500 and 450 nm for the square-planar species (1*R*,4*R*,8*S*,11*S*)-[NiL]$^{2+}$ and [Ni(cyclam)]$^{2+}$, respectively. In both Figs. 1 (A) and (B) the absorbance decreases with increasing donor solvent concentration.

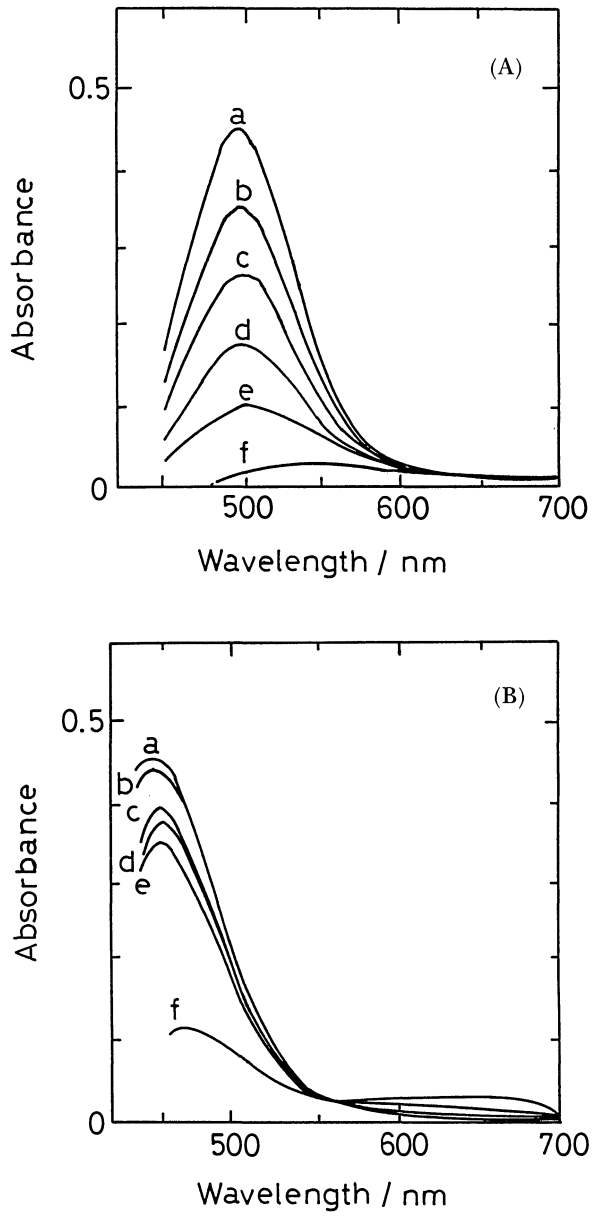

Fig. 1. (A) Variation of the visible spectrum with AN concentration for a solution of (1*R*,4*R*,8*S*,11*S*)-[NiL]$(ClO_4)_2$ (1×10^{-3} mol dm^{-3}) in NB at 25 °C. AN concentration (mol dm^{-3}): (a) 0.0, (b) 0.067, (c) 0.13, (d) 0.19, (e) 0.33, (f) neat; (B) for [Ni(cyclam)]$(ClO_4)_2$. AN concentration (mol dm^{-3}): (a) 0.0, (b) 0.32, (c) 0.54, (d) 0.71, (e) 1.0, (f) neat.

Figures 2 and 3 show variations of the molar absorptivities for (1*R*,4*R*,8*S*,11*S*)-[NiL]$^{2+}$ and [Ni(cyclam)]$^{2+}$ with the concentration of the donor solvents, respectively. The molar absorptivities for both complexes decreased with increasing donor solvent concentration. It should be noted that the decreasing ratio of AN is larger than those of DMF and DMSO for (1*R*,4*R*,8*S*,11*S*)-[NiL]$^{2+}$, but the reverse is true for [Ni(cyclam)]$^{2+}$. For [Ni(cyclam)]$^{2+}$ a small variation in the molar absorptivities was observed. The plots for BzN in which there is no variation in the molar absorptivities for [Ni(cyclam)]$^{2+}$, are omitted.

Equations 1 and 2 show the stepwise equilibria for the coordination of a solvent to the square-planar complexes,

$$(1R,4R,8S,11S)\text{-}[NiL]^{2+} + S \overset{K_{NiS1}}{\rightleftarrows} (1R,4R,8S,11S)\text{-}[NiL(S)]^{2+}, \quad (1)$$

$$(1R,4R,8S,11S)\text{-}[NiL(S)]^{2+} + S \overset{K_{NiS2}}{\rightleftarrows} (1R,4R,8S,11S)\text{-}[NiL(S)_2]^{2+}, \quad (2)$$

where S stands for the donor solvent. The molar absorptivities of the complexes are correlated to the

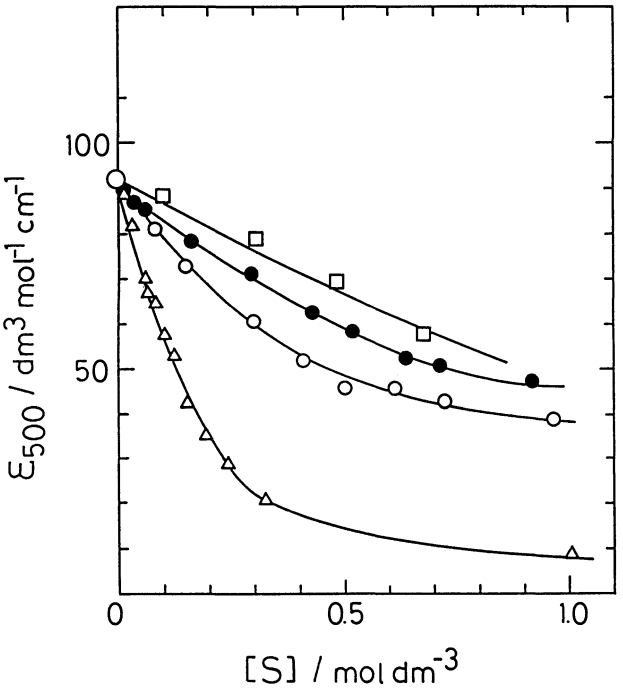

Fig. 2. Variation of molar absorptivities for (1*R*,4*R*,8*S*,11*S*)-[NiL]$^{2+}$ with the donor solvent concentration in NB at 25 °C. ○, DMSO; ●, DMF; △, AN; □, BzN.

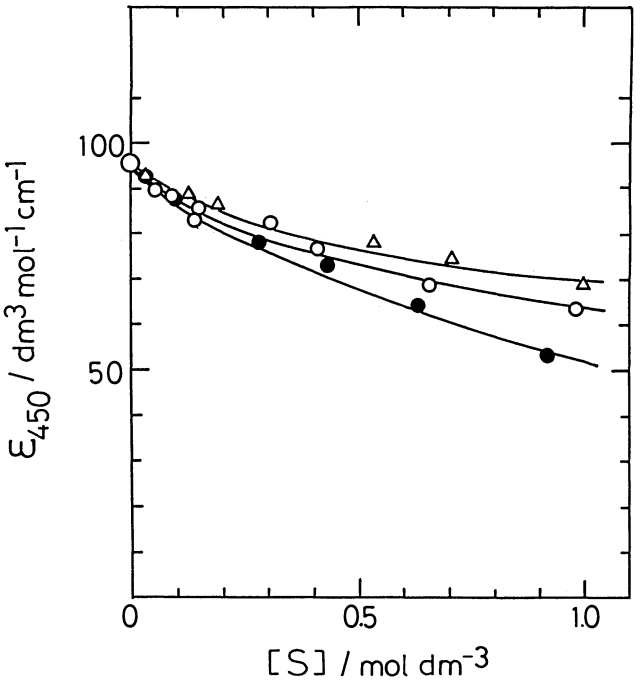

Fig. 3. Variation of molar absorptivities for [Ni(cyclam)]$^{2+}$ with the donor solvent concentration in NB at 25 °C. ○, DMSO; ●, DMF; △, AN.

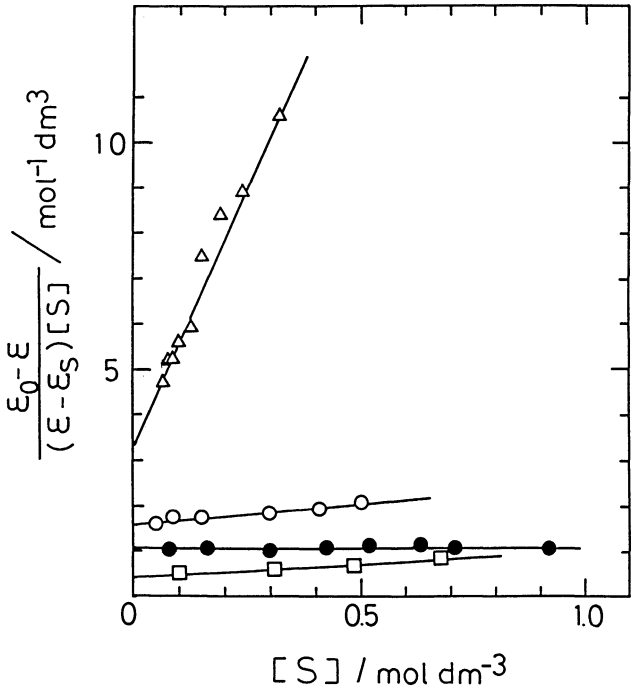

Fig. 4. Plots of $(\varepsilon_o-\varepsilon)/(\varepsilon-\varepsilon_s)$[S] for (1*R*,4*R*,8*S*,11*S*)-[NiL]$^{2+}$. ○, DMSO; ●, DMF; △, AN; □, BzN.

axial coordination constants by Eq. 3.

$$(\varepsilon_o-\varepsilon)/(\varepsilon-\varepsilon_s)[S]=K_{NiS1}+K_{NiS1}K_{NiS2}[S]. \quad (3)$$

The molar absorptivity, ε_o of square-planar species for (1*R*,4*R*,8*S*,11*S*)-[NiL]$^{2+}$ and for [Ni(cyclam)]$^{2+}$ is 92.2 dm^3 mol^{-1} cm^{-1} at 500 nm and 94.9 at 450 nm, respectively. The symbol ε is the apparent molar absorptivity, and ε_s is the combined molar absorptivity for five- and six-coordinated species and is 1.0 dm^3 mol^{-1} cm^{-1} at 500 nm for (1*R*,4*R*,8*S*,11*S*)-[NiL]$^{2+}$ and 14.2 at 450 nm for [Ni(cyclam)]$^{2+}$. A typical plot of Eq. 3 for (1*R*,4*R*,8*S*,11*S*)-[NiL]$^{2+}$ is shown in Fig. 4 where a good linear relationship is obtained for all solvents used. In all the plots of Fig. 4, the concentration of S bonded to the cation is negligible compared with that of unbonded S, since the complex cation concentration used for measurements is 1×10^{-3} mol dm^{-3}. The K_{NiS1} and K_{NiS2} values can be obtained from the intercept and slope, and the results obtained are summarized in Table 1.

The overall coordination constants for [Ni(cyclam)](ClO$_4$)$_2$ and (1*R*,4*R*,8*S*,11*S*)-[NiL](ClO$_4$)$_2$ in NB are decreased in the order DMF (0.24)>AN (0.22)>DMSO (0.021) and AN (23)>DMSO (0.80)>BzN (0.76)>DMF (0.11), respectively. In pure solvents the overall coordination constants for [Ni(cyclam)](ClO$_4$)$_2$ are decreased in the order DMF (27.15)>AN (8.85)>DMSO (2.13)>H$_2$O (0.43, 0.38).[20,21]

Coordination ability of DMSO and H$_2$O as pure solvents is less than that expected from their basicity. This is attributed to the self-association which masks the donor oxygen atom: DMSO forms a cyclic dimer and water forms a three dimensional polymer.[17]

From Table 1, it is obvious that the coordination constants for [Ni(cyclam)](ClO$_4$)$_2$ are smaller than those for (1*R*,4*R*,8*S*,11*S*)-[NiL](ClO$_4$)$_2$. This can be

Table 1. K_{NiS1} and K_{NiS2} for (1*R*,4*R*,8*S*,11*S*)-[NiL]$^{2+}$ and [Ni(cyclam)]$^{2+}$, and K_{NiS} for (1*R*,4*S*,8*R*,11*S*)-[NiL]$^{2+}$ in NB at 25 °C

Solvent	(1*R*,4*R*,8*S*,11*S*)-[NiL]$^{2+}$		[Ni(cyclam)]$^{2+}$		(1*R*,4*S*,8*R*,11*S*)-[NiL]$^{2+}$[a]
	K_{NiS1}	K_{NiS2}	K_{NiS1}	K_{NiS2}	K_{NiS}
DMSO	1.6±0.1	0.5±0.1	0.7±0.1	0	3.8
DMF	1.0±0.1	0.1±0.1	0.8±0.1	0.3±0.1	5.4
AN	3.4±0.3	6.7±0.1	0.2±0.1 0.7±0.1[b]	1.1±0.2 1.2±0.1[b]	3.1
BzN	0.4±0.1	1.9±0.1	—	—	0.4

a) Ref. 15. b) [Ni(cyclam)](BPh$_4$)$_2$.

explained, first, through the phenomenon of hydrogen bonding of the four N-H protons of $[Ni(cyclam)]^{2+}$. Effects of hydrogen bonding of N-H protons on ionic association in NB were studied.[18] The ionic association constants K_a obtained by the Fuoss-Edelson method,[22] were 0, 1190, and 11000 mol^{-1} dm^3 for $[Ni(cyclam)](BPh_4)_2$, (1*R*,4*S*,8*R*,11*S*)-$[NiL](ClO_4)_2$, and $[Ni(cyclam)](ClO_4)_2$, respectively, indicating that $[Ni(cyclam)](ClO_4)_2$ greatly associative.[15,18] The difference in K_a between BPh_4^- and ClO_4^- for $[Ni(cyclam)]^{2+}$ is slightly reflected on the K_{NiS1} values: the ClO_4^- complex gives a little smaller K_{NiS1} value compared with BPh_4^-. The basic donor solvents can be also hydrogen-bonded to the N-H protons, and their attack on the central nickel is hampered.

Secondly, the stability of square-planar configuration for $[Ni(cyclam)]^{2+}$ is considered. The logarithm of the stability constant is 8.6 for (1*R*,4*S*,8*R*,11*S*)-$[NiL]^{2+}$ and 20.1 for $[Ni(cyclam)]^{2+}$.[23] The absorption wavelength of the d-d transition observed is 450, 500, and 520 nm for $[Ni(cyclam)]^{2+}$, for (1*R*,4*R*,8*S*,11*S*)-$[NiL]^{2+}$, and for (1*R*,4*S*,8*R*,11*S*)-$[NiL]^{2+}$, respectively, indicating that the stability for the square-planar configuration decreases in the order $[Ni(cyclam)]^{2+}$>(1*R*,4*R*,8*S*,11*S*)-$[NiL]^{2+}$> (1*R*,4*S*,8*R*,11*S*)-$[NiL]^{2+}$. Cyclam is the secondary amines while L is the tertiary ones. As the coordination of the tertiary amine is stronger than the secondary one, the stability for $[NiL]^{2+}$ must be larger than that for $[Ni(cyclam)]^{2+}$.[23] However, the repulsion between the methyl groups of $[NiL]^{2+}$ leads to less stability for the square-planar configuration. In other words, it is easy for $[NiL]^{2+}$ to change its configuration from the square-planar into the square-pyramidal or the octahedral. Therefore, $[NiL]^{2+}$ easily receives the attack of the solvent.

Table 1 also compiles the coordination constants obtained together with K_{NiS} for (1*R*,4*S*,8*R*,11*S*)-$[NiL]^{2+}$. The K_{NiS1} values of DMF and DMSO are less than K_{NiS}, but those of AN and BzN are the same as K_{NiS}. The calculation of the strain energy showed that each coordination site for (1*R*,4*R*,8*S*,11*S*)-$NiL]^{2+}$ is more sterically crowded than the coordination site for (1*R*,4*S*,8*R*,11*S*)-$[NiL]^{2+}$.[3,4] It is likely that coordination of DMF and DMSO molecules with $-N(CH_3)_2$ and two $-CH_3$, respectively, is sterically hindered, and the rod-like cyano group receives little steric hindrance.

Cyano groups show a striking and different trend from other solvents. K_{NiS2} for AN is twice as large as K_{NiS1}, although K_{NiS2} for DMF is only one tenth of K_{NiS1}. This anomalous behavior of AN may refer to π-back donation. Evidence has been reported for the π-back bonding of AN: the increase of the CN stretching frequency for copper halide adducts with AN,[24] the large stability constant of bis (α-furil dioximato)-diiodocobaltate(III) in AN,[25] the large ratio of $10Dq'$ (nickel bromide AN complex)/$10Dq'$ (nickel chloride AN complex),[26] the dependence of the coordination power value (relative Gibbs free energy change for solvation of the nickel ion) on other parameters,[27] and the deviation of ν_{max} for the copper complexes in AN from a correlation of ν_{max} with solvent donor number.[28] In all these cases, AN is strongly bonded to the complex than expected from its basicity. The coordination of one AN molecule via π-back donation makes another axial trans-coordination site active (a trans-effect). On receiving the electron-pair of AN, the nickel atom loses the positive charge slightly, but when the electrons of the nickel atom flow in the AN molecule via π-back donation, the density of positive charge on nickel increases. Therefore, the larger the π-back donation becomes, the stronger the second coordination, resulting in K_{NiS2}>K_{NiS1} for nitriles. The activation enthalpy for the loss of a single solvent molecule from (1*R*,4*R*,8*S*,11*S*)-$[NiL(AN)_2]^{2+}$ and (1*R*,4*R*,8*S*,11*S*)-$[NiL(DMF)_2]^{2+}$ are 41.5 and 38.3 kJ mol^{-1}, respectively.[14] This indicates that the coordination of AN to (1*R*,4*R*,8*S*,11*S*)-$[NiL]^{2+}$ is stronger than that of DMF, thus supporting π-back donation. In addition, the wavelength of the absorption maximum is 349 and 373 nm for the octahedral species (1*R*,4*R*,8*S*,11*S*)-$[NiL(S)_2]^{2+}$ in AN and in DMF, respectively, and indicates blue-shifts in AN compared with DMF.[15]

X-Ray crystallographic data showed that the deformation in the square-planar configuration of (1*R*,4*S*,8*R*,11*S*)-$[NiL]^{2+}$ is larger for one AN molecule coordination than that of DMF,[5,29,30] hence supporting the above view. The Ni-N (ring) bond lengths for the non-coordinated, DMF-coordinated, and AN-coordinated species are 0.1960, 0.2105, and 0.2143 nm, respectively. For DMF-coordinated species the distance of nickel atom displaced from the N_4 plane is 0.029 nm, while for the AN-coordinated it is 0.034 nm. The trans non-coordinating axial site of (1*R*,4*S*,8*R*,11*S*)-$[NiL(AN)]^{2+}$ is also activated, but the solvent cannot be coordinated because of the steric hindrance of methylene groups.

Influence of the ligand trans to O_2 on the O_2 adduct formation for the square-planar complex has already been reported.[31-33] The coordination constants of O_2 (K_{O_2}) increases in the order H_2O<pyridine (Py)< imidazole (Im)<NH_3<CN^- for $[Co(cyclam)]^{2+}$, Cl^-< ClO_4^-<Br^-<Py<Im for $[Co(Me_6(14)4,11\text{-dien}\ N_4)]^{2+}$, and ClO_4^-<Cl^-<SCN^- for $[Co(C\text{-meso-}Me_6[14]\text{-}aneN_4)]^{2+}$. As a matter of fact, when the axial ligand trans to O_2 is coordinated to the cobalt atom by π-back donation (e.g. CN^-), the K_{O_2} is large. A correlation between axial ligand basicity and oxygen affinity is stronger for a fully saturated macrocycle than that for unsaturated ones.[31] It is likely that the π-electrons of the macrocycle interrupt the approaching ligand through repulsion, resulting in a large K_{NiS2} for (1*R*,4*R*,8*S*,11*S*)-$[NiL]^{2+}$ which has a saturated macro-

cyclic ligand.

Conclusion

The introduction of AN into the coordination sphere of (1*R*,4*R*,8*S*,11*S*)-$[NiL]^{2+}$ is supported by π-back donation and hence AN is strongly bonded to the nickel atom. Coordination of nitriles by π-back donation activates the opposite axial trans-site of the square-planar complexes, contrary to DMF and DMSO, where no influence on its trans position is observed. The fact that K_{NiS2} is larger than K_{NiS1} for AN in AN–NB mixture, provides conclusive evidence for π-back donation to the nickel atom.

This work was supported by a Grant-in-Aid for Scientific Research, No. 01303004, from the Ministry of Education, Science and Culture.

References

1) P. Moore, J. Sachinidis, and G. R. Willey, *J. Chem. Soc., Chem. Commun.*, **1983**, 522.
2) S. F. Lincoln, J. H. Coates, D. A. Hadi, and D. L. Pisaniello, *Inorg. Chim. Acta*, **81**, L9 (1984).
3) T. W. Hambley, *J. Chem. Soc., Chem. Commun.*, **1984**, 1228.
4) T. W. Hambley, *J. Chem. Soc., Dalton Trans.*, **1986**, 565.
5) I. S. Crick, R. W. Gable, B. F. Hoskins, and P. A. Tregloan, *Inorg. Chim. Acta*, **111**, 35 (1986).
6) P. J. Connolly and E. J. Billo, *Inorg. Chem.*, **26**, 3224 (1987).
7) E. K. Barefield and F. Wagner, *Inorg. Chem.*, **12**, 2435 (1973).
8) E. K. Barefield, F. Wagner, A. W. Herlinger, and A. R. Dahl, *Inorg. Synth.*, **16**, 220 (1975).
9) F. Wagner and E. K. Barefield, *Inorg. Chem.*, **15**, 408 (1976).
10) F. Wagner, M. T. Mocella, M. J. D'Aniello, Jr., A. H.-J. Wang, and E. K. Barefield, *J. Am. Chem. Soc.*, **96**, 2625 (1974).
11) N. Herron and P. Moore, *J. Chem. Soc., Dalton Trans.*, **1979**, 441.
12) E. H. Curzon, N. Herron, and P. Moore, *J. Chem. Soc., Dalton Trans.*, **1980**, 574.
13) J. K. Beattie, M. T. Kelso, W. E. Moody, and P. A. Tregloan, *Inorg. Chem.*, **4**, 415 (1985).
14) P. Moore, *Pure Appl. Chem.*, **57**, 347 (1985).
15) E. Iwamoto, T. Yokoyama, S. Yamasaki, T. Yabe, T. Kumamaru, and Y. Yamamoto, *J. Chem. Soc., Dalton Trans.*, **1988**, 1935.
16) I. S. Crick and P. A. Tregloan, *Inorg. Chim. Acta*, **142**, 291 (1988).
17) T. Yokoyama, E. Iwamoto, and T. Kumamaru, *J. Chem. Soc., Faraday Trans.*, **86**, 2937 (1990).
18) E. Iwamoto, K. Imai, and Y. Yamamoto, *Inorg. Chem.*, **23**, 986 (1984).
19) E. Iwamoto, S. Monya, and Y. Yamamoto, *J. Chem. Soc., Faraday Trans. 1*, **79**, 625 (1983).
20) G. S. Vigee, C. L. Watkins, and H. F. Bowen, *Inorg. Chim. Acta*, **35**, 255 (1979).
21) N. Herron and P. Moore, *Inorg. Chim. Acta*, **36**, 89 (1979).
22) R. M. Fuoss and D. Edelson, *J. Am. Chem. Soc.*, **73**, 269 (1951).
23) R. D. Hancock and A. E. Martell, *Chem. Rev.*, **89**, 1875 (1989).
24) J. Zarembowithch and R. Maleki, *Spectrochim. Acta, Part A*, **39**, 43 (1983).
25) K. Burger, F. Gaizer, E. P-Molnar, and T. T. Binth, *J. Inorg. Nucl. Chem.*, **36**, 863 (1974).
26) A. B. P. Lever, S. M. Nelson, and T. M. Shpherd, *Inorg. Chem.*, **4**, 810 (1965).
27) M. Munakata and S. Kitagawa, *Inorg. Chim. Acta*, **169**, 225 (1990).
28) Y. Fukuda, M. Cho, and K. Sone, *Bull. Chem. Soc. Jpn.*, **62**, 51 (1989).
29) I. S. Crick, B. F. Hoskins, and P. A. Tregloan, *Inorg. Chim. Acta*, **114**, L33 (1986).
30) S. F. Lincoln, T. W. Hambley, D. L. Pisaniello, and J. H. Coates, *Aust. J. Chem.*, **37**, 713 (1984).
31) G. McLendon and M. Mason, *Inorg. Chem.*, **17**, 362 (1978).
32) A. Bakac and J. H. Espenson, *Inorg. Chem.*, **29**, 2062 (1990).
33) P. D. Smith, B. R. James, and D. H. Dolphin, *Coord. Chem. Rev.*, **39**, 31 (1981).

 © 1991 The Chemical Society of Japan Bull. Chem. Soc. Jpn., 64, 469—475 (1991)

Different Kinetic Behavior of Zinc(II), Cadmium(II), and Lead(II) Porphyrins in the Ligand-Substitution Reaction with Ethylenediaminetetraacetic Acid

Masaaki TABATA* and Kazuhisa SUENAGA
Department of Chemistry, Faculty of Science and Engineering, Saga University, Honjo-machi, Saga 840
(Received September 14, 1990)

Kinetics and mechanism of the ligand-substitution reaction of Zn-, Cd-, and Pb(tpps)$^{4-}$ (H_2tpps^{4-}= 5,10,15,20-tetrakis(4-sulfonatophenyl)porphyrin) with ethylenediaminetetraacetic acid (EDTA) have been studied at 25 °C and I=0.1 mol dm^{-3} ($NaNO_3$). The rate equation for the decrease of M(tpps)$^{4-}$ is expressed as $-d[M(tpps)^{4-}]/dt=(k_1[edta^{4-}]+k_2[Hedta^{3-}]+k_3k_4[H]^2(k_{-3}+k_4[H^+])^{-1})[M(tpps)^{4-}]$, where M=$Zn^{2+}$, Cd^{2+}, and Pb^{2+}, and edta^{4-} denotes the fully deprotonated form of EDTA, respectively. The values of k_1 were found to be 0 for all of the metalloporphyrins studied, and k_2=0 mol^{-1}dm^3 s^{-1}; $k_3k_4(k_{-3})^{-1}$=8.7±0.2 mol^{-2} dm^6 s^{-1} for Zn(tpps)$^{4-}$, k_2=4.1±0.2 mol^{-1} dm^3 s^{-1}; $k_3k_4(k_{-3})^{-1}$=(8.3±0.4)×10^{12} mol^{-2} dm^6 s^{-1} for Cd(tpps)$^{4-}$ and k_2=2.0±0.1 mol^{-1} dm^3 s^{-1}; k_3(5.4±0.1)×10^7 mol^{-1} dm^3 s^{-1}; $k_3k_4(k_{-3})^{-1}$=2.0±0.1 mol^{-2} dm^6 s^{-1} for Pb(tpps)$^{4-}$, respectively. Hedta^{3-} directly attacks Cd- or Pb(tpps)^4 to form its metal complex, whereas Hedta^{3-} can not bind Zn(tpps)$^{4-}$. Zn(tpps)$^{4-}$ dissociates to aquazinc(II) by proton attack, then the aquazinc(II) reacts with Hedta^{3-}. Therefore, the ligand-substitution reaction of Zn(tpps)$^{4-}$ with EDTA is so slow that the reaction can be negligible compared with those of Cd- and Pb(tpps)$^{4-}$ in an alkaline solution. The reaction mechanism of the ligand substitution reaction and the different reactivities of the metalloporphyrins in it are discussed in detail.

Since zinc(II), cadmium(II), and lead(II) have filled d shell, they, especially zinc(II) and cadmium(II), are very similar in their chemical properties. For example, the formation constants of their metal complexes with ethylenediaminetetraacetic acid (EDTA) are $10^{16.44}$, $10^{16.36}$, and $10^{17.88}$.[1] Therefore it is difficult to determine these metal ions separately. However, the chemical properties of metalloporphyrins are different considerably. Formation constant of the metalloporphyrin of 5,10,15,20-tetrakis(4-sulfonatophenyl)-porphyrin (H_2tpps^{4-}) with zinc(II) is about 10^9 times larger than that of cadmium(II) or lead(II),[2,3] and the acid-dissociation rate of Cd(tpps)$^{4-}$ is 10^{12} times as fast as that of Zn(tpps)$^{4-}$. These large differences have been applied to the determination of zinc(II) in a large amount of cadmium(II) or lead(II) using the acid-dissociation reaction of their metalloporphyrins or the ligand-substitution reaction with EDTA.[3-5]

It has been believed that metalloporphyrins are very stable and they are hard to be replaced with EDTA.[6-8] In addition, only a few papers concerning the formation constants of metalloporphyrins have been published.[2,9-11] Because of the slow reaction rate of metalloporphyrin formation, it will take a few months or years to reach the equilibrium at room temperature except for some metalloporphyrins of such as mercury(II), cadmium(II), and lead(II). For that reason, it is ambiguous whether thermodynamically or kinetically metalloporphyrins are not replaced with EDTA. We have succeeded in determining the formation constant of Zn(tpps)$^{4-}$ using a catalytic effect of mercury(II) on the formation rate of Zn(tpps)$^{4-}$.[2] Comparing the formation constant of Zn(tpps)$^{4-}$ with that of Zn(edta)$^{2-}$, we have noticed that the conditional formation constant of Zn(tpps)$^{4-}$ is comparable to that of Zn(edta)$^{2-}$ at a neutral pH and that Zn(tpps^{4-}) should be replaced with EDTA thermodynamically in large excess of EDTA.

The present study was undertaken to clarify the reaction mechanism on the replacement of Zn(tpps)$^{4-}$ with EDTA and to get the detailed information on the large differences in the reactivities of Zn-, Cd- and Pb(tpps)$^{4-}$ which have been applied to the determination of zinc(II) in the presence of a large amount of cadmium(II) or lead(II).

Experimental

Reagents. 5,10,15,20-tetrakis(4-sulfonatophenyl)-porphyrine (TPPS) was synthesized and its sodium salt (Na_4H_2tpps) was purified by a previous method.[12] The purity was checked by thin-layer chromatography and ^{1}H NMR. Solutions of zinc(II), cadmium(II), and lead(II) were prepared from their nitrates, and the concentrations in these stock solutions were determined by EDTA titration using Xylenol Orange or Eriochrome Black T as indicators. The ionic strength of the sample solutions was held constant (0.1 mol dm^{-3}) with sodium nitrate. Sodium acetate (1×10^{-2} mol dm^{-3}) or sodium borate (1×10^{-2} mol dm^{-3}) containing nitric acid or sodium hydroxide was used as buffer solution. All reagents were of analytical reagent grade and all solutions were prepared in water deionized and then distilled from alkaline permanganate. The solutions of the metalloporphyrins were prepared just before the kinetic measurements in volumetric flasks covered with aluminum foil to shield from light. The formation of the metalloporphyrins was confirmed spectrophotometrically.

Measurement. The ligand-substitution reaction of M(tpps)$^{4-}$ (M=Zn^{2+}, Cd^{2+}, and Pb^{2+}) with EDTA was studied in a pH range 3—4.5 for Zn(tpps)$^{4-}$ and 8.0—9.3 for Cd- and Pb(tpps)$^{4-}$ at the concentrations of EDTA (1.0×10^{-3}—5.0×10^{-2} mol dm^{-3}), metal ions (Zn^{2+}, Cd^{2+}, Pb^{2+}; each at 4.0×10^{-6}—1.0×10^{-4} mol dm^{-3}) and H_2tpps^{4-} (1.0×10^{-6}—2.0×10^{-6} mol dm^{-3}). The reaction was started by mixing a

$M(tpps)^{4-}$ solution with an EDTA solution using a sample mixing device (Union Giken, MX7). The change in absorbance at Soret bands of the metalloporphyrins (421 nm for $Zn(tpps)^{4-}$, 430 nm for $Cd(tpps)^{4-}$, and 465 nm for $Pb(tpps)^{4-}$) was monitored as a function of time on a Hitachi 323 spectrophotometer. The kinetic studies for the acid-dissociation rate of Zn-, Cd-, and $Pb(tpps)^{4-}$ were carried out in a pH range of 1.2—2.0 for $Zn(tpps)^{4-}$ and that of 4.5—5.5 (acetate buffer, 10^{-2} mol dm^{-3}) for $Cd(tpps)^{4-}$ and $Pb(tpps)^{4-}$, respectively. The change in absorbance at Soret band of the metalloporphyrins was followed by a Uniongiken RA401 stopped-flow spectrophotometer at 25 °C.

The pH values were determined by a Radiometer Ion 85 Ion Analyzer with a combined electrode (GK2401C). A 1.000×10^{-2} mol dm^{-3} nitric acid solution containing 0.09 mol dm^{-3} sodium nitrate was employed as a standard hydrogen ion concentration ($-\log[H^+]=2.000$). From pH meter readings in various hydrogen ion concentrations at 0.1 mol dm^{-3} ionic strength (HNO_3-$NaNO_3$), the pH meter and electrode system was calibrated in terms of $-\log[H^+]$.

Results

Ligand-Substitution Reaction of Zn-, Cd-, and $Pb(tpps)^{4-}$ with EDTA. The reaction of $M(tpps)^{4-}$ ($M=Zn^{2+}$, Cd^{2+}, and Pb^{2+}) with EDTA was studied in large excess of EDTA at pH 3—4.5 for the reaction of $Zn(tpps)^{4-}$ and at pH 8—9.3 for that of Cd- and $Pb(tpps)^{4-}$. Under the present experimental conditions, the porphyrin is in its protonated and free base forms: H_4tpps^{2-}, H_3tpps^{3-}, and H_2tpps^{4-}, since the protonation constants for $[H_3tpps^{3-}][H^+]^{-1}[H_2tpps^{4-}]^{-1}$ and for $[H_4tpps^{2-}][H^+]^{-1}[H_3tpps^{3-}]^{-1}$ are $10^{4.99}$ and $10^{4.76}$, respectively.[2] Furthermore, the chemical species of EDTA are in the forms of H_3edta^-, H_2edta^{2-}, $Hedta^{3-}$, and $edta^{4-}$. Thus the reaction of $M(tpps)^{2-}$ with EDTA is written as

$$M(tpps)^{2-} + edta' \rightleftarrows M(edta)^{2-} + tpps', \quad (1)$$

where edta' and tpps' are all chemical species of EDTA and TPPS not bound to metal ions, respectively. The equilibrium of metalloporphyrin formation is generally given by

$$M^{2+} + H_2tpps^{4-} \rightleftarrows M(tpps)^{4-} + 2H^+, \quad (2)$$

with the equilibrium constant defined by

$$K_{MP} = \frac{[M(tpps)^{4-}][H^+]^2}{[M^{2+}][H_2tpps^{4-}]}, \quad (3)$$

and the values of K_{MP} have been found to be $10^{-0.43}$, $10^{-9.94}$, $10^{-9.97}$ for Zn-, Cd-, and $Pb(tpps)^{4-}$, respectively at 25 °C and I=0.1 mol dm^{-3}.[2,3] Moreover, the formation constants of $M(edta)^{2-}$ are respectively $10^{16.44}$, $10^{16.36}$, and $10^{17.88}$ for $M=Zn^{2+}$, Cd^{2+}, and Pb^{2+}, while the stepwise protonation constants of $edta^{4-}$ are $10^{10.17}$, $10^{6.18}$, and $10^{2.68}$.[1] Thus the equilibrium constants of Eq. 1 are calculated to be $10^{2.39}$ at pH 4 for $Zn(tpps)^{4-}$, $10^{8.13}$ at pH 8 for $Cd(tpps)^{4-}$, and $10^{8.16}$ at pH 8 for $Pb(tpps)^{4-}$, respectively. The metalloporphyrins, therefore, are completely replaced with EDTA and the reverse reaction of Eq. 1 can be neglected in large excess of EDTA compared with that of TPPS.

Thus, the pseudo-first-order kinetics was observed for the reaction of Eq. 1:

$$-d[M(tpps)^{4-}]/dt = k_0[M(tpps)^{4-}], \quad (4)$$

where k_0 denotes the conditional rate constant containing concentrations of edta', hydrogen ion, and metal ion. The k_0 values for the reactions of Cd- and $Pb(tpps)^{4-}$ increased with the edta' (Fig. 1), and this result shows that the reaction is first-order in edta'. In contrast, the k_0 values for the reaction of $Zn(tpps)^{4-}$ were independent of edta' even at its concentration of 0.05 mol dm^{-3} (Fig. 2). Figure 3 shows the dependence of rate constant on hydrogen ion concentration for the reaction of Cd- and $Pb(tpps)^{4-}$ with EDTA. The k_0 values increased with hydrogen ion concentrations and reached a plateau at pH 8, where main chemical species of EDTA is in the form of $Hedta^{3-}$. Thus the reaction mechanism to account for the kinetic data is shown in Scheme 1:

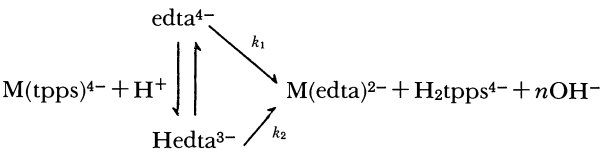

Scheme 1.

This leads to the rate equation of Eq. 5

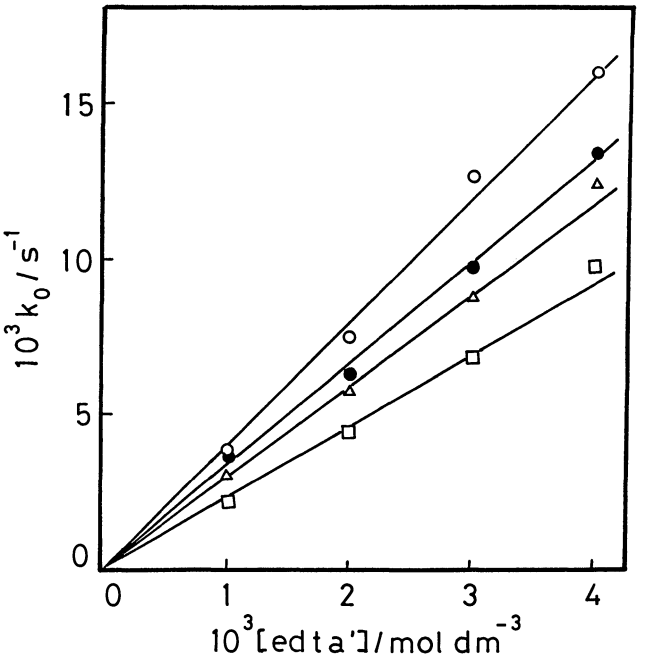

Fig. 1. Dependence of rate constants on the concentrations of edta' for the reaction of $Cd(tpps)^{4-}$ with EDTA in pH 8.01 (○), 8.48 (●), 8.69 (△), and 9.09 (□) at 25 °C and I=0.1 mol dm^{-3} ($NaNO_3$).

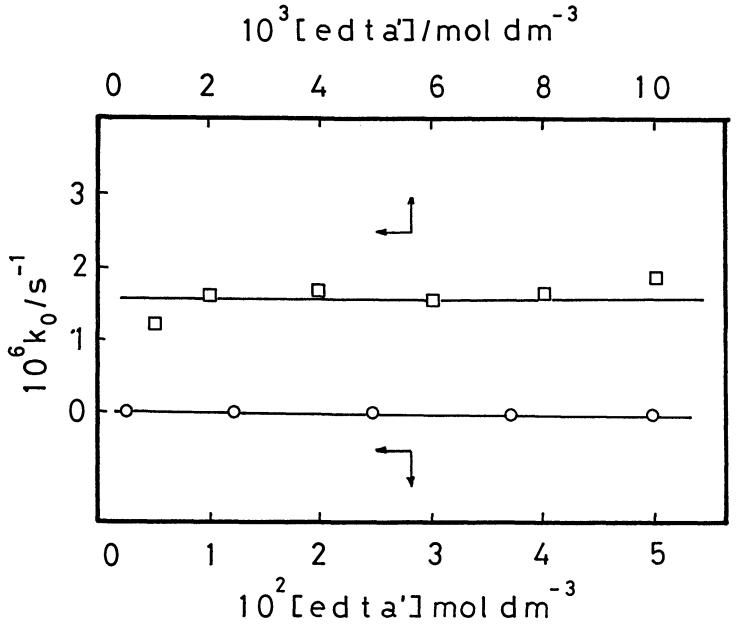

Fig. 2. Dependence of rate constants on the concentrations of edta' for the reaction of $Zn(tpps)^{4-}$ with EDTA in pH 3.30 (□) and 4.50 (○) at 25 °C and I=0.1 mol dm^{-3} ($NaNO_3$).

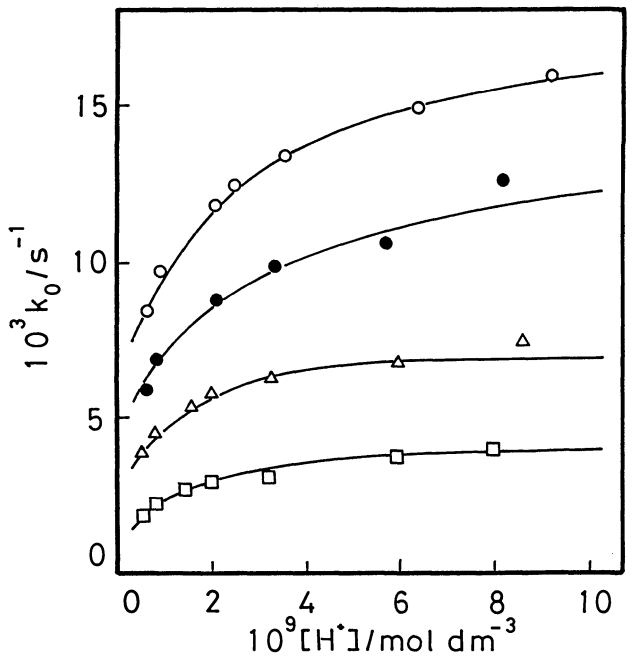

Fig. 3. Dependence of rate constants on the concentrations of hydrogen ion for the reaction of $Cd(tpps)^{4-}$ with EDTA at 25 °C and I=0.1 mol dm^{-3} ($NaNO_3$). [edta']/mol dm^{-3}=1.00×10^{-3} (□), 2.00×10^{-3} (△), 3.00×10^{-3} (●), and 4.00×10^{-3} (○).

$$k_0 = k_1[\text{edta}^{4-}] + k_2[\text{Hedta}^{3-}] \quad (5)$$

$$= \frac{(k_1 + k_2K^{H}[H^+])[\text{edta'}]}{1 + K^{H}[H^+]}, \quad (6)$$

where [edta']=[edta^{4-}]+[Hedta^{3-}]. Equation 6 is rearranged to

$$k_0(1 + K^{H}[H^+])[\text{edta'}]^{-1} = k_1 + k_2K^{H}[H^+] \quad (7)$$

where K^{H} is the protonation constant of edta^{4-}: $K^{H}=10^{10.17}$. The plots of the left-hand side of Eq. 7 against [H$^+$] give straight lines with zero intercept for Cd- and $Pb(tpps)^{4-}$ (Fig. 4). The values were found to be k_1=0 mol^{-3} dm^3 s^{-1} both for Cd- and $Pb(tpps)^{4-}$, k_2=4.1±0.2 mol^{-1} dm^3 s^{-1} for $Cd(tpps)^{4-}$ and k_2= 2.02±0.1 mol^{-1} dm^3 s^{-1} for $Pb(tpps)^{4-}$. In Fig. 5, the k_0 values are plotted against the concentrations of cadmium(II) or lead(II). The results show that the k_0 values are independent of the concentrations of these metal ions, and suggest that the metalloporphyrins do not dissociate before the attack of EDTA to Cd- or $Pb(tpps)^{4-}$.

Acid-Dissociation of Zn-, Cd-, and $Pb(tpps)^{4-}$. Protolytic demetallation of Zn-, Cd, and $Pb(tpps)^{4-}$ was studied in acidic medium. Cd- and $Pb(tpps)^{4-}$ easily dissociate in a dilute acid solution of pH 4—6 and $Zn(tpps)^{4-}$ dissociates at lower pH than 2. The observed first-order rate constants were plotted against [H$^+$]^2. The plots for Zn- and $Cd(tpps)^{4-}$ were straight lines, while those for $Pb(tpps)^{4-}$ were proportion to[H$^+$]^2 at the low concentration of hydrogen ion but suppressed at the high concentrations of hydrogen ion. This indicates that the rate for the second-proton attack to $Pb(Htpps)^{3-}$ which is formed in the first-protonation of $Pb(tpps)^{4-}$ as shown in Scheme 2 becomes comparable to that for the dissociation $Pb(Htpps)^{3-}$.

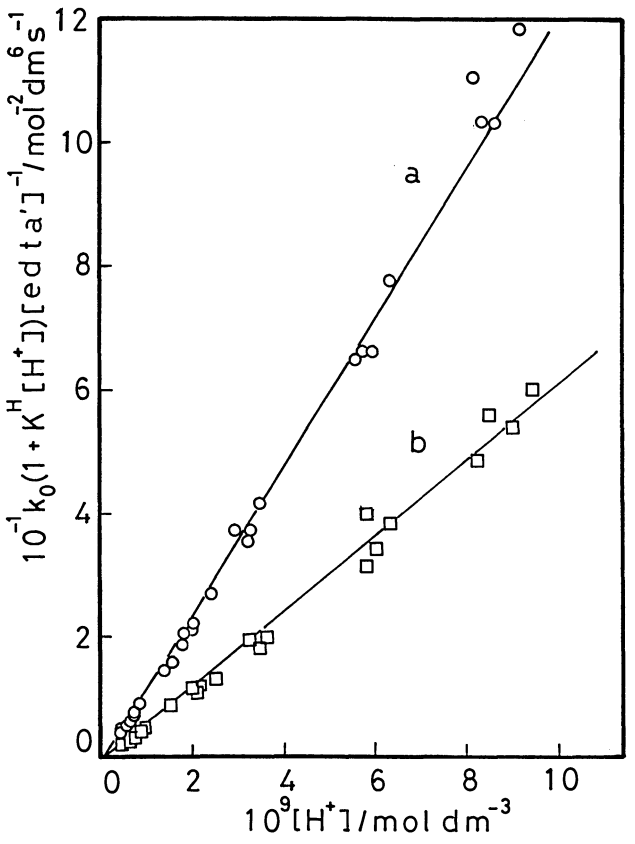

Fig. 4. Plots of 10^{-1} k_0 $(1+K^H[H^+])/[edta']$ vs. $[H^+]$ for the reaction of $Cd(tpps)^{4-}$ (a) and $Pb(tpps)^{4-}$ (b) with EDTA at 25 °C and I=0.1 mol dm^{-3} ($NaNO_3$).

$$M(tpps)^{4-} + H^+ \underset{k_{-3}}{\overset{k_3}{\rightleftarrows}} M(Htpps)^{3-} \quad (8)$$

$$M(Htpps)^{3-} + H^+ \xrightarrow{k_4} M^{2+} + H_2tpps^{4-} \quad (9)$$

$$H_2tpps^{4-} + 2H^+ \xrightarrow{fast} H_4tpps^{2-} \quad (10)$$

Scheme 2.

Applying the steady-state approximation for $M(Htpps)^{3-}$, we have Eq. 11

$$k_0 = \frac{k_3k_4[H^+]^2}{k_{-3}+k_4[H^+]}. \quad (11)$$

The equation agrees with the observed kinetic results. That is, $k_{-3} \gg k_4[H^+]$ for Zn- and $Cd(tpps)^{4-}$, and $k_{-3} \approx k_4[H^+]$ for $Pb(tpps)^{4-}$ at the high concentration of hydrogen ion. Equation 11 is rearranged to

$$[H^+]^2k_0^{-1} = k_{-3}(k_3k_4)^{-1} + k_3^{-1}[H^+]. \quad (12)$$

The plots of $[H^+]^2k_0^{-1}$ vs. $[H^+]$ are shown in Fig. 6. For Cd- and $Zn(tpps)^{4-}$, only $k_3k_4(k_{-3})^{-1}$ was found, while for $Pb(tpps)^{4-}$ both k_3 and $k_3k_4(k_{-3})^{-1}$ were determined.

Combining the rate equations both for the ligand-substitution reaction of $M(tpps)^{4-}$ with EDTA (Eq. 5) and the acid-dissociation reaction of $M(tpps)^{4-}$ (Eq. 11), we have Eq. 13 for the the rate of the decrease of $M(tpps)^{4-}$

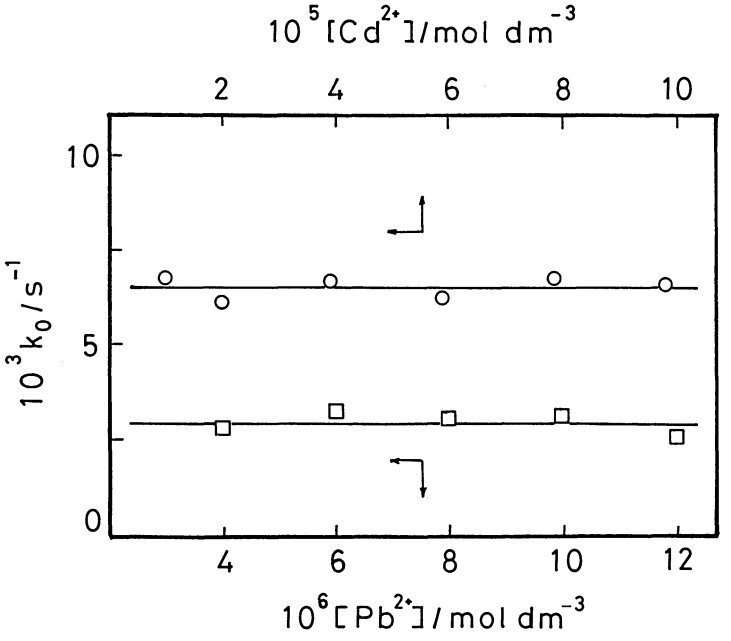

Fig. 5. Dependence of rate constants on the concentrations of cadmium(II) (○) and lead(II) (□) for the reaction of Cd- and $Pb(tpps)^{4-}$ with EDTA at 25 °C and I=0.1 mol dm^{-3} ($NaNO_3$). Concentrations of edta' (mol dm^{-3}) and pH are 2.00×10^{-3} and 8.26 for $Cd(tpps)^{4-}$, and 4.00×10^{-3} and 8.69 for $Pb(tpps)^{4-}$, respectively.

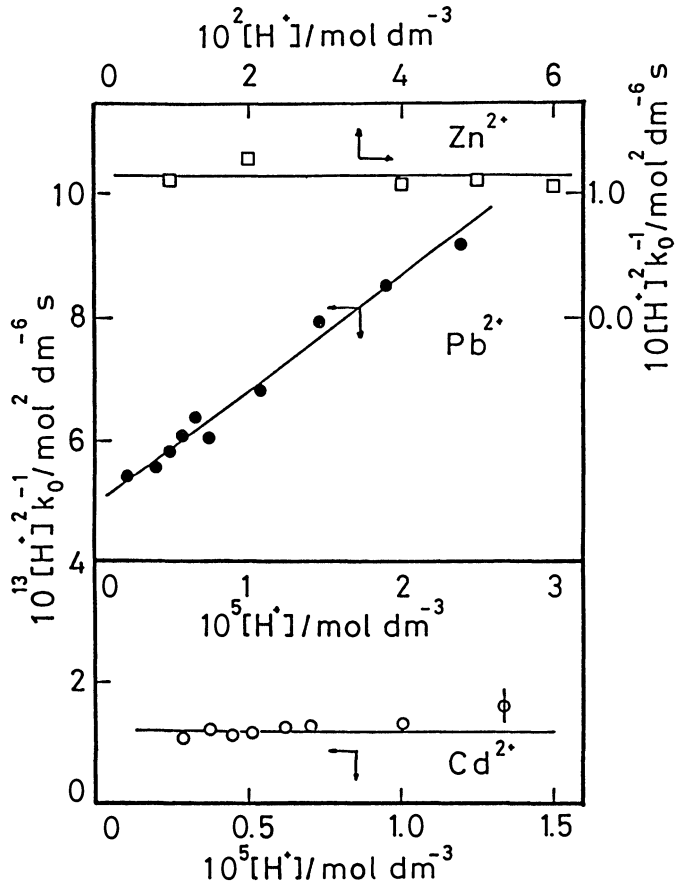

Fig. 6. Plots of $[H^+]^2(k_0)^{-1}$/mol^2 dm^{-6} s vs. $[H^+]$ for the acid-dissociation of Zn(tpps)$^{4-}$ (□), Pb(tpps)$^{4-}$ (●), and Cd(tpps)$^{4-}$ (○) at 25 °C and I=0.1 mol dm^{-3} ($NaNO_3$).

Table 1. Kinetic Parameters for the Reaction of Zn-, Cd-, and Pb(tpps)$^{4-}$ with EDTA and the Acid-Dissociation Reaction of the Metalloporphyrins at 25 °C and I=0.1 mol dm^{-3} ($NaNO_3$)

	Zn(II)	Cd(II)	Pb(II)
k_2 / mol^{-1} dm^3 s^{-1}	0.00	4.1±0.2	2.0±0.1
k_3 / mol^{-1} dm^3 s^{-1}	—	—	(5.4±0.3)×10^7
$k_3k_4(k_{-3})^{-1}$ / mol^{-2} dm^6 s^{-1}	8.7±0.2	(8.3±0.4)×10^{12}	(2.0±0.1)×10^{12}
K_{MP} / mol dm^{-3}	10$^{-0.43}$	10$^{-9.94}$	10$^{-9.97}$

$$-d[M(tpps)^{4-}]/dt = (k_1[edta^{4-}] + k_2[Hedta^{3-}] + k_3k_4[H^+]^2 \times (k_{-3} + k_4[H^+])^{-1})\,[M(tpps)^{4-}]. \quad (13)$$

In Table 1, the kinetic and the equilibrium parameters are summarized for the ligand-substitution and the acid-dissociation reactions of Cd-, Pb-, and Zn(tpps)$^{4-}$, where the values of k_1 are not shown as they were 0 for all the M(tpps)$^{4-}$.

Discussion

We can see the followings from Table 1. 1. Zn(tpps)$^{4-}$ is hard to be replaced with EDTA, whereas Cd- and Pb(tpps)$^{4-}$ are easily substituted with EDTA. 2. Acid-dissociation rate of Cd- and Pb(tpps)$^{4-}$ is 10^{12} times faster than that of Zn(tpps)$^{4-}$. 3. The formation constant of Zn(tpps)$^{4-}$ is about 10^9 times as large as those of Cd- and Pb(tpps)$^{4-}$. These large differences are discussed below.

Reaction with EDTA. The rate of the ligand-substitution reaction of Cd- or Pb(tpps)$^{4-}$ with EDTA increased linearly along with the concentrations of edta', while that of Zn(tpps)$^{4-}$ was independent of edta'. The kinetic difference between zinc(II) and cadmium(II) or lead(II) can be ascribed to their ionic radii: 109 pm for Cd^{2+}; 132 pm for Pb^{2+}; 89 pm for Zn^{2+}. Large metal ions such as cadmium(II) and lead(II) can not incorporate well into porphyrin core and just sit on the porphyrin plane. Barkigia et al. called lead(II) porphyrin a "roof complex" after X-ray

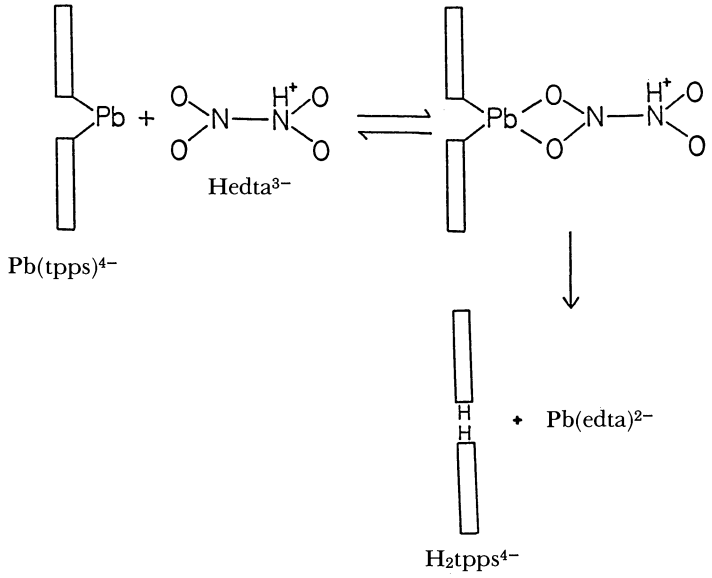

Fig. 7. Reaction mechanism for the reaction of $Pb(tpps)^{4-}$ with EDTA. ▭ H-H ▭ denotes H_2tpps^{4-}.

analysis of tetrapropylporphyrinato lead(II).[13] The roof metalloporphyrin, therefore, can be bound with a segment of $Hedta^{3-}$: two carboxylato and nitrilo groups, and then is easily replaced with $Hedta^{3-}$ (see Fig. 7). On the other hand, zinc(II) incorporates well into porphyrin core to form stable $Zn(tpps)^{4-}$.[14-16] Thus, $Hedta^{3-}$ can not pull zinc(II) away from $Zn(tpps)^{4-}$ by means of an axial ligation of $Hedta^{3-}$.

Dependence of rate constant on pH for the reaction with EDTA indicates that $Hedta^{3-}$ is more reactive than $edta^{4-}$. Similar results were also observed for the reaction of $Gd^{III}(tpps)^{4-}$ with EDTA.[17] A proton-transfer pathway might contribute to the dissociation of metalloporphyrin as in the case of the ligand-substitution reaction of metal-peptide complexes.[18-20] First, the carboxylato and the nitrilo groups of $Hedta^{3-}$ coordinate to lead(II) or cadmium(II), then the proton bound to the other nitrilo nitrogen of $Hedta^{3-}$ transfers to the pyrrole nitrogen of the porphyrin. Binding of the proton to the pyrrole nitrogen makes the demetallation of Cd- or $Pb(tpps)^{4-}$ easier (vide infra).

Proton-Assisted Demetallation. The metalloporphyrins of Cd-, Pb-, and $Zn(tpps)^{4-}$ were demetallated in acidic solution. The rate for the acid dissociation of $Cd(tpps)^{4-}$, is only four times as fast as that for $Pb(tpps)^{4-}$, while the dissociation rate for $Zn(tpps)^{4-}$ is about 10^{12} times slower than those for $Cd(tpps)^{4-}$ and $Pb(tpps)^{4-}$. The large kinetic difference also results from the ionic radii as described before. In the case of the demetallation of $Pb(tpps)^{4-}$, the present kinetic data clearly indicate that hydrogen ion attacks the

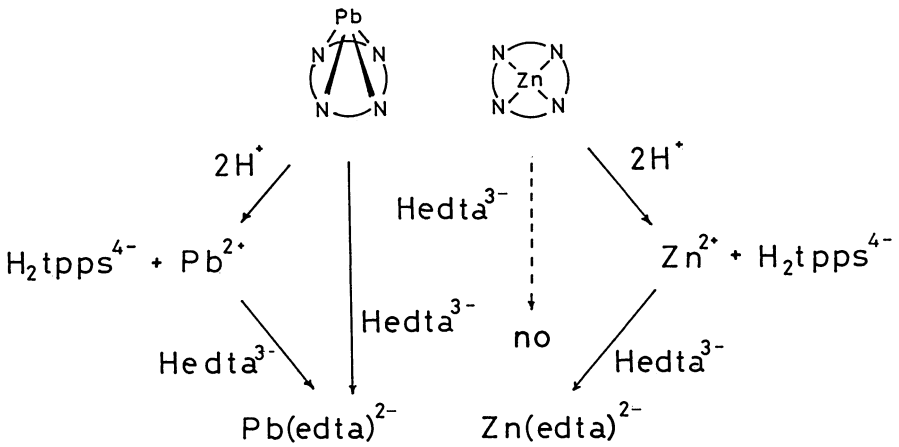

Fig. 8. Summary of the reaction pathways for the reaction of Pb- and $Zn(tpps)^{4-}$ with EDTA. $Cd(tpps)^{4-}$ goes through the same reaction pathway as $Pb(tpps)^{4-}$.

porphyrin core step by step to bind the pyrrole nitrogens. The first step is the formation of $Pb(Htpps)^{3-}$ through the protonation, and the second step is the dissociation of the metalloporphyrin after the formation of the diprotonated metalloporphyrin: $Pb(H_2tpps)^{2-}$.

Proposed reaction mechanism is shown in Fig. 8. $Hedta^{3-}$ directly attacks Pb- or $Cd(tpps)^{4-}$ to form its metal complex. On the other hand, $Hedta^{3-}$ can not bind $Zn(tpps)^{4-}$. Therefore, $Zn(tpps)^{4-}$ dissociates to aquazinc(II) and the free-base porphyrin after the proton attack, then the aquazinc(II) reacts with $Hedta^{3-}$ to form $Zn(edta)^{2-}$. Pb- and $Cd(tpps)^{4-}$ also dissociate to their aqua ions in an acidic medium. The rate-determining step for Pb- and $Cd(tpps)^{4-}$ is the $Hedta^{3-}$ attack at pH 8—9.3, which shifts to the proton attack at pH 4—6.

Present paper clearly shows the different behavior of Zn-, Cd-, and $Pb(tpps)^{4-}$ in their reaction mechanism and rate constants. $Zn(tpps)^{4-}$ is replaced with EDTA although the reaction is very slow compared with Cd- and $Pd(tpps)^{4-}$, and the rate-determining step for $Zn(tpps)^{4-}$ is the proton attack. The differences in the kinetic behavior of Zn-, Cd-, and $Pb(tpps)^{4-}$ also strongly support the experimental results in the previous analytical methods for the determination of zinc(II) in large excess of cadmium(II) and lead(II) using the ligand substitution reaction with EDTA or the acid-dissociation rate of these metalloporphyrins.

The present study was partly supported by Grant-in-Aid for Scientific Research (No. 01470030) and a Grant-in-Aid for Scientific Research (No. 02245212) on Priority Area of "Molecular Approaches to Nonequilibrium Processes in Solutions" from the Ministry of Education, Science and Culture Japan. We also wish to express our thanks for the support from Ito Foundation.

References

1) A. E. Martell and R. M. Smith, "Critical Stability Constants," Plenum Press, New York (1974), Vol. 1, pp. 204—211.
2) M. Tabata and M. Tanaka, *J. Chem. Soc., Chem. Commun.*, **1985**, 42.
3) M. Tabata and N. Kajihara, *Anal. Sci.*, **5**, 719 (1989).
4) M. Tabata, K. Oshita, and M. Tanaka, *Mikrochim. Acta Wien*, **1985 I**, 397.
5) H. Ishii and H. Tuchiai, *Anal. Sci.*, **3**, 229 (1987).
6) B. Dempsey, M. B. Lowe, and J. N. Philips, "Hematin Enzymes," ed by J. E. Falk, R. Lemberg, and R. K. Morton, Pergamon Press, London (1961), Part 1, pp. 29—40.
7) P. Hambright, "Porphyrins and Metalloporphyrins," ed by K. M. Smith, Elsevier, New York (1975), pp. 233—278.
8) D. K. Lavallee, *Coord. Chem. Rev.*, **61**, 55 (1985).
9) P. Hambright, *Inorg. Chem.*, **16**, 2987 (1977).
10) D. Brisbin and R. Balahura, *Can. J. Chem.*, **44**, 2157 (1957).
11) H. R. Jimenez, M. Julve, J. M. Moratal, and J. Faus, *J. Chem. Soc., Chem. Commun.*, **1987**, 910.
12) M. Tabata and M. Tanaka, *J. Chem. Soc., Dalton Trans.*, **1983**, 1955.
13) K. M. Barkigia, J. Fajer, A. D. Adler, and G. J. B. Wiliams, *Inorg. Chem.*, **19**, 2057 (1980).
14) W. R. Scheidt, M. E. Kastner, and Hatano, *Inorg. Chem.*, **17**, 706 (1978).
15) C. K. Schaure, O. P. Anderson, S. S. Eaton, and G. Eaton, *Inorg. Chem.*, **24**, 4082 (1985).
16) W. R. Scheidt, J. U. Mondal, C. W. Eigenbrot, A. Adler, and L. J. Radonvich, *Inorg. Chem.*, **25**, 795 (1986).
17) P. Hambright, C. Adams, and K. Vernon, *Inorg. Chem.*, **27**, 1660 (1988).
18) M. Tabata and M. Sarkar, *Can. J. Chem.*, **63**, 3111 (1985).
19) J. C. Cooper, L. F. Wong, D. L. Venezky, and D. W. Margerum, *J. Am. Chem. Soc.*, **96**, 7560 (1974).
20) C. E. Bannister, J. M. Raycheba, and D. W. Margerum, *Inorg. Chem.*, **21**, 1106 (1982).

Solvent Extraction of Dansyl-Amino Acid Anions by Dicationic Extractants

Akira OHKI,* Hiroyuki DOHMITSU, and Shigeru MAEDA
Department of Applied Chemistry, Faculty of Engineering, Kagoshima University,
1-21-40, Korimoto, Kagoshima 890
(Received September 25, 1990)

The extraction of dansyl-amino acid anions from an alkaline aqueous medium was studied by the use of dicationic anion-exchange extractants, polymethylenebis(trioctylphosphonium)s (abbreviated as C_nBPs; n=2—12). As for the extraction of dianionic species, such as dansyl-aspartic acid anion (Dns-Asp^{2-}) and dansyl-glutamic acid anion (Dns-Glu^{2-}), the dicationic extractants were greatly superior to a monocationic extractant, butyltrioctylphosphonium (BuMP). However, regarding the extraction of monoanionic species, such as dansyl-serine anion, dansyl-phenylalanine anion, and dansyl-valine anion, the extraction abilities of the dicationic extractants and the monocationic extractant were similar to one another. The extraction ability of dicationic extractants was remarkably dependent on the length of their bridge-chain, which connects the two ionic centers. For extractants having short bridge-chain (C_2BP—C_4BP), Dns-Asp^{2-} was more extracted than Dns-Glu^{2-}. On the contrary, for extractants with long bridge-chain (C_8BP—$C_{12}BP$), Dns-Glu^{2-} was more extracted than Dns-Asp^{2-}. The solvent effect on the extraction of Dns-Asp^{2-} and Dns-Glu^{2-} was also studied.

Solvent extraction using anion-exchange extractants (liquid anion-exchangers) is widely used in separation processes of analytical chemistry.[1] Not only the extraction of metal complex anions, but also that of organic anions, have been studied by many researchers. However, as for the extraction of organic anions, 1 : 1 ion-pair formation between an extractant and an extracted anion has been most extensively discussed. Few studies have been concerned with multi-point ion-pair formation within a complex. Most of the liquid anion-exchange extractants hitherto reported are monoonium salts, i.e., long-chain quaternary ammonium ions and protonated long-chain tertiary amines have been used.

In recent years, we have developed dicationic anion-exchange extractants, which are lipophilic diphosphonium ions bearing two cationic centers within a molecule.[2-5] In our previous paper,[6] the extraction of phthalate isomer dianions (phthalate, isophthalate, and terephthalate) from an alkaline aqueous medium was studied by the use of such dicationic extractants, polymethylenebis(trioctylphosphonium)s (abbreviated as C_nBPs; n=2—12; Fig. 1). Two-point ion-pair formation within a complex between the dicationic extractant and the dianionic species caused some peculiar phenomena.

In the present study we investigated the extraction of dansyl-amino acid anions by use of the dicationic extractants (C_nBPs) and a monocationic extractant, butyltrioctylphosphonium (BuMP). Dansyl-amino acids have frequently been used in the field of chromatography. However, the extraction of dansyl-amino acids from alkaline media has not yet been sufficiently studied in detail. Especially, regarding the extraction of dicarboxylates, Dns-Asp^{2-} and Dns-Glu^{2-} (Fig. 1), two-point ion-pair formation within a complex has not yet been studied.

The effect of extracting solvent is one of the important factors in anion-exchange extractions. However, this effect has not yet been studied regarding the extractions using dicationic extractants. We found and analyzed a peculiar solvent effect when the dicationic extractants were used.

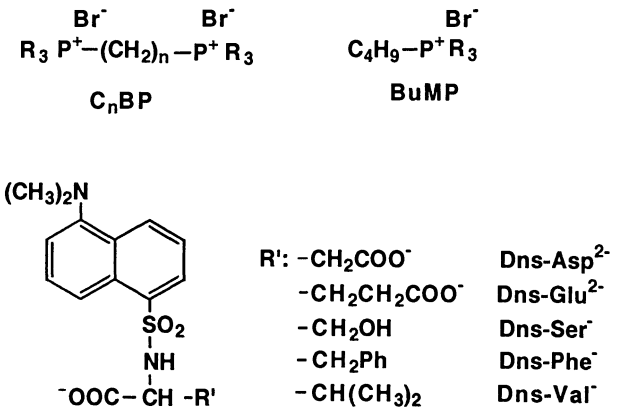

Fig. 1. Anion-exchange extractants, C_nBPs and BuMP (R=octyl; n=2—12), and dansyl-amino acid anions. The all carboxyl groups of dansyl-amino acids act as carboxylate anions under the relevant pH conditions (pH 10). Therefore, dansyl-aspartic acid, dansyl-glutamic acid, dansyl-serine, dansyl-phenylalanine, and dansyl-valine are abbreviated as Dns-Asp^{2-}, Dns-Glu^{2-}, Dns-Ser^{-}, Dns-Phe^{-}, and Dns-Val^{-}, respectively.

Experimental

Reagents. The synthesis of C_nBPs and BuMP was described in our previous paper.[5] Dansyl-amino acids (Sigma) and other chemicals were of reagent grade and used without further purification.

Extraction Procedure. An aqueous solution (10 ml) containing a 0.1 mM (1 M=1 mol dm^{-3}) dansyl-L-amino acid, sodium bromide, and 10 mM $Na_2B_4O_7$–NaOH buffer (pH 10) was shaken with an organic solution (10 ml) containing a 0.2 mM C_nBP (or 0.4 mM BuMP) in a stoppered centrifuge tube at 25 °C for 30 min. After phase separation, the con-

centration of the dansyl-amino acid anion remaining in the aqueous phase was determined by spectrophotometry using a Hitachi 228 instrument (λ_{max}=328 nm). The amount of the dansyl-amino acid anion extracted into the organic phase was taken as the difference between the amount initially added and that remaining in the aqueous phase after equilibrium. In some runs, the material balance on the distribution of dansyl-amino acid anions between the aqueous and organic phases was confirmed by back-extraction experiments.[2)]

Results and Discussion

Extraction of Dansyl-Amino Acids. The extraction of dansyl-amino acids by various anion-exchange extractants is summarized in Table 1. The concentration of the monocationic extractant (BuMP) initially added to the organic phase was twice that of the dicationic extractants (C_nBPs). Therefore, the cationic charge concentration in the aqueous phase was the same for both the monocationic and dicationic extractants.

It is reasonable to consider that the dansyl-derivatives of neutral amino acids (Dns-Ser$^-$, Dns-Phe$^-$, and Dns-Val$^-$) serve as monoanions under the relevant pH conditions (pH 10). When these dansyl-amino acids were extracted, the extraction abilities of the monocationic extractant (BuMP) and the dicationic extractants (C_4BP and $C_{10}BP$) were similar to each other.

However, when the dansyl-derivatives of acidic amino acids (Dns-Asp^{2-} and Dns-Glu^{2-}) were extracted, which serve as dianions, the extraction ability of the dicationic extractants greatly surpassed that of the monocationic extractant. These results suggest that the compatibility of the charge number between the extractant and the extracted anion greatly affects the extractability. We observed such a concept in the extraction of dianionic species including anionic metal complexes[2,4,5)] and phthalates;[6)] we call this concept "multiple charge compatibility."

A commercially available monocationic extractant, Capriquat (methyltrioctylammonium), showed a similar extraction behavior to that of BuMP in the extraction of the monoanionic dansyl-amino acids, as well as in the extraction of the dianionic dansyl-amino acids.

Table 1. % Extraction of Dansyl-Amino Acids[a)]

Dansyl-amino acid	[NaBr][b)]	Extractant		
	mM	BuMP	C_4BP	$C_{10}BP$
Dns-Asp^{2-}	1.2	3.9	57.3	26.2
Dns-Glu^{2-}	1.2	2.7	41.8	30.2
Dns-Ser$^-$	50	30.0	25.7	27.3
Dns-Phe$^-$	200	79.6	76.3	79.6
Dns-Val$^-$	200	44.3	46.7	39.1

a) Extracting Solvent: 1,2-dichloroethane. b) Sodium bromide was initially added in the aqueous phase.

Extraction Equilibrium of Dianionic Dansyl-Amino Acids. The extraction of dianionic dansyl-amino acids, Dns-Asp^{2-} and Dns-Glu^{2-}, was investigated in detail. One can assume that the extraction of the dianion (A^{2-}) by the dicationic extractant (C_nBP) involves the formation of a 1:1 ion-pair complex between C_nBP and A^{2-}. The reaction and the extraction constant (K_{ex}) can be defined as follows:

$$(Q\cdot Br_2)_o + (A^{2-})_w \rightleftarrows (Q\cdot A)_o + 2(Br^-)_w,$$

and

$$K_{ex} = [Q\cdot A]_o[Br^-]_w^2/[Q\cdot Br_2]_o[A^{2-}]_w, \quad (1)$$

where $Q\cdot Br_2$ represents C_nBP, and subscripts w and o denote the aqueous and organic phases, respectively. It can also be expressed logarithmically:

$$\log [Q\cdot A]_o/[Q\cdot Br_2]_o[A^{2-}]_w = \log K_{ex} - 2\log [Br^-]_w. \quad (2)$$

The $Q\cdot Br_2$ and the complex, $Q\cdot A$, are highly lipophilic and do not appreciably dissolve in the aqueous phase. Thus, the values of $\log [Q\cdot A]_o/[Q\cdot Br_2]_o[A^{2-}]_w$ and $\log [Br^-]_w$ in Eq. 2 can be easily obtained experimentally.

With the monocationic extractant (BuMP) calibrations were carried out in such a way that $[Q\cdot Br_2]_o$ and $[Q\cdot A]_o$ in Eq. 2 were taken as $2\times[BuMP^+\cdot Br^-]_o$ and $[(BuMP^+)_2\cdot A^{2-}]_o$, respectively.

Figure 2 shows a plot of $\log [Q\cdot A]_o/[Q\cdot Br_2]_o[A^{2-}]_w$

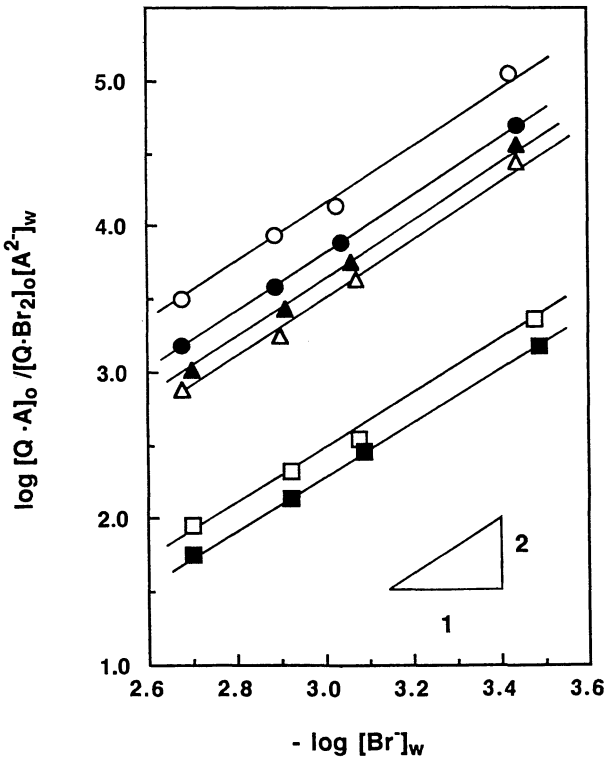

Fig. 2. Extraction of Dns-Asp^{2-} (○, C_4BP; △, $C_{10}BP$; □, BuMP) and Dns-Glu^{2-} (●, C_4BP; ▲, $C_{10}BP$; ■, BuMP) (extracting solvent: 1,2-dichloroethane).

against $-\log[Br^-]_w$ in the extractions of Dns-Asp^{2-} and Dns-Glu^{2-}; the extractants (C_4BP, $C_{10}BP$, and BuMP) were used and 1,2-dichloroethane was used as an extracting solvent (diluent). All of the plots in Fig. 2 are straight lines with a slope of 2. These results suggest that the extraction reaction proceeds via the formation of a 1 : 1 ion-pair complex between C_nBP^{2+} and A^{2-} (or a 2 : 1 complex between $BuMP^+$ and A^{2-}). These results again indicate that the dansyl-amino acids serve as dianions, so that the dissociation of the sulfonamide proton in dansyl-amino acids is negligibly small under the present conditions.

Figure 3 (a and b) shows graphical representations of the extraction constants ($\log K_{ex}$) as a function of the length of "bridge-chain" of C_nBPs; the "bridge-chain" is defined as the bridging chain connecting the two ionic centers of the extractant (or extracted anion). The bridge-chain length greatly affects the extraction ability of C_nBPs, and the plots possess maximum values at n=4 for the Dns-Asp^{2-} extraction and around n=4—6 for the Dns-Glu^{2-} extraction. Therefore, such a extraction behavior cannot be explained simply in terms of the change in the lipophilicity of C_nBPs via the change in the length of the methylene unit. We have proposed a concept called "geometrical charge distribution compatibility" regarding the extraction of phthalates; the compatibility between the ionic center distance of the dicationic extractants and that of the dianionic phthalates has fundamental significance regarding the extractability of the phthalates.[6] Obviously, the concept is at work as well concerning the present dansyl-amino acid extractions.

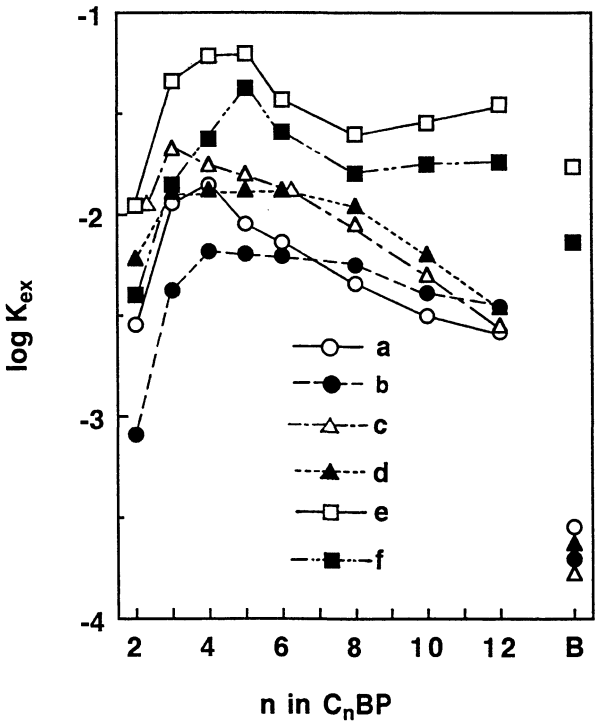

Fig. 3. Extraction constants ($\log K_{ex}$) obtained in the cases of 1,2-dichloroethane (a, Dns-Asp^{2-}; b, Dns-Glu^{2-}), 1-pentanol (c, Dns-Asp^{2-}; d, Dns-Glu^{2-}), and toluene (e, Dns-Asp^{2-}; f, Dns-Glu^{2-}). B represents BuMP.

It is noted that Dns-Asp^{2-} was more extracted than Dns-Glu^{2-} in the cases of C_2BP—C_6BP, whereas conversely Dns-Glu^{2-} was more extracted in the cases of C_8BP—$C_{12}BP$. The bridge-chain of Dns-Glu^{2-} is longer by one methylene unit than that of Dns-Asp^{2-}. Therefore, the short bridge-chain extractants (the C_nBPs possessing short bridge-chain) prefer the Dns-Asp^{2-} extraction, whereas the long bridge-chain extractants prefer the Dns-Glu^{2-} extraction.

Extranction of Dianionic Dansyl-Amino Acids with Various Extracting Solvents. 1-Pentanol and toluene were used as extracting solvents instead of 1,2-dichloroethane. Figure 3 again indicates plots of $\log K_{ex}$ vs n in C_nBP by the use of these solvents (Fig. 3, c—f). In all cases, the extraction equilibrium, Eq. 1, was confirmed to hold.

When 1-pentanol was used (Fig. 3, c and d), the order of the extractabilities of Dns-Asp^{2-} and Dns-Glu^{2-} was reversed at n=6; the short bridge-chain extractants preferred Dns-Asp^{2-} and the long bridge-chain extractants preferred Dns-Glu^{2-}. When 1-octanol was used, the extraction ability of the extractants was systematically larger than that in the extraction using 1-pentanol (see Table 2). However, the

Table 2. Extraction Constants ($\log K_{ex}$) by Use of Various Extracting Solvents

Extracting solvent	ε[a]	Dns-Asp^{2-}			Dns-Glu^{2-}		
		BuMP	C_4BP	$C_{10}BP$	BuMP	C_4BP	$C_{10}BP$
Toluene	2.4	−1.76	−1.22	−1.54	−2.14	−1.62	−1.75
Chlorobenzene	5.6	−2.78	−1.51	−1.67	−3.09	−2.06	−1.78
o-Dichlorobenzene	9.9	−3.06	−1.49	−2.01	−3.45	−2.07	−2.15
1-Octanol	10.3	−3.06	−1.23	−1.45	−2.96	−1.37	−1.33
1,2-Dichloroethane	10.4	−3.55	−1.85	−2.51	−3.71	−2.17	−2.38
1-Pentanol	13.9	−3.78	−1.75	−2.29	−3.63	−1.88	−2.19
$\Delta \log K_{ex}$[b]		2.02	0.53	0.75	1.49	0.26	0.44

a) Dielectric constant. b) $\Delta \log K_{ex}$ is defined as the difference between the $\log K_{ex}$ in the case of toluene and that in the case of 1-pentanol (see text).

extractability order of the dansyl-amino acids was similarly reversed at n=6.

When toluene was used (Fig. 3, e and f), the extractability of Dns-Asp^{2-} was greater than that of Dns-Glu^{2-} in all cases concerning the extractants. The uses of chlorobenzene and *o*-dichlorobenzene as extracting solvents resulted in a similar behavior regarding the extractability order of Dns-Asp^{2-} and Dns-Glu^{2-}; Dns-Asp^{2-} was more extracted than Dns-Glu^{2-}.

The extraction constants ($\log K_{ex}$), in terms of the use of various extracting solvents, are summarized in Table 2. The extraction ability of BuMP was remarkably dependent on the polarity of the extracting solvents. Low polar solvents, such as toluene, promote both the extractions of Dns-Asp^{2-} and Dns-Glu^{2-}. It is noted that when C_4BP was used as an extractant, the dependence of $\log K_{ex}$ on the polarity of the solvents became relatively small compared to the extractions by BuMP.

The value of $\Delta \log K_{ex}$ is defined as the difference between $\log K_{ex}$ in the case of toluene and that in the case of 1-pentanol; the former is the least polar solvent of all indicated in Table 2, while the latter is the most polar solvent. As shown in Table 2, the value of $\Delta \log K_{ex}$ decreased in the order BuMP$\gg$$C_{10}BP>$$C_4$BP in both Dns-Asp^{2-} and Dns-Glu^{2-} extractions.

"Multiple charge compatibility" can be at work when the dicationic extractants are used, and "geometrical charge distribution compatibility" can be more effectively at work in the case of C_4BP than in the case of C_{10}BP. Therefore, especially in the case of C_4BP, two-point ion-pair formation can be smoothly and compatibly carried out, so that the ion-pair is considered to be very tight. Thus, the instabilization for the ion-pair by polar solvents may be relaxed to a considerable extent, since the insertion of the solvent molecule between the cation and anion composing the complex is retarded. Such a situation leads to a lowering of the dependence of $\log K_{ex}$ on the polarity of the solvents in the case of C_4BP. The polarity and/or other solvent properties may complicatedly affect the stability of the ion-pair and, thus, the solvent effects cannot be elucidated sufficiently.

In conclusion, two-point ion-pair formation within a complex causes some unique phenomena in the extraction of Dns-Asp^{2-} and Dns-Glu^{2-}. The concepts presented in this study can be applied to chromatographic separation systems including ion-pair chromatography, and may offer a new possibility in the separation among dansyl-amino acids.

References

1) H. Green, *Talanta*, **20**, 139 (1973).
2) A. Ohki, K. Dohtsu, and M. Takagi, *Bunseki Kagaku*, **33**, E187 (1984).
3) X-L. Xiao, A. Ohki, H. Nakamura, and M. Takagi, *Anal. Sci.*, **1**, 135 (1985).
4) S. Ide, A. Ohki, and M. Takagi, *Anal. Sci.*, **1**, 349 (1985).
5) A. Ohki, M. Yamura, S. Kumamoto, S. Ide, S. Maeda, and T. Takeshita, *Solvent Extr. Ion. Exch.*, **7**, 57 (1989).
6) A. Ohki, M. Yamura, Y. Sumiyoshi, M. Takagi, and S. Maeda, *Anal. Sci.*, **6**, 291 (1990).

Association of Symmetrical *p*-Dihalobenzenes with Cyclodextrins in Aqueous Medium

Tatsuyoshi TAKUMA, Toshio DEGUCHI, and Isao SANEMASA*
Department of Chemistry, Faculty of Science, Kumamoto University, Kurokami 2-39-1, Kumamoto 860
(Received October 3, 1990)

The complex formation of cyclodextrin (CyD, host) with symmetrical *p*-difluoro-, dichloro-, dibromo-, and diiodobenzenes (guests) has been studied in aqueous medium at 25 °C by making use of the volatilization rate of guest molecules from the aqueous into gaseous phase. In the excess of the host, α- and β-CyDs form 1 : 1 and 2 : 1 (host : guest) complexes, while γ-CyD forms 1 : 1 complexes. The association constants, especially for α- and β-CyDs, increased with an increase in the size of the halogen atom. A linear relationship between the logarithm of the 1 : 1 association constant and the total surface area of guest molecule was found for CyD–monohalobenzenes and CyD–*p*-dihalobenzenes. The van der Waals force seems to be the main factor in stabilizing the associated complexes. The validity of the concept of microscopic binding constant is discussed.

We studied host-guest associations using α-, β-, and γ-cyclodextrins (CyDs) as hosts and four monohalobenzenes as guests.[1] The present work is concerned with symmetrical *p*-dihalobenzenes as analogous guests. Although complex formations of α-CyD with *p*-dichloro-, dibromo-, and diiodobenzenes have been reported,[2] there are no literature data published on other CyDs and *p*-difluorobenzene. The object of this study is to compare the association constants of monohalobenzenes with those of *p*-dihalobenzenes and to discuss the mechanism of CyD-halobenzene complexations.

Several methods are available to approach CyD-guest complexations. Of these, UV absorption and fluorescence spectroscopies are generally used; the former is based on the shift of absorption spectrum by association, and the latter on the enhancement of guest fluorescence intensity in the presence of host. These methods, however, cannot be satisfactorily applied to guests of high volatility and low aqueous solubility, because in aqueous medium it is difficult to prepare CyD-guest associated species in an appreciable amount and to maintain its concentration constant during measurements. To such guests the solubility method can be applied, which makes use of an increase in the guest solubility in water as a consequence of association with CyD. This method is usually based on a "shake-flask technique:" an excess quantity of a guest substance is added to water containing CyD of known concentration, the mixture is mechanically shaken, and then the excess guest, which may be present in water as a liquid or solid phase, is separated. The solubility method is simple and versatile, but there are some essential problems. It is difficult to separate the excess guest phase while maintaining the temperature of the aqueous solution constant. The presence of an excess guest phase is particularly troublesome: CyD (host) molecules will be adsorbed on the surface of the liquid or solid guest phase or, in an extreme case, can penetrate into the guest phase to cause modification of its physicochemical properties and consequently its aqueous solubility.

The method used in this work to determine the association constant is the same as that employed in our previous works.[3,4] This method is based on the volatility of guest in aqueous solutions. Volatile guest molecules are driven out to the gas phase by introducing an inert gas at a constant flow rate into the aqueous solution. The volatilization rate is measured with and without addition of CyD; the rate decreases as a result of the association with CyD. The method is applicable to host-guest association systems where (a) the guest molecule is volatile, (b) the concentration of host is sufficiently high in comparison with that of guest, and (c) the rate of association is rapid compared with the volatilization rate. This method has been applied to CyD associations with such guests as iodine,[5] benzene and alkyldenzenes,[3] naphthalene and its methyl derivatives,[6] polynuclear aromatic hydrocarbons,[4] carbon tetrachloride, chloroform, and dichoromethane,[7] monohalobenzenes,[1] and normal alkanes,[8] and proved to give satisfactory association constants in reasonable agreement with the literature data.

Experimental

Materials and Preparation of Sample Solutions. Deionized distilled water was used throughout the experiments. An appropriate amount of α-, β-, and γ-CyD of guaranteed grade (Nakarai Chemical Co.), dried over phosphorus pentoxide under vacuum, was weighed and dissolved in water to prepare CyD stock solutions of desired concentrations. Four guest substances, *p*-difluoro-, *p*-dichloro-, *p*-dibromo-, and *p*-diiodobenzene, were used as received; the minimum purities are 95, 98, 99, and 98%, respectively, as claimed by the manufacturers (Tokyo Kasei Kogyo Co. for the first three and Kanto Kagaku Co. for the last one). An aqueous stock solution of each guest was prepared by adding an excess of each *p*-dihalobenzene to water and stirring for at least 24 h in the dark. After leaving the mixture standing for at least 24 h, a portion of the saturated guest solution was transferred to a separatory funnel and the absorbance of its cyclohexane extract was measured to determine the guest

concentration at the following wavelengths: *p*-difluoro- at 272.4, *p*-dichloro- at 273, *p*-dibromo- at 273, and *p*-diiodobenzene at 241 nm.

A portion of the saturated guest solution was transferred into a 2.5ϕ×25 cm cylindrical glass tube for *p*-difluoro- and dichlorobenzenes, or into a round-bottom flask of 500 cm^3 capacity for the other two guests. An appropriate fraction of the CyD stock solution was then added, and the solution was diluted with water to 100 cm^3 for the former two guests or to 500 cm^3 for the latter two guests. The concentration ranges of host and guest are given in Table 1.

Apparatus and Procedures. The apparatus and the experimental procedure were the same as those described in a previous paper.[1] Nitrogen gas was bubbled into the aqueous guest solution with or without CyD placed in the cylindrical glass tube, or in the round-bottom flask immersed in a bath thermostated at 25.0±0.1 °C, at a constant flow rate suitable for each guest volatility: *p*-difluoro- at 30, *p*-dichloro- at 50, *p*-dibromo- at 400, and *p*-diiodobenzene at 400 cm^3 min^{-1}. The N_2 gas leaving the sample solution was passed through a glass column of 0.5ϕ×23 cm filled by 8 cm in length with XAD-2 resin beads (80—150 mesh). The guest adsorbed on the resin within a fixed time was eluted out with 4 cm^3 of cyclohexane, and the amount of guest, ΔQ_ϕ, was determined by UV absorption measurements.

Results

The equation derived in previous papers[3,4] was used to estimate the 1 : 1 and 2 : 1 (host : guest) association constants, K_1 and K_2:

$$\ln(C_\phi - Q_\phi V^{-1}) = -kt/(1 + K_1 C_{CyD} + K_1 K_2 C^2_{CyD}) + \ln C_\phi = -k't + \ln C_\phi, \quad (1)$$

where C_{CyD} and C_ϕ refer to the total concentration of host and that of guest, respectively, Q_ϕ is the sum of ΔQ_ϕ from time 0 to t, V is the volume of the aqueous solution, k is the rate constant for transfer of guest molecules from the aqueous to gas phase, and

$$k' = k/(1 + K_1 C_{CyD} + K_1 K_2 C^2_{CyD}). \quad (2)$$

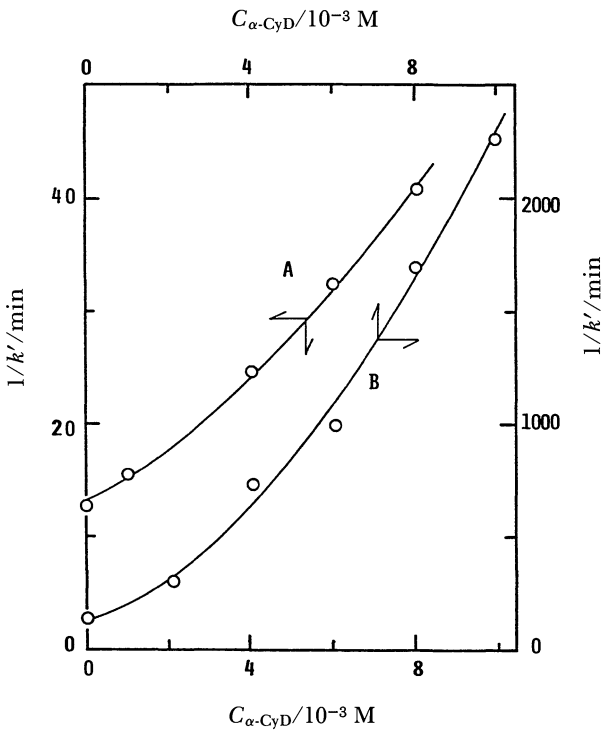

Fig. 1. Plots of $1/k'$ vs. C_{CyD}. α-CyD-*p*-difluorobenzene(A), -*p*-diiodobenzene (B).

Table 1. Concentration Ranges of Host and Guest and the Formation Constants, K_1 (1 : 1) and K_2 (2 : 1) of (Host : Guest) Complexes at 25 °C

	Concentration		Formation constant (Literature value)[a]			
	C_ϕ[b]	C_{CyD}[c]	K_1		K_2	
	10^{-5} M	10^{-2} M	M^{-1}		M^{-1}	
p-Difluorobenzene:						
α-CyD	13.2—16.4	0.974—8.03	19.6±0.3		4.9±0.8	
β-CyD	11.0—14.8	0.401—1.20	40±10		110±80	
γ-CyD	11.6—15.7	1.00—3.00	28±9		—[d]	
p-Dichlorobenzene:						
α-CyD	21.7—27.7	1.00—5.00	225±8	(232±16)	42±3	(90±12)
β-CyD	25.2—27.7	0.201—0.703	320±20		90±30	
γ-CyD	21.3—27.7	1.00—3.00	43±1		—[d]	
p-Dibromobensene:						
α-CyD	4.61—5.86	0.100—0.500	1020±60	(913±22)	100±40	(397±14)
β-CyD	5.34—6.50	0.0604—0.230	940±20		100±20	
γ-CyD	5.34—6.40	0.500—2.00	48±8		—[d]	
p-Diiodobenzene:						
α-CyD	0.132—0.295	0.0204—0.100	4200±900	(5060±940)	2000±1000	(6255±1270)
β-CyD	0.132—0.239	0.0203—0.0807	1500±200		1500±400	
γ-CyD	0.132—0.414	0.362—1.50	81±8		—[d]	

a) Literature values given in the parentheses are from Ref. 2. b) Total concentration of guest. c) Total concentration of cyclodextrin. d) K_2 was not evaluated because $1/k'$ vs. C_{CyD} plots gave a nearly straight line.

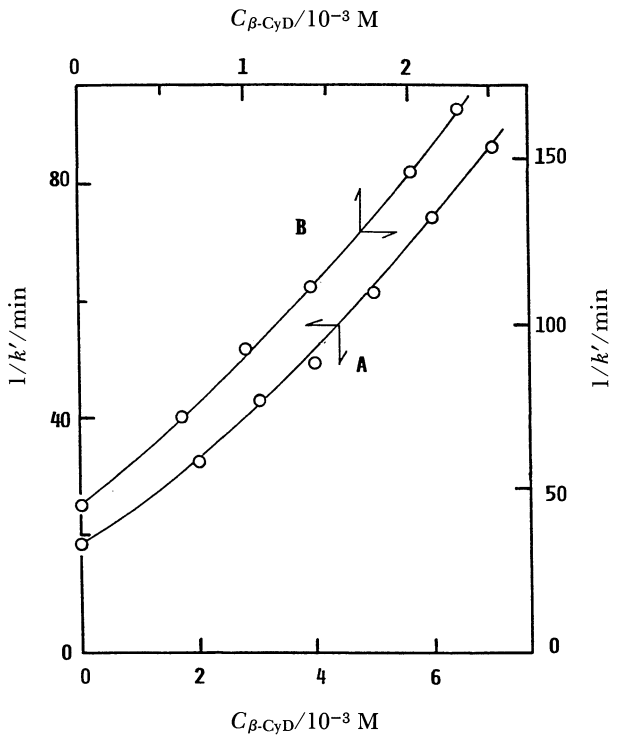

Fig. 2. Plots of $1/k'$ vs. C_{CyD}. β-CyD–*p*-dichlorobenzene (A), -*p*-dibromobenzene (B).

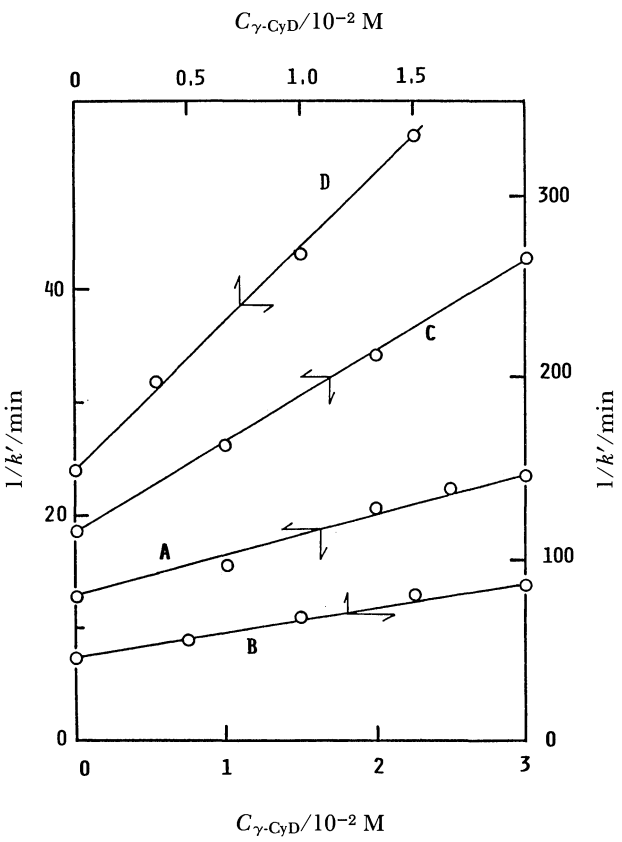

Fig. 3. Plots of $1/k'$ vs. C_{CyD}. γ-CyD–*p*-difluorobenzene (A), -*p*-dichlorobenzene (B), -*p*-dibromobenzene (C), -*p*-diiodobenzene (D).

Rearrangement of Eq. 2 yields

$$1/k' = K_1K_2C^2_{CyD}/k + K_1C_{CyD}/k + 1/k. \quad (3)$$

The plots according to Eq. 1 for all the symmetrical *p*-dihalobenzene-CyD systems examined in this work gave straight lines over the whole aeration time, during which ca. 50 to 70% of the guest molecules present initially in the sample solutions were purged. Slopes of the resulting straight lines, k' (and k), were evaluated by the least-squares method. Typical $1/k'$ vs. C_{CyD} plots are shown in Figs. 1 through 3. The plots display upward curvatures for α- and β-CyDs, indicating the formation of 1 : 1 and 2 : 1 (host : guest) complexes, whereas those for γ-CyD are linear, indicating only 1 : 1 complex formation. The K_1 and K_2 values were determined by the curve-fitting method and are summarized in Table 1, where the data obtained by solubility measurements by Connors and Pendergast[2] are also listed.

The agreement between the present and the literature K_1 values is good, in spite of an essential difference in the methods employed. As for the K_2 value, however, considerable discrepancies are noted; we have no criterion at the present stage to claim that the literature data are overestimated.

Discussion

The concept of microscopic binding constant has been proposed by Connors and Pendergast.[2] They used various kinds of symmetrical *p*-disubstituted benzenes, X-C_6H_4-X, as guests and α-CyD as host, and predicted that the 1 : 1 association constant, K_{11}^{xx}, is just twice the microscopic binding constant, $K_{x'x}$ (the binding site is indicated by a superscript prime). The concept seems reasonable when we consider that a guest molecule with two equivalent binding sites is to be accepted by a host molecule which associates with the guest at a single site (α-CyD, in the present case). There have been reported, however, few data to support directly this idea. An example which seems to support the concept is the α-CyD complex with toluene (K_1=33±3)—*p*-xylene (K_1=72±7 M^{-1})[3] (1 M=1 mol dm^{-3}). It is interesting to compare our previous data on monohalobenzenes with the present data on symmetrical *p*-dihalobenzenes and to examine whether the concept of microscopic binding constant is valid for the halobenzene series. If K_1 of a symmetrical *p*-dihalobenzene is twice that of the corresponding monohalobenzene, the concept is acceptable.

We use the following K_1 in M^{-1} for α-CyD—monohalobenzene: fluorobenzene (34±1), chlorobenzene (100±10), bromobenzene (510±10), and iodobenzene (1100±100).[1] Comparing with the corresponding K_1 value listed in Table 1, the microscopic binding concept seems to hold for chloro- and bromobenzene, but this is not the case for fluoro- and iodobenzene. The K_1 of *p*-difluorobenzene is smaller than that of mono-

fluorobenzene itself, while the K_1 of *p*-diiodobenzene is much larger than the doubled K_1 of monoiodobenzene. Although the data available at the present stage are scanty, we conclude that the microscopic binding concept does not necessarily apply to α-CyD complexations with all of symmetrical *p*-disubstituted benzenes. The physicochemical properties of the substituent such as size, polarity, and affinity to water should be taken into consideration.

If the size of the guest relative to the host cavity is considered, the microscopic binding concept seems not to be applicable to β- and γ-CyD associations with mono- and *p*-dihalobenzenes. When we compare these association constants,[1] however, the concept appears to hold for some host-guest association systems. Namely, for β-CyD, the K_1 of chlorobenzene (160±10) is just half that of *p*-dichlorobenzene, and this is also the case for the iodobenzene (K_1=800±100)—*p*-diiodobenzene combination. As for γ-CyD, in view of the range of experimental error, the K_1 of fluorobenzene (14±6), bromobenzene (39±8), and iodobenzene (30±10) are almost half that of the corresponding *p*-dihalobenzenes. These observations rather deteriorate than reinforce the validity of the concept of microscopic binding constant, because γ-CyD forms only 1 : 1 associated complexes with both mono- and *p*-dihalobenzenes.

In preceding papers,[1,3] dealing with polyaromatic hydrocarbons and monohalobenzenes as guests, we concluded that the van der Waals interaction of these guests with the CyD inner wall is the main factor to stabilize the CyD complexes. Our conclusion came from the finding that the 1 : 1 complex formation constant K_1 for the homologous guest series decreases with increasing the guest hydrophobicity estimated from the Henry's law constant, and that $\log K_1$ increases almost linearly with the surface area of guest molecule.

In Fig. 4 are plotted $\log K_1$ vs. the total surface area (TSA) of *p*-dihalobenzenes; the plots for monohalobenzenes are also shown for comparison. Linear positive relationships between $\log K_1$ and TSA are observed for the three CyDs. In analogy with monohalobenzenes, association constants of *p*-dihalobenzenes for α-CyD are most sensitive to the size of halogen atom. For γ-CyD, $\log K_1$ vs. TSA plots of mono- and *p*-dihalobenzenes fall within a single line. This means that the cavity size of γ-CyD is wide enough to allow the guest molecule to orient itself in the cavity to get as

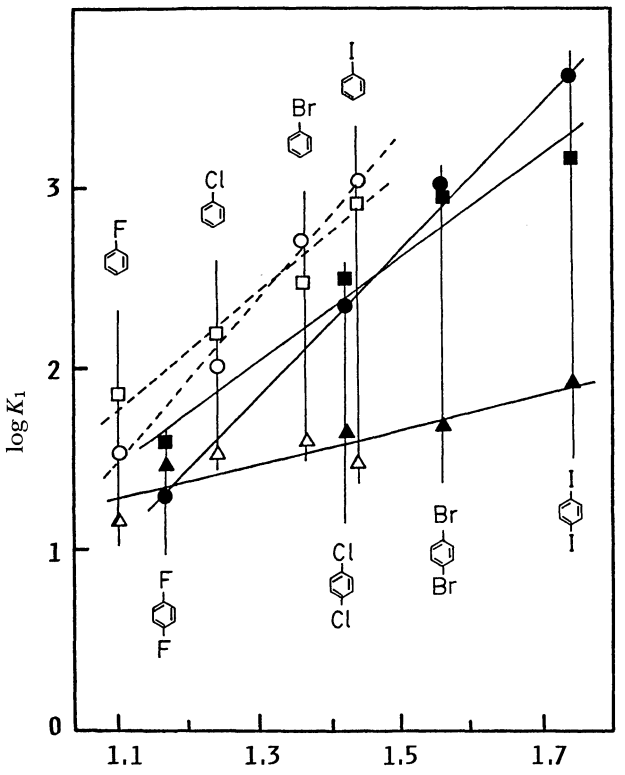

Fig. 4. Dependence of association constant on the total surface area of guest molecule. α-CyD (○, ●), β-CyD (□, ■), γ-CyD (△, ▲). Data of total surface area are from Ref. 9.

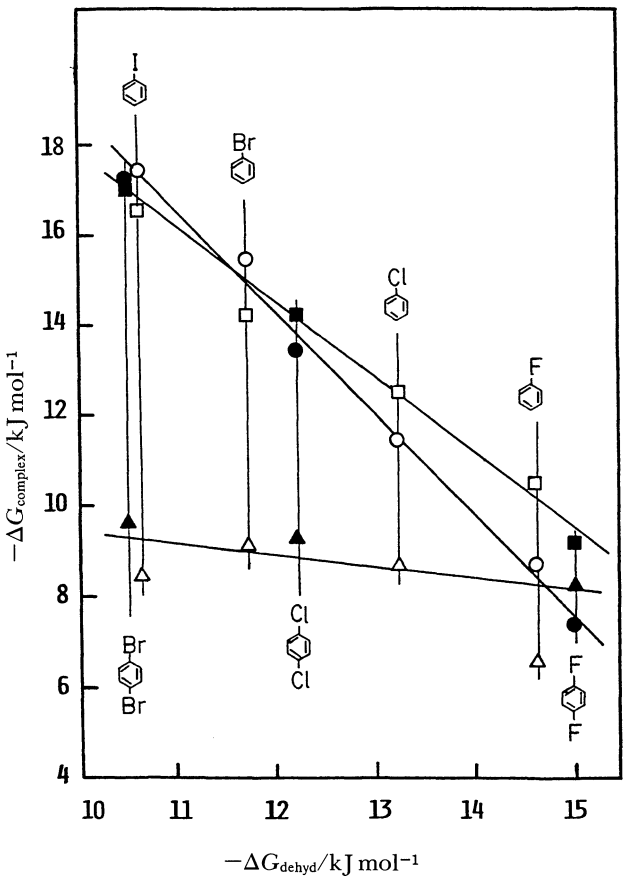

Fig. 5. Free energy changes of CyD-guest complexation, $\Delta G_{complex}$ ($=-RT \ln K_1$), and that of dehydration, ΔG_{dehyd} ($=-RT \ln K_H$) of guest. Symbols are the same as in Fig. 4.

large a contact area as possible. On the other hand, for either α- or β-CyD, the linear plot of *p*-dihalobenzenes, compared with that of monohalobenzene, shifts to the lower $\log K_1$ side. This is probably due to a difference in the 1 : 1 CyD-guest association model between mono- and *p*-dihalobenzenes, or to the affinity for water of another halogen atom substituted to monohalobenzene.

In the case of *p*-dihalobenzene, the benzene ring is situated just in the center of the cavity of β-CyD and two halogen atoms extrude equally outside the host cavity to some extent depending on the size of a particular halogen atom, whereas in the case of monohalobenzene the center of the cavity of β-CyD shifts to the halogen atom side. As for α-CyD, its cavity size is too small to include the benzene ring as a whole, but nearly equal to the diameter of the iodine atom. When the 1:1 complex is formed between *p*-dihalobenzene and α-CyD, an unassociated halogen atom might have some influence on the complex formation. That is, iodine, the most hydrophobic among halogen atoms, promotes, whereas fluorine, the most hydrophilic, depresses the association which occurs on the opposite side. This idea is not accepted in general at present, but helps us explain why the microscopic binding concept fails in the two cases mentioned above.

We previously proposed that the most reasonable parameter for the hydrophobicity of volatile solutes is the Henry's law onstant, K_H.[1,3,4] The K_H value is a measure how easily the solute is transferred from the aqueous to gas phase; a solute with the larger K_H is more hydrophobic. The free energy change in the 1 : 1 complex formation, $\Delta G_{complex}$ ($=-RT \ln K_1$), is plotted against ΔG_{dehyd} ($=-RT \ln K_H$) in Fig. 5; because of the lack of the vapor pressure data available for *p*-diiodobenzene, we cannot estimate ΔG_{dehyd} of this guest. In analogy with polyaromatic hydrocarbons,[4] almost linear relationships are observed for the three types of CyD. There are still two points to be noted.

First, as is the case of monohalobenzenes,[1] the hydrophobic interaction as a driving force of CyD complex formation is not significant for *p*-dihalobenzenes, because $-\Delta G_{complex}$ does not increase with $-\Delta G_{dehyd}$ but the situation is just the reverse. The van der Waals force seems to govern the associations of CyD with both mono- and *p*-dihalobenzenes. On an assumption that the positive relationship between $-\Delta G_{complex}$ and $-\Delta G_{dehyd}$ indicates the association being governed by the host-guest hydrophobic interaction, the negative slope of the linear plot may be taken as a measure of nonhydrophobic interaction. Namely, there is some contribution from hydrophobic interaction to γ-CyD complexations, but the least to α-CyD complexations. Secondly, regardless of the type of CyD, the plots for the two different halobenzene homologous series fall on the same linear line. We cannot elucidate this observation at the present stage.

References

1) T. Takuma, T. Deguchi, and I. Sanemasa, *Bull. Chem. Soc. Jpn.*, **63**, 1246 (1990).
2) K. A. Connors and D. D. Pendergast, *J. Am. Chem. Soc.*, **106**, 7607 (1984).
3) I. Sanemasa and Y. Akamine, *Bull. Chem. Soc. Jpn.*, **60**, 2059 (1987).
4) I. Sanemasa, T. Takuma, and T. Deguchi, *Bull. Chem. Soc. Jpn.*, **62**, 3098 (1989).
5) I. Sanemasa, Y. Nishimoto, A. Tanaka, and T. Deguchi, *Bull. Chem. Soc. Jpn.*, **59**, 2269 (1986).
6) M. Fujiki, T. Deguchi, and I. Sanemasa, *Bull. Chem. Soc. Jpn.*, **61**, 1163 (1988).
7) M. Nishimura, T. Deguchi, and I. Sanemasa, *Bull. Chem. Soc. Jpn.*, **62**, 3718 (1989).
8) I. Sanemasa, T. Osajima, and T. Deguchi, *Bull. Chem. Soc. Jpn.*, **63**, 2814 (1990).
9) R. J. Baker, B. J. Donelan, L. J. Peterson, W. W. Acree, Jr., and C.-C. Tsai, *Phys. Chem. Liq.*, **16**, 279 (1987).

Studies on Ferrocene Derivatives. VII.[1] Solvent Effect on the Oxidation Reaction of *t*-Butylferrocenes

Takatoshi HAYASHI, Yutaka OKADA,* and Tetsurou YAMASHITA†
Department of Chemistry, Faculty of Science and Engineering, Ritsumeikan University, Kita-ku, Kyoto 603
(Received September 7, 1990)

The oxidation reactivity of *t*-butylferrocenes with air was measured in 1,2-dichloroethane or 1,4-dioxane. Their reactivity in 1,2-dichloroethane was increased with increasing the number of the substituents. It was considered that the oxidation proceeds through air oxidation with catalytic proton. On the other hand, in 1,4-dioxane, the conversion amount to oxidized form of ferrocene or *t*-butylferrocene suddenly incresed in the course of the reaction. In this solvent, the ferrocene nucleus was decomposed to give Fe^{3+} ion. It seems that the substrate was oxidized by Fe^{3+} ion formed.

Ferrocene (Fc) is very stable in air, so that the oxidation from Fe(II) to Fe(III) is difficult. However, in an acidic solution, Fc is readily oxidized to ferrocenium ion[2] with air.

The oxidation reaction of ferrocene derivatives with air (or oxygen gas) in acidic solution has been investigated by several workers.[3,4] The reaction mechanism was considered as follows:[4] ferrocenonium ion[2] is formed by coordination of a proton to iron atom of Fc, and is converted continuously to ferrocenium ion with loss of hydrogen atom by the attack of oxygen (Eq. 1).

$$\mathrm{Fc} \xrightarrow{H^+} \underset{\text{ferrocenonium ion}}{[\mathrm{Fc\text{-}H}]^+} \xrightarrow{O_2} \underset{\text{ferrocenium ion}}{\mathrm{Fc}^+} \quad (1)$$

In our previous paper,[5] the oxidation reaction of (substituted phenyl)ferrocenes was discussed. It was clarified that the reactivity of (substituted phenyl)ferrocenes is influenced by a coordination facility of proton to iron atom. The coordination facility is governed by both the I-effect and the steric effect of the substituent. That is to say, the oxidation reaction proceeds through Eq. 1. In the present work, the oxidation reaction of *t*-butylferrocenes was carried out in the presence of trichloroacetic acid. The reactivity of *t*-butylferrocenes in 1,2-dichloroethane increased with the number of *t*-butyl substituents, and was governed by the coordination facility of proton to iron atom. No steric hindrance by *t*-butyl groups was observed, and the reactivity was controlled by the I-effect of *t*-butyl groups. However, in 1,4-dioxane, the order of the reactivity was different from that in 1,2-dichloroethane. In 1,4-dioxane, the reactivity of ferrocene or *t*-butylferrocene suddenly increased in the course of the reaction. In this paper, we will discuss the mechanism of the oxidation reaction of these ferrocenes in 1,4-dioxane.

Experimental

Preparation of Materials. t-Butylferrocenes were prepared by well known methods[6-9] and the method developed in our laboratory.[10]

$$\mathrm{Fc} \xrightarrow{(CH_3CO)_2O} \mathrm{Fc\text{-}COCH_3} \xrightarrow{CH_3MgI+I_2} \mathrm{Fc\text{-}C(CH_3)_3}$$

$$\mathrm{Fc} \xrightarrow{CH_3COCl} \mathrm{Fc(COCH_3)_2} \xrightarrow{2CH_3MgI+I_2} \mathrm{Fc[C(CH_3)_3]_2}$$

$$\mathrm{Fc} \xrightarrow{(CH_3)_3CCl} \mathrm{Fc[C(CH_3)_3]}_n \quad (n=3,4).$$

Table 1. Melting Points of *t*-Butylferrocenes

	Mp/°C [lit]
t-Butyl Fc[a]	—
1,1′-Di-*t*-butyl Fc[a]	28.5—29.0[28][b]
1,1′,3-Tri-*t*-butyl Fc	87.0—89.0[92][b]
1,1′,3,3′-Tetra-*t*-butyl Fc	193.0—194.0[198][b]

a) Ref. 10. b) Ref. 9.

Table 2. ^{1}H NMR Chemical Shifts of *t*-Butylferrocenes[a]

	Chemical shift/ppm[b]									
	H-1	H-2	H-3	H-4	H-5	H-1′	H-2′	H-3′	H-4′	H-5′
t-Butyl Fc[c]	—	4.07	4.01	4.01	4.07	4.14	4.14	4.14	4.14	4.14
1,1′-Di-*t*-butyl Fc[c]	—	4.07	4.01	4.01	4.07	—	4.07	4.01	4.01	4.07
1,1′,3-Tri-*t*-butyl Fc	—	3.86	—	3.94	3.94	—	4.06	4.01	4.01	4.06
1,1′,3,3′-Tetra-*t*-butyl Fc	—	3.85	—	3.92	3.92	—	3.85	—	3.92	3.92

a) Sample concentration is ca. 0.05 mol dm^{-3}. Solv.: $CDCl_3$. Temp.: ambient. b) Downfield positive, TMS internal standard. c) Ref. 10.

† Present address: Dainippon Screen Mfg. Co., Ltd., Rakusai Plant, 322 Furukawa-cho, Hazukashi, Fushimi-ku, Kyoto 612.

The compounds were identified by melting point and ^{1}H NMR, and the purity was determined by HPLC. The melting point data and ^{1}H NMR chemical shifts are shown in Tables 1 and 2.

Measurements of Oxidation Reactivity. The oxidation reaction and analysis were carried out as described in the previous paper.[5] In the case of the reaction in 1,4-dioxane, HPLC analysis was carried out as follows: after water was added to a sample, unreacted material and internal standard (nitrobenzene) were extracted with 1,2-dichloroethane from a mixture of the reaction solution and water. The extract was analyzed by HPLC as mentioned in the previous paper.[5]

Results and Discussion

Oxidation Reaction in 1,2-Dichloroethane. The conversion of the oxidation of ferrocene and *t*-butylferrocenes in 1,2-dichloroethane is shown in Fig. 1. The order of the reactivity was as follows:

Fc<*t*-Bu-Fc<1,1′-di-*t*-Bu-Fc<1,1′,3-tri-*t*-Bu-Fc
<1,1′,3,3′-tetra-*t*-Bu-Fc.

The reactivity increased with increase in the number of the substituents. The reason was considered as follows: the electron density of iron atom of ferrocene molecule increases with an increase in the number of the electron-releasing substituents (*t*-butyl groups). It seems that the coordination of catalytic proton to iron atom is accelerated by higher electron density of iron atom. It was considered that the oxidation reaction in this solvent is not controlled by the steric hindrance of *t*-butyl groups and proceeds through Eq. 1.

Oxidation Reaction in 1,4-Dioxane. The conversion of the oxidation of *t*-butylferrocenes in 1,4-dioxane is shown in Fig. 2. The reactivity of ferrocene or *t*-butylferrocene suddenly increased in the course of the reaction. The conversion amount of ferrocene was zero in 1,2-dichloroethane, but the reactivity in 1,4-dioxane was higher. The color of the reaction solution will be noticed. When no remarkable increase of the conversion amount was observed, the solution was green of ferrocenium ion. Whereas, after the conversion amount increased, the solution changed to red-violet. Therefore, it was considered that the sudden increase of the conversion amount did not proceed through Eq. 1, and another mechanism is necessary to explain this reaction.

When sodium hydroxide was added to the red-violet solution, red precipitates were produced. By the addition of potassium thiocyanate (confirmatory reagent for Fe^{3+}) and 1,10-phenanthroline (confirmatory reagent for Fe^{2+}), the solution became orange-red and red, respectively. From these results, both F^{3+} and Fe^{2+} ions must be contained in the red-violet solution after sudden increase of the conversion amounts.[11] On the other hand, in the green solution, where the remarkable increase of the conversion amounts was absent, there were neither Fe^{3+} nor Fe^{2+} ions. Therefore, it seems that the ferrocene nucleus was decom-

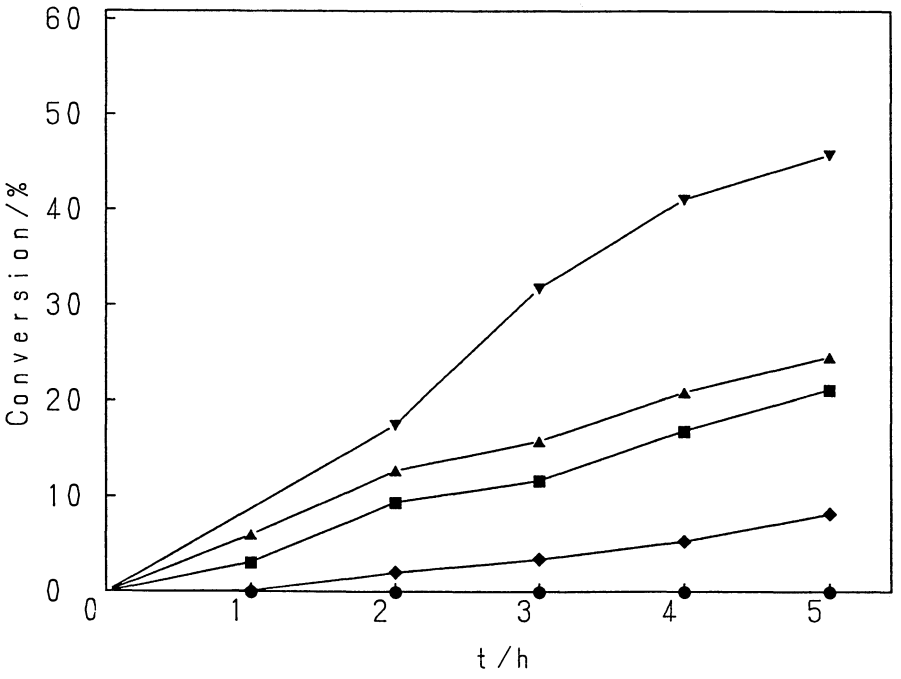

Fig. 1. Conversion of ferrocene and *t*-butylferrocenes in 1,2-dichloroethane.
(ferrocenes: trichloroacetic acid=1 : 10, reaction temperature: 40 °C).
●: ferrocene, ◆: *t*-butylferrocene, ■: 1,1′-di-*t*-butylferrocene, ▲: 1,1′,3-tri-*t*-butylferrocene, ▼: 1,1′,3,3′-tetra-*t*-butylferrocene.

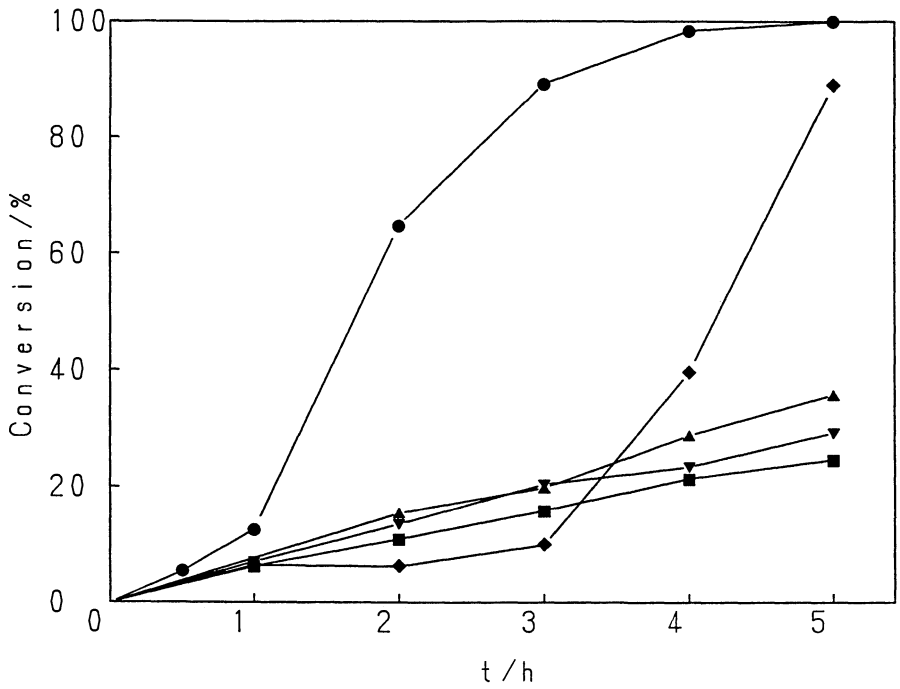

Fig. 2. Conversion of ferrocene and *t*-butylferrocenes in 1,4-dioxane. (ferrocenes: trichloroacetic acid=1 : 10, reaction temperature: 40 °C).
●: ferrocene, ◆: *t*-butylferrocene, ■: 1,1′-di-*t*-butylferrocene, ▲: 1,1′,3-tri-*t*-butylferrocene, ▼: 1,1′,3,3′-tetra-*t*-butylferrocene.

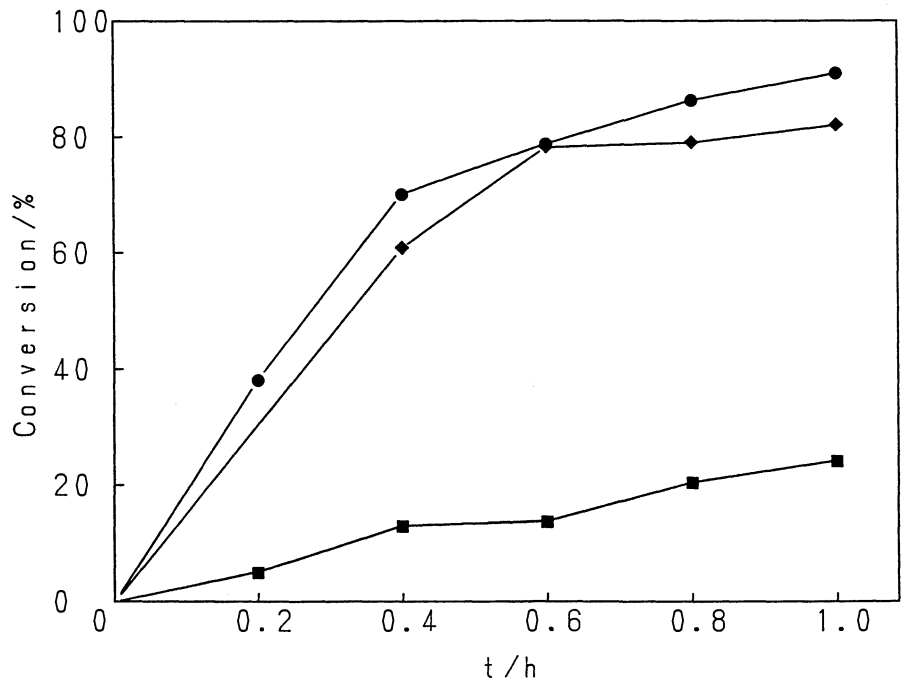

Fig. 3. Conversion of ferrocene in addition of acetic acid or salicylic acid. (ferrocene: trichloroacetic acid=1 : 5, ferrocene: acetic acid=1 : 50, ferrocene: salicylic acid=1 : 1, reaction temperature: 40 °C).
●: trichloroacetic acid, ◆: trichloroacetic acid + acetic acid, ■: trichloroacetic acid + salicylic acid.

posed in the red-violet solution.

The increase of the conversion amounts was not recognized in 1,2-dichloroethane, but it was found in 1,4-dioxane. Another ethereal solvent, dibutyl ether, was used instead of 1,4-dioxane. In a mixed solvent (dibutyl ether: 1,2-dichloroethane=1 : 9 (molar ratio)), which included only 10% ethereal solvent, it seems that the dielectric constant of the solvent is not different from that of pure 1,2-dichloroethane. As shown in Fig. 3, the increase of the conversion amounts was recognized. That is to say, the increase of the conversion amounts is recognized in the presence of ethereal solvents as 1,4-dioxane or dibutyl ether.

Trichloroacetate anion is stable in nonpolar solvent such as 1,2-dichloroethane. However, it was reported that the anion is decomposed to CCl_3^- ion with decarboxylation in aprotic polar solvent such as 1,4-dioxane.[12,13]

$$CCl_3COO^- \longrightarrow CCl_3^- + CO_2 \quad (2)$$

CCl_3^- ion is carbanion, and is a very strong nucleophilic reagent.[14] On the other hand, ferrocenium ion is decomposed by the attack of nucleophilic reagent.[15] Therefore, it seems that CCl_3^- ion is effective species for the decomposition of ferrocenium ion. It was considered that ferrocenium ion was decomposed by CCl_3^- ion.

The oxidation was carried out in methanol. The remarkable increase of the conversion amounts was not recognized as in 1,2-dichloroethane. The reason was considered as follows: CCl_3^- ion was produced even in methanol. However, the ion was converted to chloroform by the attack of methanol proton,[12] and did not act as nucleophilic reagent for ferrocenium ion. The decomposition process of ferrocenium ion by CCl_3^- ion was supported by this phenomenon observed in methanol.

The decomposition of ferrocene nucleus was confirmed by the following facts. As shown in Fig. 2, the remarkable increase of the conversion amounts was detected only for ferrocene and *t*-butylferrocene. Whereas, for 1,1′-di-, 1,1′,3-tri-, and 1,1′,3,3′-tetra-*t*-butylferrocene, such an increase was not observed. The reason was considered as follows: the Cp(cyclopentadienyl)-Fe bond is relatively strong for di-, tri-, and tetra derivatives and the steric hindrance is increased by *t*-butyl groups. Therefore, the decomposition of ferrocene nucleus of these compounds is difficult, so that the increase of the conversion amount was not remarkable for these three derivatives. The Cp-Fe bond force and the steric hindrance of ferrocene are weakest in all the ferrocenes examined in this study, and the remarkable increase occurred within 1 h from the start of the reaction. Whereas, on *t*-butylferrocene, the increase was observed after 3 h. These phenomena were explained by a similar reason to that mentioned above.

Fe^{3+} ion was formed by the decomposition of ferrocene nucleus. Fe^{3+} ion was a very strong oxidizing reagent for ferrocenes. Ferrocene and *t*-butylferrocenes examined in this study were oxidized perfectly by iron(III) chloride. Hence, when the remarkable increase of the conversion amount was recognized, the oxidation reaction by Fe^{3+} ion seems to proceed as Eq. 3.

$$Fe^{3+} + Fc \longrightarrow Fe^{2+} + Fc^+ \quad (3)$$

Furthermore, in order to block the oxidizing ability of Fe^{3+} ion, the following reaction was carried out: salicylic acid, which forms a complex between Fe^{3+} ion,[16] was added to the reaction solution together with trichloroacetic acid. No remarkable increase of the conversion amounts was recognized, and the reaction proceeded slowly (Fig. 3). (By the addition of acetic acid possessing no complex-forming ability, the increase of the conversion amounts was not stopped.) The reaction solution was washed with water, and UV spectra of the washings (light violet) showed a sharp absorption at 305.5 nm. The solution of iron(III) chloride and salicylic acid absorbed at the same position. From these results, it seems that Fe^{3+} ion formed by the decomposition of ferrocene nucleus was masked as a complex of salicylic acid in the presence of salicylic acid.

It was considered that the remarkable increase of the conversion amounts for ferrocene or *t*-butylferrocene was caused by the following mechanism: ferrocene nucleus was attacked by CCl_3^- ion formed by the decomposition of trichloroacetate ion in 1,4-dioxane. The nucleus was decomposed to form Fe^{3+} ion. Fe^{3+} ion oxidized ferrocenes, and the increase of the conversion amounts was remarkable. As mentioned above, the reaction solution contains Fe^{2+} and Fe^{3+} ions. It seems that Fe^{3+} ion was reduced to Fe^{2+} through Eq. 3 or by the action of Cp^- ion[15] formed by the decomposition of ferrocene nucleus.

Conclusion

In 1,4-dioxane, the oxidation of ferrocene or *t*-butylferrocene proceeds as follows:

1. CCl_3^- ion is produced by the decomposition of trichloroacetate ion.
2. The ferrocene nucleus is decomposed by CCl_3^- ion to form Fe^{3+} ion.
3. The substrate is oxidized faster by Fe^{3+} ion than ferrocenonium ion is oxidized by air.

Consequently, in 1,4-dioxane, the conversion amount of ferrocene or *t*-butylferrocene suddenly increases in the course of the reaction.

References

1) Part VI: Y. Okada and T. Hayashi, *Nippon Kagaku Kaishi*, **1990**, 279.
2) Ferrocenium ion: F^+, ferrocenonium ion: $[Fc\text{-}H]^+$.
3) S. Muto, H. Kochi, and Y. Kamiya, *Sekiyu Gakkai*

Shi, **17**, 50 (1974).
4) T. E. Bitterwolf and A. C. Ling, *J. Organomet. Chem.*, **40**, C29 (1972).
5) Y. Okada, N. Yamamoto, and T. Hayashi, *Bull. Chem. Soc. Jpn.*, **62**, 114 (1989).
6) Peterson and G. M. Whiteman, *J. Am. Chem. Soc.*, **79**, 3416 (1957).
7) T. S. Abram and W. E. Watts, *Synth. React. Inorg. Met-Org. Chem.*, **4**, 355 (1974).
8) M. Rosenblum and R. B. Woodward, *J. Am. Chem. Soc.*, **80**, 5443 (1958).
9) T. Leigh, *J. Chem. Soc.*, **1964**, 3294.
10) Y. Okada, N. Nakai, N. Nakamura,and T. Hayashi, *Nippon Kagaku Kaishi*, **1987**, 1567.
11) "Shin Zikken Kagaku Kouza 9. Bunseki Kagaku [I]," ed by the Chemical Society of Japan, Maruzen, Tokyo (1975), p. 327.
12) F. H. Vorhoek, *J. Am. Chem. Soc.*, **56**, 571 (1934).
13) L. W. Clark, "The Chemistry of Carboxylic Acids and Esters," ed by S. Patai, Interscience, New York (1969), p. 598.
14) N. S. Isaacs, "Reactive Intermediate in Organic Chemistry," John Wiley & Sons, New York (1974), p. 262.
15) R. Prins, A. R. Korswagen, and A. G. T. G. Kortbeek, *J. Organomet. Chem.*, **39**, 335 (1972).
16) K. Yamadera and M. Nakahara, "Mukisakutai No Kagaku," Kyoritsu Shuppan, Tokyo (1970), p. 135.

Phosphorylation of Nucleotides with Inorganic Cyclo-Triphosphate

Mitsutomo TSUHAKO,* Rumi KUNITOMI, Yoshinobu BABA, and Tohru MIYAJIMA†
Kobe Women's College of Pharmacy, Kitamachi, Motoyama, Higashinada-ku, Kobe 658
†Department of Chemistry, Faculty of Science, Kyushu University, Hakozaki, Higashi-ku, Fukuoka 812
(Received September 19, 1990)

Phosphorylation of nucleotides (nucleoside 3′- and 5′-monophosphates, and 2′-deoxynucleoside 5′-monophosphates) with inorganic sodium cyclo-triphosphate (P_{3m}) was studied in aqueous solutions under various conditions (mixing ratio of P_{3m} to nucleotides, pH, reaction temperature, and time). (1) Unprotected nucleoside 5′-monophosphates (5′-NMP's) were easily phosphorylated at the *cis*-2′,3′-diol by P_{3m} to form selectively nucleoside 2′,5′-bis(monophosphate) (2′,5′-NDP's), nucleoside 3′,5′-bis(monophosphate) (3′,5′-NDP's), and nucleoside 2′,3′-cyclic 5′-bis(monophosphate) (cNDP's). (2) The phosphorylation of 5′-NMP's was strongly dependent on mixing ratio, pH, reaction temperature, and time. Under conditions of high mixing ratios of P_{3m} to 5′-NMP's (5 : 1—10 : 1), high pH (12), and room temperature, 92—98% of 5′-NMP's was converted into 3′,5′-NDP's and 2′,5′-NDP's in roughly equimolar quantities. (3) Small quantities (5—8%) of cNDP's were formed at the initial stage of reaction of 5′-NMP's with P_{3m} but in the course of the reaction for a long period, cNDP's were hydrolyzed to 2′,5′-NDP's and 3′,5′-NDP's. (4) Nucleoside 3′-monophosphates (3′-NMP's) and 2′-deoxynucleoside 5′-monophosphates (dNMP's) could not be phosphorylated by P_{3m}, which indicates that the presence of hydroxyl groups at both 2′- and 3′-positions on nucleotides is indispensable for the phosphorylation of nucleotides with P_{3m}. (5) The mechanism of the formation of 2′,5′-NDP's, 3′,5′-NDP's, and cNDP's in the phosphorylation of 5′-NMP's with P_{3m} is discussed.

Phosphoryl chloride,[1,2] organic phosphorus compounds,[1,3,4] and polyphosphoric acid[5-8] have so far been used as phosphorylating agents of organic compounds, nucleosides, and bioorganic compounds. Since the phosphorylation with these phosphorylating agents is accompanied by various side reactions, introduction of protective groups is often required. In addition, the experimental operation of phosphorylation is extremely complicated because of its character of multi-stage reaction in organic solvents. Simple and selective phosphorylating agents have always been required.

In 1965—1969, Feldmann demonstrated that inorganic cyclo-triphosphate (P_{3m}) phosphorylated selectively some functional groups on organic compounds such as alkylamines,[9,10] alcohols,[11] sugars,[11] amino acids,[12] and phenol[13] without complicated handling. After Feldmann's work, several authors have tried to extend this technique to the phosphorylation of nucleosides.

Saffhill[14] reported that a treatment of unprotected adenosine with P_{3m} produced adenosine 2′- and 3′-monophosphates in high yield. On the other hand, Etaix and Orgel[15] reported that the reaction of 2′-deoxynucleosides with P_{3m} gave 2′-deoxynucleoside triphosphates in substantial yield, whereas a small amount of adenosine triphosphate and a large amount of adenosine 2′- and 3′-monophosphates were obtained by the reaction of adenosine with P_{3m}. There are some discrepancies in the kind and yield of products between the experimental results of Saffhill and those of Etaix and Orgel, because of some differences in their reaction conditions. Schwartz[16] produced a small amount of a mixture of 2′-deoxyadenosine 3′- and 5′-monophosphates by phosphorylating 2′-deoxyadenosine with P_{3m}.

The present authors[17] have extensively studied the phosphorylation of unprotected nucleosides with P_{3m} and its reaction mechanism. We reported that the hydroxyl groups at the 2′- and 3′-positions of ribonucleosides were selectively phosphorylated by the reaction of ribonucleosides with P_{3m} in an aqueous solution to form nucleoside 2′-, 3′-, and 2′,3′-cyclic monophosphates in high yield (80—90%). We concluded on the basis of this mechanistic study that nucleoside 2′- and 3′-triphosphates as well as nucleoside 2′,3′-cyclic monophosphates were produced as reaction intermediates.

The present authors have tried to phosphorylate nucleic acids and their related compounds with inorganic sodium cyclo-triphosphate (P_{3m}) to develop a selective phosphorylating agent for single-stage reaction in aqueous solution. In the present study, therefore, phosphorylation of nucleotides with P_{3m}, structures of reaction products, yields, and reaction mechanisms were investigated using HPLC and ^{31}P NMR.

Experimental

Chemicals. Sodium cyclo-triphosphate hexahydrate (P_{3m}), $Na_3P_3O_9 \cdot 6H_2O$, was prepared by the procedure described in our previous paper[18] and recrystallized twice from an aqueous solution. Guaranteed grade adenosine 5′-monophosphate (5′-AMP), adenosine 3′-monophosphate (3′-AMP), 2′-deoxyadenosine 5′-monophosphate (dAMP), cytidine 5′-monophosphate (5′-CMP), cytidine 3′-monophosphate (3′-CMP), 2′-deoxycytidine 5′-monophosphate (dCMP), guanosine 5′-monophosphate (5′-GMP), guanosine 3′-monophosphate (3′-GMP), uridine 5′-monophosphate (5′-UMP), uridine 3′-monophosphate (3′-UMP), and thymidine 5′-monophosphate(dTMP) were purchased from Yamasa Shoyu Co., Ltd. (Tokyo, Japan) and Sigma

Chemical Company.

Phosphorylation of Nuceotides with Inorganic Cyclotriphosphate (P_{3m}). The initial concentration of P_{3m} was fixed at a constant value of 0.5 mol dm^{-3} and those of nucleotides were varied from 0.5 to 0.05 mol dm^{-3}. Values of pH of mixed solutions were adjusted to desired values (14, 12, 10, 7, and 5) with 6 mol dm^{-3} sodium hydroxide solution or hydrochloric acid. Mixed solutions were allowed to react at room temperature (20—25 °C) or at specified temperatures (50 and 70 °C) by use of a thermostated bath controlled within ±2 °C. As the pH of the mixtures handled would gradually decrease with progress of reaction, it was kept at the prescribed value using sodium hydroxide solution during reaction.

HPLC Measurement. HPLC analysis was carried out with a JASCO HPLC-800 system (Tokyo, Japan). A column (250×4.6 mm i. d.) was packed with an anion exchanger (MCI gel, CDR-I0, Mitsubishi Chemical Industry, Tokyo, Japan), and the column temperature was maintained at 40 °C.

The linear gradient elution techique was used for the adenosine (5′-AMP, 3′-AMP, and dAMP) and cytidine (5′-CMP, 3′-CMP, and dCMP) systems, whereas the isocratic elution technique was used for the separation of guanosine (5′-GMP and 3′-GMP), uridine (5′-UMP and 3′-UMP), and dTMP systems. All eluents contained ammonium sulfate, dipotassium hydrogenphosphate, and 4% (v/v) acetonitrile. The eluent pH was kept at 10. The UV absorbance of an effluent was monitored continuously at 260 nm for the adenosine, guanosine, and uridine systems, 270 nm for the dTMP system, and 280 nm for the cytidine system.

^{31}P NMR Measurement. Pulse FT ^{31}P NMR spectra were recorded at room temperature by use of Varian XL-VX 300 (121 MHz) and Varian XL-200 (81 MHz) spectrometers. Orthophosphoric acid (85%) was used as an external standard.

Results and Discussion

Phosphorylation of 5′-AMP with P_{3m}. An aqueous reaction mixture of P_{3m} (0.5 mol dm^{-3}) and 5′-AMP (0.05 mol dm^{-3}) was allowed to react at pH 12 and room temperature. The pH of the mixed solution decreased gradually and reached about 9.9 after 1 d. Thus, the pH of the mixture was kept at 12 using sodium hydroxide solution during reaction.

Figure 1 shows the results of HPLC of the reaction products in the phosphorylation of 5′-AMP with P_{3m} at mixing ratio 10:1 (0.5 mol dm^{-3}:0.05 mol dm^{-3}), pH 12, and room temperature. With progress of reaction, the peak of 5′-AMP (retention time about 9 min) was reduced and the three peaks of the reaction products were observed at the retention times of about 26,

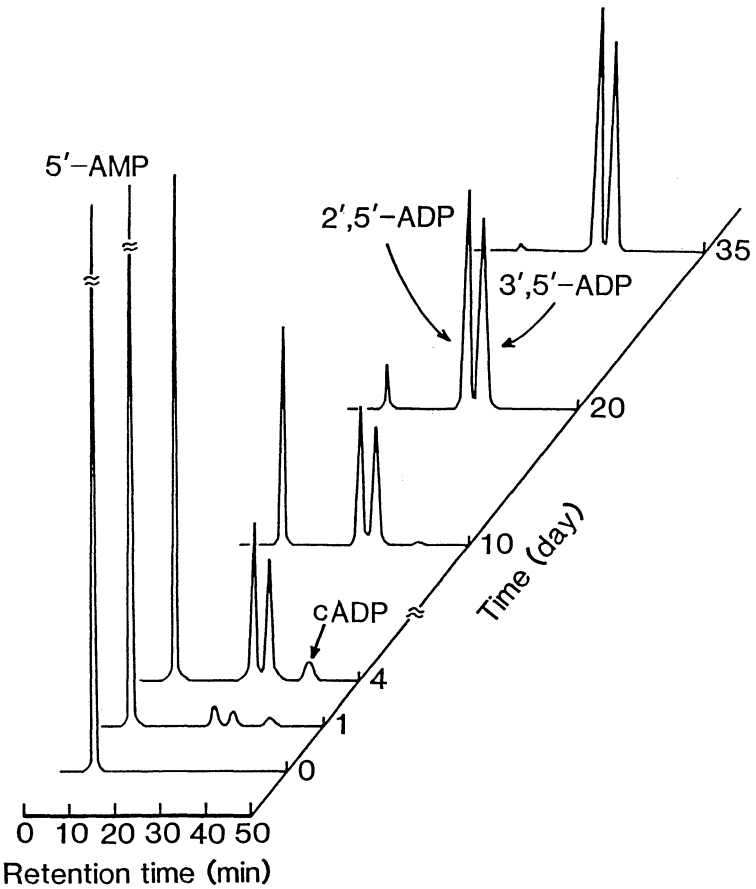

Fig. 1. Phosphorylation of 5′-AMP with P_{3m}.
P_{3m}: 5′-AMP=10:1 (0.5 mol dm^{-3}: 0.05 mol dm^{-3}), pH 12, room temperature.

30, and 38 min, respectively. These reaction products were identified to be adenosine 2′,5′-bis(monophosphate) (designated as 2′,5′-ADP), adenosine 3′,5′-bis(monophosphate) (3′,5′-ADP), and adenosine 2′,3′-cyclic 5′-bis(monophosphate) (cADP) by comparing with results of HPLC and ^{31}P NMR analyses of the authentic samples. As can be seen from the result of HPLC, two main products (2′,5′-ADP and 3′,5′-ADP) and a by-product (cADP) were produced in the phosphorylation of 5′-AMP with P_{3m} in an aqueous solution. cADP was produced at the initial stage of reaction, and it gradually decreased with reaction time and finally disappeared after 13 d. On the other hand, the amounts of 2′,5′-ADP and 3′,5′-ADP increased with elapse of reaction time and reached 46.1 and 46.3% after 20 d, respectively. Under any reaction conditions, the amounts of 2′,5′-ADP and 3′,5′-ADP were nearly equal to each other.

To establish the structure of phosphorylated products, ^{31}P NMR spectra were measured. Figure 2 shows the ^{31}P NMR spectra for the reaction mixture of P_{3m} and 5′-AMP at molar ratio 10 : 1, pH 12, and room temperature. In the ^{1}H-decoupling spectrum, four peaks due to the reaction products were observed at δ=+4.9, +4.7, +4.6, and +4.4. By comparing with the chemical shifts of the authentic samples, the peaks at δ=+4.9 and +4.7, and at δ=+4.6 and +4.4 were attributed to 3′,5′-ADP and 2′,5′-ADP, respectively. The peaks at δ=+4.9 and +4.7 split into a doublet and a triplet, respectively, in the ^{1}H-coupling spectrum. Thus, it was found that the peaks at δ=+4.9 and +4.7 were attributable to the phosphorus atoms at the 3′- and 5′-positions of ribose in 3′,5′-ADP, respectively, and the peaks at δ=+4.4 and +4.6 were attributable to the phosphorus atoms at the 2′- and 5′-positions in 2′,5′-ADP, respectively. A singlet peak corresponding to the 2′,3′-cyclic phosphate of cADP was observed at δ=+20.5 and split into a triplet due to the two protons of 2′- and 3′-positions of ribose in the ^{1}H-coupling. The singlet peak at δ=−21.4 corresponds to the starting material, P_{3m}, the peaks at δ=−4.0 and −4.3 were assigned to the terminal phosphorus atoms of triphosphate (P_3) produced by the hydrolysis of P_{3m} and those at δ=−18.2, −18.4, and −18.6 to the middle phosphorus atom of P_3. The singlet peaks at δ=+5.4 and −4.6 were attributed to ortho (P_1) and pyrophosphates (P_2), respectively.

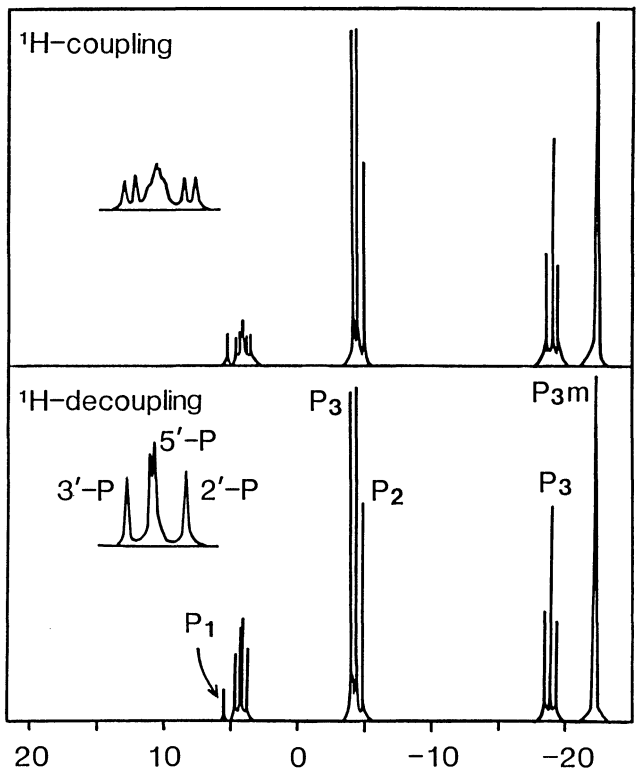

Fig. 2. ^{31}P NMR of the reaction products.
P_{3m}: 5′-AMP=10 : 1 (0.5 mol dm^{-3}: 0.05 mol dm^{-3}), pH 12, room temperature, after 30 d.

In Fig. 3, the amounts of 2′,5′-ADP, 3′,5′-ADP, and cADP, formed in the reaction of P_{3m} with 5′-AMP at mixing ratio 10 : 1, pH 12 and room temperature, are plotted as a function of time. While the starting material (5′-AMP) decreased with reaction time, each amount of 2′,5′-ADP and 3′,5′-ADP gradually increased up to the same constant value of approximately 47%. The yield of 2′,5′-ADP was nearly equal to that of 3′,5′-ADP at any reaction times. The yield of cADP reached about 5% after 1 d and decreased to zero after 13 d.

The influence of pH on the reaction of P_{3m} with 5′-AMP is shown in Fig. 4. The phosphorylation of 5′-AMP with P_{3m} proceeded faster in a high alkaline region, e.g., at pH 12, than at pH 10 and less. The phosphorylation did not proceed in an acidic medium (pH 5) at all. This fact may be explained in terms of

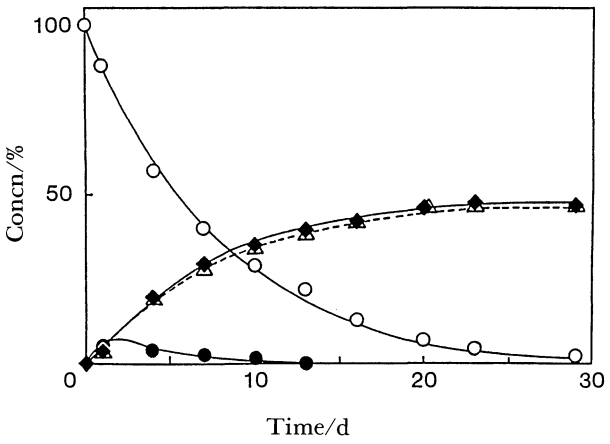

Fig. 3. Changes of the amounts of products in the reaction of P_{3m} with 5′-AMP.
P_{3m}: 5′-AMP=10 : 1 (0.5 mol dm^{-3}: 0.05 mol dm^{-3}), pH 12, room temperature.
○; 5′-AMP, ◆; 2′,5′-ADP, △; 3′,5′-ADP, ●; cADP.

such a sequence that the hydroxyl group (-OH) at the 2′- or 3′-position of ribose in 5′-AMP[19] is partially dissociated into O^- which nucleophilically attacks the phosphorus atom of P_{3m}.

We have further studied the phosphorylation of 5′-AMP at varying temperatures and mixing ratios, with the pH of reaction mixture maintained at pH 12. The yields of the 2′,5′-ADP, 3′,5′-ADP, and cADP thus obtained are summarized in Table 1. The effect of reaction temperature on maximum yield was examined for the reaction of 5′-AMP with P_{3m} at a mixing ratio of 5 : 1. As can be seen in Table 1, the best yield was obtained at room temperature after 40 d. Due to the hydrolysis of the reaction products, the maximum yield obtained at higher temperatures is lower than that obtained at room temperature. The effect of the mixing ratio of P_{3m} to 5′-AMP was tested as listed in Table 1. The ratio of P_{3m} to 5′-AMP of 10 : 1 (0.5 mol dm^{-3} : 0.05 mol dm^{-3}) is better than that of 1 : 1 (0.5 mol dm^{-3} : 0.5 mol dm^{-3}). The yield at a mixing ratio of 10 : 1 was, however, not so much different from that at 5 : 1.

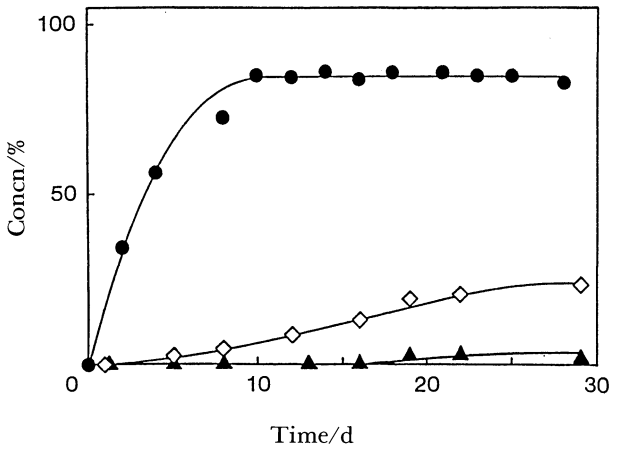

Fig. 4. Changes of the amounts of products in the reaction of P_{3m} with 5′-AMP.
P_{3m}: 5′-AMP=5 : 1 (0.5 : 0.1 mol dm^{-3}), 50 °C, ●; pH 12, ◇; pH; 10, ▲; pH 7.

The optimum conditions for the phosphorylation of 5′-AMP with P_{3m} are found to be mixing ratio 5 : 1—10 : 1, pH 12, room temperature, and reaction period 35—41 d. The total yields of 2′,5′-ADP and 3′,5′-ADP under the optimum condition were about 96.5%. On the other hand, cADP was produced only at the initial stage of reaction under any reaction conditions and its yield was about 5—6% which was much lower than those of 2′,5′-ADP and 3′,5′-ADP. The amount of cADP gradually decreased with elapse of reaction time. This is because cADP is easily hydrolyzed to give 2′,5′-ADP and 3′,5′-ADP.

The phosphorylation of 3′-AMP or dAMP with P_{3m} was also investigated under various conditions. However, these compounds could not be phosphorylated with P_{3m} at all under any conditions. This fact may suggest that the presence of the hydroxyl groups at both the 2′- and 3′-positions of ribose in 5′-AMP is required for the phosphorylation of nucleotides with P_{3m}.

Phosphorylation of 5′-CMP with P_{3m}. HPLC separations of the reaction products in the phosphorylation of 5′-CMP with P_{3m} gave the three peaks due to cytidine 2′,3′- cyclic 5′-bis(monophosphate) (designated as cCDP), cytidine 2′,5′-bis(monophosphate)

Table 1. Yields of 2′,5′-ADP, 3′,5′-ADP, and cADP

Reaction conditions				Yield/%		
Mixing ratio	pH	Temp/°C	Time/d	2′,5′-ADP	3′,5′-ADP	cADP
P_{3m} : 5′-AMP						
1 : 1 (0.5 M : 0.5 M)	12	50	3	9.3	8.1	5.6
			20	28.3	26.2	0
5 : 1 (0.5 M : 0.1 M)	12	Room	1	3.1	2.6	4.7
			41	49.3	47.2	0
	12	50	2	14.3	15.8	4.0
			14	41.1	45.1	0
	10	50	29	9.6	11.5	2.4
	7	50	29	0.6	0.8	0
	12	70	1	4.8	5.3	4.0
			6	30.2	34.0	0
10 : 1 (0.5 M : 0.05 M)	12	Room	1	3.6	3.3	4.9
			35	47.6	47.4	0
	12	50	2	17.1	18.9	2.7
			18	42.1	46.4	0
P_{3m} : 3′-AMP						
10 : 1 (0.5 M : 0.05 M)	12	Room	24	0	0	0
P_{3m} : dAMP						
10 : 1 (0.5 M : 0.05 M)	12	Room	25	—	0	—

(2′,5′-CDP), and cytidine 3′,5′-bis(monophosphate) (3′,5′-CDP). The main reaction products were identified to be 2′,5′-CDP and 3′,5′-CDP by comparing with the results of HPLC and ^{31}P NMR of the authentic samples. Although a small amount (about 5—8%) of cCDP was produced at the initial stage of reaction, it decreased rapidly with reaction time. The formation of 2′,5′-CDP and 3′,5′-CDP increasingly predominated with progress of reaction.

Table 2 lists the yields of 2′,5′-CDP, 3′,5′-CDP, and cCDP under various reaction conditions. In the reaction of 5′-CMP with P_{3m} at mixing ratio 5:1 (0.5 mol dm^{-3} : 0.1 mol dm^{-3}), pH 12, and room temperature for long time (48 d), about 92% of 5′-CMP was phosphorylated to form 2′,5′-CDP (40%) and 3′,5′-CDP (52%). The yield of 3′,5′-CDP was always a little more than that of 2′,5′-CDP, though both yields were nearly equal to each other. The phosphorylation proceeded for a short time (5 h) at 70 °C and high pH (14), and the total yields of 2′,5′-CDP, and 3′,5′-CDP reached about 66% at 5 h. The amounts of these products, however, gradually decreased with time, because they were easily hydrolyzed at pH 14 and 70 °C. The reaction rate was decreased by lowering the pH of the mixed solution. The reaction did not proceed at all in acidic medium (pH 5). Neither 3′-CMP, nor dCMP could be phosphorylated with P_{3m} under the same conditions as the phosphorylation of 5′-CMP with P_{3m}.

The experimental results indicate that the optimum conditions for the phosphorylation of 5′-CMP with P_{3m} are mixing ratio 5:1, pH 12, and room temperature.

Phosphorylation of 5′-GMP with P_{3m}. The phosphorylation of 5′-GMP with P_{3m} was carried out by the same method as that of the 5′-AMP and 5′-CMP systems. Figure 5 shows an example of HPLC analysis of the reaction products in the phosphorylation of 5′-GMP with P_{3m}. The products were guanosine 2′,5′-bis(monophosphate) (2′,5′-GDP) and guanosine 3′,5′-bis(monophosphate) (3′,5′-GDP). No guanosine 2′,3′-cyclic 5′-bis(monophosphate) (cGDP) was obtained in the phosphorylation of 5′-GMP with P_{3m} unlike those of the 5′-AMP and 5′-CMP systems. It is not clear yet whether cGDP was not formed originally or the cGDP once formed at the initial stage of the reaction was so unstable as to be immediately hydrolyzed to form 2′,5′-GDP and 3′,5′-GDP. However, it may be reasonable to consider that the latter is more probable, similarly to the case of the 5′-AMP and 5′-CMP systems.

Table 3 shows amounts of 2′,5′-GDP and 3′,5′-GDP obtained under various reaction conditions. The optimum conditions for the phosphorylation of 5′-GMP with P_{3m} are found to be mixing ratio 5:1—10:1, pH 12, room temperature, and long reaction period (28 d). The yields of the reaction products (2′,5′-GDP and 3′,5′-GDP) under the optimum conditions were approximately 97%. Also, the yield of 2′,5′-GDP was nearly equal to that of 3′,5′-GDP under any conditions. On the other hand, 3′-GDP was not phosphorylated with P_{3m} at all.

Phosphorylation of 5′-UMP with P_{3m}. In the phosphorylation of 5′-UMP with P_{3m}, the reaction

Table 2. Yields of 2′,5′-CDP, 3′,5′-CDP, and cCDP

Reaction conditions				Yield/%		
Mixing ratio	pH	Temp/ °C	Time/d	2′,5′-CDP	3′,5′-CDP	cCDP
P_{3m} : 5′-CMP						
1:1 (0.5 M : 0.5 M)	12	Room	5	4.9	6.0	6.3
			81	35.7	46.7	0
	12	50	1	2.1	3.5	5.0
			14	20.5	28.6	0
5:1 (0.5 M : 0.1 M)	12	Room	3	2.3	4.0	6.3
			48	39.7	51.6	0
	12	50	1	2.9	4.6	4.1
			21	31.3	44.4	0
	12	70	3	2.6	5.4	5.0
			12	13.6	35.1	0
	10	50	14	2.7	2.9	4.5
			41	11.4	15.5	0
	7	50	34	0.8	2.6	0
10:1 (0.5 M : 0.05 M)	14	70	5hr	28.3	38.0	0
	12	50	4	5.2	8.0	8.3
			24	32.4	46.8	0
P_{3m} : 3′-CMP						
10:1 (0.5 M : 0.05 M)	12	Room	21	0	0	0
P_{3m} : dCMP						
10:1 (0.5 M : 0.05 M)	12	Room	15	—	0	—

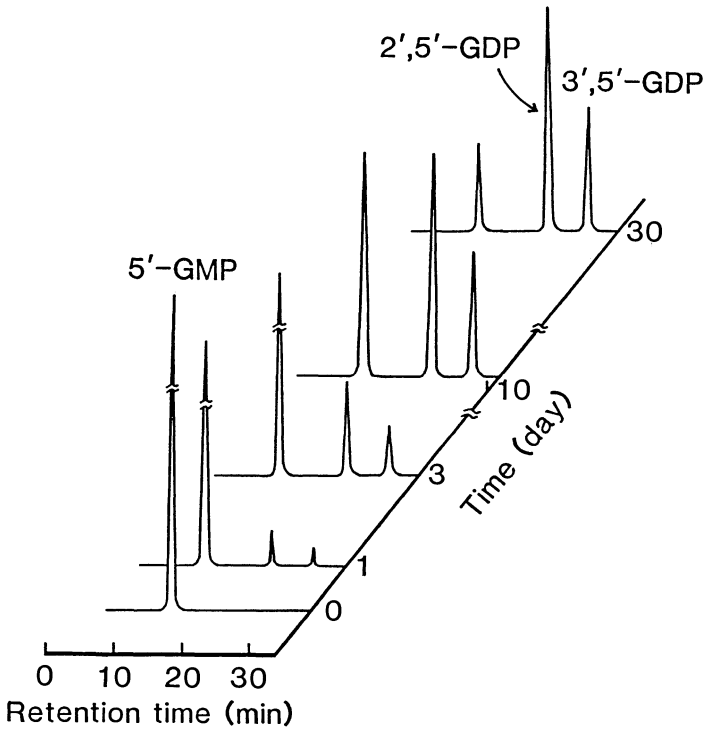

Fig. 5. Phosphorylation of 5'-GMP with P_{3m}.
P_{3m}: 5'-GMP=1 : 1 (0.5 mol dm^{-3}: 0.5 mol dm^{-3}), pH 12, room temperature.

Table 3. Yields of 2',5'-GDP and 3',5'-GDP

Reaction conditions				Yield/%	
Mixing ratio	pH	Temp/°C	Time/d	2',5'-GDP	3',5'-GDP
P_{3m} : 5'-GMP					
1 : 1 (0.5 M : 0.5 M)	12	Room	28	49.7	40.3
	12	50	19	37.4	31.4
	12	70	6	29.5	28.0
5 : 1 (0.5 M : 0.1 M)	12	Room	28	47.6	49.7
	12	50	26	43.8	47.5
	12	70	17	32.4	36.7
10 : 1 (0.5 M : 0.05 M)	12	Room	28	46.8	50.0
	12	50	21	43.8	48.3
	12	70	22	37.6	38.4
	10	50	26	33.2	30.7
	7	50	25	0	0
P_{3m} : 3'-GMP					
10 : 1 (0.5 M : 0.05 M)	12	Room	21	0	0

products were identified to be uridine 2',5'-bis(monophosphate) (2',5'-UDP), uridine 3',5'-bis(monophosphate) (3',5'-UDP), and uridine 2',3'-cyclic 5'-bis(monophosphate) (cUDP) by comparing with the data of HPLC and ^{31}P NMR of the authentic samples. Although cUDP was produced at the initial stage of the reaction, it disappeared with reaction time and the formation of 2',5'-UDP and 3',5'-UDP predominated instead.

Yields of 2',5'-UDP, 3',5'-UDP, and cUDP under various reaction conditions are summarized in Table 4. The optimum conditions for the phosphorylation of 5'-UMP with P_{3m} are mixing ratio 5 : 1—10 : 1, pH 12, and room temperature. The total yields of 2',5'-UDP and 3',5'-UDP under the optimum conditions were about 93% at the highest. 3'-UMP was not phosphorylated with P_{3m} at all, similarly to 3'-AMP, 3'-CMP, and 3'-GMP.

The ^{31}P NMR parameters of the main reaction products (2',5'-NDP's and 3',5'-NDP's) in the phosphoryl-

Table 4. Yields of 2′,5′-UDP, 3′,5′-UDP, and cUDP

Reaction conditions				Yield/%		
Mixing ratio	pH	Temp/°C	Time/d	2′,5′-UDP	3′,5′-UDP	cUDP
P_{3m} : 5′-UMP						
1 : 1 (0.5 M : 0.5 M)	12	Room	1	2.2	2.1	7.6
			55	37.5	38.8	0
	12	50	1	4.9	5.2	7.6
			25	28.2	27.5	0
	12	70	1	6.4	7.4	5.4
			24	16.6	16.8	0
5 : 1 (0.5 M : 0.1 M)	12	Room	1	1.5	1.5	6.3
			55	45.3	47.0	0
	12	50	1	2.9	3.1	6.7
			37	40.2	39.0	0
	12	70	1	4.0	4.5	6.0
			26	26.3	25.5	0
10 : 1 (0.5 M : 0.05 M)	12	Room	6	11.1	10.8	6.9
			60	46.1	47.0	0
	12	50	4	10.1	10.7	6.0
			35	40.3	39.1	0
	12	70	3	4.6	5.3	5.1
			31	28.0	27.6	0
	10	50	8	5.5	6.1	7.3
			30	19.3	21.1	4.5
	7	50	30	2.0	1.6	1.9
P_{3m} : 3′-UMP						
10 : 1 (0.5 M : 0.05 M)	12	Room	21	0	0	0

Table 5. ^{31}P NMR Parameters of Phosphorylated Products (2′,5′-NDP's and 3′,5′-NDP's)

Product	δ (2′-P)	δ (3′-P)	δ (5′-P)	$^3J_{P(2')H}$/Hz	$^3J_{P(3')H}$/Hz
2′,5′-ADP	4.4	—	4.6	6.88	—
3′,5′-ADP	—	4.9	4.7	—	7.29
2′,5′-CDP	4.0	—	4.1	6.81	—
3′,5′-CDP	—	4.2	4.1	—	7.26
2′,5′-GDP	3.7	—	4.0	6.80	—
3′,5′-GDP	—	4.2	4.0	—	7.21
2′,5′-UDP	4.1	—	4.2	6.80	—
3′,5′-UDP	—	4.4	4.3	—	7.25

ation of 5′-NMP's with P_{3m} are shown in Table 5. The measurements of ^{31}P NMR were made at pH 12.

Mechanism of Phosphorylation of 5′-NMP's with P_{3m}. In the reaction of P_{3m} and 5′-NMP's, cis-2′,3′-diol on nucleotides is phosphorylated to form 2′,5′-NDP's, 3′,5′-NDP's, and cNDP's. Considering that dNMP's and 3′-NMP's are not phosphorylated, the presence of hydroxyl groups at both 2′- and 3′-positions is indispensable for the phosphorylation of 5′-NMP's with P_{3m}.

From the above-mentioned experimental results, the authors propose the reaction mechanism shown in Fig. 6. The hydrogen bond is first formed between the hydroxyl group at the 2′- or 3′-position on nucleotides and an oxygen atom of P_{3m}, e.g., the hydrogen bond of 3′-OH with P_{3m} in Fig. 6. Closely related hydrogen-bonded intermediates have been postulated.[13,17] Then, the lone electron pair on the oxygen atom of another hydroxyl group (2′-OH in Fig. 6) nucleophilically attacks the phosphorus atom of P_{3m} to generate nucleoside 2′-triphosphates as an unstable intermediate, via the ring opening of P_{3m}. The roles of the 2′- and 3′-hydroxyl groups in hydrogen bonding and nucleophilic attack could equally be reversed, of course. An intramolecular attack of unphosphorylated hydroxyl group (3′-OH in Fig. 6) on a phosphorus atom of nucleoside 2′-triphosphates occurred to produce cNDP's as an intermediate. The cNDP's thus formed are quickly hydrolyzed to give 2′,5′-NDP's and 3′,5′-NDP's. The yields of 2′,5′-NDP's were nearly equal to those of 3′,5′-NDP's, which shows that the rate of hydrolysis at the 2′-position of cNDP's is almost the same as that at the 3′-position. Such a fact is well-known in the hydrolysis of RNA in an alkaline solution.[20]

In the 5′-GMP system, however, guanosine 2′,3′-

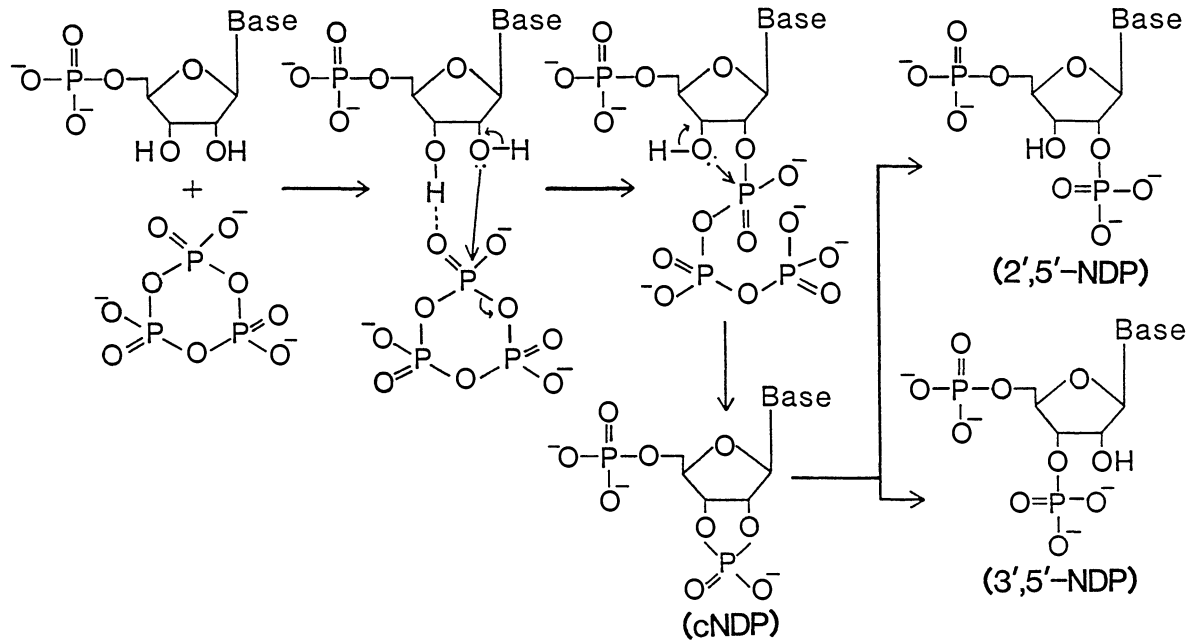

Fig. 6. Mechanism of phosphorylation of nucleotides with P_{3m}.

cyclic 5′-bis(monophosphate) (cGDP) could not be detected by HPLC or ^{31}P NMR. It is considered that cGDP is so unstable in alkaline aqueous solution that it is easily hydrolyzed to 2′,5′-GDP and 3′,5′-GDP.

References

1) M. Ikehara, T. Ueda, and E. Otsuka, "Kakusan Yuki Kagaku," Kagaku Dojin, Kyoto (1979), p. 85.

2) M. Yoshikawa, T. Kato, and T. Takenishi, *Tetrahedron Lett.*, **1967**, 5065.

3) D. W. Hutchinson, "Comprehensive Organic Chemistry," ed by E. Haslam, Pergamon Press, New York (1979), Vol. 5, p. 123.

4) Y. Mizuno, "The Organic Chemistry of Nucleic Acids," Kodansha, Tokyo (1986), p. 161.

5) R. H. Hall and H. G. Khorana, *J. Am. Chem. Soc.*, **77**, 1871 (1955).

6) E. R. Walwick, W. K. Roberts, and C. A. Dekker, *Proc. Chem. Soc.*, **1959**, 84.

7) A. W. Schwartz and C. Ponnamperuma, *Nature*, **218**, 443 (1968).

8) J. Hulshof and C. Ponnamperuma, *Origins Life*, **7**, 197 (1976).

9) W. Feldmann and E. Thilo, *Z. Anorg. Allg. Chem.*, **327**, 159 (1964).

10) W. Feldmann, *Z. Chem.*, **5**, 26 (1965).

11) W. Feldmann, *Chem. Ber.*, **100**, 3850 (1967).

12) W. Feldmann, *Z. Chem.*, **9**, 154 (1969).

13) W. Feldmann, *Chem. Ber.*, **99**, 3251 (1966).

14) R. Saffhill, *J. Org. Chem.*, **35**, 2881 (1970).

15) E. Etaix and L. E. Orgel, *J. Carbohydr. Nucleosides. Nucleotides*, **5**, 91 (1978).

16) A. W. Schwartz, *Chem. Commun.*, **1969**, 1393.

17) M. Tsuhako, M. Fujimoto, S. Ohashi, H. Nariai, and I. Motooka, *Bull. Chem. Soc. Jpn.*, **57**, 3274 (1984).

18) M. Tsuhako, N. Fujita, A. Nakahama, T. Matsuo, M. Kobayashi, and S. Ohashi, *Bull. Chem. Soc. Jpn.*, **53**, 1968 (1980).

19) W. Saenger, "Principles of Nucleic Acid Structure," Springer-Verlag, New York (1984); translated by Y. Nishimura, Springer-Verlag, Tokyo (1987), p. 104.

20) E. E. Conn, P. K. Stumpf, G. Bruening, and R.H. Doi, "Outlines of Biochemistry," John Wiley & Sons, New York (1987); translated by N. Tamiya and T. Yagi, Tokyo Kagaku Dojin, Tokyo (1988), p. 197.

Fluctuation of Local Field and Depolarization Ratio of the ν_1 Raman Line of Carbon Tetrachloride in Carbon Disulfide Solution

Shi-aki Hyodo
Toyota Central Research and Development Labs., Inc., Nagakute-cho, Aichi-gun, Aichi 480-11
(Received March 3, 1990)

The depolarization ratio of a molecule having T_d symmetry has been expressed in terms of the mean-square fluctuation of the local field which is felt by a molecule in the condensed phase. The fluctuation of the polarizability at each position in the scattering volume was found to dominantly affect local-field fluctuation. The concentration dependence of the depolarization ratio for the ν_1 Raman line of carbon tetrachloride in a carbon disulfide solution could be well described by this expression.

The depolarization ratio of Raman spectra, ρ, for linear polarized incident light sources is defined as

$$\rho=\frac{3\,\gamma^2}{45\,\bar{\alpha}^2+\gamma^2}, \tag{1}$$

where

$$\bar{\alpha}\equiv\frac{1}{3}(\alpha'_{xx}+\alpha'_{yy}+\alpha'_{zz})$$

and

$$\gamma^2\equiv[(\alpha'_{xx}-\alpha'_{yy})^2+(\alpha'_{yy}-\alpha'_{zz})^2+(\alpha'_{zz}-\alpha'_{xx})^2].$$

Here, $\alpha'_{\sigma\rho}$ is the $\sigma\rho$-component of the Raman scattering tensor. Using this relation, ρ can supply much useful information concerning molecular structure. It is easy to imagine that ρ also includes information about intermolecular interactions and/or the aggregation structure of molecules in condensed phases. The depolarization ratio of the ν_1 Raman line of liquid carbon tetrachloride is an example of such phenomena. This depolarization ratio should be exactly zero in an isolated molecule, since the relation $\alpha'_{xx}=\alpha'_{yy}=\alpha'_{zz}$ is satisfied. However, it has been reported by many authors[1-6] that the depolarization ratio has an experimental value that is not exactly zero. The isotropic effects of chlorine atoms were quantitatively analyzed and were found to contradict information regarding the origin of this finite value of ρ.[7,8] This ρ value came to be considered to originate from some intermolecular interactions. Its detailed mechanism, however, had not been discussed until a report concerning the fluctuation of the local field[9] appeared.

Hyodo and Fujiyama proposed a model for explaining this finite value of the depolarization ratio.[9] They considered that a molecule is subjected to both the direct field of a light wave and to an indirect field caused by the dipoles of surrounding molecules induced by the light wave field. Such a field as the latter is a so-called "local field." In this case, it depends only on the relative positions of the molecules surrounding the central molecule, because both the polarizability tensor and its derivative with respect to the ν_1 normal coordinate have spherical symmetry. The local field fluctuates by some magnitudes and directions because of the thermal motion of molecules, therefore causing finite depolarized scattering. Nishikawa and Iijima[10] calculated this depolarization ratio based on the formula of Hyodo and Fujiyama. Their own local-lattice structure model for liquid carbon tetrachloride was found to be quantitatively describable as the observed depolarization ratio. The pressure dependence of this depolarization ratio could be explained by a local field fluctuation up to 10^8 Pa by Ikawa and Whalley.[5] This fluctuation was also found to significantly affect the solvent-mixing fraction dependence of the depolarization ratio for the ν_1 Raman line of the perchlorate anion in mixed-solvent solutions of lithium perchlorate.[11]

On the other hand, Murphy et al. reported the concentration dependence of the depolarization ratio of the ν_1 Raman line of carbon tetrachloride in various binary solutions.[3] Unfortunately, however, the formula of Hyodo and Fujiyama was derived under the assumption that explicit information of the local structure is known. Since the proposed explicit structure models are based on X-ray diffraction data for pure liquid carbon tetrachloride,[12-14] this formula is numerically calculable. The local structure in a solution, on the other hand, seems to be very complicated because of the many possible combinations of multicomponent species. The formula of Hyodo and Fujiyama may be too hard to apply solutions.

One possible idea regarding its formulation has a similar basis as work undertaken by Ladanyi and Keyes[15-18] just before the local lattice model[9] was proposed. Their work concerned the local field effect on the Rayleigh scattering intensity. They explained and averaged from the standpoint of statistical mechanics the effect of induced polarization on each molecule, as well as the treated electric field induced from the dielectric continuum, and obtained a detailed, accurate expression of the local field effect on the light scattering intensities. The local field effect on the Raman scattering intensity seems to be explained in a similar way. However, the local field effect of Ladanyi and Keyes cannot be expected on

Raman lines in usual liquids or solutions, since the term of intermolecular interaction among permanent dipoles has significant effects on the intensity of Raman scattering in such cases. Computer simulation is an indispensable process because it gives terms which cannot be extracted from experiments.[19] In the present article, a formulation similar to that of Ladanyi and Keyes is applied to the expression of the fluctuation of the local field on the Raman scattering intensity. An equation with only experimentally observable quantities can be derived by transforming their expression into an expression that is slightly rougher.

The effect of the local field was first introduced by Kakimoto et al. in order to explain the depolarization ratio of the ν_1 Raman line of a T_d molecule with concentration dependence.[20] However, their idea included no consideration of the fluctuation in a medium. Their work caused some confusion because of its failure to consider fluctuation effects. Although the formulation of the present work is essentially different from theirs, it is much indebted to their preliminary work which established the problem.

In the present article, we have tried to express the fluctuation of the local field in a binary solution without any detailed information concerning the local structure. The local field fluctuation was formulated by including terms involving the fluctuation of the polarizability at each position in the scattering volume. A solution consisting of carbon tetrachloride and carbon disulfide was considered to be an ideal mixing solution. This is the reason why the solution was chosen in the present study.

Experimental

All of the chemicals used in the present study were commercially available products without further purifications. The concentrations of involved solutions were x_{CCl_4}=1.0, 0.8, 0.6, 0.4, and 0.2, where x_{CCl_4} is the mole fraction of carbon tetrachloride in a carbon disulfide solution.

The polarized and depolarized components of the ν_1 Raman line of carbon tetrachloride were measured with an NR-1000 system (Japan Spectroscopic Co., Ltd.). The 488 nm line of an Ar^+ laser (NEC, GLG 3300) was used as the excitation light source at 700 mW power. Polarization measurements were made using a Kenko PL filter mounted in the pathway of the scattered light. The slit widths of the double monochromator were chosen to be 250, 500 (with two slits), and 250 μm for the incident, middle and exit slits, respectively. The slit height was set at 1 mm. The Raman spectra were recorded at 25 °C.

The extinction coefficient of the polarization filter, β, and the transmittance ratio of the spectrometer for the polarized and depolarized components, γ, were simultaneously determined using a W-X lamp (The Eppley Lab., Inc.) at the peak position of a ν_1 Raman line (ca. 460 cm^{-1}) with 488 nm excitation. These instrumental factors were determined by a method which used a relation among the expected intensities from different polarization configurations. This relation with two polarization filters completely identical with each other is presented in Ref. 21 (also see Appendix). The instrumental factors, β and γ, thus obtained, were used for an intensity data correction. The depolarization ratio of a Raman line, ρ, is determined with β and γ, as

$$\rho=\frac{1}{\gamma}\frac{I_\perp-\beta I_{/\!/}}{I_{/\!/}-\beta I_\perp}, \tag{2}$$

where $I_\perp$ and $I_{/\!/}$ are the integrated depolarized and polarized intensities for this Raman line, respectively.

Theoretical

The intensity of Raman scattering is proportional to the mean-square polarization induced on molecules with a respective Raman frequency. Polarization measurements decompose this intensity to the components of a laboratory-fixed Cartesian coordinate system (X, Y, Z). When linear polarized incident light is used, the polarized and depolarized components of the scattering light are parallel and perpendicular, respectively, to the direction of the incident light polarization. For the ν_1 Raman line of a T_d molecule, the symmetry of the molecular vibration shows no intensity for the depolarized components, as can be seen from eq. 1. The possible depolarized intensity of this Raman line is produced by symmetry degradation due to some kind of intermolecular interaction or local field and its fluctuation. In order to estimate the effect of the local field on the depolarized intensity, the mean-square value of the local field is given in this section.

Consider a molecule i at a position $\boldsymbol{R}_i$ in a scattering volume v. This molecule feels a local field originating from induced polarization at each position $\boldsymbol{R}$ in v. The local field fluctuates in both magnitude and direction, depending on the molecular arrangement around $\boldsymbol{R}_i$. If we choose the incident light beam as being Z-polarized, the depolarized components of the Raman intensity are X- and Y-polarized. A component of the coordinate (X, Y, or Z) is denoted here as g. Assuming isotropic polarizability for all positions, the g-component of the local field, $F_g(\boldsymbol{R}_i)$, is expressed as

$$F_g(\boldsymbol{R}_i)=\int_v \alpha(\boldsymbol{R})\, l_{gZ}(\boldsymbol{R}-\boldsymbol{R}_i)\, d\boldsymbol{R}. \tag{3}$$

For this simplified expression, the component of the dipole operator tensor, $l_{gg'}(\boldsymbol{r})$, is defined by

$$l_{gg'}(\boldsymbol{r})=\frac{3\, r_g r_{g'}-\delta_{gg'} r^2}{r^5}, \tag{4}$$

where

$$r\equiv|\boldsymbol{r}|=\sqrt{r_X{}^2+r_Y{}^2+r_Z{}^2}.$$

Here, $\delta_{gg'}$ is the Kronecker delta. Equation 3 is integrated in order to consider the contribution of the polarizabilities on all positions. If we take the molecular viewpoint, this integration must be substi-

tuted by a summation over all positions of the molecules. However, to actually carry out this summation, detailed information is necessary concerning the molecular arrangement. Integration over all positions, including the no-molecule point, is carried out for the expression of the local field in Eq. 3. In the case of isotropic polarizability, the depolarization ratio, ρ, of the Raman line noticed here can be calculated as

$$\rho=\frac{4\langle F_{g'}{}^2\rangle}{1+4\langle F_Z{}^2\rangle}, \tag{5}$$

where g' is X or Y and the brackets $\langle\cdots\rangle$ denote the averaging value over all possible arrangements of the molecules. Factor 4 in Eq. 5 arises from the fact that the two frequency components, Rayleigh and Raman parts, of both $F_{g'}$ and F_Z contribute to the intensity of this Raman line in apparently the same way,[9] as shown in Eq. 5. Here, $\alpha(\boldsymbol{R})$ is decomposed into two parts: an invariable part, $\bar{\alpha}$, and a fluctuating part, $\Delta\alpha(\boldsymbol{R})$. $F_g(\boldsymbol{R}_i)$ can be rewritten as

$$\begin{aligned}F_g(\boldsymbol{R}_i)&=\bar{\alpha}\int_v l_{gZ}(\boldsymbol{R}-\boldsymbol{R}_i)\mathrm{d}\boldsymbol{R}+\int_v \Delta\alpha(\boldsymbol{R})\, l_{gZ}(\boldsymbol{R}-\boldsymbol{R}_i)\mathrm{d}\boldsymbol{R}\\&=\int_v \Delta\alpha(\boldsymbol{R}) l_{gZ}(\boldsymbol{R}-\boldsymbol{R}_i)\mathrm{d}\boldsymbol{R},\end{aligned} \tag{6}$$

where the integral of $l_{gZ}(\boldsymbol{R}-\boldsymbol{R}_i)$ is zero when the explicit expression of Eq. 4 is considered. If the correlation of the space dependence of $\Delta\alpha(\boldsymbol{R})$ is neglected, the mean-square value of $F_g(\boldsymbol{R}_i)$ is

$$\begin{aligned}\langle\{F_g(\boldsymbol{R}_i)\}^2\rangle&=w\int_v \mathrm{d}\boldsymbol{R}'\int_v \langle\{\Delta\alpha(\boldsymbol{R})\, l_{gZ}(\boldsymbol{R}-\boldsymbol{R}_i)\}^2\rangle\,\mathrm{d}\boldsymbol{R}\\&\quad+w\iint_{\boldsymbol{R}'\neq\boldsymbol{R}}\langle\Delta\alpha(\boldsymbol{R})\,\Delta\alpha(\boldsymbol{R}')\, l_{gZ}(\boldsymbol{R}-\boldsymbol{R}_i)\, l_{gZ}(\boldsymbol{R}'-\boldsymbol{R}_i)\rangle\,\mathrm{d}\boldsymbol{R}\,\mathrm{d}\boldsymbol{R}'\\&=w\int_v \mathrm{d}\boldsymbol{R}'\int_v \langle\{\Delta\alpha(\boldsymbol{R})\}^2\rangle\,\{l_{gZ}(\boldsymbol{R}-\boldsymbol{R}_i)\}^2\,\mathrm{d}\boldsymbol{R},\end{aligned} \tag{7}$$

where w is a statistical weight. Since the dipole operator tensor, of course, does not depend on the molecular arrangement, the averaging procedure affects only $\{\Delta\alpha(\boldsymbol{R})\}^2$ in Eq. 7. The last expression of Eq. 7 is derived from this fact. On the other hand, the homogeneity of the medium allows one to replace $\langle\{\Delta\alpha(\boldsymbol{R})\}^2\rangle$ with $\langle(\Delta\alpha)^2\rangle$, a position-independent mean-square quantity of $\Delta\alpha$. Equation 7 can be expressed by

$$\langle\{F_g(\boldsymbol{R}_i)\}^2\rangle=w\langle(\Delta\alpha)^2\rangle\int_v \mathrm{d}\boldsymbol{R}'\int_v \{l_{gZ}(\boldsymbol{R}-\boldsymbol{R}_i)\}^2\,\mathrm{d}\boldsymbol{R}. \tag{7'}$$

If the assumption of the space-independence of the $\Delta\alpha(\boldsymbol{R})$ correlation in Eq. 7 is rejected, details concerning the distribution functions are required. The contribution of the pair-distribution function is considered in Ref. 9 and that of the triplet-distribution function is discussed in Ref. 6. Equation 7′ can be calculated numerically using the formula $l_{gZ}(\boldsymbol{R}-\boldsymbol{R}_i)$. For multi-component systems, however, the integration ranges for each component are different from each other, since the radial part of this integral is restricted by the smallest distance between pairing molecules. The correlation between $\langle\{\Delta\alpha(\boldsymbol{R})\}^2\rangle$ and the integration range, therefore, still holds for multi-component systems. For one-component systems, the problem concerning the integration range is not very complicated. Equation 7′ is rewritten here for one-component systems. In order to consider the discreteness of molecules, the polarizability, α_ϕ, at a no-molecule point is introduced. At that point, α_ϕ is obviously zero. When the probability of finding a molecule at the position is denoted as P, $\bar{\alpha}$, and $\langle(\Delta\alpha)^2\rangle$ are expressed as

$$\bar{\alpha}=P\alpha_M+(1-P)\alpha_\phi=P\alpha_M \tag{8}$$

and

$$\begin{aligned}\langle(\Delta\alpha)^2\rangle&=P\,(\bar{\alpha}-\alpha_M)^2+(1-P)\,(\bar{\alpha}-\alpha_\phi)^2\\&=P\,(\bar{\alpha}-\alpha_M)^2+(1-P)\,(P\alpha_M)^2\\&=P\,(1-P)\,\alpha_M{}^2.\end{aligned} \tag{9}$$

Here, α_M is the polarizability of the molecule in this one-component system. By inserting Eq. 9 into Eq. 7′ and integrating Eq. 7′, the mean-square value of $F_g(\boldsymbol{R}_i)$ for one-component systems can be written as

$$\langle\{F_g(\boldsymbol{R}_i)\}^2\rangle=CP\,(1-P)\alpha_M{}^2N_A{}^2(d/M)^2, \tag{10}$$

where

$$C=\begin{cases}2\,\pi^2/15 & \text{for } g=x \text{ or } y.\\ 8\,\pi^2/45 & \text{for } g=z\end{cases}$$

Further, N_A, d, and M are Avogadro's number, the density of this system, and the molecular weight of the component molecule, respectively. In the derivation of Eq. 10, the following relations were used:

$$\frac{4\pi}{3}a^3N_A=\frac{M}{d}$$

and

$$w=\frac{\langle n\rangle}{v}=N_A\frac{d}{M}=\left(\frac{4\pi}{3}a\right)^{-1},$$

where a and $\langle n\rangle$ are the molecular radius and the mean-number of molecules in volume v. The range of integration, as well as the radial part of the integral in Eq. 7′, was taken from $2a$ to infinity.

The quantities of molecules are included in Eq. 10 as α_M, d, and M. A new variable, Q, is introduced in Eq. 11 in order to calculate Eq. 7′ for multi-component systems, although the problem concerning the range of integration cannot be determined yet.

$$Q\equiv\alpha_M N_A\, d/M. \tag{11}$$

Using this variable, Q, we can assume that Eq. 7 is transformed into

$$\langle\{F_g(\boldsymbol{R}_i)\}^2\rangle=C\,\langle(\Delta Q)^2\rangle. \tag{12}$$

Equation 12 is similar to Eq. 10 derived from Eqs. 8 and 9 in the relation between $\bar{Q}$ and $\langle(\Delta Q)^2\rangle$. The use of Q for each component makes it possible to express the complicated relation of Eq. 7′ without any knowledge of the correlation between $\langle(\Delta\alpha)^2\rangle$ and the range of integration in this equation. Therefore, the

following relations are expected to hold for a binary solution with A and B components:

$$\bar{Q}=P\{x_A Q_A+(1-x_A)Q_B\}+(1-P)\,Q_\phi \qquad (13)$$

and

$$\langle(\Delta Q)^2\rangle=P\{x_A(\bar{Q}-Q_A)^2+(1-x_A)(\bar{Q}-Q_B)^2\}+(1-P)(\bar{Q}-Q_\phi)^2, \qquad (14)$$

where $Q_\phi=0$ because $\alpha_\phi=0$. x_A is the mole fraction of component A. If analytical transformations are made for Eq. 14, the following relation is derived:

$$\langle\{F_g(\boldsymbol{R}_i)\}^2\rangle=C[P^2(Q_A-Q_B)^2\,x_A\,(1-x_A)+P\,(1-P)\,\{(Q_A{}^2-Q_B{}^2)\,x_A+Q_B{}^2\}]. \qquad (15)$$

The equality between Eqs. 15 and 10 is confirmed again when $x_A=1$.

A simpler formulation can be taken if the range of integration is ignored. However, the lower limit of the integration range as well as the radial part of the integral in Eq. 7′ must be given as the mean-value of the nearest-neighbor distances in this case. Since $l_{gZ}(\boldsymbol{R}-\boldsymbol{R}_i)$ takes a large value at short distances, the contribution of a component molecule of smaller size cannot be satisfactorily considered in this treatment. A schematic view of this problem is given in Fig. 1. As a possible formula based on the above simpler formulation, the following expression can be derived:

$$\langle\{F_g(\boldsymbol{R}_i)\}^2\rangle=C[P^2(\alpha_A-\alpha_B)^2\,x_A\,(1-x_A)+P\,(1-P)\,\{(\alpha_A{}^2-\alpha_B{}^2)\,x_A+\alpha_B{}^2\}]\times N_A\,[\bar{d}/\{M_A\,x_A+M_B\,(1-x_A)\}]^2, \qquad (16)$$

where $\bar{d}$ is the system density. The error originating from adopting the mean nearest-neighbor distance is not thought to be very large when $x_A\approx1$ and 0, since $\bar{d}\approx d_A$ when $x_A\approx1$ and $\bar{d}\approx d_B$ when $x_A\approx0$. On the other hand, Eq. 16 can be underestimated when $0<x_A<1$, since this equation omits part of the contribution of $l_{gZ}(\boldsymbol{R}-\boldsymbol{R}_i)$ at short distances (The shaded

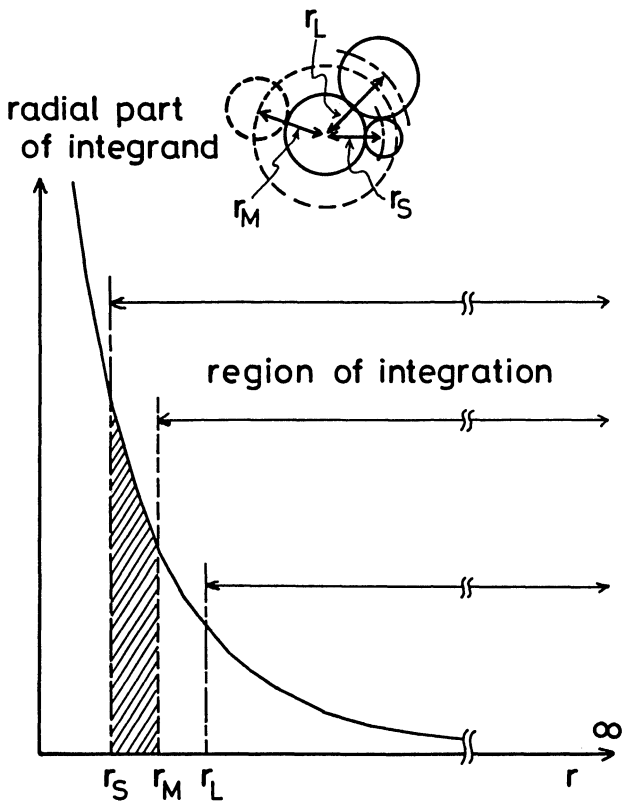

Fig. 1. Schematic view of the problem on the lower limit of the integration range along with the radial part of the integral in Eq. 7. r_M: mean-value of nearest-neighbor distances. r_S:. nearest-neighbor distance between the T_d molecule and a component molecule of smaller size. r_L: nearest-neighbor distance between the T_d molecule and a component molecule of larger size. Shaded regions were parts omitting the contribution of integrand for the formulation with the mean-value of nearest-neighbor distances.

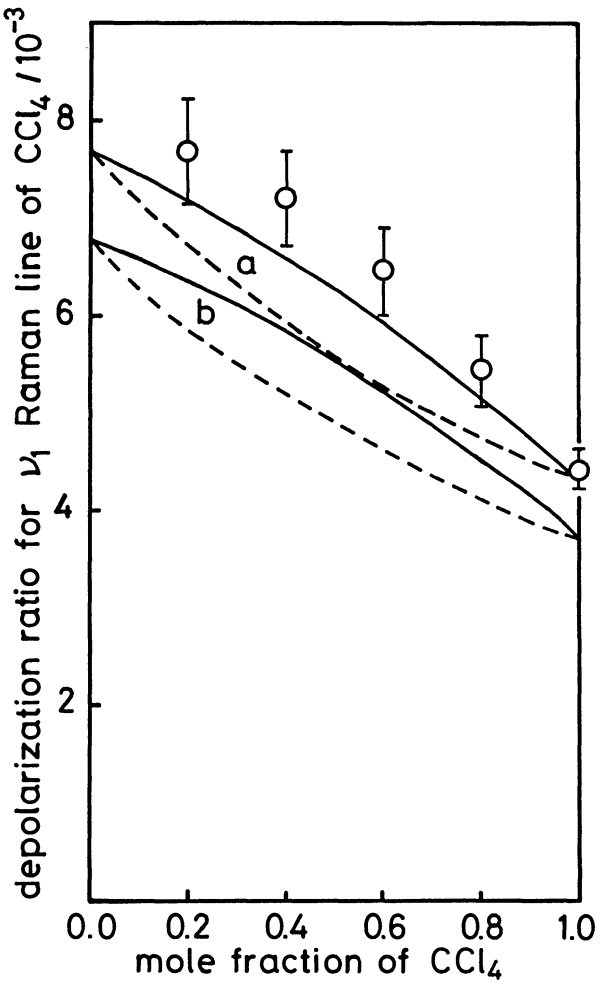

Fig. 2. Observed and calculated depolarization ratios of the ν_1 Raman line of carbon tetrachloride in carbon disulfide solution. Circles with error bars are observed values. Straight and broken lines are curves calculated by Eqs. 15 and 16, respectively. Lines marked "a" are the values for P=0.74, while those marked "b" are the values for P=0.68.

region in Fig. 1). Therefore, we must notice that Eq. 16 possibly gives less quantitative results, except for a system constructed using components of similar size.

The use of distribution functions can result in another explicit formulation of $\langle\{F_g(\boldsymbol{R}_i)\}^2\rangle$ based on some fundamentals from statistical mechanics. Equation 15 is substituted for that derived from this formulation. One example of the use of distribution functions for a pure liquid was given in a previous report.[9] However, numerical calculations using this formulation are impossible if explicit information concerning the distribution functions is not given for an object system. This proves that Eq. 15 is useful.

Results and Discussion

Figure 2 shows the depolarization ratio, ρ, of the ν_1 Raman line of carbon tetrachloride against the mole fraction, x_{CCl_4}, of carbon tetrachloride in carbon disulfide solutions. The instrumental factors of Eq. 2 for deriving the depolarization ratios, β and γ, resulted in 0.0021 and 0.360, respectively, at the wavelength of this Raman line with 488 nm excitation. The observed depolarization ratios are indicated by open circles with a vertical bar through them. These vertical bars indicate the statistic errors, which include the uncertainties of the β and γ values. The observed depolarization ratios increase with the carbon tetrachloride diluted with carbon disulfide along with a curve opening downwards. The extrapolation of this curve to infinite dilution almost duplicates the depolarization ratio of neat carbon tetrachloride. These depolarization ratios agreed fairly well with the previously reported data.[3,22]

The depolarization ratios calculated using Eqs. 15 and 5 are also shown in Fig. 2 as straight lines. The parameters used for these calculations are listed in Table 1. The density data were obtained from Ref. 24. The probability of finding a molecule, P, was defined by simple geometrical calculations for the occupation volume of hard spheres in three types of packing. Calculations regarding two cases of the P value are shown in Fig. 2. The cases for *fcc* and *hcp* are indicated as a, while that for *bcc* is indicated as b. The results obtained by using Eq. 16 are also shown in Fig. 2, as indicated by broken lines in the same manner as those from Eq. 15. The density data were interpolated between each pair of neighboring data points for calculations using Eq. 16.

The observed relation between the depolarization ratio and the mole fraction, ρ-x_{CCl_4}, can be well explained by Eq. 15, because the factor of x_A $(1-x_A)$ must have a positive value. Putting the parameters listed in Table 1 into Eq. 15, the depolarization ratio when $x_{CCl_4}\approx 0$ is found to be almost twice as large as that when $x_{CCl_4}\approx 1$. The calculated curves of Eq. 15 satisfy the experimental ρ-x_{CCl_4} relation for both the P values adopted here. An X-ray diffraction study[10] confirmed that the local structure of pure liquid carbon tetrachloride ($x_A=1$) is *bcc*. A more explicit expression for the depolarization ratio than that given in the present article resulted in 0.0042, supporting the local *bcc* model.[6,10] The calculated value for $P=0.74$ (*fcc* and *hcp* cases) at $x_A=1$ must be considered to accidentally agree with the observed value. It is not known why these two P values are adopted quantitatively. However, Eq. 15 is sufficiently qualitative to express the observed concentration dependence of the depolarization ratio.

The calculated depolarization ratios of Eq. 16 with both two P values show curves opening upwards, although those of Eq. 15 are curves opening downwards. Since the polarizability fluctuation term in Eq. 16 shows a curve opening downwards, the figured tendency that Eq. 16 shows must be dominantly described by the term involving the mean density of these solutions. The use of the mean density of the solution omits the contribution of a component at short distances, as was stated in the previous section. A qualitative disagreement of Eq. 16 with the observed data, therefore, occurs. This fact seems to stress the necessity for considering the nearest-neighbor distances in binary solutions.

It was found that Eq. 15 qualitatively predicts the fluctuation of the local field by comparing the observed and calculated depolarization ratios of the ν_1 Raman line of carbon tetrachloride in carbon disulfide solution. Also, the agreement between those values was observed within about 10% each for the cases of the different P values, although no quantita-

Table 1. Parameters in Eqs. 15 and 16 for Binary Solution of Carbon Tetrachloride and Carbon Disulfide

			CCl_4		CS_2
Polarizability[a] (α_M/Å^3)			10.5		8.74
Molecular weight (M/g mole^{-1})			154		76
Mole fraction (x_{CCl_4})	1.00	0.75	0.40	0.16	0.00
Density[b] ($\bar{d}$/g cm^{-3})	1.5845	1.5237	1.4197	1.3310	1.2558
P		0.74 for *fcc* and *hcp* packing 0.68 for *bcc* packing			

a) Ref. 23. The trace of the polarizability tensor was taken for carbon disulfide. b) Ref. 24.

tiveness of the theoretical accuracies was guaranteed. As a result, the sufficiency of Eq. 15 was not very bad regarding quantitativeness. The derivation of Eq. 15 was made for completely random mixing. Fortunately, this equation can easily be expanded to involve solutions containing an ideal associated complex[25] by redefining the concentration of the respective species under consideration in which the associating species are treated as being different ones from the individual component. This fact shows that the concentration dependences of the depolarization ratio are different, depending on the system with different association numbers. The determination of the association number must be made experimentally using Eq. 15. This determination is one of the most difficult problems to be solved, because of the insufficient experimental accuracies of our instrumental set-up.

Concluding Discussion

The fluctuation of the local field was expressed in terms of the fluctuation of the polarizability at each position in the scattering volume. The formulation was made by distinguishing the positions with the polarizabilities of molecules from that of a vacancy, in order to take the discreteness of molecules into account. This expression was found to explain well the concentration dependence of the depolarization ratio of the ν_1 Raman line for carbon tetrachloride in carbon disulfide solutions. This concentration dependence cannot be analyzed using the previously proposed local lattice model,[9] without any explicit information concerning the local structure in each solution. The shape of carbon disulfide was assumed to be spherical, and the probability of finding molecules was considered to have no concentration dependence in this formulation. Therefore, the estimation with this expression seems to be very rough. However, the result of the estimation agreed well with the observed concentration dependence of this depolarization ratio. This result indicated that the finite size of a molecule essentially affects the magnitude of the fluctuation of the local field.

The fluctuation of the local field is affected mainly by the region including the first and second nearest-neighbor molecules around each molecule, because this can be calculated using the mean-square values of the dipolar field created by surrounding molecules. Therefore, the fluctuation of the local field suggests the structure of local molecular arrangements. In the present states, the fluctuation of the local field is found to be reflected only in the depolarization ratio of the ν_1 Raman line for T_d molecules. Consequently, the present study indicates that, regardless of the above-mentioned restriction, studies concerning the local field fluctuation are useful for evaluating model systems for discussions concerning the local structure of solution states.

The author is indebted to Dr. Tomohiko Yamazaki of Toyota Central Research and Development Laboratories, Inc. (TCRDL) for his invaluable assistance with the REDUCE operations, of which results are summarized in the Appendix. The author wishes to thank Professor Tadashi Kato of Tokyo Metropolitan University for directing his attention to the papers on the Rayleigh light scattering intensity. The author also thanks Dr. S. Noda and Dr. A. Isogai of TCRDL for their encouragement of this work, and the director of TCRDL for permission to publish this work.

Appendix

This Appendix presents a determination method of the extinction coefficient of the polarization filter, β, and the transmittance ratio of the spectrometer for polarized and depolarized components, γ.

The transmittance ratio, γ, is defined by

$$\gamma \equiv \tau_\perp / \tau_{/\!/}, \tag{A1}$$

where $\tau_\perp$and $\tau_{/\!/}$ are the transmittances of linear polarized lights which are perpendicular and parallel to the slit of the spectrometer. The observed intensities of these two linear polarized components, $I_\perp^{obsd}$ and $I_{/\!/}^{obsd}$, are expressed as

$$I_\perp^{obsd} = t\,\beta\, I_{/\!/}^{\circ}\,\tau_{/\!/} + t\, I_\perp^{\circ}\,\tau_\perp \tag{A2-a}$$

and

$$I_{/\!/}^{obsd} = t\, I_{/\!/}^{\circ}\,\tau_{/\!/} + t\,\beta\, I_\perp^{\circ}\,\tau_\perp, \tag{A2-b}$$

where t is the transmittance of the polarization filter and superscript $^\circ$ denotes the true intensities. Moreover, the conditions with two polarization filters are considered. The observed intensity is denoted as $I_{\perp/\!/}^{obsd}$ when one filter is set perpendicular and the other parallel to the slit; it is denoted as $I_{\perp\perp}^{obsd}$ when both filters are set perpendicular to the slit. These two intensities are expressed as

$$I_{\perp/\!/}^{obsd} = t_1 t_2(\beta_1\, I_{/\!/}^{\circ}\,\tau_{/\!/} + \beta_2\, I_\perp^{\circ}\,\tau_\perp) \tag{A3-a}$$

and

$$I_{\perp\perp}^{obsd} = t_1 t_2(\beta_1\,\beta_2\, I_{/\!/}^{\circ}\,\tau_{/\!/} + \beta_2\, I_\perp^{\circ}\,\tau_\perp) \tag{A3-b}$$

where subscript 1 and 2 denote the two different polarization filters.

If these two polarization filters are completely identical, the following relations are satisfied:

$$t_1 = t_2 \equiv t \text{ and } \beta_1 = \beta_2 \equiv \beta. \tag{A4}$$

For this condition, the extinction coefficient of the polarization filter, β, can be expressed as

$$\beta = \frac{(1-u+v+uv) \pm \sqrt{(1-u+v+uv)^2-4u^2}}{2u}, \tag{A5}$$

where

$$u \equiv \frac{I_\perp^{obsd}}{I_{/\!/}^{obsd}} = \frac{\beta+\gamma}{1+\beta\gamma} \tag{A6-a}$$

and

$$v \equiv \frac{I_{\perp\perp}^{\text{obsd}}}{I_{\perp/\!/}^{\text{obsd}}} = \frac{\beta^2+\gamma}{\beta+\beta\gamma} \tag{A6-b}$$

Simultaneously, γ and t are

$$\gamma = \frac{u-\beta}{1-u\beta} \tag{A7}$$

and

$$\gamma = \frac{I_{/\!/}^{\text{obsd}} + \tau_{\perp}^{\text{obsd}}}{(1+\beta)I^{\text{obsd}}}, \tag{A8}$$

where I^{obsd} is the observed intensity with no polarization filter. Equations A5-A8 were previously described in Ref. 21.

However, since it is very difficult to obtain two completely identical polarization filters, we analyzed expressions of the observed intensitites without the relations A4. An analysis of the expressions was made using the following definitions:

$$u_i = \frac{\beta_i+\gamma}{1+\beta_i\gamma}, \quad (i=1, 2) \tag{A9}$$

$$v_{12} = \frac{\beta_1\beta_2+\gamma}{\beta_1+\beta_2\gamma}, \tag{A10}$$

$$\beta_1 \equiv \beta, \tag{A11}$$

and

$$\beta_2 \equiv \beta + \beta'. \tag{A12}$$

REDUCE ver. 3.0, a computer language for mathematical analysis, was operated on a computer, IBM 3083. Equations All and A12 are essential for solving the expressions, because of the complexity of the relations. The results of the analysis are

$$\begin{aligned}\beta = [&(u_1^2u_2v_{12} - u_1^2u_2 + 2u_1u_2 + u_2v_{12} + u_2 + u_1^2v_{12} - u_1^2 - 2u_1v_{12} - v_{12} - 1) \\ &\pm (u_1+1)\{(v_{12}+1)(u_1-1) \\ &\times (u_1u_2^2v_{12} - 3u_1u_2^2 - u_2^2v_{12} - u_2^2 + 2u_1u_2v_{12} + 2u_1u_2 \\ &+ 2u_2v_{12} + 2u_2 - 3u_1v_{12} + u_1 - v_{12} - 1)\}^{1/2}] \\ &\div \{2u_1(u_1u_2 + u_2v_{12} - u_1v_{12} - 1)\},\end{aligned} \tag{A13}$$

$$\beta' = \frac{(1+\beta\gamma)u_2 - (\beta+\gamma)}{1-\gamma u_2}, \tag{A14}$$

and

$$\gamma = \frac{u_1-\beta}{1-u_1\beta} = \frac{u_2-(\beta+\beta')}{1-u_2(\beta+\beta')}. \tag{A15}$$

Usually, $u_i \approx \gamma \approx 1$, $\beta \ll 1$, and $v_{12} \gg 1$. Therefore, sufficient care concerning the experimental accuracy must be taken when determinating these equations.

References

1) A. E. Douglas and D. H. Rank, *J. Opt. Soc. Am.*, **38**, 281 (1948).
2) J. Brandmüller, K. Burchardi, H. Hacker, and H. W. Schrötter, *Z. Angew. Phys.*, **22**, 177 (1967).
3) W. F. Murphy, M. W. Evans, and P. Bender, *J. Chem. Phys.*, **47**, 1836 (1967).
4) K. Fukushi and M. Kimura, *J. Raman Spectrosc.*, **8**, 125 (1979).
5) S. Ikawa and E. Whalley, *J. Chem. Phys.*, **89**, 51 (1988).
6) S. Hyodo, N. Tatsuta, and T. Okamoto, *J. Chem. Phys.*, **92**, 882 (1990).
7) G. W. Chantry, *Spectrochim. Acta*, **21**, 1007 (1965).
8) A. E. Douglas and D. H. Rank, *Nature*, **162**, 453 (1948).
9) S. Hyodo and T. Fujiyama, *Bull. Chem. Soc. Jpn.*, **53**, 2456 (1980).
10) K. Nishikawa and T. Iijima, *Bull. Chem. Soc. Jpn.*, **58**, 1220 (1985).
11) S. Hyodo, *Chem. Phys. Lett.*, **161**, 245 (1989).
12) A. H. Narten, M. D. Danford, and H. A. Levy, *J. Chem. Phys.*, **46**, 4875 (1967).
13) G. Reichelt, J-U. Weidner, and H. W. Zimmermann, *Ber. Bunsen-Ges. Phys. Chem.*, **78**, 1050 (1974).
14) K. Nishikawa and Y. Murata, *Bull. Chem. Soc. Jpn.*, **52**, 293 (1979).
15) B. M. Ladanyi and T. Keyes, *Mol. Phys.*, **33**, 1063 (1977).
16) T. Keyes and B. M. Ladanyi, *Mol. Phys.*, **33**, 1099 (1977).
17) B. M. Ladanyi and T. Keyes, *Mol. Phys.*, **33**, 1247 (1977).
18) T. Keyes and B. M. Ladanyi, *Mol. Phys.*, **33**, 1271 (1977).
19) B. M. Ladanyi and T. Keyes, *J. Chem. Phys.*, **68**, 3217 (1978).
20) M. Kakimoto, T. Fujiyama, and T. Shimanouchi, unpublished results. Bunshikōzō Sōgō Tōronkai, Nagoya, 1973.
21) T. Fujiyama and M. Tasumi, *Bunkou Kenkyu*, **20**, 28 (1971).
22) F. Iida, S. Hyodo, and T. Fujiyama, unpublished results. Bunshikōzō Sōgō Tōronkai, Fukuoka, 1980.
23) Landolt-Börnstein, "Atom und Molekül Physik," 3 Teil, Molekulen II, Springer, Berlin (1951).
24) "International Critical Tables," McGraw-Hill, New York (1928), Vol. III.
25) See for example, I. Prigofine and R. Defay, "Chemical Thermodynamics," Longmans Green and Co., London (1954). Chap. 26.

 © 1991 The Chemical Society of Japan Bull. Chem. Soc. Jpn., 64, 505—509 (1991)

Electrochemical Studies of Poly(mercaptohydroquinone) and Poly(mercapto-*p*-benzoquinone) Films Prepared by Electrochemical Polymerization. V. Spectroelectrochemistry of Ten pH Indicators in the Film

Gorou ARAI,* Kenji IMAI, Ken-ichiro TANAKA, and Iwao YASUMORI
Department of Applied Chemistry, Faculty of Engineering, Kanagawa University, Kanagawa-ku, Yokohama 221
(Received July 26, 1990)

The electroconductive, almost colorless and transparent poly(mercaptohydroquinone/mercapto-*p*-benzoquinone) film, prepared by electropolymerization of mercaptohydroquinone on an SnO_2/glass electrode, was impregnated with a pH indicator. The film exhibited a clear electrochromic behavior arising from proton release/consumption within the film by electrooxidation/reduction, as verified by spectroelectrochemical measurements. For ten different pH indicators examined, such a color change could be well repeated over a long-term continuous experiment by use of potential steps.

There has been considerable interest in examining transition metal oxides,[1] conductive polymer films prepared by electropolymerization,[2] and electrochromic active sites introdueed in polymers as the basis for electrochromic displays.[3] The spectroelectrochemical response observed with these materials comes directly from the coloration of their electrochemically reduced or oxidised form. As described in a series of papers,[4] poly(mercaptohydroquinone) (SQ_{Red}) and poly(mercapto-*p*-benzoquinone) (SQ_{Ox}) are electroconductive and almost transparent films. These redox polymers (SQ, standing for SQ_{Red} and/or SQ_{Ox}) exhibit no change in the shape of the cyclic voltammogram over more than 1000 times repetitive potential scannings from +0.7 V vs. a saturated calomel electrode (SCE) to the H_2 evolution potential. The oxidation-reduction equilibrium between SQ_{Ox} and SQ_{Red} is represented by the following scheme.

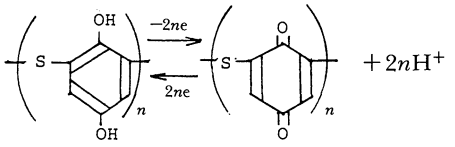

Hence, the pH value in an SQ film in contact with an aqueous solution will be decreased by oxidation, while increased by reduction of the film. When a pH indicator is incorporated into the polymer film, the film will exhibit a color change characteristic of the pH indicator by oxidation-reduction of the film. Spectroelectrochemical properties of phenolphthalein, a typical pH indicator, incorporated within the SQ film on a transparent electrode (SnO_2/glass) was briefly reported in a previous paper,[5] where phenolphthalein showed a distinct color change between red by reduction and transparent by oxidation of the film. Here we describe spectroelectrochemical behaviors of ten different pH indicators incorporated within the polymer film and the characteristics of the electrochromic electrodes thus prepared.

Experimental

Chemicals and Preparation of SQ Films. Mercaptohydroquinone was synthesized and purified according to the method described in our previous papers.[6] All of the pH indicators and inorganic reagents used here were of reagent grade and used without further purification. Deionized water was used for preparation of solutions and rinsing the SQ film. The substrate electrode was an SnO_2/glass plate (Taiyo Yuden Co.). The SnO_2/glass plate was washed with acetone and rinsed with water. The SnO_2/glass plate was coated with an SQ film by anodic polymerization of 10 mM (1 M=1 mol dm^{-3}) mercaptohydroquinone at a potential of +0.7 V vs. SCE in a Britton-Robinson buffer solution of pH 7.0 containing 20% volume fraction ethanol in an N_2-atmosphere at room temperature.

Apparatus and Procedure. Potentiostatic electrolysis and cyclic voltammetry were performed with a Toho Technical Research potentiostat/galvanostat Model 2020. The

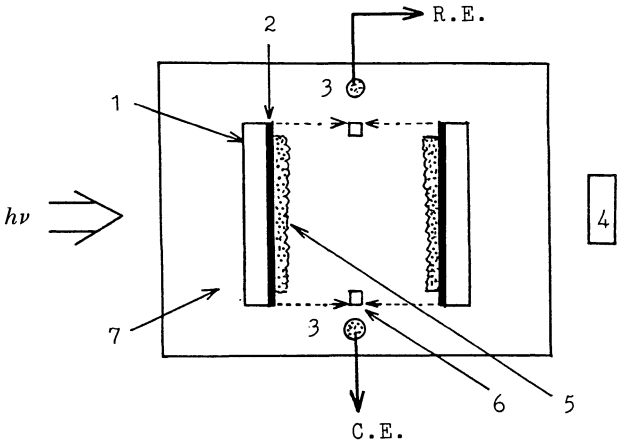

Fig. 1. Schematic view of the experimental arrangement for transmission spectroelectrochemical measurements.
1: Substrate glass, 2: SnO_2, 3: Salt bridge, 4: Detector, 5: pH indicator-impregnated SQ film, 6: Silicone rubber, 7: Supporting electrolyte solution.

electrode surface was examined with a JEOL scanning electron microscope (SEM) Model JSM-35C. Spectroelectrochemical study of the pH indicator-impregnated electrodes was done with a three-electrode system consisting of an SCE reference electrode, a Pt wire counter electrode, and an electrochromic working electrode placed in a Shimadzu spectrophotometer Model UV-240. The electrochromic working electrode consisted of a pair of pH indicator-impregnated electrodes held together face to face via two 0.5-mm thick silicone rubber spacers as shown in Fig. 1.

Incorporation of pH Indicators. Incorporation of pH indicators into the SQ films was carried out by three different methods: (1) electropolymerization of mercaptohydroquinone in a Britton-Robinson buffer solution containing 50% volume fraction of ethanol, saturated with the pH indicator, (2) dipping of the SQ film-coated SnO_2/glass electrode in an ethanol solution saturated with the pH indicator for ca. 20 h, and (3) spray of an ethanol solution containing the pH indicator on the SQ film-coated electrode. The electrochromic cells prepared by methods (1) and (2) were inferior to the cell prepared by method (3) with regard to the optical density, which depends the amount of the pH indicator incorporated within the SQ film, for all of the pH indicators examined. Moreover, the electrochromic cell prepared by method (3) exhibited good reproducibility in color change when the SQ film was repetitively oxidized/reduced. In view of this, the electrochromic cell used in this work was prepared by method (3). The SQ_{Ox} film prepared on an SnO_2/glass electrode was rinsed with methanol, washed with water, and then air-dried. A small amount (ca. 0.05 cm^3) of an ethanol solution containing 10% volume fraction of water and 2% mass fraction of a pH indicator was sprayed on a dried SQ film of 1 cm^2 in area. A pH indicator-impregnated SnO_2/glass electrode was then soaked in a 1 M KCl aqueous solution adjusted to a pH value slightly lower than the value where the indicator changes the color, by adding a small amount of an HCl and/or KOH aqueous solution, and used immediately as an electrochromic working electrode. The 1 M KCl solution thus conditioned was also used as the supporting electrolyte solution. The pH value of the 1 M KCl solution adjusted to each of the pH indicators is denoted by "pH in cell" in the last column of Table 1.

Results and Discussion

Properties of SQ Films on SnO_2/Glass. Figure 2 shows the relationship between the time of electrooxidation of mercaptohydroquinone and the amount of the SQ film formed on the SnO_2/glass electrode, calculated from their cyclic voltammograms (CV). The amount of the SQ film increased linearly with the electrolysis time up to 40 min. However, the SQ film became colored in dark yellow by electrolysis for more than ca. 20 min. Therefore, all the SQ films used in this work were prepared by 20-min electrooxidation. A typical CV of the resulting SQ film on an SnO_2/glass electrode is shown in Fig. 3. A pair of broad anodic and cathodic waves arising from reduction-oxidation of the SQ film were observed with peaks at

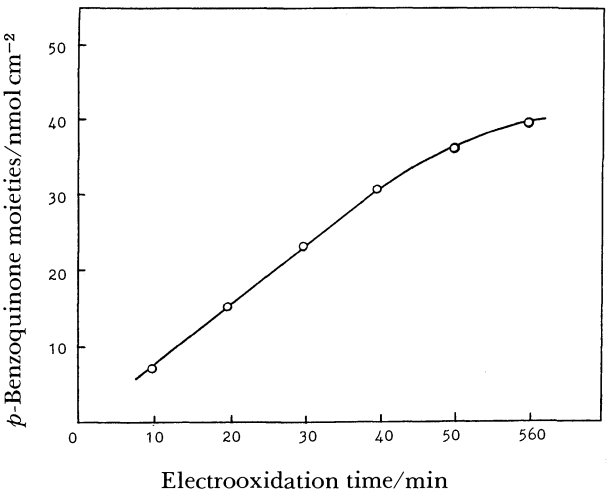

Fig. 2. Increase in the amount of quinone moieties in the SQ film on SnO_2/glass electrode with the lapse of electrooxidation time. The electrooxidation was carried out by anodic oxidation (+0.7 V vs. SCE) of 10 mM mercaptohydroquinone using Britton-Robinson buffer solution (20 vol% EtOH) in N_2 atmosphere.

Table 1. Electrochromic Characteristics of pH Indicator-Impregnated SQ Films Prepared on SnO_2/Glass Electrode[a)]

pH indicator	Color change(pH)	Response time	pH in cell
	Acid color ⟷ Basic color	s	
Bromophenol Blue[b)]	Yellow(3.0) ⟷ Blue(4.6)	5—7	2.9
Bromocresol Green[b)]	Yellow(3.8) ⟷ Green(5.4)	3—4	3.6
p-Nitrophenol	Colorless(5.0) ⟷ Yellow(7.6)	2—3	4.8
Bromothymol Blue	Yellow(6.0) ⟷ Blue(7.6)	2—3	5.8
Indooxine	Red(6.0) ⟷ Blue(8.0)	2—3	5.8
Quinoline Blue	Colorless(6.6) ⟷ Blue(8.6)	<2	6.4
Phenol Red[b)]	Yellow(6.8) ⟷ Red(8.4)	3—4	6.6
o-Cresolphthalein	Colorless(8.2) ⟷ Red(9.8)	<2	8.0
Phenolphthalein	Colorless(8.3) ⟷ Red(10.0)	<2	8.0
Thymolphthalein	Colorless(9.4) ⟷ Blue(10.6)	4—5	9.0

a) All data are average of 10 or more experiments. b) Potential stepping was carried out between −0.5 V and 0.7 V vs. SCE.

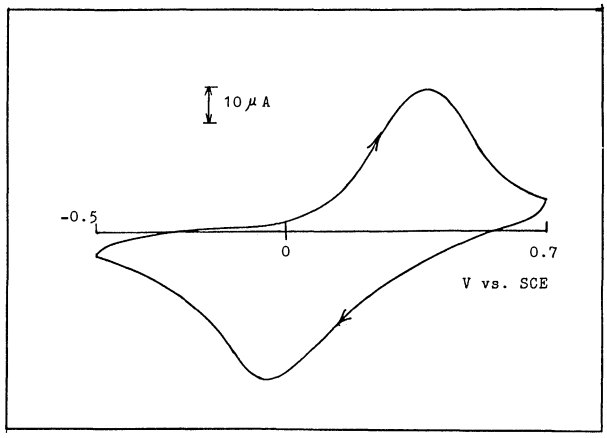

Fig. 3. Cyclic voltammogram of the SQ film prepared on SnO_2/glass electrode (1 cm^2 in area) in Britton-Robinson buffer solution (pH 5.0). The sample electrode was prepared under the same conditions as in Fig. 2.
Electrolysis time: 20 min, Sweep rate: 2 mV s^{-1}.

0.38 V and −0.05 V vs. SCE, respectively. The surface concentration of hydroquinone and/or *p*-benzoquinone moieties was calculated to be ca. 15.6 nmol cm^{-2}. This indicates that in an aqueous solution with a pH value at which one hydroquinone moiety releases two protons via a two-electron reaction, complete oxidation of SQ_{Red} to SQ_{Ox} may increase the amount of proton by 31.2 nmol, while on complete reduction of SQ_{Ox} to SQ_{Red} the same amount of proton may be lost per one sheet of electrode. Hence, in an electrochromic working electrode of 0.5 mm in thickness and 1 cm^3 in area (0.05 cm^3 in volume), the increase and/or decrease in the amount of hydrogen ion is twice this value because two sheets of working electrodes were used. Examination of the SQ film by SEM revealed that the dried film prepared by 20-min electrooxidation of mercaptohydroquinone (Fig. 4(b)) covered the whole surface of the SnO_2/glass electrode, though the film was rougher than that on a glassy carbon electrode.[7] The film thickness was estimated to be 1—2 μm and even after repeated water washings no appreciable morphological change was observed.

Spectroelectrochemical Properties. Figure 5 depicts the absorption spectrum of a colored *o*-Cresolphthalein-impregnated SnO_2/glass electrode when SQ_{Ox} was reduced to SQ_{Red} at −0.7 V, with the dashed curve showing the spectrum of an SnO_2/glass electrode coated with SQ_{Red} alone. In addition, the inset gives a typical absorption spectrum of a colored *o*-Cresolphthalein alkaline solution. The absorption maximum at 565 nm observed for the colored working electrode is in good agreement with that of colored *o*-Cresolphthalein in an alkaline solution. This indicates that the coloration observed on the working electrode is obviously due to that of *o*-Cresolphthalein within the SQ_{Red} film. When the potential of the colored working electrode was stepped to +0.7 V where SQ_{Red} was oxidized to SQ_{Ox}, the absorption spectrum based on the coloration rapidly disappeared. This spectral change was easily observed visually, namely the working electrode became red in a few seconds when reduced and colorless when oxidised. Then the potential was changed by use of square voltage pulses, and both the optical response at 565 nm and the current response were recorded. The result is illustrated in Fig. 6. The time course of absorvance response was almost the same for anodic and cathodic potential steps even after 10 min of the repetitive potential steps. But a small amount of the colored indicator was observed to seep out of the gap between the two sheets of SnO_2/glass electrodes into the solution bulk when the potential step had been continued for more than ca. 10 min.

Similar spectroelectrochemical behaviors were

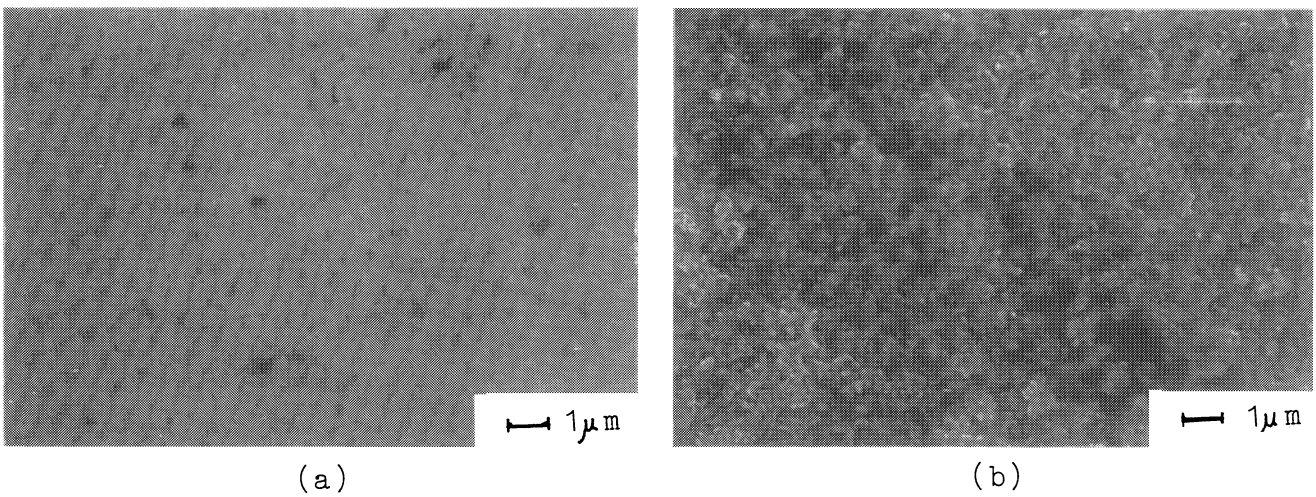

Fig. 4. SEM photograph of the bare surface (a) and the SQ film-coated surface (b) of SnO_2/glass electrode. The SQ film-coated electrode was prepared under the same conditions as in Fig. 3.

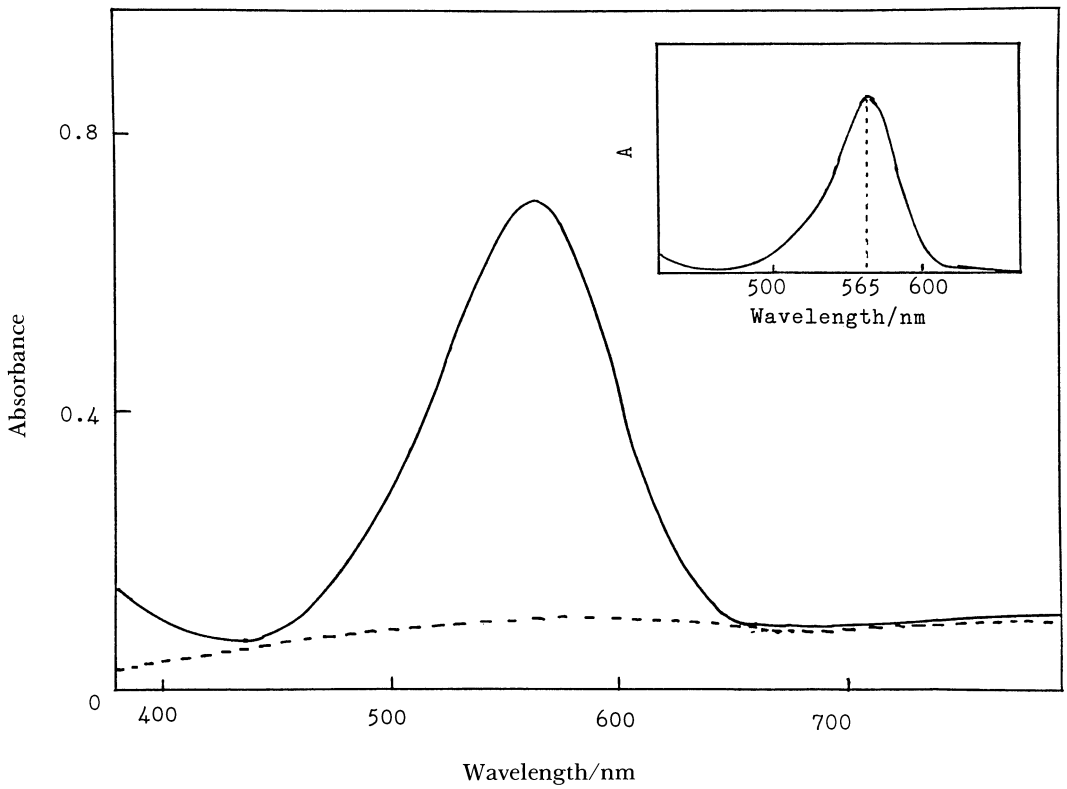

Fig. 5. Absorption spectrum of colored *o*-cresolphthalein incorporated within SQ_{Red} film on SnO_2/glass electrode (solid curve). Dashed curve represents the absorption spectrum of the SQ_{Red} film alone on SnO_2/glass electrode. Inset shows the absorption spectrum of a colored *o*-cresolphthalein alkaline solution.

observed for the other indicators incorporated within the SQ film. Their spectroelectrochemical properties are given in Table 1. Most of the pH indicators examined here exhibited their characteritic color change within ca. 5 s by a potential step of the working electrode. Almost no decrease in optical density of the colored working electrode was observed at least within 10-min run of repetitive potential steps. Moreover, the shaped CV of the SQ film on the SnO_2/glass electrode remained unchanged even after a long-term run of repetitious potential steps. This demonstrates that neither the hydroquinone nor *p*-benzoquinone moiety in the SQ film reacts with the pH indicators examined here. A slight seepage of the colored pH indicator as in the case of *o*-Cresolphthalein was observed in every case.

Bromophenol Blue, Bromocresol Green, and Phemol Red underwent electrochemical reduction in a potential range from −0.7 V to −0.5 V. Therefore, for these indicators the potential of the working electrode was stepped between −0.5 V and +0.7 V. The positive shift in the negative-end potential from −0.7 V to −0.5 V tended to lengthen the response time of the color change at basic pH's. This tendency is reasonable since the response speed of the color change may depend on the rate of reduction-oxidation of the SQ film. Bromophenol Blue which

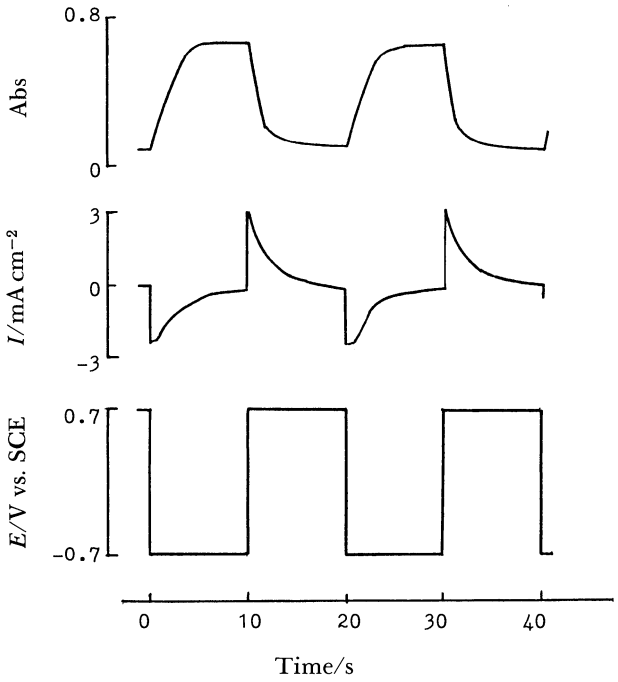

Fig. 6. Response of absorbance and current to a square voltage pulse for the *o*-cresolphthalein-impregnated SQ film (prepared on SnO_2/glass electrode under the same conditions as in Fig. 3) measured in a supporting electrolyte solution of pH 8.0 (see Table 1).

exhibits a color change in the lowest pH range among the pH indicators listed in Table 1, required the longest time for the color change. Thymol Blue, which should change color from red to yellow by a pH range from 1.2 to 2.8, showed no color change even when the potential was stepped between −0.7 V and +0.8 V vs. SCE. Hence Thymol Blue was omitted from Table 1. Judging from the estimate that the decrease in the amount of H^+ ion in the working electrode by reduction of SQ_{Ox} to SQ_{Red} is 62.4 nmol (see above), the phenomena observed for these two pH indicators may be rationalized. In line with this, a slower response in color change was observed also for Thymolphthalein, which should change color in a relatively strong alkaline range, namely between pH 9.4 and 10.6. In a previous work,[8] we found that an SQ_{Red}-coated carbon electrode showed pH response with a slope of ca. −59 mV/pH over a pH range from 1.8 to 8.5, and with a slope of ca. −30 mV/pH above pH 10. This indicates that the pK_1 of the hydroquinone moiety in the SQ film is nearly 8.5. Hence, the slow response of the color change for Thymolphthalein is understandable in this content.

The present results demonstrate that ten different pH indicators incorporated within the SQ film on an SnO_2/glass electrode show well-repetitive characteristic color changes by potential steps. In addition, the pH indicators suitable for use in the electrochromic cell employed here should change color in a pH range from 3 to 10, should not be electrochemically active over a potential range where the SQ film is oxidised or reduced, and should not chemically react with either SQ_{Red} or SQ_{Ox}.

References

1) Y. Sato, K. Ono, T. Kobayashi, H. Wakabayashi, and H. Yamanaka, *J. Electrochem. Soc.*, **134**, 570 (1987); P. Delichere, P. Falaras, and A. Goff, *Solar Energy Mater.*, **19**, 323 (1989); H. Akram, M. Kitao, and S. Yamada, *J. Appl. Phys.*, **66**, 4364 (1989); K. Machida and M. Enyo, *J. Electrochem. Soc.*, **137**, 1169 (1990).

2) K. Itaya, H. Akahoshi, and S. Toshima, *J. Electrochem. Soc.*, **129**, 762 (1982); A. Sammells and N. Pujare, *ibid.*, **133**, 1270 (1986); N. Kobayashi, N. Mineta, and R. Hirohashi, *Nippon Shashin Gakkaishi*, **52**, 314, (1989); T. Amemiya, K. Itoh, and A. Fujishima, *Ber. Bunsen-Ges. Phys. Chem.*, **93**, 682 (1989).

3) M. Kaneko, H. Nakamura, and T. Shimomura, *Makromol. Chem.*, **8**, 179 (1987); V. Gater, M. Liu, M. Love, and C. Leidner, *J. Electranal. Chem. Interfac. Electrochem.*, **257**, 133 (1988); R. Jiang and S. Dong, *J. Chem. Soc., Faraday Trans. 1*, **85**, 1585 (1989); P. Foot and R. Simon, *J. Phys. D: Appl. Phys.*, **22**, 1598 (1989).

4) G. Arai, S. Shimamura, Y. Ohtomo, and I. Yasumori, *Bull. Chem. Soc. Jpn.*, **62**, 1395 (1989), and references therein.

5) G. Arai, K. Enomoto, and I. Yasumori, *Chem. Lett.*, **1988**, 733.

6) G. Arai and M. Furui, *Nippon Kagaku Kaishi*, **1984**, 673.

7) G. Arai, K. Matsumoto, T. Murofushi, and I. Yasumori, *Bull. Chem. Soc. Jpn.*, **63**, 121 (1990).

8) G. Arai, T. Koike, and I. Yasumori, *Chem. Lett.*, **1986**, 867.

Limiting Partial Molar Volumes of Ions in Water-Methanol and Water-Acetonitrile

Fumio KAWAIZUMI,* Yoshitomo INOUE,† and Hiroyasu NOMURA†
Institute for Molecular Science, Myodaiji, Okazaki 444
†Department of Chemical Engineering, School of Engineering,
Nagoya University, Chikusa-ku, Nagoya 464-01
(Received August 22, 1990)

Measurements of densities of solution of $AgNO_3$ and $Ca(NO_3)_2$ in the mixed solvents water-methanol and water-acetonitrile were carried out at 25 °C and the partial molar volumes V_2^∞ of these electrolytes were determined by taking account of the concentration dependence of the apparent molar volumes predicted by the Debye-Hückel theory. The ionic partial molar volumes of Ag^+, Ca^{2+}, and NO_3^- were evaluated and compared with those of other ions in the two mixed solvent systems. The solvent composition dependence is more remarkable in water-acetonitrile than in water-methanol, and characteristic behavior was observed for Ag^+ and Ca^{2+} ions in water-acetonitrile system.

First light was shed on the selective solvation of ions in mixed solvent wate-acetonitrile(AN) by Schneider and Strehlow[1] more than 30 years ago. These authors argued that the ion Ag^+ is preferentially solvated by acetonitrile, while in the solvation shell of the ion NO_3^- the solvation of water molecules is preferential. In the second paper,[2] they reported the preferential solvation of water to Ca^{2+} and Cl^- ions in water-methanol mixtures. However, this second paper seems to draw less attention than their first paper. Following Schneider and Strehlow[1] a number of workers have investigated the problem of selective solvation of ions in water-acetonitrile mixture. The quantities investigated are, for example, transfers of thermodynamic function,[3-5] $\Delta_t X$ (X=G, H, S), transport numbers,[6,7] and ionic molar conductivities.[8,9]

In our series of work on solute-solvent interaction in mixed solvents,[10-13] special emphasis has been placed on the determination of the partial molar volume and partial molar adiabatic compressibility of ionic solutes and the splitting of these partial molar quantities into cationic and anionic contributions. In this paper, we will report the partial molar volumes of silver nitrate and calcium nitrate in water-methanol and water-acetonitrile systems. The dielectric behavior of these two systems is quantitatively similar up to ca. 70 mol% of water. As for solutes we must add that use of other divalent nitrates as samples was unsuccessful on account of the difficulty in obtaining completely anhydrous sample (case for $Mg(NO_3)_2$) or the limited solubility of the salts for precise measurements of the solution density (case for $Zn(NO_3)_2$, $Ba(NO_3)_2$, and $Pb(NO_3)_2$). Even for $Ca(NO_3)_2$ measurement in pure acetonitrile was impossible on account of its low solubility.

To determine the V_2^∞ values from apparent molar volumes, we adopted the theoretical coefficient S_V, the values of which for water-acetonitrile were calculated as part of this work.

To date, the partial molar volumes of electrolytes in water-acetonitrile system have been treated in the three papers.[14-16] The V_2^∞ values of 1-1 electrolytes up to 25 mol% of acetonitrile was reported recently.[14] In pure acetonitrile the ultrasonic vibration potential measurement[15] was done for the ionic division of V_2^∞ of 1-1 type salt. Using the roughly evaluated V_2^∞ values, Singh et al. reported the $\Delta_t V_2^\infty$ ($H_2O \rightarrow H_2O$/AN) for univalent ions over the whole composition of the solvent system.[16]

Experimental

Samples. Anhydrous calcium nitrate was obtained from $Ca(NO_3)_2 \cdot 4H_2O$ by keeping it in vacuo for more than 48 hours over P_2O_5. The guaranteed grade reagent methanol was dried using the molecular sieves activated at 350 °C for more than three hours. The molecular sieves were set into the solvent methanol two or three days before use and the molecular sieves were eliminated by decantation. The solvent acetonitrile was distilled with phosphorus pentaoxide which was added to the solvent in the ratio of 5 g of P_2O_5 to one dm^3 of solvent. As the anhydrous calcium nitrate is extremely hygroscopic, the sample solution of this product was prepared in a dry-box.

Measurements. As in our recent work,[11-13] densities of solution were measured with a digital vibrating density meter Anton Paar DMA-02C. All measurements were done at 298.15 K.

Results and Discussion

Partial Molar Volumes. The apparent molar volumes V_ϕ were calculated using the conventional equation

$$V_\phi = 1000\,(d_1 - d)/cd_1 + M/d_1, \qquad (1)$$

where c is the concentration of solute in mol dm^{-3} and the subscript 1 refers to solvent. The concentration dependence of V_ϕ in the experimental concentration ranges is expressed in terms of the equation

$$V_\phi - S_V c^{1/2} = V_2^\infty + hc. \qquad (2)$$

In Eq. 2 the parameter S_V is equal to $kw^{3/2}$ and the

quantities w and k are expressed as

$$w = (1/2)\sum \nu_i z_i^2, \quad (3)$$

and

$$k = 2N_o^2 e^3 (2\pi/1000RT)^{1/2} \varepsilon^{-3/2} \{(\mathrm{d}\ln\varepsilon/\mathrm{d}P) - (\kappa_T/3)\}, \quad (4)$$

where κ_T is the isothermal compressibility and other symbols have their usual meaning. The values of κ_T were obtained from the reported data.[17] From the Tait-form equation for dielectric constants found elsewhere,[18] we calculated the pressure derivatives of the dielectric constant at 0.1 MPa. Values of ε, $\mathrm{d}\ln\varepsilon/\mathrm{d}P$ and κ_T at rounded solvent composition are summarized in Table 1.

Figures 1 and 2 show the plot of Eq. 2 for the samples $AgNO_3$ and $Ca(NO_3)_2$, respectively. The parameter h of Eq. 2 is negative except for $AgNO_3$ in water-acetonitrile system. The values of h of the solute $Ca(NO_3)_2$ become negatively larger with increasing content of methanol or acetonitrile. An increase in the negative deviation from Eq. 2 with the content of organic solvent in aqueous mixed solvents has also been observed for $CaCl_2$ in water-methanol

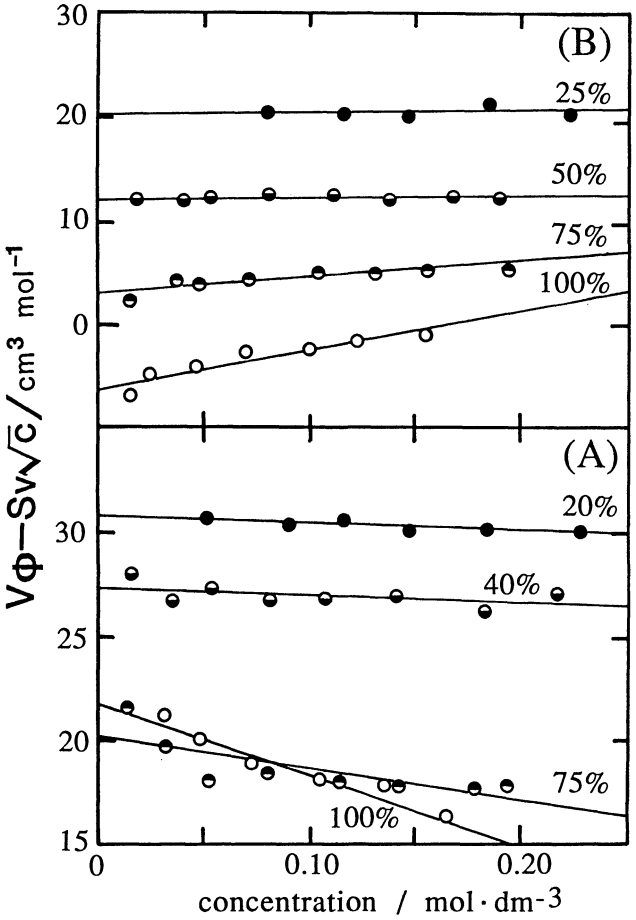

Fig. 1. Plots of $V_\phi - S_v c^{1/2}$ versus concentration c for $AgNO_3$ dissolved in the mixed solvent water-methanol(A) and water-acetonitrile(B) at 25 °C. The % in the figure refers to the acetone content (mol%) of the solvent system.

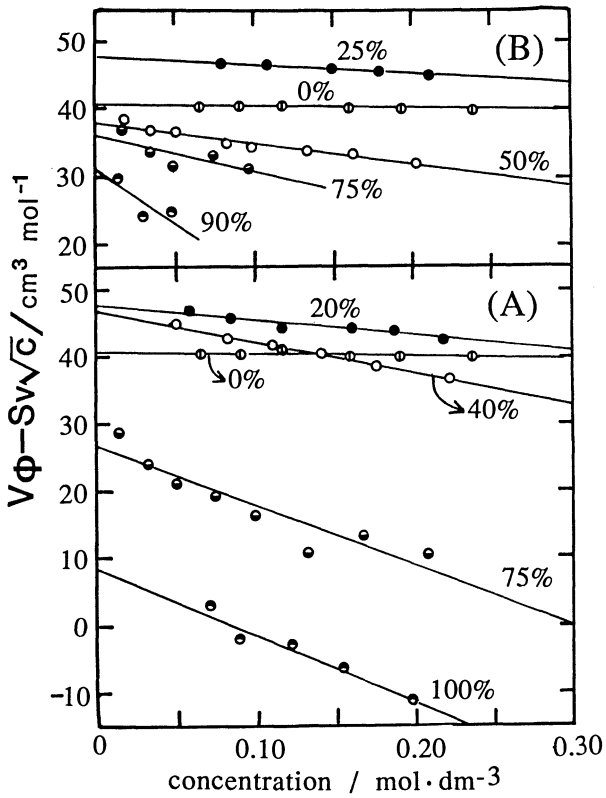

Fig. 2. Plots of $V_\phi - S_v c^{1/2}$ versus concentration c for $Ca(NO_3)_2$ dissolved in the mixed solvent water-methanol (A) and water-acetonitrile (B) at 25 °C. The % in the figure refers to the acetone content (mol%) of the solvent system.

Table 1. Numerical Values of the Coefficient k Calculated by the Debye-Hückel Theory for the Mixed Solvent Water-Acetonitrile at 25 °C

[Acetonitrile]	k	[Acetonitrile]	k
mol%	$cm^3\,mol^{-3/2}\,dm^{3/2}$	mol%	$cm^3\,mol^{-3/2}\,dm^{3/2}$
0	1.868	60	8.118
10	2.863	70	9.507
20	3.700	75	10.20
25	4.256	90	12.81
40	6.164	100	15.08
50	7.104		

Table 2. Partial Molar Volumes of $AgNO_3$ and $Ca(NO_3)_2$ in H_2O-MeOH System at 25 °C

[Methanol]	V_2^∞/cm^3 mol^{-1}		[Acetonitrile]	V_2^∞/cm^3 mol^{-1}	
mol%	$AgNO_3$	$Ca(NO_3)_2$	mol%	$AgNO_3$	$Ca(NO_3)_2$
0	27.9	40.7	0	27.9	40.7
	28.02[a]	40.164[b]		28.02[a]	40.164[b]
20	30.8	47.7	25	20.3	47.9
40	27.4	46.6	50	12.3	38.0
75	20.2	26.5	75	3.3	36.1
100	21.8	8.7	90	—	31.2
			100	−6.4	—
				−3[c]	

a) Ref. 19. b) Ref. 20. c) Ref. 16.

system.[11] Such a negative deviation observed for $Ca(NO_3)_2$ is perhaps due to the ion association, the amount of which increases with decreasing dielectric constant of the solvent. In every case represented in Figs. 1 and 2, extrapolation of V_ϕ to infinite dilution was carried out by the first order least mean-squares fitting to the experimental data.

The partial molar volumes of $AgNO_3$ and $Ca(NO_3)_2$ at infinite dilution obtained are given in Table 2 and are plotted against solvent composition in Fig. 3. In water, our partial molar volumes agree satisfactorily with those found in the literature.[19,20] Among the four systems studied, direct comparison is possible only for $AgNO_3$ in water-acetonitrile. As seen in Fig. 3, our V_2^∞ ($AgNO_3$) falls fairly well on the line connecting the values reported earlier.[16] The difference in the value of V_2^∞ ($AgNO_3$) in pure acetonitrile obtained in this work (−6.4 cm^3 mol^{-1}) and that found in the literature (−3 cm^3 mol^{-1}) is too large to accept in the discussion of the V_2^∞ values in aqueous solutions. In the case of V_2^∞ values in nonaqueous solvents, however, such a degree of difference is not rare. For example, two distinctly different values 4.73[15] and 11[16] cm^3 mol^{-1} have been reported by different authors for the V_2^∞ of sodium iodide in acetonitrile.

Ionic Partial Molar Volumes. At present, experimental techniques for the ionic division of V_2^∞ of a salt are limited to the ultrasonic vibration potential and the sedimentation potential measurements. In a previous paper[12] we measured the sedimentation potential (SP) in solutions of LiCl, NaCl, and KCl dissolved in water-methanol mixtures and split V_2^∞ of these chlorides into cationic and anionic parts. In that paper, the variation of the partial molar volumes of Cl^- as well as Li^+, Na^+, and K^+ in water-methanol system with solvent composition was represented graphically. Combination of the values V_2^∞ (MX) determined in our laboratory[10-12] and those obtained in this work with the numerical values of V_2^∞ (Cl^-) obtained in our previous work[12] permits us to evaluate the partial molar volumes of various ions in water-methanol system. The calculation procedure for the nitrate and silver ions is as follows: first, we calculate

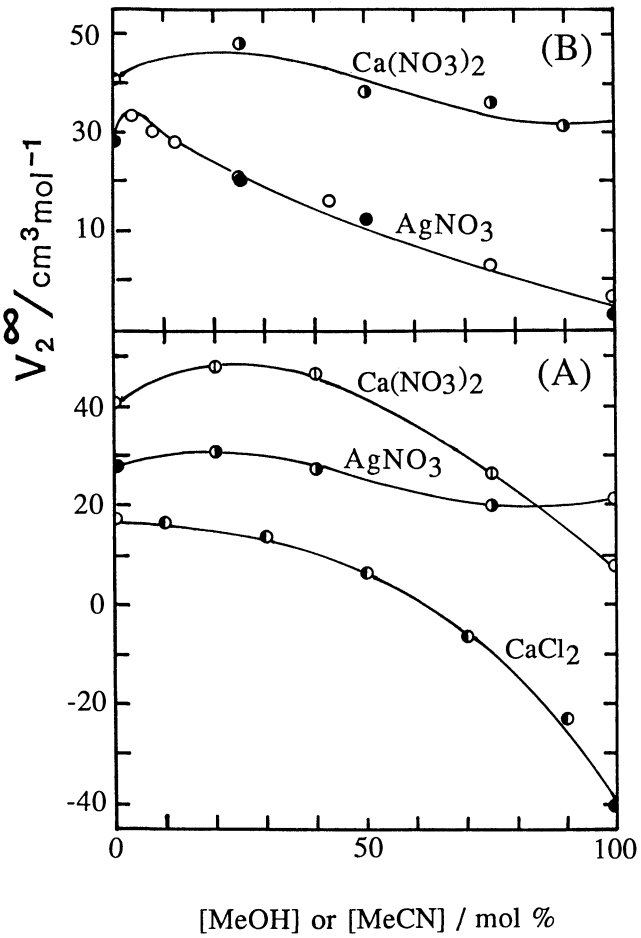

Fig. 3. Variation of the partial molar volumes with solvent composition at 25 °. (A): $Ca(NO_3)_2$, $CaCl_2$, and $AgNO_3$ in water-methanol. (B); $Ca(NO_3)_2$ and $AgNO_3$ (●; this work, ○; reported value) in water-acetonitrile.

V_2^∞ (Ca^{2+}) by subtracting V_2^∞ (Cl^-) from V_2^∞ ($CaCl_2$), then calculate V_2^∞ (NO_3^-) from V_2^∞ ($Ca(NO_3)_2$), and finally obtain V_2^∞ (Ag^+) from V_2^∞ ($AgNO_3$). The ionic partial molar volumes thus evaluated are shown in Table 4 in which the V_2^∞ values in water are included; the values in water are based on the V_2^∞ values of

Table 3. Ionic Partial Molar Volumes in Water-Methanol System Based on the Measurements of Sedimentation Potentials at 25 °C

[MeOH]	V_2^∞/cm^3 mol^{-1}							
mol%	Li^+	Na^+	K^+	Cs^+	Ag^+	Ca^{2+}	Cl^-	NO_3^-
0	−3.01	−3.39	6.85	19.15	−3.7	−22.22	20.0[a]	31.5
							23.5[b]	34.9[b]
10						−26.5	21.5[a]	
20					−7.7	(−29.4)		38.5
30	−6.9	−6.5	4.9	16.4		−32.0	22.8[a]	
40					−13.7	(−35.6)		41.1
50	−9.2	−8.5	4.7	14.9		−39.0	22.6[a]	
70	−12.3	−12.7	1.6	11.8		−48.1	20.8[a]	
75					−18.7	(−51.2)		38.9
90	−12.7	−16.1	−3.5	8.4		−57.0	16.9[a]	
100	−16.9	−15.6	−6.1	2.7	−14.9	−64.6	12.0[a]	36.7
							12.6[c]	
							13.0[d]	

a) Reference for the ionic division of V_2^∞(MX). b) Ref. 22. c) Ref. 23. d) Ref. 24.

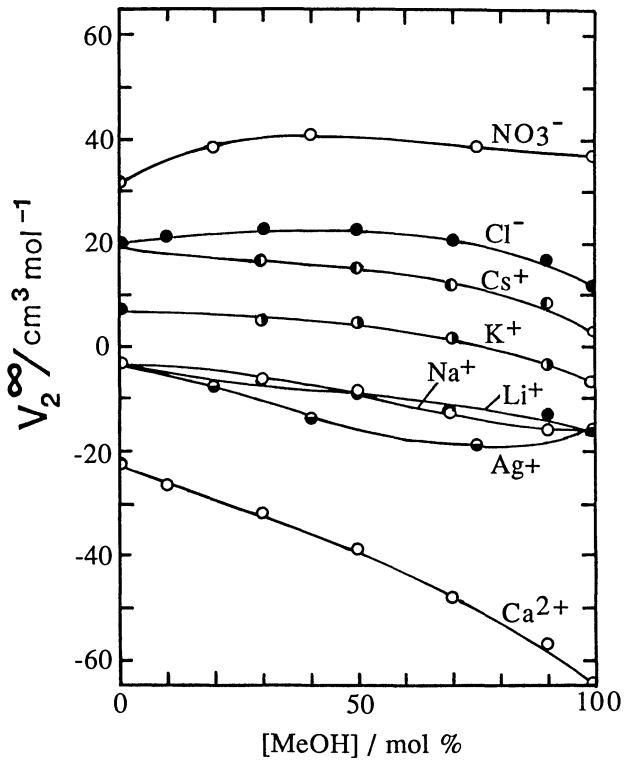

Fig. 4. Partial molar volumes of various ions dissolved in water-methanol at 25 °C.

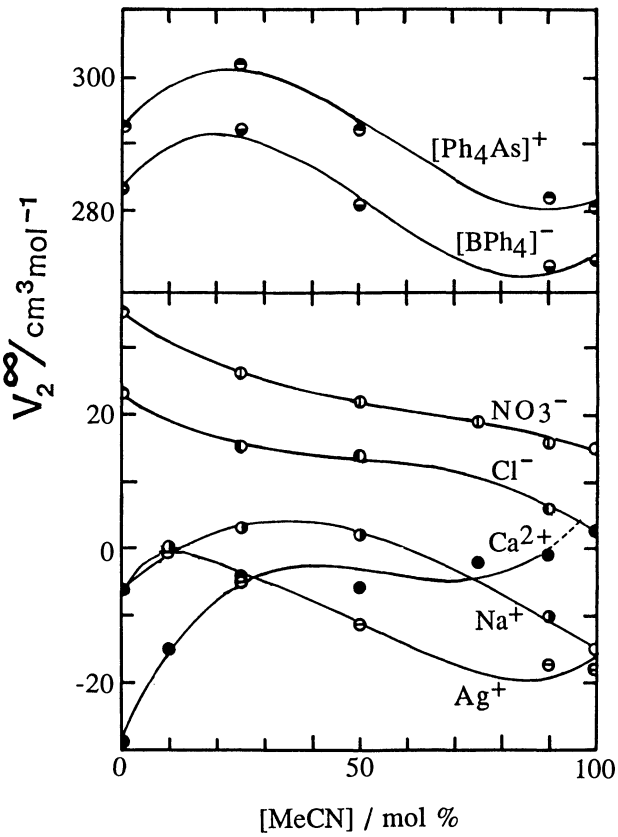

Fig. 5. Partial molar volumes of various ions dissolved in water-acetonitrile at 25 °C. The dotted line for the ion Ca^{2+} means that the partial molar volume in pure acetonitrile is unknown.

electrolytes recommended by Millero,[21] while the V_2^∞ values of salt in methanol used are those obtained by adding the most recent values of ionic partial molar volumes listed by French and Criss.[23]

The ultrasonic vibration potential or sedimentation potential method has not been applied to the system water-acetonitrile system. Here, we evaluate the partial molar volumes of ion first by interpolating the V_2^∞ values reported by Singh et al.[16] and then by using the the assumption that

$$\frac{V_2^\infty(Ph_4As^+)}{V_2^\infty(BPh_4^-)} = \frac{V_{vw}(Ph_4As^+)}{V_{vw}(BPh_4^-)} = 1.0337, \quad (6)$$

where V_{vw} means the van der Waals volume. Results of this ionic division are summarized in Table 4 and also represented in Fig. 5.

Table 4. Rounded Values of the Ionic Partial Molar Volumes in Water-Acetonitrile System at 25 °C Based on the V_2^∞ (Ph_4AsCl) and V_2^∞ ($NaBPh_4$) Data

[MeCN]	V_2^∞/cm^3 mol^{-1}						
mol%	Ph_4As^+	BPh_4^-	Na^+	Ag^+	Ca^{2+}	Cl^-	NO_3^-
0	292	283	−7	−7	−29	23	35
10	306	296	0	−1	−15	17	30
25	302	292	3	−5	−4	15	26
50	292	281	2	−11	−6	14	22
75					−2		19
90	282	272	−10	−17	1	6	16
100	281	273	−15	−18		3	15
			−21.4[a]			6.4[a]	

a) Ref. 15 determined by the ultrasonic vibration potential method.

Making allowance for uncertainties due to various factors (V_2^∞, use of the two different methods for ionic division, etc.) we can mention at least the following several characteristic features of the ion-solvents interactions in water-methanol and water-acetonitrile.

1) The partial molar volumes of metallic ions decrease with the methanol content, except for V_2^∞ (Ag^+) in solvents with 80—100 mol% of methanol. The decrease of V_2^∞ with the methanol content is most remarkable for the divalent cation Ca^{2+} indicating that the decrease of V_2^∞ is mainly electrostatic. The increase of V_2^∞ ($Ca(NO_3)_2$) observed in Fig. 3(A) is totally ascribable to the ion NO_3^-. Roughly speaking, in the mixed solvent water-methanol, the change of partial molar volume accompanying the solvent change, $\Delta_t V_2^\infty$, is similar for all the alkali metal ions (see Fig. 4).

2) In water-acetonitrile system, the solvent composition dependences of ionic partial molar volumes are drastically different from those in water-methanol. As mentioned earlier, for water-methanol and water-acetonitrile the bulk dielectric constants (ε) are similar in magnitude; the only difference is that ε is 35.9 for pure acetonitrile and 32.6 for methanol. The interpretation of the differences in the behavior of various ions represented in Figs. 4 and 5 in terms of the bulk dielectric constant of the solvents is obviously impossible. It must be stressed that the V_2^∞ of ions depends strongly on the degree of steric hindrance of the poles of the solvent molecule dipole and the properties of the solvent layer around the ion.[15,24] The acetonitrile molecule has the dipole moment μ equal to 3.913 Debye (1 Debye=3.336×10^{-30} Cm), while those of methanol and water are 1.69 and 1.94 Debye, respectively. The negative pole of the acetonitrile is located at the nitrogen atom of the -C≡N group, and in both methanol and water, the negative and positive poles are on oxygen and hydrogen atoms, respectively. Hence, the nature of solvation at the microscopic level varies to a lesser extent with the solvent composition in water-methanol than in water-acetonitrile.

3) For large univalent ions [Ph_4As^+] and [BPh_4^-] the differences between V_2^∞ ([Ph_4As^+]) and V_2^∞ ([BPh_4^-]) are independent of the solvent composition.

4) The V_2^∞ (NO_3^-) and V_2^∞ (Cl^-) decrease in a similar way with the acetonitrile content. The increase of V_2^∞ ($AgNO_3$) observed in the water-rich region in the water-acetonitrile system (see Fig. 3) is attributed not to the anion NO_3^- but to the cation Ag^+, in contrast to the case of $Ca(NO_3)_2$ in the water-methanol system mentioned above. For the ions Ag^+ and Na^+, the extremum appears in the relationship between the respective V_2^∞ values and the acetonitrile content in the solvent system. The acetonitrile content giving the maximum V_2^∞ value corresponds to the solvent composition at which the values of isothermal compressibility κ_T pass through a minimum. The fact that the acetone content for the maximum of V_2^∞ (Ag^+) is far lower than that of V_2^∞ (Na^+) demonstrates the different behavior of ion Ag^+ from the alkali metal ion.

5) The result for Ca^{2+} in water-acetonitrile is the most striking one detected by the ionic splitting of V_2^∞ of the electrolytes investigated.

References

1) H. Schneider and H. Strehlow, *Ber. Bunsen-Ges. Phys. Chem.*, **62**, 373 (1958); H. Schneider, in "Solute-Solvent Interatctions," ed by J. F. Coetzee and C. D. Ritchie, Marcel Dekker (1976), Vol. 2.

2) H. Schneider and H. Strehlow, *Ber. Bunsen-Ges. Phys. Chem.*, **66**, 309 (1962).

3) B. G. Cox, A. J. Parker, and Waghorne, *J. Phys. Chem.*, **78**, 1731 (1974).

4) B. G. Cox, R. Natarajan, and W. E. Waghorne, *J. Chem. Soc., Faraday Trans. 1*, **75**, 86 (1979).

5) K. Miyaji and K. Morinaga, *Bull. Chem. Soc. Jpn.*, **56**, 1861 (1983).

6) D. S. Gill, K. S. Arora, J. Tewari, and B. Singh, *J. Chem. Soc., Faraday Trans. 1*, **84**, 1729 (1988).

7) D. S. Gill and M. S. Bakshi, *J. Chem. Soc., Faraday Trans. 1*, **84**, 3517 (1988).

8) M. M. Sanchez, C. Moran, C. Quintana, and A. Vivo, *J. Solution Chem.*, **18**, 993 (1989).

9) K. Morinaga and K. Miyaji, *Denki Kagaku*, **50**, 736 (1982).

10) F. Kawaizumi, H. Suzuki, H. Nomura, and Y.

Miyahara, *Bull. Chem. Soc. Jpn.*, **55**, 2771 (1982).
11) H. Nomura, F. Kawaizumi, and Y. Miyahara, *Chem. Eng. Commun.*, **34**, 305, (1985).
12) H. Hirakawa, H. Nomura, and F. Kawaizumi, *J. Phys. Chem.*, **93**, 3784, (1989): The value of V_2^∞ (LiCl) in water adopted in this reference was incorrect. One should have carried out the ionic division using the generally accepted V_2^∞(LiCl) value, 16.99 $cm^3 mol^{-1}$. Therefore, the values of V_2^∞, V_+° and V_-° for LiCl at 0, 10, and 30 mol% of methanol listed in Table 2 of this reference should be modified accordingly.
13) F. Kawaizumi, F. Nakao, and H. Nomura, *J. Chem. Eng. Data*, **33**, 204 (1988).
14) G. T. Hefter, J.-P. E. Grolier, A. H. Roux, and G. Roux-Desgranges, *J. Solution Chem.*, **19**, 207, (1990).
15) R. Zana, G. Perron, and J. E. Desnoyers, *J. Solution Chem.*, **8**, 729 (1979).
16) P. Singh, I. D. MacLeod, and A. J. Parker, *Aust. J. Chem.*, **36**, 1675 (1983).
17) A. J. Easteal and L. A. Woolf, *J. Chem. Thermodyn.*, **14**, 755 (1982).
18) T. Moriyoshi and Y. Uosaki, *Zairyo*, **33**, 127 (1984).
19) G. Jones and J. H. Colvin, *J. Am. Chem. Soc.*, **62**, 338 (1950).
20) W. W. Ewing and R. J. Mikovsky, *J. Am. Chem. Soc.*, **72**, 1390 (1950).
21) F. J. Millero, in "Water and Aqueous Solutions. Structure, Thermodynamics, and Transport Processes," ed by R. A. Horne, Wiely-Interscience, (1972), Chap. 13.
22) R. Zana and E. B. Yeager, *J. Phys. Chem.*, **71**, 521 (1967).
23) R. N. French and C. M. Criss, *J. Solution Chem.*, **11**, 625 (1982).
24) F. Kawaizumi and R. Zana, *J. Phys. Chem.*, **78**, 627 (1974).

Silica-Supported Boron Phosphate Catalyst Prepared by Chemical Vapor Deposition

Satoshi SATO,* Mitsuharu HASEGAWA, Toshiaki SODESAWA, and Fumio NOZAKI
Department of Applied Chemistry, Faculty of Engineering, Chiba University, Yayoi-cho, Chiba 260
(Received September 6, 1990)

A silica-supported boron phosphate (BPO_4) catalyst was prepared by chemical vapor deposition (CVD) using mixtures of boron triethoxide and phosphoryl trimethoxide. Both the amount and the P/B ratio of deposited BPO_4 were changed with the CVD temperature and time. At the optimum CVD temperature of 300 °C, the amount of deposited BPO_4 was linearly increased with the CVD time. When alkoxide mixtures with the desired P/B ratio were used as CVD sources at 300 °C, the expected P/B ratios were available. At CVD temperatures below 300 °C, neither a sufficient amount nor a desired P/B ratio was given. On the other hand, above 325 °C, the deposition was suppressed by blocking the micropore of silica, especially for long-time CVD operation, owing to the too fast deposition. Although the resulting surface compound was amorphous, it was revealed to have microstructures of BPO_4 by means of a ^{31}P NMR measurement. The amorphous BPO_4 dispersed highly on silica exhibited a high catalytic efficiency for the isomerization of 1-butene and a simultaneous oligomerization of 1-butane in comparison with a catalyst prepared by the conventional impregnation method.

Boron phosphate (BPO_4) is known to be a solid acid which is an effective catalyst for various organic reactions such as hydration,[1] dehydration,[2-5] alkylation,[6-8] and oligomerization.[9,10] The catalytic activities depend on the ratio P/B. In a region including excess phosphorus, BPO_4 catalysts have a large percentage of Brønsted acid sites,[2,11] and exhibit catalytic activities for such reactions as the hydration of ethylene,[1] the dehydration of ethanol to ethylene,[2] and the oligomerization of 1-decene.[10] In contrast, in a region including excess boron, BPO_4 catalysts consist predominately of Lewis acid sites,[2,11] and show catalytic efficiencies for the dehydration of ethanol to diethyl ether,[2] the dehydration of 2-methylbutanal to isoprene,[5] the ethylation of phenol,[8] and the Beckmann rearrangement of cyclohexanone oxime.[2] Unsupported BPO_4, however, has a relatively small surface area and its catalytic activity is often poor. Whereas BPO_4 with surface areas of more than 100 $m^2 g^{-1}$ have been reported,[12,13] carefulness is required for any reproducible preparation. In addition, it is difficult to impregnate a support material with uniform BPO_4 because of its poor solubility.

Several attempts have been made to prepare a supported type of solid acids such as silica-supported boria,[14] alumina-supported boria,[15] and alumina-supported silica[16,17] by means of chemical vapor deposition (CVD) using the respective metal alkoxides. The alkoxides were easily decomposed into the respective metal oxide on the surface of the support in the presence of oxygen. The highly dispersed boria catalysts, having a weak interaction with the support materials, exhibited an excellent catalytic efficiency for a vapor-phase Beckmann rearrangement of cyclohexanone oxime.[14,15] The alumina-supported silica, having a strong interaction between the silica and alumina to form composite-oxides on the surface of alumina support, showed high catalytic activities for several organic reactions such as cracking, isomerization, and dehydration,[16,17] which was comparable to those of commercial silica-alumina catalyst.

In the present work, we prepared a silica-supported boron phosphate catalyst (CVD BPO_4/SiO_2) by the simultaneous deposition of boron and phosphorus components onto a silica surface using a mixed vapor of boron triethoxide and phosphoryl trimethoxide, and investigated both the structural and catalytic properties of the deposited boron phosphate.

Experimental

A CVD BPO_4/SiO_2 catalyst was prepared by bringing a mixture of boron triethoxide ($B(OEt)_3$) and phosphoryl trimethoxide ($PO(OMe)_3$) into contact with a silica (ID type gel supplied by Fuji Davison Chemical Ltd.: surface area, 145 $m^2 g^{-1}$; pore volume, 1.0 $cm^3 g^{-1}$; particle size, 0.1—0.6 mm.) in a CVD reactor described previously.[17] The mixture of alkoxides with the prescribed P/B ratio, containing 5 wt% methanol, was supplied together with air as a carrier gas (400 mmol h^{-1}) at a flow rate of 1.7—2.4 mmol h^{-1}. Both the BPO_4 loading and the P/B ratio in the catalyst sample were determined by the alkalimetric titration of H_3BO_3 and H_3PO_4, which were extracted from the sample with hot water. The extracted H_3PO_4 was titrated with sodium hydroxide, followed by titration of the extracted H_3BO_3, whose acidity was strengthened by addition of mannitol. An impregnation catalyst (IMP BPO_4/SiO_2) was obtained by immersing a silica support in an aqueous solution of H_3BO_3 and H_3PO_4, drying at 110 °C and calcining at 300 °C for 2 h.

Isomerization of 1-butene was carried out in a closed circulation system (reactor volume: 250 ml, catalyst: 0.2 g) with a butene initial pressure of 19 kPa at 50 °C. Prior to the reaction, a catalyst was heated in the reactor at 500 °C for 1 h under reduced pressure (0.1 Pa). The catalytic performance for the isomerization of 1-butene was evaluated by the 1st-order rate constant during the initial reaction period, and for a simultaneous side reaction of 1-butene oligomerization, forming mainly C_8 olefins by a conversion which was calculated from the pressure drop in the circulation system after the reaction had proceeded for 1 h.

An X-ray difractogram (XRD) was recorded using a Rigaku Giger Flex. A ^{31}P magic angle-spinning (MAS) NMR measurement was performed at 161.98 MHz at a spinning rate of 4 kHz with a Bruker AM-400, while H_3PO_4 was used as an external standard. Time intervals of 2 s were allowed between pulse sequences with 4 μs and 500 free induction decays were accumulated for each sample. The samples were used for the measurement without any further pretreatment.

The amount of chemisorbed ammonia was measured using a static volumetric method. Prior to adsorption, 0.5 g of the catalyst was evacuated at 500 °C for 1 h. A first adsorption of ammonia was performed at the prescribed temperature at pressures of about 1.2 kPa, followed by several repetitions of adsorption until obtaining a final pressure of 6.6 kPa. The amounts of physisorbed and chemisorbed smmonia were estimated by extrapolating the given isotherm. The physisorbed ammonia was desorbed by evacuating the sample at the same temperature as in the first adsorption for 1 h; then, only the physisorbed ammonia was measured with the second adsorption. The amount of chemisorbed ammonia was evaluated by the difference between the first and second adsorption of ammonia.

Results and Discussion

Deposition of Boron Phosphate. Figures 1 and 2 show the effects of the CVD temperature upon BPO_4 deposition for a source P/B ratio of 1. For a CVD time of 3 h or above, the BPO_4 loading exhibited a maximum at a CVD temperature of 300 °C, while the BPO_4 loading slightly increased with increasing CVD temperature for CVD times of 1 and 2 h (Fig. 1). This is related to the change in surface area of the catalyst, and is discussed later. At 300 °C, the BPO_4 loading was increased monotonously with a CVD time up to a maximum of 0.96 g g-silica^{-1} for 5 h. Such a large loading could not be realized by the impregnation method. The P/B ratio in the catalyst changed with both the CVD temperature and time (Fig. 2). At CVD temperatures below 300 °C, espe-

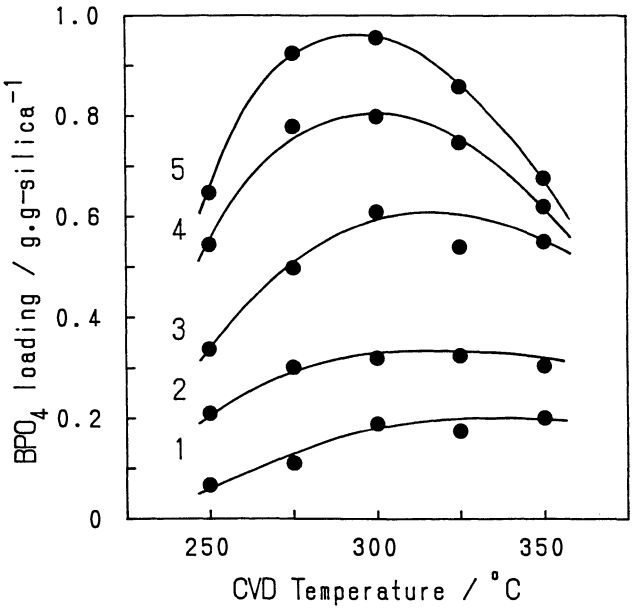

Fig. 1. Effect of CVD temparature and time on the BPO_4 deposition.
P/B ratio in CVD source is 1. Numbers show the CVD time (h).

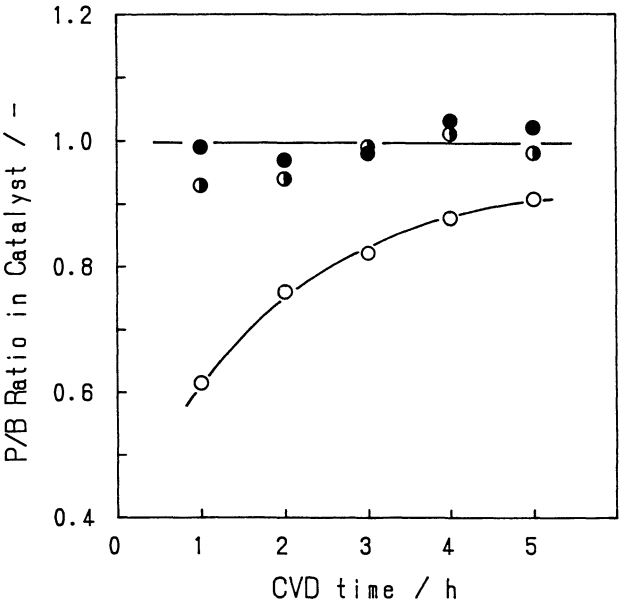

Fig. 2. Change in P/B ratio with CVD time.
○, prepared at 250 °C; ◑, 300 °C; ●, 350 °C.
P/B ratio in CVD source is 1.

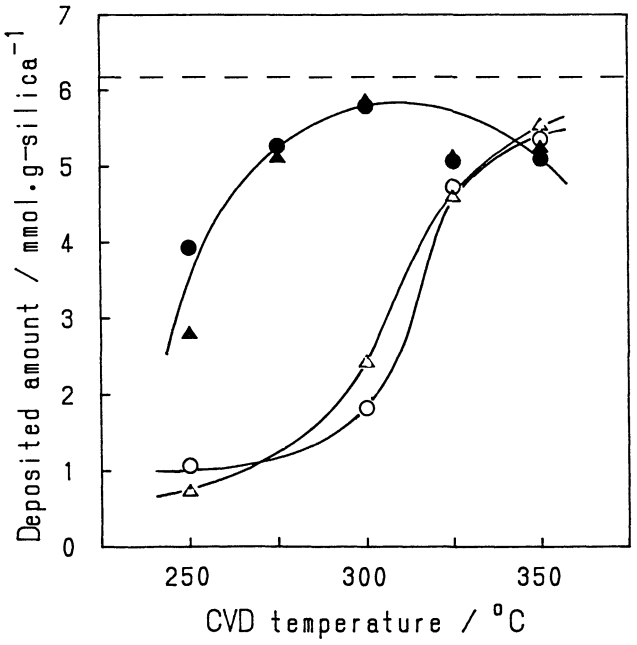

Fig. 3. Comparison of individual deposition with simultaneous deposition of B_2O_3 and P_2O_5.
○, B in B_2O_3/SiO_2; △, P in P_2O_5/SiO_2; ●, B; ▲, P in CVD BPO_4/SiO_2 (P/B=1).
Dashed line shows the maximum deposition.

cially for a short CVD time, the P/B ratio became smaller than 1. At CVD temperatures of 300 °C and above, however, the P/B ratio nearly equaled 1. Therefore, both the sufficient deposition rate and the expected P/B ratio were attained at 300 °C.

Figure 3 shows a comparison of the individual deposition with a simultaneous deposition of both the boron and phosphorus components. When either $B(OEt)_3$ or $PO(OMe)_3$ was fed individually, the deposition behavior of individual oxides was similar to each other. At a CVD temperature of 325 °C, either B_2O_3 or P_2O_5 was readily deposited on SiO_2, whereas at temperatures lower than 325 °C, the individual oxides were slowly deposited. In contrast to individual deposition, the simultaneous deposition of boron and phosphorus components satisfactorily proceeded, even at 275 °C with a P/B ratio of 1. The simultaneous supply of alkoxides drastically lowered the deposition temperature, and the deposition of BPO_4 proceeded with an excess boron component at 250 °C at which the individual oxides could hardly be deposited. Although oxygen accelerated the deposition rate of individual oxide, such as B_2O_3,[14] BPO_4 was deposited on silica even in the absence of oxygen at 300 °C. Moreover, both B_2O_3/SiO_2 and P_2O_5/SiO_2 prepared by CVD using the corresponding alkoxides at 350 °C were inactive for the isomerization of 1-butene, while the BPO_4/SiO_2 prepared at 300 °C was catalytically active. These results indicate that the deposition of BPO_4 occurred on the surface of silica with an accompanying formation of boron phosphate.

Figures 4 and 5 show the effects of the P/B ratio in the CVD source upon BPO_4 deposition. At an optimum CVD temperature of 300 °C, the BPO_4 loading almost reached the maximum deposition expressed by dashed lines for each CVD time (Fig. 4). Furthermore, the P/B ratio in the catalyst nearly equaled the source P/B ratio, whereas an excess boron component

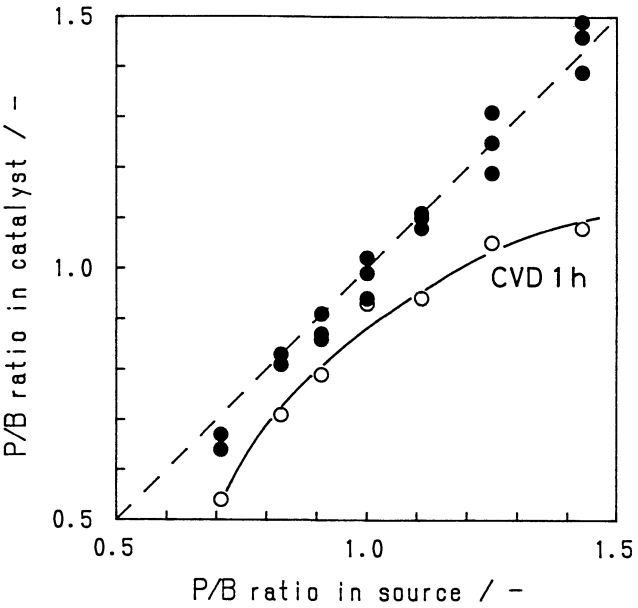

Fig. 5. Effect of P/B ratio in CVD source on P/B ratio in deposited BPO_4.
Dashed line shows the controlled composition of deposition.

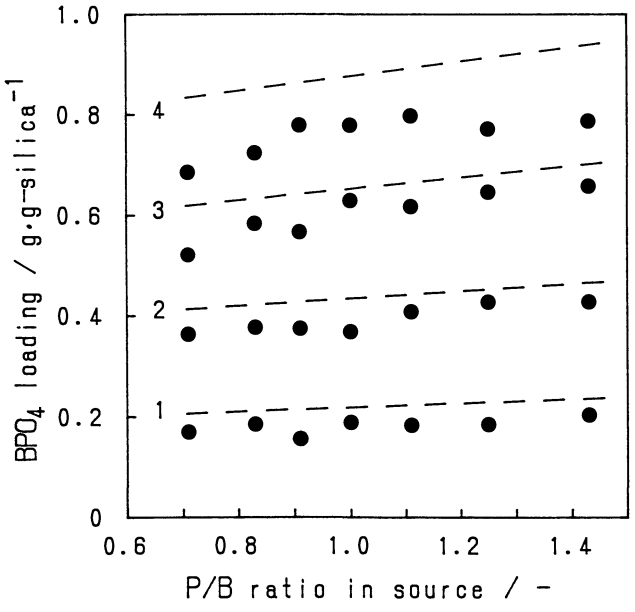

Fig. 4. Effect of P/B ratio in CVD source upon BPO_4 deposition at 300 °C.
Numbers in Figure shows the CVD time (h). Dashed line shows the maximum deposition for each CVD time.

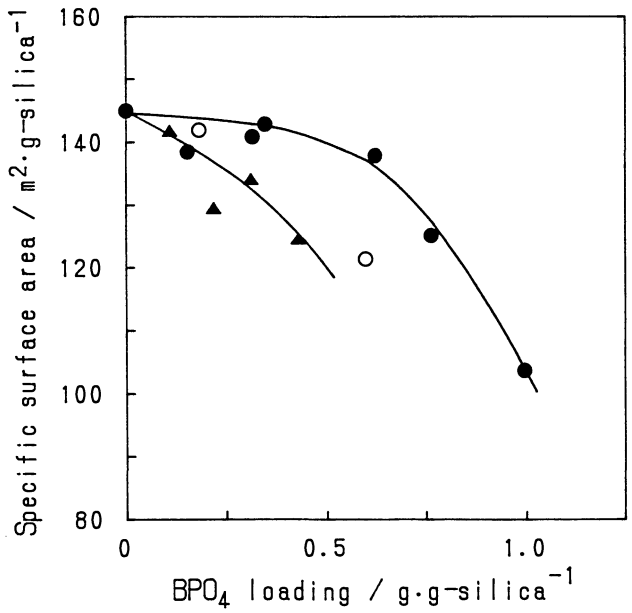

Fig. 6. Change in specific surface area with BPO_4 loading.
●, CVD BPO_4/SiO_2 prepared at 300 °; ○, at 350 °C; ▲, impregnation catalyst. The P/B ratio is 1.

was deposited for a short CVD time of 1 h (Fig. 5). Consequently, BPO_4 with the desired P/B ratio could be deposited on a silica support at 300 °C by controlling the source P/B ratio in the range between 0.7 and 1.4.

Structure of Deposited Boron Phosphate. Figure 6 shows changes in specific surface area with BPO_4 loading. For CVD BPO_4/SiO_2 catalysts prepared at 300 °C, the surface area based on the unit weight of the silica support did not change, even at a BPO_4 loading of 0.6 g g-silica^{-1}, whereas those of the impregnation catalysts linearly decreased with an increase in BPO_4 loading. Above the loading of 0.6 g g-silica^{-1}, however, it steeply decreased with an increase in BPO_4 loading. On the other hand, for CVD catalysts prepared at 350 °C, the surface area decreased with BPO_4 loading in a similar manner as those of IMP BPO_4/SiO_2 catalysts. As shown in Fig. 1, BPO_4 loading decreased at high CVD temperatures. This fact is speculated to be caused by concentrated deposition onto the entrance of the micropore of the support, followed by a closure of the micropore. These findings in Figs. 1 and 6 suggest that a uniform deposition of BPO_4 was attained at 300 °C, owing to an optimum deposition rate of BPO_4.

Figure 7 illustrates the XRD spectra of BPO_4 catalysts. An unsupported BPO_4 exhibited sharp crystalline diffraction peaks at 2θ=24.5, 40.0, and 49.0 attributed to a cristobalite-type structure[2] (Fig. 7-a). An IMP BPO_4/SiO_2 catalyst also showed the same diffraction patterns as unsupported BPO_4 with low crystallinity, even after drying at 110 °C (Fig. 7-b). None of the CVD BPO_4/SiO_2 catalysts, however, showed any diffraction peaks, indicating that the BPO_4 deposited on silica was amorphous.

The ^{31}P MAS NMR of the catalyst was measured in order to elucidate the amorphous phase of deposited BPO_4. For a P/B ratio of 1, an unsupported crystalline BPO_4 showed a sharp resonance at −29.6 ppm together with two small signals at 0.4 and −21.7 ppm (Fig. 8-a). The chemical shift at −29.6 ppm is a characteristic signal for a crystalline BPO_4, which is considered to be caused by a phosphate anion tetrahedrally coordinated by four boron atoms. An additional shift at 0.4 ppm may be attributed to a free phosphate anion, such as phosphoric acid. The silica-supported P_2O_5 had two characteristic chemical shifts at −43.9 and 0.3 ppm (Fig. 8-b). The chemical shifts of P_2O_5 are quite different from those of BPO_4.

For a P/B ratio of 1.1, the ^{31}P MAS NMR spectra of BPO_4 catalysts are shown in Fig. 9. Both the

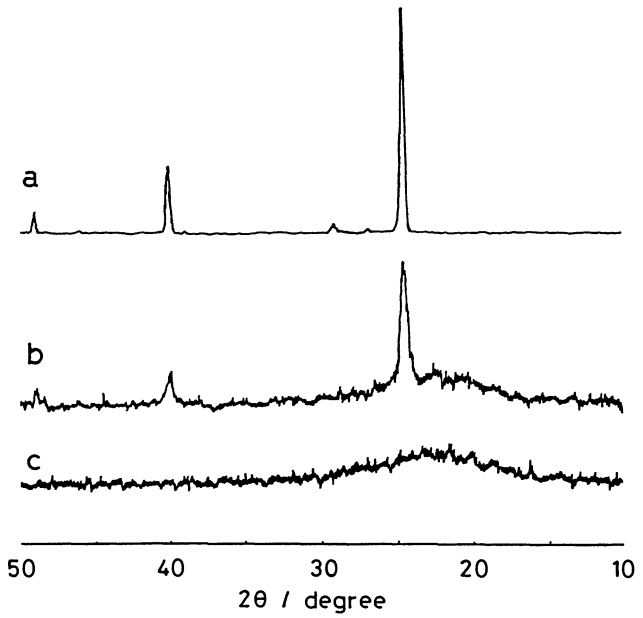

Fig. 7. XRD spectra of catalysts prepared under different conditions.
a, unsupported BPO_4 (P/B=1); b, BPO_4 (36 wt%)/SiO_2 prepared by impregnation; c, BPO_4 (36 wt%)/SiO_2 prepared by CVD.

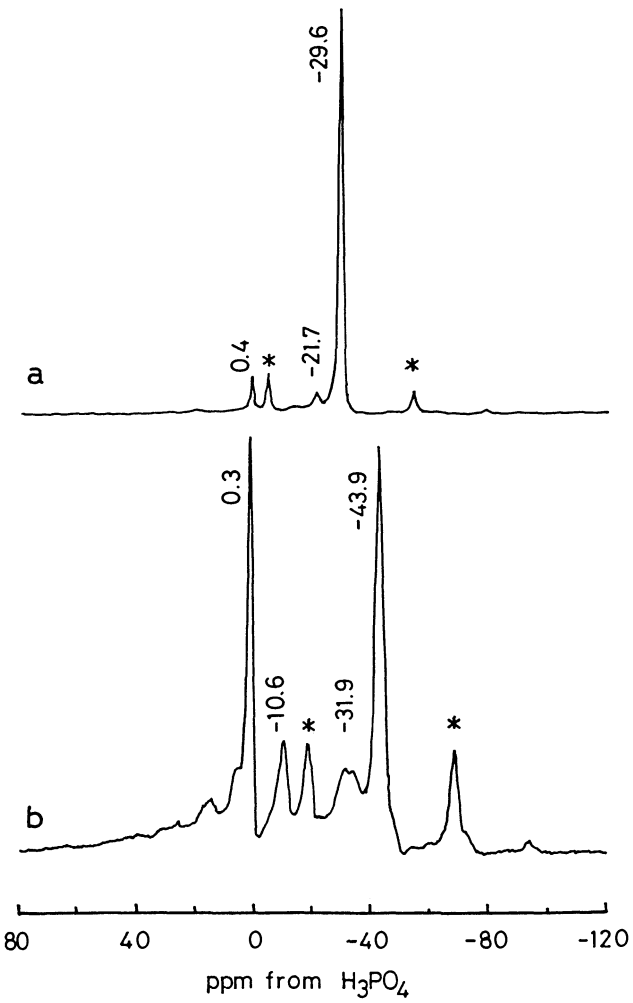

Fig. 8. ^{31}P MAS NMR spectra of phosphate catalysts.
a, unsupported BPO_4 (P/B=1); b, P_2O_5 (20 wt%)/SiO_2 prepared by impregnation.
* denotes a spinning side band.

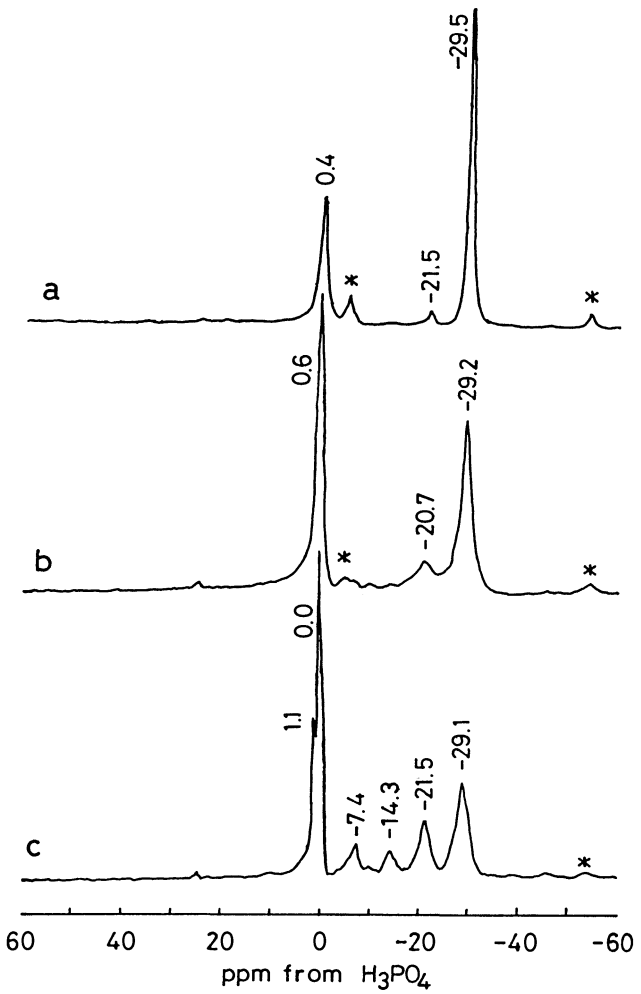

Fig. 9. ^{31}P MAS NMR spectra of BPO_4 (P/B=1.1) catalysts.
a, unsupported BPO_4; b, BPO_4 (20 wt%)/SiO_2 prepared by impregnation; c, BPO_4 (36 wt%)/SiO_2 prepared by CVD.
* denotes a spinning side band.

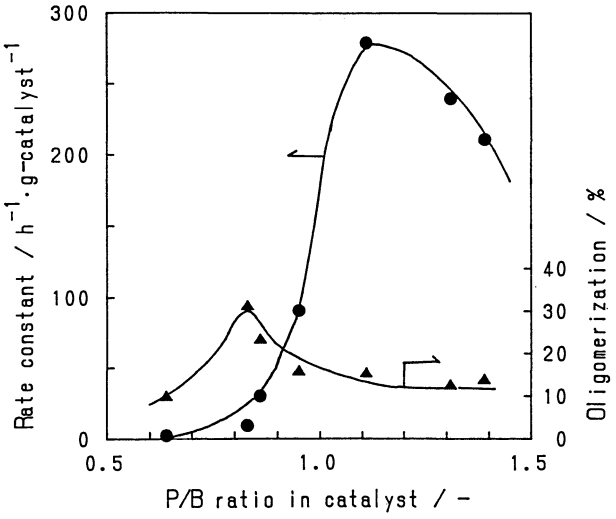

Fig. 10. Catalytic activity of CVD BPO_4/SiO_2 at 50 °C.
●, Isomerization of 1-butene; ▲, oligomerization.
CVD catalysts were prepared at 300 °C for 2 h.

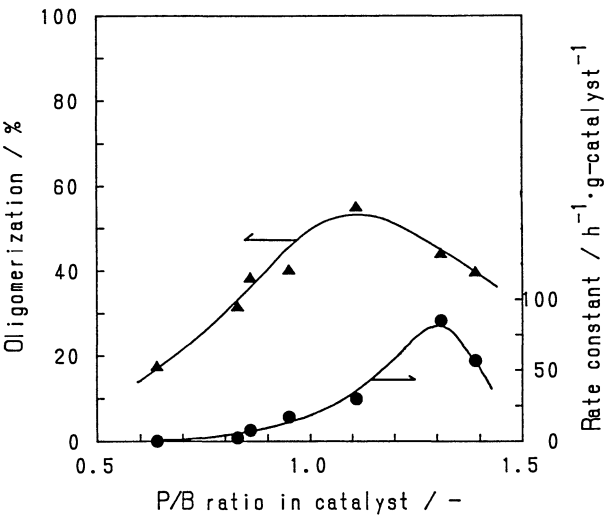

Fig. 11. Oligomerization activity of CVD BPO_4/SiO_2 at 0 °C.
Symbols as those in Fig. 10.

unsupported BPO_4 and the IMP BPO_4/SiO had three chemical shifts at −29.5, −21.5, and 0.4 ppm (Fig. 9-a and b) in similar manner as for Fig. 8-a. An increase in the phosphorus content weakened the intensity of the shift at −29.2 ppm, and strengthened that at 0.4 ppm. The CVD BPO_4/SiO_2 had two other signals at −14.3 and −7.4 ppm in addition to the above-mentioned three chemical shifts (Fig. 9-c). Further, the chemical shift at 0.4 ppm was split into two signals at 0 and 1.1 ppm. These five chemical shifts, except for that at 1.1 ppm, each appeared at about 7.2 ppm intervals between 0 and −29.1 ppm. For chemical shifts of ^{29}Si in aluminosilicates, the most characteristic trend is that substitution of the Si ions in silicate tetrahedra by Al ions leads to low-field shifts at each 4 to 6 ppm intervals.[18] The five ^{31}P chemical sifts suggest that not less than 5 different types of phosphate tetrahedra existed on the surface of the CVD BPO_4/SiO_2 catalyst. These results indicate that amorphous composite oxides, having micro-structures of BPO_4, were highly dispersed on silica for the CVD catalyst.

Catalytic Activity of CVD BPO_4/SiO_2. The catalytic activity for the isomerization of 1-butane was affected by the P/B ratio in the CVD BPO_4/SiO_2 catalyst prepared at 300 °C (Fig. 10). In the region of excess phosphorus, the activity was much higher than that in the region of excess boron, and the maximum activity was obtained at a P/B ratio near 1.1. The trans/cis ratio of product 2-butene ranged from 1.0 to 1.3 at a 1-butene conversion level of 50%, irrespective of the P/B ratio. In addition to isomerization, a small amount of butene dimers was produced with

Table 1. Acid Amount Measured by Ammonia Adsorption

BPO_4 catalyst (P/B ratio)		Content	Adsorbed amount/mmol g^{-1}	
		wt%	150 °C[a)]	300 °C[a)]
CVD	(1.0)	28	—	0.12
CVD	(0.83)	27	0.34	0.13
CVD	(1.1)	29	0.39	0.13
Impregnation	(1.1)	30	0.22	0.11
Unsupported	(1.1)	100	0.08	0.04

a) Adsorption temperature of ammonia.

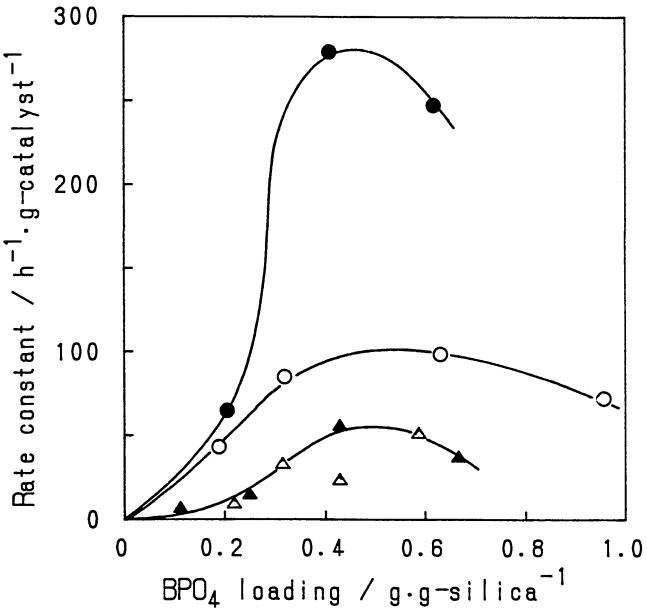

Fig. 12. Isomerization activities of various BPO_4/SiO_2 catalysts at 50 °C.
●, CVD catalyst of P/B=1.1; ○, P/B=1.
▲, Impregnation catalyst of P/B=1.1; △, P/B=1.

passing of the reaction time. The conversions of 1-butene to oligomers were 10—29% after the reaction had proceeded for 1 h. In order to clarify the catalytic behavior for oligomerization, the reaction was performed at lower temperatures. Since the isomerization activity was suppressed, the essential oligomerization activity appeared at 0 °C (Fig. 11). The maximum oligomerization activity was also observed at a P/B ratio near 1.1. This result is consistent with the catalytic behavior of unsupported BPO_4 for the liquid-phase oligomerization of 1-decene.[10)]

Figure 12 shows a comparison of CVD BPO_4/SiO_2 with the IMP BPO_4/SiO_2 catalyst regarding catalytic activity in 1-butene isomerization. For the CVD catalyst with a P/B ratio of 1, the isomerization activity increased with BPO_4 loading, passed through a maximum and then decreased above a loading of 0.6 g g-silica^{-1}. The decrease in the activity was considered to be caused by a closure of the micropore of the support, as has been described in connection with the results of the change in the specific surface area with BPO_4 loading (Fig. 6). The CVD catalysts, especially for the P/B ratio of 1.1, were much more active than both the IMP BPO_4/SiO_2 catalysts and the unsupported BPO_4 (P/B=1.1) whose rate constant for 1-butene isomerization was 89 h^{-1} g-catalys^{-1}. In addition, for the oligomerization activity, the CVD catalysts were also more active than both IMP BPO_4/SiO_2 and unsupported BPO_4 whose conversions were 6—9% at 50 °C (Fig. 10).

In order to evaluate the acid amount of catalyst, the amount of chemisorbed ammonia was measured volumetrically (Table 1). Irrespective of the P/B ratio, the amounts of ammonia chemisorbed on CVD catalysts were almost unchanged. The changes in the catalytic activity with the P/B ratio (Figs. 10 and 11) are not attributable to the acid amount, but probably to acid type (Brønsted or Lewis acid) of catalyst,[2,11)] though further work concerning the acid type and strength of CVD BPO_4/SiO_2 catalysts is in the progress. However, it has been clearly demonstrated that the acid amount of the CVD BPO_4/SiO_2 catalyst is much larger than those of both IMP BPO_4/SiO_2 and unsupported BPO_4. This tentatively explains the superiority of the CVD catalyst for the reactions mentioned above.

In conclusion, amorphous boron phosphate was deposited on a silica support with the desired P/B ratio and with high dispersion by means of a CVD method. The resulting CVD BPO_4/SiO_2 catalyst was superior to the impregnation catalyst for the isomerization of 1-butene and the simultaneous side reaction of oligomerization.

We wish to thank Mr. H. Shoji, Maruzen Petrochemical Co., Ltd., for performing the NMR measurement. The present work was partially supported by the Grant-in-Aid for Development Scientific Research No. 63750807 from the Ministry of Education, Science and Culture.

References

1) R. Tartarelli, M. Giorgini, A. Lucchesi, G. Stoppato, and F. Moreli, *J. Catal.*, **17**, 41 (1970).
2) J. Haber and U. Szybalska, *Faraday Discuss. Chem. Soc.*, **72**, 263 (1981).
3) J. B. Moffat, *Catal. Rev.-Sci. Eng.*, **18**, 199 (1978).

4) S. S. Jewur and J. B. Moffat, *J. Catal.*, **57**, 167 (1979).
5) J. B. Moffat and A. Schmidtmeyer, *Appl. Catal.*, **28**, 161 (1986).
6) F. Nozaki and I. Kimura, *Bull. Chem. Soc. Jpn.*, **50**, 614 (1977).
7) T. Sodesawa, I. Kimura, and F. Nozaki, *Bull. Chem. Soc. Jpn.*, **52**, 2431 (1979).
8) J. Morey, J. M. Marinas, and J. V. Sinisterra, *React. Kinet. Catal. Lett.*, **22**, 175 (1983).
9) Y. Imizu, S. Aoyama, H. Itoh, and A. Tada, *Chem. Lett.*,**1981**, 1455.
10) A. Tada, H. Suzuka, and Y. Imizu, *Chem. Lett.*, **1987**, 423.
1I) H. Miyata and J. B. Moffat, *J. Catal.*, **62**, 357 (1980).
12) H. L. Goltz and J. B. Moffat, *J. Catal.*, **22**, 85 (1971).
13) J. B. Moffat and J. F. Neeleman, *J. Catal.*, **31**, 274 (1973).
14) S. Sato, K. Urabe, and Y. Izumi, *J. Catal.*, **102**, 99 (1986).
15) S. Sato, S. Hasebe, H. Sakurai, K. Urabe, and Y. Izumi, *Appl. Catal.*, **29**, 107 (1987).
16 S. Sato, M. Toita, Y. Q. Yu, T. Sodesawa, and F. Nozaki, *Chem. Lett.*, **1987**, 1535.
17) S. Sato, M. Toita, T. Sodesawa, and F. Nozaki, *Appl. Catal.*, **62**,73 (1990).
18) J. M. Thomas and J. Klimowski, *Adv. Catal.*, **33**, 199 (1985).

Reaction of 1,2-Dichloroethane with Pyridine Using the 1*R*,4*S*,8*R*,11*S*-Tetramethyl-1,4,8,11-tetraazacyclotetradecanenickel(II) Cation as a Probe

Etsuro IWAMOTO, Takashi YOKOYAMA, Jun NISHIMOTO, Tamao YAMASHITA, and Takahiro KUMAMARU*
Department of Chemistry, Faculty of Sciences, Hiroshima University, Hiroshima 730
(Received September 17, 1990)

A spectral change of the title square planar cation $[Ni(tmc)]^{2+}$ by an axial ligation of the halide ions in nitrobenzene was applied to kinetic studies of pyridine and alkyl halides. The ligation of the chloride ions proceeds with a formation constant of more than 1×10^4 dm^3mol^{-1} and rapidly with a rate of less than millisecond. It was found that 1,2-dichloroethane and dichloromethane react with pyridine through the Menschutkin reaction with a rate constant of 1.2×10^{-8} and 3.7×10^{-9} $dm^3mol^{-1}s^{-1}$ at 35 °C, respectively.

1,2-Dichloroethane (DCE) is a very useful solvent with a favorable boiling point, an intermediate dielectric constant and non-hydrogen-bonding property as an inactive medium for various reactions.

It is well known that the Menschutkin reaction occurs between amines and alkyl halides.[1-9] Nevstad and Songstad[3] examined the reactivity of dichloromethane (DCM) toward amines in DCM at 25 °C and found that the reaction rate of DCM-trimethylamine is considerable: the half-life (τ) is *ca.* 18 h, while pyridine (Py) reacts exceedingly slowly with DCM (τ=ca. 9600 h). On the other hand, no kinetic study has been reported for DCE, and this solvent is widely used without the special precautions at room temperatures. Gutmann[10,11] used DCE as a standard of basicity of solvents in which enthalpy of adduct formation of $SbCl_5$ with donor solvents was measured. However, it was pointed out that DCE rapidly quaternizes triethylamine under the catalytic action of $SbCl_5$.[12,13]

In the course of study of axial coordination of donor solvents to $[Ni(tmc)]^{2+}$ (tmc=1,4,8,11-tetramethyl-1,4,8,11-tetraazacyclotetradecane) in DCE, the time-dependent spectra of the $[Ni(tmc)]^{2+}$ cation were observed when Py is present and it was found that the resultant spectrum is referred to the chloride coordinated $[Ni(tmc)Cl]^+$ cation (Scheme 1), showing the occurrence of the Menschutkin reaction between Py and DCE. Usually, the Menschutkin reaction has been examined by using conductometry and the silver nitrate titration. In this work the reaction between Py and alkyl halides in nitrobenzene (NB) as solvent was studied kinetically by using the square planar $[Ni(tmc)]^{2+}$ cation which shows color change from red to blue by an axial ligation of the halide ion.

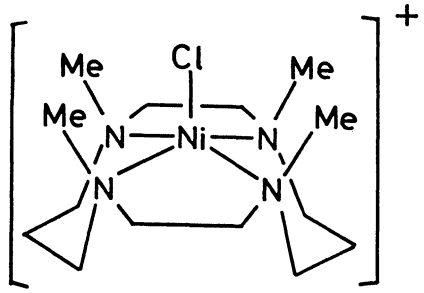

[Ni(tmc)Cl]$^+$

Scheme 1.

Experimental

The salt $[Ni(tmc)](ClO_4)_2$ with (1*R*,4*S*,8*R*,11*S*)-nitrogen configuration was prepared by the published method[14,15] and was recrystallized from acetone-diethyl ether mixtures. Purity of the salt was checked by elemental analysis and IR spectra. Tetraphenylphosphonium bromide was prepared by the reported method[16] and the crude product was recrystallized by the method described previously.[17] Tetraphenylphosphonium chloride and tetraethylammonium chloride (Wako Pure Chemical Industries Ltd.) were recrystallized from an acetone-ether mixture. Purification of Py, DCE, and NB has been described previously.[18,19] Bromoethane (BE) of reagent grade (Wako Pure Chemical Industries Ltd.) was purified by fractional distillation through a 1.2-m column without washing.

The instrumentation and the procedure used for measurements of spectra and conductance were the same as described previously.[19]

Results and Discussion

In Fig. 1 are shown the spectra of $[Ni(tmc)](ClO_4)_2$ in a Py-DCE mixed solvent at 25 °C which change with time. The absorption peak at 524 nm is assigned to the low-spin, square planar species and the peaks at 430 nm and 720 nm to the high-spin, square pyramidal species. It is clearly shown that a certain ligand which is generated with the passage of time is coordinated to form a square pyramidal species. In our previous study,[19] it was found that neither DCE nor Py are coordinated because the basicity of DCE is too low and coordination of Py is sterically hindered in spite of its high basicity. If water is contained in their mixture, water molecules hydrogen-bonded to Py can be coordinated because of

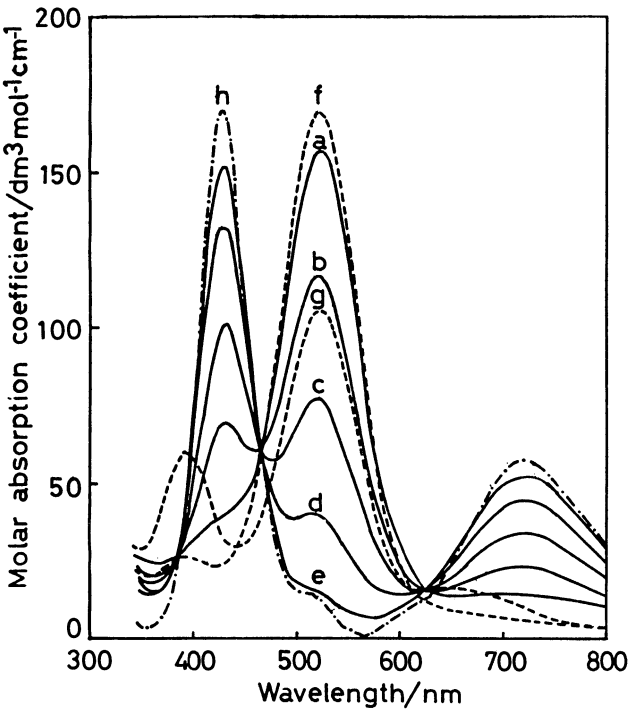

Fig. 1. Visible spectrum variation of a 1×10^{-3} mol dm^{-3} solution of $[Ni(tmc)](ClO_4)_2$ with time and water contents in Py at 25 °C. The DCE molar fraction (0.19): a, 16 min after preparation of the solution; b, 46; c, 76; d, 106; e, 136. Without DCE: f, $[H_2O]=8.6\times10^{-3}$ mol dm^{-3}; g, 5.7×10^{-2}. h, Spectrum of $[Ni(tmc)Cl]ClO_4$ in Py.

the increased basicity of water by polarization through hydrogen-bonding.[20,21] But as shown in Fig. 1, the water-coordinated species has an isosbestic point at 607 nm and absorption peaks at 390 nm and 660 nm, different from the time-dependent spectrum. Therefore, coordination of another ligand should be considered.

Alkyl halides react with amines, that is the Menschutkin reaction, forming quaternary ammonium salts with halide ions, and several works concerning this reaction of Py and alkyl halides at both atmospheric and elevated pressures have been reported.[6-9] As far as we know, however, reactivity of DCE with amines has not been examined in spite of the fact that DCE is very widely used as various reaction media.

The salt $[Ni(tmc)Cl]ClO_4$ was prepared by adding an equivalent sodium chloride to the aqueous $[Ni(tmc)](ClO_4)_2$ solution[14] and its spectrum was recorded ((h) in Fig. 1). The time-dependent spectrum which has absorption peaks at 430 nm and 720 nm coincides with that of the chloride-coordinated species. Therefore, it can be said that DCE reacts with Py to form quaternary ammonium chloride as depicted by Eq. 1. If the resultant chloride ion is

$$ClCH_2CH_2Cl + NC_5H_5 \longrightarrow ClCH_2CH_2N^+C_5H_5\ Cl^- \quad (1)$$

determined, the rate of reaction can be evaluated.

Coordination of the Chloride and Bromide Ions to $[Ni(tmc)]^{2+}$. The first ionic association constant of $[Ni(tmc)]^{2+}$ with the ClO_4^- ion is 1190 dm^3 mol^{-1} [19] in NB which indicates that 49% of $[Ni(tmc)]^{2+}$ are associated with ClO_4^- at 0.001 mol dm^{-3}. The association results from electrostatic attractive forces because of the weak basicity of ClO_4^- and the nickel complex cation remains the four-coordinated species. When a more basic solute is present, its coordination is hardly interrupted by the perchlorate association.[19]

Coordination of the chloride and bromide ions was examined spectrophotometrically by adding tetraphenylphosphonium or tetraethylammonium chloride and tetraphenylphosphonium bromide to the $[Ni(tmc)](ClO_4)_2$ solutions. Table 1 gives variation of the molar absorption coefficient (ε) of the complex cation at 524 nm with the concentration of chloride and bromide ions in DCE-NB mixed solvents. It was found that the ε values decrease linearly with increasing the halide ion concentration. The formation constant K_{NiX} was calculated by equation

$$K_{NiX}=(\varepsilon_o-\varepsilon)/(\varepsilon-\varepsilon_s)[X^-], \quad (2)$$

where ε_o is the molar absorption coefficient of the four-coordinated species at 524 nm and ε_s is the molar absorption coefficient of the five-coordinated species (ε_s=10 dm^3 mol^{-1} cm^{-1} [19]). $[X^-]$ is the concentration of the non-coordinated halide ion. The K_{NiX} values obtained are given in the last column. The activity

Table 1. Coordination of the Chloride and Bromide Ions to $[Ni(tmc)]^{2+}$ at 35 °C

X_{DCE}	Salt	$[X^-]$	$[[Ni(tmc)]^{2+}]$	ε_o	ε	K_{NiX}
		10^{-4} mol dm^{-3}	10^{-3} mol dm^{-3}	dm^3 mol^{-1} cm^{-1}		10^4 dm^3 mol^{-1}
0	Ph_4PBr	0.755	0.983	209	195	1.2
0		2.05	0.970	209	171	1.2
0.10	Ph_4PCl	1.05	1.02	207	188	1.7
0.10		1.83	1.01	207	174	1.4
0.40	Et_4NCl	4.41	1.02	199	119	7.9
0.40	Ph_4NCl	2.36	1.00	199	155	9.5
0.40		5.35	0.975	199	98	8.2

coefficient is not taken into account because a constant $[Ni(tmc)]^{2+}$ concentration of *ca.* 1×10^{-3} mol dm^{-3} was used throughout the work. It is seen that the formation constant is one order of magnitude larger than the ionic association constant for the perchlorate ion and an increase in DCE molar fraction strengthens the coordination of halide ions. The rate of coordination of Cl^- ions to $[Ni(tmc)]^{2+}$ could not be measured by the stopped-flow method, showing that it is faster than millisecond. The results obtained above show that the $[Ni(tmc)]^{2+}$ cation can be used as a probe for the Menschutkin reaction.

Estimation of the Rate Constant of the Menschutkin Reaction. For the Menschutkin reaction the second-order rate equation Eq. 2 applies,

$$dx/dt = k_2(a-x)(b-x), \quad (3)$$

and then it is rewritten as

$$\ln(b-x)/(a-x) = (b-a)k_2t - \ln a/b \quad (4)$$

where k_2 is the rate constant in dm^3 mol^{-1} s^{-1} and a and b are the initial concentrations of alkyl halide and Py, respectively, and x is the concentration of the product (ammonium salt) formed after an interval of t s. The x values are estimated by using the coordination constant K_{NiX}

$$x = m'[1 + 1/K_{NiX}(m-m')] \quad (5)$$

where m' is the concentration of five-coordinated species, and m is the initial concentration of four-coordinated species. Since the K_{NiX} values are more than 10^4 and so the contribution of the second term in Eq. 5 is very small, the K_{NiX} value in Table 1 in the solvent composition close to the solvent system in question was used for calculation.

Typical examples of plot of Eq. 4 for the DCE-Py system in NB are illustrated in Fig. 2. Good linear relationships were obtained from which the k_2 rate constants were calculated. Similar measurements were made as a reference in the DCE-NB mixture without Py and in the Py-NB mixture without DCE, and it was confirmed that the change in absorbances is negligible compared with that in the DCE-Py system.

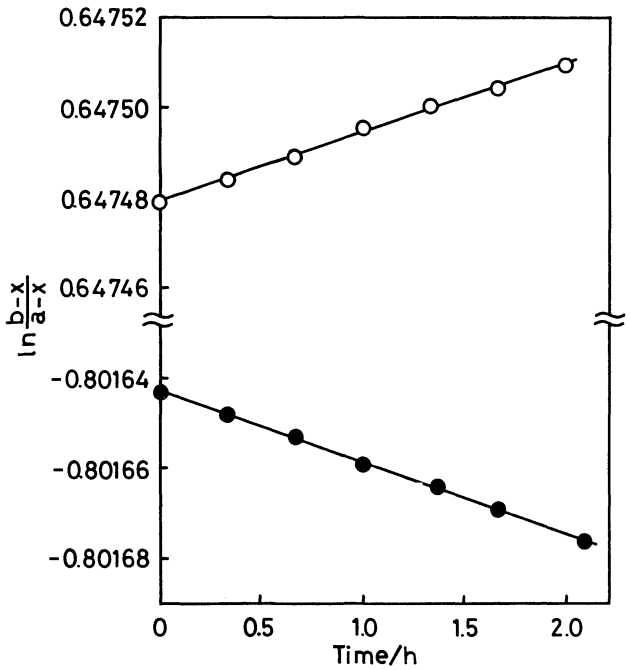

Fig. 2. Plots of $\ln(b-x)/(a-x)$ vs. t in NB at 35 °C. [DCE], [Py] in mol dm^{-3}: a, 0.411, 0.786; b, 0.844, 0.379.

Table 2. Second Order Rate Constants for the Reaction of Py with DCE, DCM, and BE in NB at 35 °C

[Py]	[DCE]	k_2
mol dm^{-3}	mol dm^{-3}	10^{-8} dm^3 mol^{-1} s^{-1}
0.0924	1.12	1.1
0.143	1.03	1.1
0.258	0.958	1.1
0.379	0.844	0.92
0.786	0.411	1.1
0.807	0.206	1.4
0.877	0.243	1.1
0.446	5.50	0.68
0.503	5.55	0.64
0.886	5.22	0.64
1.39	5.16	0.59
1.52	4.47	0.63
2.01	4.08	0.63
2.52	3.89	0.62
3.80	2.48	0.70
3.91	1.96	0.69
4.49	1.56	0.72
4.93	0.919	0.80
5.01	1.29	0.71
5.53	0.506	0.85
10.0	2.41	0.26[a]
11.4	1.02	0.27[a]
12.3	0.112	1.1[a]
[Py]	[DCM]	k_2
mol dm^{-3}	mol dm^{-3}	10^{-9} dm^3 mol^{-1} s^{-1}
0.109	0.911	2.6
0.267	0.859	2.5
0.317	0.710	2.5
0.801	0.227	3.1
0.912	0.0974	3.8
[Py]	[BE]	k_2
mol dm^{-3}	mol dm^{-3}	10^{-5} dm^3 mol^{-1} s^{-1}
0.00593	0.139	1.1
0.0240	0.116	1.0
0.0274	0.0860	1.1
0.0336	0.0415	1.1
0.0662	0.0196	1.1
0.0736	0.0325	1.1
0.0903	0.00636	1.3
0.112	0.00225	1.1
0.134	0.0103	1.1
0.137	0.00527	1.1

a) Obtained without NB at 25 °C.

The k_2 values obtained in this way are summarized in Table 2.

The conductance measurements were also carried out to evaluate the k_2 value in a different method. Figure 3 typically shows variation of the conductivity with time in a reactant composition of [DCE]=0.826 mol dm^{-3} and [Py]=0.413 mol dm^{-3} in NB at 35 °C. The chloride and bromide concentrations were approximately evaluated by using the molar conductance of tetraphenylphosphonium chloride and bromide, respectively because the corresponding salts are not available.

Figures 4 and 5 show the dependence of k_2 values obtained spectrometrically and conductometrically on the DCE fraction. A slight difference is found for conductometry, this being because the salts using for calibration are not the same as the products. It is seen that for DCE the rate constant slightly increases with decreasing the DCE fraction. This may be due to the secondary Menschutkin reaction of the DCE molecule having two reaction sites leading to the *N,N*-ethylenedipyridinium cation $H_5C_5N^+CH_2CH_2N^+C_5H_5$, in view of the fact that such dependence was not observed for BE having one reaction site. The conductance results show the same trends. In the case of the greater content of more polar NB as the diluent, that is, the lower concentration of reactants, the rate constant is large, reflecting the ionic product in the Menschutkin reaction.

Table 3 gives the rate constants according to spectrophotometry extrapolated to zero concentration of Py at which the 1:2 DCE-Py reaction is negligible. The rate of reaction for DCM is one order of magnitude smaller than that for DCE, DCM being a little more stable than DCE. Maria and Gal[22] pointed out

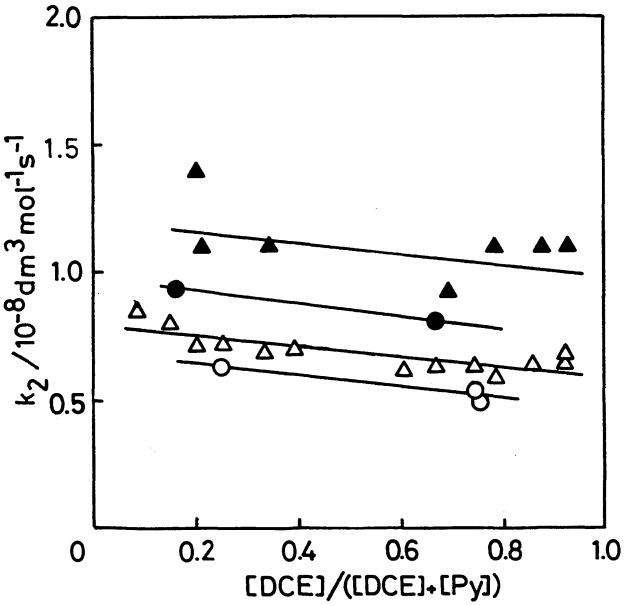

Fig. 4. Variation of the rate constant for the DCE-Py system with the DCE molar fraction in NB at 35 °C. The total concentration of DCE and Py is *ca.* 1.1 mol dm^{-3}: ▲, spectrometry; ●, conductometry. The total concentration is *ca.* 6 mol dm^{-3}: △, spectrometry; ○, conductometry.

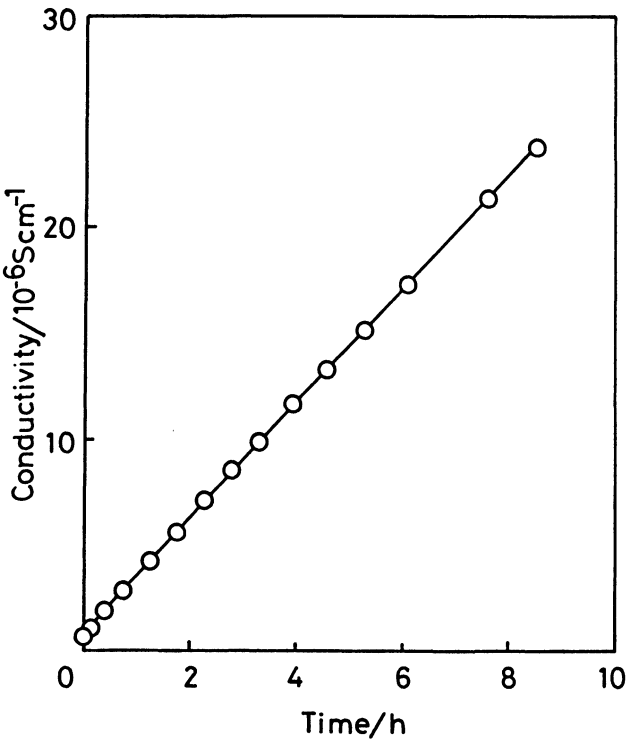

Fig. 3. Variation of the conductivity for [Ni(tmc)]$(ClO_4)_2$ with time in NB at 35 °C. [DCE]=0.826 mol dm^{-3}, [Py]=0.413 mol dm^{-3}.

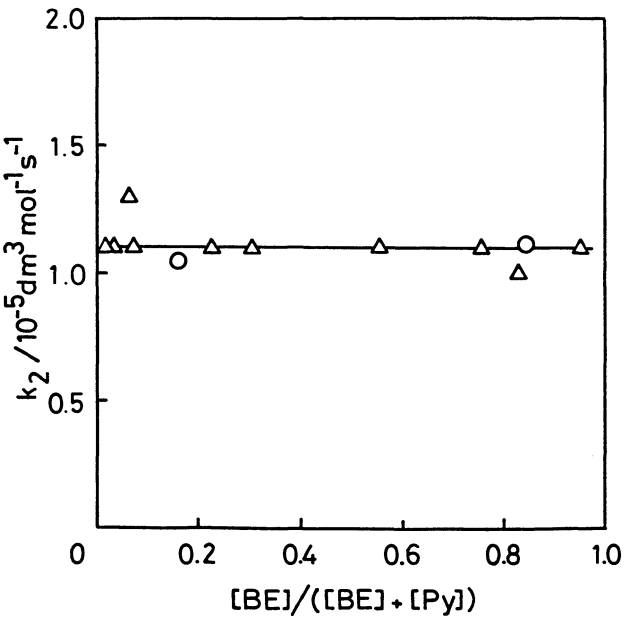

Fig. 5. Variation of the rate constant for the BE-Py system with the BE molar fraction in NB at 35 °C. △, spectrometry; ○, conductometry.

Table 3. Extrapolated Second Order Rate Constants for the Reaction of Py with DCE, DCM, and BE in NB at 35 °C

Halogeno-solvent(S)	k_2 / $dm^3\,mol^{-1}\,s^{-1}$	Initial concentration ([Py]+[S])/mol dm^{-3}
DCE	1.0×10^{-8}	1.0—1.2
	5.9×10^{-9}	5.9—6.5
DCM	2.2×10^{-9}	1.0—1.1
	5×10^{-10} a)	—
BE	1.1×10^{-5}	0.075—0.26
	8.8×10^{-6} b)	0.12

a) Measured in DCE at 25 °C. From Ref. 3. b) From Refs. 4 and 5.

that a non-negligible amount of charged species is contained in some DCE solutions of $SbCl_5$ and strong basic solute, and instead of DCE they used DCM as the solvent to establish a solvent Lewis basicity scale.

It can be concluded that although the rate of reaction is small, DCE surely reacts with Py through the Menschutkin reaction without the catalytic action of $SbCl_5$: the concentration of the chloride ions in the DCE–Py mixture amounts to 10^{-4} mol dm^{-3} level in 30 min at 25 °C.

The conductometry for the determination of halide ions suffers one disadvantage which is the difficulty in calibrating the conductivity of the salt generated in the Menschutkin reaction. The silver titration method is somewhat troublesome because it contains the procedure of extraction of the halide ions into an aqueous phase.[3] On the other hand, the present system cannot be used when the basic, coordinating solvents such as dimethyl sulfoxide, *N*,*N*-dimethylformamide, acetonitrile and water are present in the reaction system.[19] However, if such basic solvents are not, the Menschutkin reaction can be easily monitored by the spectral change of the square planar $[Ni(tmc)]^{2+}$ cation without relying on conductometry or the silver titration method.

This work was supported by a Grant-in-Aid for Scientific Research No. 01303004 from the Ministry of Education, Science and Culture.

References

1) W. C. Davies, E. B. Evans, and F. L. Hulbert, *J. Chem. Soc.*, **1939**, 412.
2) D. A. Wright and C. A. Wulff, *J. Org. Chem.*, **35**, 4252 (1970).
3) G. O. Nevstad and J. Songstad, *Acta Chem. Scand., Ser. B*, **38**, 469 (1984).
4) K. T. Leffek and A. F. Matheson, *Can. J. Chem.*, **50**, 982 (1972).
5) K. T. Leffek and A. F. Matheson, *Can. J. Chem.*, **50**, 986 (1972).
6) E. M. Arnett and R. Reich, *J. Am. Chem. Soc.*, **102**, 5892 (1980).
7) C. D. Johnson, I. Roberts, and P. G. Taylor, *J. Chem. Soc., Perkin Trans. 2*, **1981**, 409.
8) B. Almarzogi, A. V. George, and N. S. Isaacs, *Tetrahedron*, **42**, 601 (1986).
9) S. D. Yoh, J. H. Park, K. A. Lee, and I. S. Han, *Bull. Chem. Soc. Jpn.*, **60**, 1149 (1987).
10) V. Gutmann and E. Wychera, *Inorg. Nucl. Chem. Lett.*, **12**, 257 (1966).
11) V. Gutmann, "*The Donor-Acceptor Approach to Molecular Interactions*," Plenum Press, New York (1978).
12) R. W. Taft, N. J. Pienta, M. J. Kamlet, and E. M. Arnett, *J. Org. Chem.*, **46**, 661 (1981).
13) J. C. Bollinger, G. Yvernault, and T. Yvernault, *Thermochim. Acta*, **60**, 137 (1983).
14) E. K. Barefield and F. Wagner, *Inorg. Chem.*, **12**, 2435 (1973).
15) E. K. Barefield, F. Wagner, A. W. Herlinger, and A. R. Dahl, *Inorg. Syn.*, **16**, 220 (1975).
16) Von. Y. Hirusawa, M. Oku, and K. Yamamoto, *Bull. Chem. Soc. Jpn.*, **30**, 667 (1957).
17) E. Iwamoto, Y. Tanaka, H. Kimura, and Y. Yamamoto, *J. Solution Chem.*, **9**, 841 (1980).
18) S. Yamasaki, Y. Yanai, E. Iwamoto, T. Kumamaru, and Y. Yamamoto, *J. Chem. Soc., Faraday Trans. 1*, **83**, 1641 (1987).
19) E. Iwamoto, T. Yokoyama, S. Yamasaki, T. Yabe, T. Kumamaru, and Y. Yamamoto, *J. Chem. Soc., Dalton Trans.*, **1988**, 1935.
20) S. Yamasaki, E. Iwamoto, and T. Kumamaru, *J. Chem. Soc., Faraday Trans. 1*, **84**, 1679 (1988).
21) E. Iwamoto, S. Yamasaki, and T. Kumamaru, *Bull. Chem. Soc. Jpn.*, **62**, 1692 (1989).
22) P. C. Maria and J. F. Gal, *J. Phys. Chem.*, **89**, 1296 (1985).

The Electronic Structure of the Fulvene Radical Cation

Ohgi TAKAHASHI and Osamu KIKUCHI*
Department of Chemistry, University of Tsukuba, Tsukuba 305
(Received September 27, 1990)

The molecular and electronic structures of the unsubstituted fulvene radical cation, $FV^{+\cdot}$, were investigated by ab initio SCF calculations. The planar $^2A_2$ state, which corresponds to removing an electron from the butadienic moiety in the five-membered ring, was found to be the ground state of $FV^{+\cdot}$, and is more stable than the planar $^2B_1$ state, which corresponds to an olefin radical cation, by about 26 kcal mol^{-1}. The barrier to rotation around the exocyclic C-C bond in the $^2A_2$ radical cation was calculated to be about 63 kcal mol^{-1}. The importance of electronic relaxation in substituted fulvene radical cations is discussed in connection with the rotational barrier.

Fulvenes have long been a focus of interest because of their unique properties, and their molecular and electronic structures have been widely investigated both experimentally[1] and theoretically.[2] Recently, the radical cations of some fulvenes have been spectroscopically observed[3,4] and several interesting aspects appeared concerning the electronic structures of the radical cations.

Though neutral fulvene (FV) may be regarded as

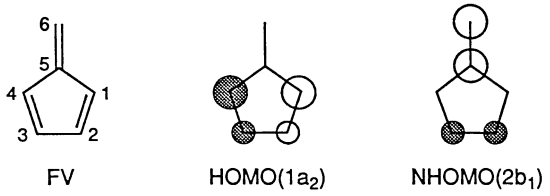

being an olefin, its HOMO ($1a_2$) is not associated with the exocyclic double bond, but extends within the butadienic moiety in the five-membered ring; the HOMO is essentially the HOMO of butadiene. The

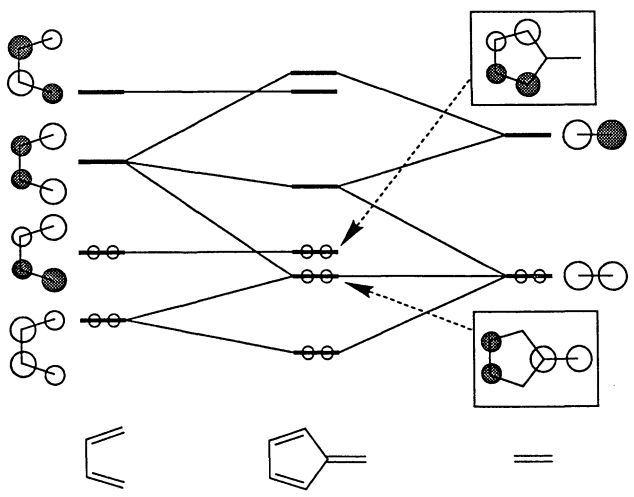

Fig. 1. Construction of π MO's of FV from those of butadiene and ethylene.

electrons associated with the exocyclic double bond are in the next to the HOMO (NHOMO), $2b_1$, which is energetically close to the HOMO. This situation of the MO levels of FV can be understood by constructing π MO's of FV from those of butadiene and ethylene, as shown in Fig. 1. The ground state of the fulvene radical cation ($FV^{+\cdot}$) is then expected to correspond to removing a π electron from the butadienic moiety ($^2A_2$ state).

Indeed, the freon matrix ESR spectrum of the radical cation of 6,6-dimethylfulvene (**1**),[3] and CIDNP observed during UV irraddiation of **1**, 6,6-diphenylfulvene (**2**), 6-phenylfulvene (**3**), (*Z*)- and (*E*)-2,6-di-*t*-butylfulvene (**4**), and (*Z*)- and (*E*)-2-*t*-butyl-6-(dimethylamino)fulvene (**5**) in the presence of electron acceptors[4] have shown that all of the radical cations of these fulvenes have a_2 or a_2-like SOMO.

On the other hand, if the electronic structure of the radical cations merely corresponds to removing an electron from the a_2-like HOMO of the neutral fulvenes, the unpaired electron and positive charge would be constrained to within the butadienic moiety and the double-bond character of the exocyclic double bond would not be reduced. Thus, it is very interesting that (*Z*)-$\mathbf{5}^{+\cdot}$ and (*E*)-$\mathbf{5}^{+\cdot}$ readily interconvert, while (*Z*)-$\mathbf{4}^{+\cdot}$ and (*E*)-$\mathbf{4}^{+\cdot}$ do not show any interconversion.[4] The electronic relaxation in substituted fulvene radical cations may be important in relation to the rotational barrier around the exocyclic double bond. In this respect, it is important to clarify the electronic structure of the unsubstituted fulvene radical cation, $FV^{+\cdot}$, at both the planar and 90°-twisted forms.

Although a semi-empirical INDO calculation on

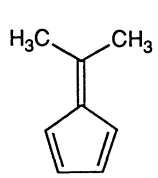

1

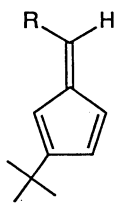

Z-4 R=-C(CH$_3$)$_3$
Z-5 R=-N(CH$_3$)$_2$

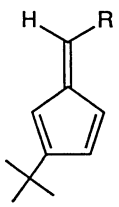

E-4 R=-C(CH$_3$)$_3$
E-5 R=-N(CH$_3$)$_2$

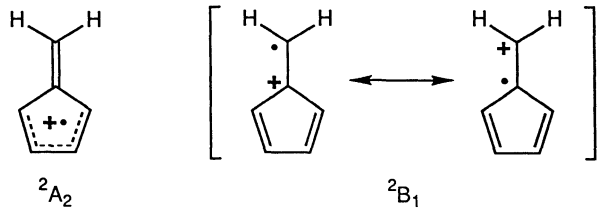

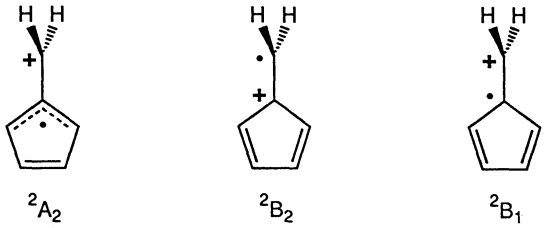

$FV^{+\cdot}$ has been carried out in connection with the photoelectron (PE) spectra of a series of alkyl-substituted fulvenes,[5] there are no ab initio level found through theoretical studies on $FV^{+\cdot}$. In this paper the electronic structures of the planar and 90°-twisted forms of $FV^{+\cdot}$ were examined using restricted open-shell Hartree-Fock (ROHF) calculations with the STO-3G[6] and 3-21G[7] basis sets. A C_{2v} symmetry was assumed for both planar and 90°-twisted forms, and the $^2A_2$ and $^2B_1$ states of the planar form and the $^2A_2$, $^2B_2$, and $^2B_1$ states of the 90°-twisted form were examined.

Results and Discussion

Planar $FV^{+\cdot}$. The two lowest energy bands in the PE spectrum of FV have been assigned to formation of the $^2A_2$ (first peak) and $^2B_1$ (second peak) states of $FV^{+\cdot}$.[5] Calculations were carried out for these two states of $FV^{+\cdot}$ using a geometry optimized for FV, so that the calculated relative energies could be compared with the vertical ionization potantials, 8.55 and 9.54 eV for the $^2A_2$ and $^2B_1$ states, respectively, measured for FV.[5] The optimized structures of FV are given in Table 1, and the energies of the two low-lying states of

Table 1. Calculated Molecular Structures of FV[a]

	3-21G	STO-3G	Exp.[b]
Bond lengths			
C_5-C_1	1.485	1.494	1.470
C_1-C_2	1.333	1.324	1.355
C_2-C_3	1.489	1.492	1.476
C_5-C_6	1.321	1.319	1.349
C_1-H_1	1.068	1.079	1.078
C_2-H_2	1.068	1.081	1.080
C_6-H_6	1.073	1.083	1.13
Bond angles			
$C_4C_5C_1$	105.2	104.6	106.6
$C_5C_1C_2$	108.3	108.5	107.7
$C_1C_2C_3$	109.1	109.2	109.0
$C_5C_1H_1$	123.8	123.4	124.7
$C_1C_2H_2$	126.9	127.3	126.4
$C_2C_6H_6$	121.7	122.0	121.5

a) Bond lengths are in Å and bond angles are in degrees. b) Ref. 8.

Table 2. Total Energies of FV and $FV^{+\cdot}$ Calculated at the Geometries Optimized for FV

Species	3-21G	STO-3G	Exp.[a]
FV	−229.35434[b]	−227.82340[b]	—
$FV^{+\cdot}(^2A_2)$	7.50[c]	6.07[c]	8.55
$FV^{+\cdot}(^2B_1)$	8.49	6.99	9.54

a) Vertical ionization potentials in eV. Ref. 5. b) Energy in a.u.. c) Energy relative to FV in eV.

Table 3. Molecular Structures of $FV^{+\cdot}$ Obtained by ROHF/3-21G and ROHF/STO-3G (in Parentheses) Calculations[a]

	C_{2v} planar		C_{2v} perpendicular		
	$^2A_2$	$^2B_1$	$^2A_2$	$^2B_2$	$^2B_1$
Bond lengths					
C_5-C_1	1.457(1.469)	1.471(1.485)	1.401(1.397)	1.472(1.487)	1.472(1.484)
C_1-C_2	1.403(1.410)	1.331(1.329)	1.464(1.469)	1.330(1.330)	1.345(1.334)
C_2-C_3	1.394(1.398)	1.546(1.546)	1.343(1.338)	1.565(1.560)	1.481(1.493)
C_5-C_6	1.333(1.339)	1.409(1.435)	1.435(1.473)	1.440(1.485)	1.411(1.458)
C_1-H_1	1.069(1.091)	1.066(1.080)	1.069(1.086)	1.065(1.080)	1.065(1.080)
C_2-H_2	1.067(1.086)	1.068(1.089)	1.067(1.082)	1.068(1.091)	1.067(1.085)
C_6-H_6	1.073(1.092)	1.072(1.092)	1.080(1.119)	1.075(1.085)	1.081(1.119)
Bond angles					
$C_4C_5C_1$	105.1(104.7)	108.7(108.4)	108.6(109.2)	109.1(108.7)	108.2(107.9)
$C_5C_1C_2$	108.4(108.4)	107.1(106.9)	107.1(106.8)	107.2(106.9)	106.2(106.2)
$C_1C_2C_3$	109.1(109.2)	108.5(109.0)	108.6(108.6)	108.2(108.8)	109.7(109.9)
$C_5C_1H_1$	125.4(125.3)	124.4(123.7)	127.0(127.1)	123.8(123.5)	124.9(124.1)
$C_1C_2H_2$	125.2(125.1)	127.7(127.9)	123.6(123.2)	128.1(128.2)	125.7(126.1)
$C_2C_6H_6$	121.6(121.7)	120.7(120.6)	121.6(122.7)	119.5(118.9)	121.3(115.5)

a) Bond lengths are in Å and bond angles are in degrees.

Table 4. Calculated Total Energies (a.u.) and Relative Energies (kcal mol^{-1}, in Parentheses) of $FV^{+\cdot}$

Structure	State	ROHF/3-21G	ROHF/STO-3G
C_{2v} planar	$^2A_2$	−229.09276(0.0)	−227.62288(0.0)
	$^2B_1$	−229.05143(25.9)	−227.58552(23.4)
C_{2v} perpendicular	$^2A_2$	−228.99294(62.6)	−227.51738(66.2)
	$^2B_2$	−229.02113(44.9)	−227.55711(41.2)
	$^2B_1$	−228.98995(64.5)	−227.51630(66.8)

$FV^{+\cdot}$ calculated using the geometries for FV are given in Table 2 along with the energies of FV and the experimental ionization potentials.[5] The calculated energy differences between the $^2A_2$ and $^2B_1$ states, 0.92 and 0.99 eV at ROHF/STO-3G and ROHF/3-21G levels, respectively, are in good agreement with the experimental value, 0.99 eV, although the ionization potentials are largely underestimated. The vertical ionization potentials estimated by the Koopmans' theorem are 7.07 and 7.96 eV (STO-3G), and 8.53 and 9.46 eV (3-21G) for the $^2A_2$ and $^2B_1$ states, respectively. These values show that the electronic reorganization energies for the $^2A_2$ and $^2B_1$ radical cations are almost the same, although the ionization that produces the $^2A_2$ radical cation is more local.[9]

The structures of the $^2A_2$ and $^2B_1$ states of the planar form of $FV^{+\cdot}$ were then optimized. The optimized structures are shown in Table 3, while the calculated total energies are given in Table 4. The calculated bond lengths well reflect the nodal properties of the MO of FV from which an electron is removed. The $^2A_2$ state is more stable than the $^2B_1$ state by about 26 kcal mol^{-1} (3-21G, 1 cal=4.184 J) when the geometries are optimized for each state, which agrees with spectroscopic observations of the spin distributions of some fulvene radical cations described above. Both the $^2A_2$ and $^2B_1$ states of the planar $FV^{+\cdot}$ correspond to energy minima as confirmed by slight twisting of the radical cations around the exocyclic C-C bond.

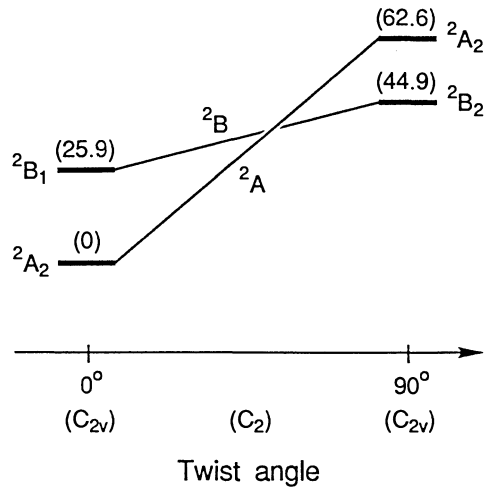

Fig. 2. A state correlation diagram for twisting of $FV^{+\cdot}$. The ROHF/3-21G energies relative to the planar $^2A_2$ state are shown in kcal mol^{-1}.

90°-Twisted $FV^{+\cdot}$. Rigid twisting of the radical cations showed that the $^2A_2$ and $^2B_1$ states of the planar $FV^{+\cdot}$ correlate with the $^2A_2$ and $^2B_2$ states of the 90°-twisted $FV^{+\cdot}$, respectively. The structures of the $^2A_2$ and $^2B_2$ states, as well as the $^2B_1$ state, of the 90°-twisted form were then optimized. The optimized structures are shown in Table 3, while the calculated total energies are given in Table 4. Figure 2 is a state correlation diagram for the double-bond twisting. For the 90°-twisted form, the $^2B_2$ state which correlates with the excited $^2B_1$ state of the planar form is the most stable; the $^2A_2$ state of the 90°-twisted form, which correlates with the $^2A_2$ ground state of the planar form, is higher in energy than the $^2B_2$ state by about 18 kcal mol^{-1} (3-21G). Both the $^2A_2$ and $^2B_2$ states of the 90°-twisted form correspond to the maxima of rotation around the exocyclic C-C bond, as confirmed by the slight untwisting of the 90°-twisted radical cations. Although the $^2B_2$ state is more stable than the $^2A_2$ state at the 90°-twisted form, rotation from the planar $^2A_2$ $FV^{+\cdot}$ is expected to proceed via the $^2A_2$ transition state, since the ^2A and ^2B states of the C_2 twisted forms prefer different molecular structures and, hence, a high barrier exists between the ^2A and ^2B valleys; the energy of the 90°-twisted $^2B_2$ state calculated at the geometry optimized for the 90°-twisted $^2A_2$ state is 88.1 kcal mol^{-1} (3-21G) relative to that of the planar $^2A_2$ ground state. Thus, the rotational barriers estimated for the planar $^2A_2$ and $^2B_1$ states are 62.6 and 19.0(=44.9−25.9) kcal mol^{-1}, respectively (3-21G).

It should be emphasized that an expression such as **I**, which was used in Ref. 4, is not appropriate for the 90°-twisted $FV^{+\cdot}$, since it does not distinguish between the $^2A_2$ and $^2B_1$ states, which are well represented by **II** and **III**, respectively. Both of the two states can be regarded as being a cyclopentadienyl radical attached by a positively charged substituent, $-CH_2$; the SOMO's of the two states stem from the doubly-degenerate SOMO of the ideal D_{5h} cyclopentadienyl

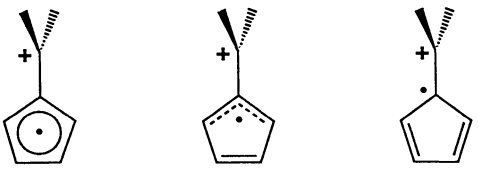

I **II**($^2A_2$) **III**($^2B_1$)

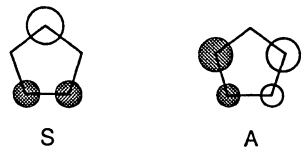

radical, the symmetric orbital (S) and the antisymmetric orbital (A).

For the 90°-twisted form, the $^2B_2$ state is calculated to be more stable than the $^2B_1$ state by about 20 kcal mol^{-1} (3-21G), although the $^2B_2$ radical cation has an antiaromatic 4π system. This result, however, is not surprising, since the positive charge in the $^2B_1$ radical cation is constrained at the C_6 atom. Furthermore, in the $^2B_2$ radical cation, two C_6–H bonds interact with the π system of the five-membered ring hyperconjugatively to spread positive charge. However, substitution by electron-donating groups at the C_6 position may reverse the relative stability of the two states, since the positive charge at C_6 in the $^2B_1$ or $^2B_1$-like radical cation is largely stabilized.

Electronic Structure of Planar $^2A_2$ State and Rotational Barrier. As described above, both the planar $^2A_2$ and $^2B_1$ $FV^{+\cdot}$ resist twisting around the exocyclic C–C bond especially in the former. Because substitution of *t*-butyl groups is expected not to greatly affect the π electron distribution of $FV^{+\cdot}$, the present computational results concerning the twisting agree with the experimental observation that (*Z*)-**4**$^{+\cdot}$ and (*E*)-**4**$^{+\cdot}$ do not show interconversion.[4] In contrast to (*Z*)-**4**$^{+\cdot}$ and (*E*)-**4**$^{+\cdot}$, (*Z*)-**5**$^{+\cdot}$ and (*E*)-**5**$^{+\cdot}$ showed ready interconversion, in spite of the spin distribution which corresponds to an $^2A_2$-like state.[4] This is partially due to the large stabilization of the 90°-twisted $^2A_2$-like state caused by an electron-donating group at C_6. On the other hand, this result can also be interpreted based on the electronic properties inherently involved in the planar $^2A_2$ state which can be described as follows.

In Table 5 the π electron and unpaired electron populations of the carbon atoms in planar $^2A_2$ and $^2B_1$ $FV^{+\cdot}$ are shown. The unpaired electron distribution in the $^2A_2$ $FV^{+\cdot}$ simply reflects the shape of the SOMO, $1a_2$; the unpaired electron is located largely on C_1 and C_4 and to a smaller degree on C_2 and C_3. Because the SOMO has a nodal plane perpendicular to the molecular plane and passing through C_5 and C_6, the unpaired electron is not located on C_5 and C_6. This spin distribution seems to correspond to a butadiene radical cation, **IV** or [**V**↔**V′**]. However, as can be seen from Table 5, the π electron density is the most dilute at C_6, which implies a significant contribution of **VI** and **VI′**. Because the SOMO has no coefficient at C_5 or C_6, the electron flow from C_6 can be attributed to π electrons other than the unpaired electron. Namely, the positively charged hole, which is made by removing an electron from the $1a_2$ HOMO of FV, is partially filled by a reorganization of π electrons other than the unpaired electron. If an electron-donating group, such as the dimethylamino group, is introduced at C_6, the contributions of **VI** and **VI′** become large, which may considerably reduce the double-bond character of the exocyclic C_5–C_6 bond and,

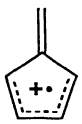

IV

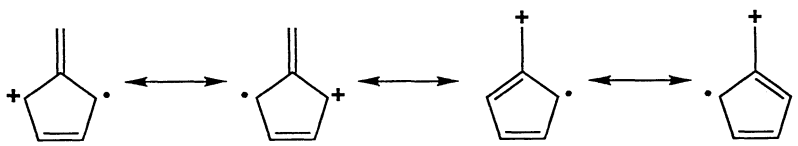

V **V′** **VI** **VI′**

Table 5. The π Electron and Unpaired Electron Populations of the Carbon Atoms in the Planar $^2A_2$ and $^2B_1$ $FV^{+\cdot}$ Obtained by ROHF/3-21G and ROHF/STO-3G (in Parentheses) Calculations

Atom	π Electron population		Unpaired electron population	
	$^2A_2$	$^2B_1$	$^2A_2$	$^2B_1$
C_1, C_4	0.696(0.702)	1.098(1.094)	0.377(0.382)	0.005(0.005)
C_2, C_3	0.896(0.892)	0.781(0.793)	0.123(0.118)	0.065(0.049)
C_5	1.151(1.120)	0.608(0.540)	0.000(0.000)	0.251(0.222)
C_6	0.665(0.693)	0.632(0.687)	0.000(0.000)	0.611(0.668)

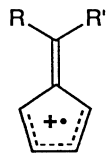

VII

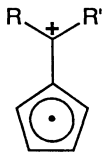

VIII

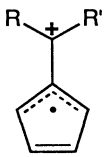

IX

hence, lower the rotational barrier.[10]

On the other hand, the $^2B_1$ state is essentially an olefin radical cation with a weakened C_5-C_6 bond, as can be seen from Tables 3 and 5. Indeed, the rotational barrier for the $^2B_1$ state is relatively small.

In Ref. 4, **VII** and **VIII** were referred to as "localized" and "relaxed" radical cations, respectively, in order to specify the possible electronic structures of the fulvene radical cations. In a "localized" radical cation, the unpaired electron and positive charge are localized in the endocyclic butadienic moiety; in a "relaxed" radical cation, the unpaired electron is located in the ring and the positive charge is located on C_6. As can be seen from the above discussion, however, both **VII** and **VIII** represent an $^2A_2$-like state with similar SOMO; as the substituent attached to the C_6 atom becomes more electron-donating, the radical cation becomes more "relaxed". Note that fulvene radical cations are more or less "relaxed", and that the boundary between the "localized" and "relaxed"radical cations is not distinct. Furthermore, it should be noted that such a representation as **VIII** used in Ref. 4 does not distinguish between the "relaxed" $^2A_2$ radical cation and the $^2B_1$ radical cation. The former may be explicitly described by **IX**. In the $^2A_2$ radical cation, the unpaired electron is not located on C_5 and C_6, while it is located mainly on C_5 and C_6 in the $^2B_1$ radical cation.

Conclusion

Ab initio SCF calculations using the STO-3G and 3-21G basis sets have shown that the ground state of the unsubstituted fulvene radical cation ($FV^{+\cdot}$) is the planar $^2A_2$ state. Though this state corresponds to removing a π electron from the butadienic moiety in the five-membered ring of FV, the positively charged hole is partially filled by a π-electron flow from the exocyclic region without any significant change in the unpaired electron distribution. The planar $^2B_1$ state, which corresponds to an olefin radical cation with a weakened exocyclic C-C bond, is higher in energy than the $^2A_2$ state by about 26 kcal mol^{-1}. Both the planar $^2A_2$ and $^2B_1$ states correspond to the minima of rotation around the exocyclic C-C bond. Although the 90°-twisted $^2A_2$ state is higher than the planar $^2A_2$ state by about 63 kcal mol^{-1}, the rotational barrier for the $^2A_2$ state was predicted to be considerably lowered by the substitution of electron-donating groups at the C_6 position.

References

1) For example, see P. Bönzli, A. Otter, M. Neuenschwander, H. Huber, and H. P. Kellerhals, *Helv. Chem. Acta*, **69**, 1052 (1986), and references cited therein.

2) O. Takahashi and O. Kikuchi, *Tetrahedron*, **46**, 3803 (1990); K. N. Houk, J. K. George, and R. E. Duke, Jr., *Tetrahedron*, **30**, 523 (1974).

3) C. J. Rhodes, *J. Chem. Soc., Chem. Commun.*, **1988**, 647.

4) C. J. Abelt and H. D. Roth, *J. Am. Chem. Soc.*, **107**, 6814 (1985).

5) F. Brogli, P. A. Clark, E. Heilbronner, and M. Neuenschwander, *Angew. Chem., Int. Ed. Engl.*, **12**, 422 (1973).

6) W. J. Hehre, R. F. Stewart, and J. A. Pople, *J. Chem. Phys.*, **51**, 2657 (1969).

7) J. S. Binkley, J. A. Pople, and W. J. Hehre, *J. Am. Chem. Soc.*, **102**, 939 (1980).

8) P. A. Baron, R. D. Brown, F. R. Burden, P. J. Domaille, and J. E. Kent, *J. Mol. Spectrosc.*, **43**, 401 (1972).

9) As to the validity of the Koopmans' theorem in connection with the fulvene radical cations, see Ref. 5.

10) The present discussion on the twisting of $FV^{+\cdot}$ reminds one of the calculations on the trimethylenemethane radical cation ($TMM^{+\cdot}$) by Du and Borden.[11] Indeed, the π system of $FV^{+\cdot}$ may be regarded as that of "$TMM^{+\cdot}$+ethylene", and the SOMO of the planar $^2A_2$ $FV^{+\cdot}$ is an in-phase combination of that of the planar $^2A_2$ $TMM^{+\cdot}$ and the LUMO of ethylene.

11) P. Du and W. T. Borden, *J. Am. Chem. Soc.*, **109**, 5330 (1987).

 © 1991 The Chemical Society of Japan Bull. Chem. Soc. Jpn., 64, 533—536 (1991)

Effect of Batch Factor on a Binary Ion Exchange Equilibrium

Koichi TANIHARA
Government Industrial Research Institute, Kyushu; Shuku-machi, Tosu 841
(Received July 9, 1990)

The relation between the distribution coefficient of Cs^+ on M^{n+} form exchanger and the ratio of the solution volume to the exchanger weight (batch factor) at a constant loading of Cs^+ has been investigated while taking the activity coefficients of ionic species into consideration when the initial concentration of Cs^+ is changed.

The effects of the batch factor on a binary ion exchange equilibrium have often been observed elsewhere[1-6] under specific experimental conditions. Until quite recently, though, very little attention has been devoted to its elucidation.[7]

There are two degrees of freedom in a binary cation exchange system at a constant temperature and pressure[8] where an ion exchanger having a constant exchange capacity is in equilibrium with an aqueous solution of two cations and one common anion. An ion exchange experiment for such a system, therefore, is usually carried out under the one degree of freedom by introducing relevant constant parameters. Taking the effects of the batch factor into consideration, the experimental conditions at a constant temperature and pressure for a binary cation exchange system can be divided into three cases depending on how one specifies the initial concentrations of two cations in the solution.

(1) The sum of the initial equivalent concentrations of two cations is kept constant, while changing the ratio:

In this case, the sum of equivalent concentrations of two cations in equlibrium with the ion exchanger is invariably constant, irrespective of the batch factor. The usual thermodynamic treatments for a binary exchange equilibrium have been conducted under this restriction.[9]

(2) The initial concentration (varied) of the "ingoing" cationic species into an exchanger is much smaller than that (kept constant) of the cationic species displaced from it:

In this case, the ingoing cationic species is a micro component and the equilibrium concentration of the displaced cationic species can be taken as being approximately constant. The distribution coefficient of the ingoing ionic species is virtually invariant with respect to the batch factor, as previously reported.[7]

(3) The initial concentration of either of the two cations is kept constant, changing that of the other:

This is the case when the effects of the batch factor are often observed. By introducing the batch factor as a second parameter, on the other hand, the present author derived a theoretical relationship between the loading of the ingoing ionic species and its equilibrium concentration in the solution, and successfully related it to the distribution coefficient of the ingoing ionic species, as previously reported.[7]

In the present paper, a refined form of theoretical equation previously reported for case (3) is derived in order to elucidate the effect of the batch factor while taking the activity coefficients into consideration.

Theoretical

The present paper is concerned with the case of an exchange involving two cations only, where a single electrolyte solution of cesium chloride is allowed to react with an ion exchanger of M^{n+} form, while changing the initial concentration at a given batch factor. The exchange reaction may be written as

$$n\mathrm{Cs}^+ + \overline{\mathrm{M}^{n+}} \rightleftarrows \overline{n\mathrm{Cs}^+} + \mathrm{M}^{n+}, \quad (1)$$

(overbar: the exchanger phase)

When the initial concentration of M^{n+} in the solution is zero, a "theoretical adsorption isotherm," as previously reported,[7] is given by

$$\frac{Q}{[\mathrm{Cs}^+]_s} = \frac{1}{n}\sqrt[n]{\frac{n\beta(C_{\mathrm{CEC}}-Q)(C_{\mathrm{CEC}}+(n-1)Q)^{n-1}}{Q}K_{\mathrm{M}^{n+}}^{\mathrm{Cs}^+}}, \quad (2)$$

where Q is the Cs^+ loading (mequiv g^{-1}), β the batch factor ($cm^3\,g^{-1}$), C_{CEC} the cation exchange capacity (mequiv g^{-1}), $[Cs^+]_s$ the equilibrium concentration of Cs^+ in the solution, and $K_{\mathrm{M}^{n+}}^{\mathrm{Cs}^+}$ a selectivity coefficient which is defined by the molarities and the mole fractions for cations in the solution and solid phases, respectively. In Eq. 2, $K_{\mathrm{M}^{n+}}^{\mathrm{Cs}^+}$ is written in terms of the thermodynamic equilibrium constant (K_c) and ionic activity coefficients as follows: $K_{\mathrm{M}^{n+}}^{\mathrm{Cs}^+} = K_c\gamma_{\mathrm{Cs}^+}^n\bar{f}_{\mathrm{M}^{n+}}/(\gamma_{\mathrm{M}^{n+}}\bar{f}_{\mathrm{Cs}^+}^n)$. The ionic activity coefficients, γ_{Cs^+} and $\gamma_{\mathrm{M}^{n+}}$, refer to the individual cations in the solution phase. They are defined so as to approach unity as $[Cs^+]_s$ and the equilibrium concentration of M^{n+} in the solution, $[M^{n+}]_s$, approach zero. The ionic activity coefficients, $\bar{f}_{\mathrm{Cs}^+}$ and $\bar{f}_{\mathrm{M}^{n+}}$ refer to the individual cations in the solid phase and are defined so as to be equal to unity for pure homo ionic exchangers in equilibrium with an infinitely dilute solution of the same ion.[10] When the exchange equilibrium is attained in a solution which is sufficiently dilute so that the imbibition of anions by the exchanger can be

neglected, the ratio $\bar{f}_{M^{n+}}/\bar{f}^n_{Cs^+}$ depends only on Q, irrespective of β, since both the ionic activity coefficients, $\bar{f}_{Cs^+}$ and $\bar{f}_{M^{n+}}$ vary with the mole fraction of Cs^+ (Q/C_{CEC}) in the solid solution of two homo-ionic exchangers. It then follows that by substituting $K_d=Q/[Cs^+]_s$ in Eq. 2, the distribution coefficient of Cs^+, K_d, can be expressed in the form

$$K_d = F(Q)\,\xi\sqrt[n]{\beta}, \tag{3}$$

where ξ denotes $\gamma_{Cs^+}/\gamma_{M^{n+}}^{1/n}$, which can be written in terms of the mean activity coefficients, $\gamma_{\pm CsCl}$ and $\gamma_{\pm MCl_n}$, of CsCl and MCl_n, respectively, as

$$\ln\xi = \ln(\gamma_{Cs^+}/\gamma_{M^{n+}}^{1/n}) = 2\ln\gamma_{\pm CsCl} - (n+1)/n\ln\gamma_{\pm MCl_n}. \tag{4}$$

On the basis of Guggenheim's theory,[11] $\gamma_{\pm CsCl}$ and $\gamma_{\pm MCl_n}$ are given by

$$\ln\gamma_{\pm CsCl} = -\frac{a\sqrt{I}}{1+\sqrt{I}} + 2\,\alpha_{Cs,Cl}[Cs^+]_s + (n\,\alpha_{Cs,Cl}+\alpha_{M,Cl})[M^{n+}]_s, \tag{5}$$

and

$$\ln\gamma_{\pm MCl_n} = -\frac{an\sqrt{I}}{1+\sqrt{I}} + \frac{2}{1+n}\left\{2n\,\alpha_{M,Cl}[M^{n+}]_s + (\alpha_{M,Cl}+n\,\alpha_{Cs,Cl})[Cs^+]_s\right\}, \tag{6}$$

where a is a constant in the Debye-Hückel formula (equal to 1.178 at 25 °C), and I the ionic strength, $\alpha_{M,Cl}$ and $\alpha_{Cs,Cl}$ the specific interaction coefficients of M^{n+} and Cs^+, respectively with Cl^-.

Eqs. 4—6 reduce to

$$\xi = \exp\left[\frac{a(n-1)\sqrt{I}}{1+\sqrt{I}} + \frac{2(n\,\alpha_{Cs,Cl}-\alpha_{M,Cl})}{n(n+1)}\left\{2+\theta(n-1)\right\}I\right], \tag{7}$$

where θ is the ionic strength fraction of CsCl.

By substituting $[M^{n+}]_s=Q/n\beta$ and $[Cs^+]_s=Q/K_d$ in the respective definition formulas, I and θ are given as

$$I = 0.5\,n(n+1)[M^{n+}]_s + [Cs^+]_s = 0.5\,Q\{(n+1)/\beta + 2/K_d\}, \tag{8}$$

and

$$\theta = [Cs^+]_s/I = 2\beta/\{2\beta+(n+1)K_d\}. \tag{9}$$

The substitution of Eqs. 7—9 in Eq. 3 indicates that K_d (also $[Cs^+]_s$) can be regarded as a function of Q and β. It is then concluded that plots of K_d/ξ vs. $\sqrt[n]{\beta}$ or $\log(K_d/\xi)$ vs. $\log\beta$ at a given Q should be a straight line passing through the origin or with a slope of $1/n$, respectively.

Experimental

Materials. As a typical organic or inorganic cation exchanger, a sulfonated polystyrene-type resin (Dowex 50W-X8, Dow Chemical Co.) and a synthetic mordenite (Zeolon 100Na, Norton Co.) were used, respectively. The Dowex 50W resin was converted to the homo ionic forms by an exhaustive treatment with the corresponding metal chloride solutions. The synthetic mordenite (Na^+ form) was used without further treatment.

Measurements and Procedures. The experimental procedures were similar to that described previously.[7] The value of $[Cs^+]_s$ for the La^{3+} form resin was determined based on the concentration of displaced La, which was measured using radiofrequency inductively coupled plasma atomic-emission spectrometry. The observed values of K_d and Q for a given β were obtained according to

$$Q = ([Cs^+]_0 - [Cs^+]_s)\beta \quad (\text{mequiv g}^{-1})$$

and

$$K_d = Q/[Cs^+]_s \quad (\text{cm}^3\,\text{g}^{-1})$$

where $[Cs^+]_0$ is the initial concentration (mol dm^{-3}) of Cs^+.

Calculation of ξ. The value of ξ at the observed point (Q, K_d) for a given β was calculated from Eqs. 7—9 where the specific interaction coefficient, that is, $\alpha_{Cs,Cl}$, $\alpha_{Na,Cl}$, $\alpha_{Ca,Cl}$, or $\alpha_{La,Cl}$ was estimated to be 0, 0.16, 1.01, or 3.88, respectively, on the basis of Eq. 5 ($[M^{n+}]_s=0$) or Eq. 6 ($[Cs^+]_s=0$), using the published values of mean activity coefficient for a single chloride solution.

Results and Discussion

Fig. 1 shows the variation of the distribution coeffi-

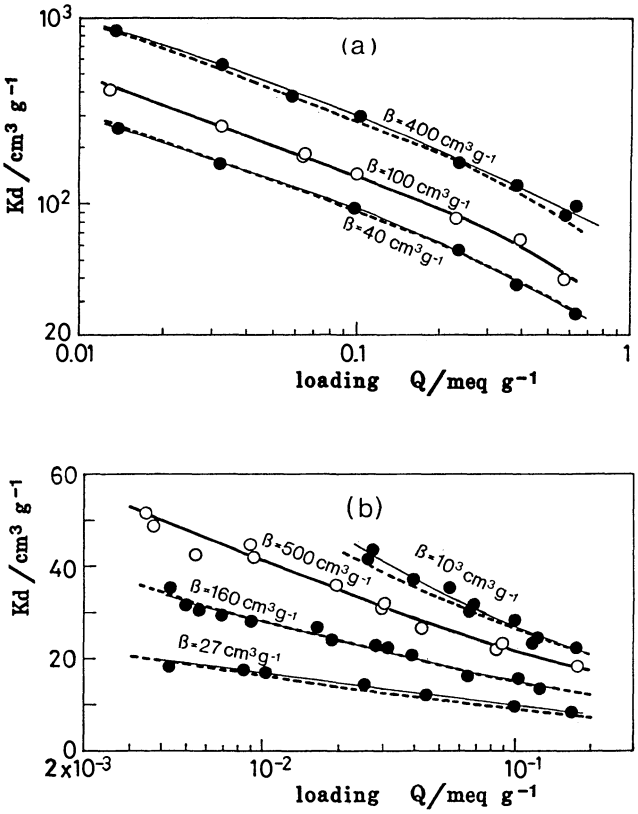

Fig. 1. Variations of K_d with Cs loading, Q, at different batch factors for Dowex 50W resin of Ca^{2+} or La^{3+} form. (a) Ca^{2+}-form, (b) La^{3+}-form. The experimental data point is indicated by a open or closed circle. The dashed curves represent the calculated curves obtained from a reference curve (denoted by a bold solid line among the open circles) at a given batch factor.

cient of cesium, K_d, with its loading, Q, at given values of the batch factor, β, for the Dowex 50W of Ca^{2+} and La^{3+} forms when Ca^{2+} and La^{3+} ions, respectively, are initially absent in the solution. In these experiments

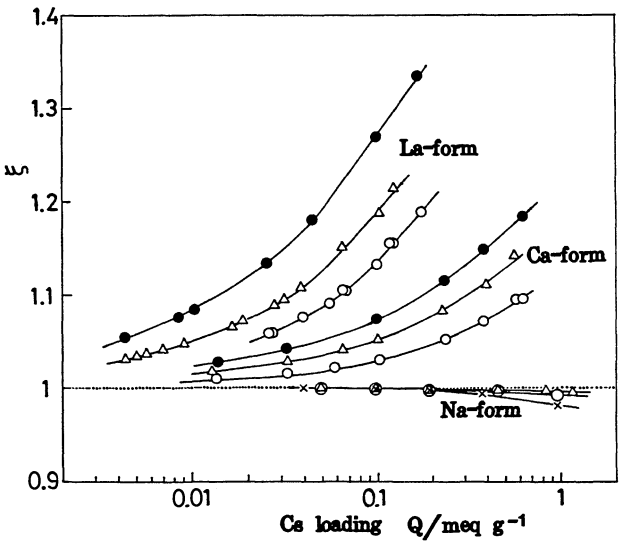

Fig. 2. Variations of ξ with the Cs loading, Q, at different batch factors for Dowex 50W resin of various ionic form: Na^+ form (β($cm^3 g^{-1}$): 20 (×); 50 (○); 100 (△)), Ca^{2+} form (β($cm^3 g^{-1}$): 40 (●); 100 (△); 400 (○)), La^{3+} form (β($cm^3 g^{-1}$): 27 (●); 160 (△); 1000 (○)).

K_d and Q at equilibrium were measured by changing the initial concentrations of Cs^+ at different fixed values of β in the ionic strength range $I<0.1$. Plots of the ξ value at each point of K_d vs. Q data in Fig. 1 and in previous paper[7] for Na^+ form reveal that the effects of Q and β on ξ greatly differ with the n values of the Dowex resin, as can be seen in Fig. 2.

The proportional expression, $K_d/\xi \propto \sqrt[n]{\beta}$, derived from Eq. 3, was verified, as shown in Fig. 3, by good linear relationships with slope of $1/n$ between $\log(K_d/\xi)$ and $\log\beta$, where K_d and β were read for an arbitrarily specified Q ranging from small to relatively large values on the basis of the graphs in Fig. 1 and those drawn in a previous paper[7] for other exchangers. These results indicate that the underlying assumptions in Eq. 3, based on a theory by Gaines and Thomas,[10] are not only valid for an exchanger of non-swelling type, such as Zeolon 100Na, but also for that of the swelling type, such as Dowex 50W, as long as the ionic strengths in the solutions are in a range less

Based on the above results, $K_d(=K_{d_i})$ vs. Q curves at different $\beta(=\beta_i)$ can be drawn from one reference curve of the K_{d_0} curve constructed at a given $\beta(=\beta_0)$, as described below.

The proportionality constant, $F(Q)$, of K_d/ξ to $\sqrt[n]{\beta}$ at an arbitrarily given Q in Eq. 3 can be determined from a point, (Q, K_{d_0}), on the reference curve for β_0 as $K_{d_0}/(\xi_0\sqrt[n]{\beta_0})$, where ξ_0 can be calculated according to

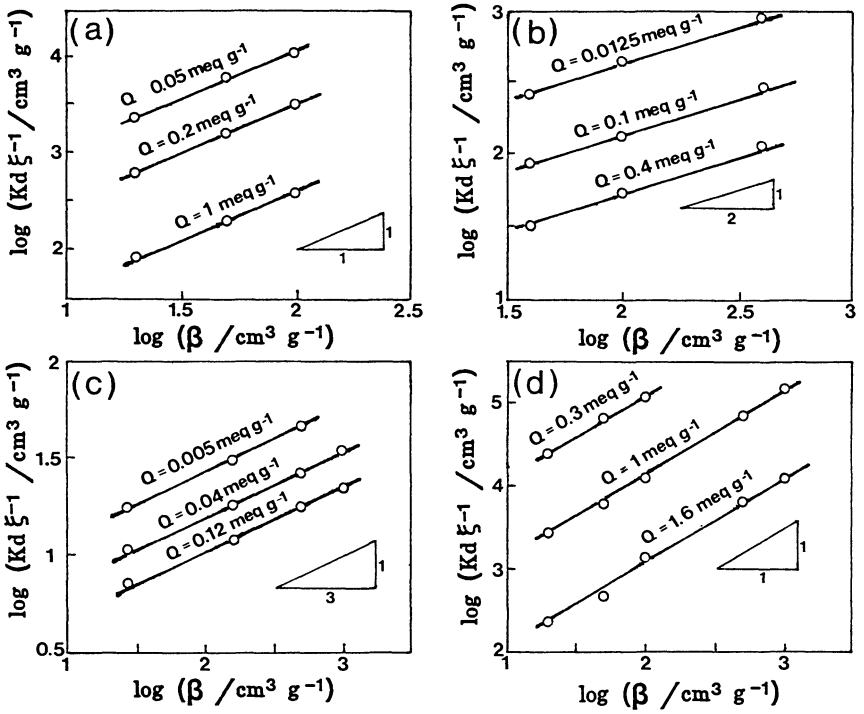

Fig. 3. Linear relationships with slope $1/n$ between $\log(K_d/\xi)$ and $\log\beta$ at different values of Q.
(a) Dowex 50W (Na^+ form), (b) Dowex 50W (Ca^{2+} form), (c) Dowex 50W (La^{3+} form), (d) Zeolon 100Na.

Eqs. 7—9 by substituting $\beta=\beta_0$ and $K_d=K_{d_0}$ into Eqs. 8 and 9. In order to calculate K_{d_i} corresponding to β_i at the given Q using Eq. 3, $\xi(=\xi_i)$ at β_i must be determined. Since the value of $K_{d_i}/\xi_i(=D_i)$ at Q and β_i can be calculated as $K_{d_0}\sqrt[n]{\beta_i}/(\xi_0\sqrt[n]{\beta_0})$ by substituting $F(Q)=K_{d_0}/(\xi_0\sqrt[n]{\beta_0})$ in Eq. 3, a transcendental equation for ξ_i is obtained when $K_d=\xi_i D_i$ and $\beta=\beta_i$ are substituted in Eqs. 8 and 9, followed by the substitutions of I and θ in Eq. 7. This equation can be readily solved by applying a numerical analysis with the aid of a personal computer when Q and β_i are given. Accordingly, K_{d_i} can be calculated as $\xi_i D_i$. As can be seen in Fig. 1, the dashed lines, which represent K_d vs. Q curves predicted from a reference curve (bold solid line) measured for a fixed β, are found to closely agree with the observed values. Similar results were obtained for the Dowex 50W of Na^+ form and Zeolon 100Na. From the K_d vs. Q curves, thus obtained, for different values of β, the corresponding Q vs. $[Cs^+]_s$ curves, that is, "adsorption isotherms" which may be distinguished from the usual "ion exchange isotherm at a constant total solution normality"[9] (independent of the batch factor), can be easily calculated for each β value using the relation $K_d=Q/[Cs^+]_s$.

As demonstrated above, K_d vs. Q curves or "adsorption isotherms" at different β can be calculated without requiring any knowledge concerning the properties of the exchanger, other than one measured K_d vs. Q curve for one value of β.

References

1) G. E. Boyd, J. Schubert, and A. W. Adamson, *J. Am. Chem. Soc.*, **69**, 2818 (1947).

2) T. Yamabe and S. Sato, *Kogyo Kagaku Zasshi*, **54**, 483 (1951).

3) S. Vlasselaer, W. D'Olieslager, and M. D'Hont, *J. Radioanal. Chem.*, **35**, 211 (1977).

4) D. Schweich and M. Sardin, *J. Hydrol.*, **50**, 1 (1981).

5) J. Lehto and R. Harjula, *Solvent Extr. Ion Exch.*, **5**, 343 (1987).

6) H. Mimura, I. Yamagishi, and K. Akiba, *Tohoku Daigaku Senko Seiren Kenkyusho Iho*, **44**, 1 (1988).

7) K. Tanihara, *Nippon Kagaku Kaishi*, **1988**, 1929.

8) e.g., A. L. Myers and S. Byington, "Ion Exchange: Science and Technology," NATO ASI Series, ed by A. E. Rodrigues, Martinus Nijhoff Publishers, Dordrecht (1986), p. 119.

9) e.g. , a) C. B. Amphlett, "Inorganic Ion Exchangers," Elsevier, Amsterdam (1964), pp. 20—29.; b) R. M. Barrer and J. Klinowski, *J. Chem. Soc., Faraday Trans. 1*, **70**, 2080 (1974).

10) G. L. Gaines, Jr. and H. C. Thomas, *J. Chem. Phys.*, **21**, 714 (1953); R. M. Barrer and R. P. Townsend, *J. Chem. Soc., Faraday Trans. 2*, **80**, 629 (1984).

11) E. A. Guggenheim, *Philos. Mag.*, **19**, 588 (1935); D. S. Flett and P. Meares, *Trans. Faraday Soc.*, **62**, 1469 (1966).

Application of the SPE Method to Organic Electrochemistry. XI. Influence of the Solvent on the Electrooxidation of Cinnamyl Alcohol on Mn,Pt-Nafion

Zhen CHEN, Toshiyuki MIZOE, Zempachi OGUMI,* and Zen-ichiro TAKEHARA
Department of Industrial Chemistry, Faculty of Engineering, Kyoto University, Sakyo-ku, Kyoto 606
(Received July 27, 1990)

The influence of organic solvents on the electrooxidation of cinnamyl alcohol on Mn,Pt-Nafion has been investigated. Though tetrahydrofuran (THF) gave a high current efficiency (90%), carbon tetrachloride gave a low current efficiency (<20%). The importance of a co-solvent for the SPE electrolyzer was proposed and substrate transport to the active site located at the interface platinum/ionic cluster region was enhanced by solvents miscible with water. Though THF behaved as a good co-solvent, carbon tetrachloride did not. A composite electrode deposited with platinum on both surfaces of Nafion was applied to oxidation. The cell voltage was as low as 2 V.

The authors have reported that the application of mediatory systems into SPE (Solid Polymer Electrolyte) electrolyzers is both effective and attractive.[1-3] In a previous paper Mn,Pt-Nafion (a manganese redox system incorporated inside Pt-Nafion prepared by the deposition of a porous platinum electrode on Nafion) was applied to the selective oxidation of cinnamyl alcohol to cinnamaldehyde.[4] Both the current efficiency and selectivity to the aldehyde were remarkably enhanced by the addition of the manganese mediatory system.

The electrode reaction of this mediatory oxidation system is as follows:

$$Mn^{2+} + 2H_2O \longrightarrow MnO_2 + 4H^+ + 2e^-. \quad (1)$$

The MnO_2 formed in this reaction reacts with the alcohol while giving aldehyde and regenerating Mn^{2+}.[5] As shown by the oxidation potential of MnO_2 described in the following equation, the activity of MnO_2 is strongly dependent on such solution properties as the pH and water content:

$$E = E^0 + \frac{RT}{2F} \ln \frac{a_{MnO_2}(a_{H^+})^4}{a_{Mn^{2+}}(a_{H_2O})^2}. \quad (2)$$

In the present work, the effect of the solvent was examined in detail.

Regarding SPE electrolyzers, it is expected that the cell voltage can be decreased by decreasing the gap between the anode and cathode. Composite electrodes deposited with an electrode on both surfaces of SPE materials would limit the electrode gap to the thickness of the SPE material. This type of composite electrode was also examined in the selective oxidation of cinnamyl alcohol.

Experimental

SPE Composite Electrodes. Pt-Nafion was prepared by the deposition of a porous platinum layer onto one surface of Nafion 415 utilizing an electroless plating method that employs hydrazine as a reductant. Details concerning the deposition method have been reported elsewhere.[6,7] Pt-Nafion-Pt, which is a composite electrode deposited with platinum on both surfaces of Nafion 415, was prepared by depositing a porous platinum layer on the second surface in the same manner as depositing one on the first surface. Incorporating a manganese redox system into Pt-Nafion and Pt-Nafion-Pt was achieved as described previously.[3,4]

Electrolysis. The experimental cell was described in a previous paper.[4] Electrolysis was carried out under potentiostatic or galvanostatic conditions.

In all experiments, 0.025 M (M=mol dm^{-3}) aqueous sulfuric acid containing 0.025 M manganese sulfate was used as a catholyte in a counter electrode compartment (CEC). Different kinds of anolytes were prepared and filled in a working electrode compartment (WEC).

Product mixtures were analyzed by an HPLC device (Hitachi 638-30) equipped with a Synchropak SCD column using internal standards.

The amount of manganese dissolved out was measured by atomic absorption spectroscopy after electrolysis under potentiostatic conditions at 1.4 V vs. Ag/AgCl.

Chemicals. All of the chemicals used were of reagent grade, and were used without further purification.

Results

Stability of Solvents. Four solvents (tetrahydrofuran (THF), diethyl ether, benzene, and carbon tetrachloride) were examined. These four solvents were stable on the anode under the experimental conditions. Since no product was isolate by HPLC, except for cinnamaldehyde and cinnamic acid, the main side reaction was considered to involve oxygen evolution.

Current Efficiency in Different Solvents. Using the four solvents, electrolysis was carried out at 1 mA cm^{-2} in 50 vol% cinnamyl alcohol, and 25 °C on Mn,Pt-Nafion. As described in Table 1, carbon tetrachloride gave the lowest current efficiency. Diethyl ether gave a current efficiency that was a little lower than THF. Benzene gave a medium value.

Since carbon tetrachloride showed the most pronounced decrease in the current efficiency, this solvent was examined in detail and compared with THF.

Table 1. Effects of Solubilities of Organic Solvents on the Current Efficiencies of Cinnamaldehyde, at 25 °C

	Solubility in water[a)]	Current efficiencies/%
CCl_4	0.077	13
Benzene	0.178	63
Diethyl ether	6.04	72
THF	Inf.	85

a) g/100 g H_2O.

Steady State Polarization Curves. Figure 1 shows steady state polarization curves for 50 vol% cinnamyl alcohol in carbon tetrachloride and THF. Curve b, obtained in the presence of a manganese mediatory system in carbon tetrachloride, shows a lower potential at a low current density than does curve a, obtained in the absence of a mediatory system in carbon tetrachloride. The difference was much smaller than in the case of using THF as a solvent (curve c). This result suggests that the mediatory system did not work as effectively in carbon tetrachloride as in THF. This ineffectiveness lowered the current efficiency of aldehyde formation. Oxygen evolution was observed in carbon tetrachloride at a high current density.

The Influence of Substrate Concentration. Generally speaking, it is favorable to increase the substrate concentration for a higher performance of electrolyzers. The influence of the substrate concentration was examined using THF and carbon tetrachloride as solvents under potentiostatic electrolysis conditions at 1.5 V. The results are shown in Fig. 2. Using THF, the current efficiency of cinnamaldehyde remained almost unchanged up to an alcohol concentration of 50%, but decreased remarkably beyond 50%. Using carbon tetrachloride as solvent, the current efficiency of aldehyde formation was much lower than the value obtained for THF, and was dependent in a different way on the concentration; the current efficiency showed a maximum at ca. 70%. The production of cinnamic acid remained almost unchanged in both solvents and oxygen evolution was observed as a side reaction.

The influence of the solvent and substrate concentration on the mediatory action and oxidation efficiency was examined in more detail using a mixed solvent of THF and carbon tetrachloride. By fixing the substrate concentration at 50%, the ratio THF/carbon tetrachloride could be changed. As shown in Fig. 3, the current efficiency of the aldehyde increased upon increasing the THF/carbon tetrachloride ratio.

Influence of Current Density. If mass transport plays an important role in the electrochemical system, the current density would provide a major influence on the current efficiency. As shown in Fig. 4, the current efficiency of cinnamaldehyde decreased rapidly from 10 mA cm^{-2} using Mn,Pt-Nafion. On the other hand, the current efficiency of cinnamic acid remained unchanged upon increasing the current density.

The Stability of Mn,Pt-Nafion. The dissolving out of incorporated manganese was also measured using carbon tetrachloride as a solvent. This dissolving out was more remarkable, by 20 to 40%, in carbon tetrachloride than in THF.[4)]

Electrolysis Using Mn,Pt-Nafion-Pt. It is favorable to use an aqueous solution in CEC, since Nafion

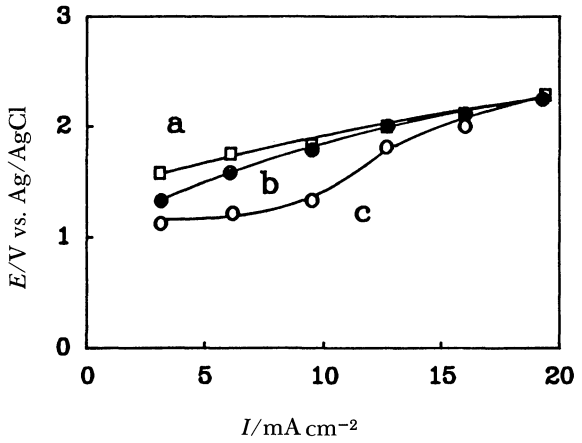

Fig. 1. Steady state polarization curves on Pt-Nafion (a), on Mn,Pt-Nafion (b) in 50 vol% cinnamyl alcohol in carbon tetrachloride, and on Mn,Pt-Nafion (c) in 50 vol% cinnamyl alcohol in THF.

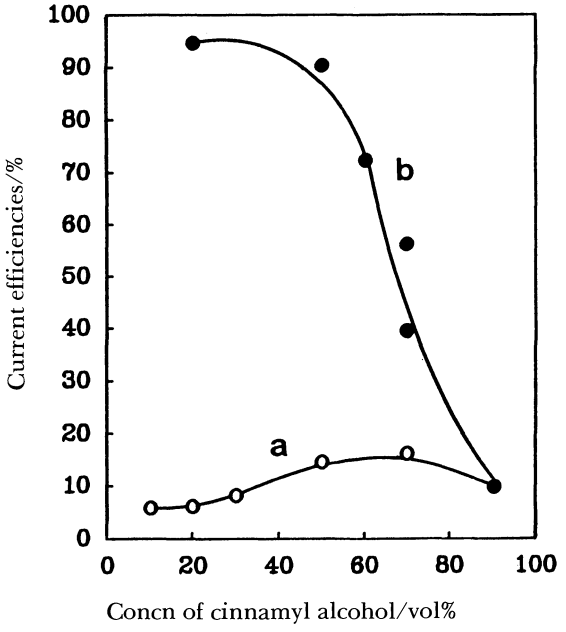

Fig. 2. Current efficiency dependencies of cinnamaldehyde production on cinnamyl alcohol concentration under potentiostatic electrolysis conditions at 1.5 V on Mn,Pt-Nafion.
a: carbon tetrachloride, b: THF.

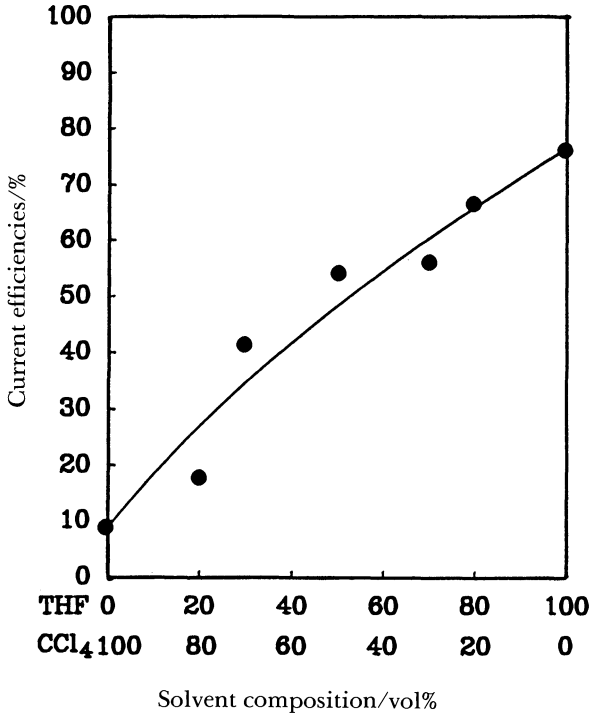

Fig. 3. The influence of THF/carbon tetrachloride ratio on the current efficiency of cinnamaldehyde under galvanostatic electrolysis conditions at 6 mA cm^{-2} on Mn,Pt-Nafion and 50 vol% cinnamyl alcohol in WEC.

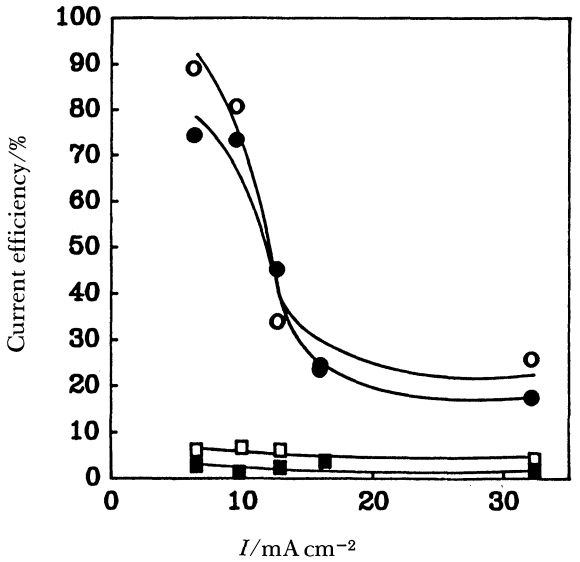

Fig. 4. Dependencies of current efficiency on current density.
open symbols: Mn,Pt-Nafion,
black symbols: Mn,Pt-Nafion-Pt,
circles: cinnamaldehyde, squares: cinnamic acid.

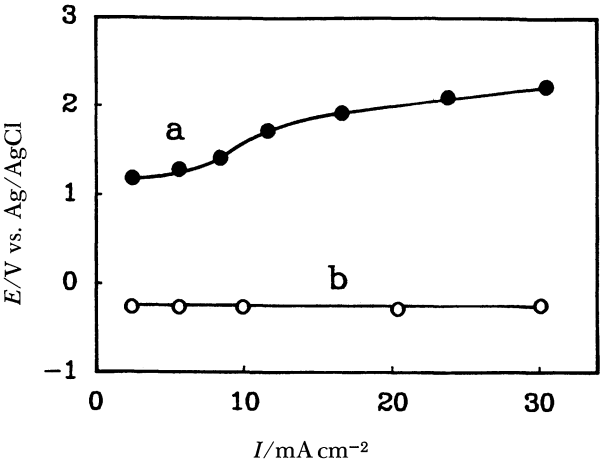

Fig. 5. Steady state polarization curves on Mn,Pt-Nafion-Pt in 50 vol% cinnamyl alcohol in THF.
(a): anode, (b): cathode.

is known to show ionic conductivity of a few orders of magnitude lower in organic solvents than in aqueous solutions.[8] Nafion shows a fairly high ionic conductivity under a humidified gas atmosphere, as investigated in fuel-cell applications. As described above and in a previous paper, the incorporated redox system tended to dissolve out into an aqueous solution in CEC. If no solution was used in the CEC, no dissolving out could occur. By using Mn,Pt-Nafion-Pt, a 50% cinnamyl alcohol solution in THF was electrolyzed. Argon was filled in CEC. The cell voltage was, however, very high for this electrolyzer and the cell temperature increased. This result suggests that the ionic conductivity of Nafion is very low under the electrolysis conditions. This type of electrolysis was not acceptable from practical viewpoints. An aqueous solution of 0.025 M sulfuric acid containing 0.025 M manganese sulfate was filled in the CEC in order to enhance the ionic conductivity of Mn,Pt-Nafion-Pt. Polarization curves for the anode and cathode are listed in Fig. 5. The electrode potential was measured using a Luggin capillary inserted in the CEC; the ohmic drop was not corrected. The difference in the anodic and cathodic potentials gives the cell voltage at each current density. At low current densities, where mediatory oxidation was predominant, the cell voltage was less than 2 V. The current efficiency for Mn,Pt-Nafion-Pt was compared with the results for Mn,Pt-Nafion. As shown in Fig. 4, Mn,Pt-Nafion-Pt showed a current efficiency change with an increase in the current density similar to that of Mn,Pt-Nafion. The current efficiency decreased abruptly at about 10 mA cm^{-2}. The critical current density corresponded to the value in the polarization curve in Fig. 5, beyond which oxygen evolution became significant.

Discussion

Electrochemical charge transfer reactions take place

at the interface between electronic and ionic conductors. This was also true in the present electrochemical system. The structure of Nafion is accepted to be microscopically separated into two phases: a hydrophilic ionic cluster and a lipophilic polytetrafluoroethylene-like backbone.[9] H. L. Yeager and co-workers have pointed out that a majority of sorbed water is incorporated in an ionic cluster region of Nafion. The ionic cluster region in the membrane is regarded as being surrounded by a lipophilic environment.[10,11] These clusters are connected to each other by a small channel. Ionic conduction of SPE composite electrodes using Nafion is based on ionic migration through the ionic cluster region where most of the ionic groups (fixed ions and counter ions) and water taken up inside the Nafion exist. Since the deposition of a porous platinum electrode on Nafion was carried out in an aqueous solution, platinum likely at least contacted the ionic cluster region. The active site for charge transfer on an SPE composite electrode is located at the platinum/Nafion interface (the interface between the platinum and the hydrophilic ionic cluster region of Nafion), since the hydrophobic region of Nafion solves neither ionic charge carriers nor polar solvents.[12] In the present system, Mn^{2+} is oxidized there to form MnO_2, which must stay in the ionic cluster region (see Fig. 6). The substrate must be transported to the ionic cluster region in order to contact and react with MnO_2, where it is oxidized. As mentioned above, the ionic cluster region is strongly hydrophilic and is considered to be in the condition of an aqueous solution. Since cinnamyl alcohol is hardly soluble in water, it is difficult for the alcohol to enter this region. Some organic solvent is required in the ionic cluster region in order to help the alcohol to penetrate into the active region, the ionic cluster. Nafion swells not only solvents having a high solubility parameter, but also those having a low solubility parameter. It was proposed that solvents with a low solubility parameter interact with the hydrophobic site of Nafion.[13] The four solvents examined here have fairly low solubility parameters. The authors have proposed the existence of a path in the amorphous hydrophobic region of Nafion for the transport of oxygen.[14] This region is responsible for the interaction with hydrophobic solvents. Since cinnamyl alcohol is hardly soluble in water, it is acceptable to consider that the alcohol does not penetrate into the hydrophilic aqueous region but, rather, stays in the hydrophobic region. This hydrophobic region corresponds to the path for oxygen and allows hydrophobic substances to remain.[6,11,14] As mentioned above, cinnamyl alcohol must be transported from a hydrophobic site to the active site of the SPE composite electrode in order to react electrochemically (Fig. 6). The difference in the current efficiency of the four solvents examined can be explained in terms of their miscibility with water. When solvents for cinnamyl alcohol is immiscible with water, transport is very difficult and is not easily oxidized on Mn,Pt-

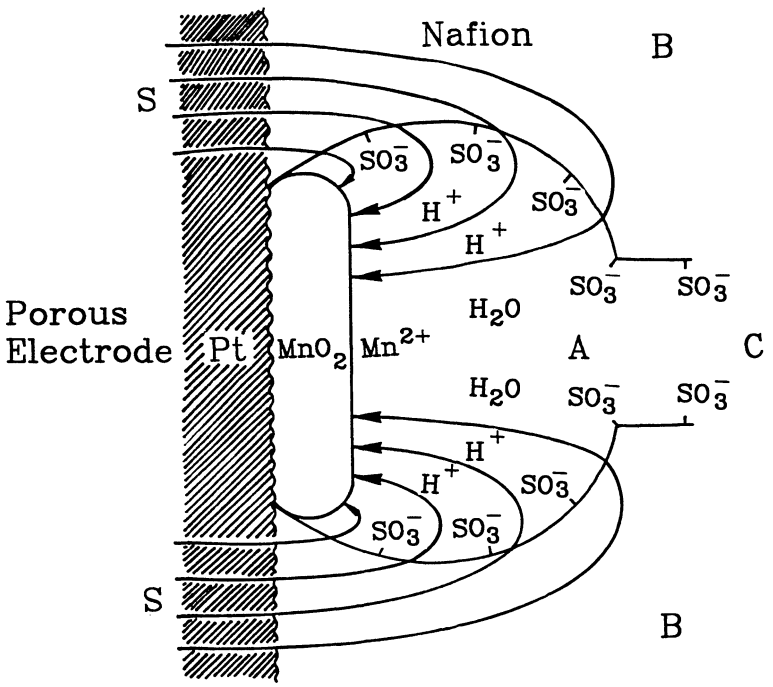

Fig. 6. Simplified schematic model of mass transfer to the active site on Mn,Pt-Nafion.
A: ionic cluster region, B: hydrophobic backbone region, C: channel, S: substrate.

Nafion. The solubilities of four solvents to water are listed in the same table. When THF is used as a solvent of anolyte, the aqueous catholyte and the anolyte mix with each other since Nafion is not a good separator for small neutral species[8] and THF is freely soluble in water; THF behaves as a co-solvent of cinnamyl alcohol and water. This mixing would increase the solubility of the substrate alcohol so that alcohol can be transported into the ionic cluster, reach MnO_2, and be oxidized to aldehyde. The product, cinnamaldehyde, is insoluble in water and mixing also increases its mass transport. Such mixing, however, also enhances the mass transport of both the substrate alcohol and the product aldehyde to the catholyte, while their transport rates are expected to remain small. This transport would make the separation processes difficult, decreasing the merit of SPE electrolyzers.

Since carbon tetrachloride is insoluble in water, on the other hand, it can neither enter into an ionic cluster nor enhance the transport of the substrate alcohol to an ionic cluster, thus differing from the case of a THF solution. The current efficiency of aldehyde formation was therefore very low in the case of carbon tetrachloride.

Benzene, the solubility of which is lower in water than THF and diethyl ether and higher than carbon tetrachloride, gave a medium current efficiency. The results given in Table 1 suggest that a mixture of benzene with water produces a sufficient flux to support mass transport at a current density as low as 1 $mA\,cm^{-1}$. When the current density is increased using benzene as a solvent, the rapid decrease in the current efficiency observed in Fig. 4 using THF appeared at a current density of about half the value for THF; a mass-transfer limitation appeared at a much lower current density for benzene than for THF. Benzene can not support such a large mass-transfer flux to the active site in the same way that THF can. This fact supports the importance of the miscibility of the solvent for mass transport. Diethyl ether has a fairly high solubility in water and gives an efficiency slightly lower than that of THF.

The increase in the substrate concentration seems to enhance its flux to the active site. This was not the case in the present system. An increase in the substrate concentration leads to a decrease in the THF (co-solvent) content. Since the substrate transport is controlled by the concentration of co-solvent around the active site of the deposited platinum electrode, a decrease in the THF content leads to a retardation of the transport of cinnamyl alcohol to the active site, and therefore lowers the current efficiency (Fig. 2). The same consideration is applicable to the result given in Fig. 3, which was obtained by changing the THF/carbon tetrachloride ratio. The decrease in the ratio lowered the THF content in the ionic cluster. This fact made the transport more difficult, decreasing the current efficiency with a decrease in the ratio.

From the above discussion, the path through which the substrate is transported to the active site of SPE composite electrodes seems to have a very large influence on the efficiency. The path includes not only the ionic cluster region, but also the porous electrode layer deposited on the Nafion. The morphology of the deposited platinum, such as its shape, size, porosity, and thickness, as well as the penetration depth of the deposited platinum particles into the Nafion, must have a very large influence on substrate transport. In order to obtain reproducible SPE composite electrodes, platinum must be deposited under controlled conditions regarding pretreatment, reductant composition, chloroplatinic acid concentration, pH, and temperature.[7] For example, the current density at which the reaction shifts from the mediatory oxidation of alcohol to oxygen evolution in a THF solution was dependent on the preparation process of the composite electrodes. On one electrode it was 12—13 $mA\,cm^{-2}$, and on the other it was 2—3 $mA\,cm^{-2}$. On the other hand, the potential at which the shift took place was independent of both the preparation process and the electrode morphology.

Conclusion

The influence of solvents on the electrooxidation of cinnamyl alcohol on Mn,Pt-Nafion was discussed. It is one of the merits of SPE electrolyzers that many different kinds of solvents can be used to dissolve the substrate. However, when an aqueous solution is used as a solution in CEC (that is favorable for electrolysis at a low cell voltage), a limitation in the selection of solvent arises in order to obtain a sufficient flux of substrate transport to the active site of the SPE composite electrode; a co-solvent for substrates and water is required. Solvents which are highly soluble in water, such as THF and diethyl ether, are useful. A composite electrode deposited with platinum on both surfaces of Nafion was applicable for the oxidation of cinnamyl alcohol. The cell voltage was as low as 2 V.

References

1) Z. Ogumi, S. Ohashi, and Z. Takehara, *Nippon Kagaku Kaishi*, **1984**, 1788.

2) Z. Ogumi, S. Ohashi, and Z. Takehara, *Electrochim. Acta*, **30**, 121 (1985).

3) Z. Ogumi, T. Mizoe, N. Yoshida, and Z. Takehara, *Bull. Chem. Soc. Jpn.*, **60**, 4233 (1987).

4) Z. Ogumi, T. Mizoe, Z. Chen, and Z. Takehara, *Bull. Chem. Soc. Jpn.*, **63**, 3365 (1990).

5) H. Lund, *Acta Chem. Scand.*, **11**, 491 (1957).

6) Z. Ogumi, Z. Takehara, and S. Yoshizawa, *J. Electrochem. Soc.*, **131**, 769 (1984).

7) P. S. Fedkiw, J. M. Potente, and W. H. Hir, *J. Electrochem. Soc.*, **137**, 1451 (1990).

8) K. A. Mauritz and A. J. Hopfinger, "Modern Aspect of

Electrochemistry," ed by J.O'M. Bockris and B. E. Conway, Plenum, New York (1982), Vol. 14, p. 425.
9) T. D. Gierke and W. Y. Hsu, "Perfluorinated Ionomer Membrane," ACS Symposium Series No. 180, American Chemical Society, Washington DC (1982), Chap. 13.
10) H. L. Yeager and A. Steck, *J. Electrochem. Soc.*, **128**, 1880 (1981).
11) C. R. Martin and H. Freiser, *Anal. Chem.*, **53**, 902 (1981).
12) Z. Ogumi, M. Inaba, S. Ohashi, M. Uchida, and Z. Takehara, *Electrochim. Acta*, **33**, 365 (1988).
13) R. S. Yeo, *Polymer*, **21**, 432 (1980).
14) Z. Ogumi, T. Kuroe, and Z. Takehara, *J. Electrochem. Soc.*, **132**, 2601 (1985).

Photocatalysis on Native and Platinum-Loaded TiO_2 and ZnO Catalysts — Origin of Different Reactivities on Wet and Dry Metal Oxides —

Masakazu ANPO,* Katsuichi CHIBA, Masanori TOMONARI,† Salvatore COLUCCIA,††
Michel CHE,††† and Marye Anne FOX††††,*
Department of Applied Chemistry, College of Engineering, University of Osaka Prefecture,
Mozu-umemachi 4-804, Sakai, Osaka 591
†Functional Materials Laboratory, Central Research Institute,
Ishihara Sangyo Kaisha, Ltd., Nishi-Shibukawa, Kusatsu, Shiga 525
††Dipartimento di Chimica Inorganica, Chimica Fisica e Chimica dei Materiali,
Universita' di Torino, Corso Massimo d'Azeglio 48, 10125 Torino, Italy
†††Laboratoire de Reactivite de Surface et Structure, Universite P. et M. Curie,
UA 1106, C. N. R. S., 4 Place Jussieu, Tour 54, 75252 Paris, Cedex 05, France
††††Department of Chemistry, The University of Texas at Austin, Austin, Texas 78712, U. S. A.
(Received September 13, 1990)

Substantial differences in photocatalytic reactivity were observed on powdered TiO_2 and ZnO, both Pt-loaded and unloaded, in the photocatalytic hydrogenation of $CH_3C{\equiv}CH$ and C_3H_6 in the presence of H_2O. Similar reactivity was observed, however, in the photocatalytic oxidation of i-C_4H_8 and C_3H_6 by O_2 on these same catalysts. Photoluminescence of TiO_2 and ZnO in the presence and the absence of H_2O and/or O_2 indicate that H_2O causes a downward band bending to increase the efficiency of recombination of photogenerated electrons and holes, with a greater effect being observed on ZnO than on TiO_2. These results, together with the direct detection of reaction intermediates by ESR, are rationalized by differences in the yields of the photogenerated intermediates, i. e., $\dot{H}$ (formed from trapped electrons) and $\dot{O}H$ (formed from trapped holes). The steady state concentrations of these intermediates depend on the degree of the positively-charged adducts on the surfaces of these oxides. The addition of O_2 causes an upward band bending of the oxide and suppresses recombination of photo-generated electrons and holes, by formation of negatively-charged surface adducts. With similar degrees of band bending, TiO_2 and ZnO produce almost the same photocatalytic reactivities as are observed for these oxides as dry systems.

Solar utilization via chemical storage can be achieved by photocatalytic and/or photoelectrochemical activation of light-sensitive semiconductor surfaces. Recent studies of photocatalysis have been focused on colloidal semiconductors,[1-4] on extremely small-sized particles in which size quantization effects are expected,[5-11] on highly dispersed well-defined supported catalysts,[12-20] and on various binary metal oxides.[21-28] Detection of the transient processes involving electron and/or energy transfer at the interfaces of the semiconducting materials has been recently contributed to a complete understanding of the true nature of the photocatalysis.[29-41]

Most photocatalytic studies on powdered semiconductors have been concerned only with analysis of reaction products and yields. These studies were mainly carried out as solid-liquid systems, where various electrochemical measurements are relatively easy but direct measurements of the intermediate species by ESR and the excited state of catalysts by photochemical techniques are difficult, compared with those in the solid-gas systems. In fact, besides a small number of mechanistic studies,[39,41-47] few photoelectrochemical measurements at the liquid-solid interface have characterized reaction intermediates or identified the excited state and/or primary processes of photocatalysis. Such mechanistic investigations would be much easier at the gas-solid interface, as has been shown in our earlier works.[4,12]

Most mechanistic studies of metal oxides have investigated on TiO_2,[1-4,12] because of its high activity and stability. A small number have been undertaken on ZnO,[46,1,48-51] although it is very similar electrochemically to TiO_2. Recently, in a preliminary study, a substantial difference in the photoreactivities of powdered TiO_2 and ZnO for the activation of H_2O and/or OH groups on the surface of these oxides has been reported despite similar reactivity for the activation of O_2 and/or lattice oxygen ions on these surfaces.[1] A detailed investigation of this different photoreactivity might clarify photocatalysis on these semiconducting materials.

In the present work we compare photocatalytic reactions on powdered TiO_2 and ZnO in the solid-gas systems in the presence (wet system) and the absence of H_2O (dry system), the effect of Pt loading on the photoreactivities of these oxides, the origin of their different reactivities, and direct measurements of the reaction intermediates by ESR and the excited state of catalysts by photoluminescence spectroscopy.

Experimental

TiO_2 (rutile) (BET surface area; 8.0 $m^2 g^{-1}$, average particle size; 1000—2000 Å) was supplied by Ishihara Sangyo Kaisha, Ltd. Kadox-25 ZnO powder (BET surface area; 8.5 $m^2 g^{-1}$, average particle size; 1000—1500 Å) was used, because it has almost the same surface area and particle size to those of TiO_2 used. Pt-loaded catalysts were prepared by

mixing the desired amount of TiO_2 (or ZnO) and Pt black powder (2.0 wt%) followed by thorough grinding in an agate mortar. $CH_3C{\equiv}CH$, C_3H_6, and i-C_4H_8 were extra pure grade from the Takachiho Kogyo Co., used without further purification. $^{18}O_2$ (90%, E. Merck Co.) was used. Deionized twice-distilled water was degassed by alternate freezing and thawing in vacuo.

The quartz cell used in the present study was about 10 cm long and 5.0 cm in diameter with a total volume of about 300 cm^3. The catalyst could be moved between the window section and the furnace section, so that its temperature could be raised from room temperature to about 1200 K. The cell was connected to a conventional vacuum system. Prior to the reaction, catalysts were degassed at 773 K for 5 h, heated in O_2 at the same temperature for 5 h, and then finally evacuated at 623 K to 10^{-6} Torr (1 Torr=133.322 Pa). After evacuation of the catalyst, water vapor (i. e., wet system) or oxygen (i. e., dry system) was introduced onto the catalyst, followed by the reactant molecules at 298 K. UV irradiation was carried out with a 75-W high-pressure mercury lamp (Toshiba SHL 100UV) through a cut-off and a water filter (λ>280 nm) at 298 K. The reaction products were collected in cold traps.

Analysis of the reaction products was carried out by gas chromatography. Quantum yields were measured at 300 nm by potassium trioxalatoferrate actinometry. Isotopic analysis of O_2 was carried out with a quadrupole mass spectrometer. ESR measurements were carried out at 77 K with a JEOL ME-1 (X-band). UV irradiation for ESR measurments was carried out using a 500-W high-pressure mercury lamp with a color filter (λ>280 nm) in a ESR cavity. Diphenylpicrylhydradyl (DPPH) was used for g values and sweep calibration. Photoluminescence spectra were measured by using a Shimadzu RF-501 spectrofluorophotometer equipped with filters to eliminate scattered light at 298 and 77 K. The amount of desorbed H_2O from the catalysts (TPD spectra) was determined by measuring the pressure of desorbed H_2O as the temperature was increased step by step from 273 to 873 K. A monolayer of H_2O had been adsorbed previously on the catalysts. Analysis of the X-ray diffraction lines of the catalysts showed that the catalysts consist of only pure rutile-type TiO_2 crystallites and pure ZnO, respectively. The particle diameters were determined by X-ray diffraction and/or transmission electron microscopy. Details of the experiments were described in the previous papers.[52-55]

Results and Discussion

1. Photocatalysis on TiO_2 and ZnO Catalysts in Wet Systems. Figure 1 shows the observed differences in the photocatalytic hydrogenation yields for the reactions of $CH_3C{\equiv}CH$ with H_2O (wet system) on Pt-free powdered TiO_2 (TiO_2), Pt-loaded powdered TiO_2 (Pt/TiO_2), Pt-free powdered ZnO (ZnO), and Pt-loaded powdered (Pt/ZnO) catalysts at 298 K. The initial rates and quantum yields of these reactions are described in Table 1. Table 2 includes these values

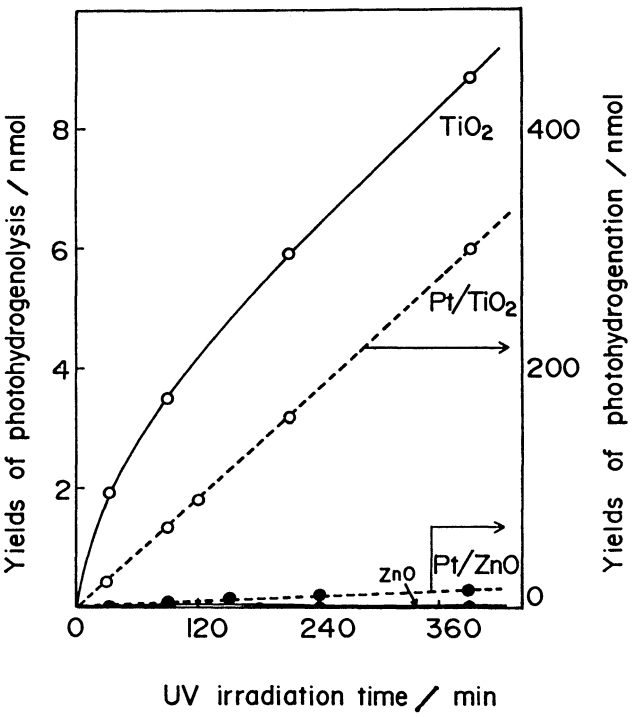

Fig. 1. Photocatalytic hydrogenation of $CH_3C{\equiv}CH$ with H_2O on Pt/TiO_2, TiO_2, Pt/ZnO, and ZnO at 298 K. (UV irradiation: 280 nm, 3 Torr C_3H_4, 8 Torr H_2O,)

Table 1. Comparison of the Rates and Quantum Yields of Photohydrogenation of $CH_3C{\equiv}CH$ with H_2O on TiO_2, Pt/TiO_2, ZnO, and Pt/ZnO Catalysts at 298 K[a]

Catalysts	Major products[b]/10^{-9} mol m^{-2} h^{-1}						
	CH_4	C_2H_4	C_2H_6	C_3H_6	C_3H_8	CO	CO_2
TiO_2	0.10	0.018	0.57	0.013	0.02	1.03	5.75
Pt/TiO_2	0.17	0.174	0.28	7.57	0.83	1.885	8.72
Quantum yields[c]	—	—	0.004	0.114	—	0.028	0.13
ZnO	0.0017	Trace	0.0094	Trace	Trace	0.034	0.107
Pt/ZnO[d]	0.002	0.0023	0.0021	0.153	0.197	0.040	0.201

a) The pressures of $CH_3C{\equiv}CH$ and H_2O were 3 and 8 Torr, respectively. b) CH_3CHO, CH_3COCH_3, $CH_3COC_2H_5$ were detected as minor oxidation products. c) Quantum yields were determined at 350±10 nm on Pt/TiO_2 at 298 K. Quantum yield=(number of photoformed product)/(number of incident photons). d) Quantum yields were too low to determine on ZnO.

Table 2. Comparison of the Rates and Quantum Yields of Photohydrogenation of C_3H_6 with H_2O on TiO_2 and Pt/TiO_2, Catalysts at 298 K[a)]

Catalysts	Major products[b)]/10^{-9} mol m^{-2} h^{-1}					
	CH_4	C_2H_4	C_2H_6	C_3H_8	CO	CO_2
TiO_2	0.21	Trace	0.67	Trace	0.76	4.33
Pt/TiO_2	0.17	Trace	0.53	5.00	1.07	6.42
Quantum yields	—	—	0.0075	0.071	0.015	0.091

a) The pressures of C_3H_6 and H_2O were 3 and 8 Torr, respectively. b) CH_3CHO, CH_3COCH_3, and $CH_3COC_2H_5$ were detected as minor oxidation products. c) Quantum yields were determined at 350±10 nm on Pt/TiO_2 at 298 K. Quantum yield=(number of photoformed product)/(number of incident photons). Rates of photohydrogenation on ZnO were too low to follow the kinetics.

for the results of the photohydrogenation reaction of C_3H_6 with H_2O on Pt-loaded and unloaded TiO_2. The rates of the photocatalytic hydrogenation of C_3H_6 with H_2O on ZnO and Pt/ZnO catalysts were too low to follow their kinetics. The major products of the photocatalytic hydrogenation of $CH_3C{\equiv}CH$ and C_3H_6 with H_2O on TiO_2 and on ZnO were C_2H_6 as hydrogenation product accompanied by the fission of the carbon-carbon bond of $CH_3C{\equiv}CH$ and C_3H_6, i. e., hydrogenolysis (CH_4 as minor product), and CO_2 as oxidation product. Ketones and aldehydes were also detected as minor photooxidation products.

The product distribution in the photocatalytic hydrogenolysis is in good agreement with that observed on TiO_2 catalysts,[52-55)] which has been attributed to a closely spaced photogenerated electron-hole pair, i. e., Ti^{3+}-$\dot{O}H$ pair species. These electron-hole pairs can interact with $CH_3C{\equiv}CH$ adsorbed on the surface to form the carbenes and/or oxygen-containing compounds via carbon-centered radicals such as $\dot{C}H$ and $CH{\equiv}\dot{C}$ formed in a manner similar to that described previously.[52,54,55)]

On the other hand, as shown in Table 1 and Fig. 1, on Pt/TiO_2 and Pt/ZnO, where the photoelectrochemical mechanism is operating, the major product was C_3H_6: that is, hydrogenation dominated over carbon-carbon bond fission while producing CO_2 as oxidation product. The rates for the photocatalytic hydrogenation are markedly enhanced on both TiO_2 and ZnO by the presence of Pt as a co-catalyst, Table 1. The rates of photocatalytic hydrogenolysis on TiO_2 and hydrogenation on Pt/TiO_2 of $CH_3C{\equiv}CH$ with H_2O are much higher than those on ZnO and Pt/ZnO, respectively, with nearly the same conversion being observed on the Pt-loaded and native systems. With TiO_2 and ZnO, the rates of oxidation are much higher than that of the hydrogenation. However, with Pt/TiO_2 and Pt/ZnO, there is no marked difference between the rates, supporting our previous assertion that photoreactions on Pt-loaded TiO_2 and ZnO are much more catalytic than those on Pt-free TiO_2 and ZnO.[53)]

Figure 2 shows a temperature-programmed desorption (TPD) spectra for desorption of H_2O from TiO_2

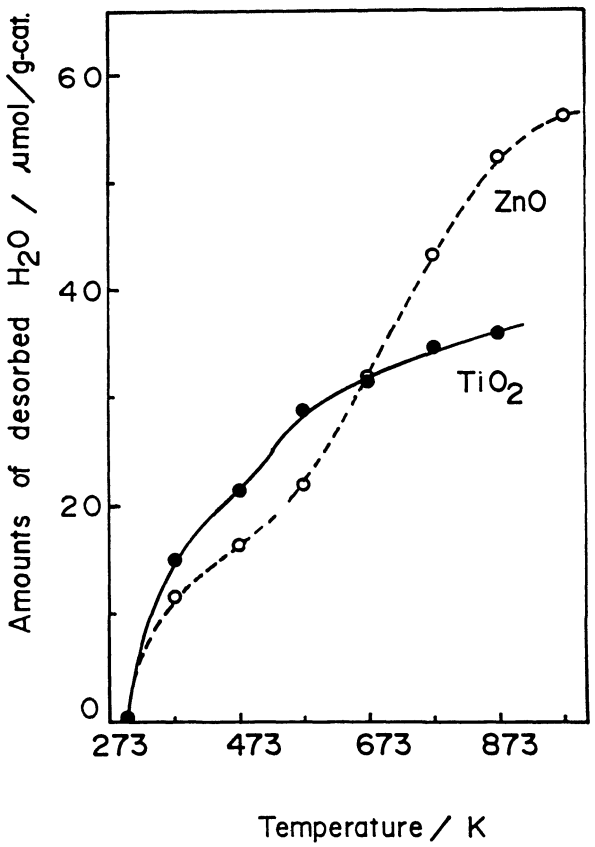

Fig. 2. Amounts of desorbed H_2O from TiO_2 and ZnO. (A monolayer of H_2O had been adsorbed previously on the oxides at 298 K.)

and ZnO after the adsorption of a monolayer of H_2O at 298 K. The amounts of water desorbed from TiO_2 and ZnO in the temperature range from 273 to 673 K are almost the same, whether native or Pt-loaded. Thus, the observed differences in rates of photocatalytic reactions do not correlate with the steady state adsorption of water.

The efficiency of photoreactions on TiO_2 is higher than that on ZnO by a factor of at least 40, irrespective of Pt loading. In these photohydrogenation reactions on TiO_2 (or ZnO) in the presence of adsorbed H_2O, it is likely that both $\dot{H}$ and $\dot{O}H$ radicals are

generated,[12,52-54] Eqs, 1 and 2, respectively, since a water dissociation preequilibrium $H_2O \rightleftarrows H^+ + OH^-$ is established on oxides.[52] Therefore, photogenerated electrons (or Ti^{3+}) are trapped by protons supplied from the acidic groups at the specific surface sites. Photogenerated holes (or O^-) are trapped at basic surface sites, though the nature of the basic OH^- groups associated with the oxidation is still unclear.

$$H^+ + e^- (Ti^{3+}) \longrightarrow \dot{H} + Ti^{4+} \quad (1)$$

$$OH^- + h^+ (O^-) \longrightarrow \dot{O}H + O^{2-} \quad (2)$$

On the Pt-free TiO_2 and ZnO, both $\dot{H}$ and $\dot{O}H$ radicals are formed on these oxides at sites close to each other, their proximity resulting in photocatalytic hydrogenolysis accompanied by the carbon-carbon bond fission, but not hydrogenation.[52-54] On the Pt-loaded TiO_2 and ZnO, however, enhancement of electron trapping by adsorbed protons on Pt results in more efficient charge separation.[53] Thus, the marked increase in the rate of photohydrogenation on Pt/TiO_2 and Pt/ZnO probably arises from addition of H atoms to $CH_3C{\equiv}CH$ and C_3H_6 on Pt particle sites but not on TiO_2 or ZnO. This results in a high efficiency for photocatalytic hydrogenation, and a much better balanced contribution of photogenerated electrons and holes to the surface reactions, i. e., a much more catalytic reactivity. The similarity in the product distribution shown in Fig. 1 and Table 1 clearly suggests that the reaction mechanisms operative on ZnO are the same as those on TiO_2, except for the much lower yields.[1]

2. Photocatalysis on TiO_2 and ZnO Catalysts in Dry Systems. UV irradiation of TiO_2 and ZnO in the presence of the mixtures of hydrocarbons and oxygen leads to the oxidation of these compounds.[1,51,56] Figure 3 shows the observed differences in the yields of the photocatalytic oxidation of i-C_4H_8 by O_2 (i. e., dry system) on Pt-free TiO_2, Pt/TiO_2, Pt-free ZnO, and Pt/ZnO catalysts at 298 K.[1] The rates and quantum yields of photooxidation of i-C_4H_8 and C_3H_6 by O_2 on these Pt-loaded and native catalysts are shown in Table 3. The major products of the photocatalytic oxidation of i-C_4H_8 are CH_3COCH_3 and CO_2 on all four catalysts, but products are formed with different rates and selectivities. In the photocatalytic oxidation of C_3H_6, various oxygen-containing compounds such as CH_3COCH_3, C_2H_5CHO and CH_3OH, in addition to the formation of CO_2, are obtained. The efficiency of TiO_2 for the photocatalytic oxidation of i-C_4H_8 and C_3H_6 is about 1.2—2 times higher than that of ZnO. These values are smaller than those obtained in wet systems by at least an order of magnitude.

UV irradiation of TiO_2 and ZnO in the presence of isotopically-labelled O_2 leads to the photocatalytic oxygen isotopic exchange,[56,57] (Fig. 4). The degassing temperature and the presence of H_2O influence the

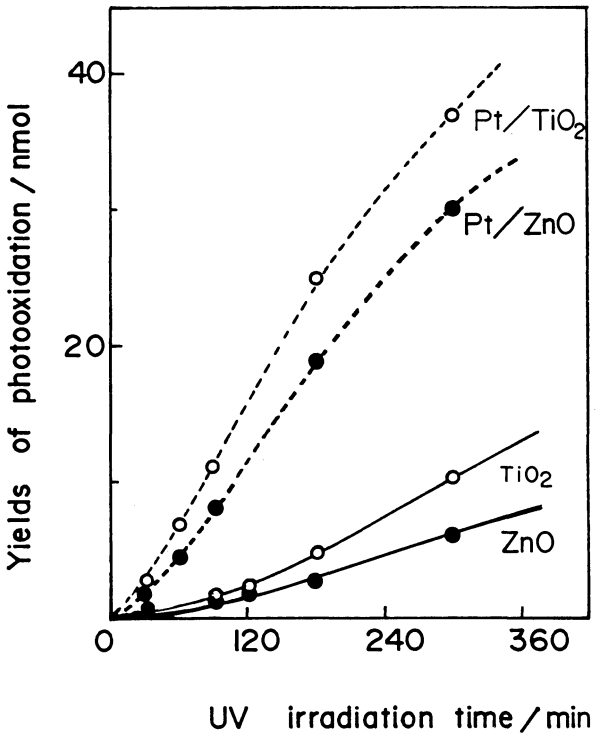

Fig. 3. Photocatalytic oxidation of i-C_4H_8 with O_2 on dry Pt/TiO_2, TiO_2, Pt/ZnO, and ZnO at 298 K. (UV irradiation: 280 nm, 6 Torr O_2, 3 Torr i-C_4H_8.)

Table 3. Comparison of the Rates and Quantum Yields of Photooxidation of i-C_4H_8 and C_3H_6 with O_2 on TiO_2, Pt/TiO_2, ZnO, and Pt/ZnO Catalysts at 298 K

Catalyst	Major products/10^{-9} mol m^{-2} h^{-1}					
	Photooxidation of i-C_4H_8[a]		Photooxidation of C_3H_6[b]			
	CO_2	CH_3COCH_3	CO_2	CH_3COCH_3	C_2H_5CHO	CH_3OH
TiO_2	2.50	0.881	3.1	0.557	0.16	0.52
Pt/TiO_2	45.1	1.863				
ZnO	1.31	0.567	1.92	0.36	0.11	0.28
Pt/ZnO	43.6	1.478				

a) The pressures of i-C_4H_8 and O_2 were 3 and 6.0 Torr, respectively. b) The pressures of C_3H_6 and O_2 were 1 and 3.0 Torr, respectively. c) The experiments of photooxidation of C_3H_6 by O_2 on Pt/TiO_2 and Pt/ZnO catalysts were not carried out yet.

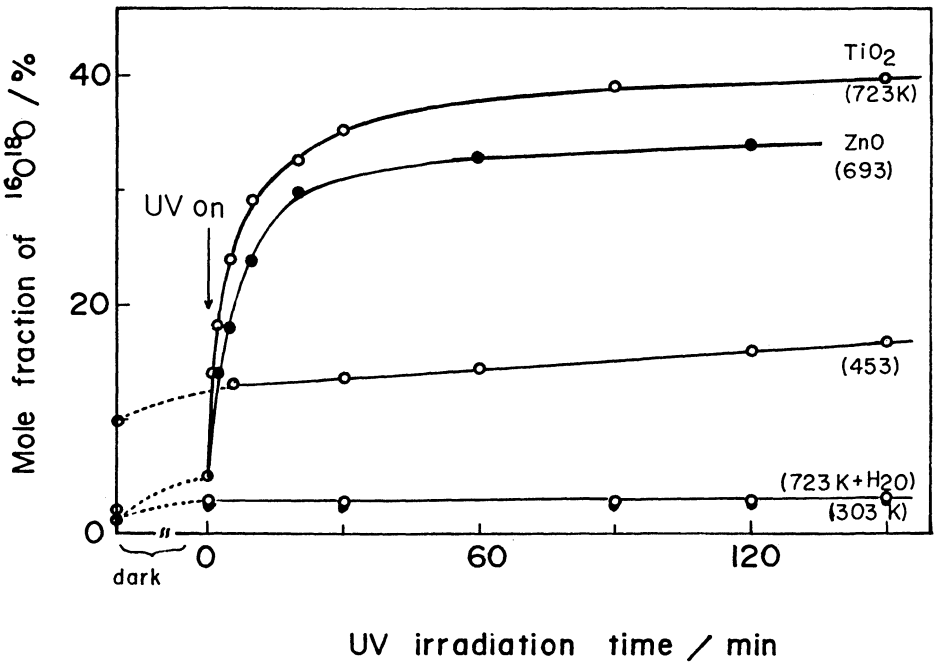

Fig. 4. Photocatalytic oxygen isotopic exchange on TiO_2 and ZnO and the effect of adsorbed H_2O on the exchange reaction on TiO_2 at 298 K. (UV irradiation: 280 nm, value in parenthesis indicates the degassing temperature of the catalyst.)

observed rates of exchange. There is only a small difference in reactivity between TiO_2 and ZnO, the reactivity of TiO_2 being higher than that of ZnO by only 1.5—2 times. Adding H_2O to the TiO_2 catalyst, which had been deggassed at 723 K, the surface OH groups markedly suppresses this reaction.

Both photocatalytic oxygen isotopic exchange and photooxidation of alkenes with O_2 on dry TiO_2 and ZnO probably proceed via O_3^- and O_2^- anion radicals, Eqs. 3 and 4:[41,42,56-58]

$$O_2 + h^+ (O^-) \longrightarrow O_3^- \quad (3)$$

$$O_2 + e^- (Ti^{3+}) \longrightarrow O_2^- \text{-} Ti^{4+} \quad (4)$$

3. Measurements of Reaction Intermediates. UV irradiation of TiO_2 in the presence of O_2 leads to the formation of O_3^- anion radicals with high efficiency, together with the formation of O_2^- anion radicals, (Fig. 5). The ESR signal assigned to O_3^- is obtained as a difference spectrum by subtracting the spectrum before irradiation from that observed after irradiation at 77 K.[54,56] The addition of O_2 to TiO_2 led to the formation of O_2^- species. The photogenerated O_3^- radicals were also observed by ESR at 77 K when ZnO was UV-irradiated in the presence of O_2. O_3^- anion radicals are probably formed via the reaction of O_2 with photogenerated O^-. This species might be formed by hole trapping on the lattice O^{2-} ions as mentioned above (i. e., reaction (3)). In the absence of O_2, the O^- species can be detected by ESR at 77 K under UV irradiation of ZnO, (Fig. 6).[59] O^- is not detected directly on TiO_2 by ESR, probably because of

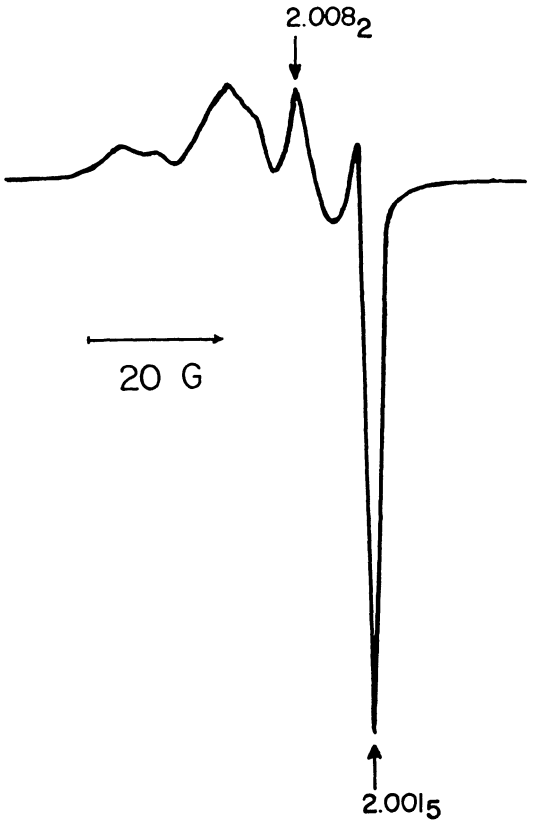

Fig. 5. ESR spectrum of the photogenerated O_3^- anion radical on TiO_2 at 77 K. (UV irradiation and ESR measurments were carried out at 77 K in the presence of O_2.)

its short lifetime even at 77 K and/or incomplete removal of the degeneracy of the p-orbitals in this species. Photogenerated electrons trapped as Ti^{3+} (or Zn^{+}) are directly associated with the photogeneration of O_2^- at Ti^{4+} sites of TiO_2 (or Zn^{2+} ions of ZnO), (Eq. 4).

In the presence of H_2O on TiO_2 and ZnO (wet systems), however, neither O_2^- nor O_3^- anion radicals could be longer detected. On extremely small TiO_2 particles (about 50 Å, and BET surface area 800 $m^2 g^{-1}$) the formation of ȮH radicals was detected by UV irradiation of the TiO_2 in the presence of a monolayer of H_2O.[60] With the present TiO_2 catalyst (2000 Å and BET surface area 8.0 $m^2 g^{-1}$), the detection of the photoformed ȮH radicals was not successful because of its lower photoactivity. Formation of these Ḣ and ȮH radicals may have occurred on these wet systems in lieu of the formation of O_2^- and O_3^-.

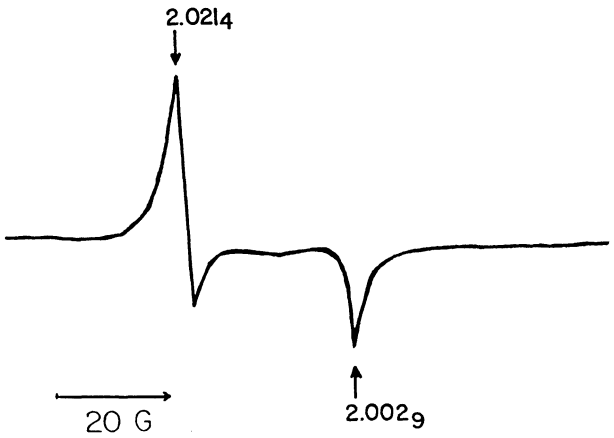

Fig. 6. ESR spectrum of the photo-generated O^- anion radical (hole trapped centers) of ZnO at 77 K. (UV irradiation and ESR measurments were carried out at 77 K in vacuo.)

4. Photoluminescence Behaviors of TiO_2 and ZnO in Dry and Wet Systems. ZnO used in the present work exhibits a high yield photoluminescence when excited with the band-gap light (about 3.2 eV=380 nm).[59] Figure 7 shows the photoluminescence spectrum of ZnO (1) at 298 K and the effect of the addition of H_2O (2—4). The addition of H_2O leads to an increase of the intensity of the photoluminescence, depending on the amounts of adsorbed H_2O. As in a previous study,[61] the addition of $CH_3C{\equiv}CH$ or H_2O onto the TiO_2 led to an enhanced photoluminescence but the magnitude of the enhancement was much smaller than that on ZnO. That is, the addition of excess H_2O led to the 1.5—2.0 times enhancement of the photoluminescence of ZnO, while on TiO_2 it was only 1.1—1.2 times.

The addition of O_2 to ZnO leads to a decrease of the intensity of the photoluminescence, its extent depending on the amounts of added O_2, Fig. 8. As reported previously,[61] the addition of O_2 to TiO_2 also led to

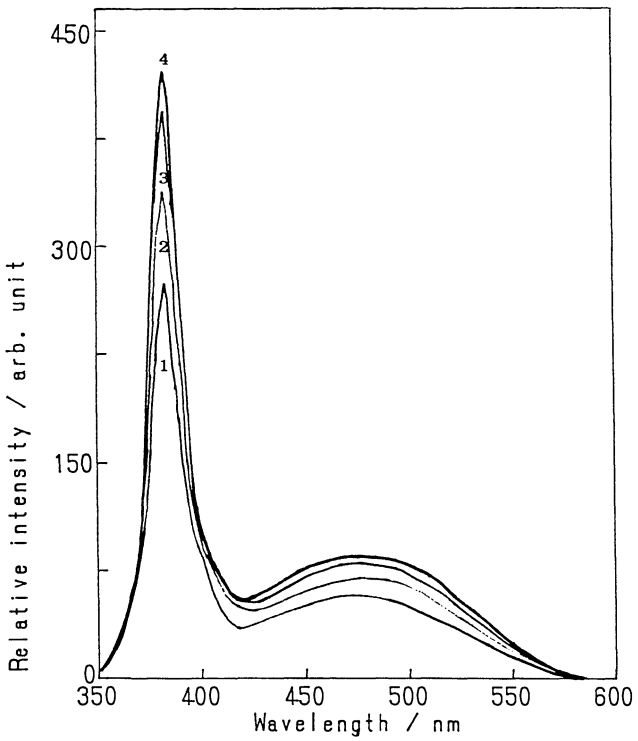

Fig. 7. Effects of H_2O on the photoluminescence of ZnO at 298 K. (Pressure of added H_2O in Torr, 1: 0.0, 2: 0.5, 3: 18, 4: excess amounts.)

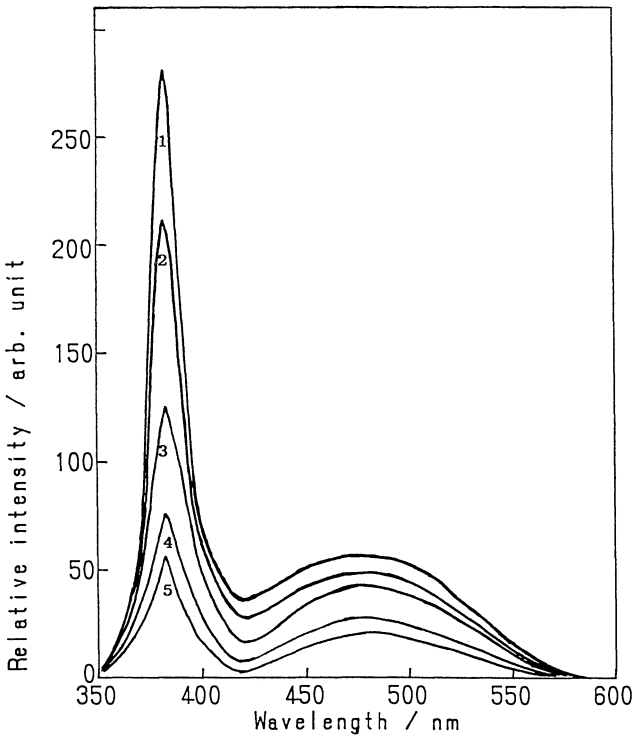

Fig. 8. Effects of O_2 on photoluminescence of ZnO at 298 K. (Pressure of added O_2 in Torr, 1: 0.0, 2: 0.5, 3: 3.5, 4: 12.0, 5: 20 or excess amounts.)

photoluminescence quenching. The addition of 3—10 Torr O_2 (even excess O_2) to TiO_2 and ZnO led to 80—95% quenching of their photoluminescence almost equally on the two oxides, though the initial yield of photoluminescence of TiO_2 is much lower than that of ZnO.

The mechanisms for the enhancement and quenching of the photoluminescence of the powdered semiconductors such as CdS and TiO_2 by added molecules are recently well explained by the models of Ellis et al.[62-64] and Anpo and Fox et al.[61] The formation of negatively-charged adducts (via electron capture) on the surfaces of semiconductors such as TiO_2 and CdS causes photoluminescence quenching, while the formation of positively-charged adducts (via hole trapping) results in an enhancement of the photoluminescence.

Bard et al.[65] have shown that the photoluminescence quenching, photoinduced oxygen adsorption, and photodecomposition observed with ZnS particles are very sensitive to surface effects and concluded that the photoluminescence can be used as a probe of electron-hole surface processes. In fact, recently, Anpo and Fox et al.[61] have found a parallel relationship between the enhancement of photoluminescence of TiO_2 by the addition of unsaturated hydrocarbons and the rates of photocatalytic hydrogenation of those same unsaturated hydrocarbons by H_2O on TiO_2. Thus, these photoinduced surface processes are closely associated with, both depending crucially on the binding of the added molecules to the TiO_2 surface. The results obtained on TiO_2 and CdS clearly suggest that the formation of adsorbed charged species plays a significant role in determining the reactivities of the photogenerated electron-hole pairs on the semiconductors.

Consequently, as shown in Fig. 9, these results suggest that the addition of H_2O and/or $CH_3C{\equiv}CH$ onto the TiO_2 and ZnO causes structural changes in surface band bending to increase the efficiency of recombination of the photogenerated electrons and holes, resulting in an enhancement of the photoluminescence, with larger effects being observed on ZnO than on TiO_2. On the other hand, the addition of O_2 onto these photocatalysts caused a suppression of the efficiency of recombination of the photogenerated electrons and holes (i. e., better charge separation), resulting in a quenching of the photoluminescence to about the same extent on TiO_2 and ZnO (Excess O_2 leads to the almost complete quenching of the photoluminescence.). Although the details are not clear at present, this photoluminescence behaviour is probably associated with the different electronic structures of the TiO_2 and ZnO surfaces, since Ti^{4+} and Zn^{2+} ions can play a significant role in forming surface adducts.

The nature of the photocatalytic action of TiO_2 and ZnO is the same for both Pt-loaded and native systems, respectively, but large differences in reactivities are

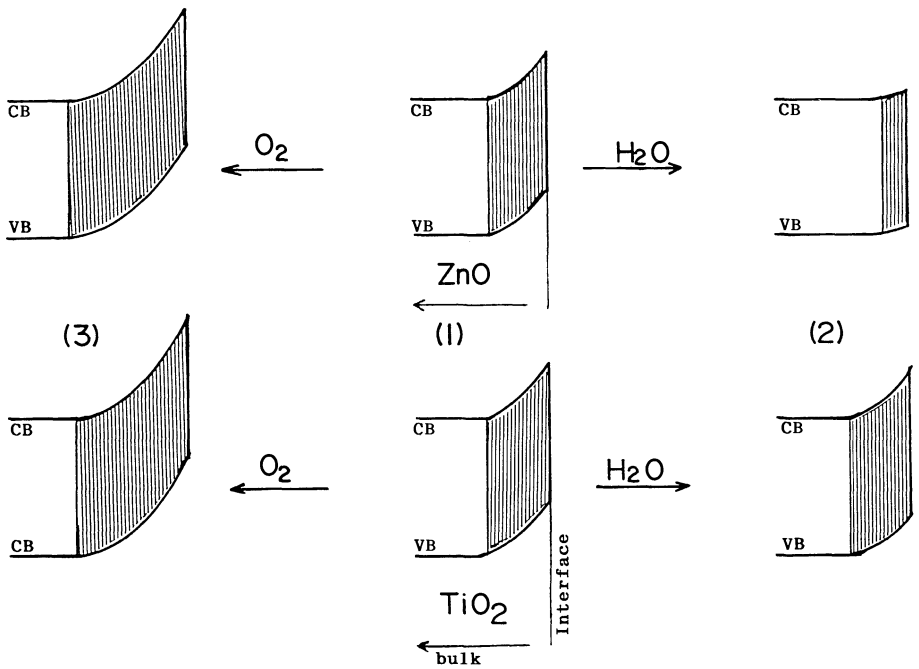

Fig. 9. Schematic description of the surface band bending of ZnO (top) and TiO_2 (bottom). (1): after degassing in vacuo (n-type semiconductors), (2): after adsorption of H_2O (decrease of band bending by formation of positively-charged species on the surfaces), (3) after adsorption of O_2 (increase of band bending by formation of negatively-charged species on the surfaces).

encountered on these catalysts. Much larger differences are observed in the activation of H_2O and/or surface OH groups, while only small differences are observed in reactions associated with the activation of O_2 in dry systems. Thus, the observed large photoreactivity differences between wet TiO_2 and ZnO arise from the much faster recombination of photogenerated electrons and holes on the surface of wet ZnO than that on TiO_2, because the formation of the positively-charged surface adducts from H_2O and/or $CH_3C{\equiv}CH$ results in much smaller upward band bending on ZnO than on TiO_2. On the other hand, in dry systems, the formation of the negatively-charged surface adducts of O_2 leads to much larger upward band bending on both TiO_2 and ZnO, producing higher photocatalytic efficiencies for TiO_2 and ZnO and negligible differences in their reactivities.

Conclusions

The photocatalytic reactivities of powdered TiO_2 and ZnO, both Pt-loaded and native, differed significantly in the photocatalytic hydrogenation of $CH_3C{\equiv}CH$ and C_3H_6 with H_2O but not in the photocatalytic oxidation of i-C_4H_8 and C_3H_6 with O_2. Photoluminescence of TiO_2 and ZnO in the presence and the absence of H_2O or O_2 indicated that addition of H_2O onto the oxides causes downward band bending to increase the efficiency of recombination of photogenerated electrons and holes, to a greater extent on ZnO than on TiO_2. On the other hand, the addition of O_2 led to upward band-bending to suppress recombination of photogenerated electrons and holes almost equally on the two oxides.

Thus, photoluminescence of TiO_2 and ZnO (as radiative recombination of photogenerated electrons and holes), together with the direct ESR detection of reaction intermediates, suggested that the large observed difference in the photoreactivity between wet TiO_2 and ZnO derives from the much faster recombination on ZnO because of the formation of positively-charged surface adducts. In dry systems, the formation of the negatively-charged O_2 proceeds nearly equivalently on these two catalysts, resulting in a net higher photocatalytic efficiencies of both TiO_2 and ZnO but little difference in their reactivities.

The photocatalytic programs in Osaka is supported in part by a Grant-in-Aid for Scientific Research No. 62550595 and 01550632) from the Ministry of Education, Science and Culture. The photocatalytic program in Austin is generously supported by the Office of Basic Energy Sciences, U.S. Department of Energy. Thanks are due to Japan/U.S. Cooperative Program in Photoconversion and Photosynthesis Research.

References

1) M. Anpo and M. Tomonari, *Denki Kagaku*, **57**, 1219 (1989).
2) "Photocatalysis, Fundamentals and Applications," ed by N. Serpone, E. Pelizzetti, Wiley, New York (1989), and references therein.
3) M. A. Fox, *Acc. Chem. Res.*, **16**, 314 (1983).
4) M. Anpo and Y. Kubokawa, *J. Surf. Sci. Soc. Jpn.* (Hyomen Kagaku), **4**, 200 (1983).
5) J. E. Brus, *J. Phys. Chem.*, **90**, 2555 (1986), and its earlier series.
6) A. Henglein, *Chem. Rev.*, **89**, 1861 (1989), and references therein.
7) I. I. Micic, M. T. Nenadovic, M. W. Peterson, and A. J. Nozik, *J. Phys. Chem.*, **91**, 1295 (1987).
8) H. J. Watzke and J. H. Fendler, *J. Phys. Chem.*, **91**, 854 (1987).
9) A. Hong, D. W. Bahnemann, and M. R. Hoffmann, *J. Phys. Chem.*, **91**, 6245 (1987).
10) C. Kormann, D. W. Bahnemann, and M. R. Hoffmann, *J. Phys. Chem.*, **92**, 5196 (1988).
11) C. Y. Liu and A. J. Bard, *J. Phys. Chem.*, **93**, 3232 (1989).
12) M. Anpo, *Res. Chem. Intermedi.*, **11**, 67 (1989), and references therein.
13) M. Anpo, M. Sunamoto, and M. Che, *J. Phys. Chem.*, **93**, 1187 (1989).
14) M. Anpo, M. Kondo, Y. Kubokawa, C. Louis, and M. Che, *J. Chem. Soc., Faraday Trans. 1*, **84**, 2771 (1989).
15) M. Anpo, M. Kondo, S. Coluccia, C. Louis, and M. Che, *J. Am. Chem. Soc.*, **111**, 8791 (1989).
16) M. Anpo and Y. Kubokawa, *Res. Chem. Intermedi.*, **8**, 105 (1987), and references therein.
17) M. A. Fox and T. L. Pettit, *Langmuir*, **5**, 1056 (1989).
18) S. Sato, A. Sobczynski, J. M. White, A. J. Bard, A. Campion, M. A. Fox, T. E. Mallouk, and S. E. Webber, *J. Photochem. Photobiol., A, Chem.*, **50**, 283 (1989).
19) Y. Wang and N. Herron, *J. Phys. Chem.*, **93**, 4988 (1989).
20) L. Kuczynski and J. K. Thomas, *J. Phys. Chem.*, **89**, 2720 (1985).
21) S. Kodama, H. Nakaya, M. Anpo, and Y. Kubokawa, *Bull. Chem. Soc. Jpn.*, **58**, 3645 (1985).
22) M. Anpo, H. Nakaya, S. Kodama, Y. Kubokawa, K. Domen, and T. Onishi, *J. Phys. Chem.*, **90**, 1633 (1986).
23) M. Anpo, T. Kawamura, S. Kodama, K. Maruya, and T. Onishi, *J. Phys. Chem.*, **92**, 438 (1988).
24) N. Kakuta, K. H. Park, M. F. Finlayson, A. Ueno, A. J. Bard, A. Campion, M. A. Fox, S. E. Webber, and J. M. White, *J. Phys. Chem.*, **89**, 732 (1985).
25) N. Kakuta, K. H. Park, M. F. Finlayson, A. J. Bard, A. Campion, M. A. Fox, S. E. Webber, and J. M. White, *J. Phys. Chem.*, **89**, 5028 (1985).
26) A. J. Frank, I. Willner, Z. Goren, and Y. Degani, *J. Am. Chem. Soc.*, **109**, 3568 (1987).
27) C. Morrison and J. Kiwi, *J. Chem. Soc., Faraday Trans. 1*, **85**, 1043 (1989).
28) M. Schiavello, V. Augugliaro, S. Coluccia, L. Palmisano, and A. Sclafani, in "Photochemistry on Solid Surfaces," ed by M. Anpo and T. Matsuura, Elsevier, Amsterdam (1989), p. 149.
29) K. R. Gopidas, and P. V. Kamat, *Langmuir*, **5**, 22 (1989).
30) W. E. Ford and P. V. Kamat, *J. Phys. Chem.*, **93**, 6423 (1989).

31) M. Neumann-Spallart, A. Schwarz, and G. J. Grabner, *J. Phys. Chem.*, **93**, 1984 (1989).
32) J. Rabani and D. Behar, *J. Phys. Chem.*, **93**, 2559 (1989).
33) S. Yanagida, Y. Ishimaru, Y. Miyake, T. Shiragami, C. Pac, K. Hashimoto, and T. Sakata, *J. Phys. Chem.*, **93**, 2576 (1989).
34) R. D. Stramel, T. Nakamura, and J. K. Thomas, *J. Chem. Soc., Faraday Trans. 1*, **84**, 1287 (1988).
35) K. Hashimoto, M. Hiramoto, A. B. P. Lever, and T. Sakata, *J. Phys. Chem.*, **92**, 1016 (1988).
36) K. Hashimoto, M. Hiramoto, T. Kajiwara, and T. Sakata, *J. Phys. Chem.*, **92**, 4636 (1988).
37) K. Itoh and A. Fujishima, *J. Am. Chem. Soc.*, **110**, 6267 (1988).
38) S. Nakabayashi, S. Komuro, Y. Aoyagi, and A. Kira, *J. Phys. Chem.*, **91**, 1696 (1987).
39) R. Rosseti and L. E. Brus, *J. Phys. Chem.*, **90**, 558 (1986).
40) Y. Nosaka and M. A. Fox, *J. Phys. Chem.*, **90**, 6521 (1986).
41) Y. Nosaka and M. A. Fox, *J. Phys. Chem.*, **92**, 1893 (1988).
42) C. D. Jaegar and A. J. Bard, *J. Phys. Chem.*, **83**, 3146 (1979).
43) J. R. Harbour and M. L. Hair, *J. Phys. Chem.*, **83**, 652 (1979).
44) C. Chen, R. P. Veregin, J. R. Harbour, M. L. Hair, S. L. Issler, and J. Tromp, *J. Phys. Chem.*, **93**, 2607 (1989).
45) S. Yamagata, S. Nakabayashi, K. M. Sancier, and A. Fujishima, *Bull. Chem. Soc. Jpn.*, **61**, 3429 (1988).
46) R. Amadelli, A. Maldotti, C. Bartocci, and V. Carassiti, *J. Phys. Chem.*, **93**, 6448 (1989).
47) D. Bahnemann, A. Henglein, J. Lilie, and L. Spanhel, *J. Phys. Chem.*, **88**, 709 (1984).
48) M. Anpo, M. Tomonari, and K. Chiba, unpublished results.
49) M. Rao, K. Rajeshwar, V. R. P. Verneker, and J. DuBow, *J. Phys. Chem.*, **84**, 1987 (1980), references therein.
50) V. Augugliaro, L. Palmisano, A. Sclafani, C. Minero, and E. Pelizzetti, *Toxicolog. Environ. Chem.*, **2**, 267 (1987).
51) P. Pichat, J. M. Herrmann, J. Disdier, and M. N. Mozzanega, *J. Phys. Chem.*, **83**, 3122 (1979).
52) M. Anpo, N. Aikawa, S. Kodama, and Y. Kubokawa, *J. Phys. Chem.*, **88**, 2569 (1984).
53) M. Anpo, N. Aikawa, and Y. Kubokawa, *J. Phys. Chem.*, **88**, 3998 (1984).
54) M. Anpo, M. Yabuta, S. Kodama, and Y. Kubokawa, *Bull. Chem. Soc. Jpn.*, **59**, 259 (1986).
55) M. Anpo, T. Shima, S. Kodama, and Y. Kubokawa, *J. Phys. Chem.*, **91**, 4305 (1987).
56) H. Courbon, M. Formenti, and P. Pichat, *J. Phys. Chem.*, **81**, 550 (1977).
57) Y. Kubokawa, M. Anpo, and C. Yun, Proc. 7th Int. Congr. Catal., Tokyo, 1980, Abstr., B 1170, and references therein.
58) M. Anpo, Y. Kubokawa, T. Fujii, and T. Suzuki, *J. Phys. Chem.*, **88**, 2572 (1984).
59) M. Anpo and Y. Kubokawa, *J. Phys. Chem.*, **88**, 5556 (1984).
60) M. Anpo, T. Shima, and Y. Kubokawa, *Chem. Lett.*, **1985**, 1799.
61) M. Anpo, M. Tomonari, and M. A. Fox, *J. Phys. Chem.*, **93**, 7300 (1989).
62) G. J. Meyer, G. C. Lisensky, and A. B. Ellis, *J. Am. Chem. Soc.*, **110**, 4914 (1988).
63) G. J. Meyer, G. C. Lisensky, and A. B. Ellis, *J. Am. Chem. Soc.*, **111**, 5146 (1989).
64) G. J. Meyer, E. R. M. Luebker, G. C. Lisensky, and A. B. Ellis, in "Photochemistry on Solid Surfaces," ed by M. Anpo and T. Matsuura, Elsevier, Amsterdam (1989), 388.
65) W. G. Becker and A. J. Bard, *J. Phys. Chem.*, **87**, 4888 (1983).

Hydrogenation of 1,3-Butadiene over CaO Catalyst Treated with Methanol

Tsuneo MATSUDA,* Masatoshi SUGIMOTO, and Hiroshi YOSHIARA
Department of Applied Chemistry, Faculty of Engineering, Saitama University, Urawa, Saitama 338
(Received October 8, 1990)

When calcium oxide was treated with methanol at low temperature, calcium methoxides i.e., calcium dimethoxide and, calcium hydroxide methoxide, could be easily formed. The catalyst produced by the thermal decomposition of these compounds exhibited remarkably high activity to the hydrogenation of 1,3-butadiene. With the aim to investigate the cause of the high activity, two other calcium oxide catalysts were used for a comparison. The cause was ascribed to the formation of a large amount of electron-donating sites, including both basic ones and those with a high surface area.

Solid base catalysts, such as CaO and MgO, are known to catalyze the isomerization of butenes,[1] the dehydrogenation of alcohols,[2] the hydrogenation of dienes,[3-6] as well as H_2-D_2[7] and CH_4-D_2[8,9] exchange reactions. Tanaka et al.[3] pointed out that CaO prepared by the evacuation of $Ca(OH)_2$ above 1073 K gave a high catalytic activity for the hydrogenation of 1,3-butadiene at 273 K. Miyahara et al.[4] have also shown that the maximum activity for the hydrogenation of 1,3-butadiene is obtained when MgO is prepared around 1073—1273 K under vacum. Thus, treatment at higher temperatures than 1073 K under vacuum are necessary for the appearance of hydrogenation activity. We recently found a remarkably highly active CaO catalyst for the hydrogenation of 1,3-butadiene. The preparation method of the catalyst does not require a higher temperature than 1073 K. By heating under vacum at a rather lower temperature (873 K) after a treatment with methanol, a very high activity could be developed. Why such a high activity appeared through such a simple method as a methanol treatment is a very interestng problem. The aim of this paper is to answer the above question by comparing the three kinds of CaO catalysts.

Experimental

Materials. Three kinds of calcium oxide catalysts were used for a comparion. The calcium oxide purchased from Wako Junyaku Co. was calcined at 1173 K for 15 h in air in order to decompose the calcium carbonate and hydroxide impurities into CaO. This is called CaO(I). The second catalyst, CaO(II), was prepared by the decomposition of $Ca(OH)_2$, which was formed by refluxing a CaO(I) suspension in water for 3 h. In place of water CaO(I) was suspended in methanol, followed by stirring for 24 h at room temperature; methanol was then removed to dryness in an evaporator at ca. 333 K. This catalyst is called CaO-M. All of the catalysts were stored in a desiccator. Just before the reaction all of the catalysts used were slowly heated *in situ* under a vacuum and increasing temperature at a rate of 5 K min^{-1} to 873 K; this temperature was maintained for 1 h. This procesure is abbreviated as a pretreatment hereafter. The surface areas of CaO(I), (II) and CaO-M were measured by the BET method, giving 7.71, 55.2 and 139 $m^2 g^{-1}$, respectively.

1.3-Butadiene (Takacio Co., more than 99% purity) was purified by a repeated freeze-and-thaw technique. Hydrogen with a purity of more than 99.9999% (Takachio Co.)was dried using a trap containig a moleculare sieve (5A) kept at 77 K.

Reaction Procedures. The reaction was carried out in an all-glass static reactor with a volume of ca. 225 ml in a closed recirculation reactor equipped with a sampling manifold. A weighed amount of catalyst specimen (0.05 g as CaO) was placed in a qualtz glass reactor. The weight loss of CaO(II) and CaO-M due to the pretreatment was examined beforehand. A typical hydrogenation mixture of 1,3-butadine : hydrogen=50 : 100 Torr, (1 Torr=133.322 Pa) was used in the reaction. The reaction was carried out at 273 K, and the reaction products analyzed by a gas chromatograph equipped with a 5 m column of VZ-7 at 313 K

IR Measurement, A thin disk of the catalyst sample was treated using the same procedure as in the pretreatment. The IR spectra were recorded with a JASCO Model 810 spectrometer without exposing the sample to air.

ESR Measurement. The ESR spectra were recorded on a Varian E-9 spectrometer (X-band with 100 kHz field modulation) at room temperature. The sample was prepared in an apparatus equipped with both greaseless stop valves and a trap used to cut the vapor from grease. For the *g*-value and spin concentration calibration, DPPH was used as a standard probe in a dual cavity. The relative concentration was estimated as being the ratio of the spin concentration per unit gram of sample vs. the spin concentration of DPPH. An approximate method to measure the spin concentration was adopted comprising the product of the square of the line width and the peak-to-peak height in order to estimate the area under the ESR absorption curve.[10] The electron-donating property of the catalysts was examined with the radical produced by the adsorption of nitrobenzene.

The sample was placed in a qualtz adsorption chamber equipped with a side ESR tube; at room temperature nitrobenzene vapor was adsorbed for 30 min and then evacuated for 15 min at the same temperature. The proper amount of the sample was transfered into the tube and then sealed for an ESR measurement.

XPS Measurement. The X-ray photoelectron spectra were recorded at room temperature on a Ulvac-Phi Model UP ESCA and Auger spectrometer using monochromatic Mg-α exciting radiation with an energy of 1253.6 eV. The spectrometer vacuum was better than 10^{-9} Torr. A thin

disk pressed from powder was treated using the same method as in the pretreatment. The Cls level of a trace of contaminant carbon, 285.0 eV, was taken as a reference.

Basicity Measurement. A CaO-M catalyst after the pretreatment showed a slight dark-gray color. Two other calcium oxide catalysts were white. Consequently, it was impossible to measure the surface basicity of CaO-M by the indicator method. Therefore, the basicity was estimated from the irreversible adsorption amount of CO_2. CO_2 was adsobed at 273 K on the catalyst sample; after attaining equilibrium, it was evacuated at 873 K for 1 h. Again, CO_2 was adsorbed on the sample at 273 K at the same presure as in the case of the initial adsorption. The irreversible adsorption amount of CO_2 was thus estimated from the difference of the adsorbed amount during the initial and secondary adsorption.

Results

Hydrogenation of 1,3-Butadiene. Carbon dioxide and oxygen inhibited the reaction when they were adsorbed on the catalysts. Hydrogenation of 1,3-butadiene over three kinds of CaO catalysts was carried out at 273 K. The conversion vs. the reaction-time plots are shown in Fig. 1. Though no reaction proceeded on CaO(I), the activity appeared on CaO(II) and CaO-M. Especially CaO-M catalyst exhibited a remarkably high activity, while attaining a conversion of 100% in only 2—3 min. Though the activity of CaO(II) was less than that of CaO-M, the conversion reached ca. 100% within 40 min after starting the reaction. The product distribution is shown in Table 1, showing that *trans*-2-butene was preferentially formed on both CaO(II) and CaO-M catalysts. This result agrees with those of Miyahara et al.[4] or of Shima and Yamaguchi.[5] The equilibrium composition of the hydrogenation products at 273 K can be calculated as 1-butene : *trans*-2-butene : *cis*-2-butene=2.3 : 76.1 : 21.6 (%). It can therefore be supposed that the experimental results regarding both CaO(II) and CaO-M catalysts nearly attained the thermodynamic equilibrium state due to the very high reaction rate. The conversion to 2-butene was higher than 96%, indicating that a 1,4-addition of hydrogen on 1,3-butadiene dominated. Strictly, it can also be considered that 1-butene was formed by a 1,2-addition during the initial stage, and then rapidly isomerized to 2-butenes, since the reaction rate was so high. However, from the results concerning the reaction of 1,3-butadiene and deuterium,[6] the 1,4-addition reaction predominantly proceeds on solid-base catalysts, such as MgO and CaO. It is consequently rational to regard that the hydrogenation in this study proceeded by the 1,4-addition mechanism. The reaction temperature of hydrogenation was so low that no further hydrogenation to butane could proceed, although CaO-M was the most active catalyst, as already described. However, if the reaction temperature was increased to as high temperature as 523 K,[11] the formation of butane would be detected. Also, in this study the rate from butenes to butane appears to be remarkably slow compared to the hydrogenation of butadiene. The initial rates of the hydrogenation, which were obtained from a decline of the linear region in 1.5-min intervals from the start of the reaction in the curve of the conversion vs. reaction time plots, are shown in Table 2. The rate on CaO-M was 2-times greater in magnitude than that on CaO(II).

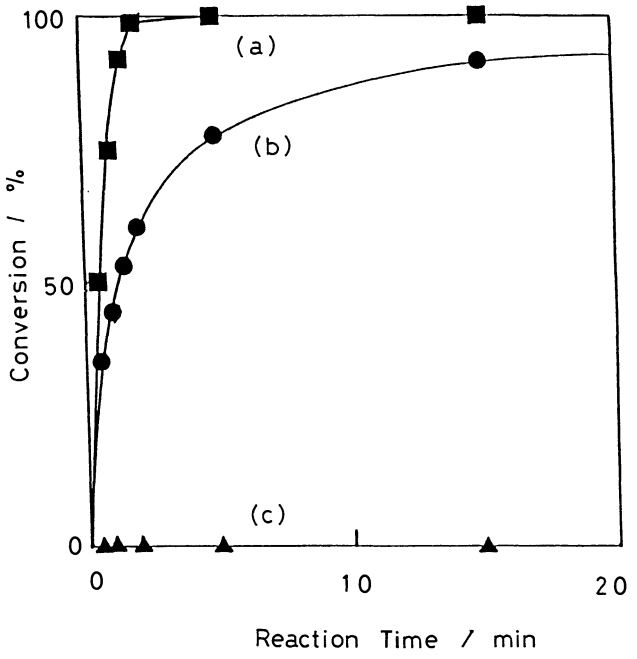

Fig. 1. The plot of conversion of 1,3-butadiene vs. reaction time.
(a) CaO-M, (b) CaO(II), (c) CaO(I).

Table 1. Product Distribution in Hydrogenation of 1,3-Butadiene

Catalyst	Reaction time/min	Conversion	Product/%		
		%	1-Butene	*trans*-2-Butene	*cis*-2-Butene
CaO-M	2	98.8	3.65	72.4	24.0
	5	100	3.26	71.8	25.0
	15	100	3.09	72.6	24.3
CaO(II)	2	60.8	3.73	72.4	22.9
	5	76.5	3.43	72.7	24.3
	15	90.9	3.16	72.3	24.6

Table 2. The Relative Spin Concentration and Initial Rate of the Hydrogenation on the Three CaO Catalysts

Catalyst	Initial rate	Relative spin concentration
	mmol g^{-1} min^{-1}	g^{-1}
CaO-M	8.93	3.59×10^{2} a)
CaO(II)	4.20	1.45×10^{2}
CaO(I)	0	4.01×10^{-2}

a) The caliblated value with the relative concentration of graphite carbon.

XRD Measurements. CaO(I) exhibited only CaO peaks as expected. Though before the pretreatment, CaO(II) mainly comprised $Ca(OH)_2$, after heating at 873 K under vacuum it turned to CaO accompanyed by a small amount of $Ca(OH)_2$, although the crystal structure was somewhat distorted. In the case of CaO-M, the XRD pattern exhibited relatively good crystallinity before the pretreatment, in which the peaks corresponded to CaO, $Ca(OH)_2$ and calcium dimethoxide, ($Ca(OCH_3)_2$) or calcium hydroxide methoxide ($Ca(OH)(OCH_3)$) were observed, as shown in Fig.2. However, $Ca(OH)(OCH_3)$ could not be distinguished from $Ca(OCH_3)_2$ by XRD. By the pretreatment the crystal state was remarkably distorted to be amorphous. Whether other alcohols, (for instance, ethanol and propanol) could similarly react with calcium oxide or not was examined. No calcium alcohoxides of ethanol and 2-propanol could be produced. Only the CaO peak was detected by XRD.

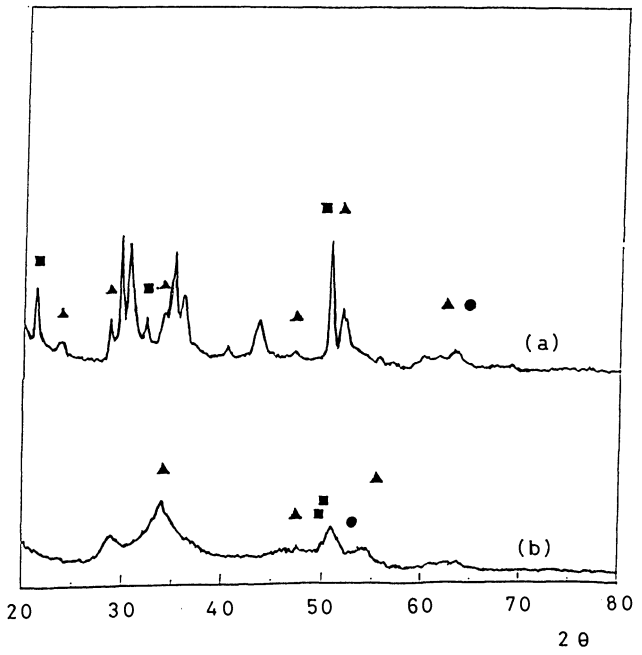

Fig. 2. XRD data of CaO-M (a) before (b) after the pretreatment.
●: CaO, ▲: $Ca(OH)_2$, ■: $Ca(OCH_3)_2$.

IR Measurement. Typical IR spectra of CaO-M measured after the treatment at room temperature and from 373 to 873 K at intervals of 100 K for 30 min under vacuum are shown in Fig. 3. From this data the formation of $Ca(OCH_3)_2$ and $Ca(OH)(OCH_3)$ could be clearly confirmed; i.e. the absorption bands at 1076 and 3640 cm^{-1} were assigned to $Ca(OH)(OCH_3)$[12] and those at 1079, 1159, 1410, 1472, 2072, 2192, 2306, 2592, 2777, 2818, 2864, and 2929 cm^{-1} also assigned to $Ca(OCH_3)_2$[13] (see Fig. 3 (a), (b), and (c)). It can be seen that both $Ca(OCH_3)_2$ and $Ca(OH)(OCH_3)$ were stable until 773 K, then gradually decreasing their strength with increasing temperature; at 873 K they were almost decomposed into CaO, leaving a small amount of $Ca(OH)_2$ (see Fig. 3(d)) which could be derived from the band at 3720 cm^{-1} shifted from 3670 cm^{-1}. The band shifted to 3720 cm^{-1} exhibits an isolated OH on the surface.[14] It is rather surprising that calcium methoxides can be eas-

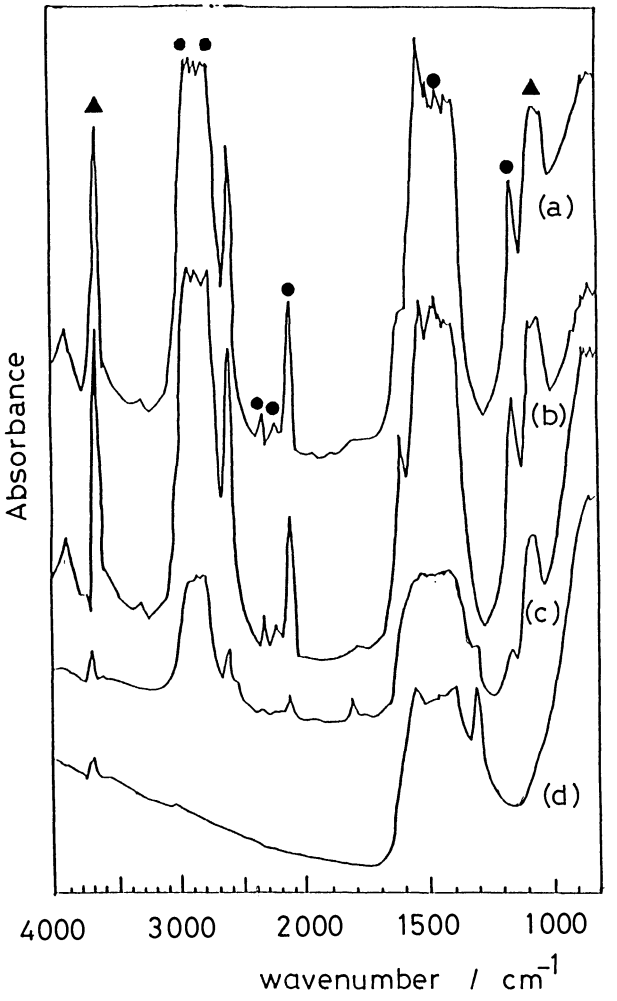

Fig. 3. IR spectra change of CaO-M treated under vacuum, (a): at room temperatures, (b): 573 K, (c): 773 K, (d): 873 K.
●: $Ca(OCH_3)_2$, ▲: $Ca(OH)(OCH_3)$.

ily produced by treatment with methanol at a relatively low temperature and are stable against heat. IR spectra of CaO(I) and (II) are also shown in Fig. 4 for a comparison. The bands between 500 and 1000 cm^{-1} characteristic for CaO, although the assignment was not known. As can be seen in CaO(II), the band at 3670 cm^{-1} can be assigned to basic OH, and that between 1300 and 1600 cm^{-1} probably to the OH of $Ca(OH)_2$.

EPMA (Electron Probe Microanalysis). The surface states of CaO(I),(II) and CaO-M were examined by EPMA. On CaO-M the deposition of free carbon was detected at the wavelength position of ca. 11.5 Å, which would cause the appearance of the dark-gray color on the catalyst after the pretreatment. On CaO(I) and (II) carbon deposition could not be entirely observed. It is therefore clear that the carbon on CaO-M is deposited by the decomposition of calcium methoxides.

ESR. The ESR spectra of CaO(I) and (II) exhibited nothing, except for that due to a Mn impurity.

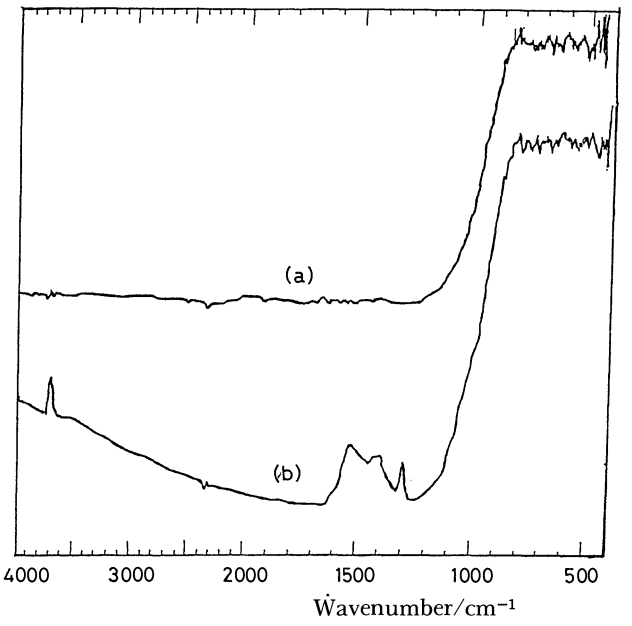

Fig. 4. IR spectra of (a) CaO(I) and (b) CaO(II) after the pretreatment.

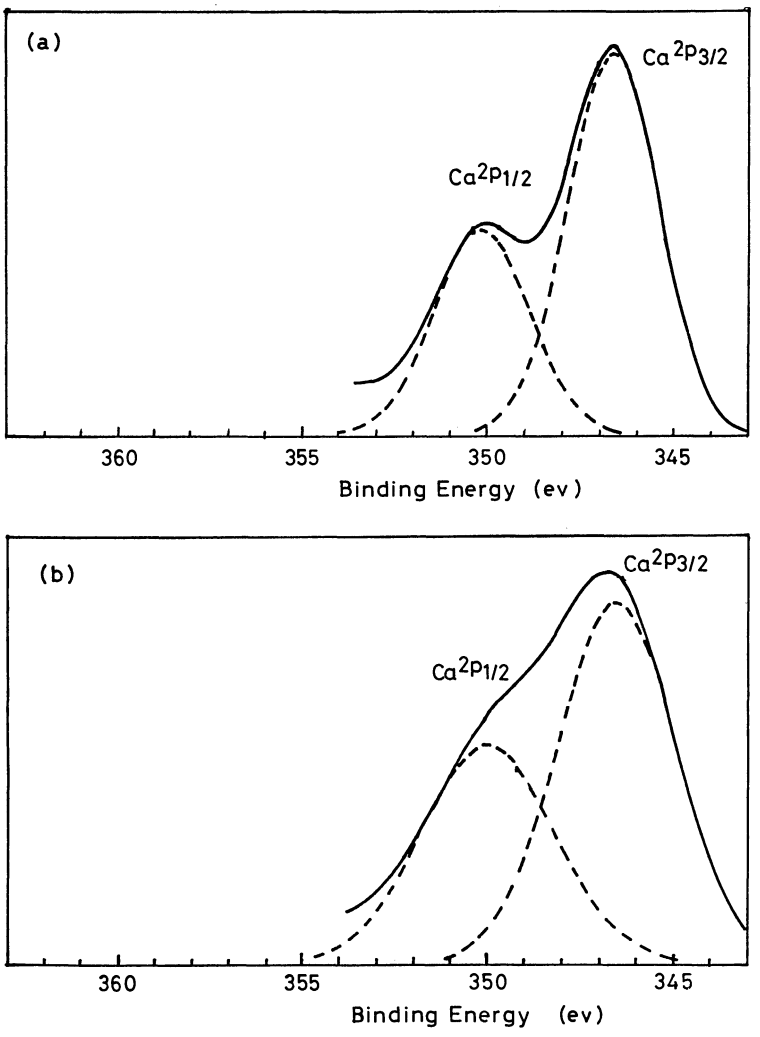

Fig. 5. XPS spectra of Ca $2P_{1/2}$ and Ca $2P_{3/2}$ of (a) CaO-M and of (b) CaO(I).

On the other hand, CaO-M gave a symmetrical Gaussian-shape signal at g=2.0033, which was assigned to graphite.[15,16] The relative spin concentration of the graphite carbon radical was estimated to be 4.31×10^2 per g of CaO-M. When butadiene, H_2 or CO_2 (being catalyst poison) was adsorbed on CaO-M, the carbon-radical signal did not entirely vary. This fact indicats that the carbon radical is not responsible for the hydrogenation. This conclusion was also derived from the fact that the carbon radical did not emerge on the CaO(II) catalyst. Therefore, other active sites should be expected to exist on the catalyst surface.

As described previously such electron-accepting molecules as oxygen inhibit hydrogenation, from which the electron-donating sites on CaO-M and CaO (II) may be active centers. It is further well-known that calcium oxides exhibit surface basicity. The basic sites are considered to be O^{2-} in the low-coordinatation sites.[17,18,19] Other electron-donating sites with the paramagnetic property, (for instance O^-) can be examined by an ESR measurement of the radical formed by the adsorption of an electron-accepting molecule, such as nitrobenzene.[14,20] When nitrobenzene was adsorbed on the three calcium oxide catalysts a relatively symmetrical signal with g=2.0048 could be detected. This also indicates that nitrobenzene adsorbs on graphite carbon on CaO-M to form its radical. By a comparison of the concentration of the nitrobenzene radical with that of DPPH, the relative spin concentrations of the electron-donating sites of these three catalysts were obtained (Table 2). The concentration of CaO-M is a value from which the value for the graphite carbon radical is subtracted. The concentration of CaO(II) and CaO-M were 3600- and 9000-times greater in magnitude than that of CaO(I). Though the existence of electron-donating sites can be detected in CaO(I), there is no hydrogenation activity. This may be due to the small amount of electron-donating sites.

XPS. Though the spectra of $Ca2P_{3/2}$, $Ca2P_{1/2}$, O1s and C1s showed similar binding energies in all samples, the size and shape of the spectra were different to some extent. In Figs. 5 and 6 the spectra derived from CaO(II) were omitted because of the similar behaviors to that of CaO-M and CaO(I). As shown in Fig. 6, the peak of O1s at 532.0 eV can be assigned to O^- derived from OH.[21,22] The peak assigned to O^{2-}, which can be seen at the position of 529.5 eV,[21,22] can not be clearly detected in Fig. 6. This seems to be due to an overlapping by the large O^- peak. The narrowest full width at half maximum (fwhm) of $Ca2P_{3/2}$, as the typical calcium band, O1s and C1s were measured and the ratios of the fwhm value of $Ca2P_{3/2}$ to O1s and to C1s, respectively, were calculated (Table 3). The ratio of $Ca2P_{3/2}$/O1s in CaO-M was the smallest, and increased in the order of CaO(II) and CaO(I). This fact indicates that the surface of CaO-M has somewhat more oxygen excess than does CaO(I) and (II). On the other hand, the ratio of $Ca2P_{3/2}$/C1s of CaO-M is smaller than that of the other two CaO catalysts. This fact indicates that carbon is deposited on the surface of CaO-M, which also agrees with the EPMA results.

Table 3. The Ratio of fwhm Values of $Ca2P_{3/2}$ to O1s and C1s

Catalyst	$Ca2P_{3/2}$/O1s	$Ca2P_{3/2}$/C1s
CaO-M	1.05	1.18
CaO(II)	1.09	1.82
CaO(I)	1.12	1.84

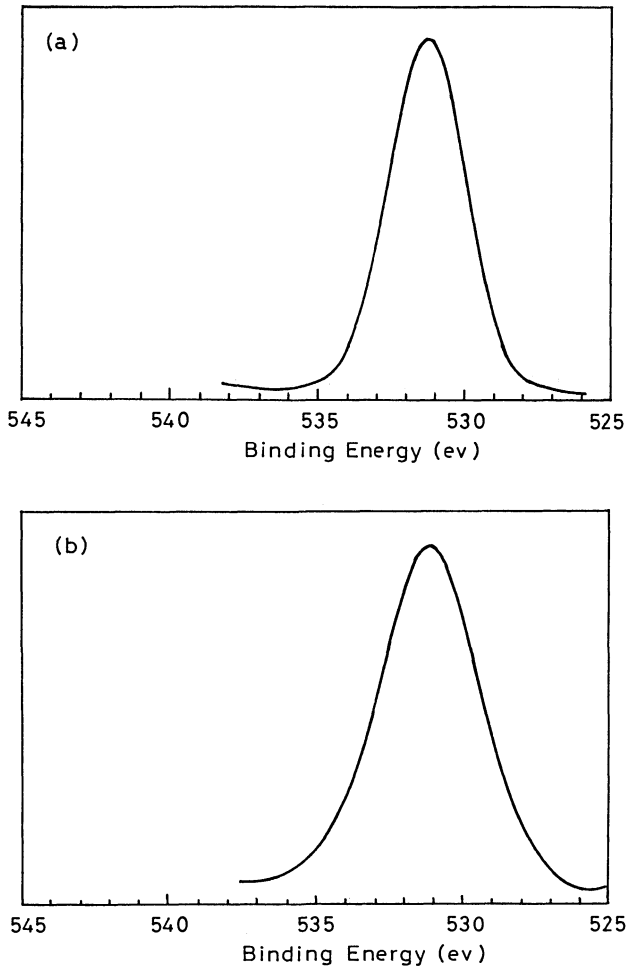

Fig. 6. XPS spectra of O1s of (a) CaO-M and of (b) CaO(I).

Basicity. A measure of the basicity from the amount of irreversible adsorption was obtained for the three CaO catalysts. The basicity of CaO-M, CaO(II) and (I) were 0.767, 0.277, and 0.019 mmol g^{-1}, respectively. As expected, the basicity of CaO-M was the largest. The correlation of the basicity between CaO-M and CaO(II) was 2.47 to 1 and that between the initial rates (Table 2) was 2.18 to 1. A relatively good

correlation could be obtained.

Discussion

Calcium oxide reacts with methanol to form calcium dimethoxide (I) and calcium hydroxide methoxide (II), as confirmed by XRD and IR measurements. These reaction schemes are described as follows, concurrently forming calcium hydroxide:

$$2CaO + 2CH_3OH \longrightarrow Ca(OCH_3)_2 + Ca(OH)_2, \quad (I)$$

and

$$CaO + CH_3OH \longrightarrow Ca(OH)(OCH_3). \quad (II)$$

When CaO treated with methanol was heated at 673 K under vacuum, the calcium methoxides remained. The CaO in this state did not entirely reveal any hydrogenation activity. This fact suggests that these calcium methoxides have no direct connection with activity. However, by a heat-treatment at 773 K under vacuum, in which the decomposition of calcium methoxides seemed to vigorously occur, a slight hydrogenation activity began to appear. At a temperature of 873 K most of the calcium methoxides converted to CaO, and remarkable activity was found. This fact indicates that the active sites are produced by the decomposition of calcium methoxides into CaO. The preparation of CaO by the decomposition of calcium methoxides is similar to the process in the sol-gel method. Generally, this method accompanying the hydrolysis of metal alcohoxides and calcination at a relative low temperature has been used to obtain both ceramics[23] and carriers[24] of high purity and activity; there has, however, been no report concerning a method to prepare highly active catalysts having a high surface area by a direct decomposition of metal alcohoxides.

Calcium hydroxide also showed activity due to a treatment at 873 K under vacuum, although the activity was low, due to an inadequate decomposition of $Ca(OH)_2$ at that temperature. As indicated in the literature,[2] it may be necessary to perform treatments at a temperature higher than 1073 K under vacuum. Martens et al [25] pointed out that the thermal decomposition of $Mg(OH)_2$ under vacuum released water and hydrogen in the temperature range, 570—970 K, leaving O^- and O^{2-} on the surface. Also, in the case of $Ca(OH)_2$, water and hydrogen are released, forming O^- and O^{2-} sites at the same time. In the case of CaO-M CH_3OH, CH_3OCH_3, and other compounds including water, CO, and hydrogen are probably released, although the decomposition process of calcium methoxides has not yet been clarified yet. Regarding the decomposition process of calcium methoxides, the growth of crystalization into CaO is probably suppressed by the release of the decomposed gases, leading to the high surface area of CaO. At the same time, it can be considered that some extent of the point defects accompanying the low coordination sites located at the edges and corners on a surface are formed. This consideration is rational, since CaO-M exhibited a distorted XRD pattern (see Fig. 2) and the surface area increased greatly. By the formation of point defects and low coordination sites, basic sites (i.e., the lattice O^{2-} and electron-donating sites accompanied by a paramagnetic property) are produced on the surface. As previously mentioned, since hydrogenation is ceased by the adsorption of CO_2, the basic sites on the surface are responsible for the hydrogenation; i.e., the O^{2-} sites are active centers. The O^- species are derived from the OH which remains on the surface in the undecomposable state, or which is derived by the adsorption of a proton—an abstracted from, for instance, hydrocarbon—on O^{2-}.[21,22] In this case, the former can be related with the formation of O^- sites. It is known that by XPS O^- and the lattice O^{2-} can be distinguished.[21,22] As shown in Fig. 6, however, the contribution of O1s of O^- at 532.0 eV was so large that the O^{2-} peak could not be found at 529.5 eV. Consequently, though there seems to be no O^{2-} sites on the surface, since CO_2 adsorption could be detected as a measure of the basicity, there must be O^{2-} sites (although the sites could not be clearly found in XPS). Iizuka et al.[14] have suggested that a nitrobenzene radical measurement revealed the property of the reducing sites on the surface and Kijenskii et al.[20] mentioned the property of the one-electron donating sites, although the detailed properties of both sites are not yet well known. If the reducing or one-electron donating sites are O^-, nitrobenezene can be adsorbed on the sites to form the nitrobenzene radical. In our study the relative spin concentration of nitrobenzene and DPPH of the three CaO catalysts were obtained (Table 2). The correlation between the relative spin concentration in the ESR measurement and the initial rate of hydrogenation on both CaO-M and CaO(II) catalysts were sought. The ratios of the relative spin concentration and the initial rate were 1 : 2.48 and 1 : 2.13, respectively. A good correlation between them was obtained. The initial rates, basicity and relative spin concentrations on CaO-M and CaO(II) per unit surface area were obtained as 6.4×10^{-2}, 7.6×10^{-2}, (mmol m^{-2} min^{-1}), 5.0×10^{-3}, 5.5×10^{-3} (mmol m^{-2}), and 2.6, 2.6 (m^{-2}), respectively. Since relatively good correlations between the rates and basicity or spin concentration per unit surface area were also found, it can be considered that the active sites on CaO-M and CaO(II) for hydrogenation consist of the same kind of sites.

It is suspected that the O^- sites are the active center. This conclusion agrees with the fact that Inoue and Yasumori[21] assumed that the active center of the hydrogeantion of ethylene would be O^-. From the results of the basicity measurement the basic sites were correlated with the initial rate, indicating that the

basic sites are also another active center. Especially in the case of CaO-M, a large amount of the active center can be produced. From the results of XPS, it was found that fwhm values of $Ca2P_{3/2}$ and O1s of the three catalysts decrease in the order CaO(I), (II) and CaO-M (see Table 3). This result is responsible for the presence of the excess amount of O^- sites on the CaO-M catalyst, which results in the high activity. It may be concluded that the hydrogenation of 1,3-butadiene proceeds at both basic and paramagnetic sites (i.e., O^{2-} and O^-), which both can be derived from the decomposition of calcium methoxides that have a strong effect on hydrogenation.

The authors gratefully thank Mr. M. Ohsima who is an assistant in the Deparment of Applied Chemistry in Saitama University, for measurements of XPS and basicity and further for drawing of the figures.

References

1) Y. Schachter and H. Pines, *J. Catal.*, **11**, 147 (1968).
2) H. Pines and W. M. Stabick, "Base Catalyzed Reactions of Hydrocarbons and Related Compounds," Academic Press, New York (1977), p. 544.
3) Y. Tanaka, H. Hattori, and K. Tanabe, *Chem. Lett.*, **1976**, 37.
4) K. Miyahara, Y. Murata, I. Toyoshima, Y. Tanaka, and T. Yokoyama, *J. Catal.*, **68**, 186 (1981).
5) H. Shima and T. Yamaguchi, *J. Catal.*, **90**, (1984).
6) H. Hattori, Y. Tanaka, and K. Tanabe, *J. Am. Chem. Soc.*, **98**, 4652 (1976).
7) M. Boudart, A. Deiboulle, E. G. Derouane, V. Indovina, and A. B. Walters, *J. Am. Chem. Soc.*, **94**, 6622 (1972).
8) M. Uchiyama, H. Hattori, and K. Tanabe, *J. Catal.*, **53**, 237 (1978).
9) M. F. Hoq and K. J. Klabunde, *J. Am. Chem. Soc.*, **108**, 2114 (1986).
10) T. Chang and A. H. Kahn, "Electron Paramagnetic Resonance Intensity," ed by National Bureau of Standards Special Publication 260-59 S, RM-2601; Description and Used p. 4 (1978).
11) H. Hattori, Y. Tanaka, and K. Tanabe, *Chem. Lett.*, **1875**, 659.
12) H. D. Lutz, *Z. Anorg. Allgem. Chem.*, **353** 207 (1967).
13) K. Kubo, K. Uchida, K. Tubozaki, and F. Hashimi *Kohgyo Kagaku Zasshi*, **73**, 75 (1970).
14) T. Iizuka, H. Hattori, Y. Ohno, J. Sohm, and K. Tanabe, *J. Catal.*, **22**, 130 (1971).
15) K. L. Collins, M. D. Bell, and G. Kaus, *J. Appl. Phys.*, **30**, 56 (1959).
16) I. F. Baycher and B. Ellis, *J. Colloid Interface Sci.*, **30**, 658 (1972).
17) A. J. Tench and R. L. Nelson, *Trans. Faraday Soc.*, **63**, 2254 (1967).
18) M. Che, C. Naccache, and B. Imelik, *J. Catal.*, **24**, 326 (1972).
19) D. Cordishi, V. Indovina, and A. Cimino, *J. Chem. Soc., Faraday Trans. 1*, **70**, 2189 (1974).
20) J. Kijenski and S. Malinowski, *Bull. Acad. Pol. Sci., Ser. Sci. Chim.*, **25**, 329, 427 (1977).
21) Y. Inoue and I. Yasumori, *Bull. Chem. Soc. Jpn.*, **54**, 1505 (1981).
22) C. T. Au, A. F. Carley, and M. W. Roberts, *Int. Rev. Phys. Chem.*, **5**, 57 (1986).
23) S. Sakka, *Bull. Inst. Chem. Res., Kyoto Univ.*, **61**, 376 (1983).
24) Y. Hirashima and A. Ueno, *Shokubai*, **28**, 250 (1986).
25) R. Martens, H. Gentsch, and F. Freund, *J. Catal.*, **44**, 366 (1976).

The Hypervirial Condition upon Coulson-Longuet-Higgins Polarizabilities in the Hückel Model

Makoto ISIHARA
Department of General Education, Shotoku-Gakuen Women's Junior College, Nakauzura 1-38, Gifu 500
(Received October 15, 1990)

This paper describes a fundamental condition upon Coulson-Longuet-Higgins polarizabilities in the Hückel model. The condition, named the hypervirial condition upon polarizabilities, consists of linear equations to be fulfilled by polarizabilities, being derivable from the hypervirial condition upon site electron densities and bond orders. The hypervirial condition upon polarizabilities can lead us to various simple relationships between polarizabilities, aided by the two auxiliary conditions stemming from the conservation of the number of electrons and from the Hellmann-Feynman theorem. The relationships, being characteristic of a system, will be useful for considering the reactivity of the system within the Hückel model. Several examples for typical systems are given to illustrate how the hypervirial and the auxiliary conditions work practically.

In the previous paper,[1] the author has derived the hypervirial condition upon p-densities[2] in the Hückel model and has set forth the significance of the condition with illustrative applications. The present paper, following the previous one, describes the hypervirial condition upon Coulson-Longuet-Higgins polarizabilities[3-6] (called merely polarizabilities below) in the Hückel model. From now on, the hypervirial conditions upon p-densities and upon polarizabilities are abbreviated to the pHVC and the πHVC, respectively.

The πHVC can lead us to various simple relationships between polarizabilities, aided by the two auxiliary conditions stemming from the conservation of the number of electrons and from the Hellmann-Feynman theorem. The relationships, being characteristic of a system, will be useful for considering the reactivity of the system within the Hückel model. The πHVC must have wide applicability as the pHVC.

We have the four sections below: The first section, deriving the πHVC from the pHVC after preparation of basic definitions, gives some general remarks on the πHVC. The second is a brief account of the symmetry condition and the intrinsic πHVC nontrivial under the symmetry condition. The third concerns the two auxiliary conditions and the last includes several examples illustrating how the πHVC and the auxiliary conditions work practically.

The Hypervirial Condition upon Polarizabilities

Let us consider the Hückel model of an electronic system of m sites. Denote the set $\{1, \cdots, m\}$ of the sites by M and the set of the up- and the down-spin states by Ω. Assume that the Hückel matrix B is real symmetric and that the Hückel model Hamiltonian $H(B)$ depends parametrically on the components $\{b_{rs}\}$ of B under the $m(m-1)/2$ constraints

$$b_{rs}=b_{sr} \qquad (r<s\in M). \tag{1}$$

Using the annihilators $\{a_{r\mu}\}$ and the creators $\{a_{r\mu}^{\dagger}\}$ for the $2m$ one-electron quantum states $\{r\mu\}$, we can write $H(B)$ explicitly as

$$H(B)=\sum_{r,s\in M} b_{rs}\rho_{rs} \tag{2}$$

with

$$\rho_{rs}=\sum_{\mu\in\Omega}(a_{r\mu}^{\dagger}a_{s\mu}+a_{s\mu}^{\dagger}a_{r\mu})/2. \tag{3}$$

For each normalized eigenstate $|B\rangle$ of $H(B)$ we have the matrix $P(B)$ of p-densities

$$p_{rs}(B)=\langle B|\rho_{rs}|B\rangle \qquad (r,s\in M). \tag{4}$$

Polarizabilities $\{\pi_{rs}^{tu}(B)\}$ are defined as[4]

$$\pi_{rs}^{tu}(B)=\frac{\partial}{\partial b_{tu}}p_{rs}(B) \qquad (r,s,t,u\in M), \tag{5}$$

which have the following inherent symmetry for interchange of subscripts.

$$\pi_{rs}^{tu}(B)=\pi_{sr}^{tu}(B)=\pi_{rs}^{ut}(B)=\pi_{sr}^{ut}(B) \tag{6}$$

and

$$\begin{cases}\pi_{rs}^{tu}(B)=\pi_{tu}^{rs}(B) & (r=s,\ t=u \text{ or } r\neq s,\ t\neq u)\\ \pi_{rr}^{tu}(B)=2\pi_{tu}^{rr}(B) & (t\neq u).\end{cases} \tag{7}$$

Let $\Pi^{tu}(B)$ be the matrix having $\pi_{rs}^{tu}(B)$ as r,s-component;

$$\Pi^{tu}(B)=\frac{\partial}{\partial b_{tu}}P(B) \qquad (t,u\in M), \tag{8}$$

which is real symmetric as well as $P(B)$.

Now, the pHVC for the Hamiltonian $H(B)$ can be written in the matrix form as[1]

$$[B, P(B)]=0. \tag{9}$$

Differentiating this with respect to b_{tu}, we obtain the πHVC

$$[B, \Pi^{tu}(B)]=\Phi^{tu}(B) \qquad (t\leqq u\in M), \tag{10}$$

where $\Phi^{tu}(B)$ is the real antisymmetric matrix having the components $\{\phi_{rs}^{tu}(B)\}$ expressible in general form as

$$\phi_{rs}^{tu}(B)=(\delta_{st}p_{ru}(B)-\delta_{rt}p_{su}(B)+\delta_{su}p_{rt}(B)-\delta_{ru}p_{st}(B))/(1+\delta_{tu}). \tag{11}$$

Each of the components is actually quite simple even if nonvanishing. The matrix $\Phi^{tu}(B)$ is invariant for interchange of subscripts tu as well as $\Pi^{tu}(B)$.

What is to be kept in mind is that the πHVC is formally common to all the eigenstates of $H(B)$ without regard to the number of electrons as the pHVC is. Say, supposing the one-electron eigenstate, we can regard polarizabilities and p-densities in the πHVC as being due to one Hückel orbital. We can suppose not only ground but also excited states. Now assume that a system in $|B\rangle$ is perturbed with the change of b_{tu} that alters B to B'. Then, the electron distribution in the system is so rearranged as to fit $|B'\rangle$. What the πHVC means here is that the rearrangement occurs keeping some detailed balance, and that the detailed balance is of the same character for all the eigenstates of $H(B)$.

So far, the Hückel matrix B remains parametric, specified only by its dimension m the number of sites. Actually, we are almost always interested in the effect of small changes of b_{tu} at certain standard "values" $\{\beta_{rs}\}$ of $\{b_{rs}\}$. Let B_0 be the Hückel matrix having the components $\{\beta_{rs}\}$ and let us omit the argument symbol (B) after the substitution of B_0. In what follows, the πHVC at $B=B_0$

$$[B_0, \Pi^{tu}] = \Phi^{tu} \qquad (t \leqq u \in M) \tag{12}$$

is considered exclusively, where B_0 reflects the structural and the symmetry features of the system. The terms "the simple Hückel model" and "the semisimple Hückel model"[7] are operative with regard to B_0. Thus, the simple Hückel model has the πHVC of the form

$$[J, \Pi^{tu}] = \Phi^{tu} \qquad (t \leqq u \in M) \tag{13}$$

Table 1. Dictionary of the Diagrammatic Representation of πHVRs in the Semisimple Hückel Model[a]

Term	Diagram	Term	Diagram
$\alpha_r \pi_{rs}^{tu}$ [b]		ϕ_{rs}^{rs}	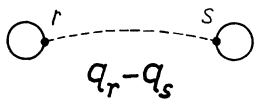
$\beta_{rs} \pi_{ss}^{tu}$ [c]	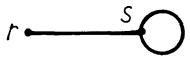	ϕ_{rs}^{rt}, ϕ_{rs}^{tr} $(t \neq s)$	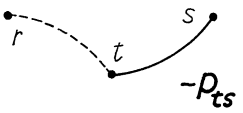
$\beta_{rv} \pi_{vs}^{tu}$ $(v \neq r,s)$		ϕ_{rs}^{st}, ϕ_{rs}^{ts} $(t \neq r)$	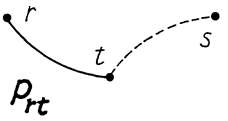
		ϕ_{rs}^{tu} $\begin{pmatrix} t \neq r,s \\ u \neq r,s \end{pmatrix}$	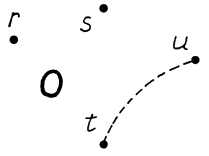
ψ_{rs}^{tu}	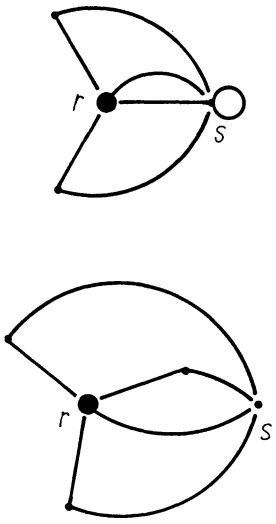	ϕ_{rs}^{rr} [d]	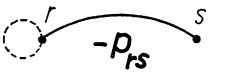
		ϕ_{rs}^{ss}	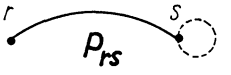
		ϕ_{rs}^{tt} $(t \neq r,s)$	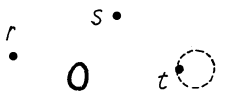

a) The symbols α_r and q_r are used instead of β_{rr} and p_{rr}, respectively. b) This term is ignorable in the simple Hückel model, canceling the corresponding term in ψ_{sr}^{tu}. c) This term appears only for adjacent rs, sharing the factor β_{rs} with the corresponding term in ψ_{sr}^{tu}. d) These three are really special cases of the above.

with the adjacency matrix J.[8] Here, Π^{tu} stands for $\beta\Pi^{tu}$ with β the sole resonance integral between adjacent sites.

The πHVC consists of linear equations to be fulfilled by polarizabilities, which can be written as

$$\psi_{rs}^{tu} - \psi_{sr}^{tu} = \phi_{rs}^{tu} \qquad (r<s,\ t\leqq u\in M) \tag{14}$$

with

$$\psi_{rs}^{tu} = \sum_{v\in M} \beta_v \pi_{vs}^{tu}. \tag{15}$$

The case of $r\geqq s$ is excluded because of the antisymmetry. Each of the equations, specified by upper tu and lower rs subscripts, is called the πHVR (hypervirial relationship between polarizabilities) for $[rs]tu$. In particular, for the simple Hückel model, we can put

$$\psi_{rs}^{tu} = \sum_{v\in C_r} \pi_{vs}^{tu}, \tag{16}$$

using the set C_r of the sites adjacent to r and rewriting $\beta\pi_{rs}^{tu}$ as π_{rs}^{tu}. Exceptional cases aside, no πHVR contains many terms in the simple Hückel model even if m becomes large. The situation is similar in the semisimple Hückel model.

We can represent πHVRs with simple diagrams on structural formulas in the semisimple Hückel model. The diagrammatic representation is especially useful for writing out πHVRs for individual systems. Table 1 is an adequate dictionary of the diagrammatic representation of πHVRs, doubling as a list of the concrete expressions of ϕ_{rs}^{tu}'s. Note that the representation of ψ_{rs}^{tu} is not affected by upper subscripts.

The Symmetry Condition and the Intrinsic πHVC

Let G be the permutation group on M that consists of all the permutations $\{x\}$ keeping B_0 invariant in the sense that[1]

$$\beta_{xrxs} = \beta_{rs} \qquad (r,s\in M). \tag{17}$$

Then, we have the permutational symmetry condition

$$\pi_{xrxs}^{xtxu} = \pi_{rs}^{tu} \qquad (r,s,t,u\in M) \tag{18}$$

for faithful states.[9] Confine ourselves to faithful states whenever the permutational symmetry is taken into account. Incorporating the inherent symmetry into the permutational symmetry condition, we have the symmetry condition.

Let us refer to the πHVR remaining nontrivial under the symmetry condition as the intrinsic πHVR. All the intrinsic πHVRs together constitute the intrinsic πHVC. As to how to draw out intrinsic πHVRs, the situation being similar to that for intrinsic pHVRs[1] (hypervirial relationships between p-densities), details are omitted here. The crucial point peculiar to intrinsic πHVRs is that the value of b_{tu} for the perturbed position tu[10] should be regarded tentatively as being off β_{tu}, and that the tentative perturbed symmetry should be considered for each tu individually.

Let G^{tu} be the subgroup of G that consists of all the permutations $\{x\}$ satisfying $x(tu)=tu$ or $x(tu)=ut$. In many cases, G^{tu} is a tiny group of order one or two, even if the order of G is large. The following guidelines will suffice to draw out intrinsic πHVRs practically. The last one is determinative.

(1) The πHVR for $[x(rs)]tu$ is identical with that for $[rs]x^{-1}(tu)$ for any $x\in G$.

(2) The πHVR for $[r's']tu$ is identical with that for $[rs]tu$ if there exists $x\in G^{tu}$ satisfying $r's'=x(rs)$.

(3) The πHVR for $[rs]tu$ is intrinsic unless there exists $x\in G^{tu}$ satisfying $sr=x(rs)$.

Apart from exceptional cases, all the intrinsic pHVRs of a system are necessarily independent.[1,11] In contrast to this, it is possible for some intrinsic πHVRs to be mutually dependent. When a system has intrinsic pHVRs, it is also possible for some intrinsic πHVRs to contain the intrinsic pHVRs implicitly. Then, reversely, the intrinsic pHVRs make the intrinsic πHVRs mutually dependent.

The symmetry condition classifies polarizabilities into sets of equivalent polarizabilities. Taking one polarizability from each set as a representative, we have the symmetry-independent representatives, which are abbreviated to the SIRs below. When we treat a lot of equations for polarizabilities simultaneously, it is helpful or rather necessary to translate the equation containing arbitrary polarizabilities into that containing only SIRs.

The Auxiliary Conditions

The analysis with the πHVC is facilitated by using the following two auxiliary conditions,[12] particularly when a system does not have many sites. Both conditions are also formally common to all the eigenstates of $H(B)$ without regard to the number of electrons.

The Number Conservation Condition. The number n of electrons can be constant for the change of b_{tu}. Hence, differentiating the number condition

$$\mathrm{Tr}(P(B)) = n \tag{19}$$

with respect to b_{tu} and substituting B_0 for B, we have the number consevation condition

$$\mathrm{Tr}(\Pi^{tu}) = 0 \qquad (t\leqq u\in M), \tag{20}$$

each constituent of which is referred to as the NCR (number conservation relationship) for tu. The NCR for $x(tu)$ is identical with that for tu for any $x\in G$.

The number conservation condition makes πHVRs for $[rs]tt$'s for arbitrary rs and all t's mutually dependent, since we have

$$\sum_{t\in M} [B_0, \Pi^{tt}] = 0 \tag{21}$$

as well as

$$\sum_{t\in M} \Phi^{tt} = 0. \tag{22}$$

The intrinsic πHVC is, therefore, not always inde-

pendent of the number conservation condition.

The Polarizability Sum Condition. It follows from the Hellmann-Feynman theorem[13] immediately that

$$(\frac{\partial}{\partial b_{tu}}\langle B|)H(B)|B\rangle+\langle B|H(B)(\frac{\partial}{\partial b_{tu}}|B\rangle)=0 \quad (t\leqq u\in M). \tag{23}$$

Using the expression

$$\pi_{rs}^{tu}(B)=(\frac{\partial}{\partial b_{tu}}\langle B|)\rho_{rs}|B\rangle+\langle B|\rho_{rs}(\frac{\partial}{\partial b_{tu}}|B\rangle) \tag{24}$$

and substituting B_0 for B, we obtain the polarizability sum condition[14]

$$\mathrm{Tr}(B_0\Pi^{tu})=0 \qquad (t\leqq u\in M), \tag{25}$$

each constituent of which is referred to as the PSR (polarizability sum relationship) for tu. The PSR for $x(tu)$ is identical with that for tu for any $x\in G$. Since

$$\sum_{t\in M}\mathrm{Tr}(B_0\Pi^{tt})=0 \tag{26}$$

holds, PSRs for tt's become mutually dependent under the number conservation condition.

By using the polarizability sum condition it is readily found that

$$\sum_{t\leqq u\in M}\beta_{tu}[B_0, \Pi^{tu}]=0, \tag{27}$$

while we obtain

$$\sum_{t\leqq u\in M}\beta_{tu}\Phi^{tu}=[P, B_0]. \tag{28}$$

That is, πHVRs for $[rs]tu$'s for arbitrary rs and all $t\leqq u$'s[15] together yield the pHVR for rs. This brings on the case that some intrinsic πHVRs become mutually dependent under the polarizability sum condition and the intrinsic pHVC.

To write out PSRs practically, it is preferable to arrange the terms as

$$\sum_{r\in M}\beta_{rr}\pi_{rr}^{tu}+2\sum_{r<s\in M}\beta_{rs}\pi_{rs}^{tu}=0 \qquad (t\leqq u\in M), \tag{29}$$

which is reduced for the simple Hückel model to

$$\sum_{r<s\in M}{}'\,\pi_{rs}^{tu}=0 \qquad (t\leqq u\in M). \tag{30}$$

Here, the prime means that the summation is restricted to adjacent sites.

It remains still possible for other additional dependence to occur in intrinsic πHVRs. However, it seems quite knotty to analyze the situation exhaustively to ascertain a fully systematic way of extracting only independent equations from all the conditions. Fortunately, this annoying point for completeness causes no serious difficulties actually.

Illustrative Examples

To treat typical systems with the πHVC and the auxiliary conditions will be the best way of understanding the nature of the conditions. Throughout this section, π_{rs}^{tu} is used for $\beta\pi_{rs}^{tu}$, being dimensionless and opposite to the original one in sign with β negative. See Fig. 1 for the numbering of sites and the notation for p-densities.

The Symmetric Two-Site System. This system provides the simplest example of the intrinsic πHVC. Let us choose π_{11}^{11}, π_{22}^{11}, π_{12}^{11}, and π_{12}^{12} as the SIRs. Even if b_{12} becomes off β, the two sites remain equivalent; if b_{11} becomes off α, the symmetry vanishes. Hence,

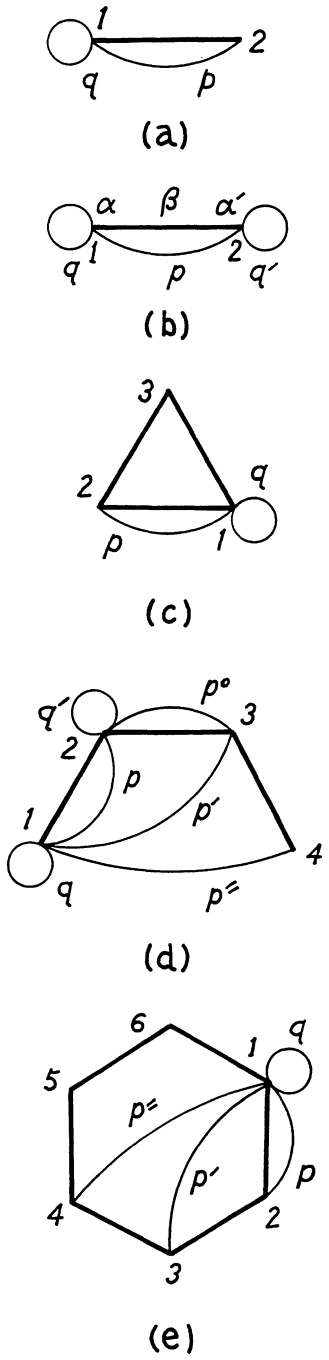

Fig. 1. The notation and the numbering of sites in the examples: (a) The symmetric two-site system, (b) The asymmetric two-site system, (c) The three-site ring, (d) The four-site linear chain, (e) The six-site ring.

only the πHVR for [12]11

$$\pi_{22}^{11}-\pi_{11}^{11}=-p \tag{31}$$

is intrinsic. From this and the NCR for 11

$$\pi_{11}^{11}+\pi_{22}^{11}=0 \tag{32}$$

it follows that

$$\pi_{11}^{11}=-\pi_{22}^{11}=p/2. \tag{33}$$

The PSRs for 11 and 12 are, in themselves,

$$\pi_{12}^{11}=\pi_{12}^{12}=0. \tag{34}$$

We have positive π_{11}^{11}, as expected, for the ground state of less than four electrons. Yet, if p is negative or zero, so is π_{11}^{11}, which is really the case for excited states.

The Asymmetric Two-Site System. This system can exemplifies the relation between the conditions concisely. Choose π_{11}^{11}, π_{22}^{11}, π_{12}^{11}, π_{22}^{22}, π_{12}^{22}, and π_{12}^{12} as the SIRs. Under the NCRs for 11, 22, and 12

$$\pi_{11}^{11}+\pi_{22}^{11}=0, \tag{35}$$

$$\pi_{22}^{11}+\pi_{22}^{22}=0, \tag{36}$$

and

$$\pi_{12}^{11}+\pi_{12}^{22}=0, \tag{37}$$

the PSRs for 11 and 22 become dependent on each other, leading to

$$\lambda\pi_{11}^{11}+\pi_{12}^{11}=0 \tag{38}$$

with

$$\lambda=(\alpha-\alpha')/2\beta. \tag{39}$$

The PSR for 12 is written, by using the NCR for 12, as

$$2\lambda\pi_{12}^{11}+\pi_{12}^{12}=0. \tag{40}$$

These five equations suffice to express all the SIRs in terms of π_{11}^{11}. The π_{11}^{11}-expression

$$\begin{cases} \pi_{22}^{22}=-\pi_{22}^{11}=\pi_{11}^{11} \\ \pi_{12}^{11}=-\pi_{12}^{22}=-\lambda\pi_{11}^{11} \\ \pi_{12}^{12}=2\lambda^2\pi_{11}^{11} \end{cases} \tag{41}$$

is instructive in itself showing the sign and the order of each SIR.

The intrinsic πHVC consists of three πHVRs. The NCRs make the πHVRs for [12]11 and [12]22 dependent on each other. Using the π_{11}^{11}-expression in the πHVR for [12]11

$$2\lambda\pi_{12}^{11}+\pi_{22}^{11}-\pi_{11}^{11}=-p, \tag{42}$$

we find

$$\pi_{11}^{11}=p/2(1+\lambda^2), \tag{43}$$

which enables us to express the other SIRs in terms of p and λ.[16] On the other hand, the πHVR for [12]12

$$2\lambda\pi_{12}^{12}+2\pi_{12}^{22}-2\pi_{12}^{11}=q-q' \tag{44}$$

results in the intrinsic pHVR[1]

$$2\lambda p=q-q'. \tag{45}$$

With this presupposed, the πHVR for [12]12 is no longer independent of the others.

The Three-Site Ring. Next, take the smallest ring in the simple Hückel model, the simplest nonalternant system. This system has the five independent equations connecting the six SIRs π_{11}^{11}, π_{22}^{11}, π_{12}^{11}, π_{23}^{11}, π_{12}^{12}, and π_{23}^{12}. Let us, therefore, find the π_{11}^{11}-expression of the SIRs. From the auxiliary conditions, we have

$$\pi_{22}^{11}=-\pi_{11}^{11}/2, \tag{46}$$

$$\pi_{12}^{11}=-\pi_{23}^{11}/2, \tag{47}$$

and

$$\pi_{23}^{12}=-\pi_{12}^{12}/2, \tag{48}$$

which are substituted into the πHVRs

$$\pi_{22}^{11}+\pi_{23}^{11}-\pi_{11}^{11}-\pi_{12}^{11}=-p \tag{49}$$

and

$$2\pi_{12}^{11}+\pi_{12}^{12}-2\pi_{23}^{11}-\pi_{23}^{12}=p \tag{50}$$

to yield

$$\pi_{23}^{11}=\pi_{11}^{11}-2p/3 \tag{51}$$

and

$$\pi_{12}^{12}=2(\pi_{11}^{11}-p/3). \tag{52}$$

Note that this system has the degeneracy causing nonfaithful states, to which the above relationships are inapplicable. The one- and the two-electron ground states, necessarily faithful, have $\pi_{11}^{11}=4p/9$ and $p=n/3$, which leads to, say,

$$\pi_{23}^{11}-\pi_{12}^{11}=-n/9 \tag{53}$$

and

$$\pi_{12}^{12}-\pi_{23}^{12}=n/9. \tag{54}$$

No explanation will be necessary as to what these mean.

The Four-Site Linear Chain. The number of the SIRs amounts to thirty-one for the four-site linear chain even in the simple Hückel model. The auxiliary conditions give seven independent equations. The number of the intrinsic πHVRs that remain independent of one another and of the auxiliary conditions is twenty-one under the intrinsic pHVC

$$\begin{cases} p'=q'-q \\ p''=p^{\circ}-p. \end{cases} \tag{55}$$

Fortunately, the thirty-one SIRs are seperated into three sets in entering twenty-eight equations because of the alternant symmetry and the number of SIRs of each set is one more than that of equations for the set. All the SIRs of each set are, hence, expressible in terms of one SIR of the set. Because each equations contains, at most, only four SIRs, it is never intractable to work out the equations in spite of the largeness of the number of SIRs.

The twelve SIRs π_{11}^{11}, π_{22}^{11}, π_{33}^{11}, π_{44}^{11}, π_{22}^{22}, π_{33}^{22}, π_{13}^{11}, π_{24}^{11}, π_{13}^{22}, π_{24}^{22}, π_{13}^{13}, and π_{24}^{13} concern the three NCRs for 11, 22, and 13

$$\pi_{11}^{11}+\pi_{22}^{11}+\pi_{33}^{11}+\pi_{44}^{11}=0, \tag{56}$$

$$\pi_{22}^{11}+\pi_{22}^{22}+\pi_{33}^{22}+\pi_{33}^{11}=0, \tag{57}$$

and

$$\pi_{13}^{11}+\pi_{13}^{22}+\pi_{24}^{22}+\pi_{24}^{11}=0, \tag{58}$$

and the eight πHVRs for [12]11, [12]33, [12]13, [23]11, [23]22, [14]11, [14]22, and [14]13

$$\pi_{22}^{11}-\pi_{11}^{11}-\pi_{13}^{11}=-p, \tag{59}$$

$$\pi_{33}^{22}-\pi_{33}^{11}-\pi_{24}^{22}=0, \tag{60}$$

$$2\pi_{13}^{22}-2\pi_{13}^{11}-\pi_{13}^{13}=-p^\circ, \tag{61}$$

$$\pi_{33}^{11}+\pi_{13}^{11}-\pi_{22}^{11}-\pi_{24}^{11}=0, \tag{62}$$

$$\pi_{33}^{22}+\pi_{13}^{22}-\pi_{22}^{22}-\pi_{24}^{22}=-p^\circ, \tag{63}$$

$$\pi_{24}^{11}-\pi_{13}^{11}=-p'', \tag{64}$$

$$\pi_{24}^{22}-\pi_{13}^{22}=0, \tag{65}$$

and

$$\pi_{24}^{13}-\pi_{13}^{13}=-p. \tag{66}$$

The last three may be suggestive by themselves. Expressing the SIRs in terms of π_{11}^{11}, we obtain the result summarized in Table 2. We can reconstruct arbitrary relationships between the SIRs using only π_{11}^{11}, p, and p°, at most. For the four-electron ground state, an easy, direct estimation[5] gives $\pi_{11}^{11}=0.626$, $p=0.894$, and $p^\circ=0.447$, which is enough to estimate the other SIRs.

On the other hand, the seven SIRs π_{12}^{12}, π_{23}^{23}, π_{23}^{12}, π_{34}^{12}, π_{14}^{12}, π_{14}^{23}, and π_{14}^{14} concern the three PSRs for 12, 23, and 14

$$\pi_{12}^{12}+\pi_{23}^{12}+\pi_{34}^{12}=0, \tag{67}$$

$$2\pi_{23}^{12}+\pi_{23}^{23}=0, \tag{68}$$

and

$$2\pi_{24}^{12}+\pi_{14}^{23}=0, \tag{69}$$

and the three πHVRs for [13]12, [13]23, and [13]14

$$\pi_{23}^{12}-\pi_{12}^{12}-\pi_{14}^{12}=-p^\circ, \tag{70}$$

$$\pi_{23}^{23}-\pi_{23}^{12}-\pi_{14}^{23}=p, \tag{71}$$

and

$$\pi_{14}^{23}-\pi_{14}^{12}-\pi_{14}^{14}=-p, \tag{72}$$

which suffice to express the SIRs in terms of π_{12}^{12}. The result is summarized in Table 3. For the four-electron ground state, we can use $\pi_{12}^{12}=0.089$ to estimate the other SIRs. As to the remaining twelve SIRs and eleven equations, the description is omitted for brevity.

It must be relevant to mention here the general features of the πHVC for alternant systems. Define the indicator σ_r of the attribute of site r as

$$\sigma_r=\begin{cases} 1 & (r \text{ starred}) \\ -1 & (r \text{ unstarred}) \end{cases} \tag{73}$$

and classify polarizabilities of an alternant system into three sets as

$$\pi_{rs}^{tu}=\begin{cases} {}^1\pi_{rs}^{tu} & (\sigma_r\sigma_s=\sigma_t\sigma_u=1) \\ {}^2\pi_{rs}^{tu} & (\sigma_r\sigma_s=\sigma_t\sigma_u=-1) \\ {}^3\pi_{rs}^{tu} & (\sigma_r\sigma_s\sigma_t\sigma_u=-1). \end{cases} \tag{74}$$

Then, the πHVRs can be classified also into three sets;

$$\sum_{v\in C_r}\beta_{rv}{}^i\pi_{vs}^{tu}-\sum_{v\in C_s}\beta_{sv}{}^i\pi_{vr}^{tu}={}^i\phi_{rs}^{tu} \qquad (i=1,2,3) \tag{75}$$

with

$$\phi_{rs}^{tu}=\begin{cases} {}^1\phi_{rs}^{tu} & (\sigma_r\sigma_s=-1;\ \sigma_t\sigma_u=1) \\ {}^2\phi_{rs}^{tu} & (\sigma_r\sigma_s=1;\ \sigma_t\sigma_u=-1) \\ {}^3\phi_{rs}^{tu} & (\sigma_r\sigma_s=\sigma_t\sigma_u). \end{cases} \tag{76}$$

The NCRs and the PSRs are classified as

$$\sum_{r\in M}{}^i\pi_{rr}^{tu}=0 \qquad (i=1,3) \tag{77}$$

and

$$\sum_{r<s\in M}{}'\beta_{rs}{}^i\pi_{rs}^{tu}=0 \qquad (i=2,3). \tag{78}$$

In particular, for the m-electron ground state of the m-site alternant system ${}^3\phi_{rs}^{tu}$'s are all vanishing and the equations for $i=3$ give nothing more than

$${}^3\pi_{rs}^{tu}=0 \tag{79}$$

a natural consequence of the fact that no perturbation at the site pair of different attributes violates the alternant symmetry.[17]

The Six-Site Ring. The last example is the simple Hückel model of the six-site ring, which has no intrin-

Table 2. The π_{11}^{11}-Expression of Some SIRs of the Four-Site Linear Chain in the Simple Hückel Model[a]

tu	rs	c_1	c_p	c_{p°
22	22	1	−1/2	1/2
11	22	−1	0	1/2
11	33	−1	1	−1/2
11	44	1	−1	0
22	33	1	−1/2	−1/2
11	13	−2	1	1/2
11	24	−2	3/2	0
22	13,24	2	−3/2	0
13	13	8	−5	0
13	24	8	−6	0

a) $\pi_{rs}^{tu}=c_1\pi_{11}^{11}+c_pp+c_{p^\circ}p^\circ$.

Table 3. The π_{12}^{12}-Expression of Some SIRs of the Four-Site Linear Chain in the Simple Hückel Model[a]

tu	rs	c_{12}	c_p	c_{p°
23	23	4	2	−4
12	23	−2	−1	2
12	34	1	1	−2
23	14	6	2	−6
12	14	−3	−1	3
14	14	9	4	−9

a) $\pi_{rs}^{tu}=c_{12}\pi_{12}^{12}+c_pp+c_{p^\circ}p^\circ$.

sic pHVR. The intrinsic πHVC gives seventeen independent equations under the auxiliary conditions consisting of seven independent equations. The thirty SIRs enter twenty-four equations, separated into three sets. We have ten, eight, and six equations, respectively, for twelve, ten, and eight SIRs. Hence, all the SIRs of each set are expressible in terms of relevantly chosen two SIRs of the set.

The description here is, however, confined to the derivation of a few relationships between atom-atom polarizabilities. Substituting the πHVR for [14]11

$$\pi_{24}^{11}-\pi_{13}^{11}=-p''/2 \tag{80}$$

into that for [12]33

$$\pi_{22}^{11}+\pi_{24}^{11}-\pi_{33}^{11}-\pi_{13}^{11}=0, \tag{81}$$

we obtain

$$\pi_{22}^{11}-\pi_{33}^{11}=p''/2. \tag{82}$$

From the πHVRs for [12]11, [12]44, and [14]22

$$\pi_{22}^{11}+\pi_{26}^{11}-\pi_{11}^{11}-\pi_{13}^{11}=-p, \tag{83}$$

$$\pi_{33}^{11}+\pi_{35}^{11}-\pi_{44}^{11}-\pi_{24}^{11}=0, \tag{84}$$

and

$$\pi_{13}^{11}+\pi_{35}^{11}-\pi_{26}^{11}-\pi_{24}^{11}=0, \tag{85}$$

it follows that

$$\pi_{11}^{11}-\pi_{22}^{11}+\pi_{33}^{11}-\pi_{44}^{11}=p, \tag{86}$$

which leads to

$$\pi_{11}^{11}-\pi_{44}^{11}=p+p''/2. \tag{87}$$

Further, using the NCR for 11

$$\pi_{11}^{11}+2\pi_{22}^{11}+2\pi_{33}^{11}+\pi_{44}^{11}=0, \tag{88}$$

we attain the π_{11}^{11}-expression

$$\begin{cases} \pi_{22}^{11}=-\pi_{11}^{11}/2+p/4+3p''/8 \\ \pi_{33}^{11}=-\pi_{11}^{11}/2+p/4-p''/8 \\ \pi_{44}^{11}=\pi_{11}^{11}-p-p''/2. \end{cases} \tag{89}$$

Note that these relationships are valid for any faithful states without regard to the number of electrons. For the six-electron ground state, although the values of all the atom-atom polarizabilities are already known,[5] the above relationships remain eloquent of how simply but delicately the polarizabilities are interrelated.

As the above treatment shows, we can often attain the result of significance only by working out some equations in the πHVC and the other conditions. This is an important advantage from an applicational point of view.

References

1) M. Isihara, *Bull. Chem. Soc. Jpn.*, **62**, 2284 (1989).

2) Site electron densities and bond orders are called generically p-densities, for convenience' sake. Ref. 11 of Ref. 1 includes the reason for the name.

3) The term "polarizability" has been used peculiarly in the Hückel model since Coulson and Longuet-Higgins' papers. The term has another meaning in the theory of dielectrics and it is prevalent to use the term fixedly for that meaning. Some authors prefer "mutability" to "polarizability." Still, we seem to have no decisive alternative at present.

4) C. A. Coulson and H. C. Longuet-Higgins, *Proc. R. Soc. London, Ser. A*, **191**, 39 (1947), the inceptive paper on polarizabilities in the Hückel model.

5) C. A. Coulson and H. C. Longuet-Higgins, *Proc. R. Soc. London, Ser. A*, **192**, 16 (1947); **193**, 447 (1948), which include the first basic applications of polarizabilities.

6) S. Aono and K. Nishikawa, *Bull. Chem. Soc. Jpn.*, **58**, 288 (1985), where polarizabilities are treated in a propagator formalism.

7) For the definition of these terms, see Ref. 1.

8) For the adjacency matrix, see, for example, Refs. 4 and 15 of Ref. 1.

9) The faithful eigenstate was introduced in Ref. 1, associated with the degeneracy, for which P.-O. Löwdin, *J. Chem. Phys.*, **21**, 496 (1953) may be suggestive.

10) Even if β_{tu} is zero, we should not ignore the change of b_{tu}. The perturbed position can be the site pair tu of vanishing β_{tu}.

11) The term "independent" is often used to mean "linearly independent" for short; so is "dependent."

12) Though Coulson and Longuet-Higgins have touched upon both conditions (Ref. 4), they have regarded the conditions only as such as checking tools for numerical calculation.

13) For example, S. T. Epstein, "The Hellmann-Feynman Theorem," in "The Force Concept in Chemistry," ed by B. M. Deb, Van Nostrand Reinhold, New York (1981).

14) This derivation is a little more transparent than Coulson and Longuet-Higgins' one.

15) The simple Hückel model allows us to replace "all $t\leqq u$" with "all adjacent $t<u$" here.

16) This does not mean that the dependence of the polarizabilities on λ is fully resolved, because p itself dependes on λ.

17) Obviously, π_{rr}^{tu} are zero for adjacent tu's, but ${}^1\pi_{rr}^{tu}$ does not vanish, in general.

Ion-Exchange Properties and Thermal Stability of Hydrous Titanium(IV)-Zirconium(IV) Oxide Ion Exchanger

Hiromichi YAMAZAKI, Yasushi INOUE,* Naoki KIKUCHI, and Hiroshi KURIHARA
Department of Nuclear Engineering, Faculty of Engineering, Tohoku University, Aramaki, Aoba-ku, Sendai 980
(Received September 11, 1990)

Ion-exchange properties and thermal stability were studied for hydrous Ti^{IV}-Zr^{IV} oxide ion exchangers with various contents of titanium. The cation-exchange capacity increased with the titanium content in the exchanger, along with a decrease in the anion-exchange capacity. Though the affinity for representative metal ions increases with the acidity of the exchange sites, no such simple relation holds for transition metal ions. Exchangers with 30 to 70 mol% Ti (the mol% of Ti to Ti+Zr) do not suffer from drastic changes in both the water content and crystallinity upon heating to 500 °C; they are much more heat-resistant than component simple hydrous metal oxides. Though the total cation-exchange capacity decreases with increasing temperature during a heat treatment, only a minute amount of the acidic sites dissociating at a pH lower than the isoelectric point of the exchangers with $\leqslant$70 mol% Ti increases upon heating. The effect of a heat treatment on the distribution coefficients of cations has been explained by these observations.

Hydrous metal oxides are sorbents with an ion-exchange selectivity peculiar to the metallic elements forming the materials.[1] However, they are thermodynamically metastable and liable to lose their ion-exchange capacity at high temperature. Tanabe et al. reported that binary metal oxides have a marked higher acidity than do component simple oxides.[2-4] It is conceivable that thermally stable hydrous metal oxides possessing a large ion-exchange capacity can be synthesized by combining more than two kinds of metallic elements. There have been few studies concerning the relation between the ion-exchange properties of binary and simple hydrous metal oxides. For this reason hydrous Si-Ti^{IV} oxides with various titanium contents were synthesized, and both their ion-exchange properties and thermal stability investigated. As a result, a hydrous Ti^{IV} oxide modified with Si, which has a higher ionic potential than does Ti^{IV}, had a larger ion-exchang capacity and was thermally more stable than simple hydrous Ti^{IV} oxide.[5]

In the present study a hydrous Ti^{IV} oxide modified with Zr^{IV}, which has a lower ionic potential than does Ti^{IV}, was investigated in order to clarify the effect of modifiers on the ion-exchange property and thermal stability of the materials.

Experimental

Reagents and Apparatus. Titanium(IV) chloride and zirconium(IV) chloride oxide octahydrate were supplied by Wako Pure Chemical Industries Ltd., and their purity was checked before use. A thermogravimetric analysis (TGA) and a differential thermal analysis (DTA) were undertaken with a Seiko micro thermal analyzer (Model SSC5020-TG/DTA300) at a heating rate of 10 °C min^{-1}. All the other apparatuses were the same as those described previously.[5]

Ion-Exchangers. A 1 M $TiCl_4$ aqueous solution and a 1 M $ZrOCl_2$ aqueous solution (1 M=1 mol dm^{-3}) were prepared by dissolving unhydrated titanium(IV) chloride and zirconium chloride oxide octahydrate in distilled water. They were mixed to make a solution with the desired molar ratio of Ti to Ti+Zr (the mixture). Hydrous Ti^{IV}-Zr^{IV} oxide was then precipitated by pouring the mixture into 1 M NaOH. The pH at precipitation was controlled within 13.0±0.1 by varying the volume ratio of the NaOH solution to the mixture. After being washed with distilled water the precipitate was filtered and dried at 70 °C. The product was immersed in distilled water to break it down into fine particles, which were subsequently dried at room temperature. The particles were then ground in a porcelain mortar and sieved to obtain the required particle size (63 to 210 mm). Hydrous Ti^{IV} and Zr^{IV} oxides were precipitated at pH 13 in the same manner as described above.

The exchanger of a desired particle size was converted to the H^+ form by treating it with 0.05 M HCl by the procedure described previously[5] and stored in a desiccator containing a saturated NH_4Cl solution (relative humidity; 79% at 25 °C).

Total Analysis of the Exchanger. A sample of 0.5 g was ignited at 850 °C; the water content was calculated from the weight loss. A part (0.1 g) of the oxide, thus formed, was decomposed by a mixture of concentrated H_2SO_4 (4 cm^3) and $(NH_4)_2SO_4$ (2.5 g) by heating, followed by dilution to 50 cm^3 with 4 M H_2SO_4. The titanium in this solution was assayed by extraction-spectrophotometry; the absorbance of the titanium-thiocyanate complex extracted from a 9 M H_2SO_4 solution by trioctylphosphine oxide in cyclohexane was measured.[6] The amount of TiO_2, thus determined, was subtracted from the mass of the calcined exchanger to obtain the amount of ZrO_2.

Titration Curves. One tenth gram of each exchanger in the H^+ form was immersed in 25 cm^3 of 0.1 M NaOH for 24 h at 25 °C; the solution pH was then measured. After every addition of a small amount of 1 M NaOH or HCl, the solution pH was measured after standing for 24 h to obtain a titration curve.

Uptake Curves. One tenth gram of each exchanger in the H^+ form was immersed in 15 cm^3 of various solutions prepared by the desired combinations of 0.1 M NaCl, and 0.1

M NaOH or 0.1 M HCl, for 7 d at 25 °C with intermittent shaking. This was followed by pH measurements and a determination of the Na^+ and Cl^-. The chloride concentration was determine by the Fajans' method after the solution had been neutralized. The sodium ions were converted to an equivalent amount of sodium chloride by evaporating the solution with HCl, and indirectly determined by titrating the Cl^-. The amount of ions taken up by the exchanger was evaluated from the difference between the initial and final concentrations of the respective ions in the solutions.

Distribution Coefficients. The distribution coefficients, K_d, were determined in the following way. The exchanger was contacted at 25 °C with a solution containing metal ions to be examined until their concentration in the supernatant solution became constant (8 to 18 d). The ratio of the solution volume (cm^3) to the amount of exchanger (g) was always kept constant at 100. The initial concentration of metal ions was 1×10^{-4} M (except carrier free ^{241}Am) and the ionic strength was adjusted to 0.1 M by using an $NaNO_3$ solution. The pH and metal ion concentration in the supernatant solution were then measured. The K_d, expressed in cm^3g^{-1}, was obtained from a calculation performed in the usual manner. Analyses of Cs, Sr, Ba, Mn, Fe, Co, Zn, Eu, and Am, respectively, were carried out radiometrically using ^{137}Cs, ^{85}Sr, ^{133}Ba, ^{54}Mn, ^{59}Fe, ^{60}Co, ^{65}Zn, ^{152}Eu, and ^{241}Am as tracers. Uranyl(VI) ions were analyzed spectrophotometrically using 2-(5-bromo-2-pyridylazo)-5-(diethylamino)phenol,[7] while the concentration of the other cations was determined by means of atomic absorption spectrophotometry.

Heat Treatment. About 5 g of each exchanger in the H^+ form were heated in air to a constant weight at a constant temperature (150, 300, and 500 °C). After being cooled over P_2O_5, the sample was weighed and then left immersed in water overnight. The sample separated from water was allowed to stand to a constant weight in a desiccator containing a saturated NH_4Cl solution (humidification). The water recovery of the heat-treated sample was calculated according to the difference in the water content between samples cooled over P_2O_5 immediately after the treatment and those subjected to humidification.

Results and Discussion

(I) Synthesis of the Exchangers. The effect of the conditions at precipitation on the yield and the acid-base property of the exchangers was first examined. It was found that exchangers with a variety of acid-base property can be synthesized by controlling the molar ratio of Ti to Ti+Zr in mixed solutions. The cation-exchange capacity of an exchanger of high titanium content increased with pH at precipitation. The total concentration of Ti plus Zr in the solution, the kind of alkali used (NaOH or NH_3), and the mixing method had little effect on the acid-base property of the exchangers. By applying the method described in Experimental, which was established by taking the yield and the convenience of the procedure into consideration, exchangers with various composition were synthesized. As is shown in Table 1, the exchangers, thus prepared, have nearly the same titanium content as that in the mixed solutions. The water content of the exchangers tends to decrease with an increase in the titanium content. Independent triplicate preparation was carried out for each of the exchangers with 50 and 90 mol% Ti (the molar percent of Ti to Ti+Zr is used to distinguish the exchangers with titanium content in the text and the molar ratio R in the figures) in order to examine the reproducibility of the synthesis. The uptake curve (Fig. 1) and the composition of the three samples agree well with each other, except for a small fluctuation in the water content, which is susceptible to environmental conditions (Table 1). The synthetic procedure, therefore, is considered to be reproducible.

The X-ray diffraction patterns of the binary and simple hydrous metal oxides showed that all of the samples were amorphous at room temperature. Being heated at 850 °C, the exchangers showed diffraction peaks: The exchanger with 90 mol% Ti crystal-

Table 1. Composition of the Exchangers

Sample No.	Ti-mol% in solution $\frac{TiO_2/mol}{(TiO_2+ZrO_2)/mol}\times100$	pH at precipitation	Ti-mol% in exchanger $\frac{TiO_2/mol}{(TiO_2+ZrO_2)/mol}\times100$	Water content H_2O/mol / $(TiO_2+ZrO_2)/mol$
1	10±1	13.06	10±1	2.44±0.01
2	30±1	13.07	30±1	2.59±0.01
3	50±1	13.04	49±1	2.16±0.01
4	50±1	13.06	49±1	2.12±0.01
5	50±1	13.05	50±1	2.14±0.01
6	70±1	13.10	70±1	1.99±0.02
7	90±1	13.10	91±1	1.33±0.01
8	90±1	13.05	91±1	1.46±0.02
9	90±1	13.00	90±1	1.28±0.01
10	Hydrous TiO_2	12.95		1.43±0.01
11	Hydrous ZrO_2	13.08		2.44±0.02

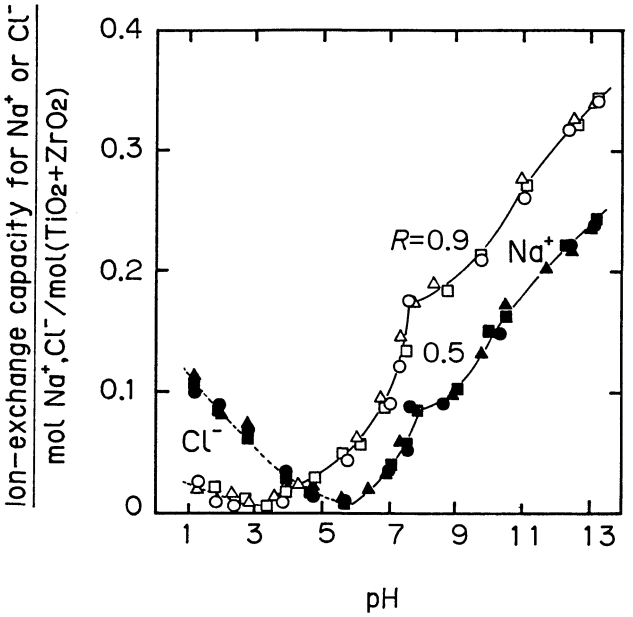

Fig. 1. Uptake curves of Na^+ or Cl^- (reproducibility of synthesis).
Ionic strength of solution: 0.1 M (HCl-NaCl-NaOH).
Exchanger, ▲: No. 3; ●: No. 4; ■: No. 5 (50 mol% Ti). △: No. 7; ○: No. 8; □: No. 9 (90 mol% Ti).

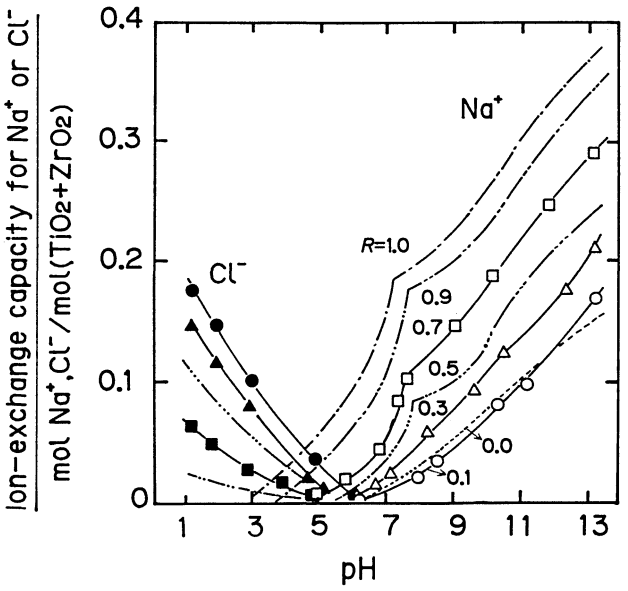

Fig. 2. Uptake curves of Na^+ or Cl^- (acid-base property as a function of titanium content).
Ionic strength of solution: 0.1 M (HCl-NaCl-NaOH).
Exchanger, ○: No. 1; △: No. 2; —···—: No. 3—5; □: No. 6; —··—: No. 7—9; —·—: No. 10; ------: No. 11. Open and Closed symbols show Na^+ and Cl^- uptake, respectively.

lized to anatase TiO_2; the hydrous Ti^{IV} oxide crystallized to the rutile form. Though the diffraction patterns of the orthorhombic (Ti, Zr)O_2 were observed in exchangers with 50 and 70 mol% Ti,[8] no pattern characteristic of the titanium-containing phase was found in exchangers with $\leqslant$30 mol% Ti; an exchanger with 30 mol% Ti crystallized to a mixture of cubic and orthorhombic ZrO_2, and that with 10 mol% Ti and the hydrous Zr^{IV} oxide crystallized to monoclinic ZrO_2.

(II) Ion-Exchange Property. (a) Acid-Base Property of the Exchangers: Figure 2 shows uptake curves of Na^+ and Cl^- on exchangers with various titanium contents, along with those on simple hydrous metal oxides. This figure reveals that all exchangers, except for the hydrous Ti^{IV} oxide, are amphoteric, and that an increase in the zirconium content reduces the cation-exchange while increasing the anion-exchange capacity. The acid-base property of hydrous Ti^{IV}-Zr^{IV} oxides might reflect that of the component simple hydrous metal oxides; the hydrous Ti^{IV} oxide is weakly acidic and the hydrous Zr^{IV} oxide is an amphoteric ion exchanger with an isoelectric point at pH 6.5, having an anion-exchange capacity larger than the cation-exchange capacity.[9,10] In exchangers with $\geqslant$30 mol% Ti, the increase in the titanium content shifted the pH, at which the sorption of Na^+ commenced, to the acidic side and increased the cation-exchange capacity in the region of pH lower than the inflection point of the uptake curves. The acidity was almost constant in exchangers with $\leqslant$30 mol% Ti, which crystallized to the form of Zr^{IV} oxides.

It is apparent from these results that both the acidity and number of OH groups in hydrous Ti^{IV} oxide decrease upon modifying the material with hydrous Zr^{IV} oxide. As has been previously reported, the hydrous Si-Ti^{IV} oxides with 37 to 67 mol% Ti possess a cation-exchange capacity that is much larger than a simple mixture of hydrous Si and Ti^{IV} oxides.[5] These facts would suggest that the cation-exchange capacity of hydrous metal oxides can be improved by modifying them with a metal element having a larger ionic potential.

(b) Selectivity for Cations: In order to examine the relation between the cation-exchange selectivity and the composition of the exchangers, the K_d's for various cations were measured as a function of pH. The pH's at which the K_d's reach 100 are shown in Table 2, as an indicator of the cation-exchange selectivity of the materials.

The pH's for representative metal ions increased with a decrease in the titanium content, while those for transition metal ions did not depend largely on the composition of the exchangers. In exchangers with $\leqslant$70 mol% Ti, the affinity was markedly higher for a transition than for representative metal ions, while in those with $\geqslant$90 mol% Ti such a relation is unclear. The selectivity series for alkali metal or alkaline earth metal ions appears to increase with the ionic potential of hydrated cations. This conforms

Table 2. Cation-Exchange Selectivities of the Exchangers[a)]

Cation	pH at which K_d reaches 100						
	No. 10[b)]	No. 9	No. 6	No. 5	No. 2	No. 1	No. 11
Li^+	6.3	7.7	9.6	x[c)]	x	x	x
K^+	5.9	6.5	7.9	x	x	x	x
Cs^+	1.8	4.1	6.5	7.8	x	x	x
Mg^{2+}	—	5.8	—	7.4	—	7.6	—
Ca^{2+}	—	5.3	—	6.5	—	7.2	—
Sr^{2+}	4.0	5.1	5.4	6.2	6.6	7.0	7.0
Ba^{2+}	3.3	4.2	4.8	5.7	6.5	6.7	6.7
Mn^{2+}	4.0	4.5	5.0	5.7	6.0	6.3	—
Co^{2+}	3.9	4.9	4.9	5.6	5.8	6.0	6.0
Zn^{2+}	3.4	4.3	4.5	4.9	5.1	5.3	5.3
Cu^{2+}	2.8	3.4	3.6	3.8	4.0	4.2	4.2
Fe^{3+}	—	2.4	2.2	2.2	2.2	2.4	2.4
Eu^{3+}	2.5	3.6	3.6	4.0	4.3	4.5	4.5
Am^{3+}[d)]	2.1	3.1	3.0	3.6	3.7	4.2	4.2
UO_2^{2+}	2.1	3.4	2.7	2.7	2.9	3.3	3.4

a) Conditions, Initial concentration of metal ion: 1×10^{-4} M; volume of solution/amount of exchanger: 100 $cm^3 g^{-1}$; ionic strength of solution: 0.1 M (HNO_3-$NaNO_3$-NaOH); Temperature: 25±1 °C. b) The numbers are the same as those in Table 1. c) The K_d is smaller than 100 in the region of pH>10. d) Tracer concentration.

to ion-hydration theory, which claims that the strength of the electrostatic interaction between hydrated cations and fixed anionic sites determines the selectivity of a strongly acidic resin.[11] On the other hand, such a simple relation does not hold for transition metal ions. Irrespective of the compositions of the exchangers, the affinity series for bipositive transition metal ions follows the Irving-Williams series: Mn<Fe<Co<Ni<Cu<Zn.[12] This order arise in part from an increase in the acidic strength of metal ions as Lewis acids. In addition, UO_2^{2+} had an affinity higher than that expected value due to the ionic charge. It may therefore be considered that in the ion-exchange reaction of transition metal ions the formation of covalent bonds between anionic sites in the exchanger and metal ions plays an important role in determining the selectivity of the exchanger, along with the remote Coulombic interaction.

These findings are consistent with the decrease in the acidity of the exchange sites with the titanium content in the exchangers (Fig. 2). Due to the higher acidity of the sites, an exchanger with a higher titanium content is preferable for the sorption of representative metal ions, since their ion-exchange reactions are governed by an electrostatic interaction between the ions and dissociated sites in the exchangers. The decrease in the acidity of exchange sites lowers the electrostatic interactions between ions and sites, but increases the ability to form a covalent bond between them. By presuming that the former effect is not completely offset by the latter, we can understand the small positive dependence of K_d on the titanium content in the ion-exchange reaction of transition metal ions. Since the acidity of the exchange sites in the hydrous Ti^{IV}-Zr^{IV} oxides depends on the titanium content, exchangers possessing a variety of selectivity series can be obtained by varying the compositions of the materials.

Table 3. Effect of Heat Treatment on the Water Content of the Exchangers

Exchanger[b)]	Water content/mol H_2O (mol(TiO_2+ZrO_2))$^{-1}$						
	Room temperature	150 °C[a)]		300 °C		500 °C	
		A	B	A	B	A	B
No. 1	2.44	0.39	1.72	0	0.98	0	0.55
No. 2	2.59	0.47	2.04	0.16	1.68	0	1.25
No. 3—5	2.12—2.14	0.31	1.82	0.06	1.58	0	1.22
No. 6	1.99	0.27	1.80	0.04	1.54	0	1.25
No. 7—9	1.28—1.46	0.27	1.12	0.04	0.98	0.05	0.51
No. 10	1.43	0.22	1.18	0.10	0.74	0.02	0.18
No. 11	2.44	0.39	1.72	0.02	0.98	0	0.55

A: Water content in the exchangers immediately after heat treatment. B: Water content in the exchangers subjected to humidification. a) Temperature for heat treatment. b) The numbers are the same as those in Table 1.

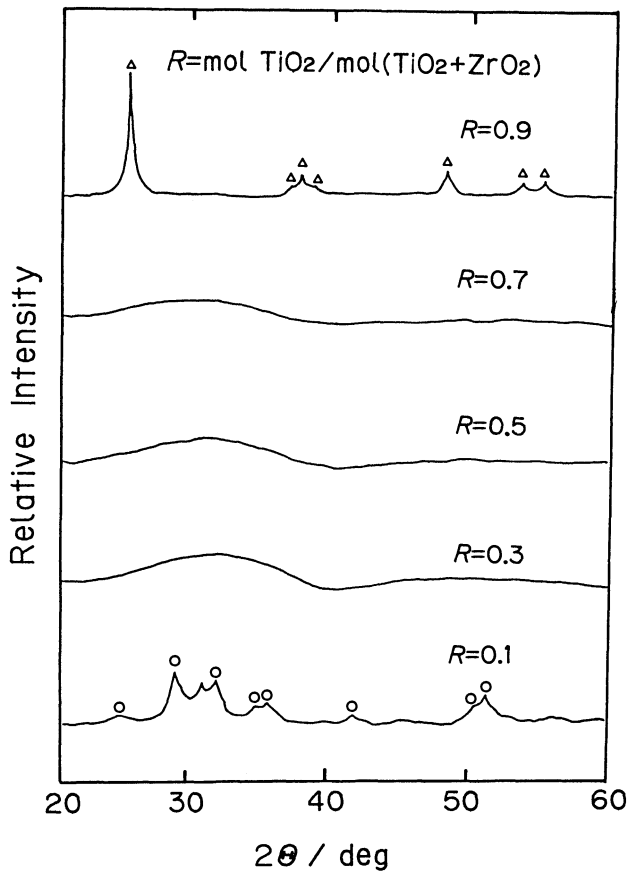

Fig. 3. X-Ray diffraction patterns of the exchangers heated at 500 °C.
○: Peaks corresponding to monoclinic ZrO_2.
△: Peaks corresponding to anatase TiO_2. Ni filtered Cu $K\alpha$-radiation was used.

(III) Effect of Heat Treatment. (a) Water Content: Table 3 shows the relation between the temperature for a heat treatment and the water content of the exchanger immediately after the treatment or being subjected to humidification. Irrespective of the titanium content, the amount of water contained in the exchangers immediately after a heat treatmen at 150 °C was reduced to <20% of the original values; it then decreased to almost zero at 300 °C. On the other hand, the water content of exchangers subjected to humidification varied with the titanium content. For exchangers with 30 to 70 mol% Ti heated at 500 °C, about 1.3 mol of water per 1 mol of the metallic elements were recovered, indicating that 50 to 65% of water lost by heating was recovered by humidification. When exchangers with a composition close to that of the simple hydrous metal oxides were heated at 500 °C, more than 75% of water originally present was released irreversibly.

As shown in Fig. 3, the X-ray diffraction patterns of exchangers with 30 to 70 mol% Ti, display an amorphous structure which did not change, even when heated at 500 °C. Heat-treated exchangers with 10 and 90 mol% Ti, respectively, showed peaks characteristic of monoclinic ZrO_2 and anatase TiO_2. These results indicate that the heat treatment hardly changed the structure of exchangers with 30 to 70 mol% Ti, but easily crystallized exchangers with a composition

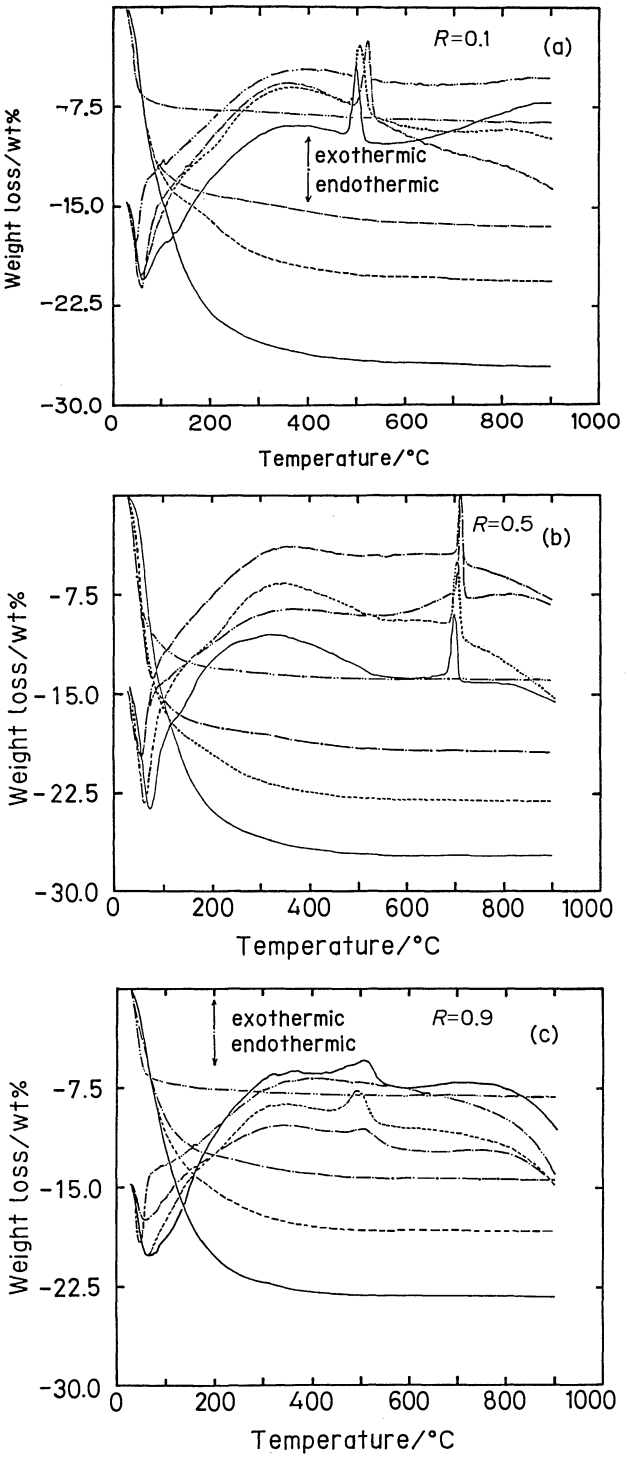

Fig. 4. TGA and DTA curves of the exchangers subjected to humidification.
Exchangers, (a): No. 1; (b): No. 3—5; (c): No. 7—9.
Temperature for heat treatment, ——: R.T.; ----: 150 °C; — · —: 300 °C; — · · —: 500 °C.

close to that of simple hydrous metal oxides.

The DTA and TGA measurements were made for the heat-treated and a humidified exchangers, along with samples without a heat treatment, as shown in Fig. 4. In the DTA curves, a large endothermic peak with a shoulder appearing in the range below 200 °C is due to a loss of water. A large exothermic peak observed at 450 °C or higher is assigned to the crystallization of exchangers as judged from X-ray data. Exchangers with 30 to 70 mol% Ti crystallized at 660 to 715 °C, while those with a composition close to that of simple hydrous oxides crystallized at a temperature below 520 °C. The large difference in the crystallization temperature reflects the difference in the structures of the exchanger matrices. The shoulder at the high-temperature side of the large endothermic peak indicates that the exchanger has at least two kinds of water having different binding energies. The large endothermic peaks at around 75 °C sharpened and the area under the shoulders decreased as the heat-treatment temperature became higher. When simple hydrous metal oxides and exchangers with 10 and 90 mol% Ti were heated at 500 °C, the water lost in regions with a temperature higher than 100 °C decreased to negligibly small amount, as can be seen from the TGA curves. Exchangers with 30 to 70 mol% Ti, heated at 500 °C, still had a small amount of water of high binding energy.

As discussed previously, the water of lower binding energy is zeolitic or adherent, while the water of higher binding energy is present as either hydroxyl groups or water bound thereto.[13-15] Accordingly, the water recoverable by humidification is considered to correspond mainly to a certain kind of zeolitic water, while the hydroxyl groups and the bound water

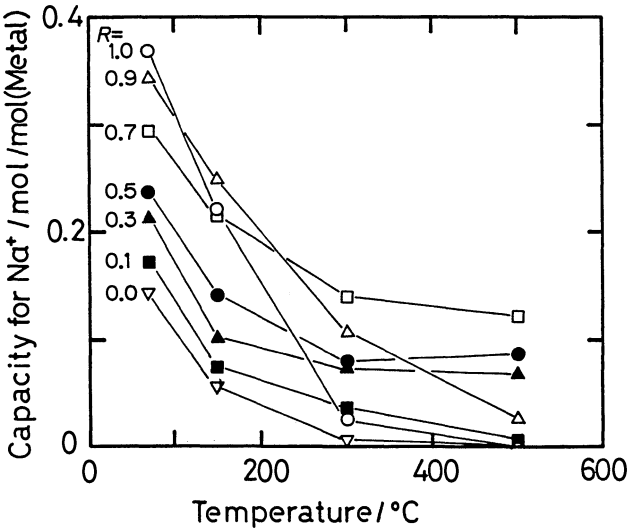

Fig. 5. Effect of heat treatment on the ion-exchange capacities for Na^+.
Exchanger, ■: No. 1; ▲: No. 2; ●: No. 3—5; □: No. 6; △: No. 7—9; ○: No. 10; ▽: No. 11.

are lost irreversibly from a heated exchanger. The irreversible loss of water of high binding energy is smaller in exchangers with 30 to 70 mol% Ti than in those with composition close to the simple hydrous metal oxides.

(b) Acid-Base Property: To examine the dependence of the thermal stability on the titanium content, the ion-exchange capacity of Na^+ was measured at pH 13 on samples with or without a heat treatment (Fig. 5). When simple hydrous metal oxides and an exchanger with 10 mol% Ti were heated at 300 °C, the capacity decreased to about ≤10% of the original values. Exchangers with 30 to 70 mol% Ti retaind larger capacity at the same temperature; an exchanger with 70 mol% Ti had the largest residual capacity. Even when heated at 500 °C, they did not lose their capacity further, which indicates that they were thermally more stable than the component hydrous metal oxides. These findings are compatible with the results of thermal analysis, which indicates that OH groups in exchangers with 30 to 70 mol% Ti once lost by heating, were recovered to a certain degree during humidification. The recovery of the exchange sites may be due to the matrices of these exchangers which are thermally more stable than those of simple hydrous metal oxides (Fig. 3).

In order to examine the effect of a heat treatment on the acid-base properties of exchangers, the pH-titration curves were measured for samples both with or without a heat treatment. Some results are shown in Fig. 6. In hydrous Ti^{IV} oxide[16] and an exchanger with 90 mol% Ti, the pH at which the sorption of Na^+ commenced, greatly shifted to the alkaline side upon heating. This indicates that the acidity of the exchange sites is decreased by a heat treatment. On the other hand, the acidity of the exchange sites in exchangers with ⩽70 mol% Ti was not affected by heating. Regardless of the composition, the exchange capacity at a pH lower than the inflection point decreased with the temperature for a heat treatment, while, in the higher pH region, the curves of samples with a given titanium content were parallel with each other. This observation indicates that a heat treatment destroys mainly the exchange sites with higher acidity.

In hydrous Ti^{IV}-Zr^{IV} oxide, the destruction of the exchange sites by heat treatment occurs mainly at more acidic sites, as in the hydrous Si-Ti^{IV} oxide.[5] The degree of the decrease in the exchange capacity by heat treatment is larger in exchangers with a higher titanium content. Hence, we can give an excellent thermal stability to hydrous Ti^{IV} oxide by modifying it with hydrous Si or Zr^{IV} oxide. The optimum titanium content for the thermal stability depends on the kind of modifiers.

(c) Distribution Coefficients: The distribution coefficients, K_d, of Cs^+, Sr^{2+}, Co^{2+}, Eu^{2+}, and UO_2^{2+} on heat-treated exchangers with various titanium con-

tents were measured at various pH's. Heat treatments did not alter the dependency of the K_d's on the pH, indicating that the stoichiometric relation governing the ion-exchange reaction does not change with a heat treatment.

Figures 7-a to 7-e show plots of the K_d's of Cs^+ and Sr^{2+} at pH 6, of Co^{2+} at pH 5.5, of Eu^{3+} at pH 3.5, and of UO_2^{2+} at pH 2.5 against the temperature for a heat treatment. The K_d's of Cs^+ and Sr^{2+} decreased with increasing temperature for the treatment, with the extent higher on the exchangers with $\geqslant$70 mol% Ti than on those with smaller titanium content (Figs. 7-a to 7-b). On an exchanger with 90 mol% Ti and hydrous Ti^{IV} oxide, the K_d's of Co^{2+} decreased consistently with temperature, while remaining nearly constant on exchangers with 50 and 70 mol% Ti or even increased somewhat on exchangers with 10 and 30 mol% Ti between 150 and 300 °C (Fig. 7-c). On hydrous Ti^{IV} oxide, the K_d's of Eu^{3+} decreased greatly

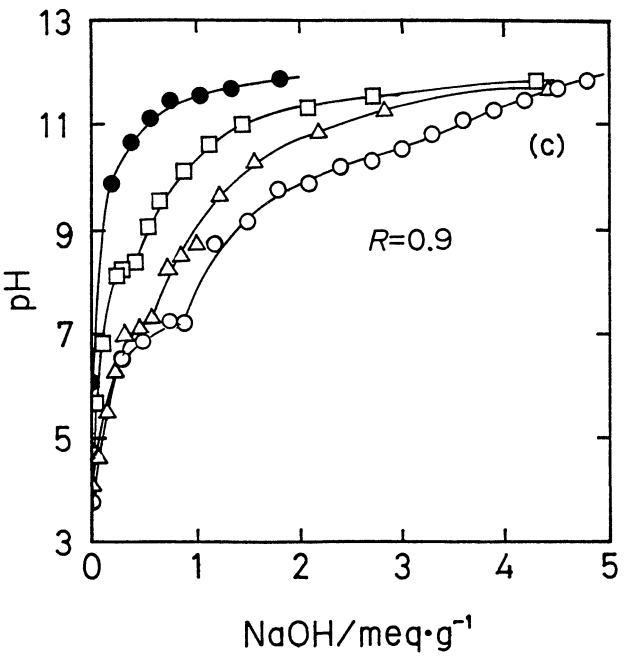

Fig. 6. Titration curves of heat-treated exchangers. Exchangers, (a): No. 2; (b): No. 6; (c): No. 7—9. Temperature for heat treatment, ○: R.T.; △: 150 °C; □: 300 °C; ●: 500 °C.

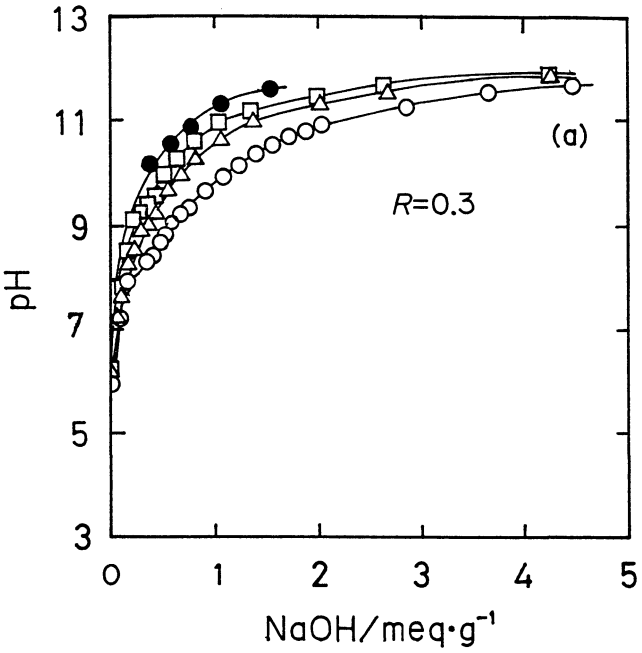

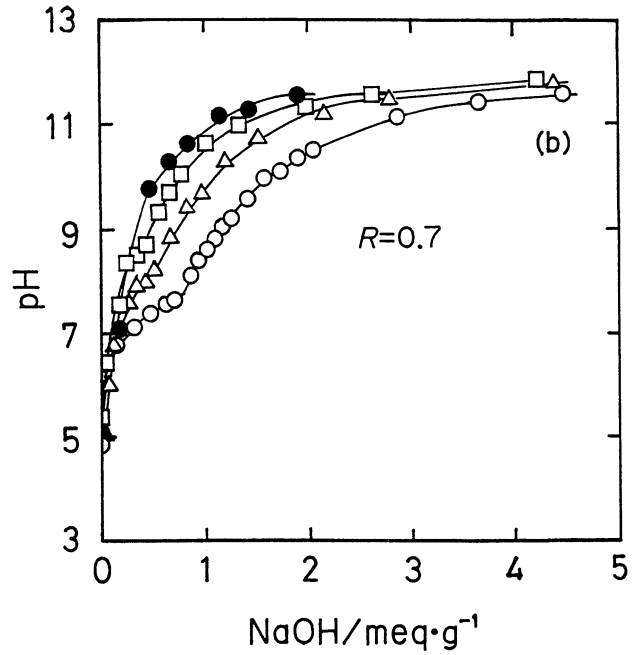

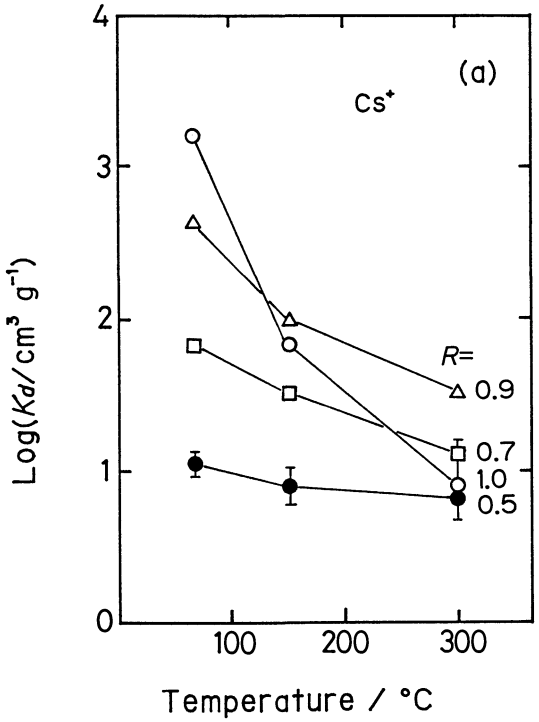

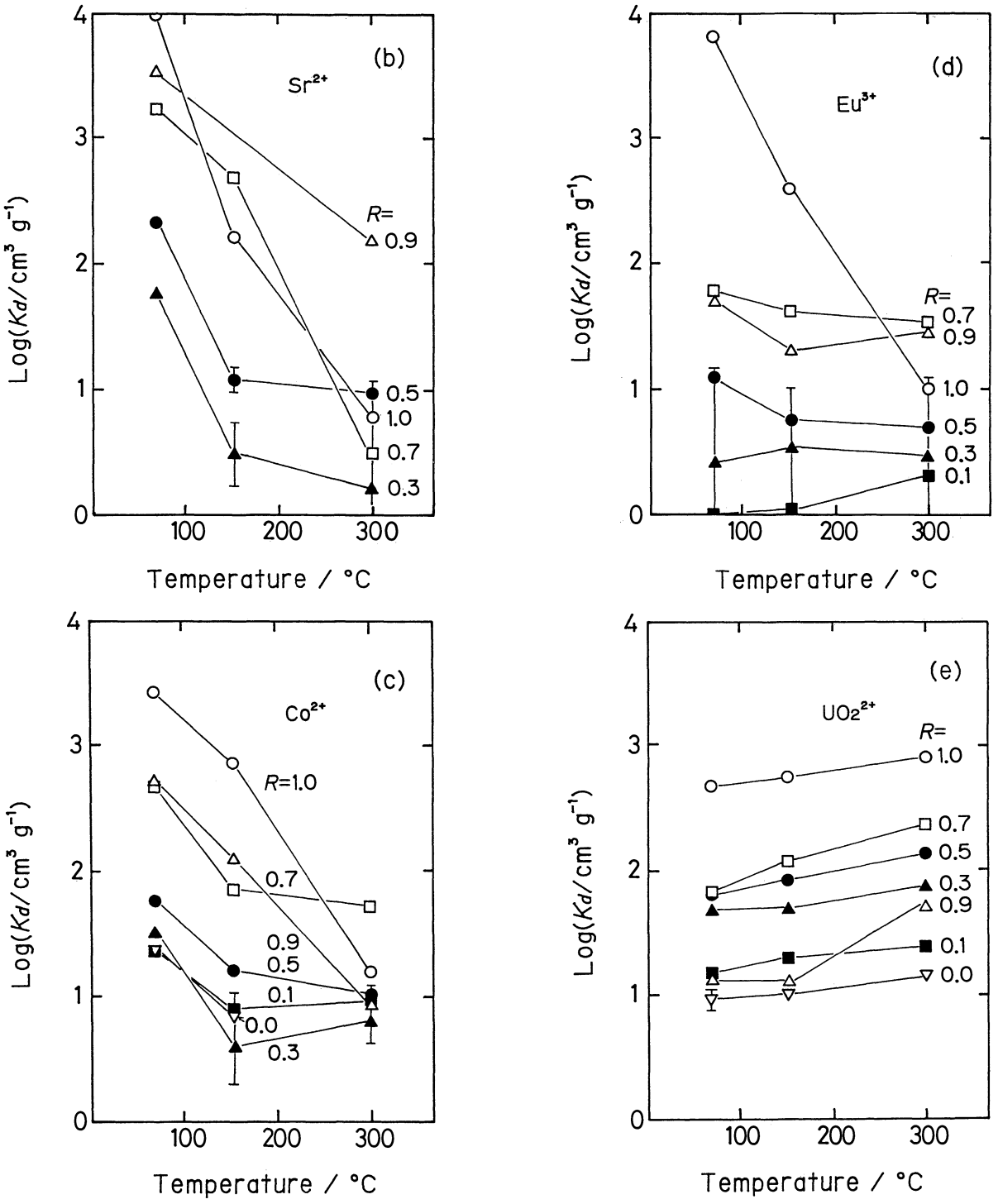

Fig. 7. Effect of heat treatment on the distribution coefficients of cations.
Cations, (a): Cs^+; (b): Sr^{2+}; (c): Co^{2+}; (d): Eu^{3+}; (e): UO_2^{2+}.
Exchanger, ■: No. 1; ▲: No. 2; ●: No. 3—5; □: No. 6; △: No. 7—9; ○: No. 10; ▽: No. 11.

with increasing temperature for a heat treatment, while on exchangers with 30 to 90 mol% Ti, they changed a little, and even somewhat increased on an exchanger with 10 mol% Ti by a heat treatment. The K_d's of UO_2^{2+} increased with the heat-treatment temperature, irrespective of the composition of the exchangers. The degree of the increase was somewhat larger on exchangers with 50 to 90 mol% Ti than on those with other compositions. These findings suggest that the exchangers after a heat treatment tend to retain their high affinity to cations, which can be sorbed from solution with a pH lower than the isoelectric point of the materials.

In order to understand these observations, the effect

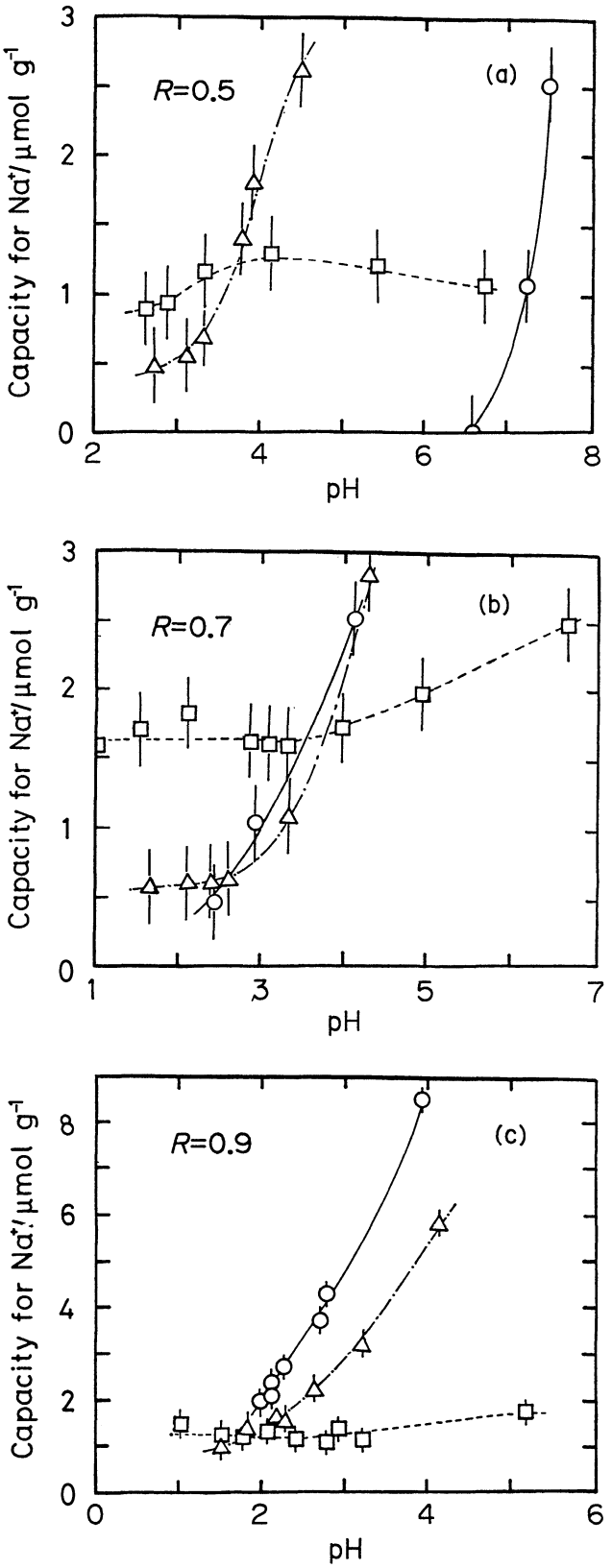

Fig. 8. Effect of heat treatment on a small amount of strongly acidic exchange sites.
Exchangers, (a): No. 3—5; (b): No. 6; (c): No. 7—9.
Temperature for heat treatment, ○: R.T.; △: 150 °C; □: 300 °C.
Solution: 2×10^{-4} M HNO_3-NaOH. Solution volume/Exchanger mass: 20 cm^3/0.2 g.

of a heat treatment on a small amount of the most acidic sites in the exchangers was examined by measuring the Na^+-uptake curve in Na^+-solutions of such low initial concentration as 2×10^{-4} M (Figs. 8-a to 8-c). In a pH range higher than 2, the amount of Na^+ sorbed on an exchanger with 90 mol% Ti and hydrous Ti^{IV} oxide decreased with increasing temperature, while at lower pH, it depended little on the temperature (Fig. 8-c). The curve of an exchanger with 70 mol% Ti was not affected by a heat treatment at 150 °C, but changed appreciably with a heat treatment at 300 °C; the amount of Na^+ sorbed was almost independent of the pH; thus, at a pH lower than 3.5 it was larger than the values for an exchanger without a heat treatment (Fig. 8-b). When exchangers with $\leqslant$50 mol% Ti were heat-treated, the pH at which the sorption of Na^+ commenced largely shifted to the acidic side and the sorption capacity in the region of pH <4 increased with temperature for a heat treatment (Fig. 8-a).

From the above-mentioned observations, the effect of a heat treatment on the distribution coefficients can be understood as follows. Although the total cation-exchange capacity decreases with increasing temperature, a heat treatment brings about a small increase in strongly acidic exchange sites, which can dissociate at a pH lower than the isoelectric point of exchangers with $\leqslant$70 mol% Ti. This is the reason why the distribution coefficients of cations with high affinity increase with a heat treatment. On the other hand, cations with low affinity are sorbed on exchangers by exchanging with hydrogens on abundant ion-exchange sites less acidic than the isoelectric point. The number of these sites determines the total cation-exchange capacity. A heat treatment, therefore, brings about a decrease in the distribution coefficients of cations with low affinity, in keeping with a decrease in the total cation exchange capacity.

References

1) M. J. Fuller, *Chromatogr. Rev.*, **14**, 45 (1971).
2) K. Shibata, T. Kiyoura, J. Kitagawa, T. Sumiyoshi, and K. Tanabe, *Bull. Chem. Soc. Jpn.*, **46**, 2985 (1973).
3) K. Tanabe, T. Sumiyoshi, and K. Shibata, *Bull. Chem. Soc. Jpn.*, **47**, 1064 (1974).
4) T. Yamanaka and K. Tanabe, *J. Phys. Chem.*, **80**, 1723 (1976).
5) H. Yamazaki, Y. Kanno, and Y. Inoue, *Bull. Chem. Soc. Jpn.*, **62**, 1837 (1989); *ibid.*, **63**, 2601 (1990).
6) J. P. Yaung and J. C. White, *Anal. Chem.*, **31**, 393 (1959).
7) D. A. Johnson and T. M. Florence, *Anal. Chim. Acta*, **53**, 73 (1971); *Talanta*, **22**, 253 (1975).
8) A. Willgallis, *Neues Jahrb. Mineral. Monatsh.*, **1983**, 151.
9) Y. Inoue and M. Tsuji, *Bull. Chem. Soc. Jpn.*, **49**, 111 (1976).
10) Y. Inoue and H. Yamazaki, *Bull. Chem. Soc. Jpn.*, **60**, 891 (1987).

11) R. Kunin, "Ion Exchange Resins," John Wiley and Sons, New York (1958), Chap. 2.
12) H. Irving and R. J. P. Williams, *Nature*, **162**, 746 (1948).
13) Y. Inoue and M. Tsuji, *Bull. Chem. Soc. Jpn.*, **51**, 479 (1978).
14) Y. Inoue, H. Yamazaki, and H. Nakamizo, *Bull. Chem. Soc. Jpn.*, **58**, 1292 (1985).
15) Y. Inoue, H. Yamazaki, and Y. Matsuda, *Bull. Chem. Soc. Jpn.*, **58**, 3225 (1985).
16) H. Yamazaki, M. Kaneda, and Y. Inoue, *Bull. Chem. Soc. Jpn.*, **63**, 3216 (1990).

Synthesis and Inclusion Properties of Sulfur-Bridged Analogs of Acyclic Phenol-Formaldehyde Oligomers

Yoshihiro Ohba, Kazuhiko Moriya, and Tyo Sone*
Department of Materials Science and Engineering, Faculty of Engineering, Yamagata University, Yonezawa 992
(Received September 10, 1990)

A series of compounds in which a part or all of the methylene bridges of acyclic *p*-methyl- and *p*-*t*-butylphenol-formaldehyde tetramers were replaced by sulfur bridge(s) was synthesized. It was found that though the sulfur-bridged tetramers formed crystalline host-guest complexes with a variety of organic compounds, they were different from the parent tetramers regarding their inclusion behavior. The number and position of the sulfur bridge(s), as well as the *p*-substituent of phenol in the tetramers, had a great influence upon the inclusion property. The thermal stability of complexes of the sulfur-bridged tetramers (**SSS-a,b**) with benzene, as estimated from their thermal dissociation rates, are lower than those of the parent tetramers (**CCC-a,b**).

We recently reported that acyclic *p*-substituted phenol-formaldehyde oligomers with methylene bridges ortho to the phenolic hydroxyl group formed crystalline inclusion compounds with many organic compounds, as did the corresponding cyclic oligomers, calixarenes.[1] The inclusion behavior of the acyclic oligomers was remarkably influenced by the *p*-substituent of phenol and the number of phenol units; tetramers and pentamers consisting of four and five phenol units with the *p*-substituent, such as the methyl, *t*-butyl, or cyclohexyl group, were very effective in complex formation. The oligomers included quite a few molecules which had no group to participate in hydrogen-bonding, suggesting that intermolecular hydrogen-bonding between the oligomers and the guest molecules was not essential for complex formation.

An X-ray crystallographic examination of the *p*-cresol tetramer (**CCC-a**)-benzene complex revealed that hydrogen-bonding between the phenolic hydroxyl groups plays a crucial role in the construction of the host lattice.[2] Namely, two molecules of the tetramer form a cyclic dimer in the crystalline complex through intramolecular hydrogen-bonding between adjacent phenolic hydroxyl groups in the molecule, as well as an intermolecular one between the phenolic hydroxyl groups of the opposite ends of the two molecules. This is in sharp contrast with the non-complexed tetramer, molecules of which are arranged in the crystalline state to chains of indefinite length by intermolecular hydrogen-bonding.[3]

These results suggest that modification in the methylene bridge of the phenol-formaldehyde oligomers affects the inclusion behavior as well. A noteworthy feature of this type of oligomer is that, owing to the bridges between the rigid aromatic skeletons, they can adapt to fit guest molecules through conformational changes in complexation. In the hope of founding a new host family based on phenol-formaldehyde oligomers, we extended our study to their sulfur-bridged analogs. In the present paper we describe the synthesis of sulfur-bridged analogs of acyclic *p*-cresol- and *p*-*t*-butylphenol-formaldehyde tetramers and their ability to form crystalline inclusion compounds with organic guest molecules.

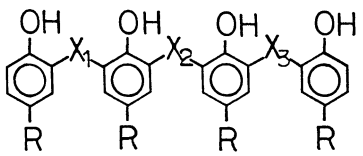

SSS: $X_1=X_2=X_3=S$
SSC: $X_1=X_2=S$, $X_3=CH_2$
SCS: $X_1=X_3=S$, $X_2=CH_2$
CSC: $X_1=X_3=CH_2$, $X=S$
SCC: $X_1=S$, $X_2=X_3=CH_2$
CCC: $X_1=X_2=X_3=CH_2$

a: R=Me
b: R=t-Bu

Results and Discussion

Synthesis of Oligomers. The sulfur-bridged analogs of *p*-cresol- and *p*-*t*-butylphenol-formaldehyde tetramers (**SSS-a,b**; **SSC-a,b**; **SCS-a,b**; **CSC-a,b**; **SCC-a,b**)[4] were synthesized as shown in Scheme 1; it involves repeated sulfuration and/or hydroxymethylation of the phenols, followed by condensation of the resulting hydroxymethyl compounds with the phenols.

The reaction of the phenols (**1a,b**) with 0.2 equivalent moles of SCl_2 in CH_2Cl_2 gave phenol-sulfur dimers (**2a,b**) together with a small amount of the corresponding trimers (**3a,b**). Further reaction of **2** (**a,b**) with SCl_2 yielded all sulfur-bridged tetramers, **SSS-a** and **SSS-b**, respectively. The NaOH-catalyzed hydroxymethylation of **3** (**a,b**) with aq formaldehyde, followed by the *p*-toluenesulfonic acid (TsOH)-catalyzed condensation of the resulting hydroxymethyl compounds (**4a,b**) with *p*-cresol (**1a**) or *p*-*t*-

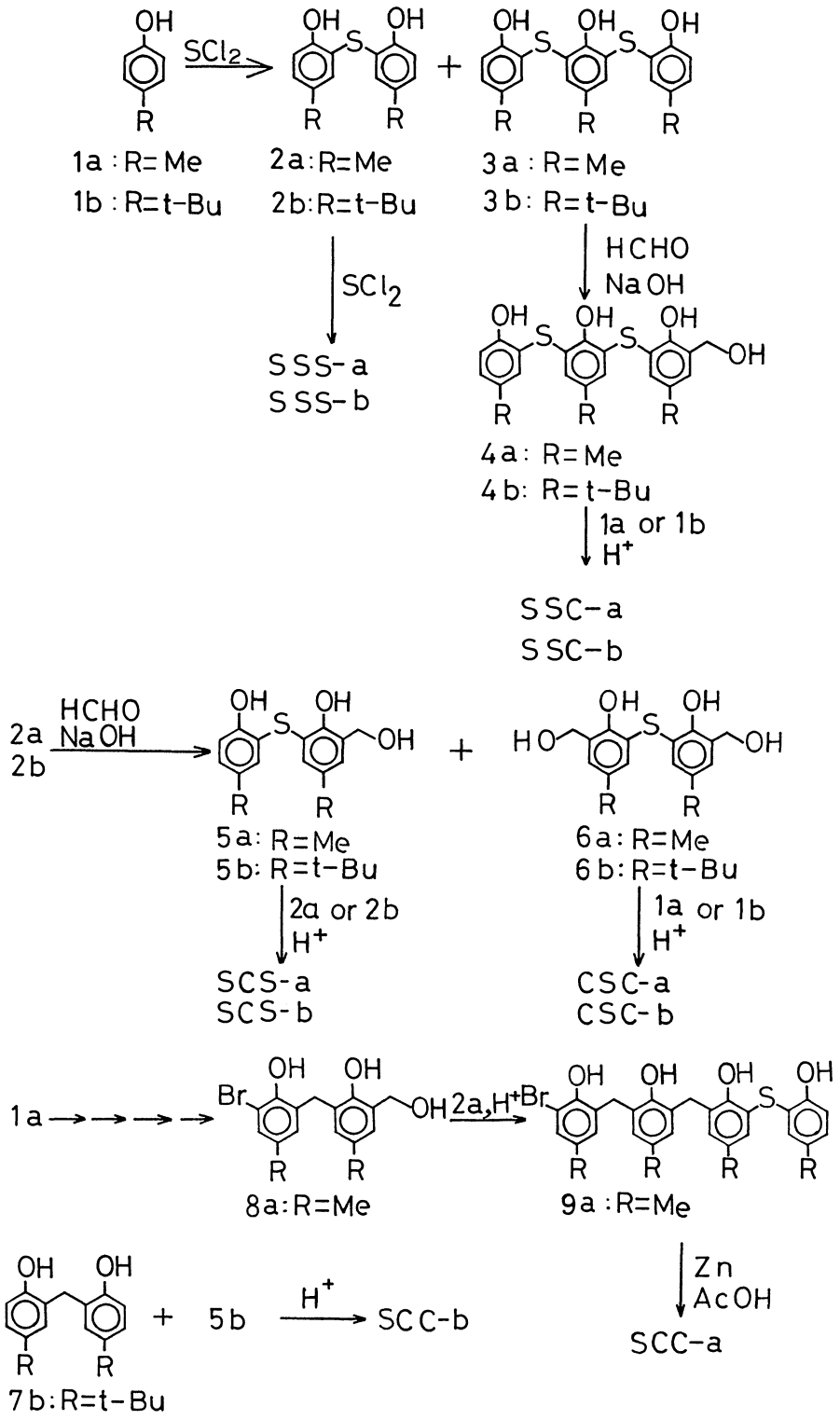

Scheme 1.

butylphenol (**1b**), gave tetramers, **SSC-a** and **SSC-b**, with two neighboring sulfur bridges and one methylene bridge. The symmetrical tetramers, **SCS-a** and **SCS-b**, with one central methylene bridge were synthesized by condensation of the hydroxymethyl derivatives (**5a,b**) of **2** (**a,b**) with an large excess of **2** (**a,b**), while the other symmetrical tetramers, **CSC-a** and **CSC-b**, with one sulfur bridge were obtained analogously from the bis(hydroxymethyl) derivatives (**6a,b**) of **2** (**a,b**) and the corresponding phenols (**1a,b**). On the other hand, treatment of the *p-t*-butylphenol-formaldehyde dimer (**7b**) with **5b** in the presence of TsOH afforded the unsymmetrical *p-t*-butylphenol tetramer, **SCC-b**. The unsymmetrical *p*-cresol tetra-

Table 1. Molar Ratio and the Melting Points of the Complexes of **SSS-a**, **SSC-a**, **SCS-a**, **CSC-a**, **SCC-a**,[a] and **CCC-a**[b]

Guest (G)	Host (H)											
	SSS-a		**SSC-a**		**SCS-a**		**CSC-a**		**SCC-a**		**CCC-a**	
	H:G	(°C)	H:G	(°C)	H:G	(°C)	H:G	(°C)	H:G	(°C)	H:G	(°C)
None		(138—140)		(163—164)		(133—134)		(152—154)		(180—185)		(174—178)
Cyclohexane	+	(140—148.5)	−		−		−		−		−	
Benzene	2:1	(141—152)	−		−		1:1	(142—149)	−		2:1	(172—175)
Toluene	+	(130—147)	−		−		−		−		−	
o-Xylene	−		−		−		−		−		−	
Thiophene	−		−		−		−		−		−	
Methanol	−		2:1	(108—111)	−		3:1		−		−	
Ethanol	−		2:1	(111—118)	−		−		−		−	
Dioxane	+	(135—145)	2:1	(141—150)	−		1:2	(97—116)	2:1	(167—180)	1:1	(142—143)
Acetone	−		−		−		−		−		−	
Dichloromethane	−		−		−		2:1	(155—158)	−		2:1	(161—162)
1,2-Dichloroethane	+		2:1	(85—93)	−		2:1	(148—152)	−		1:1	(144—146)
1,2-Dibromoethane	−		2:1	(94—97)	−		1:1	(118.5—130)	−		1:1	(152—153)
1,1,1-Trichloroethane	−		−		−		−		−		2:1	(145—147)
Diethylamine	1:2	(59—67)	1:2	(111—120)	1:2	(116—121)	1:2	(104—109)	1:2	(155—165)	1:1	(112—115)
Triethylamine	1:2	(77—88)	1:2	(85—110)	1:1	(84—91)	1:1	(181—185)	1:1	(120—128)	1:1	(94—102)

a) − : host-guest complex does not form. + : host : guest ratio is not clear. b) See Ref. 1.

Table 2. Molar Ratio and the Melting Points of the Complexes of **SSS-b**, **SSC-b**, **SCS-b**, **CSC-b**, **SCC-b**,[a] and **CCC-b**[b]

Guest (G)	Host (H)											
	SSS-b		**SSC-b**		**SCS-b**		**CSC-b**		**SCC-b**		**CCC-b**	
	H:G	(°C)	H:G	(°C)	H:G	(°C)	H:G	(°C)	H:G	(°C)	H:G	(°C)
None		(101.5—103)		(123—124)		(170—174)		(172—173.5)		(174.5 —177.5)		(210—211)
Cyclohexane	2:1	(120—126)	1:1	(118.5—122)	+	(170—173)	−		−		1:2	(105)
Benzene	1:1	(113—118)	2:1	(94—103)	2:1	(170—173)	−		−		2:1	(123—125)
Toluene	2:1	(105—108)	1:1	(100.5—103)	1:1	(173—174.5)	−		1:1	(168—171)	1:1	(133—135)
o-Xylene	1:1	(107—109.5)	−		1:1	(154—165)	−		1:1	(153—163)	2:1	(151—153)
Thiophene	1:1	(125—129)	2:1	(108.5—112)	−		−		−		−	
Methanol	−		−		3:1	(171—175)	−		−		−	
Ethanol	−		−		−		−		−		−	
Dioxane	+		−		+	(169.5—173)	+	(122—167)	−		2:1	(163—165)
Acetone	−		−		−		−		−		−	
Dichloromethane	+	(99.5—101.5)	2:1	(96.5—105)	−		−		−		−	
1,2-Dichloroethane	2:1	(109—113.5)	2:1	(104.5—110)	2:1	(168—172.5)	−		−		+	(165—167)
1,2-Dibromoethane	1:1	(110.5—113)	+		2:1	(153—165)	2:1	(95—158.5)	−		+	(152—153)
1,1,1-Trichloroethane	2:1	(124—130)	1:1	(119—124)	−		−		−		2:1	(109—110)
Diethylamine	1:1	(142—150)	1:1	(120—125)	1:1	(167.5—171)	1:2	(124—132.5)	1:1	(160—162)	1:2	(132—135)
Triethylamine	1:2	(108—123)	1:1	(104—108)	1:1	(120—128)	1:3	(144—148.5)	1:1	(133—143)	1:1	(130—133)

a) − : host-guest complex does not form. + : host : guest ratio is not clear. b) See Ref. 1.

mer, **SCC-a**, was obtained by the condensation of 3-(3-bromo-5-methylsalicyl)-2-hydroxy-5-methylbenzyl alcohol (**8a**)[5] with **2a**, and a subsequent debromination of the product (**9a**) with zinc powder in AcOH.

Inclusion Properties. The inclusion behavior of the tetramers towards organic molecules was examined by recrystallization of the tetramers from various organic solvents. The results are shown in Tables 1 and 2, together with those obtained for **CCC-a** and **CCC-b**.[1] It was found that the tetramers had an ability to form complexes with many organic compounds as the parent tetramers, and that the sulfur-bridged *p*-cresol and *p*-*t*-butylphenol tetramers were different from each other and from the parent tetramers regarding their inclusion behavior. The stoichiometries of the inclusion range from 3:1 to 1:3 (host:guest); 2:1 or 1:1 exist in most complexes, except for those with amines whose stoichiometric ratios are 1:1 or 1:2.[6]

Concerning the sulfur-bridged *p*-cresol tetramers, replacement of the methylene bridge(s) with sulfur(s) in the molecule of **CCC-a** tends to decrease the inclusion ability; **SCC-a**, **SCS-a**, and **SSS-a** are particularly poor. It seems that the position, rather than the number of the sulfur bridge(s), influences the ability. For example, while **CSC-a** is similar to **CCC-a**, **SCC-a** is decidedly inferior, both of the tetramers having one sulfur bridge. Likewise, **SSC-a** exhibits an inclusion property, whereas **SCS-a** and **SSS-a**, which have two terminal sulfur bridges, are almost ineffective. In spite of the low tendency for complex formation, the introduction of a sulfur bridge(s) in place of a methylene bridge(s) gave some of the tetramers (**SSC-a** and **CSC-a**) a new property to include alcohols.

On the other hand, sulfur-bridged *p*-*t*-butylphenol tetramers are, as a whole, superior to the corresponding *p*-cresol tetramers regarding complexation. Moreover, three (**SSS-b**, **SSC-b**, and **SCS-b**) out of the five tetramers form complexes with many more organic molecules than does the parent, **CCC-b**. For example, they form complexes with thiophene and aliphatic halogen compounds; **SSS-b** forms a 1:1 complex with 1,1,1-trichloroethylene, a water pollutant. The tetramers, **CSC-b** and **SCC-b**, with one sulfur bridge, however, show a low inclusion ability. Contrary to the observation concerning the *p*-cresol series, the number of sulfur bridge(s) seems to affect the inclusion ability in the *p*-*t*-butylphenol series.

It is interesting to note that, regardless of the *p*-substituent of the phenol, though all of the sulfur-bridged tetramers examined exhibit a high preference for aliphatic amines,[6] they lack the ability to include acetone, and neither of the tetramers of the **SCC** type in both series incorporate the aliphatic halogen compounds.

Guest preferences of the sulfur-bridged phenol tetramers, as observed, are dependent upon the *p*-substituent of the phenols, as well as both the number and position of the sulfur bridges. However, it is difficult to find an obvious rule which can explain all of the sulfur effects on the inclusion behavior. The results obtained here suggest that the tetramers build up characteristic host lattices which depend upon the combination of their building blocks. This assumption needs to be confirmed by X-ray structural studies of individual complexes.

The inclusion selectivities of **SSS-b** were examined for several equimolar mixtures of simple benzene derivatives. The results, together with those obtained for **CCC-b**, are shown in Table 3. In some cases, **SSS-b** shows a strong affinity to one guest in the guest mixtures. For example, **SSS-b** includes preferentially *o*-xylene in mixtures with benzene and *p*-xylene, and *m*-xylene in a mixture with benzene. However, **SSS-b** is generally inferior to **CCC-b** regarding inclusion selectivity. Sequences of the selectivity of **SSS-b** towards isomeric xylenes or benzene homologue are indefinite, suggesting that the conformation of the host molecule changes with the guest molecule to be accommodated.

There are only a few data available concerning the thermodynamic properties of crystalline inclusion

Table 3. Selectivity in the Complexation of **SSS-b** and **CCC-b** for an Equimolar Mixture of Guests

Guest(A)/Guest(B)	Host	
	SSS-b	**CCC-b**
	(A)/(B)	(A)/(B)
Benzene/toluene	36/64	47/53
Benzene/*o*-xylene	8/92	0/100
Benzene/*m*-xylene	6/94	79/21
Benzene/*p*-xylene	54/46	100/0
Toluene/*o*-xylene	61/39	2/98
Toluene/*m*-xylene	37/63	86/14
Toluene/*p*-xylene	45/55	99/1
o-Xylene/*m*-xylene	51/49	77/23
m-Xylene/*p*-xylene	63/37	34/66
p-Xylene/*o*-xylene	5/95	8/92

Table 4. Kinetic Data for the Thermal Dissociation of the Complexes of **SSS-a**, **SSS-b**, **CCC-a**,[a] and **CCC-b**[a] with Benzene

Complex	Temp	$k\times10^4$	$\Delta H^{\neq}$	$\ln A$
	°C	s^{-1}	kJ mol^{-1}	
SSS-a: benzene	117.1	1.881		
	123.9	3.342		
	128.1	5.835		
	132.3	10.62	145.8	35.6
SSS-b: benzene	85.2	0.2969		
	99.3	0.7506		
	106.4	3.166		
	116.7	4.939	110.0	26.4
CCC-a: benzene[a]			162.6	42.1
CCC-b: benzene[a]			123.7	33.9

a) See Ref. 1.

complexes of artificial organic hosts with organic molecules.[7] In an attempt to estimate the thermal stability of the host-guest complexes, some kinetic parameters for the dissociation of **SSS-a**-benzene (host : guest=2 : 1) and the **SSS-b**-benzene complex (host : guest=1 : 1) were obtained from their dissociation rates (Table 4). The data indicate that the **SSS-a**-benzene complex is less stable than the corresponding **CCC-a**-benzene (2 : 1) complex. Assuming that the complexation mode of **SSS-a** is similar to that of **CCC-a**, the difference between the two complexes regarding thermal stability is principally attributable to difference in the lengths of the C(aromatic)-S(bridge) and C(aromatic)-C(bridge) bonds in the two host molecules.[8] Replacement of the C-C bonds with longer C-S bonds lengthens the distance between the adjacent hydroxyl groups in the molecule of **CCC-a** and, consequently, weakens the strength of the intramolecular hydrogen bonding between the adjacent hydroxyl groups. Thus, **SSS-a** more easily undergoes a conformational change in the molecule upon heating than does **CCC-a**. Alternatively, a lattice which **SSS-a** built up is too large for the guest molecule to fit. On the other hand, difference between **SSS-a**-benzene and **SSS-b**-benzene complexes in the stability arises from difference in the complexation mode.

Experimental

All melting points are uncorrected. NMR spectra were obtained on a Hitachi R-600 spectrometer at 60 MHz, using TMS as an internal reference. IR and mass (70 eV) spectra were recorded on a Hitachi EPI-S2 and on a Hitachi UMU-6MG spectrometers, respectively. TG/DTA curves were recorded on a Seiko TG/DTA 30 instrument with a heating rate of 10 °C min^{-1} under an air stream. Gas chromatographic-analyses were performed on a Hitachi K 53 chromatograph equipped with a standard golei column, U-90 (0.25 mm×90 m).

Synthesis of 2-[3-[3-(2-Hydroxy-5-methylphenylthio)-2-hydroxy-5-methylphenylthio]-2-hydroxy-5-methylphenylthio]-4-methylphenol (SSS-a). The reaction of *p*-cresol (**1a**) with SCl_2 gave 2,2′-thiobis[4-methylphenol] (**2a**; 61%);[11] 2,6-bis(2-hydroxy-5-methylphenylthio)-4-methylphenol (**3a**) was obtained as a minor product (4%).

3a: Colorless powder (hexane), mp 160—161 °C; IR (KBr) 3250, 880, 870, and 810 cm^{-1}; ^1H NMR ($CDCl_3$) δ=2.10 (3H, s), 2.23 (6H, s), and 6.85—7.35 (8H, m); MS (70 eV) *m/z* (rel intensity) 384 (M^+, 100). Found: C, 65.53; H, 5.28%. Calcd for $C_{21}H_{20}O_3S_2$: C, 65.59; H, 5.24%.

Sulfur dichloride (0.67 g, 6.5 mmol) was added to a solution of **2a** (8.1 g, 33 mmol) in dry CH_2Cl_2 (100 ml) over a period of 35 min at 0 °C; the mixture was stirred at the same temperature for 1 h. The solvent was evaporated and the residue chromatographed on silica gel (Wako C-200; hexane/AcOEt=4/1) to give **SSS-a** (0.83 g, 24%).

SSS-a: Colorless prisms (hexane), mp 138—140 °C; IR (KBr) 3400, 880, and 820 cm^{-1}; ^1H NMR ($CDCl_3$) δ=2.12 (3H, s), 2.22 (9H, s), and 6.50—7.35 (10H, m); MS (70 eV) *m/z* 522 (M^+, 100). Found: C, 64.62; H, 5.03%. Calcd for $C_{28}H_{26}O_4S_3$: C, 64.34; H, 5.01%.

Synthesis of 2-[3-[3-(5-*t*-Butyl-2-hydroxyphenylthio)-5-*t*-butyl-2-hydroxyphenylthio]-5-*t*-butyl-2-hydroxyphenylthio]-4-*t*-butylphenol (SSS-b). Sulfur dichloride (5.1 g, 50 mmol) was added to a solution of *p*-*t*-butylphenol (**1b**; 15 g, 0.1 mol) in dry CH_2Cl_2 (100 ml) over a period of 15 min at 0 °C. After stirring for 1 h at the same temperature, the mixture was concentrated and steam-distilled to remove any unreacted **1b**. Crystallization of the residual mass from hexane yielded 2,2′-thiobis[4-*t*-butylphenol] (**2b**; 8.85 g). The mother liquor was concentrated and subjected to medium-pressure liquid column chromatography (Kieselgel 60, 230—300 mesh; hexane/AcOEt=10/1) to afford another crop of **2b** (3.5 g, 75% in total) and 2,6-bis(5-*t*-butyl-2-hydroxyphenylthio)-4-*t*-butylphenol (**3b**; 0.75 g, 6%).

2b: Colorless prism (hexane), mp 101—102 °C; IR (KBr) 3300 and 820 cm^{-1}, ^1H NMR ($CDCl_3$) δ=1.24 (18H, s), 6.28 (2H, s, OH), and 6.80—7.45 (6H, m); MS (70 eV) *m/z* 330 (M^+, 100). Found: C, 72.94; H, 8.13%. Calcd for $C_{20}H_{26}O_2S$: C, 72.69; H, 7.93%.

3b: Colorless needles (hexane), mp 129—130 °C; IR (KBr) 3350, 880, and 820 cm^{-1}; ^1H NMR ($CDCl_3$) δ=1.12 (9H, s), 1.23 (18H, s), and 6.80—7.30 (8H, m); MS *m/z* 510 (M^+, 24). Found: C, 70.29; H, 7.66%. Calcd for $C_{30}H_{38}O_3S$: C, 70.55; H, 7.50%.

Tetramer **SSS-b** was prepared in 51.5% yield by a similar procedure as described regarding the synthesis of **SSS-a** from **2a**.

SSS-b: Colorless needles (hexane), mp 101.5—103 °C; IR (KBr) 3400, 880, and 820 cm^{-1}; ^1H NMR ($CDCl_3$) δ=1.13 (18H, s), 1.25 (18H, s), and 6.70—7.65 (14H, m); MS (70 eV) *m/z* 690 (M^+, 100). Found: C, 69.57; H, 7.40%. Calcd for $C_{40}H_{50}O_4S_3$: C, 69.53; H, 7.29%.

Synthesis of 2-[3-[3-(2-Hydroxy-5-methylphenylthio)-2-hydroxy-5-methylphenylthio]-5-methylsalicyl]-4-methylphenol (SSC-a). To a solution of **3a** (2.0 g, 5.2 mmol) in MeOH (1 ml) a 10% NaOH solution (1 ml), and formalin (37%; 0.42 g, 5.2 mmol), were added under ice-cooling; the mixture was then stirred at 50 °C for 80 h in an atmosphere of N_2. The mixture was cooled to room temperature, acidified with 50% AcOH (pH 6), and extracted by $CHCl_3$. After the usual work-up, the product was subjected to medium-pressure column chromatography on silica gel (Kieselgel 60, 230—400 mesh; hexane/AcOEt=4/1) to give 3-[3-(2-hydroxy-5-methylphenylthio)-2-hydroxy-5-methylphenylthio]-2-hydroxy-5-methylbenzyl alcohol (**4a**; 0.65 g, 30%) and unreacted **3a** (0.6 g, 30 %).

4a: Colorless prisms (hexane-AcOEt), mp 163—164 °C; IR (KBr) 3400, 875, and 820 cm^{-1}; ^1H NMR ($CDCl_3$) δ=2.22 (3H, s), 2.29 (6H, s), 4.72 (2H, br s), 6.15 (1H, s, OH), and 6.60—7.35 (7H, m); MS (70 eV) *m/z* 384 (M^+, 93). Found: C, 63.99; H, 5.54%. Calcd for $C_{22}H_{22}O_4S_2$: C, 63.74; H, 5.35%.

A mixture of **4a** (0.65 g, 1.6 mmol), **1a** (2.0 g, 18.5 mmol), TsOH (50 mg), and benzene (20 ml) was refluxed for 24 h. The benzene was evaporated and excess **1a** removed by steam distillation. The residual mass was chromatographed on silica gel (Wako C-200; hexane/AcOEt=10/1) to give **SSC-a** (0.65 g, 80%).

SSC-a: Colorless needles (benzene), mp 130—131 °C; IR (KBr) 3400, 880, and 810 cm^{-1}; ^1H NMR ($CDCl_3$) δ=2.05 (3H, s), 2.10 (6H, s), 2.22 (3H, s), 4.40 (2H, s), and 6.60—7.20 (10H, m); MS (70 eV) *m/z* 502 (M^+, 100). Found: C, 68.97; H, 5.22%. Calcd for $C_{29}H_{28}O_4S_2$: C, 69.02; H, 5.59%.

Synthesis of 2-[3-[3-(5-*t*-Butyl-2-hydroxyphenylthio)-5-*t*-butyl-2-hydroxyphenylthio]-5-*t*-butylsalicyl]-4-*t*-butylphenol (SSC-b). Hydroxymethylation of **3b** by an analogy of the procedure described for **3a** yielded 3-[3-(5-*t*-butyl-2-hydroxyphenylthio)-5-*t*-butyl-2-hydroxyphenylthio]-5-*t*-butyl-2-hydroxybenzyl alcohol (**4b**; 40%) and unreacted **3b** (52%).

4b: Colorless powder (hexane), mp 84—87 °C; IR (KBr) 3370, 880, and 820 cm^{-1}; ^1H NMR ($CDCl_3$) δ=1.10 (9H, s), 1.16 (9H, s), 1.23 (9H, s), 4.80 (2H, br s), and 6.80—7.45 (7H, m); MS (70 eV) *m/z* 540 (M^+, 67). Found: C, 69.33; H, 7.34%. Calcd for $C_{31}H_{40}O_4S_2$: C, 68.85; H, 7.46%.

Tetramer **SSC-b** was prepared from **4b** and **1b** in 73% yield, as described regarding the synthesis of **SSC-a**.

SSC-b: Colorless prisms (*o*-xylene), mp 123—124 °C, IR (KBr) 3400, 880, and 820 cm^{-1}; ^1H NMR ($CDCl_3$) δ=1.12 (9H, s), 1.21 (9H, s), 1.26 (18H, s), 3.94 (2H, s), and 6.70—7.70 (10H, s); MS (70 eV) *m/z* 672 (M^+, 100). Found: C, 73.46; H, 7.98%. Calcd for $C_{41}H_{52}O_4S_2$: C, 73.17; H, 7.79%.

Synthesis of 2-[3-[3-(2-Hydroxy-5-methylphenylthio)-5-methylsalicyl]-2-hydroxy-5-methylphenylthio]-4-methylphenol (SCS-a). Formalin (37%; 11.3 g, 0.14 mol) was added to a mixture of **2a** (10 g, 0.04 mol), a 10% NaOH solution (30 ml) and MeOH (40 ml) over a period of 5 min at 0 °C in an N_2 atmosphere. After stirring at 50 °C for 26 h, the reaction mixture was cooled to room temperature, acidified to pH 5 with 10% HCl, and then extracted with $CHCl_3$. The organic layer was washed with H_2O and dried over Na_2SO_4. The solvent was removed, and the residue was chromatographed on silica gel (Wako C-200; hexane/AcOEt=2/1) to give 3-(2-hydroxy-5-methylphenylthio)-2-hydroxy-5-methylbenzyl alcohol (**5a**; 4.15 g, 37%) along with 3,3′-thiobis[2-hydroxy-5-methylbenzenemethanol] (**6a**; 6.7 g, 54%).

5a: Colorless prisms (benzene), mp 100—101 °C; IR (KBr) 3370, 850, and 820 cm^{-1}; ^1H NMR ($CDCl_3$) δ=2.12 (3H, s), 2.20 (3H, s), 4.68 (2H, br s), and 6.65—7.40 (5H, m); MS (70 eV) *m/z* 276 (M^+, 100). Found: C, 65.46; H, 5.82%. Calcd for $C_{15}H_{16}O_3S$: C, 65.19; H, 5.84%.

6a: Colorless needles ($CHCl_3$), mp 133—134 °C; IR (KBr) 3350 and 880 cm^{-1}; ^1H NMR ($CDCl_3$) δ=2.20 (6H, s), 4.00—4.70 (2H, m, OH), 4.73 (4H, s), 6.90 (2H, s), and 7.15 (2H, s); MS (70 eV) *m/z* 306 (M^+, 100). Found: C, 62.96; H, 5.94%. Calcd for $C_{16}H_{18}O_4S$: C, 62.72; H, 5.92%.

A solution of **5a** (1.0 g, 3.6 mmol), **2a** (8.0 g, 32.5 mmol), and TsOH (50 mg) in benzene (100 ml) was stirred under reflux for 16 h. The water produced during the reaction was removed by azeotropic distillation using a Dean-Stark condenser. After removing the solvent, the residue was subjected to medium-pressure liquid column chromatography (Kieselgel 60, 230—300 mesh; hexane/AcOEt=4/1) to give **SCS-a** (0.90 g, 50%).

SCS-a: Colorless powder (benzene), mp 160—161.5 °C; IR (KBr) 3350, 860, 820 cm^{-1}; ^1H NMR ($CDCl_3$) δ=2.10 (3H, s), 2.14 (9H, s), 3.70 (2H, s), 6.48—7.35 (10H, m); MS (70 eV) *m/z* 504 (M^+, 100). Found: C, 68.95; H, 5.64%. Calcd for $C_{29}H_{28}O_4S_2$: C, 69.02; H, 5.59%.

Synthesis of 2-[3-[3-(5-*t*-Butyl-2-hydroxyphenylthio)-5-*t*-butylsalicyl]-5-*t*-butyl-2-hydroxyphenylthio]-4-*t*-butylphenol (SCS-b). 2,2′-Thiobis[4-*t*-butylphenol] (**2b**) was treated with formalin and 10% NaOH in MeOH, as described for **2a**, to give 3-(5-*t*-butyl-2-hydroxyphenylthio)-5-*t*-butyl-2-hydroxybenzyl alcohol (**5b**, 47%), and 3,3′-thiobis[5-*t*-butyl-2-hydroxybenzenemethanol] (**6b**, 33%) and unreacted **2b** (15%).

5b: Colorless prisms (hexane), mp 146—146.5 °C; IR (KBr) 3280, 880, and 820 cm^{-1}; ^1H NMR ($CDCl_3$) δ=1.18 (9H, s), 1.20 (9H, s), 4.80 (2H, br s), and 6.70—7.60 (5H, m); MS (70 eV) *m/z* 360 (M^+, 48). Found: C, 69.89, H, 7.89%. Calcd for $C_{21}H_{28}O_3S$: C, 69.96; H, 7.83%.

6b: Colorless powder (hexane), mp 93—94 °C IR (KBr) 3350 and 880 cm^{-1}; ^1H NMR ($CDCl_3$) δ=1.24 (18H, s), 4.78 (4H, s), 7.15 (2H, br s), 7.35 (2H, br s), and 7.95 (2H, br s); MS (70 eV) *m/z* 390 (M^+, 88). Found: C, 67.38; H, 7.80%. Calcd for $C_{22}H_{26}O_4S$: C, 67.66; H, 7.74%.

A solution of **5b** (1.0 g, 2.8 mmol), **2b** (9.2 g, 28 mmol), and TsOH (50 mg) in benzene (70 ml) was stirred under reflux for 21 h. The reaction mixture was worked up as described regarding the synthesis of **SCS-a** to give **SCS-b** (0.8 g, 43%).

SCS-b: Corless plates (hexane), mp 170—174 °C; IR (KBr) 3370, 880, and 820 cm^{-1}; ^1H NMR ($CDCl_3$) δ=1.20 (18H, s), 1.26 (18H, s), 3.90 (2H, s), and 6.70—7.65 (10H, m); MS (70 eV) *m/z* 672 (M^+, 100). Found: C, 73.24; H, 7.95%. Calcd for $C_{41}H_{52}O_4S_2$: C, 73.17; H, 7.79%.

Synthesis of 2-[3-[3-(5-Methylsalicyl)-2-hydroxy-5-methylphenylthio]-5-methylsalicyl]-4-methylphenol (CSC-a). A solution of **6a** (3.0 g, 9.8 mmol), **1a** (15 g, 0.14 mol), and TsOH (50 mg) in benzene (100 ml) was stirred under reflux for 10 h. After evaporating the solvent excess **1a** was removed by steam-distillation. The crude product was purified by medium-pressure liquid column chromatography (Kieselgel 60, 230—300 mesh; hexane/AcOEt=4/1) to give **CSC-a** (4.1 g, 86%).

CSC-a: Colorless prisms (hexane-AcOEt), mp 157—158 °C; IR (KBr) 3250, 865, and 815 cm^{-1}; ^1H NMR ($CDCl_3$) δ=2.20 (6H, s), 2.28 (6H, s), 3.85 (4H, s), and 6.60—7.30 (10H, m); MS *m/z* (70 eV) 486 (M^+, 100). Found: C, 74.23; H, 6.23%. Calcd for $C_{30}H_{30}O_4S$: C, 74.05; H, 6.21%.

Synthesis of 2-[3-[3-(5-*t*-Butylsalicyl)-5-*t*-butyl-2-hydroxyphenylthio]-5-*t*-butylsalicyl]-4-*t*-butylphenol (CSC-b): Treatment of **6b** (3 g, 7.7 mmol) with **1b** (23 g, 0.15 mmol) in a similar manner as that described for the synthesis of **CSC-a** from **6a** gave **CSC-b** (4.3 g, 85%).

CSC-b: Colorless prisms (benzene), mp 172—173.5 °C; IR (KBr) 3370, 875, and 815 cm^{-1}; ^1H NMR ($CDCl_3$) δ=1.18 (18H, s), 1.24 (18H, s), 3.91 (4H, s), and 6.60—7.55 (10H, m); MS (70 eV) *m/z* 654 (M^+, 100). Found: C, 77.01; H, 8.39%. Calcd for $C_{42}H_{54}O_4S$: C, 77.02; H, 8.31%.

Synthesis of 2-[3-[3-(2-Hydroxy-5-methylphenylthio)-5-methylsalicyl]-5-methylsalicyl]-4-methylphenol (SCC-a). 3-(3-Bromo-5-methylsalicyl)-2-hydroxybenzyl alcohol[5] (**8a**; 5.7 g, 17 mmol), **2a** (20.8 g, 84 mmol), and TsOH (100 mg) were dissolved in benzene (50 ml); the solution was then stirred under reflux for 9 h. After the usual work-up, column chromatography (Wako Q-200, hexane/AcOEt=3/1) of the reaction mixture yielded 2-[3-[3-(3-bromo-5-methylsalicyl)-5-methylsalicyl]-2-hydroxy-5-methylphenylthio]-4-methylphenol (**9a**; 4.2 g, 43%).

9a: Colorless prism (benzene-hexane), mp 168—170 °C; IR 3340, 860, 810 cm^{-1}; ^1H NMR ($CDCl_3$) δ=2.15 (12H, s), 3.80 (4H, s), 5.30 (4H, br s, OH), and 6.30—7.30 (9H, m); MS (70 eV) *m/z* 564 (M^+, 100). Found: C, 63.88; H, 5.16%. Calcd for $C_{30}H_{29}O_4SBr$: C, 63.72; H, 5.17%.

To a refluxing solution of **9a** (1.3 g, 2.3 mmol) in 80% AcOH, zinc powder (15 g, 0.23 mol) was added over a period of 1 h with stirring. After stirring under reflux for 15 h, the

mixture was cooled to room temperature and filtered. The filtrate was extracted with $CHCl_3$. The residual zinc was extracted with $CHCl_3$ using a Soxhlet extractor. The combined extracts were concentrated and the residual oil subjected to medium-pressure liquid chromatography (Kiesel gel 60, 230—300 mesh; hexane/AcOEt=4/1) to give **SCC-a** (0.9 g, 80 %).

SCC-a: Colorless needles (benzene), mp 180—185 °C; IR 3300, 860, and 810 cm^{-1}; ^1H NMR ($CDCl_3$) δ=2.15 (3H, s), 2.20 (6H, s), 2.25 (3H, s), 3.84 (4H, s), and 6.10—7.40 (14H, m); MS (70 eV) *m/z* 486 (M^+, 57). Found: C, 73.81; H, 6.25%. Calcd for $C_{30}H_{30}O_4S$: C, 74.05; H, 6.21%.

Synthesis of 2-[3-[3-(5-*t*-Butyl-2-hydroxyphenylthio)-5-*t*-butylsalicyl]-5-*t*-butylsalicyl]-4-*t*-butylphenol (SCC-b). A solution of **5b** (2.0 g, 5.6 mmol), 2-(5-*t*-butylsalicyl)-4-*t*-butylphenol (**7b**; 17.2 g, 51 mmol), and TsOH (50 mg) in benzene (100 ml) was stirred under reflux for 40 h; the water produced during the reaction was removed by azeotropic distillation using a Dean-Stark condenser. The reaction mixture was cooled to room temperature and the precipitate filtered off. The solvent was then evaporated and the residual oil (10.6 g) chromatographed (silica gel Wako Q-200, benzene) to give **SCC-b** (2.55 g, 70%) and unreacted **2b** (7.4 g).

SCC-b: Colorless powder (benzene), mp 174.5—177.5 °C IR (KBr) 3260, 880, and 820 cm^{-1}; ^1H NMR ($CDCl_3$) δ=1.18 (9H, s), 1.26 (9H, s), 3.90 (4H, s), and 6.60—7.45 (10H, m); MS (70 eV) *m/z* 654 (M^+, 100); Found: C, 77.09; H, 8.59%. Calcd for $C_{42}H_{54}O_4S$: C, 77.02; H, 8.31%.

Preparation of Inclusion Complexes. The host oligomer was recrystallyzed using a minimum amount of organic solvent (guest). The precipitates were collected by filtration, when necessary, washed with hexane, and dried at ambient temperature overnight. The host-guest ratio was determined by means of ^1H NMR spectroscopy.

Selective guest inclusion was examined as follows: The tetramer **SSS-b** (500 mg) was dissolved in an equimolar mixture of guests by heating. The mixture was treated in a similar manner as the procedure described above. Upon heating the complex under reduced pressure, a liquid mixture was obtained by distillation. The ratio of the components in the distillate was determined by gas chromatography.

Kinetic Study. The weight-decreasing ratio of a complex was measured from the TG-DTA curve using Al_2O_3 as an reference. The programmed temperature was raised at a rate 10 °C min^{-1} up to each temperature. Based on the rate constants, thus obtained, the ΔH^*, $\ln A$ and E_a values were calculated by a least-squares method.

The authors are grateful to Professor Kenzo Matsuki and Mr. Takashi Endo for TG/DTA measurements. They would also like to thank Mr. Kazuaki Sato for elemental analyses and Mr. Hideaki Hino for his assistance in some of the experiments.

References

1) T. Sone, Y. Ohba, and H. Yamazaki, *Bull. Chem. Soc. Jpn.*, **62**, 1111 (1989).

2) Y. Fukazawa, K. Deyama, S. Usui, T. Sone, and Y. Ohba, Presented at the Annual Meeting of the Chemical Society of Japan, Kyoto, April 1989. Abstr. 2IIIA28.

3) E. Paulus and V. Böhmer, *Makromol. Chem.*, **185**, 1921 (1984).

4) The abbreviations refer to the kind and the sequence of arrangement of the bridges in the tetramers: **S**, sulfur bridge; **C**, methylene bridge; **a**, *p*-cresol tetramer; **b**, *p*-*t*-butylphenol tetramer.

5) B. T. Hayes and R. F. Hunter, *J. Appl. Chem.*, **8**, 743 (1958).

6) High preference of the sulfur-bridged tetramers for aliphatic amines suggests that the mode of the complexation with the amines is different from that with the other guests. In contrast to the complexation with the neutral guests, hydrogen-bonding between host and guest molecules may play an important role in the complexation with the amines. See, for example, J. E. Barry, M. Finkelstein, and S. D. Ross, *J. Org. Chem.*, **49**, 1669 (1984). F.Toda, K. Tanaka, T. Hyoda, and T. C. W. Mak, *Chem. Lett.*, **1988**, 107.

7) a) F. Toda, K. Tanaka, Y. Wang, and G-H. Lee, *Chem. Lett.*, **1986**, 109. b) K. Saigo, R-H. Lin, M. Kubo, A. Youda, and M. Hasegawa, *J. Am. Chem. Soc.*, **108**, 1996 (1986).

8) Diaryl sulfides have C-S bond length of 1.75 Å[9] and C-S-C bond angles of 109—113°, while 2,2′-methylenebisphenol has C-CH_2 bond length of 1.51 Å and C-CH_2-C bond angle of 113.9°.[10] Thus, the maximum distance between adjacent phenolic hydroxyl groups in the sulfur-bridged phenols is longer than that of the methylene-bridged phenols by about 0.2—0.3 Å.

9) W. A. Pryor, "Mechanisms of Sulfur Reactions," McGraw-Hill, New York (1962), pp. 18, 25.

10) G. Casiraghi, M. Cornia, G. Sartori, G. Casnati, V. Bocchi, and G. D. Andreetti, *Makromol. Chem.*, **183**, 2611 (1982).

11) A. J. Neale, P. J. S. Bain, and T. J. Rawlings, *Tetrahedron*, **25**, 4593 (1969).

 © 1991 The Chemical Society of Japan Bull. Chem. Soc. Jpn., 64, 583—587 (1991)

Synthesis and Properties of Gramicidin S Analogs Containing D-Lys Residue in Place of Orn Residue

Makoto TAMAKI,* Sadatoshi AKABORI, and Ichiro MURAMATSU†
Department of Chemistry, Faculty of Science, Toho University, Miyama, Funabashi-shi, Chiba 274
†Department of Chemistry, College of Science, Rikkyo University, Nishi-ikebukuro, Tokyo 171
(Received September 6, 1990)

[L-Lys$^{2,2'}$]-gramicidin S has been known to possess the same type activity and conformation as that of gramicidin S. The D-isomer of the Lys residue, instead of the Orn residue, was introduced to gramicidin S in order to investigate the contribution of the configurations of the Orn residue in gramicidin S to its activity and conformation. [D-Lys$^{2,2'}$]- and [D-Lys^{2}, L-Lys$^{2'}$]-gramicidin S were synthesized by a liquid-phase method. The CD spectra of these analogs showed a pattern similar to that of gramicidin S, suggesting that the conformation of these analogs at the β-turn parts around the D-Phe-Pro sequence resemble that of gramicidin S. These analogs have either a weak or no activity against the Gram-positive microorganisms tested, indicating the importance of the configuration of the Orn residue in gramicidin S for exhibiting strong activity.

Gramicidin S (GS)[1-2] is an antibiotic cyclodecapeptide isolated from *Bacillus brevis*. In studies of the relationship between the structure and antibiotic activity of GS, various analogs have been synthesized. From these studies it has been recognized that the basic amino groups of the Orn residues in GS are necessary for the activity. For example, the acylation of these amino groups caused a drastic decrease in the activity.[3] On the other hand, changes in the length of the side chain in the Orn residues[4-5] and a conversion of the amino groups into strongly basic guanidino groups[6] did not alter the activity. However, the effects of an alternation of the configuration of the Orn residues on the secondary structure and antibiotic actvity of GS have not been studied.

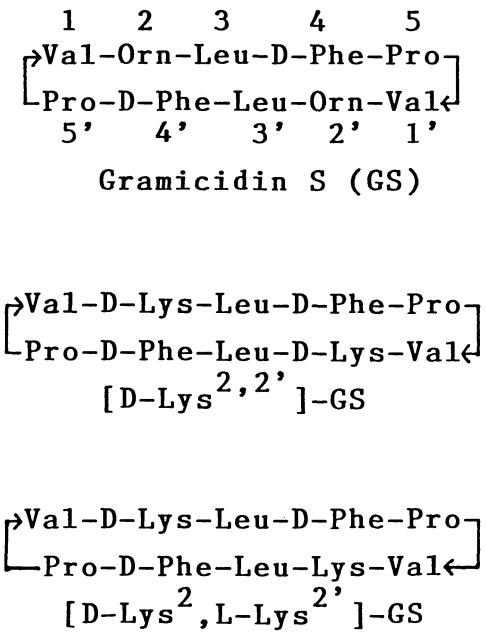

Fig. 1. Primary structure of gramicidin S and its analogs.

Waki et al.[5] synthesized [L-Lys$^{2,2'}$]-GS, in which the Orn residues at the 2- and 2'-positions are replaced with Lys residues, and reported that this analog shows the same ORD curve and antibiotic activity as those of GS.

In the present paper we describe the synthesis, antibiotic activity and CD spectra of [D-Lys$^{2,2'}$]- and [D-Lys^{2}, L-Lys$^{2'}$]-GS (Fig. 1), and discuss the structure-activity relationship of these GS analogs.

The synthetic routes of [D-Lys$^{2,2'}$]- and [D-Lys^{2}, L-Lys$^{2'}$]-GS are shown in Fig.2. In the synthesis of [D-Lys$^{2,2'}$]-GS (**5a**), the Boc-pentapeptide benzyl ester (**1a**) was synthesized from the Pro benzyl ester by a step-by-step elongation using 1-ethyl-3-(3-dimethylaminopropyl)carbodiimide hydrochloride (WSCD·HCl) and 1-hydroxybenzotriazole (HOBt), and then saponified to give Boc-pentapeptide (**2a**). A part of **2a** was converted into the corresponding succinimido ester **2a'** with WSCD·HCl and *N*-hydroxysuccinimide (HONSu). Coupling of **2a'** and the pentapeptide derived from **2a** afforded the decapeptide (**3a**), which was converted into the decapeptide succinimido ester (**3a'**). The Boc-group of **3a'** was removed by the action of trifluoroacetic acid (TFA); the succinimido ester was then cyclized under high dilution in pyridine at 45 °C for 5 h. The resulting product was purified by means of high-performance liquid chromatography (HPLC), followed by recrystallization. The cyclodecapeptide (**4a**) was obtained in 26% yield. The removal of all the masking groups of **4a** by hydrogenolysis yielded [D-Lys$^{2,2'}$]-GS (**5a**). [D-Lys^{2}, L-Lys$^{2'}$]-GS (**5b**) was synthesized in a similar manner. The yield of the cyclization of **3b** was 60%. Cyclization of **3a** using a succinimido active ester method gave a very low yield of the desired cyclic peptide, compared with that of **3b**. These phenomena indicate that the substitution of two Orn(*Z*) residues by two D-Lys(*Z*) residues induces a decrease in the chance for collisions between the N- and C-terminals in the linear decapeptide **3a**. The homogeneity of

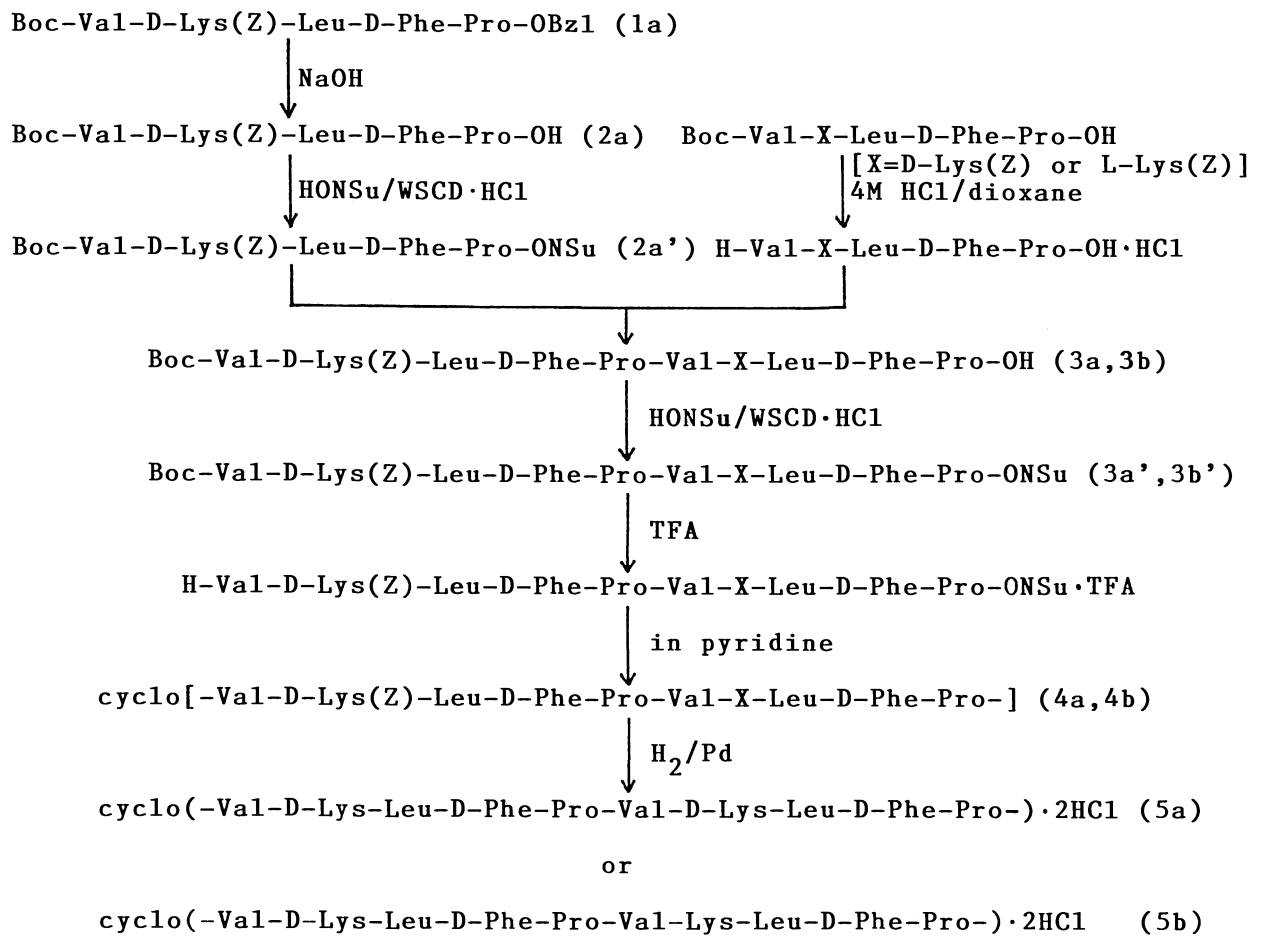

Fig. 2. Synthesis of [D-Lys$^{2,2'}$]-GS and [D-Lys^{2}, L-Lys$^{2'}$]-GS.

[D-Lys$^{2,2'}$]- and [D-Lys^{2}, L-Lys$^{2'}$]-GS was confirmed by means of thin-layer chromatography (TLC), amino acid analysis, HPLC, elemental analysis, and fast atom bombardment (FAB) mass spectrometry.

The CD spectra of GS and the analogs (**5a** and **5b**) were measured in aqueous solutions (Fig. 3). Though the shape of the CD spectrum of **5b** was similar to that of GS, each depth of the two troughs was about 1/2 that of GS. Though two troughs in the CD parttern of **5a** were also observed, their depths were much shallower. In studies regarding an alternation of the configurations of the constituent amino acid residue in GS, it was reported that [D-Val$^{1,1'}$]-,[7] [L-Phe$^{4,4'}$]-,[8] and [D-Pro$^{5,5'}$]-GS,[9] in which L-Val, D-Phe, or L-Pro residues in GS was replaced with D-Val, L-Phe, or D-Pro residues, respectively, possessed a CD spectra different from those of GS in aqueous solutions. These results indicated that the configuration of the amino acid residues at the β-turn parts of GS influences its conformation more than does that of the Orn residue. In CD studies of GS and gratisin, we also reported that their CD spectra mainly reflect the ring features near the Pro residue, but not the entire structure of the molecule.[7-10] The present results suggest that though there exists a similarity among the CD pattern of these synthetic analogs and the GS results from the presence of a D-Phe-Pro sequence of these analogs, the stability of their conformation decreases as the D-Lys residue is introduced.

The antibiotic activity of these synthetic peptides is summarized in Table 1. [D-Lys$^{2,2'}$]-GS possessed about 1/8 of the activity of the natural GS against *C. diphtheriae* P.W.8, and no activity toward the other Gram-positive microorganisms tested. On the other hand, [D-Lys^{2}, L-Lys$^{2'}$]-GS showed activity against all of the Gram-positive microorganisms tested, although it was very weak. Further, it was reported that [D-Val$^{1,1'}$]-,[7] [L-Phe$^{4,4'}$]-,[8] and [D-Pro$^{5,5'}$]-GS[9] shows either a weak or no activity. These results point out the importance of the configuration of the constituent amino acid residue of GS for exhibiting activity. In ESR studies of GS, Ovchinikov et al. reported that the average distance between the NH_3^+ groups of the Orn residues in GS and its analogs with activity is about 8—10 Å, and that the spatial situation is held by a rigid conformation containing two D-Phe-Pro type-II' β-turns.[11] From the present studies, it is deduced that the introduction of one or two D-Lys residues at

Table 1. Antibiotic Activity of GS and Its Analogs[a)]

Test organisms	GS	[D-Lys$^{2,2'}$]-	[D-Lys^{2}, L-Lys$^{2'}$]-
S. aureus MS353	3.13	>100	50
S. aureus Smith	3.13	>100	50
S. epidermidis ATCC 27626	3.13	>100	50
S. pyogenes N. Y. 5	3.13	>100	50
S. agalatiae 1020	3.13	>100	50
M. luteus ATCC 9341	3.13	>100	100
C. diphtheriae P. W. 8	3.13	25	12.5
B. subtilis ATCC 6633	3.13	100	12.5
E. coli NIHJ JC-2	>100	>100	>100
P. aeruginosa PA01	>100	>100	>100

a) The minimum inhibitory concentration ($\mu g\,ml^{-1}$) was determined by means of an agar-dilution method with 10^6 organisms per milliliter.

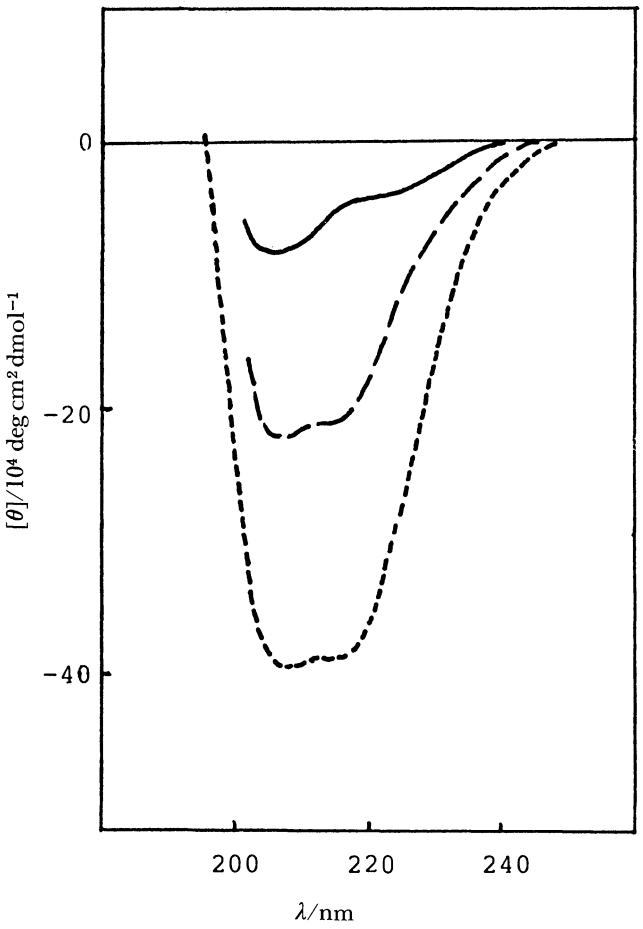

Fig. 3. CD spectra of GS and its analogs in aqueous solution.
——, [D-Lys$^{2,2'}$]-GS: ——, [D-Lys^{2}, L-Lys$^{2'}$]: ----, GS.

positions 2 and 2′ in GS decreases the stability of the type-II′ β-turn around D-Phe-Pro sequences, resulting in a distortion of the spatial arrangement of the NH_3^+ groups required for antibiotic activity.

Experimental

All melting points are uncorrected. The CD spectra were measured by a JASCO spectropolarimeter (model J-500) using a 0.5 mm quarts cell at room temperature. The CD spectroscopy of GS and its analogs was carried out as aqueous solutions of their dihydochlorides at a concentration of 1.5—2.0×10^{-4} M (1 M=1 mol dm^{-3}). The molecular weights of these synthetic peptides were determined by FAB mass spectrometry using a JEOL JMS-D-300 mass spectrometer. Amino acid analyses were carried out using a Hitachi 835 amino acid analyzer, after hydrolysis in 6 M HCl at 110 °C for 24 h. HPLC was performed by an octadecylsilica (ODS) column (φ 4.6×250 mm) using MeOH-5% $NaClO_4$aq (5:1) as an elution solvent. TLC was performed on Merck silica-gel F_{254} plates with the following solvent systems (v/v): R_f^1, $CHCl_3$-MeOH (9:1); R_f^2, $CHCl_3$-MeOH-AcOH (95:5:3); R_f^3, *n*-BuOH-AcOH-H_2O (4:1:1); R_f^4, *n*-BuOH-pyridine-AcOH-H_2O (4:1:1:2). The yields of **1a** and **1b** were calculated on the basis of the amount of Pro-OBzl as a starting material.

Boc-Val-D-Lys(Z)-Leu-D-Phe-Pro-OBzl (1a). Pro-OBzl·HCl (1.20 g, 5 mmol) was dissolved in $CHCl_3$ (20 ml). The solution was then washed with aqueous 5% Na_2CO_3 and water under cooling in an ice bath. To the organic layer were added Boc-D-Phe (1.32 g, 5 mmol), HOBt (0.75 g, 5.5 mmol) and WSCD·HCl (0.96 g, 5 mmol) at 0 °C. This solution was stirred for 1 h at 0 °C and overnight at room temperature. The reaction mixture was washed successively with aqueous 5% citric acid, water, and aqueous 5% Na_2CO_3, and water; the solvent was then evaporated in vacuo. The residue was dissolved in 4 M HCl/dioxane (20 ml) at 0 °C. After stirring for 30 min at room temperature, the solution was concentrated in vacuo. The residue was dissolved in $CHCl_3$ (30 ml); the solution was then washed with aqueous 5% Na_2CO_3 and water under cooling in an ice bath. To this solution was added Boc-Leu (1.25 g, 5 mmol), HOBt (0.75 g, 5.5 mmol) and WSCD·HCl (0.96 g, 5 mmol) at 0 °C. The same procedure as described above was repeated for this reaction mixture. Further, Boc-D-Lys(*Z*) and Boc-Val were successively coupled by the same method. All reactions were followed by TLC on a silica-gel plate. The crude protected pentapeptide obtained from the final reaction mixture was purified by chromatography on a silica-gel column (φ 1.5×60 cm) using a solvent system of $CHCl_3$-MeOH (50:1) and reprecipitation from AcOEt-ether.; overall yield, 3.38 g (73% from Pro-OBzl·HCl); mp, 70—74 °C; $[\alpha]_D^{27}$ −30.8° (*c* 1.1, DMF); R_f^1 0.90, R_f^2 0.54.

Found: C, 65.33; H, 7.65; N, 8.71%. Calcd for $C_{51}H_{70}$-

$N_6O_{10}\cdot 0.5H_2O$: C, 65.43; H, 7.64; N, 8.98%.

Boc-Val-D-Lys(Z)-Leu-D-Phe-Pro-OH (2a). To a solution of **1a** (3.00 g, 3.24 mmol) in MeOH (40 ml), 1 M NaOH (8 ml) was added; the solution was then stirred for 7 h at room temperature. After the addition of water (10 ml), the solution was concentrated in vacuo at low temperature, and aqueous 5% citric acid (100 ml) added to the reaction mixture. The resulting solid was collected by filtration, washed with water and dried. The product was recrystallized from MeOH-ether-hexane; yield, 2.64 g (97%); mp, 82—87 °C; $[\alpha]_D^{27}$ −29.6° (*c* 1.1, DMF); R_f^1 0.38, R_f^2 0.52.

Found: C, 62.47; H, 7.88; N, 9.61%. Calcd for $C_{44}H_{64}N_6O_{10}\cdot 0.5H_2O$: C, 62.47; H, 7.74; N, 9.93%.

Boc-[Val-D-Lys(Z)-Leu-D-Phe-Pro-]$_2$-OH (3a). To a solution of **2a** (800 mg, 0.96 mmol) in DMF (5 ml) were added HONSu (231 mg, 2 mmol) and WSCD·HCl (383 mg, 2 mmol) at 0 °C; the mixture was then stirred for 5 h at room temperature. After the solution was evaporated in vacuo, water was added to the residue. The resulting solid, Boc-Val-D-Lys(Z)-Leu-D-Phe-Pro-ONSu (**2a′**), was collected by filtration, washed with water and then dried. Another crop of **2a** (800 mg, 0.96 mmol) was dissolved in 4 M HCl/dioxane (15 ml) at 0 °C. After stirring at room temperature for 30 min, the solution was concentrated in vacuo. Ether (50 ml) was added to the residue, and the resulting solid was collected by filtration. To a solution of HCl·H-Val-D-Lys(Z)-Leu-D-Phe-Pro-OH (prepared as mentioned above) and triethylamine (0.26 ml, 1.92 mmol) in DMF (20 ml), **2a′** derived from **2a** at 0 °C was added. The mixture was left standing for 2 h at 0 °C and then overnight at room temperature. The solution was evaporated; aqueous 5% citric acid was then added to the residue. The resulting solid was collected by filtration, washed with water and dried. The product was recrystallized from AcOEt-ether; yield, 1.40 g (93%); mp, 120—125 °C; $[\alpha]_D^{27}$ −37.9° (*c* 1.1, DMF); R_f^1 0.40, R_f^2 0.53.

Found: C, 62.28; H, 7.70; N, 10.51%. Calcd for $C_{83}H_{118}N_{12}O_{17}\cdot 2.5H_2O$: C, 62.27; H, 7.74; N, 10.50%.

Cyclo[-Val-D-Lys(Z)-Leu-D-Phe-Pro-]$_2$ (4a). Compound **3a** (750 mg, 0.48 mmol) was converted into the *N*-hydroxysuccinimido ester (**3a′**) by methods described for **2a**. It was then dissolved in TFA (15 ml) at 0 °C. The mixture was stirred for 40 min at room temperatue and then concentrated in vacuo. The residue, the trifluoroacetate of the decapeptide active ester, was triturated with ether and collected by filtration and dissolved in DMF (10 ml). The solution was poured, dropwise, in pyridine (500 ml) at 45 °C. After stirring for 3 h at 45 °C, the solution was concentrated. The addition of water to the reisdue afforded precipitates, which were filtered and washed with water. The purification of this compound was performed by HPLC on ODS column (ϕ 7.6×250 mm) using a solvent system of MeOH-H_2O (6:1), followed by reprecipitation from MeOH-ether; yield, 180 mg (26%); mp, 220—222 °C; $[\alpha]_D^{27}$ −137.7° (*c* 0.65, DMF); R_f^1 0.83, R_f^2 0.56.

Found: C, 63.32; H, 7.64; N, 11.35%. Calcd for $C_{78}H_{108}N_{12}O_{14}\cdot 2H_2O$: C, 63.57; H, 7.66; N, 11.40%.

Cyclo(-Val-D-Lys-Leu-D-Phe-Pro-)$_2$·2HCl (5a). Compound **4a** (120 mg, 0.083 mmol) was dissolved in 90% aq MeOH (40 ml) and then 1 M HCl (0.17 ml) was added to the solution. The compound was hydrogenolyzed in the presence of palladium black for 15 h. After removing the catalyst, the filtrate was concentrated in vacuo. The product was purified by gel filtration on a Sephadex LH-20 column (ϕ 1.2×120 cm) using MeOH as a solvent, and by reprecipitation from MeOH-ether; yield, 90 mg (87%); mp, 246—248 °C; $[\alpha]_D^{27}$ −158.3° (*c* 0.70, EtOH); R_f^3 0.44, R_f^4 0.76.

Amino acid ratios: Val, 0.97; Lys, 0.98; Leu, 1.03; Phe, 1.08; Pro, 0.93. MS (FAB), *m/z* 1169 ($C_{62}H_{96}N_{12}O_{10}$, MH^+).

Found: C, 54.81; H, 8.04; N, 12.40%. Calcd for $C_{62}H_{96}N_{12}O_{10}\cdot 2HCl\cdot 6.5H_2O$: C, 54.78; H, 8.23; N, 12.36%.

Boc-Val-D-Lys(Z)-Leu-D-Phe-Pro-Val-Lys(Z)-Leu-D-Phe-Pro-OH (3b). This compound was prepared from **2a** (600 mg, 0.72 mmol) and Boc-Val-Lys(Z)-Leu-D-Phe-Pro-OH (700 mg, 0.84 mmol) in a manner similar to that described for the preparation of **3a**. Purification of the product was performed by reprecipitation from AcOEt-ether-hexane: yield, 1.03 g (92%); mp, 104—112 °C; $[\alpha]_D^{27}$ −40.9° (*c* 1.2, DMF); R_f^1 0.51, R_f^2 0.57.

Found: C, 62.87; H, 7.77; N, 10.53%. Calcd for $C_{83}H_{118}N_{12}O_{17}\cdot 1.5H_2O$: C, 62.98; H, 7.70; N, 10.62%.

Cyclo[-Val-D-Lys(Z)-Leu-D-Phe-Pro-Val-Lys(Z)-Leu-D-Phe-Pro-] (4b). This compound was prepared from **3b** (750 mg, 0.48 mmol), as described regarding the preparation of **4a**; yield, 417 mg (60%); mp, 133—137 °C; $[\alpha]_D^{27}$ −154.4° (*c* 1.0, DMF); R_f^1 0.76, R_f^2 0.55.

Found: C, 64.32; H, 7.68; N, 11.45%. Calcd for $C_{78}H_{108}N_{12}O_{14}\cdot H_2O$: C, 64.35; H, 7.62; N, 11.54%.

Cyclo(-Val-D-Lys-Leu-D-Phe-Pro-Val-Lys-Leu-D-Phe-Pro-)·2HCl (5b). This compound was prepared from **4b** (200 mg, 0.14 mmol) as described regarding the preparation of **5a**; yield, 150 mg (87%); mp, 228—235 °C; $[\alpha]_D^{27}$ −223.4° (*c* 0.82, EtOH); R_f^3 0.69, R_f^4 0.79.

Amino acid ratios: Val, 0.98; Lys, 0.99; Leu, 1.05; Phe, 1.04; Pro, 0.94.

MS(FAB), *m/z* 1169 ($C_{62}H_{96}N_{12}O_{10}$, MH^+).

Found: C, 56.51; H, 8.08; N, 12.75%. Calcd for $C_{62}H_{96}N_{12}O_{10}\cdot 2HCl\cdot 4H_2O$; C, 56.65; H, 8.13; N, 12.79%.

We are grateful to the staff of the Research Laboratories of the Toyo Jozo Co. for their elemental analysis, microbiological assays, and the measurement of the FAB mass.

References

1) A. R. Battersby and L. C. Craig, *J. Am. Chem. Soc.*, **73**, 1887 (1951).

2) Amino acid residues with no plefix are of L-configuration. The abbreviations of amino acids and peptides are in accordance with the rules of IUPAC-IBU commission of Biological Nomenclature. Abbreviations used are as follows: Boc, *t*-butoxycarbonyl; Z, benzyloxycarbonyl; OBzl, benzyloxy; DMF, *N,N*-dimethylformamide; AcOEt, ethyl acetate.

3) A. S. Kaprel' yants, V. V. Nikiforov, A. I. Miroshinov, L. G. Snezhkova, V. A. Eremin, and D. N. Ostrovski, *Biochemistry* (translated from Russian), **42**, 252 (1977).

4) R. Schwyzer and P. Sieber, *Helv. Chim. Acta*, **41**, 1582 (1958).

5) M. Waki, O. Abe, R. Okawa, T. Kato, S. Makisumi, and N. Izumiya, *Bull. Chem. Soc. Jpn.*, **40**, 2904 (1967).

6) A. B. Silaev and V. N. Stepanov, *Dokl. Acad. Nauk SSSR*, **112**, 297 (1957).

7) M. Tamaki, T. Okitsu, M. Araki, H. Sakamoto, M.

Takimoto, and I. Muramatsu, *Bull. Chem. Soc. Jpn.*, **58**, 531 (1985).
8) M. Rothe and F. Eisenbeiss, *Angew. Chem.*, **80**, 907 (1968).
9) K. Sato, R. Kato, and U. Nagai, *Bull. Chem. Soc. Jpn.*, **59**, 535 (1986).
10) M. Tamaki, *Bull. Chem. Soc. Jpn.*, **57**, 3210 (1984).
11) Yu. A. Ovchinikov and V. T. Ivanov, *Tetrahedron*, **31**, 2117 (1975).

Chemical Synthesis of Branched Oligoribonucleotides

Mitsuo SEKINE,* Jarmo HEIKKILÄ, and Tsujiaki HATA
Department of Life Science, Tokyo Institute of Technology, Nagatsuta, Midoriku, Yokohama 227
(Received September 7, 1990)

This paper describes the full detail of the chemical synthesis of branched oligoribonucleotides by use of appropriately protected adenosine 2′,3′-diphosphate derivatives (**13** and **30**), as key intermediates, which were synthesized by a series of reactions involving phosphoryl rearrangement via a new phosphorylation process. Branched triribonucleotides A^{pG}_{pC} (**21**) and A^{pG}_{pU} (**27**) were obtained by using the synthetic unit **13**. Several problems during these syntheses were discussed. The use of **30** as an improved building unit enabled us to prepare synthetic intermediates as neutral, i.e., fully esterified species which allowed facile purification of them by means of silica-gel column thin-layer chromatography throughout the synthesis of a branched hexaribonucleotide derivative $CpUpGpA^{pG}_{pC}$.

Since Wallace and Edmonds[1] discovered branched RNAs, this unique structure has been found as part of the so-called lariat structure in splicing products of messenger RNAs in a variety of eukaryotic cells.[2]

Chemical synthesis of branched RNAs has been reported in several laboratories.[3-15] In this paper,# we report the detailed study of chemical synthesis of branched oligoribonucleotides, involving the regioselective introduction of two different phosphoryl groups into the 2′- and 3′-positions of adenosine at the branched point. Preliminary results of this study have already been reported.[3,13]

Results and Discussion

To introduce a protected phosphate group into the 2′-hydroxyl group of adenosine which is the ribonucleoside found in the target branched RNA, the following method for phosphorylation of the 2′-hydroxyl group of silylated adenosine derivative (**1**) was explored. Caruthers[16] has reported the P-N bond activation of deoxyribonucleoside phosphoramidite derivatives with tetrazole for rapid internucleotidic bond formation. On the other hand, we described previously the synthesis of deoxyribonucleoside phosphonates via phosphorodiamidite intermediates.[17]

On the basis of these facts, **1** was allowed to react with 1.5 equiv of tris(diethylamino)phosphine (TEAP) in the presence of tetrazole in dichloromethane. The resulting phosphorodiamidite intermediate (**2**) was further treated with 4 equiv of aniline in the presence of 4 equiv of tetrazole for transamidation to give the phosphorodianilidite derivative (**3**). Addition of 1.5 equiv of iodine in pyridine to the mixture resulted in the phosphorylated species (**4**).

Desilylation of **4** with KF-Et_4NBr-H_2O in acetonitrile gave a mixture of the 2′,5′-diol derivative (**6a**) and 3′,5′-diol derivative (**6b**). Fortunately, the latter was easily crystallized from the mixture by evaporation of MeOH from its 1,2-dichloroethane-MeOH solution. However, the former did not crystallize from any solvents tested and decomposed upon silica-gel column chromatography. Therefore, we examined the possibility of isomerization of **6a** to **6b** in a variety of solvents. As a result, it was found that **6a** was gradually isomerized to **6b** in pyridine-water (9 : 1, v/v) at 40 °C for 1 h to attain equilibrium giving rise to a ca. 1 : 1 mixture of **6a** and **6b**. It is interesting that the above isomerization did not occur in anhydrous pyridine. Such effects of water on isomerization have also been reported in the case of the 2′-3′ silyl migration by Ogilvie and his co-workers.[18] Thus, compounds **6b** was ultimately obtained in 55% yield by repeated isomerization of the **6a**-rich filtrate followed by crystallization.

Attempts to obtain monophosphorylated adenosine derivative **8a** or **8b** by reaction of 5′-*O*: 6-*N*-bis(4,4′-dimethoxytrityl)adenosine (**7**) with *N*,*N*′-diphenylphosphorodiamidic chloride[19] failed since chromatographic separation of these compounds caused considerable decomposition.

With the hope that the isomerization could be suppressed by modification of the anilino group with an electron-donating *p*-substituent or by replacement of the P=O by the P=S bond, the corresponding 2′-[*N*,*N*′-bis(*p*-methoxyphenyl)phosphorodiamidate] (**9**) and 2′-(*N*,*N*′-diphenylphosphorodiamidothioate) (**10**) were synthesized in 84 and 75% yields from **1** via

In this paper the following abbreviations are used: Tris(diethylamino)phosphine (TEAP); 4,4′,4″-tris(4,5-dichlorophthalimido)trityl (or tris[4(4,5-dichlorophthalimido)phenyl]methyl) (CPTr); 4,4′,4″-tris(4,5-dichlorophthalimido)trityl bromide (or tris[4-(4,5-dichlorophthalimido)phenyl]methyl bromide) (CPTrBr); bis(anilino)phosphinyl (PNN); cyclohexylammonium *S*,*S*-diphenyl phosphorodithioate (PSS); *N*,*N*′-dicyclohexylcarbodiimide (DCC); mesitylenedisulfonyl dichloride (MDS); isodurenedisulfonyl dichloride (or 1,2,3,5-tetramethylbenzenedisulfonyl dichloride) (DDS); 3-nitro-1*H*-1,2,4-triazole (NT); pyridinium *m*-nitrobenzenesulfonate (PNBS); 4-methoxytrityl (MMTr); 4,4′-dimethoxytrityl (DMTr); 2-cyanoethyl (CE); *N*,*N*-diphenylcarbamoyl (DPC); propionyl (pro); benzoyl (Bz); triethylammonium hydrogencarbonate (or triethylammonium bicarbonate) (TEAB); 2,2-dimethyl-2-silapentane-5-sulfonic acid sodium salt (DSS); snake venom phosphodiesterase (VSP); calf spleen phosphodiesterase (CSP).

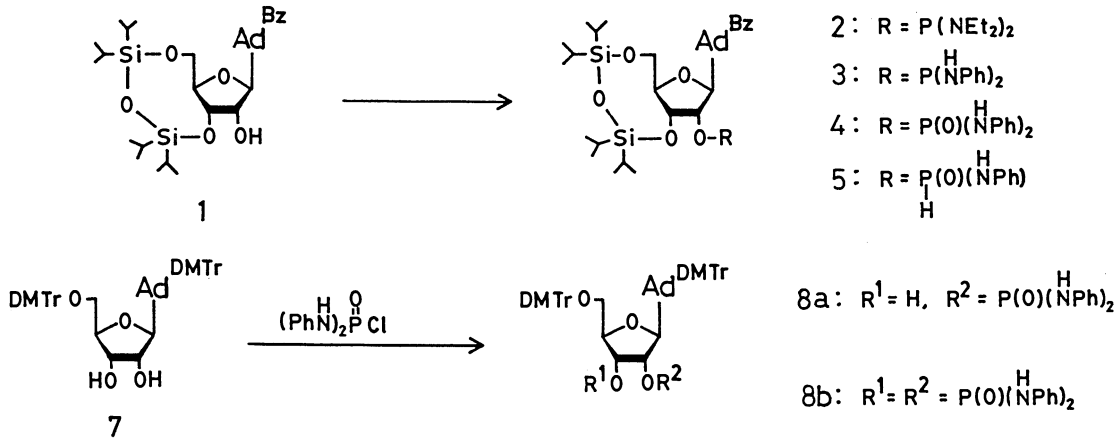

similar iodine oxidation and sulfurization, respectively. However, desilylation of **9** resulted in a similar isomerization to give **11a** and **11b** in 18% and 42% yields, respectively. Unexpectedly, desilylation of **10** caused considerable decomposition.

We tried to synthesize a branched triribonucleotide A^{pG}_{pC} by the use of the predominant product **6b** above-mentioned. The 5′-hydroxyl group of **6b** was protected with tris[4-(4,5-dichlorophthalimido)-phenyl]methyl (CPTr) which has recently been proposed as a hydrazine-labile protecting group of primary alcohols.[20] Reaction of **6b** with 2 equiv of tris[4-(4,5-dichlorophthalimido)phenyl]methyl bromide (CPTrBr) in the presence of 2 equiv of silver nitrate in *N*,*N*-dimethylformamide (DMF) gave the 5′-tritylated product (**12**) in 57% yield. Isomerization or decomposition of the 3′-bis(anilino)phosphinyl (PNN) group did not occur during the tritylation.

Phosphorylation of the 2′-hydroxyl group of **12** should be done in a manner where each protecting group of the 2′- and 3′-phosphate groups can be removed without damage of the other protecting group under different conditions in order to elongate the RNA chain in the 2′- or 3′-direction. If possible no chiral center should be introducted on the second phosphorus atom as well as the first as seen in the PNN group to avoid complexity on TLC or for analysis of further reactions. Therefore, we chose the phe-

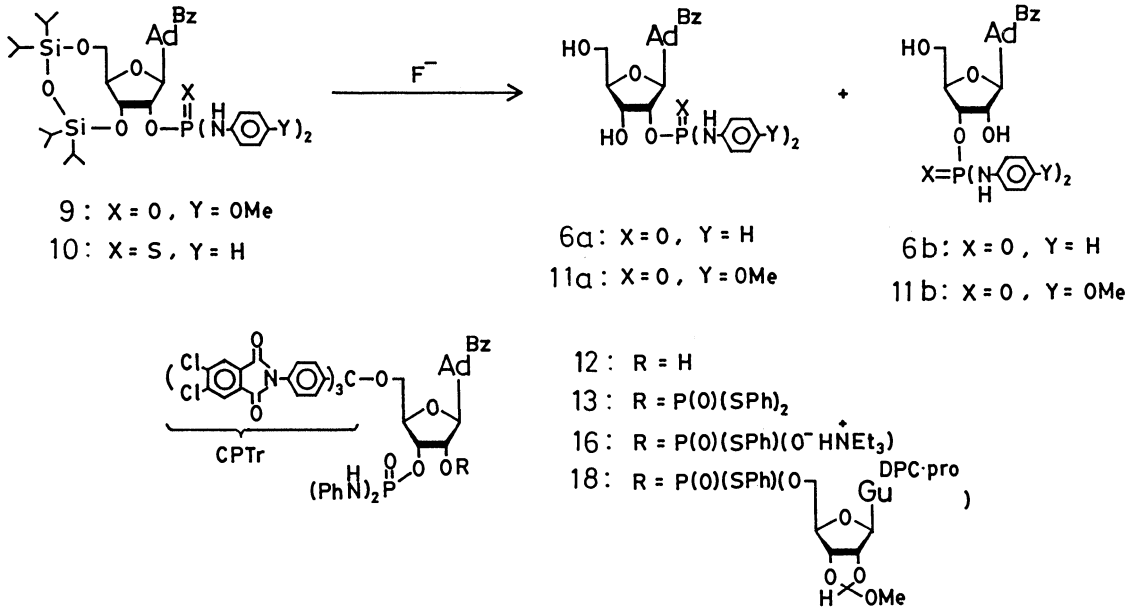

nylthio group for protection of both hydroxyl groups of the second phosphate function, since bis(phenylthio)phosphinyl group was known to be introduced rapidly into hydroxyl groups by reaction with cyclohexylammonium *S,S*-diphenyl phosphorodithioate (PSS)[21] in the presence of tetrazole[20] by use of a bifunctional condensing reagent, mesitylenedisulfonyl dichloride (MDS).[22] Application of this procedure gave a fully protected adenosine 2′,3′-diphosphate derivative (**13**) in 81% yield.

The ^{31}P NMR spectrum of **13** showed indeed two sharp resonance signals at 1.94 and 54.74 ppm. The latter signal was characteristic of *O*-alkyl *S,S*-diphenyl phosphorodithioates. For example, the resonance peak of *S,S*-diphenyl 5′-*O*-(4,4′-dimethoxytrityl)-thymidine 3′-phosphorodithioate[22] appeared at 49.63 ppm in $CDCl_3$. Thus, the homogenity of **13** could be readily ascertained by this spectroscopic analysis.

Next, we attempted to synthesize an appropriately protected adenosine 2′-phosphorothioate derivative (**14**), which seemed to be a fascinating intermediate for chain elongation in the 3′-direction since the same phosphate protecting group could be used commonly for both 2′- and 3′-side chains, from **13** by a two-step reaction. Treatment of **13** with isopentyl nitrite[23] in the presence of acetic anhydride[24] in pyridine–acetic acid for 15 h gave the 2′-unprotected adenylate derivative (**15**) in 50% yield. Under these conditions the phenylthio group was found to be stable as evidenced by ^{31}P NMR of the reaction mixture which showed a characteristic resonance peak at 51.11 ppm due to the 3′-bis(phenylthio)phosphinyl group.

However, conversion of **15** to **14** by treatment with 20 equiv each of tributylphosphine and diphenyl disulfide in acetonitrile[25] resulted in formation of an unexpected product without P–S bond formation.[26] Attempts to introduce the 2-chlorophenyl group into the 3′-phosphate of **15** have also failed. Dicyclohexylcarbodiimide (DCC) promoted reaction gave predominantly a symmetric pyrophosphate derivative of **15**.

Therefore, our attention has been turned to the selective removal of one of the two phenylthio groups from the 2′-PSS group of **13** to change our original project of the first internucleotidic bond formation from the 3′-5′ to 2′-5′ direction. Treatment of **13** with phosphinic acid in pyridine gave the 2′-phosphorothioate derivative (**16**) in 93% yield. Under these conditions the other protecting groups were found to be stable. The ^{31}P NMR spectrum of **16** showed a set of two sharp resonance signals at 15.65 and −0.19 ppm. The former peak was assigned to the 2′-phosphorus of a diester-type of phosphoromonothioate from its chemical shift. Condensation of the resulting 2′-phosphorothioate **16** with 2′,3′-*O*-methoxymethylene-2-*N*-propionyl-6-*O*-diphenylcarbamoylguanosine (**17**) in the presence of 1,2,3,5-tetramethylbenzenedisulfonyl dichloride (DDS)[22] and 3-nitro-1,2,4-triazole (NT)[27] in pyridine for 80 min gave the 2′-5′ linked triester (**18**) in 90% yield. This

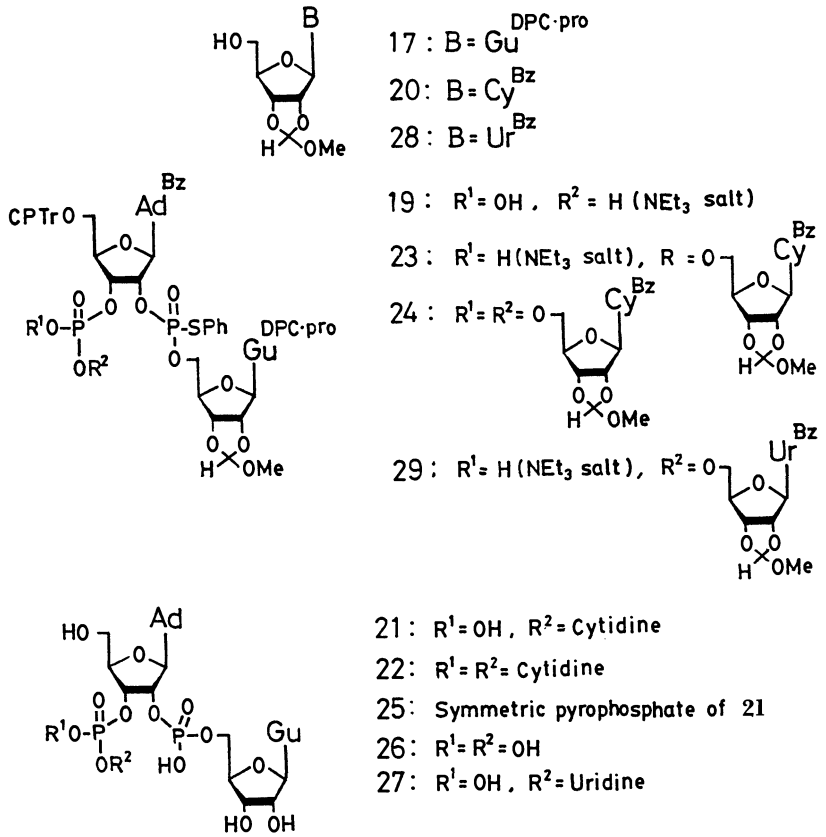

dimer should have four diastereomers due to the chirality of the trisubstituted 2′-5′ linked phosphorus and the methoxymethylene group. However, the ^{31}P NNR spectrum of **18** showed two peaks at 26.76 and 26.59 ppm and a broad signal peak at 2.23 ppm, suggesting that the methoxymethylene group did not affect the chemical shift significantly since it was remote from the diasteromeric phosphorus atom.

The anilino group was removed from **18** by the isopentyl nitrite treatment as described before to afford the 3′-unesterified phosphate (**19**) in 75% yield. An attempt to introduce the phenylthio group into the phosphate group by means of Bu_3P-PhSSPh has also failed as in the case of **15**. Therefore, direct condensation of **19** with 2′,3′-*O*-methoxymethylene-N^4-benzoylcytidine (**20**) in the phosphodiester method using DDS as the condensing reagent was performed. However, large excess amounts of **20** (8 equiv) and DDS (7 equiv) were required until **19** had disappeared (see Experimental). This reaction ultimately gave a mixture of the desired branched triribonucleotide (**21**) and a doubly esterified tetraribonucleoside diphosphate derivative (**22**) after deprotection.

Since DCC is known as the condensing agent that gives only phosphodiester products without formation of phosphotriesters,[28] the compound **22** should not be obtained when the condensing agent was changed from DDS to DCC. To ascertain this expectation, the condensation was performed in the presence of DCC. Consequently, the reaction became simpler and only two principal products were observed along with recovery of A_p^{pG}. It was indeed confirmed that compound **22** was not formed in the reaction. Since compound **19** was the triethylammonium salt which was difficult for activation with DCC, pyridinium 3-nitrobenzenesulfonate (PNBS)[29] was added as an acid catalyst. Without this salt the reaction was extremely slow to given **21** in only 2% yield after one day. With the improved condensation, the isolated yield of **21** was increased up to 29%. A significant amount of symmetrical pyrophosphate derivative (**25**) was formed as the by product. DCC-mediated condensation usually produced such relatively unreactive species.[28] In this case, it was difficult to activate the pyrophosphate intermediate **25** for condensation with **20**. Prolonged reaction for 4 days did not improve the yield of **21** although A_p^{pG} disappeared.

The structural assignment of **21** was also supported by characterization of the deprotected material of the synthetic intermediate **18**. Incubation of the product with bacterial alkaline phosphatase gave a dephosphorylated material which was digested to A and pG with snake venom phosphodiesterase and resistant to nuclease P_1. Incubation of this material with other enzymes such as Ribonucleases T1, T2, and A, and spleen phosphodiesterase did not result in any change. These properties were in agreement with those of 2′-5′ linked ApG having an internal 3′-phosphate.

In a manner similar to that described in the synthesis of **21**, A_{pU}^{pG} (**27**) was also synthesized via compound **29** which was obtained in 21% yield by DCC-mediated condensation of **19** with 2′,3′-*O*-methoxymethylene-N^3-benzoyluridine (**28**), and characterized by the enzymatic assay. Finally, the structure of A_{pC}^{pG} and A_{pU}^{pG} was confirmed by 500 MHz ^{1}H NMR. As the reference materials, linear triribonucleotide diphosphates, GpApC and GpApU were synthesized according to our method reported previously.[20]

Synthesis of Branched Ribonucleotides via a New Fully Protected Synthetic Unit (30). As described above, the condensation of **23** with **20** or **28** in the phosphodiester approach gave charged products which were bothersome for isolation and further chain elongation. Therefore, we designed a more general approach to branched oligoribonucleotides. Since the CPTr group was rather stable under the conditions of removal of the anilino group which involved pyridine buffered by acetic acid, it was employed for the synthesis of the simplest branched triribonucleotide blocks in the previous method. However, this protecting group required restricted conditions for chain elongation, especially in the 5′-direction, where the pivaloyloxymethyl, 4-methoxytrityl (MMTr), and 4,4′-dimethoxytrityl (DMTr) groups should be used for protection of the

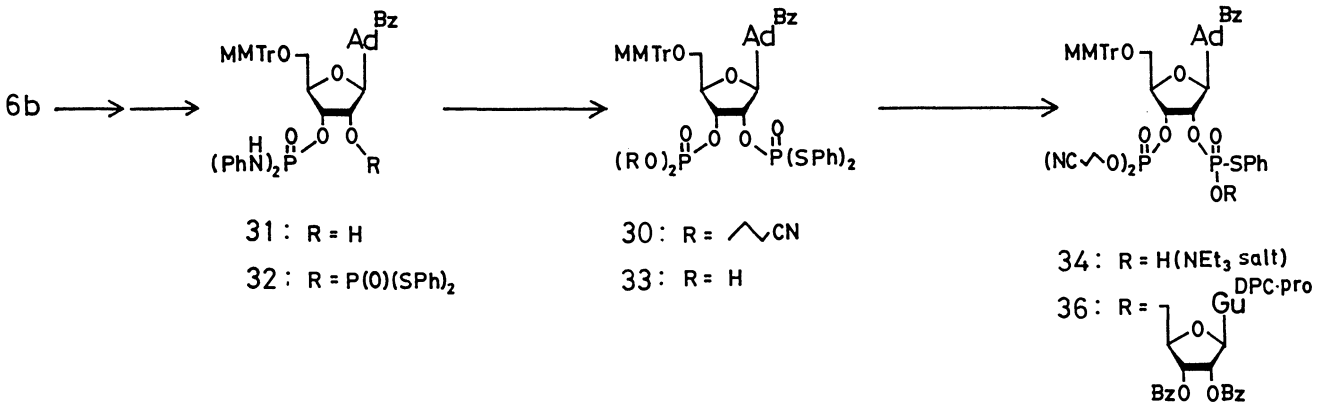

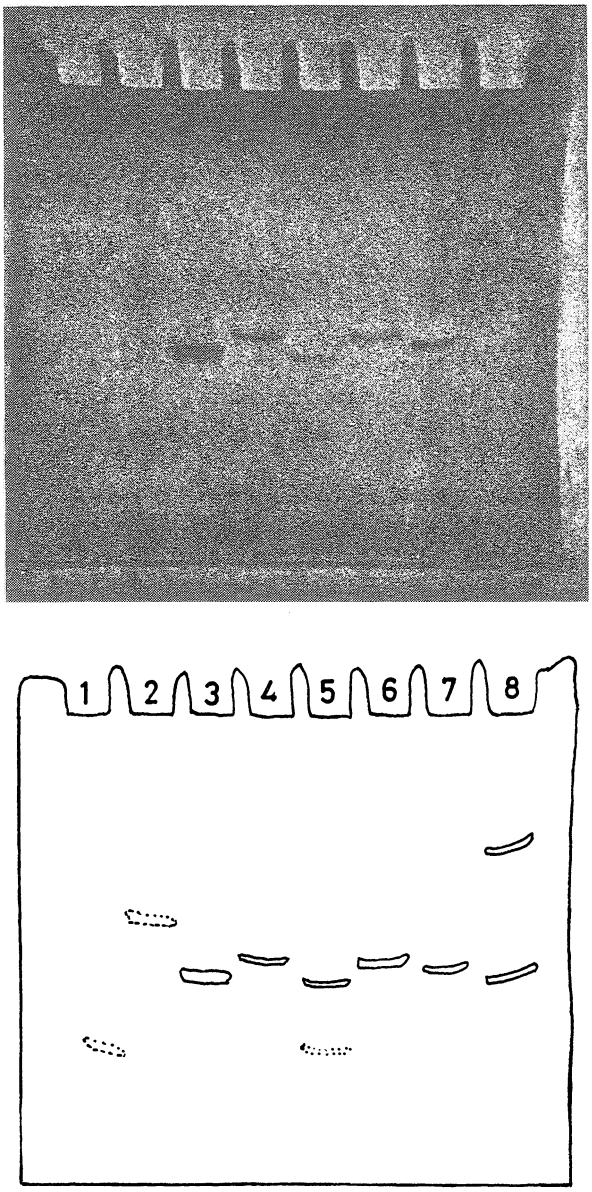

Fig. 1. 20% Polyacrylamide gel electrophoresis of branched and oligoribonucleotides and related compounds. 1: A_p^{pG} **26**; 2: $^{pG}_{(pC)_2}$ **22**; 3: A_{pC}^{pG}; 4: GpApC; 5: a ca. 4:1 mixture of A_{pU}^{pG} and A_p^{pG}; 6: GpApU; 7: $CpUpGpA_{pC}^{pG}$ 8: Bromphenol Blue and Xylene Cyanole FF as markers.

base residues of uridine, adenosine, and cytidine, respectively.[20] Since the DMTr group was somewhat too unstable during the isopentyl nitrite treatment, the MMTr group[30] was chosen as the 5′-hydroxyl protecting group. It was desirable to find more suitable protecting groups for the 3′-phosphate group since removal of the anilino group required a long time and tedious extractive workup. It was again considered that if possible no chiral centers should be produced when a new phosphate protecting group was designed.

On the basis of the above discussion, the anilino group should be changed to the 2-cyanoethyl (CE) group at the stage of the monomer building unit. The new synthetic unit at the branched point was a fully protected adenosine 2′,3′-diphosphate derivative (**30**). Reaction of **6b** with 4-methoxytrityl chloride followed by the successive phosphorylation of the resulting tritylated product (**31**) gave the fully protected adenosine derivative (**32**). Treatment of **32** with isopentyl nitrite in a manner similar to that described in the conversion of **13** to **15** gave the 3′-unesterified derivative (**33**) in 55% yield. Biscyanoethylation of **33** with excess 2-cyanoethanol in the presence of DDS in pyridine gave a fully protected adenosine 2′,3′-diphosphate derivative **30** in 67% yield. The ^{31}P NMR spectrum of **30** exhibited two sharp resonance signals at −3.10 and 51.98 ppm which were due to the 3′- and 2′-phosphoryl groups, respectively. The intermediates **32** and **33** also gave similar ^{31}P NMR spectra as summarized in Table 1.

The protection of each phosphoryl group with the same two protecting groups proved to be indeed useful for the structural assignment of synthetic interme-

Table 1. ^{31}P NMR Spectra of Synthetic Intermediates and Branched Ribonucleotide Derivatives

Compound	Solvent	Signals (ppm)		
3	$CDCl_3$	3.221		
6a	$CDCl_3$-Py (9:1, v/v)	3.003		
6b	$CDCl_3$-Py-MeOH (10:6:1, v/v/v)	2.857		
9	$CDCl_3$	5.933		
12	$CDCl_3$	2.518		
13	$CDCl_3$	1.937	54.737	
16	$CDCl_3$	−0.193	15.646	
18	$CDCl_3$	2.228	26.594 26.763	
23+24	$CDCl_3$	−3.003 −2.785 −2.640 −2.373 −2.276	24.292 24.583 24.777 25.189 25.261	25.382 25.649 25.746 25.915 26.012
30	$CDCl_3$	−3.100	51.977	
32	$CDCl_3$	3.100	55.756	
33	$CDCl_3$	−9.010	51.154	
34	$CDCl_3$	−3.234	13.374	
36	$CDCl_3$	−2.907 −3.270	24.822 25.694	
37	$CDCl_3$	−2.653	24.277 24.895	
39	$CDCl_3$	−2.216 −2.289 −2.471	24.786 24.931 25.258 25.367	

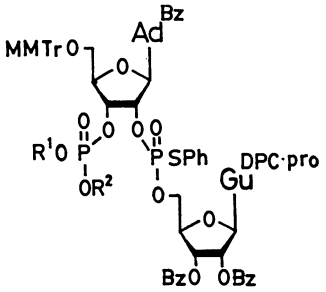

37 : R^1 = ∼CN, R^2 = H(NEt_3 salt)

39 : R^1 = ∼CN, R^2 =

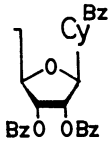

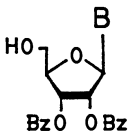

35 : B = $Gu^{DPC\cdot pro}$

38 : B = Cy^{Bz}

diates during the construction of the branched triribonucleotide block. Upon treatment of **30** with the phosphinate reagent gave quantitatively phosphodiester derivative (**34**). The high selectivity of this conversion was confirmed by ^{31}P NMR. Condensation of **34** with 2′,3′-di-*O*-benzoyl-6-*O*-diphenylcarbamoyl-2-*N*-propionylguanosine (**35**) gave the 2′-5′ linked dinucleotide derivative (**36**) in 87% yield. The decyanoethylation of **36** with *N*,*N*-diisopropylethylamine in pyridine at 40 °C for 4 h afforded the 3′-phosphodiester intermediate (**37**) which was purified by preparative TLC and obtained as triethylammonium salt in 82% yield. A similar condensation of **37** with 2′,3′-*O*: N^6-tribenzoylcytidine (**38**) gave the fully protected triribonucleotide unit (**39**) in 63% yield. This unit exhibited the ^{31}P NMR spectrum in which two kinds of resonance signals appeared at ca. −2.3 and 25.5 ppm. The former consisted of three peaks at −2.47, −2.29, and −2.22 ppm in a 2:1:1 ratio. The highest peak seemed to be imposed with

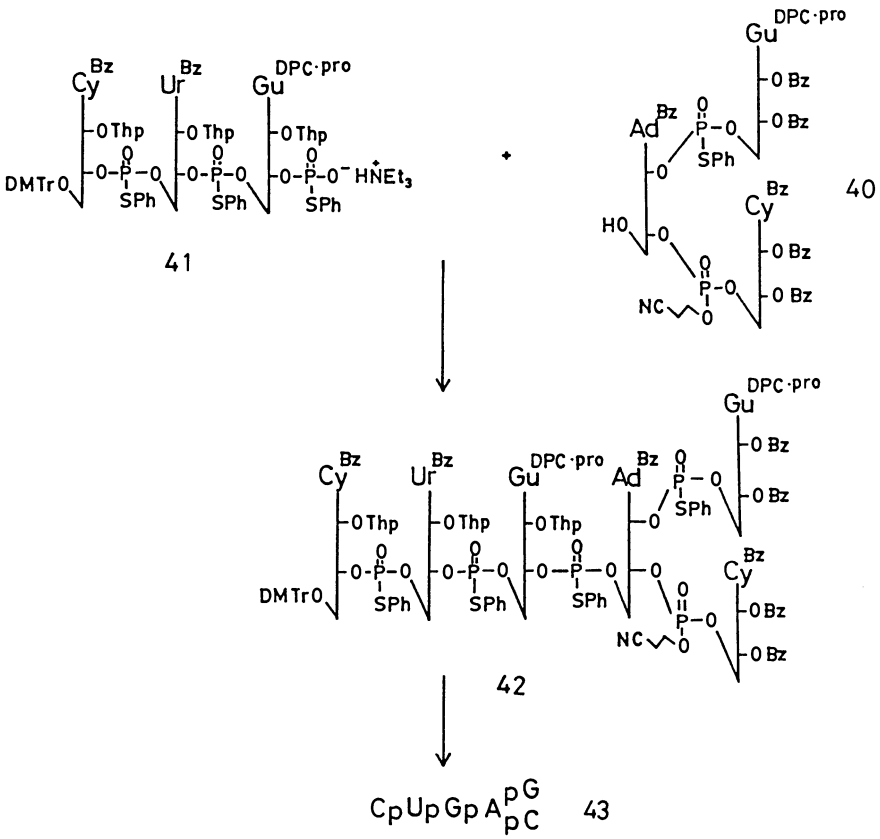

41 40 42

$CpUpGpA^{pG}_{pC}$ 43

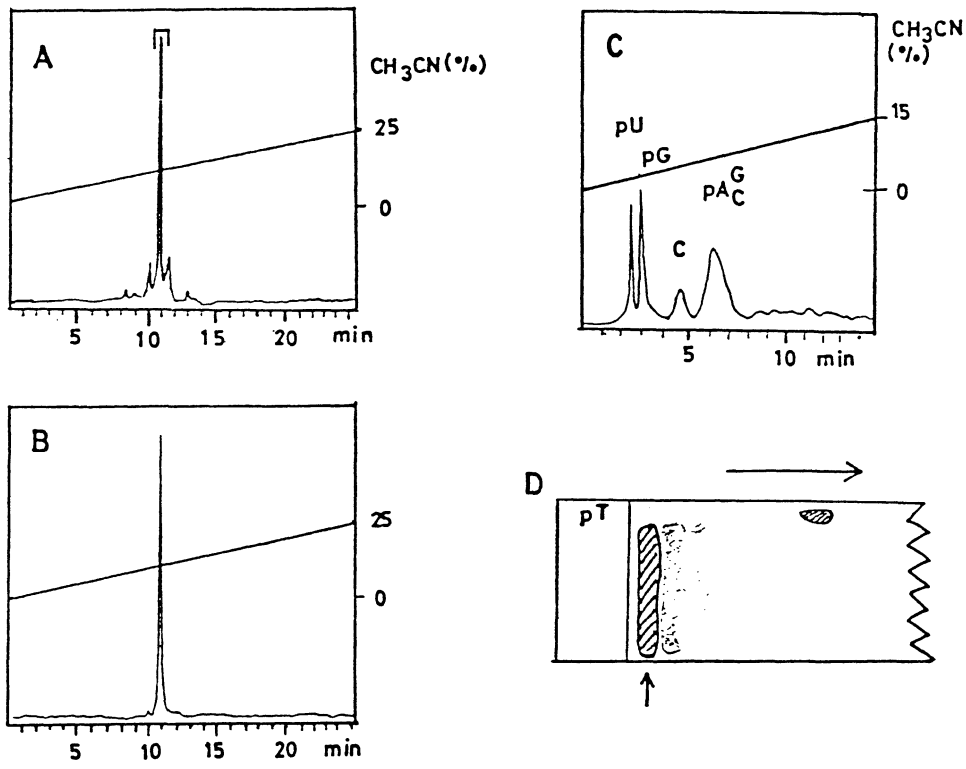

Fig. 2. A: HPLC profile of the crude branched hexaribonucleotide obtained after paper chromatography as shown in Fig. 2D. B: HPLC profile of the purified branched hexaribonucleotide. C: Enzyme analysis of the purified branched hexaribonucleotide with nuclease P_1. D: Paper chromatography of the mixture obtained by deprotection of the fully protected branched hexaribonucleotide (**42**).

two different peaks. The latter involved two sets of doublets as shown in Table 1.

Since compound **39** was neutral species unlike **23**, it was possible to extend the chain in the 5′-direction after removal of the MMTr group. Acid treatment of **39** with 1% trifluoroacetic acid gave the 5′-hydroxyl compound (**40**), which was further condensed with a triribonucleotide block (**41**) to give the fully protected hexaribonucleotide derivative (**42**) in 56% yield. The trimer **41** was synthesized according to our standard method.[31,32]

Deprotection of **42** was achieved by the following procedure: 1) 0.5 M (M=mol dm^{-3}) bis(tributyltin) oxide in pyridine r.t. 28 h.[33] 2) trimethylsilyl chloride in pyridine, r.t., 15 min. 3) concd aqueous ammonia-pyridine, r.t., 19 h. 4) 0.02 M HCl-dioxane, r.t., 48 h. 5) paper chromatography, *i*-PrOH-concd ammonia-water. Thus, the unprotected hexamer CUGA_{pC}^{pG} (**43**) was isolated in 32% yield. The HPLC profile of the mixture obtained after deprotection is shown in Fig. 2A. The peak at 10.8 min was collected and characterized by enzyme analysis as the desired branched hexaribonucleotide. As shown in Fig. 2C, digestion of this material with nuclease P1 gave four products which were identified with pU,pG, C, and pA_{pC}^{pG}. The latter was further dephosphorylated with alkaline phosphatase to give A_{pC}^{pG} which was also identified with authentic material of **21**.

The branched trimers A_{pC}^{pG} and A_{pC}^{pG} were not phosphorylated with kinase as reported by Caruthers.[5] On the other hand, the branched hexamer could be expectedly labelled with this enzyme in the presence of [γ-^{32}p]ATP to give ^{32}pCpUpGpA_{pC}^{pG} (data not shown).[34]

Finally, the synthetic branched trimers and hexamer were tested for inhibition experiments of splicing reaction using the extract from Hela cell. However, our preliminary results revealed that significant inhibitory effects were not observed under the standard conditions.[34] This is probably because the lariat structure was the ultimate deletion product and did not interact with splicing intermediates.

Conclusion

There have been reported several strategies for construction of branched ribonucleotide fragments. They are mainly classified in two types. One is the use of monomer building blocks having 2′,3′-protected phosphoryl or phosphoramidite groups represented by this research and Ogilvie's original approach.[4] The other involves condensation of 2′- or 3′-phosphorylated species with ribonucleoside 5′-

phosphoramidite units. In the former case, it is possible to add stepwise the oligonucleotide chain in any direction, as shown by the present study. However, multistep reactions for synthesis of such building units are required. Indeed, our approach involves a series of seven reactions to obtain the unit **30** from 6-*N*-benzoyladenosine. Although some improvements should be done to shorten the number of the step, the unit **30** is easy to handle and can be stored for long periods of time without decomposition since this material is a neutral species.

As one of the representative approaches for the latter classification, Kierzek and Caruthers[5] reported the regioselective condensation of 2′-side chains with 3′-5′ linked dimer derivatives in which the internal phosphate and 2′-hydroxyl groups were unprotected. In this case, the number of reactions was less than that of ours but synthetic intermediates and final products were charged molecules. Chattopadhyaya[8] has used a combination of the *p*-toluoyl and 9-phenylxanthene-9-yl groups as the 5′- and 2′-protecting groups, respectively, for his synthesis of branched trimers using a similar amidite approach. Chattopadhyaya[9] also applied the 5′-selective cleavage of Markiewicz's protecting group[35] with dilute HCl to the synthesis of branched tetramers. This method still involved a series of charged intermediates. More recently, his research group reported an improved synthesis of neutral protected branched trimer blocks from a 2′-phosphorylated 6-*N*-benzoyladenosine derivative.[15] The latter intermediate, however, was prepared via 7 step-reactions from 6-*N*-benzoyladenosine. The 3′-5′ phosphate bond formation required large excess amounts (ca. 3.5—9 equiv) of 3′-components bearing the phosphoramidite group. The other approaches reported up to date have encountered similar drawbacks. In our own approach, new methods for regioselective phosphorylation in a more straightfoward manner should be explored. We are now studying improved procedures in this direction.

Experimental

Melting points were determined on a Mitamura MELTPOINTER apparatus and are uncorrected. ^{1}H NMR spectra were recorded at 60 MHz on a Hitachi 24B spectrometer, at 100 MHz on a JEOL UNM PS-100 spectrometer, and at 270 MHz on a JEOL GX270 with Me_4Si as the internal standard and at 500 MHz on a JEOL GX500 with DDS as the internal reference. UV spectra were obtained on a Hitachi 220A spectrophotometer. Paper chromatography was performed by use of a descending technique with Whatman 3MM papers and Toyo Roshi 51A papers using the following solvent systems: Solvent I (2-propanol–concd aq ammonia–water. 7 : 1 : 2, v/v/v); Solvent II (2-propanol–concd aq ammonia–water, 6 : 1 : 3, v/v/v); Solvent III (1-propanol–concd aq ammonia–water, 55 : 10 : 35, v/v/v). Column chromatography was performed with silica gel C-200 purchased from Wako Co., Ltd., and a minipump for a goldfish bowl was conveniently used to attain sufficient pressure for rapid chromatographic separation. TLC was performed on precoated TLC plates of silica gel 60 F-254 (Merck). Reversed-phase HPLC was performed on a Waters Model A25 using a μ Bondapack C-18 column with a linear gradient starting from 0.1 M NH_4OAc, pH 7.0 and applying CH_3CN at a flow rate of 1.5 ml min^{-1} for 30 min (System A). Ribonucleosides were purchased from Yamasa Co., Ltd. Pyridine was distilled two times from *p*-toluenesulfonyl chloride and from calcium hydride and then stored over molecular sieves 3A. The linear trimers of GpApC and GpApU were prepared by condensation of $C^{P}TrG^{DPC\cdot pro}(thp)p(SPh)A^{MMTr}(thp)(O^{-}HN^{+}Et_3)$ with $C^{bz}(bz)_2$ or $U^{bz}(bz)_2$, respectively, followed by the usual deprotection procedure. The detail of these trimers will be reported elsewhere. The yields of branched oligoribonucleotides were estimated by using following ε values at λ_{max}: A_p^{pG} 29.9×10^3 at 257 nm, A_{pC}^{pG} 27.5×10^3 at 258 nm, A_{pU}^{pG} 33.5×10^3 at 256.5 nm, CpUpGpA_{pC}^{pG} 48.3×10^3 at 257 nm. Elemental analyses were performed by the Microanalytical Laboratory, Tokyo Institute of Technology, at Nagatsuta.

5′-*O*: 6-*N*-Bis(4,4′-dimethoxytrityl)adenosine (7). Adenosine (5.34 g, 20 mmol) was rendered anhydrous by repeated coevaporation with dry pyridine (50 mL×3) and finally dissolved in dry pyridine (180 mL). 4,4′-Dimethoxytrityl chloride (15.25 g, 45 mmol) was added to the pyridine solution. After being stirred for 5 h, the mixture was partitioned between CH_2Cl_2 and water. The organic phase was collected and the aqueous layer was extracted two times with CH_2Cl_2. The CH_2Cl_2 extracts were combined, dried over Na_2SO_4, filtered, and evaporated under reduced pressure. The residue was chromatographed on a column of silica gel (300 g) with CH_2Cl_2–MeOH to give the foammy material of **7**, which was reprecipitated from its CH_2Cl_2 solution into hexane to give **7** as the powder (14.5 g, 83%).

7: ^{1}H NMR ($CDCl_3$–D_2O) δ=3.31 (2H, m, 5′-H), 3.74 (6H, s, OCH_3), 3.74 (1H, m, 4-H), 4.33 (1H, m, 3′-H), 4.57 (1H, m, 2′-H), 5.83 (1H, d, J=5.83 Hz, 1′-H), 6.70 (8H, d, J=9 Hz, ArH), 7.16 (18H, m, ArH), 7.95 (1H, s, 2-H), 7.89 (1H, s, 8-H). Anal. Calcd for $C_{52}H_{49}N_5O_8$: C, 71.63, H, 5.66; N, 8.03%. Found: C, 71.40; H, 5.94; N, 7.77%.

3′,5′-*O*-(1,1,3,3-Tetraisopropyldisiloxane-1,3-diyl)-6-*N*-benzoyladenosine 2′-Phosphorodianilidate (4). A mixture of compound **1** (614 mg, 1 mmol) and tetrazole (105 mg, 1.5 mmol) was coevaporated three times with dry toluene (10 mL) and dissolved in dry 1,2-dichloroethane (10 mL). TEAP (411 μL, 1.5 mmol) was added with vigorous stirring to the solution. After the mixture was stirred for 10 min, aniline (365 μL, 4 mmol) and tetrazole (280 mg, 4 mmol) were successively added and stirring was continued for 10 min. Then a solution of iodine (381 mg, 1.5 mmol) in dry pyridine (2 mL) was added to the mixture. After being stirred for 10 min, the mixture was diluted with CH_2Cl_2 and 5% aqueous Na_2SO_3 was added to remove the excess iodine. The organic phase was collected, dried over Na_2SO_4, filtered, and concentrated under reduced pressure. The residue was chromatographed on a column of silica gel (30 g) with CH_2Cl_2–MeOH to give **4** (703 mg, 83%). **4:** ^{1}H NMR ($CDCl_3$) δ=1.03 (24H, m, $(CH_3)_2CH$), 4.10 (3H, m, 4′- and 5′-H), 5.19 (1H, m, 3′-H), 5.63 (1H, dd, $J_{2'\text{-}3'}$=5.3 Hz, $J_{P\text{-}H}$=9.3 Hz, 2′-H), 6.43 (1H, s, 1′-H), 6.80—7.27 (10H, m, ArH), 7.53 (2H, m, ArH), 8.18 (3H, m, ArH), 8.18 (1H, s, 2-H), 8.62 (1H,

s, 8-H), 8.75 (1H, s, NH).

6-*N*-Benzoyladenosine 2′-Phosphorodianilidate (6a) and Its 3′-Regioisomer (6b). Small Scale Synthesis: To a solution of **8** (591 mg, 0.7 mmol) in acetonitrile (8.4 mL) were added KF (236 mg, 4.2 mmol), Et_4NBr (883 mg, 4.2 mmol), and water (0.076 mL, 4.2 mmol). The mixture was stirred at 45 °C for 20 min and diluted with CH_2Cl_2–pyridine (2 : 1, v/v, 30 mL). The resulting solution was washed six times with water (30 mL) to remove quarternary ammonium salts. Each aqueous washing was reextracted with another CH_2Cl_2–pyridine (2 : 1, v/v, 30 mL) solution which was used commonly for six times extraction in another separatory funnel. The two extracts were combined, dried over Na_2SO_4, filtered, concentrated under reduced pressure, and coevaporated four times with toluene. The residue was dissolved in CH_2Cl_2 (15 mL). Upon standing of this solution for a few minutes a powder-like precipitate appeared. Collection of this material by filtration took ca. 1 h to give **6b** (182 mg, 43%). Concentration of the filtrate followed by preparative thin-layer chromatography with CH_2Cl_2–MeOH (8 : 1, v/v) gave **6a** (156 mg, 37%) and **6b** (56 mg, 13%).

6a: ^{1}H NMR ($CDCl_3$–CD_3OD, 5 : 1, v/v) δ=3.72 (2H, m, 5′-H), 4.21 (1H, m, 4′-H), 4.57 (1H, m, 3′-H), 5.43 (1H, m, 2′-H), 6.10 (1H, d, J=7 Hz, 1′-H), 6.37—7.20 (10H, m, ArH), 7.40 (3H, m, ArH), 7.91 (2H, m, ArH), 8.05 (1H, s, 2-H), 8.38 (1H, s, 8-H). Anal. Calcd for $C_{29}H_{28}N_7O_6P \cdot 0.5H_2O$: C, 57.05, H, 4.79; N, 16.06%. Found: C, 56.98; H, 4.76; N, 15.95%.

6b: ^{1}H NMR ($CDCl_3$–CD_3OD, 2 : 1, v/v) δ=3.72 (2H, m, 5′-H), 5.00 (2H, m, 2′- and 3′-H), 6.03 (1H, d, J=6.4 Hz, 1′-H), 6.60—7.30 (10H, m, ArH), 6.43 (3H, m, ArH), 7.91 (2H, m, ArH), 8.32 (1H, s, 2-H), 8.53 (1H, s, 8-H). Anal. Calcd for $C_{29}H_{28}N_7O_6P \cdot 0.5H_2O$: C, 57.05, H, 4.79; N, 16.06%. Found: C, 57.04; H, 4.65; N, 15.98%.

Large Scale Synthesis of 6b: The same procedure described in the small scale synthesis of **6a** and **6b** before crystallization of **6b** was done except that the scale was increased to 16 mmol. The residue containing **6a** and **6b** was dissolved in MeOH (40 mL) and 1,2-dichloroethane (360 mL). Concentration of the solution under reduced pressure to ca 200 mL followed by standing at 0 °C for 15 min resulted in crystallization of **6b**. The crystals were collected by filtration and washed with minimum amounts of 1,2-dichloroethane to give 3.67 g (38.3%) of **6b**. The filtrate, which contained a ca. 5 : 1 mixture of **6a** and **6b**, was concentrated under reduced pressure and the residue was dissolved in pyridine (60 mL) and water (6 mL). The solution was kept at 60 °C for 2 h, at which time the ratio of **6a** to **6b** was changed to ca. 1 : 1. The mixture was then evaporated and coevaporated several times with toluene. The residue was tritulated with petroleum ether (3×20 mL) to remove the remaining silyl derivative derived from the 1,1,3,3-tetraisopropyldisiloxane-1,3-diyl group, dissolved in a mixture of 1,2-dichloroethane (150 mL)–MeOH (30 mL), and the solution was passed through a column of silica gel (100 g). The column was further eluted with a mixture of 1,2-dichloroethane–MeOH (300 mL–60 mL). The eluate was concentrated and the residue was dissolved in a mixture of 1,2-dichloroethane–MeOH (250 mL–25 mL). Concentration to half the volume followed by standing for 15 min and successive collection gave the second crop of **6b** (0.75 g, 7.8%). More two times repetition of the same procedure gave additional crops (0.44 g and 0.31 g) of **6b** from each filtrate. The total yield of **6b** was 5.17 g (55%). Each crop was confirmed to be homogeneous on TLC.

3′,5′-*O*-(1,1,3,3-Tetraisopropyldisiloxane-1,3-diyl)-6-*N*-benzoyladenosine 3′-[*N*,*N*′-Bis(*p*-methoxyphenyl)phosphorodiamidate] (9). Under conditions similar to those described in the case of **4**, 759 mg (84%) of **9** was obtained from 0.4 mmol of **1**.

9: ^{1}H NMR ($CDCl_3$) δ=1.04 (24H, m, $(CH_3)_2CH$), 3.67 (6H, s, CH_3O), 4.05 (3H, m, 4′- and 5′-H), 4.80—6.00 (2H, m, 2′- and 3′-H), 6.11 (1H, s, 1′-H), 6.59 (4H, d, J=8.5 Hz, ArH), 6.90 (4H, d, J=8.5 Hz, ArH), 7.42 (3H, m, ArH), 7.88 (2H, m, ArH), 8.00 (1H, s, 2-H), 8.49 (1H, s, 8-H). Anal. Calcd for $C_{43}H_{58}N_7O_9PSi_2$: C, 57.13; H, 6.47; N, 10.84%. Found: C, 56.93; H, 6.61; N, 10.94%.

3′,5′-*O*-(1,1,3,3-Tetraisopropyldisiloxane-1,3-diyl)-6-*N*-benzoyladenosine 3′-[*N*,*N*′-Diphenylphosphorodiamidothioate] (10). This compound was synthesized by using 0.4 mmol of **1** under the same conditions as described in the case of **4** except that at the final stage the sulfurization (10 min) was undertaken by addition of elemental sulfur (38 mg, 1.2 mmol) in dry pyridine (2.5 mL) to the mixture containing **3** in place of iodine oxidation. The yield was 256 mg (75%).

10: ^{1}H NMR ($CDCl_3$) δ=1.06 (24H, m, $(CH_3)_2CH$), 4.07 (3H, m, 4′- and 5′-H), 5.15 (1H, m, 3′-H), 5.70 (1H, dd, J=5 Hz, J=13 Hz, 2′-H), 6.08 (1H, m, 1′-H), 7.05 (10H, m, ArH), 7.37 (3H, m, ArH), 7.88 (2H, m, ArH), 7.92 (1H, s, 2-H), 8.58 (1H, m, 8-H). Anal. Calcd for $C_{41}H_{54}N_7O_6PSSi_2$: C, 57.25; H, 6.33; N, 11.40; S, 3.73%. Found: C, 57.05; H, 6.42; N, 11.39%.

6-*N*-Benzoyladenosine 2′-[*N*,*N*′-Bis(*p*-methoxyphenyl)-phosphorodiamidate (11a) and Its Regioisomer (11b). These compounds were obtained by the same procedure as described in the small scale synthesis of **6a** and **6b** starting from 0.79 mmol of **10** except that the reaction was carried out at 45 °C for 45 min. The yields of **11a** and **11b** were 86 mg (18%) and 295 mg (42%), respectively.

11a: ^{1}H NNR ($CDCl_3$) δ=3.54 (6H, s, CH_3O), 3.59 (2H, m, 5′-H), 4.26 (1H, m, 4′-H), 4.73 (1H, m, 3′-H), 5.59 (1H, m, 2′-H), 6.00—7.15 (9H, m, 1′-H and ArH), 7.57 (3H, m, ArH), 8.05 (2H, m, ArH), 8.24 (1H, s, 2-H), 8.57 (1H, s, 8-H). Anal. Calcd for $C_{31}H_{32}N_7O_8P \cdot 0.5H_2O$: C, 55.52; H, 4.96; N, 14.62%. Found: C, 55.10; H, 4.92; N, 14.66%.

11b: ^{1}H NMR ($CDCl_3$–CD_3OD, 2 : 1, v/v) δ=3.73 (2H, m, 5′-H), 4.38 (1H, m, 4′-H), 5.03 (2H, m, 2′- and 3′-H), 6.02 (1H, d, J=6.5 Hz, 1′-H), 6.67 (4H, d, J=8.5 Hz, ArH), 6.95 (4H, d, J=8.5 Hz, ArH), 7.44 (3H, m, ArH), 7.95 (2H, m, ArH), 8.30 (1H, s, 2-H), 8.57 (1H, s, 8-H). Anal. Calcd for $C_{31}H_{32}N_7O_8P \cdot 0.5H_2O$: C, 55.52; H, 4.96; N, 14.62%. Found: C, 55.88; H, 5.08; N, 14.36%.

5′-*O*-[Tris[4-(4,5-dichlorophthalimido)phenyl]methyl]-6-*N*-benzoyladenosine 3′-Phosphorodianilidate (12). Compound **6b** (60 mg, 0.1 mmol) was coevaporated two times each with dry toluene and DMF and finally dissolved in dry DMF (1 mL). To the solution were added silver nitrate (34 mg, 0.2 mmol) and tris[4-(4,5-dichlorophthalimido)-phenyl]methyl bromide (193 mg, 0.2 mmol). The mixture was stirred for 45 min and then quenched with 2,6-lutidine (23 μL, 0.2 mmol). The resulting mixture was diluted with dichloromethane, filtered, transferred to a separatory funnel, and washed six times with water. Each washing was reextracted with another CH_2Cl_2. The two CH_2Cl_2 extracts were combined, dried over Na_2SO_4, and filtered. Removal of the solvent by evaporation followed by thin-layer chroma-

tography using two plates of Merck 5717 with CH_2Cl_2–MeOH gave **12** (86 mg, 57%).

12: ^1H NMR ($CDCl_3$) δ=3.35 (2H, m, 5′-H), 4.38 (1-H, m, 4′-H), 5.15 (2H, m, 2′,3′-H), 5.99 (1H, m, 1′-H), 6.50—8.00 (27H, m, ArH), 7.83 (6H, s, ArH), 8.01 (qH, s, 2-H), 8.47 (1H, s, 8-H). Anal. Calcd for $C_{72}H_{45}N_{10}O_{12}PCl_6 \cdot H_2O$: C, 57.50; H, 3.15; N, 9.31%. Found: C, 57.52; H, 3.03; N, 9.30%.

2′-*O*-Bis(phenylthio)phosphinyl-5′-*O*-[tris[4-(4,5-dichlorophthalimido)phenyl]methyl]-6-*N*-benzoyladenosine 3′-Phosphorodianilidate (13). To a pyridine solution (3 mL) of **12** (446 mg, 0.3 mmol), cyclohexylammonium *S*,*S*-dipheyl phosphorodithioate (171 mg, 0.45 mmol) and tetrazole (84 mg, 1.2 mmol) dried by repeated coevaporation with dry pyridine was added mesitylenedisulfonyl dichloride (MDS) (190 mg, 0.6 mmol). After being stirred for 15 min, the mixture was partitioned between CH_2Cl_2 and water. The organic layer was collected, washed with 5% $NaHCO_3$, dried over Na_2SO_4, filtered, and concentrated under reduced pressure. The residue was chromatographed on a column of silica gel (20 g) with CH_2Cl_2–MeOH to give **13** (423 mg, 81%).

13: ^1H NMR (270 MHz, $CDCl_3$) δ=3.48 (1H, dd, J=11 Hz, J=3.0 Hz, 5′-Ha), 3.65 (1H, d, J=11.0 Hz, 5′-b), 4.53 (1H, m, 4′-H), 5.38 (1H, m, 3′-H), 6.13 (1H, d, J=5.3 Hz, 1′-H), 6.18 (1H, m, 2′-H), 6.50—7.65 (37H, m, ArH), 7.93 (6H, s, ArH), 8.09 (1H, s, 2-H), 8.63 (1H, s, 8-H), 9.31 (1H, br, NH). Anal. Calcd for $C_{84}H_{54}N_{10}O_{13}P_2S_2Cl_6$: C, 57.65; H, 3.11; N, 8.00%. Found: C, 57.44; H. 3.16; N, 7.96%.

Triethylammonium 2′-*O*-Bis(phenylthio)phosphinyl-5′-*O*-[tris[4-(4,5-dichlorophthalimido)phenyl]methyl]-6-*N*-benzoyladenosine 3′-Phosphate (15). Compoud **13** (175 mg, 0.1 mmol) was dissolved in a mixture of pyridine–acetic acid–acetic anhydride (1 : 1 : 1, v/v/v, 3 mL) and isopentyl nitrite (100 μL) was added. After the mixture being stirred for 11 h, the mixture was diluted with CH_2Cl_2 and water was added. The CH_2Cl_2 layer was collected, washed successively with water and 0.2 M TEAB, and each aqueous layer was backextracted with another CH_2Cl_2. The combined organic phase was dried over Na_2SO_4, filtrated, concentrated under reduced pressure and coevaporated with toluene. The residue was subjected to a preparative TLC developed with CH_2Cl_2–MeOH (9 : 1, v/v) to give **15** (85 mg, 50%).

15: ^1H NMR ($CDCl_3$) δ=1.30 (9H, t, J=7 Hz, $C\underline{H}_3CH_2N$), 3.00 (6H, q, J=7 Hz, $CH_3C\underline{H}_2N$), 3.68 (2H, m, 5′-H), 4.62 (1H, m, 4′-H), 5.58 (1H, m, 3′-H), 6.28 (1H, m, 1′-H), 6.43 (1H, m, 2′-H). 6.90—8.10 (27H, m, ArH), 7.93 (6H, s, ArH), 8.24 (1H, s, 2-H), 8.69 (1H, s, 8-H).

Triethylammonium *S*-Phenyl 3′-*O*-Dianilinophosphinyl-5′-*O*-[tris[4-(4,5-dichlorophthalimido)phenyl]-methyl]-6-*N*-benzoyladenosine 2′-Phosphorothioate (16). Compound **13** (1.75 g, 1 mmol) was treated with a solution of 3 M pyridinium phosphinate (65 mmol) in dry pyridine (21.7 mL) at room temperature for 1 h. The resulting mixture was diluted with CH_2Cl_2, which was washed subsequently with water, 0.2 M TEAB (×2), and water. Each washing was backextracted with another CH_2Cl_2. The two CH_2Cl_2 extracts were combined, dried over Na_2SO_4, filtered, and concentrated under reduced pressure. Coevaporation of the residue with toluene followed by precipitation from its CH_2Cl_2 solution into hexane gave **16** as white powder (1.744 g, 99%). This material was used without further purification for the next condensation with **17**.

Synthesis of the Fully Protected 2′–5′ Linked ApG Dimer (18). A mixture of **16** (1.58 g, 0.9 mmol), **17** (778 mg, 1.35 mmol), and 3-nitro-1*H*-1,2,4-triazole (308 mg, 2.7 mmol) was rendered anhydrous by three times coevaporation with dry pyridine and finally dissolved in dry pyridine (10 ml). To the mixture was added DDS (894 mg, 2.7 mmol). After being stirred for 2 h, the extractive workup followed by column chromatography gave **18** (1.83 g, 92%).

Removal of the Anilino Group from 18 by Isopentyl Nitrite Treatment. Compound **18** (130 mg, 58.6 μmol) was treated with isopentyl nitrite (58.6 μL) in pyridine–acetic acid–acetic anhydride (1 : 1 : 1, v/v/v, 586 μL) for 16 h. Then the mixture was diluted with CH_2Cl_2, which was washed subsequently with water (×4), 0.2 M TEAB (×2), and water. Each washing was backextracted with another CH_2Cl_2. The two CH_2Cl_2 extracts were combined, dried over Na_2SO_4, filtered, and concentrated under reduced pressure. The residue was coevaporated with toluene and chromatographed on two preparative TLC plates developed with CH_2Cl_2–MeOH (6 : 1, v/v). Elution was performed with CH_2Cl_2–MeOH (4 : 1, v/v). The eluate was evaporated and the residue was partitioned between CH_2Cl_2 and 0.2 M TEAB. The CH_2Cl_2 extract was collected, dried over Na_2SO_4, and concentrated to give **19** free of silica gel as triethylammonium salt (95.3 mg, 75%).

Synthesis of the Partially Protected Branched Triribonucleotide (23). Method A: A mixture of **19** (152 mg, 70 μmol) and **20** (54.5 mg, 0.14 mmol) was rendered anhydrous by repeated coevapoartion with dry pyridine and finally dissolved in dry pyridine (1 mL), and DDS (70 mg, 0.21 mmol) was added. After 9 h, TLC showed that a product which appeared higher than **19** was formed in a considerable amount and ca. 40% of **19** remained unchanged. This faster moving material seemed to be a tetrasubstituted pyrophosphate intermediate. To make the condensation complete, **20** (54.5 mg, 0.14 mmol) and DDS (46 mg, 0.14 mmol) were added. After being stirred for an additional 2 h, DDS (46 mg, 0.14 mmol) was added to convert excess **20** to the corresponding 5′-sulfonated derivative which was hydrolyzed to a more polar sulfonic acid derivative upon addition of water. After the mixture was kept for 3 h, water (0.2 mL) was added, and the resulting mixture was stirred for 15 min and then extracted in the usual manner as described in the synthesis of **16**. Preparative TLC developed with CH_2Cl_2–MeOH (9 : 1, v/v) gave a mixture of **23** and **24** (143 mg).

Method B: A mixture of **19** (28 mg, 13 μmol), **20** (20.1 mg, 52 μmol), and pyridinium 3-nitrobenzenesulfonate (11 mg, 39 μmol) was rendered anhydrous by repeated coevapoartion with dry pyridine and finally dissolved in dry pyridine (0.2 mL). DCC (20 mg, 97 μmol) was added to the mixture. After being stirred for 36 h, the mixture was diluted with CH_2Cl_2 which was washed with 0.2 M TEAB. The organic phase was dried over Na_2SO_4, filtered, concentrated, and chromatographed on a preparative TLC with CH_2Cl_2–MeOH (7 : 1, v/v) to give the crude material of **23** (49.3 mg).

Deprotection of 23 Giving Rise to Branched Triribonucleotide (21). Part (88 mg) of the mixture of **23** and **24** obtained in Method A described in the above experiment was dissolved in pyridine (5 mL) and 0.2 M NaOH (5 mL) was added at 0 °C to the solution. The solution was stirred at 0 °C for 15 min and then neutralized with Dowex 50W X2 (pyridinium form, 5 mL). The supernatant and washing

with pyridine–water (1 : 1, 40 mL) were combined, concentrated, and the residue was dissolved in pyridine (5 mL)–concd ammonia (45 mL). After being stirred at 50 °C for 6 h, the mixture was concentrated and treated with 80% acetic acid (50 mL) for 6h. The solvent was then evaporated and the residue was chromatographed on Whatman 3MM papers developed with Solvent II to give **21** (237 A_{258}, 20%) and **22** (193 $A_{256.5}$, 14%).

21: λ_{max} 258 nm, λ_{min} 227 nm; R_f 0.61 (relative to pU) (Solvent II, R_f 0.74 (relative to pU) (Solvent III); R_m 0.47 (relative to pU) (0.03 M phosphate buffer, pH 7.1); Retension time 11.8 min (HPLC system A); ^{1}H NMR (500 MHz, D_2O/DSS) δ=3.70 (1H, dm, J=11.7 Hz), 3.79 (1H, dd, J=12.8 Hz, J=2.2 Hz, 5′-Ha of A), 3.86 (1H, d, J=12.8 Hz, J=1.3 Hz, 5′-Hb of A), 3.95 (1H, tm, J=11.7 Hz), 4.04 (1H, br. s), 4.20 (1H, m), 4.28 (2H, q, J=5.2 Hz), 4.33 (2H, m), 4.47 (1H, t, J=8.2 Hz), 4.51 (1H, d, J=2.6 Hz), 5.32 (1H, quintet, J=9.6 Hz, J=4.8 Hz, 3′-H of A), 5.64 (1H, d, J=4.9 Hz, 1′-H of G), 5.91 (1H, d, J=4.0 Hz, 1′-H of C), 5.95 (1H, d, J=7.3 Hz, 5-H of C), 6.17 (1H, d, J=5.5 Hz, 1′-H of A), 7.73 (1H, s, 8-H of G), 7.84 (1H, d, J=7.3 Hz, 6-H of C), 7.87 (1H, s, 2-H of A), 8.22 (1H, s, 8-H of A). **22:** λ_{max} 256.5 nm, λ_{min} 225 nm R_f 0.34 (relative to pU) (Solvent II), R_f 0.37 (relative to pU) (Solvent III); R_m 0.12 (relative to pU) (0.03 M phosphate buffer, pH 7.1).

In a similar manner, the partially protected branched trimer **23** (49.3 mg, 13 μmol) obtained in Method B was deprotected except that the ammonia and acid treatments were performed at room temperature for 26 h and for 11 h, respectively. The yield of **21** was 109 A_{258} (29%).

Synthesis of Branched Triribonucleotide A^{pG}_{pU} (27). A mixture of **19** (43.3 mg, 20 μmol), **28** (15.6 mg, 40 μmol), and pyridinium *m*-nitrobenzenesulfonate (16.9 mg, 60 μmol) was coevaporated three times with dry pyridine and then dissolved in dry pyridine (0.5 mL). DCC (29 mg, 0.14 mmol) was added and the solution was stirred for 4 d. The resulting mixture was diluted with pyridine (3 mL) and cooled to 0 °C. To the solution was added 0.2 M NaOH (3 mL), and the mixture was kept at 0 °C for 10 min. Then, cation-exchange DIAION resin (sulfonic acid form, 3 mL) was put to neutralize the solution, and the resin was removed by filtration and washed with pyridine–water (2 : 1, v/v, 36 mL). The eluate was evaporated and the residue was dissolved with pyridine (5 mL). Concentrated aqueous ammonia (50 mL) was added and this solution was kept for 3 d. Then the mixture was concentrated and the residue was treated with 80% acetic acid (50 mL) for 1 d. After the solvent was removed by evaporation, the residue was chromatographed on a Whatman 3MM paper developed with Solvent III to give **27** (122 A_{257}, 20%).

27: λ_{max} 257 nm; λ_{min} 227 nm; R_f 0.82 (relative to pU) (Solvent III) (55 : 10 : 35); R_m 0.71 (relative to pU) (0.03 M phosphate buffer, pH 7.1). ^{1}H NMR (500 MHz, D_2O/DSS) δ=3.60 (1H, dm, J=12.3), 3.80 (1H, d, J=12.3 Hz, 5′-Ha of A), 3.85 (1H, d, J=12.3 Hz, 5′-Hb of A), 3.92 (1H, m), 3.95 (1H, br. s), 4.20 (1H, m), 4.27 (1H, m), 4.35 (1H, quintet, J=5.0 Hz), 4.41 (1H, t, J=5.0 Hz), 4.51 (1H, br. s), 5.32 (1H, m, 2′-H of A), 5.63 (1H, d, J=5.2 Hz, 1′-H of G), 5.84 (1H, d, J=7.6 Hz, 5-H of U), 5.95 (1H, d, J=4.9 Hz, 1′-H of U), 6.20 (1H, d, J=5.8 Hz, 1′-H of A), 7.69 (1H, s, H-8 of G), 7.84 (1H, d, J=7.6 Hz, 6-H of U), 7.85 (1H, s, 2-H of A), 8.23 (1H, s, 8-H of A).

Enzymatic Analysis of 21 and 27. The branched triribonucleotide **21** (10 A_{258} unit) was incubated with snake venom phosphodiesterase (10 μL, 1 mg mL^{-1}) in 50 mM Tris-HCl (pH 7.5, 100 μL). Aliquots of the incubation mixture were analyzed after 1.5 h, 5 h, and 12 h by paper electropheresis using 0.05 M phosphate buffer (pH 8.0, 1250 V, 1 h 15 min). In paper electrophoresis done after 1.5 h and 5 h, two digestion intermediates of A(3′–5′)pC and A(2′–5′)pG were detected at R_m values 0.59 and 0.20, respectively. The ultimate ratio of pG, pC, and A, which was obtained after 12 h, was 1.0 : 1.0 : 1.1.

In a similar manner, **27** was digested under the same conditions to give pG, pU, and A in a ratio of 0.8 : 1.0 : 1.2.

Deprotection of 19 Giving Rise to 3′-*O*-Phosphinyladenylyl(2′–5′)guanylate. To a solution of compound **19** (152 mg, 70 μmol) in pyridine (10 mL) was added with stirring 0.2 M NaOH–pyridine (10 mL) at 0 °C. After being stirred at 0 °C for 15 min, the mixture was neutralized with Dowex 50W X2 (pyridinium form, 5 mL), and the resin was removed by filtration and washed with pyridine–water (1 : 1, v/v, 10 mL and 2 : 1, v/v, 36 mL). The filtrate and washing were combined, concentrated, dissolved in pyridine (10 mL), and mixed with concentrated aqueous ammonia (90 mL). The solution was kept for 24 h and evaporated. The residue was allowed to react with 80% acetic acid (50 mL) for 6 h. The solvent was removed under reduced pressure and the residue was chromatographed on Whatman 3MM papers with Solvent III. A band of R_f 0.66 relative to pU was eluted with water and lyophilized to give **26** (1464 A_{256}): R_m 0.85 (pH 7.1, 0.03 M phosphate buffer, 1 h 40 min, 1200 V).

Enzymatic Assay of 26. Compound **26** (70.4 OD at 256 nm) lyophilized was incubated with bacterial alkaline phosphatase (35.2 U/802 μL) in 50 mM Tris-HCl (pH 7.5, 704 μL) at 55 °C for 3 h. Then the incubation mixture was directly applied to a Whatman 3MM paper developed with Solvent II to give A(2′–5′)pG (62.4 $A_{255.5}$) as the sole product (λ_{max} 255.5 nm, λ_{min} 226.5 nm); R_m 0.32 (pH 7.1, 0.03 M phosphate buffer, relative to pU). The dinucleotide (5 $A_{255.5}$ each) was further incubated with RNase T_1, RNase T_2, RNase A, Nuclease P_1, snake venom phosphodiesterase (SVP), and calf spleen phosphodiesterase (CSP) at 37 °C for at least 13 h under the following conditions: 1) RNase T_1 (30 U, 6 μL), 10 mM Tris-HCl (100 μL) containing 1 mM EDTA, pH 7.5; 2) RNase T_2 (30 U, 150 μL), 20 mM NaOAc (100 μL), pH 5.5; 3) RNase A (150 μg, 15 μL), 10 mM Tis-HCl (30 μL) containing 1 mM EDTA, pH 7.5; 4) Nuclease P_1 (30 μg, 15 μL), 20 mM NaOAc (100 μL), pH 5.5; 5) SVP (30 μg, 30 μL), 50 mM Tris-HCl (100 μL), pH 7.5; 6) CSP (10 μg, 5 μL), 0.01 M pyrophosphate (50 μL) and 0.05 M ammonium acetate (100 μL), pH 6.5.

These enzyme reactions were analyzed after 1.5 h and 13 h by paper electrophoresis (0.03 M phosphate buffer, pH 7.1, 1200 V, 1 h 10 min). Among these enzymes, only SVP degraded the dinucleotide to A and pG in a ratio of 1.03 : 1.00 after 2 h. The digetion products were identified as the authentic samples by comparison of their R_f and R_m values as well as UV spectra.

***S,S*-Diphenyl 3′-*O*-Dianilinophosphinyl-5′-*O*-(4-methoxytrityl)-6-*N*-benzoyladenosine 2′-Phosphorodithioate (32).** Compound **6b** (1.21 g, 2 mmol) was rendered anhydrous by repeated coevaporation with dry pyridine and finally dissolved in dry pyridine (5 mL). 4-Methoxytrityl chloride (1.85 g, 6 mmol) was added and the mixture was stirred for 3

h. To the mixture were added successively cyclohexylammonium *S,S*-diphenyl phosphorodithioate (1.14 g, 3 mmol), tetrazole (560 mg, 8 mmol), and MDS (1.27 g, 4 mmol). The resulting mixture was stirred for 15 min and then diluted with CH_2Cl_2. After the usual workup as described in the synthesis of **13**, chromatography on a column of silica gel (100 g) with CH_2Cl_2–MeOH gave **32** (1.89 g, 83%).

32: ^{1}H NMR (500 MHz, $CDCl_3$) δ=3.43 (2H, br s, 5′-H), 3.61 (3H, s, OCH_3), 4.72 (1H, br s, 4′-H), 5.41 (1H, t, J=6.0, 3′-H), 5.98 (1H, q, J=6.0 Hz, J=6.8 Hz, 2′-H), 6.34 (1H, d, J=6.8 Hz, 1′-H), 6.75 (2H, d, J=8.79 Hz, ArH), 6.83 (2H, q, J=7.33 Hz, J=6.83 Hz, ArH), 6.88 (2H, t, J=7.32 Hz, ArH), 6.98—7.60 (31H, m, ArH), 8.07 (2H, d, J=7.8 Hz, ArH), 8.17 (1H, s, 2-H), 8.46 (1H, s, 8-H), 9.58 (1H, br, NH).

Removal of the Anilino Groups from 32. Compound **32** (1.85 g, 1.6 mmol) was allowed to react with isopentyl nitrite (1.6 mL) in pyridine–acetic acid–acetic anhydride (1 : 1 : 1, v/v/v) for 15 h. Then pyridine (5 mL) was added and the mixture was partitioned between CH_2Cl and water. The organic phase was collected and washed with water, 0.2 M TEAB (×5), water. Each washing was backextracted with another CH_2Cl_2. The two CH_2Cl_2 extracts were combined, concentrated, and the residue was chromatographed on a column of silica gel (64 g) with CH_2Cl_2–MeOH in the presence of 0.5% pyridine to give **33** as glassy material. As described in the case of **19**, further extractive workup followed by precipitation of its CH_2Cl_2 solution into hexane gave **33** as white powder (969 mg, 55%).

***S,S*-Diphenyl 3′-*O*-Bis(2-cyanoethoxy)phosphinyl-5′-*O*-(4-methoxytrityl)-6-*N*-benzoyladenosine 2′-Phosphorodithioate (30).** Compound **33** (219 mg, 0.2 mmol) was rendered anhydrous by repeated coevaporation with dry pyridine and finally dissolved in dry pyridine (4 mL). To the solution were added 2-cyanoethanol (272 μL, 4 mmol) and DDS (662 mg, 2 mmol). The resulting mixture was sitirred for 1 h and then diluted with CH_2Cl_2. The CH_2Cl_2 solution was washed with water (×2) and 5% $NaHCO_3$ (×3) and each washing was backextracted with another CH_2Cl_2. The two CH_2Cl_2 extracts were combined, dried over Na_2SO_4, filtered, concentrated, and chromatographed on a column of silica gel (20 g) with CH_2Cl_2–MeOH in the presence of pyridine to give **30** as foam (147 mg, 67%).

30: ^{1}H NMR ($CDCl_3$) δ=2.67 (4H, t, J=6 Hz, CH_2CN), 3.55 (2H, m, 5′-H). 3.74 (3H, s, CH_3O), 4.24 (4H, q, J=6 Hz, CH_2O-P), 4.45 (1H, m, 4′-H), 5.36 (1H, m, 3′-H), 6.08 (1H, m, 2′-H), 6.17 (1H, m, 1′-H), 6.73 (2H, d, J=8 Hz, 6.92—7.80 (25H, m, ArH), 7.91 (2H, m, ArH), 8.01 (1H, s, 2-H), 8.58 (1H, s, 8-H). Anal. Calcd for $C_{54}H_{49}N_7O_{10}P_2$: C, 59.94; H, 4.56; N, 9.06; S, 5.93%. Found: C, 60.31; H, 4.81; N, 8.85; S, 5.89%.

The Fully Protected 2′-5′ Linked ApG Derivative (36). A 5 M solution of pyridinium phosphinate in pyridine (1.1 mL) was mixed with triethylamine (0.55 mL) and **30** (100 mg, 91 μmol) was dissolved in this solution. After the mixture was stirred at room temperature for 30 min, the resulting mixture was diluted with CH_2Cl_2, which was washed subsequently with water, 0.2 M triethylammonium hydrogencarbonate (×2), and water. Each washing was backextracted with another CH_2Cl_2. The two CH_2Cl_2 extracts were combined, dried over Na_2SO_4, Filtered, and concentrated under reduced pressure. The residue was mixed with **35** (81 mg, 109 μmol) and 3-nitro-1*H*-1,2-4-triazole (31 mg, 0.27 mmol). The mixture was coevaporated several times with dry pyridine, dissolved in dry pyridine (1 mL), and DDS (90 mg, 0.27 mmol) was added. After the mixture was stirred for 1 h, the usual extractive workup followed by chromatography on a column of silica gel (20 g) with CH_2Cl_2–MeOH gave **36** (137 mg, 87%).

Synthesis of the Fully Protected Branched Trimer (39). The 2′-5′ linked dimer **36** (52 mg, 30 μmol) was treated with *N,N*-diisopropylethylamine (1 mL) in pyridine (2 mL) at 40 °C for 4 h. Evaporation followed by preparative TLC chromatography (CH_2Cl_2–MeOH 9 : 1, v/v) gave **37** as triethylammonium salt (44 mg, 82%).

A mixture of **37** (42 mg, 23 μmol), **38** (19.5 mg, 35 μmol), and 3-nitro-1*H*-1,2,4-triazole (24 mg, 0.21 mmol) was rendered anhydrous by repeated coevaporation with dry pyridine and finally dissolved in dry pyridine (0.5 mL). DDS (23 mg, 71 μmol) was added and the resulting mixture was stirred for 1 h. At this time the condensation was almost complete but an additional amount of DDS (23 mg, 71 μmol) was added to convert the excess hydroxy component to a sulfonate derivative. After stirring was continued for 1 h, the mixture was diluted with CH_2Cl_2, which was washed successively with water, 5% $NaHCO_3$, and water. Each washing was backextracted with another CH_2Cl_2. The two extracts were combined, dired over Na_2SO_4, filtered, concentrated and chromatographed on a preparative TLC plate developed with CH_2Cl_2–MeOH (9 : 1, v/v) to give **39** (33 mg, 63%).

Removal of the Methoxytrityl Group from 39. Compound **39** (33 mg, 15 μmol) was treated with trifluoroacetic acid (20 μL) in CH_2Cl_2 (2 mL) for 5 min. Then 5% $NaHCO_3$ was added and the mixture was extracted with CH_2Cl_2 (×3). The extracts were combined, dried over Na_2SO_4, filtered, concentrated, and chromatographed on a preparative TLC plate developed with CH_2Cl_2–MeOH (9 : 1, v/v) to give **40** (17.5 mg, 60%).

Synthesis of Fully Protected UpG Dimer. A mixture of triethylammonium *S*-phenyl 5′-*O*-(4,4′-dimethoxytiryl)-3′-*O*-(tetrahydro-2-pyranyl)-N^3-(*p*-anisoyl)uridine 3′-phosphorothioate (343 mg, 0.33 mmol) and *S,S*-diphenyl 3′-*O*-(tetrahydro-2-pyranyl)-2-*N*-propionyl-6-*O*-(diphenylcarbamoyl)guanosine 3′-phosphorodithioate (170 mg, 0.275 mmol), which were obtained from the corresponding monomer units[31,32] by treatments with phosphinate and trifluoroacetic acid, respectively, was rendered anhydrous by repeated coevaporation with dry pyridine and finally dissolved in dry pyridine (5 mL). To the solution were added 3-nitoro-1*H*-1,2,4-triazole (114 mg, 1 mmol) and DDS (331 mg, 1 mmol). After being stirred for 40 min, the mixture was quenched by the addition of water and extracted four times with CH_2Cl_2. Each CH_2Cl_2 extract was washed with 5% $NaHCO_3$. The CH_2Cl_2 extracts were combined, dried over Na_2SO_4, filtered, and evaporated under reduced pressure. The residue was chromatographed on a column of silica gel (15 g) with CH_2Cl_2–MeOH to give the fully protected UpG dimer (329 mg, 78%).

Removal of the DMTr Group of the Fully Protected UpG Dimer. The Fully protected UpG dimer (310 mg, 0.21 mmol) was dissolved in CH_2Cl_2 (20 mL) and the solution was cooled at 0 °C. Trifluoroacetic acid (100 μL) was added and the resulting mixture was kept at the same temperature for 10 min. Then 5% $NaHCO_3$ was added to neutralize the solution. The usual extract with CH_2Cl_2 followed by preparative TLC developed with CH_2Cl_2–MeOH gave the 5′-

hydroxy component of the fully protected UpG dimer (194 mg, 76%).

Synthesis of the Fully Protected CpUpG Trimer. A mixture of *S*-phenyl 5′-*O*-(4,4′-dimethoxytrityl)-3′-*O*-(tetrahydro-2-pyranyl)-N^4-benzoylcytidine 3′-phosphorothioate (174 mg, 0.173 mmol) and the 5′-hydroxy component (186 mg, 0.15 mmol) obtained in the above experiment was rendered anhydrous by repeated coevaporation with dry pyridine and finally dissolved in dry pyridine (3 mL). To the mixture were added 3-nitro-1*H*-1,2,4-triazole (51.4 mg, 0.45 mmol) and DDS (149 mg, 0.45 mmol). After being stirred for 1 h, the mixture was quenched by the addition of water. The usual workup followed by chromatography on a column of silica gel gave the fully protected CpUpG trimer (282 mg, 88%).

Removal of the 3′-Terminal Phenylthio Group from the Fully Protected CpUpG Trimer. The fully protected CpUpG trimer (106 mg, 0.05 mmol) was dissolved in a mixture of 5 M phosphinic acid (pyridine solution) and triethylamine (2:1, v/v, 0.91 mL). The mixture was kept at room temperature for 1 h. Extraction with CH_2Cl_2 as described in the synthesis of **16** was performed. Chromatography on preparative TLC plates (Merck 5717) with CH_2Cl_2–MeOH gave **41** (65 mg, 60%) as triethylammonium salt.

Synthesis of the Fully Protected Branched Hexamer (42). A mixture of **40** (10.0 mg, 5.2 μmol), **41** (14.3 mg, 6.7 μmol), and 3-nitro-1*H*-1,2,4-triazole (3.8 mg, 34 μmol) was rendered an hydrous by repeated coevaporation with dry pyridine, finally dissolved in dry pyridine (0.2 mL), and DDS (11.1 mg, 34 μmol) was added. After being stirred for 1 h, the mixture was diluted with CH_2Cl_2. Extraction followed by preparative TLC gave **42** (8.7 mg, 56%).

Full Deprotection of 42. The fully protected branched hexamer **42** (8.5 mg, 2.1 μmol) was treated with bis-(tributyl)tin oxide (0.15 mL, 0.23 mmol) in pyridine (0.25 mL) for 28 h. Then trimethylsilyl chloride (70 μL, 0.46 mmol) was added and the mixture was kept for 15 min. Pyridine (20 mL) and concentrated aqueous ammonia (20 mL) were added to the solution. After being stirred for 19 h, the mixture was evaporated and coevaporated two times with dioxane to remove the last traces of pyridine. The residue was dissolved in dioxane (20 mL) and 0.02 M HCl (20 mL) was added. The resulting solution was further arranged to pH 2.0 by addition of 0.1 M HCl and stirred for 48 h. Then the solution was neutralized by addition of concentrated aqueous ammonia, evaporated, and the residue was chromatographed on a Toyo Roshi 51A paper developed with Solvent II to give **43** (36 A_{257}, 32%): λ_{max} 257 nm, λ_{min} 226 nm; Retension time 11.0 min (HPLC System A); R_f 0.09 (Solvent II, relative to pT).

Enzyme Analysis of 43. The sample of **43** (0.1 A_{257}) purified by HPLC was incubated with nuclease P_1 (10 μL) in 10 mM sodium acetate (pH 5.5, 200 μL) at 37 °C for 15 min. The result of this enzyme reaction is depicted in Fig. 2C. The peak of pA_{pC}^{pG} was collected, desalted by repeated lyophilization from water, and incubated with bacterial alkaline phosphatase (0.3 μg/μL, 4 μL) in 50 mM Tris-HCl (pH 7.5, 30 μL) for 15 min. The peak of pA_{pC}^{pG} was completely shifted to an authentic sample of A_{pC}^{pG}.

We thank Professor Yasumi Ohshima and Dr. Akira Mayeda, Kyushu University for their helpful discussion throughout this study. This work was supported by a Grant-in-Aid for Scientific Research from the Ministry of Education, Science and Culture.

References

1) J. C. Wallace and M. Edmonds, *Proc. Natl. Acad. Sci. U.S.A.*, **80**, 950 (1983).
2) C. Weissmann, C. *Nature (London)*, **311**, 103 (1984); W. Keller, *Cell*, **39**, 432 (1984).
3) M. Sekine and T. Hata, *J. Am. Chem. Soc.*, **107**, 5813 (1985).
4) M. J. Damha, R. T. Pon, and K. K. Ogilvie, *Tetrahedron Lett.*, **26**, 4839 (1985).
5) R. Kierzek, D. W. Kopp, M. Edmonds, and M. H. Caruthers, *Nucleic Acids Res.*, **14**, 4751 (1986).
6) G. Remaud, J-M. Vial, A. Nyilas, N. Balgobin, and J. Chattopadhyaya, *Tetrahedron Lett.*, **43**, 947 (1987).
7) S. Huss, G. Gosselin, and J. L. Imbach, *Tetrahedron Lett.*, **28**, 415 (1987).
8) J-M. Vial, N. Balgobin, G. Remaud, A. Nylas, and J. Chattopadhyaya, *Nucleosides Nucleotides*, **6**, 209 (1987).
9) X-X. Zhou, A. Nyilas, G. Remaud, and J. Chattopadhyaya, *Tetrahedron*, **43**, 4685 (1987).
10) Y. Hayakawa, T. Nobori, R. Noyori, and J. Imai, *Tetrahedron Lett.*, **28**, 2623 (1987).
11) J. L. Fourrey, J. Varenne, C. Fontaine, E. Guittet, and Z. W. Yang, *Tetrahedron Lett.*, **28**, 1769 (1987).
12) S. Huss, G. Gosselin, and J. L. Imbach, *J. Org. Chem.*, **53**, 499 (1988).
13) M. Sekine, J. Heikkilä, and T. Hata, *Tetrahedron Lett.*, **28**, 5691 (1988).
14) M. J. Damha and K. K. Ogilvie, *J. Org. Chem.*, **53**, 3710 (1988).
15) X-X. Zhou, G. Remaud, and J. Chattpadhyaya, *Tetrahedron*, **44**, 6471 (1988). Several references on studies of confomational analysis of branched oligoribonucleotides are cited in this paper.
16) S. L. Beaucage and M. H. Caruthers, *Tetrahedron Lett.*, **1981**, 1859; L. J. McBride and M. H. Caruthers, *Tetrahedron Lett.*, **24**, 245 (1983); For a review see M. H. Caruthers, *Science*, **250**, 281 (1985).
17) M. Sekine, H. Mori, and T. Hata, *Tetrahedron Lett.*, **1979**, 1145.
18) K. K. Ogilvie and D. W. Entwistle, *Carbohydr. Res.*, **89**, 203 (1981).
19) J. Smrt, "Nucleic Acid Chemistry," ed by L. B. Townsend and R. Tipson, John Wiley & Sons, New York (1978), Part 2, p. 993.
20) M. Sekine and T. Hata, *J. Am. Chem. Soc.*, **106**, 5763 (1984); *ibid.*, **108**, 4581 (1986).
21) M. Sekine, K. Hamaoki, and T. Hata, *J. Org. Chem.*, **44**, 2325 (1979); *Bull. Chem. Soc. Jpn.*, **54**, 3815 (1981); K. Yamaguchi, S. Honda, I. Nakagawa, and T. Hata, *Chem. Lett.*, **1978**, 507.
22) M. Sekine, J. Matsuzaki, and T. Hata, *Tetrahedron*, **41**, 5279 (1985).
23) E. Ohtsuka, K. Murao, M. Ubasawa, and M. Ikehara, *J. Am. Chem. Soc.*, **92**, 3441 (1970).
24) M. Nishizawa, T. Kurihara, and T. Hata, *Chem. Lett.*, **1984**, 175.
25) T. Hata and M. Sekine, *Chem. Lett.*, **1974**, 837.
26) A preliminary study also showed that 3′-*O*-acetyl-

5′-*O*-[tris[4-(4,5-dichlorophtalimido)phenyl]methyl]-thymidine was modified by this oxidation-reduction reagent to give a new product which appeared higher than this substrate. These results indicated that the CPTr group was modified exclusively by this reagent.

27) C. B. Reese, R. C. Titmas, and L. Yau, *Tetrahedron Lett.*, **1978**, 2727.

28) P. T. Gilham and H. G. Khorana, *J. Am. Chem. Soc.*, **80**, 6219 (1958); H. G. Khorana, *Pure Appl. Chem.*, **17**, 349 (1968).

29) M. Sekine and T. Hata, *J. Am. Chem. Soc.*, **105**, 2044 (1983).

30) M. Smith, D. H. Rammler, I. H. Goldberg, and H. G. Khorana, *J. Am. Chem. Soc.*, **84**, 430 (1962).

31) T. Kamimura, M. Tsuchiya, K. Urakami, K. Koura, M. Sekine, K. Shinozaki, K. Miura, and T. Hata, *J. Am. Chem. Soc.*, **106**, 4552 (1984).

32) M. Sekine, S. Nishiyama, T. Kamimura, Y. Osaki, and T. Hata, *Bull. Chem. Soc. Jpn.*, **58**, 850 (1985).

33) M. Sekine, H. Tanimura, and T. Hata, *Tetrahedron Lett.*, **26**, 4621 (1985); H. Tanimura, M. Sekine, and T. Hata, *Tetrahedron*, **42**, 4179 (1986).

34) Y. Ohshima, et al. unpublished results.

35) W. T. Markiewicz, *J. Chem. Res., Miniprint*, **1979**, 181.

Selective Deoxygenation of Various N-O Bonds Catalyzed by Rhodium Carbonyl Clusters in the Presence of H_2O and CO and Their Heterogenization Using Amino-Substituted Polystyrenes

Kiyotomi KANEDA,* Kazuo FUJITA, Tetsuya TAKEMOTO, and Toshinobu IMANAKA
Department of Chemical Engineering, Faculty of Engineering Science, Osaka Univesity, Toyonaka, Osaka 560
(Received September 10, 1990)

Catalytic deoxygenation of various N-O bonds using rhodium carbonyl compounds under a water gas shift reaction was studied. A catalyst system of $Rh_6(CO)_{16}$ and *N,N,N′,N′*-tetramethyl-1,3-propanediamine was found to have high activities for the following deoxygenations: 1) conversion of nitrobenzenes to anilines, 2) aliphatic nitro compounds to nitriles, 3) oximes to nitriles, 4) hydroxylamines to amines, and 5) amine oxides to amines. The above-mentioned rhodium catalyst system was heterogenized by using amino-substituted polystyrenes. Rh_6 and Rh_{14} carbonyl clusters of $[Rh_6(CO)_{15}H]^-$, $[Rh_6(CO)_{15}]^{2-}$, and $[Rh_{14}(CO)_{25}]^{4-}$, were formed on the polymer surface. The characteristic features of the catalysis of the polymer-bound rhodium cluster complexes are described in relation to the corresponding homogeneous ones.

Metal carbonyl clusters have generated interest as catalysts from the standpoint of faciliting new organic reactions and as a model for metal catalysts.[1] Various organic reactions explored by using metal carbonyl clusters (e.g., hydroformylation, reduction, and deoxygenation) have been carried out under a CO atmosphere since the labile cluster framework consisting of metal-metal bonds must be reinforced by CO molecules.[2] We also studied the application of the water gas shift reaction (WGSR) using CO and H_2O for organic syntheses in the presence of rhodium carbonyl clusters, and found that the rhodium clusters have unique reactivities for the reduction of carbonyl compounds (e.g., aldehydes and α,β-unsaturated carbonyl compounds), carbonylation of olefins, and deoxygenation of various N-O bonds.[3] In the above-mentioned organic reactions, the amines or pyridines are an essential additive to form active species of rhodium catalysts. In order to simplify the work-up procedure, we heterogenized the rhodium catalyst systems using amino-substituted polystyrenes and the rhodium cluster anions $[Rh_6(CO)_{15}H]^-$, $[Rh_6(CO)_{15}]^{2-}$, and $[Rh_{14}(CO)_{25}]^{4-}$ which formed as ammonium salts on the polymer. In this paper, we give a detailed account of the deoxygenation of nitro compounds, oximes, hydroxylamines, and amine oxides using CO and H_2O in the presence of rhodium carbonyl clusters, e.g., $Rh_6(CO)_{16}$ and $Rh_4(CO)_{12}$.[4] Furthermore, the characteristic features of the catalysis of polymer-bound rhodium cluster complexes are mentioned in relation to the corresponding homogeneous ones.

Results and Discussion

Deoxygenation of Aromatic Nitro Compounds. Rhodium carbonyl cluster-diamine catalyst systems showed high activity for WGSR under mild conditions.[5] In relation to WGSR, we have examined the reactivity of various amines and pyridines as additives for the deoxygenation of nitrobenzene to aniline using CO and H_2O at 80 °C. Results using CO of 700 mmHg (1 mmHg=133.322 Pa) and H_2O in the presence of the $Rh_6(CO)_{16}$ cluster are shown in Table 1 together with the activities of the corresponding WGSR. Aniline was the only deoxygenation product. The formation

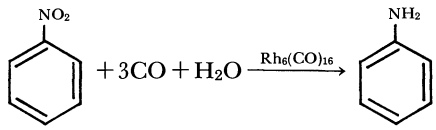

(1)

of other products (e.g., nitrosobenzene, phenylhydroxylamine, *N,N′*-diphenylurea, and cyclohexylamine) could not be observed under the reaction conditions.[6] The yields of aniline are also strongly dependent on various kinds of bases. It should be noted that there are sharp contrasts between the deoxygenation of nitrobenzene and WGSR regarding the effect of additives. The most effective additive in the deoxygenation reaction is *N,N,N′,N′*-tetramethyl-1,3-propanediamine (TMPDA), which had no activity for generation of H_2 in WGSR. Among the diamine series of $-N(CH_2)_nN-$, increasing the number (n) of methylenes and the introduction of methyl substituents on the nitrogen atoms increase the yield of aniline, respectively, while decreasing H_2 generation from WGSR. For pyridine derivatives, the introduction of electron-releasing substituents on the γ-position of pyridines increases the yields of aniline; 4-(dimethylamino)-pyridine was the most effective additive. On the other hand, methyl substituents on the α-position of pyridines decrease the yield of H_2 while an α-substituent effect could not be observed in the nitrobenzene deoxygenation. The strong basicity of the pyridines with high pK_a value is an essential factor for attaining high yields of aniline in the deoxygenation of nitrobenzene.

The catalytic behavior for nitrobenzene deoxygenation using various metal complexes was examined in the presence of TMPDA as an additive. Typical

Table 1. Additive Effect of Various Amines and Pyridines on Deoxygenation of Nitrobenzene and the Water Gas Shift Reaction Using $Rh_6(CO)_{16}$[a]

Base(pK_a)[b]	Deoxygenation		WGSR
	Reaction time	Yieid of aniline	Yield of H_2[c]
	h	%	
$NH_2CH_2CH_2NH_2$(9.97)	10	34	75
$NH_2(CH_2)_3NH_2$(10.65)	10	45	32
$NH_2(CH_2)_4NH_2$(10.84)	10	50	6.4
$CH_3NHCH_2CH_2NHCH_3$(9.5)	10	45	69
$(CH_3)_2NCH_2CH_2N(CH_3)_2$(8.97)	4	>99	2.5
$(CH_3)_2N(CH_2)_3N(CH_3)_2$(10.2)	2.5	>99	0
(5.17)	10	79	22 3[d]
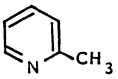 (5.97)	10	72	1
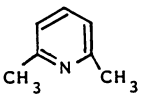 (6.75)	10	80	0
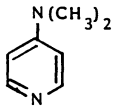 (9.70)	2.5	>99	2.8[d]
$N(C_2H_5)_3$(10.65)	10	83	0
(10.1)	5	92	2.3

a) For deoxygenation; nitrobenzene 1.5 mmol, $Rh_6(CO)_{16}$ 0.05 mmol, base 15 mmol, H_2O 0.72 ml, 2-ethoxyethanol 3 ml, P_{co}=700 mmHg, 80 °C. For WGSR: $Rh_6(CO)_{16}$ 0.05 mmol, base 85 mmol, H_2O 0.72 ml, 2-ethoxyethanol [10-base]ml, P_{co}=700 mmHg, 4 h.[5] b) The pK_a values are cited from Ref. 44. c) Yield of H_2=mol of H_2/mol of $Rh_6(CO)_{16}$ per 6 h. d) Base 17 mmol, 2-ethoxyethanol 10 ml, 12 h, 100 °C.

Table 2. Deoxygenation of Nitrobenzene with Various Metal Carbonyl Compounds in the Presence of H_2O and CO[a]

Catalyst	Aniline	
	Time/h	Yield/%
$Rh_6(CO)_{16}$	2.5	>99
$Rh_4(CO)_{12}$	3.0	>99
$Rh_2(CO)_4Cl_2$	6.0	>99
$RhCl_3 \cdot 3H_2O$	10	20
$RhCl(PPh_3)_3$	10	17
Rh_2O_3	10	4
$Ru_3(CO)_{12}$	10	18
$Fe(CO)_5$	10	54
$W(CO)_6$	10	5

a) Reaction conditions were the same as used in Table 1.

examples are summarized in Table 2. Though Rh carbonyl compounds (e.g., $Rh_6(CO)_{16}$, $Rh_4(CO)_{12}$, and $Rh_2(CO)_4Cl_2$) are good catalysts, other Rh compounds (such as $RhCl(PPh_3)_3$, $RhCl_3 \cdot 3H_2O$, and Rh_2O_3) have low catalytic activities for deoxygenation. Other transition metal carbonyl complexes of $Ru_3(CO)_{12}$, $Fe(CO)_5$, and $W(CO)_6$ are poor catalysts under the reaction conditions. All rhodium carbonyl complexes having high activities were dark brown in solution during deoxygenation. $Rh_2(CO)_4Cl_2$ had a longer induction period for deoxygenation than the Rh_6 and Rh_4 carbonyl clusters did. This phenomenon supports the idea that these rhodium complexes were changed into a common active Rh species during nitrobenzene deoxygenation.

The deoxygenation of various aromatic nitro compounds using the catalyst system of $Rh_6(CO)_{16}$ and TMPDA under 4 atm of CO is shown in Table 3, together with that in the amino-substituted polymer system. Details concerning the heterogeneous deoxygenation of nitro compounds are discussed in a latter section. In a series of *p*-substituted nitrobenzenes, electron-donating substituents decrease their reactivity for deoxygenation, which became more clear by using competitive reactions to unsubstituted nitrobenzene

Table 3. Deoxygenation of Various Nitro Compounds Using $Rh_6(CO)_{16}$ in the Presence of CO and H_2O[a]

Nitro compound	Amino-substituted product Yield[b]/%	k_x/k_H[c]
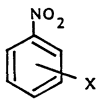 X=H	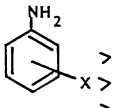 >99(>99)	1
4-Cl	>99(>99)	5.3(4)
4-CH_3	>99(65)	0.40(0.36)
4-OCH_3	65(21)	0.15(0.22)
3-CH_3	73(54)	
2-CH_3	42(23)	
2,4-CH_3	76(23)	
2,6-CH_3	10(trace)	
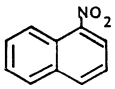	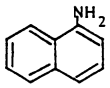 61 (60)	

a) $Rh_6(CO)_{16}$ 0.05 mmol, substrate 5 mmol, H_2O 2.88 ml, 2-ethoxyethanol 2 ml, P_{CO}=4 atm, 80 °C, *N,N,N'N'*-tetramethyl-1,3-propanadiamine (TMPDA) 5 mmol, 5 h. b) Values of parentheses are for the polymer system. Amino-substituted polymer (**Ia**, 0.8 mg-atom of N), 48 h. c) Relative rates were calculated by initial product ratios of substituted anilines to aniline.

(ρ=2.75). A similar electronic effect of substituents has been reported in the phase-transfer catalyst of $Ru_3(CO)_{12}$[2d] and $Ru(CO)_3(Ph_4C_4CO)$,[7] while in the case of $[Ru(cod)py_4]^{2+}$, electron-donating substituents accelerate the yield of aniline derivatives.[8] Nitronaphthalene also gave naphthylamine in a 61% yield under the above-mentioned conditions.[9]

Aliphatic Nitro Compounds and Oximes. The reaction of 1-nitropropane in place of aromatic nitro compounds was performed by the catalyst system of $Rh_6(CO)_{16}$ and TMPDA at 40 °C under 16 atm of CO. Unexpectedly, propionitrile was obtained as the main product, accompanied by 1-propanol and tripropylamine without propylamine. Typical results of aliphatic nitro compounds are listed in Table 4, together with those of amino-substituted polymer systems. A nitro function on the primary carbon atoms in various nitro compounds was deoxygenated to give the corresponding nitriles as the main product, respectively,

$$C_3H_7\text{-}NO_2 \xrightarrow[Rh_6(CO)_{16}\text{-diamine}]{CO,\ H_2O} C_2H_5CN + C_3H_7OH + (C_3H_7)_3N \quad (2)$$

Table 4. Deoxygenation of Various Aliphatic Nitro Compounds and Oximes Using $Rh_6(CO)_{16}$ in the Presence of CO and H_2O

Nitrogen compound	Deoxygenated products Yield[b]/%
$C_2H_5\text{-}NO_2$	CH_3CN 69 C_2H_5OH 10 2-butanone 7
$C_3H_7\text{-}NO_2$	C_2H_5CN 71(72) C_3H_7OH 15(19) $(C_3H_7)_3N$ 4(3)
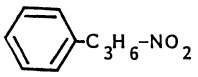	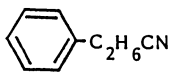 C_2H_6CN (85)
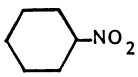	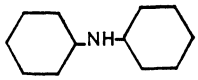 33(30) 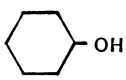 OH 29(27) 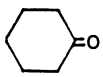
$CH_3CH{=}N\text{-}OH$	CH_3CN 64(68) C_2H_5OH 11(14) trace(trace)
$C_2H_5CH{=}N\text{-}OH$	C_2H_5CN 61(62) C_3H_7OH 20(20)
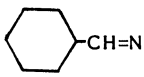	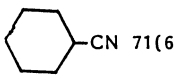 CN 71(65) 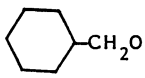 CH_2OH 12(25)
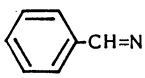	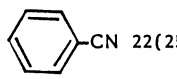 CN 22(25) 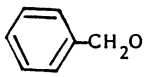 CH_2OH 75(65)
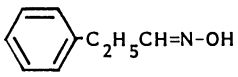	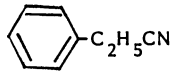 C_2H_5CN 84(84) 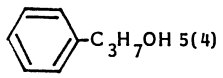 C_3H_7OH 5(4)
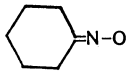	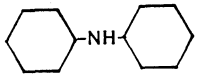 28(21) 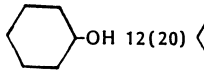 OH 12(20) 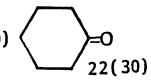 22(30)

a) Substrate 5 mmol, $Rh_6(CO)_{16}$ 0.05 mmol, 2-ethoxyethanol 2 ml, H_2O 2.88 ml, *N,N,N'N'*-Tetramethyl-1,3-propanamine (TMPDA) 5 mmol, P_{CO}=16 atm, 40 °C, 24 h. For oximes: P_{CO}=8 atm, 5 h. b) Values of parentheses are for the polymer system. Amino-substituted polymer (**Ia**, 0.8 mg-atom of N), 48 h.

while amines, alcohols, and ketones were formed in the case of secondary nitro compounds. The formations of these products are discussed (vide infra). During the initial stage of these deoxygenations, trace amounts of oximes were detected, respectively. The reaction of a prepared propionaldehyde oxime was carried out under the same conditions as in the above 1-nitropropane to give propionitrile as the main product. From the above results, a possible path for the formation of propionitrile via an oxime intermediate can be considered in Scheme 1; the deoxygenation of

$$C_3H_7\text{-}NO_2 + CO \longrightarrow C_3H_7\text{-}NO \rightleftarrows C_2H_5\text{-}CH{=}N\text{-}OH + CO_2$$
$$C_2H_5\text{-}CH{=}N\text{-}OH + CO \longrightarrow C_2H_5\text{-}CN + CO_2 + H_2$$

Scheme. 1. Deoxygenation of 1-nitropropane via an oxime intermediate.

1-nitropropane occurs to give 1-nitrosopropane, which is tautomerized to propionaldehyde oxime, and dehydration of the oxime affords propionitrile with generation of H_2 and CO_2. 1-Propanol originated from hydrolysis of propionaldehyde oxime to give propionaldehyde, followed by a reduction. We have already found that a catalyst system consisting of $Rh_6(CO)_{16}$ and TMPDA has a high catalytic activity for the reduction of formyl groups under WGSR conditions.[3b]

The results of various oximes under 8 atm of CO are also included in Table 4. Aldoximes, except for benzaldehyde oxime, were deoxygenated to selectively give the corresponding nitriles; benzaldehyde oxime afforded benzyl alcohol as the main product, because of its facile hydrolysis to benzaldehyde under the reaction conditions. Deoxygenation with a protected oxime of propionaldehyde *O*-methyloxime did not occur and the starting material was recovered. Interestingly, this nitrile synthesis from oximes is regarded as being a formal dehydration, which occurs with the formation of CO_2 and H_2 (Eqs. 3 and 4).[10]

$$R\text{-}CH{=}N\text{-}OH \longrightarrow R\text{-}CN + H_2O \quad (3)$$

$$R\text{-}CH{=}N\text{-}OH + CO \xrightarrow{Rh_6(CO)_{16}} R\text{-}CN + CO_2 + H_2 \quad (4)$$

Next, the reaction of ketoximes was performed, leading to complicated product distributions of amines, alcohols, and ketones; for example, cyclohexanone oxime gave dicyclohexylamine, cyclohexanone, and cyclohexanol in 28, 22, and 12% yields, respectively. The formation of dicylohexylamine can be explained by the following paths. The hydrogenolysis of cyclohexanone oxime yields cyclohexylamine, followed by the dehydration of cyclohexylamine with cyclohexanone to afford *N*-cyclohexylidenecyclohexylamine, which is further reduced to dicyclohexylamine. In a separate experiment, the Schiff base of *N*-cyclohexylidenecyclohexylamine could be converted into dicyclohexylamine in 83% yield under the same conditions as in the oxime reactions. We planed one-pot *N*-alkylation of amines with ketones via Schiff base intermediates. The reaction of primary amines with ketones was carried out in the presence of $Rh_6(CO)_{16}$ under WGSR conditions. The expected *N*-alkylated products of the amines were obtained in moderate yields, which is shown in Table 5.[11]

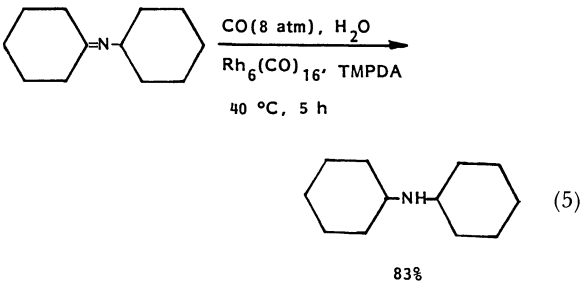

(5)

Table 5. *N*-Alkylation of Amines with Ketones Using $Rh_6(CO)_{16}$ in the Presence of CO and H_2O[a]

Amine	Ketone	N-Alkylated product Yieid[b]/%
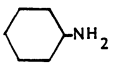		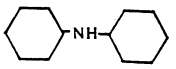 80
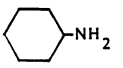	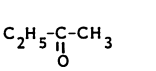	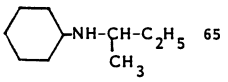 65
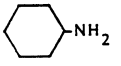	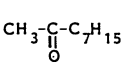	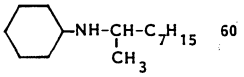 60
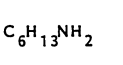	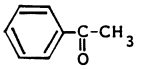	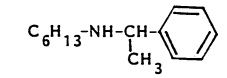 70

a) Amine 5 mmol, ketone 5 mmol, $Rh_6(CO)_{16}$ 0.05 mmol, 2-ethoxyethanol 2 ml, H_2O 1.4 ml, P_{CO}=8 atm, 80 °C, 5 h. b) Isolated yield.

Hydroxylamines and Amine Oxides. In previous sections it was revealed that a catalyst system of $Rh_6(CO)_{16}$ and TMPDA was effctive for the deoxygenation of various nitro compounds and oximes. In order to develop the deoxygenation ability of the rhodium catalyst to other nitrogen compounds having N-O bonds, many reactions of hydroxylamines and amine oxides were carried out under conditions similar to those of the above-mentioned oximes. The results are shown in Table 6. Various hydroxylamines and amine oxides were easily deoxygenated to give the corresponding amines in high yields, respectively.[12] The deoxygenation of pyridine *N*-oxide did not occur under the present conditions and the *N*-oxide was recovered quantitatively. Although there are many reagents and catalysts for the deoxygenations of oximes, hydroxylamines, and amine oxides,

Table 6. Deoxygenation of Hydroxylamines and Amine Oxides Using $Rh_6(CO)_{16}$ in the Presence of CO and H_2O[a]

Nitro compound	Amine product yield[b]/%
$(C_2H_5)_2N$-OH	$(C_2H_5)_2NH$ 93(89)
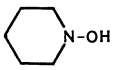	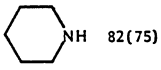 82(75)
$(CH_3)_3CN$(H)-OH	$(CH_3)_3CNH_2$ 70(80)
$(C_3H_7)_3N\rightarrow O$	$(C_3H_7)_3N$ 91(84)
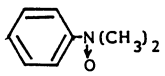	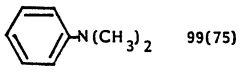 99(75)
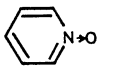	No reaction

a) Substrate 5 mmol, $Rh_6(CO)_{16}$ 0.05 mmol, 2-ethoxyethanol 2 ml, H_2O 2.88 ml, TMPDA 5 mmol, P_{co}=8 atm, 40 °C, 5 h. b) Values of parentheses are for the polymer system. Amino-substituted polymer (**Ia**, 0.8 mg-atom of N), 5 h (hydroxylamines), 24 h (amine oxides).

little has been known about such deoxygenations using a reducing agent of CO in organic synthesis.[13] It should be noted that our system of Rh carbonyl clusters and TMPDA can catalyze the deoxygenation of various nitrogen compounds using CO as an inexpensive reducing agent.

$$(C_2H_5)N\text{-}OH + CO \xrightarrow[H_2O,\ 40\,°C,\ 5\ h]{Rh_6(CO)_{16}\text{-diamine}} \underset{93\%}{(C_2H_5)_2NH} + CO_2 \quad (6)$$

$$(C_3H_7)_3N\rightarrow O + CO \xrightarrow[H_2O,\ 40\,°C,\ 5\ h]{Rh_6(CO)_{16}\text{-diamine}} \underset{91\%}{(C_3H_7)_3N} + CO_2 \quad (7)$$

Polymer System in Deoxygenation of N-O Bonds. The most practical advantage of using insoluble polymer-bound metal complexes is to simplify the work-up procedure in organic synthesis.[14] Amines and pyridines are an essential additive in the above-mentioned deoxygenations, and act as a base to induce the formation of active species of Rh carbonyl cluster anions and as an ammonium counter ion to stabilize the Rh cluster anions in an aqueous media (vide infra). We had a plan to heterogenize the $Rh_6(CO)_{16}$ catalyst system by using amino substituted organic polymers in place of TMPDA. The amino-substituted polymers were prepared by the following procedures: 1) polymerization of *p*-(chloromethyl)-styrene, followed by its treatment with amines, and 2) amination of *p*-(chloromethyl)styrene, followed by its polymerization. The above-mentioned synthetic routes are summarized in Scheme 2.

The catalytic behavior of our homogeneous $Rh_6(CO)_{16}$-amine systems is strongly dependent on various kinds of the amines, which was described in a previous section regarding nitrobenzene deoxygenation. It has been of interest whether polymer-heterogenized metal systems keep their instinctive catalytic activities of the corresponding homogeneous systems. Table 7 shows the effect of various amines on the 1-nitropropane reduction in the cases of poly-

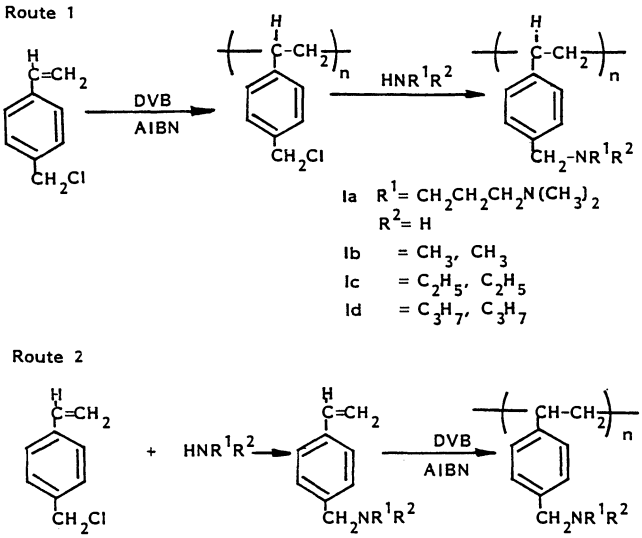

Scheme. 2. Synthetic routes of amino-substituted polystyrenes.

Table 7. Effect of Amines and Amino-Substituted Polymers on Deoxygenation of 1-Nitropropane[a]

Amine	Products yield[b]/%			
	C_2H_5CN	C_3H_5OH	3-Hexanone	$(C_3H_7)_3N$
Ⓟ-$NHC_3H_6N(CH_3)_2$ **Ia**	72	19	0	3
$(CH_3)_2NC_3H_6N(CH_3)_2$	71(44)[b]	15(20)	0(5)	4(7)
Ⓟ-$N(CH_3)_2$ **Ib**	55	32	0	3
$N(CH_3)_3$	55(48)	15(20)	0(5)	8(9)
Ⓟ-$N(C_2H_5)_2$ **Ic**	53	29	5	0
$N(C_2H_5)_3$	40	19	4	9
Ⓟ-$N(C_3H_7)_2$ **Id**	31	7	18	4
$N(C_3H_7)_3$	39(35)	16(24)	5(5)	—

a) Reaction conditions were the same as in Table 4. b) Values in parentheses are for the amine monomers of 0.4 mmol used, respectively.

mer and homogeneous systems. Both of the systems gave similar product distributions for a variety of amine additives; the use of a polymer having the diamino moiety (**Ia**) led a high yield of propionitrile, and TMPDA was the most effective additive in homogeneous systems. Various heterogeneous systems of the amino-substituted polymers showed lower reaction rates for the 1-nitropropane deoxygenation than the corresponding homogeneous ones did; the reaction times for heterogeneous reactions had to be prolonged for up to 48 h in order to attain high nitrile yields. However, a relatively small amount of the amino moiety (0.8 mg-atom of N) can cause the selective formation of nitriles, compared with homogeneous systems (10 mg-atom of N). This might be due to the location of amino moieties within a relatively small volume of the polymers;[15] the high concentration of the amines on the polymer surfaces increases the basicity of the reaction media near the polymer surfaces, which facilitates the formation of Rh carbonyl cluster anions as an active species, and also promotes the stability of the Rh cluster anions through ammonium ions.

The effect of the various polymerization degrees of polystyrene supports on the deoxygenation was examined by using polymers prepared from route 1 with *N*,*N*-dimethyl-1,3-propanediamine. In the cases of polystyrenes with M_w=7600, 8600, and 52700, heterogeneous polymer-bound Rh complexes were formed in the above-mentioned deoxygenation, and gave similar yields of the nitrile in 69, 73, and 71%, respectively. The difference of the polymerization degree did not remarkably change the product distribution of 1-nitropropane. Furthermore, the use of amino-substituted polymers having the diamino moiety (**Ia**) prepared from routes 1 and 2 gave similar yields of the nitrile of 70 vs. 75% under the conditions with an equivalent amino amount. We think that the structure of amino moieties on polymers is the crucial factor in the design of a suitable polystyrene support for the selective deoxygenation of 1-nitropropane to propionitrile.

Heterogeneous deoxygenations of nitropropane using Ia were carried out in the presence of various solvents. Since large amounts of water were required for the selective formation of the nitrile, the solvents used here had to be well miscible with organic compounds and water. These results are shown in Table 8. Alcohols having an ether function (e.g., 2-ethoxyethanol and 2-methoxyethanol) were good solvents. Although THF and dioxane have a high swelling ability for polystyrene supports,[16] the use of THF, dioxane, and a mixed solvent of 2-ethoxyethanol-THF did not lead to high yields of propionitrile in a polymer system. It seems that the swelling ability of solvents might not play an important role in the selective formation of the nitrile in the present aqueous systems.

Recycling of the polymer-bound Rh cluster catalyst was examined in the deoxygenation of 1-nitropropane. After deoxygenation, a dark-green polymer was filtered, and was then reused for deoxygenation under the same conditions as in a former reaction. The results are shown in Table 9. Reused Rh com-

Table 8. Solvent Effect of Deoxygenation of 1-Nitropropane Using Polymer-Bound Rh Complex[a]

Solvent	Products yield/%			
	C_2H_5CN	C_3H_7OH	3-Hexanone	$(C_3H_7)_3N$
2-Ethoxyethanol	72	19	0	3
2-Ethoxyethanol[b]	53	9	0	5
2-Methoxyethanol	67	17	1	4
Ethylene glycol	56	25	4	3
THF/2-ethoxyethanol	56	28	1	3
Methanol	52	19	0	3
THF	27	29	1	0

a) Nitrobenzene 5 mmol, $Rh_6(CO)_{16}$ 0.05 mmol, H_2O 2.88 ml, polymer (**Ia**, 0.8 mg-atom of N), P_{CO}=16 atm, 40 °C, 48 h. b) H_2O 1.44 ml.

Table 9. Recycling of Polystyrene-Bound Rh Cluster Complex in Deoxygenation of 1-Nitropropane[a]

Reused number	Products yield/%			
	C_2H_5CN	C_3H_7OH	3-Hexanone	$(C_3H_7)_3N$
Fresh	72	19	0	3
1	57	20	6	2
2	53	14	9	2
3	54	28	9	1

a) Initial conditions were the same as in Table 8. In the recycling study, the polymer-bound Rh catalyst filtered under an atmosphere were used and other conditions were the same as in the fresh reaction.

plexes kept their catalytic activity to give propionitrile as the main product as well as a small amount of new 3-hexanone.[17] In separated experiments, the reaction of 1-nitropropane was interrupted after 5h. A colorless filtrate was separated from the resulting heterogeneous mixture under a CO atmosphere, which did not further show any catalytic activity for deoxygenation under the same conditions as in the above 1-nitropropane reaction. It can be said that deoxygenation proceeds on polymer-bound Rh complexes.

The deoxygenation of organic compounds with various N-O bonds in the presence of the diamino-substituted polymer (**Ia**) was carried out. The results for aromatic nitro compounds, aliphatic nitro compounds, and oximes appear together with the corresponding homogeneous compounds in Tables 3 and 4, respectively. The reactions of hydroxylamines and amine oxides are summarized in Table 6. In the deoxygenations of ortho-substituted nitrobenzenes, polymeric Rh catalyst systems showed extremely low catalytic activities (Table 3) since the approach of the substrates to active metal centers is strongly influenced by the steric hindrance of polymer surfaces. The heterogenization of soluble metal catalysts using organic polymers which leads to a decreasing of their catalytic activities has been reported in many polymer-bound metal catalysts.[18]

Reaction Mechanisms for Deoxygenations. Many of the reactions of aromatic nitro compounds using CO have been studied in the presence of various transition metal carbonyl complexes, e.g., $Fe_3(CO)_{12}$, $Ru_3(CO)_{12}$, and $Rh_6(CO)_{16}$.[2] The reaction products from nitrobenzenes were anilines, isocyanides, carbamates, and ureas. All of the above-mentioned metal-catalyzed reactions proceed via nitrene species as a common intermediate derived from the deoxygenation of nitrobenzene with CO. The characterization of various isolated metal nitrene complexes and their reactivities have been actively examined.[19] The μ_3-coordination mode in nitrene complexes is the most common in low-valent organometallics and the phenylnitrene bound to metal clusters reacts with CO and hydrogen to give phenyl isocyanate and aniline, respectively. In our combined catalyst system of $Rh_6(CO)_{16}$ and diamines, aniline would be formed via the nitrene intermediate, as shown in Scheme 3: a phenylnitrene bound to Rh carbonyl clusters reacts with hydrogens generated from the water gas shift reaction to give aniline or reacts with CO to give phenyl isocyanate, followed by hydrolysis to aniline.

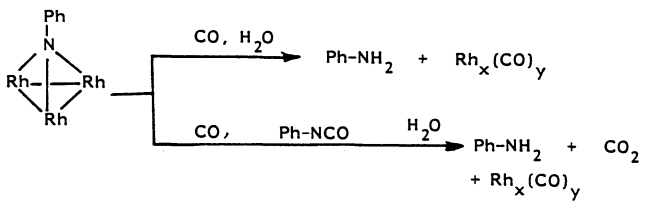

Scheme. 3. Formation of aniline via a nitrene intermeidate.

In the case of our Rh catalysts, primary aliphatic nitro compounds did not give amines but, rather, nitriles as the main product. As mentioned in a previous section, the deoxygenation of aliphatic nitro compounds affords oximes, which further react with CO to give nitriles with formations of H_2 and CO_2. One can image that the deoxygenation of oximes to nitriles is operated by a similar mechanism proposed for WGSR (Scheme 4);[20] a nucleophilic oxygen of oximes or H_2O attacks a carbonyl moiety on Rh clusters to form a metallocarboxyimine or metallocarboxylic acid intermediate, and their decarboxylation gives either nitrile and/or H_2, respectively. Since the reaction of an aldehyde *O*-methyloxime did not occur, oximes would be deprotonated by an amino moiety of additive bases to increase their nucleophilicity in the deoxygenation. The bonding mode of carbonyl moieties on Rh carbonyl clusters can be classified mainly into three types: terminal, edge-bridge, and face-bridge. A nucleophilic attack of oximes or H_2O might favor the terminal CO moiety because of the relatively weak back bonding of Rh metal to the

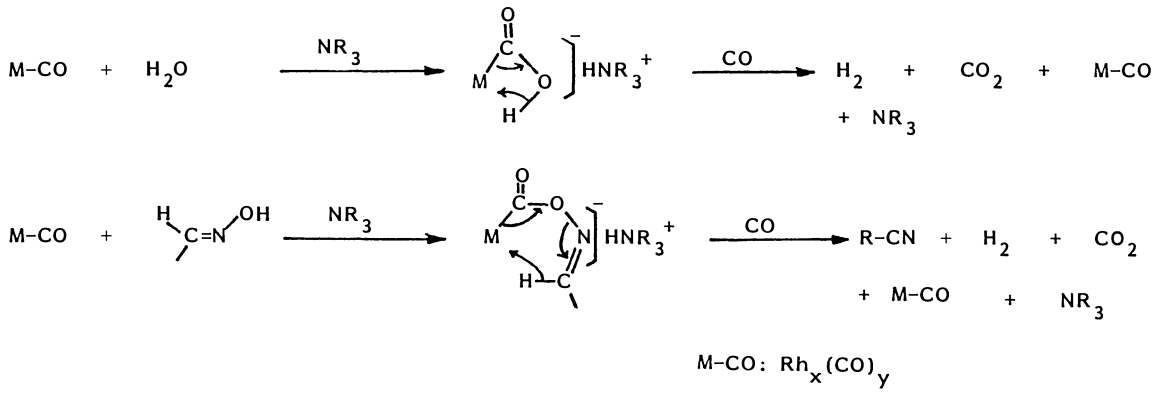

Scheme. 4. Mechanisms for the water gas shift reaction and deoxygenation of oximes.

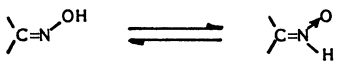

(8)

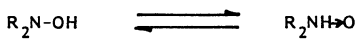

(9)

terminal CO.[21]

Next, the amine oxide forms can be thought as being the corresponding tautomers of oximes and hydroxylamines according to Eqs. 8 and 9, respectively. Recently, Basolo and co-workers have studied the mechanism for a stoichiometric deoxygenation of tertiary alkylamine N-oxides with $M_3(CO)_{12}$ (M= Fe,Ru,Os);[13] a nucleophilic oxygen of amine oxides attacks a carbonyl moiety on the metal clusters to give the corresponding amines and CO_2. Therefore, the amine oxide intermediates might also participate in the present deoxygenation of nitro compounds, oximes, and hydroxylamine using the present Rh cluster catalysts.

In the homogeneous deoxygenation of N-O bonds, e.g., aliphatic nitro compounds, oximes, hydroxylamines, and amine oxides at 40 °C, the reaction solutions had a dark-green color which changed instantly to dark brown upon exposure to air. In polymer systems (Ia), polymer-bound Rh complexes isolated from reaction mixtures were stable as dark-green powders in air for several hours.[22] The IR spectrum of the dark green powder showed the formation of $[Rh_6(CO)_{15}]^{2-}$ and $[Rh_6(CO)_{15}H]^-$ on the polymer.[23] Treatment of the Rh_6 species with aqueous KOH at room temperature gave the $[Rh_7(CO)_{16}]^{3-}$ anion. In Rh cluster chemistry, increasing the reaction temperatures tends to increase the cluster nuclearity.[24] Probably, the Rh_{14} species might be derived from a dimerization of the Rh_7 species during the nitrobenzene reaction.

Under WGSR conditions, hydridorhodium anions can be thought as being one of the important intermediates species which binds to ammonium ions to form an ion-pair complex (II) equilibrated with a dihydrido complex (III) , as shown in Eq. 10.[25] Additive bases having a strong coordinating ability, e.g. ethylenediamine, easily coordinate to Rh clusters to promote H_2 generation,[26] while additives with methyl groups on nitrogen atoms, e.g., TMPDA, can not greatly activate an intermediate species III, because of their weak coordination. Therefore, nitro compounds, oximes,

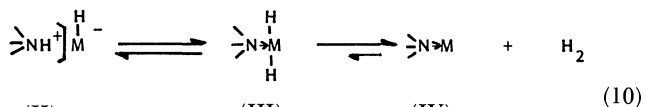

(II) (III) (IV) (10)

M=$[Rh_x(CO)_y]^{n-}$

hydroxylamimes, and amine oxides can react with the carbonyl moiety on both species of II and/or III to give deoxygenated products. Presumably, a nucleophilic oxygen attack of N-O bonds might favor the species of III over the II because the carbon atom of the CO moieties within the III species are more cationic than that of II. In the course of the deoxygenation of nitrobenzene using TMPDA or 4-(dimethylamino)-pyridine at 80 °C under 700 mmHg of CO, H_2 could not be detected and WGSR did not occur without adding nitrobenzene. Furthermore, using the catalyst system of $Rh_6(CO)_{16}$ and 4-(dimethylamino)-pyridine, only 6% nitrobenzene was reduced at 80 °C during 4 h under 700 mmHg of H_2. It can be said that deoxygenation occurs mainly not with molecular hydrogen, but with $CO+H_2O$ acting as the reducing agent.[27]

Conclusions

The catalyst system of $Rh_6(CO)_{16}$ *N,N,N′,N′*-tetramethy-1,3-propanediamine shows high activity for the deoxygenation of various N-O bonds, e.g., nitro compounds, oximes, hydroxylamines, and amine oxides in the presence of H_2O and CO. Notably, a formal dehydration of oximes to nitriles occurred selectively, even in aqueous media. The unique deoxygenation is due to the strong deoxygenating ability of the CO moiety within the Rh clusters. The Rh catalyst system can be heterogenized by using amino-substituted polystyrenes. The functions of the amines on the polymer are summarized as follows: 1) generation of OH^- in aqueous media to yield Rh-cluster anions, 2) stabilization and heterogenization of the Rh-cluster anions by forming ion-pairs, and 3) control for the reaction course through coordination of amines to Rh clusters. On the basis of the present study, we are now developing a new methodology of organic synthesis in aqueous media.

Experimental

$RhCl_3 \cdot 3H_2O$, $Fe(CO)_5$, $Mo(CO)_5$, $W(CO)_6$ were commercially available. $RhCl(PPh_3)_3$,[28] $Rh_2(CO)_4Cl_2$,[29] $Rh_4(CO)_{12}$,[30], $Rh_6(CO)_{16}$,[31] and $Ru_3(CO)_{12}$[32] were prepared by methods described in the literature. 3-Phenyl-1-nitropropane,[33] tripropylamine *N*-oxide,[34] *N,N*-dimethylaniline *N*-oxide,[35] all oximes,[36] propionaldehyde *O*-methyloxime,[37] and *N*-cyclohexylidenecyclohexylamine[38] were prepared according to published procedures. Other nitro compounds, hydroxylamines, and amine oxides were commercially available. All amines and pyridines used were also commercially available. Chloromethylated polystyrenes with M_w=7600, 8600, and 52700 were available from Toso Chemical Co. Elemental analyses were performed by Yanagimoto CHN-CORDER MT-III. The ^1H NMR spectra were recorded at 100 MHz with a Nihondenshi-JEO-JNM 4H-100 spectrometer. Infrared spectra were obtained with a Hitachi EPI-G spectrometer. Analytical GLPC was performed with a Shimadzu GC-3BT or a Shimadzu GC-8A

with a flame ionization detector,a linear temperature programe, and a Shimadzu CHROMATOPAC CR-3A integrator. The columns used were ASC-H, Apiezon L, and OV-17 for the analysis of liquid products.

Preparation of Amino-Substituted Polystyrenes. Typical examples for the title preparation are shown below. For route 1: bulk polymerization of *p*-(chloromethyl)styrene and divinylbenzenes (98/2, v/v) was carried out at 100 °C using AIBN, followed by amination with *N,N*-dimethyl-1,3-propanediamine in dioxane at room temperature. The MeOH treatment gave an amino-substituted polymer with N 8.7%. Chloromethylated polystyrenes (Toso) were aminated with *N,N*-dimethyl-1,3-propanediamine in dioxane at room temperature, which is a simiar method to that of Lieto:[39] N, 7.1% for M_w=7700; N, 9.0% for M_w=8600; N, 7.0% for M_w=52700. For route 2: reaction of *p*-(chloromethyl)styrene (Seimi Chemical) with *N,N*-dimethyl-1,3-propanediamine gave *N,N*-dimethyl-*N'*-(4-vinylphenylmethyl)-1,3-propanediamine which was identified by elemental analysis, IR, and NMR. ^{1}H NMR ($CDCl_3$) δ=1.5—1.9 (2H, m, CH_2), 2.16 (1H, s, NH), 2.20 (6H, s, $N(CH_3)_2$), 2.34 (2H, t, J=6.5 Hz, NCH_2), 2.68 (2H, t, J=6.5 Hz, NCH_2), 3.77 (2H, s, Ph-CH_2) 5.1—5.9 (2H, m, =CH_2), 6.4—7.0 (1H, m, HC=), and 7.3 (4H, s, phenyl). Bulk copolymerization of the amino-substituted styrene and divinylbenzene (98/2, v/v) was carried out at 100 °C using AIBN. After a MeOH treatment, the obtained polymer showed 11.4% of N. The above-mentioned procedures are described in the literature.[40,41] Polymers having other amino moieties (**Ib—Id**) were prepared only by the method of route 1. **Ib**; N, 7.4%, **Ic**; N, 6.6%, **Id**; N, 5.3%.

General Procedure of the Water Gas Shift Reaction. The reaction vessel was a 25 ml flask with a sidearm sealed with silicone rubber. It was attached to a closed reaction system (510 ml) with a reflux condenser, a gas circulator, and a vent. The Rh compound was placed in the vessel. The reaction system was evacuated and flushed three times with CO and then charged at room temperature to an initial CO pressure of 700 mmHg. Amine, H_2O, and 2-ethoxyethanol were added to the vessel. The solution was heated with stirring to 100 °C. The gas above the dark-brown solution was periodically sampled and analyzed by gas chromatography (3 m column of activated carbon).

General Procedure of Deoxygenation of Nitrobenzene under 700 mmHg of CO. The reaction apparatus was similar to that in the case of previous WGSR.[5] The Rh compound was placed in the vessel; the reaction system was then evacuated and flushed thee times with CO and charged at room temperature to an initial CO pressure of 700 mmHg. Nitrobenzene, 2-ethoxyethanol, amine, and H_2O were successively added to the vessel. The solution was heated with stirring to 80 °C. Both the gas and liquid phases were sampled periodically and analyzed by gas chromatography. The results are shown in Tables 1 and 2.

General Procedure of Homogeneous Deoxygenation of Nitro Compounds, Oximes, Hydorxylamines, and Amine Oxides under CO Pressure. A stainless-steel autoclave containing a Rh complex and an amine additive was evacuated and flushed three times with CO. A substrate, H_2O, and a solvent were added. The reaction was carried out with stirring under apropriate conditions (4—16 atm of CO). After the reaction, the liquid phase was analyzed by GLPC. The results are summarized in Tables 3, 4, 6, and 7.

General Procedure for the Heterogeneous Deoxygenation of Nitro Compounds, Oximes, Hydroxylamines, and Amine Oxides under CO Pressure. A method similar to the above-mentioned homogeneous reactions was used for the title heterogeneous reactions. Amino-substituted polymers (**I**) were used in place of the soluble amines. After the reaction, a polymeric Rh complex was separated by filtration. The filtrate was analyzed by GLPC and then distillated to give pure products. The Results are summarized in Tables 3, 4, 6, 7, 8, and 9. A typical isolation procedure was used for 3-phenyl-1-nitropropane. A mixture of 3-phenyl-1-nitropropane (1.65 g 10 mmol), $Rh_6(CO)_{16}$ (0.107 g, 0.10 mmol), and an amino-substituted polymer (1.6 mg-atm of N, 0.32g) in H_2O (5.76 g) and 2-ethoxyethanol (4 ml) was stirred at 40 °C under 16 atm of CO for 48 h. After the polymer-bound Rh complex was removed by filtration, the filtrate was extracted with diethyl ether. The ether layer was washed with an aqueous NaCl solution and then dried. Kugelrohr distillation afforded 0.97 g of pure nitrile (74%).

IR Measurement of Polymer-Bound Rh Complexes. After deoxygenations, polymer-bound Rh complexes were filtered and washed with 2-ethoxyethanol. The Rh complexes in KBr were measured by IR spectroscopy. All of the above-mentioned procedure were carried out under a CO atmosphere. In the deoxygenation of nitrobenzene at 80 °C under 4 atm of CO, isolated dark-brown powders showed the formation of the $[Rh_{14}(CO)_{25}]^{4-}$ species on the amino-substituted polymer (Ia). IR ν_{co} 1969, 1814 cm^{-1} for $[Rh_{14}(CO)_{25}]^{4-}$.[42] In the deoxygenations of the aliphatic nitro compounds, oximes, hydroxylamines, and amine oxides at 40 °C under 8—16 atm of CO, dark-green polymer showed formations of $[Rh_6(CO)_{15}]^{2-}$ and $[Rh_6(CO)_{15}H]^-$ species. IR ν_{co} 1989, 1960, 1765 cm^{-1} for $[Rh_6(CO)_{15}]^{2-}$;[43] 2063, 2019 cm^{-1} for $[Rh_6(CO)_{15}H]^-$.[42] A treatment of the Rh_6 species with KOH and HCl under a nitrogen atmosphere gave the $[Rh_7(CO)_{16}]^{3-}$ and $Rh_6(CO)_{16}$ species, respectively. IR ν_{co} 1951, 1763 cm^{-1} for $[Rh_7(CO)_{16}]^{3-}$.[43] The above-mentioned values due to the CO stretching frequencies were compatible with the corresponding homogeneous Rh cluster complexes.[42,43]

Reduction of *N*-Cyclohexylidenecyclohexylamine Using $Rh_6(CO)_{16}$ in the Presence of CO and H_2O. A stainless-steel autoclave of 300 ml containing $Rh_6(CO)_{16}$ (0.05 mmol) and *N,N,N',N'*-tetramethyl-1,3-propanediamine (2 ml) was evacuated and flushed three times with CO. The titile Schiff base (5 mmol), H_2O (2.8 g), and 2-ethoxyethanol (2 ml) were then added. The reaction was carried out with stirring under 8 atm of CO at 40 °C. After 5 h, the liquid phase was analyzed to give 83% of dicyclohexylamine by GLPC.

***N*-Alkylation of Amines with Ketones Using $Rh_6(CO)_{16}$ in the Presence of CO and H_2O.** The reaction of cyclohexylamine with cyclohexanone is typical. A stainless-steel autoclave (300 ml) containing a Rh complex (53 mg, 0.05 mmol) was evacuated and flushed three times with CO. Cyclohexylamine (0.496 g, 5 mmol), cyclohexanone (0.491 g, 5 mmol), H_2O (1.40 g), and 2-ethoxyethanol (2 ml) were then added. The reaction was carried out with stirring at 80 °C under 8 atm of CO. After 5 h, the resulting mixture was subjected to chromatography with Silica gel (Wakogel 200). Dicyclohexylamine of 0.72 g (80%) was isolated from hexane-dichloromethane elution. The results are shown in Table 5.

We would like to thank M. Hiraki and M. Doken for their technical assistances. One of the authors, K. Kaneda greatly acknowledges Dr. Martinengo for his helpful information concerning the characterization of Rh carbonyl clusters.

References

1) For reviews, see: a) E. L. Muettertes, T. N. Rhodin, E. Band, C. F. Brucker, and W. R. Pretzer, *Chem. Rev .*, **79**, 91 (1979). b) P. Chini, G. Longoni, and V. G. Albano, *Adv. Organomet. Chem.*, **14**, 285 (1976). c) "Chemistry of Metal Cluster," ed by S. Otsuka and H. Yamazaki, Gakukaisyuppansenta, Tokyo (1986). d) A. Fukuoka and M. Ichikawa, *Surface (Hyomen)*, **26**, 436 (1988).

2) Concerning deoxygenation of aromatic nitro compounds, aniline formation: a) A. F. M. Iqubal, *Tetrahedron Lett.*, **37**, 3385 (1971). b) K. Cann, C. W. Slegeir, and R. Pettit, *J. Am. Chem. Soc.*, **100**, 3969 (1978). c) R. C. Ryan, G. M. Wilemon, M. P. DalSanto, and C. U. Pittman, *J. Mol. Catal.*, **5**, 319 (1979). d) H. Alper and S. Amaratunga, *Tetrahedron Lett.*, **21**, 2603 (1980). e) T. Okano, K. Fujiwara, H. Konishi, and J. Kiji, *J. Bull. Chem. Soc. Jpn.*, **55**, 1975 (1982). Isocyanides, carbamates, and ureas formations: f) F. L'Eplattenier, P. Matthys, and F. Calderzzo, *Inorg. Chem.*, **9**, 342 (1970). g) H. des Abbayes and H. Alper, *J. Am. Chem. Soc.*, **99**, 98 (1977). h) H. Alper and K. E. Hashem, *J. Am. Chem. Soc.*, **103**, 6514 (1981). i) S. Cenini, M. Pizzotti, C. Crotti, F. Porta, and G. La Monica, *J. Chem. Soc., Chem. Commun.*, **1984**, 1286. For other reactions, see: j) P. C. Ford and A. Rokicki, *Adv. Organomet., Chem.*, **28**, 139 (1988); k) Y. Sugi, *Catalyst (Shokubai)*, **25**, 464 (1983) and references cited therein.

3) a) K. Kaneda, M. Hiraki, T. Imanaka, and S. Teranishi, *J. Mol. Catal.*, **12**, 385 (1981). b) K. Kaneda, M. Yasumura, T. Imanaka, and S. Teranishi, *J. Chem. Soc., Chem. Commun.*, **1982**, 93. c) K. Kaneda, M. Yasumura, T. Imanaka, and S. Teranishi, *Chem. Lett.*, **1981**, 1763. d) K. Kaneda, T. Imanaka, and S. Teranishi, *Chem. Lett.*, **1983**, 1465. e) K. Kaneda, M. Doken, and T. Imanaka, *Chem. Lett.*, **1988**, 285. f) K. Kaneda, T. Takemoto, and T. Imanaka, *Chem. Lett.*, **1988**, 1759.

4) Preliminary communications for this paper, see: Ref. 3a, 3e, and 3f.

5) K. Kaneda, M. Hiraki, K. Sano, T. Imanaka, and S. Teranishi, *J. Mol. Catal.*, **9**, 227 (1980).

6) M. Hudlicky, "Reductions in Organic Chemistry," Ellis Horwood, Chichestger (1984), p. 69.

7) Y. Shvo and D. Czarkie, *J. Organomet. Chem.*, **368**, 357 (1989).

8) R. A. Sanchez-Delgado and B. Alexis-Orgamas, *J. Mol. Catal.*, **36**, 283 (1986).

9) For typical reagents for nitrobenzene deoxygenation, see: a) Bu_3P-PhSSPh: D. H. R. Barton, W. B. Motherwell, E. S. Simon, and S. Z. Zard, *J. Chem. Soc., Perkin Trans. 1*, **1986**, 2243. b) PI_3: J. N. Denis and A. Krief, *J. Chem. Soc., Chem. Commun.*, **1980**, 544. c) Et_3N-SO_2, $(Me_2N)_3P$: G. A. Olah, Y. D. Vankar, and B. G. B. Gupta, *Synthesis*, **1979**, 36. d) PCl_3: P. A. Wehrli and S. Beatrice, *J. Org. Chem.*, **42**, 3956 (1977). e) PO_2Cl: *J. Skramstad, Acta Chem. Scand.*, **24**, 3424 (1970). f) $(C_2H_5O)_2POCl$: T. Mukaiyama and H. Nambu, *J. Org. Chem.*, **27**, 2201 (1962).

10) For typical reagents for oxime deoxygenation, see: a) Cl_3CCOCl: A. Saednya, *Synthesis*, **1983**, 748. b) TMSI: M. E. Jung and Z. Long-Mei, *Tetrahedron Lett.*, **24**, 4533 (1983). c) $(CH_3)_3N$-SO_2: G. A. Olah and Y. D. Vankar, *Synthesis*, **1978**, 702. d) SeO_2: G. Sosnovsky and J. A. Krogh, *Synthesis*, **1978**, 703.

11) Watanabe and co-wokers have reported that Rh compounds of $RhCl_3 \cdot 3H_2O$, $[Rh(cod)Cl]_2$ and $RhCl(PPh_3)_3$ catalyzed the N-alkylation of amines using 40 atm of CO at 180 °C: Y. Watanabe, M. Yamamoto, T. Mitsudo, and Y. Takegami, *Tetrahedron Lett.*, **15**, 1289 (1978).

12) For typical reagents for deoxygenation of hydroxylamines and amine oxides, see: a) NaH_2PO_2: S. K. Boyer, J. Bach, J. McKenna, and E. Jagdmann, Jr., *J. Org. Chem.*, **50**, 3408 (1985).
b) Ni-Al: G. Lunn and E. B. Sansone, *Synthesis*, **1985**, 1104. c) CH_3CO_2CHO: N. Tokitoh and R. Okazaki, *Chem. Lett.*, **1985**, 1517. d) Fe(TPP): N. Miyata, T. Santa, and M. Hirobe, *Chem. Pharm. Bull.*, **32**, 377 (1984). e) CS_2: Y. Yoshimura, K. Asada, and S. Oae, *Bull. Chem. Soc. Jpn.*, **55**, 3000 (1982). f) P_2I_4: H. Suzuki, N. Sato, and A. Osuka, *Chem. Lett.*, **1980**, 459. g) Mo(III): S. Polanc, B. Stanovnik, B., and M. Tisler, *Synthesis*, **1980**, 129. h) Bu_3SnH: S. Kozuka, T. Akasaka, and S. Furumai, *Chem. Ind.*, **1**, 452 (1974).

13) J.-K.Shen, Y.-L. Shi, Y.-C. Gao, Q.-Z. Shi, and F. Basolo, *J. Am. Chem.Soc.*, **110**, 2414 (1988), and references therein.

14) For a recent review, see: D. E. Bergbreiter, *CHEMTECH*, **6**, 686 (1987).

15) In hydroformylation of terminal olefins, phosphinated polystyrene-bound Rh catalysts favored linear aldehyde products over branched ones, compared with the corresponding homogeneous Rh catalysts within identical phosphine loading. The phenomenon has been also explained by "ligand concentration effect". C. U. Pittman and R. H. Hanes, *J. Am. Chem. Soc.*, **98**, 5402 (1976).

16) S. L. Regen, *J. Am. Chem. Soc.*, **91**, 3108 (1975).

17) A similar type product of ethyl methyl ketone was also observed in the nitroethane reaction. The mechanism of the ketone formation is under investigation.

18) Using soluble polymer-bound metal complexes could mimic catalysis of the conventional homogeneous complexes without a loss of catalytic activities in various organic reactions. See: Ref. 14.

19) For recent papers concerning the μ_3-type, see: a) J. A. Smieja and W. L. Gladfeelter, *Inorg. Chem.*, **25**, 2667 (1986). b) J. A. Smieja, J. E. Gozum, and W. L. Gladfelter, *Organometallics*, **5**, 2154 (1986). c) M. L. Blohm and E. L. Gladfelter, *Organometallics*, **5**, 1049 (1986). d) W. Bernhardt, W. Von Schenering, and H. Vahrenkamp, *Angew. Chem. Int. Ed. Engl.*, **25**, 279 (1986). e) G. D. Williams, R. R. Whittle, G. L. Geoffory, and A. L. Rheingold, *J. Am. Chem. Soc.*, **109**, 3936 (1987). f) S.-H. Hans, G. L. Geoffory, and A. L. Rheingold, *Inorg. Chem.*, **26**, 3426 (1987). g) E. J. Wucherer, M. Tasi, B. Hansert, A. K. Powell, M.-T. Garland, J-F. Halet, J.-Y. Saillard, and H. Vahren Kamp, *Inorg. Chem.*, **28**, 3564 (1989).

20) For mechanism of the WGSR, see: a) J. C. Bricker, C. C. Nagel, A. A. Bhattacharyya, and S. G. Shore, *J. Am. Chem. Soc.*, **107**, 377 (1985). b) B. H. Weiller, J.-P. Liu, and E. R. Grant, *J. Am. Chem. Soc.*, **107**, 1595 (1985).

21) K. Wade, "Transition Metal Clusters," ed by B. F. G. Johnson, John Wiley & Sons, Chichester (1980), p. 193.

22) As one of characteristic features of polymer-bound

metal complexes, use of polymer ligands can lead to facile isolation of metal species which are unstable in the corresponding homogeneous systems. For our work, see: K. Kaneda, T. Imanaka, and S. Teranishi, "Advances in Polyolefins," ed by R. B. Seymour and T. Cheng, Plenum, New York (1987), p. 203.

23) Examples for metal carbonyl cluster anions on polymers: a) A. T. Jurewicz, L. D. Rollman, and D. D. Whitehurst, *Adv. Chem. Ser.*, **132**, 240 (1974). b) T. Kitamura, T. Joh, and N. Hagihara, *Chem. Lett.*, **1975**, 203. c) Ref. 2c. d) H. Marakchi, J. B. Effa, M. Haimeur, J. Liato, and J. P. A. Aune, *J. Mol. Catal.*, **30**,101 (1985). e) S. Bhaduri and K. R. Sharma, *J. Chem. Soc., Dalton Trans.*, **1984**, 2309.

24) J. L. Vidal and R. C. Schoening, *J. Organomet. Chem.*, **241**, 395 (1983).

25) T. Cole, R. Ramage, K. Cann, and R. Pettit, *J. Am. Chem. Soc.*, **102**, 6182 (1980).

26) In the case of $Ru_3(CO)_{12}$, H_2 generation from hydrido species is a rate-limiting step. J. C. Bricker, C. C. Nagel, and S. G. Shore, *J. Am. Chem. Soc.*, **104**, 1444 (1982).

27) Using $Fe(CO)_5$ and $Rh_6(CO)_{16}$ catalysts, the aniline product contains about 90% deuterium incoporation at amino group in the presence of D_2O and H_2. See Refs. 2b and 2c, respectively.

28) J. A. Osborn and G. Wilkinson, *Inorg. Synth.*, **10**, 67 (1967).

29) J. A. McCleverty and G. Wilkinson, *Inorg. Synth.*, **8**, 211 (1966).

30) S. Martinengo, P. Chini, and G. Giordano, *J. Organomet. Chem.*, **27**, 389 (1971).

31) P. Chini and S. Martinengo, *Inorg. Chim. Acta*, **3**, 315 (1969).

32) J. L. Dawes and J. D. Holmes, *Inorg. Nucl. Chem. Lett.*, **7**, 847 (1971).

33) F. G. Bordwell and J. E. Bartmess, *J. Org. Chem.*, **40**, 1676 (1978).

34) J. T. Edward and J. Whiting, *Can. J. Chem.*, **49**, 3502 (1971).

35) D. W. Cunningham and M. O. Workman, *J. Inorg. Nucl. Chem.*, **33**, 3861 (1971).

36) H. Wieland, *Ber.*, **40**, 1676 (1907).

37) G. J. Karabatsos and N. Hsi, *Tetrahedron*, **23**, 1079 (1967).

38) K. N. Campbell, A. H. Sommers, and B. K. Campbell, *J. Am. Chem. Soc.*, **66**, 82 (1944).

39) J. Lieto, D. Milstein, R. L. Albright, J. V. Minkiewizcz, and B. C. Gates, *CHEMTECH*, **1983**, 46.

40) G. D. Jones, J. R. Runyon, and J. Ong, *J. Appl. Polym. Sci.*, **16**, 452 (1961).

41) S. Tanimoto, T. Miyake, and M. Okano, *Synth. Commun.*, **4**, 1938 (1974).

42) A personal communication from Dr. Martinengo.

43) P. Chini, S. Martinengo, and G. Giordano, *Gazz. Chim. Ital.*, **102**, 330 (1972).

44) M. Kotake, "Constants of Organic Compounds," Asakura Publishing, Tokyo (1963), p. 584.

Synthesis of α,ω-Diamino Acids via Amidocarbonylation Reaction: Novel Synthesis of Lysine, Ornithine, and Their Analogs

Yusuke AMINO and Kunisuke IZAWA*
Central Research Laboratories, Ajinomoto Co., Inc., 1-1, Suzuki-cho, Kawasaki-ku, Kawasaki 210
(Received September 18, 1990)

α,ω-Diamino acid derivatives, such as lysine and ornithine, were synthesized via amidocarbonylation (cobalt-catalyzed formation of *N*-acyl α-amino acid from aldehyde, amide and carbon monoxide) of ω-(phthalimido)alkanals in good yield. The phthalimido group was proved to be intact under the conditions of amidocarbonylation. The hydroformylation-amidocarbonylation of *N*-phthaloyl-β,γ- and *N*-phthaloyl-γ,δ-unsaturated amines proceeds very nicely to give α,ω-diamino acid derivatives with good selectivity. Selective deprotection of α-*N*-acyl-ω-*N*-phthaloyl α,ω-diamino acids was achieved using hydrazine for the *N*-phthaloyl group and aminoacylase for the *N*-acetyl group to afford the optically active α,ω-diamino acid, respectively.

The Cobalt-catalyzed amidocarbonylation (Eq. 1) discovered by Wakamatsu et al. in 1971 provides a versatile method for the synthesis of α-amino acids, including a variety of nonproteinogenic α-amino acids, from aldehyde, amide and carbon monoxide.[1] Since the reaction conditions of amidocarbonylation are almost the same as those of hydroformylation, except for the coexistence of an amide, it is possible to combine the two reactions. In fact, 2-acetamido-4-cyanobutyric acid (**2**) was synthesized from acrylonitrile (**1**) in one-pot reactions with high selectivity (Eq. 2).[2] Recently, Ojima et al. also reported that the extremely regioselective hydroformylation of trifluoropropene (**3**) was successfully combined with the amidocarbonylation to give *N*-acetyltrifluoronorvaline (**4**) with 96% selectivity (Eq. 3).[3]

As a continuation of our work directed toward the preparation of nonproteinogenic α-amino acid,[4] we intended to synthesize α,ω-diamino acids, such as lysine, ornithine and their analogs, via the amidocarbonylation of *N*-protected ω-aminoalkanals or the hydroformylation-amidocarbonylation of *N*-protected unsaturated amines.

Results and Discussion

Synthesis of Lysine, Ornithine, and Their Analogs. The choice of the *N*-protecting group was important to successfully achieve the preparation of α,ω-diamino acid derivatives from ω-aminoalkanals or unsaturated amines. We have revealed that the intramolecular amidocarbonylation of ω-(acylamino)alkanals takes place nicely to give *N*-acyl cyclic α-amino acids in good yield.[5] Furthermore, we have found that cobalt-catalyzed carbonylation of *N*-benzoylallylamine (**6**) affords 2-benzamidobutyric acid (**7**) and 3-benzamido-2-methylpropionic acid (**8**) as well as *N*-benzoylproline (**9**) (Eq. 4).[5] The formation of **7** and

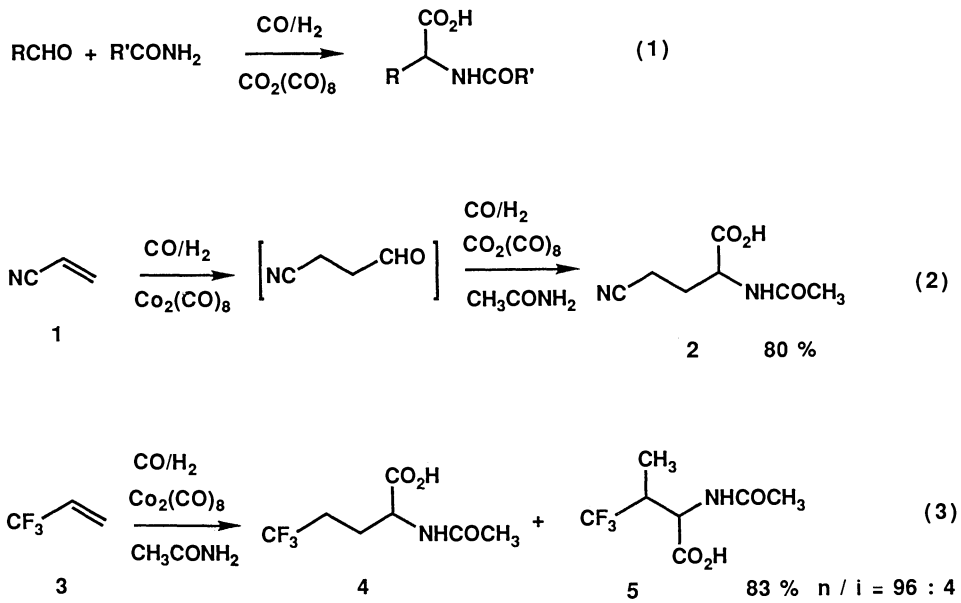

Scheme 1.

8 can be explained by the facile migration of the cobalt carbonyl moiety from the β- or γ-position to the α- or β-position of the amido group followed by CO insertion and subsequent hydrolysis.[6] Accordingly, the *N*-acyl group is inadequate as the protecting group of amino group for synthesizing the α,ω-diamino acid.

On the other hand, hydroformylation of *N*-phthaloylallylamine was previously studied by some groups,[7] in which such side reactions as migration or cyclization have not been observed. Moreover, Sato has reported that the hydroformylation of *N*-phthaloylallylamine (**10a**) took place regioselectively to give linear aldehyde, 4-phthalimidobutanal (**11a**) as the sole product.[7a] We therefore examined the synthesis of α,ω-diamino acid from ω-aminoalkanals by choosing the phthaloyl group as the N-protecting group. The results are given in equation 6.

It was thus found that the phthalimido group was intact under the conditions of amidocarbonylation and the derivatives of lysine (**13b**) and ornithine (**13a**) were obtained in moderate yield, regardless of the length of the alkyl chain and the kind of amide used.

Next, we examined the synthesis of α,ω-diamino acid derivatives from *N*-phthaloyl unsaturated amines (**10**) via hydroformylation followed by subsequent amidocarbonylation (Eq. 7). The results are shown in Table 1.

As Table 1 shows, the cobalt-catalyzed carbonylation of *N*-phthaloylallylamine (**10a**) in the presence of benzamide (initial pressure at 25 °C: CO, 65 atm; H_2, 60 atm) at 100 °C for 6 h gave α-*N*-benzoyl-δ-*N*-phthaloylornithine (**13a**) with more than 80% selectivity in 71% yield (Run 1). The reaction of the longer homolog, *N*-phthaloyl-3-butenylamine (**10b**) afforded α-*N*-acyl-ε-*N*-phthaloyllysine (**13b,c**) in similar yield (Runs 3 and 4). As shown in the previous cases, linear isomers were obtained in good selectivity, regardless of the length of the alkyl chaines and the kind of amide. The introduction of a substitution group at the 1- or 2-position of the allyl moiety of **10a** remarkably improved the selectivity (Runs 6 and 7) to give methyl substituted ornithine derivatives. Similarly, the reaction of methyl 2-phthalimido-4-pentenoate (*N*-phthaloylallylglycine methyl ester) gave the 2,6-diaminoheptandioic acid derivative with more than 95% selectivity (Run 5). As shown in the entries, since *N*-phthaloylallylamine derivatives did not give isomerization-carbonylation products, the difference in the phthalimido and acylamino groups in the cobalt-catalyzed carbonylation was revealed.

Sato exclusively obtained a linear aldehyde (**11a**) during the hydroformylation of *N*-phthaloylallylamine,[7a] whereas, in the hydroformylation-amidocarbonylation of the same substrate, we obtained a linear

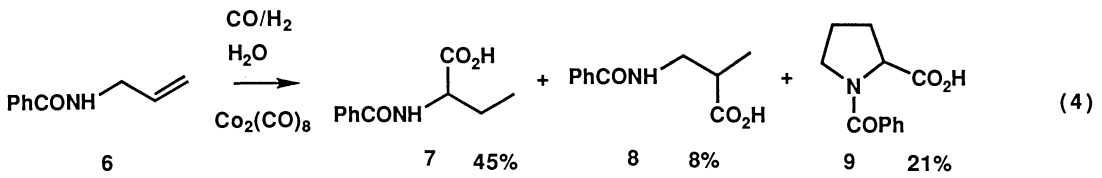

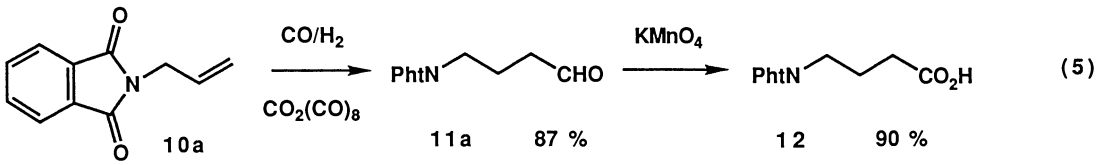

Scheme 2.

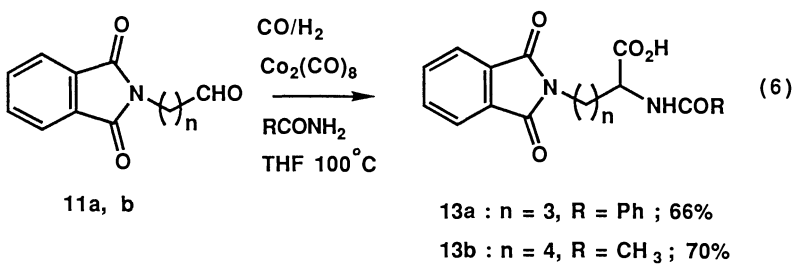

Scheme 3.

Table 1. Synthesis of α,ω-Diamino Acids

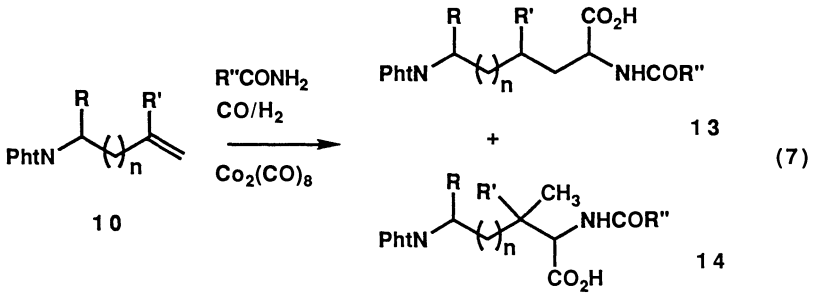

Run	10			Amide	Products	
	R	R′	n	R″	13 : 14[a]	Yield (13+14)[b]/%
1	H	H	0	Ph	5 : 1	71 (a)
2[c]	H	H	0	Ph	12 : 1	56 (a)
3	H	H	1	Ph	6 : 1	68 (c)
4	H	H	1	CH_3	5 : 1	76 (b)
5	CO_2CH_3	H	1	Ph	>20 : 1	66 (d)
6	H	CH_3	0	Ph	>100 : 1	24 (e)
7	CH_3	H	0	Ph	>20 : 1	63 (f)
8	CH_3	H	1	Ph	>10 : 1	60 (g)

a) Determined by ^{1}H NMR and/or GC-MS. b) Isolated yield after esterification with CH_2N_2.
c) Stepwise reaction; hydroformylation (100 °C, 3h), amidocarbonylation (100 °C, 3h).

Table 2. Synthesis of α,β-Diamino Acids

Run	Aldehyde **15** (yield/%)[a]	Product **16** (yield/%)[b]
1	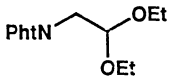	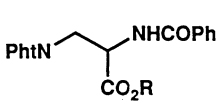 a; R=H (50) R=Et (8)
2	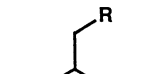 R=^{i}Pr (25)	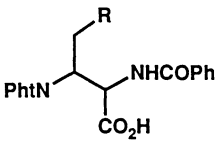 b; R=^{i}Pr (32)
3	R=Ph (35)	c; R=Ph (42)
4	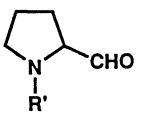 R′=CO_2Ph (70)	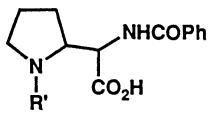 d; R′=CO_2Ph (30)
5[c]	R′=COPh (35)	e; R′=COPh (31)

a) Determined by ^{1}H NMR. Obtained by oxydation of alcohols with DMSO-SO_3·Py-Et_3N.
b) Isolated yield after esterification with CH_2N_2. c) *N*-Benzoyl-2-piperidinecarboxylic acid (20%) and α,ε-*N*,*N*′-dibenzoyllysine (3%) were also obtained.

(**13**) and branched (**14**) product (derived from a terminal and internal hydroformylated intermediate, respectively) in the ratio of *ca.* 5 : 1 (Run 1). We thought that the decrease in regioselectivity during the hydroformylation step should be attributed to the coexistence of the amide. To confirm our estimation, after the hydroformylation was almost completed acetamide was added and the reaction resumed (Run 2). The ratio of the linear and branched products was increased to 12 : 1. It is presumed that the property of the cobalt hydridocarbonyl catalyst or the solvent may be affected by the coexistence of the amide, which resulted in the decrease of the regioselectivity of hydroformylation. A similar result was previously observed in the hydroformylation-amidocarbonylation of isobutene.[6]

Since *N*-phthaloyl unsaturated amines (**10**) are easily obtained from the corresponding unsaturated alcohols or unsaturated amines, the hydroformylation-amidocarbonylation of **10** revealed a useful method for the synthesis of nonproteinogenic α-amino acid analogs of lysine and ornithine.

Synthesis of α,β-Diamino Acid Derivatives. We also examined the synthesis of α,β-diamino acid via

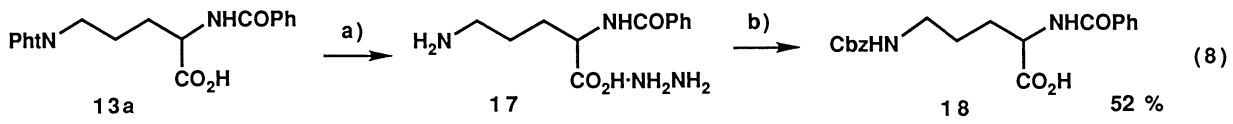

Reagents : a) 2eq NH_2NH_2, MeOH, Δ ; b) CbzCl, $NaHCO_3$, H_2O-ether.

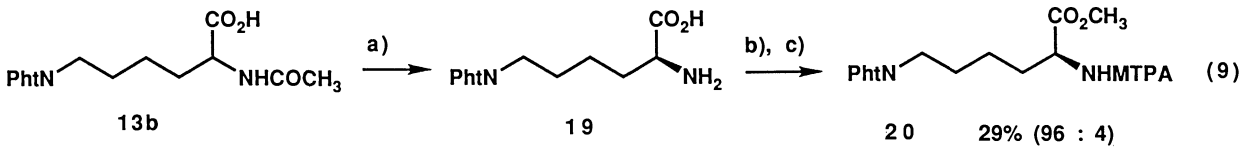

Reagents : a) acylase ; b) MTPACl, Na_2CO_3 ; c) CH_2CN_2.

Scheme 4.

amidocarbonylation starting from N-protected α-aminoalkanals (**15**), which are easily obtained from α-amino acids.[8] The preparation of β-functionalyzed α-amino acid via the amidocarbonylation of an α-functionalyzed aldehyde, such as 2-acetoxypropanal, has not yet been successful.[6] The results are shown in Table 2.

The yield of α,β-diamino acid derivatives (**16**) was not very satisfactory when compared with the α,ω-diamino acid derivatives (**13**). This low yield would be ascribed to the liability of the N-protected α-aminoalkanal (**15**) under the reaction conditions. Also, α-(phthalimido)alkanals, *N*-benzoyl- and *N*-benzyloxycarbonyl-2-pyrrolidinecarbaldehyde gave the corresponding α,β-diamino acid derivatives. However, except for the 2-pyrrolidinecarbaldehyde derivatives, the reactions of the *N*-benzoyl or *N*-benzyloxycarbonyl derivatives of acyclic α-aminoalkanal were unsuccessful. The choice of the protective group was also important to successfully achieve the preparation of α,β-diamino acid derivatives. Disappointingly, α,β-diamino acid derivatives were a diastereoisomeric mixture, in spite of the fact that optically active *N*-protected α-aminoalkanals were used; thus, the 1,2-asymmetric induction was not achieved in this process.

Selective Deprotection of α,ω-Diamino Acid Derivatives. The α,ω-diamino acid derivatives, thus obtained, should be very useful compounds, since the two amino groups are protected by different groups which can be selectively removed by conventional methods. Equation 8 shows the selective removal of the ω-phthaloyl group. The treatment of **13a** with hydrazine in methanol gave the α-*N*-benzoyl, ω-free diamino acid derivative (**17**), which was further transformed into α-*N*-benzoyl-ω-*N*-benzyloxycarbonyl-ornithine (**18**).

It is worth noting that an enantioselective hydrolysis of **13b** can be achieved by an enzyme (aminoacylase) to give ω-phthaloyl-L-lysine (**19**) in moderate yield, as shown in Eq. 9. Its optical purity proved to be more than 92% by ^1H NMR and HPLC studies after transformation to **20** by a treatment with Mosher's acid chloride, followed by esterification.

In conclusion, the synthesis of α,ω-diamino acid derivatives was achieved via the amidocarbonylation of the ω-(phthalimido)alkanals and the hydroformylation–amidocarbonylation of *N*-phthaloyl unsaturated amines. A new application of amidocarbonylation to the preparation of nonproteinogenic α-amino acid was represented.

Experimental

^1H NMR spectra were measured with a Varian XL 300 spectrometer and chemical shifts are given as δ ppm relative to tetramethylsilane (TMS) or sodium 3-trimethylsilylpropionate-2,2,3,3-d_4 (TPS) as an internal standard. Infrared (IR) spectra were recorded on a Hitachi 260-10 spcctrophotometer with samples as neat liquid or in KBr disks. Mass spectra (MS) were recorded with a JEOL DX-300 instrument by using the FAB technique. The melting points were determined with a Yanaco micro melting point apparatus and are uncorrected. GC–MS was performed on a HP 5890A-5970B with a high-performance capillary column (cross-linked methyl silicone). The thin-layer chromatographic system employed on silica gel (Merck Art. 7515). PTLC was performed with a Whatman PLK 5F. HPLC was performed on a GILSON 303 with a YMC-A312 (ODS 6×150 mm) column with a mobil phase composed of 70% MeOH-H_2O, at 25 °C. The elution rate was 0.5 ml min^{-1} and detection was carried out at ultraviolet (UV) 254 nm.

Amidocarbonylation of ω-(Phthalimido)alkanals (11). A typical procedure is described for the reaction of 4-phthalimidopentanal (**11b**) catalyzed by $Co_2(CO)_8$.

4-Phthalimidopentanal (**11b**) (1.28 g, 5.56 mmol), acetamide (328 mg, 5.56 mmol), and $Co_2(CO)_8$ (100 mg, 0.29 mmol)

were heated in a 100 ml stainless-steel autoclave with a 1 : 1 mixture of carbon monoxide and hydrogen (total pressure 120 atm, measured at room temperature) at 100 °C for 3.5 h. The autoclave was then cooled to ambient temperature and carbon monoxide and hydrogen purged out. After the solvent was removed under reduced pressure, the residue was dissolved in AcOEt (50 ml) and the insoluble material filtered off. The filtrate was extracted with 10% aqueous $NaHCO_3$ (50 ml) and the extract washed with AcOEt. Then, the aqueous phase was acidified with concentrated HCl and extracted with AcOEt (50 ml). The organic layer was washed with brine and dried over $MgSO_4$. After concentration, the residue was washed with hexane-AcOEt (1 : 1, v/v) to give α-*N*-acetyl-ε-*N*-phthaloyllysine (**13b**) as a solid (1.24 g, 3.90 mmol, 70.1%).

α-*N*-Acetyl-ε-*N*-phthalylolysine (13b): ^{1}H NMR (300 MHz, DMSO-d_6) δ=1.28—1.40 (2H, m, CH_2), 1.50—1.75 (4H, m, CH_2), 1.80 (3H, s, CH_3), 3.55 (2H, t, *J*=7.0 Hz, CH_2), 4.07—4.15 (1H, m, CH), 7.82—7.89 (4H, m, aromatic H), 8.05 (1H, d, *J*=7.6 Hz, NH); IR (KBr) 3300, 3050, 2940, 1770, 1700, 1645, 1540, 1395, 1370, 1295, 1155, 1050, 720 cm^{-1}; mp 170—172 °C (from hexane-AcOEt) ; High mass (FAB) *m/z* Calcd for $C_{16}H_{18}N_2O_5$+H: 319.1294. Found: 319.1301.

α-*N*-Benzoyl-δ-*N*-Phthaloylornithine (13a): ^{1}H NMR (300 MHz, DMSO-d_6) δ=1.60—1.85 (4H, m, CH_2), 3.62 (2H, t, *J*=5.9 Hz, CH_2), 4.35—4.45 (1H, m, CH), 7.43—7.57 (4H, m, aromatic H), 7.80—7.89 (5H, m, aromatic H), 8.57 (1H, d, *J*=7.7 Hz, NH); IR (KBr) 3350, 2940, 1780, 1710, 1645, 1520, 1400, 1050, 720 cm^{-1}; mp 190—193 °C (from hexane-AcOEt); High mass (FAB) *m/z* Calcd for $C_{20}H_{18}N_2O_5$+H: 367.1294. Found; 367.1294.

Hydroformylation-Amidocarbonylation of *N*-Phthaloyl Unsaturated Amines (10). A typical procedure is described for the reaction of *N*-phthalyl-3-butenylamine (**10b**) catalyzed by $Co_2(CO)_8$.

N-Phthalyl-3-butenylamine (**10b**) (1.0 g, 4.97 mmol), benzamide (602 mg, 4.97 mmol), and $Co_2(CO)_8$ (100 mg, 0.29 mmol) in THF (20 ml) were heated in a 100 ml stainless-steel autoclave with a 1 : 1 mixture of carbon monoxide and hydrogen (total pressure 120 atm, measured at room temperature) at 100 °C for 6 h. The autoclave was then cooled to ambient temperature and carbon monoxide and hydrogen purged out. After the solvent was removed under reduced pressure, the residue was dissolved in AcOEt (50 ml) and the insoluble material filtered off. The filtrate was extracted with 10% aqueous $NaHCO_3$ (50 ml) and the extract washed with AcOEt. The aqueous phase was acidified with concentrated HCl and then extracted with AcOEt (50 ml). The organic layer was washed with brine and dried over $MgSO_4$. After concentration, the residue was esterified with etherial CH_2N_2 to give α-*N*-benzoyl-ε-*N*-phthaloyllysine methyl ester (methyl ester of **13c**) (1.33 g, 3.36 mmol, 67.6%) as a solid.

α-*N*-Benzoly-ε-*N*-phthaloyllysine Methyl Ester (Methyl Ester of 13c): ^{1}H NMR (300 MHz, $CDCl_3$) δ=1.35—2.10 (6H, m, CH_2), 3.70 (2H, t, *J*=7.2 Hz, CH_2), 3.78 (3H, s, CH_3), 4.75—4.83 (1H, m, CH) , 6.75 (1H, d, *J*=7.2 Hz, NH), 7.40—7.55 (4H, m, aromatic H), 7.65—7.85 (5H, m, aromatic H), minor isomer 1.04 (1.5H, d, *J*=6.6 Hz, CH_3), 1.10 (1.5H, d, *J*=6.6 Hz, CH_3); IR (KBr) 3320, 2950, 1770, 1745, 1710, 1635, 1395, 1335, 1215, 1160, 720 cm^{-1}; GC-MS *m/z* 335 (M^+−59); mp 112—114 °C (from hexane-AcOEt); High mass (FAB) *m/z* Calcd for $C_{22}H_{22}N_2O_5$+H: 395.1607. Found; 395.1611.

α-*N*-Acetyl-ε-*N*-phthaloyllysine Methyl Ester (Methyl Ester of 13b): ^{1}H NMR (300 MHz, $CDCl_3$) δ=1.25—1.90 (6H, m, CH_2), 3.68 (2H, t, *J*=7.0 Hz, CH_2), 3.73 (3H, s, CH_3), 4.53—4.61 (1H, m, CH), 6.15 (1H, d, *J*=7.3 Hz, NH), 7.68—7.88 (4H, m, aromatic H), minor isomer 0.95 (1.5 H, d, *J*=6.8 Hz, CH_3), 1.02 (1.5 H, d, *J*=6.8 Hz, CH_3); IR (KBr) 3300, 3080, 2950, 2860, 1765, 1740, 1700, 1645, 1540, 1435, 1400, 1375, 1345, 1295, 1220, 1155, 1055, 720 cm^{-1}; GC-MS *m/z* 300 (M^+−18); 289 (M^+−29), 273 (M^+−45); mp 117—119 °C (from hexane-AcOEt); High mass (FAB) *m/z* Calcd for $C_{17}H_{20}N_2O_5$+H: 333.1451. Found 333.1445.

α-*N*-Benzoyl-δ-*N*-phthaloylornithine Methyl Ester (Methyl Ester of 13a): ^{1}H NMR (300 MHz, $CDCl_3$) δ=1.70—2.05 (4H, m, CH_2), 3.72 (2H, br. t, *J*=6.6 Hz, CH_2), 3.76 (3H, s, CH_3), 4.83—4.90 (1H, m, CH), 6.75 (1H, d, *J*=7.8 Hz, NH), 7.40—7.55 (4H, m, aromatic H), 7.65—7.90 (5H, m, aromatic H), minor isomer 0.98 (1.5 H, d, *J*=6.9 Hz, CH_3), 1.13 (1.5H, d, *J*=6.9 Hz, CH_3); IR (neat) 2950, 1770, 1740, 1700, 1650, 1520, 1440, 1395, 1210, 1040 cm^{-1}; GC-MS *m/z* 321 (M^+−59); High mass (FAB) *m/z* Calcd for $C_{21}H_{20}N_2O_5$+H: 381.1451. Found: 381.1434.

Dimethyl 2-Benzamido-6-phthalimidoheptandioate (Methyl Ester of 13d): ^{1}H NMR (300 MHz, $CDCl_3$) δ=1.30—2.35 (6H, m, CH_2), 3.72 (6H, s, CH_3), 4.70—4.90 (2H, m, CH), 6.64 (1H, br. t, *J*=7.0 Hz, NH), 7.35—7.55 (4H, m, aromatic H), 7.70—7.85 (5H, m, aromatic H); IR (neat) 2950, 1770, 1740, 1710, 1640, 1520, 1430, 1380, 1240 cm^{-1}; GC-MS *m/z* 393 (M^+−59); High mass (FAB) *m/z* Calcd for $C_{24}H_{24}N_2O_7$+H: 453.1662. Found: 453.1636.

α-*N*-Benzoyl-ε-methyl-ε-*N*-phthaloyllysine Methyl Ester (Methyl Ester of 13g): ^{1}H NMR (300 MHz, $CDCl_3$) δ=1.46 (1.5 H, d, *J*=6.8 Hz, CH_3), 147 (1.5 H, d, *J*=6.9 Hz, CH_3), 1.69—2.20 (6H, m, CH_2), 3.70 (1.5H, s, CH_3), 3.71 (1.5H, s, CH_3), 4.38—4.40 (1H, m, CH), 4.70—4.80 (1H, m, CH), 6.65 (1H, br.s, NH), 7.35—7.55 (4H, m, aromatic H), 7.63—7.85 (5H, m, aromatic H); IR (neat) 2950, 2860, 1770, 1740, 1710, 1360, 1325, 1210, 1160, 1040 cm^{-1}; GC-MS *m/z* 408 (M^+), 373 (M^+−32), 349 (M^+−59); High mass (FAB) *m/z* Calcd for $C_{23}H_{24}N_2O_5$+H: 409.1763. Found: 409.1781.

α-*N*-Benzoyl-δ-methyl-δ-*N*-phthaloylornithine Methyl Ester (Methyl Ester of 13f): ^{1}H NMR (300 MHz, $CDCl_3$) δ=1.46 (1.5H, d, *J*=6.8 Hz, CH_3), 1.47 (1.5H, d, *J*=6.8 Hz, CH_3), 1.80—1.91 (2H, m, CH_2), 2.14—2.35 (2H, m, CH_2), 3.73 (1.5H, s, CH_3), 3.77 (1.5H, s, CH_3), 4.30—4.42 (1H, m, CH), 4.78—4.88 (1H, m, CH), 6.70 (0.5H, d, *J*=7.7 Hz, NH), 6.76 (0.5H, d, *J*=7.5 Hz, NH), 7.40—7.55 (4H, m, aromatic H), 7.68—7.85 (5H, m, aromatic H); IR (KBr) 3320, 2950, 1770, 1740, 1695, 1630, 1520, 1385, 1360, 1200, 1050, 720 cm^{-1}; GC-MS *m/z*: 394 (M^+), 362 (M^+−32), 335 (M^+−59); mp 120—124 °C (from hexane-AcOEt); High mass (FAB) *m/z* Calcd for $C_{22}H_{22}N_2O_5$+H: 395.1607. Found: 395.1594.

α-*N*-Benzoyl-γ-methyl-δ-*N*-phthaloylornithine Methyl Ester (Methyl Ester of 13e): ^{1}H NMR (300 MHz, $CDCl_3$) δ=1.05 (3H, d, *J*=6.8 Hz, CH_3), 1.70—1.90 (2H, m, CH_2), 2.12—2.25 (1H, m, CH) , 3.58—3.67 (2H, m, CH_2), 3.74 (1.5H, s, CH_3), 3.75 (1.5H, s, CH_3), 4.87—4.95 (1H, m, CH), 6.80 (1H, br.s, NH), 7.18 (1H, br.s, NH), 7.35—7.55 (4H, m, aromatic H), 7.65—7.90 (5H, m, aromatic H); IR (neat) 3060, 2950, 1770, 1740, 1710, 1650, 1530, 1440, 1400, 1360, 1210, 1050 cm^{-1}; GC-MS *m/z* 394 (M^+), 362 (M^+−32), 335 (M^+−59); High mass (FAB) *m/z* Calcd for $C_{22}H_{22}N_2O_5$+H: 395.1607. Found 395.1604.

Amidocarbonylation of *N*-Protected α-Aminoalkanal

Derivatives (15). A typical procedure is described for the reaction of *N*-(2,2-diethoxyethyl)phthalimido (**15a**) catalyzed by $Co_2(CO)_8$.

N-(2,2-Diethoxyethyl)phthalimido (**15a**) (1.0 g, 3.8 mmol), benzamide (460 mg, 3.8 mmol), and $Co_2(CO)_8$ (100 mg, 0.29 mmol) in THF (20 ml) were heated in a 100 ml stainless-steel autoclave with a 1:1 mixture of carbon monoxide and hydrogen (total pressure 120 atm, measured at room temperature) at 100 °C for 6 h. The autoclave was then cooled to ambient temperature and carbon monoxide and hydrogen were purged out. After the solvent was removed under reduced pressure, the residue was dissolved in AcOEt (50 ml) and the insoluble material filtered off. The filtrate was washed with 10% aqueous $NaHCO_3$ (50 ml) and brine. The organic phase was dried over $MgSO_4$. The solvent was removed under reduced pressure and the residue purified by PTLC (hexane:AcOEt=3;5, v/v) to give ethyl 2-benzamido-3-phthalimidopropionate (ethyl ester of **16a**) (113 mg, 0.31 mmol, 8.1%) as an oil. The aqueous $NaHCO_3$ extract was acidified with concentrated HCl and extracted with AcOEt (50 ml). The organic layer was washed with brine and dried over $MgSO_4$. After concentration, the residue was esterified with etherial CH_2N_2 and purified by PTLC (hexane:AcOEt=3:5, v/v) to give methyl 2-benzamido-3-phthalimidopropionate (meihyl ester of **16a**) (662 mg, 1.88 mmol, 49.5%) as a solid.

Methyl 2-Benzamido-3-phthalimidopropionate (Methyl Ester of 16a): ^{1}H NMR (300 MHz, $CDCl_3$) δ=3.81 (3H, s, CH_3), 4.20—4.30 (2H, m, CH_2), 5.00—5.10 (1H, m, CH), 7.32 (1H, br.d, J=6.7 Hz, NH), 7.40—7.55 (4H, m, aromatic H), 7.70-7.90 (5H, m, aromatic H); IR (KBr) 3300, 2950, 1770, 1710, 1640, 1525, 1425, 1390, 1320, 1215, 1020, 900, 720 cm^{-1}; GC-MS m/z 293 (M^+−59); mp 123—125 °C (from hexane-AcOEt); High mass (FAB) m/z Calcd for $C_{19}H_{16}N_2O_5$+H: 353.1137. Found: 353.1138.

Ethyl 2-Benzamido-3-phthalimidopropionate (Ethyl Ester of 16a): ^{1}H NMR (300 MHz, $CDCl_3$) δ=1.30 (3H, t, J=6.8 Hz, CH_3), 4.15—4.30 (4H, m, CH_2), 5.00—5.08 (1H, m, CH), 7.30 (1H, br.d, J=6.7 Hz, NH), 7.40—7.55 (4H, m, aromatic H), 7.70—7.90 (5H, m, aromatic H); IR (neat) 3320, 2950, 1765, 1710, 1640, 1525, 1390, 1020 cm^{-1}; GC-MS m/z 293 (M^+−73).

Methyl 2-Benzamido-5-methyl-3-phthalimidohexanoate (Methyl Eester of 16b): ^{1}H NMR (300 MHz, $CDCl_3$) δ= 0.89—0.96 (6H, m, CH_3), 1.63—1.70 (2H, m, CH_2), 2.13—2.23 (0.5H, m, CH), 2.63 (0.5H, td, J=11.7 and 1.8 Hz, CH), 3.66 (1.5H, s, CH_3), 3.79 (1.5H, s, CH_3), 4.80—4.92 (0.5H, m, CH), 5.03—5.12 (1H, m, CH), 5.20 (0.5H, dd, J=8.6 and 4.8 Hz, CH), 7.11 (0.5H, d, J=7.5 Hz, NH), 7.41—7.56 (3H, m, aromatic H), 7.72—7.89 (5H, m, aromatic H), 7.97—8.00 (1H, m ,aromatic H), 8.39 (0.5H, d, J=8.6 Hz, NH); IR (neat) 2950, 1770, 1740, 1705, 1660, 1520, 1360, 1210, 1160, 1065 cm^{-1}; GC-MS m/z 377 (M^+−31), 349 (M^+−59); High mass (FAB) m/z Calcd for $C_{23}H_{24}N_2O_5$+H: 409.1763. Found: 409.1739.

Methyl 2-Benzamido-4-phenyl-3-phthalimidobutyrate (Methyl Ester of 16c): ^{1}H NMR (300 MHz, $CDCl_3$) δ=3.21—3.47 (2H, m, CH_2), 3.64 (1.5H, s, CH_3), 3.81 (1.5H, s, CH_3), 5.12 (0.5H, quint, J=5.4 Hz, CH), 5.20—5.29 (1.5H, m, CH), 7.10—7.20 (6H, m, NH and aromatic H), 7.40—7.58 (3H, m, aromatic H), 7.67—7.83 (5H, m, aromatic H), 8.03—8.06 (1H, m, aromatic H), 8.53 (0.5H, d, J=8.3 Hz, NH); IR (neat) 3030, 2950, 1775, 1740, 1710, 1660, 1520, 1485, 1385, 1360, 1210 cm^{-1}; GC-MS m/z 411 (M^+−31), 383 (M^+−59); High mass (FAB) m/z Calcd for $C_{26}H_{22}N_2O_5$+H: 443.1607. Found: 443.1592.

Methyl 2-Benzamido-2-(*N*-benzoylpyrrolidine-2-yl)ethanoate (Methyl Ester of 16e): ^{1}H NMR (300 MHz, $CDCl_3$) δ= 1.40—2.28 (3H, m, CH_2), 2.32—2.45 (1H, m, CH_2), 3.35—3.60 (2H, m, CH_2), 3.78 (1.5H, s, CH_3), 3.83 (1.5H, s, CH_3), 4.25 (0.5H, d, J=5.0 Hz, CH), 4.59—5.05 (1.5H, m, CH), 7.35—7.65 (6H, m, aromatic H), 7.70—7.98 (4H, m, aromatic H), 8.20 (0.5H, d, J=5.6 Hz, NH), 9.16 (0.5 H, d, J=7.9 Hz, NH); IR (neat) 3055, 2950, 1735, 1650, 1575, 1520, 1480, 1415, 1205 cm^{-1}; GC-MS m/z 335 (M^+−31), 307, (M^+−59); High mass (FAB) m/z Calcd for $C_{21}H_{22}N_2O_4$+H: 367.1658. Found: 367.1635.

***α,ε-N,N′*-Dibenzoyllysine Methyl Ester:** ^{1}H NMR (300 MHz, $CDCl_3$) δ=1.38—2.05 (8H, m, CH_2), 3.38—3.52 (2H, m, CH_2), 3.76 (3H, s, CH_3), 4.75—4.85 (1H, m, CH), 6.55 (1H, br.s, NH), 7.00 (1H, d, J=7.3 Hz, NH), 7.30—7.55 (6H, m, aromatic H), 7.70—7.88 (4H, m, aromatic H); IR (neat) 3070, 2950, 1753, 1640, 1535, 1490, 1440, 1310, 1210 cm^{-1}; GC-MS m/z 368 (M^+), 336 (M^+−32), 309 (M^+−59).

Methyl *N*-Benzoyl-2-piperidinecarboxylate: ^{1}H NMR (300 MHz, $CDCl_3$) δ=1.35—1.85 (4H, m, CH_2), 2.20 (0.5H, br.d, CH_2), 2.35 (1H, br.d, CH_2), 2.85 (0.5H, m,CH_2), 3.25 (1H, br.t, CH_2), 3.65 (1H, br.d, CH_2), 3.78 (3H, br.s, CH_3), 4.45—4.70 (0.5H, m, CH), 5.50 (0.5H, br.s, CH), 7.40 (5H, br.s, aromatic H); IR (neat) 2950, 2860, 1740, 1640, 1420, 1280, 1210 cm^{-1}; GC-MS m/z 247 (M^+); High mass (FAB) m/z Calcd for $C_{14}H_{17}N_1O_3$+H: 248.1287. Found 248.1278.

Methyl 2-Benzamido-2-(*N*-benzyloxycarbonylpyrrolidine-2-yl)ethanoate, (Methyl Ester of 16d): ^{1}H NMR (300 MHz, $CDCl_3$) δ=1.70—2.10 (3H, m, CH_2), 2.20—2.30 (1H, m, CH_2), 3.25—3.65 (2H, m, CH_2), 3.67 (1.5H, s, CH_3), 3.78 (1.5H, s, CH_3), 4.25—4.55 (1.5H, m, CH), 4.84 (0.5H, dd, J=7.5 and 2.4 Hz, CH), 5.07—5.22 (2H, m, CH_2), 7.20—7.55 (8H, m, aromatic H), 7.80—7.95 (2H, m, aromatic H), 8.24 (0.5H, br.d, J=4.2 Hz, NH), 8.84 (0.5H, d, J=7.2 Hz, NH); IR (neat) 2945, 1753, 1690, 1655, 1520, 1480, 1405, 1350, 1330, 1200, 1100 cm^{-1}; GC-MS m/z 365 (M^+−31), 204 (M^+−192); High mass (FAB) m/z Calcd for $C_{22}H_{24}N_2O_5$+H: 397.1763. Found 397.1766.

Deprotection of ω-*N*-Phthaloyl Group. α-*N*-Benzoyl-δ-*N*-phthaloylornithine (**13a**) (500 mg, 1.42 mmol) and hydrazine monohydrate (2.84 mmol) in MeOH (10 ml) were heated at 80 °C for 1 h. The solvent was removed under reduced pressure. The residue was dissolved in aqueous HCl and an insoluble material was filtered off. The filtrate was concentrated under reduced pressure and washed with AcOEt to give α-*N*-benzoylornithine hydrazine salt (**17**) (319 mg, 1.19 mmol, 83.8%) as a solid.

α-*N*-Benzoylornithine Hydrazine Salt (17): ^{1}H NMR (300 MHz, $CDCl_3$) δ=1.75—2.08 (4H, m,CH_2), 3.07 (2H, t, J=7.5 Hz, CH_2), 4.43 (1H, dd, J=8.0 and 5.2 Hz, CH), 7.50—7.70 (3H, m, aromatic H), 7.78—7.84 (2H, m, aromatic H); IR (KBr) 3345, 2950, 1635, 1600, 1530, 1400, 1365, 1300 cm^{-1}; mp 226—228 °C (from H_2O-MeOH); High mass (FAB) m/z Calcd for $C_{12}H_{16}N_2O_3$+H: 237.1239. Found: 237.1257.

α-*N*-Benzoylornithine hydrazine salt (**17**) (319 mg), $NaHCO_3$ (706 mg, 8.4 mmol), and benzyloxycarbonyl chrolide (toluene solution, 4.2 mmol) in H_2O (15 ml) and ether (10 ml) were stirred at room temperature for 15 h. The reaction mixture was washed with ether and acidified with concentrated HCl. The solution was extracted with AcOEt and the extract washed with brine, then dried over $MgSO_4$. After concentration, the residue was washed with hexane-

AcOEt to give α-*N*-benzoyl-δ-*N*-benzyloxycarbonylornithine (**18**) (275 mg, 0.74 mmol, 52.2%) as a solid.

α-*N*-Benzoyl-δ-*N*-benzyloxycarbonylornithine (18): ^{1}H NMR (300 MHz, DMSO-d_6) δ=1.45—1.60 (2H, m, CH_2), 1.70—1.90 (2H, m, CH_2), 2.98—3.07 (2H, m, CH_2), 4.30—4.40 (1H, m, CH), 5.00 (2H, s, CH_2), 7.20—7.58 (8H, m, aromatic H), 7.85—7.92 (2H, m, aromatic H), 8.57 (1H, d, *J*=8.1 Hz, NH); IR (KBr) 3310, 2940, 1700, 1680, 1630, 1530, 1250 cm^{-1}; mp 133—135 °C (from hexane-AcOEt); High mass (FAB) *m/z* Calcd for $C_{20}H_{22}N_2O_5$+H: 371.1607. Found: 371.1625.

Deprotection of α-*N*-Acetyl Group. A solution of α-*N*-acetyl-ε-*N*-phthaloyllysine (**13b**) (300 mg, 0.90 mmol), $CoCl_2$ (3.9 mg, 0.003 mmol), and aminoacylase (19800 u g^{-1}, 60 mg) in H_2O (30 ml) was adjusted to pH 7.0. The solution was shaken at 38 °C for 4 d. The solution was concentrated under reduced pressure. The residue was dissolved in H_2O (5 ml) and acetone (5 ml). To the solution, 1 equiv $NaHCO_3$ (2 ml) and (−)-MTPACl (methoxytrifluoromethylphenylacetyl chloride) (228 mg, 0.90 mmol) were added at 0 °C; the solution was then stirred at room temperature for 1 h. The solution was acidified with concentrated HCl and extracted with AcOEt (20 ml). The extract was washed with brine and dried over $MgSO_4$. After concentration, the residue was esterified with etherial CH_2N_2 and purified by PTLC (hexane : AcOEt=2 : 1, v/v) to give α-*N*-MTPA-ε-*N*-phthaloyl-L-lysine methyl ester (**20a**) (132 mg, 0.26 mmol, 28.9%, 92%de) as an oil.

Authentic samples of α-*N*-(−)- and -(+)-MTPA-ε-*N*-phthaloyl-L-lysine methyl ester (**20a**, **b**) were prepared starting from α-*N*-benzyloxycarbonyl-L-lysine.

ε-*N*-Phthaloyl-L-lysine (19): ^{1}H NMR (300 MHz, D_2O) δ=1.38—1.50 (2H, m, CH_2), 1.65—1.75 (2H, m, CH_2), 1.85—1.95 (2H, m, CH_2), 3.67 (2H, t, *J*=6.9 Hz, CH_2), 3.73 (1H, t, *J*=6.0 Hz, CH), (4H, m, aromatic H), 7.82 (4H, s, aromatic H); IR (KBr) 2940, 1770, 1710, 1700, 1575, 1500, 1400 cm^{-1}; mp 232—233 °C (from H_2O-MeOH); High mass (FAB) *m/z* Calcd for $C_{14}H_{16}N_2O_4$+H: 277.1188. Found: 277.1180.

α-*N*-(−)-Methoxytrifluoromethylphenylacetyl-ε-*N*-phthaloyl-L-lysine Methyl Ester (20a): ^{1}H NMR (300 MHz, $CDCl_3$) δ=1.17—1.30 (2H, m, CH_2), 1.58—1.98 (4H, m, CH_2), 3.54—3.56 (3H, m, CH_3), 3.60 (2H, t, *J*=7.3 Hz, CH_2), 3.76 (3H, s, CH_3), 4.65 (1H, td, *J*=8.2 and 5.0 Hz, CH), 7.08 (1H, d, *J*=8.1 Hz, NH), 7.35—7.74 (3H, m, aromatic H), 7.50—7.56 (2H, m, aromatic H), 7.70—7.74 (2H, m, aromatic H), 7.80—7.84 (2H, m, aromatic H); IR (neat) 3350, 2950, 2850, 1770, 1740, 1710, 1610, 1510, 1440, 1395, 1360, 1265 cm^{-1}; High mass (FAB) *m/z* Calcd for $C_{25}H_{25}N_2O_6F_3$+H: 507.1743. Found: 507.1732.

α-*N*-(+)-Methoxytrifluoromethylphenylacetyl-ε-*N*-phthaloyl-L-lysine Methyl Ester (20b): ^{1}H NMR (300 MHz, $CDCl_3$) δ=1.35—1.50 (2H, m, CH_2), 1.62—2.05 (2H, m, CH_2), 3.35—3.38 (3H, m, CH_3), 3.69 (2H, t, *J*=7.1 Hz, CH_2), 3.74 (3H, s, CH_3), 4.61 (1H, td, *J*=8.3 and 5.1 Hz, CH), 7.35—7.43 (4H, m, NH and aromatic H), 7.50—7.58 (2H, m, aromatic H), 7.70—7.74 (2H, m, aromatic H), 7.76—7.83 (2H, m, aromatic H).

References

1) H. Wakamatsu, J. Uda, and N. Yamakami, *J. Chem. Soc., Chem. Commun.*, **1971**, 1540.

2) T. Yukawa, Ph. D. Thesis, Osaka Uiversity, Osaka Japan, 1973.

3) I. Ojima, K. Hirai, M. Fujita, and T. Fuchikami, *J. Organomet. Chem.*, **279**, 203 (1985).

4) a) S. Asada, H. Izawa, T. Ineyama, and K. Izawa, 35th Symposium on Organometallic Chemistry, Osaka, Japan, Nov. 1988, Abstr., B120. b) H. Izawa and K. Izawa, 36th Symposium on Organometallic Chemistry, Tokyo, Japan, Sept. 1989, Abstr., B106.

5) S. Nishi, S. Asada, and K. Izawa, 31th Symposium on Organometallic Chemistry, Tsukuba, Japan, Oct. 1984, Abstr., B202.

6) K. Izawa, *J. Synth. Org. Chem., Jpn.*, **46**, 218 (1988).

7) a) S. Sato, *Nippon Kagaku Zasshi*, **90**, 404 (1969). b) G. Delogu, G. Fedda, and S. Gladiali, *J. Organomet. Chem.*, **268**, 167 (1984).

8) J. Jurczak and A. Golebiowski, *Chem. Rev.*, **89**, 149 (1989).

Synthesis of Proline and 2-Piperidinecarboxylic Acid via Cobalt-Catalyzed Isomerization-Carbonylation of *N*-Acyl Unsaturated Cyclic Amines

Yusuke Amino, Seiichi Nishi, and Kunisuke Izawa*
Central Research Laboratories, Ajinomoto Co., Inc., 1-1, Suzuki-cho, Kawasaki-ku, Kawasaki 210
(Received September 18, 1990)

N-Acyl derivatives of proline and 2-piperidinecarboxylic acid (pipecolic acid) were synthesized in moderate yield from *N*-acyl unsaturated cyclic amines through cobalt-catalyzed isomerization-carboxylation under hydroformylation conditions in the presence of H_2O. A possible mechanism for the process is discussed which is related to that of the amidocarbonylation (cobalt-catalyzed formation of *N*-acyl α-amino acid from aldehyde, amide and carbon monoxide).

The cobalt-catalyzed formation of amido carboxylic acid (tentatively designated as amidocarbonylation hereafter) has been developed by Wakamatsu et al. as a useful method for the synthesis of *N*-acyl α-amino acid from aldehyde, amide and carbon monoxide (Eq. 1).[1] The remarkable features of the reaction are its highly regioselective α-carbonylation and hydrolysis, rather than the hydrogenolysis of the acyl complex under hydroformylation conditions.

On the other hand, Sato has reported that *N*-acetylallylamine (**1a**) uniquely reacts with carbon monoxide to give 2-acetamidobutyric acid (**2a**) in 29%

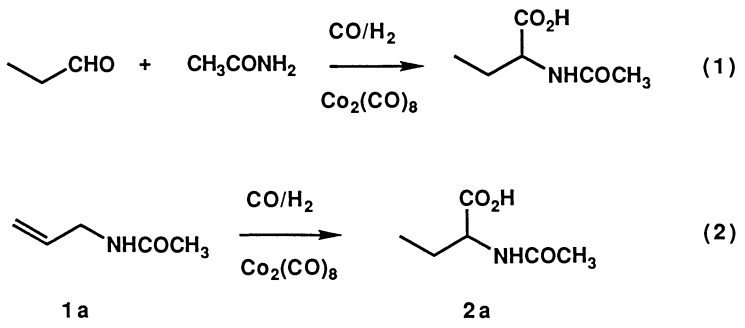

Scheme 1.

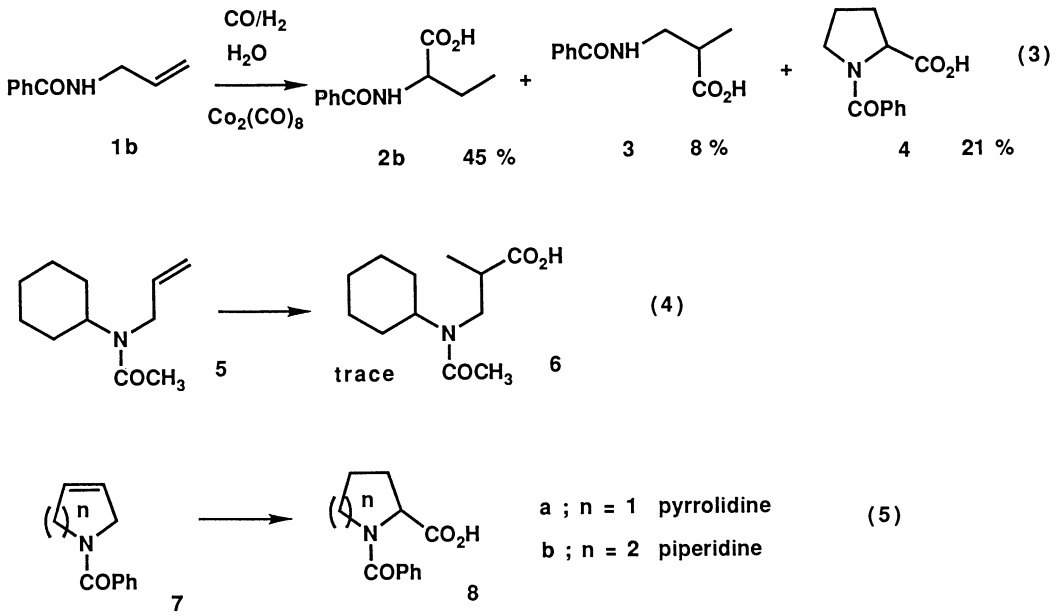

Scheme 2.

yield under hydroformylation conditions (Eq. 2).[2]

We have been interested in the fact that the product (**2a**) corresponds to the amidocarbonylation product of propionaldehyde and acetamide. The reaction can be explained by a facile migration of the cobalt carbonyl moiety from the β- or γ-position to the α-position of the acylamino group, followed by CO insertion. The resulting acyltetracarbonylcobalt intermediate [Co(RCO)(CO)$_4$] with the acylamino group on the α-carbon specifically undergoes hydrolytic cleavage to give **2a**.

Previously, the reaction of *N*-benzoylallylamine (**1b**) under hydroformylation conditions by the addition of one mole equivalent of H_2O was reinvestigated. The reaction was complicated, giving 2-benzamidobutyric acid (**2b**) and 3-benzamido-2-methylpropionic acid (**3**) as well as *N*-benzoylproline (**4**) (Eq. 3).[3] The formation of *N*-benzoylproline (**4**) can be explained by hydroformylation followed by subsequent intramolecular amidocarbonylation.

Though Magnus and co-workers examined the reaction of *N*-acetyl-*N*-cyclohexylallylamine (**5**) under hydroformylation conditions, they obtained a β-carboxylation product **6** in low yield, and could not obtain an α-carboxylation product (Eq.4).[4]

We then intended to examine the cobalt-catalyzed isomerization-hydrocarboxylation of *N*-acyl-β,γ-unsaturated cyclic amine (**7**) to obtain *N*-acylproline (**8a**) and *N*-acyl-2-piperidinecarboxylic acid (*N*-acylpipecolic acid) (**8b**) (Eq.5).

Results and Discussion

We found that the cobalt-catalyzed isomerization-hydrocarboxylation of *N*-benzoyl-β,γ-unsaturated cyclic amine (**7**) under hydroformylation conditions with the addition of two equivalents of H_2O (initial pressure at 25 °C: CO, 60 atm; H_2, 60 atm) at 100 °C for 24 h proceeded smoothly to give *N*-benzoyl cyclic α-amino acid (**8**) in moderate yield.

As shown in Table 1, *N*-benzoyl cyclic α-amino acids (**8**), as well as the isomerization-hydroformylation products (**9**) and hydrogenation products (**10**), were obtained as major products. In the case of cyclic

Table 1. Synthesis of Cyclic α-Amino Acids

Run	Substrate	Catalyst	Products, yield[a]/%		
	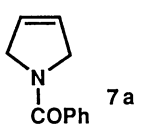 7a		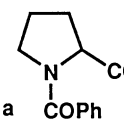 8a	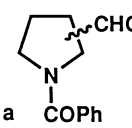 9a	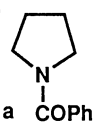 10a
1		$Co_2(CO)_8$	54	6	16
2		$Co_2(CO)_8$ + $PdCl_2(PPh_3)_2$ b)	47	22	6
3		$Co_2(CO)_8$ + CH_3CONH_2 c)	44	18	15
4	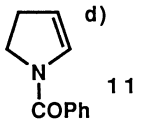 d) 11	$Co_2(CO)_8$	32	47	19
	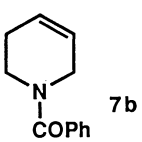 7b		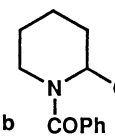 8b	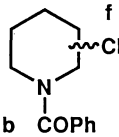 9b	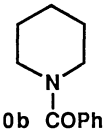 10b
5		$Co_2(CO)_8$	61	16	6
6		$Co_2(CO)_8$ + $PdCl_2(PPh_3)_2$ b)	75	16	3
7		$Co_2(CO)_8$ + $[RhH(CO)(PPh_3)_3]$ b)	55	21	6

a) Carboxylic acids were isolated as methyl esters. Neutral materials were analyzed by GC–MS. b) 0.25 equiv to $Co_2(CO)_8$. c) 5 equiv to $Co_2(CO)_8$. d) 100 °C, 2 h. e) α-Isomer>90%. f) α-: β- or γ-Isomer=1 : 1.

substrates, the only detectable hydrocarboxylation product was an α-carboxylation isomer, and the corresponding β- or γ-isomer was not obtained. It is postulated that the acylamino group of an (α-amidoalkyl)acylcobalt intermediate participated in the hydrolysis of the acyl-cobalt bond in this intermediate (Scheme 3), while the hydrolysis of sterically restricted (β- or γ-amidoalkyl)acylcobalt intermediates is thought to be difficult to give β- or γ-carboxylation products.

It is interesting that since the hydroformylation also proceeded after isomerization, the α-formyl product (**9a**) was obtained as a major isomer in the reaction of *N*-benzoyl-3-pyrroline (**7a**).

Isomerization of the alkylcobalt intermediate, a key step in this reaction, is thought to be promoted by stabilization to the (α-amidoalkyl)cobalt intermediate (similar to *N*-acyliminium cation). To accelerate isomerization, $PdCl_2(PPh_3)_2$ and $[RhH(CO)(PPh_3)_3]$, which were used by Stille and co-workers as isomerization catalysts of the unsaturated amide and imide,[5a] were added as a co-catalyst. However, the effect of the co-catalyst was not remarkable; only the addition of $PdCl_2(PPh_3)_2$ slightly increased the yield of *N*-benzoyl-2-piperidinecarboxylic acid (Run 6). Evans and co-workers reported a $PdCl_2(PPh_3)_2$ catalyzed hydroesterification [hydro(methoxycarbonyl)ation] of *N*-acetyl-1,2,3,6-tetrahydropyridine.[6] They obtained methyl *N*-acetyl-2-piperidinecarboxylate only in 12% yield, together with regioisomers (major products), *N*-acetyl-2-methoxypiperidine, and *N*-acetyl-1,2,3,4-tetrahydropyridine (minor products). These results indicate that the alkylcobalt intermediate is more liable to isomerize relative to the alkylpalladium intermediate.

The coexistence of an amide sometimes decreases the regioselectivity of the hydroformylation step in the hydroformylation-amidocarbonylation of olefins. This fact may be explained by the exchanged regioselectivity of a cobalt hydridocarbonyl catalyst in the presence of amide.[7] Though the reaction was then tried with the addition of acetamide, the reaction was not affected by the addition of acetamide (Run 3).

The reaction of previously isomerized *N*-benzoyl-2-pyrroline (**11**)[5a] under milder reaction conditions also gave the same products as did *N*-benzoyl-3-pyrroline (**7a**) in different product ratios (Run 4). It is unclear why the hydroformylation product (**9a**) was produced predominantly when **11** was used.

A possible mechanism of this reaction is shown in Scheme 3. (*N*-Benzoyl-3-pyrrolidinyl)tetracarbonylcobalt (**12**) isomerizes to the more stable (*N*-benzoyl-2-pyrrolidinyl)tetracarbonylcobalt (**13**), which then produces the (*N*-benzoyl-2-pyrrolidinoyl)tetracarbonylcobalt (**14**) through the insertion of carbon monoxide. The acyl complex (**14**) then undergoes a hydrolytic cleavage (**14**→**8a**), rather than hydrogenolysis (**14**→**9a**), to give *N*-acyl cyclic α-amino acid in a manner similar to that of amidocarbonylation. We have already proposed that cyclization to the oxazolone-like ion pair (**15**), via an intramolecular nucleophilic attack of the oxygen atom if the acylamino moiety is adjacent to the acylcobalt complex, may promote a solvolytic cleavage of the acyl-cobalt bond in the amidocarbonylation.[8] As shown in the Table 1, though the hydrolytic cleavage is the preferred route to hydrogenolysis in this process, the amount of the hydroformylation product (**9a**) is not negligible. At present, it is not clear why hydrogenolysis proceeds to such a degree.

We have already presented the preparation of *N*-acyl cyclic α-amino acid, such as proline and 2-piperidinecarboxylic acid, via the intramolecular amidocarbonylation of ω-(acylamino)alkanals[9] or cobalt-catalyzed carbonylation of *N*-acyl α-alkoxyalkylamines.[8] Another example regarding the preparation of *N*-acyl cyclic α-amino acid via the cobalt-catalyzed carbonylation was developed here.

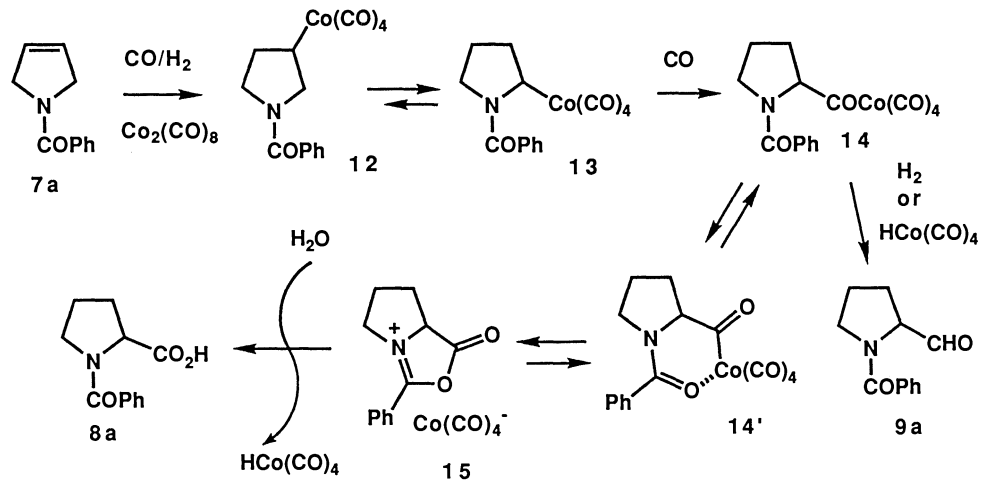

Scheme 3.

Stille and co-workers achieved proline derivative synthesis from *N*-*t*-butoxycarbonyl-3-pyrroline, which is a similar starting material to our's, through the subsequent isomerization, hydroformylation and oxidation.[5] We achieved a similar process by one-pot synthesis utilizing cobalt-catalyzed carbonylation.

Experimental

^{1}H NMR spectra were measured with a Varian XL 300 spectrometer and chemical shifts are given as δ ppm relative to tetramethylsilane (TMS) as an internal standard. Infrared (IR) spectra were recorded on a Hitachi 260-10 spectrophotometer with samples as neat liquid. Mass spectra (MS) were recorded with a JEOL DX-300 instrument by using the FAB technique. GC-MS was performed on a HP 5890A-5970B with a high-performance capillary column (cross-linked methyl silicone). The thin-layer chromatographic system employed silica gel (Merck Art. 7515). PTLC was performed with a Whatman PLK 5F.

N-Benzoyl-3-pyrroline (**7a**) and *N*-benzoyl-1,2,3,6-tetrahydropyridine (**7b**) were prepared by the reaction of amines and benzoyl chloride.

***N*-Benzoyl-3-pyrroline (7a):** ^{1}H NMR (300MHz, $CDCl_3$) δ=4.18—4.23 (2H, m, CH_2), 4.44—4.49 (2H, m, CH_2), 5.72—5.78 (1H, m, -CH=), 5.89—5.94 (1H, m, -CH=), 7.38—7.55 (5H, m, aromatic H); IR (neat) 3050, 2850, 1635, 1605, 1570, 1410 cm^{-1}; GC-MS *m*/*z* 173 (M^+).

***N*-Benzoyl-1,2,3,6-tetrahydropyridine (7b):** ^{1}H NMR (300MHz, $CDCl_3$) δ=2.25 (2H, br. s, CH_2), 3.46, 3.86, and 4.20 (4H, br. s, CH_2), 5.50—5.90 (2H, m, -CH=), 7.41 (5H, br. s, aromatic H); IR (neat) 3050, 2940, 2850, 1700, 1630, 1580, 1435, 1290, 1260 cm^{-1}; GC-MS *m*/*z* 187 (M^+).

N-Benzoyl-2-pyrroline (**11**) was prepared by isomerization of *N*-benzoyl-3-pyrroline (**7a**) with $[RhH(CO)(PPh_3)_3]$.[5a] ^{1}H NMR (300MHz, $CDCl_3$) δ=2.67—2.76 (2H, m, CH_2), 4.03 (2H, t, *J*=9.0 Hz, CH_2), 5.15—5.23 (1H, m, -CH=), 6.42—6.67 (1H, m, -CH=), 7.33—7.55 (5H, m, aromatic H); IR (neat) 1610, 1570, 1410 cm^{-1}; GC-MS *m*/*z* 173 (M^+).

Isomerization-Carboxylation of *N*-Acyl Unsaturated Cyclic Amines (7). A typical procedure is described for the reaction of *N*-benzoyl-3-pyrroline (**7a**) and carbon monoxide catalyzed by $Co_2(CO)_8$.

N-Benzoyl-3-pyrroline (**7a**) (606 mg, 3.5 mmol), $Co_2(CO)_8$ (100 mg, 0.29 mmol), and H_2O (0.13 ml, 7.2 mmol) in THF (20 ml) were heated in a 100 ml stainless-steel autoclave with a 1:1 mixture of carbon monoxide and hydrogen (total pressure 120 atom, measured at room temperature) at 110 °C for 24 h. The autoclave was then cooled to ambient temperature and carbon monoxide and hydrogen were purged out. After the solvent was removed under reduced pressure, the residue was dissolved in AcOEt (50 ml) and the insoluble material filtered off. The filtrate was extracted with 10% aqueous $NaHCO_3$ (50 ml) and brine. The organic phase was dried over $MgSO_4$. The solvent was removed under reduced pressure and the residue analyzed by GC-MS; it was then purified by PTLC (hexane : AcOEt=1 : 2, v/v) to give *N*-benzoyl-2-pyrrolidinecarbaldehyde (**9a**) (44 mg, 0.22 mmol, 6.3%) and *N*-benzoylpyrrolidine (**10a**) (98 mg, 0.56 mmol, 16.0%) as major products. The aqueous $NaHCO_3$ extract was acidified with concentrated HCl and extracted with AcOEt (50 ml). The organic layer was washed with brine and dried over $MgSO_4$. After concentration, the residue was esterified with etherial CH_2N_2 and purified by PTLC (hexane : AcOEt=1 : 2, v/v) to give *N*-benzoylproline methyl ester (methyl ester of **8a**) (443 mg, 1.90 mmol, 54.3%) as an oil.

***N*-Benzoylproline Methyl Ester (Methyl Ester of 8a):** ^{1}H NMR (300MHz, $CDCl_3$) δ=1.50—2.30 (4H, m, CH_2), 3.45—3.55 (2H, m, CH_2), 3.75 (3H, s, CH_3), 4.66 (1H, dd, *J*=5.1 and 8.3 Hz, CH), 7.30—7.58 (5H, m, aromatic H); IR (neat) 2950, 2880, 1740, 1630, 1420, 1280, 1200, 1180 cm^{-1}; GC-MS *m*/*z* 233 (M^+), 174 (M^+−59); High mass (FAB) *m*/*z* Calcd for $C_{13}H_{15}N_1O_3$+H: 234.1130. Found: 234.1136.

***N*-Benzoyl-2-pyrrolidinecarbaldehyde (9a):** ^{1}H NMR (300MHz, $CDCl_3$) δ=2.30—2.85 (4H, m, CH_2), 3.50—3.70 (2H, m, CH_2), 4.65—4.72 (1H, m, CH), 7.35—7.63 (5H, m, aromatic H), 9.68 (1H, s, CHO); IR (neat) 1730, 1625, 1580, 1420 cm^{-1}; GC-MS *m*/*z* 174 (M^+−29).

***N*-Benzoylpyrrolidine (10a):** ^{1}H NNR (300MHz, $CDCl_3$) δ=1.87 (2H, q, *J*=6.6 Hz, CH_2), 1.94 (2H, q, *J*=6.6 Hz, CH_2), 3.42 (2H, t, *J*=6.6 Hz, CH_2), 3.65 (2H, t, *J*=6.6 Hz, CH_2), 7.35—7.55 (5H, m, aromatic H); IR (neat) 3050, 2970, 2890, 1620, 1575, 1410, 1340 cm^{-1}; GC-MS *m*/*z* 175 (M^+).

Methyl *N*-Benzoyl-2-piperidinecarboxylate (Methyl Ester of 8b): ^{1}H NMR (300MHz, $CDCl_3$) δ=1.35—1.85 (4H, m, CH_2), 2.20 (0.5H, br. d, CH_2), 2.35 (1H, br. d, CH_2), 2.85 (0.5H, m, CH_2), 3.25 (1H, br. t, CH_2), 3.65 (1H, br. d, CH_2), 3.78 (3H, br. s, CH_3), 4.45—4.70 (0.5H, m, CH), 5.50 (0.5H, br. s, CH), 7.40 (5H, br. s, aromatic H); IR (neat) 2950, 2860, 1740, 1640, 1420, 1280, 1210 cm^{-1}; GC-MS *m*/*z* 247 (M^+); High mass (FAB) *m*/*z* Calcd for $C_{14}H_{17}N_1O_3$+H: 248.1287. Found 248.1278.

Mixture of *N*-Benzoyl-2-piperidinecarbaldehyde and Regioisomer(s) (9b): ^{1}H NMR (300MHz, $CDCl_3$) δ=9.50 (s, CHO); IR (neat) 1730 cm^{-1}; GC-MS *m*/*z* 217 (M^+), 216 (M^+−1), 188 (M^+−29).

***N*-Benzoylpiperidine (10b):** ^{1}H NMR (300MHz, $CDCl_3$) δ=1.45—1.80 (6H, m, CH_2), 3.34 (2H, br. s, CH_2), 3.70 (2H, br. s, CH_2), 7.38 (5H, br. s, aromatic H); IR (neat) 2940, 2850, 1630, 1575, 1440, 1275 cm^{-1}; GC-MS *m*/*z* 189 (M^+), 188 (M^+−1).

References

1) H. Wakamatsu, J. Uda, and N. Yamakami, *J. Chem. Soc., Chem. Commun.*, **1971**, 1540.

2) S. Sato, *Nippon Kagaku Zasshi*, **90**, 404 (1969).

3) S. Nishi, S. Asada, and K. Izawa, 31th Symposium on Organometallic Chemistry, Tsukuba, Japan, Oct. 1984, Abstr., B202.

4) P. Magnus and M. Slater, *Tetrahedron Lett.*, **28**, 2829 (1987).

5) a) J. K. Stille and Y. Becker, *J. Org. Chem.*, **45**, 2139 (1980); b) Y. Becker, A. Eisenstadt, and J. K. Stille, *J. Org. Chem.*, **45**, 2145 (1980).

6) E. E. Avery, M. F. Baevsky, S. J. Braswell, C. W. Duffus, G. O. Evans II, D. K. Rocha, and R. A. Wynne, *J. Mol. Catal.*, **53**, 179 (1989).

7) K. Izawa, *J. Synth. Org. Chem., Jpn.*, **46**, 218 (1988).

8) K. Izawa, S. Nishi, and S. Asada, *J. Mol. Catal.*, **41**, 135 (1987).

9) K. Izawa and S. Nishi, The 49th annual Meeting of the Chemical Society of Japan, Tokyo, Apr. 1984, Abstr., 3Z34.

Enhanced Enantioselectivity of the Lipase-Catalyzed Hydrolysis by the Addition of a Catalytic Amount of an Amino Alcohol

Toshiyuki ITOH,* Eri OHIRA, Yumiko TAKAGI, Shigenori NISHIYAMA, and Kaoru NAKAMURA†
Department of Chemistry, Faculty of Education, Okayama University, Okayama 700
†Institute for Chemical Research, Kyoto University, Uji, Kyoto 611
(Received September 27, 1990)

L-Methioninol (L-MetOH) was discovered to be an effective additive for improving the enantioselectivity of lipase-catalyzed hydrolysis. It was found that L-MetOH accelerated the enzyme-catalyzed hydrolysis of (*R*)-3-acetoxybutyronitrile (**1**) and inhibited that of (*S*)-**1**.

The synthetic value of enzymes is being increasingly recognized because enzymatic reactions are highly efficient and proceed under mild conditions.[1] One such enzyme being recommended for use by organic chemists is lipase, which is especially useful,[2] since lipases are uniquely characterized by their ability to catalyze the hydrolysis of many types of ester bonds, they can be used for the kinetic resolution of various racemic alcohols. However, there is only a limited number of commercially available lipases for practical use, and substrates which are applicable to effective kinetic resolution are limited at the present time. Therefore, a new method for improving the ability of the enzymes regarding both enantioselectivity and adaptability toward substrates, has been long awaited.

We have recently developed one such method using the modification of substrates: The introduction of a sulfur functional group to the acyl residue of a substrate increases the enantioselectivity of lipase-catalyzed hydrolysis.[3] We now wish to report here another simple method which extends the synthetic utility of a lipase, an amino alcohol which acts as a very efficient additive to increase the enantioselectivity of a lipase catalyzed hydrolysis of 3-acetoxybutyronitrile.

Results and Discussions

Recently, Sih et al.[4] reported that dextromethrophan (*d*-3-methoxy-*N*-methylmorphinan; DM) improved the enantioselectivity of lipase-catalyzed hydrolysis. Though this finding is very interesting when considering the nature of the enzyme, dextromethrophan, a derivative of morphinan, is not recommended for practical use since it lacks availability and is expensive. During our study of the lipase-catalyzed hydrolysis of 3-acetoxy nitriles, we found that the addition of a catalytic amount of diisopropylamine (33 mol% towards the substrate) considerably increased the rate of hydrolysis, although the enantioselectivity decreased.# This fact prompted us to survey other simple amines which have the ability to enhance the enantioselectivity of a lipase-catalyzed reaction. The effect of additives in lipase PS (*Pseudomonas* sp.)##-catalyzed hydrolysis of (±)-3- acetoxybutyronitrile (**1**) was examined (Eq. 1). The nitrile, **1**, should become a useful chiral building block for the synthesis of many biologically active compounds.[5] Lipase PS (30 mg) and an additive were added to a suspension of (±)-**1** (60 mg, 0.47 mmol) in a 0.1 M phosphate buffer (pH 7.2, 5.0 mL); the resulting suspension was stirred at room temperature. The reaction was monitored by silica-gel TLC and was stopped when spots due to the ester and alcohol became the same size. The optical purity of the hydrolyzed alcohol, **2**, was determined by an ^{1}H NMR analysis of the corresponding (+)-α-methoxy-α-phenyl-α-trifluoromethylacetate (MTPA).[7] The effect of various amines on the enantioselectivity of the lipase-catalyzed hydrolysis of (±)-**1** is shown in Table 1. Of the thirteen amines examined, four of them markedly enhanced the enantioselectivity of the reaction. Among them, DM (Entry 2) and (*S*)-2-amino-4-methylthio-1-butanol (L-MetOH) (Entry 8), which has been derived from L-methionine, showed a remarkable effect on the enantioselectivity. The other four amino alcohols derived from the corresponding amino acid, i.e. L-phenylalanine (Entry 12), L-leucine (Entry 13), glycine (Entry 11), and *dl*-serine (Entry 14), did not enhance the enantioselectivity of this enzyme. Since L-MetOH is easily prepared, we recommended L-MetOH be used as an additive for practical applications.

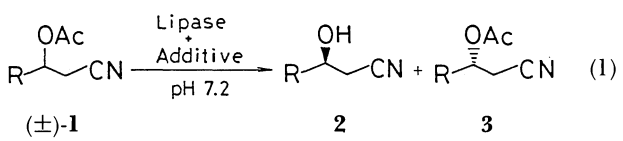

(1)

In the reaction conditions, the hydrolysis of **1** never occurred without the enzyme. Although the pH value of the reaction mixture was not affected by addition of this amount of *i*-$PrNH_2$ it seemed that this amine acted as an effective base in the enzymatic hydrolysis.

Preliminary experiments involving the hydrolysis of **1** revealed that lipase PS (Amano, *Pseudomonas* sp.) was more promising than any other of the eight enzymes tested. However, it is fair to say that the result was not satisfactory because the ratio of specificity constants for the resolution was only 7. Lipases from *Aspergillus niger* (A and A6), *Candida* sp. (MY and M10), *Rhizopus* sp. (F-AP15 and Newlase F), Porcine Pancreatin (PPL), and Hog pancreatin (F) were not stereospecific.

Table 1. Effect of Various Amines on the Lipase-Catalyzed Enantioselective Hydrolysis of (±)-3-acetoxybutyronitrile (**1**)

Entry	Additive	mol%[b]	Time/h	%ee[a] of **2** (% Conv.)	E[c]
1	None	0	10	61(45)	7
2	DM	33	2.0	82(30)	15
3	Bn_2NH	33	3.0[d]	70(46)	10
4	DAPr	33	3.0	78(31)	11
5	Et_3N	33	1.0[d]	51(35)	4
6	*i*-Pr_2NH	33	0.17[d]	0(43)	1
7	*i*-$PrNH_2$	33	2.5[d]	63(31)	5
8	L-MetOH	33	16	69(56)	14
9	DL-MetOH	33	14	61(45)	7
10	D-MetOH	33	14	55(58)	8
11	$HOCH_2CH_2NH_2$	33	2.5	53(23)	4
12	L-PheOH	33	5.0	58(51)	7
13	L-LeuOH	33	3.0	58(38)	5
14	APD	33	6.0	53(23)	4

a) Determined by 200 MHz ^{1}H NMR analysis of (+)-MTPA ester of **2**. b) Based on the substrate. Where 33 mol% corresponds 28 mM. c) Calculated by the hydrolysis ratio (% Conv.) and ee of **2**.[6] d) Reactions were carried out at 35 °C. DM: Dextromethorphan. DAPr: 1,3-Diamino-2-propanol. L-MetOH: (2*S*)-2-Amino-4-methylthio-1-butanol. D-MetOH: (2*R*)-2-Amino-4-methylthio-1-butanol. L-PheOH: (2*S*)-3-Phenyl-2-amino-1-propanol. L-LeuOH: (2*S*)-4-Methyl-2-amino-1-pentanol. APD: 2-Amino-1,3-propanediol.

Table 2. Effect of Various Concentrations of Additives on the Enantioselective Hydrolysis of (±)-**1** Catalyzed by Lipase PS (*Pseudomonas* sp.)

Entry	Additive	mol%[a]	%ee of **2** (Conv. %)	E[6]
1	None	0	68(31)	7
2	L-MetOH	10	51(63)	8
3	L-MetOH	20	50(58)	8
4	L-MetOH	33	69(56)	14
5	L-MetOH	50	50(63)	8
6	L-MetOH	100	55(59)	8
7	L-MetOH	200	29(71)	4
8	DM	10	76(46)	14
9	DM	33	82(30)	15
10	DM	100	67(49)	10
11	DM	200	72(31)	8
12	DL-MetOH	10	42(63)	5
13	DL-MetOH	33	61(45)	7
14	DL-MetOH	100	37(64)	4
15	DL-MetOH	200	30(70)	4
16	D-MetOH	10	48(61)	6
17	D-MetOH	33	55(58)	8
18	D-MetOH	100	55(61)	9
19	D-MetOH	200	49(63)	7

a) Based on the substrate.

To gain insight into the mechanism of the action of L-MetOH, the hydrolysis was studied under various concentrations of the additive (DM or MetOH) (Table 2). The results can be summarized as follows: (1) L-MetOH is the best additive among isomers of MetOH, i.e. DL-, L- and D-MetOH. (2) The enantioselectivity of the reaction increases accordingly to the amount of L-MetOH until 33 mol% of **1**; the selectivity then decreases. (3) The effects of L-MetOH are similar to those of DM.

To study the mechanism regarding the action of L-MetOH, the enantiomer of **1** ((*R*)-**1**[3a] or (*S*)-**1**[3a]) was used as the substrate. The kinetic inhibition pattern for each enantiomer of the substrates could provide us with useful information relative to the inhibition mechanism.[4] We used an ^{1}H NMR analysis for determining the rate of hydrolysis. The enantiomer of **1** was subjected to hydrolysis and the reaction was stopped after 2.5 h. The relative rate of the reaction was calculated from the conversion rate at that time, since the hydrolysis of (*S*)-**1** is too small to

Table 3. Effect of Additives on the Rate of Hydrolysis of (±)-**1** Catlyzed by Lipase PS (*Pseudomonas* sp.)

Entry	Substrate	Additive	Concentration	Conv.	Rate[a]
1	(*R*)-**1**	None	0.0 mM	76%	4.0
2	(*R*)-**1**	L-MetOH	10.4 mM[b]	90%	4.7
3	(*R*)-**1**	D-MetOH	10.4 mM	79%	4.1
4	(*R*)-**1**	DM	10.4 mM	52%	2.7
5	(*S*)-**1**	None	0.0 mM	19%	1.0
6	(*S*)-**1**	L-MetOH	10.4 mM	0%	0.0
7	(*S*)-**1**	D-MetOH	10.4 mM	13%	0.7
8	(*S*)-**1**	DM	10.4 mM	11%	0.6

a) Results of comparing the % conversion with reference rate. The reference rate appears on Entry 5. b) 33 mol% based on the substrate.

determine detailed kinetic parameters (Table 3). As can be seen in Table 3, dextromethrophan (DM) inhibited the enzyme-catalyzed hydrolysis of both enantiomers of the acetate (Entries 4 and 8)[4]. It was found that D-MetOH was inferior compared to L-MetOH regarding the inhibitory action of hydrolysis of (*S*)-**1** (Entries 6 and 7). According to the results of hydrolysis under various concentrations of additives (Table 2) the effect of L-MetOH is similar to that of DM. However, the action of L-MetOH to the rate of hydrolysis of (*R*)-**1** was found to be different to that of DM. DM inhibits the hydrolysis of both enantiomers while an enzyme-catalyzed hydrolysis of (*R*)-**1** was not inhibited by L-MetOH. On the contrary, the reaction was accelerated by the addition of L-MetOH (Entry 2). On the other hand, the hydrolysis of (*S*)-**1** was strongly inhibited by L-MetOH and the hydrolyzed product in the presence of L-MetOH was not detected (Entry 6). Evidently, L-MetOH inhibited the hydrolysis of (*S*)-**1** and accelerated that of (*R*)-**1**. It seems therefore that there is a difference in the mechanism for the action to the enzyme between DM and L-MetOH.

According to the experimental results, it seems that L-MetOH and the substrate combine independently with the enzyme at different sites. A conformational change due to the binding of L-MetOH with a certain part of the enzyme may provide a change in the affinity towards the substrates. Therefore, a change of the conformation of the enzyme may provide an increase in the hydrolysis rate of (*R*)-**1** while decreasing the rate of the hydrolysis of (*S*)-**1**. This effect may provide an enhancement of the enantioselectivity of the resolution.

It is not clear at present what geometrical change in the conformation of the enzyme causes a change in the stereoselectivity during hydrolysis. In this study, however, it was established that L-MetOH is an efficient additive that can control the enantioselectivity of a lipase. Considering the broad substrate specificities of lipases, the present method is recommended for use in obtaining optically active alcohols under mild conditions using lipases.

Experimental

Instruments and Materials. NMR spectra were recorded on JEOL MH-100 and Varian VXR-200 spectrometers in $CDCl_3$ with tetramethylsilane (TMS) as an internal reference. Solvents and commercially available starting materials were generally used without additional purification, unless otherwise indicated. TLC analyses were carried out on Merck 60 F_{254} silica-gel plates and Wako gel B-5F. Pyridine and dichloromethane were refluxed over calcium hydride for 5 h, distilled and stored under argon in the presence of 4 Å molecular sieves.

Hydrolysis of 3-Acetoxybutyronitrile (1) by Lipase PS: A suspension of 3-acetoxybutyronitrile (**1**)[8] (60 mg, 0.47 mmol), Lipase PS (30 mg, 50 w%) and L-MetOH (21 mg, 0.16 mmol) in a mixed solvent of 0.1 M phosphate buffer (pH 7.2, 5.0 mL) and acetone(0.5 mL) was stirred by a magnetic stirrer at room temperature. After 14 h, the product was extracted from the reaction mixture with ethyl acetate, the extract was then filtered through a short silica-gel column (5 cm) for removing the L-MetOH, dried over anhydrous magnesium sulfate and evaporated in vacuo to give a crude oily product (160 mg). By ^{1}H NMR analysis of this crude product, the hydrolysis ratio was determine as a 56% conversion. Separation by silica-gel TLC gave **2** (22 mg, 0.26 mmol, 55%) and **3** (20 mg, 0.16 mmol, 33%). The optical purity of the produced alcohol, **2**, was determined by an ^{1}H NMR analysis of the corresponding (+)-MTPA ester. The enantiomeric excess (ee) of the remaining ester, **3**, was also determined by a conversion to the corresponding alcohol with LAH reduction (in THF at −50 °C) and esterification with 100% excess of (*S*)-(+)-MTPA chloride. **2**; 69 %ee; $[\alpha]_D^{23}$ +3.1°(*c* 1.0, EtOH, lit,[3a] +4.1° (*R*), 84 %ee). **3**; 80 %ee; $[\alpha]_D^{23}$ −19.0° (*c* 1.0, EtOH). The (*E*) value, which was calculated by ee of **2** and ee of **3**, agreed well with that calculated from the hydrolysis ratio and ee of **2**.[6]

Preparation of (*R*)- and (*S*)-3-Acetoxybutyronitrile (1): A solution of 3-(methylthioacetoxy)butyronitrile (**4**)[3c] (10 g, 57.7 mmol) in 0.1 M phosphate buffer (pH 7.2, 100 mL) and acetone (6.0 mL) was incubated with lipase P (2.96 g)at RT for 6 h. The mixture was filtered through a celite pad, and then extracted with ethyl acetate. Using silica-gel flash column chromatography, 8.24 g of the recovered ester and 1.25 g (14.7 mmol, 25% yield) of the product, (*R*)-**2**, were obtained. (*R*)-**2** ($[\alpha]_D^{23}$ +6.8°(*c* 1.33, EtOH); The ee of (*R*)-**2** (98%) was determined by 200MHz ^{1}H NMR analysis of the corresponding (+)-MTPA ester. The produced alcohol, (*R*)-**2**, was acetylated by acetyl chloride in the presence of pyridine in a usual manner to give (*R*)-**1**; $[\alpha]_D^{23}$ +19.0° (*c* 1.0, EtOH). To obtain (*S*)-**1** with a sufficient ee for practical use, the recovered acetate (8.24 g) was incubated once more with the lipase to give 2.68 g (36% yield) of (*S*)-(methylthio) acetate; $[\alpha]_D^{23}$ −17.6° (*c* 0.945, EtOH). LAH reduction of the ester in THF at −50 °C provided 98% ee of (*S*)-**2**; $[\alpha]_D^{23}$ −7.1° (*c* 0.98, EtOH), which was acetylated to give (*S*)-**1** ($[\alpha]_D^{23}$ −18.6°, *c* 1.0, EtOH).

Kinetics Experiment: Lipase PS (1.0 g) was dissolved in 20 mL of a 0.1 M phosphate buffer (pH 7.2) and centrifuged (2000 rpm, 2 min.). The resulting supernatant liquid was diluted with the buffer solution until the total volume was doubled and used as an enzyme solution. When the lipase was added as a powder to the reaction mixture, we could not obtain reproducible results concerning the determination of the % conversion. 3-Acetoxybutyronitrile (**1**) (20 mg, 0.157 mmol) and the additive (0.0145 mmol, 33 mol% based on the substrate) were weighed directly into a flask and dissolved into 1.0 mL of acetone. The enzyme solution (4.0 mL) was added and stirred for 2.5 h at 23 °C. The reaction was stopped by the addition of crashed ice; the reaction mixture was then extracted with ethyl acetate, dried, and evaporated. The ^{1}H NMR spectrum was then taken. The hydrolysis ratio was determined by a comparison of the peak intensity of 3-H signals, i. e. alcohols **2**; 3.9—4.1 (m), and the remaining ester **3**; 4.8—5.1(m).

We are grateful to SC-NMR Laboratory of Okayama University for the NMR measurement. We thank Amano Pharmaceutical Co., Ltd. for providing the lipase.

References

1) For recent reviews see, a) J. B. Jones, *Tetrahedron*, **42**, 3351 (1986); b) D. H. G. Crout and M. Christen, "Modern Synthetic Method 1989," ed by R. Scheffold, Springer Verlag (1989), p. 1—114.

2) Recent reviews see, a) C.-S. Chen, C. J. Sih, *Angew. Chem., Int. Ed. Engl.*, **28**, 695 (1989); b) Y.-F. Wang and C.-H. Wong, *J. Org. Chem.*, **53**, 3129 (1988). Recent other examples see; c) G. Kirchner, M. P. Scollar, and A. M. Klibanov, *J. Am. Chem. Soc.*, **107**, 7072 (1985); d) C.-S. Chen, S.-H. Wu, G. Girdaukas, and C. J. Sih, *ibid.*, **109**, 2812 (1987); e) J. T. Lin, T. Yamazaki, and T. Kitazume, *J. Org. Chem.*, **52**, 4565 (1987); f) G. Sabbion and J. B. Jones, *ibid.*, **52**, 4565 (1987); g) F. Francalanci, P. Cesti, W. Cabri, D. Bianchi, T. Martinengo, and M. Foa, *ibid.*, **52**, 5079 (1987); h) R. Riva, B. Danielli, G. Lesma, and G. Palmisano, *J. Chem. Soc., Chem. Commun.*, **1987**, 299; i) S. T. Russell, J. A. Robinson, and D. J. Willliams, *ibid.*, **1987**, 351; j) C. Fuganti, O. Graselli, S. Servi, A. Lazzarin, and P. Casati, *ibid.*, **1987**, 538; M. Pottie, J. Van der Eycken, and M. Vandewalle, *Tetrahedron Lett.*, **30**, 5319 (1989); k) Z.-F. Xie, H. Suemune, and K. Sakai, *J. Chem. Soc., Chem. Commun.*, **1987**, 839; Z.-F. Xie, I. Nakamura, H. Suemune, and K. Sakai, *ibid.*, **1988**, 966; l) F. Bjorkling, J. Boutelie, M. Higlmarsson, K. Hult, and T. Norin, *ibid.*, **1987**, 1041; m) V. Kerscher and W. Kreiser, *Tetrahedron Lett.*, **28**, 531 (1987); n) Y. Kato, H. Ohta, and G. Tsuchihashi, *ibid.*, **28**, 1303 (1987); o) G. Bold, S. Chao, R. Bhide, S.-H. Wu, D. V. Patel, and C. J. Sih, *ibid.*, **28**, 1973 (1987); p) H. Hemmerle and H.-J. Gais, *ibid.*, **28**, 3471 (1987); q) E. Guibe-Jampel and G. Rousseau, *ibid.*, **28**, 3563 (1987); J. Salaun and B. Karkour, *ibid.*, **28**, 4669 (1987); r) A. L. Gutman, K. Zuobi, and A. Boltansky, *ibid.*, **28**, 3861 (1987); s) R. Roy and A. W. Roy, *ibid.*, **28**, 4935 (1987); t) D. Bianchi, W. Cabri, P. Cesti, F. Francalanci, and M. Ricci, *J. Org. Chem.*, **53**, 104 (1988); u) J. Zemlicka, L. E. Craine, M.-J. Heeg, and J. P. Oliver, *ibid.*, **53**, 937 (1988); v) Y.-F. Wang and C.-H. Wong, *ibid.*, **53**, 3129 (1988); w) D. Bianchi, P. Cesti, and E. Battistel, *ibid.*, **53**, 5531 (1988); x) V. Gotor, R. Brieva, and F. Rebolledo, *J. Chem. Soc., Chem. Commun.*, **1988**, 957; y) T. Miyazawa, T. Takitani, S. Uegi, and T. Yamada, *ibid.*, **1988**, 1215; z) M. Bucciarevi, A. Formi, I. Moretti, and F. Prati, *ibid.*, **1988**, 1614; aa) Z.-F. Xie, H. Suemune, and K. Sakai, *ibid.*, **1988**, 1638; ab) K. Faber, H. Honig, and P. S-Wasserthal, *Tetrahedron Lett.*, **29**, 1903 (1988); ac) L. Blanco, E. G-Jampel, and G. Roussean, *ibid.*, **29**, 1915 (1988); ad) D. Bianchi, W. Carbi, P. Cesti, F. Francalanci, and F. Rama, *ibid.*, **29**, 2455 (1988); ae) M. Nakada, S. Kobayashi, and M. Ohno, *ibid.*, **29**, 3951 (1988); af) A. Scilimati, T. K. Ngooi, and C. J. Sih, *ibid.*, **29**, 4927 (1988); ag) K. Okahata, Y. Fujimoto, and K. Ijiro, *ibid.*, **29**, 5133 (1988); ah) G. Zhi-Wei, T. K. Ngooi, A. Scilimati, G. Fuling, and C. J. Sih, *ibid.*, **29**, 5583 (1988); ai) C. H. Von der Osten, A. J. Sinskey, C. H. Barbas III, R. L. Pederson, Y-F. Wang, and C-H. Wong, *J. Am. Chem. Soc.*, **111**, 3924(1989); aj) T. K. Ngooi, A. Scilimati, Z.-W. Guo, and C. J. Sih, *J. Org. Chem.*, **54**, 911 (1989); ak) H. S. Berinakatti, A. A. Benerji, and R. V. Newadkar, *ibid.*, **54**, 2453 (1989); D. Bisson, S. Henrot, M. Larchereque, and R. Azerd, *Tetrahedron Lett.*, **28**, 5033 (1989); al) A. L. Gutman and T. Brardo, *J. Org. Chem.*, **54**, 4263 (1989); am) A. L. Gutman and T. Brardo, *ibid.*, **54**, 5645 (1989); an) T. Yamazaki, S. Ichikawa, and T. Kitazume, *J. Chem. Soc., Chem. Commun.*, **1989**, 934; ao) H. Yamada, S. Ohsawa, T. Sugai, H. Ohta, and S. Yoshikawa, *Chem. Lett.*, **1989**, 1775; ap) C. Feichter, K. Faber, and H. Griengel, *Tetrahedron Lett.*, **30**, 551 (1989); aq) J. Hiratake, K. Yamamoto, Y. Yamamoto, and J. Oda, *ibid.*, **30**, 1555 (1989); ar) K. Hirai, S. Miyakoshi, and A. Naito, *idid.*, **30**, 2553 (1989); as) G. Guanti, L. Banfi, and E. Narisano, *ibid.*, **30**, 2697 (1989); at) K. Burgess and I. Henderson, *ibid.*, **30**, 3633 (1989); au) S.-H. Wu, Z.-W. Guo, and C. J. Sih, *J. Am. Chem. Soc.*, **112**, 1990 (1990); av) P. Kalaritis, R. W. Regenye, J. J. Partridge, and D. K. Coffen, *J. Org. Chem.*, **55**, 812 (1990); aw) K. Burgess and L. D. Jennings, *ibid.*, **55**, 1138 (1990); ax) E. Foelsche, A. Hickel, H. Honig, and P. S-Wasserthal, *ibid.*, **55**, 1749 (1990); ay) J. S. Walle, K. B. Reda, M. E. Williams, and C. J. Morrow, *ibid.*, **55**, 3544 (1990); az) F. J. Urban, R. Breitenbach, and L. A. Vincent, *ibid.*, **55**, 3670 (1990); ba) H. Estermann, K. Prasad, M. J. Shapiro, J. J. Bolsterli, and M. D. Walkinshaw, *Tetrahedron Lett.*, **31**, 445 (1990); bb) R.-L. Gu and C. J. Sih, *ibid.*, **31**, 3283 (1990); bc) K. Nakamura, K. Ishihara, A. Ohno, M. Uemura, K. Nishimura, and Y. Hayashi, *ibid.*, **31**, 3603 (1990); bd) R. Chenevert, M. Desjardins, and R. Gagnon, *Chem. Lett.*, **1990**, 33; bd) C. Fuganti, G. Pedrocchi-Fantoni, and S. Servi, *ibid.*, **1990**, 1137; be) S. Liang and L. A. Paquette, *Tetrahedron Asym.*, **1**, 445 (1990).

3) a) T. Itoh and Y. Takagi, *Chem. Lett.*, **1989**, 1505; b) T. Itoh, K. Kuroda, M. Tomosada, and Y. Takagi, *J. Org. Chem.*, **56**, 797 (1991).

4) Z.-W. Guo and C. J. Sih, *J. Am. Chem. Soc.*, **111**, 6836 (1989).

5) G. Tennant, "Comprehensive Organic Chemistry," ed by D. Barton and D. Ollis, Pergamon Press, 1979, Vol. 2, p. 385.

6) C.-S. Chen, Y. Fujimoto, G. Girdaukas, and C. J. Sih, *J. Am. Chem. Soc.*, **102**, 7294 (1982).

7) J. A. Dale and H. S. Mosher, *J. Am. Chem. Soc.*, **95**, 512 (1972).

8) T. Kuwahara and H. Takahashi, *Bull. Chem. Soc. Jpn.*, **42**, 1745 (1969).

Mechanism of 2-Propanol Dehydrogenation with Suspended Nikel Fine-Particle Catalyst

Masaru YAMASHITA,* Feng-Yuen DAI, Minoru SUZUKI, and Yasukazu SAITO
Department of Industrial Chemistry, Faculty of Engineering, The University of Tokyo, 7-3-1 Hongo, Bunkyo-ku, Tokyo 113
(Received August 21, 1990)

Selective dehydrogenation of 2-propanol was performed with a suspended nickel fine-particle catalyst at high activity under refluxing conditions. The isotope effects, k_H/k_D, for $(CH_3)_2CDOH$ and $(CD_3)_2CDOD$ were found to be 2.56 and 2.69, respectively, in contrast to 1.68 for $(CH_3)_2CHOD$, suggesting that the C-H bond dissociation at the methine position is rate-determining. With regard to $(CH_3)_2CHOD$ and $(CH_3)_2CDOH$, a distinct difference was observed for the deuterium distributions among the liquid-phase components after the reaction, since deuterium transfer from the hydroxyl to the methyl and other groups proceeded tremendously for $(CH_3)_2CHOD$, whereas the methine group of $(CH_3)_2CDOH$ changed little, even after a 5-h reaction under refluxing conditions. This contrast was well accounted for by the difficult splitting of the methine C-H bond and the facile dissociation of the hydroxyl group, in addition to a gradual H-D exchange due to the keto-enol equilibriation of the adsorbed acetone and the hydrogen transfer from 2-propanol to acetone. Distributions of H_2, HD, and D_2 were interpreted as well, which varied with the reaction periods and the kinds of substrates. Based on the proposed mechanism, strategies for a catalyst improvement suitable for a newly-proposed chemical heat pump system are discussed.

Industrial processes concerning 2-propanol dehydrogenation are carried out on heterogeneous catalysts above 300 °C,[1] since the change in the standard Gibbs free energy becomes negative at high temperature.[2]

2-Propanol dehydrogenation over zinc oxide was investigated by Teichner et al., who concluded that the dissociation of the methine C-H bond is rate-determining.[3] The reaction mechanism was discussed later by Krylov regarding various solid catalysts; the importance of the enol-type adsorption of acetone was pointed out.[4] The dissociation of 2-propanol into isopropoxide and hydrogen surface species on zinc oxide, followed by enforced desorption of acetone with the adsorbed isoproxide species, was revealed by Tamaru et al.[5] The desorption process of 2-propanol from the zinc oxide surface, itself, was studied by Kemball et al. up to a temperature of 300 °C.[6]

Even at a temperature as low as 82.4 °C, however, the reaction can proceed under boiling conditions, since the produced hydrogen is removed from the reaction medium immediately after its formation (Eq. 1).

$$(CH_3)_2CHOH(l) \rightarrow (CH_3)_2CO(l) + H_2(g). \quad (1)$$

Actually, suspended copper chromite and Raney nickel catalysts proved to be active for 2-propanol dehydrogenation under refluxing conditions.[7,8]

Boudart et al. analyzed the reaction using a suspended nickel boride catalyst using the following equation, in which the rate retardation caused by acetone adsorption was taken into account:[9]

$$v = k/(1 + K[\text{acetone}]), \quad (2)$$

where v is the reaction rate, k the rate constant and K the equilibrium constant of acetone adsorption, respectively.

Recently, highly active nickel fine-particle catalysts (116 mmol h^{-1} g^{-1}), prepared by a gas-evaporation method,[10] were reported by Saito et al., where the same rate equation (2) was ascertained to hold for 2-propanol dehydrogenation.[11] Efficient catalysts for reaction (1) are indispensable to a newly-proposed chemical heat pump system,[12] which raises the temperature of low-quality heat from 80 °C to a more valuable temperature of 200 °C.

In the present paper, the mechanism of the nickel fine-particle catalyst is elucidated in order to obtain strategies for catalyst improvement suitable for 2-propanol dehydrogenation in the newly-proposed chemical heat-pump system.

Experimental

A prescribed amount (200 mg) of the nickel fine-particle catalyst (supplied by Vacuum Metallurgical Co. with an average particle diameter of 20 nm and a specific surface area (BET) of 43.7 $m^2 g^{-1}$, Lot. No. 2180) was laid in a Schlenk flask (20 ml). The catalyst was preheated at 160 °C for 1 min under a hydrogen atmosphere, by which a part of the surface oxide was removed from the nickel fine particles. The catalyst was well suspended in 2-propanol by an ultrasonic treatment (Kaijyo Denki Co., Sona 50a) at room temperature for 1 min under an argon atmosphere.

Three kinds of deuterium-substituted 2-propanol, i.e., $(CH_3)_2CHOD$, $(CH_3)_2CDOH$, and $(CD_3)_2CDOD$, in addition to $(CD_3)_2CO$ (all supplied by the Division of Merck, Frost Inc.) were used without further purification. After the catalyst suspension was heated at the boiling temperature with an oil bath kept at 100 °C, the amount of evolved gas was determined time-sequentially with a gas burette (250 ml) through a refluxing condenser. Gaseous products were collected at the exit of the reaction vessel.

Both gaseous and liquid-phase products were analyzed by gas chromatography with MS-5A and PEG 1000 columns,

respectively.

The deuterium distribution of molecular hydrogen was monitored by a quadrupole-type mass spectrometer (NEC Anerva Co., AQA 360), whereas an FT-NMR spectrometer (JEOL Co., GX-270) was used for analyzing the liquid-phase components both before and after the reaction.

Results

Dehydrogenation of Deuterium-Substituted 2-Propanol. The nickel fine-particle catalyst was dispersed in 2-propanol at a concentration ten-times larger than that examined previously.[11] 2-Propanol dehydrogenation proceeded at 82.4 °C under boiling conditions (heat at 100 °C) at high activity and selectivity in a densely suspended solution as well (Fig. 1). The exclusive formation of hydrogen and acetone was confirmed in the gaseous- and liquid-phase components, respectively. The reaction rates and the deuterium distributions were reproducible satisfactorily.

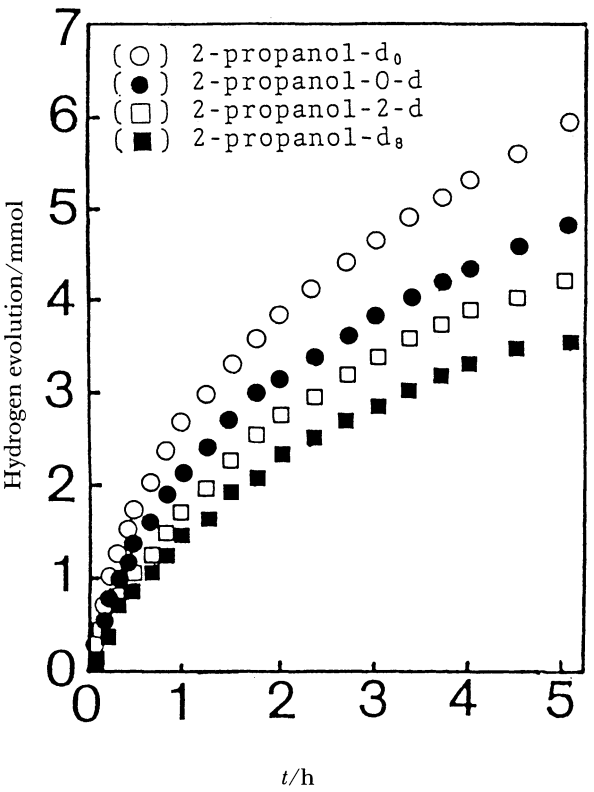

Fig. 1. Dehydrogenation of deuterium-substituted 2-propanol with the suspended nickel fine-particle catalyst (200 mg) at 82.4 °C under refluxing conditions (heat at 100 °C).

A preheat treatment of the nickel fine-particle catalyst under a hydrogen atmosphere was necessary in order to exhibit the dehydrogenation activity.[13] It was revealed that the reaction rates were substantially indifferent to the conditions of a reduction performed with either H_2 or D_2.

The initial rates of hydrogen evolution from 2-propanol-d_0, -O-d, -2-d and -d_8 are summarized in Table 1. Since the gradual decrease of the reaction rates was ascribed to retardation due to the product acetone (Eq. 2),[11] the rate constant k [mmol h^{-1} g^{-1}] was given by the observed initial reaction rate.

As shown in Table 1, the isotope effects, k_H/k_D, related to the methine hydrogen of 2-propanol were obtained as large as 2.56 and 2.69 from 2-propanol-2-d and d_8 respectively, with reference to 2-propanol-d_0 and the catalyst pre-reduced by H_2.

On the contrary, the isotope effect concerning the hydroxyl hydrogen was rather small (k_H/k_D: 1.68 for 2-propanol-O-d).

Table 2. Deuterium Distribution in the Product Hydrogen Evolved from Deuterium-Substituted 2-Propanol at 82.4 °C under Refluxing Conditions (heat at 100 °C) with Nickel Fine-Particle Catalyst

Deuterium-substituted 2-propanol	Preheated atmosphere	Product hydrogen/%		
		H_2	HD	D_2
d_0	H_2	100	0	0
d_0	D_2	100	0	0
O-d	H_2	42.2	41.2	16.6
2-d	H_2	79.0	19.8	1.2
d_8	H_2	0.73	6.37	92.7

Pretreatment of catalyst: Heated at 160 °C for 1 min under hydrogen atmosphere. Catalyst solution: Suspension of 200 mg in 2-propanol (5 ml). Reaction conditions: Refluxing for 5 h under atmospheric pressure.

Table 1. Dehydrogenation of Deuterium-Substituted 2-Propanol at 82.4 °C under Refluxing Conditions (heat at 100 °C) with Nickel Fine-Particle Catalyst and Kinetical Isotope Effect

Deuterium-substituted 2-propanol	Preheat atmosphere	Conversion	Initial rate	Isotope effect
		%	mmol g^{-1} h^{-1}	k_H/k_D
d_0[a]	H_2	9.36	81.3	—
d_0	D_2	9.33	78.1	1.04
O-d	H_2	7.68	48.5	1.68
2-d	H_2	6.71	31.8	2.56
d_8	H_2	6.39	30.2	2.69

a) -d_0 stands for undeuterated. Pretreatment of catalyst: Heated at 160 °C for 1 min under hydrogen atmosphere. Catalyst solution: Suspension of 200 mg in 2-propanol (5 ml). Reaction conditions: Refluxing for 5 h under atmospheric pressure.

Deuterium Distribution in the Product Hydrogen. Even when the catalyst was preheated under a D_2 atmosphere, the gaseous product of 2-propanol-d_0 dehydrogenation was found to be H_2 exclusively. The amount of surface deuterium species left after the pretreatment of D_2 reduction is therefore negligible.

As shown in Table 2, the gaseous products of 2-propanol-O-*d* and 2-*d* were found to be the mixture of H_2, HD, and D_2, as shown in the following equations:

$$(CH_3)_2CHOD(l) \rightarrow (CH_3)_2CO(l) + H_2, HD, D_2(g), \quad (3)$$

and

$$(CH_3)_2CDOH(l) \rightarrow (CH_3)_2CO(l) + H_2, HD, D_2(g). \quad (4)$$

The product hydrogen was more abundant with H_2 from 2-propanol-2-*d* than from 2-propanol-O-*d*.

Figure 2 shows the deuterium distribution of newly-evolved hydrogen from 2-propanol-O-*d* as a function of time. H_2 gradually increased at the expense of both HD and D_2.

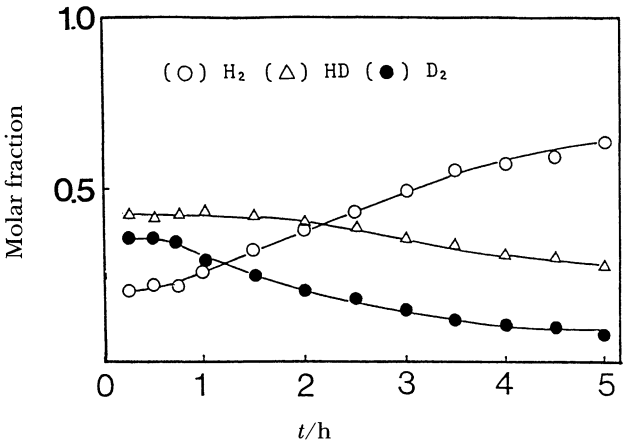

Fig. 2. Variation among the molar fractions of H_2, HD, and D_2 in hydrogen evolved from 2-propanol-O-*d* as a function of time.

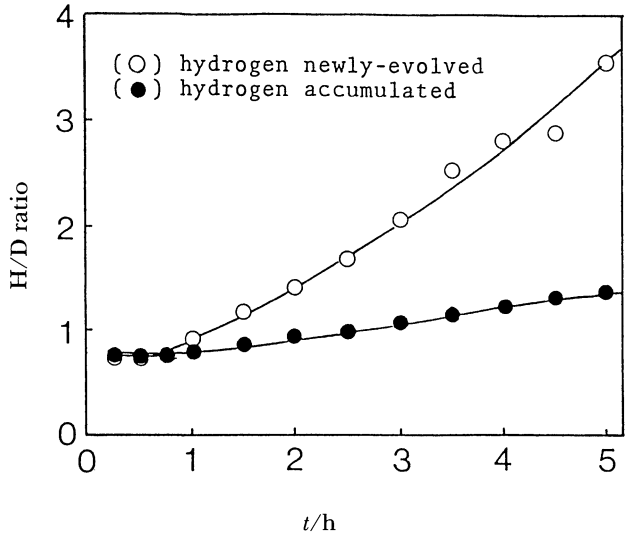

Fig. 3. H/D ratio in newly-evolved hydrogen and the one accumulated till the time concerned.

The time dependence of the deuterium distribution, represented as the H/D ratio in the product hydrogen, was more sensitive to newly-evolved hydrogen than to that accumulated in the gas burette (Fig. 3). The latter was obtained by combining the composition with the amount of hydrogen. Since the reaction rate gradually decreased, the variation of the deuterium distribution in the newly-evolved hydrogen was smoothed out in the accumulated hydrogen during the reaction period from the beginning until the time concerned.

As for 2-propanol-O-*d*, the H/D ratio of the newly-evolved hydrogen gradually increased from 0.82 at the intitial stage to 3.55 after 5 h along with the reaction progress.

Deuterium Distribution Among the Liquid-Phase Components. The ^2H NMR spectra for the solutions of 2-propanol-O-*d*, 2-*d* and d_8 after a dehydrogenation reaction for 5 h are shown in Fig. 4.

The deuterium spectral peaks changed variously. Many deuterium atoms were transferred from the hydroxyl group to the methyl and methine groups of 2-propanol-O-*d*. The strongest peak was not observed at the hydroxyl position but, rather, at the methyl position of 2-propanol (Fig. 4A). On the contrary, most of the deuterium atoms in the methine group of

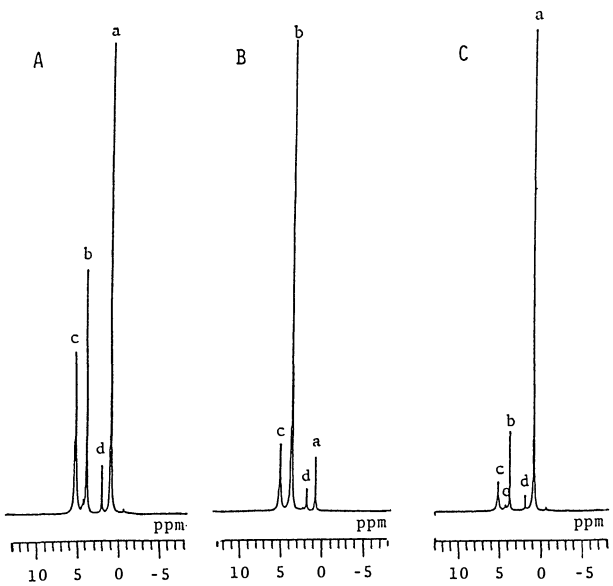

Fig. 4. ^2H NMR spectra of $(CH_3)_2CHOD$ (A), $(CH_3)_2CDOH$ (B), and $(CD_3)_2CDOD$ (C) solutions after 5-h reaction with the suspended nickel fine-particle catalyst (200 mg) at 82.4 °C under refluxing conditions (heat at 100 °C).
Peaks identified as 2-propanol methyl (a), methine (b), and hydroxyl (c) groups, acetone (d) and deuterium oxide (e).
$Si(CD_3)_4$ was used as the standard reference (0.0 ppm).

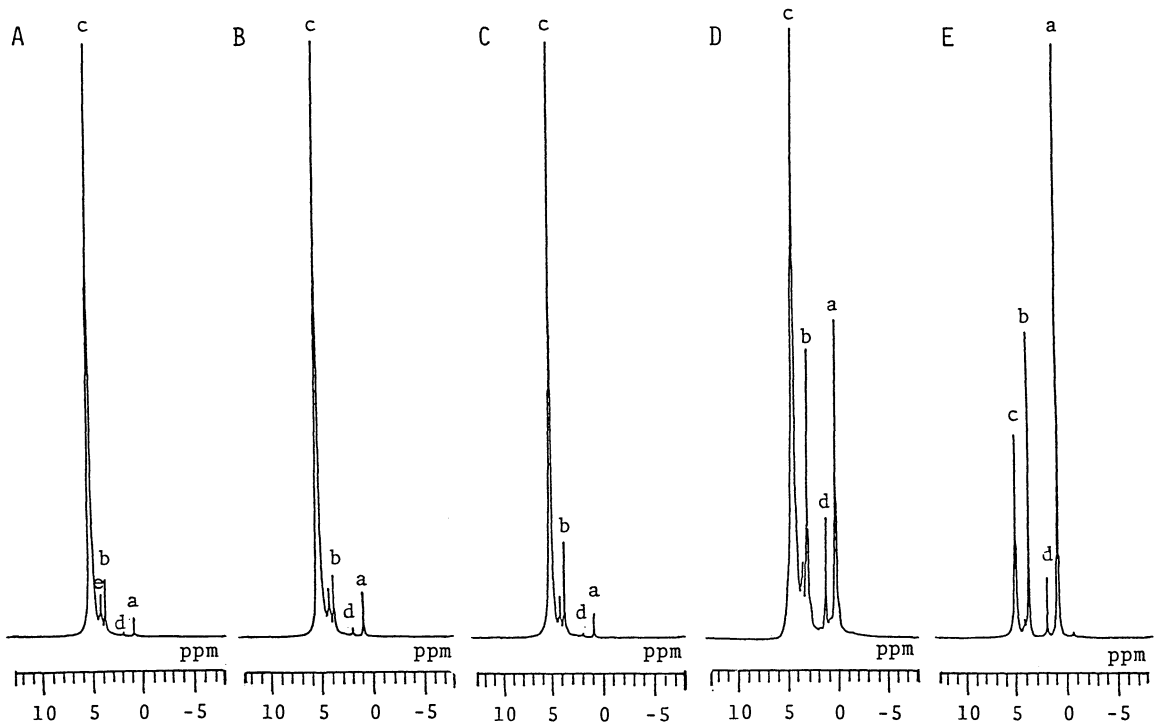

Fig. 5. ^{2}H NMR spectra of 2-propanol-O-*d* after 1/4 h (A), 1 h (B), 2 h (C), and 3 h (D) and 5 h (E) reactions with the suspended nickel fine-particle catalyst (200 mg) at 82.4 °C under refluxing conditions (heat at 100 °C).
Peaks idenified as 2-propanol methyl (a), methine (b), and hydroxyl (c) groups, acetone (d), and deuterium oxide (e) and set as 95% height for the strongest one in each chart.
$Si(CD_3)_4$ was used as the standard reference (0.0 ppm).

2-propanol-2-*d* remained unchanged, though a small amount of deuterium was found at the methyl and hydroxyl groups of 2-propanol (Fig. 4B). The deuterium transfer to acetone was clearly larger from the hydroxyl group than from the methine group of 2-propanol, corresponding to the extents of transfer to the other groups of 2-propanol. As for 2-propanol-d_8, the deuterium peak at the hydroxyl position changed rather extensively, while the other peaks exhibited the smallest variations (Fig. 4C).

A remarkable change which took place in the liquid-phase deuterium distribution of 2-propanol-O-*d* was demonstrated in the ^{2}H NMR spectra after reactions for 1/4, 1, 2, 3, and 5 h time-sequentially (Fig. 5). It should be noted that the deuterium peak at the methine position of 2-propanol increased more rapidly than did the other peaks until 2 h, whereas an extensive change of the hydroxyl peak and a simultaneous increase in the methyl deuterium of 2-propanol became apparent only after 2 h.

Rate Retardation in 2-Propanol Dehydrogenation Due to Acetone. In order to elucidate the retardation effect of acetone on the dehydrogenation rate of 2-propanol, the amounts of hydrogen evolved from solutions of 2-propanol, including acetone-d_6 of 0, 4 and 20 wt%, were pursued as a function of time (Fig. 6). A concentration of 4 wt% corresponded to the

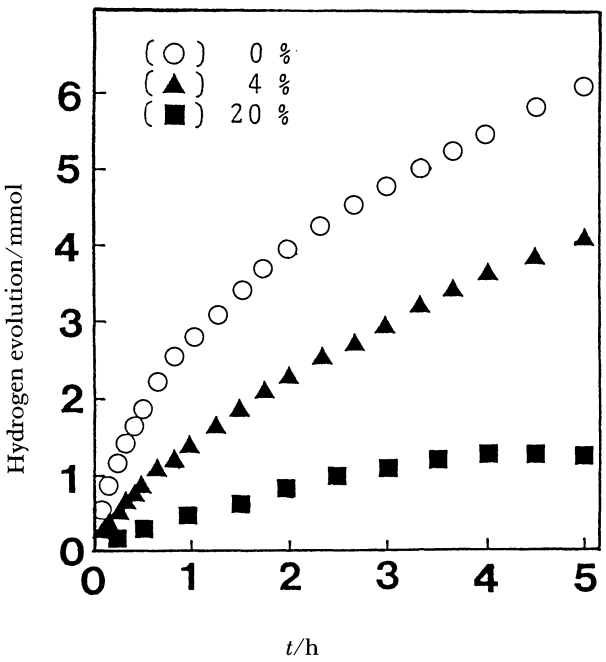

Fig. 6. Dehydrogenation of 2-propanol including acetone-d_6 of 0, 4, and 20 wt% with the suspended nickel fine-particle catalyst (200 mg) at 82.4 °C under refluxing conditions (heat at 100 °C).

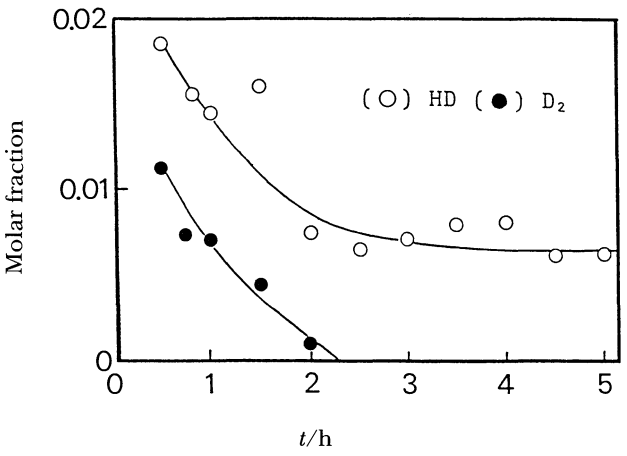

Fig. 7. Variation of HD and D_2 molar fractions in hydrogen evolved from the mixture of 2-propanol-d_0 and acetone-d_6 (4 wt%).

Table 3. Deuterium Distribution among Liquid-Phase Components Yielded from the Mixture of $(CH_3)_2CHOH$ and $(CD_3)_2CO$ (10 vol%) after 1-h or 5-h Reaction with Nickel Fine-Particle Catalyst at 82.4 °C under Refluxing Conditions (heat at 100 °C)

Reaction time/h	Deuterium distribution/% 2-propanol			Acetone
	Methyl	Methine	Hydroxyl	
0	0.00	0.00	0.00	100.00
1	49.5	3.2	19.7	27.7
5	60.1	5.1	17.2	17.7

Catalyst pretreatment: Heated at 160 °C for 1 min under H_2. Catalyst solution: Suspension of 200 mg in the mixed solution (5 ml).

amount of acetone yielded from neat 2-propanol during the 2-h reaction.

The deuterium distribution in hydrogen evolved from a mixed solution of 2-propanol and acetone-d_6 (4 wt%) showed that both HD and D_2 were appreciably formed only during the initial stage (Fig. 7). From the ^2H NMR spectra of a solution mixed with 2-propanol and acetone-d_6 (20 wt%) after the 1- and 5 h reactions, it was found that the deuterium atoms of acetone were transferred mainly to the methyl position of 2-propanol. The variations of the deuterium distribution with the reaction time are summarized in Table 3.

Discussion

Adsorbed Species on the Catalyst Surface. The relatively large molar fractions of HD and D_2 evolved from 2-propanol-O-*d* during the initial stage (Figs. 2 and 3) suggest that 2-propanol adsorbs on the catalyst surface by a facile dissociation of its hydroxyl group. The present view of easy O-D splitting is supported by the fact that an extensive HD exchange was observed among the liquid-phase components after a 5 h reaction for 2-propanol-O-*d*, in contrast to 2-*d* (Fig. 4). The methine C-H bond of adsorbed isopropoxide is rather strong and difficult for dissociation.

$$(CH_3)_2CHOD(l) \rightarrow (CH_3)_2CHO_{ads} + D_{ads}. \quad (5)$$

It is, therefore, deduced that the nickel fine-particle catalyst is covered with the isopropoxide and hydrogen surface species to appreciable extents during the reaction.

The adsorbed acetone is equilibriated rapidly between the keto and enol forms on the catalyst surface,[14] since many deuterium atoms were introduced to acetone during the dehydrogenation of 2-propanol-O-*d* (Figs. 4 and 5).

$$(CH_3)_2CO_{ads} \rightleftarrows CH_2{=}CO{-}CH_{3ads} + H_{ads}. \quad (6)$$

The appearance of deuterium during the earliest stage of the reaction as a gaseous product from acetone-d_6 confirms the view concerning the rapid keto-enol equilibrium of adsorbed acetone (Fig. 7).

Hydrogen Transfer from 2-Propanol to Acetone during 2-Propanol Dehydrogenation. The rapid conversion of acetone-d_6 (20 wt% in 2-propanol-d_0) into the methyl part of 2-propanol (Table 3) strongly suggests that hydrogen transfer from 2-propanol to acetone proceeds on the catalyst surface (Eq. 7)[15] simultaneously with hydrogen evolution.

$$(CD_3)_2CO + (CH_3)_2CHOH \rightarrow (CD_3)_2CHOH + (CH_3)_2CO. \quad (7)$$

The rapid deuterium incorporation from OD into the methine group during the early stage of 2-propanol-O-*d* dehydrogenation (<2 h, Fig. 5) supports the mechanism of hydrogen transfer from 2-propanol to acetone.

The extensive substitution of the methyl hydrogen with deuterium observed during the later stage (>2 h, Fig. 5) is well interpreted in terms of both the keto-enol equilibrium occurring in the product acetone (Eq. 6) and the hydrogen transfer from 2-propanol to acetone (Eq. 7).

These two processes (Eqs. 6 and 7) account for the gradual predominance of H to D species on the surface as well, which was demonstrated by the H/D ratio in the product hydrogen (Fig. 3), especially during the later stage of 2-propanol-O-*d* dehydrogenation.

The sharp contrast in deuterium distribution observed for the product hydrogen from 2-propanol-O-*d* and 2-*d* after the 5-h reaction (Table 2) is ascribed not only to the facile dissociation of the hydroxyl group (Eq. 5) but also to the rapid keto-enol equilibrium (Eq. 6) and the easy hydrogen transfer (Eq. 7).

Rate-Determining Step in 2-Propanol Dehydrogenation. The isotope effects, k_H/k_D, for the dehydrogenation of 2-propanol-2-*d* and d_8 were obtained at 82.4 °C as large as 2.56 and 2.69, respectively, in contrast to 2-propanol-O-*d* of 1.68 (Fig. 1 and Table 1).

The primary isotope effect for eliminating β-hydrogen from the adsorbed propyl species on an aluminium film was reported to be 2.6 at 247 °C.[16] The apparent coincidence in magnitudes suggests that the rate-determining step is the C-H bond dissociation of the methine hydrogen (Eq. 8), which is reconciled with the kinetical conclusion deduced for zinc oxide by Teichner et al.[3]

$$(CH_3)_2CHO_{ads} \rightarrow (CH_3)_2CO_{ads} + H_{ads}. \quad (8)$$

The rate-determining step of the methine C-H dissociation is succeeded by the formation and desorption step of molecular hydrogen:

$$2H_{ads} \rightarrow H_2. \quad (9)$$

Recently, the dehydrogenation rates with a ruthenium catalyst supported on carbon were revealed to be in the order $(CH_3)_2CHOH > (CH_3)_2CDOH > (CH_3)_2CHOD$ under boiling and refluxing conditions, for which the rate-determining step was deduced as the process mentioned above (Eq. 9).[17] On the other hand, the amounts of species adsorbed on the surface can affect the availability of sites for splitting the methine C-H bond of the isopropoxyl moiety. Hence, the predissociation process of the hydroxyl group (Eq. 5) would be relevant to the small, but unnegligible, isotope effects observed for $(CH_3)_2CHOD$ vs. $(CH_3)_2CHOH$ or $(CD_3)_2CDOD$ vs. $(CH_3)_2CDOH$ on the nickel fine-particle catalyst.

Strategies of Catalyst Improvement Suitable for the Newly-Proposed Chemical Heat Pump System. The newly-proposed chemical heat pump[12] requires a catalyst with high selectivity, long life and large space-time yield for 2-propanol dehydrogenation in the presence of acetone.

The strategies for catalyst improvement of the rate constant and the retardation constant consist of: (1) facilitating C-H bond splitting at the methine position and (2) obstructing acetone adsorption in order to avoid any undesirable active-site occupation and hydrogen transfer on the surface.

The reaction rate constant of the nickel fine-particle catalyst (96.9 mmol h^{-1} (metal-g)$^{-1}$) was surpassed by the Ru/carbon catalyst (4630 mmol h^{-1} (metal-g)$^{-1}$),[18] for which the formation and desorption step of molecular hydrogen was elucidated to be rate-determining.[17] Consequently, 2-propanol would be dehydrogenated rapidly as long as the methine C-H bond is easily split.

The adsorption strength of acetone seems to be large with regard to the enol-type surface species. In contrast to the nickel fine-particle catalyst, it was observed that the keto-enol isomerization occurred little on the Ru/carbon catalyst.[17] A larger retardation constant due to acetone adsorption obtained for nickel (0.066 mmol dm^{-3}) than for ruthenium (0.017 mmol dm^{-3})[18] is ascribed to the mode of adsorption (at least partly), since no enol-type species was formed for the latter, according to an ^2H NMR analysis.[17]

Conclusion

(1) The nickel fine-particle catalyst exhibited high selectivity and activity for 2-propanol dehydrogenation at concentrations ten-times larger than those examined previously, with an accompanying rate retardation due to acetone.

(2) The large isotope effects, k_H/k_D, of 2.56 and 2.69 for $(CH_3)_2CDOH$ and $(CD_3)_2CDOD$, respectively, suggested that the C-H dissociation process at the methine position is rate-determining, whereas the unnegligible magnitude of 1.68 for $(CH_3)_2CHOD$ would be related to the predissociation process of the hydroxyl group.

(3) The keto-enol equilibriation of adsorbed acetone proceeded rapidly on the catalyst surface, which would make a certain unfavorable contribution to rate retardation.

(4) The hydrogen transfer from 2-propanol to acetone proceeded simultaneously with the evolution of molecular hydrogen from 2-propanol.

(5) Catalysts more suitable for the chemical heat pump system would be developed by fascilitating methine C-H dissociation and by avoiding enol-type acetone adsorption.

The present work was supported by a Grant-in-Aid on Priority-Area Research from the Ministry of Education, Science and Culture.

References

1) E. J. Wickson, "Kirk-Othmer Encyclopedia of Chemical Technology," 2nd ed, John Willey & Sons, New York (1968), Vol. 16, pp. 564—578.

2) D. R. Stull, F. E. Westrum, Jr., and G. C. Sinke, "The Chemical Thermodynamics of Organic Compounds," John Willey & Sons, New York (1969), pp. 649—651.

3) Y. Dechatre and S. J. Teichner, *Bull. Soc. Chim. Fr.*, **8**, 2804 (1967).

4) O. V. Krylov, "Catalysis by Nonmetals," Academic Press, London (1970).

5) O. Koga, T. Onishi, and K. Tamaru, *J. Chem. Soc., Faraday Trans. 1*, **1980**, 7619.

6) D. J. Wheeler, P. W. Darby, and C. Kemball, *J. Chem. Soc.*, **1960**, 332.

7) F. Clase and J. C. Junger, *Bull. Soc. Chim. Fr., Ser. 5*, **25**, 1167 (1958).

8) F. Velasco, *Chim. Ind.*, **81**, 521 (1959).

9) D. E. Mears and M. Boudart, *AIChE J.*, **12**, 313 (1966).

10) S. Kasyu, M. Nagase, C. Hayashi, R. Uyeda, N. Wada, and N. Kamijyo, *Jpn. J. Appl. Phys.*, **24**, L3 (1985); S. Yatsuya, S. Kasukabe, and R. Ueda, *Jpn. J. Appl. Phys.*, **12**, 1675 (1987).

11) M. Noda, S. Shinoda, and Y. Saito, *Nippon Kagaku-Kaishi*, **1984**, 1017; M. Noda, S. Shinoda, Y. Saito, *Bull. Chem. Soc. Jpn.*, **61**, 961 (1988), 3421 (1988).

12) S. Fujii, H. Kameyama, K. Yoshida, and D. Kunii, *J. Chem. Eng. Jpn.*, **10**, 224 (1977); W. M. Raldow and W. E.

Wentworth, *Solar Energy*, **23**, 78 (1979); Y. Saito, H. Kameyama, and K. Yoshida, *Int. J. Energy Research*, **11**, 594 (1987); Y. Saito, M. Yamashita, and E. Ito, 8th World Hydrogen Energy Conference Honolulu, July 1990, Abstr., B1-6.

13) M. Yamashita, H. Kojima, M. Noda, M. Suzuki, and Y. Saito, *Nippon Kagaku Kaishi*, **1988**, 1292.

14) Keto-enol equilibrium of acetone adsorbed on zinc oxide was proposed previously for the mechanism of the stepwise H–D exchange between acetone-d_0 and acetone-d_6: K. Nagai, K. Tanaka, and K. Miyahara, *Bull. Chem. Soc. Jpn.*, **47**, 2847 (1974).

15) Meerwein–Ponndorf reduction of acetone with 2-propanol is known to take place at 400 °C on zinc oxide, where an enol-type adsorption was demonstrated by IR spectroscopy: K. Nagai and K. Miyahara, *J. Res. Inst. Catalysis, Hokkaido Univ.*, **23**, 98 (1975).

16) B. E. Bent, R. G. Nuzzo, and L. H. Dubois, *J. Am. Chem. Soc.*, **111**, 1634 (1989).

17) M. Yamashita, T. Kawamura, M. Suzuki, and Y. Saito, *Bull. Chem. Soc. Jpn.*, **64**, 272 (1991).

18) Y. Saito, M. Yamashita, and E. Ito, 8th World Hydrogen Energy Conference Honolulu, July 1990, Abstr., B1-6.

A Study of the Reduction of Chelated Palladium on Mercury Electrode

C. K. LAI, Y. Y. WANG,* and C. C. WAN
Department of Chemical Engineering, National Tsing Hua University, Hsinchu, Taiwan, R.O.C.
(Received March 26, 1990)

This paper investigates the reduction kinetics and mechanism of Pd(II)-ethylenediamine with cyclic voltammetry and normal pulse polarography techniques. The results indicate that the reduction is an irreversible process. The major kinetic parameters and diffusion coefficients of Pd(II)-ethylenediamine and other Pd(II)-aliphatic diamine complexes are reported. The influences of concentrations, pH values, and ligand structures on the reduction of Pd(II) complex are also discussed. The electrochemical reaction orders with respect to ethylenediamine and Pd(II)-ethylenediamine are found to be 0 and 1, respectively and these reaction orders demonstrate an undissociated complex reduction mechanism. Finally the iodide effect on normal pulse polarography is studied. The increase in current when iodide is added implies that the reduction is via the outer sphere path way.

A palladium deposit is a good substitute for gold in the electronic industry because of its lower cost and excellent chemical, physical, and electrical properties. Among various Pd plating solutions, Pd-diamine system is an important one.[1-4] Although Pd deposition has become a hot topic in recent years, the electrochemical behavior of Pd^{2+} electrolytes has not received wide attentions yet.

Early in 1945 Willis had studied the polarographic reductions of Pd(II) in various complexing agents such as ammonia, ethylenediamine(en), diethylamine, and ethanolamine. He found that the reductions are incompletely reversible two-electron processes.[5] He also found that the half-wave potentials of the reductions of these complexes are more negative as the ligand becomes more basic. Later, Simpson et al. studied the Pd(II) reductions with polarography and obtained the diffusion coefficients of Pd(II) complexes in solutions containing chloride and acetate.[6] Chakravarty also studied polarographic behavior of Pd(II) complexes and discovered that those Pd(II) complexes with ammonia or ethylenediamine as complexing agents are irreversibly reduced.[7] Hirota et al. studied reductions of Pd(II) complexes and found that the more stable the complex the more difficult the reduction.[8] The polarography studies of Gaur revealed that the reduction of Pd(II) in 0.2 M pyridine, 0.1 M HCl is a quasi-reversible process[9,10] (1 M=1 mol dm^{-3}).

The reduction mechanism of $PdCl_4^{2-}$ on some solid electrodes has been studied by some authors. Confusing results were obtained. Watt and Cunningham reported that $PdCl_4^{2-}$ is the species that was reduced.[11] Later in a series of papers published by Harrison and co-workers, $PdCl_2$ was thought to be the species that was reduced, though the prevailing ion in solution is $PdCl_4^{2-}$.[12-17]

For quantative analysis, both direct current polarography and differential pulse polarography have been used to determine Pd(II) concentration.[18-25]

There have been few studies concerning the electrochemical behavior of chelated Pd(II) though it is an important ingredient of palladium plating solution. In this work both the electrode kinetics and reduction mechanism are investigated. First we study the reduction kinetics of Pd(II) chelated with diamines on a mercury drop electrode with cyclic voltammetry(CV) and normal pulse polarography(NPP) techniques. Both kinetic parameters and diffusion coefficients are reported. The influences of concentrations, pH values, and ligand structures on the reduction of Pd(II) complex are discussed. Then we consider the reduction mechanism of $Pd(en)_2^{2+}$. In order to ascertain the reactive species of $Pd(en)_2^{2+}$ reduction, the electrochemical reaction orders with respect to en and $Pd(en)_2^{2+}$ are used as criteria. Finally the iodide effect on NPP is also investigated for a further understanding of the essence of $Pd(en)_2^{2+}$ reduction.

Experimental

A palladium stock solution was prepared by dissolving reagent grade $PdCl_2$ (Wako Co.) in deionized water with sufficient potassium chloride to enhance its solubility and stability. The Pd content was 0.06 M. NaI, KCl, en, 1,2-propanediamine (1,2-pn, Merck), 1,3-propanediamine (1,3-pn, Janssen), 1,4-butanediamine (bn, Janssen), 1,6-hexanediamine (hn, Merck) were all dissolved in deionized water to 2 M. The concentration of Triton X-100 (Merck) solution was 0.1%. The test solutions were prepared by mixing these stock solutions to desired concentrations. Hydrochloric acid and sodium hydroxide were used to adjust the pH value.

All CV and NPP experiments were performed on an EG&G Model 384B polarographic analyzer. A mercury drop electrode controlled by mechanical motions (EG&G Model 303A) was used as the working electrode (electrode area 0.009 cm^2). Platinum wire and a silver-silver chloride electrode (SSCE) were used as counter and reference electrodes, respectively. In CV experiments the scan rates ranged from 25 mV s^{-1} to 500 mV s^{-1} while the scan rate was 10 mV s^{-1} with a drop time of 1 second for all NPP experiments. Before the measurements, nitrogen purified through the vanadium (II) chloride scrubbing solution was bubbled into test solutions for 10 minutes to exclude the dissolved oxygen.

All chemicals were reagent grade and used without further purification. The complexes were identified by ultraviolet-(UV) absorption experiments (Hitachi, model 320).[26-28]

Results and Discussion

1. Fundamental Kinetic Studies. First we discuss the reversibility of the $Pd(en)_2^{2+}$ reduction process. Fig. 1 shows the cyclic voltammogram of $Pd(en)_2^{2+}$. Obviously the complex reduction is irreversible. For a totally irreversible system, peak current (I_p) is proportional to the square root of scan rate ($v^{1/2}$) which is not the case for a partially irreversible process. Figure 2 confirms this.

The kinetic parameters and diffusion coefficients were derived from NPP experiments. The normal pulse polarogram of $Pd(en)_2^{2+}$ without the addition of

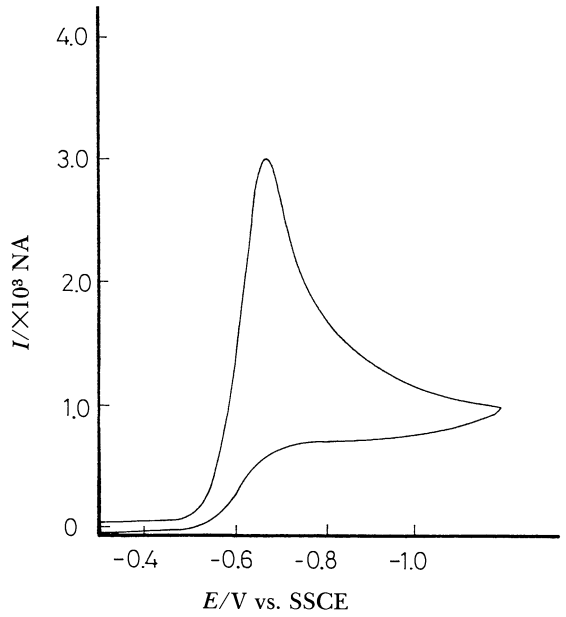

Fig. 1. Cyclic voltammogram of $Pd(en)_2^{2+}$. Solution contains 0.1 M KCl, 0.1 M en, 3×10^{-4} M $Pd(en)_2^{2+}$, scan rate 400 mV s^{-1}.

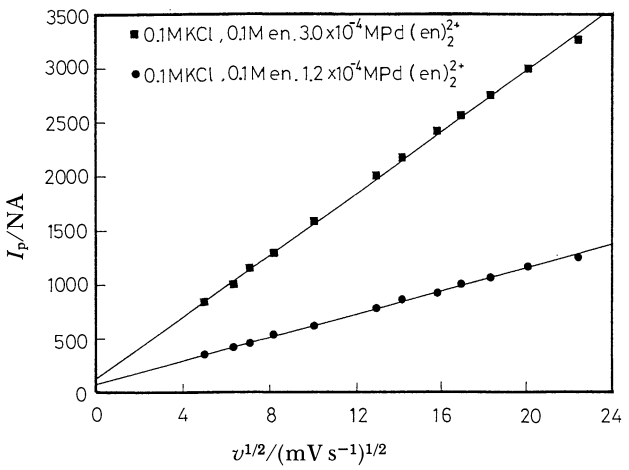

Fig. 2. Plot of I_p vs. $v^{1/2}$.

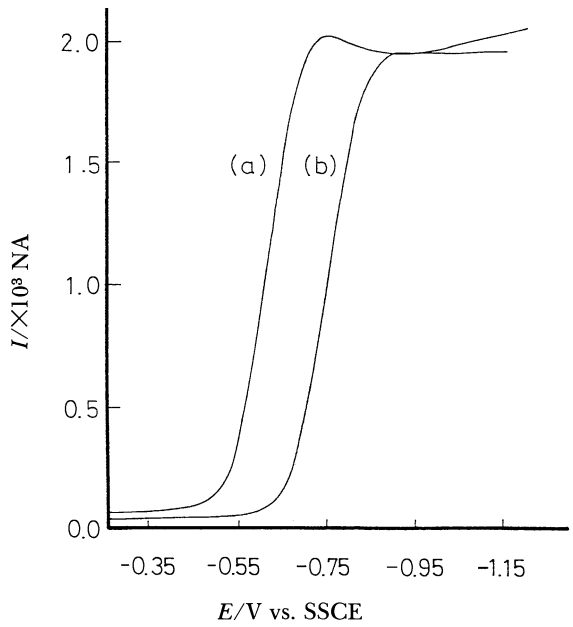

Fig. 3. Normal pulse polarogram of $Pd(en)_2^{2+}$. Solution contains 0.1 M KCl, 0.1 M en, 1.2×10^{-4} M $Pd(en)_2^{2+}$, and (a) no Triton X-100 (b) 0.003% Triton X-100.

Triton X-100 is shown in Fig. 3(a) which contains a maximum. In order to analyze the polarogram successfully, Triton X-100 was added to suppress the maximum. The result is shown in Fig. 3(b). The addition of Triton X-100 shifts the reduction toward negative direction by about 0.15 V.

The relationship between the diffusion-controlled current(I_d) and bulk solution concentration (C_b) is known as:[29]

$$I_d = \frac{nFAD_o^{1/2}C_b}{\pi^{1/2}(t-t')^{1/2}} \quad (1)$$

where n, F, and A are number of electrons transferred, faradic constant, and electrode surface area respectively, D_o is diffusion coefficient, and t-t' is the NPP sampling time (40 milliseconds). With this equation, the diffusion coefficients can be calculated.

The polarograms were analyzed according to the method proposed by Oldham and Parry for irreversible processes.[30] A plot of log $\{x^2(1.75+x^2)/(1-x)\}$ (where $x=i/i_d$) against electrode potential E should yield a straight line whose slope and intercept can be used to calculate the charge transfer coefficient α and rate constant k. All data reported below were obtained in this way and the effects of concentrations, pH values, and ligand structure will be discussed in the following sections.

1.1. The Effects of Concentrations. The effects of concentrations of $Pd(en)_2^{2+}$ and en upon kinetic parameters and diffusion coefficient were studied. It is found that both concentrations have little influences on these figures in the concentration range of 1.5×10^{-5} to 3×10^{-4} M ($Pd(en)_2^{2+}$) and 0.1 to 0.001

M(en). The αn, $E_{1/2}$, and k^r values are 0.51, −0.75 (V vs. SSCE), and 3.7×10^{-4} (cm s^{-1}) respectively. The diffusion coefficient is 1.1×10^{-5} $cm^2 s^{-1}$ which is somewhat larger than those obtained by Simpson et al.[6] ($4—8\times10^{-6}$ $cm^2 s^{-1}$, for Pd(II) in solutions containing chloride and acetate) and by Harrison et al.[13] (7×10^{-6} $cm^2 s^{-1}$, for Pd(II) in chloride solutions).

1.2. The Effects of pH Values. The normal pulse polarograms were also studied in various pH values. Surprisingly different mixing procedures gave different results. Thus it is important to identify the complexes which exist in test solutions. The results in Table 1(a) were obtained from solutions of various pH values which were prepared by adding $PdCl_2^{2-}$, then HCl (or NaOH) to en solution. It is discovered that $Pd(en)_2^{2+}$ was always formed completely since the limiting current observed was the same throughout the pH values studied. The reductions were stable in basic conditions while the half-wave potential shifted negatively with the increase of acidity in acid region. This potential change is attributed to the chloride effect introduced by the addition of HCl since similar results were observed when KCl was used in the experiments instead. It is thus concluded that the accumulation of chloride moves the reduction potential of $Pd(en)_2^{2+}$ toward the hydrogen evolution region and is unfavorable in the electroplating process.

Table 1(b) shows the NPP results obtained from the opposite mixing procedure, i.e., HCl (or NaOH) was added to en solution before the $PdCl_4^{2-}$. Different results were observed in pH 3.55 and 12.56. In acidified solutions the reduction current of $Pd(en)_2^{2+}$ decreased with increasing H^+ concentration and finally the reduction wave disappeared. This phenomenon can be explained by en protonation reported by De Waal and Robb.[31] Since

$$en + H^+ \rightleftarrows Hen^+, \quad (2)$$

$$Hen^+ + H^+ \rightleftarrows H_2en^{2+}, \quad (3)$$

the major species in an acidified en solution is H_2en^{2+}. After complete protonation, H_2en^{2+} loses its ability to form a complex with Pd(II). This en protonation results in a diminution of free en and then $Pd(en)_2^{2+}$ concentration. Finally in highly acidified solutions, the $Pd(en)_2^{2+}$ reduction current can not be found any more.

This explanation is supported by the UV absorption experiments. The pH 3.55 solution in Table 1(b) showed a λ_{max} of 280 nm with high intensity, which is characteristic of $PdCl_4^{2-}$. Obviously there was no free en to subsititute the chloride of the added $PdCl_4^{2-}$ and consequently no $Pd(en)_2^{2+}$ reduction was observed.

The polarogram in highly basic condition (pH 12.56) in Table 1(b) is presented in Fig. 4(a). A two-wave polarogram was observed. Also shown in Fig. 4(b) is the polarogram of the same solution without en (i.e., the complex in solution is $Pd(OH)_4^{2-}$). From Fig. 4(b) it is apparent that $Pd(OH)_4^{2-}$ is not reduced in the potential range studied. Thus the reduction current in Fig. 4(a) should be attributed to $Pd(en)_2^{2+}$ reduction. In fact the half-wave potential of the first wave is almost the same as that of $Pd(en)_2^{2+}$. This result may be explained qualitatively as follows. As $PdCl_4^{2-}$ was added into a highly alkaline en solution,

Table 1(a). Parameters Calculated from NPP Data in Solutions of 0.1 M KCl+0.001 M en+1.2×10^{-4} M $PdCl_4^{2-}$+0.003% Triton X-100+Various Amounts of HCl or NaOH to Desired pH Values

pH	αn	$-E_{1/2}$	$k^r\times10^{-4}$	$D_o\times10^{-5}$
		V vs. SSCE	cm s^{-1}	$cm^2 s^{-1}$
3.55	0.56	0.78	1.4	1.1
6.43	0.52	0.77	2.3	1.1
9.92	0.50	0.75	3.9	1.1
11.56	0.51	0.75	3.7	1.1
12.56	0.52	0.75	3.5	1.1

Table 1(b). Parameters Calculated from NPP Data in Solutions of 0.1 M KCl+0.001 M en+0.003% Triton X-100+Various Amounts of HCl or NaOH to Desired pH Values +1.2×10^{-4} M $PdCl_4^{2-}$

pH	αn	$-E_{1/2}$	$k^r\times10^{-4}$	$D_o\times10^{-5}$
		V vs. SSCE	cm s^{-1}	$cm^2 s^{-1}$
3.55	a)	a)	a)	a)
6.43	0.53	0.77	2.3	1.2
9.92	0.50	0.75	3.9	1.1
11.56	0.50	0.75	3.9	1.1
12.56	b)	b)	b)	b)

a) No $Pd(en)_2^{2+}$ reduction was observed. b) Two-wave polarogram was observed, see Fig. 4(a).

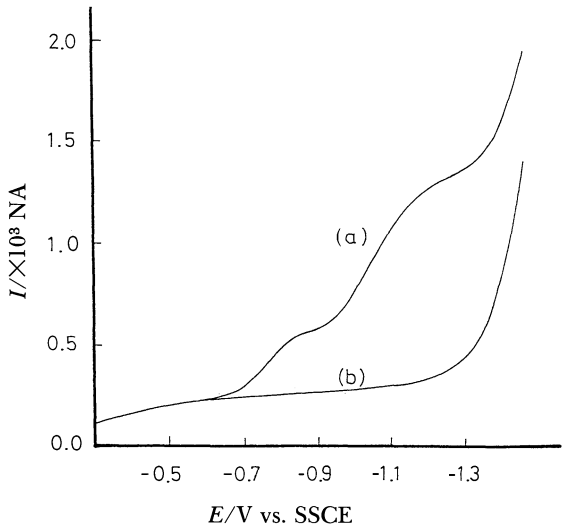

Fig. 4. Normal pulse polarograms of solutions of 0.1 M KCl, NaOH (to pH=12.56), 1.2×10^{-4} M $PdCl_4^{2-}$, 0.003% Triton X-100, and (a) 0.001 M en (b) without en.

chloride was substituted by either en or OH^- group and consequently there exist both $Pd(OH)_4^{2-}$ and $Pd(en)_2^{2+}$ in the solution. The UV absorption of the solution in Fig. 4(a) shows that the absorption maximum occurs at 365 nm, which is the same as that of the solution in Fig. 4(b), but with a smaller intensity. This observation implies that the solution in Fig. 4(a) contains both $Pd(OH)_4^{2-}$ and $Pd(en)_2^{2+}$ and the UV absorption of $Pd(en)_2^{2+}$ may be covered by that of $Pd(OH)_4^{2-}$.

Now the polarogram can be explained. In the first wave, $Pd(en)_2^{2+}$ is reduced and a limiting current which is controlled by the diffusion of $Pd(en)_2^{2+}$ is achieved. But en released due to $Pd(en)_2^{2+}$ reduction accumulates on the electrode surface and reacts with $Pd(OH)_4^{2-}$ to form more $Pd(en)_2^{2+}$. As a result the reduction current increases again and the surface concentration of $Pd(OH)_4^{2-}$ decreases as the potential increases. Finally another limiting current which is subjected to the diffusion of $Pd(OH)_4^{2-}$ appears.

1.3. The Effects of Ligand Structure. In order to investigate the effects of ligand structure on the complex reduction, we also carried out the CV and NPP experiments of Pd(II) in solutions containing aliphatic diamines with different carbon numbers. The experimental results show that they are all reduced irreversibly and the calculated parameters are summarized in Table 2.

The αn values are almost the same although the half-wave potentials do exhibit some difference between the 5 complexes. This is quite reasonable if we consider the essence of these complexes. Willis[5] reported that Pd(II) complexes have increasing negative half-wave potentials as the ligand becomes more basic. Hirota et al.[8] further pointed out that the reduction is directly related to the stability of the complex. Though the diamines studied here have greater basicity when the length of the carbon chain increases, the half-wave potential does not change significantly. This can be explained in terms of the chelate structure of the complexes. As the carbon number increases, the half-wave potential shifts in the negative direction because of the increasing basicity. However, too long a chain makes the chelate ring unstable and results in the shift of half-wave potential in the positive direction. As a result a maximum occurred at the ligand, 1,3-pn. The same effects were also observed in the rate constants.

The variation of ligand also has an influence upon diffusion coefficient as shown in Table 2. Obviously the complex with a larger volume has a smaller diffusion coefficient, which is consistent with the prediction of the Wilke-Chang equation.[32]

2. Reduction Mechanism Studies. For the reduction of $Pd(en)_2^{2+}$ on mercury electrode, we consider three possible mechanisms as follows:

$$\text{(a) } Pd(en)_2^{2+} + 2e^-(Hg) \longrightarrow \text{Pd-amalgam} + 2en, \quad (4)$$

$$\text{(b) } Pd(en)_2^{2+} \rightleftarrows Pd(en)^{2+} + en, \quad (5)$$

$$Pd(en)^{2+} + 2e^-(Hg) \longrightarrow \text{Pd-amalgam} + en, \quad (6)$$

$$\text{(c) } Pd(en)_2^{2+} \rightleftarrows Pd^{2+} + 2en, \quad (7)$$

$$Pd^{2+} + 2e^-(Hg) \longrightarrow \text{Pd-amalgam}. \quad (8)$$

Corresponding to these three mechanisms, the current-concentration relationships are:

$$I = K[Pd(en)_2^{2+}], \text{ for (a)}, \quad (9)$$

$$I = K[Pd(en)_2^{2+}][en]^{-1}, \text{ for (b)}, \quad (10)$$

$$I = K[Pd(en)_2^{2+}][en]^{-2}, \text{ for (c)}, \quad (11)$$

where K is a proportional constant and $[Pd(en)_2^{2+}]$, [en] represent concentrations of $Pd(en)_2^{2+}$ and en respectively. The difference of the electrochemical reaction orders between the three possible mechanisms are listed in Table 3.

First we carried out the NPP experiments without the addition of Triton X-100 to avoid the interference which may be introduced by surface active materials such as gelatin, Triton, etc. Figures 5 and 6 are the $\log I$ vs. $\log C$ plots derived from NPP experiments under various $Pd(en)_2^{2+}$ and en concentrations. These figures show that the electrochemical reaction orders with respect to $Pd(en)_2^{2+}$ and en are 1 and 0 respectively. Hence according to Table 3 we conclude that the reduction mechanism is mechanism (a), i.e., $Pd(en)_2^{2+}$ is reduced to Pd-amalgam directly (Eq. 4).

The influence of Triton X-100 on the reduction mechanism of $Pd(en)_2^{2+}$ was also investigated through NPP analyses. One of the polarograms is shown in Fig. 3(b). It seems that Triton X-100 shifts the reduction toward negative direction and has little effect upon its shape except in the region where diffusion becomes important. The electrochemical reaction orders with respect to $Pd(en)_2^{2+}$ and en in the presence of Triton X-100 were also calculated from $\log I$ vs. $\log C$ plots and were found to be 1 and 0 respectively.

Table 2. Parameters Calculated from NPP Data in Solutions of 0.1 M KCl, 0.003% Triton X-100, and 1.2×10^{-4} M $Pd(L)_2^{2+}$

L	αn	$-E_{1/2}$	$k^r\times10^{-4}$	$D_o\times10^{-5}$
		V vs. SSCE	cm s^{-1}	cm^2 s^{-1}
en	0.51	0.75	3.7	1.1
1,2-pn	0.53	0.73	4.7	1.0
1,3-pn	0.53	0.78	1.7	1.0
bn	0.52	0.74	3.6	0.8
hn	0.51	0.56	83	0.3

Table 3. Electrochemical Reaction Orders for Different Reduction Mechanisms

Electroactive species	Electrochemical reaction order	
	$[Pd(en)_2^{2+}]$	[en]
$Pd(en)_2^{2+}$	1	0
$Pd(en)^{2+}$	1	−1
Pd^{2+}	1	−2

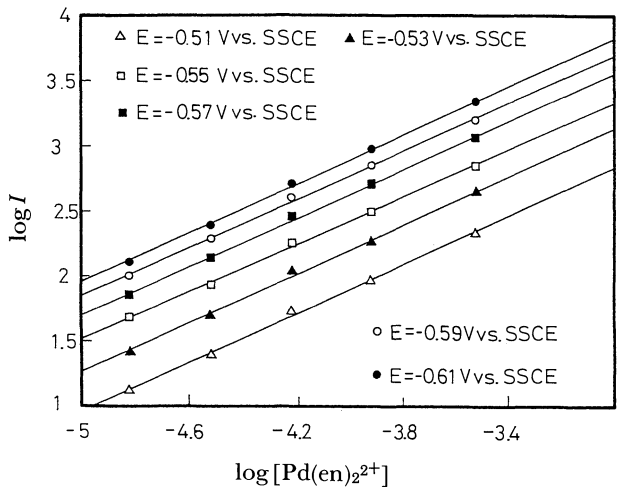

Fig. 5. Plot of $\log I$ vs. $\log[Pd(en)_2^{2+}]$. Solutions contain 0.1 M KCl, 0.1 M en, and various $Pd(en)_2^{2+}$ concentrations.

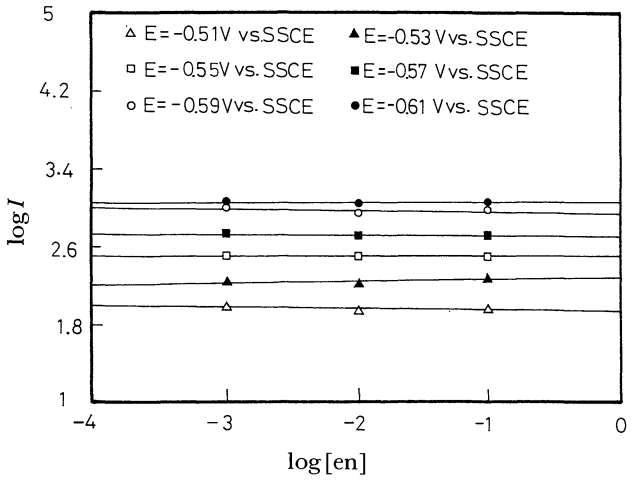

Fig. 6. Plot of $\log I$ vs. $\log[en]$. Solutions contain 0.1 M KCl, 1.2×10^{-4} M $Pd(en)_2^{2+}$, and various en concentrations.

Based on these results we know that Triton X-100 does not alter the reduction mechanism of $Pd(en)_2^{2+}$.

We also studied further the nature of the discharge complex in double layer by adding iodide into electrolyte. Because of its ability to be adsorbed strongly on mercury surface and its electrochemical inactivity,[33-36] iodide is commonly used to distinguish between the inner sphere and outer sphere mechanisms for reductions of positively charged complexes. For an inner sphere mechanism, the transition state will be formed at the inner Helmholtz Plane (IHP). The presence of iodide which is strongly adsorbed on the surface will lead to a competition for adsorption sites which should raise the energy of the transition state and produce a lower reaction rate. But if an outer sphere reaction pathway is involved, the addition of iodide should produce rate changes only if there is an alternation in the potential at the outer

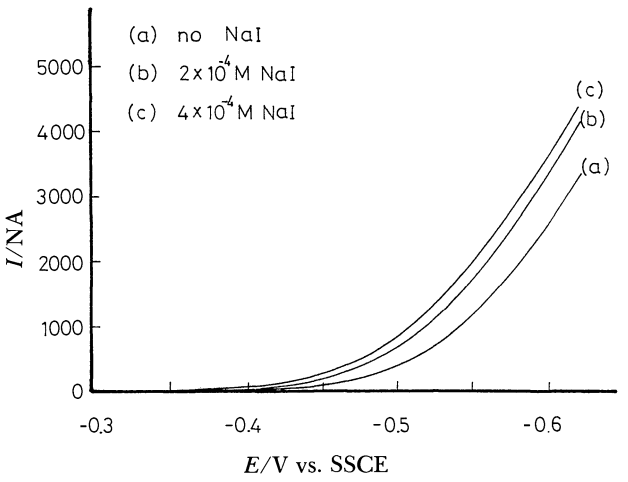

Fig. 7. Iodide effect on NPP experiments. Solutions contain 0.1 M KCl, 0.1 M en, 3×10^{-4} M $Pd(en)_2^{2+}$, and different amounts of NaI.

Helmholtz Plane (OHP). This will result in a surface concentration increase because of the greater electrostatic attraction caused by iodide adsorption. Consequently a current increase is expected.

The iodide effects on normal pulse polarograms of $Pd(en)_2^{2+}$ are shown in Fig. 7. An increase in current was observed which implies that $Pd(en)_2^{2+}$ reduction should proceed via the outer sphere mechanism. That is, the complex does not enter the inner Helmholtz Plane.

Conclusions

Both CV and NPP data show that $Pd(en)_2^{2+}$ reduction is an irreversible process. The reduction is independent of both $Pd(en)_2^{2+}$ and en concentrations. The half-wave potential is -0.75 V (vs. SSCE, in the presence of 0.003% Triton X-100) and diffusion coefficient is 1.1×10^{-5} $cm^2 s^{-1}$.

Different mixing procedures give different complexes which have been identified by UV absorption experiments. If Pd(II) is added to en solution before pH adjustment, $Pd(en)_2^{2+}$ is always formed completely. When Pd(II) is added to an acidified en solution, the $Pd(en)_2^{2+}$ reduction current decreases and finally no $Pd(en)_2^{2+}$ reduction can be observed. On the other hand, adding Pd(II) to an en solution of high OH^- concentration results in a two-wave polarogram. The two waves are controlled by the diffusion of $Pd(en)_2^{2+}$ and $Pd(OH)_4^{2-}$ respectively.

The reduction of different Pd-diamine complexes depends on the coordinated ligands. A compromise of basicity and chelate ring size results in a maximal half-wave potential at $Pd(1,3\text{-pn})_2^{2+}$.

The electrochemical reaction orders with respect to $Pd(en)_2^{2+}$ and en are 1 and 0 respectively and won't be altered by the addition of Triton X-100. The addition of iodide increases the reduction current of $Pd(en)_2^{2+}$. From these two results, we conclude that

the $Pd(en)_2^{2+}$ reduction process can be described as follows:

$$Pd(en)_2^{2+}\ (bulk) \rightleftarrows Pd(en)_2^{2+}\ (OHP),$$

$$Pd(en)_2^{2+}\ (OHP) + 2e^- (Hg) \longrightarrow Pd\text{-amalgam} + 2en.$$

References

1) S. Yoshimura, S. Chida, E. Sato, and N. Kubota, *Met. Finish.*, **84**, 39 (1986).
2) J. A. Abys and H. S. Trop, U.S. Patent 4486274 (1984).
3) R. J. Morrissey, U.S. Patent 4278514 (1981).
4) R. J. Morrissey, U.S. Patent 4406755 (1983).
5) J. B. Willis, *J. Am. Chem. Soc.*, **67**, 547 (1945).
6) R. B. Simpson, R. L. Evans, and H. A. Saroff, *J. Am. Chem. Soc.*, **77**, 1438 (1955).
7) B. Chakravarty and D. Banerjea, *J. Inorg. Nucl. Chem.*, **16**, 288 (1961).
8) M. Hirota, Y. Umezawa, M. Nakamura, and S. Fujiwara, *J. Inorg. Nucl. Chem.*, **33**, 2617 (1971).
9) J. N. Gaur, S. C. Baghel, and R. S. Sharma, *Inorg. Chim. Acta*, **30**, 65 (1978).
10) R. S. Sharma and J. N. Gaur, *Bull. Electrochem.*, **2**, 485 (1986).
11) G. W. Watt and J. A. Cunningham, *J. Electrochem. Soc.*, **110**, 716 (1963).
12) M. F. Bell and J. A. Harrison, *Electroanal. Chem. Interfacial Electrochem.*, **41**, 15 (1973).
13) J. A. Harrison, R. P. J. Hill, and J. Thompson, *Electroanal. Chem. Interfacial Electrochem.*, **47**, 431 (1973).
14) J. A. Harrison and J. Thompson, *Electrochim. Acta*, **18**, 829 (1973).
15) J. A. Harrison, H. B. Sierra Alcazer, and J. Thompson, *Electroanal. Chem. Interfacial Electrochem.*, **53**, 145 (1974).
16) J. N. Crosby, J. A. Harrison, and T. A. Whitfield, *Electrochim. Acta*, **26**, 1647 (1981).
17) J. N. Crosby, J. A. Harrison, and T. A. Whitfield, *Electrochim. Acta*, **27**, 897 (1982).
18) R. F. Wilson and R. C. Daniels, *Anal. Chem.*, **27**, 904 (1955).
19) B. K. Puri and A. Kumar, *Analyst*, **108**, 1345 (1983).
20) R. Sreenivasulu, V. S. R. Rao, and K. H. Reddy, *Analyst*, **110**, 411 (1985).
21) G. M. Rafi and A. Paul, *Curr. Sci.*, **51**, 350 (1982).
22) T. C. Childers, P. Moncuse, J. J. Reiss, and S. K. Vohra, *Am. Lab.*, **1984**, 37.
23) A. Varma, *Talanta*, **28**, 701 (1981).
24) R. J. Magee and I. A. Beattie, *Anal. Chim. Acta*, **28**, 253 (1963).
25) W. H. Douglas and R. J. Magee, *J. Electroanal. Chem.*, **5**, 171 (1963).
26) G. Anderegg, *Inorg. Chim. Acta*, **111**, 25 (1986).
27) L. Rasmussen and Chr. K. Jorgensen, *Acta Chem. Scand.*, **22**, 2313 (1968).
28) A. J. Cohen and N. Davidson, *J. Am. Chem. Soc.*, **73**, 1955 (1951).
29) A. J. Bard and L. R. Faulkner, "Electrochemical Methods, Fundamentals and Applications," Wiley (1984).
30) K. B. Oldham and E. P. Parry, *Anal. Chem.*, **40**, 65 (1968).
31) D. J. A. De Waal and W. Robb, *Int. J. Chem. Kinet.*, **6**, 309 (1974).
32) R. H. Perry and D. Green, "Perry's Chemical Engineers' Handbook," 6th ed, McGraw-Hill (1984).
33) M. J. Weaver and F. C. Anson, *Inorg. Chem.*, **15**, 1871 (1976).
34) M. J. Weaver and F. C. Anson, *J. Am. Chem. Soc.*, **97**, 4403 (1975).
35) F. C. Anson, M. G. Finn, and A. Yamada, *Inorg. Chem.*, **16**, 2124 (1977).
36) M. J. Weaver and T. L. Satterberg, *J. Phys. Chem.*, **81**, 1772 (1977).

Oxidation of *trans*-1,2-Cyclohexanediaminetetraacetatocobaltate(II) by Peroxodiphosphate Catalyzed by Ag(I) in Acetate Buffers. A Kinetic Study

Pathaneni SIVASWAROOP, Kondapi ANANDKUMAR, and Panuganti V.K. RAO*
Physical Chemistry Research Laboratories, School of Chemistry,
Andhra University, Visakhapatnam 530003, India
(Received April 9, 1990)

The kinetics of oxidation of *trans*-1,2-cyclohexanediaminetetraacetatocobaltate(II) by peroxodiphosphate (PDP) in acetate buffers was studied in the presence of Ag(I). For the first time, this study gives a clear evidence for the involvement of Ag(I)/Ag(II) cycle in the Ag(I)-catalyzed PDP oxidation reactions in acetate buffers. A plausible mechanism consistent with the observed kinetic features is proposed.

Peroxodiphosphate (PDP) is the structural and electronic analogue of peroxodisulfate (PDS). The Ag(I)-catalyzed reactions of PDP are scanty[1,2] when compared with those of PDS.[3] In acid medium, the PDP reactions are liable to occur via a hydrolytic path and the reactivity was ascribed to the hydrolytic product. In acetate buffered medium, the hydrolysis of PDP is negligible and the reactive species is PDP itself. In this medium, the uncatalyzed reactions were reported to be slow[4] and Ag(I) is recently proposed as an efficient catalyst for these reactions.[4-7] But these studies could not clearly establish whether the reaction occurs through an Ag(I)/Ag(II) cycle or via complexation of PDP with Ag(I). We report in this communication the results of our studies to clarify the role played by Ag(I) in the Ag(I)-catalyzed oxidation of *trans*-1,2-cyclohexanediaminetetraacetatocobaltate(II), $[Co(cydta)]^{2-}$ by PDP in acetate buffers.

Experimental

All the aqueous solutions were prepared afresh with double distilled deionized water. Peroxodiphosphate is a gift sample from FMC Corporation, USA and was used as such. Its aqueous solutions were standardized iodometrically.[8] *trans*-1,2-Cyclohexanediaminetetraacetic acid (H_4cydta) is an Aldrich sample and the aqueous solutions of its disodium salt were standardized against standard zinc sulfate solution in ammonical buffers (pH=10) using Eriochrome Black T as indicator. All other reagents were either AR or GR grade as the case may be. Ionic strength of the medium was maintained by using E. Merck's 'p.a.' grade sodium nitrate. The pH of the medium was maintained by varying [AcOH] and fixing [AcONa]. In all the kinetic runs, the ligand was in 10% excess to that of [Co(II)].

The kinetics of the reaction were monitored spectrophotometrically by measuring the increase in absorbance of the product, $[Co(cydta)]^-$ at 545 nm using a Carl Zeiss 'Spekol' spectrocolorimeter in conjunction with an EK_5 attachment and a Cenco circulation cum immersion thermostat. Toshniwal's CL-46 digital pH meter was used for adjusting the pH of the reaction mixtures. The reaction was initiated by adding the temperature-equilibrated Ag(I) solution to the rest of the reaction mixture kept at 30.0±0.1 °C in a black coated reaction vessel. The reaction mixture was immediately transferred to the optical cell of the spectrocolorimeter and the increase in optical density (OD) at 545 nm against the reagent blank was noted from time to time.

Results

When the spectrum of the reaction mixture in a typical kinetic run was recorded with time on a Shimadzu UV-260 spectrophotometer in the range 360—600 nm, two absorption maxima (380 and 545 nm) were noticed all through the reaction time unlike in earlier reports using other oxidants[9] where the former peak was noticed after a certain period of time since the commencement of the reaction.

The stoichiometry of the reaction was determined under the conditions: $[Co^{II}(cydta)^{2-}] \gg [PDP]$ at 30.0±0.1 °C. The amount of $[Co^{III}(cydta)^-]$ formed

Table 1. Kinetic Data for the Oxidation of $[Co(cydta)^{2-}]$ by Peroxodiphosphate Catalyzed by Ag(I) in Acetate Buffers[a]

$[Co(cydta)^{2-}]$	[PDP]	[Ag(I)]	$[H^+]$	$k_0 \times 10^7$
$\times 10^4$ M	$\times 10^3$ M	$\times 10^4$ M	$\times 10^6$ M	M s^{-1}
5.0	30.0	10.0	10.0	7.96
10.0	30.0	10.0	10.0	8.33
15.0	30.0	10.0	10.0	8.05
20.0	30.0	10.0	10.0	8.23
25.0	30.0	10.0	10.0	8.55
30.0	30.0	10.0	10.0	8.50
20.0	5.0	10.0	10.0	1.0
20.0	10.0	10.0	10.0	2.06
20.0	15.0	10.0	10.0	3.56
20.0	20.0	10.0	10.0	4.18
20.0	30.0	10.0	10.0	7.33
20.0	30.0	5.0	10.0	3.68
20.0	30.0	10.0	10.0	7.80
20.0	30.0	15.0	10.0	12.88
20.0	30.0	20.0	10.0	18.21
20.0	30.0	10.0	1.78	11.06
20.0	30.0	10.0	5.62	9.73
20.0	30.0	10.0	10.0	8.45
20.0	30.0	10.0	22.38	6.96
20.0	30.0	10.0	56.23	5.31

a) I=0.3 mol dm^{-3}: Temp=30.0±0.1 °C.

was estimated by measuring the optical density of the reaction mixture at the end of the reaction (D_∞) as indicated by its constancy with time and the molar absorbance of the [Co^{III}(cydta)$^-$]. It was observed that 2 moles of [Co^{II}(cydta)$^{2-}$] required one mole of PDP for its complete oxidation.

The progress of the reaction was monitored at 545 nm upto 80% completion of the reaction. The plots of (D_∞-D_t) versus time (where D_∞ and D_t are the optical densities of the reaction mixture after completion of the reaction and at time 't' respectively) were linear. From the slopes of these plots, the zero-order rate constants (k_0) were evaluated and are given in Table 1. The zero-order rate constants were found to be independent of [Co(cydta)$^{2-}$], suggesting the independence of the reaction rate on the [Co(cydta)$^{2-}$]. When the substrate was varied in the range (5.0—30.0)$\times10^{-4}$ mol dm^{-3}, keeping all other parameters constant, the D_∞ values were plotted against [Co(cydta)$^{2-}$], a straight line passing through origin was obtained. From the slope of this plot, the molar extinction coefficient (ε) was found to be 310±8 mol^{-1} dm^3 cm^{-1}, which is in good agreement with that reported earlier[10] for [Co(cydta)$^-$] under similar experimental conditions, thus supporting our view that the product is exclusively [Co(cydta)$^-$]. The zero-order rate constants (k_0) were found to increase with increasing [PDP] and a plot of k_0 versus [PDP] was a straight line passing through the origin, suggesting the first-order dependence of the reaction rate on [PDP]. When the kinetic runs were carried out by varying [Ag(I)] in the range (5.0—20.0)$\times10^{-4}$ mol dm^{-3}, keeping all other parameters constant, the zero-order rate constants were found to increase linearly with [Ag(I)] and a plot of k_0 versus [Ag(I)] was a straight line passing through the origin confirming that the reaction is also first-order in [Ag(I)]. Increase in pH of the reaction medium increased the rate. A plot of $k_0\{K_a+[H^+]\}$ versus [H^+], where K_a is the third acid dissociation constant of PDP,[11] was a straight line with a positive slope and positive intercept on the ordinate (Fig. 1). Sodiumacetate and disodiumhydrogenphosphate were found to have no effect on the reaction rate at fixed [H^+] where as increasing [H_2cydta^{2-}] and ionic strength had inhibitory effect on the reaction rate. The reaction mixture initiated polymerization of acrylonitrile monomer suggesting the involvement of free radical intermediates in the reaction. Although at [H^+] used in the kinetic runs, the characteristic test for Ag(II)[12] was not observed, perhaps due to unfavorable conditions for the formation of the orange red colored precipitate of Ag(II)-bipyridyl complex, it was positive when the reaction mixture was acidified.

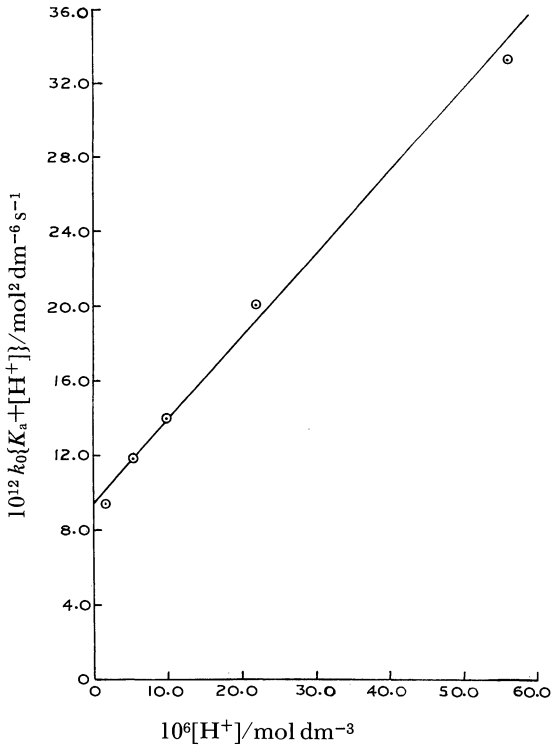

Fig. 1. Plot of $k_0\{K_a+[H^+]\}$ vs. [H^+]. [Co^{II}(cydta)$^{2-}$]= 2.0×10^{-3} M; [PDP]=3.0×10^{-2} M; [Ag(I)]=1.0×10^{-3} M; I=0.3 M; Temp=30.0±0.1 °C.

Discussion

The earlier studies on the oxidation of [Co^{II}(cydta)$^{2-}$] by various oxidants[9,10,13,14] point out to its direct oxidation by the oxidant via the formation of an innersphere complex or in a direct step. In the oxidation of [Co^{II}(cydta)$^{2-}$] by PDS, clear first-order dependence on each [reactant] was reported.[10] With periodate as the oxidant,[13] the order in [Co^{II}(cydta)$^{2-}$] was found to vary between **1** and **2**. In the present study, the direct oxidation of [Co^{II}(cydta)$^{2-}$] by PDP was not observed, thus making the presence of Ag(I) as a catalyst mandatory. This is interesting because the oxidation of metal ions and their complexes by PDP was reported to follow an innersphere path way[15] and Co(II) complexes are known to be labile. Despite this, the reaction doesnot occur in absence of a catalyst like Ag(I).

In the earlier reports[4-7] on the Ag(I) catalyzed oxidation reactions of PDP in acetate buffers, the catalytic role of Ag(I) was ascribed to its complexation with PDP rather than to the formation of higher oxidation states of Ag(I). The earlier investigators could not obtain any experimental evidence for the existence of Ag(II) or Ag(III) in the reaction, but at the same time they could not also rule out the possibility of Ag(II) or Ag(III) being involved in the reaction. In the present case, the zero-order dependence of the reaction rate on [Co(cydta)$^{2-}$] and the positive test for Ag(II) unequivocally suggests that Ag(II), which is formed as an active intermediate, is responsible for the oxidation of the substrate. Further it was observed that in absence of either PDP or Ag(I), the reaction

was negligible, thus ruling out the possibility of oxidation of [Co(cydta)$^{2-}$] by either PDP or Ag(I) alone. In the earlier studies on Ag(I) catalyzed oxidation reactions of PDP in acid media, the formation of Ag(II) as an intermediate was reported.[1,2] In the present study also in absence of the substrate, when PDP is added to Ag(I) in acetate buffers (pH=5.0) a black precipitate which slowly changes to a pale yellow was noticed. It is interesting to recall that Edwards[11] reported that this black precipitate is a peroxodiphosphate complex of silver which rapidly oxidizes water to form Ag(I). When Ag(II) generated electrolytically is added to [Co(cydta)$^{2-}$], an intense pink color characteristic of [Co(cydta)$^{-}$] was immediately noticed. A perusal of the redox potentials of the couples: PDP/PO_4^{3-} (2.01 V); Ag(II)/Ag(I) (1.98 V) and [Co(cydta)$^{-}$]/[Co(cydta)$^{2-}$] (0.62 V)# shows that the oxidation of [Co(cydta)$^{2-}$] is readily feasible. The quantitative nature of the reactions with Ag(II) either as a reactant or a product could not be established unequivocally as it is highly unstable under the experimental conditions. Although in the mechanism now proposed, the $HPO_4^{\cdot-}$ was also shown to be the reactive species responsible for the oxidation, it may be noted that it is formed along with Ag(II) in step(3). Further Michaelis-Menten type kinetic pattern characteristic of the precomplexation equilibrium was not observed. This may be due to the fact that even if the Ag(I)PDP complex is formed, it immediately decomposes to give the reactive intermediates, thus escaping its identification kinetically.

Under the experimental conditions, $H_2P_2O_8^{2-}$ and $HP_2O_8^{3-}$ are the active oxidizing species of PDP. The linearity of the plot of $k_0\{K_a+[H^+]\}$ versus $[H^+]$ suggests that both the species are reactive. Keeping in view these facts, the following mechanism is proposed.

$$H_2P_2O_8^{2-} \overset{K_a}{\rightleftharpoons} HP_2O_8^{3-} + H^+, \quad (1)$$

$$H_2P_2O_8^{2-} + Ag^+ \overset{k_1}{\longrightarrow} Ag^{2+} + HPO_4^{\cdot-} + HPO_4^{2-}, \quad (2)$$

$$HP_2O_8^{3-} + Ag^+ \overset{k_2}{\longrightarrow} Ag^{2+} + HPO_4^{\cdot-} + HPO_4^{3-}, \quad (3)$$

$$[Co^{II}(cydta)]^{2-} + Ag^{2+}/HPO_4^{\cdot-} \overset{fast}{\longrightarrow} products. \quad (4)$$

This mechanism leads to the rate law:

$$k_0 = \frac{[PDP]_t[Ag(I)]_t\{k_1[H^+]+k_2K_a\}}{\{K_a+[H^+]\}},$$

where $[PDP]_t$, $[Ag(I)]_t$ represent the total analytical concentrations of the respective reagents and K_a is the third acid dissociation constant of PDP. This rate law explains all the observed facts. From the slope and intercept values of the $k_0\{K_a+[H^+]\}$ versus $[H^+]$, the k_1 and k_2 were calculated to be: $(14.2\pm0.5)\times10^{-3}$ $mol^{-1}dm^3s^{-1}$ and (43.5 ± 0.8) $mol^{-1}dm^3s^{-1}$ at 30.0 ± 0.1 °C. This shows that $HP_2O_8^{3-}$ is ca. 10^3 times more reactive than $H_2P_2O_8^{2-}$ towards Ag(I). From the Arrhenius plot the activation parameters for the two steps were calculated to be: $E_{act}=(96.9\pm0.6)$ and (58.1 ± 0.5) kJ mol^{-1} and $\Delta S^*=+(68\pm4)$, and $-(29\pm0.2)$ J K^{-1} mol^{-1} respectively at 30.0 ± 0.1 °C.

Experimentally determined by the authors in the present study.

Two of us (PSS and KAK) are thankful to the CSIR and DAE, India for the financial assistance. Our special thanks are due to Frank Caropreso of FMC Corporation, USA for the free gift of a PDP sample.

References

1) K. J. M. Rao and P. V. Krishna Rao, *Indian J. Chem., Sect. A*, **21**, 1066 (1982).
2) K. J. M. Rao, A. S. P. Vittal, and P. V. Krishna Rao, *Inorg. Chem.*, **23**, 3212 (1984).
3) D. A. House, *Chem. Rev.*, **62**, 185 (1962).
4) Bharati Gupta, K. S. Gupta, and Y. K. Gupta, *J. Chem. Soc., Dalton Trans.*, **1984**, 1873.
5) Bharati Gupta, A. K. Gupta, K. S. Gupta, and Y. K. Gupta, *Indian J. Chem., Sect. A*, **24**, 927 (1985).
6) A. K. Gupta, K. S. Gupta, and Y. K. Gupta, *Inorg. Chem.*, **24**, 3670 (1985).
7) A. K. Gupta, K. S. Gupta, and Y. K. Gupta, *Indian. J. Chem., Sect. A*, **26**, 653 (1986).
8) S. Kapoor, P. D. Sharma, and Y. K. Gupta, *Talanta*, **22**, 765 (1975).
9) D. H. Huchital and R. J. Hodges, *Inorg. Chem.*, **12**, 998 (1973).
10) M. P. Pujari and P. Banerjee, *Trans. Met. Chem.*, **8**, 91 (1983).
11) I. I. Creaser and J. O. Edwards, *Top. Phosphorus Chem.*, **7**, 395 (1972).
12) J. A. McMillan, *Chem. Rev.*, **62**, 65 (1962).
13) A. A. Abdel-Khalek and Yousif Sulfab, *Trans. Met. Chem.*, **7**, 297 (1982).
14) W. H. Woodruff, D. W. Margerum, M. J. Milano, H. L. Pardue, and R. E. Santini, *Inorg. Chem.*, **12**, 1490 (1973).
15) E. Chaffee, I. I. Creaser, and J. O. Edwards, *Inorg. Nucl. Chem. Lett.*, **7**, 1 (1977).

On the Partitioning of the NMR B'-Coefficient. The Evaluation of Single Ion B'-Coefficients by a New Method and the Correlation with the Viscosity B-Coefficient, Partial Molal Volume and Electrostatic Entropy of Solvation of Ions in Aqueous and Nonaqueous Systems

Moni Mohan BHATTACHARYYA
Physical Chemistry Section, Department of Chemistry, University College of Science, Calcutta 700009, India
(Received July 17, 1990)

A new method of division used for the viscosity B-coefficient has now been extended to the partitioning of the NMR B'-coefficient both in aqueous and various nonaqueous systems. The derived set of B_i'-values, unlike those obtained by other methods in water are found to be quantitatively related to the ionic molal volumes obtained by the UVP method. The usual assumption of equal contributions of K^+ and Cl^- ions has been discarded. Abraham et al.'s electrostatic entropy of solvation of ions has also been found to give excellent linear correlation with the derived NMR B_i'-values in different solvents. The striking feature is that the NMR B_i'-values as derived by Abraham and coworkers by a different method are almost identical to the present values in all the nonaqueous solvents studied. The slight disagreement observed for the aqueous system has been discussed as being due to encroaching of the disordered second layer to the first layer of solvation, thereby making the absolute entropy estimates less certain. Both the cationic and anionic B_i'-values are represented by a single smooth parabolic curve against the crystal ionic radii as predicted by the theory. The hydration number for Cl^- ion as derived from this work agrees excellently with the widely accepted value.

Recently, there are many attempts[1-5] to derive the single ion values of various thermodynamic and transport properties of electrolytes both in aqueous and nonaqueous systems. However, similar activities for the NMR B'-coefficient, first introduced by Hertz and co-workers,[6] are rather limited. From the NMR measurements concerning the molecular motion in solutions, these authors proposed the following equation (1), in analogy with the viscosity B-coefficient,[7] of the relative proton relaxation rate for pure solvent $(1/T_1^\circ)$ and solution $(1/T_1)$ as a function of concentration:

$$\frac{1/T_1}{1/T_1^\circ} = 1 + B'c + C'c^2 + \cdots \quad (1)$$

The NMR B'-coefficient in equation (1) gives information about the reorientational behavior of solvent molecules in the first coordination sphere of the ions.

A survey of the literature shows that there has been no generally accepted method of division for the B'-coefficient in any solvent. In aqueous solution, Hertz et al.[6] partitioned the B'-coefficient assuming $B'_{K^+} = B'_{Cl^-}$ at all temperatures in analogy with the partitioning of the B-coefficient by Kaminsky.[8] Very recently, Sacco and co-workers[9] have utilized the same method as adopted for the B-coefficient in dimethyl sulfoxide (DMSO) by Bicknell et al.[10] for the separation of the B'-coefficient in the same solvent. Abraham and co-workers[11] have also partitioned both the NMR B' and viscosity B-coefficient by means of correspondence plots with the theoretically estimated electrostatic entropy of solvation of ions in various protic and aprotic solvents.

Very recently, a general method of separation of the viscosity B-coefficient applicable to both aqueous and various nonaqueous systems has been developed by the author.[12] Since the NMR B'-coefficient has almost all the attributes of the viscosity B-coefficient and also the fact that the NMR relaxation rate has better theoretical models than the viscosity, it is interesting to see how far the new method is applicable to the division of the B'-coefficient. Moreover, it is also imperative to study the relative merits of the various methods of division of the NMR B'-coefficient as far as the basis of suitable criteria is concerned. With these ends in view, we have compiled the various NMR B'-coefficient of different electrolytes reported by Hertz and co-workers,[6,13] Sacco and co-workers[9] in water, methanol, formamide, N-methylformamide (NMF), DMSO, and ethylene glycol at 25 °C.

Derivation of the Model

Now, that the NMR B'-coefficient is not only additive and a measure of ion-solvent interaction like the B-coefficient, but the hydration number from the two coefficients can also be evaluated from the two analogous expressions as follows:

$$B'^{\pm} = (\tau_c^{\pm}/\tau_c^\circ - 1)\, n_h^{\pm}/55.5 \quad (2)$$

$$B^{\pm} = (\eta_c^{\pm}/\eta_0 - 1)\, n_h^{\pm}/55.5 \quad (3)$$

where $\tau_c^{\pm}$ is the rotational correlation times,[6,13] $\eta_c^{\pm}$ is the coefficient of viscosity for the hydrated ions,[14] $n_h^{\pm}$ is the hydration number of ions, 55.5 and the subscript zero are respectively the number of moles of water per kg of water and the corresponding property for pure solvent.

Table 1. Single Ion Values of NMR B_i' Coefficient/kg mol^{-1}, $\overline{V}_i^\circ$/cm^3 mol^{-1}, $\Delta S_{I,II}$/cal K^{-1} mol^{-1} and B_i-Coefficient/dm^3 mol^{-1} for Monovalent Ions Together with the Estimated Values[a] in Various Solvents by Different Methods at 25 °C

Ion	Water					Methanol					Formamide				
	Present B_i' (0.075)[a]	Abraham et al. B_i'	$\overline{V}_i^\circ$ (UVP)	$\Delta S_{I,II}$	Present B_i	Present B_i' (0.034)[a]	Abraham et al. B_i'	$\overline{V}_i^\circ$ (UVP)	$\Delta S_{I,II}$	Present B_i	Present B_i' (0.014)[a]	Abraham et al. B_i'	$\overline{V}_i^\circ$ (Mukerjee)	$\Delta S_{I,II}$	Present B_i
Li^+	0.215	0.17	−11.2	−30.4	0.2015	0.259	0.25	—	−34.2	0.486	—	—	−4.0	−27.4	0.345
Na^+	0.135	0.09	−7.4	−17.4	0.1383	0.149	0.14	−18.6	−28.7	0.454	0.164	0.16	−2.5	−27.4	0.448
K^+	0.065	0.02	3.4	−1.5	0.045	0.119	0.11	−4.9	−21.7	0.422	0.089	0.08	8.4	−20.5	0.222
Rb^+	0.035	−0.01	9.0	3.1	0.022	0.089	0.08	−2.8	−17.2	—	0.074	0.06	12.4	−16.0	0.199
Cs^+	0.025	−0.02	15.5	7.1	0.007	0.079	0.07	3.3	−13.8	0.221	0.064	0.07	18.7	−12.5	0.173
$(CD_3)_4N^+$	0.255	—	—	—	—	—	—	—	—	—	—	—	—	—	—
F^-	0.065	0.11	3.3	−9.9	0.0445	—	—	−1.2	−20.7	—	—	—	—	—	—
Cl^-	−0.085	−0.04	23.7	10.6	−0.059	0.041	0.05	13.0	−9.9	0.342	0.041	0.04	23.6	−8.4	0.142
Br^-	−0.115	−0.07	30.2	15.9	−0.094	0.021	0.03	17.1	−7.0	0.318	0.021	0.03	30.0	−5.4	0.115
I^-	−0.155	−0.11	41.4	23.5	−0.1205	−0.009	0.00	30.0	−1.5	0.253	−0.004	0.005	42.4	0.2	0.07

Ion	NMF			DMSO					Ethylene glycol	
	Present B_i (0.022)[a]	Abraham et al. B_i'	$\Delta S_{I,II}$	Present B_i' (0.064)[a]	Lawrence et al. B_i'	$\overline{V}_i^\circ$ (Criss et al.[11])	$\Delta S_{I,II}$	Present B_i	Present B_i' (0.025)[a]	$\overline{V}_i^\circ$ (UVP)
Li^+	0.124	0.13	−38	—	—	−9	−42	0.508	—	−10.3
Na^+	0.094	0.11	−33	0.109	0.118	−2	−40	0.434	0.125	−4.9
K^+	0.084	0.095	−26	0.110	0.119 (0.11)[b]	2	−33	0.444	0.045	4.4
Rb^+	0.074	0.08	−22	0.096	0.105	7	−29	0.423	0.025	9.1
Cs^+	0.064	0.07	−18	0.088	0.097	8	−25	0.392	0.010	15.4
F^-	—	—	−25							12.5
Cl^-	0.056	0.04	−14	—	—	15	−21	0.358	−0.005	26.2
Br^-	0.046	0.04	−11	0.067	0.060	22	−18	0.399	−0.020	31.9
I^-	0.036	0.03	−5	0.044	0.035 (0.04)[b]	36	−12	0.372	−0.035	42.5

a) Different estimated values. b) Ref. 11.

Thus, considering the similarity of the two definitions in Eq. 2 and 3, it is now assumed that the ionic NMR B'-values like the viscosity B_i-values should be a monotonic function of crystal radii cubed, independent of the sign of the charge.[12] The above assumption is implicit in the treatment of Couture and Laidler[15] that for large monoatomic monovalent ions, B_i' like $\overline{V}_i^\circ$ is not dependent on the sign of the charge, as the two parameters are also similar in nature. Figure 1 shows two different smooth curves of B_i' versus r_i^3 plots, one for the alkali metal ions and the other for the halide ions on the basis of $B'_{K^+}=B'_{Cl^-}$[6] in aqueous system. According to the assumption, a smooth curve representing all the cations and anions is only obtained, if an estimated correction term of 0.075 is added to the cationic B_i'-values and the same is subtracted from the anionic values. The smooth fusion of the two curves into a single one as also the same derived values obtained for K^+ and F^- ions add support to the above assumption. This is also illustrated in the figure. It is striking to note that the only alkali metal ion off the curve is Cs^+, as was similarly observed for the viscosity B-coefficient in aqueous system.[12]

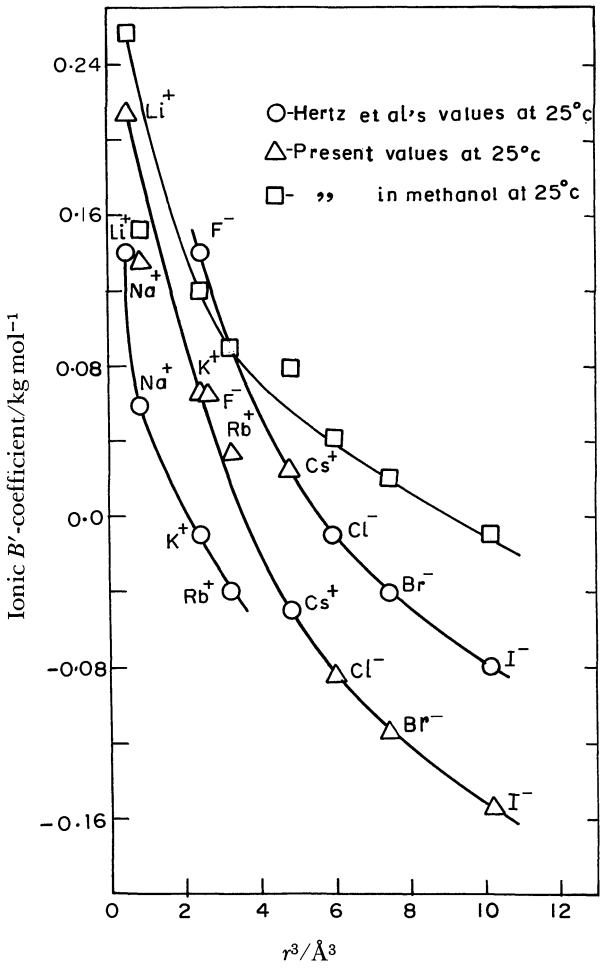

Fig. 1. The NMR B'-coefficient of alkali metal ions and halide ions plotted against r_i^3 in methanol as well as the same for two different values of B_i' based on (i) $B'_{K^+}=B'_{Cl^-}$ scale and (ii) the present scale for aqueous system.

The method of partitioning the B'-values for aqueous system at 25 °C has been extended to other temperatures also, viz. 50 °C, 80 °C with the respective correction terms being 0.080 and 0.070. Thus, in order to get B_i'-values of any ion at any temperature, one requires to add $[Z]$ times the corresponding correction term to the cationic B'-values and subtract the same from the anionic B'-values, as obtained on the assumption that $B'_{K^+}=B'_{Cl^-}$, where Z is the charge on the ion. The correction term which is the direct consequence of the assumption signifies that cations are more and anions are less solvated relative to what are obtained from the assumed equality of B_i'-values for K^+ and Cl^- ions or any other ions. Since the additivity law holds good for the B'-coefficient, the magnitude of the correction term for the oppositely charged ions becomes the same though with opposite sign.

Following the same model, the partitioning of B'-coefficient[6] in methanol, formamide, NMF, DMSO, and ethylene glycol has been carried out at 25 °C. The initial tentative B_i'-values are obtained on the basis of $B'_{Cs^+}=B'_{I^-}$ in formamide, NMF, and DMSO, whereas in methanol and ethylene glycol, $B'_{K^+}=B'_{I^-}$ and $B'_{K^+}=B'_{Cl^-}$ respectively are followed. The different correction terms estimated in various solvents are 0.034, 0.014, 0.022, 0.064, and 0.025 respectively. Also, Fig. 1 illustrates a smooth curve representing the relation between the derived B_i'-values of all the simple ions and r_i^3 in methanol only, thereby confirming the justification of the present method of division in nonaqueous systems. The thus derived B_i'-values together with the corresponding viscosity B_i-values for monovalent ions are recorded in Table 1. Also included in the table are the various ionic entropy of solvation of different ions reported by Abraham et al,[11] as also the corresponding ionic partial molal volumes mostly derived by the ultrasonic vibration potential method.[16,17]

Results and Discussion

The ionic partial molal volume also measures the ion-solvent interaction and is more akin to the B or B'-coefficient than either the more sensitive entropy of solvation[18] or the ion conductance.[19] As there are now reliable estimates of the $\overline{V}_i^\circ$-values from the definitive experimental measurements,[16,17] any quantitative correlation of this parameter with any of the derived B_i'-values by different methods would be the reasonable criterion to evaluate the relative merits of such methods. Moreover, the good linear correlations between the entropy parameter ($\Delta S_{I,II}$) and the derived B' or B-coefficient obtained by Abraham and co-workers,[11] are in fact, the direct consequence of the

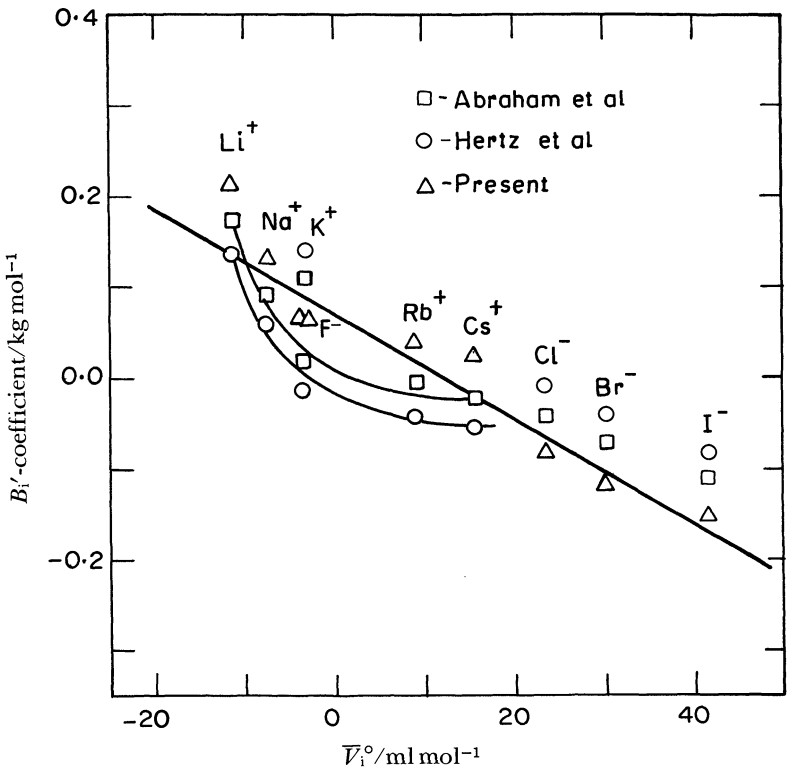

Fig. 2. Comparison of NMR B_i' versus $\overline{V}_i°$ plots for monovalent monoatomic ions between the present work and those obtained by (i) Hertz and co-workers (ii) Abraham and co-workers for aqueous system.

correspondence plots between the two parameters. In the present case, where the ionic B or B'-values are derived by an entirely different approach, any quantitative correlation between the derived B'-values and the entropy parameter ($\Delta S_{I,II}$) should demonstrate the better applicability of the present method of division.

Partial Molal Volume of Ions ($\overline{V}_i°$). Figure 2 illustrates the comparison of the various B_i' versus $\overline{V}_i°$ plots obtained by using the single ion B'-values by different methods, viz., Hertz and co-workers,[6] Abraham and co-workers[11] as well as the present method for aqueous solutions. Apart from the Li^+ ion, the B_i'-$\overline{V}_i°$ plots for all the inorganic ions studied in this work show an excellent linear correlation as anticipated, and the regression data are shown in Table 2. In comparison to this, the B_i'-values by Hertz and co-workers show a U-shaped curve indicating that the assumption $B'_{K^+}=B'_{Cl^-}$ is not satisfactory for aqueous system. Although the nonlinearity is considerably reduced in the case of B_i'-values derived by Abraham and co-workers,[11] it still deviates from the linearity shown by the present work. Exactly the same observation was also obtained in the case of viscosity B_i-$\overline{V}_i°$ plot obtained by the present method[12] in aqueous system, indicating the close similarity of the two coefficients. Moreover, the $\overline{V}_i°$ values of K^+ and F^- ions obtained by the UVP method in water are almost identical, as is similarly obtained for both the B' and B-coefficient for the same ions following the present method (Table 1).

It is striking to note that contrary to what is observed for aqueous system, the B_i'-values obtained in this work and those by Abraham and coworkers[11] are quite close in almost all the nonaqueous solvents studied here.

the B_i'-$\overline{V}_i°$ plots for all the non-aqueous solvent excepting NMF have also been studied taking different derived B_i'-values. The various $\overline{V}_i°$ values required for these plots were compiled from the UVP method for methanol[16] and ethylene glycol,[17] Mukerjee's method[20] for formamide and those reported by Abraham et al.[11] for DMSO. A comparison of B_i'-$\overline{V}_i°$ plots in methanol and formamide obtained by using B_i'-values of this work with those of Abraham et al.[11] clearly shows that the quantitative correlations are quite similar, as is evident from Table 2.

In DMSO, such comparison is made with the two different sets of B_i'-values derived by Sacco and co-workers[9] using two different reference electrolytes,[10,21] as very few data were reported by Abraham et al. in this solvent. While the B_i'-values of Sacco et al. following Lawrence et al.'s method[21] fail to correlate well with the $\overline{V}_i°$, the other set of B_i'-values[10] show comparable linear correlation with those obtained by this work (Table 2). Also, the B_i'-values of only three ions as reported by Abraham et al.[11] in this solvent are quite close to the present values.

Table 2. Regression Data for Various NMR B_i' vs. $\overline{V}_i^\circ$, NMR B_i' vs. $\Delta S_{I,II}$ and Viscosity B_i^* vs. $\Delta S_{I,II}$ Linear Plots for Simple Inorganic Ions in Various Solvents Obtained by Computerized Least Square Method

Abraham et al.	This work
Water	
—	$B'=-0.0062\overline{V}_i^\circ+0.089$ ±0.001 ±0.016
$B'=-0.0053\Delta S_{I,II}+0.016$ ±0.002 ±0.015	$B'=-0.0068\Delta S_{I,II}+0.021$ ±0.008 ±0.029
	$B^*=-0.0060\Delta S_{I,II}+0.019$ ±0.004
Methanol	
$B'=-0.0029\overline{V}_i^\circ+0.084$ ±0.002	$B'=-0.0034\overline{V}_i^\circ+0.088$ ±0.0016 ±0.007
$B'=-0.0051\Delta S_{I,II}+0.005$ ±0.0008 ±0.003	$B'=-0.0060\Delta S_{I,II}+0.016$ ±0.0007 ±0.006
Formamide	
$B'=-0.0033\overline{V}_i^\circ+0.124$ ±0.0043 ±0.016	$B'=-0.0036\overline{V}_i^\circ+0.132$ ±0.0036 ±0.013
$B'=-0.0032\Delta S_{I,II}+0.0016$ ±0.0015	$B'=-0.0044\Delta S_{I,II}+0.02$ ±0.0003
DMSO	
[a] $B'=-0.0024\overline{V}_i^\circ+0.117$ ±0.001 ±0.004	$B'=-0.0018\overline{V}_i^\circ+0.108$ ±0.001 ±0.0034
[a] $B'=-0.0032\Delta S_{I,II}+0.005$ ±0.0004 ±0.009	$B'=-0.0024\Delta S_{I,II}+0.022$ ±0.0003
NMF	
$B'=-0.0032\Delta S_{I,II}+0.0076$ ±0.0006 ±0.005	$B'=-0.0025\Delta S_{I,II}+0.02$ ±0.0003 ±0.004
Ethylene glycol	
	$B'=-0.0029\overline{V}_i^\circ+0.073$ ±0.003 ±0.019

a) Sacco et al.[9]

Electrostatic Entropy of Solvation of Ions ($\Delta S_{I,II}$). It is interesting to note that contrary to what is observed for B_i'-$\overline{V}_i^\circ$ plots in aqueous system, the B_i'-values of all the inorganic ions including Li^+ derived by the two methods give good linear correlation with the ionic entropy of solvation as shown in Table 2. A comparison of the regression data for the two linear relations, however, indicates that the Abraham et al.'s correspondence method makes the smaller ions less structure makers and the larger ions less structure breakers in water than the present method. Table 2 also reveals that the B_i'-$\Delta S_{I,II}$ correlations for the various non-aqueous systems studied here obtained by the two methods, are almost similar. However, the corresponding correlations between the viscosity-B_i versus $\Delta S_{I,II}$ also shown in Table 2 are even better than the same for the NMR B_i'-coefficient.

The striking similarity between the B_i'-values by the two methods in the nonaqueous solvents can now be explained as follows. According to Abraham et al.,[11] the entropy calculations either by one layer or two layer model in aprotic solvents result in the same value and these agree well also with the experimental values. However, this is not true in the case of hydrogen-bonded solvents, where a disordered second layer of solvation makes the calculations rather more complicated. For DMSO, NMF, methanol, and formamide, there is either no such disordered region, or the effect due to this is quite insignificant. As a result, the estimated entropy values are of the right order of magnitude. However, water being a predominantly structured solvent is also known to be highly susceptible to structure-breaking in presence of larger inorganic ions.[22] It is perhaps due to encroaching of this disordered region into the first layer that the estimated entropy values as given by Abraham et al. do not reflect satisfactorily the effective picture of ion-solvent interaction in water.

Table 3. Ionic B'-Coefficient of Higher Valent Cation and Polyatomic Anions in Aqueous Solution at 25 °C

Ion	Pauling radius / Å	B_i' / kg mol^{-1}	Ion	Pauling radius / Å	B_i' / kg mol^{-1}
Ba^{2+}	1.43	0.33	SCN^-	2.34	−0.145
Sr^{2+}	1.27	0.38	ClO_3^-	2.58	−0.155
Ca^{2+}	1.06	0.42	BrO_3^-	2.69	−0.135
Mg^{2+}	0.78	0.65	IO_3^-	2.79	−0.055
Pb^{2+}	1.32	0.35	NO_3^-	2.49	−0.125
CO_3^{2-}	2.48	0.10	$Hg(CN)_4^{2-}$	4.68	−0.26
SO_3^{2-}	2.54	0.07	CdI_4^{2-}	4.75	−0.24
SO_4^{2-}	2.89	−0.03	HgI_4^{2-}	4.85	−0.21
$S_4O_6^{2-}$	3.6	−0.10	WO_4^{2-}	3.35	+0.02

Table 4. Ratio of Rotational Correlation Times of Simple Inorganic Ions for Different Hydration Numbers by This Work as Also from Hertz et al.[6,13] (within Parentheses) in Aqueous Solution at 25 °C

Ion	Hydration numbers			
	4	6	8	10
Li^+	3.9 (2.9)	2.9 (2.3)	2.5 (2.0)	2.2 (1.8)
Na^+	2.8 (1.8)	2.2 (1.6)	1.9 (1.4)	1.7 (1.3)
K^+	1.9 (0.8)	1.6 (0.9)	1.4 (0.9)	1.3 (0.9)
Rb^+	1.5	1.3 (0.6)	1.2 (0.7)	1.2 (0.8)
Cs^+	1.3	1.2 (0.5)	1.2 (0.7)	1.1 (0.7)
F^-	1.9 (2.9)	1.6 (2.3)	1.4 (2.0)	1.3 (1.8)
Cl^-	— (0.8)	0.2 (0.9)	0.4 (0.9)	0.6 (0.9)
Br^-	— (0.4)	— (0.6)	0.2 (0.7)	0.4 (0.8)
I^-	— —	— (0.3)	— (0.4)	0.2 (0.6)

Crystal Ionic Radii (r). Engel and Hertz[6] deduced the NMR B'-coefficient as a function of ionic radius by the following equation,

$$B'^{\pm} = K(ar^2 - b|Z|e + cZ^2e^2/r^2), \quad (4)$$

where K, a, b, and c are constants, $|Z|e$ is the charge on the ion.

Equation 4 can be conveniently written as

$$B'^{\pm} = A_1r^2 - A_2|Z|e + A_3Z^2e^2/r^2, \quad (5)$$

where A_1, A_2, and A_3 are the products of the various constants.

Equation 5 is a parabolic equation such that the B_i'-coefficient has high values both for smaller and higher ionic radii and a minimum in between. The expression for r_{min} can easily be obtained by equating the first derivative of B' in Eq. 5 to zero

$$r_{min} = (A_3/A_1)^{1/4}(|Z|e)^{1/2} \quad (6)$$

and by substituting r_{min} in Eq. 5 one obtains

$$B'^{\pm}_{min} = |Z|e\,[2(A_1A_3)^{1/2} - A_2]. \quad (7)$$

Thus for a change in $|Z|e$ values, both r_{min} and $B'^{\pm}_{min}$ should change by $\sqrt{|Z|e}$ and $|Z|e$ fold respectively.

Figure 3 illustrates two smooth parabolic curves of B_i' versus r_i plots, one for the monovalent ions and the other for the divalent ions. The different B'-values for various ions for aqueous solution are derived by the present method from those reported by Hertz and co-worker,[6] and are included in Table 3. The noticeable feature is that both the cations and anions of the same valence fall on the same line of the curve. This is contrary to what was demonstrated earlier by Engel and Hertz[6] showing two separate curves for the cations and anions with the B_i'-values derived on the basis of $B'_{K^+} = B'_{Cl^-}$. It is now known that the cation-solvent and anion-solvent interactions are very similar in aqueous as also in many nonaqueous solutions.[16,23] Figure 3 also reveals that while the increase in $B'^{\pm}_{min}$ for $Z=2$ is in accordance with Eq. 7, the same for r_{min} is slightly larger than that predicted by Eq. 6.

Rotational Correlation Times and the Hydration Number. Equation 2 gives the values of $(\tau_c^{\pm}/\tau_c^{\circ})$ for various ions provided the hydration number $(n_h^{\pm})$ is known with certainty. According to Engel and Hertz,[6,13] if $\tau_c^{\pm}/\tau_c^{\circ} > 1$, then the ion is structure forming and for $\tau_c^{\pm}/\tau_c^{\circ} < 1$, the ion is structure breaking. Table 4 compares such values for simple inorganic ions calculated with B_i'-values derived by the two methods, viz., Hertz and co-workers and the present method, assuming arbitrary values of $n_h = 4,6,8$, and 10. The interesting feature of Table 4 is that only the present method rules out the possibility of hydration

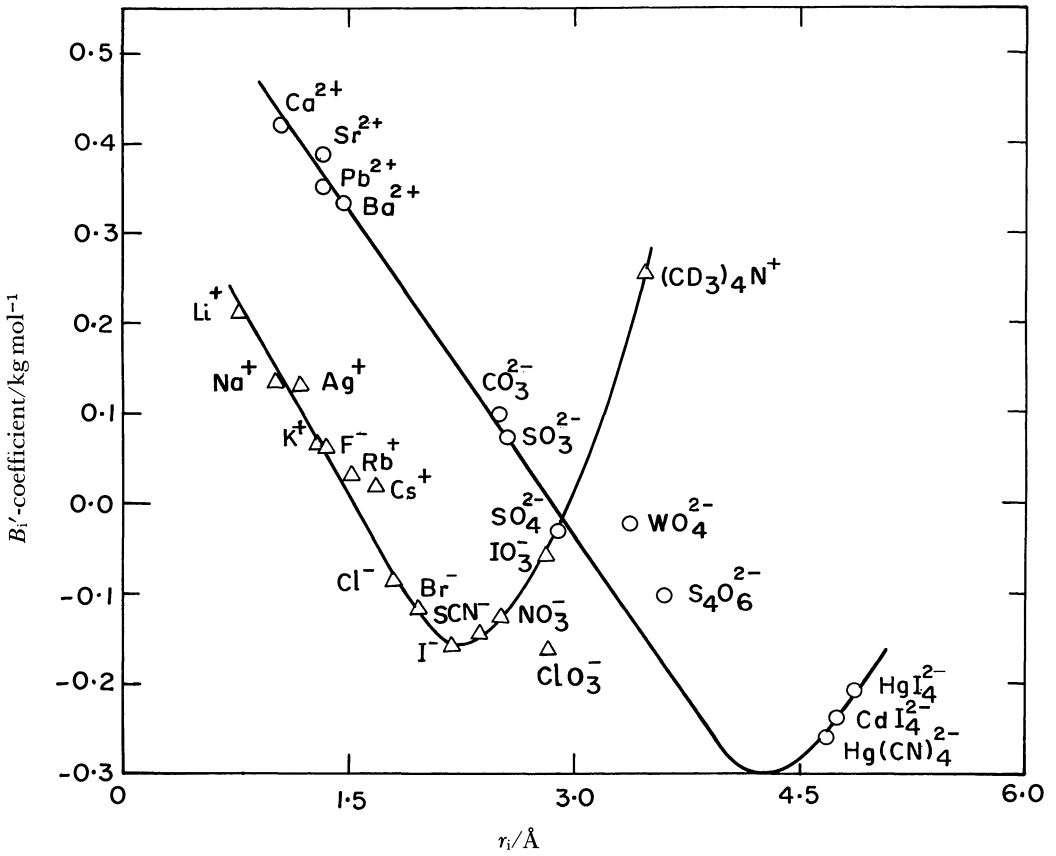

Fig. 3. Variation of ionic NMR B'-values with crystal ionic radii at 25 °C for aqueous system.

number equal to 4 for Cl^- because of the negative value obtained for $(\tau_c^{\pm}/\tau_c^{\circ})$, and agree with a value of 6 instead, which is confirmed by definitive experimental studies.[24]

Moreover, Hertz and co-workers[13] also estimated the correlation time for fluoride ion (τ_c^-) in aqueous solution, considering the unsymmetrical arrangement of water molecule in the hydration sphere (nonrigid) of the ion and the values are $\tau_c^- \approx 1 \times 10^{-11}$ s for $n_h=4$ and $\tau_c^- \approx 0.5 \times 10^{-11}$ s for $n_h=6$. The corresponding values from the proton relaxation data derived by the present method are 0.5×10^{-11} s and 0.4×10^{-11} s respectively. The fair agreement between the values in the case of $n_h=6$ thus strongly favors the latter as the hydration number for F^- ion.

The author is indebted to Professor M. Sengupta, Calcutta University, for initial inspiration in this area of chemistry, and also thankful to the referee for courteous comments.

References

1) H. Hirakawa, H. Nomura, and F. Kawaizumi, *Bull. Chem. Soc. Jpn.*, **62**, 1781 (1989).
2) B. S. Krumgalz, *J. Chem. Soc., Faraday Trans. 1*, **76**, 1275 (1980); *ibid.*, **76**, 1887 (1980).
3) H. D. B. Jenkins and M. S. F. Pritchett, *J. Chem. Soc., Faraday Trans. 1*, **80**, 721 (1984).
4) R. Zana, J. E. Desnoyers, G. Perron, R. L. Kay, and K. Lee, *J. Phys. Chem.*, **86**, 3996 (1982).
5) B. E. Conway, R. E. Verrall, and J. E. Desnoyers, *Z. Phys. Chem.*, **230**, 157 (1965).
6) G. Engel and H. G. Hertz, *Ber. Bunsen-Ges. Phys. Chem.*, **72**, 808 (1968).
7) G. Jones and M. Dole, *J. Am. Chem. Soc.*, **51**, 2950 (1929).
8) M. Kaminsky, *Discuss. Faraday Soc.*, **24**, 171 (1957).
9) A. Sacco, M. Carbonara, and M. Holz, *J. Chem. Soc., Faraday Trans. 1*, **85**, 1257 (1989).
10) R. T. M. Bicknell, K. G. Lawrence, M. A. Seeley, D. Feakins, and L. Werblan, *J. Chem. Soc., Faraday Trans. 1*, **76**, 637 (1980).
11) M. H. Abraham, J. Liszi, and E. Papp, *J. Chem. Soc., Faraday Trans. 1*, **78**, 197 (1982).
12) M. M. Bhattacharyya, *Can. J. Chem.*, **67**, 1324 (1989).
13) L. Endom, H. G. Hertz, B. Thül, and M. D. Zeidler, *Ber. Bunsen-Ges. Phys. Chem.*, **71**, 1008 (1967).
14) N. Gorski, *Z. Phys. Chem.*, **264**, 640 (1983).
15) A. M. Couture and K. J. Laidler, *Can. J. Chem.*, **34**, 1209 (1956).
16) F. Kawaizumi and R. Zana, *J. Phys. Chem.*, **78**, 627 (1974); **78**, 1099 (1974).
17) R. Zana, G. A. Lage, and C. M. Criss, *J. Solution Chem.*, **9**, 667 (1980).
18) S. W. Benson and C. S. Copeland, *J. Phys. Chem.*, **67**, 1194 (1963).
19) K. G. Lawrence and A. Sacco, *J. Chem. Soc., Faraday Trans. 1*, **79**, 615 (1983).
20) Utpal Sen, *J. Phys. Chem.*, **35**, 81 (1977).
21) K. G. Lawrence, R. T. M. Bicknell, A. Sacco, and A. Del'Atti, *J. Chem. Soc., Faraday Trans. 1*, **81**, 1133 (1985).
22) R. H. Stokes and R. Mills, "Viscosity of Electrolytes and Related Properties," Pergamon Press, Oxford (1965).
23) R. Zana, G. Perron, and J. E. Desnoyers, *J. Solution Chem.*, **8**, 729 (1979).
24) H. L. Friedman, *Chem. Scr.*, **25**, 42 (1985).

Voltammetric Studies on Some Arylhydrazones of α-Cyano Ketones and α-Cyano Esters

G. M. Abou-Elenien,* N. A. Ismail,† and T. S. Hafez††
Chemistry Department, Faculty of Science, Cairo University, Giza, A.R. Egypt
†Chemistry Department, Faculty of Science, Zagazig University, Egypt
††National Research Centre, Dokki, Giza, Egypt
(Received April 16, 1990)

The redox characteristics of the title compounds are extensively studied using DC-, cyclic voltammetry, coulometry, and controlled potential electrolysis in benzonitrile at platinum electrodes. These compounds are oxidized in one-electron transfer process followed by deprotonation which leads to dimerization. The reduction process differs according to the nature of the compound and the electron-withdrawing power of the substituent in the α-position. They can be reduced in a single two electron or two one electron waves leading in both cases to saturation of the hydrazonic moiety.

The electrochemical behavior of α-arylhydrazononitriles and their *N*-methylated derivatives has been recently reported in literature.[1-8] The increase of interest in the chemistry of this class of compounds arose from their reported biological activity.[9-13] It has been found that these compounds are more effective than cyanides in the uncoupling oxidative phosphorylation in mitoconderial systems.[14,15] In a previous investigation,[16] it has been shown that arylhydrazonomesoxalonitrile (**I**) are electrochemically active in proton-free benzonitrile. These compounds are oxidized in a single irreversible one-electron-transfer process forming the corresponding radical cation which undergoes dimerization reaction. The electrochemical reduction occurs through acceptance of two electrons in two successive irreversible one-electron waves following the well-known ECEC-mechanism. In connection with this work we report here the redox characteristics of different substituted ethyl α-cyano-α-(arylhydrazono)glyoxalates (**II**) and 2-arylhydrazono-3-oxo-3-phenylpropionitriles (**III**).

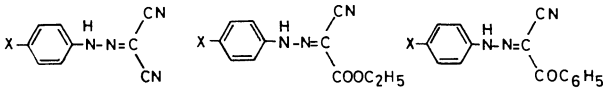

I **II** **III**

III, III	a	b	c	d	e	f	g	h
X	H	NO_2	Br	Cl	CH_3	OCH_3	NH_2	H·(N-CH_3)

Experimental

Organic Synthesis. All compounds involved in this investigation are prepared following the procedures described by Bennett[17] and Elnagdi.[18] The obtained products were purified by repeated crystallization from ethanol.

Reagents. Benzonitrile (BN) (Rotitainerm, West Germany) was purified by first distillation under vacuum from orthophosphoric acid, followed by repeated distillations from phosphorus pentaoxide and final fractional distillation from potassium metal. The supporting electrolyte tetrabutylammonium perchlorate (TBAP) (Fluka-Swiss) was crystallized several times from ethanol-water (9:1 v/v) mixture and dried in vacuum before use.

Apparatus and Instruments. The voltammetric measurements were carried out with the following apparatus:

Potential Source : Potential Scan Generator VSG 72.
Potentiostat : Potential Control Amplifier PCA 72C (Bank Electronic, Gottingen, W. Germany).
X-Y Recorder : Servoger XY (Metrawatt, Nurnberg, West Germany).
Digital Multimeter: T 2201 (Hartman & Braun, Frankfurt, West Germany).
Coulometer : (Bank Electronic, Gottingen, W. Germany).

The rotating platinum disc electrode (RDE) is mounted to a rotating motor (750 rpm) (Metrohm, Swiss).

Measurements. The electrochemical measurements were carried out in dry benzonitrile (BN) containing 0.1 M TBAP (1 M=mol dm^{-3}). The voltammetric study involved direct current (DC) voltammetry at RDE and cyclic voltammetry at a stationary platinum disc electrode. The number of electrons participating in each electrode process was obtained by the controlled potential coulometry (CPC) at a platinum sheet electrode. The electrode potentials were measured against saturated Ag/AgCl/Cl^- (BN) electrode, which was from time to time calibrated against the redox potential of cobaltocenium/cobaltocene system.[19] The standard potential of Ag/AgCl/Cl^- (BN) electrode against the normal hydrogen electrode (NHE) is −176 mV.[20,21]

Controlled Potential Electrolysis (CPE). Electrolysis of ethyl α-cyano-α-(*p*-chlorophenylhydrazono)glyoxalate (**IId**). CPE was carried out twice with 300 mg of **IId** in both acetonitrile and benzonitrile. The potential was adjusted at a value on the limiting current plateau (+2.2 V in oxidation and −1.2 V in reduction). The electrolysis was stopped after the passage of a quantity of electricity corresponding to the uptake of 1 mole of electrons per mole of product for oxidation and 2 moles at reduction. In each case, after electrolysis, the resulting solution was evaporated in vacuo and the product was extracted with ethyl acetate solvent which was evaporated in turn. The obtained mixture was chromatographed on thin-layer silica-gel plates using chloroform solvent.

The Reduction Product of CPE. A quantitative yield of the original compound **IId** was obtained. Anal. Calcd: C,

52.49; H, 3.98; Cl, 14.12; N, 16.70%. Found: C, 52.33; H, 3.84; Cl, 13.98; N, 16.80%. IR (KBr) 3220 (NH), 2220 (CN), 1760 (ester CO), 1620 cm^{-1} (C=N). ^1H NMR ($CDCl_3$, TMS) δ=1.4 (t, 3H, $\underline{CH_3}$-CH_2-), 3.6 (q, 2H, CH_3-$\underline{CH_2}$-), 7.2—7.5 (m, 4H, aromatic protons), 10.0 (s, br, 1H, NH).

The Oxidation Product of CPE. Two main products were obtained:

i) The zone with R_f value 0.68 was scraped off the plate and extracted with acetonitrile, filtered and evaporated in vacuo. The resulting solid compound (yield 55 %) was identified as compound **IV**. Anal. Calcd: C, 41.38; H, 3.13; Cl, 22.26; N, 13.17%. Found: C, 41.20; H, 3.01; Cl, 22.40; N, 13.12%. IR (KBr) 3220—3300 (two NH), 2220 (CN), 1760, 1750 (ester CO), 1630 (C=N), 1220 cm^{-1} (ClO_4^-). ^1H NMR ($CDCl_3$, TMS) δ=1.4 (t, 6H, two $\underline{CH_3}$-CH_2-), 3.6 (q, 4H, two CH_3-$\underline{CH_2}$), 7.2—7.5 (m, 8H, aromatic protons), 10.0 (s, br, 2H, two NH).

ii) The zone with R_f value 0.79 was scraped and extracted as above. The obtained product (yield 30%) was identified as compound **V**. Anal. Calcd: C, 52.69; H, 3.59; Cl, 14.17; N, 16.77%. Found: C, 52.52, H, 3.53; Cl, 14.23; N, 16.59%. IR (KBr) 3200—3300 (two NH), 2220 (CN), 1760—1750 (ester CO), 1630 cm^{-1} (C=N). ^1H NMR ($CDCl_3$, TMS) δ=1.4 (t, 6H, two $\underline{CH_3}$-CH_2-), 3.6 (q, 4H, two CH_3-$\underline{CH_2}$-), 7.2—7.4 (m, 6H, aromatic protons), 10.0 (s, br, 2H, two NH).

Results and Discussion

The voltammetric redox data of compounds (**IIa—h** and **IIIa—h**) are summarized in Table 1. Figures 1 and 2 represent typical DC- and cyclic voltammograms of the investigated compounds respectively.

Ethyl (Arylhydrazono)glyoxalate (IIa—h). All the investigated compounds **IIa—h** behave similarly in shape in both oxidation and reduction. They are oxidized in a single irreversible one-electron process which is followed by a coupled chemical reaction (EC-mechanism). This mechanism is clearly indicated by the absence of the corresponding reduction peak in the

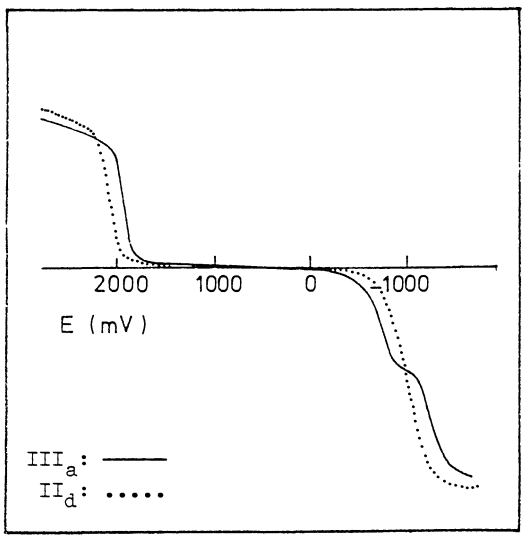

Fig. 1. DC-voltammograms of compounds **IId** and **IIIa** at RDE in benzonitrile.

Table 1. DC Voltametric Data of Ethyl (α-Cyano-α-hydrazono)glyoxalates (**IIa—h**) and 2-Arylhydrazono-3-oxo-3-phenylpropionitriles (**IIIa—h**) at RDE in Benzonitrile

Compd	Process	$E_{\frac{1}{2}}$/mV	$S^{a)}$	Compd	Process	$E_{\frac{1}{2}}$/mV	$S^{a)}$
IIa	O_I	1835	133	**IIIa**	O_I	1932	121
	R_I	−1075	114		R_I	−723	240
					R_{II}	−1170	199
IIb	O_I	2222	66	**IIIb**	O_I	2215	75
	R_I	−825	99		R_I	−428	178
	R_{II}	−1203	52		R_{II}	−1088	116
IIc	O_I	2002	196	**IIIc**	O_I	1902	84
	R_I	−1050	189		R_I	−573	215
					R_{II}	−1133	127
IId	O_I	2047	189	**IIId**	O_I	1912	92
	R_I	−980	190		R_I	−583	244
					R_{II}	−1003	86
IIe	O_I	2002	143	**IIIe**	O_I	1812	180
	R_I	−998	230		R_I	−473	176
					R_{II}	−965	62
IIf	O_I	1845	75	**IIIf**	O_I	1532	106
	R_I	−948	193		R_I	−488	181
					R_{II}	−1043	123
IIg	O_I	748	191	**IIIg**	O_I	760	183
	O_{II}	2072	176		O_{II}	2030	100
	R_I	−972	141		R_I	−505	180
					R_{II}	−1112	130
IIh	O_I	1932	130	**IIIh**	O_I	1902	97
	R_I	−1238	147		R_I	−1148	178

a) $S=dE/d\log[(i_d-i)/i]$.

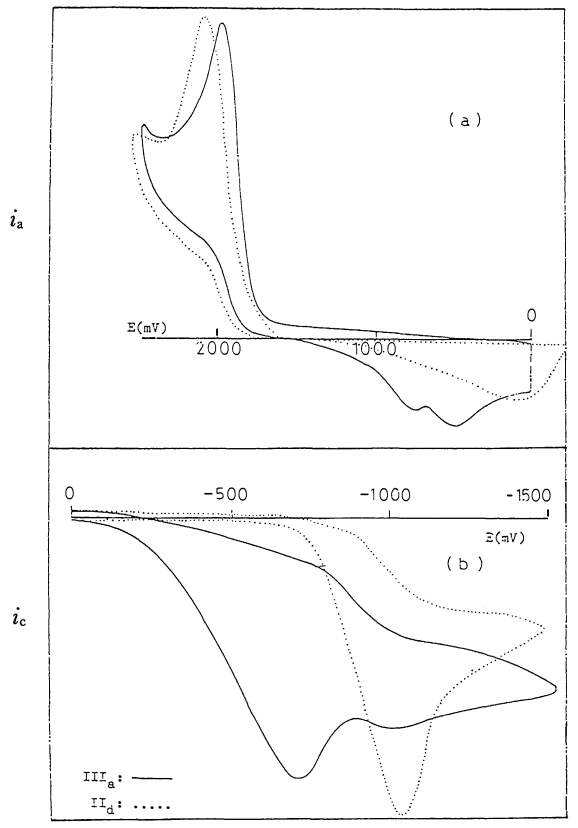

Fig. 2. Cyclic voltammograms of compounds **IId** and **IIIa** at a stationary platinum disc electrode in benzonitrile (a) Oxidation, (b) Reduction. Scan rate=100 mV s^{-1}.

reverse cycle[22] of the cyclic voltammogram (Fig. 2). The reduction process occurs through the acceptance of two electrons in a single irreversible wave following also the EC-mechanism. The irreversibility of the electrode process is obtained also from the slope of the logarithmic analysis curves[23] as shown from Table 1. The amino group in the compound (**IIg**) can be also oxidized in a first oxidation wave and the nitro group in the compound (**IIb**) reduced in the well-known reduction wave of nitro aromatic compounds.

2-Arylhydrazono-3-oxo-3-phenylpropionitrile (IIIa—h). These compounds are oxidized in the same manner as compounds (**IIa—h**) in a single irreversible one-electron transfer process following the EC-mechanism. The reduction process is markedly different: Although the total number of electrons participating in the electrode reaction is two electrons per moelcule as for compounds (**IIa—h**), these two electrons appear not as a single wave but as a two successive irreversible one-electron waves. The *N*-methyl derivative **IIIh** behaves as its similar **IIh**; the reduction occurs in a single two-electron wave.

The polarographic behavior of this class of compounds was investigated.[24-29] They are reduced in a 4-electron wave in either acidic or basic media accompanied by N-N bond cleavage to the corresponding amines. Although this reduction process has been well-documented,[30] it cannot be generalized to account for the reduction of other substituted α-arylhydrazono nitriles since these compounds are tautomeric with the corresponding azo forms. The contribution of each form would depend on the nature of substituents in the molecule. Several articles suggested the existence of certain arylhydrazono nitriles in a charge separated azo form.[31,32] Recently the different substituted (*N*-methylarylhydrazono)-mesoxalonitriles were studied in both aqueous and nonaqueous media.[33,34]

In this work, based on the careful analysis of the data obtained and the identification of the resulting product of CPE, Scheme 1 is suggested for the electrochemical oxidation of the investigated compounds.

The electrochemical oxidation (Scheme 1) proceeds through a one-electron transfer forming the radical cation with its canonical forms A and B. Mesomer A undergoes a dimerization process leading to the formation of the dication **IV** which can be stabilized through its combination with two perchlorate ions from the supporting electrolyte forming salt (**IV**). Also mesomer B may be dimerized with proton removal from the ortho-position in the phenyl ring leading

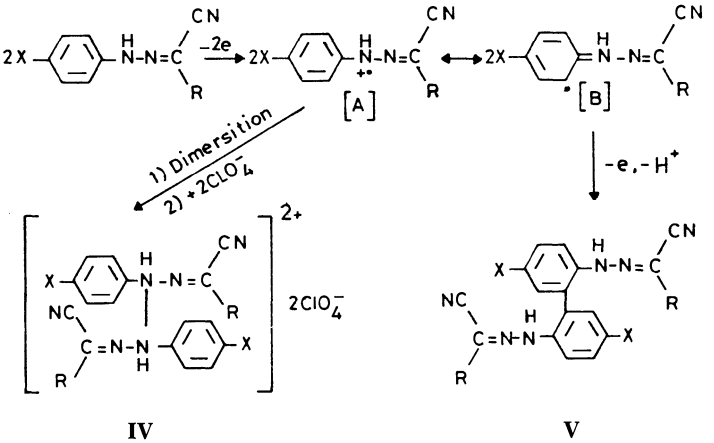

Scheme 1.

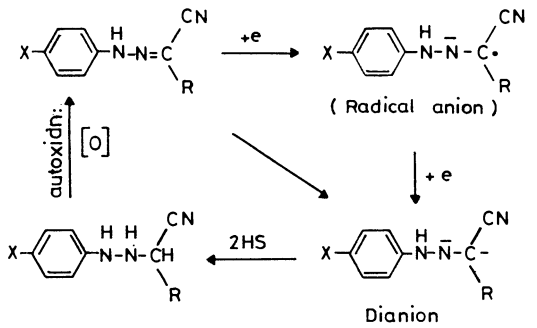

VI

Scheme 2.

to the formation of the neutral dimer **V**.

The difference in electron-withdrawing power of the $-COOC_2H_5$ and -CN or $-COC_6H_5$ groups plays a significant role in the mode of the reduction process. The high electron-withdrawing power of the -CN or $-COC_6H_5$ groups compared with that of $-COOC_2H_5$ group stabilized the firstly formed radical anion which appears in a well-defined separate one electron wave.

The reduced center in these compounds is the -N=C double bond which accepts two electrons to form the corresponding dianion. The formed dianion would be strong base enough to abstract protons from the solution (from the solvent-moisture or from the supporting electrolyte or even from the solvent itself)[35,36] forming compound **VI**. It is clear from the structure of **VI** (Scheme 2) that this compound is unstable especially in air, which can be oxidized with air oxygen to give the starting substance. This is in full agreement with the results obtained from CPE. Thus instead of the final product **VI**, a quantitative yield of the starting material was isolated.

References

1) M. H. Elnagdi and H. M. Fahmy, *J. Electroanal. Chem.*, **84**, 149 (1977).
2) H. M. Fahmy and M. H. Elnagdi, *Electrochim. Acta*, **23**, 255 (1978).
3) H. M. Fahmy, M. A. Morsi, and M. H. Elnagdi, *Gazz. Chim. Ital.*, **107**, 565 (1977).
4) G. Cauquis, H. M. Fahmy, G. Pierre, and M. H. Elnagdi, *Electrochim. Acta*, **24**, 391 (1979).
5) G. Cauquis, N. M. Fahmy, G. Pierre, and Z. E. Kandeel, *J. Electroanal. Chem.*, **124**, 133 (1981).
6) M. A. Morsi, H. M. Fahmy, M. H. Elnagdi, and M. Abdel Azzem, *J. Electroanal. Chem.*, **133**, 269 (1982).
7) M. A. Morsi, A. M. A. Helmy, and H. M. Fahmy, *J. Electroanal. Chem.*, **148**, 123 (1983).
8) N. M. Abed, N. Nashed, H. M. Fahmy, and M. Abdel Azeem, *Monatsh. Chem.*, **117**, 599 (1986).
9) T. Zsolnai, *Biochem. Pharmacol.*, **13**, 285 (1964); *Chem. Abstr.*, **60**, 13811h (1964).
10) T. Zsolnai, *Biochem. Pharmacol.*, **14**, 1325 (1965); *Chem. Abstr.*, **63**, 15467d (1965).
11) T. Zsolnai, *Biochem. Pharmacol.*, **14**, 1425 (1965); *Chem. Abstr.*, **64**, 2686h (1966).
12) M. W. Goldberg and A. I. Rachlin, U.S.P. 265889 (1953); *Chem. Abstr.*, **49**, 1103g (1955).
13) P. G. Heytler and W. W. Prichard, *Biochem. Biophys. Res. Commun.*, **1**, 272 (1962).
14) B. Dienh and G. Tollin, *Arch. Biochem. Biophys.*, **121**, 169 (1967).
15) E. S. Bamberger, C. C. Black, C. A. Fewson, and M. Gibbs, *Plant Physiol.*, **38**, 483 (1963).
16) M. A. Mohamed, M. Sc. Thesis, Zagazig University, Egypt, 1983.
17) E. L. Bennett, *J. Am. Chem. Soc.*, **74**, 2420 (1952).
18) M. H. Elnagdi, M. R. N. Elmoghayar, and D. H. Fleita, *J. Prak. Chem.*, **316**, 975 (1964).
19) W. Summerman, Ph. D. Thesis, Freiburg University, West Germany, 1970, p. 10.
20) M. H. Koepp, H. Wendt, and H. Strehlow, *Z. Electrochem.*, **64**, 483 (1960).
21) Wilkinson, *J. Am. Chem. Soc.*, **74**, 6148 (1952).
22) R. S. Nicholson and I. Shain, *Anal. Chem.*, **36**, 706 (1964); **37**, 178 (1965).
23) J. Tomes, *Collect. Czech. Chem. Commun.*, **7**, 198 (1935).
24) M. H. Fahmy and M. H. Elnagdi, *Electrochim. Acta*, **23**, 255 (1978).
25) M. H. Elnagdi, H. M. Fahmy, and M. A. Morsi, *J. Electroanal. Chem.*, **68**, 237 (1976).
26) H. M. Sammour, H. M. Fahmy, and M. H. Elnagdi, *J. Prak. Chem.*, **317**, 257 (1975).
27) M. A. Morsi, H. M. Fahmy, M. H. Elnagdi, and M. Abdel Azzem, *J. Electroanal. Chem.*, **133**, 269 (1982).
28) M. A. Morsi, A. M. A. Helmy, and H. M. Fahmy, *J. Electroanal. Chem.*, **148**, 123 (1983).
29) N. A. Abed, B. Nashed, H. M. Fahmy, and M. Abdel Azzem, *Monatsh. Chem.*, **117**, 599 (1986).
30) Yu. P. Kitaev, G. K. Bundikov, and L. I. Maslova, *Izv. Akad. Nauk SSSR, Ser. Khim.*, **1967**, 1911.
31) H. Simon and W. Modenhour, *Chem. Ber.*, **100**, 1949 (1967).
32) B. V. Loffe and V. S. Stopskij, *Tetrahedron Lett.*, **1968**, 1333.
33) H. M. Fahmy, M. H. Elnagdi, Z. E. Kandeel, and G. Pierre, *J. Chem. Technol. Biotechnol.*, **31**, 688 (1981).
34) G. Cauquis, M. H. Fahmy, G. Pierre, and Z. E. Kandeel, *J. Electroanal. Chem.*, **124**, 133 (1981).
35) J. L. Sadlev and A. J. Bard, *J. Am. Chem. Soc.*, **90**, 1979 (1968).
36) K. G. Boto and F. G. Thomas, *Aust. J. Chem.*, **26**, 125 (1973).

Separation of Scandium(III) as Ascorbato Complex by Extraction with Aliquat 336S

M. A. KARVE and S. M. KHOPKAR*
Department of Chemistry, Indian Institute of Technology, Bombay 400076, India
(Received February 8, 1990)

Scandium was quantitatively extracted with 0.1 mol dm^{-3} Aliquat 336S in xylene at pH=6.0 from 0.01 mol dm^{-3} ascorbic acid. It was stripped with 1 mol dm^{-3} hydrochloric acid and determined as its complex with Arsenazo III. It was separated from binary mixtures by exploiting the difference in the extraction behavior from ascorbic acid. Several separations were accomplished by process of selective stripping with concentrated hydrochloric acid. Many interesting separations of scandium from associated elements like yttrium, thorium, uranium, and molybdenum have been carried out.

Solvent extraction separation methods for scandium with liquid anion exchangers from organic acid media are limited. Scandium was separated from solutions of EDTA,[1] malonic,[2] citric,[3] and succinic acids.[4] 4—5% of Amberlite LA-1,[2] Aliquat 336S[3,4] was used with xylene or benzene as the diluent. 0.05—0.1 mol dm^{-3} of organic acid was employed. At pH 2.5—4.5 extraction was carried out while stripping was done from 0.5—8 mol dm^{-3} of mineral acids. However iron(III), zirconium, vanadium (V), thorium, and molybdenum showed strong interference. Similar studies from sulphate[5,6] and nitrate media were also not effective in separating scandium.

In this paper a new method is proposed for extraction of anionic complex of scandium from ascorbic acid at pH 6.0 with 0.1 mol dm^{-3} Aliquat 336S. The chief advantage of the proposed method is the possibility of separation of scandium from large number of less common elements.

Experimental

Apparatus and Reagents. An ECIL spectrophotometer GS866C with matched 10 cm corex glass cuvettes and an ECIL pH meter with combined glass electrodes as well as wrist action flask shaker were used.

A stock solution of scandium was prepared by dissolving 1.50 g of scandium oxide in 100 cm^3 of boiling nitric acid. It was diluted to one liter with distilled water and was standardized complexometrically with EDTA using xylenol orange as an indicator.[8] It contained 1.045 mg cm^{-3} of scandium. The solution containing 40 μg cm^{-3} of scandium was prepared by dilution.

Aliquat 336S (General Mills Ltd., England), Amberlite LA-1 or LA-2 (Rohm and Hass Co., U.S.A.), trioctylamine (Riedel Haen, Germany), and Primene JMT (Rohm and Hass Co., U.S.A.) were used without further purification in the ascorbate form.[9]

General Procedure. To an aliquat of solution containing 40 μg of scandium, 5 cm^3 of 0.01 mol dm^{-3} ascorbic acid was added. The pH of the solution was adjusted to 6.0 with 0.01 mol dm^{-3} ammonia or ascorbic acid. The solution was diluted to 10 cm^3. It was transferred into a separatory funnel. Then 10 cm^3 of 0.1 mol dm^{-3} Aliquat 336S in xylene was added and the solution was shaken on a wrist action flask shaker for 15 minutes. The two phases were allowed to settle and separate. Scandium from the organic phase was stripped with 10 cm^3 of 1 mol dm^{-3} hydrochloric acid. Then 2.5 cm^3 of 8% ascorbic acid, 0.5 cm^3 of 13.6% sodium acetate trihydrate, and 2 cm^3 of 0.1% Arsenazo III were added in total volume of 25 cm^3 to develop blue color. The absorbance was measured spectrophotometrically at 670 nm against a reagent blank. The concentration of scandium was computed from the calibration curve.[10]

Results and Discussion

Extraction of Scandium as a Function of pH. The pH for the quantitative extraction of scandium was ascertained by extracting scandium at pH 1—8 with 4% solutions of various liquid anion exchangers in xylene (Fig. 1). At pH 6.0 the extraction was 15% with Amberlite LA-1 while it was less than 25% with

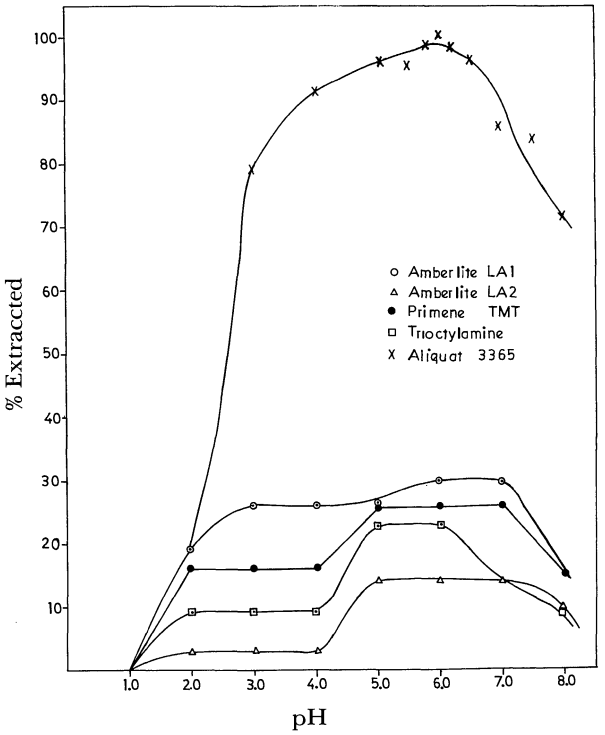

Fig. 1. Extraction of scandium as a function of pH with various liquid anion exchangers.

Primene JMT and Trioctylamine, and with Amberlite LA-1 it was 30%. Since only with Aliquat 336S extraction was quantitative this was used throughout the work.

Effect of Varying Concentration of Aliquat 336S. Scandium was extracted at pH 6.0 with 10 cm^3 of various concentrations and volume of 0.1 mol dm^{-3} Aliquat 336S in xylene. Scandium was quantitatively extracted with 10 cm^3 of 0.1 mol dm^{-3} Aliquat 336S in xylene (Table 1).

Effect of Varying Concentration of Ascorbic Acid. Scandium was extracted at pH 6.0 with 0.1 mol dm^{-3} Aliquat 336S in xylene from varying concentration of ascorbic acid (Table 2). The extraction was quantitative from 0.008 mol dm^{-3} concentration of ascorbic acid. 0.01 mol dm^{-3} ascorbic acid was used in subsequent work.

Effect of Various Diluents. Benzene, toluene, xylene, hexane, cyclohexane, chloroform, and carbon tetrachloride were used as the diluents for Aliquat 336S. The phase volume ratio was maintained as 1 : 1. The aromatic hydrocarbons proved to be efficient while hexane, chloroform, and carbon tetrachloride proved to be poor. Xylene was preferred as the diluent due to nontoxicity and clear phase separation (Table 3).

Period of Shaking. Scandium was extracted for different time of shaking ranging from 2.5, 10, 15, and 20 minutes. The corresponding extraction was 55, 90, 100, and 100% respectively. Hence 15 minutes period of equilibration was employed throughout the work.

Effect of Various Stripping Agents. After extraction, scandium was stripped with various acids and salts (Table 4). 1—8 mol dm^{-3} hydrochloric acid or 0.5—8 mol dm^{-3} sulfuric acid or nitric acid could strip scandium quantitatively. Hydrochloric acid was preferred as it facilitated direct spectrophotometric determination of scandium in the aqueous phase.

Separation from Binary Mixtures. The separation of scandium was attempted from binary mixtures. The alkali, alkaline earths, lead, or iron were not extracted with scandium. This in turn facilitated their separation. Cerium, yttrium, chromium, manganese, cobalt, nickel, copper, zinc, and aluminium formed weak complexes with ascorbic acid, but such complexes could be stripped with water before stripping of scandium with 1 mol dm^{-3} hydrochloric acid. However scandium was coextracted along with titanium, zirconium, hafnium, thorium, vanadium, or molybdenum. Therefore these separations were effected by stripping scandium with 8 mol dm^{-3}

Table 1. Effect of Varying Concentration and Volume of Aliquat 336S

Aliquat 336S	Vol	% Extracted	D
1×10^{-2} mol dm^{-3}	cm^3		
0.5	10	36	0.5
0.6	10	42	0.76
0.7	10	50	1.0
0.8	10	56	1.2
0.9	10	65	1.8
1.0	10	70	2.3
2.5	10	76	3.1
5.0	10	85	5.6
6.0	10	92	11.5
7.0	10	99.6	249
8.0	10	99.8	499
9.0	10	99.8	499
10.0	10	100	∞
10.0	4	70	2.4
10.0	6	80	4
10.0	8	92	11.5
10.0	15	100	∞

Table 2. Effect of Varying Ascorbic Acid Concentration

Ascorbic acid	% Extracted	D
1×10^{-3} mol dm^{-3}		
0.5	25.0	0.33
0.6	32.0	0.47
0.7	40.0	0.66
0.8	48.0	0.90
0.9	55.0	1.1
1.0	62.0	1.3
2.0	70.0	2.30
3.0	73.0	2.70
4.0	80.0	4.00
5.0	89.0	8.00
6.0	92.0	11.50
7.0	98.0	49.00
8.0	99.8	499
9.0	99.8	499
10.0	100.0	∞

Table 3. Effect of Various Diluents

Diluent	Dielectric constant (ε)	Extraction %	Distribution ratio (D)
Benzene	2.28	99.7	332.4
Toluene	2.38	99.0	99
Xylene	2.30	100.0	∞
Hexane	1.89	80.0	40
Cyclohexane	2.05	98.0	49
Chloroform	4.8	92.0	11.5
Carbontetrachloride	2.24	92.0	11.5

Table 4. Effect of Different Stripping Agents

Stripping agent	% Recovery					
mol dm^{-3}	0.5	1	2	4	6	8
HCl	85	100	100	100	100	100
H_2SO_4	99	100	100	100	100	100
HNO_3	100	100	100	100	100	100
HBr	—	95.0	96.0	96.0	97.0	98.0
$NaNO_3$	80.2	82.0	—	—	—	—
NH_4Br	85.0	83.0	—	—	—	—

Table 5. Effect of Diverse Ions
(Sc=20 μg, pH=6.0, 0.1 mol dm^{-3} Aliquat 336S in Xylene)

Element	Added as	Foreign ion added	Recovery	Ratio
		mg	%	
Li^+	$LiSO_4 \cdot H_2O$	6	100	1:300
Na^+	NaCl	6	100	1:300
K^+	KCl	6	100	1:300
Rb^+	RbCl	5	99.6	1:250
Mg^{2+}	$MgSO_4 \cdot 7H_2O$	4	100	1:200
Ca^{2+}	$Ca(NO_3)_2$	5	100	1:300
Sr^{2+}	$Sr(NO_3)_2 \cdot 2H_2O$	4	100	1:200
Ba^{2+}	$Ba(NO_3)_2 \cdot 4H_2O$	5	100	1:250
Fe^{2+}	$FeSO_4 \cdot 7H_2O$	1.5	99	1:75
Pb^{2+}	$Pb(NO_3)_2$	1.5	99.2	1:75
Al^{3+}	$Al(NO_3)_3 \cdot 9H_2O$	4	99.6	1:200
Co^{2+}	$Co(NO_3)_2 \cdot 6H_2O$	1	99	1:250
Ni^{2+}	$Ni(NO_3)_2 \cdot 6H_2O$	1	99	1:50
Cu^{2+}	$CuSO_4 \cdot 5H_2O$	1.8	99.2	1:90
Mn^{2+}	$MnSO_4 \cdot 7H_2O$	1.5	100	1:75
Ce^{3+}	$Ce(SO_4)_3 \cdot 8H_2O$	1	99.2	1:50
Y^{3+}	$Y(NO_3)_2 \cdot 2H_2O$	1	100	1:50
Cr^{2+}	$Cr(NO_3)_3 \cdot 9H_2O$	0.5	99	1:25
Tl^+	Tl_2SO_4	2.5	100	1:125
V^{4+}	$VOSO_4 \cdot 5H_2O$	0.100	100	1:5
Zr^{4+}	$Zr(NO_3)_4 \cdot 5H_2O$	0.500	99	1:25
Hf^{4+}	$Hf(NO_3)_2$	0.250	99	1:125
UO_2^{2+}	$UO_2(NO_3)_2 \cdot 6H_2O$	0.100	99	1:5
$Mo_7O_{24}^{6-}$	$(NO_4)_6Mo_7O_{24} \cdot 4H_2O$	0.500	100	1:25
Th^{4+}	$Th(NO_3)_2 \cdot 4H_2O$	0.025	100	1:1.25

Table 6. Separation of Scandium from Multicomponent Mixtures

Metal	Amount taken	Amount found	Recovery	Stripping agent	Chromogenic agent	λ_{max} for spectro photometer
	μg	μg	%	mol dm^{-3}		
1) Mn(II)	800	799.8	99.2	H_2O	Formaldoxime	450
Sc(III)	40	40	100	8 HCl	Arsenazo III	670
V(V)	40	40	100	0.1 HCl	Xylenolorange	520
2) Fe(II)	800	799	99.8	Unextracted	Thiocyanate	480
Sc(III)	40	39.5	99.7	10 HCl	Arsenazo III	670
Hf(IV)	100	99	99	1 HCl	Arsenazo III	625
3) Ce(III)	500	498	99.6	H_2O	Xylenolorange	575
Sc(III)	40	40	100	5 HNO_3	Arsenazo III	670
Th(IV)	25	25	100	2 HCl	Arsenazo III	650
4) Ce(III)	500	498	99.6	H_2O	Xylenolorange	575
Sc(III)	40	40	100	5 HCl	Arsenazo III	670
U(VI)	100	99	99	0.5 NaOH	Arsenazo III	665
5) Al(III)	500	498	99.6	H_2O	Alizarin RedS	520
Sc(III)	40	40	100	4 HCl	Arsenazo III	670
Mo(VI)	100	99	99	4 HNO_3	Phenylfluorone	525
U(VI)	100	99.6	99.6	0.5 NaOH	Arsenazo III	665
6) Ce(III)	500	498	99.6	H_2O	Xylenolorange	575
Sc(III)	40	40	100	5 HNO_3	Arsenazo III	670
U(VI)	100	99	99	0.5 NaOH	Arsenazo III	665
Th(IV)	25	25	100	2 HCl	Arsenazo III	650

hydrochloric acid followed by, stripping of these elements with 1 mol dm^{-3} hydrochloric acid. During stripping these elements formed anionic chlorocomplexes with hydrochloric acid and were in turn reextracted in Aliquat 336S and were back washed with 1 mol dm^{-3} hydrochloric acid.

Separation of Scandium from Multicomponent Mixtures. When a mixture of manganese, scandium, and vanadium was extracted, manganese was first stripped with water, then scandium with 8 mol dm^{-3} hydrochloric acid and finally vanadium with 0.1 mol dm^{-3} hydrochloric acid.

Iron(II), scandium(III), and hafnium(IV) were separated after extraction by first stripping scandium with 10 mol dm^{-3} hydrochloric acid, then hafnium with 1 mol dm^{-3} hydrochloric acid and finally unextracted iron was determined directly in the aqueous phase.

Cerium(III), scandium(III), and thorium(IV) were separated after extraction by stripping of scandium with 5 mol dm^{-3} nitric acid, thorium with 2 mol dm^{-3} hydrochloric acid and cerium was stripped with water.

After extraction, cerium(III), scandium(III), and uranium(VI) were separated by washing cerium with water, then stripping scandium with 8 mol dm^{-3} hydrochloric acid and finally uranium with 0.5 mol dm^{-3} sodium hydroxide.

Aluminium(III), scandium(III), molybdenum(VI), and uranium were separated after extraction, by stripping aluminium with water, scandium with 4 mol dm^{-3} hydrochloric acid, molybdenum with 4 mol dm^{-3} nitric acid and uranium with 0.5 mol dm^{-3} sodium hydroxide.

Cerium(III), scandium(III), uranium(VI), and thorium(IV) were separated by stripping cerium with water, scandium with 5 mol dm^{-3} nitric acid, uranium with 0.5 mol dm^{-3} sodium hydroxide and thorium with 2 mol dm^{-3} hydrochloric acid (Tables 5 and 6).

The proposed method is simple, rapid, selective, and applicable at tracer concentration. Scandium was separated from uranium, thorium, hafnium, molybdenum, and vanadium which are generally associated with it in fission products.

We are thankful to the Council of Scientific and Industrial Research for sponsoring this project and awarding J.R.F. to M.A.K. (This paper was awarded Professor Pandu Rang Rao memorial award at the 26th Annual Meeting of Indian Chemical Society at Indore in December 1989.)

References

1) Y. Chushiro and O. Hiroshi, *Anal. Chim. Acta*, **96**, 211 (1978).
2) M. B. Dalvi and S. M. Khopkar, *Talanta*, **26**, 892 (1979).
3) C. P. Vibhute and S. M. Khopkar, *Indian J. Chem., Sect. A*, **24**, 446 (1985).
4) D. D. Desai and V. M. Shinde, *Analyst (London)*, **106**, 806 (1981).
5) T. Shimuzu, *Jpn. Anal.*, **17**, 1187 (1968).
6) R. W. Cattrall and S. J. E. Slater, *Inorg. Chem.*, **9**, 598 (1970).
7) S. J. Stepanov, N. G. Kiyatkina, and O. N. Fedotove, *Zh. Neorg. Khim.*, **32**, 2517 (1987); *Chem. Abstr.*, **108**, 83018j (1987).
8) F. J. Welcher, "The Analytical Use of Ethylenediamine Tetraacetic Acid," D. Van Nostrand, London (1958), p. 175.
9) C. P. Vibhute and S. M. Khopkar, *J. Radioanal. Chem.*, **97**, 3 (1986).
10) F. D. Snell, "Photometric and Fluorimeteric Methods of Analysis of Metals," John Wiley and Sons, New York (1978), Part I, p. 539.

 © 1991 The Chemical Society of Japan Bull. Chem. Soc. Jpn., 64, 659—667 (1991)

Cumulene Hosts: Synthesis and Inclusion Property of Tetraaryl-Substituted Butatrienes. X-Ray Crystal Structures of an Unsolvated Host and Its 1:2 Inclusion Compounds with *o*- and *p*-Xylene

Edwin WEBER,* Wilhelm SEICHTER, Ru-Ji WANG, and Thomas C. W. MAK*,†
Institut für Organische Chemie und Biochemie der Universität Bonn,
Gerhard-Domagk-Strasse 1, D-5300 Bonn-1, FR-Germany
†Department of Chemistry, The Chinese University of Hong Kong,
Shatin, New Territories, Hong Kong
(Received April 24, 1990)

A series of tetraaryl-substituted cumulenes were synthesized and characterized by elemental analysis, ^{1}H NMR, and MS spectra. Their inclusion capabilities for a variety of organic solvents were examined. It was found that substitution on the phenyl groups connected to both ends of these cumulenes critically influences their inclusion behavior since the substituents dictate the size and shape of lattice space for accommodation of the guest molecules. The crystal structures of an unsolvated butatriene and its 1:2 inclusion compounds with *p*-xylene and *o*-xylene were determined by X-ray crystallography. The structural analysis showed that the guest molecules do not simply fit into the free space of the host lattice, but their presence rearranges the packing mode of the host molecules in the inclusion compounds.

Considerable interest in clathrates[1] and similar systems has arisen over the past few years. This has led to the development of new strategies in clathrate formation[3] and the design of novel host types.[4] Recently we have shown that allene host molecules (e.g. **1** and **2**) provide access to a new family of channel-type clathrates.[5,6] Obviously they depend on the bulk of host substituents present.

In order to ascertain whether inclusion behavior is critically effected by the special geometry and dimensions of the 1,2-diene framework,[7] we became interested in the potential host properties of cumulenes which are the higher analogs of allenes.[8] It is important to note that allenes and cumulenes have either orthogonal or co-planar pairs of substituents at both ends of the molecule depending on the number of double bonds present;[9] i.e. from allenes to the higher cumulenes orthogonal and co-planar orientations alternate. Moreover, the central axle is gradually increased on going from allenes to higher cumulenes. This will allow geometrical and dimensional tuning of possible host molecules. Representative examples illustrating these considerations are the tetraaryl-substituted cumulenes **3**—**7**, which may be contrasted with the allenes **1** and **2**.

In the present work, we describe the preparation of

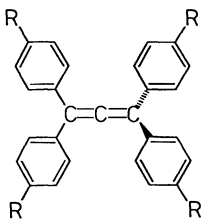

1

a: R = H
b: R = Me
c: R = CMe_3

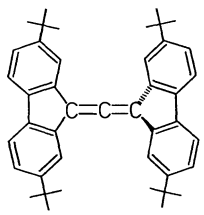

2

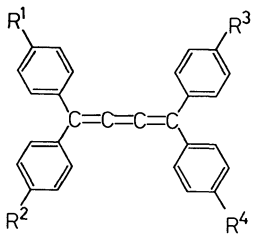

3 $R^1 = R^2 = R^3 = R^4 = H$
4 $R^1 = R^2 = R^3 = R^4 = CMe_3$
5 $R^1 = R^3 = Br$, $R^2 = R^4 = H$

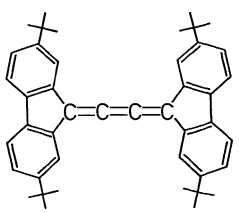

6

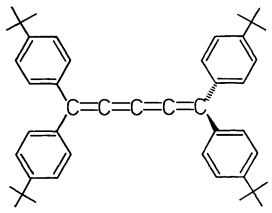

7

cumulenes **3**—**7**, report on their crystal inclusion properties, and give X-ray crystal structure demonstrations of unsolvated host **6** and of two of its isolated host-guest species, namely **6**·*o*-xylene (1 : 2) and **6**·*p*-xylene (1 : 2).

Results and Discussion

Synthesis. Except for **3**,[10] the cumulenes **4**—**7** have not been reported previously in the literature. Trienes **3**—**6** and the tetraene **7** were prepared on different synthetic routes.[10,11] For trienes **3**—**6**, vinyl bromide was treated with phenyllithium in dry ether to give dilithium acetylide. On reaction with the corresponding ketone, diols **8a**—**c** and **9** were obtained in 39—65% yield. Diols **8a**—**c** and **9** were reduced with tin(II)chloride dihydrate on powder reaction to yield the cumulenes **3**—**6** in 58—80%. For tetraene **7**, diethyl glutarate was treated with four equivalents of 4-*t*-butylphenyllithium to yield 52% of 1,4-diene **10a**. Addition of bromine gave 45% of dibromo intermediate **10b** which was bis-dehydrobrominated with methanolic potassium hydroxide to yield 70% of cumulene **7**.

Inclusion Properties. Because of the co-planar orientation of σ-bonds in the triene-type cumulenes (see above), bulky substituents are required to induce free lattice space for guest inclusion.[3] Consequently **4** and **6** which bear bulky *t*-butyl groups at each aromatic residue are optimal for clathrate formation, as both the parent **3** and lower substituted **5** do not exhibit inclusion behavior. The isolated inclusion compounds of **4** and **6** are listed in Table 1. Due to the nonpolar nature of the hosts, hydrocarbon guests are well to the fore;[12] bromobenzene, cyclopentanone, and 1,4-dioxane are exceptions. Moreover, strict discrimination effects regarding the size and shape of guest molecules are inferrable from Table 1, as will be discussed below. Table 1 makes also reference to solvents not included by **4** and **6**.

Obviously the inclusion capabilities of **4** and **6** differ from each other in more than one respect. To begin with, **4** is more efficient in clathrate formation compared with **6**, which is significantly indicated by the number of isolated complexes formed by both hosts (Table 1). In addition, host **4** forms a broader range of inclusion compounds, i.e. with solvents of different classes (see Table 1) and somewhat varying dimensions (thickness), while **6** is only successful with aromatic substances. Nevertheless, aromatic substances are also the preferred guests for **4**. These findings are in agreement with geometric parameters since bridging in **6** causes flattening of the substituents and thus reduction of the net bulkiness of the host, which is reflected in its low inclusion capability.

However, from the stoichiometric ratio point of view, **6** is superior to **4** in that **6** exclusively forms clathrates of 1 : 2 stoichiometry (high percentage of guest), whereas **4** gives 1 : 1 clathrates (lower percentage of guest) in all cases, except for mesitylene (1 : 2

Table 1. Crystalline Inclusion Compounds of Cumulene Hosts **4** and **6**

Guest component[a]	Host/guest ratio[b] in inclusion compound	
	4	**6**
Benzene	1 : 1	1 : 2
Toluene	1 : 1	—
o-Xylene	1 : 1	1 : 2
m-Xylene	c)	—
p-Xylene	1 : 1	1 : 2
Mesitylene	1 : 2	—
Bromobenzene	1 : 1	—
Cyclohexane	1 : 1	—
Cyclohexene	1 : 1	—
Cycloheptatriene	1 : 1	—
Cyclopentanone	1 : 1	—
1,4-Dioxane	1 : 1	—

a) The following solvents yield no crystalline inclusion compounds: 1,2,4,5-tetramethylbenzene, *o*-dichlorobenzene, 1,4-difluorobenzene, pyridine, cyclopentane, cycloheptane, cyclopentene, methylcyclopentane, methylcyclohexane, cyclohexanone, tetrahydrofuran, 1,3-dioxolane, morpholine. b) Determined by NMR integration of the isolated crystals (for method of preparation and drying standard, see Experimental Section). c) Difficult to crystallize.

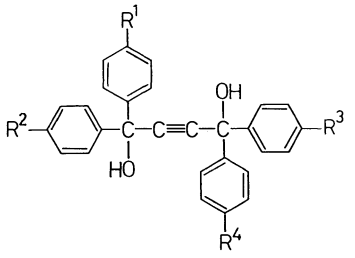

8

a: $R^1 = R^2 = R^3 = R^4 = H$

b: $R^1 = R^2 = R^3 = R^4 = CMe_3$

c: $R^1 = R^3 = Br$, $R^2 = R^4 = H$

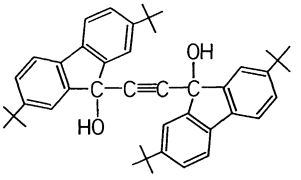

9

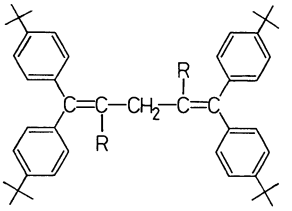

10

a: R = H

b: R = Br

Table 2. Data Collection and Processing Parameters

Compound	**6**	**6**·*p*-Xylene (1:2)	**6**·*o*-Xylene (1:2)
Molecular formula	$C_{44}H_{48}$	$C_{44}H_{48}\cdot 2C_8H_{10}$	$C_{44}H_{48}\cdot 2C_8H_{10}$
Molecular weight	576.92	789.19	789.19
Color and habit	Red polyhedron	Red polyhedron	Red polyhedron
Unit cell parameters			
a/Å	14.623(6)	9.103(1)	8.868(2)
b/Å	6.065(1)	19.440(5)	12.080(4)
c/Å	19.646(7)	14.091(4)	24.195(9)
α/°	90	90	91.43(3)
β/°	100.28(3)	96.38(2)	94.92(3)
γ/°	90	90	102.86
V/Å^3	1714(1)	2478(1)	2515(1)
Z	2	2	2
ρ_{calcd}/g cm^{-3}	1.118	1.058	1.042
Space group	$P2_1/c$ (No. 14)	$P2_1/a$ (No. 14)	$P\bar{1}$ (No.2)
Radiation	Graphite-monochromatized Mo $K\alpha$, λ=0.71073 Å		
Standard reflections	(22$\bar{8}$), (612)	(24$\bar{2}$), (312)	(122), (1$\bar{3}\bar{3}$)
Intensity variation	±3%	±2%	±2%
R_{int} (from merging of equiv reflections)	0.082	0.023	0.054
Absorption coefficient/cm^{-1}	0.6	0.5	0.5
Crystal size/mm^3	0.52×0.52×0.40	0.45×0.35×0.35	0.58×0.38×0.14
Scan type and rate/° min^{-1}	ω; 3.01—14.65	ω-2θ; 2.00—19.53	ω; 3.97—15.63
Scan range	0.65° below $K\alpha_1$ to 0.65° above $K\alpha_2$		
Background counting	Stationary counts for one-fifth of scan time at each end of scan range		
Collection range, $2\theta_{max}$	h, k, ±l, 50°	h, k, ±l, 45°	h, ±k, ±l, 45°
Unique data measured	3031	4331	4698
Obsd data [$\|F_o\|\geq 6\sigma(\|F_o\|)$], n	2126	1875	2014
No. of variables, p	199	298	297
$R_F=\sum\|\|F_o\|-\|F_c\|\|/\sum\|F_o\|$	0.087	0.073	0.159
Weighting scheme, w	Unit weight	$[\sigma^2(F_o)+0.0005\|F_o\|^2]^{-1}$	Unit weight
$R_G=[\sum w(\|F_o\|-\|F_c\|)^2/\sum w\|F_o\|^2]^{1/2}$	0.096	0.107	0.164
$S=[\sum w(\|F_o\|-\|F_c\|)^2/(n-p)]^{1/2}$	1.693	3.915	4.192
Residual extrema in final difference map/e Å^{-3}	+0.36 to −0.36	+0.31 to −0.29	+0.70 to −0.39

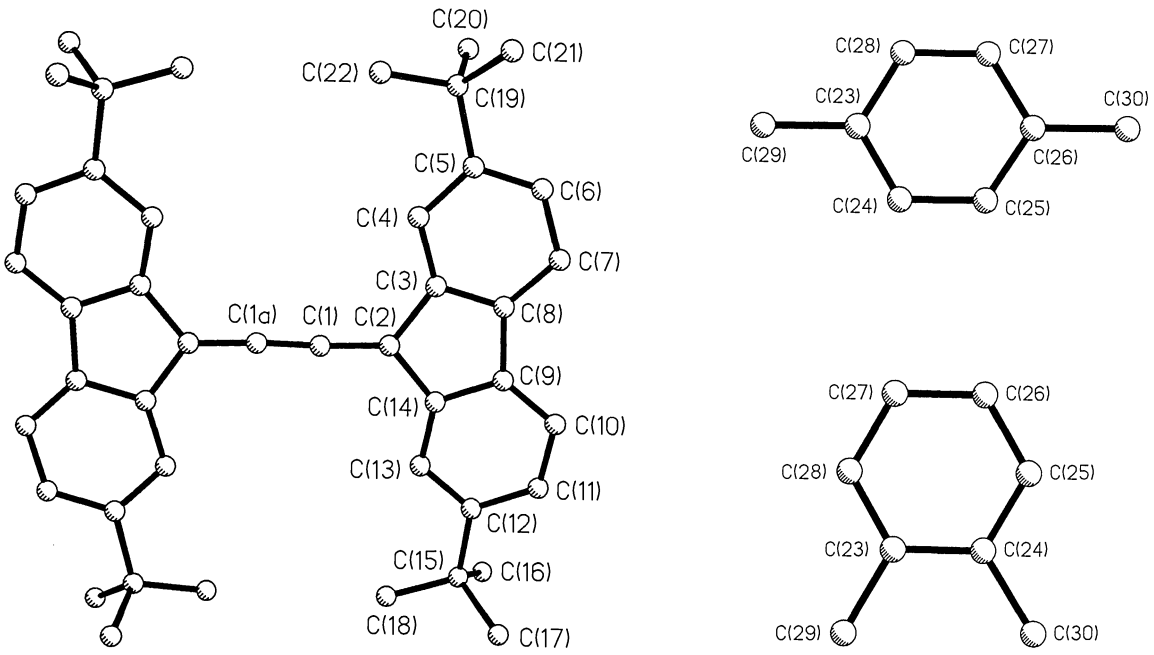

Fig. 1. Perspective view of cumulene host molecule **6** and the scheme of atom numbering. Symmetry code is given in Tables 3, 4, and 5.

Table 3. Atomic Coordinates ($\times 10^4$) and Thermal Parameters[a] ($\times 10^3$) for **6**

Atom	x	y	z	U_{eq}/Å^2
C(1)	−190(3)	4323(9)	4783(3)	37(2)
C(2)	−560(3)	2824(9)	4312(3)	33(2)
C(3)	−49(3)	1122(9)	3994(3)	33(2)
C(4)	912(3)	764(9)	4077(3)	35(2)
C(5)	1228(3)	−910(9)	3684(3)	37(2)
C(6)	594(4)	−2159(10)	3243(3)	50(2)
C(7)	−367(4)	−1861(10)	3174(3)	49(2)
C(8)	−677(3)	−178(9)	3555(3)	37(2)
C(9)	−1624(3)	645(9)	3577(3)	35(2)
C(10)	−2482(3)	−38(9)	3243(3)	41(2)
C(11)	−3265(3)	1140(9)	3345(3)	40(2)
C(12)	−3204(3)	3009(9)	3773(2)	32(2)
C(13)	−2330(3)	3666(9)	4113(2)	32(2)
C(14)	−1548(3)	2493(9)	4016(2)	31(2)
C(15)	−4104(3)	4237(9)	3847(3)	38(2)
C(16)	−4520(4)	5267(11)	3135(3)	54(2)
C(17)	−4808(4)	2588(12)	4050(4)	63(3)
C(18)	−3943(4)	6040(11)	4387(3)	55(2)
C(19)	2282(3)	−1291(9)	3724(3)	40(2)
C(20)	2557(4)	−355(12)	3057(3)	60(2)
C(21)	2482(4)	−3809(11)	3764(4)	66(3)
C(22)	2863(3)	−196(11)	4352(3)	51(2)

a) Equivalent isotropic U_{eq} defined as one third of the trace of the orthogonalized $\boldsymbol{U}$ tensor.

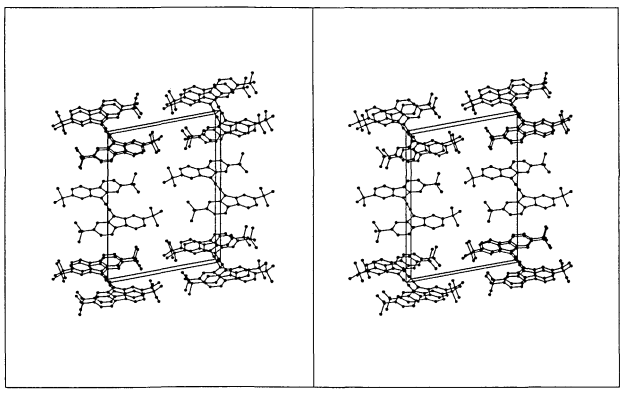

Fig. 2. Stereoview of the crystal structure of **6** parallel to the *b* axis. The origin of the unit cell lies at the upper left corner, with *a* pointing from left to right, *b* towards the reader, and *c* downwards.

stoichiometry). Considering the size of mesitylene, it is not difficult to understand why it occupies a special position. All other guests suitable for inclusion by **4** are molecules of nearly the same breadth (approximately 4.5 Å),[12] as deducible from Table 1, but in length (cf. benzene=6.9 Å with *p*-xylene=8.8 Å) and thickness (cf. benzene=3.8 Å with cyclohexane=5.6 Å) they can vary to some extent. Beyond that, it seems that **6** effects also a selection of guests via molecular thickness, since its inclusion property is limited to flat aromatic substances. This suggests different cavity dimensions and inclusion modes for the clathrates of **4** and **6**, but for the individual host species, similar inclusion structures with similar cavity dimensions

Table 4. Atomic Coordinates ($\times 10^4$) and Thermal Parameters[a] ($\times 10^3$) for **6**·*p*-Xylene (1 : 2)

Atom	x	y	z	U_{eq}/Å^2
C(1)	177(5)	4762(3)	4742(3)	38(2)
C(2)	576(6)	4253(3)	4177(3)	38(2)
C(3)	−253(6)	3993(3)	3296(3)	35(2)
C(4)	−1587(6)	4189(3)	2830(4)	41(2)
C(5)	−2131(6)	3884(3)	1964(4)	43(2)
C(6)	−1250(7)	3382(3)	1598(4)	49(2)
C(7)	99(6)	3180(3)	2058(4)	45(2)
C(8)	599(6)	3477(3)	2923(3)	38(2)
C(9)	1969(6)	3380(3)	3582(3)	39(2)
C(10)	3148(6)	2942(3)	3571(4)	46(2)
C(11)	4314(6)	2985(3)	4271(4)	50(2)
C(12)	4367(6)	3472(3)	5007(4)	45(2)
C(13)	3134(6)	3906(3)	5028(4)	41(2)
C(14)	1973(6)	3858(3)	4322(3)	36(2)
C(15)	5717(6)	3558(3)	5751(5)	59(2)
C(16A)[b]	6350(18)	4312(8)	5695(14)	78(6)
C(17A)	5290(23)	3449(11)	6775(13)	88(8)
C(18A)	7042(18)	3100(11)	5600(16)	96(9)
C(16B)	7007(17)	3813(14)	5164(14)	118(10)
C(17B)	5441(29)	3998(18)	6547(19)	177(16)
C(18B)	6223(29)	2793(9)	6036(19)	142(11)
C(19)	−3628(7)	4105(3)	1465(4)	55(2)
C(20)	−3617(9)	4886(3)	1262(6)	93(3)
C(21)	−4829(7)	3946(4)	2098(5)	88(3)
C(22)	−4041(8)	3723(4)	514(5)	88(3)
C(23)	−377(8)	4303(4)	−1519(5)	67(3)
C(24)	115(9)	4037(4)	−659(5)	79(3)
C(25)	1183(10)	3530(5)	−577(5)	85(3)
C(26)	1806(9)	3265(4)	−1346(6)	80(3)
C(27)	1285(9)	3548(4)	−2225(5)	77(3)
C(28)	221(8)	4053(4)	−2311(5)	76(3)
C(29)	−1533(9)	4858(4)	−1617(6)	99(4)
C(30)	2990(11)	2713(5)	−1253(7)	118(4)

a) Equivalent isotropic U_{eq} defined as one third of the trace of the orthogonalized $\boldsymbol{U}$ tensor. b) Atoms C(16A) to C(18B) belong to the disordered *t*-butyl group and have site occupancy factor of 0.5.

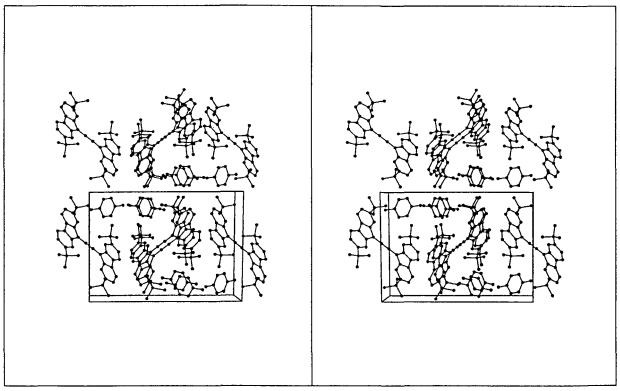

Fig. 3. Stereoview of the crystal structure of **6**·*p*-xylene (1 : 2) parallel to the *a* axis. The origin of the unit cell lies at the lower left corner, with a pointing to the reader, *b* from left to right, and *c* vertically upwards. For clarity the disordered *t*-butyl group is shown as an ordered one.

Table 5. Atomic Coordinates ($\times 10^4$) and Thermal Parameters[a] ($\times 10^3$) for **6**·*o*-Xylene (1 : 2)

Atom	*x*	*y*	*z*	U_{eq}/Å^2	Atom	*x*	*y*	*z*	U_{eq}/Å^2
					C(9B)	917(18)	6818(12)	1551(6)	48(4)
Type-A molecule of **6**					C(10B)	2024(19)	7594(13)	1919(6)	62(5)
C(1A)	5168(19)	4795(12)	5237(5)	52(5)	C(11B)	3441(22)	8130(15)	1725(7)	77(6)
C(2A)	5527(17)	4426(11)	5732(5)	42(4)	C(12B)	3845(21)	7929(14)	1193(7)	68(5)
C(3A)	4496(17)	3679(11)	6051(5)	42(4)	C(13B)	2715(19)	7133(13)	847(6)	59(5)
C(4A)	2991(19)	3089(13)	5921(6)	56(5)	C(14B)	1300(20)	6637(13)	1025(6)	60(5)
C(5A)	2141(19)	2372(13)	6311(6)	55(5)	C(15B)	−5287(20)	4045(16)	1383(8)	75(9)
C(6A)	2938(20)	2357(13)	6824(6)	61(5)	C(16B)	−6303(28)	4348(26)	1778(11)	208(20)
C(7A)	4456(19)	2979(12)	6986(6)	57(5)	C(17B)	−6116(36)	4154(25)	789(11)	207(20)
C(8A)	5223(18)	3650(12)	6584(6)	48(4)	C(18B)	−5260(31)	2841(20)	1468(15)	222(22)
C(9A)	6797(19)	4329(12)	6581(6)	54(5)	C(19B)	5363(22)	8515(16)	1004(8)	73(8)
C(10A)	8059(19)	4591(13)	6991(6)	59(5)	C(20B)	5614(39)	9785(23)	1064(14)	250(25)
C(11A)	9546(21)	5280(13)	6859(7)	67(5)	C(21B)	6815(35)	8387(30)	1387(12)	219(23)
C(12A)	9738(21)	5660(13)	6338(6)	57(5)	C(22B)	5574(29)	8236(27)	441(11)	218(20)
C(13A)	8415(20)	5430(13)	5958(7)	61(5)					
C(14A)	6989(18)	4768(12)	6062(6)	46(4)	Type-A molecule of *o*-xylene				
C(15A)	11175(20)	6372(16)	6196(9)	83(9)	C(23A)	3700(27)	1602(18)	3418(14)	229(16)
C(16A)	11588(30)	6029(28)	5615(10)	204(20)	C(24A)	3908	1299	3967	192(13)
C(17A)	11222(35)	7573(19)	6212(14)	248(26)	C(25A)	4519	354	4089	222(15)
C(18A)	12586(26)	6221(24)	6587(11)	184(17)	C(26A)	4922	−287	3661	344(26)
C(19A)	566(20)	1671(16)	6175(8)	66(8)	C(27A)	4715	17	3112	206(14)
C(20A)	−375(37)	1304(35)	6602(12)	292(30)	C(28A)	4104	961	2990	208(14)
C(21A)	−538(44)	2260(34)	5836(19)	357(36)	C(29A)	3117(56)	2356(39)	3194(16)	306(22)
C(22A)	485(34)	761(26)	5768(15)	258(24)	C(30A)	3605(54)	1934(36)	4439(15)	280(19)
Type-B molecule of **6**					Type-B molecule of *o*-xylene				
C(1B)	52(20)	5254(13)	228(5)	56(5)	C(23B)	313(34)	836(28)	1558(9)	274(20)
C(2B)	67(18)	5803(12)	739(6)	53(4)	C(24B)	−325	1789	1505	288(21)
C(3B)	−1142(18)	5542(12)	1129(6)	48(4)	C(25B)	−480	2258	988	231(16)
C(4B)	−2646(20)	4858(13)	1018(7)	69(5)	C(26B)	2	1774	524	269(19)
C(5B)	−3693(20)	4745(13)	1447(6)	59(5)	C(27B)	640	821	577	326(24)
C(6B)	−3090(21)	5375(14)	1943(7)	73(5)	C(28B)	795	352	1094	208(14)
C(7B)	−1537(19)	6070(13)	2047(6)	61(5)	C(29B)	124(52)	534(35)	2076(15)	275(19)
C(8B)	−609(18)	6164(12)	1614(6)	52(4)	C(30B)	−926(52)	2526(35)	1930(15)	275(19)

a) Equivalent isotropic U_{eq} [for C(15A)–C(22A) and C(15B)–C(22B)] defined as one third of the trace of the orthogonalized $\boldsymbol{U}$ tensor. The exponent of the isotropic temperature factor takes the form: $-8\pi^2 U \sin^2\theta/\lambda^2$.

are expected.

For the tetraene **7** which is an analog of allene **1c** elongated by two C=C bonds one would possibly anticipate a clathrate lattice suitable for inclusion of larger guest molecules. Surprisingly, however, **7** is inefficient in clathrate formation under the given solvent conditions. This compound is difficultly soluble in the low boiling solvents mentioned in Table 1. In high boiling solvents, such as xylenes or mesitylene, in which **7** is soluble, a partial decompositon of the compound prevents further inclusion studies.

X-Ray Analysis. Structure Description of Unsolvated 6, 6·*o*-Xylene (1 : 2), and 6·*p*-Xylene (1 : 2). In order to elucidate the building principles and host-guest relationships of the cumulene-type clathrates, we have carried out X-ray structural studies of free host **6** and two of its inclusion compounds, namely **6**·*o*-xylene (1 : 2) and **6**·*p*-xylene (1 : 2).

Details of crystal parameters, intensity data collection, and structure refinement are given in Table 2. The coordinates of non-hydrogen atoms for **6**, **6**·*p*-xylene (1 : 2), and **6**·*o*-xylene (1 : 2) are listed in Tables 3, 4, and 5, respectively. Table 6 shows the bond lengths and angles of host triene in the three crystals. Figure 1 is a perspective view of **6** and shows the atom labelling scheme which also applies to the host molecule in the inclusion compounds. Since there are three double bonds in the molecule of host cumulene **6**, four phenyl groups connected to both ends of the triene are almost coplanar. The center of the triene is located at a crystallographic inversion center in all three crystals.

A stereoview of the molecular packing for unsolvated host **6** is shown in Fig. 2. Figure 3 illustrates the mode of molecular packing in crystalline **6**·*p*-xylene (1 : 2). It is seen that *p*-xylene guest molecules related by the *a*-glide are accommodated in zigzag fashion within a column surrounded by *t*-butyl groups of the neighboring host molecules. In the crystal of **6**·*o*-xylene (1 : 2), the host molecules are arranged in a herringbone fashion and centered about planes of the (0 2 0) type, between which the *o*-xylene molecules are accommodated like a corrugated sheet and bounded by the *t*-butyl groups of the neighboring host molecules (Fig. 4).

Table 6. Selected Bond Lengths and Bond Angles[a)]

Atom	Bond lengths/Å			Atom	Bond lengths/Å		
	6	**6**·*p*-Xylene (1:2)	**6**·*o*-Xylene (1:2)		**6**	**6**·*p*-Xylene (1:2)	**6**·*o*-Xylene (1:2)
C(1)-C(2)	1.341(7)	1.345(7)	1.32(3)	C(9)-C(14)	1.406(7)	1.396(7)	1.39(3)
C(1)-C(1a)	1.24(1)	1.24(1)	1.22(3)	C(10)-C(11)	1.394(7)	1.369(8)	1.43(3)
C(2)-C(3)	1.477(7)	1.469(7)	1.47(3)	C(11)-C(12)	1.405(7)	1.401(8)	1.37(3)
C(2)-C(14)	1.472(6)	1.481(7)	1.47(3)	C(12)-C(13)	1.390(6)	1.408(8)	1.41(3)
C(3)-C(4)	1.403(7)	1.369(7)	1.38(3)	C(12)-C(15)	1.542(7)	1.532(8)	1.56(3)
C(3)-C(8)	1.387(7)	1.404(7)	1.42(3)	C(13)-C(14)	1.388(7)	1.372(7)	1.40(3)
C(4)-C(5)	1.402(8)	1.398(7)	1.43(3)	C(15)-C(16)	1.554(7)	1.58(2)	1.55(5)
C(5)-C(6)	1.378(7)	1.396(8)	1.40(3)	C(15)-C(17)	1.538(9)	1.55(2)	1.44(4)
C(5)-C(19)	1.547(7)	1.524(8)	1.55(3)	C(15)-C(18)	1.513(8)	1.53(2)	1.60(4)
C(6)-C(7)	1.399(8)	1.381(8)	1.37(3)	C(19)-C(20)	1.545(9)	1.545(9)	1.40(5)
C(7)-C(8)	1.388(8)	1.380(7)	1.39(3)	C(19)-C(21)	1.554(8)	1.52(1)	1.49(5)
C(8)-C(9)	1.480(7)	1.482(7)	1.46(3)	C(19)-C(22)	1.521(7)	1.542(9)	1.47(5)
C(9)-C(10)	1.372(7)	1.371(8)	1.40(3)				

Atom	Bond angles/°			Atom	Bond angles/°		
	6	**6**·*p*-Xylene (1:2)	**6**·*o*-Xylene (1:2)		**6**	**6**·*p*-Xylene (1:2)	**6**·*o*-Xylene (1:2)
C(2)-C(1)-C(1a)	177.2(7)	179.1(7)	177(2)	C(10)-C(11)-C(12)	122.2(4)	122.4(5)	121(2)
C(1)-C(2)-C(3)	126.5(4)	127.3(5)	127(2)	C(11)-C(12)-C(13)	118.3(4)	117.3(5)	120(2)
C(1)-C(2)-C(14)	127.7(5)	125.8(4)	128(2)	C(11)-C(12)-C(15)	118.8(4)	122.6(5)	123(2)
C(3)-C(2)-C(14)	105.8(4)	106.9(4)	105(2)	C(13)-C(12)-C(15)	122.9(4)	120.1(3)	117(2)
C(2)-C(3)-C(4)	129.1(4)	130.8(5)	130(2)	C(12)-C(13)-C(14)	119.7(5)	119.7(5)	119(2)
C(2)-C(3)-C(8)	109.4(4)	108.0(4)	109(2)	C(2)-C(14)-C(9)	108.4(4)	108.2(4)	109(2)
C(4)-C(3)-C(8)	121.5(5)	121.1(4)	121(2)	C(2)-C(14)-C(13)	130.5(5)	130.2(5)	130(2)
C(3)-C(4)-C(5)	118.0(4)	120.6(5)	120(2)	C(9)-C(14)-C(13)	121.1(4)	121.7(5)	121(2)
C(4)-C(5)-C(6)	119.5(5)	117.2(5)	118(2)	C(12)-C(15)-C(16)	108.3(4)	109.6(7)	111(2)
C(4)-C(5)-C(19)	120.3(4)	119.6(5)	119(2)	C(12)-C(15)-C(17)	109.4(5)	110.9(8)	111(3)
C(6)-C(5)-C(19)	120.2(5)	123.2(5)	123(2)	C(16)-C(15)-C(17)	108.7(4)	108(1)	117(3)
C(5)-C(6)-C(7)	122.8(6)	122.9(5)	123(2)	C(12)-C(15)-C(18)	112.8(4)	115.2(9)	108(2)
C(6)-C(7)-C(8)	117.5(5)	119.0(5)	119(2)	C(16)-C(15)-C(18)	109.2(5)	104(1)	100(2)
C(3)-C(8)-C(7)	120.6(5)	119.2(5)	120(2)	C(17)-C(15)-C(18)	108.4(5)	109(1)	110(2)
C(3)-C(8)-C(9)	108.0(5)	108.6(4)	107(2)	C(5)-C(19)-C(20)	108.1(4)	109.8(5)	114(2)
C(7)-C(8)-C(9)	131.4(5)	132.2(5)	134(2)	C(5)-C(19)-C(21)	109.0(5)	109.7(5)	113(2)
C(8)-C(9)-C(10)	131.6(5)	132.7(5)	131(2)	C(20)-C(19)-C(21)	109.2(5)	109.2(6)	104(3)
C(8)-C(9)-C(14)	108.4(4)	108.3(4)	110(2)	C(5)-C(19)-C(22)	112.5(5)	112.6(5)	110(2)
C(10)-C(9)-C(14)	120.0(5)	119.0(5)	120(2)	C(20)-C(19)-C(22)	109.6(5)	108.6(5)	110(3)
C(9)-C(10)-C(11)	118.8(5)	119.9(5)	119(2)	C(21)-C(19)-C(22)	108.4(5)	106.8(5)	104(3)

a) Symmetry transformation: a=(−*x*, 1−*y*, 1−*z*) for **6** and **6**·*p*-xylene (1:2); a=(1−*x*, 1−*y*, 1−*z*) for **6**·*o*-xylene (1:2). Atoms C(16), C(17), and C(18) are to be considered as C(16A), C(17A), and C(18A), respectively, for **6**·*p*-xylene (1:2), and atoms C(1)-C(22) to be considered as C(1A)-C(22A) for **6**·*o*-xylene (1:2).

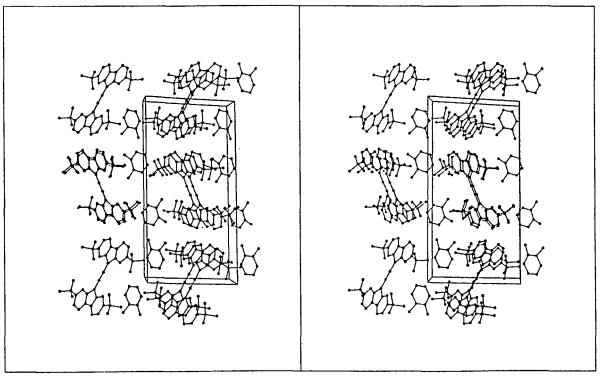

Fig. 4. Stereoview of the crystal structure of **6**·*o*-xylene (1:2) parallel to the *a* axis. The origin of the unit cell lies at the lower left corner, with *a* pointing to the reader, *b* from left to right, and *c* vertically upwards.

Conclusion

A series of cumulenes, **3**—**7**, were prepared. With a rigid backbone and dumbbell molecular shape, they are potentially useful as inclusion hosts. Substitution on the phenyl groups connected to both ends of these cumulenes critically influences their inclusion behavior since the substituents dictate the size and shape of lattice space for accommodation of the guest molecules. It was found that only cumulenes **4** and **6** with bulky *t*-butyl substituents at the phenyl rings can form inclusion compounds with various organic solvent molecules (Table 1), whereas the parent **3** and lower substituted **5** can not. The inclusion capabilities of unbridging substituted **4** differ obviously from those of bridging substituted **6**, and **4** behaves like the

analogous allenes.[5] In contrast to the closely related inclusion compounds of allenes,[5] the crystals of **6**, **6** · *p*-xylene (1 : 2), and **6** · *o*-xylene (1 : 2) not only have very different unit cells but also belong to different space groups (Table 2). The X-ray structural analysis showed that the guest molecules do not simply get into the free crystal space of the host as they do in the clathrates of allenes, but their presence rearranges the packing mode of the host molecules in the inclusion crystals. This is why **6** shows the higher selectivity in the formation of inclusion compounds and forms inclusion compounds with planar aromatic molecules only.

Experimental

General Methods and Materials. Melting points were determined with a Reichert hot-stage apparatus. IR spectra were recorded on an SP-1100 Pye-Unicam spectrometer. ^{1}H NMR spectra were measured with a Bruker WH-90 (90 MHz) spectrometer. Chemical shifts are reported in ppm (δ) down field from tetramethylsilane. Mass spectra were obtained from an A.E.I. MS 50 instrument. Elemental analyses were carried out by the Microanalytical Laboratory of the Institut für Organische Chemie und Biochemie, Universität Bonn. For column chromatography aluminum oxide (grade II—III, Merck) was used. All solvents were of reagent quality or purified by distillation before use. Starting compounds and all other reagents were purchased from Janssen unless otherwise stated.

1,1,4,4-Tetraaryl-2-butyne-1,4-diols 8a—c and 9 (General Procedure). Into a cooled solution of vinyl bromide (5.35 g, 50 mmol) in dry ether (50 ml) a solution of phenyllithium (150 mmol) in dry ether was added dropwise under N_2. The mixture was stirred for 1 h at room temperature. A solution of the corresponding ketone (90 mmol, see below) in dry ether (50 ml) was added dropwise, and the mixture was allowed to stand overnight. Hydrolysis and usual work-up[13] followed by recrystallization yielded the pure product. Specific details for each compound are given below.

1,1,4,4-Tetraphenyl-2-butyne-1,4-diol (8a). Benzophenone was reacted; recrystallization from benzene yielded 65% colorless crystals; mp 197 °C (lit,[14] 196—197 °C); ^{1}H NMR ($CDCl_3$) δ=2.90 (2H, s), 7.00—7.65 (20H, m).

1,1,4,4-Tetrakis(4-*t*-butylphenyl)-2-butyne-1,4-diol (8b). Bis(4-*t*-butylphenyl)methanone was reacted; recrystallization from ethanol/acetone yielded 39% colorless crystals; mp 280—282 °C; IR (KBr) 3650, 3100, 3000, 1120 cm^{-1}; ^{1}H NMR ($CDCl_3$) δ=1.27 (36H, s), 2.70 (2H, s), 7.27, 7.50 (16H, AA′BB′, J=10 Hz). Found: MS m/z (M^+) 614.4108. Calcd for $C_{40}H_{54}O_2$: 614.4124.

1,4-Bis(4-bromophenyl)-1,4-diphenyl-2-butyne-1,4-diol (8c). (4-Bromophenyl)phenylmethanone was reacted; recrystallization from ethanol/acetone yielded 42% colorless crystals; mp 124—125 °C; IR (KBr) 3500, 3100, 1040 cm^{-1}; ^{1}H NMR ($CDCl_3$) δ=3.03 (2H, s), 7.10—7.60 (18H, m); MS m/z 546 (M^+). Found: C, 60.92; H, 3.85%. Calcd for $C_{28}H_{20}Br_2O_2$: C, 61.34; H, 3.68%.

1,1 : 4,4-Bis(4,4′-di-*t*-butylbiphenyl-2,2′-diyl)-2-butyne-1,4-diol (9). 2,7-Di-*t*-butylfluoren-9-one was reacted; recrystallization from ethanol/acetone yielded 49% colorless crystals; mp 270 °C (decomp); IR (KBr) 3620, 3100, 3000, 1030 cm^{-1}; ^{1}H NMR ($CDCl_3$) δ=1.28 (36H, s), 2.45 (2H, s), 7.25—7.75 (12H, m). Found: MS m/z (M^+) 610.3014. Calcd for $C_{44}H_{50}O_2$: 610.3011.

1,1,4,4-Tetraarylbutatrienes 3—6 (General Procedure). Following a literature description,[15] 2.0 g of the corresponding diol (**8a—c**, **9**) was mixed with the fivefold amount of tin(II) chloride dihydrate and ground for 30 min using mortar and pistil. The powder obtained was extracted with chloroform. After removal of the solvent in vacuo, the residue was chromatographed on aluminum oxide (petroleum ether, bp 40—60 °C) and recrystallized to yield the pure product. Specific details for each compound are given below.

1,1,4,4-Tetraphenylbutatriene (3). Diol **8a** was reacted; recrystallization from ethanol/acetone yielded 80% yellow needles; mp 237 °C (lit,[15] 235—236 °C). Found: MS m/z (M^+) 356.1568; C, 94.49; H, 5.66%. Calcd for $C_{28}H_{20}$: 356.1565; C, 94.34, H, 5.66%.

1,1,4,4-Tetrakis(4-*t*-butylphenyl)butatriene (4). Diol **8b** was reacted; recrystallization from ethanol/acetone yielded 68% yellow needles; mp 281—282 °C; ^{1}H NMR ($CDCl_3$) δ=1.35 (36H, s), 7.35, 7.52 (16H, AA′BB′, J=9 Hz); MS m/z 580 (M^+). Found: C, 91.17; H, 9.25%. Calcd for $C_{44}H_{52}$: C, 90.97; H, 9.03%.

1,4-Bis(4-bromophenyl)-1,4-diphenylbutatriene (5). Diol **8c** was reacted; sublimation at 230 °C/760 Torr (1 Torr=133.322 Pa) yielded 60% yellow needles; mp 258 °C (lit,[16] 254 °C); ^{1}H NMR ($CDCl_3$) δ=7.00—7.55 (18H, m). Found: MS m/z (M^+) 511.9732; C, 64.96; H, 3.32%. Calcd for $C_{28}H_{18}Br_2$: 511.9779; C, 65.40; H, 3.53%.

1,1 : 4,4-Bis(4,4′-di-*t*-butylbiphenyl-2,2′-diyl)butatriene (6). Diol **9** was reacted; recrystallization from acetone yielded 58% red crystals; mp >320 °C; ^{1}H NMR ($CDCl_3$) δ=1.43 (36H, s), 7.25—7.95 (12H, m). Found: MS m/z (M^+) 576.3751; C, 91.70; H, 8.37%. Calcd for $C_{44}H_{48}$: 576.3756; C, 91.61; H, 8.39%.

1,1,5,5-Tetrakis(4-*t*-butylphenyl)-1,4-pentadiene (10a). Into a solution of 4-*t*-butylphenyllithium, prepared from 4-*t*-butylbromobenzene (60 g, 280 mmol) and granulated lithium (1.94 g, 280 mmol) in dry ether (300 ml), was dropped a solution of diethyl glutarate (5.3 g, 50 mmol) in dry ether (50 ml) under N_2. The mixture was heated for 2 h under reflux and then quenched with water to give a voluminous precipitate of the corresponding diol. The deposit was collected, dried, and dissolved in acetic acid (150 ml). On addition of concd sulfuric acid (0.5 ml), a dark-green solution resulted which was heated for 2 h under reflux. After cooling, the solution was diluted with water to cause a precipitate. It was collected, washed free of acid, and recrystallized from ethanol to yield 52% of colorless crystals; mp 162—164 °C; ^{1}H NMR ($CDCl_3$) δ=1.27 (18H, s), 1.30 (18H, s), 2.90 (2H, t, J=7 Hz), 5.97 (2H, t, J=7 Hz), 7.20—7.90 (16H, m); MS m/z 596 (M^+). Found: C, 90.31; H, 9.23%. Calcd for $C_{45}H_{56}$: C, 90.55; H, 9.45%.

1,1,5,5-Tetrakis(4-*t*-butylphenyl)-2,4-dibromo-1,4-pentadiene (10b). To pentadiene **10a** (20.89 g, 35.0 mmol) was added a solution of bromine (11.2 g, 70.0 mmol) in carbon tetrachloride (50 ml). Gaseous hydrogen bromide formed and a violet-colored solution resulted. After removal of the solvent in vacuo, the residue was recrystallized from ethanol/acetone to yield 45% colorless crystals, mp 225 °C; ^{1}H NMR ($CDCl_3$) δ=1.27 (36H, s), 3.80 (2H, s), 7.00—7.40 (16H, m); MS m/z 752 (M^+). Found: C, 71.35; H, 7.12%;

Calcd for $C_{45}H_{54}Br_2$: C, 71.61; H, 7.21%.

1,1,5,5-Tetrakis-(4-*t*-butylphenyl)pentatetraene (7). To a solution of dibromopentadiene **10a** (2.00 g, 2.65 mmol) in dimethylformamide (50 ml) was slowly added concd methanolic KOH (5 ml), while passing N_2 through the solution. After stirring for 10 min, methanol (20 ml) was added, followed by methanol/water (1/1 v/v, 20 ml). The precipitate formed was collected and recrystallized from benzene to yield 70% yellow needles; mp 130 °C (decomp); ^{1}H NMR ($CDCl_3$) δ=1.30 (36H, s), 7.30—7.55 (16H, m). Found: MS m/z (M^+) 592.4059. Calcd for $C_{45}H_{52}$: 592.4069.

Preparation of the Clathrates (General Procedure). The corresponding host compound (**4** or **6**) was dissolved under heating in a minimum amount of the respective guest solvent. The solution was allowed to cool down slowly. After storage for 12 h at room temperature, the crystals that formed were collected by suction filtration, washed with methanol, and dried (1 h, 15 Torr, room temperature). Host-guest stoichiometry of the isolated crystals was determined by NMR integration. Data for each compound are given in Table 1.

Crystal Structure Determination

Sample Preparation and Data Collection. Crystals suitable for X-ray diffraction were grown from the corresponding solvent. The crystals were sealed inside a Lindemann glass capillary pre-filled with a small amount of solvent at its tip portion. Raw intensities were collected on a Nicolet R3m/V four-circle diffractometer at room temperature (294 K), were processed with the profile-fitting procedure of Diamond,[17] and corrected for absorption using ψ-scan data.[18] Details of data collection and processing are listed in Table 2.

Structure Analysis and Refinement. Unsolvated Host 6. Direct phase determination[19] yielded the positions of all nonhydrogen atoms, which were subjected to anisotropic refinement. The hydrogen atoms were generated geometrically (C-H bonds fixed at 0.96 Å) and allowed to ride on their respective parent C atoms; all hydrogen atoms were assigned appropriate isotropic temperature factors and included in the structure-factor calculations.

6·*p*-Xylene (1:2). Structure solution was accomplished by direct phase determination guided by negative quartets.[19] The host molecule is located at a centrosymmmetric site, and one of the two independent *t*-butyl groups in the asymmetric units exhibits twofold orientational disorder. The six disordered carbon atoms were named C(16A), C(17A), C(18A), C(16B), C(17B), and C(18B), each of half site occupancy. In the final stage of refinement, the phenyl group of the guest molecule was constrained to be a regular hexagon with C-C bonds of 1.395(5) Å in order to overcome the problem of slight positional disorder. All C atoms were subjected to anisotropic refinement. The H atoms except those of the disordered C atoms were generated geometrically, and were included in structure-factor calculations in least-square cycles with assigned isotropic thermal parameters.

6·*o*-Xylene (1:2). The unit cell contains two independent cumulene molecules each occupying a centrosymmetric site, as well as two independent *o*-xylene molecules. Owing to the very unfavorable data-to-parameter ratio, only the C atoms of the ordered *t*-butyl groups [C(15A)-C(22A) and C(15B)-C(22B)] were varied anisotropically, whereas all other C atoms were subjected to isotropic refinement. For the cumulene molecules, the methyl groups were treated as rigid groups, and the aromatic H atoms allowed to ride on their respective parent C atoms; these H atoms were included in structure-factor calculations with assigned isotropic temperature factors. For the guest molecules, the phenyl groups were constrained to be a regular hexagon with C-C bond of 1.395(5) Å, and the distance from the methyl carbon atom to its two nearest carbon neighbors in the phenyl group were constrained to be 1.52(1) and 2.52(2) Å, respectively.

Computations were performed using the SHELTXL-PLUS program package[20] on a DEC MicroVAX-II computer. Analytic expressions of atomic scattering factors were employed, and anomalous dispersion corrections were incorporated.[21] The final atomic parameters of **6**, **6**·*p*-xylene (1 : 2), and **6**·*o*-xylene (1 : 2) are listed in Tables 3—5.[22]

The authors gratefully acknowledge financial support for this work by the Deutsche Forschungsgemeinschaft (SFB 334), the Fonds der Chemischen Industrie, and a Hong Kong UPGC Earmarked Grant for Research (Acc. No. 221300010).

References

1) "Molecular Inclusion and Molecular Recognition-Clathrates I and II," ed by E. Weber, Springer-Verlag, Berlin-Heidelberg (1987 and 1988), (Topics in Current Chemistry, Vols. 140 and 149).

2) "Inclusion Compounds," ed by J. L. Atwood, J. E. D. Davies, and D. D. MacNicol, Academic Press, London (1984), Vols. 1—3.

3) E. Weber, *J. Mol. Graphics*, **7**, 12 (1989); and references cited therein.

4) Recent examples: E. Weber, M. Hecker, I. Csöregh, and M. Czugler, *J. Am. Chem. Soc.*, **111**, 7866 (1989); b) E. Weber, N. Dörpinghaus, and I. Goldberg, *J. Chem. Soc., Chem. Commun.*, **1988**, 1566; c) F. Toda and K. Tanaka, *Tetrahedron Lett.*, **29**, 551 (1988); d) F. Toda, A. Kai, R. Toyotaka, W.-H. Yip, and T. C. W. Mak, *Chem. Lett.*, **1989**, 1921.

5) E. Weber, W. Seichter, and I. Goldberg, *J. Chem. Soc., Chem. Commun.*, **1987**, 1426.

6) E. Weber, W. Seichter, and I. Goldberg, *Chem. Ber.*, **123**, 811 (1990).

7) "The Chemistry of the Allenes," ed by S. R. Landor, Academic Press, London (1982), Vols. 1—3.

8) "The Chemistry of Ketenes, Allenes, and Related Compounds," ed by S. Patai, Wiley, New York (1980), Vols. 1 and 2.

9) E. L. Eliel, "Stereochemie der Kohlenstoffverbindungen," Verlag Chemie, Weinheim (1966).

10) R. Kuhn and H. Krauch, *Chem. Ber.*, **88**, 309 (1955).

11) R. Kuhn, H. Fischer, and H. Fischer, *Chem. Ber.*, **97**, 1760 (1964).

12) Cf. E. Weber, J. Ahrendt, I. Csöregh, and M. Czugler, *Angew. Chem.*, **98**, 719 (1986); *Angew. Chem., Int. Ed. Engl.*, **25**, 746 (1986).

13) B. Z. Wakefield, *Organomet. Chem. Rev.*, **1**, 131 (1966).

14) G. Wittig and G. Harborth, *Ber. Dtsch. Chem. Ges.*, **77**, 306 (1944); G. Wittig and G. Harborth, *ibid.*, **79**, 311 (1946).
15) R. Kuhn and H. Krauch, *Chem. Ber.*, **88**, 309 (1955).
16) P. Godineau, *C. R. Acad. Sci.*, **246**, 2499 (1958).
17) R. Diamond, *Acta Crystallogr. Sect. A*, **25**, 43 (1969).
18) G. Kopfmann and R. Hubber, *Acta Crystallogr. Sect. A*, **24**, 348 (1968).
19) G. T. DeTitta, J. W. Edmonds, D. A. Langs, and H. Hauptman, *Acta Crystallogr. Sect. A*, **31**, 472 (1975).
20) G. M. Sheldrick, In "Crystallographic Computing 3: Data Collection. Structure Determination, Proteins, and Databases," ed by G. M. Sheldrick, C. Krüger, and R. Goddard, Oxford University Press, New York (1985), pp. 175—189.
21) "International Tables for X-Ray Crystallography," Kynoch Press, Birmingham (1974), Vol. 4, pp. 55—60, 99—101, 149—150, (Now distributed by Kluwer Academic Publishers, Dordrecht).
22) Anisotropic temperature factors, hydrogen coordinates, and tables of observed and calculated structure factors for **6**, **6**·*p*-xylene (1 : 2), and **6**·*o*-xylene (1 : 2) (51 pages) are deposited as Document No. 9090 at the Office of the Editor of Bull. Chem. Soc. Jpn.

Nitriles in Heterocyclic Synthesis. Synthesis and Reactions of Pyrano[3,2-*h*]quinoline Derivatives

Z. H. KHALIL, A. A. ABDEL-HAFEZ, A. A. GEIES,* and A. M. KAMAL EL-DEAN
Chemistry Department, Faculty of Science, Assiut University, Assiut, Egypt
(Received May 14, 1990)

8-Quinolinol reacts with cinnamonitrile derivatives in presence of a basic catalyst to afford pyrano[3,2-*h*]quinolines (**3a—f**). The reaction of **3a** with reagents such as acetic anhydride/pyridine, formamide, formic acid/formamide, and carbon disulfide gave the fused heterotetracyclic systems pyrimido[4′,5′:6,5]pyrano[3,2-*h*]quinolines.

A variety of pyrans and condensed pyrans were prepared recently by utilizing nitriles as starting materials.[1-5] The cinnamonitrile derivatives react with different heterocyclic compounds containing hydroxyl group to produce condensed pyran derivatives.[6-8] Within this respect and also for continuation of our work for the synthesis of heterocycles containing the quinoline moiety,[9,10] the present work is aimed to synthesize different pyrano[3,2-*h*]quinolines.

Results and Discussion

8-Quinolinol (**1**) reacts with cinnamonitrile derivatives (**2a—f**) in an ethanolic solution in the presence of piperidine to afford 2-amino-4-aryl-4*H*-pyrano-[3,2-*h*]quinoline-3-carbonitriles (**3a—c**) or ethyl 2-amino-4-aryl-4*H*-pyrano[3,2-*h*]quinoline-3-carboxylates (**3d—f**) in moderate yield.

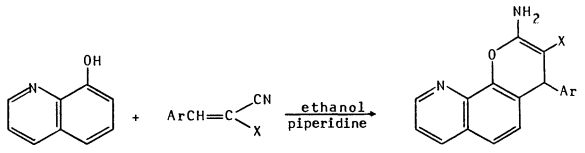

(**1**) (**2a—f**) (**3a—f**)

	X	Ar
a;	CN	C_6H_5
b;	CN	*p*-$CH_3OC_6H_4$
c;	CN	*p*-ClC_6H_4
d;	COOEt	C_6H_5
e;	COOEt	*p*-$CH_3OC_6H_4$
f;	COOEt	*p*-ClC_6H_4

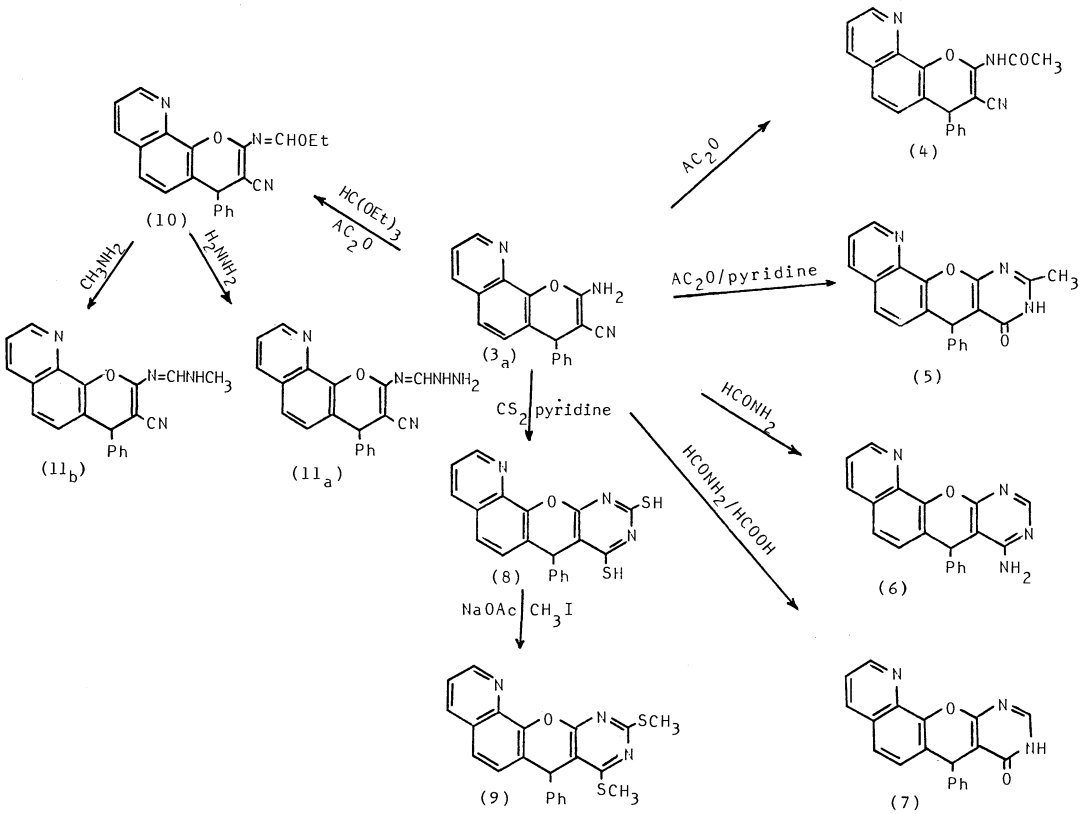

Scheme 1.

Table 1. Physical and Spectral Data of Compounds **3—12**

Compd No.	Mp/°C (Solvent)	Yield/% (Color)	Molecular formula[a)]	IR cm^{-1}	^1H NMR δ
3a	225—226 (Ethanol)	72 (Buff)	$C_{19}H_{13}N_3O$	3460, 3340 (NH_2), 2200 (CN).	(DMSO-d_6) 4.9 (s, 1H, CH pyran), 7.1 (s, 2H, NH_2), 7.2—8.9 (m, 10H, arom.).
3b	219—220 (Ethanol)	70 (Pale brown)	$C_{20}H_{15}N_3O_2$	3420, 3300 (NH_2), 2200 (CN).	(DMSO-d_6) 3.9 (s, 3H, CH_3), 5.0 (s, 1H, CH), 6.8—9.0 (m, 11H, NH_2 and arom.).
3c	223—224 (Ethanol)	68 (Buff)	$C_{19}H_{12}ClN_3O$	3460, 3320 (NH_2), 2200 (CN).	(DMSO-d_6) 5.1 (s, 1H, CH pyran), 7.0 (s, 2H, NH_2), 7.1—9.0 (m, 9H, arom.).
3d	184—185 (Ethanol)	74 (Pale yellow)	$C_{21}H_{18}N_2O_3$	3400, 3300 (NH_2), 1680 (C=O).	($CDCl_3$) 1.3 (t, 3H, CH_3), 4.1 (q, 2H, CH_2), 5.1 (s, 1H, CH), 6.7 (s, 2H, NH_2) 7.1—8.9 (m, 10H, arom.).
3e	193—194 (Ethanol)	66 (Yellow)	$C_{22}H_{20}N_2O_4$	3420, 3300 (NH_2), 1690 (C=O).	($CDCl_3$) 1.3 (t, 3H, CH_3), 3.9 (s, 3H, CH_3), 4.1 (q, 2H, CH_2), 5.0 (s, 1H, CH), 6.6 (s, 2H, NH_2), 6.8—8.9 (m, 9H, arom.).
3f	197—198 (Ethanol)	62 (Pala yellow)	$C_{21}H_{17}ClN_2O_3$	3400, 3300 (NH_2), 1680 (C=O).	($CDCl_3$) 1.3 (t, 3H, CH_3), 4.1 (q, 2H, CH_2), 5.0 (s, 1H, CH), 6.7(s, 2H, NH_2), 6.7—8.9 (m, 9H, arom.).
4	257—258 (Acetic acid)	85 (Pale yellow)	$C_{21}H_{15}N_3O_2$	3200 (NH), 2220 (CN), 1700 (C=O).	(DMSO-d_6) 2.3 (s, 3H, CH_3), 4.9 (s, 1H, CH), 7.0—8.9 (m, 10H, arom.), 9.2 (s, 1H, NH).
5	356—357 (Acetic acid)	52 (Brown)	$C_{21}H_{15}N_3O_2$	3100 (NH), 1660 (C=O).	(CF_3COOH) 2.8 (s, 3H, CH_3), 5.1 (s, 1H, CH), 6.9—9.0 (m, 10H, arom.).
6	333—334 (Ethanol)	50 (Brown)	$C_{20}H_{14}N_4O$	3420, 3300 (NH_2).	(DMSO-d_6) 5.1 (s, 1H, CH), 6.8—9.1 (m, 13H, NH_2 and arom.).
7	281—282 (Ethanol)	66 (White)	$C_{20}H_{13}N_3O_2$	3100 (NH), 1650 (C=O).	(DMSO-d_6) 4.9 (s, 1H, CH), 6.2 (s, 1H, NH), 7.1—9.1 (m, 11H, CH and arom.).
8	284—285 (Dioxane)	68 (Yellow)	$C_{20}H_{13}N_3OS_2$	3120, 3100 (2NH), 1230 (C=S).	(CF_3COOH) 5.2 (s, 1H, CH), 6.9—9.1 (m, 10H, arom.).
9	194—195 (Ethanol)	84 (White)	$C_{22}H_{17}N_3OS_2$	2990 (CH, aliph.), 1630 (C=N).	($CDCl_3$) 2.6 (s, 6H, $2CH_3$), 5.0 (s, 1H, CH), 7.2—9.0 (m, 10H, arom.).
10	147—148 (Ethanol)	82 (Pale yellow)	$C_{22}H_{17}N_3O$	2220 (CN).	($CDCl_3$) 1.3 (t, 3H, CH_3),4.3 (q, 2H, CH_2), 4.9 (s, 1H, CH), 7.1—8.9 (m, 11H, CH and arom.).
11a	211—212 (Ethanol)	80 (White)	$C_{20}H_{15}N_5O$	3380, 3300 ($NHNH_2$), 2200 (CN).	(DMSO-d_6) 4.9 (s, 1H, CH), 5.3 (s, 1H, NH), 5.8 (s, 2H, NH_2), 7.1—9.0 (m, 11H, CH and arom.).
11b	177—178 (Ethanol)	74 (White)	$C_{21}H_{16}N_4O$	3320 (NH), 2200 (CN).	($CDCl_3$) 3.3 (s, 3H, CH_3), 4.9 (s, 1H, CH pyran), 5.6 (s, 1H, NH), 7.1—9.2 (m, 11H, CH and arom.).

a) All products gave satisfactory microanalysis (C, ±0.36; H, ±0.22; N, ±0.23; S, ±0.28%).

Compound **3** was subjected for further reactions to produce fused heterotetracyclic systems incorporating pyrimidine nucleus in addition to pyranoquinoline moiety. Thus the reaction of **3a**, with acetic anhydride/pyridine mixture gave pyrimidopyranoquinoline **5**, while reaction of **3a** with acetic anhydride alone gave the acetamido derivative **4**. Interaction of **3a** with formamide afforded aminopyrimidine derivative **6**, while the reaction with formamide/formic acid mixture gave pyrimidinone derivative **7**.

The reaction of **3a** with carbon disulfide in pyridine proceeded through the addition of CS_2 on the amino group followed by cyclization by nucleophilic attack of the sulfur atom on the cyano group which underwent rearrangement to give pyrimidinedithiol derivative **8**.[11,12] Compound **8** reacted smoothly with methyl iodide in ethanol containing anhydrous sodium acetate to give bis(methylthio) derivative **9**.

Also, refluxing of **3a** with ethyl orthoformate in acetic anhydride gave the corresponding ethoxymethyleneamino derivative **10**. The latter compound further reacted with hydrazine hydrate or methylamine to give the corresponding derivatives **11a,b**, respectively. Attempts to cyclize compound **11a** by refluxing in ethanol containing piperidine and/or pyridine were unsuccessful.

Experimental

Melting points are uncorrected. IR spectra were recorded (KBr) on a Pye Unicam spectrophotometer. ^{1}H NMR spectra were obtained on 90 MHz Varian spectrometer in suitable deutrated solvent using TMS as internal standard. Analytical data were obtained by the microanalytical data Unit at Assiut University.

2-Amino-4-aryl-4*H*-pyrano[3,2-*h*]quinoline-3-carbonitriles (3a—c) and Ethyl 2-Amino-4-aryl-4*H*-pyrano[3,2-*h*]-quinoline-3-carboxylates (3d—f). General Procedure. A mixture of cinnamonitrile derivative (**2a—f**) (0.01 mol) and 8-quinolinol (0.01 mol) was refluxed in absolute ethanol (50 ml) containing a catalytic amount of piperidine for 5 h. The reaction mixture was concentrated, cooled and the precipitated product was collected by filtration. The physical and spectral data are summarized in Table 1.

2-Acetamido-4-phenyl-4*H*-pyrano[3,2-*h*]quinoline-3-carbonitrile (4). A mixture of **3a** (0.01 mol) was refluxed in acetic anhydride for 3 h, then cooled and poured onto ice/water mixture. The solid product thus formed was filtered off and washed several times with water.

10-Methyl-7-phenyl-7*H*-pyrimido[4′,5′:6,5]pyrano[3,2-*h*]quinolin-8(9*H*)-one (5). A solution of **3a** (0.01 mol) in Ac_2O/pyridine mixture (30 ml, 2:1 v/v) was heated on a water bath for 8 h, then cooled, and poured into ice/water mixture. The precipitate thus formed was collected by filtration and washed several times with water.

8-Amino-7-phenyl-7*H*-pyrimido[4′,5′:6,5]pyrano[3,2-*h*]-quinoline (6). A mixture of **3a** (0.01 mol) and formamide (20 ml) was refluxed for 1 h. After cooling the precipitated brown crystalline product was filtered off and washed several times with cold ethanol.

7-Phenyl-7*H*-pyrimido[4′,5′:6,5]pyrano[2,3-*h*]quinolin-8(9*H*)-one (7). A mixture of **3a** (0.01 mol) and formic acid (5 ml) in formamide (20 ml) was refluxed for 2 h. After cooling the reaction mixture was poured onto ice/water mixture and the solid product thus formed was filtered off.

7-Phenyl-7*H*-pyrimido[4′,5′:6,5]pyrano[3,2-*h*]quinolin-8,10-dithiol (8). A mixture of **3a** (0.01 mol) and carbon disulfide (5 ml) in pyridine (30 ml) was heated on water bath for 8 h. The solid product thus formed was filtered off while hot and washed several times with ethanol.

8,10-Bis(methylthio)-7-phenyl-7*H*-pyrimido[4′,5′:2,3]-pyrano[3,2-*h*]quinoline (9). A mixture of **8** (0.001 mol) and methyl iodide (2 ml) in ethanol (30 ml) in the presence of anhydrous sodium acetate (2 g) was refluxed for 2 h. The reaction mixture was concentrated, poured into cold water and the solid product was collected by filtration.

2-(Ethoxymethyleneamino)-4-phenyl-4*H*-pyrano[3,2-*h*]quinoline-3-carbonitrile (10). A mixture of **3a** (0.01 mol) and ethyl orthoformate (2 ml) in acetic anhydride (10 ml) was refluxed for 1 h. After cooling the precipitated pale yellow crystalline product was filtered off and washed severl times with cold ethanol.

2-(Hydrazinomethyleneamino)-4-phenyl-4*H*-pyrano[3,2-*h*]quindine-3-carbonitrile (11a) and 2-(Methylaminomethyl-eneamino)-4-phenyl-4*H*-pyrano[3,2-*h*]quinoline-3-carbonitrile (11b). General Procedure: A mixture of **10** (0.01 mol) and hydrazine hydrate or methylamine (0.01 mol) in absolute ethanol (50 ml) was stirred at room temperature for 15 min. The precipitated products (**11a** or **11b**) were collected by filtration.

References

1) L. Juergen and H. Horst, Ger. Offen. 106331 (1974); *Chem. Abstr.*, **82**, 97939 (1975).
2) P. Czerney and H. Hartmann, *J. Prakt. Chem.*, **324**, 21 (1982).
3) O. H. Hartwig and S. Herbert, *Monatsh. Chem.*, **110**, 279 (1979).
4) M. Quinteiro, C. Seoane, and J. L. Soto, *Tetrahedron Lett.*, **1977**, 1835.
5) M. Quinteiro, C. Seoane, and J. L. Soto, *J. Heterocycl. Chem.*, **15**, 57 (1978).
6) S. Abdou, S. M. Fahmy, K. U. Sadek, and M. H. Elnagdi, *Heterocycles*, **16**, 2177 (1981).
7) Z. E. Kandeel, K. M. H. Hilmy, F. M. Abdel-Razek, and M. H. Elnagdi, *Chem. Ind. (London)*, **1984**, 33.
8) H. A. Daboun, S. E. Abdou, M. M. Husein, and M. H. Elnagdi, *Synthesis*, **6**, 502 (1982).
9) Z. H. Khalil, A. S. Yanni, A. A. Khalaf, A. A. Abdel-Hafez, and R. F. Abdo, *Bull. Chem. Soc. Jpn.*, **61**, 1345 (1988).
10) Z. H. Khalil, A. A. Abdel-Hafez, A. S. Yanni, and A. M. Moharam, *Bull. Chem. Soc. Jpn.*, **61**, 4143 (1988).
11) E. C. Taylor, A. Mckckillop, and R. N. Warrener, *Tetrahedron*, **23**, 891 (1967).
12) A. Aviran and S. Vramer, *Chem. Ind. (London)*, **1967**, 1452.

 © 1991 The Chemical Society of Japan Bull. Chem. Soc. Jpn., 64, 671—673 (1991)

Synthesis of Dimethylsilyl Bis-Enol Ethers Derived from Aldehydes

Z. A. FATAFTAH,* M. R. IBRAHIM, and H. N. ABDEL-RAHMAN
Department of Chemistry, Yarmouk University, Irbid, Jordan
(Received May 28, 1990)

Two procedures for the prepation of dimethylsilyl bis-enol ethers from aldehydes, through enolization, are described. Dimethylsilyl bis-enol ethers, derived from propanal, butanal, 2-methylpropanal, pentanal, hexanal, and heptanal have been synthesized by refluxihg a mixture of triethylamine, dichlorodimethylsilane and the corresponding aldehyde in tetrahydrofuran for 18—38 h. The yields are in the range of 75—90%. Alternatively, a stronger base, lithium 2,2,6,6-tetramethylpiperidide (LiTMP) is used for deprotonation of the above mentioned aldehydes at −23 °C. The enolates are then quenched with dichlorodimethylsilane. The small aldehydes, propanal, butanal, and 2-methylpropanal fail to give the desired products, while the others gave a very good yields (56—85%). Ethanal fails to give the product in either of the two procedures. A competitive rate of polymerization with the rate of proton abstraction or with the rate of mixing of the reactants could explain these failures. The silyl bis-enol ethers have been characterized on the basis of their NMR, IR, and elemental analysis data.

Trimethylsilyl enol ethers were originally introduced as precursors for specific enolates[1,2] and much of their chemistry is like that of enol. Their usefulness surpasses that of all other derivatives,[3] because of their ease of preparation, clean reactions, and the mildness of desilylation processes: They also combine a reasonable reactivity with a high selectivity. Silyl enol ethers' reactions have been widely used as part of synthetic routes to natural products and other complex molecules[4] as well as simple coupling reactions.[5-7] Silyl enol ethers as synthetic reagents have been noted in the regeneration of enolates to react with electrophiles under basic conditions or direct reaction with electrophiles under neutral or acidic (Lewis acid) conditions. Although a great deal of attention has been paid to silyl enol ethers[4,8] derived from ketones and esters (silyl ketene acetals) very limited reports mentioned indirectly the silyl enol ethers derived from aldehydes.[8-10] The reason behind this ignorance of aldehydes is a theoretical problem. These reactions cannot be utilized with the enolates of reactive aldehydes, due to facile base-catalyzed polymerization of the starting material and/or product.[11] For this reason, various indirect methods have been developed for the alkylation of aldehydes, e.g., enamines[12] and imine anions.[13]

In earlier study[14] the preparation and characterization of some dimethylsilyl bis-enol ethers derived from ketones have been reported. The aim of the present work is to synthesize dimethylsilyl bis-enol ethers derived from aldehydes, in which two reactive aldehyde enolates are trapped in the same molecule as shown by Eq. 1. In this paper the preparation methods that we employed and the characterization of various dimethylsilyl bis-enol ethers derived from some aldehydes are described.

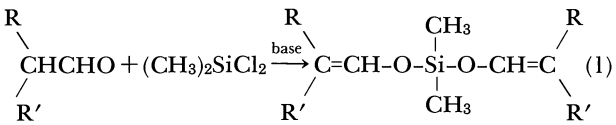

Results and Discussion

The first preparative method employed for dimethylsilyl bis-enol ethers derived from aldehydes involves preliminary treatment of a solution of LiTMP in tetrahydrofuran, generated from tetramethylpiperidine and butyllithium at 0 °C under nitrogen, with aldehydes to convert them completely into their enolate anions. Subsequent reaction of the enolate anions with dichlorodimethylsilane has produced the dimethylsilyl bis-enol ethers. Unfortunately the yields are low compared to yields in case of ketones. A better yield was obtained when the reaction temperature is changed to −23 °C instead of 0 °C and the aldehyde to dichlorodimethylsilane ratio is increased to 2 : 1. The results are summarized in Table 1. The small aldehydes fail to give the desired product. Dilution of these small aldehydes with tetrahydrofuran and then addition slowly to the base (LiTMP) do not produce any product either. It seees that in case of small aldehydes a competitive rate of aldol condensation and polymerization with the rate of proton abstraction or with the rate of mixing of the reactants. As the aldehydes get larger, the aldol condensation or polymerization is slowed down to such a degree that dimethylsilyl bis-enol ethers predominate.

In an effort to produce products with the small aldehydes we examined an alternative method in which the quenching reagent, dichloromethylsilane, is added before enolate formation. In this case triethylamine as a base in tetrahydrofuran was the reagent of choice. The silyl bis-enol ethers were prepared by refluxing the mixture of the aldehyde, dichlorodimethylsilane, and three fold excess triethylamine in tetrahydrofuran for 18—38 h. The yields are in the range of 75—90%. In this way the preparation of dimethylsilyl bis-enol ethers (**1—6**) were accomplished regardless the size of the aldehyde. Evidently, in this case, the rate of the reaction of aldehyde enolates with dichlorodimethylsilane is faster than the

Table 1. Characterization and Properties of the Products (**1**—**6**)

Entry	Product R	Product R′	Preparative method[a] (reaction time/h) yield[b]/%	$\bar{\nu}_{C=C}$ (CCl_4) cm^{-1}	NMR spectrum δ ($CDCl_3$) vinyl[c] CH (*Z* of *E*)	
1	CH_3	H	B (18) 90	1660	4.60 (d of q, *J*=6 and 6.8)	*Z*
					5.07 (d of q, *J*=12 and 6.8)	*E*
2	CH_3CH_2	H	B (24) 84	1665	4.55 (d of t, *J*=5.9 and 7.1)	*Z*
					5.16 (d of t, *J*=12.1 and 7.1)	*E*
3	CH_3	CH_3	B (38) 77	1680	—	
4	$CH_3(CH_2)_2$	H	A (24) 56	1655	4.54 (d of t, *J*=6.2 and 7.2)	*Z*
			B (24) 82		5.06 (d of t, *J*=12.1 and 7.2)	*E*
5	$CH_3(CH_2)_3$	H	A (24) 85	1650	4.58 (d of t, *J*=5.9 and 7.2)	*Z*
			B (30) 75		—	
6	$CH_3(CH_2)_4$	H	A (24) 83	1655	4.54 (d of t, *J*=5.9 and 7.3)	*Z*
			B (30) 79		—	

a) In procedure A, the enolate, formed by initial reaction of the aldehyde with LiTMP in THF, was quenched with $(CH_3)_2SiCl_2$. In procedure B, the aldehyde was refluxed with a mixture of Et_3N and $(CH_3)_2SiCl_2$. b) GC yields. c) The aldehydic vinyl protons are shown in the experimental section.

rate of polymerization. Ethanal, however, fails to give product in either of the two methods. This result is not unexpected since it is reported[1] that the indirect methods of enolization of aldehydes have never been successfully extended to the alkylation of ethanal, the simplest carbonyl compound having α-hydrogens.

It is interesting to note that the time required for synthesis of dimethylsilyl bis-enol ethers derived from aldehydes (1—2 days) is much shorter than the time required for the synthesis of dimethylsilyl bis-enol ethers derived from ketones (2—20 days).[14] We believe that the reason behind this is the fact that aldehyde enolates are more reactive than ketone enolates.

The dimethylsilyl bis-enol ethers derived from propanal, butanal, pentanal, and heptanal show geometrical isomers (Eq. 2). NMR analysis for the vinylic protons shows the predominance of *Z*-protons in these derivatives under thermodynamic conditions (triethylamine method). Under kinetic conditons, the NMR analysis for the vinylic protons of pentanal derivative showed the predominance of the *E*-protons which is in agreement with literature reports[14,15] of ketone enolates under similar conditions.

Experimental

All boiling points are uncorrected. The infrared spectra were determined with a Pye-Unican SP3-100 spectrophotometer. The NMR spectra were determined at Bruker WP 80 EY spectrometer. Vapor phase chromatographic analysis and preparative work were carried out on a Varian Aerograph 1400 thermal conductivity chromatogram. The microanalysis were performed by M-H-W Laboratories, Phoenix AZ.

Commercial samples of aldehyses were purified by redistillation and stored over molecular sieve. Triethylamine and tetrahydrofuran were distilled from $LiAlH_4$ and stored under nitrogen over molecular sieve. Dichlorodimethylsilane was distilled prior to use. Commerical 2,2,6,6-tetramethylpiperidine and a solution of butyllithium were used without further purification.

Illustrative Procedures for the Preparation of the Dimethylsilyl Bis-Enol Ethers. Procedure A. A 250 ml round bottom flask equipped with a magnetic stir bar, septum and a reflux condenser fitted with a calcium chloride tube was flame dried while a stream of nitrogen gas was flowing through the system. 80 ml of tetrahydrofuran was introduced followed by 80 mmol (5.77 ml) of propanal, three fold excess of triethylamine (240 mmol) and 40 mmol (4.8 ml) of dichlorodimethylsilane. The resulting mixture was

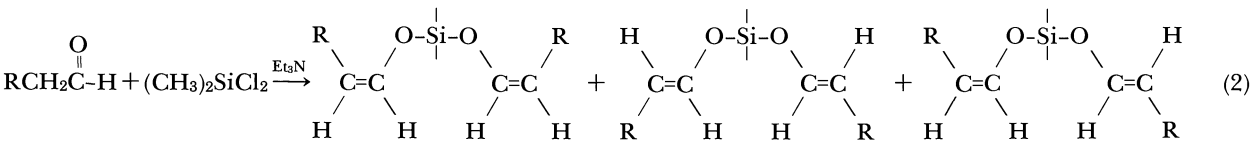

(2)

refluxed and followed by GLC analysis (2.5% SE-30, 1/8 in×5ft column). After two hours a peak different from starting materials was noticed. Then the reaction was refluxed for 18 h. The reaction mixture was cooled, diluted with petroleum ether (40—60 °C) and washed with cold saturated solution of sodium hydrogen carbonate. The organic layer was separated and dried over anhydrous sodium carbonate. Then the solvent was removed by simple distillation and residue was vacuum distilled or chromatographed using 40 cm×2 cm column packed with 60/120 mesh silica gel and petroleum ether (40—60 °C). A sample for analysis was prepped from a GLC column (2.5% SE-30, 1/4 in×3 ft, 1 in=2.54 cm, 1 ft=30.48 cm).

Procedure B. A 50 ml flask equipped with a magnetic stir bar, septum, gas inlet valve and mercury bubbler, was flame dried under nitrogen. A 5.0 ml (8 mmol) of butyllithium (1.6 M, 15% in hexane, M=mol dm^{-3}) was added to the flask. The flask was immersed in an ice bath and 1.34 ml (8 mmol) of 2,2,6,6-tetramethylpiperidine was added dropwise over 2 min. Following the addition, the viscous mixture was stirred for an additional 10 min, after which the hexane was removed under reduced pressure at 0 °C. The flask was refilled with nitrogen and the residual white solid was redissolved in sufficient dry THF at 0 °C to give approximately 1 M solution. When dissolution was complete, the ice bath was replaced by CCl_4/liq N_2(−23 °C) bath. The reaction mixture was stirred for 10 min, and then 0.98 ml (8 mmol) of hexanal was added dropwise over 3 min. The mixture was stirred for 20 min, then quenched with 0.24 ml (2 mmol) of dichlorodimethylsilane all added at once at −23 °C. The reaction mixture was removed from the bath and to room temperature with stirring. An internal standard $C_{16}H_{34}$ (2 mmol) was added. The highest yield (85%) was obtained after 24 h of stirring at room temperature.

Dimethylsilyl Bis-Enol Ether Derived from Propanal (1): Bp 23 °C (2 mmHg, 1 mmHg=133.322 Pa); density=0.896 g cm^{-3}; NMR ($CDCl_3$) δ=0.26 (s, 6H), 1.55 (m, 6H), 4.60, 5.07 (two multiplets 70:30, 2H), 6.24 (m, 2H); IR(CCl_4) 3040, 2960, 1660, 1450, 1065, 875, and 815 cm^{-1}. Calcd for $C_8H_{16}O_2Si$: C, 55.76; H, 9.36%. Found: C, 55.87; H, 9.27%.

Dimethylsilyl Bis-Enol Ether Derived from Butanal (2): Bp 30—32 °C (0.7 mmHg), density=0.865 g cm^{-3}, NMR ($CDCl_3$) δ=0.25 (s, 6H), 0.96 (t, 6H), 2.11 (m, 4H), 4.55, 5.16 (two multiplets 80:20, 2H) 6.18 (m, 2H); IR(CCl_4) 3020, 2960, 1655, 1450, 1260, 1070, 850, and 810 cm^{-1}. Calcd for $C_{10}H_{20}O_2Si$: C, 59.95%; H, 10.06%. Found: C, 60.09; H, 9.93%.

Dimethylsilyl Bis-Enol Ether Derived from 2-Methylpropanal (3): Bp 34—36 °C (0.6 mmHg), density=0.865 g cm^{-3}, NMR ($CDCl_3$) δ=0.22 (s, 6H), 1.56 (d, 6H), 1.61 (d, 6H), 6.09 (m, 2H); IR (CCl_4) 2960, 1680, 1450, 1260, 1070, 890, and 800 cm^{-1}. Calcd for $C_{10}H_{20}O_2Si$: C, 59.95; H, 10.06%, Found: C, 60.15; H, 10.09%.

Dimethylsilyl Bis-Enol Ether Derived from Pentanal (4): Bp 48.51 °C (0.6 mmHg), density=0.861 g cm^{-3}, NMR ($CDCl_3$) δ=0.24 (s, 6H), 0.95 (t, 6H), 1.41 (m, 4H), 2.02 (m, 4H), 4.54, 5.06 (two multiplets 76:24, 2H), 6.25 (m, 2H); IR (CCl_4) 2960, 1655, 1450, 1260, 1050, 860, and 810 cm^{-1}. Calcd for $C_{12}H_{24}O_2Si$: C, C, 63.10; H, 10.59% Found: C, 62.91; H, 10.31%.

Dimethylsilyl Bis-Enol Ether Derived from Hexanal (5): Bp 58—60 °C (0.6 mmHg), density=0.893 g cm^{-3}, NMR ($CDCl_3$) δ=0.25 (s, 6H), 0.90 (t, 6H), 1.31 (m, 8H), 2.10 (m, 4H), 4.58 (m, 2H), 6.24 (m, 2H); IR (CCl_4) 2960, 1650, 1455, 1260, 1070, 865, and 810 cm^{-1}. Calcd for $C_{14}H_{28}O_2Si$: C, 65.56; H, 11.00%. Found: C, 65.44; H, 10.86%.

Dimethylsilyl Bis-Enol Ether Derived from Heptanal (6): Bp 68.73 °C (0.6 mmHg), density=1.104 g cm^{-3}, NMR ($CDCl_3$) δ=0.24 (s, 6H), 0.88 (t, 6H), 1.30 (m, 12H), 2.08 (m, 4H), 4.54 (m, 2H), 6.22 (m, 2H); IR (CCl_4) 3025, 2950, 1655, 1260, 1080, 865, and 810 cm^{-1}. Calcd for $C_{16}H_{32}O_2Si$: C, 67.54; H, 11.34%. Found: C, 67.38; H, 11.09%.

The authors would like to thank Yarmouk University for financial support.

References

1) H. O. House, L. J. Czuba, M. Gali, and H. D. Olmstead, *J. Org. Chem.*, **34**, 2324 (1969).
2) G. Stork and P. Hudrlik, *J. Am. Chem. Soc.*, **90**, 4462 (1968).
3) I. Fleming, *Chimia*, **1980**, 265.
4) P. Brownbridge, *Synthesis*, **1983**.
5) T. X. Chen et al., *Tetrahedron Lett.*, **1979**, 4029.
6) Y. Ito, T, Konoike, and T. Saegusa, *J. Am. Chem. Soc.*, **97**, 649 (1975).
7) Y. Kobayashi, T. Taguchi, and E. Tokuno, *Tetrahedron Lett.*, **1977**, 3741; Y. Kobayashi et al., *Chem. Pharm. Bull.*, **28**, 262 (1980).
8) J. K. Rasmussen, *Synthesis*, **1977**, 91.
9) E. W. Colvin, *Chem. Soc. Rev.*, **7**, 15 (1978).
10) R. D. Miller and D. R. McKean, *Synthesis*, **1979**, 730.
11) M. E. Jung and R. B. Blum, *Tetrahedron Lett.*, **43**, 3791 (1977).
12) G. Stork, A Brizzolara, H. K. Landesmann, J. Szumszkovicz, and R. Terrell, *J. Am. Chem. Soc.*, **85**, 207 (1963).
13) G. Stork and S. R. Dowd, *J. Am. Chem. Soc.*, **85**, 2178 (1963); G. Witting and H. Reiff, *Angew. Chem., Int. Ed. Engl.*, **7**, 7 (1968).
14) Z. A. Fataftah, M. R. Ibrahim, and M. S. Abu-Agil, *Tetrahedron Lett.*, **27**, 4067 (1986).
15) Z. A. Fataftah, I. E. Kopka, and M. W. Rathke, *J. Am. Chem. Soc.*, **102**, 3959 (1980).

Synthesis and Aldol Stereoselectivity of 2-Oxazolidinones Derived from L-Histidine

Francisco BERMEJO GONZALEZ,* Julia PEREZ BAZ, Fabio SANTINELLI, and Fernando MAYOR REAL†
Departamento de Química Orgánica, Facultad de Químicas, Universidad de Salamanca,
Pza de los Caídos 1-5, 37008 Salamanca, Spain
†Departamento de Química Inorgánica, Facultad de Ciencias, Universidad de Valladolid, 47005 Valladolid, Spain
(Received June 21, 1990)

The regiospecific synthesis of the 2-oxazolidinones **5b**, **7**, **12a**, and **12b** starting from L-histidine **1a** is described. The stereoselectivity in the dibutyl(trifluoromethylsulfonyloxy)borane promoted aldol condensation between the chiral imides **13a** and **13b** and benzaldehyde was also studied. The formation of a cationic imidazole-boron complex, **14a**, occurs before the aldol condensation between **13a** and benzaldehyde takes place. However, the condensation between **13b** and benzaldehyde occurs without the formation of any boron complex. The steric hindrance of the substituent at C-4 may account for this difference in behavior.

As part of a program aimed at the discovery and development of novel drugs with potential muscarinic activity, our laboratory has examined the preparation of 2-oxazolidinones derived from the naturally occurring amino acid L-histidine **1a**.

As far as we know, the preparation of N^{π}- and N^{τ}-alkyl-substituted 2-oxazolidinones (The N-2 and N-4 positions in the imidazolyl group are tentatively denoted as N^{π} and N^{τ}-, respectively) derived from L-histidine has no precedents in the literature, even though the regiospecific functionalization on the imidazole moiety has been previously resolved.[1-6] We now wish to report our first results on this topic. Our interest in the potential aldol diastereoselectivity exhibited by chiral imides such as **13a** and **13b** lay in the previously announced feature of the amine-boron complexation.[7] These imides display a very different behavior when treated with dibutyl(trifluoromethylsulfonyloxy)borane. While **13a** leads to the formation of a cationic imidazole-boron complex **14a** before the aldol condensation with benzaldehyde takes place, the chiral imide **13b** undergoes aldol condensation without complexing; the steric hindrance at C-4[8] may account for this different behavior. However, since the stereoselectivity obtained in both cases is remarkable, we assume that an important role of the boron complexation on the aldol steroselectivity in the former case seems unlikely.

Results and Discussion

Preparation of the N^{π}-Ethyl 2-Oxazolidinone Derived from L-Histidine 5b. Preparation of the N^{π}-ethyl-substituted 2-oxazolidinone **5b** was achieved using the same synthetic sequence that we have recently reported for the preparation of the N^{π}-methyl-substituted 2-oxazolidinone, **5a**, in the course of the synthesis of some (+)-pilocarpine analogs[9] (Scheme 1).

The reaction of N^{α}-benzoyl-N^{π}-ethyl-L-histidine

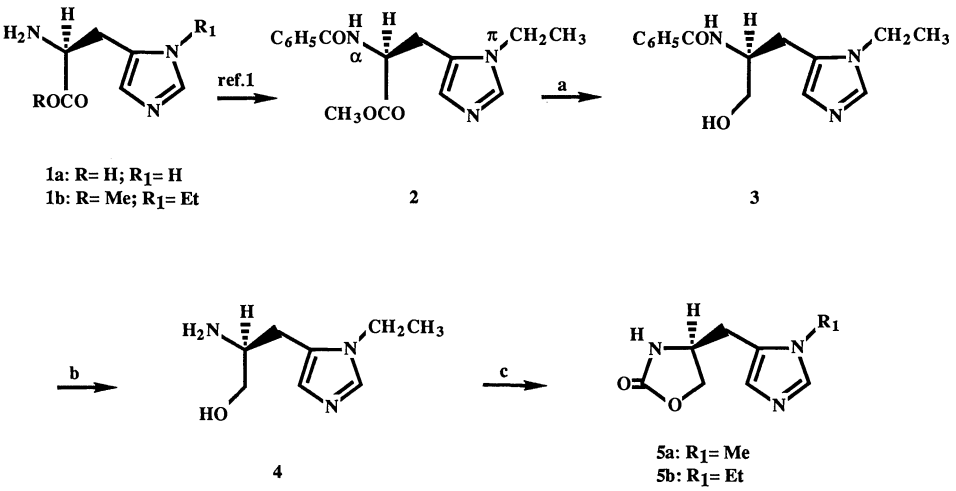

a: LAH(4 eq,), THF, 0 °C, 45 min. (90%); b: 1) 6N HCl, 80 °C, 6h.; 2) 1N KOH (EtOH) (95%); c: $(EtO)_2CO$ (1.2 equiv), CH_3OH reflux, $NaCH_3O$ (2 equiv), 1h. (70%)

Scheme 1.

(**2**)[1a] with 4 equiv of LAH in freshly distilled THF at 0 °C (45 min.) yielded a crude material from which the reduction product **3** was isolated by flash chromatography (90%). Hydrolysis of **3** by treatment with 6 M HCl (1 M=mol dm^{-3}) at 80—90 °C afforded the N^{π}-ethyl-L-histidinol dihydrochloride **4·2HCl**. Neutralization of **4·2HCl** with 1 M ethanolic KOH led to the free base **4**, after removal of the KCl and evaporation of the solvent. The structural change was confirmed by the upfield displacement of the signals corresponding to the two aromatic protons from δ H_2^{im}=8.81 and δ H_5^{im}=7.39 in **4·2HCl** to δH_2^{im}=7.51 and δH_5^{im}=6.69 in **4**. Reaction of **4** with 1.2 equiv of diethyl carbonate in refluxing methanol, using CH_3ONa as a base, afforded a crude material from which it was possible to isolate the 2-oxazolidinone **5b** by flash chromatography (70%). The presence of a signal at δ=161.8 in the ^{13}C NMR spectrum confirmed the presence of the cyclic carbamate functionality.

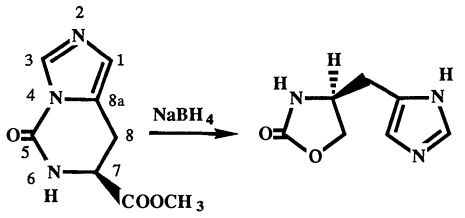

6 **7**

Scheme 2.

Preparation of the 2-Oxazolidinone 7. The starting material to obtain our next target molecule was the oxoimidazo[1,5-*c*]pyrimidine **6**[2] (Scheme 2). Reduction of **6** with an excess of $NaBH_4$[10] afforded the 2-oxazolidinone **7** (80%) (Scheme 2). We assumed that the carbonyl group belonging to the cyclic urea function of **6** undergoes nucleophilic attack by the alkoxide resulting from the reduction of the ester function. The acyl migration is helped by the good leaving character of the imidazole ring. The structural change was confirmed by the displacement of the ^{13}C NMR signals corresponding to the carbonyl groups from δ=149 in the urea **6** to δ=162 in the cyclic carbamate **7**. This result provides a very interesting alternative to the previously reported LAH reduction of **6**.[11]

Preparation of the N^{τ}-Alkyl-Substituted 2-Oxazolidinones Derived from L-Histidine 12a and 12b. The experience gained on the reduction of the oxoimidazo-[1,5-*c*]pyrimidine **6** prompted us to prepare the imidazolium iodides **8a** and **8b**[2] (Scheme 3) and to attempt the cyclization under the conditions described for **6** in an effort to prepare **12a** and **12b**. We expected that the imidazolinium functionality of both molecules would accelerate the process, due to the increased leaving character of the aromatic moiety. However, $NaBH_4$ reduction of **8a** led to a complicated mixture from which the hydroxy-substituted formamide **9** was isolated by flash chromatography (65%). The spectroscopic properties obtained for the new reduction product provided enough evidence for the presence of

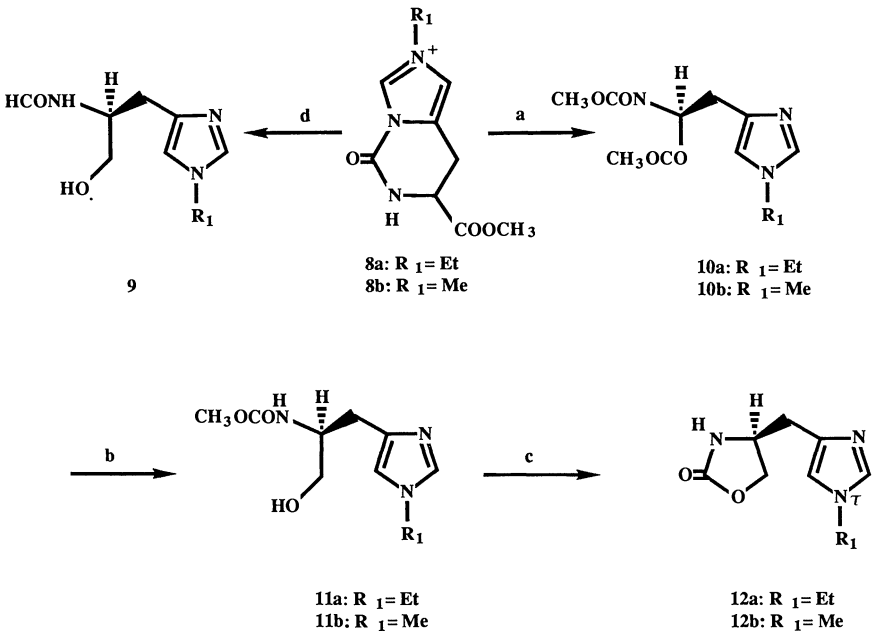

9

8a: R 1= Et
8b: R 1= Me

10a: R 1= Et
10b: R 1= Me

11a: R 1= Et
11b: R 1= Me

12a: R 1= Et
12b: R 1= Me

a: $NaCH_3O$ (1.1 equiv), CH_3OH, 24 °C, 2h. (95%); **b**: $NaBH_4$ (5 equiv), CH_3OH, 0 °C, 5h. (70%); **c**: $NaCH_3O$ (2 equiv), CH_3OH, 24 °C, 5h. (87%); **d**: $NaBH_4$

Scheme 3.

the hydroxy (^{13}C NMR: δ=63.95; ^{1}H NMR: δ=3.50 (d, J=7.5 Hz, 2H)) and the formamide moieties (^{13}C NMR: δ=163.8 (CH); ^{1}H NMR: δ=7.95 (s, 1H)). We were able to detect traces of the desired 2-oxazolidinone **12a** by ^{1}H NMR analysis of some of the minor components, but the yield was unacceptable.

This disappointing result led us to attempt the transformation of **8a** into the carbamate **10a**.[6] Treatment of **8a** with 1.1 equiv of CH_3ONa in absolute methanol at room temperature afforded a crude product from which it was possible to isolate the carbamate **10a** by flash chromatography (95%). The presence of two singlets at δ=3.63 and 3.60 in the ^{1}H NMR spectrum together with the appearance of two signals at δ=172 and 156 in the ^{13}C NMR spectrum allowed us to confirm the presence of the two desired functionalities; the methyl ester and the methyl carbamate.

$NaBH_4$ reduction of **10a** led to the isolation of the hydroxy-substituted carbamate **11a** by flash chromatography (70%). The ^{13}C NMR spectrum of **11a** showed only one carbonyl absorption at δ=156 together with a new methylene absorption at δ=64.14 corresponding to the hydroxymethyl group; this allowed us to confirm the chemoselective reduction of the methyl ester functionality.

Base-promoted cyclization of **11a** was successfully achieved with an excellent yield. The treatment of the hydroxy carbamate **11a** with CH_3ONa in methanol at room temperature led to the isolation of the N^{τ}-ethyl-substituted 2-oxazolidinone **12a** (87%). The structural change was confirmed by the displacement of the signals corresponding to the absorption of the carbonyl and hydroxymethyl groups in the ^{13}C NMR spectrum from δ=156 and 64 in **11a** to δ=159 and 68 in **12a**, respectively. Application of the same three-step sequence to the imidazolium iodide **8b** afforded the N^{τ}-methyl-substituted 2-oxazolidinone **12b** with 63% overall yield.

In summary, the effective regioselective synthesis of **12a** and **12b** proceeded in five steps from the methyl ester of L-histidine **1b** with 60% and 58% overall yields, respectively.

Stereoselection in the Aldol Condensation between the Chiral Imides 13a and 13b with Benzaldehyde. In order to test the induction of the stereoselectivity of these 2-oxazolidinones in the aldol condensation with aldehydes and to see what role the imidazole moiety might play in this type of process, we decided to analyze the reaction of the N-acyl-2-oxazolidinones **13a** and **13b** with benzaldehyde via the boron enolate.

Treatment of **5a**[9] and **12b** with HaH (1.1 equiv) in DMF followed by addition of propionyl chloride (1.1 equiv) led to the imides **13a** (80%) and **13b** (85%), respectively.

Treatment of the chiral imide **13a** with 1 equiv of dibutyl(trifluoromethylsulfonyloxy)borane, followed by addition of benzaldehyde under the conditions described by Evans[7] led to the isolation of a white solid **14b** (Scheme 4), which was soluble in chloroform and could be purified by crystallization in dry THF; flash chromatography of the crude product led also to pure **14b** with partial decomposition. Spectroscopic analysis (IR, ^{1}H NMR, and ^{13}C NMR) clearly showed that the condensation reaction did not take place. The ^{13}C NMR spectrum of the new product exhibited two signals corresponding to two carbonyl groups (δ=174.30 and 153.16) and three upfield signals corresponding to three methyl groups (δ=33.23, 13.93, and 8.14), one of them belonging to a butyl moiety, as the presence of three new methylene signals (δ=26.76, 26.06, and 21.03) seemed to confirm. The ^{1}H NMR spectrum exhibited the presence of the three methyl groups (signals at δ=3.81 (s), 1.11 (t), and 0.80 (t)) and pointed to a structural change in the imidazole ring by the downfield displacement of the aromatic protons from δ H_2^{im}=7.35 and δ H_5^{im}=6.76 in **13a** to δ H_2^{im}=8.02 and δ H_5^{im}=6.85 in **14b**.

According to the assumption of Evans that the ineffectiveness of bases such as pyridine in the enolization process of this type of chiral imides can be attributed to the irreversible amine-boron complexation,[7] we first thought of the formation of an sp^3-hybridized cationic boron complex **14a**;[12] which under the usual workup conditions would undergo metathesis to the phosphate **14b**.[13] The obtained MS (FAB) spectrum for **14b** comfirmed our assumption. The presence of two peaks at m/z: 599 (45%) and 362 (100%) proved the presence of the boron cation in the complex and the loss of an imide fragment, respectively.

Treatment of the imide **13a** with 1 equiv of dibutyl(trifluoromethylsulfonyloxy)borane at 0 °C gave **14b** (80%) after quenching the reaction with phosphate buffer. Apparently, the formation of the boron complex occurred prior to any condensation process.

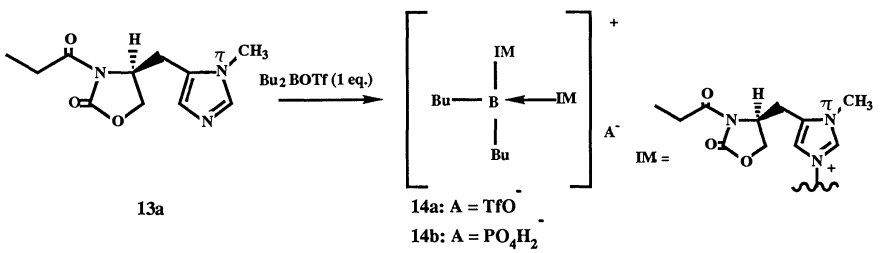

13a

14a: A = TfO

14b: A = PO_4H_2

Scheme 4.

Since the imidazole base present in **13a** scavenged half of one equiv of the triflate, the use of al least 1.5 equiv of the reagent was necessary to promote the aldol condensation with benzaldehyde. Treatment of **13a** with 2 equiv of dibutyl(trifluoromethylsulfonyloxy)-borane followed by addition of benzaldehyde led to the condensation product **15** (Scheme 5) after the usual work up conditions.

Spectroscopic analysis of the aldol product **15a** excluded the presence of threo isomers and confirmed the formation of the imidazol-boron complex by the downfield shifts obtained for the imidazole protons (δ H_2^{im}=7.98 and δ H_5^{im}=6.84) by comparison with the above-mentioned values exhibited by **13a**.[16]

Transformation of the crude aldol product into the possible mixture of erythro isomers of methyl 3-hydroxy-2-methyl-3-phenylpropionate **16a** by the classical procedure[7] allowed us to obtain an optical value of $[\alpha]_D^{24}$=−18.1° (*c* 1.74, $CHCl_3$), which led us to establish the absolute configuration of the major erythro isomer as (2*S*, 3*S*) **16a** and to determine the optical puriry of the aldol condensation product as >94% in accordance with the data in the literature.[17,18]

Treatment of the chiral imide **13b** (Scheme 6) with 1 equiv of dibutyl(trifluoromethylsulfonyloxy)borane followed by addition of benzaldehyde led to the aldol product **15b** (86%) whose spectroscopic properties excluded the existence of threo isomers in the reaction product. However, in this case the chemical shifts obtained for the imidazole protons at δ H_5^{im}=6.69 and δ H_2^{im}=7.41 excluded the imidazol-boron complexation. We assume that the steric hindrance at C-4 may account for the difficulties of the chiral imide **13b** in undergoing the imidazole-boron complexation.

Transformation of **15b** into **16b** by the reported procedure[7] led us to obtain an optical value of $[\alpha]_D^{21}$=−17.3° and enabled us to determine the optical purity of the aldol product as >90%, in agreement with the data in the literature.[17]

Conclusion

The synthesis of **5b**, **7**, **12a**, and **12b** from L-histidine was successfully achieved. These compounds are useful chiral auxiliaries from which imides such as **13a** and **13b** can be prepared and used in aldol reactions. Since the imidazole base present in the histidine-derived auxiliary **13a** scavenged half of one equiv of the triflate reagent, the use of 1.5 equiv of dibutyl(trifluoromethylsulfonyloxy)borane to promote the aldol condensation between **13a** and benzaldehyde was necessary. However, the chiral imide **13b** led to the aldol product **15b** by treatment with 1 equiv of the boron triflate followed by addition of benzaldehyde. Since the aldol stereoselectivity was remarkable in both cases we assume that the imidazole-boron complexation displayed by **13a** plays no significant role in the high stereoselectivity observed with this chiral imide.

Experimental

Organic extracts were dried with commercially dried Na_2SO_4 and evaporated under reduced pressure below 40 °C. Melting points were determined on a Kofler hot-stage apparatus and are uncorrected. Optical rotations were determined on a digital Perkin-Elmer 241 polarimeter in a 1-dm cell. The ^1H and ^{13}CNMR spectra were recorded on a Bruker WP-200-SY spectrometer operating at 200 MHz and 50.3 MHz respectively. All ^{13}CNMR spectra were obtained using deuteriochloroform as solvent unless otherwise stated; for ^{13}CNMR spectra in D_2O, 1,4-dioxane (δ=67.6) was used as the internal standard. The IR spectra were determined on a Beckman 33-IR spectrophotometer as indicated in each case. Mass spectra were recorded on a Kratos MS-25 instrument operating with either EI (70 eV) or FAB ionization (8 kV, using Xe and $(HOCH_2CH_2S)_2$ as matrix). Elemental analyses were carried out using a Perkin-Elmer 240 B Analyzer. Conductimetric measurements were made on a Crison 522 conductimeter. All compounds discussed in this paper were obtained in a chromatographically homogeneous state.

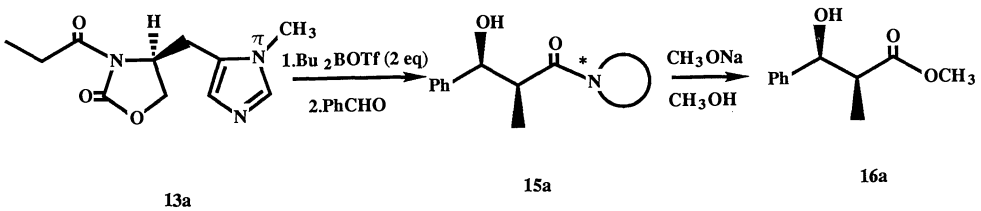

Scheme 5.

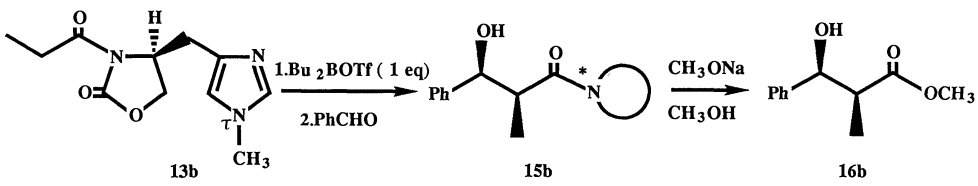

Scheme 6.

N^{α}-Benzoyl-N^{π}-ethyl-L-histidinol: (3). A solution of **2**[1] (5 g, 16.6 mmol) in freshly distilled THF (100 mL) was added dropwise to a stirred suspension of $LiAlH_4$ (1.3 g, 33.2 mmol) in anhydrous THF (100 mL) under a nitrogen atmosphere. After 45 min of stirring the reaction was worked up as usual to obtain a residue (4.2 g) which was fractionated by flash chromatography on silica gel. Elution with chloroform–methanol (80:20) yielded **3** (4.1 g, 90%); $[\alpha]_D^{20}$ −49.3° (*c* 1.02, CH_3OH); IR ν_{max} ($CDCl_3$) 3600—3000, 2950, 1640, 1540, 1230, 1040, 940, and 710 cm^{-1}; ^1H NMR (200 MHz, $CDCl_3$) δ=1.39 (3H, t, *J*=7 Hz, $NCH_2\underline{CH_3}$), 2.94 (2H, m, $\underline{CH_2}Ar$), 3.68 (2H, m, $\underline{CH_2}OH$), 4.06 (2H, q, *J*=7 Hz, $N\underline{CH_2}CH_3$), 4.14 (1H, m, CH), 6.73 (1H, s, CCHN), 7.36 (3H, m, Ar), 7.44 (1H, s, NCHN), 7.72 (2H, m, Ar); ^{13}C NMR (50.3 MHz, $CDCl_3$) δ=16.54 (q, $NCH_2\underline{CH_3}$), 26.30 (t, $\underline{CH_2}Ar$), 40.63 (t, $N\underline{CH_2}CH_3$), 52.53 (d, CH), 64.25 (t, CH_2OH), 127.49 (d, Ar), 128.24 (d, Ar), 129.39 (d, Ar), 130.00 (s, C_4^{im}), 132.51 (d, C_5^{im}), 135.89 (s, Ar), 138.00 (d, C_2^{im}) 170.28 (s, Ar$\underline{CO}$). Anal. Calcd for $C_{15}H_{19}N_3O_2$ (M. W. 273): C, 65.93; H, 6.96; N, 15.38%. Found: C, 65.87; H, 6.90; N, 15.32%.

N^{π}-Ethyl-L-histidinol Dihydrochloride: (4·2HCl) and N^{π}-Ethyl-L-histidinol: (4). A solution of **3** (5 g, 18.3 mmol) in 6 M HCl (350 mL) was heated under reflux for 6 h in a nitrogen atmosphere. The volume of water was reduced (to 50 mL) by evaporation of the solvent. Benzoic acid was removed by extraction of the aqueous solution with ether (3×15 mL). The aqueous solution was evaporated to dryness to afford **4·2HCl** (4 g, 90%); $[\alpha]_D^{21}$ 3.3° (*c* 1.6, CH_3OH); IR ν_{max} (Nujol) 3300, 3030, 2950, 1540, 1470, 1380, 1060, and 860 cm^{-1}; ^1H NMR (200 MHz, CD_3OD) δ=1.35 (3H, t, *J*=7 Hz, $NCH_2\underline{CH_3}$), 3.0 (2H, m, $\underline{CH_2}Ar$), 3.48 (1H, m, CH), 3.58 (2H, m, $\underline{CH_2}OH$), 4.11 (2H, q, *J*=7 Hz, $N\underline{CH_2}CH_3$), 7.39 (1H, s, CCHN), 8.81 (1H, s, NCHN); ^{13}C NMR (50.3 MHz, CD_3OD) δ=15.48 (q, $NCH_2\underline{CH_3}$), 24.27(t, $\underline{CH_2}Ar$), 43.63 (t, $N\underline{CH_2}CH_3$), 52.79 (d, CH), 61.18 (t, CH_2OH), 119.98 (d, C_5^{im}), 130.70 (s, C_4^{im}), 136.22 (d, C_2^{im}). Anal. Calcd for $C_8H_{15}N_3O\cdot 2HCl\cdot 2H_2O$ (M. W. 278): C, 34.53; H, 7.55; N, 15.11%. Found: C, 34.49; H, 7.50; N, 15.06%.

Treatment of **4·2HCl** (4 g, 16.5 mmol) with 1 M ethanolic KOH (33 mL) led to the isolation of the free base **4** (2.8 g, 100%); $[\alpha]_D^{20}$ −15.1° (*c* 1.44, CH_3OH), after filtration of the KCl and evaporation of the solvent; IR ν_{max} (film) 3600—3000, 2900, 1490, 1050 cm^{-1}; ^1H NMR (200 MHz, D_2O) δ=1.30 (3H, t, *J*=7 Hz, $NCH_2\underline{CH_3}$), 2.62 (2H, m, $\underline{CH_2}Ar$), 2.97 (1H, m, CH), 3.41 (2H, m, $\underline{CH_2}OH$), 3.92 (2H, q, *J*=7 Hz, $N\underline{CH_2}CH_3$), 6.71 (1H, s, CCHN), 7.53 (1H, s, NCHN); ^{13}C NMR (50.3 MHz, D_2O) δ=16.7 (q, $NCH_2\underline{CH_3}$), 28.57 (t, $\underline{CH_2}Ar$), 40.62 (t, $N\underline{CH_2}CH_3$), 53.27 (d, CH), 66.38 (t, CH_2OH), 127.32 (d, C_5^{im}), 129.98 (s, C_4^{im}), 137.87 (d, C_2^{im}). Anal. Calcd for $C_8H_{15}N_3O$ (M. W. 169): C, 56.80; H, 8.88; N, 24.85%. Found: C, 56.76; H, 8.79; N, 24.81%.

(4*S*)-4-[(3-Ethyl-3*H*-imidazol-4-yl)methyl]-2-oxazolidinone: (5b). Diethyl carbonate (4.3 mL, 35.5 mmol) and 1.78 g (59.2 mmol) of NaH (80%) were added to a solution of **4** (5 g, 29.6 mmol) in absolute methanol (20 mL) under a nitrogen atmosphere. When addition had finished, the reaction mixture was heated to 100 °C for 1 h. Evaporation of the solvent at reduced pressure afforded a residue which was fractionated by flash chromatography on silica gel. Elution with chloroform–methanol (70:30) afforded **5b** (4 g, 70%); mp 111—113 °C (CH_3OH); $[\alpha]_D^{21}$ −12.8° (*c* 1.31, CH_3OH); IR ν_{max} (Nujol) 2950, 1750, 1450, 1360, 1050 cm^{-1}; ^1H NMR (200 MHz, CD_3OD) δ=1.32 (3H, t, *J*=7 Hz, $NCH_2\underline{CH_3}$), 2.82 (2H, d, *J*=6.2 Hz, $\underline{CH_2}Ar$), 3.93 (2H, q, *J*=7 Hz, $N\underline{CH_2}CH_3$), 4.07 (2H, m, CH_2OCO), 4.45 (1H, m, CH), 6.74 (1H, s, CCHN), 7.57 (1H, s, NCHN); ^{13}C NMR (50.3 MHz, CD_3OD) δ=16.56 (q, $NCH_2\underline{CH_3}$), 30.40 (t, $\underline{CH_2}Ar$), 40.74 (t, $N\underline{CH_2}CH_3$), 52.81 (d, CH), 71.01 (t, $\underline{CH_2}OCO$), 127.35 (d, C_5^{im}), 128.21 (s, C_4^{im}), 138.24 (d, C_2^{im}), 161.81 (s, CO); MS *m/z*, (%) 196 (M^++1, 1.5), 195 (4.9), 111 (9), 110 (100), 109 (96.7), 86 (6.3), 82 (43.3), 81 (58.0). Anal. Calcd for $C_9H_{13}N_3O_2$ (M. W. 195): C, 55.38; H, 6.67; N, 21.54%. Found: C, 55.30; H, 6.64; N, 21.50%.

(4*S*)-4-[(4-Imidazolyl)methyl]-2-oxazolidinone: (7). A solution of **6**[2] (5 g, 25.6 mmol) in absolute methanol (100 mL) at 0 °C under a nitrogen atmosphere was added dropwise to a suspension of $NaBH_4$ (4.8 g, 130 mmol) in absolute methanol (100 mL). The reaction mixture was stirred for 30 min at room temperature and was quenched by addition of an aqueous saturated NH_4Cl solution (30 mL). The reaction volume was then reduced (to ca. 50 mL) by evaporation of the solvent at reduced pressure and the aqueous solution was extracted with mixtures of chloroform–methanol (30:10) (5×25 mL). Evaporation of the organic solvent led to the isolation of **7** (3.4 g, 80%); mp 150—152 °C (Hexane); $[\alpha]_D^{23}$ −7.2° (*c* 1.5, CH_3OH); IR ν_{max} (film) 3600—3000, 1750, 1540, 1410, 1240, 1020, 760 cm^{-1}; ^1H NMR (200 MNz, D_2O) δ=2.73 (2H, d, *J*=5.5 Hz, $\underline{CH_2}Ar$), 4.05 (2H, m, CH_2OCO), 4.35 (1H, m, CH), 6.95 (1H, s, CCHN), 7.89 (1H, s, NCHN); ^{13}C NMR (50.3 MHz, D_2O) δ=31.11 (t, $\underline{CH_2}Ar$), 52.45 (d, CH), 70.73 (t, $\underline{CH_2}OCO$), 118.02 (d, C_5^{im}), 131.47 (s, C_4^{im}), 135.80 (d, C_2^{im}), 162.19 (s, CO); MS *m/z* (%) 168 (M^++1, 10), 136 (12), 123 (80), 96 (75), 82 (100). Anal. Calcd for $C_7H_9N_3O_2$ (M. W. 167): c, 50.30; H, 5.39; N, 25.15%. Found: C, 50.26; H, 5.32; N, 25.08%.

N^{τ}-Ethyl-N^{α}-methoxycarbonyl-L-histidine Methyl Ester: (10a). A solution of imidazolium iodide **8a**[2] (5 g, 14.2 mmol) in absolute methanol (35 mL) was added dropwise to a suspension of CH_3ONa (842.4 mg, 15.6 mmol) in absolute methanol at 0 °C under a nitrogen atmosphere. The reaction was stirred for 2h at room temperature and was quenched by addition of an aqueous saturated NH_4Cl solution (50 mL). Evaporation of the methanol at reduced pressure and extraction of the aqueous solution with chloroform led to the isolation of crude **10a** after evaporation of the solvent. Fractionation of the crude was performed by flash chromatography on silica gel. Elution with chloroform–methanol (90:10) yielded **10a** (3.6g, 100%); $[\alpha]_D^{24}$ +1.0° (*c* 1.04, $CHCl_3$); IR ν_{max} (film) 3600—3000, 2950, 1720, 1500, 1450, 1050, and 780 cm^{-1}; ^1H NMR (200 MHz, $CDCl_3$) δ=1.35 (3H, t, *J*=7 Hz, $NCH_2\underline{CH_3}$), 2.98 (2H, m, $\underline{CH_2}Ar$), 3.60 (3H, s, $NHCOO\underline{CH_3}$), 3.63 (3H, s, $COO\underline{CH_3}$), 3.85 (2H, q, *J*=7 Hz, $N\underline{CH_2}CH_3$), 4.5 (1H, m, CH), 6.62 (1H, s, CCHN), 7.3 (1H, s, NCHN); ^{13}C NMR (50.3 MHz, $CDCl_3$) δ=15.72 (q, $NCH_2\underline{CH_3}$), 29.67 (t, $\underline{CH_2}Ar$), 41.34 (t, $N\underline{CH_2}CH_3$), 51.64 (q, $COO\underline{CH_3}$+q, $NHCOO\underline{CH_3}$), 53.90 (d, CH), 115.76 (d, C_5^{im}), 135.98 (d, C_2^{im}), 137.08 (s, C_4^{im}), 156.35 (s, $\underline{CO}N$), 171.98 (s, $\underline{CO}OCH_3$). Anal. Calcd for $C_{11}H_{17}N_3O_4$ (M. W. 255): C, 51.76; H, 6.67; N, 16.47%. Found: C, 51.70; H, 6.61; N, 16.43%.

N^{α}-Methoxycarbonyl-N^{τ}-methyl-L-histidine Methyl Ester: (10b). Prepared under the same conditions as described for **10a**. Flash chromatography on silica gel. Eluent chloroform–methanol (90:10); **10b** (3.4 g, 96%); $[\alpha]_D^{22}$ +2.3° (*c* 1.03, $CHCl_3$); IR ν_{max} (film) 3600—3000, 1725, 1500, 1450, 1050, and 760 cm^{-1}; ^1H NMR (200 MHz, $CDCl_3$) δ=2.96 (2H, m,

$\underline{CH_2}Ar$), 3.54 (3H, s, NCH_3), 3.59 (3H, s, $NHCOO\underline{CH_3}$), 3.63 (3H, s, $COO\underline{CH_3}$), 4.48 (1H, m, CH), 6.57 (1H, s, CCHN), 7.24 (1H, s, NCHN) ^{13}C NMR (50.3 MHz, $CDCl_3$) δ=29.91 (t, $\underline{CH_2}Ar$), 33.02 (q, NCH_3), 51.91 (q, $NHCOO\underline{CH_3}$+q, $COO\underline{CH_3}$), 53.95 (d, CH), 117.59 (d, C_5^{im}), 137.45 (d, C_2^{im}+s, C_4^{im}), 156.59 (s, NCO), 172.11 (s, $\underline{CO}OCH_3$). Anal. Calcd for $C_{10}H_{15}N_3O_4$ (M. W. 241): C, 49.79; H, 6.22; N, 17.43%. Found: C, 49.76; H, 6.18; N, 17.39%.

N^{τ}-Ethyl-N^{α}-methoxycarbonyl-L-histidinol: (11a). A solution of **10a** (5 g, 19.6 mmol) in absolute methanol (50 mL) at 0 °C under a nitrogen atmosphere was added to a suspension of $NaBH_4$ (3.7 g, 98 mmol) in absolute methanol (25 mL). The reaction mixture was stirred for 5 h at room temperature. The reaction was then quenched by addition of an aqueous saturated NH_4Cl solution (30 mL). The organic solvent was evaporated at reduced pressure and the aqueous layer was extracted with $CHCl_3$. The combined organic layers were dried over Na_2SO_4 and evaporated to afford a crude **11a** which was fractionated by flash chromatography on silica gel. Elution with chloroform–methanol (90:10) afforded **11a** (3.1 g, 70%); $[\alpha]_D^{24}$+3.4° (*c* 1.6, $CHCl_3$); IR ν_{max} (film) 3600—3000, 2950, 1700, 1520, 1260, and 1060 cm^{-1}; ^{1}H NMR (200 MHz, $CDCl_3$) δ=1.4 (3H, t, *J*=7 Hz, $NCH_2\underline{CH_3}$), 2.8 (2H, m, $\underline{CH_2}Ar$), 3.60 (3H, s, OCH_3), 3.65 (2H, m, $\underline{CH_2}OH$), 3.85 (1H, m, CH), 3.88 (2H, q, *J*=7 Hz, $N\underline{CH_2}CH_3$), 6.70 (1H, s, CCHN), 7.35 (1H, s, NCHN); ^{13}C NMR (50.3 MHz, $CDCl_3$) δ=16.03 (q, $NCH_2\underline{CH_3}$), 30.23 (t, $\underline{CH_2}Ar$), 41.77 (t, $N\underline{CH_2}CH_3$), 51.84 (q, OCH_3), 52.24 (d, CH), 64.14 (t, CH_2OH), 116.46 (d, C_5^{im}), 135.79 (d, C_2^{im}), 138.17 (s, C_4^{im}), 156.89 (s, CO). Anal. Calcd for $C_{10}H_{17}N_3O_3$ (M. W. 227): C, 52.86; H, 7.49; N, 18.50%. Found: C, 52.82; H, 7.41; N, 18.48%.

N^{α}-Methoxycarbonyl-N^{τ}-methyl-L-histidinol: (11b). Prepared under the same conditions as described for **11a**. Flash chromatography on silica gel. Eluent: chloroform–methanol (90:10); **11b** (3.1 g, 70%); $[\alpha]_D^{22}$+10° (*c* 1.2, $CHCl_3$); IR ν_{max} (film) 3550—3000, 1724, 1480, 1450, 1050, and 760 cm^{-1}; ^{1}H NMR (200 MHz, $CDCl_3$) δ=2.76 (2H, m, $\underline{CH_2}Ar$), 3.54 (3H, s, NCH_3), 3.55 (3H, s, $NHCOO\underline{CH_3}$), 3.83 (2H, m, $\underline{CH_2}OH$), 4.10 (1H, m, CH), 6.63 (1H, s, CCHN), 7.27 (1H, s, NCHN); ^{13}C NMR (50.3 MHz, $CDCl_3$) δ=29.78 (t, $\underline{CH_2}Ar$), 33.02 (q, NCH_3), 51.60 (q, $NHCOO\underline{CH_3}$), 52.29 (d, CH), 63.64 (t, CH_2OH), 117.92 (d, C_5^{im}), 136.94 (d, C_2^{im}), 138.28 (s, C_4^{im}), 156.74 (s, CO). Anal. Calcd for $C_9H_{15}N_3O_3$ (M. W. 213): C, 50.70; H, 7.04; N, 19.72%. Found: C, 50.74; H, 7.07; N, 19.69%.

(4*S*)-4-[(1-Ethyl-1*H*-imidazol-4-yl)methyl]-2-oxazolidinone: (12a). Sodium methoxide (2.4 g, 44 mmol) was added to a solution of **11a** (5 g, 22 mmol) in absolute methanol (40 mL) at room temperature under a nitrogen atmosphere. The reaction mixture was stirred for 5 h at room temperature. The reaction was then quenched by addition of aqueous saturated NH_4Cl solution (15 mL). The aqueous phase was extracted with $CHCl_3$ (3×25 mL). The combined organic layers were dried over Na_2SO_4 and evaporated to afford **12a** (3.7 g, 87%); mp 102 °C (Hexane); $[\alpha]_D^{24}$−44.3° (*c* 1.05, $CHCl_3$); IR ν_{max} (film) 3600—3000, 2950, 1750, 1500, 1400, 1250, 1020 940, and 760 cm^{-1}; ^{1}H NMR (200 MHz, $CDCl_3$) δ=1.38 (3H, t, *J*=7 Hz, $NCH_2\underline{CH_3}$), 2.74 (2H, d, *J*=6 Hz, $\underline{CH_2}Ar$), 3.90 (2H, q, *J*=7 Hz, $N\underline{CH_2}CH_3$), 4.14 (2H, m, CH_2OCO), 4.47 (1H, m, CH), 6.27 (1H, s, NH), 6.69 (1H, s, CCHN), 7.34 (1H, s, NCHN); ^{13}C NMR (50.3 MHz, $CDCl_3$) δ=15.39 (q, $NCH_2\underline{CH_3}$), 32.99 (t, $\underline{CH_2}Ar$), 41.05 (t, $N\underline{CH_2}CH_3$), 51.86 (d, CH), 68.97 (t, $\underline{CH_2}OCO$), 115.65 (d, C_5^{im}), 135.63 (d, C_2^{im}), 136.49 (s, C_4^{im}), 159.13 (s, CO); MS *m/z* (%) 196 (M^++1, 1), 195 (0.4), 111 (7.2), 110 (100), 109 (33.3), 95 (1.6), 82 (5.8), 81 (59.6). Anal. Calcd for $C_9H_{13}N_3O_2$ (M. W. 195): C, 55.38; H, 6.67; N, 21.50%. Found: C, 55.32; H, 6.61; N, 21.50%.

(4*S*)-4-[(1-Methyl-1*H*-imidazol-4-yl)methyl]-2-oxazolidinone: (12b). Prepared under the same conditions as described for **12a**. (92%); mp 132—134 °C (Hexane); $[\alpha]_D^{22}$−9.8° (*c* 1.6, $CHCl_3$); IR ν_{max} (film) 3600—3000, 1750, 1420, 1240, 1010, and 756 cm^{-1}; ^{1}H NMR (200 MHz, $CDCl_3$) δ=2.76 (2H, d, *J*=6 Hz, $\underline{CH_2}Ar$), 3.61 (3H, s, NCH_3), 4.13 (2H, m, CH_2OCO), 4.46 (1H, m, CH), 6.1 (1H, s, NH), 6.68 (1H, s, CCHN), 7.32 (1H, s, NCHN); ^{13}C NMR (50.3 MHz, $CDCl_3$) δ=32.84 (q, NCH_3), 33.14 (t, $\underline{CH_2}Ar$), 52.11 (d, CH), 69.22 (t, $\underline{CH_2}OCO$), 117.61 (d, C_5^{im}), 136.66 (s, C_4^{im}), 137.20 (d, C_2^{im}), 159.33 (s, CO); MS *m/z* (%) 182 (M^++1, 10), 181 (12), 150(10), 137 (25), 121 (20), 109 (30), 96 (100), 81 (30). Anal. Calcd for $C_8H_{11}N_3O_2$ (M. W. 181): C, 53.04; H, 6.08; N, 23.20%. Found: C, 53.09; H, 6.02; N, 23.23%.

(4*S*)-4-[(3-Methyl-3*H*-imidazol-4-yl)methyl]-3-propionyl-2-oxazolidinone: (13a). A solution of **5a** (5 g, 27.6 mmol) in DMF (100 mL) was added to a suspension of NaH (80%) (0.9 g, 30.4 mmol) in anhydrous DMF (6 mL) at room temperature under nitrogen atmosphere.

The reaction mixture was stirred for 30 min at the same temperature; it was then chilled at 0 °C and propionyl chloride (2.6 mL, 30.4 mmol) was added dropwise.

The reaction mixture was stirred at room temperature for 15 h. Then, a sat. NH_4Cl solution (25 mL) was added. The organic layer was separated, dried and evaporated under reduced pressure to give a crude residue which was fractionated by flash chromatography on silica gel. By elution with chloroform–methanol (80:20) a pale yellow solid **13a** (5.2 g, 80%), was obtained; mp 110—111 °C ($CHCl_3$); $[\alpha]_D^{20}$+76.9° (*c*, 1.52, CH_3OH); IR ν_{max} (film) 3100, 2950, 1780, 1770, 1680, 1440, 1360, 1050, 1010, 990, 940, 910, and 740 cm^{-1}; ^{1}H NMR (200 MHz, $CDCl_3$) δ=1.11 (3H, t, *J*=7 Hz, $COCH_2\underline{CH_3}$), 2.72 (1H, dd, J_1=15 Hz, J_2=10 Hz, $\underline{CH_2}Ar$), 2.88 (2H, dq, J_1=3 Hz, J_2=7 Hz, $CO\underline{CH_2}CH_3$), 3.17 (1H, dd, J_1=15 Hz, J_2=3 Hz, $\underline{CH_2}Ar$), 3.60 (3H, s, NCH_3), 4.14 (1H, dd, J_1=3 Hz, J_2=9 Hz, CH_2OCO), 4.23 (1H, t, *J*=7 Hz, CH_2OCO), 4.46 (1H, m, CH), 6.76 (1H, s, CCHN), 7.35 (1H, s, NCHN); ^{13}C NMR (50.3 MHz, $CDCl_3$) δ=7.75 (q, $COCH_2\underline{CH_3}$), 26.45 (t, $CO\underline{CH_2}CH_3$), 28.53 (t, $\underline{CH_2}Ar$), 30.91 (q, NCH_3), 52.51 (d, CH), 66.22 (t, $\underline{CH_2}OCO$), 125.49 (s, C_4^{im}), 127.54 (d, C_5^{im}), 138.41 (d, C_2^{im}), 152.72 (s, $N\underline{CO}O$), 173.66 (s, $\underline{CO}N$); MS *m/z* (%) 238 (M^++1, 10), 181 (80), 96 (100), 77 (40), 64 (80). Anal. Calcd for $C_{11}H_{15}N_3O_3$ (MW. 237): C, 55.69; H, 6.32; N, 17.72%. Found: C, 55.61; H, 6.27; N, 17.69%.

(4*S*)-4-[(1-Methyl-1*H*-imidazol-4-yl)methyl]-3-propionyl-2-oxazolidinone: (13b). Prepared under the same conditions as described for **13a** (85%). $[\alpha]_D^{22}$+72.4° (*c* 1.04, $CHCl_3$); IR ν_{max} (film) 3600—3000, 2900, 1780, 1700, 1380, 1020, and 750 cm^{-1}; ^{1}H NMR ($CDCl_3$) δ=1.15 (3H, t, *J*=7 Hz, $NCOCH_2\underline{CH_3}$), 2.95 (3H, m, CHAr+$CO\underline{CH_2}CH_3$), 3.05 (1H, dd, J_1=15 Hz, J_2=3 Hz, CHAr), 3.92 (3H, s ,NCH_3), 4.29 (1H, t, *J*=8 Hz, CHOCO), 4.54 (1H, dd, J_1=7 Hz, J_2=3 Hz, CHOCO), 4.65 (1H, m, CH), 6.68 (1H, s, CCHN), 7.38 (1H, s, NCHN); ^{13}C NMR ($CDCl_3$) δ=8.27 (q, $COCH_2\underline{CH_3}$), 29.01 (t, $CO\underline{CH_2}CH_3$), 30.17 (t, CH_2Ar), 41.72 (q, NCH_3), 54.13 (d, CH), 66.66 (t, CH_2OCO), 116.50 (s, C_5^{im}), 136.34 (d, C_2^{im}+s, C_4^{im}), 153.76 (s, $N\underline{CO}O$), 173.98 (s, $\underline{CO}CH_2CH_3$). Anal.

Calcd for $C_{15}H_{15}N_3O_3$ (M. W. 237): C, 55.69; H, 6,32: N, 17.72%. Found: C, 55.61; H, 6.28; N, 17.65%.

Formation of the Cationic Boron Complex: (14b). A 1 M solution of dibutyl(trifluoromethylsulfonyloxy)borane (4.2 mL, 4.2 mmol) in dichloromethane was added drpwise to a stirred solution of triethylamine (0.6 mL, 4.2 mmol) in dichloromethane (5 mL). Then, a solution of **13a** (1 g, 4.2 mmol) in dichloromethane (5 mL) was added dropwise at 0 °C under an argon atmosphere. The reaction mixture was stirred at 0 °C for 1 h and then quenched by addition to pH=7 phosphate buffer. The mixture was extracted twice with dichloromethane and the combined extracts were washed with brine and concentrated in vacuo. The crude oil was then dissolved in methanol (15 mL) at 0 °C and 30% hydrogen peroxide (4.5 mL) was added. After the mixture had been stirred at room tempetrature for 2h, water (20 mL) was added; the mixture was concentrated and extracted twice with dichloromethane. The combined extracts were washed with brine and concentrated in vacuo. The crude oil was then dissolved in methanol (15 mL) at 0 °C and 30% hydrogen peroxide (4.5 mL) was added. After the mixture had been stirred at room tempetrature for 2h, water (20 mL) was added; the mixture was concentrated and extracted twice with dichloromethane. The combined organic layers were washed with 5% aqueous sodium hydrogencarbonate and brine, dried (Na_2SO_4), and concentrated in vacuo to afford 1.30 g of crude product. By digestion in ethyl acetate, a white solid (mp 131—134 °C) was separated which was recrystallized in THF to give **14b** (1.16 g, 80%); mp 135—136 °C (THF); $[\alpha]_D^{20}$+42.4° (*c*, 1.13, $CHCl_3$); IR ν_{max} ($CHCl_3$) 3600—3200, 3180, 2980, 1790, 1720, 1600, 1550, 1460, 1400, 1280, 1160, 1100, 1020, 770, and 460 cm^{-1}; ^1H NMR (200 NHz, $CDCl_3$) δ=0.81 (3H, t, J=7 Hz, $(CH_2)_3\underline{CH_3}$), 1.11 (3H, t, J=7 Hz, $COCH_2\underline{CH_3}$), 2.86 (3H, m, $CO\underline{CH_2}CH_3$+$\underline{CH}$Ar), 3.17 (1H, dd, J_1=15 Hz, J_2=3 Hz, $\underline{CH}$Ar), 3.81 (3H, s, NCH_3), 4.13 (1H, dd, J_2=2 Hz, J_2=10 Hz, CH_2OCO), 4.37 (1H, t, J=8 Hz, CH_2OCO), 4.66 (1H, m, CH), 6.85 (1H, s, CCHN), 8.02 (1H, s, NCHN); ^{13}C NMR (50.3 MHz, $CDCl_3$) δ=8.14 (q, $COCH_2\underline{CH_3}$), 13.93 (q, $(CH_2)_3\underline{CH_3}$), 21.03 (t, BCH_2), 26.06 and 27.27 (dt, $BCH_2(\underline{CH_2})_2CH_3$), 26.76 (t, $CO\underline{CH_2}CH_3$), 28.92 (t, $\underline{CH_2}$Ar), 33.23 (q, NCH_3), 52.39 (d, CH), 66.89 (t, $\underline{CH_2}OCO$), 121.47 (d, C_5^{im}), 129.00 (s, C_4^{im}), 137.57 (d, C_2^{im}), 153.18 (s, $N\underline{C}OO$), 174.20 (s, $\underline{C}ON$); MS (FAB) *m/z* (%) 599 (45), 362 (100), 250 (90); MS (EI) *m/z* (%) 237 (60), 138 (90), 96 (100). Anal. Calcd for $C_{30}H_{50}O_{10}N_6BP$ (MW: 696): C, 51.73; H, 7.18; N, 12.07%. Found: C, 51.69; H, 7.09; N, 11.96%.

Condensation of 13a with Benzaldehyde via the Formation of the Cationic Boron Complex: (15a). A 1 M solution of dibutyl(trifluoromethylsulfonyloxy)borane (6.3 mL, 6.3 mmol) in dichloromethane was added dropwise to a stirred solution of triethylamine (0.9 mL, 6.3 mmol) in dichloromethane (4 mL) was added dropwise. Then, a solution of **13a** (0.75 g, 3.15 mmol) in dichloromethane (5 mL) was dropwise added at 0 °C under argon atmosphere. The reaction mixture was stirred at 0 °C for 1 h, cooled to −78 °C and a solution of benzaldehyde (0.30 mL, 3.15 mmol) in dichloromethane (5 mL) was added. This mixture was stirred for 30 min at −78 °C and 1 h at 0 °C. The reaction was quenched by addition to pH=7 phosphate buffer. The mixture was extracted twice with dichloromethane and the combined extracts were washed with brine and concentrated in vacuo. The crude was then dissolved in methanol (10 mL) at 0 °C and 30% hydrogen peroxide (4.5 mL) was added. After the mixture had been stirred at room temperature for 2 h, water (20 mL) was added; the mixture was concentrated and extracted twice with dichloromethane. The combined organic layers were washed with 5% aqueous sodium hydrogencarbonate and brine, dried (Na_2SO_4) and concentrated in vacuo to afford **15a** (1.14 g, 80%); mp 95—97 °C (EtOAc); $[\alpha]_D^{20}$+69.1° (*c* 1.38, $CHCl_3$); ^1H NMR (200 MHz, $CDCl_3$) δ=0.81 (3H, t, J=7 Hz, $(CH_2)_3\underline{CH_3}$), 1.06 (3H, d, J=7 Hz, $CH\underline{CH_3}$),2.81 (1H, dd, J_1=15 Hz, J_2=10 Hz, $\underline{CH}$Ar), 3.12 (1H, dd, J_1=15 Hz, J_2=3 Hz, $\underline{CH}$Ar), 3.79 (3H, s, NCH_3), 4.02 (2H, m, $\underline{CH}OCO$+$\underline{CH}CH_3$), 4.22 (1H, dd, J_1=7 Hz, J_2=9 Hz, $\underline{CH}OCO$), 4.59 (1H, m, $\underline{CH}CH_2$Ar), 5.03 (1H, d, J=3.8 Hz, Ar$\underline{CH}$OH), 6.83 (1H, s, CCHN), 7.3 (5H, m, Ar), 7.98 (1H, s, NCHN); ^{13}C NMR (50.3 MHz, $CDCl_3$) δ=10.51 (q, $\underline{CH_3}CH$), 13.96 (q, $(CH_2)_3\underline{CH_3}$), 21.07 (t, BCH_2), 26.06 and 26.85 (dt, $BCH_2(\underline{CH_2})_2CH_3$), 27.30 (t, $\underline{CH_2}$Ar), 33.29 (q, NCH_3), 44.88 (d, $CH_3\underline{CH}$), 52.70 (d, $\underline{CH}CH_2$Ar), 66.90 (t, $\underline{CH_2}OCO$), 73.52 (d, Ar$\underline{CH}$OH), 121.52 (d, C_5^{im}), 125.98 (d, Ar), 127.48 (d, Ar), 128.21 (d, Ar), 129.04 (s, C_4^{im}), 137.40 (d, C_2^{im}), 141.58 (s, Ar), 152.87 (s, $N\underline{C}OO$), 176.29 (s, $\underline{C}ON$); MS (EI) *m/z* (%) 889 (M^++1−H_2O, 10), 739 (30), 614 (50), 475 (85), 237 (100), 107 (80). Anal. Calcd for $C_{44}H_{62}O_{12}N_6BP$ (MW. 908): C, 58.14; H, 6.82; N, 9.25%. Found: C, 57.96; H, 6.76; N, 8.97%.

Condensation of 13b with Benzaldehyde: (15b). Prepared under the same conditions as described for **15a** using one equiv of the boron triflate (86%). $[\alpha]_D^{21}$+75° (*c* 1.0, $CHCl_3$); ^1H NMR ($CDCl_3$) δ=1.14 (3H, d, J=7 Hz, $CH\underline{CH_3}$), 2.95 (2H, m, CH_2Ar), 3.90 (3H, s, NCH_3), 2.95 (2H, m, CH_2Ar), 3.90 (3H, s, NCH_3), 4.55 (1H, dq, J_1=7 Hz, J_2=3.8 Hz, $CHOH\underline{CH}CH_3$), 4.17 (1H, t, J=8.5 Hz, CH_2OCO), 4.59 (1H, m, $N\underline{CH}(CH_2O)CH_2$), 5.05 (1H, d, J=3.8 Hz, CHOH), 6.69 (1H, s, CCHN), 7.4 (5H, m, Ar), 7.41 (1H, s, NCHN); ^{13}C NMR ($CDCl_3$) δ=15.79 (q, $CH\underline{CH_3}$), 29.74 (t, $\underline{CH_2}$Ar), 42.19 (q, NCH_3), 44.54 (q, $CH\underline{CH_3}$), 54.07 (t, $NCH\underline{CH_2}$), 66.66 (t, $\underline{CH_2}OCO$), 73.62 (d, CHOH), 116.98 (d, C_5^{im}), 136.22 (d, C_2^{im}), 141.64 (s, C_4^{im}), 153.17 (s, $N\underline{C}OO$), 176.57 (s, $\underline{C}ONCOO$). Anal. Calcd for $C_{18}H_{21}O_4N_3$ (M. W. 343) C, 62.97; H, 6.12; N, 12.24%. Found C, 62.92; H, 6.16; N, 12.26%.

Methyl (2*S*,3*S*)-3-Hydroxy-2-methyl-3-phenylpropanoate: (16a). Sodium hydride (180 mg, 80%) was carefully added to methanol (10 mL) under an argon atmosphere. Then, a solution of **15b** (1.4 g, 2 mmol) in methanol (50 mL) was added dropwise at 0 °C. The reaction mixture was stirred 15 min at 0 °C. Addition of an aqueous sat. NH_4Cl solution (25 mL) was followed by extraction with chloroform. The combined organic layers were dried evaporated to afford a crude which was purified by flash chromatography. Elution with hexane-ethyl acetate (80:20) gives **16b** (760.5 mg, 98%); $[\alpha]_D^{20}$−18.1° (*c* 1.7, $CHCl_3$); ^1H NMR (200 MHz, $CDCl_3$), δ=1.10 (3H, d, J=7 Hz, $CH\underline{CH_3}$), 2.78(1H, m, $\underline{CH}CH_3$), 3.65 (3H, s, $COO\underline{CH_3}$), 5.08 (1H, d, J=3.6 Hz, $\underline{CH}$OH), 7.31 (5H, m, Ar); ^{13}C NMR (50.3 MHz, $CDCl_3$) δ=10.81 (q, $CH\underline{CH_3}$), 46.51 (d, $\underline{CH}CH_3$), 51.71 (q, $COO\underline{CH_3}$), 73.76 (d, CHOH), 125.97 (d, Ar), 127.47 (d, Ar), 128.22 (d, Ar), 141.57 (s, Ar), 175.97 (s, CO). Anal. Calcd for $C_{11}H_{14}O_3$ (MW. 194): C, 68.04; H, 7.21%. Found: C, 68.06; H, 7.15%.

Compound **16b** was prepared under the same conditions as described for **16a** staring from **15b** (97%). $[\alpha]_D$−17.3° (*c* 1.89, $CHCl_3$) with identical spectroscopic properties as those described for **16a**.

We thank Dr. Gabriel Tojo Suárez (Univ. Santiago, Spain) for his help on the MS experiments. F. Santinelli wishes to thank The European Foundation for a Grant (Erasmus Program. Contract Nr. ICP-88-092-E). Permanent address: Dipartimento di Chimica; V. Elce di Sotto 8, 06100 Perugia (Italy).

References

1) H. C. Beyerman, L. Maat, and A. van Zon, *Recl. Trav. Chim. Pays-Bas*, **91**, 246 (1972).

2) A. Noordam, L. Maat, and H. C. Beyerman, *Recl. Trav. Chim. Pays-Bas*, **97**, 293 (1978).

3) J. C. Hodges, *Synthesis*, **1987**, 20.

4) J. H. Jones, D. L. Rathbone, and P. B. Wyatt, *Synthesis*, **1987**, 1110.

5) K. Barlos, J. Hondrelis, G. Lonergan, J. Matsoukas, and Ch. Sanida, *Liebigs Ann. Chem.*, **1989**, 387.

6) C.J.Chivikas and J. C. Hodges, *J. Org. Chem.*, **52**, 3591 (1987).

7) D. A. Evans, J. V. Nelson, E. Vogel, and T. R. Taber, *J. Am. Chem. Soc.*, **103**, 3099 (1981).

8) L-Histidine numbering: "Nomenclature of a-Amino Acids (Recomendations, 1974)," IUPAC Commission on the nomenclature of organic chemistry and IUPAC-IUB Commission on Biochemical nomenclature, *Biochemistry*, **14**, 449 (1975).

9) F. Bermejo González, J. P. Baz, and M. I. R. Espina, *Tetrahedron Lett.*, **30**, 2145 (1989).

10) M. S. Brown and H. Rapoport, *J. Org. Chem.*, **28**, 3261 (1963).

11) G. Gerhard and W. Schunack, *Arch. Pharm. (Weinheim)*, **313**, 780 (1980).

12) J. M. Davidson and C. M. French, *J. Chem. Soc.*, **1962**, 3364.

13) The measurement of the molar conductivity L=69.8 ($ohm^{-1}cm^2mol^{-1}$) for a 10^{-3} M solution of **14b** in nitromethane is in agreement with the conductance range to be expected for a typical 1 : 1 electrolyte.[14,15]

14) W. J. Geary, *Coord. Chem. Rev.*, **1971**, 81.

15) J. F. Coetzee and G. P. Cunningham, *J. Am. Chem. Soc.*, **87**, 2529 (1965).

16) The ^{1}H NMR (200 MHz) spectrum of **15a** exhibited only one doublet centered at δ=4.98 (J=4.8 Hz) to be assigned to the benzylic methine of an erythro aldol stereoisomer.

17) D. A. Evans, J. Bartroli, and T. Shih, *J. Am. Chem. Soc.*, **103**, 2127 (1981).

18) The ^{1}H NMR (200 MHz) spectrum of the phenylpropionic derivative **16a** exhibited only one doublet at δ=5.08 (J=4 Hz) which, considering the limits of NMR detection, excluded the presence of the possible threo isomers. The ^{13}C NMR spectra of both products **15a** and **16a** (see Experimental) confirmed the presence of only one diastereomer in the aldol.

Theoretical Study on the Formation of Spherical Micelles

Noriaki FUNASAKI* and Sakae HADA
Kyoto Pharmaceutical University, Yamashina-ku, Kyoto 607
(Received September 4, 1990)

Synopsis. From the Tanford theory for the formation of spherical micelles and a modification of this theory, the aggregation number n_w and monomer concentration x_1 are calculated as a function of total surfactant concentration x. The definition of cmc of $d^3x_1/dx^3=0$ is adequate. Empirical equations for the estimation of n_w and cmc are obtained.

When the concentration of surfactant is raised above the critical micelle concentration (cmc), to a first approximation all added molecules go into micelles. Then the question arises if the micelles grow in size or if only the number of the micelle is increased.[1] Recently, a number of experimental researches have been done, but there is still a matter of controversy whether the micelle of nonionic surfactant grows with increasing concentration or not.[2] Another question arises if the monomer concentration of the surfactant remains constant above the cmc.[3]

By gel-filtration chromatography, we determined the monomer concentration as a function of total surfactant concentration and further calculated the micellar aggregation number from this result.[3-5] These data may be used to test several theories for micellization or to estimate the micelle size distribution and other properties on the basis of these theories. Among these theories, the Tanford theory seems to be of greatest promise.[6] Warr and White modified it for computational simplicity and calculated the concentration dependence of the monomer concentration and aggregation number for spherical micelles.[7]

In this work we compare these theories and obtain useful relations to fit these theories to our experimental data.

Thermodynamic Basis

According to Tanford,[6] the free energy (per RT) of transfer of i surfactant molecules to a spherical micelle of aggregation number i may be expressed as[7,8]

$$\Delta G_i^\circ = -ai + bi^{2/3} + ci^{4/3} - (-a+b+c). \quad (1)$$

This equation holds for all micelles of aggregation number greater than unity. The coefficient a is a bulk free-energy term for transfer of an alkyl chain from water into the micelle core, b is the surface free energy per surfactant at the micelle/solution interface, and c is a term for repulsions etc. between the head groups in the micelle. The mole fraction of micelles of aggregation number i may be given by

$$x_i = x_1{}^i \exp(-\Delta G_i^\circ). \quad (2)$$

Using this equation, one can express the total surfactant mole fraction x and the weight average aggregation number n_w as

$$x = \sum_{i=1}^{\infty} i x_i, \quad (3)$$

and

$$n_w = \sum_{i=2}^{\infty} i^2 x_i / \sum_{i=2}^{\infty} i x_i. \quad (4)$$

From Eqs. 1 and 2, one can obtain a scaled mole fraction of i-mer as a function of a scaled monomer concentration from

$$x_i e^a = (x_1 e^a)^i \exp[-b(i^{2/3}-1) - c(i^{4/3}-1)]. \quad (5)$$

Furthermore Tanford defined the cmc as x at which $x_1/x=0.95$.[6]

For computational simplicity Warr and White modified Eq. 1 as

$$\Delta G_i^\circ = -a(i-1) + b(i-1)^{2/3} + c(i-1)^{4/3}, \quad (6)$$

and gave useful expressions for the cmc and other properies.[7] They defined scaling parameters for ΔG_i° and i:

$$\Gamma = b^2/c, \quad (7)$$

and

$$I = (b/c)^{3/2}. \quad (8)$$

The Γ value varies linearly with ΔG_i° and I gives a rough value of n_w. Furthermore they considered cmc values on the basis of the following equation:

$$d^3x_1/dx^3 = 0. \quad (9)$$

This is a form of the general definition of cmc by Phillips.[9] From Eq. 2 we can obtain

$$d^3x_1/dx^3 = M/x_1{}^2 [\sum_{i=1}^{\infty} i^2 x_1{}^{i-1} \exp(-\Delta G_i^\circ)]^5, \quad (10)$$

where

$$M = 3[\sum_{i=1}^{\infty} i^2 (i-1) x_1{}^{i-1} \exp(-\Delta G_i^\circ)]^2 - [\sum_{i=1}^{\infty} i^2(i-1)(i-2) x_1{}^{i-1} \exp(-\Delta G_i^\circ)] [\sum_{i=1}^{\infty} i^2 x_1{}^{i-1} \exp(-\Delta G_i^\circ)]. \quad (11)$$

From Eq. 9 the cmc is the value of x at which $M=0$.

Results and Discussion

Figure 1 shows plots of n_w against the logarithm of total concentration scaled by exp a in the case of $I=60$. The solid lines were calculated from the Tanford theory, viz., Eq. 1 and the dashed lines were from the Warr and White theory, viz., Eq. 6. The numerals attached to these lines denote the Γ values. Results similar to Fig. 1 were obtained in the cases of $I=20$ and 150. As Fig. 1 shows, at high concentrations the I value is similar to the n_w values calculated from the Warr and White theory, but is slightly larger than

those from the Tanford theory. These results are useful to estimate the values of b and c from observed n_w values and show that n_w is determined by the balance of the b term to the c term in Eqs. 1 and 6.

Figure 2 shows plots of monomer concentration against total concentration calculated from Eq. 1 (solid lines) and Eq. 6 (dashed lines) in the cases of I=60. Similar results were obtained in the cases of I=20 and 150. The monomer concentrations calculated from Eq. 1 are smaller than those from Eq. 6.

Figure 3 shows the logarithm of cmc against the square root of the product bc, calculated from Eq. 1. The filled symbols denote the cmc values calculated from the definition by Tanford, viz., x_1/x=0.95 and the hollow symbols are those from the definition of Eq. 9. Similar results were obtained from Eq. 6. The plots in Fig. 2 show part of these results. Empirically, these cmc values are expressed by the following equation:

$$\ln x_{cmc} = -a + \beta(bc)^{1/2} + \gamma. \quad (12)$$

Table 1 shows the coefficients β and γ in Eq. 12 and the correlation coefficient of linearity determined by a linear least-squares method. In the case of Eq. 6, the cmc values determined by the two definitions are close to each other and also close to the predictions by Eq. 12, as can be seen from the values of the correlation coefficient and the standard deviations of β and γ in Table 1. In the case of Eq. 1 the cmc values determined by the two definitions are far, as shown in Fig. 2 and Table 1. From Fig. 2 we can conclude that the definition of cmc by Eq. 9 is better than that by Tanford. Figure 1 shows the n_w values predicted by Eq. 1 are smaller than those by Eq. 6. As a result, in the case of Eq. 1 the cmc values defined by Tanford

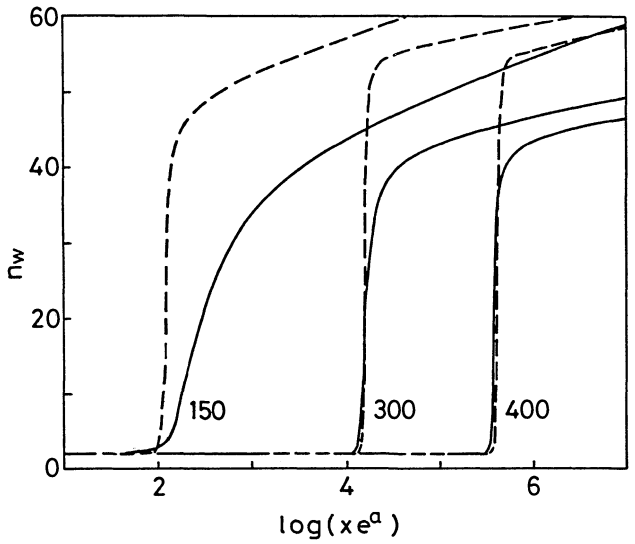

Fig. 1. Weight average aggregation numbers calculated from Eqs. 1 (solid lines) and 6 (dashed lines) as a function of the logarithm of scaled total concentration at different Γ values for I=60.

Table 1. The Coefficients β and γ and the Correlation Coefficient r Fitted to Eq. 12

Eq	Definition	$\beta\pm$sd[a)]	$\gamma\pm$sd[a)]	r
1	x_1/x=0.95	1.96±0.04	−1.23±0.82	0.9978
1	Eq. 9	1.87±0.01	0.25±0.26	0.9998
6	x_1/x=0.95	1.99±0.01	−0.12±0.13	0.9999
6	Eq. 9	1.98±0.00	−0.10±0.10	1.0000

a) Standard deviation.

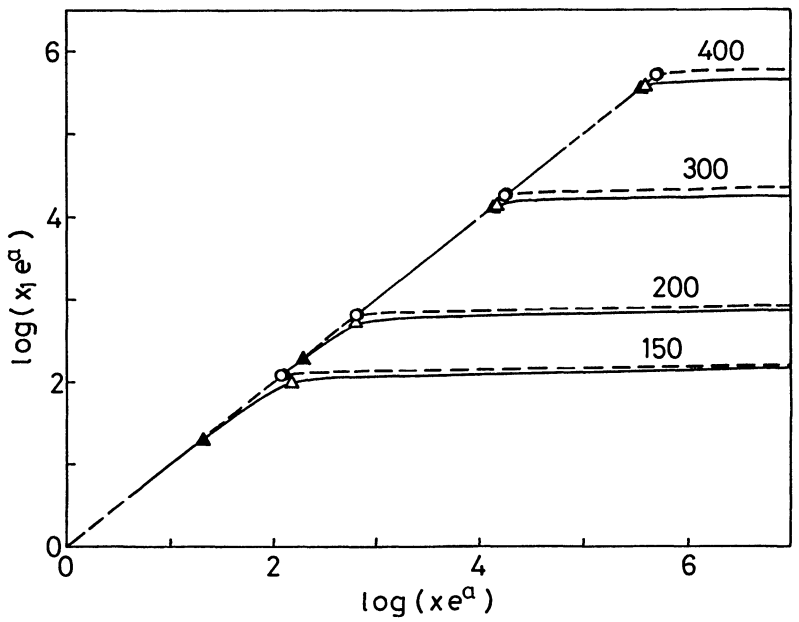

Fig. 2. Plots of scaled monomer concentrations against scaled total concentrations, calculated from Eqs. 1 (solid lines) and 6 (dashed lines) for I=60 at different Γ values. The hollow symbols ○ and △ show the cmc values defined by Eq. 9 and the filled symbols ● and ▲ show those defined by x_1/x=0.95.

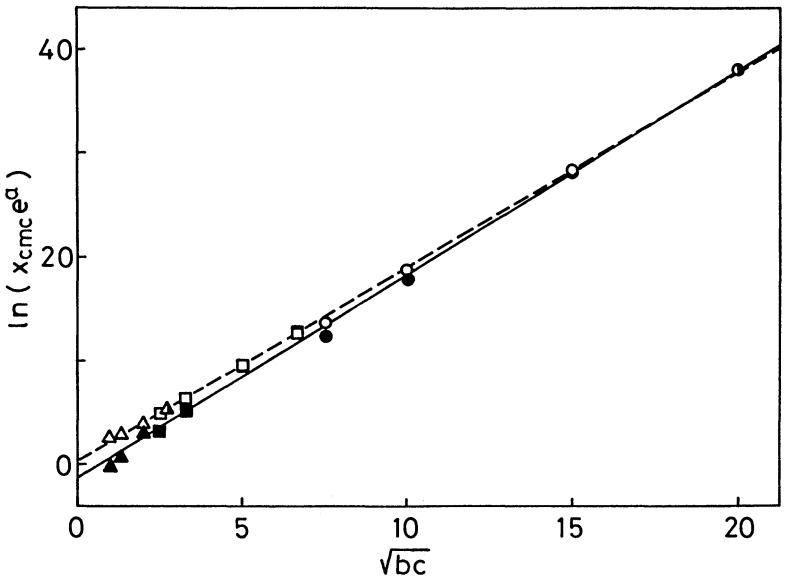

Fig. 3. Plots of scaled cmc values against the square root of the product bc for Eq. 1, calculated from the definitions of Eq. 9 (hollow symbols) and $x_1/x=0.95$ (filled symbols) at different I values: ○ and ●; I=20, □ and ■; I=60, △ and ▲; I=150. The dashed line is fitted to the hollow symbols and the solid line is fitted to the filled symbols.

become too small. From Eq. 12 we can see that the cmc value is controlled mainly by term a viz., interactions between alkyl groups and water, and further by terms b and c, viz., interactions between head groups at the micellar surface. The definition of cmc by Ruckenstein and Nagarajan,[8] viz., $d^2\Delta G_i^\circ/di^2=0$, yielded too small cmc values (data not shown).

In conclusion, the Warr and White theory (Eq. 6) is simple and useful to understand the predictions from the Tanford theory (Eq. 1). In Eq. 1 as well as in Eq. 6, the micelle size parameter I is a good measure of n_w, and the cmc value is empirically given by Eq. 12. These results are useful to fit Eqs. 1 and 6 to experimental data of cmc and n_w.[10] The values of n_w and x_1 predicted by Eq. 1 are significantly different from those predicted by Eq. 6. This result means that the physical meanings of the coefficients a, b, and c in Eq. 1 are different from, though similar to, those in Eq. 6. Therefore Eq. 6 is not a very good approximation of Eq. 1. The definition of cmc by Eq. 9 gives reasonable cmc values for both Eqs. 1 and 6.

Thanks are due to Mr. Shimada and Mr. Yamana for some preliminary calculations.

References

1) H. Wennerström and B. Lindman, *Phys. Rep.*, **52**, 1 (1979).
2) N. Funasaki, S. Hada, and S. Neya, *Bull. Chem. Soc. Jpn.*, **62**, 1725 (1989), and references cited therein.
3) N. Funasaki, S. Hada, and S. Neya, *J. Phys. Chem.*, **92**, 7112 (1988).
4) N. Funasaki, S. Hada, and S. Neya, *Chem. Lett.*, **1990**, 1075.
5) N. Funasaki, S. Hada, and S. Neya, *J. Phys. Chem.*, **94**, 8322 (1990).
6) C. Tanford, *J. Phys. Chem.*, **78**, 2469 (1974).
7) G. G. Warr and L. R. White, *J. Chem. Soc., Faraday Trans. 2*, **81**, 549 (1985).
8) E. Ruckenstein and R. Nagarajan, *J. Phys. Chem.*, **79**, 2622 (1975).
9) J. N. Phillips, *Trans. Faraday Soc.*, **51**, 561 (1955).
10) N. Funasaki, H.-S. Shim, and S. Hada, *J. Chem. Soc., Faraday Trans.*, in press.

Chemical Shift Standards in High-Resolution Solid-State NMR (1) ^{13}C, ^{29}Si, and ^{1}H Nuclei

Shigenobu HAYASHI* and Kikuko HAYAMIZU
National Chemical Laboratory for Industry, Tsukuba, Ibaraki 305
(Received September 17, 1990)

Synopsis. The resonance frequencies of ^{13}C, ^{29}Si, and ^{1}H nuclei in pure tetramethylsilane have been measured accurately by spinning the liquid sample at the magic angle, which are free from the effects of the bulk magnetic susceptibility and the solvent. Using the above resonance positions, the chemical shifts of several second shift-standard materials have been determined with much improved accuracy and precision.

The chemical shift can be expressed as the deviation of the resonance frequency from that of a standard sample. An external reference is usually used in solid-state NMR, where we should be careful of the effect of the bulk magnetic susceptibility.[1,2] In high-resolution solid-state NMR of ^{13}C, ^{29}Si, and ^{1}H, few papers have been presented, in which the chemical shifts have been determined accurately by directly referring to the signal of tetramethylsilane (TMS), except for the Earl and VanderHart's work.[3] In our previous paper,[4] we have reported chemical shift values of several second shift-standard materials in ^{13}C, ^{29}Si, ^{31}P, ^{23}Na, ^{27}Al, and ^{11}B NMR, although the accuracies were not so good as in solution NMR.

In the present work, we can trace the spectra of pure tetramethylsilane with high resolution in the instrumental set-up for solid-state NMR by the magic-angle spinning (MAS) of the liquid sample, to the extent that the error in the first standard is negligible. The resonance position obtained by the above method is free from the solvent effect and the effect of the bulk magnetic susceptibility. Thus, we can determine the "absolute chemical shifts" of the materials to be investigated with markedly improved accuracy.

Experimental

Materials were available commercially. They were used as supplied.

The instrument used for the NMR measurements was a Bruker MSL400 pulsed spectrometer, whose magnetic field strength was 9.4 T. The resonance frequencies were 100.614, 79.496, and 400.136 MHz for ^{13}C, ^{29}Si, and ^{1}H, respectively. The commercial MAS probehead supplied by Bruker was used, in which a double-bearing type rotor made of zirconia was spun at spinning rates between 3 and 4 kHz for solid samples. Sealed inserts which fit the inside of the rotor[5] were used to spin the liquid samples at spinning rates of 0.5 to 1 kHz. A spherical container made of Pyrex was also used to check the effect of the bulk magnetic susceptibility. One did not need to remove the probehead from the magnet bore when the sample was exchanged, which excluded the error in the chemical shift caused by the replacement of the probehead. Temperature was 294 K. Before the NMR measurements, the magnetic field was carefully shimmed to achieve a linewidth less than 0.010 ppm for liquid samples when the magic-angle spinning was applied.

The chemical shifts were determined by use of an external reference. The drift of the magnetic field was less than 0.006 ppm per day, and thus, the drift of the magnetic field was negligible compared to the other experimental errors during a day. Most part of the experimental errors came from the residual linewidth and the line shape both of which caused by the field inhomogeneity and the sample nature.

Results and Discussion

Accurate Determination of Chemical Shifts. TMS can be used as the first standard in ^{13}C, ^{29}Si, and ^{1}H measurements, where pure liquid should be used to avoid the solvent effect. TMS is highly volatile, and a resonance line with a relatively broad linewidth is obtained for a sealed sample in the static state. On the other hand, we can get a very sharp line by spinning the sealed sample at the magic angle. The residual linewidths are 0.008 ppm in the decoupled spectra of ^{13}C and ^{29}Si, and 0.012 ppm in the ^{1}H spectra. Small peaks are observed on both sides of the intense peak in the ^{13}C spectra, which are originated from the coupling with ^{29}Si, where the coupling constant $^{1}J(^{13}C-^{29}Si)$ is 51.4 Hz. The coupling constants with ^{1}H can be determined accurately from the ^{1}H-coupled spectrum, which are $^{1}J(^{13}C-^{1}H)=118.06\pm0.03$ Hz, $^{3}J(^{13}C-^{1}H)=2.16\pm0.03$ Hz, and $^{2}J(^{29}Si-^{1}H)=6.59\pm0.01$ Hz. This high resolution enables the accurate determination of the chemical shifts.

Tables 1 and 2 summarize the results on the second standard materials frequently used in high-resolution

Table 1. ^{13}C Chemical Shifts[a]

Compounds	δ[b] ppm	FWHM[c] ppm
[Pure liquids]		
Tetramethylsilane	0	0.008
Benzene	128.475 (0.005)	0.006
Chloroform	77.966 (0.005)	0.020
[Solids]		
Adamantane	38.520 (0.005)	0.050
	29.472 (0.004)	0.049
Glycine	176.46 (0.02)	0.40
	43.67 (0.01)	0.90
Hexamethylbenzene	132.07 (0.04)	0.83
	17.17 (0.02)	0.80
Tetrakis(trimethylsilyl)silane	3.517 (0.005)	0.077
Silicone rubber	[d] 1.422 (0.004)	0.030
	[e] 1.412 (0.004)	0.030

a) All the samples are spinning at the magic angle. b) Numbers in the parentheses are experimental errors. c) Full width at half maximum. d) $\nu_r \leqslant 1.0$ kHz. e) $\nu_r \geqslant 2.5$ kHz.

Table 2. ^{29}Si Chemical Shifts[a]

Compounds	δ ppm	FWHM ppm
[Pure liquids]		
Tetramethylsilane	0	0.008
Hexamethyldisiloxane	6.679 (0.004)	0.011
[Solids]		
Sodium 3-(trimethlsilyl)-propionate-d_4[b]	1.669 (0.022)	0.17
	1.445 (0.012)	0.16
	av. 1.50 (0.03)	
Sodium 3-(trimethylsilyl)-propionate[b]	1.682 (0.022)	0.24
	1.459 (0.012)	0.17
	1.158 (0.022)	0.28
	av. 1.50 (0.03)	
Sodium 3-(trimethylsilyl)-propane-1-sulfonate[b]	1.534 (0.012)	0.22
	av. 1.46 (0.03)	
Hexamethylcyclotrisiloxane	−9.66 (0.05)	1.0
Tetrakis(trimethylsilyl)silane	−9.843 (0.006)	0.040
	−135.402 (0.007)	0.059
Silicone rubber	[c] −22.319 (0.005)	0.030
	[d] −22.333 (0.008)	0.031

a) All the samples are spinning at the magic angle. b) Shift values of main peaks are listed. Average values indicated by av. are determined by artificial broadening. c) $\nu_r \leqslant 1.0$ kHz. d) $\nu_r \geqslant 2.0$ kHz.

Table 3. ^{1}H Chemical Shifts[a]

Compounds	δ ppm	FWHM ppm
[Pure liquids]		
Tetramethylsilane	0	0.012
Benzene	6.771 (0.005)	0.011
Chloroform	7.392 (0.005)	0.006
Cyclohexane	1.482 (0.005)	0.014
Water	4.877 (0.005)	0.024
[Solids]		
Adamantane	1.85 (0.15)	2.5[b]
d-Camphor	1.1 (0.1)	2.7[b]
Tetrakis(trimethylsilyl)silane	0.247 (0.011)	0.80[b]
Silicone rubber	[c] 0.123 (0.003)	0.048
	[d] 0.119 (0.003)	0.047

a) All the samples are spinning at the magic angle. b) The linewidth depends on the spinning rate. The listed values were obtained at ν_r=4.04, 3.59, and 4.01 kHz for adamantane, *d*-camphor, and tetrakis(trimethylsilyl)silane, respectively. c) $\nu_r \leqslant 1.0$ kHz. d) $\nu_r \geqslant 2.5$ kHz.

solid-state ^{13}C and ^{29}Si NMR. Among the solid materials, adamantane, tetrakis(trimethylsilyl)silane (Si(Si$(CH_3)_3)_4$; TKS),[6] and silicone rubber have markedly narrow resonance lines, where the dipolar coupling with ^{1}H nuclei is weak due to fast molecular motions. Cross polarization (CP) is not efficient in TKS and silicone rubber. On the other hand, glycine and hexamethylbenzene need cross polarization to get ^{13}C signals with a good signal to noise ratio. To set up the ^{29}Si CP/MAS experiment, sodium 3-(trimethylsilyl)propionate-d_4 ($(CH_3)_3SiCD_2CD_2COONa$; TSPA-d_4), sodium 3-(trimethylsilyl)propionate ($(CH_3)_3SiCH_2CH_2COONa$; TSPA), and sodium 3-(trimethylsilyl)propane-1-sulfonate (sodium 4,4-dimethyl-4-silapentane-1-sulfonate; $(CH_3)_3SiCH_2CH_2CH_2SO_3Na$; DSS) are suitable. However, they have a fine structure in the spectra, as shown in Fig. 1, which is considered to be caused by the crystallographic inequivalence in the solid state. The most intense peaks have chemical shift values of 1.445, 1.459, and 1.534 ppm in TSPA-d_4, TSPA, and DSS, respectively.

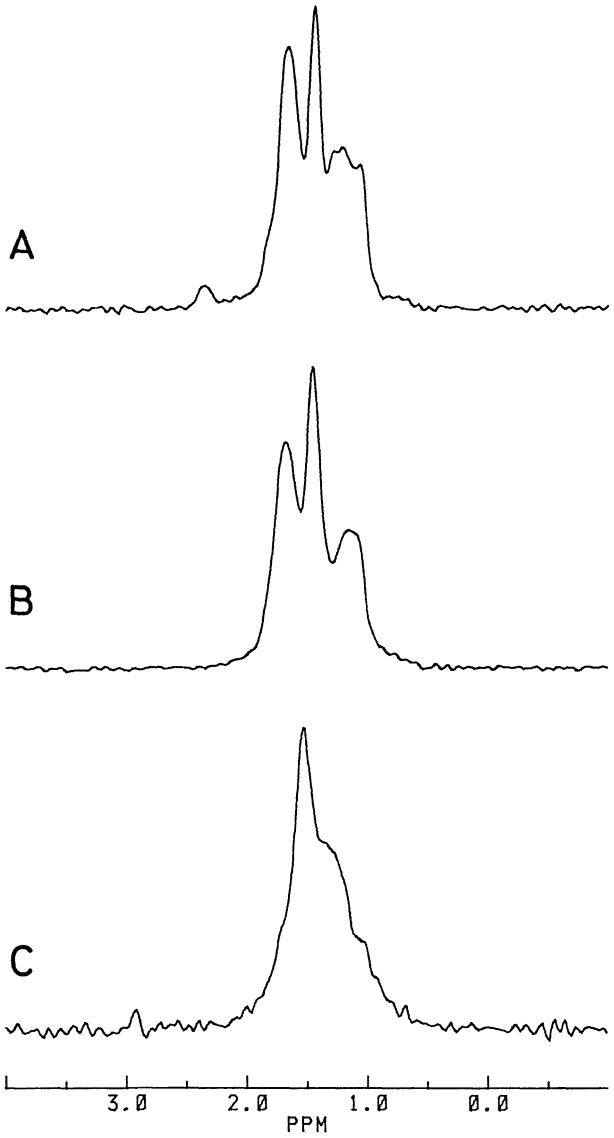

Fig. 1. ^{29}Si CP/MAS NMR spectra of (A) TSPA-d_4, (B) TSPA, and (C) DSS, measured at ν_0=79.496 MHz.

The homonuclear dipole-dipole interaction between ^{1}H spins cannot be usually suppressed by the magic-angle spinning of the normal rate. In this work, the chemical shift values of weakly-coupled ^{1}H are determined only by MAS, which results are summarized in Table 3.

The spectra of silicone rubber have a fine structure in the range of the spinning rate between 1.4 and 2.0 kHz, while only one component is observed outside the range. Thus, the shift values outside the above range are listed in the tables.

Table 4. Summary of the Experiments on the Effect of the Bulk Magnetic Susceptibility[a)]

Nucleus	Shape	Mode	δ	FWHM
			ppm	ppm
^{13}C	Cylinder	MAS	128.475 (0.005)	0.006
	Cylinder	Static	128.51 (0.05)	0.22
	Sphere	Static	128.45 (0.05)	0.19
^{1}H	Cylinder	MAS	6.771 (0.005)	0.011
	Cylinder	Static	6.78 (0.03)	0.22
	Sphere	Static	6.76 (0.02)	0.050

a) The sample is pure benzene.

Effect of Bulk Magnetic Susceptibility on the Shift. Earl and VanderHart[3)] have suggested that the bulk magnetic susceptibility effect is negligible for an infinitely long cylinder spinning about its cylindrical axis which is inclined at the magic angle from the direction of the field. Even if the length of the cylinder is finite, the susceptibility effect is expected to be negligible in the MAS experiment, being derived from VanderHart et al.[7)]

We have checked the above suggestions in practical samples. Three types of experiments have been carried out: First, the resonance frequency of a cylindrical sample is measured under MAS, using the sealed insert with a cylindrical hole. Second, the resonance frequency of a cylindrical sample is measured without the spinning. Third, the spectra of a spherical sample is measured in the static state. In the first and the second experiments, the cylindrical axis is inclined at the magic angle from the direction of the field.

We have measured ^{13}C and ^{1}H signals of pure benzene, the results of which are summarized in Table 4. The resonance positions of the spherical samples are free from the susceptibility effect. As shown in table, the effect is negligible for the cylindrical sample under MAS as well as in the static state. The inclination of the cylindrical axis might be important to cancel the effect. Thus, the MAS experiment can determine "the absolute chemical shift" free from the susceptibility effect and the solvent effect.

References

1) J. R. Zimmerman and M. R. Foster, *J. Phys. Chem.*, **61**, 282 (1957).
2) D. H. Live and S. I. Chan, *Anal. Chem.*, **42**, 791 (1970).
3) W. L. Earl and D. L. VanderHart, *J. Magn. Reson.*, **48**, 35 (1982).
4) S. Hayashi and K. Hayamizu, *Bull. Chem. Soc. Jpn.*, **62**, 2429 (1989).
5) L. H. Merwin and A. Sebald, *J. Magn. Reson.*, **84**, 367 (1989).
6) J. V. Muntean and L. M. Stock, *J. Magn. Reson.*, **76**, 540 (1988).
7) D. L. VanderHart, W. L. Earl, and A. N. Galloway, *J. Magn. Reson.*, **44**, 361 (1981).

Chemical Shift Standards in High-Resolution Solid-State NMR (2) ^{15}N Nuclei

Shigenobu HAYASHI* and Kikuko HAYAMIZU
National Chemical Laboratory for Industry, Tsukuba, Ibaraki 305
(Received September 18, 1990)

Synopsis. ^{15}N NMR spectra of the shift standard compound, pure nitromethane, have been measured with high resolution by spinning the liquid sample at the magic angle. Using the precise resonance position of nitromethane, the chemical shifts of the solid second-standard materials such as ammonium salts and glycine have been measured with great precision.

High-resolution solid-state NMR has been widely used recently. Many of them are concerned with ^{13}C and ^{29}Si nuclei, while measurements of ^{15}N nuclei are rather limited.[1] One of the reasons is that the sensitivity of ^{15}N nuclei is very low because of the low natural abundance and the low gyromagnetic ratio. However, the ^{15}N nuclei is important for the studies of biosubstances such as proteins, polypeptides, and amino acids.

The chemical shift can be expressed as the deviation of the resonance frequency from that of a standard material. In solution ^{15}N NMR, pure nitromethane is widely used as the first standard.[1] On the other hand, various materials have been used for the first standard in high-resolution solid-state ^{15}N NMR. NH_4Cl[2] and glycine[3] have been used as the solid shift standards, and various liquid samples used in solution NMR have also been used as the first standard; for example, HNO_3 aqueous solution, NH_4NO_3 saturated aqueous solution, and liquid NH_3.

In our previous paper,[4] we have reported precise chemical shift values of several second standard materials in ^{13}C, ^{29}Si, and ^{1}H NMR determined with respect to pure tetramethylsilane. In the present work, we have extended the previous work to ^{15}N NMR. The key point is how we measure the peak position of the first standard precisely.

Experimental

Materials were available commercially; CH_3NO_2 from Tokyokasei, $HCONH_2$ and $NH_4H_2PO_4$ from Kokusankagaku, $^{15}NH_4Cl$, NH_4Cl (10at.% ^{15}N), $^{15}NH_4NO_3$, and Glycine-^{15}N from Aldrich, NH_4Cl from Mitsubishikasei, NH_4NO_3 and $(NH_4)_2SO_4$ from Nacalai, and glycine from Wako. They were used as supplied.

The instrument used for the NMR measurements was a Bruker MSL400 pulsed spectrometer, whose magnetic field strength was 9.4 T (the resonance frequency, 40.561 MHz). The detail of the hardware has been described previously.[4] The rotor was spun at spinning rates of about 3 kHz and 0.5—1.0 kHz for solid and liquid samples, respectively. Temperature was 294 K, unless otherwise stated.

INEPT pulse sequences with and without ^{1}H decoupling[5] were used for liquid samples as well as the ordinary single pulse sequence. Two kinds of pulse sequences were used for solid samples; single pulse with ^{1}H decoupling only during the data acquisition, and cross polarization (CP) from ^{1}H to ^{15}N with ^{1}H decoupling during acquisition. CP was always used for the unenriched solid samples, in which the contact time was 3 ms, the recycle time was 8—10 s, and the number of scans was 100—200.

Results and Discussion

^{15}N Spectra of Nitromethane and Formamide. Nitromethane is the first standard, and formamide is used as the liquid second standard. Table 1 summarizes the chemical shifts and linewidths obtained in this work. The resonance frequency of pure nitromethane measured without decoupling and with MAS is assumed to be 0 ppm throughout this work, the reason of which is described below.

Figure 1 shows the spectra of pure nitromethane without and with ^{1}H decoupling. Linewidths less than 0.010 ppm have been obtained by the initial careful shimming. Figure 1A shows XH_3 pattern, in which the coupling constant between X and H is 2.33±0.01 Hz. This value agrees excellently with that of Strelenko et al.[6] Figure 1B shows the decoupled spectrum, and only one sharp resonance line can be observed. However, note that the resonance position of the decoupled spectrum does not

Table 1. Results of Pure Nitromethane and Formamide

Shape	Spinning	^{1}H Coupling	δ[a] ppm	FWHM[b] ppm
[Nitromethane]				
Cylinder	MAS	Coupled	0[c]	0.007
		Decoupled	−0.03 (0.01)	0.008
Sphere	Static	Coupled	0.04 (0.05)	0.20
Cylinder	Static	Coupled	0.00 (0.02)	0.20
[Formamide]				
Cylinder	MAS	Coupled	−266.712 (0.006)	0.018
		Decoupled	−267.02 (0.10)	0.082

a) Higher frequecy side is expressed as positive. Values in the parentheses are experimental errors.
b) Full width at half maximum. c) Assumed to be 0 ppm.

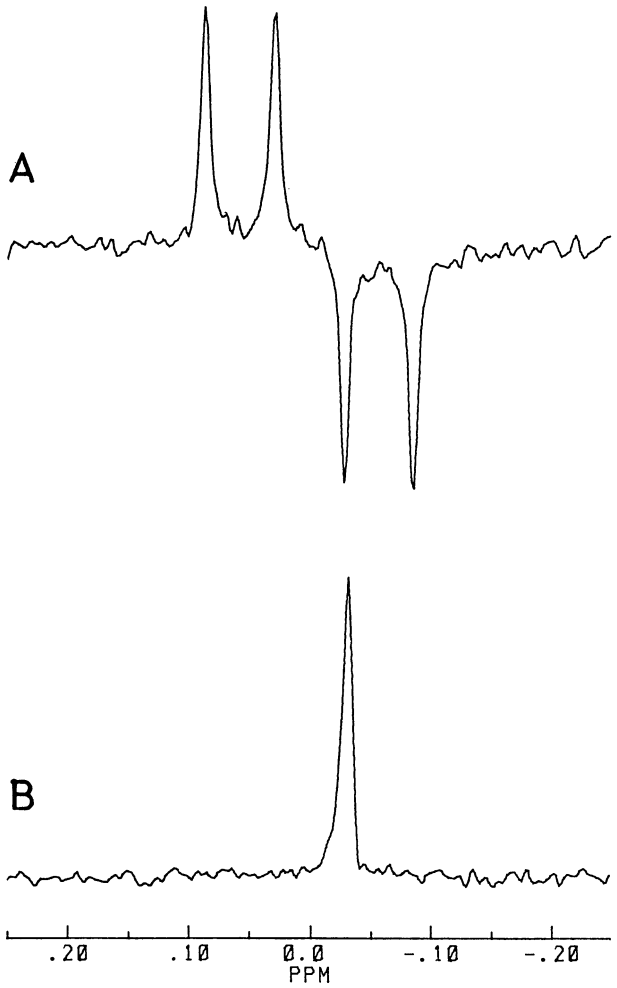

Fig. 1. ^{15}N MAS NMR spectra of neat nitromethane. (A) INEPT without decoupling, and (B) refocused INEPT with ^{1}H decoupling. Experimental parameters are as follows; 100 scans, τ (=1/4J) 109 msec, spectral width 1250 Hz, data size 32 kwords, and line broadening 0.1 Hz.

agree to the center of the coupled spectrum. We have repeated these measurements several times, including the single-pulse-sequence measurements with and without decoupling, and conclude that the deviation is not the experimental error. The deviation ranges from 0.026 to 0.037 ppm, depending on the experiment.

Which spectrum is independent of the measurement, the decoupled or coupled spectrum? The answer comes from the similar measurements on formamide, $HCONH_2$. The coupled spectrum shows XH_2 pattern accompanied by a long-range splitting. The coupling constants are $^{1}J(^{15}N-^{1}H)=89.21\pm0.02$ Hz and $^{2}J(^{15}N-^{1}H)=14.03\pm0.02$ Hz. The decoupling induces a shift of -0.30 ± 0.10 ppm. This deviation is much larger than that observed in nitromethane, and the fluctuation from experiment to experiment is also larger. We have compared the spectra of nitromethane with those of formamide. The difference in the resonance frequency between the coupled spectra of the two compounds are always constant, while the difference between the decoupled specta fluctuates up to 0.20 ppm. Consequently, the coupled spectrum is independent of the experiment. Thus, the coupled spectrum should be taken as the shift standard. In the present work, the center of the coupled spectrum of pure nitromethane (Fig. 1A) is assumed to be 0 ppm.

The origin of the decoupling induced shift is discussed briefly. The most possible mechanism is that the decoupling induces temperature increase in the sample, resulting in the resonance frequency shift. Nitromethane and formamide have large dielectric constants,[7] and thus the decoupling pulse loses its energy, which converts into heat. The heating effect is largely dependent on the experimental conditions, and the shift in the decoupled spectrum fluctuates from experiment to experiment. To check the above hypothesis, we have measured the temperature dependence of the ^{15}N chemical shifts in nitromethane and formamide under the MAS condition. The temperature range studied is between 294 and 304 K. The resonance lines shift towards lower frequency as the temperature increases, which direction is the same as the decoupling induced shift. The magnitudes of the tempearture dependence are -0.0045 and -0.0089 ppm K^{-1} for nitromethane and formamide, respectively. A simple calculation indicates that the decoupling increases the temperature of the sample by 6—8 K and 23—45 K in nitromethane and formamide, respectively. The specific inductive capacities of the two compounds are 35.8 (30 °C) and 111.0 (20 °C).[7] Since the dielectric constant of formamide is markedly large, the decoupler heating is very efficient in this compound. The linewidth in the decoupled spectrum of formamide (0.082 ppm) is much broader than in the coupled spectrum (0.018 ppm). The decoupler heating might produce chemical shift dispersion in the sample.

Anderson and Freeman[8] have proposed a mechanism of the decoupling induced shift, called "Bloch-Siegert shift." However, this mechanism cannot be applied to the present case, since the estimated shift is

Table 2. ^{15}N Chemical Shifts in Solids[a]

Compounds	δ[b] ppm	FWHM[c] ppm
$^{15}NH_4Cl$	−341.168 (0.011)	0.077
NH_4Cl (10at.% ^{15}N)	−341.168 (0.011)	0.085
NH_4Cl	−341.15 (0.02)	0.14
$^{15}NH_4NO_3$	−358.45 (0.01)	0.30
NH_4NO_3	−4.98 (0.06)	0.50
	−358.43 (0.03)	0.27
$NH_4H_2PO_4$	−356.88 (0.02)	0.20
$(NH_4)_2SO_4$	−355.70 (0.01)	0.13
	−355.98 (0.01)	0.12
Glycine-^{15}N	−347.54 (0.03)	0.57
Glycine	−347.58 (0.05)	0.70

a) Measured at ν_0=40.561 MHz with MAS. b) With respect to the resonance frequency of pure nitromethane measured under MAS without ^{1}H decoupling. The values in the parentheses are experimental errors. c) Full width at half maximum.

much smaller than the experimental shift.

Next the effect of the bulk magnetic susceptibility is checked and discussed for pure nitromethane. The procedure is the same as the previous work,[4] which results are summarized in Table 1. Although the experimental error is large for the static samples, the observed values demonstrate that the effect of the bulk magnetic susceptibility is negligible within the experimental error in MAS NMR. Furthermore, the susceptibility effect is negligible in the static cylinder whose cylindrical axis is inclined at the magic angle.

Second Shift Standards. Practically, solid materials are adequate in order to set up the instrument. We have measured ^{15}N CP/MAS NMR spectra of various ammonium salts and glycine, and have determined their chemical shifts with respect to pure nitromethane. Table 2 summarizes the obtained chemical shifts and linewidths. Cross polarization is not always necessary for the ^{15}N-enriched compounds, while it is indispensable for the compounds with the natural-abundance ^{15}N. Although $^{15}NH_4NO_3$ has two kinds of N atoms, only the chemical shift of $^{15}NH_4$ is listed in the table, since NO_3 was not observed in a few scans. $(NH_4)_2SO_4$ has two peaks originated from crystallographycally inequivalent sites.[9] Since this work delas with the shift standard, detailed discussion on the correlation between the chemical shifts and the structure will be published elsewhere. For routine use, we recommend to use $^{15}NH_4Cl$ and NH_4Cl (10 at.%^{15}N) to set up the instrument and as the second shift standard. The linewidths are smallest among the solid materials measured.

References

1) M. Witanowski, L. Stefaniak, and G. A. Webb, *Ann. Rep. NMR Spectrosc.*, **18**, 1 (1986).
2) C. I. Ratcliffe, J. A. Ripmmester, and J. S. Tse, *Chem. Phys. Lett.*, **99**, 177 (1983).
3) L. J. Mathias, D. G. Powell, J.-P. Autran, and R. S. Porter, *Macromolecules*, **23**, 963 (1990).
4) S. Hayashi and K. Hayamizu, *Bull. Chem. Soc. Jpn.*, **64**, 685 (1991).
5) J. K. M. Sanders and B. K. Hunter, "Modern NMR Spectroscopy," Oxford University, Oxford (1987), p. 81.
6) Yu. A. Strelenko, V. N. Torocheshnikov, and N. M. Sergeyev, *J. Magn. Reson.*, **89**, 123 (1990).
7) The Chemical Society of Japan, "Kagakubinran," 3rd ed, Maruzen, Tokyo (1984), p. II-501.
8) W. A. Anderson and R. Freeman, *J. Chem. Phys.*, **37**, 85 (1962).
9) M. L. H. Gruwel, M. S. McKinnon, and R. E. Wasylishen, *Chem. Phys. Lett.*, **139**, 321 (1987).

Synthesis and Molecular Structure of Europium(III) Complex with 2,6-Diacetylpyridine Bis(2-pyridylhydrazone)

Masatomi SAKAMOTO,* Naohide MATSUMOTO,*,† and Hisashi ŌKAWA†
Department of Industrial Chemistry, Faculty of Engineering, Ehime University, Matsuyama 790
†Department of Chemistry, Faculty of Science, Kyushu University, Hakozaki, Higashi-ku, Fukuoka 812
(Received August 6, 1990)

Synopsis. The title complex, $[Eu(NO_3)_2(L)(CH_3OH)]NO_3$, has been synthesized and its molecular structure has been determined by a single crystal X-ray analysis, where L denotes 2,6-diacetylpyridine bis(2-pyridylhydrazone). The complex has a ten-coordinate structure with quinquedentate L, two bidentate NO_3^- ions, and monodentate CH_3OH.

Lanthanoid ions are classified into "hard acids" in the HSAB sence and generally have a low affinity toward nitrogen donor atom. Therefore, lanthanoid complexes derived from nitrogenous ligands (with only nitrogen donor atoms) are still limited to those of phthalocyanine, porphyrines, *o*-phenanthroline, 2,2′-bipyridyl, and aliphatic polyamines.

In 1979, Backer-Dirks et al.[1a] reported the synthesis of lanthanum(III) complex of a Schiff base derived from 2,6-diacetylpyridine and ethylenediamine. Thereafter some synthetic investigations of lanthanoid complexes have been undertaken using related nitrogenous ligands.[1-4] Those previous studies suggest that despite low affinity to nitrogen donor atom lanthanoid ions form significantly stable complexes when a multidentate nitrogenous ligand is appropriately chosen. In this study a quinquedentate nitrogenous ligand, 2,6-diacetylpyridine bis(2-pyridylhydrazone) (abbreviated as L), obtained by the condensation of 2,6-diacetylpyridine and 2-pyridylhydrazine in the 1 : 2 ratio, has been utilized for the synthesis of europium(III) complex. This paper describes the synthesis and single crystal X-ray analysis of $[Eu(NO_3)_2(L)(CH_3OH)]NO_3$.

Experimental

Synthesis of Ligand (L). To a solution of 2,6-diacetylpyridine (10 mmol) and 2-pyridylhydrazine (20 mmol) in ethanol (25 cm^3) was added one drop of concentrated hydrochloric acid, and the mixture was heated at about 60 °C with stirring to give a pale yellow precipitate. After further heating with stirring at this temperature for 1 h, the mixture was allowed to stand overnight at room temperature. The precipitate was collected by filtration, washed with ethanol, and dried in the open air. The yield was 2.3 g (60%).

Found: C, 60.08; H, 5.89; N, 25.72%. Calcd for $C_{19}H_{19}N_7 \cdot 2H_2O$: C, 59.83; H, 6.08; N, 25.70%.

$[Eu(NO_3)_2(L)(CH_3OH)]NO_3$. To a solution of the ligand (L, 1 mmol) in hot methanol (90 cm^3) was added europium(III) nitrate hexahydrate (1 mmol) in methanol (10 cm^3). The solution was refluxed with stirring for 2 h and set aside at room temperature overnight to give orange crystals, which were collected on a glass filter, washed with methanol, and dried in the open air. The yield was 0.54 g (77%).

Found: C, 32.58; H, 3.09; N, 19.72; Eu, 21.49%. Calcd for $C_{19}H_{21}EuN_{10}O_{10}$: C, 32.54; H, 3.02; N, 19.97; Eu, 21.67%.

Recrystallization of the above complex from hot methanol formed single crystals suitable for X-ray analysis.

Measurements. Elemental analyses were carried out at Advanced Instrumentation Center for Chemical Analysis, Ehime University. Molar conductances were measured in methanol (concn 1×10^{-3} mol dm^{-3}) at 25 °C with a Toa CM-S Conductivity Meter. Infrared spectra were recorded on KBr disks with a JASCO IR-G Spectrometer.

X-Ray Crystallography. Reflection data were measured on a Rigaku Denki AFC-5 automated four-circle diffractometer with graphite-monochromatized Mo $K\alpha$ radiation at room temperature. The details of data collection and crys-

Table 1. Positional Parameters

Atom	x	y	z	B_{eqv}/Å^2
Eu	0.15267(5)	0.28634(4)	0.54933(5)	2.0
N1	−0.0208(9)	0.2661(6)	0.6007(10)	2.9
N2	0.0140(9)	0.1288(7)	0.6406(10)	3.0
N3	0.1008(8)	0.1403(6)	0.5994(9)	2.4
N4	0.2732(8)	0.1707(6)	0.5196(8)	2.2
N5	0.3288(8)	0.3223(6)	0.5216(9)	2.6
N6	0.3559(8)	0.4026(6)	0.5311(10)	2.8
N7	0.2099(8)	0.4307(6)	0.6097(9)	2.5
C1	−0.0848(12)	0.3277(10)	0.6055(13)	3.7
C2	−0.1742(11)	0.3210(10)	0.6461(13)	3.8
C3	−0.2030(11)	0.2454(11)	0.6846(13)	4.2
C4	−0.1408(11)	0.1803(10)	0.6806(13)	3.7
C5	−0.0520(10)	0.1934(8)	0.6385(11)	2.8
C6	0.1520(10)	0.0779(8)	0.5817(11)	2.6
C7	0.1225(13)	−0.0076(8)	0.6087(14)	3.7
C8	0.2458(10)	0.0923(7)	0.5319(10)	2.4
C9	0.3012(12)	0.0287(8)	0.4951(13)	3.5
C10	0.3856(12)	0.0446(9)	0.4487(14)	3.7
C11	0.4169(12)	0.1264(9)	0.4416(13)	3.6
C12	0.3587(10)	0.1862(8)	0.4817(10)	2.4
C13	0.3896(10)	0.2732(8)	0.4830(11)	2.5
C14	0.4887(11)	0.2946(9)	0.4548(15)	5.3
C15	0.2936(9)	0.4565(7)	0.5739(10)	2.2
C16	0.3207(12)	0.5392(8)	0.5799(13)	3.4
C17	0.2599(13)	0.5912(8)	0.6281(13)	3.8
C18	0.1720(12)	0.5652(8)	0.6685(12)	3.5
C19	0.1511(11)	0.4834(8)	0.6567(12)	3.0
OM	0.0804(7)	0.2152(6)	0.3680(8)	3.3
CM	−0.0164(13)	0.2220(11)	0.3156(16)	5.2
N8	0.1031(10)	0.4028(8)	0.3591(11)	4.0
O1	0.1836(7)	0.3697(6)	0.3636(8)	3.4
O2	0.0777(13)	0.4523(11)	0.2824(14)	9.5
O3	0.0460(7)	0.3853(6)	0.4346(8)	3.1
N9	0.2019(9)	0.3017(6)	0.8053(9)	3.1
O4	0.2592(8)	0.2709(6)	0.7380(8)	3.5
O5	0.1170(7)	0.3137(6)	0.7596(8)	3.5
O6	0.2246(11)	0.3181(8)	0.9077(9)	5.5
N10	0.0861(9)	0.0421(7)	1.2183(10)	3.2
O7	0.0464(10)	−0.0075(8)	1.1521(12)	6.1
O8	0.1178(11)	0.1061(8)	1.1821(14)	7.0
O9	0.0929(11)	0.0286(9)	1.3244(10)	6.2

tallographic data are as follows:

$[Eu(NO_3)_2(L)(CH_3OH)]NO_3$, formula=$C_{20}H_{23}EuN_{10}O_{10}$, F.W.=715.4, monoclinic, space group $P2_1/n$, a=13.978(4), b=16.487(4), c=11.443(2) Å, β=95.02(2)°, V=2626.9(11) Å^3, D_x =1.808 g cm^{-3}(Z=4), crystal size 0.3×0.3× 0.4 mm, μ(Mo $K\alpha$) =18.16 cm^{-1}, scan mode θ-2θ, scan range 2.5—52°, scan width (1.2+0.35 tan θ)°, octant measured $+h$, $+k$, $\pm l$, number of observed reflections with $|F_o|>3\sigma$ ($|F_o|$) 4284, R=7.22%, R_w=8.81%, highest peak on the final D-Fourier 4.3 e Å^{-3} around Eu atom.

The intensity data were corrected for Lorentz and polarization effects but not for absorption and extinction effects. The structure was solved by the standard heavy-atom method and refined by the block-diagonal least-squares method, in which the function minimized was $\sum w(|F_o|-|F_c|)^2$ and the equal weight w=1 was adopted for all the reflections. The atomic scattering factors were taken from Ref. 5. All computations were performed on a FACOM M 780 computer at the Computer Center of Kyushu University using UNICS III program system.[6] The final atomic coordinates are given in Table 1. Tables of observed and calculated structure factors, listing of atomic positional and anisotropic thermal parameters, and complete lists of bond distances and angles with their estimated standard deviations have been deposited as Document No. 9101 at the office of the Editor of Bull. Chem. Soc. Jpn.

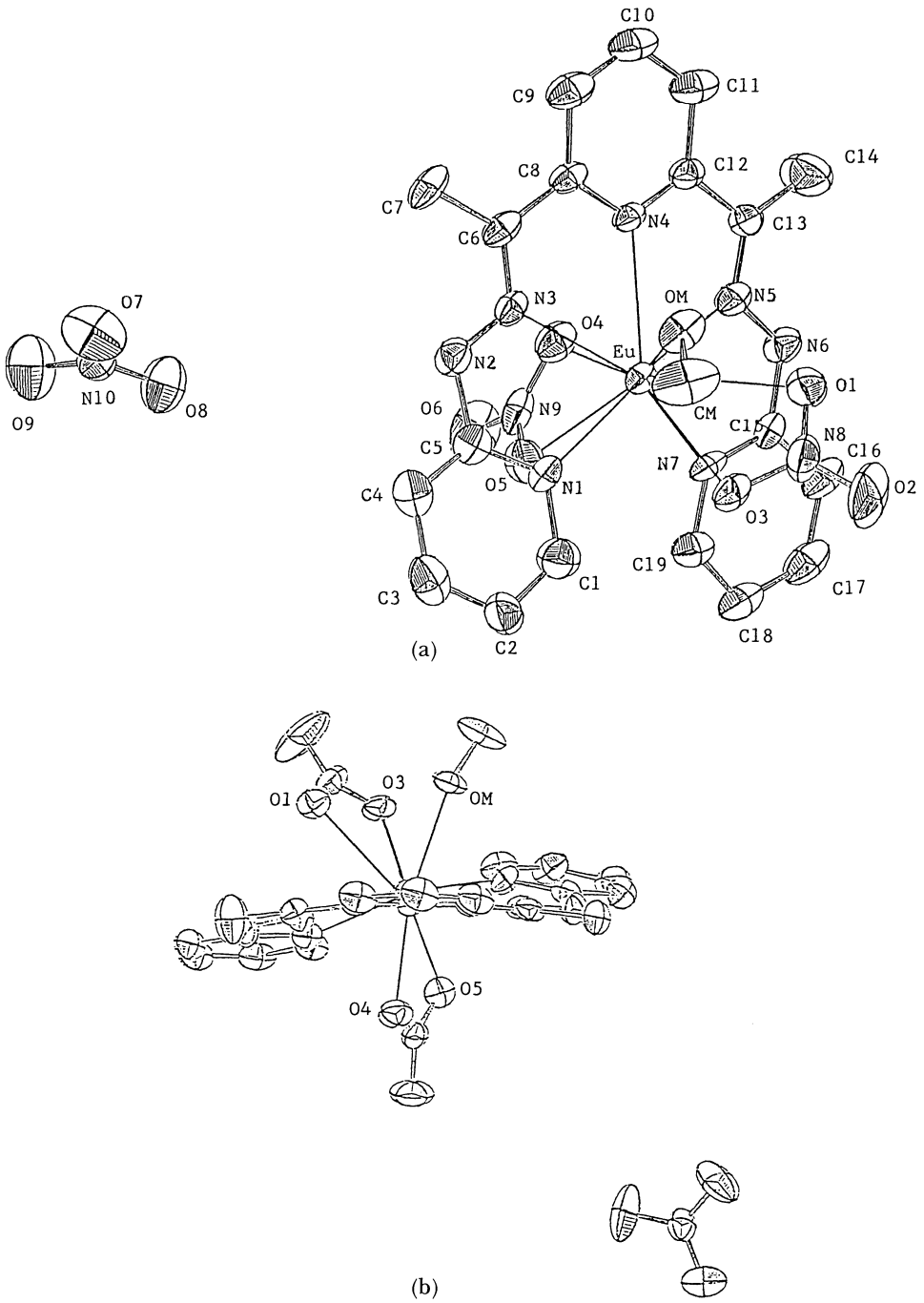

Fig. 1. Molecular structure of $[Eu(NO_3)_2(L)(CH_3OH)]$ NO_3 (a) and the side view (b) drawn by ORTEP.

Table 2. Selected Bond Distances(Å) and Angles(deg)

(a) Bond distance/Å					
Eu-N1	2.566(12)	Eu-N3	2.594(10)	Eu-N4	2.587(10)
Eu-N5	2.579(11)	Eu-N7	2.585(9)	Eu-O1	2.599(9)
Eu-O3	2.503(9)	Eu-O4	2.526(9)	Eu-O5	2.540(9)
Eu-OM	2.516(9)				
(b) Bond angle/deg					
N1-Eu-N3	62.6(3)		N3-Eu-N4	62.7(3)	
N4-Eu-N5	60.9(3)		N5-Eu-N7	62.9(3)	
N1-Eu-N7	109.6(3)		O1-Eu-O3	50.2(3)	
O4-Eu-O5	50.1(3)		Eu-OM-CM	127(1)	

Results and Discussion

Some typical IR bands of the free ligand shifted significantly on complexation: ν(C=N), from 1600 cm^{-1} to 1575 cm^{-1}; skeletal bands of pyridine, from 1565 and 1575 cm^{-1} to 1595 and 1612 cm^{-1}, respectively. The shifts of the skeletal bands toward higher frequencies suggest the coordinations of pyridine rings.[2b,d,e] Two nitrate vibrations were observed around 1450 and 1380 cm^{-1}, suggesting the presence of bidentate and non-coordinating groups within a molecule.[1b,2c-e,3b,7] Electrical conductivity in methanol was 101 $S\,cm^2\,mol^{-1}$, indicating that the complex functions as a 1 : 1 electrolyte in this solvent.[8]

The ORTEP drawing of the complex with atom numbering scheme is shown in Fig. 1. The selected bond distances and angles with standard deviations are given in Table 2.

The X-ray structural result demonstrates that the geometry around the europium(III) ion is of ten-coordination with quinquedentate L, two bidentate nitrate ions, and a methanol oxygen. The quinquedentate ligand L forms the basal coordination plane, in which the atoms N_1, N_3, N_4, N_5, and N_7 deviate by −0.27, 0.30, −0.08, −0.16, and 0.23 Å from the best plane of the basal donor atoms, respectively. The third nitrate ion is free from coordination and captured in the crystal lattice. One of the bidentate nitrate ions is situated on one side of the coordination plane formed by the ligand L, with similar Eu-O4 and Eu-O5 bond distances (2.526 and 2.540 Å, respectively). Another bidentate nitrate ion and the methanol molecule are situated on the other side, with the Eu-O1 and Eu-O3 bond distances of 2.599 and 2.503 Å, respectively, and the Eu-OM distance of 2.516 Å. The Eu-O1 bond is significantly elongated probably because of a steric effect from the neighboring methanol molecule. The Eu-N bond distances fall in the range 2.566—2.594 Å, which are short compared with the Sm-N bond distances (2.620—2.655 Å) found for a samarium(III) complex of 3,6,14,17,23,24-hexaazatricyclo[17.3.1.$1^{8,12}$]tetracosa-1(23),2,6,8,10,12(24),13,17,19,21-decaene[3b] but long on the whole compared with the Gd-N bond distances (2.500—2.606 Å) found for a gadolinium(III) complex of *N,N'*-bis(2-pyridylmethylene)ethylenediamine.[9] This trend is in line with that ionic radii of lanthanoid ions decrease with increasing atomic number (lanthanide contraction), i.e., r(Sm)>r(Eu)>r(Gd).

References

1) a) J. D. J. Backer-Dirks, C. J. Gray, F. A. Hart, M. B. Hursthause, and B. C. Schoop, *J. Chem. Soc., Chem. Commun.*, **1979**, 774; b) A. M. Arif, J. D. J. Backer-Dirks, C. J. Gray, F. A. Hart, and M. B. Hursthouse, *J. Chem. Soc., Dalton Trans.*, **1987**, 1665; c) C. J. Gray and F. A. Hart, *ibid.*, **1987**, 2289.

2) a) W. Radecka-Paryzek, *Inorg. Chim. Acta*, **35**, L349 (1979); **45**, L147 (1980); b) W. Radecka-Paryzek, *ibid.*, **52**, 261 (1981); c) W. Radecka-Paryzek, *ibid.*, **54**, L251 (1981); **109**, L21 (1985); d) W. Radecka-Paryzek and E. Jankowska, *ibid.*, **134**, 179 (1987); e) W. Radecka-Paryzek, E. Jankowska, and E. Luks, *Polyhedron*, **7**, 439 (1988).

3) a) K. K. Abid and D. E. Fenton, *Inorg. Chim. Acta*, **95**, 119 (1984); b) K. K. Abid, D. E. Fenton, U. Casellato, P. A. Vigato, and R. Graziani, *J. Chem. Soc., Dalton Trans.*, **1984**, 351.

4) a) G. Bombieri, F. Benetollo, A. Polo, L. De Cola, D. L. Smailes, and L. M. Vallarino, *Inorg. Chem.*, **25**, 1127 (1986); b) De Cola, D. L. Smailes, and L. M. Vallarino, *ibid.*, **25**, 1729 (1986).

5) "International Tables for X-Ray Crystallography," Kynoch Press, Burmingham, England (1974), Vol. IV.

6) T. Sakurai and K. Kobayashi, *Rikagaku Kenkyusho Houkoku*, **55**, 69 (1979); S. Kawano, *Rep. Comput. Kyushu Univ.*, **13**, 39 (1980).

7) K. Nakamoto, "Infrared and Raman Spectra of Inorganic and Coordination Compounds," 4th ed, John Wiley & Sons, Inc., New York (1986), p. 124 and pp. 254—257.

8) W. J. Geary, *Coord. Chem. Rev.*, **7**, 81 (1971).

9) M.-ul-Haque, F. A. Hart, and C. N. Caughlan, *J. Chem. Soc., Chem. Commun.*, **1970**, 1240; G. D. Smith, C. N. Caughlan, M.-ul-Haque, and F. A. Hart, *Inorg. Chem.*, **12**, 2654 (1973).

Synthetic Inorganic Ion-Exchange Materials LX. Ion Exchange and Chromatographic Separation of Alkali Metal Ions on Cubic Ammonium Molybdate — A Novel Cation Exchanger

Abdul Jabbar KHAN,* Mitsuo ABE, Masamichi TSUJI, and Yasushi KANZAKI
Department of Chemistry, Faculty of Science, Tokyo Institute of Technology, 2-12-1 Ookayama, Meguro-ku, Tokyo 152
(Received August 29, 1990)

Synopsis. The ion-exchange selectivity of H^+-form of cubic ammonium molybdate (H-CAM) was studied for alkali metal ions in both HNO_3 and NH_4NO_3 media. Ideal ion-exchange reaction was observed in both the media with high selectivity for Rb^+ and Cs^+. The selectivity sequence was found to be $Li^+<Na^+<K^+<Rb^+<Cs^+$ in accordance with the Eisenman sequence-1 in both the media, with separation factors greater than the commercial polystyrene strong acid exchange resin. Efficient separation of alkali metal ions could be achieved on H-CAM column.

The inorganic ion-exchange materials possess significant superiority over the commercial organic ion-exchange resins at high temperatures and ionizing radiations. Some of these materials are very selective showing greater exchange capacity for certain metal ions.[1-4] Abe and Ito[5] studied adsorption properties of various metal oxides and hydrous oxides. An insufficient information about the ion-exchange properties of hexavalent metal hydrous oxides could also be found in the literature.[6] The isopolymolybdates and tungstates have been reviewed by Tytko and Glemser.[7] The heteropoly acid salts of molybdenum have been sufficiently worked on for their ion-exchange properties.[8,9] The acid salts and hydrated compounds of Mo(VI) have drawn a considerable interest for their catalytic properties too. However, less attention has been given to the work concerning the ion-exchange properties of these materials.

The previously reported results[10] indicated that cubic ammonium molybdate (CAM), prepared by the reaction of HNO_3 and hexaammonium heptamolybdate under controlled temperature conditions and reagent specifications, showed a reversible NH_4^+/H^+ exchange reaction. This paper describes the ion-exchange behaviour of H^+-form of CAM (H-CAM) cation exchanger along with some chromatographic separations of alkali metal ions.

Experimental

Synthesis of CAM and H-CAM. CAM was synthesized under optimum conditions and reagent specifications by the reaction of hexaammonium heptamolybdate tetrahydrate and HNO_3 (Wako Pure Chemical Ind., Japan) at 60 °C, following the previously described procedure.[10] The H^+ form (H-CAM) was obtained by conditioning CAM with 0.5 M (M=mol dm^{-3}) HNO_3 by using a column. H-CAM was used throughout the investigations reported here.

Rate of Adsorption and Ion-Exchange Selectivity. The rate of adsorption of alkali metal ions on H-CAM was investigated by equilibrating 0.25 g of the exchanger with 25 cm^3 of 10^{-4} M alkali metal ion solutions containing different concentrations of HNO_3 or $*NH_4NO_3$ (*=NH_4NO_3 solutions in 10^{-2} M HNO_3).

The distribution coefficients (K_d) for alkali metal ions were determined batchwise by equilibrating 0.10 g of H-CAM with 10 cm^3 of 10^{-4} M alkali metal ions in different concentrations of HNO_3 or $*NH_4NO_3$ at 30±0.5 °C with intermittent shaking. The metal ion concentrations in the equilibrated solutions were determined by a Varian Techtron-1100 atomic absorption spectrophotometer using air-acetylene flame. The K_d (cm^3 g^{-1}) values were calculated by the following equation,

$$K_d = \frac{\bar{X}}{X} \times \frac{V}{W},$$

where $\bar{X}$ and X are the amounts of metal ion in exchanger and solution respectively. V is the volume of equilibrated solution and W stands for the weight of H-CAM.

Chromatographic Separations. Separations of mixed alkali metal ions were conducted on H-CAM column (2.5—3.5 cm×0.5 cm i.d.). A mixed solution containing 1.0 μmol of each metal ion was loaded at the top of the column, kept for 12—14 h (to assure complete adsorption of metal ions on H-CAM) and then eluted with HNO_3 or $*NH_4NO_3$ solutions of various concentration. A continuous charging of the eluents was carried out through a high-pressure pump (Nihon Seimitsu Kagaku, model NP-DX-2). The effluent fractions were collected with the help of a fraction collector (Ohtake Works, model UM-160) and analyzed for the metal ion concentrations.

Results and Discussion

Specification of CAM and H-CAM. CAM was a yellowish granular material which could be ground even to <40 mesh size. Characterization of CAM and H-CAM showed the same results as reported previously.[10] Both CAM and H-CAM possessed a body-centered cubic structure with crystal lattice of 12.94±0.005 Å. The chemical formulae of CAM and H-CAM could be represented as $[(NH_4)_{0.78}(NH_4)_2]$-$O_{1.39} \cdot 14.16MoO_3 \cdot 6.08H_2O$ and $[H_{0.68}(NH_4)_2]O_{1.34} \cdot 14.16MoO_3 \cdot 6.92H_2O$, respectively. The H^+ of H-CAM was found to be reversibly exchanged with NH_4^+ with an exchange capacity of 0.31 mequiv g^{-1} for the latter ion.[10]

Exchange Equilibria and Ion Selectivity. The time required for the equilibration of alkali metal ions was determined through the rate of sorption of these ions on H-CAM in HNO_3 and $*NH_4NO_3$ media. The exchanger showed a fair rate of adsorption for all the alkali metal ions. The rate of adsorption in $*NH_4NO_3$ medium was slower for all alkali metal ions by one day as compared to HNO_3 medium. The ion-exchange reaction for all the ions was relatively fast in HNO_3 medium, except Na^+. About 1—2 days were required for ion-exchange equilibria of Li^+, K^+, Rb^+, and Cs^+, whereas for Na^+ it took>2 days.

The ion-exchange reaction where the exchange of micro-amounts of n-valent cations (M^{n+}) follows the stiochiometric ion-exchange mechanism rather than specific adsorption, can be represented as follows,

$$n\overline{H^+} \text{ or } n\,\overline{NH_4^+} + M^{n+} \rightleftarrows \overline{M^{n+}} + n\,H^+ \text{ or } n\,NH_4^+, \quad (1)$$

where bar denotes the exchanger phase then,

$$\log K_d = -n \log\{[H^+] \text{ or } [NH_4^+]\} + \text{const.} \quad (2)$$

The log-log plot of K_d vs. [*NH_4NO_3] (Fig. 1) showed a linear relationship with a slope of -1 for all the alkali metal ions indicating the 1:1 ideal ion-exchange reaction with greater separation factors. The selectivity increased in the order of $Li^+ < Na^+ < K^+ < Rb^+ < Cs^+$ in accordance with the Eisenman sequence-1.[11]

The above mentioned requirements (Eq. 2), however, are not always met with, either due to the nature of the exchanger[12] or the nature of the small number of groups (contained in the exchanger) which interact specifically with the trace ion.[13] The log-log plot of K_d vs. [HNO_3] (Fig. 2-dotted lines) was also linear with a slope of -1 for all the alkali metal ions except K^+. The selectivity sequence was found to be the same as in *NH_4NO_3 medium with very high K_d values for Rb^+ and Cs^+ even in 8.0 M HNO_3 solution. For K^+ the slope was observed to be <-1 due to its greater exchange affinity for the structural NH_4^+ in H-CAM (irrespective of H^+ concentration of equilibrated K^+ solution) owing to the almost same crystal ionic radii,[14,15] The most probable ion-exchange reaction of the K^+ could be described as,

$$\overline{H^+} + K^+ \rightleftarrows \overline{K^+} + H^+, \quad (3)$$

$$\overline{NH_4^+} + K^+ \rightleftarrows \overline{K^+} + NH_4^+, \quad (4)$$

where $\overline{NH_4^+}$ represents the structural NH_4^+ in H-CAM.

A fractional contribution of the process (4) seems to be responsible for the slope of <-1 for K^+ exchange. Almost same behaviour was expected for Rb^+ too, however the selectivity of ions at SA-site seems to be different for K^+ and Rb^+ (or Cs^+) at low metal ion concentration. The ideal exchange of K^+ (slope -1) and greater separation factor for Rb^+ and Cs^+ in *NH_4NO_3 medium may also be due to the same fact mentioned above. The K_d and separation factors for the alkali metal ions in both the media were found to be greater than that of ion-exchange resin (Table 1).

The K_d values for all the alkali metal ions were observed to be inversely dependent on the initial concentrations of metal ions (Fig. 2) indicating the Langmuir-type ion-exchange reaction.[17] The log-log plots of K_d vs. $[H^+]$ were linear indicating an ideal exchange reaction, however the slope of plots decreased than unity with increasing metal ion concentration. This fact can be explained on the basis of following equations. For the ion-exchange reaction,

$$n\overline{H^+} + M^{n+} \rightleftarrows \overline{M^{n+}} + nH^+, \quad (5)$$

where bar represents the exchanger phase and M^{n+} as n-valent cation, at lower $[M^{n+}]$ e.g. 10^{-4} M $[M^{n+}]$, $[H^+]^n \gg [M^{n+}]$ and $\overline{[H^+]^n} \gg \overline{[M^{n+}]}$ then,

$$K_d = \text{constant} \times \frac{1}{[H^+]^n}, \quad (6)$$

and the slope of equation (6)$=-1$ if $n=1$. However, when $[M^{n+}]$ increases e.g. $10^{-3} \rightarrow 10^{-2}$ etc, $\overline{[M^{n+}]} \gg \overline{[H^+]^n}$ and $\overline{[H^+]^n}$ is a variable depending on $\overline{[M^{n+}]}$ then,

$$K_d = \text{constant} \times \frac{\overline{[H^+]^n}}{[H^+]^n}, \quad (7)$$

and slope of equation (7)<-1 depending on the increase in metal ion concentration.

Similar observations have also been reported by Abe et al.[12,18,19] in the ion-exchange isotherms for some inorganic ion exchangers. This fact indicated the rigid structure of H-CAM. Moreover, the strong dependence of K_d on initial metal ion concentration (Fig. 2) which was observed to be stronger for K^+, Rb^+, and Cs^+ shows that, besides the ordinary exchange site {H^+-site or H^+ exchangeable NH_4^+-site (EA-site) in CAM}, H-CAM also contain an additional functional group {structural NH_4^+-site (SA-site)} of high affinity to certain cations e.g. K^+, Rb^+, and Cs^+.

Chromatographic Separations. In view of the K_d values and separation factors for the neighboring ion pairs, separation of alkali ions was carried out with both HNO_3 and *NH_4NO_3 solutions (eluents) of different concentrations at ambient temperature.

Table 1. K_d Values and Separation Factors (α)[a] on H-CAM and BIO-RAD AG 50W-X8[16]

Exchanger	Medium	Parameter	Li		Na		K		Rb		Cs
H-CAM	1 M HNO_3	K_d	1.23×10^{-1} [b]		2.46		6.86×10^2		1.56×10^4		2.0×10^4
		α		2.0×10^2		28		22.8		1.2	
	0.01 M NH_4NO_3 + 0.01 M HNO_3	K_d	*7.2×10^{-3} [b]		6.0		4.9×10		6.4×10^2		4.6×10^3
		α		8.3×10^2		8.2		13.0		7.2	
BIO-RAD AG 50W-X8	1 M HNO_3	K_d	3.9		6.3		11.4		13.4		16.8
		α		1.6		1.8		1.1		1.2	

a) $\alpha = K_{dB}/K_{dA}$. b) Extrapolated values to 1.0 M HNO_3.

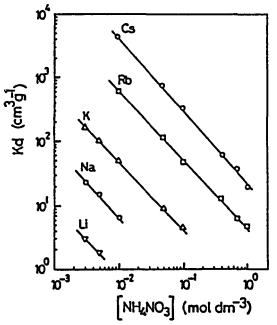

Fig. 1. Distribution coefficients (K_d) for alkali metal ions on H-CAM as a function of [NH_4NO_3] (contained in 0.01 M HNO_3). H-CAM: 0.10 g, Init. [M^+]: 10^{-4} M, Soln vol: 10 cm^3, Temp: 30±0.5 °C.

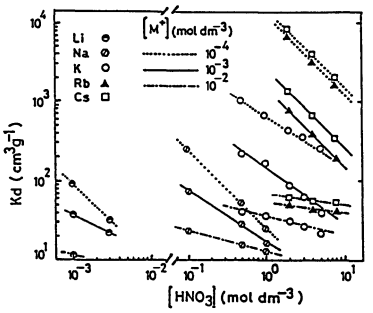

Fig. 2. Distribution coefficients (K_d) for alkali metal ions on H-CAM as a function of HNO_3 concentration and dependence of K_d on the initial concentrations of metal ions. H-CAM: 0.10 g, Soln vol: 10 cm^3, Temp: 30±0.5 °C.

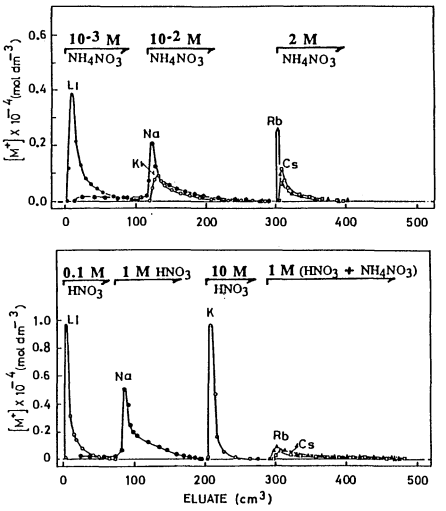

Fig. 3. Chromatographic separations of alkali metal ions on H-CAM. Top—Eluent: NH_4NO_3 soln (in 0.01 M HNO_3), H-CAM: 0.7637 g., Bottom—Eluent: HNO_3, H-CAM: 0.9209 g, Loading: 1 μmol of each M^+, Flow rate: 0.05 $cm^3\,min^{-1}$.

Figure 3(top) indicates the separation chromatogram with *NH_4NO_3 as an eluent. Li^+ was separated with 99% recovery from the Na^+-K^+ and Rb^+-Cs^+ groups with tailing rears. A long leading front was also observed for Na^+.

Successful separation of Li^+, Na^+, and K^+ with a respective recovery of 99.9, 100, and 82% was achieved with HNO_3 of different concentrations (Fig. 3-bottom). A tailing rear was observed for all the ions and long leading front for Na^+ in addition to the tailing rear. The long leading front for Na^+ was observed to be due to some solubility of H-CAM in HNO_3 eluent as well as slow rate of adsorption of the ion on H-CAM.

It has been known that the shape of elution curve depends on the type of ion-exchange isotherm.[20] The retention time may be a function of loading on the exchanger. The peak with a sharp front and a tailing rear (Langmuir type) for the alkali metal ions in the elution curves were evident from the strong dependence of K_d on the initial concentrations of metal ions (Fig. 2).

Complete separation of Rb^+ and Cs^+ was not possible even with concentrated HNO_3 or *NH_4NO_3 solutions. However the recovery of these ions in a mixed eluent {1 M (NH_4NO_3+HNO_3)} was better. The low recovery of Rb^+ (35%) and Cs^+ (25%) with 2.0 M *NH_4NO_3 and 60% and 54% respectively with the mixed eluent may be due to migration of these ions to the less accessible sites, or alternatively that strong bonding forces are involved for low loading.

In conclusion H-CAM (or CAM) can be used as a selective cation exchanger for heavy alkali metal ions even at higher acid concentrations. The very high selectivity of H-CAM towards Cs^+ will enable the latter to be quantitatively removed from the nuclear wastes, rain (fall-out Cs) or even sea water despite a large amount of matrix to Cs^+. It can work as a reliable material for the solid state storage of radioactive cesium at lower cost. H-CAM can be employed to separate K^+ and Rb^+ efficiently which are usualy difficult to do on some of the inorganic ion exchangers.

References

1) M. Abe, in "Inorganic Ion Exchange Materials," ed by A. Clearfield, CRC Press, Boca Raton, FL. (1982), pp. 160 and 190.
2) C. B. Amphlett, "Inorganic Ion Exchangers," Elsevier Pub. Co., N. Y. (1964).
3) V. Vesely and V. Pekarek, *Talanta*, **19**, 219 (1972).
4) A. K. De and A. K. Sen, *Sep. Sci. Tech.*, **13**, 517 (1978).
5) M. Abe and T. Ito, *Kogyo Kagaku Zasshi*, **86**, 817 (1965).
6) A. K. De and N. D. Chowdhary, *Chromatographia*, **11**, 586 (1978).
7) K. Tytko and O. Glemser, *Adv. Inorg. Chem. Radiochem.*, **19**, 239 (1976).
8) V. Pekarek and V. Vesely, *Talanta*, **19**, 1245 (1972).
9) A. Clearfield, G. H. Noncollas, and R. H. Blessing, in "Ion Exchange and Solvent Extraction," ed by J. A. Marinsky and Y. Marcus, Marcel Dekker, N. Y. (1973), Vol. 5, p. 69.
10) A. J. Khan, M. Tsuji, and M. Abe, *Bull. Chem. Soc. Jpn.*, **62**, 3457 (1989).
11) G. Eisenman, *Biophys. J.*, **2**, 259 (1962).
12) M. Abe, M. Tsuji, S. P. Qureshi, and H. Uchikoshi, *Chromatographia*, **13**, 626 (1980).
13) F. Helfferich, "Ion Exchange," McGraw-Hill, N. Y. (1962), pp. 153—155.
14) R. D. Shannon, *Acta Cryst., Sect. A*, **32**, 751 (1976); R. D. Shannon and C. T. Prewitt, *ibid., Sect. B*, **25**, 925 (1969).
15) R. M. Barrer, R. Pardopoulos, and L. V. C. Rees, *J. Inorg. Nucl. Chem.*, **29**, 2047 (1967).
16) F. W. E. Strelow, R. Rethemeyer, and C. J. C. Bothma, *Anal. Chem.*, **37**, 106 (1965).
17) K. Dorfner, "Ion Exchangers—Properties and Applications," Ann Arbor Sci. Pub. Inc., Michigan (1972), pp. 198 and 205.
18) M. Abe, E. A. A. Ichsan, and K. Hayashi, *Anal. Chem.*, **52**, 524 (1980).
19) M. Abe and K. Uno, *Sep. Sci. Tech.*, **14**, 355 (1979).
20) J. A. Dean, "Chemical Separation Methods," Van Norstrand Reinhold Co., N. Y. (1969), p. 66.

A Polarographic Study of the Glycine Complexes of Copper(II), Lead(II), Cadmium(II), and Manganese(II)

Hiroshi YAMASHITA,* Toru NOZAKI, Yoshihito FUKUDA, and Toshiyuki KABATA
Department of Resources Chemistry, Faculty of Engineering, Ehime University, Bunkyo-cho, Matsuyama 790
(Received September 10, 1990)

Synopsis. From the polarographic behavior of copper (II), lead(II), cadmium(II), and manganese(II) in aqueous glycine solutions at an ionic strength of 0.4 mol dm^{-3} adjusted with sodium perchlorate, the species of the metal complexes and their stability constants were determined.

Glycine (abbreviated to HL) is included in industrial waste solutions treated by the hydrolysis of protein. Many studies[1,2] on both the compositions and stability constants of the glycine complexes have been carried out by means of a pH titration method, polarography, calorimetry, etc. However, both the species and the stability constants of the mixed-ligand hydroxo-complexes have remained unknown.

In the present work, both the species and stability constants were determined by means of polarography with respect to the copper(II), lead(II), cadmium(II), and manganese(II) complexes. From the experimental results, it is pointed out that those complexes would be formed within high pH ranges.

Experimental

Apparatus. Current-potential curves were obtained using Yanagimoto (Model PA-102) polarographic analyzer. The used dropping mercury-electrodes (DME) had mercury flow rates (m) of 1.273 to 2.758 mg s^{-1}. The drop time (t) was between 2.70 and 5.82 s in distilled water at −1.0 V vs. SCE. The mercury reservoir was 60 cm in height. The DME potential was referred to at the saturated calomel electrode (SCE). The temperatures of the solutions were maintained by the use of a water thermostat at 25±0.1 °C. High-purity nitrogen gas was bubbled through the solutions in order to remove any oxygen gas dissolved in the solutions. The pH values of the solutions were measured after polarographic measurements with a Toa Electronics Ltd. (Model HM-30S) pH meter.

Reagents. Stock solutions of metal ions were prepared by converting metal nitrates into perchlorates with perchloric acid, which had been redistilled under 50—70 mmHg (1 mmHg=133.322 Pa) at 40 °C. The solutions were diluted to a constant volume with redistilled water and were standardized by chelatometric titration with EDTA. A standard solution of glycine was prepared by dissolving a weighed amount of glycine in redistilled water.

Procedures. Acid dissociation-constants of glycine were measured by means of pH titration[3] at an ionic strength of 0.4 mol dm^{-3} and 25 °C. Both the compositions and stability constants of the glycine complexes were determined by a dc polarographic method under the following conditions: an ionic strength of 0.4 mol dm^{-3}; a metal concentration of 8.0×10^{-5} mol dm^{-3}; glycine concentrations from 8.0×10^{-3} to 2.0×10^{-1} mol dm^{-3}, and a temperature of 25 °C. The ionic strengths of the solutions were adjusted with sodium perchlorate.

Results and Discussion

Reversibility of the Electrode Reactions. The reversibility of the electrode reaction was tested under the following conditions: in the cadmium(II) system, pH values from 2.4 to 12.5; in the manganese(II) system, from 6.3 to 9.1; in the copper(II) system, both from 2.1 to 4.0 and from 8.0 to 12.7; and in the lead(II) system, both from 2.1 to 7.0 and from 11.5 to 12.4.

As mentioned in the procedues section, plots of the potential (E) vs. $\log i/(i_l-i)$ exhibited straight lines under the experimental conditions with respect to polarograms of copper, lead, cadmium, and manganese in the aqueous glycine solutions. The slopes of the lines were from 29.0 to 33.2 mV of the potential so that electrode reactions could be regarded as reversible.

Compositions and Stability Constants of the Complexes. At constant metal and glycine concentrations, the dependence of the half-wave potential, $E_{1/2}$, on the pH is shown in Fig. 1. In the ranges of the dashed lines in Fig. 1, polarograms of the complexes could not to be analyzed due to both poor reversibility in the copper system and the formation of a precipite in the lead system. The half-wave potential, $E_{1/2}$, shifted more negatively with increasing pH, and reached a constant value in the high pH ranges. Beyond about 12.0, the potential, moreover, shifted negatively. In Fig. 2 at pH>12.0, the dependence of the half-wave potential on the pH is shown for various glycine concentrations. From their results, it is

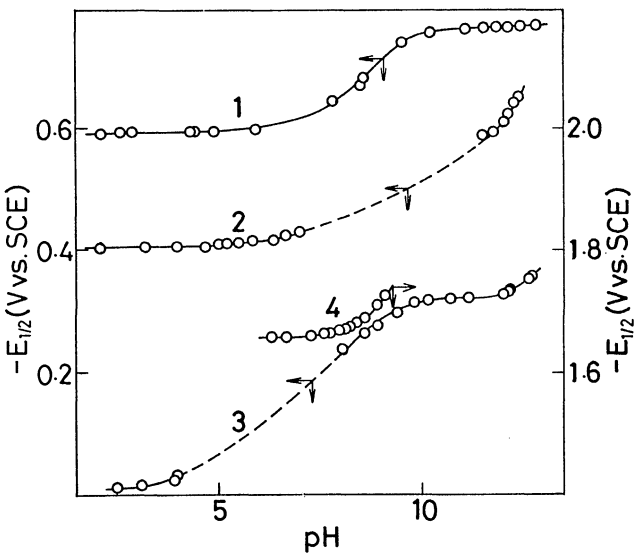

Fig. 1. Effect of pH on the half-wave potential ($-E_{1/2}$).
1: Cd(II), 2: Pb(II), 3: Cu(II), 4: Mn(II), [M(II)]= 8.0×10^{-5} mol dm^{-3}.
[Glycine] (mol dm^{-3}) 1 : 4.0×10^{-2}, 2 : 8.0×10^{-3}, 3 : 4.0×10^{-3}, 4 : 2.0×10^{-1}.
I=0.4 mol dm^{-3}, 25 °C.

Table 1. Stability Constants of Complexes (I=0.4 mol dm^{-3}, 25 °C)

$\log \beta_{ij}$	Cu(II)	Pb(II)	Cd(II)	Mn(II)
ML	8.26±0.1 8.46(I=0.2)[a] 8.14±0.02(I=0.5)[b]	5.3±0.1 5.11(I=1.0)[a] 5.47(I=0)[b]	4.94±0.1 6.0(I=0.1)[a] 4.14(I=1.0)[b]	0.94±0.2 2.65(I=0.5)[a]
ML_2	15.42±0.1 15.29(I=0.2)[a] 14.97±0.1(I=0.5)[b]	7.8±0.1 7.08(I=1.0)[a] 8.86(I=0)[b]	8.30±0.1 8.08(I=1.0)[a] 7.60(I=1.0)[b]	4.7(I=0.5)[a]
ML_3	17.34±0.1 16.25(I=0.1)[a]	10.0±0.1	9.73±0.1 9.78(I=1.0)[a] 9.74(I=1.0)[b]	
M(OH)L	14.59±0.1	9.9±0.1	6.57±0.1	6.65±0.2
$M(OH)L_2$	17.31±0.1	11.1±0.1	9.59±0.1 9.27(I=1.0)[a]	
$M(OH)_2L$	15.86±0.1	12.7±0.1	9.31±0.1	
$M(OH)_2L_2$	18.85±0.1	13.6±0.1	11.81±0.1	
$M(OH)_3L$	17.85±0.1	14.7±0.1		
$M(OH)_4L$		17.3±0.1		

a) Ref. 1. b) Ref. 2.

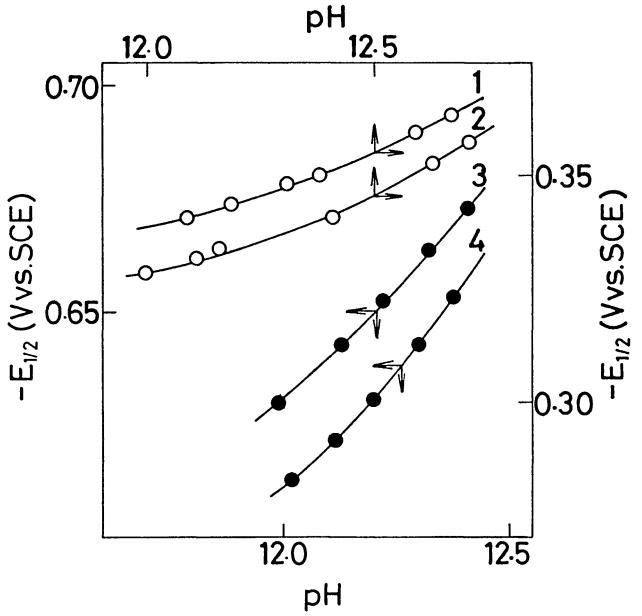

Fig. 2. Effect of pH on the half-wave potential ($-E_{1/2}$).
○: Cu(II), ●: Pb(II), [M(II)]=8.0×10^{-5} mol dm^{-3}.
[Glycine] (mol dm^{-3}) 1: 6.0×10^{-3}, 2: 4.0×10^{-3}, 3: 3.0×10^{-2}, 4: 8.0×10^{-3}.
I=0.4 mol dm^{-3}, 25 °C.

considered that mixed-ligand hydroxo-complexes coordinated both L^- and OH^- to their metals, according to Eq. 1. Therefore, both the compositions and over-all stability constants, β_{ij}, of mixed complexes were determined as described previously.[4] In this method, Eq. 2 was used while also applying the Schaap's equation:[5]

$$M^{2+} + iOH^- + jL^- \rightleftarrows M(OH)_iL_j^{2-(i+j)} \quad (1)$$

$$F_{00}(OH, L) \equiv \sum \beta_{ij}[OH]^i[L]^j = \text{antilog}[0.435(nF/RT)\{(E_{1/2})_s - (E_{1/2})_c\} + \log I_s/I_c], \quad (2)$$

where $(E_{1/2})_s$ is the half-wave potential of simple metal ions, $(E_{1/2})_c$ is the potential of the metal complexes, I_s is the diffusion current-constants of the metal ions, and I_c is a constant of the metal complexes. By considering the coordination number of metal ions, OH^- and L^-, the values of β_{ij} were determined by a previously described method.[4] Both the compositions and stability constants of the complexes, thus obtained in this work, are shown in Table 1 together with the values obtained in the literature. The β_{ij} values of copper(II), lead(II), and cadmium(II) were in fair agreement with the values found in the literature. The complexing ability of glycine with their metals increased in the following order: manganese(II)< cadmium(II)<lead(II)<copper(II). From the results, it is considered that the reactivity of glycine with its metals contributed to the electrostatic effect.

References

1) L. G. Sillén and A. E. Martell, "Stability Constants of Metal-Ion Complexes," Supplement No. 1, Chem. Soc., London (1971), pp. 265—268.
2) A. E. Martell and R. M. Smith, "Critical Stability Constants," Plenum Press, New York and London (1982), Vol. 1, p. 1 and 2.
3) S. Chaberek and A. E. Martell, *J. Am. Chem. Soc.*, **74**, 5052 (1952).
4) T. Nozaki, M. Sakamoto, J. Nakaki, and M. Miyake, *Nippon Kagaku Kaishi*, **1979**, 891.
5) W. B. Schaap and D. L. McMasters, *J. Am. Chem. Soc.*, **83**,4699 (1961).

A New Type of Reductive Cleavage of Disulfide in Quadruply ortho-Substituted Diphenyl Disulfide by Neighboring Thiolate Anion

Hisashi FUJIHARA,* Jer-Jye CHIU, and Naomichi FURUKAWA*
Department of Chemistry, University of Tsukuba, Tsukuba, Ibaraki 305
(Received August 1, 1990)

Synopsis. The reaction of bis[2,6-bis(bromomethyl)-phenyl] disulfide with thiourea or sodium sulfide showed an unusual reductive cleavage of disulfide linkage with elimination of bromine by neighboring-group participation of the generated thiolate anion. Its reaction gave the structurally intriguing thiols which indicated the facile anodic oxidation.

Studies of intramolecular interactions and reactions have provided numerous informations on the structures and reactivities of linear and cyclic compounds containing sulfur atoms.[1-3] It has been reported that the oxidative cleavage of disulfides having neighboring nucleophiles (e.g., amide) provides a facile route to the formation of heterocyclic intermediates and products.[4] The intramolecular redox reactions between disulfides and thiols are of considerable important from a biological point of view.[5] Meanwhile, we described an unusual sulfur extrusion in a new quadruply ortho-bridged biphenyl compounds with disulfide linkage, methanodithiomethano-bridged dibenzotrithionin, via the sulfur-sulfur bond formation.[6] Its analogous compounds exhibit interesting physical and chemical properties on account of their unique arrangement of functional groups and heteroatoms in space. This paper presents that the reaction of bis[2,6-bis(bromomethyl)phenyl] disulfide (**1**) with thiourea gave the structurally interesting redox products, thiol-disulfide and trithiol, with the elimination of bromine. The electrochemical and chemical oxidations of their thiols are also described.

The compound **1** was prepared by photobromination using *N*-bromosuccinimide of bis(2,6-dimethyl-

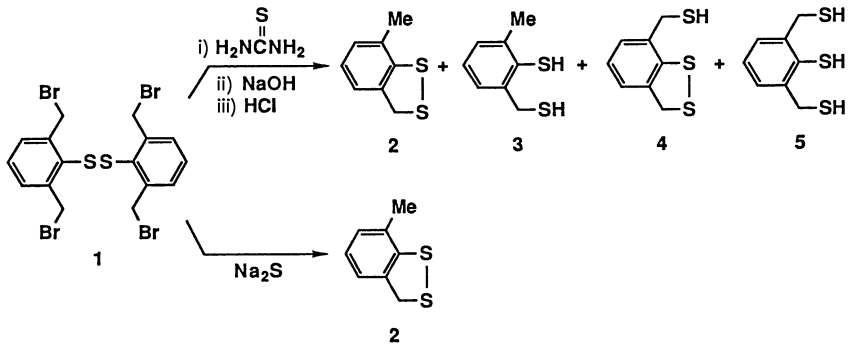

Scheme 1.

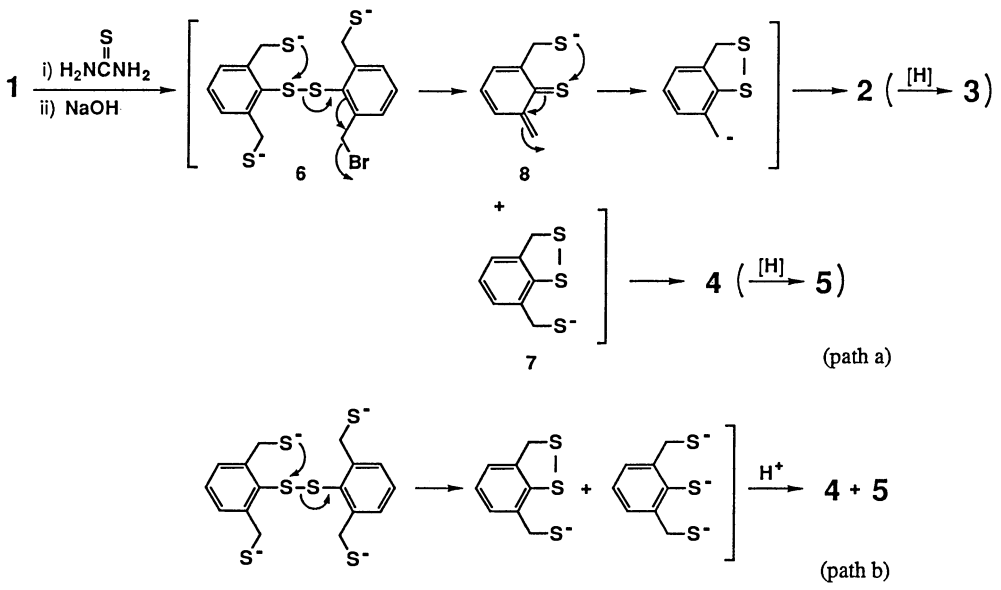

Scheme 2.

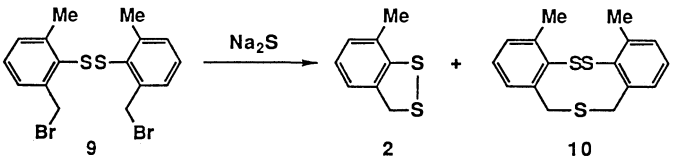

Scheme 3.

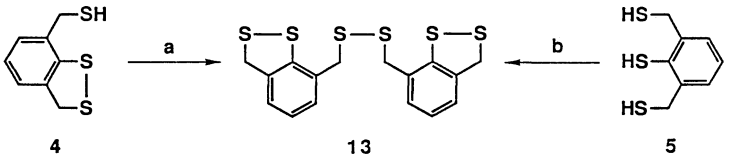

Scheme 4. a) pyridine in $CHCl_3$ under air, b) I_2, Et_3N in $CHCl_3$.

phenyl) disulfide (**14**) which was obtained by oxidation of 2,6-dimethylbenzenethiol with I_2. The reduction of disulfide linkage in **1** was found in the following reactions (Scheme 1). Treatment of **1** with thiourea in ethanol, followed by adding with aqueous sodium hydroxide solution, resulted in formation of four products, disulfide **2** (19%), dithiol **3** (27%), thioldisulfide **4** (18%), and trithiol **5** (25%). The plausible mechanism for formation of the compounds **2**—**5** can be explained as follows (Scheme 2). The reaction of **1** with thiourea produces the thiol **6** via isothiouronium salt whose third stage proceeds intramolecularly and leads to formation of the cyclic disulfide **7** and thione intermediate **8** like quinodimethane with the elimination of bromine. Subsequently, **8** converts to **2** and **3**, and **7** changes finally to **4** and **5**, respectively (Scheme 2, path a). The path b in Scheme 2 is also conceivable mechanism for the formation of **4** and **5**.

On the other hand, when the compound **1** was allowed to react with Na_2S in the presence of tetrabutylammonium bromide as a phase-transfer catalyst in benzene-water at 80 °C for 8 h, disulfide **2** was obtained in 38% yield (Scheme 1). This reaction may proceed likely as shown in Scheme 2.

Meanwhile, bis(2-bromomethyl-6-methylphenyl) disulfide (**9**) was reacted with Na_2S to give the cyclic disulfide **2** (45%) and the nine-membered ring, dibenzotrithionin **10** (14%) (Scheme 3).

The electrochemical oxidations of thiols (**3**, **5**, **11**, and **12**) were studied by cyclic voltammetry. Peak potentials of the first oxidation peak were determined at a glassy carbon working electrode (scan rate; 100 $mV\,s^{-1}$) in CH_3CN-0.1 M $NaClO_4$ vs. Ag/0.01 M $AgNO_3$ as reference electrode (1 M=1 $mol\,dm^{-3}$). The peak potentials (E_p) showed the following values: 0.78 V for **3**, 0.75 V for **5**, 1.35 V for **11**, and 1.52 V for **12**. These anodic oxidations were irreversible at scan rates of 1 $V\,s^{-1}$. There are dramatic shifts in the peak potentials toward more cathodic values for the thiols **3** and **5**. Comparison of the thiols **5** with **11** showed a peak potential ca. 600 mV more cathodic for the former, indicating that **5** is oxidized more readily.

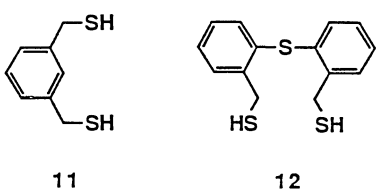

Structural Formula 1.

The oxidation of **4** in the presence of pyridine in chloroform under air at room temperature gave the oxidative dimer **13** in 74% yield (Scheme 4). Trithiol **5** also afforded the oxidation product **13** in 91% yield upon treatment with I_2 in the presence of triethylamine in chloroform at room temperature.

Experimental

^1H and ^{13}C NMR spectra were measured on Hitachi R-600 FT-NMR and Bruker AM 500 spectrometer. The IR spectra were obtained on JASCO A-3 spectrometer. Mass spectra were taken by Hitachi M-80B mass spectrometer. Elemental analyses were carried out by the Chemical Analytical Center at University. For cyclic voltammetry measurements, a Hokuto Denko Co. Model HB-104 electrochemical apparatus was used in conjunction with a Yokokawa Co. Model 3025A X-Y recorder.

Bis(2,6-dimethylphenyl)disulfide (14). To a stirred solution of 2,6-dimethylbenzenethiol[3a] (44.5 g, 0.32 mol) and triethylamine (32.6 g, 0.32 mol) in chloroform (500 ml) was added a solution of iodine (40.6 g, 0.16 mol) in chloroform (150 ml) at 0 °C. The whole mixture was stirred at room temperature for 1 h. The mixture was washed with aqueous sodium thiosulfate solution and the organic layer was dried over anhydrous $MgSO_4$. After evaporation of the solvent, the residue was purified by silica-gel column chromatography (eluent, hexane) to give the disulfide **14** in 89% yield. The compound **14** was recrystallized from hexane: White crystals; mp 103—104 °C; ^1H NMR ($CDCl_3$) δ=2.22 (s, 12H, CH_3) and 7.02 (br s, 6H, ArH). Found: C, 69.99; H, 6.57; S, 23.40%. Calcd for $C_{16}H_{18}S_2$: C, 70.02; H, 6.61; S, 23.36%.

Bis[2,6-bis(bromomethyl)phenyl]disulfide (1) and Bis(2-bromomethyl-6-methylphenyl)disulfide (9). A solution of disulfide **14** (7 g, 25.5 mmol) and *N*-bromosuccinimide (NBS; 18.2 g, 102 mol) in dry carbon tetrachloride (150 ml) was stirred under an Ar atmosphere at 15 °C while being irradiated with a high-pressure mercury lamp for 7 h. The resulting solid was separated by filtration, and the filtrate was concentrated under reduced pressure. The residue was purified by silica-gel column chromatography (eluent, hex-

ane-$CHCl_3$=1 : 1) to afford the tetrabromide **1** in 11% and bisbromide **9** in 52% yields.

1: White crystals; mp 186.5—187 °C; ^{1}H NMR (500 MHz, $CDCl_3$) δ=4.42 (s, 8H, CH_2), 7.38 (t, J=8 Hz, 2H, ArH), and 7.45 (d, J=8 Hz, 4H, ArH); ^{13}C NMR (125 MHz, $CDCl_3$) δ=31.3, 131.2, 131.6, 134.4, and 143.5. Found: C, 32.60; H, 2.64%. Calcd for $C_{16}H_{14}Br_4S_2$: C, 32.57; H, 2.39%.

9: White crystals; mp 121—121.5 °C; MS m/z 432 (M^+); ^{1}H NMR ($CDCl_3$) δ=2.40 (s, 6H, CH_3), 4.25 (s, 4H, CH_2), and 7.22 (s, 6H, ArH). Found: C, 44.11; H, 3.61%. Calcd for $C_{16}H_{16}Br_2S_2$: C, 44.46; H, 3.73%.

Reaction of Bis[2,6-bis(bromomethyl)phenyl]disulfide (1) with Thiourea. A solution of **1** (750 mg, 1.25 mmol) and thiourea (490 mg, 6.40 mmol) in ethanol (500 ml) was stirred for 12 h under reflux. After concentration of the solution, 6% sodium hydroxide solution (1 l) was added to the residue. The mixture was refluxed for 8 h under an Ar atmosphere and then cooled in an ice-water bath; cooled aqueous hydrochloric acid was then added dropwise. The reaction mixture was extracted with chloroform and the extract was dried over $MgSO_4$. After removal of the solvent, the residue was separated by silica-gel column chromatography (eluent, hexane-$CHCl_3$=1 : 1) and further purified by preparative liquid chromatography to give disulfide **2** in 19%, dithiol **3** in 27%, thiol-disulfide **4** in 18%, and trithiol **5** in 25% yields. Yields of **2—5** are in 1/2 mol%.

2: Yellow oil; MS, m/z 168 (M^+); ^{1}H NMR (500 MHz, $CDCl_3$) δ=2.31 (s, 3H, CH_3), 4.49 (s, 2H, CH_2), 6.96 (d, J=7 Hz, 1H, ArH); 7.00 (t, J=7 Hz, 1H, ArH), and 7.09 (d, J=7 Hz, 1H, ArH); ^{13}C NMR (125 MHz, $CDCl_3$) δ=21.2, 44.1, 122.0, 125.5, 128.4, 132.7, 138.8, and 141.7. Found: C, 56.75; H, 4.75%. Calcd for $C_8H_8S_2$: C, 57.10; H, 4.79%.

3: Yellow oil; MS, m/z 170 (M^+); ^{1}H NMR (500 MHz, $CDCl_3$) δ=1.86 (t, J=7 Hz, 1H, SH), 2.40 (s, 3H, CH_3), 3.61 (s, 1H, SH), 3.67 (d, J=7 Hz, 2H, CH_2), 7.06 (t, J=7 Hz, 1H, ArH), 7.10 (d, J=7 Hz, 1H, ArH), and 7.13 (d, J=7 Hz, 1H, ArH); ^{13}C NMR (125 MHz, $CDCl_3$) δ=22.2, 29.2, 126.0, 127.0, 129.3, 130.1, 138.3, and 139.9. Found: C, 56.46; H, 5.82%. Calcd for $C_8H_{10}S_2$: C, 56.43; H, 5.92%.

4; Yellow oil; MS, m/z 200 (M^+); ^{1}H NMR (500 MHz, $CDCl_3$) δ=1.67 (t, J=7 Hz, 1H, SH), 3.75 (d, J=7 Hz, 2H, CH_2SH), 4.47 (s, 2H, CH_2), 7.04 (t, J=7 Hz, 1H, ArH), 7.10 (d, J=7 Hz, 1H, ArH), and 7.17 (d, J=7 Hz, 1H, ArH); ^{13}C NMR (125 MHz, $CDCl_3$) δ=28.9, 43.7, 123.4, 126.0, 127.2, 136.2, 140.5, and 141.4. Found: C, 47.92; H, 3.89%. Calcd for $C_8H_8S_3$: C, 47.96; H, 4.03%.

5: Yellow oil; MS, m/z 202 (M^+); ^{1}H NMR (500 MHz, $CDCl_3$) δ=1.88 (t J=7 Hz, 2H, SH), 3.92 (d J=7 Hz, 4H, CH_2), 4.10 (s, 1H, SH), 7.14 (t, J=7 Hz, 1H, ArH), and 7.21 (d, J=7 Hz, 2H, ArH); ^{13}C NMR (125 MHz, $CDCl_3$) δ=29.1, 126.0, 127.0, 128.4, 129.4, and 141.9. Found: C, 47.58; H, 4.94%. Calcd for $C_8H_8S_3$: C, 47.49; H, 4.98%.

Reaction of Bis[2,6-bis(bromomethyl)phenyl]disulfide (1) with Sodium Sulfide. To a solution of **1** (5 g, 8.5 mmol) and tetrabutylammonium bromide (0.27 g, 0.85 mmol) in benzene (1000 ml) and water (50 ml) was added a solution of sodium sulfide (6.36 g, 25.5 mmol) in water (150 ml). The reaction mixture was stirred at 80 °C for 8 h. The organic layer was separated, washed with water, and dried over $MgSO_4$. After removal of the solvent, the residue was separated by silica-gel column chromatography (eluent, $CHCl_3$) and further purified by preparative liquid chromatography to afford disulfide **2** in 38% yield. Yield of **2** is in 1/2 mol%.

Reaction of Bis(2-bromomethyl-6-methylphenyl)disulfide (9) with Sodium Sulfide. The reaction was performed according to the method described in the reaction of **1** with sodium sulfide. The compound **2** and dibenzotrithionin **10** were obtained in 45% and in 14% yields, respectively. Yield of **2** is in 1/2 mol%, while yield of **10** is in mol%.

10: Off white crystals; mp 140—141 °C; MS m/z 304 (M^+); ^{1}H NMR ($CDCl_3$) δ=2.64 (s, 6H, CH_3), 4.10 (s, 4H, CH_2), and 6.85—7.34 (m, 6H, ArH). Found: C, 63.39; H, 5.32%. Calcd for $C_{16}H_{16}S_3$: C, 63.12; H, 5.30%.

Oxidation of Thiol-Disulfide 4. A solution of **4** (50 mg, 0.25 mmol) and pyridine (39.5 mg, 0.5 mmol) in chloroform (30 ml) was stirred for 12 h under air. After removal of the solvent, the crude product was purified by preparative liquid chromatography to give the compound **13** in 74% yield: Yellow oil; ^{1}H NMR (500 MHz, $CDCl_3$) δ=3.72 (s, 4H, CH_2), 4.46 (s, 4H, CH_2), 7.01 (d, J=7 Hz, 2H, ArH), 7.07 (t, J=7 Hz, 2H, ArH), and 7.20 (d, J=7 Hz, 2H, ArH); ^{13}C NMR (125 MHz, $CDCl_3$) δ=43.2, 43.8, 123.8, 125.6, 129.1, 132.5, 140.5, and 142.4. Found: C, 47.87; H, 3.41%. Calcd for $C_{16}H_{14}S_6$: C, 48.21; H, 3.54%.

Oxidation of Trithiol 5. The oxidation was carried out according to the same method of the preparation of disulfide **14**. The reaction gave the compound **13** in 91% yield.

Electrochemical Study. Cyclic voltammetry (CV) was performed with 10 ml portions of 2 mM solutions of thiol in CH_3CN and 0.1 M $NaClO_4$. The CV cell was equipped with an Ag/0.01 M $AgNO_3$ in CH_3CN reference electrode in a reference well separated from the analyte by a cracked glass bead junction, a Pt wire counter electrode, and a glassy-carbon working electrode polished before use with alumina.

This work was supported by the Grant-in-Aid for Scientific Research on Priority Area of Organic Unusual Valency No. 02247101 from the Ministry of Education, Science and Culture.

References

1) a) W. K. Musker, *Acc. Chem. Res.*, **13**, 200 (1980); b) R. S. Glass, M. Hojjatie, A. Petsom, G. S. Wilson, M. Gobl, S. Mahling, and K.-D. Asmus, *Phosphorus Sulfur*, **23**, 143 (1985).

2) K. Ohkata, K. Okada, and K. Akiba, *Tetrahedron Lett.*, **26**, 4491 (1985).

3) a) H. Fujihara, J.-J. Chiu, and N. Furukawa, *J. Am. Chem. Soc.*, **110**, 1280 (1988); b) H. Fujihara, J.-J. Chiu, and N. Furukawa, *Tetrahedron Lett.*, **30**, 2805 (1989), c) H. Fujihara, R. Akaishi, and N. Furukawa, *Tetrahedron Lett.*, **30**, 4399 (1989).

4) W. K. Musker and J. T. Doi, in "Reviews on Heteroatom Chemistry," ed by S. Oae, MYU, Tokyo (1988), Vol. 1, p. 120.

5) A. L. Fluharty, in "The Chemistry of the Thiol Group," ed by S. Patai, John Wiley & Sons, New York (1974), Chap. 13.

6) H. Fujihara, J.-J. Chiu, and N. Furukawa, *Tetrahedron Lett.*, **30**, 7441 (1989).

Synthesis of 2-(Trimethylsilyl)ethyl Benzenesulfenate and Benzeneselenenate and Their Reaction with Some Electrophiles in the Presence of Tetrabutylammonium Fluoride

Tatsuo OIDA, Atsushi OHNISHI, Toshiharu SHIMAMAKI,† Yoshiyuki HAYASHI,† and Shigeo TANIMOTO*
Institute for Chemical Research, Kyoto University, Uji, Kyoto 611
†Department of Materials Science and Technology, Faculty of Engineering and Design, Kyoto Institute of Technology, Matsugasaki, Sakyo-ku, Kyoto 606
(Received August 13, 1990)

Synopsis. 2-(Trimethylsilyl)ethyl benzenesulfenate was allowed to react with several halides in the presence of tetrabutylammonium fluoride (TBAF) to afford the corresponding phenyl sulfoxides as the main product. In the reaction of 2-(trimethylsilyl)ethyl benzeneselenenate and several halides with TBAF, the corresponding alcohols were obtained as the main product.

When an arenesulfenyl or areneselenenyl halide is allowed to react with an alcohol in order to synthesize the corresponding arenesulfenate or areneselenenate ester, the reaction would rarely be achieved as desired if the halide has no electron-withdrawing group, such as a nitro or keto group on its arene nucleus.[1] Among the arenesulfenate esters[2] isolated previously, only three arenesulfenate esters (methyl benzenesulfenate,[3] methyl and benzyl *p*-toluenesulfenates[4]) were those derived from arenesulfenyl halides having no electron-withdrawing group on their arene nuclei. Also, all of the hitherto isolated areneselenenate esters[5] possess one or two electron-withdrawing groups in their areneselenenic acid moiety. Thus, except methyl alcohol, such alcohol that is capable of converting benzenesulfenyl and/or benzeneselenenyl chlorides, which may be regarded as the parent compounds of arenesulfenyl and/or areneselenenyl halides, to the corresponding benzenesulfenate and/or benzeneselenenate esters has not been found. We propose here 2-(trimethylsilyl)ethyl benzenesulfenate (**1**) and 2-(trimethylsilyl)ethyl benzeneselenenate (**2**) as a new class of arenesulfenate and areneselenenate esters.

The reaction of benzenesulfenyl chloride with 2-(trimethylsilyl)ethanol proceeded by using butyllithium to give **1** in 81% yield after distillation. By the same procedure using benzeneselenenyl chloride instead of benzenesulfenyl chloride, although requiring a relatively lower reaction temperature, **2** was obtained in 56% yield after distillation. The employment of butyllithium in such a condensation reaction has already been reported.[6] It is likely that compound **1** or **2** is structurally a masked benzenesulfenic or benzeneselenenic acid, respectively. Trimethylsilyl 2-nitrobenzenesulfenate[7] is found in the literature as only one example of such a masked sulfenic acid. If the removal of the 2-(trimethylsilyl)ethyl group from **1** or **2** is possible, in analogy with a 2-(trimethylsilyl)ethyl carboxylate,[8] the reaction of the generated benzenesulfenate or benzeneselenenate ion with an appropriate electrophile is expected to occur. Thus, the reactions of **1** or of **2** with some electrophiles in the presence of TBAF were investigated.

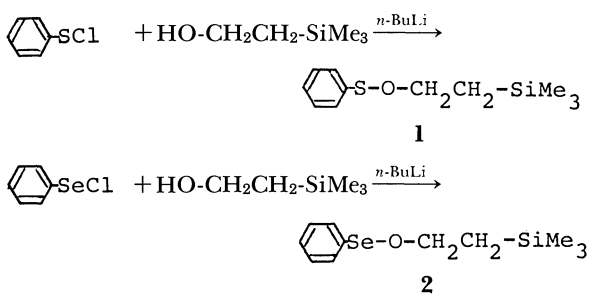

1 **2**

When a mixture of **1** and any one of alkyl iodides, alkyl bromides, and allyl bromides was allowed to react with TBAF according to Procedure A, the reaction proceeded at room temperature to provide the compounds listed in Table 1. In these cases, except for Run 2 [only in this case, tris(dimethylamino)sulfonium (trimethylsilyl)difluoride was used instead of TBAF], TBAF was used as the fluoride ion source. As can be seen from Table 1, the reaction of **1**, TBAF and an alkyl iodide provided the corresponding alkyl phenyl sulfoxide as the main product. This was also the same as in the reaction of **1**, TBAF and benzyl bromide or an allyl bromide. The reaction seems to proceed via a process involving an initial attack of the fluoride ion and a subsequent elimination of the trimethylsilyl group and the ethylene molecule, leading to a benzenesulfenate ion which is trapped by the electrophile. The removal of the 2-(trimethylsilyl)-ethyl group by a fluoride ion is well-known, although it concerns only the 2-(trimethylsilyl)ethyl carboxylates.[9,10] Probably, **1** is decomposed in a similar manner to the carboxylates by a fluoride ion generated from TBAF. Also, the experimental fact that the yield of alkyl phenyl sulfoxide obtained in the reaction using an alkyl iodide decreases with increasing its molecular weight is consistent with the proposed mechanism. When a solution of **1** (0.113 g, 0.5 mmol) in tetrahydrofuran (THF) (2.5 ml) was mixed initially with a 1.0 M solution (1.5 ml, 1.5 mmol, M=mol dm^{-3}) of TBAF in anhydrous THF and (after stirring for 30 min) methyl iodide (0.036 g, 2.5 mmol) was added followed by stirring for 2 h, methyl phenyl sulfide, butyl phenyl sulfide, diphenyl disulfide(**3**), and methyl phenyl sulfone(**4**) were obtained in 10, 12, 18, and 31% yields, respectively. It is likely that the reaction of the intermediate benzenesulfenate ion with **1**, itself, providing unstable[11] *S*-phenyl benzenethiosulfinate occurred in competition with the reaction of the sulfenate ion with methyl iodide. The thiosulfinate is probably converted to **3**.[11] However, the process by which **4** has been produced remains equivocal.

When a mixture of **1** and an acetylenic compound having one or two electron-withdrawing groups was

Table 1. Reaction of **1** with a Halide or with an Acetylenic Compound in the Presence of TBAF

Run	Halide or acetylenic compound	Procedure	Reaction time / h	Isolated products[a] (Yield/%)[b]
1	MeI	A	2	PhS(O)Me(66), PhSMe(3), PhS-*n*-Bu(16)
2[c]	MeI	A	11	PhS(O)Me(59), PhSMe(7)
3	EtI	A	6	PhS(O)Et(38), PhSEt(5), PhS-*n*-Bu(15)
4	*n*-PrI	A	2	PhS(O)-*n*-Pr(26), PhS-*n*-Pr(5), PhS-*n*-Bu(15)
5	*n*-BuI	A	24	PhS(O)-*n*-Bu(21), PhS-*n*-Bu(18)
6	$PhCH_2Br$	A	4	$PhS(O)CH_2Ph$(54), $PhSCH_2Ph$(8)
7		A	4	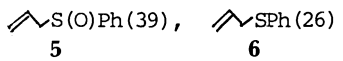 **5** **6**
8		A	4	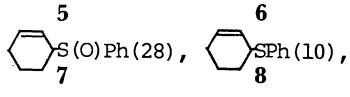 **7** **8** **9**
9	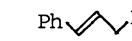	A	4	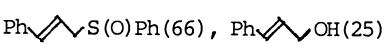 **10**
10	$PhC{\equiv}CCO_2Et$	B	4	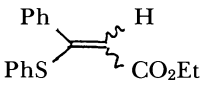 (28) **11**
11	$EtO_2CC{\equiv}CCO_2Et$	B	4	$PhSC{\equiv}CCO_2Et$ (67) **12**
12	$PhC{\equiv}CH$	B	4	$PhC{\equiv}C\text{-}SPh$ (62), **13** 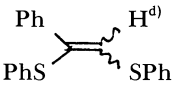 (9) **14**

a) The products **5**—**14** were confirmed by their spectral and analytical data. The sulfides among the other products were confirmed by direct comparison with the commercially available samples. And, the sulfoxides among the other products were comfirmed by direct comparison with the authentic samples prepared by the known method.[13] The compound **13** was also confirmed by direct comparison with the authentic sample prepared by the known method.[14] b) Isolated yield by column chromatography on silica gel using ethyl acetate as eluent. c) Only in Run 2, tris(dimethylamino)sulfonium (trimethylsilyl)difluoride was used instead of TBAF. d) Compound **14** showed the presence of two components on GLC analyses. Further, it was estimated to be a mixture of cis- and trans-isomer with the help of its mass and ^1H NMR spectra.

allowed to react with TBAF according to Procedure B, the reaction proceeded at room temperature or −78 °C to provide the compounds listed also in Table 1. If TBAF was omitted from the reaction system, almost all of the starting substrates were recovered, suggesting the participation of TBAF in these reactions. As can be seen from Table 1, the obtained products varied, depending upon the acetylenic compounds used. Also, the reaction using phenylacetylene provided α,β-bis(phenylthio)styrene (**14**), although it is not the main product. In a somewhat analogous reaction[7] of trimethylsilyl 2-nitrobenzenesulfenate with methyl propynoate, the 2-nitrobenzenesulfinyl moiety of the former had been introduced to the latter. Under our conditions, however, the products obtained were such compounds that the benzenethio moiety of **1** was introduced to the acetylenic compounds used.

When a mixture of **2** and one of benzyl bromide, cinnamyl bromide, 1-chloro-, 1-bromo-, and 1-iodododecane was allowed to react with TBAF according to Procedure C, the reaction proceeded at room temperature to provide the compounds listed in Table 2. As can be seen from Table 2, the obtained products were alcohols which correspond to the halides employed as the trapping agent. Also, in Runs 3—5, a small amount of 1-fluorododecane (**16**) was isolated as a by-product. It is likely that the benzeneselenenate ion formed from **2** and TBAF attacks the halide providing benzeneselenenate ester which is hydrolyzed to the corresponding alcohol together with unstable benzeneselenenic acid. It is likely that the intermediate benzeneselenenate ion attacks a halide used with its oxygen atom. If the ion attacks the halide with its selenium atom, the corresponding phenyl selenoxide would be formed as an intermediate. For example, in Run 1, benzyl phenyl selenoxide would be formed and isolated without any further alteration due to its invariability. However, none of benzyl phenyl selenoxide was obtained in Run 1. This suggests that the benzeneselenenate ion has a pair of available electrons only on its oxygen atom as a nucleophile. In a separate experiment, a solution containing benzyl phenyl selenoxide[12] (0.13 g, 0.5 mmol), a 1.0 M solution (1.0 ml, 1.0 mmol) of TBAF in anhydrous THF and tetrabutylammonium bromide (0.16 g, 0.5 mmol) in THF (2.5 ml) was stirred at room temperature for 7 h. The forma-

Table 2. Reaction of **2** with a Halide in the Presence of TBAF

Run	Halide	Procedure	Reaction time (h)	Isolated product[a] (Yield/%)[b]
1	$PhCH_2Br$	C	7	$PhCH_2OH$ (100)
2		C	7	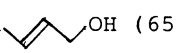 (65)
3	$Me(CH_2)_{11}Cl$	C	48	$Me(CH_2)_{11}OH$ (19), $Me(CH_2)_{11}F$(2), **15** **16** $Me(CH_2)_{11}Cl$[c] (36)
4	$Me(CH_2)_{11}Br$	C	7	**15**(43), **16**(2), $Me(CH_2)_9CH{=}CH_2$(trace)
5	$Me(CH_2)_{11}I$	C	7	**15**(49), **16**(3)

a) Except **16**, the products in this table were confirmed by direct comparison with the commercially available samples. The compound **16** was confirmed by its spectral and analytical data. b) Yields of alcohols were determined by GLC analysis with 1-tetradecanol as an internal standard. Other yields were obtained by column chromatography on silica gel using hexane or 10% ethyl acetate-hexane as eluent. c) Recovered 1-chlorododecane.

tion of benzyl alcohol, however, could not be recognized after a similar work up as in Procedure C. This experimental fact seems to support the above suggestion.

Experimental

Synthesis of 1. To a stirred, cooled (−78 °C) solution of 2-(trimethylsilyl)ethanol (2.03 g, 17.2 mmol) in ether (110 ml) was added (during 5 min, by syringe under nitrogen) a 1.6 M solution of butyllithium (11.7 ml, 18.7 mmol) in hexane. This mixture was stirred under nitrogen for 30 min at the same temperature and a solution of benzenesulfenyl chloride (2.26 g, 15.6 mmol) in ether (20 ml) was then dropped in. This mixture was allowed to warm to room temperature, stirred for 4 h, filtered, and concentrated in vacuo to give a residue which was distilled, bp, 74—80 °C/2 Torr (1 Torr=133.322 Pa), yield 81%. ^1H NMR ($CDCl_3$) δ=0.01 (s, 9H), 1.1—1.2 (m, 2H), 3.8—3.9 (m, 2H), and 7.1—7.4 (m, 5H).

Synthesis of 2. To a stirred, cooled (−78 °C) solution of 2-(trimethylsilyl)ethanol (1.36 g, 11.5 mmol) in ether (100 ml) was added (during 5 min, by syringe under nitrogen) a 1.6 M solution (7.2 ml, 11.5 mmol) of butyllithium in hexane. The mixture was stirred under nitrogen for 30 min at −78 °C and a solution of benzeneselenenyl chloride (2.20 g, 11.5 mmol) in ether (40 ml) was dropped in. Then, the mixture was stirred for 4 h, during which time it was allowed to slowly warm to −30 °C. The mixture was concentrated in vacuo at −30 °C to give a residue. After adding a large quantity of pentane to the residue, it was filtered and concentrated in vacuo to give the crude product which was distilled, bp 77—83 °C/2 Torr, yield 56%. ^1H NMR ($CDCl_3$) δ=0.01 (s, 9H), 1.0—1.1 (m, 2H), 3.9—4.0 (m, 2H), 7.2—7.5 (m, 3H), and 7.5—7.6 (m, 2H).

Reaction of 1 and a Halide with TBAF (Procedure A). To a stirred solution of **1** (0.113 g, 0.5 mmol) and any one of alkyl iodides (2.5 mmol), alkyl bromides (2.5 mmol), and allyl bromides (1.2 mmol) in THF (2.5 ml) was added, under nitrogen, a 1.0 M solution (1.5 ml, 1.5 mmol) of TBAF in anhydrous THF. The mixture was stirred under nitrogen at room temperature. After adding excess ether to the mixture, it was filtered, and evaporated in vacuo to give a residue which was subjected to column chromatography on silica gel.

Reaction of 1 and an Acetylenic Compound with TBAF (Procedure B). To a cooled (−78 °C), stirred solution of **1** (0.113 g, 0.5 mmol) and an acetylenic compound (1.0 mmol) in THF (2.5 ml) was added, under nitrogen, a 1.0 M solution (1.5 ml, 1.5 mmol) of TBAF in anhydrous THF. The mixture was stirred under nitrogen for 4 h at −78 °C (Run 11) or at room temperature (Runs 10 and 12) after being allowed to warm to that temperature, and worked up in a similar manner as mentioned above.

Reaction of 2 and a Halide with TBAF (Procedure C). To a stirred solution of **2** (0.156 g, 0.55 mmol) in THF (2.5 ml) was added successively, under nitrogen, a halide (0.77 mmol) and a 1.0 M solution (1.65 ml,1.65 mmol) of TBAF in anhydrous THF. The mixture was stirred under nitrogen at room temperature. After adding excess ether to the mixture, it was filtered, washed with water, dried over Na_2SO_4, and evaporated in vacuo to give a residue which was subjected to column chromatography on silica gel.

References

1) D. R. Rayner, E. G. Miller, P. Bickart, A. J. Gordon, and K. Mislow, *J. Am. Chem. Soc.*, **88**, 3138 (1966); R. Tang and K. Mislow, *ibid.*, **92**, 2100 (1970); O. Behaghel and W. Müller, *Ber.*, **68**, 1540 (1935).

2) H. Sayo, Y. Yamada, and T. Michida, *Chem. Pharm. Commun.*, **1970**, 1466; F. K. Learmonth and S. Smiles, *J. Chem. Soc.*, **1936**, 327; N. Kharasch, D. P. McQuarrie, and C. M. Buess, *J. Am. Chem. Soc.*, **75**, 2658 (1953); D. Peters and N. Kharasch, *J. Org. Chem.*, **21**, 590 (1956); K. Fries, *Ber.*, **45**, 2965 (1912); R. Matsueda and E. T. Kaiser, *Heterocycles*, **51**, 1089 (1981).

3) H. Lechner, F. Holschneider, K. Köberle, W. Speer, and P. Stöcklin, *Ber.*, **58**, 409 (1925).

4) E. G. Miller, D. R. Rayner, and K. Mislow, *J. Am. Chem. Soc.*, **88**, 3139 (1966).

5) G. Hölzle and W. Jenny, *Helv. Chim. Acta*, **41**, 331 (1958); W. S. Cook and R. A. Donia, *J. Am. Chem. Soc.*, **73**, 2276 (1951); W. Jenny, *Helv. Chim. Acta*, **35**, 845 and 1433 (1952).

6) E. G. Miller, D. R. Rayner, H. T. Thomas, and K. Mislow, *J. Am. Chem. Soc.*, **90**, 4861 (1968).

7) F. A. Davis and A. J. Friedman, *J. Org. Chem.*, **41**, 897 (1976).

8) H. Gerlach, *Helv. Chim. Acta*, **60**, 3039 (1977).

9) B. H. Lipshutz and J. J. Pegram, *Tetrahedron Lett.*, **21**, 3343 (1980).

10) F. J. Corey and A. Venkateswarlu, *J. Am. Chem. Soc.*, **94**, 6190 (1972).

11) F. A. Davis, A. J. Friedman, and U. K. Nadir, *J. Am. Chem. Soc.*, **100**, 2844 (1978).

12) M. Cinquini, S. Colonna, and R. Giovini, *Chem. Ind. (London)*, **48**, 1737 (1969).

13) N. J. Leonard and C. R. Johnson, *J. Org. Chem.*, **27**, 282 (1962).

14) W. E. Truce, H. E. Hill, and M. M. Boudakian, *J. Am. Chem. Soc.*, **78**, 2760 (1956).

Thermochromism of Metal Complexes of Cresolphthalein Dye. Solvent Effect on Temperature-Dependence and Reversibility

Masato NANASAWA,* Mitsuo WADA, and Hiroyoshi KAMOGAWA
Department of Applied Chemistry and Biotechnology, Faculty of Engineering,
Yamanashi University, Takeda-4, Kofu 400
(Received August 24, 1990)

Synopsis. The thermochromism of metal complexes of cresolphthalein dye was studied in organic solvents in the presence of pyridine derivatives. Remarkable thermochromic changes were observed for complexes with nickel(II) and magnesium(II) ion; a large temperature dependence was found in a polar aprotic solvent.

Organic erasable-direct-read-after-write (EDRAW) media have received much attention regarding their application to recording devices with high storage density and responsibility. These include heating-mode recording system employing the abrasive recording of pigments,[1] phase conversion of liquid crystals,[2] and color change of thermochromic compounds.[3] The thermochromism of metal complexes with triphenylmethane dyes observed in aqueous buffer solution[4,5] was also possible in the solid state, and its thermochromic behavior was found to depend distinctly on the kind of polymer matrix employed.[3] This paper describes the thermochromism of cresolphthalein (PC) complexon with various bivalent metal ions and discusses the solvent effect on its temperature-dependence and reversibility.

Results and Discussion

The 2:1-metal complexes of the multidentate ligands of triphenylmethane dyes indicate thermochromism by protolytic equilibrium.[3,4] The reversible color change of a PC-dye was investigated in H_2O, ethylene glycol (EG), and *N*-methylpyrrolidone (NMP) containing pyridine derivatives as organic base, using metal ions having four coordination number such as Cd(II), Co(II), Cu(II), Mg(II), Mn(II), Ni(II), Pb(II), and Zn(II).

Metal ions, Co(II) and Cu(II), formed a complex with an organic solvent to induce an intensive color, and the complex of Fe(III) ion revealed a strong absorption at 517 nm (ε=1600 $dm^3 mol^{-1} cm^{-1}$) in NMP and 532 nm (ε=1400) in EG without the addition of the pyridine derivative. The color development of a PC-metal complex was observed only slightly in the case of PC-Zn(II) possessing a large value of stability constant against PC-dye ($K_{stab.}$).[6] The magnitude of the absorptivity difference between 25 and 80 °C was in the following order: Ni(II), Mg(II)≫Cd(II)> Mn(II), Pb(II)>Zn(II).[7] Proton dissociation of PC-metal complexes to induce thermochromism is not correlated to the value of $K_{stab.}$, but seems to relate to the affinity constant against OH^- ions (K_{OH}) and the metal ionic radius.[8] An intensive reversible color change was obtained with metal ions possessing 2.5—4.0 of pK_{OH} value and approximately 0.7 Å ionic radius.

In Fig. 1, the absorbances of the PC-Mg complex are plotted against the proton dissociation constants of the conjugated acid of pyridine derivatives (K_{py}).[9] The absorbance at 25 °C increased with an increase in the pK_{py} value, and also increased in the order NMP<EG<H_2O. This order is consistent with the values of the proton dissociation constant of relatively low molecular weight phenol derivatives.[10] Since color development takes place by the dissociation of the phenolic proton from a PC-metal complex, its absorbance depends on the stability of a combination of metalloquinonoid anion (PC^--M) and the protonated pyridinium derivatives (Py^+H). Since the salt comprising PC^--M and a pyridinium cation with higher pK_{py} is more stable, its absorbance is large at 25 °C. However, upon heating, a marked increase in the absorbance was observed for the solution of PC-Mg(II) in NMP. Table 1 shows the acid dissociation constant of a PC-metal complex (K_c) and the thermodynamic parameter ΔH and ΔS for the following equation: PC-M⇄PC^--M+H^+ (2). The value of K_c was determined by the following equation $\log K_c = \log K + \log K_{py}$ (3), where K indicates the equilibrium constant for Eq. 1. The values of ΔH and ΔS were determined by plotting the value of $\log K_c$ against

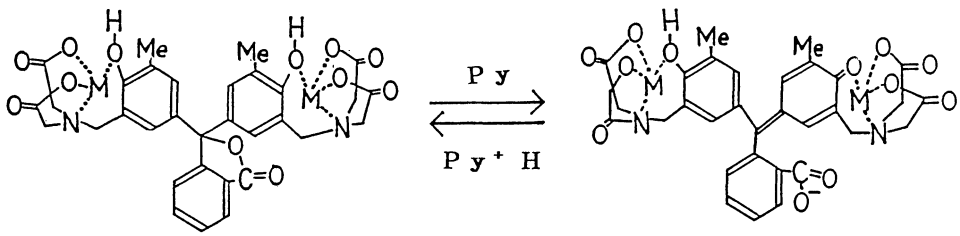

PC-M + Py ⇄ PC^--M + Py^+H (1)

Scheme 1.

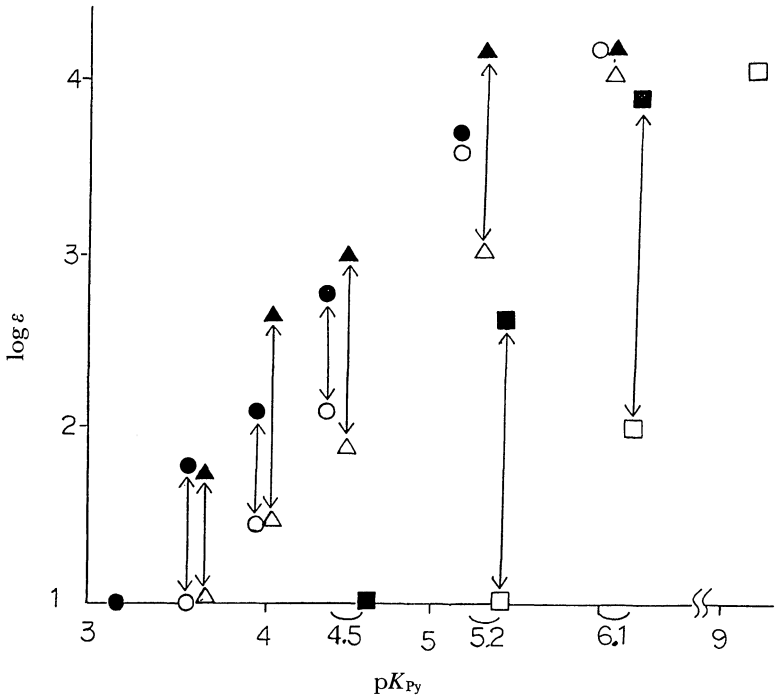

Fig. 1. Temperature-Dependence of PC-Mg(II) Complex with Pyridine Derivatives. ○⟷● indicates the reversible absorption difference at 566 nm between 25 and 80 °C in H_2O; △⟷▲ at 573 nm in EG; □⟷■ at 576 nm in NMP. PC-dye, 1.5×10^{-3} mol dm^{-3}; metal ions, 9×10^{-3}; pyridine derivative, 7.5×10^{-2} mol dm^{-3}.

Table 1. Thermodynamic Parameters for the Proton Dissociation of PC-Metal in Different Solvents[a)]

	PC-Ni(II)			PC-Mg(II)		
	H_2O	EG	NMP	H_2O	EG	NMP
p(K_c[b])/mol dm^{-1})	6.6	7.9	10.2	7.8	8.5	10.7
ΔH[c])/kJ mol^{-1}	27	55	78	29	51	75
ΔS[c])/JK^{-1} mol^{-1}	−37	−15	37	−13	−20	30
ΔG_{298}/kJ mol^{-1}	38	37	36	31	42	31
ΔG_{333}	40	28	15	33	37	16
$\Delta\Delta G$[d])	−2	9	21	−2	5	15

a) Calculated for the Eq. 2: PC-dye, 1.5×10^{-3} mol dm^{-3}; metal ions, 9×10^{-3} mol dm^{-3}; 3-Acetylaminopyridine, 7.5×10^{-2} mol dm^{-3} for PC-Ni(II), 4-Acetylaminopyridine for PC-Mg(II). b) Calculated from Eq. 3 at 25 °C. c) Average values for the range 25—80 °C, deviation ±5% in H_2O; ±15% in EG; ±35% in HMP. d) Difference in ΔG-values between 25 °C and 60 °C.

Table 2. Rate Constants for the Reversible Reaction of PC-Ni(II) in Different Solvents[a)]

	H_2O	EG	NMP
k_1/dm^3 mol^{-1} s^{-1}	8.4×10^{-4}	5.1×10^{-4}	1.5×10^{-5}
k_{-1}/dm^3 mol^{-1} s^{-1}	2.2×10^{-1}	1.0×10^{-1}	1.2×10^{-3}
k_{-1}/k_1	3.8×10^{-3}	5.1×10^{-3}	1.3×10^{-2}

a) at 60 °C, PC-dye, 1.5×10^{-3} mol dm^{-3}; Ni(II) ions, 9×10^{-3} mol dm^{-3}; *N*-methylniconinamide, 7.5×10^{-2} mol dm^{-3}.

$1/T$. However, the plot of $\log k_c$-$1/T$ in an organic solvent does not give a straight line, but the gradient increases with a decrease in $1/T$. Although the value of ΔH, or ΔS, was calculated by supposing that the variation of ΔS, or ΔH, with the temperature would be small in the same solvent,[11,12] the errors of both values in EG and NMP amounted to more than 15- and 35 percent, respectively. Accordingly, the values of the Gibbs function are shown in Table 1.

The value of pK_c of PC-dye with Ni(II) and Mg(II) is of the order H_2O<EG<NMP. This order is different from those of the phenol derivatives having a relatively bulky molecular size.[10] Presumably, PC-metal is fully solvated with the H-donor solvent at complexed sites, so that difference in solvation for its conjugated base is small. The values of ΔH of PC-Ni(II) and -Mg(II) in H_2O resemble that of Xylenol orange(XO) with Cu(II) ion.[5] Although the deviation of the estimated values of ΔH and ΔS were large for the equilibrium reaction in EG and NMP, the ΔH-value increased in the order H_2O<EG<NMP. These results correspond to the intensive reversible color change observed for Eq. 1. The ΔS-value is large compared with that of XO-Cu in buffer solution of sodium perchlorate. The difference might be caused by a color development obtained by using the pyridine derivatives as proton acceptor.

The reversibility of the thermochromism of a PC-metal complex is also affected by the kind of solvent. Table 2 shows the reaction rate at 60 °C for Eq. 1.

The amount of the pyridine derivative employed was 50-molar equivalent for the PC-metal complex, so that the rate constants were estimated for the forward reaction(k_1) as the first order and the reverse(k_{-1}) one as the second order.[13] The value of $\Delta\Delta G$ (temperature-dependence) and the ratio of k_1 to k_{-1} (fixing of colored species) were large in a polar aprotic solvent. Since a protic solvent solvates the PC^-–M and Py^+H combination strongly and increases the anion content, strong absorption is induced even at a low temperature.[14] On the other hand, a polar aprotic solvent appears to predominantly solvate the pyridinium cation formed by protonation at an elevated temperature, as compared with an undissociated metallophthalein having a bulky molecular size. This causes a large temperature dependence of thermochromism in an aprotic solvent. The predominant solvation with an aprotic solvent stabilizes the pyridinium cation, so that proton recombination may be retarded in a polar aprotic solvent.[15]

Experimental

Solvents were purified by distillation under reduced pressure. All chemicals were used as supplied. Visible absorption spectra were recorded on a Hitachi 200-10 and a Shimadzu UV-160 spectrophotometer. Absorbance was measured for 1.5×10^{-3} mol dm^{-3} dye solution (2:98 H_2O–solvent) containing 9×10^{-3} mol dm^{-3} metal nitrate and 7.5×10^{-2} mol dm^{-3} pyridine derivative at a given temperature.

References

1) A. Kuroiwa, K. Nanba, A. Asami, T. Aoi, T. Takahashi, and S. Nakagawa, *Jpn. J. Appl. Phys.*, **22**, 340 (1983).
2) H. J. Coles, *Polym. Sci. Technol.*, **28**, 351 (1985).
3) M. Nanasawa, T. Narita, and H. Kamogawa, *Polym. J.*, **20**, 715 (1988).
4) S. Nakada, M. Yamada, T. Ito, and M. Fujimoto, *Bull. Chem. Soc. Jpn.*, **52**, 766 (1979).
5) S. Nakada, M. Yamada, T. Ito, and M. Fujimoto, *Bull. Chem. Soc. Jpn.*, **53**, 2252 (1980).
6) A. Ringbom, "Complexation in Analytical Chemistry," John Wiley and Sons, New York (1963).
7) Absorption maxima of metalloquinonoid in EG: Ni, 595 nm; Mg, 573 nm; Cd, 582 nm; Mn, 584 nm; Pb, 586 nm; Zn, 573 nm.
8) R. D. Hancock and A. E. Martell, *Chem. Rev.*, **89**, 1875 (1989).
9) Y. Okamoto, "Acids and Bases," Tokyo Kagaku Dojin, Tokyo (1970).
10) B. W. Clare, D. Cook, E. C. F. Ko, Y. C. Mac, and A. J. Parker, *J. Am. Chem. Soc.*, **88**, 1911 (1966).
11) A. J. Ellis, *J. Chem. Soc.*, **1963**, 2299.
12) E. J. Laidler, *Trans. Farady Soc.*, **55**, 1725 (1959).
13) S. Koshiyama, "Physical Chemistry II," Tokai University Pub., Tokyo (1974).
14) D. A. Hinckley, P. G. Seybold, and D. P. Borris, *Spectrochim. Acta, Part A*, **42**, 747 (1986).
15) R. G. Pearson and D. C. Vogelsong, *J. Am. Chem. Soc.*, **80**, 1038 (1958).

The Reaction of Diphenyl(trimethylsilylmethyl)phosphine with Carbonyl Compounds in the Presence of Fluorides

Takayuki KAWASHIMA,* Noriaki MITSUDA, and Naoki INAMOTO
Department of Chemistry, Faculty of Science, The University of Tokyo, Hongo, Bunkyo-ku, Tokyo 113
(Received August 28, 1990)

Synopsis. Diphenyl(trimethylsilylmethyl)phosphine (**1**) was allowed to react with benzophenone in the presence of CsF in *N,N*-dimethylformamide to give a mixture of methyldiphenylphosphine (**2**), (2,2-diphenyl-2-trimethylsiloxyethyl)diphenylphosphine (**3**) and (2-hydroxy-2,2-diphenylethyl)diphenylphosphine (**4**) in good yield. The use of about 10 mol% of CsF gave **3** with fairly good selectivity. The reaction with benzaldehyde gave a similar result, but only protodesilylation occurred in the reaction with enolizable carbonyl compounds.

The direct deprotonation of methyldiphenylphosphine was achieved successfully by using organolithium compounds with a help of *N,N,N′,N′*-tetramethylethylenediamine. However, it was accompanied by the substitution reaction at the phosphorus atom because of their nucleophilicity enhanced by the disaggregation.[1] In the course of our studies on the Horner-Emmons reaction, we uncovered the fluoride induced Horner-Emmons reaction.[2] We decided to examine the generation of diphenylphosphinomethyl anion by the fluoride-induced desilylation and the olefination via quaternalization from its carbonyl adduct. In this paper we wish to report on the results.

Results and Discussion

The Reaction of Diphenyl(trimethylsilylmethyl)phosphine (1) with Carbonyl Compounds in the Presence of CsF. Diphenyl(trimethylsilylmethyl)phosphine (**1**) was allowed to react with benzophenone in the presence of CsF in *N,N*-dimethylformamide (DMF) to afford a mixture of methyldiphenylphosphine (**2**), a protodesilylation product of **1**, (2,2-diphenyl-2-trimethylsiloxyethyl)diphenylphosphine (**3**), and (2-hydroxy-2,2-diphenylethyl)diphenylphosphine (**4**). The results are shown in Table 1. Sulfurization of the reaction mixture followed by usual workup gave a mixture of methyldiphenylphosphine sulfide (**5**) and (2-hydroxy-2,2-diphenylethyl)diphenylphosphine sulfide (**6**).[3] The signal due to **3** decreased with an increase in that of **4** with the elapse of the reaction time, indicating the hydrolysis of **3** occurred under the conditions. About 10 mol% of CsF is enough to complete the reaction, indicating that the present reaction proceeds as shown in the following scheme. An alternative mechanism where the resulting **8** reacts with **1** to afford **3** and **7** cannot be ruled out. It is interesting to point out that the carbanion **7** can be generated in the present system in spite of the lack of carbanion-stabilizing ability compared with cases of phosphonio[4,5] or phosphoryl derivatives[2] and that the yield of **7** is very high, though a part of **7** reacts with water existing in the system to give **2**.

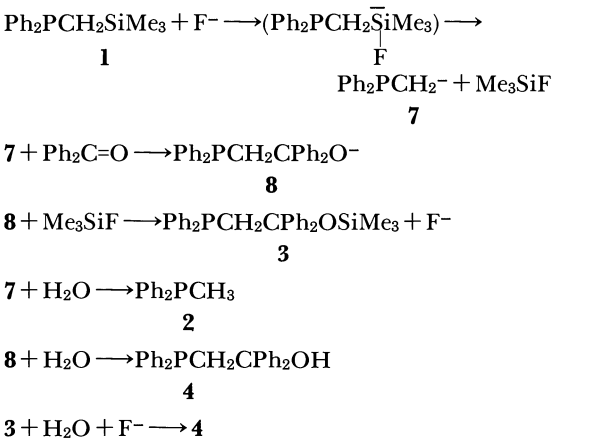

The use of LiF or NaF as a fluoride ion source gave no adduct (**3** or **4**) besides a small amount of **2**, presumably because of its poorer solubility. The use of HMPA as a solvent gave almost the same results, but the reaction using an ethereal solvent such as tetrahydrofuran or diethylene glycol dimethyl ether was unsuccessful. An addition of molecular sieves 4A to remove water caused a decrease in the yields of the products as well as a reduction in the rate of the reaction.

In the case of the reaction of **1** with 1,5-diphenyl-3-pentanone in the presence of CsF the resulting carban-

Table 1. The Reaction of **1** with Benzophenone in the Presence of CsF in DMF

Entry	**1**/mmol	CsF[a]/mmol	Temp/°C	Time/h	**2**:**3**:**4**[b]
1	1.5	2.6	40	24	60:10:30
2	0.75	0.79	90	3	29:40:31
3	0.75	0.38	60	2	24:72:4
4	0.75	0.10	60	4	14:82:4
5	0.75	0.10	50	6	19:75:7[c]

a) Dried by heating with a heat gun under vacuum. b) The ratio of peak heights of signals at δ_P=−27.7, −26.3, and −24.8 due to **2**, **3**, and **4**, respectively. c) About 9% of **1** (δ_P=−22.7) remained.

ion acts as a base to afford only protodesilylation product **2**. Considering the fact that the reaction of dimethyl lithiomethylphosphonate gives the corresponding adduct in 95% yield,[6] it is concluded that unexpectedly low nucleophilicity for the present reactive species is probably attributed to the following reason: It may not be a free carbanion but solvated one, or it exists in equilibrium with "silicon ate complex".

$$\underset{\mathbf{1}}{Ph_2PCH_2SiMe_3} + Me_2NCHO \xrightarrow{F^-}$$

$$Ph_2PCH_2CH(NMe_2)OSiMe_3 \xrightarrow{-Me_3SiOH}$$

$$\underset{\mathbf{9}}{Ph_2PCH{=}CHNMe_2} \xrightarrow{S_8} \underset{\mathbf{10}}{Ph_2P(S)CH{=}CHNMe_2}$$

In the reaction with sterically hindered carbonyl compounds such as (−)-fenchone the desired adduct was not obtained, but a new peak appeared at δ_P=−14.0 besides −27.7 in the ^{31}P NMR spectrum, which is assignable to 1-dimethylamino-2-diphenylphosphinoethylene (**9**), a reaction product with DMF, from the following facts: 1) The chemical shift (δ_P=−14.0) is similar to that of diphenylvinylphosphine (δ_P=−11.7).[7] 2) Sulfurization of the reaction mixture gave **5** and trans-1-dimethylamino-2-(diphenylphosphinothioyl)ethylene (**10**).[8]

Olefination via P-Methylation. The reaction mixture which was obtained by the reaction of **1** with benzophenone in the presence of CsF was treated with iodomethane (1.1 equiv) and subsequent CsF-H_2O (1 equiv) to give 1,1-diphenylethylene (**11**). The isolated yield of **11** and the reaction conditions are summarized in Table 2.

$$Ph_2PCH_2\overset{OSiMe_3}{\overset{|}{C}}Ph_2 \xrightarrow[2)\ H_2O/F^-]{1)\ MeI} Ph_2P^+CH_2\overset{OH}{\overset{|}{C}}Ph_2\ I^- \xrightarrow{F^-} \underset{\mathbf{11}}{CH_2{=}CPh_2} + Ph_2\overset{O}{\overset{\|}{P}}Me$$

Besides the desired olefination side reactions such as the C-C bond cleavage (Entry 2) and the dehydration (Entry 3) occurred depending on the reaction conditions. Interestingly, an addition of more than 1.5 equivalents of water gave good results. A similar effect of water was reported in the case of the conversion of β-hydroxyalkylphosphonates into the corresponding olefins.[6,9] The ^{31}P NMR shows siloxyphosphonium salt is converted into the hydroxyphosphonium salt before the olefination.

Experimental

All melting points and boiling points are not corrected. ^{1}H NMR and ^{31}P NMR spectra were measured with a JEOL FX-90Q using tetramethylsilane as an internal standard and 85% H_3PO_4 as an external standard, respectively.

Preparation of Diphenyl(trimethylsilylmethyl)phosphine (1). To a solution of chlorodiphenylphosphine (5.1 g, 23 mmol) in dry ether (50 ml) was added dropwise an ethereal solution[10] of trimethylsilylmethylmagnesium chloride (1 M, 1 M=1 mol dm^{-3}, 23 mmol) at −78 °C under Ar. The reaction mixture was allowed to warm to room temperature and the resulting precipitates were filtered under Ar. The filtrate was evaporated under reduced pressure and the residue was distilled under vacuum with Kugelrohr to give **1** in 76% yield. Bp 105—110 °C/0.03 Torr (1 Torr=133.322 Pa) (lit,[11] bp 139—143 °C/0.6 Torr). ^{31}P NMR ($CDCl_3$) δ_P=−21.6. ^{1}H NMR ($CDCl_3$) δ=−0.05 (9H, s, Si(CH_3)$_3$), 1.3 (2H, d, J=1 Hz, P-CH_2-Si), and 7.0—7.5 (m, 10H, 2×Ph).

Reaction of 1 with Carbonyl Compounds in the Presence of CsF. Benzophenone: In a two-necked flask CsF (0.03 g, 0.1 mmol) was placed and heated by a heat gun under vacuum. A mixed solution of **1** (0.20 g, 0.75 mmol) and benzophenone (0.24 g, 1.3 mmol) in dry DMF (10 ml) was added to the flask and the mixture was heated at 60 °C for 4 h. The ^{31}P NMR spectrum of the reaction mixture showed three signals at δ_P=−27.7, −26.3, and −24.8 due to methyldiphenylphosphine (**2**), (2,2-diphenyl-2-trimethylsiloxyethyl)-diphenylphosphine (**3**), and (2-hydroxy-2,2-diphenylethyl)-diphenylphosphine (**4**) in a ratio of peak heights of 14 : 82 : 4, respectively.[12] Sulfurization of the reaction mixture by treatment with excess of sulfur, followed by usual workup afforded a mixture of methyldiphenylphosphine sulfide (**5**) and (2-hydroxy-2,2-diphenylethyl)diphenylphosphine sulfide (**6**), which could be separated by preparative high-pressure liquid chromatography (LC) (Japan Analytical Industries: JAIGEL 1H, 2H).

5 (10%):[13] ^{1}H NMR ($CDCl_3$) δ=2.27 (3H, d, $^2J_{H,P}$=13.4 Hz, PCH_3), 7.39—7.54 (6H, m, para and meta), and 7.65—7.97 (4H, m, ortho). ^{31}P NMR ($CDCl_3$) δ_P=35.81.

6 (80%): mp 151—152.5 °C (hexane) (lit,[1] mp 142—145 °C). ^{1}H NMR ($CDCl_3$) δ=3.64 (2H, d, $^2J_{H,P}$=10.3 Hz, PCH_2), 6.63 (1H, s, OH), 6.98—7.18 (5H, m, Ph), 7.18—7.50 (11H, m, Ph′ and para and meta of PPh), and 7.50—7.80 (4H, m, ortho of PPh). ^{31}P NMR ($CDCl_3$) δ_P=34.66. The results of the reactions carried out under various conditions are shown in Table 1.

Benzaldehyde: A mixture of **1** (0.10 g, 0.38 mmol), benzaldehyde (0.04 g, 0.38 mmol), and CsF (0.03 g, 0.19 mmol) was heated in DMF (8 ml) at 0 °C for 2 h. The ^{31}P NMR spectrum of the reaction mixture showed three signals at δ_P=−27.7, −22.3, and −21.6 due to **2**, (2-phenyl-2-trimethyl-

Table 2. Isolated Yield of **11** and the Reaction Conditions

Entry	CsF[a]/mmol	H_2O/mmol	Temp/°C	Time/h	**11**[b]/%
1	0.79	—	R.T.	24	49
2	0.79	—	60	1.5	28[c]
3	0.79	—	0	12	—[d]
4	0.79	1.19	R.T.	2	60
5	0.83	2.49	R.T.	12	53
6	0.83	7.47	R.T.	12	58

a) Dried by heating with a heat gun under vacuum. b) Isolated yield based on **1**. c) The formations of benzophenone and dimethyldiphenylphosphonium iodide[14] were observed. d) Methyl(2,2-diphenylethenyl)diphenylphosphonium iodide was formed.[15]

siloxyethyl)diphenylphosphine, (2-hydroxy-2-phenylethyl)-diphenylphosphine in a ratio of peak heights of 12:15:74, respectively. Sulfurization of the mixture as described above, followed by LC gave (2-hydroxy-2-phenylethyl)-diphenylphosphine sulfide (**12**) in 83% yield.

12: Mp 90—91 °C (hexane). ^{1}H NMR ($CDCl_3$) δ=2.88 (2H, dd, $^3J_{H,H}$=6.0 Hz, $^2J_{H,P}$=9.6 Hz, PC$\underline{H}_2$), 4.29 (1H, s, O$\underline{H}$), 5.15 (1H, dt, $^3J_{H,H}$=6.0 Hz, $^3J_{H,P}$=11.8 Hz, C$\underline{H}$OH-), 7.24—7.33 (5H, m, CPh), 7.38—7.59 (6H, m, meta and para of PPh), and 7.61—8.06 (4H, m, ortho of PPh). ^{31}P NMR ($CDCl_3$) δ_P=38.43. High-resolution mass spectrum (HRMS) (70 eV): *m/z* Found: 338.0913. Calcd for $C_{20}H_{19}OPS$: 338.0895.

(−)-Fenchone: The reaction using **1** (0.20 g, 0.75 mmol), (−)-fenchone (0.14 g, 0.93 mmol), and CsF (0.05 g, 0.33 mmol) in DMF (10 ml) gave a mixture of **2** and trans-2-dimethylamino-1-diphenylphosphinoethylene (**9**), which was sulfurized and subjected to LC to afford trans-dimethylamino-1-diphenylphosphinothioylethylene (**10**) in 36% yield.

9: ^{31}P NMR (DMF) δ_P=−14.0.

10: Mp 99—101 °C (hexane). ^{1}H NMR ($CDCl_3$) δ=2.92 (6H, s, NMe_2), 4.48 (1H, dd, $^2J_{H,P}$=13.5 Hz, $^3J_{H,H}$=17.2 Hz, PC$\underline{H}$=CH), 7.24 (1H, dd, $^3J_{H,P}$=14.0 Hz, $^3J_{H,H}$=17.2 Hz, =C$\underline{H}$NMe_2), 7.31—7.56 (6H, m, meta and para), and 7.62—7.96 (4H, m, ortho). ^{31}P NMR ($CDCl_3$) δ_P=37.49. HRMS (70 eV): *m/z* Found: 287.0907. Calcd for $C_{16}H_{18}NPS$: 287.0897.

Olefination via P-Methylation. To the reaction mixture which was obtained by the reaction of **1** (0.20 g, 0.75 mmol) with benzophenone (0.20 g, 1.1 mmol) in the presence of CsF (0.06 g, 0.38 mmol) were added iodomethane (1.1 equiv), CsF (0.20 g, 0.75 mmol), and H_2O (1.19 mmol). After stirring for 2 h at room temperature the reaction was quenched with water, and then the reaction mixture was extracted with dichloromethane. After removal of the solvent the residue was subjected to dry column chromatography (SiO_2) to give 1,1-diphenylethylene (**11**) in 60% yield. The isolated yield of **11** and the reaction conditions are summarized in Table 2.

The authors wish to express their thanks to Shinetsu Kagaku Co. for a gift of chlorotrimethylsilane. The present work was partially supported by a Grant-in-Aid for Scientific Research No. 61540365 from the Ministry of Education, Science and Culture.

References

1) D. J. Peterson, *J. Organomet. Chem.*, **8**, 199 (1967).
2) T. Kawashima, T. Ishii, and N. Inamoto, *Tetrahedron Lett.*, **24**, 739 (1983), *idem.*, *Bull. Chem. Soc. Jpn.*, **60**, 1831 (1987).
3) Diphenyl(2,2-diphenyl-2-trimethylsiloxyethyl)phosphine sulfide was hydrolyzed to give **6** during the workup.
4) E. Vedejs and G. R. Martinez, *J. Am. Chem. Soc.*, **101**, 6452 (1979).
5) H. J. Bestmann and A. Bomhard, *Angew. Chem., Int. Ed. Engl.*, **21**, 545 (1982).
6) T. Kawashima, T. Ishii, and N. Inamoto, *Chem. Lett.*, **1983**, 1375.
7) S. O. Grim, W. McFarlane, and E. F. Davidoff, *J. Org. Chem.*, **32**, 781 (1967).
8) A similar reaction with DMF was observed in the reaction of dialkyl α-lithioalkylphosphonates: E. E. Aboujaoude, N. Collignon, and P. Savignac, *Synthesis*, **1983**, 634.
9) T. Kawashima, T. Ishii, and N. Inamoto, *Chem. Lett.*, **1984**, 1097.
10) F. C. Whitemore and L. H. Sommer, *J. Am. Chem. Soc.*, **68**, 481 (1946).
11) D. J. Peterson, *J. Org. Chem.*, **33**, 780 (1968).
12) The proton-noise decoupled ^{31}P NMR spectra were taken under the following conditions: Spectral width (5000 Hz); flip angle (45° pulse); pulse delay (1 s).
13) D. J. Peterson and H. R. Hays, *J. Org. Chem.*, **30**, 1939 (1965).
14) R. Davidson, R. Sheldon, and S. Trippett, *J. Chem. Soc. C*, **1966**, 722.
15) The structure was estimated by the following NMR spectral data: ^{1}H NMR ($CDCl_3$) δ=2.3 (3H, d $^2J_{H,P}$=14 Hz, PC$\underline{H}_3$) and 6.7—7.9 (21H, m, C$\underline{H}$=CPh_2 and 4×Ph). ^{31}P NMR ($CDCl_3$) δ_P=12.9.

Revised Structure of 2-Cyclohexyl-3,4-diphenyl-1,2-oxaphosphetane 2-Oxide

Takayuki KAWASHIMA,* Shigenobu NAKAYAMA, Masaaki YOSHIFUJI, Renji OKAZAKI, and Naoki INAMOTO
Department of Chemistry, Faculty of Science, The University of Tokyo, Hongo, Bunkyo-ku, Tokyo 113
(Received September 10, 1990)

Synopsis. The correct structure of the title compound was elucidated to be cyclohexyl(2,2-diphenyl-1-hydroxyethyl)phosphine oxide, which seems to be formed via migration of a phenyl group, from the NMR spectral data and synthesis of the dimethyl derivative.

In the course of our study on the reactions of phosphinylidenes and phosphinothioylidenes,[1] we have reported that 1,2-oxaphosphetane derivative (**1**) was formed in the reaction of cyclohexylphosphonic dichloride (**2**) with magnesium in the presence of *trans*-stilbene oxide (**3**) as shown in the following scheme.[2]

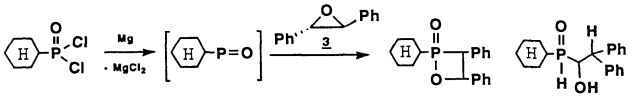

2 **1** **4**

Further investigation on this compound allows us to reach the conclusion that the product is not 1,2-oxaphosphetane 2-oxide (**1**), but an acyclic secondary phosphine oxide (**4**), which seems to be formed via migration of a phenyl group. In this paper we wish to revise the structure.

Results and Discussion

In order to confirm whether the sample, which was obtained previously,[2] remains unchanged as it was or not, we took a ^{1}H NMR spectrum (90 MHz). Its spectrum showed the same signals as taken previously except a double doublet with a large coupling constant, indicating the existence of a direct P-H bond. We overlooked a double doublet in the 60 MHz-^{1}H NMR spectrum, because a lower field signal had appeared about δ=9.7 and upper one, which was expected to appear at δ=2.2, was unfortunately superimposed with the signals of the cyclohexyl group. In the IR spectrum the stretching frequencies for O-H and P-H bonds had been observed at 3150 and 2330 cm^{-1}, respectively. However, the former band had been assigned to that of water of crystallization, as expected from the results of elemental analysis, and the latter band had been completely neglected because the presence of P-H bond was beyond the consideration. Judging from the existence of P-H bond we at first presumed Structure A, which is considered to be formed by the reduction and the subsequent ring opening by hydrolysis of the oxaphosphetane.

The ^{13}C NMR spectrum showed the signals due to three methine groups at δ_C=34.54 (J=65.4 Hz), 53.31 (J=3.4 Hz), and 69.74 (J=74.5 Hz). The chemical shifts are reasonable for the carbons bonding to a phosphorus, phosphorus, and oxygen atom, respectively, but the magnitudes of coupling constant with

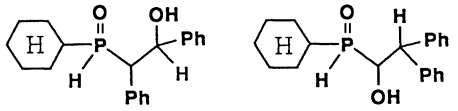

Structure A Struucture B (**4**)

Fig. 1. Possible Structures of the Product.

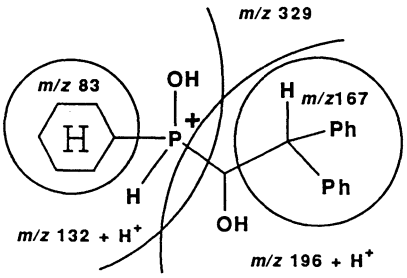

Fig. 2. Fragmentation of **4**.

phosphorus nucleus cannot be explained for Structure A at all. From the data a phosphorus atom must directly be attached to the carbon bonded with an oxygen atom. Structure B (**4**) is consistent with these facts (see Fig. 1).

The ^{31}P NMR spectrum showed a very small peak at δ_P=44.96 (<1/18) due to a minor diastereomer besides a major peak at δ_P=39.11. A negligibly small doublet was observed at δ=6.14 in the ^{1}H NMR spectrum, suggesting the formation of diastereomer also. Interesting features in the NMR spectrum are nonequivalences in cyclohexane ring carbons and in two phenyl groups, because of neighboring chiral center.

On the other hand the mass spectrum measured by electron impact ionization gave no parent peak, as mentioned previously,[2] but in the chemical ionization mass spectrum using methane gas the protonated molecular peak was observed at m/z 329 (7%). The base peak was m/z 105, which is assigned to a rearranged fragment ($PhCO^+$). Peaks at m/z 197 (14%), 167 (44%), 133 (46%), and 83 (51%) were also observed, supporting the structure **4** (see Fig. 2).

Methylation of 4. Compound **4** was allowed to react with 2 equivalents of *n*-BuLi at −78 °C in tetrahydrofuran (THF) and with excess iodomethane to afford a mixture of cyclohexyl(methyl)(2,2-diphenyl-1-methoxyethyl)phosphine oxides (**5a** and **5b** in 3 : 1

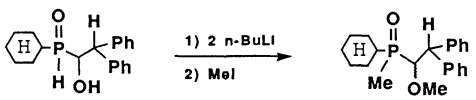

4 **5a** and **5b**

diastereomer ratio. The structure of **5** was determined by the observations of a pair of doublets at δ=0.84 and 0.98 due to PMe groups and a pair of singlets at δ=3.22 and 3.30 due to OMe groups instead of the signals due to PH and OH groups in the ^{1}H NMR spectrum. In the ^{13}C NMR spectrum of **5** the signals of the minor diastereomer could not be observed clearly, because of an insufficient amount of the sample, but those of the major one support the structure **5**. The high resolution mass spectrum gave the exact mass number of the parent peak. The change in the diastereomer ratio can be explained reasonably if one considers the difference in sterical bulkiness between hydrogen atom and methyl group.

It is very surprising that such a secondary alkylphosphine oxide remains without any change even after being exposed to air for 14 years. Unexpected stability of this compound having a readily oxidizable moiety seems to come from the following factors: intramolecular hydrogen bonding stabilizes a pentavalent tautomer and a reaction center is hindered by two bulky substituents.

Experimental

^{1}H NMR spectra were measured with a Bruker AM-500 (500.13 MHz) spectrometer using tetramethylsilane (TMS) as an internal standard. ^{13}C NMR spectra were taken with a Bruker AM-500 (125.77 MHz) spectrometer using TMS as an internal standard. ^{31}P NMR spectra were obtained with a JEOL FX-90Q spectrometer using 85% H_3PO_4 as an external standard. IR spectra were taken with a Hitachi 260-30 spectrophotometer. Mass spectra were recorded with a JEOL 300-D mass spectrometer.

The sample stored in a vial, which was reported to be 2-cyclohexyl-3,4-diphenyl-1,2-oxaphosphetane 2-oxide (**1**),[2] was used after confirming it remains unchanged as it was.

Spectral Data of the Compound 4. ^{1}H NMR ($CDCl_3$)[3] (500.13 MHz) δ=1.10—1.14 (4H, m, C(2)H$_2$, ax. H-C(3′), and eq. H-C(4) of c-Hex), 1.65—1.70 (2H, m, C(3)H$_2$ of c-Hex), 1.70—1.80 (3H, m, C(2′)H$_2$ and eq. H-C(4) of c-Hex), 1.80—1.95 (1H, m, C(1)H of c-Hex), 1.95—2.05 (1H, m, eq. H-C(3′) of c-Hex), 4.25 (1H, s, OH), 4.50—4.60 (2H, m, CHCHOH), 6.02 (1H, dd, $^3J_{H,H}$=4.8 Hz, $^1J_{H,P}$=451.1 Hz, PH), 7.20—7.25 (2H, m, para-H of Ph and Ph′), 7.28—7.31 (2H, m, meta-H of Ph), 7.32—7.36 (4H, m, meta and ortho-H of Ph′), and 7.43—7.45 (2H, m, ortho-H of Ph). A small doublet appeared at δ=6.14 ($^1J_{H,P}$=458.6 Hz). ^{13}C NMR ($CDCl_3$)[3] δ_C=25.16 (s,[4] C-4 of c-Hex), 25.22 (d, $^3J_{C,P}$=2.9 Hz, C-3′of c-Hex), 25.73 (s, C-2 of c-Hex), 25.80 (d, $^3J_{C,P}$=14.8 Hz, C-3 of c-Hex), 25.91 (d, $^2J_{C,P}$=12.8 Hz, C-2′ of c-Hex), 34.54 (d, $^1J_{C,P}$=65.4 Hz, C-1 of c-Hex), 53.31 (d, $^2J_{C,P}$=3.4 Hz, PCHCHPh$_2$), 69.74 (d, $^1J_{C,P}$=74.5 Hz, PCHOH), 126.92 (s, para-C of Ph), 127.48 (s, para-C of Ph′), 128.49 (s, ortho-C of Ph′), 128.69 (s, ortho-C and meta-C of Ph), 129.06 (meta-C of Ph′), 139.91 (s), and 140.35 (d, $^3J_{C,P}$=10.5 Hz) (ipso-C of Ph and Ph′). ^{31}P NMR ($CDCl_3$) δ_P=39.11 and 44.96 (>18:1). Mass spectrum (chemical ionization: Methane gas): m/z 329 (M^++1, 7%), 197 (HCOCHPh$_2$+H$^+$, 14), 167 (CH$^+$Ph$_2$, 44), 133 (c-C$_6$H$_{11}$P(O)H$_2$+H$^+$, 46), 105 (PhCO$^+$, 100), and 83 (c-C$_6$H$_{11}^+$, 51). IR (KBr disc) ν_{OH}=3150 cm^{-1} and ν_{PH}=2330 cm^{-1}.

Methylation of 4. To a solution of **4** (7.2 mg, 0.022 mmol) in THF (2 ml) was added dropwise *n*-BuLi (0.96 M hexane solution, 0.05 ml, 0.048 mmol) at −78 °C with stirring, then excess of iodomethane (0.1 ml, 1.6 mmol) was added to the solution. The reaction mixture was allowed to warm to room temperature, treated with aq NH_4Cl. Organic layer was extracted with dichloromethane and dried over anhydrous $MgSO_4$. After removal of the solvent the residue was subjected to high-pressure liquid chromatography (column: Japan Analytical Industries (JAIGEL 1H, 2H)) to give a diastereomer mixture of cyclohexyl(methyl)(2,2-diphenyl-1-methoxyethyl)phosphine oxides (**5a** and **5b**) (2.0 mg, 26%) as viscous oil in a ratio of 3:1. **5:** ^{1}H NMR ($CDCl_3$) δ=0.84 (d, $^2J_{H,P}$=12.4 Hz, PCH$_3$ of **5b**), 0.98 (d, $^2J_{H,P}$=11.9 Hz, PCH$_3$ of **5a**), 0.80—1.35 (m) and 1.55—1.92 (m) (c-C$_6$H$_{11}$ of **5a** and **5b**), 3.22 (s, OCH$_3$ of **5b**), 3.30 (s, OCH$_3$ of **5a**), 4.26 (dd, $^3J_{H,H}$=7.1 Hz, $^2J_{H,P}$=4.9 Hz, PCHOMe of **5a**), 4.29 (t, $^3J_{H,H}$=$^3J_{H,P}$=5.1 Hz, PCHOMe of **5b**), 4.56 (t, $^3J_{H,H}$=$^3J_{H,P}$=7.1 Hz, CHPh$_2$ of **5a**), 4.66 (t, $^3J_{H,H}$=$^3J_{H,P}$=5.1 Hz, CHPh$_2$ of **5b**), 7.20—7.24 (m, all para-H), 7.24—7.35 (m, all meta-H), 7.42—7.46 (m, ortho-H of Ph of **5a** and **5b**), 7.52—7.55 (m, ortho-H of Ph′ of **5a**), and 7.57—7.62 (m, ortho-H of Ph′ of **5b**). ^{13}C NMR ($CDCl_3$) δ_C=10.13 (d, $^1J_{C,P}$=59.9 Hz, PCH$_3$), 24.76 (d $^4J_{C,P}$=3.6 Hz, C-4 of c-Hex), 25.98 (d, $^3J_{C,P}$=2.5 Hz, C-3′ of c-Hex), 26.23 (d, $^3J_{C,P}$=8.4 Hz, C-3 of c-Hex), 26.31 (s, C-2 of c-Hex), 26.35 (d, $^2J_{C,P}$=4.9 Hz, C-2′ of c-Hex), 36.71 (d, $^1J_{C,P}$=64.0 Hz, C-1 of c-Hex), 51.11 (d, $^2J_{C,P}$=5.8 Hz, CHPh$_2$), 60.68 (s, OCH$_3$), 83.36 (d, $^1J_{C,P}$=76.3 Hz, PCHOMe), 127.00 (s, para-C of Ph), 127.07 (s, para-C of Ph′), 128.44 (s, ortho-C of Ph), 128.73 (s, meta and ortho-C of Ph′), 129.53 (s, meta-C of Ph), 140.29 (s), and 141.3 (d, $^3J_{C,P}$=5.7 Hz) (ipso-C of Ph and Ph′). ^{31}P NMR ($CDCl_3$) δ_P=51.28 and 51.64 (ca. 3:1). High resolution mass spectrum (70 eV): m/z Found: 356.1895. Calcd for $C_{22}H_{29}O_2P$: 356.1905.

The authors wish to express their thanks to Tosoh Akzo Co. for a gift of *n*-BuLi and also to Dr. Hiroshi Hirota, The University of Tokyo, for his measuring chemical ionization mass spectrum. This work was partially supported by the Grant-in-Aid for Scientific Research on Priority Area of Organic Unusual Valency No. 02247205 from the Ministry of Education, Science and Culture.

References

1) For examples see: M. Yoshifuji, S. Nakayama, R. Okazaki, and N. Inamoto, *J. Chem. Soc., Perkin Trans. 1*, **1973**, 2065, 2067 and references cited therein.

2) S. Nakayama, M. Yoshifuji, R. Okazaki, and N. Inamoto, *Bull. Chem. Soc. Jpn.*, **49**, 1173 (1976).

3) These assignments are supported by ^{1}H-{^{31}P} and ^{13}C-{^{31}P} NMR and two-dimensional NMR (H,H-COSY and C,H-COSY (correlation spectroscopy)) spectroscopies.

4) Abbreviation shows a coupling manner with a phosphorus nucleus.

The Correct Structure of Cyclic Adducts of (Diphenylmethylene)-oxophenylphosphorane with Aromatic Aldehydes

Takayuki KAWASHIMA* and Naoki INAMOTO
Department of Chemistry, Faculty of Science, The University of Tokyo, Hongo, Bunkyo-ku, Tokyo 113
(Received September 10, 1990)

Synopsis. The title cyclic adducts have been reported to be 4-aryl-2,3,3-triphenyl-1,2-oxaphosphetane 2-oxides. However, these compounds are concluded not to be the 1,2-oxaphosphetanes, but 1-aryl-3,4-diphenyl-3,4-dihydro-1*H*-2,3-benzoxaphosphorin 3-oxides from our detailed NMR studies and the investigation of the chemical behavior of the adduct of benzaldehyde.

Recently, pentacoordinate 1,2-oxaphosphetanes have attracted much attention as the reactive intermediates of the Wittig reaction, which can be observed by the low temperature NMR spectroscopies.[1] 1,2-Oxaphosphetane 2-oxides, their tetracoordinate analogs, were known to be much more stable in the earlier time. Since the compound, which we reported previously as an example,[2] was not 1,2-oxaphosphetane 2-oxides, as mentioned in the preceding paper,[3] we decided to prepare 4-aryl-2,3,3-triphenyl-1,2-oxaphosphetane 2-oxides (**1**), which were reported as other examples of stable oxaphosphetane oxide,[4] in order to investigate their chemical behavior toward various nucleophiles. However, we have found that the compound prepared by the method reported in the literature are not 1,2-oxaphosphetane 2-oxides (**1**), but 3,4-dihydro-1*H*-2,3-benzoxaphosphorin 3-oxides (**2**). Here, we wish to report on the results.

Results and Discussion

(Diphenylphosphinyl)phenyldiazomethane (**3**) was irradiated in benzene at room temperature in the presence of aromatic aldehydes (**4**) according to the literature,[4] to give a complex mixture, which was treated with MeOH to afford 1-aryl-3,4-diphenyl-3,4-dihydro-1*H*-2,3-benzoxaphosphorin 3-oxides (**2**) instead of 4-aryl-2,3,3-triphenyl-1,2-oxaphosphetane 2-oxides (**1**) as reported previously.[4]

In order to confirm the structure ^{13}C NMR spectrum was taken in various measuring modes. In the proton-noise decoupled ^{13}C NMR signals due to PC and CO were observed at the expected positions for the structure of **1**, but these signals also appeared in its DEPT (distortionless enhancement by polarization transfer) spectrum, indicating that both of them are not signals due to quaternary carbon. In the detailed study of the ^{1}H NMR spectrum of **1a**, the existence of a doublet was elucidated in the region of aromatic protons. This coupling was confirmed to be that with a phosphorus nucleus by the ^{1}H-{^{31}P} NMR spectroscopy. Thus, it was clarified from both ^{1}H and ^{13}C NMR spectral data that this compound has two methine groups except aromatic protons in the molecule. In order to assign the signals, two-dimensional NMR spectra were taken. Figure 1 shows the C,H-COSY (correlation spectroscopy) spectrum of **2a**, indicating that two doublets at δ=4.7 and 6.7 correlate with two doublets at δ_C=49 and 78, respectively. From the magnitudes of coupling constants the following conclusion were drawn: one methine group is bonded directly with a phosphorus atom and the other is attached to an oxygen atom. These methines must not be bonded with each other. These facts cannot be explained from Structure **1**, but they are consistent with Structure **2**. Four continuous proton system of benzo moiety was elucidated by the H,H-COSY spectrum of **2a** as shown in Fig. 2.

Although the fragmentation pattern of mass spectrum was used as evidence for Structure **1**,[4] observation of the fragment (M^+-$PhPO_2$) can also be explained nicely as Structure **2**, by considering that the fragmentation takes place via the retro-Diels-Alder reaction. In order to undergo thermally this retro-Diels-Alder reaction **2a** was heated at 250 °C in toluene-d_8 in a sealed NMR tube. High-pressure liquid chromatography gave 9-phenyl-9,10-dihydroanthracene (**5**) and 9-phenylanthracene (**6**), oxidation product of **5**, in 26 and 13% yields, respectively. Dihydro compound **5** seems to be formed by the cyclization of the first product **7** of the retro-Diels-Alder reaction of **2a**. A similar result has been reported by Cava and his co-workers in the thermolysis of 1,3-

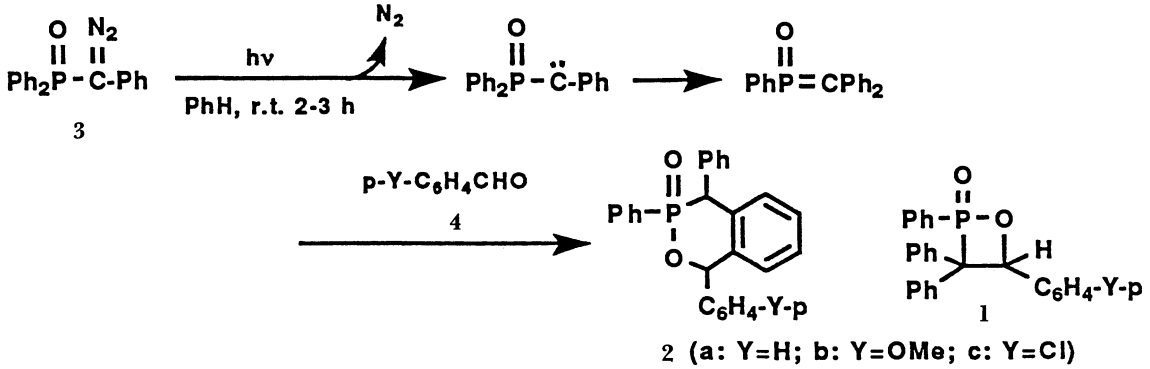

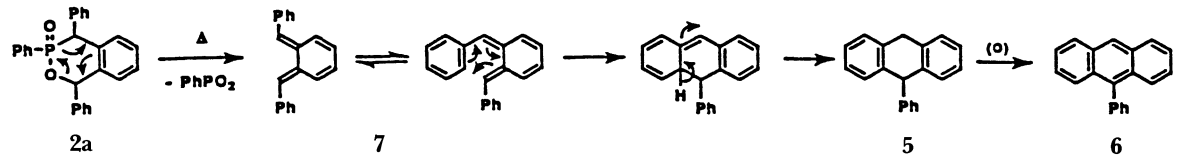

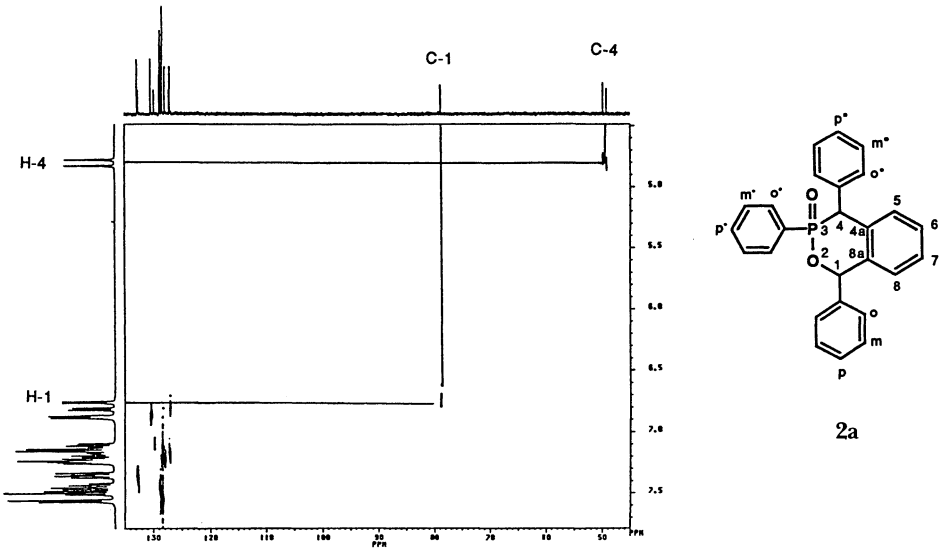

Fig. 1. The C,H-COSY Spectrum of **2a**.

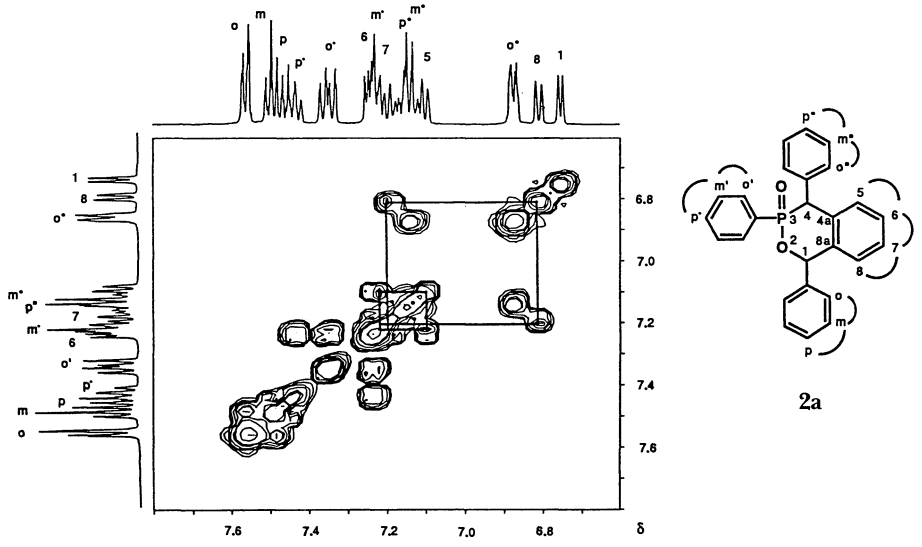

Fig. 2. The Partially H,H-COSY Spectrum of **2a**.

diphenyl-1,3-dihydrobenzo[*c*]thiophene 2,2-dioxide (**8**).[5] The structure with a fused benzene ring for **2a** is strongly supported by the fact that 9-phenyl-9,10-dihydroanthracene was obtained in its thermolysis. Judging from these spectral data and chemical behavior it is reasonably concluded that the compound is not 1,2-oxaphosphetane 2-oxide, but 2,3-benzoxaphosphorin 3-oxide. For 2,3-benzoxaphosphorin ring system only one example has been reported until now.[6]

The stereochemistry of **2a** was also studied. The NOESY (nuclear Overhauser effect spectroscopy) spectrum of **2a** (Fig. 3) shows the cross peaks between H-1 and H-4 and between ortho-protons of three phenyl groups, indicating that all phenyl groups are cis.

Experimental

All melting points are uncorrected. ^{1}H NMR spectra were measured with a Bruker AM-500 (500.13 MHz) spectrometer using tetramethylsilane (TMS) as an internal standard. ^{13}C NMR and ^{31}P NMR spectra were taken with a Bruker AM-500 (125.77 MHz) using TMS as an internal standard and with a JEOL FX-90Q spectrometer using 85% H_3PO_4 as an external standard, respectively. Mass spectra were recorded with a JEOL 300-D mass spectrometer.

Photolysis of (Diphenylphosphinyl)phenyldiazomethane (3) in the Presence of Aromatic Aldehydes (4). A benzene (20 ml) solution of **3** (0.207 g, 0.649 mmol), which was prepared by the method described in the literature using *n*-BuLi instead of PhLi,[7] and benzaldehyde (**4a**) (0.198 ml,

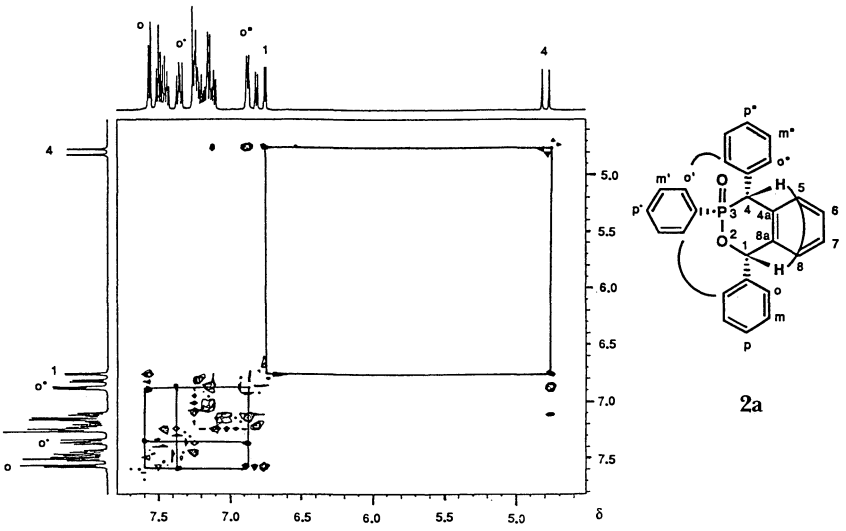

Fig. 3. The NOESY Spectrum of **2a**.

1.95 mmol) was irradiated with a 100-W medium-pressure mercury arc lamp for 2.5 h at room temperature under nitrogen atmosphere. After removal of the solvent the residue was treated with methanol to give crude 1,3,4-triphenyl-3,4-dihydro-1*H*-2,3-benzoxaphosphorin 3-oxide (**2a**), whose physical and spectral data agreed with those reported as 2,3,3,4-tetraphenyl-1,2-oxaphosphetane 2-oxide. Recrystallization from methanol afforded pure **2a** in 14% yield.

2a: mp 254—257 °C (decomp). ^{1}H NMR ($CDCl_3$)[8] δ= 4.80 (1H, d, $^2J_{H,P}$=24.4 Hz, PCHPh), 6.75 (1H, d, $^3J_{H,P}$=5.8 Hz, POCHPh), 6.81 (1H, d, $^3J_{H,H}$=7.6 Hz, H-8), 6.86—6.89 (2H, m, ortho-H of C(4)-Ph), 7.10 (1H, d, $^3J_{H,H}$=7.5 Hz, H-5), 7.11—7.27 (7H, m, H-6, H-7, meta and para-H of C(4)-Ph, and meta-H of P-Ph), 7.33—7.38 (2H, m, ortho-H of P-Ph), 7.41—7.52 (4H, m, para-H of P-Ph, meta and para-H of C(1)-Ph), and 7.54—7.58 (2H, m, ortho-H of C(1)-Ph). ^{13}C NMR ($CDCl_3$)[8] δ_C=49.47 (d,[9] $^1J_{C,P}$=81.1 Hz, PCHPh), 78.73 (d, $^2J_{C,P}$=8.0 Hz, POCHPh), 127.04 (s, C-7 and C-8), 127.19 (d, $^5J_{C,P}$=3.3 Hz, para-C of C(4)-Ph), 127.94 (d, $^3J_{C,P}$=13.3 Hz, meta-C of P-Ph), 128.33 (s, ortho-C of C(1)-Ph), 128.35 (d, $^4J_{C,P}$=3.8 Hz, meta-C of C(4)-Ph), 128.43 (d, $^1J_{C,P}$=140.2 Hz, ipso-C of P-Ph), 128.50 (s, C-6), 128.90 (s, para-C of C(1)-Ph), 129.75 (d, $^3J_{C,P}$=9.0 Hz, C-5), 130.35 (d, $^3J_{C,P}$=5.2 Hz, ortho-C of C(4)-Ph), 132.51 (d, $^4J_{C,P}$=2.7 Hz, para-C of P-Ph), 132.71 (d, $^2J_{C,P}$=9.4 Hz, ortho-C of P-Ph), 134.17 (d, J=4.8 Hz), 134.82 (d, J=4.7 Hz), 137.29 (d, J=5.7 Hz) (C-4a, C-8a, ipso-C of C(1)-Ph), and 138.55 ($^3J_{C,P}$=9.5 Hz, ipso-C of C(1)-Ph). ^{31}P NMR ($CDCl_3$) δ_P=35.47. Compounds **2b** and **2c** were obtained in 12 and 14% yields, respectively, as described above.[10]

Thermolysis of 2a. A solution of **2a** (10 mg, 0.025 mmol) in d_8-toluene (1 ml) was heated at 250 °C for 7 h in a degased sealed NMR tube until starting material disappeared completely. ^{1}H NMR showed a new AB quartet at δ=3.92. The solvent was distilled with a Kugelrohr to give tarry material, which was subjected to high-pressure liquid chromatography (column: Japan Analytical Industries: JAIGEL 1H, 2H) to afford 9-phenyl-9,10-dihydroanthracene (**5**)[11] and 9-phenylanthracene (**6**) in 26 and 13% yields, respectively. Besides these hydrocarbons some of unidentified products containing a phosphorus atom were obtained. Dihydro compound **5** was oxidized readily on silica gel to afford **6**.

5: ^{1}H NMR ($CDCl_3$) δ=3.91 (1H, d, $^2J_{H,H}$=18.1 Hz, CHH'), 4.02 (1H, d, $^2J_{H,H}$=18.1 Hz, CHH'), 5.26 (1H, s, CHPh), 7.06—7.09 (2H, m, ortho-H of Ph), 7.12—7.16 (1H, m, para-H of Ph), 7.19—7.23 (6H, m, meta-H of Ph, H-1, H-2, H-7, H-8), 7.29—7.33 (4H, m, H-3, H-4, H-5, H-6). ^{13}C NMR ($CDCl_3$) δ_C=35.65 (t,[12] C-10), 51.42 (d, C-9), 126.19 (d), 126.35 (d), 126.40 (d), 127.75 (d), 128.04 (d), 128.41 (d), 128.43 (d), 136.42 (s), 139.48 (s), 143.57 (s). High-resolution mass spectrum (70 eV): m/z Found: 256.1244. Calcd for $C_{20}H_{16}$: 256.1250. Compound **6** agreed with authentic sample.

The authors wish to express their thanks to Tosoh Akzo Co. for a gift of *n*-BuLi. This work was partially supported by the Grant-in-Aid for Scientific Research on Priority Area of Organic Unusual Valency No. 02247205 from the Ministry of Education, Science and Culture.

References

1) E. Vedejs and K. A. Snoble, *J. Am. Chem. Soc.*, **95**, 5778 (1973); A. B. Reitz, M. S. Mutter, and B. E. Maryanoff, *J. Am. Chem. Soc.*, **106**, 1873 (1984); B. E. Maryanoff and A. B. Reitz, *Phosphorus Sulfur*, **27**, 167 (1986), and references cited therein.

2) S. Nakayama, M. Yoshifuji, R. Okazaki, and N. Inamoto, *Bull. Chem. Soc. Jpn.*, **49**, 1173 (1976).

3) T. Kawashima, S. Nakayama, M. Yoshifuji, R. Okazaki, and N. Inamoto, preceding paper.

4) M. Regitz, H. Scherer, W. Illger, and H. Eckes, *Angew. Chem., Int. Ed. Engl.*, **12**, 1010 (1973): M. Regitz and H. Eckes, *Chem. Ber.*, **113**, 3303 (1980).

5) P. Cava, M. J. Mitchell, and A. A. Deana, *J. Org. Chem.*, **25**, 1481 (1960).

6) F. Mathey and F. Mercier, *J. Chem. Soc., Chem. Commun.*, **1980**, 191.

7) M. Regitz and W. Anschütz, *Chem. Ber.*, **102**, 2216 (1969).

8) These assignments are supported by ^{1}H-{^{31}P} and ^{13}C-{^{31}P} NMR spectra and two-dimensional NMR (H,H-COSY and C,H-COSY) spectroscopies.

9) Abbreviations show a coupling manner with a phosphorus nucleus.

10) The physical and spectral data of **2b** and **2c** are deposited as Document No. 9100 at the Office of the Editor of Bull. Chem. Soc. Jpn.

11) A. W. Brinkmann, M. Gordon, R. G. Harvey, P. W. Rabideau, J. B. Stothers, and A. L. Ternay, Jr., *J. Am. Chem. Soc.*, **92**, 5912 (1970).

12) Abbreviations show a coupling manner with proton.

On the Mechanism of the Cleavage Reaction of (Methylthio)methyl Ether with Triphenylmethyl Cation

Haruki NIWA* and Yasuyoshi MIYACHI
Department of Chemistry, Faculty of Science, Nagoya University, Chikusa, Nagoya 464
(Received September 21, 1990)

Synopsis. The cleavage reaction of a (methylthio)methyl (MTM) ether with triphenylmethyl cation was not initiated by the previously proposed hydride abstraction with triphenylmethyl cation but promoted by the coordination of triphenylmethyl cation as a Lewis acid to the sulfur atom in the MTM group.

In the synthesis of polyfunctional molecules, (methylthio)methyl (MTM) ethers have been recognized as excellent protecting groups for hydroxyl functions, especially for tertiary alcohols owing to their facile formation and unique stability characteristics.[1] Although there have been reported various methods for removing the MTM protecting groups,[2] the reaction with triphenylmethyl tetrafluoroborate (Ph_3CBF_4)[2g] seems to be the most efficient and promising procedure owing to the mild reaction conditions, the simple procedure, and the wide applicability to polyfunctional molecules.[3] The mechanism of cleavage reaction of the MTM group has been thought *a priori* to be the same as proposed by Barton[4] for the oxidative cleavage of methylenedioxy ($O-CH_2-O$) groupings with Ph_3CBF_4: The initial step is abstraction of a hydride anion from MTM ether **A** with triphenylmethyl (trityl) cation to form intermediate **B**, which upon hydrolysis (workup) gave parent alcohol **C** (Scheme 1).[2g] However, we have found that this cleavage reaction is not initiated by hydride abstraction with trityl cation but promoted by the coordination of trityl cation to the sulfur in the MTM group.

As the substrate for the present investigation, we have chosen 1-adamantanol (tricyclo[3.3.1.1^{3,7}]decan-1-ol) MTM ether (**1**) prepared from 1-adamantanol (**2**) by Yamada's procedure (Ac_2O-DMSO).[2b] The reaction of **1** with 1.05 equiv of Ph_3CBF_4 in CH_2Cl_2 at room temperature for 10 min followed by quenching with aqueous $NaHCO_3$ (workup) provided 1-adamantanol (**2**) (88%) together with Ph_3COH (**6**) (77%) and Ph_3CSCH_3 (**8**) (16%) (Scheme 2). However, Ph_3CH was detected in only trace amounts (<1%). When the cleavage reaction of **1** with Ph_3CBF_4 was quenched with a large excess of methanol prior to aqueous workup, **2** was again obtained in 87% yield together with 1-adamantanol MOM ether (**3**) (11%), Ph_3COCH_3 (**7**) (84%), and Ph_3CSCH_3 (**8**) (8%). Only trace amounts (<1%) of Ph_3CH was again detected.

The above results clearly indicate that the cleavage of the MTM ether **1** with Ph_3CBF_4 is not initiated by hydride abstraction with trityl cation as proposed previously.[2g] Although trityl cation is well-documented[5] as a hydride ion acceptor, it has been also known to behave as a Lewis acid.[6] Therefore, the initial step in the cleavage reaction of the MTM ether **1** with Ph_3CBF_4 is supposed to be the complexation of trityl cation to the sulfur atom in the MTM group, forming the sulfonium salt **9** (Scheme 3).[6] Then, the sulfonium salt **9** comes to equilibrium with the collapsed oxonium salt **10** and Ph_3CSCH_3(**8**). During workup the sulfonium salt **9** and oxonium salt **10** may be decomposed via two competing reaction pathways [**a** and **b**]. When the reaction is quenched with H_2O (aqueous workup) (R=H) route **a** gives rise to the parent alcohol **2** and Ph_3COH (**6**) via **11**, whereas route **b** affords also **2** along with Ph_3CSCH_3 **8** through the intermediate **12** generated from **10**. On the other hand, quenching the reaction with methanol ($R=CH_3$) prior to aqueous workup provides the MOM ether **3** arising from the intermediate **10**, and again Ph_3CSCH_3 **8** in a ratio of ca. 1:1 through route **b**, whereas route **a** provides the parent alcohol **2** and

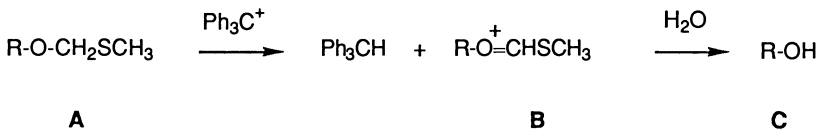

Scheme 1.

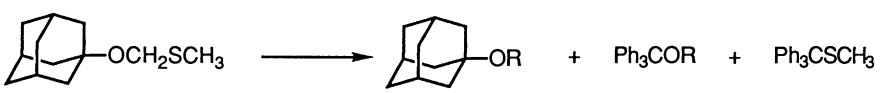

1

2 R = H
3 R = CH_2OCH_3
4 R = CPh_3
5 R = CH_3

6 R = H
7 R = CH_3

8

Scheme 2.

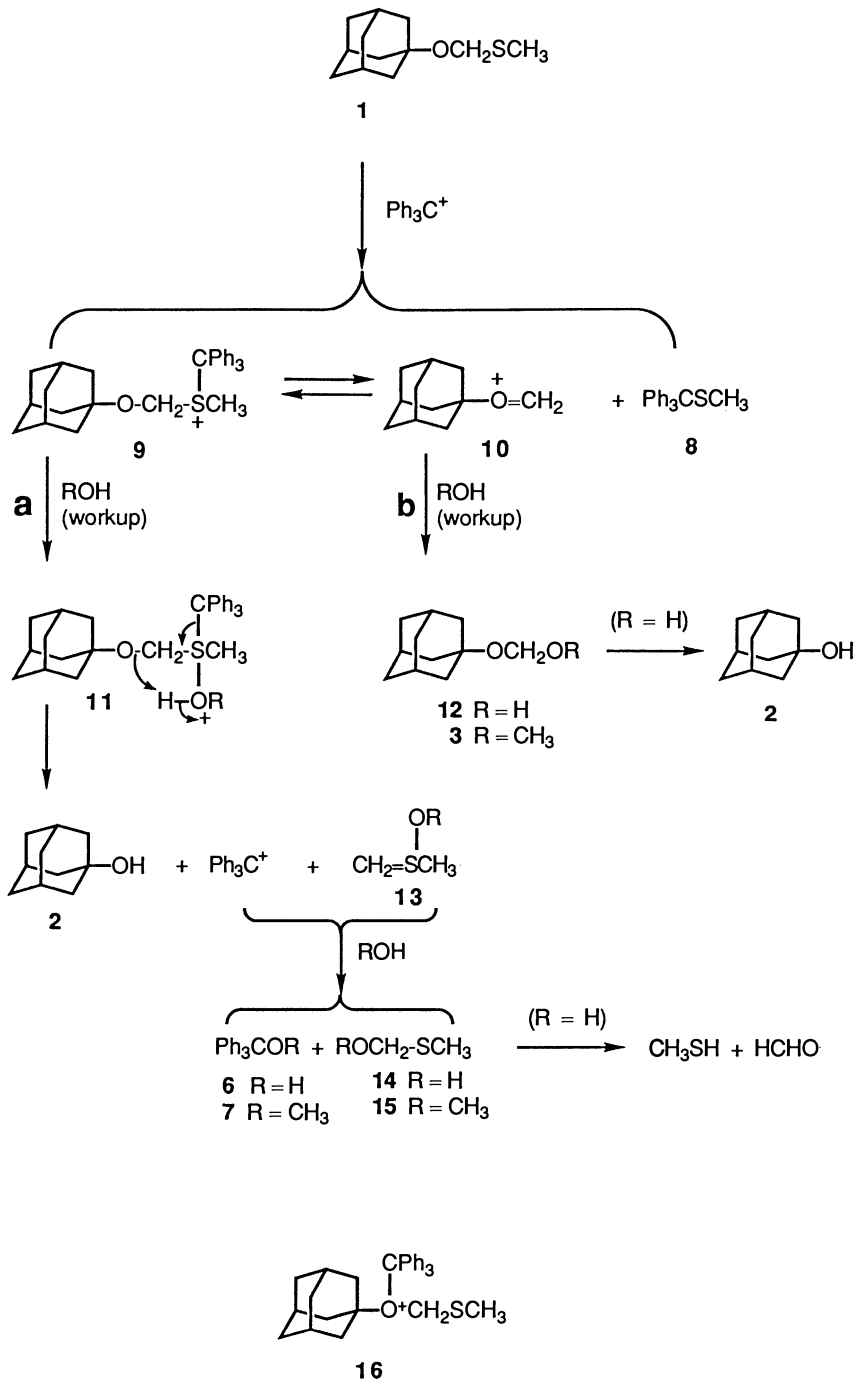

Scheme 3.

Ph_3COCH_3 (**7**) in a ratio of ca. 1:1. These experimental results suggest that the cleavage of the MTM ether **1** with Ph_3BF_4 predominantly proceeds through route **a**. The clean generation of the parent alcohol **2** without forming the corresponding trityl ether **4** precludes the intervention of the oxonium intermediate **16** during the course of the cleavage reaction. Intervention of 1-adamantyl cation is also ruled out because none of 1-adamantyl methyl ether (**5**) was formed on treatment of the reaction mixture with MeOH prior to aqueous workup. The reported results[2g,3] also indicate that the MTM groups can be removed with the complete retention concerning the configuration of the corresponding hydroxyl groups, precluding intervention of carbocation intermediates during the cleavage reactions.

Based on our understanding of the mechanism of this cleavage reaction, one would expect that Ph_3CClO_4 is also effective reagent to cleave the MTM ether **1**. Our experimental results on the reaction of **1** with Ph_3CClO_4 agree with this prediction, giving the similar result as the cleavage of **1** with Ph_3CBF_4 (see Experimental section).

In summary, the cleavage reaction of the MTM

ether **1** with Ph_3CBF_4 or Ph_3CClO_4 is found to be promoted by the coordination of trityl cation to the sulfur in the MTM group and not initiated by hydride abstraction with trityl cation.

Experimental

Infrared (IR) spectra were recorded on a JASCO Model IR-810 spectrophotometer in $CHCl_3$. Proton nuclear magnetic resonance (^1H NMR) spectra were determined on a JEOL FX-90QE (90 MHz) spectrometer in $CDCl_3$. Chemical shifts are expressed in ppm downfield from internal tetramethylsilane using the δ scale. The low (EIMS) and high resolution (HREIMS) mass spectra were measured on a JEOL-LG2000 instrument. Fuji-Davison silica gel BW-820-MH was used for column chromatography. Merck precoated silica gel 60 F_{254} plates, 0.25 mm thickness, were used for analytical thin-layer chromatography. Unless otherwise stated, materials were obtained from commercial suppliers and used without further purification. Trityl tetrafluoroborate (Ph_3CBF_4)[6] and trityl perchlorate (Ph_3CClO_4)[7] were purified by the reported procedures, respectively. Dichloromethane was freshly distilled from CaH_2. Methanol was distilled from magnesium methoxide. The organic solutions obtained by extractive workup were washed with saturated brine, dried over anhydrous sodium sulfate, and concentrated with a rotary evaporator under reduced pressure.

1-[(Methylthio)methoxy]tricyclo[3.3.1.1^{3,7}]decane (1). A mixture of tricyclo[3.3.1.1^{3,7}]decan-1-ol (**2**) (200 mg, 1.32 mmol), dimethyl sulfoxide (2.5 mL), and acetic anhydride (2.5 mL) was stirred at room temperature for 19 h and then 40 °C for 4 h.[2b] After cooling, the mixture was concentrated in vacuo and the resulting oily residue was purified by column chromatography on silica gel (1 : 1 benzene–ethyl acetate) to give **1** (141 mg, 51%) as a colorless oil: IR 1450, 1355, 1300, 1070, 1035 cm^{-1}; ^1H NMR δ=4.60 (s, 2H), 2.0—2.3 (m, 3H), 2.19 (s, 3H), 1.86 (m, 6H), 1.64 (m, 6H); EIMS *m/z* (rel intensity) 212 (M^+; 7), 182 (9), 165 (5), 152 (10), 136 (15), 135 (100), 95 (28), 79 (16). HREIMS. Found: *m/z* 212.1252. Calcd for $C_{12}H_{20}OS$: M, 212.1235.

Cleavage Reaction of 1 with Ph_3CBF_4. A. Quenching with Saturated $NaHCO_3$ Solution. To a stirred solution of **1** (93 mg, 0.44 mmol) in dichloromethane (4 mL) under nitrogen was added Ph_3CBF_4 (152 mg, 0.46 mmol) at room temperature. After being stirred for 15 min at room temperature, the reaction mixture was diluted with saturated $NaHCO_3$ solution (3 mL) and the mixture was stirred for 10 min and extracted with chloroform (3×10 mL). The combined organic layers were washed with saturated $NaHCO_3$ solution and saturated brine, dried and concentrated. The crude product was purified by column chromatography on silica gel (2 : 1 hexane–chloroform→chloroform) to provide 1-adamantanol (**2**) (59 mg, 88%), trityl alcohol (**6**) (92 mg, 77%), and methyl trityl sulfide (**8**) (22 mg, 16%). The spectral (IR , ^1H NMR, MS) properties of these compounds were identical with those of the authentic samples, respectively.

B. Quenching with MeOH Prior to Aqueous Work Up. After reaction of **1** (82 mg, 0.39 mmol) with Ph_3CBF_4 (134 mg, 0.41 mmol) in dichloromethane (4 mL) for 10 min at room temperature, the reaction mixture was diluted with MeOH (1 mL). After being stirred for 10 min at room temperature, the mixture was diluted with H_2O (5 ml) and extracted with chloroform (4×7 mL). The combined organic solutions were washed with saturated $NaHCO_3$ solution and saturated brine, dried, and concentrated. Purification of the resulting crude product by column chromatography on silica gel (2 : 1 hexane–chloroform→chloroform) afforded **2** (51 mg , 87%), 1-(methoxymethoxy)tricyclo-[3.3.1.1^{3,7}]decane (**3**) (8 mg, 11%), methyl trityl ether (**7**) (93 mg, 84%), and **8** (9 mg, 8%). **3**: A colorless oil; IR 1455, 1355, 1145, 1035, 910 cm^{-1} ^1H NMR δ=4.77 (s, 2H), 3.37 (s, 3H), 2.0—2.3 (m, 3H), 1.82 (m, 6H), 1.63 (m, 6H); EIMS *m/z* (rel intensity) 196 (M^+; 76), 166 (37), 139 (47), 135 (100), 109 (78), 107 (63), 95 (44), 79 (33). HREIMS. Found: *m/z* 196.1491. Calcd for $C_{12}H_2O_2$: M, 196.1463.

Cleavage Reaction of 1 with Ph_3CClO_4. To a stirred solution of **1** (44 mg, 0.21 mmol) in dichloromethane (2 mL) under nitrogen was added Ph_3CClO_4 (78 mg, 0.23 mmol) at room temperature. After being stirred for 30 min, the reaction mixture was diluted with saturated $NaHCO_3$ solution (3 mL). The mixture was vigorously stirred for 10 min and extracted with chloroform (4×10 mL). The combined organic solutions were washed, dried and concentrated. Purification of the crude residue by column chromatography on silica gel (2 : 1 hexane–chloroform→chloroform) provided **2** (27 mg, 85%), **6** (44 mg, 75%), and **8** (17 mg, 25%).

We are deeply indebted to Professor Kiyoyuki Yamada for the valuable discussions and the encouragement for the present research.

References

1) T. W. Greene, "Protective Groups in Organic Synthesis," Wiley-Interscience, New York (1981).

2) a) E. J. Corey and M. G. Bock, *Tetrahedron Lett.*, **1975**, 3269. b) K. Yamada, K. Kato, H. Nagase, and Y. Hirata, *Tetrahedron Lett.*, **1976**, 65. c) P. M. Pojer and S. J. Angyal, *Tetrahedron Lett.*, **1976**, 3067. P. M. Pojer and S. J. Angyal, *Aust. J. Chem.*, **31**, 1031 (1978). d) R. A. Holton and R. G. Davis, *Tetrahedron Lett.*, **1977**, 533. 4) H. Niwa and M. Kurono, *Chem. Lett.*, **1979**, 23. f) Y. Guindon, H. E. Morton, and C. Yoakim, *Tetrahedron Lett.*, **24**, 3969 (1983). Y. Guindon, C. Yoakim, and H. E. Morton, *J. Org. Chem.*, **49**, 3912 (1984). g) P. K. Chowdhury, R. P. Sharma, and J. N. Baruah, *Tetrahedron Lett.*, **24**, 4485 (1983). h) N. C. Barua, R. P. Sharma, and J. N. Baruah, *Tetrahedron Lett.*, **24**, 1189 (1983). D. N. Sarma, N. C. Barua, and R. P. Sharma, *Chem. Ind.*, **1984**, 223.

3) Recent application to the synthesis of a polyfunctional natural product: H. Niwa, Y Miyachi, Y. Uosaki, A. Kuroda, H. Ishiwata, and K. Yamada, *Tetrahedron Lett.*, **27**, 4609 (1986).

4) D. H. R. Barton, P. D. Magnus, G. Smith, G. Streckert, and D. Zurr, *J. Chem. Soc., Perkin Trans. 1*, **1972**, 542.

5) C. D. Nenitzescu, "Intermolecular Hydride Transfer Reactions Involving Carbonium Ion in Carbonium Ions," ed by G. A. Olah and P. von R. Schleyer, Wiley-Interscience, New York (1970), Vol. 2.

6) A synthetic reaction promoted by complexation of trityl cation to the sulfur in the thioacetal has been reported: M. Ohshima, M. Murakami, and T. Mukaiyama, *Chem. Lett.*, **1985**, 1871, and references cited therein.

7) H. J. Dauben, Jr., L. R. Honnen, and K. M. Harmon, *J. Org. Chem.*, **25**, 1442 (1960).

Preparation of Pyrazoles Using Hydrazyl Radicals Initiated by DPPH

Nobutoshi YOSHIHARA,* Tadashi HASEGAWA, and Sadao HASEGAWA
Department of Chemistry, Tokyo Gakugei University, Nukuikitamachi, Koganei, Tokyo 184
(Received September 28, 1990)

Synopsis. Hydrazyl radicals, initiated by DPPH, reacted with α,β-unsaturated ketones without any good leaving group on their β-positions to yield pyrazoles regioselectively.

Recently, though free radicals have been actively used as intermediates in organic synthesis.[1] only a little is known about the application of such a reaction to the synthesis of heteroaromatics. The physical properties of these hydrazyl radicals have been well studied;[2,3] nevertheless, these radicals have not been used in any successful organic synthesis. The hydrazyl radicals can be expected to be useful as synthetic intermediates for introducing a nitrogen-nitrogen chromophore in the synthesis of such heteroaromatics as pyrazoles, which are important and useful compounds in organic and drug synthesis.[4] The widely accepted methods for the synthesis of pyrazoles involve the reaction of hydrazines with bifunctional compounds, such as 1,3-diketones[5] or α,β-unsaturated ketones with good leaving groups on their β-positions.[5] Unsaturated ketones without any good leaving group on their β-positions have been scarecely used in the synthesis of pyrazoles. We report here on a novel, convenient method for the synthesis of pyrazoles using hydrazyl radicals, initiated by 2,2-diphenyl-1-picrylhydrazyl (DPPH), and simple α,β-unsaturated ketones without any good leaving groups on the β-positions.

The reaction of methylhydrazine (**1a**) with 4-phenyl-3-buten-2-one (**3a**) in the presence of DPPH at −78 °C proceeded resioselectively to give 1,5-dimethyl-3-phenyl-1*H*-pyrazole (**4a**) in 12% yield. Only a trace amount of an isomeric pyrazole, 1,3-dimethyl-5-phenyl-1*H*-pyrazole (**5a**), was detected. Similarly, the reaction of **1a** with 3-buten-2-one (**3b**) under the same conditions gave dimethylpyrazoles **4b** and **5b** in 50 and 7% yields, respectively. The reaction of **1a** with 1,3-diphenyl-2-propen-1-one (**3c**) under the same conditions also gave 1-methyl-3,5-diphenyl-1*H*-pyrazole (**4c**) in 30% yield. The structures of the pyrazoles, **4a—c** and **5a—b**, were determined by a comparison with authentic samples.[6-8]

In these pyrazole formations, the role of DPPH is quite important. No pyrazoles were produced when DPPH was absent. Methylhydrazine did not react with **5a** at −78 °C. When a mixture of **1a** and **3a** was refluxed in benzene, 1,3-dimethyl-5-phenyl-2-pyrazoline (**6**) was obtained in 92% yield. The structure of the pyrazoline **6** was determined by a comparison with an authentic sample.[9] The pyrazoline **6** may be considered to be a precursor of the pyrazoles. However, this idea can be excluded for the following reasons: 1) The resioselectivity of pyrazoline formation is completely reversed to that in the pyrazole formation. The dehydrogenation of the pyrazoline **6** should give a minor isomer of the pyrazoles **5a**. 2) When **6** was stirred with DPPH, no pyrazoles were formed. Pyrazoline formation can be explained in terms of the 1,2-addition of the hydrazine **1a** to the α,β-unsaturated ketones **3** followed by cyclization and dehydration.

Table 1. Yields of the Reaction of **1** with **3** in the Presence of DPPH

	R	R^1	R^2	Yield/%	
				4	**5**
a	Me	Me	Ph	12	Trace
b	Me	Me	H	50	7
c	Me	Ph	Ph	30	
d	H	Me	Ph	27	
e	H	Me	H	24	
f	H	Ph	Ph	23	

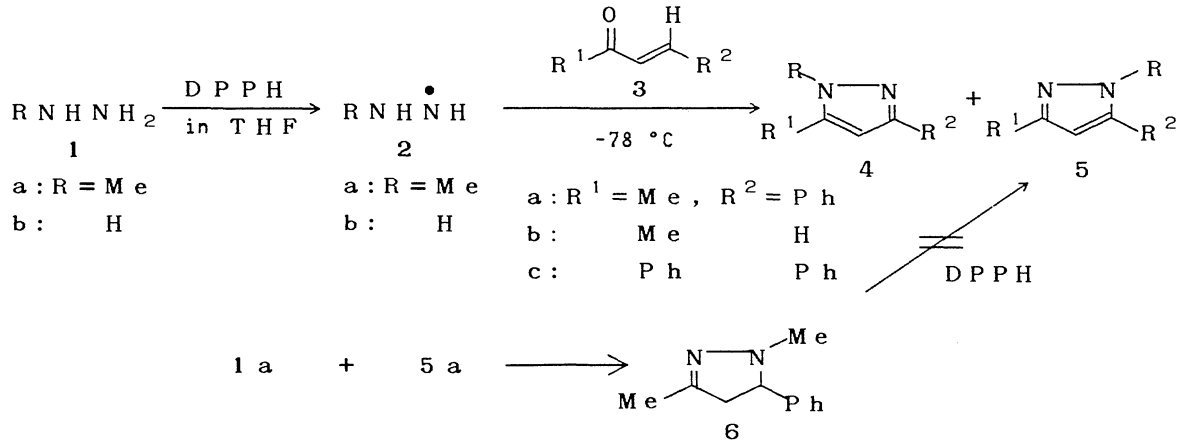

Scheme 1.

The behavior of **1a** in the pyrazole formation should be quite different from that in pyrazoline formation. When **1a** was added to a THF solution of DPPH, a purple color characteristic of the DPPH radical in THF changed to the brown characteristic of $DPPH_2$. This implies that DPPH abstracts hydrogen from **1a** to form $DPPH_2$ and the 2-methylhydrazyl radical. Both of the hydrogens on and N_1 and N_2 in 1-methylhydrazine (**1a**) may be abstractable by DPPH. However, sterically less hindered hydrogen on N_2 seems to be predominantly abstracted by the sterically hindered DPPH radical. The 2-methylhydrazyl radical (**2a**) is probably an intermediate in pyrazole formation. The quite different regioselectivlty in pyrazole formation from that in a normal Michael addition[10] can be reasonably explained in terms of the addition of radical **2a** to the β-position of enones.

Hydrazine itself (**1b**) could also be used as a radical precursor. The hydrazyl radical (**2b**) was easily prepared by the addition of DPPH to a THF solution of **1b** at −78 °C. The reactions of **2b** with the enones **3a**, **3b**, and **3c** gave the corresponding pyrazoles **4d**, **4e**, and **4f** in 27, 24, and 23% yields, respectively. The structures of **4d—f** were determined by a comparison with authentic samples.[1]

The hydrazyl radicals, initiated easily and rapidly by DPPH, reacted with simple α,β-unsaturated ketones without any good leaving group on their β-positions. The hydrazyl radicals can be used as reagents for introducing a nitrogen-nitrogen chromopher in the synthesis of heteroaromatics.

Experimental

General Procedure for Preparation of Pyrazoles. To the solution of a hydrazine (0.75—1.5 mmol) dissolved in 30 cm^3 of THF and cooled to −78 °C, was added DPPH (0.75—1.5 mmol) with stirring. The mixture was cooled to −78 °C and added dropwise to a solution of enones (0.5—1 mmol) in 50 cm^3 of THF at −78 °C. The mixture was stirred for 2 h at the same temperature. After concentration in vacuo, the residue was chromatographed on a silica-gel column (Merck Kieselgel 60). Elution with benzene or a mixture of benzene–ethyl acetate gave **4** and/or **5**. The structures of **4a-f** and **5a-b** were determined by a comparison with direct comparisons with authentic samples.[6,7,8,11]

Preparation of 1,3-Dimethyl-5-phenyl-2-pyrazoline (6). A solution of benzalacetone (0.50 g, 3.4 mmol) and methylhydrazine (0.51 g, 4.7 mmol) in 50 cm^3 of benzene was refluxed overnight. The mixture was poured into water and extracted three times with 30 cm^3 of dichloromethane. The dichloromethane solution was washed with water and then dried over magnesium sulfate. After filtration and removal of the solvent, the residue was chromatographed on a silica-gel column (Merck Kieselgel 60). Elution with benzene gave **6** (0.54 g, 3.1 mmol, 92%): 131 °C/25 mmHg (lit,[9] 123—4 °C/20 mmHg) (1 mmHg=133.322 Pa). The structure of **6** was determined by a comparison with an authentic sample.[9]

References

1) B. Giese, "Radicals in Organic Synthesis; Formation of Carbon-Carbon Bonds," Pergamon Press, New York (1986).

2) E. Hayon and M. Simic, *J. Am. Chem. Soc.*, **94**, 42 (1972).

3) a) D. E. Wood, C. A. Wood, and W. A. Lathan, *J. Am. Chem. Soc.*, **94**, 9278 (1972); b) S. F. Nelsen and R. T. Landis, II, *ibid.*, **95**, 2719 (1973); *ibid.*, **95**, 6451 (1973); *ibid.*, **96**, 1788 (1974); c) R. A. Kaba, L. Lunazzi, D. Lindsay, and K. U. Ingold, *ibid.*, **97**, 6762 (1975).

4) J. Eleguro, "Comprehensive Heterocyclic Chemistry," ed by A. R. Katritzky and C. W. Rees, Pergamon Press, New York (1984), Vol. 5, p. 167.

5) a) F. G. Badder, F. H. Al-Hajjar, and N. R. El-Rayyes, *J. Heterocycl. Chem.*, **13**, 257 (1976); b) H. Dorn, *Chem. Heterocycl. Compd.*, **16**, 1 (1980).

6) J.-L. Aubagnac, J. Elguero, and R. Jacquier, *Bull. Soc. Chim. Fr.*, **1969**, 3306.

7) G. Coispeau and J. Elguero, *Bull. Soc. Chim. Fr.*, **1970**, 2717.

8) J. Elguero and R. Jacquler, *Bull. Soc. Chim. Fr.*, **1966**, 2832.

9) J. L. Aubagnac, P. Bouchet, J. Elguero, R. Jacquier, and C. Marzin, *J. Chim. Phys. Phys.-Chim. Biol.*, **64**, 1649 (1967).

10) E. Benary and W. Kerckckoff, *Ber.*, **59**, 2548 (1926).

11) K. van Auwers and Th. Breyhan, *J. Prakt. Chem.*, **143**, 259 (1935).

Synthesis of Lateral Root-Inducing Compounds Using an Efficient Coupling Reaction of Chiral Triflates

Hiyoshizo KOTSUKI,* Aya MIYAZAKI, Masamitsu OCHI, and James J. SIMS†
Department of Chemistry, Faculty of Science, Kochi University, Akebono-cho, Kochi 780
†Department of Plant Pathology, University of California, Riverside, CA 92521, U.S.A.
(Received October 1, 1990)

Synopsis. Lateral root-inducing compounds, isolated from the bacterium *Erwinia quercina*, have been synthesized by using a coupling reaction of chiral triflates derived from L- or D- tartrates and their biological activities examined.

Recent studies in our laboratories have revealed that the copper(I)-catalyzed coupling reaction of chiral trifluoromethanesulfonates (triflates) with Grignard reagents is a powerful technique to synthesize optically active natural products.[1] As an extension of these studies, we herein wish to describe a new versatile strategy towards lateral root-inducing compounds isolated from the bacterium *Erwinia quercina*.[2] Sims et al. reported that these compounds are a mixture of two diastereomers of 4,5-dihydroxy-6-phenylhexanoic acid; synthetically, they confirmed that all four possible chiral isomers possess biological activity.[2] However, their synthesis involves a non-stereoselective reduction step and, hence, requires an unavoidable separation stage from the diastereomeric mixture. Compared with this example, our route is of great advantage for deriving these compounds in complete enantioselectivity while providing a rapid means for bioassay.[3]

A concise route to (4*S*,5*S*)- and (4*S*,5*R*)-isomers (**1a** and **1b**)[4] is shown in Scheme 1. Utilizing the strategy already developed in these laboratories,[1d] mono-*p*-toluenesulfonate (tosylate) **2** was converted into the key intermediate **4** either stepwise or by a one-pot double alkylation method.

Thus, the reaction of **2** with allylmagnesium bromide (7 equiv) in the presence of a catalytic amount of CuBr produced **3** in 83% yield. Triflation followed by treatment with PhMgBr (3 equiv)-CuBr gave the

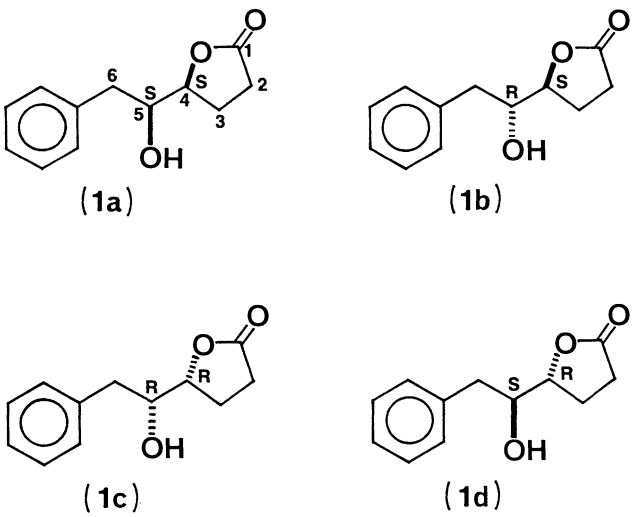

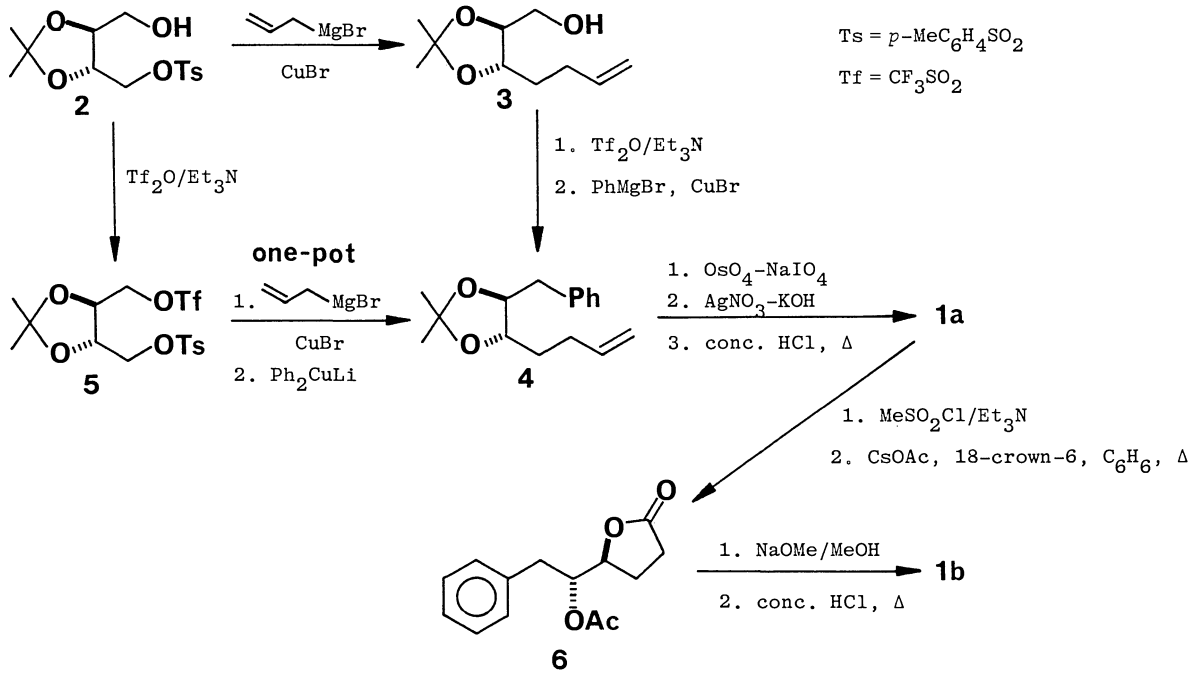

Scheme 1.

required intermediate **4** in 71% yield. Alternatively, after conversion of **2** into the corresponding tosyltriflate derivative **5**, one-pot double alkylation first with allylmagnesium bromide (1.1 equiv)-CuBr (at 0 °C for 1 h) and secondly with Ph_2CuLi (3.0 equiv) (at −15 °C for 4 h) afforded **4** in 33% yield from **2**. In contrast to the stepwise method, unfortunately, this one-pot double alkylation procedure could not improve so much the overall yield. This, however, does not loose its synthetic superiority from the viewpoint of the experimental simplicity as well as the economical usage of two kinds of alkylating agents.

The double bond in **4** was smoothly oxidized to the corresponding carboxylic acid (OsO_4-$NaIO_4$ then $AgNO_3$-KOH), which underwent lactonization under acidic conditions to give the (4*S*,5*S*)-isomer (**1a**) {$[\alpha]_D^{21}$ +59.8° (*c* 1.04, $CHCl_3$); lit,[2] $[\alpha]_D$ +49.06° (*c* 1.28, $CHCl_3$)} in 91% yield from **4**. Applying the Ikegami's inversion technique,[5] **1a** was efficiently converted into acetate **6**, which was further treated with NaOMe in MeOH to afford the (4*S*,5*R*)-isomer (**1b**) {$[\alpha]_D^{20}$ +34.0° (*c* 0.96, $CHCl_3$); lit,[2] $[\alpha]_D$ +29.22° (*c* 0.84, $CHCl_3$)} in 69% yield from **1a**.

The application of the same synthetic procedure on the enantiomer of **2**, available from D-tartrates, furnished the (4*R*,5*R*)-isomer (**1c**) {$[\alpha]_D^{21}$ −60.0° (*c* 0.5, $CHCl_3$); lit,[2] $[\alpha]_D$ −50.77° (*c* 0.2, $CHCl_3$) and also the (4*R*,5*S*)-isomer (**1d**) {$[\alpha]_D^{20}$ −34.2° (*c* 1.20, $CHCl_3$); lit,[2] $[\alpha]_D$ −29.23° (*c* 0.2, $CHCl_3$) in good overall yields.

A comparison of the specific rotation of our samples with literature data showed a higher optical purity for all of our chiral isomers. These results prompted us to reexamine the structure-activity relationship of these molecules.[6] However, we found that all of our compounds were active at 10^{-5} M (1 M=1 mol dm^{-3}), with only a slight difference between isomers.[7] These results are compatible with previous evidence.[2] Apparently, the stereochemistry of the compounds is not critical to the activity. One possibility is that the chirality is changed or destroyed by metabolism in the carrot discs; a bioassay required 10 days to complete. Further experiments are required to clarify this observation and to identify the actual active compound.

Experimental

All melting points are uncorrected. The NMR spectra were recorded on a Hitachi R-90H spectrometer (90 MHz for ^{1}H NMR analysis and 22.6 MHz for ^{13}C NMR analysis). All NMR spectra were taken in a $CDCl_3$ solution and tetramethylsilane was used as an internal standard. The IR spectra were measured with a JASCO Model FT/IR-5000 Fourier Transform Infrared spectrometer. High-resolution mass spectra were obtained with a JEOL HX-100 spectrometer. Optical rotations were measured on a Union PM-101 polarimeter. Thin-layer chromatography was conducted by using Merck precoated Kieselgel 60F-254 plates (0.25 mm). Column chromatography was carried out on a Wakogel C-300, and for flash chromatography, Merck Kieselgel (230—400 mesh) was employed.

All solvents were dried immediately before use. Et_2O, C_6H_6 and tetrahydrofuran (THF) were distilled from sodium diphenylketyl; dichloromethane and triethylamine were distilled from CaH_2. All Grignard and organolithium reagents were titrated before use according to methods described in the literature.[8] All reactions were carried out in a nitrogen or argon atmosphere.

Preparation of 3 from 2. To an ice-cooled suspension of CuBr (65 mg, 0.45 mmol) in 1.5 ml of dry Et_2O was added 0.39 M of an allylmagnesium bromide/Et_2O solution (5.4 ml, 2.1 mmol), followed by the introduction of an Et_2O solution (1.5 ml) of monotosylate **2** (95 mg, 0.3 mmol); the mixture was then stirred for 1 h. During the reaction a black insoluble substance was gradually formed. The reaction was quenched by the addition of aqueous NH_4Cl-aqueous NH_3 (9:1); the mixture was then filtered through Celite. The filtrate was extracted with Et_2O, and the combined extracts were washed with aqueous saturated $NaHCO_3$ and brine, and dried over Na_2SO_4. Evaporation of the solvent gave a crude product which was purified by column chromatography (C-300; from hexane/Et_2O=2:1 to 1:1) to give 46 mg (83%) of **3** as a colorless oil.

3: R_f 0.49 (Et_2O); $[\alpha]_D^{23}$ −27.1° (*c* 1.1, $CHCl_3$); IR (neat) 3500, 1644, 1054, 913, and 855 cm^{-1}; ^{1}H NMR δ=1.41 (6H, s), 1.5—1.8 (2H, m), 1.88 (1H, s), 2.05—2.4 (2H, m), 3.5—4.0 (4H, m), 4.98 (1H, brd, *J*=10.0 Hz), 5.02 (1H, brd, *J*=17.2 Hz), 5.84 (1H, ddt, *J*=17.2, 10.0, 6.5 Hz); ^{13}C NMR δ=27.03, 27.33, 29.98, 32.30, 62.06, 76.39, 81.42, 108.56, 114.87, 137.64. Found: *m/z* 186.1248. Calcd for $C_{10}H_{18}O_3$: M, 186.1256.

Enantiomer of **3**: $[\alpha]_D^{19}$ +27.3° (*c* 1.1, $CHCl_3$).

Preparation of 4 from 3. To a mixture of alcohol **3** (520 mg, 2.8 mmol) and Et_3N (1.2 ml, 8.6 mmol) in 9 ml of dry CH_2Cl_2 was added dropwise a CH_2Cl_2 solution (3 ml) of $(CF_3SO_2)_2O$ (710 μl, 4.2 mmol) at −15 °C; the mixture was then stirred for 20 min. After dilution with CH_2Cl_2, the mixture was treated conventionally. The crude product was dried azeotropically with toluene and used in the following step.

To an ice-cooled suspension of CuBr (80 mg, 0.56 mmol) in 6 ml of dry THF was added 1.6 M of PhMgBr/Et_2O solution (5.3 ml, 8.5 mmol) followed by the introduction of a THF solution (12 ml) of the triflate (obtained as mentioned above); the mixture was then stirred at 0 °C for 8 h. The reaction was quenched by the addition of aqueous NH_4Cl-aqueous NH_3 (9:1), the mixture filtered through Celite. After removing the solvent, the residue was extracted with Et_2O. After the usual workup, the crude product was purified by column chromatography (flash silica gel; hexane/Et_2O=50:1) to give 495 mg (72%) of **4** as a colorless oil.

4: R_f 0.60 (hexane/Et_2O=2:1); $[\alpha]_D^{23}$ −28.0° (*c* 2.0, $CHCl_3$); IR (neat) 2988, 2936, 1642, 1497, 1456, 1375, 1058, and 913 cm^{-1}; ^{1}H NMR δ=1.36 (6H, s), 1.2—1.6 (2H, m), 1.9—2.3 (2H, m), 2.81 (1H, dd, *J*=14.0, 5.3 Hz), 2.94 (1H, dd, *J*=14.0, 5.7 Hz), 3.55—4.0 (2H, m), 4.8—5.1 (1H, m), 5.75 (1H, ddt, *J*=17.1, 9.6, 6.1 Hz), 7.24 (5H, s); ^{13}C NMR δ=27.27, 27.39, 30.05, 32.12, 39.38, 79.87, 80.99, 108.04, 114.72, 126.33, 128.19(×2), 129.23(×2), 137.49, 137.86. Found: *m/z* 246.1601. Calcd for $C_{16}H_{22}O_2$: M, 246.1620.

Enantiomer of **4**: $[\alpha]_D^{22}$ +28.4° (*c* 2.0, $CHCl_3$).

Preparation of 5 from 2. To a mixture of monotosylate **2** (116 mg, 0.37 mmol) and Et_3N (155 μl, 1.1 mmol) in 2 ml of dry CH_2Cl_2 was added dropwise a CH_2Cl_2 solution (1 ml) of $(CF_3SO_2)_2O$ (95 μl, 0.56 mmol) at −15 °C; the mixture was then stirred for 20 min. After dilution with CH_2Cl_2, the mixture was treated conventionally and the crude tosyltriflate **5** was used in the following step, as described above.

Preparation of 4 from 5. To an ice-cooled suspension of CuBr (10 mg, 0.07 mmol) in 1.5 ml of dry Et_2O was added a 0.39 M allylmagnesium bromide/Et_2O solution (1 ml, 0.39 mmol), followed by the introduction of an Et_2O solution (0.5 ml) of tosyl-triflate **5** (obtained as mentioned above); the mixture was then stirred at 0 °C for 1 h. During the reaction, a black insoluble substance was gradually formed.

Then, Ph_2CuLi (prepared from CuI (211 mg, 1.11 mmol) and 1.19 M of PhLi/Et_2O solution (1.9 ml, 2.26 mmol) in dry Et_2O (3 ml)) was introduced at −15 °C; the mixture was then stirred at this temperature for 4 h. The reaction was quenched by the addition of aqueous NH_4Cl-aqueous NH_3 (9:1) and the mixture filtered through Celite. After the usual workup, the crude product was purified by column chromatography (flash silica gel; hexane/Et_2O=50:1) to give 30 mg (33%) of **4** as a colorless oil.

Preparation of 1a from 4. The starting material **4** (74 mg, 0.3 mmol) was dissolved in 9 ml of THF/H_2O (5:4) and an Et_2O solution of OsO_4 (5 mg in 0.5 ml) was added at room temperature. After stirring for 10 min, $NaIO_4$ (330 mg, 1.5 mmol) was added and the mixture stirred for 0.5 h. The mixture was then quenched by the addition of brine, and the conventional treatment gave a crude aldehyde which was subjected to the next reaction.

To a stirred solution of the aldehyde obtained above in 2.5 ml of MeOH were successively added $AgNO_3$ (102 mg, 0.6 mmol) in 1.5 ml of H_2O and KOH (67 mg, 1.2 mmol) in 1 ml of H_2O. After stirring for 0.5 h at 0 °C, the mixture was acidified with concentrated HCl and heated at 50 °C for 0.5 h. After removing the insoluble substance by filtration through Celite, the filtrate was concentrated in vacuo. The usual treatment of the residue gave a crude product which was purified by column chromatography (flash silica gel; from hexane/Et_2O=1:2 to Et_2O only) to give 56 mg (91%) of **1a** as a colorless oil.

1a: R_f 0.26 (Et_2O); $[\alpha]_D^{21}$ +59.8° (*c* 1.04, $CHCl_3$); IR (neat) 3500, 1769, and 1191 cm^{-1}; ^1H NMR δ=2.0—2.4 (2H, m), 2.4—2.7 (2H, m), 2.58 (1H, s), 2.91 (2H, d, *J*=7.0 Hz), 3.80 (1H, dt, *J*=6.8, 3.1 Hz), 4.42 (1H, dt, *J*=7.1, 3.3 Hz), 7.27 (5H, s); ^{13}C NMR δ=23.92, 28.55, 39.89, 74.26, 81.21, 126.61, 128.53(×2), 129.26(×2), 137.19, 177.43. Found: *m/z* 206.0932. Calcd for $C_{12}H_{14}O_3$: M, 206.0943.

1c, enantiomer of **1a**: $[\alpha]_D^{21}$ −60.0° (*c* 0.5, $CHCl_3$).

Preparation of 1b from 1a. To an ice-cooled mixture of alcohol **1a** (65 mg, 0.32 mmol), Et_3N (88 µl, 0.63 mmol) and a catalytic amount of 4-(dimethylamino)pyridine in 3.0 ml of dry CH_2Cl_2 was added methanesulfonyl chloride (30 µl, 0.39 mmol); the mixture was then stirred at room temperature for 1 h. The usual workup gave a crude methanesulfonate which was used without further purification in the following step.

A mixture of the methanesulfonate (obtained as mentioned above), CsOAc (200 mg, 1.0 mmol) and 18-crown-6 (100 mg, 0.38 mmol) was refluxed in dry C_6H_6 (9 ml) for 12 h. After dilution with Et_2O, the organic layer was treated conventionally and the crude product was purified by column chromatography (flash silica gel; hexane/Et_2O=1:2) to give 56 mg (71%) of acetate **6** as colorless needles (recrystallized from Et_2O-hexane).

6: Mp 75.0—76.0 °C; R_f 0.40 (Et_2O); $[\alpha]_D^{19}$ +43.1° (*c* 0.52, $CHCl_3$); IR ($CHCl_3$) 1779, 1744, 1236, and 1044 cm^{-1}; ^1H NMR δ=2.00 (3H, s), 2.1—2.4 (2H, m), 2.4—2.7 (2H, m), 2.91 (1H, dd, *J*=14.3, 6.6 Hz), 2.98 (1H, dd, *J*=14.3, 6.6 Hz), 4.47 (1H, dt, *J*=6.6, 5.1 Hz), 5.28 (1H, dt, *J*=6.6, 4.8 Hz), 7.24 (5H, m). Found: C, 67.77; H, 6.51%. Calcd for $C_{14}H_{16}O_4$: C, 67.73; H, 6.50.

Enantiomer of **6**: Mp 74.5—75.0 °C; $[\alpha]_D^{19}$ −41.8° (*c* 1.3, $CHCl_3$).

Preparation of 1b from 6. To a solution of acetate **6** (80 mg, 0.32 mmol) in 5 ml of absolute MeOH was added 0.4 M NaOMe/MeOH (1 ml, 0.4 mmol) at 0 °C and the mixture was stirred at the same temperature for 1 h. At the end of the reaction the mixture was acidified with concentrated HCl and heated at 50 °C for 0.5 h. After removing most of the organic solvent, the residue was extracted with AcOEt. The usual workup gave a crude product which was purified by column chromatography (flash silica gel, hexane/Et_2O=1:4) to afford 64 mg (97%) of **1b** as colorless needles (recrystallized from Et_2O-hexane).

1b: Mp 60.0—61.0 °C (lit,[2] 59—60 °C); R_f 0.30 (Et_2O); $[\alpha]_D^{20}$ +34.0° (*c* 0.96, $CHCl_3$); IR ($CHCl_3$) 3434, 1775, and 1187 cm^{-1}; ^1H NMR δ=1.8—2.7 (6H, m), 4.10 (1H, ddd, *J*=7.7, 5.7, 4.4 Hz), 4.41 (1H, dt, *J*=7.0, 4.0 Hz), 7.27 (5H, m); ^{13}C NMR δ=21.60, 28.49, 39.01, 72.52, 81.85, 126.64, 128.53(×2), 129.14(×2), 136.94, 177.37. Found: C, 69.89; H, 6.86. Calcd for $C_{12}H_{14}O_3$: C, 69.88; H, 6.84.

1d, enantiomer of **1b**: Mp 58.0—60.5 °C; $[\alpha]_D^{20}$ −34.2° (*c* 1.20, $CHCl_3$).

The authors are grateful to Dr. Ayumi Ohsaki of Kinki University for the measurements of high-resolution mass spectra. We also thank Central Glass Co., Ltd., for partial support of this work.

References

1) a) H. Kotsuki, I. Kadota, and M. Ochi, *Tetrahedron Lett.*, **30**, 1281 (1989). b) H. Kotsuki, I. Kadota, and M. Ochi, *ibid.*, **30**, 3999 (1989). c) H. Kotsuki, Y. Ushio, I. Kadota, and M. Ochi, *J. Org. Chem.*, **54**, 5153 (1989). d) H. Kotsuki, I. Kadota, and M. Ochi, *ibid.*, **55**, 4417 (1990). e) H. Kotsuki, I. Kadota, and M. Ochi, *Tetrahedron Lett.*, **31**, 4609 (1990). f) H. Kotsuki, in "Research Trends-Organic Chemistry," Council of Scientific Research Integration, Trivandrum, India; in press.

2) A. E. Wright, M. Schäfer, S. Midland, D. E. Munnecke, and J. J. Sims, *Tetrahedron Lett.*, **30**, 5699 (1989).

3) As the target molecules we chose lactones **1** which were isolated as artifacts of 4,5-dihydroxy-6-phenylhexanoic acid. See Ref. 2.

4) For the convenience, the numbering of these compounds is based on their parent molecule of 4,5-dihydroxy-6-phenylhexanoic acid.

5) Y. Torisawa, H. Okabe, and S. Ikegami, *Chem. Lett.*, **1984**, 1555.

6) "Stereochemistry and Biological Activity of Drugs," ed by E. J. Ariens, W. Soudijn, and P. B. M. W. M. Timmermans, Blackwell Scientific Publications, Oxford (1983).

7) For the procedure of bioassay, see Ref. 2.

8) "Yukikagaku Jikken no Tebiki," ed by T. Goto, T. Shiba, and T. Matsuura, Kagakudojin, Kyoto (1988), Vol. 1.

Photoinduced Intramolecular Cyclization Reaction of 2-(2-Alkenoyl)-3-isopropylthio-1,4-benzoquinones to Heterocyclic Compounds

Hidetoshi IWAMOTO* and Akio TAKUWA
Department of Chemistry, Faculty of Science, Shimane University, Matsue 690
(Received October 8, 1990)

Synopsis. Irradiation of 2-acryloyl- and 2-(1-cycloalkenylcarbonyl)-3-isopropylthio-1,4-benzoquinones in benzene gave tricyclic and tetracyclic compounds in good yields, respectively.

We recently reported that photochemical reactions of 3-alkoxy- (**1**, X=O)[1] and 3-alkylthio-2-cinnamoyl-1,4-benzoquinones (**1**, X=S)[2] give tricyclic compounds (**5**, X=O or S) in good yields together with other minor secondary products.[2,3] In these reactions, the biradical intermediate **2** generated by an intramolecular hydrogen abstraction of **1** easily cyclizes with the carbonyl oxygen of the cinnamoyl group to give another cyclic intermediate **3**; it finally yields the tricyclic product **5** (Eq. 1).[1,2] For an extension of this cyclization reaction, we examined the photochemical reaction of 2-acryloyl- (**6**) and 2-(1-cycloalkenylcarbonyl)-3-isopropylthio-1,4-benzoquinones (**11**).

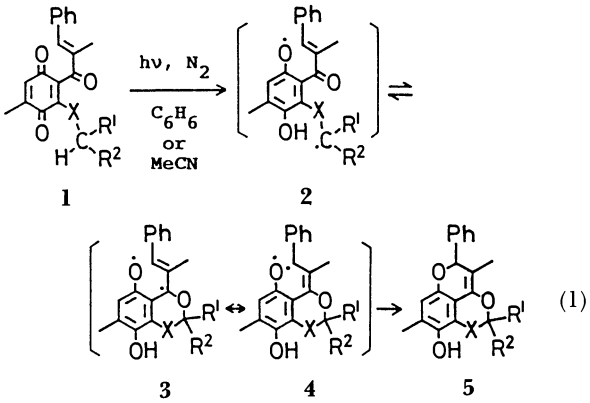

(1)

X=O or S; R^1=R^2=H, R^1=Me, R^2=H, R^1=R^2=Me

Results and Discussion

Irradiation of a benzene solution of **6** (0.01 mol dm^{-3}) with light of wavelength longer than 410 nm under a nitrogen atmosphere for 1 h afforded a mixture of **7**, **8**, **9**, and/or **10** (Eq. 2, Table 1), which were separated by column chromatography on silica gel. The tricyclic product **7** was a major product. A structural identification of these products was elucidated by spectral analyses and a chemical transformation. For example, the IR spectrum of **7** showed the presence of a hydroxyl group at ca. 3500 cm^{-1} and the absence of a carbonyl group. The ^{1}H NMR spectrum of **7** showed the presence of two methyl groups arising from the isopropylthio group at δ ca. 1.69 (6H, s), and also suggested a change in the alkenoyl group to the corresponding enol type, as shown in the Experimental section. The ^{1}H NMR spectra of **8** and **9** also agreed with the proposed structures (Experimental section).

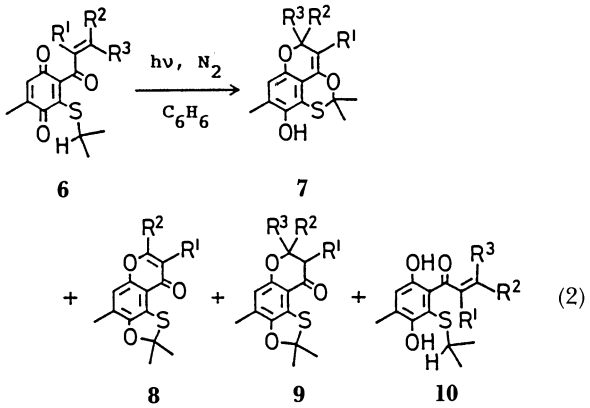

(2)

a: R^1=Me, R^2=R^3=H; **b**: R^1=R^2=Me, R^3=H;
c: R^1=R^2=R^2=Me; **d**: R^1=R^3=H, R^2=Me;
e: R^1=H, R^2=R^3=Me

On the basis of the following results and a comparison with the reaction of **1**,[2,3] products **8** would be oxidation products of **7**, and **9** would be an isomerization product of **7**. As shown in Table 1, the formation of **8** was always accompanied by hydroquinone **10** (Runs 1, 2, and 4). These results indicate that the quinone **6** oxidized product **7** to give **8**, together with

Table 1. Photochemical Reaction of **6**

Run	Quinone	Substituents			Yields of prodicts/%[a]			
		R^1	R^2	R^3	**7**	**8**	**9**	**10**
1	**6a**	Me	H	H	80	11	0	6
2	**6b**	Me	Me	H	82	10	0	5
3	**6c**[b]	Me	Me	Me	79	0	0	0
4	**6d**[b]	H	Me	H	49	17	11	14
5	**6e**[b]	H	Me	Me	77	0	8	0

a) Isolated yields based on the quinone used. b) The starting quinones **6c**, **6d**, and **6e** were recovered in 9%, 4%, and 12% yields, respectively.

10. The amount of **8** is always greater than that of hydroquinone **10** (Runs 1, 2, and 4), suggesting that product **7** can also be oxidized with air.

Since hydrogen at the R^3-position of **7a**, **b**, or **d** is situated in both the allylic and α-alkoxyl positions, it should easily be abstracted by the quinone.[4] This idea is supported by the fact that **7c** and **e**, which have no hydrogen at R^3-position, afforded neither **8** nor **10** (Runs 3 and 5).

Product **9** was observed only in the reactions of **6d** and **e** (Runs 4 and 5). Therefore, products **7d** and **e**, which have a hydrogen at the R^1-position, may be less stable than **7a**, **b**, and **c**, which have a methyl group (Runs 1, 2, and 3).[5]

Irradiation of **11** under the same conditions gave the corresponding tetracyclic product **12** in good yield together with **13** and **15** (Eq. 3, Table 2). Since the structures of **11a—c** agreed with the type of **6b**, the isomerization product **14** was not obtained.[5] The amounts of the oxidation products, **13b** and **c**, were larger than that of **13a**. This result indicates that products **12b** and **c**, which have a six- or seven-membered ring, are more reactive than **12a**, which has a five-membered ring.[6]

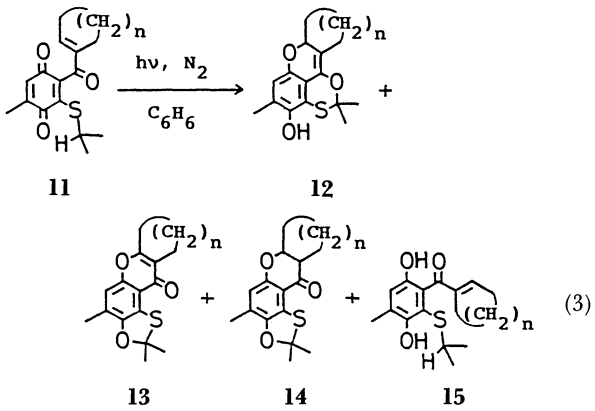

(3)

a: n=1; **b**: n=2; **c**: n=3

Table 2. Photochemical Reaction of **11**

Run	Quinone	$(CH_2)_n$ n	Yields of products/%[a]			
			12	**13**	**14**	**15**
6	**11a**	1	90	5	0	4
7	**11b**	2	63	21	0	14
8	**11c**	3	69	20	0	10

a) Isolated yields based on the quinone used.

In any event, these cyclization paths can be consistently explained by a modification of Eq. 1, and the irradiation of 2-(2-alkenoyl)-3-isopropylthio-1,4-benzoquinones which have an α,β-unsaturated carbonyl group as an alkenoyl side chain, should generally give the corresponding cyclization product in good yield.

Experimental

All of the melting points are uncorrected. The ^{1}H NMR spectra were measured using a JEOL JNM-GX 270 spectrometer in $CDCl_3$ using TMS. The IR (CCl_4) spectra were recorded on a Hitachi 260-50 spectrometer. Elemental analyses (C and H) were agreed within ±0.3%.

Quinones **6** and **11** were prepared by modified methods of Farina and Valderrama[7] and Jacob et al.,[8] as described in a previous paper.[2] The characteristic physical properties of **6** and **11** are described.

3-Isopropylthio-3-methacryloyl-5-methyl-1,4-benzoquinone (6a): Red oil; IR (CCl_4) 1660 cm^{-1}; ^{1}H NMR (270 MHz, $CDCl_3$) δ=1.24 (6H, d, J=6.8 Hz, SCHMe$_2$), 2.01 (3H, dd, J=1.5 and 0.7 Hz, COCMe=CH$_2$), 2.12 (3H, d, J=1.7 Hz, CH=CMe), 3.96 (1H, m, J=6.8 Hz, SCHMe$_2$), 5.74 (1H, m, J=0.7 Hz, COCMe=CHH), 6.02 (1H, m, J=1.5 Hz, COCMe=CHH), 6.61 (1H, q, J=1.7 Hz, CH=CMe). Anal. ($C_{14}H_{16}O_3S$) C, H.

6b: Red oil; IR 1675 cm^{-1}; ^{1}H NMR δ=1.89 (3H, d, J=7.3 Hz), 1.90 (3H, d, J=1.7 Hz), 6.47 (1H, mq, J=7.3 and 1.7 Hz). Anal. ($C_{15}H_{18}O_3S$) C, H.

6c: Red oil; IR 1665 cm^{-1}; ^{1}H NMR δ=1.85 (3H, d-like, J=1.2 Hz), 1.91 (3H, s), 2.11 (3H, d-like, J=1.2 Hz). Anal. ($C_{16}H_{20}O_3S$) C, H.

6d: Orange prisms, mp 70—72 °C; IR 1670 cm^{-1}; ^{1}H NMR δ=1.96 (3H, dd, J=6.8 and 1.5 Hz), 6.28 (1H, dq, J=15.9 and 1.5 Hz), 6.71 (1H, dq, J=15.9 and 6.8 Hz). Anal. ($C_{14}H_{16}O_3S$) C, H.

6e: Orange prisms, mp 55—56 °C; IR 1650 cm^{-1}; ^{1}H NMR δ=1.95 (3H, d, J=1.2 Hz), 2.25 (3H, d, J=1.0 Hz), 6.11 (1H, m). Anal. ($C_{15}H_{18}O_3S$) C, H.

2-(1-Cyclopentenylcarbonyl)-3-isopropylthio-5-methyl-1,4-benzoquinone (11a): Orange needles, mp 87—89 °C; IR 1660 cm^{-1}; ^{1}H NMR δ=1.95—2.10 (2H, m, J=7.6 Hz), 2.50—2.75 (4H, m), 6.54 (1H, ms). Anal. ($C_{16}H_{18}O_3S$) C, H.

11b: Orange prisms, mp 78—80 °C; IR 1670 cm^{-1}; ^{1}H NMR δ=1.6—1.75 (4H, m), 2.23 (2H, bs), 2.36 (2H, bs), 6.63 (1H, ms). Anal. ($C_{17}H_{20}O_3S$) C, H.

11c: Orange prisms, mp 67—69 °C ; IR 1660 cm^{-1}; ^{1}H NMR δ=1.52—1.62 (4H, m), 1.75—1.85 (2H, m), 2.30—2.40 (2H, m), 2.60—2.65 (2H, m), 6.79 (1H, t J=6.6 Hz). Anal. ($C_{18}H_{22}O_3S$) C, H.

Photochemical Reaction of 6. A solution of **6** (0.3 mmol) in 30 cm^3 of benzene was degassed under reduced pressure and replaced with N_2, and then irradiated with a 300-W halogen lamp through a yellow glass filter (<410 nm cut off) at room temperature for 1 h. After irradiation, the solvent was removed in vacuo and the resulting oil chromatographed on a silica-gel column with benzene as the eluent. The first yellow component was **7** and/or **9**, the second was **8**, and the third was **10**. The yields of products **7**, **8**, **9**, and **10** are summarized in Table 1.

2,2,4,8-Tetramethyl-5*H*-pyrano[4,3,2-*de*][3,1]benzoxathiin-9-ol (7a): Oil; IR 3500, 1670 (w), 1180 cm^{-1}; ^{1}H NMR δ=1.69 (6H, s, 2-Me$_2$), 1.70 (3H, d, J=1.2 Hz, 4-Me), 2.18 (3H, s, 8-Me), 4.65 (1H, bs, 9-OH), 4.70 (2H, bs, 5-H$_2$), 6.41 (1H, s, 7-H).

2,2,4,8-Tetramethyl-9*H*-oxathiolo[4,5-*f*][1]benzopyran-9-one (8a): Pale yellow prisms, mp 131—132 °C; IR 1650, 1430 cm^{-1}; ^{1}H NMR δ=1.85 (6H, s, 2-Me$_2$), 1.99 (3H, d, J=1.0 Hz, 8-Me), 2.29 (3H, s, 4-Me), 6.86 (1H, s, 5-H), 7.67 (1H, q, J=1.0 Hz, 7-H). Anal. ($C_{14}H_{14}O_3S$) C, H.

7b: Oil; IR 3510, 1665 (w), 1180 cm^{-1}; ^{1}H NMR δ=1.34 (3H, d, J=6.6 Hz), 1.62 (3H, s), 4.65 (1H, s), 4.82 (1H, q, J=6.6 Hz).

8b: Pale yellow needles, mp 182-183 °C; IR 1635, 1430 cm^{-1}; ^{1}H NMR δ=2.01 (3H, s), 2.35 (3H, s). Anal. ($C_{15}H_{16}O_3S$) C, H.

7c: Oil; IR 3510, 1650 (w), 1185 cm^{-1}; ^{1}H NMR δ=1.40 (6H, s), 1.74 (3H, s), 4.47 (1H, s).

9c: Pale yellow oil; IR 1680, 1610, 1420 cm^{-1}; ^{1}H NMR δ=1.19 (3H, d, J=7.1 Hz), 1.27 (3H, s), 1.46 (3H, s), 2.67 (1H, q, J=7.1 Hz). Anal. ($C_{16}H_{20}O_3S$) C, H.

7d: Oil; IR 3500, 1670 (w), 1185 cm^{-1}; ^1H NMR δ=1.42 (3H, d, J=6.3 Hz), 4.73 (1H, bs), 5.00 (1H, d, J=3.2 Hz), 5.00—5.10 (1H, m, 5-H).

8d: Pale yellow needles, mp 140—141 °C; IR 1650, 1420 cm^{-1}; ^1H NMR δ=2.31 (3H, s), 6.05 (1H, s). Anal. ($C_{14}H_{14}O_3S$) C, H.

2,2,4,7-Tetramethyl-7*H*-oxathiolo[4,5-*f*][1]benzopyran-9(8*H*)-one (9d): Pale yellow prisms, mp 94—95 °C; IR 1685, 1615, 1415 cm^{-1}; ^1H NMR δ=1.47 (3H, d, J=6.3 Hz, 7-Me), 1.81 (6H, s, 2-Me_2), 2.19 (3H, d, J=0.7 Hz, 4-Me), 2.55—2.70 (2H, m, 8-H_2), 4.40—4.55 (1H, m, 7-H), 6.43 (1H, q, J=0.7 Hz, 5-H).

7e: Oil, IR 3500, 1645 (w), 1185 cm^{-1}; ^1H NMR δ=1.42 and 1.43 (6H, each s), 4.55 (1H, s), 4.99 (1H, s).

9e: Pale yellow prisms, mp 118—119 °C; IR 1680, 1615, 1415 cm^{-1}; ^1H NMR δ=1.41 (6H, s), 2.55 (2H, s). Anal. ($C_{15}H_{18}O_3S$) C, H.

A photochemical reaction of **11** was similarly carried out for **6** described above. On the column, the first yellow component was **12**, the second was **13**, and the third was **15**. The yields of products **12**, **13**, and **15** are summarized in Table 2.

2,2,5-Trimethyl-7a,8,9,10-tetrahydrocyclopenta[5,6]-pyrano[4,3,2-*de*][3,1]benzoxathiin-4-ol (12a): Oil; IR 3500, 1680 (w), 1180 cm^{-1}; ^1H NMR δ=1.55—2.0 (4H, m), 2.25—2.60 (2H, m), 4.75 (1H, bs), 5.07 (1H, t-like).

2,2,4-Trimethyl-7,8,9,10-tetrahydrocyclopenta[*b*][3,1]-oxathiolo[4.5-*f*][1]benzopyran-10-one (13a): Yellow needles, mp 236—238 °C; IR 1630, 1440 cm^{-1}; ^1H NMR δ=2.09 (2H, m, 7.5 Hz), 2.81 (2H, t-like, J=7.5 Hz), 2.92 (2H, t-like, J=7.5 Hz). Anal. ($C_{16}H_{16}O_3S$) C, H.

12b: Oil; IR 3500, 1665 (w), 1185 cm^{-1}; ^1H NMR δ=1.15—1.45 (2H, m), 1.55—1.90 (4H, m), 2.15—2.25 (1H, m), 2.95 (1H, bd, J=14.0 Hz), 4.55 (1H, s), 4.92 (1H, dd, J=11.0 and 5.4 Hz).

13b: Pale yellow needles, mp 149—151 °C; IR 1630, 1430 cm^{-1}; ^1H NMR δ=1.65—1.9 (4H, m), 2.51 (2H, t-like, J=6.3 Hz), 2.59 (2H, t-like, J=6.3 Hz). Anal. ($C_{17}H_{18}O_3S$) C, H.

12c: Oil; IR 3500, 1645 (w), 1190 cm^{-1}; ^1H NMR δ=1.5—2.1 (7H, m), 2.65—2.75 (1H, m), 4.70 (1H, s), 4.92 (1H, dd, J=6.5 and 3.5 Hz).

13c: Pale yellow prisms, mp 173—174 °C; IR 1615, 1420, 1205 cm^{-1}; ^1H NMR δ=1.55—1.9 (6H, m), 2.70—2.80 (4H, m). Anal. ($C_{18}H_{20}O_3S$) C, H.

References

1) K. Maruyama, H. Iwamoto, O. Soga, A. Takuwa, and A. Osuka, *Chem. Lett.*, **1985**, 1675.

2) H. Iwamoto, *Bull. Chem. Soc. Jpn.*, **62**, 3479 (1989).

3) The minor product corresponds to **8** in Eq. 2. H. Iwamoto, *Chem. Express*, **4**, 145 (1989).

4) The oxidation reaction of **5S** with quinone has been examined, and the possible reaction mechanism for **7** can be proposed to Eq. 4 as described in previous paper.[3]

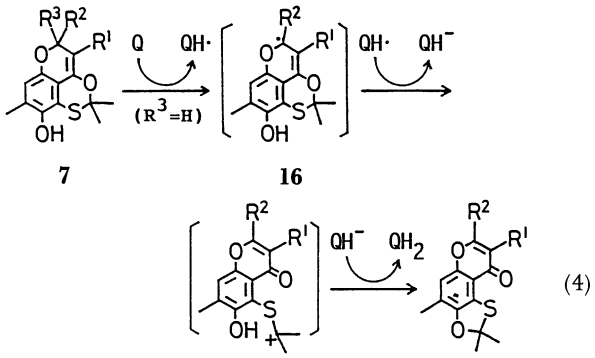

(4)

Q=Quinone

5) The isomerization of **7** to **9** was accelerated by the presence of a weak acid as described in previous paper.[2] The other **7a—c** and **12a—c**, of course, can be respectively converted into **9a—c** and **14a—c** in the presence of a weak acid.

6) Probably, the radical intermediate of type **16** from **12b** must be more stable than that from **12a**, because the former having six-membered ring is more flexible than the latter having five-membered ring. c.f. R. Srinivasan and F. I. Sonntag, *J. Am. Chem. Soc.*, **89**, 407 (1967).

7) F. Farina and J. Valderrama, *Synthesis*, **1971**, 315.

8) P. Jacob, III, P. S. Callery, A. T. Shulgin, and N. Castagnoli, Jr., *J. Org. Chem.*, **41**, 3627 (1976).

Indium-Induced Reaction of Phenacyl Iodide. Deiodinative Dimerization to β,γ-Epoxy Ketone and Aldol Condensation with Aldehydes

Shuki ARAKI* and Yasuo BUTSUGAN
Department of Applied Chemistry, Nagoya Institute of Technology, Gokiso-cho, Showa-ku, Nagoya 466
(Received October 15, 1990)

Synopsis. The reaction of phenacyl iodide with indium metal gave 3,4-epoxy-1,3-diphenyl-1-butanone which, on treatment with silica gel, gave 2,4-diphenylfuran and 2,4-diphenyl-4-oxobutanal. Metallic indium as well as indium(I) iodide were found to mediate the aldol condensation between α-halo ketone and aldehyde.

We have recently reported that activated halides such as allylic halides[1] and α-iodoacetate[2] react with metallic indium to form organoindium compounds and these reagents have been proved to be useful in organic synthesis. In order to extend the synthetic utility of organoindium reagents, we have studied the generation and reaction of indium enolates of ketones. We describe here the reaction of phenacyl iodide with indium metal which leads to a β,γ-epoxy ketone. The same reaction in the presence of an aldehyde gave aldol condensation products. The aldol reaction using indium(I) iodide is also described.

An exothermic reaction of phenacyl iodide and indium powder took place in DMF at room temperature. Aqueous workup and distillation gave 3,4-epoxy-1,3-diphenyl-1-butanone (**1**) (57% yield) together with small amounts (<3%) of acetophenone and 1,2-dibenzoylethane. The epoxy ketone **1** is acid-labile; by adsorption on silica gel, **1** was completely converted to 2,4-diphenylfuran (**2**) and 2,4-diphenyl-4-oxobutanal (**3**), in 40 and 48% yields, respectively. The above transformations are illustrated in Scheme 1, in which the indium enolate **4** is postulated as an intermediate.

The syntheses of 2,4-disubstituted furans from the reaction of α-halo ketones have been performed by using magnesium,[3] zinc,[4] tetracarbonylnickel(0),[5] or copper(I) chloride.[6] Yoshisato and Tsutsumi have reported the synthesis of β,γ-epoxy ketone from aliphatic α-bromo ketone and realized its thermal transformation to 2,4-dialkylfuran.[5b] However, the compound **1** has never been obtained so far by the reactions of the metal enolates derived from phenacyl bromide,[5a,6,7] probably owing to its instability.

When the above reaction of phenacyl iodide with indium was conducted in the presence of an aldehyde, the aldol condensation proceeded; i.e., with benzaldehyde were formed β-hydroxy ketone **5** and chalcone (**6**) in 53 and 17% yields, respectively. Octanal gave similar results (Eq. 1).

$$\mathrm{PhCOCH_2I + RCHO} \xrightarrow[\mathrm{DMF}]{\mathrm{In}} \mathrm{PhCOCH_2CH(OH)R + PhCOCH{=}CHR} \quad (1)$$

5 (R=Ph) 53% **6** (R=Ph) 17%
7 (R=heptyl) 43% **8** (R=heptyl) 17%

It has previously been shown that indium(I) iodide can be used for oxidative addition to allylic halides and α-iodoacetate in place of metallic indium.[8] Indium(I) iodide has now been found to be effective also for the formation of the indium enolate from phenacyl iodide. Thus, refluxing of a mixture of phenacyl iodide and indium(I) iodide in THF for 12 h and aqueous workup of the reaction mixture gave

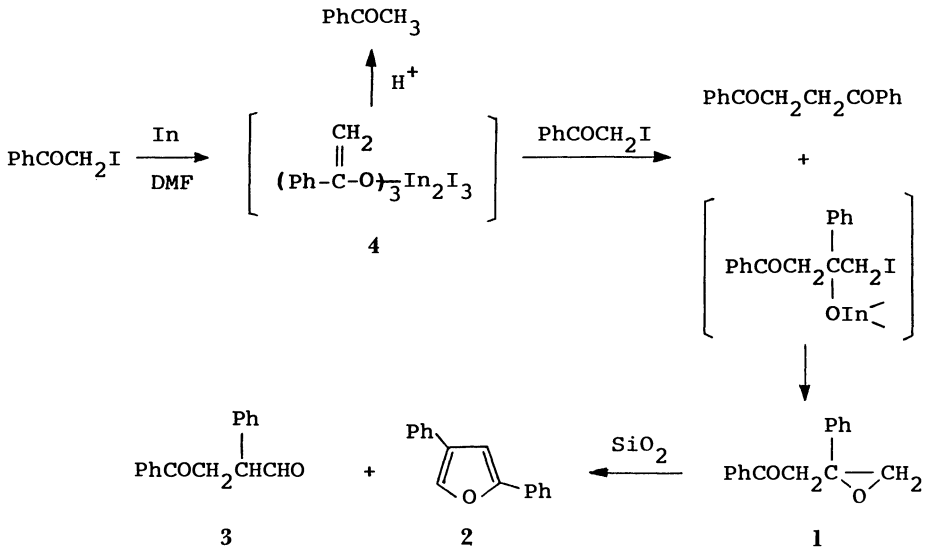

Scheme 1.

Table 1. Indium(I) Iodide-Induced Condensation of α-Bromo Ketones with Aldehydes

α-Bromo Ketone	Aldehyde	Product	Yield/%
$PhCOCH_2Br$	PhCHO	PhCOCH=CHPh (**6**)	74
$PhCOCH_2Br$	*p*-ClC_6H_4CHO	PhCOCH=CHC_6H_4Cl-*p* (**10**)	75
$PhCOCH_2Br$	$CH_3(CH_2)_6CHO$	PhCOCH=$CH(CH_2)_6CH_3$ (**8**)	77
$PhCOCH_2Br$	PhCH=CHCHO	PhCOCH=CHCH=CHPh (**11**)	53
p-$BrC_6H_4COCH_2Br$	*p*-ClC_6H_4CHO	*p*-BrC_6H_4COCH=CHC_6H_4Cl-*p* (**12**)	63
CH_3COCH_2Br	PhCHO	CH_3COCH=CHPh (**13**)	40
CH_3COCH_2Br	$CH_3(CH_2)_6CHO$	CH_3COCH=$CH(CH_2)_6CH_3$ (**14**)	52

$$PhCOCH_2I \xrightarrow[THF]{InI} Ph\text{-}C(O\text{-}InI_2)=CH_2 \quad (2)$$

9

acetophenone in 75% yield together with a trace amount of 1,2-dibenzoylethane. This supports the in situ formation of the indium enolate **9** (Eq. 2). Phenacyl bromide was equally reactive to the iodide. When the reaction of α-bromo ketones and indium(I) iodide was carried out with aldehydes, α,β-unsaturated ketones were obtained. Table 1 summarizes the results. Both aromatic and aliphatic α-bromo ketones gave moderate yields of α,β-unsaturated ketones. The corresponding β-hydroxy ketones were not found in the reaction mixtures owing to a facile dehydration under the reaction conditions employed.

Experimental

General. Melting points were determined with a Mitamura Riken micro melting point apparatus and are uncorrected. IR spectra were taken with a JASCO A-102 spectrophotometer. Mass spectra (MS) were recorded with a Hitachi M-2000 instrument at 70 eV. ^1H NMR spectra were obtained with a Hitachi R-90 (90 HMz) spectrometer. ^{13}C NMR spectra were obtained with a Varian XL-200 (50.3 MHz) spectrometer. Elemental analyses were performed at Elemental Analysis Center of Kyoto University. Indium powder (99.99%, stabilized by 0.5% MgO) was obtained from Nacalai Tesque Co., Ltd. THF (tetrahydrofuran) and DMF (*N,N*-dimethylformamide) were distilled from lithium aluminum hydride and calcium hydride, respectively. All reactions were conducted under argon.

Reaction of Phenacyl Iodide with Indium. To a suspension of indium powder (114 mg, 1 mmol) in DMF (1 cm^3) was added phenacyl iodide (492 mg, 2 mmol) at room temperature. An exothermic reaction started immediately. The mixture was stirred at room temperature for 100 min. Water was added and the products were extracted with ether. The extracts were washed with water and dried over anhydrous sodium sulfate. Evaporation of the solvent left an oil which was distilled (Kugelrohr) to give acetophenone [bp 100 °C/1 Torr (1 Torr=133.322 Pa), bath temperature] (8 mg, 3%) and **1** (bp 190 °C/1 Torr, bath temperatures) (136 mg, 57%). The latter contained a trace amount of 1,2-dibenzoylethane which was crystallized and filtered (mp 142 °C, lit,[5a] mp 145 °C).

3,4-Epoxy-1,3-diphenyl-1-butanote (1). Colorless oil; IR (neat) 1680 cm^{-1} (C=O); ^1H NMR ($CDCl_3$) δ=2.97 (1H, d, *J*=5 Hz, OCH_2), 3.10 (1H, d, *J*=5 Hz, OCH_2), 3.58 (1H, d, *J*=17 Hz, $PhCOC\underline{H}_2$), 3.77 (1H, d, *J*=17 Hz, $PhCOC\underline{H}_2$), 7.36 (8H, m, aromatic), and 7.95 (2H, m, aromatic); ^{13}C NMR ($CDCl_3$) δ=45.3 (t), 55.3 (t), 57.1 (s), 125.8 (d), 127.8 (d), 128.3 (d), 128.4 (d), 128.6 (d), 133.4 (d), 136.8 (s), 139.6 (s), and 196.8 (s); MS *m/z* 238 (M^+); Found: C, 80.56; H, 5.98%. Calcd for $C_{16}H_{14}O_2$: C, 80.65; H, 5.92%.

Treatment of 1 with Silica Gel. A solution of **1** (114 mg, 0.48 mmol) in dichloromethane was adsorbed on a silica-gel column. After 1.5 h at room temperature, the column was eluted with acetone. The eluate showed two spots on a thin-layer chromatogram, which were separated by column chromatography on silica gel (hexane-dichloromethane gradient) to give **2** (42 mg, 40%) and **3** (55 mg, 48%).

2,4-Diphenylfuran (2). Colorless crystals; mp 111 °C (lit,[5a] mp 111 °C); ^1H NMR ($CDCl_3$) δ=6.95 (1H, d, *J*=1 Hz, H^3), 7.38 (8H, m, aromatic), 7.70 (2H, m, aromatic), and 7.75 (1H, d, *J*=1 Hz, H^5).

2,4-Diphenyl-4-oxobutanal (3). Colorless oil; IR (neat) 1722 (aldehyde C=O) and 1680 cm^{-1} (ketone C=O); ^1H NMR ($CDCl_3$) δ=3.30 (1H, dd, *J*=18, 5 Hz, CH_2), 3.93 (1H, dd, *J*=18, 8 Hz, CH_2), 4.41 (1H, dd, *J*=8, 5 Hz, $C\underline{H}CHO$), 7.31 (8H, m, aromatic), 7.98 (2H, m, aromatic), and 9.81 (1H, bs, CHO); ^{13}C NMR ($CDCl_3$) δ=39.3 (t), 53.5 (d), 127.8 (d), 128.0 (d), 128.5 (d), 129.0 (d), 129.2 (d), 133.2 (d), 135.3 (s), 136.3 (s), 197.2 (s), and 198.9 (d); MS *m/z* 238 (M^+); Found: C, 80.39; H, 5.72%. Calcd for $C_{16}H_{14}O_2$: C, 80.65; H, 5.92%.

Indium-Induced Reaction of Phenacyl Iodide with Aldehydes. To a mixture of indium powder (114 mg, 1 mmol) and benzaldehyde (159 mg, 1.5 mmol) in DMF (1 cm^3) was added phenacyl iodide (246 mg, 1 mmol) at room temperature. After a reaction started (exothermic), the mixture was cooled to 0 °C and stirred for 70 min. Water was added and the products were extracted with ether. Extracts were dried (Na_2SO_4) and evaporated. The residue was chromatographed on silica gel (eluent: CH_2Cl_2) to give **5** (120 mg, 53%) and **6** (35 mg, 17%). The reaction with octanal was similarly carried out.

3-Hydroxy-1,3-diphenyl-1-propanone (5). Colorless oil; (lit,[9] mp 50—50.5 °C); ^1H NMR ($CDCl_3$) δ=3.35 (2H, d, *J*=6 Hz, CH_2), 3.40 (1H, bs, OH), 5.32 (1H, t, *J*=6 Hz, CH), 7.38 (8H, m, aromatic), and 7.90 (2H, m, aromatic).

Chalcone (6). Yellow crystals; mp 55 °C (lit,[10] mp 56—58 °C); ^1H NMR ($CDCl_3$) δ=7.50 (10H, m, =CH- and aromatic) and 7.97 (2H, m, aromatic).

3-Hydroxy-1-phenyl-1-decanone (7). Colorless crystals; mp 48 °C; IR (KBr) 3420 (OH) and 1672 cm^{-1} (C=O); ^1H NMR ($CDCl_3$) δ=0.90 (3H, bt, *J*=6 Hz, Me), 1.30 (12H, m, CH_2), 2.90 (1H, bs, OH), 3.08 (1H, dd, *J*=18, 7 Hz, $COCH_2$), 3.13 (1H, dd, *J*=18, 4 Hz, $COCH_2$), 4.20 (1H, m, $C\underline{H}(OH)$), 7.53 (3H, m, aromatic), and 7.97 (2H, m, aromatic); MS *m/z* 230 ($M-H_2O$); Found: C, 77.02; H, 9.95%. Calcd for $C_{16}H_{24}O_2$: C, 77.38; H, 9.74%.

1-Phenyl-2-decen-1-one (8). Colorless oil; IR (neat) 1668 and 1620 cm^{-1} (CH=CH-C=O); ^1H NMR ($CDCl_3$) δ=0.88 (3H, bt, *J*=6 Hz, Me), 1.30 (10H, m, CH_2), 2.32 (2H, bq, *J*=6 Hz, CH_2), 6.87 (1H, d, *J*=15 Hz, =CH-), 7.00 (1H, dt, *J*=15, 6 Hz, =CH-), 7.50 (3H, m, aromatic), and 7,93 (2H, m, aromatic); MS *m/z* 230 (M^+); Found: C, 82.70; H, 9.69%. Calcd

for $C_{16}H_{22}O$: C, 83.43; H, 9.63%.

Reaction of Phenacyl Iodide with Indium(I) Iodide. A mixture of phenacyl iodide (123 mg, 0.5 mmol) and indium(I) iodide[11] (130 mg, 0.54 mmol) in THF (5 cm^3) was heated at reflux for 12 h. Hydrochloric acid (3%) was added and the products were extracted with dichloromethane. The extracts were dried (Na_2SO_4) and evaporated. The residue was chromatographed on silica gel (eluent: CH_2Cl_2) to give acetophenone (45 mg, 75%) and a trace amount of 1,2-dibenzoylethane (ca. 3 mg).

Indium(I) Iodide-Induced Reaction of α-Bromo Ketones with Aldehydes. General Procedure: A mixture of α-bromo ketone (0.8 mmol), aldehyde (0.5 mmol), and indium(I) iodide (0.8 mmol) was refluxed in THF (5 cm^3) for 12—17 h. Diluted hydrochloric acid (3%) was added and the product was extracted with dichloromethane. The extracts were dried (Na_2SO_4) and evaporated. The residue was chromatographed on silica gel (eluent: CH_2Cl_2) to give α,β-unsaturated ketone.

3-(4-Chlorophenyl)-1-phenyl-2-propen-1-one (10). Yellow crystals; mp 112 °C (lit,[10] mp 114—115 °C); ^1H NMR ($CDCl_3$) δ=7.55 (9H, m, =CH- and aromatic) and 7.99 (2H, m, aromatic).

1,5-Diphenyl-2,4-pentadien-1-one (11). Yellow crystals; mp 100 °C (lit,[12] mp 102—103 °C); ^1H NMR ($CDCl_3$) δ=6.9—7.7 (12H, m, =CH- and aromatic) and 7.95 (2H, m, aromatic).

1-(4-Bromophenyl)-3-(4-chlorophenyl)-2-propen-1-one (12). Yellow crystals; mp 161 °C (lit,[13] mp 167—168 °C); ^1H NMR ($CDCl_3$) δ=7.3—7.9 (m, 10H, =CH- and aromatic).

4-Phenyl-3-buten-2-one (13). Yellow crystals; mp 40 °C (lit,[14] mp 41.5—42 °C); ^1H NMR ($CDCl_3$) δ=2.37 (3H, s, Me), 6.73 (1H, d, J=16 Hz, =CH-), and 7.45 (6H, m, =CH- and Ph).

3-Undecen-2-one (14).[15] Colorless oil; ^1H NMR ($CDCl_3$) δ=0.90 (3H, bt, J=6 Hz, Me), 1.30 (10H, m, CH_2), 2.23 (5H, m, CH_2 and COMe), 6.07 (1H, d, J=16 Hz, =CH-), and 6.80 (1H, dt, J=16, 7 Hz, =CH-).

References

1) S. Araki, H. Ito, and Y. Butsugan, *J. Org. Chem.*, **53**, 1831 (1988).

2) S. Araki, H. Ito, and Y. Butsugan, *Synth. Commun.*, **18**, 453 (1989).

3) J. E. Dubois and J. Itzkowitch, *Tetrahedron Lett.*, **1965**, 2839.

4) T. A. Spencer, R. W. Britton, and D. S. Watt, *J. Am. Chem. Soc.*, **89**, 5727 (1967).

5) a) E. Yoshisato and S. Tsutsumi, *J. Chem. Soc., Chem. Commun.*, **1968**, 33; b) *idem.*, *J. Am. Chem. Soc.*, **90**, 4488 (1968).

6) H. Nozaki, T. Shirafuji, K. Kuno, and Y. Yamamoto, *Bull. Chem. Soc. Jpn.*, **45**, 856 (1972).

7) For the formation of β,γ-epoxy ketones from *p*-halophenacyl bromides and pentacarbonyliron(0), see: H. Alper and E. C. H. Keung, *J. Org. Chem.*, **37**, 2566 (1972).

8) S. Araki, H. Ito, N. Katsumura, and Y. Butsugan, *J. Organomet. Chem.*, **369**, 291 (1989).

9) H. O. House, D. S. Crumrine, A. Y. Teranishi, and H. D. Olmstead, *J. Am. Chem. Soc.*, **95**, 3310 (1973).

10) H. H. Szmant and A. J. Basso, *J. Am. Chem. Soc.*, **74**, 4397 (1952).

11) L.-C. Chao and R. D. Rieke, *J. Organomet. Chem.*, **67**, C64 (1974).

12) H. Scholtz, *Chem. Ber.*, **28**, 1726 (1895).

13) D. E. Applequist and R. D. Gdanski, *J. Org. Chem.*, **46**, 2502 (1981).

14) G. Lardelli and O. Jeger, *Helv. Chim. Acta*, **32**, 1817 (1949).

15) S. Yanashita and M. Shimano, *Nippon Kagaku Kaishi*, **63**, 1338 (1942).

Reversible Color Changes of Polydiacetylene Induced by Monomer Solid Phase Transition

Kotaro ARAYA
Advanced Research Laboratory, Hitachi Ltd., Hatoyama, Saitama 350-03
(Received August 23, 1990)

Synopsis. Color change associated with solid phase transition is observed in the diacetylene derivatives, partially polymerized 4,6-decadiyne-1,10-bis(propylurethane). Moreover, the temperature of this color change can be altered by mixing with other derivatives.

Polydiacetylene,-(-RC=C=C=CR-)$_n$-, belongs to a unique class of polymers obtained by topochemical polymerization of a diacetylene(1,4-disubstituted 1,3-butadiyne) monomer in the solid state upon either thermal annealing or exposure to high energy radiation.[1] The polymers are colored either red, purple, or blue because π-electrons are delocalized along the conjugated backbone. The polymers also exhibit several types of color change; namely, thermochromism,[2,3] solvatochromism,[4-6] and photochromism.[7,8]

This paper reports a color change triggered by a solid phase transition of a diacetylene monomer. Color changes of polydiacetylene are understood to be due to changes in the length of the conjugated chain and/or in the planality of the polymer backbone. Therefore, the change would be caused by differences in the packing condition of the conjugated backbone. In the partially polymerized diacetylene, the polymer chain is dissolved in a monomer matrix and it forms a solid solution with a monomer. If a diacetylene monomer has a solid phase transition, changes in the packing condition of the polymer chains would be induced, leading to a color change. This type of color change has been reported only for the partially polymerized 1,6-di(1-carbazolyl)-2,4-hexadiyne.[9] The transition temperature, however, is very low (142 K) and, of course, unchangeable. This low temperature constrains other measurements and applications.

With this in mind, diacetylenes have been extensively synthesized in search of a diacetylene with a solid phase transition at a proper temperature, which would make this transition temperature changeable. Suitable diacetylenes are reported here. These compounds are 4,6-decadiyne-1,10-bis(propylurethane), R=-$(CH_2)_3$-$CONHC_3H_7$ and 4,6-decadiyne-1,10-bis(butylurethane), R=-$(CH_2)_3$-$CONHC_4H_9$. Hereafter, these compounds are designated as 3PU and 3BU, respectively. These compounds were prepared according to a procedure reported by Patel.[10] The calorimetric data were recorded with a Perkin-Elmer DSC-7 differential scanning calorimeter (DSC). The respective melting points of 3PU and 3BU were 117.6 °C and 110.0 °C. The solid phase transition of 3PU was observed at 76.6 °C and it was reversible.

A crystalline 3PU monomer is a white powder and turns blue upon exposure to daylight. The polymer content of this partially polymerized sample is about 1 wt%. The polymer conversion was determined by extracting a monomer with acetone using a Soxhlet extractor and weighing the residual polymer. Solid state absorption spectra were measured using a Hitachi U-3400 spectrophotometer with reflectmetric

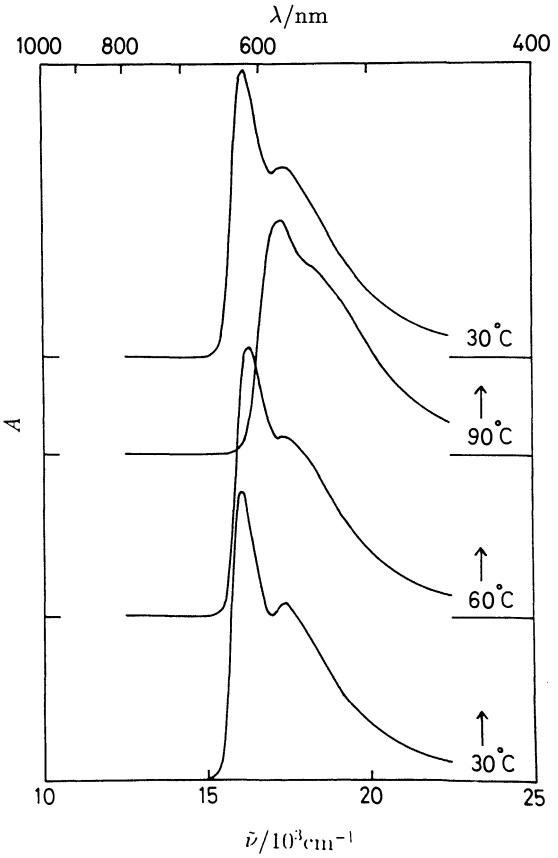

Fig. 1. Absorption spectra of partially polymerized 3PU.

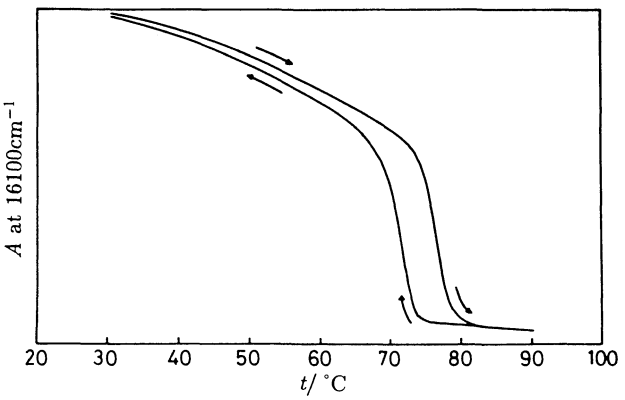

Fig. 2. Temperature dependence of absorbance at 16100 cm^{-1} of partially polymerized 3PU.

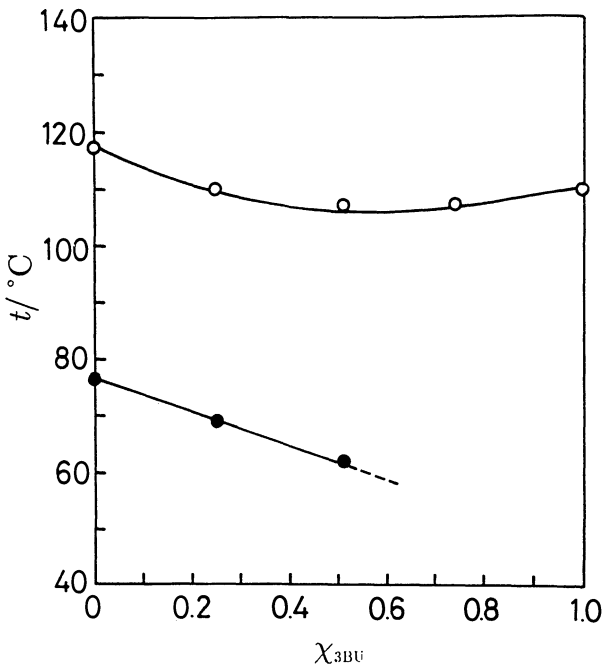

Fig. 3. Phase diagram of the 3PU-3BU system. Open circles: melting points. Closed circles: solid phase transition temperatures.

equipment, and were derived from diffuse reflection spectra of the solid dispersed in powdered sodium chloride. The temperature dependences of the absorption spectra are shown in Fig. 1. The maximum at 30 °C is located at 16100 cm^{-1} (620 nm). The spectrum at 60 °C is almost the same as at 30 °C. A large blue shift, however, is observed at 90 °C, when the color changed to purple. The maximum is shifted to 17200 cm^{-1} (580 nm). The spectral shift amounts to about 1100 cm^{-1}. When the solid is cooled to 30 °C again, the maximum turns back to 16100 cm^{-1}. For a detailed study of the temperature dependences of these spectra, the absorbance at 16100 cm^{-1} was monitored as a function of temperature. The results are shown in Fig. 2. During heating, absorbance drastically decreases at 76 °C and falls to almost zero at 80 °C. During cooling, absorbance sharply increases at 75 °C. This spectral change is reversible, and the temperature coincides with the solid phase transition temperature of 3PU, 76.6 °C. It is therefore concluded that the spectral change is induced by the monomer phase transition.

The most interesting feature of this diacetylene derivative is that the temperature of this color change can be changed. The 3PU and 3BU compounds form a solid solution over the entire composition. The phase diagram of the 3PU-3BU system determined by DSC is shown in Fig. 3. The phase transition of 3PU observed at 76.6 °C is also clearly observed up to 50 mol% of 3BU. The transition temperature is reduced to 62.0 °C at 50 mol% of 3BU. Accordingly, the temperature of the color change can be varied from 76.6 °C to 62.0 °C. If many diacetylenes having a phase transition were found, the color change of this type would be attained at a desired temperature and could be more effectively applied, for example, as a thermoindicator.

Although many types of color change have already been reported, a detailed understanding of this phenomenon has not been attained. The system reported here may help in understanding the relationship between the electronic state and the structure of polydiacetylenes.

References

1) V. Enkelmann, "Polydiacetylenes," ed by H. J. Cantow, Springer-Verlag, Berlin (1984), pp. 91—136.
2) R. R. Chance, R. H. Baughman, H. Muller, and J. Eckhardt, *J. Chem. Phys.*, **67**, 3616 (1977).
3) R. R. Chance, G. N. Patel, and J. D. Witt, *J. Chem. Phys.*, **71**, 206 (1979).
4) G. N. Patel, R. R. Chance, and J. D. Witt, *J. Chem. Phys.*, **70**, 4387 (1979).
5) G. N. Patel, R. R. Chance, and J. D. Witt, *J. Polym. Sci., Polym. Lett. Ed.*, **16**, 607 (1978).
6) R. R. Chance, J. M. Sowa, and J. Eckhardt, *J. Phys. Chem.*, **90**, 3031 (1986).
7) T. Kanetake, Y. Tokura, and T. Koda, *Solid State Commun.*, **56**, 803 (1985).
8) Y. Tokura, S. Nishikawa, and T. Koda, *Solid State Commun.*, **59**, 393 (1986).
9) R. J. Kennedy, I. F. Chalmers, and D. Bloor, *Makromol. Chem., Rapid Commun.*, **1**, 357 (1980).
10) G. N. Patel, *Radiat. Phys. Chem.*, **14**, 1678 (1975).

Preparation and Property of Zirconia-Pillared Montmorillonite Having Different Pillar Populations

Kenzi SUZUKI, Masakazu HORIO, Hiroyuki MASUDA, and Toshiaki MORI*
Government Industrial Research Institute, Nagoya, Hirate-cho, Kita-ku, Nagoya 462
(Received August 29, 1990)

Synopsis. Zirconia-pillared clay was prepared by ion-exchanging montmorillonites having different cation exchange capacities (CEC's) in an aqueous solution of $ZrOCl_2$. The amount of zirconia incorporated as pillars varied depending on the CEC of the starting clay. The interlayer distance was almost the same: ca., 0.8 nm. These findings suggest that the distance between pillars or the lateral distance should be different from one zirconia-pillared clay to another. As a result of pillaring the surface area was 200—260 $m^2 g^{-1}$. The thermal stability was examined in terms of a decrease in the surface area after heating at elevated temperatures.

By pillaring with alumina,[1] zirconia,[2] chromia,[3] titania,[4] or other kinds of oxide clusters,[5] a swellable layered clay mineral has been converted to a zeolite-like high surface area material. The resultant pillared clay has pores with sizes comparable to the dimension of many simple molecules. It is, therefore, expected that pillared clay can be used as a shape-selective catalyst or a molecular sieving separation material.[6,7]

The pore structure of pillared clay is characterized by both the distances between the silicate layers and between pillars, which are called, respectively, the interlayer distance and the lateral distance. It is not easy to prepare pillared clay with the desired interlayer distances. On the other hand, the lateral distance may be readily altered by altering the number of pillars: i.e., the lateral distance should be smaller in pillared clay with a larger number of pillars, as long as the interlayer distance is the same. By pillaring a montmorillonite having different CEC's with alumina we prepared a pillared clay with different lateral distances and studied its catalytic property.[7,8]

In the present study we similarly altered the pillar population in zirconia-pillared montmorillonite in order to change the lateral distance. Thermal stability was also investigated by measuring the surface area after heating at elevated temperatures.

Experimental

Na-montmorillonite [Kunipia-F, CEC; 1.28 mequiv g^{-1}] was obtained from Kunimine Industries, Co. The CEC was similarly altered by partially exchanging Na-montmorillonite with Ni^{2+}, followed by heating.[9] Zirconia-pillared clay was prepared by suspending the (Na, Ni)-montmorillonite with the CEC previously altered from 1.28 to 0.51 mequiv g^{-1} in an aqueous solution of $ZrOCl_2$, followed by washing chlorine free, drying at 333 K overnight and then calcined at elevated temperatures for 2 h. The amount of zirconia incorporated as pillars was determined by inductively coupled plasma (ICP) emission spectrometry (Shimadzu, ICPQ-1000). X-Ray powder diffraction was taken using a diffractometer with Ni-filtered monochromatic Cu $K\alpha$ radiation (Philips, APD-1700). The surface area was measured using an automatically controlled nitrogen-adsorption apparatus (Carlo Erba, Sorptomatic 1800).

Results and Discussion

Incorporation of Zirconia. The amount of zirconia introduced in the clay is plotted in Fig. 1 as a function of the CEC of the starting montmorillonite. Above 0.5 mequiv g^{-1}, the amount of zirconia increased linearly with increasing CEC, which is natural, since zirconia pillars are introduced in clay via ion-exchange. The tetrameric cation, $[Zr_4(OH)_{14}(H_2O)_{10}]^{2+}$ has been proposed as a plausible precursor for the zirconia pillar.[2a,d] Therefore, the number of zirconia pillars observed can be compared with the number expected from the divalent tetrameric cation. For a CEC of 1.28 mequiv g^{-1}, the observed number was 338 mg-ZrO_2 g^{-1}, while that expected was 315 mg-ZrO_2 g^{-1}, showing good agreement. However, it is obvious from a precise examination of Fig. 1 that when CEC decreased, the amount of observed zirconia was smaller than that expected, the possible reason for

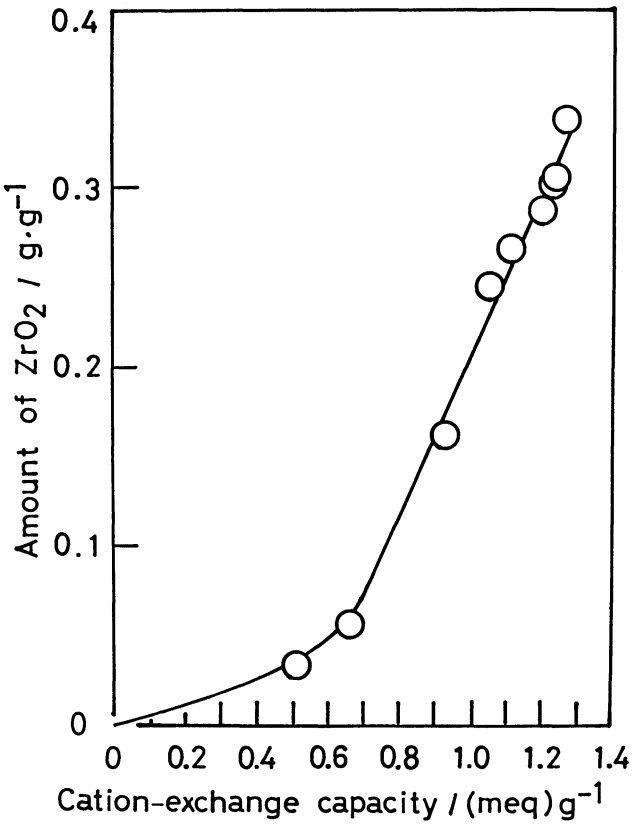

Fig. 1. The amount of ZrO_2 incorporated in montmorillonite with various CEC.

which is discussed below.

X-Ray Powder Diffraction. Since, as described below, the present zirconia-pillared montmorillonite was less thermally stable, X-ray powder diffraction was taken mainly for samples before calcination. Figure 2 summarizes the results. A diffraction peak, attributable to the 0 0 1 reflection, was observed at 4.5—5° for the CEC of the starting montmorillonite from 1.28 to 0.93 mequiv g^{-1}. The intensity of the 0 0 1 reflection increased with decreasing CEC to 1.06 mequiv g^{-1} and then decreased again for a CEC of 0.93 mequiv g^{-1}. Alumina-pillared montmorillonite also showed a similar variation in the intensity of the 0 0 1 reflections.[8] The intensity of the 0 0 1 reflection indicates the extent of the long-range ordering of the stacking of the silicate layers. Therefore, a favorable range of CEC seems to be present for preparing pillared clay well ordered in the longrange. From 0.93 to 1.28 mequiv g^{-1} of CEC, an additional peak also appeared at 8—9°, probably attributable to the 0 0 2 reflection. The variation in the intensity of the 0 0 2 reflection was found to be similar to that in the intensity of the 0 0 1 reflection, which may support the validity of the attribution.

For a CEC of 0.66 or 0.51 mequiv g^{-1}, a new main peak appeared at 9°, accompanying a very broad peak at 4.5—5°. The latter peak is again attributed to the 0 0 1 reflection. The diffraction for Ni-montmorillonite indicates that the former main peak is attributed to the 0 0 1 reflection of the non-pillared montmorillonite. The non-pillared portion present explains why the number of zirconia pillars was smaller than that expected. The reduced charge montmorillonite was reported to show a heterogeneous property with respect to a layer charge reduction.[9] This heterogeneity may be responsible for the presence of the non-pillared portion.

Interlayer Distance and Lateral Distance. The 0 0 1 basal spacing, d(0 0 1), was about 1.8 and 1.0 nm for the peak at 4.5—5 and at 9°, respectively. Since the thickness of the silicate layer was 0.96 nm, the respective interlayer distance was ca. 0.8 and 0.05 nm. The former interlayer distance assures pillaring, while the latter assures non-pillaring.

Figures 1 and 2 show that the number of zirconia pillars varied with the CEC of the starting montmorillonite from 1.28 to 0.93 mequiv g^{-1}, while the interlayer distance was virtually the same: ca., 0.8 nm. This suggests that the lateral distance is different from one zirconia-pillared montmorillonite to another: i.e., the greater number of zirconia pillars, the smaller is the lateral distance.

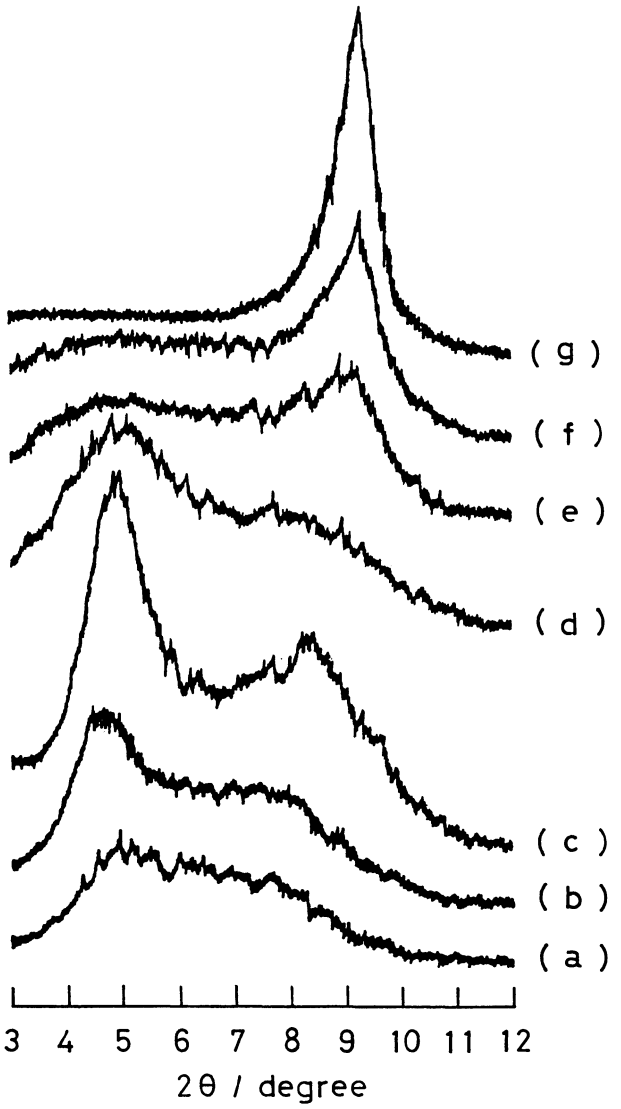

Fig. 2. X-Ray powder diffractions for the montmorillonite involving zirconium tetrameric cations in it. The CEC of the starting montmorillonite is 1.28 (a), 1.21 (b), 1.06 (c), 0.929 (d), 0.660 (e), and 0.506 mequiv g^{-1} (f). X-ray powder diffraction was taken for Ni-montmorillonite in a different scale (g).

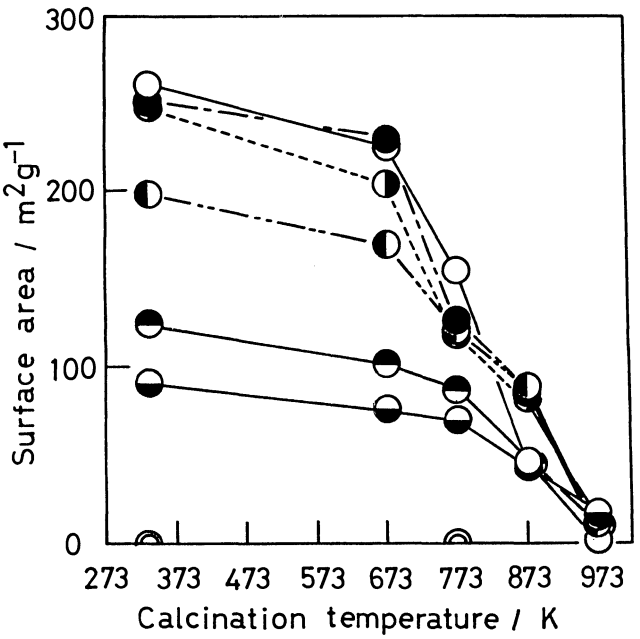

Fig. 3. Surface areas varied with calcination temperatures for typical zirconia-pillared montmorillonites. The CEC of the starting montmorillonite is 1.28 (◐), 1.21 (●), 1.06 (○), 0.929 (◑), 0.660 (◒), and 0.506 mequiv g^{-1} (◒). ◎; Ni-montmorillonite.

Surface Area Varied with Calcination at Elevated Temperatures. As a result of pillaring, the surface area was 200—260 $m^2 g^{-1}$. The surface area of montmorillonite partially pillared was also much larger than that of Ni-montmorillonite: 120 or 90 $m^2 g^{-1}$ vs. >1 $m^2 g^{-1}$. The surface area is plotted in Fig. 3 as a function of the calcination temperature. For all pillared montmorillonites, the surface area slightly decreased up to 673 K accompanying a drastic decrease for a further elevation of the calcination temperature.

Our previous study showed that the decrease in the surface area caused by high-temperature calcination was much less pronounced for an alumina-pillared montmorillonite: the surface area was 285, 260, and 180 $m^2 g^{-1}$ after calcination at 773, 873, and 973 K, respectively.[10] Compared with this pillared montmorillonite, the thermal stability of the present zirconia-pillared montmorillonite does not seem to be high. Here, the thermal stability was evaluated on the basis of a decrease in the surface area caused by high-temperature calcination. It is known that for zirconia-pillared clay the preparation method strongly affects the thermal stability.[2d] Samples synthesized from refluxed $ZrOCl_2$ solutions were reported to have higher surface areas than those prepared using fresh, unrefluxed solutions. The highest thermal stability was obtained by refluxing a $ZrOCl_2$ solution prior to mixing with dispersed clay, combined with a subsequent refluxing of the mixture, while the lowest stability was produced by using a fresh solution followed by mixing at room temperature. Lower thermal stability of the present zirconia-pillared montmorillonite may be due to the preparation method: the fresh solution was used followed by mixing at room temperature.

References

1) a) G. W. Brindley and R. E. Semples, *Clay Miner.*, **12**, 229 (1977); b) N. Lahav, U. Shani, and J. Shabtai, *Clays Clay Miner.*, **26**, 107 (1978); c) M. L. Occelli and D. H. Finseth, *J. Catal.*, **99**, 316 (1986); d) G. Poncelet and A. Schutz, "Chemical Reactions in Organic and Inorganic Constrained Systems," ed by R. Setton, Reidel, Dordrecht (1986), pp. 165—178; e) K. Suzuki, T. Mori, K. Kawase, H. Sakami, and S. Iida, *Clays Clay Miner.*, **36**, 147 (1988); f) J. Guan, E. Min, and Z. Yu, "Proc. 9th Int. Congr. Catal.," ed by M. J. Phillips and M. Ternan, Chem. Inst. Canada,(1988), Vol. 1, pp. 104—111.

2) a) S. Yamanaka and G. W. Brindley, *Clays Clay Miner.*, **27**, 119 (1979); b) R. Burch and C. I. Warburton, *J. Catal.*, **97**, 503 (1986); c) G. J. J. Burtley and R. Burch, *Appl.Catal.*, **19**, 175 (1985); d) G. J. J. Burtley, *Catal. Today*, **2**, 233 (1988).

3) a) T. J. Pinnavaia, M. S. Tzou, and S. D. Landau, *J. Am. Chem. Soc.*, **107**, 4785 (1985); b) M. S. Tzou and T. J. Pinnavaia, *Catal. Today*, **2**, 243 (1988).

4) J. Sterte, *Clays Clay Miner.*, **34**, 658 (1986).

5) a) S. P. Christiano, J. Wang, and T. J. Pinnavaia, *Inorg. Chem.*, **24**, 1222 (1985); b) C. I. Warburton, *Catal. Today*, **2**, 271 (1988).

6) a) D. E. W. Vaughan and R. J. Lussier, "Proc. 5th Int. Conf. on Zeolite," ed by L. V. C. Rees, Heydon, London (1980), pp. 94—101; b) J. Shabtai, R. Lazar, and A. G. Oblad, "Proc. 7th Int. Congr. Catal.," ed by T. Seiyama and K. Tanabe, Elsevier, Amsterdam (1981), pp. 828—837; c) J. Shabtai, F. B. Massoth, M. Tokarz, G. M. Tzai, and J. McCayley, "Proc. 8th Int. Congr. Catal.," Verlag Chemie, Weinheim (1984), Vol. IV, pp. 735—745; d) E. Kikuchi and T. Matsuda, *Catal. Today*, **2**, 297 (1988).

7) a) T. Mori and K. Suzuki, *Chem. Lett.*, **1989**, 2165; b) *idem.*, Program/Abstracts 1st Tokyo Conf. Adv. Catal. Sci. Tech., P-14 (1990).

8) K. Suzuki, M. Horio, and T. Mori, *Mater. Res. Bull.*, **23**, 1711 (1988).

9) D. M. Clementz and M. M. Mortland, *Clays Clay Miner,*, **22**, 223 (1974).

10) K. Suzuki and T. Mori, *Appl. Catal.*, **63**, 181 (1990).

Catalytic Activity of Bismuth(III) Chloride for Dehydrochlorination of Poly(vinyl chloride)

Yoshio UEMICHI,* Kazuhiko TAKUMA,† Masatoshi SUGIOKA, and Takaji KANAZUKA
Department of Applied Chemistry, Muroran Institute of Technology, Mizumoto, Muroran 050
(Received August 30, 1990)

Synopsis. Bismuth(III) chloride was found to be highly active as a catalyst for the dehydrochlorination of poly(vinyl chloride). The degree of dehydrochlorination was 97% at the highest. The catalyst showed high activity even in water vapor.

It is well-known that many metal chlorides with surface acidity catalyze various reactions such as alkylation, acylation, isomerization, polymerization, halogenation, etc.[1,2] In particular, chlorides of Fe, Al, Sb, Sn, and Ti are effective catalysts. However, there have been few reports to date on the catalytic activity of bismuth(III) chloride. In this paper, we report that $BiCl_3$ is an active catalyst for the dehydrochlorination of poly(vinyl chloride) (PVC). The reaction has recently attracted considerable attention in connection with the disposal of PVC waste[3] or the transformation of PVC into a polyene material which is one of the electrically conductive polymers.[4]

Experimental

Guaranteed-grade $BiCl_3$ purchased from Kishida Chemical Co. was used as catalyst after grinding it into a fine powder of 160 mesh or under. The chloride was so hygroscopic that it was handled in a dry nitrogen atmosphere. A commercial PVC (Aldrich Chemical Co.) was used without further purification. Its particle size and average molecular weight were 100—160 mesh and 48,000, respectively.

The dehydrochlorination of PVC was carried out at 100—175 °C in a stream of He (30 $ml \cdot min^{-1}$). A powdered mixture of PVC (5.6 mmol in monomer units) and $BiCl_3$ (0.3—2.2 mmol) was loaded into a U-shaped glass tube reactor. The reaction was started by immersing the reactor in an oil bath with a prescribed temperature. The evolved HCl gas was absorbed by water and the aqueous solution was periodically titrated with a sodium hydroxide solution. The total HCl consisted of HCl evolved from PVC and that from $BiCl_3$. The amount of HCl from the reaction of $BiCl_3$ with trace amounts of H_2O adsorbed on the chloride was evaluated from the decrease in the Cl content of catalyst. The content was determined by the Mohr's method; $BiCl_3$ was dissolved in water and the free Cl^- ions were titrated with silver nitrate after filtration of the precipitated BiClO. In some cases, the Cl content in dehydrochlorinated PVC was measured by combustion of the sample, followed by titration with silver nitrate. The total fraction of the eliminated plus residual Cl was 95% or more.

Results and Discussion

The experimental data showing the HCl evolution from PVC and $BiCl_3$ are given in Table 1. The dehydrochlorination of PVC in the absence of catalyst scarcely occurred at 175 °C, while in the presence of $BiCl_3$ it readily proceeded even at lower temperatures. However, HCl was also formed from the catalyst according to the reaction:

$$BiCl_3 + H_2O \longrightarrow BiClO + 2HCl \quad (1)$$

since the $BiCl_3$ originally contained trace amounts of water. The occurrence of Eq. 1 has been verified experimentally; i.e., the amount of HCl evolved from $BiCl_3$ agreed with the decrease in the Cl content of catalyst on heating $BiCl_3$ alone. Therefore, the net HCl from PVC was calculated by subtracting this decrease from the total HCl evolved.

Table 1 indicates that a considerable amount of HCl was evolved when only $BiCl_3$ was heated, but with the mixture of PVC and $BiCl_3$ the HCl evolution from the catalyst decreased remarkably. This result could be

Table 1. HCl Evolution from PVC and $BiCl_3$ at 125 °C

Sample	Bi/PVC	Reaction time	Total HCl	Cl decrease in $BiCl_3$/mmol	HCl from PVC[a]
	mol/mol	h	mmol		mmol
PVC[b]	—	3	0.03	—	0.03 (0.5)
$BiCl_3$[c]	—	6	0.65	0.66	—
$BiCl_3$[c,d]	—	6	0.64	0.63	—
PVC+$BiCl_3$	0.1	6	2.33	0.14	2.19 (39.1)
PVC+$BiCl_3$	0.2	6	3.35	0.03	3.32 (59.3)
PVC+$BiCl_3$	0.3	6	3.38	trace	3.38 (60.4)
PVC+$FeCl_3$	0.2[e]	20	4.50	3.53[f]	0.97 (17.3)

a) Values in parentheses denote the degree of dehydrochlorination (%). b) At 175 °C. c) 1.1 mmol was used: the same applies to the case of Bi/PVC=0.2 for PVC+$BiCl_3$ samples. d) Outgassed under vacuum at room temperature for 4 h prior to use. e) Fe/PVC molar ratio. f) Cl decrease in $FeCl_3$.

† Present address: Hokkaido Technological Research Laboratory, Sumitomo Coal Mining Co., Ltd., Akabira 079-11.

rationalized as follows. Eq. 1 is a reversible reaction, so that the equilibrium between $BiCl_3$ and BiClO favors the former in the presence of HCl eliminated from PVC. This explanation was supported by the result shown in Fig. 1, in which the evolution of HCl from $BiCl_3$ at 150 °C started after about 3 h where the dehydrochlorination of PVC, and hence the HCl evolution from PVC, became very slow. This also suggests that a significant amount of water remained on the catalyst surface even after 3 h. Therefore, water is probably not desorbed from the surface as separate molecules. Hydrolysis of $BiCl_3$ resulted in the formation of BiClO and HCl. The catalytic activity of bismuth chloride oxide will be commented on later.

The degree of dehydrochlorination of PVC was heavily dependent on the reaction conditions. Table 1 shows that the degree of dehydrochlorination increases by raising the molar ratio of $BiCl_3$ to the vinyl chloride unit of PVC (Bi/PVC), but the increase is almost saturated at the molar ratio of 0.2. Figure 1 illustrates the time course of PVC dehydrochlorination at various temperatures. A significant dehydrochlorination activity of the $BiCl_3$ catalyst was observed at temperatures higher than 125 °C, while a sublimation of catalyst took place at 175 °C. The degree of dehydrochlorination increased almost linearly up to about 60% with the reaction time. This result suggests that no essential deactivation of the catalyst occurred. Nevertheless, complete dehydrochlorination was not attained under the conditions employed in this study. The degree of dehydrochlorination was 97% at the highest at 150 °C and Bi/PVC=0.4. The existence of the limit of the dehydrochlorination level may be attributed to the formation of Cl atoms isolated from reactive neighbors, such as -CH=CH-CH(Cl)-CH=CH-, by random elimination of HCl.[5] In the course of the reaction, the PVC sample rapidly turned from white to black. This color development seems to be a result of the formation of polyene sequences. In thermal dehydrochlorination of PVC without any additive, PVC particles strongly adhered each other and to the reactor wall. The adhesion made it difficult to handle the dehydrochlorinated residue. In the presence of $BiCl_3$, in contrast, the PVC residue remained fine powdery throughout.

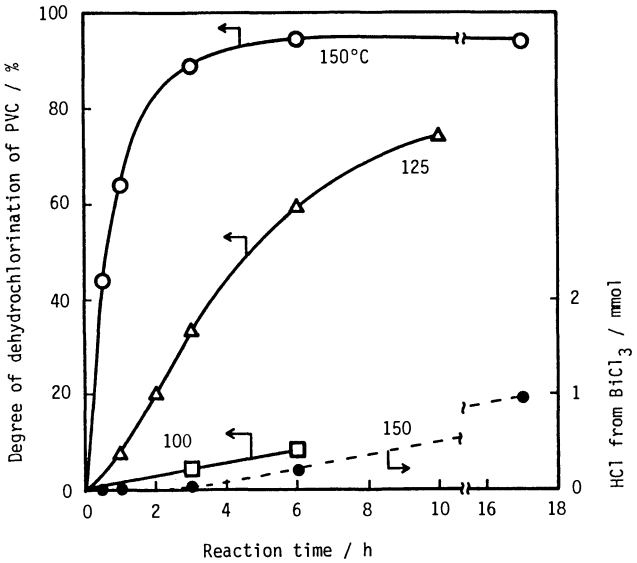

Fig. 1. Time course of PVC dehydrochlorination at various reaction temperatures. Bi/PVC=0.2.

Thus, $BiCl_3$ is active as a catalyst for dehydrochlorination of PVC. There have been many studies on the stabilization of PVC. In this regard, oxides or chlorides of Al, Cd, Fe, Mo, and Zn[6-10] were found to catalyze dehydrochlorination of PVC although their catalytic activities were not always assayed quantitatively. Silica-supported $FeCl_3$ was claimed to be an active catalyst for dehydrochlorination of PVC; the degree of dehydrochlorination was about 90% at 200 °C in 3 h under air, while it was 50% in a N_2 stream.[8] In this study, the catalytic activity of $BiCl_3$ was compared with that of $FeCl_3$ (Merck Co.). The latter was slightly more active than the former in the initial stage of the reaction. However, a rapid reduction in the reaction rate with time was observed and consequently the final dehydrochlorination level was much lower with $FeCl_3$ as catalyst (Table 1). Hence the overall catalytic activity is higher for $BiCl_3$ than for $FeCl_3$.

To obtain further information about the catalysis by $BiCl_3$, the effects of adsorbed pyridine and water on its activity were examined. The results are summarized in Table 2. $BiCl_3$ was treated with 4 Torr (1 Torr=133.322 Pa) of pyridine at room temperature for 10 min in a vacuum system, followed by outgassing at the same temperature for 30 min. After pyridine adsorption the activity of catalyst was reduced by roughly an order-of-magnitude. This strongly suggests that the acidic property of $BiCl_3$ is responsible for the dehydrochlorination activity. In general, the catalytic activity of solid acids is remarkably influenced by addition of water. Since $BiCl_3$ used in this study contained water, removal of water was attempted by outgassing the catalyst at room temperature for 4 h. However, this pretreatment exerted little effect on the catalytic activity, due probably to strong adsorption of the water molecules. The strong adsorption is also substantiated by the observation that no decrease in the amount of HCl evolved from

Table 2. Dehydrochlorination Activity of $BiCl_3$ after Various Treatments

Treatment	Activity/%[a]
None	59.3
After pyridine adsorption at room temperature	6.5
After outgassing at room temperature	58.5
After treatment with water vapor (3 mol% in He) at 125 °C	0.5
In the presence of water vapor (3 mol% in He)	55.5

a) At 125 °C for 6 h.

$BiCl_3$ took place by the outgassing (Table 1). On the other hand, when $BiCl_3$ was treated with water vapor (3 mol% in He) at 125 °C for 10 h prior to use, the catalytic activity disappeared almost completely. During the pretreatment $BiCl_3$ was transformed mostly into BiClO according to Eq. 1, and the resulting chloride oxide showed no catalytic activity for dehydrochlorination of PVC. This was the reason for the complete loss of the catalytic activity. Then, water vapor was introduced into the reaction system simultaneously with the start of PVC dehydrochlorination and was continuously supplied throughout the reaction. Here the formation of BiClO occurred only to a small extent, most probably because the HCl eliminated from PVC interfered with the formation of the chloride oxide. Owing to this behavior, which is advantageous on a practical viewpoint, the $BiCl_3$ catalyst remains sufficiently active even in the presence of water.

References

1) T. Asaoka, "Oyo Shokubai Kagaku," Sankyo Shuppan, Tokyo (1967), Chaps. 7—9.
2) K. Tanabe and T. Takeshita, "San Enki Shokubai," Sangyo Tosho, Tokyo (1966), Chap. 3.
3) R. C. Poller, *J. Chem. Tech. Biotechnol.*, **30**, 152 (1980).
4) "Pori Enka Biniru-Sono Kiso To Oyo," ed by Kinki Kagaku Kyokai Biniru Bukai, Nikkan Kogyo Shinbunsha, Tokyo (1988), Chap. 7.
5) C. S. Marvel, J. H. Sample, and M. F. Roy, *J. Am. Chem. Soc.*, **61**, 3241 (1939).
6) J. C. Bevington and R. G. W. Norrish, *J. Chem. Soc.*, **1948**, 771.
7) R. Nagatomi and Y. Saeki, *Kogyo Kagaku Zasshi*, **65**, 393 (1962).
8) Y. Uegaki and T. Nakagawa, *J. Appl. Polym. Sci.*, **21**, 965 (1977).
9) R. P. Lattimer and W. J. Kroenke, *J. Appl. Polym. Sci.*, **26**, 1191 (1981).
10) E. D. Owen and K. J. Msayib, *J. Polym. Sci., Part A, Polym. Chem.*, **27**, 399 (1989).

Sorption of Anionic Surfactants with Wood Charcoal

Itsusei FUJITA,* Jyo TOMOOKA, and Tsugiharu SUGIMURA
Kumamoto Prefectural Institute of Public Health, 4-33 Minamisendanbata-machi, Kumamoto 860
(Received August 20, 1990)

Synopsis. The possibility of wood charcoal as an adsorbent, not as an energy source as in the past, was confirmed by the use of an anionic surfactant as the model adsorbate, and a trial sorption of polluting substances in an actual river by a wood charcoal column was conducted.

The rapidly progressing population centralization and the change of life style in urban areas are today having an extremely adverse effects on river environments. Although this has been caused by a delayed construction of basic social facilities (such as sewage disposal facilities) to cope with the increasing population, hasty perfection of social facilities would be difficult in view of the present status of Japan. In order to improve the water environment, it is therefore necessary to reduce the pollution loading amount at each disposal point. As one possible measure, there have been movements to recommend a reduction of polluting materials discarded by each home. In some parts of the country there have also been trial installations of simplified water-purification facilities at disposal points of homes or at nearby small rivers. Simplified water purification facilities include those utilizing catalytic oxidation and those using hydrophytes.

The catalytic oxidation method is a method for cleaning water by the utilization of a self-purifying action of water ways packed with contracting materials covered with a biomembrane. As contracting materials gravel[1] and wood charcoal have commonly been tried.

Wood charcoal, with a history going back to the Heian Era in Japan, was one of national necessaries of life until about 30 years ago. Its annual production sharply decreased from 2 million tons around 1955 to 40 thousand tons at present. The development of new applications of wood charcoal, therefore, not only activates its business circle, but is also expected to stimulate the average person's concern for wood as well as for the concept of "green", leading to a heightened movement fowards "green" cultivation. Wood charcoal has had two major uses: one as an energy source, and the other as a carbon material. The characteristics of wood charcoal as a carbon material are: a large inner surface area with both high reactivity and adsorptivity, high content of valuable minerals, and only a small content of hazardous components. The incorporation of wood charcoal, to which microorgraisms readily adhere, into soil improves the filtration ability and water retention of soil; efficient farming producers, therefore, have applied wood charcoal into soil. From long ago wood charcoal has been used for the filtration of well water; there has also been an idea[2] to use wood charcoal as a water-purifying agent. However, systematic studies concerning the water-purifying function of wood charcoal, which have rarely been carried out, are strongly desired. In the present study, in terms of the abovementioned background, the possibility of wood charcoal as an adsorbent was investigated using anionic surfactants found in river water as a model substance.

Experimental

Materials and Reagents. The wood charcoal used for the adsorption experiment, a product made from lumber produced by thinning, was presented by the Federation of Kumamoto Forestry Association. The sodium alkylbenzenesulfonate, an anionic surfactant that was used for a batch process experiment, has an alkyl chain of C_{11} to C_{14} and is made by Nacalai Tesque, Inc. The other reagents used were of special reagent grade obtained from commercial sources.

Determination of Surfactants. The determination of surfactants was made by highperformance liquid chromatography.[3] Along with the method using 225 nm ultraviolet absorption, fluorescence spectroscopy using on excitation wavelength of 225 nm and fluorescence light at 285 nm was employed.

Determinations of Other Items. The determination of COD, pH, total nitrogen(T-N), ammonium nitrogen (NH_4-N), nitrite nitrogen (NO_2-N), nitrate nitrogen (NO_3-N), phosphate phosphorus (PO_4-P), and total phosphorus (T-P) was conducted according to Japan Industrial Standad (JIS) K0102. The determination of the chloride ion was made by Mohrs's method.

Sorption Study by Batch Process. One gram of crashed wood charcoal was put into a 300 cm^3 conical flask, and then 100 ml of sodium alkylbenzenesulfonate solution was added. The flask was shaken at 25 °C for 24 h, and the wood charcoal separated by centrifugation. The concentration of sodium alklbenzenesulfonate in the supernatant was measured.

Experimental Conditions of the Wood Charcoal Column for the Adsorption of River Water. A glass column packed with wood charcoal was 15 mm in inner diameter and 500 mm in length. The wood charcoal packed was of crashed irregular shapes with an average diameter of 5 mm. The packed height was 200 mm, and the temperature 25 °C. A 250 cm^3 sample of river water was filtered by suction through a GF/B glass filter, which was washed in 1 ml of methanol and 50 cm^3 of distilled water. The filtrate was passed through a wood charcoal column at a rate of 5 $cm^3 min^{-1}$ to adsorb chemical components in river water; the column effluent was collected at 200 cm^3. Similarly, the filtrate was passed through the activated-carbon column. This column-sorption experiment was triplicated, respectively. The mean concentrations of the chemical components in the eluate are tabulated in the table.

Results and Discussion

Table 1 shows data concerning the wood charcoal used: the specific surface area, ion exchange capacity,[4] chloride ion adsorption, and nitrogen content by ele-

Table 1. Physicochemical Properties of Wood Charcoal

Capacity of anion exchange	8.82×10^{-5} equiv g^{-1}
Sorbed amount of chloride	9.51×10^{-6} mol g^{-1}
Specific surface area	3.57 $m^2 g^{-1}$
N content (elemental analysis)	0.31%

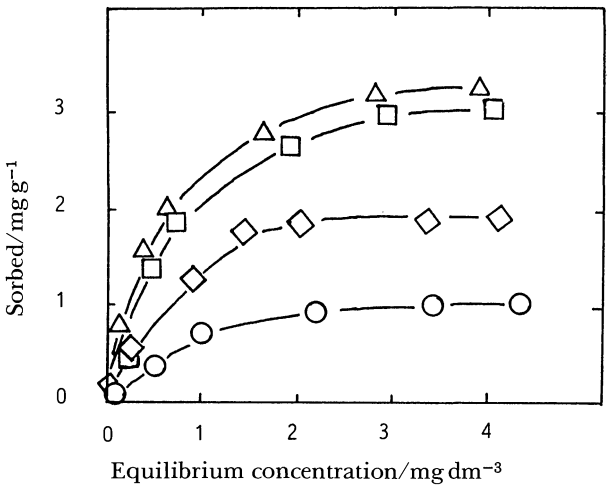

Fig. 1. Sorption isotherm at 25 °C for alkylbenzenesulfonates with wood charcoal.
○: $CH_3(CH_2)_{10}C_6H_4SO_3Na$,
△: $CH_3(CH_2)_{11}C_6H_4SO_3Na$,
□: $CH_3(CH_2)_{12}C_6H_4SO_3Na$,
◇: $CH_3(CH_2)_{13}C_6H_4SO_3Na$.

mental analysis. The specific surface area[5-8] was smaller compared to that of the powdery activated carbon generally used as an adsorbent. Basic groups, the presence of which in low-temperature (300 °C)-treated activated carbon has been reported,[5,6] are supposed to also exist in wood charcoal as a possible precursor of activated carbon.

A surfactant (more specifically, sodium alkylbenzenesulfonate in this experiment), commonly used in adsorption experiments, was used as a model organic substance to be adsorbed by wood charcoal. The experiment was conducted in a batch process. Figure 1 shows the adsorption isotherm, a general means for a comprehensive expression of the adsorption capacity or adsorbed amount of an adsorbent. The adsorbed amount did not show such an increase corresponding to the increase in the length of the alkyl chain of the surfactant.

Figure 2 and Table 2 show the results of an investigation involving the application of Freundlich's adsorption equation, which has been applied to activated carbon. In an adsorbed amount, though wood charcoal showed lower values than did activated carbon, the $1/n$ value which expresses the readiness for adsorption, showed values paralleling those of a previous evaluations.[7]

Wood charcoal, found to have the function described above, was then subjected to an investigation concerning its adsorption capacity in a column of actual river water. Generally, though the particle diameter of an adsorbent to be packed in a column is

Table 2. Freundlich's Absorption Constant

	k	$1/n$
Wood charcoal	4.46×10^{-3}	0.307

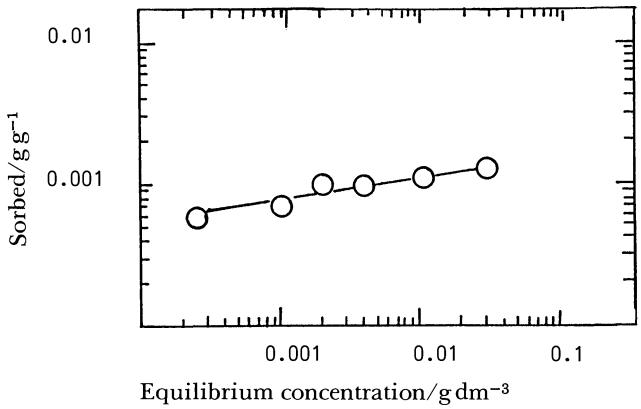

Fig. 2. Sorption isotherm at 25 °C for undecylbenzenesulfonate with wood charcoal.

desinably very small, considering practical applications (to avoid column choking by suspended matter and the removal of river water pollution by the whole experiment system) wood charcoal was powdered to an average diameter of 5.0 mm. Evaluations of the overall pollution loading amount from organic materials in river water has generally been made in terms of the biochemical oxygen demand (BOD); in this experiment, however, it was made in terms of the chemical oxygen demand (COD) owing to its operation simplicity. Evaluations were also made for linear alkylbenzenesulfonate sodium salt (LAS), the principal component of detergents deemed as a model substance of pollution loading by waste water from living, and for nutrient salts (N, P), the loading of which in lakes and ponds is becoming a problem. Water samples taken at Kengun river in a new residential quarter where there were no public water-treatment facilities, were subjected to an investigation concerning their sorption by the wood charcoal column developed in this study.

As can be seen in Table 3, wood charcoal is considered to be efficient as a factor only for the overall removal by sorption. Regarding ionic adsorption of the surfactant, NO_3^-, NO_2^-, and PO_4^{2-}, however, the values remain at the level of about 1/5 of the ion exchange capacity (Table 1). The contact time in the column is very deeply related to this.

The main purpose of using natural materials in conventional water purification processes has been as the carrier of a biomembrane for biological catalytic oxidation. In recent years there have been examples of using wood charcoal for such catalytic oxidation. There have been a number of reports stating that wood charcoal has a greater specific surface area than do conventional materials for catalytic oxidation and is excellent concerning the living conditions of soil bacteria.[2] Wood charcoal might therefore possibly become more useful through additional detailed

Table 3. Sorption of Chemical Components in River Water

	LAS	NH_4-N	NO_2-N	NO_3-N	PO_4-P	T-N	T-P	COD	pH
	mg dm^{-3}	mg dm^{-3}	mg dm^{-3}	mg dm^{-3}	mg dm^{-3}	mg dm^{-3}	mg dm^{-3}	mg dm^{-3}	
Original	1.338	5.40	0.09	1.82	0.73	9.20	1.68	30.5	7.7
Elution[a)]	0.706	4.27	0.08	1.41	0.68	7.34	1.58	28.5	7.9
Elution[b)]	0.342	4.87	0.02	0.41	0.57	6.50	1.32	25.6	7.8

a) Wood charcoal. b) Activated carbon.

investigations of the application conditions. Because an improvement in the adsorption activity by a simple treatment was claimed for activated carbon,[5] such an improvement for wood charcoal is also of interest as a future theme of investigation.

References

1) M. Ohya and K. Enda, *Yokohamashi Kougai Kenkyu-shohou*, **13**, 157 (1967).
2) G. Sugiura and I. Furuya, "Mokutan ha yomigaeru (Charcoal Revives)," Zenkoku Ringyo Fukyu Sosho (A Series for Growth of National Forestry Business), Tokyo, (1988).
3) I. Fujita, Y. Ozasa, T. Tobino, and T. Sugimura, *Chem. Pharm. Bull.*, **38**, 1025 (1990).
4) M. Honda, H. Kakihana, and Y. Yoshino, "Ion Koukan Jyusi (Ion-exchange Resins)," Hirokawa Shoten, Tokyo (1976).
5) Y. Fujita and S. Okazaki, *Nippon Kagakukai Shi*, **1990**, 352.
6) K. Kamegawa and H. Yoshida, *Nippon Kagakukai Shi*, **1989**, 789.
7) R. Leyva-Ramos and F. J. Molina-Segura, World Congress III of Chemical Engineering, Tokyo, 1986, Abstr., p. 813.
8) F. Kitahara, "Kaimenkasseizai (Surfactans)," Kodan Sha, Tokyo (1988).

Effects of Pretreatment of Yubari Coal by Solvent-Extraction on the Reductive Alkylation with Molten Potassium and Iodoethane

Mikio MIYAKE,* Kazushi TAMADA, Hiroo MINAMI, and Masakatsu NOMURA*
Department of Applied Chemistry, Faculty of Engineering, Osaka University, 2-1, Yamada-oka, Suita, Osaka 565
(Received September 29, 1990)

Synopsis. Effects of pretreatments of Yubari coal by solvent-extraction on the reductive alkylation with molten potassium and iodoethane have been investigated by comparing the reactions with and without ultrasonic irradiation. Important roles of electron-transfer agents and secondary bonds between coal macromolecules on the anionization were elucidated.

The Sternberg's method of reductive alkylation[1] has been accepted as one of the most effective procedures for the coal solubilization in conventional organic solvents under mild reaction conditions.[2] We have demonstrated previously that highly efficient coal anionization with molten potassium in refluxing tetrahydrofuran (THF)[3] can be further enhanced by ultrasonic irradiation.[4,5] For example, ethylated Yubari coal, prepared by anionization for only 10 min under ultrasonic irradiation, followed by alkylation with iodoethane, yielded 70 wt% of benzene-soluble materials, compared with 41 wt% obtained without ultrasonic irradiation under otherwise the same conditions.[5] Prolonged anionization time both with and without ultrasonic irradiation showed an increase in solubility of alkylated products. Nearly quantitative solubilization in benzene was achieved within 1 h by ultrasonic irradiation but more than 6 h were necessary without the irradiation.[3,5]

In this study, two reactions mentioned above were carried out for the residues of Yubari coal after extraction with different solvents. Such an approach will enable us to assess the role of solvent-extractable constituents in coal on the reactions and to elucidate the reason why ultrasonic irradiation leads to highly efficient reductive alkylation.

Experimental

Pulverized Yubari and Kairan coal samples (−200 mesh) were dried at 110 °C under vacuum overnight. Elemental analyses (dry ash-free basis) are as follows: C, 87.3; H, 6.1; N, 2.0; O (difference), 4.6 wt% for Yubari coal and C, 87.6; H, 4.8; N, 1.5; O (difference), 6.1 wt% for Kairan coal. Extraction solvents (hexane, heptane, chloroform, and benzene) and potassium metal were used as received. Naphthalene used as an electron-transfer agent was purified by recrystallization from ethanol. Purification procedures of THF and iodoethane were described elsewhere.[3-5]

Yubari coal was thoroughly extracted with heptane, chloroform, or benzene using a Soxhlet apparatus for one week. The extract and the residue were dried overnight at 90 °C under vacuum.

A typical reductive alkylation procedure is as follows: a three-necked flask containing THF (50 cm^3) and potassium metal (4 g) was heated in an oil bath until potassium melted and dispersed completely in the refluxing THF. Then, the coal or residue sample (3 g) was added into the flask and agitated by a magnetic stirrer for 6 h under a stream of dry argon. After the anionization of the coal or residue sample with molten potassium, the flask was cooled to 0 °C and then a large excess of iodoethane was added dropwise to the reaction mixture. The resulting mixture was stirred overnight at room temperature.[3] This procedure using molten potassium is called the M-K method. The same procedure was carried out under ultrasonic irradiation by immersing the flask in a heated water bath of an ultrasonic laboratory cleaner (Bransonic B-220, 100 W, 45 kHz, 0.5 W cm^{-2}).[4,5] This procedure under ultrasonic irradiation is called the M-K/US method. Kairan coal sample (3 g) in the presence or absence of naphthalene (0.3 g) was made to react with molten potassium metal (2.4 g) for 2 h under otherwise the same conditions as the M-K and M-K/US methods. It should be mentioned that molten potassium is explosive when exposed to atmosphere. Ethylated products, after repeated washing with deionized water, were subjected to Soxhlet extraction with hexane and benzene for 48 h, and the soluble materials were named Hexane solubles (HS) and Benzene solubles (BS), respectively. Procedures were described in detail elsewhere.[3-5]

The Curie-point pyrolysis of the coal extract (3 mg) was done at 670 °C for 3 s by a pyrolyzer (Japan Analytical Industry Co., model JHP-3). Volatile pyrolysates were analyzed by GLC (Hewlett-Packered, model 5970) and mass spectrometer (JEOL, model DX-303) which were connected to the pyrolyzer, as described in detail elsewhere.[6] The number of ethyl groups per 100 carbon atoms was determined from an increase in weight of the ethylated products.[3]

Results and Discussion

The yield of the extract from Yubari coal increased in the order, heptane (1 wt%) < chloroform (5 wt%) < benzene (12 wt%). The heptane extract showed a high H/C value (1.222) and a low N/C value (0.005), whereas the chloroform extract showed a high N/C value (0.014). In order to characterize the extracts obtained by nonpolar solvents (heptane and benzene), the Curie-point pyrolysis-GC/MS analysis was carried out, indicating that the heptane extract is predominantly composed of long-chain alkanes and that the benzene-extract contains alkylbenzenes in addition to long-chain alkanes. Thus, each extraction solvent (heptane, chloroform, and benzene) may remove aliphatic compounds especially long-chain alkanes, polar compounds containing heteroatoms, and aromatic compounds in addition to heptane solubles, respectively.

Table 1 summarizes properties of Yubari coal, the solvent-extracted residues, and their ethylation products. The properties given are H/C ratio, number of ethyl groups per 100 carbon atoms, and solubility in hexane and benzene (HS and BS, respectively). By the M-K method with molten potassium and iodoethane in THF, ethylated products from the original

Table 1. Properties of Yubari Coal, Residues, and Ethylated Products

Sample	Reaction method[a)]	Atomic H/C	No. of Et added per 100 C[b)]	Solubility/wt%	
				HS[c)]	BS[d)]
Original coal	—	0.84	—	Tr.[e)]	5
Et-product	M-K	1.20	20	36	78
Et-product	M-K/US	1.32	31	60	85
Heptane residue	—	0.84	—	—	—
Et-product	M-K	1.16	14	35	79
Chloroform residue	—	0.82	—	—	—
Et-product	M-K	1.24	19	49	83
Benzene residue	—	0.83	—	—	—
Et-product	M-K	1.02	3	11	63
Et-product	M-K/US	1.20	16	33	83

a) Sample (3 g) was anionized with molten potassium (4 g) using magnetic stirrer (M-K method) or under ultrasonic irradiation (M-K/US method) for 6 h, followed by alkylation with iodoethane. b) Estimated by an increase in weight. c) Hexane-soluble fraction obtained by Soxhlet extraction for 48 h. d) Benzene-soluble fraction obtained by Soxhlet extraction for 48 h. e) Less than 0.5 wt%.

Table 2. Properties of Original and Ethylated Kairan Coals

Sample	Reaction method[a)]	Naphthalene	Atomic H/C	No. of Et added per 100 C[b)]	Solubility/wt%	
					HS[b)]	BS[b)]
Original coal	—	—	0.66	—	2	6
Et-product	M-K	No	0.77	4	6	20
Et-product	M-K	Yes	0.94	12	27	72
Et-product	M-K/US	No	1.05	15	34	75
Et-product	M-K/US	Yes	1.07	18	37	75

a) Kairan coal (3 g) was anionized in the presence or absence of naphthalene (0.3 g) with molten potassium (2.4 g) using magnetic stirrer (M-K method) or under ultrasonic irradiation (M-K/US method) for 2 h, followed by alkylation with iodoethane. b) See Table 1.

coal and the heptane-extracted residue showed a similar solubility in hexane (HS yields were 36 and 35 wt%, respectively) and in benzene (BS yields were 78 and 79 wt%, respectively). The results indicate that long-chain alkanes, which were removed by heptane-extraction, affect little on the reaction. On the other hand, the chloroform-extracted residue gave the product with the highest HS and BS yields (49 and 83 wt%, respectively), whereas the product from the benzene-extracted residue showed the lowest HS and BS yields (11 and 63 wt%, respectively). In contrast, the product from the benzene-extracted residue obtained by the M-K/US method (under ultrasonic irradiation, otherwise the same conditions as the M-K method) sustained rather high HS and BS yields (33 and 83 wt%, respectively), although these values were lower than those of the original coal (60 and 85 wt%, respectively).

The restricted reaction of the benzene-extracted residue by the M-K method (Table 1) may be related to the removal of aromatic compounds from coal by benzene-extraction. In the M-K method, these extracted aromatic compounds may play an important role as electron-transfer agents from molten potassium to bulk constituents in coal. An enhancement of coal anionization with molten potassium in THF in the presence of 18-crown-6, which is known to accelerate the formation of solvated electrons,[7)] suggests the importance of an electron carrier, even for the system with molten potassium. In the case of the M-K/US method, however, the benzene-extractable materials as electron-transfer agents may play a less important role in the anionization reaction (Table 1).

In order to examine the effects of an electron-transfer agent on the coal anionization by both the M-K and M-K/US methods, Kairan coal was subjected to reductive ethylation in the presence and absence of naphthalene as an electron-transfer agent. The results are summarized in Table 2. By the M-K method in the absence of naphthalene, number of ethyl groups added per 100 carbon atoms was 4, and the yields of the HS and BS were 6 and 20 wt%, respectively. By the M-K/US method, number of ethyl groups added (15) and the yields of HS and BS (34 and 75 wt%, respectively) were much higher than those by the M-K method in the absence of naphthalene (Table 2). In the case of the M-K method, however, the presence of naphthalene significantly enhanced the extent of the reaction; The number of ethyl groups added per 100 carbon atoms increased 3 times and the yields of HS and BS increased more than 3.5 times. In contrast, only a small degree of enhancement of the reaction was observed by the M-K/US method. Thus, the results in Table 2 demonstrate that by using the M-K method electron-transfer agents enhance coal anionization with molten potas-

sium compared to the reaction solely with solvated electrons produced in THF. Such acceleration effect of electron-transfer agents has been commonly observed in the reduction of various organic compounds with alkali metal in THF.[8-10] Under ultrasonic irradiation, however, reductive alkylation of Yubari coal in Na/HMPA system has been reported to proceed more efficiently than that in Na/THF/naphthalene system,[11] suggesting that anionization via solvated electrons is more important than that via electron-transfer agents by the M-K/US method.

Since extraction with chloroform was carried out extensively for one week, significant amount of polar compounds, which form secondary bonds (e.g., hydrogen bond) between macromolecules in coal, will be removed for the chloroform-extracted residue. Although THF as the reaction solvent may also remove polar compounds similarly to chloroform, such an effect of THF may be ignored because of much shorter reaction time (6 h) than the Soxhlet extraction with chloroform (one week). The absence of secondary bonds prevents the formation of associated macromolecules to increase mobile constituents in the chloroform-extracted residue[12] compared to the case of the original coal and the heptane-extracted residue, resulting in efficient diffusion of electron-transfer agents to bulk constituents in the residue. This seems to be a reason why the ethylation product from the chloroform-extracted residue shows the highest HS yield among those prepared by the M-K method (Table 1).

The ultrasonic energy adopted in the present study (0.5 $W\,cm^{-2}$) is reported to be too weak to cleave covalent bonds in coal constituents, but strong enough to destruct secondary bonds between coal constituents.[13] Destruction of such secondary bonds by ultrasonic irradiation may make essentially the same effect as the removal of polar compounds mentioned above. In addition, cavitation induced by ultrasonic irradiation leads to highly efficient diffusion of solvent molecules[14] and presumably of solvated electrons into bulk constituents in coal. This will be the major reason why the M-K/US method leads to the efficient reaction of the benzene-extracted residue as well as the original coal containing polar compounds (Table 1).

References

1) H. W. Sternberg, C. L. Delle Donne, P. Pantages, E. C. Moroni, and R. E. Markby, *Fuel*, **50**, 432 (1971).
2) L. M. Stock, *Coal Sci.*, **2**, 161 (1982).
3) M. Miyake, M. Sukigara, M. Nomura, and S. Kikkawa, *Fuel*, **59**, 637 (1980). *J. Chem. Soc. Jpn.*, **1980**, 939.
4) M. Miyake, S. Yamamoto, and M. Nomura, *Fuel Process. Technol.*, **14**, 206 (1986).
5) M. Miyake, S. Yamamoto, and M. Nomura, *Fuel*, **67**, 589 (1988).
6) M. Nomura, T. Ida, M. Miyake, T. Kikukawa, and T. Shimono, *Chem. Lett.*, **1989**, 645.
7) M. Miyake, T. Ohsaki, and M. Nomura, *J. Fuel Soc. Jpn.*, **66**, 441 (1987).
8) M. Itoh, S. Yoshida, T. Ando, and N. Miyaura, *Chem. Lett.*, **1976**, 271.
9) N. L. Holy, *Chem. Rev.*, **74**, 243 (1974).
10) J. Eisch, *J. Org. Chem.*, **27**, 707 (1963).
11) M. Miyake, R. Uematsu, and M. Nomura, *Chem. Lett.*, **1984**, 535.
12) J. W. Larsen, T. K. Green, and J. Kovac, *J. Org. Chem.*, **50**, 4729 (1985).
13) N. E. Cooke and R. P. Gaikwad, *Can. J. Chem. Eng.*, **61**, 697 (1983).
14) H. Tsuboi, K. Nagoya, M. Nagai, M. Nakano, and M. Kasagi, *J. Fuel Soc. Jpn.*, **57**, 918 (1978).

Gold(III) Complexes of 2-Amino-4,6-dimethylpyrimidine

Dimitra KOVALA-DEMERTZI
Laboratory of Inorganic Chemistry, Department of Chemistry, University of Ioannina, Ioannina 45110, Greece
(Received March 26, 1990)

Synopsis. The reactions of Au(III) with 2-amino-4,6-dimethyl pyrimidine (ADMPY) are reported. Complexes of Au(III) with ADMPY have been isolated from reactions in aqueous and in methanolic solutions, and characterized by elemental analysis, IR spectra ^{1}H NMR spectra, electronic absorption spectra, conductivity in DMF solutions, and thermal gravimetric analysis.

The pyrimidine ring system present in nucleic acids, several vitamins, coenzymes, and antibiotics etc., provides potential binding sites for metal ions and any information on their coordinating properties is important as a means of understanding the role of metal ions in biological systems. The interaction of metal ions with nucleic acids constituents has been the subject of extensive investigations in recent years.[1,2]

The gold complexes are interesting in biological chemistry.[3] Many gold compounds were recently found to be strong antitumor agents,[4] more promising were found the binuclear gold complexes.[4] Gold complexes with nitrogen donor ligands[3,5] have been considered suitable for modern chrysotherapy associated with the treatment of rheumatoid arthritis. The gold antiarhritic compounds include important examples of inorganic-based pharmaceuticals.[6,7]

Experimental

Preparation of the Complexes. Au(ADMPY)Cl$_3$. (1) and Au(ADMPY)Br$_3$, (2). The complexes were prepared by mixing aqueous solutions of the ligand and $HAuCl_4$. aq or $AuBr_3$ [1 : 1 ligand to metal molar ratio]. The reaction mixture was stirred for 2h at room temperature. The precipitate was filtered off, washed with small amounts of ice-cold water and dried in vacuum over silica gel. Compound **1**; yellow powder, Found: C, 16.48; H, 2.04; N, 9.80; Au, 45.80; Cl, 24.80%. Calcd for C, 16.89; H, 2.12; N, 9.85; Au, 46.18; Cl, 24.93%. Compound **2**. red-brown powder, Found: C, 12.30; H, 1.15; N, 7.20; Au, 35.32; Br, 42.02%. Calcd for C, 12.87; H, 1.62; N, 7.50; Au, 35.17; Br, 42.82%.

[Au(ADMPY)$_2$Br]$_2$Br$_4$ (3). The complex was prepared by mixing methanolic solutions of the ligand and $AuBr_3$ [3 : 1 or 2 : 1 ligand to metal molar ratio]. After stirring for 24h at room temperature no precipitate was separated. The yellow solution was evaporated to dryness under reduced pressure. When the residual was dissolved in a small volume of CH_2Cl_2 and an excess of C_6H_6 was added, a red powder was precipitated. After filtration the powder was again dissolved in CH_2Cl_2 and precipitated by C_6H_6. The complex was washed with petroleum ether and dried as before. Compound **3**. Found: C, 21.20; H, 2.77; N, 12.64; Au, 28.64; Br, 34.65%. Calcd for C, 21.10; H, 2.63; N, 12.30; Au, 28.84; Br, 35.09%.

[Au(ADMPY)$_2$Cl$_2$](ADMPY)Cl · 2H$_2$O (4). The complex was prepared by mixing methanolic solutions of the ligand and $HAuCl_4$. aq [3 : 1 or 2 : 1 ligand to metal molar ratio]. When the reaction mixture was stirred for 24 h at room temperature, no precipitate was separated. The clear solution was evaporated to a small volume (2—3 ml CH_3OH) under reduced pressure. With addition of an excess of ether, a yellow powder was precipitated. After filtration the powder was redissolved in methanol and precipitated with ether. Compound **4**. Found: C, 30,08; H, 4.02; N, 17.67; Au, 27.50; Cl, 14.80%. Calcd for C, 30.54; H, 4.37; N, 17.81; Au, 27.82; Cl, 15.02%.

Physical Measurements. Infrared spectra were recorded on a Perkin-Elmer 580 spectrophotometer on KBr pellets in the 4000—400 cm^{-1} region and on Nujol mulls supported by polyethylene windows in the 500—200 cm^{-1} region. The electronic absorption spectra of the solution in dimethylformamide were recorded on Hitachi 100-70 and Cary 17D spectrophotometers. Solid state electronic reflectance spectra were run on Varian 634 and Cary 14 spectrophotometers. Analyses and other experimental techniques were as described previously.[8,9]

Results and Discussion

The complexes **1** and **2** were non conductors in dimethylformamide solutions in agreement with their four coordination and square planar geometry. The complex **3** was 1 : 2 electrolyte while the complex **4** was 1 : 1 electrolyte in DMF solution.[10] Λ_m **1**=9; Λ_m **2**=21; Λ_m **3**=108; Λ_m **4**=46 S cm^2 mol^{-1}.

The significant bands observed in the IR spectra of the ligand and their complexes are presented in Table 1. All the complexes showed reductions in the observed values of $\nu_{as}(NH_2)$, $\nu_s(NH_2)$ by 25—60 cm^{-1}, but they were not as large as expected if coordination of the -NH_2 nitrogen atom occurs,[9] indicating the presence of intermolecular hydrogen bonding of the -NH_2 protons.[11] No appreciable changes were observed in the 700—1000 cm^{-1} region, in which coordinated water bands appeared.[12] On the other hand, various IR absorptions of free ADMPY, corresponding to ring vibrations modes underwent more sizeable shifts and occasional splittings in the spectra of the new complexes, this is consistent with coordination of the ADMPY through ring nitrogen in the complexes.[8] The complexes **1** and **2** showed one strong band at 367 and 251 cm^{-1} respectively, which were assigned to the asymmetric stretching vibration of the X-Au-X group possibly coinciding with the ν(Au-X) of the same motion.[13] The ν(Au-Cl) stretching vibration was assigned to the very strong band at 360 cm^{-1} for the complex **4**. The appearence of one band may indicate a trans rather a cis square planar structure. The complexes exhibited an intense infrared band in the 400—430 cm^{-1} region, but no bands are observed in the spectra of the ligand in this region, this band thus must have a large ν(Au-N) character.[8]

The ^{1}H NMR spectrum of the ligand in DMSO-d_6 showed a peak at 2.15 ppm downfield from TMS, which assigned to the equivalent C_4-CH_3 and C_6-CH_3 group protons, a sharp singlet at 6.48 ppm was

Table 1. Spectra IR Data of the Ligand and Its Complexes

Compound	$\nu_s(NH_2)$ $\nu_{as}(NH_2)$		$\delta(NH_2)$	I Ring vibr. II Ring vibr. III Ring vibr.	ν(Au-N)	ν(Au-X)
ADMPY	3416vs	3390sh	1646sh	1606vs		
	3325ms	3200s	1637ms	1572m		
				1472s		
1	3422vs	3330ms	1664sh	1610vs	432msbr	367s
	3260	3170s	1655s	1560s		341w
				1490m		
2	3418vs	3320ms	1655sh	1610vs	430msbr	251s
	3240sh	3160s	1646s	1580m		246s
				1540s		
				1482w		
3	3380vs	3340sh	1680sh	1640vs	426wbr	—
	3270ms	3180s	1670s	1600ms		
				1520m		
4	3390vs	3320s	1688s	1640vs	465ms	360s
	3280sh	3210s		1602ms		
				1590ms		
				1565m		

Table 2. Electronic Spectra of Square Planar Au(III) Complexes

Compound	Absorption in solution energy (ε/cm^{-1} mol^{-1} dm^3)	Reflectance in the solid	Assignment	Reference to exp. work
Au(py)Cl_3		20.833sh		30
(Chloroform soln)	27.472sh	26.315sh		
	32.050(1.400)	31.250	$^1A_{1g}\rightarrow{}^1E_g$	
Au(py)$_2Cl_3$		21.740sh		30
		24.390sh		
		30.300	$^1A_{1g}\rightarrow{}^1E_g$	
ADMPY(DMF soln)	35.114(3.300)		$n\rightarrow\pi^*$	This work
1		20.830sh	$^1A_{1g}\rightarrow{}^3B_{1g}$	This work
(DMF soln)		26.370	$^1A_{1g}\rightarrow{}^1E_g$	
	34.480(5.700)		$n\rightarrow\pi^*$	
4	30.769sh(2.700)	25.860	$^1A_{1g}\rightarrow{}^1E_g$	This work
(DMF soln)	35.087(12.400)		$n\rightarrow\pi^*$	
Au(py)Br_3	19.320sh	19.604sh		30
(Chloroform soln)	21.980sh			
	25.125(1.500)	25.000	$^1A_{1g}\rightarrow{}^1E_g$	
	29.410	28.570sh		
Au(py)$_2Br_3$		20.000sh		30
		24.390sh		
		29.410	$^1A_{1g}\rightarrow{}^1E_g$	
2		18.180sh	$^1A_{1g}\rightarrow{}^3A_{2g}$	This work
(DMF soln)	21.050sh(150)	20.120	$^1A_{1g}\rightarrow{}^3B_{1g}$	

assigned to the $-NH_2$ protons and another sharp singlet at 6.38 ppm was assigned to the C_5-H proton. The ^1H NMR spectra of the complexes **1** and **2** showed a downfield shift of the signal of the C_4-CH_3 and C_6-CH_3 protons and splitting of the signal was observed it can be noted that the symmetry of the pyrimidine molecule is disturbed. The protons of the amino groups exhibit characteristic downfield shifts by ca. 1.0—2.0 ppm in all the complexes indicating the occurrence protonation and/or coordination.[9] The spectra of the complex **4** showed two broad peaks centered at 7.4 and 6.1 ppm, assigned to the protons of the amino groups coordinate and free respectively.

The electronic absorption spectral data of square planar Au(III) complexes and the assignments of the observed bands are given in Table 2. The band at ca. 25.000—26.000 cm^{-1} is assigned to the $^1A_{1g}\rightarrow{}^1E_g$ transition. Brown, McKinlay, and Smith reported[14] that the positions and intensities of the lowest energy band $^1A_{1g}\rightarrow{}^1E_g$ appear to depend on the nature of the com-

plexing species. For the complexes of Au(III) with pyrimidine derivatives it was shown that, the intensity of the lowest energy band $^1A_{1g} \rightarrow {}^1E_g$ depended on the nature of the complexing species. The intensity range was much greater for the chlorides than the bromides (Table 2).

The thermal decomposition of the complex **4** was also studied by TG/DTG technique the TG and DTG curves showed that the dehydration process took place in two steps at 100 and 110 °C, and the dehydrated compound decomposed in the temperature range of 125—500 °C. The anhydrous compound $[Au(ADMPY)_2Cl_2]Cl$ (ADMPY) dissociated in three steps, two fast decomposition between 125—225 °C and 355—500 °C and another slow one between 225—340 °C. The complex **4** underwent and the endothermic reaction at 100—110 °C with mass loss corresponding to two molecules of water and also two endothermic and one exothermic reactions at 175 and 300 and at 440 °C respectively, with mass loss corresponding to the pyrimidine ring and halogen. The residue obtained at the end of the pyrolysis at 500 °C was 27.90% of the original weight, corresponding to Au(theoretical value 27.82%).

In accordance with the trans effect, the cis Pt(II), Pd(II), and Au(III) complexes can be synthesized directly from the $[MCl_4]^{2-}$ ions by reaction with N-donor ligand in methanolic or aqueous media, indicating that Cl^- has a greater trans effect compared to the N-donor ligand (L). While the replacement of chloride ions from $[MCl_4]^{2-}$ by (L) molecules give the cis isomer for the Pt(II) complexes, when $[AuCl_4]^-$,[15] $[PdCl_4]^{2-}$ [16] ions react with N-donor ligands (L) cis-trans isomerisation took place because of the higher stability of the trans-isomer. The *trans*-$Pd(L)_2Cl_2$[16] and *trans*-$[Au(L)_2Cl_2]Cl$ [15] isomers were thermodynamically more stable, so the *trans*-$[Au(ADMPY)_2Cl_2]Cl : ADMPY : 2H_2O$ isomer was precipitated instead of cis-isomer. The uncoordinated molecule of pyrimidine probably gives more stability to the compound. The failure to isolate $[Au(ADMPY)_4]Cl_3$ complexes is attributed to steric hindrance effects.

In the solid state, the ADMPY acts as unidentate through the endocyclic nitrogen N_1 or N_3 than through the nitrogen of the amino group. ^1H NMR data obtained for the diamagnetic complexes in DMSO-d_6 solution suggests a different coordination mode in which ADMPY coordinates via amino group nitrogen atom.[17] The most plausible structures for the isolated new complexes, based on the above results, are monomeric for **1**, **2**, and **4**. The latter complex exists rather in the trans form in view of the single band observed in the far ir spectra.[15] Considering the high value of molar conductivity in DMF solution and that there are no bands in the far IR spectra assignable to ν(Au-Br), the new complex $Au(ADMPY)_2Br_3$ seems to have a dimeric square planar structure $[Au(ADMPY)_2Br]_4$.

Finally it is worth noting that the four new compounds are possible candidate for antiarthritic activity[3,6,7] while the compounds **3** and **4** are possible candidate for antitumor activity.[4,18]

References

1) B. Martin, *Met. Ions Biol. Syst.*, **8**, 56 (1979).
2) D. J. Hodgson, *Prog. Inorg. Chem.*, **23**, 211 (1976).
3) P. J. Sadler, *Struct. Bonding (Berlin)*, **28**, 171 (1976).
4) I. Haiduc and C. Silvestri, *Coord. Chem. Rev.*, **99**, 253 (1990).
5) A. Lorber and T. M. Simon, *Gold Bull.*, **12**, 149 (1979).
6) R. C. Elder and M. K. Eidsness, *Chem. Rev.*, **87**, 1027 (1987).
7) B. M. Sutton, "Platinum, Gold, and Other Metal Chemotherapeutic Agents," ed by S. J. Lippard, A. C. S. Symposium Series 209, Washington DC (1983), p. 355.
8) D. Kovala-Demertzi, J. M. Tsangaris, H. O. Desseyn, and B. J. Van der Veken, *Bull. Soc. Chim. Belg.*, **96**, 7 (1987).
9) D. Kovala-Demertzi, N. Hadjiliadis, and J. M. Tsangaris, *J. Less-Common. Met.*, **115**, 1 (1986).
10) W. J. Geary, *Coord. Chem. Rev.*, **7**, 81 (1981).
11) S. Souza, J. A. Carcia Vasquez, and J. R. Massaguer, *Trans. Met. Chem.*, **8**, 140 (1983).
12) J. Fujita, K. Nakamoto, and M. Kobayashi, *J. Am. Chem. Soc.*, **78**, 3963 (1956).
13) T. Boshi, B. Crociani, L. Cattalini, and G. Marangoni, *J. Chem. Soc., A*, **1970**, 2408.
14) D. H. Brown, C. C. McMinlay, and W. E. Smith, *Inorg. Chim. Acta*, **32**, 117 (1979).
15) V. Hans-Norbert Adams and J. S. Strahle, *Z. Anorg. Allg. Chem.*, **485**, 65 (1982).
16) Y. N. Kukushkin, G. N. Sedova, L. Y. Pyzhova, R. A. Vlasova, and A. D. Garnovskii, *Russ. J. Inorg. Chem.*, **24**, 1257 (1979).
17) D. Kovala-Demertzi and D. Nicholls, *J. Coord. Chem.*, **17**, 297 (1988).
18) C. Dragulescu, J. Heller, A. Maurer, S. Policec, V. Topcui, M. Csalci, S. Kirschner, S. Kravitz, and R. Moraski, Int. Coord. Chem. Conf. XVI, January 1974, Abstr., p. 99.

Organophosphorus Chemistry. XV.[1] The Reaction of 10-Dicyanomethylene-9(10*H*)-phenanthrenone with Alkyl Phosphites

Wafaa M. Abdou,* Neven A. F. Ganoub, and Mohamed R. Mahran
Department of Pesticide Chemistry, National Research Centre, Cairo, Egypt
(Received November 30, 1989)

Synopsis. The titled compound **5a** reacts with trialkyl phosphites and dialkyl phosphonates to give, in each case, two conformers (**A**+**B**) of the corresponding phosphonate **8** and **9**. The yields of the two isomers were estimated on the basis of ^{31}P NMR data. Besides, structures **8** and **9** were supported by analytical and spectroscopic measurements of the major isomer **8A** and **9A**. The rotational isomers were assigned in terms of the Newman projection and NMR data. Relative ratios were studied in the light of dynamic NMR spectroscopy.

Recently,[2] we have reported on the reaction of trialkyl phosphites with 3-cyanomethylene-1,3-dihydro-2*H*-indol-2-ones (**2**) which offered a new pattern of attack by these reagents on α, β-unsaturated carbonyl systems. The initially observed *C*-alkylation at the phosphonium intermediate **3**, accounted for the formation of the 1 : 1 phosphonate adducts **4** (Scheme 1).

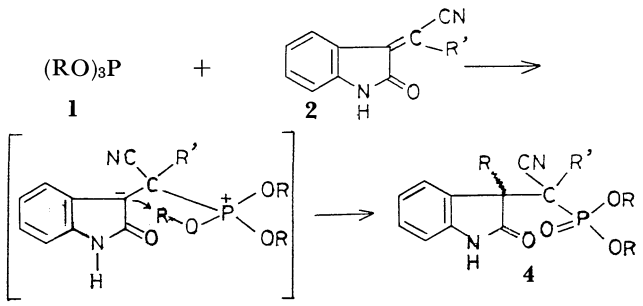

Scheme 1.

This, together with the growing interest[3] in this area of research, has prompted us to study the behavior of 10-dicyanomethylene-9(10*H*)-phenanthrenone (**5a**) with trialkyl phosphites (**1a—c**) and with dialkyl phosphonates (**6a—c**).

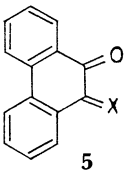

5

5	X
a	$C(CN)_2$
b	NH
c	NOH

$(RO)_2P(O)H$

6

6	R
a	CH_3
b	C_2H_5
c	i-C_3H_7

Results and Discussion

Treatment of **5a** with trimethyl phosphite yielded a reaction mixture with two resonances at δ=29.47 and 26.31 in its ^{31}P NMR.[4] These absorptions were assigned to two phosphonate 1 : 1 conformers (**8Aa**+**8Ba**). The relative percentages were 70% and 30% respectively. The ^{1}H NMR spectrum of this material had signals at δ=3.49 (s, -COCH$_3$) and 3.89 [d, -P(OCH$_3$)$_2$][5] assigned to the major isomer **8Aa**, as well as, at δ=3.85 and 4.1 assigned to -COCH$_3$ and -P(OCH$_3$)$_2$, respectivley for the minor conformer **8Ba**.

The possible interconversion for the rotational isomers **8Aa**$\rightleftarrows$**8Ba** was studied by variable temperature ^{31}P NMR spectral measurements. At −20 °C, a marked increase was shown in the signal around δ=26 with recording a proportion of **8Aa** : **8Ba**=15 : 85. On the

Table 1. ^{31}P and ^{1}H NMR Data of Diastereomeric Mixtures **8** and **9** Derived from the Reaction of 10-Dicyanomethylene-9(10*H*)-phenanthrenone(**5a**) with Trialkyl Phosphites(**1**) and Dialkyl Phosphonates(**6**)

Compound	Major **A** (trans)					Minor **B** (cis)				
	^{31}P	^{1}H				^{31}P	^{1}H			
8a	29.47		3.49s	3.89 & 4.16 (2d)		26.31		3.365	3.85 & 4.1 (2d)	
			-OCH$_3$	POCH$_3$				-OCH$_3$	POCH$_3$	
8b	28.6	0.95 t	1.19 t	3.97 q	4.2 qt	23.14	0.91 t	1.12 t	3.78 qt	4.1 qt
		=···CH$_3$	P···CH$_3$	-OCH$_2$	P·CH$_2$		=···CH$_3$	P···CH$_3$	-OCH$_2$	P·CH$_2$
8c	29.53	0.90 d	1.95 d	4.07 sept	4.6 sept	25.4	0.8 d	1.28 d	3.75 sept	4.5 sept
		=···CH$_3$	P···CH$_3$	-OCH	POCH		=···CH$_3$	P···CH	OCH	POCH
9a	27.20		3.12 & 3.58 (2d)		6.49 d[a]	21.77		3.09 & 3.52 (2d)		6.41 d[b]
			POCH$_3$		-CH			POCH$_3$		-CH
9b	25.35	1.29 t	4.1 qt		5.52 d[a]	22.16	1.06 t	3.85 qt		5.74 d[b]
		P-CH$_3$	POCH$_2$		-CH		P-CH$_3$	POCH$_2$		-CH
9c	25.07	1.15 d	3.92 sept		5.47 d[a]	21.92	0.96 d	3.49 sept		5.39 d[b]
		P···CH$_3$	POCH		-CH		P···CH$_3$	POCH		-CH

qt=quintet. a) $^3J_{HP}$=ca. 13 Hz. b) J_{HP}=ca. 15 Hz.

other hand, at 100 °C, the relative ratio of the same isomers became 90 : 10. At this stand point, it could be concluded that the first product, less stable, is the kinetic product and that the isomerization occurs, for steric reasons, to the thermodynamically stable product.[6] The activation energy, computed for the ^{31}P NMR spectra for the process of retention of configuration is $\Delta G=8$ kcal mol^{-1}. The incomplete permutational isomerization is verified by the variable temperature ^{1}H NMR studies which gave the same results.

On the basis of these observations, and by an inspection of a model, drawn by Newman projection,[7] there is no plausible alternative structure for **8** other than the staggered conformers, which could exist as **A** [vicinal trans, (anti), major] or **B** [gauche, minor].

However, only the major rotational isomers (**8Aa—c**) could be obtained in pure form (CH_2Cl_2), which gave compatible analytical and spectroscopic measurement for the assigned structure (see Tables 2 and 3). On the other hand, all attempts to isolate **8B** in a pure analytical form were not successful, even by chromatographic technique.

Formation of the vinyl ether phosphonate 1 : 1 adducts **8** is believed to involve 1,4-carbophilic addition by the tervalent phosphite ester on the α,β-unsaturated carbonyl system in **5a** by Arbuzov-like rearrangement[8] of the resulting dipolar intermediate **7**.

Next, we have studied the behavior of **5a** toward dialkyl phosphonates (**6a—c**). When **5a** was heated with dimethyl phosphonate a non-crystalline material

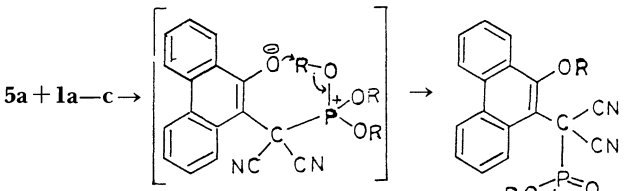

7 **8(A and B)**

8A	R	%	8B	R	%
a	CH_3	70	a	CH_3	30
b	C_2H_5	77	b	C_2H_5	23
c	i-C_3H_7	89	c	i-C_3H_7	11

Scheme 2.

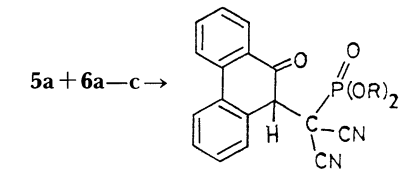

9

9A	R	%	9B	R	%
a	CH_3	70	a	CH_3	30
b	C_2H_5	75	b	C_2H_5	25
c	i-C_3H_7	80	c	i-C_3H_7	20

Scheme 3.

was obtained. Its ^{31}P NMR spectrum showed two resonances at $\delta=+27.20$ (major) and +21.77 (minor) which correspond to two possible phosphonate conformers **9A,B**. The relative ratio, on the basis of ^{31}P NMR, is **9Aa : 9Ba**=70 : 30). Only the major isomers (**9Aa—c**) could be obtained in pure forms (CH_2Cl_2).

Further, the conformational analyses of **9a** by an inspection of a model, drawn by Newman projection and the variable temperature (−27 °C to 100 °C)

Table 2. Characteristics of Compounds **8Aa—c** and **9Aa—c**

Compound[a]	% [b]	Mp °C	Mol. form. Mol wt calcd	MS *m/z*
8A a	76.69	167	$C_{20}H_{17}N_2O_4P$ 380.352	380
8A b	75.5	290	$C_{23}H_{23}N_2O_4P$ 422.433	422
8A c	72.22	204	$C_{26}H_{29}N_2O_4P$ 464.514	464
9A a	77.64	203	$C_{19}H_{15}N_2O_4P$ 366.325	366
9A b	74.76	202	$C_{21}H_{19}N_2O_4P$ 394.379	394
9A c	73.17	265	$C_{23}H_{23}N_2O_4P$ 422.433	422

a) The reaction was carried out in CH_2Cl_2. b) Yields are based on the isolated diastereomeric mixture. c) Solvent of crystallization is CH_2Cl_2. d) Compounds **8Aa—c** and **9Aa—c** gave satisfactory elemental analyses for C, H, N. e) IR spectra of compounds **8Aa—c** and **9Aa—c** gave characteristic bands at ca. 2200 (C≡N), ca. 1260 (P=O) and at ca. 1040 (P-OR) while **9Aa—c** showed bands at ca. 1700 (C=O). f) Presence of $\underline{C}OCH_3$ and $CO\underline{C}H_3$ carbon atoms in **8Aa** were supported by a signal at $\delta=157.8$ and 54.5 respectively, in its ^{13}C NMR spectrum. g) Presence of C=O group in **9Aa** was also attested by a signal at $\delta=169$ in its ^{13}C NMR spectrum.

Table 3. ^{31}P and ^{1}H NMR Spectral Data[a]

Compound[b]	$^{31}P/\delta$	^{1}H NMR					
8A a	29.7	3.48 s 3H $COC\underline{H}_3$			3.98 & 4.55 (2d) J_{HP}=12 Hz 6H P·$C\underline{H}_3$		7.54—8.76 m 8H arom.
8A b	28.2	0.92 t J_{HH}=4.5 Hz 3H $CO\cdot\cdot C\underline{H}_3$	1.17 t J_{HP}=11.5 Hz 6H P···$C\underline{H}_3$	3.87 q J_{HH}=4.5 Hz 2H C·$C\underline{H}_2$	4.2 qt J_{HP}=11.5 Hz 4H P·$C\underline{H}_2$		7.61—8.71 m 8H arom.
8A c	27.3	0.93 d J_{HP}=6 Hz 6H C··$C\underline{H}_3$	1.24 d J_{HP}=13.5 Hz 12H P···$C\underline{H}_3$	4.11 sept J_{HH}=6 Hz 1H C·$C\underline{H}$	4.68 sept 2H P·$C\underline{H}$		7.50—8.68 m 8H arom.
9A a	27.9				3.18 & 3.52 (2d) J_{HP}=12 Hz 6H P·CH_3	6.48 d J_{HP}=12 Hz 1H -$C\underline{H}$	7.41—8.37 m 8H arom.
9A b	26.8		1.19 t J_{HP}=12.5 Hz 6H P···$C\underline{H}_3$		3.97 qt J_{HH}=12.5 Hz 4H P·$C\underline{H}_2$	5.52 d J_{HR}=12.5 Hz 1H -$C\underline{H}$	7.46—8.14 m 8H arom.
9A c	25.9		1.09 d J_{HP}=13 Hz 12H P···$C\underline{H}_3$		3.87 sept 2H P·$C\underline{H}$	5.47 d J_{HR}=13 Hz 1H -$C\underline{H}$	7.37—8.97 m 8H arom.

a) See experimental for details of NMR experiments. b) The solvent is $CDCl_3$, qt.=quintet, sept.=septet.

^{1}H NMR and ^{31}P NMR spectra of **9a** showed that it was possible, as in case of **8a**, to change only the proportion of **9A** and **9B** in the mixture of **9a**, but with incomplete interconversion. Thus, the ligand rearrangement should be intramolecular in nature due to fluxioning of the molecule and does not involve any ionization process. The well-established structures for the two isomers are **9A** and **9B**.

Structural assignments for **9Aa—c** were supported by the mass spectra, IR, ^{1}H, ^{13}C, and ^{31}P NMR spectral data, and analyses which obtained for the new products **9Aa—c** (see, Tables 2 and 3).

Conclusion

It is evident that the initial step in the reaction of trialkyl phosphites with both **2** and **5a** is a carbophilic attack by the P(III) reagent on the most electrophilic carbon atom of the exo-conjugated system to yield phosphonium betaines **3** and **7**, respectively. However, while **3** is stabilized by *C*-alkylation (1,2-pattern) to give adducts **4**,[2] betaine **7** is stabilized by *O*-alkylation (1,4-pattern) to afford adducts **8**. In this respect, the behavior of **5a** toward trialkyl phosphites is also in great disparity to 9,10-phenanthrenequinone-monoimine (**5b**) and 9,10-phenanthrenequinone-monoxime (**5c**) which produce cyclic phosphorane structures with the same phosphite esters.[9,10]

Experimental

All melting points are uncorrected. The IR spectra were run on a Perkin-Elmer Infracord Spectrometer 157 (Grating) in KBr. Variable temperature, ^{1}H NMR and ^{31}P NMR spectra, were taken on a Varian Model FT-80 Spectrometer equipped with a 5 or 10 mm variable temperature, broad band probe. The mass spectra were performed at 70 eV on MS-50 Kratos (A.E.I.) Spectrometer. All reactions were carried out under N_2 atmosphere.

1. Reaction of 10-Dicyanomethylene-9(10*H*)-phenanthrenone (5a) with Trialkyl Phosphites (1a—c). General Procedure: To a stirred solution of **5a**[11] (0.01 mol) in 20 ml of CH_2Cl_2 (ether, acetonitrile, or toluene) at 0—5 °C were added a solution of TAP [TMP, TEP, and/or $(i\text{-PrO})_3$P (**1a—c**), respectively] (0.02 mol) in the same solvent (5 ml). After being warmed to room temperature, the reaction mixture was stirred for 10 h. The volatile materials were removed at 30 °C (first at 20 mm, then at 0.5 mm Hg, 1 mmHg=133.322 Pa) and the mixture of diastereomers **8** was collected. ^{31}P and ^{1}H NMR spectra of compounds **8** are collected in Table 1. Proportions of **8A**:**8B** are listed in Scheme 2. The mixture of isomers was redissolved in CH_2Cl_2 and kept at −10 °C for 3 days. The solvent was decanted and the procedure was repeated with fresh CH_2Cl_2. Crystals that separated out were collected and proved to be the major isomer (**8A**). Percentage yields (based on the isolated mixtures), physical and analytical data for compounds **8Aa—c** are presented in Tables 2 and 3.

The CH_2Cl_2 mother liquor was evaporated to give a colorless substance which still has two isomers **8A** and **B** in equal proportion (^{31}P NMR).

2. Reaction of 10-Dicyanomethylene-9(10*H*)-phenanthrenone (5a) with Dialkyl Phosphonates (6). General Procedure: A mixture of **5a** (0.01 mol) and dialkyl phosphonates [dimethyl, diethyl, and/or diisopropyl phosphonate] (4 ml) was heated at 100 °C in absence of solvent for 8—10 h (TLC). Excess DAP was distilled off to give a mixture of rotational isomers (**9A** and **B**) as a colorless substance. Compounds **9a—c** neither dissolve in NaOH (10%) solution nor respond to the $FeCl_3$ 1% color reaction. ^{31}P and ^{1}H NMR data for mixtures **9a—c** are given in Table 1. For **9A**:**9B** ratio in the diastereomeric mixture, see Scheme 3.

Working up the reaction mixture **9** in the same way as described in the case of **8**, resulted in isolation of **9Aa—c** in a pure form, see Tables 2 and 3.

Thermal Decomposition of the Adduct 9a. Compound **9a** (0.5 g) was heated in a cold finger sublimator at 220 °C (bath temperature) for about 30 minutes under reduced pressure (0.5 mm Hg). The substance that sublimed was boiled in light petroleum, filtered and recrystallized from cyclohexane to give (0.3 g, 85%) of **5a**, identified by mp, mixed mp and comparative IR spectra.[11] **6a** was detected in the receiver by the development of a violet color on addition of 3,5-dinitrobenzoic acid in the presence of alkali.[12]

Action of Diazomethane on 9Aa. **9Aa** (0.5 g) in ether (10 ml) was treated at 5 °C with an ethereal diazomethane solution (from 3 g, *N*-nitroso-*N*-methyl urea). The mixture was then kept at room temperature for 3 h. After removal of CH_2Cl_2, the residual substance was recrystallized from ether to give **8Aa** (0.46 g, 88.6%) (mp, mixed mp 167 °C, and comparative IR spectra).

References

1) For part XIV see, M. R. Mahran, W. M. Abdou, and M. D. Khidre, *Chem. Ind.* (1989), in press.
2) M. R. Mahran, W. M. Abdou, N. M. Abdel Rahman, and M. M. Sidky, *Phosphorus Sulfur*, **45**, 47 (1989).
3) M. R. Mahran, W. M. Abdou, N. A. F. Ganoub, and M. M. Sidky, *Phosphorus Sulfur*, **40**, 19 (1988).
4) M. M. Crutchfield, O. H. Dungan, J. H. Letcher, V. Mark, and J. R. van Wazer, "Topics in Phosphorus Chemistry," Interscience Publishers, a Division of John Wiley and Sons (1967), Vol. 5, ^{31}P Nuclear Magnetic Resonance, Chap. 4 (Compilation of ^{31}P NMR Data), pp. 227—447.
5) R.M. Silverstein, G. C. Bassler, and T. C. Morrill, "Spectroscopic Identification of Organic Compounds," John Wiley and Sons, Inc. (1981), Chap. 4, p. 229.
6) D. D. Denney, D. Z. Denney, P. J. Hammond, and Y. P. Wang, *J. Am. Chem. Soc.*, **103**, 1785 (1981).
7) I. L. Finar, "Organic Chemistry," The English Language Book Society, and Longman Group Limited, Britain, Vol. 1, pp. 77—82.
8) R. R. Hindersinn and R. S. Ludington, *J. Org. Chem.*, **30**, 4020 (1965).
9) M. M. Sidky and M. F. Zayed, *Tetrahedron Lett.*, **25**, 2313 (1971).
10) M. M. Sidky, M. F. Zayed, A. A. El-Kateb, and I. T. Hennawy, *Phosphorus Sulfur*, **9**, 343 (1981).
11) H. Junek and H. Hambock, *Mikrochim. Acta (Wien)*, **1966**, 522.
12) B. C. Saunders and B. P. Stark, *Tetrahedron*, **4**, 197 (1958).

Studies on 4-Thiazolidinones. IX.[1] The Conversion of 5-Substituted 2-Thioxo-4-thiazolidinones into Corresponding 2,4-Thiazolidinediones

Mohamed T. Omar,* Abd-Elrehiem Fouli, and Mahmoud Z. El-Garhi
Chemistry Department, Faculty of Science, Ain Shams University, Abbassia, Cairo, Egypt
(Received June 4, 1990)

Synopsis. The thioxo to oxo conversion in a variety of 2-thioxo-4-thiazolidinones **1** and **2** has been achieved simply by treating with bromine. A postulate for the route of interconversion is given and structures of all products are evidenced by analytical and spectral data.

Several methods have been used to effect the thioxo to oxo conversion in 2-thioxo-4-thiazolidinones. Thus, chloroacetic acid in aqueous solution[2] and hydrogen peroxide[3] were used successfully with 2-thioxo-4-thiazolidinone and its 5-alkylidene derivatives. However, the insolubility of many aryl-substituted 2-thioxo-4-thiazolidinones in aqueous chloroacetic acid prevents its use to effect the required transformation.[4] Furthermore, hydrogen peroxide may further oxidize the formed 2,4-dione into sulfoxides, sulfones, and even to sulfate ion.[3,5] The thioxo to oxo conversion has been achieved in 5-arylmethylene-2-thioxo-4-thiazolidinones via two step processes involving first conversion into 2-alkylthio-,[6] 2-(disubstituted amino)[7] 2-thiazolin-4-ones or 2-arylimino-4-thiazolidinones,[6] then treating the product with a hydrolyzing agent.[6,8] The use of the two-step method is somewhat limited as the first step affords mixture of products.

Now, we report an easy method for the conversion of aryl-substituted 2-thioxo-4-thiazolidinones into corresponding 2,4-thiazolidinediones. The reaction is carried out by treating the thioxo compound with bromine in 90% acetic acid solutions. The versatility of this method is illustrated by the successful results obtained upon application on a variety of 2-thioxo derivatives comprising 5-aroylmethyl-3-benzyl-, (*E,Z*)-5-aroylmethylene-3-benzyl-, 5-aroylmethyl- and (*E,Z*)-5-arylmethylene-2-thioxo-4-thiazolidinones (compounds **1a—e** and **2a,b,f,g**). Thus, refluxing the acetic acid solutions of **1a** and **2a** and of **1b** and **2b** with bromine for 2h gives 5-benzoylmethylene- and 5-(4-methylbenzoylmethylene)-3-benzyl-2,4-thiazolidinediones (**3a** and **3b**), respectively. The reaction of the 3-unsubstituted derivatives **1c—g** with bromine is faster than with the 3-benzyl counterparts and the reaction is completed after warming for 5 min in the case of **1c,d,e** and 15 min in the case of **2f,g**, affording the 2,4-diones **3c,d,e** and **3f,g**, respectively. However, treatment of **1c,d** with bromine at room temperature yielded 5-benzoylmethylene- and 5-(4-methylbenzoylmethylene)-2-thioxo-4-oxo-1,3-thaizolidinones, respectively. This latter method represents a new route to synthesize the hitherto unknown 5-aroylmethylene-2-thioxo-4-thiazolidinones **2c,d**.

Conversion of **1** into **3** has occurred, most probably, via the dehydrogenated product **2** since it has been reported that **2a** is formed upon treating **1a** with bromine for 5 min.[9] This is supported chemically by the independent transformation of **2a** and **2b** into **3a** and **3b**, respectively.

The structures of **3f,g** are based exclusively on comparsion (mp and IR) with authentic samples[10,11] and that of **3c** is rigidly confirmed by identity (mp and IR) with the (*E*)-isomer isolated from the (*E,Z*)-mixture obtained upon treating 2,4-thiazolidinedione with phenylglyoxal. The structures of **3a,b,c,d,e,g** and **2c,d** are deduced from analytical data and infrared spectra. All the spectra of **3** show the complex carbonyl pattern extending to 1745 cm^{-1} consistent with the stretching vibrations of coupled carbonyl groups and those of **2** show one carbonyl group stretching vibration at ca. 1680 cm^{-1}. Moreover, compounds **2** give the color reaction reported previously by Turkevich et al.[12] to characterize the 2-thioxo-4-thiazolidinones.

The problem of configurational assignment to **2c** and **3c,f,g** has been solved by ^1H NMR spectroscopy. The (*E*)-configuration has conferred to **2c** and **3c** as they are identical with the (*E*)-isomers isolated from

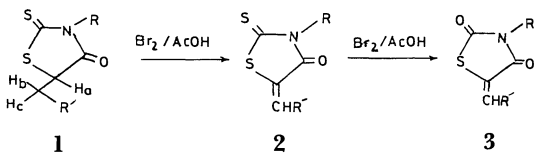

1 **2** **3**

a R=CH_2Ph; R′=C_6H_5CO
b R=CH_2Ph; R′=4-CH_3-C_6H_4CO
c R=H; R′=C_6H_5CO
d R=H; R′=4-CH_3-C_6H_4CO
e R=H; R′=4-Br-C_6H_4CO
f R=H; R′=C_6H_5
g R=H; R′=4-CH_3O-C_6H_4

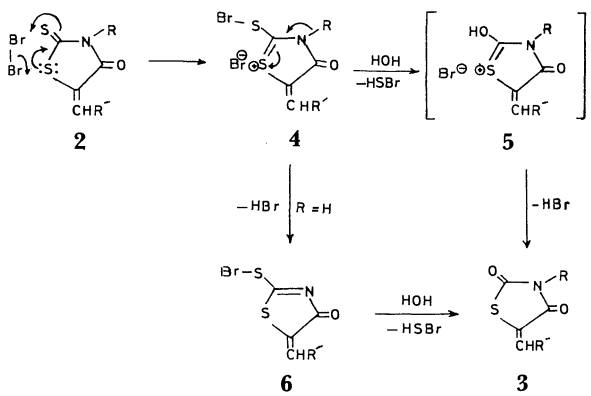

2 **4** **5**

6 **3**

Scheme 1.

Table 1. Some Data of the Newly Synthesized Compounds

Compd No.	Mp °C	Yield %	Formula[q]	^{1}H NMR Spectral data					
				Olefinic hydrogen	Aromatic hydrogen[k]		N-CH_2Ph	CH_3	Exchangable H
1b	137—138[a]	70	$C_{19}H_{17}NO_2S_2$						
1c	164—165[b]	65	$C_{11}H_9NO_2S_2$						
1d[j,l]	172—173[b]	60	$C_{12}H_{11}NO_2S_2$	—	7.85 d, 2H	7.30 d, 2H	—	2.45 s	9.30 br s
1e	192—193[b]	70	$C_{11}H_8BrNO_2S_2$						
2b	215—217[c]	90(90)[g]	$C_{19}H_{15}NO_2S_2$	7.85 s	7.88 d, 2H	7.35—7.05 m, 7H	5.30 br s	2.23 s	—
(*E*)-**2c**[p]	284—286[d]	85	$C_{11}H_7NO_2S_2$	7.85 s	8.10 dt, 2H	7.62 m, 3H	—	—	3.50 br s
(*Z*)-**2c**	236—238[e]	—	$C_{11}H_7NO_2S_2$	7.93 s	8.16 dt, 2H	7.62 m, 3H	—	—	3.57 br s
2d	254—255[c]	85	$C_{12}H_9NO_2S_2$	7.95 s	7.80 d, 2H	7.25 d, 2H	—	2.30 s	3.10 br s
3a	157—159[a]	85(83)[h]	$C_{18}H_{13}NO_3S$	8.13 s	8.03 dt, 2H	7.20—7.70 m, 8H	4.80 br s	—	—
3b	154—155[a]	80(80)[h]	$C_{19}H_{15}NO_3S$	8.20 br s	8.00 d, 2H	7.60 d, 7H	4.80 br s	2.32 s	—
(*E*)-**3c**	219—221[a]	90	$C_{11}H_7NO_3S$	7.82 s	8.10 m, 2H	7.60—7.80 m, 3H	—	—	7.50 br s
(*Z*)-**3c**	202—203[f]	—	$C_{11}H_7NO_3S$	8.03 s	8.10 dt, 2H	7.55 dt, 3H	—	—	3.25 br s
3d	219—220[c]	85	$C_{12}H_9NO_3S$						
3e	250—252[c]	90	$C_{11}H_6BrNO_3S$	7.95 s	8.00 d, 2H	7.70 d, 2H	—	—	3.25 br s
(*E*, *Z*)-**3f**	238—239[c]	75(70)[i]	$C_{10}H_7NO_2S$	7.85[m] s 7.75[m] s	7.10 br s, 5H		—	—	11.80 br s
(*E*, *Z*)-**3g**	211—212[c]	80(78)[i]	$C_{11}H_9NO_3S$	7.80[n] s 7.75[n] s	7.55 d, 2H	7.07 d, 2H	—	3.90[n,o] s 3.80[n,o] s	12.40 br s

a) Glacial acetic acid. b) Methanol. c) Toluene. d) Dioxane. e) 1-Butanol. f) Benzene. g) Yield obtained upon treating **1b** with one molar proportion of bromine. h) Yields obtained upon treating **2a** and **2b** with 1 or 2 molar proportions of bromine. i) Yields obtained upon treating **3f** and **3g** with one molar proportion of bromine. j) Measured in $CDCl_3$. k) All aromatic d show J=7.0 Hz. l) The spectrum shows also the following signals: δ=4.75 (dd, H_a), 3.95 (dd, H_c), 3.60 (dd, H_b). J_{H_a,H_b}=9.0 Hz, J_{H_a,H_c}=3.50 Hz, J_{H_c,H_b}=1.8 Hz. m) Characteristic of (*Z*)- and (*E*)-isomers with the integrated proton ratios of 3 : 7, respectively. n) Characteristic of (*Z*)- and (*E*)-isomers with the integrated proton ratios of 1 : 9 respectively. o) The methoxyl proton signal. p) ^{13}C NMR (DMSO-d_6) δ=200.5 (s), 187.7 (s), 168.7 (s), 144.0 (s), 135.9 (s), 133.9 (d), 128.8 (d), 128.5 (d), 116.4 (d). q) Satisfactory analytical data (within 0.3% for C, H, and N) were obtained for all new compounds.

the (*E,Z*)-mixtures obtained upon condensing 2-thioxo-4-thiazolidinone and 2,4-thiazolidinedione with phenylglyoxal. However, **3f,g** are (*E,Z*)-mixtures and integrated proton ratios show that the (*Z*)-isomers constitute 10% and 30%, respectively. The (*E*)- and (*Z*)-configurations are deduced by comparing the observed chemical shift values of the exocyclic olefinic protons with the incremented values.[13] The olefinic proton is relatively deshielded in the (*Z*)-rather than the (*E*)-isomers.

The thioxo to oxo conversion may be visualized to occur via the route represented in Scheme 1. The possibility of formation of **3** via the action of water on 5-aroylmethylene-2-bromothio-2-thiazolin-4-one (**6**) which is believed to be formed via elimination of hydrogen bromide directly from **4**, in compounds having no substituents at the 3-position, cannot be ruled out, especially that easy displacement of the 2-alkylthio group by nucleophiles in similar systems has been reported.[6] A chemical support for the formation of **4** is gained from the isolation of semisolids containing bromine upon treating **1a** and **2g** with bromine in chloroform. Formation of sulfonium salts is well-known upon treating sulfides with N-halo amides, but to our knowledge, formation of it upon treating with bromine is not reported.

The 5-aroylmethyl- and 5-aroylmethyl-3-benzyl-2-thioxo-4-thiazolidinones **1b—e** are synthesized by treating the respective 3-aroylacrylic acids[15] with ammonium dithiocarbamate and benzyl dithiocarbamate.

The structures of **1b—e** are based on microanalysis, infrared and ^{1}H NMR spectroscopy. The structures of **2a,b** are based on analytical and infrared spectral data which show the stretching absorptions consistent with ketonic and amidic C=O groups.

Experimental

All melting points are uncorrected. IR spectra were measured on a Unicam SP 1200 spectrometer as KBr discs. ^{1}H NMR were recorded in DMSO-d_6 on a Varian EM 390, 90 MHz instrument except those of **2c** which were recorded on a JEOL FX-900, 90 MHz apparatus, using TMS as an internal standard with chemical shifts (δ) expressed in ppm downfield from it. ^{13}C NMR was recorded on a JEOL FX-900, 22.5 MHz instrument. Mass spectrum was measured on a Varian MAT SM 1 spectrometer. The term acetic acid used herein refered to a 90% (v/v) solution.

Starting Materials. The following compounds were prepared as described previously: 5-Benzoylmethyl-3-benzyl-2-thioxo-4-thiazolidinone (**1a**).[9] 5-Benzoylmethylene-3-benzyl-2-thioxo-4-thiazolidinone (**2a**).[9] 5-Benzylidene-2-thioxo-4-thiazolidinone (**2f**).[16] 5-(4-Methoxybenzylidene)-2-thioxo-4-thiazolidinone (**2g**).[17]

5-(4-Methylbenzoylmethyl)-3-benzyl-2-thioxo-4-thiazolidinone (1b) and 5-Aroylmethyl-2-thioxo-4-thiazolidinones (1c—e). A solution of ammonium benzyldithiocarbamate or ammonium dithiocarbamate (10 mmol) in ethanol (10 ml) was added to a stirred solution of 3-benzoyl-, 3-(4-methylbenzoyl)- or 3-(4-bromobenzoyl) acrylic acid (10 mmol) in ethanol (10 ml) at room temperature. Stirring was continued for 30 min, then concentrated hydrochloric acid (3.0 ml) was added in three portions during 30 min and the pale yellow solid prepicipitated after stirring for 2 h was filtered off, washed successively with water, dried and recrystallized from the proper solvent to give the title compounds.

Conversion of 1c,d into 2c,d. Bromine (20 mmol) was added to a solution of each of **1c,d** (10 mmol) in acetic acid (20 ml) and the mixture left to stand at room temperature for 1 h during which hydrogen bromide gas evolved. The reaction mixture was poured into cold water and the precipitated solid was filtered off, washed several times with cold water, dried and recrystallized from the proper solvent to give the respective **2c,d**

Conversion of 1b into 2b. A solution of **1b** (10 mmol) in glacial acetic acid (20 ml) was heated with bromine (10 or 20 mmol) for 5 min. The reaction mixture was treated with charcoal, concentrated and the faint yellow crude product was recrystallized from toluene to give 5-(4-methylbenzoylmethylene)-3-benzyl-2-thioxo-4-thiazolidinone (**2b**).

5-Aroylmethylene-3-benzyl- (3a,b), 5-Aroylmethylene- (3c,d,e), and 5-Arylmethylene-2,4-dioxo-1,3-thiazolidinediones (3f,g). A solution of **1** (10 mmol) or **2** (10 or 20 mmol) in acetic acid (20 ml) was heated with bromine (20 mmol) for the time required. The reaction mixture was treated with charcoal, concentrated and the pale yellow crude product was filtered off, washed several times with small portions of ice-cold diethyl ether and dried.

Compounds **1a** and **2a** and **1b** and **2a** were refluxed for 2 h and afforded **3a** and **3b**, respectively.

Compounds **1c,d,e** were refluxed for 5 min and gave **3c,d,e** respectively.

Compounds **2f,g** were refluxed for 15 min and gave **3f,g** respectively.

Synthesis of Authentic Samples. A mixture of 2,4-thiazolidinedione or 2-thioxo-4-thiazolidinone (10 mmol), phenylglyoxal (10 mmol), anhydrous sodium acetate (30 mmol), and glacial acetic acid (50 ml) was refluxed for 40 min. The reaction mixture was poured into ice-cold water and the precipitated solid was filtered off, washed successively with water and dried. The faint brown crude product (80%) melted at 200—205 °C obtained from 2,4-thiazolidinedione is found to be a mixture of the (*Z*)- and the (*E*)-isomers in the ratio of 1 : 9, respectively, by ^{1}H NMR spectroscopy. Separation of the isomers was attained by dissolving the crude product in glacial acetic acid and allowing to stand overnight. The faint brown crystals which separated are filtered off and recrystallized from glacial acetic acid to give (*E*)-5-benzoylmethylene-2,4-thiazolidinedione (**3c**), 90%.

Dilution of the original mother liquor with water precipitated a faint brown solid which was recrystallized from benzene to give the (*Z*)-isomer 10%.

The crude yellowish brown product (80%), mp 214—220 °C obtained from 2-thioxo-4-thiazolidinone was found to be a mixture of (*Z*)- and (*E*)-5-benzoylmethylene-2-thioxo-4-thiazolidinones (**2c**) in the ratio of 3 : 7, respectively, as evidenced by ^{1}H NMR spectroscopy. The fraction which precipitated upon allowing the 1-butanol extract to cool was filtered off and recrystallized from 1-butanol to give (*Z*)-**2c** 30%.

The insoluble fraction was recrystallized from dioxane to give (*E*)-**2c** 70%.

Reactions of 1a and 2g with Bromine in Chloroform. A mixture of **1a** or **2g** (5 mmol), bromine (10 mmol) and chloroform (20 ml) was refluxed for 3 h. Evaporation of the solvent using rotary evaporator left a viscous oil. Trituration with light petroleum (bp 40—60 °C) followed by recrystallization from toluene failed to give a pure praduct. The faint yellow crystals obtained upon dissolution in 90% acetic acid solution was filtered off, dried and recystallized from glacial acetic acid.

Compound **1a** gave a product (70%) identical (mp and IR) with **3a**.

Compound **2g** afforded **3g** (70%), identical (mp and IR) with an authentic sample.[11]

Authors are grateful to Dr. H. Fröhlich, Institute of Organic Chemistry, University of Vienna for Microanalysis, ^{1}H NMR and ^{13}C NMR measurements of compound **2c**.

References

1) Part VIII: M. T. Omar, M. M. Habashy, A. M. Youssif, and F. A. Sherif, *J. Prakt. Chem.*, **331**, 393 (1989).
2) W. J. Croxall, C. P.-Lo, and E. Y. Shropshire, *J. Am. Chem. Soc.*, **75**, 5419 (1953); F. Everes, *Ber.*, **21**, 962 (1888).
3) R. Kitamura, *J. Pharm. Soc. Jpn.*, **58**, 804 (1938); H. Taniyama, K. Hagiwara, H. Okada, and H. Uchida, *Yakugaku Zasshi*, **77**, 1236 (1957); *Chem. Abstr.*, **52**, 6322 (1958).
4) E. V. Vladzimirskaya, *Zh. Obshch. Khim.*, **29**, 2795 (1959); *Chem. Abstr.*, **54**, 10997c (1960).
5) M. Suesse and H. Dehne, *Z. Chem.*, **15**, 303 (1975); *Chem. Abstr.*, **84**, 43923e (1976).
6) M. T. Omar and F. A. Sherif, *J. Prakt. Chem.*, **322**, 835 (1980).
7) A. R. A. Raouf, M. T. Omar, S. M. A. Omran, and K. E. El-Bayoumy, *Acta Chim. (Budapest)*, **83**, 359 (1974).
8) M. T. Omar, M. M. Habashy, and M. A. Kasem, *J. Prakt. Chem.*, **324**, 483 (1982).
9) H. Nagase, *Chem. Pharm. Bull.*, **22**(**7**), 1661 (1974).
10) R. Andreasch, *Monatsh Chem.*, **38**, 206 (1917).
11) C.P.-Lo, E.Y. Shropshire, and W. J. Croxall, *J. Am. Chem. Soc.*, **75**, 4845 (1953).
12) N. M. Turkevich and M. P. Makukha, *Zh. Anal. Khim.*, **6**, 308 (1951); *Chem. Abstr.*, **46**, 1924 (1952).
13) V. C. Pascual, J. Meier, and W. Simon, *Helv. Chem. Acta*, **49**, 164 (1966).
14) H. Kise, G. E. Whitfield, and D. Swern, *J. Org. Chem.*, **37**, 1121 (1972).
15) H. G. Oddy, *J. Am. Chem. Soc.*, **45**, 2156 (1923).
16) G. Bargellini, *Gazz. Chim. Ital.*, **36**(**II**), 129 (1906).
17) M. Girard, *Ann. Chim.*, **16**, 326 (1941).

Depth Profiling of Ultra Thin Film Using Laser Induced Fluorescence Spectroscopy under Normal Incidence Conditions Based on the Reciprocal Principle

Xing-Zheng Wu, Takehiko Kitamori, Norio Teramae,† and Tsuguo Sawada*
Department of Industrial Chemistry, Faculty of Engineering,
The University of Tokyo, 7-3-1 Hongo, Bunkyo, Tokyo 113
† Department of Applied Chemistry, Faculty of Engineering,
Nagoya University, Hurouchou 1, Chigusa-ku, Nagoya 464
(Received September 12, 1990)

Depth profiling for thin film sample using laser induced fluorescence spectroscopy under normal incidence conditions, based on the principle of reciprocity, was studied. A laminated Langmuir–Blodgett model film sample (187 nm in thickness) with a concentration depth profile which varies as a stair-like function with 20.8 nm steps was prepared. Using this model film sample, observation angle dependence of fluorescence intensity was compared with theoretical results based on the principle of reciprocity, and it was shown that the principle held for the thin film sample having a continuous concentration depth profile. Secondly, these data were used to reconstruct the concentration depth profile by the least square method. The quantitative concentration depth profiling results obtained for the model film sample were satisfactory. This method can be used for film samples thinner than the wavelength of the excitation light and its spatial resolution in the depth direction is estimated to be in the order of a nanometer.

The importance of measurements of local concentration depth profiles and three-dimensional profiles with resolution in submicrometer or nanometer regions has been emphasized in many technological fields such as electronic devices,[1] solid surface physics,[2] and cell biology.[3] Optical spectroscopical concentration depth profiling methods should be non-destructive, non-contact methods without using a high vacuum system. Attenuated total reflection infrared (ATR IR) adsorption spectroscopy[4] and total internal reflection fluorescence spectroscopy[3] are well known non-destructive depth profiling methods. Although it is estimated theoretically that the ATR IR method has a depth resolution about one-tenth that of the wavelength,[5] practical analysis for thin film samples thinner than the wavelength used is difficult. Total internal reflection fluorescence spectroscopy has been used to determine concentration depth profiling of proteins adsorbed at a solid/liquid interface,[6] depth distribution of fluorescent species in silk fabrics,[7] and the concentration ratio of a fluorophore between a two layer film sample.[8] However, until now only qualitative results or results for a simple concentration depth profile model, such as a uniform concentration distribution, have been reported.

Recently, Suci and Reichert[9] have studied the reciprocity in an angular pattern of fluorescence, and they have investigated the possibility of depth profiling, using Langmuir–Blodgett (LB) films, for the sample having a uniform concentration depth profile.[10] For such film samples in which fluorophores were uniformly distributed over a range of 52.8 nm, i.e., a rectangular profile, the central position of the rectangular profile could be accurately determined, which demonstrated the possibility of determining the width of the rectangular distribution profile. This depth profiling method using variable angle fluorescence date is attractive, since it can be used for the concentration depth profile of a film sample thinner than the wavelength of the excitation light, with highest sensitivity applying laser as the beam source. However, as actual samples usually have a complicated concentration distribution, it is important to study the validity of this method for the thin film sample which has a concentration depth profile varying continuously with distance from the surface.

In the present study, a 187 nm thick LB film sample, having a concentration depth profile which varies as a stair-like function with 20.8 nm steps, was prepared as the model sample. By using variable observation angle fluorescence data obtained under normal incidence conditions, it is shown that the reciprocal principle holds for the sample having a nonuniform concentration depth profile. Then the profile is determined by applying this method.

Method Outline

According to the reciprocal principle for fluorometry proposed by Suci and Reichert,[9] as shown in Fig. 1, fluorescence intensity $F(\theta)$ measured at the observation angle θ under normal incidence conditions is expressed as,

$$F(\theta) = k\int_0^t C(z)T(\theta, z)\mathrm{d}z, \quad (1)$$

where $C(z)$ is the concentration distribution in the depth direction z, t is the thickness of the sample, and k is a constant related to spectroscopical parameters such as absorption coefficient and fluorescence quantum yield. The function $T(\theta, z)$ is defined as a transmission function, and its functional form has been given by a

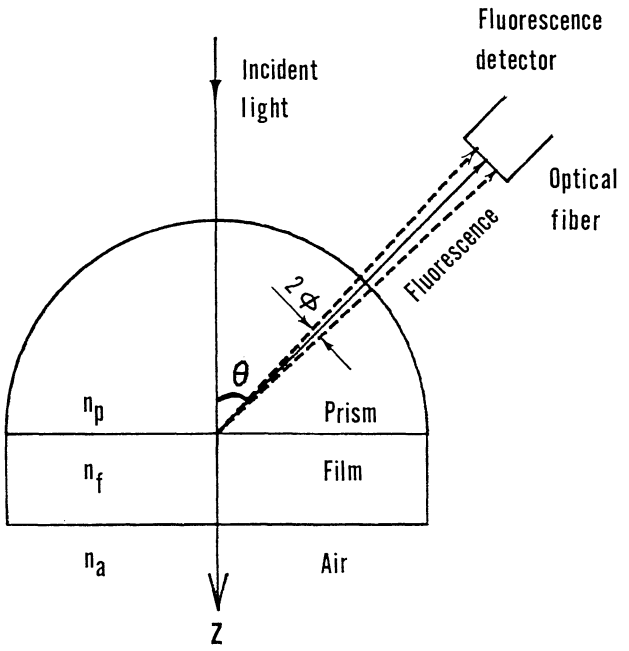

Fig. 1. Schematic of laser induced fluorescence spectroscopy under normal incidence conditions based on the reciprocal principle.

theoretical analysis of the multiple reflection of the electromagnetic waves between the prism/film and film/air interfaces.[9]

Suci and Reichert verified the propriety of the reciprocity described by Eq. 1 using the sample in which a fluorophore is localized at a certain distance z_0 from the surface. As the fluorophore localizes at z_0, the concentration distribution $C(z)$ becomes $C_0\delta(z-z_0)$, and Eq. 1 becomes

$$F(\theta, z_0) = kC_0T(\theta, z_0). \quad (2)$$

They measured the observation angle dependence of the fluorescence intensity $F(\theta, z_0)$ and compared it with the calculated value of $T(\theta, z_0)$ to show the propriety of the transmission function $T(\theta, z)$. In addition, they applied it to a uniform concentration distribution with which $F(\theta)$ is the integrated form of $T(\theta, z)$.[10]

In the present study, we tried to obtain the concentration distribution $C(z)$ from the measured data $F(\theta)$ and the relationships described in Eq. 1. The function $C(z)$ can be obtained by solving the inverse integral of Eq. 1, because $T(\theta, z)$ is known theoretically and $F(\theta)$ is given experimentally. However, the inverse problem of the convolutions, as it well known, does not always have an analytical solution, and the numerical method is frequently confronted with the problem of divergence and precision. Then, a numerical fitting method was applied to obtain $C(z)$. If the physical and chemical processes leading to the concentration distribution can be guessed, a general functional form of $C(z)$ is roughly estimated. For example, $C(z)$ is an error function type for a diffusion limiting process, and an exponential one for a chemical kinetics system. Hence, an exact function $C(z)$ is obtained by the following numerical fitting, which utilizes the least square method. The functions $F_{cal}(\theta)$ and $F_{mea}(\theta)$ are defined as the calculated function $F(\theta)$ for a guessed or trial function $C(z)$ and an experimentally obtained one, respectively. The exact form of $C(z)$ is determined by minimizing the following value of s,

$$s = \sum_i [F_{mea}(\theta_i) - F_{cal}(\theta_i)]^2/g_{\theta_i}, \quad (3)$$

where i means the i-th measurement data, and g_{θ_i} is a weight factor. In the present report, this fitting method was used to obtain $C(z)$.

Experimental

A block diagram of the experimental set up is shown in Fig. 2-A. An argon-ion laser provided the excitation light (λ_i=488 nm). The laser output power was adjusted to about 10 mW. A quarter-wave plate and a polarizer were used to adjust the polarization of incident light. The laser beam was modulated with a chopper. The chopped beam was focused on the focal plane of hemicylindrical prism (n_p=1.88 at 587.6 nm). The prism was 1 cm in diameter and 2 cm in length. The hemicylidrical prism was mounted on the rotating stages as shown in Fig. 2-B. Both the rotating stages and hemicylindrical prism were coaxially adjusted. An optical lightguide (50 cm length; 0.11 cm bundle diameter; step index type glass fiber; 0.57 numerical aperture) was used to collect the fluorescence transmitted through the prism. One end of the optical lightguide was fixed at the focal plane of the prism and the other end was coupled with a monochromator. A film polarizer was placed in front of the optical lightguide. The film polarizer restricted the collected fluorescence to the perpendicularly polarized component. A photomultiplier (Hamamatsu R928) was used as a detector. The signal from the photomultiplier was fed into and amplified with a lock-in amplifier.

The incident angle and the observation angle can be varied by adjusting the relative position of the two rotating stages. In the experiment, the incident angle was kept at 0°, while the observation angle θ was changed from 15° to 80° with 1° steps. The absolute value of the observation angle was determined as follows; rotating the upper stage from the location at which the laser beam is in normal incidence condition to that at which the reflected beam irradiated on the center of the fiber. The value of the observation angle is double the upper rotating stage angle. As shown in Fig. 1, the uncertainty ϕ at the observation angle θ is determined by the fiber bundle size and the distance between the fiber and the irradiation point. For this system, ϕ is estimated to be ±0.7°.

Sample. The method of Langmuir-Blodgett deposition used was the same as described elsewhere.[11] The two species used to fabricate the model film sample were icosanoic acid (eicosanoic acid) (analytical grade, Kanto Kagaku) and *N,N'*-dioctadecylrhodamine B (DORB) (Nippon Kankoh-Shikiso Kenkyusho).[12] Aqueous cadmium sulfate solutions (5×10^{-5} mol dm^{-3}) was used as a subphase. A benzene solution of

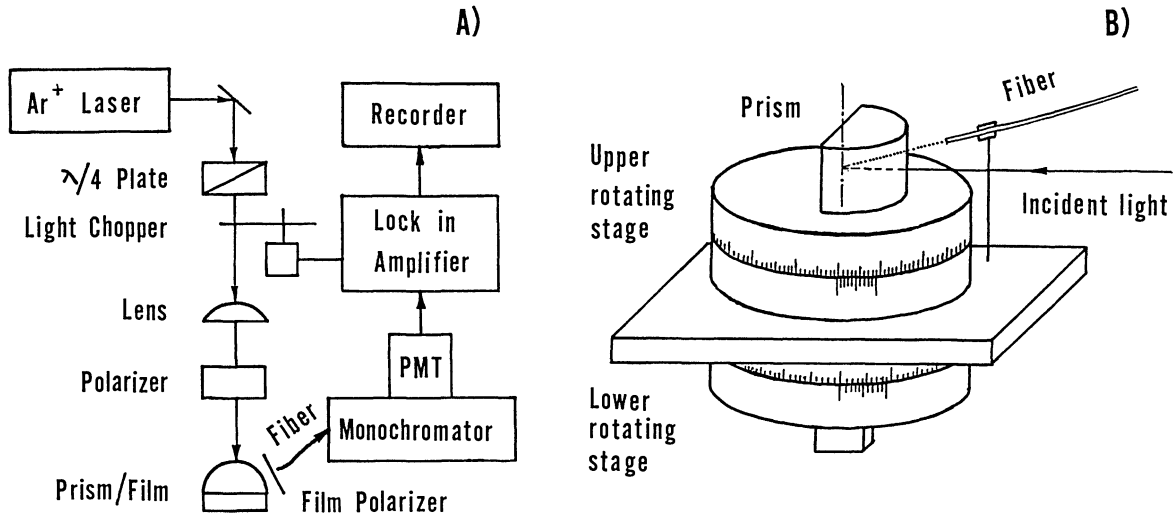

Fig. 2. Schematic diagram of the experimental setup including a detailed optical arrangement of the detection unit.

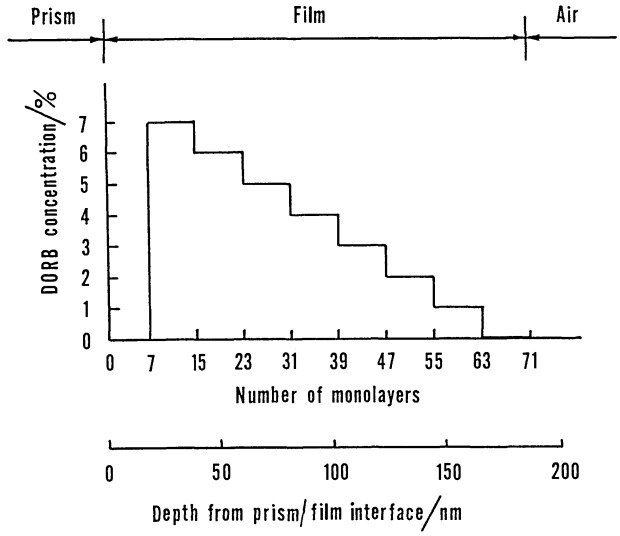

Fig. 3. Concentration depth profile of the model LB film sample.

icosanoic acid and mixtures of icosanoic acid and DORB with a certain molar ratio were spread on the subphase in a Langmuir trough (Kyouwakagaku). The LB layers were deposited onto the prism at a film pressure of 25—30×10^{-3} N m^{-1}. The prism surface was first precoated with seven layers of cadmium icosanoate to ensure the surface was uniform and hydrophobic. Secondly, eight layers of 7% DORB (the unit of DORB concentration is the molar percent) and cadmium icosanoate mixture were deposited. Then another eight layers of 6% DORB and cadmium icosanoate mixture were deposited. This procedure was repeated eight times to laminate layers of DORB in which the concentration was being changed from 7% to 0% as shown in Fig. 3. The total number of monolayers was 71.

When the molar ratio of dye to icosanoic acid is less than 10%, the mixed monolayers and multilayers have a similar structure to cadmium icosanoate LB films.[11,13] The reported thickness of a monolayer of cadmium icosanoate and the refractive index of the multilayers are 2.64 nm and 1.53, respectively.[11] Thus the total film thickness can be estimated from the number of monolayers, and it was calculated to be 187 nm. The multilayers deposited onto the curved part of the prism were removed with an acetone-soaked wadding[14] to prevent interference with the fluorescence measurement.

The fluorescence peak of the model sample appeared at 580 nm, and this peak was used in the following experiments.

Results and Discussion

To verify the propriety of the reciprocity for a nonuniform $C(z)$, fluorescence dependence on the observation angle was measured for the model sample under normal incident conditions, and the results were compared with the theoretical values calculated using Eq. 1. The experimental results are plotted in Fig. 4. As the concentration distribution $C(z)$ for the model sample shown in Fig. 3 is written as follows,

$$C(z) = \begin{cases} 0\% & 0 \leqslant z \leqslant 7d \\ (8-j) & 8jd \leqslant z \leqslant 8(j+1)d,\ j = 1, 2, 3, \cdots, 8 \end{cases} \quad (4)$$

where d is the thickness of the monolayer, 2.64 nm, then the theoretical value $F_{cal}(\theta)$ can be calculated by substituting Eq. 4 into Eq. 1 (the values of the parameters and material constants are described in the experimental section). The calculated results are shown by a solid line in Fig. 4. The theoretical values agree well with the experimental results, where the most appropriate value of k in Eq. 1 is 2.3×10^{-3} (%$^{-1}$ nm^{-1}). Therefore, the propriety of the reciprocity is confirmed for the nonuniform concentration distribu-

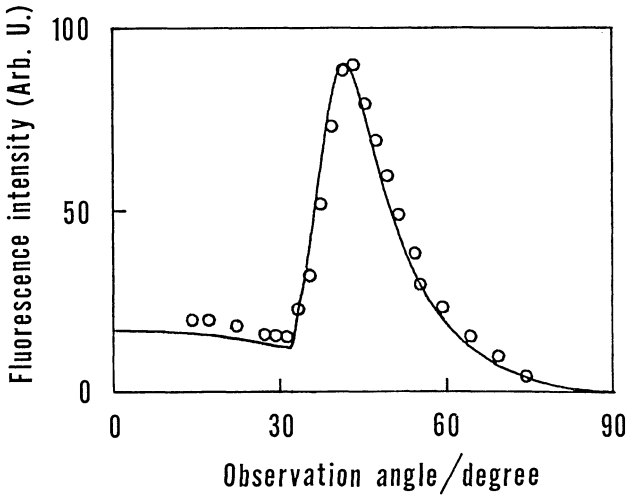

Fig. 4. Theoretical and experimental results of the angular dependency of the fluorescence intensity measured for the model sample. The theoretical values are described by the solid line, and the experimental results are plotted as circles.

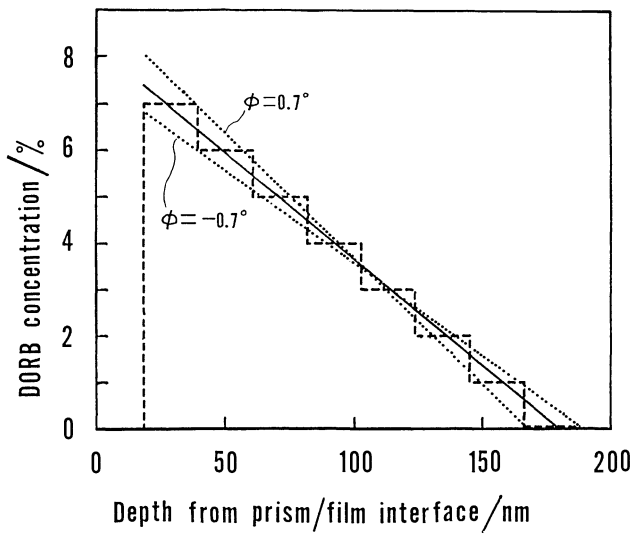

Fig. 5. Reconstructed concentration depth profile for the model film sample. The solid and dashed lines represent reconstructed and actual $C(z)$ values, respectively. The dotted lines represent the error region of the reconstructed results given by the experimental uncertainty of the observation angles.

tion, and it is proved that the reciprocity described in Eq. 1, which has been partially verified for localized and uniform concentration distribution, is applicable to a general functional form of $C(z)$. These results suggest that the arbitrary concentration depth profile $C(z)$ can be obtained from Eq. 1.

Next, concentration depth profiling which was proposed in the method outline section, based on the reciprocal theory, was examined. As mentioned in the method outline section, $C(z)$ can be obtained from the least square method of Eq. 3, when the functional form of $C(z)$ is roughly estimated. In the present case, the linear function,

$$C(z) = Az + B, \tag{5}$$

is assumed to be a trial function, and the constants A (% nm^{-1}) and B (%) which give the nearest form to the actual distribution shown in Fig. 3 are tentatively obtained from Eq. 3. Using the data presented in Fig. 4 and the most appropriate value of k obtained above, the constants A and B are obtained as $-0.04\%\ \mathrm{nm}^{-1}$ and 8.0%, respectively, and the reconstructed line is shown in Fig. 5 with the actual distribution indicated by a dashed line. The obtained result $C(z)$ reconstructs well the absolute value of the concentration, and shows the decreasing profile. Hence the calculated concentration depth profile of DORB in the model sample is considered to be reasonable, and the propriety of the present depth profiling method is verified.

The main experimental error factor of this system is the uncertainty of the observation angle. As stated in the experimental section, the uncertainty ϕ at observation angle was estimated to be $\pm 0.7°$. The reconstructed results in which uncertainty was taken into consideration are shown in Fig. 5 with dotted lines. These reconstructed results become better when a fiber with smaller bundle size is used to reduce the uncertainty of the observation angle. In this experiment, the concentration changes of 20 nm steps in a 187 nm thick sample shown in Fig. 3 can be recognized. Considering the experiment errors in Fig. 5, although the exact value of the spatial resolution in the depth direction is not given, a resolution of less than 20 nm can be expected for the present method. It is no exaggeration to say that the present experiment is the first which obtains a quantitative depth profile for a thin film thinner than the excitation wavelength using a nondestructive spectroscopic technique. For thin film samples with thickness on the order of a wavelength or thinner, this method is particularly meaningful, since other optical depth profiling methods such as photoacoustic spectroscopy[15] cannot easily yield information on depth profiling for such thin film samples.

As stated above, the reconstructed concentration depth profiling results would become better when a fiber with a smaller bundle size is used. A smaller bundle size also leads to a decreased signal to noise ratio. A detailed discussion on the application limits of the present method, which are considered to be restricted by the experimental conditions such as the uncertainty and accuracy of the observation angle and signal to noise ratio, will be reported elsewhere.

Althouth the absolute value of A (% nm^{-1}) and B (%) were obtained for the present model film sample, it is generally difficult to known k for the actual samples.

Hence only a relative concentration depth profile can be obtained using the least square method.

The present method is similar to the conventional ATR method, where variable incident angle data are used to reconstruct $C(z)$.[4,5,7] For a bulk sample, the ATR method has been proved to be effective. However, in the conventional ATR method, only total internal reflection occurring at the prism/film interface shown in Fig. 1 is considered, thus only the data obtained beyond the critical angle can be used to reconstruct $C(z)$. For the film sample with a thickness on the order of the incident light wavelength or the thinner, such as our model film sample, the conventional ATR method in which only consider evanescent wave decays from prism/film interface exponentially cannot be applied. It is also necessary to consider the reflection effect which occurs at the film/air interface for the evanescent wave. On the other hand, in the present method, $T(\theta, z)$ is derived by considering multiple reflection occurring at the interfaces of the prism/film and film/air shown in Fig. 1,[10] so data at any observation angle can be applied to samples which are thinner than the excitation wavelength or the evanescent wave.

In summary, concentration depth profiling using fluorescence spectroscopy under normal incidence conditions based on the reciprocal principle was demonstrated for a 187 nm thick film sample. The present depth profiling method had a high spatial resolution and could be used for ultra thin film samples. Using normal incidence conditions, it was possible to obtain a local three-dimensional profile by scanning the excitation beam. In addition, dynamics and kinetics of the fluorophore can be measured if array detectors are applied to obtain various angular data simultaneously. Therefore, this method is expected to be a useful one for analytical and spectroscopical studies of thin films and surfaces.

The authors wish to express their thanks to Professor Y. Gohshi of the University of Tokyo, for his useful advices in preparation of model LB film sample.

References

1) Y. Ago, *J. Appl. Phys.*, **64**, 3760 (1988).
2) Y. Okajima, *Kinzoku Hyomen Gijutsu*, **36**, 501 (1985).
3) D. L. Taylor and Y-L Wang, "Methods in Cell Biology, Vol. 30: Fluorescence Microscopy of Living Cells in Culture, Pt. B: Quantitative Fluorescence Microscopy-Imaging and Spectroscopy," Academic Press, Inc., London (1989).
4) N. J. Harrick, "Internal Reflection Spectroscopy," Interscience-Wiley, New York (1967).
5) T. Hirschfeld, *Appl. Spectrosc.*, **31**, 289 (1977).
6) W. M. Reichert and P. A. Suci, *Appl. Spectrosc.*, **41**, 503 (1987).
7) A. Kurahashi, A. Itaya, and H. Masuhara, *Chem. Lett.*, **1986**, 1413.
8) H. Masuhara, S. Tazuke, N. Tamai, and I. Yamazaki, *J. Phys. Chem.*, **90**, 5830 (1986).
9) P. A. Suci and W. M. Reichert, *Appl. Spectrosc.*, **42**, 120 (1988).
10) P. A. Suci and W. M. Reichert, *Langmuir*, **4**, 1131 (1988).
11) K. H. Drexhage, "Progress in Optics," ed by E. Wolf, North-Holland Press, New York (1974), Vol. XII, pp. 164—232.
12) N. Tamai, T. Yamazaki, and I. Yamazaki, *Chem. Phys. Lett.*, **147**, 25 (1988).
13) I. Yamazaki, N. Tamai, and T. Yamazaki, *Bunkou Kenkyuu*, **37**, 167 (1988).
14) O. Wolfbeis and B. H. Schaffar, *Anal. Chim. Acta*, **198**, 1 (1987).
15) A. Harata and T. Sawada, *J. Appl. Phys.*, **65**, 959 (1989).

X-Ray Crystal Structures of Ti(IV)-4,4′-Methylenebis(antipyrine) Complexes, $[Ti(dam)_3](ClO_4)_4$. Formation of Eight-Membered Chelate Rings and Aromatic Ring Stacking Responsible for Characteristic Coloration

Akio YUCHI,* Motoo SHIRO,† Hiroko WADA, and Genkichi NAKAGAWA
Department of Applied Chemistry, Nagoya Institute of Technology, Gokiso, Showa, Nagoya 466
† Shionogi Research Laboratory, Shionogi & Co., Ltd., Fukushima, Osaka 553
(Received September 28, 1990)

X-Ray crystallographic studies have been made for two Ti(IV) complexes with 4,4′-methylenebis(antipyrine) (so-called diantipyrylmethane, abbreviated to dam) used for spectrophotometry of Ti(IV). The crystal data and final R values are: $[Ti(dam)_3](ClO_4)_4$ (**1**), triclinic, $P\bar{1}$, a=15.099(2), b=22.308(2), c=14.015(2) Å, α=100.00(1), β=116.68(1), γ=87.16(1)°, V=4151(1) Å^3, Z=2, R=0.124 for 8060 reflections; $[Ti(dam)_3](ClO_4)_4 \cdot H_2O$ (**2**), monoclinic, $P2_1/c$, a=14.075(3), b=29.127(7), c=21.386(6) Å, β=122.42(1)°, V=7401(3) Å^3, Z=4, R=0.105 for 6685 reflections. The reagent dam acts as a bidentate ligand to form eight-membered chelate rings. Between a pyrazolone moiety of one ligand and a phenyl ring of another prevails aromatic ring stacking, which gives extra stability to these complexes and is responsible for the characteristic charge transfer band around 385 nm.

4,4′-Methylenebis(antipyrine) (so-called as diantipyrylmethane abbreviated to dam; Fig. 1) reacts with titanium(IV) in a strongly acidic medium to form a yellow complex having an absorption maximum at around 385 nm. This reaction has widely been used for selective photometric determination of titanium(IV).[1–10]

Although the metal-to-ligand ratio of the species was determined to be 1:3, the exact composition including the hydrolysis degree of Ti(IV) center has been unknown. Provided dam forms a chelate ring (Fig. 1), it will be a large one containing not less than eight members, which is known to be hardly formed.[11,12] Furthermore, the mechanism for strong coloration upon coordination to titanium(IV) is not clear.

Preparative works in a strongly acidic medium used for spectrophotometry afforded two kinds of crystalline compounds having the composition of $[Ti(dam)_3](ClO_4)_4$. To elucidate the points mentioned above, we have made X-ray crystal structure analysis for these compounds and found unusual eight-membered chelate rings and remarkable aromatic ring stacking responsible for the coloration.

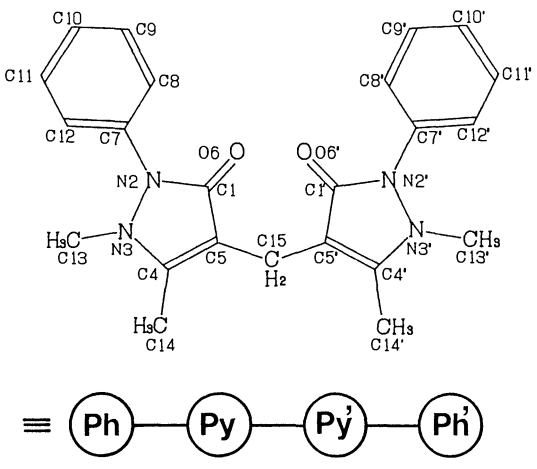

Fig. 1 Atom-numbering system of diantipyrylmethane.

Experimental

Preparation of the Complexes. Titanium(IV) tetrachloride was reacted with 4,4′-Methylenebis(antipyrine) in perchloric acid solution. Slow evaporation gave only small amounts of orange crystals(**1**) together with yellow powder. We could not perform chemical analysis for the complex **1**.

After these were filtered off, the filtrate was further stood to give larger amounts of violet crystals(**2**). Found: C, 50.53; H, 4.57; N, 10.41%. Calcd for $[Ti(dam)_3](ClO_4)_4 \cdot H_2O$: C, 50.86; H, 4.59; N, 10.32%. The water content determined by Karl Fischer's method (1.1%) was in good agreement with the calculated value (1.11%). The compound **2**, when ground, changes in color to orange similar to crystalline **1**.

X-Ray Analysis. Crystallographic details for **1** and **2** are given in Table 1. The space group of **1** was possible to be either $P1$ or $P\bar{1}$, but was determined to be the latter, after the structure refinement, on the basis of the significance test of the R values for the respective space groups. Intensity data were collected on a Rigaku AFC-5R diffractometer with graphite-monochromatized Cu $K\alpha$ radiation (λ=1.54178 Å). The ω–2θ scan technique was employed with an ω-scan width of $(1.2+0.2 \tan\theta)$ deg at a scan rate of 6 deg min^{-1} with 5 s background counts. No significant variations in intensities of 3 standard reflections monitored every 100 measurements were observed during data collection.

The structures were solved by the conventional heavy-atom method. In difference Fourier maps for **1** and **2** synthesized without the contributions of the perchlorate O atoms, five or more peaks were found around respective Cl atoms. We assumed the O atoms to be disordered, but could not clearly interpret the arrangement of peaks on the basis of any superpositions of the disordered anions. For each anion, four rather high peaks exhibiting an approximate configuration of the anion were adopted and kept fixed during refinement. The geometries thus obtained are of less accuracy: mean Cl–O=1.43 Å (ranging in 1.29—1.66 Å),

Table 1. Crystallographic Details for **1** and **2**

	1	**2**
Formula	$C_{69}H_{72}N_{12}O_{22}Cl_4Ti$	$C_{69}H_{74}N_{12}O_{23}Cl_4Ti$
Formula weight	1611.1	1629.1
Crystal system	Triclinic	Monoclinic
Space group	$P\bar{1}$	$P2_1/c$
a/Å	15.099(2)	14.075(3)
b/Å	22.308(2)	29.127(7)
c/Å	14.015(2)	21.386(6)
α/deg	100.00(1)	—
β/deg	116.68(1)	122.42(1)
γ/deg	87.16(1)	—
V/Å^3	4151(1)	7401(3)
Z	2	4
ρ_{calcd}/g cm^{-3}	1.289	1.462
μ(Cu $K\alpha$)/cm^{-1}	27.3	30.8
Crystal size/mm	0.3×0.2×0.1	0.3×0.1×0.1
$2\theta_{max}$/deg	110	120
No. of unique reflections	10417	10993
No. of observed reflections with $F_o>3\sigma(F_o)$	8363	6874
R	0.124	0.105
R_w	0.180	0.148
S (goodness of fit)	1.145	1.253
No. of reflections used at the last stage of refinement	8060	6685

1.37 Å (1.18—1.46 Å); mean O-Cl-O=108° (83—137°), 109° (99—122°) for **1** and **2**, respectively. Though the results of Karl Fischer's method suggested the crystal of **2** to be monohydrated, we could not locate any water molecule in a difference Fourier map.

The structures were refined by the block-diagonal least-squares technique using the positional and anisotropic thermal parameters for the non-H atoms excluding disordered perchlorate O atoms for which only isotropic temperature factors were refined. No H atoms were located. Absorption corrections were applied after isotropic least-squares refinement by an empirical method based on the differences between the observed and calculated structure factors.[13] Atomic scattering factors were evaluated by analytical procedures, $f=\sum[a_i \exp(-b_i\lambda^{-2}\sin^2\theta)]+c$ (i=1, ··, 4).[14] Weights were taken as $w=[\sigma^2(F_o)+c^2|F_o|^2]^{-1}$ for the reflections with $w^{1/2}|\Delta F|<4$, and w=0 otherwise. The values of c^2 were 0.02297 and 0.00966 for **1** and **2**, respectively. No peaks larger than 0.5 e Å^{-3} were found in the last difference electron density maps of **1** and **2**. Comparatively large R values for **1** and **2** may be due to the poor quality of intensity data measured by using very small and inferior crystals and to the disordered structures of ClO_4 anions. Computations using the programs of PLUTO and XPACK86 SHIONOGI were performed on a FACOM M-730 computer at Shionogi Research Laboratories.[15]

Results and Discussion

Atomic coordinates and equivalent isotropic temperature factors for **1** and **2** are listed in Table 2. Stereoscopic views of the cations are represented in Fig. 2. The atoms of one ligand referred to as (A) in the respective complex ions are numbered as shown in Fig. 1, and those of the other two ligands (B and C) are represented by the corresponding numbers of 100 and 200 levels. The ClO_4 anions are given by the numbers

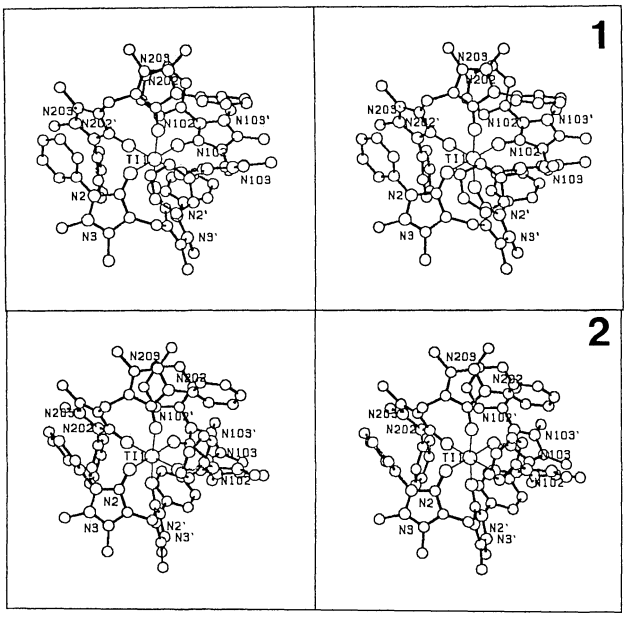

Fig. 2 Stereoscopic views of **1** and **2**.

of 300 level. The four anions of **1** are statistically distributed at five locations: two of them labeled as Cl(300) and Cl(310) are fully occupied and the other three labeled as Cl(320), Cl(330), and Cl(340) with partial occupancy of 2/3.

Coordination Geometry around Ti(IV). The metal-ligand distances and angles for **1** and **2** are summarized in Table 3. The Ti–O distances (av 1.93 Å for **1** and 1.94 for **2**) are shorter than those of other Ti(IV) complexes hexa-coordinated only by oxygen atoms, such as $Ti_2O_2(acac)_4$ (2.01 Å; acac=acetylacetonate),[16] $Ti(OR)_2(acac)_2$ (1.96 Å; OR=2,6-diisopropyl-

Table 2. Atomic Coordinates ($\times 10^4$) and Equivalent Isotropic Temperature Factors (Å$^2\times 10$) with esd Values in Parentheses for **1** and **2**

Atom	**1**				**2**			
	x	y	z	B_{eq}/B[a)]	x	y	z	B_{eq}/B[a)]
Ti	2621.8(7)	2689.6(5)	7969.5(8)	29.2(4)	4742(1)	975.3(5)	7102.3(8)	26.1(5)
C(1)	3821(4)	3516(3)	10059(5)	31(2)	3277(7)	1133(3)	5436(5)	34(3)
N(2)	3620(4)	3822(3)	10867(4)	39(2)	2724(6)	870(3)	4827(4)	38(3)
N(3)	4470(4)	3858(3)	11824(4)	44(2)	1982(6)	1150(3)	4244(4)	44(3)
C(4)	5193(5)	3602(3)	11608(5)	41(2)	2081(7)	1577(4)	4513(5)	41(4)
C(5)	4818(5)	3383(3)	10512(5)	36(2)	2860(7)	1579(3)	5249(5)	36(3)
O(6)	3123(3)	3408(2)	9065(3)	33(1)	4072(4)	951(2)	6066(3)	33(2)
C(7)	2661(5)	4002(3)	10786(6)	37(2)	2857(8)	396(3)	4730(5)	40(4)
C(8)	2313(6)	3787(4)	11414(7)	51(3)	2384(10)	62(4)	4953(6)	63(5)
C(9)	1408(7)	3982(5)	11365(8)	66(4)	2548(11)	−397(5)	4877(7)	79(6)
C(10)	859(8)	4364(5)	10621(10)	77(5)	3151(12)	−522(5)	4567(7)	73(6)
C(11)	1197(8)	4551(5)	9961(9)	74(4)	3597(14)	−206(4)	4338(10)	85(9)
C(12)	2145(6)	4387(3)	10073(7)	51(3)	3460(12)	262(4)	4432(8)	69(7)
C(13)	4563(7)	4265(4)	12825(6)	62(3)	1206(11)	942(6)	3507(6)	83(6)
C(14)	6238(6)	3576(4)	12498(7)	60(3)	1402(9)	1965(4)	4029(7)	60(5)
C(15)	5388(5)	3056(3)	9926(6)	42(3)	3282(8)	1985(3)	5765(5)	40(4)
C(1′)	4423(5)	2036(3)	9345(5)	36(2)	2938(6)	1697(3)	6773(5)	32(3)
N(2′)	4643(4)	1434(3)	9306(5)	40(2)	2356(6)	1840(2)	7084(4)	37(3)
N(3′)	5638(4)	1395(3)	9677(5)	47(2)	1879(7)	2264(3)	6767(5)	44(3)
C(4′)	6053(5)	1964(4)	10001(6)	41(3)	2086(8)	2348(3)	6236(6)	45(4)
C(5′)	5296(5)	2380(3)	9775(5)	38(2)	2776(7)	2015(3)	6227(5)	39(4)
O(6′)	3508(3)	2206(2)	9005(4)	37(2)	3510(5)	1325(2)	7002(3)	35(2)
C(7′)	3948(5)	938(3)	8721(6)	41(3)	2544(8)	1697(3)	7786(6)	43(4)
C(8′)	3213(7)	869(4)	8998(8)	54(4)	2815(8)	2034(3)	8314(6)	46(4)
C(9′)	2506(8)	382(4)	8436(10)	69(5)	3035(9)	1896(4)	9011(6)	54(5)
C(10′)	2593(8)	−22(4)	7589(8)	66(4)	2979(10)	1425(4)	9139(7)	59(5)
C(11′)	3326(8)	47(4)	7334(8)	65(4)	2708(10)	1108(4)	8600(7)	56(5)
C(12′)	4033(7)	538(3)	7904(7)	55(3)	2483(9)	1250(3)	7902(6)	47(5)
C(13′)	6141(7)	830(4)	10062(8)	69(4)	882(11)	2420(5)	6783(8)	73(6)
C(14′)	7154(6)	2081(5)	10506(8)	63(3)	1585(11)	2765(4)	5752(8)	67(6)
C(101)	3848(5)	2746(3)	6741(5)	35(2)	6222(7)	1831(3)	7620(5)	32(3)
N(102)	4151(5)	3245(3)	6524(5)	46(2)	7098(6)	1984(2)	7572(5)	40(3)
N(103)	4417(5)	3054(3)	5701(5)	52(3)	7726(7)	2287(3)	8147(5)	49(4)
C(104)	4228(6)	2452(4)	5388(7)	53(3)	7218(8)	2328(3)	8543(6)	44(4)
C(105)	3883(5)	2239(3)	6036(5)	39(2)	6279(7)	2055(3)	8219(5)	36(4)
O(106)	3664(3)	2790(2)	7565(3)	38(2)	5528(4)	1535(2)	7147(3)	33(2)
C(107)	4516(7)	3816(4)	7269(7)	54(3)	7436(8)	1853(3)	7078(6)	42(4)
C(108)	5497(8)	3915(5)	7877(8)	71(4)	6738(10)	1924(4)	6327(6)	54(5)
C(109)	5881(10)	4413(5)	8687(11)	89(6)	7125(12)	1784(4)	5867(7)	65(6)
C(110)	5141(12)	4833(6)	8794(10)	98(6)	8169(12)	1627(4)	6157(9)	70(7)
C(111)	4211(13)	4734(6)	8246(13)	101(8)	8871(12)	1542(4)	6913(10)	79(8)
C(112)	3796(8)	4193(4)	7386(9)	70(5)	8515(10)	1654(4)	7398(8)	62(6)
C(113)	4743(9)	3484(6)	5253(10)	83(5)	8464(12)	2619(5)	8102(9)	79(8)
C(114)	4409(8)	2106(6)	4491(8)	74(5)	7677(10)	2628(4)	9205(7)	62(5)
C(115)	3761(5)	1594(3)	6127(6)	43(3)	5427(7)	2029(3)	8432(5)	35(4)
C(101′)	2074(5)	1524(3)	6145(5)	34(2)	5551(7)	1169(3)	8748(5)	37(3)
N(102′)	1236(4)	1153(3)	5603(4)	39(2)	5729(6)	905(2)	9330(4)	36(3)
N(103′)	1332(5)	772(3)	4770(5)	45(2)	5948(6)	1203(3)	9893(4)	37(3)
C(104′)	2252(5)	863(3)	4876(6)	44(3)	5841(7)	1637(3)	9652(5)	36(3)
C(105′)	2717(5)	1347(3)	5703(5)	38(2)	5586(7)	1629(3)	8933(5)	33(3)
O(106′)	2112(4)	1960(2)	6890(4)	47(2)	5441(5)	978(2)	8168(3)	37(2)
C(107′)	309(5)	1253(3)	5645(6)	39(2)	6030(7)	432(3)	9430(5)	36(4)
C(108′)	280(6)	1323(4)	6613(6)	49(3)	7084(9)	301(4)	9999(6)	51(4)
C(109′)	−602(6)	1436(5)	6649(8)	62(3)	7349(11)	−175(4)	10021(8)	69(6)
C(110′)	−1469(6)	1491(4)	5703(9)	65(4)	6600(11)	−467(4)	9471(7)	62(6)
C(111′)	−1432(6)	1416(4)	4765(8)	66(4)	5543(12)	−320(4)	8906(7)	61(6)
C(112′)	−542(6)	1307(4)	4684(7)	52(3)	5245(9)	137(3)	8890(5)	43(4)
C(113′)	745(7)	189(4)	4262(8)	58(4)	5970(11)	1035(4)	10549(6)	58(5)
C(114′)	2589(8)	494(5)	4117(10)	80(5)	6067(10)	2041(4)	10157(6)	57(5)
C(201)	852(5)	3096(3)	6193(5)	41(2)	6574(6)	259(3)	7574(5)	31(3)
N(202)	530(4)	2859(3)	5120(4)	45(2)	7627(6)	236(2)	8218(4)	39(3)
N(203)	−518(4)	2859(3)	4644(5)	48(2)	7940(6)	−227(3)	8319(5)	46(3)
C(204)	−791(5)	3078(4)	5381(6)	48(3)	7072(7)	−473(3)	7788(6)	44(4)

Table 2. (Continued)

Atom	1				2			
	x	y	z	B_{eq}/B[a)]	x	y	z	B_{eq}/B[a)]
C(205)	39(5)	3247(3)	6390(6)	44(3)	6230(7)	−181(3)	7292(5)	39(4)
O(206)	1792(3)	3163(2)	6847(4)	43(2)	6104(4)	646(2)	7300(3)	34(2)
C(207)	1060(6)	2824(4)	4498(6)	45(3)	8432(7)	583(3)	8583(5)	39(3)
C(208)	1116(6)	2275(4)	3890(6)	50(3)	8326(10)	901(4)	9039(6)	55(5)
C(209)	1592(8)	2258(5)	3243(8)	65(4)	9125(11)	1231(4)	9390(7)	68(6)
C(210)	2065(8)	2759(5)	3271(8)	73(4)	10087(10)	1252(4)	9344(8)	73(6)
C(211)	2013(8)	3318(5)	3893(8)	69(4)	10178(10)	936(5)	8916(8)	73(6)
C(212)	1503(8)	3345(4)	4502(6)	61(3)	9368(8)	599(4)	8517(7)	54(5)
C(213)	−1094(6)	2674(5)	3471(7)	64(3)	8904(9)	−383(4)	9028(6)	61(5)
C(214)	−1858(7)	3130(5)	5178(9)	74(4)	7111(11)	−988(3)	7778(8)	68(6)
C(215)	67(6)	3574(4)	7422(6)	49(3)	5124(7)	−286(3)	6610(5)	39(4)
C(201′)	884(5)	2748(3)	8600(6)	36(2)	3737(6)	−17(3)	6974(5)	30(3)
N(202′)	691(4)	2485(3)	9306(5)	43(2)	2990(6)	−218(2)	7107(4)	35(3)
N(203′)	−133(5)	2724(3)	9349(6)	53(3)	2910(6)	−682(2)	6921(5)	39(3)
C(204′)	−487(6)	3137(4)	8665(8)	59(4)	3679(7)	−768(3)	6736(5)	36(3)
C(205′)	127(5)	3171(4)	8193(6)	45(3)	4210(6)	−368(3)	6772(4)	31(3)
O(206′)	1602(3)	2582(2)	8389(4)	37(2)	3970(5)	415(2)	7098(3)	33(2)
C(207′)	1252(6)	2023(3)	9915(6)	43(3)	2065(7)	−18(3)	7123(5)	37(4)
C(208′)	2258(6)	2143(4)	10598(6)	53(3)	1303(8)	265(3)	6527(6)	42(4)
C(209′)	2779(8)	1701(6)	11204(8)	82(5)	372(9)	429(4)	6521(7)	57(5)
C(210′)	2317(10)	1158(6)	11118(10)	90(6)	246(9)	322(4)	7101(8)	60(6)
C(211′)	1334(11)	1041(5)	10389(10)	92(6)	1007(10)	64(4)	7684(7)	53(5)
C(212′)	777(8)	1482(5)	9786(9)	68(5)	1944(8)	−103(3)	7704(5)	44(4)
C(213′)	−431(8)	2622(6)	10182(9)	73(5)	2180(9)	−1005(3)	6990(7)	56(5)
C(214′)	−1393(8)	3503(6)	8537(10)	79(5)	3805(10)	−1233(3)	6492(7)	54(5)
Cl(300)	9412(2)	889(1)	1499(2)	58(1)	4186(2)	1766(1)	4060(2)	50(1)
O(301)	8817	970	2092	113(2)	4247	2022	4643	71(2)
O(302)	10418	827	2197	137(4)	4291	1304	4217	80(2)
O(303)	9548	1544	1431	195(6)	4950	1935	3938	71(2)
O(304)	9106	341	766	252(9)	3138	1788	3447	88(3)
Cl(310)	5769(2)	1819(2)	2669(2)	74(1)	4802(3)	3186(1)	6546(2)	59(1)
O(311)	6614	1879	2511	109(3)	4471	2987	7017	113(3)
O(312)	5139	2292	2532	116(3)	5065	3627	6678	127(4)
O(313)	6162	1603	3714	135(4)	4159	3109	5814	130(4)
O(314)	5130	1307	1786	126(3)	5860	2973	6734	190(7)
Cl(320)	6780(3)	1988(2)	7383(3)	70(1)	−77(2)	1302(1)	5035(2)	55(1)
O(321)	7759	1876	8037	92(3)	−1073	1130	4859	111(3)
O(322)	6408	2505	7807	128(5)	−62	1661	4665	101(3)
O(323)	6150	1604	7527	208(10)	753	995	5156	131(4)
O(324)	6441	1730	6334	222(10)	331	1443	5769	141(5)
Cl(330)	7044(3)	4759(1)	5807(3)	66(1)	9279(3)	1348(1)	1431(2)	74(1)
O(331)	6859	5371	6038	106(4)	10395	1453	1731	149(5)
O(332)	6511	4279	5184	131(4)	8500	1449	743	149(5)
O(333)	8136	4670	6507	134(5)	9315	903	1535	199(7)
O(334)	6913	4560	6786	205(9)	8974	1579	1745	209(8)
Cl(340)	8503(2)	4136(2)	1777(3)	61(2)				
O(341)	7769	4497	1508	188(9)				
O(342)	9407	4100	1763	238(11)				
O(343)	8706	4111	2873	146(6)				
O(344)	7884	3502	999	205(8)				

a) $B_{eq}=4/3\sum_i\sum_j \beta_{ij}\boldsymbol{a}_i\boldsymbol{a}_j$.

phenolate),[17] $(Et_3NH)_2[Ti(cat)_3]$ (1.97 Å; cat=catecholate), $K_4[TiO(cat)_2]_2\cdot 9H_2O$ (1.97 Å), and $(Et_3NH)_2$-$[TiH(dtbc)_3]\cdot 2CHCl_3$ (1.97 Å; dtbc=3,5-di-*t*-butylcatecholate).[18]

The bite angles of dam (av 91° for **1** and 93° for **2**) are much larger than those of catecholate (78—80°) forming a five-membered ring or acetylacetonate (83°) forming a six-membered ring.[16–18] The Ti atoms are located at various distances from six pyrazolone planes, 1.136, 1.128, 0.744, 0.341, 1.429, and 0.260 Å for **1** and 0.518, 0.542, 0.915, 0.283, 1.033, and 0.054 Å for **2**.

Ligand Conformation and Aromatic Ring Stacking. Chelate rings of medium size (eight- to eleven-membered rings) are known to be hardly formed

Table 3. Metal-Ligand Distances (Å) and Angles (°) with esd Values in Parentheses for **1** and **2**

Compound	**1**	**2**
Ti-O(6)	1.929(5)	1.888(7)
Ti-O(6′)	1.929(6)	1.922(7)
Ti-O(106)	1.930(5)	1.943(7)
Ti-O(106′)	1.938(6)	1.939(7)
Ti-O(206)	1.958(6)	1.976(7)
Ti-O(206′)	1.917(6)	1.958(7)
O(6)-Ti-O(6′)	89.3(2)	92.1(3)
O(6)-Ti-O(106)	89.8(2)	90.1(3)
O(6)-Ti-O(106′)	178.7(3)	178.0(3)
O(6)-Ti-O(206)	92.7(2)	92.9(3)
O(6)-Ti-O(206′)	90.2(2)	92.1(3)
O(6′)-Ti-O(106)	88.1(2)	91.0(3)
O(6′)-Ti-O(106′)	90.0(3)	89.3(3)
O(6′)-Ti-O(206)	174.9(3)	174.4(3)
O(6′)-Ti-O(206′)	90.9(3)	88.6(3)
O(106)-Ti-O(106′)	91.3(2)	91.3(3)
O(106)-Ti-O(206)	87.3(2)	86.3(3)
O(106)-Ti-O(206′)	179.0(3)	177.7(3)
O(106′)-Ti-O(206)	88.1(3)	85.8(3)
O(106′)-Ti-O(206′)	88.7(3)	86.5(3)
O(206)-Ti-O(206′)	93.7(3)	93.9(3)

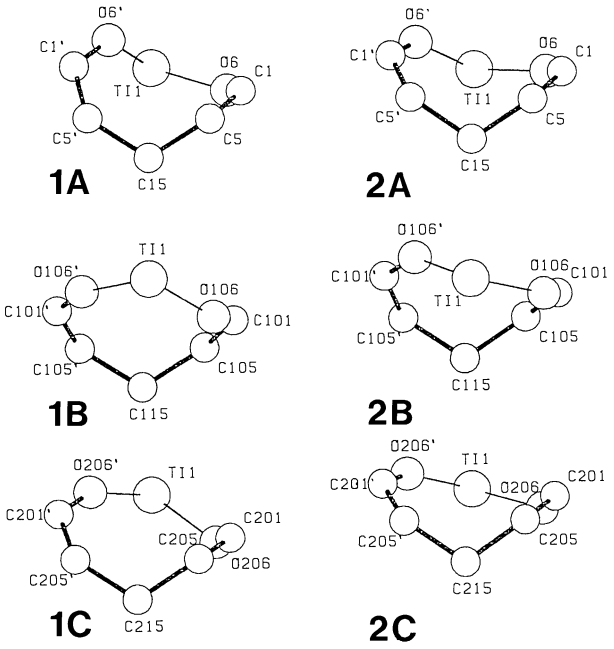

Fig. 3 Projection of the eight-membered chelate rings on the C(5)–C(15)–C(5′) planes.

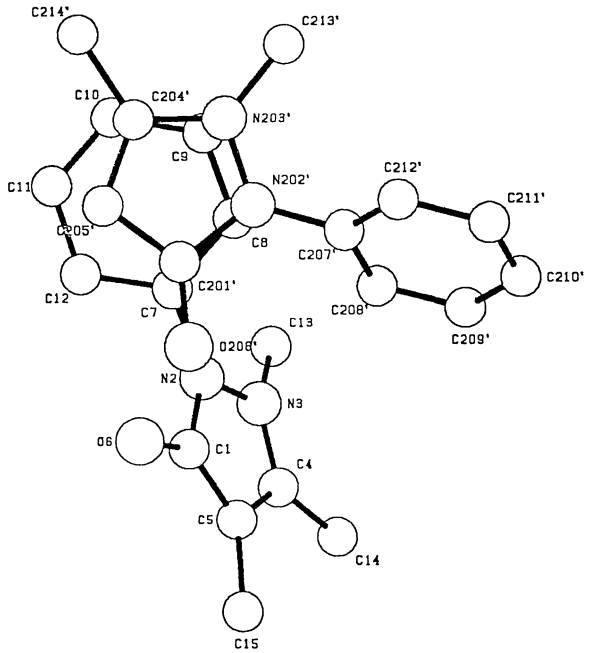

Fig. 4 Projection of the phenyl ring (Ph of A) on the least squares plane of the pyrazolone moiety (Py of C) for **1**.

because of ring strain and entropy factor in the ring closure process.[11,12] In **1** and **2**, however, dam acts as a bidentate ligand to construct an eight-membered ring. It is partly because of the rigidity of this ligand; free rotation is possible only for C(5)–C(15) and C(5′)–C(15). Six eight-membered rings adopt varying conformation as shown in Fig. 3. Within a ligand, one pyrazolone moiety is almost perpendicular to the plane through C(5), C(15), and C(5′), whereas the other not. Dihedral angles between two pyrazolone moieties within a ligand are between 61.4—70.1° (av 65°) except ligand B of **1**, which has an exceptionally small value of 47.0°.

Another striking feature of these complexes is aromatic ring stacking between a pyrazolone moiety of one ligand and a phenyl ring of another. An example for **1** is shown in Fig. 4, and relationship between twelve rings is schematically presented in Fig. 5, together with the closest interatomic distances and dihedral angles between rings. To bring about this stacking, phenyl groups are not coplanar with pyrazolone moieties within a ligand as shown by dihedral angles(47.5—77.3°, av 60°) in Fig. 5.

It is evident that the stacking is more pronounced for the complex **1** than for **2**; for example, that between phenyl group of B and pyrazolone ring of C (Fig. 2). Such stacking not only facilitates the formation of eight-membered rings, but also contributes to the whole stability of these complexes.

Implication for the Coloration. When both crystals were suspended in 1 mol dm^{-3} hydrochloric acid solution, **1** was rapidly and **2** was slowly dissolved to give a solution having an absorption maximum at 385 nm, which agrees well with that of the species used for photometric determination of Ti(IV).

In the ternary systems of Cu–an aromatic amine–a nucleotide, a phenylalkanecarboxylate or an aromatic amino acid, a single well-defined absorption peak appears around 360 nm, which is ascribed to a CT

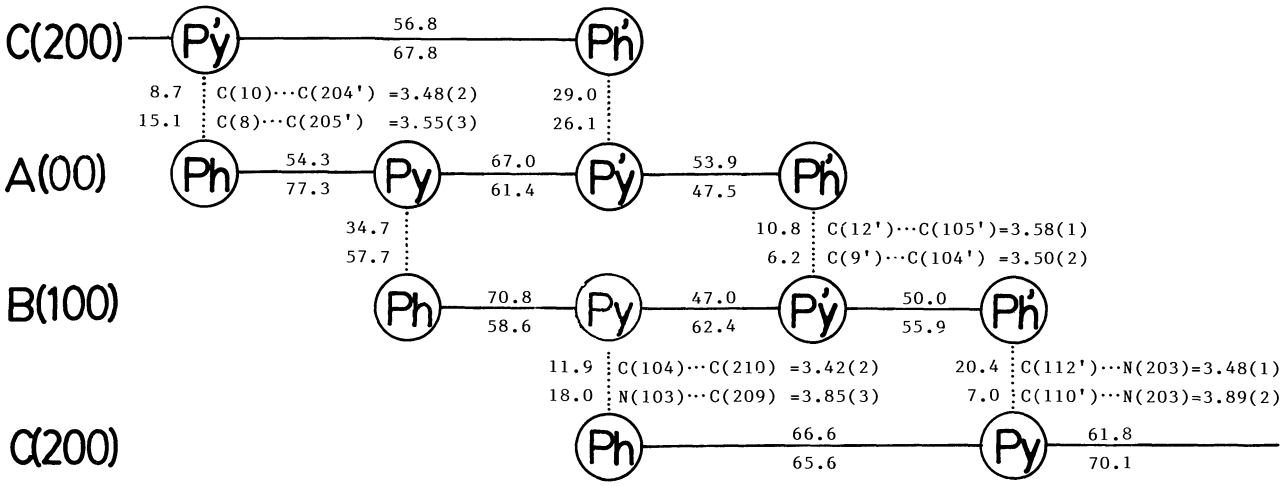

Fig. 5 Relationship between twelve aromatic rings. Ⓟh, Ⓟh′: phenyl group; Ⓟy, Ⓟy′: pyrazolone moiety. Solid line: covalent bond; dotted line: aromatic ring stacking. The closest interatomic distances are given for appreciable ring-overlapping. Other numbers are dihedral angles between two rings. Upper: **1**; lower: **2**.

band.[19–23] X-ray crystal structures just demonstrate the intramolecular aromatic ring stacking in Cu–phenanthroline–tryptophan.[24,25]

Since Ti-dam has several stacking of appreciable ring overlapping, the absorption band at around 385 nm is likewise assigned to a CT band. The electron flows from phenyl groups to pyrazolone moieties made electron-deficient by the coordination to Ti(IV) center.

References

1) A. A. Minin, *Uch. Zap. Permsk. Gos. Univ.*, **9**, 177 (1955). *Chem. Abstr.*, **52**, 8826d (1958).
2) A. A. Minin, *Uch. Zap. Permsk. Gos. Univ.*, **15**, 95 (1958). *Chem. Abstr.*, **54**, 15059c (1960).
3) A. A. Minin and S. A. Erofeeva, *Uch. Zap. Permsk. Gos. Univ.*, **19**, 97 (1961); *Anal. Abstr.*, **10**, 92 (1963).
4) L. Ya. Polyak, *Zh. Anal. Khim.*, **17**, 206 (1962).
5) L. Ya. Polyak, *Zh. Anal. Khim.*, **18**, 956 (1963).
6) L. Ya. Polyak, *Zh. Anal. Khim.*, **19**, 1468 (1964).
7) P. G. Jeffery and G. R. E. C. Gregory, *Analyst (London)*, **90**, 177 (1965).
8) V. I. Lazareva and A. I. Lazarev, *Zh. Anal. Khim.*, **21**, 172 (1966).
9) H. Ishii, *Bunseki Kagaku*, **16**, 110 (1967).
10) R. Kajiyama and K. Yamaguchi, *Bunseki Kagaku*, **16**, 908 (1967).
11) H. Ogino and J. Fujita, *Bull. Chem. Soc. Jpn.*, **48**, 1836 (1975).
12) H. Ogino, *Bull. Chem. Soc. Jpn.*, **50**, 2459 (1977).
13) N. Walker and D. Stuart, *Acta Crystallogr., Sect. A*, **39**, 158 (1983).
14) "International Tables for X-Ray Crystallography," Kynoch Press, Birmingham (1974), Vol. IV. (Present distributor Kluwer Academic Publishers, Dordrecht).
15) PLUTO: W. D. S. Motherwell and W. Clegg, "Program for Plotting Molecular and Crystal Structures," Univ. of Cambridge(1978). XPACK86 SHIONOGI: H. Nakai, T. Sato, and M. Shiro, "Program Pack for X-Ray Structure Analysis," Shionogi Res. Lab. (1986).
16) G. D. Smith, C. N. Caughlan, and J. A. Campbell, *Inorg. Chem.*, **11**, 2989 (1972).
17) P. H. Bird, A. R. Fraser, and C. F. Lau, *Inorg. Chem.*, **12**, 1322 (1973).
18) B. A. Borgias, S. R. Cooper, Y. B. Koh, and K. N. Raymond, *Inorg. Chem.*, **23**, 1009 (1984).
19) C. F. Naumann and H. Sigel, *J. Am. Chem. Soc.*, **96**, 2750 (1974).
20) E. Dubler, U. K. Haring, K. H. Scheller, P. Baltzer, and H. Sigel, *Inorg. Chem.*, **23**, 3785 (1984).
21) R. Malini-Balakrishnan, K. H. Schller, U. K. Haring, R. Tribolet, and H. Sigel, *Inorg. Chem.*, **24**, 2067 (1985).
22) O. Yamauchi and A. Odani, *J. Am. Chem. Soc.*, **107**, 5938 (1985).
23) A. Odani and O. Yamauchi, *Nippon Kagaku Kaishi*, **1987**, 336.
24) K. Aoki and H. Yamazaki, *J. Chem. Soc., Dalton Trans.*, **1987**, 2017.
25) H. Masuda, O. Matsumoto, A. Odani, and O. Yamauchi, *Nippon Kagaku Kaishi*, **1988**, 783.

A Facile Synthesis of 2-Aza-1,3-butadienes

Hidenori OKAMOTO and Shozo KATO
Tsukuba Research Lab., Tokuyama Soda Co., Ltd., 40 Wadai, Tsukuba, Ibaraki 300-42
(Received August 29, 1990)

2-Aza-1,3-butadienes bearing alkoxyl substituent were obtained easily by the reaction of ketimines with orthoesters. The reaction proceeded smoothly by the addition of small amount of *p*-toluenesulfonic acid. When acetals were used in place of orthoesters, the corresponding 2-aza-1,3-butadienes were similarly prepared.

Due to the usefulness in various organic syntheses, several reports have been published on 2-aza-1,3-butadienes.[1] However, there have been few reports about 2-aza-1,3-butadienes bearing an alkoxyl group at the end position. For example, Saegusa and co-workers[2] reported that the reaction of vinyl isocyanide with alcohols in the presence of Cu(I) catalyst gives the corresponding 1-alkoxy-2-aza-1,3-butadienes.

$$CH_2{=}CHNC + ROH \xrightarrow{Cu_2O} CH_2{=}CHN{=}CHOR \quad (R = Me, Et, C_6H_{11} \text{ etc.})$$

Aue and co-worker[3] described that thermolysis of 2-methyl-1-azetine affords 1-alkoxy-2-aza-1,3-butadienes via electrocyclic ring opening followed by a 1,5-hydride shift.

Brown and co-worker[4] reported that the reaction of the orthoester with an enamino nitrile gives rise to the corresponding ethoxy derivative. This method, however, is only applicable to the enamines having electron-withdrawing groups.

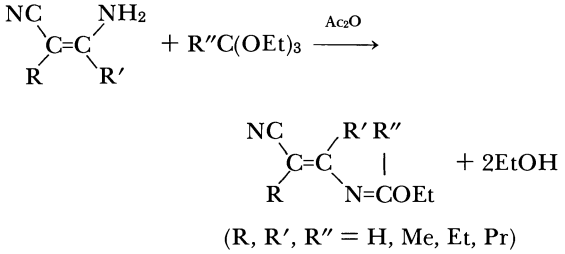

(R, R′, R″ = H, Me, Et, Pr)

Although a number of reactions of orthoesters with amine compounds have been reported,[5] little has been known of the reaction with ketimines. During the course of our study on ketimine compounds, we found that ketimines easily react with orthoesters and acetals to give 2-aza-1,3-butadienes.

In this paper, we wish to report a facile, extensive synthesis of 2-aza-1,3-butadienes having alkoxyl substituent or dialkylamino substituent.

Results and Discussion

1-Alkoxy-2-aza-1,3-butadienes (**1**) were prepared from 1-aryl-2-methyl-1-propanimines and orthoesters as shown in Scheme 1.

General procedure is as follows. To a flask equipped with distillation head were added 1-aryl-2-methyl-1-propanimines, orthoester and a small amount of *p*-toluenesulfonic acid (PTS). The mixture was heated in an oil bath (120—160 °C) for about 10—20 min until the corresponding alcohol, which was formed during the reaction, was distilled out. The resulting mixture afforded a colorless, pale yellow or yellow liquid after distillation under a reduced pressure.

These results are summarized in Table 1. As can be seen in the Table, 2-aza-1,3-butadienes, having branched alkoxyl group, especially isopropoxyl group, were obtained in good yields (Entry No. **1e—j**). Furthermore, 2-aza-1,3-butadienes derived from triethyl orthoacetate and triethyl orthopropionate were formed in considerable yields (Entry No. **1m** and **1n**). These results seemed to be attributed to the steric protection around the carbon–nitrogen double bond. Good results were obtained by use of excess amount of orthoesters in the cases of trimethyl orthoformate and triethyl orthoformate because of their low boiling points. When the reaction was carried out for a long time, polymeric substance was obtained.

Although this condensation reaction proceeded without catalyst, the presence of a small amount of PTS was favorable to afford good yields. For instance, the reaction of 2-methyl-1-phenyl-1-propanimine (**2**) with triethyl orthoacetate or triethyl orthopropionate in the presence of a small amount of PTS at 120 °C for 15 min gave the products **1m** and **1n** in 70 and 63% yields, respectively, while in the absence of PTS at 120 °C for 3h **1m** and **1n** were obtained in yields of 30 and 20%, respectively.

The 2-aza-1,3-butadiene (**3**), which is the dimer of **2**, was produced as a by-product in the reaction of **2** with orthoesters. Dimerization of ketimines has been

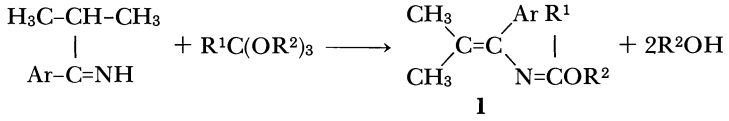

1

Scheme 1.

Table 1. 2-Aza-1,3-butadienes (**1**)

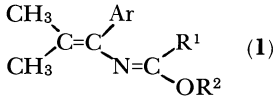

(**1**)

No.	Ar	R^1	R^2	Method[a]	Yield/%	Bp/°C/mmHg
a	5-Me-2-thienyl	H	Me	A	25	75—76/0.1
b	2-Me-C_6H_4	H	Et	C	53	75—76/0.2
c	3-Me-C_6H_4	H	Et	C	52	92—94/0.6
d	3-CF_3-C_6H_4	H	Et	B	49	73—75/0.3
e	C_6H_5	H	*i*-Pr	A	62	79—82/0.15
f	2-Me-C_6H_4	H	*i*-Pr	A	87	65—69/0.1
g	4-F-C_6H_4	H	*i*-Pr	A	71	69—70/0.1
h	2-Furyl	H	*i*-Pr	A	71	57—58/0.2
i	2-Thienyl	H	*i*-Pr	A	68	66/0.12
j	3-MeO-2-thienyl	H	*i*-Pr	A	69	94/0.1
k	C_6H_5	H	*s*-Bu	A	56	82—83/0.15
l	C_6H_5	Me	Me	C	40	73—75/0.35
m	C_6H_5	Me	Et	B	70	80—82/0.4
n	C_6H_5	Et	Et	B	63	82—83/0.25
o	C_6H_5	*n*-Pr	Me	B	55	84—86/0.5

a) Method A: PTS catalyst at 150—160°C for 10—15 min; Method B: PTS catalyst at 120—130°C for 5—15 min; Method C: No catalyst at 110—120°C for 2—8 h.

previously accomplished by refluxing a THF solution of ketimines in the presence of trifluoroacetic acid.[6] When **2** was heated at 150 °C in the presence or absence of PTS, **3** was obtained along with the evolution of ammonia.

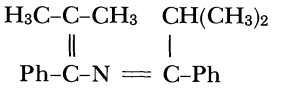

(**3**)

To synthesize 1-phenoxy-2-aza-1,3-butadiene (R^2= Ph), diethyl phenyl orthoformate (**4**) was allowed to react with **2**. However, this reaction was failed to give 2-ethoxy-2-aza-1,3-butadiene as shown in the following scheme because of higher ability of elimination of phenol.

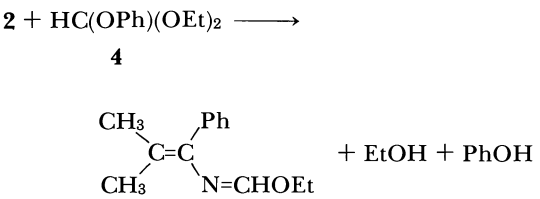

Table 2. 2-Aza-1,3-butadienes (**5**)[a]

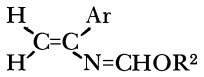

(**5**)

No.	Ar	R^2	Yield/%	Bp/°C/mmHg
a	C_6H_5	Et	11	65—66/0.15
b	2-Me-C_6H_4	Et	20	86—90/1.0
c	C_6H_5	*i*-Pr	28	76—78/0.15
d	2-Me-C_6H_4	*i*-Pr	55	74—75/0.1

a) Reaction was carried out in the presence of small amount of PTS at 140—160°C for 5 min.

We carried out the reaction between 1-aryl-1-ethanimines and orthoesters. 1-Alkoxyl-2-aza-1,3-butadienes (**5a—d**) were obtained similarly as described in Table 2. The yield seemed to become higher with the increase of the steric protection around the carbon–nitrogen double bond to suggest the importance of the steric factor in these reactions. When 1-phenyl-1-pentanimine (**6**) was treated with triisopropyl orthoformate, a mixture of two isomers (**7a**:**7b**=2:1) were formed. The isomer ratio was determined by ^{1}H NMR.

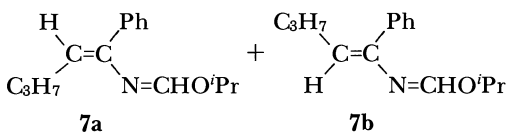

In the course of extention of 2-aza-1,3-butadiene synthesis using ketimines, we have investigated the reaction of ketimines with acetals instead of orthoesters. When *N*,*N*-dimethylformamide dimethylacetal was allowed to react with **2**,1-amino-2-aza-1,3-butadiene (**9**) was obtained as shown in Scheme 2. In this reaction, the formation of intermediate (**8**) proceeded smoothly. Subsequent reaction which involves removal of the methanol from **8** was slow. It was

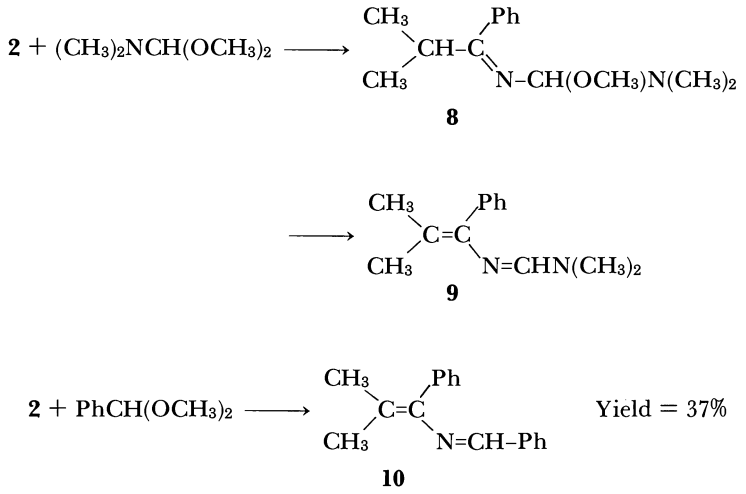

Scheme 2.

difficult to separate these two compounds (**8** and **9**) by vacuum distillation. To make the reaction complete, longer reaction time at high temperature was required. It was also effective to carry out the reaction under a reduced pressure. R. Gompper and co-worker[7] have reported the synthesis of 4-amino-2-aza-1,3-butadienes by the reaction of *N,N*-dimethylformamide diethylacetal with azomethines. Moreover, the treatment of benzaldehyde dimethylacetal with **2** in a similar manner gave 1-phenyl-2-aza-1,3-butadiene (**10**). Since the condensation was rather slow in comparison with that of orthoesters, the competitive formation of **3** and **10** was observed. They could not be separated with each other by distillation under a reduced pressure. These results indicate that acetals, as well as orthoesters, react with ketimine to give 2-aza-1,3-butadienes. Although **10** was similarly prepared by the reaction of **2** with benzaldehyde, the yield was only 5% at 160 °C for 30 min.

In conclusion, the present reaction affords a facile and useful preparative method for 2-aza-1,3-butadienes bearing an alkoxyl or an amino group at the end position. At present, we are trying to prepare biologically active compounds by use of thus obtained 2-aza-1,3-butadienes.

Experimental

The IR spectra were measured with a Hitachi I-2000 spectrometer. The ^{1}H NMR spectra were measured in a $CDCl_3$ solution with a Hitachi R-1500 spectrometer using tetramethylsilane as an internal standard. The mass spectra were obtained on a Hitachi M-80 spectrometer. Elemental analysis data (C, H, and N) agreed within ±0.3% for the calculated values.

Materials. Most of the orthoesters and acetals were commercially available. Triisopropyl orthoformate and tri-*s*-butyl orthoformate were prepared by the transesterification of trimethyl orthoformate and triethyl orthoformate with 2-propanol and 2-butanol, respectively.

Synthesis of Ketimines.[8] Some compounds were prepared by the reaction of benzonitrile with methyllithium or *n*-butyllithium, followed by the addition of ice at low temperature. Some compounds were synthesized by the reaction of aryllithium with isobutyronitrile. The other compounds were prepared by the reaction of aryl Grignard reagent with isobutyronitrile or isopropyl Grignard reagent with arylnitrile.

Synthesis of 2-Aza-1,3-butadienes (1). Method A: A typical procedure is as follows. To a 100 ml flask equipped with distillation head were added 1-(3-methoxy-2-thienyl)-2-methyl-1-propanimine (6.11 g, 33 mmol), triisopropyl orthoformate (6.98 g, 36 mmol) and a small amount of PTS. The mixture was heated in an oil bath (160 °C) for about 20 min until 2-propanol, which was formed during the reaction, was distilled out. The resulting mixture afforded a yellow liquid (5.82 g, 69%) of 1-isopropoxy-3-(3-methoxy-2-thienyl)-4,4-dimethyl-2-aza-1,3-butadiene which boiled at 94 °C/0.1 mmHg (1 mmHg=133.322 Pa) (Table 1, **1j**). ^{1}H NMR ($CDCl_3$) δ=1.28 (6H, d, J=6 Hz, CH_3×2), 1.68 (3H, s, CH_3), 2.00 (3H, s, CH_3), 3.74 (3H, s, OCH_3), 5.10 (1H, quint., J=6 Hz, OCH), 6.76 (1H, d, J=5 Hz, thienyl H), 7.12 (1H, d, J=5 Hz, thienyl H), 7.27 (1H, s, N=CHO); IR(KBr) 1630 cm^{-1} (N=CHO); MS m/z 253 (M^+), 210 ([$M-C_3H_7$]$^+$). Found: C, 61.73; H, 7.53; N, 5.49%. Calcd for $C_{13}H_{19}NO_2S$: C, 61.63; H, 7.56; N, 5.53%.

Method B: A typical procedure is as follows. To a 100 ml flask equipped with distillation head were added 1-phenyl-2-methyl-1-propanimine (10.44 g, 71 mmol), triethyl orthoacetate (15.90 g, 98 mmol) and a small amount of PTS. The mixture was heated in an oil bath (120 °C) for about 15 min until ethanol, which was formed during the reaction, was distilled out. The resulting mixture afforded a pale yellow liquid (10.84 g, 70%) of 1-ethoxy-1,4,4-trimethyl-3-phenyl-2-aza-1,3-butadiene which boiled at 80—82 °C/0.4 mmHg (Table 1, **1m**). ^{1}H NMR ($CDCl_3$) δ=1.25 (3H t, J=7 Hz, CH_3), 1.63 (3H, s, CH_3), 1.73 (6H, s, CH_3×2), 4.13 (2H, q, J=7 Hz, OCH_2), 7.12 (5H, s, aromatic H); IR(KBr) 1670 cm^{-1} (N=CMeO); MS m/z 217 (M^+), 188 ([$M-C_2H_5$]$^+$). Found: C, 77.59; H, 8.66; N, 6.34%. Calcd for $C_{14}H_{19}NO$: C, 77.37; H,

8.81; N, 6.45%.

Method C: A typical procedure is as follows. To a 100 ml flask equipped with distillation head were added 1-(3-methylphenyl)-2-methyl-1-propanimine (10.10 g, 63 mmol) and triethyl orthoformate (10.34 g, 70 mmol). The mixture was heated in an oil bath (110 °C) for about 3 h until ethanol, which was formed during the reaction, was distilled out. The resulting mixture afforded a pale yellow liquid (7.10 g, 52%) of 1-ethoxy-4,4-dimethyl-3-(3-methylphenyl)-2-aza-1,3-butadiene which boiled at 92—94 °C/0.6 mmHg (Table 1, **1c**). ^{1}H NMR ($CDCl_3$) δ=1.28 (3H, t, J=7 Hz, CH_3), 1.59 (3H, s, CH_3), 1.96 (3H, s, CH_3), 2.30 (3H, s, CH_3), 4.20 (2H, q, J=7 Hz, OCH_2), 6.80—7.33 (5H, m, N=CHO and aromatic H); IR(KBr) 1625 cm^{-1} (N=CHO); MS m/z 217 (M^+), 188 ([M−C_2H_5). Found: C, 77.25; H, 8.78; N, 6.50%. Calcd for $C_{14}H_{19}NO$: C, 77.37; H, 8.81; N, 6.45%.

Synthesis of 3. To a 100 ml flask were added **2** (5.06 g, 34 mmol) and a small amount of PTS. The mixture was heated in an oil bath (150 °C) for about 20 min. The resulting mixture afforded a yellow viscous liquid (1.65 g, 35%) of 1-isopropyl-4,4-dimethyl-1,3-diphenyl-2-aza-1,3-butadiene which boiled at 123 °C/0.3 mmHg. ^{1}H NMR ($CDCl_3$) δ=1.18 (6H, d, J=6 Hz, CH_3×2), 1.59 (3H, s, CH_3), 1.65 (3H, s, CH_3), 2.85 (1H, quint., J=6 Hz, OCH), 6.80—7.80 (10H, m, aromatic H); IR(KBr) 1632 cm^{-1} (N=C); MS m/z 277 (M^+).

Synthesis of 5d. To a 100 ml flask equipped with distillation head were added 1-(2-methylphenyl)-1-ethanimine (4.55 g, 39 mmol), triisopropyl orthoformate (8.25 g, 43 mmol) and a small amount of PTS. The mixture was heated in an oil bath (140—150 °C) for about 5 min until 2-propanol was distilled out. The resulting mixture afforded a pale yellow liquid (4.33 g, 55%) of 1-isopropoxy-3-(2-methylphenyl)-2-aza-1,3-butadiene which boiled at 74—75 °C/0.1 mmHg (Table 2, **5d**). ^{1}H NMR ($CDCl_3$) δ=1.27 (6H, d, J=6 Hz, CH_3×2), 2.32 (3H, s, CH_3), 4.56 (1H, s, =CH), 4.92 (1H, s, =CH), 5.10 (1H, quint., J=6 Hz, OCH), 7.19 (4H, m, aromatic H), 7.43 (1H, s, N=CHO); IR(KBr) 1622 cm^{-1} (N=CHO); MS m/z 203 (M^+). Found: C, 76.55; H, 8.32; N, 7.04%. Calcd for $C_{13}H_{17}NO$: C, 76.81; H, 8.43; N, 6.89%.

Synthesis of 7. To a 100 ml flask equipped with distillation head were added **6** (4.93 g, 31 mmol), triisopropyl orthoformate (7.89 g, 41 mmol) and a small amount of PTS. The mixture was heated in an oil bath (160 °C) for about 5 min until 2-propanol was distilled out. The resulting mixture afforded a yellow liquid (3.03 g, 42%) of 1-isopropoxy-4-propyl-3-phenyl-2-aza-1,3-butadiene which boiled at 92 °C/0.15 mmHg. ^{1}H NMR ($CDCl_3$) δ=0.94 (t, J=7 Hz, CH_3), 1.25 (d, J=6 Hz, CH_3×2), 1.35 (d, J=6 Hz, CH_3×2), 1.40—1.70 (m, CH_2), 1.90—2.30 (m, CH_2), 5.11 (quint., J=6 Hz, OCH), 5.24 (t, J=7 Hz, C=CH), 5.45 (t, J=7 Hz, C=CH), 7.10—7.50 (m, N=CHO and aromatic H); IR(KBr) 1648 cm^{-1} (N=CHO); MS m/z 231 (M^+). From the NMR spectrum and GC of the mixture, it was assigned as being a 2:1 mixture of **7a** and **7b**.

Synthesis of 9. To a 100 ml flask were added **2** (4.05 g, 28 mmol), *N*,*N*-dimethylformamide dimethylacetal (3.77 g, 32 mmol) and a small amount of PTS. The mixture was heated in an oil bath (130—150 °C) for about 1h until methanol was distilled out. The resulting mixture afforded a yellow liquid (3.10 g, 56%) of 4,4-dimethyl-1-dimethylamino-3-phenyl-2-aza-1,3-butadiene which boiled at 88 °C/0.15 mmHg. ^{1}H NMR ($CDCl_3$) δ=1.53 (3H, s, CH_3), 2.02

Table 3. ^{1}H NMR Data of 2-Aza-1,3-butadienes

Compound	^{1}H NMR ($CDCl_3$, δ)
1a	1.77 (3H, s, CH_3), 1.94 (3H, s, CH_3), 2.43 (3H, s, CH_3), 3.79 (3H, s, OCH_3), 6.61 (2H, s, thienyl H), 7.42 (1H, s, N=CHO)
1b	1.26 (3H, t, J=7 Hz, CH_3), 1.45 (3H, s, CH_3), 2.01 (3H, s, CH_3), 2.09 (3H, s, CH_3), 4.18 (2H, q, J=7 Hz, OCH_2), 6.90—7.05 (2H, m, aromatic H), 7.08 (2H, s, aromatic H), 7.14 (1H, s, N=CHO)
1d	1.30 (3H, t, J=7 Hz, CH_3), 1.59 (3H, s, CH_3), 1.96 (3H, s, CH_3), 4.25 (2H, q, J=7 Hz, OCH_2), 7.16 (1H, s, N=CHO), 7.43 (4H, brs, aromatic H)
1e	1.25 (6H, d, J=6 Hz, CH_3×2), 1.57 (3H, s, CH_3), 1.96 (3H, s, CH_3), 5.08 (1H, quint., J=6 Hz, OCH), 7.00—7.40 (6H, m, N=CHO and aromatic H)
1f	1.26 (6H, d, J=6 Hz, CH_3×2), 1.47 (3H, s, CH_3), 2.03 (3H, s, CH_3), 2.29 (3H, s, CH_3), 5.07 (1H, quint., J=6 Hz, OCH), 6.95 (1H, s, N=CHO), 7.15 (4H, brs, aromatic H)
1g	1.28 (6H, d, J=6 Hz, CH_3×2), 1.58 (3H, s, CH_3), 1.96 (3H, s, CH_3), 5.10 (1H, quint., J=6 Hz, OCH), 7.01 (2H, s, aromatic H), 7.13 (3H, s, N=CHO and aromatic H)
1h	1.30 (6H, d, J=6 Hz, CH_3×2), 1.87 (6H, s, CH_3×2), 5.16 (1H, quint., J=6 Hz, OCH), 6.17 (1H, d, J=3 Hz, furyl H), 6.34 (1H, t, J=3 Hz, furyl H), 7.35 (2H, s, N=CHO and furyl H)
1i	1.29 (6H, d, J=6 Hz, CH_3×2), 1.76 (3H, s, CH_3), 1.92 (3H, s, CH_3), 5.11 (1H, quint., J=6 Hz, OCH), 6.80—7.25 (3H, m, thienyl H), 7.30 (1H, s, N=CHO)
1k	0.90 (3H, t, J=7 Hz, CH_3), 1.25 (3H, d, J=6 Hz, CH_3), 1.35—1.80 (2H, m, CH_2), 1.58 (3H, s, CH_3), 1.95 (3H, s, CH_3), 4.89 (1H, q, J=6 Hz, CH), 7.00—7.42 (6H, m, N=CHO and aromatic H)
1l	1.62 (3H, s, CH_3), 1.69 (3H, s, CH_3), 1.74 (3H, s, CH_3), 3.64 (3H, s, OCH_3), 7.12 (5H, s, aromatic H)
1n	0.90 (3H, t, J=7 Hz, CH_3), 1.25 (3H, t, J=7 Hz, CH_3), 1.64 (3H, s, CH_3), 1.75 (3H, s, CH_3), 2.09 (2H, q, J=7 Hz, CH_2), 4.14 (2H, q, J=7 Hz, OCH_2), 7.13 (5H s, aromatic H)
1o	0.73 (3H, t, J=6 Hz, CH_3), 1.10—1.60 (2H, m, CH_2), 1.63 (3H, s, CH_3), 1.75 (3H, s, CH_3), 1.90—2.25 (2H, m, CH_2), 3.67 (3H, s, OCH_3), 7.12 (5H, s, aromatic H)
5a	1.36 (3H, t, J=7 Hz, CH_3), 4.32 (2H, q, J=7 Hz, OCH_2), 4.54 (1H, s, =CH), 4.95 (1H, s, =CH), 7.20—7.80 (6H, m, N=CHO and aromatic H)
5b	1.29 (3H, t, J=7 Hz, CH_3), 2.34 (3H, s, CH_3), 4.23 (2H, q, J=7 Hz, OCH_2), 4.58 (1H, s, =CH), 4.94 (1H, s, =CH), 7.19 (4H, s, aromatic H), 7.47 (1H, s, N=CHO)
5c	1.35 (6H, d, J=6 Hz, CH_3×2), 4.53 (1H, s, =CH), 4.94 (1H, s, =CH), 5.18 (1H, quint., J=6 Hz, OCH), 7.20—7.70 (6H, m, N=CHO and aromatic H)

(3H, s, CH_3), 2.84 (6H, s, CH_3×2), 6.90 (1H, s, N=CHN), 7.00—7.50 (5H, m, aromatic H); IR(KBr) 1626 cm^{-1} (N=C); MS *m/z* 222(M^+).

Synthesis of 10. To a 100 ml flask were added **2** (4.27 g, 29 mmol), benzaldehyde dimethylacetal (4.68 g, 31 mmol) and a small amount of PTS. The mixture was heated in an oil bath (160 °C) for about 30 min until methanol was distilled out. The resulting mixture afforded a yellow viscous liquid (3.60 g) of 4,4-dimethyl-1,3-diphenyl-2-aza-1,3-butadiene which boiled at 120—125 °C/0.15 mmHg. The obtained liquid contained 70% of **10** and 30% of **3**, which was confirmed by GC. The other 2-aza-1,3-butadienes were prepared by the methods described above. Their ^1H NMR data are summarized in Table 3.

References

1) K. Dietliker and H. Heimgartner, *Helv. Chim. Acta*, **66**, 262 (1983); A. Dehnel, J. P. Finet, and G. Lavielle, *Synthesis*, **1977**, 474; J. Baum, D. Scholz, F. Tataruch, and H. G. Viehe, *Chimia*, **29**, 514 (1975) and references cited therein.

2) T. Saegusa, I. Murase, and Y. Ito, *J. Org. Chem.*, **36**, 2876 (1971).

3) D. H. Aue and D. Thomas, *J. Org. Chem.*, **40**, 1349 (1975).

4) D. J. Brown and K. Ienega, *J. Chem. Soc., Perkin Trans. 1*, **1974**, 372.

5) L. A. Pavlova, Yu. A. Davidovich, and S. V. Rogozhin, *Usp. Khim.*, **55**, 1803 (1986); R. S. Hosmane, *Tetrahedron Lett.*, **25**, 363 (1984).

6) J. Barluenga, J. Joglar, S. Fustero, V. Gotor, C. Krueger, and M. J. Romao, *Chem. Ber.*, **118**, 3652 (1985).

7) R. Gompper and U. Heinemann, *Angew. Chem., Int. Ed. Engl.*, **20**, 296 (1981).

8) P. L. Pickard and D. J. Vaughan, *J. Am. Chem. Soc.*, **72**, 876 (1950); I. Pattison, K. Wade, and B. K. Wyatt, *J. Chem. Soc. A*, **1967**, 837.

Formation and Molecular Structure of the 2:1-Adducts of 1-Alkoxy-2-benzopyrylium-4-olates with Carbon Disulfide

Hirofumi NAKANO, Hatsue TAMURA, and Toshikazu IBATA*
Institute of Chemistry, College of General Education, Osaka University, Toyonaka, Osaka 560
(Received September 14, 1990)

The $Rh_2(OAc)_4$-catalyzed decomposition of alkyl *o*-(diazoacetyl)benzoates in the presence of carbon disulfide gave two 2:1-adducts of the intermediate 1-alkoxy-2-benzopyrylium-4-olates with carbon disulfide together with a small amount of 5-(*o*-alkoxycarbonylphenyl)-1,3-oxathiole-2-thiones. The intramolecular carbene-carbonyl reaction of the carbenoid generated by the decomposition of the diazo ketones was clarified to be much faster than the intermolecular attack on carbon disulfide. The molecular structure of the major 2:1-adduct of 1-methoxy-2-benzopyrylium-4-olate with carbon disulfide was determined by means of X-ray crystallography. The crystals of the adduct are triclinic with space group $P\bar{1}$, and with the unit-cell dimensions of a=12.213(1), b=11.846(1), c=7.0403(2) Å, α=93.395(6), β=102.147(5), γ=109.536(7)°, and Z=2. The final R value is 0.044 for 2597 observed reflections. The structure was confirmed to be (S-*endo*, S′-*endo*).

Recently, formation of carbonyl ylides by carbene–carbonyl reaction,[1] and their 1,3-dipolar cycloaddition with various types of dipolarophiles have been studied extensively from the synthetic interests.[2] The authors reported previously the 1,3-dipolar cycloaddition of 1-methoxy-2-benzopyrylium-4-olate (**3a**), which was formed by the intramolecular carbene–carbonyl reaction of the carbenoid **2a**, with ethylenic,[1b,3] acetylenic,[1b,4] and carbonyl compounds.[5] In the continuation of these studies we report here the reaction of **3** with carbon disulfide as an example of dipolarophiles having a C–S double bond.

Results and Discussion

The Catalytic Decomposition of Alkyl *o*-(Diazoacetyl)benzoates (1) in the Presence of Carbon Disulfide. The medium pressure column chromatography of the $Rh_2(OAc)_4$-catalyzed reaction mixture of methyl *o*-(diazoacetyl)benzoate (**1a**) with carbon disulfide at 46 °C gave two 2:1-adducts **5a** of the corresponding carbonyl ylide intermediate **3a** with carbon disulfide along with 5-(*o*-methoxycarbonylphenyl)-1,3-oxathiole-2-thione (**6a**). The formation of **6a** was described in the previous papers.[6,7]

Elemental analysis of the 2:1-adducts **5a** indicates that they contain two molecules of **3a** and a molecule of carbon disulfide. The NMR spectra of the major 2:1-adduct (**5a-A**; 64.5% yield) showed that two moieties of **3a** are equivalent each other in **5a-A**. For example, the ^1H NMR spectrum of **5a-A** has only one signal of methine protons at δ=5.01 and that of methoxyl-protons at δ=3.95. Similarly, the ^{13}C NMR spectrum of **5a-A** also exhibited only one signal for each pairs of methoxyl-carbons (δ=53.41), methine-

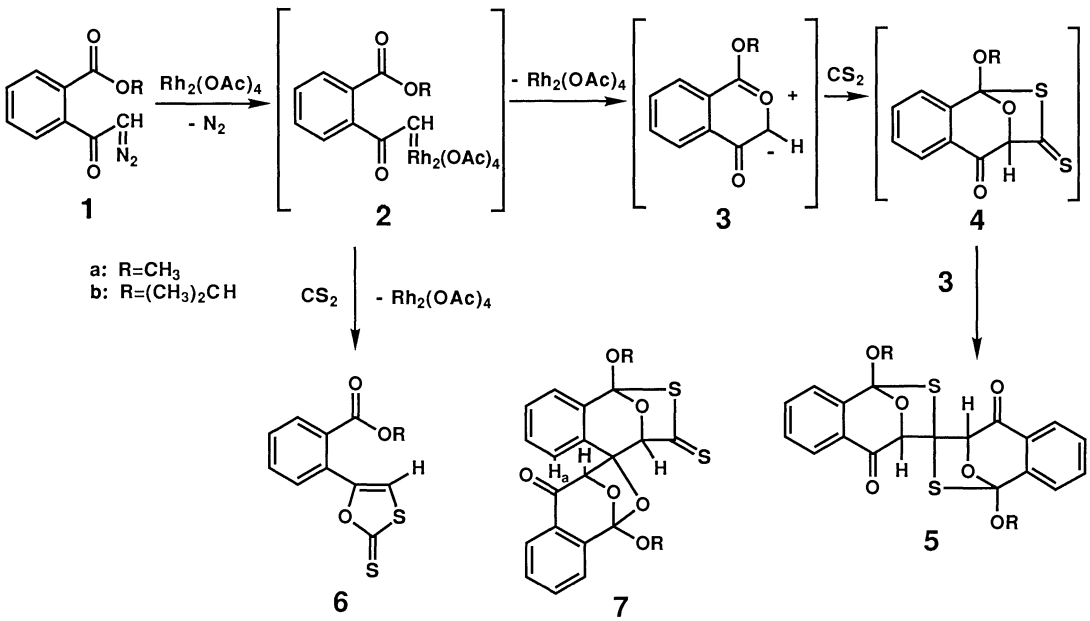

Scheme 1.

Table 1. NMR Data of 2:1-Adducts

Major 2:1-adduct **5a-A**		Minor 2:1-adduct **5a-B**	Major 2:1-adduct **5b-A**		Minor 2:1-adduct **5b-B**
^{1}H NMR ($CDCl_3$)					
OCH_3 (s)	3.95 (6H)	3.74 (3H)	CH_3 (d)	1.43 (6H, J=6.2 Hz)	1.26 (3H, J=6.2 Hz)
		3.87 (3H)			1.39 (3H, J=6.2 Hz)
CH (s)	5.01 (2H)	5.08 (1H)		1.44 (6H, J=6.2 Hz)	1.41 (3H, J=6.2 Hz)
		5.29 (1H)			1.48 (3H, J=6.2 Hz)
arom-H (m)	7.42—7.62 (6H)	7.41—7.63 (6H)	CH (s)	4.98 (2H)	5.04 (1H)
	8.03—8.05 (2H)	7.96—8.03 (2H)			5.30 (1H)
			CH (sept)	5.03 (2H, J=6.2 Hz)	4.51 (1H, J=6.2 Hz)
					4.76 (1H, J=6.2 Hz)
			arom-H (m)	7.40—8.04 (8H)	7.38—8.01 (8H)
^{13}C NMR ($CDCl_3$)					
OCH_3 (q)	63.41	52.52	CH_3 (q)	23.26	23.06
		52.69		23.88	23.31
spiro-C (s)	70.91	75.78			23.71
CH	89.86[a]	83.62[b]			23.94
		94.35[c]	spiro-C (s)	71.00	75.89
S-C-O (s)	117.40	117.06	OCH (d)	71.31	70.77
		117.50			71.04
arom-CH (d)	120.76	120.47	CH	89.58[d]	83.07[e]
		120.63			94.17[f]
arom-C (s)	127.23	127.00	S-C-O (s)	116.97	116.76
		127.60			117.07
arom-CH (d)	127.45	127.71	arom-CH (d)	121.08	120.78
		127.74			120.90
arom-CH (d)	128.85	128.84	arom-C (s)	127.10	126.63
		129.06			127.27
arom-CH (d)	134.77	134.57	arom-CH (d)	127.36	127.55
		134.70			127.60
arom-C (s)	147.77	147.97	arom-CH (d)	128.35	128.62
		148.35			128.86
C=O (s)	188.89	189.97	arom-CH (d)	134.72	134.58
		190.38			134.72
			arom-C (s)	148.34	148.52
					148.79
			C=O (s)	188.97	189.96
					190.26

a) dd, $^3J_{CH}$=3.4 Hz. b) d, $^3J_{CH}$=0 Hz. c) dd, $^3J_{CH}$=3.1 Hz. d) dd, $^3J_{CH}$=3.4 Hz. e) d, $^3J_{CH}$=0 Hz. f) dd, $^3J_{CH}$=3.1 Hz.

carbons (δ=89.86), carbonyl-carbons (δ=188.89), and other carbons of two benzopyrylium-olate moieties as are shown in Table 1. On the other hand, in the minor 2:1-adduct (**5a-B**; 10.8% yield) two **3a** moieties involved are not equivalent each other, and the corresponding protons and carbons of two **3a** moieties show their signals at different positions in its ^{1}H and ^{13}C NMR spectra (Table 1).

Quite similar results were also obtained in the $Rh_2(OAc)_4$-catalyzed decomposition of isopropyl *o*-(diazoacetyl)benzoate (**1b**) in the presence of carbon disulfide.

In these reactions of **1a** and **1b**, no 1:1-adduct **4** between **3** and carbon disulfide was observed in spite of the detailed inspection of the reaction mixture by column chromatography. This indicates that the second cycloaddition of **3** with the 1:1-adducts **4** is much faster than the first attack of **3** on carbon disulfide.

There are two sites of the second attack of **3** in a molecule of the 1:1-adduct **4**. One is thiocarbonyl group to give **5**, and the other is carbonyl group to give **7**. From our previous studies,[5c,8] **7** should show a signal of an aromatic proton H_a at high field in its ^{1}H NMR spectrum due to the ring current of the neighboring aromatic ring system. The fact that our major and minor 2:1-adducts show no such a high field signal indicates that the second attack of **3** to give these 2:1-adducts did not occur on the carbonyl group but occurred on the thiocarbonyl group of **4**. Absence of a signal of thiocarbonyl carbon in the ^{13}C NMR spectra of these adducts in the region of δ=202—203[7] also supports the reaction site described above. The regiochemistry of the first and the second cycloadditions of **3** is consistent with the presence of singlet signals of nonaromatic quaternary carbons having orthothioformate structure at near δ=117 in the ^{13}C NMR spectra of **5**.[5]

These 1,3-dipolar cycloadditions of carbonyl ylides have been found to proceed through the interaction

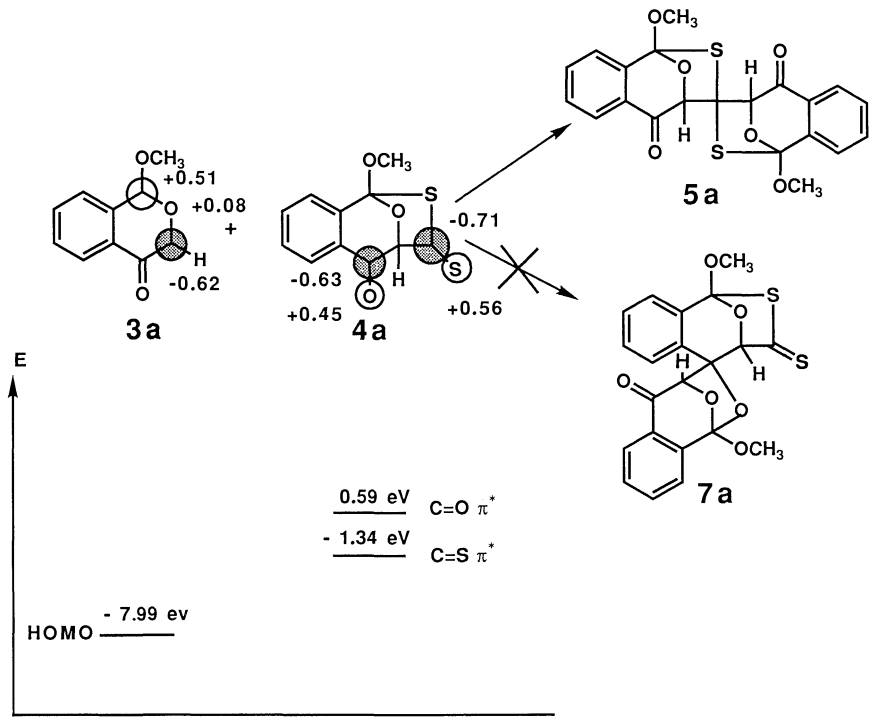

Fig. 1. The energy levels and atomic orbital coefficients of frontier orbitals of **3a** and **4a**.

controlled by carbonyl ylide-HOMO and dipolarophile-LUMO.[5b,9] In order to presume the reaction site of the second attack of **3a** toward 1:1-adduct **4a**, energy levels of the C=O π^* and C=S π^* of **4a** were calculated together with HOMO level of **3a**. Results of MNDOC calculation[10] shown in Fig. 1 revealed that the energy level of C=S π^* (−1.34 eV) is lower than that of C=O π^* (0.59 eV). This indicates that the reaction site is not the C=O group but the C=S group affording the 2:1-adducts **5** as is described above. The atomic orbital coefficients of the related frontier orbitals of **3a** and **4a** also explain the regiochemistry of the cycloaddition.[5b]

There are four possibilities in the second attack of **3** on C–S double bond of the 1:1-adduct **4** in a regiochemistry similar to that of the first cycloaddition to afford four stereoisomers, **5-A** (*S-endo, S′-endo*),[11] **5-B** (*S-endo, S′-exo*), **5-C** (*S-exo, S′-endo*), and **5-D** (*S-exo, S′-exo*) as shown in Fig. 2. In these four isomers, **5-B** and **5-C** are enantiomers each other, and the two benzopyrylium-4-olate moieties of **5-B** (=**5-C**) are not equivalent. Therefore, the minor 2:1-adduct can be assigned to the structure **5-B**. On the other hand, both **5-A** and **5-D** have a symmetric structure having a C_2-axis through spiro-carbon bisecting both S–C–S and CO–C–CO planes. Because the two benzopyrylium-4-olate moieties are equivalent in **5-A** and **5-D**, the structural assignment for the major 2:1-adducts to **5-A** or **5-D** was not successful on the basis of the NMR data. Single crystal X-ray analysis of the major 2:1-adduct **5a-A** was therefore studied.

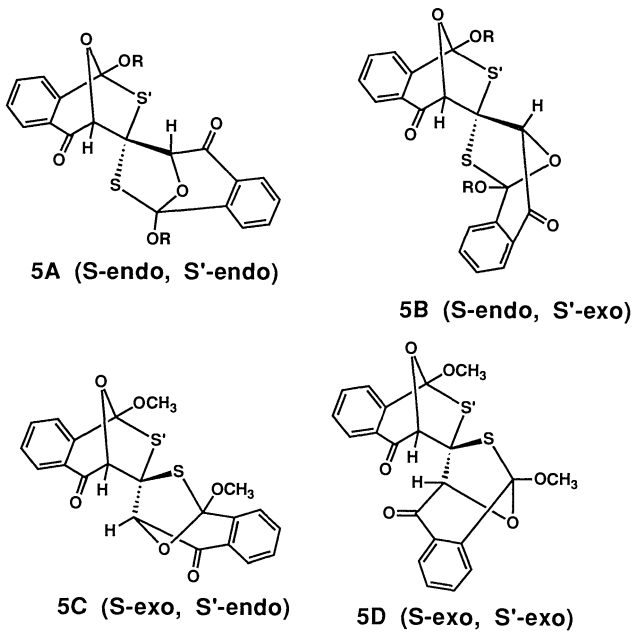

Fig. 2. Possible four structures of the 2:1-adduct **5**.

X-Ray Crystallography of the 2:1-Adduct 5a-A. The crystal data of **5a-A** are listed in Table 2 along with the experimental details. The ORTEP[12] drawing (see Fig. 3) shows that the major 2:1-adduct **5a-A** has the symmetric structure **5-A** (*S-endo, S′-endo*).

Inspection of the CPK model of **5-A** and **5-D** indicates that carbonyl groups of two benzopyrylium-

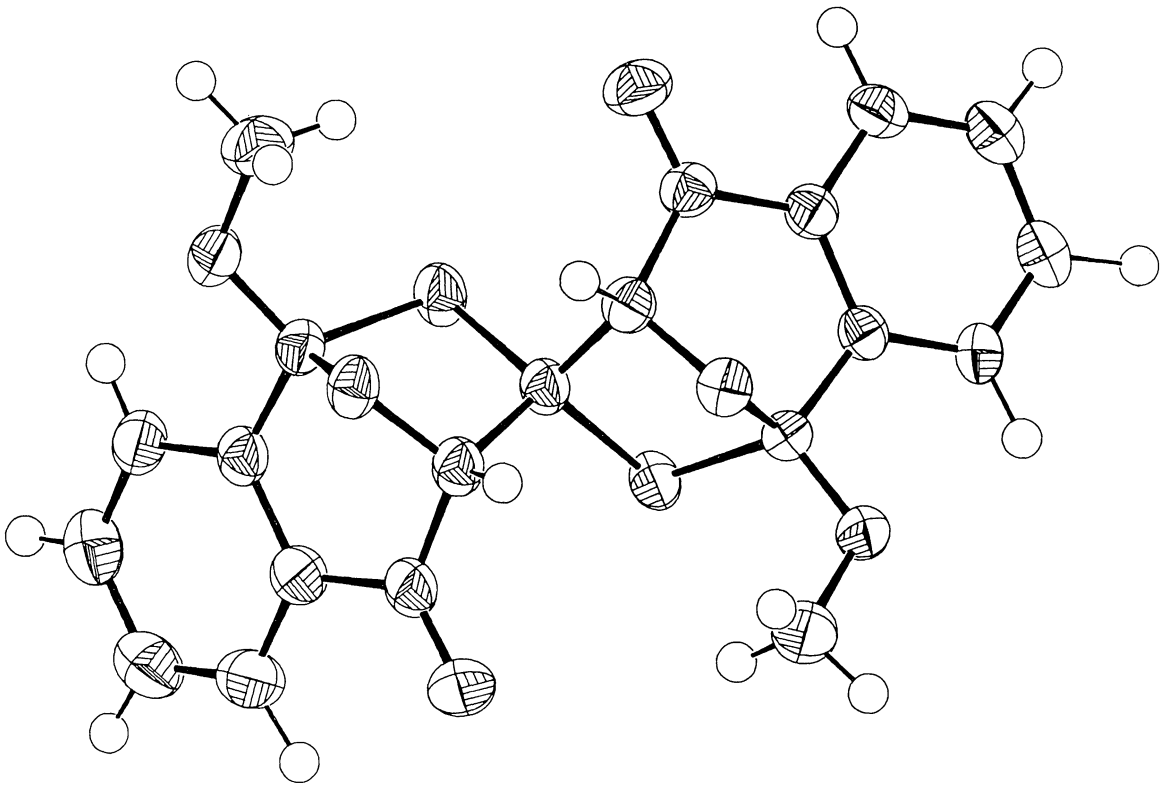

Fig. 3. ORTEP drawing of the 2:1-adduct **5a-A**.

Table 2. Crystal Data and Experimental Details of **5a-A**

Molecular formula	$C_{21}H_{16}O_6S_2$
Molecular weight	428.49
Crystal system	Triclinic
Space group	$P\bar{1}$
a	12.213(1) Å
b	11.846(1) Å
c	7.0403(2) Å
α	93.395(6)°
β	102.147(5)°
γ	109.536(7)°
V	929.1(1) Å^3
Z	2
D_m	1.550(2) Mg m^{-3}
D_x	1.532 Mg m^{-3}
μ (Cu $K\alpha$)	28.551 cm^{-1}
Scan method	ω–2θ
Scan speed in ω	4° min^{-1}
Scan width	(1.1+0.15 tan θ)°
Back ground	2×4 s
Number of reflections	2753
	2597 ($\|F_o\| \geqq 2\sigma(F_o)$)
R	0.044
Crystal size	0.3×0.2×0.2 mm
$2\theta_{max}$	120°

olate moieties of **5-D** come in the region of van der Waals radii of these groups, and that the approach to give **5-D** is hindered by the steric repulsion. On the other hand, isomers **5-A** and **5-B** (=**5-C**) are free from this sort of steric repulsion. The model of **5-B** is a little crowded than that of **5-A**. These facts will explain the product ratio of the reactions described above.

Experimental

Melting points were measured with a Yanagimoto Melting Point Apparatus and are not corrected. IR spectra were recorded on a Perkin-Elmer Model 983. ^{1}H NMR and ^{13}C NMR spectra were measured on a Varian EM 390 and a Brucker AM 360 spectrometers in a $CDCl_3$ solution using TMS as an internal standard.

Materials. Methyl *o*-(diazoacetyl)benzoate (**1a**) and isopropyl *o*-(diazoacetyl)benzoate (**1b**) were prepared by the procedure described in the previous paper.[5b] Benzene and carbon disulfide were purified by distillation over CaH_2 and P_2O_5, respectively.

General Procedure of the $Rh_2(OAc)_4$-Catalyzed Decomposition of 1 in the Presence of CS_2. A benzene solution (10 ml) of **1** (3.00 mmol) was added dropwise into a solution of $Rh_2(OAc)_4$ (1.6 mg, 3.62×10^{-3} mmol) in carbon disulfide (20 ml) at 46 °C under stirring in a N_2 atmosphere. After being refluxed for about 1 h, the reaction mixture was concentrated under reduced pressure, and the residue was separated by medium pressure column chromatography over silica gel using hexane–benzene as an eluent. Two types of 2:1-adducts **5-A** and **5-B** were obtained together with 1,3-oxathiole-2-thione derivative **6**.

Major 2:1-Adduct 5a-A: Yield 64.5% from **1a**; colorless crystals; mp 236.1—237.0 °C (from benzene–hexane); IR (KBr) 1697 (C=O), 1597, 1456, 1308, 1292, 1272, 1237, 1206, 1149, 1097, 1075, 1054, 1042, 1022, 968, 846, 756, 740, and

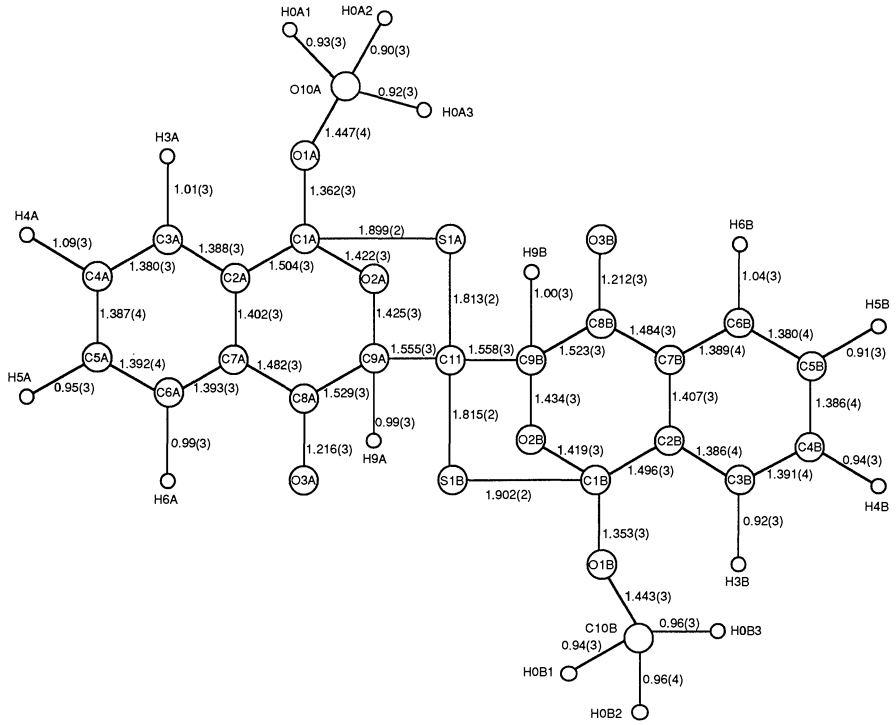

Fig. 4-a. Bond lengths of **5a-A**.

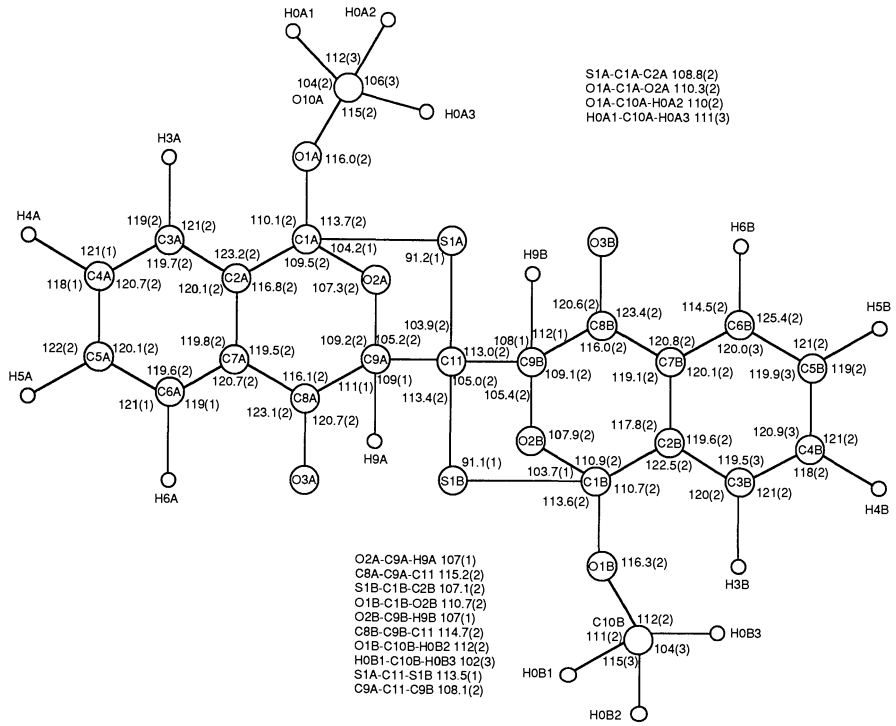

Fig. 4-b. Bond angles of **5a-A**.

656 cm^{-1}; MS (EI) 328 (1.4%, M^+), 396 (8.4), 176 (100), 133 (8), and 77 (10). Found: C, 58.93; H, 3.77%. Calcd for $C_{21}H_{16}O_6S_2$: C, 58.87; H, 3.76%.

Minor 2:1-Adduct 5a-B: Yield 10.3% from **1a**; colorless crystals; mp 200—202 °C (from benzene–hexane); IR (KBr) 2985, 2942, 1700 (C=O), 1598, 1455, 1435, 1318, 1291, 1267, 1242, 1202, 1146, 1085, 1058, 1021, 1009, 980, 962, 904, 849, 794, 765, 852, 711, and 655 cm^{-1}; MS (EI) 423 (3.4%, M^+), 396 (8.4), 176 (3), 163 (100), 133 (8), and 77 (8).

5-(*o*-Methoxycarbonylphenyl)-1,3-oxathiole-2-thione (6a):

Yield 6.3% from **1a**; pale yellow crystals; mp 120.1—121.0 °C (from benzene–hexane).[7]

Major 2:1-Adduct 5b-A: Yield 65.7% from **1b**; colorless crystals; mp 211.0—211.8 °C (from acetone); IR (KBr) 3070, 2977, 1700 (C=O), 1598, 1456, 1384, 1371, 1294, 1270, 1236, 1190, 1171, 1140, 1095, 1074, 1053, 998, 968, 914, 894, 885, 834, 807, 775, 758, 747, 688, and 653 cm^{-1}. MS (EI) 484 (3%, M^+), 452 (7), 424 (6), 382 (14), 367 (7), 349 (6), 323 (7), 294 (9), 252 (7), 234 (19), 191 (17), 149 (100), 133 (7), 111 (6), and 104 (8). Found: C, 61.87; H, 5.23%. Calcd for $C_{25}H_{24}O_6S_2$: C, 61.96; H, 4.99%.

Minor 2:1-Adduct 5b-B: Yield 8.8% from **1b**; colorless crystals; mp 210.8—211.2 °C (from benzene–hexane); IR (KBr) 3191, 3073, 2975, 1697 (C=O), 1598, 1457, 1383, 1371, 1292, 1269, 1243, 1191, 1171, 1141, 1111, 1099, 1079, 1056, 993, 926, 903, 854, 836, 792, 753, 720, 701, 669, and 653 cm^{-1}; MS (EI) 484 (8%, M^+), 452 (5), 424 (10), 382 (7), 377 (7), 349 (5), 294 (10), 251 (8), 234 (19), 191 (13), 162 (6), 149 (100), 133 (5), 111 (4), and 104 (11). Found: C, 62.16; H, 5.04%. Calcd for $C_{25}H_{24}O_6S_2$: C, 61.96; H, 4.99%.

5-(*o*-Isopropoxycarbonylphenyl)-1,3-oxathiole-2-thione (6b): Yield 8.8% from **1b**; yellow oil.[7]

X-Ray Crystallography of the 2:1-Adduct 5a-A. Single crystals of **5a-A** recrystallized from a mixed solvent of benzene–hexane were used for X-ray analysis. Intensity data were measured on a Rigaku four-circle diffractometer with Ni-filtered Cu $K\alpha(\lambda=1.5418$ Å) radiation. The reflections of 2752 with $|F_o|\geq 2\sigma(F_o)$ were used in the structure determination. The space group $P\bar{1}$ was confirmed by the statistical distribution of E values and a successful refinement of the structure.

Table 3. Atomic Positional and Thermal Parameters for the Non-Hydrogen Atoms of **5a-A**

Atom	x	y	z	B_{eq}/Å^2
S(1A)	0.87328(4)	0.26793(4)	0.38567(8)	3.18
S(1B)	0.63559(5)	0.18057(5)	0.49898(9)	4.00
O(1A)	0.9683(1)	0.2391(1)	0.0732(2)	3.81
O(2A)	0.7647(1)	0.1583(1)	0.0244(2)	3.11
O(3A)	0.5752(1)	−0.0769(1)	0.2076(3)	4.21
O(1B)	0.4266(1)	0.2271(1)	0.4372(2)	3.77
O(2B)	0.5483(1)	0.2938(1)	0.2372(2)	3.50
O(3B)	0.8233(2)	0.5226(2)	0.2867(3)	5.32
C(1A)	0.8776(2)	0.1791(2)	0.1555(3)	2.88
C(2A)	0.8870(2)	0.0602(2)	0.2033(3)	2.77
C(3A)	0.9934(2)	0.0372(2)	0.2296(3)	3.22
C(4A)	0.9944(2)	−0.0749(2)	0.2710(3)	3.69
C(5A)	0.8904(2)	−0.1651(2)	0.2875(4)	3.80
C(6A)	0.7840(2)	−0.1423(2)	0.2648(3)	3.51
C(7A)	0.7821(2)	−0.0293(2)	0.2231(3)	2.92
C(8A)	0.6693(2)	−0.0039(2)	0.1926(3)	3.00
C(9A)	0.6757(2)	0.1196(2)	0.1325(3)	3.05
C(10A)	0.9622(2)	0.3486(2)	−0.0017(5)	5.31
C(1B)	0.5419(2)	0.2783(2)	0.4271(3)	3.19
C(2B)	0.6022(2)	0.3963(2)	0.5600(3)	3.31
C(3B)	0.5657(2)	0.4219(2)	0.7261(4)	4.01
C(4B)	0.6279(2)	0.5325(2)	0.8454(4)	4.81
C(5B)	0.7263(2)	0.6168(2)	0.8022(4)	4.78
C(6B)	0.7626(2)	0.5923(2)	0.6364(4)	4.37
C(7B)	0.7016(2)	0.4823(2)	0.5151(3)	3.54
C(8B)	0.7419(2)	0.4521(2)	0.3403(4)	3.66
C(9B)	0.6715(2)	0.3270(2)	0.2242(3)	3.38
C(10B)	0.3571(2)	0.1141(2)	0.3106(4)	4.66
C(11)	0.7117(2)	0.2239(2)	0.3046(3)	3.05

$B_{eq}=(4/3)\{a^2B_{11}+b^2B_{22}+c^2B_{33}+ab\cos\gamma\,(B_{12}/2)+ac\cos\beta(B_{13}/2)+bc\cos\alpha\,(B_{23}/2)\}$.

The crystal structure was determined by direct methods with the program of MULTAN 80.[12] The E-map computed with the phase set of the highest combined figure of merit (2.864) revealed the positions of all the non-hydrogen atoms. The hydrogen atoms were located on a difference map and their positional parameters were refined together with isotropic thermal parameters, while the other atoms were refined anisotropically by block-diagonal least-squares. The final R value was 0.044. The function minimized was $\sum w(|F_o|-k|F_c|)^2$ with the following weighting scheme: $w=1/(\sigma^2(F_o)+0.0476|F_o|+0.0041|F_o|^2)$.

All the atomic scattering factors were taken from the "International Tables for X-Ray Crystallography".[14] The computations were carried out with "The Universal Crystallographic Computing System-Osaka"[15] on an ACOS-S930 computer at the Research Center for Protein Engineering, Institute for Protein Research, Osaka University. Table 3 lists the final atomic and thermal parameters with their estimated standard deviations. The bond distances and angles are given in Fig. 4.[16]

The authors are grateful to Mr. Yoshio Takai, Institute of Scientific and Industrial Research, Osaka University for the measurement of ^{13}C NMR spectra, and to Mr. Hiroshi Moriguchi, Faculty of Engineering, Osaka University for obtaining mass spectra.

References

1) a) M. Takebayashi, T. Ibata, and K. Ueda, *Bull. Chem. Soc. Jpn.*, **43**, 1500 (1970); b) K. Ueda, T. Ibata, and M. Takebayashi, *Bull. Chem. Soc. Jpn.*, **45**, 2779 (1972).

2) R. Huisgen, *Angew. Chem., Int. Ed. Engl.*, **16**, 572 (1977); M. Bekhazi and J. Warkentin, *J. Am. Chem. Soc.*, **105**, 1289 (1983); A. Gillon, D. Ovadia, M. Kapon, and S. Bien, *Tetrahedron*, **38**, 1477 (1982); M. E. Maier and K. Evertz, *Tetrahedron Lett.*, **29**, 1677 (1988); A. Padwa and D. C. Dean, *J. Org. Chem.*, **55**, 406 (1990) and references cited therein.

3) T. Ibata and K. Jitsuhiro, *Bull. Chem. Soc. Jpn.*, **54**, 240 (1981).

4) T. Ibata and K. Jitsuhiro, *Bull. Chem. Soc. Jpn.*, **52**, 3582 (1979).

5) a) T. Ibata and J. Toyoda, *Chem. Lett.*, **1983**, 1453; b) T. Ibata and J. Toyoda, *Bull. Chem. Soc. Jpn.*, **58**, 1787 (1985); c) T. Ibata and J. Toyoda, *Bull. Chem. Soc. Jpn.*, **59**, 2489 (1986).

6) T. Ibata and H. Nakano, *Chem. Express*, **1989**, 93.

7) T. Ibata and H. Nakano, *Bull. Chem. Soc. Jpn.*, **63**, 3096 (1990).

8) J. Toyoda, T. Ibata, H. Tamura, and K. Ogawa, *Bull. Chem. Soc. Jpn.*, **58**, 2212 (1985).

9) K. N. Houk, J. Sims, C. R. Watts, and L. J. Luskus, *J. Am. Chem. Soc.*, **95**, 7301 (1973).

10) W. Thiel, *J. Am. Chem. Soc.*, **103**, 1413 (1981); W. Thiel, QCPE #438; T. Takagi, A. Tanaka, S. Matsuo, S. Maeda, H. Maesaki, M. Tani, and Y. Sasaki, *Bulletin of Computation Center, Osaka University*, **16**, 83 (1987).

11) The notation (S-*endo*, S′-*endo*) means that the sulfur atoms S and S′ bind to *endo* directions to each 1,3-

oxathiolane in the spiro ring system of **5**.

12) C. K. Johnson, ORTEP-II: A FORTRAN Thermal-Ellipsoid Plot Program for Crystal Structure Illustrations, ORNL-5138, March 1976, Oak Ridge National Laboratory.

13) P. Main, S. J. Fiske, S. E. Hull, L. Lessinger, G. Germain, J-P. Declercq, and M. M. Woolfson, "MULTAN 80. A system of Computer Programs for the Automatic Solution of Crystal Structures from X-Ray Diffraction Data," Univs. of York, England and Louvain, Belgium (1980).

14) "International Tables for X-Ray Crystallography," Kynoch Press, Birmingham (1974), Vol. IV, p. 71.

15) T. Ashida, "The Universal Crystallographic Computing System-Osaka," The Computation Center, Osaka University (1979), HBLS V, p. 53 and DAPH, p. 61.

16) The tables of the observed and calculated structure factors, the best planes, anisotropic thermal parameters for non-H atoms, and atomic parameters of hydrogen atoms are deposited as Document No. 9104 at the Office of the Editor of Bull. Chem. Soc. Jpn.

Strong van der Waals Interactions in Water. Molecular Complexes of Porphyrins and Quinones in Organic and Aqueous Media

Koji KANO,* Tadashi HAYAKAWA, and Shizunobu HASHIMOTO
Department of Applied Chemistry, Faculty of Engineering, Doshisha University, Kamikyo-ku, Kyoto 602
(Received October 6, 1990)

The stability of the molecular complexes between 5,10,15,20-tetraarylporphyrins and quinones in organic solvents has been compared with that in water. 5,10,15,20-Tetrakis(mono-substituted phenyl)porphines (RTPPs) hardly form molecular complexes with *p*-benzoquinone (BQ), 2,3,5,6-tetramethyl-*p*-benzoquinone (DQ), and 2,3,5,6-tetrachloro-*p*-benzoquinone (CQ) in dichloromethane ($K<10$ mol^{-1} dm^3). In contrast, the stability constants ($K>60$ mol^{-1} dm^3) for the molecular complexes of cationic porphyrins (TMPyP and TAPP) with BQ in water are much larger than those in methanol. The thermodynamic parameters clearly indicate that complexation in water is an enthalpically favorable process, suggesting that the van der Waals interactions are the main binding forces and that hydrophobic interaction does not play an important role in complex formation in water. The larger stability of the molecular complexes in water can be interpreted in terms of the nature of water, as demonstrated by Smithrud and Diederich (D. B. Smithrud and F. Diederich, *J. Am. Chem. Soc.*, **112**, 339 (1990)). The microscopically hydrophobic porphyrin ring many hardly be hydrated and interact with BQ through the van der Waals interactions without an extensive dehydration process. The water molecules bound to BQ should be released upon complexation, and the released water molecules may be incorporated tightly into the hydrogen-bonding networks of water. Such complexation in water seems to be an enthalpically favorable process.

We have demonstrated that anionic and cationic porphyrins in water tend to form molecular complexes with guest aromatics throught van der Waals interactions.[1-5] Enthalpic (ΔH) and entropic changes (ΔS) in the complexation of water-soluble porphyrins are summarized in Table 1. In all of the cases shown in Table 1, the complexation of water-soluble porphyrins with guest aromatics is an enthalpically favorable process. This suggests that the main binding forces for molecular association in water are the van der Waals interactions. During these studies, we came to recognize that the association between anionic and/or cationic porphyrins and various aromatics, as well as the porphyrin dimerization,[5-7] is strictly suppressed in organic solvents (the results have not been published except for dimerization of a cationic porphyrin[6]). Why are the van der Waals interactions so strong in water? Answering this question is the aim of the present study.

Table 1. Enthalpic (ΔH) and Entropic Changes (ΔS) for Molecular Complex Formation of 5-Phenyl-10,15,20-tris(4-sulfophenyl)porphine Trisodium Salt ($TPPS_3$) and TMPyP in Water

Porphyrin	Guest[a]	$-\Delta H$/kJ mol^{-1}	$-\Delta S$/J mol^{-1} K^{-1}	Ref
$TPPS_3$	AQαS	10.5	−19.1	2
$TPPS_3$	AQβS	17.7	−11.0	2
$TPPS_3$	AQDS	34.9	53.1	2
$TPPS_3$	PyS	18.9	0.2	2
$TPPS_3$	AnS	12.7	−13.0	2
$TPPS_3$	MV	22.3	19.3	2
TMPyP	PFl	29.3	34.9	3
TMPyP	PNP	46.1	99.9	4

a) AQαS; sodium 9,10-anthraquinone-1-sulfonate, AQβS; sodium 9,10-anthraquinone-2-sulfonate, AQDS; disodium 9,10-anthraquinone-2,6-disulfonate, PyS; sodium 1-pyrenesulfonate, AnS; sodium 2-anthracenesulfonate, MV; 1,1′-dimethyl-4,4′-dipyridinium dichloride, PFl; 2,6-diaminoacridinium hydrogensulfate, PNP; *p*-nitrophenol.

At first, in order to known the extent of the van der Waals interactions in an organic solvent, we investigated the complex formation of 5,10,15,20-tetrakis(mono-substituted phenyl)porphines (RTPPs) with quinones, such as *p*-benzoquinone (BQ), 2,3,5,6-tetramethyl-*p*-benzoquinone (DQ), and 2,3,5,6-tetrachloro-*p*-benzoquinone (CQ), in dichloromethane (CH_2Cl_2). The quinones were chosen as guests because ground-state complexes can be detected easily by measuring the static fluorescence quenching of prophyrins by quinones. The substituents (R) attached to the phenyl groups at the meso positions seem to alter the electron density of the porphyrin ring. It is expected, therefore, that the substituent effects on the formation of molecular complexes with quinones through the van der Waals interactions can be studied. We also presumed that a charge-transfer interaction may act as an cooperative force for forming stable molecular complexes, since porphyrin and quinone can behave as an electron donor and acceptor, respectively. Moreover, some tetrakis(*o*-substituted phenyl)porphines have a possibility to bind with quinones through hydrogen bonding.

Second, the stability of the molecular complexes of cationic porphyrins, such as 5,10,15,20-tetrakis(1-methyl-4-pyridinio)porphine tetrachloride (TMPyP) and 5,10,15,20-tetrakis[4-(trimethylammonio)phenyl]-porphine tetrachloride (TAPP), and BQ in methanol was compared with that in water. Although the experiments were limited due to the solubilities of

porphyrins and quinones in organic and/or aqueous media, we expected to obtain information about the specialty of water as a solvent for molecular complex formation through van der Waals interactions.

Experimental

RTPPs (R=*o*-, *m*-, *p*-OH, *o*-, *m*-, *p*-CH_3, *o*-, *m*-, *p*-OCH_3, *o*-NH_2, *o*-$NHCOCH_3$, *o*-, *m*-, *p*-Cl, *o*-Br, *o*-, *p*-NO_2, *p*-$COOCH_3$, *p*-CN) were prepared according to the procedures described in the literatures.[8] The TMPyP[7] and TAPP[5] employed were previously described. BQ, DQ, CQ,

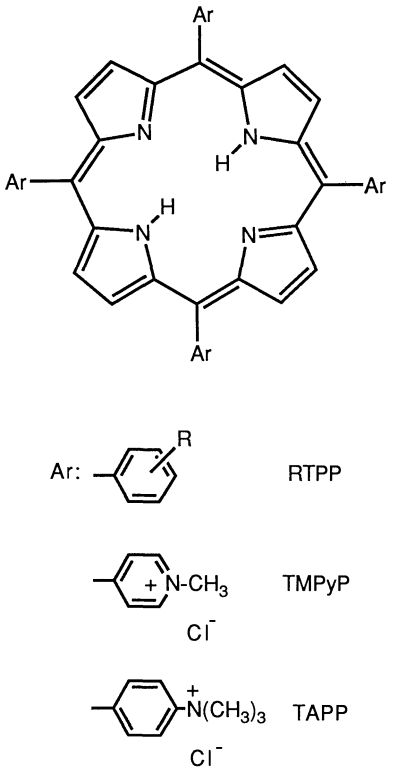

and 1,4-naphthoquinone (NQ) were purchased from Nacalai Tesque (Kyoto) and purified by sublimation in vacuo.

The absorption and fluorescence spectra were measured on a Shimadzu UV-2100 spectrophotometer and a Hitachi 650-60 spectrofluorometer (uncorrected, band width=5 nm), respectively, whose cell holders were thermostated. The 400 MHz ^{1}H NMR spectra in $CDCl_3$ were recorded with a JEOL GX-400 spectrometer at 23±0.5 °C using TMS as an internal standard. The fluorescence lifetimes of RTPPs were determined by an Ortec-PRA single-photon counting apparatus, as described previously.[7] The cyclic voltammograms (CV) of RTPPs were taken in CH_2Cl_2 containing tetrapropylammonium perchlorate as a supporting electrolyte at 10 °C with a CV-1B voltammograph manufactured by Bioanalytical Systems. Platinum and silver-silver chloride electrodes were used as the working and reference electrodes, respectively. All samples containing both porphyrin and quinone were prohibited from exposure to room light.

Results and Discussion

Substituent Effects on ^{1}H NMR and CV of RTPPs. The complexation of porphyrin with quinone through van der Waals and/or charge-transfer interactions should be affected by the electron density of the porphyrin ring. Worthington et al.[9] have determined the reduction potentials ($E_{1/2}^r$) of various RTPPs in DMSO and found that the electron density on the porphyrin ring is slightly affected by the substituent attached to the phenyl group at the meso position.

We measured ^{1}H NMR in $CDCl_3$ and the oxidation potentials ($E_{1/2}^o$) in CH_2Cl_2 in order to determine the effects of the substituents (R) on the electron density of the porphyrin ring. The chemical shifts of the β-protons of pyrrole, as well as of the N–H protons of RTPPs, are expected to be the measures of the π-electron density on the porphyrin ring. The chemical shifts of the β-protons (δ_{CH}) and the N–H protons (δ_{NH}) and the first ($E_{1/2}^o(1)$) and second oxidation potentials ($E_{1/2}^o(2)$) of RTPPs are listed in Table 2.

Although δ_{CH} tends to shift to a lower magnetic field upon increasing the electron-donating ability of R, no clear relationship has been found between δ_{CH} as well as δ_{NH} and Hammett's σ-values. Figure 1 shows a plot of $E_{1/2}^o(1)$ vs. Hammett's σ-values. A linear relationship was found ($E_{1/2}^o(1)=0.38\sigma+1.05$, $R=0.980$), suggesting that the substituent at the phenyl group of RTPP regularly alters the electron density on the porphyrin ring.

Molecular Complexes of RTPPs with Quinones in Organic Solvents. It has been well-known that the fluorescent states of the porphyrins and their metal complexes are quenched by quinones and that an electron transfer from photoexcited porphyrin to quinone can be accounted for by a quenching mechanism.[10] For dynamic fluorescence quenching, a

Table 2. Chemical Shifts (δ_{CH}, δ_{NH}) and Oxidation Potentials ($E_{1/2}^o$) of RTPPs

R	δ_{CH}/ppm	δ_{NH}/ppm	$E_{1/2}^o(1)$/V	$E_{1/2}^o(2)$/V
H	8.85	−2.78	1.05	1.26
o-OH			0.85	1.29
m-OH	8.91	−2.99	0.83	1.28
p-OH	8.89	−2.89	0.90	1.15
o-CH_3	8.66	−2.68	1.07	1.40
m-CH_3	8.85	−2.79	1.03	1.24
p-CH_3	8.85	−2.78	1.05	1.30
o-OCH_3	8.72	−2.63	1.06	1.20
m-OCH_3	8.89	−2.80	1.07	1.28
p-OCH_3	8.86	−2.76	0.92	1.07
o-NH_2	8.90	−2.73	1.03	1.22
o-Cl	8.69	−2.67	1.20	
m-Cl	8.87	−2.89	1.19	
p-Cl	8.84	−2.87	1.14	1.28
o-Br	8.67	−2.63		
p-CN	8.80	−2.83	1.30	
o-NO_2	8.62	−2.57		
m-NO_2	8.82	−2.81		

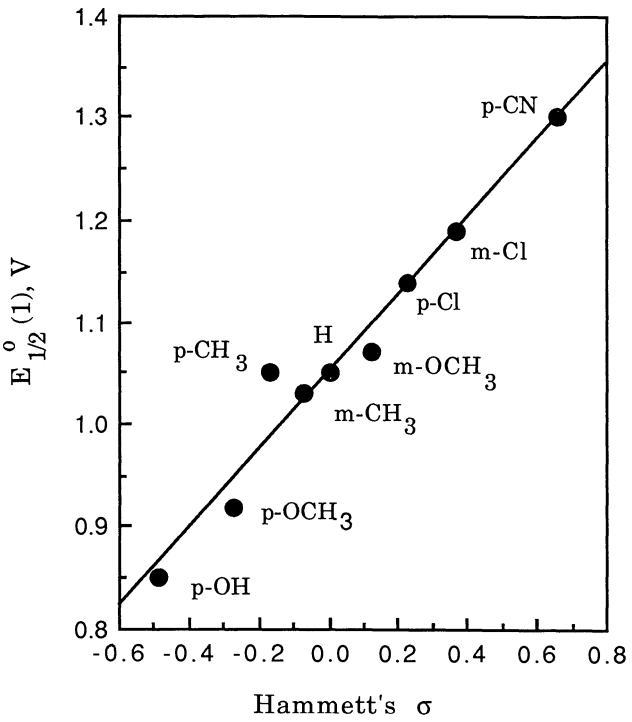

Fig. 1. Plot of $E_{1/2}^{o}$ (1) of RTPPs in CH_2Cl_2 vs. Hammett's σ.

Stern–Volmer linear relationship can be applied:

$$I_0/I = \tau_0/\tau = 1 + K_{SV}[Q] = 1 + k_q\tau_0[Q], \quad (1)$$

where I_0 and I are the fluorescence intensities in the absence and the presence of a quencher (Q), respectively; K_{SV} is the Stern–Volmer constant, k_q is the rate constant for fluorescence quenching, and τ_0 and τ are the fluorescence lifetimes in the absence and the presence of Q, respectively. If static quenching due to the formation of nonfluorescent ground-state complex competes with a dynamic type, the Stern–Volmer equation is modified as[11]

$$I_0/I = (1 + K(\varepsilon_2/\varepsilon_1)[Q])(1 + K_{SV}^{\tau}[Q]), \quad (2)$$

where K is the binding constant of the ground-state complex, K_{SV}^{τ} is the Stern–Volmer constant for dynamic quenching, and ε_1 and ε_2 are the extinction coefficients of fluorophore and complex at the excitation wavelength, respectively. In the case where Eq. 2 can be applied, the absorption spectral change should be observed. When the fluorophore is excited at an isosbestic point, Eq. 2 can be simplified as

$$I_0/I = (1 + K[Q])(1 + K_{SV}^{\tau}[Q]). \quad (3)$$

The fluorescence quenching technique is very convenient for determining molecular complex formation as well as the binding constant, K, when a Benesi–Hildebrand plot[12] for an absorption spectral change cannot be applied for reasons such as a small change in the optical density upon complexation.

Table 3. Fluorescence Quenching of RTPPs by DQ, BQ, and CQ in Dichloromethane at 10 °C

R	τ_0/ns	$10^{-9}\,k_q$/mol^{-1} dm^3 s^{-1}		
		DQ	BQ	CQ
H	7.1	5.1	16.0	31.7
o-NH_2	3.9	6.7	30.8	45.1
o-OH	5.4	10.0	26.0	25.9
m-OH	5.1	13.0	31.0	35.3
p-OH	9.0	8.3	22.0	31.0
o-CH_3	5.0	5.0	23.0	36.0
m-CH_3	6.5	5.8	17.0	28.6
p-CH_3	4.1	8.5	26.0	44.4
o-Cl	3.3	6.1	20.0	40.6
m-Cl	4.4	4.2	15.0	29.1
p-Cl	2.9	8.4	23.0	46.9
o-OCH_3	7.1	3.2	13.0	25.4
m-OCH_3	7.5	3.2	14.0	24.8
p-OCH_3	6.8	4.9	16.0	27.6
p-NO_2	5.4	0.6	8.7	26.3
p-$COOCH_3$	5.2	3.7	14.0	28.8
p-CN	5.2	2.5	11.0	36.2

We initially sought RTPP–quinone pairs which form molecular complexes in an organic solvent by using the 17 RTPPs listed in Table 3 as well as BQ, DQ, and CQ. Dichloromethane (CH_2Cl_2) was used as an organic solvent. The $E_{1/2}^{r}$(1) of DQ, BQ, and CQ determined using a cyclic voltammograph are −1.08, −0.72, and −0.10 V, respectively, at 10 °C. Contrary to expectations, linear Stern–Volmer plots were obtained for all cases when the fluorescence emissions from RTPPs (4×10^{-5} mol dm^{-3}) were quenched by the quinones at concentrations below 1×10^{-2} mol dm^{-3}. This indicates that only dynamic fluorescene quenching takes place and that no appreciable amounts of the ground-state complexes of RTPPs with quinones are formed at the concentration range of the quinone below 1×10^{-2} mol dm^{-3}. The results of fluorescence quenching are shown in Table 3. Of course, no absorption spectral change was measured under the same conditions as those for fluorescence quenching. In the cases of DQ and BQ, the k_q value tends to increase with decreasing $E_{1/2}^{o}$(1) of RTPP. This should be ascribed to fluorescence quenching via an electron transfer from photoexcited RTPP to the quinone. Meanwhile, no correlation was observed between k_q and $E_{1/2}^{o}$(1) in fluorescence quenching by CQ. This result can be interpreted as meaning that the fluorescence quenching by CQ proceeds at a diffusion-controlled rate because of the large electron affinity of this quinone.

At BQ concentrations above 1×10^{-2} mol dm^{-3}, however, the absorption spectra of the several RTPPs regularly changed upon addition of BQ. An example is shown in Fig. 2, which shows the absorption

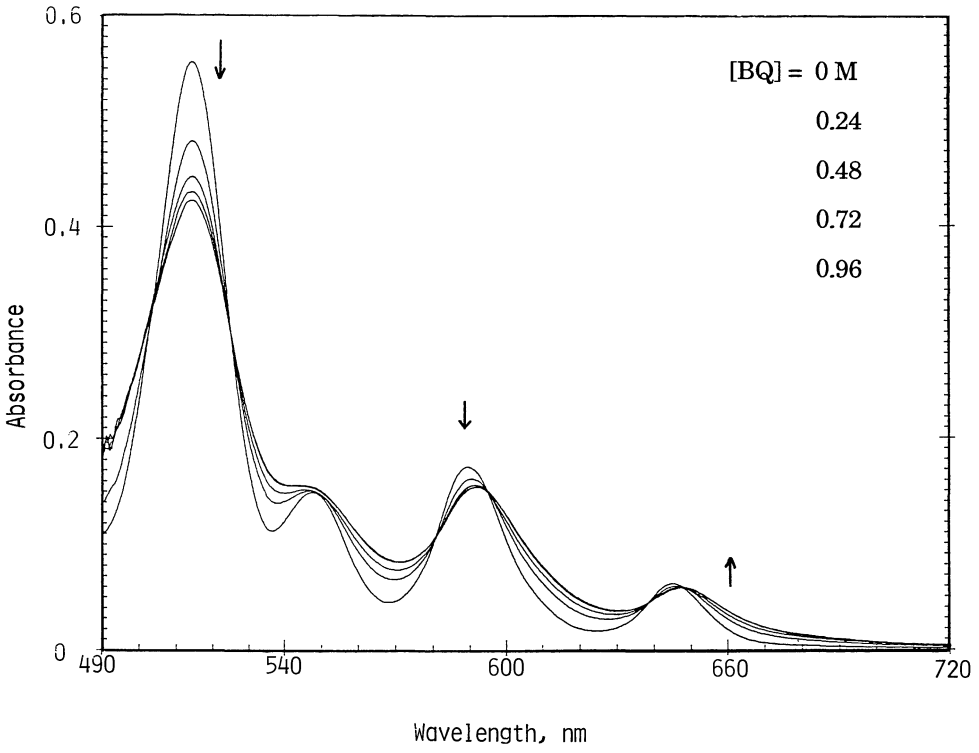

Fig. 2. Absorption spectral change of *o*-$NHCOCH_3TPP$ (4×10^{-5} mol dm^{-3}) in CH_2Cl_2 upon addition of BQ at 7 °C.

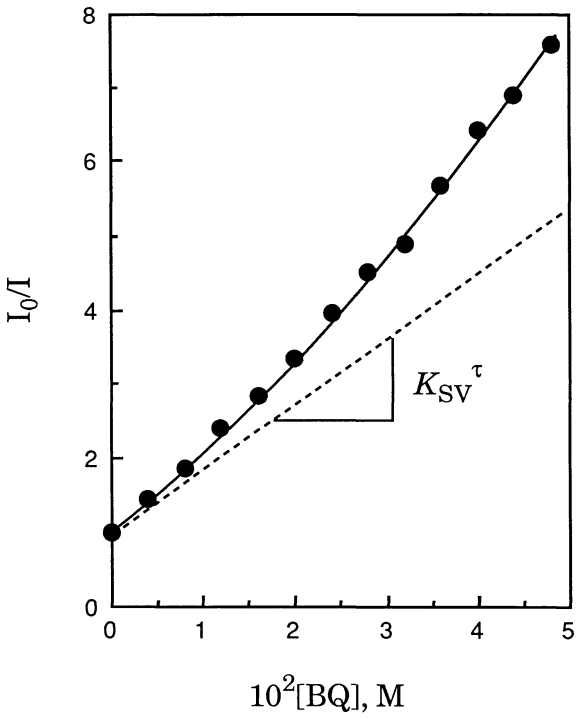

Fig. 3. Stern-Volmer plot for the fluorescence quenching of *o*-$NHCOCH_3TPP$ (4×10^{-5} mol dm^{-3}) by BQ in CH_2Cl_2 at 7 °C. The porphyrin was excited at 581 nm and the fluorescence intensities were followed at 652 nm.

Table 4. Binding Constants (K) for Complexation of RTPPs with BQ in Organic Solvents

R	Solvent	Temperature/°C	K/mol^{-1} dm^3
H	CH_2Cl_2	15	0.6
o-$NHCOCH_3$	CH_2Cl_2	7	7.8
o-$NHCOCH_3$	CH_3CN	15	4.1
o-OH	CH_3CN	15	3.2
m-OH	CH_3CN	15	2.4
o-NH_2	CH_3CN	15	0.02

spectral change of *o*-$NHCOCH_3TPP$ in CH_2Cl_2 upon addition BQ at 7 °C. The spectra are of the differential type obtained by substracting the BQ contribution. The Stern-Volmer plot for the fluorescence quenching deviates upward from a straight line, as predicted by Eq. 2 (Fig. 3). These results clearly indicate the formation of a ground-state complex of *o*-$NHCOCH_3$-TPP and BQ. The binding constant, K, determined by a Benesi-Hildebrand plot for the absorption spectral change is 7.8 mol^{-1} dm^3 at 7 °C (Table 4). HTPP (5,10,15,20-tetraphenylporphine) also shows a similar behavior (K=0.6 mol^{-1} dm^3 at 15 °C). A molecular complex with a very small K has also been reported for the *p*-CH_3TPP-BQ system in acetone (K=0.5 mol^{-1} dm^3 at 25 °C).[13]

In order to evaluate the contribution of a charge-transfer interaction to complexation, CH_2Cl_2 was replaced by an aprotic polar solvent, acetonitrile. The

results obtained for *o*-$NHCOCH_3$TPP, *o*-OHTPP, and *m*-OHTPP are shown in Table 4. Since the *K* value (4.1 mol^{-1} dm^3 at 15 °C) for the *o*-$NHCOCH_3$-TPP–BQ system in acetonitrile is almost the same as that in CH_2Cl_2, a charge-transfer interaction may not play an important role in complexation. *o*-$NHCOCH_3$-TPP, *o*-OHTPP, and *o*-NH_2TPP were used to study the possibility for the formation of hydrogen-bonded complexes between these porphyrins and BQ. However, no appreciable difference was observed for the *K* values between these ortho-substituted porphyrins and HTPP and *m*-OHTPP. The *K* value for the *o*-OHTPP–BQ system was too small to be determined accurately. It, therefore, seems that the hydrogen bonding as well as the charge-transfer interaction scarcely participate in the complex formation of organic solvents. Therefore, it may be reasonable to assume that the main binding forces for the unstable complexes of RTPPs with quinones are van der Waals interactions.

Molecular Complexes of TMPyP and TAPP with BQ in Organic and Aqueous Media. In spite of the electrostatic repulsion, both cationic porphyrins, TMPyP and TAPP, associate with a cationic dye, 2,6-diaminoacridinium hydrogensulfate (PFl), in water to form relatively stable molecular complexes (*K* for TMPyP=2161 mol^{-1} dm^3 at 25 °C, *K* for TAPP=800 mol^{-1} dm^3 at room temperature).[3,5] *p*-Nitrophenol (PNP) can also act as a guest molecule in complexation with TMPyP in water (K=550 mol^{-1} dm^3 at 25 °C).[4] On the basis of the thermodynamic parameters determined for these systems (see Table 1), we have claimed that the van der Waals interactions are the main binding forces.[4,5]

We initially expected that relatively stable molecular complexes of these cationic porphyrins should be formed in organic solvents, as long as van der Waals interactions are the binding forces. We then compared the stability of the TMPyP- and TAPP–BQ complexes in methanol and water. The determined *K* values are listed in Table 5. The *K* values in methanol were evaluated from Benesi–Hildebrand plots for the absorption spectral changes, and those in water were determined from data regarding fluorescence quenching using Eq. 3. We confirmed that both methods can provide almost the same *K* values. For example, the *K* values evaluated from the Benesi–Hildebrand plots for the TMPyP–BQ and TAPP–BQ systems at 20 °C are 79 and 151 mol^{-1} dm^3, respectively, and are in good agreement with the *K* values determined from the fluorescence quenching (see Table 5).

Table 5. Binding Constants (*K*) for Complexation of TMPyP and TAPP with BQ and NQ in Methanol and Water

Porphyrin	Quinone	Solvent	Temperature/°C	K/mol^{-1} dm^3
TMPyP	BQ	CH_3OH	20	4.0
TAPP	BQ	CH_3OH	20	2.7
TMPyP	NQ	CH_3OH	20	7.6
TAPP	NQ	CH_3OH	20	13.0
TMPyP	BQ	H_2O	20	73
TMPyP	BQ	H_2O	25	70
TMPyP	BQ	H_2O	30	67
TMPyP	BQ	H_2O	35	63
TAPP	BQ	H_2O	20	147
TAPP	BQ	H_2O	25	85
TAPP	BQ	H_2O	30	84
TAPP	BQ	H_2O	35	80

As Table 5 indicates, complexes formed in water are much more stable than those formed in methanol. The *K* values in methanol are comparable to those of the RTPP–BQ systems in CH_2Cl_2 or acetonitrile. NQ, which has a more expanded π-conjugated system compared with BQ, also shows small *K* values. From these results it can be concluded that the cationic porphyrins, as well as RTPPs, cannot form stable molecular complexes with quinones in organic solvents through van der Waals interactions. Meanwhile, the *K* values in water are much larger than those in methanol. The van't Hoff plots for the data shown in Table 5 provide ΔH and ΔS for complexation of TMPyP and TAPP with BQ in water, ΔH and ΔS being −28 kJ mol^{-1} and −56 J mol^{-1} deg^{-1}, respectively, for TMPyP and −34 kJ mol^{-1} and −73 J mol^{-1} deg^{-1}, respectively, for TAPP. It is clear that the complex formation of these cationic porphyrins with BQ in water is the enthalpically favorable process. This finding is the same as that obtained for other systems investigated previously (see Table 1). If we define that complexation through hydrophobic interaction is favorably dominated by an entropy term, it can be concluded that the hydrophobic interaction does not contribute to the complexation of these cationic porphyrins with BQ in water. The charge-transfer, hydrophobic, and, in some special cases, hydrogen-bonding interactions can be excluded from the main binding forces. The van der Waals interactions may mainly participate in the complexation of cationic porphyrins with BQ in water. However, in order to conclude that the van der Waals interactions are the main binding forces, we have to explain the reason why these interactions are so strong in water compared with in organic solvents.

Quite recently, Smithrud and Diederich[14] reported the solvent effects on complex formation of a macrocyclic cyclophane host and a pyrene guest and found a linear relationship between $-\Delta G°$ for complexation and Dimroth's $E_T(30)$ values of the solvents. They explained the largest binding constant in water in terms of such water properties as low molecular polarizability and a high cohesive interaction that promote the strongest van der Waals interactions between an apolar host and an apolar guest in water. A similar explanation may be possible

Table 6. Average Molecular Polarizabilities (α)

Molecule	α (calcd)/Å^3	α (exp)/Å^3	Ref
H_2O	1.47	1.45	15
CH_3OH	3.28	3.26	15
CH_3CN	4.86		This work
CH_2Cl_2	6.38	6.48	15
HTPP	74.9		This work
$TMPyP^{4+}$[a)]	75.4		This work
BQ	10.7		This work

a) The α value was calculated for the cation ($TMPyP^{4+}$) and no contribution of Cl^- was considered.

for our systems.

The London dispersion force, as well as the dipole-induced dipole interaction, becomes remarkable when host and/or guest molecules have large molecular polarizabilities. The average molecular polarizability, α, can be calculated using the following equation:[15)]

$$\alpha = (4/N)(\sum \tau_A)^2 \ (\text{Å}^3), \tag{5}$$

where N is the number of electrons in the molecule and τ_A is the atomic hybrid components of α for each atom in a particular hybrid configuration. The calculated polarizabilities of the molecules which were used in this study are summarized in Table 6. The molecular polarizability of H_2O is lowest amongst the solvent molecules in Table 6, which means that the van der Waals interactions between apolar solute and solvent molecules are weakest in water. Both TMPyP and TAPP are regarded as being amphiphilic molecules and the hydrophobic porphyrin rings of these porphyrins may not strongly interact with water molecules through van der Waals interactions, while the hydrophilic peripheries are extensively hydrated through an ion–dipole interaction. The association of the cationic porphyrins and BQ in water, therefore, may be a process which does not require extensive dehydration from the porphyrin rings. Since TMPyP and TAPP have large molecular polarizabilities, BQ is also polarizable and the carbonyl groups of BQ have dipoles, molecular association between these hosts and the guest seems to occur through dipole-induced dipole and London dispersion interactions in water as an enthalpically favorable process.

Meanwhile, BQ is hydrated through both hydrogen bonding and dipole–dipole interactions. Dehydration from the BQ molecules, therefore, needs to form a complex with porphyrin as an endothermic process. The water molecules released from BQ, however, may be incorporated tightly into hydrogen-bonding networks of water as an exothermic process. This strong cohesive interaction of water may compensate for any energetic disadvantage due to dehydration. Sinanoglu[18)] has developed a theory regarding solvophobic interaction. In this theory an apolar solute molecule is regarded as being a cavity. The dissolution of a solute molecule in a solvent causes an increase in the surface area of the solvent, which requires energy to work against the strong cohesive interaction of water. The association of two solute molecules, therefore, is energetically favorable since the surface area of the solvent is reduced upon complexation. Margalit and Rotenberg[19)] have applied this theory to explain the dimerization of porphyrin in water. The strong solvophobic interaction in water is ascribed to a strong cohesive interaction of this solvent, and may also participate in the complexation of the cationic porphyrins with BQ in water.

The large stability of the complexes of TMPyP with PF1 and PNP[3–5)] as well as of the complexes of $TPPS_3$ with various aromatics[1,2)] in water may be interpreted in the same manner. We have claimed that TMPyP dimerizes in water, even at very low concentrations ([TMPyP]$>2\times10^{-7}$ mol dm^{-3}).[3–7)] Our dimer model for TMPyP contradicts the conclusion presented by Hambright and Fleischer[16)] as well as Pasternack and his co-workers.[17)] The novel dimerization of TMPyP can also be explained by strong van der Waals interactions which are ascribed to the nature of water, such as the low molecular polarizability and the strong cohesive interaction of water.

We believe that the stoichiometries of the complexes of TMPyP and TAPP with BQ are 2:1 and 1:1, respectively, in water while the 1:1 complexes of both porphyrins are formed in methanol. In previous papers we confirmed that TMPyP and TAPP exist as a dimer and monomer, respectively, in water under the present conditions ([porphyrin]$=4\times10^{-5}$ mol dm^{-3})[5)] and that the TMPyP dimer associates with PF1.[3)] Although we attempted to obtain a correlation between $\Delta G°$ for the complexation of TMPyP with BQ and $E_T(30)$ in aqueous methanol, we did not succeed because of the partial dissociation of the TMPyP dimer to the monomer in aqueous methanol.

This work was supported by Grant-in-Aid for Science Research on Priority Areas, "Multiplex Organic Systems" No. 01649006, from the Ministry of Education, Science and Culture.

References

1) K. Kano, T. Sato, S. Yamada, and T. Ogawa, *J. Phys. Chem.*, **87**, 566 (1983).

2) T. Sato, T. Ogawa, and K. Kano, *J. Phys. Chem.*, **88**, 3678 (1984).

3) K. Kano, T. Nakajima, and S. Hashimoto, *J. Phys. Chem.*, **91**, 6614 (1987).

4) K. Kano and S. Hashimoto, *Bull. Chem. Soc. Jpn.*, **63**, 633 (1990).

5) K. Kano, M. Takei, and S. Hashimoto, *J. Phys. Chem.*, **94**, 2181 (1990).

6) K. Kano, T. Miyake, K. Uomoto, T. Sato, T. Ogawa, and S. Hashimoto, *Chem. Lett.*, **1983**, 1867.

7) K. Kano, T. Nakajima, M. Takei, and S. Hashimoto,

Bull. Chem. Soc. Jpn., **60**, 1281 (1987).

8) A. D. Adler, F. R. Longo, J. D. Finarelli, J. Goldmacher, J. Assour, and L. Korsakoff, *J. Org. Chem.*, **32**, 476 (1967). K. Hatano, K. Anzai, T. Kubo, and S. Tamai, *Bull. Chem. Soc. Jpn.*, **54**, 3518 (1981). R. A. Freitag and D. G. Whitten, *J. Phys. Chem.*, **87**, 3918 (1987).

9) P. Worthington, P. Hambright, R. F. X. Williams, J. Reid, C. Burnham, A. Sharnim, J. Turay, D. M. Bell, R. Kirkland, R. Little, N. Datta-Gupta, and U. Eisner, *J. Inorg. Biochem.*, **12**, 281 (1980).

10) For example: Y. Sakata, S. Nakashima, Y. Goto, H. Tatemitsu, and S. Misumi, *J. Am. Chem. Soc.*, **111**, 8979 (1989), and references cited therein.

11) T. L. Nemzek and W. R. Ware, *J. Chem. Phys.*, **62**, 477 (1975).

12) K. A. Connors, "Binding Constants. The Measurements of Molecular Complex Stability," Wiley, New York (1987), p. 141.

13) S. Yamada, T. Sato, K. Kano, and T. Ogawa, *Photochem. Photobiol.*, **37**, 257 (1983).

14) D. B. Smithrud and F. Diederich, *J. Am. Chem. Soc.*, **112**, 339 (1990).

15) K. J. Miller and J. A. Savchik, *J. Am. Chem. Soc.*, **101**, 7206 (1979).

16) P. Hambright and E. B. Fleischer, *Inorg. Chem.*, **9**, 1757 (1970).

17) R. F. Pasternack, P. R. Huber, P. Boyd, G. Engesser, L. Francesconi, E. Gibbs, P. Fasella, G. C. Venturo, and L. deC. Hinds, *J. Am. Chem. Soc.*, **94**, 4511 (1972). R. F. Pasternack, E. J. Gibbs, A. Gaudemer, A. Autebi, S. Bassner, L. De Poy, D. H. Yurner, A. Williams, F. Laplace, M. H. Lansard, C. Merrience, and M. Perree-Fauvet, *ibid.*, **107**, 8179 (1985).

18) O. Sinanoglu, *Int. J. Quant. Chem.*, **18**, 381 (1981), and references cited therein.

19) R. Margalit and M. Rotenberg, *Biochem. J.*, **219**, 445 (1984).

Kinetic Studies on the Cobalt(II) Naphthenate Catalyzed Decomposition of "Cumene Hydroperoxide" in Benzene

Hideo SAWADA,* Hideyo ISHIGAKI,† Mitsukuni KATO,† and Masaharu NAKAYAMA
Tsukuba Research Laboratory, Nippon Oil & Fats Co., Ltd.,
Tokodai, Tsukuba, Ibaraki, 300-26
† Chemicals & Explosives Research Laboratory, Nippon Oil & Fats Co., Ltd.,
Taketoyo, Aichi 470-23
(Received October 3, 1990)

The cobalt(II) naphthenate[$Co(Nap)_2$] catalyzed decomposition of cumene hydroperoxide(CHP) gave a mixture of α-cumyl alcohol, acetophenone and di-α-cumyl peroxide in benzene at 25 °C. All experimentally observed time courses of disappearing CHP and an increasing of three products compared well with theoretical values.

Much attention has been paid to the metal-ion-catalyzed decomposition of organic hydroperoxides, which are important intermediates in both the oxidation of lipids *in vivo*[1] and the autoxidation of hydrocarbons.[2] Numerous attempts have been made to obtain a mechanism for the metal-ion-catalyzed decomposition of organic hydroperoxides.[3] Previously, Hiatt et al. proposed a radical chain mechanism for a metal-catalyzed decomposition of *t*-alkyl hydroperoxides, based on kinetic data regarding only the disappearance of the peroxides, due to a lack of detailed kinetic data concerning each product.[4] Thus, in order to examine the Hiatt mechanism, which seemed to be the most plausible one among hitherto proposed mechanisms, we initiated a detailed products analysis of a cobalt naphthenate catalyzed decomposition of 1-methyl-1-phenylethyl hydroperoxide ("cumene hydroperoxide," abbreviated as CHP) and kinetic studies of not only the disappearance of CHP, but also each product formation.

Results and Discussion

When the $Co(Nap)_2$ catalyzed decomposition of CHP was carried out in benzene at 25 °C, 1-methyl-1-phenylethyl alcohol (α-cumyl alcohol, abbreviated as CA) was obtained as the major product, with acetophenone (AP) and di-α-cumyl peroxide (DCP) as minor products.

$$\underset{\textbf{CHP}}{PhCMe_2OOH} \xrightarrow[\text{In benzene}]{Co(Nap)_2} \underset{\textbf{CA}}{PhCMe_2OH} + \underset{\textbf{AP}}{PhCOMe} + \underset{\textbf{DCP}}{PhCMe_2OOCMe_2Ph}$$

The effect of the initial concentration of CHP on the product distribution is shown in Fig. 1. The products which resulted from the solvent could not be detected. CA, AP, and DCP explained about 100% of the CHP consumed in all reactions, with different initial [CHP] ranging from 0.59 M to 5.35 M (M=mol dm^{-3}) (Table 1).

According to Hiatt's mechanism (Scheme 1), the processes of a cobalt(II) naphthenate catalyzed decomposition of CHP consist of the following three classes of reactions: (1) Cobalt(II)-ion-catalyzed decomposi-

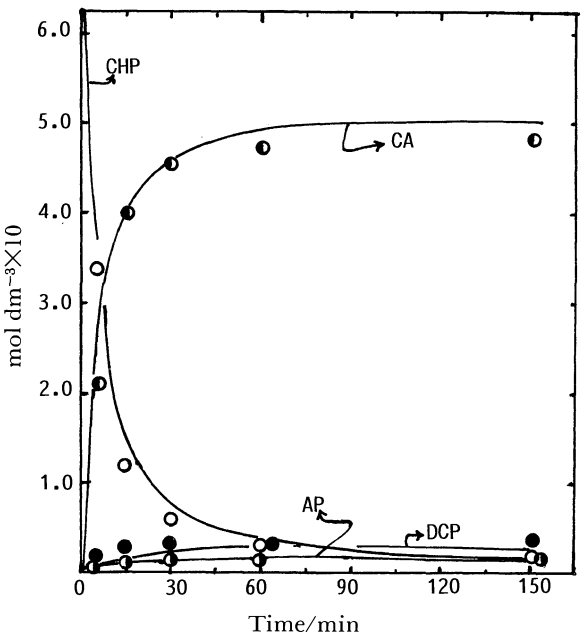

Fig. 1. $Co(Nap)_2$ catalyzed decomposition of CHP in benzene at 25 °C with $[CHP]_0$=0.59 mol dm^{-3} and $[Co(Nap)_2]_0=4.48\times10^{-3}$ mol dm^{-3}. Experimental observed value: CHP, ○; CA, ◐; AP, ◑; DCP, ●. Each solid line is theoretical (k_1=3.4 l mol^{-1} min^{-1}, k_4'=16, k_3'=145 l mol^{-1}).

Table 1. Effect of the Concentration of CHP on $Co(Nap)_2$[a] Catalyzed Decomposition of CHP in Benzene at 25 °C for 60 min

Initial concn of CHP/M	Products/M			
	CA	AP	DCP	CHP[b]
0.59[c]	0.40	0.01	0.03	0.12
3.80	2.98	0.11	0.54	0.10
5.35	3.80	0.17	1.20	0.16

a) Concentration of $Co(Nap)_2$: 4.47 mM. b) Concentration of residual CHP. c) Reaction time: 15 min.

$$PhCMe_2OOH + Co^{2+} \xrightarrow{k_1} PhCMe_2O\cdot + OH^- + Co^{3+} \quad (1)$$

$$PhCMe_2OOH + Co^{3+} \xrightarrow{k_2} PhCMe_2OO\cdot + H^+ + Co^{2+} \quad (2)$$

$$PhCMe_2O\cdot + PhCMe_2OOH \xrightarrow{k_3} PhCMe_2OH + PhCMe_2OO\cdot \quad (3)$$

$$2PhCMe_2OO\cdot \xrightarrow{k_4} 2PhCMe_2O\cdot + O_2 \quad (4)$$

$$2PhCMe_2OO\cdot \xrightarrow{k_5} PhCMe_2OOCMe_2Ph + O_2 \quad (5)$$

$$PhCMe_2O\cdot \xrightarrow{k_6} PhCOMe + Me\cdot \xrightarrow{O_2} MeOO\cdot \quad (6)$$

$$MeOO\cdot + PhCMe_2OO\cdot \xrightarrow{k_7} HCHO + O_2 + PhCMe_2OH \quad (7)$$

Scheme 1.

tions of CHP to provide α -cumyloxyl radical (Eq. 1) and α-cumylperoxyl radical (Eq. 2). (**2**) Chain reaction carried by α-cumyloxyl radical (Eqs. 3 and 4). (**3**) Termination reactions: reactions 6 and 7, to which Hiatt did not pay any attention, were newly added as some of termination reactions, in addition to reaction 5, since formation of a certain amount of AP was observed in this investigation.

Assuming steady states for [$PhCMe_2O\cdot$], [$PhCMe_2OO\cdot$], [$MeOO\cdot$], [Co^{2+}], and [Co^{3+}], Eqs. 8—11 are derived from the decomposition mechanism of CHP shown in Scheme 1.

$$k_1[CHP][Co^{2+}] = k_2[CHP][Co^{3+}] \quad (8)$$

$$d[MeOO\cdot]/dt = k_6[PhCMe_2O\cdot] - k_7[MeOO\cdot][PhCMe_2OO\cdot] = 0 \quad (9)$$

$$d[PhCMe_2O\cdot]/dt = k_1[CHP][Co^{2+}] - k_3[PhCMe_2O\cdot][CHP] + 2k_4[PhCMe_2OO\cdot]^2 - k_6[PhCMe_2O\cdot] = 0 \quad (10)$$

$$d[PhCMe_2OO\cdot]/dt = k_1[PhCMe_2OOH][Co^{2+}] + k_3[PhCMe_2O\cdot][CHP] - 2k_4[PhCMe_2OO\cdot]^2 - 2k_5[PhCMe_2OO\cdot]^2 - k_7[MeOO\cdot][PhCMe_2OO\cdot]^2 = 0 \quad (11)$$

$$[PhCMe_2O\cdot] = \{(2k_1k_4 + k_1k_5) / (2k_4k_6 + k_5k_6 + k_3k_5[CHP])\}[CHP][Co^{2+}] \quad (12)$$

From Eqs. 8, 9, 10, 11, and 12, the disappearance rate of CHP and rates of formations of CA, AP, and DCP are written as follows:

$$-d[CHP]/dt = 2k_1[CHP][Co^{2+}] + k_3[RO\cdot][CHP] = [\{2k_1(k_4' + 1) + k_1k_3'(2k_4' + 3)[CHP]\} / \{(2k_4' + 1) + k_3'[CHP]\}][CHP][Co^{2+}] \quad (13)$$

$$d[CA]/dt = k_3[RO\cdot][CHP] + k_7[MeOO\cdot][ROO\cdot] = [\{k_1(2k_4' + 1)(1 + k_3'[CHP])\} / \{(2k_4' + 1) + k_3'[CHP]\}][CHP][Co^{2+}] \quad (14)$$

$$d[AP]/dt = k_6[RO\cdot] = [\{k_1(2k_4' + 1)/\{(2k_4' + 1) + k_3'[CHP]\}][CHP][Co^{2+}] \quad (15)$$

$$d[DCP]/dt = 2k_5[ROO\cdot]^2 = [2k_1k_3'/\{(2k_4' + 1) + k_3'[CHP]\}][CHP]^2[Co^{2+}], \quad (16)$$

where R=$PhCMe_2$, $k_3'=k_3/k_6$, $k_4'=k_4/k_5$.

Assuming that the initiation rate, k_1[CHP][Co ion], where $k_1=k_2$ and [Co ion] is ([Co^{2+}]+[Co^{3+}]), derived from Eqs. 1, 2, and 8 is equal to the sum of termination rates (Eqs. 5, 6, and 7), the specific rate of reaction (1), k_1, is calculated to be 3.40 l mol^{-1} min^{-1}. This value was chosen to fit the experimental yields of the termination products by applying simplex optimization.[5] The values of k_3' and k_4' were successfully estimated to be 145 and 16 l mol^{-1}, respectively, by applying the Rung-Kutta-Gill method[6] for the experimental data given in Table 1 and k_1=3.4 l mol^{-1} min^{-1}, so as to fit the theoretical time courses of both disappearing CHP and appearing products in the experimental values. As shown in Fig. 1, the theoretical curves (solid line) are in accord with the

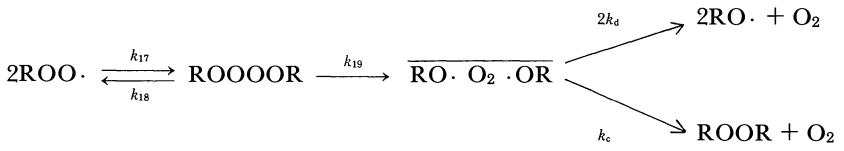

Scheme 2.

experimental values depicted by circles, revealing that the mechanisms shown in Scheme 1 is reasonable. Bimolecular reactions of ROO· (Eqs. 4 and 5) are known to proceed by the mechanism shown in Scheme 2.[7]

Eqs. 20 and 21 are obtained under a steady state condition for [ROOOOR] and [$\overline{\text{RO}\cdot\ \text{O}_2\ \cdot\text{OR}}$].

$$k_4 = (k_d k_{17} k_{19})/\{(2k_d + k_c)(k_{18} + k_{19})\} \quad (20)$$

$$k_5 = (k_c k_{17} k_{19})/\{2(2k_d + k_c)(k_{18} + k_{19})\} \quad (21)$$

The ratio of dissociation to cage recombination, k_d/k_c, can be obtained from Eqs. 20 and 21:

$$k_4' = 2k_d/k_c = 6.7. \quad (22)$$

The fraction of cage collapse, F, i.e. $k_c/(2k_d+k_c)$, is calculated as 0.13 from Eq. 22. This value agrees well with that of the caged t-butyloxyl radical pairs formed by the decomposition of di-t-butyl hyponitrite (DBH) in "isooctane" (F=0.098) at 45.0 °C (Scheme 3),[8] supporting the mechanism given in Scheme 1. The small difference in the two F values can be rationalized in terms of an easier diffusion out of the t-butyloxyl radical pair from the solvent cage than that from sterically bulky α-cumyloxyl radical pair.

Eqs. 23 is obtained from Eqs. 14 and 15, suggesting that plots of d[CA]/d[AP] against [CHP] fall on a straight line with a slope of, k_3' (145 l mol^{-1}).

$$\text{d[CA]/d[AP]} = k_3'[\text{CHP}]_t + 1 \quad (23)$$

The terms involved in Eq. 23 may be substituted using experimentally observable values, i.e. $\Delta[\text{CA}]_{ij}/\Delta[\text{AP}]_{ij}$ and $[\text{CHP}]_{ij}$, to obtain the following equation:

$$\Delta[\text{CA}]_{ij}/\Delta[\text{AP}]_{ij} \simeq k_3'[\text{CHP}]_{ij} + 1 \quad (24)$$

Here, $\Delta[\text{CA}]_{ij}$ and $\Delta[\text{AP}]_{ij}$ represent the concentrations of CA and AP, which increased for a time between i and j, while $[\text{CHP}]_{ij}$ denotes the average [CHP] for the same time, approximated as $([\text{CHP}]_i+[\text{CHP}]_j)/2$. These values were calculated from the experimental data given in Fig. 1, and plotted as shown in Fig. 2. The straight line shown in Fig. 2 has a slope of 145 mol l^{-1}. Considering the limited number of a vailable data, one can say that Fig. 2 well satisfies the relationship given by Eq. 23.

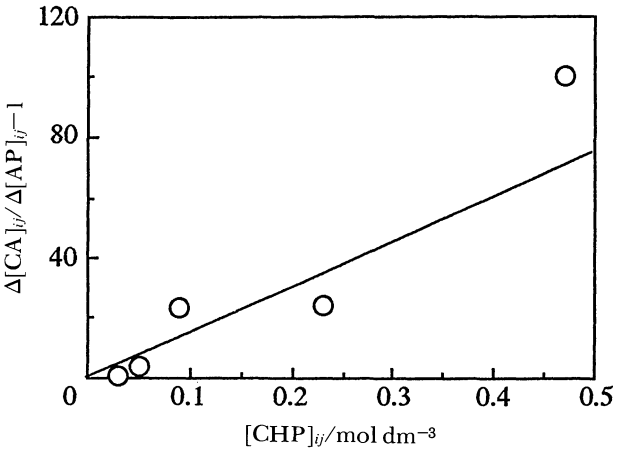

Fig. 2. Relationship between $\Delta[\text{CA}]_{ij}/[\text{AP}]_{ij}$ and $[\text{CHP}]^{av}$ on Co(Nap)_2 catalyzed decomposition of $[\text{CHP}]^{av}$ in benzene at 25 °C with $[\text{CHP}]_o$=0.59 mol dm^{-3}.

The mechanism of Scheme 1 previously proposed by Hiatt[4] has been verified by our new kinetic investigations which included both the disappearance of CHP and the formation of CA, AP, and DCP in the Co(Nap)_2 catalyzed decomposition of CHP in benzene.

Experimental

GC-analysis was performed on a Shimadzu GC-8A gas chromatography with 1.5 m glass column(silicon OV-210, 10%). GC-MS spectra were recorded on a JEOL DX-500 spectrometer.

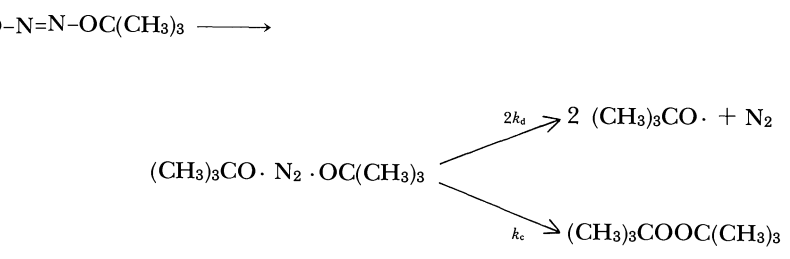

Scheme 3.

"Cumene hydroperoxide" (commercial grade of Nippon Oil & Fats Co.) was purified via sodium salt by a method described in the literature.[9]

A $Co(Nap)_2$ catalyzed decomposition of CHP was started by the addition of CHP to a catalyst, and an internal standard (benzil)-containing benzene solution immersed in a constant-temperature bath (25.0±0.2 °C) under nitrogen. Each sample was removed by syringe after an appropriate time interval. The residual CHP concentration was determined iodometrically.[10] The concentrations of CA, AP, and DCP were determined by GC after treating with triphenylphosphine to convert CHP to a stable compound, CA.

We thank Dr. Ken Fujimori of University of Tsukuba for his helpful advice and encouragement to this work.

References

1) E. Niki and H. Shimazaki, "Kassei Sanso," Ishiyaku Syupan, Tokyo (1987).

2) L. F. Martin, "Organic Peroxide Technology," Noyes Data Corporation, New Jersey (1973).

3) a) H. E. DeLaMare, J. K. Kochi, and F. F. Rust, *J. Am. Chem. Soc.*, **85**, 1437 (1963); b) A. M. Trzeciak, R. Grobelny, A. Mackowiak, and J. J. Ziolkowski, *Oxid. Commun.*, **7**, 283 (1984); c) Yu. S. Zimin, E. P. Talzi, V. M. Nekipelov, V. D. Chinakov, and K. I. Zamaraev, *React. Kinet. Catal. Lett.*, **29**, 225 (1985). d) W. H. Richardson, *J. Am. Chem. Soc.*, **87**, 247, 1096 (1965); e) J. W. L. Fordham and H. L. Williams, *J. Am. Chem. Soc.*, **73**, 1634 (1951); f) J. K. Kochi and P. E. Mocadlo, *J. Org. Chem.*, **30**, 1134 (1965); g) M. Hronec and R. Svehlik, *React. Kinet. Catal. Lett.*, **29**, 181 (1985); h) N. G. Ariko, G. V. Putyrshaya, T. P. Kenigsberg, and N. I. Mitskevich, *Oxid. Commun.*, **6**, 161 (1984); i) G. K. Zhavnerko, G. V. Butovskaya, V. E. Agabekov, and G. N. Supichenko, *React. Kinet. Catal. Lett.*, **29**, 129 (1985); j) M. Hronec, A. Stasko, L. Malik, and A. S. Herrera, *Oxid. Commun.*, **3**, 125 (1983); k) I. M. Kolthoff and A. Z. Medalia, *J. Am. Chem. Soc.*, **71**, 3789 (1949); l) R. Hiatt, T. Mill, and F. R. Mayo, *J. Org. Chem.*, **33**, 1416 (1968); m) M. S. Kharasch and A. Fono, *J. Org. Chem.*, **24**, 72 (1959).

4) R. Hiatt, K. C. Irwin, and C. W. Gould, *J. Org. Chem.*, **33**, 1430, (1968).

5) A. Yamaguchi, "LA Programing Giho," Information Science Co., Tokyo (1986), p. 57.

6) S. Gill, *Proc. Cambridge Philos. Soc.*, **47**, Part I, 96 (1951).

7) J. A. Howard, "Advances in Free-Radical Chemistry IV," ed by G. H. Williams, Academic Press, New York (1972), Chap. II.

8) H. Kiefer and T. G. Traylor, *J. Am. Chem. Soc.*, **89**, 6667 (1967).

9) M. S. Kharasch, A. Fono, and W. N. Nudenberg, *J. Org. Chem.*, **16**, 113 (1951).

10) W. H. Richardson, *J. Am. Chem. Soc.*, **87**, 247 (1964).

 © 1991 The Chemical Society of Japan Bull. Chem. Soc. Jpn., 64, 789—795 (1991)

Thermally Irreversible Photochromic Systems. Reversible Photocyclization of Non-Symmetric Diarylethene Derivatives

Yasuhide NAKAYAMA, Koichiro HAYASHI, and Masahiro IRIE*,†
The Institute of Scientific and Industrial Research, Osaka University,
Mihogaoka 8-1, Ibaraki, Osaka 567
† Institute of Advanced Material Study, Kyushu University,
Kasuga-Koen 6-1, Kasuga, Fukuoka 816
(Received October 25, 1990)

Non-symmetric diarylethenes with an indole ring on one end and a thiophene, a benzo[*b*]thiophene, or a pyrrole ring on the other end of the double bond were synthesized in an attempt to get thermally irreversible photochromic compounds having absorption bands at longer wavelengths. 2-(1,2-Dimethyl-3-indolyl)-3-(2,4,5-trimethyl-3-thienyl)maleic anhydride(**8a**) underwent photoinduced cyclization/ring-opening reactions with relatively high quantum yields (cyclization quantum yield: 0.15; ring-opening quantum yield: 0.40), and the both isomers were thermally stable. The closed-ring form had the absorption maximum at 595 nm with the edge extending to 760 nm. Cyclization/ring-opening reactions of **8a** and 2-(1,2-dimethyl-3-indolyl)-3-(2-methyl-3-benzo[*b*]thienyl)maleic anhydride (**9a**) were induced by Ar ion (488 nm) and He–Ne (633 nm) lasers.

A photochromic material is characterized by its ability to undergo a reversible transformation between two different chemical forms. Such a transformation is induced by irradiation with an appropriate wavelength.[1] The instant image-forming property without processing has led to the consideration of the use in rewritable direct read after write memory systems.[2] Despite favorable situations provided by recent progress of optical memory technology, organic photochromic compounds have found little applications in optical information storage media. The limitation is due to the lack of suitable compounds which fulfill the requirements for the reversible recording media. Among the requirements the most important one is the thermal stability.[3]

Recently, a new type of thermally stable photochromic compounds, diarylethenes with heterocyclic rings, was developed such as 1,2-dicyano-1,2-bis(2,4,5-trimethyl-3-thienyl)ethene (**1a**), and 2,3-bis(2,4,5-trimethyl-3-thienyl)maleic anhydride (**3a**).[4] Compounds

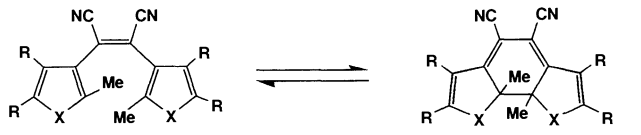

1a, X=S; R=CH_3 **1b**, X=S; R=CH_3
2a, X=NCH_3; **2b**, X=NCH_3;
R⌒R=CH=CH–CH=CH R⌒R=CH=CH–CH=CH

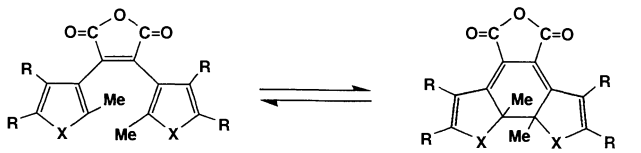

3a, X=S; R=CH_3 **3b**, X=S; R=CH_3
4a, X=NCH_3; **4b**, X=NCH_3;
R⌒R=CH=CH–CH=CH R⌒R=CH=CH–CH=CH

1a—4a are not thermochromic, even at 300 °C, and the colored closed-ring forms **1b** and **3b** are stable for more than 3 months at 80 °C.[2g] The compounds fulfill the most important condition for optical data storage media. The absorption edges of the closed-ring forms, however, do not extend to 700 nm. This precludes isomerization of the compounds by conventional diode laser light ($780<\lambda<840$ nm). The compounds lack the important requirement of photosensitivity at diode laser wavelengths.

In order to gain access to compounds which have sensitivity at longer wavelengths, symmetric diarylethenes with various heterocyclic rings have been synthesized.[5] Replacing the thiophene rings with indole rings, i.e. 1,2-dicyano-1,2-bis(1,2-dimethyl-3-indolyl)ethene (**2a**) and 2,3-bis(1,2-dimethyl-3-indolyl)maleic anhydride (**4a**), shifts the absorption maxima to longer wavelengths. Compound **4b** has an absorption edge extending to 800 nm and the ring-opening reaction was effected with 780 nm diode laser. The closed-ring forms, **2b** and **4b**, were, however, thermally unstable, reverting in the dark to **2a** and **4a**. The absorption intensity of **4b** decreased to 50% of the initial intensity in 3 h at 80 °C. The thermal stability difference between the diarylethenes with thiophene and indole rings was interpreted by the difference in aromatic stabilization energy of the rings.[6]

In the present study, we synthesized unsymmetrically substituted non-symmetric diarylethene derivatives having an indole ring on one end and a thiophene, a benzo[*b*]thiophene, or a pyrrole ring on the other end of the double bond in an attempt to get thermally stable photochromic compounds having the absorption bands at longer wavelengths.

Results and Discussion

Diarylethene Derivatives with Dicyano Group. Substituted non-symmetric diaryldicyanoethenes

having an indole ring on one end and a thiophene, a benzo[*b*]thiophene, or a pyrrole ring on the other end of the double bond were prepared by a coupling reaction of 3-(cyanomethyl)-1,2-dimethylindole and 3-(cyanomethyl)-2,4,5-trimethylthiophene, 3-(cyanomethyl)-2-methyl-benzo[*b*]thiophene or 3-(cyanomethyl)-1,2,4,5-tetramethylpyrrole, respectively.

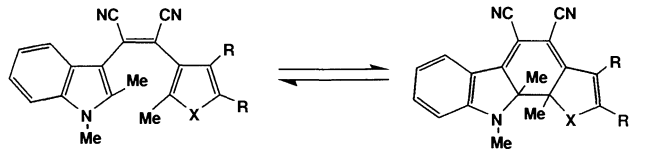

5a, X=S; R=CH_3
6a, X=S; R⌒R=CH=CH-CH=CH
7a, X=NCH_3; R=CH_3
5b, X=S; R=CH_3
6b, X=S; R⌒R=CH=CH-CH=CH
7b, X=NCH_3; R=CH_3

In the case of a coupling reaction of equimolar (cyanomethyl)indole and (cyanomethyl)pyrrole approximately equal amounts of **7a** and **2a** were obtained. (Cyanomethyl)pyrrole reacted more efficiently with (cyanomethyl)indole than (cyanomethyl)pyrrole. The self coupling product of the pyrrole compounds, 1,2-dicyano-1,2-bis(1,2,4,5-tetramethyl-3-pyrrolyl)ethene, was formed in very low yield. The mixture of **7a** and its trans form, and **2a** and its trans form was separated by silica-gel chromatography using benzene as an eluent. The trans and cis mixture of the indolyl-pyrrolylethene derivative was dissolved in acetonitrile and exposed to ultraviolet-visible light (λ>350 nm). The irradiation converted a large part of the trans form to the cis form. The cis form was isolated by high-performance liquid chromatography (HPLC, 5 μm silica gel/benzene) and purified by recrystallization from a hexane–ether mixture.

The coupling reaction of equimolar (cyanomethyl)-indole and (cyanomethyl)thiophene yielded the mixture of **5a**, **1a**, and **2a** (4:20:1 including the trans forms). The mixture was separated by the same procedure used for **7a**. Compound **6a** was also prepared by the similar coupling reaction as used for **7a**. The structures of the above compounds were fully characterized by spectroscopic methods.

Non-symmetric diarylethenes with the dicyano group underwent the cyclization to produce the cyclohexadiene-type derivatives.[7] Figure 1 shows the absorption spectral change of a dilute benzene solution of **5a** (1.0×10^{-4} mol dm^{-3}) by photoirradiation with 436 nm light. Irradiation of the yellow benzene solution in the presence of air with 436 nm light leads to the decrease of the absorption at 412 nm ($\varepsilon=1.0\times10^4$ l mol^{-1} cm^{-1}) and formation of a brown solution, in which a visible absorption at 549 nm ($\varepsilon=5.4\times10^3$ l mol^{-1} cm^{-1}) was observed. The closed-ring form **5b** shows a 37 nm bathochromic shift compared with **1b**. Isosbestic points are observed at 382 and 458 nm. The spectra indicate that the cis to trans isomerization is negligible when the sample is irradiated at 436 nm. Upon irradiation with light of wavelengths longer than 520 nm, the brown color of

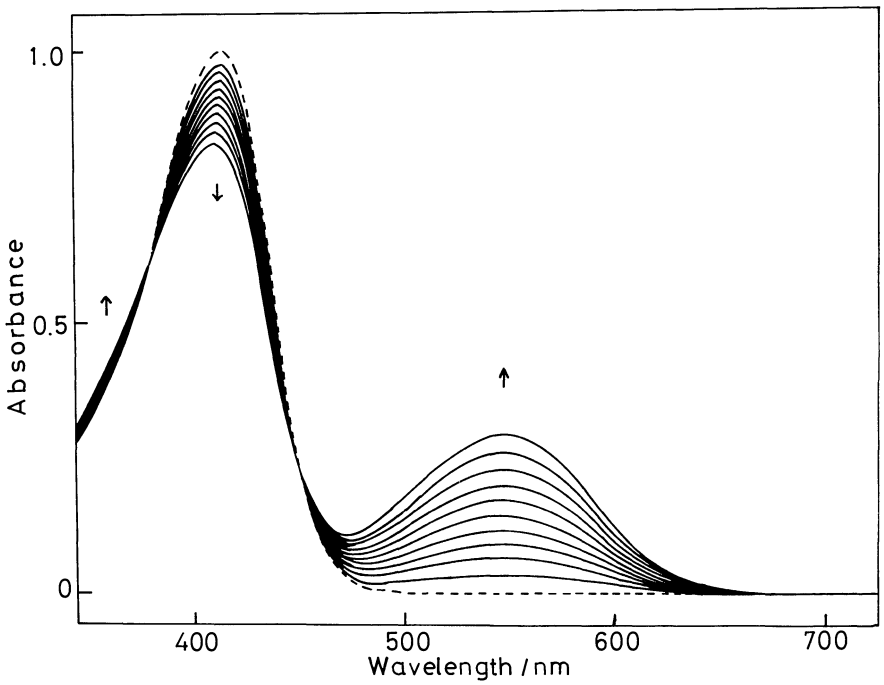

Fig. 1. Absorption spectral change of benzene solution of **5a** (1.0×10^{-4} mol dm^{-3}) (---) induced by irradiation with 436 nm light. Irradiation time; 25, 50, 80, 110, 150, 195, 261, 333, 471, and 855 s.

5b disappeared, and the initial cis form absorption was restored. The conversion of **5a** to **5b** at the photostationary state was estimated to be 55% by comparing the absorption intensity at 549 nm with that of **5b**, which was isolated from the photoirradiated sample by HPLC.

The absorption maximum of **1b** was observed at 512 nm,[1] while that of **2b** was 575 nm.[5] The absorption maximum of **5b** was in between those of **1b** and **2b**.[7] This indicates that donor-acceptor conjugation over two heterocyclic rings does not play an important role in this compound.

By replacing the thiophene ring of **5b** with a benzo[*b*]thiophene or a pyrrole ring, the absorption maximum of the closed-ring forms of the dicyano derivatives shifted to longer wavelengths, 558 and 575 nm, respectively. The absorption maxima and the conversions of the cis forms to the closed-ring forms at the photostationary state are summarized in Table 1. The conversions were determind by comparing the absorption maximum intensities at the photostationary state with those of the isolated closed-ring forms. The closed-ring forms were easily isolated from the photoirradiated samples by HPLC equipped with a visible absorption monitor. Conversions over 50% are observed for the non-symmetric dicyano derivatives. In order to shift the absorption band further to longer wavelengths and to prevent the cis to trans isomerization completely, the dicyano group was converted to an oxydicarbonyl group.

Table 1. Absorption Maxima of the Closed-Ring Forms and Photochromic Property of Non-Symmetric Diarylethenes in Benzene Solution

Compd	λ_{max}	Conversion[b]	Exciting wavelength
	nm	%	nm
5b	547	55	436
6b	558	50	440
7b	575	59	440
8b	595	58	491
8b[a]	578	70	450
9b	597	26	480
9b[a]	583	66	470

a) In hexane solution. b) At photostationary state.

Maleic Anhydride Derivatives. The dicyano derivatives were converted to maleic anhydride derivatives by hydrolysis with KOH in ethylene glycol monoethyl ether–water mixture. The 2,3-diarylmaleic anhydrides were purified by column chromatography using benzene as an eluent, and were recrystallized from a hexane–chloroform mixture.

Their structures were fully characterized by spectroscopic methods. The non-symmetric 2,3-diarylmaleic anhydride underwent cyclization reactions to produce the cyclohexadiene-type derivatives. Figure 2 shows the spectra of **8a** and **8b**, and the spectrum at the photostationary state under irradiation with 491 nm light in benzene. Upon irradiation with 491 nm light in the presence of air, the solution turned green and a new peak appeared at 595 nm (ε=5.5×10^3 l mol^{-1} cm^{-1}). Isosbestic points are observed at 437 and

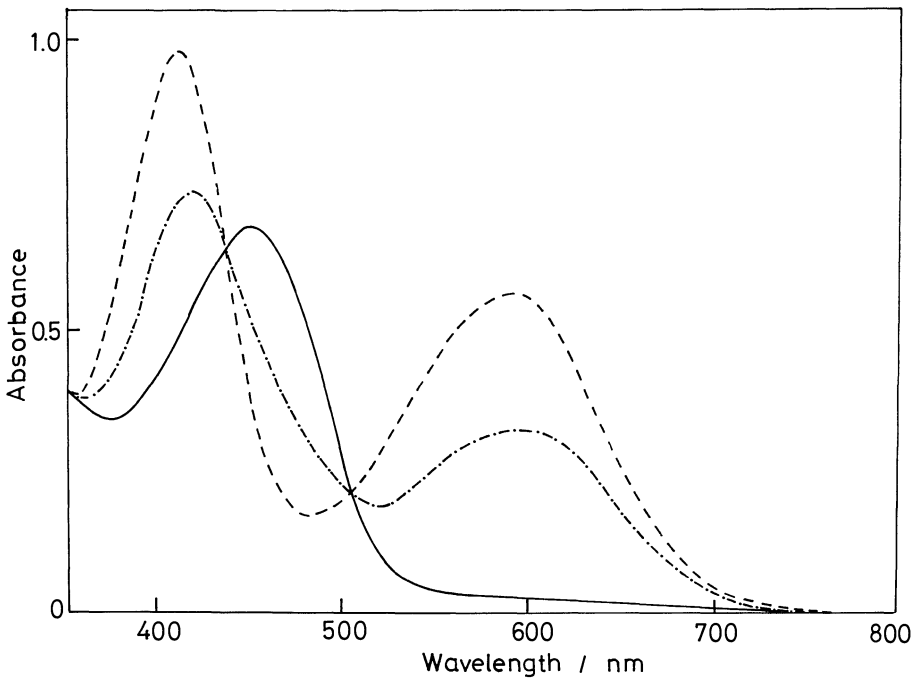

Fig. 2. Absorption spectra of benzene solution of **8a** (1.0×10^{-4} mol dm^{-3}) (——) and **8b** (1.0×10^{-4} mol dm^{-3}) (---) and a mixture of **8a** and **8b** at the photostationary stae (—·—) under irradiation with 491 nm light.

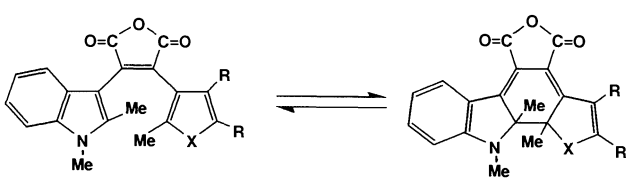

8a, X=S; R=CH_3 **8b**, X=S; R=CH_3
9a, X=S; R⌒R=CH=CH-CH=CH **9b**, X=S; R⌒R=CH=CH-CH=CH

504 nm. The absorption maximum shifts to longer wavelengths by 56 nm in comparison with the dicyano derivative **5b**. On exposure to visible light (λ>560 nm), the solution again became yellow, and the initial absorption of **8a** was restored. The absorption maxima of **3b** and **4b** were observed at 560 nm and 620 nm, respectively.[4,5] The absorption maximum of **8b**, 595 nm, was in between those of **3b** and **4b**.

The cyclization reaction was also induced by irradiation with 488 nm light of Ar ion laser. The photogenerated green color disappeared on exposure to 633 nm He–Ne laser. Compound **9a** underwent similar cyclization/ring-opening reactions upon irradiation with 488 and 633 nm lights.

The absorption maxima of the closed forms of symmetric diarylethenes showed red shifts with increasing electron-donating ability of the heterocyclic groups and with increasing electron-accepting ability of 1,2-substituents by replacing the dicyano group with oxydicarbonyl group.[4,5,8] The absorption maxima of the closed-ring forms of dicyano derivatives increased in the following order; dithienylethene≈bis(benzo[*b*]thienyl)ethene<diselenenylethene<diindolylethene.[4,5,8] The maleic anhydride derivatives showed a bathochromic shift in comparison with the dicyano derivatives as much as 50 nm.

For the non-symmetric diarylethenes with an indole ring on one end of the double bond, the absorption maximum was also controlled by the electron-donating ability of the other heterocyclic rings. The absorption maximum showed red shift in the order of **5b**<**6b**<**7b**. The result suggests that donor–acceptor type interaction between heterocyclic groups and the dicyano or the oxydicarbonyl group plays an important role in determining the position of the absorption band.

The absorption spectra of the closed-ring forms are dependent on the polarity of the medium. Figure 3 shows the absorption spectra of **7a**+**7b** at the photostationary state in several solvents. The absorption maximum of **7b** in hexane at 554 nm shifts to 574 nm in benzene. In hexamethylphosphoric triamide (HMPA), the closed-ring form has a deep blue color, and the absorption maximum is observed at 603 nm. The dramatic red-shift of the absorption band indicates that $S_0 \rightarrow S_1$ band of **7b** has charge-transfer character and the S_1 is polar state. The invariance of the second band of **7b** with solvent polarity suggests that the band is due to the transition to a less polar

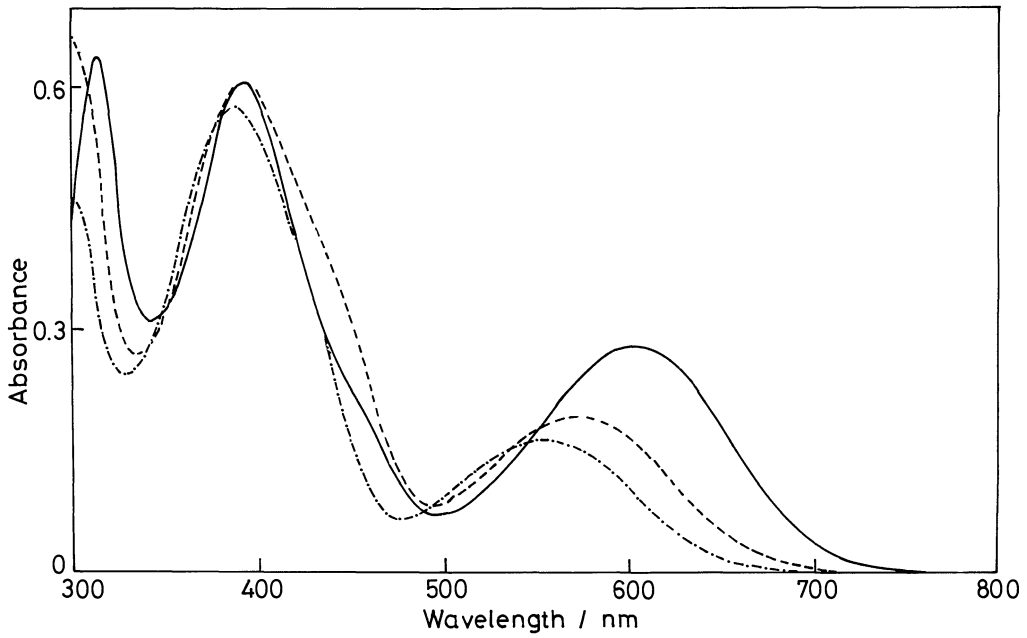

Fig. 3. Absorption spectra of **7a**+**7b** (total concentration, 1.0×10^{-4} mol dm^{-3}) at the photostationary state in hexane (—·—), in benzene (----), and in HMPA (——). Conversion from the open-ring to the closed-ring form was 39% in hexane, 44% in benzene, and 75% in HMPA. The absorption bands longer than 500 nm and at around 400 nm are ascribable to **7b**, and shoulders at around 450 nm to **7a**.

excited state.

Thermal Stability of Closed-Ring Forms. Figure 4 illustrates the thermal stability of the closed-ring forms **5b**, **6b**, **7b**, **8b**, and **9b** at 80 °C in the dark. The value of A/A_0 was plotted against storage time, where A_0 is the initial absorbance at the absorption maximum of the closed-ring form, and A the absorbance after t hours at 80 °C. As seen in Fig. 4, the photogenerated closed-ring forms, **5b**, **6b**, **8b**, and **9b** are stable, and maintain a constant absorption intensity for more than 12 h at 80 °C, whereas **7b** is thermally unstable. The absorption intensity of **7b** decreases to 75% of the initial intensity in 12 h at 80 °C.

In a previous paper,[6] we showed that the thermal stability of the closed-ring forms of symmetric diarylethene derivatives is dependent on the aromatic stabilization energy of the aryl groups. When the aryl groups of the compounds have low aromatic stabilization energy, the closed-ring forms are thermally stable, while they become thermally unstable when they contain benzene or pyrrole rings with high aromatic stabilization energy. The experimental results presented in this paper indicate that the closed-ring forms of non-symmetric diarylethenes are thermally stable when at least one of the heterocyclic rings has low aromatic stabilization energy. Note that the non-symmetric compound having aryl groups with high aromatic stabilization energy for both substituents, e.g. **7b**, is thermally unstable.

Quantum Yield. The quantum yields of cyclization and ring-opening reactions were measured in benzene and hexane solutions. A xenon lamp equipped with a monochromater (Jovin Yvon H10-UV) was used as the light source. The light intensity was determined with a photometer (International Light, IL-700). Table 2 summarizes the result. The cyclization quantum yields of **5a** and **8a** in benzene are below 0.1. The values are similar to those observed for **2a** and **3a**.

The cyclization quantum yield was strongly dependent on the polarity of solvents. The quantum yield in hexane is 3 times larger than the value observed in benzene. Similar solvent dependence of the quantum yield was observed for the thiophene derivatives.[4] The cyclization quantum yield of **3a** decreases from 0.13 to 0.003 by increasing the solvent polarity from hexane to acetonitrile.[9] These solvent dependences suggest that there exist two kinds of excited states with different polarity, and the less polar

Table 2. Quantum Yields for Cyclization and Ring-Opening Reactions of Non-Symmetric Diarylethenes

	Excitation wavelength	Solvent	
	nm	Benzene	Hexane
5a→**5b**	405	0.08	a)
8a→**8b**	405	0.06	0.15
	450	a)	0.14
	490	0.05	a)
5b→**5a**	546	0.56	a)
8b→**8a**	546	0.40	a)

a) Not measured.

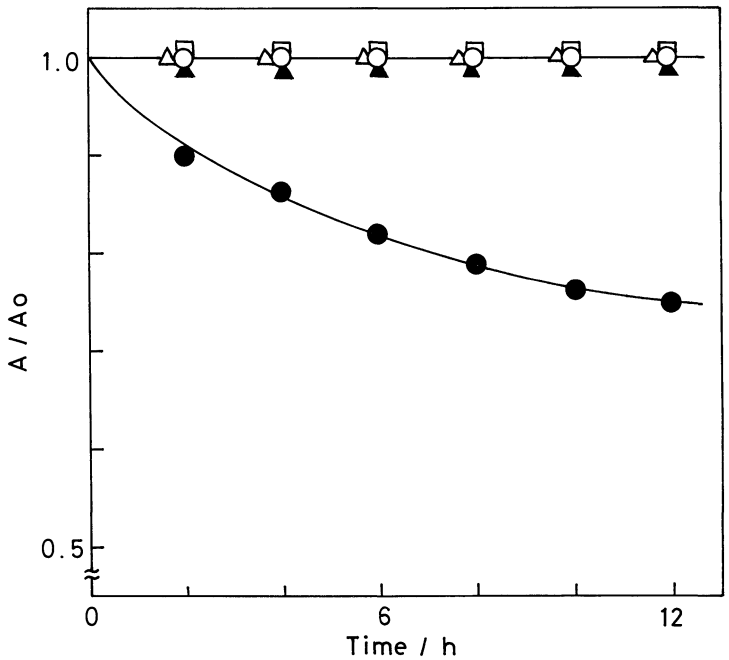

Fig. 4. Thermal stability of the closed ring forms in toluene at 80 °C in deaerated conditions. Compounds **5b** (□), **6b** (○), **7b** (●), **8b** (△), and **9b** (▲).

state is responsible to the photocyclization.

The ring-opening quantum yields of **5b** and **8b** in benzene are quite high. The value of **8b** is 3 times larger than the value observed for the ring-opening reaction of **3b**. Replacement of one of the thiophene rings with an indole ring increased the ring-opening quantum yield. Similar increase of the ring-opening quantum yield was observed for bis(benzo[*b*]thienyl)-ethene.[8] The introduction of a rigid indole (or benzo[*b*]thiophene) ring possibly destabilizes the closed-ring forms, and increases the ring-opening quantum yield.

Summary

Non-symmetric diarylethenes with an indolyl group on one end and a thienyl, a benzo[*b*]thienyl or a pyrrolyl group on the other end were synthesized. The diaryldicyano- and diaryl(oxydicarbonyl)ethenes **5a**, **6a**, **8a**, and **9a** underwent thermally irreversible photochromic reactions. Although these compounds still are not sensitive to wavelengths of diode lasers, both the open-ring and closed-ring forms have absorption bands in the visible region, and the cyclization/ring-opening reactions of **8a** and **9a** were induced by Ar ion (488 nm) and He–Ne (633 nm) lasers.

Experimental

^{1}H NMR spectra (360 MHz) were recorded in $CDCl_3$ with a Brucker WN-360 instrument. All chemical shifts were expressed in parts per million (ppm) downfield from internal tetramethylsilane. Mass spectra and elemental analysis were performed in the Material Analysis Center of Osaka University. High-performance liquid chromatography (HPLC) was carried out on a JASCO 800 instrument. For isolation and purification of samples, a column (10×250 mm) packed with silica gel (JASCO, Fine SIL-5) was used.

Absorption spectra were measured with a spectrophotometer (Shimadzu MPS-200). Photoisomerization was carried out in solution in the presence of air. A Ushio mercury lamp (1 kW) or a EWIG XC-500 xenon lamp equipped with a monochromater (Jovin Yvon 10H-UV) were used as the light sources. Quantum yields were determined by measuring the rate of isomerization in the initial stage of the reaction at low concentration (absorbance at the irradiation wavelength<0.2). The light intensity was measured with a photometer (International Light IL700).

Materials. 3-(Cyanomethyl)-1,2-dimethylindole,[5] 3-(cyanomethyl)-2,4,5-trimethylthiophene,[4] 3-(cyanomethyl)-2-methylbenzo[*b*]thiophene,[8] and 3-(cyanomethyl)-1,2,4,5-tetramethylpyrrole[10,11] were prepared by the reported procedures.

A general procedure for the preparation of 1,2-diaryl-1,2-dicyanoethenes and 2,3-diarylmaleic anhydrides is illustrated by the following scheme.

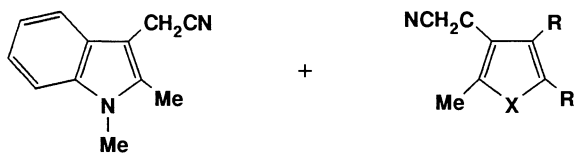

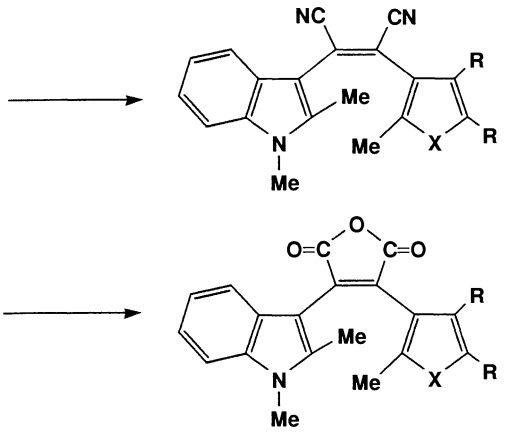

1,2-Dicyano-1-(1,2-dimethyl-3-indolyl)-2-(2,4,5-trimethyl-3-thienyl)ethene(5a). To a mixed solution of CCl_4 (1.58 ml) and benzene (1.58 ml) containing 0.07 g (0.22 mmol) of tetrabutylammonium bromide, 0.5 g (2.7 mmol) of 3-(cyanomethyl)-1,2-dimethylindole and 0.45 g (2.7 mmol) of 3-(cyanomethyl)-2,4,5,-trimethylthiophene was added at 40 °C 1.09 ml of 50% NaOH aqueous solution. The reaction mixture was heated to 45 °C for 3 h, and then cooled to room temperature. The solution was poured into water, and the aqueous layer was extracted with $CHCl_3$. The organic phase was dried over $MgSO_4$ and filtered. After the solvent was removed, the mixtures of **5a** and its trans form, **1a** and its trans form, and **3a** and its trans form were separated by column chromatography on silica gel (30 μm) using benzene as an eluent. The trans and cis mixture of the indolylthienylethene derivative was dissolved into acetonitrile and exposed to ultraviolet-visible light (λ>350 nm). The irradiation converts a large part of the trans form to the cis form. After evaporation of the solvent, the trans and the cis forms were isolated by column chromatography (HPLC, 5 μm silica gel/benzene). The closed-ring form **5b** was also isolated by HPLC (5 μm silica gel/benzene). HPLC retention times (flow rate 1 ml min^{-1}): **5a** 14.9 min, the trans form 7.9 min, **5b** 20.0 min. The cis form was further purified by recrystallization from a hexane–ether mixture yielding 0.1 g (10%) of **5a**.

5a: IR(KBr, cm^{-1}) 2240; ^{1}H NMR δ=1.92 (s, 3H, CH_3), 1.95 (s, 3H, CH_3), 2.07 (s, 3H, CH_3), 2.20 (s, 3H, CH_3), 3.63 (s, 3H, CH_3), 7.10 (dd, J=8.1, 6.8 Hz, 1H), 7.21 (dd, J=8.1, 6.8 Hz, 1H), 7.25 (d, J=8.1 Hz, 1H), 7.39 (d, J=8.1 Hz, 1H); MS m/z (rel intensity) 345 (M^+, 100), 330 (45), 315 (17); HRMS Found: m/z 345.1320. Calcd for $C_{21}H_{19}N_3S$: M, 345.1299. Anal. Calcd for $C_{21}H_{19}N_3S$: C, 73.01; H, 5.54; N, 12.16; S, 9.28%. Found: C, 73.06; H, 5.40; N, 12.15%.

1,2-Dicyano-1-(1,2-dimethyl-3-indolyl)-2-(2-methyl-3-benzo[*b*]thienyl)ethene (6a). This was prepared by a coupling reaction of 3-(cyanomethyl)-1,2-dimethylindole and 3-(cyanomethyl)-2-methylbenzo[*b*]thiophene, and isolated in 19% yield. HPLC retention times (silica gel/benzene, flow rate 1 ml min^{-1}): **6a** 13.0 min, the trans form 7.2 min, **6b** 9.3 min.

6a: IR(KBr, cm^{-1}) 2240; ^{1}H NMR δ=2.00 (s, 3H, CH_3), 2.12 (s, 3H, CH_3), 3.55 (s, 3H, CH_3), 6.99—7.70 (m, 8H); HRMS Found: m/z 367.1116. Calcd for $C_{23}H_{17}N_3S$: M, 367.1142. Anal. Calcd for $C_{23}H_{17}N_3S$: C, 75.18; H, 4.66; N, 11.43; S, 8.72%. Found: C, 75.23; H, 4.52; N, 11.37%.

1,2-Dicyano-1-(1,2-dimethyl-3-indolyl)-2-(1,2,4,5-tetramethyl-3-pyrrolyl)ethene (7a). This was prepared by a coupling reaction of 3-(cyanomethyl)-1,2-dimethylindole and 3-(cyanomethyl)-1,2,4,5-trimethylpyrrole, and isolated in 5% yield. HPLC retention times (silica gel/benzene, flow rate 1 ml min^{-1}): **7a** 19.8 min, the trans form 10.0 min. Isolation of **7b** by the silica-gel column was failed. The conversion from **7a** to **7b** at the photostationary state was estimated by measuring the HPLC intensity change of **7a** by photoirradiation.

7a: IR(KBr, cm^{-1}) 2240; ^1H NMR δ=1.72 (s, 3H, CH_3), 1.77 (s, 3H, CH_3), 2.00 (s, 3H, CH_3), 2.15 (s, 3H, CH_3), 3.19 (s, 3H, CH_3), 3.63 (s, 3H, CH_3), 7.03 (dd, J=9.0, 6.8 Hz, 1H), 7.16 (dd, J=8.2, 6.8 Hz, 1H), 7.22 (d, J=8.2 Hz, 1H), 7.27 (d, J=9.0 Hz, 1H); MS m/z (rel intensity) 342 (M^+, 100), 327 (57), 312 (12); HRMS Found: m/z 342.1875. Calcd for $C_{22}H_{22}N_4$: M, 342.1843. Anal. Calcd for $C_{22}H_{22}N_4$: C, 77.16; H, 6.48; N, 16.36%. Found: C, 77.42; H, 6.68; N, 16.26%.

2-(1,2-Dimethyl-3-indolyl)-3-(2,4,5-trimethyl-3-thienyl)-maleic Anhydride (8a).[12] Compound **5a** (630 mg, 1.8 mmol) and ethylene glycol monoethyl ether (1.53 ml) were added to a solution of 0.73 g of potassium hydroxide in 1.53 ml of water. The solution was refluxed for 24 h. The reaction mixture was poured into water and 20% hydrochloric acid was added until the mixture became acidic. The red precipitate was extracted with $CHCl_3$. The organic phase was dried over $MgSO_4$ and filtered. After the solvent was removed **8a** was isolated by HPLC (5 μm silica gel/benzene) and purified by recrystallization from a ether–hexane mixture, yielding 110 mg (16%) of **8a**. HPLC retention times (flow rate 1 ml min^{-1}): **8a** 8.8 min, **8b** 13.4 min.

8a: IR(KBr, cm^{-1}) 1760, 1820; ^1H NMR δ=1.87 (s, 3H, CH_3), 1.95 (s, 3H, CH_3), 2.17 (s, 3H, CH_3), 2.25 (s, 3H, CH_3), 3.70 (s, 3H, CH_3), 7.03 (dd, J=8.1, 7.2 Hz, 1H), 7.13 (d, J=8.1 Hz, 1H), 7.19 (dd, J=8.1, 7.2 Hz, 1H), 7.26(d, J=8.1 Hz, 1H); MS m/z (rel intensity) 365 (M^+, 100), 650 (8); HRMS Found: m/z 365.1103. Calcd for $C_{21}H_{19}NO_3S$: M, 365.1085. Anal. Calcd for $C_{21}H_{19}NO_3S$: C, 69.02; H, 5.24; N, 3.83; O, 13.13; S, 8.77%. Found: C, 68.89; H, 5.01, N, 3.57%.

2-(1,2-Dimethyl-3-indolyl)-3-(2-methyl-3-benzo[*b*]thienyl)-maleic Anhydride (9a). This was prepared by the hydrolysis of **6a**. HPLC retention times (flow rate 1 ml min^{-1}): **9a** 7.8 min, **9b** 5.6 min.

9a: IR(KBr, cm^{-1}) 1760; ^1H NMR δ=2.09 (s, 3H, CH_3), 2.21 (s, 3H, CH_3), 3.62 (s, 3H, CH_3), 6.97—7.72 (m, 8H); MS m/z 387 (M^+); HRMS Found: m/z 387.0954. Calcd for $C_{23}H_{17}NO_3S$: M, 387.0928. Anal. Calcd for $C_{23}H_{17}NO_3S$: C, 71.30; H, 4.42; N, 3.62; O, 12.39; S, 8.27%. Found: C, 71.26; H, 4.33; N, 3.33%.

References

1) a) H. Dürr, *Angew. Chem.*, **101**, 427 (1989). b) H. Dürr, H. Bouas-Laurent, "Photochromism—Molecules and Systems," Elsevier, Amsterdam (1990).

2) a) Y. Hirschberg, *J. Am. Chem. Soc.*, **78**, 2304 (1956). b) P. J. Darcy, H. G. Heller, P. J. Strydom, and J. Whittall, *J. Chem. Soc., Perkin Trans. 1*, **1981**, 202. c) H. G. Heller and J. R. Langan, *J. Chem. Soc., Perkin Trans. 2*, **1981**, 341. d) H. G. Heller, *IEEE Proc.*, **130**, 209 (1983), and references cited in. e) H. Suzuki, A. Tomoda, M. Ishizuka, A. Kaneko, M. Furui, and R. Matsushima, *Bull. Chem. Soc. Jpn.*, **62**, 3968 (1989), and references cited in. f) Y. Yokoyama, T. Iwai, N. Kera, I. Hitomi, and Y. Kurita, *Chem. Lett.*, **1990**, 263, and references cited in. g) M. Irie, *Jpn. J. Appl. Phys.*, **28-3**, 215 (1989).

3) A. E. J. Wilson, *Phys. Technol.*, **15**, 232 (1984).

4) M. Irie and M. Mohri, *J. Org. Chem.*, **53**, 803 (1988).

5) Y. Nakayama, K. Hayashi, and M. Irie, *J. Org. Chem.*, **55**, 2592 (1990).

6) S. Nakamura and M. Irie, *J. Org. Chem.*, **53**, 6136 (1988).

7) R. M. Kellogg, M. B. Groen, and H. Wynberg, *J. Org. Chem.*, **32**, 3093 (1967).

8) K. Uchida, Y. Nakayama, and M. Irie, *Bull. Chem. Soc. Jpn.*, **63**, 1311 (1990).

9) K. Sayo and M. Irie, unpublished result.

10) D. M. Young and C. F. Allene, *Org. Synth.*, Coll. Vol. II, 219 (1943).

11) W. Herz and R. L. Settine, *J. Org. Chem.*, **24**, 201 (1959).

12) M. A. Goldberg, E. P. Ordas, and G. Carsch, *J. Am. Chem. Soc.*, **69**, 260 (1947).

A New Oxidizing System for Aromatic Alcohols by the Combination of *N*-Oxoammonium Salt and Electrosynthesized Tetraalkylammonium Tribromide

Tsutomu INOKUCHI, Sigeaki MATSUMOTO, Mitsuhiro FUKUSHIMA, and Sigeru TORII*
Department of Applied Chemistry, Faculty of Engineering,
Okayama University, Okayama 700
(Received October 29, 1990)

A combination of 2,2,6,6-tetramethyl-1-piperidinyloxyl and tetraalkylammonium tribromides (R_4NBr_3), which are available from the corresponding tetraalkylammonium bromides via electrooxidation with potassium bromide, has proved to be useful for oxidations of primary and secondary alcohols to the corresponding aldehydes and ketones, respectively. The oxidation reaction proceeds smoothly even with a 0.5—1.0 mol% of *N*-oxyl compounds and 1.5—2.0 equivalents of tetraalkylammonium tribromides in an aqueous-organic two-phase solution buffered at pH 8.0—8.6. This recyclable oxidant/co-oxidant combination system may involve the formation of *N*-oxoammonium salts, actual oxidizing agents of alcohols, by the action of hypobromite species generated from R_4NBr_3 in the binary solution. Utility of the method is highlighted by the selective oxidation of benzylic alcohols bearing electron-releasing groups on the aromatic nucleus to the corresponding aldehydes or ketones without any bromination and overoxidation.

N-Oxoammonium salts have attracted increasing attention as a nonmetallic oxidizing reagent for alcohols to the corresponding carbonyl compounds.[1] The attractiveness of this oxidant may stem from the following characteristic features: (a) the advantage of recycling the reagent by the aid of a co-oxidant (stoichiometric), (b) high selectivity attainable in favor of a primary hydroxyl group for the competitive oxidation of mixed polyols, and (c) easy operation and workup not to produce any hazardous wastes. In the preceding paper, we reported a catalytic procedure for the oxidation of alcohols by using the combination of *N*-oxyl compounds and co-oxidant such as sodium bromite ($NaBrO_2$) and calcium hypochlorite ($Ca(OCl)_2$).[1a] However, this method was faced with a problem that undesired $NaBrO_2$-based bromination of the benzene nucleus proceeded considerably in competition with normal oxidation with *in situ* generated *N*-oxoammonium salts when aromatic alcohols bearing electron-releasing groups were oxidized. We, therefore, turned our attention to a new oxidizing system and examined the combination of *N*-oxyl compound and tetraalkylammonium tribromides (R_4NBr_3) as a co-oxidant for oxidation of aromatic alcohols, because these are considered to be more controllable than $NaBrO_2$ in terms of their reactivity.

Tetraalkylammonium tribromides (R_4NBr_3) have mainly been used for brominations of unsaturated compounds[2,3a] and ketones,[3b] and sometimes for the oxidation of amines[4] and amides,[3c] but, to the best of our knowledges, there was no precedent entry for a catalytic oxidation system. These tribromide salts are soluble in polar solvents such as CH_2Cl_2, $CHCl_3$, and AcOEt, but insoluble in H_2O, and exhibit long-term stability on exposure to air. Although tetraalkylammonium tribromides are available from the corresponding tetraalkylammonium bromides (R_4NBr) by various bromination methods,[2] we employed an electrooxidation method for their preparation starting from tetraalkylammonium bromides and potassium bromide.[5] R_4NBr_3 can undergo disproportionation in an aqueous basic solution to give hypobromite and Br^-, and hypobromite species thus generated is known to be a powerful oxidizing agent with redox potential of 0.71 V vs. NHE.[6] Consequently, these properties of R_4NBr_3 are expected to be of benefit to the present purpose as a co-oxidant for *N*-oxoammonium-mediated oxidations, which indeed resulted in a dramatic improvement in circumventing the problem mentioned above.

Results and Discussion

In order to know a general trend for *N*-oxyl compound **5** (oxidant)/Bu_4NBr_3 (co-oxidant) combination, we firstly examined the oxidation of 1-undecanol (R^1=*n*-$C_{10}H_{21}$, **1a**) in an aqueous-organic two phase solution. To our delight, it turned out that the oxidation proceeded rather rapidly without any dimeric ester as a by-product (Scheme 1).

The reaction was carried out by employing 1.5—2.0 equivalents of Bu_4NBr_3 and a mixture of **1a** and **5** in a two phase solution consisted of CH_2Cl_2 and an aqueous buffer solution at 20 °C. Time-dependent curves of yields of the desired aldehyde **2a** (R^1=*n*-$C_{10}H_{21}$) are shown for various pH values in Fig. 1. The enhanced oxidizing ability of the combination of *N*-oxyl **5** and Bu_4NBr_3 is clearly indicated at pH 8.6 (aqueous $NaHCO_3$ solution) and more significantly at pH 8.0 (aqueous AcONa solution). An aqueous-organic two-phase solution was essential for the present purpose, otherwise no reaction was effected. Indeed, an attempted oxidation of **1a** in a single phase system of CH_2Cl_2 resulted in an almost quantitative recovery of **1a**. Neither higher (11) nor lower (4—7) pH than the values indicated above afforded the

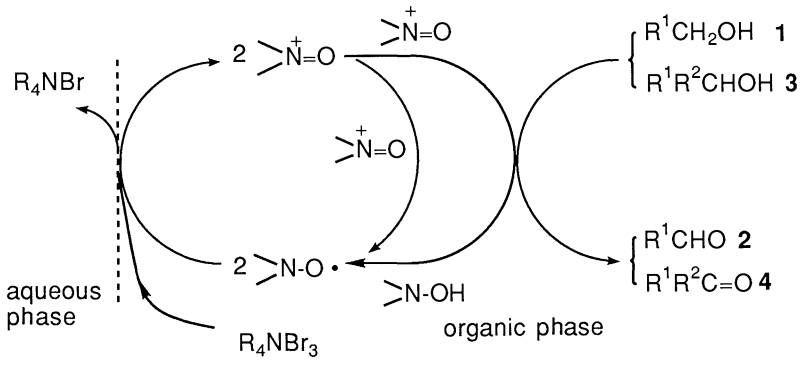

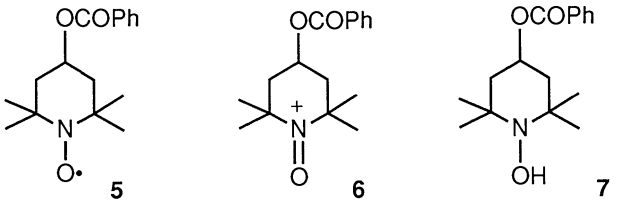

Scheme 1.

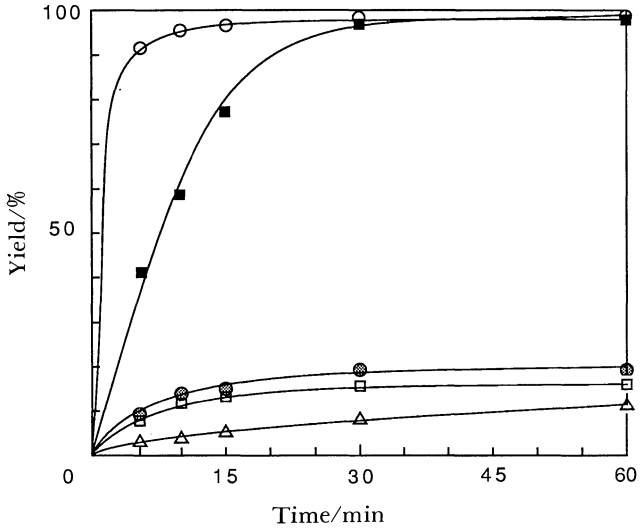

Fig. 1. Time-yield curves for the oxidation of **1a** with a **5**–Bu_4NBr_3 system under various pH values. Symbols are as follows: pH; 4 (△), pH; 7 (□), pH; 8.0 (○), pH; 8.8 (■), pH; 11 (●). Data points were obtained by GC analyses based on an internal standard (octyl acetate) method.

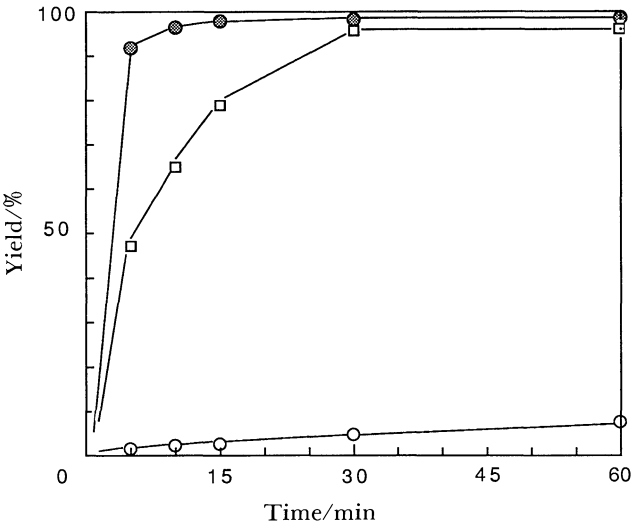

Fig. 2. Time-yield curves for the oxidation of **1a** and Bu_4NBr_3 (2.0 equiv) under various amounts of **5**. Symbols are as follows: 1 mol% of **5** (●); 0.5 mol% of **5** (□); in the absence of **5** (○). Analyzed by GC based on an internal standard (octyl acetate) method.

reasonable levels of yield, only reaching 20% or less. Furthermore, only 0.5—1.0 mol% of the *N*-oxyl compound **5** was enough for the oxidation to be completed within 35 minutes under the conditions indicated (Fig. 2).

Although the detailed mechanism on the present oxidation must wait future studies, we can point out its some aspects. Based on the amount of Bu_4NBr_3 as well as the fact that the oxidation can be enhanced in a two-phase solution buffered at pH 8.0—8.6, it is proposed that this reaction would involve the formation of hypobromite species from Bu_4NBr_3 at the initial stage.[7] Thus, the disproportionation of Bu_4NBr_3 led to hypobromite HOBr as a source of positively charged bromine species, the reaction of which with **5** gave rise to *N*-oxoammonium salt that is responsible for the oxidation of substrates in the organic phase. In contrast to the trimeric structure of $NaBrO_2$[8] as a versatile co-oxidant in the *N*-oxoammonium/*N*-oxyl redox system,[1a] Bu_4NBr_3 dissolved in the organic phase of a binary system may exist as a monomer and be more stable than $NaBrO_2$.[7b] In these respects R_4NBr_3 is highly amenable to the

Table 1. Oxidation of Aromatic Alcohols with **5** and Various Oxidizing Reagents[a]

Entry	Substrate	Oxidizing reagents	Products (Yield/%)
1	**1b**	Bu_4NBr_3 (1.5 equiv)[b]	**2b** (88) **8b** (—)
2	**1b**	$PhCH_2Bu_3NBr_3$ (1.5 equiv)[b]	**2b** (87) **8b** (—)
3	**1b**	$NaBrO_2$ (5.0 equiv)[c]	**2b** (39) **8b** (44)
4	**1b**	Electrolysis (4.0 F mol^{-1})[d]	**2b** (9) **8b** (78)
5	**3a**	Bu_4NBr_3 (3.0 equiv)[b]	**4a** (92) **9a** (—)
6	**3a**	Electrolysis (10.0 F mol^{-1})[d]	**4a** (—) **9a** (87)

a) Substrates (1 mmol) were allowed to react in the presence of *N*-oxyl **5** (0.01 mmol). b) Carried out in a CH_2Cl_2–5% AcONa (6:14 v/v) solution. c) Carried out in a CH_2Cl_2–5% $NaHCO_3$ (5:10 v/v) solution. d) Electrolyzed in a CH_2Cl_2–25% NaBr (5:10 v/v)-(Pt) system.

present redox system, which, in turn, implies that it can provide the splended oxidative ability.

In contrary to the selective oxidation with Bu_4NBr_3, our attempt to employ pyridinium tribromide (Py·HBr·Br_2) as an alternative co-oxidant for the present reaction system was unsuccessful. For instance, the similar oxidation of **1a** with a combination of **5** (catalytic) and Py·HBr·Br_2 (1.6 equivalent) was carried out in an aqueous 5% AcONa–CH_2Cl_2 system, affording a mixture of **2a** and the dimeric ester such as undecyl undecanoate, in 11% and 22% yields, respectively.

Since R_4NBr_3 is a good brominating agent applicable to a variety of unsaturated compounds including arenes,[2] there is a fear of an unfavorable bromination on the aromatic ring in the oxidation of benzylic alcohols. However, the present oxidizing system consisted of an *N*-oxyl **5** (catalytic) and R_4NBr_3 (stoichiometric) turned out to be promising for the selective oxidation of various benzylic alcohols even though the aromatic rings were substituted with electron-releasing groups. In a previous work, we observed that bromination on the aromatic nucleus of *m*-methoxybenzyl alcohol (**1b**) became a predominant process (44% bromination in addition to 39% of the normal oxidation)[1a] under the conditions employing *N*-oxyl **5** and $NaBrO_2$. It was also the case for an indirect electrooxidation with a two redox couples of *N*-oxoammonium/*N*-oxyl and [Br^+ or $Br^\cdot$]/Br^- (78% bromination).[9] As shown in Entries 1 and 2, Table 1, to our delight, such a bromination process was almost completely suppressed by use of a combination of *N*-oxyl **5** and tetraalkylammonium tribromide such as Bu_4NBr_3 (88% yield) or $PhCH_2Bu_3NBr_3$ (87% yield).

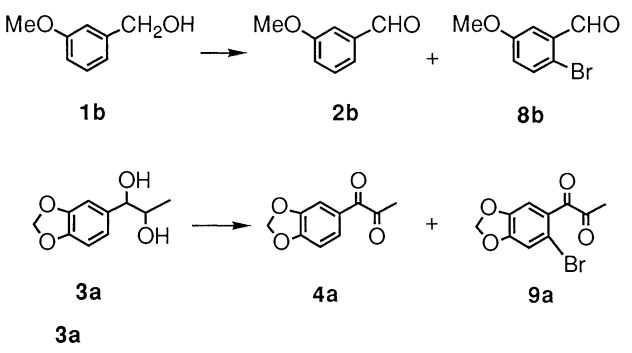

Furthermore, the oxidation of the aromatic diol **3a** by the combination of *N*-oxyl **5** and Bu_4NBr_3 afforded the corresponding 1,2-diketone **4a**, selectively (Entry 5),

Table 2. Oxidation of Primary and Secondary Alcohols by an *N*-Oxyl **5**-Bu_4NBr_3 System[a]

Entry	Substrate	Bu_4NBr_3, equiv/reaction time/h	Product (Yield/%)[b]
1	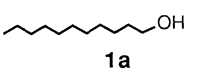 **1a**	1.5/1.0	**2a** (95)
2	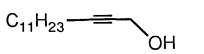 **1c**	2.3/1.0	**2c** (16) (79)
3[c]	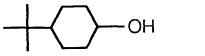 **3b**	2.0/2.5	**4b** (95)
4	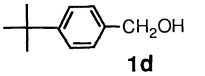 **1d**	1.5/1.0	**2d** (93)
5	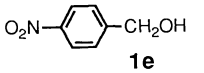 **1e**	1.5/1.0	**2e** (96)
6	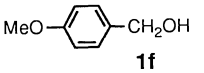 **1f**	1.5/1.0	**2f** (92)
7	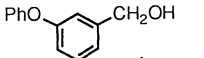 **1g**	1.5/1.0	**2g** (92)
8	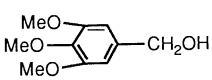 **1h**	1.5/2.0	**2h** (76)[d]
9	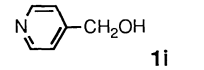 **1i**	1.5/1.5	**2i** (94)
10	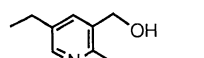 **1j**	1.5/1.5	**2j** (90)

a) Substrates (1—2 mmol) were allowed to react with **5** (0.01—0.02 mmol) in a CH_2Cl_2 (3 ml)-aqueous 5% NaOAc system (7—14 ml). b) Yields based on isolated products. c) Aqueous saturated $NaHCO_3$ was used instead of aqueous 5% NaOAc. d) Contaminated with brominated product (18%).

while the indirect electrooxidation of **3a** with *N*-oxyl **5** as a mediator in an aqueous NaBr–CH_2Cl_2 solution resulted in the bromination concurrent with the oxidation to give **9a**, exclusively (Entry 6).

We applied this oxidation method to a variety of primary and secondary alcohols and the results are shown in Table 2. A triple bond adjacent to the hydroxyl group undergoes a competitive bromination under these conditions in the extent that products are consisted of an unseparable 17:83 mixture of the alkynal **2c** and 2,3-dibromo-2-tetradecenal (Entry 2). However, benzylic alcohols are oxidized to the corresponding aldehydes without any bromination on the rings. The yields are reproducible and as high as 90%. Some of the entries in Table 2 should be useful as an intermediate of agrochemicals (Entries 6 and 9) and drugs (Entry 7).

In conclusion, the present catalytic oxidation method is useful since R_4NBr_3 can easily be obtained by the electrooxidation of the corresponding R_4NBr with potassium bromide. Furtheremore, tetraalkylammonium bromide salts were recovered after the oxidation reaction by a chromatographic separation and then R_4NBr_3 were regenerated by their electrooxidation. This combined system of *N*-oxyl compound **5** and tetraalkylammonium tribromides can highly promote oxidation of alcohols as compared with the combination of **5** and $NaBrO_2$, which is advantageous in terms of durability of the recyclable *N*-oxyl compounds.

Experimental

All reactions were carried out under an argon atmosphere. Boiling points indicated by an air-bath temperature and melting points were uncorrected. Starting alcohols were purified by distillation or column chromatography (SiO_2) prior to use. GC analyses were carried out on a "Quadrex" Bond-Fused Silica capillary column (Methyl Silicone: 0.25 μm film thickness, 25 m×0.25 mm I. D.). ^1H NMR and ^{13}C NMR spectra were recorded in $CDCl_3$. Elemental analyses were performed in our laboratory.

Preparation of Tetrabutylammonium Tribromide. A cylindrical two compartment electrolysis cell, in which anodic room (200 ml volume) and the cathodic room (80 ml) were separated by a porous glass filter (20 mm in diameter, Type 5G). A platinum foil (4 cm×3 cm) and a lead plate (4 cm×3 cm) were used for the anode and the cathode, respectively. In the anodic compartment were placed Bu_4NBr (9.76 g, 30 mmol) and water (100 ml), and in the cathodic chamber were placed potassium bromide (3.57 g, 30 mmol) and water (40 ml). The mixture was electrolyzed at a constant current density of 25 mA cm^{-2} on warming at 40—50 °C. Orange crystals have precipitated on the surface of the anode upon charging the electricities and the reaction was terminated when 4 F mol^{-1} of electricity had been passed. To the anodic compartment was added CH_2Cl_2 (30 ml) to dissolve the orange solids and the aqueous phase was extracted with CH_2Cl_2. The combined extracts were dried ($MgSO_4$) and concentrated to dryness. The product was purified by recrystallization from CH_2Cl_2–Et_2O (1:1 v/v, 7 ml) to give 11.6 g (80%) of Bu_4NBr_3 as orange solids; mp 72—74 °C (lit,[11] 73—76 °C); IR (KBr) 2928, 2860, 1464, 1377, 1029, 880, 801, 741 cm^{-1}; ^1H NMR (200 MHz) δ=1.04 (t, 12, CH_3), 1.52 (m, 8, N-C-C-CH_2), 1.71 (m, 8, N-C-CH_2), 3.25 (t, 8, N-CH_2); ^{13}C NMR (50 MHz) δ=13.7, 19.8, 24.1, 59.1. Found: C, 39.9; H, 7.7; N, 3.0%. Calcd for $C_{16}H_{36}Br_3N$: C, 39.9; H, 7.5; N, 2.9%.

Similarly, benzyltributylammonium tribromide ($PhCH_2Bu_3NBr_3$) was obtained in 60—70% yields from $PhCH_2Bu_3NBr$; mp 93—94 °C; IR (KBr) 3382, 1481, 1470, 1458, 1406, 891, 777, 725, 704 cm^{-1}; ^1H NMR (500 MHz) δ=1.03 (t, 9, CH_3), 1.46 (m, 6, N-C-C-CH_2), 1.84 (m, 6, N-C-CH_2), 3.22 (m, 6, N-CH_2), 4.62 (s, 2, CH_2Ph), 7.47—7.51 (m, 5, ArH); ^{13}C NMR (126 Hz) δ=13.7, 19.8, 24.4, 58.7, 63.1, 126.6, 129.7, 131.1, 132.4.

Oxidation of Primary Alcohols to Aldehydes. A Typical Procedure. In a round-bottomed flask were succesively placed 1-undecanol (**1a**, 172 mg, 1.0 mmol), 4-benzoyloxy-2,2,6,6-tetramethyl-1-piperidinyloxyl (**5**, 2.8 mg, 0.01 mmol), and CH_2Cl_2 (3 ml). The mixture was covered with aqueous 5% CH_3CO_2Na (7 ml) and the tack was purged with argon. After agitating vigorously, to this mixture was added portionwise Bu_4NBr_3 (709 mg, 2.0 mmol). The mixture was stirred for 1 h at room temperature and the reaction was quenched with ethanol (0.2 ml). The organic layer was separated and the aqueous layer was extracted with CH_2Cl_2. The combined extracts were dried (Na_2SO_4), and concentrated. Flash chromatography (SiO_2, hexane–AcOEt 10:1 v/v) of the crude product gave 163 mg (95%) of undecanal (**2a**) as an oil; bp 113 °C (9 Torr, 1 Torr=133.322 Pa); IR (film) 2718, 1729 (C=O), 1466 cm^{-1}; ^1H NMR (500 MHz) δ=0.88 (t, *J*=7.0 Hz, 3, CH_3), 1.26 (brs, 14, CH_2), 1.62 (m, 2, CH_2), 2.41 (dt, *J*=7.3, 2.0 Hz, 2, CH_2CO), 9.76 (t, *J*=2.0 Hz, 1, CHO); ^{13}C NMR (126 MHz) δ=14.1, 19.2, 22.1, 22.7, 29.29, 29.34, 29.4, 29.5, 31.9, 43.9, 203.0.

Oxidation of Secondary Alcohols to the Ketones. A Typical Procedure. A solution of 4-*t*-butylcyclohexanol (**3b**, 156 mg, 1 mmol) and **5** (2.8 mg, 0.01 mmol) in CH_2Cl_2 (6 ml) was covered with aqueous saturated $NaHCO_3$ (12 ml). To this biphase mixture was added portionwise Bu_4NBr_3 (709 mg, 2.0 mmol) under a vigorous stirring at 40 °C. The mixture was stirred for an additional 2.5 h. The mixture was worked up in the usual manner and the crude products were purified by column chromatography to give 146 mg (95%) of 4-*t*-butylcyclohexanone (**4b**) as solids; mp 48—49 °C (from hexane) (lit,[16] 47.5—48.5 °C).

Properties and spectral data of the compounds in Table 1 and Table 2 are as follows.

3-Methoxybenzaldehyde (**2b**): Bp 141—142 °C (50 Torr) (lit,[12] 126—127 °C (25 Torr)).

4-Bromo-3-methoxybenzaldehyde (**8b**): Mp 71—73 °C (from hexane) (lit,[13] 74 °C); IR (KBr) 1601 (C=O), 1572, 1475, 1286, 934, 822, 648, 598 cm^{-1}; ^1H NMR (500 MHz) δ=3.828, 3.834 (s, 3, MeO), 7.01 (m, 1. ArH), 7.40 (m, 1, ArH), 7.45 (m, 1, ArH), 10.29 (d, *J*=4 Hz, 1, CHO); ^{13}C NMR (126 MHz) δ=55.7, 112.6, 117.9, 123.1, 133.9, 134.5, 159.2, 191.7.

A mixture of 2-Tetradecynal (**2c**)[14] and 2,3-Dibromo-2-tetradecenal: IR (film) 2858, 1700 (C=O), 1673, 1578, 1466, 1379, 1139, 1096 cm^{-1}; ^1H NMR (200 MHz, peaks due to the major component) δ=0.87 (t, *J*=6.7 Hz, 3), 1.26 (brs, 14, CH_2), 1.69 (m, 2, CH_2), 2.96, 3.00 (d, *J*=8.0 Hz, 2, CH_2), 9.81

(s, 1, CHO); ^{13}C NMR (50 MHz, peaks due to the major component) δ=14.1, 22.7, 27.2, 28.7, 29.25, 29.29, 29.4, 29.6 (2C), 31.9, 43.2, 120.7, 144.7, 185.6.

4-*t*-Butylbenzaldehyde (**2d**): Bp 89—90 °C (33 Torr).[15]

4-Nitrobenzaldehyde (**2e**): Mp 103—104 °C (lit,[16] 104—105 °C).

4-Methoxybenzaldehyde (**2f**): Bp 103—104 °C (33 Torr) (lit,[17] 248 °C).

3-Phenoxybenzaldehyde (**2g**): Bp 180—184 °C (14 Torr) (lit,[18] 175—176 °C (11 Torr)); IR (film) 3066, 2818, 2734, 1694 (C=O), 1582, 1483, 1452, 1390, 1164, 1131, 944 cm^{-1}; ^{1}H NMR (500 MHz) δ=7.04 (d, J=7.4 Hz, 2), 7.17 (t, J=7.4 Hz, 1), 7.29 (dd, J=7.8, 2.2 Hz, 1), 7.38 (t, J=7.8 Hz, 2), 7.46 (m, 1), 7.50 (t, J=7.8 Hz, 1), 7.60 (d, J=7.4 Hz, 1), 9.96 (s, 1, CHO); ^{13}C NMR (126 MHz) δ=118.1, 119.5, 124.2, 124.6, 124.7, 130.0, 130.4, 138.0, 156.2, 158.4, 191.6.

3,4,5-Trimethoxybenzaldehyde (**2h**): Mp 72—74 °C (lit,[19] 73—74 °C).

3-Pyridinecarbaldehyde (**2i**): Bp 83—85 °C (33 Torr) (lit,[20] 102—103 °C (20 Torr)).

5-Ethyl-2-methyl-3-pyridinecarbaldehyde (**2j**): Bp 115—117 °C (15 Torr) (lit,[1a] 115—117 °C (15 Torr)).

1-(3,4-Methylenedioxyphenyl)-1,2-propanedione (**4a**): Bp 108—111 °C (1 Torr) (lit,[21] 115—117 °C (1—2 Torr)); IR (film) 2916, 1715 (C=O), 1661 (C=O), 1605, 1506, 1491, 1446, 1354, 1267, 1038, 932 cm^{-1}; ^{1}H NMR (500 MHz) δ=2.49 (s, 3, CH_3), 6.07 (s, 2, CH_2), 6.87 (d, J=8 Hz, 1, PhH), 7.47 (d, J=1.6 Hz, 1, PhH), 7.62 (dd, J=8, 1.5 Hz, 1, PhH); ^{13}C NMR (126 MHz) δ=26.5, 102.1, 108.3, 109.0, 126.3, 128.0, 148.4, 153.1, 189.7, 200.8.

Recovery Experiment of Tetrabutylammonium Tribromide after the Oxidation Reaction of Alcohol. A mixture of EtOH (96 mg, 2.8 mmol) and the *N*-oxyl **5** (5.8 mg, 0.02 mmol) was treated with Bu_4NBr_3 (1.02 g, 2.12 mmol) in a suspension of CH_2Cl_2 (9 ml) and aqueous 5% AcONa (27 ml) for 30 min at room temperature. An aqueous phase was extracted with CH_2Cl_2 and the combined organic layers were dried (Na_2SO_4), and concentrated under vacuum. The residual solids were passed through a short column (SiO_2, AcOEt/hexane and then MeOH as an eluent) to give 657 mg of Bu_4NBr; IR (KBr) 2922, 2962, 2876, 1475, 1168, 1110, 897, 884, 739 cm^{-1}; ^{1}H NMR (500 MHz) δ=0.90 (t, J=7.4 Hz, 12, CH_3), 1.36 (m, 8, N-C-C-CH_2), 1.59 (m, 8, N-C-CH_2), 3.28 (m, 8, N-CH_2); ^{13}C NMR (126 MHz) δ=13.4, 19.5, 23.9, 58.7. Found: C, 59.2; H, 12.0; N, 4.3%. Calcd for $C_{16}H_{36}BrN$: C, 59.6; H, 11.3; N, 4.3%. The solids were electrolyzed with KBr (250 mg, 2.1 mmol) in water (50 ml) in the anodic compartment of the divided cell. Passage of 4.0 F mol^{-1} of electricity at 25 mA cm^{-2} at room temperature gave 663 mg (67%) of Bu_4NBr_3 as orange solids.

The present work was partially supported by a Grant-in-Aid for Developmental Scientific Research No. 63850172 from the Ministry of Education, Science and Culture. We are grateful to the SC-NMR laboratory of Okayama University for experiments with Varian VXR-500 and -200 instruments.

References

1) a) T. Inokuchi, S. Matsumoto, T. Nishiyama, and S. Torii, *J. Org. Chem.*, **55**, 462 (1990); b) M. Yamaguchi, T. Takata, and T. Endo, *ibid.*, **55**, 1490 (1990); c) P. L. Anelli, C. Biffi, F. Montanari, and S. Quici, *ibid.*, **52**, 2559 (1987); d) R. Siedlecka, J. Skarzewski, and J. Mlochowski, *Tetrahedron Lett.*, **31**, 2177 (1990); e) T. Suzuki, K. Iizuka, T. Nabeshima, and Y. Yano, *Chem. Lett.*, **1990**, 1497, and references cited therein.

2) S. Kajigaeshi and T. Kakinami, *J. Synth. Org. Jpn.*, **46**, 986 (1988).

3) a) J. Berthelot, C. Guette, M. Essayegh, P. L. Desbene, and J. Basselier, *Synth. Commun.*, **16**, 1641 (1986); b) S. Kajigaeshi, T. Kakinami, H. Tokiyama, T. Hirakawa, and T. Okamoto, *Bull. Chem. Soc. Jpn.*, **60**, 2667 (1987); c) S. Kajigaeshi, K. Asano, S. Fujisaki, T. Kakinami, and T. Okamoto, *Chem. Lett.*, **1989**, 463.

4) T. Inokuchi, S. Matsumoto, S. Tanigawa, M. Fukushima, and S. Torii, Unpublished results.

5) M. J. Schuler and K. C. Smeltz, U. S. Patent 3432409 (1969); *Chem. Abstr.*, **71**, 9130r (1969).

6) a) CH. S. Reddy and E. V. Sundaram, *Tetrahedron*, **45**, 2109 (1989); b) W. A. Latimer, "Oxidation Potentials," 2nd ed, Prentice Hall, Englewood Cliffs, N. J. (1952).

7) a) H. A. Liebhafsky, *J. Am. Chem. Soc.*, **56**, 1500 (1934); b) G. Bellucci, R. Bianchini, C. Chiappe, and R. Ambrosetti, *ibid.*, **111**, 199 (1989).

8) M. Okawara, *J. Synth. Org. Jpn.*, **42**, 751 (1984).

9) a) T. Inokuchi, S. Matsumoto, T. Nishiyama, and S. Torii, *Synlett*, **1990**, 57; b) T. Inokuchi, S. Matsumoto, and S. Torii, *J. Org. Chem.*, **56** (1991), in press.

10) T. Kageyama and T. Yamamoto, *Chem. Lett.*, **1980**, 671.

11) S. Winstein and N. J. Holness, *J. Am. Chem. Soc.*, **77**, 5562 (1955).

12) R. E. Buckles, M. P. Bellis, and Wm. D. Coder, Jr., *J. Am. Chem. Soc.*, **73**, 4972 (1951).

13) H. H. Hodgson and H. G. Beard, *J. Chem. Soc.*, **1925**, 875.

14) P. C. Wailes, *Aust. J. Chem.*, **12**, 173 (1959).

15) I. Wender, H. Greenfield, S. Metlin, and M. Orchin, *J. Am. Chem. Soc.*, **74**, 4079 (1952).

16) H. C. Brown and B. C. Subba Rao, *J. Am. Chem. Soc.*, **80**, 5377 (1958).

17) "Encyclopedia of Chemical Technology," John Wiley & Sons, New York (1975), Vol. 1, p. 791.

18) M. Tomita, S. Edatsune, and S. Iwata, *J. Pharm. Soc. Jpn.*, **75**, 1021 (1955).

19) K. R. Kavanaph and J. M. Pepper, *Can. J. Chem.*, **33**, 24 (1955).

20) W. Mathes and W. Sauermilch, *Chem. Ber.*, **85**, 1008 (1952).

21) F. Dallacker, J. Thoma, and M. Lipp, *Ann.*, **663**, 67 (1963).

Structure and Optical Properties of Thermochromic Schiff Bases. Charge Transfer Interaction and Proton Transfer in the *N*-Tetrachlorosalicylideneaniline and *N*-Tetrachlorosalicylidene-1-pyrenylamine Crystals

Tamotsu INABE,* Isabelle GAUTIER-LUNEAU,†,†† Naomi HOSHINO,††† Kaoru OKANIWA,†
Hiroshi OKAMOTO, Tadaoki MITANI, Umpei NAGASHIMA, and Yusei MARUYAMA*
Institute for Molecular Science, Myodaiji, Okazaki 444
† Graduate University for Advanced Studies and Institute for Molecular Science, Myodaiji, Okazaki 444
(Received June 22, 1990)

Two kinds of *N*-salicylideneaniline derivatives, *N*-tetrachlorosalicylideneaniline (CL4SA) and *N*-tetrachlorosalicylidene-1-pyrenylamine (CL4SPY), have been prepared and subjected to structural and optical studies in the crystalline state. A thermochromic-type behavior of the former crystal has been observed as a shift of the absorption edge, while that of the latter crystal is much less pronounced. Fairly short O-H···N hydrogen bonds have been found in both compounds through crystallographic studies, which may be mainly due to a steric effect of chlorine substituents. The difference in the proton transfer behavior of CL4SA and CL4SPY should presumably be caused by an intermolecular charge-transfer interaction in the latter crystal.

N-Salicylideneaniline derivatives have been known to show a self-isomerization induced by an intramolecular proton transfer from the hydroxyl oxygen to the imine nitrogen through the O-H···N hydrogen bond. Since this type of proton transfer process involves a π-electron configurational change, the two isomers produced by the proton transfer have different electronic states. Sometimes, this self-isomerization is observed in the crystalline state as thermochromism or photochromism.[1] We have recently carried out structural and optical studies of the thermochromism of *N,N'*-disalicylidene-*p*-phenylenediamine (BSP) crystals.[2] In this crystal the planar BSP molecules are stacked one-dimensionally with a short interplanar spacing (3.29 Å at room temperature and 3.26 Å at 108 K[3]). These relatively short distances suggest that some intermolecular interaction operates in the crystal; we have assigned it to a charge-transfer interaction.

We are particularly interested in the case where the intermolecular interaction is sufficiently strong that the electronic properties of the crystal may be modulated by proton motion. This coupling between protons and electrons may utilized for designing materials which have novel types of electronic properties.[4] From this point of view, the introduction of a sufficiently strong charge-transfer interaction into the *N*-salicylideneaniline system is supposed to be an effective approach. In this paper we report the synthesis of the title compounds, in which an *o*-chloranil-like acceptor portion and aromatic-amine-like donor portions are produced when the proton transfers to the imine nitrogen (NH form). The structural and optical properties of the CL4SA and CL4SPY crystals are also described with emphasis on the nature of their fairly strong hydrogen bonds.

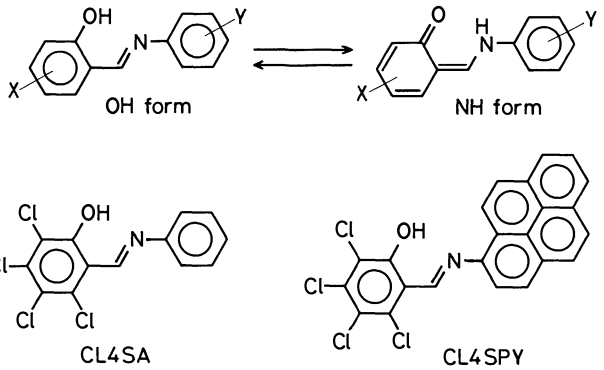

Experimental

Materials. CL4SA was prepared by the condensation of tetrachlorosalicylaldehyde and aniline in refluxed methanol, and was recrystallized from benzene. Tetrachlorosalicylaldehyde was synthesized from tetrachlorophthalic anhydride by following a method reported by Heaney et al.[5] Needle-like single crystals of CL4SA were obtained by slow evaporation of the benzene solution.

CL4SPY was prepared by the condensation of tetrachlorosalicylaldehyde and 1-pyrenylamine in the same manner as CL4SA, and was recrystallized from chlorobenzene. Needle-like single crystals of CL4SPY were grown by slow cooling of a chlorobenzene solution.

Optical Measurements. The infrared and visible absorption as well as the emission spectra were measured using single-crystal specimens and the same methods as reported before.[2]

X-Ray Structure Analyses. The data-collection conditions and the crystal data are summarized in Table 1. In both cases, the measurements were carried out at room temperature with graphite monochromatized Mo$K\alpha$ radiation (λ=0.71073 Å). The intensities of the three standards used (monitored every 100 data measurements) remained constant within 3% for both crystals.

†† Present address: LIESG, ENSEEG, Domaine Universitaire BP75, 38402 Saint-Martin D'Heres, France.
††† Present address: Department of Chemistry, Faculty of Science, Hokkaido University, Sapporo 060.

Table 1. Data-Collection Conditions and Crystal Data

	CL4SA	CL4SPY
Diffractometer	Rigaku AFC-5	Rigaku AFC-5R
2θ range	$<60°$	$<50°$
Range of h, k, and l	$-19\leqq h\leqq 19$ $0\leqq k\leqq 34$ $0\leqq l\leqq 5$	$-17\leqq h\leqq 17$ $0\leqq k\leqq 17$ $0\leqq l\leqq 9$
Scan width/°	$1.2+0.5\tan\theta$	$1.2+0.5\tan\theta$
Scan mode	θ-2θ	θ-2θ
Scan rate/θ° min^{-1}	3	4
Number of unique reflections measured	3995	3447
Number of independent relections observed ($\|F_o\|>3\sigma(F_o)$)	1021	1280
Background count time/sec	8—21.4	5—14.9
Lattice parameter measurement		
2θ range/°	$20<2\theta<30$	$20<2\theta<27$
Number of reflections	25	25
Chemical formula	$C_{13}H_7NOCl_4$	$C_{23}H_{11}NOCl_4$
Molecular weight	335.017	459.159
Crystal color	Orange	Dark red
Crystal size/mm	0.1×0.1×0.7	0.06×0.06×0.5
Crystal system	Monoclinic	Monoclinic
Space group	$P2_1/a$	$P2_1/a$
a/Å	14.117(7)	15.135(3)
b/Å	24.240(9)	15.298(4)
c/Å	3.898(2)	8.197(2)
β/deg	93.62(5)	100.05(2)
V/Å^3	1331.2(10)	1868.9(7)
Z	4	4
D_c/g cm^{-3}	1.672	1.633
μ(Mo$K\alpha$)/cm^{-1}	8.81	6.51
R	0.046	0.035
R_w	0.063	0.034
Weighting factor (g) [$w^{-1}=\sigma^2+(gF)^2$]	0.040	0.015

Table 2. Atomic Parameters for CL4SA (×10^4)

Atom	x	y	z	B_{eq}/Å^2[a)]
Cl(1)	10622 (1)	1092 (1)	−1198 (6)	5.2
Cl(2)	9047 (2)	384 (1)	2012 (5)	5.0
Cl(3)	7086 (1)	903 (1)	3217 (5)	4.6
Cl(4)	6693 (1)	2132 (1)	1223 (5)	4.7
O(5)	10027 (3)	2190 (2)	−3079 (13)	4.2
N(6)	8904 (4)	2996 (2)	−3685 (14)	3.5
C(7)	8465 (4)	2160 (3)	−1068 (16)	2.7
C(8)	9350 (4)	1912 (3)	−1593 (17)	3.2
C(9)	9526 (5)	1366 (3)	−588 (17)	3.2
C(10)	8828 (4)	1060 (3)	893 (17)	3.4
C(11)	7954 (4)	1296 (3)	1430 (16)	2.8
C(12)	7775 (4)	1837 (3)	523 (16)	3.0
C(13)	8273 (5)	2717 (3)	−2138 (17)	3.5
C(14)	8755 (5)	3540 (3)	−4926 (17)	3.3
C(15)	7869 (5)	3788 (3)	−5376 (19)	4.2
C(16)	7811 (5)	4321 (3)	−6600 (20)	4.5
C(17)	8608 (6)	4620 (3)	−7334 (20)	4.7
C(18)	9476 (6)	4360 (4)	−6960 (22)	5.3
C(19)	9563 (5)	3827 (3)	−5740 (19)	4.3

a) $B_{eq}=4/3\sum_i\sum_j\beta_{ij}\boldsymbol{a}_i\boldsymbol{a}_j$.

Both crystal structures were solved by a direct method,[6] and the positions of all hydrogen atoms were determined from difference synthesis maps. A block-diagonal least-squares technique (UNICS III[7]) with anisotropic thermal

Table 3. Atomic Parameters for CL4SPY (×10^4)

Atom	x	y	z	B_{eq}/Å^2
Cl(1)	680 (1)	−2937 (1)	6206 (2)	4.6
Cl(2)	2654 (1)	−2721 (1)	7983 (2)	4.4
Cl(3)	3760 (1)	−1088 (1)	7303 (2)	4.7
Cl(4)	2839 (1)	399 (1)	5040 (2)	4.3
O(5)	0 (2)	−1460 (2)	4144 (4)	3.8
N(6)	99 (2)	−24 (3)	2645 (5)	2.9
C(7)	1332 (3)	−596 (3)	4579 (6)	2.5
C(8)	841 (3)	−1358 (3)	4863 (6)	3.0
C(9)	1274 (3)	−2009 (3)	5919 (6)	2.7
C(10)	2157 (3)	−1911 (3)	6679 (6)	2.9
C(11)	2651 (3)	−1171 (3)	6413 (6)	2.9
C(12)	2237 (3)	−527 (3)	5378 (6)	2.8
C(13)	916 (3)	55 (3)	3439 (6)	3.1
C(14)	−334 (3)	590 (3)	1488 (6)	2.9
C(15)	91 (3)	1340 (3)	1065 (7)	3.6
C(16)	−336 (3)	1930 (3)	−67 (7)	3.9
C(17)	−1223 (3)	1814 (3)	−784 (6)	3.0
C(18)	−1676 (3)	1051 (3)	−378 (6)	2.6
C(19)	−1223 (3)	423 (3)	743 (5)	2.4
C(20)	−1703 (4)	2426 (3)	−1957 (6)	3.8
C(21)	−2583 (4)	2316 (3)	−2585 (6)	3.9
C(22)	−3064 (3)	1572 (3)	−2169 (6)	3.2
C(23)	−3982 (4)	1448 (4)	−2796 (7)	5.1
C(24)	−4424 (3)	703 (4)	−2408 (7)	5.0
C(25)	−3971 (4)	65 (4)	−1392 (7)	4.3
C(26)	−3056 (3)	167 (3)	−725 (6)	3.1
C(27)	−2571 (3)	−464 (3)	358 (6)	3.3
C(28)	−1705 (3)	−349 (3)	1060 (6)	3.2
C(29)	−2596 (3)	930 (3)	−1090 (6)	2.8

parameters for non-hydrogen atoms and isotropic for hydrogen atoms was employed for the structure refinement.

Results

Structures. The atomic parameters of CL4SA and CL4SPY obtained by X-ray analyses are listed in Tables 2 and 3, respectively. Both molecular structures are shown in Fig. 1; the bond lengths and angles are listed in Table 4. The dihedral angle between two aromatic groups connected by the azomethine group is 15° for CL4SA and 2.3° for CL4SPY. These values are much smaller compared with that of *N*,*N*′-disalicylidene-1,6-pyrenediamine, DSPY (42°), in which proton transfer is suppressed.[3]

The most noticeable point commonly observed for both compounds is the quite short distance of O(5)···N(6) (2.517(7) Å for CL4SA and 2.534(7) Å for CL4SPY), which form the hydrogen bond. The corresponding distances are in the range between 2.58 and 2.62 Å for other *N*-salicylideneanilines.[2,3,9,10] The O(5)–C(8) bond lengths (1.332(8) Å for CL4SA and 1.316(5) Å for CL4SPY) are also shorter than those of BSP, DSPY, 2-chloro-*N*-salicylideneaniline,[9] and *N*-(5-chlorosalicylidene)aniline,[10] in which the values are in the range between 1.350 and 1.365 Å. This contraction obviously indicates that there exists a resonance contribution from the quinonoid structure, which is produced when a proton transfers from the hydroxyl oxygen to the imine nitrogen. A corresponding alternation of the bond lengths of the benzene ring expected for a quinonoid structure has been observed for both compounds.

The crystal structures of CL4SA and CL4SPY are shown in Figs. 2(a) and (b), respectively. The CL4SA molecules are translationally stacked along the *c*-axis; the interplanar distances are 3.44 Å between the tetrachlorophenol rings and 3.64 Å between the benzene rings of the aniline side. On the other hand, the

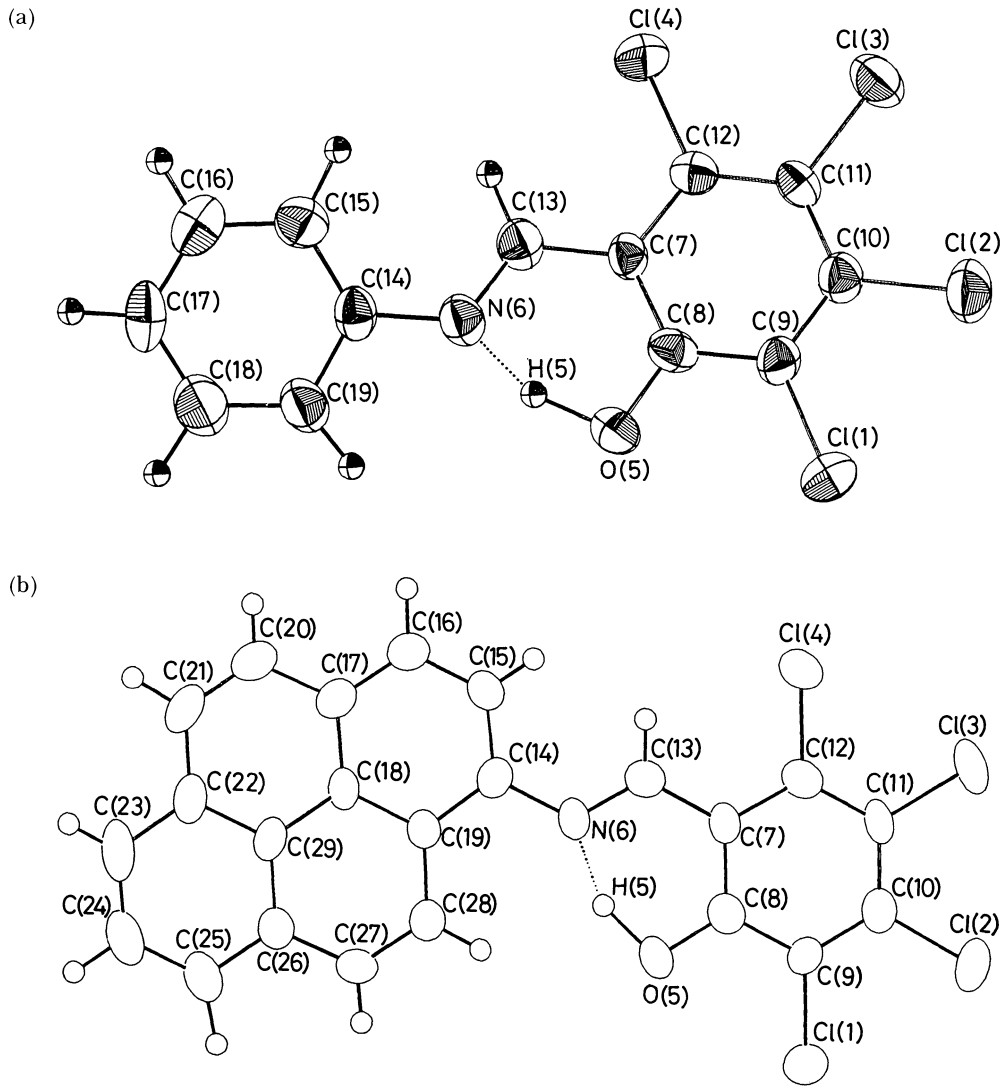

Fig. 1. ORTEP drawing[16] of CL4SA (a) and CL4SPY (b) showing the atom numbering scheme.

Table 4. Bond Lengths and Angles of CL4SA and CL4SPY

	CL4SA	CL4SPY		CL4SA	CL4SPY
Distance	*l*/Å	*l*/Å	C(7)–C(8)–C(9)	120.3(6)	118.8(4)
Cl(1)–C(9)	1.715(7)	1.719(5)	Cl(1)–C(9)–C(8)	118.2(5)	118.1(3)
Cl(2)–C(10)	1.718(7)	1.721(5)	Cl(1)–C(9)–C(10)	121.4(5)	121.1(4)
Cl(3)–C(11)	1.731(7)	1.715(4)	C(8)–C(9)–C(10)	120.3(6)	120.8(4)
Cl(4)–C(12)	1.724(7)	1.732(5)	Cl(2)–C(10)–C(9)	119.6(5)	119.0(4)
O(5)–C(8)	1.332(8)	1.316(5)	Cl(2)–C(10)–C(11)	120.1(5)	119.6(3)
N(6)–C(13)	1.298(9)	1.298(6)	C(9)–C(10)–C(11)	120.2(6)	121.4(4)
N(6)–C(14)	1.414(9)	1.413(6)	Cl(3)–C(11)–C(10)	119.5(5)	120.3(4)
C(7)–C(8)	1.412(9)	1.423(7)	Cl(3)–C(11)–C(12)	120.2(5)	121.0(4)
C(7)–C(12)	1.422(9)	1.415(6)	C(10)–C(11)–C(12)	120.3(6)	118.6(4)
C(7)–C(13)	1.435(9)	1.434(7)	Cl(4)–C(12)–C(7)	118.7(5)	118.8(4)
C(8)–C(9)	1.399(9)	1.405(6)	Cl(4)–C(12)–C(11)	120.2(5)	119.2(3)
C(9)–C(10)	1.387(9)	1.380(6)	C(7)–C(12)–C(11)	121.0(6)	122.0(4)
C(10)–C(11)	1.388(9)	1.394(7)	N(6)–C(13)–C(7)	120.2(6)	122.3(4)
C(11)–C(12)	1.380(9)	1.378(7)	N(6)–C(14)–C(15)	124.1(6)	122.4(4)
C(14)–C(15)	1.390(10)	1.389(7)	N(6)–C(14)–C(19)	116.0(6)	118.0(4)
C(14)–C(19)	1.390(10)	1.400(6)	C(15)–C(14)–C(19)	120.0(7)	119.6(4)
C(15)–C(16)	1.378(11)	1.373(7)	C(14)–C(15)–C(16)	118.9(7)	121.8(4)
C(16)–C(17)	1.382(12)	1.379(7)	C(15)–C(16)–C(17)	122.1(7)	120.8(5)
C(17)–C(18)	1.378(12)	1.422(7)	C(16)–C(17)–C(18)	118.0(7)	118.6(4)
C(18)–C(19)	1.379(11)	1.420(6)	C(17)–C(18)–C(19)	121.6(8)	120.6(4)
C(17)–C(20)	—	1.444(7)	C(16)–C(17)–C(20)	—	122.7(5)
C(18)–C(29)	—	1.425(6)	C(18)–C(17)–C(20)	—	118.7(4)
C(19)–C(28)	—	1.436(7)	C(17)–C(18)–C(29)	—	119.2(4)
C(20)–C(21)	—	1.352(7)	C(19)–C(18)–C(29)	—	120.2(4)
C(21)–C(22)	—	1.424(8)	C(14)–C(19)–C(18)	—	118.5(4)
C(22)–C(23)	—	1.408(7)	C(14)–C(19)–C(28)	—	123.5(4)
C(22)–C(29)	—	1.423(7)	C(18)–C(19)–C(28)	—	118.1(4)
C(23)–C(24)	—	1.387(8)	C(17)–C(20)–C(21)	—	121.4(5)
C(24)–C(25)	—	1.385(8)	C(20)–C(21)–C(22)	—	121.3(5)
C(25 –C(26	—	1.407(7)	C(21)–C(22)–C(23	—	122.3(5
C(26)–C(27)	—	1.426(7)	C(21)–C(22)–C(29)	—	118.7(4)
C(26)–C(29)	—	1.417(7)	C(23)–C(22)–C(29)	—	119.1(5)
C(27)–C(28)	—	1.348(7)	C(22)–C(23)–C(24)	—	120.8(5)
O(5)–H(5)	1.18 (9)	1.17 (6)	C(23)–C(24)–C(25)	—	120.6(5)
N(6)···H(5)	1.38 (9)	1.44 (7)	C(24)–C(25)–C(26)	—	120.4(5)
			C(25)–C(26)–C(27)	—	122.1(5)
Angle	*θ*/°	*θ*/°	C(25)–C(26)–C(29)	—	119.8(4)
C(13)–C(6)–C(14)	123.6(6)	124.4(4)	C(27)–C(26)–C(29)	—	118.1(4)
C(8)–C(7)–C(12)	117.8(6)	118.5(4)	C(26)–C(27)–C(28)	—	122.2(5)
C(8)–C(7)–C(13)	120.7(6)	119.5(4)	C(19)–C(28)–C(27)	—	121.2(4)
C(12)–C(7)–C(13)	121.5(6)	121.9(4)	C(22)–C(29)–C(26)	—	119.3(4)
O(5)–C(8)–C(7)	120.8(6)	121.0(4)	C(18)–C(29)–C(22)	—	120.6(4)
C(5)–C(8)–C(9)	118.8(6)	120.2(4)	C(18)–C(29)–C(26)	—	120.1(4)

CL4SPY molecules are stacked with an alternating orientation. As shown in Fig. 2(c), this stacking mode leads to an effective intermolecular overlapping of the donor and acceptor parts. Consequently, the interplanar distances between the mean planes of the entire molecule are short, i.e., 3.37 and 3.39 Å, and there are several short interatomic distances between stacked molecules (Fig. 2(c)). The intermolecular contacts in CL4SA are longer than the sum of the van der Waals radii, except for Cl(2)···C(11) (3.489(7) Å).

Optical Properties. The polarized infrared spectra of the CL4SA single crystal at room temperature are shown in Fig. 3(a). An extremely broad band centered at ca. 2700 cm^{-1} is observed when the polarization is perpendicular to the *c*-axis. Since the hump at 3030 cm^{-1} is undoubtedly assigned to the CH stretching mode, this broad molecular in-plane component is assignable to the OH stretching mode. Compared with BSP and DSPY, the intensity is considerably weak, although the position and the half width (ca. 600 cm^{-1}) is comparable. Figure 3(b) shows the infrared spectra of the CL4SPY single crystal at room temperature. A broad OH stretching band was observed at ca. 2600 cm^{-1}. The half width is ca. 700 cm^{-1}, which is slightly larger than that of CL4SA. The intensity seems to be even weaker, compared with the normalized intensity of the CH stretching mode at 3030 cm^{-1}.

Figure 4(a) shows the absorption spectra of the CL4SA single crystal at various temperatures. The

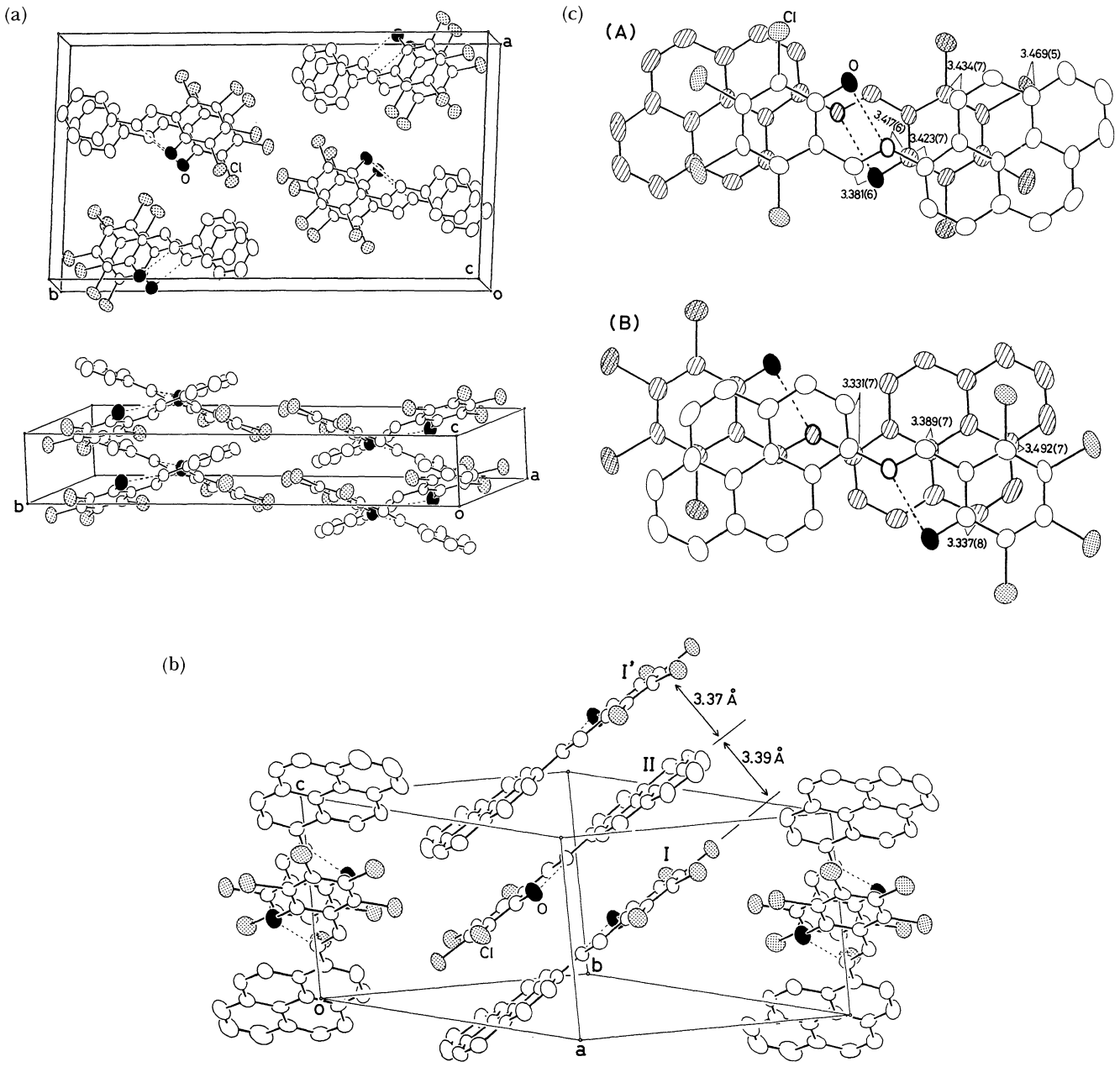

Fig. 2. Crystal structures of CL4SA (a) and CL4SPY (b); symmetry code, I (x, y, z), II ($1-x$, $1-y$, $1-z$), I′ (x, y, $1+z$), and molecular overlapping between the CL4SPY molecules, I and II (A) and II and I′ (B) and some short interatomic distances (Å) (c).

thermochromic-type behavior is observed as a shift of the absorption edge with temperature. This behavior represents a different type of thermochromism from that ordinarily observed for other *N*-salicylideneanilines. For example, in BSP, a new band appeared in the lower-energy region grows with increasing temperature.[2] The emission spectra of CL4SA (Fig. 4) show a Stokes shift (0.35 eV at 6 K and 0.25 eV at 300 K from the absorption edge). No noticeable change of the band profile was observed with changing temperature.

The visible region absorption spectra of the CL4SPY single crystal is shown in Fig. 4(b). Though a shift in the absorption edge due to a temperature change was observed, the energy of a shift was about half that observed in CL4SA over the same temperature range. On the other hand, the emission spectra showed a complicated change with the temperature. At 8 K, five peaks were observed at 2.04, 1.99, 1.85, 1.70, and 1.55 eV. With increasing temperature, the first peak merged into the second peak. The other three peaks, which are equally separated by 0.15 eV, shifted slightly towards higher energy by 132 K, then merged into one band at 1.83 eV. The intensities decreased rather

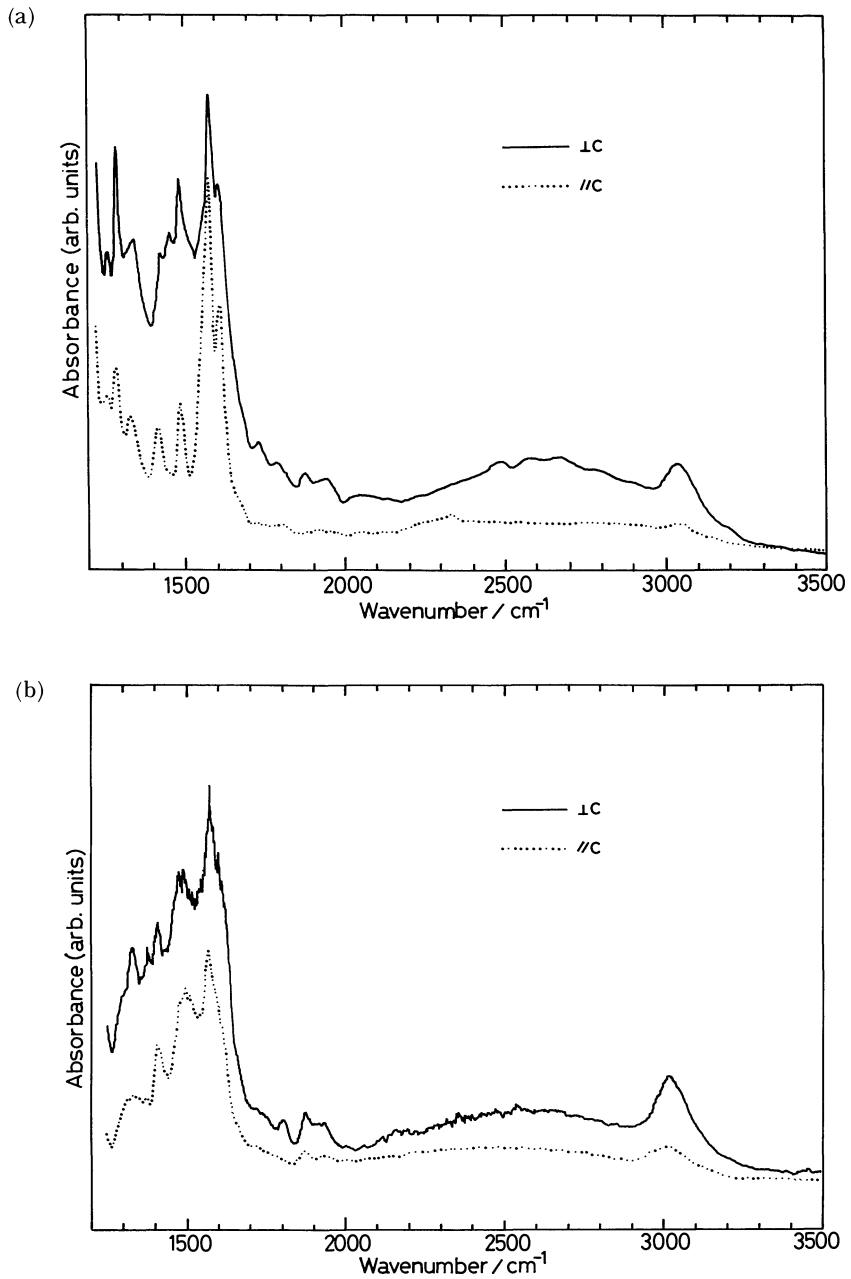

Fig. 3. Single-crystal infrared spectra for CL4SA (a) and CL4SPY (b) at room temperature.

rapidly with increasing temperature to 74 K, then decreased gradually.

Discussion

When the O···N distance is short enough to make the energy difference and the barrier height appreciably small, in reference to the thermal energy, the proton transfer is thermally allowed in *N*-salicylideneanilines. In both CL4SA and CL4SPY, the O···N distances are considerably short compared with other thermochromic *N*-salicylideneanilines. This shortening results, partly at least, from the substitution of chlorine atoms.

Firstly, we examined this substitution effect by means of MNDO calculations of the single molecules. Since all geometric parameters were fully optimized at a certain NH distance in these calculations, the optimized conformations might correspond to an isolated molecule, which is known to be nonplanar.[11] The deformation of the hydrogen-bond structure due to this nonplanarity may be substantially small, because the major deformation from the planar conformation is a rotation of the aromatic ring at the aniline side. Therefore, the substitution effect is expected to appear to a large extent by this type of calculation. Figure 5 shows the results for CL4SA,

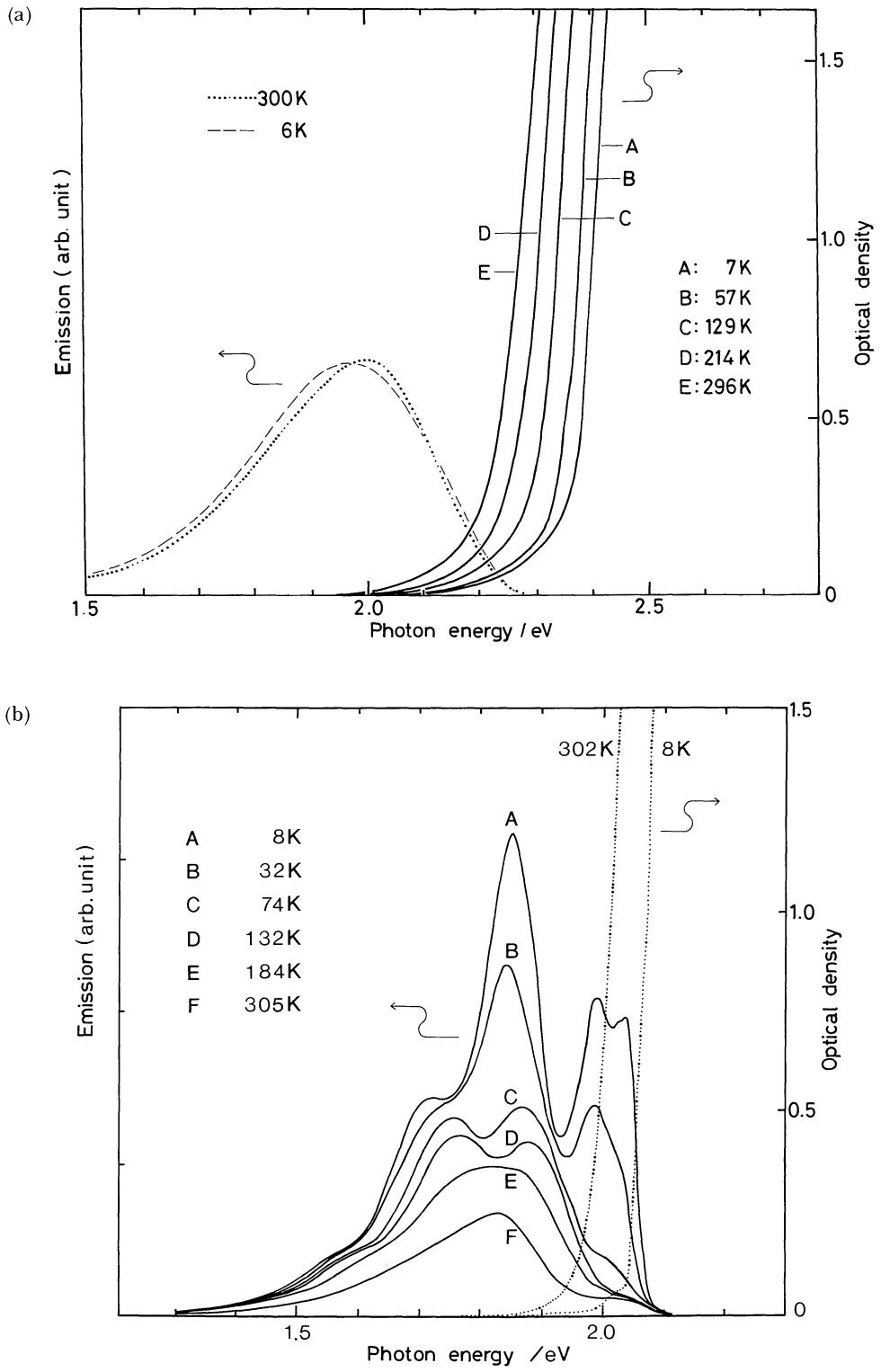

Fig. 4. Single-crystal absorption and emission spectral changes with temperature for CL4SA (a) and CL4SPY (b).

CL4SPY, and nonsubstituted *N*-salicylideneaniline. It can be seen that the space separation between two minima becomes smaller by the introduction of chlorine substituents. The energy difference between the two minima is also smaller in chlorinated compounds. On the other hand, the difference between the aniline side structures, i.e., 1-pyrenyl and phenyl, has almost no influence on the potential

Table 5. Distances and Angles Related to the Steric Effect

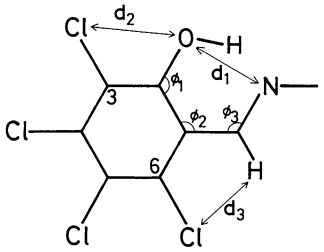

	CL4SA		CL4SPY		*N*-salicylideneanilines[a]	
	Obsd	Calcd[b]	Obsd	Calcd[b]	Obsd	Calcd[b]
d_1/Å	2.512(7)	2.84	2.534(5)	2.90	2.58—2.62	2.98
d_2/Å	2.874(5)	2.90	2.902(4)	2.88	—	—
d_3/Å	2.61(7)	2.40	2.59(3)	2.37	—	—
$\phi_1+\phi_2+\phi_3$/°	361.4	371	362.8	373	364—367	376

a) Values for other derivatives which have no substituents at the 3 and 6 positions. b) Values obtained by MNDO calculations at the most stable conformation in Fig. 5.

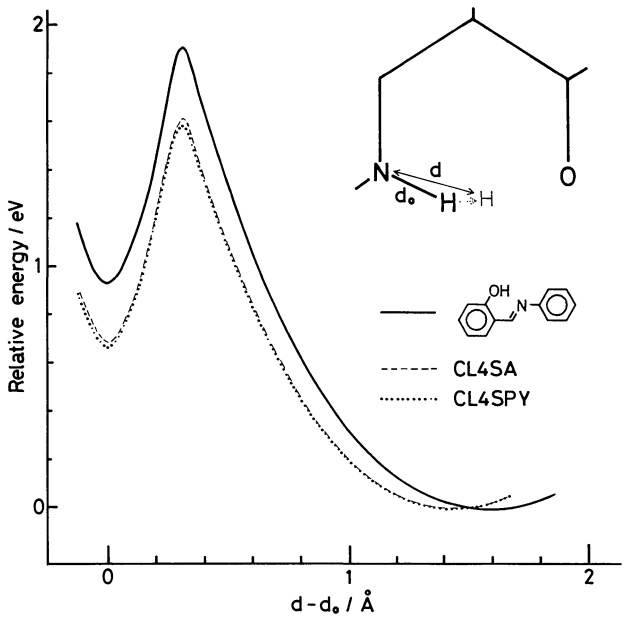

Fig. 5. Potential energy diagram calculated by an MNDO method. The energy is standardized at the OH form minima. The abscissa is the difference from the distance between N and H to that of the NH form minima.

surface of the proton.

The most notable effect of the chlorine substituents is considered to be a steric one; as shown in Table 5, the substituents at the 3 and 6 positions of the benzylidene side cause a contraction of the O···N distance due to a steric repulsion. A similar steric effect of the substituents on the hydrogen-bond structure was noticed in β-diketones[12] and salicylaldehydes.[13] Besides the steric effect, there might be an electronic effect of the substituents, as found for β-diketones.[12] However, in CL4SA and CL4SPY, this effect is supposed to be negligibly small,[14] as far as single molecules are concerned. Consequently, the shortening of the hydrogen bond in CL4SA and CL4SPY can be considered to result from a steric effect of the chlorine substituents.

From the above arguments, CL4SA and CL4SPY should have the same strength as that of the hydrogen bond. The O···N distances are actually not so different in these two molecules. However, the spectroscopic studies for both crystals suggest that there is a substantial difference in the nature of the hydrogen bond in the crystalline state. It has also been noticed that the C(8)–O(5) distance of CL4SPY is considerably shorter than that of CL4SA. This indicates that the resonance contribution from the *o*-quinonoid structure in the NH form is larger in CL4SPY than in CL4SA. Although the N(6)–C(13) distance is also expected to be longer in CL4SPY than in CL4SA, this bond may not be so sensitive, due to a delocalization effect.

On the same basis, the observed optical properties can be interpreted as described below. Firstly, the intensity of the hydrogen stretching mode in these compounds may be considered to depend on the position of the hydrogen in the hydrogen bond. When the hydrogen vibrates near the center of the hydrogen bond, the induced dipole moment can be very weakly changed due to the delocalization of electrons in the entire chelate ring system.[15] Therefore, when the hydrogen-bond structure is closer to the intermediate one, the intensity becomes weaker.

Secondly, the temperature dependence of the visible absorption spectra must be considered. The thermochromic behavior is usually observed as a growth of new bands. When the energy difference between the thermochromic state and the thermal ground state is smaller or comparable to the thermal energy, the

thermochromic band has an appreciable intensity, even at low temperatures. Contrary to the case in BSP which shows a typical thermochromic-type behavior, the energy difference between the NH and OH forms is much smaller in both CL4SA and CL4SPY. This means that the content of the NH form is still large at the lowest temperatures in these measurements. Since the measurements were carried out by using single-crystal specimens, such intense absorption can hardly be observed as a clear peak. Thus, the initial growth or a peak profile of the thermochromic band could not be observed. In such a case, the approximate temperature dependence of the thermochromic band can be estimated from the shift of the absorption edge.[16] The relatively large shift in CL4SA indicates that the thermochromic band grows with increasing temperature, and this crystal can be regarded as being an ordinary thermochromic type. On the other hand, the smaller shift in CL4SPY in the same temperature range suggests that the growth approaches some degree of saturation. Such a situation is expected when the energy difference between the OH and NH forms is extremely small. The smaller Stokes shift compared with CL4SA also suggests a large contribution of the NH form in CL4SPY at low temperature.

From these structural and optical data, the energy difference between the two minima in the potential energy surface is considered to be much smaller in CL4SPY than in CL4SA. Considering the structural difference between the CL4SA and CL4SPY crystals, it is reasonable to assume that the intermolecular charge-transfer interaction operates in the CL4SPY crystal. This interaction is expected to make the ground state slightly polarized as a consequence of mixing with the excited state. Although this originates purely from a π–π interaction, it may cause a change in the net charge on the N and O atoms. Such an excess charge effect has been calculated and found to have great influence on the potential surface of the proton.[17]

Since our interest lies in the influence on proton motion, we have tried to visualize the hydrogen in the

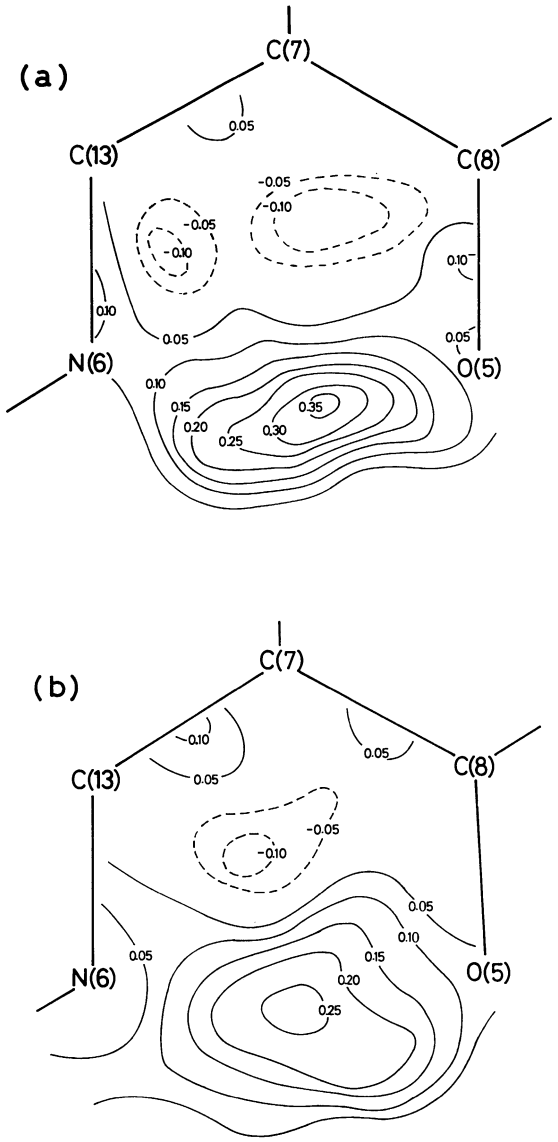

Fig. 6. Difference synthesis maps of the hydrogen bonded chelate ring (e Å^{-3}) of CL4SA (a) and CL4SPY (b).

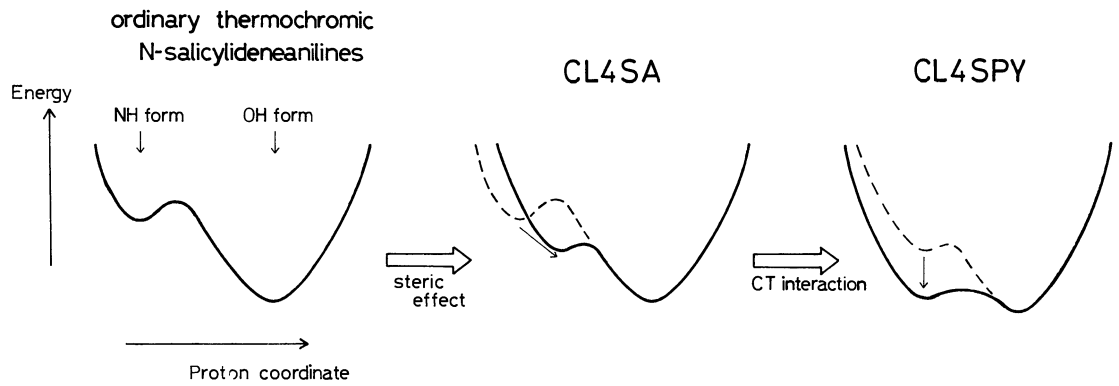

Fig. 7. Schematic representation of the potential energy surface of the proton modified by the steric effect and the intermolecular charge transfer (CT) interaction.

hydrogen bond. The method is the same as that performed for BSP and DSPY;[3] the difference syntheses are calculated by taking the parameters of the hydroxyl hydrogen out of the refined structure. The obtained electron-density maps are shown in Fig. 6. In both compounds, a broad peak appears at nearly the center of the hydrogen bond, which is quite different from the situation in ordinary thermochromic *N*-salicylideneanilines. The difference between CL4SA and CL4SPY may not be clearly seen due to the limitation of accuracy.

In conclusion, the strong hydrogen bonds in CL4SA and CL4SPY have mainly been attributed to a steric effect of the chlorine substituents at the 3 and 6 positions of the bezylidene side. In addition to this effect, the intermolecular charge-transfer interaction makes contribution from the NH form larger in CL4SPY, which makes the hydrogen-bond structure nearly intermediate between the NH and OH forms. These situations are schematically summarized in Fig. 7. The coupling between the proton transfer and the intermolecular π–π interaction may provide a hopeful prospect for the realization of the system proposed in the Introduction.

This work was partly supported by Scientific Resesarch Grants-in-Aid No. 02804032 from the Ministry of Education, Science and Culture.

References

1) M. D. Cohen, G. M. J. Schmidt, and S. Flavian, *J. Chem. Soc.*, **1964**, 2041.
2) N. Hoshino, T. Inabe, T. Mitani, and Y. Maruyama, *Bull. Chem. Soc. Jpn.*, **61**, 4207 (1988).
3) T. Inabe, N. Hoshino, T. Mitani, and Y. Maruyama, *Bull. Chem. Soc. Jpn.*, **62**, 2245 (1989).
4) T. Inabe, submitted to *New J. Chem.*; T. Mitani, *Mol. Cryst. Liq. Cryst.*, **171**, 343 (1989).
5) H. Heaney, J. M. Jablonski, and C. T. McCarty, *J. Chem. Soc., Perkin 1*, **1972**, 2903.
6) P. Main, L. Lessinger, M. M. Woolfson, G. Germain, and J. -P. Declercq, MULTAN78, Univs. of York, England, and Louvain, Belgium (1978).
7) T. Sakurai and K. Kobayashi, *Rep. Inst. Phys. Chem. Res.*, **55**, 69 (1979).
8) The lists of structure factors, anisotropic thermal parameters for non-hydrogen atoms, and parameters for hydrogen atoms are deposited as Document No. 9102 at the Office of the Editor of Bull. Chem. Soc. Jpn.
9) J. Bregman, L. Leiserowitz, and K. Osaki, *J. Chem. Soc.*, **1964**, 2986.
10) J. Bregman, L. Leiserowitz, and G. M. J. Schmidt, *J. Chem. Soc.*, **1964**, 2068.
11) M. D. Cohen and S. Flavian, *J. Chem. Soc. B*, **1967**, 321.
12) J. Emsley, *Struct. Bonding*, **57**, 147 (1984), and references therein.
13) D. C. Nonhebel, *Tetrahedron*, **24**, 1869 (1968).
14) In the case of CL4SA or CL4SPY, both inductive and mesomeric effects of substituents are considered to be too small to change the electronegativities of the O and N atoms.
15) S. F. Tayyari, Th. Zeegers-Huyskens, and J. L. Wood, *Spectrochim. Acta, Part A*, **35**, 1289 (1979).
16) This behavior was confirmed by the measurements of BSP using a thick crystal or with increasing temperature well above room temperature.
17) M. Hasegawa, K. Daiyasu, and S. Yomosa, *J. Phys. Soc. Jpn.*, **28**, 1304 (1970).
18) C. K. Johnson, ORTEP, Report ORNL-3794, Oak Ridge National Laboratory, Tennessee (1976).

Electrical Conductivity of Black Phosphorus-Germanium Compound

Yusei MARUYAMA,* Tamotsu INABE, Lin HE, Toshifumi TERUI,† and Kokichi OSHIMA††
Institute for Molecular Science, Myodaiji, Okazaki 444
† Graduate University for Advanced Studies, Myodaiji, Okazaki 444
†† Department of Physics, Okayama University, Tsushimanaka, Okayama 700
(Received October 4, 1990)

Single crystals of a new material, black phosphorus doped with germanium, have been prepared by a bismuth-flux method. Germanium atoms are incorporated into the black phosphorus in 2 to 4 atomic percent. The resistivity is reduced by two to three orders (ρ=6×10^{-3} Ω cm) compared with the pure black phosphorus, and its temperature dependence is metallic at low temperatures. There is no magnetoresistance up to 12 T at 0.6 K in striking contrast to the pure black phosphorus which shows negative magnetoresistance in this region. The crystal lattice constants decrease with germanium doping, especially in the interlayer direction. These facts indicate the enhanced three dimensionality with germanium doping.

Black phosphorus discovered by Bridgman in 1914[1] has been known to be a layered structure narrow gap semiconductor[2] and to have interesting properties, such as pressure-induced structural phase transitions,[3] anomalous superconductivity,[4] and two-dimensional Anderson localization.[5] A chemical modification of black phosphorus is a potentially promising strategy to realize a metallic phase in black phosphorus under normal pressure.

As the first approach to prepare new chemical species based on black phosphorus we have tried to synthesize black phosphorus intercalation compounds with cesium[6] and iodine.[7] The second trial was a doping of silicon, a IV group element, to increase the positive hole character in black phosphorus (a V group element). The doping of silicon realized a somewhat metallic character in black phoshporus.[8]

In this report we describe the effect of germanium doping into black phosphorus. Almost metallic temperature dependence was observed for the electrical resistivity at low temperatures, and no magnetoresistance was found out. Substantial decrease in the lattice constants was recognized with germanium doping, especially in the interlayer direction.

Experimental

Doping of germanium was carried out by mixing it into melted bismuth with black phosphorus powder. By very slow cooling of the melt very tiny crystals were obtained (typical size: 500×15×3 μm^3). The incorporated amount of germanium was detected by an Electron-Probe-Micro-Analysis technique (EPMA).

Electrical resistivity and its temperature dependence were measured with a four-probe method from 300 to 0.6 K in the ^{3}He cryostat system. Magnetoresistance was also examined by the use of a superconducting magnet up to 12 T at low temperatures. The change in lattice constants caused by the incorporation of germanium was detected by an X-ray diffraction analysis.

Results and Discussion

The resistivity of a germanium doped single crystal at room temperature is lower by almost three orders compared with a pure black phosphorus: ρ(RT)=6×10^{-3} Ωcm. The relative amount of germanium which is incorporated in black phosphorus was roughly estimated to be 2 to 4 atomic percent from the result of EPMA. The corresponding amount of silicon which was included in black phosphorus-silicon was about 0.01 atomic percent.[8] Germanium is far better introduced into black phosphorus compared with silicon in spite of larger covalent radius of the former, and this causes the remarkable reduction in the resistivity.

The lattice constants of a single crystal of germanium doped black phosphorus, PGe$_x$ (x=0.03±0.01), were found by an X-ray diffraction analysis and

Table 1. Comparison of the Lattice Constants of PGe$_x$ (x=0.03±0.01) and Those of Black P

	a/Å	b/Å	c/Å
Black P[9]	3.3136	10.478	4.3763
PGe$_x$	3.310	10.42	4.364
Difference	−0.004	−0.058 (0.6%)	−0.012 (0.3%)

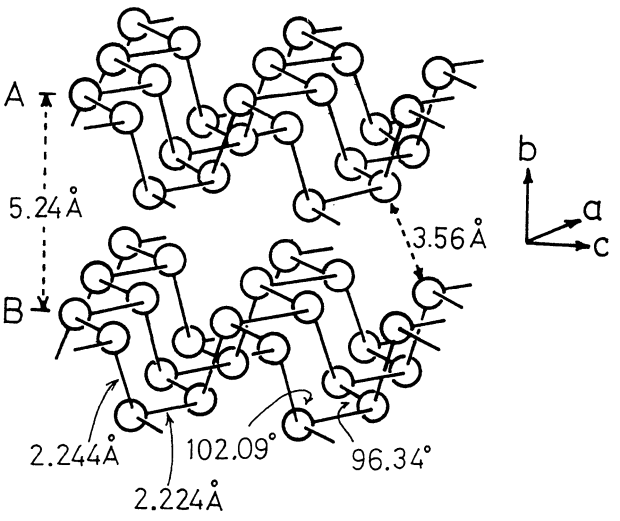

Fig. 1. Crystal structure of black phosphorus.[9]

they are shown in Table 1 together with those of black phosphorus.[9] All lattice constants become shorter, especially in the b-axis, interlayer direction (Fig. 1), substantially shorter. In the c-axis direction, the rate of reduction is almost the same order as in the b-axis direction, and in the a-axis direction there is almost no reduction within the experimental error. This fact is just corresponding to the pressure dependence of the

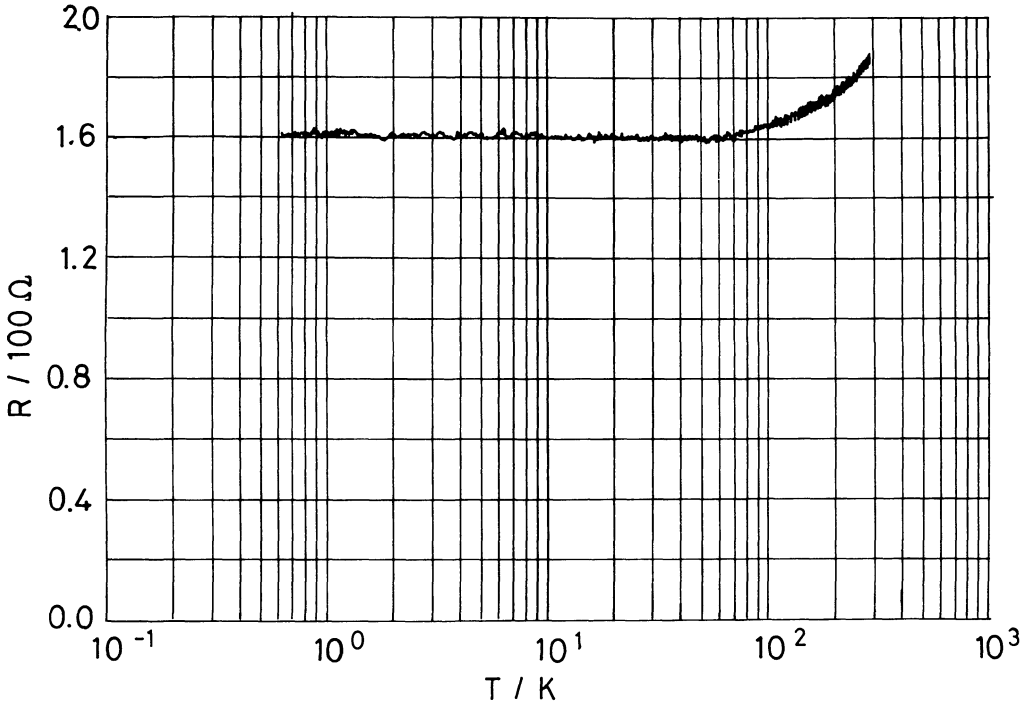

Fig. 2. Temperature dependence of the resistance of PGe_x (x=0.03±0.01).

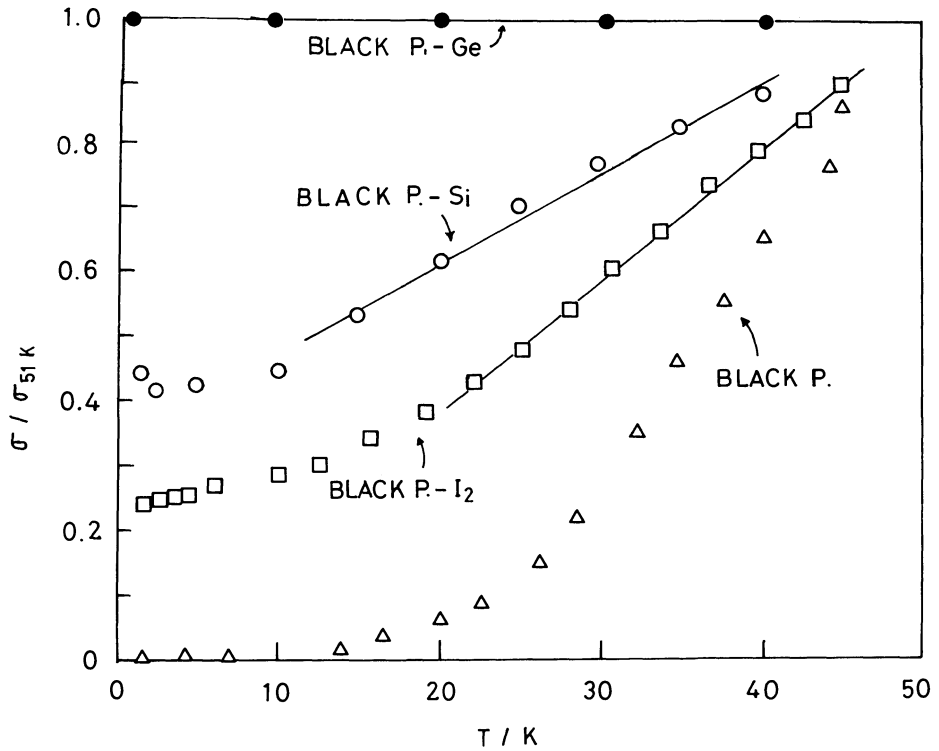

Fig. 3. Temperature dependence of the normalized conductivities (σ(T)/σ(51 K)) of black phosphorus, black phosphorus–I_2, black phosphorus–Si, and black phosphorus–Ge.

lattice constants of black phosphorus.[10] In pure black phosphorus, the semiconducting gap energy is strongly dependent on the interlayer interaction, and thus the reduction in the b-axis length of PGe_x may lead reasonably to lower resistivity.

The temperature dependence of the resistances of PGe_x (x=0.03±0.01) is shown in Fig. 2. It shows almost metallic behavior from 300 to 0.6 K, and below 50 K the resistance is almost constant. This behavior clearly contrasts with the case of pure black phosphorus in which the resistivity has an exponential rise at low temperatures. Even in PSi_x there is small rise in the resistivity at low temperatures. Figure 3 shows the different behaviors of the conductivity ratios (σ(T)/σ (51 K)) below 50 K in pure black phosphorus and its intercalated or doped compounds.

The magnetoresistance of PGe_x was investigated at 0.6 K up to 12 T applying the magnetic field along the b-axis with the electric current along the a-axis since black phosphorus is known to have negative magnetoresistance at low temperatures.[2,5] There is, however, no indication of magnetoresistance in PGe_x at all in this range of magnetic field at 0.6 K.

These two findings, metallic behavior and no magnetoresistance, may be partly ascribed to the enhancement of three dimensional character due to the reduction in the interlayer distance with the doping of germanium. It was reported that the semiconducting energy gap of black phosphorus is dependent on pressure and it vanishes over 1.8 GPa.[11] The reduction of the lattice constants around 2.0 GPa is about 2.5% in b or c-axis. The differences in the corresponding lattice constants are about 0.3—0.6% in Table 1. The reduction of the lattice constants is not large enough for vanishing the semiconducting gap of black phosphorus, but the enhanced number of holes in the filled band may be responsible for the appearance of metallic nature in PGe_x.

In conclusion, we have succeeded in the synthesis of germanium doped black phosphorus, and determined the composition, $PGe_{0.03\pm0.01}$, and the lattice constants of the new compound. The metallic behavior was observed by the temperature dependence of the resistivity at low temperatures, and such behavior is reasonably explained by referring to the change in the lattice constants on doping.

References

1) P. W. Bridgman, *J. Am. Chem. Soc.*, **36**, 1344 (1914).
2) Y. Maruyama, S. Suzuki, K. Kobayashi, and S. Tanuma, *Physica B*, **105**, 99 (1981).
3) S. Narita, S. Terada, S. Muro, Y. Akahama, and S. Endo, *J. Phys. Soc. Jpn.*, **52**, 3544 (1983).
4) H. Kawamura, I. Shirotani, and K. Tachikawa, *Solid State Commun.*, **49**, 879 (1984).
5) N. Iwasaki, Y. Maruyama, S. Kurihara, I. Shirotani, and M. Kinoshita, *Chem. Lett.*, **1985**, 119.
6) Y. Maruyama, S. Suzuki, T. Osaki, H. Yamaguchi, S. Sakai, K. Nagasato, and I. Shirotani, *Bull. Chem. Soc. Jpn.*, **59**, 1067 (1986).
7) T. Nishii, Y. Maruyama, T. Inabe, and I. Shirotani, *Synth. Met.*, **18**, 559 (1987).
8) Y. Maruyama, T. Inabe, T. Nishii, L. He, A. J. Dann, and I. Shirotani, *Synth. Met.*, **29**, F213 (1989).
9) A. Brown and S. Rundqvist, *Acta Cryst.*, **19**, 684 (1965).
10) L. Cartz, S. R. Srimivasa, R. J. Riednev, J. D. Jorgensen, and T. G. Worlton, *J. Chem. Phys.*, **71**, 1718 (1979).
11) Y. Akahama, S. Endo, and S. Narita, *J. Phys. Soc. Jpn.*, **52**, 2148 (1983).

A Stopped-Flow Kinetic Study of the Solubilization of Acridine Orange and Its 10-Alkyl Derivatives into the Micelle of Sodium Dodecyl Sulfate

Yukio KUBOTA,* Naofumi OMURA, and Kiyofumi MURAKAMI
Department of Chemistry, Faculty of Science, Yamaguchi University, Yamaguchi 753
(Received August 27, 1990)

Stopped-flow method has been used to investigate the kinetics of the solubilization of Acridine Orange (AO, 3,6-bis(dimethylamino)acridinium chloride) and its 10-alkyl derivatives into the micelle of sodium dodecyl sulfate (SDS). The reaction curves of the SDS–AO and SDS–10-alkyl AO systems were characterized by single and double exponential functions, respectively. It was found that all the time constants are concentration dependent and approach limiting values at high reactant concentrations. The data were fitted by a minimal mechanism in which a rapid bimolecular step is followed by one (AO) or two (10-alkyl derivatives of AO) sequential isomerizations. All the rate constants determined for this mechanism markedly decrease with an increase in the length of the introduced alkyl chain. The equilibrium constants for the bimolecular and first isomerization steps do not highly depend on the size of the alkyl chain, while the equilibrium constant for the second isomerization step progressively increases with increasing it. The spectral changes with time indicate that the bound dye gradually migrates to more hydrophobic environment inside the micelle. These results lead to the conclusion that the steps in the proposed mechanism correspond to rapid adsorption of the dye to the micelle surface site, followed by reorientation of the dye and then migration of its alkyl chain into the hydrophobic region of the micelle.

The most important properties of micellar systems are their ability to solubilize a variety of molecules and their catalytic effects on many reactions occurring at the micelle surface and inside.[1–3] In order to better understand the nature of this solubilization and the physicochemical behavior of solubilized molecules, it is of fundamental significance to obtain information concerning the structure of micelles and the location or relative orientation of solubilized molecules.[4,5] For this purpose, several spectroscopic techniques such as NMR,[6,7] ESR,[8] and fluorescence[9–13] have been employed so far.

Kinetic methods, though helpful in understanding the solubilization mechanism, have rarely been applied to the solubilization phenomena.[14–19] Robinson and co-workers[16,17] proposed a mechanism in which rapid adsorption of dye on the micelle surface is followed by slow penetration into the hydrocarbon interior of the micelle. On the other hand, Takeda et al.[14] proposed the rapid initial formation of a dye-surfactant salt which then penetrates the palisade layer of the micelle. However, there is no extensive discussion based on the evaluation of equilibrium and rate constants for each step.

This paper describes detailed results on the kinetics of the solubilization of Acridine Orange (AO) and its 10-alkyl derivatives into the micelle of sodium dodecyl sulfate (SDS), studied by stopped-flow method with absorption and fluorescence detection. The aim of the present study is to establish the mechanism of the solubilization through the evaluation of equilibrium and rate constants. Among the results, it is revealed that the solubilization process consists of rapid initial adsorption of the dye on the micelle surface and one (AO) or two subsequent isomerizations (10-alkyl derivatives of AO).

Experimental

AO (3,6-bis(dimethylamino)acridinium chloride) was purchased from Merck. The 10-alkyl derivatives of AO (methyl-AO, propyl-AO, pentyl-AO, octyl-AO, and decyl-AO) were synthesized according to the method of Miethke and Zanker.[20] All dyes were purified by repeated recrystallizations and column chromatography; no trace of impurity was detected by the method of thin-layer chromatography for each dye. SDS (specially pure grade >99%) was obtained from Nakarai Chemicals and used without further purification. All other chemicals were reagent grade and deionized redistilled water was used for the preparation of all aqueous solutions.

Absorption and fluorescence spectra were measured with a Shimadzu UV-200S spectrophotometer and a Hitachi MPF-2A fluorescence spectrophotometer, respectively. The critical micelle concentration (cmc) of SDS in the absence and presence of dye was determined by the conductometric method. Kinetic measurements were made on a Union Giken RA-601 rapid-scanning stopped-flow spectrophotometer using both absorbance and fluorescence detection, a 1:1 mixing ratio, and a 2 mm path-length cell. The dead time of the instrument was 0.6 ms, as judged from the reduction reactions of 2,6-dichloroindophenol by L-ascorbic acid.[21] In the kinetic experiments, the initial concentration of SDS was always maintained in large excess of that of the dye. The resulting reaction curves were subjected to multiexponential analysis with a nonlinear least-squares regression program based on the Marquardt algorithm.[22] All measurements were carried out at 25±0.2 °C.

All the calculations were accomplished with an Acos-850 computer system (NEC Corporation) and/or a PDP 11 minicomputer (Digital Equipment Corporation).

Results and Discussion

Electronic Spectra and CMC. The alkyl derivatives of AO when mixed with SDS solutions showed absorp-

tion and fluorescence changes similar to those reported for AO.[16,17,23] Figure 1 displays typical absorption spectra obtained with pentyl-AO (1.0×10^{-5} M) in the presence of SDS. The spectra are characterized by two absorption bands; one is the monomer band at 495 nm and the other (470 nm) is the band due to the dimer or higher aggregates.[16,23] Below the cmc, the spectrum of pentyl-AO exhibits both a reduction of the band at 495 nm and an enhancement of the band at 470 nm with increasing SDS concentration. This behavior is ascribed to the ion pair (or salt) formation between the dye cation and the SDS anion, followed by the formation of mutual induced aggregates. In the vicinity of the cmc, the monomer band markedly increases and then the shape of spectrum remains unchanged above the cmc. The absorption maximum above the cmc shifts toward longer wavelengths compared to that of free dye in aqueous solutions (492 nm). The fluorescence quenching of the dye below the cmc and the strong enhancement of its fluorescence above the cmc were observed for all dyes; above the cmc, a blue shift and a narrowing of the fluorescence band were also observed when compared to that of free dye in aqueous solutions. These absorption and fluorescence properties above the cmc suggest that the dye is solubilized in a hydrophobic region of the micelle and exists as a monomeric form.[9,16,23]

The cmc of SDS solution, in agreement of the literature value,[24] was 8.0×10^{-3} M (1 M=1 mol dm^{-3}) and the presence of dye (1.0×10^{-5} M) had no appreciable influence on cmc irrespective of the dye structure.

Kinetics of Solubilization. It is well-known that AO and its alkyl derivatives aggregate in aqueous solutions at higher concentrations.[17,25,26] To minimize the effect of dye aggregation, kinetic measurements were made on solutions in which dye concentrations were kept below 10^{-5} M; in fact, the kinetic behavior was idependent of dye concentrations in the range of 2.5×10^{-6} to 2.0×10^{-5} M. Figure 2 displays typical time courses of absorbance changes after mixing an equal volume of AO and SDS solutions (curve a) and of pentyl-AO and SDS solutions (curve b). The reaction curve of the AO–SDS system was characterized by a single-exponential function, while that of the pentyl-AO–SDS system by a double-exponential one. Figures 3 and 4 show the dependence of the reciprocal of the time constant (τ^{-1}; apparent rate constant) on [SDS]—cmc for the AO–SDS and pentyl-AO–SDS systems respectively; here, [SDS] stands for the total SDS concentration. It can be seen that τ^{-1} increases with an increase in the SDS concentration and reaches a

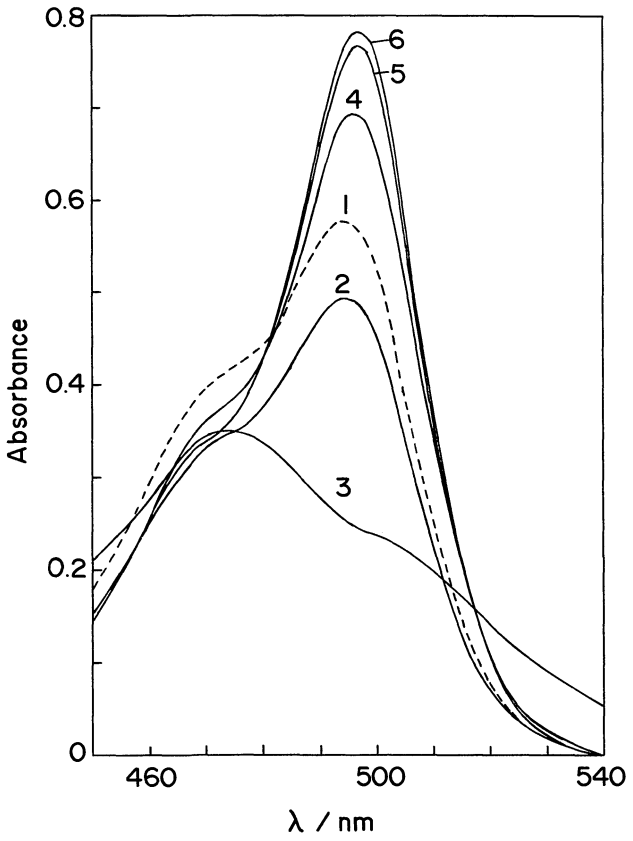

Fig. 1. Absorption spectra of pentyl-AO (1.0×10^{-5} M) in the presence of various concentrations of SDS at 25 °C. [SDS]/M: (1) 0; (2) 1.0×10^{-5}; (3) 2.0×10^{-3}; (4) 6.0×10^{-3}; (5) 8.0×10^{-3}; (6) 2.0×10^{-2}.

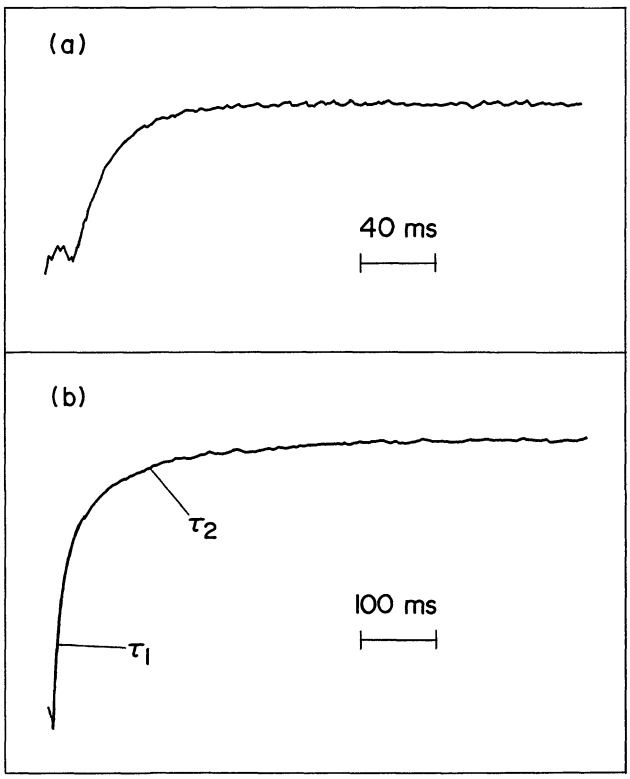

Fig. 2. Typical time courses of absorbance changes observed at 498 nm after mixing of (a) [AO]=2.0×10^{-5} M and [SDS]=5.0×10^{-2} M and (b) [pentyl-AO]=2.0×10^{-5} M and [SDS]=4.0×10^{-2} M.

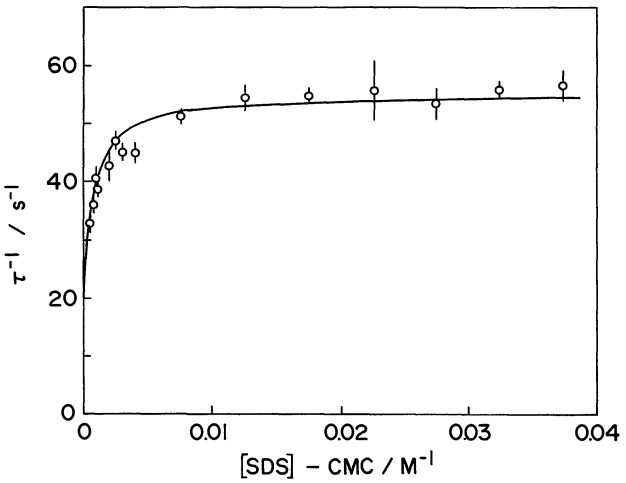

Fig. 3. Dependence of τ^{-1} on [SDS]—cmc for the AO–SDS system. The concentration of AO was 1.0×10^{-5} M. The line is drawn using Eq. 4 with parameters listed in Table 1.

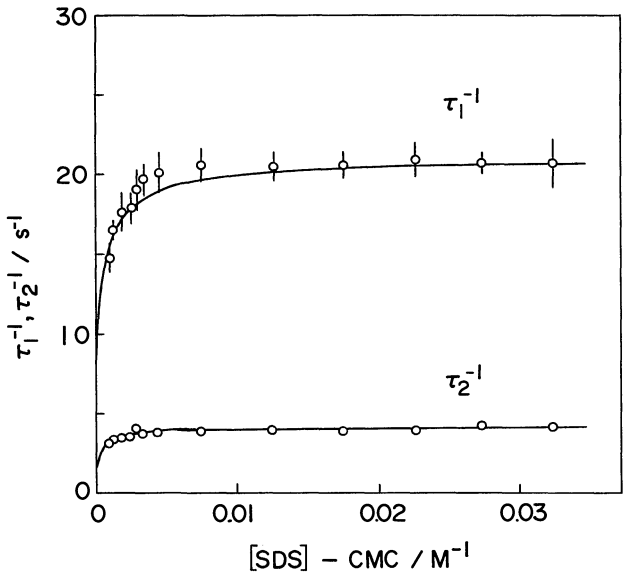

Fig. 4. Dependence of τ_1^{-1} and τ_2^{-1} on [SDS]—cmc for the pentyl-AO–SDS system. The concentration of pentyl-AO was 1.0×10^{-5} M. The lines are drawn using Eq. 5 with parameters listed in Table 1.

limiting value (Figs. 3 and 4). The reaction of SDS with propyl-AO or decyl-AO was also examined with fluorescence detection. As Fig. 5 shows the result obtained with the decyl-AO–SDS system, the time constants determined from absorbance and fluorescence changes agree well with each other. This implies that absorbance and fluorescence changes reflect the same reaction process. In the case of octyl-AO or decyl-AO, additional rapid changes in both the absorbance and the fluorescence intensity were observed. Their magnitudes, however, were too small to

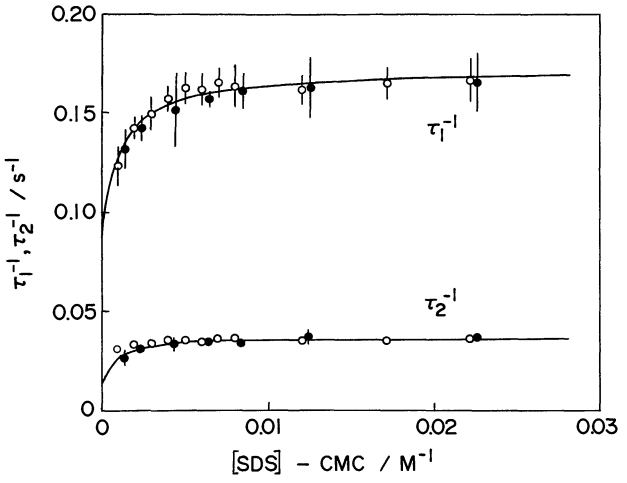

Fig. 5. Dependence of τ_1^{-1} and τ_2^{-1} on [SDS]—cmc for the decyl-AO–SDS system: (○) absorbance detection; (●) fluorescence detection. The concentration of decyl-AO was 1.0×10^{-5} M for absorbance detection and 5.0×10^{-6}M for fluorescence detection. The lines are drawn using Eq. 5 with parameters listed in Table 1.

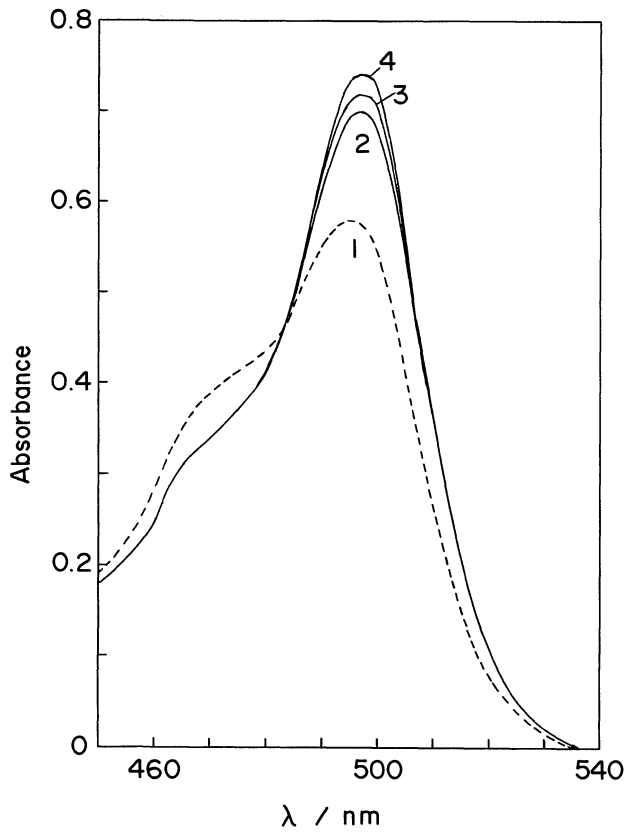

Fig. 6. Spectral change of pentyl-AO (1.0×10^{-5} M) after mixing with SDS (2.0×0^{-2} M). (1) spectrum of pentyl-AO in the absence of SDS; (2) t=12.5 ms; (3) t=32.5 ms; (4) t=152.5 ms. t denotes the time after mixing.

determine the accurate time constant.

To see the time course of spectral changes in the solubilization process, stopped-flow rapid scanning spectroscopy was employed. Figure 6 depicts a typical result obtained with the pentyl-AO–SDS system. It can be seen that the absorbance at the monomer band increases and the absorption maximum shifts toward a longer wavelength with time. This result supports that the dye is solubilized into the hydrophobic environment of the micelle in a monomeric form.[9,16,23]

Mechanism of Solubilization. Some mechanisms for the solubilization of dye into the surfactant micelle have been proposed. Hoffmann[15] suggested that the rapid formation of a dye-surfactant ion pair is followed by a stepwise accumulation of surfactant monomers around the ion pair until a dye-containing micelle is built up. Robinson and co-workers[16,17] observed that the reaction curve for the 10-alkyl AO–SDS system is approximately characterized by a single-exponential function and the first-order rate constant markedly decreases with increasing the size of the alkyl chain. Their observation argues against the suggestion of Hoffmann,[15] that the micelle breakdown is the rate-determining step, since such a process should be fast and independent of the dye structure. Therefore, they proposed another mechanism in which rapid adsorption of the dye on the micelle surface is followed by slow penetration of the dye into the hydrophobic region of the micelle;[16,17] the concentration dependence of the rate constant was consistent with that expected for the slow step.

The results obtained in this study clearly indicate that the reaction of SDS with AO is characterized by one time constant, whereas the reactions of SDS with 10-alkyl derivatives of AO by two time constants. The latter finding is distinguishable from that of Robinson et al.[17] To interpret the present data, we propose the following schemes for the solubilization of the dye into the surfactant micelle: for AO,[16]

$$\mathrm{D} + \mathrm{M} \underset{k_{-2}}{\overset{K_1}{\rightleftharpoons}} \mathrm{DM}_1 \underset{}{\overset{K_2,\ k_2}{\rightleftharpoons}} \mathrm{DM}_2, \qquad (1)$$

and for 10-alkyl derivatives of AO,

$$\mathrm{D} + \mathrm{M} \underset{k_{-2}}{\overset{K_1}{\rightleftharpoons}} \mathrm{DM}_1 \underset{k_{-3}}{\overset{K_2,\ k_2}{\rightleftharpoons}} \mathrm{DM}_2 \underset{}{\overset{K_3,\ k_3}{\rightleftharpoons}} \mathrm{DM}_3, \qquad (2)$$

where D, M, and DM_i denote the dye, the micelle surface site and the i-th dye-surfactant complex, respectively, and K_i, k_i, and k_{-i} are equilibrium, forward rate and backward rate constants for the i-th step, respectively. The first step can be assigned to the adsorption of the dye on the micelle surface and the subsequent ones to the isomerizations of the complexes. Since the initial binding of the dye to the micelle is considered to be electrostatic in nature and there is no restriction of a single site on each micelle, the concentration of the micelle surface site ([M]) can be defined as[16]

$$[\mathrm{M}] = \alpha([\mathrm{SDS}] - \mathrm{cmc}), \qquad (3)$$

where α is the fraction of micelle surface charge which is not neutralized by Na^+ counterion; the value of α was evaluated to be 0.168 by dividing the surface charge of the SDS micelle by its association number.[27] On the assumption that the bimolecular adsorption step is faster than the isomerization step and [M]≫[D], the time constant for the second step in Scheme 1 is simply expressed by[28]

$$\tau^{-1} = k_2K_1[\mathrm{M}]/(1 + K_1[\mathrm{M}]) + k_{-2}. \qquad (4)$$

To secure the requirement [M]≫[D], experimental conditions were regulated in such a way that there is always an excess of micelle sites. Under these conditions the possible complication due to dye–dye interactions on the micelle surface is eliminated.

Estimating the starting values from the intercept and initial slope of a plot of τ^{-1} versus [M] and from the plateau value of τ^{-1}, kinetic parameters (K_1, k_2, and k_{-2}) were determined by a nonlinear regression analysis so as to fit the expression of τ^{-1} (Eq. 4) to the observed data.[22] The results are summarized in Table 1. It is found that the k_2 value for AO (40 s^{-1}) is very similar to the value (47.6 s^{-1}) reported by Robinson et

Table 1. Equilibrium and Rate Constants at 25 °C

Dyes	K_1 / $M^{-1}\times10^{-3}$	K_2	k_2 / s^{-1}	k_{-2} / s^{-1}	K_3	k_3 / s^{-1}	k_{-3} / s^{-1}	K_T / $M^{-1}\times10^{-4}$
AO	11	2.6	40	15				3.8
Methyl-AO	9.5	1.8	79	43	1.9	65	35	6.0
Propyl-AO	11	1.7	41	24	4.2	29	7.0	11
Pentyl-AO	12	2.5	14	5.6	5.1	4.6	0.89	19
Octyl-AO	12	2.5	0.75	0.30	6.1	0.27	0.044	22
Decyl-AO	5.8	2.3	0.11	0.047	12	0.049	0.004	18

al.[16]

For the 10-alkyl AO–SDS systems (Scheme 2), the time constants for the two isomerization steps can be expressed by[28]

$$\tau_1^{-1},\ \tau_2^{-1} = \frac{1}{2}[(a_{11} + a_{22}) \pm \{(a_{11} - a_{22})^2 + 4a_{12}a_{21}\}^{1/2}], \quad (5)$$

where

$$a_{11} = k_2K_1[\mathrm{M}]/(1 + K_1[\mathrm{M}]) + k_{-2} + k_3, \quad (6)$$

$$a_{12} = k_2K_1[\mathrm{M}]/(1 + K_1[\mathrm{M}]) - k_{-3}, \quad (7)$$

$$a_{21} = -k_3, \quad (8)$$

$$a_{22} = k_3. \quad (9)$$

It should be noted that Eq. 5, as in the case of Eq. 4, holds on the assumption [M]≫[D] which is the case in this study. Equation 5 is a complex expression, but the problem can easily be solved by considering the following expressions:

$$\tau_1^{-1}\cdot\tau_2^{-1} = (k_3 + k_{-3})(\tau_1^{-1} + \tau_2^{-1}) - (k_3 + k_{-3})k_2 - k_{-2}k_{-3}, \quad (10)$$

$$\tau_1^{-1} + \tau_2^{-1} = k_2K_1[\mathrm{M}]/(1 + K_1[\mathrm{M}]) + k_{-2} + k_3 + k_{-3}. \quad (11)$$

In the same manner as Eq. 4, the curve-fitting analysis of Eq. 11 gives K_1, k_2, and $k_{-2}+k_3+k_{-3}$. Then, the values of k_{-2}, k_3 and k_{-3} are determined from the slope and intercept of a plot of $\tau_1^{-1}\cdot\tau_2^{-1}$ against $(\tau_1^{-1}+\tau_2^{-1})$. The kinetic parameters thus obtained are listed in Table 1. The solid lines in Figs. 3—5 represent the theoretical ones calculated on the basis of kinetic parameters in Table 1; there is a satisfactory agreement between observed and calculated values.

Takeda et al.[14] found that when pinacyanol solution is mixed with the solution containing SDS micelles, the absorption band characteristic of the surfactant-dye salt appears and this is progressively replaced by the monomer band of the dye with time. To interpret the kinetics of the solubilization of pinacyanol into the SDS micelle, they proposed the rapid initial formation of the salt which then penetrates the palisade layer of the micelle.[14] A similar mechanism was also suggested for the solubilization of an anthraquinone acidic dye into the micelle of hexadecyltrimethylammonium bromide (HTAB).[19] Since hydrophobic interactions between hydrocarbon chain attached to AO and surfactant stabilize the salt, it is expected that the salt formation might be pronounced with an increase in the length of the alkyl chain. In the present systems, unambiguous evidence for the salt formation was not obtained from both the rapid-scanning spectroscopy (Fig. 6) and the wavelength dependence of optical changes in reaction curves. Nevertheless, it seems worthwhile to examine some possibility of the salt formation, since this is anticipated to be a very rapid process outside the time range of stopped-flow measurements. In such a case, the following kinetic scheme should be considered:

$$\mathrm{D} + x\mathrm{S} \overset{K_0}{\rightleftharpoons} \mathrm{DS}_x,$$

$$\mathrm{DS}_x + \mathrm{M} \overset{K_1}{\rightleftharpoons} \mathrm{DM}_1 \overset{K_2}{\rightleftharpoons} \mathrm{DM}_2 \overset{K_3}{\rightleftharpoons} \mathrm{DM}_3. \quad (12)$$

In Scheme 12, S is the surfactant monomer, DS_x is the salt of dye with surfactant molecules, x is a small integer, and K_0 is the equilibrium constant for the salt formation. If we assume that both the salt formation and the adsorption of the salt on the micelle surface are rapid, we can find that the time constants for the isomerization steps are also expressed by Eq. 6. In the expressions for τ_1^{-1} and τ_2^{-1},

$$a_{11} = k_2K_1[\mathrm{M}]/\{(1 + 1/K_0[\mathrm{S}]^x) + K_1[\mathrm{M}]\} + k_{-2} + k_3, \quad (13)$$

$$a_{12} = k_2K_1[\mathrm{M}]/\{(1 + 1/K_0[\mathrm{S}]^x) + K_1[\mathrm{M}]\} + k_{-3}, \quad (14)$$

$$a_{21} = -k_3, \quad (15)$$

$$a_{22} = k_{-3}. \quad (16)$$

If the salt formation predominatly occurs, that is, $K_0[\mathrm{S}]^x \gg 1$, Eqs. 13—16 are reduced to Eqs. 6—9. In this case, two schemes (Scheme 2 and Scheme 12) can not kinetically be distinguished. Here, it should be noted that K_1 in Scheme 12 is the equilibrium constant for the adsorption of the salt (DS_x). Since D having a positive charge is more accessible to the negatively charged micelle surface than DS_x which is neutral or negatively charged, K_1 for DS_x (Scheme 12) is expected to be smaller than that for D (Scheme 2). Table 1 indicates that K_1 does not depend on the length of the alkyl chain except decyl-AO. This finding suggests that not hydrophobic but eletrostatic interactions make major contributions to the driving force for the adsorption process. The smaller value for decyl-AO is presumably a result of appreciable formation of the salt which leads to weakening the electrostatic force. Moreover, the additional rapid reaction observed for decyl-AO dye or octyl-AO may be attributed to the adsorption of the salt and/or to its dissociation on the micelle surface which takes place rapidly prior to the penetration of the dye into the micelle. In view of the considerations stated above, it seems reasonable to conclude that Scheme 2 prevails for the AO derivatives with shorter alkyl chains, whereas Scheme 12, in addition to Scheme 2, makes some contributions to the kinetics of the solubilization for the AO derivativs with longer alkyl chains.

K_2 has similar values for all dyes, whereas the

forward and backward rate constants of the second step (k_2 and k_{-2}) gradually decrease with increasing the length of the alkyl chain (Table 1). This result shows that the second step is not driven by hydrophobic force, but the alkyl chain plays an important role for the activation of the second step. One possible mechanism is the reorientation of the dye at the micelle surface which includes partial penetration of the alkyl chain through the surface layer of the micelle. This process must be accompanied by the release of hydrated water molecules surrounding the alkyl chain.[29] Therefore, the rate constants for the second step are expected to decrease with increasing the size of the alkyl chain.

Table 1 also indicates that both the equilibrium and the rate constants for the third step highly depend on the length of the alkyl chain; K_3 increases with increasing the size of the alkyl group, while k_3 and k_{-3} decrease. This result suggests that the final form of the complex is stabilized by the hydrophobic force. On the other hand, the spectral change of the dye with time (Fig. 6) obviously shows that the dye is solubilized into the hydrophobic environment. In view of these results, it seems reasonable to assign the third step to the migration of the alkyl chain from the micelle surface to the *inner* hydrophobic site of the micelle.

Figure 7 displays the standard free energy changes ($\Delta G_2°$, $\Delta G_3°$, $\Delta G_{2+3}°$) for the second and third steps in Schemes 1 and 2 as a function of the number of carbon atoms in the alkyl chain (n); $\Delta G_{2+3}°$ corresponds to the standard free energy changes for the overall isomerization process. The free energy of transfer of a methylene group to the inside of the micelle can be estimated

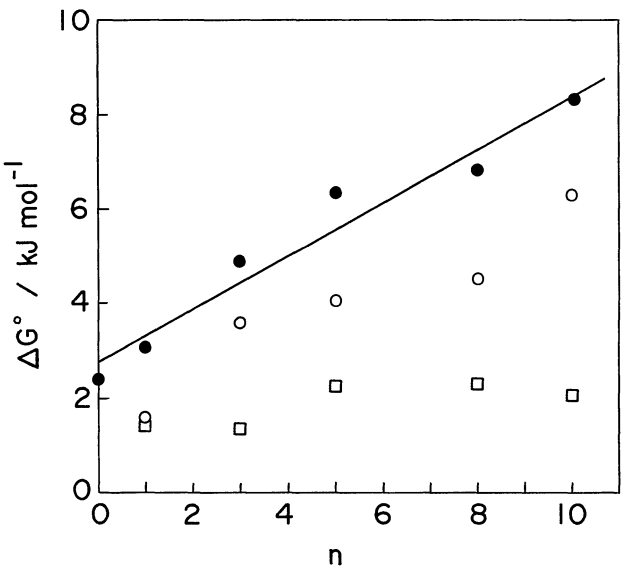

Fig. 7. The standard free energy changes for the isomerization steps as a function of the number of carbon atoms in the alkyl chain (n). (□) $\Delta G_2°$; (○) $\Delta G_3°$; (●) $\Delta G_{2+3}°$. The line is the least-squares fit for $\Delta G_{2+3}°$.

from the slope of a linear plot of $\Delta G_{2+3}°$ versus n;[29] the value was found to be about 0.6 kJ mol^{-1}. This value is about a half to one third of that estimated for the transfer of a hydrocarbon to the SDS micelle.[29] Possibly this smaller value of the free energy of transfer is due to the presence of the bulky acridine head group.

The overall binding constant K_T can be defined by

$$K_T = K_1(1 + K_2 + K_2K_3). \quad (17)$$

As shown in Table 1, the K_T values are the order of 10^4 to 10^5 M^{-1}. To confirm the mechanism of the solubilization, it is necessary to determine binding constants for micelles by means of other techniques. In spite of the desire to have useful, general methods for obtaining such constants, the present state of affairs remains difficult. Fluorescence techniques have been applied to evaluate rough binding constants, but their number is quite limited.[10,11,30] Chiang and Lukton[10] reported $K_T \approx 2\times10^3$ M^{-1} for the binding of 6-(*p*-toluidino)-2-naphthalenesulfonate to the SDS micelle. On the other hand, Reed et al.[11] estimated the following association constants of Rose Bengal binding to HTAB and SDS micelles; $K_T(\text{HTAB}) \geqq 10^4$ M^{-1} and $K_T(\text{SDS}) \geqq 10^2$ M^{-1}. By employing the fluorescence quenching method, Zoltewicz and Munoz[30] have recently reported that the association constants of heterocyclic cations such as 10-methylacridinium and ethidium bromide to the SDS micelle range between 1.0×10^4 and 1.4×10^5 M^{-1}. This method gives more accurate binding constants and its application to our systems will be an interesting subject. The above results suggest that the magnitude of K_T, when the charges of the dye and micelle are opposite, is much larger ($\geqq 10^4$—10^5 M^{-1}) compared to that ($\approx 10^3$ M^{-1}) with the same charge. It is worth noting that the K_T values in this study are to be expected for the binding of cationic dyes to the anionic micelle. As can be seen from Table 1, K_T increases with increasing the size of the alkyl chain except a somewhat smaller value for decyl-AO. This behavior can be understood in terms of the combined effect of the electrostatic interaction, which is responsible for K_1, and of the hydrophobic interaction, which predominantly affects K_3.

In conclusion, the stopped-flow kinetic study reveals that the solubilization of AO and its 10-alkyl derivatives into the SDS micelle consists of a rapid initial adsorption of the dye on the micelle surface and two sequential isomerization steps; one is the reorientation of the dye at the micelle surface and the other is the migration of its alkyl chain into the inner hydrophobic region of the micelle.

References

1) J. H. Fendler and E. J. Fendler, "Catalysis in Micellar and Macromolecular Systems," Academic Press, New York (1975).

2) J. H. Fendler, "Membrane Mimetic Chemistry,"

Wiley, New York (1982).
3) J. H. Fendler, *Ann. Rev. Phys. Chem.*, **35**, 137 (1984).
4) M. A. Chaiko, R. Nagarajan, and E. Ruckenstein, *J. Colloid Interface Sci.*, **99**, 168 (1984).
5) N. Ramnath, V. Ramesh, and V. Ramamurthy, *J. Photochem.*, **31**, 75 (1985).
6) Y. Chevalier and C. Chachaty, *J. Phys. Chem.*, **89**, 875 (1985).
7) J. F. Ellena, R. Dominay, and D. S. Cafiso, *J. Phys. Chem.*, **91**, 131 (1987).
8) M. F. Ottaviani, P. Baglioni, and G. Martini, *J. Phys. Chem.*, **87**, 3146 (1983).
9) Y. Kubota, M. Kodama, and M. Miura, *Bull. Chem. Soc. Jpn.*, **46**, 100 (1973).
10) H. C. Chiang and A. Lukton, *J. Phys. Chem.*, **79**, 1935 (1975).
11) W. R. Reed, M. J. Politi, and J. H. Fendler, *J. Am. Chem. Soc.*, **103**, 4591 (1981).
12) E. Blatt and W. H. Sawyer, *Biochim. Biophys. Acta*, **822**, 43 (1985).
13) A. Malliaris, *Adv. Colloid Interface Sci.*, **27**, 153 (1987).
14) K. Takeda, N. Tatsumoto, and T. Yasunaga, *J. Colloid Interface Sci.*, **47**, 128 (1974).
15) H. Hoffmann, in "Chemical and Biological Applications of Relaxation Spectroscopy," ed by E. Wyn-Jones, Reidel, Dordrecht (1975), pp. 181—193.
16) B. H. Robinson, N. C. White, and C. Mateo, *Adv. Mol. Relaxation Processes*, **7**, 321 (1975).
17) A. D. James and B. H. Robinson, *Adv. Mol. Relaxation Processes*, **8**, 287 (1976).
18) A. D. James, B. H. Robinson, and N. C. White, *J. Colloid Interface Sci.*, **59**, 328 (1977).
19) Y. Miyashita and S. Hayano, *Bull. Chem. Soc. Jpn.*, **54**, 3249 (1981).
20) E. Miethke and V. Zanker, *Z. Phys. Chem. (Frankfurt am Main)*, **18**, 375 (1958).
21) B. Tonomura, H. Nakatani, M. Ohnishi, J. Yamaguchi-Ito, and K. Hiromi, *Anal. Biochem.*, **84**, 370 (1978).
22) P. R. Bevington, "Data Reduction and Error Analysis for the Physical Sciences," McGraw-Hill, New York (1969), pp. 187—246.
23) A. Yamagishi, *J. Colloid Interface Sci.*, **81**, 511 (1981).
24) P. Mukerjee and K. J. Mysels, *J. Am. Chem. Soc.*, **77**, 2937 (1955).
25) V. Zanker, *Z. Phys. Chem. (Leipzig)*, **199**, 225 (1952).
26) K. Murakami, K. Mizuguchi, Y. Kubota, and Y. Fujisaki, *Bull. Chem. Soc. Jpn.*, **59**, 3393 (1986).
27) K. J. Mysels and L. H. Princen, *J. Phys. Chem.*, **63**, 1696 (1959).
28) K. Hiromi, "Kinetics of Fast Enzyme Reactions," Halsted Press, New York (1979), Chap. 6.
29) C. Tanford, "The Hydrophobic Effect," 2nd ed, Wiley-Interscience, New York (1980), pp. 60—78.
30) J. A. Zoltewicz and S. Munoz, *J. Phys. Chem.*, **90**, 5820 (1986).

The 2.0 Å Crystal Structure of Cyanide Metmyoglobin Reconstituted with 5,10,15,20-Tetrapropylhemin

Tadashi HATA,* Yasuo HATA,† Takao SATO,†† Nobuo TANAKA,†† Saburo NEYA,††† Noriaki FUNASAKI,††† and Yukiteru KATSUBE†

Analytical and Metabolic Research Laboratories, Sankyo Co., Ltd., Hiromachi, Shinagawa-ku, Tokyo 140
† Institute for Protein Research, Osaka University, Yamadaoka, Suita, Osaka 565
†† Department of Life Science, Faculty of Bioscience and Biotechnology, Tokyo Institute of Technology, Midori-ku, Yokohama, Kanagawa 227
††† Department of Physical Chemistry, Kyoto Pharmaceutical University, Yamashina, Kyoto 607

(Received September 7, 1990)

Sperm whale metmyoglobin reconstituted with 5,10,15,20-tetrapropylhemin was crystallized in the space group $P2_12_12_1$, which was different from the space group $P2_1$ of the native. The crystal structure of the reconstituted metmyoglobin was determined by the molecular replacement method. The atomic coordinates were refined to R=0.209 at 2.0 Å resolution. The overall structure is essentially the same as that of the native. The pronounced structural change is observed in the side-chain orientation of Arg 45 moving to the surface of the molecule. This conformational change may reflect a side-chain fluctuation that allows the small ligands to approach the heme pocket from the outside of the protein. The porphyrin ring does not rotate freely about the Fe–N^{ε} (His 93) bond in the crystalline state, although temperature-dependent NMR spectra suggest its free rotation in solution.

It is well-known that stereospecific interactions of the heme with globin play important roles in the functional behavior of hemoproteins. Various kinds of reconstituted myoglobins and hemoglobins have been prepared with modified protohemes to investigate the relationship between the structure and the function. The major modification has been performed mainly at the vinyl positions of protoheme, to discern whether the electronic characters or the steric effects of substituents are responsible for the oxygen-binding property.[1–3] On the other hand, 5,10,15,20-tetraalkylporphyrins do not have any substituent at the pyrrole carbons, rather they bear four alkyl groups on 5,10,15,20-positions, as shown in Fig. 1. This difference between 5,10,15,20-tetraalkylporphyrin and protoheme is expected to affect the heme-globin interactions in different ways.

Proton NMR spectra of cyanide metmyoglobin reconstituted with 5,10,15,20-tetraalkylhemin resolved the pyrrole-proton signals of porphyrins in the −5 to −15 ppm region as a singlet, a doublet, and a quartet for the methyl, ethyl, and propyl group, respectively. These peaks of ethyl- or propyl- derivative, however, coalesce into a sharp singlet at 61 °C, suggesting dynamic free rotation of the porphyrin rings about the Fe–N^{ε} (His–F8)bond.[4,5] Such a large fluctuation in amplitude of the porphyrin ring has never been appreciated. The structural perturbation in reconstituted metmyoglobin with 5,10,15,20-tetrapropylhemin is expected to be larger than that in the ethyl derivative. This paper deals with the results of structural studies of cyanide metmyoglobin reconstituted with 5,10,15,20-tetrapropylhemin (R=Pr, in Fig. 1) using X-ray crystallographic analysis. This is the first analysis of myoglobin containing 5,10,15,20-tetraalkylporphyrin.

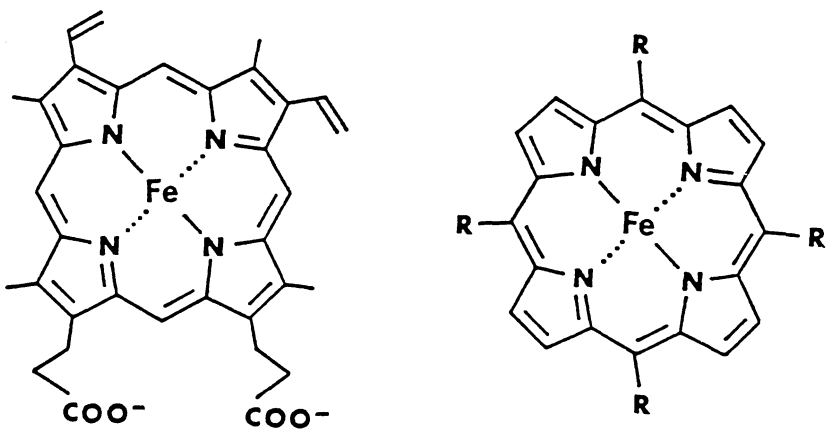

Protoheme

5,10,15,20-Tetraalkylporphyrinatoiron(III)
R=Me, Et, and Pr

Fig. 1. Chemical structures of protoheme and 5,10,15,20-tetraalkylporphyrinatoiron(III).

Materials and Methods

Crystallization. Reconstituted sperm whale metmyoglobin was prepared as described previously[4,5] and stocked in a 10 mM (1 M=1 mol dm^{-3}) Tris-KCN buffer solution (pH 7.0). Crystals of cyanide metmyoglobin reconstituted with 5,10,15,20-tetrapropylhemin were obtained by a dialysis of 0.5 mM protein solution against a saturated ammonium sulfate solution containing 10 mM KCN. The pH of the outer solution was adjusted to 6.5—7.0 with HCl.

The crystals belong to the orthorhombic space group $P2_12_12_1$ with the unit cell dimensions a=58.39(2), b=76.15(2), and c=33.86(2) Å. There are 4 molecules per unit cell, which gives the V_m value of 2.1 $Å^3$/dalton. The unit cell dimensions were determined by the least-squares method using the observed setting angles of 25 reflections collected on a Rigaku AFC-5 four-circle diffractometer. Native sperm whale metmyoglobin has been known to crystallize in two forms: a monoclinic form with space group $P2_1$ from an ammonium sulfate solution, and an orthorhombic form of $P2_12_12_1$ from a phosphate buffer solution.[6] Contrary to expectations, the cell dimensions of reconstituted metmyoglobin with 5,10,15,20-tetrapropylhemin are similar not to those of the previous orthorhombic form, but to those of blue whale myoglobin.[6]

Data Collection and Processing. Crystals with typical dimensions of 0.4×0.4×1.2 mm were sealed in glass capillaries with the mother liquid and used for data collections. Diffraction data were collected at 10 °C on a diffractometer using a nickel-filtered Cu $K\alpha$ radiation produced by a rotating anode X-ray generator operated at 40 kV and 300 mA. The diffraction pathway was kept in vacuo with an evacuated beam tunnel extending from the vicinity of the crystal to the counter, to improve the S/N ratio of data by reducing the X-ray scattering and/or the absorption of air.

Reflection intensities were measured in a continuous omega-scan of approximately 0.8° in width at a scanning speed of 4° min^{-1}. Background counts were measured for 4 seconds at both ends of each scan. Three standard intensities were checked every 100 reflections during data collection to monitor the decay intensity and crystal slippage. Crystals were exchanged as soon as any one of the standard intensities was reduced by 10%. The intensity data were corrected for absorption using an empirical correction curve obtained by measuring the intensity of a phi-independent reflection in 36 consecutive positions of 10° phi-intervals.[7] The correction for crystal damage due to X-ray irradiation was made as a function of the elapsed time. Diffraction intensities were scaled among different data sets by the method of Rollett and Sparks.[8] The final R_{merge} value was 3.1% for 10331 unique reflections up to 2.0 Å resolution, where $R_{merge}=\Sigma|<F>-F_i|/\Sigma F_i$, and $<F>$ is the average of F_i.

Structure Determination. The structure was solved by the molecular replacement method.[9,10] The structure of native sperm whale metmyoglobin in a $P2_1$ form[11] was used as the reference molecule, and its atomic coordinates were obtained from the Protein Data Bank.[12] The reference molecule without the prosthetic group was positioned in an arbitrary $P1$ unit cell with dimensions of $a=b=c$=100 Å and $\alpha=\beta=\gamma$=90°. The structure factors were calculated in the resolution range of 10 to 6 Å, the overall temperature factor being assumed to be 25 $Å^2$. To determine the orientation of the reference molecule in the observed unit cell, the fast rotation function[13] was calculated using Crowther's Eulerian angles with 5° grid intervals. The lengths of the vectors to be searched were limited to within 30 Å, and origin removal was applied. The peak coordinates found in the calculation are given in Table 1 for the two kinds of reference molecules; one reference molecule consisted of all atoms of globin, the other contained only the main chain and the C^β carbon atoms. The fourth peak of the former corresponds to the secondary peak of the latter. This orientation was accepted in the next step.

Table 1. Peak Coordinates in Rotation Functions[a]

	Peak	Peak height	β	α	γ
Case 1	1	62.9	55.0	120.0	60.0
	2	57.8	5.0	50.0	−105.0
	3	57.5	40.0	140.0	165.0
	4	53.0	35.0	40.0	170.0
	5	46.9	80.0	140.0	−15.0
Case 2	1	57.9	10.0	130.0	170.0
	2	47.6	35.0	45.0	165.0
	3	39.8	60.0	120.0	−120.0

a) α, β, and γ are Crowther's Eulerian angles. As the reference molecule, all atoms were included in Case 1, and only the main chain and C^β atoms were in Case 2. The orientation of Peak 2 in Case 2, which corresponds to that of Peak 4 in Case 1, was submitted to a translation search

The translation search was performed by the R-factor map procedure.[14,15] In this step, porphyrin with the Fe atom (R=H, in Fig. 1) was added to the whole globin as the prosthetic group. The reference molecule was located in the orientation obtained in the previous step. The structure factors were calculated separately for each symmetry operation of the space group $P2_12_12_1$. These partial structure factors were merged using relative phase angles calculated by placing the reference molecule in various positions. The R factor at 6 Å resolution was calculated at 1 Å grids over the range of 0—1/2 lattice along the three crystallographic axes. Some short intermolecular contacts were found at the position of the lowest R value, 0.51. After a packing analysis was carried out to check intermolecular contacts, a rigid body refinement was performed to improve the results obtained from the coarse grid searches of rotation and translation about several reasonable positions. Three rotational and three translational parameters were refined to minimize the R value by the simplex method,[16] which is well-suited for searching the minimum point around the initial parameters over a wide range. The lowest R factor after this refinement was 0.38 for 186 large reflections in the resolution range of 8 to 5 Å, while R factors of the others were more than 0.41. The new position was obtained by improving the initial parameters by −3.7, 12.6, and 0.2° in rotation of the Eulerin angles and −0.2, 1.1, and 0.0 Å in translation along the three crystallographic axes. Successive rigid body refinements resulted in R values of 0.34 for 351 large reflections of 4.5—4.0 Å resolution, and 0.32 for 266 large reflections between 3.15 and 3.0 Å resolution. The position of the heme iron atom was also confirmed by the

anomalous difference Patterson map based on the intensity data which were measured using the synchrotron radiation (λ=1.74 Å) at Tsukuba Photon Factory.

Structure Refinement. Refinement of the structure was carried out by a restrained least-squares technique according to the Hendrickson-Konnert method.[17] The resolution in the refinement was gradually improved from 3 Å to 2 Å. A hundred and twelve refinement cycles were done to the convergence at 2.0 Å resolution. The temperature factors were refined independently for the individual atoms after 12 cycles. Forty-three water molecules were found in the $2F_o-F_c$ electron density map calculated after 26 cycles and included as the oxygen atoms in the following refinement. After the 20th, 38th, 48th, and 78th cycles, the refined model was modified by fitting it to the respective $2F_o-F_c$ maps with the color graphics display system. The four propyl groups of 5,10,15,20-tetrapropylhemin were not introduced into the refinement because no remarkable peaks were found in their corresponding positions on electron density maps. The final crystallographic R-factor was 0.209 for 4926 reflections with F_o larger than $3\sigma(F_o)$ at the resolution of 5.5 to 2.0 Å. The rms deviations from their ideal values are 0.013 Å for bond distances, 0.031 Å for angle distances, and 0.037 Å for planar 1-4 distances.

Results and Discussion

Heme and Its Environment. The electron density of the heme in reconstituted metmyoglobin is not so clear, as shown in Fig. 2, and the cyano group coordinating to the iron atom does not appear on the Fourier map, although the electronic absorption spectra indicate the presence of CN^- anion.[4,5] The temperature factors of the atoms in the porphyrin ring are 17 to 20 Å^2, which are slightly larger than the mean value of the overall molecular structure (15 Å^2), indicating disorder and/or vibration. Surprisingly, pyrrole B, located at the bottom of the heme pocket, has larger thermal factors (19—20 Å^2) than any other pyrrole, and the corresponding electron density becomes much lower. On the contrary, pyrrole D, located at the entrance to the heme pocket, represents the smallest thermal motion. Myoglobin, as is well-known, has some interior spaces, or cavities, in the vicinity of the heme.[18] These facts suggest that the cavity at the bottom of the heme pocket is much wider than that at the entrance which is reduced by two imidazole rings of His 64 (E7) and His 97 (FG2), and that the bottom part of the porphyrin ring, such as pyrrole B, swings up and down in the direction normal to the ring, in addition to the oscillatory movement of the heme about the Fe–N$^\varepsilon$ (His 93) bond. However, the free rotation of the heme about the Fe–N$^\varepsilon$ (His 93) bond, which was suggested by proton NMR spectra,[4,5] is not observed in the crystalline state.

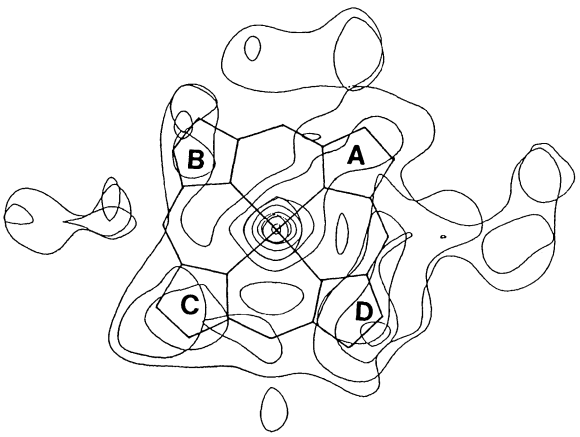

Fig. 2. $2F_o-F_c$ electron density map of the heme. The −2—2 sections parallel to the mean heme plane at intervals of 1 Å are superposed. The heme plane is located on the 0 section. Contours are drawn at arbitrary levels. The four pyrrole rings of porphyrin are labelled by the symbols A, B, C, and D.

The distance between the iron atom and N$^\varepsilon$ of His 93 (F8) is 2.01 Å, which is comparable to 2.13 Å in the native. The iron atom is displaced by 0.2 Å from the mean plane of the porphyrin ring, and by 0.1 Å from the imidazole plane of His 93 (F8). The angle between the Fe–N$^\varepsilon$ (His 93) bond and the axis normal to the mean pyrrole plane is 11.0°, which is comparable with 3.9° in the native. The imidazole ring of His 93 (F8) makes an angle of 35° to the plane composed of the iron atom and two nitrogens of pyrroles B and D. Since the corresponding angle in native myoglobin is 19°, the porphyrin ring in reconstituted metmyoglobin is rotated by 16° about the Fe–N$^\varepsilon$ (His 93) bond.

Rotation of the Heme Group. Temperature-dependent NMR spectroscopy suggested that the heme group of reconstituted myoglobin with 5,10,15,20-tetrapropylhemin freely rotates about the Fe–N$^\varepsilon$ (His 93) bond in solution at high temperature.[4,5] However, this free rotation has not been observed in the crystalline state. In order to check for the possibility of such rotation, the energy barrier for the rotational movement of the heme group about the Fe–N$^\varepsilon$ (His 98) bond was elucidated by calculating the conformational energy with the MM2′ program.[19] The sixteen amino acid residues around the heme were used in the calculation and fixed during energy minimization. The positions of the four propyl groups attached to the heme group were estimated from the standard geometry of 5,10,15,20-tetrapropylporphyrin.[20] All hydrogen atoms were located at the ideal positions. In order to estimate the energy barrier of the heme rotation, the heme group was rotated at 10° steps from 0° to 90° about the Fe–N$^\varepsilon$ (His 93) bond, considering the four-fold rotation symmetry of 5,10,15,20-tetrapropylporphyrin, and used in energy minimization.

The resulting energy variation is shown in Fig. 3 as a function of the His 93C$^\varepsilon$–His 93N$^\varepsilon$–Heme Fe–Heme CCD torsional angle, ϕ. The curve of reconstituted myoglobin with 5,10,15,20-tetrapropylhemin has a

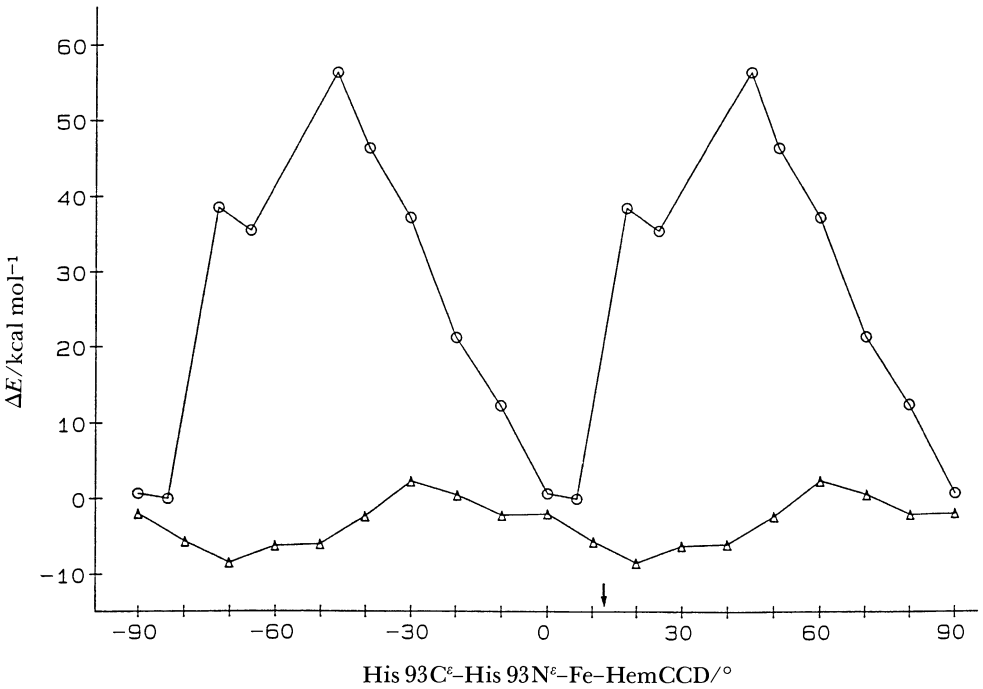

Fig. 3. The variation of the potential energy with rotational angle (ϕ) about His 93C^{ε}–His 93N^{ε}–Fe–Hem CCD for reconstituted metmyoglobin with 5,10,15,20-tetrapropylhemin (circles) and porphyrin (triangles). The potential energy is subtracted by the minimum comformation energy of reconstituted metmyoglobin with 5,10,15,20-tetrapropylhemin. The arrow indicates the observed rotational angle for reconstituted metmyoglobin with 5,10,15,20-tetrapropylhemin.

minimum at ϕ value close to the observed angle of 12.5° and a maximum between −40° and −50°. In these position, the propyl groups of the heme must pass through the narrow spaces composed of Leu 72 (E15) and Phe 138 (H15), and Tyr 103 (G4) and Ile 107 (G8), which are paired above and below the heme plane, respectively; there are short interatomic distances of Leu 72$C^{\delta 1}$···Phe 138C^{ζ} (3.75 Å), Tyr 103O···Ile 107N (3.16 Å) and Tyr 103O···Ile 107$C^{\gamma 2}$ (3.27 Å). Moreover, Lys 42 (C7) and Phe43 (CDl) also prevent the heme group from rotating. Thus, the energy barrier is so high that the heme group could not freely rotate in the crystalline state.

The potential energy curve of reconstituted metmyoglobin with porphyrin (R=H, in Fig. 1) is also plotted in Fig. 3. In this case, the minimum is at ϕ=20 which is different by about 10° from that of reconstituted myoglobin with 5,10,15,20-tetrapropylhemin. Since the energy barrier at ϕ=30° is 11 kcal mol^{-1}, which is much less than that of reconstituted metmyoglobin with 5,10,15,20-tetrapropylhemin, the porphyrin ring might freely rotate about the Fe–N^{ε} (His 93) bond even in the crystalline state. Actually the weak and flat electron density of heme has been observed in the crystal structure of reconstituted metmyoglobin with porphyrin, suggesting rotation and/or vibration of the heme group.[21]

Structural Comparison with Native Metmyoglobin. The overall structure of reconstituted metmyoglobin with 5,10,15,20-tetrapropylhemin is essentially the same as that of the native. Before quantifying the structural differences between the two proteins, a least-square superposing procedure based on the positions of the C^{α} atoms was performed, to get the best fit between them. The resulting superposition of the C^{α}-tracings of the two molecules is illustrated in Fig. 4, and the positional deviations of the amino acid residues are plotted in Fig. 5. The root mean square deviation between the corresponding C^{α} atoms is 0.6 Å. These two figures show that the most pronounced change occurs at the C-terminal region (0.9—3.7 Å), and the next at the N-terminal (1.9 Å). The other residues that move more than 0.77 Å are located at the CD-loop and the E-helix regions: Lys 47 (CD5), His 48 (CD6), and Asp 60 (E3). These regions construct the entrance and/or exit channel through which small diatomic or triatomic ligands move from the outside of the protein to the distal heme pocket.[22]

The mean temperature factors of the backbone atoms (N, C^{α}, C, and O) in each amino acid residue are also plotted in Fig. 5, with the corresponding positional deviations. This figure shows a measure of the flexibility of the polypeptide chain by the relationship between the average temperature factor

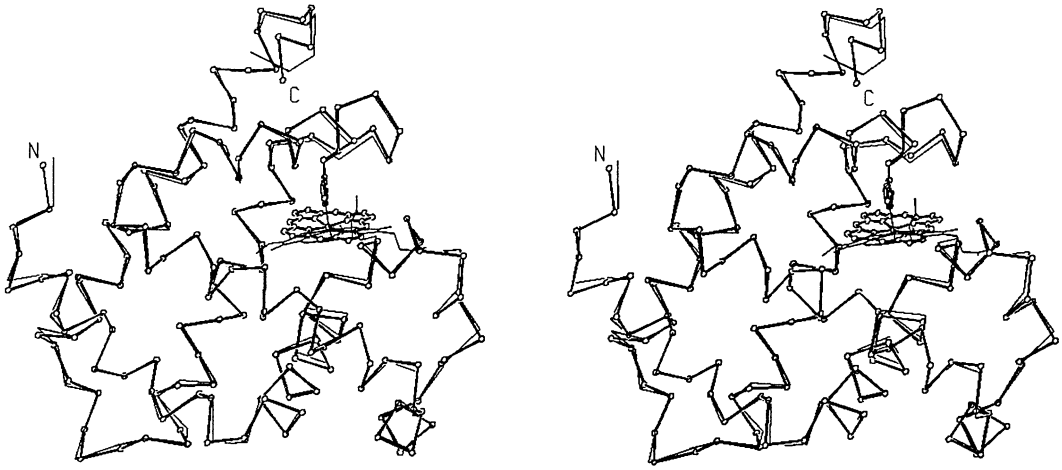

Fig. 4. The conformations of the C^{α} backbone, the heme moiety, and the heme linkage to His 93 in reconstituted metmyoglobin with 5,10,15,20-tetrapropylhemin (thick lines) and native metmyoglobin (thin lines). The amino and carboxyl termini are labelled by N and C.

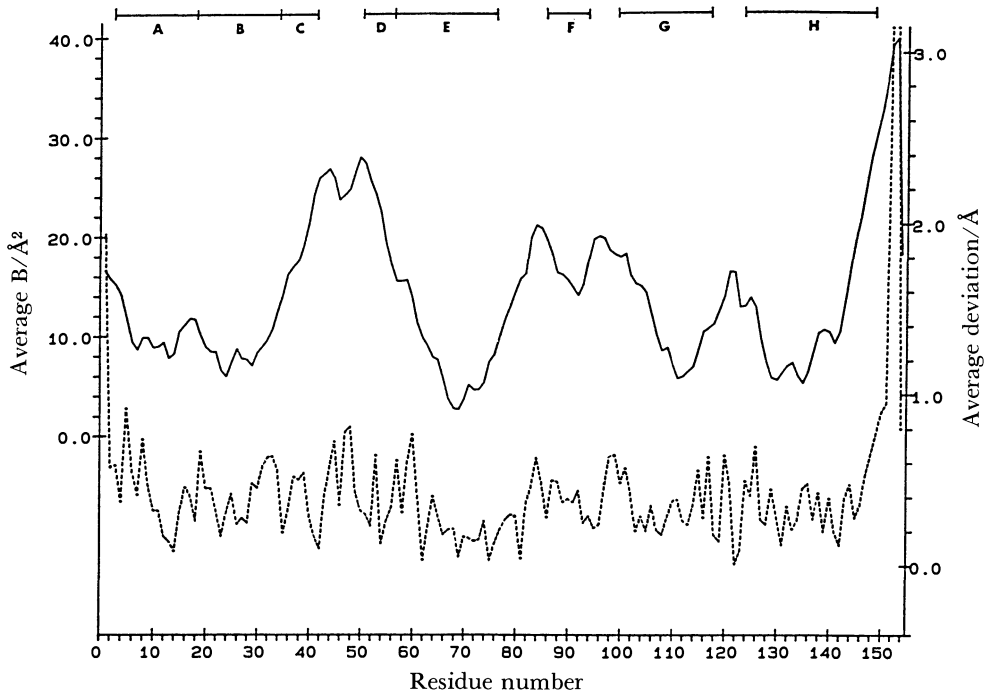

Fig. 5. Plots of the mean temperature factors for each amino acid residue of the main chain in reconstituted metmyoglobin with 5,10,15,20-tetrapropylhemin (solid line) and the positional deviations in the corresponding C^{α}-atoms between reconstituted metmyoglobin with 5,10,15,20-tetrapropylhemin and native metmyoglobin (a dotted line). Bars drawn on the upper part of the graph represent the regions of alpha-helical structure.

and the posisional deviation. The average temperature factors of the overall main chain is 14.1 Å², but considerable variablity is observed along the course of the polypeptide chain. The highest thermal motion is observed in atoms of the C-terminal region. Main-chain atoms in the loops, especially in the CD-loop, have considerably high temperature factors and have been shown to be particularly mobile by temperature-dependent X-ray diffractions of myoglobin.[23] These flexible regions of a polypeptide chain might be able to move easily and to adopt different conformations depending on their circumstances, such as existence of the heme ligand.

Although the structural changes of the main chain

are small, except for the amino and carboxyl termini, a number of pronounced changes occur at the side groups. The side chain of Arg 45 (CD3) dramatically moves toward the outside of the protein. The guanidino group of Arg 45 (CD3) in native metmyoglobin forms two hydrogen bonds: to the carboxyl groups of Asp 60 (E3) and 6-propionic acid of protoheme. In reconstituted metmyoglobin, the latter hydrogen bond is ruptured because of the lack of a carboxyl group of the heme, and the guanidino group is rotated by ca. 170° about the C^{α}–C^{β} bond, to shift its terminal nitrogen atom by 6 Å. As a result, the side chain of Arg 45 (CD3) is no longer stabilized by the hydrogen bond to Asp 60 (E3). Structural differences between phenyl-ligated metmyoglobin and native metmyoglobin have been observed in the side-chain orientation of Arg 45 (CD3), His 64 (E7), and Val 68 (E11) around the distal His 64 (E7), suggesting that these amino acid residues may play an important role in forming the pathway through which small ligands have been presumed to enter the distal heme pocket from the outside of the protein.[22] In reconstituted metmyoglobin, however, only the side group of Arg 45 (CD3) swings out, and those of His 64 (E7) and Val 168 (E11) do not significantly move.

The other drastic changes are observed mainly at the side chains located at the surface of the protein. The maximum deviations in each side chain of Glu 83 (EF6), Lys 96 (FG1), Lys 98 (FG3), and Lys 147 (H24) are all more than 4.0 Å. Among these residues, only Lys 96 (FG1) is situated in the vicinity of the heme pocket. Crystallographic study of sperm whale metmyoglobin reconstituted with 2,4-diisopropyldeuterioheme or 2-isopropyl-4-vinyldeuterioheme has elucidated that the introduction of a bulky isopropyl group to the 2-position of the heme forces the phenyl group of Phe 138 (H15) to rotate around the C^{α}–C^{β} and C^{β}–C^{γ} bonds, resulting in the average deviation of 4 Å by the phenyl atoms.[24] In reconstituted metmyoglobin with 5,10,15,20,-tetrapropylhemin, this rotation of the phenyl group does not occur, although the porphyrin ring has propyl groups.

The superposition of the heme moieties of reconstituted metmyoglobin with 5,10,15,20-tetrapropylhemin and native metmyoglobin is illustrated in Fig. 6. The iron atoms are deviated by 0.8 Å from each other. The porphyrin ring is rotated by 33° within the plane of the ring, and the dihedral angle between these porphyrin planes is 13°. Among four carbons to which the propyl groups are attached, the CDA atom between the pyrrole rings D and A in Fig. 6 is positioned only 1.2 Å from the C-6 position of protoheme in the native. Consequently, it is expected that the propyl group bonded to the CDA atom might be located at the position of 6-propionic acid. On the other hand, the position of the 7-propionic acid is not occupied by any propyl group of 5,10,15,20-tetrapropylporphyrin.

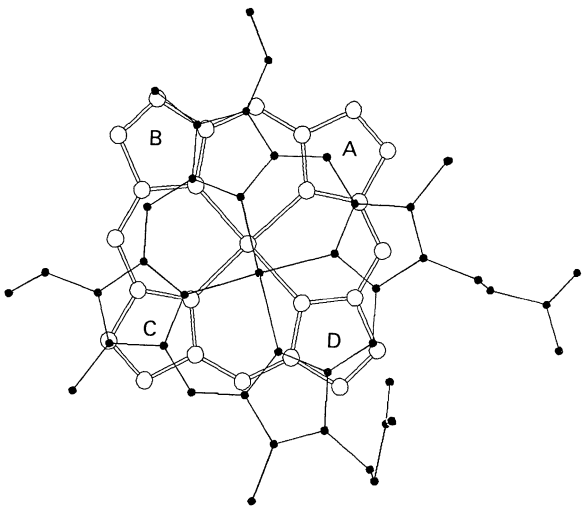

Fig. 6. Superposition of the heme moieties of reconstituted metmyoglobin with 5,10,15,20-tetrapropylhemin (large opened circles) and native metmyoglobin (small full circles). The four pyrrole rings of reconstituted metmyoglobin with 5,10,15,20-tetraproylhemin are labelled by the symbols A, B, C, and D.

The structure of metmyoglobin shows that the pathway of the ligand from the surface of the molecule into the distal heme pocket is shielded by side chains of His 64 (E7) and several other residues, as shown in Fig. 7. In order to form an open channel to the surface, the imidazolyl group of His 64 (E7) has to rotate after the side chain of Arg 45 (CD3) moves toward the outside, as suggested by Nobbs.[25] This mechanism may be regarded as the "double door" mechanism. A structure analysis of reconstituted metmyoglobin reveals that only the side chain of Arg 45 (CD3) moves toward the outside of the molecule to open the "outer door" of the channel. Once the "outer door" is opened, ligands are expected to move inside through the channel in order to open the "inner door" by rotating the imidazole ring of His 64 (E7). Finally, the channel is opened completely. Crystallographic study of phenyl-ligated metmyoglobin,[22] which has a bulky ligand, reveals that the binding of the ligand to the distal position of iron atom makes the side chains of His 64 (E7) and Arg 45 (CD3) move aside and the channel open to the surface.

The guanidino group of Arg 45 (CD3) in native metmyoglobin is locked by two hydrogen bonds to the carboxyl groups of Asp 60 (E3) and 6-propionic acid of the heme. One of the four propyl groups in the porphyrin ring of reconstituted metmyoglobin with 5,10,15,20-tetrapropylhemin occupies the position of the 6-propionic acid of the heme in native metmyoglobin, resulting in a breakage of the hydrogen bond between Arg 45 (CD3) and the 6-propionic acid. In addition, the replacement of the carboxyl group by the

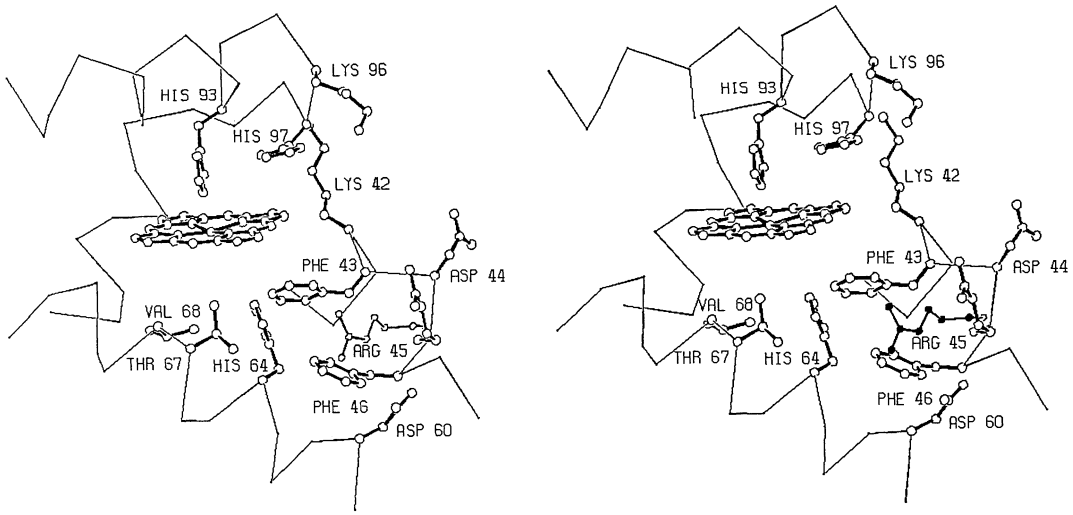

Fig. 7. Drawing of the C^{α}-tracing and the amino acid residues around the heme pocket in reconstituted metmyoglobin with 5,10,15,20-tetrapropylhemin. The pathway through which small ligands have been presumed to enter the ligand pocket lies among Arg 45 (CD3), His 64 (E7), Val 68 (E11), and the heme.[22] The guanidino group of Arg 45 (CD3) moves to the surface of the protein molecule from its position in native metmyoglobin (small full circles).

alkyl group makes the hydrophilic environment change to a hydrophobic one. As the reusult, the hydrophilic guanidino group might be turned toward the hydrophilic globin surface.

As to the opened "outer door", an alternative explanation could been made as follows. Since the amino acid residues of Arg 45 (CD3) and Asp 60 (E3), which are hydrogen-bonded to each other, are located on the surface of the molecule, they are highly influenced by a change of the environment, such as the solvent. If these are species around the protein that are more preferable to the hydrogen bond than Asp 60 (E3), the guanidino group of Arg 45 (CD3) may move outwards to form hydrogen bond with them after breakage of the previous hydrogen bonds. In reconstituted metmyoglobin, there are a large number of the potassium cations and cyano anions around the protein molecule. Such changes in the outer environment may be responsible for the opening and shutting of the "outer door". In addition, the conformational changes observed here should account for the polymorphism of myoglobin depending on the conditions for crystallization.

We would like to thank Dr. Akio Takenaka of the Tokyo Institute of Technology for kindly supplying the rotational and translational search programs and for useful discussions.

References

1) T. Asakura and M. Sono, *J. Biol. Chem.*, **249**, 7087 (1974).

2) H. Yamamoto and T. Yonetani, *J. Biol. Chem.*, **249**, 7964 (1974).

3) R. K. Dinello and D. H. Dolphin, *J. Biol. Chem.*, **256**, 6903 (1981).

4) S. Neya and N. Funasaki, *J. Biol. Chem.*, **262**, 6725 (1987).

5) S. Neya and N. Funasaki, *Biochim. Biophys. Acta*, **952**, 150 (1988).

6) J. C. Kendrew, R. G. Parrish, J. R. Marrack, and E. S. Orlans, *Nature*, **174**, 946 (1954).

7) A. C. T. North, D. C. Phillips, and F. S. Mathews, *Acta Crystallogr., Sect. A*, **24**, 351 (1968).

8) J. S. Rollett and R. A. Sparks, *Acta Crystallogr.*, **13**, 273 (1960).

9) M. G. Rossmann, "The Molecular Replacement Method," ed by M. G. Rossmann, Gordon & Breach, New York (1972), pp. 1—42.

10) A. Takenaka, K. Kizawa, T. Hata, S. Sato, E. Misaka, C. Tamura, and Y. Sasada, *J. Biochem.*, **103**, 463 (1988).

11) T. Takano, *J. Mol. Biol.*, **110**, 537 (1977).

12) F. C. Bernstein, T. F. Koetzle, G. J. B. Williams, E. F. Meyer, Jr., M. D. Brice, J. R. Rodgers, O. Kennard, T. Shimanouchi, and M. Tasumi, *J. Mol. Biol.*, **112**, 535 (1977).

13) R. A. Crowther, "The Molecular Replacement Method," ed by M. G. Rossmann, Gordon & Breach, New York (1972), pp. 173—178.

14) R. E. Nixon and A. C. T. North, *Acta Crystallogr., Sect. A*, **32**, 320 (1976).

15) Z. S. Derewenda, E. J. Dodson, G. C. Dodson, and A. M. Brzozowski, *Acta Crystallogr., Sect. A*, **37**, 407 (1981).

16) "HITAC Mathematical Subprogram Library," Hitachi, Tokyo (1978), Part 3.

17) W. A. Hendrickson and J. H. Konnert, "Biomolecular Structure, Function, Conformation and Evolution," ed by R. Srinivasan, Pergamon Press, Oxford (1981), Vol. 1, pp. 43—57.

18) R. F. Tilton, Jr. and G. A. Petsko, *Biochemistry*, **27**,

6574 (1988).
19) C. Jaime and E. Ōsawa, *Tetrahedron*, **39**, 2769 (1983).
20) P. W. Codding and A. Tulinsky, *J. Am. Chem. Soc.*, **94**, 4151 (1972).
21) T. Sato, A. Tekenaka, N. Tanaka, S. Neya, N. Funasaki, and T. Hata, Protein Engineering '89 Second International Conference, Kobe, August 1989, Abstr., p. 183.
22) D. Ringe, G. A. Petsko, D. E. Kerr, and P. R. Ortiz de Montellano, *Biochemistry*, **23**, 2 (1984).
23) H. Frauenfelder, G. A. Petsko, and D. Tsernoglou, *Nature*, **280**, 558 (1979).
24) K. Miki, S. Harada, Y. Hato, S. Iba, Y. Kai, N. Kasai, Y. Katsube, K. Kawabe, Z. Yoshida, and H. Ogoshi, *J. Biochem.*, **100**, 277 (1986).
25) C. D. Nobbs, "Hemes and Hemoproteins," ed by B. Chance, R. W. Estabrook, and T. Yonetani, Academic Press, New York (1966), pp. 143—147.

 © 1991 The Chemical Society of Japan Bull. Chem. Soc. Jpn., 64, 829—836 (1991)

Resonance Raman Active Vibrations of Rubredoxin. Normal Coordinate Analysis of a 423-Atom Model

Hiroshi SAITO, Takeo IMAI, Kaori WAKITA, Akio URUSHIYAMA,* and Tatsuhiko YAGI†
Department of Chemistry, College of Science, Rikkyo University, Nishiikebukuro 3, Toshima-ku, Tokyo 171
†Department of Chemistry, Shizuoka University, 836 Oya, Shizuoka 422
(Received September 17, 1990)

Normal coordinate analyses were performed on three molecular models of the rubredoxin of *Desulfovibrio vulgaris, Desulfovibrio gigas,* and *Clostridium pasteurianum.* The total 1081, 1093, and 1148 internal coordinates were specified by the X-ray analyzed coordinates of the 390, 399, and 423 atoms, respectively, in a mass-group approximation. The appropriately assumed values of Urey–Bradley force constants as well as some diagonal values of out-of-plane bending and torsional forces gave 146, 146, and 148 normal modes, respectively, in 250—450 cm^{-1} region. These are the deformational vibrations within the peptide skeleton of the protein molecules. The Fe–S stretching displacements of the FeS_4 core contribute to a limited number of these vibrations. The modes having a totally symmetric Fe–S stretching contribution confined within a frequency region of 290—330 cm^{-1} in which the principal resonance Raman band of rubredoxin has been reported, and the several minor resonance Raman bands reported in the higher frequency region of 330—420 cm^{-1} were assigned to noraml modes having a non-totally symmetric Fe–S stretching character. The PED values indicated that all of these modes are constructed mostly by the deformational displacements in the peptide skeleton widely spread into the molecule around the FeS_4 core. This feature is very similar to the case of the blue-copper protein studied previously.

In a previous study,[1] a normal coordinate analysis of the blue-copper protein was carried out on molecular models constructed using a maximum of 169 atoms including the blue-copper site. The analysis showed that the resonance Raman (RR) active modes comprise a dominant contribution of the bond angle bending displacements in the particular part of the peptide skeleton including side chains around the blue-copper site. A sensitive variation in the RR spectra of the type-1 blue-copper proteins was ascribed to a conformational difference in the protein skeleton around the blue-copper site.

In the present study, this work was extended to rubredoxin, which is the initial member of a class of non-heme iron-containing proteins having the simplest Fe–S(cysteine)$_4$ core in the molecule. Long et al.[2,3] first reported the RR effect of oxidized rubredoxin of *Clostridium pasteurianum* in both crystalline and solution phases. The spectra in both phases contain several components: a dominant band (polarized) at 314 cm^{-1}, a moderate band (depolarized) at 368 cm^{-1}, and a weak broad band (depolarized) at 126 cm^{-1} with a shoulder at 150 cm^{-1} upon excitation within a visible Fe←S charge-transfer absorption band centered at 490 nm. Subsequently, Yachandra et al.[4] have found a small shoulder at 325 cm^{-1} in the higher envelope of the main band and an evident splitting by 12 cm^{-1} of the moderate band, commonly found in the RR spectra of rubredoxin of four different bacterial species. They assigned the main band (at 312 cm^{-1}) to the A_1 breathing mode of the FeS_4 core and the shoulder (at 325 cm^{-1}) and the split bands (at 359 and 371 cm^{-1}) to the $B_1+B_2+A_1$ components of the $T_2(T_d)$ Fe–S stretching vibration under the C_{2v} effective symmetry of the core. However, they did not succeed in the reproduction of such a large splitting of the T_2 mode employing any variation of the Urey–Bradley force constant values, considering the actual lowering of the FeS_4 core symmetry in their normal coordinate analyses on a maxinum of thirteen-atom molecular model.

We performed normal coordinate analyses of the molecular models constructed by the three X-ray analyzed molecules of oxidized rubredoxin, from *Desulfovibrio vulgaris* (Rd:Dv),[5] *Desulfovibrio gigas* (Rd:Dg),[6] and *Clostridium pasteurianum* (Rd:Cp),[6] on 390-, 399-, and 423-atom systems, respectively. The results clearly indicated an extensive coupling between the Fe–S stretching vibration and bond angle bending displacements in the polypeptide skeleton widely spread into the molecule around the FeS_4 core. The vibrational characteristics of the RR active modes will be discussed from a different point of view from that by Yachandra et al.[4]

Material and Measurements

Rubredoxin from *Desulfovibrio vulgaris* Miyazaki (Rd:DvM) was isolated as described elsewhere.[18] The 495/280 nm absorbance ratio of the purified protein was ca. 0.4. The RR signals were detected with a backscattering technique from the surface of a dried protein film on a small iron plate which was wholly immensed into liquid nitrogen within a quartz Dewar. All sampling procedures were carried out in an oxygen-free dry box. The Ar^+ 4880 Å line (350 mW) was used as an excitation source. The spectra were well reproduced during a prolonged acquisition time of about eight hours.

Computation

Our view concerning a normal coordinate analysis of protein molecules in which various subsidiary forces work within the molecules was discussed in a

previous study.[1] While the RR effects of rubredoxin appear to be in a somewhat lower wavenumber region (mainly in 290—430 cm^{-1}) than that of the blue-copper proteins (mainly in 360—450 cm^{-1}) previously studied, a similar basis of the approximation, ignoring the hydrogen-bonding potential, charge potential, van der Waals potential, potential due to solvent molecules, and almost of torsional potentials, was also employed in the present study. No particular remark concerning the anharmonicity of the principal RR active vibration of 312 cm^{-1} was reported while assigning the overtone and combination signals. This has been reconfirmed in the present measurement in the overtone region (Fig. 1). The lowest RR bands of rubredoxin detected in 120—160 cm^{-1} region, which were assigned to the S–Fe–S deformational modes ($\nu_2(E)+\nu_4(T_2)$) of the tetrahedral FeS_4 core, must be greatly influenced by the low-frequency "concerted motion" of the protein skeleton, which is believed to have frequencies of up to ca. 100 cm^{-1}. Therefore, the normal coordinates of these deformational modes must not be correctly deduced, although an apparent coincidence between the calculated and observed values could be obtained when the values of the bending and repulsive forces were adjusted. Thus, the discussion is almost limited to within the Fe–S stretching region of vibration studied in the present work.

Totals of 1081 (Rd:Dv), 1093 (Rd:Dg), and 1148 (Rd:Cp) internal coordinates involving all possible bond-stretching and bond-angle-bending coordinates, as well as some selected coordinates of the out-of-plane bending regarding the C_α–C(CO)–N part in the peptide bonding and the CH_n–, OH–(benzene ring) part in the side chain (and the corresponding part in the tryptophan residue) as well as the torsion around N–C_α bond in the peptide bonding, were specified from the X-ray determined 390, 399, and 423 non-hydrogen atoms, respectively. A mass-group approximation in which the mass of all hydrogen atoms is included into those of the attached atoms was employed similarly to the previous work.

The geometrical parameters of the molecules of rubredoxins from *Desulfovibrio vulgaris* (Rd:Dv), *Desulfovibrio gigas* (Rd:Dg) and *Clostridium pasteurianum* (Rd:Cp) consisting of 52, 52, and 54 amino acid residues, respectively, were obtained from the Protein Data Bank (PDB). The primary structure (amino acid sequences) of Rd:Dv is shown in Fig. 4. The Urey–Bradley force constant values as well as diagonal values of the out-of-plane bending and the torsional forces used in the present work are essentially the same as those used in the previous work. The Fe–S(cysteine) stretching force was set to be K(Fe–S)=1.36 mdyn $Å^{-1}$ after several trial calculations to obtain a better fitting to the observed RR spectra. This value is somewhat larger than that proposed by Yachandra et al. This is due to the extensive coupling of the Fe–S stretching

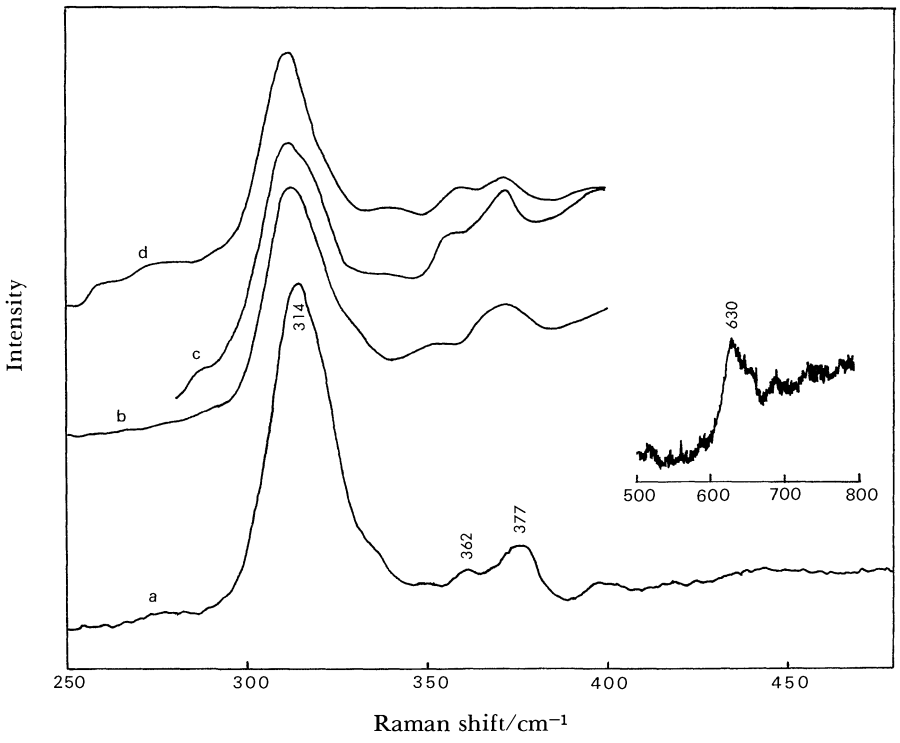

Fig. 1. Resonance Raman spectra of rubredoxin. (a) *Desulfovibrio vulgaris* Miyazaki at 77 K (present measurement). (b) *Megasphera elsdenii*.[4] (c) *Desulfovibrio sulfricans*.[4] (d) *Desulfovibro gigas*.[4]

displacements to the skeletal deformational modes (see below).

The computer programs used for normal coordinate analyses are the same as those used in the previous study. All computational work was done on M682H and S-820 computers at the Computer Center of the University of Tokyo.

Results and Discussion

The resonance and preresonance Raman mechanisms have been discussed in the literature.[7,8] Resonance enhancement is primarily sensitive to a displacement of potential surface of the electronic excited states, which is concerned with the Raman excitation, in totally symmetric normal coordinate space (Albrecht's A term).

The RR spectrum of the oxidized Rd:Dv is shown in Fig. 1, in which the spectra of those from several other bacterial species already reported are also included. The essentially similar spectrum of Rd:Cp has been shown in the literature.[3] The sequence resemblances between the rubredoxins were shown,[10,11] in which, especially, the sequential difference ratio between Rd:Dv and Rd:DvM was found to be only 5/52. The invariant nature in the over-all folding and Fe–S_4 environment in the three-dimensional X-ray structures of Rd:Dv, Rd:Cp, and Rd:Dg has also been described.[11] The present measurement confirms the presence of additional weak bands at ca. 397, ca. 420, and ca. 440 cm^{-1}, while the main part of the spectra (290—390 cm^{-1}) is quite similar to those reported for other species. A distinct overtone signal of the main band (314 cm^{-1}) was detected at 630 cm^{-1}.

The excitation profile of the Raman bands of rubredoxin was discussed by Long et al. The characteristic intense absorption bands of oxidized rubredoxin centered at 20000 and 27000 cm^{-1} can be correlated with charge-transfer transitions from the bonding molecular orbitals localized mainly at the sulfur ligands to the non-bonding orbitals of the iron 3d orbitals[9] of the tetrahedral FeS_4 core; the Fe–S displacement must be therefore occur in the totally symmetric normal coordinate space associated with these electronic transitions (elongation of the Fe–S bondings in the

Table 1. Important Normal Mode Frequencies (in 250—450 cm^{-1}) and Their PED Values of Four Fe–S Stretching Coordinates in Rubredoxin[a]

Normal coord.	Frequency	PED[b] of Fe–S stretching coordinates			
	cm^{-1}	Cys6–Fe	Cys9–Fe	Cys39–Fe	Cys42–Fe
Q 616	419.1	−4.33	1.31	6.27	−1.27
Q 617	416.8	19.27	−6.78	−11.06	4.67
Q 621	412.9	18.55	−7.14	−16.66	6.42
Q 622	412.7	−9.84	7.03	3.38	−1.99
Q 623	388.2	12.12	−7.79	32.25	−0.65
Q 637	378.5	1.96	2.99	0.18	−8.29
Q 639	372.7	−1.67	−0.46	4.18	5.61
Q 641	370.5	−0.00	−6.41	1.39	2.91
Q 642	368.4	−3.71	25.71	−4.23	−0.68
Q 647	357.4	−0.47	29.97	−40.48	7.58
Q 649	356.0	−4.18	−1.51	4.10	1.79
Q 651	354.8	−17.98	−0.27	5.57	15.43
Q 652	351.7	6.28	−0.58	0.00	−4.00
Q 655	342.0	1.49	3.17	−0.00	1.61
Q 662	340.2	−0.02	−6.64	0.05	−9.75
Q 664	335.4	−6.16	0.00	4.34	10.21
Q 670	330.9	−4.28	−1.07	−0.41	0.06
Q 672	329.8	13.55	2.74	2.70	−1.46
Q 673	326.1	−11.13	−10.51	−7.35	−3.54
Q 675	322.5	2.69	0.92	1.07	3.27
Q 678	308.3	−0.22	0.88	−1.12	−10.67
Q 690	302.0	5.05	14.55	5.43	10.75
Q 694	293.8	1.27	0.82	1.44	5.41

a) Rubredoxin of *Desulfovibrio vulgaris*: (minus) signs represent the (minus) sign of the corresponding L-matrix elements, l_{in}; only normal vibrations having total PED value of the four Fe–S stretching coordinates exceed 5.8 are presented; Urey-Bradley force constant values are K(Fe–S)=1.360 mdyn $Å^{-1}$, H(Fe–S–CH_2)=0.150, F(Fe–S–CH_2)=0.040, H(S–Fe–S)=0.085, F(S–Fe–S)=0.085 mdyn $Å^{-1}$, and other skeletal forces were set as the same values as the previous analysis of the blue-copper proteins[1] (see text). b) Definition PED=$(F_{ii}l_{in}^2/\sum F_{ii}l_{in}^2)\times 100$ is employed here.

#) While a correction of Thr21 to Asp21 was pointed out on the basis of the DNA sequence (Ref. 10), the original Thr21 is used here as the X-ray structure of Rd:Dv.

electronic excited state). Therefore, the principal RR effect observed at 314 cm^{-1} upon the visible excitation must be primarily related to the totally symmetric Fe–S stretching component in normal coordinates.

The present calculational evidence can be divided into the following four categories:

(1) The totals of 146 (Q_{594}—Q_{739}) modes for Rd:Dv, 146 (Q_{605}—Q_{750}) for Rd:Dg, and 148 (Q_{634}—Q_{781}) for Rd:Cp were obtained in the RR interesting region of the 250—450 cm^{-1}, respectively. The frequency positions of these normal modes are shown in Figs. 2—4. These modes all comprise, principally, deformational displacements within the peptide skeleton, having a minor contribution of skeletal bond stretching coor-

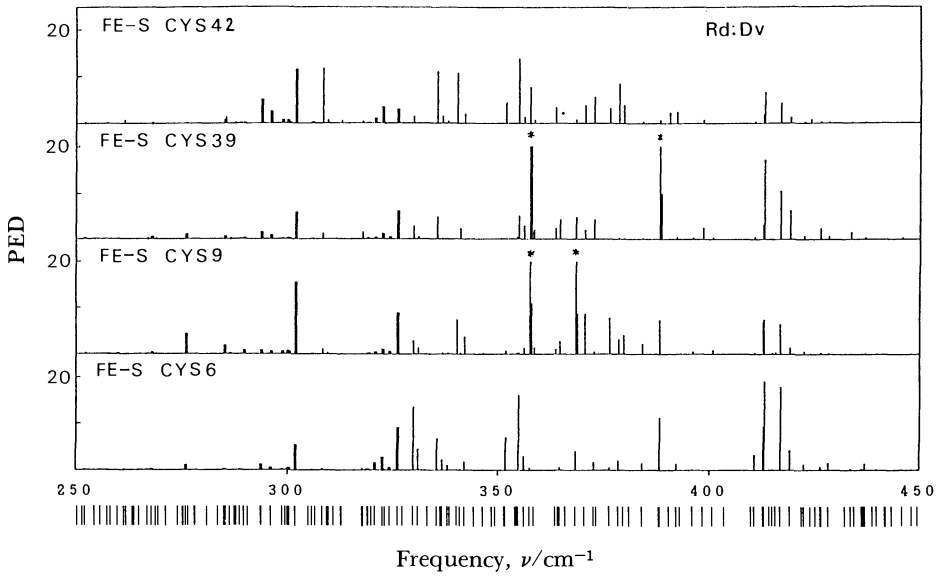

Fig. 2. PED of the four Fe–S stretching coordinates of Rd : Dv. The bold and thin lines denote the normal modes including totally symmetric (with all the same sign of the corresponding L-matrix elements, L_{in}) and non-totally symmetric (with not the same sign) of Fe–S stretching displacements, respectively. The short vertical lines below each figures denote the frequency positions of the normal vibrations. The values exceed 20.0 (asterisked) are depicted by double lines.

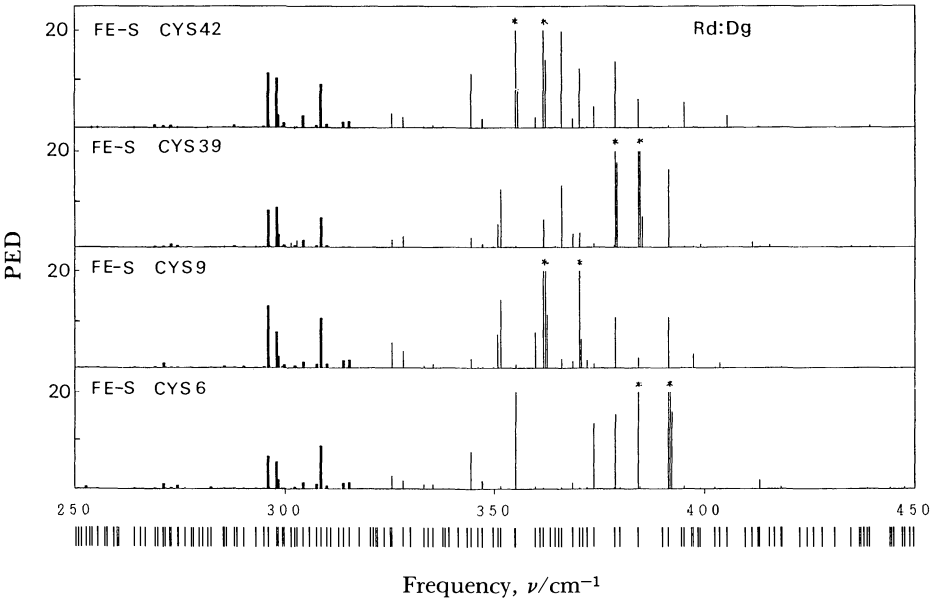

Fig. 3. PED of the four Fe–S stretching coordinates of Rd : Dg. The notation is similar to Fig. 1.

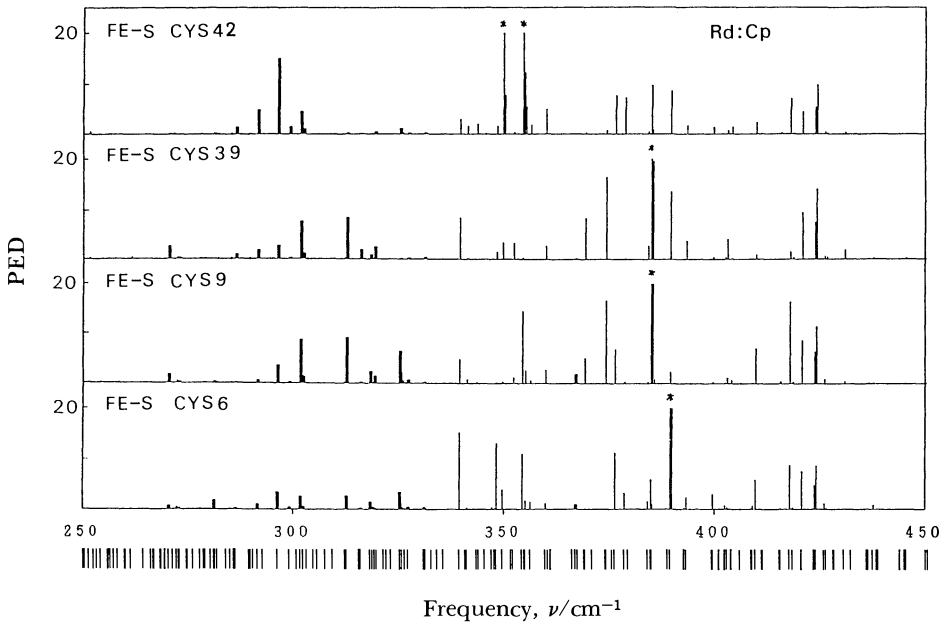

Fig. 4. PED of the four Fe–S stretching coordinates of Rd : Cp. The notation is similar to Fig. 1.

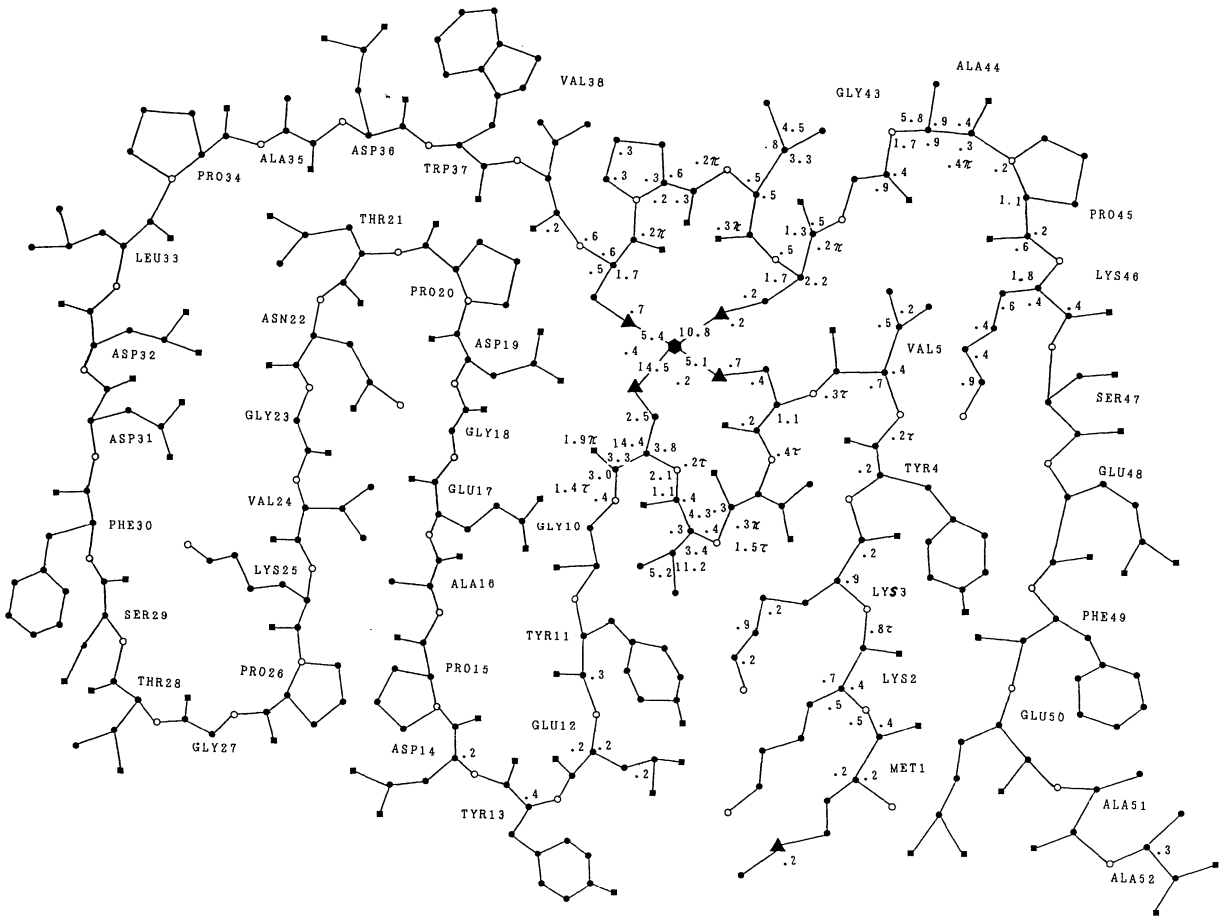

Fig. 5. PED values of the deformational coordinates (bond angle bending, out-of-plane bending: π, and torsional: τ) of the Q_{690} (302.0 cm^{-1}) of Rd : Dv (●: carbon; □: oxygen; ○: nitrogen; ▲: sulfur; ⬢: iron). The values exceed 0.2 are depicted.

dinates (vide infra).

(2) Among the above-mentioned normal vibrations, limited modes involve an actual contribution of the Fe–S stretching displacements (Table 1). In Figs. 2—4. are illustrated the PED values of the four Fe–S(cysteine) stretching coordinates for the normal modes in the 250—450 cm^{-1} region. There is no mode which comprises almost a pure contribution of the Fe–S stretching vibration.

(3) The normal modes involving a totally symmetric Fe–S stretching character, which means in the present study those modes having the same sign as all four corresponding L-matrix elements, appear in the lower-wavenumber region (280—330 cm^{-1}) than those of the non-totally symmetric Fe–S stretching character (not the same sign of all the four corresponding L-matrix elements) (330—450 cm^{-1}). The frequency positions of the former have been confined in the region where the principal RR band was observed, as shown in Fig. 1. The latter well interprets the minor RR bands appearing in the higher-frequency region (including the newly detected bands in the present measurement). An interpretation of the RR intensity of the non-totally symmetrical Fe–S stretching vibrations is possible if the actual reduction of the FeS_4 core symmetry is taken into account. In fact, the 1.2 Å refined X-ray structure of Rd:Cp indicates the smallest and largest S–Fe–S angles of 103.7(4) and 114.3(4) degree and the shortest and longest Fe–S bond lengths of 2.24(1) and 2.39(1) Å, respectively. In C_1, the actual symmetry of the FeS_4 core, all vibrational modes can be RR enhanced.

(4) Normal vibrations having a large (totally or non-totally symmetric) Fe–S stretching contribution comprise skeletal deformational displacements over a considerably wide range of the protein skeleton around the FeS_4 center. The PED values of the 302.0 cm^{-1} mode of Rd:Dv, for example, which has the largest totally-symmetric Fe–S stretching character, are depicted in Fig. 5; the PED values of the bond-angle-bending coordinates (including out-of-plane bending and torsion) summed up for the four normal modes having a large Fe–S stretching character are shown in Fig. 6. Essentially similar figures were obtained for the non-totally symmetric Fe–S stretching vibrations (Fig. 7). It was found that the interaction occurs with the deformational coordinates, roughly speaking, in more than 15 amino acid residues around the FeS_4

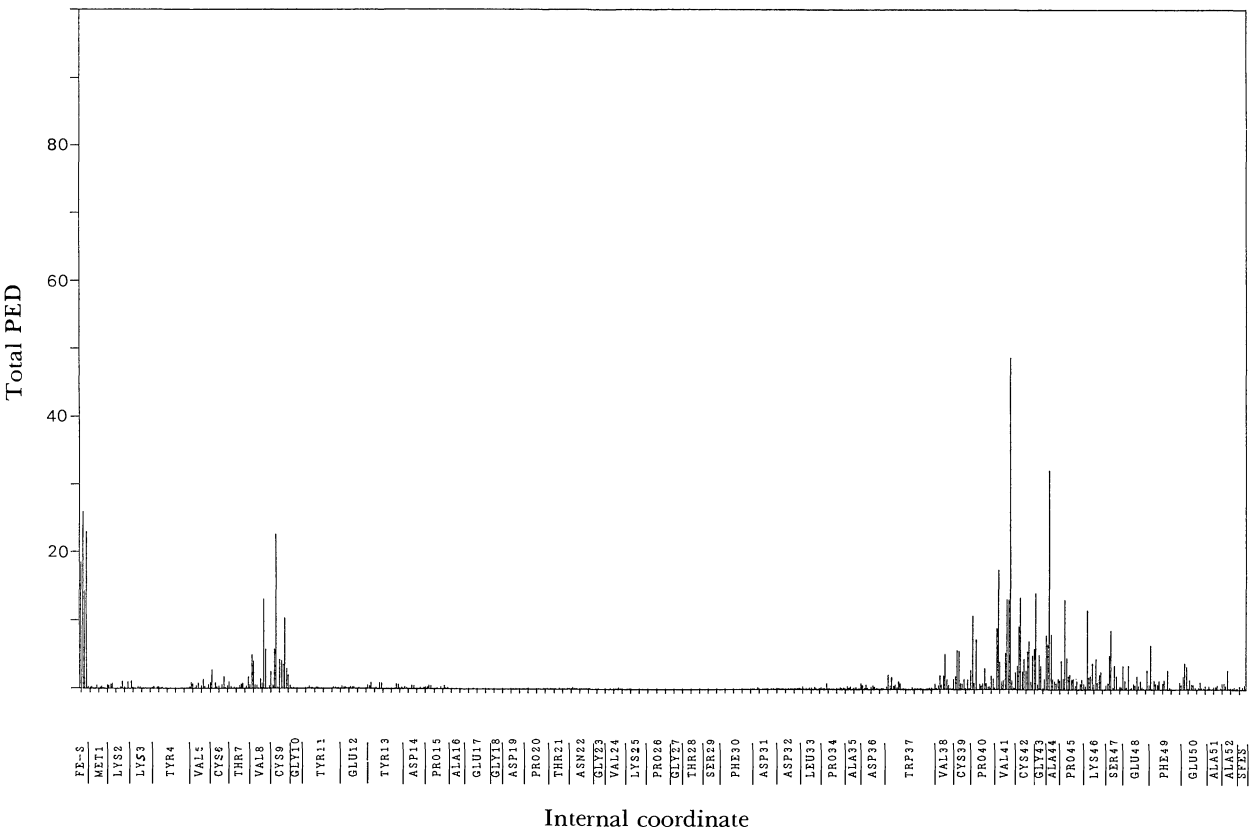

Fig. 6. PED of the deformational coordinates defined in the amino acid residues in the primary structure of Rd : Dv. The Fe–S stretching and S–Fe–S bending coordinates are included at the first top and the last end of the internal coordinates, respectively. The values depicted are those summed up the four normal modes, Q_{673} (326.1 cm^{-1}), Q_{675} (322.5), Q_{690} (302.0), and Q_{694} (293.8) which involve totally symmetric displacements of the Fe–S stretching coordinates.

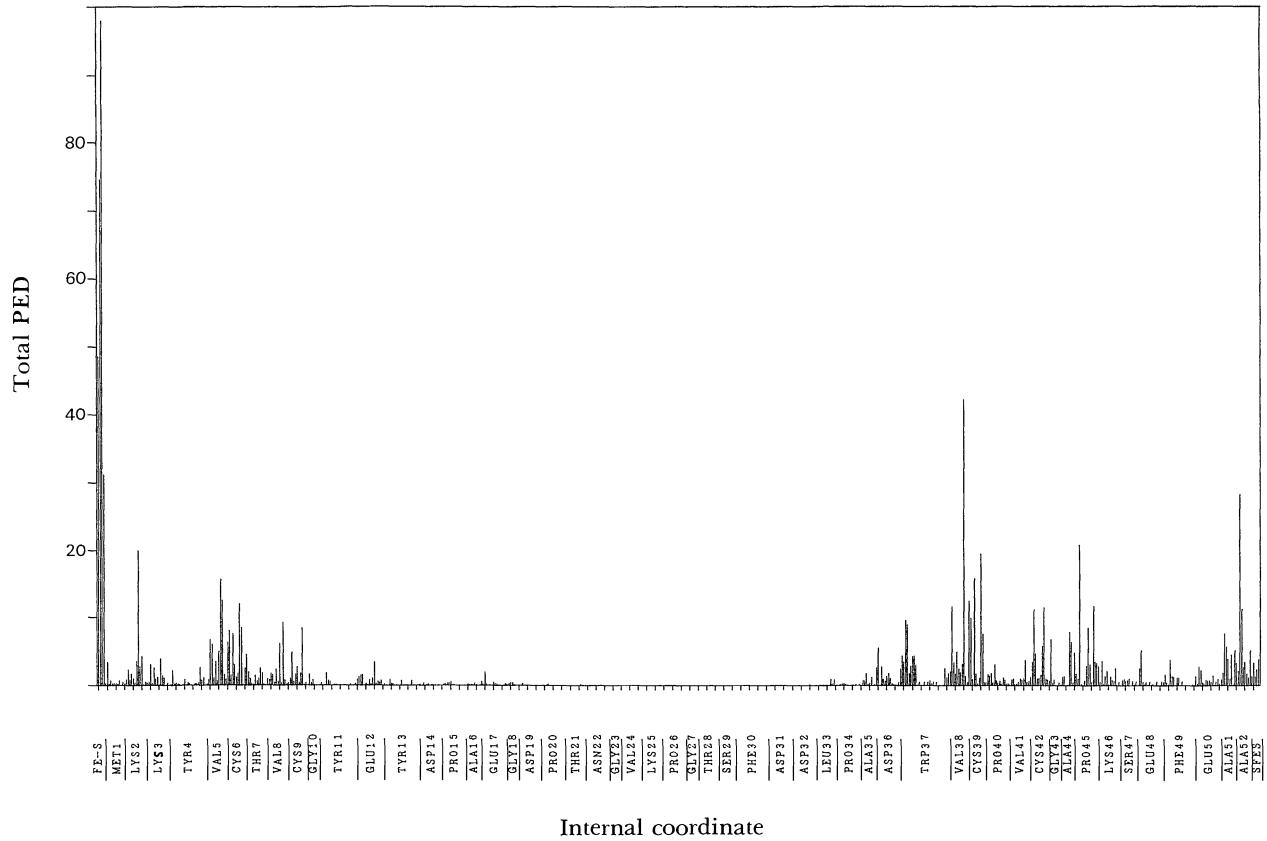

Fig. 7. PED of the deformational coordinates Rd : Dv. The notation is similar to Fig. 4. The values depicted are those summed up the six normal modes, Q_{621} (412.9 cm^{-1}), Q_{623} (388.2), Q_{642} (368.4) and Q_{647} (357.4), Q_{652} (351.7), Q_{664} (335.4) which involve non-totally symmetric displacements of the Fe–S stretching coordinates.

center. The PED ratio of the skeletal bond stretching, (four) Fe–S stretching and skeletal bending coordinates (including out-of-plane bending and torsion) is 8.99:35.77:55.24 for the Q_{693} (302.0 cm^{-1}) modes of Rd:Dv. These strong cooperations between Fe–S stretching and skeletal deformational displacements are not accidental with the particular set value of the force constants. We carried out many trial calculations in which all of the force constant values were either increased or decreased from the original force constant set, while the K(Fe–S) and H, F(S–Fe–S) values are kept constant. Extensive mixing between the Fe–S stretching and the bond angle bending displacements always appeared. In other words, the vibrational characteristics mentioned above, (1)—(4), are retained unless extraordinary small values of the skeletal deformational force constants are employed.

Conclusion

The present assignments differ from those reported by Yachandra et al. regarding the following two points:

(1) The main band at 312 cm^{-1} including the shoulder at ca. 325 cm^{-1}, is assigned to skeletal deformational vibrations having totally symmetrical Fe–S stretching displacements confined to within this frequency region. Moderate bands at ca. 360 and ca. 370 cm^{-1} and newly detected bands in the 390—450 cm^{-1} region are the skeletal deformational modes having non-totally symmetrical Fe–S stretching contributions. Whereas, Yachandra et al.[18] assigned the main band at 312 cm^{-1} to the FeS_4 breathing modes and the shoulder at ca. 325 cm^{-1} and the moderate peaks at ca. 360 and ca. 370 cm^{-1} to split components ($B_1+B_2+A_1$) of the degenerate (T_2:T_d) Fe–S stretching vibration in the C_{2v} effective symmetry of the FeS_4 core. Still, they were puzzled by such a large splitting of the $T_2(T_d)$ vibration.

(2) They suggested the importance of coupling between Fe–S stretching and the Fe–S–C_β (cysteine) and/or S–C_β–C_α (cysteine) bending displacements in order to account for the extraordinary large splitting of the $B_1+B_2+A_1$ components, in addition to accounting for the actual reduction of the FeS_4 core symmetry. The nearly planer geometry of the Fe–S–C_β–C_α sequences present in the proteins has been considered to be advantageous for these couplings. However, our calculational results show no particular impor-

tance of these couplings (Figs. 3—5). They do evidence an extensive coupling between the Fe–S stretching and skeletal deformations around the FeS_4 core.

Though a precise determination of the normal coordinates of the large molecules of the proteins is not the present purpose, a new standpoint for understanding the RR spectra of the rubredoxins is presented regarding the extensive mixing of the Fe–S stretching and the skeletal deformational displacements in the peptide skeleton around the FeS_4 core. The resonance Raman spectroscopy has been believed to constitute the most poweful method for identifying the iron-sulfur core in ferredoxins.[12–17] However, there are still problems remaining to be analyzed: for example, concerning the not negligible difference in the RR spectra between the ferredoxin from spinach and adrenodoxin,[13] both of which were proven to have similar Fe_2S_6 cluster, and in the RR spectra of the 4Fe-type ferredoxins and HiPIP-type,[16] especially, in the higher wavenumber Fe–S(terminal thiolate) stretching region of 350—400 cm^{-1}. This work will be extended to ferredoxins which contain a multi-iron cluster. A theoretical base for a further utilization of the RR spectroscopy will also be developed.

References

1) A. Urushiyama and J. Tobari, *Bull. Chem. Soc. Jpn.*, **63**, 1563 (1990).

2) T. V. Long, II and T. M. Loehr, *J. Am. Chem. Soc.*, **92**, 6384 (1970).

3) T. V. Long, II, T. M. Loehr, J. R. Allkins, and W. Lovenberg, *J. Am. Chem. Soc.*, **93**, 1809 (1971).

4) V. K. Yachandra, J. Hare, I. Moura, and T. G. Spiro, *J. Am. Chem. Soc.*, **105**, 6455 (1983).

5) E. T. Adman, L. C. Sieker, L. H. Jensen, M. Bruschi, and J. LeGall, *J. Mol. Biol.*, **112**, 113 (1977).

6) K. D. Watenpaugh, L. C. Sieker, and L. H. Jensen, *J. Mol. Biol.*, **138**, 615 (1980).

7) M. Tsuboi and A. Hirakawa, *J. Raman Spectrosc.*, **5**, 75 (1976).

8) T. G. Spiro and P. Stein, *Ann. Rev. Phys. Chem.*, **28**, 501 (1977).

9) J. V. Pivnichny and H. H. Brintzinger, *Inorg. Chem.*, **12**, 839 (1973).

10) F. Shimizu, M. Ogata, T. Yagi, S. Wakabayashi, and H. Matsubara, *Biochimie*, **71**, 1171 (1989).

11) M. Frey, L. Sieker, F. Payan, R. Haser, M. Bruschi, G. Pepe, and J. Legall, *J. Mol. Biol.*, **197**, 525 (1987).

12) R. W. Lane, J. A. Ibers, R. B. Frankel, G. C. Papaefthymiou, and R. H. Holm, *J. Am. Chem. Soc.*, **99**, 84 (1977).

13) V. K. Yachandra, J. Hare, A. Gewirth, R. S. Czernuszewicz, T. Kimura, R. H. Holm, and T. G. Spiro, *J. Am. Chem. Soc.*, **105**, 6462 (1983).

14) R. W. Lane, J. A. Ibers, R. B. Frankel, and R. H. Holm, *Proc. Nat. Acad. Sci. USA*, **72**, 2868 (1975).

15) J. -M. Moulis, J. Meyer, and M. Lutz, *Biochemistry*, **23**, 6605 (1984).

16) R. S. Czernuszewicz, K. A. Macor, M. K. Johnson, A. Gewirth, and T. G. Spiro, *J. Am. Chem. Soc.*, **109**, 7178 (1987).

17) M. K. Johnson, R. S. Czernuszewicz, T. G. Spiro, J. A. Fee, and W. V. Sweeney, *J. Am. Chem. Soc.*, **105**, 6671 (1983).

18) S. Han, R. S. Czernuszewicz, and T. G. Spiro, *J. Am. Chem. Soc.*, **111**, 3496 (1989).

19) M. Frey, L. Sieker, F. Payan, R. Haser, M. Bruschi, G. Pepe, and J. L. Gall, *J. Mol. Biol.*, **197**, 525 (1987).

The Fifth Overtone Spectra of C-H Stretching Vibrations of C_6H_5X in Nonpolar Solvents

Kazuhiko ITAYA, Takao NASU, Jun SAKAI,† and Mikio KATAYAMA*,†
Department of Pure and Applied Sciences, College of Arts and Sciences,
The University of Tokyo, Komaba, Meguro-ku, Tokyo 153
(Received September 26, 1990)

The fifth overtone spectra of aryl C-H stretching vibrations of fluorobenzene, chlorobenzene, and bromobenzene in nonpolar solvents were observed using photoacoustic spectroscopy. In a nonpolar solvent, such as hexane, the three components of the overtones of the *o*-, *m*-, and *p*-C-H stretching vibrations could be easily decomposed owing to line-width narrowing. We could therefore obtain more detailed information concerning the chemical properties of these C-H bonds.

A number of investigations on the high overtone spectra of C-H stretching vibrations have elucidated that the spectra can be interpreted on the basis of a local mode model.[1,2] According to the local mode model, equivalent C-H bonds have the same vibrational frequency. For example, all of the six C-H bonds of benzene are equivalent, and their high overtones are observed at the same frequencies. On the other hand, for molecules of monosubstituted benzene having the three types of C-H bonds (*o*-, *m*-, and *p*-) three different frequencies must be observable in the region of the high overtone of the C-H stretching vibrations. It is, however, rather difficult to determine their frequencies.

As far as we know, there have been few reports in which the different frequencies of the three components of the overtone of the C-H stretching vibrations have been observed in the neat liquid states of monosubstituted benzenes. Mizugai and Katayama previously observed the frequency shifts of the overtones of monosubstituted benzene from that of benzene; they found that the shifts are related to the chemical and physical properties of the C-H bonds.[3] Furthermore, a doublet structure was observed in the overtone spectra of para-substituted benzenes.[4] However, it was impossible to distinguish the three components of the overtone spectra in monosubstituted benzenes, since the line width of the overtone spectrum becomes wider in the neat liquid state due to an intermolecular interaction.

In the present article we report on the experimental results of the high overtone spectra of the C-H vibrations of halobenzenes in nonpolar solvents using a photoacoustic technique; the observed results for the fifth overtone spectra of the C-H stretching vibrations elucidated that it is possible to distinguish the frequencies of three components of the overtones which correspond to the *o*-, *m*-, and *p*-C-H bonds.

Because the fifth overtone spectra of the C-H stretching vibrations are very broad and have almost 100 cm^{-1} width, even in the vapor phase,[5] the overtone spectra which we observed using a nonpolar solvent, did not split into three components, though considerable changes of the spectral shape upon dilution were observed. We can thus distinguish the three frequencies by means of a least-square method using the fifth overtone spectra of benzene in a nonpolar solvent as an elemental spectral line shape. Linear relations were found between the frequency shifts of the overtones from that of benzene $\Delta\tilde{\nu}_{\mathrm{I}}$, $\Delta\tilde{\nu}_{\mathrm{II}}$, or $\Delta\tilde{\nu}_{\mathrm{III}}$ and the inductive contribution of Hammett σ of halogen atoms. The values of $\Delta\tilde{\nu}_{\mathrm{I}}/\Delta\tilde{\nu}_{\mathrm{II}}$ and $\Delta\tilde{\nu}_{\mathrm{III}}/\Delta\tilde{\nu}_{\mathrm{II}}$ were found to be 1.7 and 0.43, respectively, and were independent of F, Cl, and Br substituents.

Our results indicate that we can measure the frequencies of the overtone spectra rather precisely in a nonpolar solvent, and that more detailed information concerning the chemical and physical properties of *o*-, *m*-, and *p*-C-H bonds in monosubstituted benzenes can easily be obtained.

Experimental

The extremely weak absorption of the fifth overtone of the C-H vibrations of benzene or substituted benzenes in various solvents can be observed relatively easily using photoacoustic spectroscopy with a pulsed dye laser light source and a piezoelectric transducer detector.[6]

Figure 1 shows our experimental arrangement. A flash lamp-pumped dye laser (Chromatix CMX-4) was used to excite the liquid samples. A laser pulse of 3—5 mJ output, 1 μs width and 5 Hz repetition rate was incident on the quartz cell which was loaded with the sample. The piezoelectric transducer (obtained from TOKIN Co., Ltd.) was attached to one side of the cell with thin layer of vacuum grease. The photoacoustic signal was detected by using the piezoelectric detector; after being amplified with a low-noise amplifier and gated through a box car averager, the signal intensity was normalized through a signal from the power monitor. The samples were either spectrograde or guaranteed reagent grade and were obtained from Tokyo Kasei Co., Ltd.

Results and Discussion

Figure 2 shows changes in the fifth overtone spectra of the C-H stretching vibrations of fluorobenzene

† Present address: Teikyo University of Technology.

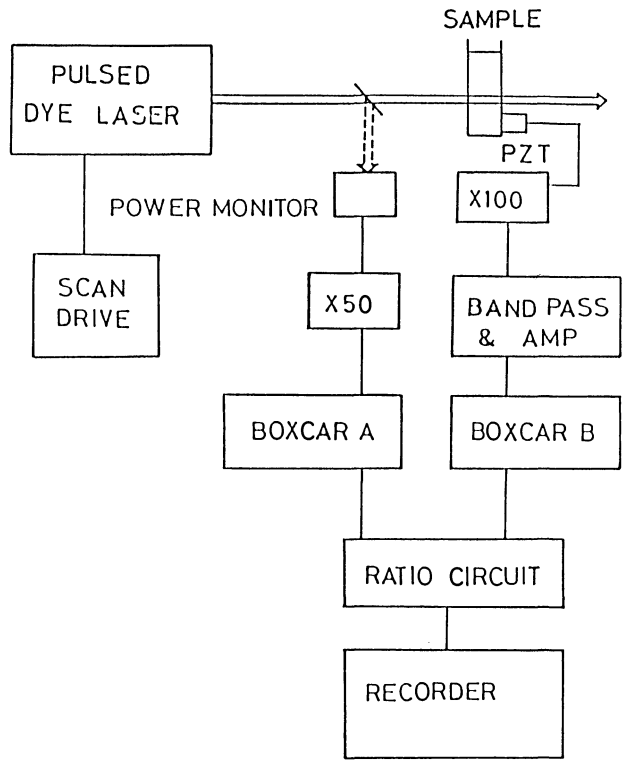

Fig. 1. Experimental arrangement.

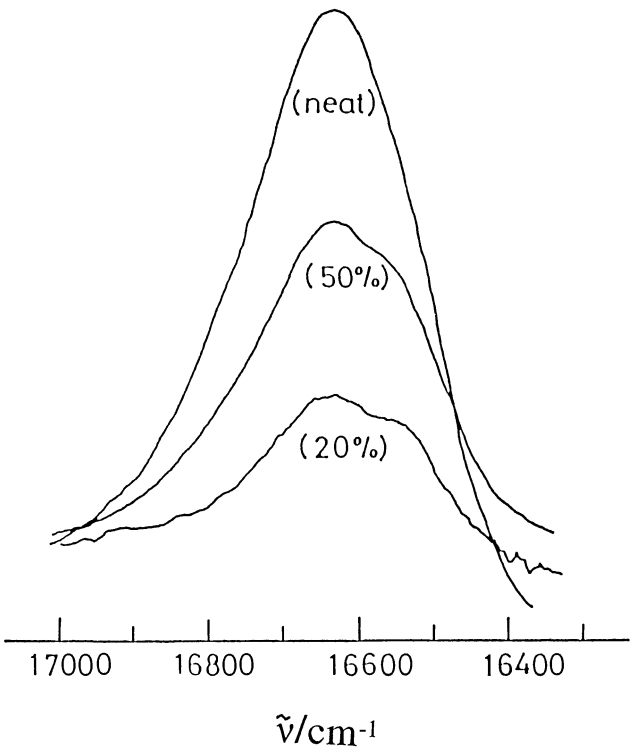

Fig. 2. The fifth overtone spectra of the C–H stretching vibrations of fluorobenzene diluted with hexane.

Table 1. Frequencies and the Line Widths of the Fifth Overtones of C–H Stretching Vibrations of Benzene in the Neat Liquid State and in Hexane Solutions of Various Concentrations

Concentration	Frequency	Linewidth
%	cm^{-1}	cm^{-1}
Neat	16475	270
50	16475	260
30	16480	250
10	16485	235
5	16485	230

when diluted with hexane. Though the spectrum in the neat liquid state conprises a single broad band centered at 16620 cm^{-1}, its line shape at 50% dilution with hexane exhibits a shoulder on the lower frequency side. In a 20% solution, the shoulder becomes more prominent and shifts by about 10 cm^{-1} to the blue side. The spectra of the fifth overtone of the C–H stretching vibrations of benzene in hexane also change upon dilution. The width becomes narrower and the peak of the spectrum is observed at the higher frequency when diluted. Table 1 represents our experimental results. Patel and Tam have also reported similar data for a CCl_4 solution.[6] The decrease in the interaction between the molecules gives rise to linewidth narrowing, and shifts of the the absorption frequency are induced by a change in the refractive index of the solution.[7]

Although fluorobenzene has three nonequivalent aryl C-H bonds, the frequency differences of their vibrational overtones are far smaller than the absorption linewidth in the neat liquid, and it is impossible to determine the frequencies of the three components of the overtone. When diluted with hexane, however, a decrease in the molecular interaction gives rise to a narrowing of the spectrum width and , hence, the rather complex absorption spectra are obtained (Fig. 2). The structures of the spectra correspond to the overtones of the three components of the C–H stretching vibrations. It must be mentioned that the shift of the peak of the overtone spectra of fluorobenzene in a hexane solution is not so evident, presumably because the difference in the refractive indices between hexane and fluorobenzene is relatively small, i.e., 1.3723 and 1.4683, respectively.

In order to analyze the observed overtone spectra, the shape of the spectra was calculated using appropriate assumptions: (1) the widths of the fifth overtone spectra of the *o*-, *m*-, and *p*-C–H stretching vibrations of fluorobenzene in hexane solutions are somewhat smaller than those of the corresponding overtones of benzene in its neat liquid state, and (2) the intensity ratio of the overtones of the *o*-, *m*-, and *p*-C–H stretching vibrations is 2:2:1. Furthermore, the peaks of the absorptions are assumed to be at 16665, 16580,

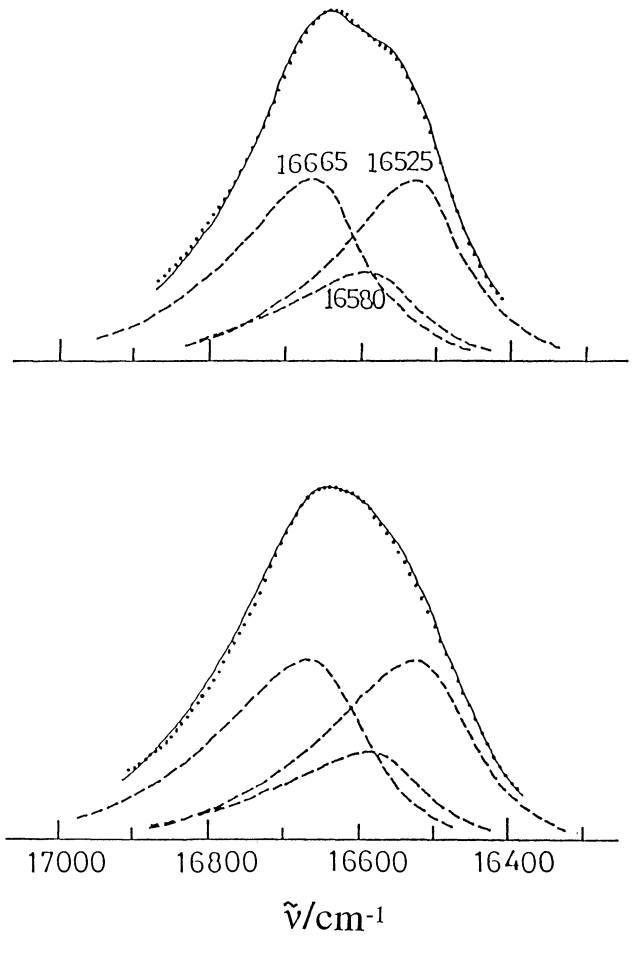

Fig. 3. Observed line shape of the spectra of the fifth overtone of the C–H stretching vibration of fluorobenzene and the calculated results, upper; 50% in hexane, lower; neat liquid state. Dashed curves; the calculated spectra of *o*-, *m*-, and *p*-components, solid curve; whole spectrum, dotted line; the observed spectrum.

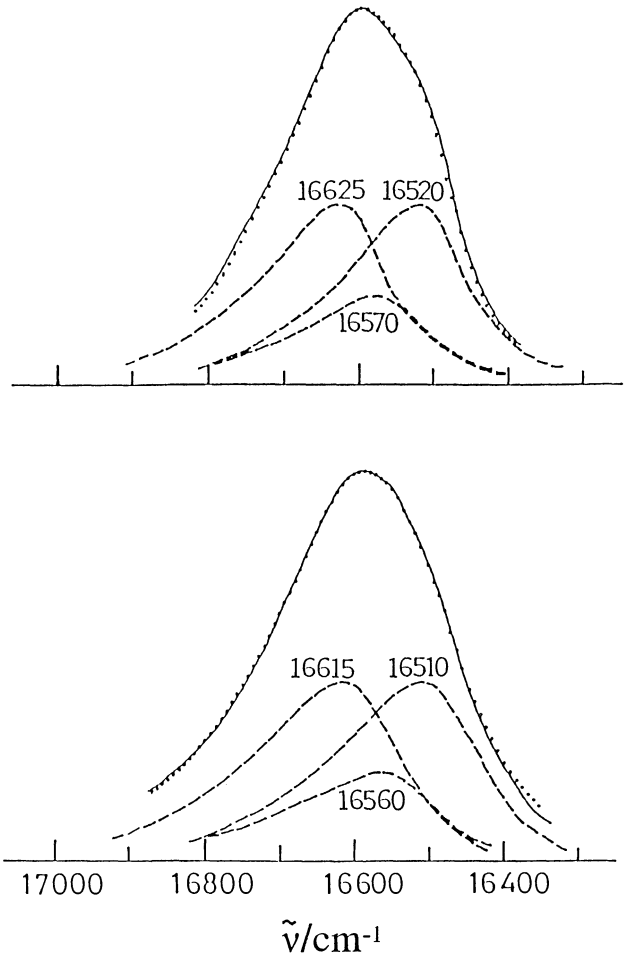

Fig. 4. Observed line shape of the spectra of the fifth overtone of the C–H stretching vibration of chlorobenzene and the calculated results, upper; 20% in hexane, lower; neat liquid state. Dashed curves; the calculated spectra of *o*-, *m*-, and *p*-components, solid curve; the whole spectrum, dotted line; the observed spectrum.

and 16525 cm^{-1} with an intensity ratio of 2:1:2; the width (fwhm) of the absorption is considered to be 235 cm^{-1}, as is shown by the dashed curves in the upper part of Fig. 3. The calculated shape of the entire spectrum was obtained as exhibited by the solid line of this figure; the results are in good agreement with those observed.

If we assume that each component has a width wider than 265 cm^{-1} in the neat liquid state, the superposed spectrum would not show any structure. Substantial agreement between the calculated and observed spectra was obtained, as is shown in the lower part of Fig. 3.

The overtone spectra of chlorobenzene slightly varies with the concentration in a hexane solution; though little change was observed in a 50% solution, we could see a slight modification of the line shape in a 20% solution. The observed line shapes are indicated by the dotted lines in Fig. 4; the solid curves indicate the calculated line shapes of the overtone of chlorobenzene, the upper part for a 20% solution in hexane, the lower part for the neat liquid state. In a hexane solution of chlorobenzene the frequency shift is not negligible; in a 20% solution the blue shift is about 10 cm^{-1}.

The overtone spectra of bromobenzene and iodobenzene in hexane solutions were also observed. Though for bromobenzene, quite similar results to the fluorobenzene case were obtained, for iodobenzene the line shape did not show any appreciable vibration with dilution up to a concentration of 5%, and we were unable to determine the frequencies of their three components.

The frequencies of the three components of the fifth overtones of fluorobenzene, chlorobenzene, and bromobenzene determined by the present analysis are listed in Table 2; the frequency shifts from that of

Table 2. Frequencies and the Shifts of Three Components of the Fifth Overtones of C–H Stretching Vibrations of Halobenzens and σ_I Values of Halogen Atoms

Molecules		Frequencies	Shift	σ_I values
		cm^{-1}	cm^{-1}	
Fluorobenzene	$\tilde{\nu}_I$	16665	190	0.56
	$\tilde{\nu}_{II}$	16580	105	
	$\tilde{\nu}_{III}$	16525	50	
Chlorobenzene	$\tilde{\nu}_I$	16615	140	0.51
	$\tilde{\nu}_{II}$	16560	85	
	$\tilde{\nu}_{III}$	16510	35	
Bromobenzene	$\tilde{\nu}_I$	16605	130	0.50
	$\tilde{\nu}_{II}$	16550	75	
	$\tilde{\nu}_{III}$	16505	30	

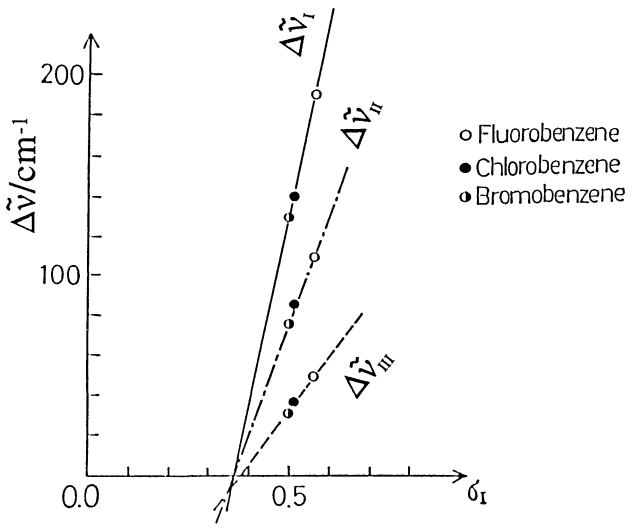

Fig. 5. The relation between the frequency shifts and σ_I of the substituents.

benzene, $\Delta\tilde{\nu}_I$, $\Delta\tilde{\nu}_{II}$, and $\Delta\tilde{\nu}_{III}$ are also presented.

Though it is obvious that the three components are due to the *o*-, *m*-, and *p*-C–H bonds, it is not easy to assign the frequency of each component to individual bonds. However, the results of the calculation mentioned above indicate that the component $\Delta\tilde{\nu}_{II}$ can be ascribed to the *p*-C–H vibration. With regard to the other components, it was difficult from the present analysis to determine to what type of C–H bond the $\tilde{\nu}_I$ and $\tilde{\nu}_{III}$ frequencies can be ascribed, though we may tentatively assume that $\tilde{\nu}_I$, the higher frequency vibration, results from the *o*-C–H bond.

Mizugai and Katayama[3] have reported that the shift of the $\Delta\tilde{\nu}$ frequency is proportional to σ_I, an inductive contribution of the Hammett σ. Having determined the frequencies of the three components of the C–H overtone in halobenzenes, we plotted the $\Delta\tilde{\nu}_I$, $\Delta\tilde{\nu}_{II}$, and $\Delta\tilde{\nu}_{III}$ frequency shifts as a function of σ_I, respectively. Figure 5 shows their relations. The present results indicate that a linear relation can be established between the frequency shift of each component and σ_I of the substituent. The straight lines for $\Delta\tilde{\nu}_I$ $\Delta\tilde{\nu}_{II}$, and $\Delta\tilde{\nu}_{III}$ in Fig. 5 intersect at around 3.5 of the σ_I value, but not at the origin of the figure, in contrast with the results for the overtone spectra of the aryl C–H vibration of $C_6H_5CH_{3-n}Cl_n$;[8] almost the same results were obtained in our previous report[3] concerning the C–H overtone spectra of the neat liquid state of C_6H_5X. Our present proposition is, however, an extension of the conclusion derived by Mizugai and Katayama. Since the σ_I value of an I atom is 0.43, the relative frequency shifts of the overtone spectra of iodobenzene are expected to be small. This is the reason that we were unable to resolve the three components of the C–H overtone vibration in the present experiment. It is reasonable to assume that since the inductive contribution of the substituent to the *o*-C–H bond is larger than that to the *m*-C–H bond, the higher frequency $\tilde{\nu}_I$ of the overtone of the C–H vibration may be attributed to the *o*-C–H bond and that the lower frequency $\tilde{\nu}_{III}$ belongs to the *m*-C–H bond.

We can derive another conclusion from the results of Fig. 5, that the ratio $\Delta\tilde{\nu}_I:\Delta\tilde{\nu}_{II}:\Delta\tilde{\nu}_{III}$ is independent of the substituents; the following two relations were obtained:

$$\Delta\tilde{\nu}_I/\Delta\tilde{\nu}_{II} = 1.7$$

and

$$\Delta\tilde{\nu}_{III}/\Delta\tilde{\nu}_{II} = 0.43\,.$$

These relations indicate that the relative shifts of the three components of the overtone frequencies are independent of the substituted atoms; we thus confirmed from the observed results of the high overtone of the C–H stretching vibrations that almost the same behavior can be expected in certain types of C–H bonds of the halobenzenes. Consequently, we can see that the specific C–H bonds of halobenzenes have the same chemical and physical properties.

Conclusion

We have demonstrated that the frequencies of the three components of the fifth overtone of aryl C–H vibrations of halobenzenes can be distinguished by using hexane as a solvent. These results can help us to understand the properties of the *o*-, *m*-, and *p*-C–H bonds respectively.

References

1) B. R. Henry and W. Siebrand, *J. Chem. Phys.*, **49**, 5369 (1968).

2) R. L. Swofford, M. E. Lang, and A. C. Albrecht, *J. Chem. Phys.*, **65**, 179 (1976).
3) Y. Mizugai and M. Katayama, *J. Am. Chem. Soc.*, **102**, 6424 (1981).
4) Y. Mizugai and M. Katayama, *J. Am. Chem. Soc.*, **103**, 5061 (1981).
5) R. G. Bray and M. J. Berry, *J. Chem. Phys.*, **71**, 4909 (1979).
6) C. K. N. Patel and A. C. Tam, *Rev. Mod. Phys.*, **53**, 517 (1981).
7) E. Bauer and M. Magat, *J. Phys. Radium*, **9**, 319 (1938).
8) Y. Mizugai and M. Katayama, *Bull. Chem. Soc. Jpn.*, **53**, 2081 (1980).

Rearrangement of 4-Perfluoroalkyl Quinols

Hidemitsu UNO,* Yasukazu SHIRAISHI, Yuji MATSUSHIMA,
Ayumi YAYAMA, and Hitomi SUZUKI*,†
Advanced Instrumentation Center for Chemical Analysis, Ehime University,
Bunkyo-cho 2-5, Matsuyama 790
† Department of Chemistry, Faculty of Science, Kyoto University,
Sakyo-ku, Kyoto 606
(Received September 3, 1990)

Treatment of 4-perfluoroalkyl-4-hydroxy-2,5-hexadien-1-one (4-perfluoroalkyl-4-quinol), prepared from the reaction of 1,4-benzoquinone with perfluoroalkyllithium, with acetic anhydride–sulfuric acid gave a mixture of 2,4-diacetoxy-1-perfluoroalkylbenzene and 1,2-diacetoxy-4-perfluoroalkylbenzene in a comparable ratio. When 4-perfluoroalkyl-4-quinols bearing a methyl group ortho to the perfluoroalkyl group were subjected to the rearrangement, acetoxymethyl compounds were obtained in addition to diacetoxybenzene derivatives. Only 1,3-migration was observed in the cases of 2,4-di-*t*-butyl-4-perfluorooctyl-4-quinol and 4-hydroxy-4-perfluoroalkyl-1(4*H*)-naphthalenone, while the reaction of 2,6-dimethyl and 2-methoxy derivatives gave only 1,2-shift products. Reaction routes to the apparent 1,2- and 1,3-acetoxyl migration products are discussed.

The quinol rearrangement and Thiele–Winter acetoxylation are very useful methods for the preparation of polyhydroxybenzenes.[1,2] These cationic rearrangements are considered to proceed via cyclohexadienyl cations, stability of which affects product distributions. Migratory aptitude of substituents is also important in the quinol rearrangement. On treatment with sulfuric acid in methanol, 4-alkyl-4-hydroxy-2,5-hexadiene-1-ones (abbreviated to 4-alkyl-4-quinols throughout this paper) undergo rearrangement followed by aromatization to give alkylhydroquinones,[3] while the reaction in acetic anhydride–sulfuric acid takes another route to afford 4-alkylresorcinol diacetates via 1,2-migration of acetoxyl group rather than alkyl group.[4] Unusual 1,3-acetoxyl migration has been observed in the rearrangement of quinols derived from *o*-quinones[5] and sterically hindered 4-quinols.[6] Acid treatment of 2,6-di-*t*-butyl-4-phenyl-4-quinol in acetic anhydride was reported to give 3,4-diacetoxy-5-*t*-butylbiphenyl.[6] We reported the preliminary findings that the acid-catalyzed rearrangement of 4-perfluoroalkyl-4-quinols **1a—d** in acetic anhydride gave a comparable mixture of 1,3-diacetoxy-4-perfluoroalkylbenzenes **3a—d** and 1,2-diacetoxy-4-perfluoroalkylbenzenes **5a—d**. The apparent 1,3-migration of acetoxyl group giving **5a—d** is quite interesting in the rearrangement of simple quinols. From the synthetic point of view, this quinol rearrangement may offer a new useful method for the synthesis of polyhydroxylated perfluoroalkylbenzenes.[8] In this paper, we described the acid-catalyzed rearrangement of 4-perfluoroalkyl-4-quinols.

Results and Discussion

Preparation of 4-Perfluoroalkyl-4-quinols. We first examined the preparation of 4-perfluoroalkyl-4-quinols **1** by the perfluoroalkylation of several quinones with perfluoroalkyllithiums (Eq. 1). The reaction was carried out under slightly modified conditions of the reported procedure,[9] because of low solubility of quinones in ether at low temperatures. We used dichloromethane or toluene as a co-solvent and a Dry Ice–acetone bath was substituted for a Dry Ice–acetonitrile bath to prevent precipitation of quinones upon cooling. Although the stability of perfluoroalkyllithiums decreased sharply with increase of the reaction temperature,[10] yields of quinols obtained were comparable under these modified conditions (Table 1). The yields were not improved by the uses of 0.5 to 2 equivalents of quinone to perfluoroalkyllithium.

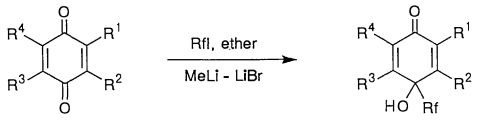

(1)

1

A regioisomeric problem arose from perfluoroalkylation of unsymmetrically substituted quinones. Perfluorooctyllithium reacted with methyl-1,4-benzoquinone almost equally at both carbonyls to give an isomeric mixture of **1a** and **1b** (**1a**:**1b**=ca. 7:6, determined by GC), which could be easily separated by column chromatography (**1a**, 20%; **1b**, 21%). The reaction of 2,6-dimethyl-1,4-benzoquinone and 2-methoxyl-1,4-benzoquinone with perfluoroalkyllithium also afforded the isomeric quinols (**1h**, 37%; **1i**, 12% and **1m**, 7%; **1n**, 42%, respectively). On the other hand, perfluorooctyllithium added selectively to the less hindered carbonyl of 2-*t*-butyl- and 2,6-di-*t*-butyl-1,4-benzoquinone to afford **1j** and **1l** in 46% and 77% yields, respectively. Quinols **1g**, **1k**, and **1o** were obtained from 2,5-dimethyl-, 2,5-di-*t*-butyl-, and 2,5-dichloro-1,4-benzoquinones in respective yields of 36%, 40%, and 14%. The low yield observed in the perfluoroalkylation of dichloroquinone may be attributed to its high oxidation potential.[11] Naphtho-

Table 1. Rearrangement of 4-Perfluoroalkyl-4-hydroxy-2,5-cyclohexadien-1-ones

	Quinol **1**						Ratio[b]					Combined Yield[c]/%
								1,2-Rearr.		1,3-Rearr.		
	R^1	R^2	R^3	R^4	Rf	Yield[a]/%	**2**	**3**	**4**	**5**	**6**	**7**
a	H	H	H	H	*n*-C_8F_{17}	50		57		43			87
b	H	H	H	H	*n*-C_6F_{13}	43		57		43			83
c	H	H	H	H	*n*-C_4F_9	56		57		43			98
d	H	H	H	H	C_2F_5	56		57		43			99
e	Me	H	H	H	*n*-C_8F_{17}	20		78	13		9		85
f	H	Me	H	H	*n*-C_8F_{17}	21	34		2	24	5	34	86
g	Me	H	Me	H	*n*-C_8F_{17}	36		77			17	6	83
h	Me	H	H	Me	*n*-C_8F_{17}	32		100					97
i	H	Me	Me	H	*n*-C_8F_{17}	12						100	92
j	*t*-Bu	H	H	H	*n*-C_8F_{17}	46			13	60	27		86
k	*t*-Bu	H	*t*-Bu	H	*n*-C_8F_{17}	40	13		87				93
l	*t*-Bu	H	H	*t*-Bu	*n*-C_8F_{17}	77				100			80
m	OMe	H	H	H	*n*-C_4F_9	7			100				79
n	H	OMe	H	H	*n*-C_4F_9	42	100						73
o	Cl	H	Cl	H	*n*-C_8F_{17}	14	100						87
p	H	H	-CH=CH-CH=CH-		*n*-C_6F_{13}	41	38			62			99

a) Isolated yield based on the quinone. b) Determined by NMR analysis of the reaction mixture. c) Combined yield of **2**—**7**.

quinone also reacted with perfluorooctyllithium to give **1p** in a 41% yield.

Rearrangement of Quinols. The acid-catalyzed rearrangement of various quinoles was examined under the following general conditions; To a quinol in acetic anhydride (0.033 M) were added several drops of concd sulfuric acid (one drop per 0.33 mmol) at ambient temperature. The progress of reaction was monitored by TLC and GC. After one day, the reaction was quenched by adding saturated aqueous sodium hydrogencarbonate. The results are summarized in Table 1 and Chart 1.

Rearrangement of methyl-4-quinol **1e** was completed within a similar period of time as quinol **1a—d** (overnight). Proton NMR analysis of the product mixture from **1e** showed the presence of three diacetoxybenzenes **3e**, **4e**, and **6e** in a ratio of 78:13:9. Major product **3e** was isolated in 69% yield by column chromatography. On the other hand, the rearrangement of isomeric methyl-4-quinol **1f** was incomplete under the standard conditions and appreciable amounts of quinol acetate **2f** remained unchanged in the reaction mixture (**2f**:**4f**:**5f**:**6f**:**7f**=34:2:24:5:34). When this mixture was treated with Ac_2O/H_2SO_4 overnight at 80—90 °C, the rearrangement of the remaining quinol acetate was completed (**4f**:**5f**:**6f**:**7f**=4:35:8:53). Chromatography of the latter product mixture gave acetoxymethyl derivative **7f** and a mixture of diacetoxybenzenes **5f** and **6f** in 30% and 31% yields, respectively. Attempted isolation of diacetoxybenzenes **4f—6f** was unsuccessful.

Under the standard conditions, dimethyl-4-quinols **1g**, **1h** and **1i** underwent smooth rearrangement within 1 h. The reaction of **1g** afforded a mixture of **3g**, **6g**, and **7g**, the ratio of which was 77:17:6 based on both

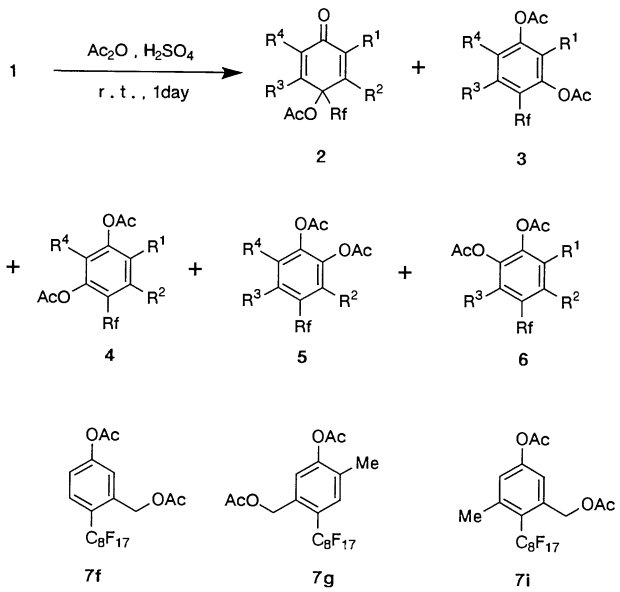

Chart 1.

^1H NMR and capillary GC determinations. Major components **3g** and **6g** were isolated in 69% and 14% yields, respectively. The acid-catalyzed rearrangement of **1h** and **1i** gave **3h** and **7i** as the sole product respectively in isolated yields of 97% and 93%. One of the *t*-butyl groups was replaced by acetoxyl group on the acid treatment of di-*t*-butyl-4-quinols **1k** and **1l**. In the reaction of 2-*t*-butyl-4-quinol **1j** the displacement of the *t*-butyl group was the major reaction to give 1,2-diacetoxy-4-perfluorooctylbenzene (**5j**=**5a**) predominantly. 2-Methoxy-4-quinol **1m** was susceptible to 1,2-acetoxyl migration to afford **4m** in a 79% yield. In contrast, 3-methoxy-4-quinol **1n** resisted such

rearrangement and only the corresponding acetate **2n** was obtained. Similar resistance toward aromatization was encountered in the reaction of quinol **1o**, where only quinol acetate **2o** was obtained in almost quantitative yield. It is worthy to mention that the Thiele–Winter type acetoxylation did not take place with the parent quinone, 2,5-dichloro-1,4-benzoquinone.[12] Quinol **1p** derived from 1,4-naphthoquinone underwent the apparent 1,3-acetoxyl migration to give **5p** in 61% yield together with quinol acetate **2p** (38%). The rearrangement of quinol acetate **2p** did not proceed under the usual conditions. Using perchloric acid in place of sulfuric acid caused the complete disappearance of **1p**, giving **5p** in 86% yield.

Hydrolysis of Diacetoxybenzenes. We reported that the hydrolysis of 4-perfluorobutylresorcinol diacetate (**3c**) and 4-perfluorobutylcatechol diacetate (**5c**) with potassium hydroxide in THF–methanol brought about simultaneous substitution of benzylic fluorine atoms to give perfluorobutanoyl derivatives.[7] When heated in methanol in the presence of *p*-toluenesulfonic acid (PTSA), however, these diacetates were readily hydrolyzed to parent resorcinol **8** and catechol **9** (Eq. 2; Table 2). The resorcinols and catechols were separated by column chromatography on silica gel, although the isolated yields of the latter compounds were low probably due to their air-sensitive property. In order to isolate the catechols more efficiently from the hydrolyzed mixture, the catechols were protected as acetonides before chromatography. Thus, an original mixture of **8a** and **9a** was heated under reflux in acetone[13] and the resulting product was chromatographed on silica gel to obtain an intimate mixture of catechol acetonide **10** and unexpected product **11** in very poor yields, along with resorcinol **8a** intact (Eq. 3). Separation of **11** from **10** was performed by preparative GPC and the structure of **11** was established by analytical and spectroscopic data (NMR, IR, and MS) as an acetal derived from catechol **5a** and mesityl oxide.

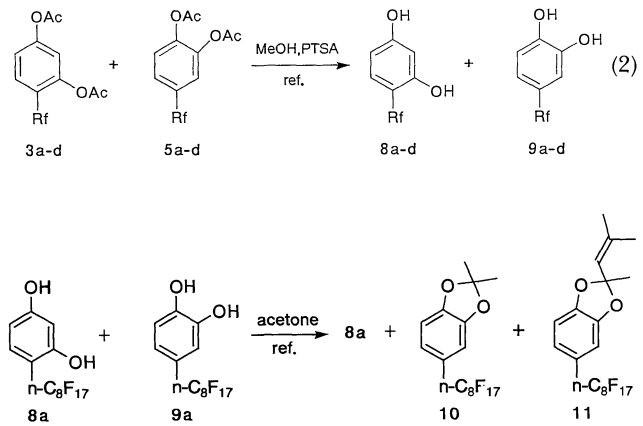

(3)

Table 2. Preparation of Perfluoroalkyl Resorcinols and Catechols

Quinol	Yield[a]/%	
	8	**9**
1a	87	
1b	49	17
1c	51	35
1d	51	11
2a	50	12

a) Yield refer to isolated ones.

Mechanism of the Acid-Catalyzed Rearrangement. We would like to discuss the mechanistic aspects of the acid rearrangement of quinols. Our proposal of this rearrangement is shown in scheme 1. 1,2-Acetoxyl migration of 4-perfluoroalkyl-4-quinols may occur via benzenium ions **12** (R=H or Ac) and **16** similarly in the cases 4-alkyl- and 4-aryl-4-quinols. However, when perfluoroalkyl groups were introduced, energy gap between the two benzenium ions **12** and **16** becomes considerably large because of destabilization, leading to other pathway. When R^2 is methyl, **12** loses a proton to give quinol tautomer **15**, which is subject to a facile allylic rearrangement to afford acetoxymethyl derivative **7**.[14] It is noteworthy that such an acetoxylation on methyl group was not observed in the Thiele–Winter acetoxylation on mono- and dimethyl-1,4-quinones.[1] Another pathway leading to catechol

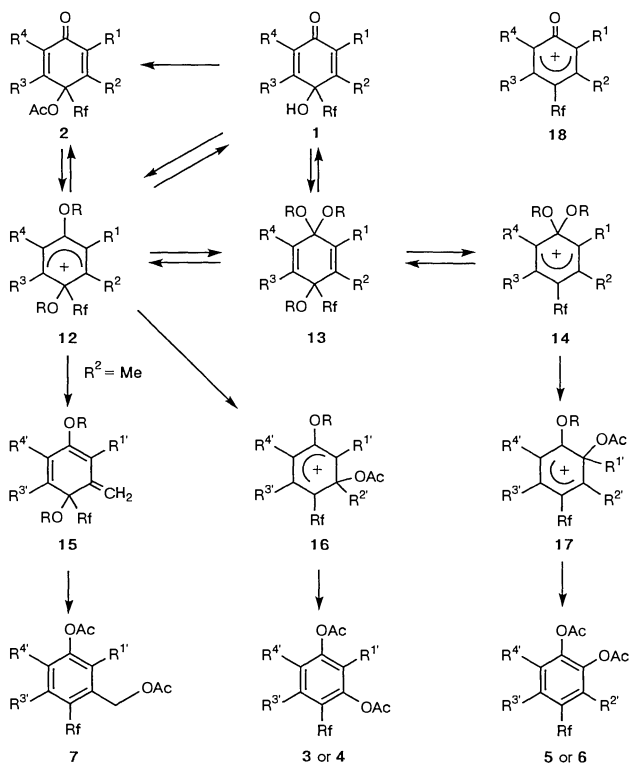

Scheme 1.

derivatives **5** and **6** may be thought as follows: sp^3-hydridization of the carbonyl carbon of **1** takes place to afford (hemi)acetal **13**. Then, **13** loses an RO group at 4 position to give rather unstable benzenium ion **14** of which acetoxyl group migrates to give **5** or **6** via benzenium ion **17**. This proposal is based on the fact that carbonyl functional groups tend to be hydrated or acetalized when electron-withdrawing groups are attached. Moreover, benzenium ion **18** doubly destabilized by perfluoroalkyl and carbonyl groups is unlikely.[15] If the benzenium ion **16** is stabilized by electron-donating $R^{1'}$ and $R^{4'}$, the pathway to give **3** or **4** is dominant (**1g**, **1h**, and **1m**). In the case of **1n**, as benzenium ion **12** is strongly stabilized by R^2 (MeO), the rearrangement to **16** becomes disadvantageous. sp^3-Hybridization of the carbonyl to **13** is also unfavorable, because the carbonyl is considered as vinylogous ester. Thus, the rearrangement of **1n** did not proceed and quinol acetate **2n** was obtained quantitatively.

Bulky *t*-butyl group disfavors acetoxyl group migrating vicinal to it and tends to be replaced.[1] In the case of **1k**, an interesting point is that *t*-butyl group is substituted by acetoxyl group. Steric hindrance between the vicinal *t*-butyl and perfluoroalkyl groups is very severe when they are linked by two sp^2 carbons. Therefore, the pathway via **12** to **16** ($R^{2'}=R^{4'}=t$-Bu) may be more favorable than that via **14** to **17** ($R^{1'}=R^{3'}=t$-Bu). Formation of quinol acetal **13** from **1l** ($R^1=R^4=t$-Bu) would be expected to encounter large steric hindrance by the two *t*-butyl groups. However, the CPK model structure can be build up if at least one of OR groups at C-1 is OH. It should be noted that quinol acetates **2l** and **2p** did not react, while the corresponding quinols **1l** and **1p** did undergo only 1,3-migration to give **5l** and **5p** under the same conditions. On the other hand, the reaction of simple quinol acetates **2a—d** gave the same results as those obtained from the reaction of quinols **1a—d**. These facts might be interpreted if we take it into account that sp^3-hybridization of the carbonyl group to **13** is sterically interfered by C-4 substituents (acetoxyl and perfluoroalkyl). In the reaction of methyl-4-quinols **1e** and **1f**, regioselectivity of the acetoxyl migration shows sharp contrast to that observed in the Thiele-Winter reaction of the parent quinone, where acetoxylation occurs mainly para to the methyl group.[1] The reason for the difference is nuclear at present.

Experimental

Melting points were measured with a Yanagimoto micromelting point apparatus and are uncorrected. Unless otherwise noted, all NMR spectra were observed with a GSX-270 spectrometer by using $CDCl_3$ as solvent, tetramethylsilane as an internal standard for ^1H and ^{13}C, and $CFCl_3$ for ^{19}F. Mass spectra were measured with a Hitachi M80LCAPI spectrometer under the following ionizing conditions: EI (electron impact ionization, 20 eV) and CI (chemical ionization, 70 eV, methane as CI gas). IR spectra were recorded on a Hitachi 270-30 spectrophotometer. Column chromatogaphy was carried out using Wakogel C-200. Preparative GPC was performed using JAI LC-80 with JAI-1H (20 mmID×60 cm) and JAI-2H (20 mmID×60 cm) columns. Diethyl ether was distilled from sodium benzophenone ketyl. Dichloromethane and toluene were distilled from calcium hydride and stored over 4A molecular sieves. Perfluoroalkyl iodides were purified by simple distillation. Methyllithium was titrated prior to use. Other commercially available materials were used without further purification.

Perfluoroalkylation of 1,4-Quinones. General Procedure: A 1,4-quinone (10 mmol) and a perfluoroalkyl iodide (12 mmol) are dissolved in a mixture of 100 ml of dry ether and 50 ml of dry toluene (or dichloromethane), and cooled down to −40—−50 °C by a Dry Ice-acetonitrile bath. In case the quinone begins to separate, dry toluene (or dichloromethane) is added to keep the solution homogenous. An ethereal solution of methyllithium-lithium bromide (11 mmol) is added at given temperature range over 30 min. During the course of addition, the yellow solution turned to a bluish purple suspension. After stirring for 1 h, the reaction is quenched with aqueous NH_4Cl. The organic phase is separated and the aqueous phase is extracted with ether. The combined extracts are washed with brine and dried over Na_2SO_4. The solvent is evaporated and the residue is chromatographed on silica gel ($CHCl_3$–ether). The quinol obtained is recrystallized from chloroform/hexane or dichloromethane/hexane.

4-Hydroxy-4-perfluorooctyl-2,5-cyclohexadien-1-one (1a). Colorless needles (chloroform), mp 132—133 °C.[9]

4-Hydroxy-4-perfluorohexyl-2,5-cyclohexadien-1-one (1b). Colorless crystals (chloroform), mp 111—113 °C. ^1H NMR (acetone-d_6) δ=6.42 (2H, d, J=10.4 Hz), 6.49 (1H, s), and 7.09 (2H, d, J=10.4 Hz); ^{13}C NMR (acetone-d_6) δ=72.44 (tt, J=24 and 1 Hz), 105—125 (6C), 132.25, 143.11 (m), and 184.91; ^{19}F NMR (acetone-d_6) δ=−81.65 (3F, tt, J=10 and 2 Hz), −117.94 (2F, m), −118.42 (2F, m), −121.27 (2F, m), −122.24 (2F, m), and −125.70 (2F, m); IR (KBr) 3228vs, 1674vs, 1628vs, 1406m, 1390m, 1366m, 1318m, and 1300—1100vs cm^{-1}; MS (CI) m/z 429 (M^++1, 100), 411 (26), 393 (11), 138 (18), and 109 (72). Found: C, 33.62; H, 1.23%. Calcd for $C_{12}H_5F_{13}O_2$: C, 33.66; H, 1.18%.

4-Hydroxy-4-perfluorobutyl-2,5-cyclohexadien-1-one (1c). Colorless needles (dichloromethane/hexane), mp 88—90 °C. ^{19}F NMR δ=−80.73 (3F, tt, J=10 and 3 Hz), −118.21 (2F, m), −119.46 (2F, m), and −125.59 (2F, m); IR (KBr) 3220vs, 1674vs, 1628vs, 1408m, 1392m, 1358m, and 1300—1100vs cm^{-1}; MS (CI) m/z 329 (M^++1, 100), 311 (29), 293 (6), 138 (19), and 109 (59). Found: C, 36.66; H, 1.59%. Calcd for $C_{10}H_5F_9O_2$: C, 36.60; H, 1.54%.

4-Hydroxy-4-perfluoroethyl-2,5-cyclohexadien-1-one (1d). Colorless needles (dichloromethane/hexane), mp 47—48 °C. ^{19}F NMR δ=−78.45 (3F, s) and −122.18 (2F, m); IR (KBr) 3232vs, 1672vs, 1626vs, 1402m, 1384m, 1344s, and 1300—1100vs cm^{-1}; MS (EI) m/z 228 (M^+, 4), 202 (1), 133 (3), and 109 (100). Found: C, 41.88; H, 2.28%. Calcd for $C_8H_5F_5O_2$: C, 42.12; H, 2.21%.

4-Hydroxy-2-methyl-4-perfluorooctyl-2,5-cyclohexadien-1-one (1e). Colorless crystals (dichloromethane/hexane), mp 69—70 °C. ^1H NMR (acetone-d_6) δ=1.86 (3H, s), 3.50 (1H, br s), 6.33 (1H, d, J=9.8 Hz), 6.77 (1H, m), and 6.97 (1H, dm,

J=9.8 Hz); ^{13}C NMR (acetone-d_6) δ=16.17, 72.80 (t, J=24 Hz), 105—125 (8C), 132.10, 138.14, 139.36 (m), 143.11 (t, J=2 Hz), and 186.65; ^{19}F NMR (acetone-d_6) δ=−80.69 (3F, tt, J=10 and 2 Hz), −117.91 (2F, m), −118.47 (2F, m), −120.8—−121.8 (6F, m), −122.27 (2F, m), and −125.75 (2F, m); IR (KBr) 3416vs, 1678vs, 1642s, 1408m, 1372m, 1330s, and 1300—1100vs cm^{-1}; MS (EI) m/z 542 (M^+, 4), 525 (1), 523 (2), 475 (1), and 123 (100). Found: C, 32.93; H, 1.42%. Calcd for $C_{15}H_7F_{17}O_2$: C, 33.23; H, 1.31%.

4-Hydroxy-3-methyl-4-perfluorooctyl-2,5-cyclohexadien-1-one (1f). Colorless crystals (dichloromethane/hexane), mp 122—123 °C. ^{1}H NMR (acetone-d_6) δ=2.13 (3H, m), 6.20 (1H, m), 6.30 (1H, dm, J=10.1 Hz), 6.40 (1H, br s), and 7.00 (1H, dm, J=10.1 Hz); ^{13}C NMR (acetone-d_6) δ=19.73, 74.07 (tm, J=24 Hz), 105—125 (8C), 131.00, 131.88, 143.97 (m), 155.27, and 185.43; ^{19}F NMR (acetone-d_6) δ=−80.83 (3F, tt, J=10 and 2 Hz), −114.30 (1F, dm, J=279 Hz), −116.61 (1F, dm, J=279 Hz), −118.88 (2F, m), −120.8—−121.8 (6F, m), −122.37 (2F, m), and −125.87 (2F, m); IR (KBr) 3416vs, 1676vs, 1632vs, 1448m, 1400m, 1372m, 1330s, and 1300—1100vs cm^{-1}; MS (EI) m/z 542 (M^+, 1), 523 (1), 475 (1), and 123 (100). Found: C, 33.38; H, 1.35%. Calcd for $C_{15}H_7F_{17}O_2$: C, 33.23; H, 1.31%.

4-Hydroxy-2,5-dimethyl-4-perfluorooctyl-2,5-cyclohexadien-1-one (1g). Colorless crystals (dichloromethane/hexane), mp 91—92 °C. ^{1}H NMR (acetone-d_6) δ=1.84 (3H, d, J=1.2 Hz), 2.11 (3H, m), 6.18 (2H, m), and 6.75 (1H, m); ^{13}C NMR (acetone-d_6) δ=19.73 (m), 74.07 (ddm, J=22 and 21 Hz), 105—125 (8C), 130.99, 131.88, 143.96 (m), 155.26, and 185.43; ^{19}F NMR (acetone-d_6) δ=−80.65 (3F, tm, J=10 Hz), −114.29 (1F, dm, J=278 Hz), −116.47 (1F, dm, J=278 Hz), −118.99 (2F, m), −121.0—−121.5 (6F, m), −122.27 (2F, m), and −125.72 (2F, m); IR (KBr) 3396vs, 1678m, 1634vs, 1456m, 1398m, 1378m, 1328m, and 1300—1100vs cm^{-1}; MS (CI) m/z 557 (M^++1, 54), 539 (23), 166 (22), and 137 (100). Found: C, 34.41; H, 1.64%. Calcd for $C_{14}H_5F_{17}O_2$: C, 34.55; H, 1.63%.

4-Hydroxy-2,6-dimethyl-4-perfluorooctyl-2,5-cyclohexadien-1-one (1h). Colorless crystals (dichloromethane/hexane), mp 86—87 °C. ^{1}H NMR δ=1.94 (6H, s), 4.40 (1H, br s), and 6.72 (2H, s); ^{13}C NMR δ=16.07, 71.13 (t, J=24 Hz), 105—125 (8C), 135.35, 138.78, and 185.17; ^{19}F NMR δ=−81.25 (3F, tt, J=10 and 2 Hz), −119.50 (4F, m), −121.9—−122.5 (6F, m), −123.21 (2F, m), and −126.61 (2F, m); IR (KBr) 3424vs, 1676s, 1644vs, 1446s, 1396vs, and 1300—1100vs cm^{-1}; MS (CI) m/z 557 (M^++1, 47), 539 (37), 166 (9), and 137 (100). Found: C, 34.31; H, 1.66%. Calcd for $C_{14}H_5F_{17}O_2$: C, 34.55; H, 1.63%.

4-Hydroxy-3,5-dimethyl-4-perfluorooctyl-2,5-cyclohexadien-1-one (1i). Colorless crystals (dichloromethane/hexane), mp 104—106 °C. ^{1}H NMR (acetone-d_6) δ=2.15 (6H, s), 6.18 (2H, s), and 6.22 (1H, s); ^{13}C NMR (acetone-d_6) δ=19.90 (t, J=4 Hz), 76.69 (tt, J=20 and 2 Hz), 105—125 (8C), 131.54, 155.71, and 185.22; ^{19}F NMR (acetone-d_6) δ=−80.65 (3F, tt, J=10 and 2 Hz), −111.75 (2F, m), −119.35 (2F, m), −120.95 (2F, m), −121.39 (4F, m), −122.29 (2F, m), and −125.76 (2F, m); IR (KBr) 3364vs, 1672vs, 1626vs, 1450m, 1386s, 1356s, 1328m, and 1300—1100vs cm^{-1}; MS (CI) m/z 557 (M^++1, 68), 539 (12), 537 (29), 166 (29), and 137 (100). Found: C, 34.42; H, 1.51%. Calcd for $C_{14}H_5F_{17}O_2$: C, 34.55; H, 1.63%.

2-*t*-Butyl-4-hydroxy-4-perfluorooctyl-2,5-cyclohexadien-1-one (1j). Colorless crystals (dichloromethane/hexane), mp 92 °C. ^{1}H NMR δ=1.25 (9H, s), 2.74 (1H, br s), 6.33 (1H, d, J=10.1 Hz), 6.63 (1H, s), and 6.77 (1H, d, J=10.1 Hz); IR (KBr) 3216vs, 2964m, 1672vs, 1626vs, 1460m, 1368s, and 1300—1100vs cm^{-1}. MS (CI) 585 (M^++1, 8), 567 (59), 165 (100), and 123 (52). Found: C, 36.93; H, 2.18%. Calcd for $C_{18}H_{13}F_{17}O_2$: C, 37.00; H, 2.24%.

2,5-Di-*t*-butyl-4-hydroxy-4-perfluorooctyl-2,5-cyclohexadien-1-one (1k). Colorless crystals (dichloromethane/hexane), mp 164—165 °C. ^{1}H NMR δ=1.23 (9H, s), 1.35 (9H, s), 2.81 (1H, s), 6.37 (1H, s), and 6.50 (1H, s); IR (KBr) 3220vs, 2969s, 1658s, 1618vs, 1468s, 1370s, and 1300—1100vs cm^{-1}; MS (CI) 641 (M^++1, 11), 623 (13), 585 (15), 250 (20), and 222 (100). Found: C, 41.20; H, 3.27%. Calcd for $C_{22}H_{21}F_{17}O_2$: C, 41.26; H, 3.31%.

2,6-Di-*t*-butyl-4-hydroxy-4-perfluorooctyl-2,5-cyclohexadien-1-one (1l). Colorless crystals (dichloromethane/hexane), mp 82—83 °C. ^{1}H NMR δ=1.24 (18H, s), 3.30 (1H, br s), and 6.52 (2H, s); ^{13}C NMR δ=29.04, 35.29, 71.97 (t, J=24 Hz), 105—125 (8C), 132.34, 150.94, and 185.56; ^{19}F NMR δ=−81.27 (3F, tt, J=10 and 3 Hz), −118.76 (2F, m), −119.53 (2F, m), −122.24 (6F, m), −123.21 (2F, m), and −126.62 (2F, m); IR (KBr) 3496vs, 2964vs, 1672s, 1648vs, 1486m, 1464m, 1366s, and 1300—1100vs cm^{-1}; MS (CI) 641 (M^++1, 57), 625 (13), 623 (11), 599 (9), 597 (10), 222 (100), 221 (64), and 111 (38). Found: C, 41.37; H, 3.37%. Calcd for $C_{22}H_{21}F_{17}O_2$: C, 41.26; H, 3.31%.

4-Hydroxy-2-methoxy-4-perfluorobutyl-2,5-cyclohexadien-1-one (1m). Colorless crystals (dichloromethane/hexane), mp 69—71 °C. ^{1}H NMR δ=3.28 (br s), 3.74 (3H, s), 5.76 (1H, m), 6.41 (1H, d, J=10.1 Hz), and 6.94 (1H, m); ^{13}C NMR δ=55.36, 73.07 (t, J=24 Hz), 105—125 (4C), 107.82, 130.48, 141.71, 152.52, and 179.41; ^{19}F NMR δ=−81.31 (3F, tt, J=10 and 3 Hz), −119.23 (2F, m), −120.29 (2F, m), and −126.43 (2F, m); IR (KBr) 3544s, 3454s, 3088s, 1672m, 1623s, 1437m, 1353s, and 1300—1100vs cm^{-1}; MS (CI) m/z 359 (M^++1, 71), 341 (46), 327 (53), 168 (21), and 139 (100). Found: m/z 358.0258. Calcd for $C_{11}H_7F_9O_3$: M, 358.0251.

4-Hydroxy-3-methoxy-4-perfluorobutyl-2,5-cyclohexadien-1-one (1n). Colorless crystals (dichloromethane/hexane), mp 76—77 °C. ^{1}H NMR δ=3.85 (3H, s), 5.68 (1H, d, J=1.5 Hz), 6.36 (1H, dd, J=10.1 and 1.5 Hz), and 6.73 (1H, dd, J=10.1 and 1.2 Hz); ^{13}C NMR δ=56.31, 72.00 (t, J=23 and 2 Hz), 103.16, 108.48 (tm, J=270 Hz), 111.23 (ttt, J=269, 37, and 31 Hz), 115.18 (tt, J=270 and 32 Hz), 117.22 (qt, J=288 and 33 Hz), 130.52, 138.14 (dt, J=3 and 1 Hz), 168.81 (d, J=2 Hz), and 186.49; ^{19}F NMR δ=−81.37 (3F, tt, J=10 and 3 Hz), −116.80 (1F, dm, J=279 Hz), −118.20 (1F, dm, J=279 Hz), −121.72 (2F, m), −126.20 (1F, dddt, J=293, 20, 11, and 3 Hz), −126.60 (1F, dddt, J=293, 19, 14 and 3 Hz); IR (KBr) 3252vs, 1672vs, 1636s, 1608vs, 1356s, and 1300—1100vs cm^{-1}; MS (CI) m/z 359 (M^++1, 100), 343 (11), 341 (30), 339 (14), 327 (59), 323 (21), 313 (36), 168 (35), 140 (77), and 139 (76). Found: C, 36.59; H, 1.87%. Calcd for $C_{11}H_7F_9O_3$: C, 36.89; H, 1.97%.

2,5-Dichloro-4-hydroxy-4-perfluorooctyl-2,5-cyclohexadien-1-one (1o). Colorless crystals (ether/hexane), mp 98—99 °C. ^{1}H NMR (acetone-d_6) δ=6.83 (1H, s), 7.32 (1H, m), and 7.41 (1H, br s); ^{13}C NMR (acetone-d_6) δ=75.94 (t, J=23 Hz), 105—125 (8C), 131.49, 135.78, 139.18 (m), 152.29, and 176.85; ^{19}F NMR (acetone-d_6) δ=−80.61 (3F, tm, J=10 Hz), −114.06 (1F, dm, J=279 Hz), −115.80 (1F, dm, J=279 Hz), −118.69 (2F, m), −121.00 (2F, m), −121.30 (4F, m), −122.21 (2F, m), and −125.69 (2F, m); IR (KBr) 3860s, 1682vs, 1600s, 1332m, 1332m, and 1300—1100vs cm^{-1}; MS

(CI) *m/z* 601 (6), 599 (37), 597 (56), 581 (20), 579 (36), 577 (27), 563 (21), 543 (24), 180 (100), and 178 (98). Found: C, 27.90; H, 0.66%. Calcd for $C_{14}H_3Cl_2F_{17}O_2$: C, 28.16; H, 0.51%.

4-Hydroxy-4-perfluorohexyl-1(4*H*)-naphthalenone (1p). Colorless crystals (dichloromethane/hexane); mp 91.5 °C. ^{1}H NMR δ=3.32 (1H, s), 6.57 (1H, d, J=10.4 Hz), 7.04 (1H, dm, J=10.4 Hz), 7.58 (1H, td, J=7.6 and 1.2 Hz), 7.69 (1H, td, J=7.6 and 1.5 Hz), 7.89 (1H, dm, J=7.9 Hz), and 8.12 (1H, dd, J=7.6 and 1.5 Hz); ^{13}C NMR δ=72.61 (dd, J=25 and 22 Hz), 105—125 (6C), 126.91, 127.92 (t, J=3 Hz), 130.15, 130.89 (m), 131.95, 133.10, 137.37, 142.17 (m), and 183.38; ^{19}F NMR δ=−81.32 (3F, tt, J=10 and 2 Hz), −116.26 (1F, dm, J=278 Hz), −118.66 (1F, dm, J=278 Hz), −118.77 (2F, m), −122.30 (2F, m), −123.27 (2F, m), and −126.63 (2F, m); IR (KBr) 3312vs, 1666s, 1634s, 1602s, 1308s, and 1300—1100vs cm^{-1}; MS (CI) *m/z* 479 (M^++1, 41), 461 (20), 188 (10), and 159 (100). Found: C, 39.94; H, 1.53%. Calcd for $C_{16}H_7F_{13}O_2$: C, 40.19; H, 1.48%.

4-Acetoxy-4-perfluorooctyl-2,5-cyclohexadien-1-one (2a). Colorless crystals (dichloromethane/hexane), mp 50—51 °C. ^{1}H NMR δ=2.17 (3H, s), 6.53 (2H, d, J=10.1 Hz), and 6.84 (2H, d, J=10.1 Hz); ^{13}C NMR δ=20.87 (m), 77.22 (tt, J=26 and 3 Hz), 105—125 (8C), 132.98, 138.88, 167.47, and 183.56; ^{19}F NMR δ=−81.24 (3F, tt, J=10 and 2 Hz), −116.46 (2F, m), −118.84 (2F, m), −122.15 (6F, m), −123.17 (2F, m), and −126.62 (2F, m); IR (KBr) 1774vs, 1680vs, 1636s, 1374s, and 1300—1100vs cm^{-1}; MS (EI) *m/z* 570 (M^+, 3), 528(3), 512 (6), 492 (23), and 173 (100). Found: C, 33.30; H, 1.23%. Calcd for $C_{16}H_7F_{17}O_3$: C, 33.70; H, 1.24%.

4-Acetoxy-4-perfluorohexyl-2,5-cyclohexadien-1-one (2b). Colorless oil. ^{19}F NMR δ=−81.39 (3F, tt, J=10 and 3 Hz), −116.44 (2F, m), −118.82 (2F, m), −122.19 (2F, m), −123.10 (2F, m), and −126.62 (2F, m); IR (KBr) 1776vs, 1680vs, 1640s, 1370s, and 1300—1100vs cm^{-1}; MS (EI) *m/z* 470 (M^+, 2), 428 (4), 412 (16), and 143 (100). Found: *m/z* 470.0225. Calcd for $C_{14}H_7F_{13}O_3$: M, 470.0187.

4-Acetoxy-4-perfluorobutyl-2,5-cyclohexadien-1-one (2c). Colorless oil. ^{19}F NMR δ=−81.21 (3F, tt, J=10 and 3 Hz), −116.72 (2F, m), −119.89 (2F, m), and −126.46 (2F, m); IR (KBr) 1776vs, 1678vs, 1640s, 1386m, 1372m, 1356m, and 1300—1100vs cm^{-1}; MS (EI) *m/z* 370 (M^+, 19), 328 (26), 312 (26), 300 (27), and 143 (100). Found: *m/z* 370.0251. Calcd for $C_{14}H_7F_9O_3$: M, 370.0250.

4-Acetoxy-4-perfluoroethyl-2,5-cyclohexadien-1-one (2d). Colorless oil. ^{19}F NMR δ=−78.76 (3F, s) and −120.99 (2F, s); IR (KBr) 1776vs, 1680vs, 1640s, 1370s, and 1300—1100vs cm^{-1}; MS (EI) *m/z* 270 (M^+, 19), 228 (100), 208 (11), and 159 (24). Found: *m/z* 270.0293. Calcd for $C_{10}H_7F_5O_3$: M, 270.0314.

4-Acetoxy-3-methyl-4-perfluorooctyl-2,5-cyclohexadien-1-one (2f). Colorless crystals (dichloromethane/hexane), mp 89—91 °C. ^{1}H NMR δ=2.05 (3H, d, J=1.2 Hz), 2.22 (3H, s), 6.38 (1H, m), 6.45 (1H, dd, J=10.3 and 1.8 Hz), and 6.81 (1H, dt, J=10.3 and 2.8 Hz); ^{13}C NMR δ=19.08 (t, J=4 Hz), 20.69, 78.96 (t, J=24 Hz), 105—125 (8C), 131.68, 132.05, 139.80, 150.31, 167.49, and 184.28; ^{19}F NMR δ=−81.27 (3F, t, J=10 Hz), −115.56 (2F, m), −118.94 (2F, m), −122.13 (2F, m), −123.19 (2F, m), and −126.59 (2F, m); IR (KBr) 1754vs, 1672s, 1640vs, 1366s, and 1300—1100vs cm^{-1}; MS (CI) 585 (M^++1, 31), 543 (38), 527 (60), 507 (69), and 157 (100). Found: C, 34.95; H, 1.51%. Calcd for $C_{17}H_9F_{17}O_3$: C, 34.95; H, 1.55%.

4-Acetoxy-2,5-di-*t*-butyl-4-perfluorooctyl-2,5-cyclohexadien-1-one (2k). Colorless crystals (dichloromethane/hexane), mp 95—97 °C. ^{1}H NMR δ=1.22 (9H, s), 1.26 (9H, m), 2.19 (3H, s), 6.36 (1H, dd, J=5.2 and 3.0 Hz), and 6.52 (1H, s); IR (KBr) 2972s, 1782s, 1754s, 1714s, 1666s, 1640s, 1370s, and 1300—1100vs cm^{-1}; MS (CI) 683 (M^++1, 26), 667 (6), 655 (13), 640 (28), 627 (100), 623 (43), 607 (33), and 585 (59). Found: C, 42.38; H, 3.49%. Calcd for $C_{24}H_{23}F_{17}O_3$: C, 42.24; H, 3.40%.

4-Acetoxy-2,6-di-*t*-butyl-4-perfluorooctyl-2,5-cyclohexadien-1-one (2l). Colorless crystals (dichloromethane/hexane), mp 53—54 °C. ^{1}H NMR δ=1.24 (18H, s), 2.15 (3H, s), and 6.43 (2H, s); ^{13}C NMR δ=21.18, 28.98, 35.42, 78.04, (t, J=24 Hz), 105—125 (8C), 130.51, 151.40, 167.43, and 185.68; ^{19}F NMR δ=−81.26 (3F, tt, J=10 and 3 Hz), −116.80 (2F, m), −118.96 (2F, m), −122.15 (2F, m), −122.36 (4F, m), −123.30 (2F, m), and −126.63 (2F, m); IR (KBr) 2960s, 1764vs, 1672s, 1648s, 1462s, 1368s, 1330s, and 1300—1100vs cm^{-1}; MS (CI) 683 (M^++1, 3), 663 (2), 655 (3), 627 (100), 623 (57), 607 (46), and 584 (71). Found: C, 41.87; H, 3.43%. Calcd for $C_{24}H_{23}F_{17}O_3$: C, 42.24; H, 3.40%.

4-Acetoxy-3-methoxy-4-perfluorobutyl-2,5-cyclohexadien-1-one (2n). Colorless crystals (hexane), mp 29—30 °C. ^{1}H NMR δ=2.18 (3H, s), 3.78 (3H, s), 5.78 (1H, d, J=1.5 Hz), 6.44 (1H, dd, J=10.1 and 1.5 Hz), and 6.60 (1H, d, J=10.1 Hz); ^{13}C NMR δ=20.38 (m), 56.48 (m), 76.96 (tt, J=23 and 2 Hz), 105.00, 105—125 (4C), 132.67, 135.56 (m), 166.16, 167.34, and 185.49; ^{19}F NMR δ=−81.28 (3F, tt, J=10 and 2 Hz), −116.08 (1F, dm, J=280 Hz), −116.73 (1F, dm, J=280 Hz), −120.98 (2F, m), and −126.27 (2F, m); IR (KBr) 1764vs, 1666s, 1606vs, 1354s, and 1300—1100vs cm^{-1}; MS (CI) *m/z* 401 (M^++1, 100), 359 (38), 358 (46), 339 (17), and 323 (40). Found: C, 38.70; H, 2.23%. Calcd for $C_{13}H_9F_9O_4$: C, 39.02; H, 2.27%.

4-Acetoxy-2,5-dichloro-4-perfluorooctyl-2,5-cyclohexadien-1-one (2o). Colorless crystals (dichloromethane/hexane); mp 91—92 °C. ^{1}H NMR δ=2.26 (3H, s), 6.84 (1H, s), and 7.00 (1H, m); ^{13}C NMR δ=20.48, 78.71 (t, J=25 Hz), 105—125 (8C), 131.58, 134.75, 136.06 (m), 147.55, 167.20, and 175.78; ^{19}F NMR δ=−81.30 (3F, tm, J=10 Hz), −115.25 (2F, m), −118.87 (1F, m), −119.07 (1F, m), −121.86 (2F, m), −122.12 (2F, m), −122.33 (2F, m), −123.19 (2F, m), and −126.61 (2F, m); IR (KBr) 3064m, 1770vs, 1686vs, 1602s, 1372s, 1332m, and 1300—1100vs cm^{-1}; MS (EI) *m/z* 640 (2), 638 (4), 582 (9), 580 (15), 213 (63), and 212 (100). Found: C, 30.09; H, 0.77%. Calcd for $C_{16}H_5Cl_2F_{17}O_{15}$: C, 30.03; H, 0.79%.

4-Acetoxy-4-perfluorohexyl-1(4*H*)-naphthalenone (2p). Colorless oil. ^{1}H NMR δ=2.20 (3H, m), 6.64 (1H, d, J=10.4 Hz), 6.99 (1H, dm, J=10.4 Hz), 7.61 (3H, m), and 8.18 (1H, dm, J=7.9 Hz); ^{13}C NMR δ=21.05, 77.71 (t, J=25 Hz), 105—125 (6C), 126.27 (t, J=3 Hz), 127.24, 130.12, 131.84 (2C), 132.59, 134.78, 140.39, 167.30, and 183.09; ^{19}F NMR δ=−81.31 (3F, tt, J=10 and 2 Hz), −116.14 (2F, t, J=15 Hz), −118.36 (2F, m), −122.21 (2F, m), −123.14 (2F, m), and −126.59 (2F, m); IR (neat) 3072m, 1770vs, 1680vs, 1638s 1600vs, 1460m, 1370s, and 1300—1100vs cm^{-1}; MS (CI) *m/z* 521 (M^++1, 23), 507 (8), 479 (35), 461 (33), 443 (19), and 159 (100). Found: C, 41.40; H, 1.69%. Calcd for $C_{18}H_9F_{13}O_3$: C, 41.56; H, 1.74%.

Acid Treatment of Quinols. General Procedure: To an acetic anhydride solution (30 ml) of a quinol (1 mmol) was added three drops of concd H_2SO_4 at room temperature. After stirring overnight, the reaction was quenched by careful addition of a saturated aqueous solution of $NaHCO_3$

and the mixture was stirred until gas evolution ceased. The mixture was extracted with ether and the ethereal extract was washed by brine, dried with Na_2SO_4, and evaporated. The residue was chromatographed on silica gel (hexane–hexane/ether).

2,4-Diacetoxy-1-perfluorooctylbenzene (3a) and 1,2-Diacetoxy-4-perfluorooctylbenzene (5a=5j). Colorless crystals (dichloromethane/hexane); mp 56—58 °C. ^{19}F NMR δ= −81.34 (both 3F, t, J=10 Hz), −108.79 (**5a**, 2F, t, J=13 Hz), −110.77 (**3a**, 2F, t, J=13 Hz), −121.70 (both 2F, m), −121.8—−122.4 (6F, m), −123.18 (both 2F, m), and −126.61 (both 2F); IR (neat) 1772vs, 1374s, and 1300—1100vs cm^{-1}; MS (EI) m/z 612 (M^+, 2), 570 (20), 528 (68), 509 (5), and 154 (100). Found: C, 35.36; H, 1.41%. Calcd for $C_{18}H_9F_{17}O_4$: C, 35.31; H, 1.48%.

2,4-Diacetoxy-1-perfluorohexylbenzene (3b) and 1,2-Diacetoxy-4-perfluorohexylbenzene (5b). Colorless crystals (hexane); mp 38—40 °C. ^{19}F NMR δ=−81.32 (both 3F, tt, J=10 and 2 Hz), −108.81 (**5b**, 2F, t, J=15 Hz), −110.81 (**3b**, 2F, m), −121.7—−122.3 (both 4F, m), −123.23 (both 2F, m), and −126.59 (both 2F, m); IR (neat) 1782vs, 1374s, and 1300—1100vs cm^{-1}; MS (EI) m/z 512 (M^+, 2), 470 (26), 428 (77), 160 (8), and 159 (100). Found: C, 37.54; H, 1.71%. Calcd for $C_{16}H_9F_{13}O_4$: C, 37.52; H, 1.77%.

2,4-Diacetoxy-1-perfluorobutylbenzene (3c) and 1,2-Diacetoxy-4-perfluorobutylbenzene (5c).[7] Colorless oil. MS (EI) m/z 412 (M^+, 4), 370 (13), 329 (12), 328 (100), and 159 (96). Found: C, 41.90; H, 2.35%. Calcd for $C_{14}H_9F_9O_4$: C, 40.79; H, 2.20%.

2,4-Diacetoxy-1-perfluoroethylbenzene (3d) and 1,2-Diacetoxy-4-perfluoroethylbenzene (5d). Colorless oil. ^{19}F NMR δ=−84.79 (**3d**, 3F, t, J=2 Hz), −85.10 (**4d**, 3F, t, J=2 Hz), −112.92 (**3d**, 2F, m), and −114.77 (**4d**, 2F, m); IR (neat) 1780vs, 1614m, 1510m, 1426s, 1374s, 1338s, and 1300—1100vs cm^{-1}; MS (EI) m/z 312 (M^+, 5), 270 (44), 229 (9), 228 (100), and 159 (45). Found: C, 45.77; H, 2.83%. Calcd for $C_{12}H_9F_5O_4$: C, 46.17; H, 2.91%.

1,3-Diacetoxy-2-methyl-4-perfluorooctylbenzene (3e). Colorless crystals (dichloromethane/hexane), mp 75—76 °C. ^{1}H NMR δ=2.02 (3H, s), 2.31 (3H, s), 2.36 (3H, m), 7.14 (1H, d, J=8.9 Hz), and 7.46 (3H, d, J=8.9 Hz); ^{13}C NMR δ=10.19, 20.16, 20.60, 105—125 (8C), 118.81 (t, J=23 Hz), 120.11, 126.50, 126.62 (t, J=8 Hz), 148.73 (t, J=3 Hz), 152.97, 168.03, and 168.19; ^{19}F NMR δ=−81.29 (3F, t, J=10 Hz), −107.5 (1F, dm, J=ca. 265 Hz), −110.5 (1F, dm, J=ca. 265 Hz), −121.47 (2F, m), −122.2—−122.3 (6F, m), −123.26 (2F, m), and −126.62 (2F, m); IR (KBr) 1764vs, 1606m, 1590m, 1430s, 1368s, and 1300—1100vs cm^{-1}; MS (EI) 626 (M^+, 0.7), 607 (0.8), 584 (32), 542 (100), 523 (10), and 173 (96). Found: 36.73; H, 1.77%. Calcd for $C_{19}H_{11}F_{17}O_4$: C, 36.44; H, 1.77%.

1,5-Diacetoxy-2-methyl-4-perfluorooctylbenzene (4e) and 1,2-Diacetoxy-3-methyl-5-perfluorooctylbenzene (5e). Colorless oil. ^{1}H NMR **4e**: δ=2.23 (3H, s), 2.27 (3H, s), 2.34 (3H, s), 7.31 (1H, m), and 7.35 (1H, m); **5e**: δ=2.05 (3H, s), 2.25 (3H, s), 2.27 (3H, s), 7.05 (1H, s), and 7.45 (1H, s); ^{13}C NMR **4e**: δ=16.21, 20.33, 20.56, 105—125 (8C), 118.82, 123.48 (t, J=23 Hz), 128.62, 130.83 (t, J=9 Hz), 147.29 (t, J=3 Hz), 152.26 (t, J=1 Hz), 168.12, and 168.62; **5e**: (typical signals) δ=15.68, 20.04, 133.46, 142.71, 144.10, 167.35, and 167.84; ^{19}F NMR **4e**: (typical signal) δ=−108.86; **5e**: (typical signal) δ=−110.96.

1,5-Diacetoxy-3-methyl-2-perfluorooctylbenzene (4f), 1,2-Diacetoxy-3-methyl-4-perfluorooctylbenzene (5f), and 1,2-Diacetoxy-4-methyl-5-perfluorooctylbenzene (6f). Colorless oil. ^{1}H NMR **4f**: δ=2.26 (3H, s), 2.30 (3H, s), 2.50 (3H, t, J=4.6 Hz), 6.90 (1H, m), and 6.97 (1H, m); **5f**: δ=2.31 (3H, m), 2.31 (3H, s), 2.35 (3H, m), 7.21 (1H, d, J=8.9 Hz), and 7.47 (1H, d, J=8.9 Hz); **6f**: δ=2.30 (6H, m), 2.47 (3H, t, J=3.0 Hz), 7.14 (1H, s), and 7.35 (1H, s); ^{13}C NMR **4f**: δ=20.56, 21.04, 21.83 (m), 105—125 (8C), 116.36, 120.80, 123.29, 125.13 (t, J=23 Hz), 141.98, 152.73, 168.31, and 168.75; **5f**: δ=12.99 (tt, J=5 and 3 Hz), 20.18, 20.67, 105—125 (8C), 120.80, 125.77 (t, J=23 Hz), 126.75, (t, J=10 Hz), 133.50 (t, J=2 Hz), 141.97, 145.29, 167.63, and 167.67; **6f**: δ=20.02 (m), 20.46, 20.61, 105—125 (8C), 124.05 (t, J=9 Hz), 125.13 (t, J=23 Hz), 127.34, 137.32 (t, J=2 Hz), 139.94, 144.41, 167.67, and 167.90; ^{19}F NMR **4f**: (typical signal) δ=−103.51 (m); **5f**: δ=−81.27 (3F, tt, J=10 and 2 Hz), −105.51 (2F, m), −121.02 (2F, m), −121.94 (2F, m), −122.33 (4F, m), −123.19 (2F, m), and −126.61 (2F, m); **6f**: (typical signal) δ=−106.75 (m).

4-Acetoxy-2-acetoxymethyl-1-perfluorooctylbenzene (7f). Colorless crystals (dichloromethane/hexane), mp 74—75 °C. ^{1}H NMR δ=2.14 (3H, s), 2.34 (3H, s), 5.27 (2H, s), 7.24 (1H, dd, J=8.5 and 2.1 Hz), 7.35 (1H, d, J=2.1 Hz), and 7.61 (1H, d, J=8.5 Hz); ^{13}C NMR δ=20.79, 21.08, 62.53 (tt, J=7 and 3 Hz), 105—125 (8C), 121.43, 123.07, 123.70 (t, J=23 Hz), 130.31, (t, J=9 Hz), 138.02 (t, J=2 Hz), 153.49, 168.67, and 170.38; ^{19}F NMR δ=−81.26 (3F, tt, J=10 and 2 Hz), −105.70 (2F, t, J=14 Hz), −121.16 (2F, m), −121.82 (2F, m), −122.31 (2F, m), −123.19 (2F, m), and −126.60 (2F, m); IR (KBr) 1740vs, 1610m, 1586s, 1370s, and 1300—1100vs cm^{-1}; MS (EI) 626 (M^+, 6), 584 (23), 542 (100), 153 (24), and 123 (13). Found: C, 36.39; H, 1.81%. Calcd for $C_{18}H_{11}F_{17}O_4$: C, 36.44; H, 1.77%.

1,3-Diacetoxy-2,5-dimethyl-4-perfluorooctylbenzene (3g). Colorless crystals (dichloromethane/hexane), mp 115—117 °C. ^{1}H NMR δ=1.95 (3H, s), 2.26 (3H, s), 2.31 (3H, s), 2.45 (3H, t, J=4.6 Hz), and 6.94 (1H, s); ^{13}C NMR δ=9.93, 20.01, 20.53, 21.42 (m), 105—125 (8C), 117.54 (t, J=21 Hz), 123.87, 124.09, 138.56 (t, J=2 Hz), 149.92 (t, J=4 Hz), 152.00, 168.17, and 168.22; ^{19}F NMR δ=−81.40 (3H, tm, J=10 Hz), −102.23 (1F, dm, J=289 Hz), −104.83 (1F, dm, J=289 Hz), −120.82 (1F, m), −121.09 (1F, m), −122.30 (6F, m), −123.17 (2F, m), and −126.64 (2F, m); IR (KBr) 1764vs, 1580m, 1372s, and 1300—1100vs cm^{-1}; MS (EI) m/z 640 (M^+, 4), 598 (15), 556 (100), 537 (7), and 187 (63). Found: C, 37.67; H, 2.08%. Calcd for $C_{20}H_{13}F_{17}O_4$: C, 37.52; H, 2.05%.

2,3-Diacetoxy-1,4-dimethyl-5-perfluorooctylbenzene (6g). Colorless crystals (dichloromethane/hexane), mp 73—75 °C. ^{1}H NMR δ=2.22 (3H, s), 2.23 (3H, s), 2.33 (3H, s), 2.34 (3H, s), and 7.33 (1H, s); ^{13}C NMR δ=12.81 (m), 16.08, 20.21, 20.27, 105—125 (8C), 125.51 (t, J=22 Hz), 128.30 (t, J=9 Hz), 129.84, 130.54 (t, J=2 Hz), 142.44, 144.25, 167.41, and 167.73; ^{19}F NMR δ=−81.25 (3F, tm, J=10 Hz), −105.58 (2F, m), −120.94 (2F, m), −121.95 (2F, m), −122.32 (4F, m), −123.19 (2F, m), and −126.58 (2F, m); IR (KBr) 1780vs, 1490m, 1458m, 1430m, 1374s, 1320s, and 1300—1100vs cm^{-1}; MS (EI) m/z 640 (M^+, 3), 598 (12), 556 (100), 537 (6), and 187 (52).

1-Acetoxy-5-acetoxymethyl-2-methyl-4-perfluorooctylbenzene (7g). ^{1}H NMR (typical signals) δ=5.24 (2H, m), 7.29 (1H, s), and 7.46 (1H, s).

2,4-Diacetoxy-1,3-dimethyl-5-perfluorooctylbenzene (3h). Colorless crystals (dichloromethane/hexane), mp 72—74 °C. ^{1}H NMR δ=1.97 (3H, s), 2.20 (3H, s), 2.29 (3H, s), 2.37 (3H, s), and 7.31 (1H, s); ^{13}C NMR δ=10.51 (m), 16.34 (m), 20.28

(m), 20.38 (m), 118.71 (t, J=23 Hz), 126.51, 127.94 (tm, J=8 Hz), 128.93, 146.39 (t, J=3 Hz), 151.69 (t, J=1 Hz), 167.78, and 168.28; ^{19}F NMR δ=−81.25 (3F, tt, J=10 and 2 Hz), −107.65 (1F, dm, J=267 Hz), −110.88 (1F, dm, J=267 Hz), −121.42 (2F, m), −122.27 (6F, m), −123.21 (2F, m), and −126.60 (2F, m); IR (KBr) 1768vs, 1604m, 1374s, 1330s, 1300—1100vs cm^{-1}; MS (EI) m/z 640 (8), 598 (20), 556 (100), and 167 (88). Found: C, 37.67; H, 2.08%. Calcd for $C_{20}H_{13}F_{17}O_4$: C, 37.52; H, 2.05%.

5-Acetoxy-1-acetoxymethyl-3-methyl-2-perfluorooctylbenzene (7i). Colorless crystals (dichloromethane/hexane), mp 78—80 °C. ^{1}H NMR δ=2.13 (3H, s), 2.32 (3H, s), 2.51 (3H, mt, J=4.6 Hz), 5.24 (2H, t, J=3.0 Hz), 7.05 (1H, s), and 7.21 (1H, s); ^{13}C NMR δ=20.82, 21.03, 22.12 (tt, J=7 and 4 Hz), 63.62 (tt, J=10 and 4 Hz), 105—125 (8C), 121.24, 122.45 (t, J=22 Hz), 125.78, 139.45 (t, J=3 Hz), 142.04 (t, J=4 Hz), 152.61, 168.71, and 170.33; ^{19}F NMR δ=−81.29 (3F, tt, J=10 and 2 Hz), −99.59 (2F, m), −120.42 (2F, m), −122.09 (6F, m), −123.15 (2F, m), and −126.57 (2F, m); IR (KBr) 1764vs, 1738s, 1602s, 1462m, 1386s, 1372s, 1328m, and 1300—1100vs cm^{-1}; MS (CI) m/z 641 (M^++1, 100), 621 (76), 599 (46), 585 (16), 579 (37), 557 (49), 556 (47), 271 (9), and 187 (73). Found: C, 37.45; H, 2.03%. Calcd for $C_{20}H_{13}F_{17}O_4$: C, 37.52; H, 2.05%.

1-*t*-Butyl-2,4-diacetoxy-5-perfluorooctylbenzene (4j=4k). Colorless crystals (dichloromethane/hexane), mp 76—77 °C. ^{1}H NMR δ=1.37 (9H, s), 2.27 (3H, s), 2.35 (3H, s), 7.03 (1H, s), and 7.57 (1H, s); IR (KBr) 2960m, 1774vs, 1612m, 1580m, 1502m, 1404m, 1372s, and 1300—1100vs cm^{-1}; MS (EI) m/z 668 (M^+, 1), 653 (0.4), 649 (1), 626 (12), 584 (41), and 569 (100). Found: C, 39.74; H, 2.53%. Calcd for $C_{22}H_{17}F_{17}O_4$: C, 39.54; H, 2.56%.

1-*t*-Butyl-2,3-diacetoxy-5-perfluorooctylbenzene (6j=5l). Colorless crystals (dichloromethane/hexane), mp 61—63 °C. ^{1}H NMR δ=1.37 (9H, s), 2.28 (3H, s), 2.36 (3H, s), 7.38 (1H, m), and 7.47 (1H, m); ^{13}C NMR δ=20.69, 20.83, 30.00, 35.20, 105—125 (8C), 120.63 (t, J=7 Hz), 122.93 (t, J=7 Hz), 126.19 (t, J=25 Hz), 143.08, 144.08 (t, J=2 Hz), 144.21, 167.52, and 167.58; ^{19}F NMR δ=−81.25 (3F, tt, J=10 and 3 Hz), −110.83 (2F, t, J=13 Hz), −121.85 (4F, m), −122.35 (4F, m), −123.20 (2F, m), and −126.59 (2F, m); IR (KBr) 2984s, 1762s, 1428s, 1370s, and 1300—1100vs cm^{-1}; MS (EI) m/z 668 (M^+, 7), 626 (8), 584 (100), and 569 (49). Found: C, 39.51; H, 2.60%. Calcd for $C_{22}H_{17}F_{17}O_4$: C, 39.54; H, 2.56%.

1,5-Diacetoxy-2-methoxy-4-perfluorobutylbenzene (4m). Colorless crystals (dichloromethane/hexane), mp 73—74 °C. ^{1}H NMR δ=2.26 (3H, s), 2.32 (3H, s), 3.87 (3H, s), 7.01 (1H, s), and 7.09 (1H, s); ^{13}C NMR δ=20.50, 20.52, 56.40, 105—125 (4C), 111.62 (t, J=9 Hz), 118.44 (t, J=23 Hz), 119.91, 142.10 (t, J=3 Hz), 142.78, 149.15, 167.86, and 168.82; ^{19}F NMR δ=−81.41 (3F, tt, J=10 and 3 Hz), −109.08 (2F, m), −122.58 (2F, m), and −126.43 (2F, m); IR (KBr) 1774vs, 1516s, 1410s, 1374s, 1350s, and 1300—1100vs cm^{-1}; MS (EI) m/z 442 (M^+, 3), 401 (3), 358 (100), and 189 (51). Found: C, 40.78; H, 2.45%. Calcd for $C_{15}H_{11}F_9O_5$: C, 40.72; H, 2.51%.

1,2-Diacetoxy-4-perfluorohexylnaphthalene (5p). Colorless crystals (dichloromethane/hexane), mp 89—90 °C. ^{1}H NMR δ=2.33 (3H, s), 2.46 (3H, s), 7.58 (2H, m), 7.73 (1H, s), 7.59 (1H, m), and 8.22 (1H, m); ^{13}C NMR δ=20.27, 20.50, 105—125 (8C), 121.98, 123.35 (t, J=23 Hz), 124.62 (t, J=11 Hz), 125.08 (m), 127.42, 127.86, 128.63, 129.37, 137.83, 140.63 (t, J=1 Hz), 167.44, and 167.95; ^{19}F NMR δ=−81.28 (3F, tt, J=10 and 2 Hz), −104.62 (2F, t, J=15 Hz), −120.32 (2F, t, J=12 Hz), −121.90 (2F, m), −123.10 (2F, m), and −126.53 (2F, m); IR (KBr) 2950m, 1770vs, 1634m, 1614m, 1588m, 1520m, 1472m, 1436m, 1374s, 1354s, and 1300—1100vs cm^{-1}; MS (EI) m/z 562 (M^+, 3), 520 (12), 478 (100), 459 (5), 458 (5), 239 (9), and 209 (97). Found: C, 42.46; H, 2.06%. Calcd for $C_{20}H_{11}F_{13}O_4$: C, 42.72; H, 1.97%.

Deacetylation of Diacetoxybenzenes. General Procedure: A mixture of **3a—d** and **5a—d** (ca. 1:1, derived from 1 mmol of quinols) was dissolved in 20 ml of methanol containing 100 mg (1 mmol) of *p*-toluenesulfonic acid hydrate. The methanol solution was refluxed for 1 d under a nitrogen atmosphere. After the solvent was removed in vacuo, the residue was dissolved in ether. The solution was washed with water and brine, dried over Na_2SO_4, and evaporated to give an almost quantitative yields of benzenediols. Separation of isomeric benzenediols was carried out by chromatography of the residue on silica gel (CH_2Cl_2–ether). Resorcinol and catechol derivatives were obtained from less and more polar fractions, respectively. In the case of perfluorooctyl derivatives, fractional crystallization of **8a** from $CHCl_3$ was performed prior to the chromatographic separation.

4-Perfluorooctyl-1,3-benzenediol (8a). Colorless crystals (dichloromethane/hexane), mp 118—119 °C; ^{1}H NMR (acetone-d_6) δ=6.45 (1H, dd, J=8.6 and 2.0 Hz), 6.49 (1H, d, J=2 Hz), 7.24 (1H, d, J=8.6 Hz), 8.99 (1H, br s), and 9.11 (1H, br s); ^{13}C NMR (acetone-d_6) δ=105.15, 107.32 (t, J=23 Hz), 108.67, 105—125 (8C), 131.42, (t, J=8 Hz), 159.60 (t, J=3 Hz), and 163.41; ^{19}F NMR (acetone-d_6) δ=−81.85 (3F, tt, J=10 and 2 Hz), −106.11 (2F, t, J=14 Hz), −120.76 (2F, m), −121.43 (6F, m), −122.23 (2F, m), and −125.85 (2F, m); IR (KBr) 3216vs, 1612vs, 1318vs, and 1300—1100vs cm^{-1}; MS (EI) m/z 528 (M^+, 14), 159 (100), and 119 (3). Found: C, 31.61; H, 1.32%. Calcd for $C_{14}H_5F_{17}O_2$: C, 31.84; H, 0.95%.

4-Perfluorooctyl-1,2-benzenediols (9a). Colorless crystals (dichloromethane/hexane), mp 94—95 °C. ^{1}H NMR δ=6.90 (2H, m) and 6.96 (1H, s); ^{13}C NMR δ=105—125 (8C), 115.43 (t, J=7 Hz), 117.10, 120.70 (t, J=7 Hz), 121.31 (t, J=25 Hz), 147.61, and 151.15 (t, J=1 Hz); ^{19}F NMR δ=−80.80 (3F, t, J=10 Hz), −108.76 (2F, t, J=14 Hz), −120.80 (2F, m), −121.43 (6F, m), −122.21 (2F, m), and −125.75 (2F, m); IR (KBr) 3536s, 3476vs, 1614m, 1530m, 1448s, 1394s, 1314vs, and 1300—1100vs cm^{-1}; MS (EI) m/z 528 (M^+, 19), 509 (5), 508 (5), 189 (14), and 159 (100). Found: m/z 528.0028. Calcd for $C_{14}H_5F_{17}O_2$: M, 528.0017.

4-Perfluorohexyl-1,3-benzenediol (8b). Colorless crystals (dichloromethane/hexane), mp 70 °C; ^{19}F NMR (acetone-d_6) δ=−80.66 (3F, tt, J=10 and 3 Hz), −106.03 (2F, tt, J=15 and 3 Hz), −120.79 (2F, m), −121.40 (2F, m), −122.26 (2F, m), and −125.75 (2F, m); IR (KBr) 3212vs, 1614vs, 1536m, 1468s, 1394s, 1364s, 1316s, and 1300—1100vs cm^{-1}; MS (CI) m/z 429 (M^+, 2), 406 (100), and 159 (99). Found: m/z 428.0094. Calcd for $C_{12}H_5F_{13}O_2$: M, 428.0081.

4-Perfluorohexyl-1,2-benzenediol (9b). Colorless crystals (dichloromethane/hexane), mp 77—78 °C. ^{19}F NMR δ=−80.99 (3F, tt, J=10 and 3 Hz), −108.78 (2F, tt, J=15 and 3 Hz), −121.18 (2F, m), −121.60 (2F, m), −122.54 (2F, m), and −126.00 (2F, m); IR (KBr) 3416vs, 1614m, 1532m, 1448m, 1356s, 1316s, and 1300—1100vs cm^{-1}; MS (EI) m/z 428 (M^+, 4), 407 (3), 406 (18), 387 (3), 209 (7), 159 (13), and 137 (100). Found: m/z 428.0087. Calcd for $C_{12}H_5F_{13}O_2$: M, 428.0081.

4-Perfluorobutyl-1,3-benzenediol (8c). Colorless crystals

(dichloromethane/hexane), mp 52—53 °C. ^{19}F NMR δ=−80.85 (3F, tt, J=10 and 3 Hz), −106.26 (2F, tq, J=13 and 3 Hz), −121.66 (2F, m), and −125.60 (2F, m); IR (KBr) 3504s, 3224vs, 1612vs, 1466s, 1394s, 1356m, 1318m, and 1300—1100vs cm^{-1}; MS (EI) m/z 328 (M^+, 22), 309 (3), 308 (2), 289 (1), and 159 (100). Found: m/z 328.0143. Calcd for $C_{10}H_5F_9O_2$: M, 328.0144.

4-Perfluorobutyl-1,2-benzenediol (9c). Colorless crystals (dichloromethane/hexane), mp 67—68 °; ^{19}F NMR (acetone-d_6) δ=−80.92 (3F, tt, J=10 and 2 Hz), −108.74 (2F, tt, J=13 and 3 Hz), −122.38 (2F, m), and −125.25 (2F, m); IR (KBr) 3460vs, 1614s, 1534s, 1448s, 1356s, 1316s, and 1300—1100vs cm^{-1}; MS (EI) m/z 328 (M^+, 27), 309 (4), 308 (4), 189 (7), and 159 (100). Found: m/z 328.0165. Calcd for $C_{10}H_5F_9O_2$: M, 328.0144.

4-Perfluoroethyl-1,3-benzenediol (8d). Colorless needles (hexane). ^{19}F NMR (acetone-d_6) δ=−83.95 (3F, t, J=2 Hz) and −110.32 (2F, q, J=2 Hz); IR (KBr) 3420vs, 1616s, 1580s, 1500m, 1446m, 1406s, 1336s, and 1300—1100vs cm^{-1}; MS (CI) m/z 229 (M^++1, 100), 211 (34), 209 (16), 110 (50), and 109 (67). Found: m/z 228.0258. Calcd for $C_8H_5F_5O_2$: M, 228.0210.

4-Perfluoroethyl-1,2-benzenediol (9d). Colorless oil. ^{19}F NMR δ=85.14 (3F, t, J=3 Hz) and −113.13 (2F, m). MS (EI) m/z 228 (100), 208 (41), 180 (40), and 159 (64). Found: m/z 228.0237. Calcd for $C_8H_5F_5O_2$: M, 228.0210.

Treatment of Benzenediols 8a and 9a with Acetone: A mixture of (**8a** and **9a** obtained from 100 mg of **3a** and **5a** as described above was dissolved in acetone (10 ml) and refluxed for 3 d under a nitrogen atmosphere. The solvent was removed and the residue was chromatographed on silica gel (hexane–CH_2Cl_2/ether) to give **8a** (38 mg, 43%), **9a** (17 mg, 17%), and a mixture of **10** and **11**. Further separation of the last mixture on GPC gave 2 mg of **10** and 6 mg of **11**.

5-Perfluorooctyl-2,2-dimethyl-1,3-benzodioxole (10). Colorless crystals (dichloromethane/hexane), mp 58—59 °C. ^{1}H NMR δ=1.71 (6H, s), 6.80 (1H, d, J=8.2 Hz), 6.91 (1H, d, J=1.8 Hz), and 7.05 (1H, dd, J=8.2 and 1.8 Hz); ^{13}C NMR δ=25.87, 105—125 (8C), 106.94 (t, J=7 Hz), 108.07, 119.51, 121.08 (t, J=7 Hz), 121.65 (t, J=25 Hz), 147.78, and 150.42; ^{19}F NMR δ=−81.24 (3F, t, J=10 Hz), −109.51 (2F, t, J=15 Hz), −121.81 (2F, m), −122.28 (6F, m), −123.21 (2F, m), and −126.59 (2F, m); IR (KBr) 3004m, 1634m, 1614m, 1512s, 1454s, 1372s, 1330s, and 1300—1100vs cm^{-1}; MS (EI) m/z 568 (M^+, 51), 553 (100), 549 (5), 199 (51), and 159 (40).

5-Perfluorooctyl-2-methyl-2-(2-methyl-1-propenyl)-1,3-benzodioxole (11). Colorless crystals (dichloromethane/hexane), mp 100—101 °C. ^{1}H NMR δ=1.76 (3H, s), 1.78 (3H, d, J=1.5 Hz), 1.83 (3H, d, J=1.5 Hz), 5.50 (1H, m), 6.81 (1H, d, J=8.2 Hz), 6.93 (1H, d, J=1.8 Hz), and 7.05 (1H, dd, J=8.2 and 1.8 Hz); ^{13}C NMR δ=19.15, 26.64, 105—125 (8C), 106.87 (t, J=7 Hz), 107.99, 118.36, 121.11 (t, J=7 Hz), 121.64 (t, J=25 Hz), 123.94 (m), 140.68 (m), 147.70, and 150.33; ^{19}F NMR δ=−81.26 (3F, t, J=10 Hz), −110.11 (2F, t, J=14 Hz), −121.80 (2F, m), −122.40 (6F, m), −123.22 (2F, m), and −126.62 (2F, m); IR (KBr) 2984m, 2932s, 1678m, 1504vs, 1452vs, 1372s, 1300—1100vs cm^{-1}; MS (EI) 608 (M^+, 100), 593 (99), 589 (15), 565 (43), and 553 (32).

This work is partially supported by a Grant-in-Aid for Scientific Research No. 02750619 from the Ministry of Education, Science and Culture. We thank Dr. Kazuhiro Shimokawa (Daikin Kogyo Co. Ltd.) for a generous gift of perfluoroalkyl iodides.

References

1) J. F. M. McOmie and J. M. Blatchly, *Org. React.*, **19**, 199 (1972).

2) A. Planas, J. Tomas, and J. -J. Bonet, *Tetrahedron Lett.*, **28**, 471 (1987), and references cited therein.

3) W. Metlesics, F. Wesseley, and H. Budzikiewicz, *Tetrahedron*, **6**, 345 (1959).

4) S. Goodwin and B. Witkop, *J. Am. Chem. Soc.*, **79**, 179 (1957); E. Hecker and E. Meyer, *Chem. Ber.*, **97**, 1926 and 1940 (1964).

5) H. Budzikiewicz and J. Gunawan, *Z. Naturforsch., B*, **30**, 437 (1975); H. Budzikiewicz and J. Gunawan, *Monatsh. Chem.*, **104**, 876 (1973).

6) G. G. I. Moore and A. R. Kirk, *J. Org. Chem.*, **44**, 925 (1979).

7) H. Suzuki, Y. Shiraishi, K. Shimokawa, and H. Uno, *Chem. Lett.*, **1988**, 127.

8) C. Zhao, G. M. El-Taliawi, and C. Walling, *J. Org. Chem.*, **48**, 4908 (1983); M. Yoshida, H. Amemiya, M. Kobayashi, H. Sawada, H. Hagii, and K. Aoshima, *J. Chem. Soc., Chem. Commun.*, **1985**, 234; H. Sawada, M. Yoshida, H. Hagii, K. Aoshima, and M. Kobayashi, *Bull. Chem. Soc. Jpn.*, **59**, 215 (1986); G. V. D. Tiers, *J. Am. Chem. Soc.*, **82**, 5513 (1960); A. B. Cowell and C. Tamborski, *J. Fluorine Chem.*, **17**, 345 (1981); C. Wakselman and M. Tordeux, *J. Chem. Soc., Chem. Commun.*, **1987**, 1701; K. M. Yagupolskii, I. I. Maletina, N. V. Kondratenko, and V. V. Orda, *Synthesis*, **1978**, 835; T. Umemoto, Y. Kuriu, and H. Shuyama, *Chem. Lett.*, **1981**, 1663.

9) H. Uno, Y. Shiraishi, and H. Suzuki, *Bull. Chem. Soc. Jpn.*, **62**, 2636 (1989).

10) P. G. Gassman and N. J. O'Reilly, *J. Org. Chem.*, **52**, 2481 (1987).

11) G. P. Stahly and D. R. Bell, *J. Org. Chem.*, **54**, 2873 (1989).

12) J. Thiele and F. Gunther, *Ann.*, **349**, 45 (1906).

13) K. Ogura and G. -i. Tsuchihashi, *Tetrahedron Lett.*, **1971**, 3151.

14) L. F. Fieser and C. K. Bradsher, *J. Am. Chem. Soc.*, **61**, 417 (1939).

15) K. M. Koshy and T. T. Tidwell, *J. Am. Chem. Soc.*, **102**, 1261 (1980); M. N. Paddon-Row, C. Santiago, and K. N. Houk, *ibid.*, **102**, 6561 (1980).

Reactions of Methoxynaphthalenes with Active Methylene Compounds in the Presence of Manganese(III) Acetate

Katsunori TSUNODA, Mitsuyoshi YAMANE, Hiroshi NISHINO, and Kazu KUROSAWA*
Department of Chemistry, Faculty of Science, Kumamoto University,
Kurokami 2-39-1, Kumamoto 860
(Received September 12, 1990)

The reaction of methoxynaphthalenes with malonamide in the presence of magnanese(III) acetate gives 2-acetoxy-2-(1-naphthyl)propanediamides and 2-hydroxy-2-(1-naphthyl)propanediamides. It was found that the propanediamidation reaction did occur when naphthalenes have electron-donating substituents, such as a methoxyl group. The reactions of methoxynaphthalenes with ethyl 3-oxobutanoate, 2-cyanoacetamide, and malononitrile in the presence of manganese(III) acetate also yielded the corresponding substituted naphthalenes, ethyl 2-(acetoxymethyl)naphtho[2,1-*b*]furan-1-carboxylates, and/or a 4-methylene-1(4*H*)-naphthalenone. The reaction mechanisms are discussed.

Although the reactions of alkenes with active methylene compounds in the presence of manganese(III) acetate have been well documented,[1] the reaction of aromatic substrates with manganese(III) acetete–active methylene compounds has received less attention than alkenes, probably because of the lower reactivity of the aromatic compounds towards the reagents. The authors have reported that the reactions of naphthalenes, anthracene, and other aromatic substrates with tris(2,4-pentanedionato)manganese(III), and with malonic acid in the presence of manganese(III) acetate,[2] gave diacetylmethylated arenes[3] and formylated arenes,[4] respectively. Citterio et al.[5,6] have also reported that the reactions of alkoxynaphthalenes with diethyl malonates, ethyl 3-oxobutanoate and ethyl 2-cyanoacetate in the presence of manganese(III) acetate gave aromatic substitution products. In view of the potential synthetic utility of these reactions, which could functionalize aromatic compounds, we then investigated the reactions involved in incorporating other carbonyl functions into naphthalenes and other aromatic substrates. We describe here the reactions of methoxy-substituted naphthalenes with malonamide, ethyl 3-oxobutanoate, 2-cyanoacetamide, and malononitrile in the presence of manganese(III) acetate.

Results

2,7-Dimethoxynaphthalene (**1a**) was selected as an aromatic substrate in a reaction aimed at optimizing the reaction conditions since the reaction products could be readily separated and characterized by spectroscopic methods. The reaction of **1a** with malonamide in the presence of manganese(III) acetate gave an acetate (**2a**) as the major product after purification on preparative TLC. The ^{1}H NMR spectrum of **2a** ($C_{17}H_{18}N_2O_6$ based on elemental analysis and M^+=346 in the MS spectrum) exhibited an AB (δ_A=7.24 and δ_B=7.86, J_{AB}=8.79 Hz) and an ABC spin system (δ_A=7.03, δ_B=7.42, δ_C=7.78, J_{AB}=2.20, J_{AC}=7.89, J_{BC}=0 Hz) due to aromatic protons. The J value for the AB spin system indicated the presence of H-3 and H-4. The peaks at δ=2.38 (3H, singlet), 3.76 (3H, singlet), and 3.79 (3H, singlet) are assigned to an acetoxyl group and two methoxyl groups, respectively. There are four peaks at δ=6.86, 7.87, 7.95, and 9.66 assigned to two NH_2, which disappeared upon deuteration. The IR spectrum showed absorptions at 1685 and 3100—3500 cm^{-1} due to amide functions. These spectral properties indicate the structure of 2-acetoxy-2-(2,7-dimethoxy-1-naphthyl)-propanediamide for **2a**. There was a minor product (**3a**) which showed an ^{1}H NMR spectrum similar to that of **2a**, except for the presence of a hydroxyl group and

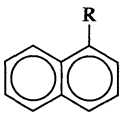

1 : R=H
2 : R=C(OAc)($CONH_2$)$_2$
3 : R=C(OH)($CONH_2$)$_2$
4 : R=C(OAc)($COCH_3$)CO_2Et
7 : R=C(OAc)(CN)$CONH_2$

a : 2,7-(OMe)$_2$
b : 4-OMe
c : 2-OMe
d : 2,6-(OMe)$_2$
e : 4,6-(OMe)$_2$
f : 6,7-(OMe)$_2$

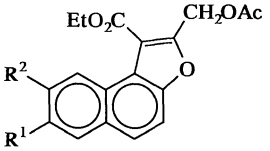

5a : R^1=H, R^2=OMe
5c : R^1=R^2=H
5d : R^1=OMe, R^2=H

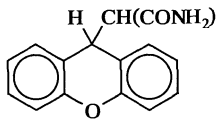

6

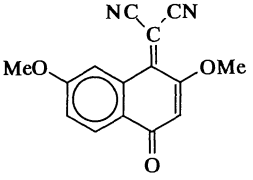

8

Fig. 1.

Table 1. Reactions of Methoxynaphthalenes with Active Methylene Compounds in the Presence of Manganese(III) Acetate in Acetic Acid[a]

Entry	Substrate	Active methylene	Molar ratio[b]	Time	Composition of products (%)[c]				
				min	Substrate	Acetate	Alcohol	Furan	Others
1	**1a**	$CH_2(CONH_2)_2$	1:8:8	3	**1a** (4)	**2a** (52)	**3a** (19)		
2	**1a**	$CH_2(CONH_2)_2$	1:8:8[d]	3		**2a** (61)	**3a** (7)		
3	**1b**	$CH_2(CONH_2)_2$	1:8:8	3	**1b** (3)	**2b** (38)	**3b** (10)[e]		
4	**1c**	$CH_2(CONH_2)_2$	1:8:8	3	**1c** (5)	**2c** (55)	**3c** (9)[e]		
5	**1d**	$CH_2(CONH_2)_2$	1:8:8	3	**1d** (15)	**2d** (37)	**3d** (9)		
6	**1e**	$CH_2(CONH_2)_2$	1:8:8	3	**1e** (6)	**2e** (17)	**3e** (8)[e]		
7	**1f**	$CH_2(CONH_2)_2$	1:8:8	3	**1f** (19)	**2f** (35)	**3f** (22)		
8	**1a**	$CH_3COCH_2CO_2Et$	1:4:12	15	**1a** (4)	**4a** (46)		**5a** (2)	
9	**1c**	$CH_3COCH_2CO_2Et$	1:4:12	5		**4c** (49)		**5c** (12)	
10	**1d**	$CH_3COCH_2CO_2Et$	1:4:12	3		**4d** (19)		**5d** (11)	
11	**1a**	$NCCH_2CONH_2$	1:8:8	3		**7a** (25)			
12	**1a**	$CH_2(CN)_2$	1:8:8	3	**1a** (44)				**8** (9)

a) The reactions were carried out at the reflux temperature. b) Substrate : active methylene compound : Mn(III). c) Isolated yield based on the amount of substrate added. d) Ac_2O (2 cm^3) was added. e) Yield was estimated from the ^1H NMR spectra.

the absence of an acetoxyl group. The structure was then assigned to be 2-hydroxy-2-(2,7-dimethoxy-1-naphthyl)propanediamide (**3a**) (Fig. 1).

The reaction was carried out at various molar ratios of **1a**: malonamide: manganese(III); we found that the reaction at a molar ratio of 1:8:8 at the reflux temperature for 3 min gave the maximum yield for **2a** (Table 1, Entry 1). The reactions were then examined for 1-methoxynaphthalene (**1b**), 2-methoxynaphthalene (**1c**), 2,6-dimethoxynaphthalene (**1d**), 1,7-dimethoxynaphthalene (**1e**), and 2,3-dimethoxynaphthalene (**1f**) at a molar ratio of 1:8:8 at reflux temperature for 3 min. The results are shown in Table 1. The 2-hydroxy derivatives were not always obtained as a pure substance because of contamination with the acetates. The yields of some 2-hydroxy derivatives (**3b**, **3c**, **3e**) were estimated from the intensities of the hydroxyl group in **3** and the acetoxyl group in **2**, which are well separated from the other signals in their ^1H NMR spectra. In order to prevent the formation of the 2-hydroxy derivative (**3a**), a reaction was conducted which added acetic anhydride. The yield of **2a** was slightly improved (by 9%) at the expense of **3a**; the yield of which was lowered by 12% (Entry 2). It was shown that an aromatic ring having a methoxyl group in naphthalene is always active towards the reaction, except for **1f** (2,3-dimethoxynaphthalene). In the case of **1f**, the propanediamide moiety is introduced into the unsubstituted ring. The reaction of unsubstituted naphthalene with manganese(III) acetate–$CH_2(CONH_2)_2$ gave a small amount of products along with the unchanged material. The products could not be characterized. The reactions of anthracene and pyrene also gave a complex mixture which could not be identified.

We then looked into the reactions of 2,7-dimethoxynaphthalene (**1a**), 2-methoxynaphthalene (**1c**), and 2,6-dimethoxynaphthalene (**1d**), with ethyl 3-oxobutanoate in the presence of manganese(III) acetate that gave ethyl 2-acetoxy-2-(1-naphthyl)-3-oxobutanoates (**4a**, **4c**, **4d**) and ethyl 2-(acetoxymethyl)naphtho[2,1-*b*]-furan-1-carboxylates (**5a**, **5c**, **5d**) (Entries 8—10). The isolated yield of **4c** (ethyl 2-acetoxy-2-(2-methoxy-1-naphthyl)-3-oxobutanoate) was better than the yield (20%) reported by Citterio et al.,[5] who obtained **4c** in a reaction at 80 °C. The IR and ^1H NMR spectra of compound **5d**, which has a molecular formula $C_{19}H_{18}O_6$ (analysis and M^+=342), indicated the presence of 1,2,6-trisubstituted naphthalene, a methoxy group (δ=3.90 (3H, s)), an ethoxycarbonyl group (1710 cm^{-1}, δ=4.50 (2H, q) and δ=1.45 (3H, t)), an acetoxyl group (1732 cm^{-1}, δ=2.12 (3H, s)), and a methylene group (δ=5.52 (2H, s)). The ^{13}C NMR spectrum showed two methylene groups at δ=58.297, 61.374 that finally confirmed the structure of ethyl 2-(acetoxymethyl)-7-methoxynaphtho[2,1-*b*]furan-1-carboxylate for **5d**. The structures of **5a** and **5c** were similarly determined on the basis of the presence of acetoxymethyl group in their ^1H NMR spectra. The reactions of **1a** with 2-cyanoacetamide, and malononitrile in the presence of manganese(III) acetate at a molar ratio of 1:8:8 at reflux temperature were also carried out (Entries 11, 12). The products were found to be 2-acetoxy-2-cyano-(2,7-dimethoxy-1-naphthyl)acetamide (**7a**) and 4-(dicyanomethylene)-3,6-dimethoxy-1(4*H*)-naphthalenone (**8**). The yields were rather poor and much of the unchanged **1a** was recovered in the reaction of malononitrile.

Discussion

It has been reported that diacetylmethylation using tris(2,4-pentanedionato)manganese(III) (abbreviated [Mn(acac)$_3$]) is effective when the ionization potential of the aromatic compound is lower than 8.28 eV.[3] The reaction could be accounted for in terms of a radical reaction initiated by the diacetylmethyl radical, ·CH-

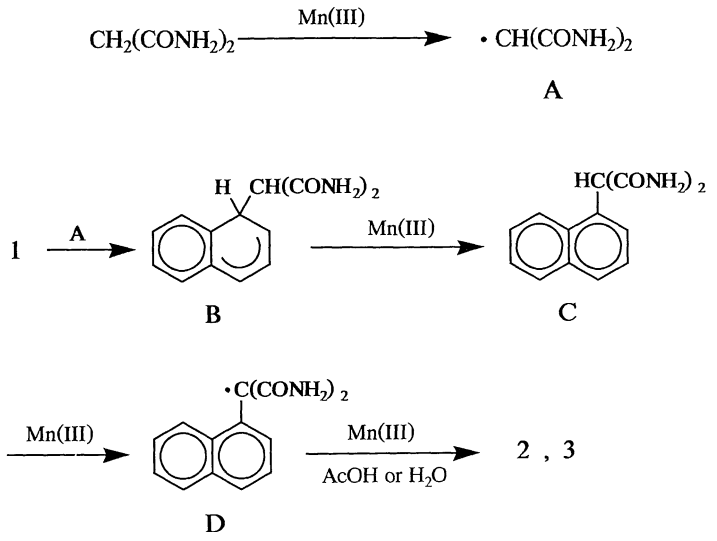

Scheme 1.

$(COCH_3)_2$, which is formed by the thermal decomposition of [Mn(acac)3], and subsequently attacks the aromatic nucleus, followed by further oxidation by [Mn(acac)3] to give products.[3] In an analogy to the above-mentioned mechanism, the reaction of aromatic compounds with malonamide in the presence of manganese(III) acetate could be envisaged as being initiated by a propanediamide radical, $\cdot CH(CONH_2)_2$ (**A**), which is formed by an interaction with manganese(III) acetate and $CH_2(CONH_2)_2$. In an attempt to obtain information concerning the complex formation between Mn(III) and $CH_2(CONH_2)_2$ though the visible spectra of manganese(III) acetate in AcOH were taken in both the presence and absence of three equivalents of $CH_2(CONH_2)_2$ at room temperature, no appreciable change could be observed. However, the formation of **A** was substantiated by the fact that xanthene gave a 2-(9-xanthenyl)propanediamide (**6**) in 81% yield when treated with manganese(III)–$CH_2(CONH_2)_2$ (Fig. 1). The propanediamide radical (**A**) seems to have an electrophilic nature as well as do $\cdot CH_2CO_2H$ and other radicals which have carbonyl functions attached to the radical carbon. Thus, **A** attacks the α-position in naphthalenes to give radicals (**B**), which could be subsequently oxidized with excess manganese(III) acetate present in the oxidation system to give 2-(1-naphthyl)propanediamide (**C**). Compound **C** could not be isolated, probably because **C** has a hydrogen on a tertiary carbon which may more easily be oxidized than the methylene group in $CH_2(CONH_2)_2$ to give radical (**D**). Radical (**D**) is further oxidized to a corresponding cation, which takes up either an acetate ion or water to yield **2** and **3**, respectively (Scheme 1). The acetate (**2a**) was fairly stable and could not be hydrolyzed, even with 50% aqueous acetic acid containing a small amount of hydrochloric acid at room temperature for 12 h. It is therefore reasonable to assume that **3a** was not formed from **2a** by hydrolysis during the work-up but, rather, was formed from the intermediate **D** and water contained in the reaction medium.

The formation of ethyl 2-(acetoxymethyl)naphtho-[2,1-*b*]furan-1-carboxylates (**5a**, **5c**, and **5d**) in the reactions of methoxynaphthalenes (**1a**, **1c**, and **1d**) with ethyl 3-oxobutanoate reveals another interesting feature of the reaction. The removal of the methoxyl group has been observed in the reactions of 2-hydroxy-2′-methoxybenzophenones with manganese(III) acetate that yielded 9-xanthenones,[7] and in the reaction of **1c** (2-methoxynaphthalene) with dimethyl malonate.[6] The formation of **5a**, **5c**, and **5d** could be accounted for by the fact that the substituted product (**E**) was cyclized to give **F**, which was subsequently acetoxylated with manganese(III) acetate (Scheme 2). The intermediates, **E** and **F**, could not be isolated from the reaction mixture, probably because we were using excess manganese(III) acetate (1:12 molar equivalent ratio).

The reactions of **1a** (2,7-dimethoxynaphthalene)

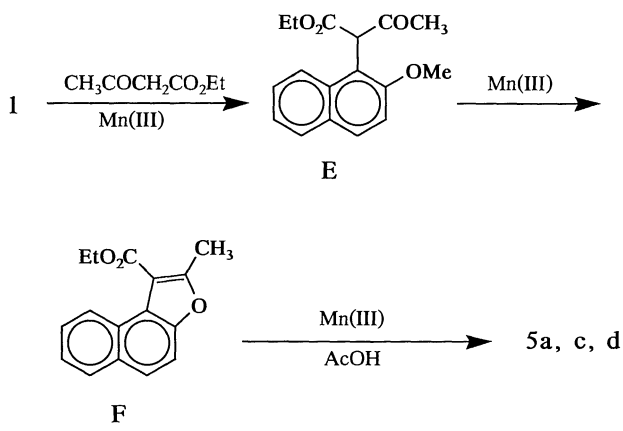

Scheme 2.

with 2-cyanoacetamide and malononitrile could also be accounted for by similar mechanisms initiated with the $\cdot CH(CN)CONH_2$ and $\cdot CH(CN)_2$ radical, respectively. The low yields are probably due to the less reactive nature of 2-cyanoacetamide and malononitrile than malonamide towards manganese(III) acetate.

It can thus be concluded that a radical substitution reaction occurred only at the α-position and that the substitution reaction occurs at the unsubstituted nucleus in the case of **1f** (2,3-dimethoxynaphthalene) that may be due to a steric hindrance caused by the two methoxyl groups at the C-2 and C-3 position. It should be emphasized that this new direct incorporation of C_3 and C_4 units using manganese(III) acetate–active methylene compounds takes place in the electron-rich aromatic compounds having such an electron-donating group as the methoxyl group. These reactions could be utilized in organic syntheses.

Experimental

Measurements. All the ^1H and ^{13}C NMR spectra were taken with JNM PMX-60SI (60 MHz), JNM EX-90 (90 MHz for ^1H and 22.4 MHz for ^{13}C), and JNM GX-400 (400 MHz) FT NMR spectrometers with tetramethylsilane used as the internal standard. The IR spectra were measured on a JASCO A-102 IR spectrometer. The mass spectra were obtained on a JMS-DX303 HF mass spectrometer using a direct-insertion probe at an ionizing voltage of 70 eV. The melting points were determined with a Yanagimoto micro-melting point apparatus.

Materials. Methoxynaphthalenes (**1a—f**) were synthesized by the methylation of the corresponding naphthols with dimethyl sulfate. The other aromatic compounds were commercially available. Manganese(III) acetate was prepared by a method described in the literature.[8]

Reaction of Aromatic Compounds with Malonamide in the Presence of Manganese(III) Acetate. The typical procedure for the reaction of aromatic compounds with malonamide in the presence of manganese(III) acetate was as follows. To a heated solution of an aromatic compound (1 mmol) and malonamide (8 mmol) in acetic acid (30 cm^3), manganese(III) acetate (1.98 g, 8 mmol as Mn(III)) was added. The reaction mixture was heated under reflux until the dark-brown color of the solution turned opaque white. The solvent was then removed in vacuo, and the residue triturated with 2 M (1 M=1 mol dm^{-3}) hydrochloric acid (50 cm^3), followed by extraction with ethyl acetate. The solvent was removed again in vacuo and the products separated on a silica-gel plate while eluting with chloroform. Yields are summarized in Table 1.

Products. 2-Acetoxy-2-(2,7-dimethoxy-1-naphthyl)propanediamide (2a): Mp 184.5—185.5 °C (from chloroform–ethyl acetate); IR(KBr) ν 1685, 1726 ($-CONH_2$), 1755 (-OAc), 3100—3500 ($-NH_2$) cm^{-1} ; ^1H NMR (400 MHz, DMSO-d_6) δ=2.38 (3H, s, -OAc), 3.76 (3H, s, $-OCH_3$) 3.79 (3H, s, $-OCH_3$), 6.86 (1H, s, NH), 7.03 (1H, dd, J=7.89, 2.20 Hz, H-6), 7.24 (1H, d, J=8.79 Hz, H-3), 7.42 (1H, d, J=2.20 Hz, H-8), 7.78 (1H, d, J=7.89 Hz, H-5), 7.86 (1H, d, J=8.79 Hz, H-4), 7.87 (1H, s, -NH), 7.95 (1H, s, -NH), and 9.66 (1H, d, -NH); MS m/z (rel intensity)=346 [M^+] (100), 285 (100), 255 (44), 215 (67), 199 (51), and 185 (87). Found: C, 58.85; H, 5.25; N, 8.06%. Calcd for $C_{17}H_{18}O_6N_2$: C, 58.95; H, 5.24; N, 8.09%.

2-Hydroxy-2-(2,7-dimethoxy-1-naphthyl)propanediamide (3a): Mp 211—214 °C (from ethyl acetate); IR(KBr) ν 1705 ($-CONH_2$), 3100—3500 ($-NH_2$, -OH) cm^{-1}; ^1H NMR (400 MHz, DMSO-d_6) δ=3.80 (3H, s, $-OCH_3$) 3.82 (3H, s, $-OCH_3$), 6.07 (1H, br. s, -OH), 6.86—8.12 (4H, br. 2×$-NH_2$), 7.07 (1H, dd, J=8.6, 2.0 Hz, H-6), 7.26 (1H, d, J=9.0 Hz, H-3), 7.51 (1H, d, J=2.2 Hz, H-8), 7.81 (1H, d, J=8.6 Hz, H-5), and 7.88 (1H, d, J=9.0 Hz, H-4). Found: C, 59.30; H, 5.29; N, 9.30%. Calcd for $C_{15}H_{16}N_2O_5$: C, 59.20; H, 5.30; N, 9.21%.

2-Acetoxy-2-(4-methoxy-1-naphthyl)propanediamide (2b): Mp 196.5—197.5 °C (from chloroform–ethyl acetate); IR (KBr) ν 1682 ($-CONH_2$), 1763 (-OAc), 3100—3500 ($-NH_2$) cm^{-1}; ^1H NMR (400 MHz, DMSO-d_6) δ=2.34 (3H, s, OAc), 3.97 (3H, s, $-OCH_3$), 6.95 (1H, d, J=8.43 Hz, H-3), 7.01 (1H, s, -NH), 7.38 (1H, d, J=8.42 Hz, H-4), 7.47—7.54 (2H, m, H-6, H-7), 7.70 (1H, s, -NH), 8.02 (1H, s, -NH), 8.10—8.12 (1H, dd, H-5), 8.20—8.22 (1H, dd, H-8), and 10.25 (1H, s, -NH); MS m/z (rel intensity) 316 [M^+] (13), 272 (13), 255 (37), 231 (19), and 185 (100). Found: m/z 316.1054. Calcd for $C_{16}H_{16}O_5N_2$: M, 316.1059.

2-Acetoxy-2-(2-methoxy-1-naphthyl)propanediamide (2c): Mp 205 — 206 °C (from chloroform–ethyl acetate); IR(KBr) ν 1691 ($-CONH_2$), 1766 (-OAc), 3100 — 3500 ($-NH_2$) cm^{-1}; ^1H NMR (400 MHz, DMSO-d_6) δ=2.08 (3H, s, OAc), 3.82 (3H, s, $-OCH_3$), 7.30 — 7.45 (7H, m, 2×$-NH_2$, 3×arom. H), 7.81 — 7.83 (1H, dd, H-5), 7.93 (1H, d, J=8.79 Hz, H-4), and 8.35 — 8.37 (1H, dd, H-8). Found: C, 60.66; H, 5.14; N, 8.86%. Calcd for $C_{16}H_{16}O_6N_2$: C, 60.75; H, 5.10; N, 8.86%.

2-Acetoxy-2-(2,6-dimethoxy-1-naphthyl)propanediamide (2d): Mp 199 — 200 °C (from chloroform–ethyl acetate); IR(KBr) ν 1690 ($-CONH_2$), 1730 (-OAc), 3100 — 3500 ($-NH_2$) cm^{-1}; ^1H NMR (400 MHz, DMSO-d_6) δ=2.37 (3H, s, -OAc), 3.74 (3H, s, $-OCH_3$), 3.83 (3H, s, $-OCH_3$) 6.87 (1H, s, -NH), 7.10 (1H, dd, J=9.53, 2.93 Hz, H-7), 7.30 (1H, d, J=2.57 Hz, H-5), 7.37 (1H, d, J=8.80 Hz, H-3), 7.72 (1H, s, -NH), 7.85 (1H, d, J=7.89 Hz, H-4), 7.96 (1H, d, J=9.16 Hz, H-8), 8.31 (1H, s, -NH), and 9.65 (1H, s, -NH). Found: C, 58.81; H, 5.24; N, 8.06%. Calcd for $C_{17}H_{18}O_6N_2$: C, 58.95; H, 58.24; N, 8.09%.

2-Hydroxy-2-(2,6-dimethoxy-1-naphthyl)propanediamide (3d): Mp 228 — 230 °C (from ethyl acetate); IR(KBr) ν 1670, 1687 ($-CONH_2$), 3100 — 3500 ($-NH_2$, -OH) cm^{-1}; MS m/z (rel intensity)=304 [M^+] (46), 261 (49), 215 (100), 201 (18), and 157 (23). Found: m/z 304.1032. Calcd for $C_{15}H_{16}O_5N_2$: M, 304.1059.

2-Acetoxy-2-(4,6-dimethoxy-1-naphthyl)propanediamide (2e): Mp 187—188 °C (from chloroform–ethyl acetate); IR(KBr) ν 1690, 1712 ($-CONH_2$), 1730 (-OAc), 3100—3500 ($-NH_2$) cm^{-1}; ^1H NMR (400 MHz, DMSO-d_6) δ=2.33 (3H, s, -OAc),3.86 (3H, s, $-OCH_3$), 3.97 (3H, s, $-OCH_3$), 6.90 (1H, d, J=8.06 Hz, H-2), 6.98 (1H, s, -NH), 7.18 (1H, d, J=9.15 Hz, H-8), 7.19 (1H, dd, J=9.16, 2.93 Hz, H-7), 7.39 (1H, d, J=8.06 Hz, H-3), 7.51 (1H, d, J=2.93 Hz, H-5), 7.59 (1H, s, -NH), 7.74 (1H, s, -NH), and 9.86 (1H, s, -NH). Found: C, 58.66; H, 5.28; N, 8.00%. Calcd for $C_{17}H_{18}O_6N_2$: C, 58.95; H, 5.24; N, 8.09%.

2-Acetoxy-2-(6,7-dimethoxy-1-naphthyl)propanediamide (2f): Mp 215—216 °C (from chloroform–ethyl acetate); IR(KBr) ν 1680 ($-CONH_2$), 1738 (-OAc), 3100—3500 ($-NH_2$) cm^{-1}; ^1H NMR (400 MHz, DMSO-d_6) δ=2.21 (3H, s, -OAc),

3.82 (6H, s, 2×-OCH_3), 7.13—7.34 (2H, m, H-3, -NH), 7.32 (1H, s, H-5), 7.51—7.53 (1H, dd, H-2), 7.67 (1H, s, H-8), 7.75—7.79 (1H, dd, H-4), 7.92 (2H, s, 2×-NH), and 8.20 (1H, s, -NH); MS *m/z* (rel intensity) 346 [M^+] (70), 304 (44), 285 (100), 261 (100), 216 (100), and 188 (90). Found: *m/z* 346.1141. Calcd for $C_{17}H_{18}O_6N_2$: M, 346.1165.

2-Hydroxy-2-(6,7-dimethoxy-1-naphthyl)propanediamide (3f): Mp 229.5—230.5 °C (from chloroform–ethyl acetate); IR(KBr) ν 1680 (-$CONH_2$), 3100—3500 (-NH, -OH) cm^{-1}; ^1H NMR (400 MHz, DMSO-d_6) δ=3.81 (3H, s, -OCH_3) 3.87 (3H, s, -OCH_3), 6.21 (1H, s, -OH), 7.25 (1H, t, *J*=7.33 Hz, H-3), 7.27—7.29 (1H, dd, H-2), 7.28 (1H, s, -NH), 7.31 (1H, s, H-5), 7.58 (1H, s, -NH), 7.62 (1H, s, H-8), 7.70—7.73 (1H, dd, H-4), and 7.93 (2H, s, -NH_2). MS *m/z* (rel intensity) 304 [M^+] (100), 285 (34), 261 (100), 216 (100), and 188 (100). Found: *m/z* 304.1050. Calcd for $C_{15}H_{16}O_5N_2$: M, 304.1069.

Reaction of Xanthene with Malonamide in the Presence of Manganese(III) Acetate. To a heated solution of xanthene (1 mmol) and malonamide (8 mmol) in acetic acid (30 cm^3), manganese(III) acetate (8 mmol as Mn(III)) was added. The reaction mixture was heated under reflux for 1 min. The solvent was removed under reduced pressure and the residue treated with 2 M hydrochloric acid (50 cm^3). The precipitate was collected and recrystallized from a mixture of chloroform and ethyl acetate to give 9-xanthenone (11%) and 2-(9-xanthenyl)propanediamide (**6**) (81%): Mp 281—282 °C; IR(KBr) ν 1675 (-$CONH_2$), 3100—3500 (-NH_2) cm^{-1}; ^1H NMR (60 MHz, DMSO-d_6) δ=3.10 (1H, d, *J*=10.8 Hz, >CH-), 4.60 (1H, d, *J*=10.8 Hz, >CH-), and 6.87—7.41 (12H, m, 2×-NH_2, arom. H). Found: C, 67.81; H, 5.05; N, 9.84%. Calcd for $C_{16}H_{14}O_3N_2$: C, 68.07; H, 5.00; N, 9.92%.

Reactions of Methoxynaphthalenes (1a, 1c, and 1d) with Ethyl 3-Oxobutanoate in the Presence of Manganese(III) Acetate. A mixture of a methoxynaphthalene (1 mmol), ethyl 3-oxobutanoate (4 mmol), and manganese(III) acetate (12 mmol for Mn(III)) in acetic acid (30 cm^3) was heated under reflux until the dark-brown color of the solution turned colorless. The reaction mixture was poured into water (50 cm^3) and then extracted with chloroform (50 cm^3). The chloroform and the unchanged ethyl 3-oxobutanoate was removed under reduced pressure; the residue was then chromatographed on a silica-gel plate while eluting with chloroform. The products were further purified by repeated TLC or by recrystallization.

Products. Ethyl 2-Acetoxy-2-(2,7-dimethoxy-1-naphthyl)-3-oxobutanoate (4a): Liquid; IR($CHCl_3$) ν 1720, 1743, 1750 (≥C=O) cm^{-1}; ^1H NMR (60 MHz, $CDCl_3$) δ=1.28 (3H, t, *J*=7.0 Hz, -$OCH_2\underline{CH_3}$), 2.20 (3H, s, -$COCH_3$), 2.28 (3H, s, -$COCH_3$), 3.83 (3H, s, -OCH_3) 3.87 (3H, s, -OCH_3), 4.30 (2H, q, *J*=7.0 Hz, -$O\underline{CH_2}CH_3$), 6.98 (1H, dd, *J*=9.0, 2.0 Hz, H-6), 7.10 (1H, d, *J*=9.0 Hz, H-3), 7.42 (1H, d, *J*=2.0 Hz, H-8), 7.62 (1H, d, *J*=9.0 Hz, H-4 or H-5), and 7.74 (1H, d, *J*=9.0 Hz, H-5 or H-4). MS *m/z* (rel intensity) 374 [M^+] (8), 332 (19), 289 (13), and 215 (100). Found: *m/z* 374.1330. Calcd for $C_{20}H_{22}O_7$: M, 374.1366.

Ethyl 2-(Acetoxymethyl)-8-methoxynaphtho[2,1-*b*]furan-1-carboxylate (5a): Mp 92—93 °C (from ethanol); IR ($CHCl_3$) ν 1717 (-CO_2Et), 1742 (-OAc) cm^{-1}; ^1H NMR (90 MHz, $CDCl_3$) δ=1.463 (3H, t, *J*=7.03 Hz, -$OCH_2\underline{CH_3}$), 2.148 (3H, s, -OAc), 3.996 (3H, s, -OCH_3) 4.511 (2H, q, *J*=7.03 Hz, -$O\underline{CH_2}CH_3$), 5.559 (2H, s, -CH_2-), 7.170 (1H, dd, *J*=9.09, 2.49 Hz, H-7), 7.474 (1H, d, *J*=9.09 Hz, H-4 or H-5), 7.735 (1H, d, *J*=9.09 Hz, H-5 or H-4), 7.826 (1H, d, *J*=9.09 Hz, H-6), and 8.691 (1H, d, *J*=2.49 Hz, H-9). MS *m/z* (rel intensity) 342 [M^+] (100), 283 (20), 255 (33), 254 (24), and 253 Found: *m/z* 342.1085. Calcd for $C_{19}H_{18}O_6$: M, 342.1104.

Ethyl 2-Acetoxy-2-(2-methoxy-1-naphthyl)-3-oxobutanoate (4c): Mp 146—147 °C (from ethanol); IR($CHCl_3$) ν 1720, 1742, 1750 (>C=O) cm^{-1}; ^1H NMR (60 MHz, $CDCl_3$) δ=1.28 (3H, t, *J*=7.0 Hz, -$OCH_2\underline{CH_3}$), 2.20 (3H, s, -$COCH_3$), 2.28 (3H, s, -$COCH_3$), 3.91 (3H, s, -OCH_3), 4.17 (2H, q, *J*=7.0 Hz, -$O\underline{CH_2}CH_3$), 7.27 (1H, d, *J*=9.0 Hz, H-3), 7.87 (1H, d, *J*=9.0 Hz, H-4), and 7.3—8.2 (4H, m, H-5—H-8). MS *m/z* (rel intensity) 344 [M^+] (21), 302 (63), 260 (17), 259 (22), 256 (23), 229 (18), 214 (27), 187 (27), 186 (26), and 185 (100). Found: C, 66.23; H, 5.84%. Calcd for $C_{19}H_{20}O_6$: C, 66.27; H, 5.85%.

Ethyl 2-(Acetoxymethyl)naphtho[2,1-*b*]furan-1-carboxylate (5c): Colorless liquid; IR($CHCl_3$) ν 1722 (-CO_2Et), 1745 (-OAc) cm^{-1}; ^1H NMR (60 MHz, $CDCl_3$) δ=1.46 (3H, t, *J*=7.0 Hz, -$OCH_2\underline{CH_3}$), 2.13 (3H, s, -OAc), 4.53 (2H, q, *J*=7.0 Hz, -$O\underline{CH_2}CH_3$), 5.56 (2H, s, -CH_2-), 7.4—8.1 (5H, m, H-4—H-8), and 9.15 (1H, m, H-9). MS *m/z* (rel intensity) 312 [M^+] (95), 270 (38), 269 (28), 253 (22), 225 (30), 224 (30), and 223 (100). Found: *m/z* 312.1002. Calcd for $C_{18}H_{16}O_5$: M, 312.0998.

Ethyl 2-Acetoxy-2-(2,6-dimethoxy-1-naphthyl)-3-oxobutanoate (4d): Liquid; IR($CHCl_3$) ν 1725, 1745, 1760 (>C=O) cm^{-1}; ^1H NMR (60 MHz, $CDCl_3$) δ=1.29 (3H, t, *J*=7.0 Hz, -$OCH_2\underline{CH_3}$), 2.20 (3H, s, -$COCH_3$), 2.29 (3H, s, -$COCH_3$), 3.87 (6H, s, 2×-OCH_3), 4.33 (2H, q, *J*=7.0 Hz, -$O\underline{CH_2}CH_3$), 7.0—7.2 (2H, m, H-5, H-7), 7.22 (1H, d, *J*=9.0 Hz, H-3), 7.73 (1H, d, *J*=9.0 Hz, H-4), and 8.00 (1H, d, *J*=10.0 Hz, H-8). MS *m/z* (rel intensity) 374 [M^+] (36), 332 (66), 217 (31), 216 (21), and 215 (100). Found: *m/z* 374.1356. Calcd for $C_{20}H_{22}O_7$: M, 374.1366.

Ethyl 2-(Acetoxymethyl)-7-methoxynaphtho[2,1-*b*]furan-1-carboxylate (5d): Mp 112—113 °C (from ethanol); IR ($CHCl_3$) ν 1710 (-CO_2Et), 1732 (-OAc) cm^{-1}; ^1H NMR (60 MHz, $CDCl_3$), δ=1.45 (3H, t, *J*=7.0 Hz, -$OCH_2\underline{CH_3}$), 2.12 (3H, s, -OAc), 3.90 (3H, s, -OCH_3), 4.50 (2H, q, *J*=7.0 Hz, -$O\underline{CH_2}CH_3$), 5.52 (2H, s, -CH_3-), 7.18 (1H, d, *J*=2.0 Hz, H-6), 7.21 (1H, dd, *J*=8.2, 2.0 Hz, H-8), 7.53 (1H, d, *J*=9.0 Hz, H-4 or H-5), 7.62 (1H, d, *J*=9.0 Hz, H-5 or H-4), and 9.00 (1H, d, *J*=8.2 Hz, H-9); ^{13}C NMR (22.4 MHz, $CDCl_3$) δ=14.246 (1C, -$CH_2\underline{C}H_3$), 20.705 (1C, -$OCO\underline{C}H_3$), 55.269 (1C, -OCH_3), 58.297 (1C, -CH_2-), 61.370 (1C, -CH_2-), 107.868 (1C, =CH-), 112.239 (1C, =CH-), 114.730 (1C, =C-), 118.266 (1C, =CH<), 120.130 (1C, =C<), 122.845 (1C, =C<), 126.754 (1C, =CH-), 127.500 (1C, =CH-), 132.766 (1C, =C<), 151.502 (1C, =C<), 155.798 (1C, =C<), 156.947 (1C, =C<), 164.033 (1C, -$O\underline{C}OCH_3$), and 170.313 (1C, -$\underline{C}OOEt$). MS *m/z* (rel intensity) 342 [M^+] (88), 300 (19), 283 (20), 253 (100), and 215 (44). Found: C, 66.64; H, 5.27%. Calcd for $C_{19}H_{18}O_6$: C, 66.66; H, 5.30%.

Reactions of 2,7-Dimethoxynaphthalene (1a) with 2-Cyanoacetamide and Malononitrile in the Presence of Manganese(III) Acetate. Reactions of **1a** with the active methylene compounds in the presence of manganese(III) acetate were carried out in a manner similar to that of malonamide at a molar ratio of 1:8:8.

Products. 2-Acetoxy-2-cyano-2-(2,7-dimethoxy-1-naphthyl)acetamide (7a): Mp 169 °C (from ethanol); IR($CHCl_3$) ν 1708 (-$CONH_2$), 1765 (-OAc), 2230 (C≡N) cm^{-1}; ^1H NMR

(400 MHz, $CDCl_3$) δ=2.15 (3H, s, -OAc), 3.84 (3H, s, $-OCH_3$), 3.94 (3H, s, $-OCH_3$), 7.08 (1H, dd, J=8.79, 2.20 Hz, H-6), 7.31 (1H, d, J=8.80 Hz, H-3), 7.46 (1H, d, J=2.20 Hz, H-8), 7.81 (1H, d, J=8.79 Hz, H-5), 7.93 (1H, d, J=8.79 Hz, H-4), 8.18 (1H, s, -NH), and 8.39 (1H, s, -NH). MS m/z (rel intensity) 328 [M^+] (21), 301 (10), 285 (9), 242 (39), 226 (13), and 215 (100). Found: C, 62.21; H, 4.89; N, 8.52%. Calcd for $C_{17}H_{16}O_5N_2$: C, 62.19; H, 4.91; H, 8.53%.

4-Dicyanomethylene-3,6-dimethoxy-1(4*H*)-naphthalenone (8): Mp 166—167 °C (from ethanol); IR($CHCl_3$) ν 1618 (C=C), 1676 (>C=O), 2220 (C≡N) cm^{-1}; ^1H NMR (60 MHz, $CDCl_3$) δ=3.95 (3H, s, $-OCH_3$) 3.98 (3H, s, $-OCH_3$), 6.84 (1H, s, =CH-), 7.20 (1H, dd, J=9.0, 2.4 Hz, H-7), 7.72 (1H, d, J=2.4 Hz, H-5), and 8.73 (1H, d, J=9.0 Hz, H-8). Found: C, 67.55; H, 3.89; N, 10.55%. Calcd for $C_{15}H_{10}O_3N_2$: C, 67.66; H, 3.79; N, 10.52%.

The authors wish to thank Mr. Yasunori Sudoh of Taiho Pharmaceutical Co., Ltd., Tokushima, for his assistance in measuring the mass spectra.

References

1) W. J. de Klein, "Reactions with Manganese(III) Acetate," in "Organic Syntheses by Oxidation with Metal Compounds," ed by W. J. Mijs and C. R. H. J. de Jonge, Plenum Press, New York (1986), pp. 261—314.

2) W. E. Fristad and S. S. Hershberger, *J. Org. Chem.*, **50**, 1026 (1985). The formula of manganese(III) acetate has been reported to be $[Mn_3O(OAc)_6(OAc)(HOAc)]5H_2O$, where all manganese are in the state of Mn(III).

3) H. Nishino, *Bull. Chem. Soc. Jpn.*, **59**, 1733 (1986).

4) H. Nishino, K. Tsunoda, and K. Kurosawa, *Bull. Chem. Soc. Jpn.*, **62**, 545 (1989).

5) A. Citterio, D. Fancelli, R. Santi, A. Pagani, and S. Bonsignore, *Gazz. Chim. Ital.*, **118**, 405 (1989).

6) A. Citterio, R. Santi, T. Fiorani, and S. Strologo, *J. Org. Chem.*, **54**, 2703 (1989).

7) S. Ueda and K. Kurosawa, *Bull. Chem. Soc. Jpn.*, **50**, 193 (1977).

8) P. Andrulis, Jr., M. J. S. Dewar, R. Dietz, and R. Hunt, *J. Am. Chem. Soc.*, **88**, 5473 (1966).

Structures of the Polymers Obtained by the Solid-State Polymerization of Diyne, Triyne, and Tetrayne with Long-Alkyl Substituents

Shuji Okada,* Kikuko Hayamizu,† Hiro Matsuda, Atsushi Masaki, and Hachiro Nakanishi
Research Institute for Polymers and Textiles, 1-1-4 Higashi,
Tsukuba, Ibaraki 305
† National Chemical Laboratory for Industry, 1-1-5 Higashi,
Tsukuba, Ibaraki 305
(Received September 27, 1990)

Structures of the polymers obtained by solid-state polymerization of diyne, triyne, and tetraynes substituted by long chain alkyl groups were investigated by solid-state ^{13}C NMR spectroscopy. Assignment of all peaks in the spectra were made successfully, referring to those of the monomers and the polydiacetylenes of known structures. It was clearly shown that the backbone of these polymers has always the same structure of $\rangle C{=}C{-}C{\equiv}C{-}C{=}\langle$. This fact suggests that only 1,4-addition polymerization takes place in the similar way for the diyne, the triyne and the tetraynes, excluding many other possible addition schemes, and the tetraynes give an interesting polydiacetylene with butadiynyl substituents. This exclusive 1,4-addition can be explained in terms of topochemical control.

Conjugated polymers are interesting for their superior third-order nonlinear optical properties. Among them, polydiacetylenes were the first conjugated polymer whose third-order nonlinear optical property was reported with expectation to surpass the semiconductors.[1] To achieve enlarged third-order susceptibilities, polydiacetylenes having π-conjugations between polymer backbone and side chains might be better candidates than those with no such π-conjugations because of increased numbers of π-electrons per repeating unit.[2,3] We have succeeded in the preparation of several series of new polydiacetylenes with aromatic rings directly bound to the main chains by proper crystal engineering.[4–9] In this context, especially interesting are the polydiacetylenes with acetylenic substituents directly bound to the main chain, since we can expect perfect π-conjugation between the main chain and substituents. Recently, we have synthesized a triyne[9] and tetraynes[10] with long-alkyl substituents and confirmed their solid-state polymerizabilities. However, the structures of these polymers were not determined exactly. This paper concerns with the detailed structural analysis of the polymers by solid-state ^{13}C NMR spectroscopy and some other measurements.

Experimental

Spectroscopy and X-Ray Diffraction. IR spectra, Visible spectra, and solution ^1H NMR spectra were measured by a JASCO IR-810, a Shimadzu UV-3100S, and a Nicolet NT-360, respectively. Transmitted X-ray diffraction patterns were recorded on a powder diffractometer (Philips PW-1700) using Cu $K\alpha$ radiation.

Solid-state high resolution ^{13}C NMR spectra were obtained by use of a JEOL FX-200 at 50.10 MHz with the cross-polarization (CP)/ magic angle spinning (MAS) method. The 90° pulse for the ^{13}C resonance was 4.5 μs and the MAS speed was between 4.8 and 5.5 kHz. The CP time was changed from 1 to 10 ms to observe the relative intensities. Dipole-dephasing spectra were measured with the delayed time of 40 μs for the assignment. Also the single pulse measurement with ^1H decoupling and MAS was carried out to observed mobile carbons. The ^{13}C chemical shifts were referred to external adamantane, where the CH_2 peak was set as 29.5 ppm. Solution-state ^{13}C NMR spectra were also observed by the same spectrometer. Chloroform-*d* including a small amount of tetramethylsilane was used as a solvent.

Synthesis of Monomers. The synthetic procedures of the compounds used were shown in Fig. 1. 10,12,14-Nonacosatriynoic acid (14-3A-8C), as a triyne compound, was prepared according to the procedure described before.[9] Tetrayne compounds of 15,17,19,21-hexatriacontatetrayne (14-4A-14) and 19,21,23,25-tetratetracontatetrayne (18-4A-18) were also synthesized as described before.[10] 15,17-Dotriacontadiyne (14-DA-14) was synthesized as a reference of this series of compounds, according to the procedure described below.

14-DA-14. To a solution of *N,N,N′,N′*-tetramethylethylenediamine (580 mg, 5 mmol) and copper(I) chloride (500 mg, 5 mmol) in tetrahydrofuran (150 cm^3), 1-hexadecyne (11.1 g, 50 mmol) was added. While it was stirred for one day at ambient temperature, oxygen was bubbled into the solution. After evaporating the solvent, hydrochloric acid solution was added to the residue and the mixture was extracted with hexane. The hexane layer was dried with anhydrous sodium sulfate. After filtration, the solvent was removed in vacuo and the residue was purified by column chromatography (silica gel, hexane) to give 9.90 g, (90%) of 14-DA-14. After recrystallization from hexane, 3.59 g of pure 14-DA-14 was obtained. Mp 50—51 °C; IR(KBr) 2950, 2924, 2857, 2179 (weak), 2146 (weak), 1473, 1418, 718 cm^{-1}; ^1H NMR ($CDCl_3$) δ=0.88 (6H, t, J=6.4 Hz), 1.26 (40H, m), 1.37 (4H, m), 1.51 (4H, tt, J=7.1, 6.7 Hz), 2.24 (4H, t, J=6.7 Hz). Found: C, 86.80; H, 13.20%. Calcd for $C_{32}H_{58}$: C, 86.68; H, 13.43%.

Polymerization. Absorption spectral changes of the compounds during photopolymerization were followed using KBr-pelletized specimens under the irradiation of an 8 W UV lamp (Tokyo Kogaku Kikai K. K. PUV-1A) at the distance of 2 cm. Polymers were obtained by γ-ray induced polymerization. The doses of ^{60}Co γ-ray were 112 Mard for 14-DA-14, 57 Mrad for 14-3A-8C, 31 Mrad for 14-4A-14 and 47 Mrad for 18-4A-18, respectively, with the dose rate of ca. 0.15 Mrad h^{-1}. Since the polymers are insoluble in the organic solvents

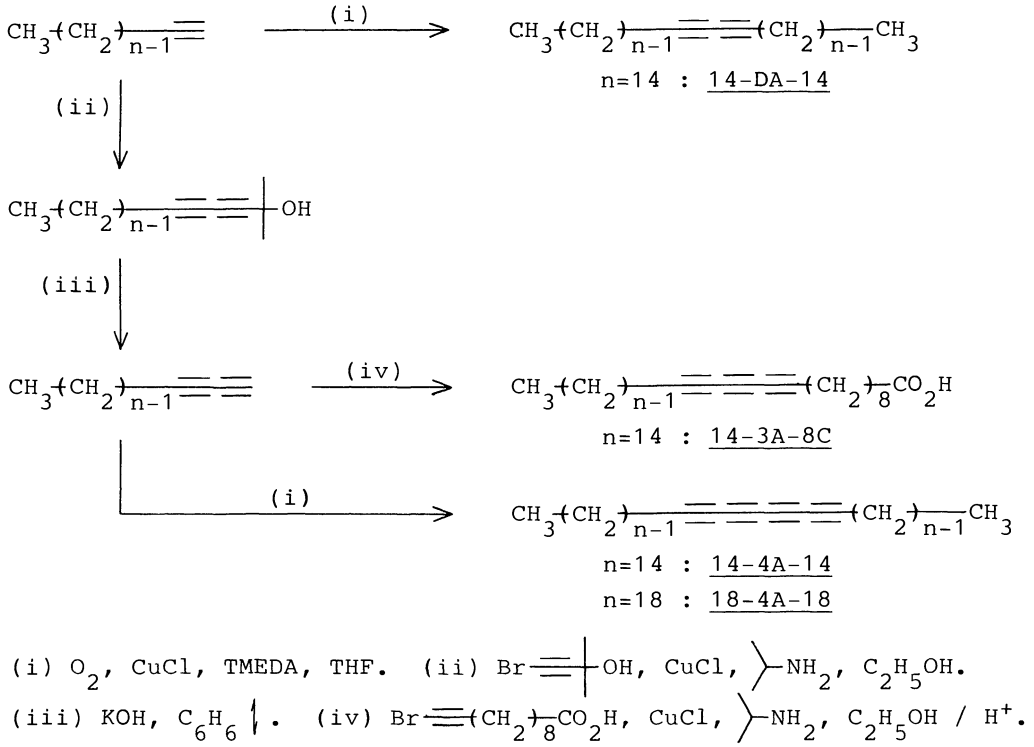

Fig. 1. Synthetic procedure of the monomers.

which can dissolve the monomers, the polymer conversion was determined gravimetrically after the solvent extraction of the monomers. Although the 14-4A-14 and 18-4A-18 were polymerized almost quantitatively, the conversion of 14-DA-14 and 14-3A-8C were 57% (after hexane extraction) and 86% (after chloroform extraction), respectively.

Results and Discussion

Visible and IR Spectra and X-Ray Diffraction. Figure 2 shows the visible absorption spectral change of 14-DA-14 during photopolymerization. The characteristic absorption maximum of polydiacetylene as a conjugated polymer was observed around 635 nm. 14-3A-8C, 14-4A-14, and 18-4A-18 were also polymerized by UV irradiation to become deep blue-colored polymers. Table 1 shows the comparison of the absorption maxima at the longest wavelength of the polymers from 14-DA-14, 14-3A-8C, 14-4A-14, and 18-4A-18. The absorption maxima of the polymers shifts to the longer wavelength as the number of acetylene units in the corresponding monomers increases. The increase of the acetylene units in the monomer brings the more extended π-conjugation and narrower band gap in the polymers synthesized by the solid-state polymerization.

IR spectra of 14-3A-8C, 14-4A-14, and 18-4A-18 monomers show a strong absorption in the stretching band region of acetylenic triple bonds. In their polymers, the stretching band becomes weaker but remains. If all the acetylene units were included in the polymer backbone, the bands should disappear because of the symmetric structure around acetylene

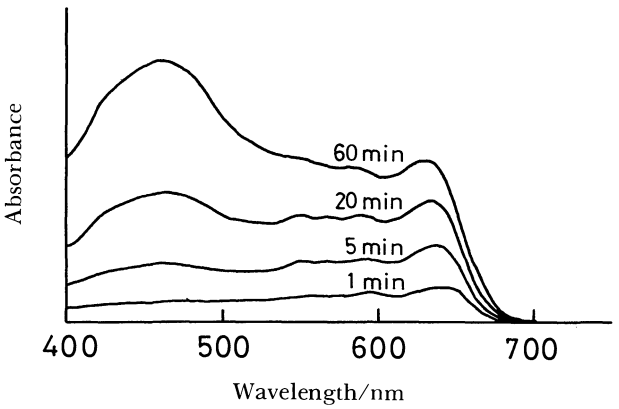

Fig. 2. Visible spectral change of 14-DA-14 depending on UV irradiation time.

Table 1. The Longest-Wavelength Absorption Maxima at the Initial Stage of Polymerization

Compound	λ_{max}/nm
14-DA-14	640—630
14-3A-8C	670—660
14-4A-14, 18-4A-18	710—700

units. Thus, one or more acetylene bonds must be in the side chains.

Crystallinity was checked by X-ray powder diffraction analysis. All the monomers showed several sharp diffraction peaks. The polymers of 14-3A-8C, 14-4A-14, and 18-4A-18, however, showed only broad peaks and the largest main peak was around 19—20°. This peak corresponds to the spacing of ca. 0.45 nm indicating that regularity between adjacent alkyl chains was maintained even in these polymers. On the contrary, the polymer of 14-DA-14 showed several sharp peaks, reflecting the high crystallinity.

^{13}C NMR Spectra. Tables 2, 3, and 4 show the ^{13}C chemical shifts of the monomers of 14-DA-14, 14-3A-8C, and 14-4A-14, respectively, in the solution and in the solid-state. The assignment was first carried out for the monomers in solution. The acetylenic carbons were assigned from ^{1}H undecoupled spectra. For instance, 14-4A-14 monomer gives the four ^{13}C peaks at 80.5, 65.7, 61.4, and 60.6 ppm, corresponding to the existence of four pairs of nonequivalent acetylenic carbons. It is known that the coupling constants of those carbons with α-methylene protons decrease with the numbers of the bonds between them. Since the coupling constants of the signals at 80.5, 65.7, 61.4, and 60.6 ppm were 5.5 Hz, 4.6 Hz, 3.7 Hz, and undetectable, respectively, the four peaks in the above order were easily identified to the four nonequivalent acetylenic carbons, i.e., from the outer most to the inner most ones in the same order. This trend is the same as the di-*t*-butyl-substituted octatetrayne.[11]

The ethynylene group causes the higher field shift of about 10 ppm to α-CH_2 but none to β- and γ-CH_2. Thus, among many carbon atoms in the alkyl chains, α-CH_2 can be identified. Though the monomer of 14-3A-8C in solution showed three pairs of acetylenic carbon peaks with small splittings because of its unsymmetrical structure, the differences were very small and less than 0.5 ppm and their assignments were straightforward as shown in Table 3. The ^{13}C spectral patterns of the monomers in chloroform-*d* solution are saved in the Spectral Database System (SDBS) constructed by National Chemical Laboratory for Industry[12].

The solid-state ^{13}C spectra of the 14-DA-14 and 14-4A-14 monomers observed by single-pulse MAS method with ^{1}H decoupling resemble to the corresponding solution-state spectra, and this suggests that these monomer contain very mobile molecules within

Table 2. ^{13}C Chemical Shifts of 14-DA-14 Monomer

Solution-state	Solid-state		Assignment[a]
	MAS	CP/MAS	
77.5	76.8 sharp	78.7 broad	6 -C≡
65.4	66.8 sharp	65.0 broad	7 -C≡
32.0	32.7	—[b]	3 CH_2
—	—	34.0	4 CH_2 stacked
29.7[c] broad	30.5	30.5	4 CH_2
		25.7	2 CH_2 rigid
22.7	23.4	23.4	2 CH_2 mobile
		22.1	5 CH_2 rigid
19.3	19.9	20.0	5 CH_2 mobile
		15.4	1 CH_3 rigid
14.1	14.6	14.7	1 CH_2 mobile

a) CH_3-CH_2-CH_2-(CH_2)$_{10}$-CH_2-C≡C-C≡C-(CH_2)$_{13}$-CH_3.
1 2 3 4 5 6 7
b) Overlapped with the carbons 4. c) Many peaks overlapped.

Table 3. ^{13}C Chemical Shifts of 14-3A-8C Monomer

Solution-state	Solid-state[a]		Assignment[b]
	MAS[c]	CP/MAS	
179.9	182.5	182.2	11 -CO_2H
79.3[d]	81 w	81.1	6 -C≡
	78 vw	78 vw	
65.7[d]	67 w	67.1	7 -C≡
	65 vw	66 vw	
60.4[d]	62 w	62.3	8 -C≡
	60 vw	60 vw	
34.0	35.7	35.6	10 CH_2
31.9	—[e]	—[e]	3 CH_2
	34.3 vs	34.3 vs	4 CH_2
28.4[f] broad	30 w	30.4 w	
24.6		26.6	9 CH_2
22.7	25.8 s	25.8	2 CH_2
19.4	22 w	21.9	5 CH_2
14.1	16.0 s	15.9	1 CH_3

a) vw: very weak, w: weak, s: strong, vs: very strong.
b) CH_3-CH_2-CH_2-(CH_2)$_{10}$-CH_2-C≡C-C≡C-C≡C-
1 2 3 4 5 6 7 8 8 7 6
CH_2-(CH_2)$_5$-CH_2-CH_2-CO_2H. c) Very intensive.
5 4 9 10 11
d) Average of two peaks. See text. e) Overlapped with the carbons 4. f) Many peaks overlapped.

Table 4. ^{13}C Chemical Shifts of 14-4A-14 Monomer

Solution-state	Solid-state		Assignment[a]
	MAS	CP/MAS	
80.5	80.5 sharp	82 broad	6 -C≡
65.7	66.8 sharp	67 broad	7 -C≡
61.4	62.4 sharp	62 broad	8 -C≡
60.6	61.5 sharp	62 broad	9 -C≡
32.0	32.7	—[b]	3 CH_2
		33.8	4 CH_2 stacked
28.0[c] broad	30.5	30.6	4 CH_2 mobile
		25.4	2 CH_2 rigid
22.7	23.4		2 CH_2 mobile
		22	5 CH_2 rigid
19.5	20.2		5 CH_2 mobile
14.1	14.7	15.4	1 CH_3

a) CH_3-CH_2-CH_2-(CH_2)$_{10}$-CH_2-C≡C-C≡C-C≡C-C≡
1 2 3 4 5 6 7 8 9
C-(CH_2)$_{13}$-CH_3. b) Overlapped with the carbons 4.
c) Many peaks overlapped.

the crystals. In the CP/MAS ^{13}C spectra of these monomers, the line widths are broader and a large peak of the alkyl chain carbons in the stacked state can be observed at 33—34 ppm in addition to the mobile carbons signals at about 30 ppm. In the CP/MAS spectrum of the 14-DA-14 monomer, the signals of the mobile acetylene carbons were not observed, while the both signals of the mobile and the rigid carbons in the alkyl chains were observed as shown in Table 2. Then it is clear that the alkyl-chain carbons are more flexible than the acetylenic carbons in the 14-DA-14 monomer in the solid-state. Similarly, the CP/MAS spectrum of the 14-4A-14 monomer contains both signals of the mobile and the rigid alkyl-chain carbons, but the ratio of the mobile carbons decreases. Then the molecular motions of 14-4A-14 monomer may become slower compared with the 14-DA-14 monomer. On the other hand, the single-pulse MAS spectrum of the 14-3A-8C monomer was very intensive suggesting that the crystal structure is rigid. The reduced molecular motion in the 14-3A-8C monomer can be attributed to hydrogen bonding between carboxyl groups contained in the molecule. The magnitudes of the alkyl-chain motion of these three monomers coincide to the order of their melting points, i.e., melting points of the monomers are 50—51 °C for 14-DA-14, 58—59 °C for 14-4A-14, and 78—79 °C for 14-3A-8C, respectively. The lower melting point the monomer has, the more mobile its alkyl chain is. In 14-3A-8C, shoulders were observed in the three acetylenic carbon peaks in the MAS and CP/MAS spectra. This may be due to inhomogenious circumstances around the acetylenic carbons in 14-3A-8C monomer.

Figure 3 shows the CP/MAS ^{13}C spectra of the polymers in olefinic and acetylenic region and Table 5 lists up the chemical shifts of all the peaks. The backbone structure of 14-DA-14 polymer is

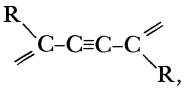

where the two acetylenic carbons and two olefinic carbons are equivalent. Actually, in Fig. 3(a), only two peaks at 101.6 and 130.2 ppm were observed. They were easily assigned to be acetylenic and olefinic carbons, respectively, which agree with those of so-far known polydiacetylenes[13–16] as summarized in Table 6.

In the polymer of 14-3A-8C, six peaks, of which two peaks around 103.9 ppm are considered to overlap because of the twice intensity, were observed (Fig. 3(b)). If they were polymerized symmetrically by 1,6-addition, the number of the peaks in this region should be three. The result clearly indicates that 14-3A-8C are polymerized unsymmetrically by 1,4-addition and therefore the backbone structure of 14-3A-8C polymer is

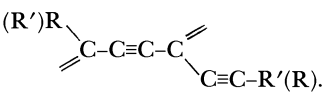

The same polymerization scheme was reported for a hexatriyne derivative with urethane substituents based

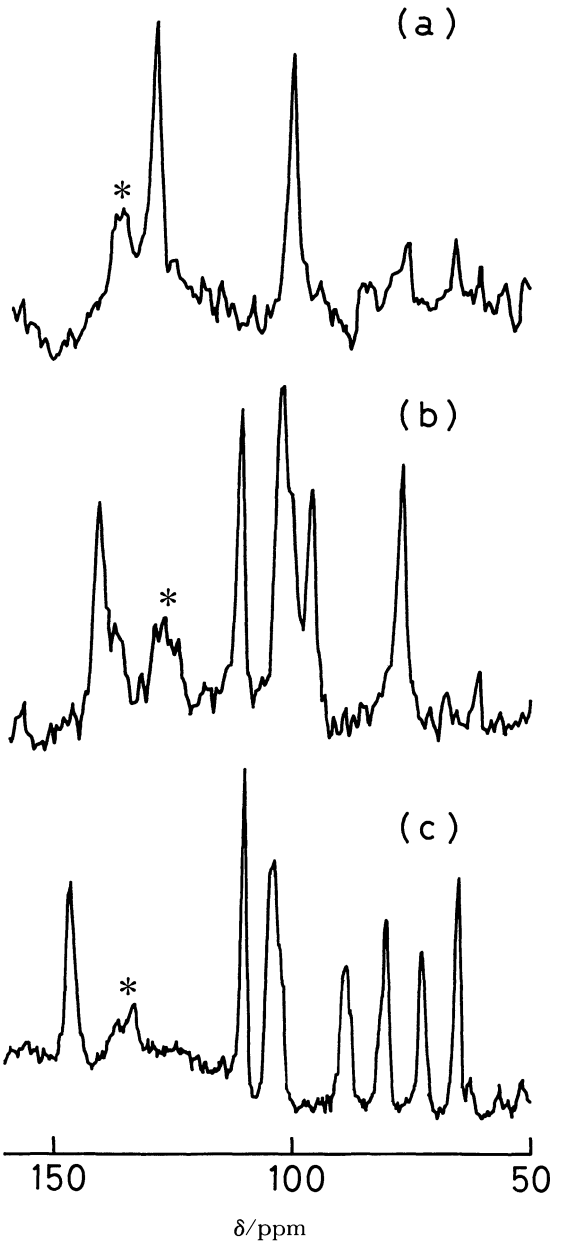

Fig. 3. ^{13}C CP/MAS spectra in the olefinic and acetylenic region of the polymers of 14-DA-14 (a), 14-3A-8C (b), and 14-4A-14 (c). Asterisks indicate background or spinning side bands.

Table 5. ^{13}C Chemical Shifts (CP/MAS) of Polymers

14-DA-14	14-3A-8C	14-4A-14	18-4A-18	Assignment[a]
	181.8			13 $-CO_2H$
130.2	141.9	147.3	147.0	4 >C=
	112.0	110.3	110.5	6 >C=
101.6	103.9	105.0	104.7	5 -C≡
		89.5	89.5	10 -C≡
	97.4	80.6	80.6	8 -C≡
	77.9	72.7	72.7	7 -C≡
		65.2	65.4	9 -C≡
33.3	33.4	33.6	33.6	3 CH_2 mainly stacked
30.9				3 CH_2 mobile
	26.5			12 CH_2
23.5	24.2	24.6	24.7	2 CH_2 mobile
	21.8	22.2	22.5	11 CH_2
14.8	14.6	15.0	15.0	1 CH_3 mobile

a) For 14-DA-14:

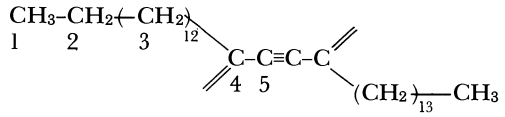

For 14-3A-8C:

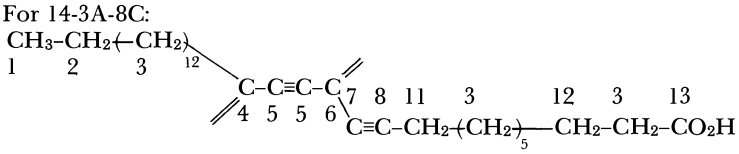

or

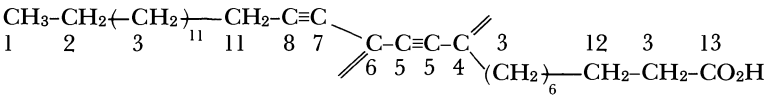

For 14-4A-14 and 18-4A-18:

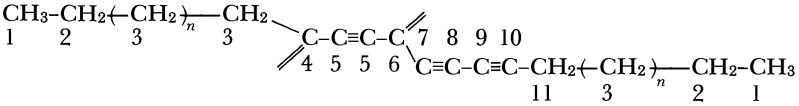

(n=11 for 14-4A-14 and n=15 for 18-4A-18)

Table 6. ^{13}C Chemical Shifts of the Backbone of Polydiacetylenes

Polydiacetylene	Measuring condition	δ/ppm		Reference
		>C=	-C≡	
4BCMU	$CDCl_3$ (30°C)	129.3	99.3	13)
PTS-12	$CDCl_3$	129	99.4	14)
DCHD	CP/MAS	129.0	104.3	15)
ETCD	CP/MAS	131.6	107.4	16)
14-DA-14	CP/MAS	130.2	101.6	This work

on the X-ray diffraction analysis.[17] The two olefinic carbons of the main chain of 14-DA-14 polymer are equivalent to give one peak at 130.2 ppm, whereas those of 14-3A-8C are not equivalent to give two peaks, i.e., one at the higher and the other at the lower field. It is known that an acetylenic group, compared with an alkyl group, attached to the olefinic moiety bring the chemical shift of the olefinic α-carbon to about 20 ppm higher field, as shows in the following example;

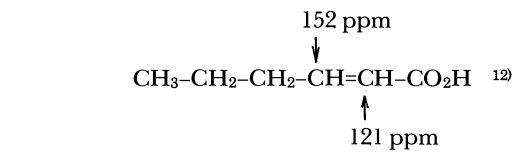

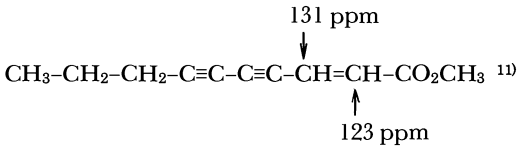

Thus, the higher field peak about 112 ppm was assigned to the olefinic carbon attached to the acetylenic side chain, and the lower field peak about 142 ppm to that attached to the simple alkyl chain. However, the splitting of the two peaks is quite large, i.e., 30 ppm for 14-3A-8C polymer whereas about 20 ppm for the typical case which is expected from the difference of the chemical shift of the two molecules shown above. This will be mentioned later again.

The peak at 103.9 ppm with larger intensity is assigned to the two backbone acetylenic carbons and is not so moved from 101.6 ppm of the acetylenic carbons of 14-DA-14. For the acetylenic side chain, the peaks at 97.4 ppm and 77.9 ppm were assigned to the β- and α-carbons from the polymer backbone, respectively, because the alkyl-attached acetylenic carbon shows the peak in the lower field as discussed in the case of the monomers.

In the same manner, the assignment of the peaks for polymers of 14-4A-14 and 18-4A-18 was performed as listed in Table 5. The spectra of 14-4A-14 and 18-4A-18 are the same except in peak intensity for the carbons of long-alkyl groups. As the chemical shifts of the three peaks in the lower field of Fig. 3(c) which correspond to the polymer backbone are similar to those of Fig. 3(b), it was estimated that 14-4A-14 and 18-4A-18 also are polymerized unsymmetrically by 1,4-addition just like 14-3A-8C. Thus, the backbone structure of 4A polymers is

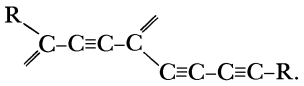

The splitting of the chemical shifts between two olefinic carbons are about 37 ppm and larger than that of 14-3A-8C. One of the plausible explanation of this splitting may be the polarization of the main chain as follows;

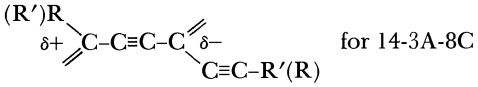

for 14-3A-8C

and

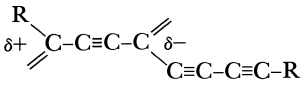

for 14-4A-14 and 18-4A-18,

respectively. This polarization should be enhanced in 14-4A-14 and 18-4A-18 polymers because of the more conjugated side chains.

The diacetylenic side chain was assigned by referring the following example;[11]

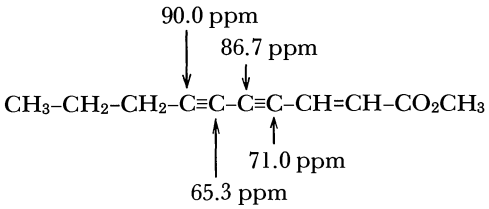

The peaks at about 90, 81, 72, and 65 ppm in 14-4A-14 and 18-4A-18 polymers are for the carbons at δ-, β-, α-, and γ-positions from the polymer backbone, respectively.

From these results, it has been clarified that only 1,4-polymerization occurs even in triyne and tetrayne compounds. This can be explained by so-called "topochemical control"; that is, the molecular arrangement in the crystal geometrically allows only the exclusive reaction path among many possible paths since the molecular movements are very restricted in the crystal.[18] It is known that the solid-state polymerizability of diacetylene monomers to the well-known polydiacetylene structure via 1,4-addition can be characterized by the stacking distance of the monomer array (d) and by the angle between the diacetylene rod and stacking axis (Φ).[19] And the maximal reactivity is expected for $d \approx 0.5$ nm and $\Phi \approx 45°$. When 14-4A-14 molecules are packed, using a space-filling model, without any gaps between molecules, the perpendicular distances of adjacent alkyl groups and adjacent tetraacetylenic moieties are 0.45 nm and 0.34 nm, respectively. Under this condition, d and Φ

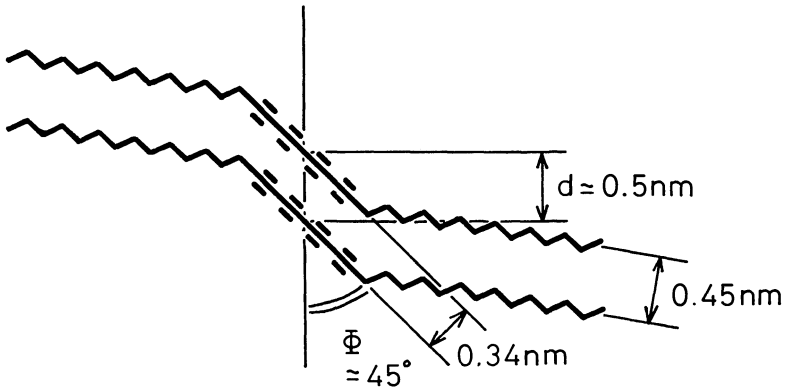

Fig. 4. Molecular packing scheme of 14-4A-14.

become ca. 0.5 nm and ca. 45°, respectively, as shown in Fig. 4. This is the case of the alkyl-substituted diynes and triynes, and the packing is exactly the best one for the 1,4-addition and not for other schemes such as 1,2-, 1,6-, and 1,8-additions.

For the tetrayne compounds, two different types of 1,4-polymerization are possible as mentioned in the previous paper,[10] i.e., the unsymmetrical polymerization as shown in this work and the symmetrical polymerization to give a di(1-alkynyl)-substituted polydiacetylene. The distance between the reacting carbons of the adjacent molecules are the same for the both polymerization procedures because tetrayne moiety stacks parallel. Only difference between two possible schemes is the existence of the reactive carbon with an alkyl chain in the case of unsymmetrical polymerization. Since the alkyl chain is more mobile than the acetylene moiety, the acetylenic carbon bound to an alkyl group can be assumed to become a starting point of the polymerization which results in the present unsymmetrical polydiacetylene structures.

In conclusion, the structures of the polymers from alkyl-substituted triyne and tetraynes were analyzed especially by solid-state ^{13}C NMR spectra. It has been found that triyne and tetraynes are polymerized unsymmetrically via 1,4-addition to give the polydiacetylene with acetylenic side chains and the polydiacetylenes with diacetylenic side chains, respectively. As the structure of the polydiacetylenes with diacetylenic side chains are confirmed, polymerization of the diacetylene moieties in side chain seems to be interesting to obtain a novel class of π-conjugated polymers and the investigation is currently in progress.

References

1) C. Sauteret, J. P. Hermann, R. Fray, F. Pradere, D. Ducuing, R. H. Baughman, and R. R. Chance, *Phys. Rev. Lett.*, **36**, 956 (1976).

2) B. J. Orchard and S. K. Tripathy, *Macromolecules*, **19**, 1844 (1986).

3) S. B. Clough, S. Kumar, X. F. Sun, S. Trypathy, H. Matsuda, H. Nakanishi, S. Okada, and M. Kato, "Nonlinear Optics of Organics and Semiconductors (Springer Proceeding in Physics, Vol. 36)," ed by T. Kobayashi, Springer-Verlag, Berlin (1989), p. 149.

4) H. Nakanishi, H. Matsuda, S. Okada, and M. Kato, "Frontiers of Macromolecular Science," ed by T. Saegusa, T. Higashimura, and A. Abe, Blackwell Scientific Publications, Oxford (1989), p. 469.

5) H. Matsuda, H. Nakanishi, T. Hosomi, and M. Kato, *Macromolecules*, **21**, 1238 (1988).

6) H. Matsuda, H. Nakanishi, N. Minami, and M. Kato, *Mol. Cryst. Liq. Cryst.*, **160**, 241 (1988).

7) H. Nakanishi, H. Matsuda, S. Okada, and M. Kato, "Nonlinear Optics of Organics and Semiconductors (Springer Proceeding in Physics, Vol. 36)," ed by T. Kobayashi, Springer-Verlar, Berlin (1989), p. 155.

8) S. Okada, M. Ohsugi, A. Masaki, H. Matsuda, S. Takaragi, and H. Nakanishi, *Mol. Cryst. Liq. Cryst.*, **183**, 81 (1990).

9) S. Okada, H. Matsuda, H. Nakanishi, M. Kato, and M. Otsuka, *Thin Solid Films*, **179**, 423 (1989).

10) S. Okada, H. Matsuda, H. Nakanishi, and M. Kato, *Mol. Cryst. Liq. Cryst.*, **189**, 57 (1990).

11) R. Zeisberg and F. Bohlmann, *Chem. Ber.*, **107**, 3800 (1974).

12) The ^{13}C spectrum can be obtained from Spectral Database System (SDBS) constructed by National Chemical Laboratory for Industry; O. Yamamoto, K. Someno, N. Wasada, J. Hiraishi, K. Hayamizu, K. Tanabe, T. Tamura, and M. Yanagisawa, *Anal. Sci.*, **4**, 233 (1988); O. Yamamoto, K. Hayamizu, and M. Yanagisawa, *Anal. Sci.*, **5**, 645 (1989), and references therein.

13) G. E. Babbitt and G. N. Patel, *Macromolecules*, **14**, 554 (1981).

14) G. Wenz, M. A. Muller, M. Schmidt, and G. Wegner, *Macromolecules*, **17**, 837 (1984).

15) H. Eckert, J. P. Yesinowski, D. J. Sandman, and C. S. Velazquez, *J. Am. Chem. Soc.*, **109**, 761 (1987).

16) H. Tanaka, M. A. Gomez, A. E. Tonelli, and M. Thakur, *Macromolecules*, **22**, 1208 (1989).

17) J. Kiji, J. Kaiser, G. Wegner, and R. C. Schulz, *Polymer*, **14**, 433 (1973).

18) M. D. Cohen and G. M. J. Schmidt, *J. Chem. Soc.*, **1964**, 1996.

19) R. H. Baughman and K. C. Yee, *J. Polym. Sci., Macromol. Rev.*, **13**, 219 (1978); V. Enkelmann, "Polydiacetylenes (Advamces in Polymer Science, Vol. 63)," ed by H.-J. Cantow, Springer-Verlag, Berlin (1984), p. 91.

Synthesis of 3,4′-Diaryl- and 4,4′-Diaryl-2,2′-bithienyls from 2,5-Dichlorothiophene[1)]

Tyo Sone,* Yasuhiro Umetsu, and Kazuaki Sato
Department of Materials Science and Engineering, Faculty of Engineering,
Yamagata University, Yonezawa 992
(Received October 19, 1990)

3,4′-Diaryl-, and 4,4′-diaryl-2,2′-bithienyls, new classes of mixed thiophene–arene oligomers, were synthesized from 2,5-dichlorothiophene via 4-aryl-2-chlorothiophene in three and two steps, respectively. Namely, a Friedel–Crafts type self-condensation of 4-aryl-2-chlorothiophene, followed by catalytic dechlorination, yielded unsymmetrical bithienyls. Homocoupling of 4-aryl-2-chlorothiophene using a nickel–phosphine catalyst gave symmetrical bithienyls.

Although the syntheses and properties of oligophenylenes have been systematically investigated, the chemistry of their thiophene analogues, thiophene oligomers and mixed thiophene–arene oligomers, has not yet been fully explored. Oligomers with definite structure, corresponding to quaterphenyl or its higher homologues, are rather limited in number; only a few of those containing 2,3′-bithienyl or 3-arylthiophene unit have been known.[2–5)] As for diarylbithienyls, one of the simplest classes of oligomers, for example, only two (5,5′-diaryl-[3)] and 3,3′-diphenyl-2,2′-bithienyl[4)]) have been reported. We have reported the synthesis of a series of unsymmetrical 5,5′-diaryl-2,3′-bithienyls by acid-catalyzed coupling of 2-arylthiophenes.[5)] Some of the oligomers have recently attracted attention in connection with their potential electric conductivity.[6)]

During the course of the studies on the acid-catalyzed reactions of thiophene nuclei, we found that, in the presence of $AlCl_3$, the chlorine atom of chlorothiophenes was sufficiently reactive; 2-chlorothiophene gave the corresponding 2-arylthiophenes with some aromatic compounds,[7)] while 2, 5-dichlorothiophene gave 4-aryl-2-chlorothiophenes (**1**) unexpectedly.[8)] These findings suggest a simple route to certain arylthiophenes starting from readily available chlorothiophenes. As an extension of the studies,

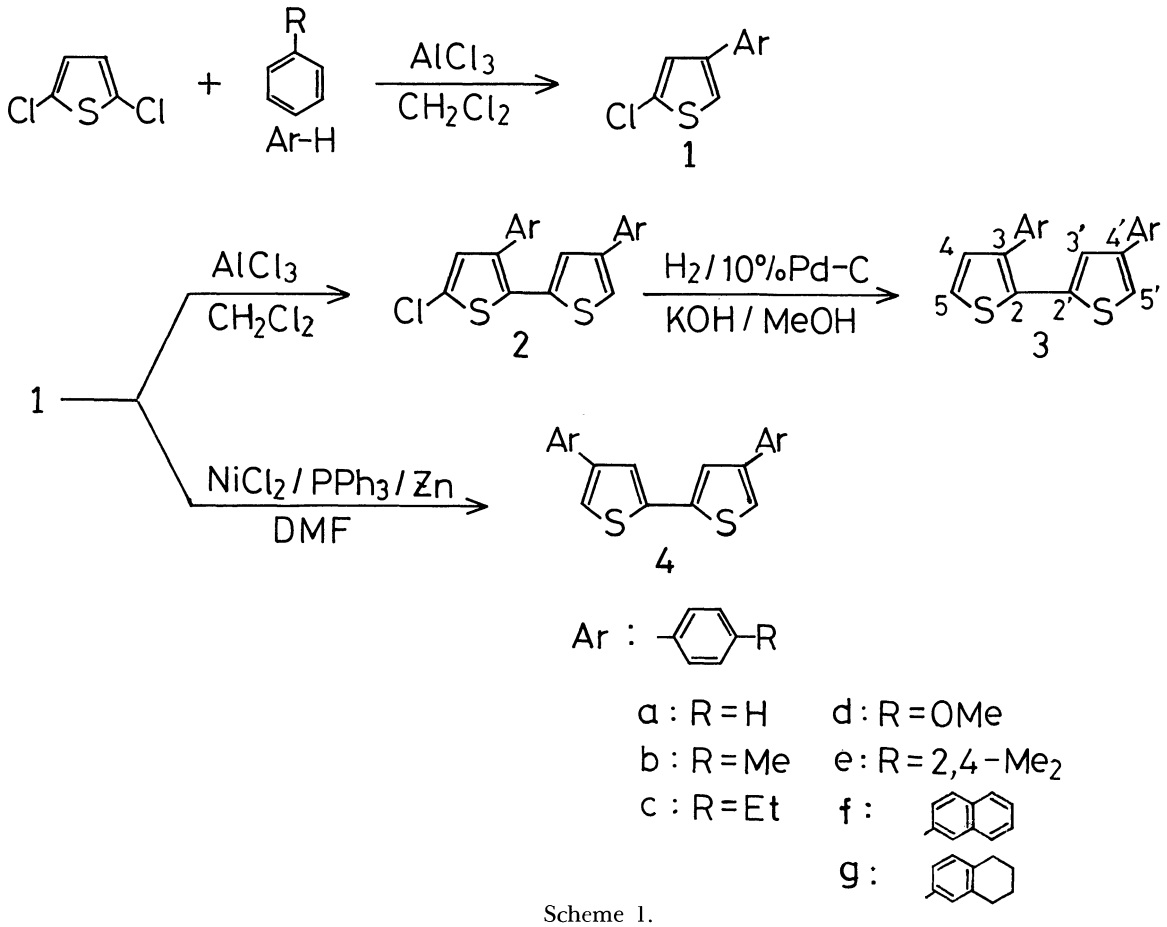

Scheme 1.

we found a convenient method for the synthesis of unsymmetrical 3,4′-diaryl-2,2′-bithienyls (**3**) from **1**. Furthermore, a series of symmetrical 4,4′-diaryl-2,2′-bithienyls (**4**) has been synthesized by homo-coupling of **1** using a nickel–phosphine catalyst. Besides forming new classes of mixed thiophene–arene oligomers, these compounds are interesting as potential key building blocks for well-ordered β-arylthiophene oligomers from the viewpoint of electrochemical properties.

Results and Discussion

In order to find a simple route to 2,4-diarylthiophenes which were not easily accessible by traditional methods, the Friedel–Crafts type reaction of **1** with aromatic compounds was investigated. When reacted with such an active compound as anisole, however, **1** were found to undergo self-condensation with the elimination of HCl to give, instead of the expected product, 5-chloro-3,4′-diaryl-2,2′-bithienyls (**2**). This prompted us to apply the procedure for the synthesis of the unsymmetrical bithienyls, **3**. Self-condensation products, **2**, precursors of **3**, could be synthesized by this procedure in satisfactory yields. The results are summarized in Table 1.

The procedure of the Friedel–Crafts type reaction is simple; a mixture of **1** and an equimolar amount of $AlCl_3$ in CH_2Cl_2 or in CH_2Cl_2–benzene was stirred below 40 °C for a total of 2 h.

The assignment of the 3,4′-diaryl-2,2′-bithienyl structure is based on the NMR spectra of the self-condensation products, **2**, and those of the dechlorination products, **3**. The AB quartets with coupling constants J=1.3—1.7 Hz, observed in the aromatic region of the spectra of **2**, indicate the presence of a 2,4- disubstituted thiophene ring in the molecules. Moreover, the two sets of coupling constants, 1.5—1.6 and 5.0—5.3 Hz, observed in the aromatic region of the spectra of **3** are apparently derived from 2,4-di- and 2,3-disubstituted thiophene ring protons, respectively.[9]

The probable mechanism for self-condensation is shown in Scheme 2; this requires an initial protonation of **1** to form the thiophenium ion **A** as the

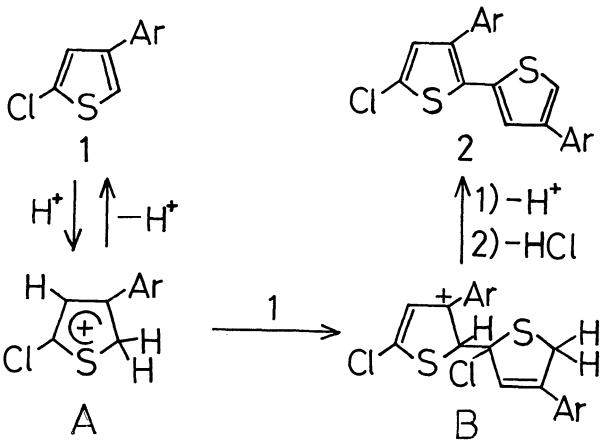

Scheme 2.

electrophile. It is generally accepted that $AlCl_3$, when coming into contact with H_2O in moist air or HCl, produces a hypothetical species, such as $[H]^+[AlCl_3OH]^-$ or $[H]^+[AlCl_4]^-$ which acts as a proton source. Once the reaction occurs, it can provide HCl, which, together with $AlCl_3$, stimulates a further reaction. The existence of such a protonated species as **A** was confirmed by a direct NMR spectroscopic observation;[10] the spectrum of the thiophenium ion (**A**, **Ar**=Ph) produced from 2-chloro-4-phenylthiophene (**1a**) in HSO_3F at 32 °C shows, in addition to signals at 7.7—8.4 ppm due to the phenyl protons, two signals at 5.82 and 8.32 ppm with a relative intensity of 2:1. An attack of the thiophenium ion, **A** on the 5-position of **1**, followed by elimination of a proton and a HCl molecule, yields the self-condensation product, **2**.

The chlorine atom of the self-condensation products, **2**, could be easily removed by catalytic hydrogenation under atmospheric pressure using 10% Pd–C as a catalyst to give the unsymmetrical bithienyls, **3**, in satisfactory yields. The results are summarized in Table 1.

Symmetrical diarylbithienyls can be obtained by homo-coupling of the corresponding aryl-substituted halothiophenes. 3,3′-Diphenyl-2,2′-bithienyl was prepared by a Ullmann reaction of 3-phenyl-2-iodothiophene, though in low yield.[4] Efficient methods for

Table 1. Friedel–Crafts Type Self-Condensation of 4-Aryl-2-chlorothiophenes (**1**) and Catalytic Dechlorination of the Products (**2**)

1 Ar	**2** Yield[a]/%	**2** Mp (θ_m/°C)	**3** Yield[a]/%	**3** Mp (θ_m/°C)
a R=H	59	69—70 (hex)[b]	86	113—114 (hex–chl)
b R=Me	63	101—102 (hex)	90	161—162 (hex–chl)
c R=Et	69	Oil	75	Oil
d R=OMe	68	103—104 (ac–MeOH)	71	92—93 (MeOH)
f 2-Naphthyl	65	151—152 (hex–chl)	77	155—156 (hex–chl)

a) Isolated yields based on **1** or **2** used. b) Solvent for recrystallization: hex=hexane, ac=acetone, chl=chloroform, MeOH=methanol.

Table 2. Coupling of 4-Aryl-2-chlorothiophenes (**1**)

1 Ar	**4** Yield[a]/%	Mp (θ_m/°C)
a R=H	63	224—225 (ben)[b]
b R=Me	75	220—221 (chl)
c R=Et	65	181—182 (hex-ben)
d R=OMe	65	289—291[d]
e R=2,4-Me_2	59	101—102 (hex)
f 2-Naphthyl	82	268—269 (chl)
g 2-Tetrahydro-2-naphthyl[c]	85	151—152 (hex-ben)

a) Isolated yields based on **1** used. b) Solvent for recrystallization: hex=hexane, ben=benzene, chl=chloroform. c) 5,6,7,8-Tetrahydro2-naphthyl. d) Purified by sublimation under reduced pressure (240 °C/1 mmHg).

coupling aryl halides have recently been developed using zerovalent nickel complexes. This method was applied to **1** for the synthesis of the symmetrical bithienyls, **4**. The nature of the zerovalent nickel complex used has been known to play an important role in nickel-mediated coupling. In addition, the amount of nickel complexes used is dependent upon the situation; in catalytic or stoichiometric amount. 4-Aryl-2-chlorothiophenes **1** were successfully coupled to **4** by using stoichiometric amounts of the nickel-phosphine complex prepared in situ from $NiCl_2$/PPh_3/Zn at a molar ratio of 1/4/1 in *N*,*N*-dimethylformamide (DMF) at 50 °C.[11] The results are summarized in Table 2. It has been reported that aryl chlorides, which tend to give unsatisfactory results in nickel-mediated reactions, can be efficiently coupled to diaryls by using catalytic amounts of the nickel complex in the presence of excess zinc.[12] Application of the catalytic method, however, led to the dechlorination of **1** in preference to coupling.

The structures of symmetrical bithienyls, **4**, were confirmed by their ^{1}H NMR spectra, which showed in the aromatic region an AB quartet with a coupling constant, J=1.4—1.5 Hz, characteristic of 2,4-dosibstituted thiophenes.[9]

Under the conditions employed for the synthesis of the symmetrical bithienyls, **4**, the nickel-mediated coupling of 2,5-dichloro-3-phenylthiophene was slow, affording 5-chloro-4,4′-diphenyl-2,2′-bithienyl (15%) together with the starting substance (25%) and 2-chloro-3-phenylthiophene (30%) instead of the expepcted 5,5′-dichloro-3,3′-diphenyl-2,2′-bithienyl, a precursor of the isomeric 3,3′-diphenyl-2,2′-bithienyls, in a prolonged reaction (12 h). A similar reaction (5 h) of 2-chloro-3-phenylthiophene did not give the desired 3,3′-diphenyl-2,2′-bithienyl, either, but yielded 3-phenylthiophene (25%) along with the starting substance (ca. 40%). These results indicate that steric hindrance plays an important role in nickel-mediated coupling.

In summary, we could synthesize 3,4′-diaryl-(**3**) and 4,4′-diaryl-2,2′-bithienyls (**4**), new classes of mixed thiophene–arene oligomers, which would be accessible only through many steps by other routes, in good yields in 3 and 2 steps, respectively, from readily available 2,5-dichlorothiophene. 4-Aryl-2-chlorothiophenes, **1**, which are obtained in one step from 2,5-dichlorothiophene by the Friedel–Crafts type reaction, serves as the key intermediates, suggesting the synthetic versatility of **1**.

Experimental

All of the melting and boiling points are uncorrected. The UV and MS spectra were obtained on a Hitachi 228A and a Hitachi RMU-6M (70 eV, unless otherwise noted), respectively. The ^{1}H NMR spectra were recorded on a Hitachi R-90H (90 MHz) or a Varian XL-200 (200 MHz) spectrometer using TMS as an internal reference.

4-Aryl-2-chlorothiophenes (**1**) were prepared from 2,5-dichlorothiophene by a previously described method.[8] Commercial $AlCl_3$ was used without special precautions against moisture.

Self-Condensation of 4-Aryl-2-chlorothiophene (1). Pulverized $AlCl_3$ (1.38 g, 10 mmol) was added in portions to an ice-cooled solution of **1** (10 mmol) in CH_2Cl_2 (10 ml) over ca. 5 min periods. The solution developed a dark-brown color. The reaction mixture was stirred in an ice-bath for 30 min, then at room temperature for 60 min, and finally at the reflux temperature of the solvent for an additional 30 min. The reaction mixture was poured into ice water (ca. 40 ml) and extracted with $CHCl_3$ (10 ml×3). The extracts were combined, washed successively with water, 5% $NaHCO_3$ solution, and water and dried. After removing the solvent, the residue was chromatographed (silica gel/hexane or hexane–$CHCl_3$) to afford, together with a small amount of unreacted **1**, 5-chloro-3,4′-diaryl-2,2′-bithienyl (**2**). In reactions with **1a** and **1f**, which are less soluble in CH_2Cl_2 under cooling, a mixture of CH_2Cl_2 (10 ml) and benzene (3—8 ml) was used as the solvent. In the case of **1d**, the reaction was carried out for 1 h in a mixed solvent of CH_2Cl_2 (10 ml) and anisole (10 ml) at room temperature, and then at ca. 40 °C for 30 min. Analytical samples were purified by recrystallization or chromatography.

5-Chloro-3,4′-diphenyl-2,2′-bithienyl (2a). UV (MeOH) 235 (log ε 4.44), 243 (sh, 4.43), 266 (sh, 4.36), and 320 nm (3.94); ^{1}H NMR (90 MHz; acetone-d_6) δ=7.06 (1H, s, 4-H), 7.28 (1H, d, J=1.7 Hz, 3′-H), and 7.3—7.65 (11H, m including d at 7.53, J=1.7 Hz, phenyl and 5′-H); MS *m/z* (rel intensity) 352 (M^+, 100). Found: C, 68.18; H, 3.58%. Calcd for $C_{20}H_{13}ClS_2$: C, 68.07; H, 3.71%.

5-Chloro-3,4′-di-*p*-tolyl-2,2′-bithienyl (2b). UV (MeOH) 240 (log ε 4.45), 247 (4.45), 271 (sh, 4.36), and 325 nm (3.91); ^{1}H NMR (90 MHz; acetone-d_6) δ=2.26 and 2.27 (6H, s each, CH_3), 7.00 (1H, s, 4-H), 7.09 and 7.18 (4H, AA′BB′m, *p*-phenyl), 7.20 and 7.29 (2H, AA′BB′m, *p*-phenyl), 7.33 (1H, d, J=1.3 Hz, 3′-H), and 7.4—7.5 (3H, m consisting of AA′BB′m at 7.40 and 7.49, and d at 7.50, J=1.3 Hz, *p*-phenyl and 5′-H); MS *m/z* (rel intensity) 380 (M^+, 100). Found: C, 69.40; H, 4.20%. Calcd for $C_{22}H_{17}ClS_2$: C, 69.36; H, 4.50%.

5-Chloro-3,4′-bis(*p*-ethylphenyl)-2,2′-bithienyl (2c). UV (MeOH) 244 (log ε 4.27), 271 (sh, 4.36), and 325 nm (3.73);

^{1}H NMR (90 MHz; $CDCl_3$) δ=1.19 (6H, t, J=6.8 Hz, CH_2CH_3), 2.64 (4H, q, J=6.8 Hz, CH_2CH_3), 6.90 (1H, s, 4-H), and 7.05—7.65 (10H, m, p-phenyl, 3′-H, and 5′-H); MS m/z (rel intensity) 408 (M^+, 100). Found: C, 70.22; H, 5.08%. Calcd for $C_{24}H_{21}ClS_2$: C, 70.48; H, 5.18%.

5-Chloro-3,4′-bis(p-methoxyphenyl)-2,2′-bithienyl (2d). UV (MeOH) 245 (sh, log ε 4.40), 254 (4.43), 273 (4.42), and 318—331 nm (3.89); ^{1}H NMR (90 MHz; acetone-d_6) δ=3.77 (6H, s, OCH_3), 6.85 and 6.95 (4H, AA′BB′m, p-phenyl), 7.02 (1H, s, 4-H), and 7.2—7.6 (6H, m including AA′BB′m at 7.24 and 7.34, and 7.47 and 7.57, p-phenyl, 3′-H and 5′-H); MS m/z (rel intensity) 412 (M^+, 100). Found: C, 63.99; H, 4.11%. Calcd for $C_{22}H_{17}ClO_2S_2$: C, 63.99; H, 4.15%.

5-Chloro-3,4′-di(2-naphthyl)-2,2′-bithienyl (2f). UV (MeOH) 222 (log ε 4.72), 243 (4.71), 290 (4.35), and 301 nm (sh, 4.29); ^{1}H NMR (90 MHz; $CDCl_3$) δ=7.00 (1H, s, 4-H) and 7.2—7.9 (16H, m, naphthyl, 3′-H, and 5′-H); MS m/z (rel intensity) 452 (M^+, 100). Found: C, 74.17; H, 3.59%. Calcd for $C_{28}H_{17}ClS_2$: C, 74.27; H, 3.78%.

Catalytic Dechlorination of 5-Chloro-3,4′-diaryl-2,2′-bithienyls (2). A mixture of **2** (3 mmol), KOH (1.5 g), 10% Pd–C (0.6 g), and MeOH (50 ml; MeOH (25 ml) and dioxane (50 ml) in the case of **2b** and **2d**) was stirred at room tempeprature under an atmosphere of H_2 in an atmospheric-pressure hydrogenation apparatus. After the calculated amount of H_2 was taken up (usually within 1 h), the catalyst was removed by filtration and washed with MeOH (20 ml; dioxane (20 ml) in the case of **2b** and **2d**). The combined filtrate and washings were evaporated to ca. 20 ml. Water (40 ml) was added to the residue and the resulting crystalline materials were removed by filtration, washed with a little water, dried, and chromatographed (silica gel/hexane–$CHCl_3$) to give 3,4′-diaryl-2,2′-bithienyls (**3**). The analytical sample was purified by recrystallization, sublimation under reduced pressure, or chromatography.

3,4′-Diphenyl-2,2′-bithienyl (3a). UV (MeOH) 249 (sh, log ε 4.42), 263 (4.48), and 318 nm (sh, 3.87); ^{1}H NMR (200 MHz; acetone-d_6) δ=7.17 (1H, d, J=5.2 Hz, 4-H), and 7.25—7.7 (13H, m including d at 7.53, J=5.2 Hz, 3′-H, 5′-H, 5-H, and p-phenyl); MS m/z (rel intensity) 318 (M^+, 100). Found: C, 75.16 H, 4.48%. Calcd for $C_{20}H_{14}S_2$: C, 75.43; H, 4.43%.

3,4′-Di-p-tolyl-2,2′-bithienyl (3b). UV (MeOH) 250 (sh, log ε 4.19), 265 (4.26), and 320 nm (sh, 3.74); ^{1}H NMR (200 MHz; acetone-d_6) δ=2.33 and 2.35 (6H, s each, CH_3), 7.15 (1H, d, J=5.2 Hz, 4-H), 7.19 and 7.23 (4H, AA′BB′m, p-phenyl), 7.29 and 7.33 (2H, AA′BB′m, p-phenyl), 7.39 (1H, d, J=1.5 Hz, 3′-H), 7.5—7.55 (3H, m including d at 7.52, J=5.2 Hz, and AA′BB′m at 7.53, 5-H and p-phenyl), and 7.58 (1H, d, J=1.5 Hz, 5′-H); MS m/z (rel intensity) 346 (M^+, 100). Found: C, 75.96; H, 5.15%. Calcd for $C_{22}H_{18}S_2$: C, 76.26; H, 5.24%.

3,4′-Bis(p-ethylphenyl)-2,2′-bithienyl (3c). UV (MeOH) 250 (sh, log ε 4.47), 266 (4.51), and 320 nm (sh, 3.84); ^{1}H NMR (200 MHz; acetone-d_6) δ=1.20 and 1.22 (6H, t each, J=7.6 Hz, CH_2CH_3), 2.62 and 2.64 (4H, q each, J=7.6 Hz, CH_2CH_3), 7.13 (1H, d, J=5.3 Hz, 4-H), 7.19 and 7.23 (4H, AA′BB′m, p-phenyl), 7.25—7.45 (3H, m, 3′-H and p-phenyl), and 7.5—7.7 (4H, m, 5-H, 5′-H, and p-phenyl); MS m/z (rel intensity) 374 (M^+, 100). Found: C, 76.81; H, 5.92%. Calcd for $C_{24}H_{22}S_2$: C, 76.96; H, 5.92%.

3,4′-Bis(p-methoxyphenyl)-2,2′-bithienyl (3d). UV (MeOH) 232 (sh, log ε 4.38), 250 (4.42), 272 (4.48), and 333 nm (sh, 3.76); ^{1}H NMR (200 MHz; acetone-d_6) δ=3.79 and 3.80 (6H, s each, OCH_3), 6.91 and 6.96 (4H, AA′BB′m, p-phenyl), 7.12 (1H, d, J=5.0 Hz, 4-H), 7.31 and 7.35 (2H, AA′BB′m, p-phenyl), 7.37 (1H, d, J=1.6 Hz, 3′-H), 7.46 and 7.47 (2H, d each, J=1.6 Hz, J=5.0 Hz, 5′-H and 5-H), and 7.53 and 7.57 (2H, AA′BB′m, p-phenyl); MS m/z (rel intensity) 378 (M^+, 100). Found: C, 69.87; H, 4.72%. Calcd for $C_{22}H_{18}O_2S_2$: C, 69.81; H, 4.79%.

3,4′-Di(2-naphthyl)-2,2′-bithienyl (3f). UV (MeOH) 222 (log ε 4.79), 244 (sh, 4.71), 263 (sh, 4.63), and 290 nm (sh, 4.45); ^{1}H NMR (200 MHz; acetone-d_6) δ=7.33 (1H, d, J=5.2 Hz, 4-H), 7.45—7.6 (4H, m, naphthyl), 7.62 (1H, d, J=5.2 Hz, 5-H), 7.66 (1H, d, J=1.6 Hz, 3′-H), 7.77 (1H, d, J=1.6 Hz, 5′-H), 7.8—8.2 (10H, m, naphthyl); MS m/z (rel intensity) 418 (M^+, 100). Found: C, 80.07; H, 4.17%. Calcd for $C_{28}H_{18}S_2$: C, 80.34 H, 4.33%.

Coupling of 4-Aryl-2-chlorothiophenes (1). The procedure is a modification of the one described by Tiecco et al.[11] for the preparation of bipyridyls, in which $NiCl_2$ is used instead of $NiCl_2 \cdot 6H_2O$. To a solution of $NiCl_2$ (0.65 g, 5 mmol) and PPh_3 (5.2 g, 20 mmol) in N,N-dimethylformamide (25 ml), Zn powder (0.32 g, 5 mmol) was added under an N_2 atmosphere. The mixture was stirred at 50 °C for 1 h. 4-Aryl-2-chlorothiophene (**1**; 5 mmol) was added to the resulting red brown solution. After stirring for 30 min, the mixture was poured into H_2O (50 ml). The precipitate was filtered, washed with H_2O (20 ml), and dried.

(a) When the coupling product was soluble in $CHCl_3$, as were the cases with **4e** and **4g**, the precipitate was directly chromatographed (silica gel/hexane–$CHCl_3$ (3:2)), giving **4e** or **4g** together with PPh_3 and a small amount of the dechlorination product of **1e** or **1g**. (b) When the coupling product was less soluble in $CHCl_3$ (**4d** and **4f**), the precipitate was washed with the solvent (20 ml×2) and the PPh_3-free residue was then sublimed under reduced pressure (230 °C (bath)/1 mmHg; 1 mmHg=133.322 Pa) or treated with hot 10% HCl (20 ml) and washed with H_2O to give **4d** or **4f**. (c) In the cases with **1a**, **1b**, and **1c**, the precipitate was extracted with $CHCl_3$ (20 ml×2). The undissolved solid was recrystallized from $CHCl_3$ to yield the coupling product. Evaporation of the combined extracts followed by column chromatography (silica gel/hexane–$CHCl_3$ (3: 1—2)) gave another crop of the product.

The analytical samples were purified by recrystallization.

4,4′-Diphenyl-2,2′-bithienyl (4a). UV (MeOH) 258 (log ε 4.74) and 323 nm (4.06); ^{1}H NMR (90 MHz, $CDCl_3$); δ=7.2—7.7 (m, phenyl, 3-H, 3′-H, 5-H, and 5′-H); MS m/z (rel intensity) 318 (M^+, 100). Found: C, 75.51; H, 4.27%. Calcd for $C_{20}H_{14}S_2$: C, 75.43; H, 4.43%.

4,4′-Di-p-tolyl-2,2′-bithienyl (4b). UV (MeOH) 261 (log ε 4.71) and 325 nm (3.96); ^{1}H NMR (90 MHz, $CDCl_3$) δ=2.38 (6H, s, CH_3), 7.1—7.3 (6H, m including AA′BB′m at 7.16 and 7.25, and d at 7.28, J=1.6 Hz, p-phenyl, 3-H, and 3′-H), and 7.3—7.55 (6H, m including AA′BB′m at 7.46 and 7.55, p-phenyl, 5-H, and 5′-H); MS m/z (rel intensity) 346 (M^+, 100). Found: C, 76.23; H, 5.24%. Calcd for $C_{22}H_{18}S_2$: C, 76.26; H, 5.24%.

4,4′-Bis(p-ethylphenyl)-2,2′-bithienyl (4c). UV (MeOH) 260 (log ε 4.78) and 325 nm (4.02); ^{1}H NMR (90 MHz, $CDCl_3$) δ=1.26 (6H, t, J=7.6 Hz, CH_2CH_3), 2.67 (4H, q, J=7.6 Hz, CH_2CH_3), 7.05—7.3 (6H, m including AA′BB′m at 7.17 and

7.27, and d at 7.28, J=1.5 Hz, p-phenyl, 3-H, and 3′-H), and 7.35—7.65 (6H, m including d at 7.46, J=1.5 Hz, and AA′BB′m at 7.47 and 7.57, 5-H, 5′-H, and p-phenyl); MS m/z (rel intensity) 374 (M^+, 100). Found: C, 77.16; H, 5.86%. Calcd for $C_{24}H_{22}S_2$: C, 77.16; H, 5.92%.

4,4′-Bis(p-methoxyphenyl)-2,2′-bithienyl (4d). UV (MeOH; molar extinction coefficients were not determined because of low solubility) 265 and 302 nm (sh); ^{1}H NMR (90 MHz, pyridine-d_5 peak intensities were not determined because of low solubility) δ=3.75 (s, OCH_3), 7.09 and 7.18 (AA′BB′m p-phenyl), 7.76 and 7.85 (AA′BB′m, p-phenyl), 7.77 (d, J=1.4 Hz, 3-H and 3′-H), and 7.90 (d, J=1.4 Hz, 5-H and 5′-H); MS m/z (rel intensity) 378 (M^+, 100). Found: 69.95; H, 4.67%. Calcd for $C_{22}H_{18}O_2S_2$: C, 69.81; H, 4.67%.

4,4′-Bis(2,4-dimethylphenyl)-2,2′-bithienyl (4e). UV (MeOH) 253 (log ε 4.45) and 322 nm (4.20); ^{1}H NMR (90 MHz, $CDCl_3$) δ=1.50 (12H, s, CH_3), 6.85—7.4 (10H, m including d at 7.03 and 7.21, J=1.4 Hz, 3-H, 3′-H, 5-H, 5′-H, and trisubstituted phenyl); MS m/z (rel intensity) 374 (M^+, 100). Found: C, 77.26; H, 5.92%. Calcd for $C_{24}H_{22}S_2$: C, 76.96; H, 5.92%.

4,4′-Di(2-naphthyl)-2,2′-bithienyl (4f). UV (MeOH; molar extinction coefficients were not determined because of low solubility) 257, 290, and 306 nm (sh); ^{1}H NMR (90 MHz, pyridine-d_5; peak intensities were not determined because of low solubility) δ=7.4—8.4 (m including d at 7.87 and 8.08, J=1.5 Hz each, naphthyl, 3-H, 3′-H, 5-H, and 5′-H); MS m/z (rel intensity) 418 (M^+, 100). Found: C, 80.47; H, 4.12%. Calcd for $C_{28}H_{18}S_2$: C, 80.34; H, 4.33%.

4,4′-Bis(5,6,7,8-tetrahydro-2-naphthyl)-2,2′-bithienyl (4g). UV (MeOH) 252 (sh, log ε 4.61), 258 (sh, 4.75), 264 (4.75), and 326 nm (4.00); ^{1}H NMR (90 MHz, $CDCl_3$) δ=1.6—1.95 (8H, m, $PhCH_2CH_2$), 2.78 (8H, br s, $PhCH_2$), 6.9—7.35 (8H, m including d at 7.24, J=1.5 Hz, 3-H, 3′-H, and trisubstituted phenyl), and 7.43 (2H, d, J=1.5 Hz, 5-H and 5′-H); MS m/z (rel intensity) 426 (M^+, 100). Found: C, 79.09; H, 6.09%. Calcd for $C_{28}H_{26}S_2$: C, 78.83; H, 6.14%.

2,5-Dichloro-3-phenylthiophene. Sulfonyl chloride (8.1 g, 60 mmol) was added to a stirred solution of **1** (7.8 g, 40 mmol) in CCl_4 (60 ml) over ca. 5 min period and the mixture refluxed for 60 h. The reaction mixture was poured into ice water (ca. 40 ml) and extracted with CCl_4 (15 ml×3). The extracts were combined, washed successively with water, 5% $NaHCO_3$ solution, and water again, and dried. After evaporating the solvent, the residue was chromatographed (silica gel/hexane) to afford 2,5-dichloro-3-phenylthiophene (4.6 g, 50%) as an oil. UV (MeOH) 233 (log ε 4.33) and 260 nm (3.92); ^{1}H NMR (90 MHz, CCl_4) δ=6.83 (1H, s, 4-H), 7.21—7.49 (5H, m, phenyl); MS m/z (rel intensity) 230 (M^++2, 69), 228 (M^+, 100). Found: C, 52.45; H, 2.50%. Calcd for $C_{10}H_6Cl_2S$: C, 52.42; H, 2.64%.

Coupling of 2,5-Dichloro-3-phenylthiophene. 2,5-Dichloro-3-phenylthiophene (0.8 g, 3.5 mmol) was subjected to coupling under the conditions described above, except for the reaction period (12 h instead of 1 h). A work-up and repeated chromatography (silica gel/hexane) of the reaction mixture gave 5-chloro-4,4′-diphenyl-2,2′-bithienyl (0.1 g, 15%) together with 2,5-dichloro-3-phenylthiopheene (0.2 g, 25%) and 2-chloro-3-phenylthiophene (0.2 g, 30%). The structure of the 5-chloro-4,4′-diphenyl-2,2′-bithienyl was confirmed by its catalytic dechlorination, which gave the known 4,4′-diphenyl-2,2′-bithienyl.

5-Chloro-4,4′-diphenyl-2,2′-bithienyl. Pale yellow needles, mp 144—145 °C (hexane–$CHCl_3$); UV (MeOH) 254 (log ε 4.63), 328 (4.11), and 351 nm (sh, 3.78); ^{1}H NMR (90 MHz, $CDCl_3$) δ=7.23 (1H, s, 3-H), 7.35—7.8 (12H, m including d at 7.48 and 7.63, J=1.7 Hz each, phenyl, 3′-H, and 5′-H); MS m/z (rel intensity) 354 (M^++2, 40), 352 (M^+, 100). Found: C, 68.07; H, 3.48%. Calcd for $C_{20}H_{13}ClS_2$; C, 68.07; H, 3.71%.

The authors would like to thank Professor Kensuke Takahashi of Nagoya Institute of Technology for recording the NMR spectrum of the protonated 2-chloro-4-phenylthiophene and the 200 MHz spectra of 3,4′-diaryl-2,2′-bithienyls.

References

1) Acid-catalyzed Reactions of Thiophene Nuclei. VII. Presented in parts at the 9th International Congress of Heterocyclic Chemistry, Tokyo, August 1983, Abstr., p. 178 and at the 57th Annual Meeting of the Chemical Society of Japan, Sendai, September 1988, Abstr., p. 561. Part VI. Ref. 8.

2) J. Nakayama, S. Murabayashi, and M. Hoshino, *Heterocycles*, **26**, 2599 (1987). Y. Nakamura, S. Murabayashi, J. Nakayama, and M. Hoshino, the 52nd Annual Meeting of Chemical Society of Japan, Tokyo, 1986, Abstr. II, p. 1248; S. Murabayashi, J. Nakayama, and M. Hoshino, *ibid.*, p. 1247.

3) W. Steinkopf, R. Leitsmann, and K. H. Hoffmann, *Ann.*, **546**, 180 (1941); A. I. Kosak, *J. Am. Chem. Soc.*, **76**, 4450 (1954).

4) A. L. Jonson, *J. Org. Chem.*, **41**, 1320 (1976).

5) T. Sone, M. Kubo, and T. Kanno, *Chem. Lett.*, **1982**, 1195. In connection with the study 5,5′-Diphenyl-3,3′-bithienyl has also been prepared.

6) 2,5-Thienylene based oligomers with aryl group at the 3-position, for example, M. Sato, S. Tanaka, and K. Kaeriyama, *J. Chem. Soc., Chem. Commun.*, **1987**, 1725; M. Sato, S. Tanaka, and K. Kaeriyama, *Makromol. Chem.*, **190**, 1233 (1989).

7) T. Sone, R. Yokoyama, Y. Okuyama, and K. Sato, *Bull. Chem. Soc. Jpn.*, **59**, 83 (1986).

8) T. Sone, M. Inoue, and K. Sato, *Bull. Chem. Soc. Jpn.*, **61**, 3779 (1988).

9) S. Gronowitz, "Advances in Heterocyclic Chemistry," ed by A. R. Katritzky, Academic Press, New York (1963), Vol. 1, p. 7.

10) The spectrum was taken at 60 MHz in a similar manner as described previously; Y. Yokoyama, Y. Yamashita, K. Takahashi, and T. Sone, *Bull. Chem. Soc. Jpn.*, **56**, 2208 (1983).

11) M. Tiecco, L. Testaferri, M. Tingoli, D. Chianelli, and M. Montanucci, *Synthesis*, **1984**, 737.

12) I. Colon and D. R. Kelsey, *J. Org. Chem.*, **51**, 2627 (1986); P. Caubere, *Angew. Chem.*, **95**, 597 (1983).

 © 1991 The Chemical Society of Japan Bull. Chem. Soc. Jpn., 64, 869—876 (1991)

Synthesis of 5,6-Dideoxy-5-phenylphosphinyl-L-galactopyranoses. The P-in-Ring Sugar Analogs of L-Fucose

Tadashi HANAYA, Hiroshi YAMAMOTO, Takeshi OHMAE, Heizan KAWAMOTO, Margaret-Ann ARMOUR,† Alan M. HOGG,† and Hiroshi YAMAMOTO*
Department of Chemistry, Faculty of Science, Okayama University, Tsushima, Okayama 700
† Department of Chemistry, University of Alberta, Edmonton, Alta., T6G 2G2, Canada
(Received November 5, 1990)

1,2-*O*-Isopropylidene-3-*O*-methyl-6-*O*-tosyl-β-D-*arabino*-hexofuranos-5-ulose (**9a**) and its 3-*O*-benzyl congener (**9b**) were prepared from 1,2:5,6-di-*O*-isopropylidene-β-D-altrofuranose in 4 steps. Addition of methyl phenylphosphinate to **9a** and **9b** in the presence of DBU, followed by reduction with Raney Ni, afforded (5*R* and 5*S*)-5,6-dideoxy-1,2-*O*-isopropylidene-5-[(methoxy)phenylphosphinyl]-3-*O*-methyl-β-D-*arabino*-hexofuranose (**11a**) and 3-*O*-benzyl congener (**11b**), respectively. The latter compound (**11b**) was debenzylated to 3-*O*-unsubstituted hexofuranose **11d**. By reduction with sodium dihydrobis(2-methoxyethoxy)aluminate, followed by acid hydrolysis, these key intermediates **11a**, **11b**, and **11d** provided the title L-fucoses **13** (together with a minor proportion of D-altropyranoses **14**) having as phenylphosphinylidene group in place of the ring oxygen. Compounds **13** and **14** were converted into per-*O*-acetyl derivatives for structural and conformational analysis by spectroscopy.

Sugar analogues having a phosphorus atom in the hemiacetal ring have been prepared in recent years;[1] e.g., those corresponding to D-ribofuranoses **1**[2] and D-glucopyranoses **2**.[3] These P-in-ring sugars have drawn interest in view of their physicochemical properties as well as potential biological activity. In the mean time, 1,5-imino-L-fucitol (**3**)[4] and 5-thio-L-fucose (**4**)[5] were synthesized and both compounds have been proven to inhibit L-fucosidase. We describe herein a detailed synthetic study on the first P-in-ring L-fucose analogues by placing phenylphosphinylidene in the hemiacetal ring as a model functional group.[6]

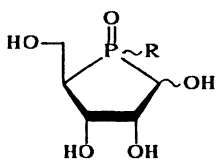

1 R=Et, Ph, OH

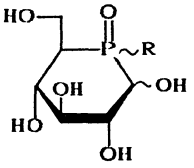

2 R=Et, OH

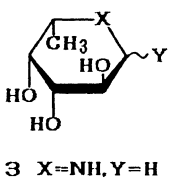

3 X=NH, Y=H
4 X=S, Y=OH

Results and Discussion

1,2:5,6-Di-*O*-isopropylidene-β-D-altrofuranose (**5**)[7] (available from D-glucose) served as the starting material for preparation of the important key intermediate, 3-*O*-substituted 1,2-*O*-isopropylidene-6-*O*-tosyl-β-D-*arabino*-hexofuranos-5-uloses (**9a—c**), by the sequence illustrated in Scheme 1.

Thus, 3-*O*-methylation of **5** using NaH–MeI in 1,2-dimethoxyethane (DME) was found to furnish a higher yield of 3-*O*-methyl derivative **6a** than that by the previously reported method (MeI–Ag_2O in DMF).[8] The selective deprotection of **6a** with acid afforded 1,2-*O*-isopropylidene-3-*O*-methyl-β-D-altrofuranose (**7a**),[8] which was then treated with tosyl chloride in pyridine to give the 6-*O*-tosyl derivative **8a**. Oxidation of **8a** with pyridinium chlorochromate (PCC) in dichloromethane in the presence of molecular sieves (3A) gave 3-*O*-methyl-5-ulose **9a** in 95% yield.

The reaction of **9a** with methyl phenylphosphinate in DME in the presence of DBU gave 5,6-anhydro-5-[(methoxy)phenylphosphinyl] compound (**10a**) as a mixture of the diastereomers with regard to C-5 and P atom. Hydrogenation of **10a** in the presence of Raney-Ni (W-4) in ethanol afforded the 5,6-dideoxy derivative **11a**.

Compound **11a** was reduced with dihydrobis(2-methoxyethoxy)aluminate (SDMA) to give the unstable 5,6-dideoxy-5-phenylphosphinyl derivative **12a**, which was immediately treated with ethanolic 0.5 M hydrochloric acid (1 M=1 mol dm^{-3}) at 90 °C, thus affording a crude mixture of 5,6-dideoxy-3-*O*-methyl-5-phenylphosphinyl-L-galacto- (L-fucose, **13a**) and -D-altropyranoses (**14a**) as shown in Scheme 1.

These products were characterized after having been converted into the corresponding tri-*O*-acetyl derivatives **15** and **16** by the usual method. By purification in a silica-gel column, the presence of the following five diastereomers was confirmed, although some of the minor products were not completely separable (see the Experimental section): 5,6-dideoxy-5-[(*R*)-phenylphosphinyl]-α-L-galactopyranose (**15A**, 9.8% overall yield from **11a**), the β-anomer **15B** (2.1%), the 5-[(*S*)-*P*]-α-isomer **15C** (7.1%), 5,6-dideoxy-5-[(*S*)-phenylphosphinyl]-α-D-altropyranose (**16A**, 2.1%), the β-anomer **16B** (9.1%). Structures and the preferable conformations of these products were established on the basis of high-resolution mass spectrometry and 500 MHz ^1H NMR spectral data (see below).

Similarly, synthesis of 3-*O*-benzyl congeners **13b** and **14b** was performed by the sequence of **5**→**6b**→**7b**→**8b**→**9b**→**10b**→**11b**→**12b**→**13b** and **14b**. The unambiguous structural assignments of **13b** and **14b** were

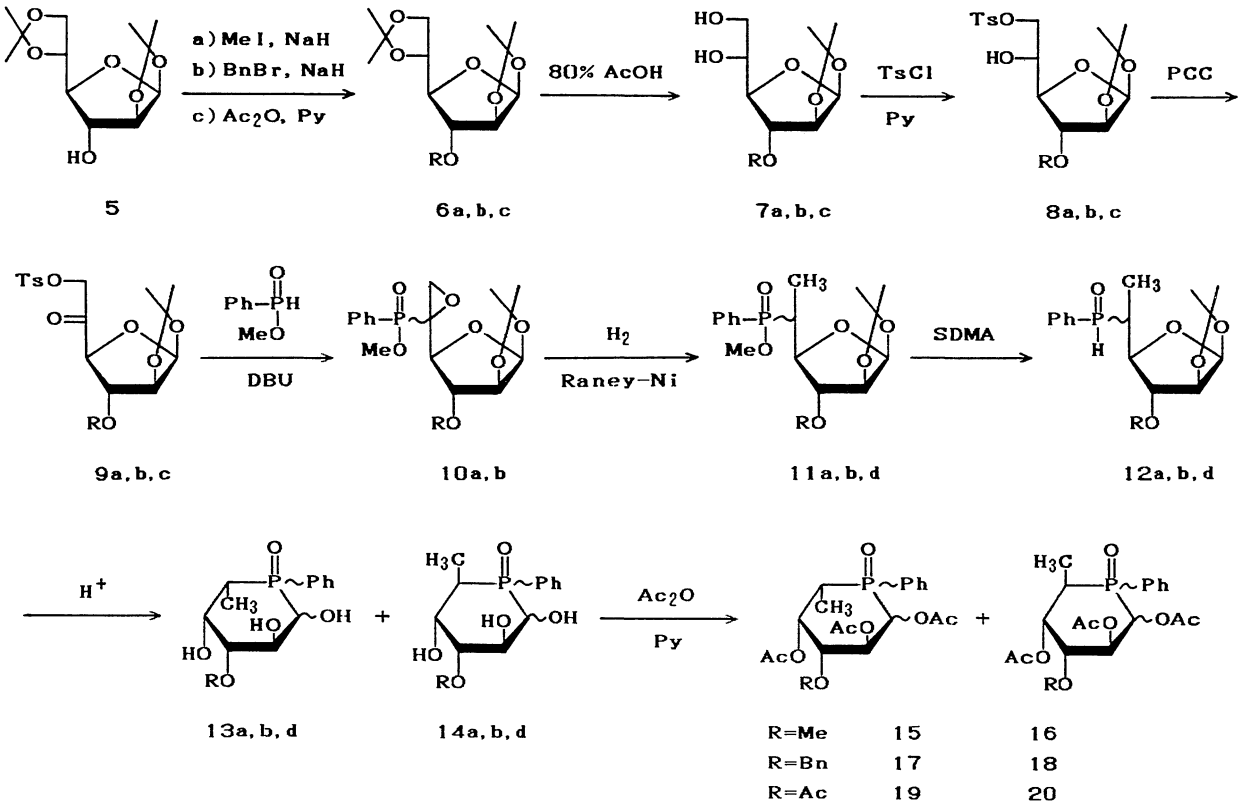

Scheme 1. Synthesis of 5,6-dideoxy-5-phenylphosphinyl-L-galacto- and -D-altropyranoses. **a**: R=Me. **b**: R=Bn. **c**: R=Ac. **d**: R=H.

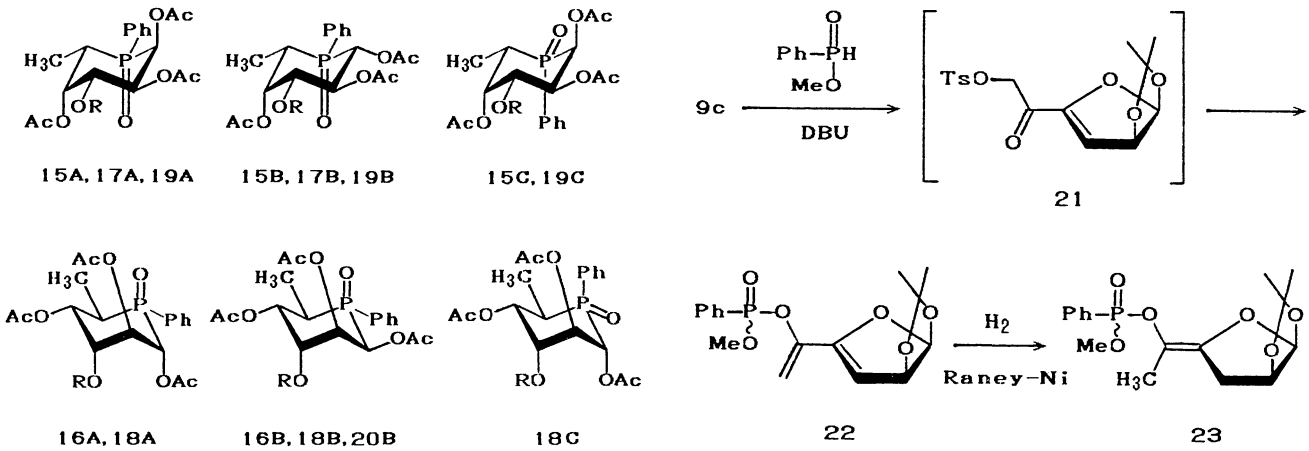

Scheme 2.

made by converting them into their triacetates **17** and **18**, which were separated into five diastereomers: **17A** (4.4% overall yield from **11b**), **17B** (1.1%), **18A** (1.3%), **18B** (9.3%), and **18C** (4.4%).

These successful synthesis of 3-*O*-alkyl-L-fucose analogues **13a** and **13b** prompted us to prepare 3-*O*-unsubstituted compound **13d**. Thus, following the synthetic scheme analogous to that used for **9a**, **b**, we prepared 3-*O*-acetyl-5-ulose **9c** from **5** by the sequence of **5**→**6c**[9]→**7c**→**8c**→**9c**. However, when **9c** was treated with methyl phenylphosphinate and DBU in DME as in the cases of **9a** and **9b**, the main product turned out to be the enol phosphonate **22**. This is presumably formed from **9c** as the result of the prior elimination of AcOH by the action of DBU to give an activated α-tosyloxycarbonyl compound **21**, which in turn undergoes the Perkow[10] type reaction with methyl phenylphosphinate to afford **22** as illustrated in Scheme 2. Although many examples are well known for the Perkow reactions of α-halo-, α-acetoxy-,[11] and α-tosyloxycarbonyl compounds[12] with trialkyl phosphites, the reactions with alkyl phosphinate appear to be rare, to our knowledge. The catalytic hydrogen-

ation of **22** in the presence of Raney-Ni afforded hex-4-enofuranose **23**.

Therefore, we turned our attention to another approach for preparation of **13d**: namely, from **11b** in stead of **9c**. Debenzylation of **11b** by catalytic hydrogenation over 20% $Pd(OH)_2$–C in ethanol smoothly provided **11d**. By the same procedures described above, compound **11d** was converted into a mixture of **13d** and **14d** via **12d** (Scheme 1). The structures of **13d** and **14d** were similarly established by derivatization into tetraacetates **19** and **20** that were separated by column chromatography into four diastereomers: **19A** (11% overall yield from **11d**), **19B** (2.7%), **19C** (4.2%), and **20B** (3.5%).

^{1}H NMR Spectral Analysis of Per-*O*-acetyl-5,6-dideoxy-5-phenylphosphinyl-L-galactopyranoses (15A—C, 17A,B, 19A—C) and D-Altropyranoses (16A,B, 18A—C, 20B). For structural assignments of these new products **15—20**, the chemical shift of each proton signal of their NMR spectra and the dependence of the $^2J_{H,P}$, $^3J_{H,P}$, and $^3J_{H,H}$ values on their dihedral angles were carefully taken into consideration. The precise parameters thereby obtained for the these compounds are summarized in Table 1. Since the parameters for 5,6-dideoxy-5-phosphinyl-L-galacto- and -D-altropyranoses have been obtained for the first time in the present study, some characteristic features of **15—20** are discussed here in detail. These parameters are instructive in determining the structures of other similar phosphinyl-in-ring sugar analogues, preparation of which is currently under investigation.

(1) A series of compounds **15**, **17**, and **19** characteristically show small values of $J_{4,5}$ (2.3—3.0 Hz) and $J_{2,P}$ (0—4 Hz) and large values of $J_{2,3}$ (9.8—10.9 Hz) and $J_{4,P}$ (28—31 Hz), whereas another series of compounds **16**, **18**, and **20** exhibit opposite magnitudes of the

Table 1. ^{1}H NMR (500 MHz) Parameters for **15—20** in $CDCl_3$

Compd	Chemical shift (δ)											
	H-1	H-2	H-3	H-4	H-5	H-6	MeO-3 (CH_2O-3)[c]	Ac-1,2,4[a] (Ac-1,2,3,4)	Ph(*o*)	Ph(*m*)	Ph(*p*)[b]	^{31}P
5,6-Dideoxy-5-phenylphosphinyl-L-galactopyranoses												
15A	5.77	5.85	3.68	5.87	2.61	1.19	3.46	2.23, 2.00, 1.95	7.75	7.51	7.59	30.9
15B	5.62	5.90	3.50	5.79	2.30	1.17	3.44	2.24, 2.04, 1.95	7.76	7.51	7.58	33.2
15C	6.17	5.57	3.74	5.61	2.73	1.28	3.43	2.24, 2.11, 1.65	7.76	7.51	7.58	30.9
17A	5.78	5.90	3.92	5.89	2.59	1.19	(4.76, 4.54)	2.23, 1.96, 1.89	7.74	7.49	7.58 d)	30.4
17B	5.57	5.96	3.70	5.80	2.30	1.16	(4.75, 4.49)	2.25, 1.97, 1.96	7.74	7.50	7.57 d)	32.7
19A	5.80	5.95	5.39	5.76	2.72	1.15		(2.23, 2.03, 1.97, 1.95)	7.75	7.52	7.59	30.5
19B	5.64	6.05	5.16	5.66	2.29	1.12		(2.25, 2.02, 2.00, 1.95)	7.76	7.53	7.61	30.4
19C	6.24	5.65	5.41	5.49	2.82	1.30		(2.26, 2.06, 1.98, 1.61)	7.94	7.57	7.62	30.1
5,6-Dideoxy-5-phenylphosphinyl-D-altropyranoses												
16A	5.37	5.49	3.80	5.60	3.02	1.16	3.60	2.18, 2.09, 1.96	7.80	7.51	7.59	35.2
16B	5.69	5.77	3.85	5.64	2.70	1.10	3.61	2.23, 2.13, 1.94	7.76	7.51	7.57	30.1
18A	5.38	5.50	4.01	5.58	3.10	1.15	(4.74, 4.63)	2.20, 2.07, 1.97	7.80	7.51	7.59 d)	35.0
18B	5.82	5.77	4.04	5.59	2.76	1.09	(4.86, 4.67)	2.22, 1.98, 1.96	7.76	7.50	7.57 d)	29.9
18C	5.94	5.75	3.89	5.60	3.16	1.23	(4.83, 4.67)	2.07, 1.97, 1.73	7.96	7.53	7.59 d)	33.2
20B	5.70	5.59	5.57	5.66	2.59	1.14		(2.25, 2.24, 2.00, 1.96)	7.76	7.53	7.61	29.6

Compd	Coupling constant (Hz)									
	$J_{1,2}$	$J_{1,P}$	$J_{2,3}$	$J_{2,P}$	$J_{3,4}$	$J_{3,P}$	$J_{4,5}$	$J_{4,P}$	$J_{5,6}$	$J_{5,P}$	$J_{6,P}$
5,6-Dideoxy-5-phenylphosphinyl-L-galactopyranoses											
15A	2.9	11.8	10.4	0	2.8	0	2.7	27.9	7.3	6.7	14.8
15B	11.1	2.7	9.9	2.3	2.8	0	2.5	29.1	7.2	5.0	14.7
15C	3.1	8.6	9.8	4.2	2.8	0	2.9	29.6	7.3	21.2	14.6
17A	2.9	11.7	10.4	0	3.0	0	3.0	27.9	7.3	6.6	15.0
17B	11.0	2.8	9.9	2.4	2.8	0	2.3	29.5	7.2	5.0	14.5
19A	2.9	11.7	10.9	0	3.0	0	2.9	28.2	7.3	5.9	15.0
19B	11.1	2.8	10.4	2.3	2.7	0	2.8	29.3	7.3	5.0	14.7
19C	3.0	9.6	10.7	0	2.8	0	2.5	30.7	7.3	20.7	14.2
5,6-Dideoxy-5-phenylphosphinyl-D-altropyranoses											
16A	3.4	9.6	4.7	20.1	2.3	1.0	11.5	6.4	7.2	6.1	14.9
16B	3.5	0.5	5.2	24.9	2.3	1.8	12.0	4.1	7.2	4.1	14.8
18A	3.4	9.5	4.5	20.2	2.2	1.2	11.8	6.8	7.2	6.5	14.9
18B	3.5	0.5	5.0	24.7	2.3	1.8	12.3	4.0	7.1	4.1	15.0
18C	3.9	13.8	5.1	27.6	2.2	1.8	12.7	3.2	7.2	20.9	15.3
20B	3.5	0.8	5.0	25.3	2.5	1.8	12.1	4.0	7.2	4.1	14.8

a) The assignments of acetoxyl groups may have to be interchanged. b) J values for *P*-Ph: $J_{P,o}$=12.5, $J_{P,m}$=3.5, $J_{P,p}$=1.5, $J_{o,m}$=$J_{m,p}$=7.5, and $J_{o,p}$=1.5 Hz. c) $^2J_{CH_2}$=11.9 Hz. d) *C*-Ph: δ=7.29—7.41 (5H, m).

corresponding coupling constants, namely relatively large values of $J_{4,5}$ (11.5—12.7 Hz) and $J_{2,P}$ (20—28 Hz) and small values of $J_{2,3}$ (4.5—5.2 Hz) and $J_{4,P}$ (3.2—6.8 Hz). By applying the arguments similar to these employed for distinction between 5-deoxy-5-phosphinyl-L-gulo- and -D-mannopyranoses,[13] the above two series of compounds **15,17,19** and **16,18,20** can be assigned to have structures of L-galactopyranose predominantly in the $^1C_4$(L) conformation and D-altropyranose in the $^4C_1$(D) conformation, respectively.

(2) As the H-5 of **15—20** is all in axial position, the magnitudes of $J_{5,P}$ values establishes the orientation of the ring P=O group in these compounds. The small values of $J_{5,P}$ (4.1—6.7 Hz) are indicative of the anti orientation of H-C(5)-P=O for **15—19A,B** and **20B**. On the other hand, because of the large values of $J_{5,P}$ (20.7—21.2 Hz), the equatorial P=O orientation is assigned to **15C**, **18C**, and **19C**. The orientation of the ring P=O group in these compounds should also be derived by examining the δ values of H-2 for **15**, **17**, and **19** and of H-4 for **16**, **18**, and **20**, although care must be taken when the inclination of the axially oriented *P*-phenyl ring exerts an anisotropic effect on H-2 and/or H-4 of 1,3-diaxial position.[14] An appreciable downfield shift (0.3—0.4 Hz) is observed for **15A,B**, **17A,B**, and **19A,B** (compared with the chemical shifts of **15C** and **19C**), thus confirming the axial orientation of the ring P=O for the compounds of the former group (**A** and **B**).

(3) The anomeric orientation of C-1 is derived from the values of $J_{1,P}$ and $J_{1,2}$ and also in some cases the δ values of H-5. Namely, the small values of $J_{1,P}$ (0.5—2.8 Hz) of **15—20B** and the large $J_{1,P}$ values (8.6—13.8 Hz) of **15—19A,C** suggest respectively the anti and gauche connection of H-C(1)-P=O for these compounds. The large value of $J_{1,2}$ (11 Hz) of **15—20B** confirms the axial H-1 orientation for **15B**, **17B**, and **19B**, whereas the smaller $J_{1,2}$ value (3 Hz) points out the equatorial H-1 configuration for **15A,C**, **17A**, and **19A,C** in the L-galactopyranose series. For a series of the D-altropyranoses whose H-2 are in the equatorial position and thus $J_{1,2}$ values are all similar and small (ca. 3.5 Hz), an appreciable downfield shift (0.3—0.4 ppm) of H-5 caused by the axially situated AcO group on C-1 can be used for distinction between the α-anomers (**16A** and **18A,C**) and β-anomers (**16B**, **18B**, and **20B**).

Present work thus demonstrates a possible way for preparation of 5,6-dideoxy-5-phosphinyl-L-galactopyranoses from appropriate intermediates. Extension of this work including preparative studies on improved product ratios of the L-fucose type analogues in conection with other kinds of substituents at P-5 and O-3 of the precursors **11** and **12**, as well as biological evaluation of the compounds, is in progress.

Experimental

Melting points were determined with a Yanagimoto MP-S3 instrument and are uncorrected. All reactions were monitored by TLC (Merck silica gel 60F, 0.25 mm) with (*A*) 1:1 AcOEt–hexane or (*B*) AcOEt as the eluant; components were detected by exposing the plates to a UV light (254 nm) and/or by spraying them with 20% sulfuric acid–ethanol, with subsequent heating. Column chromatography was performed on Wako C-200 silica gel. Optical rotation were measured with a Nihon-Bunko DIP-4 polarimeter at 25 °C. The IR spectra were taken with a Hitachi 260-105 infrared spectrophotometer. The ^{1}H and ^{31}P NMR spectra were measured in $CDCl_3$ with Varian VXR-500 and VXR-200 instruments (500 and 81 MHz, respectively, the SC-NMR Lab., Okayama Univ. at 21 °C) or with a Hitachi R-600 (60 MHz, FT) spectrometer. Chemical shifts are reported as δ values relative to tetramethylsilane (internal standard for ^{1}H) and 85% phosphoric acid (external standard for ^{31}P). The assignments of all signals obtained at 500 MHz were made by employing a first-order analysis with the aid of decoupling technique and, if necessary, two-dimensional COSY measurements; the parameters were confirmed by a computer-assisted simulation analysis. The mass spectra were taken on an A.E.I. MS 50 ultrahigh resolution instrument and were given in terms of *m/z* (rel intensity) compared with the base peak.

1,2:5,6-Di-*O*-isopropylidene-3-*O*-methyl-β-D-altrofuranose (6a)[8] and Its 3-*O*-Benzyl Congener (6b). The following procedures resulted in a better yield of **6a** than the reported method using MeI–Ag_2O.[8] Thus, to a solution of **5**[7] (1.35 g, 5.19 mmol) in DME (10 ml) was added, with stirring, sodium hydride [500 mg, 60% in mineral oil (which was washed with DME), 2.4 equiv] in small portions at 0 °C under an argon atmosphere. To this suspension was dropwise added methyl iodide (1.00 ml, 16.1 mmol) at 0 °C. The mixture was stirred at 25 °C for 2 h and then methanol (8 ml) was added at 0 °C. The mixture was stirred at 25 °C for 0.5 h and evaporated in vacuo. The residue was dissolved in CH_2Cl_2, washed with water, dried (Na_2SO_4), and evaporated in vacuo. The residue was purified by column chromatography, giving **6a** (1.37 g, 96%) as a colorless syrup (cf. lit,[8] 88% yield): R_f=0.73 (*A*).

The procedures similar to those for **6a** from **5** were employed for preparation of **6b**. Thus, **5** (510 mg, 1.96 mmol) was treated with sodium hydride (60% in oil, 200 mg, 2.6 equiv) and benzyl bromide (0.47 ml, 3.95 mmol) at 25 °C for 3 h. Purification by column chromatography gave **6b** (625 mg, 91%) as a colorless syrup: R_f=0.80 (*A*); $[\alpha]_D$+4.0° (*c* 1.20, $CHCl_3$); ^{1}H NMR (500 MHz) δ=1.31, 1.51 (3H each, 2s, Me_2C-O-1,2), 1.35, 1.43 (3H each, 2s, Me_2C-O-5,6), 3.99 (1H, dd, $J_{6,6'}$=8.8, $J_{5,6'}$=4.9 Hz, H-6'), 4.03 (1H, dd, $J_{4,5}$=9.3, $J_{3,4}$=1.6 Hz, H-4), 4.11 (1H, dd, $J_{5,6}$=6.2 Hz, H-6), 4.19 (1H, d, $J_{2,3}\approx$0 Hz, H-3), 4.25 (1H, ddd, H-5), 4.58, 4.60 (1H each, 2d, ^2J=11.7 Hz, CH_2O-3), 4.64 (1H, d, $J_{1,2}$=3.8 Hz, H-2), 5.89 (1H, d, H-1), 7.34 (5H, m, Ph); MS *m/z* 335 (M-CH_3; 2.7), 292 (1.5), 249 (4.1), 221 (2.5), 163 (2.5), 129 (3.0), 105 (12), 91 (100). Found: *m/z* 335.1494. Calcd for $C_{18}H_{23}O_6$: M-CH_3, 335.1494.

General Procedures for the Preparation of 3-*O*-Substituted 1,2-*O*-Isopropylidene-β-D-altrofuranoses (7a—c). A mixture of **6** (4.78 mmol) and 80% aqueous acetic acid (15 ml) was stirred at 60 °C for 2 h. The solution was evaporated in vacuo and the residue was purified by use of column

chromatography on silica gel, giving **7**.

3-*O*-Methyl Derivative (7a):[8] Colorless syrup (83% from **6a**, lit,[8] 79%); R_f=0.14 (*A*).

3-*O*-Benzyl Derivative (7b): Colorless needles (85% from **6b**); mp 68—69 °C (from AcOEt–hexane); R_f=0.23 (*A*); $[\alpha]_D$+4.2° (*c* 1.33, $CHCl_3$); ^1H NMR (500 MHz) δ=1.33, 1.52 (3H each, 2s, CMe_2), 2.15 (2H, br s, HO-5,6), 3.72 (1H, dd, $J_{6,6'}$=11.3, $J_{5,6'}$=5.4 Hz, H-6′), 3.76 (1H, dd, $J_{5,6}$=3.9 Hz, H-6), 3.91 (1H, ddd, $J_{4,5}$=7.5 Hz, H-5), 4.05 (1H, dd, $J_{3,4}$=2.9 Hz, H-4), 4.21 (1H, d, $J_{2,3}$≈0 Hz, H-3), 4.60, 4.62 (1H each, 2d, ^2J=11.6 Hz, CH_2O-3), 4.67 (1H, d, $J_{1,2}$=4.1 Hz, H-2), 5.89 (1H, d, H-1), 7.35 (5H, m, Ph); MS *m/z* 310 (M^+; 0.1), 295 (1.8), 249 (4.7), 221 (3.5), 193 (2.5), 163 (3.1), 91 (100). Found: *m/z* 310.1419. Calcd for $C_{16}H_{22}O_6$: M, 310.1416.

3-*O*-Acetyl Derivative (7c): Colorless needles (84% from **6c**[9]); mp 85—86 °C (from AcOEt–hexane); R_f=0.13 (*A*); $[\alpha]_D$−196° (*c* 1.00, $CHCl_3$); ^1H NMR (500 MHz) δ=1.31, 1.52 (3H each, 2s, CMe_2), 2.10 (3H, s, AcO-3), 2.28 (2H, br s, HO-5,6), 3.73 (1H, dd, $J_{6,6'}$=11.5, $J_{5,6'}$=4.7 Hz, H-6′), 3.82 (1H, dd, $J_{5,6}$=3.7 Hz, H-6), 3.93 (1H, ddd, $J_{4,5}$=9.1 Hz, H-5), 4.04 (1H, dd, $J_{3,4}$=1.3 Hz, H-4), 4.63 (1H, d, $J_{1,2}$=3.9, $J_{2,3}$≈0 Hz, H-2), 5.28 (1H, d, H-3), 5.92 (1H, d, H-1); MS *m/z* 247 (M−CH_3; 29), 231 (2.3), 201 (49), 187 (4.5), 173 (28), 143 (100), 127 (33), 113 (41). Found: *m/z* 247.0819. Calcd for $C_{10}H_{15}O_7$: M−CH_3, 247.0818.

General Procedures for the Preparation of 3-*O*-Substituted 1,2-*O*-Isopropylidene-6-*O*-tosyl-β-D-altrofuranoses (8a—c). To a solution of **7** (8.30 mmol) in dry pyridine (40 ml) was added tosyl chloride (1.8 g, 9.5 mmol) at 0 °C. The mixture was stirred at 25 °C for 8 h and then water (2 ml) was added at 0 °C. The mixture was evaporated in vacuo. The residue was dissolved in CH_2Cl_2, washed with water, dried (Na_2SO_4), and evaporated in vacuo. The residue was chromatographed on silica gel to give **8**.

3-*O*-Methyl Derivative (8a): Colorless syrup (86% from **7a**); R_f=0.48 (*A*); $[\alpha]_D$+33° (*c* 0.89, $CHCl_3$); ^1H NMR (500 MHz) δ=1.29, 1.43 (3H each, 2s, CMe_2), 2.05 (1H, br s, HO-5), 2.45 (3H, s , MeC_6-*S*), 3.38 (3H, s, MeO-3), 3.88 (1H, dd, $J_{4,5}$=8.5, $J_{3,4}$=1.7 Hz, H-4), 3.98 (1H, d, $J_{2,3}$≈0 Hz, H-3), 4.04 (1H, m, H-5), 4.06, 4.30 (1H each, 2m, H-6,6′), 4.54 (1H, d, $J_{1,2}$=3.9 Hz, H-2), 5.82 (1H, d, H-1), 7.35, 7.80 (2H each, 2d, *J*=8.5, C_6H_4-*S*); MS *m/z* 373 (M−CH_3; 13), 345 (2.7), 327 (1.4), 281 (4.6), 245 (10), 215 (5.3), 173 (93), 155 (30), 91 (41), 87 (100). Found: *m/z* 373.0951. Calcd for $C_{16}H_{21}O_8S$: M−CH_3, 373.0958.

3-*O*-Benzyl Derivative (8b): Colorless syrup (95% from **7b**); R_f=0.80 (*A*); $[\alpha]_D$+8.7° (*c* 1.71, $CHCl_3$); ^1H NMR (500 MHz) δ=1.28, 1.43 (3H each, 2s, CMe_2), 2.44 (3H, s, MeC_6-*S*), 2.63 (1H, br s, HO-5), 3.99 (1H, dd, $J_{4,5}$=7.1, $J_{3,4}$=1.5 Hz, H-4), 4.05—4.07 (2H, m, H-5,6′), 4.21 (1H, d, $J_{2,3}$≈0 Hz, H-3), 4.31 (1H, m, H-6), 4.56, 4.58 (1H each, 2d, ^2J=11.7 Hz, CH_2O-3), 4.62 (1H, d, $J_{1,2}$=3.9 Hz, H-2), 5.85 (1H, d, H-1), 7.30—7.35 (5H, m, Ph-C), 7.33, 7.79 (2H each, 2d, *J*=8.3 Hz, C_6H_4-*S*); MS *m/z* 449 (M−CH_3; 0.1), 295 (1.2), 249 (5.4), 221 (2.5), 193 (1.5), 163 (2.7), 91 (100). Found: *m/z* 449.1299. Calcd for $C_{22}H_{25}O_8S$: M−CH_3, 449.1270.

3-*O*-Acetyl Derivative (8c): Colorless syrup (88% from **7c**); R_f=0.50 (*A*); ^1H NMR (60 MHz) δ=1.28, 1.43 (3H each, 2s, CMe_2), 2.10 (3H, s, AcO-3), 2.46 (3H, s, MeC_6-*S*), 3.00 (1H, m, HO-5), 4.05—4.35 (3H, m, H-4,6,6′), 4.60 (1H, d, $J_{1,2}$=4.0, $J_{2,3}$≈0 Hz, H-2), 5.35 (1H, d, $J_{3,4}$=1.5 Hz, H-3), 5.89 (1H, d, H-1), 7.35, 7.80 (2H each, 2d, *J*=8.5 Hz, C_6H_4-*S*).

General Procedures for the Preparation of 3-*O*-Substituted 1,2-*O*-Isopropylidene-6-*O*-tosyl-β-D-*arabino*-hexofuranos-5-uloses (9a—c). To a stirred suspension of **8** (0.59 mmol) and finely powdered molecular sieves 3A (500 mg) in dry CH_2Cl_2 (2 ml) was added PCC (254 mg, 1.18 mmol) at 0 °C. The mixture was stirred at 25 °C for 4 h and then 2-propanol (0.5 ml) was added at 0 °C. The mixture was stirred at 25 °C for 1 h and diluted with ether. The precipitates were filtered off through activated carbon. The filtrate was evaporated in vacuo and the residue was purified by short-path chromatography with 1:1 AcOEt–hexane as an eluant, giving **9**.

3-*O*-Methyl Derivative (9a): Colorless syrup (95% from **8a**); R_f=0.55 (*A*); $[\alpha]_D$+2.4° (*c* 1.47, $CHCl_3$); IR (neat) ν 1740 (C=O), 1360 (ν_{as} SO_2), 1170 cm^{-1} (ν_s SO_2); ^1H NMR (500 MHz) δ=1.24, 1.25 (3H each, 2s, CMe_2), 2.45 (3H, s, MeC_6-*S*), 3.40 (3H, s, MeO-3), 4.24 (1H, br s, $J_{3,4}$=0.5, $J_{2,3}$≈0 Hz, H-3), 4.52 (1H, br s, H-4), 4.55 (1H, d, $J_{1,2}$=3.9 Hz, H-2), 4.95, 5.26 (1H each, 2d, $J_{6,6'}$=17.7 Hz, H-6,6′), 5.95 (1H, d, H-1), 7.35, 7.83 (2H each, 2d, *J*=8.5 Hz, C_6H_4-*S*); MS *m/z* 386 (M^+; 0.5), 371 (9.0), 343 (11), 313 (2.1), 255 (13), 185 (2.2), 173 (100), 155 (23), 145 (11), 115 (25), 91 (39). Found: *m/z* 386.1036. Calcd for $C_{17}H_{22}O_8S$: M, 386.1036.

3-*O*-Benzyl Derivative (9b): Colorless syrup (86% from **8b**); R_f=0.49 (*A*); $[\alpha]_D$−6.1° (*c* 2.60, $CHCl_3$); IR (neat) ν 1740 (C=O), 1360 (ν_{as} SO_2), 1170 cm^{-1} (ν_s SO_2); ^1H NMR (500 MHz) δ=1.24, 1.26 (3H each, 2s, CMe_2), 2.45 (3H, s, MeC_6-*S*), 4.47 (1H, br s, $J_{3,4}$=0.5, $J_{2,3}$≈0 Hz, H-3), 4.58 (2H, s, CH_2O-3), 4.60 (1H, br s, H-4), 4.62 (1H, d, $J_{1,2}$=3.9 Hz, H-2), 4.95, 5.25 (1H each, 2d, $J_{6,6'}$=17.6 Hz, H-6,6′), 5.98 (1H, d, H-1), 7.30—7.35 (5H, m, Ph), 7.35, 7.83 (2H each, 2d, *J*=8.3 Hz, C_6H_4-*S*); MS *m/z* 447 (M−CH_3; 0.2), 230 (2.9), 172 (1.9), 155 (18), 122 (7.4), 105 (31), 91 (100). Found: *m/z* 447.1120. Calcd for $C_{22}H_{23}O_8S$: M−CH_3, 447.1114.

3-*O*-Acetyl Derivative (9c): Colorless syrup (97% from **8c**); R_f=0.45 (*A*); $[\alpha]_D$−2.1° (*c* 1.54, $CHCl_3$); IR (neat) ν 1740 (C=O), 1730 (ester C=O), 1355 (ν_{as} SO_2), 1170 cm^{-1} (ν_s SO_2); ^1H NMR (500 MHz) δ=1.23, 1.25 (3H each, 2s, CMe_2), 2.09 (3H, s, AcO-3), 2.45 (3H, s, MeC_6-*S*), 4.56 (1H, d, $J_{1,2}$=3.9, $J_{2,3}$≈0 Hz, H-2), 4.59 (1H, br s, $J_{3,4}$=0.5 Hz, H-4), 4.95, 5.21 (1H each, 2d, $J_{6,6'}$=17.4 Hz, H-6,6′), 5.55 (1H, br s, H-3), 5.98 (1H, d, H-1), 7.35, 7.83 (2H each, 2d, *J*=8.2 Hz, C_6H_4-*S*); MS *m/z* 399 (M−CH_3; 0.4), 201 (5.4), 185 (1.2), 161 (1.4), 149 (5.1), 43 (100). Found: *m/z* 399.0749. Calcd for $C_{17}H_{19}O_9S$: M−CH_3, 399.0750.

(5*R* and 5*S*)-5,6-Anhydro-1,2-*O*-isopropylidene-5-[(*R* and *S*)-(methoxy)phenylphosphinyl]-3-*O*-methyl-β-D-*arabino*-hexofuranoses (10a) and Their 3-*O*-Benzyl Congeners (10b). To a solution of **9a** (123 mg, 0.322 mmol) and methyl phenylphosphinate (0.065 ml, 0.49 mmol) in DME (1 ml) was dropwise added a solution of DBU (74 mg, 0.49 mmol) in DME (1 ml) at −40 °C. The mixture was stirred at the same temp for 1 h and the concentrated in vacuo. The residue was dissolved in CH_2Cl_2 and saturated aq $NaHCO_3$ was added. After stirring at 25 °C overnight, the organic layer was separated and the aq layer was extracted twice with CH_2Cl_2. The combined organic layers were dried (Na_2SO_4) and evaporated in vacuo. The residue was chromatographed in a column of silica gel, giving **10a** (65 mg, 55%) as a colorless syrup: R_f=0.27 (*A*); ^1H NMR (60 MHz) δ=1.31, 1.51 (3H each, 2s, CMe_2), 2.75, 3.20 (1H each, 2m, H-6,6′), 3.13, 3.36 (3H, 2s, MeO-3), 3.70, 3.78 (3H, 2d, J_{POMe}=10.8 Hz, POMe), 3.80—4.10 (1H, m, H-3), 4.25—4.55 (2H, m, H-2,4),

5.18, 5.25 (1H, 2d, $J_{1,2}$=4.0 Hz, H-1), 7.40—8.05 (5H, m, Ph); MS *m/z* 370 (M^+; 0.9), 355 (19), 340 (9.2), 312 (5.5), 294 (6.4), 281 (16), 253 (12), 227 (100), 211 (20), 155 (76). Found: *m/z* 370.1174. Calcd for $C_{17}H_{23}O_7P$: M, 370.1181.

By the use of the same procedures described above, **9b** (2.86 g, 6.18 mmol) was treated with methylphenylphosphinate (1.65 ml, 12.4 mmol) and DBU (1.0 ml, 6.7 mmol) at −40 °C for 1 h. Purification by column chromatography gave **10b** (1.37 g, 50%) as a colorless syrup: R_f=0.43 (*A*); ^{1}H NMR (60 MHz) δ=1.28, 1.50 (3H each, 2s, CMe_2), 2.75, 3.17 (1H each, 2m, H-6,6′), 3.68, 3.70 (3H, 2d, J_{POMe}=10.8 Hz, POMe), 4.00—4.60 (3H, m, H-2,3,4), 4.54 (2H, s, CH_2O-3), 5.67, 5.75 (1H, 2d, $J_{1,2}$=4.0 Hz, H-1), 7.30 (5H, s, Ph-C), 7.30—8.00 (5H, m, Ph-P); MS *m/z* 431 ($M-CH_3$; 2.5), 355 (3.1), 340 (4.8), 297 (6.8), 281 (7.2), 253 (3.6), 227 (8.4), 198 (15), 156 (34), 91 (100). Found: *m/z* 431.1254. Calcd for $C_{22}H_{24}O_7P$: $M-CH_3$, 431.1260.

(5*R* and 5*S*)-5,6-Dideoxy-1,2-*O*-isopropylidene-5-[(*R* and *S*)-(methoxy)phenylphosphinyl]-β-D-*arabino*-hexofuranoses (11d) and 3-*O*-Methyl and 3-*O*-Benzyl Derivatives (11a and 11b). Compound **10a** (256 mg, 0.691 mmol) dissolved in ethanol (2 ml) was hydrogenated in the presence of Raney-Ni (W-4) (730 mg) at 24 °C under an atmospheric pressure of H_2. After 4 h, the mixture was centrifuged to remove the catalyst; the precipitate was twice extracted with ethanol. The combined organic layers were evaporated in vacuo. The residue was chromatographed on silica gel to give **11a** (108 mg, 44%) as a pale yellow syrup: R_f=0.31—0.24 (*B*); ^{1}H NMR (60 MHz) δ=1.11 (3H, dd, $J_{6,P}$=17.0, $J_{5,6}$=7.4 Hz, H$_3$-6), 1.32, 1.40, 1.48 (6H, 3s, CMe_2), 2.10—2.65 (1H, m, H-5), 3.37, 3.40 (3H, 2s, MeO-3), 3.65, 3.68, 3.76 (3H, 3d, J_{POMe}=10.8 Hz, POMe), 3.90—4.55 (3H, m, H-2,3,4), 5.60—5.85 (1H, m, H-1), 7.35—7.95 (5H, m, Ph).

By the same procedures described above, **10b** (247 mg, 0.553 mmol) was treated with Raney-Ni (W-4) (600 mg) for 7 h under H_2. Purification by column chromatography gave **11b** (98 mg, 41%) as a colorless syrup: R_f=0.36—0.26 (*B*); ^{1}H NMR (500 MHz) for the two predominant components of **11b** δ=1.06, 1.21* (3H, 2dd, $J_{6,P}$=17.5, $J_{5,6}$=7.0 Hz, H-6), 1.25, 1.30,* 1.45, 1.50* (6H, 4s, CMe_2), 2.45,* 2.50 (1H, 2dq, $J_{5,P}$=14.5,* 14.7, $J_{4,5}$=7.7,* 8.2 Hz, H-5), 3.62,* 3.64 (3H, 2d, J_{POMe}=11.0 Hz, POMe), 3.92, 4.32* (1H, 2ddd, $J_{4,P}$=6.8, 5.9,* $J_{3,4}$=4.0 Hz, H-4), 4.02, 4.08* (1H, 2d, $J_{2,3}\approx$0 Hz, H-3), 4.54, 4.59,* 4.62, 4.62* (2H, 4d, *J*=11.7 Hz, CH_2O-3), 4.58 (1H, d, $J_{1,2}$=3.8 Hz, H-2), 5.81,* 5.84 (1H, 2d, H-1), 7.36 (5H, m, Ph-C), 7.46 [2H, m, Ph(*m*)-P], 7.55 [1H, m, Ph(*p*)-P], 7.73, 7.76* [2H, 2m, Ph(*o*)-P], *for another diastereomer (the assignment of some of the δ values may have to be interchanged); MS *m/z* 432 (M^+; 0.3), 417 (2.8), 341 (5.2), 326 (7.4), 303 (2.1), 283 (7.5), 267 (8.9), 213 (23), 184 (28), 155 (29), 91 (100). Found: *m/z* 432.1699. Calcd for $C_{23}H_{29}O_6P$: M, 432.1702.

Compounds **11b** (103 mg, 0.238 mmol) dissolved in ethanol (1 ml) was hydrogenated in the presence of 20% $Pd(OH)_2$–C (80 mg) at 25 °C under an atmospheric pressure of H_2. After 1.5 h, the catalyst was filtered off through celite, and the filtrate was evaporated in vacuo. The residue was purified by column chromatography, giving **11d** (78 mg, 96%) as a colorless syrup: R_f=0.25—0.19 (*B*); ^{1}H NMR (60 MHz) δ=0.96, 1.19 (3H, 2dd, $J_{6,P}$=17.4, $J_{5,6}$=7.4 Hz, H$_3$-6), 1.36, 1.40, 1.45 (6H, 3s, CMe_2), 2.00—2.75 (1H, m, H-5), 3.20—3.50 (1H, m, HO-3, D_2O exchangeable), 3.59, 3.67 (3H, 2d, J_{POMe}=10.8 Hz, POMe), 3.95—4.75 (3H, m, H-2,3,4), 5.72 (1H, d, $J_{1,2}$=4.0 Hz, H-1), 7.30—7.95 (5H, m, Ph-P); MS *m/z* 342 (M^+; 1.6), 327 (6.1), 295 (1.2), 267 (3.4), 239 (2.9), 213 (61), 173 (9.8), 155 (52), 100 (100). Found: *m/z* 342.1235. Calcd for $C_{16}H_{23}O_6P$: M, 342.1232.

1,2,4-Tri-*O*-acetyl-5,6-dideoxy-3-*O*-methyl-[(*R* and *S*)-phenylphosphinyl]-L-galactopyranoses (15) and -D-Altropyranoses (16). To a solution of **11a** (227 mg, 0.637 mmol) in dry benzene (3 ml) was added, with stirring, a solution of SDMA (3.4 M in toluene, 0.5 ml, 2.5 equiv) in dry benzene (1 ml), in small portions at 5 °C under an argon atmosphere. The mixture was stirred at this temp for 1.5 h, and then water (1 ml) was added to decompose excess SDMA. The mixture was centrifuged and the precipitate was extracted with several portions of benzene. The organic layers were combined and evaporated in vacuo, giving (5*R* and 5*S*)-5,6-dideoxy-1,2-*O*-isopropylidene-3-*O*-methyl-5-[(*R* and *S*)-phenylphosphinyl]-β-D-*arabino*-hexofuranoses (**12a**) as a colorless syrup.

The syrup was immediately treated with 1:1 ethanol–0.5 M hydrochloric acid (6 ml) at 90 °C for 3 h under an argon atmosphere. After cooling, the reactants were neutralized with Amberlite IRA-45. The resin was filtered off and washed with aq ethanol. The filtrate was evaporated in vacuo to give a mixture of 5,6-dideoxy-3-*O*-methyl-5-[(*R* and *S*)-phenylphosphinyl]-α, β-L-galactopyranoses (**13a**) and -D-altropyranoses (**14a**) as a colorless syrup.

This was dissolved in dry pyridine (4 ml) and acetic anhydride (2 ml) at 0 °C. The mixture was stirred at 25 °C overnight, diluted with a small amount of cold water, and concentrated in vacuo. The residue was dissolved in CH_2Cl_2 and washed with water. The organic layer was dried (Na_2SO_4) and evaporated in vacuo, giving a mixture of triacetates **15** and **16**, which were separated by column chromatography with a gradient eluant of 3:1 AcOEt–hexane→AcOEt into four fractions A—D.

Fraction A [R_f=0.44 (*B*)] gave 5-[(*R*)-phenylphosphinyl]-α-L-galactopyranose (**15A**) as colorless needles: 26.7 mg (9.8% from **11a**); mp 260—261 °C (from AcOEt–hexane); ^{1}H and ^{31}P NMR, see Table 1; MS *m/z* 369 (M–Ac; 1.1), 353 (11), 338 (3.6), 327 (1.2), 312 (21), 279 (8.8), 269 (19), 251 (27), 211 (40), 182 (21), 169 (24), 129 (70), 85 (100). Found: *m/z* 369.1098. Calcd for $C_{17}H_{22}O_7P$: $M-CH_3CO$, 369.1103.

Fraction B [R_f=0.38 (*B*)] gave 5-[(*S*)-*P*]-α-D-altropyranose **16A** as a colorless syrup: 5.4 mg (2.1% from **11a**); ^{1}H and ^{31}P NMR, see Table 1; MS *m/z* 413 (M+1; 0.7), 412 (M^+; 0.2), 353 (11), 311 (13), 269 (11), 251 (22), 183 (10), 169 (24), 115 (38), 85 (100). Found: *m/z* 412.1311. Calcd for $C_{19}H_{25}O_8P$: M, 412.1287.

Fraction C [R_f=0.30 (*B*)] gave a colorless syrup (29.5 mg) which consisted of 5-[(*R*)-*P*]-β-D-altro isomer **16B** (9.1% from **11a**) and 5-[(*R*)-*P*]-β-L-galacto isomer **15B** (2.1%), the relative amounts being determined by the intensity ratio of their MeO-3 signals: ^{1}H and ^{31}P NMR, see Table 1.

Fraction D [R_f=0.25 (*B*)] gave 5-[(*S*)-*P*]-α-L-galacto isomer **15C** as a colorless syrup: 18.6 mg (7.1% from **11a**); ^{1}H and ^{31}P NMR, see Table 1; MS *m/z* 353 (M−AcO; 4.9), 311 (5.9), 292 (2.5), 269 (10), 251 (12), 169 (19), 129 (11), 85 (100). Found: *m/z* 353.1154. Calcd for $C_{17}H_{22}O_6P$: M−AcO, 353.1154.

1,2,4-Tri-*O*-acetyl-3-*O*-benzyl-5,6-dideoxy-5-[(*R* and *S*)-phenylphosphinyl]-α,β-L-galactopyranoses (17) and -D-Altropyranoses (18). By the same procedures described for **15** and **16**,

compound **11b** (266 mg, 0.615 mmol) was converted into a mixture of triacetates **17** and **18** via **12b** and **13b/14b**. This was separated by column chromatography into four fractions A—D.

Fraction A [R_f=0.61 (*B*)] gave 5-[(*R*)-phenylphosphinyl]-α-D-altropyranose (**18C**) as a colorless syrup: 14.6 mg (4.4% from **11b**); ^{1}H and ^{31}P NMR, see Table 1; MS *m/z* 489 (M+1; 0.1), 429 (7.5), 387 (1.3), 327 (3.2), 323 (29), 280 (5.4), 221 (11), 125 (13), 91 (100). Found: *m/z* 489.1680. Calcd for $C_{25}H_{30}O_8P$: M+1, 489.1678.

Fraction B [R_f=0.55 (*B*)] gave 5-[(*R*)-*P*]-α-L-galacto isomer **17A** as colorless needles: 18.3 mg (6.1% from **11b**); mp 242—244 °C (from AcOEt–hexane); $[\alpha]_D$−78° (*c* 0.56, $CHCl_3$); ^{1}H and ^{31}P NMR, see Table 1; MS *m/z* 429 (M−AcO; 1.3), 323 (51), 280 (15), 263 (15), 238 (12), 221 (26), 125 (14), 91 (100). Found: *m/z* 429.1452. Calcd for $C_{23}H_{26}O_6P$: M−AcO, 429.1467. Anal. ($C_{25}H_{29}O_8P$) C, H.

Fraction C [R_f=0.45 (*B*)] gave a colorless syrup (7.2 mg) which consisted of 5-[(*R*)-*P*]-β-L-galacto isomer **17B** (1.1% from **11b**) and 5-[(*S*)-*P*]-α-D-altro isomer **18A** (1.3%), the relative amounts being determined from the integral ratio of ^{31}P signals: ^{1}H and ^{31}P NMR, see Table 1.

Fraction D [R_f=0.38 (*B*)] gave 5-[(*S*)-*P*]-β-D-altro isomer (**18B**) as colorless needles: 27.8 mg (9.3% from **11b**); mp 268—269 °C (from AcOEt–hexane); $[\alpha]_D$−28° (*c* 0.64, $CHCl_3$); ^{1}H and ^{31}P NMR, see Table 1; MS *m/z* 429 (M−AcO; 14), 387 (3.0), 369 (1.3), 327 (5.0), 280 (5.3), 125 (10), 91 (100). Found: *m/z* 429.1463. Calcd for $C_{23}H_{26}O_6P$: M−AcO, 429.1467.

1,2,3,4-Tetra-*O*-acetyl-5,6-dideoxy-5-[(*R* and *S*)-phenylphosphinyl]-α,β-L-galactopyranoses (19) and -D-Altropyranoses (20). By the same procedures described above, compound **11d** (264 mg, 0.771 mmol) was converted into a mixture of tetraacetates **19** and **20** via **12d** and **13d/14d**. This was separated by column chromatography into four fractions A—D.

Fraction A [R_f=0.60 (*B*)] gave 5-[(*R*)-phenylphosphinyl]-α-L-galactopyranose (**19A**) as a colorless syrup: 36.6 mg (11% from **11d**); ^{1}H and ^{31}P NMR, see Table 1; MS *m/z* 441 (M+1; 1.6), 398 (7.4), 381 (13), 356 (10), 339 (73), 296 (24), 279 (86), 253 (19), 237 (100), 209 (29), 184 (25), 159 (25), 141 (31), 125 (73). Found; *m/z* 441.1297. Calcd for $C_{20}H_{26}O_9P$: M+1, 441.1314.

Fraction B [R_f=0.53 (*B*)] gave a colorless syrup (10.3 mg, 3.0% from **11d**) which consisted of three isomers among **19** and **20**, the exact structures of which, however, have remained unassignable; ^{31}P NMR δ=34.4, 33.0, and 31.0 (1:1:2).

Fraction C [R_f=0.48 (*B*)] gave a colorless syrup (21.0 mg) which consisted of 5-[(*R*)-*P*]-β-L-galacto isomer **19B** (2.7% from **11d**) and 5-[(*S*)-*P*]-β-D-altro isomer **20B** (3.5%), the relative amounts being determined from the integral ratio of ^{31}P signals; ^{1}H and ^{31}P NMR, see Table 1; MS *m/z* 441 (M+1; 2.7), 398 (6.2), 381 (10), 356 (7.5), 339 (88), 296 (23), 279 (59), 237 (100), 209 (26), 184 (24), 159 (21), 141 (27), 125 (60). Found: *m/z* 441.1302. Calcd for $C_{20}H_{26}O_9P$: M+1, 441.1314.

Fraction D [R_f=0.43 (*B*)] gave 5-[(*S*)-*P*]-α-L-galacto isomer **19C** as a colorless syrup: 14.3 mg (4.2% from **11d**); ^{1}H and ^{31}P NMR, see Table 1; MS *m/z* 441 (M+1; 0.7), 440 (M^+; 0.7), 398 (6.9), 381 (11), 356 (7.1), 339 (85), 296 (24), 279 (55), 237 (100), 209 (30), 184 (23), 159 (27), 142 (33), 125 (74). Found: *m/z* 440.1255. Calcd for $C_{20}H_{25}O_9P$; M, 440.1236.

3,6-Dideoxy-1,2-*O*-isopropylidene-5-*O*-[(*R* and *S*)-(methoxy)phenylphosphinyl]-α-L-*glycero*-hexa-3,5-dienofuranoses (22). The procedures similar to those for **10a** from **9a** were eomployed. Thus, **9C** (333 mg, 0.803 mmol) was treated with methyl phenylphosphinate (0.20 ml, 1.5 mmol) and DBU (0.14 ml, 0.94 mmol) at −40 °C for 1 h. Purification of the crude product by column chromatography gave **22** (227 mg, 83%) as an inseparable mixture (1:1 epimers with respect to the phosphorus atom): Colorless syrup; R_f=0.46 (*A*); ^{1}H NMR (500 MHz) δ=1.29, 1.40,* 1.42, 1.43* (6H, 4s, CMe_2), 3.84, 3.86* (3H, 2d, J_{POMe}=11.2 Hz, POMe), 5.20, 5.24,* 5.24, 5.27* (2H, 4t, $J_{6,6'}=J_{6,P}$=2.3 Hz, H-6,6′), 5.31, 5.34* (1H, 2dd, $J_{1,2}$=5.2, $J_{2,3}\approx$2.5 Hz, H-2), 5.41, 5.43* (1H, 2d, H-3), 6.075, 6.08* (1H, 2d, H-1), 7.48, 7.49* [2H, 2m, Ph(*m*)], 7.58, 7.59* [1H, 2m, Ph(*p*)], 7.83, 7.83* [2H, 2m, Ph(*o*)], *for another diastereomer (the assignment of some of the δ values may have to be interchanged).

3,6-Dideoxy-1,2-*O*-isopropylidene-5-*O*-[(*R* and *S*)-(methoxy)phenylphosphinyl]-α-L-*glycero*-hex-4-enofuranoses (23). The procedures similar to those for **11a** from **10a** were employed. Thus, **22** (79 mg, 0.233 mmol) was treated with Raney-Ni(W-4) (70 mg) under H_2 for 5 h. Purification of the crude product by column chromatography gave **23** (35 mg, 44%) as an inseparable mixture (1:1) of *P*-epimers: Colorless syrup; R_f=0.40 (*A*); ^{1}H NMR (500 MHz) δ=1.35, 1.36,* 1.40,* 1.42 (6H, 4s, CMe_2), 1.87,* 2.02 (3H, 2t, $J_{3S,6}=J_{6,P}$=2.0 Hz, H_3-6), 2.51, 2.71* (1H, 2dddq, $J_{3R,3S}$=17.1, $J_{2,3S}$=5.7, $J_{3S,P}$= 3.7 Hz, H-3S), 2.87, 2.92* (1H, 2br d, $J_{3R,P}$=0.5 Hz, $J_{2,3R}\approx$0 Hz, H-3R), 3.79, 3.795* (3H, 2d, J_{POMe}=11.2 Hz, POMe), 4.67, 4.72* (1H, 2dd, $J_{1,2}$=3.6 Hz, H-2), 5.92, 5.93* (1H, 2d, H-1), 7.47, 7.47* [2H, m, $J_{o,m}=J_{m,p}$=7.5, $J_{m,P}$=4.4 Hz, Ph(*m*)], 7.57, 7.57* [1H, m, $J_{o,p}=J_{p,P}$=1.5 Hz, Ph(*p*)], 7.82, 7.82* [2H, m, $P_{o,P}$=13.6 Hz, Ph(*o*)], *for another diastereomer.

References

1) For reviews, see H. Yamamoto and T. Hanaya, "Studies in Natural Products Chemistry," ed by T. I. Attaur-Rahman, Elsevier, Amsterdam (1990), Vol. 6, pp. 351—384; H. Yamamoto and S. Inokawa, *Adv. Carbohydr. Chem. Biochem.*, **42**, 135 (1984); Z. J. Witczak and R. L. Whistler, *J. Carbohydr. Chem.*, **2**, 351 (1983).

2) T. Hanaya and H. Yamamoto, *Bull. Chem. Soc. Jpn.*, **62**, 2320 (1989); P. Luger, E. Müller, H. Yamamoto, and S. Inokawa, *Carbohydr. Res.*, **145**, 25 (1985); H. Yamamoto, Y. Nakamura, S. Inokawa, M. Yamashita, M.-A. Armour, and T. T. Nakashima, *J. Org. Chem.*, **49**, 1364 (1984).

3) T. Richter, P. Luger, T. Hanaya, and H. Yamamoto, *Carbohydr. Res.*, **193**, 9 (1989); H. Yamamoto, T. Hanaya, H. Kawamoto, and S. Inokawa, *J. Org. Chem.*, **53**, 4790 (1988); H. Yamamoto, T. Hanaya, H. Kawamoto, S. Inokawa, M. Yamashita, M.-A. Armour, and T. T. Nakashima, *ibid.*, **50**, 3516 (1985); H. Yamamoto, K. Yamamoto, S. Inokawa, M. Yamashita, M.-A. Armour, and T. T. Nakashima, *ibid.*, **48**, 435 (1983).

4) G. W. J. Fleet, A. N. Shaw, S. V. Evans, and L. E. Fellows, *J. Chem. Soc., Chem. Commun.*, **1985**, 841.

5) H. Hashimoto, T. Fujimori, and H. Yuasa, *J. Carbohydr. Chem.*, **9**, 683 (1990).

6) A part of the results have been reported as a communication: T. Hanaya, T. Ohmae, H. Kawamoto, and H. Yamamoto, *Chem. Lett.*, **1990**, 1359.

7) K. N. Slessor and A. S. Tracey, *Can. J. Chem.*, **47**, 3989 (1969); T. S. Fuller and R. V. Stick, *Aust. J. Chem.*, **33**, 2509

(1980).

8) F. H. Newth, *J. Chem. Soc.*, **1953**, 2504.

9) L. D. Hall, S. A. Black, K. N. Slessor, and A. S. Tracey, *Can. J. Chem.*, **50**, 1912 (1972).

10) W. Perkow, K. Ullerich, and F. Meyer, *Naturwissenschaften*, **39**, 353 (1952); for a review, see F. W. Lichtenthaler, *Chem. Rev.*, **61**, 607 (1961).

11) M. Sekine, M. Nakajima, and T. Hata, *J. Org. Chem.*, **46**, 4030 (1981).

12) J. Thiem, D. Rasch, and H. Paulsen, *Chem. Ber.*, **109**, 3588 (1976).

13) The parameters are examined with respect to the corresponding vicinal dihedral angles (namely, whether the H–C–C–P and H–C–P=O groups are in the anti or gauche connection): see T. Hanaya, K. Ohmori, H. Yamamoto, M.-A. Armour, and A. M. Hogg, *Bull. Chem. Soc. Jpn.*, **63**, 1174 (1990) and references cited therein.

14) A characteristic upfield shift (0.2—0.4 ppm) is also noticed for signals of axially situated AcO-4 of **15C** and **19C** and AcO-2 of **18C**, supporting the axial orientation of *P*-phenyl group in these compounds: see T. Hanaya, N. Shigetoh, and H. Yamamoto, *Bull. Chem. Soc. Jpn.*, **61**, 2499 (1988) and references cited therein; T. Richter, P. Luger, T. Hanaya, and H. Yamamoto, *Carbohydr. Res.*, in press (RJ-1797).

Cobalt(III)-tren Complexes of 3-Formylcamphor[1)]

Yoshiharu NAKANO,* Yuzo YOSHIKAWA,† Shigeo MASUHARA, and Shoichi SATO††,2)
Department of Chemistry, Faculty of Science, Ibaraki University, Bunkyo 2-2-1, Mito 310
† Department of Chemistry, Faculty of Science, Okayama University, Tsushima, Okayama 700
†† The Institute for Solid State Physics, The University of Tokyo, Roppongi 7-22-1, Tokyo 106
(Received August 7, 1990)

3-Formylcamphor Co(III) complexes of a tripod-like ligand, tren, were prepared and the two possible geometrical isomers were separated successfully. The crystal structure of one of them was determined by X-ray diffraction. A red plate-like crystal was monoclinic, space group $P2_1$, a=12.401 (2), b=9.9400 (7), c=10.932 (1) Å, β=108.44 (1)°, and Z=2. The structure was refined to R=0.047 on 2818 reflections. The geometrical isomers were compared sepectroscopically.

There have been few reports on Co(III)-tren complexes compared to those of Co(III)-trien. Until now, the Co(III)-tren complexes containing amino acids, diamines,[3)] and β-diketones[4)] have been reported. The tren complexes are much more suitable for model compounds to study the optical activities of such complexes. Because the trien complexes have two asymmetric centers and, thus, extra isomerisms occur. We have investigated both the crystal structure and optical activity of the Co(III)-tren complexes of unsymmetrical β-diketone type ligands.[4e)] In these complexes a pair of geometrical isomers is possible. If the coordinating atoms are of the same kind as in this case, it is very difficult to differentiate the geometrical structure spectroscopically, due to a lack of fundamental data concerning Co(III)-tren complexes. In the present work, Co(III)-tren complexes of 3-formylcamphorato(fc) were studied. Two geometrical isomers, **I** and **II**, (as shown in Fig. 1) were successfully separated by cation exchange chromatography. Contrary to tris(fc)metal complexes, only little regioselectivity was observed in this case.[5)] We determined the crystal structure of an isomer, **II**, $[Co(fc)(tren)](ClO_4)_2 \cdot H_2O$, eluted slowly on the column of cation-exchanging resin by an X-ray diffraction method, because of the inability to use various forms of spectroscopy.

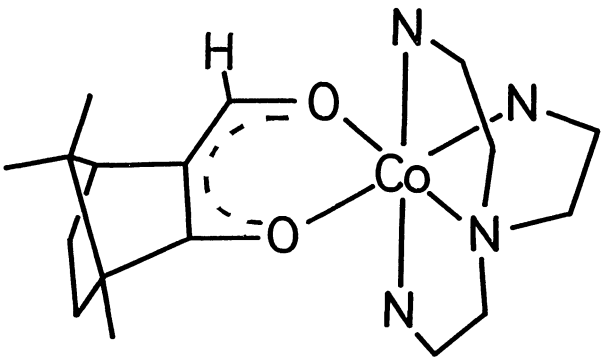

I

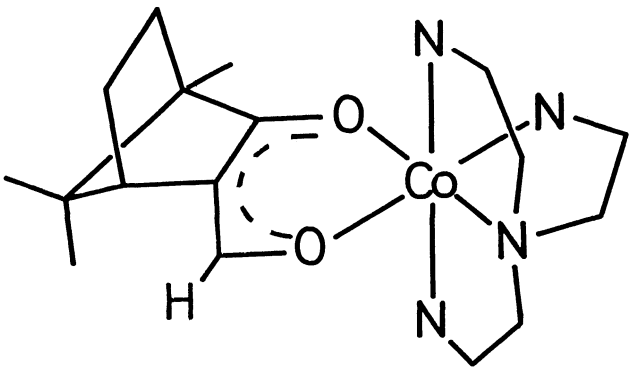

II

Fig. 1. Geometrical isomers of $[Co(fc)(tren)]^{2+}$.

The ^1H NMR and ^{13}C NMR spectra of the two isomers were measured, and almost all of the signals could be assigned. They showed significant differences in the ^1H NMR, ^{13}C NMR, and CD spectra. The geometrical structure of Co(III)-tren complexes can be determined through comparison with the chemical shifts of the carbonyl carbons. The CD spectra can be discussed in terms of both vicinal and quasienantiomeric effects. The vicinal effect is more important than the quasienantiomeric effect in the case of 3-formylcamphor.

Experimental

Materials. a) Preparation of Ligands. Hfc was prepared by the Claisen Reaction of camphor with pentyl formate.[6)] The resulting white powder was confirmed through a measurement of the ^1H NMR. The starting complex, $[Co(CO_3)(tren)]^+$, was prepared as before.[4)]

b) Preparation of the Isomers, I and II. An isomeric mixture of fc complexes was prepared (as described previously) and separated by cation-exchanging chromatography using a 0.5 M (1 M=1 mol dm^{-3}) sodium chloride solution.[4)] A solution of the mixture (3 mmol in each column) was poured into an SP-Sephadex (C-25, 3×150 cm) column. The isomers were eluted by a 0.25 M sodium sulfate solution and completely separated into two bands, which were named **I** and **II** in the order of elution. After excess sodium sulfate was removed by adding ethanol to each eluted solution, six equivalents of sodium perchlorate were added. The resulting perchlorate crystals of each isomer, **I** or **II**, were filtered. The two isomers were recrystallized from a 5% aqueous solution of sodium perchlorate. IR (KBr) 3100—

3300 cm^{-1} broad peak (N–H stretching), 1610 cm^{-1} (carbonyl stretching). Yield: 19% from the beginning of preparation of complex mixtures. Relative ratio of **I**:**II**=45:55. Found for **I**: C, 33.87; H, 5.85; N, 9.30%. Found for **II**: C, 33.73; H, 5.80; N, 9.19%. Calcd for $[Co(fc)(tren)](ClO_4)_2 \cdot H_2O = C_{17}H_{33}N_4O_{10}Cl_2Co \cdot H_2O$: C, 33.84; H, 5.85; N, 9.29%.

Physical Measurement. The absorption spectra were recorded on a Hitachi 200-10 spectrophotometer and the CD spectra on a JASCO J-500A spectropolarimeter. All measurements were carried out in aqueous solution at room temperature. The ^1H and ^{13}C NMR spectra were recorded in deuterium oxide on a Hitachi R-20, JEOL JNM-FX90, and GX-400 NMR spectrometer at room temperature. The internal reference used was dioxane (methylene protons and carbons were assumed as 3.71 and 67.40 ppm, respectively). Calculations for structure analyses were carried out on a HITAC M-680 computer at the University of Tokyo.

Table 1. Atomic Parameters[a)]

Atom	x	y	z	B_{eq}
Co	30704(4)	50000	23261(5)	209(1)
Cl(1)	62749(14)	98600(19)	26900(15)	447(4)
Cl(2)	20410(12)	96688(15)	25786(14)	383(4)
O(1)	1530(3)	5502(4)	1976(4)	31(1)
O(2)	3154(3)	3728(4)	3652(3)	28(1)
O(3) m1	6697(9)	8601(12)	2625(10)	59(3)
O(4) m1	5747(12)	10341(13)	1462(7)	83(4)
O(5) m1	5435(12)	9501(19)	3249(11)	87(5)
O(6) m1	6927(9)	10790(11)	3596(11)	61(3)
O(7) m2	2176(20)	10924(13)	2314(19)	122(9)
O(8) m2	967(11)	9554(43)	2452(21)	199(17)
O(9) m2	2101(21)	8790(16)	1613(14)	141(9)
O(10) m2	2516(13)	9011(14)	3773(9)	79(4)
O(11)	1453(5)	4584(6)	−1318(5)	58(2)
O(12) m3	6398(32)	10662(35)	3674(13)	213(17)
O(13) m3	7131(13)	8752(19)	2862(13)	71(5)
O(14) m3	6425(36)	10682(29)	1690(24)	168(17)
O(15) m3	5124(18)	9721(29)	2486(57)	258(26)
O(16) m4	2600(13)	8880(19)	2017(15)	74(5)
O(17) m4	896(15)	9896(46)	2005(18)	170(15)
O(18) m4	2759(25)	10875(25)	2835(36)	167(17)
O(19) m4	2261(21)	9772(56)	3987(19)	163(15)
N(1)	4660(3)	4702(4)	2496(4)	26(1)
N(2)	2706(4)	3461(5)	1142(4)	30(1)
N(3)	3044(4)	6269(5)	978(4)	28(1)
N(4)	3621(4)	6323(5)	3733(4)	33(1)
C(1)	4743(4)	3240(6)	2162(6)	33(1)
C(2)	3767(5)	2926(6)	959(5)	34(1)
C(3)	5018(5)	5596(7)	1583(5)	34(1)
C(4)	4201(5)	6767(6)	1147(6)	36(1)
C(5)	5313(4)	4993(8)	3868(4)	35(1)
C(6)	4901(5)	6325(7)	4221(5)	37(1)
C(7)	2304(5)	3463(6)	4051(5)	31(1)
C(8)	1250(5)	4029(7)	3574(6)	35(1)
C(9)	941(3)	4984(6)	2604(4)	25(1)
C(10)	−275(4)	5399(6)	2414(5)	32(1)
C(11)	−169(6)	6234(10)	3623(8)	53(2)
C(12)	113(7)	5257(17)	4733(8)	76(4)
C(13)	211(6)	3873(11)	4031(8)	63(3)
C(14)	−753(5)	4022(9)	2653(9)	56(2)
C(15)	−770(8)	2964(10)	1694(13)	81(4)
C(16)	−1953(7)	4113(17)	2777(15)	104(5)
C(17)	−858(5)	6113(9)	1155(7)	49(2)

a) Positional parameters are multiplied by 10^5 for Co, Cl, 10^4 for O, N, C. $B_{eq}=4/3 \cdot a(\text{beta}) \cdot \boldsymbol{a}$ are multiplied by 10^2 for Co, Cl, 10^1 for O, N, C. m_j indicate multiplicities of each atom. m1=0.56, m2=0.54, m3=0.44, m4=0.46.

X-Ray Data Collection. The unit cell-parameters and reflection data using a single crystal (ca. 0.42×0.37×0.47 mm) were measured on a Rigaku four-circle diffractometer (AFC-3) with graphite-monochromatized Mo $K\alpha$ rediation at The Institute for Solid State Physics. The cell dimensions were determined by least-squares calculations based on 40 reflections ($15.2<\theta<24.9$). Systematic absences of 0, k, 0 ($k=2n+1$) led to the space group $P2_1$.

Crystal data: $C_{17}H_{35}N_4O_{11}Cl_2Co$, M.W.=603.33, space group $P2_1$, a=12.401(2), b=9.9396(7), c=10.932(1) Å, β=108.44(1)°, V=1278.3(2) $Å^3$, Z=2, D_x=1.568, D_m=1.562 g cm^{-3} (by the floatation), (Mo $K\alpha$)=9.710 cm^{-1}, $F(000)$=628. The intensity data were collected by the θ-2θ scan technique up to $2\theta=55°$ with a scan rate of 2° min^{-1} in θ. The intensity data were converted to F_o data in the usual manner. A total of 2818 independent reflections with $|F_o|>2.5\sigma$ $|F_o|$ of the measured 3347 reflections were considered, as observed, and used for the structure analysis. Absorption was not corrected.

Determination of the Crystal Structure of the Isomer II. The structure was solved by a heavy-atom method using the UNICS III program system. All of the non-hydrogen atoms were refined by block-diagonal least squares with anisotropic thermal parameters. Hydrogen atoms were located using difference Fourier maps, except for the hydrogens of water, which were included in a refinement with isotropic thermal parameters. At a later stage of the refinement, the oxygen atoms of two perchlorate ions were found to have disordered dispositions. The final positional parameter shifts of almost all atoms, except for the oxygen atoms of the perchlorate, were less than the standard deviations. The final residual values were R=0.047 and R_w=0.066, where the weights are $w=1/(1.0+0.011|F_o|^2)$ for $|F_o|<15.0$ and $w=1/(\sigma^2/|F_o|+0.011|F_o|^2)$ for $F_o>15.0$. The final defference Fourier map showed a peak of 0.6 e $Å^{-3}$. The map showed several peaks less than 0.3 e $Å^{-3}$. The configuration was assigned on the basis of the known configuration of d-camphor. The y-coordinate of the cobalt

Table 2. Interatomic Distances and Bond Angles for $[Co(fc)(tren)](ClO_4)_2 \cdot H_2O$

Bond distances/Å			
Co–O(1)	1.893(4)	Co–O(2)	1.901(4)
Co–N(1)	1.943(4)	Co–N(2)	1.962(5)
Co–N(3)	1.933(5)	Co–N(4)	1.974(6)
O(1)–C(9)	1.260(7)	O(2)–C(7)	1.289(7)
C(8)–C(9)	1.384(9)	C(7)–C(8)	1.366(8)
C(9)–C(10)	1.513(8)	C(8)–C(13)	1.530(13)
C(7)–H(C-7)	1.07(10)		
Bond angles/degree			
O(1)–Co–O(2)	97.9(2)	O(1)–Co–N(1)	171.1(2)
O(2)–Co–N(1)	91.0(2)	O(2)–Co–N(3)	177.7(2)
N(1)–Co–N(2)	87.7(2)	N(1)–Co–N(3)	86.8(2)
N(1)–Co–N(4)	86.3(2)	Co–O(1)–C(9)	120.3(4)
N(2)–Co–N(4)	169.8(2)	O(1)–C(9)–C(8)	129.1(6)
C(7)–C(8)–C(9)	125.1(6)	O(2)–C(7)–C(8)	124.9(6)
Co–O(2)–C(7)	122.8(4)	O(1)–C(9)–C(10)	122.6(5)
C(7)–C(8)–C(13)	129.5(7)		
O(2)–C(7)–H(C-7)	118(5)	C(8)–C(7)–H(C-7)	117(5)

atom was fixed at 0.5. The final positional paprameters of non-hydrogen atoms and selected bond distances and angles are listed in Tables 1 and 2. The positional parameters of hydrogen atoms (Table a), the thermal parameters of all the atoms (Table b), structure factors (Table c), and nonessential interatomic distances and angles (Table d) are being kept as Document No. 9103 at the Office of the Editor of Bull. Chem. Soc.

Results and Discussion

The Crystal Structure of Complex II. Two rod-like complex cations lie along the *a*-axis on different levels along the *b*-axis by $y=0.5$, and the remaining space is filled with two water molecules and four perchlorate ions. As is often observed in other perchlorate salts, the perchlorate ions have disordered positions; furthermore, several interatomic distances and angles of the perchlorate ions deviate from the normal values and the thermal parameters of several oxygen atoms are unreasonably large.

A perspective drawing of the complex cation is shown in Fig. 2. The cobalt atom is octahedrally surrounded by two oxygen and four nitrogen atoms. Since the three primary nitrogen atoms are constrained to approach the tertiary nitrogen (N(1)) to form three five-membered chelate rings (denoted as A, B, and C as shown in Fig. 2), the angles subtended at the cobalt atom by the chelate rings are compressed to an average angle of 87.0°, and the interatomic distance of Co–N(3) is significantly short compared with those of Co–N(2) and Co–N(4). The two chelate rings, B and C, have an almost symmetrical conformation. These features are very similar to those of other tren complexes. Although the six-membered chelate ring adopts an almost planar conformation, the atoms with large thermal parameters within fc group are rather flexible perpendicularly to the ring as a whole, as is obseved in the ellipsoid of each atoms. This flexibility might be responsible for the relatively large standard deviation of several interatomic distances and angles (C(12), C(13), C(15), and C(16)).

Characterization of I and II. Though the infrared spectra of the two isomers showed only general features of β-diketonatocobalt(III) complexes, no notable difference was observed between them. Several significant differences were observed in the ^{1}H NMR, ^{13}C NMR, CD spectra. Upon assigning the NMR spectra, we had to refer to the assignment of $[Co(acac)(tren)]^{2+}$ and camphor. Twelve protons and six carbons of the tren part in $[Co(acac)(tren)]^{2+}$ were assigned based on the H–H and C–H cosy spectra; the results are shown in Table 3. The same names were used as those used in the crystal structure for the non-hydrogen atoms, and all of the protons were indicated with the names of non-hydrogen atoms to which the protons were attached. We assumed that the four protons of the four methylene group of the B and C ring facing the acac ring shifted by more than the opposite four protons. Refering to the tren and camphor parts, the essential peaks of the two isomers could be assigned as shown in Table 4. Within the chelate ring of 3-formylcamphor in **I** and **II**, the carbon atoms in the trans side to the tertiary nitrogen

Table 3. NMR Spectra of $[Co(acac)(tren)]^{2+}$[a)]

Carbon number	^{1}H	^{13}C
C(1) or C(5)	2.742, 3.581	61.749
C(2) or C(6)	3.076, 3.396	45.400
C(3)	3.244 (triplet)	61.292
C(4)	2.910	43.827

a) Chemical shifts were given in ppm.

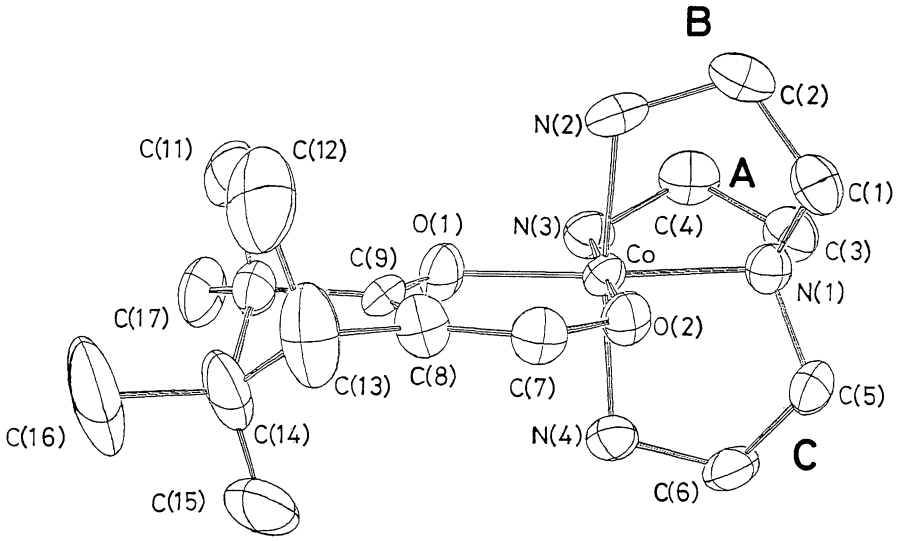

Fig. 2. Perspective drawing of the cobalt complex, **II**. Atom numbering scheme and chelate ring name of tren were shown.

Table 4. Comparison of Two Isomers, **I** and **II** in ^{1}H and ^{13}C NMR

Carbon number	Isomer, **I**		Isomer, **II**	
	^{1}H	^{13}C	^{1}H	^{13}C
C(1) or C(5)	2.807	61.877	2.703	61.882
	3.573		3.519	
C(2) or C(6)	3.207	45.601	3.068	45.707
	3.444	45.765	3.409	45.817
C(3)	3.287	61.822	3.257	61.708
C(4)	2.921	43.863	2.941	44.046
C(7)	6.980	173.123	6.831	170.238
C(8)		117.436		117.001
C(9)		205.145		207.158
C(10)		60.231		60.174
C(11)	1.281	31.171	1.110	31.239
	1.765		1.691	
C(12)	1.281	28.099	1.293	28.203
	2.042		2.018	
C(17)	1.073	9.098	0.957	9.103

a) Chemical shifts were given in ppm.

atom of tren were deshielded more than those in the cis side.

All of the complexes of $[Co(3\text{-}X\text{-}acac)(tren)]^{2+}$(X=H, naphthyl, 2,4-dinitro-1-naphthyl, etc.) previously prepared showed two peaks for the methyl groups in ^{1}H NMR and ^{13}C NMR, and for the carbonyl carbons in ^{13}C NMR.[4] This is probably due to an electronic deformation of the coordination sphere produced by the three five-membered chelate rings of tren. Thus, the remaining coordination site in the Co(tren) system became unbalanced, resulting in a magnetically different field. If these observations are also true for other Co(III)-tren complexes, and the assignments of carbonyl carbons can be established, the geometrical structure can be determined in terms of the chemical shifts of the carbonyl carbons. Limitations of this assumption, however, have to be ascertained. Since we could not find any papers in the literature that describes any clearly assigned ^{13}C peaks of the carbon atoms (carbonyl or thiocyanato group) of the tren and trien complexes in a similar environment, the problems remained unsolved.

Absorption and Circular Dichroism Spectra of the Isomers. Both of the spectra are shown in Fig. 3. Since the absorption spectra of the isomers **I** and **II** were superimposable to each other, only that of isomer **I** is shown. Though they resembled that of $[Co(acac)(tren)]^{2+}$, but all of the transition peaks shifted slightly to a lower-wave number region. Especially, the charge-transfer band shifted to 29.4×10^{3} cm^{-1}, probably because the chelate ring of fc was strained and the antibonding π-orbitals levels decreased. The CD spectra of **I** and **II** were compared with that of $[\{Co(tren)\}_2(tae)]^{4+}$.[4d] Two electronic transitions regions, at $17\text{—}21\times10^{3}$ cm^{-1} and $23\text{—}27\times10^{3}$ cm^{-1}, were assigned to the d-d* transitions of the first and the second absorption bands, respectively. The CD

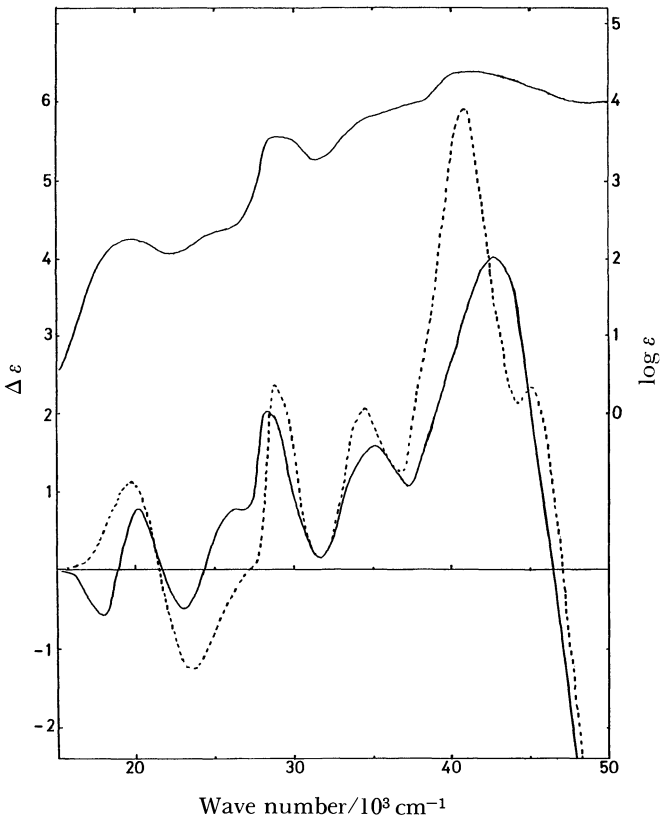

Fig. 3. Absorption and CD spectra.

spectra showed that the electronic transitions of present complexes shifted to a lower wave-number region compared with the corresponding transition of $[\{Co(tren)\}_2(tae)]^{4+}$. The origin of every transitions became obscure at region higher than 40×10^{3} cm^{-1}, due to the overlap of various transition.

Akamatsu et al. reported that vicinal and quasi-enantiomeric effects can contribute to the CD spectra in the case of Co(III)-tren complexes containing optically active amino acids and diamines.[3b] They claimed that the latter effect is dominant. If the quasi-enantiomeric effect is also dominant in the present complex, almost all of the corresponding CD peaks would show opposite signs to each other. The CD spectra of the isomeric complexes, **I** and **II**, resembled each other as a whole, and showed peaks of the same sign. This fact indicates that the vicinal effect is dominant, in contrast to the case of amino acids and diamines. In the present fc complexes, bulky alkyl groups which cause chirality are incorporated directly into the chelate ring. The vicinal effect may be more important in this case.

This work was supported in part by the Joint Research Project of the Institute for Solid State Physics, the University of Tokyo.

References

1) Following abreviations were used in this report; trien for triethylenetetramine, tren for tris(2-aminoethyl)amine, Hfc for 3-formylcamphor, and fc for 3-formylcamphorate, Hacac for acetylacetone, H_2tae for tetraacetylethane.

2) Dr. S. Sato retired from the Institute at March 1990. Present address is as follows. Kasahata 5024-467, Kawagoe, Saitama 350.

3) a) Y. Mitsui, Y. Iitaka, Y. Kushi, and E. Kimura, *J. Chem. Soc., Dalton Trans.*, **1976**, 2095. b) K. Akamatsu, T. Komorita, and Y. Shimura, *Bull. Chem. Soc. Jpn.*, **54**, 3000 (1981).

4) a) Y. Nakano and S. Sato, *Inorg. Chem.*, **19**, 3391 (1980); b) Y. Nakano and S. Sato, *Inorg. Chem.*, **21**, 1315 (1982); c) Y. Nakano and S. Sato, *Bull. Chem. Soc. Jpn.*, **55**, 1683 (1982); d) Y. Nakano, Y. Yoshikawa, and H. Kondo, *J. Am. Chem. Soc.*, **108**, 7630 (1986); e) Y. Nakano, Y. Yoshikawa, J. Hasegawa, T. Asano, Y. Igarashi, and S. Masuhara, *J. Chem. Soc., Chem. Commun.*, **1987**, 1481.

5) Y. T. Chen and G. W. Everett, *J. Am. Chem. Soc.*, **90**, 6660 (1968).

6) A. W. Bishop, L. Claisen, and W. Sinclair, *Justus Liebigs Ann. Chem.*, **281**, 314 (1894).

7) L. F. Johnson and W. C. Jankowski, "Carbon-13 NMR Spectra," John Wiley and Sons, New York (1972), p. 397.

Solvent Extraction of the Hexaaquarhodium(III) Ion from Halogenated Carboxylate Solutions with Trioctylphosphine Oxide

Hisanori IMURA,† Hiromi TAKAHASHI, and Nobuo SUZUKI*
Department of Chemistry, Faculty of Science, Tohoku University, Sendai 980
(Received September 4, 1990)

The extraction equilibrium of the inert hexaaquarhodium(III) ion has been studied. Rhodium(III) was quantitatively and rapidly extracted from 0.10 mol dm^{-3} trichloroacetate (TCA) or 0.010 mol dm^{-3} pentadecafluorooctanoate solutions to heptane containing 0.10 mol dm^{-3} trioctylphosphine oxide (TOPO) at pH 3—5. The extraction equilibria were achieved within 1 min at 298 K. From the equilibrium study in the TCA–TOPO system, the rhodium(III) species extracted into heptane was found to be Rh·3TCA·4TOPO, and the extraction constant was $10^{12.29}$. The rhodium(III) species in the organic phase was suggested to be the hexaaquarhodium(III) complex associated with TCA and TOPO.

Recently, much attention has been focused on the separation of metals of the platinum group. Solvent extraction is one of the powerful separation methods and is widely used in fundamental analytical chemistry and applied fields, such as hydrometallurgy. The various extraction systems which have been reported for the separation of the platinum metals were summarized in both a monograph[1] and a review.[2] The poor extractability of rhodium has often been pointed out. This is primarily ascribed to the very inert tendency of rhodium(III) toward the ligand substitution reactions with extracting agents. Thus, a thorough investigation of the extraction chemistry of rhodium(III) is inevitable.

In the extraction of such inert metals as rhodium(III), the chemical form of the metal in an aqueous solution seems to be of great importance. In this work a hexaaquarhodium(III) ion was prepared and used. Only a few papers have appeared concerning the extraction of hexaaquarhodium(III), in which it has been extracted into the inverted micelles of the organic solution formed by dinonylnaphthalenesulfonic acid.[3,4]

In the present study the extraction of the hexaaquarhodium(III) ion was studied with such halogenated carboxylic acids as trichloroacetic acid (HTCA) and pentadecafluorooctanoic acid (HPDFO) in the presence of a hydrophobic base, trioctylphosphine oxide (TOPO), in nonpolar solvents at 298 K. The trichloroacetic acid–TOPO system has been used by one of the authors in the extraction of inert chromium(III) ions.[5] The extraction equilibrium of hexaaquarhodium(III) ions in this system was studied in detail, and the composition of the extracted species as well as the extraction constant were determined.

Experimental

Reagents. Radioisotopes, ^{101m}Rh and ^{102m}Rh, were produced by 50 MeV bremsstrahlung irradiation of high-purity rhodium (99.99%) with the linear electron accelerator of Tohoku University. The rhodium target was dissolved in concentrated sulfuric acid with heating, neutralized with a sodium hydroxide solution to precipitate rhodium(III) hydroxide, and aged at 328—333 K for 24 h. To prepare a hexaaquarhodium(III) solution, the precipitate of rhodium(III) hydroxide was dissolved in concentrated perchloric acid, heated at 433—443 K for ca. 40 h, and diluted to be 0.2 mol dm^{-3} perchloric acid solution. The rhodium(III) species in the aqueous solution was ascertained to be the hexaaquarhodium(III) ion by the electronic absorption spectrum.[6,7]

Trioctylphosphine oxide was obtained from Dojindo laboratories and purified as follows: a hexane solution (ca. 0.2 mol dm^{-3} TOPO) was washed with 0.5 mol dm^{-3} sodium hydroxide in 50% (v/v) methanol/water and then with water several times. After evaporation of hexane, the residue (purified TOPO) was dried over diphosphorus pentaoxide under vacuum.

Trichloroacetic acid was of guaranteed reagent grade and used as obtained. Sodium trichloroacetate solutions were prepared by mixing a trichloroacetic acid solution standardized by the acid–base titration and sodium hydroxide solutions. Pentadecafluorooctanoic acid (98% purity) was used without further purification.

Benzene and heptane were purified by ordinary methods. Water was doubly distilled and deionized. All other reagents used were of analytical reagent grade.

Extraction and Back Extraction of Rhodium(III). An aqueous solution (5 cm^3) of 4×10^{-3}—1×10^{-1} mol dm^{-3} halogenated carboxylate containing 8×10^{-5} mol dm^{-3} hexaaquarhodium(III) labeled with ^{101m,102m}Rh was shaken for 1 min to 3 h with an organic solution (5 cm^3) containing 5×10^{-3}—1×10^{-1} mol dm^{-3} TOPO at 298 K. After centrifugation, an aliquot of each phase was taken. The γ-activity was measured with a well-type NaI(Tl) scintillation counter and the distribution ratio (D_M) calculated. The pH value of the aqueous phase was measured immediately after shaking. The ionic strength was adjusted to 0.1 mol dm^{-3} with sodium nitrate.

For back extraction, the organic phase (5 cm^3) containing rhodium(III), prepared by the forward extraction described above, was shaken with the aqueous phase (5 cm^3) preequilibrated with an organic solution of TOPO. The distribution ratio and the equilibrium pH value were measured in the same manner as that described above.

Extraction of Trichloroacetic Acid. An aqueous solution

† Present address: Department of Chemistry, Faculty of Science, Ibaraki University, Mito 310.

of 0.1 mol dm^{-3} trichloroacetate was shaken with a heptane solution of 2×10^{-3}—1×10^{-1} mol dm^{-3} TOPO for 5 min at 298 K. After centrifugation, an aliquot of the organic phase was taken, added to a small volume of water, and titrated with the standardized sodium hydroxide solution with vigorous agitation. The distribution ratio of trichloroacetic acid was calculated from the concentration of trichloroacetic acid extracted into the organic phase and the initial concentration of trichloroacetate in the aqueous phase.

Results and Discussion

Extraction Behavior of Rhodium(III). The extraction of hexaaquarhodium(III) from trichloroacetate or pentadecafluorooctanoate solutions into various organic solvents containing TOPO was tried at 298 K. The agitation of both phases was carried out for only 5 min. The results for the 0.10 mol dm^{-3} trichloroacetate–0.10 mol dm^{-3} TOPO system are shown in Fig. 1. A quantitative extraction of rhodium(III) can be accomplished using heptane as a diluent of TOPO; rhodium(III) of more than 99% is readily extracted at pH 3—5. However, rhodium(III) is scarcely extracted into chloroform. The extraction increases in the following order: chloroform<1,2-dichloroethane<nitrobenzene≈benzene<heptane. This order agrees with that observed in the extraction of chromium(III) with trichloroacetate and TOPO,[5] as well as in the synergic extraction of europium(III) with 4,4,4-trifluoro-1-(2-thienyl)-1,3-butanedione and TOPO.[8] Such a large observed solvent effect reveals the importance of the reaction between the extracted metal species and TOPO in the organic phase, e.g., solvation or adduct formation. The lowering of extraction in the low- and high-pH region is ascribed to the extraction of trichloroacetic acid with TOPO in the organic phase and the hydrolysis of rhodium(III) ion in the aqueous phase, respectively (vide infra).

Figure 2 shows the extraction curves of rhodium(III) in the 0.010 mol dm^{-3} pentadecafluorooctanoate–0.10 mol dm^{-3} TOPO system. The distribution ratio was independent of the shaking time from 1 to 180 min. The extraction increases in the following order: chloroform<nitrobenzene≈benzene≈1,2-dichloroethane<heptane. Though the extraction behavior is quite similar to that in the trichloroacetate–TOPO system, rhodium(III) could be quantitatively extracted into most of the solvents studied. Since pentadecafluorooctanoic acid has a larger molecular size and a higher hydrophobic character than does trichloroacetic acid, the extraction ability of the former is much higher.

A further study concerning the extraction equilibrium of the hexaaquarhodium(III) ion was made (see below) in the trichloroacetate–TOPO–heptane system in order to elucidate the composition of the extractable rhodium(III) species.

Extraction Equilibrium of Trichloroacetic Acid with TOPO. The extractability of rhodium(III) seems to be significantly affected by the extraction of

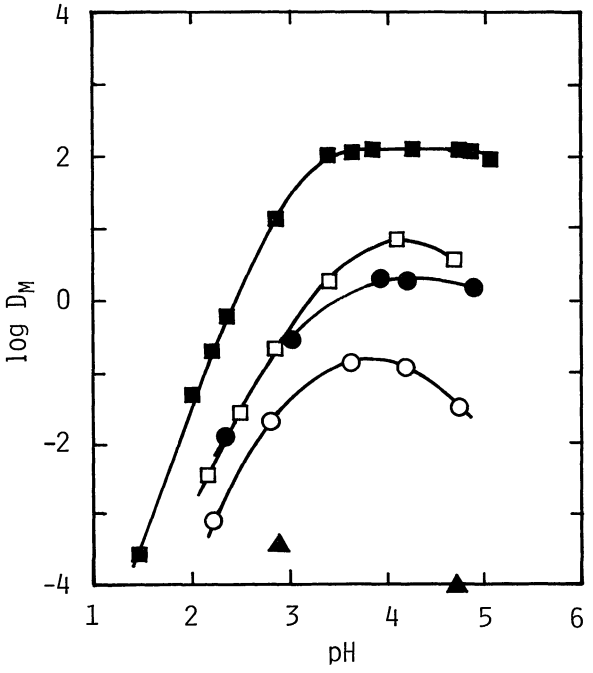

Fig. 1. Extraction of rhodium(III) from 0.10 mol dm^{-3} trichloroacetate solutions into various organic solvents containing 0.10 mol dm^{-3} TOPO. Shaking time: 5 min. ■, Heptane; □, benzene; ●, nitrobenzene; ○, 1,2-dichloroethane; ▲, chloroform.

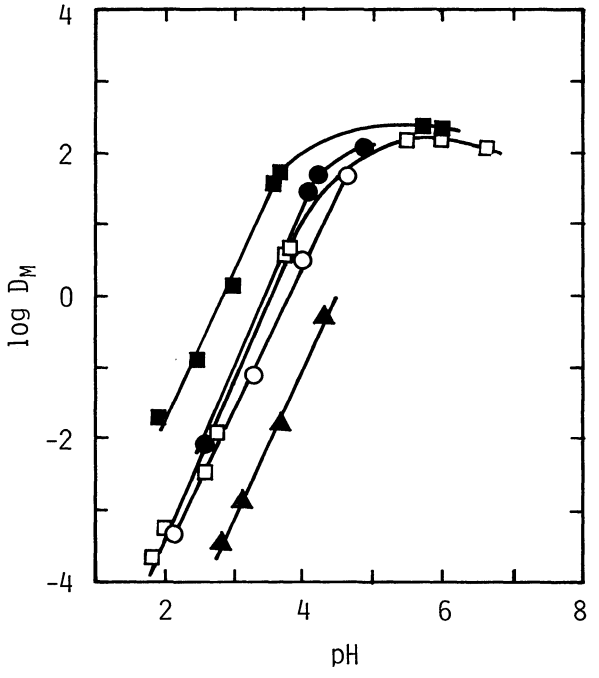

Fig. 2. Extraction of rhodium(III) from 0.010 mol dm^{-3} pentadecafluorooctanoate solutions into various organic solvents containing 0.10 mol dm^{-3} TOPO. Shaking time: 5 min. ■, Heptane; □, benzene; ●, nitrobenzene; ○, 1,2-dichloroethane; ▲, chloroform.

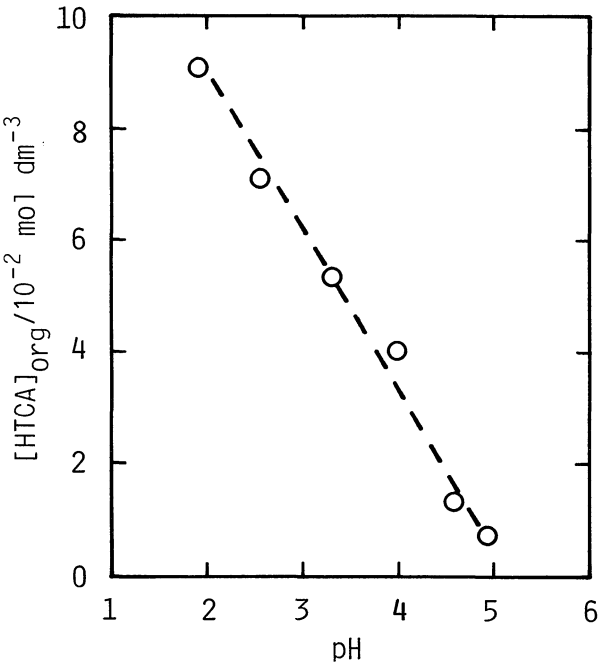

Fig. 3. Variation of the trichloroacetic acid concentration in the heptane phase with pH in the 0.10 mol dm^{-3} trichloroacetate–0.10 mol dm^{-3} TOPO system.

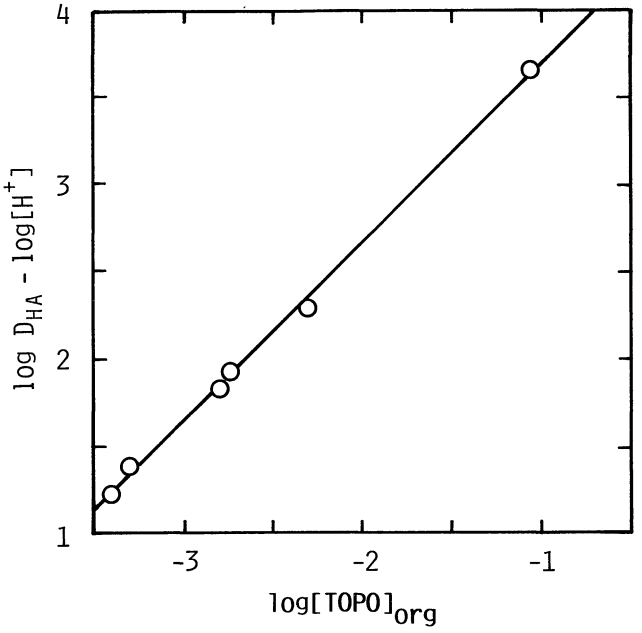

Fig. 4. Effect of the equilibrium concentration of TOPO in the organic phase on the distribution ratio of trichloroacetic acid. 0.10 mol dm^{-3} trichloroacetate, 0.0025—0.10 mol dm^{-3} TOPO. pH 2.80—4.58.

trichloroacetic acid with TOPO. Figure 3 shows the variation of the concentration of trichloroacetic acid extracted into the heptane phase at various pH. The acid concentration in the organic phase increases with a decrease in the pH, and reaches about 0.09 mol dm^{-3} at pH 2, i.e., 90% of the total concentration of trichloroacetate. Since trichloroacetic acid is a strong acid (pK_a=−0.46[9]), it should be completely dissociated in the aqueous phase within such a pH range. Hence, the extraction of trichloroacetic acid is not ascribed to the protonation of trichloroacetate following the distribution of the acid into heptane, but to the association among protons, trichloroacetate, and TOPO in the organic phase, as was previously discussed regarding the extraction of trichloroacetic acid with TOPO[5] and various acids with organophosphorus extractants.[10] The equilibrium concentrations of the trichloroacetate ion in the aqueous phase and of TOPO in the organic phase are lowered by association from the initial concentration of the respective agents. Thus, the extraction equilibrium of trichloroacetic acid with TOPO must be clarified in order to obtain the equilibrium concentration of the trichloroacetate ion and TOPO. The extraction equilibrium can be written as

$$H^+ + TCA^- + i\,TOPO_{org} \rightleftharpoons HTCA\cdot i\,TOPO_{org}, \quad (1)$$

$$K_{ex,HA} = \frac{[HTCA\cdot i\,TOPO]_{org}}{[H^+][TCA^-][TOPO]_{org}{}^i}, \quad (2)$$

where $K_{ex,HA}$ stands for the extraction constant of trichloroacetic acid and the subscript org, the organic phase. The distribution ratio (D_{HA}) of trichloroacetic acid can be given as

$$D_{HA} = \frac{[HTCA\cdot i\,TOPO]_{org}}{[TCA^-]}. \quad (3)$$

From Eqs. 2 and 3, the following equation is derived:

$$\log D_{HA} = i \log [TOPO]_{org} + \log [H^+] + \log K_{ex,HA}. \quad (4)$$

Using this equation, the equilibrium concentration of TOPO in the organic phase was calculated by deducing the amount of TOPO associated with trichloroacetic acid in the organic phase from that of TOPO initially taken. Figure 4 shows a plot of $\log D_{HA}$–$\log [H^+]$ against $\log [TOPO]_{org}$, which was obtained by setting i=1. The plot is a straight line with a slope of 1.0, as was expected. When i=2 or i=3 was assumed, no slope corresponding to the each assumption was obtainable. Consequently, the extracted species was found to be HTCA·TOPO and the extraction constant, $\log K_{ex,HA}$=4.66±0.05, was obtained. The equilibrium concentration of TOPO and trichloroacetate can be readily calculated using this value.

Extraction Equilibrium of Rhodium(III) with Trichloroacetate and TOPO. Figure 5 shows both the extraction and back extraction of hexaaquarhodium-

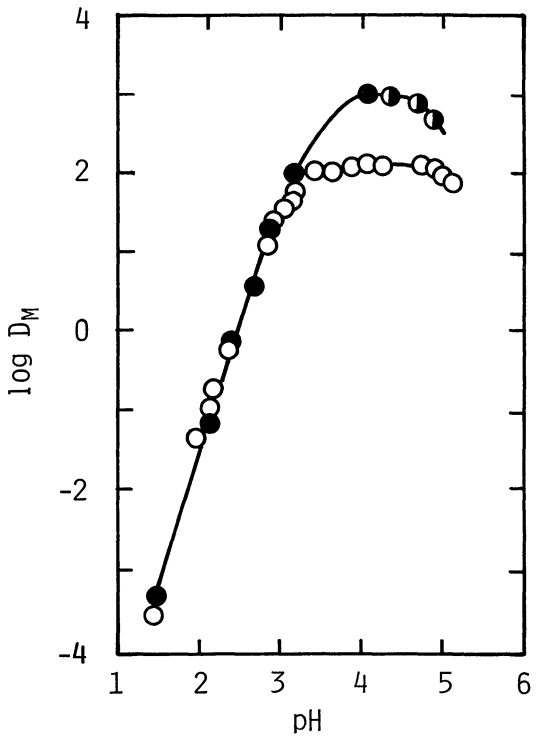

Fig. 5. Forward and backward extraction of rhodium(III) in the 0.10 mol dm^{-3} trichloroacetate–0.10 mol dm^{-3} TOPO–heptane system. ○, Forward extraction at the shaking time 5 min; ●, backward extraction at the shaking time 5 min; ◑, backward extraction at the shaking time 30 min.

(III). The distribution ratio of rhodium(III) was independent on the shaking time in a pH region lower than about 3; that is, the logarithmic values of the distribution ratio in forward extraction at pH 2.57 for three different shaking time (1, 5, and 30 min) were −2.44, −2.46, and −2.47, respectively; the same was true in backward extraction. In Fig. 5 the distribution ratio obtained from forward extraction is in good agreement with that obtained from backward extraction. These facts demonstrate that the extraction equilibrium in the present system was completely achieved within an agitation time of only 1 min. The extraction of the inert hexaaquarhodium(III) ion is surprisingly rapid in this trichloroacetate–TOPO system.

On the other hand, a disagreement between the distribution ratio in forward extraction and that in backward extraction at around pH 4 was observed. This difference in the distribution ratios was gradually reduced with the shaking time; the log D_M values in both forward and backward extraction at pH 3.9 were almost consistent at 2.7 after shaking for 27 h. This phenomenon can be ascribed to a slow extraction reaction, which may be caused by the hydrolysis and polymerization of hexaaquarhodium(III) ion in the aqueous phase within such a pH range.[11] Hence, equilibrium studies regarding the extraction of rhodium(III) were performed below pH 3 at which the rapid equilibrium could be always achieved.

The effect of the rhodium(III) concentration on the distribution ratio of rhodium(III) was examined in the 0.10 mol dm^{-3} trichloroacetate–0.10 mol dm^{-3} TOPO system at pH 2.90. The logarithmic values of the distribution ratio were 1.28, 1,28, and 1.26 at 8.1×10^{-6}, 8.1×10^{-5}, and 8.1×10^{-4} mol dm^{-3} of the rhodium(III) concentration, respectively. Since the distribution ratio is independent on the rhodium(III) concentration, no polymerization of the extracted species occurs in the organic and the aqueous phase.

The extraction equilibrium of rhodium(III) with the trichloroacetate ion (TCA^-) and TOPO can be expressed as

$$Rh^{3+} + m\,TCA^- + n\,TOPO_{org} \rightleftharpoons Rh\cdot m\,TCA\cdot n\,TOPO_{org}, \quad (5)$$

$$K_{ex,M} = \frac{[Rh\cdot m\,TCA\cdot n\,TOPO]_{org}}{[Rh^{3+}][TCA^-]^m[TOPO]_{org}^n}, \quad (6)$$

where $K_{ex,M}$ stands for the extraction constant of rhodium(III). The distribution ratio of rhodium(III) under the present experimental conditions can be written as

$$D_M = \frac{[Rh\cdot m\,TCA\cdot n\,TOPO]_{org}}{[Rh^{3+}]}. \quad (7)$$

Therefore,

$$\log D_M = m\log[TCA^-] + n\log[TOPO]_{org} + \log K_{ex,M}. \quad (8)$$

Figure 6 shows a plot of $\log D_M - 3\log[TCA^-]$ against the logarithmic value of the equilibrium concentration of TOPO in the organic phase, where it was assumed that the number of TCA molecules associated with the rhodium(III) ion, m, is three, based on the electrical neutrality with respect to the extractable species. The plot gives a straight line with a slope of 3.8 in the low-concentration region of TOPO, where the extraction of trichloroacetic acid with TOPO is negligible and the ionic strength in the aqueous phase is almost constant. Therefore, the rhodium(III) ion is solvated with four molecules of TOPO in the organic phase.

To ascertain that the number of the trichloroacetate molecules associated with the rhodium(III) ion is three, a plot of $\log D_M - 4\log[TOPO]_{org}$ against $\log[TCA^-]$ was made using $n=4$. The result is shown in Fig. 7. A straight line with a slope of 2.7 was obtained; the result is compatible with that expected, $m=3$. Therefore, the rhodium(III) species extracted into

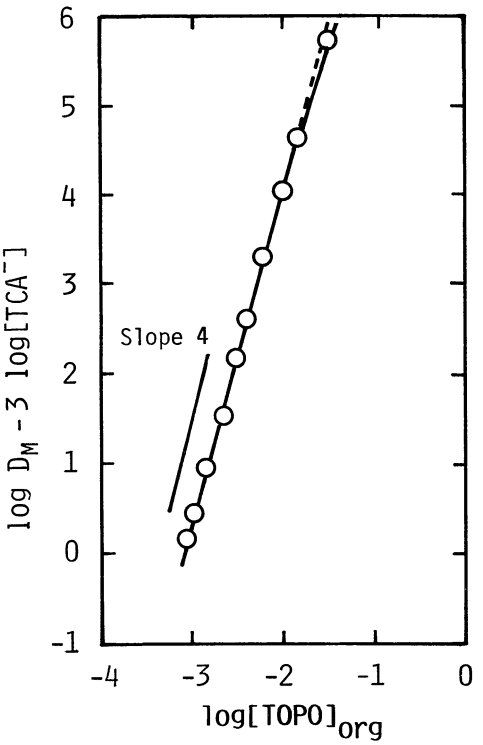

Fig. 6. Effect of the equilibrium concentration of TOPO in the organic phase on the distribution ratio of rhodium(III). 0.10 mol dm^{-3} trichloroacetate, pH 2.90, shaking time: 5 min.

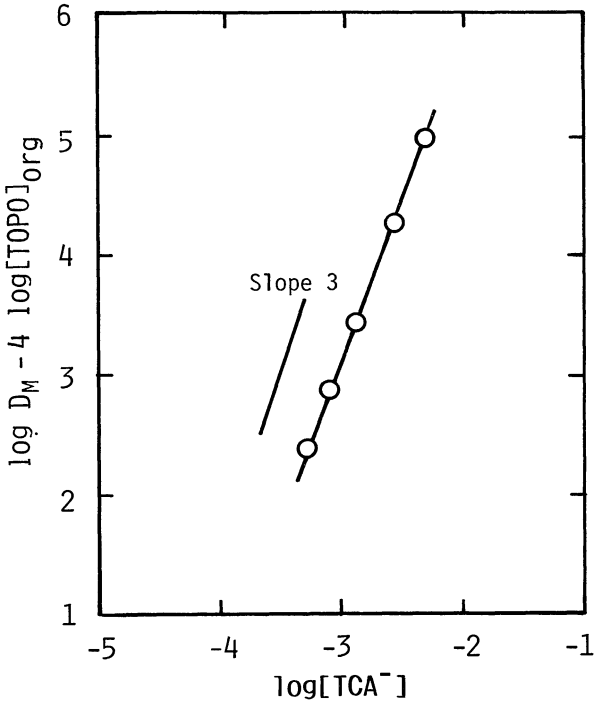

Fig. 7. Effect of the equilibrium concentration of trichloroacetate in the aqueous phase on the distribution ratio of rhodium(III). 0.10 mol dm^{-3} TOPO, pH 2.90, 0.10 mol dm^{-3} $NaNO_3$, shaking time: 5 min.

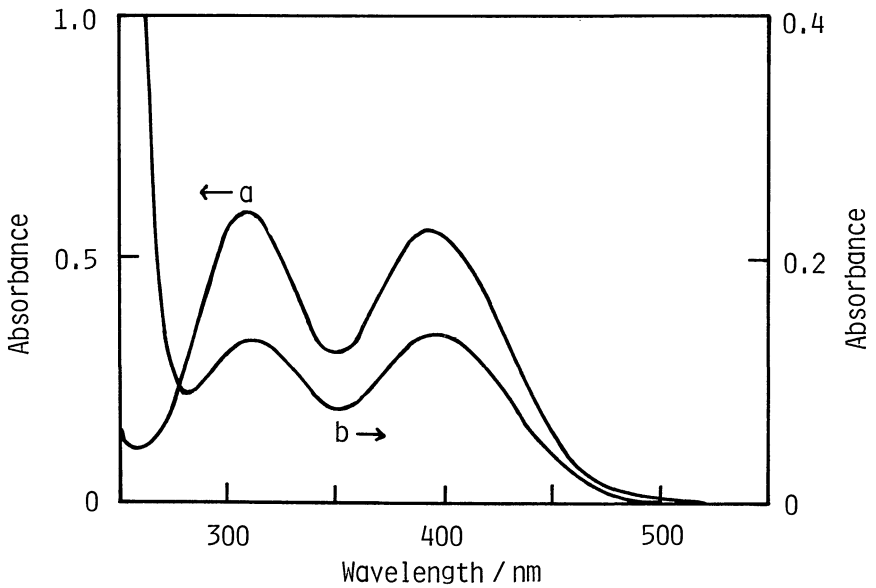

Fig. 8. Absorption spectra of the hexaaquarhodium(III) ion in perchloric acid solution and the rhodium(III) species extracted into the heptane phase containing 0.10 mol dm^{-3} TOPO from a 0.10 mol dm^{-3} trichloroacetate solution at pH 3.18. a, 1.1×10^{-2} mol dm^{-3} hexaaquarhodium(III) ion; b, 2.2×10^{-3} mol dm^{-3} rhodium(III) extracted.

heptane was found to be Rh·3TCA·4TOPO, and the extraction constant, log $K_{ex,M}$=12.29±0.06, was obtained. The composition of the extractable species was the same as that in the rhodium(III)–2,4,6-trinitrophenol–TOPO system.[12]

The electronic absorption spectrum of the rhodium(III) species extracted into heptane was measured and compared with that of the hexaaquarhodium(III) ion in an aqueous perchlorate solution. The spectra of both rhodium(III) species shown in Fig. 8 are very similar to each other. Taking account of the very inert property of the hexaaquarhodium(III) ion, it is impossible to rapidly exchange the coordinated water molecules with TOPO or TCA^- molecules. Consequently, in the present extraction system rhodium(III) is extracted as a hexaaquarhodium(III) complex, which is associated with the four molecules of TOPO and the three molecules of trichloroacetate ions. This extractable species can be considered to be an outer-sphere complex and the following model may be speculated: four TOPO and three trichloroacetate molecules may be present on the octahedral faces of the hexaaquarhodium(III) ion to most effectively interact with the central metal, as well as the coordinated water by coulombic and charge-dipole interaction, hydrogen bonding, etc.

In conclusion, an inert rhodium(III) species, could be very rapidly and quantitatively extracted in an ion-association system comprising the halogenated carboxylates and TOPO at room temperature. This rapidity of the extraction could be explained in terms of the extraction of the hydrated rhodium(III) without any ligand substitution. The present system is very useful for the extraction of such inert metal ions.

References

1) L. M. Gindin, "Solvent Extraction of Elements of the Platinum Group," in "Ion Exchange and Solvent Extraction," ed by J. M. Marinsky and Y. Marcus, Marcel Dekker Inc., New York (1981), Vol. 8, Chap. 4, pp. 311—368.

2) S. J. Al-Bazi and A. Chow, *Talanta*, **31**, 815 (1984).

3) M. A. Khan and D. F. C. Morris, *J. Less-Common Met.*, **13**, 53 (1967).

4) N. M. Patel and J. R. Thornback, *Solv. Extr. Ion Exch.*, **5**, 633 (1987).

5) H. Imura, T. Kiba, and T. Honjo, *Bull. Chem. Soc. Jpn.*, **52**, 2563 (1979).

6) C. K. Jorgensen, *Acta Chem. Scand.*, **10**, 500 (1956).

7) W. C. Wolsey, C. A. Reynolds, and J. Kleinberg, *Inorg. Chem.*, **2**, 463 (1963).

8) K. Akiba, M. Wada, and T. Kanno, *J. Inorg. Nucl. Chem.*, **43**, 1031 (1981).

9) D. D. Ensor and G. R. Choppin, *J. Inorg. Nucl. Chem.*, **42**, 1477 (1980).

10) Y. Marcus and A. S. Kertes, "Ion Exchange and Solvent Extraction of Metal Complexes," Wiley, London (1969), pp. 650—694.

11) J. S. Forrester and G. H. Ayres, *J. Phys. Chem.*, **63**, 1979 (1959).

12) H. Takahashi, H. Imura, and N. Suzuki, *Res. Rep. Lab. Nucl. Sci., Tohoku Univ.*, **22**, 181 (1989).

Synthesis and Coordination Behaviors of New Double-Sided Porphyrinatoiron(II) Complexes: Effect of the Pocket-Size for Imidazole on Dioxygen Binding

Eishun TSUCHIDA,* Etsuo HASEGAWA, Teruyuki KOMATSU, Taisaku NAKATA, Keisuke NAKAO, and Hiroyuki NISHIDE
Department of Polymer Chemistry, Waseda University, Shinjuku, Tokyo 169
(Received September 21, 1990)

The synthesis and characteristic ligation behaviors of new "double-sided porphyrinatoiron(II) complexes" having two pockets of different spacing-size on each side of a ring plane and a larger sized one on both sides of a macrocycle, are described. The equilibrium constants for the imidazole derivatives to the four-coordinated porphyrinatoiron(II)s were increased in proportion to the size of the pocket-space, which is reflected by the ΔH term. The five-coordinated complexes of the porphyrinatoirons, obtained by the addition of 1,2-dimethylimidazole (1,2-dmin) in a toluene solution, formed stable and reversible dioxygen adducts at 25 °C. The oxygen affinities for the iron(II) complexes increased as the steric bulk on the rear side of the porphyrin plane was relieved. These changes in the oxygen affinity are attributed to the strength of the π-electron donation from the imidazole to the central iron ion.

Simple porphyrinatoiron(II)s are well known to react rapidly with dioxygen to form irreversible μ-oxo-iron(III) dimers. A number of synthetic analogs of oxygen-carrying hemoproteins have been synthesized to inhibit such undesirable bimolecular reactions and have demonstrated a dramatic variation in O_2 affinities due to the nature of the pocket structure and/or the effect of the proximal base.[1-9]

Single-face highly modified porphyrinatoiron(II)s (picket-fence, capped, and pocket porphyrins) having an appropriate cavity on the ring plane, bind dioxygen reversibly in aprotic organic solvents containing an excess of axial base; their dioxygen adducts are stable against irreversible oxidation.[1-5] However, these iron(II) complexes have a very short lifetime under conditions in which the axial base concentration is very low, since the μ-oxo dimer can be formed through the unprotected side of a heme.

It is therefore necessary to modify the rear side of the porphyrin plane; the proximal imidazole binding site. Both-faces hindered porphyrinatoiron(II) (bis-pocket and basket-handle porphyrin) have been synthesized in order to sterically prevent irreversible oxidation and to perform a unique feature for dioxygen binding.[3,4] The preparation of such derivatives, however, is generally not easy and the yield is rather low.

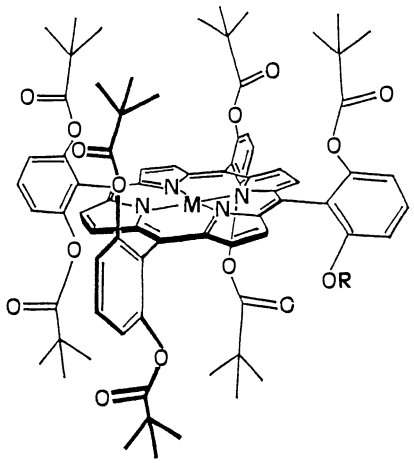

R;		-H	-C(=O)C(CH$_3$)$_3$
M;	H	1a	3a
	Fe(III)	1b′	3b′
	Fe(II)	1b	3b

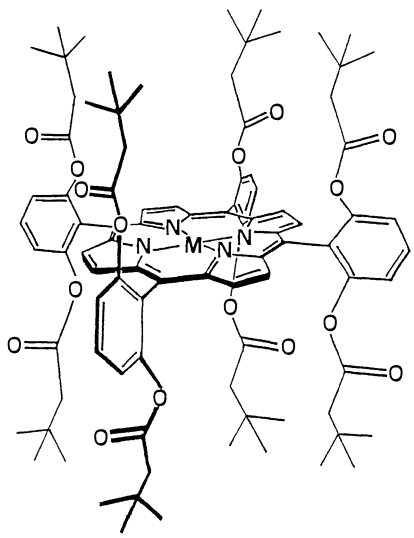

M;	H	2a
	Fe(III)	2b′
	Fe(II)	2b

On the other hand, in recent years many of the dioxygen-carrier model derived from 5,10,15,20-tetrakis(*o*-aminophenyl)porphyrin have amide residues, which have been suggested to interact with bound dioxygen (hydrogen bonding, local polarity effect, etc.) and to contribute to the stability of oxygen-adduct formation.[1-3,7] In some cases, the oxygen-binding affinity of the porphyrinatoiron complex is surely affected by the polarity of the environment around the binding site.[2-4]

We recently reported a new methodology for the synthesis of both-faces hindered and highly symmetric porphyrin, 5,10,15,20-tetrakis[2,6-bis(pivaloyloxy)phenyl]porphyrinatoiron (**3b**), which is much simpler and gives higher yields in comparison with the previous models.[10] Our results have shown that an ester-fenced porphyrin without amide groups can form a stable, reversible dioxygen adduct at 25 °C in toluene, suggesting that an electrostatic interaction between the fence residues and the bound dioxygen is not essential for the formation of a dioxygen adduct. However, the double-sided porphyrinatoiron(II) and porphyrinatocobalt(II) complexes quantitatively showed a steric hindrance of the bulky ester fences on both sides of the porphyrin plane when axial ligands bind. Generally, π-electron donation from the axial base to the metal can be varied with the binding character of the base ligand, making it possible for the oxygen-affinities of metalloporphyrins to be controlled by changes in the strength of the metal-base bonding.[3,5,8,9] It is therefore considered that the low oxygen affinity of the **3b** complex can be attributed to a decrease in the π-electron flow from the axial base to the bound dioxygen due to a steric interaction between the axial base and the bulky ester groups. In order to increase the oxygen affinity of this porphyrin, we designed and synthesized new "double-sided porphyrins", 5,10,15-tris[2,6-bis(pivaloyloxy)phenyl]-20-[(2-hydroxy-6-pivaloyloxy)phenyl]porphyrinatoiron (**1b**) and 5,10,15,20-tetrakis[2,6-bis(3,3-dimethylbutyryloxy)phenyl]porphyrinatoiron (**2b**), each having a larger cavity for axial base binding on the ring plane. Their characteristic ligation properties with imidazole derivatives or dioxygen have been clarified by spectroscopic measurements. We now wish to report on the effects of a steric change in the fences on the rear side of the ring plane, both on the binding of the axial base and on the oxygen affinities for the double-sided porphyrinatoirons.

Experimental

General. A Shimadzu UV-2100 highly-sensitive spectrophotometer equipped with a thermostatted cell holder and bath (±0.2 °C) was used for spectroscopic measurements. Infrared spectra (IR) were taken with a JASCO IR-810 spectrometer. ^{1}H NMR and ^{13}C NMR spectra were recorded on a JEOL GSX-400 instrument. Chemical shifts are expressed in parts per million downfied from Me_4Si as an internal standard. FAB MS spectra were measured with a JEOL DX-303 spectrometer. Elemental analyses were performed on a Yanagimoto MT3 CHN corder. Thin-layer chromatography (TLC) was carried out on 0.2 mm precoated plates of silica gel 60 F-254 (Merck). Products purification was performed by silica gel 60 (Merck) column chromatography. Solvents were evaporated with a type-N2 Tokyo Rikakikai rotary evaporator.

Materials and Solvents. 1-Methylimidazole (1-mim) and 1,2-dimethylimidazole (1,2-dmim) were purified before use by distillation in vacuo under reduced pressure. Pivaloyl chloride, 4-(dimethylamino)pyridine, 3,3-dimethylbutyric acid, and thionyl chloride are commercially available as special grade and were used without further purification. Tetrahydrofuran (thf) and toluene were purified immediately before use by distillation from sodium and benzophenone uder argon.

The synthetic routes for the complexes (**1b′**) and (**2b′**) are as follows.

5,10,15,-Tris[2,6-bis(pivaloyloxy)phenyl]-20-[(2-hydroxy-6-pivaloyloxy)phenyl]porphyrin (1a). 5,10,15,20-Tetrakis(2,6-dihydroxyphenyl)porphyrin ($H_2T_{(OH)_2}PP$)[10] (1.0 g, 1.35 mmol) and 4-(dimethylamino)pyridine (1.18 g, 9.69 mmol) were dissolved in dry thf (200 ml). To this ice-cooled solution pivaloyl chloride (1.19 cm^3, 9.69 mmol) was added dropwise with stirring under an argon atmosphere; the reaction mixture was stirred for 1 h at room temperature. The solution was further stirred for 12 h at 60 °C, then brought to dryness on a rotary evaporator and extracted with $CHCl_3$. The organic layer was washed, first with dilute hydrochloric acid and then with aqueous ammonia. The organic phase dried over anhydrous Na_2SO_4 was concentrated and the residue was chromatographed on a silica-gel column using $CHCl_3$–diethyl ether, 10:1 (v/v), as the eluent. The second elution band was collected and reduced to a small volume on a rotary evaporator. The residue was then dried at room temperature for several hours in vacuo to give a purple crystalline product (**1a**) (0.17 g, 9.3%). R_f 0.45 $CHCl_3$–diethyl ether, 10:1 (v/v). Anal. Found: C, 70.45; H, 6.77; N, 4.03%. Calcd for $C_{79}H_{86}N_4O_{15}\cdot H_2O$: C, 70.35; H, 6.58; N, 4.15%. FAB MS $[M]^+$ 1331. IR (KBr); 3450 cm^{-1} (ν_{OH}), 1760 cm^{-1} (ν_{CO}(ester)). ^{1}H NMR ($CDCl_3$) δ=−2.9 (2H, s, inner H), −0.5—−1.0 (63H, m, pivaloyl), 7.4—8.0 (12H, m, phenyl H), 8.8 (8H, d, pyrrole β-H). VIS. ($CHCl_3$) 636, 583, 538, 506, and 412 nm.

5,10,15-Tris[2,6-bis(pivaloyloxy)phenyl]-20-[(2-hydroxy-6-pivaloyloxy)phenyl]porphyrinatoiron(III) Bromide (1b′). The synthetic procedure for complex **1b′** was similar to that used for **1a**, except for using 5,10,15,20-tetrakis(2,6-dihyroxyphenyl)porphyrinatoiron bromide ($FeT_{(OH)_2}PP$)[10] (1.0 g). Finally, dark-purple crystalline products **1b′** (83.6 mg, 5.0%) were obtained. R_f 0.25 ($CHCl_3$–CH_3OH, 100:1 (v/v)). Anal. Found: C, 65.22; H, 6.30; N, 3.83%. Calcd for $C_{79}H_{84}N_4O_{15}FeBr\cdot 0.5C_6H_6$: C, 65.47; H, 5.83; N, 3.72%. FAB MS $[M-Br]^+$ 1385. IR (KBr); 3450 cm^{-1} (ν_{OH}), 1760 cm^{-1} (ν_{CO}(ester)). VIS. ($CHCl_3$) 680, 649, 586, 507, and 411 nm.

5,10,15,20-Tetrakis[2,6-bis(3,3-dimethylbutyryloxy)phenyl]-porphyrin (2a). 3,3-Dimethylbutyric acid (15 cm^3, 0.12 mol) was suspended in thionyl chloride (10.0 cm^3, 0.11 mol); the mixture was refluxed for 2.5 h and distilled in vacuo: colorless oil, yield 12.1 g (76.2%), bp 58 °C/69 mmHg

(1 mmHg=133.322 Pa). The acid chloride (3.62 g, 26.9 mmol) was added dropwise with stirring to an ice-cooled mixture of $H_2T_{(OH)_2}$ PP (1.0 g, 1.35 mmol) and 4-(dimethylamino)pyridine (3.29 g, 26.9 mmol) in dry thf (200 cm^3) under argon. The mixture was stirred further at room temperature for 1 h and at 50 °C for 12 h. The solution was brought to dryness on a rotary evaporator and extracted with $CHCl_3$. The organic layer was washed, first with dilute hydrochloric acid and then with aqueous ammonia. The organic phase dried over anhydrous Na_2SO_4 was concentrated and the residue chromatographed on a silica gel column using $CHCl_3$–diethyl ether, 30:1 (v/v), as the eluent. The eluent was collected and reduced to small volume on a rotary evaporator. The residue was then dried at room temperature for several hours in vacuo, to give a purple crystalline product (**2a**) (0.69 g, 33.6%). R_f 0.34 ($CHCl_3$–diethyl ether, 30:1 (v/v)). Anal. Found: C, 70.59; H, 7.33; N, 3.37%. Calcd for $C_{92}H_{110}N_4O_{16}\cdot 0.3CHCl_3$: C, 70.90; H, 7.11; N, 3.58%. FAB MS $[M]^+$ 1526. IR (KBr); 1760 cm^{-1} (ν_{CO}(ester)). ^1H NMR ($CDCl_3$) δ=−3.0 (2H, s, inner H), −0.2 (72H, s, $C(C\underline{H}_3)_3$), 1.2 (16H, s, $C(=O)C\underline{H}_2-$), 7.4—7.9 (12H, m, phenyl H), 8.8 (8H, s, pyrrole β-H). ^{13}C NMR ($CDCl_3$) δ=28.6 (methyl), 29.9 (quaternary carbon), 46.0 (methylene), 109.1 (5,10,15,20-C), 130.8 (pyrrole β-carbon), 146.9 (pyrrole α-carbon), 120.2, 128.5, 129.6, 152.0 (phenyl), 169.6 (carbonyl). VIS. ($CHCl_3$) 653, 583, 534, 506, and 413 nm.

5,10,15,20-Tetrakis[2,6-bis(3,3-dimethylbutyryloxy)phenyl]-porphyrinatoiron(III) Bromide (2b′). The synthetic procedure for complex **2b′** was similar to that used for **2a**, except for using $FeT_{(OH)_2}$ PP (1.0 g). Finally, dark-purple crystalline products **2b′** (0.22 g, 11.5%) were obtained. R_f 0.61 ($CHCl_3$–diethyl ether, 30:1 (v/v)). Anal. Found: C, 66.73; H, 6.84; N, 3.59%. Calcd for $C_{92}H_{108}N_4O_{16}FeBr$: C, 66.50; H, 6.55; N, 3.37%. FAB MS $[M]^+$ 1661, $[M-Br]^+$ 1580. IR (KBr); 1760 cm^{-1} (ν_{CO}(ester)). VIS. ($CHCl_3$) 675, 644, 577, 506, and 412 nm.

Iron(II) Complex. An iron(III) complex (0.1 μmol) was dissolved in toluene (8 cm^3) and the solution bubbled with argon to removed any oxygen. Then, a deoxygenated aqueous $Na_2S_2O_4$ solution (8 cm^3) was added. The mixture vigorously stirred for 1 h and the red-orange organic layer was collected and dried over anhydrous Na_2SO_4. After filtration from Na_2SO_4 under argon, a toluene solution of a four-coordinated porphyrinatoiron(II) (20 μmol dm^{-3}) was obtained.

Base Equilibrium Measurement. The equilibrium constants of the bases were determined at 25 °C under argon by titration of the four-coordinated porphyrinatoiron(II)s with aliqouts of an imidazole derivative in deoxygenated toluene. For the bases there are two possible equilibria, (1) and (2).

$$P + B \overset{K^B}{\rightleftarrows} P(B) \quad (1)$$

$$P(B) + B \overset{K_B{}^B}{\rightleftarrows} P(B)_2 \quad (2)$$

When $K_B{}^B$=0, the titration shows isosbestic points. However, no isosbestic ones were observed when the three species (P, P(B), and $P(B)_2$) were simultaneously present. The corresponding thermodynamic parameters (ΔH, ΔS) were calculated using the equilibrium constants at various temperatures and van't Hoff plots. The temperature of the solution was maintained to a precision of ±0.2 °C. In general, porphyrinatoiron(II) concentrations of 20 μmol dm^{-3} were used, and the spectra were recoorded within the range of 650—360 nm.

Dioxygenation of Porphyrinatoiron(II). Dioxygenation of porphyrinatoiron(II) complexes can be expressed by equation (3).

$$P(B) + O_2 \overset{K_B{}^{O_2}}{\rightleftarrows} P(B)O_2 \quad (3)$$

The oxygen-binding affinity (oxygen pressure at half oxygen binding for the porphyrinatoiron(II), ($P_{1/2}(O_2)=1/K_B{}^{O_2}$) was determined from the spectral changes at various partial pressures of dioxygen, using an equation employed by Collman et al.[11] The thermodynamic parameters (ΔH, ΔS) of dioxygenation were calculated by the oxygen-binding affinity at various temperatures, using van't Hoff plots of $\ln(760/P_{1/2}(O_2))$ vs. $1/T$. The temperature of the solution was maintained to a precision of ±0.2 °C. In general porphyrinatoiron(II) concentrations of 20 μmol dm^{-3} were used; the spectra were recorded within the range of 650—360 nm.

Results and Discussion

In this study, we designed and synthesized new double-sided porphyrinatoiron complexes (**1b** and **2b**), having large pockets for axial base binding on the rear side of the ring plane, respectively. The **1b′** complex, which has four and three pivaloyloxy groups on each side of a macrocycle, was synthesized by the reaction of $FeT_{(OH)_2}PP$ with a 7.2-times molar quantity of pivaloyl chloride. During purification on a silica-gel column, the first band, which was the least polar porphinatoiron, was identified as **3b′**. The **1b′** complex corresponded to the second band. The **2b′** complex was obtained by the coupling of $FeT_{(OH)_2}$ PP with 3,3-dimethylbutyryl chloride. Kyuno et al. reported that picket-fence type porphyrinatocobalt, having only one cavity comprising four 3,3-dimethylbutyryl amides on one side of the ring plane, was easily dissolved in organic solvents and had a higher oxygen affinity than did the picket-fence porphyrinatocobalt.[12]

The identification and structural assignments of these complexs were based on some physicochemical analyses.

The both-faces protected structure must have a similar effect as that of the protein in natural dioxygen carriers (hemoglobin and myoglobin), which forms a hydrophobic pocket around the heme, and inhibits the contact necessary for oxidation reactions. However, axial base binding to porphyrinatoiron is depressed with an increase in the steric bulk of the fences appended to the ring plane. In both planes of highly modified complexes, the effect of a steric hindrance on the protected distal face can be investigated using external nitrogenous ligands bound to the protected face of the porphyrins.[4]

The equilibrium constants were measured for the ligation of the double-sided porphyrinatoirons. Large changes in the absorption spectra occur upon titration of a toluene solution of iron(II) four-coordinate species with imidazole derivatives under an argon atmosphere. For the less-hindered base, 1-mim, these iron(II) complexes bind to a second base more strongly than does the first one due to the accompanying electron-spin changes in going from five- to six-coordinate iron(II) ($K_B^B > K^B$). In the addition of 2-substituted imidazole, 1,2-dmim, to **1b** or **2b**, however, gives only five-coordinate high-spin species cleanly ($K_B^B \ll K^B$); well defined isosbestic points are observed in the visible absorption spectra during titration (Figure 1). In order to study the oxygenation equilibrium [equation (3)], the condition must be chosen so as to ensure that the dominant species is the five-coordinate P(B). The values for the equilibrium constants for base additions to complexes **1b** and **2b** are given in Table 1.

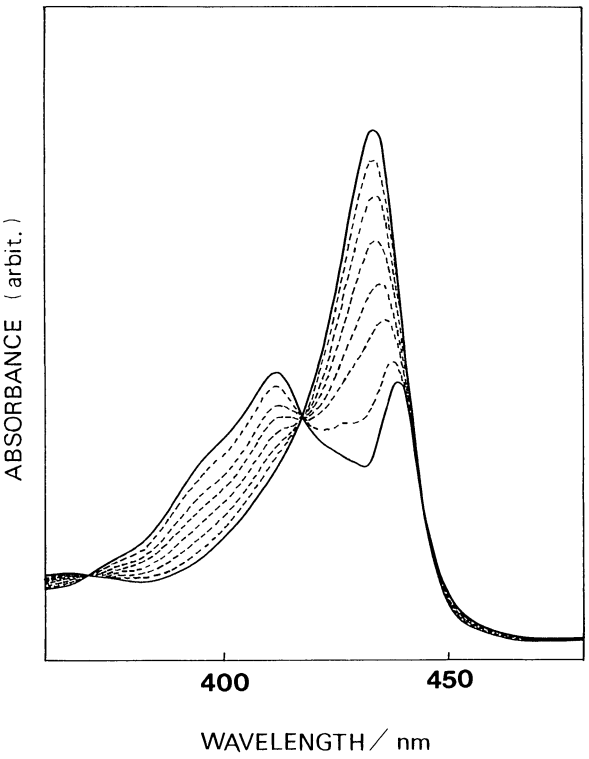

Fig. 1. Visible absorption spectral changes occurring upon titration of a 20 μmol dm^{-3} toluene solution of **2b** with 1,2-dmim (the final base concentration=12.8 mmol dm^{-3}) at 25 °C.

In a previous study we reported that the **3b** complex, having two highly modulated cavities on both sides of the porphyrin plane, showed significantly decreased values of K_B, due to their great steric hindrance afforded by the 2,6-bis(pivaloyl ester) groups held rigidly around the coordination cavities.[10] These results indicated that **3b** binds nitrogenous bases more weakly than do other unhindered porphyrin complexes.

Table 1 shows that the values of K^B for the binding of 1,2-dmim to each of the three complexes (**1b**, **2b**, and **3b**), having different pocket-space for axial base binding, are increased in the order of pocket-size, **2b**≫**1b**>**3b**. Since the K^B of complex, **1b** is slightly larger than that of **3b**, it can be said that 1,2-dmim distinguishes the two different pockets regarding size and micropolarity on each side of the ring plane in **1b**. The discriminative ligation of 1,2-dmim to this complex must be attributed to a reduction of the steric hindrance by substituting one pivaloyl group by hydrogen and to the polar nature of the rear side. The value of K^B for **2b**, having a large or flexible pocket constructed by 3,3-dimethylbutyryloxy groups is 1.3×10^3 (M^{-1}) (1 M=1 mol dm^{-3}), which is one order of magnitude lower than that for single-face hindered porphyrin (picket-fence porphyrin, etc.) or flat-open TPP. This large K^B value indicates that the unfavorable steric factor on the rear side of **2b** is appreciably weakened.

It is therefore concluded that the coordination of double-sided porphyrin to an axial base can be presumed to be controlled by the nature and structure of the rear side pocket.

Table 1 also gives thermodynamic parameters for

Table 1. Equilibrium Constants and Thermodynamic Parameters for the Binding of Axial Base to Fe(II) Porphyrin Complexes in Toluene at 25 °C

Porphyrin	Ligand	K^B / dm^3 mol^{-1}	ΔH / kcal mol^{-1}[a]	ΔS / cal K^{-1} mol^{-1}	Ref
1b	1,2-dmim	60	−8.5	−21	This work
2b	1,2-dmim	1.3×10^3	−9.8	−18	This work
3b	1,2-dmim	36	−6.9	−16	This work
TPP	2-mim[b]	2.4×10^4	—	—	11
$T_{piv}PP$[c]	1,2-dmim	3.2×10^4	—	—	d)
$T_{bp}PP$[e]	1,2-dmim	2.7×10^4	—	—	4
$T_{cap}PP$[f]	1,2-dmim	7.9×10^2	−6.1	−7	g)

a) cal=4.184 J. b) 2-mim; 2-methylimidazole. c) $T_{piv}PP$: picked-fence porphyrinatoiron(II). d) Collman et al., *J. Am. Chem. Soc.*, **105**, 3038 (1983). e) $T_{bp}PP$: bis-pocket porphyrinatoiron(II). f) $T_{cap}PP$: capped porphyrinatoiron(II). g) Basolo et al., *J. Am. Chem. Soc.*, **102**, 1889 (1980).

base binding, derived from the van't Hoff plots of $\log K^B$ vs. $1/T$ (15—30 °C). The order of enthalpy changes for 1,2-dmim binding is **3b>1b>2b**, indicating the enthalpy dependence of the free energy changes in this system.

Kyuno et al. discussed the thermodynamic parameters for base and dioxygen binding to four atropisomers of the picket-fence porphyrinatocobalt(II).[12] The higher base affinities of the *trans*-α^2 complex, compared with the α^4 complex, were due to an increase in the binding energies of the bases, although a substantial decrease in entropy change also occurs. They concluded that the stabilization of the base binding by the pickets was attributed to an intermolecular interaction between the ligated base and the *t*-butyl groups.

Indeed, entropy changes of double-sided porphyrins are small because the orientation of the 1,2-dmim plane is regulated by the fence through the process of binding to porphyrinatoiron. However, the existence of four and three bulky ester residues around the base binding site might overcome, or even cancel out, the advantageous intermolecular stabilization effect of the pocket.

The new double-sided porphinatoiron complexes (**1b** and **2b**) with 1-mim or 1,2-dmim gave stable and reversible dioxygen adducts in toluene at 25 °C. Spectrophotomeric dioxygen titrations of **1b**/1,2-dmim and **2b**/1,2-dmim were carried out under conditions of excess base. The isosbestic points were maintained in all titrations. The dioxygen complex changed to the corresponding CO adduct upon bubbling carbon monoxide gas through the solution. The electron-absorption spectral data are listed in Table 2. The values for $P_{1/2}(O_2)$ were found to be independent of the wavelength used to determined the extent of dioxygenation, and are shown in Table 3 (Figure 2).

For complexes **1b** and **2b**, the bulky ester groups on both sides of the porphyrin plane impede the formation of an intermolecular μ-dioxo dimer, as did **3b**. The $P_{1/2}(O_2)$ values of the double-sided type porphyrins were large compared to those of the corresponding adducts having intermolecular polar amido groups. Our previous study, with regard to **3b** complex, suggested that the unfavorable steric repulsions from bulky fences with imidazole must play a major role in the reduced oxygen-binding affinity.[10]

It is well known that the dioxygen affinities of porphyrinatoiron increase with increasing σ- and π-electron donation of an axial ligand.[1-3,8,9] Walker et al. reported that the rotation of 1-mim in *trans*-α^2 picket-fence porphyrinatoiron(III)(1-mim)$_2$ was restricted by pivaloyl groups, and that the dihedral angle of the bound 1-mim plane with respect to the Np–Fe–Np

Table 2. Electron-Absorption Spectra of Fe(II) Porphyrin Complexes in Toluene at 25 °C

Porphyrin	Ligand	λ_{max}/nm		
		Deoxy	Oxy	Carbonyl
1b	None	565, 532, 438, 410	—	—
	1-mim	562, 536, 430	546, 423	542, 423
	1,2-dmim	557, 535, 434	543, 423	541, 421
2b	None	565, 532, 438, 411	—	—
	1-mim	557, 530, 423	542, 419	538, 419
	1,2-dmim	554, 532, 433	545, 419	535, 419
3b	None	565, 535, 440, 411	—	—
	1-mim	561, 535, 429	544, 423	542, 424
	1,2-dmim	558, 535, 436	545, 422[a]	542, 422
$T_{piv}PP$[b]	None	565, 535, 435, 415	—	—
	1-mim	562, 537, 432	548, 429	542, 427
	1,2-dmin	562, 535, 439	544, 421	542, 424

a) At −20 °C. b) See c) of Table 1. Ref. 1.

Table 3. Oxygen-affinity and Thermodynamic Parameters for Oxygenation of Fe(II) Porphyrin Complexes in Toluene at 25 °C

Porphyrin	Ligand	$P_{1/2}(O_2)$	ΔH	ΔS	Ref
		mmHg[a]	kcal mol^{-1}[b]	cal K^{-1} mol^{-1}	
1b	1,2-dmim	503	−13.0	−43	This work
2b	1,2-dmim	229	−14.1	−45	This work
3b	1,2-dmim	866	−9.3	−31	10
$T_{piv}PP$[c]	1,2-dmim	38	−14.3	−42	1
$T_{bp}PP$[d]	1,2-dmim	508	−14.4	−47	4
$T_{cap}PP$[e]	1,2-dmim	4.0×10^3	−9.7	−49	5

a) mmHg=133 Pa. b) cal=4.184 J. c), d), e) See c), e), f) of Table 1.

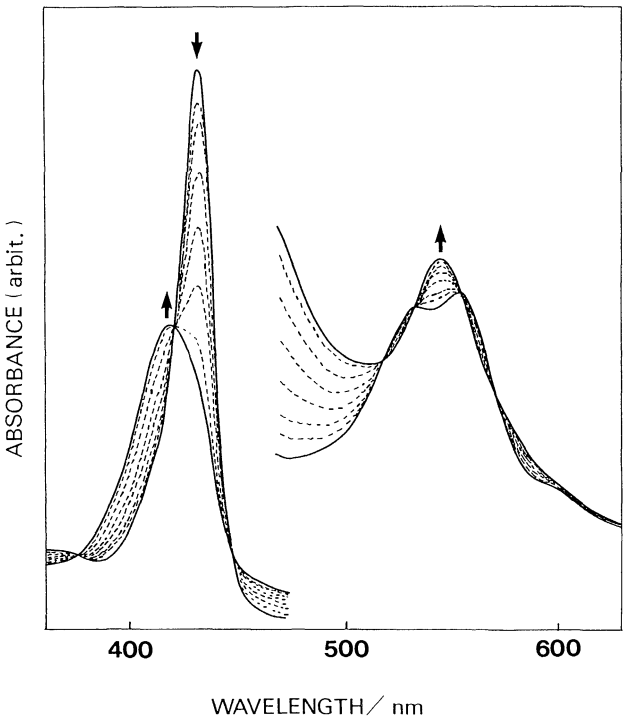

Fig. 2. Visible absorption spectral changes in the dioxygen binding to **2b**/1,2-dmim complex in toluene at 25 °C. Arrows indicate the changes with increasing dioxygen pressures.

direction is equal to 45°.[13] The lobe of the Fe dπ (d_{xz} or d_{yz}) orbitals therefore point to the pyrrole nitrogen and the lobe of pπ (p_x or p_y) orbitals on the nitrogen of 1-mim point of 135°.

Kyuno et al. suggested that the decreased oxygen affinities of "jellyfish type porphyrinatocobalt(II) complexes" can be attributed to the regulated orientation of 1-mim plane (ϕ=45°), in which π–π interaction between metal and 1-mim reaches a minimum due to the steric repulsions with appended fence groups.[14] However, the oxygen and carbon monoxide affinities for the corresponding porphyrinatoiron(II) complexes did not exhibit a similar trend to that observed for the oxygen affinities for the Co(II) complexes. They suggested that conformational changes in the cavity, constructed strapped methylene chain, were concerned with reduced oxygen and carbon monoxide affinities.

In the case of the **3b** complex, since the dihedral angle may be equal to 0°, the π-electron donation of 1,2-dmim is expected to be at the maximum because of the maximum π-overlap with the Fe dπ orbitals. Although the favorable orientation of the axial base, accelerating π–π interaction between Fe and the axial base, the $P_{1/2}(O_2)$ values were low in comparison to those of other models.

In order to quantitatively clarify the correlation $P_{1/2}(O_2)$ with the pocket-space on the rear side of the macrocycle for imidazole binding, the oxygen affinities of **1b**, **2b**, and **3b** complexes were compared.

The oxygen-binding affinities of the double-sided porphyrinatoirons were of the order **2b**>**1b**>**3b**, in proportion to the spacing-size of the rear pocket space. This result indicates that oxygen affinities for the iron(II) complexes increased as the unfavorable steric bulk on rear side of the porphyrin plane was relieved. That is, in spite of the orientation of the axial base plane to π-orbital, great steric hindrance of ester fences reduced their π-bond character in the Fe(II)-base. The oxygen affinities decrease in the order of the repulsion of the substituents, and can be controlled by the pocket-size for axial base binding.

On the other hand, the oxygen affinity is surely attributed to the nature of the hydrophobic pocket for dioxygen binding ((1) steric effect, (2) solvation effect, and (3) local polarity).[1–5,15] (1) The steric hindrance significantly influences the $P_{1/2}(O_2)$ of the protected porphyrin. But the "central" and "peripheral" effects, proposed by Basolo, might not be found in the pivaloyloxy type.[5] (2) Among the "protected" heme, a small difference in the solvation effect has no significant meaning on $P_{1/2}(O_2)$. In double-sided porphyrinatoiron complexes, the solvation effects were considered to be almost the same for the other protected models. (3) The polarity of the dioxygen binding site considerably influences the oxygen affinity. From structural studies and ^{17}O NMR spectroscopic data of picket-fence porphyrin, though there is no hydrogen-bonding between the amido proton and bound dioxygen, these amide groups can be expected to increase the polarity at the binding site.[7,16] Bis-pocket and ether hanging-base porphyrin which had a nonpolar pocket, showed a low oxygen affinity in comparison to the amide handle derivatives.[3,4] Therefore, the low oxygen affinity of the double-sided porphyrins systems might be the result of a smaller polar pocket effect around the oxygen-binding site. However, from the quantitative results for a series of this type of porphyrins, it is concluded that the oxygen affinity can be controlled by the pocket-size for imidazole binding.

Chang et al. have determined the individual contribution of dipole–dipole interactions in stabilizing the Fe–O_2 cmplex.[17] A disadvantageous dipole–dipole orientation may exist between FeO_2 and the ester moieties of the double-sided porphyrin.

Table 3 also shows the enthalpy and entropy changes of the dioxygenation equilibrium of the **1b**/1,2-dmim and **2b**/1,2-dmim complex determined from van't Hoff plots (15—30 °C). The thermodynamic values given in Table 3 show that a major difference in dioxygen binding is manifested in the enthalpy terms. Among the double-sided porphyrins, the order of $P_{1/2}(O_2)$ was **3b**>**1b**>**2b**. A similar tendency was also found for the ΔH, indicating the enthalpy dependence of the free energy changes in this

system.

This work was partially supported by a Grant-in-Aid in science research on a priority area, "Macromolecular Complexes", from the Ministry of Education, Science and Culture.

References

1) J. P. Collman, R. R. Gagne, C. A. Reed, T. R. Halbert, G. Lang, and W. T. Robinson, *J. Am. Chem. Soc.*, **97**, 1427 (1975); J. P. Collman, J. I. Brauman, B. L. Iverson, J. L. Sessler, R. M. Morris, and Q. H. Gibson, *ibid.*, **105**, 3052 (1983).

2) T. G. Traylor, S. Tsuchiya, D. Campbell, M. Mitchel, D. Styness, and N. Koga, *J. Am. Chem. Soc.*, **107**, 614 (1985); T. G. Traylor, N. Koga, and L. A. Deardurff, *ibid.*, **107**, 6504 (1985).

3) M. M. Momenteau, *Pure Appl. Chem.*, **58**, 1493 (1986).

4) K. S. Suslick and M. M. Fox, *J. Am. Chem. Soc.*, **105**, 3507 (1983); K. S. Suslick, M. M. Fox, and T. J. Reinnert, *ibid.*, **106**, 4522 (1984).

5) T. Hashimoto, R. L. Dyer, M. J. Crossley, J. E. Baldwin, and F. Basolo, *J. Am. Chem. Soc.*, **104**, 2101 (1982); J. E. Baldwin, J. H. Cameron, M. J. Crossly, I. J. Daugly, and T. Klose, *J. Chem. Soc., Dalton Trans.*, **1984**, 1739.

6) A. R. Battersby, S. A. J. Bartholomew, and T. Nitta, *J. Chem. Soc., Chem. Commun.*, **1983**, 1291.

7) M. Momenteau, B. Loock, C. Tatreau, D. Lavalette, A. Croisy, C. Scheaeffer, C. Huel, and J-M. Lhoste, *J. Chem. Soc., Perkin Trans. 2*, **1987**, 249; I. P. Gerothanasis, M. Momenteau, and B. Loock, *J. Am. Chem. Soc.*, **111**, 7006 (1989).

8) J. P. Collman, J. I. Brauman, K. M. Doxsee, J. L. Sessler, R. M. Morris, and Q. H. Gibson, *Inorg. Chem.*, **22**, 1427 (1983).

9) C. K. Chang and T. G. Traylor, *Proc. Natl. Acad. Sci. U.S.A.*, **72**, 1166 (1975).

10) T. Komatsu, E. Hasegawa, H. Nishide, and E. Tsuchida, *J. Chem. Soc., Chem. Commun.*, **1990**, 66; E. Tsuchida, T. Komatsu, E. Hasegawa, and H. Nishide, *J. Chem. Soc., Dalton Trans.*, **1990**, 2713; E. Tsuchida, E. Hasegawa, T. Komatsu, K. Nakao, and H. Nishide, *Chem. Lett.*, **1990**, 1071.

11) J. P. Collman, J. I. Brauman, K. M. Doxsee, T. R. Halbert, S. E. Hayes, and K. S. Suslick, *Proc. Natl. Acad. Sci. U.S.A.*, **564**, 75 (1978).

12) H. Imai, K. Nakata, A. Nakatsubo, S. Nakagawa, Y. Uemori, and E. Kyuno, *Synth. React. Inorg. Met.-Org. Chem.*, **13**, 761 (1983); H. Imai and E. Kyuno, *Inorg. Chim. Acta*, **453**, 175 (1988); H. Imai and E. Kyuno, *Inorg. Chim. Acta*, **153**, 183 (1988).

13) F. A. Walker, J. Buehler, J. T. West, and J. L. Hinds, *J. Am. Chem. Soc.*, **105**, 6923 (1983).

14) Y. Uemori, H. Miyasaka, and E. Kyuno, *Inorg. Chem.*, **27**, 377 (1988); Y. Uemori and E. Kyuno, *Inorg. Chem.*, **28**, 1690 (1989).

15) S. Takagi, K. Miyamoto, and Y. Sasaki, *Bull. Chem. Soc. Jpn.*, **58**, 447 (1985).

16) G. B. Jameson and R. S. Drago, *J. Am. Chem. Soc.*, **107**, 3017 (1985).

17) C. K. Chang, *J. Macromol. Sci., Chem.*, **A25(10&11)**, 1307 (1988).

Preparations, Properties, and Crystal Structures of *trans*-[Rh(CN)$_2$(NH$_3$)$_4$]Cl·H$_2$O and *trans*-[Rh(CN)$_2$(en)$_2$]Cl

Kiyohiko Yoshida, Takayuki Kitada, Naomi Odano, Mayumi Kashiwagi, Kazumasa Harada, Akio Urushiyama,* and Masayoshi Nakahara
Department of Chemistry, College of Science, Rikkyo University, Nishiikebukuro 3, Toshima-ku, Tokyo 171
(Received October 29, 1990)

Syntheses of the title new complex compounds of Rh(III) were successful. Single, sharp IR peaks of ν (C≡N) were observed at 2130 cm^{-1} (*trans*-[Rh(CH)$_2$(NH$_3$)$_4$]Cl·H$_2$O) and 2170 cm^{-1} (*trans*-[Rh(CN)$_2$(en)$_2$]Cl), respectively. The values of the ligand field tetragonal parameter D_t were estimated to be −366 and −377 cm^{-1}, respectively, based on the $^1E_g{}^a$ (D_{4h})←$^1A_{1g}$ transition (37100 cm^{-1}: *trans*-[Rh(CN)$_2$(NH$_3$)$_4$]$^+$; 37000 cm^{-1}: *trans*-[Rh(CN)$_2$(en)$_2$]$^+$). The X-ray crystal data are: for *trans*-[Rh(CN)$_2$(NH$_3$)$_4$]Cl·H$_2$O, orthorhombic, *Cmcm*, a=7.961(3), b=17.295(2), c=7.436(3) Å, D_c=1.79, D_m=1.79 g cm^{-3}, Z=4; for *trans*-[Rh(CN)$_2$(en)$_2$]Cl, monoclinic, $P2_1/n$, a=9.665(4), b=9.107(3), c=6.779(3) Å, β=109.68(2)°, D_c=1.85, D_m=1.83 g cm^{-3}, Z=2. The N≡C–Rh–C≡N sequence of *trans*-[Rh(CN)$_2$(NH$_3$)$_4$]$^+$ lies in a line of $m2m$ symmetry in the crystal. The central Rh atom of *trans*-[Rh(CN)$_2$(en)$_2$]$^+$ occupies the special position of inversion symmetry. The important geometrical data of the complexes are Rh–N=2.07(1), Rh–C=2.02(3) Å, N–Rh–N=88.0(5)° (*trans*-[Rh(CN)$_2$(NH$_3$)$_4$]$^+$) and Rh–N=2.080(3), 2.072(3), Rh–C=2.047(4) Å, N–Rh–N (within chelate ring)=82.7(1)° (*trans*-[Rh(CN)$_2$(en)$_2$]$^+$).

A variety of Rh(III) complex compounds have been prepared and studied regarding their spectroscopic properties[1] and kinetic mechanisms of photochemical reactions.[2] However, investigations have not been developed to include the structurally rather familiar complexes of *trans*-[Rh(CN)$_2$N$_4$]$^+$ (N$_4$: (NH$_3$)$_4$, (en)$_2$, (tn)$_2$), since synthetic methods have not yet been established.

Here, we report on the syntheses, spectroscopic identification, and X-ray crystal structures of the title new complex compounds of Rh(III).

Experimental

Preparation. *trans*-[Rh(CN)$_2$(NH$_3$)$_4$]Cl·H$_2$O. Five grams of *trans*-[Rh(CN)Cl(NH$_3$)$_4$]Cl·1.5H$_2$O[3] and 3.0 g of NaCN in 300 ml DMSO were heated at 85 °C for 1.5 h. A crude product which precipitated was collected by filtration and washed by ethanol and air-dried (2.8 g). This was dissolved in 100 ml H$_2$O and, after filtration, pure chloride was obtained upon the addition of concd HCl. Yield. 2.5 g (50%). Found: C, 8.60; H, 5.09; N, 30.06%. Calcd for [Rh(CN)$_2$(NH$_3$)$_4$]Cl·H$_2$O=C$_2$H$_{14}$N$_6$OClRh: C, 8.68; H, 5.10; N, 30.39%. The water of crystallization was easily lost in air at room temperature. An elemental analysis was also performed for the anhydrate. Found, 9.24; H, 4.37; N, 32.38%. Calcd for [Rh(CN)$_2$(NH$_3$)$_4$]Cl=C$_2$H$_{12}$N$_6$ClRh: C, 9.29; H, 4.68; N, 32.51%.

***trans*-[Rh(CN)$_2$(NH$_3$)$_4$](ClO$_4$).** The immediate crystallization of the perchlorate occured when perchloric aicd was poured into an equeous solution of the chloride. Found: C, 7.49; H, 3.83; N, 25.98%. Calcd for [Rh(CN)$_2$(NH$_3$)$_4$](ClO$_4$)=C$_2$H$_{12}$N$_6$O$_4$ClRh: C, 7.45; H, 3.75; N, 26.06%.

***trans*-[Rh(CN)Cl(en)$_2$](ClO$_4$).** To an aqueous solution (500 ml) containing 6.0 g of *trans*-[RhCl$_2$(en)$_2$](NO$_3$),[4] 6.0 g of Na$_2$SO$_3$ was added. After the solution was heated to 80 °C, 3.0 g of NaCN was added. The characteristic yellow color of the starting dichlorocomplex was soon lost. After being cooled to room temperature, the solution was passed through a columun of anion-exchange resin (Cl$^-$ form, MCL GEL CA08P), followed by a cation columun (Li$^+$ form, Dowex 50-X8). Complete evaporation of the solution left a white powder (*trans*-[Rh(CN)(SO$_3$)(en)$_2$]+LiCl). The obtained cyanosulfitocomplex was easily converted to the cyanochlorocomplex by treatment with concd HCl (20 ml) at 60 °C. Within ten minutes, when SO$_2$ gas evolution ceased, to the resultant clear solution* 50 ml perchloric acid (70%) was added by ice cooling to give a mixture of solid LiClO$_4$ and a white crystalline powder, which was collected on a filter and washed by ethanol to remove LiClO$_4$ (the suction flask should be emptied before ethanol washing!) and air dried. Yield. 1.0 g (15%). Found: C, 15.38; H, 4.25; N, 18.07%. Calcd for [Rh(CN)Cl(en)$_2$](ClO$_4$)=C$_5$H$_{16}$N$_5$OCl$_2$Rh: C, 15.46; H, 4.20; N, 18.24%.

*Sometimes a mixture of *trans*-[Rh(CN)Cl(en)$_2$]Cl and LiCl was precipitated at this stage. This was filtered and redissolved in water; perchloric acid was then added to convert to the perchlorate.

***trans*-[Rh(CN)$_2$(en)$_2$]Cl.** One gram of *trans*-[Rh(CN)Cl(en)$_2$](ClO$_4$) and 1.5 g of NaCN were mixed in 25 ml DMSO. The produced white precipitate was filtered, washed by ethanol and air-dried (*trans*-[Rh(CN)Cl(en)$_2$](CN), 0.7 g). This was suspended in 25 ml DMSO–H$_2$O (10:1 in volume ratio) medium. After the addition of 1.5 g of NaCN, the mixture was heated to 90 °C for 2 h. The obtained white solid was collected, washed by ethanol and dried. This was dissolved in 7 ml of H$_2$O and filtered once (if the solution is alkaline, acidify by concd HCl. Warning! HCN gas evolved). The addition of ethanol caused the precipitation of white crystalline powder. This was adsorbed on a cation-exchange columun (Li$^+$ form, Dowex 50-X8) and eluted by 0.2 mol dm^{-3} LiCl. From the concentrated solution a white crystalline powder was separated, filtered, washed with ethanol. Yield 0.5 g (62%). Found: C, 23.34; H, 5.40; N, 27.44%. Calcd for [Rh(CN)$_2$(en)$_2$]Cl=C$_6$H$_{16}$N$_6$ClRh: C, 23.19; H, 5.19; N, 27.06%.

***trans*-[Rh(CN)$_2$(en)$_2$](ClO$_4$).** A white crystalline powder of the perchlorate was obtained by the addition of perchloric acid (70%) to the above-mentioned filtrate, or an aqueous solution of the chloride. Found: C, 19.43; H, 4.58; N, 22.70%. Calcd for [Rh(CN)$_2$(en)$_2$](ClO$_4$)=C$_6$H$_{16}$N$_6$O$_4$ClRh: C, 19.22;

H, 4.31; N, 22.44%.

Spectroscopic Measurements and Thermogravimetric Measurement. IR, Raman, and UV spectroscopies were performed using a Perkin-Elmar 1600 FTIR spectrometer, a Jobin-Yvon Ramanor 1000 monochromator equipped with an NEC GLG3300 laser (Ar^+: 5145 Å), and a Hitachi U-3400 spectrometer, respectively. The Raman apparatus was also employed for luminescence measurements by excitation of the 312 nm line of a high-pressure mercury lamp. ^1H and ^{13}C NMR measurements were accomplished by a JOEL GSX 400 spectrometer. A TGA curve was taken with a Shinkuriko TGD-7000 RH thermogravimeter.

X-Ray Crystal Structure Analyses. X-Ray crystallographic studies were carried out using a Rigaku AFC-5 four-circle automated diffractometer. Graphite monochromated Mo $K\alpha$ (λ=0.71073 Å) was used as the X-ray source. A crystal of *trans*-$[Rh(CN)_2(NH_3)_4]Cl \cdot H_2O$ was sealed into a silica glass capillary (ϕ=0.7 mm). Experimental details, crystallographic data and the R factors of the final refinements are shown in Table 1. All computational studies were carried out on a FACOM M760 computer at the Computer Center of Rikkyo University, using universal X-ray crystal structure analysis program (UNICSIII, MULTAN, ORTEP).[5] An absorption correction was employed (North et al.[6]). The atomic scattering factors were taken from "International Tables for X-Ray Crystallography," Vol. IV, Kynoch Press, Birmingham (1974). The initial phases of the structure factor determined by a direct method were refined by cycles of a block-matrix least-square method. The positions of the hydrogen atoms were obtained by difference-Fourier syntheses. The final full-matrix treatments sufficiently decreased the R factors (Table 1).

The position of the water of crystallization of *trans*-$[Rh(CN)_2(NH_3)_4]Cl \cdot H_2O$ was not clearly revealed on the difference-Fourier maps. If an oxygen atom was placed at a special position (2/m, multiplicity: 0.25) of (0.5, 0, 0), for which the maximum residual electron density (1.86 e Å^{-3}) was yielded, a rather large value of the isotropic temperature factor was obtained after a sufficient number of cycles of a least-square treatment. However, this point is recognized as being a vacant hole in the crystal; the shortest contact distance from this point to a non-hydrogen atom is 3.54 Å (to N(1) of the complex cation). The TGA curve indicated a weight loss corresponding to ca. 1 mol of crystallization water below 60 °C. It is therefore believed that almost all of the water molecules were lost from this point before the X-ray study, although the sample crystal was sealed into a small capillary. The observed density (1.77 g cm^{-3}) of the freshly prepared crystal is slightly smaller than the calculated value (1.79 g cm^{-3}), based on monohydrated stoichiometry.

Tables of the observed and calculated structure factors are deposited as Document No. 9105 at the Office of the Editor of Bull. Chem. Soc. Jpn.

Results and Discussion

Baranovskii et al.[7,8] and Skibsted et al.[9] have reported the syntheses of several cyanoammine complexes of Rh(III), which involve $[Rh(CN)(NH_3)_5]Cl_2$, *trans*-$[Rh(CN)(SO_3)(NH_3)_4] \cdot 2H_2O$, *trans*-$[Rh(CN)Cl(NH_3)_4]Cl$, and $[Rh(CN)_3(NH_3)_3]$. However, Baranovskii et al.[12] have mentioned that an attempt to introduce a second CN^- to *trans*-$[Rh(CN)(SO_3)(NH_3)_4]$ with excess CN^- was not successful in an aqueous solution. Subsequently, Kane-Maguire et al.[10] synthesized *trans*-$[Rh(CN)_2(cyclam)](ClO_4)$ by a reaction of the corresponding dichlorocomplex and CN^- in an aqueous solution. A direct synthesis[11,12] of *trans*-

Table 1. Summary of X-Ray Data Collections, Crystal Data, and Structure Refinements

	trans-$[Rh(CN)_2(NH_3)_4]Cl \cdot H_2O$	*trans*-$[Rh(CN)_2(en)_2]Cl$
Formula	$RhC_2N_6H_{14}OCl$	$RhC_6N_6H_{16}Cl$
F. W.	276.54	310.59
Crystal system	Orthorhombic	Monoclinic
Space group	$Cmcm$	$P2_1/n$
a/Å	7.961(3)	9.665(4)
b/Å	17.295(2)	9.107(3)
c/Å	7.436(3)	6.779(3)
β/degree		109.68(2)
V/Å^3	1023.8(6)	561.8(4)
Z	4	2
D_x/g cm^{-3}	1.79	1.85
D_m/g cm^{-3}	1.77	1.83
μ(Mo$K\alpha$)/cm^{-1}	18.6	17.1
Crystal size/mm	0.43×0.20×0.15	0.48×0.35×0.10
Scan mode	$\omega(2\theta \leqq 25°)$, ω-$2\theta(25° < 2\theta \leqq 55°)$	$\omega(2\theta \leqq 25°)$, ω-$2\theta(25° < 2\theta \leqq 55°)$
Scan width/deg	1.2+0.5tan θ	1.2+0.5tan θ
Scan speed/deg min^{-1}	4	4
No. of refl. measd.	1092	1868
No. of unique refl. with $F_o \geqq 3\sigma(F_o)$	970	1375
Max. min. residual electron density/(e Å^{-3})	1.86, −0.82	1.00, −1.46
Max (shift/esd)	0.29	0.22
Weighting scheme	Unit weight	Unit weight
R	0.0442	0.0289
R_w	0.0804	0.0315

$[Co(CN)_2(N)_4]^+$ ($(N)_4$: $(NH_3)_4$, $(en)_2$, $(tn)_2$) from the corresponding dichlorocomplex is also possible in DMSO or a methanol medium.

We first studied the direct reaction of *trans*-$[RhCl_2(NH_3)_4]Cl$ and NaCN under various conditions (concentrations, temperatures, and media). However, this reaction yielded only uncharacterizable insoluble solids, even in cases where the reaction occured.

For the corresponding Co(III) complex, Maki et al.[13] employed the reaction of *trans*-$[Co(CN)Cl(NH_3)_4]$-Cl+NaCN to obtain *trans*-$[Co(CN)_2(NH_3)_4]$ in DMSO. Therefore, we have studied this type of reaction, i.e., *trans*-$[Rh(CN)Cl(N)_4]Cl$+NaCN ($(N)_4$: $(NH_3)_4$, $(en)_2$), in DMSO. It was found that, while the ligand substitution of Cl^- by CN^- hardly proceeded in a pure DMSO medium, especially for the ethylenediamine complex, the reaction easily occured in a DMSO–H_2O mixed medium to give the desired *trans*-dicyano complex compounds (see experimental section). An attempt to synthesize the corresponding tn (1,3-propanediamine) complex, *trans*-$[Rh(CN)_2(tn)_2]^+$, is now proceeding using a similar ligand-substitution reaction in either a DMSO–H_2O or ethanol medium.

The IR and Raman spectra of the present Rh(III) complexes are very similar to the corresponding Co(III) complexes.[14–16] The numerical data are summerized in Table 2; some possible assignments are included. It was mentioned[13] in a study of the

Table 2. Principal IR and Raman Bands (cm^{-1}) of *trans*-$[Rh(CN)_2(NH_3)_4]Cl\cdot H_2O$ and *trans*-$[Rh(CN)_2(en)_2]Cl$

trans-$[Ph(CN)_2(NH_3)_4]^+$			*trans*-$[Rh(CN)_2(en)_2]^+$		
IR	Raman	Assignment[a]	IR	Raman	Assignment[a]
278		δ (N-Rh-N)		216	
283	285	δ (N-Rh-N)			
				253	δ (cycle)
387		δ (Rh-C≡N)		321	
	417	ν (Rh-C)	360		
456		ν (Rh-N)	390		
	478	ν (Rh-C)		421	ν (Rh-C)
	497	ν (Rh-N)	440		
824		ρ ($Rh-NH_3$)		453	
1310		δ_s (H-N-H)	486		ν (Rh-N)
1690		δ_a (H-N-H)	518		ν (Rh-C)
				542	δ N-Co-C
			582		δ N-C-C
2125		ν (C≡N)	2126		ν (C≡N)

a) Ref. 14—16.

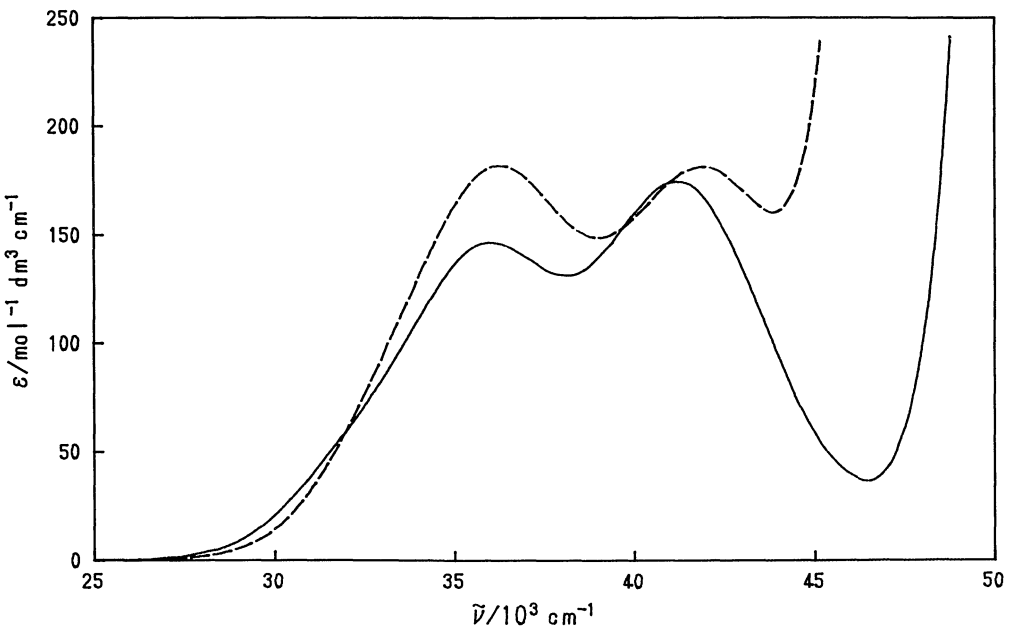

Fig. 1. Electronic absorption spectra of cyanoammine complexes of Rh(III) in aqueous solution. (a) —— *trans*-$[Rh(CN)_2(NH_3)_4]Cl\cdot H_2O$; (b) ----- *trans*-$[Rh(CN)_2(en)_2]Cl$.

corresponding Co(III) complexes that no splitting feature of the sharp IR line due to C≡N stretching vibration appeared between 2100—2200 cm^{-1} is diagnostic to the *trans*-isomer. In accord with this statement, the present *trans*-dicyano complexes of Rh(III) did not show any splitting of the C≡N band.

The UV absorption spectra were shown in Fig. 1, and the numerical data are summerized in Table 3, in which the ligand field assignments in the D_{4h} effective site symmetry are included. The lowest spin-allowed component of $^1A_{2g}(D_{4h})\leftarrow{}^1A_{1g}$ was not clearly observed for the present Rh(III) complexes compared to the corresponding Co(III) complexes.[14–16] If the energy of the $^1A_{2g}\leftarrow{}^1A_{1g}$ is approximated[17] to be that of the $^1T_{1g}(O_h)\leftarrow{}^1A_{1g}$ transition of $[Rh(NH_3)_6]^{3+}$ (32800 cm^{-1}) and/or $[Rh(en)_3]^{3+}$ (33200 cm^{-1}), the values of the tetragonal parameter, D_t, are estimated to be −366 cm^{-1} and −377 cm^{-1}, respectively, for *trans*-$[Rh(CN)_2(NH_3)_4]^+$ and *trans*-$[Rh(CN)_2(en)_2]^+$.

The present Rh(III) complexes exhibited a visible luminescence with ultraviolet irradiation (Hg 312 nm line). The band maxima of *trans*-$[Rh(CN)_2(NH_3)_4]^+$ and *trans*-$[Rh(CN)_2(en)_2]^+$ are located at 18300 cm^{-1} (10 K) and 17500 cm^{-1} (77 K), respectively. The band of *trans*-$[Rh(CN)_2(NH_3)_4]^+$ showed a resolved vibrational fine structure at low temperatures. Details will be reported elsewhere.[18]

The ammine ^1H NMR signal was detected as a single peak at 3.5 ppm for *trans*-$[Rh(CN)_2(NH_3)_4]Cl$ (in D_2O) suggesting that all of the ammine ligands are magnetically equivalent in the *trans*-form. For *trans*-$[Rh(CN)_2(en)_2]^+$, methylene and amido ^1H signals were observed at 2.8 and 5.1 ppm, respectively. It has been confirmed[19] that the methylene ^1H signal is a sharp singlet in *trans*-$[Co(CN)_2(en)_2]^+$, while *cis*-$[Co(CN)_2(en)_2]^+$, exhibits a complicated split pattern. The methylene ^{13}C NMR signal of *trans*-$[Rh(CN)_2(en)_2]^+$ was quite normally identified as being a single peak at 48.9 ppm.[20] On the other hand, the cyano-carbon signal was clearly split into two components of nearly equal strength for the present complexes (at 140.3 and 140.6 ppm for *trans*-$[Rh(CN)_2(NH_3)_4]^+$ and at 140.2 and 140.6 ppm for *trans*-$[Rh(CN)_2(en)_2]^+$). This experimental finding must be further investigated regarding the solution chemistry of the *trans*-dicyano-type metal complexes.

The crystal structures of the present new complex compounds were determined. Of course, the well

Table 3. Ligand Field Absorption Bands (cm^{-1}) of *trans*-$[Rh(CN)_2(NH_3)_4]^+$, *trans*-$[Rh(CN)_2(en)_2]^+$, and Related Complexes

Complex	I $^1E_g{}^a\leftarrow{}^1A_{1g}$	II $^1E_g{}^b\leftarrow{}^1A_{1g}$	Ref.
$[Rh(CN)(NH_3)_5]^{2+}$	34800	40700	8
trans-$[Rh(CN)Cl(NH_3)_4]^+$	33100	38600	8
trans-$[Rh(CN)Cl(en)_2]^+$	33500	39000	This work
trans-$[Rh(CN)_2(NH_3)_4]^+$	36000	41500	This work
trans-$[Rh(CN)_2(en)_2]^+$	36500	42500	This work
trans-$[Rh(CN)_2(cyclam)]^+$	37500	45900	10

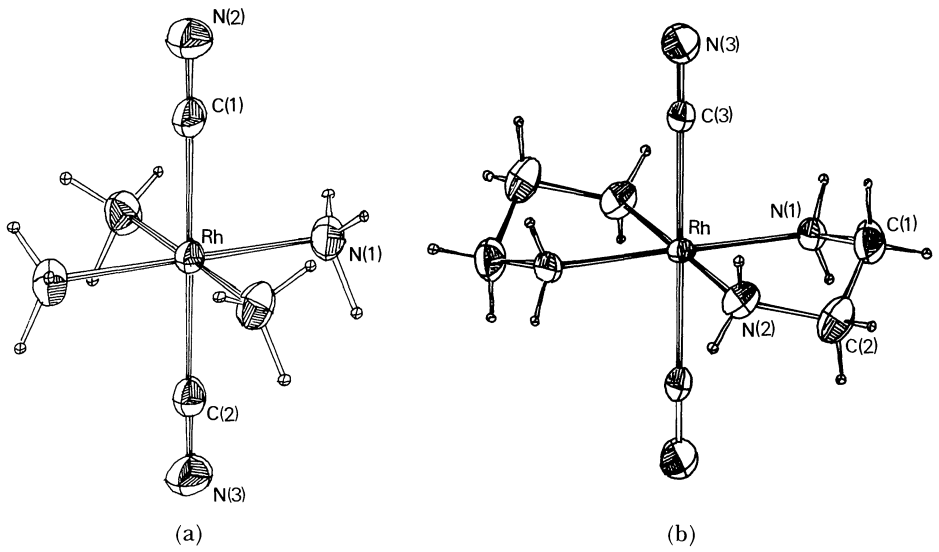

Fig. 2. ORTEP drawings of (a) *trans*-$[Rh(CN)_2(NH_3)_4]^+$ and (b) *trans*-$[Rh(CN)_2(en)_2]^+$ cations.

discrete complex cations in the *trans*-geometry were identified in both crystals (Fig. 2), being consistent with spectroscopic evidence. The positional parameters are summarized in Table 4. The bond distances and angles are included in Table 5, in which the reported values for *trans*-$[Co(CN)_2(en)_2](ClO_4)$ are also included.

In a crystal of *trans*-$[Rh(CN)_2(NH_3)_4]Cl\cdot H_2O$, the N≡C–Rh–C≡N molecular axis lies in a line with a special symmetry of *m*2*m*. The four N atoms of the ammonia ligands are required to form a rectangular plane perpendicular to the molecular axis. Therefore, the crystallographically required symmetry of the complex is C_{2v}. In the case of *trans*-$[Rh(CN)_2(en)_2]Cl$, the Rh atom occupies a special position with inversion symmetry. Therefore, the two Rh-en rings are in the $\delta\lambda$ conformation. The positional parameters of the complex (Table 4) indicate the C_{2h} effective point symmetry of the complex (all ∠C–Rh–N fall ca. 90° and all Rh–N fall ca. 2.07 Å). In comparision to the geometrical data of the corresponding Co(III) complex,[21] the Rh–C and Rh–N bonds are elongated by about 5%. This amount of the M–L bond length increase from the Co(III) complexes to the Rh(III) complexes is identical with that found in another comparison by Hambley et al.[22] On the other hand, the intra-ligand parameters of the en (N–C and C–C bond distances and N–C–C angles) are well retained in the Co(III) and Rh(III) complexes. This conservative nature of the intra-ligand structure of en accompanies a reduction of the ∠N–Rh–N chelate angles in the Rh(III) complex (82.7°), compared with those in the Co(III) complex (86.4°).

Table 4. Positional Parameters ($\times 10^4$) of *trans*-$[Rh(CN)_2(NH_3)_4]\ Cl\cdot H_2O$ and *trans*-$[Rh(CN)_2(en)_2]Cl$

Atom	*x*/*a*	*y*/*b*	*z*/*c*	B_{eq}(Å^2)[a]
		trans-$[Rh(CN)_2(NH_3)_4]Cl\cdot H_2O$		
Rh	0	1417(1)	2500	1.7
Cl	−5000	2337(4)	2500	2.5
N(1)	−1809(18)	1416(8)	493(17)	2.7
N(2)	0	3252(16)	2500	3.4
N(3)	0	−403(16)	2500	3.8
C(1)	0	2588(17)	2500	2.5
C(2)	0	249(17)	2500	2.3
		trans-$[Rh(CN)_2(en)_2]Cl$		
Rh	0	5000	5000	1.3
Cl	0	0	5000	5.3
N(1)	817(3)	3246(3)	3764(5)	1.9
N(2)	2131(3)	5770(4)	5724(5)	2.2
N(3)	820(4)	3361(4)	9344(5)	3.3
C(1)	2444(4)	3325(5)	4568(7)	2.8
C(2)	2875(4)	4905(6)	4508(7)	3.0
C(3)	544(4)	3933(4)	7817(5)	1.9

a) The isotropic equivalent thermal parameters is given as $B_{eq}=4/3(\sum_i\sum_j B_{ij}\boldsymbol{a}_i\boldsymbol{a}_j)$.

Conclusion

Two new cyanoammine-rhodium(III) complexes, *trans*-$[Rh(CN)_2(NH_3)_4]^+$ and *trans*-$[Rh(CN)_2(en)_2]^+$, were synthesized in a DMSO–H_2O mixed medium. X-Ray crystal structure analyses of *trans*-$[Rh(CN)_2(NH_3)_4]Cl\cdot H_2O$ and *trans*-$[Rh(CN)_2(en)_2]Cl$ showed well discrete complex cations in *trans*-dicyano geometry. The UV, IR, Raman, ^1H- and ^{13}C NMR spectroscopic data were characterized.

This work was financially supported by Grant-in-Aid for Scientific Research No. 02640485 from the Ministry of Education, Science and Culture. The authors express thanks to Mr. Hiroshi Tomizawa for his help with the IR and NMR measurements.

References

1) a) M. K. DeArmond and J. E. Hillis, *J. Chem. Phys.*, **54**, 2247 (1971); b) T. R. Thomas and G. A. Crosby, *J. Mol. Spectrosc.*, **38**, 118 (1971); c) P. E. Hoggard and H.-H. Schmidtke, *Ber. Bunsen-Ges. Phys. Chem.*, **77**, 1052 (1973); d) W. Blanchard and W. R. Mason, *Inorg. Chem.*, **28**, 159 (1978); e) K. Hakamata, A. Urushiyama, and H. Kupka, *J. Phys. Chem.*, **85**, 1983 (1981); f) M. Maestri, D. Sandrine, V. Balzani, U. Maeder, and A. Von Zelewsky, *Inorg. Chem.*, **26**, 1323 (1987), and references cited in these reports.

2) a) L. H. Skibsted, M. P. Hancock, D. Magde, and D. A.

Table 5. Relevant Bond Distances (Å) and Angles (deg.) of *trans*-$[M(CN)_2N_4]^+$

	trans-$[Rh(CN)_2(NH_3)_4]^+$	*trans*-$[Rh(CN)_2(en)_2]^+$	*trans*-$[Co(CN)_2(en)_2]^+$[b]
M–C	2.02(3), 2.02(3)	2.047(4)	1.91(1)
M–N	2.07(1)	2.080(3), 2.072(3)	1.99(1), 1.99(1)
C≡N	1.15(4), 1.13(4)	1.109(5)	1.16(2)
N–C(en)		1.482(5), 1.488(6)	1.50(2), 1.49(2)
C–C		1.503(7)	1.54(2)
M–C≡N	180	179.0(4)	178.8(11)
N–M–C	90.1(4), 89.9(4)	89.9(1), 91.0(1)	90.0(4), 89.1(4)
N–M–N	92.0(5), 88.0(5)	82.7(1)[a]	86.4(4)[a]
M–N–C		108.3(2), 108.5(2)	108.1(7), 108.9(7)
N–C–C		107.9(3), 107.6(4)	107.1(10), 107.1(10)

a) In chelate. b) Ref. 21.

Sexton, *Inorg. Chem.*, **23**, 3735 (1984); b) D. A. Sexton, L. H. Skibsted, D. Magde, and P. C. Ford, *Inorg. Chem.*, **23**, 4533 (1984); c) L. H. Skibsted, D. Magde, and D. A. Sexton, *Inorg. Chem.*, **26**, 1708 (1987), and references cited in these reports.

3) S. Anderson and F. Basolo, *J. Am. Chem. Soc.*, **82**, 4423 (1960).

4) "Inorg. Synth.," Vol. VII, p. 217.

5) T. Sakurai and K. Kobayashi, *Rep. Inst. Phys. Chem. Rev.*, **55**, 69 (1979).

6) A. T. C. North, D. C. Phillips, and F. S. Mathews, *Acta Crystallogr., Sect. A*, **24**, 351 (1968).

7) I. B. Baranovskii, *Nh. Neorg. Khim.*, **14**, 222 (1969).

8) I. B. Baranovskii and A. V. Babaeva, *Russ. J. Inorg. Chem. (Engl. Transl.)*, **13**, 1624 (1968).

9) L. H. Skibsted and P. C. Ford, *Inorg. Chem.*, **22**, 2749 (1983).

10) N. A. P. Kane-Maguire, P. K. Miller, and L. S. Trzupek, *Inorg. Chim. Acta*, **76**, L179 (1983).

11) M. Muto, T. Baba, and H. Yoneda, *Bull. Chem. Soc. Jpn.*, **41**, 2918 (1968).

12) H. Kawaguchi and S. Kawaguchi, *Bull. Chem. Soc. Jpn.*, **46**, 3453 (1973).

13) N. Maki, S. Ito, and S. Sakuraba, *Bull. Chem. Soc. Jpn.*, **41**, 3033 (1968).

14) A. Urushiyama, H. Kupka, J. Degen, and H.-H. Schmidtke, *Chem. Phys.*, **67**, 65 (1982).

15) K. Hakamata, A. Urushiyama, J. Degen, H. Kupka, and H.-H. Schmidtke, *Inorg. Chem.*, **22**, 3519 (1983).

16) H. Kupka, J. Degen, A. Urushiyama, K. Angermund, and C. Krueger, *Inorg. Chem.*, **25**, 3294 (1986).

17) A. B. P. Lever, "Inorganic Electronic Spectroscopy," Elsevier, Amsterdam-London-New York (1968), p. 312.

18) to be published.

19) M. Muto, T. Baba, and H. Yoneda, *Bull. Chem. Soc. Jpn.*, **41**, 2918 (1968).

20) G. H. Searle and T. W. Hambley, *Aust. J. Chem.*, **35**, 2399 (1982).

21) H. Bunderlich, *Acta Crystallogr., Sect. C*, **43**, 1209 (1985).

22) T. W. Hambley and P. A. Lay, *Inorg. Chem.*, **25**, 4553 (1986).

Effect of Chloride Ion on Lead Signal Appearance in the Co-Existence of Iron in Electrothermal Graphite Furnace Atomic Absorption Spectrometry

Shoji IMAI, Masayoshi ICHINOSEKI, Yasuko NISHIYAMA, and Yasuhisa HAYASHI*
Department of Chemistry, Joetsu University of Education, Yamayashiki-machi, Joetsu, Niigata 943
(Received November 2, 1990)

The atomic absorption signals for lead were measured in various chloride matrices at a charring temperature of 700 K. A typical double-peak signal was observed with iron(III) chloride, while a single peak was observed with iron(III) nitrate. At a charring temperature of 1440 K, the first peak disappeared and only the second peak remained; the atomization temperature of the latter was in agreement with that in the iron matrix. The larger content of the chloride ion increased the first peak absorption and decreased the second peak absorption without any shift of the peak temperatures, showing that one species for the second peak was converted to the same species for the first peak by the addition of a chloride ion. The appearance temperature of the first peak signal in the X^-–Fe^{3+} matrix system increased in the order $Cl^- < Br^- < I^-$. It was concluded that the appearance of the first peak is caused by the dissociation of lead halide.

Although graphite furnace atomic absorption spectrometry (GFAAS) is favorable for an analysis of a trace amount of lead, severe matrix interference[1,2] decrease its sensitivity by diversifying the mechanism of metal vapor formation. The mechanism of interference elimination has been discussed from the viewpoint of kinetics.[1]

The chloride ion is one of the most unfavorable matrices, because of the formation of volatile lead chloride. Wendl and Müller-Vogt[2] investigated the reaction of lead in a chloride matrix by X-ray diffraction and molecular absorption for PbCl, and proposed the following reaction processes:

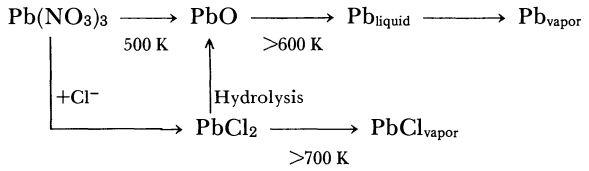

This mechanism shows that interference from chlorides is caused by volatilization of lead chloride at a temperature lower than that required to decompose the compound on the graphite surface. Frech and Cedergren[3–5] also concluded from a high-temperature gas-phase equilibrium calculation that the formation of the volatile lead chlorides, such as $PbCl_2$ and PbCl, should result in decreasing the signal of lead.

L'vov et al.[6] reported the appearance of double-peak signals of lead in sodium chloride. They considered that the second peak was caused by a revolatilization of lead condensed with a matrix on the cooler outer ends of the furnace tube. McLaren and Wheeler[7] also reported the appearance of double-peak signals in the ascorbic acid matrix, which resulted from the formation of the massicot and litharge dimorphic forms of PbO in a furnace. Salmon et al.[8] also proposed that the double-peak signal for lead was caused by two major types of active sites which chemisorbed oxygen on the graphite tube.

It was also found in this work that a double-peak signal for lead appeared in the presence of iron(III) chloride; that the chloride ion was responsible for the appearance of the first peak and that the iron caused each peak to shift to the higher temperature side; and that two different types of atomization mechanisms might exist. The mechanism that caused the appearance of the first peak is discussed in the present paper.

Experimental

Apparatus and Materials. A Hitachi Model Z-8000 flame and graphite furnace atomic absorption spectrometer equipped with a Zeemann-effect background corrector and an optical temperature controller was used. The term of the maximum heating mode was defined as the mode of maximum heating feasible with the optical temperature controller used in the present work. The sample was injected by an automatic sampler. The peak height and area were automatically printed out and displayed using a Hitachi Data Processor. The time-absorbance signals sent to an OKI Model if-800 personal computer through RS-232C could also be stored on a diskette at 20 ms intervals. The temperature of the graphite tube was recorded at 4 ms intervals using the optical temperature controller; its analog output data were converted to digital data and stored on a diskette using an OKI personal computer. The temperature was calibrated using a CHINO Model IR-AH1S radiation thermometer with a radiation factor of one.

The standard instrumental conditions were 120 °C (setting) and 30 s for the drying stage, 800 K, ramp time 20 s and hold time 5 s for the charring, 2700 K, ramp time 0 s and hold time 2 s for the atomizing. The reproducibility of the atomization temperature for the nonpyrolytic graphite (NPG) tube was 0.3% at 1419 K (n=10). When the maximum heating mode was used, the heating rates were 1450 K s^{-1} for the NPG tube and 1200 K s^{-1} for pyrolytic graphite (PG). Coating of the NPG tube with iron oxide was carried out by charring 20 μl of an iron(III) nitrate solution (1000 mg l^{-1} of

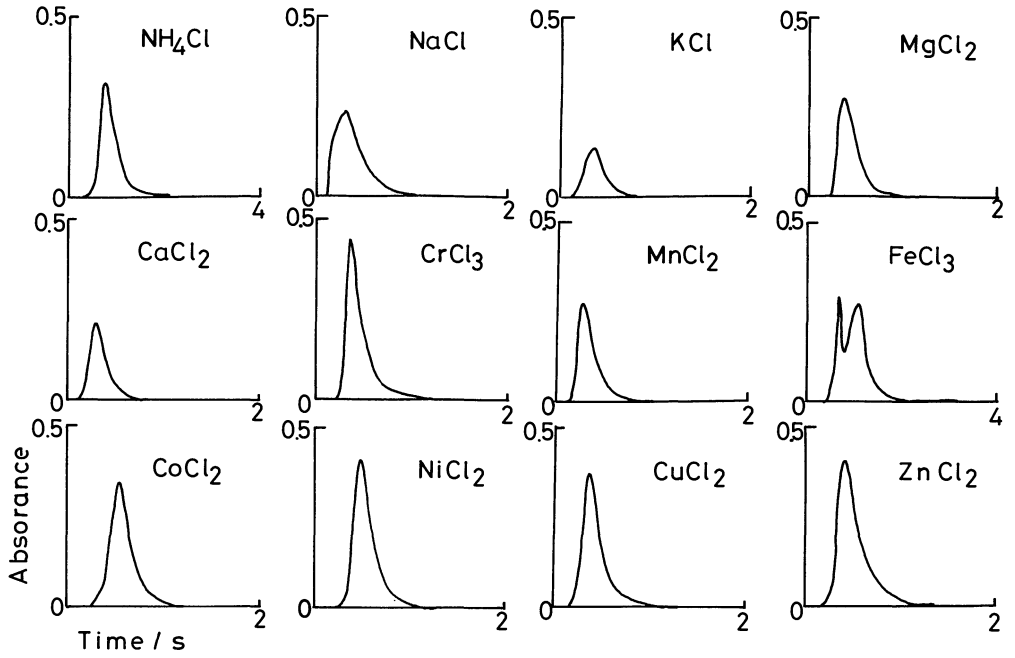

Fig. 1. Atomic absorption signals for lead in various chloride matrices. Analyte; Pb 1 ng with 20 μg of cation, atomization temperature; 3270 K (normal heating) for iron chloride and ammomium chloride matrices and 2700 K (maximum heating) for others, tube; NPG.

iron). The spectral line and slit width were 283.3 and 1.3 nm for Pb and 248.3 and 1.3 nm for Fe, respectively.

A stock solution (1 mol l^{-1} HNO_3 soln), 1000 mg kg^{-1} for the Pb used, was a commercially available standard solution (Wako Pure Chemical Industry, Ltd.). An aliquot of this solution was diluted with water to a suitable concentration before use. The iron hydroxide sample which occluded lead was prepared from an aqueous solution of 1000 mg l^{-1} of Fe(III) as its nitrate or chloride containing 100 μg l^{-1} of Pb, using aqueous ammonia. All other reagents were of analytical reagent grade. Distilled water was purified by a Milli-Q system.

Results and Discussion

Atomic Absorption Signals for Lead. The atomic absorption signals for lead were measured in various chloride matrices: ammonium, sodium, potassium, magnesium, calcium, chromium(III), manganese, iron-(III), cobalt(II), nickel, copper, and zinc chlorides. The observed signals are shown in Fig. 1. A typical double-peak signal was observed in iron(III) chloride, where the initial and latter peaks referred to the first and second peaks, respectively. In cobalt(II), sodium and potassium chlorides matrices, signals with a shoulder were also observed. In the present study, the mechanism of double-peak formation was studied because iron is an important component in biological materials, steel and so on.

Appearance of Double Peaks in the Iron(III) Chloride Matrix. Typical atomic absorption signals for lead in the iron(III) nitrate and chloride matrices

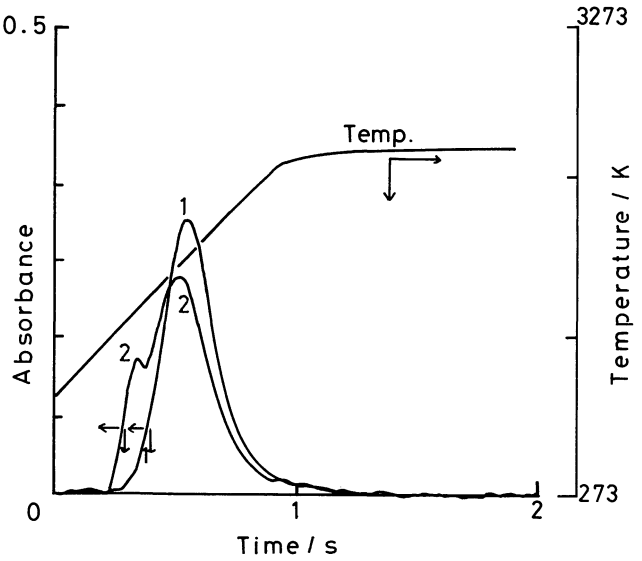

Fig. 2. Atomic absorption signals for lead in iron(III) nitrate (1) and chloride (2) matrices and time-temperature profile. Analyte; Pb 1 ng with 20 μg of Fe, atomization temperature; 2700 K, charring temperature; 800 K, tube: NPG.

are shown in Fig. 2, together with the temperatue profile for the NPG tube. With the chloride ion, a double-peak signal was observed, but not with the nitrate. The appearance temperature (T_{app}) of the signal was 1217±22 K in the iron(III) chloride matrix

and 1304±8 K in iron(III) nitrate. Fig. 2 shows that the position of the second peak is in agreement with the position of the peak in iron(III) nitrate.

As shown in Fig. 3, for a PG tube, double peaks (signal 1) were also observed in the iron(III) chloride matrix, but not in the nitrate. The second peak, which is in agreement with the peak in iron(III) nitrate (signal 2), appeared as a shoulder at a heating rate of 1200 K s^{-1} for atomizing, while only the first peak (signal 3) was observed at 362 K s^{-1}. The appearance temperature was 1157±5 K in the iron(III) chloride and 1306±5 K in the iron(III) nitrate. Thus, the chloride matrix atomizes lead at a lower temperature than does the nitrate for both the NPG and PG tubes.

Both the charring temperature and time affected the peak shape of the atomic absorption signal for lead in iron(III) chloride. Fig. 4 shows the effect of the charring temperature on the peak shape, where the

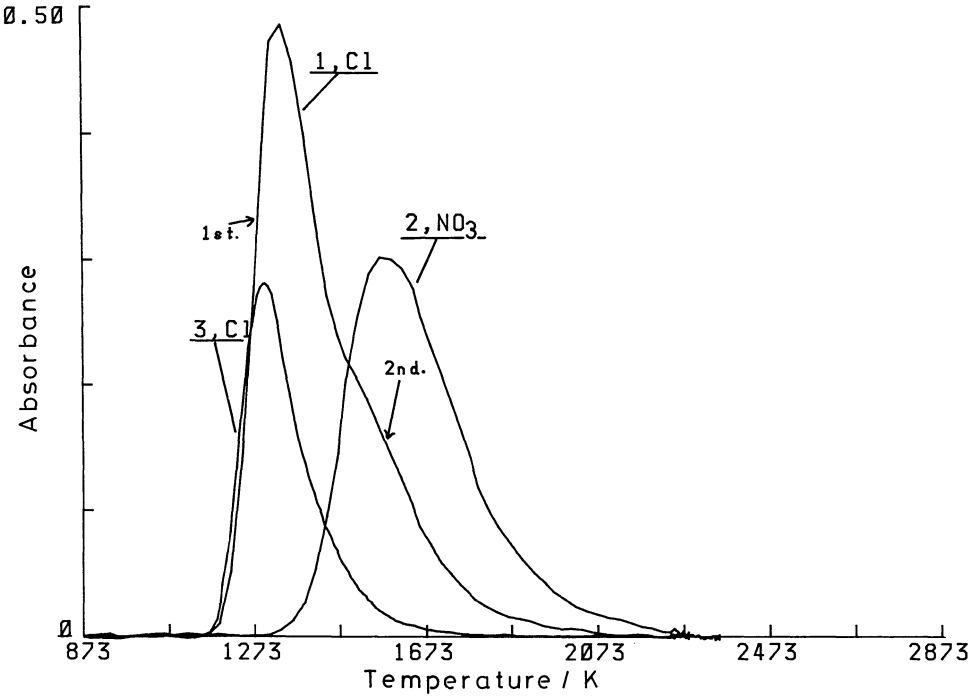

Fig. 3. Atomic absorption signals for lead (Pb: 1 ng) using the PG tube. Charring temperature; 800 K. 1: $FeCl_3$ 0.2 μg of Fe; atomization temperature; 2700 K, 2: $Fe(NO_3)_3$ 0.2 μg of Fe; 2700 K, 3: $FeCl_3$ 0.2 μg of Fe, 3000 K.

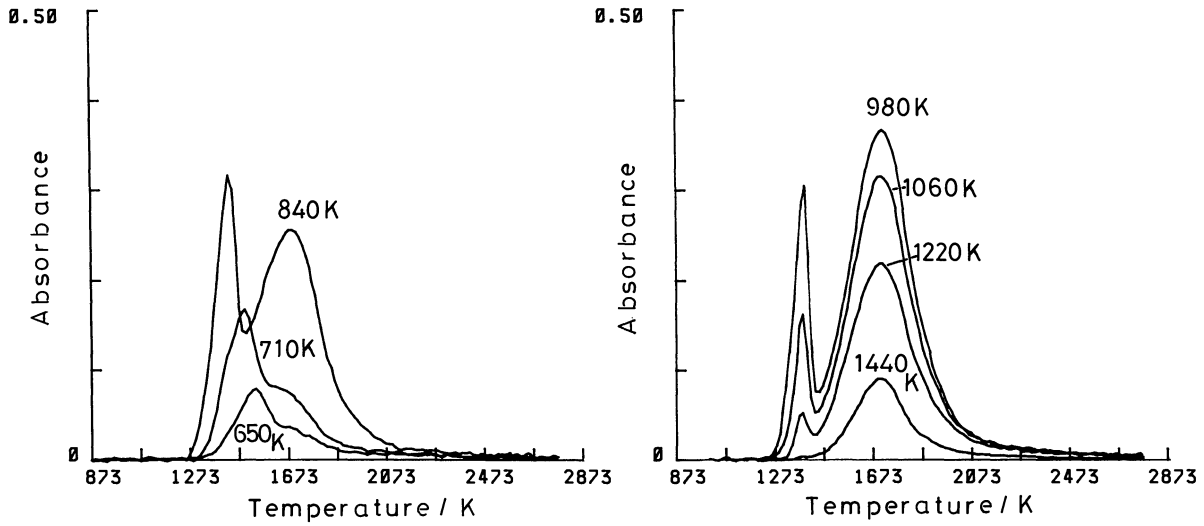

Fig. 4. Effect of the charring temperature on the peak shape. Analyte: Pb 1 ng with 20 μg of Fe($FeCl_3$), atomization temperature; 3200 K, hold time in charring step; 5 s, tube; NPG.

signals in the range of 650—840 K are indicated in the left-hand figure and those in the range of 980—1440 K in the right-hand figure. Fig. 4 shows that at a charring temperature of 710 K double peaks are clearly observed, while at 1440 K the first peak disappeared and only the second remained. The appearance temperature of the isolated second peak (1308±4 K) is also in agreement with that (1304±8 K) in the iron(III) nitrate matrix. Furthermore, Fig. 5 shows that with a hold time of 5 s in the charring stage (charring temp.: 1060 K), double peaks can be clearly seen. On the other hand, within 20 s the first peak almost disappeared and the second one remained without a change in absorbance. This result suggests that an intermediate compound for the first peak is more volatile than that for the second.

Effect of Iron and Chloride Ions on the Peak Shape. The effects of iron and chloride ions on the atomic absorption signals for lead are shown in Fig. 6; a charring temperature of 800 K was used. The concentrations of iron(III) and chloride ions were controlled with iron(III) nitrate and ammonium chloride, respectively, since both nitrate and ammonium ions scarcely contribute to lead atomic absorption.

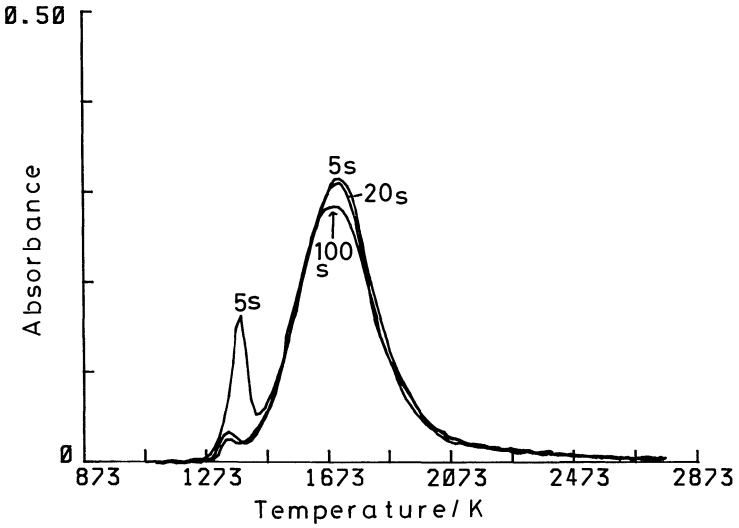

Fig. 5. Effect of the hold time in the charring step on the peak shape. Analyte; Pb 1 ng with 20 μg of Fe($FeCl_3$), atomization temperature; 3270 K (normal heating), charring temperature; 1060 K, tube; NPG.

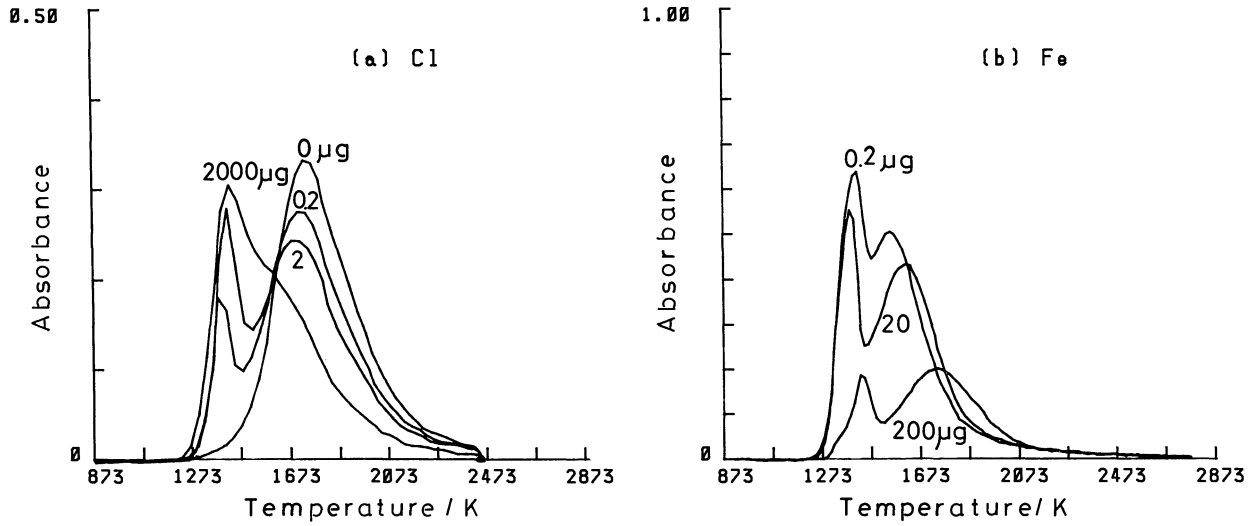

Fig. 6. Dependence of atomic absorption signals for lead on chloride and iron(III) ions added. Charring temperature; 800 K, tube; NPG. (a) Pb, 1 ng; $Fe(NO_3)_3$, 20 μg of Fe; NH_4Cl, varied. (b) Pb 2 ng; NH_4Cl, 20 μg of Cl; $Fe(NO_3)_3$, varied. Atomization temperature: (a) 2700 K (maximum heating); (b) 3270 K (normal heating).

Fig. 6(a) shows that increasing the chloride ion content under a constant amount of iron causes an increase in the first peak height and a decrease in the second peak height, with a 12% decrease of the peak area from 0 to 2000 μgCl and without any shift of the peak temperature. The atomic absorption signal for iron in the matrix is shown in Fig. 7, together with that for lead, showing that lead atomizes at the same temperature as does iron. Fig. 6(b) shows that an increase in the iron content shifts the double peaks to the higher temperature side.

Double Peaks for Another Halide Ions. Fig. 8 shows the atomic absorption signal for 2 ng of lead in the presence of ammonium chloride, ammonium bromide, and ammonium iodide with iron(III) nitrate. Double-peak signals were observed in the presence of ammonium bromide and iodide as well as chloride. The values of T_{app} for the first peak are given in Table 1. The T_{app} value is higher in the following order: Cl^- (1214±26 K)<Br^- (1268±11 K)<I^- (1284±10 K).

Recently, Holcombe[9] discussed the use of Ahrrenius-type plots employing the leading edge of the absorbance signal using data from computer simulations; they concluded that the extraction energetics of the gas-phase dissociation processes are likely to be in error. However, in practice, such a method has been applied extensively to the elucidation of the atomization process and has provided valuable information. In the present work we therefore tried to use a similar method. If the intermediate compound leading to the formation of lead halide is responsible for the first peak, the E_a value should be influenced by the variety of halogen. A kinetic analysis of the first peak was carried out by using a correction method;[10,11] the obtained E_a values are also given in Table 1. The E_a values for chloride, bromide, and iodide were 290±17, 258±5, and 252±11 kJ mol^{-1}, respectively. The E_a value decreases in the order $Cl^->Br^-\geqq I^-$. The tendency for the decrease of E_a is in agreement with that for the bond energy: 316±29 for PbCl(g), 262±38 for PbBr(g), and 213±38 for PbI(g) in kJ mol^{-1} at 1250 K.[12]

Therefore, the above results are, at least, compatible with the inference drawn here: the first peak may be caused by the dissociation of lead halide.

Effect of Iron on Appearance of the First Peak.

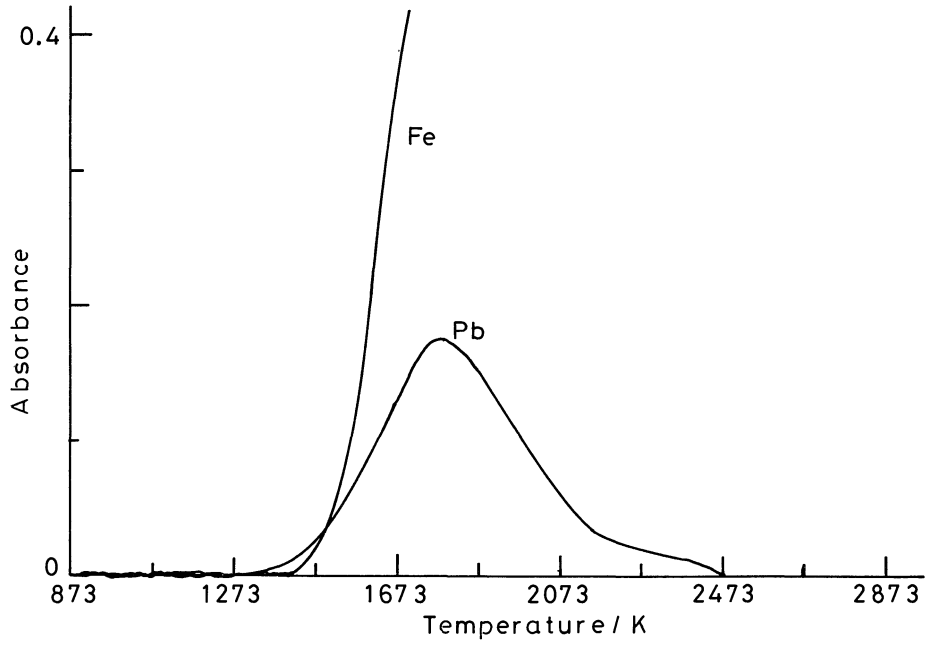

Fig. 7. Atomic absorption signal profiles for lead and iron. Pb: 1 ng; $Fe(NO_3)_3$, 20 μg of Fe. Atomization temperature; 3270 K (maximum heating), charring temperature; 800 K, tube; NPG.

Table 1. Signal Appearance Temperature (T_{app}) and Activation Energy (E_a) for the First Peak

Halogen[a]	T_{app}/K	E_a/kJ mol^{-1}	Bond energy[b] at 1250 K/kJ mol^{-1}
Cl	1214±26	290±17	316±29 Pb-Cl
Br	1268±11	258±5	262±38 Pb-Br
I	1284±10	252±11	252±11 Pb-I

a) 2 ngPb with 20 μgCl, 45 μgBr, or 72 μgI as ammonium salt, and 20 μgFe as nitrate. b) Data from Ref. 12.

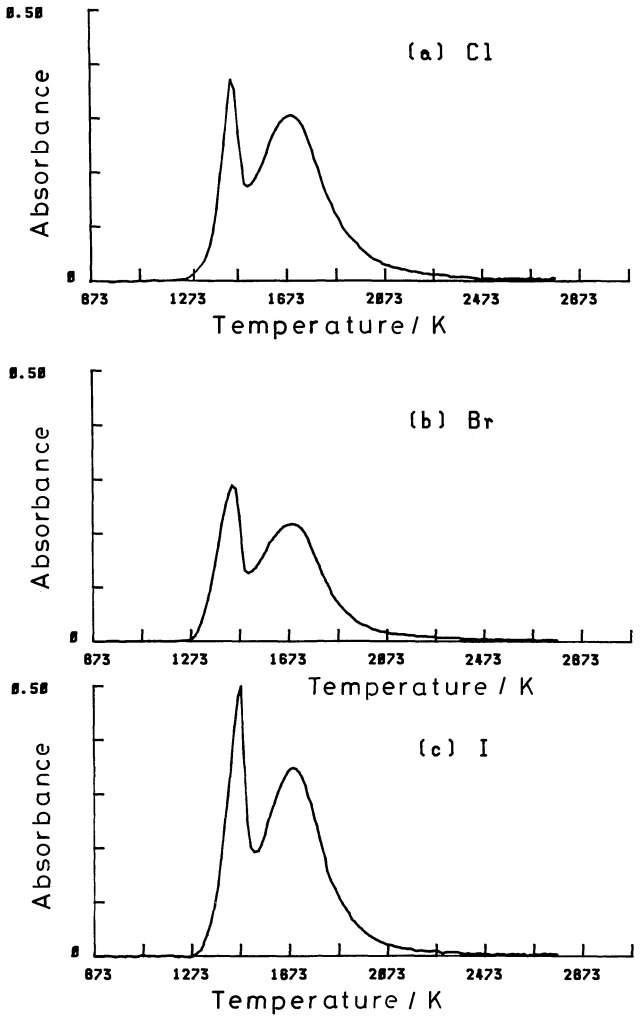

Fig. 8. Atomic absorption signal for lead (Pb: 2 ng) in a matrix of iron(III) nitrate and ammonium halide. (a) $Fe(NO_3)_3$, 20 μg of Fe; NH_4Cl, 20 μg of Cl. (b) $Fe(NO_3)_3$, 20 μg of Fe; NH_4Br, 45 μg of Br. (c) $Fe(NO_3)_3$, 20 μg of Fe; NH_4I, 72 μg of I. Atomization temperature; 3270 K (normal heating), charring temperature; 800 K, tube: NPG.

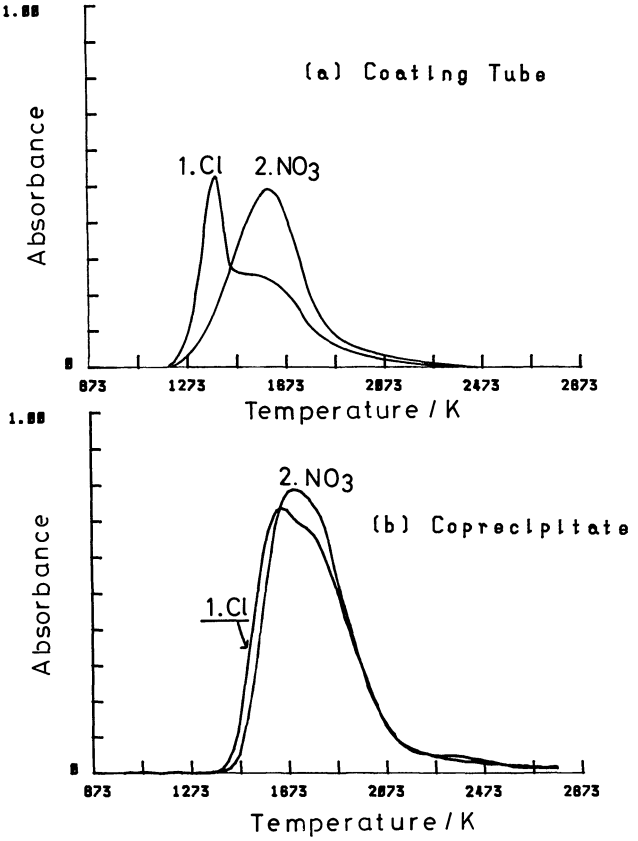

Fig. 9. Comparison between atomic absorption signals for lead. Atomization temperature: 3270 K (normal heating). Charring temperature: 800 K. (a) 1: Pb 3 ng; NH_4Cl, 20 μg of Cl; 2: Pb 1 ng, tube; NPG coated with iron oxide. (b) Lead in the coprecipitate with iron(III) hydroxide from iron(III chloride (1) and iron(III) nitrate (2) using aqueous ammonia, tube; NPG.

Wendl and Müller-Vogt[2] reported that some lead chloride was hydrolyzed to PbO, and that the others were removed as PbCl vapor at temperatures greater than 700 K. In this work, however, a reduction of the first peak which resulted from lead chloride was not observed until 900 K in the iron(III) chloride matrix. Frech and Cedergren[3] examined the interference mechanism of iron with the chloride ion and concluded that the formation of volatile lead chlorides, $PbCl_2$ and PbCl, in the gas phase resulted in a reduction of the signal of lead in steel, where high-temperature equilibrium calculations were made under the assumption that $FeCl_2$ and $FeCl_3$ were in the gas, liquid, and solid phases and that Fe_2O_4, Fe_3O_4, FeO, and Fe were in the solid phase. In the present work, as mentioned in Fig. 6(b), an increase of the iron content shifted both peaks in the double-peak signal to a higher temperature, indicating that iron also affected the atomic vapor formation of lead.

Iron hydroxide, oxide, and chloride are produced in the drying stage from an iron(III) chloride aqueous solution; the hydroxide changes to the oxide during the charring stage by a reaction with either oxygen or water. At first, in order to investigate the effect of iron oxide on the atomic absorption signal for lead, measurements were performed for two types of solution samples with and without ammonium chloride, using an NPG tube coated with iron oxide. The result is shown in Fig. 9(a). The figure shows that a double-peak signal is observed for lead with the ammonium chloride solution, while a single-peak signal is observed for lead without ammonium chloride. The E_a and T_{app} values (294±15 kJ mol^{-1} and 1214±26 K) for the first peak in the ammonium chloride matrix are in agreement with those values (290±17 kJ mol^{-1} and 1217±22 K) for the first peak in the iron(III) chloride matrix within experimental error. These agreements

of the E_a and T_{app} values show that the first peak in the ammonium chloride matrix is due to the same mechanism as the first peak in the iron(III) chloride matrix. In the second, in order to investigate the effect of iron hydroxide, measurements were performed for lead coprecipitated with iron hydroxide from either iron(III) chloride or iron(III) nitrate solutions. The result is shows in Fig. 9(b). The atomic absorption signals are not in agreement with the first peak mentioned above. These results, thus, indicate that iron oxide formed on the charring stage inhibits vaporization of lead chlorides, leading to the appearance of only the first peak.

In conclusion, atomic absorption signals with double peaks were observed for lead in an iron(III) chloride matrix and the chloride ion was responsible for the appearance of the first peak resulting from thermal dissociation of lead chloride. The iron was also responsible for shifting each peak to a higher temperature; the iron oxide formed during charring inhibited the charring loss of lead chloride.

References

1) M. Suzuki, K. Ohta, and K. Isobe, *Anal. Chim. Acta*, **173**, 321 (1985).
2) W. Wendl and G. Müller-Vogt, *J. Anal. At. Spectrosc.*, **3**, 63 (1988).
3) W. Frech and A. Cedergren, *Anal. Chim. Acta*, **82**, 83 (1976).
4) W. Frech and A. Cedergren, *Anal. Chim. Acta*, **82**, 93 (1976).
5) W. Frech, E. Lundberg, and A. Cedergren, *Prog. Anal. At. Spectrosc.*, **8**, 257 (1985).
6) B. V. L'vov, L. A. Pelieva, and A. I. Sharnopolski, *Zh. Prikl. Spectrosk.*, **27**, 395 (1977).
7) J. W. McLaren and R. C. Wheeler, *Analyst*, **102**, 542 (1977).
8) S. G. Salmon, R. H. Davis, Jr., and J. A. Holcombe, *Anal. Chem.*, **53**, 324 (1981).
9) J. A. Holcombe, *Spectrochim. Acta, Part B*, **44**, 975 (1989).
10) Chan-huan Chung, *Anal. Chem.*, **56**, 2714 (1984).
11) E. Iwamoto, N. Miyazaki, S. Ohkubo, and T. Kumamaru, *J. Anal. At. Spectrosc.*, **4**, 433 (1989).
12) "Handbook of Chemistry and Physics," 67th ed, ed by R. C. Weast, Chemical Rubber Co., Cleveland, Ohio (1986).

Kinetics and Mechanisms of the Photo-Induced Oxidation of Ascorbic Acid by Molecular Oxygen Catalyzed by Ruthenium(II) Complexes Containing 2,2′-Bipyridine and 2,2′-Bipyrazine

Keiichi TSUKAHARA,* Yuuko WADA, and Masaru KIMURA*
Department of Chemistry, Faculty of Science, Nara Women's University, Nara 630
(Received November 6, 1990)

Hydrogen peroxide was efficiently produced by the irradiation of visible light on aqueous acid solutions containing ascorbic acid, molecular oxygen, and ruthenium(II) complexes: $[Ru(bpy)_x(bpz)_{3-x}]^{2+}$ (x=0—3, bpy=2,2′-bipyridine, and bpz=2,2′-bipyrazine). The formation of hydrogen peroxide and the decay of ascorbic acid were followed by polarography during continuous irradiation by visible light of the solution. The rate constants of the quenching reaction of the excited triplet state of the ruthenium(II) complexes by ascorbate and molecular oxygen obtained from the initial rate method were in good agreement with those obtained from luminescence quenching experiments. The initiation reaction in the photo-induced reaction mechanism changes from the oxidative quenching of $*[Ru(bpy)_3]^{2+}$ by molecular oxygen to the reductive quenching of $*[Ru(bpy)_2(bpz)]^{2+}$, $*[Ru(bpy)(bpz)_2]^{2+}$, or $*[Ru(bpz)_3]^{2+}$ by ascorbate. Such a change in the mechanism arises from a difference in the redox potentials, $E^0(Ru^{3+}/*Ru^{2+})$ and $E^0(*Ru^{2+}/Ru^{+})$, for each ruthenium(II) species containing bpy and bpz. The detailed mechanisms are discussed.

Photo-induced electron-transfer reactions involving ruthenium(II) polypyridine complexes have received considerable attention for both fundamental reasons and their practical application to solar energy conversion.[1,2] Tris(2,2′-bipyridine)ruthenium(II) ion ($[Ru(bpy)_3]^{2+}$) has been one of the most studied photosensitizers. Visible-light irradiation of aqueous solutions of $[Ru(bpy)_3]^{2+}$, triethanolamine, and methylviologen (1,1′-dimethyl-4,4′-bipyridinium cation, MV^{2+}) yielded the methylviologen radical cation (MV^{+}) with a quantum yield of 0.19;[3] the production of MV^{+} led to hydrogen evolution from water by the use of PtO_2 or colloidal Pt.[4,5] A tris(2,2′-bipyrazine)ruthenium(II) ion ($[Ru(bpz)_3]^{2+}$) is a superior photosensitizer over the $[Ru(bpy)_3]^{2+}$ ion for the production of MV^{+}, with a quantum yield of 0.77.[3] The reaction mechanisms are quite different. The photo-excited state of the $[Ru(bpy)_3]^{2+}$ ion, i.e., $*[Ru(bpy)_3]^{2+}$, is oxidatively quenched by a quencher (Q), such as MV^{2+} (Reaction 1):

$$*[Ru(bpy)_3]^{2+} + Q \longrightarrow [Ru(bpy)_3]^{3+} + Q^{-}. \quad (1)$$

On the other hand, the $*[Ru(bpz)_3]^{2+}$ ion is reductively quenched by a quencher, such as triethanolamine (Reaction 2):

$$*[Ru(bpz)_3]^{2+} + Q \longrightarrow [Ru(bpz)_3]^{+} + Q^{+}. \quad (2)$$

The difference in mechanisms is considered to arise from a positive shift of about 0.5 V in the redox potential of the ruthenium(II) complexes for the latter, compared with the former.[3]

We previously studied such visible-light induced redox and substitution reactions of inorganic compounds using $[Ru(bpy)_3]^{2+}$ and $[Ru(bpz)_3]^{2+}$ ions.[6] Rillema et al.[7] have prepared the mixed-ligand ruthenium(II) complexes containing bpy and bpz, $[Ru(bpy)_2(bpz)]^{2+}$ and $[Ru(bpy)(bpz)_2]^{2+}$. Although the redox and excited-state properties of these complexes have been also investigated,[7-9] the redox quenching reaction has not been examined. It would be interesting to know the changing point from oxidative to reductive quenching mechanisms of the ruthenium(II) complexes by replacing 2,2′-bipyridine with 2,2′-bipyrazine. We therefore investigated the kinetics of the photo-induced oxidation of ascorbic acid by molecular oxygen catalyzed by the ruthenium(II) complexes, $[Ru(bpy)_x(bpz)_{3-x}]^{2+}$ (x=0—3), in an aqueous acid solution.

Although autoxidation of ascorbic acid to dehydroascorbic acid in an aqueous acid solution (Reaction 3)

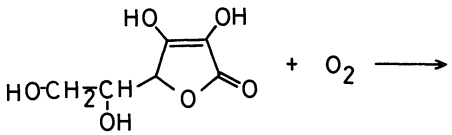

ascorbic acid

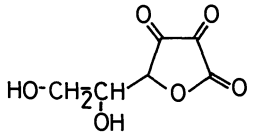

(3)

dehydroascorbic acid

is very slow, in the presence of these ruthenium(II) complexes, irradiation with visible light induced the oxidation of ascorbic acid and the formation of hydrogen peroxide. Such a photo-induced oxidation of ascorbic acid by the $[Ru(bpy)_3]^{2+}$ ion has already been studied by Kurimura et al.,[10] in which an oxidative quenching mechanism of $*[Ru(bpy)_3]^{2+}$ by

molecular oxygen has been proposed. In the present work we have also found that the formation of hydrogen peroxide by use of the $[Ru(bpz)_3]^{2+}$ ion as a photocatalyst is most efficient among the four ruthenium(II) complexes.

Experimental

Materials. Tris(2,2′-bipyrazine)ruthenium(II) chloride 3.5 hydrate ($[Ru(bpz)_3]Cl_2 \cdot 3.5H_2O$),[11] 2,2′-bipyrazinebis(2,2′-bipyridine)ruthenium(II) hexafluorophosphate ($[Ru(bpy)_2(bpz)](PF_6)_2$),[7] and bis(2,2′-bipyrazine)(2,2′-bipyridine)ruthenium(II) hexafluorophosphate ($[Ru(bpy)(bpz)_2](PF_6)_2$)[7] were prepared and purified as in previously reported methods. Tris(2,2′-bipyridine)ruthenium(II) chloride hexahydrate ($[Ru(bpy)_3]Cl_2 \cdot 6H_2O$) obtained from Aldrich Chemical Company, Inc. was used without further purification. L-Ascorbic acid and sodium L-ascorbate were purchased from Wako Pure Chemical Industries, Ltd. and used without further purification. All other chemicals used were of guaranteed grade. All of the solutions used for measurements were prepared from redistilled water. A solution of ascorbic acid and sodium ascorbate was freshly prepared just before measurements.

Procedure. Kinetic measurements during irradiation with visible light were employed by using the same method as reported previously.[6a] A sample solution was continuously irradiated with visible light from two 100 W tungsten lamps at 30 °C under various pH conditions (an acetate buffer); ionic strengths (adjusted with sodium perchlorate); and concentrations of Ru(II), ascorbic acid, and oxygen. Oxygen or air was continuously bubbled through the solution. Aliquot samples were withdrawn at appropriate times after reaction initiation; a Dowex 50W-X8 cation-exchange resin (200—400 mesh, H^+ form) was added in order to remove the ruthenium(II) complexes. After filtration and washing the resins with water, the concentrations of hydrogen peroxide formed and of ascorbic acid remaining in the solutions were measured using a Yanagimoto PA-102 polarograph at 25 °C and pH 4.6 (a 0.1 mol dm^{-3} acetate buffer containing a 0.01% gelatin) under nitrogen gas. The potentials were set at −1.25 V and 0.15 V vs. SCE (a saturated calomel electrode) for hydrogen peroxide and ascorbic acid, respectively. The concentrations of ruthenium(II) ions were determined spectrophotometrically by the use of Shimadzu UV-200S and UV-240 spectrophotometers. The light intensity absorbed in the solution was determined by the use of potassium tris(oxalato)ferrate(III) trihydrate as an actinometer.[12] The iron(II) content was determined spectrophotometrically in the form of a tris(1,10-phenanthroline)iron(II) ion at 510 nm with a molar absorption coefficient of 1.11×10^4 dm^3 mol^{-1} cm^{-1}.

The luminescence quenching experiments of the ruthenium(II) complexes with ascorbic acid and molecular oxy gen were carried out at 30 °C, pH 4.6 (a 0.1 mol dm^{-3} acetate buffer), and an ionic strength (I) of 0.10 mol dm^{-3} ($NaClO_4$) under argon gas by the use of a Hitachi 850 spectrofluorometer. The exciting wavelengths were 450 nm ($[Ru(bpz)_3]^{2+}$), 469 nm ($[Ru(bpy)(bpz)_2]^{2+}$), 406 nm ($[Ru(bpy)_2(bpz)]^{2+}$), and 452 nm ($[Ru(bpy)_3]^{2+}$), respectively. The emission intensities were monitored at wavelengths of 604 nm ($[Ru(bpz)_3]^{2+}$), 646 nm ($[Ru(bpy)(bpz)_2]^{2+}$), 707 nm ($[Ru(bpy)_2(bpz)]^{2+}$), and 608 nm ($[Ru(bpy)_3]^{2+}$), respectively.

The pH of the solutions was measured on a Hitachi-Horiba F-7LC pH meter. The internal solution of the reference electrode was a 3.33 mol dm^{-3} NaCl solution saturated with AgCl.

Results and Discussion

Although the oxidation of ascorbic acid by molecular oxygen at pH 3.9—5.6 was very slow in the absence of the ruthenium(II) complexes, or in the presence of the complexes in the dark, it was accelerated by irradiation with visible light of the solution in the presence of the ruthenium(II) complexes (Fig. 1). The absorption spectra of the ruthenium(II) complexes did not change during the reactions, indicating that the ruthenium(II) complexes act as homogeneous catalysts.

Both plots of the concentrations of ascorbic acid remained, and those of hydrogen peroxide formed against time were linear during the initial part of the reaction (up to 1 h). The initial reaction rate was, therefore, obtained from the initial slope of this line. The ratio of the concentrations of ascorbic acid reacted

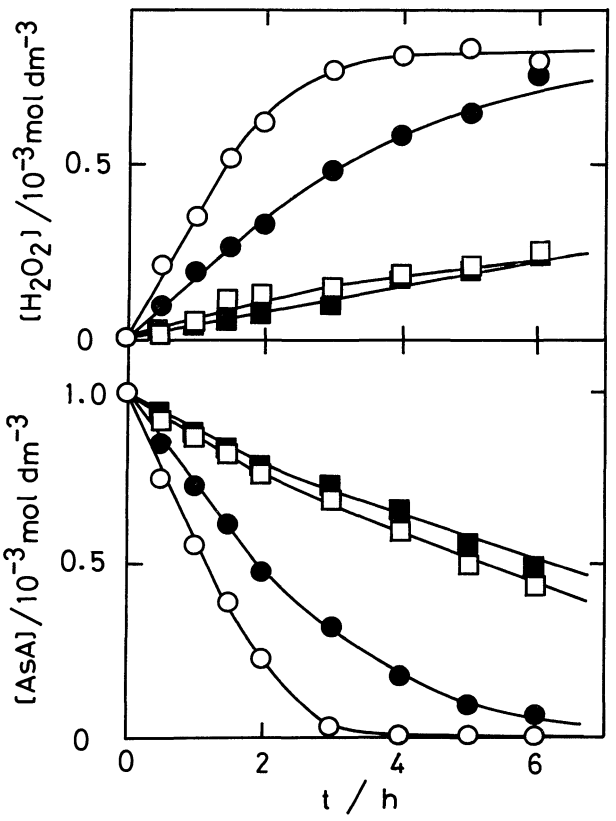

Fig. 1. The formation of hydrogen peroxide and the decay of ascorbic acid during the photo-induced oxidation of ascorbic acid by molecular oxygen in the presence of the ruthenium(II) complex at 30 °C, pH 4.60, and I=0.10 mol dm^{-3}. $[Ru(II)]=5.00 \times 10^{-5}$ mol dm^{-3}, $[AsA]_i=1.00 \times 10^{-3}$ mol dm^{-3}, and $[O_2]=2.28 \times 10^{-4}$ mol dm^{-3}. ○: $[Ru(bpz)_3]^{2+}$, ●: $[Ru(bpy)(bpz)_2]^{2+}$, □: $[Ru(bpy)_2(bpz)]^{2+}$, and ■: $[Ru(bpy)_3]^{2+}$.

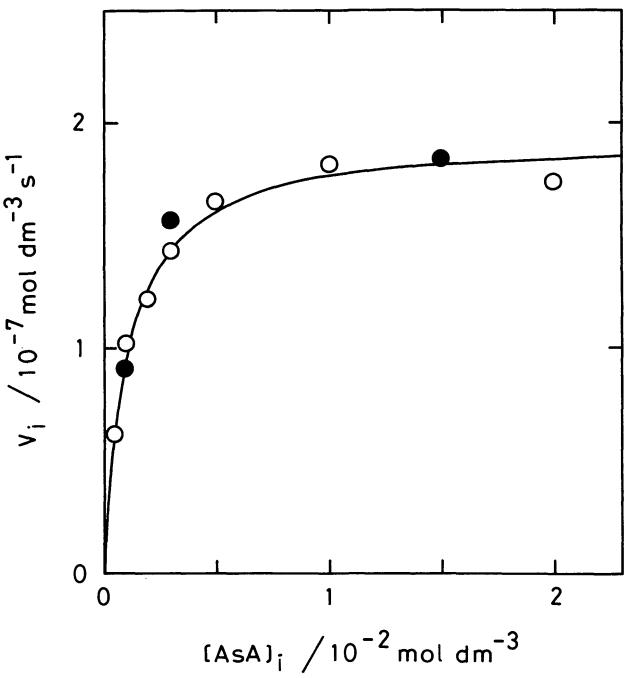

Fig. 2. Plots of V_i vs. [AsA]$_i$ for the photo-induced oxidation of ascorbic acid by molecular oxygen in the presence of $[Ru(bpz)_3]^{2+}$ ions. The initial rate V_i is the mean value for the formation of hydrogen peroxide and the decay of ascorbic acid. ○: $[O_2]=2.28\times10^{-4}$ mol dm^{-3} and ●: $[O_2]=1.16\times10^{-3}$ mol dm^{-3}. Other conditions are the same as in Fig. 1.

to those of hydrogen peroxide formed was near unity at low concentrations of ascorbic acid, but increased to about 2.5 at high concentrations. This indicates that the reaction of ascorbic acid with hydrogen peroxide occurs slowly. We found that the initial rate of the reaction between ascorbic acid and hydrogen peroxide with 1.00×10^{-3} mol dm^{-3} in each was $(9.0\pm1.0)\times10^{-9}$ mol dm^{-3} s^{-1} at pH 4.6, 30 °C, and I=0.10 mol dm^{-3} in an air-saturated solution. The autoxidation of ascorbic acid in the dark was accelerated by decreasing the ionic strength. Moreover, the reaction between ascorbic acid and hydrogen peroxide was accelerated by increasing the ionic strength. Therefore, most of the experiments in the present study were carried out at I=0.10 mol dm^{-3}, adjusted with $NaClO_4$.

Dependence of Concentrations of Ascorbic Acid. The reaction rate increased with increasing concentrations of ascorbic acid, and reached a constant value at higher concentrations of ascorbic acid. One of the examples is shown in Fig. 2 for the $[Ru(bpz)_3]^{2+}$ system. Numerical rate data are given in Table 1 for the ruthenium(II) complexes.

Effect of Oxygen. In the absence of oxygen the reaction did not occur for all of the ruthenium(II) systems. In the $[Ru(bpz)_3]^{2+}$ and $[Ru(bpy)(bpz)_2]^{2+}$ systems the reaction rate in the air-saturated solution was close to that in the oxygen-saturated solution. On the other hand, the rate of reaction in the oxygen-saturated solution was greater than that in the air-saturated solution for the other ruthenium(II) systems, $[Ru(bpy)_2(bpz)]^{2+}$ and $[Ru(bpy)_3]^{2+}$.

Table 1. Initial Rate of Reaction for the Formation of Hydrogen Peroxide and the Decay of Ascorbate in the Photo-Induced Oxidation of Ascorbic Acid by Molecular Oxygen Catalyzed by Ruthenium(II) Complexes[a]

[AsA]$_i$	$V_i(H_2O_2)$		V_i(AsA)	
10^{-3} mol dm^{-3}	10^{-7} mol dm^{-3} s^{-1}		10^{-7} mol dm^{-3} s^{-1}	
	Air satd[b]	O_2 satd[c]	Air satd[b]	O_2 satd[c]
	$[Ru(bpz)_3]^{2+}$			
0.50	0.57		0.66	
1.00	0.89	0.81	1.14	1.00
2.00	1.04		1.40	
3.00	1.16	1.33	1.69	1.80
5.00	1.27		2.03	
5.00	1.70[d]		2.50[d]	
5.00	0.61[e]		1.10[e]	
10.0	1.35		2.28	
10.0	2.00[d]		3.10[d]	
10.0	0.72[e]		2.00[e]	
15.0		1.30		2.37
20.0	1.28		2.20	
	$[Ru(bpy)(bpz)_2]^{2+}$			
1.00	0.44	0.69	0.70	0.82
2.00	0.91		1.30	
5.00	1.37		1.94	
10.0	1.38		2.77	
20.0	1.78	2.90	4.80	5.25
	$[Ru(bpy)_2(bpz)]^{2+}$			
1.00	0.21	0.23	0.26	0.30
2.00	0.29		0.41	
5.00	0.51		1.07	
10.0	0.85		1.73	
20.0	1.45	1.97	2.81	3.70
	$[Ru(bpy)_3]^{2+}$			
1.00	0.13	0.20	0.25	0.30
2.50	0.20	0.40	0.40	0.65
5.00	0.26	0.53	0.56	0.93
10.0	0.32	0.60	0.72	1.23
20.0	0.36	0.70	0.95	1.50

a) At 30 °C, pH 4.60, I=0.10 mol dm^{-3} ($NaClO_4$), and [Ru(II)]=5.00×10^{-5} mol dm^{-3}. b) In air-saturated solutions which contain 2.28×10^{-4} mol dm^{-3} O_2. c) In O_2-saturated solutions which contain 1.16×10^{-3} mol dm^{-3} O_2. d) At I=0.050 mol dm^{-3}. e) At I=0.50 mol dm^{-3}.

Dependence of Concentrations of Ruthenium(II). The effect of the concentrations of the $[Ru(bpz)_3]^{2+}$ ions on the reaction rate is shown in Fig. 3, indicating that it gradually increases with increasing concentrations of $[Ru(bpz)_3]^{2+}$ ions, reaching a constant at more than 5.00×10^{-5} mol dm^{-3} of ascorbic acid. This behavior can be accounted for by a Lambert-Beer's law (Eq. 4):

$$I_a = I_0(1 - \exp(-\gamma[[Ru(bpz)_3]^{2+}]), \quad (4)$$

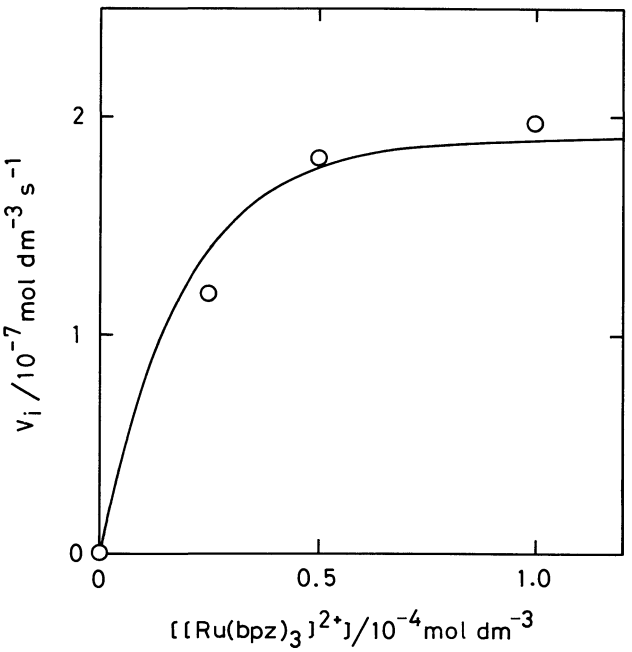

Fig. 3. Plots of V_i vs. [[Ru(bpz)$_3$]$^{2+}$] for the photo-induced oxidation of ascorbic acid by molecular oxygen at [AsA]$_i$=1.00×10^{-2} mol dm^{-3}. Other conditions are the same as in Fig. 1. The solid curve is calculated according to Eq. 4 with γ=5.3×10^4 dm^3 mol^{-1} and I_0=1.85×10^{-7}mol dm^{-3} s^{-1}.

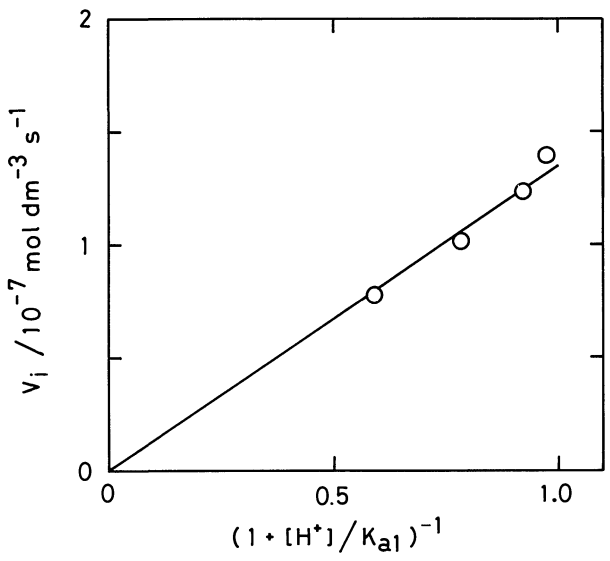

Fig. 4. Plots of V_i vs. (1+[H$^+$]/K_{a1})$^{-1}$ for the photo-induced oxidation of ascorbic acid by molecular oxygen in the presence of [Ru(bpz)$_3$]$^{2+}$ ions at [AsA]$_i$=1.00×10^{-3} mol dm^{-3}. Other conditions are the same as in Fig. 1.

where I_a and I_0 are the light intensities absorbed and irradiated, respectively, and γ is a constant including a molar absorption coefficient of the [Ru(bpz)$_3$]$^{2+}$ ion and the optical path length of the reacting solution. Saturation of the initial reaction rate corresponds to that of the light intensity absorbed in the [Ru(bpz)$_3$]$^{2+}$ solution. The solid line in Fig. 3 is a calculated one according to Eq. 4 with γ=5.3×10^4 dm^3 mol^{-1} and I_0=1.85×10^{-7} mol dm^{-3} s^{-1}. The light intensity absorbed in a reacting solution containing 5.0×10^{-5} mol dm^{-3} of the [Ru(bpz)$_3$]$^{2+}$ ion was determined to be (1.76±0.09)×10^{-7} mol dm^{-3} s^{-1} by using a tris(oxalato)-ferrate(III) actinometer. This value is very close to the mean value of the initial rates of reaction obtained from the decay of ascorbic acid and the formation of hydrogen peroxide at high concentrations of ascorbic acid ((1.8±0.4)×10^{-7} mol dm^{-3} s^{-1}).

pH Dependence. The effect of pH on the reaction rate for the [Ru(bpz)$_3$]$^{2+}$ system was studied at 30 °C, pH 3.9—5.6 (a 0.10 mol dm^{-3} acetate buffer), and I=0.10 mol dm^{-3} (NaClO$_4$) in an air-saturated solution. The reaction rate increased with increasing pH at the initial concentration of ascorbic acid, [AsA]$_i$= 1.00×10^{-3} mol dm^{-3}. The acid-dissociation constant of the *[Ru(bpz)$_2$(Hbpz)]$^{3+}$ ion is 10^{-2} mol dm^{-3},[3b] indicating that the predominant species is the *[Ru(bpz)$_3$]$^{2+}$ ion at pH 3.9—5.6. The pH dependence can be explained by considering the following acid-base equilibrium of ascorbic acid (H$_2$A):

$$H_2A \rightleftarrows HA^- + H^+ \quad [K_{a1} = 9.16 \times 10^{-5} \text{ mol dm}^{-3}].^{13)} \quad (5)$$

The molar fraction of the HA$^-$ ion is represented by

$$[HA^-]/([H_2A] + [HA^-]) = (1 + [H^+]/K_{a1})^{-1}. \quad (6)$$

Plots of the initial reaction rate vs. (1+[H$^+$]/K_{a1})$^{-1}$ was linear with a zero intercept (Fig. 4), indicating that the reacting species is the HA$^-$ ion. At a 1.00×10^{-2} mol dm^{-3} ascorbic acid the reaction rate was independent of pH, consistent with the results that the initial reaction rate is independent of the concentrations of ascorbic acid at more than 1.00×10^{-2} mol dm^{-3}.

The effect of the ionic strength on the initial reaction rate for the [Ru(bpz)$_3$]$^{2+}$ system, in which the reaction rate decreases with an increase in the ionic strength, also supports the idea that the reactive species are oppositely charged (Table 1).

Quenching of Excited State of Ruthenium(II) Complexes by Ascorbic Acid and Molecular Oxygen. The metal-to-ligand excited triplet state of [Ru(bpy)$_3$]$^{2+}$ and [Ru(bpz)$_3$]$^{2+}$ ions is quenched by ascorbic acid and molecular oxygen through an oxidation-reduction mechanism.[3,14–16] We also measured the luminescence quenching by ascorbic acid and molecular oxygen of *[Ru(bpy)$_2$(bpz)]$^{2+}$ and *[Ru(bpy)(bpz)$_2$]$^{2+}$ ions along with *[Ru(bpy)$_3$]$^{2+}$ and *[Ru(bpz)$_3$]$^{2+}$ ions under our experimental conditions.

Stern-Volmer plots for quenching by ascorbic acid are shown in Fig. 5. The rate constants of the quenching by ascorbic acid and molecular oxygen (k_{q1} and k_{q2}, respectively) were obtained by the use of the lifetime for the excited triplet state of ruthenium(II) complexes (Table 2). The lifetime of the *[Ru(bpy)(bpz)$_2$]$^{2+}$ ion in an aqueous solution is unknown and was therefore estimated from the value in propylene carbonate, compared with data for the *[Ru(bpy)$_2$(bpz)]$^{2+}$ ion in aqueous and propylene carbonate solutions.[7,9] The lifetime of the *[Ru(bpy)$_2$(bpz)]$^{2+}$ ion at pH 4.6 (a 0.1 mol dm^{-3} acetate buffer) was estimated from the ratio of the luminescence intensity at pH 4.6 to that in H_2O. The lifetime of the *[Ru(bpy)$_2$(bpz)]$^{2+}$ ion in H_2O has been reported to be 88 ns.[9]

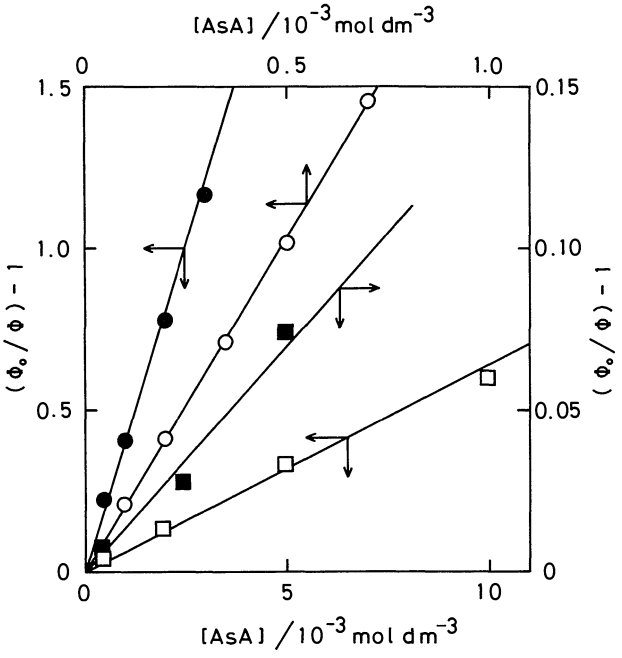

Fig. 5. Stern-Volmer plots for the luminescence quenching of the excited-triplet states of the ruthenium(II) complexes by ascorbic acid at 30°C, pH 4.60, and I=0.10 mol dm^{-3} under an argon atmosphere. ○: [Ru(bpz)$_3$]$^{2+}$, ●: [Ru(bpy)(bpz)$_2$]$^{2+}$, □: [Ru(bpy)$_2$(bpz)]$^{2+}$, and ■: [Ru(bpy)$_3$]$^{2+}$.

Mechanism of Reaction. The obtained results are accounted for by the following reaction mechanism:

$$\mathrm{Ru(II)} \xrightarrow{h\nu} \mathrm{*Ru(II)} \qquad I_a\phi \quad (7)$$

$$\mathrm{*Ru(II)} \longrightarrow \mathrm{Ru(II)} \qquad k_0 \quad (8)$$

$$\mathrm{*Ru(II) + HA^- \longrightarrow Ru(I) + A^{\cdot-} + H^+} \qquad k'_{q1} \quad (9)$$

$$[\mathrm{HA^{\cdot} \rightleftarrows H^+ + A^{\cdot-}} \quad pK_a = -0.45][17]$$

$$\mathrm{*Ru(II) + O_2 \longrightarrow Ru(III) + O_2^{\cdot-}} \qquad k'_{q2} \quad (10)$$

$$[\mathrm{HO_2 \rightleftarrows H^+ + O_2^{\cdot-}} \quad pK_a = 4.8][18]$$

$$\mathrm{Ru(III) + HA^- \longrightarrow Ru(II) + A^{\cdot-} + H^+} \qquad k_1 \quad (11)$$

$$\mathrm{Ru(I) + O_2 \longrightarrow Ru(II) + O_2^{\cdot-}} \qquad k_2 \quad (12)$$

$$\mathrm{2A^{\cdot-} \xrightarrow{H^+} A + HA^-} \qquad k_3 \quad (13)$$

$$\mathrm{2O_2^{\cdot-}\ (and/or\ HO_2) \longrightarrow H_2O_2 + O_2} \qquad k_4 \quad (14)$$

$$\mathrm{HA^- + O_2^{\cdot-}\ (and/or\ HO_2) \longrightarrow A^{\cdot-} + H_2O_2} \qquad k_5 \quad (15)$$

The reaction between the ascorbate radical and molecular oxygen might be very slow, on the basis of their redox potentials (E^0(A/A$^{\cdot-}$)=−0.14 V and E^0($O_2/O_2^{\cdot-}$)=−0.16 V).[19,20] When the decays of the ascorbate radical and the superoxide anion are very fast and the steady state assumption for *Ru(II), Ru(III), and Ru(I) is adopted, the following rate law can be derived:

$$-\frac{d[AsA]}{dt} = \frac{d[H_2O_2]}{dt} = \frac{(k'_{q1}[AsA] + k'_{q2}[O_2])I_a\phi}{k_0 + k'_{q1}[AsA] + k'_{q2}[O_2]}. \quad (16)$$

The rate constants of Reactions 11—15 have been reported: k_1=1.7×10^9 dm^3 mol^{-1} s^{-1} ([Ru(bpy)$_3$]$^{3+}$),[21] k_2=5.8×10^8 dm^3 mol^{-1} s^{-1} ([Ru(bpz)$_3$]$^+$),[22] k_3=1×10^8 dm^3 mol^{-1} s^{-1} (at pH 4.6),[23] k_4=9×10^7 dm^3 mol^{-1} s^{-1} (at pH 4.6),[24] and k_5=8×10^5 dm^3 mol^{-1} s^{-1} (at pH 4.6).[25] Then, Eq. 16 can be rewritten as

Table 2. Rate Constants of the Luminescence Quenching by Ascorbic Acid and Molecular Oxygen of the Excited-Triplet State of Ruthenium(II) Complexes at 30°C, pH 4.60, and I=0.10 mol dm^{-3}

Complex	k_{q1}(AsA) dm^3 mol^{-1} s^{-1}	k_{q2}(O_2) dm^3 mol^{-1} s^{-1}	E^0(Ru$^{*2+/+}$)[a] V	E^0(Ru$^{3+/*2+}$)[a] V
*[Ru(bpz)$_3$]$^{2+}$	(2.0±0.1)×10^9 3.0×10^9[b]	(3.8±0.1)×10^8 5.5×10^8[c]	1.64 (1.64)	0.14 (0.08)
*[Ru(bpy)(bpz)$_2$]$^{2+}$	(1.5±0.1)×10^9	(5.3±0.3)×10^8	(1.42)	(−0.03)
*[Ru(bpy)$_2$(bpz)]$^{2+}$	(2.3±0.1)×10^9	(2.3±0.1)×10^9	(1.28)	(−0.11)
*[Ru(bpy)$_3$]$^{2+}$	(2.2±0.6)×10^7 2×10^7[d]	(3.4±0.2)×10^9 3.3×10^9[e]	0.84 (0.78)	−0.84 (−0.87)

a) Ref. 2. The value in parentheses is in acetonitrile. b) At pH 5—10. Ref. 16. c) In H_2O. Ref. 16. d) In H_2O. Ref. 15. e) In H_2O. Ref. 14.

$$\frac{1}{V_i} = \frac{1}{I_a\phi} + \frac{k_0}{(k'_{q1}[AsA] + k'_{q2}[O_2])I_a\phi}, \quad (17)$$

where V_i denotes the initial rate of reaction. Since the condition $k'_{q1}[AsA] \gg k'_{q2}[O_2]$ holds for the $[Ru(bpz)_3]^{2+}$ and $[Ru(bpy)(bpz)_2]^{2+}$ systems (see Table 2), Eq. 17 can be simplified to

$$\frac{1}{V_i} = \frac{1}{I_a\phi} + \frac{k_0}{k'_{q1}I_a\phi} \cdot \frac{1}{[AsA]}. \quad (18)$$

Plots of V_i^{-1} vs. $[AsA]^{-1}$ were linear, as is shown in Fig. 6. The values of $I_a\phi$ and k'_{q1}/k_0 were, respectively, obtained from the intercept and slope of this line. The values of k'_{q1} are $(1.0\pm0.3)\times10^9$ dm^3 mol^{-1} s^{-1} and $(7.7\pm1.2)\times10^8$ dm^3 mol^{-1} s^{-1} for $[Ru(bpz)_3]^{2+}$ and $[Ru(bpy)(bpz)_2]^{2+}$, respectively. The value of $I_a\phi$ for the $[Ru(bpz)_3]^{2+}$ system ($(2.0\pm0.5)\times10^{-7}$ mol dm^{-3} s^{-1}) is in agreement with that obtained from an experiment using a tris(oxalato)ferrate(III) actinometer ($(1.76\pm0.09)\times10^{-7}$ mol dm^{-3} s^{-1}), suggesting that the quantum yield ϕ is ca. 1.

In continuous photolysis, half of the ascorbic acid is consumed and half of the hydrogen peroxide is produced against the photo-excited state of the ruthenium(II) complexes. The values of $2k'_{q1}$ and $2k'_{q2}$, therefore, correspond to those of k_{q1} and k_{q2} for luminescence quenching of the excited state of the ruthenium(II) complexes, respectively. The former values are in good agreement with the latter ones, indicating that the above-mentioned mechanism is reasonable.

From luminescence-quenching experiments for the $*[Ru(bpy)_2(bpz)]^{2+}$ ion, the value of k_{q1} is nearly equal to that of k_{q2}. Therefore, Eq. 16 for the $[Ru(bpy)_2(bpz)]^{2+}$ system is simplified to

$$\frac{1}{V_i} = \frac{1}{I_a\phi} + \frac{k_0}{k'_{q1}([AsA] + [O_2])I_a\phi}. \quad (19)$$

Plots of V_i^{-1} vs. $([AsA]+[O_2])^{-1}$ were linear and the values of $I_a\phi$ and k'_{q1}/k_0 were, respectively, obtained from the intercept and slope of this straight line (Fig. 7): $I_a\phi=(1.7\pm0.8)\times10^{-7}$ mol dm^{-3} s^{-1} and $k'_{q1}=k'_{q2}=(3.1\pm1.9)\times10^9$ dm^3 mol^{-1} s^{-1}.

In the $[Ru(bpy)_3]^{2+}$ system the condition $k'_{q2}[O_2] \gg k'_{q1}[AsA]$ holds (see Table 2). Therefore, the reaction rate should therefore be independent of the concentrations of ascorbic acid, when Reaction 11 is very fast:

$$V_i = \frac{k'_{q2}[O_2]I_a\phi}{k_0 + k'_{q2}[O_2]}. \quad (20)$$

The initial reaction rate was, however, dependent on the concentrations of ascorbic acid and reached a constant value at high concentrations of ascorbic acid. A linear dependence of the initial of reaction rate on the concentrations of ascorbic acid for this system has already been reported by Kurimura et al.[10] They have suggested that the reaction rate must reach a constant value at high concentrations of ascorbic acid, and pro-

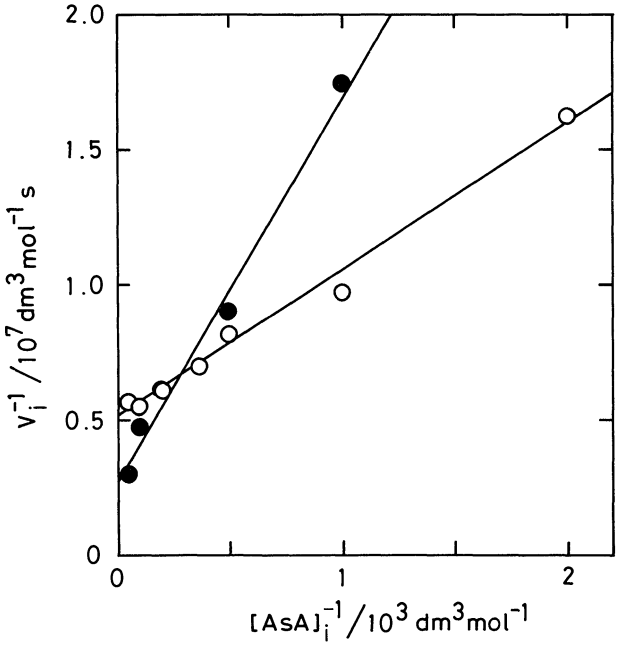

Fig. 6. Plots of V_i^{-1} vs. $[AsA]_i^{-1}$ for the photo-induced oxidation of ascorbic acid by molecular oxygen in the presence of the ruthenium(II) complexes. Experimental conditions are the same as in Fig. 1. ○: $[Ru(bpz)_3]^{2+}$ and ●: $[Ru(bpy)(bpz)_2]^{2+}$.

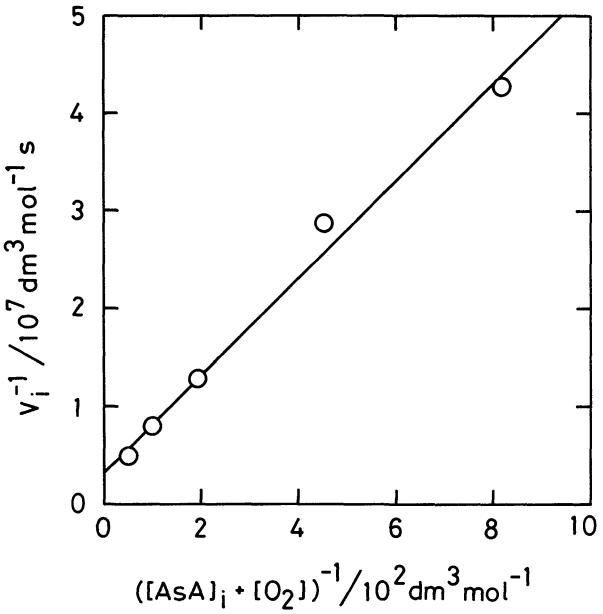

Fig. 7. Plots of V_i^{-1} vs. $([AsA]_i+[O_2])^{-1}$ for the photo-induced oxidation of ascorbic acid by molecular oxygen in the presence of $[Ru(bpy)_2(bpz)]^{2+}$ ions. Experimental conditions are the same as in Fig. 1.

posed a mechanism in which Reaction 11 competes with the back reaction for oxidative quenching by oxygen (Reaction 21):

$$[Ru(bpy)_3]^{3+} + O_2^{\cdot-} \longrightarrow [Ru(bpy)_3]^{2+} + O_2. \quad (21)$$

The rate constant of Reaction 21 has been reported to be 1.4×10^{10} dm^3 mol^{-1} s^{-1}.[26] The formation of hydrogen peroxide suggests that the reaction of superoxide ions with ascorbate and/or the disproportionation of superoxide ions must occur competitively in Reactions 11 and 21. At high concentrations of ascorbic acid, where the reaction rate is indenpendent of the concentrations of ascorbic acid, the initial rate can be simplified, as in Eq. 20. The value of k'_{q2}, obtained from air- and oxygen-saturated solutions, is $(3.0\pm 2.0)\times10^9$ dm^3 mol^{-1} s^{-1}, but has a large error due to the use of only two determinations.

Difference in Mechanisms of Reaction for $[Ru(bpy)_x(bpz)_{3-x}]^{2+}$ Ions. Hydrogen peroxide was efficiently produced during the photo-induced oxidation of ascorbic acid by molecular oxygen catalyzed by $[Ru(bpy)_x(bpz)_{3-x}]^{2+}$ (x=0—3) ions. The $[Ru(bpz)_3]^{2+}$, $[Ru(bpy)_2(bpz)]^{2+}$, and $[Ru(bpy)(bpz)_2]^{2+}$ ions are superior to the $[Ru(bpy)_3]^{2+}$ ion for the formation of hydrogen peroxide. This can be explained by a difference in the quenching rate constants of the excited triplet state of these complexes by ascorbic acid and molecular oxygen. Under the present experimental conditions $k'_{q1}[AsA]$ is larger than $k'_{q2}[O_2]$ for the $[Ru(bpz)_3]^{2+}$, $[Ru(bpy)(bpz)_2]^{2+}$, and $[Ru(bpy)_2(bpz)]^{2+}$ ions, indicating that the reductive quenching process is predominant (Scheme 1). On the other hand, $k'_{q2}[O_2]$ is larger than $k'_{q1}[AsA]$ for the $[Ru(bpy)_3]^{2+}$ ion, in which the oxidative quenching process is predominant (Scheme 2). For the $[Ru(bpy)_2(bpz)]^{2+}$ ion the value of k_{q1} is the same as that of k_{q2}. Therefore, the change in the reaction mechanisms from the oxidative to reductive might occur in the $[Ru(bpy)_2(bpz)]^{2+}$ complex. The redox potentials of couples Ru^{3+}/Ru^{*2+} and Ru^{*2+}/Ru^{+} have been reported, as given in Table 2. The excited triplet state of the $[Ru(bpy)_2(bpz)]^{2+}$ ion is considered to be in the metal-to-ligand charge transfer (MLCT) state of $[Ru^{III}(bpy)_2(bpz^{\cdot-})]^{2+}$, where an electron is localized in the bpz ligand.[7,8] The value of E^0 ($Ru^{3+/*2+}$) for the $*[Ru(bpy)_3]^{2+}$ ion is much lower than that for the other ruthenium(II) complexes containing the bpz ligand, indicating that the $bpz^{\cdot-}$ ligand is more stable during electron transfer than is the $bpy^{\cdot-}$ ligand. Therefore, the electron of the $bpz^{\cdot-}$ ion in the MLCT state of the ruthenium(II) complexes might not be easily transferred, being compared with the $bpy^{\cdot-}$ ion in the $[Ru(bpy)_3]^{2+}$ system. The order of k_{q1} is almost parallel to that of the redox potential, $E^0(Ru^{*2+/+})$, and the order of k_{q2} is inversely dependent on $E^0(Ru^{3+/*2+})$. However, the quenching reaction between Ru(II) complexes, except for the $*[Ru(bpy)_3]^{2+}$ ion and ascorbate, is almost of a diffusion- controlled rate and, therefore, the difference in the rate is much smaller than that expected from the difference in the redox potentials. This trend is similar to the oxidative quenching reaction by molecular oxygen. For example, though the quenching rate constants (k_{q1} and k_{q2}) for the $[Ru(bpy)_2(bpz)]^{2+}$ system are the same, the values of the free energy change of the reaction are quite different: -0.60 eV (1 eV=9.65×10^4 J mol^{-1}) for reductive quenching by ascorbate ($E^0(HA^{\cdot}/HA^-)$= 0.68 V)[19] and 0.05 eV for oxidative quenching by O_2 ($E^0(O_2/O_2^{\cdot-})=-0.16$ V).[20]

This research was partly supported by a Grant-in-Aid for Scientific Research No. 01470051 from the Ministry of Education, Science and Culture.

References

1) K. Kalyanasundaram, *Coord. Chem. Rev.*, **46**, 159 (1982).

2) A. Juris, V. Balzani, F. Barigelletti, S. Campagna, P. Belser, and A. von Zelewsky, *Coord. Chem. Rev.*, **84**, 85 (1988).

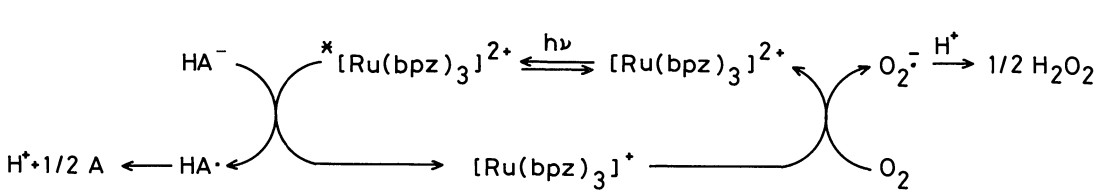

Scheme 1.

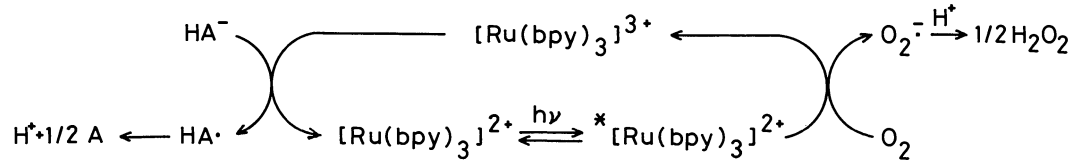

Scheme 2.

3) a) R. J. Crutchley and A. B. P. Lever, *J. Am. Chem. Soc.*, **102**, 7128 (1980); b) R. J. Crutchley, N. Kress, and A. B. P. Lever, *J. Am. Chem. Soc.*, **105**, 1170 (1983).
4) K. Kalyanasundaram, J. Kiwi, and M. Grätzel, *Helv. Chim. Acta*, **61**, 2720 (1978).
5) A. Moradpour, E. Amouyal, P. Keller, and H. Kagan, *Nouv. J. Chim.*, **2**, 547 (1978).
6) a) M. Kimura and S. Doi, *J. Chem. Soc., Dalton Trans.*, **1983**, 37; b) M. Kimura, T. Yamashita, and S. Nishida, *Inorg. Chim. Acta*, **89**, 193 (1984); c) M. Kimura and S. Nishida, *J. Chem. Soc., Dalton Trans.*, **1985**, 355; d) M. Kimura, M. Yamashita, and S. Nishida, *Inorg. Chem.*, **24**, 1527 (1985); e) M. Kimura, M. Yamamoto, and A. Nagai, *Inorg. Chim. Acta*, **117**, 169 (1986); f) S. Nishida and M. Kimura, *J. Chem. Res., Synop.*, **1986**, 336; g) S. Nishida and M. Kimura, *Bull. Chem. Soc. Jpn.*, **60**, 2367 (1987); h) M. Kimura, T. Nakamura, H. Nakamura, and S. Nishida, *Polyhedron*, **6**, 1571 (1987).
7) D. P. Rillema, G. Allen, T. J. Meyer, and D. Conrad, *Inorg. Chem.*, **22**, 1617 (1983).
8) G. H. Allen, R. P. White, D. P. Rillema, and T. J. Meyer, *J. Am. Chem. Soc.*, **106**, 2613 (1984).
9) a) K. Shinozaki, Y. Kaizu, H. Hirai, and H. Kobayashi, *Inorg. Chem.*, **28**, 3675 (1989); b) K. Shinozaki, O. Ohno, Y. Kaizu, H. Kobayashi, M. Sumitani, and K. Yoshihara, *Inorg. Chem.*, **28**, 3680 (1989).
10) Y. Kurimura, H. Yokota, and Y. Muraki, *Bull. Chem. Soc. Jpn.*, **54**, 2450 (1981).
11) R. J. Crutchley and A. B. P. Lever, *Inorg. Chem.*, **21**, 2276 (1982).
12) C. G. Hatchard and C. A. Parker, *Proc. R. Soc. London, Ser. A*, **235**, 518 (1956).
13) M. M. Taqui Khan and A. E. Martell, *J. Am. Chem. Soc.*, **89**, 4176 (1967).
14) C. -T. Lin and N. Sutin, *J. Phys. Chem.*, **80**, 97 (1976).
15) C. Creutz, N. Sutin, and B. S. Brunschwig, *J. Am. Chem. Soc.*, **101**, 1297 (1979).
16) G. Neshvad and M. Z. Hoffman, *J. Phys. Chem.*, **93**, 2445 (1989).
17) G. P. Laroff, R. W. Fessenden, and R. H. Schuler, *J. Am. Chem. Soc.*, **94**, 9062 (1972).
18) B. H. J. Bielski and A. O. Allen, *J. Phys. Chem.*, **81**, 1048 (1977).
19) C. Creutz, *Inorg. Chem.*, **20**, 4449 (1981).
20) D. T. Sawyer and J. S. Valentine, *Acc. Chem. Res.*, **14**, 393 (1981).
21) D. H. Macartney and N. Sutin, *Inorg. Chim. Acta*, **74**, 221 (1983).
22) D. R. Prasad and M. Z. Hoffman, *J. Am. Chem. Soc.*, **108**, 2568 (1986).
23) B. H. J. Bielski, D. A. Comstock, and R. A. Bowen, *J. Am. Chem. Soc.*, **93**, 5624 (1971).
24) B. H. J. Bielski, *J. Photochem. Photobiol.*, **28**, 645 (1978).
25) A. D. Nadezhdin and H. B. Dunford, *Can. J. Chem.*, **57**, 3017 (1979).
26) S. S. Miller, K. Zahir, and A. Haim, *Inorg. Chem.*, **24**, 3978 (1985).

Determination of Magnetic Susceptibility of Liquids by a Sensitive Viscometer Method

Kazuo SUEOKA
Department of Chemistry, Josai University, Keyakidai, Sakado, Saitama 350-02
(Received August 10, 1990)

A sensitive viscometer method is presented for precise measurements of the magnetic susceptibility of liquids. This method can be applied to a determination of the diamagnetic susceptibilities of various materials and the temperature dependence of the susceptibility for water. Measurements show that this method has a sensitivity of ±0.005% and a reproducibility of ±0.02%.

Various methods have been proposed for the precise measurement of the magnetic susceptibility.[1-5] Recently, a highly sensitive susceptometer based on a superconducting quantum interference device (SQUID) appeared.[6] This method can be used to detect susceptibility changes of ±0.0001% of a sample; in susceptibility measurements, the reproducibility (± 0.02%) is limited by the sample preparation technique, and the precision is limited by the availability of a standard reference value and density data regarding the conversion to mass susceptibility. Previously, the present author and a co-worker reported an improved viscometer method,[9,10] which is adaptable for both pure liquids and solutions, in addition to gas in the dead space of a measuring cell. This method gives the mass susceptibility without a density conversion that is accurate to within ±0.05%. Additional advantages of the method are: 1) the influence of dissolved air in a liquid sample can be easily almost completely eliminated; 2) a small size magnet can be used; 3) a definite sample volume is unnecessary; and 4) automatic measuring is possible. Since the susceptibility can be easily obtained precisely, it is possible to improve the method's sensitivity for a more precise measurement of the susceptibility.

In this paper, a new type cell is discussed which was designed to improve the sensitivity; its performance is also demonstrated.

Theoretical

A capillary cell is placed in a magnetic field so that the lower end is in the center of a gap between the pole pieces of an electromagnet, while its upper grobular part is outside the field. The susceptibility of a liquid, χ_L, may be written as

$$\chi_L = \frac{2g\tilde{h}}{H^2}\tau_L + (1 - \beta_G)\frac{\rho_G}{\rho_L}\chi_G + \frac{\rho_V}{\rho_L}\chi_V, \quad (1)$$

where

$$\tau_L = (t_0 - t_H)/t_H. \quad (2)$$

Here, t_0 and t_H are the flowing times in the absence and the presence of the field, H, respectively; g the acceleration of gravity; $\tilde{h}$ the mean-effective-head of the liquid; ρ the density; and β the gas solubility in the liquid. Subscripts, L, V, and G indicate the values for the sample liquid, the liquid vapor, and the operating gas, respectively.

Regarding a relative measurement of sample 1 and sample 2, considering $\chi_V \simeq \chi_L$ for each sample,

$$\frac{\chi_L(1)}{\chi_L(2)} = \frac{\tau_L(1)}{\tau_L(2)}[1 + P(1) - P(2)], \quad (3)$$

where

$$P(1) = \frac{\rho_G(1)\chi_G}{\rho_L(1)\chi_L(1)}[1 - \beta_G(1)] + \frac{\rho_V(1)}{\rho_L(1)}, \quad (4\text{-a})$$

and

$$P(2) = \frac{\rho_G(2)\chi_G}{\rho_L(2)\chi_L(2)}[1 - \beta_G(2)] + \frac{\rho_V(2)}{\rho_L(2)}. \quad (4\text{-b})$$

When sample 2 is taken as a standard reference, the following equation may be practically used instead of Eq. 4-a:

$$P(1) = \frac{\rho_G(1)\tau(2)\chi_G}{\rho_L(1)\tau(1)\chi_L(2)}[1 - \beta_G(1)] + \frac{\rho_V(1)}{\rho_L(1)}. \quad (4\text{-c})$$

Allowing for a deviation of ±0.01% (approximately $\pm 0.0001 \times 10^{-6}$ emu/g†), the P(1)—P(2) term of Eq. 3 is negligible, and one can use

$$\frac{\chi_L(1)}{\chi_L(2)} = \frac{\tau_L(1)}{\tau_L(2)}. \quad (5)$$

The sensitivity, K, of this method is

$$K = \frac{\Delta\tau_L}{\Delta\chi_L} = \frac{H^2}{2g\tilde{h}}, \quad (6)$$

where the second and third terms of Eq. 1 are considered to be negligible. Then, a more sensitive

† Note that cgs units are used hereafter. In SI units the volume susceptibility is dimensionless and numerically equal to 4π times the cgs value.

method must be obtained by designing the measuring cell that gives a more reduced mean-effective-head.

Experimental

Materials. The water was purified by sub-boiling distillation from a quartz still after deionization. Acetic acid was purified by distillation from the Wako Guaranteed reagent. Methanol, carbon tetrachloride, and benzene were Dotite Primasol solvents (Dojindo Co.) and were used without purification. Nitrogen was obtained from commercial sources with purities exceeding 99.9%.

Capillary Cell. A horizontal-type capillary cell equipped with a thermostat jaket was fixed to a magnet so that the exit end of its capillary part was located at the center of the pole gap, while its inlet part protruded out of the magnetic field through the inhomogeneous region of the field. Figure 1 shows the experimental equipment. A capillary cell made of Pyrex glass is fixed upright in duplicated water jacket cabinets made of poly(vinyl chloride). These cabinets are covered with foam polystyrene. Detectors for meniscus-passage are attached at positions a and b of the cell. The detectors comprise two pairs of light-emission diodes and photo transistors molded in poly(vinyl chloride). A vertical-type capillary cell used for a comparison was the same as that used in previous studies.[9,10]

Magnet. The electromagnet is the same type as that used in previous studied.[9,10] The pole gap was set to approximately 7 mm. The magnetic field-strength available at a maximum current of 4 A was 19.7 kOe (1 kOe=$(1/4\pi)\times 10^3$ A m^{-1}), calibrated with a Yokogawa gauss meter (Type 3251). The magnetizing current was controlled using a regulated Kikusui (Model PAD-110-5L) power supply (±0.01%), throughout the measurements.

Measurements. Prior to the measurements, any air dissolved in the liquid sample and the cell dead space was fully replaced by nitrogen by means of an operation tube connected to the cell. A detailed description of this procedure was given in a previous paper.[9] The time of liquid flow was measured to an accuracy of ±0.001 s. The electronic apparatus to measure the flow time was made by the present author. The temperature around the cell was monitored by a Takara Kogyo (Model D111) thermistor thermometer. The thermometer was calibrated against a mercury standard thermometer with 0.1 °C divisions. The stability of the temperature was controlled to be ±0.01 °C. Measurements of the flow time were repeated alternately in both the presence and absence of the magnetic field, and the τ-value was calculated for each step. The polarity of the magnetic field was alternately changed for each step by turnning the direction of the magnetizing current. Fifty measurements were averaged in order to calculate the magnetic susceptibility.

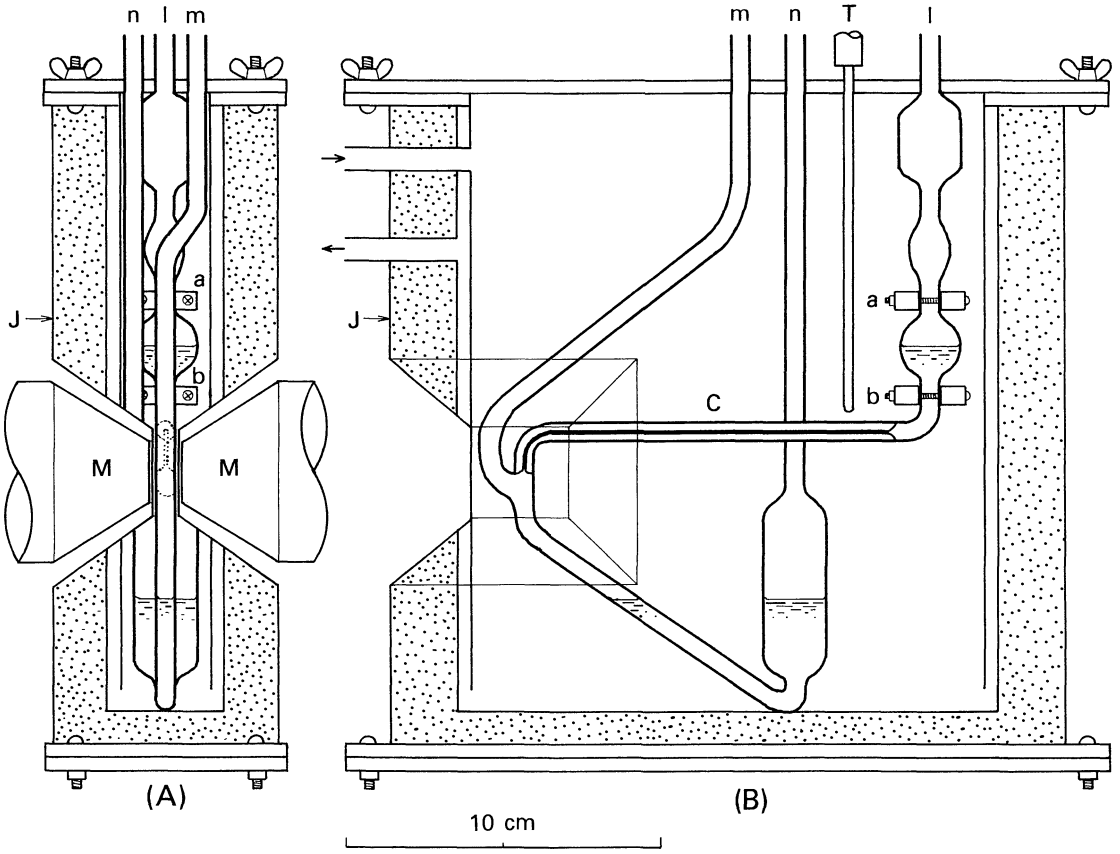

Fig. 1. Experimental setup, A, Front view, and B, side view. C, Capillary of about 0.5 mm (i.d.); a and b, detectors for meniscus passage; M, magnet; J, cabinet made of poly(vinyl chloride) covered with foam polystyrene; T, thermistor. The openings, l, m, and n, connected to the operation tube.[9]

Results and Discussion

The experimental results for water obtained by means of this cell for different magnetic field strengths are shown in Fig. 2, in comparison with the previous cell. A straight line passing through the origin and having a large slope can be seen, the slope of which is expressed from Eq. 1 as

$$\alpha = \frac{1}{2g\tilde{h}}\left[\chi_L - (1-\beta_G)\frac{\rho_G}{\rho_L}\chi_G - \frac{\rho_V}{\rho_L}\chi_V\right]. \quad (7)$$

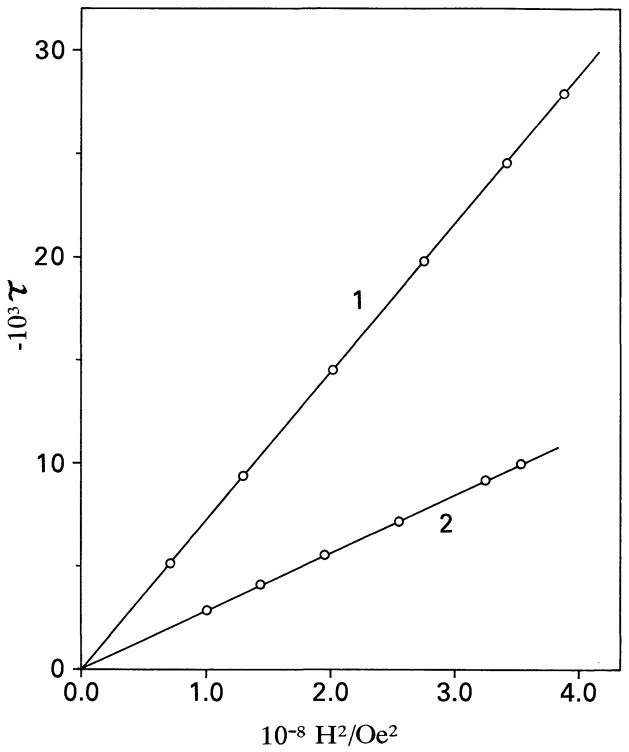

Fig. 2. Relationship between τ-value and the external magnetic field-strength measured for water: 1, this cell; 2, previous cell.

The sensitivity ratio at the same magnetic field strength between the different types of cells can be written using the respective α-values for the same material, as $K_H/K_V=\alpha_H/\alpha_V$. Here, H and V indicate the respective types of cells in the present and previous studies. The α-values for various materials obtained by this cell are listed in Table 1, and are compared with those of the previous cell. It may be seen that the sensitivity is higher than that of the previous cell by about 2.56 times, and that the ratio reproducible in different materials is within ±0.05%. The accuracy of these values is limited by the reproducibility of magnetic field-strength measurements.

The τ-values for various liquids measured at maximum magnetic field strength are listed in Table 2; the field strength was kept constant during all measurements. In the case of water under this condition, the difference in the flow times, t_0-t_H, was about −10 s, for a flow time of about 400 s. From Eq. 2, the deviation of the τ-value for water may be evaluated to be ±0.01% when the error of the flow time is ±0.001 s. The reproducibility of the values for different samples of the same material was at least ±0.02% for water and benzene, while it was ±0.05% for the other organic liquids. Since the allowance of Eq. 5

Table 1. Comparison of the α-Values for Various Liquids Measured by Different Cells at 20°C

Materials	$-10^{11}\alpha$/dyn^{-1} cm²		α_H/α_V
	This cell	Previous cell	
Water	7.182	2.803	2.562
Methanol	6.833	2.668	2.561
Acetic acid	5.380	2.099	2.563
Carbon tetrachloride	4.427	1.729	2.560
Benzene	7.094	2.769	2.562
Mean			$2.561_6(1_0)$[a]

a) The uncertainty in parenthesis is one standard deviation in units of the last quoted mean value.

Table 2. Diamagnetic Susceptibilities of Liquids Measured by Different Cells in emu at 20°C

Materials	This cell		Previous cell		Literature[a]
	$-10^3\tau$	$-10^6\chi$	$-10^3\tau$[b]	$-10^6\chi$	$-10^6\chi$
Water	27.860	0.7192[c]	9.90_7	0.7192[c]	0.7192[c]
Methanol	26.505	0.6842	9.43_0	0.684_6	0.661—0.675
Acetic acid	20.868	0.5387	7.42_0	0.538_7	0.527—0.532
Carbon tetrachloride	17.174	0.4433	6.11_0	0.443_6	0.432—0.438
Benzene	27.520	0.7104	9.78_6	0.710_4	0.700—0.704

a) Landolt-Börnstein, "Zahlenwerte und Funktionen aus Physik, Chemie, Astronomie, Geophysik und Technik," II Band, 10 Teil, Springer Verlag, Berlin (1967). b) Measured in 18.8 kOe. c) Taken as the standard.

(±0.01%) exceeds the best reproducibility, one can use this equation to calculate the magnetic susceptibilities of each material. The results are listed in Table 2. A good agreement between the values measured using the previous cell can be seen, while the literature values are slightly smaller than the results by an amount corresponding to the effect due to dissolved air.[9,11] In the present method, dried nitrogen was used as the operating gas and no continuous change of the τ-value was observed. Therefore, the error due to the effect of dissolved air can be almost completely excluded. However, the organic liquids used here absorbed a slight amount of moisture when exposed to air. Thus, the smaller reproducibility for the organic liquids may be mainly caused by the irregular contamination due to atmospheric moisture during sampling. In fact, good reproducibility was obtained for benzene, owing to the small difference in its susceptibility compared to that of water. The method's reproducibility when using this cell is considered to be within ±0.02% (±1.5×10^{-10} emu g^{-1}); such a value was obtained for water. It is difficult to estimate the absolute accuracy of the susceptibility since the absolute value of the susceptibility of water is poorly known.[12]

The diamagnetic susceptibility of a liquid slightly changes with the temperature.[13,14] In particular, accurate coefficients using the susceptibility change of water have been determined using the SQUID method.[7] If the $H^2/2g\tilde{h}$ term in Eq. 1 is kept constant for different temperatures, the present cell may be applicable to measure the temperature dependence of the susceptibilities of diamagnetic liquids. The change in g is negligibly small (≦1×10^{-6} m s^{-2}) and the value of H can be held practically constant throughout a measurement. Moreover, the change in the mean-effective-head is small, since it is of the order of the linear expansion coefficient of a cell made of Pyrex glass, about 3.3×10^{-6} K^{-1}. Thus, one may test the sensitivity by measuring the temperature coefficients for water. In this case, Eq. 3 may be written as

$$\frac{\chi(T)}{\chi(20)} = \frac{\tau(T)}{\tau(20)}\left[0.999317 + 0.60 \times \frac{\rho_G(T)}{\rho_L(T)}\right], \quad (8)$$

where the ratio of the susceptibility at T in °C to that at 20 °C is taken. The experimental results are listed in Table 3, and are in good agreement with those obtained by the SQUID method.[7] The observed $\chi(T)/\chi(20)$ ratios are fitted to a palabolic equation,

$$\chi(T)/\chi(20) = 1 + a(T - 20) + b(T - 20)^2, \quad (9)$$

by a least-squares method and the analyzed result is shown in Fig. 3. The temperature coefficients are listed in Table 4, and are compared with the reported values obtained by various observers. Earlier studies have been contradicted due to oxygen contamination of samples as well as to instrumental imprecision.[11]

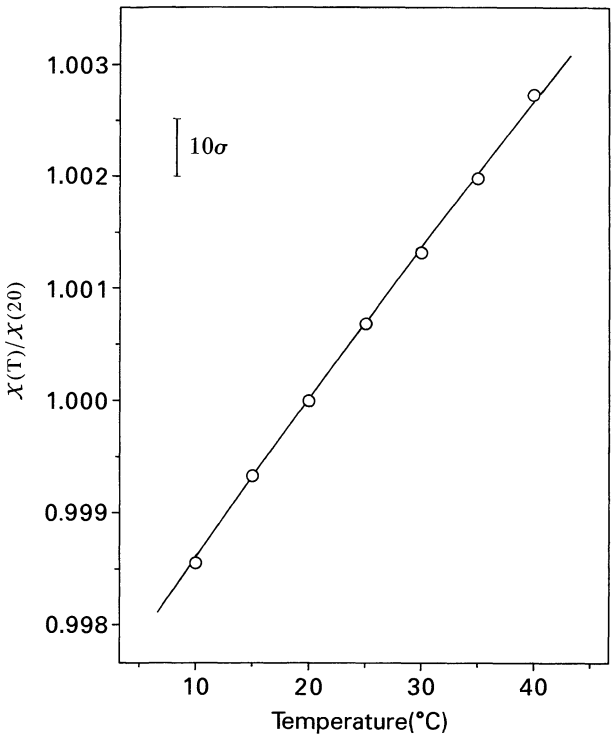

Fig. 3. Change in the mass susceptibility of water with temperature, relative to the value at 20 °C. The solid line is a best fit second-order polynomial, Eq. 9. The half diameter of the circle is approximately one standard deviation of the data points.

Table 3. Susceptibilities for Water Observed at Various Temperatures

Temperature °C	$-10^3\tau(T)$	$\tau(T)/\tau(20)$	$\chi(T)/\chi(20)$ This work	$\chi(T)/\chi(20)$ SQUID[a]
10.0	27.819	0.99852_8	0.99855	0.99860
15.0	27.841	0.99931_8	0.99932	0.99930
20.0	27.860	1.00000_0	1.00000	1.00000
25.0	27.879	1.00068_2	1.00067	1.00069
30.0	27.897	1.00132_8	1.00131	1.00138
35.0	27.916	1.00201_0	1.00198	1.00206
40.0	27.937	1.00276_4	1.00273	1.00273

a) Values calculated using a third-order polynomial, reported in Ref. 7.

Table 4. Comparison of the Temperature-Coefficients for Water Measured by Different Observers Using Different Methods[a]

Observers	$10^4a/K^{-1}$	$10^6b/K^{-2}$	$100\sigma[n]$[b]	Method	References
Cabrera and Fahlenbrach (1933)	1.15			Faraday	Ref. 1
Auer (1933)	1.26			Quinke	Ref. 2
Wills and Boeker (1934)	1.30	−0.7		Quinke	Ref. 3
Seely (1937)	1.423(58)[c]	−1.05(33)	0.009_0[4]	Quinke	Ref. 4
Cini and Torrini (1968)	1.363(22)	0.11(14)	0.008_4[49]	Gouy	Ref. 5
Philo and Fairbank (1980)	1.38954(78)	−0.1251(47)	0.0001_0[16]	SQUID	Ref. 7
Day (1980)	1.3687(39)	−0.073(23)	0.0002_8[6]	SQUID	Ref. 8
This author	1.383(29)	−0.22(18)	0.005_1[7]		

a) The values for Refs. 4, 5, 7, and 8 were recalculated using data in the range 10—40 °C, presented in respective papers. b) σ is the standard deviation of the fit and n is the number of data included in the calculation. c) The uncertainty in parentheses is one standard deviation in units of the last quoted coefficient.

The present results are in good agreement with the most pricise data[7] within each uncertainty. As estimated from the standard deviation, the sensitivity, or limit, of detection of the method is considered to be ±0.005% (±0.4×10^{-10} emu g^{-1}); this represents the best performance among various methods based on classical principles. The higher sensitivity than the stability of the magnetizing current used here may be interpreted in terms of the performance: that the method gives a susceptibility that is measured in a time-averaged magnetic field. The accuracy of the susceptibility determined by this method is seriously limited by the availability of a standard value. It is reasonable to use water as a standard in order to maximize the precision, since its nature is never influenced by atmospheric moisture and the best reproducibility available.

The author wishes to thank the late emeritus Prof. T. Ikeda of Shizuoka University for his helpful discussion while in life.

References

1) B. Cabrera and H. Fahlenbrach, *Z. Phys.*, **82**, 759 (1933).
2) H. Auer, *Ann. Phys.*, **5**, 593 (1933).
3) A. P. Wills and G. F. Boeker, *Phys. Rev.*, **46**, 907 (1934).
4) S. Seely, *Phys. Rev.*, **52**, 662 (1937).
5) R. Cini and M. Torrini, *J. Chem. Phys.*, **49**, 2826 (1968).
6) J. S. Philo and W. M. Fairbank, *Rev. Sci. Instrum.*, **48**, 1529 (1977).
7) J. S. Philo and W. M. Fairbank, *J. Chem. Phys.*, **72**, 4429 (1980).
8) E. P. Day, *J. Chem. Phys.*, **72**, 4434 (1980).
9) K. Sueoka and T. Ikeda, *Bull. Chem. Soc. Jpn.*, **50**, 2124 (1977).
10) K. Sueoka and T. Ikeda, *Bull. Chem. Soc. Jpn.*, **52**, 659 (1979).
11) B. C. Eggleston, D. F. Evans, and R. E. Richards, *J. Chem. Soc.*, **1956**, 941.
12) P. W. Selwood, "Magnetochemistry," Interscience, New York (1956), pp. 85—87.
13) Ref. 12, p. 88.
14) A. Weiss and H. Witte, "Magnetochemie," Verlag Chemie, Weinheim (1973), pp. 106—107.

Electronic Properties of One-Dimensional Iodine Complex. Benzo[*b*]phenothiazine-$I_{2.5}$

Taro SOMENO, Taketoshi HOSHIZAKI, Kozo KOZAWA, Tokiko UCHIDA,* Hakuro HAYASHI,†
Tadashi SUGANO,† and Minoru KINOSHITA†
Department of Industrial and Engineering Chemistry, Faculty of Science and Technology, Science University of Tokyo, 2641, Yamazaki, Noda, Chiba 278
†The Institute for Solid State Physics, The University of Tokyo, Roppongi, Minato-ku, Tokyo 106
(Received August 18, 1990)

One-dimensional metallic conductance was observed along the c axis of a single crystal of benzo[*b*]phenothiazine–iodine complex, $(B[b]PT)_2(I_3^-)(I)_2$, the crystal structure of which was preliminarily determined by X-ray analysis. Its metal-insulator transition was observed around 235 K, and the sign of the carriers seemed to be positive above 250 K. From the reflection spectra, with polarized light parallel to the c axis, a plasma-edge-like dispersion was observed in near IR region. Several parameters were evaluated by assuming a tight binding band model. The EPR spectra of this complex consist of only one broad signal (peak-to-peak width at room temperature 250×10^{-4} T) in the temperature range from 4 K to 296 K (g=1.998±0.002).

Since more than two decades, phenothiazine (PT) and its derivatives have been known to make semiconductive complexes with iodine.[1–15] None of them, however, has ever been structurally analyzed even if the complex was obtained as single crystals. Many reasons would be considerable about it. For example, there are so many crystallographically independent chemical entities in a large unit cell for 10-methylphenothiazine–iodine complex.[16] Moreover, PT derivatives–iodine complexes usually consist of several kinds of compounds having various mole ratios in spite of being composed of the same donor and acceptor.

We found that benzo[*b*]phenothiazine (B[*b*]PT) and iodine formed only one kind of complex compound with the composition, $(B[b]PT)_2(I_3)(I)_2$ (hereafter abbreviated as B[*b*]PT–$I_{2.5}$), and that it showed metallic behavior around room temperature and transferred to insulator at low temperature. This is the first case where metallic conduction has been observed among the complexes of PT derivatives. In this paper, we present the preliminary crystal structure, and electrical, magnetic, and optical properties of B[*b*]PT–$I_{2.5}$, and discuss the electronic structure and nature of the phase transition of this complex.

Experimental

B[*b*]PT was synthesized by the method of Van Allen et al.,[17] and purified by sublimation in vacuo (mp 291 °C, lit,[17] 278 °C). Commercially obtained iodine was also purified by sublimation.

Single crystals of B[*b*]PT–$I_{2.5}$ were prepared by diffusion method using a Y-shape tube with benzene as the solvent. The crystals were black prisms with metallic luster, having typical size of $0.5\times0.4\times1.0$ mm^3. Prior to each measurement described below, all the crystals were identified to be isostructural by X-ray photographs.

The electrical resistivity and thermoelectric power were observed over the range from 90 K to room temperature along the three crystal axes of single crystal. The resistivity along the most conductive c axis, growing direction, was measured by four-probe dc technique and those along the other two axes by two-probe technique. Carbon paint was applied as the contacts between electrodes (ϕ 30 μm gold wire) and crystal samples. In the case of thermoelectric power measurement, the electrodes were attached to two copper heat sinks, and the temperature difference between the sinks was controlled within 5 degrees.

The polarized reflection spectra were measured on the (010) crystal face for the incident light polarized parallel to the a and c axes. The measurement for the infrared region from 750 cm^{-1} to 6000 cm^{-1} was performed by using a Perkin–Elmer 1760-X FT-IR spectrometer and a Spectra-tech IR-PLAN$_{TM}$ infrared microscope. For the near-infrared and visible regions from 4500 cm^{-1} to 27500 cm^{-1}, measurements were carried out by using a Carl–Zeiss Universal microscope equipped Jobin–Yvon H-20V and H-20FIR monochromators. The spectra were calibrated for a gold evaporated mirror or a silicon crystal according to the observed regions.

EPR spectra for polycrystalline complexes were recorded over the temperature range of 4 K to 296 K using a JEOL JES-FE1XG X-band (9.1 GHz) EPR spectrometer equipped with an Air Products LTR 3-110 continuous-flow cryostat and Scientific Instrument Series 3700 digital temperature controller. Temperature was measured using a (0.07 at.% iron)-gold–chromel thermocouple, and controlled within 0.5 K. The g value was determined by comparing the resonance position with that of Mn^{2+}/MgO. The modulation width was kept much less than one-tenth of absorption line width during the measurements, in order to prevent distortion of line shape by overmodulation.

DSC for polycrystalline samples was measured from 173 K to 293 K with a Rigaku DSC-8240B at the scan speed of 1 deg min^{-1}.

Results and Discussion

Crystal Structure. The crystal data are as follows: $C_{16}H_{11}NS\cdot I_{2.5}$, F.W.=566.6, orthorhombic, *Pnmm*, a=13.976(1), b=17.824(1), c=6.434(1) Å, V=1602.7(3) Å^3,

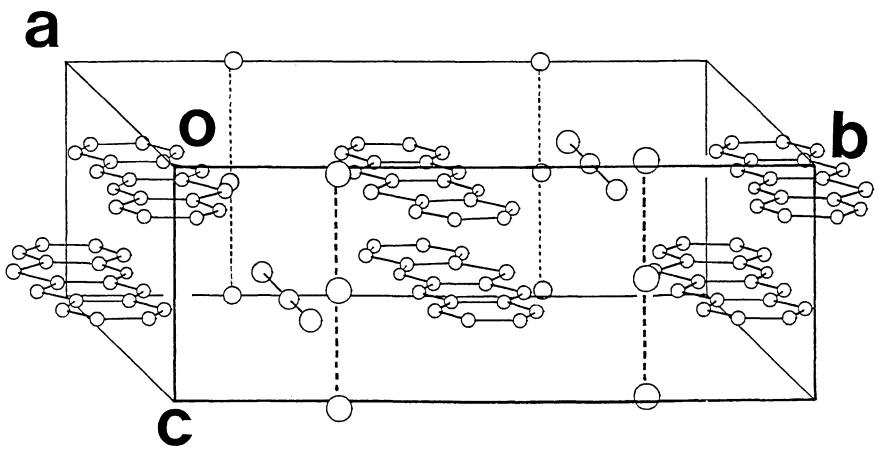

Fig. 1. The crystal structure of B[*b*]PT-$I_{2.5}$, a perspective view of the packing arrangement.

Table 1. Electrical Properties of B[*b*]PT-$I_{2.5}$

Direction	σ (300 K)/S cm^{-1}	S (300 K)/μV K^{-1}	E_a/eV
// a	3×10^{-2}	5×10^{1}	0.02
// b	2×10^{-2}	1×10^{2}	0.03
// c	3×10^{1}	3	Metallic

Z=4. At present, R=0.061 for 1133 reflections.[18] Figure 1 shows view of the crystal structure. The crystal consists of B[*b*]PT molecules, triiodide anions, and linear polyiodide chains. B[*b*]PT molecules, located on the crystallographic mirror plane [parallel to (001)], stack in face-to-face manner to form one-dimensional columns along the c axis. Spacing between B[*b*]PT planes is 3.22 Å, which is comparable with that of TTF, 3.47 Å in TTF-TCNQ.[19] There are two kinds of chemical species of iodine in this complex; one is linear I_3^- anion being parallel to the a axis, and the other is "linear polyiodide chain" being elongated along the c axis. The Fourier analysis indicates that one linear chain consists of iodine atoms arranging with almost equal intervals (3.207(6) and 3.227(6) Å, alternately).[20]

Electrical Conductivity and Seebeck Coefficient. The values of electrical transport properties of B[*b*]PT-$I_{2.5}$, summarized in Table 1, indicate that this complex is highly anisotropic and possesses one-dimensional character. Figure 2 shows temperature dependence of the electrical conductivity along the c axis. The conductivity slightly increases as temperature is lowered down to 235 K, where metal-insulator transition occurs. Below 200 K the conductivity decreases in an activated manner with a very small activation energy of E_a=0.01 eV. In the range 300—250 K, the Seebeck coefficient linearly falls with decreasing temperature and its extrapolation approaches zero at 0 K, as illustrated in Fig. 3. These

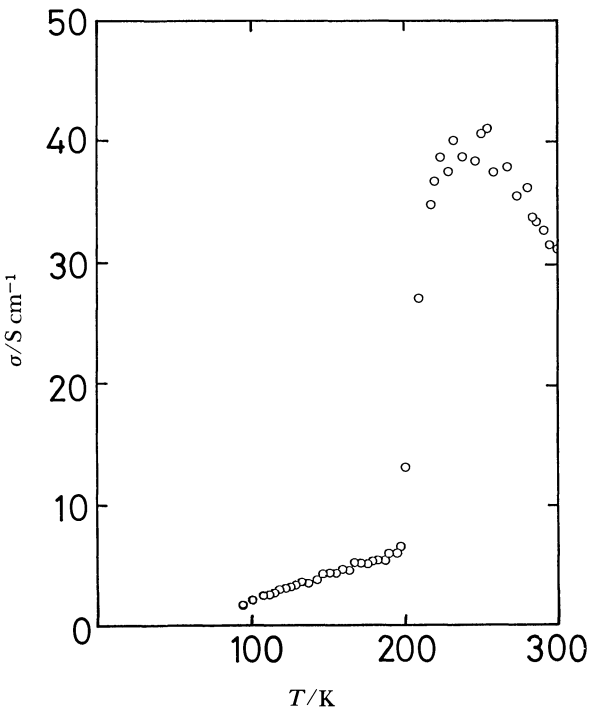

Fig. 2. Temperature dependence of electric conductivity of a single crystal of B[*b*]PT-$I_{2.5}$ measured along its c axis.

results mean that B[*b*]PT-$I_{2.5}$ is in metallic state above 250 K. The positive values of Seebeck coefficient so far measured, suggest that the B[*b*]PT stacks are more conductive than the polyiodide chains.

Polarized Reflection Spectra. Figure 4 shows the polarized reflection spectra of B[*b*]PT-$I_{2.5}$ at room temperature. The long-axes of both B[*b*]PT molecule and triiodide anion are parallel to the crystal a axis, as stated above, and the stacking direction of B[*b*]PT molecules and the linear chain direction of poly-

iodides are both parallel to the most conductive c axis. When the light polarization is parallel to the a axis, two sharp dispersions appear at 14500 and 25000 cm^{-1}. The former band (14500 cm^{-1}) can be assigned to the molecular excitation of B[*b*]PT cation radical polarized to the long axis of the molecule, as the band is also observed in the absorption spectrum of B[*b*]PT cation radical prepared by the electrochemical oxidation of B[*b*]PT in an acetonitrile solution.[21] The dispersion at 25000 cm^{-1} is safely assigned to the low-lying σ_g–σ_u* transition of triiodide anion.[22] When the incident light polarized parallel to the c axis, a plasma-edge-like dispersion appears in the near infrared region. So, it is confirmed that B[*b*]PT-$I_{2.5}$ is in metallic state at room temperature, as being in good agreement with the electrical measurements. In addition to this plasma-edge-like dispersion, a strong dispersion around 16000 cm^{-1} is observed in the //c spectrum. Since the polarization direction of this dispersion is parallel to the stacking direction of B[*b*]PT and/or polyiodide chain, the dispersion can be interpreted as the charge-transfer transition between iodide ions within the chain. Moreover, since the wavenumber of this band is lower than that of the isolated triiodide anion observed in the //a spectrum, the polyiodide would possess more stable electronic state than that of the isolated triiodide.

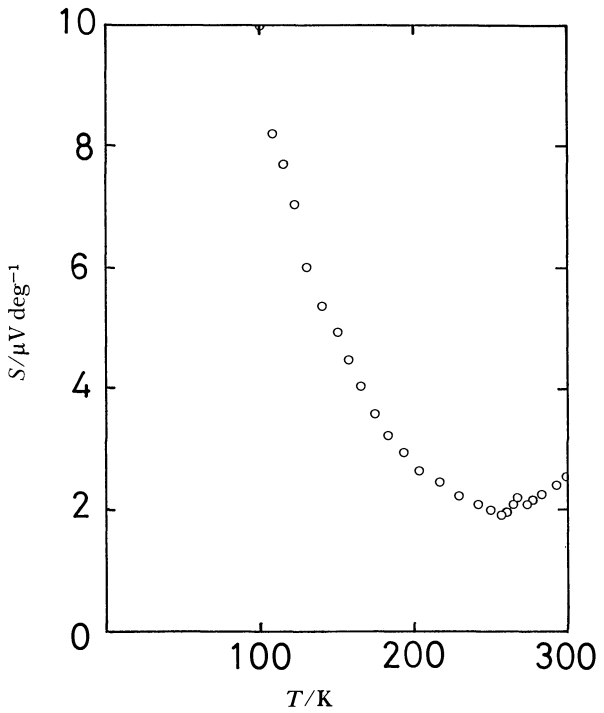

Fig. 3. Temperature dependence of Seebeck coefficient of a single crystal of B[*b*]PT-$I_{2.5}$ measured along its c axis.

Next, we have employed Drude-Lorentz model to analyze the //c spectrum assuming Lorentz oscillator around 16000 cm^{-1}. This procedure consists of the following dielectric function;

$$\varepsilon(\omega) = \varepsilon_{core} - \frac{\omega_p^2}{\omega(\omega + i\tau)} - \frac{f_1}{\omega(\omega + i\tau_1) - \omega_1^2}, \quad (1)$$

where ω_p is the plasma frequency, f_1 is the oscillator strength, ε_{core} is the residual dielectric constant at high frequency, and τ and τ_1 are the relaxation time of carriers and the oscillator, respectively. For the analysis of the //c spectrum, we adopted only the reflectance spectrum from 1900 to 27500 cm^{-1}, since the reflectance spectrum of the region lower than 1900 cm^{-1} would be influenced by intramolecular

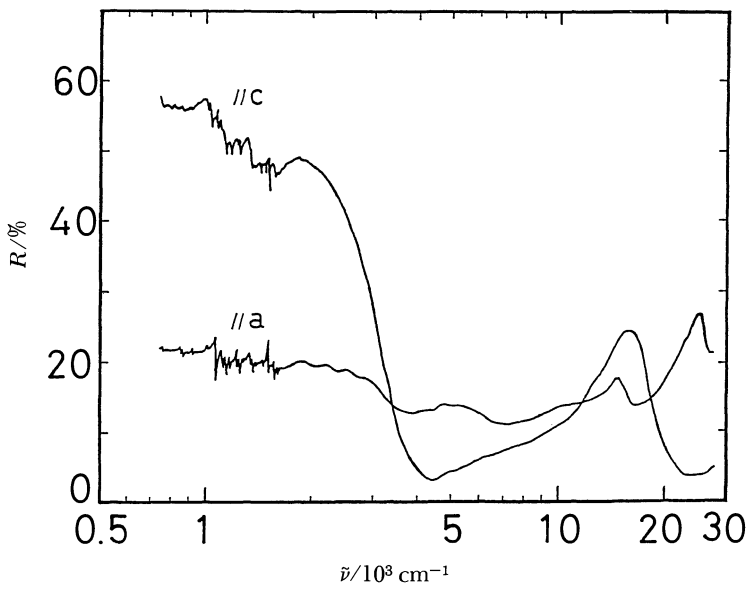

Fig. 4. Polarized reflection spectra of B[*b*]PT-$I_{2.5}$.

vibration of B[*b*]PT and/or coupling up the vibration to conduction electron. By assuming a tight-binding band, the experimentally evaluated parameter ω_p may be related to the tight-binding band width 4t by the equation.

$$\omega_p^2 = \frac{16tNe^2d^2 \sin(\pi\rho/2)}{h^2}, \quad (2)$$

where N is the number density of molecules, ρ is the number of carriers per molecule, and d is the molecular period along the polarization direction of incident light. ω_p may also be related to the optical effective mass m^* and optical conductivity at zero frequency $\sigma_{opt}(0)$ by the following equations,

$$\omega_p^2 = \frac{4\pi ne^2}{m^*} = \frac{4\pi\sigma_{opt}(0)}{\tau}, \quad (3)$$

where n is the number density of free carriers. For the tight-binding band, the Fermi velocity V_F and the mean free path Λ are derived from $4t$ and τ by the equations,

$$V_F = \frac{2td}{h}, \qquad \Lambda = V_F\tau. \quad (4)$$

By using the values N=2.50×10^{21} cm^{-3}, d=3.22 Å, and ρ=0.5, assumed that there are equal numbers of neutral and cation radical B[*b*]PT molecules in the crystal, the transport parameters are calculated from these equations by the analysis of the //c spectrum. They are summarized in Table 2 with the corresponding data of (perylene)$_2$(PF$_6$)$_{1.1}$·0.8CH$_2$Cl$_2$[23] and TTF-TCNQ[24-26]. B[*b*]PT-I$_{2.5}$ represents intermediate values of ω_p and 4t between those of them, and it suggests that B[*b*]PT-I$_{2.5}$ has intermediate property between them.

EPR Measurement. It was observed that the EPR spectra of B[*b*]PT-I$_{2.5}$ consisted of only one signal, and its shape was slightly asymmetric Lorentzian under all the observed temperature range from 4 K to 296 K. At room temperature the observed peak-to-peak linewidth ΔB, 250 G (1 G=10^{-4} T), is rather broad as an aromatic cation radical including sulfur.[27-29] The *g*-value was found to be 1.998±0.002, being slightly smaller than that of free electron. Both values imply that there is an interaction between the radical electron on B[*b*]PT cation radical and iodine atoms, because the latter has a large spin-orbit coupling constant. Magnetic susceptibilities obtained from the EPR intensity is 1×10^{-4} emu mol^{-1} at 296 K. Figure 5 illustrates the temperature dependence of the magnetic susceptibility. Below 50 K the susceptibility nearly follows Curie's low, and above this temperature it behaves in an activated manner with a slight change around 235 K. Since this temperature agrees with that of metal-insulator transition observed in the electrical measurement, it is suggested that the magnetic property of this complex also changes around 235 K. Judging from no discontinuous change in the temperature dependence of susceptibility around this temperature, the metal-insulator transition would not be a first-order phase transition. In the very low temperature region, the observed susceptibility was assumed to come from paramagnetic impurities, the contribution of which was estimated ($C=\chi/T$, C=17 emu mol^{-1}) and shown by solid line in Fig. 5. Deducting this contribution from observed susceptibilities, the activation energy was found to be 0.06±0.02 eV. The peak-to-peak linewidth ΔB increases approximately linearly with temperature up to 300 K, as shown in

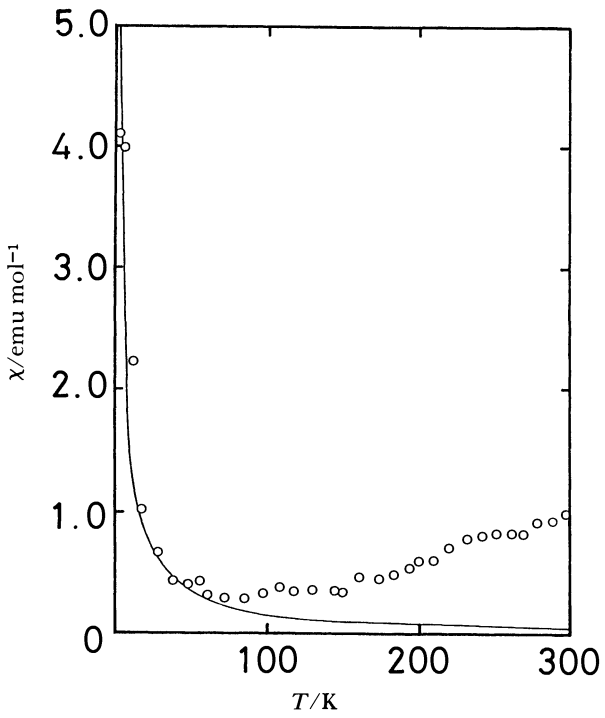

Fig. 5. Temperature dependence of magnetic susceptibility of B[*b*]PT-I$_{2.5}$.

Table 2. Transport Parameters Obtained from the Analysis of the Reflectance Data

Compound	$\omega_P/2\pi$	τ	n	m^*/m_e	$4t$	Λ	$\sigma_{opt}(0)$
	cm^{-1}	10^{-15} s	10^{21} cm^{-3}		eV	Å	S cm^{-1}
(Pe)$_2$(PF$_6$)$_{1.1}$·0.8CH$_2$Cl$_2$	(7400)	4.4	1.42	0.91	1.1		1900
B[*b*]PT-I$_{2.5}$	7720	2.9	1.25	1.9	0.87	4.3	550
TTF-TCNQ	9500	4	2.8	3	0.43		1200

The value derived from their data is given in parentheses.

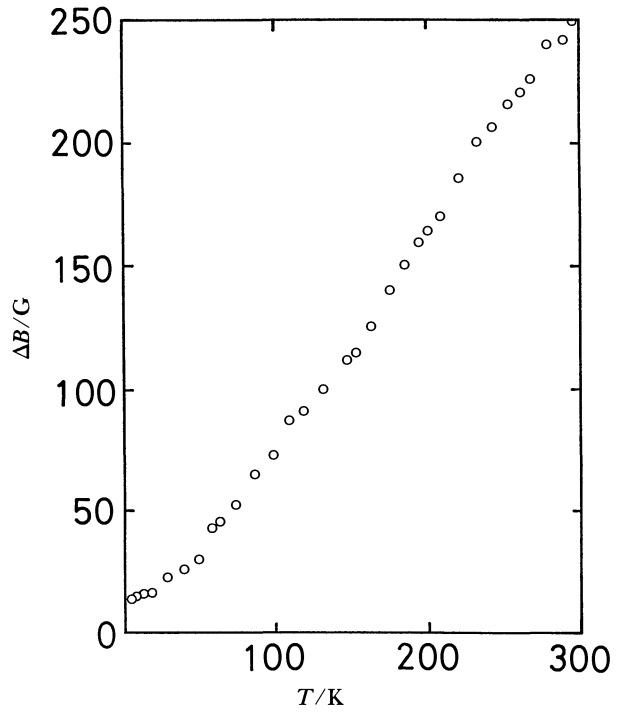

Fig. 6. The EPR peak-to-peak line width vs. temperature observed about B[*b*]PT-$I_{2.5}$.

Fig. 6, although a slight change in slope appears around 235 K. This temperature corresponds to that observed when the temperature dependence of the susceptibility was measured.

DSC Measurement. DSC measurements showed neither endothermic nor exothermic peak around 235 K. Therefore, it was found that the metal-insulator transition observed in the measurement of electrical properties was not first-order transition with latent heat.

Summary and Conclusions

B[*b*]PT-$I_{2.5}$ exhibits a metallic state in the high temperature phase, but has electrical and magnetic activation energies in the low temperature phase. The transition temperature was observed around 235 K. However, no discontinuous change of the magnetic susceptibility and the EPR linewidth, and no latent heat on DSC measurements were observed around the transition temperature. These facts would imply that the transition is attributed to the Peierls-type transition around 235 K. The electronic state of B[*b*]PT would be a mixed state of cation radical and neutral one. However, a quantitative estimation of this mixed state is hardly established, since the information about electronic state of the linear polyiodide chain is insufficient at this stage.

The authors express their hearty thanks to Dr. Koichi Nishikida of Perkin-Elmer Japan for the measurement of polarized reflection spectra in the infrared region.

References

1) R. Pummerer and S. Gassner, *Ber.*, **6**, 2310 (1913).
2) F. Kehrmann and L. Diserens, *Ber.*, **48**, 318 (1915).
3) Y. Matsunaga, *Helv. Phys. Acta*, **36**, 800 (1963).
4) Y. Matsunaga, *Nippon Kagaku Zasshi*, **89**, 905 (1968).
5) Y. Matsunaga and K. Shono, *Bull. Chem. Soc. Jpn.*, **43**, 2007 (1970).
6) M. Sano, K. Ohno, and H. Akamatu, *Bull. Chem. Soc. Jpn.*, **44**, 3269 (1971).
7) K. Kan and Y. Matsunaga, *Bull. Chem. Soc. Jpn.*, **45**, 2096 (1972).
8) Y. Matsunaga and Y. Suzuki, *Bull. Chem. Soc. Jpn.*, **45**, 3375 (1972).
9) Y. Matsunaga and Y. Suzuki, *Bull. Chem. Soc. Jpn.*, **46**, 719 (1973).
10) Y. Matsunaga, Energy Charge Transfer Org. Semicond., Proc. U.S.-Jpn. Semin., 1973, Abstr. (Pub. 1974), 189.
11) G. Dix, *Phys. Status Solidi A*, **24**, 139 (1974).
12) A. Kehl and H. W. Helberg, *Phys. Status Solidi A*, **27**, 509 (1975).
13) S. Doi, T. Inabe, and Y. Matsunaga, *Bull. Chem. Soc. Jpn.*, **50**, 837 (1977).
14) T. Matsumoto and Y. Matsunaga, *Bull. Chem. Soc. Jpn.*, **54**, 648 (1981).
15) A. T. Oza, *Mol. Cryst. Liq. Cryst.*, **104**, 377 (1984).
16) H. Kobayashi, private communication.
17) J. A. Van Allan, G. A. Reynolds, and R. E. Adel, *J. Org. Chem.*, **27**, 1659 (1962).
18) The precise structural report will be published separately, since there still exists an insoluble problem about disorder of "linear polyiodide chain", mentioned in the text. Nevertheless, the crystal structure, cited here, is essentially correct.
19) T. J. Kistenmacher, T. E. Phillips, and D. O. Cowan, *Acta Crystallogr., Sect. B*, **30**, 763 (1974).
20) The oscillation photographs along the c axis displayed very weak diffuse streaks with incommensurate with Bragg lattice. However, The spacings of them could not be assigned directly to the presence of the iodine species such as I_2, I^-, I_3^-, or I_5^-.
21) N. Urasaki and T. Uchida, unpublished result.
22) M. Mizuno, J. Tanaka, and I. Harada, *J. Phys. Chem.*, **85**, 1789 (1981).
23) H. P. Geserich, R. Wilckens, W. Ruppel, V. Enkelmann, G. Wegner, G. Wieners, D. Schweitzer, and H. J. Keller, *Mol. Cryst. Liq. Cryst.*, **93**, 385 (1983).
24) D. B. Tanner, C. S. Jacobsen, A. F. Garito, and A. J. Heeger, *Phys. Rev. B*, **13**, 3381 (1976).
25) C. S. Jacobsen, "Quasi One-Dimensional Conductors I," ed by S. Barisic et al., Springer Verlag, Berlin (1979), p. 223.
26) A. A. Bright, A. F. Garito, and A. J. Heeger, *Solid State Commun.*, **13**, 943 (1973).
27) Y. Tomkiewicz, B. A. Scott, L. J. Tao, and R. S. Title, *Phys. Rev. Lett.*, **32**, 1363 (1974).
28) T. Sugano, G. Saito, and M. Kinoshita, *Phys. Rev. B*, **34**, 117 (1986).
29) T. Sugano, G. Saito, and M. Kinoshita, *Phys. Rev. B*, **35**, 6554 (1987).

Photoreduction and Emission of Solid Europium(III) Chloride in KBr by Laser Irradiation at 308 nm

Yasuhiro YAMADA* and Shin-ichi OHNO
Department of Chemistry, Japan Atomic Energy Research Institute,
Tokai-mura, Naka-gun, Ibaraki 319-11
(Received September 7, 1990)

The emission and transient absorption spectra of solid europium irradiated with laser light at 308 nm were measured. $EuCl_3 \cdot 6H_2O$ in a KBr disk was photoreduced to form excited Eu^{2+}, and the emission from excited Eu^{2+} was observed directly after a reduction of Eu^{3+}. Since Eu^{2+} was not stabilized in the KBr disk sample, it oxidized rapidly to form Eu^{3+}. From a discussion concerning the temperature dependence of the rate constants of the reduction and deexcitation, it is shown that the reduction rate increases at higher temperature.

We studied the lifetimes of the excited states of the f-f transitions and photochemical reactions of lanthanide compounds induced by f-d or charge transfer transitions in order to investigate element selective photochemical reactions of lanthanide elements by multiphotoexcitation of f-f transitions. The lanthanide elements have complicated optical spectra because of the 4f shell; their absorption and fluorescence properties have been studied by many workers.[1,2] Europium has unique properties in that it is exceptionally stable in the divalent state (besides the trivalent state), while most lanthanide elements are stable only in the trivalent state in solution.

The photochemical separation of lanthanide elements in solution has been studied by some workers. Since most of the lanthanide elements are stable in the trivalent state in a solution system, separation is initiated by stabilizing divalent lanthanides in solution. Eu^{2+} produced by photoreduction is stabilized using either SO_4^{2-}[3] or 18-crown-6 ether[4] for the separation.

The optical absorption, emission and Zeeman splittings have been studied for Eu^{2+} substituted in NaCl, KCl, and KBr crystals.[5,6] Divalent europium was prepared by chemical reduction, and was then doped in alkali halide crystals.

We report here on laser irradiation (308 nm) of solid trivalent europium chloride $EuCl_3 \cdot 6H_2O$ in KBr which was used to investigate the photoreduction of Eu^{3+} in a solid system and discuss the emission of Eu^{2+}. This emission from Eu^{2+} in a solid sample may be a useful method to detect two-step excitation through f-f levels.

Experimental

We employed the XeCl excimer-laser (Lambda Physik EMG201MSC) for the irradiation of ultra-violet light at 308 nm (output energy: 400 mJ $pulse^{-1}$, pulse width: 20 ns). The emissions at the desired delayed time after laser pulse irradiation were measured by a diode array multichannel detector (Princeton Instruments SMA) with a 120 nm wavelength width and a 50 ns detection time width. These signals were integrated several hundred times in order to obtain a time-resolved emission spectrum. We also employed a photomultiplier (Hamamatu R928), a monochromator (ISA HR-320) and a fast transient digitizer (Tektronix 7912HB) to detect a single emission signal at the wavelength induced by pulse irradiation.

For the detection of the transient absorption, the probe light from a pulsed high-pressure xenon flash lamp (Tokyo Instruments XF-150) traversed the sample at right angles to the excitation laser light. The transient absorbance at various wavelengths was measured with a photomultiplier placed in the analyzing beam behind the sample disk. In order to eliminate the emission of a sample by laser irradiation, the emission signal obtained without probing light was subtracted from the observed signal of the transmitted probe light with laser irradiation. The transient absorbance was calculated from this signal and the reference signal of probe light without laser irradiation. We employed a spectrometer (JASCO Ubest-30) to measure the standard UV-visible absorption spectra.

As a sample disk, $EuCl_3 \cdot 6H_2O$ was ground and mixed with KBr, and then pressed to form a 1 cm diameter disk. Thick samples ($EuCl_3 \cdot 6H_2O$:0.04 g, KBr:0.10 g) for emission measurements and thin samples ($EuCl_3 \cdot 6H_2O$:0.005 g, KBr: 0.10 g) used to transmit probe light for absorption measurements were employed. The laser light was slightly focussed by a convex lens (f=150 mm) and laser spot at the sample disk was 0.1 cm^2.

Results and Discussion

The time-resolved emission spectra induced by 308 nm irradiation was observed by an SMA detector (Figs. 1 and 2), accumulating the signals for 300 pulses for each spectrum. The change in the intensity of these signals at a wavelength were fitted by a single exponential curve in order to obtain the emission lifetimes. $EuCl_3$ has a broad absorption band assigned to either f-d or a charge-transfer band in the ultraviolet region. Upon irradiation of 308 nm light, a broad absorption band was excited, followed by deexcitation to a lower f-f transition level; sharp emissions from Eu^{3+} (assigned to the f-f transition) were observed (Fig. 1). These spectra were consistent with the emissions observed after a direct excitation of the f-f transition of Eu^{3+} ($^7F_0 \rightarrow {}^5D_2$) at 465 nm. The lifetimes of these transition, $^5D_1 \rightarrow {}^7F_j$ and $^5D_0 \rightarrow {}^7F_j$, are 6.9 and 120 μs,

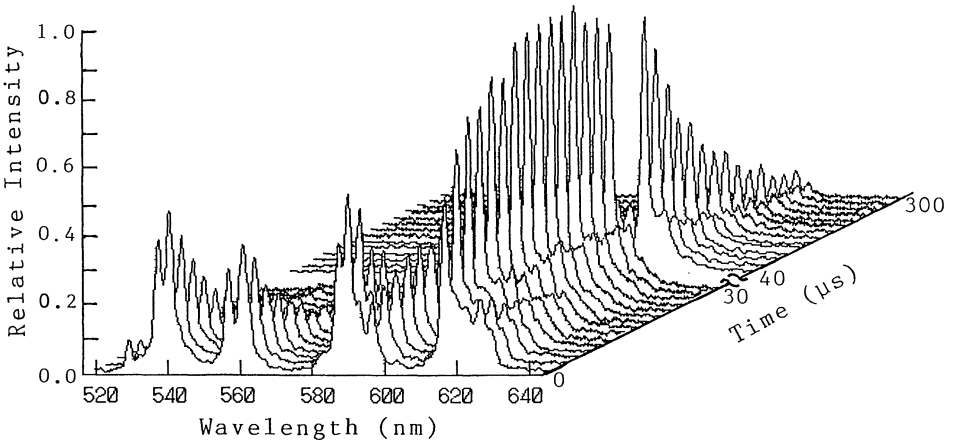

Fig. 1. The time-resolved emission spectra assigned to f-f transitions ($^5D_1$, $^5D_0 \rightarrow {}^7F_j$) of $EuCl_3 \cdot 6H_3O$ in KBr disk irradiated by 308 nm laser light.

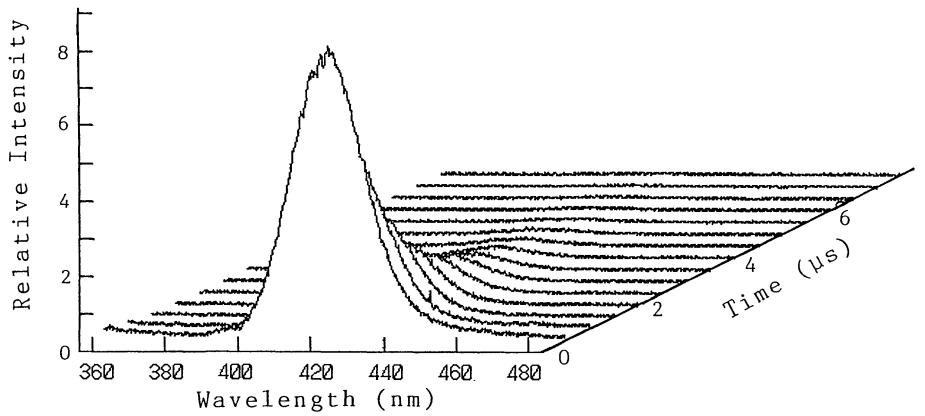

Fig. 2. The time-resolved emission spectra assigned to transition in Eu^{2+} ($4f^65d \rightarrow 4f^7$) by irradiating $EuCl_3 \cdot 6H_3O$ in KBr disk with 308 nm laser light.

respectively, and are the same as those obtained from 465 nm excitation. Besides the emission from f-f transitions, a broad intense emission band at 420 nm assigned to the transition of Eu^{2+} ($4f^65d \rightarrow 4f^7$) was observed (Fig. 2). The measured lifetime from this time-resolved emission spectra was 1.0 μs. When a disk sample of pure $EuCl_3 \cdot 6H_2O$ without KBr was irradiated by 308 nm laser light, the emissions due to the f-f transitions of Eu^{3+} were merely observed and the emission at 420 nm from Eu^{2+} was not observed. It thus seems that the KBr matrix temporarily donates an electrons to reduce $EuCl_3 \cdot 6H_2O$ in the KBr disk upon laser irradiation, and that the absorbed photon energy is transferred for both the reduction and fluorescence of the f-f transitions.

The standard absorption spectra of the disk sample was measured both before and after photoirradiation, and no change due to the production of Eu^{2+} was observed. Thus, photoreduced Eu^{2+} may not be stabilized in a KBr disk sample for a long time (the measuring time was shorter than 3 min). Also, the intensity of 420 nm emission during pulse-irradiation did not change, measured by accumulating the number of pulse-irradiations with a photomultiplier. Thus, photoreduced Eu^{2+} was not integrated but was oxidized to form Eu^{3+} rapidly, since electrons might not disperse or stabilize in a solid system. The reduction of Eu^{3+} and emission from Eu^{2+} was observed in a single 20 ns pulse.

The transient absorbance of Eu^{2+} produced by photoreduction was observed by a photomultiplier and transient digitizer at some wavelengths at room temperature (Fig. 3). The lifetimes of these signals were (1.0±0.2) μs, the same as for emission from Eu^{2+} at 420 nm. The produced Eu^{2+} may therefore be oxidized rapidly after deexcitation to the ground state. The intensity spectrum of this transient absorption signal is demonstrated in Fig. 4. This absorption spectrum corresponds to the absorption spectrum of Eu^{2+} given in the literature;[5,6] absorption was

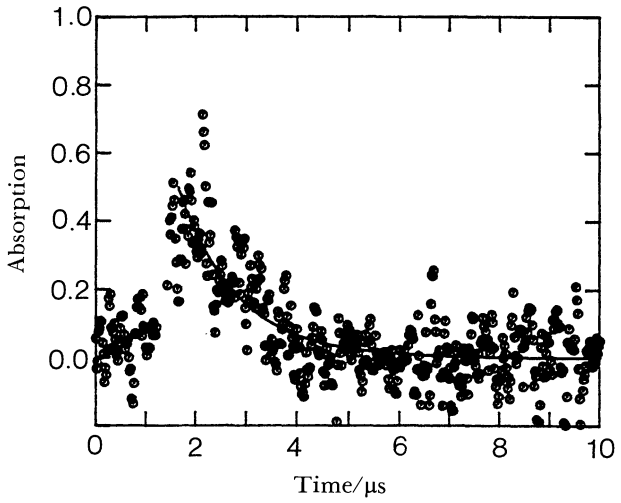

Fig. 3. The transient absorption at 340 nm of $EuCl_3 \cdot 6H_3O$ in KBr disk irradiated by 308 nm laser light.

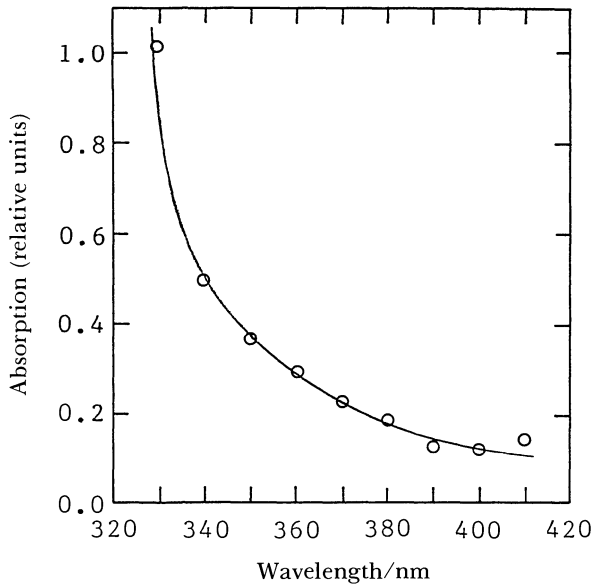

Fig. 4. The trasient absorption spectrum of $EuCl_3 \cdot 6H_2O$ in KBr disk irradiated by 308 nm laser light.

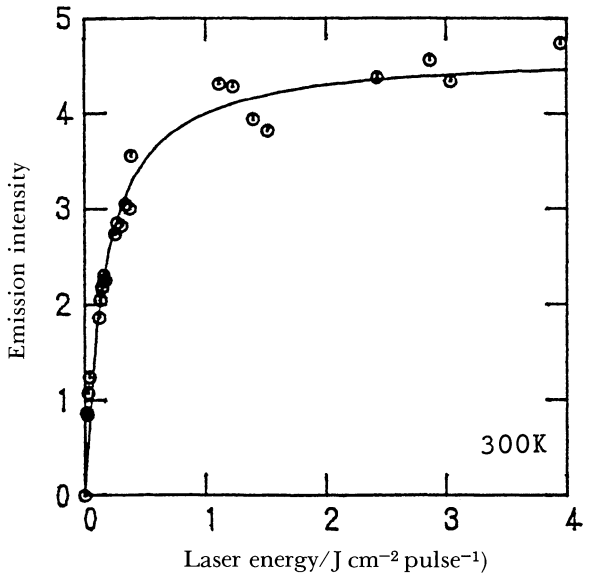

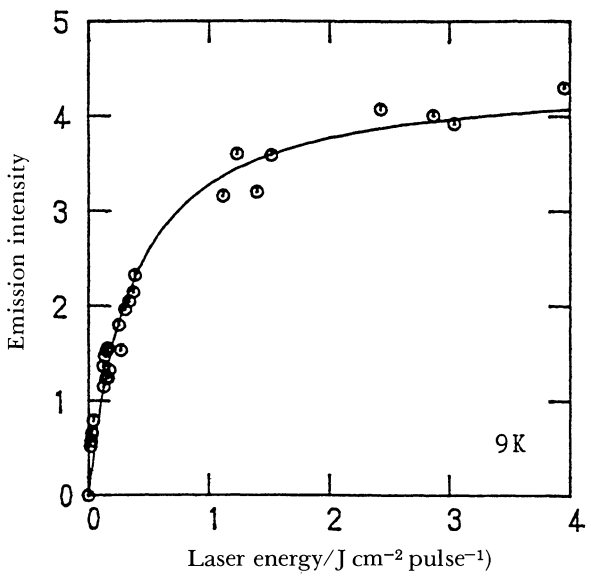

Fig. 5. The emission intensity at 420 nm and the irradiating laser energy (308 nm) of $EuCl_3 \cdot 6H_2O$ in KBr disk at 300 K and 9 K.

observed at shorter wavelengths than 410 nm, having maximum near 320 nm.

The production mechanism of excited Eu^{2+} that radiates fluorescence at 420 nm may estimated in two ways: 1) the excited Eu^{2+} is produced directly after the photoreduction of Eu^{3+} or 2) the ground state of Eu^{2+} produced by the photoreduction of Eu^{3+} is further excited. To examine which process actually takes place, we observed the relation between the laser energy and the emission intensity. The laser energy was varied by means of beam splitters and the emissions at 420 nm were detected by a photomultiplier at various laser intensities and temperatures. From the relationship between the laser energy and the emission intensity of Eu^{2+} (Fig. 5), the number of photons that induce emission from Eu^{2+} could be determined. From Fig. 5 a linear relation between the laser energy and the emission intensity of Eu^{2+} was observed at a lower laser energy, less than 0.5 J cm^{-2}-$pulse^{-1}$. Therefore, the reduction of Eu^{3+} and the emission of Eu^{2+} were induced by one photon absorption. At higher laser energy, the emission intensity saturates because of the rate constants of excitation and that deexcitations of Eu^{3+} become parallel.

To understand the relationship between the laser energy and the emission intensity of Eu^{2+}, we assumed

a simplified energy diagram of reactions and emissions of this system, as demonstrated in Fig. 6. The levels are designated as follows: Level 1 is the ground state of Eu^{3+}; 2 is the excited f-d or charge-transfer state of Eu^{3+}; 3 is the fluorescence level of Eu^{3+}; 5 is the excited and fluorescence level of Eu^{2+}, assigned to $4f^65d$; and 4 is the ground state of Eu^{2+}, assigned to $4f^7$.

The mathematical treatment of the kinetics is simplified by assuming the existence of a steady state, as discussed by Maiman.[7] The transition probabilities are also indicated in Fig. 6: I is the irradiation laser energy; σ is the absorption cross section of Eu^{3+}; k_{21} is the radiationless deexcitation probability; k_{23} and k_{31} are the transition probabilities for radiationless and radiative deexcitation in Eu^{3+} transitions; k_{25} is the transition probability for reduction to the excited level of Eu^{2+} ($4f^65d$); k_{54} is the transition probability for the fluorescence of the excited level to the ground level of Eu^{2+}; and k_{41} is the transition probability of oxidation from the ground level of Eu^{2+} to Eu^{3+}. The real energetic scheme of f-f transition in Eu^{3+} may be complicated by many levels of f-f transitions: level 3, k_{23}, k_{31}, and k_{21} should separated into some components to illustrate actual emission spectra of f-f transition in Eu^{3+}. In order to discuss the emission of Eu^{2+} we simplified the f-f transitions, as shown in Fig. 6.

In terms of this model, the steady-state rate equations are:

$$dN_2/dt=I\sigma N_1-(k_{21}+k_{23}+k_{25})N_2=0,$$
$$dN_3/dt=k_{23}N_2-k_{31}N_3=0,$$
$$dN_4/dt=k_{54}N_5-k_{41}N_4=0,$$
$$dN_5/dt=k_{25}N_2-k_{54}N_5=0,$$

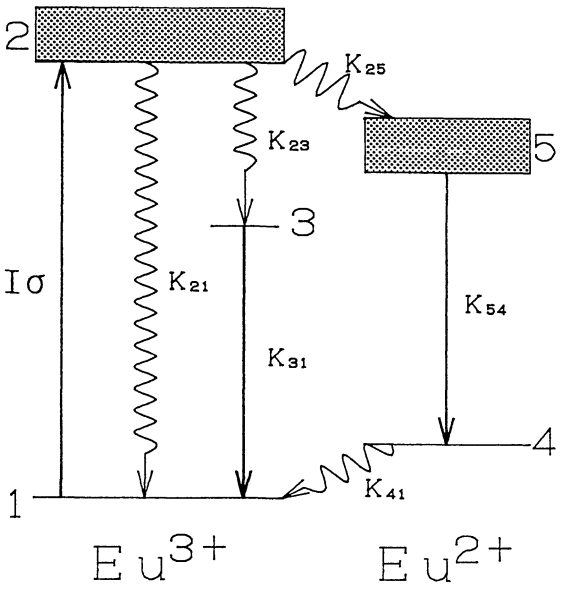

Fig. 6. The energy diagram of the system.

and

$$N_0=N_1+N_2+N_3+N_4+N_5,$$

where N_i is the population of the ith state and N_0 is the total concentration.

I and N_5 correspond to the laser energy and the emission intensity of Eu^{2+}, respectively. The steady-state solution to this set of equations is given by

$$N_5=(k_{25}N_0/(k_{54}A))/(k_2/(A\sigma I)+1),$$

where $k_2=k_{21}+k_{23}+k_{25}$ and $A=1+k_{23}/k_{31}+k_{23}/k_{41}+k_{25}/k_{54}$. The observed data were fitted by a computer least-square method which varied two parameters: $a=k_{25}N_0/(k_{54}A)$ and $b=k_2/(A\sigma)$. Here, a represents the emission intensity at the saturated region, and b represents the gradient of the curve at the region in which the emission intensity and laser energy have a linear relationship. The fitted curves are also indicated in Fig. 5; this model explains these data very well.

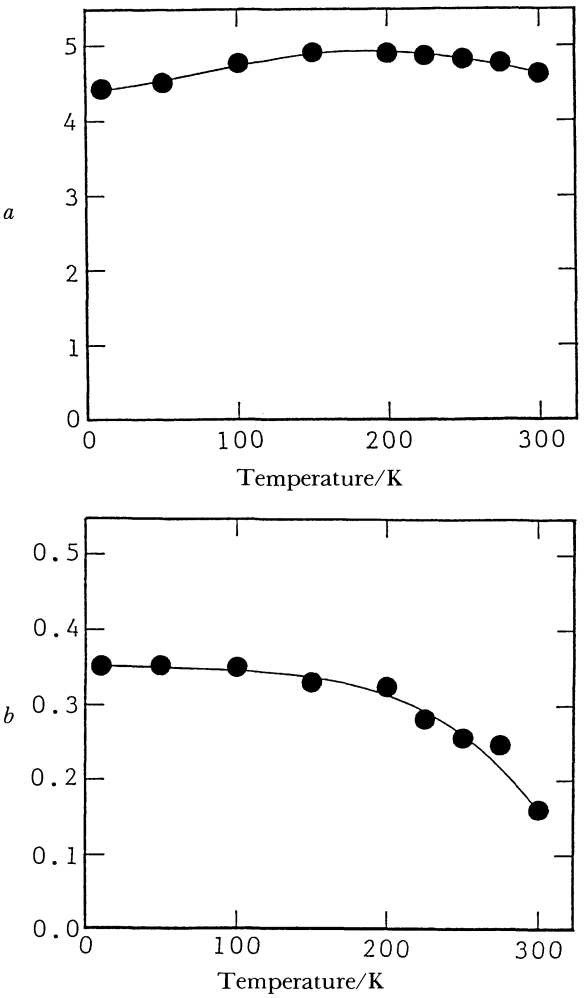

Fig. 7. The a and b obtained by fitting of the relation between the emission intensity at 420 nm and the laser energy of various temperature.

This relation was observed in various temperatures from 300 K to 9 K and the spectrum at each temperature was fitted by the formula. The lifetime of this emission at 420 nm was (1.0±0.2) μs and was independent of both the excitation intensity and temperature. The rate constants of the reduction or some transitions may be influenced by the temperature, and the relation between irradiation intensity and emission intensity may change upon varying the temperature. The obtained a and b in the temperature range 9 K to 300 K are given in Fig. 7. While a has little temperature dependence, b become smaller at higher temperature.

Considering the value k_{54} (10^6 s^{-1}), N_0 and σ are constant and independent of the temperature; the value $a/b=k_{25}N_0\sigma/(k_2k_{54})$ indicates the k_{25}/k_2 which corresponds to the rate of reduction to the total deexcitation process in excited Eu^{3+}. Though the absolute value could not be obtained from this measurement, the relative rate was obtained. From the temperature dependence of a/b, the probability to reduce excited Eu^{3+} became larger at higher temperatures.

References

1) K. A. Gschneidner, Jr. and L. Eyring, "Handbook on the Physics and Chemistry of Rare Earths," North-Holland Publishing Company, Amsterdam (1979), p. 171.
2) F. S. Richardson, *Chem. Rev.*, **82**, 541 (1982).
3) T. Donohue, *J. Chem. Phys.*, **67**, 5402 (1977).
4) T. Donohue, *Chem. Biochem. Appl. Lasers*, **5**, 239 (1980).
5) R. Reisfeld and A. Glasner, *J. Opt. Soc. Am.*, **54**, 331 (1964).
6) J. Hernandez A., W. K. Cory, and J. Rubio O., *J. Chem. Phys.*, **72**, 198 (1980).
7) T. H. Maiman, *Phys. Rev.*, **123**, 1145 (1961).

 © 1991 The Chemical Society of Japan Bull. Chem. Soc. Jpn., 64, 931—937 (1991)

Pressure Effect on Proton Jumps in *t*-Butyl Alcohol–Water Mixtures at 25 °C

Masakatsu Ueno,* Kazuhito Matsukawa, Noriaki Tsuchihashi, and Kiyoshi Shimizu
Department of Applied Chemistry, Faculty of Engineering, Doshisha University,
Karasuma Imadegawa, Kamigyo-ku, Kyoto 602
(Received September 7, 1990)

The limiting molar conductances, $\Lambda°$, of hydrochloric acid and potassium chloride in 2,3,5,7,10, and 25 mol% *t*-butyl alcohol (TBA)–water mixtures were determined at 25 °C as a function of the pressure up to 2000 kgf cm^{-2} (1 kgf cm^{-2}=0.9807×10^5 Pa) from the conductances measured within a dilute concentration range. In each solvent mixture the value of $\Lambda°$(HCl) was about three- to five-times larger than that of $\Lambda°$(KCl). The anomalous excess proton conductance, $\lambda°_E$, as estimated by the equation [$\lambda°_E=\Lambda°(HCl)-\Lambda°(KCl)$], was found to increase with increasing pressure in 2,3,5,and 7 mol% TBA–water mixtures, but to decrease in 10 and 25 mol% TBA–water mixtures. The rate of increase with pressure of the excess proton conductance normalized to the molar concentration of water in the mixture was largest in a 2 mol% TBA mixture, and its magnitude decreased in the order: 2>3>0>5≫7≫10≫25 mol% of TBA. These results are compared with those obtained in ethanol–water mixtures and are discussed in relation to the effect of alcohol molecules on the water structure in the mixtures: the three-dimensional network of water in TBA–water mixtures is more stable at a lower mol% of alcohol, and collapses more rapidly with increasing alcohol content than in ethanol–water mixtures.

The proton is much more useful than any other ion for dynamic studies of the structure of water; this is because the reorientation of water molecules has been considered to be the rate-determining step in the proton-jump mechanism.[1,2] The structure of water is dominated by the directional attractive intermolecular potential and is sensitive to any change in the pressure and/or temperature. An X-ray study on the effect of pressure on the structures of both light and heavy water,[3] as well as molecular dynamic simulation studies on liquid water under high compression,[4–6] shows that the hydrogen bonds in water become distorted at high pressure. The distortion of hydrogen bonds accelerates the rotation of water molecules. In accordance with the pressure effect on the reorientation of water molecules,[7,8] the excess proton conductance, $\lambda°_E$, due to proton jumping increases with increasing pressure; the rate of increasing $\lambda°_E$ with pressure becomes more prominent at lower temperature.[9] That is, the more significant is the water structure at atmospheric pressure, the larger is the pressure effect on $\lambda°_E$.[2] In a previous study,[10] this relation was tested in ethanol–water mixtures; it has been confirmed that a small addition of ethanol to water stabilizes the three-dimensional network of water. In the present work we extend this to *t*-butyl alcohol (TBA)–water mixtures.

The thermodynamic properties of TBA–water mixtures have been studied in order to elucidate the nature of hydrophobic hydration; thermodynamic data indicate that TBA is one of the most powerful structure makers in the water-rich region.[11–14] In addition to the unique effect of TBA molecules on the structure of water, the self-association of TBA molecules in water has been suggested to account for the following phenomena: an excess heat capacity maximum,[15] a large ultrasonic absorption,[16] a remarkable increase in light scattering,[17] and anomalies in the reaction rate[18,19] in TBA–water mixtures in a composition range of 3—5 mol% of TBA. Computer experiments have also shown the promotion of the water structure and the self-association of TBA molecules due to a hydrophobic interaction in a 3 mol% TBA–water mixture.[20] Therefore, it is considered that the water structure in these mixtures changes drastically in the dilute solution region. It was the purpose of the present study to examine whether the pressure dependence of the excess proton conductance sensitively reflects the above-mentioned anomalies or not, and whether excess proton conductance is a good measure of the structure of water.

Experimental

Conductivity water was prepared by passing distilled water through an ion-exchange resin; its conductivity was about 1.0×10^{-6} S cm^{-1} at 25 °C and 1 atm. *t*-Butyl alcohol (TBA) of guaranteed reagent obtained from Nacalai Tesque was used without further purification, and showed a water content of less than 0.2 wt% in the Karl Fischer test (MK-AII type, Kyoto Electronics MFG Co., Ltd.). Hydrochloric acid and potassium chloride of high quality were supplied from Merck. The latter was dried above 130 °C prior to use. Aqueous stock solutions of KCl [2×10^{-2} M (1 M=1 mol dm^{-3})] were made up using measuring flasks; those of HCl (ca. 1×10^{-2} M) were prepared by diluting concentrated HCl with conductivity water. Accurate concentrations of HCl stock solutions were determined by measuring the conductances of the solutions and by using the empirical equation of conductance for a HCl solution proposed by Shedlovsky.[21] All of the dilute solutions of HCl and KCl were prepared gravimetrically by diluting stock solutions of HCl and KCl with conductivity water and TBA. The concentrations of the dilute solutions at each pressure were determined by using the densities of the aqueous stock solutions at atmospheric pressure and those of the dilute solutions at each pressure, as

described below. The densities of the stock solutions were calculated for HCl using Eq. 1 in Ref. 10 and for KCl using Eq. 1 with a standard deviation of 5×10^{-6} g cm^{-3}, which can be expressed by

$$\rho(\mathrm{KCl/H_2O}) = 0.9970_5 + 0.046_9 m. \quad (1)$$

Here, ρ is the density in g cm^{-3} and m is the concentration in mol (kg H_2O)$^{-1}$. Equation 1 was obtained from measurements in the range m=0.01—0.1 mol (kg H_2O)$^{-1}$ at 25 °C and 1 atm by means of a digital vibrating densimeter (SS-D-200 twin type, the Shibayama Scientific Co., Ltd.). On the other hand, the densities of the dilute solutions at each pressure were assumed to be equal to those of the solvent mixtures at each pressure because the measured solutions were dilute. All solutions of HCl were treated in a dry box under a nitrogen atmosphere.

Table 1 summarizes the physical properties of the TBA–water mixtures used in this work, such as the density (ρ), viscosity (η), dielectric constant (ε), molar concentration of water in the mixture [$c(H_2O)$], and the observed solvent conductivity (κ).

An acid-proof Teflon cell and a glass cell were employed, respectively, for HCl and KCl solutions. The procedure and apparatus used here for conductance measurements at high pressure were the same as those in previous studies.[10,22] The molar conductances, Λ, obtained by subtrating the solvent conductivity were reproducible within ±0.1%. When ions were not associated, the Fuoss-Onsager equation of conductance[23,24] was used to determine the limiting molar

Table 1. Properties of *t*-Butyl Alcohol–Water Mixtures at 25 °C under High Pressure

P / kgf cm^{-2}	ρ[a] / g cm^{-3}	η[b] / cP	ε[c]	$c(H_2O)$ / mol dm^{-3}	$10^6\kappa$ / S cm^{-1}
		2 mol% of *t*-Butyl Alcohol			
1	0.9849	1.315	73.3	50.44	1.0
500	1.0035	1.336	75.0	51.39	1.3
1000	1.0209	1.362	76.5	52.28	1.5
1500	1.0373	1.393	77.9	53.12	1.8
2000	1.0528	1.423	79.3	53.91	2.1
		3 mol% of *t*-Butyl Alcohol			
1	0.9801	1.575	70.8	48.26	0.9
500	0.9989	1.624	72.6	49.19	1.1
1000	1.0160	1.674	74.2	50.03	1.3
1500	1.0318	1.728	75.7	50.81	1.5
2000	1.0465	1.778	77.1	51.51	1.7
		5 mol% of *t*-Butyl Alcohol			
1	0.9707	2.130	65.8	44.29	0.8
500	0.9892	2.227	67.7	45.14	1.0
1000	1.0059	2.309	69.4	45.90	1.2
1500	1.0211	2.377	70.9	46.59	1.4
2000	1.0351	2.430	72.3	47.23	1.6
		7 mol% of *t*-Butyl Alcohol			
1	0.9593	2.610	60.8	40.66	0.6
500	0.9790	2.848	62.8	41.49	0.6
1000	0.9962	3.080	64.5	42.22	0.7
1500	1.0116	3.307	66.0	42.88	0.8
2000	1.0256	3.529	67.3	43.47	0.9
		10 mol% of *t*-Butyl Alcohol			
1	0.9417	3.219	53.6	35.87	0.4
500	0.9631	3.688	55.8	36.69	0.4
1000	0.9813	4.193	57.7	37.38	0.5
1500	0.9972	4.684	59.3	37.99	0.5
2000	1.0113	5.189	60.7	38.52	0.6
		25 mol% of *t*-Butyl Alcohol			
1	0.8801	4.805	31.0	20.60	0.1
500	0.9059	6.488	33.4	21.20	0.1
1000	0.9268	8.418	35.3	21.69	0.1
1500	0.9443	10.53	36.9	22.10	0.1
2000	0.9596	12.87	38.4	22.46	0.1

a) H. Kubota, Y. Tanaka, and T. Makita, *Int. J. Thermophys.*, **8**, 47 (1987). b) Ref. 28 for 1 atm and Y. Tanaka, Y. Matsuda, H. Fujiwara, H. Kubota, and T. Makita, *Int. J. Thermophys.*, **8**, 147 (1987) for high pressure. c) Ref. 28 for 1 atm and T. Moriyoshi, T. Ishii, Y. Tamai, and M. Tado, *J. Chem. Eng. Data*, **35**, 17 (1990) for high pressure.

conductance Λ°:

$$\Lambda = \Lambda^\circ - Sc^{1/2} + Ec\log c + Jc, \quad (2)$$

where c is the molar concentration (M), and S, E, and J have their usual meanings. In the presence of ion pairs, data analysis using Eq. 2 gave a very low value of the ion-size parameter, $\mathring{a}$, involved in J. In this case, the Shedlovsky equation[25] was employed,

$$1/\Lambda S(z) = 1/\Lambda^\circ + K_A c\Lambda S(z) f_\pm^2/\Lambda^{\circ 2}, \quad (3)$$

where

$$S(z) = \{z/2 + [1 + (z/2)^2]^{1/2}\}^2, \quad (4)$$

$$z = [8.204\times10^5 \Lambda^\circ/(\varepsilon T)^{3/2} + 82.5/\eta(\varepsilon T)^{1/2}](c\Lambda/\Lambda^{\circ 3})^{1/2}, \quad (5)$$

and

$$-\log f_\pm^2 = 3.649 \times 10^6[c\Lambda S(z)/\Lambda^\circ]^{1/2}/(\varepsilon T)^{3/2}. \quad (6)$$

Here, $f_\pm$ is the mean activity coefficient, as determined by the Debye–Hückel limiting law, and T is the absolute temperature.

Results and Discussion

The molar conductances, Λ, of HCl and KCl in TBA–water mixtures up to 25 mol% of TBA were measured at five different concentrations in the range $(0.6—5.0)\times10^{-3}$ M for HCl and $(0.4—1.6)\times10^{-3}$ M for KCl at 25 °C as a function of the pressure up to 2000 kgf cm^{-2}.[26] The data for Λ were analyzed with Eq. 2 or 3 to obtain the limiting molar conductances, Λ°, at each solvent and pressure. The results are shown in Table 2 together with the related parameters. Although HCl was completely dissociated in all of the

Table 2. Limiting Molar Conductances (Λ°/S cm^2 mol^{-1}), Ion-Size Parameters ($\mathring{a}$/Å), Association Constants (K_A/mol^{-1} dm^3), and Standard Deviation of Λ (σ_Λ/S cm^2 mol^{-1}) of HCl and KCl in t-Butyl Alcohol–Water Mixtures as a Function of the Pressure at 25 °C

P/kgf cm^{-2}	Λ° (HCl)	$\mathring{a}$	σ_Λ	Λ° (KCl)	$\mathring{a}$	K_A	σ_Λ
			2 mol% of t-Butyl Alcohol				
1	339.3	2.8	0.11	110.0	0.7		0.02
500	350.4	4.6	0.25	110.7	0.7		0.09
1000	356.5	3.8	0.26	110.6	2.0		0.07
1500	362.3	4.3	0.10	110.2	5.2		0.10
2000	365.6	5.0	0.24	108.7	1.2		0.11
			3 mol% of t-Butyl Alcohol				
1	304.2	1.0	0.39	96.44	0.9		0.05
500	311.8	1.1	0.40	96.28	2.1		0.08
1000	317.6	1.3	0.44	95.89	2.0		0.01
1500	322.0	2.0	0.46	95.02	3.8		0.02
2000	324.8	2.6	0.44	93.88	7.1		0.02
			5 mol% of t-Butyl Alcohol				
1	245.3	2.8	0.16	76.73		6.3	0.002
500	249.3	2.2	0.36	74.31		5.5	0.07
1000	251.2	3.3	0.38	72.46		5.3	0.08
1500	252.8	4.8	0.54	70.45		3.2	0.05
2000	253.9	5.0	0.44	68.49	1.5		0.06
			7 mol% of t-Butyl Alcohol				
1	211.3	1.7	0.15	65.22		10.1	0.02
500	209.3	1.6	0.14	61.31		10.0	0.07
1000	207.5	1.8	0.13	57.93		9.8	0.07
1500	206.2	1.7	0.06	54.92		9.7	0.08
2000	204.6	3.7	0.26	51.78		2.6	0.05
			10 mol% of t-Butyl Alcohol				
1	170.4	3.5	0.07	53.77		14.1	0.05
500	164.9	5.9	0.14	49.03		9.1	0.12
1000	160.0	7.8	0.22	44.90		7.9	0.08
1500	155.5	8.4	0.11	41.34		7.1	0.07
2000	151.5	7.8	0.37	38.20		5.7	0.06
			25 mol% of t-Butyl Alcohol				
1	76.40	3.9	0.09	26.32		30.5	0.002
500	70.54	4.0	0.06	22.81		27.0	0.04
1000	65.31	3.5	0.10	19.77		21.8	0.04
1500	60.62	4.5	0.14	17.26		19.6	0.05
2000	56.07	3.6	0.16	15.04		16.3	0.04

solutions studied, KCl was slightly associated in TBA–water mixtures containing above 5 mol% of TBA. The obtained values of Λ° at 1 atm were larger on the average by 1.4% for HCl and by 0.4% for KCl than those estimated by interpolation of literature data.[27,28] No high-pressure data are available for a comparison.

As shown in Table 2, the value of Λ°(HCl) is three- to five-times larger than that of Λ°(KCl) in each solvent mixture studied. Furthermore, while Λ°(KCl) in each mixture, except for 2 mol% of TBA, decreases with increasing pressure in accordance with the variation of the solvent fluidity ($1/\eta$) with pressure, Λ°(HCl) increases with increasing pressure in 2,3,and 5 mol% TBA–water mixtures. These results indicate that a special mechanism called "proton jump" plays an important role in TBA–water mixtures.

So far, no exact way to exclusively measure the anomalous excess proton conductance, λ°_E, due to proton jumping has been invented, and an empirical method is often used. The quantity

$$\lambda^\circ_E = \lambda^\circ(H^+) - \lambda^\circ(K^+) = \Lambda^\circ(HCl) - \Lambda^\circ(KCl) \quad (7)$$

is taken here as being a measure of the anomalous conductance. Although Li^+ and Na^+ ions are chosen elsewhere,[1,29] instead of the K^+ ion, as a measure of the translational mobility of a proton (i.e., the oxonium ion, H_3O^+), the K^+ ion is more appropriate because its ionic size is closer to that of the H_3O^+ ion than are the smaller ions. The values of λ°_E, thus obtained, are listed in Table 3.[30]

The distribution of the protons between water and alcohol molecules for the reaction

$$ROH_2^+ + H_2O \rightleftharpoons ROH + H_3O^+ \quad (8)$$

has been examined in the alcohol-rich region by the conductivity method.[31] The equilibrium constants for the reaction $K=c(ROH)c(H_3O^+)/c(ROH_2^+)c(H_2O)$, where c(i) is the concentration of the species i in M, are 139 for methanol, 250 for ethanol, 392 for 1-propanol, 765 for 1-butanol, and 1130 for isobutyl alcohol. Assuming that the value of K does not differ so much among isomers, we can estimate the percentage of protons present as $(CH_3)_3COH_2^+$ to be about (0.03—0.04)%, even in a 25 mol% TBA–water mixture. It is therefore reasonable to consider that almost all of the protons were present as H_3O^+ in the TBA–water mixtures studied here, and were transferred from the oxonium ions to adjacent water molecules. Thus, we can regard that the excess proton conductance reflects a variation of the rotational mobility of water molecules in hydrogen-bond networks with the alcohol content and/or pressure.

As shown in Table 3, the value of λ°_E, itself, decreases markedly with an increase in the TBA content at each pressure. One of the main factors for the decrease in λ°_E with an increase in the TBA content would be a decrease in the concentration of water in a solvent mixture. That is, the fraction of water molecules adjacent to the H_3O^+ ion decreases with an increase in the TBA content and, consequently, the

Table 3. Excess Proton Conductances (λ°_E/S cm^2 mol^{-1}), Excess Proton Conductances Normalized to the Molar Concentration of Water $\{[\lambda^\circ_E/c(H_2O)]/10^3$ S cm^5 mol$^{-2}\}$, and the Ratios of $R=[\lambda^{\circ(P)}/c(H_2O)^{(P)}]/[\lambda^{\circ(1)}/c(H_2O)^{(1)}]$ in t-Butyl Alcohol-Water Mixtures as a Function of the Pressure at 25 °C

P/kgf cm^{-2}	λ°_E	$\lambda^\circ_E/c(H_2O)$	R
	Water[a]		
1	276.3	4.993	1.000
500	286.5	5.070	1.015
1000	294.5	5.116	1.025
1500	301.6	5.152	1.032
2000	307.4	5.172	1.036
	2 mol% of t-Butyl Alcohol		
1	229.3	4.546	1.000
500	239.7	4.664	1.026
1000	245.9	4.704	1.035
1500	252.1	4.746	1.044
2000	256.9	4.765	1.048
	3 mol% of t-Butyl Alcohol		
1	207.8	4.306	1.000
500	215..5	4.381	1.017
1000	221.7	4.431	1.029
1500	227.0	4.468	1.038
2000	230.8	4.479	1.040
	5 mol% of t-Butyl Alcohol		
1	168.6	3.807	1.000
500	175.0	3.877	1.018
1000	178.7	3.893	1.023
1500	182.3	3.913	1.028
2000	185.4	3.925	1.031
	7 mol% of t-Butyl Alcohol		
1	146.1	3.593	1.000
500	148.0	3.567	0.993
1000	149.6	3.543	0.986
1500	151.3	3.528	0.982
2000	152.8	3.515	0.978
	10 mol% of t-Butyl Alcohol		
1	116.6	3.251	1.000
500	115.9	3.159	0.972
1000	115.1	3.079	0.947
1500	114.2	3.006	0.925
2000	113.3	2.941	0.905
	25 mol% of t-Butyl Alcohol		
1	50.08	2.431	1.000
500	47.73	2.251	0.926
1000	45.54	2.100	0.864
1500	43.36	1.962	0.807
2000	41.03	1.827	0.752

a) Ref. 10.

frequency of the proton transfer from the H_3O^+ ion to the water molecules diminishes with an increase in the TBA content. Therefore, to evaluate the contribution of water in the mixture to λ°_E, the values of λ°_E normalized to the molar concentration of water in the mixture, i.e., $\lambda^\circ_E/c(H_2O)$, were calculated and are shown in Fig. 1 together with the values for those in ethanol–water mixtures.[32] Figure 1 shows that the value of $\lambda^\circ_E/c(H_2O)$ decreases with an increase in the alcohol content, and that the rate of decrease with the alcohol content is larger in TBA–water mixtures than in ethanol–water mixtures. If the contribution of water in the mixture to λ°_E were the same as that in pure water, $\lambda^\circ_E/c(H_2O)$ would not depend on the alcohol content. Thus, to explain the decrease in λ°_E with an increase in the alcohol content, another factor must be considered in addition to a decrease in the concentration of water in the mixture: the reorientation of water molecules adjacent to the H_3O^+ ion, which is the rate-determining step in the proton-jump mechanism,[1] becomes slower with an increase in the alcohol content, as suggested by the dielectric relaxation time measured in ethanol–water mixtures at 25 °C and 1 atm,[33] and the reorientational correlation time may be longer in TBA–water mixtures than in ethanol–water mixtures because of the higher viscosity of TBA–water mixtures.

In a previous study,[10] the excess proton conductance normalized to its value at 1 atm, $\lambda^\circ_E{}^{(p)}/\lambda^\circ_E{}^{(1)}$, were examined as a function of the pressure as a step toward determining the pressure effect on the excess proton conductance for one rotator, i.e., one water molecule adjacent to the H_3O^+ ion. It is more appropriate, however, to take into consideration the change in the concentration of water at high pressure and to examine the pressure dependence of $R=[\lambda^\circ_E{}^{(p)}/c(H_2O)^{(p)}]/[\lambda^\circ_E{}^{(1)}/c(H_2O)^{(1)}]$ for the purpose mentioned above, since the concentration of water affects λ°_E considerably. As shown in Fig. 2, R increases with increasing pressure in (0—5) mol% of TBA, but decreases in above 7 mol% of TBA. These results suggest that the rotation of water molecules adjacent to the H_3O^+ ion is accelerated by pressure in mixtures up to 5 mol% of TBA as well as in pure water, but is retarded in mixtures above 7 mol% of TBA. Figure 2 also shows that the rate of an increase in R with pressure is largest in a 2 mol% TBA–water mixture, and that its magnitude decreases in the order: 2>3>0>5≫7≫10≫25 mol% of TBA.[34] It is shown from studies on λ°_E in pure water[2,9] that the increase in R with pressure becomes larger with a decrease in temperature. Therefore, the pressure dependence of R is considered to be closely related to the stability of the

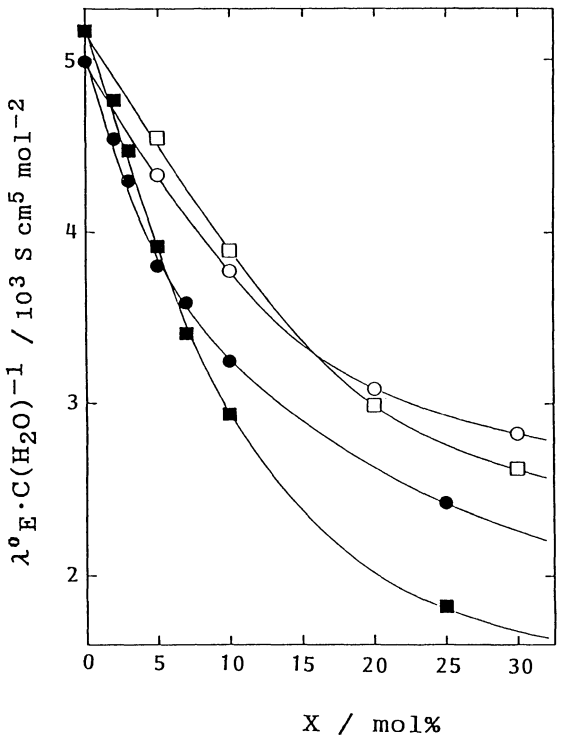

Fig. 1. Variation of the excess proton conductance normalized to the molar concentration of water with t-butyl alcohol and ethanol content at 1 and 2000 kgf cm^{-2}. t-Butyl alcohol (●: 1, ■: 2000 kgf cm^{-2}); ethanol (○: 1, □: 2000 kgf cm^{-2}).

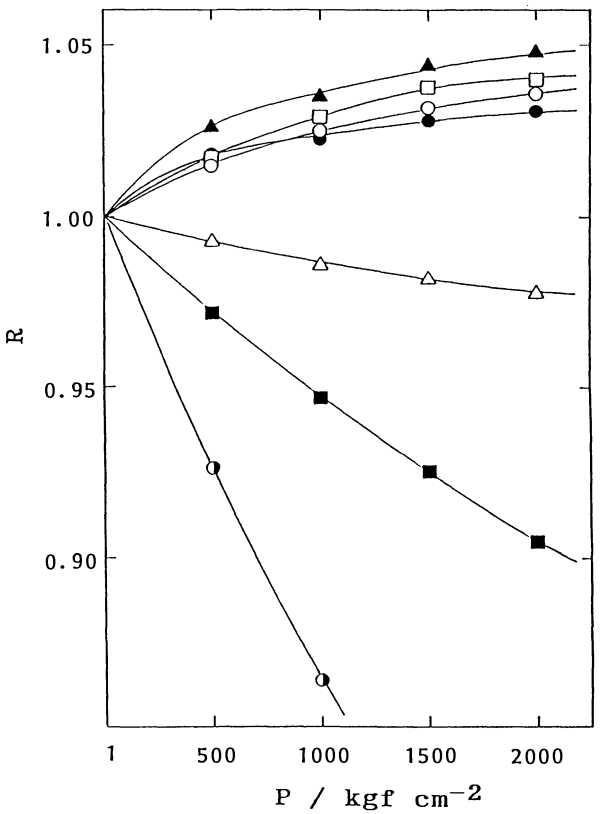

Fig. 2. Ratios of $\lambda^\circ_E/c(H_2O)$ at pressure P to that at 1 atm as a function of the pressure. ○: Water, ▲: 2 mol%, □: 3 mol%, ●: 5 mol%, △: 7 mol%, ■: 10 mol%, ◑: 25 mol% of t-butyl alcohol.

water structure: the more stable are the hydrogen bonds between water molecules at atmospheric pressure, the more prominent is the pressure effect on R. If this finding is applied to the results found for TBA–water mixtures, we can draw a conclusion that below 3 mol% of TBA the three-dimensional network of water is stabilized by the addition of TBA to water due to hydrophobic hydration around the t-butyl group. However, a large increase in the TBA content begins to make it difficult to form stable hydrogen bonds between water molecules, as can be seen in 7, 10, and 25 mol% TBA–water mixtures: R decreases with increasing pressure. Computer simulations[20,35] have shown the stabilization and promotion of the water structure by TBA molecules in a 3 mol% TBA–water mixture as well as an infinitely dilute aqueous solution, and at the same time the association of TBA molecules due to the hydrophobic interaction in a 3 mol% TBA–water mixture. This kind of association is promoted with an increase in the TBA content; the structural stabilization of water due to hydrophobic hydration rapidly decreases because TBA–water interactions are replaced by TBA–TBA interactions.

According to a previous study on proton jumping in ethanol–water mixtures at high pressure,[10] it was disclosed that the rate of increase in R with pressure is most prominent in a 5 mol% ethanol–water mixture.[32] Apparently, the rate of increase in R with pressure becomes maximum at a lower mol% of alcohol, and decreases more rapidly with an increase in the alcohol content in TBA–water mixtures than in ethanol–water mixtures. These trends are consistent with those observed regarding such properties of alcohol–water mixtures as the partial molar volumes of alcohols,[12] the temperature of maximum density,[13] and the velocity of sound.[36] The present results therefore indicate that the three-dimensional network of water in TBA–water mixtures is more stable at a lower mol% of alcohol and begins to collapse more rapidly with increasing alcohol content than in ethanol–water mixtures, since the association of alcohol molecules due to the hydrophobic interaction occurs at a lower mol% of alcohol with an increase in the surface area of the alkyl group.

Conclusions

The present experimental study has disclosed that the pressure effect on the excess proton conductance normalized to the molar concentration of water, $\lambda^\circ_E/c(H_2O)$, drastically changes with the alcohol content in TBA–water mixtures in comparison with ethanol–water mixtures. $\lambda^\circ_E/c(H_2O)$ in 2 and 3 mol% TBA–water mixtures increases with increasing pressure at a larger rate than that in pure water. However, the rate of increase in $\lambda^\circ_E/c(H_2O)$ with pressure decreases with an increase in the alcohol content, and in mixtures above 7 mol% TBA–water $\lambda^\circ_E/c(H_2O)$ decreases with increasing pressure, in contrast to the finding that $\lambda^\circ_E/c(H_2O)$ increases with pressure in ethanol–water mixtures up to at least 10 mol% of ethanol. In conclusion, these results reflect a difference in the stability of hydrogen bonds between water molecules in these mixtures at atmospheric pressure; the variation of $\lambda^\circ_E/c(H_2O)$ with pressure becomes a good measure of the stability of the water structure at atmospheric pressure.

References

1) B. E. Conway, J. O'M. Bockris, and H. Linton, *J. Chem. Phys.*, **24**, 834 (1956).
2) M. Nakahara and J. Osugi, *Rev. Phys. Chem. Jpn.*, **50**, 66 (1980).
3) G. A. Gaballa and G. W. Neilson, *Mol. Phys.*, **50**, 97 (1983).
4) F. H. Stillinger and A. Rahman, *J. Chem. Phys.*, **61**, 4973 (1974).
5) R. W. Impey, M. L. Klein, and I. R. McDonald, *J. Chem. Phys.*, **74**, 647 (1981).
6) G. Pálinkás, P. Bopp, G. Jancsó, and K. Heinzinger, *Z. Naturforsch. Teil A*, **39**, 179 (1984); G. Jancsó, P. Bopp, and K. Heinzinger, *Chem. Phys.*, **85**, 377 (1984).
7) J. Jonas, T. DeFries, and D. J. Wilber, *J. Chem. Phys.*, **65**, 582 (1976).
8) R. Pottel and E. Asselborn, *Ber. Bunsen-Ges. Phys. Chem.*, **83**, 29 (1979).
9) M. Ueno, M. Nakahara, and J. Osugi, *J. Soln. Chem.*, **8**, 881 (1979).
10) M. Ueno, K. Ito, N. Tsuchihashi, and K. Shimizu, *Bull. Chem. Soc. Jpn.*, **59**, 1175 (1986).
11) F. Franks and D. J. G. Ives, *Quart. Rev. London*, **20**, 1 (1966); F. Franks and D. S. Reid, "Water, A Comprehensive Treatise," ed by F. Franks, Plenum, New York (1973), Vol. 2, Chap. 5.
12) K. Nakanishi, *Bull. Chem. Soc. Jpn.*, **33**, 793 (1960).
13) G. Wada and S. Umeda, *Bull. Chem. Soc. Jpn.*, **35**, 646, 1797 (1961).
14) F. Franks and H. T. Smith, *Trans. Faraday Soc.*, **64**, 2962 (1968).
15) G. Roux, D. Roberts, G. Perron, and J. E. Desnoyers, *J. Soln. Chem.*, **9**, 629 (1980).
16) M. C. R. Symons and M. J. Blandamer, "Hydrogen-Bonded Solvent Systems," ed by A. K. Convington and P. Jones, Taylor and Francis, London (1968), p. 211.
17) K. Iwasaki and T. Fujiyama, *J. Phys. Chem.*, **83**, 463 (1979).
18) J. B. Hyne, in Ref. 16, p. 99.
19) R. E. Robertson and S. E. Sugamori, *J. Am. Chem. Soc.*, **91**, 7254 (1969).
20) H. Tanaka, K. Nakanishi, and H. Touhara, *J. Chem. Phys.*, **81**, 4065 (1984).
21) T. Shedlovsky, *J. Am. Chem. Soc.*, **54**, 1141 (1932).
22) M. Ueno, N. Tsuchihashi, and K. Shimizu, *Bull. Chem. Soc. Jpn.*, **58**, 2929 (1985).
23) R. M. Fuoss and F. Accascina, "Electrolytic Conductance," Interscience, New York (1959), Chap. 15.
24) P. C. Carman, *J. Phys. Chem.*, **74**, 1653 (1970).
25) T. Shedlovsky, *J. Franklin Inst.*, **225**, 739 (1938); R. M. Fuoss and T. Shedlovsky, *J. Am. Chem. Soc.*, **71**, 1496 (1949).

26) The complete data on the molar conductances Λ of HCl and KCl are deposited as Document No. 9106 at the Office of the Editor of Bull. Chem. Soc. Jpn.
27) A. R. Tourky, S. E. Mikhali, and A. A. Abdel-Hamid, *Z. Phys. Chem.*, **252**, 289 (1973).
28) T. L. Broadwater and R. L. Kay, *J. Phys. Chem.*, **74**, 3802 (1970).
29) W. Strauss, *Aust. J. Chem.*, **10**, 277 (1957).
30) According to Ref. 28, to replace the K^+ ion in Eq. 7 by smaller ions makes the values of λ°_E larger by about 12% for the Li^+ ion and by about 7% for the Na^+ ion at 1 atm.
31) R. De Lisi and M. Goffredi, *Electrochim. Acta*, **16**, 2181 (1971).
32) The values of $\lambda^\circ_E/c(H_2O)$ are obtained from the data in Ref. 10.
33) D. E. Buck, *U. S. Govt. Res. Develop. Rept.*, **40**, 59 (1965).
34) This order will not be affected so much by replacing the K^+ ion in Eq. 7 with smaller ions, since the replacement of the K^+ ion with the Na^+ ion in ethanol–water mixtures changes the order of $5>0>10\gg20\gg30$ mol% of ethanol to that of $5>10\approx0\gg20\gg30$ mol% of ethanol according to unpublished data.
35) K. Nakanishi, K. Ikari, S. Okazaki, and H. Touhara, *J. Chem. Phys.*, **80**, 1656 (1984).
36) C. J. Burton, *J. Acoust. Soc. Am.*, **20**, 186 (1948).

Thermal Dehydrogenation of Cyclooctane by Supported Noble Metal Catalysts

Takahiro FUJII, Kiyoshi YUKAWA, and Yasukazu SAITO*
Department of Industrial Chemistry, Faculty of Engineering, University of Tokyo, Hongo, Bunkyo-ku, Tokyo 113
(Received October 12, 1990)

Under boiling and refluxing conditions, cyclooctane has been dehydrogenated to cyclooctene and molecular hydrogen selectively with carbon- and alumina-supported Pd, Ph, and Ru catalysts. The activity order among these metal catalysts was Pd>Rh>Ru. The most active carbon-supported Pd catalyst was least sensitive to the rate retardation caused by cyclooctene adsorption. Desorption of molecular hydrogen from the Pd catalyst surface was deduced to proceed rapidly after the rate-determining step.

The reaction of alkane dehydrogenation yielding alkene and molecular hydrogen (Eq. 1) is highly endothermic.[1]

$$\text{alkane} \longrightarrow \text{alkene} + H_2. \quad (1)$$

High temperatures were required for this reaction in general,[2] as exemplified by styrene formation from ethylbenzene,[3] and with the various processes for petroleum reforming[4] due to the high endothermicity and the increase in the number of molecules. On the contrary, homogeneous transition metal catalysts dehydrogenated alkanes under mild temperatures, where photoirradiation was considered to be indispensable.[5]

It is possible, however, to get rid of the equilibrium restriction imposed at mild temperatures, as long as the product hydrogen is somehow removed from the reaction medium. The boiling and refluxing conditions fulfill the present requirement for the reaction. (Eq. 1) Under boiling conditions, the vapor phase in contact with the catalyst solution is full of the solvent components, whereas the refluxing procedure separates molecular hydrogen from the vapor phase. Since hydrogen is eliminated from the solution after its catalytic generation and is not allowed to dissolve into the solution, alkane dehydogenation can proceed catalytically at mild temperatures without photoirradiation, if we have any suitable catalyst. Recently, in fact, we observed the catalytic dehydrogenation of cyclooctane at 151 °C, yielding cyclooctene and molecular hydrogen (Eq. 2) using Wilkinson complex $RhCl(PR_3)_3$.[6]

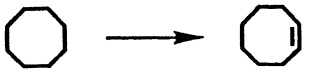

(2)

It is quite conceivable that the reaction (Eq. 2) is catalyzed by various kinds of catalysts, either homogeneous or heterogeneous. The metallic hydrogenation catalyst is a good candidate, since the metallic surface sites of hydrogenation catalysts are capable of dissociating the C–H bonds of alkane and to form molecular hydrogen from surface hydrogen species.

In the present study we attempted to find supported metal catalysts for cyclooctane dehydrogenation under boiling and refluxing conditions.

Experimental

After the treating with a mixture of concd H_2SO_4 and HNO_3 in order to remove unsaturated hydrocarbon impurities, cyclooctane was dried over $CaCl_2$ and distilled under a nitrogen atmosphere in the presence of metallic sodium. The 5 wt% supported noble metal catalysts (metals: Pd, Rh, and Ru; supports: carbon and alumina) were provided from N. E. Chemcat Co. Carbon-supported catalysts were preliminarily dried by heating in N_2 stream for about 1 h and under vacuum for about 30 min at 180 °C. All of the catalysts were pretreated with H_2 (1 atm, 180 °C, 30 min), followed by evacuation (180 °C, 10 min) before use.

All manipulations were carried out under a nitrogen atmosphere. The catalysts (0.2 mmol-metal) were suspended in cyclooctane (100 ml) in a Schlenk tube (200 ml). The suspension was heated with an oil bath (180 °C) and kept boiling at 151 °C. After the suspension began to boil, the amount of evolved gas was measured by a gas buret (50 ml) through a reflux condenser; the gas composition was analyzed by gas chromatography using an active carbon column. After the reaction, the solution from which the catalyst was removed by sedimentation was analyzed by GC (OV-1 and PEG-20M capillary columns).

Results and Discussion

Dehydrogenation of Cyclooctane under Boiling and Refluxing Conditions. The time courses of gas evolution are shown in Fig. 1. Hydrogen was yielded exclusively with the Pd/C catalyst, whereas the Ru/Al_2O_3 catalyst gave methane as a by-product at a 10% level. Gaseous products from the other four catalysts were mainly hydrogen and methane (under 0.2%). On the other hand, only cyclooctene was detected as the dehydrogenation product in the liquid phase. The amounts of hydrogen and cyclooctene produced after a 24 h reaction are show in Table 1. The stoichiometric coincidence was satisfactory. Since the turnover number (per metal-mol) was apparently over 1, the reaction of alkane dehydrogenation (Eq. 1) was demonstrated to proceed catalytically, even under

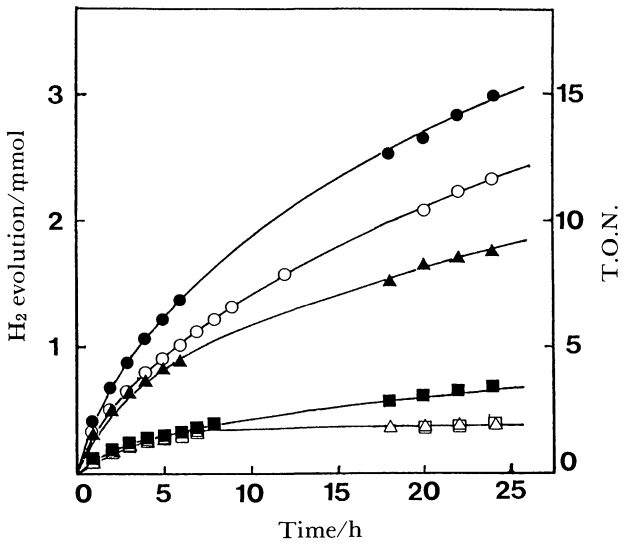

Fig. 1. Time-course plots of H_2 evolution from cyclooctane suspended with Pd (5%)/C (●), Pd (5%)/Al_2O_3 (○), Rh (5%)/C (▲), Rh (5%)/Al_2O_3 (△), Ru (5%)/C (■), and Ru (5%)/Al_2O_3 (□) at the concentration of 0.2 mmol metal/100 ml under boiling and refluxing conditions (151 °C).

Table 1. Dehydrogenation Products of Cyclooctane with Suspended Noble Metal Catalyst under Boiling and Refluxing Conditions

Catalyst	H_2/mmol	Cyclooctene/mmol
Pd (5%)/C	2.97	2.88
Pd (5%)/Al_2O_3	2.30	2.20
Rh (5%)/C	1.74	1.57
Rh (5%)/Al_2O_3	0.37	0.36
Ru (5%)/C	0.59	0.52
Ru (5%)/Al_2O_3	0.36	0.34

Catalyst concentration: 0.2 mmol metal/100 ml; Reaction temperature: 151 °C; Reaction time: 24 h.

mild conditions at 151 °C.

The activity order was Pd>Rh>Ru,[7] where the carbon-supported catalysts were more active than the alumina-supported ones. This activity order among metals was completely different from that of 2-propanol dehydrogenation (Ru>Rh>Pt>Pd),[8] and rather similar to that of cyclohexanol dehydrogenation (Pd>Rh>Pt>Ru).[9] Since the reaction temperatures (boiling point) of cyclooctane (151 °C) and cyclohexanol (161 °C) are comparable, whereas that of 2-propanol (82.4 °C) is considerably low, the low reaction rate for the Pd catalysts to evolve hydrogen from 2-propanol may be ascribed to the high stability of hydrogen in the metal hydride phase at low-temperature regions.[10]

Retardation Effects of Added Cyclooctene. The retardation effects of product cyclooctene on the reaction rates were examined about Pd/C, Pd/Al_2O_3, and Rh/C catalysts, which exhibited relatively high activities. Figure 2 shows the time courses of hydrogen evolution from the suspensions containing cyclooctene at various concentrations with these catalysts. Little retardation was found for the most active Pd/C catalyst, while the Pd/Al_2O_3 and Rh/C catalysts were considerably inhibited by added cyclooctene.

The relationship between the initial rates of hydrogen evolution (v) and the concentrations of added cyclooctene ([COE]) was analyzed with Eq. 3 while taking account of retardation due to cyclooctene adsorption.

$$v = k/(1 + K[\mathrm{COE}]). \quad (3)$$

As shown in Fig. 3, plots of $1/v$ and [COE] gave straight lines; the values of k and K are summarized in Table 2. The order of the rate constant (k) was Pd/C>Pd/Al_2O_3>Rh/C, whereas the retardation con-

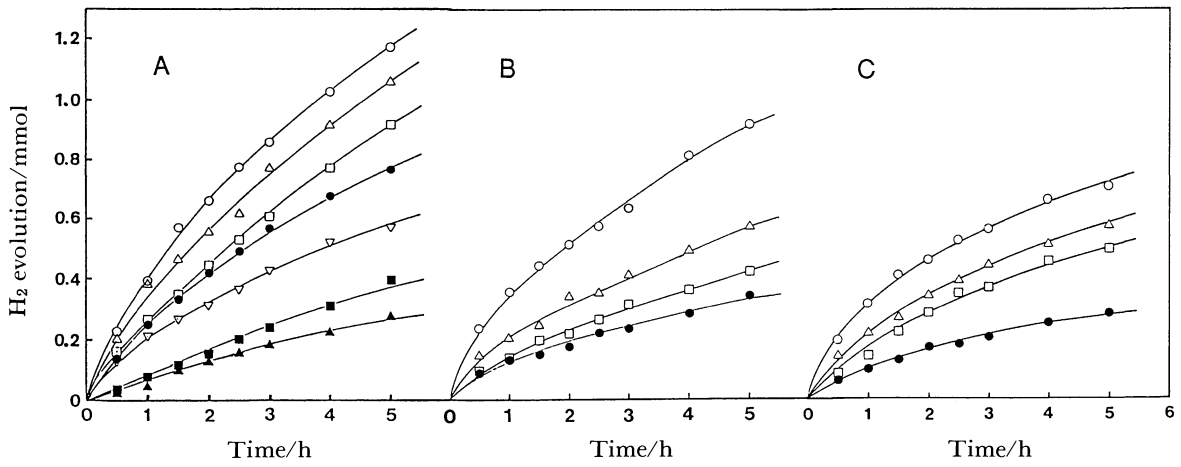

Fig. 2. Effect of cyclooctene addition on H_2 evolution from cyclooctane suspended with noble metal catalysts (0.2 mmol metal/100 ml) under boiling and refluxing conditions (151 °C). Catalyst: (A) Pd/C, (B) Pd/Al_2O_3, and (C) Rh/C. Addition of cyclooctene: 0 μl (○), 25 μl (△), 50 μl (□), 100 μl (●), 150 μl (▽), 300 μl (■), and 450 μl (▲).

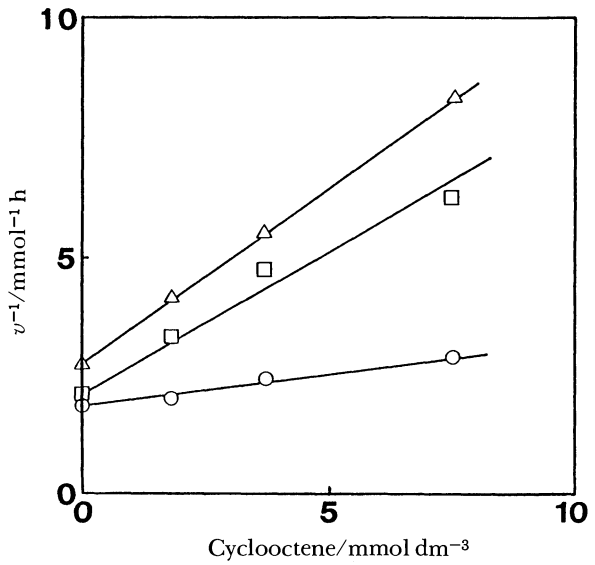

Fig. 3. Rate retardation due to cyclooctane analyzed with equation 3 for Fig. 2. Catalyst: Pd/C (○), Pd/Al_2O_3 (□), and Rh/C (△).

Table 2. Rate Constant (k) of Cyclooctane Dehydrogenation and Retardation Constant due to Cyclooctene Absorption (K) Calculated from Fig. 3

Catalyst	k/mmol h^{-1} g^{-1}	K/mmol^{-1} dm^3
Pd/C	26	0.075
Pd/Al_2O_3	22	0.270
Rh/C	17	0.250

stant (K) of the Pd/C catalyst was extremely smaller than those of the other catalysts, indicating the facile desorption of alkene from the Pd/C catalyst surface.

Rate Retardation Caused by 1-Nonene Addition. 1-Nonene (0.58 mmol, corresponding to the amount of added cyclooctene in the former section) was added to cyclooctane suspended with the Pd/Al_2O_3 catalyst, since this catalyst exhibited a relatively high activity for cyclooctane dehydrogenation and rate retardation due to added cyclooctene. Hydrogen evolved from a solution containing 0.58 mmol of 1-nonene and from one containing 0.78 mmol of cyclooctene; after reaction for 3 h it amounted to 0.20 mmol and 0.24 mmol, respectively, indicating that the rate retardations caused by these alkenes are comparable to each other.

Figure 4 shows the amounts of hydrogen evolved and the reaction products in solution, allowing a comparison of the effect of added 1-nonene with that of no alkene added.

Both hydrogen evolution (0.20 mmol) and intermolecular hydrogen transfer from cyclooctane to 1-nonene (0.30 mmol) proceeded simultaneously, while 1-nonene was isomerized exclusively to *cis*-2-nonene (0.11 mmol). It is noteworthy that the intermolecular hydrogen transfer proceeds more rapidly than does

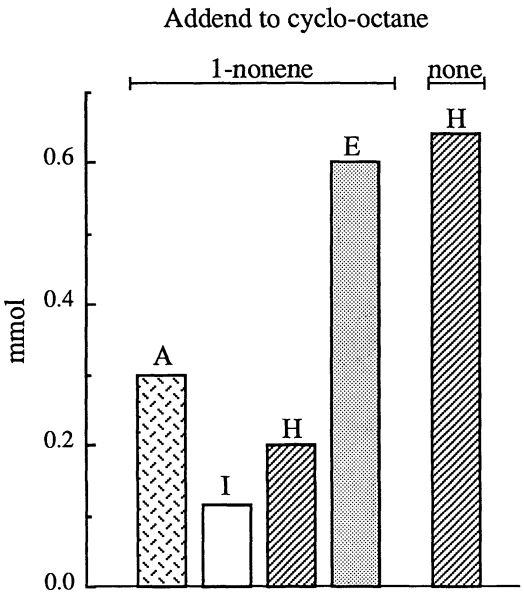

Fig. 4. Effect of alkene addition to hydrogen evolution or transfer from cyclooctane with suspended Pd catalyst under boiling and refluxing conditions. H: hydrogen, A: nonane, E: cyclooctene, I: isomerized nonene (exclusively *cis*-2-nonene). Catalyst: Palladium (5%)/alumina 0.2 mmol. Substrate: Cyclooctane (100 ml). Added alkene: 1-nonene (0.58 mmol). Reaction temperature: 151 °C, Reaction time: 3 h.

isomerization. The total amounts of nonane and hydrogen (0.5 mmol) were nearly equal to that of cyclooctene (0.60 mmol) produced. The coincidence of these magnitudes with that of hydrogen evolved from alkene-free cyclooctane (0.64 mmol) indicates that both hydrogen evolution and transfer proceed at common active sites.

Reaction Mechanism of Dehydrogenation. The mechanism of alkane dehydrogenation on heterogeneous catalysts, yielding alkene and molecular hydrogen via adsorbed species on the active site (ads), has been proposed at high temperature regions:[11]

$$\text{alkane} \longrightarrow \text{alkane(ads)}, \quad (4)$$

$$\text{alkane(ads)} \longrightarrow \text{alkyl(ads)} + \text{H(ads)}, \quad (5)$$

$$\text{alkyl(ads)} \longrightarrow \text{alkene(ads)} + \text{H(ads)}, \quad (6)$$

$$\text{alkene(ads)} \longrightarrow \text{alkene}, \quad (7)$$

and

$$2\text{H(ads)} \longrightarrow \text{H}_2. \quad (8)$$

As for dehydrogenation using homogeneous catalysts, the reaction schemes on the reductive elimination of ligand hydrides under photoirradiation, as well as thermal hydrogen transfer from alkane to alkene and the photocatalytic cycle of hydrogen evolution from alkane, have been discussed.[12] In view of endother-

micity, the evolution of molecular hydrogen from the hydride intermediate species is more difficult than hydrogen transfer to alkane.

Nonane formation from 1-nonene by the intermolecular hydrogen transfer strongly suggests the possibility for a hydrogen species on the catalyst surface to react with not only 1-nonene, but also cyclooctene, which remains on the dehydrogenation site or is adsorbed from the solution bulk. Cyclooctane should be regenerated from the surface hydrogen species and cyclooctene by hydrogen-transfer, since nonane was formed from 1-nonene.

$$\text{alkene} \longrightarrow \text{alkene(ads)}, \quad (9)$$

$$\text{alkene(ads)} + 2\text{H(ads)} \longrightarrow \text{alkane}. \quad (10)$$

It is therefore reasonable to assume that the rate retardation for hydrogen evolution caused by alkenes is brought about from a consumption of adsorbed hydrogen species by forming alkane, in addition to the site-occupation effect, owing to alkene adsorption. Since they are commonly governed by the amounts of adsorbed alkene, these retardation effects are expressed by the same rate equation (Eq. 3). In view of the standard Gibbs energy changes, the hydrogen transfer from cyclooctane to 1-nonene or from cyclooctane to cyclooctene (Eq. 11) proceeds more rapidly than does hydrogen evolution (Eq. 2) in this reaction temperature region.

$$\text{alkane} + \text{alkene}' \longrightarrow \text{alkene} + \text{alkane}'. \quad (11)$$

Provided that the hydrogen evolution step (Eq. 8) is rate-determining in the hydrogen evolution reaction, the adsorbed hydrogen species would be abundant on the catalyst surface, being sufficiently supplied from cyclooctane. The exothermic and facile nonane formation from 1-nonene would surpass the endothermic molecular hydrogen formation from the surface hydrogen species. However nearly equal rates were observed for nonane formation and hydrogen evolution in the absence of alkene, indicating that the step of molecular hydrogen formation is preceded by the rate-determining step. With regard to the reaction of molecular hydrogen formation from cyclooctane using the suspended Pd/Al_2O_3 catalyst, it is therefore plausible that either C–H bond cleavage of cyclooctane or β-hydrogen elimination of the adsorbed cyclooctyl species is rate-determining.

References

1) O. R. Stull, E. F. Westrum, Jr., and G. C. Sinke, "The Chemical Thermodynamics of Organic Compounds," John Wiley, New York (1969), pp. 422—439.

2) A. E. Shilov, "Activation of Saturated Hydrocarbons by Transition Metal Complexes," Reidel, Dordrecht (1982), pp. 55—57. New York (1980), pp. 55—85.

3) P. J. Lewis, C. Hagopian, and P. Koch, "Encyclopedia of Chemical Technology," 3rd ed, ed by Kirk–Othmer, John Wiley, New York (1983), Vol. 21, pp. 770—801.

4) C. E. Jahinig, "Encyclopedia of Chemical Technology," 3rd ed, ed by Kirk-Othmer, John Wiley, New York (1982), Vol. 17, pp. 195—256.

5) a) M. J. Burk, R. H. Crabtree, and D. V. McGrath, *J. Chem. Soc., Chem. Commun.*, **1985**, 1829; b) K. Nomura and Y. Saito, *J. Chem. Soc., Chem. Commun.*, **1988**, 161; c) T. Sakakura, T. Sodeyama, Y. Tokunaga, and M. Tanaka, *Chem. Lett.*, **1988**, 263; d) J. A. Maguire, W. T. Boese, and A. S. Goldman, *J. Am. Chem. Soc.*, **111**, 7088 (1989).

6) T. Fujii and Y. Saito, *J. Chem. Soc., Chem. Commun.*, **1990**, 757.

7) The rates of hydrogen evolution on the carbon- and alumina-supported Pt catalysts were the highest. However, Pt was not included to the comparison among these metals, because the dehydrogenated products were too complex. For example, Pt/Al_2O_3 catalyst yielded not only cyclooctene but also ethylcyclohexane, ethylbenzene, and other unidentified products from cyclooctane.

8) Y. Saito, M. Yamashita, and E. Ito, 8th World Hydrogen Energy Conference, Honolulu, July 1990, Abstr., B1-6.

9) Y. Saito, M. Yamashita, and Y. Ichinohe, 1st Tokyo Conference on Advanced Catalytic Science and Technology, Tokyo, July 1990, Abstr., P-56.

10) H. Brodowsky, *Z. Phys. Chem., N. F.*, **44**, 129 (1965).

11) a) S. Carra and L. Forni, *Catal. Rev.*, **5**, 159 (1972); b) I. Suzuki and Y. Kaneko, *J. Catal.*, **47**, 239 (1977).

12) a) R. H. Crabtree, *Chem. Rev.*, **85**, 245 (1985); b) M. J. Burk and R. H. Crabtree, *J. Am. Chem. Soc.*, **109**, 8025 (1987); c) K. Nomura and Y. Saito, *J. Mol. Catal.*, **54**, 57 (1989); d) T. Sakakura, T. Sodeyama, and M. Tanaka, *New J. Chem.*, **13**, 737 (1989); e) J. A. Maguire, W. T. Boese, M. E. Goldman, and A. S. Goldman, *Coord. Chem. Rev.*, **97**, 179 (1990).

Interactions between an Anionic Porphyrin and Cationic Surfactants in Water

Toshihiro TOMINAGA,* Satoshi ENDOH, and Hiroaki ISHIMARU
Department of Applied Chemistry, Okayama University of Science,
1-1 Ridai-cho, Okayama 700
(Received October 15, 1990)

Interactions between decyl-, dodecyl-, and tetradecyltrimethylammonium bromide (DeTAB, DTAB, and TTAB) and an anionic porphyrin, 5,10,15,20-tetrakis(4-sulfonatophenyl)porphine (H_2TPPS^{4-}), have been studied in water at 298.2 K. Precipitate formation constants between the surfactant cations and the H_2TPPS^{4-} anion have been obtained. The precipitates were resolubilized by a further addition of the surfactants at concentrations close to the critical micelle concentrations (cmc) in DeTAB, and below the cmc's in DTAB and TTAB solutions. Surface tension and conductance measurements show that the effects of H_2TPPS^{4-} on the cmc's are very small. The fluorescence of H_2TPPS^{4-} is quenched in both water and sodium dodecyl sulfate solutions by the methylviologen cation, but not in cationic surfactant solutions. The diffusion coefficients were measured in a system containing H_2TPPS^{4-} and TTAB; the results show the existence of large premicellar aggregates.

Because of their importance in biological and photochemical processes, porphyrins and metalloporphyrins have attracted much interest. Recently, water-soluble porphyrins have been shown to interact with 1,10-phenanthroline (phen) and pyridine derivatives,[1] amino acids,[2] and other ionic species.[3] Dimerization[4] and counterion-induced dimerization[5] of cationic and anionic porphyrins have been studied. Photoinduced electron-transfer and charge-separation processes have been studied extensively in microheterogeneous solutions including micelles and vesicles.[6–8] To understand these processes, an elucidation of the interactions of porphyrins with surfactants is essestial. Although there have been studies on the interactions between water-soluble porphyrins and polymers,[9,10] there have been no systematic studies on the interactions between ionic porphyrins and surfactants.

We report here on the interactions between an anionic porphyrin, 5,10,15,20-tetrakis(4-sulfonatophenyl)porphine (H_2TPPS^{4-}), and cationic surfactants in water. In acidic solutions, the predominant species of the porphyrin is H_4TPPS^{2-};[4b,9a] it tends to aggregate.[4a,4b] We have studied systems where H_2TPPS^{4-} is the predominant species. Measurements were made on precipitate formation and resolubilization concentrations, surface tension, conductance, fluorescence quenching , and diffusion coefficient. In a previous paper, we reported interactions between a metal chelate cation, $[Fe(phen)_3]^{2+}$, and anionic surfactants.[11] The present results are compared with the previous ones.

Experimental

Materials and Preparation of Solutions. H_6TPPS (Tokyo Kasei, specially prepared analytical reagent), sodium dodecyl sulfate (NaDS) (BDH, 99.0%), decyltrimethylammonium bromide (DeTAB), dodecyltrimethylammonium bromide (DTAB), and tetradecyltrimethylammonium bromide (TTAB) (Tokyo Kasei, guaranteed reagents) were used as received. Water was distilled twice. A stock solution of H_2TPPS^{4-} was prepared by neutralizing the H_6TPPS solution with NaOH. This solution was used to prepare buffered and nonbuffered solutions of the desired concentrations. The absence of H_4TPPS^{2-} was checked by the absorption spectrum, which showed a maximum at 413 nm, but no peak at 434 nm at the Soret bands.[12] Metalloporphyrin solutions were prepared by adding a trace amount of $Cd(NO_3)_2$ to the solution of H_2TPPS^{4-} as a catalyst,[13] and then adding equivalent amounts of the respective metal ions. The porphyrin and metalliporphyrin solutions were protected from light.

Measurements. All measurements were made at 298.2 K. For determining precipitate formation and the resolubilization concentrations, solutions of both H_2TPPS^{4-} and an alkyltrimethylammonium bromide were placed in a water thermostat controlled to ±0.1 K. After temperature equilibration, solutions of H_2TPPS^{4-} and the surfactant were mixed and replaced in the bath. The solubilization limit was determined by observing the presence or absence of precipitates, or turbidity. The absorption and fluorescence spectra were measured by using a Hitachi 228A spectrophotometer and a Hitachi F-2000 fluorescence spectrophotometer, respectively. The surface tensions of surfactant solutions were measured by using a De Nouy-type tensiometer (Furukawa Seisakusho). The solution conductivities were measured at 5 kHz by means of a linear-bridge conductometer (Huso Model 360 B) in an oil thermostat controlled to ±0.005 K.[11]

The diffusion coefficients were measured by the Taylor dispersion method.[14] In this method a small amount of solution is injected into a solvent flowing through a capillary tube. The solute is dispersed along the tube. From the concentration profile at the end of the tube the difussion coefficient can be calculated. For tracer diffusion measurements, the solvent flowing through the capillary contained a specified amount of TTAB; the injected solution contained the same amount of TTAB and 10 μM (1 M=1 mol dm^{-3}) H_2TPPS^{4-}. Because the H_2TPPS^{4-} concentration was well below that of TTAB, the diffusion coefficient could be taken as the tracer diffusion coefficient. (Note that the concentration of the solute is further diluted as it flows through the capillary tube.) For interdiffusion between metalloporphyrins, the solvent flowing through the capillary contained a spec-

ified amount of TTAB and 50 μM $[Mn^{III}(tpps)]^{3-}$; the injected solution contained the same amount of TTAB as the solvent and 50 μM $[M^{II}(tpps)]^{4-}$, where M stands for Cu or Ni. This was possible because $[Mn^{III}(tpps)]^{3-}$ has a weak absorption at 413 nm where $[Ni^{II}(tpps)]^{4-}$ and $[Cu^{II}(tpps)]^{4-}$ have an intense absorption. The concentration profile of the metalloporphyrin was monitored by spectrophotometric detectors, either Waters-490 or UVIDEC 100-IV. Other details concerning the measurements have been described.[11,15]

Results and Discussion

Precipitate Formation and Resolubilization. When a cationic surfactant was added to a fixed concentration of H_2TPPS^{4-}, a precipitate appeared, which was then resolubilized by a further addition of the surfactant. Figure 1 shows a phase diagram for precipitate formation and resolubilization for TTAB. Regions A and C correspond to clear solutions and region B corresponds to turbid (two-phase) systems. A similar phase diagram has been shown for the $[Fe(phen)_3]^{2+}$–DS^- system.[16] In an ammonium buffer (pH=8.0, I (ionic strength) =0.1 M), precipitate formation concentrations were larger and the resolubilization concentrations lower than in water. Figure 2 shows the effect of the surfactant chain length. With increasing surfactant chain length, both precipitate formation and resolubilization concentrations decrease. In Figs. 1 and 2, the cmc's of the surfactants determined from surface tension measurements are shown. For DTAB and TTAB, the resolubilization of the precipitate occurs at surfactant concentrations below their cmc's. This will be discussed later; we first examine the precipitate formation process. The precipitate formation reaction may be written as

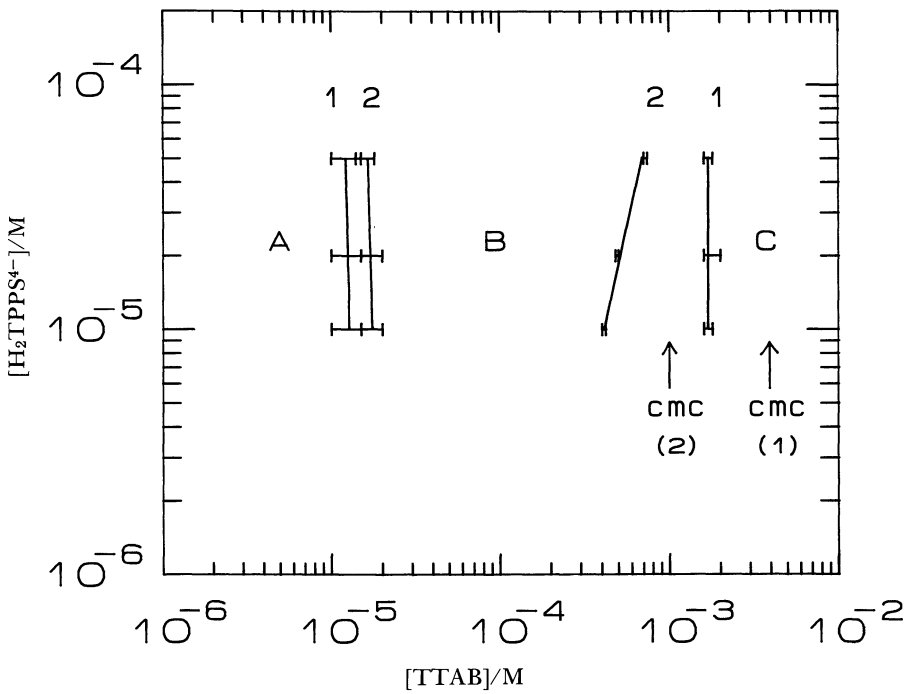

Fig. 1. Phase diagram for the precipitate formation and resolubilization for H_2TPPS^{4-} and TTAB at 298.2 K. Regions A and C correspond to the one-phase clear solutions and region B corresponds to the two-phase system. 1, In water (without added salt); 2, in ammonium buffer (pH=8.0, I=0.1 M). Arrows indicate cmc's of TTAB in water and in the ammonium buffer.

Table 1. Values of log K for the Precipitate Formation Reaction between C_nTA^+ and H_2TPPS^{4-} (Eq. 1) in Water at 298.2 K

Surfactant	log K		
	I=0.1 M[a]	No added salt	No added salt[b]
$C_{10}TAB$	18.19±0.12	19.82±0.17	13.37±0.36
$C_{12}TAB$	20.49±0.15	21.83±0.21	18.13±0.19
$C_{14}TAB$	23.71±0.38	24.32±0.45	22.20±0.34

a) Ammonium buffer (pH=8). b) The values for the reaction between C_nTA^+ and $[Fe(bpso)_3]^{4-}$ (Ref. 17).

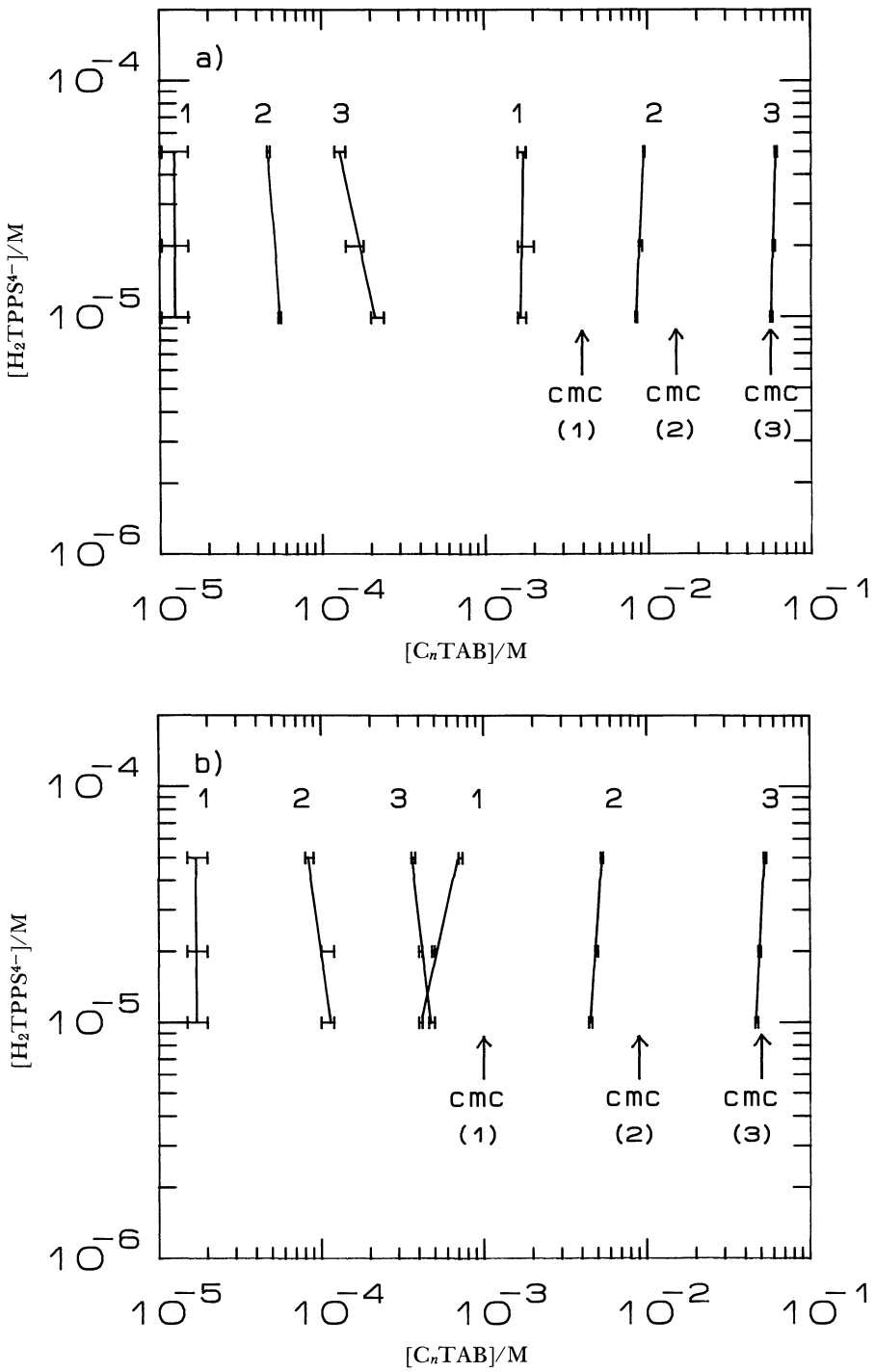

Fig. 2. Phase diagram for the precipitate formation and resolubilization for H_2TPPS^{4-} and TTAB (1), DTAB (2), and DeTAB (3) in water (without added salt) (a), and in ammonium buffer (pH= 8.0, I=0.1 M) (b) at 298.2 K. Arrows indicate cmc's of the respective surfactants.

$$4C_nTA^+ + H_2TPPS^{4-} \overset{K}{\rightleftharpoons} (C_nTA)_4 \cdot H_2TPPS, \quad (1)$$

where C_nTA^+ stands for $DeTA^+$ (n=10), DTA^+ (n=12), or TTA^+ (n=14), and $K=1/\{[C_nTA^+]^4[H_2TPPS^{4-}]\}$.

Table 1 lists the values of log K. The standard Gibbs energy of transfer from the aqueous state to the solid state can be calculated as

$$\Delta G^\circ_{aq\rightarrow solid} = -RT\ln K, \quad (2)$$

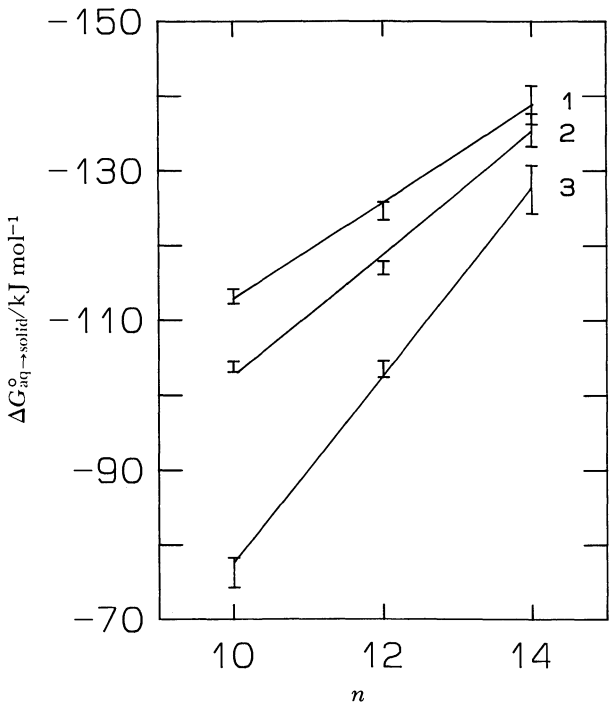

Fig. 3. Standard Gibbs energy of transfer of $(C_nTA)_4$·H_2TPPS and $(C_nTA)_4$·[Fe(bpso)$_3$] from the aqueous state to the solid state at 298.2 K. 1, $(C_nTA)_4$·H_2TPPS in water (without added salt); 2, $(C_nTA)_4$·H_2TPPS in ammonium buffer (I=0.1 M); 3, $(C_nTA)_4$·[Fe(bpso)$_3$] in water (without added salt).

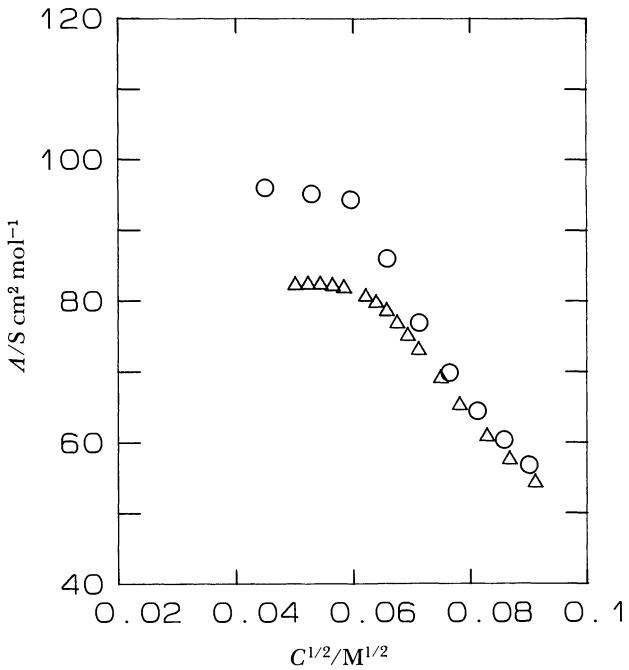

Fig. 4. Molar conductivities of TTAB in water (○) and in 0.1 mM H_2TPPS^{4-} solution (△) as a function of the TTAB concentration at 298.2 K.

where R is the gas constant. In Fig. 3, the $\Delta G^{\circ}_{aq\rightarrow solid}$ values are plotted against the surfactant chain length. The results may be regarded as being linear within experimental uncertainties. From the slopes, the values for $\Delta G^{\circ}_{aq\rightarrow solid}$ per methylene group can be obtained, and are −6.4 and −7.9 kJ mol^{-1} in the cases of no added salt and I=0.1 M (ammonium buffer, pH=8), respectively. Also shown in Fig. 3 is the result for $[Fe(bpso)_3]^{4-}$ (bpso=4.7-diphenyl-1,10-phenanthroline-disulfonate).[17] The $\Delta G^{\circ}_{aq\rightarrow solid}$ value for the methylene group for this system is −12.8 kJ mol^{-1}; it is twice as large as that for the H_2TPPS^{4-} case. This difference reflects differences in the standard Gibbs energy in the two kinds of solids.

Surface Tension and Conductivity. The cmc values shown in Figs. 1 and 2 were determined from the break point of the surface tension vs. concentration curve. They are 57 mM, 16 mM, and 4.0 mM in water, and 50 mM, 9.0 mM, and 1.0 mM in the ammonium buffer for DeTAB, DTAB, and TTAB, respectively. Resolubilization of the precipitate occurs at surfactant concentration below their cmc's for DTAB and TTAB, though it occurs close to the cmc's for DeTAB. In order to determine whether the cmc's decrease in the presence of H_2TPPS^{4-}, surface tension measurements were made for DTAB and TTAB solutions in the presence of 5×10^{-5} M H_2TPPS^{4-}. The results showed that the presence of H_2TPPS^{4-} had negligible effects on the cmc values. Figure 4 shows the molar conductivities of TTAB in the presence (0.1 mM) and absence of H_2TPPS^{4-}. From the break point, the cmc of TTAB in water is found to be 3.8 mM, which is close to the value obtained from the surface-tension measurement (4.0 mM). As can be seen from the figure, the break point is not lowered, even in the presence of 0.1 mM H_2TPPS^{4-}. These results suggest that, at surfactant concentrations below the cmc's and above the resolubilization concentrations, there is no "normal" micelle, but there are premicellar aggregates which may be expressed as $(TTA)_x(H_2TPPS)_yBr_z^{(x-4y-z)+}$. Premicellar aggregates have been known for other ionic dyes, and are sometimes called "dye-rich induced micelles."[18–20]

Fluorescence Quenching. In order to obtain information about premicellar aggregates, fluorescence quenching experiments were carried out. If H_2TPPS^{4-} is associated with cationic surfactants, a cationic quencher may have difficulty in approaching the H_2TPPS^{4-} ion. In addition to cationic surfactant solutions, measurements were also made in water and in NaDS solutions; the results are shown in Fig. 5. In the case of no surfactant, the plot for the quenching of H_2TPPS^{4-} (maximum at 640 nm) by the methylviologen ion (MV^{2+}) does not give a straight line. This reflects the fact that there are ion pairs between MV^{2+} and the ground state H_2TPPS^{4-}, and that static quenching in addition to dynamic quenching ocurrs.[6] In fact, Schmehl and Whitten have obtained a value of 647 M^{-1} for the ion-pair formation constant between

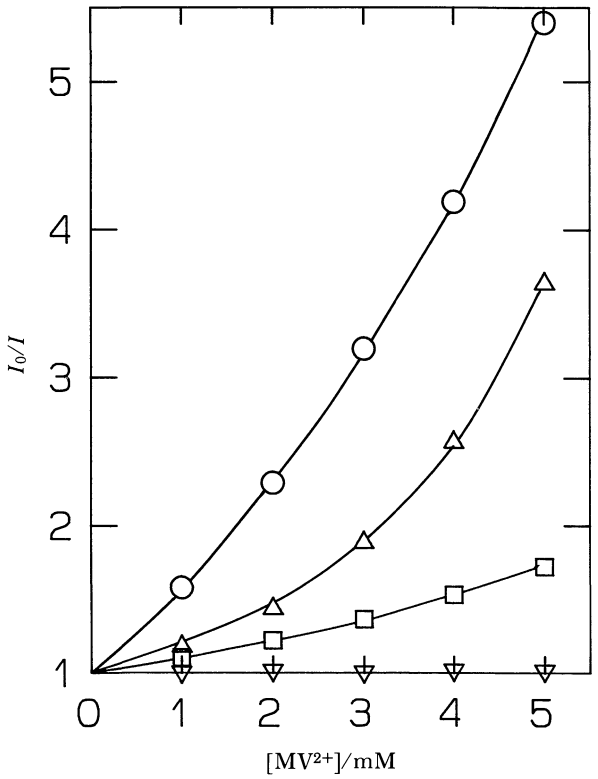

Fig. 5. Stern–Volmer plots for the quenching of H_2TPPS^{4-} by MV^{2+} in 0.1 M ammonium buffer (pH=8.0). ○, No surfactant; △, in 0.02 M NaDS; □, in 0.1 M NaDS; ▽, in 0.0005 M TTAB solutions at 298.2 K.

H_2TPPS^{4-} and MV^{2+} in 0.05 M NaCl.[6] In NaDS (0.02 M NaDS+0.05 M NaCl), although most of the MV^{2+} ions are bound to the micelles (>98%), they have estimated that the contribution to quenching is in the following order: static quenching>dynamic quenching by free MV^{2+}> dynamic quenching by micelle-bound MV^{2+}.[6] This makes plots in NaDS nonlinear also (Fig. 5). In 8 mM NaDS, the results were close to those in water (not shown in Fig. 5). With increasing NaDS concentration, the degree of quenching becomes smaller (Fig. 5), since more MV^{2+} ions are bound to the micelles.

In the case of 0.5 mM TTAB, fluorescence (maximum at 647 nm) is not quenched at all. It is unlikely that there are fewer free MV^{2+} ions in the TTAB solutions than in the NaDS solutions, since MV^{2+} ions must be less bound to TTA^+ ions than to NaDS micelles. The result therefore suggests that H_2TPPS^{4-} ions are associated with TTA^+ ions, and that the overall charge of an aggregate is positive. This prevents MV^{2+} ions from comming close to the H_2TPPS^{4-} ions and, as a result, electron transfer from the exited H_2TPPS^{4-} ion to the MV^{2+} ion does not occur. The results for 2 and 20 mM TTAB (above the cmc) and 10 mM DTAB (close to the cmc) also showed no quenching (not shown in Fig. 5).

Diffusion Coefficient. The final step in this study was to obtain information about the size of the aggregates. Figure 6 shows the tracer diffusion coefficients for H_2TPPS^{4-} and the interdiffusion

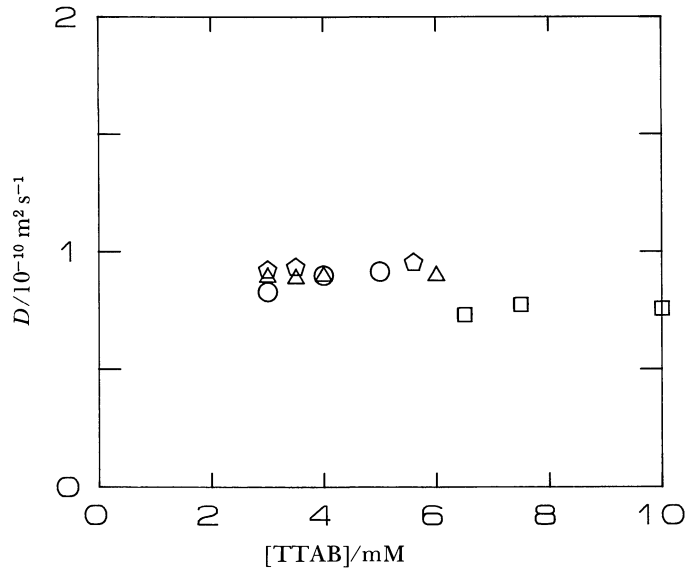

Fig. 6. Diffusion coefficients of H_2TPPS^{4-}, metalloporphyrins, and micelles in TTAB solutions at 298.2 K. ⬠, Tracer diffusion coefficients of H_2TPPS^{4-}; △, interdiffusion coefficients of $[Ni^{II}(tpps)]^{4-}$ and $[Mn^{III}(tpps)]^{3-}$; ○, interdiffusion coefficients of $[Cu^{II}(tpps)]^{4-}$ and $[Mn^{III}(tpps)]^{3-}$; □, tracer diffusion coefficients of the TTAB micelles.

coefficients for pairs of metalloporphyrins in TTAB solutions. When the TTAB concentration is zero, the tracer diffusion coefficient of the H_2TPPS^{4-} ion is 2.8×10^{-10} m^2 s^{-1} (not shown in Fig. 6), which was estimated from the limiting molar conductivity using the Nernst equation.[21] In 3—6 mM TTAB solutions, the tracer diffusion coefficient for H_2TPPS^{4-} is $(0.94\pm0.01)\times10^{-10}$ m^2 s^{-1}, and is significantly low when compared to the value in the absence of TTAB. The interdiffusion coefficient between $[M^{II}(tpps)]^{4-}$ (M=Cu or Ni) and $[Mn^{III}(tpps)]^{3-}$ in 3—6 mM TTAB is $(0.89\pm0.02)\times10^{-10}$ m^2 s^{-1}, and is close to the tracer diffusion coefficient for H_2TPPS^{4-}.[22] These values are compared with the tracer diffusion coefficient for the TTAB micelle, $(0.75\pm0.02)\times10^{-10}$ m^2 s^{-1} at 6.5—10 mM, which was obtained by measuring the diffusion of pyrene solubilized in the micelle.

By a comparison of the diffusion coefficients of the aggregate and the micelle (Fig. 6), the value of x must be large but smaller than 70, which is the agreegation number of the TTAB micelle.[23] In the case of a 3 mM TTAB solution, the mole ratio of TTA^+ to H_2TPPS^{4-} is 300 at the time of injection, and increases with time for tracer diffusion measurements, while the mole ratio of TTA^+ to $[M(tpps)]^{n-}$ (n=3 or 4) is 60 throughout the measurement for the metalloporphyrin interdiffusion cases. In the tracer diffusion case, therefore, there are sufficient TTA^+ ions to bind with the H_2TPPS^{4-} ion and form large aggregates. For the interdiffusion case, however, the maximum value of x is 60, where all TTA^+ ions are bound to $[M(tpps)]^{n-}$ ions. This suggests that the value of y is larger than one. Such kinds of premicellar aggregates are, as mentioned before, sometimes called "dye-rich induced micelles".[18—20] As we have seen, the tracer diffusion coefficients of H_2TPPS^{4-} and the interdiffusion coefficients of the metalloporphyrins are very close in magnitude. This suggests that the size of the premicellar aggregates of H_2TPPS^{4-}, $[M^{II}(tpps)]^{4-}$, and $[Mn^{III}(tpps)]^{3-}$ are similar.

Comparison with Related Studies. Schmehl and Whitten have found that precipitate formation and resolubilization occurs for H_2TPPS^{4-} and hexadecyltrimethylammonium chloride (CTAC).[6] They have mentioned that, in the presence of H_2TPPS^{4-}, micellization of CTAC occurs significantly below the cmc of CTAC in the absence of added ions. Although we have not studied CTAC, our results suggest that in the presence of H_2TPPS^{4-} although the cmc is not significantly changed (i.e., there is no normal micelle), the premicellar aggregates, each having at least one H_2TPPS^{4-} ion, exist below the cmc.

In a previous study, we measured the tracer diffusion coefficients for the $[Fe(phen)_3]^{2+}$ ion in anionic surfactant solutions.[11] In solutions of sodium 1-dodecanesulfonate (NaDSO), no precipitate forms between $[Fe(phen)_3]^{2+}$ and DSO^-, at least when the $[Fe(phen)_3]^{2+}$ concentration is lower than 2 mM and the DSO^- concentration is lower than 7 mM. The tracer diffusion coefficient of $[Fe(phen)_3]^{2+}$ (which is the tracer diffusion coefficient of the aggregate $Na_z[Fe(phen)_3]_x(DSO)_y^{(y-2x-z)-}$) decreased monotonically with increasing concentration of NaDSO. When NaDS is added to a fixed concentration of $[Fe(phen)_3]^{2+}$, precipitates of $[Fe(phen)_3](DS)_2$ form, which are resolubilized upon further addition of NaDS below its cmc. In 3—8 mM NaDS (below the cmc), the tracer diffusion coefficient of $[Fe(phen)_3]^{2+}$ (which is the tracer diffusion coefficient of the aggregate $Na_z[Fe(phen)_3]_x(DS)_y^{(y-2x-z)-}$) was lower than the tracer diffusion coefficient of the NaDS micelle. Although the cases of H_2TPPS^{4-} and TTAB are similar to that of $[Fe(phen)_3]^{2+}$ and NaDS, in that in both systems a precipitate forms which is then resolubilized below cmc's of the surfactants, the tracer diffusion of H_2TPPS^{4-}, i.e., that of the $(TTA)_x(H_2TPPS)_yBr_z^{(x-4y-z)+}$ aggregates, is not smaller than that of the tracer diffusion coefficient of the TTAB micelles.

It would be of interest to see if the diffusion coefficient of the premicellar aggregates between $[Fe(bpso)_3]^{4-}$ and TTAB is larger or smaller than that of the TTAB micelles. However, the resolubilization of the $(TTA)_4[Fe(bpso)_3]$ precipitates occurs at a TTAB concentration close to its cmc,[17] and we have not been able to tell the difference in the diffusion coefficients of the premicellar aggregates and the micelles.

The authors wish to thank Dr. Masaaki Tabata of Saga University for his helpful discussions. This work was partially supported by a Grant-in Aid for Scientific Research on Priority Area of "Molecular Approaches to Non-equilibrium Processes in Solutions" No. 02245101 from the Ministry of Education, Science and Culture.

References

1) J. A. Shelnutt, *Inorg. Chem.*, **22**, 2535 (1983); K. Kawamura, H. Kasahara, S. Igarashi, and T. Yotsuyanagi, *Chem. Lett.*, **1987**, 2365.

2) M. Tabata and M. Tanaka, *Inorg. Chem.*, **27**, 203; 3190 (1988); M. Tabata and A. Shimada, *Bull. Chem. Soc. Jpn.*, **63** 672 (1990).

3) T. Sato, T. Ogawa, and K. Kano, *J. Phys. Chem.*, **88**, 3678 (1984); K. Kano, T. Nakajima, and S. Hashimoto, *J. Phys. Chem.*, **91**, 6614 (1987); M. Tabata and I. Yamada, *Bull. Chem. Soc. Jpn.*, **60**, 3525 (1987).

4) a) A. Corsini and O. Herrmann, *Talanta*, **33**, 335 (1986); b) E. B. Fleisher, J. M. Palmer, T. S. Srivastava, and A. Chatterjee, *J. Am. Chem. Soc.*, **93**, 3162 (1971); c) M. Krishnamurthy, J. R. Sutter, and P. Hambright, *J. Chem. Soc., Chem. Commun.*, **1975**, 13; d) K. Kano, M. Takei, and S. Hashimoto, *J. Phys. Chem.*, **94**, 2181 (1990).

5) T. K. Chandrashekar, H. van Willigen, and M. H. Ebersole, *J. Phys. Chem.*, **88**, 4326 (1984); P. Firman, R. G.

Wilkins, and S. P. Kasprzyk, *J. Am. Chem. Soc.*, **111**, 4990 (1989).

6) R. H. Schmehl and D. G. Whitten, *J. Phys. Chem.*, **85**, 3473 (1981).

7) J. K. Hurst, L. Y. C. Lee, and M. Gratzel, *J. Am. Chem. Soc.*, **105**, 7048 (1983).

8) T. Nagamura, N. Takeyama, K. Tanaka, and T. Matsuo, *J. Phys. Chem.*, **90**, 2247 (1986); A. Uehata, H. Nakamura, S. Usui, and T. Matsuo, *J. Phys. Chem.*, **93**, 8197 (1989).

9) a)F. M. El Torki, P. J. Casano, W. F. Reed, and R. H. Schmehl, *J. Phys. Chem.*, **91**, 3686 (1987); b) M.D. Yanuck and R.H. Schmehl, *Chem. Phys. Lett.*, **122**, 133 (1985).

10) J. Bielec, B. Pilas, T. Sarna, and T. G. Truscott, *J. Chem. Soc., Faraday Trans. 2*, **82**, 1469 (1986).

11) T. Tominaga, T. Maruyama, T. Koshiba, and Y. Yamamoto, *Bull. Chem. Soc. Jpn.*, **62**, 1745 (1989).

12) When TTAB was added to an acidic solution containing H_4TPPS^{2-}, the absorption peak at 434 nm disappeared and the peak at 416—417 nm (2—4 mM TTAB), which corresponds to H_2TPPS^{4-}, appeared. It is worth noting that the total charge of the porphyrin increases in spite of the fact that the microscopic dielectric constant around the porphyrin decreases as a result of the interaction with TTAB. This means that what is important is microscopic charge of the central porphyrin ring, but not the total charge of the porphyrin. Similar result has been reported for the interaction of H_4TPPS^{2-} with poly(*N*-vinylpyrrolidone).[9a]

13) M. Tabata and M. Tanaka, *J. Chem. Soc., Dalton Trans.*, 1955 (1983); M. Tanaka, *Pure Appl. Chem.*, **55**, 151 (1983).

14) G. I. Taylor, *Proc. R. Soc. London, Ser. A*, **219**, 186 (1953); **225**, 473 (1954); H. J. V. Tyrrell and K. R. Harris, "Diffusion in Liquids. A Theoretical and Experimental Study," Butterworths, London (1984), p. 193.

15) T. Tominaga, S. Matsumoto, T. Koshiba, and Y. Yamamoto, *J. Chem. Soc., Faraday Trans. 1*, **84**, 4261 (1988).

16) D. Lemordant and R. Gaboriaud, *Fluid Phase Equilib.*, **20**, 269 (1985).

17) K. Osafune, T. Maruyama, and T. Tominaga, 58th National Meeting of the Chemical Society of Japan, April 1989, Abstr., No. 3IIB30.

18) P. Mukerjee and K. J. Mysels, *J. Am. Chem. Soc.*, **77**, 2937 (1955).

19) J. H. Baxendale and M. A. J. Rodgers, *Chem. Phys. Lett.*, **72**, 424 (1980); *J. Phys. Chem.*, **86**, 4906 (1982).

20) Y. Kusumoto and H. Sato, *Chem. Phys. Lett.*, **68**, 13 (1979); H. Sato, M. Kawasaki, and K. Kasatani, *J. Phys. Chem.*, **87**, 3759 (1983); H. Sato, M. Kawasaki, M. Haga, K. Kasatani, T. Ban, H. Suenaga, and N. Kitamura, *Nippon Kagaku Kaishi*, **1984**, 51.

21) R. A. Robinson and R. H. Stokes, "Elctrolyte Solutions," 2nd ed, Butterworth, London (1970), Chap. 11.

22) If the Charges of the interdiffusing pair of metalloporphyrins are the same, the interdiffusion coefficient may be regared as the intradiffusion coefficient under the assumption that the diffusion coefficient is insensitive to the central metal ion.[11,15] However, we were unable to find a pair of tetraanionic metalloporphyrins which have sufficiently different absorption spectra so that the interdiffusion coefficient can be measured. For the definition of intradiffusion coefficient, see; R. Mills, *J. Phys. Chem.*, **69**, 3116 (1965).

23) P. Lianos and R. Zana, *J. Colloid Interface Sci.*, **84**, 100 (1981); D. D. Miller, L. J. Magid, and D. F. Evans, *J. Phys. Chem.*, **94**, 5921 (1990).

 © 1991 The Chemical Society of Japan Bull. Chem. Soc. Jpn., 64, 949—953 (1991)

Preparation of Metallosilicates with ZSM-5 Type Structure by Atom-Planting Method

Kouji YAMAGISHI, Seitaro NAMBA,* and Tatsuaki YASHIMA
Department of Chemistry, Tokyo Institute of Technology, Ookayama, Meguro-ku, Tokyo 152
(Received October 18, 1990)

Aluminosilicates, gallosilicates, and indosilicates with the ZSM-5 type structure were prepared by the "Atom-Planting method". The introduction of metal cations into the framework of highly siliceous ZSM-5 zeolites was confirmed by IR and unit cell volume measurements. The acidic properties of these metallosilicates were examined by pyridine-IR and NH_3-temperature programmed desorption spectroscopies. The increasing order of the acid strengths of the metallosilicates is indosilicate<gallosilicate<aluminosilicate.

The framework composition of molecular-sieve materials is an important factor which can affect the physical and chemical properties of these materials. An aluminosilicate zeolite offers the ion-exchange properties, high acidity, and shape-selective structural features desired by those working in the areas of adsorption and catalysis. However, modifications and subsequent improvements of these properties have served as a driving force for changing the composition of the zeolites. There have been many studies in which silicon or aluminium in the framework of synthetic zeolites were replaced by some elements such as B, Be, Cr, Ge, Fe, Ga, P, Ti, V, Zr, etc.[1] These molecular sieves are generally synthesized hydrothermally. Jacobs et al. have discussed the probability of an isomorphous substitution of an element on the basis of a simplified version of Pauling's minimum radius ratio; they concluded that molecular sieves having elements with ionic radii between 0.020 and 0.061 nm can be obtained.[2] Since trivalent ions, such as aluminium ions, replace tetravalent silicium ions at the tetrahedral framework positions, the framework bears a net negative charge, which must be compensated for by counter cations. Brønsted acid sites occur in metallosilicates when the cations balancing the framework anionic charge are protons. Chu and Chang have reported that the strength of Brønsted acid sites on a series of the metallosilicates with the ZSM-5 type structure increases according to B(OH)Si≪Fe(OH)Si<Ga(OH)Si<Al(OH)Si.[3]

It has been reported that aluminium atoms are introduced into the framework of a highly siliceous ZSM-5 zeolite by alumination with $AlCl_3$ vapor at elevated temperatures,[4–10] and that not only Brønsted acid sites, but also Lewis acid sites, are generated.[6–9] For the introduction of aluminium into the framework, Chang et al. have reported that aluminium atoms can be introduced by the reaction of four terminal SiOH groups, the so-called "hydroxyl nest", with $AlCl_3$.[4] We have also discussed the mechanism for alumination, suggesting that aluminium atoms can be introduced into defect sites (including the hydroxyl nests) of the framework.[9,10] Kraushaar et al. have carried out a silylation of the highly siliceous ZSM-5 with trimethylchlorosilane, analyzed the products by ^{29}Si cross polarization MAS NMR, and proposed the existence of hydroxyl nests in the zeolitic framework.[11]

If some atoms other than silicon and aluminium can be introduced into the defect sites of the framework by treatments with metal chloride at elevated temperature, it will be possible to obtain metallosilicates. We call the preparation method the "Atom-Planting method". We have succeeded in obtaining an antimonosilicate with the ZSM-5 type structure by means of this atom-planting method.[12] The antimonosilicate has never been synthesized hydrothermally, probably because the antimony(III) cation is too large (0.090 nm). In a similar way, Kraushaar and van Hooff have reported that titanosilicate can be prepared by a subsequent dealumination of a ZSM-5 zeolite having a relatively high aluminium content with hydrochloric acid and reaction with titanium tetrachloride vapor at high temperatures.[13]

In this paper, we report that the preparation of not only aluminosilicate, but also gallosilicate and indosilicate, with the ZSM-5 type structure by the atom-planting method. Moreover, we discuss the acidic properties of these metallosilicates.

Experimental

Materials. High-purity grade gallium trichloride and indium trichloride were used without further purification. Aluminium trichloride was sublimed in order to remove any impurities. High-purity grade pyridine was thoroughly degassed several times by condensing with liquid nitrogen, and then evacuated and melted before use.

The parent highly siliceous ZSM-5 zeolite was prepared in the laboratory as previously described.[14] The Si/Al atomic ratio of the parent ZSM-5 zeolite was 870.

Atom-Planting Procedure. A 2 g sample of the parent highly siliceous ZSM-5 zeolite (powder form) was placed in a vertical quartz tube reactor and dehydrated for 4 h at 773 K in a stream of dry helium. After dehydration, the temperature was brought to an atom-planting temperature, 923 K; dry helium was then passed through a metal chloride container. The metal chloride container was heated to achieve a vapor pressure of 11 kPa. The gas line between the container and the reactor was heated to prevent vapor condensation. The

parent ZSM-5 was treated with metal chloride for 2 h and then purged with dry helium at the atom-planting temperature for 1 h to remove any residual metal chloride. The samples, thus treated, were then cooled to room temperature in dry helium stream. These samples were transformed into the NH_4^+-form by a cation-exchange procedure with 0.1 M NH_4NO_3 at 343 K for 36 h (1 M=1 mol dm^{-3}), washed with a large amount of deionized water and then dried in air at 383 K for 16 h.

Analysis of Samples. The amounts of metals in the bulk phase were determined by atomic absorption spectrophotometry. X-Ray diffraction was used to determine the crystallinity and unit-cell volumes of samples. Lead nitrate was used as an internal standard for the determination of the unit-cell volumes. The surface area of the samples were determined by applying the N_2 adsorption method at 77 K.

Infrared Measurements. Infrared spectra were measured at 4 cm^{-1} resolution on a JASCO IR-810 Spectrometer. The IR cell used was fitted with KBr windows and connected to a high-vacuum system. A 20 mg sample of the zeolite powder was accurately weighed, and then pressed into a 15 mm-diameter self-supported wafer. This wafer was placed in the IR cell and evacuated at 773 K for 1.5 h before measurements. In observations of adsorbed pyridine on samples, a wafer evacuated at 773 K for 1.5 h was exposed to pyridine vapor (1.3 kPa) at 423 K for 1 h; the IR cell was then evacuated at 423 K for 1 h, followed by desorption succesively at 523, 623, 673, 723, 773 K for 1 h in each case. All IR spectra were recorded at room temperature.

Temperature Programmed Desorption (TPD) of Ammonia. Ammonia-TPD experiments were performed using a conventional static-adsorption system connected to a quadrupole mass spectrometer through a high-vacuum line. Samples evacuated at 773 K for 1 h were exposed to a 21 kPa of ammonia gas at 423 K for 0.5 h, evacuated for 1 h at 423 K, and then cooled to room temperature. Spectra were obtained at a heating rate of 10 K min^{-1} from 314 to 848 K.

Results and Discussion

Preparation of Metallosilicates. The amounts of metals in the bulk phase of the atom-planted samples are shown in Table 1. The samples planted with aluminium, gallium, and indium are denoted by AP(Al)-Z, AP(Ga)-Z, and AP(In)-Z, respectively. The order of the amounts of introduced metals in the bulk phase were AP(Al)-Z>AP(Ga)-Z>AP(In)-Z, when these samples were prepared under the same conditions. Samples treated with metal chlorides were rinsed with 0.1 M NH_4NO_3. Therefore, the introduced metals existed in the framework sites of the ZSM-5 zeolite and/or non-framework sites except ion-exchange sites. These atom-planted sample were checked by powder X-ray diffraction for crystallinity, which was uniformly good. Moreover, the surface areas of the atom-planted samples were almost the same as that of the parent ZSM-5, as shown in Table 1. Consequently, the structure of the ZSM-5 zeolite was not destroyed by the atom-planting method.

Since trivalent ions are introduced into the tetrahedral framework sites, acidic OH groups responsible for the Brønsted acid sites should be generated. In addition, the frequency of the acidic OH groups in the IR spectra can be varied by substitution with Me^{3+} of different nature. The IR spectra in the hydroxyl stretching region for the parent highly siliceous ZSM-5 (Si/Al=870) and the atom-planted samples [AP(Al)-Z, AP(Ga)-Z, and AP(In)-Z] are depicted in Fig. 1. The parent ZSM-5 (spectrum a) showed only one band at 3740 cm^{-1} due to non-acidic silanol groups.[15] The IR

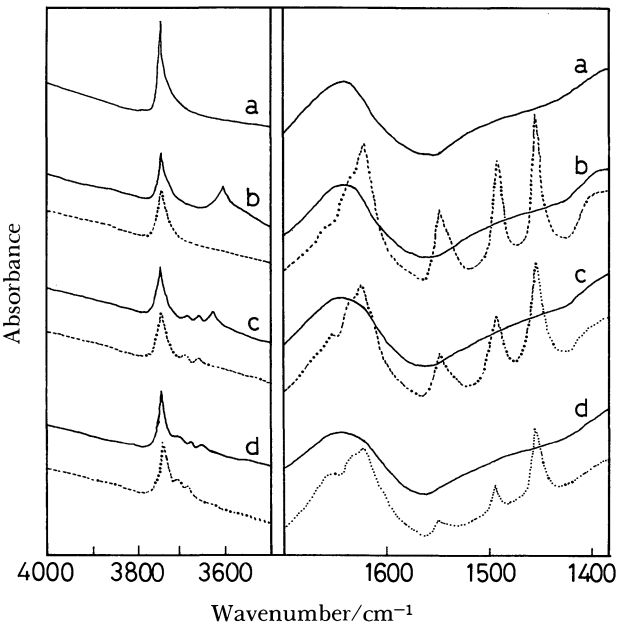

Fig. 1. Infrared spectra in the hydroxyl stretching region for parent ZSM-5 and the atom-planted samples: (a) parent (Si/Al=870), (b) AP(Al)-Z, (c) AP(Ga)-Z, (d) AP(In)-Z. Dotted lines show IR spectra following pyridine adsorption.

Table 1. Chemical and Physical Properties of the Samples Investigated

Sample	Metal concn / mmol g^{-1}	Surface area / m^2 g^{-1}	Unit-cell Dimensions/Å a	b	c	Vol/Å^3	Amount of acid sites/mmol g^{-1}
Parent ZSM-5	0.02 (Al)	448	20.22	20.11	13.08	5320	0.01
AP(Al)-Z	0.74 (Al)	415	20.28	20.18	13.04	5336	0.29
AP(Ga)-Z	0.30 (Ga)	422	20.32	20.10	13.11	5354	0.16
AP(In)-Z	0.24 (In)	431	20.40	20.09	13.13	5382	0.14

spectrum for the AP(Al)-Z exhibited a new band at 3610 cm^{-1} together with the band at 3740 cm^{-1}. The 3610 cm^{-1} band is attributed to the framework Al(OH)Si groups responsible for Brønsted acid sites.[15] In the IR spectrum of pyridine adsorbed on AP(Al)-Z, we observed an absorption band at 1545 cm^{-1}, which was attributed to pyridinium ion;[16] the absorption band at 3610 cm^{-1} disappeared. These facts show the introduction of the Al^{3+} into the framework by the atom-planting method.

The IR spectrum for the AP(Ga)-Z exhibited new bands at 3625, 3660, and 3690 cm^{-1} together with the band at 3740 cm^{-1}. On the IR spectrum of pyridine adsorbed on the AP(Ga)-Z, we observed the 1545 cm^{-1} band; the band at 3625 cm^{-1} disappeared. Chu and Change have demonstrated that in a gallosilicate with the ZSM-5 type (MFI) structure, the H^+ form has a characteristic band at 3620 cm^{-1} attributable to the framework Si(OH)Ga.[3] These facts indicate the introduction of Ga^{3+} into framework by the atom-planting method.

The spectrum of the AP(In)-Z exhibited new bands at 3650, 3680, and 3705 cm^{-1}, together with the 3740 cm^{-1} band. In the IR spectrum of pyridine adsorbed on the AP(In)-Z, we observed the 1545 cm^{-1} band; the 3650 cm^{-1} band disappeared. This fact suggests that the introduction of In^{3+} into the framework by the atom-planting method.

When aluminium, gallium, and indium atoms are introduced into the framework of the parent ZSM-5, the unit-cell volumes of the atom-planted samples should become more than that of the parent ZSM-5, because the ionic radii of Al^{3+} (0.053 nm), Ga^{3+} (0.061 nm), and In^{3+} (0.076 nm) are larger than that of Si^{4+} (0.040 nm). As shown in Table 1, the unit-cell volumes of these atom-planted samples were more than that of the parent ZSM-5. These facts also suggest that aluminium, gallium, and indium are introduced into the framework. From these results, it is apparent that aluminosilicate, gallosilicate, and indosilicate with the ZSM-5 type structure can be prepared by the atom-planting method.

The bands at 3660 and 3690 cm^{-1} for the AP(Ga)-Z, and at 3680 and 3705 cm^{-1} for the AP(In)-Z were attributed to non-acidic OH groups, since these bands were not affected by the adsorption of pyridine. Metal atoms may be introduced not only into the framework sites, but also into the non-framework sites, as was observed in the case of the aluminium-planting.[9] The bands responsible for the non-acidic OH groups may be due to some hydroxylated metal-containing species in the non-framework. In the spectra of the pyridine adsorbed on the AP(Al)-Z, AP(Ga)-Z, and AP(In)-Z, we also observed the adsorption band of the pyridine coordinated with Lewis acid sites at 1455 cm^{-1}.[16] These facts indicate that not only Brønsted acid sites but also Lewis acid sites are generated by the atom-planting method. A part of metal introduced into the non-framework sites may be responsible for the Lewis acid sites.

We have discussed the mechanism for alumination (Al-planting) of the highly siliceous ZSM-5 with $AlCl_3$, and suggested that aluminium atoms are introduced into defect sites of the highly siliceous ZSM-5.[9,10] The amount of defect sites in the framework of highly siliceous ZSM-5 can be changed by controlling the synthetic conditions of the zeolites.[10,17] The amount of defect sites was measured through the exchange of oxygen isotopes between the zeolitic framework and $C^{18}O_2$.[10,17,18] When the plantings of gallium and indium into the highly siliceous ZSM-5 with a very small amount of the defect sites were carried out at 923 K, the adsorption bands attributed to the acidic OH groups could not be detected. Hence, gallium and indium could be poorly introduced into the framework of the highly siliceous ZSM-5 with a very small amount of the defect sites. Endoh et al. have reported the galliation of the highly siliceous ZSM-5 by a treatment with NaOH solution containing gallium ions, and concluded that the reactivity of the zeolite for the galliation may depend upon the amount of the defect sites.[18] Consequently, for the mechanism of the planting of gallium and indium atoms in the zeolitic framework, we suggest that gallium and indium atoms are planted solely in the defect sites of the zeolite.

We have also reported that a considerable amount of aluminium is introduced into the non-framework sites by alumination, and that the introduction of aluminium into the non-framework occurs by a reaction of the terminal SiOH groups on the external surface and/or non-intact Si–O–Si bonds with $AlCl_3$.[9,10] In the IR spectra, changes in the terminal SiOH region may provide information related to the mechanism of the introduction of atoms into the non-framework sites. We have reported that the band at 3740 cm^{-1} can be attributed not to hydroxyl nests (defect sites), but to both isolated SiOH groups on the external surface and intracrystalline isolated SiOH groups.[17] Due to the atom-planting, the intensity of the 3740 cm^{-1} band decreased. This fact suggests that a part of the metal atoms in the non-framework sites is caused by a reaction of the terminal SiOH groups on the external surfaces with metal chlorides.

The amount of the Brønsted acid sites may correspond to the amount of the metal in the framework sites. The relative amount of the Brønsted acid sites was roughly estimated on the basis of the integrated absorbances of the acidic OH bands. The area of the Al(OH)Si band for the AP(Al)-Z was about 2 times as much as that of the Ga(OH)Si band for the AP(Ga)-Z, and was about 5 times as much as that of the In(OH)Si band for the AP(In)-Z. These facts suggest the order of the amonts of metal atoms introduced into the framework were AP(Al)-Z>AP(Ga)-Z>AP(In)-Z,

although each parent ZSM-5 has the same amount of defect sites. This order may be explained as follows: the larger radius of metal cation corresponds to the lower thermostability of the metallosilicate or to the less amount of defect sites available for the atom planting.

Acidic Properties of Metallosilicates. The acidic properties of metallosilicates AP(Al)-Z, AP(Ga)-Z, and AP(In)-Z were examined from the infrared spectra of the adsorbed pyridine and the spectra of temperature-programmed desorption for ammonia. In the IR spectra in the OH stretching region, we observed a band at 3610 cm^{-1} due to Al(OH)Si, a band at 3625 cm^{-1} due to Ga(OH)Si, and a band at 3650 cm^{-1} due to In(OH)Si. The fact that the 3625 cm^{-1} band due to Ga(OH)Si and the 3650 cm^{-1} band due to In(OH)Si appear at higher frequencies than the 3610 cm^{-1} band due to Al(OH)Si indicates that the OH bonds in the Ga(OH)Si and In(OH)Si are more covalent than those in the Al(OH)Si and, hence, less acidic.

The strength distribution of Brønsted and Lewis acid sites can be measured from the thermodesorption of pyridine. On IR spectra of pyridine adsorbed on metallosilicates, we can observe the absorption bands of pyridinium ion (PyH^+) at 1545 cm^{-1} and of the pyridine coordinated with Lewis acid sites (PyL) at 1455 cm^{-1}. As the desorption temperature increases, only pyridine molecules adsorbed on stronger sites will remain. Figure 2 shows the absorbances of the PyH^+ and PyL bands for the AP(Al)-Z, AP(Ga)-Z, and AP(In)-Z after pyridine was desorbed at progressively higher temperatures. As shown in Fig. 2a, it is apparent that the order of the acid strength of Brønsted acid sites are In(OH)Si<Ga(OH)Si<Al(OH)Si. These results are consistent with the hypothesis from the IR spectra in the OH stretching region. In addition, as shown in Fig. 2b, it is apparent that these metallosilicates prepared by the atom-planting method have a large amount of Lewis acid sites, and that the order of the acid strength of Lewis acid sites are AP(In)-Z< AP(Ga)-Z<AP(Al)-Z.

The ammonia-TPD spectra for the AP(Al)-Z, AP(Ga)-A, and AP(In)-Z are depicted in Fig. 3. The spectrum for the AP(Al)-Z had not only a main peak at 543 K but also a shoulder peak at 643 K. We have reported that AP(Al)-Z has stronger acid sites than those on ZSM-5 zeolites, which are prepared by hydrothermal synthesis. The shoulder peak at 643 K indicates that the strong acid sites are generated by the

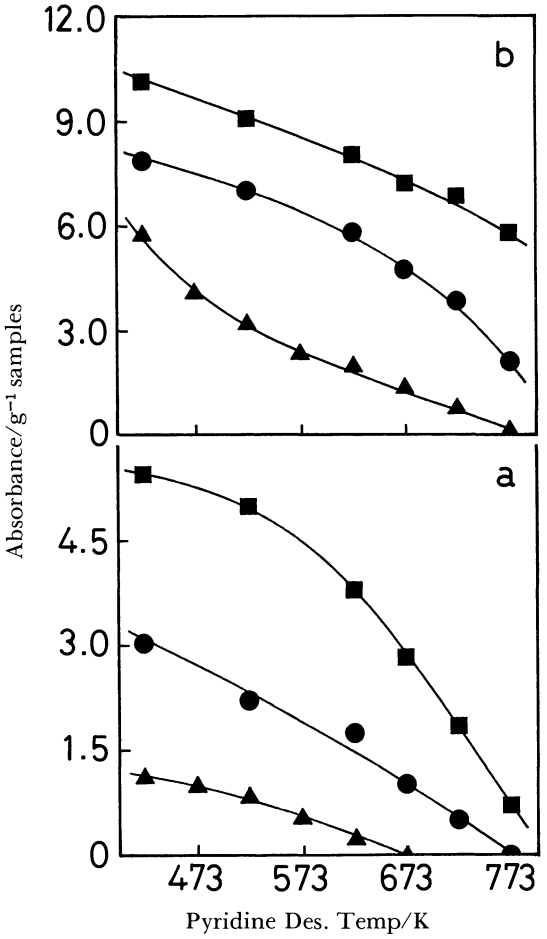

Fig. 2. Absorbance per gram of the AP(Al)-Z (■), the AP(Ga)-Z (●), and the AP(In)-Z (▲) on Brønsted acid sites (band at 1545 cm^{-1}); (a), and Lewis acid sites (band at 1455 cm^{-1}); (b), after desorption at 423—773 K.

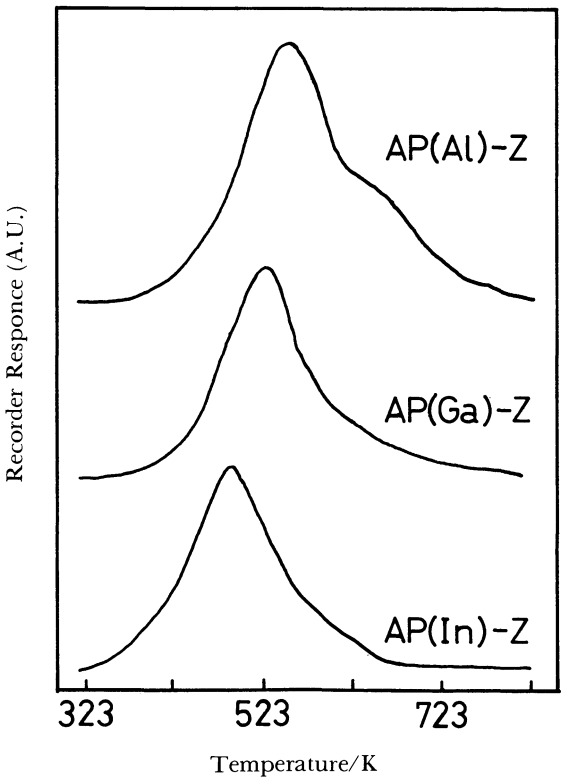

Fig. 3. NH_3-TPD spectra for the AP(Al)-Z, AP(Ga)-Z, and AP(In)-Z.

Al-planting. The spectra for the AP(Ga)-Z and for the AP(In)-Z had a single peak at 523 K and a single peak at 483 K, respectively. These facts indicate that the acid strength of the metallosilicates is ordered as follows: AP(In)-Z<AP(Ga)-Z<AP(Al)-Z.

The amount of acid sites was evaluated from the amount of ammonia desorbed during the TPD measurements. The evaluated amounts of acid sites on the metallosilicates are given in Table 1, together with the amounts of bulk metals. The amount of metal in the bulk phase was 1.7—2.5 times as much as that of the acid sites. Therefore, a part of the introduced metals does not contribute to the generation of the Brønsted or Lewis acid sites.

References

1) R. M. Barrer, "Hydrothermal Chemistry of Zeolites," Academic Press, London (1982), p. 251.
2) N. Tielen, M. Geelen, and P. A. Jacobs, *Acta Phys. Chem.*, **31**, 1 (1985).
3) C. T. -W. Chu and C. D. Chang, *J. Phys. Chem.*, **89**, 1569 (1985).
4) C. D. Change, C. T. -W. Chu, J. N. Miale, R. F. Bridger, and R. B. Calvent, *J. Am. Chem. Soc.*, **106**, 8143 (1984).
5) R. M. Dessau and G. T. Kerr, *Zeolites*, **4**, 315 (1984).
6) M. W. Auderson, J. Klinowski, and L. Xinsheng, *J. Chem. Soc., Chem. Commun.*, **1984**, 1596.
7) S. Namba, K. Yamagishi, and T. Yashima, *Chem. Lett.*, **1987**, 1109.
8) T. Yashima, K. Yamagishi, S. Namba, S. Nakata, and S. Asaoka, *Stud. Surf. Sci. Catal.*, **37**, 175 (1988).
9) K. Yamagishi, S. Namba, and T. Yashima, *J. Catal.*, **121**, 47 (1990).
10) K. Yamagishi, S. Namba, and T. Yashima, *Shokubai*, **30**, 440 (1988).
11) B. Kraushaar, L. J. M. Van de Ven, J. W. De Haan, and J. H. C. Van Hooff, *Stud. Surf. Sci. Catal.*, **37**, 167 (1988).
12) K. Yamagishi, S. Namba, and T. Yashima, *Stud. Surf. Sci. Catal.*, **48**, 459 (1989).
13) B. Kraushaar and J. H. C. Van Hooff, *Catal. Lett.*, **1**, 81 (1988).
14) T. Yashima, Y. Sakaguchi, and S. Namba, *Stud. Surf. Sci. Catal.*, **7**, 739 (1980).
15) P. A. Jacobs and R. Von Ballmoos, *J. Phys. Chem.*, **86**, 3050 (1982).
16) E. P. Parry, *J. Catal.*, **2**, 371 (1963).
17) K. Yamagishi, S. Namba, and T. Yashima, *J. Phys. Chem.*, **95**, 872 (1991).
18) A. Endoh, K. Nishimiya, K. Tsutsumi, and T. Takaishi, *Stud. Surf. Sci. Catal.*, **46**, 779 (1989).

Detection of Surface Resistance in a Gas/Porous-Adsorbent System by Frequency Response Method

Yusuke YASUDA
Faculty of Science, Toyama University, Toyama 930
(Received August 1, 1990)

The frequency-response (FR) method for studying an X⇌C system (Yasuda, 1982) has been extended to an $X \overset{I}{\rightleftharpoons} A \overset{II}{\rightleftharpoons} C$ system, where X denotes a molecule in the gas phase, A is an adspecies on the external surface of a porous adsorbent, and C is an adspecies within micropores. Based on the characteristic functions for a system derived analytically, it is shown that both rate constants for steps I and II can be determined separately from the FR data. According to actual data of CH_4/5A zeolite systems, it has been confirmed that both the adsorption and desorption rate constants for step I, k_a and k_d, respectively, and also the Fickian diffusional time constant at step II, $\widetilde{D}$, can be evaluated. The present method is expected to provide quantitative information conerning the existence and intensity of surface barriers of zeolite crystals.

A frequency-response (FR) method has been applied in order to determine the Fickian diffusivity in zeolite crystals of a pure gas[1] and a binary gas mixture.[2] With zeolites, however, the transport resistance of an adsorbate at the outside of individual crystals occurs due to deposition of an impenetrable material, hydrothermal pretreatment,[3,4] or changes in the crystal structure by a chemical vapor deposition method.[5] Therefore, studying the 'skin' effects seems of interest not only in fundamental research[6] but also regarding industrial applications. Although a micro-dynamic model has recently been proposed for describing the mass-transfer resistance,[7] the six parameters involved in the model seem to be too many to be determined by traditional methods based on time-response data.

The FR method is compared with the standard methods in Table 1, the important characteristic of which is in the volume variation illustrated in Fig. 1; since this method is a resonance-type method, both rate processes during steps I and II could be investigated.

After equilibrium was attained, the gas space of the system V is changed sinusoidally as

$$V(t) = V_e(1 - ve^{i\omega t}), \tag{1}$$

where V_e denotes the equilibrium volume, $v(\ll 1)$ the relative amplitude of the volume change, and ω the angular frequency. The response of the system may be observed in terms of pressure variation, which can generally be expressed by

$$P(t) = P_e\{1 + pe^{i(\omega t + \varphi)}\}, \tag{2}$$

where P_e denotes the equilibrium pressure, p the relative amplitude of the pressure variation, and φ the phase lag between the volume and pressure variation. The dependence of p and φ on ω would reflect the kinetic behavior of the system.

In the present article a theoretical treatment for the system given in Fig. 1 is carried out and some actual data concerning CH_4/5A systems are analyzed in order to confirm the applicability of this new method.

Table 1. Classification of Various Experimental Methods

	Non-equilibrium	Equilibrium
Time-response	Uptake-rate Method Chromatographic Method	NMR Method
Frequency-response		FR Method

Theoretical

Characteristic Functions. The FR of the system may be given by the following in-phase and out-of-phase components, respectively:

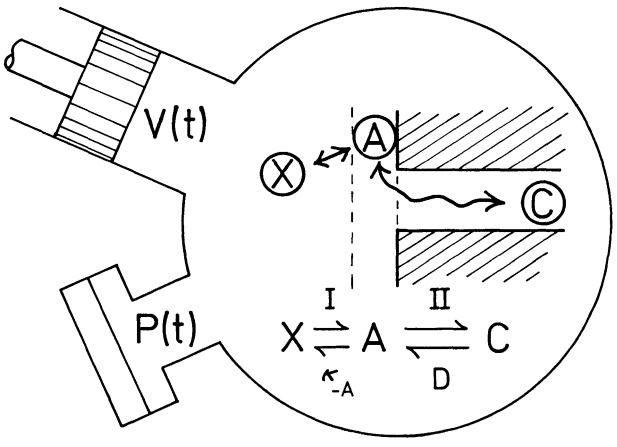

Fig. 1. Schematic diagram of the FR method applied to an X⇄A⇄C system; X denotes the adsorbate in the gas phase, A is the adspecies on the external surface, and C is the adspecies within the porous adsorbent. By measuring the pressure response $P(t)$ to the volume change $V(t)$, the two rate constant κ_{-A} and D at the steps I and II may be determined.

$$(v/p)\cos\varphi - 1 = K \cdot f_c(\omega) \tag{3}$$

and

$$(v/p)\sin\varphi = K \cdot f_s(\omega), \tag{4}$$

where K denotes the asymptote of the in-phase component as $\omega \to 0$. The value of K is expected to agree with K_e given by[1,8]

$$K_e = \left(\frac{RT_0}{V_e}\right)\left\{\frac{d(A+C)}{dP}\right\}_e, \tag{5}$$

where $\{d(A+C)/dP\}_e$ is the gradient of the adsorption isotherm and (RT_0/V_e) is the conversion factor; adspecies on the external surface are denoted by A(and/or B); the adspecies within the porous media are denoted by C.

In the extreme case, where either step I or II is rate-controlling, the present X⇌A⇌C system may be regarded as being an X⇌A or X⇌C system, each of which has been considered previously.[1,8] On the basis of these results, the present complex system can be analytically treated as follows:

(1) In the case of X⇌A, the time course of the A species, $A(t)$, associated with those of $V(t)$ and $P(t)$ in Eqs. 1 and 2 may be described by (Appendix 1)

$$A(t) = A_e[1 + m\{\alpha_c(\kappa_{-A}; \omega) - i\alpha_s(\kappa_{-A}; \omega)\}pe^{i(\omega t + \varphi)}], \tag{6}$$

where

$$m \equiv (d\ln A/d\ln P)_e \tag{7}$$

and A_e denotes the amount of A species at equilibrium.

The FR data of systems f_c and f_s may be expressed in this case by

$$f_c(\omega) = \alpha_c(\kappa_{-A}; \omega) \tag{8}$$

and

$$f_s(\omega) = \alpha_s(\kappa_{-A}; \omega), \tag{9}$$

where the characteristic functions, α_c and α_s, involving one parameter κ_{-A} are given by

$$\alpha_c(\kappa_{-A}; \omega) = \kappa_{-A}^2/(\kappa_{-A}^2 + \omega^2) \tag{10}$$

and

$$\alpha_s(\kappa_{-A}; \omega) = \kappa_{-A}\omega/(\kappa_{-A}^2 + \omega^2). \tag{11}$$

These functions are illustrated in Fig. 2.

2) A more complex system of X⇌A⇌B containing a precursor, A, has also been considered.[8]

The FR data of the system may be described by (Appendix 2)

$$f_c(\omega) = \alpha\alpha_c(\kappa_{-A}, \kappa_{-B}; \omega) \tag{12}$$

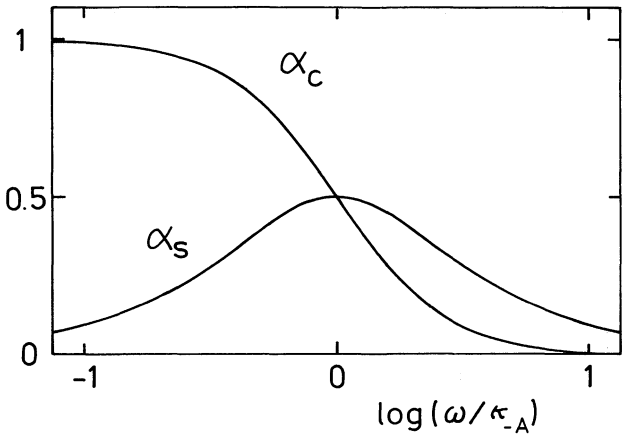

Fig. 2. Characteristic functions for an X⇄A system, $\alpha_c(\kappa_{-A}; \omega)$ and $\alpha_s(\kappa_{-A}; \omega)$; the system corresponds to the extreme case of step I being rate-controlling in Fig. 1.

and

$$f_s(\omega) = \alpha\alpha_s(\kappa_{-A}, \kappa_{-B}; \omega), \tag{13}$$

where the characteristic functions, $\alpha\alpha_c$ and $\alpha\alpha_s$, involving two parameter κ_{-A} and κ_{-B} are given by

$$\alpha\alpha_c(\kappa_{-A}, \kappa_{-B}; \omega) = (a\kappa_{-A}/\omega)^2\{a + b\alpha_c(\kappa_{-B}; \omega)\}/\Phi \tag{14}$$

and

$$\alpha\alpha_s(\kappa_{-A}, \kappa_{-B}; \omega) = (a\kappa_{-A}/\omega)[1 - (a\kappa_{-A}/\omega)\{(a\kappa_{-A}/\omega) + b\alpha_s(\kappa_{-B}; \omega)\}/\Phi]. \tag{15}$$

Here, a short notation is introduced:

$$\Phi \equiv \{(a\kappa_{-A}/\omega) + b\alpha_s(\kappa_{-B}; \omega)\}^2 + \{a + b\alpha_c(\kappa_{-B}; \omega)\}^2. \tag{16}$$

(3) In the case of X⇌C on the other hand, the time course of the C species, $C(t)$, associated with those of $V(t)$ and $P(t)$ in Eqs. 1 and 2 may be described as[1]

$$C(t) = C_e[1 + m'\{\delta_{nc}(\widetilde{D}; \omega) - i\delta_{ns}(\widetilde{D}; \omega)\}pe^{i(\omega t + \varphi)}] \quad (n = 1 \text{ or } 3), \tag{17}$$

where

$$m' \equiv (d\ln C/d\ln P)_e \tag{18}$$

and C_e denotes the amount of C species at equilibrium.

The FR data of the system may be expressed in this case by

$$f_c(\omega) = \delta_{nc}(\widetilde{D}; \omega) \tag{19}$$

and

$$f_s(\omega) = \delta_{ns}(\widetilde{D}; \omega). \tag{20}$$

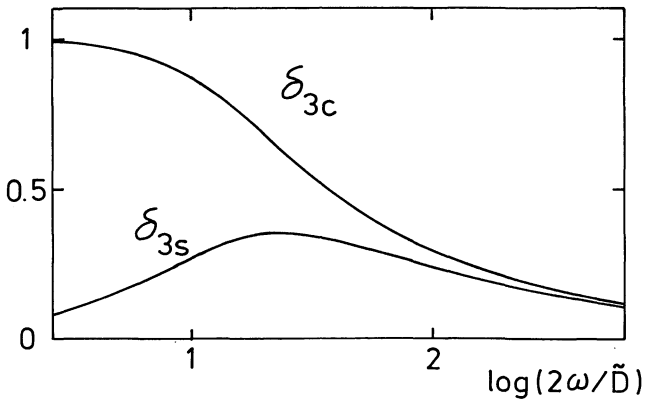

Fig. 3. Characteristic functions for an X⇄C system, $\delta_{3c}(\widetilde{D};\omega)$ and $\delta_{3s}(\widetilde{D};\omega)$; the system corresponds to the extreme case of step II being rate-controlling in Fig. 1.

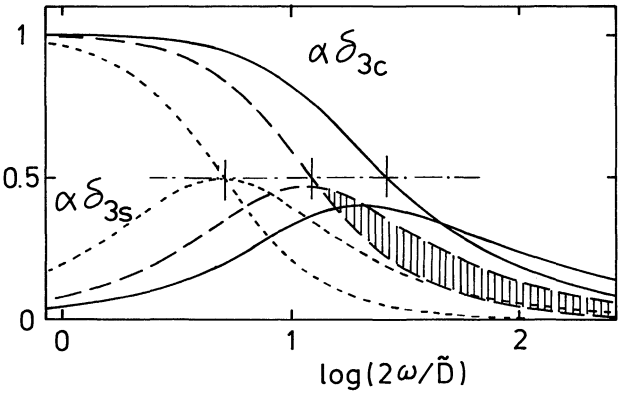

Fig. 4. Characteristic functions for an X⇄A⇄C system, $\alpha\delta_{3c}(\zeta, \widetilde{D};\omega)$ and $\alpha\delta_{3s}(\zeta, \widetilde{D};\omega)$; the parameter ζ is 50 (——), 10 (----), and 3 (……). It is demonstrated by the shaded area that these curve are intermediate between those in Fig. 2 and in Fig. 3.

The characteristic functions, δ_{nc} and δ_{ns}, involving one parameter, $\widetilde{D}$, are analytically given in Ref. 1; δ_{1c} and δ_{1s} are based on a plane sheet model, and δ_{3c} and δ_{3s} on an isotropic sphere model. The latter functions are applicable to this work with 5A; they are illustrated in Fig. 3.

(4) The FR data of the X⇌A⇌C system are assumed to be expressed by

$$f_c(\omega) = \alpha\delta_{nc}(\kappa_{-A}, \widetilde{D};\omega) \tag{21}$$

and

$$f_s(\omega) = \alpha\delta_{ns}(\kappa_{-A}, \widetilde{D};\omega). \tag{22}$$

The characteristic functions, $\alpha\delta_{nc}$ and $\alpha\delta_{ns}$, involving two parameters, κ_{-A} and $\widetilde{D}$, may be derived from Eqs. 14 and 15 by an analogy between

$$\{\alpha_c, \alpha_s\} \text{ for } X \rightleftharpoons A \rightarrow \{\alpha\alpha_c, \alpha\alpha_s\} \text{ for } X \rightleftharpoons A \rightleftharpoons B$$

and

$$\{\delta_{nc}, \delta_{ns}\} \text{ for } X \rightleftharpoons C \rightarrow \{\alpha\delta_{nc}, \alpha\delta_{ns}\} \text{ for } X \rightleftharpoons A \rightleftharpoons C,$$

since Eq. 17 is similar in form to Eq. 6.

Consequently, we have the final results

$$\alpha\delta_{nc}(\kappa_{-A}, \widetilde{D};\omega) = (a\kappa_{-A}/\omega)^2\{a + c\,\delta_{nc}(\widetilde{D};\omega)\}/\Theta \tag{23}$$

and

$$\alpha\delta_{ns}(\kappa_{-A}, \widetilde{D};\omega) = (a\kappa_{-A}/\omega)[1 - (a\kappa_{-A}/\omega)\{(a\kappa_{-A}/\omega) + c\,\delta_{ns}(\widetilde{D};\omega)\}/\Theta]. \tag{24}$$

Here, a short notation is introduced:

$$\Theta \equiv \{(a\kappa_{-A}/\omega) + c\delta_{ns}(\widetilde{D};\omega)\}^2 + \{a + c\,\delta_{nc}(\widetilde{D};\omega)\}^2 \tag{25}$$

and

$$c \equiv (dC/dP)_e/\{d(A + C)/dP\}_e \equiv 1 - a. \tag{26}$$

Three typical curves of $\alpha\delta_{3c}$ and $a\delta_{3s}$ for different choices of the values for $a\kappa_{-A}$ and $\widetilde{D}$ are compared in Fig. 4, where $a \ll 1$; that $c \fallingdotseq 1$ are assumed, because they are usually satisfied with zeolites (as discussed below). The shaded area demonstrates that these functions are intermediate in shape between the curves given in Fig. 2 and those in Fig. 3. It is worth noting that the shaded area, or the peak height of $\alpha\delta_{3s}$ depends on the ratio of ζ, defined by

$$\zeta \equiv a\kappa_{-A}/\widetilde{D}. \tag{27}$$

The Fickian diffusional time constant, $\widetilde{D}$, is given in the case of the isotropic sphere model by[1]

$$\widetilde{D} = D/r_m^2, \tag{28}$$

where D is the Fickian diffusivity and r_m is the radius of the sphere. On the other hand, the fraction, a, is expected to be approximately proportional to r_m^{-1}, since the ratio of the external surface area to the volume of the sphere is $3/r_m$. We, thus, have

$$\zeta \propto (\kappa_{-A}/D)r_m, \tag{29}$$

suggesting that 'skin' effects depend not only on the ratio of the rate constants at steps I and II, κ_{-A}/D, but also on the size of the crystals, which is in accordance with experimental findings.[3a]

Crystal-Size Distribution. The microcrystal sizes of synthetic zeolites are usually not identical, but distributed. The distribution may be regarded as being almost normal.[9] In a data analysis, therefore, δ_{nc} and δ_{ns} in Eqs. 23 and 24 should be modified as

$$\bar{\delta}_{nj}\left(\frac{D}{r_m^2};\omega\right)=\frac{1}{(2\pi)^{\frac{1}{2}}\sigma}\int_0^\infty \delta_{nj}\left(\frac{D}{r^2};\omega\right)\exp\left\{-\frac{(r-r_m)^2}{2\sigma^2}\right\}dr \quad (j=\text{c or s}), \tag{30}$$

where σ is the standard deviation and r_m is the mean radius, provided that $n=3$.

Evidently, when the crystal-size distribution is considered, Eqs. 21 and 22 should be modified as

$$f_c(\omega)=\alpha\bar{\delta}_{nc}(\zeta,\widetilde{D};\omega) \tag{31}$$

and

$$f_s(\omega)=\alpha\bar{\delta}_{ns}(\zeta,\widetilde{D};\omega), \tag{32}$$

where

$$\alpha\bar{\delta}_{nc}(\zeta,\widetilde{D};\omega)=(a\kappa_{-A}/\omega)^2\{a+c\,\bar{\delta}_{nc}(\widetilde{D};\omega)\}/\bar{\Theta} \tag{33}$$

and

$$\alpha\bar{\delta}_{ns}(\zeta,\widetilde{D};\omega)= (a\kappa_{-A}/\omega)[1-(a\kappa_{-A}/\omega)\{(a\kappa_{-A}/\omega)+c\,\bar{\delta}_{ns}(\widetilde{D};\omega)\}/\bar{\Theta}]. \tag{34}$$

Here, a short notation is introduced:

$$\bar{\Theta}\equiv\{(a\kappa_{-A}/\omega)+c\bar{\delta}_{ns}(\widetilde{D};\omega)\}^2+\{a+c\,\bar{\delta}_{nc}(\widetilde{D};\omega)\}^2. \tag{35}$$

Equations 31—35, after substitution of $n=3$ and $c=1$, were applied to a data analysis of CH_4/5A systems in this work.

It is worth noting that if the kinetic behavior at step I is described by a *Langmuir-type* rate equation, κ_{-A} may be given by[8]

$$\kappa_{-A}=k_aP_e+k_d, \tag{36}$$

where k_a and k_d denote the adsorption and desorption rate constants, respectively.

Experimental

Materials. A synthetic zeolite (5A) was supplied by Tosoh Corporation (A-30; designated as Linde 5A); its properties are summarized in Table 2. For a comparison, Linde 5A supplied commercially was used after the preparation described previously.[10]

Methane in a commercial cylinder (99.99% pure; data in catalogue) was used without any further purification.

Table 2. Properties of A-30

Cation exchange	$CaO/(CaO+Na_2O)=0.70$
Mean edge length	3.0 μm
Pretreatment	(i) pelleted with binder, (ii) calcined at 400—500°C for 1—2 h, (iii) moistened with water, and (iv) calcined again.

Apparatus and Procedure. Both the FR apparatus and procedure were similar to those described previously;[1,11] blank experiments were carried out with He under almost the same conditions as those with CH_4.

Results and Discussion

(1) A-30 Systems. Changes in the FR data at different equilibrium temperatures (T_e) are shown in Figs. 5—8; these data were divided by the value of K_F given in Table 3. The value of K_e evaluated from the adsorption isotherm according to Eq. 5 is also given in Table 3. The agreement between K_F and K_e suggests that all FR data of the system were detected in the ω-region scanned.

All solid curves represent the calculated results from Eqs. 33 and 34, where the value of σ/r_m concerned with the crystal-size distribution was assumed to be 0.4.[9b] Two parameters, ζ and $\widetilde{D}$, were determined on a trial-and-error basis from the shape of f_c and f_s; the value of ζ was easily estimated from the area corresponding to

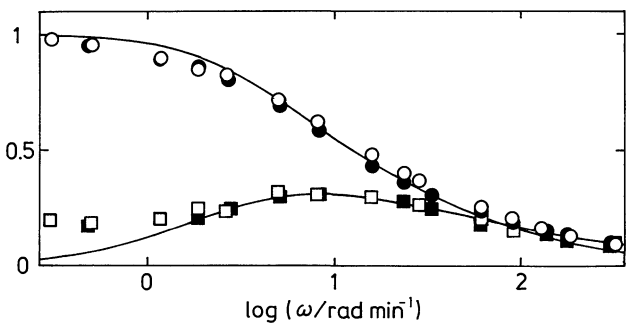

Fig. 5. FR data of CH_4/A-30 systems at −78°C; the in-phase and the out-of-phase components, f_c and f_s, are represented by the circles and the squares, respectively; each component was divided by K_F given in Table 3. ● and ■ represent the data obtained under P_e=2.7 Torr; ○ and □, those under P_e=4.5 Torr. The solid curve are calculated from Eqs. 33 and 34 of which parameters, ζ and $\widetilde{D}$, are given in Table 3.

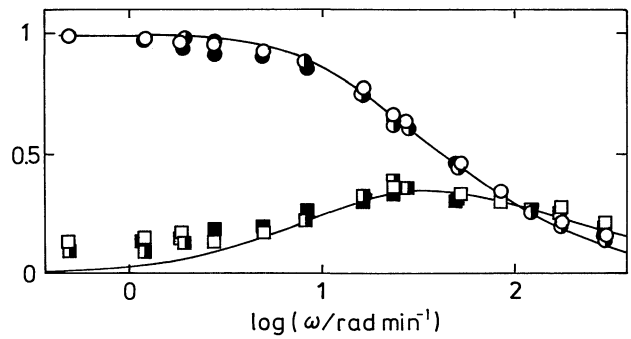

Fig. 6. FR data of CH_4/A-30 systems at T_e=−50°C. ● and ■ represent the data under P_e=3.0 Torr; ◑ and ◨, those under P_e=5.8 Torr; ○ and □, those under P_e=7.3 Torr. Notation is that of Fig. 5.

the shaded area in Fig. 4. The results are summarized in Table 3; the shift of the peak maximum of f_s has revealed an increase of $\widetilde{D}$ with increasing T_e, while an increase in the overlapping area leads to a decrease in ζ.

The deviation of f_s from the theoretical curves in the lower ω-region in Fig. 5 decreased with increasing T_e; the disagreement of K_F with K_e also decreased. This fact suggests that although the model in Fig. 1 is valid at higher T_e, the contribution of another immobile adspecies besides A and C increased with the decreasing T_e.

Arrhenius plots of the values of $a\kappa_{-A}$ ($=\zeta\widetilde{D}$; Eq. 27) and $\widetilde{D}$ are shown in Fig. 9; the activation energy of the intracrystalline diffusion, E_D, evaluated from the solid straight line was 19.1 kJ mol^{-1}, which was comparable with the heat of adsorption, ($-\Delta H=$) 19.8 kJ mol^{-1}, calculated from K_e's at $T_e=-50$ and -21 °C in Table 3 according to Clausius–Clapeyron equation.

The dependence of f_c and f_s on P_e was so slight (Fig. 8) that it was difficult to directly evaluate k_a and k_d from Eq. 36. However, on the basis of the shift indicated by the light lines in Fig. 8, we can estimate the values of k_a and k_d as follows:

(i) $\omega_{\frac{1}{2}}$ is introduced by

$$\alpha\bar{\delta}_{3c}(\zeta, \widetilde{D}; \omega_{\frac{1}{2}}) = \frac{1}{2} \tag{37}$$

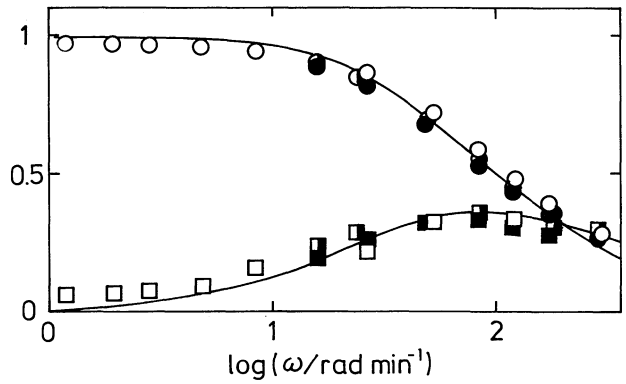

Fig. 7. FR data of CH_4/A-30 systems at $T_e=-21$ °C. ● and ■ represent the data under $P_e=3.0$ Torr; ◑ and ◨, those under $P_e=4.3$ Torr; ○ and □, those under $P_e=6.7$ Torr. Notation is that of Fig. 5.

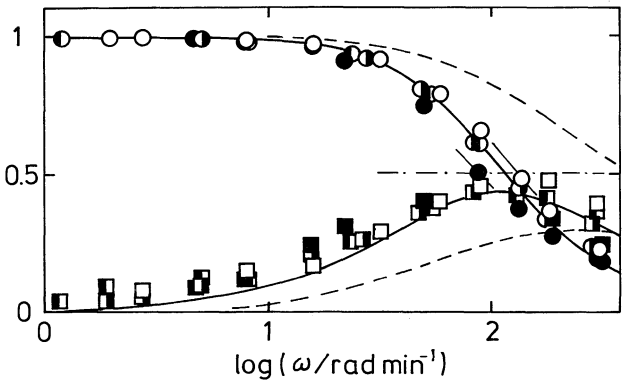

Fig. 8. FR data of CH_4/A-30 systems at $T_e=0$ °C. ● and ■ represent the data under $P_e=1.6$ Torr; ◑ and ◨, those under $P_e=3.0$ Torr; ◐ and ◧, those under $P_e=3.4$ Torr; ○ and □, those under $P_e=4.8$ Torr. Notation is that of Fig. 5. The additional dotted curves of Eq. 30 represent the extreme case of $\zeta\to\infty$; the difference between the two kinds of curves demonstrates, therefore, the transport resistance at step I.

Table 3. Experimental Conditions and Rate Constants Derived

Zeolite	m[a]	T_e	P_e	K_e	K_F	ζ	$\widetilde{D}$	$a\kappa_{-A}$[c]$\times10^{-3}$	$ak_a\times10^{-2}$	$ak_d\times10^{-2}$
	g	°C	Torr[b]				min^{-1}	min^{-1}	Torr^{-1} min^{-1}	min^{-1}
A-30	13.75	−78	2.7	—	11.4	2×10²	0.63	0.13	—	—
			4.5	—	8.4					
	25.82	−50	3.0	7.5	4.9					
			5.8	7.5	4.6	6×10	2.7	0.17	—	—
			7.3	7.5	4.5					
	25.82	−21	3.0	2.2	2.1					
			4.3	2.2	2.0	4×10	7.5	0.30	—	—
			6.7	2.2	1.7					
	101.74	0	1.6	4.2	4.8			0.15		
			3.0	4.2	6.0	10	18.8	0.19	0.3	1.0
			3.4	4.2	4.8					
			4.8	4.2	4.4			0.24		
Linde-5A	24.30	0	3.4	0.73	0.60	4×10		0.28		
			4.4	0.73	0.67	6×10	7.1	0.43	1.2	ca. 0
			9.0	0.73	0.90	2×10²		1.42		

a) The weight of the adsorbent in a dehydrated state. b) 1 Torr=133.3 Pa. c) $a\fallingdotseq6\times10^{-3}$.

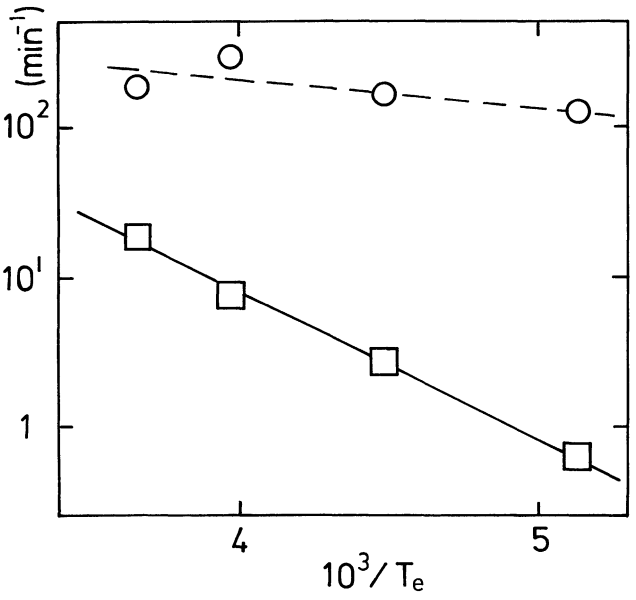

Fig. 9. Arrhenius plots of the parameters, a κ_{-A} (○) and $\widetilde{D}$ (□), derived from the solid theoretical curves shown in Figs. 5—8.

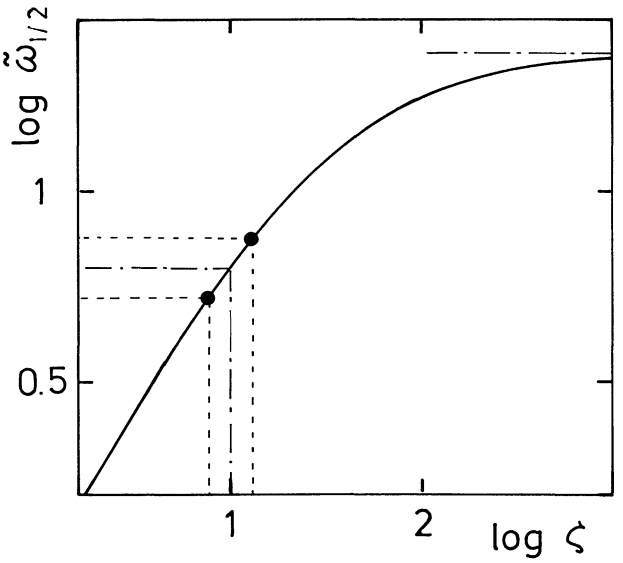

Fig. 10. The center position of the theoretical curve $\alpha\delta_{3c}(\zeta, \widetilde{D}; \omega)$ represented by $\widetilde{\omega}_{1/2}$ versus ζ; the shifts are demonstrated by the vertical lines in Fig. 4. The asymptote indicated on the right is 1.363.

and $\widetilde{\omega}_{\frac{1}{2}}$ is defined by

$$\widetilde{\omega}_{\frac{1}{2}} = \omega_{\frac{1}{2}}/\widetilde{D}. \tag{38}$$

(ii) $\widetilde{\omega}_{\frac{1}{2}}$ depends on ζ, as demonstrated by the vertical lines in Fig. 4. The extended dependence is illustrated in Fig. 10.

(iii) The shift of $\log \omega_{\frac{1}{2}}$ in Fig. 8, indicated by the two light lines, was 0.17.

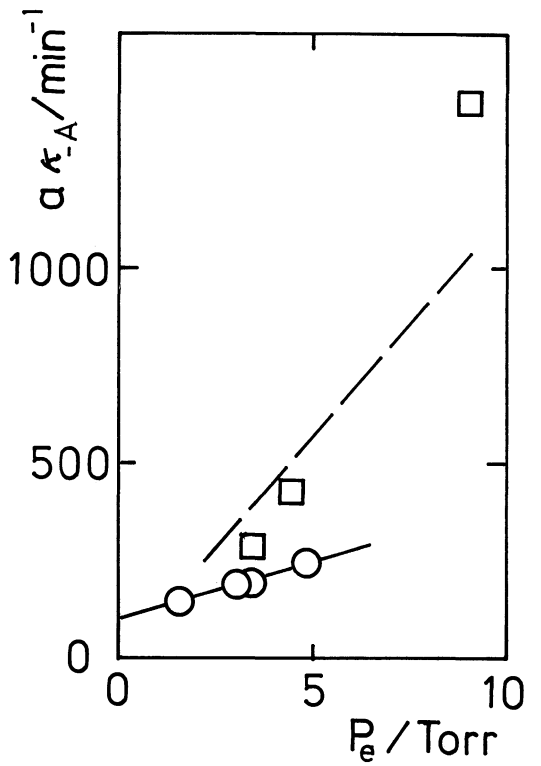

Fig. 11. Rate constant at step I, a κ_{-A}, versus P_e. ○'s represent the results of A-30; □'s, those of Linde 5A. The straight lines lead to the values of ak_a and ak_d given in Table 3.

(iv) The mean value of ζ was 10 (see Table 3).

(v) A shift by 0.17 of $\Delta\log \omega_{\frac{1}{2}}(=\Delta\log \widetilde{\omega}_{\frac{1}{2}})$ leads to 0.22 for $\Delta\log \zeta$, indicated by the solid circles in Fig. 10.

(vi) Consequently, we have (1 Torr=133.322 Pa)

$$\zeta = \begin{cases} 13 & \text{at } P_e = 4.8 \text{ Torr} \\ 7.8 & \text{at } P_e = 1.6 \text{ Torr.} \end{cases} \tag{39}$$

(vii) The values of $a\kappa_{-A}(P_e)$ evaluated from $\zeta(P_e)\times\widetilde{D}$ are plotted in Fig. 11; since the adsorption isotherm at T_e=0 °C was proportional to P_e, $\widetilde{D}$ was assumed to be independent of P_e.[12]

(viii) Under the assumption of Eq. 36, we found the values of ak_a and ak_d from the straight line in Fig. 11; they are given in Table 3.

(2) Linde 5A Systems. In order to determine the effects of a hydrothermal pretreatment of A-30, additional experiments were carried out. The FR data of Linde 5A (without the hydrothermal pretreatment) are shown in Fig. 12.

The dashed and the solid curves were calculated from Eqs. 33 and 34 under the assumption that σ/r_m=0.5.[10] In this case, the pressure dependence of $\zeta(P_e)$ was determined directly by curve fittings under the assumption of constant $\widetilde{D}$; these results are given in Table 3.

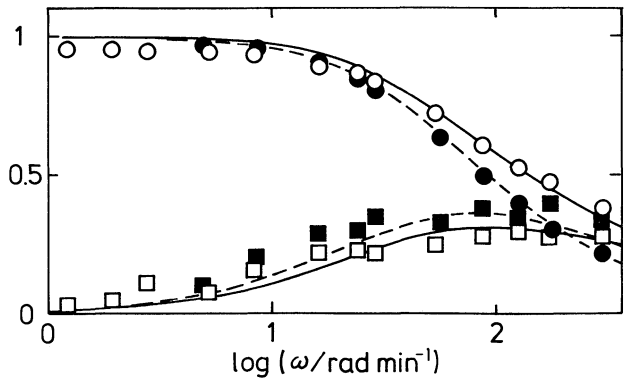

Fig. 12. FR data of CH_4/Linde 5A systems at T_e= 0°C. ● and ■ represent the data under P_e=3.4 Torr; ○ and □, those under P_e=9.0 Torr. The dashed and the solid curves are calculated from Eqs. 33 and 34, of which parameters are given in Table 3.

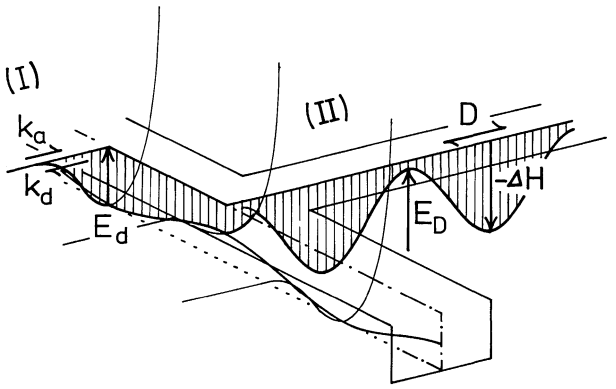

Fig. 13. The potential energy distribution of the X⇄A⇄C system in Fig. 1. Every six constant characteristic of the adsorbate-adsorbent system may be evaluated from the FR data analysis: k_a and k_d denote adsorption and desorption rate constants, respectively; E_d is the activation energy of the desorption; D is the Fickian diffusivity; E_D is the activation energy of the diffusion; $-\Delta H$ corresponds to the heat of adsorption.

The values of $a\kappa_{-A}(P_e)$ evaluated from ζ and $\widetilde{D}$ are plotted in Fig. 11. Though the results seem to be scattered, it may be concluded that the value of k_a is considerably larger than that of A-30, whereas k_d is very smaller than that of A-30; it is worth noting that Eq. 36 is valid only if the Langmuir-type equation is accepted.

The value of a is expected to be about 6×10^{-3}, since the external BET surface area of 5A zeolites was 0.6% of the entire surface area.[13] The absolute value of k_d is, therefore,

$$k_d = 1.7 \times 10^4 \text{ min}^{-1} \text{ for A-30.} \quad (40)$$

The mean lifetime of A-species, τ_A, can be given by the inverse of k_d,

$$\tau_A = 4 \times 10^{-3} \text{ s.}$$

Since k_d of the Linde 5A system was considerably smaller than that of A-30, a hydrothermal pretreatment made the lifetime of the A-species considerably shorter.

(3) Effect of Intercrystalline Diffusion. The theoretical curves based on the model in Fig. 1 without intercrystalline diffusion were valid for explaining all of the FR data given in Figs. 5—8 and Fig. 12. Therefore, the resistance due to intercrystalline diffusion may be neglected. The large difference of ak_a or ak_d in Table 3 with respect to the different adsorbents also supports this conclusion, since A-30 is designated as Linde 5A.

Conclusion

According to the theoretical procedure proposed in this work, the potential energy distribution illustrated in Fig. 13 may be derived from FR data, though we have no information about surface diffusion along the external surface. It is worth noting that all six constants do not depend on the amount of adsorbent but, rather, on the structure. Therefore, the present method would provide quantitative information concerning the existence and intensity of surface barriers of zeolite crystals.

Appendix 1

The variation of the A-species may be expressed as

$$A(t) = A_e\{1 + ae^{i(\omega t + \varphi - \psi)}\}. \quad (A1)$$

According to the result in Eq. 19 of Ref. 8, we find

$$a = mp\kappa_{-A}/(\kappa_{-A}^2 + \omega^2)^{\frac{1}{2}}. \quad (A2)$$

On the other hand, we have the result

$$\tan\psi = \omega/\kappa_{-A}. \quad (A3)$$

Substitution of Eqs. A2 and A3 into Eq. A1 leads to Eq. 6.

Appendix 2

The FR of an X⇌A⇌B system has been considered[8] and the results are rewritten in terms of α_c and α_s defined by Eqs. 10 and 11:

$$(v/p)\cos\varphi - 1 = K_A(\kappa_{-A}^2/\omega^2)\{1 + K_B\alpha_c(\kappa_{-B};\omega)\}/\Phi' \quad (A4)$$

and

$$(v/p)\sin\varphi = K_A(\kappa_{-A}/\omega)[1 - (\kappa_{-A}/\omega)\{(\kappa_{-A}/\omega) + K_B\alpha_s(\kappa_{-B};\omega)\}/\Phi'], \quad (A5)$$

where the relation of $\kappa_q/\kappa_{-q}=K_q$ in Eq. 18 of Ref. 8 is considered and a short notation is introduced:

$$\Phi' \equiv \{(\kappa_{-A}/\omega) + K_B\alpha_s(\kappa_{-B};\omega)\}^2 + \{1 + K_B\alpha_c(\kappa_{-B};\omega)\}^2. \quad \text{(A6)}$$

Considering the asymptote as $\omega\to 0$ in Eq. A4, we have

$$\lim_{\omega\to 0}(v/p)\cos\varphi - 1 = K_A(1 + K_B). \quad \text{(A7)}$$

On the other hand, the asymptote may be correlated with the gradient of the adsorption isotherm:[8]

$$\lim_{\omega\to 0}(v/p)\cos\varphi - 1 = (RT_0/V_e)\{d(A + B)/dP\}_e \ (\equiv K_e'). \quad \text{(A8)}$$

A comparison of Eq. A7 with Eq. A8 leads to

$$K_A = aK_e' \quad \text{and} \quad K_B = b/a, \quad \text{(A9)}$$

where a short notation is introduced:

$$a \equiv (dA/dP)_e/\{d(A + B)/dP\}_e \equiv 1 - b. \quad \text{(A10)}$$

Substitution of the relation in Eq. A9 into Eqs. A4 and A5 leads to the final results of Eqs. 12—16.

References

1) Y. Yasuda, *J. Phys. Chem.*, **86**, 1913 (1982).

2) Y. Yasuda and K. Matsumoto, *J. Phys. Chem.*, **93**, 3195 (1989).

3) a) M. Bülow, P. Struve, G. Finger, C. Redszus, K. Ehrhardt, and W. Schirmer, *J. Chem. Soc., Faraday Trans. 1*, **76**, 597 (1980), b) M. Bülow, P. Struve, and S. Pikus, *Zeolites*, **2**, 267 (1982).

4) a) J. Kärger, W. Heink, H. Pfeifer, and M. Rauscher, *Zeolites*, **2**, 275 (1982), b) J. Kärger and H. Pfeifer, *Zeolites*, **7**, 90 (1987).

5) M. Niwa, M. Kato, T. Hattori, and Y. Murakami, *J. Phys. Chem.*, **90**, 6233 (1986).

6) J. Crank, "The Mathematics of Diffusion," Clarendon Press, Oxford (1964), p. 195.

7) M. Kocirik, P. Struve, K. Fiedler, and M. Bülow, *J. Chem. Soc., Faraday Trans. 1*, **84**, 3001 (1988).

8) Y. Yasuda, *J. Phys. Chem.*, **80**, 1867 (1976).

9) a) K. F. Loughlin, R. I. Derrah, and D. M. Ruthven, *Can. J. Chem. Eng.*, **49**, 66 (1971), b) Y. Yasuda and S. Shinbo, *Bull. Chem. Soc. Jpn.*, **61**, 745 (1988).

10) a) Y. Yasuda and G. Sugasawa, *J. Catal.*, **88**, 530 (1984), b) Y. Yasuda and A. Yamamoto, *J. Catal.*, **93**, 176 (1985).

11) Y. Yasuda, Y. Yamada, and I. Matsuura, "Proceeding of the 7th International Zeolite Conference," ed by Y. Murakami, A. Iijima, and J. W. Ward, Kodansha-Elsevier, Tokyo (1986), p. 587.

12) D. M. Ruthven, "Principles of Adsorption and Adsorption Processes," John Wiley & Sons, New York (1984), p. 124.

13) I. Suzuki, S. Oki, and S. Namba, *J. Catal.*, **100**, 219 (1986).

Flash Photolysis Study for Halogen Abstraction of $Ph_3Sn\cdot$ and $Ph_3Si\cdot$ from Alkyl Halides

Osamu Ito* Kiyohiko Hoteiya, Akira Watanabe, and Minoru Matsuda
Chemical Research Institute of Non-Aqueous Solutions, Tohoku University, Katahira, Aoba-ku, Sendai 980
(Received September 6, 1990)

The reaction rate constants for halogen abstraction of $Ph_3Sn\cdot$ and $Ph_3Si\cdot$ have been determined by xenon-flash photolysis method. The absolute rate constants for the reactivity of $Ph_3Sn\cdot$ with several alkyl halides have been compared with the relative ones; the agreement between the both methods was fairly good. For $Ph_3Sn\cdot$, the rate constant (in unit of $mol^{-1}\,dm^3\,s^{-1}$) of *n*-BuCl (5.2×10^2) was smaller than that of *n*-BuBr (3.1×10^6) by a factor of ca. $1/10^4$. With changing the alkyl halides, the rate constants for $Ph_3Si\cdot$ and $Ph_3Sn\cdot$ varied similarly, although the rate constants for $Ph_3Si\cdot$ were larger than those for $Ph_3Sn\cdot$ by factors of 50—100. The reactivity of alkyl halides increased with a decrease in the bond-dissociation energy of the R–X (X=Cl, Br).

The high reactivities of organostannyl and organosilyl radicals in halogen abstraction reactions have been well-known and utilized widely in synthetic chemistry.[1] The relative reactivities were evaluated by various methods such as product analysis[2] and ESR spectroscopy.[3] Some of them were converted into absolute rate constants by Carlsson and Ingold using the rotating sector/competitive method.[4] In order to obtain the absolute rate constants, the laser-flash photolysis has been applied to radical reactions including the organometallic radicals.[5–10] Although the usefulness of this method has been widely proved, it is hard to evaluate the rate constants smaller than ca. $10^5\,mol^{-1}\,dm^3\,s^{-1}$. For such relatively slow reactions, the xenon-flash photolysis would be expected to be useful.[11,12]

In this study, we report the absolute rate constants evaluated by following the direct decay of transient absorption bands due to $Ph_3Sn\cdot$ and $Ph_3Si\cdot$ in the presence of various alkyl halides. The absolute rate constants thus evaluated are compared with the relative rate constants obtained by a competitive method. Furthermore, we attempted to clarify the factors determining the reactivities.

Experimental

$Ph_3SnSnPh_3$ and $Ph_3SiSiPh_3$ used as the radical sources were prepared by refluxing Ph_3MCl (M=Sn, Si) with sodium metal in toluene under N_2.[13] Alkyl halides and solvents were purified by distillation before use.

Xenon-flash photolysis apparatus was of the standard design equipped with two xenon-flash lamps (Xenon Corp., N-851C); the half-duration of the lamp was ca. 8 μs. The solution containing the radical source was photodecomposed with the light longer than 270 nm which was selected by the cut-off light filter; thus, alkyl halides having absorption band shorter than 270 nm were chosen as substrates in this study. The solution was degassed up to ca. 10^{-2} Pa. All measurements were performed at 23 °C.

For competitive experiments to evaluate the relative reaction rate constants, the following chain reactions were used (Scheme 1).

$$(CH_3)_2(CN)CN{=}NC(CN)(CH_3)_2 \xrightarrow{h\nu} 2\ (CH_3)_2(CN)C\cdot + N_2 \quad (1)$$

$$(CH_3)_2(CN)C\cdot + Ph_3SnH \longrightarrow Ph_3Sn\cdot + (CH_3)_2(CN)CH \quad (2)$$

$$Ph_3Sn\cdot + RX \xrightarrow{k_X^r} Ph_3SnX + R\cdot \quad (3)$$

$$R\cdot + Ph_3SnH \longrightarrow RH + Ph_3Sn\cdot \quad (4)$$

Scheme 1.

By using azobisisobutyronitrile as a photo-initiator, which was decomposed with the light longer wavelength than 350 nm, one could obtain the relative rates for the alkyl halides with absorption band at longer wavelength than 270 nm. For such alkyl halides, it was difficult to obtain the absolute rate constants by the xenon-flash photolysis method. RH and RX were analyzed by gas chromatography; the relative rate constants were computed by the Ingold and Shaw method.[14]

Results and Discussion

Figure 1 shows the transient absorption spectra produced by the flash photolysis of $Ph_3SnSnPh_3$ and $Ph_3SiSiPh_3$ in degassed cyclohexane solution. The main peak appeared at 320—330 nm with the broad band near 450 nm. The main peaks at 320—330 nm are similar to the reported absorption bands for $Ph_3Sn\cdot$ and $Ph_3Si\cdot$ by Chatgilialoglu et al.[8]

$$Ph_3MMPh_3 \underset{k_b}{\overset{h\nu}{\rightleftharpoons}} 2\ Ph_3M\cdot \quad (5)$$

(M = Si, Sn)

By the photolysis of some disilanes and digermanes, the biradical formation via the ipso addition was reported.[10,15] It is presumed that these species also show the absorption band at ca. 330 nm, although the decay rate was slower than that of the metal centered radicals.[10] However, in the case of photolysis of

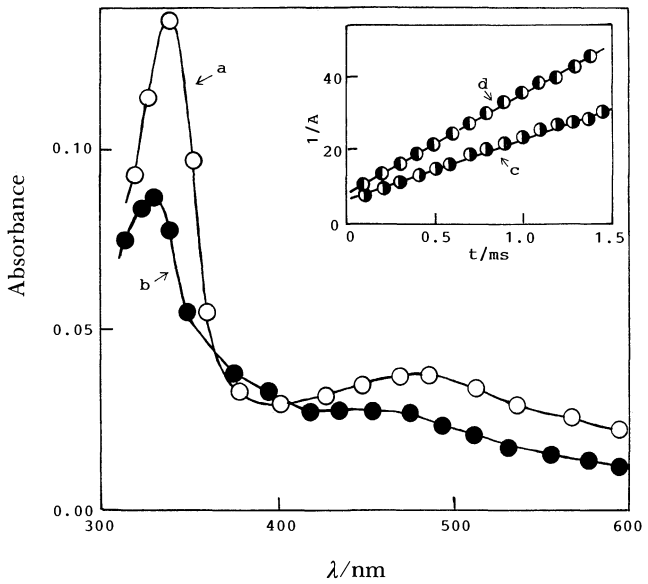

Fig. 1. Transient absorption spectra immediately after flash photolysis of 10^{-4} mol dm^{-3} of (a) $Ph_3SiSiPh_3$ and (b) $Ph_3SnSnPh_3$ in degassed cyclohexane in a cylindrical flash cell (10 cm optical path). Insert: Second-order plot at 330 nm of $Ph_3Sn\cdot$; (c) in cyclohexane and (d) in hexane.

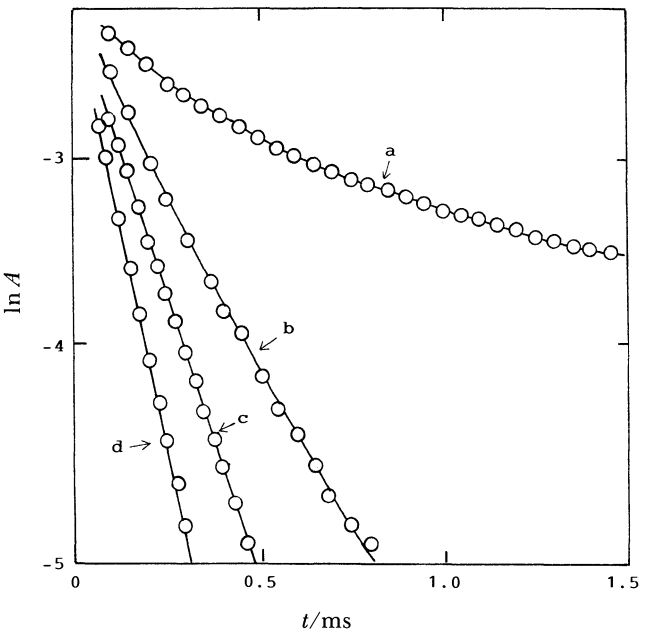

Fig. 2. First-order plots for decay of $Ph_3Sn\cdot$ (at 330 nm) in the presence of *t*-BuCl in degassed cyclohexane; (a) 0, (b) 0.21, (c) 0.47, and (d) 0.70 mol dm^{-3}.

$Ph_3SnSnPh_3$ and $Ph_3SiSiPh_3$, the formation of the biradicals may not be the main path because of the steric hindrance of many phenyl groups. The broad weak absorption band near 450 nm produced by the photolysis of the disilane was attributed to the free silanediyl (R_2Si:),[16] or to the rearrangement product.[17]

When *n*-donor solvent was used, the absorption of R_2Si: shifts to 320—330 nm by the complex formation.[18] Thus, we used cyclohexane as a solvent throughout this study. We followed predominately the decay of the main band at 320—330 nm to determine the reaction rates of $Ph_3Sn\cdot$ and $Ph_3Si\cdot$ with alkyl halides.

The insert of Fig. 1 shows the second-order plots (1/absorbance vs. time) for $Ph_3Sn\cdot$. The linear lines indicate that $Ph_3Sn\cdot$ predominately returns to Ph_3Sn-$SnPh_3$. The slope of the second-order plot, which refers to the ratio of $2k_b$ to the extinction coefficient (ε), varies with solvent viscosity, suggesting that k_b is near a diffusion controlled limit. The $2k_b/\varepsilon$ value in hexane is 3.5×10^5 cm^{-1} s^{-1}, which is close to the reported one by the laser flash photolysis.[8] On assuming k_b=ca. 2×10^9 mol^{-1} dm^3 s^{-1} which is about a half of $(C_2H_5)_3Si\cdot$, ε can be calculated to be ca. 10^4 cm^{-1} mol^{-1} dm^3; thus, the initial concentration of $Ph_3Sn\cdot$ produced by one flash exposure can be calculated from Fig. 1 to be ca. 10^{-6} mol dm^{-3}. In the case of $Ph_3Si\cdot$, the decay kinetics deviated from the second-order kinetics, suggesting that $Ph_3Si\cdot$ reacts with the phenyl group of the radical source.[8] On addition of small amount of oxygen, $Ph_3Sn\cdot$ and $Ph_3Si\cdot$ decayed rapidly; the rate constant for this reaction may be larger than 10^9 mol^{-1} dm^3 s^{-1}.

By the addition of appropriate concentration of alkyl halides to degassed solution, decay kinetics of $Ph_3Sn\cdot$ changed into first-order kinetics as shown in Fig. 2 for the reaction with *t*-butyl chloride. The decay rates were accelerated by the addition of the alkyl hafides; thus, the following halogen abstraction reaction occurs.

$$Ph_3M\cdot + RX \xrightarrow{k_X} Ph_3MX + R\cdot \qquad (6)$$

When the concentration of RX was properly high, the first-order part became predominant as shown in Fig. 2, in which the slope refers to as $k_{\text{first-order}}$. When the concentration of RX was low, the contribution of the first-order term to the whole decay was small; for such case, the first-order term was separated from the mixed-order kinetics by a computer simulation method.[19,20] Figure 3 shows the pseudo-first-order plots for some reaction systems; the slope gave the k_X value. The k_X values for various alkyl halides are summarized in Table 1 for $Ph_3Sn\cdot$ and $Ph_3Si\cdot$.

The relative halogen abstraction reactivities (k_X^r) of alkyl halides by $Ph_3Sn\cdot$ were determined by the competitive experiment described in the experimental section. They are also summarized in Table 1, in which the k_X^r value of CH_2Cl_2 was set to be 1.0. In Fig. 4, these k_X^r values are plotted against the k_X values; a linear relation is seen, showing the reliability of the

Table 1. Absolute Rate Constants (k_x) and Relative Rate Constants (k_x^r) for Halogen Abstraction of $Ph_3Sn\cdot$ and $Ph_3Si\cdot$ from RX in Cyclohexane at 23 °C

RX	$Ph_3Sn\cdot$		$Ph_3Si\cdot$	IE[c]
	k_x[a]	k_x^r[b]	k_x[a]	
	$mol^{-1}\,dm^3\,s^{-1}$		$mol^{-1}\,dm^3\,s^{-1}$	eV
n-BuCl	5.2×10^2	0.038	6.3×10^4	10.67
c-$C_6H_{11}Cl$		0.054		
$(CH_2Cl)_2$	4.5×10^3	0.15	5.7×10^5	11.12
t-BuCl	1.4×10^4	0.43	8.0×10^5	10.61
CH_2Cl_2	3.2×10^4	1.0	3.4×10^6	11.35
$PhCH_2Cl$		7.7		9.17
$CHCl_3$	2.0×10^6	55	1.1×10^8	11.42
n-BuBr	3.1×10^6	150		10.125
c-$C_6H_{11}Br$		250		

a) Each k_x value contains estimated error of ca. 10%. b) Estimation error of k_x^r is ca. 5%. c) Ionization energy from "Handbook of Chemistry and Physics," CRC Press, Bacon Raton, FL (1984), p. E-40.

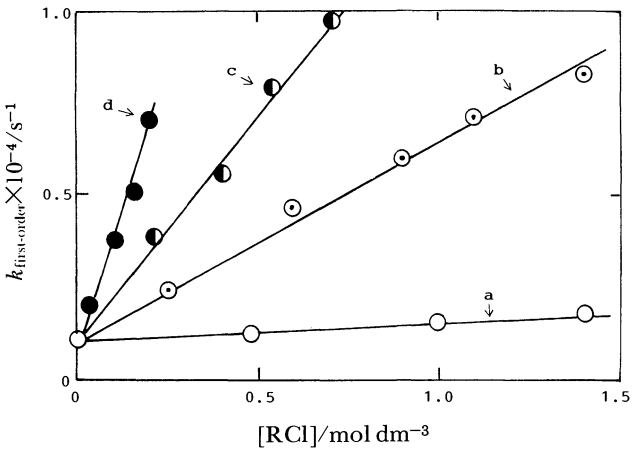

Fig. 3. Plots of pseudo-first-order rate constants ($k_{first\text{-}order}$) of $Ph_3Sn\cdot$ vs. concentration of alkyl halides; (a) *n*-BuCl, (b) $(CH_2Cl)_2$, (c) *t*-BuCl, and (d) CH_2Cl_2.

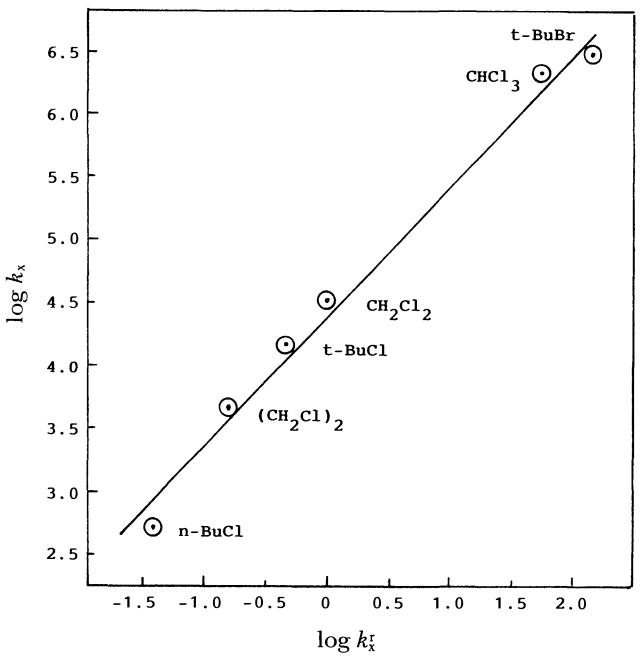

Fig. 4. Plot of log k_X (absolute rate constants) vs. log k_x^r (relative rate constant) for $Ph_3Sn\cdot$.

reaction rate constants obtained by the both methods. The k_X value for the reaction system of $Ph_3Sn\cdot$-*t*-BuCl obtained in this study ($1.4\times10^4\,mol^{-1}\,dm^3\,s^{-1}$) was similar to the reported one ($2.0\times10^4\,mol^{-1}\,dm^3\,s^{-1}$) which was determined with the rotating sector/ESR method reported by Carlsson and Ingold.[4]

For $Ph_3Sn\cdot$, the following orders in the reactivities were confirmed; RCl<RBr, $R_{primary}$-Cl<$R_{tertiary}$-Cl< cyclic halide. In order to investigate the factor controlling the reactivities, the k_X values are plotted against the bond-dissociation energy (BDE) of R-X.[21] In Fig. 5, linear correlations are found for the both radicals; the weaker the R-X bond is, the higher the reactivity is. A typical example is shown for the reactivity of RCl<RBr. Within the same halogen series, the low BDE value of R-X implies that the carbon radical (R·) is stable. Thus, the order of $R_{primary}$-Cl<$R_{tertiary}$-Cl is attributed to higher stability of tertiary carbon radical than the primary one. The α-halogen effect is more effective than the β-effect [$k_X(CH_2Cl_2)/k_X((CH_2Cl)_2)$=ca. 7]. The α-effect is intensified with additional halogen atom [$k_X(CHCl_3)/k_X(CH_2Cl_2)$=ca. 60].[22] Since the k_r values of these compounds are also on the line of Fig. 5, these effects can be interpreted by the stability of the carbon centered radicals; some of the resonance structures can be written as follows;

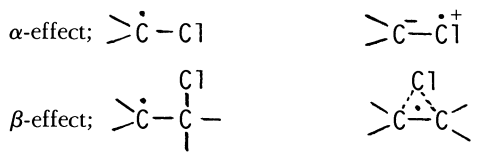

As for the polar contribution to the transition states of these reactions, charge transfer from the radical

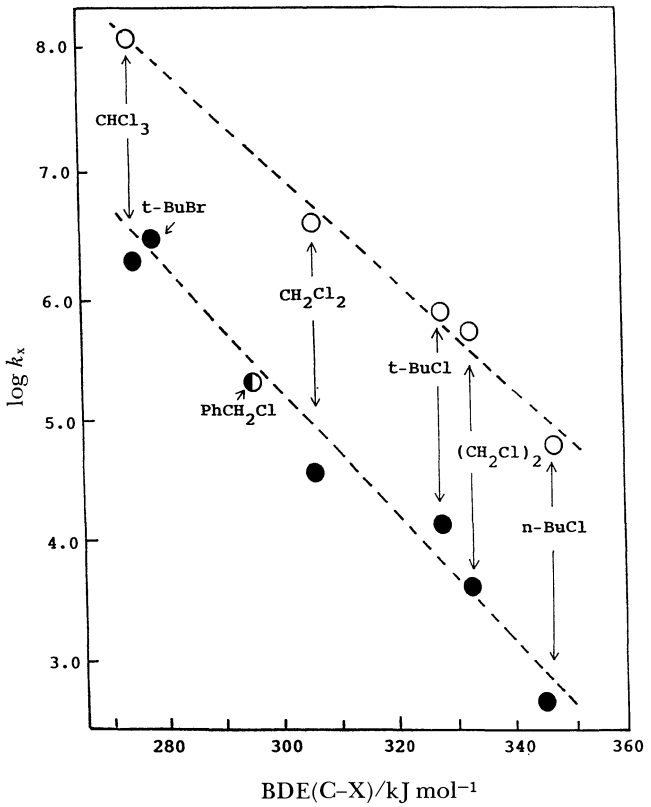

Fig. 5. Plots of log k_X vs. bond-dissociation energy of R–X [BDE(C–X)]. (●) $Ph_3Sn\cdot$ and (○) $Ph_3Si\cdot$; (◐) k_x for $PhCH_2Cl$ was evaluated from Fig. 4.

center to RX has been presumed from the Hammett plot by Chatgilialoglu et al.[23] In Table 1, however, no clear tendency that k_X values increase with the ionization energy can be found. This suggests that the polar effect is not the main factor in determining the reactivity, when a wide range of RX is compared.

From Table 1 and Fig. 5, it is confirmed that the reactivity of $Ph_3Si\cdot$ is higher than that of $Ph_3Sn\cdot$; this tendency is in agreement with the order of reactivities in the halogen abstraction of n-$Bu_3Sn\cdot$ and $Et_3Si\cdot$.[8] The order of the reactivity of $R_3Sn\cdot$ and $R_3Si\cdot$ can be well interpreted by the thermodynamic data; i.e., in the case of $(CH_3)_3MCl$, BDE of Sn–Cl (422 kJ mol^{-1}) is smaller than that of Si–Cl (485 kJ mol^{-1}),[24] which indicates that Cl-abstraction of $(CH_3)_3Sn\cdot$ is more endothermic than that by $(CH_3)_3Si\cdot$. Although the thermodynamic data for Ph_3MX are not available, this tendency is in good agreement with our observed tendency in the reactivities of $Ph_3Sn\cdot$ and $Ph_3Si\cdot$ for halogen abstraction.

The k_X value for $Ph_3Sn\cdot$–n-BuBr is ca. 1/10 of n-$Bu_3Sn\cdot$, in which the latter rate constant was determined by the laser-flash probe method.[6] The k_X value for $Ph_3Si\cdot$–t-BuCl is also ca. 1/10 of $Et_3Si\cdot$–t-BuCl.[7] The slightly lower reactivity of $Ph_3M\cdot$ compared with the corresponding $R_3M\cdot$ can be confirmed in this study. In the case of the $Ph_3C\cdot$ and $R_3C\cdot$, the former is extremely less reactive than the latter, because of the delocalization of the unpaired electron into the phenyl groups even though the π-orbitals are not in the same plane. On the other hand, the delocalization of the unpaired electron would not be expected for $Ph_3Sn\cdot$ and $Ph_3Si\cdot$, because of the small overlap between the orbitals of unpaired electron of the central atom [Si(3p) or Sn(5p)] and phenyl 2p-orbital. Thus, the difference in the reactivity between $Ph_3M\cdot$ and $R_3M\cdot$ is quite small.

References

1) a) H. G. Kuivila, L. W. Menapace, and C. R. Warner, *J. Am. Chem. Soc.*, **84**, 3584 (1963); b) H. G. Kuivila and L. W. Menapace, *J. Org. Chem.*, **28**, 2165 (1963).
2) L. W. Menapace and H. G. Kuivila, *J. Am. Chem. Soc.*, **86**, 3047 (1964).
3) J. Cooper, A. Hudson, and R. A. Jackson, *J. Chem. Soc., Perkin Trans. 2*, **1973**, 1056.
4) D. J. Carlsson and K. U. Ingold, *J. Am. Chem. Soc.*, **90**, 7047 (1968).
5) H. Paul, R. D. Small, Jr., and J. C. Scaiano, *J. Am. Chem. Soc.*, **100**, 4520 (1978).
6) C. Chatgilialoglu, K. U. Ingold, and J. C. Scaiano, *J. Am. Chem. Soc.*, **104**, 5123 (1982).
7) K. U. Ingold, J. Lusztyk, and J. C. Scaiano, *J. Am. Chem. Soc.*, **106**, 343 (1984).
8) C. Chatgilialoglu, K. U. Ingold, J. Lusztyk, A. S. Nazran, and J. C. Scaiano, *Organometallics*, **2**, 1332 (1983).
9) C. Chatgilialoglu, K. U. Ingold, J. C. Scaiano, and H. Woynar, *J. Am. Chem. Soc.*, **103**, 3231 (1981).
10) K. Mochida, M. Wakasa, Y. Nakadaira, Y. Sakaguchi, and H. Hayashi, *Organometallics*, **7**, 1869 (1988).
11) O. Ito, *J. Am. Chem. Soc.*, **105**, 850 (1983).
12) O. Ito and M. Matsuda, *J. Polym. Sci. Part. A, Polym. Chem. Ed.*, **28**, 1947 (1990).
13) H. Gilman and S. D. Rosenberg, *J. Am. Chem. Soc.*, **74**, 531 (1952).
14) C. K. Ingold and F. R. Shaw, *J. Chem. Soc.*, **1927**, 2918.
15) H. Sakurai, *J. Organomet. Chem.*, **200**, 261 (1980); **110**, 6270 (1988).
16) G. R. Gillette, G. H. Noren, and R. West, *Organometallics*, **6**, 2617 (1987).
17) H. Shizuka, K. Okazaki, M. Tanaka, M. Ishikawa, M. Sumitani, and K. Yoshihara, *Chem. Phys. Lett.*, **113**, 89 (1985).
18) T. Akasaka, S. Nagase, A. Yabe, and W. Ando, *J. Am. Chem. Soc.*, **110**, 6270 (1988).
19) E. F. Zwicker and L. I. Grossweiner, *J. Phys. Chem.*, **67**, 549 (1963).
20) G. L. Closs and B. E. Rabinow, *J. Am. Chem. Soc.*, **98**, 8190 (1976).
21) S. W. Benson, "Methods for the Estimation of Thermochemical Data and Rate Parameters," Wiley, New York (1971).
22) F. W. Evance and M. Szwarc, *Trans. Faraday Soc.*, **57**, 1905 (1961).
23) C. Chatgilialoglu, K. U. Ingold, and J. C. Scaiano, *J. Org. Chem.*, **52**, 938 (1987).
24) R. A. Jackson, *J. Organomet. Chem.*, **166**, 17 (1979).

The Carboxylation of Active Methylene Compounds with Carbon Dioxide in the Presence of Diphenylcarbodiimide and Potassium Carbonate[1)]

Koji CHIBA,* Hideyuki TAGAYA,* Masa KARASU, Tsuyoyuki ONO, Kazumi HASHIMOTO, and Yasusi MORIWAKI
Department of Materials Science and Engineering, Faculty of Engineering, Yamagata University, Jonan, Yonezawa 992
(Received September 10, 1990)

Active methylene compounds were effectively carboxylated with carbon dioxide in the presence of diphenylcarbodiimide (DPC) as a biotin model and potassium carbonate. Fluorene was carboxylated even under a nitrogen atmosphere in the presence of DPC, indicating that a carbonate ion was the carbon source. The reaction occurred even in the presence of water. It was considered that reaction intermediates are stable to water and that the concentration of the carbonate ion is important for carboxylation.

The fixation of carbon dioxide has been attempted by many researchers, since carbon dioxide is a considerable natural source of carbon.[2–6)] Furthermore, the greenhouse effect due to carbon dioxide has gained much attention and decreasing atmospheric carbon dioxide is a critical problem.[7)] Carbon dioxide can be converted into useful forms of organic compounds by coupling with an organic substance. However, in order to do so, carbon dioxide and/or the organic substances must be activated. One example of the former way is the activation of carbon dioxide by a transition metal.[2,3)] The photocarboxylation of aromatic compounds represents latter examples in which the anion radicals of aromatic compounds react with carbon dioxide.[8,9)]

It has been well established that biotin is required as a cofactor in a number of enzymatic carboxylation reactions.[6)] One of us has already reported that active methylene compounds are carboxylated by employing a reagent system, 1,3-diphenylurea (DPU), as a biotin model compound, potassium carbonate and carbon dioxide.[10,11)] Also, Otsuji and co-workers have reported that a number of active methylene compounds are carboxylated by employing the reagent system benzyltrimethylammonium hydroxide–dicyclohexylcarbodiimide and carbon dioxide.[12)] In these carboxylations, carbon dioxide is activated at the imidazole moiety. We recently found that diphenylcarbodiimide (DPC) is an effective biotin model as a carrier of carbon dioxide to active methylene compounds.[1)] We have undertaken to construct a model reaction for biotin-promoted carboxylations, whereby the chemical mechanism of the reaction may be elucidated. Mainly, we used fluorene as an active methylene compound, since fluorene-9-carboxylic acid (9-FLC) is easy to treat after the reaction.

Results and Discussions

Carboxylation of Fluorene with Imine and Carbon Dioxide. Fluorene was carboxylated with carbon dioxide and potassium carbonate to yield 9-FLC, even if no biotin model (imine) was present. However, the yield was as low as 4.8% (Table 1). It is well known that a strong base, like 1,8-diazabicyclo[5,4,0]undec-7-ene (DBU), abstracts a proton from an active methylene compound.[13,14)] In this reaction carbonate ion might abstract a proton from fluorene, while producing the fluorenyl anion ((1) in the Scheme). Since fluorenyl anion reacts with carbon dioxide to give carboxylic acid, water must be an inhibitor. Certainly, no 9-FLC was obtained when water was added. It is reported that dicyclohexylcarbodiimide was an effective imine for the carboxylation of an active methylene compound in the presence of quaternary ammonium salt.[12)] However, a low yield was obtained when potassium carbonate was used instead of quaternary ammonium salt. Also, phenyl isocyanate was not a good biotin model for this carboxylation. More than 35% of the fluorene was carboxylated with carbon dioxide in the presence of DPC. The yield was seven-times larger than that using dicyclohexylcarbodiimide. Furthermore, fluorene was carboxylated even under a nitrogen atmosphere. Without DPC, no 9-FLC was obtained if under a nitrogen atmosphere. These facts indicate that if DPC was present, potassium carbonate was able to be a source of carbon dioxide. We considered reaction mechanism (2) in the Scheme. A carbonate ion attacks an imine carbon to give anionic intermediates. The results in a non-carbon dioxide atmosphere indicated that such intermediates can donate carbon dioxide to an active methylene compound. The high yield under a carbon dioxide atmosphere suggested that such intermediates react further with carbon dioxide to give the reactive intermediates shown in the Scheme. These results are interesting examples of carboxylation under a nitrogen atmosphere as the model of an enzyme system. The yield of 9-FLC in air was 18.1%. The value was larger than 6.6% in a nitrogen atmosphere. Air might include moisture. Drying of air decreased the yield, indicating that water was a positive factor. The effect

Table 1. Carboxylation of Fluorene Using Imine as a Model of the Biotin Enzyme Active Site[a)]

Imine	Atmosphere (1 atom)	Reaction time/h	Yield of 9-FLC/%[b)]
None	CO_2	2	4.8
None[c)]	CO_2	2	0.0
None	N_2	2	0.0
Dicyclohexylcarbodiimide	CO_2	2	4.8
Diphenylcarbodiimide	CO_2	2	35.2
Diphenylcarbodiimide	Air	2	18.1
Diphenylcarbodiimide	Closed[d)]	2	10.5
Diphenylcarbodiimide	N_2	2	6.6
Diphenylcarbodiimide	N_2	5	5.7
Diphenylcarbodiimide[e)]	CO_2	2	10.3
Bis(*o*-methylphenyl)carbodiimide	CO_2	2	0.0
Bis(*m*-methylphenyl)carbodiimide	CO_2	2	32.2
Bis(*p*-methylphenyl)carbodiimide	CO_2	2	42.6
Bis(*o*-chlorophenyl)carbodiimide	CO_2	2	5.5
Bis(*o*-chlorophenyl)carbodiimide	N_2	2	0.0
Bis(*m*-chlorophenyl)carbodiimide	CO_2	2	23.8
Bis(*p*-chlorophenyl)carbodiimide	CO_2	2	15.1
Phenyl isocyanate	CO_2	5	5.2

a) Fluorene, 5 mmol; imine, 16.8 mmol; potassium carbonate, 30 mmol; DMSO, 25 ml; reaction temp, 20 °C. b) The yields were calculated on the basis of fluorene used. c) Water was added. d) Reaction was carried out with closing the reactor. e) Dimethylforamide was used as a solvent.

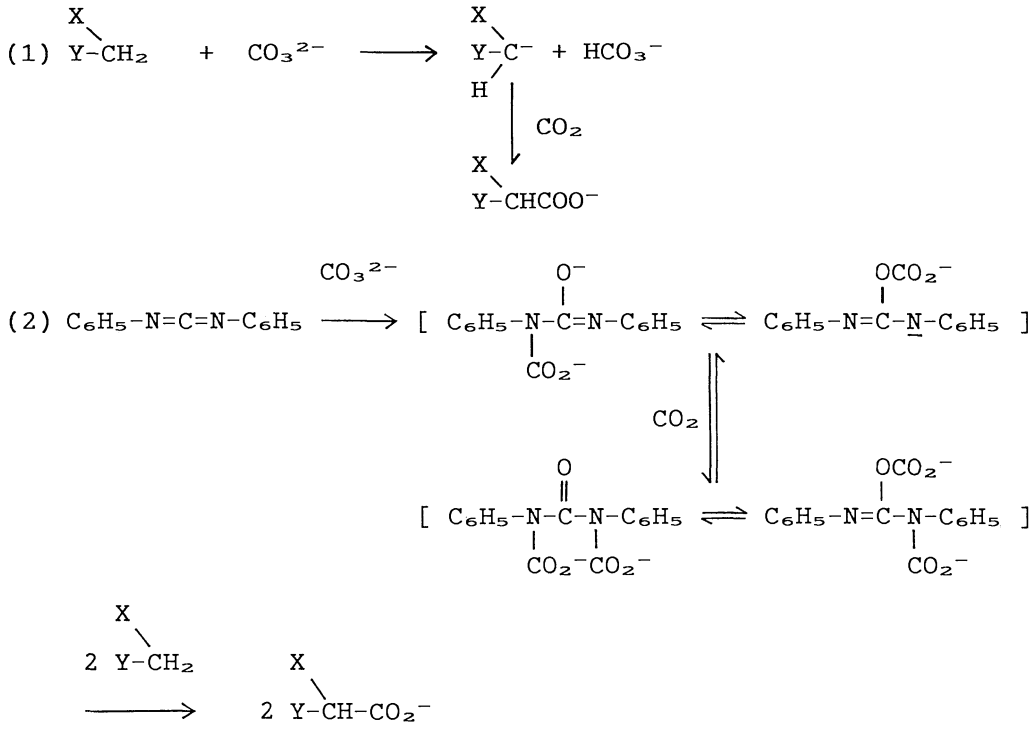

Scheme.

of water addition is discussed later. *o*-Substituents in the phenyl moieties of DPC were harmful for carboxylation, the same results as those using DPU.[10)]

If carbon dioxide is activated by transference to the imidazole moiety, as shown in the Scheme (2), *o*-substituents in the phenyl moieties of DPC interferred with the carboxylation reaction. Such a steric effect may be present.

Carboxylation of Active Methylene Compounds with DPC and Carbon Dioxide. Twelve active methylene compounds were carboxylated with carbon dioxide in the presence of DPC and potassium carbonate (Table 2). The highest yield was obtained in the carboxylation of indene. Though the yields were from 0.0 to 53.8%, there was no correlation between pK_a and the yield. In the case that a strong base is used

Table 2. Carboxylation of Active Methylene Compounds in a Carbon Dioxide Atmosphere[a]

Substrate (pK_a[16,17])	Yield of carboxylic acid/%[b]
Indene (21)	53.8
Indanone	45.5
Fluorene (25)	35.2
Phenylacetonitrile	29.2
Acetophenone (19)	28.7
1-Tetralone	21.5
p-Methoxyacetophenone	14.4
Cyclohexanone	14.0
Xanthene (29)	0.5
Acetonitrile (25)	Trace
Diphenylmethane (35)	0.0
4,4′-Dinitrodiphenylmethane (16)	0.0

a) Substrate, 5 mmol; diphenylcarbodiimide, 16.8 mmol; K_2CO_3, 30 mmol; DMSO, 25 ml; reaction temp, 20 °C; reaction time, 2 h. b) The yields of carboxylic acid were calculated on the basis of substrate used. The products were monocarboxylic acids. They were identified by comparison of IR spectra with those of the authentic samples, after esterification with diazomethane, if necessary.

without a biotin model, proton abstraction by the base should be a rate-determining step and pK_a an important factor.[14] Our results indicate that since proton abstraction is not a rate-determining step it is not an important factor. After the reaction we confirmed the presence of DPU. In the case of fluorene, one fourth of the DPC converted to DPU after a 2 hour reaction. Though we measured the ^1H NMR of the reaction solution, we could not confirm the presence of DPU during the reaction. During the post-treatment, the reaction mixture was poured into ice-cold water. There is a possibility that the reaction intermediates reacted with protons at this point to give DPU.

The Effects of Reaction Time and Carbon Dioxide Pressure on the Carboxylation of Fluorene. In the case of DPU, the yield of carboxylic acid increased with an increase in the reaction time.[10,11] However, the maximum yield of 9-FLC was obtained at ca. 2 h in the case of DPC; the yield decreased slightly after 2 h (Table 3). This suggests the presence of undesirable reactions, such as a reverse reaction and/or an adduct reaction between DPC and 9-FLC. Actually, 55% of 9-FLC changed to unknown compounds in the reaction of 9-FLC with DPC for 2 h, although no reaction was observed when 9-FLC alone was reacted in DMSO. Although the reaction mechanism is not clear, the production of fluorenone was confirmed. We could also obtain the trimer of DPC by a reaction at 80 °C for 9 h. The production was confirmed by MS. The yield of 9-FLC when the DPC trimer was used instead of DPC was only 10.1% at 20 °C for 2 h. If the oligomerization of DPC occurs, elongation of reaction time is not preferable.

Table 3. Effects of the Reaction Time and CO_2 Pressure on the Carboxylation of Fluorene Using Diphenylcarbodiimide[a]

Pressure	Reaction time/h					
MPa[b]	0.5	1	2	4	5	7
0	15.2	28.7	35.2	22.5	16.1	16.0
	25.2	24.3		29.7		
1		20.8	10.5	13.9		15.9
2		25.3	16.5		10.4	12.0
			17.6			
4		8.7	9.8	18.6	12.3	12.3

a) Fluorene, 5 mmol; diphenylcarbodiimide, 16.8 mmol; K_2CO_3, 30 mmol; DMSO, 25 ml; reaction temp, 20 °C. b) Gauge pressure.

Table 4. Effects of Alkali Carbonate on the Carboxylation of Fluorene Using Diphenylcarbodiimide (DPC)[a]

Alkali carbonate	Solubility[b] mmol	Amounts of CO_2 absorption[c]	Yield of 9-FLC[d] %
None		17.1	0.0
Li_2CO_3	0.32	18.3	6.3
Na_2CO_3	0.62	16.8	1.9
K_2CO_3	3.68	15.1	35.2
K_2CO_3[e]			38.3
Rb_2CO_3	12.6	18.3	26.8
Cs_2CO_3	13.8	64.0	71.6

a) Fluorene, 5 mmol; diphenylcarbodiimide, 16.8 mmol; alkali carbonate, 30 mmol; DMSO, 25 ml; reaction temp, 20 °C; reaction time, 2 h. b) Solubility of alkali carbonates in DPC and DMSO 100 ml. c) The amount of CO_2 absorption (mmol) in the solution of alkali carbonate, DPC, and DMSO 100 ml. d) The yields of fluorene-9-carboxylic acid (9-FLC) were calculated on the basis of fluorene used. e) 60 mmol of K_2CO_3 was used.

It has been reported that carboxylation using DBU is influenced by the pressure of carbon dioxide.[6] Active methylene compounds give carboxylated products in much higher yield under higher pressure carbon dioxide. However, in the case of DPC, the carbon dioxide pressure was not effective on the yield of 9-FLC (Table 3). It has already been reported that in the absence of any catalyst equilibrium between two phenyl isocyanate molecules and DPC, carbon dioxide exists far on the side of phenyl isocyanate.[15] There is a possibility of a reaction of DPC with carbon dioxide to give phenyl isocyanate. Phenyl isocyanate was not a good imine, as mentioned earlier (Table 1).

The Effects of Alkali Carbonate on the Carboxylation of Fluorene. The yield of 9-FLC depended upon the nature of alkali carbonate (Table 4). Lithium and sodium carbonates were not effective; cesium salt was the most effective. The yields are well related to the solubility of alkali carbonate and the amount of

Table 5. Effects of Water Addition on the Yield of 9-FLC in Carboxylation for 2 h Using Diphenylcarbodiimide and K_2CO_3[a)]

Conditions	Amount of water added/mmol					
	0	5	10	15	20	30
A	10.5	13.5	24.3	10.8	0.1	
B	35.2	35.4	42.8	41.6	37.5	30.5
C	27.4	29.9	42.6	44.4	25.3	19.2

A; reactor was closed. B; reactor was bubbled by CO_2. C; reactor was pretreated by bubbling CO_2 for 1 h before adding fluorene and after then closed. a) Fluorene, 5 mmol; diphenylcarbodiimide, 16.8 mmol; K_2CO_3, 30 mmol; DMSO, 25 ml; reaction temp, 20 °C.

carbon dioxide absorbed in the reaction solution. The solubility of potassium carbonate was 3.68, larger than those of lithium and sodium carbonates by a factor of five to ten. The solubilities of rubidium and cesium carbonates were about three- to four-times larger than that of potassium carbonate. The concentration of carbanion is critical. Without an alkali carbonate, 17.1 mmol of carbon dioxide was absorbed in DMSO. This indicates that the carbonates, except cesium carbonate, did not contribute to the increase in the amount of carbon dioxide absorption. The highest yield of 71.6% with cesium carbonate is attributable to the high solubility in DMSO and the great ability to absorb carbon dioxide in conjunction with DPC.

The Effects of Water Addition on the Carboxylation of Fluorene. 1 g of potassium carbonate is soluble in 2.8 g of water. The solubility of potassium carbonate increased from 3.68 to 8.79 upon the addition of 10 mmol water to the DMSO solution of DPC. Water is known to be an inhibitor in many carboxylation reactions, as mentioned previously. However, the yield of 9-FLC in air was larger than that in drying air (Table 1), indicating that, at least, water was not an inhibitor. We have found the very interesting fact that in this study the addition of water accelerated the carboxylation yield (Table 5). Though without carbon dioxide the yield of 9-FLC without water was 10.5%, the value increased to 24.3% upon the addition of 10 mmol water. A maximum yield was obtained at 10 to 15 mmol addition of water in the case of bubbling carbon dioxide. The addition of more water than 15 mmol was not effective. The solubility of potassium carbonate increased upon the addition of water. Although the concentration of carbonate ions increased upon the addition of water, water addition lowered the solubility of fluorene in DMSO. Carbanion reacted with a proton to give a less-reactive compound. Our results suggest that if the reaction intermediates, as shown in the Scheme (2), reacted with water, their carboxylation activity did not become lower.

Conclusions

DPC was an effective carbon dioxide carrier for the carboxylation of active methylene compounds as a biotin model. Carboxylation of fluorene, even under a nitrogen atmosphere, is a very interesting reaction, since DPC can react with the carbonate ion directly, although DPU can not.[10,11] This indicates the possibility of an effective usage of carbonate ions in which more than 99.9% of the carbon dioxide exists as calcium carbonate. The carboxylation reaction of fluorene occurred even in the presence of water, suggesting that the reaction intermediates shown in the Scheme are stable to water. It was considered that the concentration of carbonate ions determined the reaction. In a biological system, the carboxylation reaction occurs in the presence of water without carbon dioxide. Our results indicate that the carboxylation of fluorene using DPC occurs under similar conditions as those of biological systems.

Experimental

DPC and substituted DPC were synthesized according to a method of Campbell et al.[15] 1-Ethyl-3-methyl-3- phospholene 1-oxide was used as a catalyst. Active methylene compound and DPC were dissolved in DMSO (25 ml); to this solution powdered alkali carbonate was added. Dry carbon dioxide was then passed into the mixture. The reaction mixture was poured into ice-cold water and the precipitate filtered off (active methylene compound and DPU etc.). The filtrate was extracted with ether. Acidification of the aqueous solution with hydrochloric acid gave a white precipitate. The precipitate was carboxylic acid. The ether extract was dried over anhydrous sodium sulfate and the solvent evaporated. The residue and above-mentioned precipitate were identified by a comparision of the IR spectra and melting points with those of carboxylic acids. A reaction under pressure was carried out using a 100 ml magnet-driven autoclave and treated in the same manner as mentioned above. The solubilities of alkali carbonates were determined by titration using HCl after filtration.

The amounts of carbon dioxide absorption in a DMSO solution containing DPC were determined by measuring the weight both before and after carbon dioxide bubbling.

References

1) A part of the results has been preliminary presented: K. Chiba, H. Tagaya, M. Karasu, T. Ono, and M. Kugiya, *Chem. Lett.*, **1990**, 39.

2) A. Behr, *Angew. Chem., Int. Ed. Engl.*, **27**, 661 (1988).

3) P. Braunstein, D. Matt, and D. Nobel, *Chem. Rev.*, **88**, 747 (1988).

4) M. Aresta and G. Forti, "Carbon Dioxide as a Source of Carbon. Biochemical and Chemical Uses," Kluwer Academic Publishers, Hague (1987).

5) W. M. Ayers, "Catalytic Activation of Carbon Dioxide," *ACS Symp. Ser.*, **363**, (1988).

6) S. Inoue and N. Yamazaki, "Organic and Bioorganic Chemistry of Carbon Dioxide," Kodansha, Tokyo (1982).

7) B. Hileman, *Chem. Eng. News*, **1989**, March 13, 25.
8) H. Tagaya, M. Onuki, Y. Tomioka, Y. Wada, M. Karasu, and K. Chiba, *Bull. Chem. Soc. Jpn.*, **63**, 3233 (1990).
9) S. Tazuke and H. Ozawa, *J. Chem. Soc., Chem. Commun.*, **1975**, 237.
10) K. Chiba, T. Akama, K. Sakakibara, and K. Horie, *Chem. Lett.*, **1978**, 1387.
11) K. Chiba, K. Sakakibara, and A. Ohta, *Nippon Kagaku Kaishi*, **1983**, 118.
12) Y. Otsuji, M. Arakawa, N. Matsuyama, and E. Haruki, *Chem. Lett.*, **1973**, 1193.
13) E. Haruki, M. Arakawa, N. Matsumura, Y. Otsuji, and E. Imoto, *Chem. Lett.*, **1974**, 427.
14) E. J. Corey and R. H. K. Chen, *J. Org. Chem.*, **38**, 4086 (1973).
15) T. W. Campbell, J. J. Monagle, and V. S. Foldi, *J. Am. Chem. Soc.*, **84**, 3673 (1962).
16) F. G. Bordwell, "Organic Chemistry," Macmillan, New York (1963), pp. 867—873.
17) H. Mori, H. Yamamoto, and T. Kwan, *Chem. Pharm. Bull.*, **20**, 2440 (1972).

 © 1991 The Chemical Society of Japan Bull. Chem. Soc. Jpn., 64, 971—982 (1991)

The Synthesis and Properties of Cyclohepta[*a*]phenalene-6,10-, -6,12-, -7,10-, and -7,12-diones and Their Dicationic and Dianionic Species

Shigeyasu KURODA,* Yoshinobu KANBATA, Yuriko FUKUYAMA, Syuzi HIROOKA, Hideya TAKEDA, Tomohiko TSUCHIDA, Yoko FURUKI, Takayuki SUMI, Osamu HANIDA, Masaki YAMADA, and Ichiro SHIMAO

Department of Materials Science and Engineering, Faculty of Engineering, Toyama University, Gofuku 3190, Toyama 930

(Received October 8, 1990)

The titled new non linear non benzenoid quinone compounds of cyclohepta[*a*]phenalene-6,10-, -6,12-, -7,10-, and -7,12-diones have been synthesized. The dicationic species formed from quinones by protonation in a strong acid were revealed as diatropic compounds instead of a 16-pi electron system by an examination of spectral measurements, such as the ^{1}H NMR and UV spectra. The stability of these quinones, dicationic species, and dianonic species electrically derived from quinones depends upon the positions of carbonyl groups with both steric and electronic factors.

Much attention has recently been focused on quinones and quinodimethane compounds from the viewpoint of advanced materials as organic superconductors by forming CT complexes.[1] Most of these quinones, however, are linear and benzenoid compounds.[2] According to the Trost's definition of quinones,[3] poly condensed nonbenzenoid conjugated dicarbonyl compounds are also included in the quinone category. However, little is known about polycyclic nonbenzenoid quinones containing more than four rings.[4] It is thus of interest to investigate the properties of non linear four-ring-fused quinones of cyclohepta[*a*]phenalenediones as well as their dicationic species expected to be formed by protonation in strong acidic media,[5] with two electrons less than that of the corresponding neutral species of cyclohepta[*a*]-phenalene. Furthermore, to examine the influence of steric and electronic factors of the carbonyl groups on the stability of the quinones and their dicationic species, which is correlated with the planarity of the molecule, quinones having carbonyl groups at the 7- and 12-positions and at positions other than the 7- and 12-positions were required. Because the distances between the peri positions of the 6- and 7-, 7- and 8-positions, as well as the 1- and 12-positions are very close, the proton and the carbonyl group located at these positions are repulsive, causing destabilization by a distortion of the molecule. Furthermore, an electrical reduction of the quinones, measured by cyclic voltammetry, would also be indicative of the stability of their dianionic species.

Herein we wish to report the synthesis and properties of four positional isomers of the quinones of cyclohepta[*a*]phenalene-6,10- (**1**), 6-,12- (**2**)[6], -7,10- (**3**), and -7,12-diones (**4**), their dicationic species **1′**, **2′**, **3′**, and **4′** and dianionic species **1″**, **2″**, **3″**, and **4″**.

Results and Discussion

Synthesis. Syntheses of the four title quinones were successfully carried out as follows, and are illustrated in Schemes 1 and 2. First, the synthesis of a quinone having one carbonyl group at the 6-position, cyclohepta[*a*]phenalene-6,12-dione (**2**), is described. The condensation of 2,2-diethoxycycloheptanone (**6**)[7] with 2-methoxy-1-naphthaldehyde (**5**) in the presence of sodium methoxide in refluxing dry tetrahydrofuran (THF) for 3.5 h gave ketone **7** in 65% yield. When **7** was treated with 85% sulfuric acid, the expected compound **9** was obtained, though in very low yield. It might be considered that one of the isomers (*E*-isomer) around the double bond of the enone moiety does not cyclize, and decreases the yield. This double bond was therefore saturated by catalytic hydrogenation. The reaction of **7** in ethyl acetate (AcOEt) in the presence of PtO_2 under a hydrogen atmosphere at 2.7 atm gave saturated ketone **8** almost quantitatively. Cyclodehydration of **8** with about 10-times excess in weight of 85% sulfuric acid a 45 °C for 30 min successfully furnished phenalenone derivative **9** in 65% yield. To introduce two double bonds to the seven-membered ring for full conjugation, α,α-dibromination and didehydrobromination reactions were carried out. Bromination of **9** with pyridinium tribromide always gave 4,5,11,11-tetrabromo compound **10** as the main product along with a small amount of 4,5,11,-tribromo, 11,11-dibromo compounds. Because 5-bromo derivative **12** is sometime predominant in the following dehydrobromination reaction, an alternative method for bromination was employed. Bromination of **9** with $CuBr_2$[8] in refluxing chloroform for 16 h gave only 11,11-dibromide **11** in 75% yield. Dehydrobromination of **11** with LiCl[9] in DMF at 140 °C for 40 min gave **2** in 95% yield. As mentioned above, 5-bromo derivative **12** was prepared under similar conditions as mentioned above from dione **9** via the tetrabromo compound **10** in 79% yield.

The other isomer, cyclohepta[*a*]phenalene-6,10-dione (**1**), was synthesized by using intermediate **9**. The

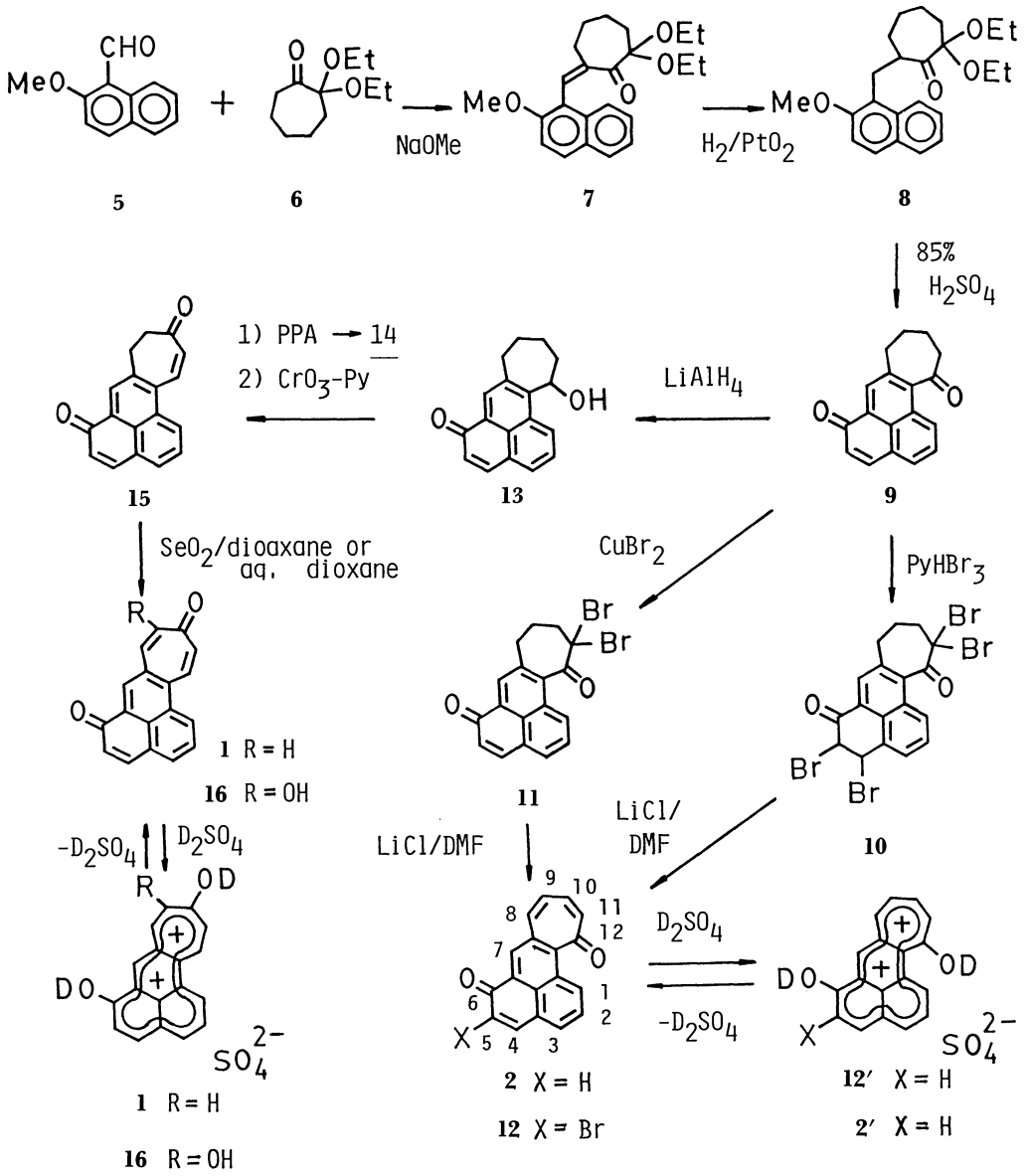

Scheme 1.

introduction of a carbonyl group at the 10-position was achieved as follows. The reduction of the carbonyl group at the 12-position of **9** with $LiAlH_4$ gave alcohol **13** in 67% yield. The reaction of **13** with an excess amount of polyphosphoric acid (PPA) at 100 °C for 1 h gave a dehydrated compound **14** in 76% yield. The allylic oxidation of **14** with pyridinium dichromate at room temperature (r. t.) overnight gave dione **15** in 34% yield. Dehydrogenation of **15** was performed by the use of SeO_2 in refluxing dioxane for 3 h to give **1** in 78% yield. When this dehydrogenation was performed[10] by using aqueous dioxane as a solvent, 9-hydroxycyclohepta[*a*]phenalene-6,10-dione (**16**) was obtained in 13% yield.

Two other quinones having one carbonyl group at the 7-position were synthesized as follows. To introduce one carbonyl group at the 7-position, ethyl 1-naphthoate (**17**) was chosen as the starting material. The reaction of **17** with cycloheptanone **18** in the presence of 1.5 equiv of sodium hydride in refluxing dry benzene for 2 h gave dione **19** in 58% yield. The bromination of **19** by using $CuBr_2$ in refluxing chloroform for 5 h furnished **20** exclusively as a colorless oil in 63% yield. The reason for this regioselective bromination is considered to be as follows. Since the ^1H NMR spectrum of **19** showed a signal for an enol proton resonating at δ=16.6, indicating the existence of a table enol form, shown in Scheme 1, a second enolization was induced at the 7-position of the cycloheptanone moiety. Thus, the more reactive 7-position of the cycloheptenone moiety was brominated to give **20**. The cyclodehydration of

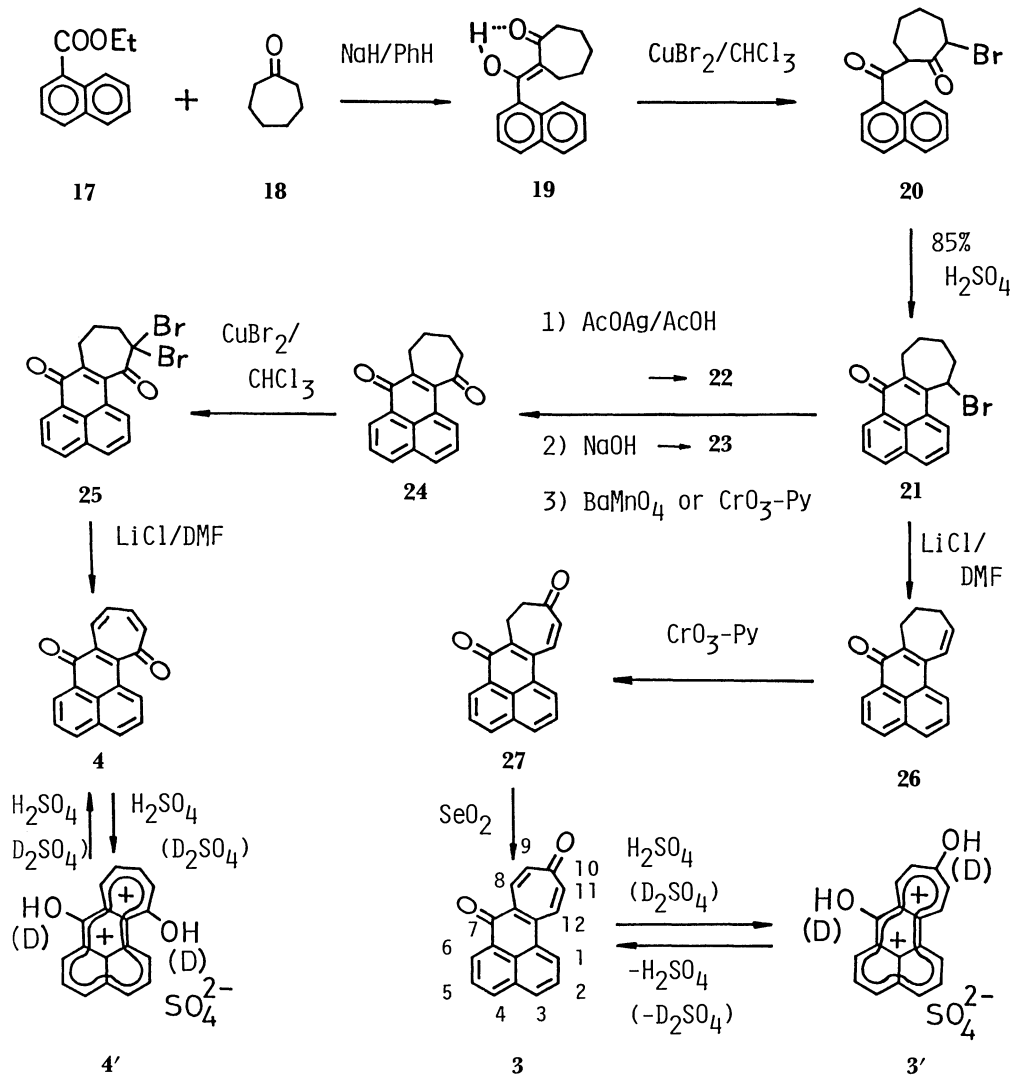

Scheme 2.

20 by 90% sulfuric acid at 40—50 °C for 30 min gave a bromo-substituted phenalenone derivative **21** in 81% yield. The reaction of **21** with 1.5 equiv of silver acetate in a solution of acetic acid and acetic anhydride at 110 °C for 24 h gave acetate **22** as a yellow oil in 85% yield. The reaction of **22** with sodium hydroxide in aqueous THF at 50—60 °C for 24 h gave alcohol **23** in 96% yield. Treatment of **23** with pyridinium dichromate[11] of $BaMnO_4$[12] at r. t. for 1 d furnished dione **24** and **23** in 75 and 97% yield, respectively. The bromination of **24** with $CuBr_2$ in refluxing $CHCl_3$ for 1 d gave **25** in 60% yield. The dehydrobromination of **25** was effected by the reaction of LiCl in DMF at 100—110 °C for 3 h to give the desired quinone **4** in over 90% yield.

The synthesis of another isomer of cyclohepta[*a*]-phenalene-7,10-dione (**3**) was started from **21** as follows. The reaction of **21** with LiCl in DMF at 110 °C for 40 min gave a dehydrobrominated compound **26** in 81% yield. An allylic oxidation of **26** with pyridinium dichromate at 50—60 °C for 7 h gave **27** in 16% yield, along with 56% of recovered **26**. The dehydrogenation of **27** was accomplished by using selenium dioxide in refluxing dioxane for 1 h to give cyclohepta[*a*]phenalene-7,10-dione (**3**) in 42% yield.

NMR Spectra of Quinones and Their Dicationic Species. Generally, in the ^1H NMR spectra of four quinones (**1**, **2**, **3**, and **4**) in $CDCl_3$, signals for the protons on the tropone moiety were observed at around δ=7.00,[13] and those of the phenalenone moiety in a range δ=7.10—8.70.[14] Furthermore, in the IR spectra the absorption bands of the carbonyl groups (ν 1595—1585 for tropone moiety and ν 1645—1625 for phenalenone moiety) are similar to those of the corresponding tropone (ν 1582)[15] and phenalenone (ν 1635),[16] respectively. This indicates that these quinones mainly comprise of tropone and phenalenone moieties, though the contribution of the

dipolar structure of quinone was suggested by the electronic absorption spectroscopic measurements. The differences of the ^{1}H-chemical shift averages in $CDCl_3$ from those in D_2SO_4 were evaluated by two methods. In the first one, a comparison was made by using the ^{1}H-chemical shift averages of all protons. In the other one, a comparison was made by using those of selected protons in which protons adjacent to the carbonyl groups were excluded in order to avoid any local anisotropy effects of the carbonyl groups. There was little difference in cases. Further, since these quinones are isomers of the carbonyl groups in the same ring system, the degree of diatropicity of the dicationic species might be estimated by simply making a comparison of the ^{1}H-chemical shifts averages. Since larger values of the ^{1}H-chemical shifts averages of the quinones indicate a greater contribution of the dicationic structures, the order of the stability of the quinones was known to be **3**, **1**, **4**, **2** by a comparison of their ^{1}H-chemical shift averages in $CDCl_3$ (Table 1). Although Wilcox et al. have reported[4a] that the protonated species of cycloocta-[*def*]biphenylene-1,4-dione does not show any significant down-field shift in the ^{1}H NMR spectrum due to a distortion of the molecule as a tab-shaped structure, the ^{1}H NMR spectra of the dicationic species formed from the quinones by protonation in a strong acidic media, such as D_2SO_4 showed large down-field shifts, as listed in Table 1 and can be seen in Figs. 1 and 2, chosen as typical examples. The ^{1}H-chemical shifts of the hydroxytropilium cation (δ=8.50),[13] hydroxyphenalenium cation (δ=8.66),[14] and 6-hydroxy-12-oxo-8,9,10,11-tetrahydrocyclohepta[*a*]phenalenium cation (**9′**) (δ=8.63) formed by protonation of tropone, phenalenone and **9** in strong acid, respectively, are higher than those of the dicationic species: **1′**, **2′**, **3′**, and **4′**. The ^{1}H-chemical shift differences of the dicationic species from the quinones (1.27—1.53 ppm) are larger than those of the evaluated value ($\Delta\delta$=10.6×

Table 1. 90 MHz ^{1}H NMR Chemical Shifts (δ) and the Chemical Shifts Averages of Quinones **1**—**4** (in $CDCl_3$) and Dicationic Species **1′**—**4′** (in D_2SO_4)

H-	1	1′	2	2′	3	3′	4	4′
1	8.73	10.27	8.67	10.16	8.10	9.17	8.63	10.09
2	7.82	8.52	7.67	8.42	7.68	8.67	7.71	9.06
3	7.82	8.93	7.54	8.90	8.38	9.49	8.18	9.68
4	7.82	9.26	7.70	9.34	8.25	9.69	7.98	8.94
5	6.77	7.84	6.65	7.85	7.80	8.67	7.53	8.52
6	—	—	—	—	8.67	9.79	8.43	9.50
7	8.80	10.21	8.62	10.25	—	—	—	—
8	7.82	9.52	7.48	9.36	8.15	10.10	8.13	9.88
9	7.03	8.38	6.92	8.62	7.17	8.37	6.89	8.52
10	—	—	6.92	8.90	—	—	6.89	8.52
11	7.17	8.52	6.92	8.70	7.02	8.40	6.89	8.52
12	8.68	9.71	—	—	8.44	10.15	—	—
$\delta_{average}$	7.85	9.12	7.51	9.05	7.97	9.24	7.72	9.12

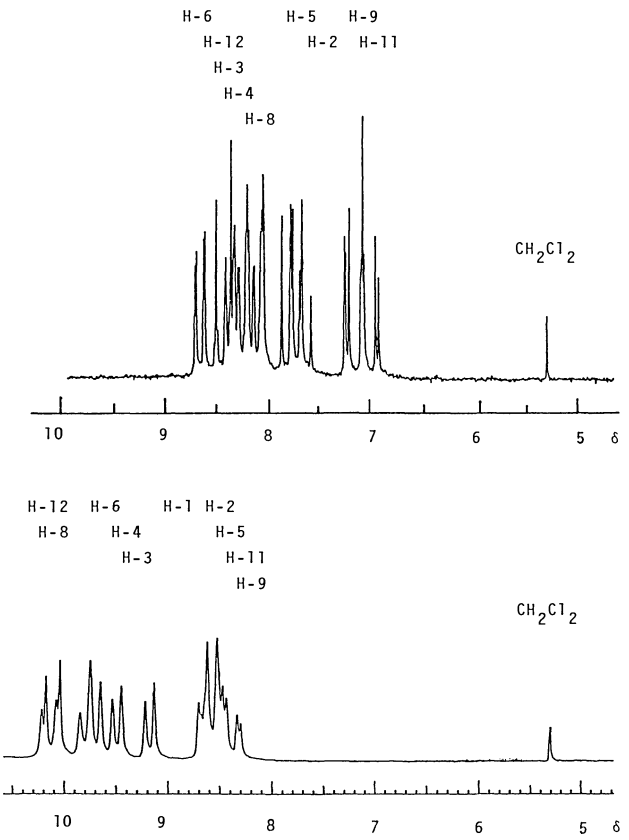

Fig. 1. ^{1}H NMR spectra of **3** in $CDCl_3$ (above) and its dication **3′** in D_2SO_4 (below) at 90 MHz.

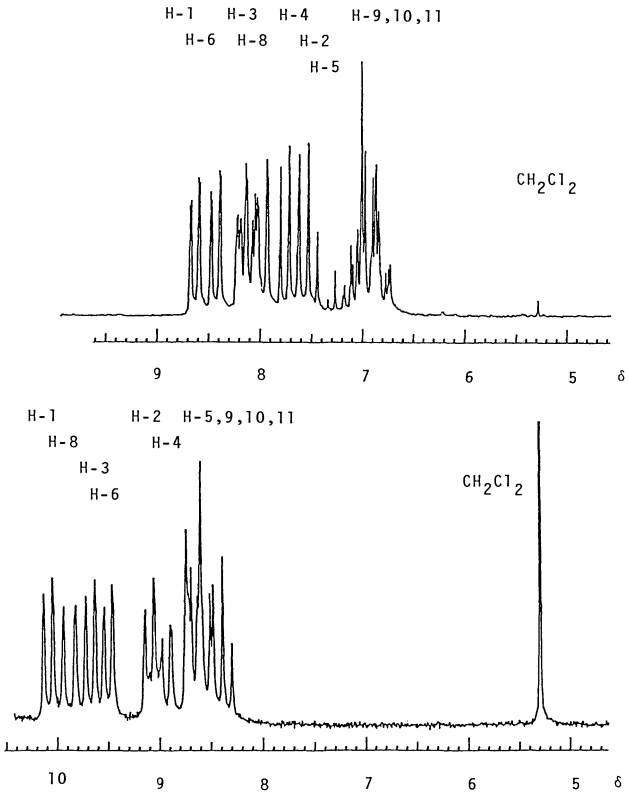

Fig. 2. ^{1}H NMR spectra of **4** in $CDCl_3$ (above) and its dication **4′** in D_2SO_4 (below) at 90 MHz.

2/18=1.18 ppm).[17] In consideration of the above-mentioned results, the larger down-field shifts of these dicationic species are only explained in terms of an induced diatropic ring current with the planarity of the molecule, excluding the structure in which two positive charges are localized at the carbonyl carbons. Based on the ^{1}H-chemical shift averages of dicationic species, the diatropicity falls off in the sequence **3′>1′>4′>2′**, similar to the result obtained for the quinones. The reason for this order might be that a steric repulsion of the carbonyl group at the 12-position and the proton on the 1-position prevents the planarity of the molecules in the formation of dicationic species. This is also supported by the electrochemical results shown later. In the ^{13}C NMR spectra, the chemical shifts of the carbonyl carbons at the 12-position in both **2** and **4** are similar and fairly lower than those of the 10-position in **1** and **3**. Since the positive charge is more localized at the carbonyl carbon in the distorted molecule than that in the planar one,[18] in the ^{13}C NMR spectra the chemical shifts of the carbonyl carbons in the distorted molecules are observed at a lower field than those in the planar molecules. The order of the ^{13}C NMR chemical shifts of both carbonyl carbons in quinones is thus **3**, **1**, **4**, **2** from a high field to a low field, indicating the order of planarity. It is also consistent with the above result obtained by a comparison of the ^{1}H NMR spectra of quinones **1**, **2**, **3**, and **4**, suggesting that the steric repulsion between the carbonyl group at the 12-position and the proton on the 1-position distorts the seven-membered-ring of **2** and **4**. The ^{13}C NMR chemical shifts of the carbonyl carbons of the quinones in D_2SO_4, were observed at a higher field than those in $CDCl_3$ indicating the formation of a dicationic species. Although the ^{13}C NMR chemical shifts of the carbonyl carbons at each of the 12-, 10-, 6-, and 7-positions in the dications are similar, those of the 12- and 7-positions are higher than those of the 10-and 6-positions. The reason for the higher chemial shifts of the 7-positions than those of the 6-positions is conceivablly as follows. The carbonyl group at the 7-positions are forced to maintain coplanarity with the adjacent two rings by a condensation of the two rings through the carbonyl group at the 7-positions. However, no clear explanation could be given for the higher chemical shifts of the 12-positions than those of the 10-positions. The ^{1}H NMR chemical shifts of 5-bromo and 9-hydroxy derivatives of quinones **12** and **16** in $CDCl_3$ are observed at a lower field than those of **2**. Especially, in the 9-hydroxy derivative **16**, though the large ^{1}H–^{1}H coupling constant on the 11- and 12-positions (J=13.0 Hz) are similar to that of 4,5-benzotropone (J=12.8 Hz),[19] indicating a smaller contribution of tautomerization, the larger downfield shift indicates a greater contribution of the dipolar structure of the quinone compared to that of **2** by hydrogen bonding between the hydroxyl and carbonyl groups.[20] Since the ^{1}H NMR chemical shifts of the dicationic species, **12′** and **16′**, are similar to those of **2′**, only slight effects of the substituents on the diatropicity of the dicationic species were noticed. Moreover, the regeneration of the quinones by the addition of a large excess of water to a solution of the dicationic species in conc sulfuric acid indicates the stability of the dicationic species under NMR measurement conditions.

Electronic Absorption Spectra of Quinones and Dicationic Species. The electronic absorption spectra of **1**—**4** in CH_2Cl_2 and conc sulfuric acid are shown in

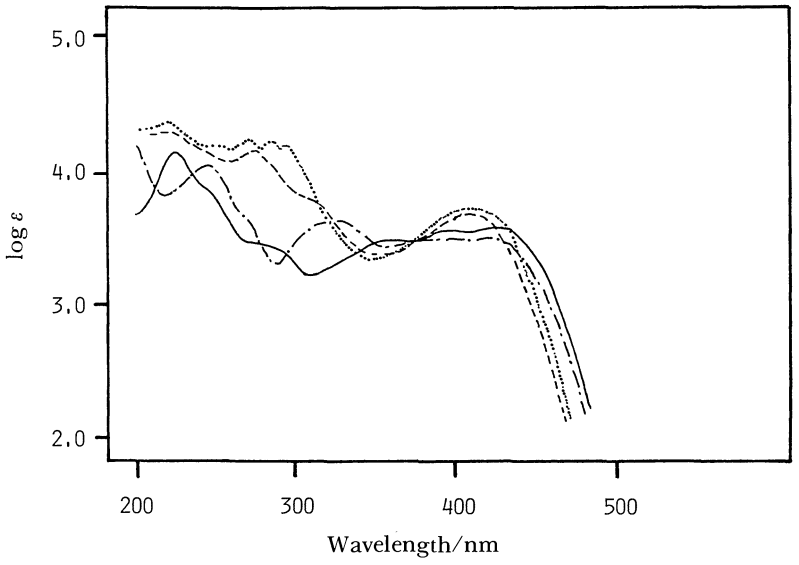

Fig. 3. Electronic absorption spectra of 6,10-dione **1** (·····), 6,12-dione **2** (-----), 7,10-dione **3** (-·-·-·-·), and 7,12-dione **4** (———) in CH_2Cl_2.

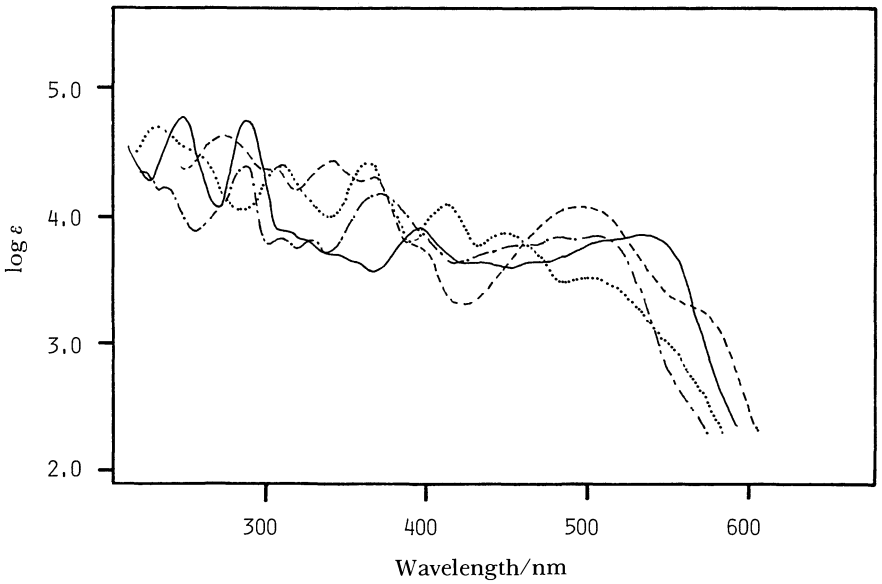

Fig. 4. Electronic absorption spectra of dication **1′** (·····), **2′** (-----), **3′** (-·-·-·-·), and **4′** (———) in conc. H_2SO_4.

Figs. 3 and 4, respectively. Although they are essentially identical, the spectra of **1** and **2** are quite different from those of **3** and **4**. The longest absorption maxima of **3** and **4** are slightly larger (ca. 10 nm) than those of **1** and **2** in CH_2Cl_2. It should be noted that the longest absorption maxima of **1**—**4** in conc sulfuric acid are larger than those in CH_2Cl_2 by ca. 80—100 nm and that the pK_a values of diones **2** and **4**, chosen as examples, were estimated as −2.3 and −1.4, respectively, by a UV method[21a,21b] in sulfuric acid at various concentrations. Since there were no clear two isobestic points in the UV spectra of **2′** and **4′** protonation to two carbonyl groups does not take place stepwise but gradually. These results indicate the formation of a dicationic species and the existence of equilibrium between the quinone and their dicationic species.[4a,5,22] These pK_a values lie between those of tropone (pK_a=−0.86)[21a] and benzanthrone (pK_a=−3.2),[22] and higher than those of the such quinones as *p*-naphthoquinone, anthraquinone, perylenequinone (their pK_a values are in a range −5.5 to −8.5).[21] This indicates a greater stability of the dicationic species **2′** and **4′** than those of the dicationic species formed by protonation of the corresponding above-mentioned quinones. The longest absorption maxima of dications **2′** and **4′**, having a carbonyl group at the 12-position are larger than those of **1′** and **3′**, having a carbonyl group at the 10-position by ca. 10 nm. It is interesting that the absorption maxima are influenced by the positions of the carbonyl groups, especially at the phenalenone moiety. However, the red shifts of the absorption maxima in sulfuric acid are influenced by the position of the carbonyl group on the seven-membered ring. The influenece of other substituents, such as the 5-bromo and 9-hydroxyl groups, on the absorption maxima are only effected so as to cause a slight red shift.

Table 2. Cyclic Voltammetric Data for Quinones (in Volts vs. SCE)

Quinone	$^1E_{1/2}$	$^2E_{1/2}$	$^1E_{1/2}-^2E_{1/2}$
1	−0.77	−1.11	0.34
2	−0.83 (−1.05)[a]	−1.30 (−1.44)[a]	0.47
3	−0.77	−1.36	0.59
4	−0.81	−1.45	0.64
1,4-Naphthoquinone[23]	−0.58	−1.29	0.71
9,10-Anthraquinone[24]	−0.78	−1.45	0.67

a) The values are measured in acetonitrile.

Electrochemistry (CV Spectra) of Quinones 1—4. These compounds showed two reversible half-wave reduction potentials, indicating the formation of stable radical anions and dianions, as shown in Scheme 3. The first and second half-wave reduction potential values, $^1E_{1/2}$ and $^2E_{1/2}$ (V vs. SCE), of the quinones shown in Table 2 indicate the stability of the reduced radical anion and dianionic species of the quinones. The first reduction potential values of quinones **1** and **3** are similar and more positive than those of **2** and **4**. This can be explained by the higher planarity in the radical anions of **1** and **3** than that of **2** and **4**.[2] The order of the first reduction potentials correlated with the planarity (stability) is **3**=**1**>**4**>**2**, from positive to negative. This relation is similar to that obtained by a comparison of the ^{1}H NMR chemical shift averages described above. A comparison of the second reduction potentials and the

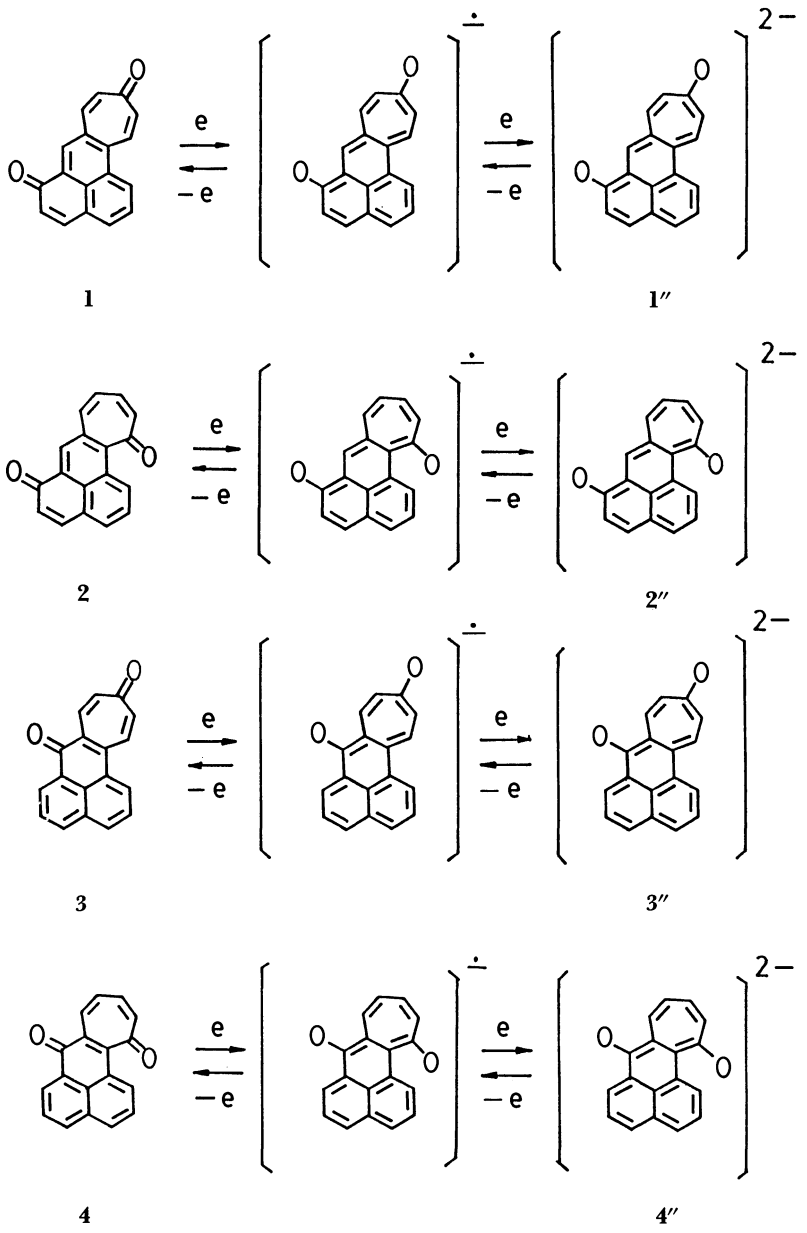

Scheme 3.

differences between $^{1}E_{1/2}$ and $^{2}E_{1/2}$ suggest the order of the stability of dianions formed from radical anions to be 6,10-(**1″**)>6,12-(**2″**)>7,10-(**3″**)>7,12-dione (**4″**). This order is different from that of dicationic species. The reason for the smaller stability of dianions having a carbonyl group at the 7-position, compared to those at the 6-position, is considered to be due to the electron-donating oxido-group at the 7-position, which destabilizes the heptafulvene moiety to a greater extent than that at the 6-position. On the other hand, the oxido group at the 12-position destabilizes the seven-membered ring to a greater extent than that at the 10-position due to a steric repulsion, as shown in Fig. 5.

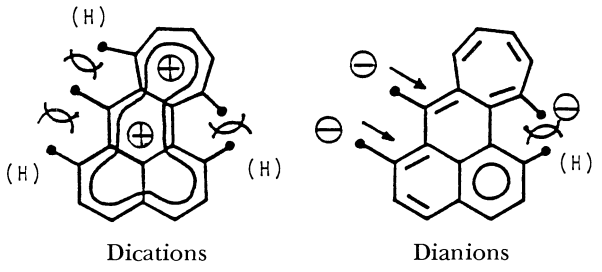

Fig. 5. The steric repulsion and electronic effects of carbonyl, hydroxyl and oxido groups.

Experimental

All melting points are uncorrected. The ^1H NMR spectra were taken on a Hitachi-60 (60 MHz) and on a JEOL-FX90 (90 MHz) spectrometers in chloroform-*d* (TMS as the internal standard) and deuteriosulfuric acid (dichloromethane, δ=5.30, as the internal standard). The ^{13}C NMR spectra were taken on a JEOL-FX90 (23 MHz) spectrometer, in the above two solvents. The mass spectra were taken on a JEOL-OISG-2 mass spectrometer. The UV and IR spectra were taken on a Hitachi EPS-3T spectrometer and on a IR-810 spectrometer, respectively. Cyclic voltammetric measurements were performed on a Yanaco P-1100. A standard three-electrode cell configuration was employed using a glassy carbon disk working electrode, at Pt wire auxiliary electrode, and a Ag wire as a Ag/Ag^+ quasireference electrode. The reference electrode was calibrated at the completion of each measurement to a saturated calomel electrode (SCE). Solvent and supporting electrode for electrochemistry were purified before use. Reduction potentials of quinones were measured by cyclic voltammetry using dimethyl sulfoxide containing tetrabutylammonium perchlorate (0.1 mol dm^{-3}) as solvent.

2,2-Diethoxycyloheptanone (6). A solution of 1,2-cycloheptanedione (30 g, 23.8 mmol), ethylorthoformate (105 g, 71.4 mmol) and a catalytic amount of *p*-toluenesulfonic acid (100 mg) in dry ethanol (300 mL) was stirred at room temperature for 12 h. The reaction mixture was poured into 15% sodium hydrogenbicarbonate solution and extracted with ether (200 mL×3). The combined organic layers were washed with water and brine twice each, and dried over anhyd $MgSO_4$. After removal of the solvent by evaporation in vacuo, the residue was distilled to give **6** (45.2 g, 95%): colorless oil, bp 110—115 °C (15 mmHg, 1 mmHg=133.322 Pa); IR (film) 2940s, 1723s, 1138m, 1120m, 997m cm^{-1}; ^1H NMR ($CDCl_3$) δ=3.42 (q, *J*=6.0 Hz, 4H, $-OCH_2-$), 2.46 (bt, *J*=6.0 Hz, 2H, H-7), 1.62 (m, 8H), 1.15 (t, *J*=6.0 Hz, $-CH_3$). MS *m/z* 200 (M^+, 100%).

2,2-Diethoxy-7-[(2-methoxy-1-naphthyl)methylene]cycloheptanone (7). To a suspension of sodium methoxide (1.00 g, 18 mmol) in dry THF (70 mL) were added a solution of **5** (3.00 g, 16 mmol) and **6** (3.22 g, 16 mmol) in dry THF (30 mL). The mixture was refluxed for 3.5 h. After cooling, it was poured into dil HCl (200 mL) and extracted with benzene (50 mL×3). The combined organic layers were washed with brine three times and dried over anhyd $MgSO_4$. The solvent was removed in vacuo, and the residue was chromatographed on silica gel to give **7** (5.23 g, 80%) from benzene elution: pale yellow oil; IR (film) 3027w, 2980w, 1705s, 1258s, 1176m, 1125s, 957m, 803m, 743m cm^{-1}; ^1H NMR ($CDCl_3$) δ=7.48 (m, 7H), 3.95 (s, 3H), 3.74 (q, *J*=6.0 Hz, 4H), 2.45 (t, *J*=3.6 Hz, 2H), 1.83 (m, 6H), 1.44 (t, *J*=6.0 Hz, 6H); MS *m/z* 368 (M^+, 85%). Found: *m/z* 360.3856. Calcd for $C_{23}H_{20}O_2$: M, 360.3900.

2,2-Diethoxy-7-[(2-methoxy-1-naphthyl)methyl]cycloheptanone (8). To a solution of **7** (18.3 g, 49.7 mmol) in AcOEt (100 mL) was added a catalytic amount of PtO_2 (10 mg) and the mixture was hydrogenated under hydrogen atmosphere at 2.7 atm for 5 h. The reaction mixture was filtered and the solvent was removed by evaporation to give **8** in an almost quantitative yield: colorless oil; IR (film) 3030w, 2970m, 2930m, 1697s, 1612m, 1584s, 1482s, 1250vs, 951m, 858m, 801m, 743m cm^{-1}; ^1H NMR ($CDCl_3$) δ=7.70 (m, 2H), 7.10 (m, 4H), 3.75 (s, 3H), 3.53 (q, *J*=6.0 Hz, 4H), 2.90—2.30 (m, 5H), 1.70 (m, 6H), 1.27 (t, *J*=6.0 Hz, 6H); MS *m/z* 370 (M^+, 78%). Found: *m/z* 362.4076. Calcd for $C_{23}H_{30}O_4$: M, 362.4048.

8,9,10,11-Tetrahydrocyclohepta[*a*]phenalene-6,12-dione (9). A mixture of 85% sulfuric acid (100 mL) and **8** (10 g) was heated with stirring at 45 °C for 30 min. After cooling, the reaction mixture was poured onto ice (ca. 1 Kg) and extracted with CH_2Cl_2 (200 mL×3). The combined organic layer was washed with water and brine twice each, and dried over anhyd $MgSO_4$. After removal of the solvent by evaporation, the residue was chromatographed on silica gel to give **9** (2.29 g, 32.5%) from CH_2Cl_2 elution: yellow needles, mp 174 °C (CH_2Cl_2–hexane); IR(KBr) 3020w, 2938m, 1678vs, 1626vs, 1580vs, 1400m, 1262s, 1120s, 838s, 762s cm^{-1}; ^1H NMR ($CDCl_3$) δ=8.45 (s, 1H), 8.13 (dd, *J*=1.8 & 8.1 Hz, 1H), 7.78 (d, *J*=9.9 Hz, 1H), 7.66 (m, 2H), 6.74 (d, *J*=9.9 Hz, 1H), 3.12 (t, *J*=6.4 Hz, 2H), 2.81 (t, *J*=6.4 Hz, 2H), 1.93 (m, 4H), (D_2SO_4–CH_2Cl_2) δ=9.35 (s, H-7), 9.02 (bd, 9.8 Hz, H-4), 8.82 (bd, *J*=5.4 Hz, H-1), 8.64 (m, H-3), 8.21 (bdt, *J*=5.4 & 5.0 Hz, H-2), 7.73 (bd, *J*=9.8 Hz, H-5), 3.30 (m, H-8), 2.1 (m, H-9 & -10) (signals for 11-position could not be observed by the substitution of deuterium); MS *m/z* 262 (M^+, 100%), 234 (90%); HRMS Found: 262.0956. Calcd for $C_{18}H_{14}O_2$: 262.0991. Found: C, 82.53; H, 5.42%. Calcd for $C_{18}H_{14}O_2$: C, 82.42; H, 5.38%.

Bromination of 9. A) To a solution of **9** (0.20 g, 0.76 mmol) in $CHCl_3$ was added $PyHBr_3$ (3.7 g, 2.28 mmol) and the mixture was stirred at 10 °C for 12 h. The solid of PyHBr was filtered off and the filtrate was washed with water twice and dried over anhyd $MgSO_4$. The solvent was removed by evaporation, and the residue was chromatographed on silica gel to give **10** (0.19 g, 23%) from benzene elution and **11** (0.51 g, 63%) from CH_2Cl_2 elution.

B) To a solution of **9** (2.30 g, 8.7 mmol) in chloroform (30 mL) was added $CuBr_2$ (11.66 g, 5.2 mmol) and the mixture was refluxed for 16 h. After cooling, the solid was filtered off and the filtrate was concentrated by evaporation. The residue was chromatographed on silica gel to give **11** (2.74 g, 75%).

10: Pale yellow plates, mp 158—167 °C (CH_2Cl_2–hexane); IR(KBr) 3030w, 2930w, 1700m, 1684vs, 1608w, 1500w, 1400m, 1222m, 1032m, 892m, 782m, 772m cm^{-1}; ^1H NMR ($CDCl_3$) δ=8.22 (s, 1H), 8.02 (dd, *J*=2.0 & 7.7 Hz, 1H), 7.71 (m, 2H), 5.89 (d, *J*=3.1 Hz, 1H), 5.51 (d, *J*=3.1 Hz, 1H), 2.92 (m, 4H), 2.14 (m, 2H); MS *m/z* 422, 420, 418 (M^+-Br_2, 10.2, 19.2, 10.2%), 233 (100%). Found: C, 37.85; H, 2.09%. Calcd for $C_{18}H_{12}O_2Br_4$: C, 37.28; H, 2.17%.

11: Yellow needles, mp 220—223 °C (CH_2Cl_2–hexane); IR(KBr) 3030w, 2951w, 1718s, 1650vs, 1588s, 1420m, 1120m, 912m, 839m, 792m, 771m cm^{-1}; ^1H NMR ($CDCl_3$) δ=8.18 (s, 1H), 7.82 (dd, *J*=1.2 & 7.6 Hz, 1H), 7.53 (d, *J*=9.8 Hz, 1H), 7.50 (m, 2H), 6.53 (d, *J*=9.8 Hz, 1H), 2.98 (mt, 2H), 2.69 (mt, 2H), 2.10 (m, 2H); MS *m/z* 422, 420, 418 (M^+, 9.4, 16.9, 9.4%), 233 (100%). Found: *m/z* 421.9077, 419.9102, 417.9172. Calcd for $C_{18}H_{12}Br_2O_2$: M, 421.9163, 419.9183, 417.9202.

Cyclohepta[*a*]phenalene-6,12-dione (2). A mixture of **11** (2.20 g, 5.24 mmol) and lithium chloride (2.40 g, 5.22 mmol) in dry DMF (21 mL) was heated at 100—110 °C with stirring for 3 h. After cooling, the mixture was poured onto ice-

water. The solid was filtered, and then dissolved in CH_2Cl_2. The resulting solution was dried over anhyd $MgSO_4$ and concentrated in vacuo. The residue was chromatographed on silica gel to give **2** (1.12 g, 80%) from CH_2Cl_2 elution: yellow needles, mp 209—212 °C (CH_2Cl_2–hexane); IR(KBr) 3040w, 1640s, 1618s, 1580s, 840m cm^{-1}; ^1H NMR ($CDCl_3$) δ=8.67 (dd, J=8.5 & 1.5 Hz, 1H), 8.62 (s, 1H), 7.70 (d, J=9.8 Hz, 1H), 7.67 (m, 2H), 7.54 (m, 3H), 7.48 (d, J=10.0, 1H), 6.92 (m, 3H), 6.65 (d, J=9.8 Hz, 1H), (D_2SO_4) δ=10.25 (s, H-7), 10.16 (d, J=8.7 Hz, H-1), 9.36 (bd, J=10.1 Hz, H-8), 9.34 (bd, J=9.3 Hz, H-4), 8.90 (dd, J=10.9 & 8.8 Hz, H-10), 8.90 (d, J=7.8 Hz, H-3), 8.70 (d, J=10.9 Hz, H-11), 8.62 (dd, J=10.1 & 8.8 Hz, H-9), 8.42 (dd, J=8.7 & 7.8 Hz, H-2), 7.85 (d, J=9.3 Hz, H-5); ^{13}C NMR ($CDCl_3$) δ=191.2, 184.7, 143.1, 137.1, 134.5, 133.0, 132.7, 131.9, 130.4, 128.8, 128.4, 127.6, 140.0, 133.4, 130.8, 130.6, 128.4, 128.0, (D_2SO_4–CH_2Cl_2) δ=182.7 (C–OH, C-12), 181.9 (C–OH, C-6), 165.2 (C-4), 154.9 (C-10), 152.5 (C-8), 148.0 (C-1), 146.9 (C-3), 141.8 (C-7), 138.5 (C-5), 132.7 (C-11), 131.4 (C-9), 120.1 (C-2), 140.2, 138.1, 129.7, 127.2, 126.4, 125.0 (quart. C); ES (EtOH) λ_{max} 416 (log ε=3.86), 319 (3.97), 268 nm (4.14), (CH_2Cl_2) λ_{max} 400 (log ε=4.00), 313 (4.09), 290 (4.26), (concd H_2SO_4) λ_{max} 560 sh (log ε=3.26), 490 (3.86), 340 nm (4.18), The pK_a value was measured by UV method. Acidity dependency of the molar extinction coefficients at 486.2 nm in sulfuric acid of various concentrations (97%, 85%, 75%, 62%, 54%, 48%, 45%, 38%, 35%, 28%, and 16%) was measured. The pK_a value was estimated by measuring the inflection point of the sigmoid curve obtained from the above method.[21a,21b]; MS m/z 258 (M^+, 69%), 230 (100%). Found: m/z 258.0672. Calcd for $C_{18}H_{10}O_2$: M, 258.0679. Found: C, 83.79; H, 3.82%, Calcd for $C_{18}H_{10}O_2$: C, 83.71; H, 3.90%.

5-Bromocyclohepta[*a*]phenalene-6,12-dione (12). 5-Bromo derivative **12** was prepared in 79% yield by the treatment of **10** with LiCl in the similar conditions as in the case of **2**: yellow needles, mp 225 °C (decomp, CH_2Cl_2–hexane); IR(KBr) 3020w, 1655s, 1610s, 1582m, 795m cm^{-1}; ^1H NMR ($CDCl_3$) δ=8.85 (s, H-7), 8.67 (dd, J=8.0 & 1.8 Hz, H-1), 8.27 (s, H-4), 7.78 (dd, J=8.0 & 1.8 Hz, H-3), 7.64 (t, J=8.0 Hz, H-2), 7.60 (dd, J=10.5 & 2.0 Hz, H-8), 6.98 (m, H-9, 10, 11), (D_2SO_4–CH_2Cl_2) δ=10.39 (s, H-7), 10.23 (d, J=8.6 Hz, H-1), 9.65 (s, H-4), 9.41 (d, J=10.0 Hz, H-8), 9.03 (md, H-3, H-10), 8.72 (m, H-9 & -11), 8.48 (dd, J=8.5 & 7.5 Hz, H-2); ^{13}C NMR spectrum of **12** colud not be measured owing to its low solubility in many solvents, (D_2SO_4–CH_2Cl_2) δ=182.9 (C–OH, C-12), 176.2 (C–OH, C-6), 165.9 (C-4), 155.6 (C-10), 152.5 (C-8), 150.3 (C-1), 139.0 (C-3), 138.9 (C-7), 132.1 (C-11), 131.9 (C-9), 114.8 (C-2), 140.3, 138.5, 130.0, 127.2, 126.3, 123.9 (quart. C); ES (CH_2Cl_2) λ_{max} 425 (log ε=4.08), 332 (4.08), 295 nm (4.28), (concd H_2SO_4) λ_{max} 588 (log ε=3.62), 504 (4.26), 392 (4.40), 376 (4.46), 350 (4.43), 312 (4.58), 265 nm (4.63); MS m/z 338, 336 (M^+, 91%, 100%), 310 (61%), 308 (53%). Found: C, 64.12; H, 2.70%. Calcd for $C_{18}H_9BrO_2$: C, 64.09; H, 2.67%.

12-Hydroxy-8,9,10,11-tetrahydrocyclohepta[*a*]phenalen-6-(12*H*)-one (13). To a suspension of $LiAlH_4$ (0.343 g, 90.4 mmol) in dry THF (100 mL) was dropwise added **9** (6.321 g, 24 mmol) in dry THF (50 mL) over a period of 1 h under ice cooling. The mixture was allowed to stand for 1 h at room temperature with stirring and then poured slowly into 3M HCl (150 mL, M=mol dm^{-3}). The solution was extracted with CH_2Cl_2 (50 mL×3). The combined organic layers were washed with water and brine twice each and dried over anhyd $MgSO_4$. After removal of the solvent, the residue was chromatographed on silica gel to give **13** (4.213 g, 66.5%) from CH_2Cl_2–AcOEt (3:1) elution: Yellow needles, mp 171.5—172.5 °C (benzene); IR(KBr) 3380m, 2925m, 1635s, 1582s, 1566s, 1403m, 996m, 829s, 746m cm^{-1}; ^1H NMR ($CDCl_3$) δ=8.37 (t, =5.3 Hz, 1H), 7.94 (s, 1H), 7.47 (d, J=5.3 Hz, 1H), 7.33 (d, J=9.7 Hz, 1H), 6.24 (d, J=9.7 Hz, 1H), 6.00 (d, J=6.7 Hz, 1H), 3.77 (t, J=12.3 Hz, 1H), 3.72 (bs, 1H), 2.88 (dd, J=7.0 & 6.1 Hz, 1H), 2.35 (m, 2H), 2.04 (m, 1H), 1.76 (m, 2H), 1.45 (q, J=12.0 Hz, 1H); MS m/z 264 (M^+, 27%), 246 (100%). Found: m/z 264.1095. Calcd for $C_{18}H_{16}O_2$: M, 264.1138. Found: C, 81.76; H, 6.00%. Calcd for $C_{18}H_{16}O_2$: C, 81.81; H, 6.06%.

8,9-Dihydrocyclohepta[*a*]phenalen-6(10*H*)-one (14). A solution of **13** (1.136 g, 4.30 mmol) in PPA (12 mL) was heated at 100 °C for 1 h. The reaction mixture was poured onto ice-water (100 mL) and extracted with CH_2Cl_2 (20 mL× 3). The combined organic layer was washed with water, brine twice each and dried over anhyd $MgSO_4$. After removal of the solvent in vacuo, the residue was chromatographed on silica gel to give **14** (0.698 g, 66%) from benezene–CH_2Cl_2 (8:1) elution: yellow needles, mp 120 °C (CH_2Cl_2–hexane); IR(KBr) 3030w, 2840w, 1638vs, 1580vs, 1402m, 1360m, 1278s, 835s, 755m cm^{-1}; ^1H NMR ($CDCl_3$) δ=8.47 (s, 1H), 8.25 (dd, J=8.1 & 1.6 Hz, 1H), 7.72 (d, J=9.7 Hz, 1H), 7.60 (m, 2H), 7.29 (d, J=11.5 Hz, 1H), 6.70 (d, J=9.7 Hz, 1H), 6.54 (dt, 11.5 & 5.5 Hz, 1H), 2.90 (m, 2H), 2.25 (m, 4H); MS m/z 246 (M^+, 100%), 231 (69%). Found: C, 87.68; H, 6.10%. Calcd for $C_{18}H_{14}O$: C, 87.80; H, 5.69%.

8,9-Dihydrocyclohepta[*a*]phenalene-6,10-dione (15). To a pyridine solution of pyridinium dichromate prepared by the addition of CrO_3 (1.425 g, 14.2 mmol) to dry pyridine (15 mL) under ice cooling was added **14** (0.701 g, 2.85 mmol) in pyridine (25 mL) with stirring, and the stirring was continued for 22 h at room temperature. The reaction mixture was diluted with water and extracted with CH_2Cl_2 (30 mL×3). The combined organic layers were washed with 3M HCl three times, water twice, brine twice and dried over anhyd $MgSO_4$. The solvent was evaporated in vacuo and the residue was chromatographed on silica gel to give **15** (0.140 g, 19%) from benzene–CH_2Cl_2 (2:3) elution: Yellow needles, mp 179—181 °C (CH_2Cl_2–hexane); IR(KBr) 3039w, 1660vs, 1650vs, 1578vs, 1402s, 1197s, 837s, 759s cm^{-1}; ^1H NMR ($CDCl_3$) δ=8.43 (s, 1H), 8.24 (dd, J=7.6 & 2.3 Hz, 1H), 7.90 (d, J=12.9 Hz, 1H), 7.68 (d, J=9.7 Hz, 1H), 7.62 (m, 1H), 6.68 (d, J=9.7 Hz, 1H), 6.55 (d, J=12.9 Hz, 1H), 3.21 (m, 2H), 2.85 (m, 2H); MS m/z 260 (M^+, 68%), 231 (100%). Found: C, 82.92; H, 4.55%. Calcd for $C_{18}H_{12}O_2$: C, 82.06; H, 4.65%.

Cyclohepta[*a*]phenalene-6,10-dione (1). A mixture of **15** (88 mg, 0.338 mmol) and SeO_2 (45 mg, 0.406 mmol) in dioxane (8 mL) was refluxed for 3.5 h. After cooling, the solid of Se was filtered off. The filtrate was concentrated in vacuo, and the residue was chromatographed on silica gel to gave **1** (65 mg, 74.4%) from CH_2Cl_2 elution: Yellow needles, mp 231.5—233 °C (CH_2Cl_2–hexane); IR(KBr) 3038w, 1650s, 1630s, 1585vs, 1254m, 848m, 766m cm^{-1}; ^1H NMR ($CDCl_3$) δ=8.80 (s, 1H), 8.73 (dd, J=7.7 & 2.4 Hz, 1H), 8.64 (d, J=10.0 Hz, 1H), 7.82 (m, 4H), 7.17 (dd, J=10.0 & 3.0 Hz, 1H), 7.03 (dd, J=10.0 & 3.0 Hz, 1H), 6.77 (d, J=10.0 Hz, 1H), (D_2SO_4–CH_2Cl_2) δ=10.27 (bd, J=8.0 Hz, H-1), 10.21 (s, H-7), 9.71 (bd, J=12.5 Hz, H-12), 9.52 (bd, J=12.5 Hz, H-8), 9.26

(bd, J=7.8 Hz, H-4), 8.93 (bd, J=8.0 Hz, H-3), 8.52 (m, H-2 & -11), 8.38 (bd, J=12.5 Hz, H-9); ^{13}C NMR ($CDCl_3$) δ=187.4, 184.6, 142.8, 141.9, 138.5, 137.1, 135.4, 135.2, 132.6, 132.2, 132.1, 130.1, 129.0, 128.4, 128.37, 128.1, 127.2, (D_2SO_4-CH_2Cl_2) δ=184.8, 181.7, 148.4, 148.2, 148.0, 144.7, 138.3, 137.5, 134.4, 132.2, 130.9, 126.9, 126.1, 125.0, 120.6; ES (CH_2Cl_2) λ_{max} 412 (log ε=4.03), 308 (4.34), 295 (4.21), 248 nm (4.34), (concd H_2SO_4) λ_{max} 548sh (log ε=2.88), 518 (3.48) 448 (4.24), 398 (4.32), 338 (4.67), 270 nm (4.35); MS m/z 258 (M^+, 27%), 230 (100%). Found: m/z 258.0686. Calcd for $C_{18}H_{10}O_2$: M, 258.0681. Found: C, 83.75; H, 3.80%. Calcd for $C_{18}H_{10}O_2$: C, 83.71; H, 3.90%.

9-Hydroxycyclohepta[*a*]phenalene-6,12-dione (16). A mixture of **15** (90 mg, 0.34 mol) and SeO_2 (50 g, 0.56 mol) in aqueous dioxane (2:8) was refluxed for 3.5 h. Compound **16** was obtained by the similar work-up as in the case of **1** in 35% yield: Yellow needles, mp 240—265 °C (decomp, CH_2Cl_2–hexane); IR(KBr) 3298m, 1626s, 1586s, 1499m, 1458m, 1301s, 1223s, 836s cm^{-1}; ^{1}H NMR ($CDCl_3$) δ=8.97 (d, J=13.1 Hz, H-12), 8.84 (s, H-7), 8.73 (d, J=4.8 Hz, H-1), 7.91—7.81 (m, H-2, -3), 7.83 (d, J=9.9 Hz, H-4), 7.54 (d, J=13.1 Hz, H-11), 6.77 (d, J=9.9 Hz, H-5), (D_2SO_4–CH_2Cl_2) δ=10.34 (d, J=12.9 Hz, H-12), 10.18 (s, H-7), 9.69 (d, J=9.0 Hz, H-1), 9.35 (s, H-8), 9.29 (d, J= 8.6 Hz, H-4), 8.91 (d, J=7.7 Hz, H-3), 8.80 (d, J=12.9 Hz, H-11), 8.48 (t, J=7.5 Hz, H-2), 7.83 (d, J=8.6 Hz, H-5); ^{13}C NMR (D_2SO_4–CH_2Cl_2) δ=181.9 (C-OH, C-10), 172.3 (C-OH, C-6), 164.3 (C-OH, C-9), 155.6, 148.8, 145.9, 145.8, 141.0, 139.6, 137.4, 137.0, 132.2, 130.7, 130.4, 126.9, 126.6, 124.0, 120.3; ES (CH_2Cl_2) λ_{max} 430sh (log ε=3.30), 419 (3.46), 348 (3.78), 321 (4.03), 306 (4.10), 252 (3.97), 231 nm (4.16), (concd H_2SO_4) λ_{max} 499 (log ε=3.49), 399 (3.57), 338 (4.25), 286 (4.10), 270 (4.00), 214 nm (3.85); MS m/z 274 (M^+, 54%), 246 (100%). Found: C, 78.78; H, 3.68%. Calcd for $C_{18}H_{10}O_3$: C, 78.83; H, 3.65%.

2-(1-Naphthoyl)cycloheptan-1-one (19). To a suspension of sodium hydride (7.8 g, 160 mmol) in dry benzene (100 mL) was added a mixture of ethyl 1-naphthonate **17** (20 g, 110 mmol) and cycloheptanone **18** (12 g, 110 mmol) in dry benzene (30 mL) dropwise at room temperature with stirring for 30 min. The mixture was refluxed for 3.5 h. After cooling, it was poured into 3M hydrochloric acid (150 mL) and extracted with benzene (30 mL×2). The combined organic layers were washed with saturated $NaHCO_3$ (30 mL×2), brine twice (20 mL), and dried over anhyd $MgSO_4$. After removal of the solvent by evaporation, the residue was chromatographed on silica gel to give **19** (17.0 g, 58%) from benzene elution: Colorless needles, mp 70—71 °C (CH_2Cl_2–hexane); IR(KBr) 3040w, 2920s, 1600s, 1560s, 770s cm^{-1}; ^{1}H NMR ($CDCl_3$) δ=16.56 (s, 1H), 7.86 (m, 3H), 7.44 (m, 4H), 2.69 (m, 2H), 2.13 (m, 2H), 1.57 (m, 6H); MS m/z 266 (M^+, 42%), 155 (100%). Found: m/z 266.1305. Calcd for $C_{18}H_{18}O_2$: M, 266.1305. Found: C, 81.02; H, 6.69%. Calcd for $C_{18}H_{18}O_2$: C, 81.17; H, 6.80%.

2-Bromo-7-(1-naphthoyl)cycloheptanone (20). A solution of **19** (6.0 g, 23 mmol) and $CuBr_2$ (8.9 g, 40 mmol) in chloroform (100 mL) was refluxed with stirring for 3 h. After cooling, the mixture was filtered and the filtrate was evaporated in vacuo. The residue was chromatographed on silica gel to give **20** (5.0 g, 63%) from benzene elution: Colorless oil; IR(film) 3050w, 2950s, 1715vs, 1580s, 780s cm^{-1}; ^{1}H NMR ($CDCl_3$) δ=7.84 (m, 3H), 7.53 (m, 4H), 4.88 (dd, J=4.8 & 4.6 Hz, 1H), 2.61—1.48 (m, 9H); MS m/z 346, 344 (M^+, 11.3%, 11.7%), 155 (100%). Found: m/z 346.0252, 344.0233. Calcd for $C_{18}H_{17}BrO_2$: M, 346.0390, 344.0410.

12-Bromo-9,10,11,12-tetrahydrocyclohepta[*a*]phenalen-7(8*H*)-one (21). To 90% sulfuric acid (190 mL) was added **20** (18.9 g, 54.8 mmol) all at once. The mixture stirred at 45—50 °C for 30 min, poured onto ice (ca, 1.5 kg) and extracted with dichloromethane (50 mL×3). The organic layer was washed with water three times, brine twice, and dried over anhyd $MgSO_4$. After removal of the solvent by evaporation in vacuo, the residue was chromatographed on silica gel to give **21** (11.0 g, 61.5%) from CH_2Cl_2 elution: Yellow needles, mp 130—131 °C (CH_2Cl_2–hexane); IR(KBr) 3100w, 2860s, 1640s, 1580s, 790s cm^{-1}; ^{1}H NMR ($CDCl_3$) δ=8.60 (dd, J=7.2 & 1.5 Hz, 1H), 8.13 (dd, J=8.0 & 1.5 Hz, 2H), 7.95 (d, J=7.2 Hz, 1H), 7.69 (dd, J=8.1 & 7.7 Hz, 1H), 7.59 (dd, J=7.9 & 7.2 Hz, 1H), 6.05 (bd, J=5.9 Hz, 1H), 3.55 (dd, J=14.0 & 7.2H, 1H), 2.82 (m, 7H); MS m/z 328, 326 (M^+, 1.2%, 1.2%), 231 (100%). Found: m/z 328.0234, 326.0312. Calcd for $C_{18}H_{15}BrO$: M, 328.0284, 326.0317. Found: C, 66.29; H, 4.7%. Calcd for $C_{18}H_{15}BrO$: C, 66.07; H, 4.62%.

12-Acetoxy-9,10,11,12-tetrahydrocyclohepta[*a*]phenalen-7-(8*H*)-one (22). To a mixture of acetic anhydride (20 mL) and acetic acid (20 mL) were added **21** (3.5 g, 10.7 mmol) and silver acetate (2.7 g, 16.2 mmol), and the resulting mixture was heated at 100—110 °C with stirring for 22 h. After cooling, the solid was filtered off, and the filtrate was evaporated to dryness. The residue was chromatographed on silica gel with CH_2Cl_2–benzene as an eluent to give **22** (2.8 g, 85%): Orange oil; IR(film) 2920w, 1740s, 1630s, 1590s, 780s cm^{-1}; ^{1}H NMR ($CDCl_3$) δ=8.58 (dd, J=7.5 & 1.3 Hz, 1H), 8.13 (d, J=7.6 Hz, 1H), 8.05 (dd, J=7.5 & 1.3 Hz, 1H), 7.87 (d, J=7.6 Hz, 1H), 7.63 (t, J=7.5 Hz, 1H), 7.52 (t, J=7.6 Hz, 1H), 6.71 (d, J=6.4 Hz, 1H), 3.48 (dd, J=15.0 & 6.4 Hz, 1H), 2.86 (m, 1H), 2.13 (s, 3H), 2.40—1.40 (m, 6H); MS m/z 306 (M^+, 6.8%), 246 (100%). Found: m/z 306.1242. Calcd for $C_{20}H_{18}O_3$: M, 306.1253.

12-Hydroxy-9,10,11,12-tetrahydrocyclohepta[*a*]phenalen-7-(8*H*)-one (23). To a solution of **22** (2.77 g, 6.8 mmol) in THF (20 mL) was added a solution of sodium hydroxide (5.44 g, 22.7 mmol) in water (25 mL). The mixture was heated with stirring at 50—60 °C for 24 h. After cooling, it was neutralized with dil HCl, concentrated in vacuo to remove THF, and extracted with CH_2Cl_2 (30 mL×3). The organic layer was washed with water and brine twice each, and dried over anhyd $MgSO_4$. After removal of the solvent by evaporation in vacuo, the residue was chromatographed on silica gel to give **23** (1.73 g, 96%) from CH_2Cl_2 elution: Yellow needles; mp 159—160 °C (CH_2Cl_2–hexane); IR(KBr) 3350m, 2920m, 1620s, 1590s, 780s cm^{-1}; ^{1}H NMR ($CDCl_3$) δ=8.29 (dd, J=8.1 & 1.3 Hz, 1H), 8.14 (d, J=7.5 Hz, 1H), 7.91 (dd, J=8.1 & 1.3 Hz, 1H), 7.78 (d, J=7.5 Hz, 1H), 7.45 (t, J=8.1 Hz, 1H), 7.44 (t, J=7.5 Hz, 1H), 5.59 (d, J=6.1 Hz, 1H), 3.08 (m, 3H), 2.30—1.30 (m, 6H); MS m/z 264 (M^+, 26%), 181 (100%). Found: m/z 264.1111. Calcd for $C_{18}H_{16}O_3$: M, 264.1148. Found: C, 82.16; H, 6.08%. Calcd for $C_{18}H_{16}O_3$: C, 81.82; H, 6.06%.

8,9,10,11-Tetrahydrocyclohepta[*a*]phenalene-7,12-dione (24). A) To a solution of pyridinium dichromate prepared by the addition of chromium trioxide (CrO_3) (5.5 g, 55 mmol) to pyridine (50 ml) was added **23** (2.97 g, 11.3 mmol) in pyridine (10 mL). The mixture stirred at room temperature for overnight, poured onto ice-water, and extracted with

CH_2Cl_2 (50 mL×3). The organic layer was washed with dil HCl three times, brine twice, and dried over anhyd $MgSO_4$. After removal of the solvent by evaporation, the residue was chromatographed on silica gel to give **24** from CH_2Cl_2 elution. Recrystallization from CH_2Cl_2–hexane gave pure **24** (2.22 g, 75%).

B) To a solution of **23** (2.6 g, 9.83 mmol) in CH_2Cl_2 (100 mL) was added $BaMnO_4$ (27 g) and the mixture was refluxed with stirring for 6 h. The solid was filtered, and the filtrate was evaporated in vacuo. The residue was chromatographed on silica gel to give **24** (2.5 g, 97%) from CH_2Cl_2 elution: Yellow needles, mp 84—85 °C; IR(KBr) 2920m, 1690s, 1630s, 1570s, 780s cm^{-1}; ^1H NMR ($CDCl_3$) δ=8.16 (dd, J=7.6 & 1.3 Hz, 1H), 8.15 (dd, J=7.9 & 1.5 Hz, 1H), 7.95 (dd, J=7.6 & 1.3 Hz, 1H), 7.71 (dd, J=7.9 & 1.5 Hz, 1H), 7.71 (t, J=7.6 Hz, 1H), 7.51 (t, J=7.9 Hz, 1H), 2.84 (m, 4H), 1.95 (m, 4H); MS m/z 262 (M^+, 100%), 219 (87%). Found: m/z 262.0950. Calcd for $C_{18}H_{14}O_2$: M, 262.0991. Found: C, 82.31; H, 5.54%. Calcd for $C_{18}H_{14}O_2$: C, 82.42; H, 5.83%.

11,11-Dibromo-8,9,10,11-tetrahydrocyclohepta[*a*]phenalene-7,12-dione (25). To a solution of **24** (2.18 g, 8.32 mmol) in chloroform (50 mL) was added $CuBr_2$ (11.2 g, 49.9 mmol), and the mixture was refluxed for overnight. After cooling, the solid was filtered off and the filterate was evaporated in vacuo. The residue was chromatographed on silica gel to give **25** (3.2 g, 92%) from CH_2Cl_2 elution: Orange needles, mp 157—158 °C (CH_2Cl_2–hexane); IR(KBr) 1710m, 1630s, 1570s, 780m cm^{-1}; ^1H NMR ($CDCl_3$) δ=8.61 (dd, J=7.7 & 1.4 Hz, 1H), 8.18 (dd, J=7.6 & 1.3 Hz, 1H), 8.00 (dd, J=7.7 & 1.4 Hz, 1H), 7.76 (dd, J=7.6 & 1.3 Hz, 1H), 7.72 (t, J=7.7 Hz, 1H), 7.58 (t, J=7.6 Hz, 1H), 3.80—2.30 (m, 2H), 2.02 (m, 2H); MS m/z 422, 420, 418 (M^+, 7%, 12%, 7%). Found: m/z 421.9200, 419.9182, 417.9256. Calcd for $C_{18}H_{12}Br_2O_2$: M, 421.9165, 419.9183, 417.9205. Found: C, 51.50; H, 2.91%. Calcd for $C_{18}H_{12}Br_2O_2$: C, 51.43; H, 2.86%.

Cyclohepta[*a*]phenalene-7,12-dione (4). A mixture of **25** (1.00 g, 2.38 mmol) and lithium chloride (1.00 g, 23.5 mmol) in dry DMF (10 mL) was heated at 100—110 °C with stirring for 3 h. After cooling, the mixture was poured onto ice-water and the solid was filtered. The solid was dissolved in CH_2Cl_2 and dried over anhyd $MgSO_4$. The solvent was evaporated and the residue was chromatographed on silica gel to give **4** (0.70 g, 96%) from CH_2Cl_2 elution: Orange needles, mp 176—177 °C (CH_2Cl_2–hexane); IR(KBr) 3050w, 1640s, 1570s, 760s cm^{-1}; ^1H NMR ($CDCl_3$) δ=8.63 (dd, J=7.6 & 1.3 Hz, H-1), 8.43 (dd, J=7.7 & 1.2 Hz, H-6), 8.18 (dd, J=7.6 & 1.3 Hz, H-3), 8.13 (dd, J=10.2 & 1.1 Hz, H-8), 7.98 (dd, J=7.7 & 1.2 Hz, H-4), 7.71 (t, J=7.6 Hz, H-2), 7.53 (t, J=7.7 Hz, H-5), 6.89 (m, H-9, -10, -11), (D_2SO_4–CH_2Cl_2) δ=10.09 (d, J=8.11 Hz, H-1), 9.88 (d, J=10.7 Hz, H-8), 9.68 (d, J=8.1 Hz, H-3), 9.50 (d, J=7.0 Hz, H-6), 9.06 (t, J=8.1 Hz, H-2), 8.94 (d, J=7.0 Hz, H-4), 8.56 (ddd, J=10.7, 9.6, & 2.9 Hz, H-9), 8.54 (m, 10-H), 8.52 (t, J=7.0 Hz, H-5); ^{13}C NMR ($CDCl_3$) δ=190.1 (C-12), 183.3 (C-7), 143.8, 136.1, 133.8, 132.5, 132.4, 131.1, 130.6, 128.0, 127.8, 126.8, 124.4, (D_2SO_4–CH_2Cl_2) δ=181.6 (C-OH, C-12), 178.6 (C-OH, C-7), 156.5 (C-4), 155.6 (C-6), 147.5 (C-5), 146.1 (C-1), 143.6 (C-2), 142.9 (C-3), 140.1 (C-8), 134.2 (C-10), 131.9 (C-11), 130.5 (C-9), 144.6, 134.4, 126.5, 123.7, 120.5 (quart. C); ES (CH_2Cl_2) λ_{max} 432 (log ε=3.72), 382 (3.68), 296sh (3.56), (concd H_2SO_4) λ_{max} 540 (log ε=4.10), 395 (4.12), 307 (4.15), 283 (5.19), 237 nm (5.20), The pK_a value was obtained by the similar manner as **2**; MS m/z 258 (M^+, 100%), 230 (97%). Found: m/z 258.0685. Calcd for $C_{18}H_{10}O_2$: M, 258.0680. Found: C, 83.59; H, 4.09%. Calcd for $C_{18}H_{10}O_2$: C, 83.71; H, 3.90%.

9,10-Dihydrocyclohepta[*a*]phenalen-7(8*H*)-one (26). A mixture of **21** (9.04 g, 27.6 mmol) and lithium chloride (1.6 g, 41.1 mmol) in DMF (20 mL) was heated at 100—110 °C with stirring for 1 h. After cooling, the mixture was poured onto ice-water and extracted with CH_2Cl_2 (30 mL×3). The organic layer was washed with water and brine twice each and dried over anhyd $MgSO_4$. The solvent was removed by evaporation and the residue was chromatographed on silica gel to give **26** (5.5 g, 81%) from CH_2Cl_2 elution: Yellow needles, mp 73—74 °C (CH_2Cl_2–hexane); IR(KBr) 2920w, 1630s, 1565s, 785s cm^{-1}; ^1H NMR ($CDCl_3$) δ=8.65 (dd, J=7.2 & 1.3 Hz, 1H), 8.13 (dd, J=8.1 & 1.3 Hz, 1H), 7.91 (m, 1H), 7.88 (d, J=1.1 Hz, 1H), 7.75 (s, J=8.1 Hz, 1H), 7.63 (t, J=7.9 Hz, 1H), 6.97 (d, J=11.3 Hz, 1H), 6.61 (dt, J=11.3 & 5.9 Hz, 1H), 4.78 (m, 2H), 2.82 (m, 4H); MS m/z 246 (M^+, 40.3%), 219 (100%). Found: m/z 246.1042. Calcd for $C_{18}H_{14}O$: M, 246.1042. Found: C, 87.48; H, 5.77%. Calcd for $C_{18}H_{14}O$: C, 87.78; H, 5.73%.

8,9-Dihydrocyclohepta[*a*]phenalene-7,10-dione (27). To a solution of pyridinium dichromate in pyridine prepared by addition of CrO_3 (17.1 g, 170 mmol) to pyridine (50 mL) at ca. 5 °C was added **26** (8.53 g, 34.7 mmol) dissolved in pyridine (20 mL). The mixture heated at 50—60 °C with stirring for 7 h, diluted with dil HCl (500 mL), and extracted with CH_2Cl_2 (50 mL). The organic layer was washed with dil HCl twice and brine twice, and dried over anhyd $MgSO_4$. The solvent was evaporated and the residue was chromatographed on silica gel to give **27** (0.59 g, 16%) from CH_2Cl_2 elution along with the recovered starting material **26** (4.85 g, 56.8%). Compound **27**: Yellow needles, mp 177—178 °C (CH_2Cl_2–hexane); IR(KBr) 1660s, 1630s, 1570s, 785s cm^{-1}; ^1H NMR ($CDCl_3$) δ=8.65 (dd, J=7.2 & 1.3 Hz, 1H), 8.19 (dd, J=7.9 & 1.3 Hz, 1H), 8.01 (d, J=7.9 Hz, 1H), 7.99 (d, J=6.6 Hz, 1H), 7.76 (dd, J=7.5 & 7.0 Hz, 1H), 7.61 (d, J=12.5 Hz, 1H), 7.59 (dd, J=7.9 & 7.7 Hz, 1H), 6.58 (d, J=12.5 Hz, 1H), 3.17 (m, 2H), 2.77 (m, 2H); MS m/z 260 (M^+, 81.5%), 231 (100%). Found: m/z 260.0778. Calcd for $C_{18}H_{12}O_2$: M, 260.0835. Found: C, 82.78; H, 4.72%. Calcd for $C_{18}H_{12}O_2$: C, 83.06; H, 4.65%.

Cyclohepta[*a*]phenalene-7,10-dione (3). A mixture of **27** (0.64 g, 2.46 mmol) and SeO_2 (0.37 g, 2.95 mmol) in dioxane (30 mL) was refluxed for 3 h. The mixture was filtered and the filtrate was evaporated to dryness. The residue was dissolved in CH_2Cl_2, washed with saturated aq $NaHCO_3$ twice and brine twice, and dried over anhyd $MgSO_4$. The solvent was evaporated in vacuo and the residue was chromtographed on silica gel to give **3** (0.38 g, 60%) from CH_2Cl_2 elution, along with the recovered starting material **27** (0.15 g, 23%). Compound **3**: Yellow needles, mp 246—247 °C (CH_2Cl_2–hexane); IR(KBr) 3050w, 1640s, 1600s, 1570s, 765s cm^{-1}; ^1H NMR ($CDCl_3$) δ=8.67 (dd, J=13.5 & 1.3 Hz, H-6), 8.44 (d, J=12.9 Hz, H-12), 8.38 (bd, J=7.6 Hz, H-3), 8.25 (dd, J=7.6 & 1.3 Hz, H-4), 8.10 (bd, J=7.6 Hz, H-1), 7.80 (t, J=7.6 Hz, H-5), 7.68 (t, J=7.6 Hz, H-2), 7.17 (dd, J=13.5 & 3.1 Hz, H-9), 7.02 (dd, J=12.9 & 3.1 Hz, H-11), (D_2SO_4–CH_2Cl_2) δ=10.15 (d, J=12.3 Hz, H-12), 10.10 (d, J=12.1 Hz, H-8), 9.79 (d, J=9.0 Hz, H-6), 9.69 (d, J=8.8 Hz, H-4), 9.49 (d, J=7.5 Hz, H-3), 9.17 (d, J=7.7 Hz, H-1), 8.61 (d, J=7.7 & 7.5 Hz, H-2), 8.61 (dd, J=9.0 & 8.8 Hz, H-5), 8.40 (d,

J=12.3 Hz, H-11), 8.37 (d, J=12.1 Hz, H-9); ^{13}C NMR ($CDCl_3$) δ=187.0 (C-10), 182.9 (C-7), 143.2, 142.3, 138.3, 136.1, 134.5, 134.1, 133.2, 132.6, 131.6, 128.9, 128.0, 127.8, 127.6, 127.0, (D_2SO_4) δ=184.7 (C-OH, C-10), 178.7 (C-OH, C-7), 155.4 (C-4), 150.3 (C-3), 147.9 (C-1), 147.4 (C-6), 143.3 (C-8), 143.0 (C-12), 137.2 (C-9 or C-11), 131.4 (C-11 or C-9), 131.4 (C-5), 131.2 (C-2), 150.3, 131.9, 131.3, 126.3, 125.5, 120.9 (quart. C); ES (CH_2Cl_2) λ_{max} 432 (log ε=3.48), 390 (3.46), 340 (3.69), 254 (4.22), 228 nm (4.05), (concd H_2SO_4) λ_{max} 520 (log ε=4.05), 489 (4.01), 370 (3.89), 330 (3.94), 282 (4.58), 230 nm (4.30); MS m/z 258 (M^+, 10.2%), 230 (100%). Found: m/z 258.0702. Calcd for $C_{18}H_{10}O_2$: M, 258.0723. Found: C, 83.49; H, 4.15%. Calcd for $C_{18}H_{10}O_2$: C, 83.71; H, 3.90%.

We are grateful to the Science and Technical Foundation of Asahi Glass Co. Ltd., for the financial support (1987—1988).

References

1) A. F. Garito and A. J. Heeger, *Acc. Chem. Res.*, **7**, 232 (1974); J. H. Perlstein, *Angew. Chem.*, **89**, 534 (1977); *Angew. Chem., Int. Ed. Engl.*, **16**, 519 (1977); D. O. Cowan, P. Shu, C. Hu, W. Krug, T. Carruthers, T. Poehler, and A. N. Bloch in "Chemistry and Physics of One-Dimentional Metals," ed by H. J. Keller, Plenum Press, New York (1977), pp. 1—25; J. B. Torrance, *Acc Chem. Res.*, **12**, 79 (1979); D. O. Cowan, A. Kini, L. Y. Chiang, K. Lerstrup, D. R. Talham, T. O. Poehler, and A. N. Bloch, *Mol. Cryst. Liq. Cryst.*, **86**, 1 (1982); R. C. Wheland and J. L. Gillson, *J. Am. Chem. Soc.*, **98**, 3916 (1976).

2) N. Martin, R. Rhenisch, and M. Hanack, *J. Org. Chem.*, **54**, 2563 (1989), and references cited therein.

3) T. A. Turney, "The Chemistry of the Quinoid Compounds," ed by S. Patai, John Wiley & Sons Interscience, New York (1974), pp. 857—876.

4) a) C. F. Wilcox, Jr., K. R. Lassila, G. VanDuyne, H. Lu, and J. Clardy, *J. Org. Chem.*, **54**, 2190 (1989); b) J. W. Lown and A. S. K. Aidoo, *Can. J. Chem.*, **49**, 1861 (1971); c) B. M. Trost, *J. Am. Chem. Soc.*, **88**, 853 (1966); d) B. M. Trost, *ibid.*, **91**, 918 (1969); e) B. M. Trost, *ibid.*, **93**, 3823 (1971); f) V. Boekelheide and J. B. Phillips, *ibid.*, **98**, 1695 (1967).

5) For example, see S. Kuroda and T. Asao, *Tetrahedron Lett.*, **1977**, 289.

6) A part of this work has been reported in a preliminary form: S. Kuroda, Y. Fukuyama, T. Tsuchida, E. Tanaka, and S. Hirooka, *Angew. Chem.*, **97**, 770 (1985); *Angew. Chem., Int. Ed. Engl.*, **24**, 757 (1985).

7) 2,2-Dimethoxycycloheptanone: M-C. Carre, B. Gregoire, and P. Caubere, *J. Org. Chem.*, **49**, 2050 (1984).

8) L. C. King and G. K. Ostrum, *J. Org. Chem.*, **29**, 3459 (1964); H. C. Brown, M. M. Rogi, and M. W. Rathe, *J. Am. Chem. Soc.*, **90**, 6218 (1968).

9) E. W. Collinton and G. Jones, *Chem. Commun.*, **1968**, 958.

10) H. Christol, Y. Delhoste, and M. Mousseren, *Bull. Soc. Chim. Fr.*, **1959**, 1238.

11) G. I. Poos, G. E. Arth, R. E. Beyer, and L. H. Sarett, *J. Am. Chem. Soc.*, **75**, 422 (1953).

12) H. Stamm, *Z. Angew. Chem.*, **47**, 791 (1930); H. Prinzbach and E. Ghaderi, *Tetrahedron Lett.*, **1978**, 839.

13) D. J. Bertelli, T. G. Andrews, and P. O. Crews, *J. Am. Chem. Soc.*, **91**, 5286 (1969); for synthesis, see K. M. Harmon, A. B. Harmon, T. Y. Coburn, and J. M. Fisk, *J. Org. Chem.*, **33**, 2567 (1968).

14) H. Prinzbach, V. Freudenberger, and U. Sheidegger, *Helv. Chim. Acta*, **50**, 1087 (1967).

15) W. von E. Doering and F. L. Detert, *J. Am. Chem. Soc.*, **73**, 876 (1951).

16) D. H. Reid, *Quart. Rev.*, **19**, 274 (1965).

17) H. Spieseke and W. G. Schneider, *Tetrahedron Lett.*, **1961**, 868; P. Garratt and M. V. Sargent, "Nonbenzenoid Aromatics," ed by J. P. Snyder, Academic Press, New York (1971), Vol. 2, p. 227.

18) For example, see K. S. Dhami and J. B. Stothers, *Tetrahedron Lett.*, **1964**, 632; J. B. Stothers, "Carbon-13 NMR Spectroscopy," Academic Press Inc., New York (1972), p. 427.

19) D. J. Bertelli, J. T. Gerig, and J. M. Herberlin, *J. Am. Chem. Soc.*, **90**, 107 (1968); for the synthesis, see D. S. Tarbell and J. C. Bill, *ibid.*, **74**, 1234 (1952).

20) H. P. Koch, *J. Chem. Soc.*, **1951**, 512; K. Kuratani, M. Tsuboi, and T. Shimamouchi, *Bull. Chem. Soc. Jpn.*, **25**, 250 (1952); Y. Ikegami, "Infrared Spectroscopy," Nankodou, Tokyo (1959), No. 8, p. 33.

21) a) H. Hosoya and S. Nagakura, *Bull. Chem. Soc. Jpn.*, **39**, 1414 (1966); b) M. A. Paul and F. A. Long, *Chem. Rev.*, **57**, 1 (1957).

22) T. Honda, *Bull. Chem. Soc. Jpn.*, **28**, 483 (1955); L. A. Flexser, L. P. Hammett, and Dingmall, *J. Am. Chem. Soc.*, **57**, 2103 (1935).

23) T. Fujinaga, K. Izutsu, and T. Nomura, *J. Electroanal. Chem.*, **29**, 203 (1971).

24) S. F. Nelson, B. M. Trost, and D. H. Evans, *J. Am. Chem. Soc.*, **89**, 3034 (1967).

Thermal Behavior and Characterization of Poly[1,3-phenylenebis (methylene)adipamide]

Choichiro SHIMASAKI,* Hisashi SANAGI, Akira UNISHI, Hisakimi NOTOYA, Eiichi TSUKURIMICHI, and Toshiaki YOSHIMURA
Faculty of Engineering, Toyama University, Gofuku, Toyama 930
(Received October 9, 1990)

Thermal degradation of poly[1,3-phenylenebis(methylene) adipamide] (MXD-6) was investigated by DTA-TG, FT-IR, TG-GC/MS, and mass spectroscopy. The DTA-TG/DTG curve showed that the thermal decomposition of MXD-6 occurred in two stages. MXD-6 melted at about 235 °C and decomposed to the oligomer or monomer with a weight loss of about 40% in the temperature region from 330 to 400 °C during the first stage. A TG effluent gas was collected in a cold trap and then directly injected into a GC for separation, the MS for an unequivocal identification. The eleven effluent compounds from the thermal degradation of MXD-6 were identified. The main fragmentation mechanism by electron impact for MXD-6 consisted of two processes: simple cleavage and a rearrangement reaction. The activation energy of the thermal decomposition was estimated to be 230 during the first stage and 150 kJ mol^{-1} during the second stage. From the value of the activation energy in each stage, the kinetic data for MXD-6 was elucidated.

The structual characterization of Poly[1,3-phenylenebis(methylene)adipamide] (MXD-6) has attracted much attention recently, since this material is an important member of a family of polyamides. This family has potential for both thermohardening materials and important commercial polymers. Its, thus, thermal decomposition mechanism is of practical and theoretical relevance. Serveral thermal decomposition products have been identified in a flash pyrolysis GC study of several nylons.[1] Since the advent of modern direct pyrolysis mass spectrometry techniques, the thermal degradation of polyamides has been the subject of several publications.[2] The polymer (**I**) of isophthalic acid and hexamethylenediamine is amorphous and has relatively low melting and heat destortion temperatures.[3] MDX-6 shows the effects caused by a reversal of the position of the carbonyl groups relative to the amide nitrogen, in comparison with **I**.[4] It was of interest to investigate the thermal properties of MXD-6 in question be applying both TG and DTA techniques. Also, since little is known about the thermal behavior, such as the TG-GC/Mass, detailed degradation studies were performed; the results are discussed.

Experimental

Materials. MXD-6 polyamide (**II**) was produced by Mitsubishi Gasukagaku Co., Ltd. The following samples were selected for the present work. Sample (**IIa**): The powdered sample was prepared by cutting the rod of **II** with a saw. Sample (**IIb**): A powdered sample was prepared by refluxing in dimethylformamide solvent, then evaporating to dryness under reduced pressure. Sample (**IIc**): A colloidal solution after refluxing of **IIb** was filtered, washed with chloroform, and dried in air. Sample (**IId**): Powdered sample was prepared by sawing a rod of **II** with an electromobile high-speed saw. The elemental analyses of each sample are summarized, together with the calculated value of the monomer of **II** in Table 1.

All other chemicals were of the highest commercially available purity and were used without further purification, unless otherwise stated.

Thermal Analysis. Thermal analyses were performed using a Rigaku Denki thermogravimetry-differential thermal analysis (TG-DTA) and a differential scanning calorimetry (DSC) apparatus in air at various heating rates. Calcinated alumina was used as the reference material. TG-TRAP-GC/MS was carried out with a Shimadzu combined system in stationary helium gas at a heating rate of 10 °C min^{-1}. Separation and identification of the pyrolysis products were carried out by using a gas chromatograph coupled with a mass selective detector. A Shimadzu gas chromatograph, containing a capillary column of porous polymer beads of poly[oxy(2,6-diphenyl-1,4-phenylene)] (TENAX GC), coupled with a mass selective detector was used. The injector and detector temperatures were maintained at 230 and 250 °C.

Spectroscopic Measurements. A double-focussing JEOL-JMS-D300 mass spectrometer, equipped with the standard EI was used to obtain the mass spectra. The instrument was scanned from m/z 20 to 1000 at a scan rate of 10 s/decade; perfluorokerosene (PFK) was used for the computor calibration. The ion source was maintained at 200 °C. Polymers were pyrolyzed directly in the ion source using direct probes, heated from 20 to 350 °C at a heating rate of 10 °C min^{-1}.

Table 1. Elemental Analysis of **II**

Sample	N/%	C/%	H/%
IIa	10.58	64.11	7.50
IIb	10.98	60.80	7.19
IIc	10.94	63.89	7.49
IId	11.07	64.99	7.46
Monomer[a)]	10.60	63.61	7.63

a)

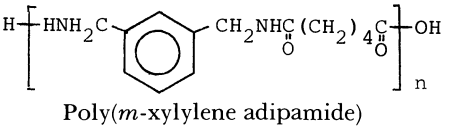

Poly(m-xylylene adipamide)
n=1: Monomer

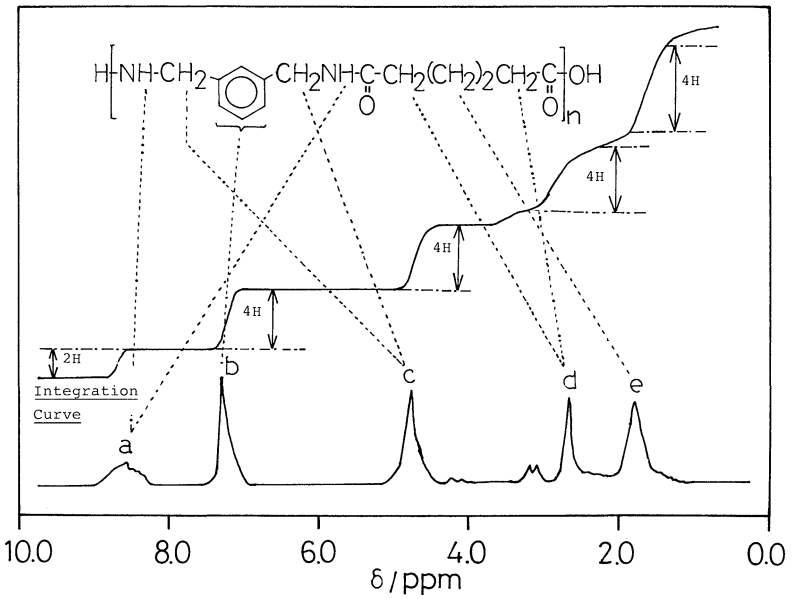

Fig. 1. ^{1}H NMR spectrum of **II**.

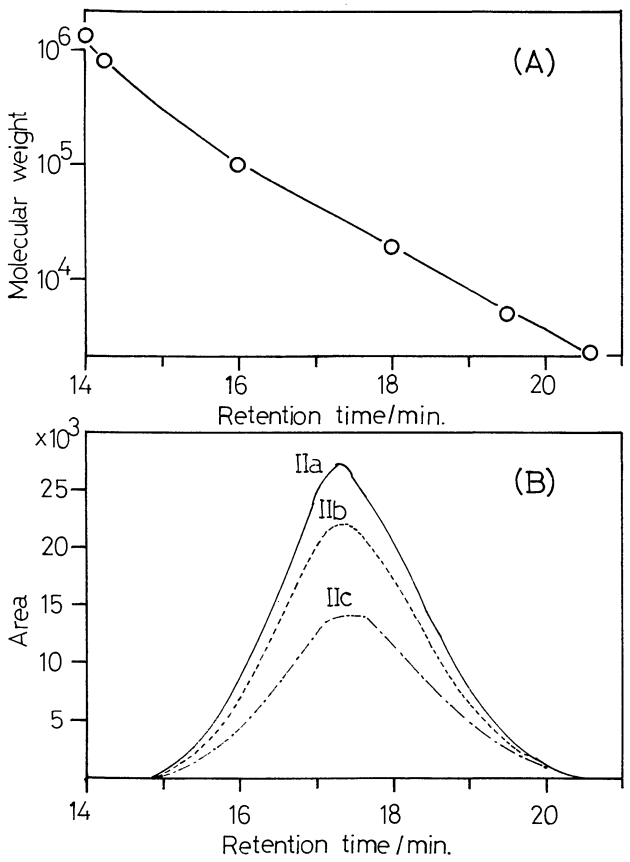

Fig. 2. GPC measurements for **II**. (A) Calibration curves of molecular weight with poly(methyl methacryrate). (B) Distribution curves of molecular weight for **II**.

Table 2. Molecular Weight for **II** by the GPC Measurement

Sample	MW[a]	MN[b]	MZ[c]	MW/MN
IIa	39250	19397	75589	2.02
IIb	38801	18934	74584	2.05
IIc	36525	16920	71459	2.16

a) MW=Weight-average molecular weight. b) MN=Number average molecular weight. c) MW=Z average molecular weight.

The IR spectrum was recorded using a JASCO FT-IR-3 type for both powder and thin films. The ^{1}H and ^{13}C NMR spectra were measured in trifluoroacetic acid using a JNM-FX-90-FT-NMR instrument. TMS was used as a reference. For the NMR spectrometric detection and identification of **II**, a solution containing trace amounts of insoluble materials was filtered with a molecular sieve. The ^{1}H NMR spectra given in Fig. 1 shows that **II** contains the constituent functional groups. The steps in the integration curve in Fig. 1 provide the ratios for the different kinds of protons in the molecule. These can be compared with the proton count obtained from the off-resonance decoupled ^{13}C spectrum.

GPC Analysis. A Waters 6000A apparatus equipped with a gel permeation chromatography (GPC) HFIP-80M column was used. A differential refractometer was used as the detector. Analyses were performed at 40 °C in 1,1,1,3,3,3,-hexafluoro-2-propanol (HFIP) as the eluent at a flow rate of 0.5 ml min^{-1}. The working curve was obtained by a calibration with poly(methyl methacrylate) of known molecular weight, as shown in Fig. 2(A). Also, Fig. 2(B) shows the relationship between the area and the retention time with the GPC measurements. The experimental data of each molecular weight for **II** are summarized in Table 2.

Results and Discussion

Thermal Analysis. The TG-DTA curves relative to **IIa** and **IId** are shown in Fig. 3. Figure 3 shows that a melting points are present in the DTA curves for **IIa** and **IId** at 234.6 and 235.5 °C, respectively. From the measurement of DSC, the heat of fusion for **II** was estimated to be about 42 J g^{-1}. The TG-DTA curves of **IIa**, **IIb**, and **IIc** are practically coincident, and the maximum volatilization rate was observed at about 370 and 470 °C. It is borne by changes in the IR spectra both before and after the heating of **II**. Figure 4 shows the change of the IR spectra between room temperature and 400 °C. For the IR spectrum of **II**, the absorption band between 1000 and 1200 cm^{-1} is assigned to the C–N stretching vibration. This absorption grew weaker at 400 °C. At about 2400 cm^{-1} the absorption band attributed to the N–H stretching vibration grew strong, showing that the cleavage of C–N proceeded. Upon further heating, the less-stable aliphatic groups were preferentially decomposed through the homolytic cleavages of the C–C, C–H, C–N, and N–H bonds. Since the thermal degradation in the present work was carried out in a static air medium, it can be said that atmospheric oxygen is consumed before combustion is completed, and that the remainder decomposes afterwards in an inert medium. The last exotherm on the DTA curve of **IId** represents a crosslinking and aromatization of the char in an inert medium.

To investigate the thermal decomposition processes which cause the DTA and the TG curves over the range from 200 to 500 °C for **II**, TG-TRAP-GC/MS was carried out in stationary He. In many cases the TG effluent gas was comprised of various components. The identification of less-abundant components became increasing difficult. Another approach is to collect the pyrolysis products and then to analyze this collected material by GC. This method has been applied to the analysis of thermal degradation products.[5] Figure 5 shows a mass chromatogram of the liberated decomposition products of **II** with a tandem thermogravimetric analyzer–gas chromatograph–mass spectrometer system. The thermally degraded products of **II** consist of about eleven components. These components were identified by measuring the mass spectrum of the liberated gas from

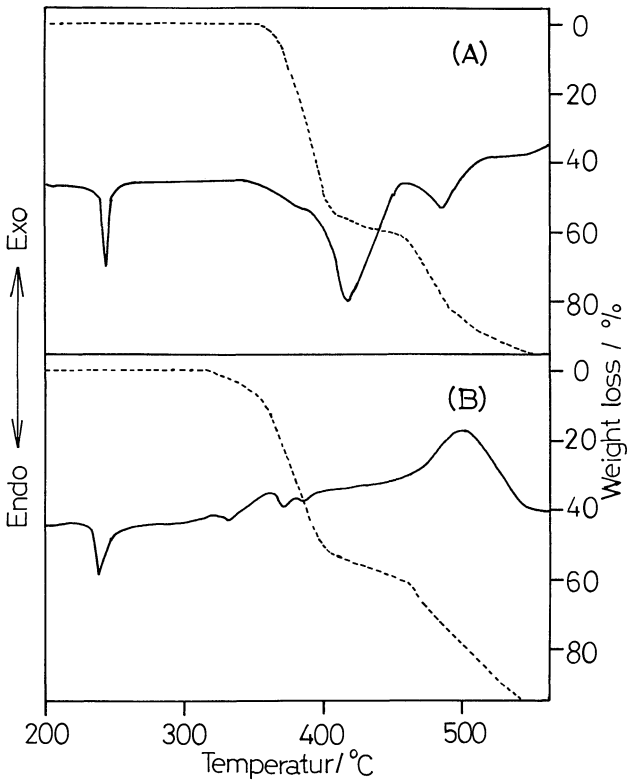

Fig. 3. Effect of pretreatment method on the DTA curves of **II**. (A) **IIa**: Powdered sample prepared by sawing rod of **II** with saw. (B) **IId**: Powdered sample prepared by sawing rod of **II** with the electromobile high speed saw.

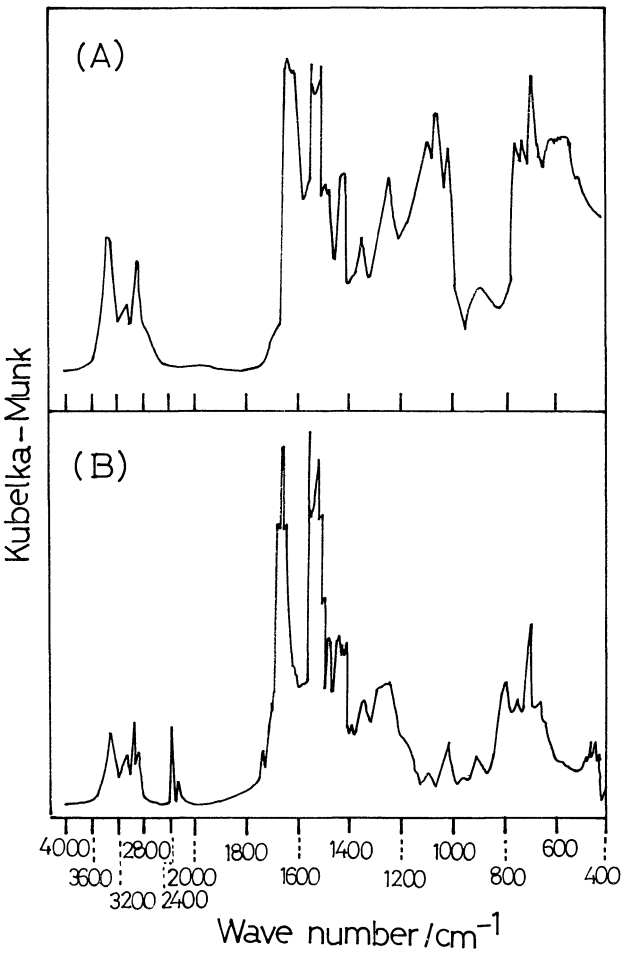

Fig. 4. Effect of heating temperature on the FT-IR spectra of **II**. (A) Sample at the room temperature. (B) Sample heated at 400 °C.

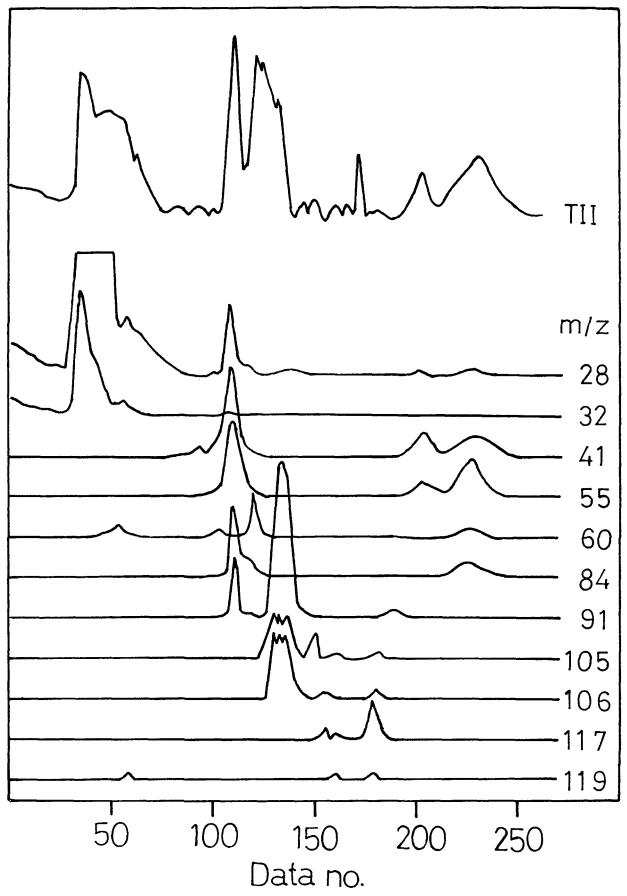

Fig. 5. Mass chromatogram of the decomposition products of **II** with TG-TRAP-GC/MS. TII=Total Ion Intensity.

the principal portion of the weight loss on the TG curve between 300 and 500 °C. The peaks at *m/z* 28 and 32 due to N_2 (or CO) and O_2 were the most intense. The peak at *m/z* 119 due to $C_8H_9N^+$ was the apparent maximum mass number in the liberated decomposition products of **II**. Other thermally degraded products of **II** consists of a complex mixture of seven components: $(C_7H_7NH_2)^+$ *m/z* 106→$(C_7H_7NH)^+$ *m/z* 105; $(C_7H_7)^+$(Tropylium ion) *m/z* 91; $(C_4H_4CO)^+$ *m/z* 84; $(C_4H_7)^+$ *m/z* 55→$(C_3H_5)^+$ *m/z* 41→$(C_2H_4)^+$ *m/z* 28. These components were identified by measuring the mass chromatograms of the decomposition products of **II** (Fig. 5). This result shows that the thermal degradation of **II** takes place through two alternative pathways. The first one dominates below 300 °C and involves dehydration, rearrangement, evolution of carbon monooxide and carbon dioxide, and the formation of carbonaceous residue. The second one, which starts at about 400 °C and overshadows the first one at higher temperatures, involves cleavages of the *m*-phenylenebis(methyleneimino) units by intramolecular rearrangements and the formation of a tar mixture and some randomly linked low molecular weight aliphatic derivatives, which then evaporate.

Mass Spectrum. The thermal decomposition process may be directly predictable from the corresponding mass spectrum. The main mass spectral data of low- and high-resolution is shown in Table 3. This table tabulates *m/z*, its corresponding elemental composition, and the probable molecular structure of each of the identified components. The ion of largest

Table 3. Mass Spectral Data for **II**

m/z[a]	Relative intensity[b]	Sigma/%[c]	Observed molecular weight	U.S.[e]	Probable ion composition
55	701.1	8.05	55.0188 (55.0183)[d]	2.5	C_3H_3O
			55.0578 (55.0546)	1.5	C_4H_7
56	276.9	3.18	56.0269 (56.0261)	2.0	C_3H_4O
			56.0631 (56.0624)	1.0	C_4H_8
77	23.1	0.26	77.0349 (77.0390)	4.5	C_6H_5
78	12.9	0.14	78.0485 (78.0468)	4.0	C_6H_6
79	46.1	0.52	79.0514 (79.0546)	3.5	C_6H_7
82	104.8	1.20	82.0637 (82.0654)	2.5	C_5H_8N
84	419.3	4.81	84.0560 (84.0573)	2.0	C_5H_8O
91	140.2	1.61	91.0510 (91.0546)	4.5	C_7H_7
104	262.7	3.01	104.0636 (104.0624)	5.0	C_8H_8
105	166.1	1.98	105.0636 (105.0576)	5.0	C_7H_7N
106	469.5	5.39	106.0659 (106.0654)	4.5	C_7H_8N
118	274.4	3.15	118.0712 (118.0654)	5.5	C_8H_8N
119	1000.0	11.48	119.0733 (119.0732)	5.0	C_8H_9N
120	420.7	4.83	120.0846 (120.0810)	4.5	$C_8H_{10}N$
133	173.4	1.99	133.0695 (133.0762)	5.5	$C_8H_9N_2$
134	133.5	1.53	134.0854 (134.0840)	5.0	$C_8H_{10}N_2$
135	193.0	2.21	135.0930 (135.0918)	4.5	$C_8H_{11}N_2$
146	92.5	1.06	146.0587 (146.0603)	6.5	C_9H_8NO
161	134.2	1.54	161.0676 (161.0711)	6.5	$C_9H_9N_2O$
189	129.7	1.48	189.1079 (189.1023)	6.5	$C_{11}H_{13}N_2O$
218	197.2	2.26	218.1399 (218.1413)	6.0	$C_{13}H_{18}N_2O$
246	174.8	2.00	246.1408 (246.1362)	7.0	$C_{14}H_{18}N_2O_2$

a) The $(M-H_2O)^+$ of monomer is underlined. b) Relative intensity referred to base peak of spectrum as 1000. c) Peak hights expressed in per cent of total ionization. d) Calculated values. e) U.S.=Degree of unsaturation.

intensity in the spectrum was selected in order to obtain the relative intensity of the raw peak height of the fragment ion. The intensity of this ion peak is called the base peak intensity. The base peak appeared at m/z 119 due to $C_8H_9N^+$. The spectrum also indicates that the peak of the maximum mass number is the $(M-H_2O)^+$ of monomer. The observed mass spectrum is an averaged recording of the results of a host of fragmentation events, most of which represent only the results of a relatively few successive fragmentations to a given moiety. A compound of **II** after ionization of the $(M-H_2O)^+$ can produce cleavages to produce fragment of m/z 100, 119, 134, 161, 189, 218, and 246, as shown in Fig. 6. Simple cleavages, such as fragment ion 1, 2, 5, and 6, as indicated by the wave line, of an even-electron ion produce another even-electron ion and a neutral olefin or other neutral particles. In fragment ion 3,4, and 7, however, the cleavage is due to the well-known McLafferty rearrangement process.

Kinetic Analysis of the Thermal Decomposition. The kinetic discussion was carried out in terms of the thermal analysis according to the Ozawa method.[6] The sample was lightly packed with the aid of a special holder into an aluminum pan. Thermal decomposition was studied at heating rates of 1.0, 3.0, 5.0, 7.0, and 10.0 °C min^{-1}. Figure 7 shows the TG curves for **II**, as determined at different heating rates. According to the Ozawa theory, the weight loss (θ) at a constant heating rate can be expressed by

$$\theta = \Delta E/aR \cdot P(\Delta E/RT), \quad (1)$$

where ΔE is the activation energy; a, the heating rate, and R, the gas constant. Also, in the case $60 > \Delta E/RT > 20$,

$$\log P(\Delta E/RT) = -\log a - 0.456\Delta E/RT. \quad (2)$$

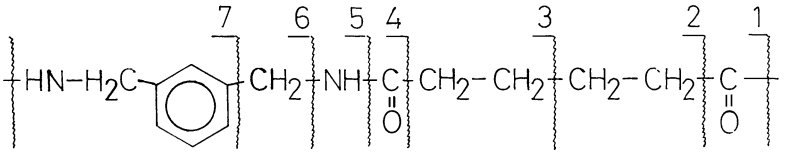

Fragment ions

1. $C_{14}H_{18}N_2O_2^+$ m/z 246
2. $C_{13}H_{18}N_2O^+$ m/z 218
3. $C_{11}H_{13}N_2O^+$ m/z 189
4. $C_9H_9N_2O^+$ m/z 161
5. $C_8H_{10}N_2^+$ m/z 134
6. $C_8H_9N^+$ m/z 119
7. $C_7H_8N^+$ m/z 100

Fig. 6. Main fragment ions by the electron impact for **II**.

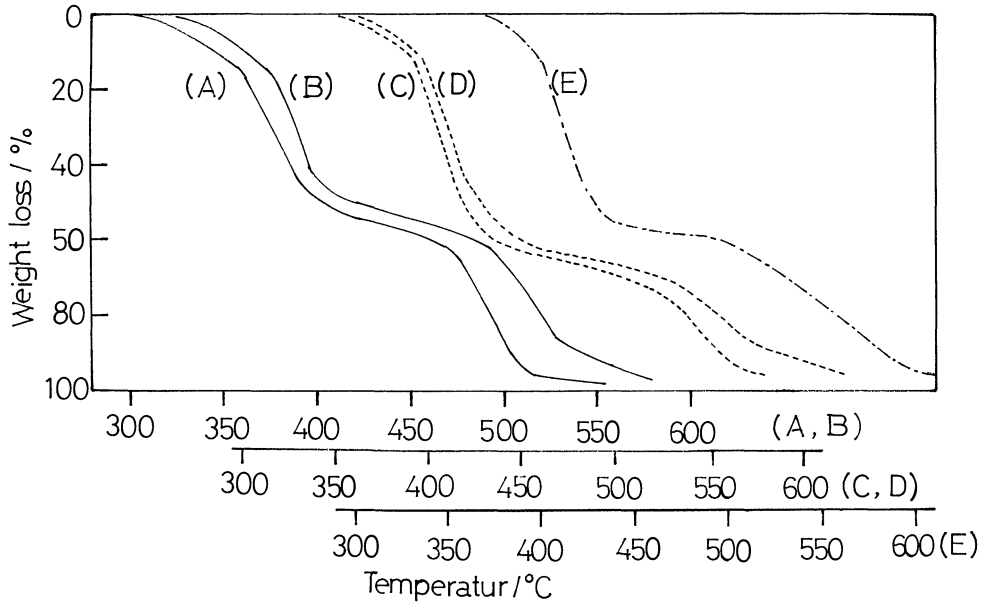

Fig. 7. TG curves for **II** at various heating rates. (A) 1.0, (B) 3.0, (C) 5.0, (D) 7.0, (E) 10.0 °C min^{-1}.

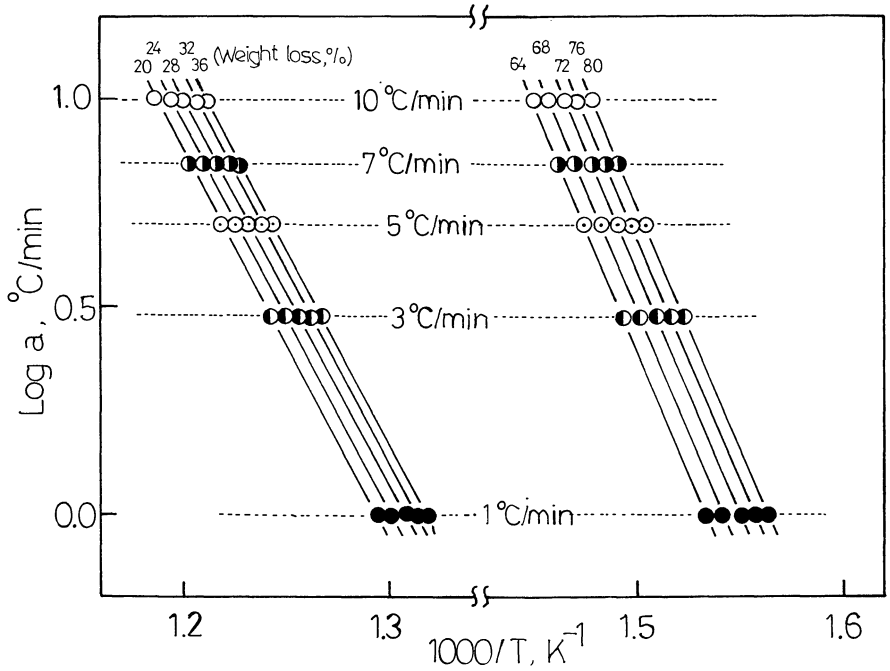

Fig. 8. Plots of logarithms of heating rate versus the reciprocal of absolute temperature for the given conversation of pyrolysis of **II**.

Table 4. Activation Energy for the Thermal Decomposition Process of **II**

Weight loss/%[a]	ΔE/kJ mol^{-1}[b]	r[c]	Process[d]
10	139	0.959	
20	188	0.987	
30	196 (203)	0.970	First stage
40	226	0.980	
50	399	0.941	
60	921	0.596	Flat portion
70	200	0.979	
80	146 (168)	0.988	Second stage
90	113	0.943	

a) Weight loss on the TG curve. b) Calculated by Ozawa's method. The values in parenthese were graphically calculated. c) Linear correlation coefficient. d) Each process on the TG curve.

Table 5. Kinetic Data for the Thermal Decomposition Process on the TG Curve for **II**

Thermal decomposition process	Reaction order	Frequency factor
First stage	0.974	0.88×10^{10}
Second stage	0.531	0.12×10^{9}

From plots of the logarithms of the heating rate versus the reciprocal of the absolute temperature for the given residual weight, the activation energy was obtained by the slope of the straight lines. In Fig. 8 is shown Ozawa's plot of the logarithmic heating rate versus the reciprocal absolute temperature. Table 4 shows the values of the activation energy, which was calculated from each weight loss on the TG curves. The activation energies of the first and second stage average 230 and 150 kJ mol^{-1}, respectively. The former was due to the main thermal decomposition while the latter resulted in an oxidative reaction. For nylon, the activation energy was evaluated to be 155 kJ mol^{-1} in Inoue and Sumoto's paper,[7] in which the mechanism of the unzipping of the monomer from carboxyl ends was postulated. The difference between the result in the first stage of this paper and in Inoue et al. paper is dependent upon the complexity of the group attached to the carbonyl carbon atom. It is possible to estimate the reaction order and the frequecy factor in each stage of the thermal decomposition process for **II** by employing the values of activation energy and the direct search method. The results are summarized in Table 5. This thermal decomposition process for **II** obeys a first-order rate law during the first stage and 1/2 order during the second stage. In order to examine the kinetic data, the present authors compared the observed value of the reaction rate and the frequecy factor with the calculated value. The results given in Table 6 agree with the expectations.

We wish to thank Miss Misao Shinoda for the Mass spectra and Mr. Yoshiharu Yoneyama for NMR measurements.

Table 6. Applicability of the Equation of $dX/dt=A\exp(-E/RT)X^n/B$, $B=1.0\,^\circ C\,min^{-1}$

TG curve[a)]	Temperature/K	Partial fraction of residue weight X	dX/dT	
			Observed	Calculated
First stage	579	0.956	$0.3250\ 10^{-2}$	$0.2467\ 10^{-2}$
	609	0.849	$0.6330\ 10^{-2}$	$0.9107\ 10^{-2}$
	628	0.698	$0.1537\ 10^{-1}$	$0.1726\ 10^{-1}$
	643	0.398	$0.2303\ 10^{-1}$	$0.1858\ 10^{-1}$
	653	0.202	$0.1388\ 10^{-1}$	$0.1429\ 10^{-1}$
	672	0.031	$0.4000\ 10^{-3}$	$0.4746\ 10^{-2}$
Seond stage	688	1.000	$0.1650\ 10^{-2}$	$0.3680\ 10^{-2}$
	713	0.920	$0.4370\ 10^{-2}$	$0.8227\ 10^{-2}$
	731	0.799	$0.1237\ 10^{-1}$	$0.1353\ 10^{-1}$
	749	0.467	$0.2065\ 10^{-1}$	$0.1729\ 10^{-1}$
	768	0.133	$0.1330\ 10^{-1}$	$0.1475\ 10^{-1}$
	783	0.0001	$0.1810\ 10^{-2}$	$0.3817\ 10^{-3}$

a) Measured at heating rate of $1.0\,^\circ C\,min^{-1}$.

References

1) H. Ohtani, T. Nagaya, Y. Sugimura, and S. Tsuge, *J. Anal. Appl. Pyrolysis*, **4**, 117 (1982).

2) I. Luderwald and H. R. Kricherdorf, *Angew. Makromol. Chem.*, **56**, 173 (1976); I. Luderwald, F. Merz, and H. Rothe, *ibid.*, **67** 193 (1978); I. Luderwald and F. Merz, *ibid.*, **74**, 165 (1978); U. Bahr, I. Luderwald, R. Muller, and R. H. Shulten, *ibid.*, **120**, 163 (1984); R. H. Shulten and H. J. Dussel, *J. Anal. Appl. Pyrolysis*, **2**, 293 (1980); A. Ballistreli, D. Garozzo, M. Giuffrida, and G. Montaudo, *Macromolecules*, **20**, 2991 (1987).

3) F. G. Lum and E. F. Carlston, *Ind. Eng. Chem.*, **44**, 1595 (1952).

4) E. F. Carlston and F. G. Lum, *Ind. Eng. Chem.*, **49**, 1239 (1957).

5) E. A. Boettner, G. Ball, and B. Weiss, *J. Appl. Polym. Sci.*, **13**, 377 (1969); W. H. Hale, A. G. Farham, R. N. Johnson, and R. A. Clendiving, *J. Polym. Sci., Part A-1*, **5**, 2399 (1967); J. Chia, *Thermochim. Acta*, **1**, 231 (1970); J. Chiu, *Anal. Chem.*, **40**, 1516 (1968).

6) T. Ozawa, *Bull. Chem. Soc. Jpn.*, **38**, 1881 (1965); T. Ozawa, *J. Therm. Anal.*, **2**, 301 (1970).

7) R. Inoue and M. Sumoto, *Chem. High Polym.*, **11**, 169 (1954).

Bismuth Trichloride as a New Efficient Catalyst in the Aldol Reaction and the Michael Reaction

Makoto WADA,* Eiji TAKEICHI,† and Takashi MATSUMOTO†
Department of Chemistry, College of General Education, University of Tokushima, 1-1, Minamijosanjima, Tokushima 770
† Department of Applied Material Science, Faculty of Integrated Arts and Science, University of Tokushima, 1-1, Minamijosanjima, Tokushima 770
(Received November 7, 1990)

In the presence of a catalytic amount of bismuth(III) trichloride (5 mol%), silyl enol ethers react with aldehydes at room temperature in dichloromethane to give the corresponding aldols in good yields. Silyl enol ethers also have been found to react with α,β-unsaturated ketones at room temperature in dichloromethane to afford the corresponding 1,5-dicarbonyl compounds, the Michael adducts in good yields. The intermediate adducts of the aldol reaction (the silyl ethers) and the Michael reaction (the silyl enol ethers) were also obtained in good yields.

In view of elemental resources for the future, it is important to use various elements for organic synthesis. Among group 15 elements, bismuth metal is cheaper and less toxic than arsenic or antimony and can be expected to play some role in organic synthesis according to its enhanced metallic character. To our knowledge, however, organic synthesis, especially carbon–carbon bond forming reaction by using bismuth and bismuth compounds has been scarcely studied.[1] Recently, the first example of chemoselective metallic bismuch[2] and bismuth (III) chloride ($BiCl_3$)–metallic zinc-,[3] iron-,[3] or aluminium[4]-mediated allylation of aldehydes with allylic halides to homoallylic alcohols was reported by us.[5] We also found that $BiCl_3$ (5 mol%) promotes aldol reaction between silyl enol ethers and aldehydes in CH_2Cl_2 at room temperature.[6] In the course of our continuous investigations, we have found that $BiCl_3$ activates α,β-unsaturated ketones. Herewith, we wish to disclose in full the $BiCl_3$ catalyzed aldol reaction and Michael reaction.

Results and Discussion

Bismuth Trichloride ($BiCl_3$) Promoted Aldol Reaction between Silyl Enol Ethers and Aldehydes. The aldol reactions is one of the standard tools for creating new carbon–carbon bonds, and numerous methods have been developed[7] including the catalytic aldol reaction by the aid of TBAF (tetrabutylammonium fluoride),[8] TASF [Tris(diethylamino)sulfonium (TAS) difluorotrimethylsiliconate],[9] trityl perchlorate,[10] and rhodium complex.[11] Concerning the cross-aldol reaction using silyl enol ethers,[12] the $TiCl_4$-promoted reaction (Mukaiyama method) is the first example, and the reaction has been carried out at −78 °C using an equimolar amount of $TiCl_4$ in most cases to obtain the aldols in good yields.[13] However, it is still desirable to find a new efficient catalyst of cross-aldol reaction between silyl enol ethers and aldehydes under extremely mild conditions (room temperature and weak acid).

In relation to aldol reaction by using bismuth and bismuth compounds, the reaction between 1-trimethylsiloxy-1-cyclohexene and benzaldehyde in the presence of $BiCl_3$ (5 mol%) in $CDCl_3$ at room temperature was monitored by ^1H NMR spectroscopy. The NMR signals at 0.17 ppm (s, O–Si<u>Me</u>$_3$), 4.87 ppm (t, vinyl-<u>H</u>), and 10.00 ppm (s, aldehyde-<u>H</u>) disappeared within 1 h, and new signals appeared at −0.02 ppm (s, O–Si<u>Me</u>$_3$ of the threo product), 0.03 ppm (s, O–Si<u>Me</u>$_3$ of the erythro product), 5.10 ppm (d, O–C<u>H</u> of the threo product, J=7.91 Hz), and 5.37 ppm (d, O–C<u>H</u> of the erythro product, J=3.95 Hz). The above results illustrate that the silyl enol ether reacts with benzaldehyde smoothly under the influence of a catalytic amount (5 mol%) of $BiCl_3$, giving the aldol silyl ether.

Practically, the reaction of 1-phenyl-1-trimethylsiloxyethylene and benzaldehyde followed by the quenching of the reaction mixture using pyridine gave 78% isolated yield of the corresponding silyl ether (Eq. 1). The corresponding aldol was obtained in 94% yield when the reaction mixture was treated with CH_3OH/1M HCl (10/1, 1 M=1 mol dm^{-3}), then H_2O was added.

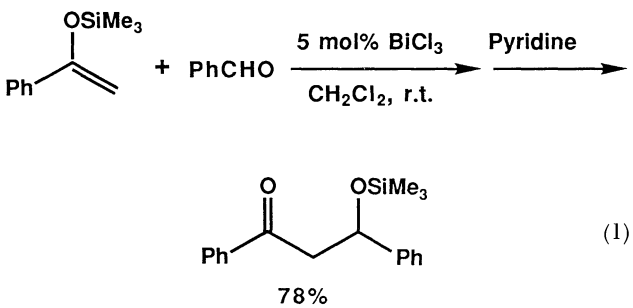

(1)

The overall reaction is shown in Scheme 1 and typical results are summarized in Table 1. Silyl enol ethers of acetophenone, propiophenone, cyclohexanone, and methyl phenylacetate could be used. Both benzaldehyde and butanal are usable to obtain aldols

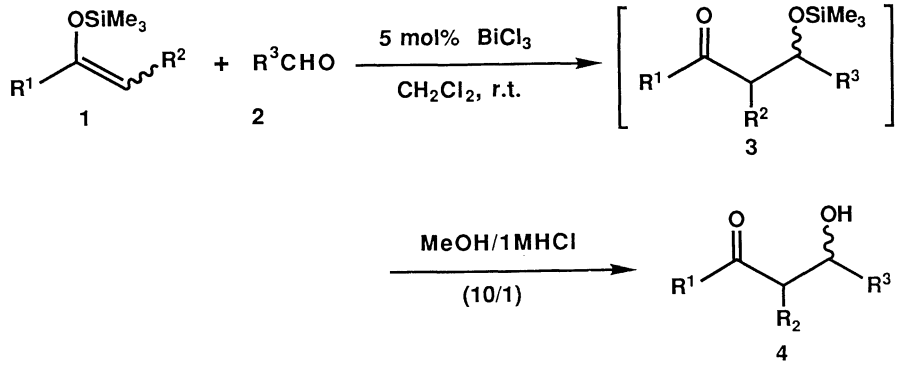

Scheme 1.

Table 1. $BiCl_3$ Mediated Synthesis of Aldols (**4**)

Entry	Silyl enol ether	Receptor	Reaction time	Product (**4**)	Yield[a]/%
1		PhCHO	25 min	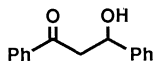	94
2		PhCHO	25 min	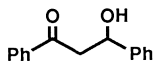	0[b]
3	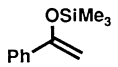	$CH_3(CH_2)_2CHO$	40 min	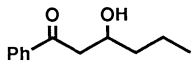	85
4		$PhCOCH_3$	6 h	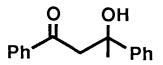	65
5		$PhCOCH_3$	11 h	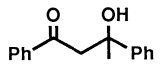	73[c]
6	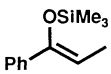	PhCHO	50 min	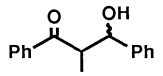	95 (56: 44)[d]
7		$PhCOCH_3$	40 h	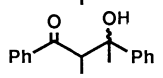	22[e]
8	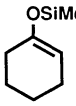	PhCHO	1 h	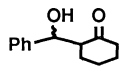	84 (25: 75)[d]
9		$PhCOCH_3$	11 h	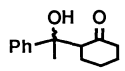	Low yield[f]
10	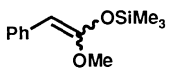	PhCHO	1 h	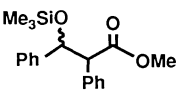	40[e,g] 32[e,g]
11	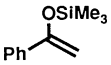	$CH_3CH(OEt)_2$	6 h	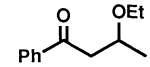	41

a) Isolated yields are given. b) The reaction was carried out at −78 °C and quenched at that temperature. c) 20 mol% $BiCl_3$ was used. d) The ratio of erythro: threo determined by ^1H NMR. e) The ratio of diastereomers was not determined. f) One equivalent of $BiCl_3$ was used. g) The reaction mixture was treated with H_2O instead of MeOH/1 M HCl for the workup.

in good yields, and an aldehyde serves naturally as a better receptor than acetophenone (Entries 4, 5, 7, and 9). The reaction proceeded very sluggishly at −78 °C and an ambient reaction temperature was required (Entry 2). 1-Phenyl-1-trimethylsiloxyethylene/acetaldehyde dimethyl acetal reaction gave the aldol-type product in 41% unoptimized yield (Entry 11).

In the connection of studies concerning the interaction of silyl enol ethers with Lewis acids, Kuwajima and Nakamura found that the transmetallation reaction occurs via either and O- or a C-metalation pathway, in which $SnCl_4$, $TeCl_4$, and $SbCl_5$ took the former pathway and $TiCl_4$ took the latter.[14] Based on the above results, the reaction between 1-trimethylsiloxy-1-cyclohexene and one equivalent of $BiCl_3$ in $CDCl_3$ at room temperature was monitored by ^1H NMR spectroscopy. We found that the transmetalation reaction does not occur, and consequently, it is of note that the active intermediate of the present reaction is not the bismuth enolate. Although the reaction mechanism of the catalytic $BiCl_3$ mediated aldol reaction is not clear, a catalytic cycle can be presumed in which the carbonyl compounds activated by $BiCl_3$, react with silyl enol ethers to give the aldol silyl ethers by Prins or Friedel–Crafts type reaction, regenerating $BiCl_3$.

Bismuth Trichloride ($BiCl_3$) Promoted Michael Reaction. In the course of our continuous investigations to explore useful synthetic reactions using $BiCl_3$, we have found that it also activates α,β-unsaturated aldehydes and ketones.[15] Herewith, we wish to describe the $BiCl_3$ catalyzed Michael reaction, and also the isolation of the intermediate adduct, the synthetically valuable silyl enol ether.

When 1-phenyl-1-trimethylsiloxyethylene was reacted with crotonaldehyde in the presence of $BiCl_3$ (5 mol%) in CH_2Cl_2 at room temperature, 1,2-addition product and 1,4-addition product were obtained in 68% and 31% yields, respectively. Noteworthy is the fact that 1,5-dicarbonyl compound, the Michael adduct, was obtained in good yield, and 1,2-addition product was not detected by the reaction of a silyl enol

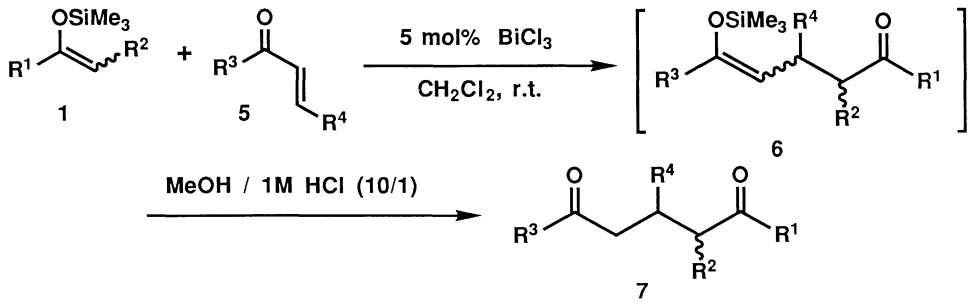

Scheme 2.

Table 2. $BiCl_3$ Mediated Synthesis of 1,5-Dicarbonyl Compounds (**7**)

Entry	Enone	Silyl enol ether	Product (**7**)	Yield[a]/%
a	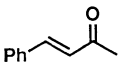	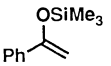	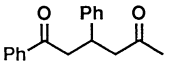	80
b	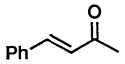		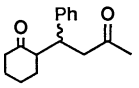	79[b]
c	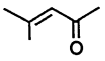	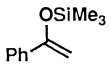	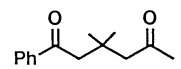	75
d	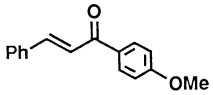	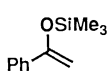	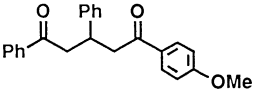	70
e		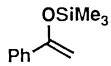	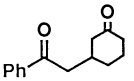	65
f		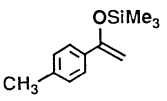	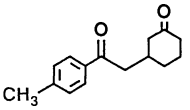	71

a) Isolated yields are given. b) The ratio of diastereomers was not determined.

Table 3. Isolation of the Silyl Enol Ethers (**6**)

Entry	Enone	Silyl enol ether	Product (**6**)	Yield[a]/%
a	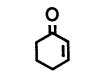	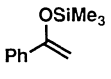	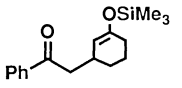	70
b	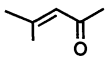	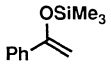	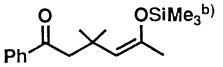	75
c	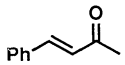	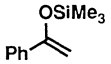	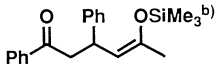	77

a) Isolated yields are given. b) The geometry of the double bond was presumed to be cis by comparing the ^{1}H NMR data with those reported.[15,16]

ether with an α,β-unsaturated ketone. The overall reaction is shown in Scheme 2 and typical results are summarized in Table 2.

Quenching of the reaction mixture using pyridine gave the satisfactory yield of the intermediate silyl enol ether. Some of the results are summarized in Table 3.

The present reaction is the first example of the cross-aldol reaction and the Michael reaction using $BiCl_3$. It should be stressed that cheap and commercially available $BiCl_3$ is a new efficient catalyst of the present reaction under extremely mild conditions [room temperature and weak acid ($BiCl_3$ is a weak Lewis acid)].

Experimental

General Methods. Infrared spectra were recorded on a Hitachi 215 spectrophotometer. ^{1}H NMR spectra were recorded with JEOL PMX 60Si spectrometer and chemical shifts (δ) were reported in ppm using internal tetramethylsilane. Bismuth (III) chloride was commercial material and used without further purification. Aldehydes and α,β-unsaturated ketones were distilled before use. Trimethylsilyl enol ethers were prepared following the procedure of House.[17]

Isolation of the Aldol Silyl Ether. Bismuth (III) chloride (0.1 mmol) was placed in a 50 ml two-necked flask and dried in vacuo by heating. Anhydrous CH_2Cl_2 (10 ml) was introduced under nitrogen, and then, using a syringe 1-phenyl-1-trimethylsiloxyethylene (2.0 mmol) and benzaldehyde (2.0 mmol) were added at room temperature. The reaction mixture was stirred for 1 h at that temperature and quenched with pyridine (1 ml) followed by the treatment of water (10 ml). The organic materials were extracted with Et_2O (20 ml×3). After drying ether layer over anhydrous $MgSO_4$, the solvent was evaporated to give the oily product in 78% yield. This product was pure by ^{1}H NMR without purification, and it was identified by comparison with an authentic sample prepared from the known procedure.[10]

General Procedure of the Aldol Reaction. In a 50 ml two-necked flask under nitrogen atmosphere, were placed bismuth (III) chloride (0.05 mmol) and dry CH_2Cl_2 (3 ml). Then, an aldehyde (1.1 mmol) and a silyl enol ether (1.0 mmol) were added sequentially at room temperature, and the reaction mixture was stirred at that temperature. The resulting reaction mixture was treated with CH_3OH/1M HCl (10/1, 0.1 ml), then H_2O (10 ml) was added, and the product was extracted with CH_2Cl_2 (10 ml×3). After drying the CH_2Cl_2 layer over anhydrous $MgSO_4$, the solvent was evaporated in vacuo. The crude product was purified on thin-layer chromatography to afford the corresponding aldol in good yield.

3-Hydroxy-1,3-diphenyl-1-propanone: Purified by thin-layer chromatography (SiO_2, hexane:AcOEt=8:1), 94% yield. This product was identified by comparison with an authentic sample prepared from the known procedure.[13b]

3-Hydroxy-1-phenyl-1-hexanone: Purified by thin-layer chromatography (SiO_2, hexane:AcOEt=9:1), 85% yield. This product was identified by comparison with an authentic sample prepared from the known procedure.[13b]

3-Hydroxy-1,3-diphenyl-1-butanone: Purified by thin-layer chromatography (SiO_2, hexane:AcOEt=9:1), 73% yield. This product was identified by comparison with an authentic sample prepared from the known procedure.[18]

3-Hydroxy-2-methyl-1,3-diphenyl-1-propanone: Purified by thin-layer chromatography (SiO_2, hexane:AcOEt=7:1), 95% yield. This product was identified by comparison with an authentic sample prepared from the known procedure.[13b]

3-Hydroxy-2-methyl-1,3-diphenyl-1-butanone: Purified by thin-layer chromatography (SiO_2, hexane:AcOEt=9:1), 22% yield. This product was identified by comparison with an authentic sample.[18]

2-(α-Hydroxybenzyl)-1-cyclohexanone: Purified by thin-layer chromatography (SiO_2, hexane:Et_2O=5:1), 84% yield. This product was identified by camparison with an authentic sample.[10a]

Methyl 3-Hydroxy-2,3-diphenylpropionate: Purified by thin-layer chromatography (SiO_2, CH_2Cl_2), 32% yield. This product was identified by comparison with an authentic sample prepared from the known procedure.[19]

3-Ethoxy-1-phenyl-1-butanone: Purified by thin-layer chromatography (SiO_2, hexane:AcOEt=15:1), 41% yield. This product was identified by comparison with an authentic sample prepared from the known procedure.[20]

Isolation of an Intermediate of the Michael Reaction, an Silyl Enol Ether. Bismuth(III) chloride (0.05 mmol) was placed in a 50 ml two-necked flask and dried in vacuo by heating. Anhydrous CH_2Cl_2 (5 ml) was introduced under nitrogen, and then, using a syring a silyl enol ether (1.0 mmol) and an α,β-unsaturated ketone (1.1 mmol) were added at room temperature. The reaction mixture was stirred for 1 h at that temperature and quenched with pyridine (1 ml) followed by the treatment of water (10 ml).

The organic materials were extracted with Et_2O (20 ml×3). After drying the ether layer over anhydrous $MgSO_4$, the solvent was evaporated to give the oily product in good yield. This product was pure by ^1H NMR without purification. This product was identified by comparison with an authentic sample.

The Silyl Enol Ether (6a): Purified by thin-layer chromatography (SiO_2, hexane:AcOEt=9:1), 70% yield. This product was identified by comparison with an authentic sample prepared from the known procedure.[15]

The Silyl Enol Ether (6b): Purified by thin-layer chromatography (SiO_2, hexane:AcOEt=9:1), 75% yield. This product was identified by comparison with an authentic sample.[15]

The Silyl Enol Ether (6c): Purified by thin-layer chromatography (SiO_2, hexane:AcOEt=9:1), 77%. This product was identified by comparison with an authentic sample. [15]

General Procedure of the Michael Reaction. In a 50 ml two-necked flask under nitrogen atmosphere, were placed bismuth(III) chloride (0.05 mmol) and dry CH_2Cl_2 (3 ml). Then, an α,β-unsaturated ketone (1.1 mmol) and a silyl enol ether (1.0 mmol) were added sequentially at room temperature, and the reaction mixture was stirred for 6 h at that temperature. The resulting mixture was treated with CH_3OH/1M HCl (10/1, 0.1 ml), then H_2O (10 ml) was added and the product was extracted with CH_2Cl_2 (10 ml×3). After drying the CH_2Cl_2 layer over anhydrous $MgSO_4$, the solvent was evaporated in vacuo. The crude product was purified on thin-layer chromatography to afford the corresponding 1,5-dicarbonyl compound in good yield.

The 1,5-Dicarbonyl Compound (7a): Purified by thin-layer chromatography (SiO_2, hexane:AcOEt=7:1), 80% yield. This product was identified by comparison with an authentic sample.[15]

The 1,5-Dicarbonyl Compound (7b): Purified by thin-layer chromatography (SiO_2, hexane:AcOEt=9:1), 79% yield. This product was identified by comparison with an authentic sample prepared from the known procedure.[15]

The 1,5-Dicarbonyl Compound (7c): Purified by thin-layer chromatography (SiO_2, hexane:AcOEt=9:1), 75% yield. This product was identified by comparison with an authentic sample.[15]

The 1,5-Dicarbonyl Compound (7d): Purified by thin-layer chromatography (SiO_2, hexane:AcOEt=9:1), 70% yield. This product was identified by comparison with an authentic sample prepared from the known procedure.[15]

The 1,5-Dicarbonyl Compound (7e): Purified by thin-layer chromatography (SiO_2, hexane:AcOEt=8:1), 65% yield. This product was identified by comparison with an authentic sample.[15]

The 1,5-Dicarbonyl Compound (7f): Purified by thin-layer chromatography (SiO_2, hexane:AcOEt=9:1), 71% yield. This product was identified by comparison with an authentic sample prepared from the known procedure.[15]

References

1) Recently, Barton and Finet reported the functional group oxidation and the phenylation by pentavalent organobismuth reagents. a) D. H. R. Barton and J-P. Finet, *Pure Appl. Chem.*, **59**, 937 (1987), b) J-P. Finet, *Chem. Rev.*, **89**, 1487 (1989), and references cited therein. Suzuki et al. reported the chemistry of bismuth ylide. c) H. Suzuki, T. Murafuji, and T. Ogawa, *Chem. Lett.*, **1989**, 847, 849. See also, d) G. O. Doak and L. D. Freedman, *J. Organomet. Chem.*, **361**, 35 (1990); *ibid.*, **360**, 297 (1989). e) M. Wada and H. Ohki, *Yuki Gosei Kagaku Kyokai Shi*, **47**, 425 (1989).

2) M. Wada and K-y. Akiba, *Tetrahedron Lett.*, **26**, 4211 (1985).

3) M. Wada, H. Ohki, and K-y. Akiba, *Tetrahedron Lett.*, **27**, 4771 (1986).

4) M. Wada, H. Ohki, and K-y. Akiba, *J. Chem. Soc., Chem. Commun.*, **1987**, 708.

5) M. Wada, H. Ohki, and K-y. Akiba, *Bull. Chem. Soc. Jpn.*, **63**, 1738 (1990).

6) H. Ohki, M. Wada, and K-y. Akiba, *Tetrahedron Lett.*, **29**, 4719 (1988).

7) a) H. O. House, "Modern Synthetic Reactions," 2nd ed, W. A. Benjamin, Menlo Park (1972), pp. 629—682. b) K Narasaka, *Yuki Gosei Kagaku Kyokai Shi*, **37**, 307 (1979). c) T. Mukaiyama, *Org. React.*, **28**, 203 (1982).

8) a) R. Noyori, K. Yokoyama, J. Sakata, I. Kuwajima, E. Nakamura, and M. Shimizu, *J. Am. Chem. Soc.*, **99**, 1265 (1977). b) E. Nakamura, M. Shimizu, I. Kuwajima, J. Sakata, K. Yokoyama, and R. Noyori, *J. Org. Chem.*, **48**, 932 (1983).

9) R. Noyori, I. Nishida, and J. Sakata, *J. Am. Chem. Soc.*, **105**, 1598 (1983).

10) a) T. Mukaiyama, S. Kobayashi, and M. Murakami, *Chem. Lett.*, **1983**, 447. b) S. Kobayashi, M. Murakami, and T. Mukaiyama, *ibid.*, **1985**, 1535.

11) a) S. Sato, I. Matsuda, and Y. Izumi, *Tetrahedron Lett.*, **27**, 5517 (1986). b) M. T. Reetz and A. E. Vougioukas, *ibid.*, **28**, 793 (1987). c) S. Sato, I. Matsuda, and T. Izumi, *ibid.*, **28**, 6657 (1987).

12) Aldol-type condensation of silyl enol ethers and acetals catalyzed by trimethylsilyl trifluoromethanesulfonate has been reported. S. Murata, M. Suzuki, and R. Noyori, *J. Am. Chem. Soc.*, **102**, 3248 (1980).

13) a) T. Mukaiyama, K. Narasaka, and K. Banno, *Chem. Lett.*, **1973**, 1011. b) T. Mukaiyama, K. Banno, and K. Narasaka, *J. Am. Chem. Soc.*, **96**, 7503 (1974). c)T. Mukaiyama, *Angew. Chem., Int. Ed. Engl.*, **16**, 817 (1977). In the connection of a catalytic aldol reaction, Mukaiyama and his co-workers found that 1-trimethylsiloxy-1-cyclopentene reacted with 3-phenylpropionaldehyde in the presence of a catalytic amount of $TiCl_4$ (13 mol%) in CH_2Cl_2 at −78 °C to give the corresponding aldol product in 80% yield.[13b] However, we found that the expected aldol was obtained only in 35% yield, when 1-phenyl-1-trimethylsiloxyethylene was reacted with benzaldehyde at room temperature in CH_2Cl_2 under the influence of a catalytic amount (5 mol%) of $TiCl_4$.

14) I. Kuwajima and E. Nakamura, *Acc. Chem. Res.*, **18**, 181 (1985).

15) Mukaiyama et al. reported the trityl perchlorate catalyzed Michael reaction. S. Kobayashi, M. Murakami, and T. Mukaiyama, *Chem. Lett.*, **1985**, 953.

16) C. H. Heathcock, C. T. Buse, W. A. Kleschick, M. C. Pirrung, J. E. Sohn, and J. Lampe, *J. Org. Chem.*, **45**, 1066 (1980).

17) H. O. House, L. J. Czuba, M. Gall, and H. D. Olmstead, *J. Org. Chem.*, **34**, 2324 (1969).

18) R. W. Stevens, N. Iwasawa, and T. Mukaiyama, *Chem. Lett.*, **1982**, 1459.

19) K. Saigo, M. Oosaki, and T. Mukaiyama, *Chem. Lett.* **1975**, 989.

20) T. Mukaiyama and M. Hayashi, *Chem. Lett.*, **1974**, 15.

Differential Thermal Analysis of Polyacrylonitrile in the Presence of Chlorine-Containing Polymers

Masao Okamoto,* Ken-ichiro Saito, and Sadayuki Motoishi
Department of Polymer Materials Engineering, Faculty of Engineering, Yamagata University, Jonan, Yonezawa 992
(Received September 20, 1990)

A differential thermal analysis (DTA) of polymer blends of polyacrylonitrile (PAN) with poly (α-chloroacrylonitrile) (PCAN) and poly (vinyl chloride) (PVC), prepared by coprecipitation from a solution containing both polymers, was carried out under nitrogen. Even if a small amount of PCAN or PVC was added to PAN, the exotherm peak position due to violent polymerization of the cyano groups, which appears at ca. 260 °C in pure PAN, shifts to the higher-temperature side by ca. 40 °C and its intensity becomes lower. Moreover, a new generation of heat is observed above ca. 220 °C and ca. 260 °C in the case of PAN–PCAN and PAN–PVC, respectively. These results were associated with the HCl generated during the heating process, since the chlorine atom formed by the reaction of a thermally degraded PAN polymer radical with HCl can both initiate polymerization of the cyano groups in PAN and terminate progress in polymerization by combination. Namely, DTA behavior could be explained by the effect of initiation (in the case of PAN–PCAN) and termination (in the case of PAN–PVC) upon the polymerization of cyano groups both below and above the temperature, respectively, at which PAN begins to be subjected to a sharp transition.

Hydrogen chloride has the effect of changing the thermal degradation behavior of polyacrylonitrile (PAN).[1] This effect is observed even when differential thermal analysis (DTA) is carried out under nitrogen for copolymers of acrylonitrile with chlorine-containing monomers; the exothermic polymerization of cyano groups is delayed and the differential temperature is reduced, as compared with the DTA curve for pure PAN.[1–3] However, there is a great difference between comonomers concerning the effect.[3] This proved to be caused by a difference in the temperature at which each comonomer unit is dehydrochlorinated; HCl accelerates and retards the polymerization of cyano groups below and above the temperature, respectively, at which pure PAN begins to be subjected to a sharp transition.[1,4]

The purpose of the present paper is to report on the DTA behavior of the two binary polyblends, namely, PAN–poly(α-chloroacrylonitrile) (PCAN) and PAN–poly(vinyl chloride) (PVC), and then to verify the above-mentioned conclusion on the effect of HCl. So far the DTA behavior of a 1:1 by weight of the PVC–PAN mixture has been reported by McNeill et al.[5] Their result shows that when HCl evolution has almost ceased, polymerization of the cyano groups begins to reach a significant rate; this is in accordance with our expectation, since the degradation of the two homopolymers suggests a considerable overlap in their main volatilization reactions.

Experimental

Preparation of Polymer Blends. A polymer blend was prepared by the coprecipitation of two polymers from a solution containing PAN[6] and PCAN[7] or PAN and PVC (Geon 103 EP-8). The powder mixture given in Table 1 was dissolved in 26 cm³ of *N,N*-dimethylformamide (DMF); the solution obtained was then poured into 520 cm³ of methanol at −60 °C. The precipitate was filtered, washed with methanol and dried in a vacuum at 50 °C for eight days to constant weight.

Chlorine Analysis. The method was reported in a previous paper.[7]

Thermogravimetry (TG). A Shimadzu DTG-20 was used. Five milligrams of PAN, PCAN, and PVC were packed in quartz sample holders measuring 5 mm in diameter and 2 mm deep; the measurement was carried out under dynamic nitrogen flow (60 cm³ min⁻¹) at a heating rate of 5 °C min⁻¹.

Differential Thermal Analysis (DTA). A Rigaku CAT. No. 8001 Thermoflex was used. Fifty milligrams of powdered samples were employed and heated to 320 °C at a rate of 5 °C min⁻¹ under nitrogen.

Results and Discussion

Chlorine Content of Polymer Blends. PAN–PVC samples were white, but PAN–PCAN samples became light purple. Figure 1 shows the relationship between

Table 1. Preparation of Polymer Blends

Sample	Composition			Chlorine content
	PAN	PCAN	PVC	
	mg	mg	mg	wt%
PAN	500.2			
PAN–PCAN-1	504.2	15.4		1.06
PAN–PCAN-2	501.9	30.8		1.92
PAN–PCAN-3	502.8	60.7		3.67
PAN–PCAN-4	501.0	120.5		6.71
PAN–PVC-1	500.6		5.1	
PAN–PVC-2	500.4		10.1	
PAN–PVC-3	505.0		18.4	1.77
PAN–PVC-4	509.0		30.1	2.94
PAN–PVC-5	500.8		61.0	6.12
PAN–PVC-6	508.5		120.2	10.98

the actual chlorine content given in Table 1 and the value calculated on the basis of a composition of each sample. Though the two values, Cl_A and Cl_C, in Fig. 1, in the PAN–PVC system agreed with each other, in the case of the PAN–PCAN system the actual value of Cl_A was smaller by ca. 15% than the calculated value of Cl_C. This indicates that PCAN is partially dehydrochlorinated in the course of the preparation of polymer blends. The fact that PCAN is dehydrochlorinated in DMF has been reported before.[7,8] It is clear that coloration in PAN–PCAN samples is caused by such dehydrochlorination.

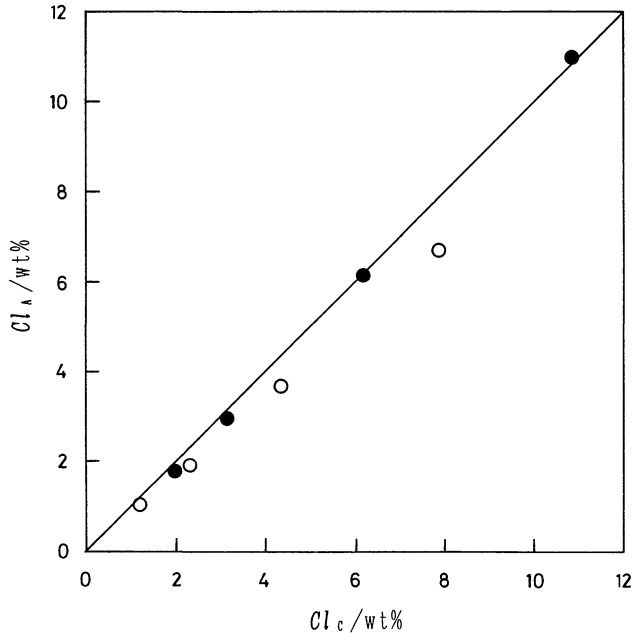

Fig. 1. Actual chlorine content (Cl_A) vs. calculated content (Cl_C). O: PAN-PCAN, ●: PAN-PVC.

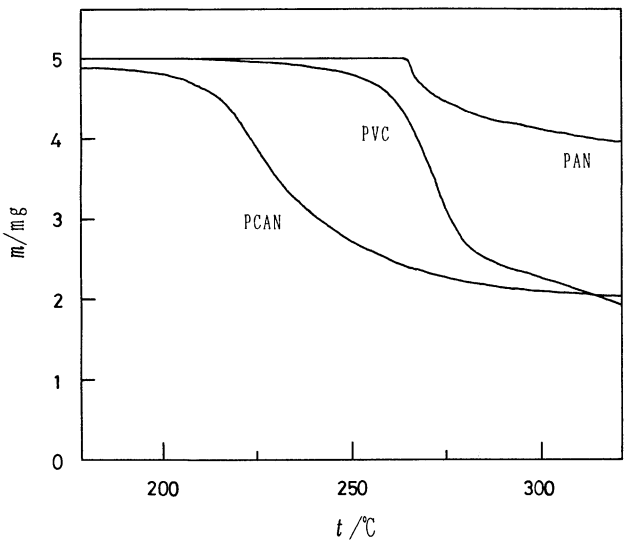

Fig. 2. TG curves for PAN, PVC, and PCAN.

Dehydrochlorination of Chlorine-Containing Polymers during Heating Process. TG curves for PAN, PVC, and PCAN are shown in Fig. 2. The temperature range in which PVC is dehydrochlorinated corresponds to that of the sharp PAN breakdown transition, whereas PCAN shows a weight loss due to dehydrochlorination in a much lower temperature range than PVC. As mentioned in the preceding section, PCAN is partially dehydrochlorinated in the course of preparation of polymer blends. Such PCAN is more easily dehydrochlorinated than the original PCAN.[9] Thus, in the case of the PAN–PCAN system, HCl exists below the temperature at which pure PAN begins to be subjected to a sharp transition, accompanied by an exothermic polymerization of the cyano groups.

Effect of the Composition in PAN-PCAN System on the Exothermic Polymerization of Cyano Groups. DTA curves for PAN–PCAN samples are shown in Fig. 3. As the composition increases in PCAN, the exotherm peak position due to violent polymerization of the cyano groups shifts to the higher-temperature

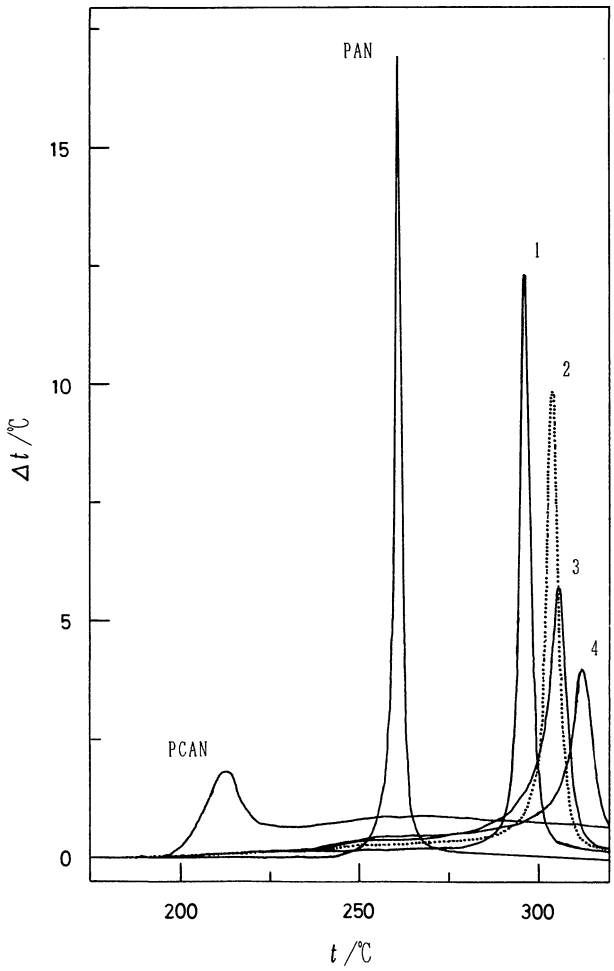

Fig. 3. DTA curves for PAN, PCAN, and PAN–PCAN samples. 1, 2, 3, and 4: PAN–PCAN-1, -2, -3, and -4 shown in Table 1, respectively.

side, and its intensity becomes lower than in the case of PAN. Moreover, in the cases of PAN–PCAN-3 and -4, a broad exotherm appears clearly above ca. 220 °C. This exotherm is due to a polymerization of the cyano groups which is closely associated with HCl generated during the heating process.[1] The mechanism has been explained by the action of a chlorine atom, which was formed by the reaction of thermally degraded polymer radical (P·) with HCl:

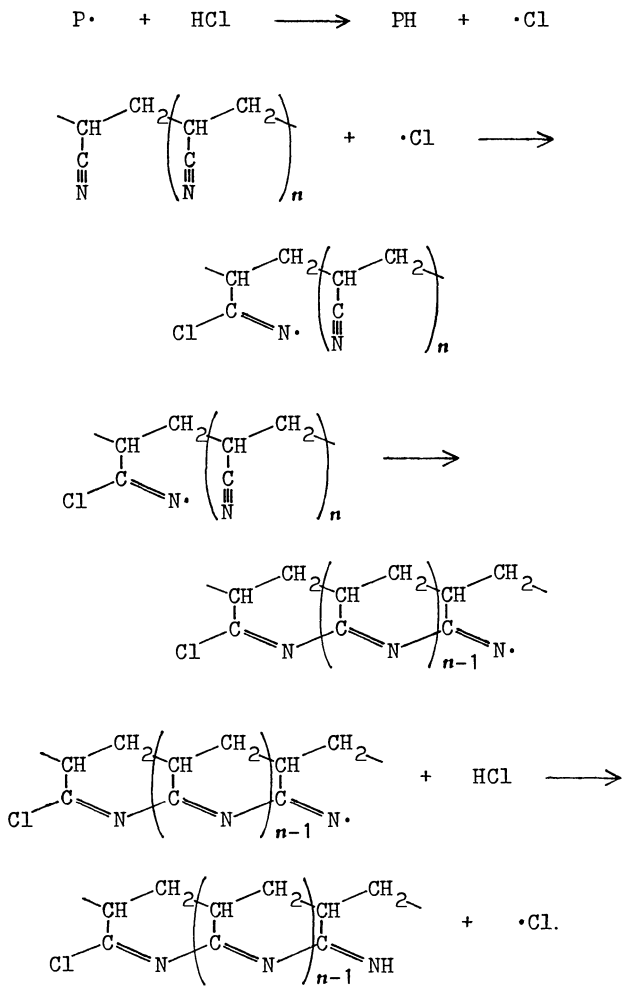

Since the chlorine atom is much more mobile at ca. 220 °C than the polymer radical, polymerization of the cyano groups is promoted in the presence of HCl. When the moieties subjected to such polymerization exist in the polymer chain, they should prevent the progress of a rapid polymerization of the cyano groups with which fragmentation[10] in PAN is usually accompanied. This effect is expected to increase in proportion to the PCAN content, since the more HCl that is generated, the more are chlorine atoms formed. Actually, the exotherm peak position due to violent polymerization of the cyano groups shifts to the higher-temperature side with increasing PCAN content (Fig. 3). Such behavior corresponds to that found in DTA curves for the acrylonitrile–α-chloroacrylonitrile copolymers in which the mole fraction of α-chloroacrylonitrile units is below 0.1.[1]

Thermal Degradation Behavior of PAN in PAN–PVC System. DTA curves for PAN–PVC-1— -3 and -4— -6 are shown in Figs. 4 and 5, respectively. Even the DTA behavior of PAN–PVC-1 (the chlorine content being ca. 0.6 wt%) changed remarkably. Namely, the exotherm peak position due to a violent polymerization of the cyano groups shifted to the higher-temperature side than that for pure PAN by ca. 40 °C; its intensity became about 1/3 compared with that for pure PAN. This change is similar to that for PAN–PCAN-3 (the chlorine content being ca. 3.7 wt%), although no broad exotherm was observed below 260 °C. It is evident that there is a great difference between PVC and PCAN concerning the effect on the thermal degradation of PAN. This seems to have been caused by a difference in the temperature range associated with dehydrochlorination. In the case of PAN–PVC-2, -3, or -4, the exotherm peak position is identical with that for PAN–PVC-1 and its intensity

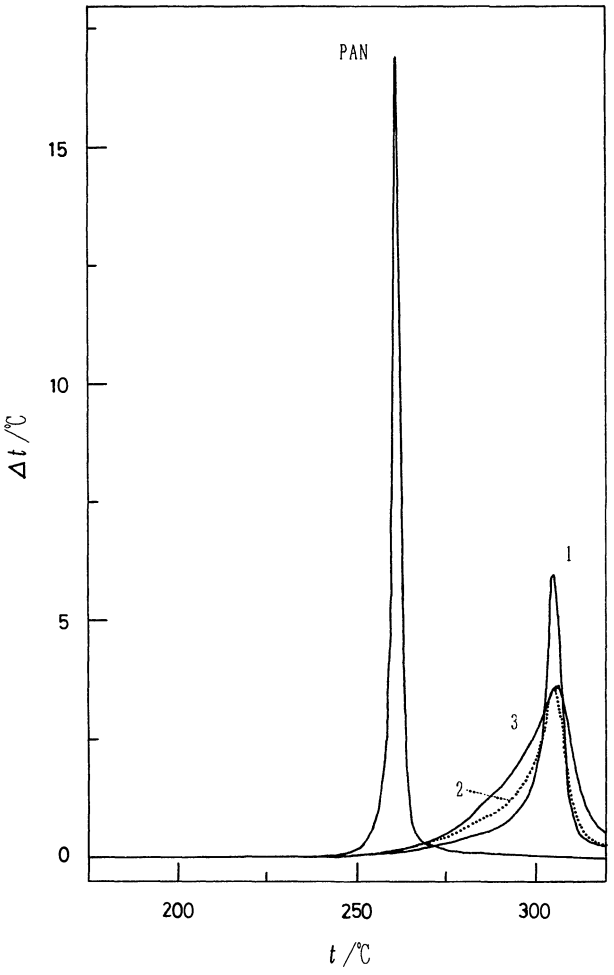

Fig. 4. DTA curves for PAN and PAN–PVC samples. 1, 2, and 3: PAN–PVC-1, -2, and -3 shown in Table 1, respectively.

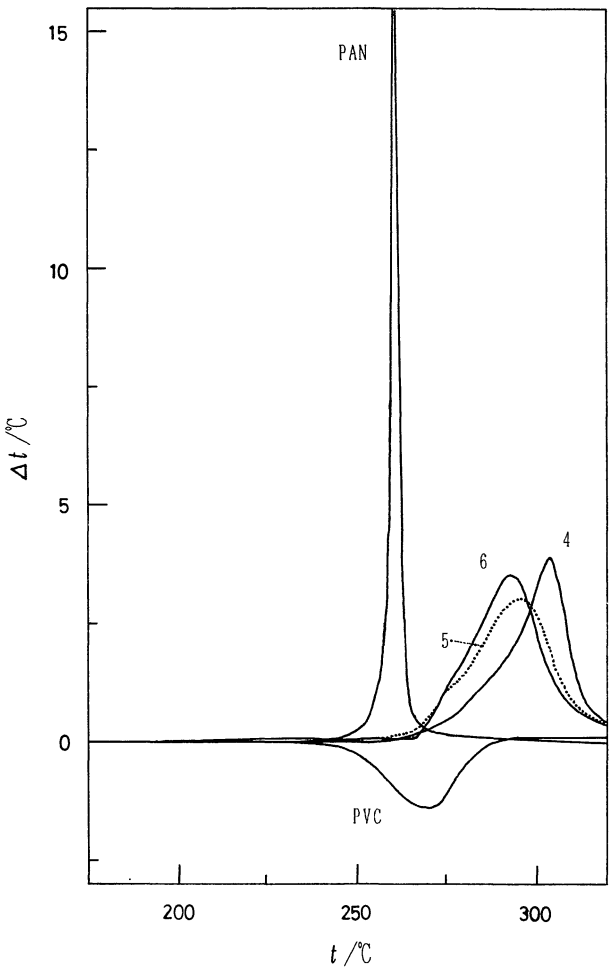

Fig. 5. DTA curves for PAN, PVC, and PAN–PVC samples. 4, 5, and 6: PAN–PVC-4, -5, and -6 shown in Table 1, respectively.

decreases to about 1/5 in comparison with that for pure PAN. This indicates that a very small amount of PVC in the PAN–PVC system is sufficient to change the behavior of the thermal degradation of PAN. It also proved that polymerization of the cyano groups cannot make rapid progress until HCl generated from PVC escapes out of the PAN–PVC system.

The generation of heat was observed in the 260—300 °C range, and increased in proportion to the PVC content (Fig. 4). We cannot conclude that this is due to only polymerization of the cyano groups. In PAN the thermally degraded polymer radicals are much more in number and are much more mobile at 260 °C than at 220 °C. Therefore, in the case of pure PAN, polymerization of the cyano groups progresses rapidly at ca. 260 °C. In the PAN–PVC system, since HCl exists in PAN above 260 °C, chlorine atoms are formed along with the disappearance of an equal number of polymer radicals. At this time although the number of active centers which initiate polymerization of the cyano groups does not change, chlorine atoms can also terminate progress in the polymerization of the cyano groups:

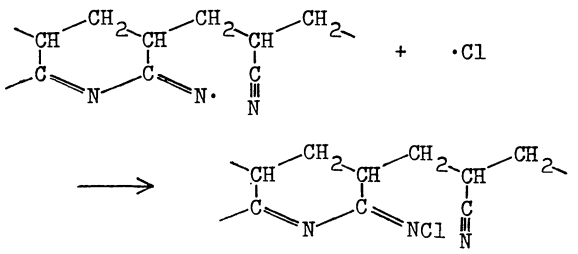

Since this reaction can take place frequently with increasing concentration of chlorine atoms, polymerization of the cyano groups should progress slowly with increasing the PVC content. Therefore, if the generation of heat in the 260—300 °C range is due to only polymerization of the cyano groups, it must decrease in proportion to the PVC content. This is contrary to the facts.

It is clear that the above-mentioned termination reaction is exothermic because of a combination of two active species. The heat of reaction must become larger as the composition increases in PVC. This is not contrary to the results shown in Figs. 4 and 5. In DTA curves for PAN–PVC-5 and -6, the exotherm peak is not observed at ca. 305 °C, but ca. 295 °C (Fig. 5). The magnitude of this broad exotherm is worth noticing. It was not reduced in spite of both a diminished content of PAN and an enlarged influence of the endotherm due to PVC. It can thus be concluded that the termination reaction is considerably exothermic.[11]

The DTA behavior of the PAN–PVC system is similar to that of acrylonitrile–allyl chloride copolymers.[3] This is thought to be attributable to a close resemblance between the two dehydrochlorination behaviors.[4]

Chlorine Content of Polymer Blends Heated to 320 °C. After DTA of polymer blends, a chlorine analysis of the residual products was carried out. The values obtained from PAN–PCAN-4 and PAN–PVC-5 were 0.35 and 2.32 wt%, respectively. These original chlorine contents are 6.71 and 6.12 wt%, respectively, (Table 1) and though they nearly resemble each other, there is a very great difference between the chlorine contents of residual products. In the case of the PAN–PVC system, as mentioned in preceding section, chlorine atoms terminate progress in the polymerization of the cyano groups. Since the termination reaction takes place frequently in the case of PAN–PVC-5 or -6 (Fig. 5), chlorine atoms combined as terminal points are the prime consideration with an increase in residual chlorine. The chlorine content of PAN–PVC-6 heated to 320 °C was 3.07 wt%, and more than that in the case of PAN–PVC-5. This comes up to our expectations, because the generation of heat in the

260—300 °C range is larger than that for PAN–PVC-5 (Fig. 5). Such a change in the residual chlorine is similar to that of the acrylonitrile–allyl chloride copolymers heated to 350 °C.[3] This indicates that these copolymers were also subjected to the above-mentioned termination reaction.

References

1) M. Okamoto, T. Ogura, R. Ashikawa, and O. Ishizuka, *Nippon Kagaku Kaishi*, **1983**, 566.

2) N. Grassie and R. McGuchan, *Eur. Polym. J.*, **9**, 507 (1973).

3) M. Okamoto, K. Suenaga, and O. Ishizuka, *Bull. Chem. Soc. Jpn.*, **59**, 1545 (1986).

4) M. Okamoto and S. Kashiwagura, *Nippon Kagaku Kaishi*, **1988**, 81.

5) I. C. McNeill, N. Grassie, J. N. R. Samson, A. Jamieson, and T. Straiton, *J. Macromol. Sci., Chem.*, **A12 (4)**, 503 (1978).

6) M. Okamoto, R. Yamada, and O. Ishizuka, *Bull. Chem. Soc. Jpn.*, **54**, 1227 (1981).

7) M. Okamoto, C. Aoki, and O. Ishizuka, *Nippon Kagaku Kaishi*, **1977**, 103.

8) G. A. Chukhadzhyan, A. Ye. Kalaidzhyan, and V. A. Petrosyan, *Vysokomol. Soedin., Ser. A*, **12**, 171 (1970).

9) M. Okamoto, C. Aoki, and O. Ishizuka, *Nippon Kagaku Kaishi*, **1978**, 433.

10) M. Okamoto, *Bull. Chem. Soc. Jpn.*, **56**, 2802 (1983).

11) McNeill et al.[5] thought, in the case of a 1:1 PVC–PAN mixture, the heat of polymerization of cyano groups is increased by some 50% compared to PAN alone; we believe that the termination reaction is, however, the prime consideration with an increase in the heat of reaction.

The Effect of the Reactor Type on the Selectivity of Thermal Reactions of *p*-Xylene in Temperature Gradient Systems

Shigenobu KAWAKAMI, Shingo IWAKI, Masahiro NAKADA, and Tatsuaki YAMAGUCHI*
Laboratory of Chemistry, Chiba Institute of Technology, Tsudanuma, Narashino-shi, Chiba 275
(Received October 17, 1990)

Thermal reactions of *p*-xylene were investigated in two kinds of reactors, batch type and flow type, with a large temperature gradient. Excellent differences of the resulting products were observed between these two types of reactors. As for a batch type reactor, 4,4′-dimethylbibenzyl was produced in a high yield with [2.2]paracyclophane and toluene as by-products, and as for a flow type reactor, toluene was obtained as a major product with a low selectivity of 4,4′-dimethylbibenzyl, respectively. These results were different from those of the conventional fast flow pyrolysis method in which [2.2]paracyclophane or poly(3,6-dimethylene-1,4-cyclohexadiene) was formed as a major product. These differences can be accounted for by the partial separation of a reaction mixture caused by the thermal diffusion effect, which arises when the mixture is subject to a temperature gradient.

Thermal diffusion arises when a mixture is subjected to a temperature gradient, leading to partial separation of the components. In a reactor, which has a large temperature gradient, partial separation of the components of the reaction mixture due to the thermal diffusion effect prevents such side reactions as reverse reactions and successive reactions. By such a reactor, the reaction products are expected to be different from those in the conventional ones. In 1941 Hirota reported the formation of oily aromatic hydrocarbons and hydrogen from methane using a Clusius–Dickel type thermal diffusion column as a reactor.[1–3] His success in getting the oil in a high yield was attributable to the prevention of the recombination reaction by the instant separation of produced hydrogen from hydrocarbon residues owing to thermal diffusion effect caused by the temperature gradient. His works ought to be regarded as one of the earliest examples of application of a thermal diffusion column as a reactor. However, they had been left unnoticed until very recently. In 1988 Yamaguchi (one of the authors) reexamined Hirota's process, confirming the conversion of methane to C2 compounds.[4] The thermal reactions of simple aromatic hydrocarbons in a temperature gradient system were developed in this laboratory.[5–7] In the preceding paper,[6] we reported the formation of 4,4′-dimethylbibenzyl in a high selectivity by the dehydrogenative coupling of *p*-xylene in a temperature gradient system. The present paper deals with the thermal reactions of *p*-xylene using two kinds of reactors (termed as a batch type reactor and a flow type reactor in this paper), in which the thermal diffusion effect is expected.

Experimental

Batch Type Reactor. The reactions were carried out in a reaction system shown in Fig. 1, where a steep temperature gradient was expected between the surface of the heater and the cold wall of the flask. The spiral heater, made of a nickel chromium steel wire of 0.5 mm in diameter and 25 cm in length was placed horizontally inside of a 1 L three-necked separable flask fitted with a reflux condenser. This reactor is termed as a batch type reactor in this paper, and is characterized by the vertical contact of *p*-xylene vapor with the heater. The flask containing 1 mole of *p*-xylene was heated by a heating mantle under nitrogen. After the boiling of *p*-xylene was started, the power of the heater inside was turned on, and vapored *p*-xylene was contacted with the heater. The surface temperature of the heater was measured

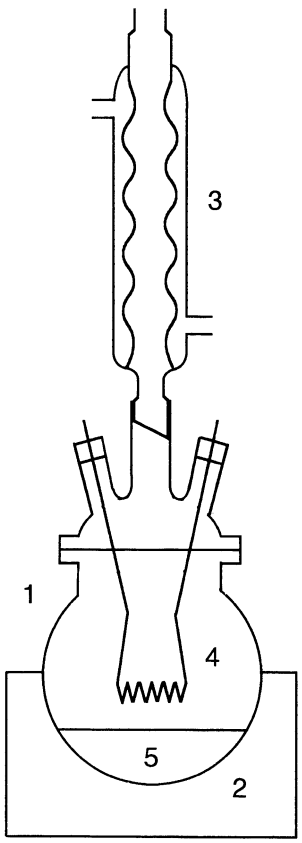

Fig. 1. Batch type reactor. 1: Separable flask, 2: Heating mantle, 3: Reflux condenser, 4: Heater, 5: Reactant.

by a radiation pyrometer (Minolta IR-120) and set at a desired reaction temperature. During the reaction the temperature was monitored by the radiation pyrometer and controlled. The reaction products were identified by GC-MS and GC-IR analysis using authentic samples. After the reaction, the reaction mixture was mixed with chloroform of twice volume of originally employed xylene to dissolve solid products, and analyzed by a gas chromatograph. Gaseous products were also analyzed by a gas chromatograph.

Flow Type Reactor. The flow type reactor used in this experiment is schematically shown in Fig. 2. In brief, the reactor consists of a Pyrex glass-made Liebig condenser (60 cm in length and 5.0 cm in inner diameter) and a heater made of a nickel chromium steel wire (42 cm length and 1.0 mm diameter) mounted at the axis of the condenser. In the flow type reactor, *p*-xylene vapor flowed parallel to the heater. The inlet of *p*-xylene and the outlet of gaseous product were placed at the level 2 cm lower from the top of the heater. The air in the reactor was first replaced by nitrogen and cooling water was supplied. The power of the heater was turned on. The temperature of the heater was measured by a radiation pyrometer and set at a desired temperature. *p*-Xylene was charged downward at a constant rate, and the surface temperature of the heater was further monitored and controlled. The heater was kept at the temperature for two hours by maintaining the voltage and the currency of the electric current. Reaction products were collected every 30 minutes; gaseous products from the upper outlet and liquid products from the lower outlet, and analyzed by gas chromatography.

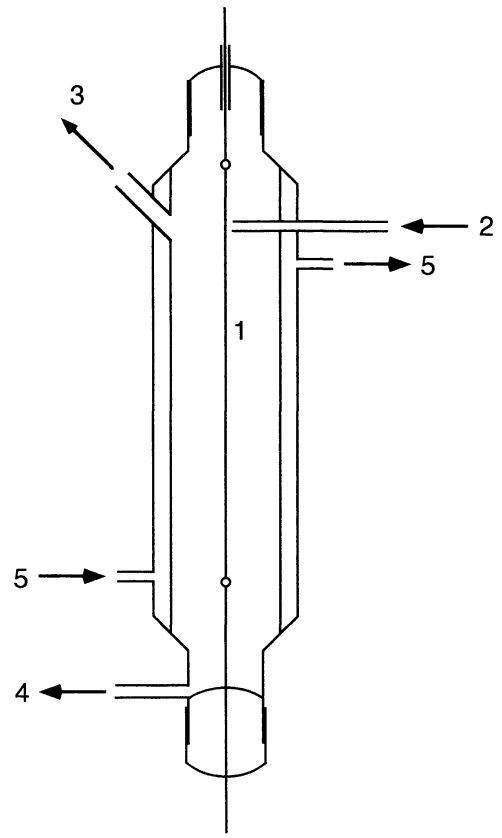

Fig. 2. Flow type reactor (Thermal diffusion column). 1: Heater, 2: *p*-Xylene, 3: Gaseous products, 4: Liquid products, 5: Cooling water.

Results and Discussion

Products of the Batch Type Reactor. The results of the batch type reactor are summarized in Table 1 with experimental details. The reaction started substantially at 1000°C, producing two ring aromatic compounds for the most part. The main product from *p*-xylene was 4,4′-dimethylbibenzyl (**1**). Among other major products were [2.2]paracyclophane (**2**), bis(4-methylphenyl)methane (**3**), *p*-methylstyrene, and toluene. The product, which remained insoluble in the reaction mixture after the addition of chloroform, was identified as poly(3,6-dimethylene-1,4-cyclohexadiene) (**4**) by IR analysis. With the raise of temperature, the selectivity of **1** decreased, while that of **3**, and the sum of **2**+**4** increased. As long as the reaction temperature remained unchanged, the constant selectivity of the products was obtained, even when the conversion of *p*-xylene increased with the prolonged reaction time.

It was shown by GC analysis that the main gaseous products were hydrogen and methane with a small amount of ethane and ethylene. The ratio of hydrogen to methane was approximately 6 to 4, which was consistent with other previous experimental results.[8,9] It should be noted that this ratio slightly decreased with the increase of the conversion of *p*-xylene by the temperature raise.

The formation of hydrogen is best accounted for by the reactions (Eqs. 1 and 2) postulated by Szwarc.[8] Most of the components of the reaction mixture can be traced to a common intermediate, *p*-methylbenzyl radical. This intermediate is formed by thermal scission of the benzylic hydrogen. Most of these radicals recombines to form **1** (Eq. 3), the product of the highest selectivity in the present temperature gradient system. Some of these radicals are converted to 3,6-dimethylene-1,4-cyclohexadiene by dispropor-

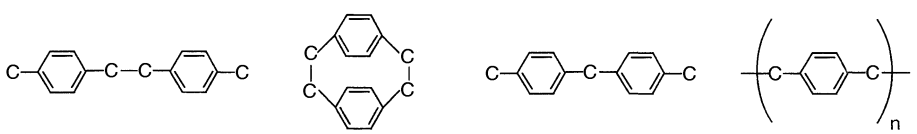

1 2 3 4

Table 1. The Thermal Reactions of *p*-Xylene in a Batch Type Thermal Diffusion Reactor

Reaction Temp./°C	1050	1050	1100	1150	1150
Reaction time/h	5	10	5	2	5
Conversion/%	5.0	10.2	10.9	12.8	32.7
Selectivity/%[a]					
Benzene	0.2	0.3	0.8	1.0	1.1
Toluene	20.1	20.0	20.3	22.1	22.0
o-Xylene	1.9	2.0	1.7	1.3	1.3
m-Xylene	2.3	2.3	2.2	2.3	2.4
Styrene	1.9	1.8	2.0	2.3	2.2
p-Methylstyrene	3.2	3.3	3.6	5.0	5.1
Naphthalene	ND[b]	ND	TR[c]	0.2	0.3
Methylnaphthalenes	ND	ND	TR	0.1	0.1
Biphenyl	ND	ND	0.1	0.1	0.1
Methylbiphenyls	ND	ND	0.2	0.5	0.6
Diphenylmethane	ND	ND	TR	0.2	0.2
Fluorene	ND	ND	0.2	0.5	0.5
Dimethylbiphenyls	ND	ND	0.2	0.5	0.4
Bibenzyl	ND	ND	0.1	0.1	0.1
Methylbibenzyls	1.1	1.1	1.3	1.7	1.8
Bis(4-methylphenyl)methane	5.9	5.8	6.1	6.6	6.6
4,4′-Dimethylbibenzyl	44.2	44.0	42.7	33.2	33.1
[2.2]Paracyclophane	10.0	9.8	9.3	8.4	8.4
Poly(3,6-dimethylene-1,4-cyclohexadiene)	1.7	1.9	2.0	6.0	6.2
Dimethylanthracenes	0.5	0.6	0.7	1.1	1.2
Others	7.1	7.1	6.5	6.8	6.3
Selectivity of gaseous product/mol%					
H_2	61.6	61.5	60.7	57.0	56.8
CH_4	37.9	37.8	38.6	42.5	42.4
Others	0.5	0.7	0.7	0.5	0.8

a) Values for selectivity were based on the weight of the products. b) Not detected. c) Trace.

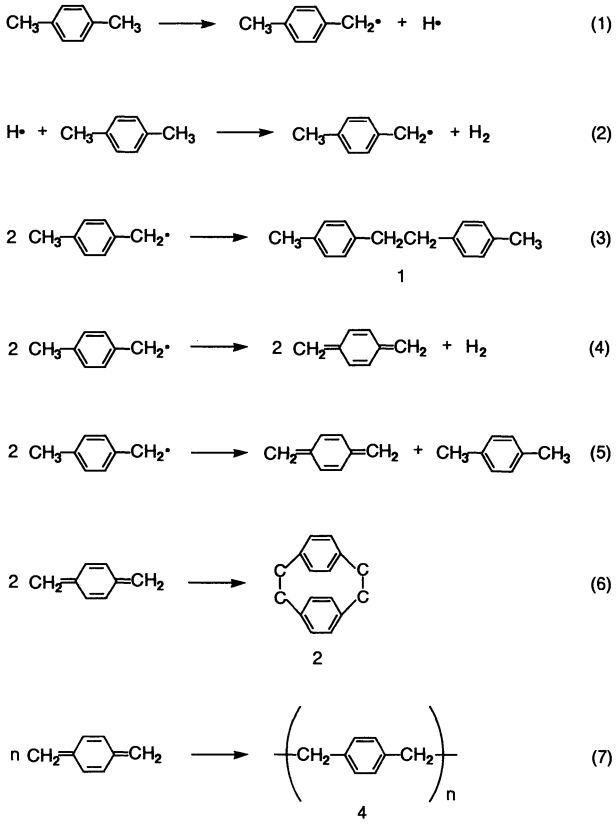

tionation (Eq. 4) or further dehydrogenation of the radicals (Eq. 5).[8,10] 3,6-Dimethylene-1,4-cyclohexadiene is either converted to **2** (Eq. 6) or polymerized to **4** (Eq. 7).

The formation of methane can be accounted for by the reaction (Eq. 8) as suggested by Szwarc[8] or by the reaction (Eq. 9) as suggested by Schaefgen.[9] The *p*-methylphenyl radical thus formed is further converted to toluene (Eq. 10), some of which is further changed to benzene. The radical is also responsible for the formation of **3**.

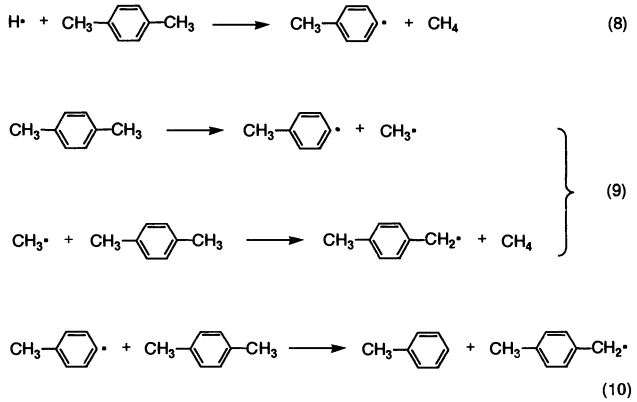

Comparison with the Results of Fast Flow Pyrolysis. In a conventional reaction method such as fast

flow pyrolysis, where *p*-xylene was pyrolyzed in a vapor phase without temperature gradient, the main products were [2.2]paracyclophane (**2**) and poly(3,6-dimethylene-1,4-cyclohexadiene) (**4**), supposed to be derived from 3,6-dimethylene-1,4-cyclohexadiene.[8–13] 4,4′-Dimethylbibenzyl (**1**) was described as only one of the by-products, the selectivity of which was only 2.9%,[12] although some reference was made to the formation of the compound.[9,11–13]

Contrary to these results, **1** was the main product in the present experiment. The high selectivity of **1** should be attributable to the thermal diffusion effect. In the conventional method, where little temperature gradient is present, *p*-methylbenzyl radical can accept enough energy to undergo dehydrogenation (Eq. 4) or disproportionation (Eq. 5) to be converted to 3,6-dimethylene-1,4-cyclohexadiene, the predecessor of **2** and **4**. Moreover, if **1** is produced from *p*-methylbenzyl radical, it is subject to successive reactions,[9] resulting in the low selectivity of **1**.

On the other hand, in the temperature gradient system as shown in Fig. 1, the thermal diffusion effect, caused by the temperature gradient between the surface of the heater and the cold wall of the vessel, brings about the quenching of the components of the reaction mixture immediately after their production. Thanks to the effect, *p*-methylbenzyl radical leaves the heated surface of the heater for the cold wall to be prevented from further conversion to 3,6-dimethylene-1,4-cyclohexadiene. No process other than the coupling to **1**, which requires almost no reaction energy, should be allowed for the quenched *p*-methylbenzyl radical. 4,4′-Dimethylbibenzyl (**1**), thus produced, is prevented from successive reactions due to the thermal diffusion effect, leading to its high selectivity.

Results of the Flow Type Thermal Diffusion Reactor. Table 2 lists the results of the flow type reactor (a thermal diffusion column), which were quite different from those of the batch type reactor. Toluene was the main product of the reaction under the reaction conditions studied. Only a few quantities of 4,4′-dimethylbibenzyl (**1**), which was the main product of the batch type reactor, was produced. As for gaseous products, a sample (corresponding to the experiment of the fifth column from the left in Table 2) comprised 61.6% of methane, 36.0% of hydrogen, 0.3% of ethane, and 2.1% of butanes. These results contrasted sharply with those of the batch type reactor (shown in Table 1), in which hydrogen occupied about 60% of gaseous products. The results of the flow type thermal diffusion reactor were also inconsistent with those of the conventional fast flow pyrolysis where **2** and **4** were major reaction products.

Thermal Diffusion Effect in the Reactors with the Temperature Gradient. The high selectivity of toluene should also be attributable to the thermal diffusion effect. Thermal diffusion arises when a mixture is subjected to a temperature gradient leading to partial separation of the components. In this process, the component of smaller molecular weight concentrates in the hotter region. In the thermal diffusion reactor of our experiment, molecular hydrogen or atomic hydrogen, evolved in the course of reactions, are separated and concentrated on the surface of the heater

Table 2. The Thermal Reactions of *p*-Xylene in a Flow Type Thermal Diffusion Reactor

Reaction temp.	1080	1080	1150	1150	1240	1240
Flow rate/mol h^{-1}	0.054	0.102	0.104	0.181	0.105	0.191
Conversion/%	6.6	4.2	12.7	8.2	24.2	16.4
Selectivity/%[a]						
Benzene	4.1	2.9	9.1	8.9	16.2	16.0
Toluene	60.5	60.7	51.3	53.2	39.8	40.9
o-Xylene	6.2	8.0	4.2	5.0	2.8	3.2
m-Xylene	2.3	3.6	1.9	2.6	1.4	1.5
Styrene	4.8	4.8	7.7	8.4	10.4	12.0
Trimethylbenzenes	10.6	8.7	6.3	5.8	3.9	2.8
p-Methylstyrene	4.5	3.1	4.9	3.1	3.9	2.7
Indene	1.1	0.5	4.6	3.3	7.0	7.4
Naphthalene	0.5	TR[c]	1.6	2.0	4.5	5.5
Methylnaphthalenes	ND[b]	ND	ND	ND	0.5	0.4
Biphenyl	ND	ND	ND	ND	1.2	0.4
Methylbiphenyls	ND	ND	ND	ND	0.7	TR
Diphenylmethane	ND	ND	ND	ND	0.1	ND
Fluorene	ND	ND	ND	0.2	0.7	0.6
Dimethylbiphenyls	ND	ND	ND	ND	0.2	ND
Bibenzyl	ND	ND	ND	ND	ND	ND
Methylbibenzyls	0.3	ND	0.5	0.4	0.2	ND
Bis(4-methylphenyl)methane	ND	ND	ND	ND	ND	ND
4,4′-Dimethylbibenzyl	2.0	3.4	1.9	2.2	0.7	0.6
[2.2]Paracyclophane	2.7	4.1	3.2	2.6	0.7	0.6
Unidentified	0.4	0.2	2.6	2.5	5.1	5.4

a) Values for selectivity were based on the weight of the products. b) Not detected. c) Trace.

due to thermal diffusion effect. They can retard the formation of *p*-methylbenzyl radicals (Eq. 2) and 3,6-dimethylene-1,4-cyclohexadiene (Eq. 4), and promote the production of *p*-methylphenyl radicals by hydrogenolysis of *p*-xylene (Eq. 8), resulting in the high selectivity of toluene. In other words, in the thermal diffusion column, *p*-xylene appears to have undergone hydrogenative cracking due to the condensation of hydrogen, without supplying hydrogen as a reactant. The analysis of the gaseous products also supports the consumption of hydrogen and the formation of methane. Furthermore, when half amount of hydrogen was added to *p*-xylene at 1150 °C (corresponding to the third column of Table 2), the selectivity of toluene rose to 83.7%, suggesting that hydrogen was responsible for the demethylation.[14]

In the batch type reactor, where the heater was placed horizontally as shown in Fig. 1, gaseous products leave the high temperature region around the heater more immediately than in the flow-type reactor, on account of their low weight and the upward flow of *p*-xylene vapor convection. Hydrogen is less concentrated in the vicinity of the heater and less *p*-methylphenyl radicals are formed in the former reactor than in the latter reactor. This difference of hydrogen concentration is responsible for the difference of products distribution between the two reactors.

Conclusions

Thermal diffusion effect can account for the following difference of product of thermal reactions of *p*-xylene. In a temperature gradient system, *p*-xylene gave as a major product 4,4′-dimethylbibenzyl in the batch type reactor and toluene in the flow type reactor, respectively. However, thermal diffusion effect worked differently, in each reactor in a temperature gradient system. In the former, the effect brought about the quenching of *p*-methylbenzyl radical which was converted to 4,4′-dimethylbibenzyl. In the latter, the effect resulted in the concentration of hydrogen around the heater, and caused *p*-xylene to undergo hydrogenative cracking. Anyway, both results contrast sharply to those of the conventional fast flow pyrolysis of *p*-xylene, where [2.2]paracyclophane and poly(3,6-dimethylene-1,4-cyclohexadiene) were produced mainly, probably because of the little temperature gradient.

The authors wish to express their heartful thanks to Professor Emeritus Kozo Hirota of Osaka University for his useful and informative discussions, and to Mr. Aiming Yu for his helpful assistance.

References

1) K. Hirota, *Bull. Chem. Soc. Jpn.*, **16**, 274 (1941).
2) K. Hirota, *Nippon Kagaku Zasshi*, **62**, 392 (1941).
3) K. Hirota and K. Oguro, *Nippon Kagaku Zasshi*, **47**, 9 (1943).
4) T. Yamaguchi and C. Saito, *Bull. Chem. Soc. Jpn.*, **61**, 2649 (1988).
5) M. Nakada, Y. Aiming, S. Kawakami, and T. Yamaguchi, *Bull. Chem. Soc. Jpn.*, **62**, 3392 (1989).
6) S. Kawakami, S. Iwaki, Y. Aiming, M. Nakada, and T. Yamaguchi, *Chem. Lett.*, **1990**, 893.
7) S. Kawakami, M. Nakada, and T. Yamaguchi, *Chem. Express*, **5**, 395 (1990).
8) M. Szwarc, *J. Chem. Phys.*, **16**, 128 (1955).
9) J. R. Schaefgen, *J. Polym. Sci.*, **15**, 203 (1955).
10) M. Szwarc, *J. Polym. Sci.*, **6**, 319 (1951).
11) R. S. Corley, H. C. Hass, M. W. Kane, and D. I. Livingstone, *J. Polym. Sci.*, **13**, 137 (1954).
12) L. A. Errede and J. P. Cassidy, *J. Am. Chem. Soc.*, **82**, 3653 (1960).
13) L. A. Errede, R. S. Gregorian, and J. M. Hoyt, *J. Am. Chem. Soc.*, **82**, 5218 (1960).
14) A. Amano, O. Horie, Y. Sato, and T. Katayose, *Sekiyu Gakkaishi*, **15**, 125 (1972).

Temperature-Programmed Desorption of Dimethylpyridine Adsorbed on Silica-Alumina Prepared by Chemical Vapor Deposition

Satoshi SATO,* Masahiro TOKUMITSU, Toshiaki SODESAWA, and Fumio NOZAKI
Department of Applied Chemistry, Faculty of Engineering,
Chiba University, Yayoi-cho, Chiba 260
(Received August 13, 1990)

Synopsis. A temperature-programmed desorption of adsorbed dimethylpyridine clarified the characteristic changes in acid type, acid strength, and acid amount of silica-alumina prepared by depositing silica on an alumina support. Lewis acid sites of the alumina changed into Brønsted acid sites together with a change in the acid strength with increasing silica deposition.

We previously prepared a supported type of silica-alumina by depositing silica on an alumina surface by means of chemical vapor deposition (CVD).[1,2] Silica was effectively deposited on alumina using tetraethoxysilane in the presence of oxygen at 240 °C, and silica loading was readily controlled by the CVD time. The resulting silica-alumina (CVD SiO_2/Al_2O_3) exhibited high catalytic activities for several types of organic reactions such as 2-butanol dehydration, *m*-xylene isomerization, cumene cracking, and heptane cracking. The catalytic activity for 2-butanol dehydration varied with silica loading, and was correlated to the amount of Brønsted acid determined from the extent of the liberated proton in the phase of an aqueous solution.[2]

However, the acid property, especially acid strength, in the absence of water has not been clarified. In this work, a temperature-programmed desorption (TPD) of dimethylpyridine (DMP) adsorbed on a CVD SiO_2/Al_2O_3 catalyst using a conductivity cell immersed in a dilute H_2SO_4 solution was carried out in order to evaluate the entire acid property, including acid type (Brønsted or Lewis), acid strength, and acid amount.

Experimental

Alumina supplied by Dia Catalyst & Chemicals Ltd. (DC-2282: specific surface area, 203 $m^2 g^{-1}$; pore volume, 0.72 ml g^{-1}; granule size, 24—60 mesh.) was used as a support. A CVD SiO_2/Al_2O_3 catalyst was prepared by contacting tetraethoxysilane vapor with the alumina support in a CVD reactor which comprised a glass column rotating in an electrical furnace inclined at 45° at 240 and 300 °C for a prescribed time in a stream of air and nitrogen, respectively;[2] the flow rates of tetraethoxysilane and carrier gas were 2.7 and 400 mmol h^{-1}, respectively. The silica loading was determined by measuring the weight increase of the alumina support after CVD operation followed by calcination at 550 °C for 3 h. K^+ ion-exchange was performed by immersing a sample in 2 mol dm^{-3} potassium chloride solution at room temperature for 2 h.

After a sample (50 mg) placed in a quartz tube (i.d. 4 mm) with quartz wool had been evacuated at 500 °C for 1 h, excess DMP was injected via a microsyringe at 200 °C, and then evacuated at 200 °C for 1 h. A TPD measurement was carried out from 100 to 600 °C at a heating rate of 5 °C min^{-1} in a nitrogen flow of 30 ml min^{-1}. The desorbed DMP was monitored by a conductivity cell immersed in aqueous sulfuric acid (1/2000 mol dm^{-3}). A cumulative amount of desorbed DMP as a function of the desorption temperature was recorded, then differentiated to give the acid strength distribution. Independently, desorbed molecules were collected at −196 °C, then analyzed by GLC.

The isomerization of 1-butene was carried out in a closed circulation system (reactor volume, 200 ml; catalyst, 0.05 g) under the conditions of a 1-butene initial pressure of 19 kPa at 0 °C. Prior to the reaction, the catalyst was preheated at 500 °C under reduced pressure (0.1 Pa). The catalytic activity was evaluated in terms of the first-order rate constant during the initial reaction period.

Results and Discussion

Decomposition of DMP was preliminarily examined. In the TPD process above 500 °C, about 30% of the 3,5-DMP desorbed from the alumina was decomposed into 3-methylpyridine and pyridine. The desorbed amines were detected by the change in the conductivity of a cell solution in which protons are neutralized with them. The conductivity detector was sensitive to such amines as pyridine and DMP, but insensitive to desorbed water as well as to such neutral molecules as benzene and ethanol. In addition, the sensitivity for DMP was almost the same as those for methylpyridine and pyridine. The conductivity detector, therefore, is convenient for the TPD measurement of adsorbed DMP.

Figure 1 shows the cumulative amounts of DMP desorbed from the catalysts. For the alumina support, itself, the cumulative amounts of desorbed DMP were 106 and 14 μmol g^{-1} for 3,5- and 2,6-DMP, respectively. For the CVD SiO_2 (12wt%)/Al_2O_3 prepared at 240 °C

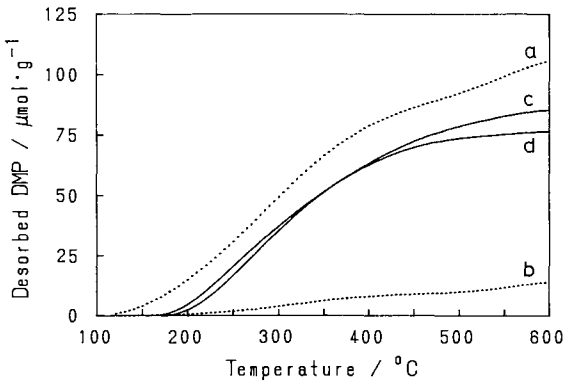

Fig. 1. Cumulative amount of desorbed dimethylpyridine (DMP). Alumina: a, 3,5-DMP; b, 2,6-DMP; CVD SiO_2 (12.4 wt%)/Al_2O_3: c, 3,5-DMP; d, 2,6-DMP.

in air, they were 85 and 77 μmol g^{-1} for 3,5- and 2,6-DMP, respectively. 2,6-DMP is known to selectively adsorb on Brønsted acid sites because of the steric hindrance arising from the two methyl groups, each of which is located adjacent to the nitrogen atom, whereas non-hindered 3,5-DMP is capable of adsorbing on both Lewis and Brønsted acid sites.[3-5] The adsorption of 2,6-DMP on the alumina was seriously restricted, compared to that of 3,5-DMP. The acid amounts measured by 3,5-DMP were also comparable to the amount measured by pyridine.

Figures 2 and 3 show the acid strength distribution of the catalysts. The alumina had a large desorption peak of 3,5-DMP at 300 °C with a shoulder at 570 °C, whereas two small desorption peaks of 2,6-DMP appeared at 300 and 560 °C (Fig. 2). The small peak of 2,6-DMP at 300 °C (Fig. 2b) appears to be caused by desorption from weak Brønsted acid sites. The small peak at 560 °C (Fig. 2b), however, seems to be attributable not to strong Brønsted acid sites, but to strong Lewis acid sites, since alumina has no strong Brønsted acid sites.[2,6] Additionally, IR spectroscopic observations have revealed that 2,6-di-*t*-butylpyridine is strongly adsorbed on alumina,[7] and that 2,6-DMP adsorb on Lewis acid sites together with weak Brønsted acid sites,[8] whereas they have not dealt with the quantitative aspects. Although the TPD of adsorbed 2,6-DMP tends to overestimate the Brønsted acid sites, the large difference between the distribution curves for 3,5- and 2,6-DMP indicates clearly that the acid sites of the alumina are predominantly composed of the Lewis type. On the other hand, the CVD SiO_2 (12wt%)/Al_2O_3 had a wide distribution at a peak top of 250 and 275 °C for 3,5- and 2,6-DMP, respectively (Fig. 3). Since there is no significant difference between two distribution curves for 3,5- and 2,6-DMP, the CVD SiO_2/Al_2O_3 catalyst has a large amount of Brønsted acid sites together with a small amount of strong Lewis acid sites.

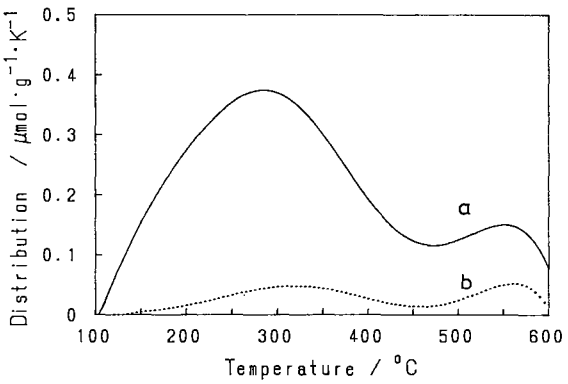

Fig. 2. TPD profiles of alumina. a, 3,5-DMP; b, 2,6-DMP.

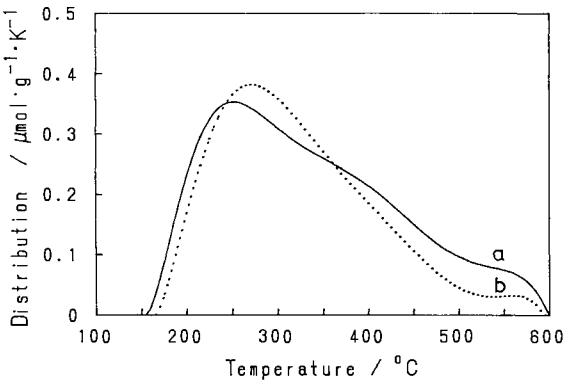

Fig. 3. TPD profiles of CVD SiO_2 (12.4 wt%)/Al_2O_3. a, 3,5-DMP; b, 2,6-DMP.

Figure 4 shows the change in the acid strength distribution measured by the desorption of 2,6-DMP for CVD catalysts prepared at 240 °C in air. When a small amount of silica (5 wt%) was deposited on alumina, the amount of 2,6-DMP desorbed near 250 °C was drastically increased (Fig. 4b). A further increase in silica deposition induced an increase in the strong acid sites represented by desorption around 400 °C; both the highest acid strength and the maximum amount of desorbed 2,6-DMP were attained at a silica loading of 12 wt% (Fig. 4c). Above 12 wt%, the amount was decreased with increasing silica loading, together with a small change in the acid strength (Fig. 4d). On the other hand, the desorption behavior of 3,5-DMP was similar to that of alumina, as is shown in Figs. 2 and 3.

Figure 5 shows changes in the amount of desorbed DMP with silica loading. The amount of desorbed 3,5-DMP was almost unchanged up to about 10 wt% of silica; above this loading it slightly decreased with increasing silica loading. In contrast, the amount of desorbed 2,6-DMP exhibited a maximum at a silica loading of 12 wt%. According to a preliminary ^{31}P magic-angle spinning NMR experiment of chemisorbed trimethylphosphine, the alumina had predominately Lewis acid sites, and Brønsted acid sites were generated on the CVD SiO_2/Al_2O_3, accompanying the disappearance of the Lewis acid sites.[2] The TPD results are consistent with the ^{31}P NMR results, and are allowed to characterize the strength of Brønsted acid sites of the CVD SiO_2/Al_2O_3 catalysts.

For the isomerization of 1-butene, the catalytic

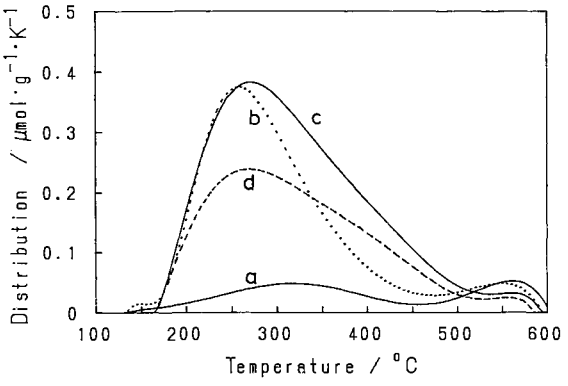

Fig. 4. TPD profiles of 2,6-dimethylpyridine adsorbed on CVD SiO_2/Al_2O_3. Silica loading: a, 0 wt%; b, 5.1 wt%; c, 12.4 wt%; d, 20.3 wt%.

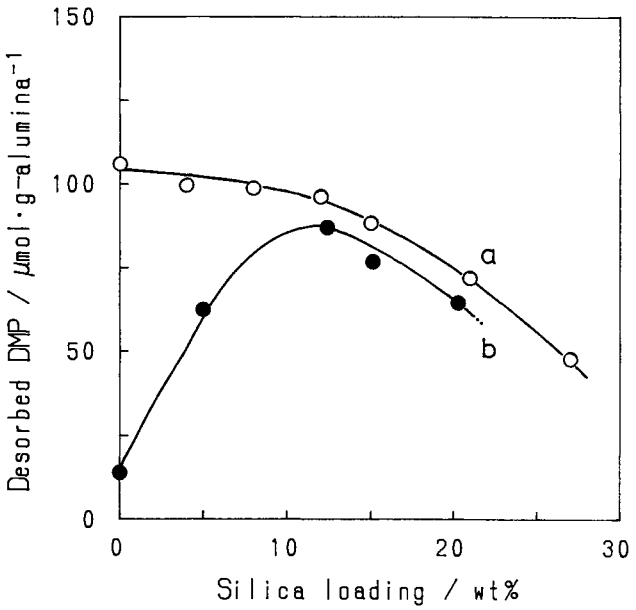

Fig. 5. Change in the total amount of desorbed DMP with silica loading. a, 3,5-DMP; b, 2,6-DMP.

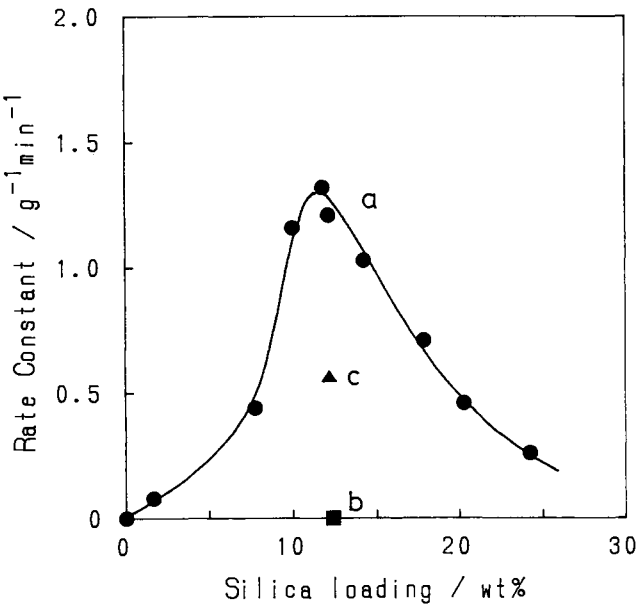

Fig. 6. Change in the initial rate constant for 1-butene isomerization. a, CVD SiO_2/Al_2O_3 prepared at 240°C in air; b, CVD SiO_2 (12.4 wt%)/Al_2O_3 exchanged with 0.11 mmol g^{-1} of K^+ ion; c, CVD SiO_2 (12.2 wt%)/Al_2O_3 prepared at 300°C in nitrogen.

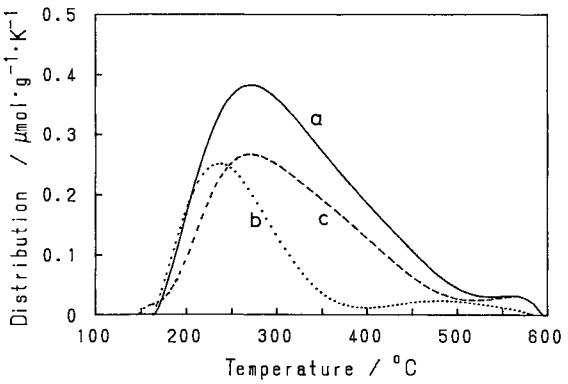

Fig. 7. TPD profiles of 2,6-DMP for various CVD SiO_2 (12 wt%)/Al_2O_3 catalysts. Symbols as those in Fig. 6.

activity was changed with silica loading (Fig. 6), and was maximized at a silica loading of 12 wt%, at which both the acid strength and amount measured by 2,6-DMP desorption showed maxima. Moreover, the CVD SiO_2/Al_2O_3 catalyst has a cation-exchange ability,[2] and an exchange of a proton with the K^+ ion suppressed the catalytic activity for 1-butene isomerization (Fig. 6b). The K^+ ion-exchange decreased both the acid strength and the amount (Fig. 7b), and the amount of desorbed 2,6-DMP drastically decreased at temperatures higher than 400 °C. In addition, a CVD SiO_2/Al_2O_3 catalyst prepared at 300 °C in nitrogen, which had a smaller amount of desorbed 2,6-DMP (Fig. 7c), was less active than that prepared at 240 °C in air (Fig. 6c). The catalytic behavior are well correlated with the Brønsted acidity measured by 2,6-DMP desorption.

References

1) S. Sato, M. Toita, Y. Q. Yu, T. Sodesawa, and F. Nozaki, *Chem. Lett.*, **1987**, 1535.
2) S. Sato, M. Toita, T. Sodesawa, and F. Nozaki, *Appl. Catal.*, **62**, 73 (1990).
3) H. A. Benesi, *J. Catal.*, **28**, 176 (1973).
4) S. L. Soled, G. B. McVicker, L. L. Murrell, L. G. Sherman, N. C. Dispenziere, Jr., S. L. Hsu, and D. Waldman, *J. Catal.*, **111**, 286 (1988).
5) L. L. Murrell and N. C. Dispenziere, Jr., *J. Catal.*, **117**, 275 (1989).
6) K. Tanabe, M. Misono, Y. Ono, and H. Hattori, *Stud. Surf. Sci. Catal.*, **51**, 82 (1989).
7) J. Dewing, G. T. Monks, and B. Youll, *J. Catal.*, **44**, 226 (1976).
8) A. Corma, C. Rodellas, and V. Fornes, *J. Catal.*, **88**, 374 (1984).

ESR Study on Free Radicals Produced from Hexane by Vacuum-Ultraviolet Photolysis, Sensitized Photolysis, and γ-Radiolysis

Hitoshi KOIZUMI,* Takehito YAMAGUCHI,† and Hiroshi YOSHIDA
Faculty of Engineering, Hokkaido University, Kita-ku, Sapporo 060
(Received August 17, 1990)

Synopsis. The free radicals generated from polycrystalline hexane at 77 K by photolysis with vacuum-ultraviolet light, sensitized photolysis, and γ-radiolysis were compared with each others using the ESR method. The selectivity of radical formation was found to depend on the excitation method.

Although the free radicals produced from saturated hydrocarbons have been extensively studied using ionizing radiation combined with ESR measurements, the mechanism for radical formation has not yet been fully understood.[1,2] Ionizing radiation generates primarily electrons, ions, and excited states, and possibly initiates several reaction channels which produce free radicals; thus, elucidating the reaction mechanism may be both complex and difficult. It seems to be helpful to produce free radicals with different excitation methods in order to obtain a deeper insight into the mechanism of free-radical formation.

In the present investigation free radicals generated from polycrystalline hexane by different methods were compared. The methods of radical generation used were direct photolysis with vacuum-ultraviolet (VUV) light from a Xe resonance lamp, sensitized photolysis with benzene and biphenyl as sensitizers, and radiolysis with ^{60}Co γ-rays. Direct photolysis with a proper wavelength of VUV-light brings hexane molecules to selected excited states either below or above the ionization threshold, from which radical formation proceeds. Although VUV-photolysis combined with ESR spectroscopy is expected to help elucidate the mechanism of radical formation, the reported studies have been scanty[3–6] because of experimental difficulties. Sensitized photolysis results in radical formation from hexane, either through energy transfer from the excited sensitizer or abstraction of an H atom by the excited sensitizer.

Experimental

All chemicals were of spectroscopic grade from Wako Pure Chemical Ind., Ltd. and were used without further purification after deaerating by freezing-thawing-pumping cycles. All irradiations and ESR measurements with an X-band spectrometer (Varian, Model E109) were made at 77 K.

A Xe electrodeless lamp constructed according to a method described in the literature[7] was used as the source of VUV light. Hexane was slowly condensed on the cold finger under vacuum of 10^{-5} Torr for one hour and then irradiated with VUV light. The irradiated sample was protected by covering with further condensation and was quickly transferred into a quartz Dewar vessel for ESR measurements.

For the sensitized photolysis, hexane with dissolved benzene (0.01—1 mol dm^{-3}) or biphenyl (0.1—1 mol dm^{-3}) was deaerated, sealed in a quartz ESR tube, and frozen at 77 K. The samples were irradiated with light from a Xe-Hg lamp through a Toshiba UV-D33S filter (250—400 nm) for one hour.

The γ-radiolysis was made with a ^{60}Co source with a dose of 1—4 kGy for hexane both in the sample tube and on the cold finger.

Results and Discussion

Typical examples of ESR spectra observed for the various radical generation methods are shown in Fig. 1. The spectra are generally a superposition of component spectra due to the hexyl, 1-methylpentyl, and 1-ethylbutyl radicals generated by the loss of an H atom from hexane. The component spectrum due to the hexyl radical is weak, since it is unstable and readily transforms into the 1-methylpentyl radical.[8]

For sensitized photolysis, the observed spectra is partly due to cyclohexadienyl-type and/or phenyl-type radicals originating from sensitizer molecules. However, the component spectra of these radicals are confined to the central, narrow region of the total spectral patterns. The yield of the sensitizer radicals was found to decrease with a decrease in the sensitizer concentration, and to be less for biphenyl than for benzene. Actually, the radicals from sensitizer benzene at 1 mmol dm^{-3} were almost ignored, compared to those from solvent hexane. These results indicate that the formation of radicals from hexane is not due to the hydrogen abstraction by the excited sensitizer but, rather, to the scission of a C–H bond of hexane caused by an energy transfer from the excited sensitizer. The formation of sensitizer radicals (cyclohexadienyl-type and phenyl-type) is due to a reaction between excited and ground-state sensitizer molecules, which can occur due to the heterogeneous dissolution at high sensitizer concentration.

The variation of the spectral shape of the solvent radicals depending on the generation method, as shown in Fig. 1, was found to be essentially due to the varying ratio of the 1-methylpentyl radical to the 1-ethylbutyl radical: the observed spectral shapes could be reproduced by superposing the theoretical shapes simulated for the 1-methylpentyl and 2-ethylbutyl radicals[8,9] and a broad spectrum due to radical pairs.[9] The 1-methylpentyl/2-ethylbutyl yield ratio was determined to be 3/2, 4/1, and 9/1 for VUV photolysis, biphenyl-sensitized photolysis, and γ-radiolysis, respectively.

The spectral shape observed for benzene-sensitized photolysis (Fig. 1d) comprises eight equally-spaced

† Present address: Chemical Products Division, Ricoh Company, Ltd., 16-1 Honda-machi, Numazu-shi, Shizuoka, 410.

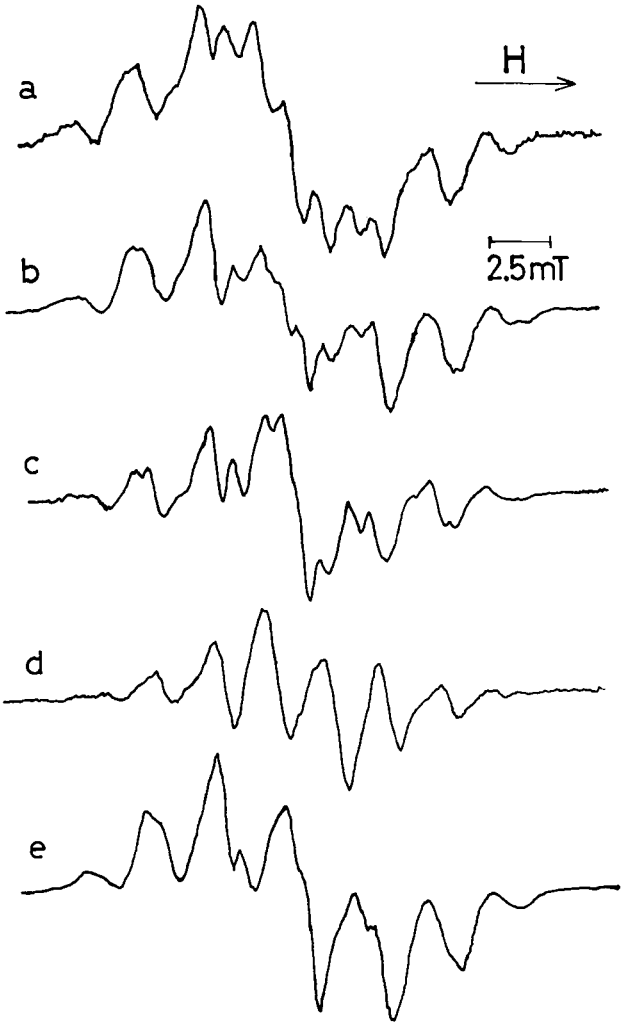

Fig. 1. ESR spectra observed at 77 K for hexane (a) photolyzed with Xe resonance lamp, (b) irradiated with γ-rays on the cold finger, (c) photolyzed by the biphenyl-photosensitization, (d) photolyzed by the benzene-photosensitization, and (e) γ-irradiated in a seal ESR tube.

hyperfine lines. This cannot be reproduced by any ratio of the 1-methylpentyl to 2-ethylbutyl radicals with normal conformation. Based on the McConell's relation, $a_\beta(\theta)=B\cos^2\theta$,[10] the distortion of the conformation by rotating about the C_α–C_β bond by 20° changes the hyperfine coupling constants of the β-CH_2 protons to 4.27 and 1.82 mT. These coupling constants well reproduce the observed spectral shape. Therefore, the free radicals generated by the benzene-sensitized photolysis are attributable to the 1-methylpentyl radicals with a distorted conformation.

A mechanism for radical formation from γ-irradiated n-alkanes has previously been proposed by Iwasaki et al.,[9]

$$RH \longrightarrow (RH^+)^* + e^-, \quad (1)$$

$$(RH^+)^* \longrightarrow R_I^+ + H \xrightarrow{+e^-} R_I + H, \quad (2)$$

$$(RH^+)^* \xrightarrow{+e^-} RH^* \longrightarrow R_I + H, \quad (3)$$

$$(RH^+)^* \xrightarrow{+RH} RH_2^+ + R_I \xrightarrow{+e^-} 2R_I + H_2 \text{ or } RH + H + R_I, \quad (4)$$

and

$$H + RH \longrightarrow R_{II},\ R_{III} + H_2. \quad (5)$$

They claimed that C–H bond scission by ionizing radiations occurs primarily at the chain-end, forming the terminal alkyl radical (R_I, $\dot{C}H_2CH_2$–) and a hydrogen atom, by one of the charge recombinantion processes: (2), (3), or (4). The terminal alkyl radical readily abstracts a hydrogen atom from a neighboring molecule to form a penultimate alkyl radical (R_{II}, $CH_3\dot{C}HCH_2$–) at 77 K in triclinic crystals of linear hydrocarbons with an even number of carbon atoms. The liberated H atom abstracts a hydrogen atom from a nearby molecule to form either R_{II} or an internal radical (R_{III}, –$CH_2\dot{C}HCH_2$–) secondarily (reaction 5).

In contrast, the present VUV-photolysis is a nonionic process, since the photon energy from the Xe resonance lamp (8.43 eV) is lower than the ionization threshold of hexane (10.06 eV in gas phase). The formation of hexyl radicals originates from the excitation:

$$RH + h\nu \longrightarrow RH^* \longrightarrow R + H. \quad (6)$$

Subsequent hydrogen abstraction (reaction 5) is also a possible source of hexyl radicals in VUV-photolysis. Assuming that the excited states in γ-radiolysis and VUV-photolysis (RH* in reaction paths (3) and (6)) are identical, the smaller R_{II}/R_{III} radical yield ratio for VUV-photolysis than for γ-radiolysis seems to results from a comparatively efficient formation of R_{III} through reaction path (3), compared with paths (2) and (4) for radiolysis. Iwasaki et al presumed that all of the reaction paths ((2),(3), and (4)) result in the formation of R_I, which then transforms into R_{II} at 77 K.[9] The present results, however, indicate that the dissociation of excited hexane into R_{III} cannot be ignored.

Kuwata et al.[4] previously reported that the VUV-photolysis of n-alkanes (C_5—C_8) with the Lyman-α line from a hydrogen discharge lamp gives ESR spectra with six hyperfine lines due to R_{III}. Their result is essentially consistent with the present result that the R_{II}/R_{III} yield ratio is comparatively low for VUV-photolysis, compared with γ-radiolysis.

In sensitized photolysis as well, radical formation occurs nonionically through reaction (7), followed by reaction (5),

$$RH + S^* \longrightarrow RH^* + S \longrightarrow R + H + S. \quad (7)$$

It was previously reported that an energy transfer from a benzene or biphenyl molecule occurs from its second or higher triplet state created by T–T absorption.[12] In benzene-sensitized photolysis, the influence of energy-

donating benzene causes a selective formation of R_{II} with a distorted conformation. Takeshita and Tsuji previously observed the selective formation of the 1-methylpentyl radical from hexane by photolysis with benzoic acid used as sensitizer.[13]

In conclusion, the selectivity in radical formation from polycrystalline solid hexane depends on the excitation method used, VUV-photolysis, sensitized photolysis, or γ-radiolysis. This is in contrast with the absence of selectivity reported for 3-methylpentane in the amorphous state.[12,14-17] It is not presently known whether the difference observed between hexane and 3-methylpentane can be attributed to differences in molecular structure or differences in the aggregation state.

It is thankfully acknowledged that this work was partly supported by the Kurata Research Grant to H. K.

References

1) S. Ya. Pshezhetskii, A. G. Kotov, V. K. Milinchuk, V. A. Roginskii, and V. I. Tupikov, "ESR of Free Radicals in Radiation Chemistry," John Wiley & Sons, New York (1974).

2) J. E. Willard, in "Radiation Chemistry, Principle and Application," ed by Farhataziz and M. A. J. Rodgers, VCH Publishers, New York (1987), p. 395.

3) M. D. Sevilla and R. A. Holroyd, *J. Phys. Chem.*, **74**, 2459 (1970).

4) K. Kuwata, Y. Kotake, K. Inada, and M. Ono, *J. Phys. Chem.*, **76**, 2061 (1972).

5) D. Bhattacharya, H. Wang, and J. E. Willard, *J. Phys. Chem.*, **85**, 1310 (1981).

6) A. Wakahara, T. Miyazaki, and K. Fueki, *J. Phys. Chem.*, **86**, 1781 (1982).

7) J. R. McNesby and H. Okabe, *Adv. Photochem.*, **3**, 157 (1964).

8) T. Gillbro and A. Lund, *Int. J. Radiat. Phys. Chem.*, **8**, 625 (1976).

9) M. Iwasaki, K. Toriyama, M. Fukaya, H. Muto, and K. Nunome, *J. Phys. Chem.*, **89**, 5278 (1985).

10) C. Heller and H. M. McConnel, *J. Chem. Phys.*, **32**, 1535 (1960).

11) P. B. Ayscough and C. Thomson, *Trans. Faraday Soc.*, **58**, 1477 (1962).

12) N. N. Shelimov, N. V. Fok, and V. V. Voevodskii, *Dokl. Akad. Nauk SSSR*, **144**, 596 (1962).

13) T. Takeshita and K. Tsuji, *J. Phys. Chem.*, **78**, 105 (1974).

14) B. Brocklehurst, W. A. Gibbons, F. T. Land, G. Porter, and M. I. Savadatti, *Trans. Faraday Soc.*, **62**, 1793 (1966).

15) D. J. Henderson and J. E. Willard, *J. Am. Chem. Soc.*, **91**, 3014 (1969).

16) N. Bremer, B. J. Brown, G. H. Morine, and J. E. Willard, *J. Phys. Chem.*, **79**, 2189 (1975).

17) T. Ichikawa and N. Ohta, *J. Phys. Chem.*, **81**, 560 (1977).

Catalytic Isomerization of Trimethylbenzenes over a Graphite-Sulfuric Acid

Susumu TSUCHIYA,* Kenji FUJII, Tadashi MITSUNO, Yoshihisa SAKATA, and Hayao IMAMURA
Department of Industrial Chemistry, Faculty of Engineering,
Yamaguchi University, Tokiwadai, Ube, Yamaguchi 755
(Received September 6, 1990)

Synopsis. The isomerization of 1,2,3- and 1,2,4-trimethylbenzene took place over a graphite–sulfuric acid to form 1,2,4- and 1,2,3-trimethylbenzene, respectively, but that of 1,3,5-trimethylbenzene was not observed.

Since Kondow et al.[1] found that the equilibration of protium–deuterium took place over a caesium–graphite intercalation compound (GIC), much attention has been paid to the characteristic properties of graphite intercalation compounds, and their catalytic properties have been investigated extensively in various reactions.[2,3] Watanabe et al.[4] reported a molecular-sieving-type physisorption of alkali metal graphites at 77 K.Tsuchiya et al.[5,6] have observed structure-selectivity in the hydrogenation and the isomerization of olefins over alkali metal graphites. The results have been explained on the basis of the molecular-sieving-like effect of the compound.

Because the molecular-sieving-like effect has been observed in the case that the intercalant of GIC is basic substances,[5,6] a similar effect would be expected in the case that the intercalant is an acidic substance. Trimethylbenzenes (1,2,3-, 1,2,4-, and 1,3,5-trimethylbenzene) are catalytically isomerized over an acid catalyst.[7] It can therefore be expected that a certain isomer of trimethylbenzene might be selectively formed over a graphite–acid with molecular-sieving effects. In this study interest was centered on a graphite–sulfuric acid.

A closed recirculation system using greaseless stopcocks was employed in order to follow the progress of the reaction; helium was used as the diluent. The reaction mixtures were occasionally analyzed by means of gas chromatography. The graphite–sulfuric acid used as the catalyst was prepared according to Takemoto et al.,[8] and identified by XRD. A bundle of glass-wool impregnated with sulfuric acid was used as "H_2SO_4-cat". Trimethylbenzenes were obtained from Tokyo Kasei Kogyo Co., Ltd., and their purity, more than 99%, was confirmed by gas chromatography.

Four kinds of reactions can be expected over an acid catalyst, as follows:

1) Disproportionation of trimethylbenzenes (1,2,3-, 1,2,4-, and 1,3,5-trimethylbenzene) to form dimethylbenzenes (1,2-, 1,3-, and 1,4-dimethylbenzene) and tetramethylbenzenes (1,2,3,4-, 1,2,3,5-, and 1,2,4,5-tetramethylbenzene).
2) Isomerization of trimethylbenzenes.
3) Isomerization of dimethylbenzenes.
4) Isomerization of tetramethylbenzenes.

Table 1 lists the equilibrium composition, assuming that these four kinds of reactions are in equilibrium. These values were calculated on the basis of reported API thermodynamic data.[9]

Figure 1 shows a typical result, when 1,2,3-trimethylbenzene was introduced over graphite-sulfuric acid at 373 K. 1,3,5-Trimethylbenzene was not observed. Neither dimethylbenzenes nor tetramethylbenzenes were detected. From a thermodynamic analysis the formation of 1,3,5-trimethylbenzene would be expected, if the interconversion of three isomers of

Table 1. Equilibrium Composition

Component	Composition C/mol%		
	300 K	400 K	500 K
1,2,3-Trimethylbenzene	1.38	2.13	2.71
1,2,4-Trimethylbenzene	29.27	29.31	28.74
1,3,5-Trimethylbenzene	19.56	15.59	13.11
1,2-Dimethylbenzene	4.06	5.02	5.86
1,3-Dimethylbenzene	14.89	15.05	15.18
1,4-Dimethylbenzene	5.94	6.42	6.69
1,2,3,4-Tetramethylbenzene	2.00	2.87	3.65
1,2,3,5-Tetramethylbenzene	13.15	13.82	14.28
1,2,4,5-Tetramethylbenzene	9.75	9.80	9.79

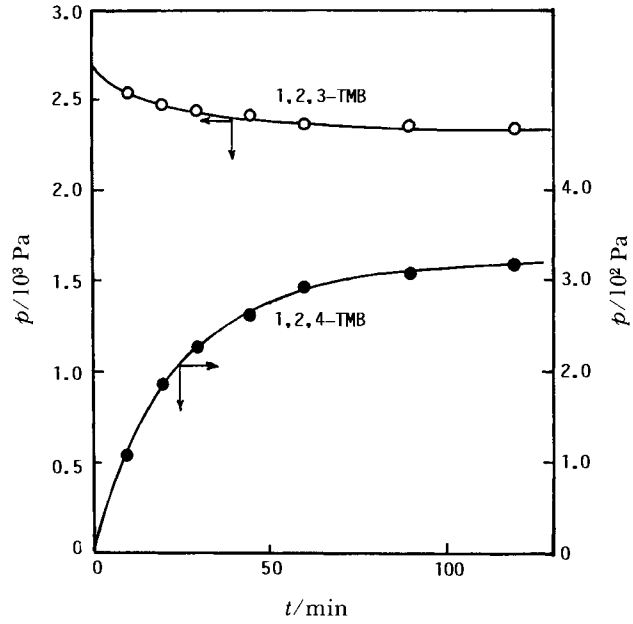

Fig. 1. Isomerization of 1,2,3-trimethylbenzene over a graphite–sulfuric acid at 373 K.

trimethylbenzenes take place. If the disproportionation of 1,2,3-trimethylbenzene takes place, dimethylbenzenes and tetramethylbenzenes might be expected. However, only 1,2,4-trimethylbenzene was selectively formed. This result suggests that only the isomerization of 1,2,3-trimethylbenzene to form 1,2,4-trimethylbenzene took place.

When 1,2,4-trimethylbenzene was the reactant, 1,2,3-trimethylbenzene was only observed as an aromatic compound. The formation of 1,3,5-trimethylbenzene, dimethylbenzenes, and tetramethylbenzenes was not detected. This result suggests that the isomerization of 1,2,4-trimethylbenzene to form 1,2,3-trimethylbenzene took place, and that the disproportionation of 1,2,4-trimethylbenzene did not take place. Another product observed was methane, the amount of which was less than 10% of the 1,2,3-trimethylbenzene formed. Methane might be formed by the decomposition of the reactant.

When 1,3,5-trimethylbenzene was the reactant, any hydrocarbon other than the reactant was observed at 373 K. This result suggests that 1,3,5-trimethylbenzene did not react under the present experimental conditions. Because neither dimethylbenzenes nor tetramethylbenzenes was observed, it is reasonably concluded that the disproportionation of trimethylbenzenes did not take place over the graphite–sulfuric acid under the present experimental conditions. At 413 K, methane was observed, the amount of which was ca. 20% of the reactant at 2 h. The methane might be formed by decomposition, as mentioned above. If the amount of methane is small, the formation of methane is an important problem, since carbon depositing on the catalyst surface might take place. In order to elucidate this point, further investigations are certainly necessary and should be carried out.

The widths of 1,2,3-, 1,2,4-, and 1,3,5-trimethylbenzene are 8.1, 7.6, and 8.6 Å, respectively. Since the interlayer distance of a graphite–sulfuric acid is 11.3 Å, wider molecules probably have more difficulty to penetrate into and move within the space between the graphite layers than do narrow molecules. Accordingly, the present experimental results, that the formation and conversion of 1,3,5-trimethylbenzene were not observed, are reasonably explained on the basis of a size effect of the molecules.

When 1,2,3-trimethylbenzene was introduced over H_2SO_4-cat, on the other hand, both dimethylbenzens and tetramethylbenzenes were observed. This result suggests that the disproportionation reaction took place over H_2SO_4-cat. Accordingly, the catalytic selectivity of H_2SO_4 was varied by forming such intercalation compounds as graphite–sulfuric acid.

In conclusion, graphite–sulfuric acid has shown high catalytic selectivity for the reaction of trimethylbenzenes.

This work was partially supported by General Sekiyu Research and Development Encouragement and Assistance Foundation, for which the authors' thanks are due.

References

1) T. Kondow, H. Inokuchi, and N. Wakayama, *J. Chem. Phys.*, **43**, 3766 (1965).

2) M. A. M. Boersma, "Catal. Rev. Sci. Eng.," ed by H. Heinemann and J. J. Carberry, Marcel Dekker, New York (1974), Vol. 10, p. 243.

3) M. A. M. Boersma, "Advanced Materials in Catalysis," ed by J. J. Burton and R. L. Garten, Academic Press, New York (1977), p. 67.

4) K. Watanabe, T. Kondow, M. Soma, T. Onishi, and K. Tamaru, *Proc. Roy. Soc., Ser. A*, **333**, 5 (1973).

5) S. Tsuchiya, A. Fukui, A. Hara, and H. Imamura, Proc. 8th Inter. Congr. Catal., West Berlin, 1984, Abstr., Vol. IV, p. 635.

6) S. Tsuchiya, K. Konishi, T. Kawashita, and H. Imamura, Bicentenary Catalysis-1988, Australia, Sydney, 1988, Abstr., p. 93.

7) e. g. E. Kikuchi, T. Matsuda, H. Fujii, and Y. Morita, *Appl. Catalysis*, **11**, 331 (1984).

8) A. Takemoto and Y. Mizutani, *Nippon Kagaku Kaishi*, **1983**, 1124.

9) "API 44 Tables. Selected Values of Properties of Hydrocarbons and Related Compounds," American Petroleum Institute Research Project 44, Thermodynamics Research Center, Texas A & M University, 1981 (final correction).

Photofading Reaction of Bis[1-(4-dimethylaminophenyl)-2-phenylethanedithione]nickel(0) in the Presence of *N,N'*-Dimethylformamide

Koe ENMANJI* and Kenzou TAKAHASHI
The Materials and Electronic Devices Laboratory, Mitsubishi Electric Co.,
Tsukaguchi-Honmachi, Amagasaki 661
(Received September 11, 1990)

Synopsis. Bis[1-(4-dimethylaminophenyl)-2-phenylethanedithione]nickel(0) was found to undergo photofading in the presence of dimethylformamide, by the action of photogenerated superoxide. Addition of a detergent suppressed the formation of superoxide, with an efficiency paralleling the fatty acid chain length.

We previously found that bis[1-(4-dimethylaminophenyl)-2-phenylethanedithione]nickel(0) (BDN), a Q-switch dye for neodimium laser was bleached in the presence of peroxide compounds[1] presumably via oxidation of BDN by peroxide. This bleaching was inhibited by inclusion of BDN into β-cyclodextrin.[1] BDN was also faded under darkness in the presence of *N,N'*-dimethylformamide (DMF).[2] In this case, BDN was reduced to its anion radical and the fading was not inhibited by inclusion into cyclodextrin but rather promoted in its presence.[3]

In addition we found that the reductive fading of BDN was promoted by illumination in the presence of DMF, and the mechanism of this reaction is the subject of the present work. Photo-generation of superoxide was expected to be the main cause as in the photofading of other dyes.[4,5] The authors incidentally found that singlet oxygen generation was inhibited by addition of a detergent in a Methylene Blue aqueous solution.[6] In view of this, the effect of detergents was also examined in the present BDN–DMF system.

Experimental

BDN was purchased from Kodak Co., and DMF, toluene, adrenalin, sodium dodecyl sulfate (SDS), sodium octyl sulfate (SOS), and sodium hexadecyl sulfate (SCS) were obtained from Nakarai Chemical Co.

Electronic spectra were measured with a Shimadzu spectrophotometer MPS-5000. The photochemical reaction system was illuminated with an Ushio high-pressure mercury lamp Model 500 equipped with a Toshiba VY-50 filter.

The photofading rate was estimated by the photodecoloration ratio, r, defined by

$$r = \frac{OD^0 - OD}{OD^0} \quad (1)$$

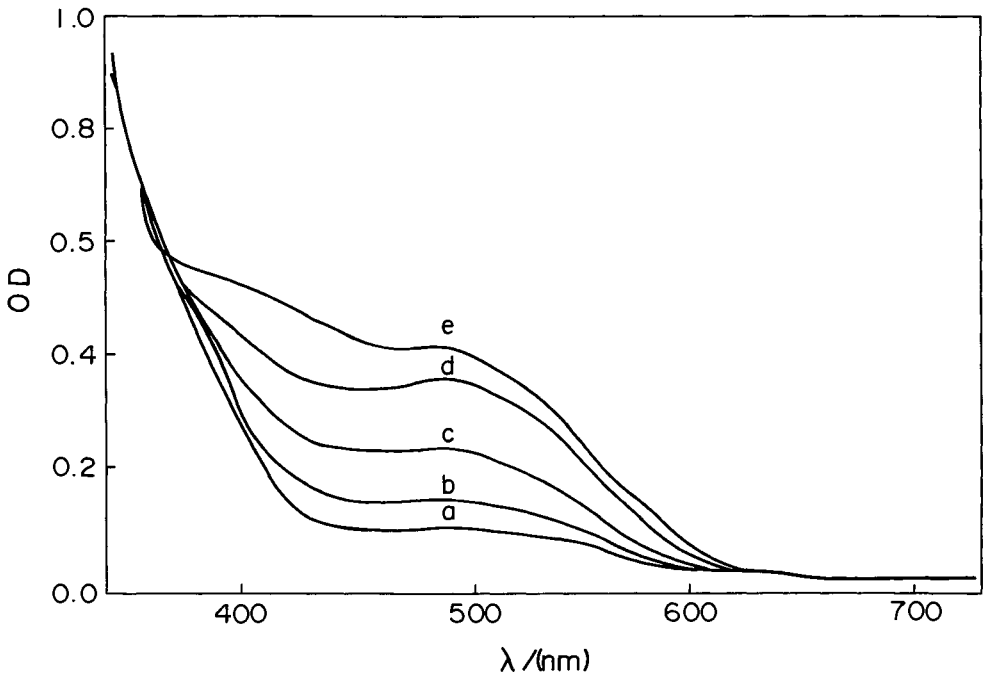

Fig. 1. Photooxidation of adrenalin to adrenochrome. [DMF]=5 mol dm^{-3}, [BDN]=10^{-5} mol dm^{-3}, [Adrenalin]=50 mmol dm^{-3}, I=69.4 mW cm^{-2}. a: 0 min, b: 15 min, c: 30 min, d: 45 min, e: 60 min.

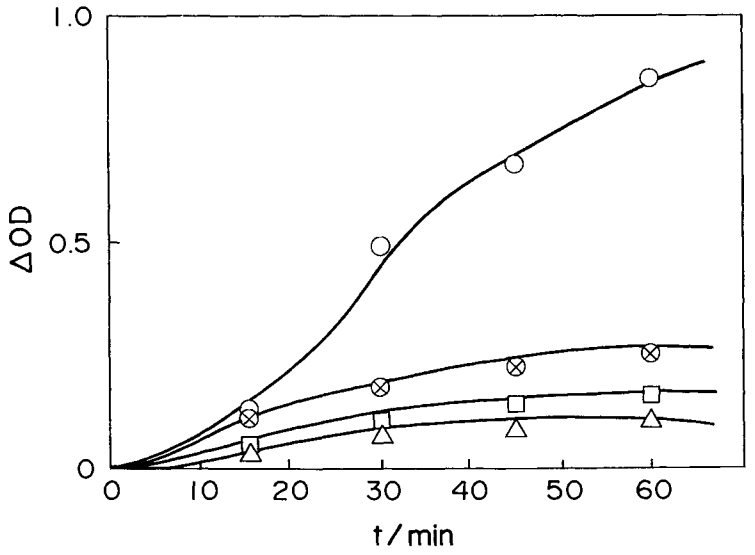

Fig. 2. Effect of detergents on the oxidation rate of adrenalin to adrenochrome. —○—: BDN alone, —⊗—: sodium octyl sulfate, 10^{-2} mol dm^{-3}, —□—: sodium dodecyl sulfate, 10^{-2} mol dm^{-3}, —△—: sodium hexadecyl sulfate, 10^{-2} mol dm^{-3}.

where, OD^0 and OD are the optical density at 1100 nm before illumination and that after t-min illumination, respectively.

Results and Discussion

In darkness BDN fades in DMF via the formation of its anion radical. Illumination in DMF accelerated this reaction yielding the same product, BDNH, as in the fading in darkness. This was ensured by observing a common R_f value (0.79) of the product by alumina thin layer chromatography (TLC), with DMF : toluene : methanol=1 : 0.75 : 1 as developer.

The generation of superoxide in this reaction system was suggested by the oxidative conversion of adrenalin to adrenochrom exihibiting an absorbance maximum at 490 nm (Fig. 1).[7] The following result also indicates the existence of superoxide. The photodecoloration ratio (r) of BDN in a DMF–water system ([DMF]=5 mol dm^{-3}) was 0.065 at 10-min illumination. The value of r was 0.000 in the presence of 75000 units superoxide dismutase, which is a good quencher of superoxide.

It was found that r of BDN was proportional to both the DMF concentration and the light intensity.

The maximum wavelength in the action spectrum of the BDN photofading was estimated to be about 300 nm, through experiments with a series of cutoff filters.

As in other photolysis systems[4,5] the following reaction sequence appears to hold for the present system.

$$\mathrm{BDN} \xrightarrow{h\nu} {}^1\mathrm{BDN} \quad (2)$$

$${}^1\mathrm{BDN} \longrightarrow {}^3\mathrm{BDN} \quad (3)$$

$${}^3\mathrm{BDN} + \text{solvent} \longrightarrow \mathrm{BDN}^{+}\cdot + \mathrm{e(solvent)} \quad (4)$$

$$\mathrm{BDN}^{+}\cdot + \mathrm{e(solvent)} \longrightarrow \mathrm{BDN}\cdot + \text{solvent} \quad (5)$$

$$2\mathrm{BDN}\cdot + \mathrm{H_2O} \longrightarrow \mathrm{BDNH} + \mathrm{BDN}^{+}\cdot + \mathrm{OH}^{-} \quad (6)$$

$$\mathrm{e(solvent)} + \mathrm{O_2} \longrightarrow \mathrm{O_2}^{-}\cdot + \text{solvent} \quad (7)$$

This scheme is supported by the identifying BDNH as a final product by TLC. This compound may be an anion radical of BDN.

To estimate the rate of superoxide penetration through the micellar layer of a detergent, as in the case of singlet oxygen in Methylene Blue–detergent system, the effect of detergents to the BDN system on the oxidation of adrenalin to adrenochrome was investigated in the presence of a small amount of DMF. As seen in Fig. 2, the rate of adrenalin oxidation is in order SOS>SDS>SCS. Probably superoxide is generated in the center of micelles containing BDN molecules, and the triplet ground state oxygen is supplied sufficiently through the micelle membrane. The generated superoxide penetrates through the micelle membrane but it may disappear partly in the course of this penetration. When the micellein membrane is thicker, namely the fatty acid chain of detergent is longer, the disappearing fraction of superoxide is larger and hence the oxidative adrenalin-to-adrenochrome conversion is less efficient. The results in Fig. 2 are in line with this speculation.

References

1) K. Enmanji and H. Yamaguchi, *Nippon Kagaku Kaishi*, **1985**, 128.
2) K. Enmanji, *Nippon Kagaku Kaishi*, **1985**, 2094.
3) K. Enmanji, *Bull. Chem. Soc. Jpn.*, **60**, 3087 (1987).
4) N. Kuramoto and T. Kitao, *J. Soc. Dyers Colour.*, **98**, 159 (1982).
5) N. S. Allen, *Dyes Pigm.*, **2**, 31 (1976).
6) K. Enmanji, K. Takahashi, and K. Nomura, *Nippon Kagaku Kaishi*, **1990**, 1315.
7) H. P. Misra and I. Fridovich, *J. Biol. Chem.*, **247**, 3170 (1972).

Belousov-Zhabotinskii Reaction with 2,3-Diones

Masao TSUKADA* and Naoki INAMOTO
Department of Chemistry, Juntendo University, Inba-gun, Chiba 270-16
(Received September 13, 1990)

Synopsis. 2,3-Butanedione and 2,3-pentanedione have been found to generate chemical oscillations in 2,3-dione/BrO_3^-/Ce^{4+}/H_2SO_4 system. The concentration range within which the oscillatory behavior can be observed for each reactant is reported.

The Belousov-Zhabotinskii(BZ) reaction is probably the best studied chemical oscillation reaction.[1] In BZ reaction, malonic acid is oxidized by bromate ions in sulfuric acid medium in the presence of cerium(IV) ions. After an induction period, the concentration of bromide ions and the redox ratio (=log [Ce^{4+}]/[Ce^{3+}]) oscillate with a frequency and an amplitude which depend on the initial composition of system and temperature. It has been known that cerium(IV) ion, malonic acid, and sulfuric acid in this oscillating system may be replaced by the other appropriate compounds. Most of the organic species capable of replacing malonic acid contain an "active" methylene group. The use of acetone alone as the substrate does not yield any oscillations, but generates oscillations in mixed-substrate BZ systems.[2] We have examined the effects of replacing malonic acid with 2,3-butanedione or 2,3-pentanedione which is of interest in a similarity to acetone.

Experimental

All reagents used were the highest grade commercially available except for 2,3-butanedione which was purified by vacuum distillation. The redox potential was monitored with a platinum electrode. A double junction Hg/Hg_2SO_4/K_2SO_4 electrode was used as a reference. In most experiments, the reaction was performed in a glass container with magnetic stirrer under aerobic conditions.

Results and Discussion

Typical responses of platinum and bromide selective electrodes in the dione/BrO_3^-/Ce^{4+}/H_2SO_4 system are shown in Figs. 1 and 2 along with the oscillations of the malonic acid system for a comparison. In the case of diketone system its oscillatory state consists of a dozen oscillations, while in the malonic acid substrate its oscillation continues for about three hours. On comparing the two systems, each level of bromide ion concentrations overlaps with the other, although the oscillation range of redox potential is considerably different. It has been shown that bromide ion concentration plays a vital role in the BZ system.[1] Thus it could be suggested that dione substrate plays a similar role to malonic acid. There was no gas evolution

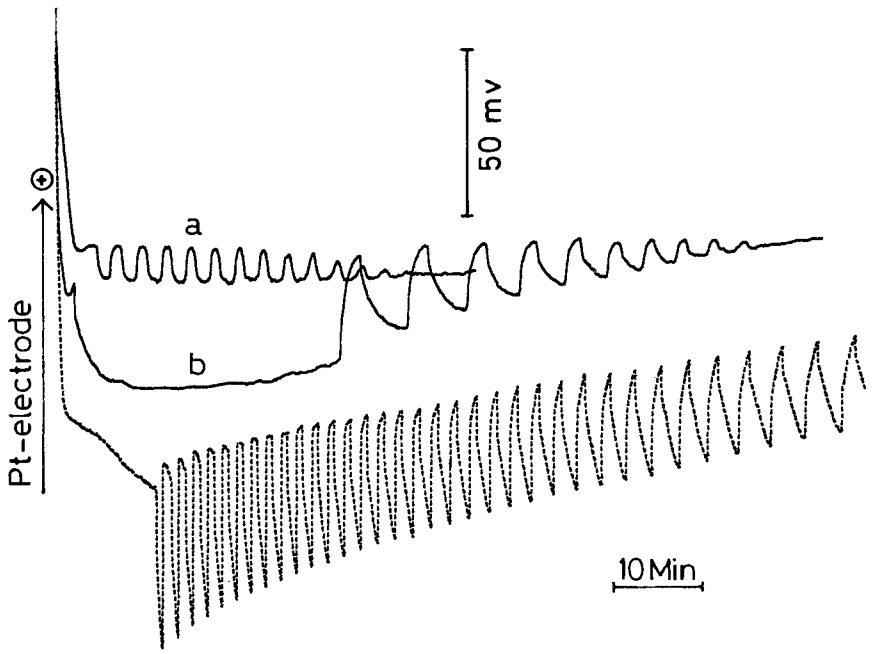

Fig. 1. Uncalibrated potential of platinum electrode in the system of following initial composition: 0.0014 M $Ce(SO_4)_2$, 0.14 M $KBrO_3$, 0.74 M H_2SO_4, and 0.032 M organic substrate. Full curve: (a) 2,3-butanedione, (b) 2,3-pentanedione; dotted curve: malonic acid. At 30 °C. The arrow indicates the direction in which the potential becomes more positive. M= mol dm^{-3}.

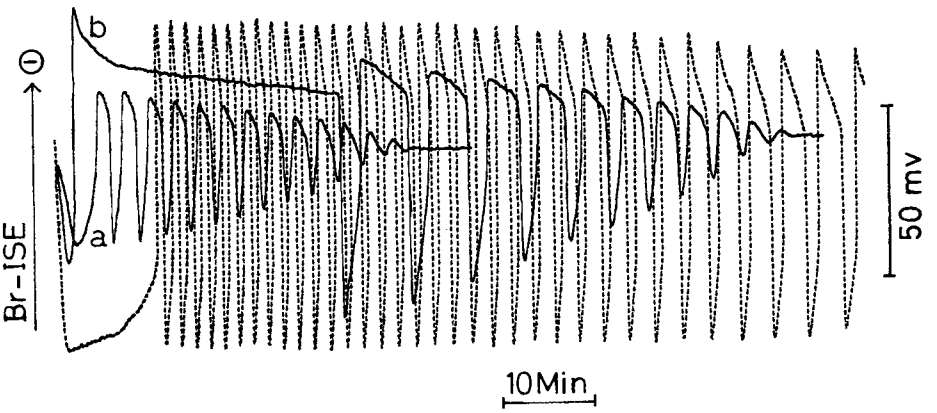

Fig. 2. Uncalibrated potetial of bromide-selective electrode (Br-ISE) in the same system as that in Fig. 1. The arrow indicates the direction in which the potential becomes more negative.

Table 1. Conditions for Oscillating Reaction[a)]

	2,3-Butanedione	2,3-Pentanedione
[Dione]/10^{-2} M	2.3 —3.8	1.3 —5.1
[H_2SO_4]/M	0.69—0.81	0.64—1.1
[$KBrO_3$]/M	0.13—0.15	0.12—0.19
[$Ce(SO_4)_2$]/10^{-3} M	0.84—2.0	0.28—3.4
Temp/°C	29—33	28—40

a) M=mol dm^{-3}.

during the oscillating reaction. In view of this fact, 2,3-dione behaves in a similar fashion to 2,4-pentanedione.[3)]

Chemical oscillations were observed in a definite range of initial concentrations for the four components, $KBrO_3$, $Ce(SO_4)_2$, H_2SO_4, and dione. We adopted the concentrations used for the reaction shown in Fig. 1 as a standard condition. The range of concentrations is shown in Table 1 where the concentration of one of the four components was varied under the fixed concentrations of the other three components at the standard condition. It is remarkable that the concentration range in which oscillations appear is very narrow for both $KBrO_3$ and H_2SO_4 in the case of 2,3-butanedione.

The induction period (t_{ind}) and the period of oscillation(t_{osc}) varied with temperature. The plots of log ($1/t_{ind}$) and of log ($1/t_{osc}$) were linear with inverse of absolute temperature in the range shown in Table 1. The values of two activation energies, E_{ind} and E_{osc} which correspond to t_{ind} and t_{osc} respectively, were found to be 68±6 and 69±8 kJ mol^{-1} for 2,3-butanedione, 67±9 and 71±7 kJ mol^{-1} for 2,3-pentanedione. E_{osc} can be attributed to the reduction reaction of BrO_3^- with brominated substrate which requires an activation energy between 60 and 70 kJ mol^{-1}.[4)] The value of E_{osc} obtained by us lies in this range.

The induction period depends on the concentrations of dione and of Ce^{4+}, but it is not affected by the concentrations of BrO_3^- and of H^+. This means that the reaction of dione with Ce^{4+} is closely related to the induction period. It has been found that acetone does not yield oscillations when acetone is used alone in the cerium(IV) ion catalyzed BZ system, because acetone can be brominated but is not oxidized.[5)] In the case of dione, it could form a five-membered chelate ring by the coordination of Ce^{4+} with its two carbonyl groups and the complex thus formed would initiate oxidation of dione.

It has been known that mechanical stirring can, in some cases, sensibly affect the oscillation.[6)] For example, in the case of malonic acid substrate system, the oscillations stop suddenly without a change of amplitude when the stirring rate rises more than a threshould and immediately start again when the stirring rate falls below the threshold. In the dione system, more rapid stirring than a threshold resulted in termination of the oscillations, but a switch to slow stirring did not cause the oscillation again. It was also observed that the addition of dione after damping of the oscillations does not regenerate the oscillations, but that under nitrogen atmosphere the addition of dione cause the oscillations again. It would be sure that some mechanical stirring effects are attributed to an increased oxygen transfer into the system. Thus the results suggest that some reaction products formed by oxygen inhibit the oscillation.

Further detailed studies on the mechanism in this system are in progress.

References

1) R. J. Field and M. Burger, "Oscillations and Traveling Waves in Chemical Systems," John Wiley & Sons, New York (1985).
2) Z. Noszticzius, *Magy. Kem. Foly.*, **85**, 330 (1979).
3) E. J. Heilweil, M. J. Henchman, and I. R. Epstein, *J. Am. Chem. Soc.*, **101**, 3698 (1979).
4) M. Burger and E. Körös, *J. Phys. Chem.*, **84**, 496 (1980).
5) R. M. Noyes, *J. Am. Chem. Soc.*, **102**, 4644 (1980).
6) V. J. Farage and D. Janjic, *Chimia*, **34**, 342 (1980).

Mixture Dependences of OH($^2\Sigma$) Produced in the Oxidations of C_2H_2 and C_2H_6 in Shock Waves

Tohru KOIKE
Department of Chemistry, National Defense Academy, Hashirimizu, Yokosuka 239
(Received October 17, 1990)

Synopsis. The OH($^2\Sigma$) emissions from shock-heated mixtures of C_2H_2/O_2, $C_2H_2/C_2H_6/O_2$, and C_2H_6/O_2 diluted in Ar were observed and the mixture dependences of the emissions were obtained. OH($^2\Sigma$) production, depending on the test gas mixture, could be in accordance with the view-point that the two oxidations of C_2H_2 and C_2H_6 progress by influencing each other.

The reaction on OH($^2\Sigma$), hereafter abbreviated as OH*, at high temperatures (above 1000 K) has been studied for many reaction systems using shock-tube techniques.[1,2] As for OH* in hydrocarbon oxidation, only single hydrocarbon/O_2 systems, excepting multi-hydrocarbon/O_2 systems, have been investigated.[3]

The temperature reached by hydrocarbon combustion is high due to their large exothermicity. The hydrocarbons used for fuels therefore decay to smaller species, thermally, as well as by oxidation processes. Acetylene is one of the primary products given by such thermal decay. Thus, at high temperatures acetylene could be present from the beginning of combustion; hydrocarbon combustion seems to proceed by self decay, as mentioned above, influenced by acetylene combustion.

We paid attention to the OH* produced in a C_2H_2+C_2H_6 systems, studying it in comparison with those in the C_2H_2 and C_2H_6 systems. The time parameters and intensities of OH* emission were investigated in relation to the test gas compositions used. The production of OH* could be understood by considering that the two oxidations of C_2H_2 and C_2H_6 progress by influencing each other.

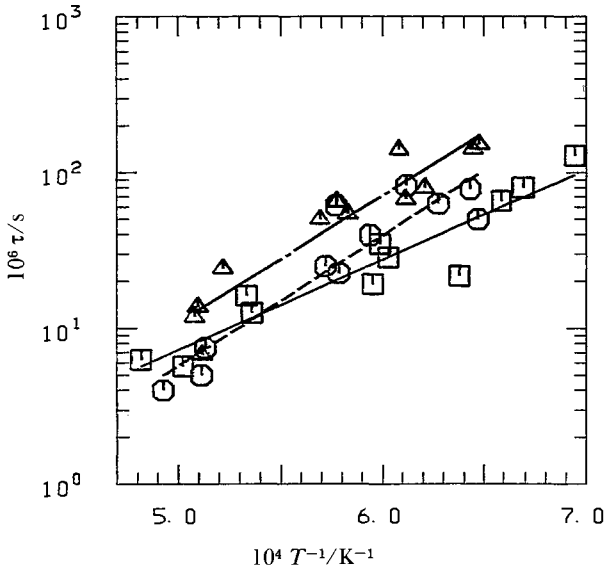

Fig. 1. Induction times, τ, vs. $10^4/T$. Symbols used are; □: $C_2H_2/O_2/Ar$=1/2.5/96.5, ○: $C_2H_2/C_2H_6/O_2/Ar$=1/1/6/92, △: $C_2H_6/O_2/Ar$=1/3.5/95.5. Lines through each data point show least squares fit.

Experimental

The rectangular shock tube used in the present study for incident shock waves was detailed in previous papers.[3,4]

OH* emission at 306.4 nm was observed using a monochromator (Jarrell-Ash, JE-25) and a photomultiplier (Hamamatsu, R-208). The output signal of the photomultiplier was fed into an operational amplifier and then recorded on a digital-oscilloscope (Iwatsu, DS-6121).

The purities of the element gases used for the test gas were; C_2H_2, 99.5% pure; C_2H_6, 99.3% pure; O_2, 99.999% pure; and Ar, 99.999% pure. The compositions of the test gas mixture are shown in the footnote of Fig. 1.

Results and Discussion

The obtained oscillograms show that after shock arrival at the observation window of the shock tube, OH* emission can not be observed for a reaction period (induction time), but increases abruptly to a maximum value and finally decays. Although the time profile and intensity of OH* emission changes depending on the temperature and the test gas mixture examined (as shown below), such profiles of OH* emission are common for the three mixtures, as well as for other hydrocarbons.[1,3]

We evaluated three parameters from these oscillograms: (1) induction time(τ),[3] (2) reaction time at which the emission intensity reaches a miximum (t_m), (3) the maximum emission intensity (I_m).[3] The time parameters, τ and t_m, were evaluated on the laboratory time base. The I_m values are proportional to [OH*].

Figure 1 shows the relation between τ and $10^4/T$. Except for high temperatures (around 2000 K), the dependence of τ on the test gas mixture was found to be $\tau(C_2H_6)>\tau(C_2H_2+C_2H_6)>\tau(C_2H_2)$, where the species in parenthes identifies the hydrocarbons contained in the test gas mixtures used. Such a mixture dependence on τ is in accord with the experimental results reported for both C_2H_2 and CH_4 oxidation:[3,5] that $\tau(CH_4)>\tau(C_2H_2+CH_4)>\tau(C_2H_2)$. Since C_2H_2 and CH_4 oxidation was confirmed to progress by influencing each other in a C_2H_2+CH_4 mixture,[5] in a C_2H_2+C_2H_6 mixture the C_2H_2 and C_2H_6 oxidation are also expected to proceed similarly and to affect the production of OH*.

It should be pointed out here that the values of τ evaluated at high temperatures are not accurate as those evaluated at lower temperatures, since τ at high temperatures becomes small and is hard to estimate from each oscillogram with sufficient precision. In contrast to such a time parameter as τ, both the t_m and

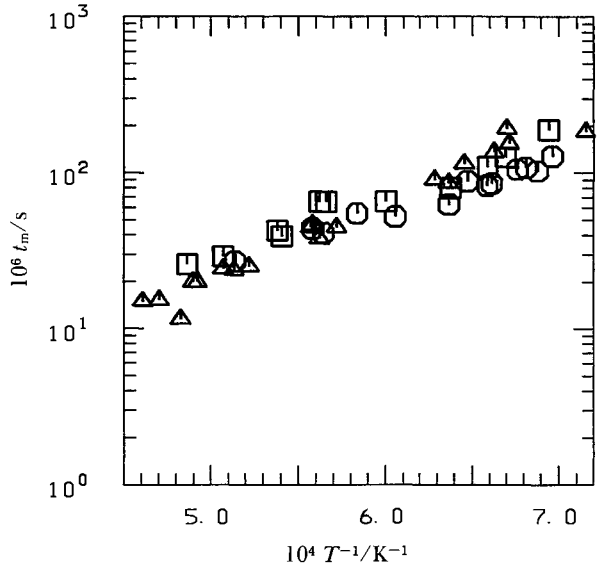

Fig. 2. Reaction times, t_m, vs. $10^4/T$. Symbols used are the same as those in Fig. 1.

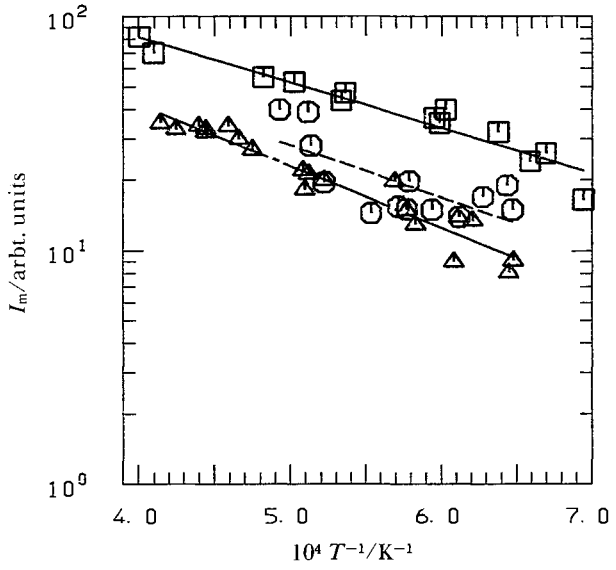

Fig. 3. Maximum emission intensity, I_m, vs. $10^4/T$. Symbols used are the same as those in Fig. 1.

I_m values could be evaluated precisely even at high temperature.

Figure 2 shows the relation between t_m and $10^4/T$. The difference of the t_m values between the three mixtures is not so clear and, thus, the influential relation between C_2H_2 and C_2H_6 oxidation to produce OH* seems to proceed much more.

Figure 3 shows the relation between I_m vs. $10^4/T$. In accordance with the former experimental results regarding I_m for C_2H_2 and CH_4 oxidation,[3] that $I_m(C_2H_2)>I_m(CH_4)$, the mixture dependence $I_m(C_2H_2)>I_m(C_2H_6)$ can be seen. If C_2H_2 and C_2H_6 oxidation could progress independently in a C_2H_2+C_2H_6 mixture, the relation $I_m(C_2H_2+C_2H_6)\approx I_m(C_2H_2)+I_m(C_2H_6)$ would be expected, since t_m is almost same for all three mixtures. The result is that the $I_m(C_2H_2+C_2H_6)$ values lie between those in the other two mixtures.

Taking into account the temperature dependences of the time parameters, τ and t_m, and the I_m values, the production of OH* can be seen to proceed rapidly and violently at high temperature. Such results may support the viewpoint that the difference in the heat of combustion between the two oxidations affects the production of OH* much more than does the difference of the generated radicals between them. As for the reaction temperature in the C_2H_2+C_2H_6 mixture, it must reach the highest value among the three mixtures, and the observed I_m values in the mixture could be largest. The result shown in Fig. 3 does not seem to be in accord with these hypotheses. Therefore, it can be concluded that in OH* production the two oxidations of C_2H_2 and C_2H_6 in the C_2H_2+C_2H_6 mixture proceed with any influence other than the thermal effect.[5] Such influences could arise due to chemical coupling of the generated radicals in each oxidation.

It is also informative regarding the existence of chemical coupling that the time variation of OH* emission is also very smooth in a test gas mixture of C_2H_2+C_2H_6. If C_2H_2 and C_2H_6 oxidation could proceed independently, two peaks of maximum emission, attributed to the two oxidations, should appear.

Although the producing step of OH* in hydrocarbon oxidation is still controversial, the fate of OH* is mentioned here briefly. If OH* is produced by the process CH+O_2=OH*+CO, as proposed by Gaydon,[6] the I_m values should be proportional to the concentration product of [CH][O_2].[1,3] It was, however, found that the I_m does not increase simply with increasing [O_2] in the mixture used. We can thus say that the producing step of OH* depends greatly on the value of [CH].

Shock tube studies concerning the production of OH* in other hydrocarbon mixtures are in progress and the results may appear elsewhere.

The present author wishes to thank Professor Kihei Morinaga, National Defense Academy, for many helpful discussions and also the reviewer for a comment on the OH* production in the present reaction system.

References

1) W. C. Gardiner, Jr., W. G. Mallard, K. Morinaga, D. L. Ripley, and B. F. Walker, 11th. Int. Symp. Combust., The Combustion Institute, Pittsburgh (1967), p. 1151.

2) Y. Hidaka, H. Takuma, and M. Suga, *J. Phys. Chem.*, **89**, 4903 (1985).

3) T. Koike and K. Morinaga, *Memoirs of the National Defense Academy*, **29**, 59 (1989), and references therein.

4) T. Koike and K. Morinaga, *Bull. Chem. Soc. Jpn.*, **49**, 1457 (1976).

5) K. S. Krishnan, R. Ravikumar, and K. A. Bhaskaran, *Combust. Flame*, **49**, 41 (1983).

6) A. G. Gaydon, "The Spectroscopy of Flames," Wiley, New York (**1957**).

Infrared Spectra of SiO_2 Coating Films Prepared from Various Aged Silica Hydrosols

Masaaki MUROYA
Osaka Electro-Communication University, 18-8 Hatsu-cho, Neyagawa, Osaka 572
(Received October 18, 1990)

Synopsis. Measurements have been made of the vibrational absorption bands of silica films. The results have been used to examine the importance of the polymerization of silica. Seven other absorption bands, which are related to the Si-O group, were clearly found in the region from 1300 to 400 cm^{-1}. A band at a wave number of 1069 cm^{-1} increased with increasing the viscosity of the hydrosol. The band at 974 cm^{-1} was substantially sensitive in intensity to the heat-treatment and the rehydration of silica film, can be assigned to the Si-O stretching vibration of the surface silanol since the intensity of its band is influenced by both the heat-treatment(dehydration) and rehydration.

It has been indicated by several workers[1-4] that silica-coating films can be prepared using several methods. Such silica films have been convenient for investigating the surface properties of silica, and may also be suitable for controlling the transmittance and refractive index in optics materials. It is known that the surface silanols on silicas, such as silica gel, pyrogenic silica and porous glass, play a central role as the active center regarding the adsorption properties, ion-exchange in solutions containing some cations, and surface modification of their materials using surface reactions.[5] Examinations using infrared spectroscopy have proved to be among the most effective means to investigate the bond nature of surfaces and substrate structures in materials.[6] The infrared spectra of such surface-active materials as silicas were normally taken in vacuo since the surface silanol is sensitive to the moisture in air, and the clearness of the spectrum is dependent on the sample preparation for infrared experiments.[7,8] The infrared spectra of the silicas can be clearly measured in the range of about 4000 to 3000 cm^{-1}, the wave number region of which corresponds to the stretching vibration of the O-H in surface silanols and the adsorbed water on such materials.[7] Indistinct spectra were found for the silicas when infrared measurements were carried out over a range of about 2000 to 400 cm^{-1}. This is due to the intense absorption efficiency of silica in this region. However, it could be expected that the problem has been solved by using silica films.

In order to understand the polymerization process of silica in its hydrosol stage, we measured the FT-IR spectra of silica films which were prepared by ageing the silica hydrosol obtained from the hydrolysis of tetraethyl orthosilicate. Moreover, the relationship between the formations of siloxane and the surface silanol and the remarkable feature of absorption bands is discussed in this report.

Experimental

Silica hydrosols were prepared by the hydrolysis of tetraethyl orthosilicate.[7] In this work, solutions of redistilled tetraethyl orthosilicate, ethyl alcohol, and distilled water adjusted to pH 2 by using a hydrochloric acid were mixed in volume ratio, $Si(OC_2H_5)_4$: C_2H_5OH: H_2O=5: 1: 0.5, and then heated at 65 °C for 60 min. After its sol had formed, the hydrolsol was allowed to stand for a long time at room temperature in air; that is, the hydrosol aged with the elapse of time. Metal plate (20×30 mm wide and 0.3 mm thickness), which is stainless steel (SUS 304) pretreated before use, was steeped in such hydrosol for 30 min in air, at a relative humidity of about 50%; its plate was then pulled from the hydrosol at a rate of 1.0 mm s^{-1} and dried at 170 °C for 1 h in air. A filmy specimen with the hues of a rainbow and about 0.9μm thickness, was obtained from the procedures mentioned above. For a pretreatment, the metal plate was immersed into a 2% NaOH solution, washed with distilled water, steeped in acid adjusted with sulfuric acid at 10%, washed with distilled water, and dried at 110 °C for 1 h. A Japan Spectroscopy Co. 5MP FT-1R spectrometer was used for the measuring on the silica films, spectra of which were taken with a polarizing reflection technique.[8]

Results and Discussion

Figure 1 shows the infrared absorption spectra of the silica coating films obtained from various ageing of the hydrosol. A number of absorption bands were found in the range from about 4300 to 400 cm^{-1}. A broad absorption band ranging from 3800 to 3000 cm^{-1}, which was ascribed to the O-H stretching vibration mode,[7,9] was found in a specimen aged for 1536 h. The intensity of this band depended on the time required for ageing. A few absorption bands around 2900 and 1400 cm^{-1}, which were assigned to C-H stretching and deformation vibrations, changed in intensity as a function of the ageing period. It can therefore be understood that the formation of the OH radical and the alkylation occurred at the same time on the surface of particles and that the contents of their chemical species in the films were dependent on the ageing. The very weak band at the water-bending vibration is ascribed to adsorbed water, since the band appeared at its wave number when the specimen was exposed to water vapor. The very strong bands at 1215 and 1069 cm^{-1} can be assigned to the asymmetrical stretching vibration of SiOSi in the layer structure of silica[10,11] and of the ≡Si-O-Si≡ bridge which is formed between particles or small spherical polymer, since the intensity of the band is enhanced with increased ageing with the elapse of time. The assignments of these bands are not in agreement with those found in the literature.[12] These bands were also indicated by Hino et al.,[13] the wave numbers of their bands are not clear due to an overlap of these bands as a result of the high concentration of Si-O species in a disordered structure. The specimens used in the literature[12,13]

were of the silica xerogel, which consist of a rigid three-dimentional network of contiguous particles of colloidal silica; in the filmy silica used in this study it is quenched during the early or middle stage of polymerization. In the later case, when polysilicic acid is formed at low pH (the pH value of the present sol was about 2.8), polymer particles are formed, and the polymerization is sufficiently slow to allow the early stage. When the particles are not charged, they link together into branched chains to form three-dimension network regions in the sol. Such a polymerization process can be followed by taking the spectra of skeletal vibrations of filmy silica prepared from the sol. In a previous study,[8] it was suggested that the 1069 cm^{-1} band is mainly related to polymerization. Actually, the intensity of this band was substantially

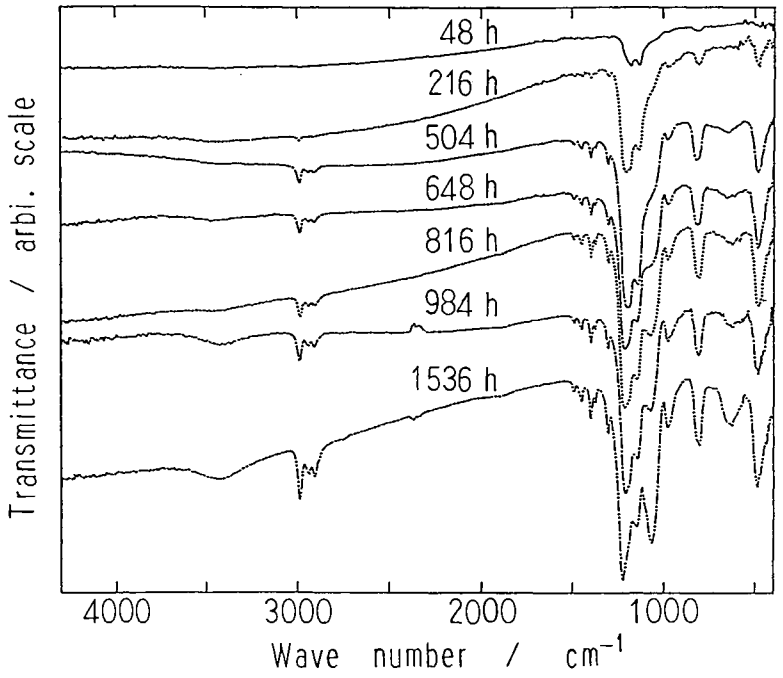

Fig. 1. Spectra of the silica films prepared from the silica hydrosol.

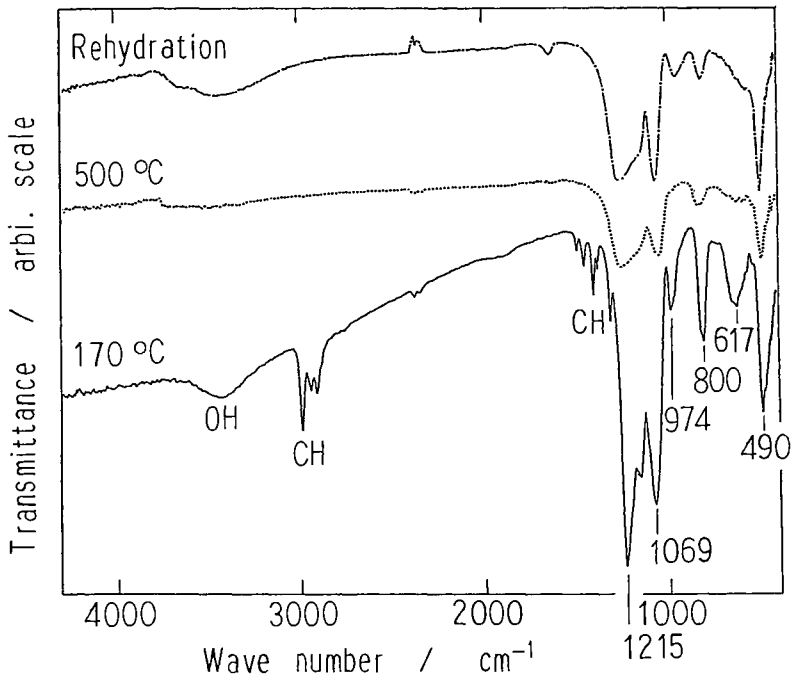

Fig. 2. Spectra of the silica films heat-treated at 500 °C in air and rehydrated with saturated water vapor after its heat-treatment.

sensitive to the elapse of time, as can be seen in Fig. 1. It is therefore thought that a measurement of the intensity change of such a band can be used as an indication of the polymerization rate.

In order to determine the nature of the bands in the lower wave number region of about 1000 to 400 cm^{-1}, a heat-treatment and rehydration experiments were performed on film specimens; their spectra are shown in Fig. 2. When heating a specimen at 500 °C for 1 h in air, both the O–H and the C–H bands disappeared, and the bands at 974 and 617 cm^{-1} also faded out. It is known that the 974 cm^{-1} band weakens as Si–OH groups condense to form Si–O–Si bands.[12,13] When such a specimen is exposed to saturated water vapor, a band at 974 cm^{-1} is recovered and, of course, the O–H stretching broad band at about 3800—3000 cm^{-1} is also observed, though the band at 617 cm^{-1} and the C–H vibration bands are not restored. These results indicate that the bands at 974 and 617 cm^{-1} can be assigned to the Si–O stretching vibration of the silanol and the absorption band related to the C–H vibration, respectively. The assignment of the 974 cm^{-1} band is in good agreement with values found in literature.[12,13] Though the sharp bands at about 800 and 490 cm^{-1} are not clear regarding their origins, they are probably associated with the typical structure of four-coordinate silica.

Stable silica films were formed on a metal plate surface by a dip-coating method from the silica hydrosol obtained from the hydrolysis of tetraethyl orthosilicate. The FT-IR spectra were measured on those films. Two remarkable bands were found at 1069 and 974 cm^{-1}. Among them, the band at 1069 cm^{-1}, which can be assigned to the stretching vibration of the ≡Si–O–Si≡ bridge, is related to the polymerization of silica particles, by which smaller molecular units are linked together into large ones. On the other hand, the band at 974 cm^{-1} is assigned to Si–O stretching vibration of the silanol and in sensitive to a thermal treatment and the rehydration.

References

1) H. Schroder, "Physics of Thin Films 5," Academic Press, New York (1969), p. 87.
2) M. Nogami and Y. Moriya, *Yogyo Kyokai Shi*, **85**, 448 (1971).
3) Y. Yamamoto, K. Kamiya, and S. Sakka, *Yogyo Kyokai Shi*, **90**, 328 (1982).
4) M. Murakami, K. Izumi, T. Deguchi, A. Morita, N. Toge, and T. Minami, *Nippon Seramikkusu Kyokai Gakujutsu Ronbunshi*, **97**, 91 (1988).
5) R. K. Iler, "The Chemistry of Silica," John Wiley, New York (1979).
6) A. V. Kiselev and V. I. Lygin, "Infrared Spectra of Surface Compound," John Wiley, New York (1975).
7) S. Kondo, M. Muroya, and K. Fujii, *Bull. Chem. Soc. Jpn.*, **47**, 553 (1974).
8) M. Muroya, S. Yasuda, and K. Yaguchi, *Shikizai Kyokaishi*, **63**, 251 (1990).
9) M. Muroya and S. Kondo, *Shikizai Kyokaishi*, **55**, 374 (1982).
10) B. D. Saksena, *Trans. Faraday Soc.*, **57**, 242 (1961).
11) A. M. Prima, *Opt. Spectrosc.*, **9**, 236 (1961).
12) T. Takamura, H. Yoshida, and K. Inazuka, *Kolloid Z. Z. Polym.*, **195**, 12 (1963).
13) M. Hino and T. Sato, *Bull. Chem. Soc. Jpn.*, **44**, 33 (1971).

Mass Spectral Study of Ionized-Hydroxyacetone Dissociation

Ryuichi ARAKAWA
College of Biomedical Technology, Osaka University,
1-1, Machikaneyamacho, Toyonaka 560
(Received November 13, 1990)

Synopsis. The ionization and appearance energies of hydroxyacetone (CH_3COCH_2OH) were obtained. The metastable dissociation of ionized hydroxyacetone involves the loss of a hydrogen atom and CHO. The results of the metastable-ion intensity and collisional activation indicate that the hydroxyacetone ion does not isomerize to the enol tautomers prior to dissociation.

The unimolecular gas-phase chemistry of ions containing oxygen atoms, such as $C_3H_6O_2^{+\cdot}$ isomers,[1-7] is usually complex in a multistep isomerization/dissociation pattern. Interest has been directed toward determining the configuration of the reacting precusor or the key intermediate. Recently, distonic ions in which the charge and radical sites are separated and/or the ion-dipole complexes have been shown to be the reacting precursor from collisional activation (CA) experiments and theoretical calculations. For instance, in an *ab initio* calculation of ionized methyl acetate,[4] a hydrogen-bridged radical ion/dipole complex, $[CH_3CO\text{–}H\text{–}OCH_2]^{+\cdot}$, is probably a precursor ion which decomposes to the observed $CH_3CO^+ + \cdot CH_2OH$. In the case of ionized propanoic acid, a deuterium-labeling experiment[5] and metastable ion fragmentation[7] indicated that a water-loss reaction involves isomerization to an enol form prior to dissociation. The enol form was found to be ca. 1 eV more stable than the corresponding keto form.

Some of the $C_3H_6O_2^{+\cdot}$ isomers show metastable dissociation, although the activation energy is less than 1 eV. Observation of a metastable ion requires a rate in the $10^5\,s^{-1}$ range. However, the predicted RRKM rate is much greater than $10^7\,s^{-1}$. One explanation for this problem is that the reaction involves isomerization to an energetically stable isomer prior to dissociation. The dissociation of this isomer is a rate-determining step.

The dissociation of ionized hydroxyacetone is within the same category mentioned above. Generally, the ionized enol form is more stable than the keto form, while for the neutral keto and enol form the thermodynamic stability is in reverse order. It is thus possible for the keto ion to isomerize to two kinds of ions (enol-1 or enol-2) by transferring a different hydrogen atom. In this paper interest is focused on the participation of the enol forms shown below as the reacting precursor in the metastable dissociation of ionized hydroxyacetone:

$[CH_3\text{–}CO\text{–}CH_2OH]^{+\cdot}$ keto

$[CH_2{=}C(OH)\text{–}CH_2OH]^{+\cdot}$ enol-1

$[CH_3\text{–}C(OH){=}CHOH]^{+\cdot}$ enol-2

Experimental

The metastable-ion intensities and the CA spectra were measured with a home-made tandem-type mass spectrometer. The CA spectra were measured at a 30% decrease in the main beam intensity by increasing the He gas pressure in the collision cell. The time-dependent appearance energies (*AE*) were measured by an ion-storage technique, which is the same as that described in detail by Herod and Harrison.[8] The enol-1 and enol-2 ions were generated by a McLafferty rearrangement from $(CH_3)_2CH(CH_2)_2COCH_2OH$ (HyMH) and $CH_3(CH_2)_2CH(OH)COCH_3$ (HyH). These precursors were prepared according to the procedure of Stansburg and Proops,[9] and of Baldwin et al.[10]

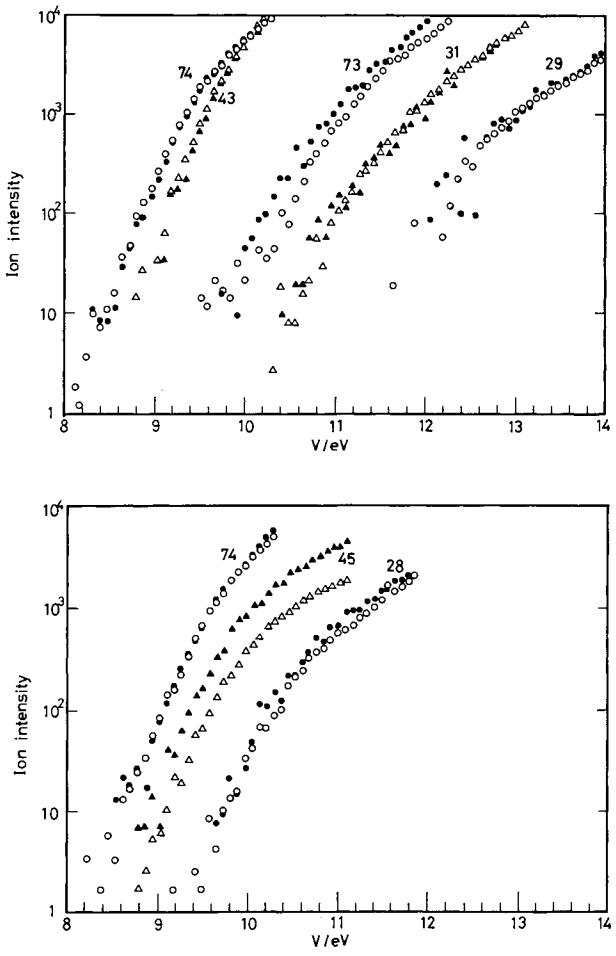

Fig. 1. The semi-log plots of the ion intensity vs. the nominal electron energy, *V* for hydroxyacetone; the storage times of $t=0$ (open mark) and 900 μs (closed mark).

Results and Discussion

Figure 1 shows semi-log plots of the ion intensity vs. the nominal electron energy at ion-storage times of t=0 and 900 μs. These curves were measured with a constant detection sensitivity. The efficiency of ion storage decreases with an increase in the storage time. Thus, the intensity curves for t=900 μs were corrected using the parent ion intensity. The distribution of electron energy was estimated to be ca. 1 eV at the full width of half maximum. The *AE*s were determined by comparing the ion intensity with the reference intensity of a known critical energy at a sensitivity of 10^2. In Fig. 2, the ionization energy (*IE*) of hydroxyacetone was estimated using CH_3OH and CH_3CN as the energy of calibration; their *IE*s are 10.85 and 12.19 eV, respectively.[11] The results of *IE*/*AE* are listed in Table 1.

A shift in the ion-intensity curve with the storage time was observed for m/z 73 and 45 ion. This is a so-called kinetic shift, which increases as the rising slope of the rate vs. energy curve decreases. Ions of m/z 73 and 45 are significant metastable peaks for hydroxyacetone. This is therefore consistent with observations of the kinetic shift. However, a question arises concerning m/z 43: its observed *AE* was almost equal to that of m/z 45. If this is correct, it seems that the dissociations for m/z 43 and 45 are not competitive, since m/z 43 is not metastable. Such nonstatistical behavior is often explained by the formation of two different electronic states during the initial ionization process: one of these states dissociates rapidly, while the other dissociates via an electronic predissociation, though there is no supporting evidence.

Shown in Fig. 3 is an energy diagram constructed from recently published energetic information[11] and the heat of formation, ΔH_f, for the keto and enol ions.

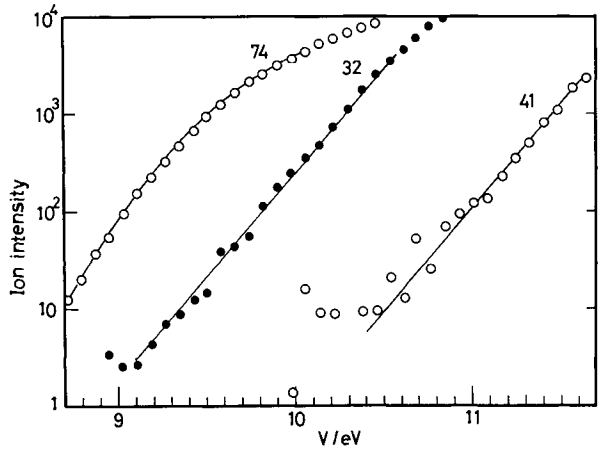

Fig. 2. The semi-log plots of the ion intensity of hydroxyacetone (74), methanol (32), and acetonitrile (41).

Table 1. Ionization and Appearance Energies in the Mass Spectra of Hydroxyacetone

Ions		*AE*/eV	
m/z		t=0 μs	t=900 μs
74	$CH_3COCH_2OH^+$	10.0±0.1	
73	$C_3H_5O_2^+$	11.8	11.6
45	$C_2H_5O^+$	10.5	10.3
43	CH_3CO^+	10.3	10.3
31	CH_3O^+	12.4	12.4
29	$C_2H_5^+$ CHO^+	13.7	13.7
28	$C_2H_4^+$ CO^+	11.3[b]	11.3
74→45*[a]		10.5	

a) The *AE* for the metastable ion was obtained from the procedure of Burgers and Holmes[15] using ethyl acetate as a reference standard. b) For example, *IE*s for N_2 and CO are 15.58 and 14.01 eV, respectively.[11]

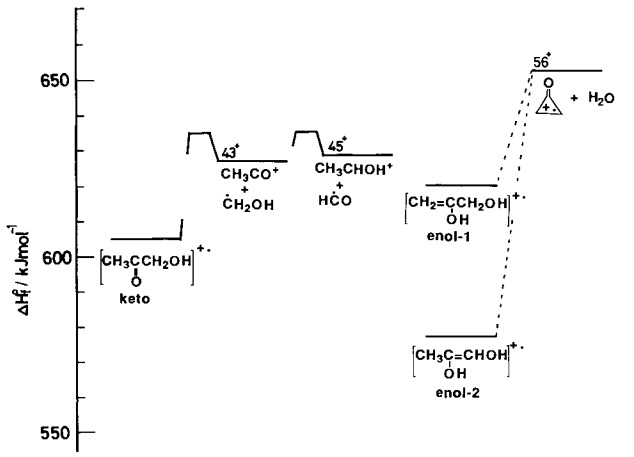

Fig. 3. A potential energy diagram of ionized hydroxyacetone and its enol isomers.

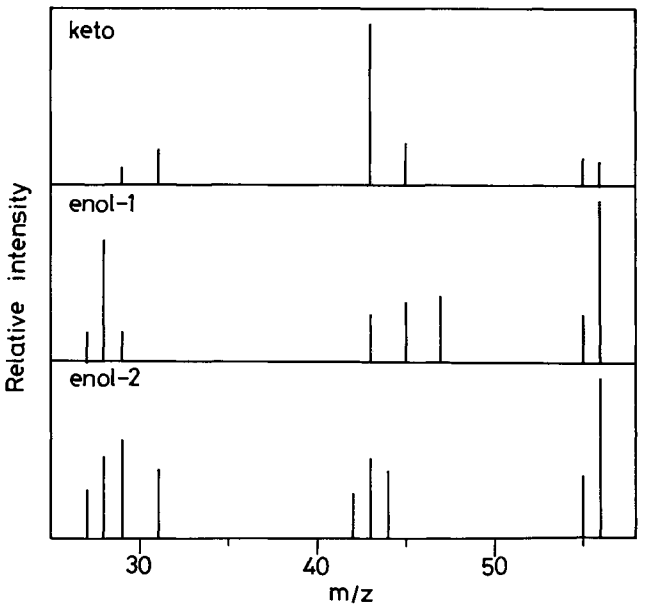

Fig. 4. Collisional activation spectra of ionized hydroxyacetone and its enol isomers.

Table 2. Metastable Ion Intensities and Kinetic Energy Releases for the Keto and Enol Forms

	Intensity ratio			
m/z	73	56	45	28
Keto (Hydroxyacetone)	1 (<10)[a]		9 (<10)	
Enol-1 (HyMH)	1 (<10)	0.5 (30±10)		
Enol-2 (HyH)		1 (<10)		0.09

a) The parentheses are $T_{0.5}$/meV.

These values were obtained from ΔH_f (neutral) estimated by the additivity rule[12] and measured *IE*/*AE*; the estimated values of ΔH_f (neutral) for hydroxyacetone, HyMH and HyH are −360, −459, and −446 kJ mol^{-1}, respectively. The *AE*s of enol-1 and enol-2 were 11.0 and 10.8 eV. The transition-state energies are those derived from the present *AE* measurements. The energy states of products were obtained assuming plausible ion structures, as shown in Fig. 3. Taking the estimation error into account, two enol forms are not so stable relative to the keto form. The activation energies relative to those of the enol isomers are still less than 1 eV. It is therefore difficult to explain the metastable rate based on isomerization prior to dissociation.

As can be seen in Fig. 4, the CA spectrum of the keto form is significantly different from the enol forms. Moreover, the results in Table 2 show that the metastable-ion intensities of hydroxyacetone are different from those of both enols. These results indicate that neither of the enols takes part in the metastable dissociation of ionized hydroxyacetone. The small kinetic energy release for *m/z* 45 is due to the low reverse activation energy (Fig. 3).

Finally, it is concluded that the hydroxyacetone ion does not isomerizes to the enol forms prior to dissociation. In addition, the previous results[1] concerning the metastable and CA spectra indicated that the hydroxyacetone ion was substantially different from the isomer structures produced from various esters, and $CH_3C(=OH^+)$–$CH_2O^\cdot$ from 2-acetoxy-2-methyloxirane. As a result, the keto form seems to be the precursor ion. Therefore, another reason for the slow metastable dissociation should be presented. The tunneling effect through a potential barrier[13] and participation of an anharmonic interaction potential[14] have been studied regarding the origin of slow dissociation. These mechanisms are, however, inadequate for an application to the present system. One possible mechanism for explaining such non-RRKM behavior is a slow predissociation due to an electronic spin-forbidden transition.

The author wishes to thank Dr. M. Hamaguchi for preparation of HyMH and HyH, and Dr. M. Arimura for helpful discussion.

References

1) C. Wesdemiotis, R. Csencsits, and F. W. McLafferty, *Org. Mass Spectrom.*, **20**, 98 (1985).
2) J. L. Holmes, C. E. C. A. Hop, and J. K. Terlouw, *Org. Mass Spectrom.*, **21**, 776 (1986).
3) P. C. Burgers, J. L. Holmes, C. E. C. A. Hop, and J. K. Terlouw, *Org. Mass Spectrom.*, **21**, 549 (1986).
4) N. Heinrich, J. Schmidt, H. Schwarz, and Y. Apeloig, *J. Am. Chem. Soc.*, **109**, 1317 (1987).
5) D. J. McAdoo and D. N. Witiak, *Org. Mass Spectrom.*, **13**, 499 (1978).
6) J. L. Holmes and F. P. Lossing, *J. Am. Chem. Soc.*, **102**, 1519 (1980).
7) R. Arakawa, *Bull. Chem. Soc. Jpn.*, **63**, 754 (1990).
8) A. A. Herod and A. G. Harrison, *Int. J. Mass Spectrom. Ion Phys.*, **4**, 415 (1970).
9) H. A. Stansbury, Jr. and W. R. Proops, *J. Org. Chem.*, **27**, 279 (1962).
10) J. E. Baldwin, G. A. Hofle, and O. W. Lever, Jr., *J. Am. Chem. Soc.*, **96**, 7125 (1974).
11) S. G. Lias, J. E. Bartmess, J. F. Liebman, J. L. Holmes, R. D. Levin, and W. G. Mallard, *J. Phys. Chem. Ref. Data, Suppl.*, **17**, 1 (1988).
12) S. W. Benson, F. R. Cruickshank, D. M. Golden, G. R. Haugen, H. E. O'Neal, A. S. Rodger, R. Shaw, and R. Walsh, *Chem. Rev.*, **69**, 279 (1969).
13) J. H. Beynon, A. E. Fontaine, and G. R. Lester, *Int. J. Mass Spectrom. Ion Phys.*, **1**, 1 (1986); A. J. Illies, M. F. Jarrold, and M. T. Bowers, *J. Am. Chem. Soc.*, **104**, 3587 (1982).
14) J.-D. Shao, T. Baer, J. C. Morrow, and M. L.-Monteiro, *J. Chem. Phys.*, **87**, 5242 (1987).
15) P. C. Burgers and J. L. Holmes, *Org. Mass Spectrom.*, **17**, 123 (1982).

Characteristics of Semiconductor and Ion-Sensitive Layers That Affect Response of Ion-Sensing Devices Based on n-SnO_2/Ion-Exchange Membrane Junction

Keiichi KIMURA,* Yoshiaki KAWASAKI, and Masaaki YOKOYAMA
Chemical Process Engineering, Faculty of Engineering, Osaka University, Yamada-oka, Suita, Osaka 565
(Received October 3, 1990)

Synopsis. The carrier density and thickness of both the semiconductor and ion-sensing membrane were found to significantly affect the sensitivity of ion-sensing devices with a junction of n-type SnO_2 and cation-selective plasticized polymeric membranes. When an anion-selective membrane was employed instead, the resulting device responded in a different way from the corresponding cation-sensing device.

Ion-selective electrodes constitute a group of the most developed ion sensors. They, however, still have some drawbacks, such as high membrane impedance and limited miniaturization. Semiconductors are useful materials for various sensors as well as for ion-sensing devices. Ion-sensitive field-effect transistors are typical ion-sensing devices based on semiconductor/insulator/ion-sensitive membrane/solution junctions,[1-3] which allow the use of high-impedance membranes and the construction of miniaturized multi-ion sensors. Recently, Okawa et al. fabricated ion-sensing devices with semiconductor/ion-sensitive layer junctions, using n-type SnO_2 as the inorganic semiconductor and a polymeric cation-exchanger,[4] valinomycin-containing poly(vinyl chloride) (PVC) film,[5] or crown ether Langmuir-Blodgett film[6] as the cation-sensitive layer. The stimulating research got us interested in the type of ion-sensing device, to which various materials can be applied, while being easy to fabricate.

We have fabricated n-SnO_2-based ion-sensing devices, using the semiconductors with various thicknesses and carrier densities and a typical cation-selective membrane. An anion-selective membrane was also tested as an ion-sensing layer of the device. This paper is concerned with the effects of the semiconductor characteristics and the ion-sensing membranes on the SnO_2-based ion-sensing device.

Experimental

Materials. Dibenzo-30-crown-10 (DB30C10) was prepared according to Pedersen's procedure.[7] Trioctylmethylammonium chloride (TOMACl) was employed as received from Tokyo Kasei. Poly(vinyl chloride) (PVC, polymerization degree of 1100) was purified by reprecipitation from tetrahydrofuran (THF) in methanol. Dioctyl sebacate (2-ethylhexyl sebacate, DOS) was distilled under vacuum. The semiconductors, n-type SnO_2 with thickness of 12—41 nm and carrier density of 1×10^{20} and 4×10^{20} cm^{-3}, which were formed on glass substrates (2×2.5 cm) by chemical mist deposition, were kindly supplied by Taiyoyuden Corporation. The metal salts employed here were of analytical grade. Water was deionized.

Device Fabrication and Measurements. The SnO_2-based ion-sensing devices were constructed with reference to a procedure from the literature.[5] A cutaway view of the device is illustrated in Fig. 1. The SnO_2 layer on the glass was etched to a 1×2.5 cm strip in the center of the glass substrate by treating with dil HCl-Zn powder. The ion-sensing membranes were cast separately. The typical cation- and anion-sensitive membranes of about 0.2 mm thickness were cast by pouring THF solutions (4 ml) of 100 mg PVC/200 mg DOS/10 mg DB30C10 (32.3/64.5/3.2 wt%) and 100 mg PVC/200 mg TOMACl (33/67 wt%) into a flat Petri dish of 43 mm inner diameter, followed by air drying of the THF at room temperature. A square of 1.3×1.3 cm was cut out from the membrane and then placed just at the center of the semiconductor substrate. The thinner cation-sensitive layers were cast or spin-coated directly on the substrate from THF solutions with the same composition as those for the thick membrane. Copper leads were contacted ohmically to each end of the SnO_2 strip by Ag paste and then fixed by an epoxy resin. The resulting device was covered by encapsulation with a silicon rubber (Shin-Etsu, KE44T), except for the ion-sensitive membrane section, the exposed area being about 1×1 cm. The device was soaked in 1×10^{-3} M (1 M=1 mol dm^{-3}) KCl solution in order to condition the ion-sensitive membrane. Electrical conductance measurements were carried out at room temperature according to a reported procedure.[4] The sample solutions did not contain any special pH buffer. The current between the two terminals of the semiconductor part (I_D) was measured with a small applied voltage (V_D), while the electrode potential (V_W) vs. Ag-AgCl was controlled potentiostatically using a double-junction reference electrode (1 M CH_3CO_2Li/3 M KCl/AgCl-Ag). The I_D readings were made in 2 min after changing the applied voltages. Since the relationship between I_D and V_D is ohmic in the V_D range of 0—100 mV, the conductance (G) was calculated from I_D values at V_D of 10 mV. The percent variation of the conductance was

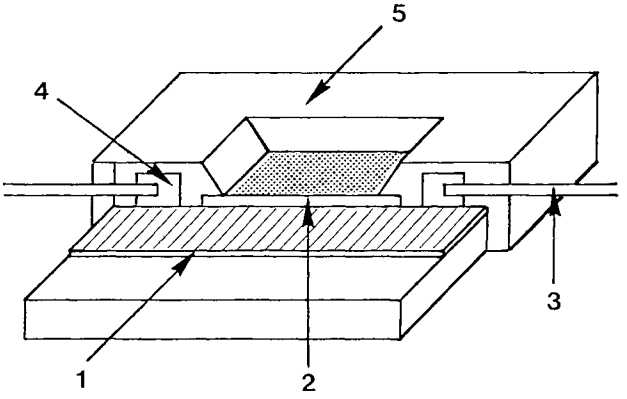

Fig. 1. Cutaway view of schematic diagram for ion-sensing device. 1: semiconductor, 2: ion-sensitive membrane, 3: copper lead, 4: Ag paste, 5: encapsulation.

obtained as 100×[G(at 1×10^{-1} M KCl)−G(at 1×10^{-4} M KCl)]/G(at 1×10^{-4} M KCl). The membrane potentials were measured by using a cell assembly of Ag–AgCl/1×10^{-3} M KCl/membrane/test solution/1 M CH_3CO_2Li/3M KCl/AgCl–Ag and an electrometer. The flatband potentials were measured by using Mott–Schottky plots.[8]

Results and Discussion

A typical response to the K^+ concentration in measured aqueous solutions for the cation-sensing device based on a SnO_2–DB30C10/DOS/PVC membrane junction is shown in Fig. 2. Increasing the cation concentration enhanced the electrical conductance of the device; a greater positive electrode potential resulted in a lower conductance. This was the case in previous SnO_2-based cation-sensing devices.[4,5] It was then proposed that their conductance response to the cation concentration is ascribable to a thickness change in a space-charge layer of the semiconductor, which is in turn caused by a cation-concentration-induced potential change of the ion-sensitive layer. If this response mechanism is reasonable, the sensitivity of ion-sensing devices based on a SnO_2–ion-sensitive membrane junction must appreciably depend upon the characteristics of the semiconductors and ion-sensitive membranes employed. We applied SnO_2 with different thicknesses and carrier densities to our cation-sensing device, using a DB30C10/DOS/PVC membrane with a thickness of 200 μm as the ion-sensitive membrane. The percent variations of conductance for the cation-sensing devices are summarized as a measure of device sensitivity in Table 1. The thinner SnO_2 layers generally afforded a higher percent variation of the conductance in the SnO_2-based cation-sensing device. This suggests that the conductance for thin semiconductors (12—19 nm thickness) are more sensitive to a potential-drop-induced change of the space-charge layer thickness than that for thick types (41 nm thickness). Moreover, low-carrier-density SnO_2 with 12 nm thickness gave better results regarding device sensitivity than did the high-donor-density type with the same thickness. This result may reflect the general observation that the higher carrier density in n-type semiconductors results in a thinner space-charge layer.

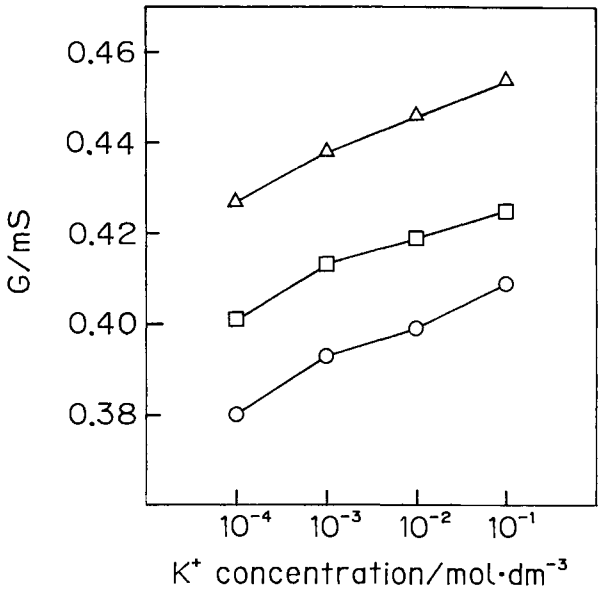

Fig. 2. Conductance response to K^+ concentration for cation-sensing device with SnO_2–DB30C10/DOS/PVC junction. V_w: 0.3 V (○), 0.1 V (□), −0.1 V (△) vs. Ag–AgCl. SnO_2: 19 nm thickness and 4×10^{20} cm^{-3} carrier density. PVC membrane: 200 μm thickness.

Table 1. Dependence of Characteristics of Semiconductor and Ion-Sensitive Layer upon Sensitivity of Ion-Sensing Devices Based on SnO_2–DB30C10/DOS/PVC Junction

Semiconductor		Ion-sensitive layer	Percent variation of conductance[a]
Donor density	Thickness	Thickness	
10^{20} cm^{-3}	nm	μm	%
4	19	200	6.1
4	19	10	1.2
4	19	0.5	1.2
4	19	0.05	1.5
4	12	200	14.4
1	41	200	5.7
1	14	200	20.0
1	12	200	21.2

a) At an electrode potential (V_w) of −0.1 V vs. Ag–AgCl.

The characteristics of the ion-sensitive membrane also affected the response of the SnO_2-based ion-sensing device. Cation-sensitive membranes of DB30C10/DOS/PVC with various thicknesses were tested regarding their conductance response of the resulting device to a K^+ concentration change (Table 1). Only an ion-sensitive membrane of 200 μm thickness allowed good sensitivity (high percent variation of conductance) in the ion-sensing device. Much thinner membranes brought about only poor sensitivity. In separate experiments for measuring the membrane potential, the 200-μm membrane exhibited a near-Nernstian response on the K^+ concentration in test solutions, whereas the thinner ones did not. A substantial thickness of the ion-sensitive layer of the plasticized PVC is, therefore, required to realize a potential drop comparable to the Nernstian response, which in turn causes a significant conductance change accompanied by a space-charge-layer thickness change. The ion selectivity of the ion-sensitive layer should be naturally reflected in the device selectivity, since its potential drop is essentially governed by its ion-exchange selectivity. An ion-sensing device based on SnO_2–DB30C10/DOS/PVC membrane junction is, thus, highly selective to K^+, as shown in Fig. 3.

It is of much interest to see how the SnO_2-based device responds when the cation-sensitive membrane is replaced by an anion-sensitive one. Increasing the Cl^- concentration diminished the electrical conductance in an anion-sensing device based on a SnO_2–TOMACl/PVC junction (Fig. 4). This anion-concentration

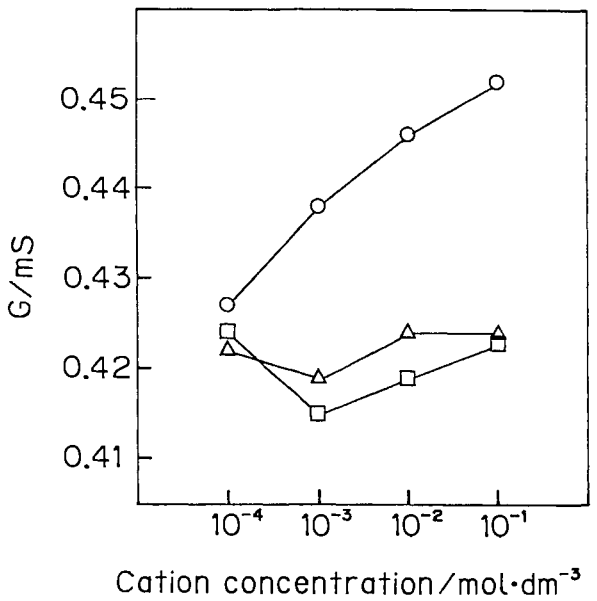

Fig. 3. Ion selectivity of cation-sensing device with SnO_2–DB30C10/DOS/PVC junction. K^+ (○), Na^+ (□), Li^+ (△). V_w: −0.1 V (△) vs. Ag–AgCl. The characteristics for the semiconductor and ion-sensitive layers are the same as for Fig. 2.

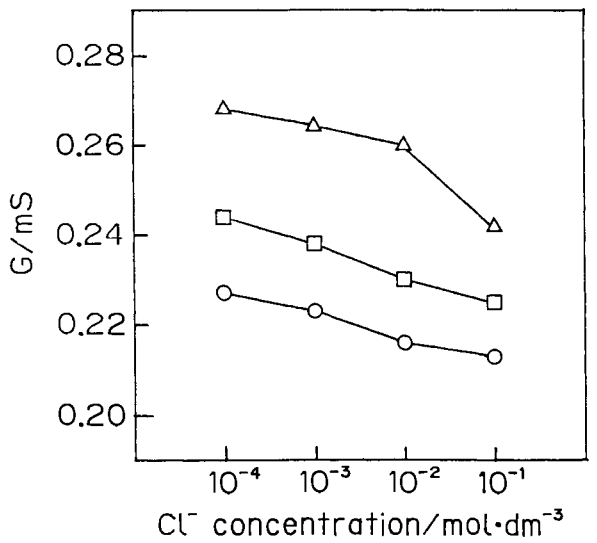

Fig. 4. Conductance response to Cl^- concentration for anion-sensing device with SnO_2–TOMACl/PVC junction. V_w: 0.3 V (○) 0.1 V (□), −0.1 V (△) vs. Ag–AgCl. SnO_2: 19 nm thickness and 4×10^{20} cm^{-3} donor density. PVC membrane: 200 μm thickness.

dependence of the conductance was contrary to the cation-concentration dependence found in the cation-sensing devices, i.e. the conductance decreased with increasing the anion concentration. The anion-sensing device, however, showed the same relationship between the electrode potential (V_W) and the conductance, i.e. the positive shift in the electrode potential diminished the conductance. The near-Nernstian response in the flatband potential of the semiconductor, as depicted in Fig. 5, confirms a response mechanism that the semiconductor conductance change is induced by a potential change in the anion-sensitive layer and, thereby, the space-charge-layer thickness change in the semiconductor.[4]

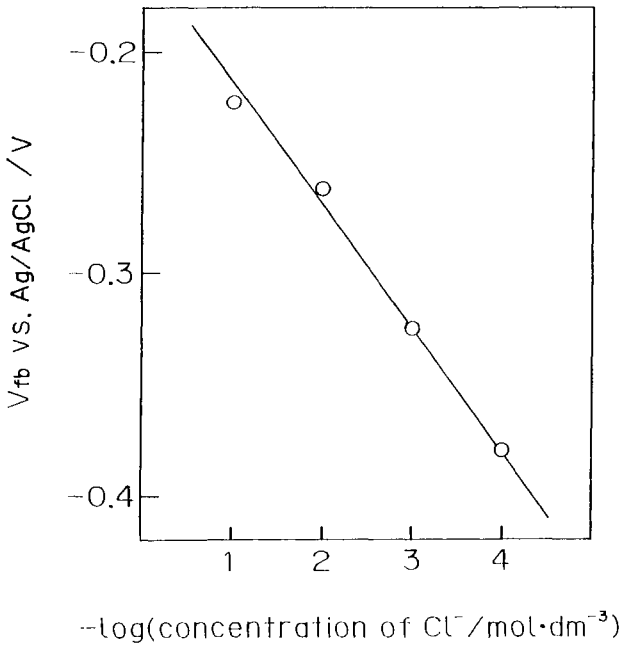

Fig. 5. Dependence of flatband potential of semiconductor upon Cl^- concentration in anion-sensing device with SnO_2–TOMACl/PVC junction. The characteristics for the semiconductor and ion-sensitive layers are the same as for Fig. 4.

In conclusion, the characteristics of the semiconductor and ion-sensitive layer significantly alters the sensitivity of ion-sensing devices based on SnO_2–ion-sensitive PVC membrane junctions; the choice of materials for the semiconductor and ion-sensitive membrane seems to be quite important for designing this type of ion-sensing device.

The authors gratefully acknowledge Dr. Shoichiro Yoshida, Institute of Industrial Science, The University of Tokyo, for his helpful discussion.

References

1) P. Bergveld, *IEEE Trans. Biomed. Eng.*, **BME-17**, 70 (1970).
2) H. Abe, M. Esashi, and T. Matsuo, *IEEE Trans. Electron Devices*, **ED-26**, 1939 (1979).
3) S. D. Moss, C. C. Johnson, and J. Janata, *IEEE Trans. Biomed. Eng.*, **BME-25**, 49 (1978).
4) M. Sukigara, Y. Aikawa, M. Kimura, and Y. Okawa, *Nippon Kagaku Kaishi*, **1987**, 484.
5) Y. Okawa, M. Sukigara, S. Yoshida, and T. Watanabe, *Bull. Chem. Soc. Jpn.*, **61**, 1175 (1988).
6) S. Yoshida, Y. Okawa, T. Watanabe, S. Inokuma, and T. Kuwamura, *Chem. Lett.*, **1989**, 243.
7) C. J. Pedersen, *J. Am. Chem. Soc.*, **89**, 7017 (1967).
8) J. M. Bolts and M. S. Wrighton, *J. Phys. Chem.*, **80**, 2641 (1976).

Hexaammineruthenium Complex as Two-Electron Catalyst for Oxygen Evolution by Homogeneous and Heterogeneous Water Oxidation

Ramasamy RAMARAJ, Masao KANEKO,*,† and Akira KIRA†
School of Chemistry, Madurai Kamaraj University, Madurai 625 021, India
† The Institute of Physical and Chemical Research (RIKEN), Wako, Saitama 351-01
(Received October 16, 1990)

Synopsis. The $[Ru(NH_3)_6]^{3+}$ complex is shown to be a two-electron catalyst for homogeneous as well as heterogeneous water oxidation to evolve dioxygen. The oxygen evolution is proposed to proceed by two molecules of the complex through a peroxo-bridged intermediate involving higher oxidation state $[Ru^V(NH_3)_6]^{5+}$.

The mechanism of oxygen evolution in plant photosynthesis still remains unsolved. According to the present knowledge, dioxygen evolves as a result of water photooxidation in the active center of photosystem II (PS II) with the participation of Mn ions which are weakly bound to the protein part of PS II.[1,2] Since oxygen evolution by water oxidation is a four-electron process (Eq. 1) only few artificial catalysts have been

$$2H_2O \longrightarrow O_2 + 4H^+ + 4e^- \quad (1)$$

known, because of the difficulty to couple an one-electron reaction with a four-electron process.[3] It is now known that $[Ru(bpy)_3]^{3+}$ is capable of bringing about a four-electron oxidation of water to oxygen if it is coupled with a solid catalyst such as RuO_2, PtO_2, and MnO_2.[4-6] However, these catalysts can not be used as models to elucidate photosynthetic oxygen evolution, since the redox chemistry on their surface is difficult to study.[7] Therefore, the design and synthesis of chemical models of PS II and the study of water oxidation in nonbiological systems by utilizing metal complexes are the best ways to elucidate the mechanism of the photosynthetic oxygen evolution.

The present authors could show that oxygen evolution by water oxidation can be achieved by four-electron oxidation catalysts, in both homogeneous and heterogeneous media.[9-13] Oxygen evolution could be realized, even by two-electron oxidation catalysts, if two molecules of the catalyst can interact with each other under homogeneous as well as heterogeneous conditions to enable four-electron oxidation of two water molecules.[8-13] These catalysts have been successfully applied in a photoelectrochemical system to photolyze water for simultaneous oxygen and hydrogen evolution which mimics PS II.[14] We have already reported[10,12] the catalytic activity of water-coordinated dinuclear ($[(bpy)_2(H_2O)RuORu(H_2O)(bpy)_2]^{4+}$) and mononuclear ($[Ru(NH_3)_5(H_2O)]^{3+}$) ruthenium complexes where the coordinated water molecules are involved in the water oxidation to evolve dioxygen. It is interesting and important to study whether a mononuclear metal complex, whose coordination sites are entirely occupied by ligands other than water, is active as a water oxidation catalyst. From this point of view we studied the catalytic activity of the $[Ru(NH_3)_6]^{3+}$ complex. Although the solution chemistry of ruthenium–ammine complexes has been studied extensively,[15,16] attention has not been focused on redox chemistry involving the higher oxidation states (e.g., Ru(IV) and Ru(V)). In this paper we report on both the homogeneous and heterogeneous catalytic activities of hexaammineruthenium(III) towards water oxidation to evolve dioxygen.

Experimental

Materials. $Ru(NH_3)_6Cl_3$ (Aldrich), ammonium cerium(IV) nitrate (Wako Pure Chemicals Co.) and kaolin clay (Nakarai Chemicals Ltd.) were used as received. The $[Ru(NH_3)_6]^{3+}$ complex was adsorbed into clay by mixing known amounts of clay and the ruthenium complex in deionized water. The mixture was stirred until complete adsorption was indicated by the disappearance of the solution color. The clay was filtered after adsorption, washed with deionized water and dried at 25 °C in air.

Instruments. Uv-visible spectra were recorded using a Hitachi 330 spectrometer. Cyclic voltammograms were run using a function generator (model HB-104) and a potentiostat/galvanostat (model HA-301) from Hokuto Denko Ltd. The electrode used to record the cyclic voltammograms was Nafion-coated basal plane pyrolytic graphite (BPG). Platinum wire was used as a counter electrode and a saturated calomel electrode (SCE) as reference electrode.

Oxygen Evolution. Oxygen evolution by water oxidation catalyzed by $[Ru(NH_3)_6]^{3+}$ was investigated by adding excess Ce(IV) as oxidant to an aqueous solution of $[Ru(NH_3)_6]^{3+}$ in a closed, deaerated vessel. The gas evolved by the reaction was analyzed by a gas chromatograph (Shimadzu GC-4C) as described earlier.[11] Repeated experiments showed that the results are reproducible with a 5% difference in the turnover values.

Results and Discussion

Although the uncoated BPG electrode gave a large catalytic current due to water oxidation, the Nafion-coated BPG electrode gave a better cyclic voltammogram for the $[Ru(NH_3)_6]^{3+}$ complex, probably because of the complex concentration into the coated Nafion film. The $[Ru(NH_3)_6]^{3+/2+}$ couple was observed in the potential region from −0.6 to 0.2 V vs. SCE and in the positive potential region (+0.6 to 1.5 V vs. SCE) two oxidative waves are observed, while their reduction waves were not clear (Fig. 1). These irreversible oxidations in the anodic region must be due to a reduction of the higher oxidation state of ruthenium (Ru(V)) by water rather than by electrochemical reduction. Based on the present results, the various redox processes occurring in $[Ru(NH_3)_6]^{3+}$ would be given by

$$[Ru^{V}(NH_3)_6]^{5} \underset{+e^-}{\overset{+e^-}{\rightleftharpoons}} [Ru^{IV}(NH_3)_6]^{4+} \underset{+e^-}{\overset{+e^-}{\rightleftharpoons}}$$

+1.32 V +1.04 V

$$[Ru^{III}(NH_3)_6]^{3+} \underset{-e^-}{\overset{+e^-}{\rightleftharpoons}} [Ru^{II}(NH_3)_6]^{2+}. \quad (2)$$

−0.22 V

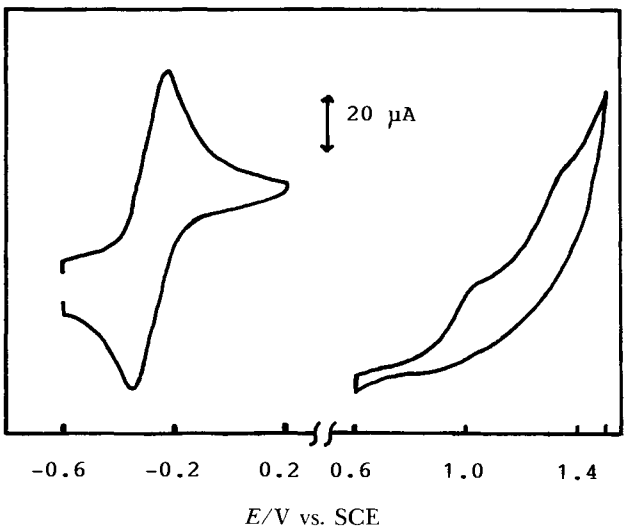

Fig. 1. Cyclic voltammogram of $[Ru(NH_3)_6]^{3+}$ in 0.1 M KNO_3 at Nafion coated BPG at a scan rate of 50 mV s^{-}.

The $[Ru(NH_3)_6]^{3+}$ complex easily forms Ru(V) upon oxidation, and the redox potentials of the complex show that it can be used as a two-electron oxidant for water oxidation. Water oxidation to evolve oxygen was investigated by adding excess ammonium cerium (IV) nitrate as an oxidant to an aqueous solution containing the ruthenium complex. Gas bubbles were readily observed in solution upon the addition of excess (Ce(IV) ion. The experimental results regarding a homogeneous catalysis of water oxidation by the monomeric ruthenium complex was treated with great caution, since decomposition of the complex may produce ruthenium oxide, which is catalytically active for water oxidation.[4,6,7] No ruthenium oxide deposition, however, could be observed after the water oxidation experiment. Though the complex turned over after oxygen evolution, the complex lost catalytic activity after 8—9 turnovers, possibly due to a slow formation of colorless Ru(III) ions from $[Ru(NH_3)_6]^{3+}$ by decomposition during the process.[12]

The amount oxygen evolved with various concentrations of $[Ru(NH_3)_6]^{3+}$ and Ce(IV) in homogeneous and heterogeneous clay-adsorbed states and the turnover numbers of the catalysts towards water oxidation are given in Tables 1 and 2. In both the homogeneous and heterogeneous systems, $[Ru(NH_3)_6]^{3+}$ worked as a catalyst to evolve oxygen by water oxidation. A maximum turnover number of 8.3 was obtained for a homogeneous catalysis and 8.7 for a heterogeneous catalysis.

The higher oxidation state ruthenium-ammine complex ($[Ru^{V}(NH_3)_6]^{5+}$) produced upon the addition of excess Ce(IV) would oxidize water to oxygen (Eqs. 3

Table 1. Oxygen Evolution by Water Oxidation Using $[Ru(NH_3)_6]^{3+}$ under Homogeneous and Heterogeneous Conditions at 25 °C[a]

$[Ru(NH_3)_6]^{3+}$ mole (M)	$[Ru(NH_3)_6]^{3+}$ in water		$[Ru(NH_3)_6]^{3+}$ in kaolin clay	
	O_2[b] 10^{-6} dm^3	Turnover number	O_2[c] 10^{-6} dm^3	Turnover number
2×10^{-6} (2×10^{-4})	162	6.7	209	8.7
4×10^{-6} (4×10^{-4})	332	6.8	340	7.0
6×10^{-6} (6×10^{-4})	405	5.7	324	4.5

a) Ru: Ce^{IV}, 1: 300 (molar ratio) (Ru=$[Ru(NH_3)_6]^{3+}$); kaolin clay, 300 mg; solution volume, 10 cm^3. b) Reaction time, 60 min. c) Reaction time, 90 min.

Table 2. Oxygen Evolution by Water Oxidation Using $[Ru(NH_3)_6]^{3+}$ under Homogeneous and Heterogeneous Conditions at 25 °C[a]

Ru:Ce^{IV} Molar ratio	$[Ru(NH_3)_6]^{3+}$ in water		$[Ru(NH_3)_6]^{3+}$ in kaolin clay	
	O_2 10^{-6} dm^{-3}	Turnover number	O_2 10^{-6} dm^{-3}	Turnover number
1: 50	117	2.4	—	—
1:100	281	5.8	—	—
1:200	400	8.3	326	6.7
1:300	386	8.0	340	7.0
1:400	—	—	370	7.6

a) Ru=$[Ru(NH_3)_6]^{3+}$, 4×10^{-6} mole (4×10^{-4} M); kaolin clay, 300 mg; solution volume, 10 cm^3; reaction time, 90 min.

and 4):

$$[Ru^{III}(NH_3)_6]^{3+} + 2Ce(IV) \longrightarrow [Ru^{V}(NH_3)_6]^{5+} + 2Ce(III) \quad (3)$$

$$2[Ru^{V}(NH_3)_6]^{5+} + 2H_2O \longrightarrow 2\left[Ru^{V}(NH_3)_6]^{5+} \atop \vdots \atop H_2O\right.$$

$$\xrightarrow{-4H^+} [(NH_3)_6Ru^{V}\text{-}O\text{-}O\text{-}Ru^{V}(NH_3)_6]^{8+}$$

$$\longrightarrow 2[Ru^{III}(NH_3)_6]^{3+} + O_2 \quad (4)$$

Endicott and Taube, who studied[17] the oxidation–reduction reactions of mononuclear ruthenium–ammine complexes, suggested that a spin-paired d^4 ion (Ru(IV)) is well-suited to accommodate seven groups in the coordination sphere of the complex. Ru(III) also forms seven-coordinated species as kinetic intermediates.[18,19] Earley and Fealey have studied[20] the kinetics of the reduction of the trinuclear ruthenium–ammine complex, and showed that Ru(III) and Ru(IV) can accommodate the seventh coordination site in the intermediate step. Such a seven-coordinated intermediate has already been proposed for oxygen evolution by water oxidation using di- and trinuclear ruthenium complexes.[11] Taking these facts into consideration, the involvement of two water molecules in the catalytic water oxidation process to evolve one molecule of oxygen in the absence of any other external catalyst can be explained as follows. The water molecule would form a loose coordination bond with the $[Ru^{V}(NH_3)_6]^{5+}$ complex, and two such intermediates of the water-coordinated monomeric Ru(V) complex would interact to form a Ru–O–O–Ru bonded intermediate upon the removal of 4 protons, which could release one molecule of oxygen. Although such a peroxo-bridged Ru–O–O–Ru intermediate complex is not known, an oxo-bridged stable dinuclear ruthenium complex, $[(NH_3)_5Ru\text{-}O\text{-}Ru(NH_3)_5]^{4+}$, is known.[21] Renger has proposed a model for the water splitting complex that is in better agreement with the reported experimental findings,[22] postulating a dinuclear manganese complex in which water ligands are finally oxidized to oxygen via the stage of a bridging peroxo ligand. The formation of an O–O bond in an intermediate has already been proposed to explain oxygen evolution by water oxidation using other metal complex systems.[8,12]

Our earlier studies[9,12] and the present observations show that one-electron oxidants can mediate oxygen evolution from water only in the heterogeneous state,[9,23] whereas two- and four-electron oxidants can catalyze oxygen evolution from water in the homogeneous state itself.[10–12] This leads to the conclusion that the two molecules of a two-electron oxidant, such as monomeric Ru(V), upon water coordination, can easily interact to form Ru–O–O–Ru with the removal of 4 protons which can spontaneously liberate oxygen. This scheme is supported by the fact that such an interaction was hindered by increasing the ionic strength of the reaction medium.[12,24]

Ramasamy Ramaraj acknowledges The Institute of Physical and Chemical Research (RIKEN) for providing the financial support for a three months stay at RIKEN.

References

1) Y. Inoue, A. P. Crofts, Govindjee, N. Murata, N. Renger, and K. Satoh, "The Oxygen Evolving Systems of Photosynthesis," Academic Press, New York (1983).
2) J. Deisenhofer, O. Epp, K. Miki, R. Huber, and H. Michel, *Nature*, **318**, 618 (1985).
3) J. R. Norris, Jr. and D. Meisel, "Photochemical Energy Conversion," Elsevier, New York (1989).
4) J. Kiwi and M. Graetzel, *Angew. Chem., Int, Ed. Engl.*, **17**, 860 (1978); **18**, 1979 (1979).
5) V. Ya. Shafirovich, N. K. Kannanov, and A. E. Shilov, *J. Inorg. Biochem.*, **15**, 113 (1981).
6) M. Kaneko, N. Awaya, and A. Yamada, *Chem. Lett.*, **1982**, 619; **1982**, 1647.
7) M. Graetzel, "Energy Resources through photochemistry and Catalysis," Academic Press, New York (1983).
8) J. A. Gilbert, D. S. Eggleston, W. R. Murphy, Jr., D. A. Geselowitz, S. W. Gersten, D. T. Hodgson, and T. J. Meyer, *J. Am. Chem. Soc.*, **107**, 3855 (1985).
9) R. Ramaraj, A. Kira, and M. Kaneko, *Angew. Chem., Int. Ed. Engl.*, **25**, 825 (1986).
10) R. Ramaraj, A. Kira, and M. Kaneko, *J. Chem. Soc., Faraday Trans. 1*, **82**, 3515 (1986).
11) R. Ramaraj, A. Kira, and M. Kaneko, *J. Chem. Soc., Faraday Trans. 1*, **83**, 1539 (1987).
12) R. Ramaraj, A. Kira, and M. Kaneko, *J. Chem. Soc., Chem. Commun.*, **1987**, 227.
13) G. J. Yao, A. Kira, and M. Kaneko, *J. Chem. Soc., Faraday Trans. 1*, **84**, 4451 (1988).
14) M. Kaneko, G. J. Yao, and A. Kira, *J. Chem. Soc., Chem. Commun.*, **1989**, 1338.
15) P. C. Ford, *Coord. Chem. Rev.*, **5**, 75 (1970).
16) A. B. P. Lever, *Inorg. Chem.*, **29**, 1271 (1990).
17) J. F. Endicott and H. Taube, *Inorg. Chem.*, **4**, 437 (1965).
18) P. C. Ford, J. R. Kuempel, and H. Taube, *Inorg. Chem.*, **7**, 1976 (1968).
19) H. Scheiddizer, J. Armor, and H. Taube, *J. Am. Chem. Soc.*, **90**, 5828 (1968).
20) J. E. Earley and T. Fealey, *Inorg. Chem.*, **12**, 323 (1973).
21) J. A. Baumann and T. J. Meyer, *Inorg. Chem.*, **19**, 345 (1980).
22) G. Renger, "Photosynthetic Water Oxidation," Academic Press, New York (1978), p. 229; G. Renger, *FEBS Lett.*, **81**, 223 (1977).
23) R. Ramaraj, A. Kira, and M. Kaneko, *Chem. Lett.*, **1987**, 261.
24) M. Kaneko, R. Ramaraj, and A. Kira, *Bull. Chem. Soc. Jpn.*, **61**, 417 (1988).

Photoinduced Alkylation Reaction of Benzo[*f*]indole-4,9-dione with Arylalkenes

Katsuhiko NAKAGAWA
Department of Industrial Chemistry, Niihama National College of Technology, Niihama, Ehime 792
(Received August 27, 1990)

Synopsis. Photoreaction of 1-alkyl-2-methyl-1*H*-benz[*f*]-indole-4,9-diones (indolequinones) with arylalkenes in benzene gave 3-alkylated products. Irradiation of 1-allyl substituted indolequinone in benzene gave 1,3-hydrogen shift product in the presence or absence of arylalkenes. The fluorescence of 1,2-dimethyl-1*H*-benz[*f*]indole-4,9-dione exhibits a large bathochromic shift in polar solvents, indicating polar charge-transfer character for its S_1-state.

Photochemistry of quinones has been a subject of many extensive investigations. As a result, a variety of photoreactions of quinones, including photoreduction, photocycloaddtion, photoisomerization, and photosubstitution have appeared in the literature.[1] However, photochemical alkylation reaction of quinones has been much less characterized so far.

Recently, we developed a convenient synthetic method of 1*H*-benz[*f*]indole-4,9-dione (**2**) by the thermal condensation reaction of 2-acetonyl-3-methoxy-1,4-naphthoquinone (**1**) with primary aliphatic

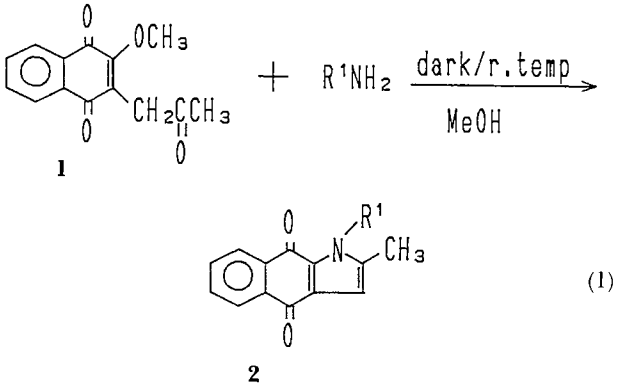

(1)

amines.[2] The compound **2** has an interesting structure containing pyrrole ring fused with naphthoquinone necleus. Since the naphthoquinone structure is electron-deficient and the pyrrole ring is electron-rich, the former ring is expected to be potential electron acceptor for the latter, thus achieving an intramolecular charge-transfer state.

Described herein is a novel photoinduced alkylation of **2** with arylalkenes.

Results and Discussion

Photochemical Alkylation Reactions of 1,2-Dimethyl-1*H*-benz[*f*]indole-4,9-dione (2a) 2-Methyl-1-propyl-1*H*-benz[*f*]indole-4,9-dione (2b) with Arylakenes (3a—c). Irradiation of **2a** (1.2 mmol dm^{-3}) in the presence of 1,1-diphenylethylene (**3a**)(1.5 mmol dm^{-3}) in benzene followed by separation by column chromatography (silica gel) afforded 1,2-dimethyl-3-(2,2-diphenylethyl)-1*H*-benz[*f*]indole-4,9-dione (**4a**) as the sole photoproduct in a 40% isolated yield at 50% conversion of **2a**. The structure of **4a** was determined by its spectroscopic analysis and elemental analysis.

Similary, **2a** was photochemically alkylated at the 3-position with 2-phenyl-1-propene (**3b**) and styrene (**3c**), giving **4b** and **4c** in 38 and 28% yields, respectively. In an analogous fashion, **2b** underwent the photoalkylation at the 3-position upon irradiation

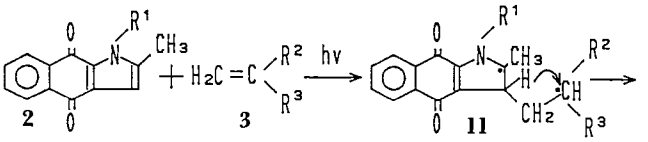

	R^1
2a	CH_3
2b	nPr

	R^2	R^3
3a	Ph	Ph
3b	Ph	CH_3
3c	Ph	H

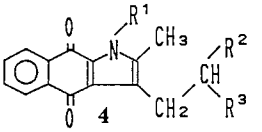

(2)

	R^1	R^2	R^3
4a	CH_3	Ph	Ph
4b	CH_3	Ph	CH_3
4c	CH_3	Ph	H
4d	nPr	Ph	Ph
4e	nPr	Ph	CH_3
4f	nPr	Ph	H

Table 1. Photochemical Alkylation Reaction of **2a** and **2b** with Arylalkene (**3a—c**) in Benzene

Quinone	Olefins	Irr. time/h	Conv.[a] %	Yields[b] of **4**/%
2a	**3a**	1	50	40
2a	**3b**	1	60	38
2a	**3c**	1	48	28
2b	**3a**	0.3	45	31
2b	**3b**	0.3	57	29
2b	**3c**	0.3	39	16

a) Conversion of **2a** and **2b**. b) Isolated yields were based on the consumed amounts of **2a** and **2b**.

in the presence of **3a—c** in benzene. Results are summarized in Table 1. No photochemical alkylation of **2a** and **2b** did not take place with 2-methyl-1-propene, 2-methoxy-1-propene and methyl acrylate. Interestingly, the alkylation products **4** were formed only in nonpolar solvents such benzene and dichloromethane.

Photochemical Isomerization of 1-Allyl-2-methyl-1*H*-benz[*f*]indole-4,9-dione (2c). Irradiation of the *N*-allyl quinone **2c** in benzene solution led to the formation of 2-methyl-1-(1-propenyl)-1*H*-benz[*f*]indole-4,9-dione (**5**) in 52% yield at 55% conversion of **2c**. The structure of **5** was assigned on the basis of its spectroscopic properties and elemental analysis. The ^{1}H NMR spectrum of **5** showed the presence of *N*-(1-propenyl) substituent at δ=1.95 (N-CH=CH-$\underline{CH}_3$), 5.85 (N-CH=C$\underline{H}$-CH$_3$), and 7.1 (N-C$\underline{H}$=CH-CH$_3$); the mass spectrum showed a peak at 251 (M^+). The

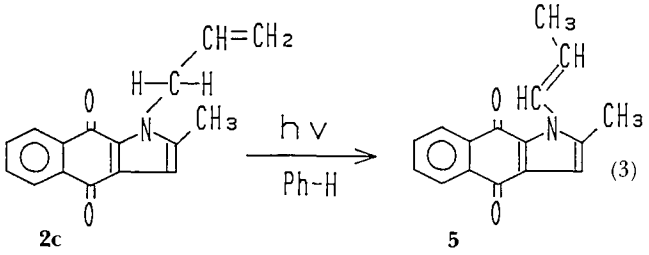

2c **5**

photoisomerization product **5** can be regarded as an intramolecular 1,3-hydrogen shift product. Irradiation of **2c** in the presence of **3a** did not give the photoalkylation product but gave **5** in 10% yield.

Absorption and Fluorescence Spectra of 2a. The shape and wavelength maxima(λ_{max}) of **2a** and **2c** in the absorption spectra of **2a** and **2c** do not exhibit substratial solvent polarity dependence. In contrast, the fluorescence of **2a** was found to undergo a large bathochromic shift upon the increase of solvent polarity (Table 2). The fluorescence of **2a** in benzene exhibited a broad band centered at λ_{max} 500 nm with lifetime of 3.1 ns at room temperature, while the fluorescence maximum in acetonitrile was observed at 526 nm with lifetime of 4.5 ns. These results suggest that the lowest singlet excited state (S_1) of **2a** has a partially charge transfer character.[3] Importantly, the floresence of **2a** was not quenched by **3a—c** in benzene.

Mechanistic Consideration of the Photoinduced Alkylation Reaction of 2 with 3a—c. The fact that the fluorescence of **2a** was not quenched by **3a—c** strongly indicated the triplet origin for the formation of **4**. In accord with this consideration, the photoinduced alkylation reaction was sensitized by benzil (E_T=53 kcal mol^{-1}),[4] but was efficiently quenched by anthracene (E_T=42 kcal mol^{-1}).[4] In ether–isopentane–ethanol (EPA) matrix at 77 K, a broad phosphorescence band of **2a** was observed at λ_{max} 564 nm. Thus, the energy of the lowest triplet excited state(T_1) of **2a** estimated from 0–0 phosphorescence band was ca 51.2 kcal mol^{-1}. In the presence of **3a**, this phosphorescence band was very weakened as compared with that in the absence of **3a**, indicating a decaying path for T_1-state of **2a** through the intereraction of **3a**. Electron transfer from **3a—c** to ^{3}(**2a**)* may be excluded, since the Rehn–Weller estimation[5] of free energy charges (ΔG) associated with the triplet electron transfer gives rather high positive values(+8—+10 kcal mol^{-1}).[6] A plausible mechanism for the formation of **42** is shown in Eq. 2. The reaction of T_1 of **2a** with **3** leads to the formation of 1,4-biradical **11**, which will give the 3-alkylated product **4** by disproportionation. When the photoreaction of **2a** with **3a—c** was conducted in benzene-d_6, no incorporation of deuterium atom in **4** was observed. Therefore, intramolecular 1,3-hydrogen shift may be predominant for the pathway from the intermediate **11** to **4**. In the *N*-allyl compound **2c**, the intramolecular hydrogen adstraction[7] by the quinone carbonyl group from the γ-position and subsequent disproportionation may account for the formation of **5**. Probably, this intramolecular process is much faster as compared to the intermolecular quenching by **3a—c**.

Table 2. Fluorescence Maxima of **2a** in Various Solvents[a,b]

Solvent	Maxima wavelength (λ_{max}/nm)	τ/ns
Benzene	500	3.1
Chloroform	510	5.9
Acetone	519	4.9
Acetonitrile	526	4.5

a) Excited wavelength, 326 nm. b) In air-saturated solvents at room temperature; [**2a**]=4.4×10^{-5} mol dm^{-3}.

Experimental

Apparatus. Melting points were measured on Yanagimoto micro-melting points apparatus and uncorrected. Infrared spectra were taken on a JASCO-IR-1A spectrometer. Fluorescence spectra and lifetimes were measured by a JASCO FP-550 spectrometer and a Horiba NAES-1100 timeresolved spectrofluorimeter, respectively. Phosphorescence spectra were measured by a Shimazu RF-502A spectrometer. NMR spectra were recorded on a JEOL GX-400 (400 MHz), a JEOL GX-270 (270 MHz), and a JEOL FX-900 (90 MHz) spectrometer with use of tetramethylsilane as an internal standard and the chemical shifts are expressed in δ values. UV spectra were taken by using a JASCO UVIDEC-1 spectrometer. Elemental analyses were performed at the Microanalytical Laboratory of Kyoto University and Advanced Instrumentation Center for Chemical Analysis, Ehime University. Mass spectra were recorded on a Hitachi M-2000 spectrometer.

Materials. 1-Alkyl-3-methyl-1*H*-benz[*f*]indole-4,9-dione **2a—c** were prepared according to a procedure in the literature.[2] Alkenes **3a—c** were commercially available and purified by distillation.

General Procedure for the Photochemical Reaction of 1-Alkyl-3-methyl-1*H*-benz[*f*]indole-4,9-dione 2 with Alkenes 3 and Product Isolation: A degassed solution of **2** (1.50 mmol) and **3** (1.80 mmol) in 300 cm^3 of benzene in a Pyrex vessel, using a 300-W high-pressure mercury lamp. The progress of the reaction was followed by TLC (Merck, Kieselgel 60F_{254}), or NMR. After evaporation of the solvent, the residual oil was separated by column chromatography on silica gel (Wakogel C-200, 74-149 μm) with benzene/dichloromethane as an eluent.

Physical Properties of Photoproducts. 1,2-Dimethyl-3-(2,2-diphenylethyl)-1*H*-benz[*f*]indole-4,9-dione (4a): Mp

217—219 °C; ^{1}H NMR (270 MHz, $CDCl_3$) δ=1.90 (3H, s), 3.50 (2H, d, J=7.6 Hz), 3.90 (3H, s, NMe), 4.40 (1H, t, J=7.6 Hz), 7.20 (10H, s), 7.6—7.7 (2H, m), 8.1—8.2 (2H, m); ^{13}C NMR (22.5 MHz, $CDCl_3$) δ=19.0 (q), 31.9 (q), 32.7 (t), 51.2 (d), 121.8 (s), 125.2 (s), 126.1 (d), 128.2 (d), 128.4 (d), 129.9 (s), 130.6 (s), 134.3 (s), 138.6 (s), 144.6 (s), 175.4 (s, C=O), 181.8 (s, C=O); IR (KBr) 1646, 1588, 1470, 1258, 722, 706 cm^{-1}. MS (20 eV), m/z 405(M^+); UV (λ_{max}, nm (log ε), CH_3CN) 270 (4.53), 334 (3.66), 431 (3.74). Found: C, 82.84; H, 5.70; N, 3.41%. Calcd for $C_{28}H_{23}N_1O_2$: C, 82.94; H, 5.72; N, 3.45%.

1,2-Dimethyl-3-(2-phenylpropyl)-1*H*-benz[*f*]indole-4,9-dione (4b): Mp 148—149 °C; ^{1}H NMR (270 MHz, $CDCl_3$) δ=1.36 (2H, d, J=6.7 Hz), 1.79 (3H, s), 2.83 (1H, m), 3.10 (1H, dd, J=5.5 and 13 Hz), 3.18 (1H, dd, J=7 and 12 Hz), 3.93 (3H, s), 7.2 (5H, s), 7.6—7.7 (2H, m), 8.1—8.2 (2H, m); IR (KBr) 2960, 2924, 1646, 1590, 1498, 1252, 1178, 980, 722, 700 cm^{-1}. MS (20 eV) m/z 343 (M^+); UV(λ_{max} nm (log ε), CH_3CN) 270 (4.69), 366 (3.82), 428 (3.87). Found: C, 80.60; H, 6.01; N, 4.19%. Calcd for $C_{23}H_{21}N_1O_2$; C, 80.44; H, 6.16; N, 4.08%.

1,2-Dimethyl-3-(2-phenylethyl)-1*H*-benz[*f*]indole-4,9-dione (4c): Mp 146—147 °C; ^{1}H NMR (270 MHz, $CDCl_3$) δ=1.85 (3H, s), 2.90 (2H, t, J=7.5 Hz), 3.1 (2H, t, J=7.5 Hz), 3.95 (3H, s), 7.2 (5H, s), 7.6—7.7 (2H, m), 8.1—8.2 (2H, m); ^{13}C NMR (22.5 MHz, $CDCl_3$) δ=9.2 (q), 27.5 (t), 32.8 (q), 36.5 (t), 123.2 (s), 125.8 (d), 126.2 (d), 128.3 (d), 128.9 (d), 132.7 (d), 132.8 (d), 134.4 (s), 137.9 (s), 142.2 (s), 175.5 (s, C=O), 181.9 (s, C=O); IR (KBr) 1645, 1587, 1498, 1410, 1249, 1196, 956, 790, 725, 705 cm^{-1}. MS (20 eV) m/z 329 (M^+); UV (λ_{max}, nm (log ε), CH_3CN) 269 (4.49), 335 (3.50), 426 (3.53). Found: C, 80.08; H, 5.70; N, 4.19%. Calcd for $C_{22}H_{19}N_1O_2$: C, 80.22; H, 5.81; N, 4.25%.

1-Propyl-2-methyl-3-(2,2-diophenylethyl)-1*H*-benz[*f*]indole-4,9-dione (4d): Mp 181—182 °C; ^{1}H NMR (90 MHz, $CDCl_3$) δ=0.8 (3H, t, J=7.3 Hz), 1.5—1.8 (2H, m), 1.6 (3H, s), 3.45 (2H, d, J=7.7 Hz), 4.1—4.4 (3H, m), 7.2 (10H, s), 7.5—7.7 (2H, m), 8.0—8.2 (2H, m); IR (KBr) 2960, 2920, 1645, 1588, 1495, 1288, 720, 700 cm^{-1}. MS (20 eV) m/z 433 (M^+); UV (λ_{max}, nm (log ε), CH_3CN) 271 (4.87), 336 (4.04), 432 (4.10). Found: C, 83.20; H, 6.23; N, 3.33%. Calcd for $C_{30}H_{27}N_1O_2$: C, 83.11; H, 6.28; N, 3.23%.

1-Propyl-2-methyl-3-(2-phenylpropyl)-1*H*-benz[*f*]indole-4,9-dione (4d): Mp 79—81 °C; ^{1}H NMR (270 MHz, $CDCl_3$) δ=0.91 (3H, t, J=7.3 Hz), 1.40 (3H, dd, J=7.0 Hz), 1.66 (2H, m), 1.72 (3H, s), 2.76 (1H, m), 3.11 (1H, dd, J=6.7 and 13.7 Hz), 3.21 (1H, dd, J=6.3 nad 12.7 Hz), 4.20 (1H, m), 4.38 (1H, m), 7.2 (5H, s), 7.5—7.7 (2H, m), 8.0—8.2 (2H, m); IR (KBr) 2966, 2934, 1651, 1591, 1497, 1460, 1251, 1172, 988, 762, 719, 702 cm^{-1}. MS (20 eV) m/z 371 (M^+); UV (λ_{max}, nm (log ε), CH_3CN) 271 (4.49), 337 (3.66), 429 (3.70). Found: C, 81.11; H, 6.84; N, 3.72%. Calcd for $C_{25}H_{25}N_1O_2$: C, 80.83; H, 6.78; N, 3.77%.

1-Propyl-2-methyl-3-(2-phenylethyl)-1*H*-benz[*f*]indole-4,9-dione (4f): Mp 116—117 °C; ^{1}H NMR (90 MHz, $CDCl_3$) δ=0.9 (3H, t, J=7.0 Hz), 1.62 (2H, m), 1.80 (3H, s), 3.0—3.2 (4H, m), 4.3 (2H, t, J=7.0 Hz), 7.2 (10H, s), 7.5—7.7 (2H, m), 8.0—8.2 (2H, m); IR (KBr) 2920, 1640, 1590, 1492, 1459, 1430, 1228, 720, 695 cm^{-1}. MS (20 eV) m/z 357 (M^+); UV (λ_{max}, nm (log ε), CH_3CN) 271 (4.70), 335 (3.87), 429 (3.90). Found: C, 80.90; H, 6.67; N, 3.93%. Calcd for $C_{24}H_{23}N_1O_2$: C, 80.64; H, 6.48; N, 3.92%.

1-(1-Propenyl)-2-methyl-1*H*-benz[*f*]-indole-4.9-dione (5): Mp 154—156 °C; ^{1}H NMR (400 MHz, $CDCl_3$) δ=1.95 (3H, d, J=0.92 Hz), 2.35 (3H, s), 5.86 (1H, sext, J=7 Hz), 6.55 (1H, s), 7.16 (1H, dd, J=7 and 1 Hz), 7.6—7.7 (2H, m), 8.1—8.2 (2H, m); IR (KBr) 3120, 2920, 1657, 1621, 1585, 1500, 1415, 1235, 980, 710 cm^{-1}. MS (20 eV) m/z 251 (M^+); UV (λ_{max}, nm (log ε), CH_3CN) 260 (4.60), 326 (3.88), 408 (3.62). Found: C, 76.56; H, 5.23; N, 5.61%. Calcd for $C_{16}H_{13}N_1O_2$: C, 76.48; H, 5.21; N, 5.57%.

In this investigation I am particularly indebted to Professor K. Maruyama of Kyoto University for his valuable suggestions and encouragement and to Dr. A. Osuka of Kyoto University for his helpful discussions. Helps given by Dr. H. Uno at Advanced Instrumentation Center for Chemical Analysis, Ehime University will be greatly appreciated.

References

1) K. Maruyama and A. Osuka, "Recent Advances in Photochemistry of Quinone," in "The Chemistry of Quinonoid Compounds," ed by S. Patai and Z. Rappaport, John Wiley, London (1988), Vol. II, pp. 759—766.

2) K. Maruyama, A. Osuka, K. Nakagawa, T. Nabeshima, and K. Tabuchi, *Synthesis*, **1989**, 628.

3) The value of the dipole moment of the singlet excited state of **2a** (μ_e) was estimated to be ca. 7D by A. Weller's equation. (H. Beens, H. Knibbe, and A. Weller, *J. Chem. Phys.*, **47**, 1183 (1967).)

4) S. L. Murov, "Hand book of photochemistry," Marcel Dekker, New York (1973), Sect. 1.

5) D. Rehn and A. Weller, *Isr. J. Chem.*, **8**, 259 (1970).

6) E(A$^-$/A)=−1.26 V(**2a**), E(D/D$^+$)=1.38 V(**3a**), 1.40(**3b**), 1.50(**3c**) were determined by cyclic voltammetry using Ag/0.1 mol dm^{-3} $AgClO_4$ (in CH_3CN) as a reference electrode.

7) A. Padwa and D. Eastman, *J. Am. Chem. Soc.*, **91**, 462 (1969).

The Effects of Aromatic Compounds on the Hydrogen-Transfer Reaction to Coal Model Compounds

Koji CHIBA,* Hideyuki TAGAYA,* Toru SUZUKI, and Shimio SATO
Department of Materials Science and Engineering, Faculty of Engineering, Yamagata University, Jonan, Yonezawa 992
(Received September 3, 1990)

Synopsis. A hydrogen-transfer reaction from a hydrogen molecule to benzophenone in 1-methylnaphthalene without a donor was accelerated in the presence of anthracene. Phenanthrene and pyrene were detrimental to the reaction. Dibenzyl ether conversion was also accelerated by the addition of anthracene, pyrene, and fluorene. Conversions of coal model compounds in 1-methylnaphthalene under a hydrogen atmosphere correlated well with conversions in tetralin under a nitrogen atmosphere.

In coal liquefaction the solvent plays a vital role as both a hydrogen donor and a reaction medium to dissolve reactants and products.[1] The selection of the solvent is an important factor for effective coal liquefaction. Hydroaromatic compounds, such as tetralin, are known to be donors.[2] We have already reported that aromatic compounds, such as anthracene and fluorene, are effective hydrogen shuttlers in hydrogen-transfer reactions from a donor, tetralin, to coal model compounds.[3] Such hydrogen-shuttling reactions contribute to an increase in the net amounts of transferred hydrogen from donors to coal.[4] Furthermore, it is well-accepted that the reactive coal fragments not only abstract hydrogen from the donor solvent, but also react with dissolved hydrogen molecules to yield liquefaction products.[5] For example, in the pyrolysis of bibenzyl without a catalyst, significant amounts of benzene and ethylbenzene have been produced, indicating a mechanism involving the direct participation of hydrogen molecules in free-radical reactions.[6] Ouchi and Makabe reported that naphthalene as a model of solvent did not convert under a hydrogen atmosphere without a catalyst.[7] However, recycle solvents include many compounds, and the role of solvent on the reaction of coal with hydrogen molecules has not been clearly understood.

Though it is appropriate to use coal model compounds, in many cases the effectiveness of various hydrogen-donor solvents were investigated. In this study, in order to understand the function and importance of coal liquefaction solvents, the reactions of coal model compounds were performed in the presence of aromatic compounds with hydrogen molecules without a donor and a catalyst.

Experimental

Reagent grade benzophenone and dibenzyl ether were used. All of the reactions were carried out in magnetdriven stainless-steel autoclave according to a method described previously.[3] The liquid products after reactions were washed from the autoclave with acetone and analyzed by gas chromatography (GC).

Results and Discussion

Six aromatic compounds were used in the reaction of benzophenone as a coal model. 1-Methylnaphthalene was used as a diluent since the hydrogen-shuttling ability of 1-methylnaphthalene is very low, as already reported.[3] When no aromatic compound was added, the conversions of benzophenone were 43 to 45% (Table 1). These values were larger than 9.3%, in which initial hydrogen pressure was 2.0 MPa and reaction time was 0.5 h.[9] No benzhydrol was observed in the products. The highest conversion was obtained

Table 1. The Effects of Aromatic Compounds on the Hydrogen Transfer Reaction[a] to Benzophenone (BZP)

Run No.	Aromatic compound	Conv. of BZP	Yield of DPM[b]
		mol%	mol%
1	1-Methylnaphthalene	42.9, 45.0	32.9, 35.4
2	Anthracene	52.4	43.1
3	Phenanthrene	23.8	21.9
4	Pyrene	29.9, 26.4	24.4, 22.6
5	Fluorene	44.7	38.3
6	Diphenylmethane	45.9	31.0
7	Triphenylmethane	43.2	32.9
8	Dihydroanthracene	52.2	52.2
9	Dihydroanthracene[c]	31.3	23.6
10	Dihydrophenanthrene	38.8	38.8
11	Dihydrophenanthrene[c]	9.8	9.8

a) Aromatic compound (1.00 g), 1-methylnaphthalene (10.00 g) and benzophenone (1.00 g) were used. Reaction temperature 430 °C; initial hydrogen pressure 3 MPa; reaction time 1 h. b) DPM=Diphenylmethane. c) Under a nitrogen atmosphere.

by adding anthracene (Run 2). It was confirmed that, in the absence of benzophenone, 47% of the anthracene was hydrogenated to dihydroanthracene (DHA; 44%) and tetrahydroanthracene (3%) in 1-methylnaphthalene under a hydrogen atmosphere at 430 °C. DHA was a good donor for benzophenone (Runs 8 and 9). Certainly, no DHA was observed in the reaction of benzophenone with 1-methylnaphthalene and anthracene. This shows that hydrogen transfer from DHA to benzophenone came to completion if DHA was produced. It was considered that a positive effect of anthracene on the hydrogen-transfer reaction was given by its high ability to accept hydrogen. Lower conversions of 20 to 30% than without additive were obtained when phenanthrene or pyrene was used as an aromatic compound(Runs 3 and 4). The facts indicated that pyrene and phenanthrene had negative effects on the conversion of benzophenone. When pyrene alone was reacted under a hydrogen atmosphere, 2% of the pyrene was hydrogenated to give dihydropyrene. In the same reaction, 1% of the phenanthrene was hydrogenated. They have lower abilities to accept hydrogen than does anthracene. However, the presence of 2% dihydrophenanthrene after the reaction of benzophenone in 1-methylnaphthalene and phenanthrene was observed. The presence of dihydrophenanthrene after the reaction and low benzophenone conversion indicated that phenanthrene was hydrogenated in preference to benzophenone and that hydrogen transfer from dihydrophenanthrene to benzophenone was slow. Conversions with additives of fluorene, diphenylmethane and triphenylmethane were the same without additives (Runs 5—7). Their abilities to accept hydrogen may be very low in consideration of their structures.

Dibenzyl ether easily decomposed at 375 °C. About 15% of the dibenzyl ether converted to toluene and benzaldehyde in 1-methylnaphthalene alone (Run 12). No benzyl alcohol was observed in the products. An intramolecular reaction of dibenzyl ether does not give toluene and benzaldehyde through free radicals. On the other hand, two free radicals result from an intermolecular reaction. It is considered that highly reactive radicals would participate in the reaction with hydrogen molecules directly. Simmons and Klein reported that a free-radical chain reaction occurred in preference to an intramolecular type reaction. They evaluated it at 400 °C. However, the exact intermolecular/intramolecular reaction ratio under our reaction conditions has not been estimated. Phenanthrene, diphenylmethane, and triphenylmethane were not effective additives (Runs 14, 17, and 18). These results indicate that the hydrogen-transfering ability of such aromatic compounds is fairly small. On the other hand, the conversion increased to 40% upon the addition of anthracene (Run 17). The high hydrogen-accepting ability of anthracene must contribute to the high conversion. Fluorene and pyrene were also effective additives for the conversion of dibenzyl ether (Runs 15 and 16).

Figure 1 shows the relationship between the conversion of coal model compounds in 1-methylnaphthalene under a hydrogen atmosphere and conversion in tetralin under a nitrogen atmosphere. The hydrogen shuttling ability and the hydrogen-transfer ability from hydrogen molecules are considered to be different. However, the correlation factor between them was as

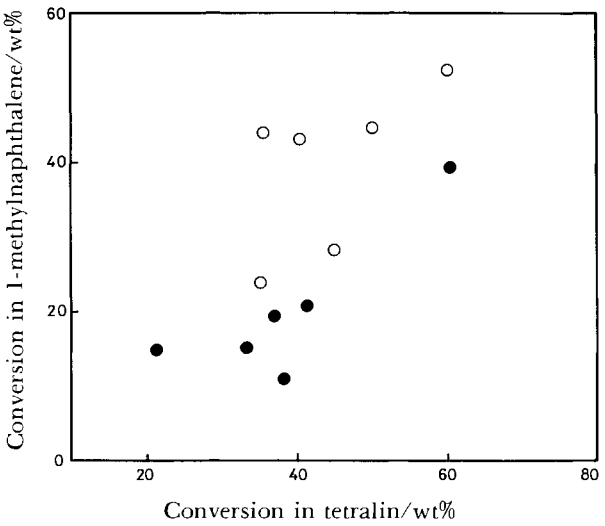

Fig. 1. The relationship between conversion of benzophenone (○), dibenzyl ether (●) in 1-methylnaphthalene under a hydrogen atmosphere and conversion in tetralin under a nitrogen atmosphere.

Table 2. The Effects of Aromatic Compounds on the Hydrogen-Transfer Reaction[a] to Dibenzyl Ether (DBE)

Run No.	Aromatic compound	Conv. of DBE	Yield of TOL[b]	Yield of BZA[b]
		mol%	mol%/2	mol%/2
12	1-Methylnaphthalene	14.6, 15.0	8.9, 9.5	5.7, 5.5
13	Anthracene	39.2	12.7	7.8
14	Phenanthrene	15.2	8.2	4.9
15	Pyrene	19.7	8.9	5.6
16	Fluorene	20.7	11.6	9.1
17	Diphenylmethane	13.8	8.6	3.8
18	Triphenylmethane	12.9	6.9	4.0

a) Aromatic compound (1.00 g), 1-methylnaphthalene (10.00 g) and dibenzyl ether (1.00 g) were used. Reaction temperature 375 °C; initial hydrogen pressure 3 MPa; reaction time 1 h. b) TOL=Toluene. BZA=Benzaldehyde.

high as 0.68. This indicates that the role of aromatic compounds in the hydrogen-transfer reaction with a donor solvent is similar to that with hydrogen molecules.

It is suggested from our results that anthracene has both the highest hydrogen-shuttling ability[3] and the highest ability to transfer hydrogen molecule. Coal liquefaction with an aromatic compound under an argon atmosphere has been reported.[11] In the report coal conversions based on quinoline-insoluble matter with anthracene were 31—34%. The conversions were lower than 48.1% with 1-methylnaphthalene. This indicated that anthracene might play an important role in coal conversion when anthracene is mixed with other compounds as the solvent.

Though the participation of hydrogen molecules in coal liquefaction is fairly complex, we believe that our methods to evaluate the abilities of hydrogen shuttling from a solvent[3] and the transference of hydrogen molecules are appropriate for evaluating solvent abilities.

Technical assistance by Mr T. Suzuki and H. Ando is greatfully acknowledged.

References

1) H. Tagaya, K. Takahashi, K. Hashimoto, and K. Chiba, *Energy Fuels*, **3**, 345 (1989); K. Chiba, H. Tagaya, and N. Saito, *Energy Fuels*, **1**, 338 (1987); K. Chiba, H. Tagaya, T. Kobayashi, and Y. Shibuya, *Ind. Eng. Chem. Res.*, **26**, 1329 (1987); M. L. Gorbatty, J. W. Larsen, and I. Wender, "Coal Science," Academic Press, New York (1983), Vol. 2, p. 65.

2) C. W. Curtis, J. A. Guin, and K. C. Kwon, *Fuel*, **63**, 1404 (1984).

3) K. Chiba, H. Tagaya, T. Suzuki, and T. Suzuki, *Bull. Chem. Soc. Jpn.*, **60**, 2669 (1987).

4) S. Futamura, S. Koyanagi, and Y. Kamiya, *Fuel*, **68**, 130 (1989).

5) S. V. Panvelker, Y. T. Shah, and D. C. Cronauer, *Ind. Eng. Chem. Fundam.*, **21**, 236 (1982).

6) L. W. Vernon, *Fuel*, **59**, 102 (1980).

7) K. Ouchi and M. Makabe, *Fuel*, **67**, 1536 (1988).

8) H. Tagaya, T. Ono, and K. Chiba, *Ing. Eng. Chem. Res.*, **27**, 895 (1988); K. Chiba, H. Tagaya, T. Yamauchi, and Y. Tsukahara, *Chem. Lett.*, **1985**, 945. K. Chiba, H. Tagaya, T. Yamauchi, and S. Sato, *Ind. Eng. Chem. Res.*, in press; D. Cronauer, D. M. Jewell, Y. T. Shah, and R. J. Modi, *Ind. Eng. Chem. Fundam.*, **18**, 153 (1979); T. Yao and Y. Kamiya, *Bull. Chem. Soc. Jpn.*, **52**, 492 (1979).

9) Y. Kamiya, S. Futamura, T. Mizuki, M. Kajioka, and K. Koshi, *Fuel Process. Technol.*, **14**, 79 (1986).

10) M. B. Simmons and M. T. Klein, *Ind. Eng. Chem. Fundam.*, **24**, 55 (1985).

11) G. O. Davies, F. J. Derbyshire, and R. Price, *J. Inst. Fuel*, **50**, 121 (1977).

A Convenient Preparation of 3,5-Disubstituted 1,2,4-Selenadiazoles from Primary Selenoamides by Treatment with *N*-Bromosuccinimide

Kazuaki SHIMADA, Yoichi MATSUDA, Shigeki HIKAGE, Yoshiyuki TAKEISHI, and Yuji TAKIKAWA*

Department of Applied Chemistry, Faculty of Engineering, Iwate University, Morioka, Iwate 020

(Received September 17, 1990)

Synopsis. A convenient preparation of 3,5-disubistituted 1,2,4-selenadiazoles was achieved by treatment of various primary selenoamides with *N*-bromosuccinimide.

The syntheses and transformation of selenium atom-containing heterocycles are of current interest in organic chemistry, and various methods for the synthesis of these compounds have been reported within the past several years;[1-6] nonetheless detailed investigation on the reactivities and the synthetic applications of selenazoles and selenadiazoles has been limited owing to the difficulty in preparation of the selenium-containing starting materials. It has been widely known that the most suitable starting material for these selenium-containing heterocycles are primary selenoamides **1**.[7-9] However, the preparation of these primary selenoamides **1** is impeded by the higher lability of **1** toward bases and oxidants, and few methods have so far been reported.[10-16] Cohen reported the synthesis of **1** from nitriles[15] and the subsequent transformation of **1** to the corresponding 3,5-disubstituted 1,2,4-selenadiazoles **2** by using I_2, but the yields of **2** were modest and the reactions were successful only in the cases of aromatic selenoamides **1**.[7]

In our previous paper we also provided a convenient synthesis of primary aromatic or aliphatic selenoamides, selenourea, and selenothiocarbamate by treatment of the corresponding nitriles, cyanamide, or thiocyanate with $(Me_3Si)_2Se$ in the presence of $BF_3{\cdot}OEt_2$.[17] It was naturally regarded that **1** would act as starting materials for the synthesis of 3,5-disubstituted 1,2,4-selenadiazoles **2** possessing various substituents by treatment with oxidizing reagents.[4,7] In this paper we would like to describe a convenient preparation of 3,5-disubstituted 1,2,4-selenadiazoles **2** by treatment of primary selenoamides **1** with *N*-bromosuccinimide (NBS).

Results and Discussion

A general procedure in the preparation of 3,5-disubstituted 1,2,4-selenadiazoles **2** is as follows. To a $CHCl_3$ solution of primary selenoamides **1**, 1.1 equiv

Table 1. Preparation of 3,5-Disubstituted 1,2,4-Selenadiazoles by Treatment of Selenoamides with Oxidizing Reagents[a]

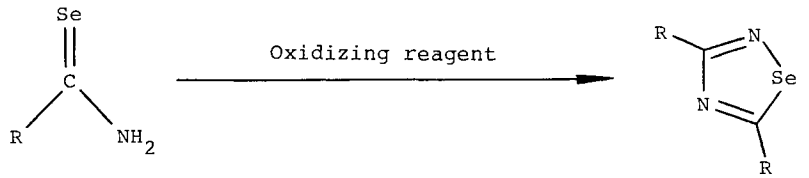

1 **2**

Run	Substrate/R		Oxidizing reagent (equiv)		Solvent	Temp/°C	Time/h	Yield/% of **2**
1	C_6H_5	(**1a**)	NBS	(1.1)	$CHCl_3$	R.T.	1	76
2	C_6H_5	(**1a**)	DMSO[b]	(Excess)	CH_2Cl_2	R.T.	9	23
3	*p*-$CH_3C_6H_4$	(**1b**)	NBS	(1.1)	$CHCl_3$	R.T.	1	72
4[c]	*p*-$CH_3C_6H_4$	(**1b**)	NBS	(1.1)	CH_2Cl_2	−78	40 min	87
5	*p*-$CH_3C_6H_4$	(**1b**)	30% H_2O_2	(2.0)	MeOH	0	10 min	66
6	*p*-$CH_3OC_6H_4$	(**1c**)	NBS	(1.1)	$CHCl_3$	0	1	70
7	*p*-ClC_6H_4	(**1d**)	NBS	(1.1)	$CHCl_3$	0	1	82
8	$CH_3CH_2CH_2$	(**1e**)	NBS	(1.1)	CH_2Cl_2	−90	6	25
9	$CH_3(CH_2)_3CH_2$	(**1f**)	NBS	(1.1)	CH_2Cl_2	−78	30 min	42
10	$CH_3(CH_2)_5CH_2$	(**1g**)	NBS	(1.1)	CH_2Cl_2	−78	1	63
11	Me_2N	(**1h**)	NBS	(1.2)	CH_2Cl_2	−78	5	36
12	Me_2N	(**1h**)	30% H_2O_2	(2.0)	MeOH	0	30 min	37
13	Me_2N	(**1h**)	MCPBA	(1.2)	MeOH	0	30 min	32
14	$C_6H_5CH_2S$	(**1i**)	NBS	(1.1)	CH_2Cl_2	−90	2	3[d]

a) The corresponding nitriles were obtained in all runs. b) One equiv of 1-methyl-2-chloropyridinium iodide was added. c) Five equiv of styrene was added. d) Benzyl thiocyanate was obtained in 80% yield.

of NBS in $CHCl_3$ was added dropwise under nitrogen atmosphere at 0 °C and stirred for 1 h. The reaction mixture was then quenched with 10% NaOH solution. After the usual work-up and purification by SiO_2 column chromatography, the resulting 3,5-disubstituted 1,2,4-selenadiazoles **2** were isolated in good to moderate yields as air-stable products. These results are shown in Table 1. By-products of the reaction were the corresponding nitriles in all cases owing to the facile selenium-extrusion of **1**. The physical properties of the obtained products **2** possessing aromatic substituents were identical in all respects with those reported by Cohen.[7] The structures of new products **2** having various aliphatic or heteroatom substituents were confirmed by ^1H NMR, IR, MS, and elemental analyses.

New products possessing heteroatom substituents, 3,5-bis(dimethylamino)-1,2,4-selenadiazole **2h** and 3,5-bis(benzylthio)-1,2,4-selenadiazole **2i**, were also obtained by this method. However, the yield of **2h** from *N,N*-dimethylselenourea **1h** was low, and only a trace amount of **2i** was formed from the corresponding selenothiocarbamate **1i** where benzyl thiocyanate was obtained in 80% yield. No improvement in the yield of **2h** could be achieved by using 30% H_2O_2 or MCPBA in place of NBS. The low yield of **2i** by treatment with NBS might be attributed to the higher affinity of the starting materials to the soft oxidizing reagent. Electron-donating substituents such as the dimethylamino group are expected to accelerate the chemical reactivities of 1,2,4-selenadiazole rings toward electrophilic reagents or Diels–Alder reactions,[18,19] and the introduction of such substituents to the rings would afford possibilities for the further conversions of this ring system to several heterocycles.

Other reagents for the oxidative dimerization of **1** were also investigated for the optimization of the preparation of **2**. However, unlike the synthesis of 3,5-disubstituted 1,2,4-thiadiazoles from primary thioamides,[20] treatment of **1a** with DMSO/1-methyl-2-chloropyridinium iodide system was not fully effective for the synthesis of 3,5-dipheyl-1,2,4-selenadiazole **2a** (Run 2 in Table 1). As was successful in the synthesis of 3,5-disubstituted 1,2,4-thiadiazoles, primary selenoamide Se-oxides were also expected to provide 1,2,4-selenadiazoles **2** by treatment with electrophilic reagents such as H^+. Although attempts for the isolation of *p*-methylselenobenzamide Se-oxide by the reaction of *p*-methylselenobenzamide **1b** with 30% H_2O_2 in MeOH at 0 °C were not successful, 3,5-di-*p*-tolyl-1,2,4-selenadiazole **2b**, *p*-methylbenzonitrile, and elemental selenium were obtained in 66, 27, and 64% yields, respectively.

In these reactions, several points are worth nothing: (1) Among the several reagents, NBS gives good results for the synthesis of 1,2,4-selenadiazoles **2** from primary selenoamides **1** except **1h** and **1i**. (2) The yields of 1,2,4-selenadiazoles **2** possessing aromatic substituents were generally high when NBS was used. On the other hand, aliphatic and heteroatom analogues **2** were obtained in moderate to low yields owing to the facile decomposition of selenoamides **1** to nitriles caused by the reagents.

The oxidative dimerization of selenoamides **1** was assumed to proceed via a similar mechanism that form 3,5-disubstituted 1,2,4-thiadiazoles reported previously by us.[20]

Conclusively, we have established a convenient one-step synthesis of 3,5-disubstituted 1,2,4-selenadiazoles **2** by treatment of primary selenoamides **1** with NBS. These products are expected to promote further chemical conversions by the use of reactivities of carbon–selenium or nitrogen–selenium bonds in the aromatic ring as well as the introduction of various functionalities to the 3- and 5-positions of the nucleus. Chemical conversion of 1,2,4-selenadiazoles **2** toward novel heterocyclic ring systems is now in progress in our laboratory.

Experimental

General. The starting selenoamides **1** were prepared by treatment of the corresponding nitriles with $(Me_3Si)_2Se$ in the presence of $BF_3{\cdot}OEt_2$.[17] The other reagents were commercial reagent grade materials and were purified by recrystallization or by distillation prior to use. IR spectra were recorded with a Hitachi 295 infrared spectrophotometer. ^1H NMR spectra were recorded with a Hitachi R-22 (90 MHz) spectrometer in deuteriochloroform solution containing tetramethylsilane as an internal standard. MS spectra were recorded with a Hitachi RMU-6M and Hitachi M-2000 spectrometer, with a direct inlet system, operating at 20 or 70 eV.

General Procedure for the Reaction of Primary Selenoamides 1 with NBS. A typical procedure is described below for the preparation of 3,5-diphenyl-1,2,4-selenadiazole **2a**. A solution of 196 mg (1.1 mmol) of NBS in 50 ml of $CHCl_3$ was added dropwise to a solution of 184 mg (1 mmol) of selenobenzamide **1a** in 50 ml of $CHCl_3$ at room temperature under nitrogen atmosphere, and was stirred for 1 h. The reaction mixture was then quenched with excess amount of 2M NaOH solution (1M=1 mol dm^{-3}). Precipitated elemental selenium was separated by filtration, and the filtrate was extracted with $CHCl_3$. The organic layer was washed with water and dried over anhydrous sodium sulfate. After removal of $CHCl_3$, the residue was purified by SiO_2 column chromatography using benzene as an eluent to give 3,5-diphenyl-1,2,4-selenadiazole **2a** in 76% yield.

2a: Colorless needles; mp 85 °C (lit, 85 °C);[7] IR (KBr) 1515, 1480, 1440, 1420, 1320, 1278, 1218, 1094, 1068, 1025, 1000, 970, 870, 760, and 680 cm^{-1}; ^1H NMR δ=7.43—7.53 (m, 6H), 7.93—8.05 (m, 2H), and 8.34—8.47 (m, 2H).

2b: Colorless needles; mp 122 °C (lit, 122 °C);[7] IR (KBr) 2925, 2830, 1600, 1482, 1410, 1320, 1300, 1280, 1240, 1160, 1090, 1020, 965, and 822 cm^{-1}; ^1H NMR δ=2.37 (s, 3H), 2.38 (s, 3H), 7.33 (d, J=8 Hz, 2H), 7.34 (d, J=8 Hz, 2H), 7.83 (d, J=8 Hz, 2H), and 8.27 (d, J=8 Hz,2H).

2c: Colorless needles; mp 139 °C (lit, 139 °C);[7] IR (KBr) 2925, 2840, 1600, 1485, 1318, 1245, 1165, 1095, 1022, 965, and 822 cm^{-1}; ^1H NMR δ=3.80 (s, 3H), 3.82 (s, 3H), 6.89 (d, J=8 Hz, 2H), 6.95 (d, J=8 Hz, 2H), 7.83 (d, J=8 Hz, 2H), and 8.30 (d, J=8 Hz, 2H).

2d: Colorless needles; mp 168 °C (lit, 168 °C); IR (KBr) 1590, 1510, 1475, 1400, 1310, 1280, 1230, 1165, 1090, 1015, 970, 875, 830, 735, and 685 cm^{-1}; ^1H NMR δ=7.24 (d, J=8 Hz, 4H), 7.87 (d, J=8 Hz, 2H), and 8.27 (d, J=8 Hz, 2H).

2e: Pale yellow oil; MS (m/z, ^{80}Se) 218 (M^+, 1%); IR (neat) 2950, 2860, 1700, 1515, 1450, 1375, 1268, 1195, 1142, 1080, 1052, 1025, 945, and 850 cm^{-1}; ^1H NMR δ=0.98 (t, J=7 Hz,

3H), 1.06 (t, J=7 Hz, 3H), 1.85 (sextet, J=7 Hz, 4H), 2.92 (t, J=7 Hz, 2H), and 3.06 (t, J=7 Hz, 2H). Found: C, 43.53; H, 6.52; N, 12.44%. Calcd for $C_8H_{14}N_2Se$; C, 44.25; H, 6.50; N, 12.90%.

2f: Pale yellow oil; MS (m/z, ^{80}Se) 274 (M^+, 14%); IR (neat) 2920, 2850, 1510, 1450, 1375, 1260, 1190, 1140, 1055, 940, 720, and 580 cm^{-1}; ^1H NMR δ=0.83—0.98 (m, 6H), 1.27—1.99 (m, 12H), 2.94 (t, J=7 Hz, 2H), and 3.07 (t, J=7 Hz, 2H). Found: C, 52.32; H, 8.27; N, 10.10%. Calcd for $C_{12}H_{22}N_2Se$; C, 52.74; H, 8.11; N, 10.25%.

2g: Pale yellow oil; MS (m/z, ^{80}Se) 330 (M^+, 11%); IR (neat) 2920, 2850, 1510, 1450, 1375, 1265, 1140, 1070, and 720 cm^{-1}; ^1H NMR δ=0.80—0.95 (m, 6H), 1.10—1.19 (m, 20H), 2.93 (t, J=7 Hz, 2H), and 3.07 (t, J=7 Hz, 2H). Found: C, 58.01; H, 9.41; N, 8.33%. Calcd for $C_{16}H_{30}N_2Se$: C, 58.34; H, 9.18; N, 8.50%.

2h: Colorless needles; 49—50 °C, MS (m/z, ^{80}Se) 220 (M^+, 99%); IR (KBr) 2910, 2850, 1590, 1510, 1370, 1330, 1250, 1190, 1110, 1050, 1020, 850, and 720 cm^{-1}; ^1H NMR δ=3.08 (s, 6H) and 3.11 (s, 6H). Found: C, 32.83; H, 5.50; N, 26.39%. Calcd for $C_6H_{12}N_4Se$: C, 32.88; H, 5.52; N, 25.57%.

2i: Colorless oil; MS (m/z, ^{80}Se) 378 (M^+); IR (neat) 3040, 2890, 1490, 1440, 1370, 1160, 990, and 690 cm^{-1}; ^1H NMR δ=4.41 (s, 2H), 4.42 (s, 2H), and 7.20—7.45 (m, 10H). Found: C, 50.57; H, 3.71; N, 7.24%. Calcd for $C_{16}H_{14}N_2S_2Se$: C, 50.92; H, 3.74; N, 7.42%.

Preparation of 3,5-Diphenyl-1,2,4-selenadiazole 2a by DMSO/1-Methyl-2-chloropyridinium Iodide. A solution of 7.36 g (40 mmol) of selenobenzamide **1a**, 25 ml of DMSO, and 10.32 g (40 mmol) of 1-methyl-2-chloropyridinium iodide in 300 ml of CH_2Cl_2 under nitrogen atmosphere was stirred at room temperature for 9 h, and the reaction mixture was then filtered. After removal of CH_2Cl_2 and DMSO, the residue was recrystallized from EtOH to give 3,5-diphenyl-1,2,4-selenadiazole **2a** in 23% yield.

Preparation of 3,5-Disubstituted 1,2,4-selenadiazoles 2 by 30% H_2O_2. A typical procedure is described below for the preparation of 3,5-di-*p*-tolyl-1,2,4-selenadiazole **2b**. To a solution of 198 mg (1 mmol) of *p*-methylselenobenzamide **1b** in 20 ml of MeOH, a solution of 227 mg (2 mmol) of H_2O_2 in 5 ml of MeOH was added at 0 °C. Immediately a reddish solid precipitated. The reaction mixture was then separated by filtration to give 153 mg of solid **A**, and the filtrate was extracted with CH_2Cl_2. The organic layer was washed with water and dried over anhydrous sodium sulfate. After removal of the solvent, the residue was purified by SiO_2 column chromatography using hexane as an eluent to give *p*-methylbenzonitrile in 27% yield. The solid **A** was treated with CH_2Cl_2 to separate 3,5-di-*p*-tolyl-1,2,4-selenadiazole **2b** and elemental selenium in 66 and 64% yields, respectively.

Preparation of 3,5-Bis(dimethylamino)-1,2,4-selenadiazole 2h by MCPBA. To a solution of 151 mg (1 mmol) of *N,N*-dimethylselenourea **1h** in 5 ml of MeOH, a solution of 258 mg (1.2 mmol) of 80% MCPBA in 5 ml of CH_2Cl_2 was added at 0 °C, and stirred for 30 min. The reaction mixture was then quenched with saturated sodium sulfite solution, and extracted with $CHCl_3$. The organic layer was washed with water and dried over anhydrous sodium sulfate. After removal of the solvent, the residue was separated by SiO_2 column chromatography using hexane/ether (2/1) as an eluent giving 3,5-bis(dimethylamino)-1,2,4-selenadiazole **2h** and dimethylcyanamide in 32 and 23% yields, respectively.

References

1) T. Ueda, Y. Shibata, J. Sakakibara, M. Inoue, and T. Ishida, *Chem. Pharm. Bull.*, **30**, 3424 (1982).
2) M. Yokoyama, K. Kumata, H. Hatanaka, and T. Shiraishi, *Bull. Chem. Soc. Jpn.*, **59**, 2909 (1986).
3) T. Ueda, S. Kawai, and J. Sakakibara, *Chem. Pharm. Bull.*, **35**, 398 (1987).
4) I. Shibuya, *Nippon Kagaku Kaishi*, **1987**, 1691.
5) V. Bertini, A. De Munno, N. Picci, F. Lucchesini, and M. Pocci, *Heterocycles*, **26**, 2153 (1987).
6) M. Renson, "The Chemistry of Organic Selenium and Tellurium Compounds," ed by S. Patai and Z. Rappoport, John Wiley and Sons, Chichester (1986), Vol. 1, p. 399.
7) V. I. Cohen, *Synthesis*, **1978**, 768.
8) V. I. Cohen, *J. Heterocycl. Chem.*, **16**, 365 (1979).
9) V. I. Cohen, *Synthesis*, **1979**, 66.
10) F. v. Dechend, *Chem. Ber.*, **7**, 1273 (1874).
11) K. Kindler, *Liebigs Ann. Chem.*, **431**, 187 (1923).
12) L. G. S. Brooker, G. H. Keyers, and F. L. White, *J. Am. Chem. Soc.*, **57**, 2492 (1935).
13) W. Walter and G. Maerten, *Liebigs Ann. Chem.*, **669**, 66 (1963).
14) K. A. Jensen and P. H. Nielsen, *Acta Chem. Scand.*, **20**, 597 (1966).
15) V. I. Cohen, *Synthesis*, **1978**, 668.
16) A. Ogawa, J. Miyake, Y. Karasaki, S. Murai, and N. Sonoda, *J. Org. Chem.*, **50**, 384 (1985).
17) K. Shimada, S. Hikage, Y. Takeishi, and Y. Takikawa, *Chem. Lett.*, **1990**, 1403.
18) M. P. Cava and L. E. Saris, *J. Chem. Soc., Chem. Commun.*, **1975**, 617.
19) K. T. Potts, F. Huang, and R. K. Khattak, *J. Org. Chem.*, **42**, 1644 (1977).
20) Y. Takikawa, K. Shimada, K. Sato, S. Sato, and S. Takizawa, *Bull. Chem. Soc. Jpn.*, **58**, 995 (1985).

Synthesis of α-Amino Acids Containing a Cyclopropane Ring via Cobalt-Catalyzed Carbonylation-Amidocarbonylation of Cyclopropanemethanols

Yusuke AMINO and Kunisuke IZAWA*
Central Research Laboratories, Ajinomoto Co., Inc.,
1-1, Suzuki-cho, Kawasaki-ku, Kawasaki 210
(Received September 18, 1990)

Synopsis. *N*-Acetyl-3-cyclopropylalanine and 2-acetamido-3-cyclopropylbutyric acid were prepared under cobalt-catalyzed amidocarbonylation conditions from cyclopropanemethanol and α-methylcyclopropanemethanol, respectively. The reaction has been estimated to comprise the *in situ* formation of aldehyde from alcohol by cobalt-catalyzed hydrocarbonylation followed by subsequent amidocarbonylation.

Some α-amino acids containing a cyclopropane ring are natural products.[1] Their unique structures have been of interest from a physiological viewpoint.

We have prepared various nonproteinogenic α-amino acids utilizing cobalt-catalyzed amidocarbonylation from amide, aldehyde, and carbon monoxide (Scheme 1).

An attempt to prepare an α-amino acid containing a cyclopropane ring from cyclopropanecarbaldehyde via amidocarbonylation was unsuccessful, giving a complex mixture. The reactive cyclopropane ring adjacent to the formyl group did not remain intact under amidocarbonylation conditions. We then turned our attention to alternative routes for the preparation of α-amino acids containing a cyclopropane ring via carbonylation-amidocarbonylation of cyclopropanemethanols.

Results and Discussion

It is well known that the cobalt-catalyzed homologation of alcohol under synthesis gas proceeds through aldehyde formation followed by hydrogenation. Benzyl alcohol having electron-releasing substituents and *t*-butyl alcohol, which easily generate a stable carbonium ion, gave homologated alcohol in good yield.[3]

Since the reaction conditions of the amidocarbonylation is the same as those of the oxo synthesis, except for the coexistence of an amide, alcohol can be carbonylated to give corresponding aldehyde, which subsequently reacts with amide and carbon monoxide to afford *N*-acyl α-amino acid under amidocarbonylation conditions. Yukawa et al. demonstrated the preparation of *N*-acetyl-*O*-methyltyrosine in 50% yield from *p*-methoxybenzyl alcohol under hydroformylation conditions in the presence of acetamide.[4] Cobalt hydridocarbonyl ($HCo(CO)_4$), which behaves as a strong acid in a polar solvent,[5] is generated *in situ* and plays an important role in giving an alkylcobalt tetracarbonyl intermediate (or a carbonium ion) from alcohol in this process. Moreover, the coexistence of an amide is essential to proceed the reactions successfully, since gas absorption could not be observed under the above-mentioned reaction conditions without acetamide, while *p*-methoxyphenylacetaldehyde was obtained in good yield using *N,N*-dimethylformamide in place of acetamide.[4]

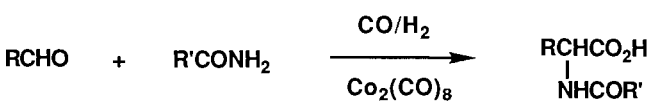

Scheme 1.

The cyclopropylmethyl cation, as well as the benzyl and *t*-butyl cations, are known to be stable carbonium ions. Whereas, the charge of the cyclopropylmethyl cation is delocalized on each of its four carbons. Namely, acidic hydrolysis of cyclopropylmethyl halide proceeds through a so-called "bicyclobutonium ion" to give cyclopropanemethanol, cyclobutanol, and 3-buten-1-ol.[6]

We tried to examine the use of cyclopropanemethanol (**1**) as a source for the carbonylation-amidocarbonylation. Although we had anticipated that the carbonylation-amidocarbonylation of cyclopropanemethanol (**1**) would give a mixture of *N*-acyl α-amino acids, **1** was transformed to *N*-acetyl-3-cyclopropylalanine (**4**) as the sole isolable *N*-acyl α-amino acid under amidocarbonylation conditions (see the experimental section) in ca. 8% yield. A possible mechanism for the formation of **4** is shown in Scheme 2. Changes in the reaction conditions (temperature, reaction time) as well as the addition of I_2 or CoI_2, did not increase the yield. Chloromethylcyclopropane did not give *N*-acyl α-amino acid under the same reaction conditions.

The yield of *N*-acyl α-amino acid was increased to 37% when the reaction was carried out under the following reaction conditions {$CO : H_2 = 3 : 1$ (80 atm at 25 °C), $Co_2(CO)_8$ (0.5 equiv), acetamide (2.0 equiv) at 120 °C for 18 h}. However, the product consisted of *N*-acetyl-3-cyclopropylalanine (**4**), *N*-acetylnorleucine (**9**), and *N*-acetylisoleucine (**10**) in a 1 : 1.5 : 1 ratio.

The formation of the latter two leucine derivatives can be explained as follows. Alkylcobalt tetracarbonyl intermediate (**2**) is considered to be in equilibrium with **5** and **6**. Intermediates (**7**) and (**8**) are generated by the hydrogenation of **5**, being accompanied by isomerization. Carbonylation-amidocarbonylation of **7** and **8** gives leucine derivatives, as shown in Scheme 2. Interestingly, an appreciable amount of 2-acetamido-2-cyclobutylacetic acid was not obtained, though the

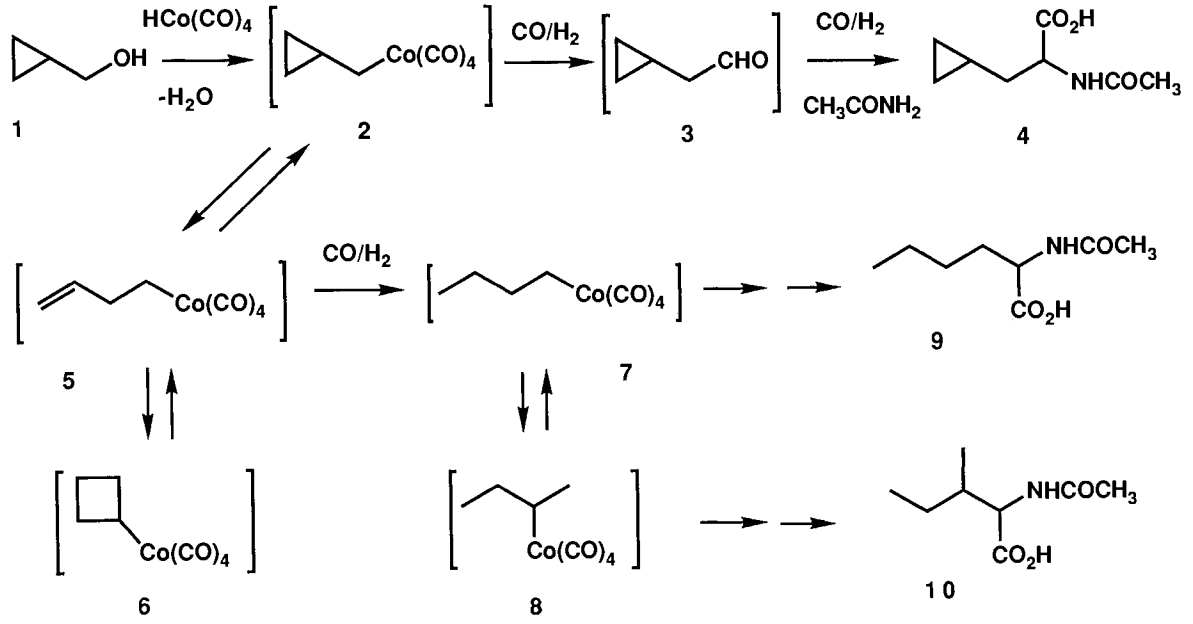

Scheme 2.

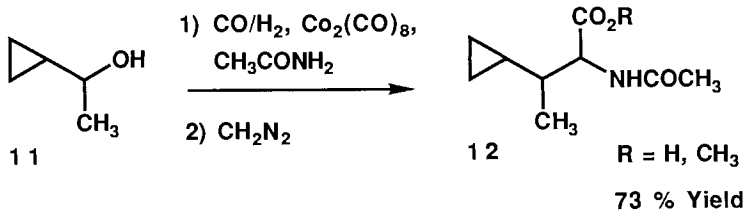

Scheme 3.

possible involvement of intermediate (**6**) would not be excluded.

Next, the reaction of α-methylcyclopropanemethanol (**11**), which is known to give the 1-cyclopropylethyl cation stabilized by a hyper-conjugation of the cyclopropyl and methyl groups, was successfully revealed, giving *threo*- and erythro-2-acetamido-3-cyclopropylbutyric acid (**12**) in 73% yield. Increasing the stability of the carbonium ion (or the alkylcobalt tetracarbonyl intermediate) resulted in a selective *in situ* generation of the desired aldehyde, which is effectively incorporated into subsequent amidocarbonylation.

The usefulness of amidocarbonylation for the synthesis of nonproteinogenic α-amino acid was demonstrated by a facil preparation of *N*-acetyl derivatives of 3-cyclopropylalanine and 2-amino-3-cyclopropylbutyric acid from cyclopropanemethanols via carbonylation followed by amidocarbonylation.

Isolation of these unique α-amino acids from *Amanita echinocephala* and *A. sp.*, as well as their inhibitory activities against spore germination of *Piricularia oryzae*, were previously reported by Nozoe et al.[7]

Experimental

^{1}H NMR spectra were measured with a Varian XL 300 spectrometer and chemical shifts are given as δ ppm relative to tetramethylsilane (TMS) as an internal standard. Infrared (IR) spectra were recorded on a Hitachi 260-10 spectrophotometer with samples as neat liquid. Mass spectra (MS) were recorded with a JEOL DX-300 instrument using the FAB technique. GC–MS was performed on an HP 5890A–5970B, with a high-performance capilary column (cross linked methyl silicone). The thin-layer chromatographic system employed silica gel Merck Art. 7515. PTLC was performed with a Whatman PLK 5F.

Reaction of Cyclopropanmethanol (1), Carbon Monoxide, and Acetamide Catalyzed by $Co_2(CO)_8$. A mixture of cyclopropanemethanol (**1**) (500 mg, 6.93 mmol), acetamide (409 mg, 6.93 mmol) and $Co_2(CO)_8$ (120 mg) in acetone (20 ml) was heated in a 100 ml stainless-steel autoclave with a 1 : 1 mixture of carbon monoxide and hydrogene (total pressure at 25 °C: 120 atm) at 100 °C for 20 h. The autoclave was then cooled to ambient temperature and depressurized. After the solvent was removed under reduced pressure, the residue was treated with 10% aqueous $NaHCO_3$ (50 ml) and an insoluble material filtered off. The filtrate was washed with AcOEt (50 ml) to remove neutral materials and acidified with concentrated HCl. The solution was extracted with AcOEt (50 ml); the extract was washed with brine, then dried over $MgSO_4$. After concentration of the solution, the residue

was esterified with ethereal diazomethane and purified by PTLC (developed with hexane : AcOEt=1 : 2, v/v) to give *N*-acetyl-3-cyclopropylalanine methyl ester (methyl ester of **4**) (105 mg, 0.57 mmol, 8.2%) as an oil.

***N*-Acetyl-3-cyclopropylalanine Methyl Ester (Methyl Ester of 4):** ^{1}H NMR (300 MHz, $CDCl_3$) δ=0.01—0.13 (2H, m, CH_2), 0.40—0.52 (2H, m, CH_2), 0.60—0.73 (1H, m, CH), 1.62—1.75 (2H, m, CH_2), 2.03 (3H, s, CH_3), 3.75 (3H, s, CH_3), 4.69 (1H, td, J=6.0 and 7.8 Hz, CH), 6.25 (1H, br. d, J=6.0 Hz, NH); IR (neat) 3280, 3060, 3000, 2950, 1740, 1650, 1540, 1435, 1375, 1205, 1160, 1008 cm^{-1}; GC-MS m/z 153 (M^+ −32), 142 (M^+ −43), 126 (M^+ −59). High mass (FAB) m/z Calcd for $C_9H_{15}N_1O_3$+H: 186.1130. Found: 186.1123; R_f 0.63 ($CHCl_3$: MeOH=10 : 1, v/v on silica gel).

Methyl 2-Acetamido-3-cyclopropylbutyrate (Methyl Ester of 12): ^{1}H NMR (300 MHz, $CDCl_3$) δ=0.01—0.22 (2H, m, CH_2), 0.42—0.51 (2H, m, CH_2), 0.57—0.63 (1H, m, CH), 1.01 (3H, d, J=6.9 Hz, CH_3), 1.15—1.38 (1H, m, CH), 2.04 and 2.05 (3H, s, CH_3), 3.73 and 3.74 (3H, s, CH_3), 4.71 (1H, m, CH), 6.10 and 6.19 (1H, d, J=6.9 Hz, NH); IR (neat) 3300, 3060, 2990, 2950, 1740, 1650, 1435, 1430, 1370, 1205, 1145, 1005 cm^{-1}; GC-MS m/z 167 (M^+ −32), 156 (M^+ −43), 140 (M^+ −59). High mass (FAB) m/z Calcd for $C_{10}H_{17}N_1O_3$+H: 200.1287. Found: 200.1300; R_f 0.70 ($CHCl_3$: MeOH=10 : 1, v/v on silica gel).

***N*-Acetylnorleucine Methyl Ester (Methyl Ester of 9):** ^{1}H NMR (300 MHz, $CDCl_3$) δ=0.89 (3H, t, J=6.9 Hz, CH_3), 1.26—1.35 (4H, m, CH_2), 1.58—1.85 (2H, m, CH_2), 2.03 (3H, s, CH_3), 3.75 (3H, s, CH_3), 4.60 (1H, td, J=7.2 and 6.0 Hz, CH), 6.03 (1H, br. d, J=3.9 Hz, NH); IR (neat) 2960, 1745, 1660, 1540, 1440, 1380, 1220, 1160 cm^{-1}. GC-MS m/z 187 (M^+), 155 (M^+ −32), 140 (M^+ −43), 128 (M^+ =59).

***N*-Acetylisoleucine Methyl Ester (Methyl Ester of 10):** ^{1}H NMR (300 MHz, $CDCl_3$) δ=0.85—0.95 (6H, m, CH_3), 1.10—1.25 (1H, m, CH_2), 1.38—1.50 (1H, m, CH_2), 1.80—1.92 (1H, m, CH), 2.03 (3H, s, CH_3), 3.74 (3H, s, CH_3), 4.60 (0.5H, dd, J=9.0 and 5.4 Hz, CH), 4.72 (0.5H, dd, J=9.0 and 4.2 Hz, CH), 6.06 (1H, br. d, J=8.1 Hz, NH); IR (neat) 2960, 1740, 1650, 1540, 1435, 1380, 1205, 1150 cm^{-1}; GC-MS m/z 155 (M^+ −32), 144 (M^+ −43), 128 (M^+ −59).

References

1) I. Wagner and H. Musso, *Angew. Chem., Int. Ed. Engl.*, **22**, 816 (1983).

2) a) H. Wakamatsu, J. Uda, and N. Yamakami, *J. Chem. Soc., Chem. Commun.*, **1971**, 1540. b) K. Izawa, *Yuki Gosei Kagaku Kyokai Shi*, **46**, 218 (1988).

3) a) I. Wender, H. Greenfield, S. Metlin, and M. Orchin, *J. Am. Chem. Soc.*, **74**, 4079 (1952). b) F. Piacenti and M. Bianchi, "Carbonylation of Saturated Oxygenated Compounds," in "Organic Synthesis via Metal Carbonyls," ed by I. Wender and P. Pino, John Wiley & Sons, New York (1977), Vol. 2, p. 1. c) H. Bahrmann and B. Cornils, "Homologation of Alcohols," in "New Synthesis with Carbon Monoxide," ed by J. Falbe, Springer-Verlag, Berlin Heidelberg (1980), Chap. 2.

4) T. Yukawa, N. Yamakami, M. Honma, Y. Komachiya, and H. Wakamatsu, Japan Patent 49-85011 (1974).

5) H. W. Sternberg, I. Wender, R. A. Friedel, and M. Orchin, *J. Am. Chem. Soc.*, **75**, 2717 (1953).

6) a) J. D. Roberts and R. H. Mazur, *J. Am. Chem. Soc.*, **73**, 2509 (1951). b) E. Renk and J. D. Roberts, *J. Am. Chem. Soc.*, **83**, 878 (1961).

7) a) T. Ohta, S. Nakajima, and S. Nozoe, The 103th Annual Meeting of the Pharmaceutical Society of Japan, Tokyo, April 1983, Abstr., 5C 2-1. b) T. Ohta, S. Nakajima, Z. Sato, T. Aoki, S.-I. Hatanaka, and S. Nozoe, *Chem. Lett.*, **1986**, 511.

Unambiguous Proof of Nitrile Formation from Pyrazine Skeleton through Photo-Oxidative Degradation. Isolation and Structural Determination of Photodegraded Product of Amorphous Poly(2,5-distyrylpyrazine)

Yukihiko HASHIMOTO, Yutaka ADEGAWA, Masaki HASEGAWA,* Kazuyuki ONODERA,†
Hirochika SAKURAGI,† and Katsumi TOKUMARU†
Department of Synthetic Chemistry, Faculty of Engineering, The University of Tokyo, Hongo, Bunkyo-ku, Tokyo 113
† Department of Chemistry, University of Tsukuba, Tsukuba, Ibaraki 305
(Received October 5, 1990)

Synopsis. In the presence of oxygen, amorphous poly(2,5-distyrylpyrazine) film was readily photodegraded, accompanied by cleavage of the pyrazine rings in the main chain. From the photodegraded film, *t*-2,*c*-4-diphenylcyclobutane-*r*-1,*t*-3-dicarbonitrile was isolated in 13% yield.

Various kinds of diolefinic compounds have been known to photopolymerize in the crystalline state into crystalline polymers having cyclobutane rings in the main chain. For example, 2,5-distyrylpyrazine (DSP) photopolymerizes in the crystalline state to give a high molecular weight liner polymer, poly(2,5-distyrylpyrazine) (poly-DSP).[1]

Thermal and photochemical behavior of poly-DSP has already been reported.[2–4] The crystalline poly-DSP is thermally depolymerized to the monomer in high yield.[2] In contrast, the photochemical reactivity of poly-DSP is affected by the matrix.[3] While poly-DSP is photodepolymerized in trifluoroacetic acid solution, it is highly stable photochemically in the crystalline state.[3] Furthermore, amorphous poly-DSP film is readily photodegraded with sunlight under air (Scheme 1). Such a high contrast in reactivity among the amorphous, crystalline, and solution states of the same polymer is quite unique in polymeric materials.

In this paper, we describe isolation and determination of one of the major degradation products of the amorphous poly-DSP film.

Results and Discussion

When poly-DSP film was stored in air under sunlight, absorption bands ascribable to hydroxyl, carbonyl, and cyano groups appeared in the IR spectrum.[3] Considering the structure of the polymer, the generation of nitrile compounds should be attributed to cleavage of the pyrazine rings in the main chain. On irradiation of amorphous poly[ethyl 4-[2-(2-pyrazinyl)ethenyl]cinnamate] (**1**) film, the nitrile formation was also observed in the IR spectrum.[5] A similar photodegradation was reported in the case of poly[2-(*p*-methoxycarbonylstyryl)-5-styrylpyrazine] (**2**).[6]

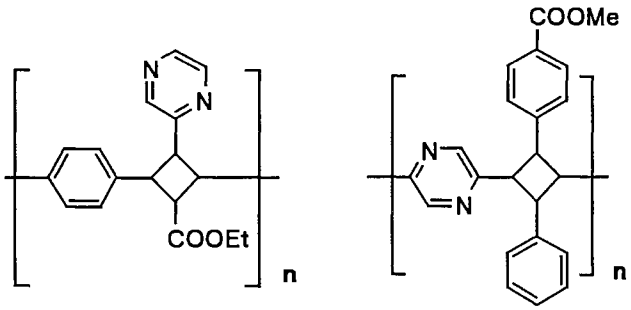

1 **2**

In order to confirm the generation of cyano groups and to throw light on the mechanism of photodegradation of the pyrazine ring, the photoreaction of substituted pyrazines such as 2,5-dimethylpyrazine was studied as a model of photodegradation of poly-DSP film.[3,4] In the case of low molecular weight azaaromatics, however, few reports have described on the nitrile formation through photoreaction.[7] Recently, we studied the photoreaction of 2,3,5,6-tetraphenylpyrazine from the viewpoint of a hindered pyrazine ring. On irradiation of the tetraphenylpyrazine in dichloromethane, a trace amount of benzonitrile was formed as detected by thin layer and gas chromatog-

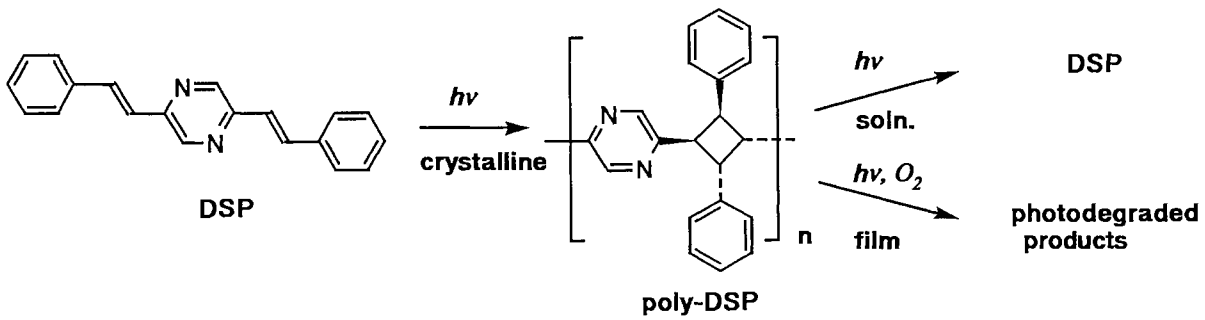

Scheme 1.

raphy. Nevertheless, the tetraphenylpyrazine was not suitable for a model of poly-DSP since the yield of products was not sufficient to attain our aim mentioned above.

Therefore, we tried to isolated directly degradation products of the poly-DSP film. The film was irradiated under oxygen with a super-high-pressure mercury lamp and extracted with chloroform. Evaporation of the solvent and separation with thin layer chromatography afforded a white powder as a product. This compound (**3**) was identified as 2,4-diphenylcyclobutane-1,3-dicarbonitrile by IR, ^{1}H and ^{13}C NMR, and mass spectra as follows. Namely, the IR spectrum of **3** represented the presence of cyano groups (2230 cm^{-1}) and the absence of pyrazine rings. In the ^{1}H NMR spectrum, a multiplet at ca. δ=7.5, and two double doublets at δ=4.3 and 4.0 indicated a diphenylcyclobutane skeleton for **3**. Furthermore, the ^{13}C NMR spectrum was consistent with the above formulation. The peaks at δ=135.19—127.01, 117.80, and 43.59—33.56 indicated the carbons of phenyl rings, of cyano groups, and of cyclobutane rings, respectively. The molecular weight 258 ($C_{18}H_{14}N_2$) for **3** was also confirmed by the mass spectrum. In EI-MS for **3**, a strong peak at *m/z* 129 corresponding to the fragmentation of $[M/2]^+$ (cinnamonitrile) was observed. Furthermore, CI-MS (isobutane) showed significant peaks at *m/z* 315, 259, and 130 corresponding to the fragmentation of $[M+C(CH_3)_3]^+$, $[M+H]^+$, and $[M/2+H]^+$, respectively.

The configuration of **3** was finally confirmed as shown in Fig. 1 by direct comparison of ^{1}H and ^{13}C NMR spectra with those of an authentic sample (**3'**) derived from α-truxillic acid. Consequently, the photodegradation of poly-DSP proceeds with retention of configuration around the cyclobutane rings of the starting polymer.

Although the photo-oxidative degradation mechanism and the origin of simultaneously generated carbonyl and hydroxyl groups have not been clarified yet, the present result is unambiguous proof of generation of cyano groups from pyrazine rings on irradiation under oxygen. Further interest is that a photodegradation product of polymeric material was readily isolated in a significant yield.

Experimental

Infrared spectra were recorded on a JASCO IR-810 spectrometer. ^{1}H and ^{13}C NMR spectra were obtained by using JEOL GX-400 instruments. Melting points were determined by a Laboratory Devices MEL-TEMP and were uncorrected. DSP and poly-DSP were prepared as described in the literature.[2]

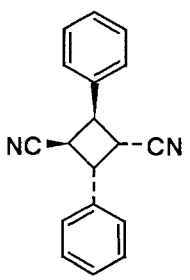

Fig. 1. Configuration of the isolated compound **3**.

Photodegradation of Amorphous Poly-DSP Film. Since crystalline poly-DSP is insoluble in usual organic solvents, trifluoroacetic acid was used as the solvent of poly-DSP. Amorphous poly-DSP film was prepared by casting its trifluoroacetic acid solution on glass plates. After the solvent was removed in vacuo, the film was washed with ethanol. The poly-DSP film (200 mg) in the flask with quartz beads was degassed by means of vacuum line and replaced by oxygen gas. The flask was sealed, and irradiated with stirring by light from a 500 W super-high-pressure mercury lamp through a water filter. After 120 h, the contents were extracted with chloroform (200 ml). The insoluble residue weighed about 40 mg. Separation of the soluble part of the products was carried out by preparative thin layer chromatography (49 : 49 : 2 $CHCl_3$/benzene/Et_2O and then 1 : 1 benzene/hexane), to give a white powder (**3**, 24 mg) as a main product, which was identified as 2,4-diphenylcyclobutane-1,3-dicarbonitrile on the basis of IR, ^{1}H and ^{13}C NMR, and mass spectra: IR (KBr) 3100—2850, 2230, 1495, 1450, 745, 700, and 660 cm^{-1}; ^{1}H NMR ($CDCl_3$) δ=7.52—7.39 (10H, m), 4.31 (2H, dd, J=7 and 9 Hz), and 4.03 (2H, dd, J=7 and 9 Hz); ^{13}C NMR ($CDCl_3$) δ=135.19, 129.31, 128.89, 127.01, 117.80, 43.59, and 33.56; MS (EI) *m/z* (rel intensity) 129 (100) and 102 (12); (CI, isobutane) *m/z* (rel intensity) 315 (35), 259 (20), and 130 (100).

Preparation of Authentic Sample of 2,4-Diphenylcyclobutane-1,3-dicarbonitrile. To a stirred suspension of α-truxillic acid (3.0 g, 10 mmol) in benzene (50 ml) was added an excess amount of thionyl chloride in the presence of DMF as a catalyst. The mixture was refluxed for 3 h. The resulting solution was concentrated in vacuo and the residual thionyl chloride was removed as the benzene azeotrope. The corresponding acid dichloride was obtained as a brown solid mass and used directly in the following step without further purification.

To 500 ml of concentrated aqueous ammonia was added dropwise, with vigorous stirring, a solution of the crude dichloride in benzene (60 ml). The reaction mixture was stirred until the precipitation was completed. Filtration followed by crystallization of the precipitate from ethanol–benzene gave the corresponding diamide (1.9 g, 65%).

To a suspension of the diamide (0.15 g, 0.50 mmol) in dichloromethane (100 ml) and DMF (8 ml) was added an excess amount of phosphoryl chloride. The mixture was refluxed for 8 h. The resulting solution was concentrated and the residual oil was poured into water. Filtration and crystallization of the precipitate from dichloromethane–hexane gave colorless plates (**3'**) (66 mg, 51%): Mp (CH_2Cl_2/hexane) 239—240 °C; IR (KBr) 3100—2850, 2230, 1490, 1460, 745, 700, and 660 cm^{-1}; ^{1}H NMR ($CDCl_3$) δ=7.50—7.39 (10H, m), 4.31 (2H, dd, J=7 and 9 Hz), and 4.02 (2H, dd, J=7 and 9 Hz); ^{13}C NMR ($CDCl_3$) δ=135.22, 129.31, 128.89, 127.03, 117.84, 43.56, and 33.56. Found: C, 83.39; H, 5.51: N, 10.95%. Calcd for $C_{18}H_{14}N_2$: C, 83.69; H, 5.46; N, 10.84%.

The authors are pleased to acknowledge Mitsui Toatsu Chemicals, Inc., for the measurement of mass spectrometry.

References

1) M. Hasegawa, *Chem. Rev.*, **83**, 507 (1983).
2) M. Hasegawa, Y. Suzuki, F. Suzuki, and H. Nakanishi, *J. Polym. Sci., Part A-1*, **7**, 743 (1969).

3) M. Sakuragi, M. Hasegawa, and M. Nishigaki, *J. Polym. Sci., Polym. Chem. Ed.*, **14**, 521 (1976); Y. Suzuki, T. Tamaki, and M. Hasegawa, *Bull. Chem. Soc. Jpn.*, **47**, 210 (1974).

4) K. Onodera, Thesis for M. Sc., University of Tsukuba, 1980.

5) For the preparation of **1**, see, M. Hasegawa, M. Aoyama, Y. Maekawa, and Y. Ohashi, *Macromolecules*, **22**, 1568 (1989).

6) M. Hasegawa, T. Katsumata, Y. Ito, K. Saigo, and Y. Iitaka, *Macromolecules*, **21**, 3134 (1988).

7) K. L. Wierzchowski, D. Shugar, and A. R. Katritsky, *J. Am. Chem. Soc.*, **85**, 827 (1963); K. L. Wierzchowski and D. Shugar, *Photochem. Photobiol.*, **2**, 377 (1963).

Oxidation of *s*-Alcohols with "Oxone" in Aprotic Solvents in the Presence of Wet-Aluminium Oxide

Masao HIRANO, Masaki OOSE, and Takashi MORIMOTO*
Department of Applied Chemistry, Faculty of Technology, Tokyo University of Agriculture and Technology, Koganei, Tokyo 184
(Received October 16, 1990)

Synopsis. The oxidation of secondary aliphatic, alicyclic, and benzylic alcohols with Oxone in aprotic solvents in the presence of "wet-aluminum oxide" afforded the corresponding ketones in good yields under mild conditions.

"Oxone" (**1**), a white free-flowing powder, is a stable double salt, consisting of potassium hydrogenperoxomonosulfate ($KHSO_5$), potassium hydrogensulfate, and potassium sulfate in 2 : 1 : 1 molar ratio.[1] Recent development in Oxone chemistry has been exclusively based on the behavior of **1**, intimately analogous to conventional peracids.[2,3] Thus, **1** has been conveniently used for oxygen-transfer-type reactions; viz. epoxidation of olefins,[4,5] allylic alcohols,[6] and unsaturated acid,[7] and oxidation of sulfides to sulfoxides[8] and/or sulfones[9] etc. However, the reactions with **1** so far studied were usually carried out in mixed solvents with water,[2-10] because of the negligible solubility of **1** in organic solvents; to our knowledge, the only exceptional case in a water-free solvent is the oxidation of sulfides mediated by a quarternary ammonium salt.[11] This paper describes the oxidation of various *s*-alcohols with Oxone in aprotic solvents under mild conditions in the presence of aluminium oxide (referred as Alumina). This reaction might be expected to provide a readily available methodology for Oxone oxidations with simple manipulation, and also with facile product isolation.

Results and Discussion

The oxidation was conducted by mixing **1**, an alcohol, and an aprotic solvent in the presence or absence of Alumina. The heterogeneous mixture was stirred under argon in order to exclude any influence of autoxidation. It should be noted that sufficiently effective stirring throughout a given period is essential to ensure a smooth, reproducible (±5%<) reaction. The progress of the reaction can easily be followed by GLC analysis of the supernatant withdrawn at intervals. The analysis revealed that in the absence of Alumina, the oxidation of 2-methylcyclohexanol (**2**) at 25°C in dichloromethane gave no detectable amount of 2-methylcyclohexanone (**3**), even within 24 h. The reaction with commercial "dry-Alumina" for 24 h led to the result that only 15% of **3** was obtained; 85% of **2** remained unreacted (GLC). On the other hand, a substantial consumption of 2 (92%) was observed for only 2 h in the presence of "wet-Alumina" (see Experimental), resulting in a dramatical increase of **3** (80%; isolated yield). Thus, "wet-Alumina" was proved to play an essential role in the oxidation. In the last case, it was observed that **2** is consumed as soon as the reaction started and that **3** increases with the progress of the reaction. There was no extensive formation of a by-product.

The oxidation was also conducted in acetonitrile and hexane in the presence of "wet-Alumina". In acetonitrile, Oxone showed a higher reactivity than in dichloromethane, and the substrate was almost consumed within 2 h at 25°C. However, a considerable formation of a by-product was observed, giving an inferior yield of **3** (35%) to that in dichloromethane. This compound also increased with a prolonged reaction and/or with the increased concentration of the oxidant at the expense of **3**, clearly indicating that **3** is susceptible to further oxidation in acetonitrile. An extensive formation of unknown by-products was also observed during the oxidations of 3- and 4-methyl, and 4-*t*-butylcyclohexanol in acetonitrile.# The oxidation in hexane was considerably slow under similar conditions, affording only a poor yield of **3**. Thus, dichloromethane might be a solvent of choice for the reactions of Entries 1—4.

The oxidation of the other alcohols (Entries 5—12) was performed in a manner similar to that of **2**, except that acetonitrile was used as a solvent in the place of dichloromethane, since a selective formation of the corresponding ketones, as well as much faster reactions than in dichloromethane, was observed in this solvent.

All of the tabulated alcohols underwent smooth oxidation in the presence of "wet-Alumina" and afforded the corresponding ketones in good yields. The results are presented in Table 1. A steric hindrance of an alkyl substituent on a cyclohexane-ring is small (Entries 1—3 and 6); even **2** or menthol, having a methyl and an isopropyl group adjacent to the hydroxyl groups, gave **3** or menthone, respectively, in high yield.

The present reaction is fairly clean and procedures for the isolation of a product are facile. Insoluble reagents can be readily removed by filtration, and the product can be isolated by evaporation of the solvent. Hence, it is emphasized that this system may be treated in a way quite similar to supported reagents comprising Alumina and various oxidants,[12-14] except that the present procedure can be instantly carried out without any laborious impregnation of the oxidant onto the support. When the purification

Identification of these compounds is now under way independently and will be reported in due course.

Table 1. Oxidation of *s*-Alcohols with Oxone in Aprotic Solvents in the Presence of "Wet-Alumina"[a]

Entry No.	Alcohols	Solvents[b]	Temp °C	Time h	Ketones %[c]
1	2-Methylcyclohexanol	DM	25	2	80
2	3-Methylcyclohexanol	DM	25	2	91
3	4-Methylcyclohexanol	DM	25	2	80
4	4-*t*-Butylcyclohexanol	DM	30	2	74
5	Cyclododecanol	AN	30	5	84
6	*l*-Menthol	AN	30	2	87
7	Borneol	AN	30	5	70
8	2-Heptanol	AN	30	2	80
9	2-Octanol	AN	30	2	85
10	1-Phenylethanol	AN	30	5	88
11	Diphenylmethanol	AN	30	5	89
12	Benzoin	AN	30	5	96

a) Under argon, 0.3 g of alcohol and 2.4 g of "wet-Alumina" were used in every run; [Oxone]/[Alcohol]=2.5 (mole ratio). b) 10 cm^3 of dichloromethane (DM) or acetonitrile (AN) was used. c) Isolated yield.

of carbonyl compounds, so obtained, was necessary due to contamination with parent alcohols and/or by-products, the crude products could be chromatographed immediately after evaporation of the solvent. Moreover, the reaction could be performed in an organic solvent, which overcomes the limited solubility of an organic substrate and/or an undesirable loss of water-miscible product attendant on the conventional reaction in a water-mixed solvent. Hence, this procedure serves as a novel and convenient tool for Oxone oxidation and may be a promising approach for the transformation of a variety of functional groups as well.

Experimental

^1H NMR spectra were measured with a JEOL PMX-60 model spectrometer for solutions in carbon tetrachloride or deuterated chloroform. IR spectra were recorded for thin films (neat or Nujol mull) on a JASCO A-100 spectrophotometer. GLC was carried out on a Shimadzu GC-4CM instrument with a 2 m column packed with 5% PEG-20M on Chromosorb GAW-DMCS, with temperature programming.

Materials. Oxone purchased from Aldrich Chemical Co., Inc. was used without purification. All of the alcohols were also commercially available. Solvents were rigorously dried and distilled. "Wet-Alumina" was prepared by vigorous shaking of commercial super-dried aluminium oxide (ICN BIOMEDICALS Alumina A, Super I; 20 g) with distilled water (4 g) untill a free-flowing powder was obtained.

General Oxidation Procedures. The following procedures are representative. To a heterogeneous mixture of "wet-Alumina" (2.4 g) and Oxone (2.5 times moles of an alcohol) in dichloromethane (10 cm^3) in a round-bottomed flask was added 2-methylcyclohexanol (0.3 g) in one portion with magnetic stirring. The flask was flushed with dry argon and then tightly sealed with a silicon-rubber septum, through which the supernatant was withdrawn by a microsyringe in the course of the reaction. The oxidation was conducted at a controlled temperature in a thermostat with efficient stirring. After a given period, the cooled mixture was filtered through a Pyrex Buchner funnel with a fritted disk, and the residue was repeatedly washed with either a solvent or dry ether. Evaporation of the combined filtrate on a rotary evaporator in vacuo gave an oil, which was chromatographed on silica gel eluted with hexane and ethyl acetate, giving pure **3** (0.236 g; 80%).

The purities of the products were checked by GLC: they were identified by a comparison of the GLC retention times, and the NMR and IR spectra with those of authentic samples.

The partial financial support for this research which came from Nippon Silica Kogyo Co., Ltd. and Daicel Chemical Industries, Ltd. is greatly acknowledged.

References

1) L. F. Fieser and M. Fieser, "Reagents for Organic Synthesis," John Wiley & Sons, New York (1967), Vol. 1, p. 952.

2) Concerning with the oxidations of olefins and sulfides (Ref. 3) with peracids, see the following reviews for comparison: a) B. Plesnicar, "Oxidation in Organic Chemistry," Part C, ed by W. S. Trahanovsky, Academic Press, New York (1978), p. 225. b) S. N. Lewis, "Oxidation," ed by R. L. Augustine, Marcel Dekker, Inc., New York (1969), Vol. 1, p. 223. c) D. Swern, "Organic Reactions," Vol. 7 (1953), p. 378.

3) (4a) p. 280. (4b) p. 244.

4) R. Bloch, J. Abecassis, and D. Hassan, *J. Org. Chem.*, **50**, 1544 (1985).

5) R. Curci, M. Fiorentino, L. Troisi, J. O. Edwards, and R. H. Pater, *J. Org. Chem.*, **45**, 4758 (1980).

6) G. Cicala, R. Curci, M. Fiorentino, and O. Laricchiuta, *J. Org. Chem.*, **47**, 2670 (1982).

7) P. F. Corey and F. E. Ward, *J. Org. Chem.*, **51**, 1925 (1986).

8) F. A. Davis, S. G. Lal, and H. D. Durst, *J. Org. Chem.*, **53**, 5004 (1988).

9) B. M. Trost and D. P. Curran, *Tetrahedron Lett.*, **22**, 1287 (1981).

10) R. J. Kennedy and A. M. Stock, *J. Org. Chem.*, **25**, 1901 (1960).

11) B. M. Trost and R. Braslau, *J. Org. Chem.*, **53**, 532 (1988).

12) A. Mckillop and D. W. Young, *Synthesis*, **1979**, 401 and 481.

13) G. H. Posner, *Angew. Chem., Int. Ed. Engl.*, **17**, 487 (1978).

14) G. H. Posner, "Preparative Chemistry Using Supported Reagents," ed by P. Laszlo, Academic Press, Inc., San Diego (1987), p. 287.

New Curvularin-Type Metabolites from the Hybrid Strain ME 0005 Derived from *Penicillium Citreo-viride* B. IFO 4692 and 6200

Sheng LAI, Yoshikazu SHIZURI, Shosuke YAMAMURA,* Kazuaki KAWAI,† and Hideyuki FURUKAWA†
Department of Chemistry, Faculty of Science and Technology, Keio University, Hiyoshi, Kohoku-ku, Yokohama 223
† Faculty of Pharmacy, Meijo University, Tenpaku-ku, Nagoya 468
(Received October 24, 1990)

Synopsis. Four new curvularin-type metabolites (11-α-methoxycurvularin, 11-β-methoxycurvularin, 11,12-dihydroxycurvularin, and 12-hydroxy-10,11-*trans*-dehydrocurvularin) have been isolated from the mycelium of the hybrid strain ME 0005 derived from *Penicillium citreo-viride* B. IFO 4692 and 6200. And β-hydroxycurvularin, the biologically active principle from *Alternaria tomato*, was identified as 11-β-hydroxycurvularin.

Curvularin-type macrolides are 12-membered ring keto lactones containing a fused 1,3-dihydroxybenzene ring. Because of an interesting macrocyclic skeleton adopting some flexible conformations and novel biological properties as described later, curvularin (**1**) and related macrolides have been receiving much attention of synthetic chemists[1] since the first isolation of curvularin and α,β-dehydrocurvularin (**2**) from *Curvularia* species.[2] These macrolides have also been found later in *Penicillium gilmanii*[3] and in *Alternaria* species.[4,5] Quite recently, six novel curvularin-type metabolites have been isolated by us from a hybrid strain ME 0005 derived from *Penicillium citreo-viride* B. IFO 4692 and 6200.[6]

Last decades, Hyeon et al.[7] isolated β-hydroxycurvularin and α,β-dehydrocurvularin as sporulation-suppressing factors from *Alternaria tomato* and recently Kobayashi et al.[8] also reported the isolation of β-hydroxycurvularin, β-methoxycurvularin[9] as well as curvularin and α,β-dehydrocurvularin as unique spindle poisons from *Penicillium* sp. 511. β-Hydroxycurvularin[7] was idenfied as 11-β-hydroxycurvularin (**3**) by comparison of its spectroscopic data, particularly ^{1}H NMR spectrum, with those of 11-β-hydroxycurvularin and 11-α-hydroxycurvularin (**4**),[10] but no stereochemical evidence of the compound β-methoxycurvularin[8,9] has been revealed. In the continuation of our study on the metabolites of the hybrid strain ME 0005, a mixture of methoxycurvularins was also obtained. It was, therefore, considered desirable to make a detailed investigation, which led to the isolation of 11-β-methoxycurvularin (**5**) and 11-α-methoxycurvularin (**6**) together with 11,12-dihydroxycurvularin (**7**) and 12-hydroxy-10,11-*trans*-dehydrocurvularin (**8**) as follows.

According to essentially the same procedure as described in the previous papers,[6] the EtOAc extract was chromatographed on silica gel (Katayama Chemicals, Type 60) using a gradient solvent of MeOH–$CHCl_3$ (1—10%). Each fraction was further separated by repeated preparative TLC and/or HPLC to give four new compounds (**5**, **6**, **7**, and **8**), in addition to the known metabolites *cis*-dehydrocurvularin, citreofuran, and 12-oxocurvularin (see Experimental).

Compounds **5** and **6** are quite similar to each other in their ^{1}H NMR spectral data. Both have a methoxyl

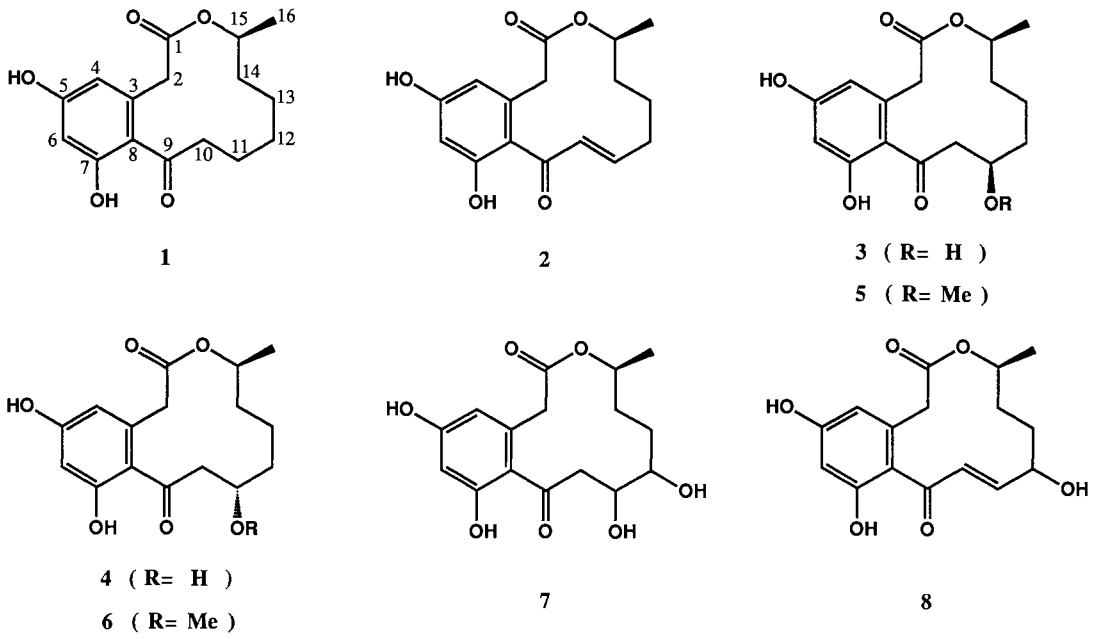

Scheme 1.

Table 1. Comparison of ^{1}H NMR Data of 11-Methoxycurvularins with 11-Hydroxycurvularins[a]

	11-β-Hydroxycurvularin (**3**)	11-α-Hydroxycurvularin (**4**)	11-β-Methoxycurvularin (**5**)	11-α-Methoxycurvularin (**6**)
H-10	*δ 3.63 (dd, J=13.7, 3.2)	* 3.23 (2H, br. d, J=6.8)[b]	* 3.88 (dd, J=13.3, 2.5)	* 3.38 (dd, J=14.2, 2.9)
	2.86 (dd, J=13.7, 10.3)		2.60 (dd, J=13.3, 10.1)	3.04 (dd, J=14.2, 10.3)
	** 3.48 (dd, J=13.6, 2.6)	3.25 (dd, J=14.2, 3.4)	3.64 (br. dd)	3.37 (dd, J=14.2, 2.9)
	2.85(overlapped)	3.03 (dd, J=14.2, 9.8)	2.56 (br. dd)	2.90 (dd, J=14.2, 10.2)
H-11	* 4.08 (1H, m)	4.09 (1H, m)	3.64 (1H, m)	3.66 (1H, m)
	** 4.02 (1H, m)	3.94 (1H, m)	3.62 (1H, m)	3.55 (1H, m)
H-15	* 4.87 (1H, m)	4.98 (1H, m)	4.81 (1H, m)	4.96 (1H, m)
	** 4.78 (1H, m)	4.90 (1H, m)	4.76 (1H, m)	4.90 (1H, m)

a) J values were given in Hz. * in CD_3OD; ** in acetone-d_6. b) This J value is an apparent one, because of the close similarity in the chemical shifts.

group [δ=3.33 (3H, s) for **5** and δ=3.25 (3H, s), for **6**] in the spectra which resemble broadly those of 11-hydroxycurvularins (**3** and **4**).[6] They also share the same mass spectrum, showing a molecular ion at m/z 322, and fragment ions at m/z 290, 203, 195, 177, 167, and 150, as that of α,β-dehydrocurvularin.[2] The formation of the prominent ion at m/z 290 (M^+—MeOH) and the ion at m/z 203 requires the presence of the methoxyl group at C-11. Thus, the structures of both **5** and **6** were deduced as 11-methoxycurvularins and were confirmed by chemical transformation of α,β-dehydrocurvularin (**2**) to these two stereoisomers. When treated on SiO_2 with MeOH–EtOAc (1 : 1) at room temperature for 5 d, α,β-dehydrocurvularin was slowly converted into a mixture of **5** and **6** in the ratio of 2 : 3[11] as a colorless oil, which was separated by HPLC to afford two pure 11-methoxycurvularins (**5** and **6**) which were identical with the two natural compounds, respectively. Finally, the stereostructures of the two isomers were determined by comparing their ^{1}H NMR data with those of 11-β-hydroxycurvularin and 11-α-hydroxycurvularin as shown in Table 1, wherein the chemical shifts of the protons at C-10 of the formers are quite different while those of the latters are close or identical to each other.

Compounds **7** and **8** show close similarities in their mass spectra, except for different molecular ions (m/z 324 for **7** and m/z 306 for **8**). Both show a predominent peak at m/z 288 originated from dehydration and the fragment peaks (m/z 203, 195, 177, 167, and 150) characteristic of α,β-dehydrocurvularin[2] and 11-methoxycurvularins (**5** and **6**), strongly suggesting that there should be an olefinic group adjacent to the aromatic carbonyl group or a hydroxyl group at C-11-position. The ^{1}H NMR spectra of **7** and **8** are also similar to each other and similar to curvularin-type compounds[2,6] including 11-methoxycurvularins in spite of somewhat differences as follows. Compound **7** shows two NMR signals at δ=5.25 (1H, m) and 5.46 (1H, m) in addition to δ=4.97 (1H, m), coupled with the molecular ion at m/z 324 in its mass spectrum, indicating the presence of two hydroxyl groups in the molecule. Irradiation of the multiplet at δ=5.25 collapsed the doublet at δ=3.46 (2H, d, J=8.8 Hz) into a singlet and caused partial collapse of the signal at δ=5.46, suggesting that the two hydroxyl groups are adjacent to each other and one should be located at C-11, the other at C-12. Thus, **7** was unambiguously determined as 11,12-dihydroxycurvularin.[12] As for compound **8**, the most significant difference between **7** and **8** is the virtual absence of two adjacent hydroxyl groups in the latter, but instead **8** has one hydroxyl group adjacent to a *trans*-1,2-disubstituted double bond (δ=6.61, 1H, dd, J=15.6, 1.0 Hz; δ=6.68, 1H, dd, J=15.6, 4.4 Hz). Irradiation of the multiplet at δ=4.54 collapsed the olefinc protons to doublets (J=15.6 Hz) and caused changes at δ=2.17 (1H, m) and 1.82 (1H, m). Therefore, compound **8** was unambiguously determined as 12-hydroxy-10,11-*trans*-dehydrocurvularin.[12]

Experimental

Melting points were determined on a Mitamura Riken apparatus and uncorrected. Optical rotations were determined with a JASCO DIP-360 polarimeter. IR spectra were taken on a JASCO A-202 spectrophotometer. ^{1}H NMR spectra were recorded on a JEOL JNM-GX 400 NMR spectrometer in $CDCl_3$ with tetramethylsilane as the internal standard unless otherwise noted. Mass spectra were measured on a Hitachi M-80 GC-MS spectrometer, operating with an ionization energy at 70 eV.

Incubation. Polished rice (600 g) in deionized water (ca. 1600 ml) was cooked using an electric cooker (99 °C, ca. 20 min) and transfered into two Erlenmyer flasks (5 l), which were pasteurized at 120 °C for 20 min at 2 atm. After inoculated with a suspension of the mycelium of the hybrid strain ME 0005 in sterilized water, the rice was incubated stationarily at 25 °C for 23 d and extracted with acetone.

Isolation and Separation. The acetone extract suspended in water (500 ml) was extracted with EtOAc (200 ml×5). The EtOAc extract (dark brown syrup, 4.85 g) was chromatographed on silica gel (300 g, Katayama Chemicals, Type 60) using $CHCl_3$ (2000 ml) and then a gradient solvent of MeOH–$CHCl_3$ (1% MeOH–$CHCl_3$ 2000 ml; 2—10% MeOH–$CHCl_3$ 500 ml for each). Elution with 3—4% MeOH–$CHCl_3$ afforded a dark brown oil, which was separated by repeated preparative TLC (Kieselgel 60 PF_{254}) using hexane–EtOAc (2 : 1), $CHCl_3$–acetone (2 : 1), and $CHCl_3$–MeOH (10 : 1), and then by preparative TLC (Kieselgel 60 F_{254}) using $CHCl_3$–MeOH [(15 : 1)×2], to afford compound **7** (0.02%) in addition to the known compounds *cis*-dehydrocurvularin (0.15%) and citreofuran (0.26%).[6] Elution with 6—7% MeOH–$CHCl_3$ gave a dark brown oil. When subjected to preparative TLC (Kieselgel 60 PF_{254}), developed with $CHCl_3$–acetone (2 : 1),

$CHCl_3$–MeOH (15 : 1), hexane–EtOAc (1 : 1) and then subjected to preparative TLC (Kieselgel 60 F_{254}) using $CHCl_3$–MeOH [(15 : 1)×2], the oil afforded compound **8** (0.15%) and the known 12-oxocurvularin (0.27%),[6] together with a mixture of **5** and **6** in the ratio of 2 : 1[11] as a colorless oil (16.25 mg, 0.34%). The mixture was further separated by HPLC (Unisil Q PH; ϕ 6.0×250 mm) using MeOH–H_2O (3 : 7) (flow rate: 0.5 ml min^{-1}; Detector: UV 250 nm), giving rise to compounds **5** (4.4 mg) and **6** (2.5 g).[13]

Conversion of α,β-Dehydrocurvularin (2) into 11-Methoxycurvularins. α,β-Dehydrocurvularin (**2**) (23.88 mg) in MeOH–EtOAc (1 : 1) (12 ml) was absorbed on SiO_2 (5 g) at room temp for 5 d, and then concentrated to dryness. The residue was subjected to preparative TLC (Kieselgel F_{254}), using $CHCl_3$–MeOH (10 : 1) and then hexane–acetone (2 : 1), to give a mixture of **5** and **6** in the ratio of 2 : 3[11] as a colorless oil (9.56 mg, 36%, c.y. 70%), which afforded compounds 11-β-methoxycurvularin (**5**) and 11-α-methoxycurvularin (**6**) when subjected to HPLC under the same conditions as mentioned above.

Compound 5 (11-β-Methoxycurvularin). Colorless oil; $[\alpha]_D^{23}$ −21.3° (*c* 0.22, EtOH); IR (film) 3300, 2935, 1700, 1656, 1608, 1590, 1460, 1265, 1165, 1132, 1080, 1020, 848, and 760 cm^{-1}; ^1H NMR δ=1.21 (3H, d, *J*=6.35 Hz), 1.4—1.8 (6H, complex), 3.06 (1H, dd, *J*=15.14, 7.81 Hz), 3.27 (1H, dd, *J*=15.14, 4.88 Hz), 3.33 (3H, s), 3.64 (1H, d, *J*=16.30 Hz), 3.81 (1H, m), 3.91 (1H, d, *J*=16.30 Hz), 4.98 (1H, m), 6.17 (1H, d, *J*=2.20 Hz), 6.30 (1H, d, *J*=2.20 Hz), 6.75 (1H, br. s), and 8.50 (1H, br. s); ^1H NMR (CD_3OD) δ=1.12 (3H, d, *J*=6.16 Hz), 1.2—1.7 (6H, complex), 2.60 (1H, dd, *J*=13.25, 10.10 Hz), 3.36 (3H, s), 3.58 (1H, d, *J*=15.40 Hz), 3.64 (1H, m), 3.88 (1H, dd, *J*=13.25, 2.50 Hz), 3.94 (1H, d, *J*=15.40 Hz), 4.81 (1H, m), 6.20 (1H, d, *J*=2.20 Hz), and 6.27 (1H, d, *J*=2.20 Hz); MS (*m/z*) 322 (M^+), 290 (M^+—MeOH, base peak), 203, 195, 177, 167, and 150. Found: *m/z* 290.1156. Calcd for $C_{16}H_{18}O_5$: M^+—MeOH, 290.1153.

Compound 6 (11-α-Methoxycurvularin). Colorless oil; $[\alpha]_D^{26}$ −4.2° (*c* 0.24, EtOH); IR (film) 3300, 2935, 1700, 1656, 1608, 1588, 1460, 1270, 1162, 1080, 986, 845, and 755 cm^{-1}; ^1H NMR δ=1.25 (3H, d, *J*=6.34 Hz), 1.4—1.95 (6H, complex), 3.12 (1H, dd, *J*=13.67, 8.31 Hz), 3.25 (3H, s), 3.34 (1H, dd, *J*=13.67, 4.88 Hz), 3.59 (1H, d, *J*=15.87 Hz), 3.77 (1H, m), 3.95 (1H, d, *J*=15.87 Hz), 5.14 (1H, m), 5.98 (1H, d, *J*=2.20 Hz), 6.36 (1H, d, *J*=2.20 Hz), 6.95 (1H, br. s), and 8.97 (1H, br. s); ^1H NMR (CD_3OD) δ=1.11 (3H, d, *J*=6.35 Hz), 1.44 (4H, m), 1.64 (2H, m), 3.04 (1H, dd, *J*=14.16, 10.26 Hz), 3.32 (3H, s), 3.38 (1H, dd, *J*=14.16, 2.93 Hz), 3.60 (1H, d, *J*=15.14 Hz), 3.66 (1H, m), 3.95 (1H, d, *J*=15.14 Hz), 4.96 (1H, m), 6.22 (1H, d, *J*=2.44 Hz), and 6.28 (1H, d, *J*=2.44 Hz); MS (*m/z*) 322 (M^+), 290 (M^+—MeOH, base peak), 203, 195, 177, 167, and 150. Found: *m/z* 290.1151. Calcd for $C_{16}H_{18}O_5$: M^+—MeOH, 290.1152.

Compound 7 (11,12-Dihydroxycurvularin). Brownish needles; mp 168—170°C (from $CHCl_3$–MeOH). $[\alpha]_D^{25}$ +69.3° (*c* 0.224, EtOH). IR (film) 3350, 1700, 1638, 1610, and 1590 cm^{-1}; ^1H NMR (CD_3OD) δ=1.14 (3H, d, *J*=6.35 Hz), 1.58 (1H, m), 1.63 (1H, m), 2.00 (1H, m), 2.27 (1H, m), 3.46 (2H, d, *J*=8.8 Hz), 3.50 (2H, s), 4.97 (1H, m), 5.25 (1H, m), 5.46 (1H, m), 6.24 (1H, d, *J*=1.95 Hz), 6.26 (1H, d, *J*=1.95 Hz). MS (*m/z*) 324 (M^+), 288 (M^+−2×H_2O, base peak), 203, 195, 177, 167, and 150. Found: *m/z* 288.0945. Calcd for $C_{16}H_{16}O_5$: M^+−2×H_2O, 288.0996.

Compound 8 (12-Hydroxy-10,11-*trans*-dehydrocurvularin). Yellowish powder, $[\alpha]_D^{26}$ −49.5° (*c* 0.86, EtOH). IR (film) 3350, 1705, 1638, 1610, and 1590 cm^{-1}. ^1H NMR (CD_3OD) δ=1.30 (1H, d, *J*=6.35 Hz), 1.70 (1H, m), 1.82 (1H, m), 2.00 (1H, m), 2.17 (1H, m), 3.48 (1H, d, *J*=15.38 Hz), 3.61 (1H, d, *J*=15.38 Hz), 4.54 (1H, m), 4.96 (1H, m), 6.38 (1H, d, *J*=1.95 Hz), 6.43 (1H, d, *J*=1.95 Hz), 6.61 (1H, dd, *J*=15.62, 0.98 Hz), 6.68 (1H, dd, *J*=15.62, 4.40 Hz). MS (*m/z*) 306 (M^+), 288 (M^+—H_2O, base peak), 203, 195, 177, 167, and 150. Found: *m/z* 288.0985. Calcd for $C_{16}H_{16}O_5$: M^+—H_2O, 288.0996.

References

1) R. H. Boeckman and M. Goldstein, "The Total Synthesis of Natural Products," ed by J. W. ApSimon, Wiley-Interscience, New York (1988), Vol. VII, pp. 20—23, and many references cited therein.

2) a) O. C. Musgrave, *J. Chem. Soc.*, **1956**, 4301; *ibid.*, **1957**, 1104; b) A. J. Birch, O. C. Musgrave, R. W. Rickards, and H. Smith, *ibid.*, **1959**, 3146; c) H. D. Munro, O. C. Musgrave, and R. Templeton, *ibid.*, **1967**, 947.

3) H. Raistrick and F. A. H. Rice, *J. Chem. Soc. C*, **1971**, 3069.

4) D. J. Robeson and G. A. Strobel, *Z. Naturforsch., C, Biosci.*, **36C**, 1081 (1981).

5) D. J. Robeson, G. A. Strobel, and R. N. Strange, *J. Nat. Prod.*, **48**, 139 (1985).

6) S. Lai, Y. Shizuri, S. Yamamura, K. Kawai, Y. Terada, and H. Furukawa, *Tetrahedron Lett.*, **30**, 2241 (1989); *Chem. Lett.*, **1990**, 589.

7) S. B. Hyeon, A. Ozaki, A. Suzuki, and S. Tamura, *Agric. Biol. Chem.*, **40**, 1663 (1976).

8) a) A. Kobayashi, T. Hino, K. Uneyama, and K. Kawazu, 27th Symposium on the Chemistry of Natural Products, Hiroshima, October 1985, Abstr., pp. 343—350; b) A. Kobayashi, S. Yata, T. Hino, and K. Kawazu, *Agric. Biol. Chem.*, **51**, 2857 (1987); c) A. Kobayashi, T. Hino, S. Yata, T. J. Itoh, and H. Sato, *ibid.*, **52**, 3119 (1988).

9) Expected to be identical with one of our 11-methoxycurvularins, but the compound β-methoxycurvularin is quite different from both 11-α-methoxycurvularin and 11-β-methoxycurvularin in both the optical rotation property and ^1H NMR data. As ^1H NMR spectrum of α-methoxycurvularin was recorded in $CDCl_3$ with a JEOL FX 100,[8] we also carefully measured ^1H NMR spectra of 11-α-methoxycurvularin and 11-β-methoxycurvularin in $CDCl_3$ on a JEOL FX 90A NMR spectrometer. These data are in accordance with those reported already in the Experimental, while they are still quite different from that of β-methoxycurvularin cited in the Ref. 8.

10) In order to establish the stereostructure of β-hydroxycurvularin, ^1H NMR spectra of 11-α-hydroxycurvularin and 11-β-hydroxycurvularin were also measured using acetone-d_6. The spectra are quite similar to each other except for the following points. 11-α-hydroxycurvularin: δ=3.25 (1H, dd, *J*=14.2, 3.4 Hz) (H-10β), 3.03 (1H, dd, *J*=14.2, 9.8 Hz) (H-10α), 3.94 (1H, m) (H-11β); 11-β-hydroxycurvularin: δ=3.48 (1H, dd, *J*=13.6, 2.6 Hz) (H-10α), 2.85 (overlapped with the signal of H_2O) (H-10β), and 4.02 (1H, m) (H-α). The spectral data of 11-β-hydroxycurvularin were indistinguishable from those of β-hydroxycurvularin.[7] Thus the latter was identified as 11-β-hydroxycurvularin.[6]

11) Based on the integration heights of their methoxyl groups in ^1H NMR spectra and supported by the calculated results according to the optical rotation of 11-β-methoxycurvularin (**5**, $[\alpha]_D^{23}$=−21.3°) and 11-α-methoxycurvularin (**6**, $[\alpha]_D^{26}$−4.2°): **5** : **6**=1.85 : 1 in the natural mixture ($[\alpha]_D^{25}$−15.3°), while **5** : **6**=0.8 : 1 in the synthetic mixture $[\alpha]_D^{27}$−11.8°).

12) The stereostructures of **7** and **8** have not yet been determined because of the flexible conformations of these new compounds.

13) 11-Methoxycurvularins are very unstable and easily dehydrated to give α,β-dehydrocurvularin during separation on preparative TLC plates or HPLC column.

New Synthesis and Diels-Alder Reactions of 2-Aminomethyl-1,3-butadienes and Related 1,3-Dienes

Akira HOSOMI,* Toshiyuki MASUNARI,† Yoshinori TOMINAGA,† and Makoto HOJO
Department of Chemistry, University of Tsukuba, Tsukuba, Ibaraki 305
† Faculty of Pharmaceutical Sciences, Nagasaki University, Nagasaki 852
(Received November 2, 1990)

Synopsis. 2-Aminomethyl-1,3-butadienes and 2,3-bis-(aminomethyl)-1,3-butadienes, readily prepared by the Grignard cross-coupling reaction of 2-bromo-2-aminopropene and vinylic bromides, are good Diels-Alder dienes toward various activated dienophiles to afford aminomethyl-substituted cyclohexenes.

The Diels-Alder reaction is important and convenient for the stereo- and regioselective construction of six-membered ring compounds and many efforts have been directed to prepare new 1,3-dienes.[1] We have shown that the organosilyl and organostannyl groups on the methyl group of isoprene dramatically improve both reactivity and regioselectivity, and that these reagents are an excellent building block for the synthesis of isoprene derivatives.[2] Furthermore 2-aminomethyl-3-silylmethyl-1,3-butadiene acts formally as the synthetic equivalent of the 2,2′-bis(allyl) diradical and zwitterion.[3] As a part of a program aimed at exploring a new class of 1,3-dienes, we report here the preparation of new aminomethyl-substituted 1,3-dienes and their cycloaddition.

The starting 1,3-dienes **1** were readily prepared by the cross-coupling of the Grignard reagent **2** with vinylic bromide as shown in Scheme 1.

1,3-Dienes **1**, thus obtained, react smoothly with various dienophiles to give the corresponding cycloadducts **5**. The results are listed in Table 1. In all cases aminomethyl-substituted cyclohexenes were obtained in good yield. The reaction proceeded in a stereospecific mode as it was seen in the reaction with dimethyl fumarate and dimethyl maleate which gave exclusively a *trans* and *cis* adduct, respectively. However the regioselectivity in this reaction with methyl acrylate (3-Me_2NCH_2-:4-Me_2NCH_2-=38:62) decreased presumably due to the electronegative amino

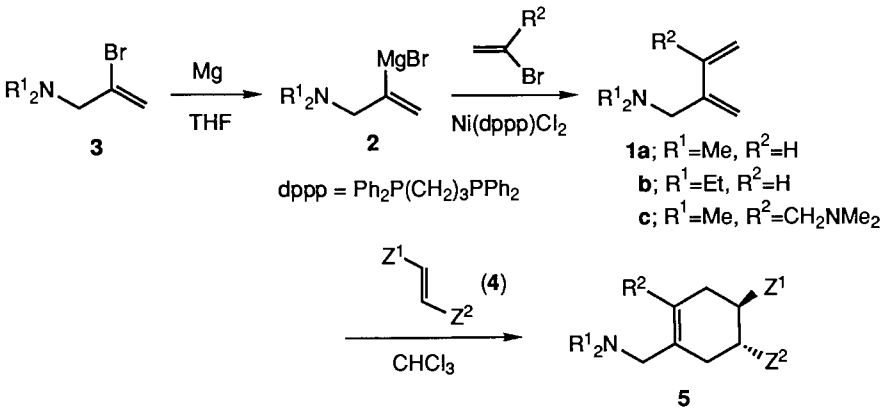

Scheme 1.

Table 1. The Diels-Alder Reaction of **1**[a]

Entry	Diene **1**	Dienophile **4**	Product **5** (Yield/%)[b]
1	**1a** (R^1=Me, R^2=H)	Dimethyl fumarate (**4a**)	**5a** (*trans*) (92)
2	**1a**	Dimethyl maleate (**4b**)	**5b** (*cis*) (67)
3	**1a**	Methyl acrylate (**4c**)	**5c**[c] (95)
4	**1a**	Ethyl acrylate (**4d**)	**5d** (80)
5	**1a**	3-Buten-2-one (**4e**)	**5e**[d] (98)
6	**1a**	Dimethyl acetylenedicarboxylate (**4f**)	**5f** (73)
7	**1b** (R^1=Et, R^2=H)	**4a**	**5g** (*trans*) (92)
8	**1b**	**4b**	**5h** (*cis*) (50)
9	**1b**	**4f**	**5i** (83)
10	**1c** (R^1=Me, R^2=CH_2NMe_2)	**4a**	**5j** (*trans*) (83)
11	**1c**	**4b**	**5k** (*cis*) (79)
12	**1c**	**4c**	**5l** (85)
13	**1c**	**4f**	**5m** (84)

a) In $CHCl_3$ at reflux for 20 h. b) Isolated by TLC. c) 3-Me_2NCH_2-:4-Me_2NCH_2=38:62. d) A mixture of regioisomers.

group, compared with the results using isoprene (30:70),[4] 2-silylmethyl-1,3-butadiene (16:84) and 2-stannylmethyl-1,3-butadiene (8:92).[2] The ratio was further close to ca. 1:1 when the reaction was carried out in the presence of a Lewis acid (44:56 for $AlCl_3$ and 43:57 for BF_3OEt_2) or hydrochloric acid (47:53). This result can be reasonably explained by the formation of more electronegative ammonium ion or a Lewis acid–amine complex.

The cycloadducts **5** include an allylamine unit which would form an electrophilic part after quaternization with an alkyl halide.[3] Therefore we studied the reaction of **5** with nucleophilic reagent. Thus, diethyl sodiomalonate reacted with the ammonium salt of **5c** in the presence of a catalytic amount of tetrakis(triphenylphosphine)palladium to give the substitution product **6** in 77% yield (Eq. 1).

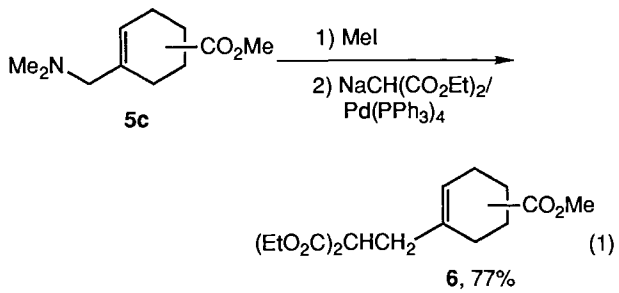

Thus, **1** is an important reagent for construction of aminomethyl-substituted six-membered ring products which are further subjected to electrophilic reactions.

Experimental

The IR spectra were recorded on a Shimadzu IR-460 spectrometer. The NMR spectra were determined on JEOL-JMN-60SI, FX-90Q spectrometers using TMS(tetramethylsilane) as an internal standard. MS spectra were recorded on JEOL-DX303 and Shimadzu QP2000 spectrometers. The microanalyses were performed at the Analytical Center of Nagasaki University and University of Tsukuba. Ether and tetrahydrofuran were distilled from sodium diphenylketyl. All experiments were carried out under an argon atmosphere. Purification of the product was carried out by thin layer chromatography (TLC) on silica gel. Unless otherwise noted, chemicals were purchased from commercial suppliers and used without further purification.

Synthesis of Aminomethyl-Substituted 1,3-Butadienes 1. A Typical Procedure. A Grignard reagent **2**,[3] readily prepared from 2-bromo-3-dimethylaminopropene (**3a**, R^1= Me) (16.4 g, 0.10 mol) and magnesium (4.8 g, 0.20 mol) in THF (10 ml), was added to vinyl bromide (12.8 g, 0.12 mol) in the presence of dichloro[1,3-bis(diphenylphosphino)propane]nickel (200 mg, 0.37 mmol) in THF (10 ml) at 0 °C. After stirring for 17 h at room temperature, hydrolysis of the reaction mixture and successive usual workup were carried out. After evaporation of solvent, the residue was distilled to give a colorless **1a** (9.8 g, 0.088 mol) in 88% yield. Bp 56 °C (1.24×10^4 Pa). Similarly, **1b**, and **1c**, bp 84 °C (5.6×10^3 Pa) and bp 85 °C (5.3×10^3 Pa), were prepared from the corresponding starting materials in 47 and 75% yields, respectively.

2-Dimethylaminomethyl-1,3-butadiene (1a): ^{1}H NMR ($CDCl_3$, 90 MHz) δ=2.22 (s, 6H), 2.99 (s, 2H), 4.97 (1H, d, J=12 Hz), 5.14 (2H, s), 5.38 (1H, d, J=18 Hz), 6.37 (1H, dd, J=12 and 18 Hz); IR (neat) 3030, 2980, 2860, 2830, 2780, 1810, 1457 cm^{-1}. MS m/z 111 (M^+, 100), 96 (13), 67 (16). Found: m/z 111.1053. Calcd for $C_7H_{13}N$: 111.1048. Anal. ($C_7H_{13}N$) C, H, N.

2-Diethylaminomethyl-1,3-butadiene (1b): ^{1}H NMR ($CDCl_3$, 90 MHz) δ=1.04. (t, J=7 Hz, 6H), 2.50 (q, J=7 Hz, 4H), 3.14 (bs, 2H), 4.90—5.70 (4H, m), 6.35 (1H, dd, J=10.5 and 16 Hz); MS m/z 139 (M^+, 73), 124 (100). Found: m/z 139.1339. Calcd for $C_9H_{17}N$: 139.1361. Anal. ($C_9H_{17}N$) C, H, N.

2,3-Bis(dimethylaminomethyl)-1,3-butadiene (1c): ^{1}H NMR (CCl_4, 60 MHz) δ=2.20 (s, 12H), 3.05 (s, 4H), 5.05 (bs, 2H), 5.30 (bs, 2H); IR (neat) 2975, 2895, 2860, 2820, 1598, 1457, 1357, 1265, 1177, 1034, 902, 855 cm^{-1}; MS m/z 168 (M^+, 6), 108 (17), 58 (100). Anal. ($C_{10}H_{20}N$) C, H, N.

General Procedure for the Diels–Alder Reaction of 1. In a 20 ml flask a mixture of a 1,3-diene **1** (0.5 mmol) and a dienophile (1.0 mmol) was heated at reflux in chloroform (3 ml) for 20 h. After the solvent was evaporated, the product was purified by TLC on silica gel. The physical properties and analytical data of the adducts obtained are listed below.

Dimethyl 4-Dimethylaminomethyl-4-cyclohexene-*trans*-1,2-dicarboxylate (5a): ^{1}H NMR (CCl_4, 90 MHz) δ=2.15 (s, 6H), 2.3—2.8 (m, 6H), 2.90 (s, 2H), 3.70 (s, 6H), 5.55 (bs, 1H); IR (CCl_4) 2950, 2015, 1738, 1674, 1257, 1234, 1107, 1030 cm^{-1}; MS m/z 255 (M^+, 36), 240 (7), 224 (8), 196 (26), 151 (8), 58 (100). Anal. ($C_{13}H_{21}NO_5$) C, H, N.

Dimethyl 4-Dimethylaminomethyl-4-cyclohexene-*cis*-1,2-dicarboxylate (5b): ^{1}H NMR (CCl_5, 90 MHz) δ=2.05 (s, 6H), 2.2—2.7 (m, 6H), 2.90 (s, 2H), 3.80 (s, 6H), 5.50 (bs, 1H); IR (CCl_4) 2975, 2855, 1741, 1679, 1027 cm^{-1}; MS m/z 255 (M^+, 39), 240 (6), 224 (6), 196 (31), 180 (4), 168 (3), 151 (10), 110 (13), 117 (39), 59 (100). Anal. ($C^{13}H_{21}NO_2$) C, H, N.

Methyl 3- and 4-Dimethylaminomethyl-3-cyclohexene-1-carboxylates (5c, as a Mixture): ^{1}H NMR (CCl_3, 90 MHz) δ=2.15 (s, 6H), 2.0—2.6 (m, 7H), 2.75 (s, 2H), 3.66 (s, 3H×0.38), 3.68 (s, 3H×0.62), 5.30 (bs, 1H); IR (CCl_4) 2975, 2855, 1793, 1673, 1256, 1150, 1021 cm^{-1}. Anal. ($C_{11}H_{19}NO_2$) C, H, N.

Ethyl 3- and 4-Dimethylaminomethyl-3-cyclohexene-1-carboxylates (5d, as a Mixture): ^{1}H NMR ($CDCl_3$, 90 MHz) δ=1.25 (3H, t, J=7 Hz), 1.55—2.64 (7H, m), 2.15 (6H, s), 2.75 (2H, s), 4.31 (2H, q, J=7 Hz), 5.56 (1H, s); MS m/z 211 (M^+, 27), 138 (11), 93 (18), 50 (100). Found: m/z 211.1562. Calcd for $C_{12}H_{21}NO_2$: 211.1573.

4- and 5-Acetyl-1-dimethylaminomethyl-1-cyclohexenes (5e, as a Mixture): ^{1}H NMR (CCl_4, 90 MHz) δ=1.64—2.73 (m, 7H), 2.15 (s, 3H), 2.76 (s, 2H), 5.58 (bs, 1H); IR (CCl_4) 2945, 1713, 1455, 1356, 1180, 1023 cm^{-1}; MS m/z 181 (M^+, 64), 166 (5), 110 (13), 93 (17), 59 (100). Found: m/z 181.1481. Calcd for $C_{11}H_{19}NO$: 181.1466. Anal. ($C_{11}H_{19}NO$) C, H, N.

Dimethyl 4-Dimethylaminomethyl-1,4-cyclohexadiene-1,2-dicarboxylate (5f): ^{1}H NMR (CCl_4, 60 MHz) δ=2.10 (s, 6H), 2.80 (s, 2H), 3.15 (bs, 4H), 4.80 (s, 6H), 5.65 (bs, 1H); IR (CCl_4) 2955, 2820, 1742, 1655, 1214, 1165, 1020 cm^{-1}. Anal. ($C_{13}H_{19}NO_4$) C, H, N.

Dimethyl 4-Diethylaminomethyl-4-cyclohexene-*trans*-1,2-dicarboxylate (5g) ^{1}H NMR (CCl_4, 60 MHz) δ=1.33 (6H, t, J=7 Hz), 2.2—2.8 (6H, m), 2.45 (4H, q, J=7 Hz), 2.85 (2H, bs), 3.70 (6H, s), 5.53 (1H, bs). Anal. ($C_{15}H_{23}NO_4$) C, H, N.

Dimethyl 4-Diethylaminomethyl-4-cyclohexene-*cis*-1,2-dicarboxylate (5h): ^{1}H NMR (CCl_4, 60 MHz) δ=0.96 (6H, t, J=7 Hz), 1.98—2.67 (10H, m), 2.80 (2H, bs), 3.77 (6H, s), 5.75 (1H, bs); MS m/z 283 (M^+, 42), 268 (96), 151 (100). Anal. ($C_{15}H_{23}NO_4$) C, H, N.

Dimethyl 4-Diethylaminomethyl-1,4-cyclohexadiene-1,2-dicarboxylate (5i): ^{1}H NMR ($CDCl_3$, 60 MHz) δ=0.97 (6H, t, J=7 Hz), 1.77—2.83 (8H, m), 2.93 (2H, s), 3.63 (6H, s), 5.83

(1H, bs); MS *m/z* 281 (M^+, 51), 266 (25), 222 (100). Found: *m/z* 281.1623. Calcd for $C_{15}H_{23}NO_2$: 281.1672.

Dimethyl 4,5-Bis(dimethylaminomethyl)-4-cyclohexene-*trans*-1,2-dicarboxylate (5j): ^1H NMR (CCl_4, 60 MHz) δ=2.05 (s, 12H), 2.80 (s, 4H), 2.9—3.2 (m, 6H), 3.6 (s, 6H); IR (CCl_4) 2975, 2355, 1738, 1457, 1197, 1172, 1012 cm^{-1}; MS *m/z* 312 (M^+, 1), 281 (19), 236 (17), 220 (85), 58 (100). Anal. ($C_{16}H_{28}N_2O_4$) C, H, N.

Dimethyl 4,5-Bis(dimethylaminomethyl)-4-cyclohexene-*cis*-1,2-dicarboxylate (5k): ^1H NMR (CCl_4, 60 MHz) δ=2.1 (s, 12H), 2.8 (s, 4H), 2.9—3.3 (m, 6H), 3.7 (s, 6H); IR 2975, 2860, 1738, 1458, 1440, 1260, 1198, 1173, 1023, 785, 761 cm^{-1}; MS *m/z* 312 (M^+, 2), 280 (29), 268 (85), 252 (85), 192 (54), 108 (57), 58 (100). Anal. ($C_{16}H_{28}N_2O_4$) C, H, N.

Methyl 3,4-Bis(dimethylaminomethyl)-3-cyclohexene-1-carboxylate (5l): ^1H NMR (CCl_4, 60 MHz) δ=2.05 (s, 12H), 2.91 (s, 4H), 2.95—3.2 (m, 7H), 3.6 (s, 3H); IR 2975, 2855, 1737, 1457, 1438, 1259, 1108, 1020 cm^{-1}; MS *m/z* 254 (M^+, 2), 166 (6), 195 (100), 134 (90), 117 (100). Anal. ($C_{14}H_{26}O_2N_2$) C, H, N.

Ethyl 3,4-Bis(dimethylaminomethyl)-3-cyclohexene-1-carboxylate (5m): ^1H NMR ($CDCl_3$, 90 MHz) δ=1.28 (3H, t, *J*=7 Hz), 2.22 (12H, s), 2.0—2.8 (7H, m), 2.90 (4H, bs), 4.14 (2H, q, *J*=7 Hz). Anal. ($C_{14}H_{26}N_2O_2$) C, H, N.

Synthesis of Methyl 3- and 4-[2,2-Bis(ethoxycarbonyl)-ethyl]-3-cyclohexene-1-carboxylates (6, as a Mixture). After **5c** (50 mg, 0.25 mmol) was quaternized with excess methyl iodide in THF (5 ml) at room temperature, a THF solution (10 ml) of sodiomalonate, prepared from diethyl malonate (1.6 g, 10 mmol) and sodium hydride (50% in paraffin, 0.48 g, 10 mmol), was added in the presence of tetrakis(triphenylphosphine)palladium (20 mg) and the mixture was stirred for 18 h at room temperature. After usual hydrolysis workup, **6** (60 mg, 0.193 mmol) was isolated by TLC (hexane/ether 1:1, R_f 0.3) in 77% yield. ^1H NMR (CCl_4, 60 MHz) δ=1.2 (t, *J*=7 Hz, 6H), 2.1—3.2 (m, 10H), 3.6 (s, 3H), 4.1 (q, *J*=7 Hz, 4H), 5.4 (bs, 1H); IR (CCl_4) 2920, 2860, 1738, 1450, 1250, 1120, 1012 cm^{-1}; MS *m/z* 312 (M^+, 28), 267 (7), 239 (14), 201 (52), 119 (100). Anal. ($C_{14}H_{20}O_6$) C, H.

References

1) B. Potthoff and E. Brietmaier, *Chem. Ber.*, **120**, 255 (1987); Y. S. Kulkarni and B. B. Snider, *Org. Prep. Proced. Int.*, **18**, 7 (1986); H. J. Reich, K. E. Yelm, and I. L. Reich, *J. Org. Chem.*, **49**, 3438 (1984); S.-S. P. Chou and C.-Y. Tsai, *ibid.*, **53**, 5305 (1988) and references cited therein.

2) A. Hosomi, M. Saito, and H. Sakurai, *Tetrahedron Lett.*, **21**, 355 (1980); A. Hosomi, H. Iguchi, J. Sasaki, and H. Sakurai, *ibid.*, **23**, 551 (1982); A. Hosomi, Y. Sakata, and H. Sakurai, *ibid.*, **26**, 5175 (1985); A. Hosomi, *Acc. Chem. Res.*, **21**, 200 (1988); A. Hosomi, T. Masunari, Y. Tominaga, T. Yanagi, and M. Hojo, *Tetrahedron Lett.*, **31**, 6201 (1990).

3) A. Hosomi, K. Otaka, and H. Sakurai, *Tetrahedron Lett.*, **27**, 2881 (1986); A. Hosomi, K. Hoashi, S. Kohra, Y. Tominaga, K. Otaka, and H. Sakurai, *J. Chem. Soc., Chem. Commun.*, **1987**, 570.

4) T. Inukai and T. Kojima, *J. Org. Chem.*, **31**, 1121 (1966).

Synthesis of 3- and 4-(ω-Phenylalkyl)catechols, the Sap Exuded from a Burmese Lac Tree, *Melanorrhoea Usitate*

Tetsuo MIYAKOSHI,* Yumin DU,†† and Ju KUMANOTANI†
Department of Industrial Chemistry, Meiji University,
Higashimita, Tama-ku, Kawasaki 214
†Faculty of Engineering, Ehime University,
Bunkyo-cho, Matsuyama, Ehime 790
(Received September 12, 1990)

Synopsis. The presence of 3- and 4-(ω-phenylalkyl)-catechols in Burmese lac has been confirmed by their synthesis. 3-(ω-Phenylalkyl)veratroles were synthesized by alkylation of ω-phenylalkyl bromide with aryl lithium derived from veratrole. 4-(ω-Phenylalkyl)veratroles were similarly obtained from ω-phenylalkyl bromide and 4-bromoveratrole. Demethylation of 3- and 4-(ω-phenylalkyl)-veratroles with boron tribromide gave the corresponding catechols in good yields.

In Asian countries, the exuded fluid sap from several kinds of lac trees is used as a preservative surface coating material for wood, porcelain, and metallic wares.[1,2] The sap of a Burmese lac tree, *Melanorrhoea usitate*, has been used as a naturally occurring phenolic coating material. In 1922, Majima reported that 4-substituted catechols having an n-C_{17} alkyl side chain were the main constituents of the sap of *Melanorrhoea usitate*,[3] but little is known about the other compounds of the sap of this plant. We executed an intensive compositional investigation of the sap of the Burmese lac tree by use of liquid chromatography, and isolated 3- (**1**) and 4-(ω-phenylalkyl)catechols (**2**), phenolic lipids with novel structure.[4-6] These compounds are included in about 40% in the sap of the Burmese lac tree. Novel structures **1** and **2** and their characteristic properties as phenolic coating materials have promptes us to synthesize **1** and **2**. We describe here the total syntheses of **1** and **2** on the basis of the cross coupling reaction previously developed in our laboratory for the synthesis of terpenoids.[7]

Results and Discussion

ω-Phenyl-1-alkanols (**4**) are useful intermediates in organic synthesis.[8] ω-Phenyl fatty acids are also important compounds in studies of metabolism.[8,9] Generally, **4** were prepared through reduction of ω-phenyl fatty acids[10] starting from the half ester

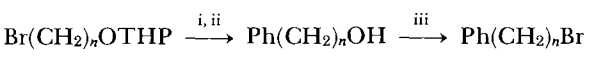

(**3**) (**4**) (**5**)

a: n=10, b: n=12

Scheme 1. Reagents: i, PhMgBr, CuCl, THF; ii, PPTS, MeOH; iii, HBr, H_2SO_4.

chloride of aliphatic dicarboxylic acid[11] and benzene, or ω-phenylalkyl bromide and diethyl malonate.[12] In the present case, we needed an efficient and mild procedure for the preparation of **4**. We recently reported a new synthetic method[7] of terpenoids using the copper(I) salt-catalyzed Grignard cross coupling reaction.[13] Based on these, we now report here analogous convenient synthesis of **4** as shown in Scheme 1.

The reaction of ω-bromo-1-(2-tetrahydropyranyloxy)-alkanes (**3**)[14-16] with phenylmagnesium bromide in the presence of copper(I) chloride in THF at reflux temperature gave exclusively cross coupling products, which were then hydrolyzed to the desired **4** in 78—80% isolated yields.

The reaction of 2,3-dimethoxyphenyllithium, prepared from veratrole and butyllithium with 1-bromo-10-phenyldecane (**5a**) gave 3-(10-phenyldecyl)veratrole (**6a**) in 74% yield.[17,18] 3-(12-Phenyldodecyl)veratrole (**6b**) was also prepared in the same manner from veratrole and 1-bromo-12-phenyldodecane (**5b**) in 76% yield (see Scheme 2).

Demethylation of **6a** using boron tribromide[19] yielded 3-(10-phenyldecyl)catechol (**1a**) in 86% yield.

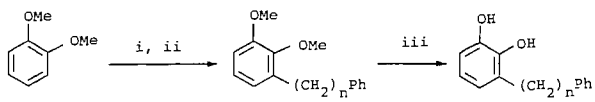

(**6**) (**1**)

a: n=10, b: n=12

Scheme 2. Reagents: i, BuLi, THF; ii, $Ph(CH_2)_nBr$, THF; iii, BBr_3, CH_2Cl_2.

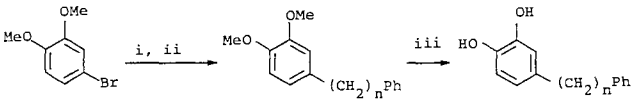

(**7**) (**2**)

a: n=10, b: n=12

Scheme 3. Reagents: i, BuLi, THF; ii, $Ph(CH_2)_nBr$, THF; iii, BBr_3, CH_2Cl_2.

†† Permanent address: Department of Chemistry, Wuhan University, Wuchang, China.

Similarly, 3-(12-phenyldodecyl)catechol (**1b**) was prepared in 87% yield. The IR, ^{1}H NMR, and EI-MS spectra of these products were in good agreement with those of the reported data.[4]

In a next stage, 4-(10-phenyldecyl)- (**7a**) and 4-(12-phenyldodecyl)veratrole (**7b**) were obtained by the coupling reaction of 3,4-dimethoxyphenyllithium[20] with 1-bromo-10-phenyldecane (**5a**) and 1-bromo-12-phenyldecane (**5b**), respectively (see Scheme 3).

Demethylation of **7a** and **7b** using BBr_3 yielded 4-(10-phenyldecyl)- (**2a**) and 4-(12-phenyldodecyl)catechol (**2b**) in 83 and 85% yield, respectively. The IR, NMR, and EI-MS spectra of **2** were in agreement with those of authentic sample. The ^{1}H NMR spectrum of **2** in $CDCl_3$ showed two triplets at δ=2.47 (2H, α-methylene protons of catechol group) and δ=2.57 (2H, α-methylene protons of phenyl group). On the other hand, the ^{1}H NMR spectrum of **1a** and **1b** in $CDCl_3$ each showed a triplet at δ=2.51 (4H, α-methylene protons of catechol and phenyl group).

The presence of **1** and **2** in the Burmese lac was confirmed using GLC by separate co-injection of their synthetic compounds with the natural products.

Experimental

Melting points were determined with a Yanagimoto micromelting point apparatus and were not corrected. IR spectra were measured on a Shimadzu IR-435 spectrometer in a liquid film or in KBr disc. All ^{1}H NMR spectra were taken in deuteriochloroform or carbon tetrachloride with tetramethylsilane as internal standard on a Varian EM 390 spectrometer (90 MHz) or JEOL GSX-270 spectrometer (270 MHz). Low resolution mass spectra were taken on a JEOL DX-300 mass spectrometer at 70 eV or with an emission current of 100 μA. High-performance liquid chromatography (HPLC) was performed on a Gilson liquid chromatograph with a Unisil ODS reverse phase column (4.6 mm×2.5 cm, 5 μm) or Develosil silica gel (4.6 mm×25 cm, 5 μm). Thin-layer chromatography (TLC) was run with precoated silica-gel plates (Merck, Art 5554). Spot detection was carried out with visualization by UV light and/or iodine vapor. Flash column chromatography was performed with glass column packed with Merck silica gel 60 (230—400 mesh). Capillary gas chromatography was performed on a Hewlett-Packard 5890A gas chromatograph using a DB-1 column (25 mm×0.25 mm).

Materials. ω-Bromo-1-(2-tetrahydropyranyloxy)alkane (**3**) were obtained from α,ω- alkanediol in good yields via ω-bromoalkyl alcohols.[14—16]

10-Phenyl-1-decanol (4a). A Grignard reagent was prepared from bromobenzene (7.07 mg, 45 mmol) and magnesium turning (0.96 g, 40 mmol) in dry THF (20 mL) with a small amount of I_2 as starter at 20—25 °C under dry nitrogen. To this Grignard solution, a solution of a mixture of 1-bromo-10-(2-tetrahydropyanyloxy)decane (**3a**) (9.63 g, 30 mmol) and CuCl (20 mg, 0.2 mmol) in dry THF (10 mL) was added at 0 °C for 10 min. The mixture was stirred for 5 h at reflux temperature. Then the ice-cooled reaction mixture was carefully added dropwise to a cold saturated NH_4Cl aq solution. The THF layer was separated and the aqueous layer was extracted with diethyl ether. The combined organic layer was washed with brine, dried (K_2CO_3) and concentrated in vacuo to give 9.8 g of crude cross-coupling product. This was employed in the next step without further purification.

A solution of the cross coupling product 9.8 g and *p*-toluenesulfonic acid (0.5 g, 2.4 mmol) in methanol (50 mL) were stirred for 8 h at room temperature. The mixture was neutralized with potassium carbonate and filtered through Celite. After removal of methanol in vacuo from the filtrate, the residual oil was purified by silica-gel column chromatography. Biphenyl as a by-product was obtained from the eluate with hexane–benzene (1:1) in 18% yield. The pure **4a** was obtained by chromatography over silica gel eluting with benzene–ethyl acetate (9:1) to give a compound (**4a**) (5.62 g) as oil. Yield: 80% from **3a** by 135—138 °C/2 Torr (1 Torr=133.322 Pa), R_f=0.38 (hexane–diethyl ether=1:1); IR (neat) 3300, 1600, 1500, and 700 cm^{-1}; ^{1}H NMR (CCl_4/TMS) δ=0.9—1.8 (br. s, 16H, CH_2), 2.54 (t, J=7 Hz, 2H, CH_2Ar), 2.91 (br. s, 1H, OH, D_2O exchangeable), 3.51 (t, J=6 Hz, 2H, CH_2O), and 6.9—7.3 (m, 5H, ArH). EI-MS *m/z* (rel intensity, %) 234 (M^+, 9), 216 (5), 117 (19) 104 (90), and 91 (100). Found: C, 81.87; H, 11.25%. Calcd for $C_{16}H_{26}O$: C, 81.99; H, 11.18%.

12-Phenyl-1-dodecanol (4b): In the same manner as described for compound (**4a**), 1-bromo-12-(2-tetrahydropyranyloxy)alkane (**3**) was converted to compound (**4b**). Yield: 80%, mp 37—38 °C (Lit,[9] mp 38—40 °C).

ω-Phenylalkyl Bromide (5). Compounds (**5**) were prepared from the ω-phenylalkyl alchols (**4**) and hydrobromic acid in the presence of sulfuric acid by mechanical stirring for 4 h at reflux temperature according to the general procedure reported in the literature.[21]

10-Phenyldecyl Bromide (5a). Yield: 81%, bp 145—146 °C/3 Torr, R_f=0.53 (hexane); IR (neat) 1600, 1500, 700, and 640 cm^{-1}; ^{1}H NMR (CCl_4/TMS) δ=1.15—2.0 (m, 16H, CH_2), 2.58 (t, J=7 Hz, 2H, CH_2Ar), 3.35 (t, J=7 Hz, 2H, CH_2Br), and 7.0—7.3 (m, 5H, ArH). EI-MS *m/z* (rel intensity, %) 298 (M^+, 17), 296 (M^+, 16), 133 (8), 105 (9) 92 (100), and 91 (74). Found: C, 64.54; H, 8.40%. Calcd for $C_{16}H_{25}Br$: C, 64.64; H, 8.48%.

12-Phenyldodecyl Bromide (5b). Yield: 83%, bp 155 °C/3 Torr, R_f=0.54 (hexane); IR (neat) 1600, 1500, 700, and 640 cm^{-1}; ^{1}H NMR (CCl_4/TMS) δ=1.13—2.0 (br. s, 20H, CH_2), 2.58 (t, J=7 Hz, 2H, CH_2Ar), 3.35 (t, J=7 Hz, 2H, CH_2Br), and 7.0—7.3 (m, 5H, ArH). EI-MS *m/z* (rel intensity, %) 326 (M^+, 13), 324 (M^+, 12), 133 (11), 104 (13), 92 (99), and 91 (100). Found: C, 66.48; H, 8.87%. Calcd for $C_{18}H_{29}Br$: C, 66.45; H, 8.99%.

3-(10-Phenyldecyl)veratrole (6a). Ten milliliters of butyllithium (1.6 M in hexane) was added to a stirred solution veratrole (6.62 g, 48 mmol) in dry THF (20 mL) at 0 °C under a nitrogen atmosphere (M=mol dm^{-3}). After stirring for 1 h at room temperature, a solution of 1-bromo-10-phenyldecane (**5a**) (4.75 g, 16 mmol) in dry THF (20 mL) was added and the mixture was refluxed for 4 h. The mixture was then poured into a saturated NH_4Cl aq solution and extracted with ethyl acetate. The ethyl acetate solution was washed with brine, dried (K_2CO_3), and concentrated in vacuo to give crude compound (**6a**). The residual oil was chromatographed over silica gel eluting with hexane to give tetradecylbenzene (15% yield). Compound (**6a**) was obtained from chromatography over silica gel eluting with hexane–benzene (5:95) to give 4.19 g (74% yield) of compound (**6a**) as a colorless liquid. IR (neat) 1600, 1585, 1500, 1080, 740, and 700 cm^{-1}; ^{1}H NMR (CCl_4/TMS) δ=1.1—1.6 (m, 16H, CH_2), 2.50 (t, J=7 Hz, 4H, CH_2Ar, CH_2Ph), 3.70 (s, 3H, CH_3O), 3.75 (s, 3H, CH_3O), 6.6—6.9 (m, 3H, ArH), and 7.1 (br. s, 5H, ArH). EI-MS *m/z* (rel intensity) 354 (M^+, 60), 151 (95), 120 (55), 91 (80), and 73 (100). Found: C, 81.22; H, 9.50%. Calcd for $C_{24}H_{34}O_2$: C, 81.31; H, 9.67%.

3-(12-Phenyldodecyl)veratrole (6b) was obtained by the reaction of compound (**5b**) (3.12 g, 9.6 mmol) with veratrole (3.97 g, 28.8 mmol) and butyllithium (6 ml, 9.6 mmol) in THF (20 mL). Yield 2.79 g (76%), IR (neat) 1600, 1585, 1500,

1080, 740, and 700 cm^{-1}; ^1H NMR (CCl_4/TMS) δ=1.1—1.6 (m, 20H, CH_2), 2.50 (t, J=7 Hz, 4H, CH_2Ar, CH_2Ph), 3.70 (s, 3H, CH_3O), 3.75 (s, 3H, CH_3O), 6.6—6.9 (m, 3H, ArH), and 7.1 (br. s, 5H, ArH). EI-MS m/z (rel intensity, %) 382(M^+, 50), 152 (48), 124 (30), and 91 (100). Found: C, 81.55; H, 9.95%. Calcd for $C_{26}H_{38}O_2$: C, 81.62; H, 10.01%.

4-(10-Phenyldecyl)veratrole (7a). To a solution of butyllithium (2.5 ml, 4 mmol) in dry THF (10 ml) was added 4-bromoveratrole (0.44 g, 2 mmol) in dry THF (10 mL) under nitrogen atmosphere. The mixture is stirred for 1 h at room temperature and then compound (**5a**) (0.60 g, 2 mmol) in dry THF (5 mL) was added under vigorous stirring. The reaction mixture was refluxed for 3 h. Then the mixture was allowed to cool to room temperature, and immediately hydrolyzed by pouring onto an iced NH_4Cl aq solution. The aqueous solution was acidified with hydrochloric acid. The mixture was then extracted with 50 mL of ethyl acetate. The ethyl acetate layer was separated, dried and evaporated. The residue was chromatographed over silica gel eluting with hexane–benzene (5:95) to give 0.43 g (61% yield) of compound (**7a**) as a colorless liquid. R_f=0.61 (hexane–benzene=5:95); IR (neat) 1600, 1520, 1260, 1230, 1140, 1020, 810, and 710 cm^{-1}; ^1H NMR (CCl_4/TMS) δ=1.3—1.8 (m, 16H, CH_2), 2.50 (t, J=7 Hz, 2H, CH_2Ar), 2.53 (t, J=7 Hz, 2H, CH_2Ar), 3.70 (s, 3H, CH_3O), 3.73 (s, 3H, CH_3O), and 6.6—7.3 (m, 8H, ArH). EI-MS m/z (rel intensity, %) 354 (M^+, 80), 151 (100), and 91 (90). Found: C, 81.19; H, 9.58%. Calcd for $C_{24}H_{34}O_2$: C, 81.31; H, 9.67%.

4-(12-Phenyldodecyl)veratrole (**7b**) was obtained by the reaction of compound (**5b**) with 4-bromoveratrole and butyllithium in dry THF. Yield 65%, R_f=0.65 (hexane–benzene=5:95); IR (neat) 1600, 1520, 1260, 1230, 1140, 1020, 810, and 710 cm^{-1}; ^1H NMR (CCl_4/TMS) δ=1.3—1.8 (m, 20H, CH_2), 3.73 (t, J=7 Hz, 2H, CH_2Ar), 2.53 (t, J=7 Hz, 2H, CH_2Ar), 3.70 (s, 3H, CH_3O), 3.73 (s, 3H, CH_3O), and 6.6—7.3 (m, 8H, ArH). EI-MS m/z (rel intensity, %) 382 (M^+, 45), 151 (56), and 91 (100). Found: C, 81.49; H, 10.12%. Calcd for $C_{26}H_{38}O_2$: C, 81.62; H, 10.01%.

3-(10-Phenyldecyl)catechol (1a). To a stirred solution of boron tribromide 0.7 g (2.8 mmol) in dichloromethane 5 mL was added dropwise a solution of compound (**6a**) (0.39 g, 1.1 mmol) in dichloromethane (20 mL) for 1 h at −10 °C. The mixture was allowed to warm up to room temperature slowly over 12 h. The mixture was hydrolyzed with water, diluted with dichloromethane. The dichloromethane layer was separated, washed with brine, dried ($MgSO_4$), and concentrated in vacuo below 30 °C. The residual oil was chromatographed on silica gel eluting with hexane–diethyl ether to give 0.31 g of compound (**1a**). Yield 86%, bp 185 °C/3 Torr, R_f=0.46 (hexane–diethyl ether=1:1); IR (neat) 3400, 1600, 1500, 780, and 730 cm^{-1}; ^1H NMR ($CDCl_3$/TMS) δ=1.1—1.8 (m, 16H, CH_2), 2.51 (t, J=7 Hz, 4H, CH_2Ar, CH_2Ph), 5.05, 5.18 (br. s, 1H, OH, D_2O exchangeable), 6.4—6.7 (m, 3H, ArH), and 6.9—7.3 (m, 5H, ArH). EI-MS m/z (rel intensity, %) 326 (M^+, 48), 124 (100), 123 (96), and 91 (47). Found: C, 80.89; H, 9.20%. Calcd for $C_{22}H_{30}O_2$: C, 80.93; H, 9.26%.

3-(12-Phenyldodecyl)catechol (**1b**) was obtained by the reaction of compound (**6b**) with boron tribromide. Yield 87%, R_f=0.58 (hexane–diethyl ether=1:1), mp 36.5 °C; IR (KBr) 3400, 1600, 1500, 780, and 730 cm^{-1}; IR (neat) 3400, 1600, 1500, 780, and 730 cm^{-1}; ^1H NMR ($CDCl_3$/TMS) δ=1.10—1.82 (m, 20H, CH_2), 2.51 (t, J=7 Hz, 4H, CH_2Ar, CH_2Ph), 5.15, 5.71 (br. s. 1H, OH, D_2O exchangeable), 6.44—6.68 (m, 3H, ArH), and 6.93—7.30 (m, 5H, ArH). EI-MS m/z (rel intensity, %) 354(M^+, 97), 124 (100), 123 (100), and 91 (87). Found: C, 81.25; H, 9.59%. Calcd for $C_{24}H_{34}O_2$: C, 81.31; H, 9.67%.

4-(10-Phenyldecyl)catechol (**2a**) was obtained by the reaction of compound (**7a**) with boron tribromide. Yield 83%, mp 56—57 °C, R_f=0.51 (benzene–ethyl acetate=1:1), IR (KBr) 3300, 1600, 1500, 1100, 800, and 700 cm^{-1}; ^1H NMR ($CDCl_3$/TMS) δ=1.2—1.8 (m, 16H, CH_2), 2.47 (t, J=7 Hz, 2H, CH_2), 2.57 (t, J=7 Hz, 2H, CH_2), 5.52 (br. s, 2H, OH, D_2O exchangeable), 6.5—6.8 (m, 3H, ArH), and 7.1—7.3 (m, 5H, ArH). EI-MS m/z (rel intensity, %) 326 (M^+, 55), 123 (100), and 91 (65). Found: C, 80.98; H, 9.19%. Calcd for $C_{22}H_{30}O_2$: C, 80.93; H, 9.26%.

4-(12-Phenyldodecyl)catechol (**2b**) was obtained by the reaction of compound (**7b**) with boron tribromide. Yield 85%, mp 62 °C, R_f=0.58 (benzene–ethyl acetate=1:1), IR (KBr) 3300, 1600, 1500, 1100, 800, and 700 cm^{-1}; ^1H NMR ($CDCl_3$/TMS) δ=1.2—1.8 (m, 20H, CH_2), 2.47 (t, J=7 Hz, 2H, CH_2Ar), 2.57 (t, J=7 Hz, 2H, CH_2Ar), 5.68 (br. s, 2H, OH, D_2O exchangeable), 6.5—6.8 (m, 3H, ArH), and 7.1—7.3 (m, 5H, ArH). EI-MS m/z (rel intensity, %) 354 (M^+, 55), 123 (100), and 91 (72). Found: C, 81.30; H, 9.75%. Calcd for $C_{24}H_{34}O_2$: C, 81.31; H, 9.67%.

The present work was financially supported in part by a Grant-in-Aid for General Scientific Research from the Ministry of Education, Science and Culture. We also thank Dr. Ryuichi Oshima, the University of Tokyo, for scientific discussions and encouragement.

References

1) J. H. P. Tyman, *Chem. Soc. Rev.*, **8**, 499 (1979).
2) J. Kumanotani, "Polymer Application of Renewable Resource Materials," ed by C. E. Carraher and L. H. Sperling, Plenum Press, New York (1983), pp. 225—248.
3) R. Majima, *Ber.*, **55B**, 191 (1922).
4) Y. Du, R. Oshima, Y. Yamauchi, J. Kumanotani, and T. Miyakoshi, *Phytochem.*, **25**, 2211 (1986).
5) Y. Du, R. Oshima, Y. Yamauchi, and J. Kumanotani, *J. Chem. Soc., Chem. Commun.*, **1985**, 630.
6) Y. Du and R. Oshima, *J. Chromatogr.*, **318**, 378 (1985).
7) T. Miyakoshi, H. Takazawa, and M. Hagimoto, *Yukagaku*, **39**, 83 (1990).
8) D. R. Elmaleh, E. Livni, R. Okada, F-L. Needham, J. Schleuederberg, and H. W. Strauss, *Nucl. Med. Commun.*, **6**, 287 (1985).
9) H. Oura, J. Hase, and K. Honda, *J. Pharm. Soc. Jpn.*, **71**, 1071 (1956).
10) J. Hase and H. Ohura, *Pharm. Bull. Jpn.*, **2**, 368 (1954).
11) P. Papa, *J. Am. Chem. Soc.*, **69**, 3018 (1947).
12) V. R. Huisgen, W. Rapp, I. Ugi, H. Walz, and I. Glogger, *Justus Liebigs Ann. Chem.*, **586**, 52 (1954).
13) E. Erdik, *Tetrahedron*, **40**, 641 (1984).
14) S-K. Kang, W-S. Kim, and B-H. Moon, *Synthesis*, **1985**, 1161, and reference cited therein.
15) T. Ando, Y. Kurotsu, M. Kaiya, and M. Uchiyama, *Agr. Biol. Chem.*, **49**, 1418 (1985).
16) F. Camps, J. Coll, A. Guerrero, and M. Riba, *J. Chem. Ecol.*, **9**, 869 (1983).
17) H. Halim, H. D. Lockaley, and J. J. Memon, *J. Chem. Soc., Perkin Trans. 1*, **1980**, 1331.
18) G. P. Ng and C. R. Dawson, *J. Org. Chem.*, **43**, 3205 (1978).
19) L. S. Kiong and J. H. P. Tyman, *J. Chem. Soc., Perkin Trans. 1*, **1981**, 1942.
20) R. Adams, "Organic Reactions," ed by R. G. Jones and H. Gilman, John Wiley & Sons, New York (1951), Vol. 6, pp. 339—366.
21) R. Adams, "Organic Reactions," ed by H. Gilman, John Wiley & Sons, New York (1948), Coll. Vol. 1, pp. 28—35.

Optical Resolution by Replacing Crystallization of Ammonium Salts of *N*-Acetyl-DL-2-aminobutanoic Acid, *N*-Acetyl-DL-norvaline, and *N*-Acetyl-DL-norleucine

Tadashi SHIRAIWA,* Masahiro YAMAUCHI, Takatoshi YAMAUCHI, Takao YAMANE, Makoto NAGATA, and Hidemoto KUROKAWA
Faculty of Engineering, Kansai University, Yamate-cho, Suita, Osaka 564
(Received October 12, 1990)

Synopsis. Ammonium salts of *N*-acetyl-DL-2-aminobutanoic acid, *N*-acetyl-DL-norvaline (DL-AcNva·AM salt), and *N*-acetyl-DL-norleucine were optically resolved by replacing crystallization in the presence of the ammonium salt of *N*-acetyl-L-alanine to give their salts with L-configuration. The optical resolution of the DL-AcNva·AM salt, espcially, gave the optically pure L-AcNva·AM salt by purification in 80% yield based on the half amount of the DL-salt used as the starting material.

Ammonium salts of *N*-acetyl-DL-2-aminobutanoic acid (denoted by DL-AcAbu·AM salt), *N*-acetyl-DL-norvaline (DL-AcNva·AM salt), and *N*-acetyl-DL-norleucine (DL-AcNle·AM salt) exist in conglomerates at room temperature and have been optically resolved by preferential crystallization.[1,2] Optical resolution by replacing crystallization is another procedure for obtaining one enantiomer from a conglomerate. Since this optical resolution is based on interactions between each of the enantiomers and an optically active cosolute,[3] it may give a clue to elucidate the chiral interaction in a solution. We, therefore, have been engaged in studying the optical resolution by replacing crystallization.[4] Optical resolutions by replacing crystallization of the DL-AcAbu·AM, DL-AcNva·AM, and DL-AcNle·AM salts were attempted as a part of our study program. This optical resolution seems to give a good result when we employ an optically active cosolute whose structure is similar to that of the racemate. In addition, the cosolute must be more soluble in the solvent than the racemate because crystallization of the cosolute makes it difficult to separate the crystallized mixture into the cosolute and the enantiomer. The ammonium salt of *N*-acetyl-L-alanine (L-AcAla·AM salt) is readily available and seems to be more soluble in ethanol than the DL-AcAbu·AM, DL-AcNva·AM, and DL-AcNle·AM salts. Hence we have been chosen the L-AcAla·AM salt as a cosolute and optically resolved the DL-AcAbu·AM, DL-AcNva·AM, and DL-AcNle·AM salts by replacing crystallization in ethanol.

Experimental

Materials. DL-2-Aminobutanoic acid, DL-norvaline, and DL-norleucine were purchased from Sigma Chemicals, and L-alanine from Wako Pure Chemicals, Ind. DL-AcAbu, DL-AcNva, DL-AcNle, and L-AcAla were obtained, respectively, by acetylating the corresponding compounds in a usual manner.[1,2,5,6] These were then converted to the DL-AcAbu·AM, DL-AcNva·AM, and DL-AcNle·AM, and L-AcAla·AM salts by the procedure described in previous papers.[1,2] L-AcAla·AM salt: Found: C, 40.70; H, 8.24; N, 18.77% (Calcd for $C_5H_{12}N_2O_3$: C, 40.53; H, 8.16; N, 18.91%); mp 161—162 °C; $[\alpha]_D^{20}$ +11.6° (*c* 1.00, ethanol).

Optical Resolution. The DL-AcAbu·AM salt 10.00 mmol (1.622 g), the DL-AcNva·AM salt 10.00 mmol (1.762 g), or the DL-AcNle·AM salt 10.00 mmol (1.902 g) and the L-AcAla·AM salt were dissolved in ethanol at 40 °C; the amounts of the L-AcAla·AM salt and ethanol used were 10.00 mmol (1.482 g) and 100 cm³, 2.00—10.00 mmol (0.296—1.482 g) and 40 cm³, and 8.000 mmol (1.185 g) and 55 cm³, respectively, for the optical resolution of the DL-AcAbu·AM, DL-AcNva·AM, and DL-AcNle·AM salts. The solution was slowly cooled to 5 °C and then stirred for 10—60 min. The precipitated L-salt was collected by filtration, washed with a small amount of cold ethanol, and dried. The optical purities were estimated on the basis of the specific rotations of the L-AcAbu·AM salt ($[\alpha]_D^{20}$ +20.7° (*c* 1.00, ethanol)),[2] L-AcNva·AM salt ($[\alpha]_D^{20}$ +19.7° (*c* 1.00, ethanol)),[2] and L-AcNle·AM salt ($[\alpha]_D^{20}$ +22.8° (*c* 1.00, methanol)),[1] respectively. The degree of resolution was calculated from the equation.

$$\text{Degree of resolution/\%} = [\text{Yield/g} \times \text{Optical purify/\%}]/M,$$

where *M* is the half amount (5.00 mmol) of the DL-salt used as the starting material. The ^{1}H NMR spectra of the L-salt obtained were measured without recrystallization and showed that the L-salts were free from the L-AcAla·AM salt. The L-salts were recrystallized from ethanol;[1,2] the L-AcAbu·AM salt (optical purity 73%) 1.50 g, the L-AcNva·AM salt (optical purity 82%) 3.00 g, and the L-AcNle·AM salt (optical purity 50%) 1.30 g yielded, respectively, 1.05, 2.39, and 0.625 g of the optically pure L-salt.

Measurements. Optical rotation was measured with a Union Giken digital polarimeter PM-101 with a quartz cell of 5.00 cm path length. ^{1}H NMR spectra were recorded on a JEOL NMR spectrometer JNM-PMX 60 in deuterium oxide without internal standard.

Results and Discussion

Optical Resolution of Ammonium Salts of *N*-Acetyl-DL-2-aminobutanoic Acid and *N*-Acetyl-DL-norleucine. The results are summarized in Table 1. Optical resolution of the DL-AcAbu·AM salt gave the L-salt with 70—75% optical purity at 50% or higher degree of resolution in 20—40 min. The L-salt was recrystallized from ethanol to give the optically pure L-AcAbu·AM salt. The yield was estimated to be 50%, based on the half amount (5.00 mmol, 0.811 g) of the DL-salt used as the starting material. In contrast, optical resolution by preferential crystallization of the DL-AcAbu·AM salt gave the D- or L-salt only in 10% yield though its enantiomer can easily be obtained from a mother liquor.[2] Replacing crystallization thus appears to be superior to preferential crystallization for optical resolution of the DL-AcAbu·AM salt.

The result of optical resolution of the DL-AcNle·AM

Table 1. Replacing Crystallization of Ammonium Salts of *N*-Acetyl-DL-amino Acids[a]

Ammonium salt[b]	Resolution time	L-Salt		
	min	Yield	Optical purity	Degree of resolution
		g	%	%
AcAbu·AM salt[c]	10	0.500	73.7	45.5
	20	0.582	74.2	53.3
	30	0.611	70.9	53.5
	40	0.612	74.8	56.0
	50	0.654	63.0	50.8
	60	0.707	56.4	49.2
AcNva·AM salt[d]	10	0.433	73.1	35.9
	20	0.736	78.6	65.6
	30	0.881	83.8	83.8
	40	0.886	83.8	84.6
	50	0.919	80.2	83.4
	60	0.920	81.2	84.4
AcNle·AM salt[e]	10	0.232	50.0	12.2
	20	0.507	50.9	27.2
	30	0.528	50.9	28.3
	40	0.592	50.0	31.2
	50	0.611	40.4	26.0
	60	0.620	37.3	24.4

a) Ammonium salt of *N*-acetyl-DL-amino acid 10.00 mmol; temperature 5 °C. b) AcAbu·AM salt=Ammonium salt of *N*-acetyl-2-aminobutanoic acid; AcNva·AM salt=Ammonium salt of *N*-acetylnorvaline; AcNle·AM salt=Ammonium salt of *N*-acetylnorleucine. c) Ammonium salt of *N*-acetyl-L-alanine (L-AcAla·AM salt) 10.00 mmol; ethanol 100 cm³. d) L-AcAla·AM salt 8.000 mmol; ethanol 40 cm³. e) L-AcAla·AM salt 8.000 mmol; ethanol 55 cm³.

salt was not better than that of the DL-AcAbu·AM salt; purification of the L-AcNle·AM salt with 50% optical purity obtained in 20—40 min gave the optically pure L-salt and the yield was estimated to be 25%.

Optical Resolution of Ammonium Salts of *N*-Acetyl-DL-norvaline. Optical resolution of the DL-AcNva·AM salt gave a better result than those of the DL-AcAbu·AM and DL-AcNle·AM salts. Optimization regarding the mixing ratio was attempted by stirring 10.00 mmol of the DL-AcNva·AM salt with 2.00—10.00 mmol of the L-AcAla·AM salt in 40 cm³ of ethanol for 20 min at 5 °C. The degrees of crystallization of the D- and L-AcNva·AM salts ($DC_{(D)}$ and $DC_{(L)}$/%) were calculated from the equations

$$DC_{(D)}/\% = (1/2)[\text{Yield/g} \times (100 - \text{Optical purity}/\%)]/0.881,$$

$$DC_{(L)}/\% = \text{Yield/g}/0.881 - DC_{(D)},$$

where 0.881 (g) corresponds to the half amount (5.00 mmol) of the DL-AcNva·AM salt used. The dependencies of the $DC_{(L)}$ and $DC_{(D)}$ values on the amount of the L-AcAla·AM salt are shown in Fig. 1.

The D-AcNva·AM salt did not rapidly crystallize under these conditions, because the $DC_{(D)}$ value ranged from 3 to 10%, and the L-AcNva·AM salt obtained was of 76—83% optical purity. When 2.00—7.00 mmol of the L-AcAla·AM salt was used, the $DC_{(L)}$ value increased with an increase in the amoun of the L-AcAla·AM salt. The $DC_{(L)}$ value, however, was approximately constant (75%) in the range of 7.00—10.00 mmol of the L-AcAla·AM salt. Optical resolution at 10—60 min, therefore, was performed with

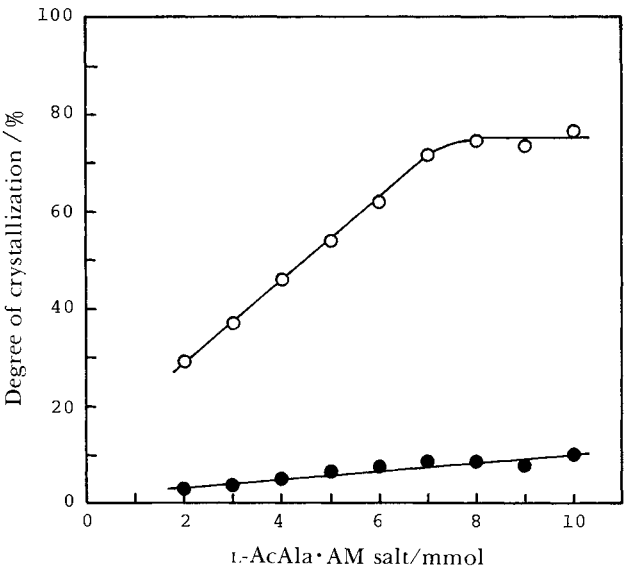

Fig. 1. Influence of the amount of the L-AcAla·AM salt on replacing crystallization of the DL-AcNva·AM salt. Conditions: DL-AcNva·AM salt 10.00 mmol; ethanol 40 cm³; temperature 5 °C; stirring time 20 min. Degree of crystallization: ○ L-AcNva·AM salt; ● D-AcNva·AM salt.

8.00 mmol of the L-AcAla·AM salt for 10.00 mmol of the DL-AcNva·AM salt. The result is listed in Table 1.

The L-AcNva·AM salt rapidly crystallized and the $DC_{(L)}$ value reached 92—94% at 30—60 min, whereas the crystallization of the D-salt was slow at 10—60 min. Optical resolution at 30—60 min gave the L-AcNva·AM salt with 81—84% optical purity at 84% degree of resolution. This L-AcNva·AM salt was recrystallized from ethanol to give the optically pure L-salt. The yield was estimated to be 80%. This result is far better than that by the optical resolution by preferential crystallization[2] and seems to be comparable to that attained by a diastereomeric procedure.

References

1) T. Shiraiwa, H. Yoshida, K. Mashima, and H. Kurokawa, *Nippon Kagaku Kaishi*, **1986**, 177.
2) T. Shiraiwa, H. Yoshida, M. Tsuda, and H. Kurokawa, *Bull. Chem. Soc. Jpn.*, **60**, 947 (1987).
3) K. Amaya, *Bull. Chem. Soc. Jpn.*, **34**, 1803 (1961).
4) T. Shiraiwa, M. Yamauchi, Y. Yamamoto, and H. Kurokawa, *Bull. Chem. Soc. Jpn.*, **63**, 3296 (1990).
5) P. Alaupovic, *Croat. Chim. Acta*, **29**, 131 (1957).
6) R. Marshall, S. M. Birnbaum, and J. P. Greenstein, *J. Am. Chem. Soc.*, **78**, 4636 (1956).

Oxidation Using Quaternary Ammonium Polyhalides. IX.[1] Oxidation of Hindered Phenols with Benzyltrimethylammonium Tribromide

Shoji KAJIGAESHI,* Yukihiro MORIKAWA, Shizuo FUJISAKI,
Takaaki KAKINAMI,† and Keigo NISHIHIRA††
Department of Industrial Chemistry, Faculty of Engineering, Yamaguchi University, Tokiwadai, Ube 755
† Department of Chemical and Biological Engineering, Ube Technical College, Tokiwadai, Ube 755
†† Ube Chemical Factory, Ube Industries Ltd., Kogushi, Ube 755
(Received November 5, 1990)

Synopsis. Reactions of hidered phenols, such as 2,6-di-*t*-butyl-4-methylphenol, 3,5-di-*t*-butyl-4-hydroxybenzyl alcohol, and 2,6-di-*t*-butylphenol, with benzyltrimethylammonium tribromide were carried out in dichloromethane in the presence of water, *t*-butyl alcohol, or aqueous sodium hydroxide at room temperature. Sequential reaction processes were provided by the obtained products.

Though the preparation of such hindered phenolic benzaldehyde as 3,5-di-*t*-butyl-4-hydroxybenzaldehyde by the usual methods is appreciably difficult, Coppinger el al. have already obtained this compound from a reaction of 2,6-di-*t*-butyl-4-methylphenol, with bromine in *t*-butyl alcohol.[2] In recent years we have found that benzyltrimethylammonium tribromide (BTMA Br_3) is a useful oxidizing agent.[3] In this paper we wish to report on the oxidation of hindered phenols by the use of BTMA Br_3, instead of bromine.

Results and Discussion

A reaction of 2,6-di-*t*-butyl-4-methylphenol (**1**) with an equimolar amount of BTMA Br_3 in dichloromethane in the presence of water at room temperature for 30 min gave 3,5-di-*t*-butyl-4-hydroxybenzyl alcohol (**2**) in quantitative yield. The reaction scheme can be represented as follows:

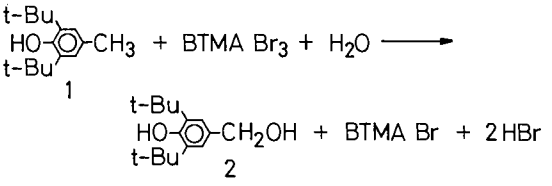

Scheme 1.

In this case, with only a 2-min reaction time, a mixture of **2** and 4-bromo-2,6-di-*t*-butyl-4-methyl-2,5-cyclohexadienone (**3**) was obtained. A mixture of **2** and **3** changed into a mixture of **2** and 4-bromomethyl-2,6-di-*t*-butylphenol (**4**) by a treatment with column chromatography on silica gel. Incidentally, the reaction of **1** with 1.0 equiv of BTMA Br_3 in methanol at 40 °C for 1 h gave 2,6-di-*t*-butyl-4-methoxy-4-methyl-2,5-cyclohexadienone (**5**) in good yield.

The reaction of **1** with 2.0 equiv of BTMA Br_3 and water in dichloromethane at room temperature for 3 h gave a mixture of 3,5-di-*t*-butyl-4-hydroxybenzaldehyde (**6**) and 4-bromo-4-bromomethyl-2,6-di-*t*-butyl-2,5-cyclohexadienone (**7**). In this case, when the reaction was carried out in the presence of *t*-butyl alcohol, compound **6** was obtained in satisfactory yield. Furthermore, when a large excess of BTMA Br_3 was used, compound **7** was obtained in quantitative yield.

The reaction of **2** with 1.0 equiv of BTMA Br_3 and water in dichloromethane at room temperature for 2 min gave a mixture of **6** and **7**. When the reaction of **2** with about 2 equiv of BTMA Br_3 was carried out for 1 h, compound **6** was obtained in good yield. That is, hindered phenolic benzaldehyde **6** was not oxidized into benzoic acid at room temperature, no matter how large was the excess of BTMA Br_3 used.[4]

The results described above are summarized in Table 1; the products might be derived from **1** and **2** through the following sequential reactions:

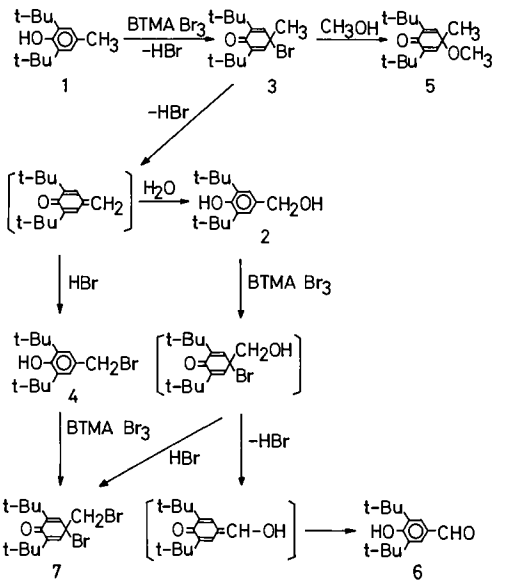

Scheme 2.

We have previously reported that the reaction of several substituted benzyl alcohols with 1 equiv of BTMA Br_3 in carbon tetrachloride in the presence of water or aqueous sodium hydroxide gave the corresponding benzaldehydes.[3b] In these cases, the obtained benzaldehydes should have been derived by an elimination of the hydrogen bromide from benzyl

Table 1. Oxidation of Hindered Phenols with BTMA Br_3

Run	Substrate	Molar ratio[a]	Solvent etc.	Reaction conditions		Product[b]	Yield[c]
				Temp/°C	Time		%
1	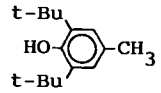 **1**	1.0	CH_2Cl_2/H_2O	R.t.	30 min	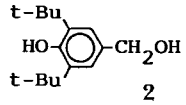 **2**	97
2[d]		1.0	CH_2Cl_2/H_2O	R.t.	2 min	**2** 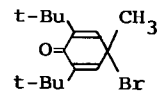 **3**	—[e] —[e]
3		1.0	CH_3OH	40	1 h	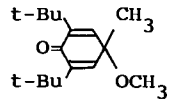 **5**	87
4[d]		2.0	CH_2Cl_2/H_2O	R.t.	3 h	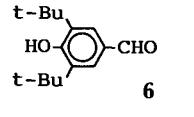 **6** 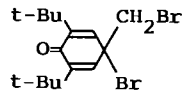 **7**	—[f] —[f]
5		2.0	$CH_2Cl_2/H_2O/t$-BuOH	R.t.	10 h	**6**	70
6		4.0	CH_2Cl_2/H_2O	R.t.	3 h	**7**	98
7[d]	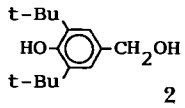 **2**	1.0	CH_2Cl_2/H_2O	R.t.	2 min	**6** **7**	—[g] —[g]
8		2.0	CH_2Cl_2/H_2O	R.t.	1 h	**6**	90
9	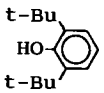 **8**	1.0	CH_2Cl_2/H_2O/NaOH	R.t.	5 h	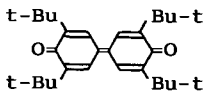 **9**	61

a) BTMA Br_3/substrate. b) Products were characterized by comparing ^1H NMR spectra and mp with those of authentic samples or reported data. c) Yield of isolated product. d) Product was obtained as a mixture, and its ratio was determined by ^1H NMR spectrum. e) **2**/**3**=1/1. f) **6**/**7**=4/5. g) **6**/**7**=2/1.

hypobromites (R–C_6H_4–CH_2OBr), which are produced from benzyl alcohols with Br^+. However, in the reaction of **2** with BTMA Br_3, it is reasonable to consider that the reaction proceeded via an intermediate, 4-bromo-4-hydroxymethyl-2,6-di-*t*-butyl-2,5-cyclohexadienone, as shown in Scheme 2, since compound **7** is also obtain together with **6** when the reaction is run for a short time (Run 7). That is, compound **2**, a hindered phenolic benzyl alcohol, should first react with Br^+ at the 1-position, affording the intermediate.

Otherwise, it has already been reported that the reaction of 2,6-di-*t*-butylphenol (**8**) with oxygen in the presence of a base gives 3,5,3′,5′-tetra-*t*-butyl-4,4′-diphenoquinone (**9**).[5] This compound **9** has also been obtained by the oxidation of **6**, **8**, and 3,5-di-*t*-butyl-4-hydroxybenzoic acid with alkaline hexacyanoferrate (III) or lead dioxide in the absence of molecular oxygen.[6] We have now found that the reaction of **8** with 1.0 equiv of BTMA Br_3 in dichloromethane in the presence of aqueous sodium hydroxide at room temperature for 5 h gives **9** in satisfactory yield. This reaction may be included a dimerization of the corresponding phenoxyl radical.[6]

We believe that the main active species for oxidation in the presence of water is probably hypobromous acid, which may be produced from a reaction of

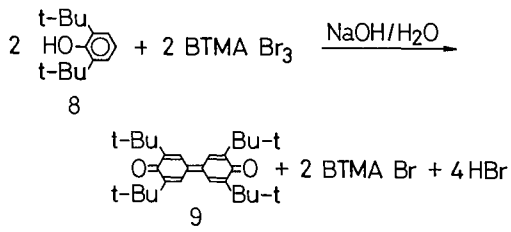

Scheme 3.

$$\text{BTMA Br}_3 + \text{H}_2\text{O} \rightarrow \text{BTMA Br} + \text{HOBr} + \text{HBr}$$

Scheme 4.

BTMA Br_3 with water. The oxidation of 1,4-benzenediols to 2,5-cyclohexadiene-1,4-diones with BTMA Br_3 in aqueous acetic acid was reported in our previous paper.[1] Similarly, it is almost certain that *t*-butyl hypobromite and sodium hypobromite are the main active oxidizing species for the reaction in *t*-butyl alcohol and in aqueous sodium hydroxide, respectively.

Furthermore, the reaction of phenols, which did not have a bulky *t*-butyl group at both *o*-positions for the hydroxyl group, with BTMA Br_3 gave electrophilic bromo-substituted products. For example, the reaction of 4-hydroxy-3-methoxybenzyl alcohol (vanillyl alcohol) with 1.0 equiv of BTMA Br_3 in dichloromethane in the presence of *t*-butyl alcohol gave 3-bromo-4-hydroxy-5-methoxybenzyl alcohol (60% yield).

We emphasize that the stable solid reagent BTMA Br_3 is a useful oxidizing agent for the hindered phenols, since it can be treated safely and quantitatively in comparison with toxic liquid bromine.

Experimental

Oxidation of 2,6-Di-*t*-butyl-4-methylphenol (1) with 1.0 equiv of BTMA Br_3 and Water (Table 1, Run 1): To a solution of BTMA Br_3 (1.17 g, 3.0 mmol) in dichloromethane (10 ml) was added **1** (0.66 g, 3.0 mmol) and water (10 ml). The mixture was stirred at room temperature for 30 min until the initial orange color faded. The water layer was then filtered through wet filter paper. The separated organic layer was washed with water and dried over $MgSO_4$, filtered, and evaporated in vacuo to give 3,5-di-*t*-butyl-4-hydroxybenzyl alcohol (**2**) as a yellow solid; yield 0.69 g (97%); mp 133—135 °C (lit,[2] mp 137.7—138.1 °C).

Oxidation of 1 with 1.0 equiv of BTMA Br_3 in Methanol (Table 1, Run 3): To a solution of **1** (0.66 g, 3.0 mmol) in methanol (30 ml) was added BTMA Br_3 (2.34 g, 6.0 mmol). The mixture was stirred for 1 h at 40 °C. After the reaction mixture was concentrated in vacuo, a yellow solid obtained was extracted with ether (10 ml×3), and the organic layer was evaporated in vacuo to give 2,6-di-*t*-butyl-4-methoxy-4-methyl-2,5-cyclohexadienone (**5**) as colorless needles; yield 0.29 g (87%); mp 95—97 °C (lit,[2] mp 94 °C).

Oxidation of 1 with 2.0 equiv of BTMA Br_3 and *t*-Butyl Alcohol-Water (Table 1, Run 5): To a solution of BTMA Br_3 (2.34 g, 6.0 mmol) in dichloromethane (10 ml) was added **1** (0.66 g, 3.0 mmol), water (10 ml) and *t*-butyl alcohol (10 ml). The mixture was stirred at room temperature for 10 h until the initial orange color faded completely. The mixture was then treated by a similar procedure to that described as Run 1. Thus, 3,5-di-*t*-butyl-4-hydroxybenzaldehyde (**6**) was obtained as colorless crystals; yield 0.49 g (70%); mp 191—193 °C (lit,[2] mp 189 °C).

Oxidation of 1 with Large Excess of BTMA Br_3 and Water (Table 1, Run 6): To a solution of BTMA Br_3 (4.68 g, 12 mmol) in dichloromethane (10 ml) was added **1** (0.66 g, 3.0 mmol), and water (20 ml). The mixture was stirred at room temperature for 3 h. The mixture was then treated by a similar procedure to that described as Run 1. Thus, 4-bromo-4-bromomethyl-2,6-di-*t*-butyl-2,5-cyclohexadienone (**7**) was obtained as yellow crystals; yield 1.11 g (98%); mp 132—134 °C (lit,[5] mp 118 °C). ^{1}H NMR ($CDCl_3$) δ=1.27 (18H, s, $2C_4H_9$), 3.96 (2H, s, CH_2Br), 6.61 (2H, s, Harom). Found: C, 48.74; H, 5.58%. Calcd for $C_{15}H_{22}OBr_2$: C, 47.64; H, 5.86%.

Oxidation of 3,5-Di-*t*-butyl-4-hydroxybenzyl Alcohol (2) with 2.0 equiv of BTMA Br_3 and Water (Table 1, Run 8): To a solution of BTMA Br_3 (2.34 g, 6.0 mmol) in dichloromethane (10 ml) was added **2** (0.71 g, 3.0 mmol) and water (10 ml). The mixture was then stirred at room temperature for 1 h. The mixture was treated as Run 1. Thus, compound **6** was obtained as colorless crystals; yield 0.63 g (90%); mp 191—193 °C.

Reaction of 2,6-Di-*t*-butylphenol (8) with 1.0 equiv of BTMA Br_3 and Aqueous Sodium Hydroxide (Table 1, Run 9): To a solution of BTMA Br_3 (1.17 g, 3.0 mmol) in dichloromethane (20 ml) was added **8** (0.62 g, 3.0 mmol) and aqueous sodium hydroxide (NaOH; 0.25 g, 6.3 mmol, H_2O; 14 ml). The mixture was stirred at room temperature for 5 h. The organic layer was then separated, washed with water, dried over $MgSO_4$, and evaporated in vacuo to give crude 3,5,3′,5′-tetra-*t*-butyl-4,4′-diphenoquinone (**9**) as a brown-red solid. The crude product was purified through a column packed with silica gel using hexane as a developing solvent. Thus, **9** was obtained as purple columnar crystals; yield 0.37 g (61%); mp 255—257 °C (lit,[5] mp 246 °C). IR (KBr) 1598 (C=O); ^{1}H NMR ($CDCl_3$) δ=1.35 (36H, s, 4 C_4H_9), 7.64 (4H, s, Harom). Found: C, 81.98; H, 10.21%. Calcd for $C_{28}H_{40}O_2$: C, 82.28; H, 9.89%.

References

1) Part VIII of this series: S. Kajigaeshi, Y. Morikawa, S. Fujisaki, T. Kakinami, and K. Nishihira, *Bull. Chem. Soc. Jpn.*, **64**, 336 (1991).

2) G. M. Coppinger and T. W. Campbell, *J. Am. Chem. Soc.*, **75**, 734 (1953).

3) a) S. Kajigaeshi, K. Asano, S. Fujisaki, T. Kakinami, and T. Okamoto, *Chem. Lett.*, **1989**, 463; b) S. Kajigaeshi, T. Kakinami, T. Yamaguchi, T. Uesugi, and T. Okamoto, *Chem. Express*, **4**, 177 (1989); c) S. Kajigaeshi, H. Kawamukai, and S. Fujisaki, *Bull. Chem. Soc. Jpn.*, **62**, 2585 (1989); d) S. Kajigaeshi, K. Murakawa, K. Asano, S. Fujisaki, T. Kakinami, and T. Okamoto, *J. Chem. Soc., Perkin Trans., 1*, **1989**, 1702; e) S. Kajigaeshi, K. Murakawa, S. Fujisaki, and T. Kakinami, *Bull. Chem. Soc. Jpn.*, **62**, 3376 (1989); f) T. Okamoto, T. Uesugi, T. Kakinami, T. Utsunomiya, and S. Kajigaeshi, *Bull. Chem. Soc. Jpn.*, **62**, 3748 (1989).

4) We previously reported that the reaction of several substituted benzyl alcohols with 2 equiv of BTMA Br_3 in aqueous sodium hydroxide gave sodium benzoates in good yields.[3f]

5) M. S. Kharasch and B. S. Joshi, *J. Org. Chem.*, **22**, 1439 (1957).

6) C. D. Cook, E. S. English, and B. J. Wilson, *J. Org. Chem.*, **23**, 755 (1958).

Oxidation of Cycloalkanes in a Radiofrequency Plasma

Meguru TEZUKA* and Tatsuhiko YAJIMA
Saitama Institute of Technology, Okabe, Saitama 369-02
(Received November 13, 1990)

Synopsis. Cyclopentane, cyclohexane, cycloheptane, and cyclooctane were reacted in a radiofrequency plasma containing oxygen to give mixtures of the corresponding cycloalkanones and cycloalkanols. Tetralin was also oxidized to 1-tetralone and 1-tetralol. Based on the effects of reaction variables on the oxidation rate, the reaction scheme involving the autoxidation of cycloalkyl radicals was proposed.

In the recent decades, much interest of organic chemists has been devoted to nonequilibrium plasma as a novel synthetic tool, since there are molecules activated by energetic electron bombardment to yield a diversity of reactive species which might not be readily generated by conventional chemical methods. Of late, a microwave or radiofrequency (rf) plasma was utilized for the purpose of partial oxidation of hydrocarbons. In this case, the effluents from the plasma containing atomic oxygen were passed over the organic substrates either dissolved in nonvolatile solvents[1,2] or adsorbed on solid supports.[3] Separately, we have also exerted ourselves to exploit a versatile oxidation process using plasma and reported that aromatic hydrocarbons could be effectively hydroxylated when the vaporized substrates flowed together with oxygen gas through an rf plasma.[4]

In this paper, we describe the oxidation of cycloalkanes in the plasma. For the mechanistic study, cycloalkanes were supposed to be suitable as starting materials, because they would yield less complicated products than other saturated hydrocarbons. It seems of not only scientific but also practical significance to establish the fundamental knowledge about the direct partial oxidation of saturated hydrocarbons.

Results and Discussion

The reactions of cyclopentane, cyclohexane, cycloheptane, cyclooctane, and tetralin with oxygen in an rf plasma were investigated. As major organic liquid products, the corresponding cycloalkanone(**1**) and cycloalkanol(**2**) were produced in comparable amounts. Their formation was favored under the conditions giving the conversions below ca. 20%. Typical results are listed in Table 1. The higher conversion was, on the whole, unfavorable, since it tended to induce the formation of tars. However, the ratio of products(**1**/**2**) was mostly unchanged regardless of kind of cycloalkanes and their conversion. The compounds which should be preferably formed in the plasma reactions without oxygen, for example, bicyclohexyl or cyclohexene from cyclohexane were not detected when oxygen was fed sufficiently. As for tetralin, the oxidation took place exclusively on the carbons of 1-position. In addition, the formation of considerable amounts of carbon dioxide and water was observed in each run.

Table 1. Oxidation of Cycloalkanes in an rf Plsma[a]

Substrate	Conversion/%	Product yield[b]/%	
		1	**2**
Cyclopentane	16	12	9
Cyclohexane	19	13	14
Cycloheptane	12	20	15
Cyclooctane	22	26	19
Tetralin	26	9	13

a) Radiofrequency power: 20 W; oxygen flow rate: 5 mmol min^{-1}; substrate flow rate: 0.5—1.5 mmol min^{-1}. b) Based on moles of substrate reacted.

In order to get mechanistic insight into the reaction of cycloalkanes in the plasma containing oxygen, effects of reaction variables, i.e., an rf power, and flow rates of the starting materials and oxygen in the oxidation of cyclohexane were examined in detail. With increasing power, the conversion of cyclohexane rose almost linearly (Fig. 1), while it diminished exponentially as the flow rate of cyclohexane was enhanced (Fig. 2). In practice, such a dependence of the conversion on the power and flow rate is so general in organic plasma chemistry,[5] and has been reasonably interpreted on the basis of a theorem that the

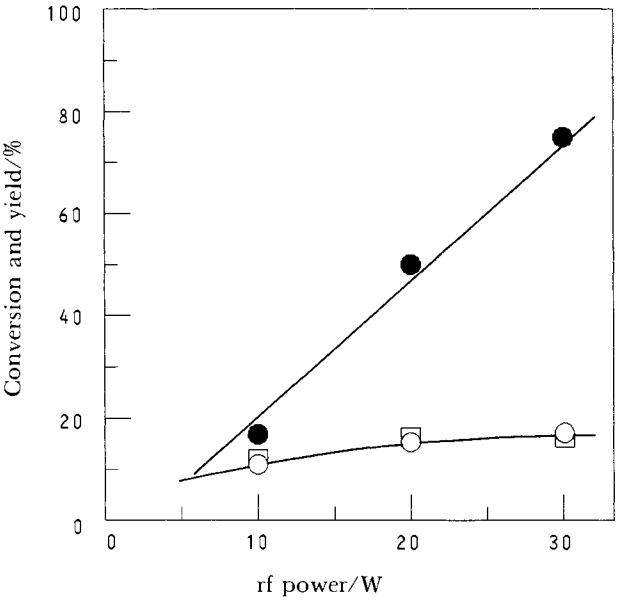

Fig. 1. Oxidation of cyclohexane in an rf plasma. Oxygen flow rate: 5 mmol min^{-1}; cyclohexane flow rate: 0.7 mmol min^{-1}; ●: cyclohexane conversion; ○: cyclohexanone yield; □: cyclohexanol yield.

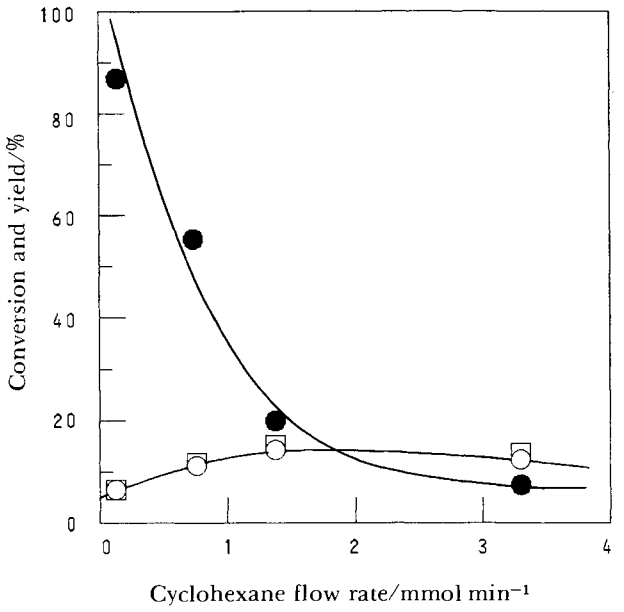

Fig. 2. Oxidation of cyclohexane in an rf plasma. Oxygen flow rate: 5 mmol min^{-1}; rf power: 20 W; ●: cyclohexane conversion; ○: cyclohexanone yield; □: cyclohexanol yield.

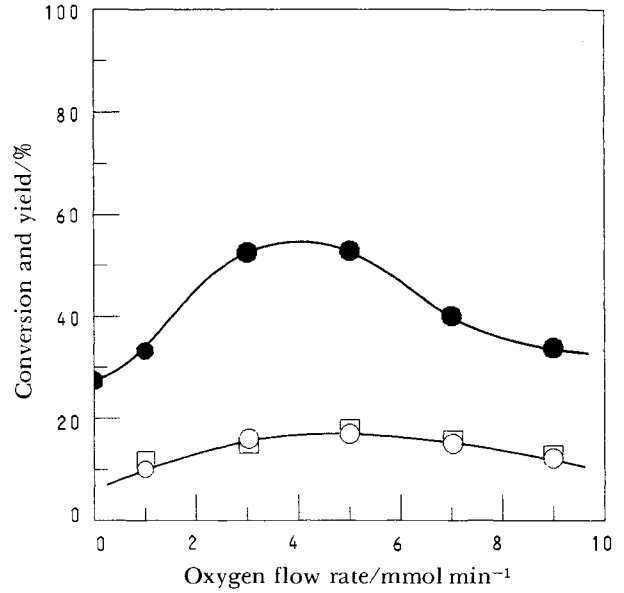

Fig. 3. Oxidation of cyclohexane in an rf plasma. Cyclohexane flow rate: 0.7—1.1 mmol min^{-1}; rf power: 20 W; ●: cyclohexane conversion; ○: cyclohexanone yield; □: cyclohexanol yield.

density and average energy of free electrons which should be most responsible for initiating chemical changes in nonequilibrium plasmas can be primarily controlled by these variables.[6] Thus, one might conclude that the rate-determining step still involves the collision of energetic electron onto molecules even in the presence of oxygen.

An interesting fact is revealed in Fig. 3; cyclohexane underwent the fragmentation or condensation principally in the plasma without oxygen and the conversion was around twenty percents under the conditions therein stated. As oxygen was added, the conversion gradually swelled and culminated around 4 mmol min^{-1} of oxygen flow rate. With a further addition of oxygen, it descended eventually close to the prime value. In contrast, as seen in Figs. 1, 2, and 3, the product yields were not substantially influenced by either of these variables. This can be understood by noting that the yield is based on the product against the starting material reacted. The final products such as **1** or **2** would be yielded through a complex of elementary chemical reactions following the initiation step caused by electron collision, and the relative importance of chemical processes is not supposed to be greatly affected by plasma parameters.

The formation of cyclohexanol and cyclohexanone in almost equimolar amounts strongly suggests that the oxidation involves the autoxidation of cyclohexyl radical as a key step. The cyclohexyl radical might be generated from cyclohexane through either C–H bond cleavage induced by electron bombardment or H abstraction by atomic oxygen. Although it is taken for granted that the latter process is most crucial in the oxidation of organic solids using oxygen plasmas, the former one seems rather superior in the system where organic substrates exist in the gas phase. Nevertheless, Fig. 3 demonstrates that the role of oxygen atom might not be neglected under the appropriate conditions, where the H abstraction should compete with the addition to O_2 giving ozone which is poorly reactive to saturated hydrocarbons. Consequently, the conversion of cyclohexane rose initially with increase in O_2 flow rate and then began to reverse in the presence of large excess O_2.

From the above discussion, the following reaction scheme could be proposed for the oxidation of cyclohexane in an rf plasma;

$$O_2 \xrightarrow{rf} 2O\cdot$$

$$C_6H_{12} \xrightarrow{rf} C_6H_{11}\cdot + H\cdot$$

$$C_6H_{12} + O\cdot \longrightarrow C_6H_{11}\cdot + \cdot OH$$

$$O\cdot + O_2 \longrightarrow O_3$$

$$C_6H_{11}\cdot + O_2 \longrightarrow \longrightarrow \mathbf{1} + \mathbf{2}$$

It seems undoubted that the analogous reaction steps proceed also in the oxidation of other cycloalkanes, since the effects of reaction variables on the products and oxidation rate were essentially identical to those in the cyclohexane oxidation.

Experimental

All of organic substrates and oxygen were of reagent grade from commercial sources and used without further purification.

The assembly and equipment of reaction apparatus are quite similar to those stated in the literature.[7] A starting material and oxygen flowed simultaneously through a plasma zone in a 40 cm×4.5 cm i.d. Pyrex reactor tube at

pressure below a few hundreds Pa. The flow rate of oxygen was controlled with a gas needle valve and monitored with a float-type flowmeter; the flow rate of substrate was controlled with a Teflon needle valve and determined from the quantity of material lost from a reactant reservoir and the elapsed time. Energy was supplied by an inductively coupled 13.56 MHz generator and in every run the impedance matching was conducted so that the reflected power was negligible. The products and recovered starting material were collected in cold traps on liquid nitrogen. The controlled variables were the applied power (10—30 W), the oxygen flow rate (1—8 mmol min^{-1}), and the flow rate of starting material (0.1—3 mmol min^{-1}).

Analysis of organic liquid products was carried out by means of GC(PEG 20 M). Identification of the products was achieved by coinjection of authentic samples with product mixtures and confirmed by GC-MS. For the quantitative analysis, toluene was used as an internal standard. Gaseous products and polymeric deposits on the reactor wall were not analyzed. The product yields were based on the starting material reacted.

Financial support from Grant-in-Aid for General Scientific Research, The Ministry of Education, Science and Culture was acknowledged.

References

1) E. Zadok, S. Rubinraut, F. Frolow, and Y. Mazur, *J. Am. Chem. Soc.*, **107**, 2489 (1985).
2) H. Suhr and H. Pfreundschuh, *Plasma Chem. Plasma Process.*, **8**, 67 (1988).
3) E. Zadok, S. Rubinraut, F. Frolow, and Y. Mazur, *J. Org. Chem.*, **50**, 2647 (1985).
4) M. Tezuka, T. Yajima, and A. Tsuchiya, *Chem. Lett.*, **1982**, 1437.
5) L. L. Miller, *Acc. Chem. Res.*, **16**, 194 (1983).
6) M. Tezuka and L. L. Miller, *J. Am. Chem. Soc.*, **100**, 4201 (1978).
7) T. Yajima, A. Tsuchiya, and M. Tezuka, *Nippon Kagaku Kaishi*, **1984**, 1677.

Vinyl Polymers Bearing Pyrrole Ring: I. Syntheses of Pyrroles Having 3-Substituent Bearing Vinyl Group

Hiroyoshi KAMOGAWA,* Takuharu NAKATA, Shin OHORI, and Sei KOMATSU
Department of Applied Chemistry, Yamanashi University, Takeda 4, Kofu 400
(Received November 14, 1990)

Synopsis. Pyrroles having 3-substituent bearing the vinyl group with an ester or amide spacer were synthesized starting with 1-(phenylsulfonyl)pyrrole. Homopolymerization of the vinyl monomers thus synthesized provided cross-linked insoluble polymers, but their copolymers with 1-vinyl-2-pyrrolidone were soluble in common solvents.

3-Substituted pyrroles have been little synthesized, since, in pyrrole, 2-position is the most reactive for electrophilic attacks such as preparation of 5,10,15,20,-tetraphenylporphyrins and polymerization.[1)]

In the present note, we wish to report the first synthesis of pyrroles having 3-substituent bearing a vinyl group. Accordingly, 3-substituted pyrroles reactive in both vinyl group and the 2-position of the pyrrole ring were obtained and their free-radical polymerization characteristics were investigated.

Pyrroles bearing a styrenic double bond **6** and **7a,b**, **11** and **12a,b**, and **16** and **17a,b**, were synthesized taking advantage of a high electrophilic reactivity at the 3 position of the pyrrole ring of **2** according to Eqs. 1, 2, and 3, respectively.

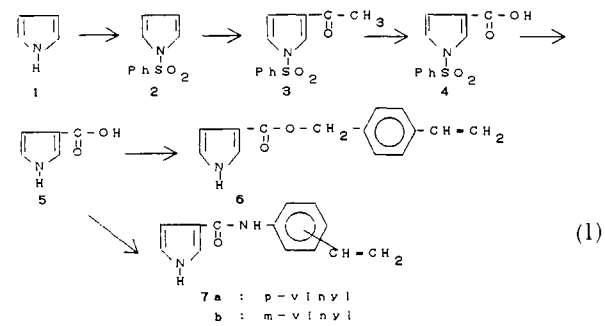

(1)

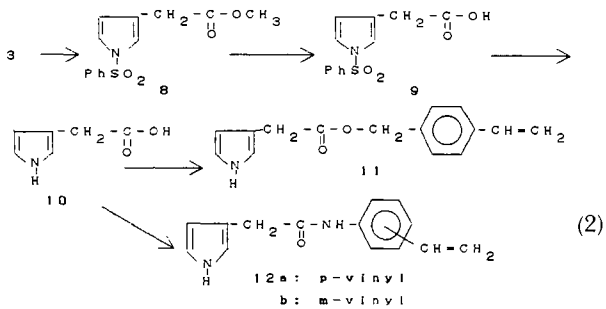

(2)

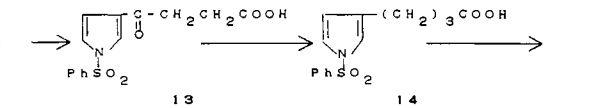

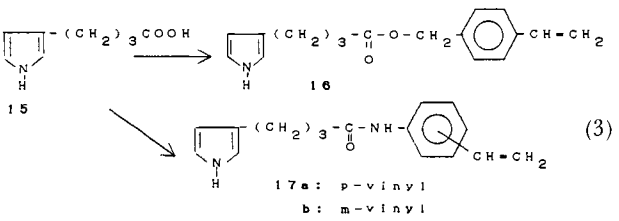

(3)

Results and Discussion

Vinyl monomer **6** was prepared by the reaction of **5**, synthesized following the route shown in Eq. 1, with *p*-vinylbenzyl chloride in DMF in the presence of triethylamine (TEA) as HCl-acceptor. Amide monomers **7a** and **7b** were prepared also by treatment of **5** with methyl chloroformate in the presence of TEA to afford a mixed anhydride, followed by addition of *p*- and *m*-vinylanilines.

Vinyl monomers **11** and **12a,b** were synthesized following the route shown in Eq. 2 in the same manners as those for **6** and **7a,b**. The last synthesis of monomers bearing a trimethylene group (**16** and **17a,b**) consisted of the application of the same ester and amide formation procedures as those for **6** and **7a,b** to **15**, synthesized following the route shown in Eq. 3. Ester and amide monomers thus prepared were subjected to free radical polymerization under conventional conditions. The results thus obtained are summarized in Table 1.

It is known from this Table 1 that homopolymerization only afforded cross-linked insoluble polymers for all monomers (Exp. Nos. 1—9), indicating that the reactive 2-position of the pyrrole ring of the monomer and/or the resulting polymer reacted each other during polymerization. Thus, copolymerizations with a large excess of 1-vinyl-2-pyrrolidone (VP) (Exp. Nos. 10—15) were carried out to provide soluble polymers, although their molecular weights, as judged from the values of intrinsic viscosity [η], and conversions were low, as was often the case with copolymerization of VP.[2)]

Conversions for *m*-vinyl polymers (Exp. Nos. 11, 13, and 15) were higher than those for *p*-vinyl ones (10, 13, and 15). In IR spectra, absorptions at 990 and 910 cm^{-1}, attributable to the vinyl group, no longer exist and a large absorption around 1650 cm^{-1}, due to the VP portion in polymer, is discernible, thereby indicating that polymerization took place.

In conclusion, it can be said generally that, by copolymerization of the monomers synthesized as above, vinyl polymers bearing the pyrrole ring as pendant of polymer molecular chain are obtained

Table 1. Polymerization Behavior of Ester and Amide Monomers[a]

Expt No.	Monomer M	VP/M mol/mol	Polymer Conversion	Polymer Solubility	Polymer $[\eta]$[b] dl g^{-1}
1	**6**	0	34	Insoluble	—
2	**11**	0	4	Insoluble	—
3	**16**	0	41	Insoluble	—
4	**7a**	0	18	Insoluble	—
5	**7b**	0	33	Insoluble	—
6	**12a**	0	47	Insoluble	—
7	**12b**	0	39	Insoluble	—
8	**17a**	0	41	Insoluble	—
9	**17b**	0	39	Insoluble	—
10	**7a**	20	21	Soluble in $CHCl_3$, MeOH, EtOH, DMF, H_2O	0.12
11	**7b**	20	26	Soluble in the same solv. as those for No. 10 and acetone	0.18
12	**12a**	20	17	Soluble in the same solv. as those for No. 10	0.15
13	**12b**	20	31	Soluble in the same solv. as those for No. 11	0.16
14	**17a**	20	18	Soluble in the same solv. as those for No. 10	0.16
15	**17b**	20	33	Soluble in the same solv. as those for No. 11	0.16

a) 20 wt% total monomers in DMF; 3% AIBN/monomers; 50 °C, 72 h. b) Intrinsic viscosity in DMF at 25 °C.

leaving the reactive 2-position intact for further electophilic reactions.

Experimental

p- and *m*-Vinylanilines were synthesized according to the methods of Kamogawa[3] and Manecke,[4] respectively. 1-(Phenylsulfonyl)pyrrole (**2**), 3-acetyl-1-(phenylsulfonyl)pyrrole (**3**), methyl 1-(phenylsulfonyl)-3-pyrrolylacetate (**8**), 3-pyrrolylacetic acid (**10**), and 4-[1-(phenylsulfonyl)-3-pyrroly]butyric acid (**14**), were also synthesized following known methods.[5,6]

1-Phenylsulfonyl-3-pyrrolecarboxylic Acid (4). The haloform reaction was applied to **3**. Thus, to an alkaline solution of bromine (4.7 g) in H_2O–dioxane (1:1, 40 ml) cooled with ice was added a solution of **3** (3.0 g, 12 mmol) in dioxane (5 ml), followed by stirring for 5 h. The reaction mixture was diluted with cold water and extracted with ether. The aqueous layer was acidified with 6M H_2SO_4 and extracted with ether(1 M=1 mol dm^{-3}), followed by working-up to afford crystalline powder of mp 146—148 °C in 68% yield. IR (KBr) 3420 cm^{-1}. NMR ($CDCl_3$-DMSO-d_6) δ=9.0 (B, 1H).

***p*-Vinylbenzyl 3-Pyrrolecarboxylate (6).** *p*-Vinylbenzyl chloride (3.1 g, 20 mmol) was added to a solution of **5** (1.1 g, 10 mmol), prepared by alkaline hydrolysis of **4**, and triethylamine (TEA; 1.5 g, 15 mmol) in DMF (10 ml) and the mixture was stirred at 20 °C for 24 h with exclusion of moisture. The reaction mixture was poured into water and extracted with ether (150 ml). The organic layer was washed first with 5% aq Na_2CO_3, then with water, and worked up. Silica-gel (WAKOGEL C-300) column chromatography gave fluid in 45% yield. IR ($CHCl_3$) 3450, 1710, 990, 900 cm^{-1}. NMR ($CDCl_3$) δ=5.3 (s, 2H), 5.6 (q, 2H), 6.9 (q, 1H), 6.3—8.0 (m, 8H).

***N*-(*p*-Vinylphenyl)-3-pyrrolecarboxamide (7a).** Methyl chloroformate (0.9 g, 10 mmol) was gently added to a solution of **5** (1.1 g, 10 mmol) and TEA (1.4 ml, 10 mmol) in anhyd. THF (20 ml) at −15—−5 °C with vigorous shaking. Upon stirring for 10 min, a solution of *p*-vinylaniline (1.2 g, 10 mmol) and TEA (1.4 ml, 10 mmol) in $CHCl_3$ (20 ml) was further added below 0 °C with shaking, followed by stirring at this temperature for one hour and subsequent stirring at 20 °C for 24 h. The reaction mixture was poured into water and extracted with $CHCl_3$. The organic layer was worked up and recrystallization from benzene–hexane provided crystalline powder of mp 64—66 °C in 33% yield. Found: C, 73.26; H, 5.60; N, 13.11%. Calcd for $C_{13}H_{12}N_2O$: C, 73.58; H, 5.66; N, 13.21%. IR (KBr) 3440, 1680, 990, 900 cm^{-1}. NMR (DMSO-d_6–$CDCl_3$) δ=5.4 (q, 2H), 6.7 (q, 1H), 6.5—8.0 (m, 8H), 9.5 (s, 1H). MS *m/z* 212 (M^+).

***N*-(*m*-Vinylphenyl)-3-pyrrolecarboxamide (7b).** The same procedure as that for **7a** provided viscous mass in 19% yield. Found: C, 73.66; H, 5.50; N, 13.09%. MS *m/z* 212 (M^+).

***p*-Vinylbenzyl 3-Pyrrolylacetate (11).** The same procedure as that for **6** was applied to afford fluid in 53% yield. IR ($CHCl_3$) 3480, 1730, 990, 900 cm^{-1}. NMR ($CDCl_3$) δ=3.5 (s, 2H), 5.1 (s, 2H), 5.5 (q, 2H), 6.6 (q, 1H), 6.6—9.0 (m, 8H).

***N*-(*p*-Vinylphenyl)-3-pyrrolylacetamide (12a).** The same procedure as that for **7a** provided crystalline powder of mp 86—87 °C in 66% yield. Found: C, 74.32; H, 6.20; N, 12.17%. Calcd for $C_{14}H_{14}N_2O$: C, 74.34; H, 6.19; N, 12.39%. IR (KBr) 1650, 990, 900 cm^{-1}. NMR ($CDCl_3$—SO-d_6) δ=3.5 (s, 2H), 5.4 (q, 2H), 6.5 (d, 3H), 6.7 (q, 1H), 7.0—7.8 (m), 9.6 (s, 1H), 10.4 (b, 1H). MS *m/z* 226 (M^+).

***N*-(*m*-Vinylphenyl)-3-pyrrolylacetamide (12b).** The same procedure as that for **7b** afforded viscous mass in 21% yield. Found: C, 74.62; H, 6.29; N, 12.01%. MS *m/z* 226 (M^+).

4-(3-Pyrrolyl)butyric Acid (15). Prepared in the same manner as that for **10**. Care was taken so as to keep the pH value of the solution at 2—3 in the isolation of the free acid **15**. Crystalline powder of mp 89—91 °C in 31% yield. Found: C, 62.37; H, 7.52; N, 9.52%. Calcd for $C_8H_{11}NO_2$: C, 62.75; H, 7.19; N, 9.15%. IR (KBr) 3400, 1700 cm^{-1}. NMR (DMSO-d_6–$CDCl_3$) δ=1.0—2.8 (m, 6H), 5.5—6.8 (d, 3H), 9.0—10.6 (b, 2H).MS *m/z* 153(M^+).

***p*-Vinylbenzyl 4-(3-Pyrrolyl)butyrate (16).** The same procedure as that for **6** provided viscous mass in 34% yield. IR ($CHCl_3$) 3480, 1730, 990, 900 cm^{-1}. NMR ($CDCl_3$) δ=1.0—2.8 (m, 6H), 5.1 (s, 2H), 5.5 (q, 2H), 6.7 (q, 1H), 5.8—8.0 (m, 8H).

***N*-(*p*-Vinylphenyl)-4-(3-pyrrolyl)butyramide (17a).** The same procedure as that for **7a** afforded crystalline powder of mp 71—72 °C in 59% yield. Found: C, 75.40; H, 7.02; N,

11.05%. Calcd for $C_{16}H_{18}N_2O$: C, 75.59; H, 7.09; N, 11.02%. IR (KBr) 1650, 990, 900 cm^{-1}. NMR (DMSO-d_6–$CDCl_3$) δ=1.4—3.6 (m, 6H), 5.4 (q, 2H), 6.7 (q, 1H), 5.8—7.7 (m, 7H), 9.8—10.7 c(b, 2H). MS m/z 254 (M^+).

***N*-(*m*-Vinylphenyl)-4-(3-pyrrolyl)butyramide (17b).** The same procedure as that for **7b** provided viscous mass in 16% yield. Found: C, 75.62; H, 7.28; N, 11.11%. MS m/z 254 (M^+). IR and NMR for **7b**, **12b**, and **17b** were essentially the same as those for **7a**, **12a**, and **17a**, respectively.

Polymerization of Pyrrole Monomers. In a typical example, a pyrrole monomer, with or without addition of comonomer, 1-vinyl-2-pyrrolidone (VP), and α,α'-azobisisobutyronitrile (AIBN; 3%/monomer) were dissolved in *N*,*N*-dimethylformamide (DMF; 3 ml) so as to afford 20 wt% monomer concentration. The solution was put into a glass ampule, which was then sealed under N_2 in a conventional manner. The sealed tube was kept at 50 °C for 72 h and the content was poured into ether to precipitate the polymerization product. IR (KBr) 1650 cm^{-1}.

References

1) P. G. Sammes, "Comprehensive Organic Chemistry," Pergamon Press, Oxford (1979), Vol. 4, p. 275.

2) R. H. Yocum and E. B. Nyquist, "Functional Monomers II," Marcel Dekker, New York (1974), p. 142.

3) H. Kamogawa, *J. Polym. Sci., Part A-1*, **7**, 725 (1969).

4) G. Manecke and G. Rossmehl, *Markomol. Chem.*, **70**, 112 (1964).

5) J. Rokach, P. Hamel, M. Kakushima, and G. M. Smith, *Tetrahedron Lett.*, **22**, 4901 (1981).

6) M. Kakushima, P. Hamel, R. Frenette, and J. Rokach, *J. Org. Chem.*, **48**, 3214 (1983).

The Photosensitized Oxygenation of Furanoeremophilanes. III.[1,2] The Transformations to the Skeletally Isomeric Lactones from Furanofukinol[3]

Keizo NAYA,* Mitsuaki SHIMIZU, Hideki NISHIO, Motonori TAKEDA, Shogo OKA, and Keiji HIROTA
Department of Chemistry, Faculty of Science, Kwansei Gakuin University, Uegahara, Nishinomiya, Hyogo 662
(Received May 14, 1990)

Pairs of the skeletal isomers of eremophilane-type lactones were synthesized from furanofukinol via photosensitized oxygenation, followed by lactone cleavage and reformation. Their stereochemistry has been clarified so as to be consistent with a classification method outlined in our earlier papers.[1,2]

Most of the naturally occurring eremophilane-type lactones possessing *cis*-decalin rings have 8β-substituents,[4,5] except for quite a few recent examples;[6] consequently, the synthesis of 8α-substituted lactone would not, hitherto, be attempted.[7] In previous papers[1,2] we reported on the photosensitized oxygenation of furanoeremophilanes in MeOH, followed by dehydration with Ac_2O-pyridine to yield, quantitatively, an epimeric mixture of 8α- and 8β-methoxylactones, in a ratio of ca. 1 : 1.[8] We have also proposed a procedure to distinguish the stereochemistry of the epimers, that is, 8α-nonsteroidal or 8β-steroidal A/B *cis* chair/chair configurations, according to the substitution mode at C-8.

The present paper deals with syntheses of novel nonsteroidal 8α-substituted eremophilenolides, termed epieremophilenolides, by the photosensitized oxygenation of furanofukinol (**1**) followed by dehydration, as well as by hydrolytic cleavage of lactones, recyclization and further chemical modifications. Recyclization to a nonsteroidal-type 8α-substituted lactone was achieved for the first time by a steric effect due to the 3β-hydroxyl group in furanofukinol (**1**).

Thus, the most simple lactone pair **13a,b** and the four 3-hydroxy skeletal diastereomers, **9a,b** and **16a,b,** were synthesized by recyclization; a further detailed comparison of the spectral data (cf. Tables 1 and 2) between the corresponding pairs was made in order to ascertain the classification procedure[1,2] proposed previously.

Furanofukinol (**1**) was isolated as a minor component from *Petasites japonicus* Maxim. rhizomes,[9] and the major components were its esters, 6-*O*-angeloylfuranofukinol: 6-*O*-[(*Z*)-2-methyl-2-butenoyl] furanofukinol (**2**) and *S*-furanopetasitin: 6-*O*-[(*Z*)-2-methyl-2-butenoyl]-3-*O*-[(*Z*)-3-methylthioacryloyl]furanofukinol (**3**). Hence, the starting material **1** was prepared by the alkaline hydrolysis of **2** and **3**. The stereochemis-

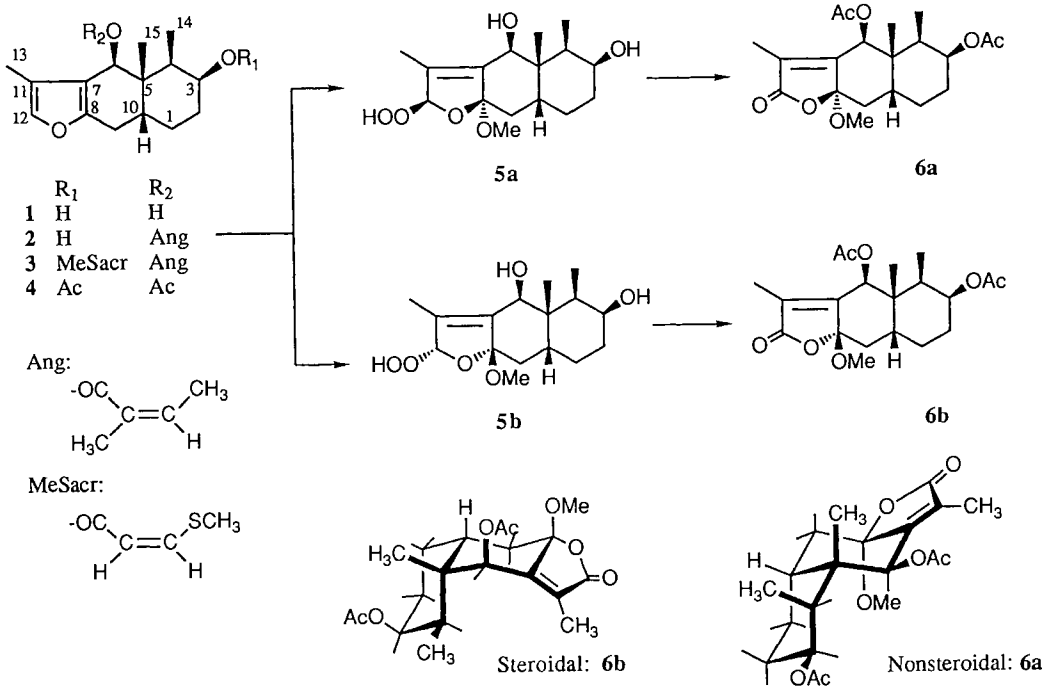

Scheme 1.

try of **1**, possessing a nonsteroidal conformation, has been unambiguously established by a combination of spectroscopic and chemical methods.[10]

A mixture of **1** and methylene blue in MeOH was irradiated with a circular fluorescent lamp (30 W×2) under bubbling air through the solution, affording quantitatively a crystalline product. The product showed two spots on TLC (R_f 0.09 and 0.29, benzene–AcOEt 2 : 1); the mixture was separated on the basis of solubilities in benzene, followed by careful recrystallization which afforded two isomeric hydroperoxides, a less soluble, polar isomer **5a**, mp 165.0—165.5 °C (decomp) and a soluble, less polar isomer **5b**, mp 94.0—96.0 °C (decomp), in a ratio of 2 : 1. Both were positive to peroxide tests, KI–AcOH and $Fe(SCN)_2$.

A mixture of **5a,b** was subsequently treated with Ac_2O–pyridine to give quantitatively an epimeric mixture, which was separated to afford the less polar (R_f 0.60, light petroleum–ether 1 : 1) 3β,6β-diacetoxy-8α-methoxyepieremophilenolide (**6a**), mp 132.5—133.0 °C and the polar (R_f 0.51) 3β,6β-diacetoxy-8β-methoxyeremophilenolide (**6b**), mp 139.0—140 °C, in a ratio of 3 : 1. Meanwhile, **5a** alone was exclusively converted to **6a** in the similar manner as described above (cf. Scheme 1).

The assigned stereoformulas of pairs of **5a,b** and **6a,b** were readily drawn from the coupling pattern of 3α-H in ^1H NMR and, furthermore, from the physical properties along with the generalization reported before.[1,2] Only the nonsteroidal **5a** and **6a** showed homoallylic couplings[2,11] between 13-Me and 6α-H (the mutual dihedral angle=ca. 90°), indicating 8α-configuration (cf. Scheme 1 and Exptl.).

An alkaline hydrolysis of a mixture of **6a,b** gave an 8-oxodienoic acid **7**, mp 163.5—164.0 °C, as a sole product in 85% yield. The Na salt of **7** in MeOH was refluxed with MeI to furnish an ester **8**, mp 114.5—115.5 °C, in 83% yield. Reduction of the ester **8** with $NaBH_4$ in MeOH gave an oily mixture, which was separated by chromatography upon silica gel, followed by recrystallization, to give 3β(*equatorial*)-hydroxyepieremophilenolide (**9a**), mp 167.0—168.0 °C, and 3β(*axial*)-hydroxyeremophilenolide (**9b**), mp 169.5—170.5 °C, in a ratio of 1 : 1; the more bulky 3-*O*-tetrahydropyranyl ether **10** prepared from **8** was subjected to a similar reduction with $NaBH_4$ as mentioned above, giving **9a** and **9b** in a ratio of 5 : 2 (cf. Scheme 2).

Jones' and PDC oxidations of **9a** and **9b** furnished the 3-oxo derivatives, **11a** mp 131.5—132.5 °C and **11b** mp 155.5—156.5 °C in good yields, respectively. However, product **11a** prepared by a Jones oxidation exhibited signals due to 14-Me (δ=1.06 and 1.20, each d, J=6.5 Hz) and 15-Me (δ=0.91 and 1.03, each s). This might be caused by epimerization of 14-Me in an acidic medium.

The dithioacetalization of **11a** and **11b**, and the subsequent desulfurization of dithioacetals **12a** and **12b** with Raney nickel furnished epieremophilenolide (**13a**), mp 86.0—86.5 °C, and eremophilenolide (**13b**), mp 123.5—124.5 °C, respectively.

In additional routes to **13a** and **13b**, the tosylation of **9a** and a subsequent treatment with NaI in acetone resulted in an elimination of the tosyl group, while affording a 3,4-dehydro compound **15a**. The mesylation of **9a** or **9b** also caused dehydration, directly

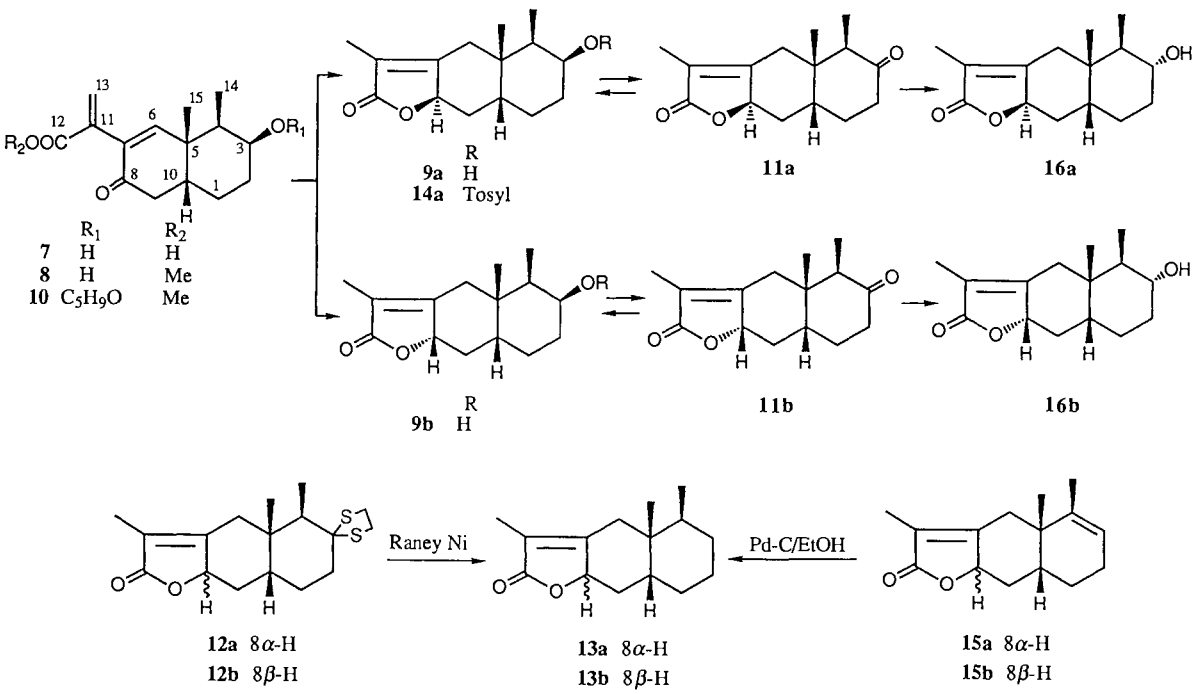

Scheme 2.

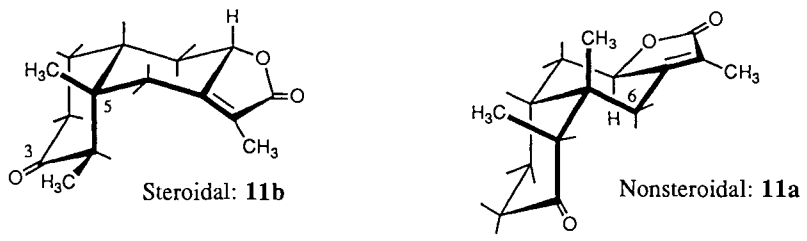

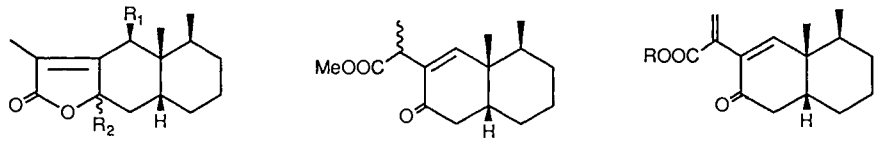

	R_1	R_2
17b	OH	β-H
19a,b	H	α,β-OMe
20b	H	β-OH

18

	R
21	H
22	Me

17b $\xrightarrow{(i)}$ **18** $\xrightarrow{(ii)}$ **13b** $\xleftarrow{(ii)}$ **22** $\xleftarrow{(iii)}$ **21** **19a,b** $\xrightarrow{(iv)}$ **20b**

Scheme 3. (i) 2 M KOH-MeOH, CH_2N_2-ether; (ii) $NaBH_4$; (iii) NaOMe-MeOH, MeI; (iv) 1.5 M KOH-MeOH, 10% H_2SO_4 (1M=1 mol dm^{-3}).

affording 3,4-dehydro compounds, **15a** or **15b**. The hydrogenation of **15a** and **15b** furnished **13a** and **13b** as predominant products, respectively. This result revealed that the addition of hydrogen to the double bond proceeded preferentially from the concave side of the *cis*-decalin ring.

A further approach to the syntheses of all four possible diastereomers of the 3-hydroxy lactones was attempted in order to explore the stereoselectivity upon reduction of the prochiral 3-oxo groups with $NaBH_4$ in MeOH as follows. Thus, **11a** gave a nonsteroidal 3α(*axial*)-OH isomer **16a**, mp 138.5—139.5 °C (56.3%), and the regenerated 3β(*equatorial*)-OH isomer **9a** (36.9%). Similarly, **11b** gave a new steroidal 3α(*equatorial*)-OH isomer **16b**, mp 158.0—159.0 °C (10%) together with the original 3β(*axial*)-OH isomer **9b** (80%). The above-mentioned results can be predicted by an observation of stereoformulas **11a** and **11b**. The 3-oxo groups in **11a** and **11b** were preferentially attacked with $NaBH_4$ from the convex and concave sides of the *cis*-decalin ring, so as to avoid 1,3-diaxial interactions with the 6-CH_2 and 15-Me groups, respectively (cf. stereoformulas **11a** and **11b** in Scheme 3).

For a comparison of the stereoselectivity upon recyclization to lactones, the natural 6β-hydroxyeremophilenolide (**17b**)[1] was subjected to alkaline hydrolysis followed by esterification with CH_2N_2 in diethyl ether, and then by reduction with $NaBH_4$ in a similar manner as in the transformation from 3β-hydroxydienoic ester **8** to **9a** and **9b**. Thus, only eremophilenolide **13b** was obtained via an enoic ester **18**, bp 116—118 °C/0.3 mmHg (40 Pa), in 86% overall yield. In a previous study,[2] 8β-hydroxyeremophilenolide (**20b**) was quantitatively synthesized from a mixture of 8α- and 8β-methoxy lactones **19a,b** by alkaline lactone cleavage, followed by acidic recyclization.

In addition, dienoic acid **21**[1,2] prepared previously from petasalbin (6β-hydroxyfuranoeremophilane) and furanofukinin (6β-methoxyfuranoeremophilane) was transformed into the methyl ester **22**, followed by a treatment with $NaBH_4$ in MeOH in a similar manner as that for ester **8** to furnish only steroidal **13b** (92%).

Therefore, the above-mentioned successful methods for the first preparation of epieremophilenolides by recyclization could be achieved by a steric effect based on the greater stability of the 3β(*equatorial*)-hydroxy group in a nonsteroidal conformation, more than the 3β(*axial*)-hydroxy group in a steroidal conformation, where 3β-substituent has a 1,3-diaxial interaction with 15β-methyl.

Now, the stereochemistry of the above-mentioned products can be clearly assigned by means of a general procedure.[1,2] In Table 1,[12] the 8α-substituted lactones (suffix a-series) showed chemical shifts due to 14-methyls at a lower field than those due to 15-methyls; this relation of the chemical shifts between 14- and 15-methyls is reversed in the 8β-series (suffix b-series). These variations in the chemical shifts could be accounted for in terms of an alteration in the geometric orientations of the 14- and 15-methyls, accompanied by a skeletal change between the steroidal and nonsteroidal conformations.[13] Also, the coupling patterns[14] of the protons at C-3 in the 3-hydroxy lactones, consisting of rigid[15] chair forms, practically serve to define the absolute configuration of 3-hydroxy substituents as well as a determination of the nonsteroidal and steroidal conformations of the

Table 1. Comparison of ^{1}H NMR Chemical Shifts (δ), Specific Rotations, CD Maxima and R_f Values of the Corresponding Isomers

Compound [mp/°C]	15-Me	14-Me $CDCl_3$	13-Me	3-H	$[\alpha]_D$/° $CHCl_3$	CD MeOH λ/nm ($\Delta\varepsilon$)	R_f	C_6H_6 : AcOEt
6a	0.92s	0.93d	1.87d	4.85ddd	−198	244 (−5.15)[a]	0.60	
[133]		J=7	J=1.8	J=6,6,12				1 : 1[c]
6b	1.24s	0.92d	2.01s	4.99ddd	+180	263 (+1.06)[a,b]	0.51	
[140]		J=7		J=3,3,3				
9a	0.85s	0.97d	1.79t	4.10ddd	−157	253 (+0.10)	0.27	
[168]		J=7	J=1.6	J=5.5,5.5,11				2 : 1
9b	1.29s	1.01d	1.80t	3.81ddd	+196	248 (+3.09)	0.60	
[170.5]		J=6.8	J=1.8	J=4,4,5				
11a	0.89s	1.20d	1.79t		−157	241 (−0.20)	0.70	
[132.5]		J=6.5	J=1.8					2 : 1
11b	1.00s	0.96d	1.83t		+154	245 (+2.05)	0.75	
[156.5]		J=7	J=1.3					
13a	0.88s	0.92d	1.80t		−127	248 (−0.54)	0.57	
[86.5]		J=6.6	J=1.5					30 : 1
13b	1.04s	0.80d	1.80t		+163	248 (+2.40)	0.55	
[124.5]		J=5.9	J=1.4					
16a	0.80s	0.95d	1.78t	3.97ddd	−138	248 (−0.04)	0.43	
[139.5]		J=7.3	J=1.5	J=3,3,3				2 : 1
16b	1.05s	1.01d	1.81t	3.61ddd	+214	252 (+0.38)	0.45	
[159]		J=8.5	J=1.5	J=5,10.3,10.3				

a) Measured with JASCO J-600 spectropolarimeter. b) Hexane. c) Light petroleum : ether, 1 : 1.

Table 2. The ^{13}C NMR Chemical Shifts of the Corresponding Isomers

C	**6a**	**6b**	**9a**	**9b**	**16a**	**16b**	**11a**	**11b**	**13a**	**13b**
1	24.9	21.0	27.3	21.7	22.8	25.0	28.1	26.9	29.1	30.7
2	26.6	24.6	29.2	28.3	28.9	30.1	34.0[a]	35.0[a]	26.6	20.6
3	71.5	73.2	68.6	71.6	73.9	72.4	213.6	211.0	27.1	26.7
4	34.9	32.1	44.7	33.9	44.7	38.1	55.4	45.6	41.4	30.0
5	45.8	42.0	41.0	39.9	38.9	41.0	42.6	44.5	40.3	39.8
6	71.0	70.7	34.7	37.4	35.1	36.6	34.4[a]	36.8[a]	31.0	36.5
7	154.8	150.0	162.1	161.0	163.3	160.5	160.2	159.1	163.0	161.0
8	106.6	106.6	77.7	80.2	78.1	80.2	77.1	79.6	78.0	80.3
9	37.8	38.0	33.7	35.0	35.1	35.1	36.9	36.1[a]	36.1	35.2
10	35.2	34.5	35.5	39.9	36.8	39.6	35.3	39.5	42.9	40.3
11	126.3	130.8	122.0	120.4	121.0	120.9	122.7	121.8	121.6	120.6
12	170.7	170.2	174.7	174.8	175.2	174.8	174.1	174.1	175.0	174.8
13	8.2	8.9	8.0	8.2	8.0	8.2	8.0	8.4	8.0	8.2
14	8.4	12.3	7.5	12.3	15.2	11.1	13.9	7.6	16.0	16.0
15	20.5	18.0	25.0	25.1	25.4	22.9	23.1	23.2	24.4	21.6
3-MeCO	19.2	20.7								
6-MeCO	21.2	21.3								
3-MeCO	170.2	170.4								
6-MeCO	170.3	170.4								
OMe	50.3	50.5								

a) Assignments may be interchanged in each column.

chair-chair *cis*-decalins in 8α- and 8β-isomers, respectively.

The paired lactones exhibited CD spectra with opposite signs (Table 1), which can be rationalyzed by the opposite helicities in the α,β-unsaturated carbonyl moieties caused by lactone ring fusion. Thus, the 8β-isomers possessing a right-handed helix showed positive Cotton effects centered near 240—260 nm corresponding to the π-π^* transition,[16] while the 8α-isomers with a left-handed helix showed negative Cotton effects in the same region, except for the compound **9a** (cf. Table 1).

In the ^{13}C-chemical shifts (Table 2), the comparative chemical shifts between the paired isomers proved, on the whole, to be qualitatively in accord with the empirical calculation presented by Beierbeck et al.,[17] except for the chemical shifts of 9-C and the olefinic carbons, 7-C and 11-C. The chemical shifts of 7-C could not also be rationalized by the diamagnetic γ-effect[18] of the 15(*axial*)-Me group in the 8α-H

isomers. The chemical shifts of the olefinic carbons, 7-C and 11-C, at a higher field in the 8β-H isomers are clearly reflected by shielding of the carbon atoms in the steroidal *cis*-type (*cis-syn-cis*) ring relative to its nonsteroidal *trans*-type (*cis-anti-cis*) ring in 8α-H isomers[19] (cf. stereoformulas **6a,b** and **11a,b**).

Experimental

All of the melting points are uncorrected. The IR, UV, CD, and MS spectra were taken with Hitachi EPI-G3, Cary 118, JASCO Model ORD/CD-5, and JEOL JMS-D300 spectrophotometers, respectively. The ^{1}H and ^{13}C NMR spectra were recorded with a JEOL FX-90Q (90 and 22.5 MHz) spectrometer, and the chemical shifts are reported in δ values (with TMS as the internal reference). The optical rotations were measured with a Perkin-Elmer 141 polarimeter. The TLC were run on a Kieselgel G (Merck).

Isolation of Furanofukinol (1), 6-*O*-Angeloylfuranofukinol (2), and *S*-Furanopetasitin (3). The dried rhizomes of *Petasites japonicus* Maxim. ("Aichiwasebuki" cultivated in Osaka Prefecture) (36 kg) were extracted with benzene (85 l) at room temperature for 12 days. The extract was concentrated in vacuo in order to remove the solvent. The residue was dissolved in ether, washed with saturated $NaHCO_3$ aqueous solution, then with water, dried over anhydrous Na_2SO_4 and evaporated in vacuo, leaving a dark oil (473 g). This oil (100 g) was chromatographed on deactivated alumina (1 kg, grade III). Elution with benzene, and then benzene-ethyl acetate (2:1), afforded a mixture of *S*-furanopetasitin (**3**) and 6-*O*-angeloylfuranofukinol (**2**) (45 g), as well as furanofukinol (**1**) (120 mg). The mixture of **2** and **3** was repeatedly chromatographed on alumina (grade III), and elution with light petroleum-ether (20:1) gave both **3** (11 g, 11% yield based on the crude extract) and **2** (16 g, 16% yield).

Furanofukinol (1): Mp 178.0—180 °C (decomp), colorless needles (from MeOH); $[\alpha]_D^{25}$ −18° (*c* 0.97, dioxane); UV (EtOH) 219 nm (ε 6720); IR (KBr) 3367, 3323 (OH), 1648, 1569 cm^{-1} (furan); ^{1}H NMR ($CDCl_3$) δ=7.06 (q, *J*=1.3 Hz, 12-H), 4.90 (br s, 6α-H), 4.21 (ddd, *J*=5, 5, 10 Hz, 3α-H), 2.07 (d, *J*=1.3 Hz, 13-Me), 0.97 (d, *J*=7.3 Hz, 14-Me), 0.95 (s, 15-Me); ^{13}C NMR (pyridine-d_5) δ=27.0 (t, 1-C), 28.2 (t, 2-C), 68.1 (d, 3-C), 39.3 (d, 4-C), 43.0 (s, 5-C), 66.8 (d, 6-C), 121.4 (s, 7-C), 149.5 (s, 8-C), 30.4 (t, 9-C), 37.0 (d, 10-C), 119.5 (s, 11-C), 138.4 (d, 12-C), 7.7 (q, 13-C), 9.1 (q, 14-C), 20.1 (q, 15-C).

Found: C, 71.82; H, 8.75%. Calcd for $C_{15}H_{22}O_3$: C, 71.97; H, 8.86%.

6-*O*-Angeloylfuranofukinol: 6-*O*-[(*Z*)-2-Methyl-2-butenoyl]furanofukinol (2): A colorless oil (purified by HPLC, μ-Bondapak C_{18}, MeOH-H_2O 8:1); $[\alpha]_D^{25}$ −41.4° (*c* 0.91, $CHCl_3$); UV (EtOH) 215 nm (ε 17150); IR (film) 3440 (OH), 1700, 1640, 1230 cm^{-1} (α,β-unsaturated ester); ^{1}H NMR ($CDCl_3$) δ=7.07 (q, *J*=1.2 Hz, 12-H), 6.50 (s, 6α-H), 6.14 (slightly splitted q, *J*=7.0 Hz, 3-H in butenoyl), 4.40 (ddd, *J*=5.5, 5.5, 10.5 Hz, 3α-H), 2.02 (br d, *J*=7.5 Hz, 4-Me in butenoyl), 1.98 (br s, 2-Me in butenoyl), 1.83 (d, *J*=1.2 Hz, 13-Me), 1.03 (s, 15-Me), 0.95 (d, *J*=6.0 Hz, 14-Me); ^{13}C NMR ($CDCl_3$) δ=27.5 (t, 1-C), 26.9 (t, 2-C), 68.9 (d, 3-C), 39.2 (d, 4-C), 42.0 (s, 5-C), 68.5 (d, 6-C), 115.2 (s, 7-C), 150.4 (s, 8-C), 28.9 (t, 9-C), 36.9 (d, 10-C), 119.6 (s, 11-C), 138.8 (d, 12-C), 7.0 (q, 13-C), 8.5 (q, 14-C), 20.4 (q, 15-C), butenoyl: 168.1 (s, CO), 127.8 (s, 2-C), 138.4 (d, 3-C), 16.0 (q, 2-Me), 20.7 (q, 4-Me).

Found: *m/z* 333.2045 (MH^+). Calcd for $C_{20}H_{28}O_4$: MH, 333.2058.

***S*-Furanopetasitin: 6-*O*-[(*Z*)-2-Methyl-2-butenoyl]-3-*O*-[(*Z*)-3-methylthioacryloyl]furanofukinol (3):** Mp 107.0—108.0 °C, colorless prisms (from ethyl acetate-diisopropyl ether), $[\alpha]_D^{24}$ −60.5° (*c* 1.0, $CHCl_3$); UV (EtOH) 216 (ε 21000), 287.5 nm (14340); IR ($CHCl_3$) 1704, 1694, 1644, 1230—1215 br (two α,β-unsaturated esters), 1603, 1573 cm^{-1} (furan); ^{1}H NMR ($CDCl_3$) δ=7.08 (q, *J*=1.0 Hz, 12-H), 7.03 (d, *J*=11.0 Hz, Me-S-C<u>H</u>=), 6.50 (s, 6α-H), 6.12 (slightly splitted q, *J*=8.0 Hz, 3-H in butenoyl), 5.82 (d, *J*=11.0 Hz, Me-S-CH=C<u>H</u>-), 5.40 (ddd, *J*=4.5, 4.5, 9.0, 3α-H), 2.38 (s, <u>Me</u>-S-), 2.03 (d, *J*=8.0 Hz, 4-Me in angelate), 1.96 (br s, 2-Me in angelate), 1.87 (d, *J*=1.0 Hz, 13-Me), 1.07 (s, 15-Me), 0.98 (d, *J*=7.0 Hz, 14-Me); ^{13}C NMR ($CDCl_3$) δ=25.8 (t, 1-C), 26.3 (t, 2-C), 72.3 (d, 3-C), 35.9 (d, 4-C), 41.7 (s, 5-C), 68.4 (d, 6-C), 115.6 (s, 7-C), 150.5 (s, 8-C), 30.0 (t, 9-C), 36.5 (d, 10-C), 119.8 (s, 11-C), 138.3 (d, 12-C), 8.5 (q, 13-C), 8.8 (q, 14-C), 19.9 (q, 15-C), butenoyl: 167.5 (s, CO), 127.9 (s, 2-C), 138.1 (d, 3-C), 15.8 (q, 2-Me), 20.7 (q, 4-Me); 3-MeS-acryloyl: 165.6 (s, CO), 113.5 (d, α-C), 151.0 (d, β-C), 19.0 (q, S-Me).

Found: C, 66.88; H, 7.39: S, 7.64%. Calcd for $C_{24}H_{32}O_5S$: C, 66.64; H, 7.46; S, 7.41%.

Preparation of Furanofukinol (1). a) Alkaline Hydrolysis of the Mixture of 2 and 3. Aqueous 20% NaOH (134 ml) was added, drop by drop, to a stirred mixture of **2** and **3** (37 g) in DMSO (240 ml). The mixture was then warmed at 60—65 °C for 9 h under N_2. After dilution with ice-water and acidification with 6 M H_2SO_4 aqueous solution (1 M=1 mol dm^{-3}), the reaction mixture was adjusted to pH 7—8 with a saturated $NaHCO_3$ aqueous solution and kept under cooling to deposit a brownish solid. After working up using the usual method, the crude furanofukinol (**1**) (23 g) was crystallized from MeOH as colorless prisms (11 g), mp 178—180 °C (decomp).

b) To a stirred solution of 1M *t*-BuOK (1 M=1 mol dm^{-3}) in anhydrous DMSO (100 ml) was added a solution of **2** (15 g) in anhydrous DMSO (150 ml) at room temperature over a 0.5 h period under N_2. After stirring for further 12 h, the reaction mixture was diluted with ice-water (300 g) and acidified with 1 M H_2SO_4 to deposit a solid, which was worked up in the usual manner. The crude product **1** was recrystallized from MeOH as colorless prisms (8.7 g); mp 178.0—180.0 °C (decomp). Both of the above-mentioned products were identical in all respects with the natural furanofukinol **1**.

Furanofukinol Diacetate (4). Furanofukinol **1** (100 mg) was treated with pyridine (1 ml) and acetic anhydride (1 ml) at room temperature for 48 h. The usual workup yielded the diacetate **4** (130 mg); mp 144.0—145.0 °C, colorless prisms (MeOH); $[\alpha]_D^{22}$ −53.7° (*c* 0.95, $CHCl_3$); UV (EtOH) 217.5 nm (ε 7720); IR (KBr) 1720, 1253, 1230 (acetate), 1640, 1565 cm^{-1} (furan); ^{1}H NMR ($CDCl_3$) δ=6.98 (q, *J*=1.1 Hz, 12-H), 6.28 (s, 6α-H), 5.28 (ddd, *J*=5.5, 5.5, 10 Hz, 3α-H), 2.11 (s, OAc), 2.00 (s, OAc), 1.82 (d, *J*=1.1 Hz, 13-Me), 0.98 (s, 15-Me), 0.93 (d, *J*=6.0 Hz, 14-Me); ^{13}C NMR ($CDCl_3$) δ=25.6 (t, 1-C), 26.0 (t, 2-C), 72.1 (d, 3-C), 36.0 (d, 4-C), 41.7 (s, 5-C), 68.9 (d, 6-C), 115.8 (s, 7-C), 150.1 (s, 8-C), 26.5 (t, 9-C), 36.4 (d, 10-C), 119.5 (s, 11-C), 138.9 (d, 12-C), 8.5 (q, 13-C), 8.5 (q, 14-C), 19.6 (q, 15-C), 170.3 and 169.1 (each s, Me<u>C</u>OO), 21.2 and 20.8 (each q, <u>C</u>H$_3$COO).

Found: C, 68.24; H, 7.82%. Calcd for $C_{19}H_{26}O_5$: C, 68.24;

H, 7.84%.

Photosensitized Oxygenation of Furanofukinol (1). A stirred solution of **1** (487 mg) and Methylene Blue (2 mg) in anhydrous MeOH (80 ml) was irradiated with two circular fluorescent lamps (30 W×2) for 55 min under air bubbling. After evaporation of the solvent in vacuo, the crystalline residue (603 mg, quantitative yield) showed two spots on TLC (R_f 0.29 and 0.09, benzene-ethyl acetate 2 : 1), and was positive to peroxide tests: KI-AcOH and $Fe(SCN)_2$ reagents. The above-mentioned crystalline mixture was separated into less and readily soluble hydroperoxides, (**5a**, R_f 0.09) (337 mg, 55%) and (**5b**, R_f 0.29) (157 mg, 27%), according to the solubility in benzene, followed by fractional crystallization.

8α-Methoxy-12β-hydroperoxide (5a): Mp 165.0—165.5 °C (decomp), colorless prisms (MeOH-acetone); $[\alpha]_D^{25}$ −20.0° (*c* 0.92, MeOH); positive to peroxide tests; IR (KBr) 3530, 3410 (OH), 1085, 1030 cm^{-1} (ether); ^1H NMR (acetone-d_6) δ=11.40 (s, OOH); (pyridine-d_5) δ=6.20 (s, 12-H), 5.12 (q, *J*=1.8 Hz, 6α-H), 4.47 (ddd, *J*=5.5, 5.5, 10.5 Hz, 3α-H), 3.29 (s, OMe), 2.33 (d, *J*=1.8 Hz, 13-Me), 1.23 (d, *J*=7.0 Hz, 14-Me), 1.11 (s, 15-Me).

Found: C, 61.12; H, 8.50%. Calcd for $C_{16}H_{26}O_6$: C, 61.13; H, 8.34%.

8β-Methoxy-12α-hydroperoxide (5b): Mp 94.0—96.0 °C (decomp), colorless needles (benzene-pentane); $[\alpha]_D^{22}$ +57° (*c* 0.93, MeOH); positive to peroxide tests; IR (KBr) 3430, 3200sh (OH), 1045 cm^{-1} (ether); ^1H NMR ($CDCl_3$) δ=10.08 (s, OOH), 5.80 (s, 12-H), 4.27 (br m, 6-H and H_2O), 3.79 (ddd, *J*=3, 3, 3 Hz, 3α-H), 3.30 (s, OMe), 1.81 (s, 13-Me), 1.31 (s, 15-Me), 0.95 (d, *J*=6.0 Hz, 14-Me).

Found: C, 60.90; H, 8.35%. Calcd for $C_{16}H_{26}O_6$: C, 61.13; H, 8.34%.

Acetylation of Hydroperoxides, 5a,b. a) A mixture of hydroperoxides, **5a,b** (3.4 g) prepared from **1** (2.7 g), was dissolved in pyridine (35 ml) and acetic anhydride (45 ml). The mixture was left overnight at room temperature. The usual type workup gave quantitatively a crude oily product (4.0 g), which showed two spots on TLC (R_f 0.51 and 0.60, light petroleum-ether 1 : 1). The crude product (1 g) was chromatographed on silica gel (20 g) with light petroleum-ether (10 : 1) to afford a less polar isomer **6a** (772 mg, 60% yield) and a polar isomer **6b** (245 mg, 20% yield), each of which was crystallized from diisopropyl ether.

b) Hydroperoxide **5a** (50 mg) was treated with pyridine (5 ml) and acetic anhydride (5 ml), as mentioned above, to afford an oily product (74 mg, quantitatively). Recrystallization from diisopropyl ether gave **6a**, mp 132.0—133.0 °C (34 mg), which was identical with the above-mentioned sample **6a**, obtained by acetylation of the hydroperoxides mixture (mixed-melting point determination and a comparison of IR spectra).

3β,6β-Diacetoxy-8α-methoxyepieremophilenolide (6a): Mp 132.5—133.0 °C, colorless prisms; $[\alpha]_D^{23}$ −198° (*c* 1.045, $CHCl_3$); UV (MeOH) 220.6 nm (ε 13900); CD (*c* 3.96×10^{-5}, MeOH, 25°) $[\theta]_{244}$ −17000; IR (CCl_4) 1770, 1695 (α,β-unsaturated γ-lactone), 1750, 1730, 1236 cm^{-1} (OAc); ^1H NMR ($CDCl_3$) δ=5.89 (d, *J*=1.8 Hz, 6-H), 4.85 (ddd, *J*=6, 6, 12 Hz, 3α-H), 3.22 (s, OMe), 2.23 and 2.02 (each s, OAc), 1.87 (d, *J*=1.8 Hz, 13-Me), 0.93 (d, *J*=7 Hz, 14-Me), 0.92 (s, 15-Me); ^{13}C NMR (Table 2).

Found: C, 63.08; H, 7.64%. Calcd for $C_{20}H_{28}O_7$: C, 63.14; H, 7.42%.

3β,6β-Diacetoxy-8β-methoxyeremophilenolide (6b): Mp 139.0—140.0 °C, colorless needles; $[\alpha]_D^{26}$ +180° (*c* 1.0, $CHCl_3$); UV (MeOH) 219.9 nm (ε 11540); CD (*c* 1.43×10^{-4}, hexane, 25°) $[\theta]_{263}$ +3500; IR (CCl_4) 1770, 1695 (α,β-unsaturated γ-lactone), 1735, 1233 cm^{-1} (OAc); ^1H NMR ($CDCl_3$) δ=5.65 (s, 6-H), 4.99 (ddd, *J*=3, 3, 3 Hz, 3α-H), 3.08 (s, OMe), 2.12 and 2.08 (each s, OAc), 2.01 (s, 13-Me), 1.24 (s, 15-Me), 0.92 (d, *J*=7 Hz, 14-Me); ^{13}C NMR (Table 2).

Found: C, 63.20; H, 7.65%. Calcd for $C_{20}H_{28}O_7$: C, 63.14; H, 7.42%.

Alkaline Hydrolysis of a Mixture of Lactones, 6a,b. A mixture (9.30 g) of 8α- and 8β-methoxy lactones, **6a,b** was dissolved in a 1.685 M KOH-MeOH solution (190 ml) and then left at room temperature for 16 h. After evaporation of the solvent in vacuo and dilution with water, the solution was acidified with aqueous 10% H_2SO_4, and then extracted with ethyl acetate. The usual workup gave an unsaturated acid (5.50 g, 85%) as the sole product, which was crystallized from ethyl acetate to afford a pure acid **7**, mp 163.5—164.0 °C, colorless prisms; $[\alpha]_D^{20}$ −42.5° (*c* 0.89, MeOH); UV (MeOH) 218 (ε 8250), 243 nm (9140); IR (KBr) 3650—2250, 3360, 1703, 1670 (α,β-unsaturated acid), 1618, 945 cm^{-1} (conjugated diene); ^1H NMR (acetone-d_6) δ=6.98 (m, COOH and OH), 6.69 (d, *J*=1.5 Hz, 6-H), 6.11 (d, *J*=1.5 Hz, 13-H), 5.68 (d, *J*=1.5 Hz, 13-H), 3.76 (ddd, *J*=5.5, 6, 6 Hz, 3α-H), 1.28 (s, 15-Me), 0.98 (d, *J*=7.4 Hz, 14-Me); ^{13}C NMR (pyridine-d_5) δ=26.9 (1-C), 28.5 (2-C), 69.9 (3-C), 44.9 (4-C), 40.4 (5-C), 156.7 (6-C), 141.1 (7-C), 197.0 (8-C), 40.7 (9-C), 36.7 (10-C), 136.6 (11-C) , 168.7 (12-C), 125.6 (13-C), 8.2 (14-C), 25.0 (15-C).

Found: C, 68.00; H, 7.84%. Calcd for $C_{15}H_{20}O_4$: C, 68.16; H, 7.63%.

Esterification of the Unsaturated Acid 7. The above-mentioned dienoic acid **7** (1.235 g) in MeOH (1 ml) was neutralized by a dropwise addition of a 1 M NaOMe-MeOH solution using phenolphthalein as the indicator, followed by the addition of MeI (15 g) over a 5 min period. The solution was refluxed for 9 h, and concentrated in vacuo, diluted with water, and extracted with ethyl acetate. The usual workup gave the crude methyl ester **8** (1.081 g, 83%), which was crystallized from ethyl acetate-diisopropyl ether as colorless needles (670 mg, 51.6%), mp 114.5—115.5 °C; $[\alpha]_D^{25}$ −40° (*c* 1.04, $CHCl_3$); UV (MeOH) 242 nm (ε 8870); IR ($CHCl_3$) 3420 (OH), 1715 (ester), 1670 (ketone), 1610, 942 cm^{-1} (conjugated diene); ^1H NMR ($CDCl_3$) δ=6.64 (d, *J*=1.5 Hz, 6-H), 6.20 (d, *J*=1.5 Hz, 13-H), 5.65 (d, *J*=1.5 Hz, 13-H), 3.72 (s, CO_2Me), ca. 3.7 (m, $W_{1/2}$=15 Hz, 3α-H), 1.29 (s, 15-Me), 1.00 (d, *J*=7 Hz, 14-Me); ^{13}C NMR ($CDCl_3$) δ=26.5 (t, 1-C), 27.9 (t, 2-C), 70.6 (d, 3-C), 44.5 (d, 4-C), 40.3 (s, 5-C), 156.9 (d, 6-C), 138.2 (s, 7-C), 197.3 (s, 8-C), 40.2 (t, 9-C), 36.0 (d, 10-C), 135.7 (s. 11-C), 166.8 (s, 12-C), 127.0 (t, 13-C), 7.5 (q, 14-Me), 25.0 (q, 15-C), 52.1 (q, OMe).

Found: C, 69.01; H, 8.19%. Calcd for $C_{16}H_{22}O_4$: C, 69.04; H, 7.97%.

Reduction of Dienoic Ester 8 with Sodium Borohydride. A solution of $NaBH_4$ (700 mg) in MeOH (10 ml) was added over a 5 min period at 60 °C into a solution of dienoic ester **8** (1.0 g) in MeOH (20 ml). After stirring for an additional 1.5 h under the same conditions, the reaction mixture was concentrated in vacuo and diluted with water. Extraction with ethyl acetate gave a colorless oil (1.166 g, quantitatively), which showed two spots on TLC (R_f 0.27 and 0.60, benzene-ethyl acetate 2 : 1), and was chromatographed on silica gel (21 g). Elution with benzene-ethyl acetate (15 : 1)

afforded the less polar **9b** (308 mg, 33.8%) and the polar isomer **9a** (305 mg, 33.5%), each of which was recrystallized from the ethyl acetate-diisopropyl ether.

Reduction of 3-*O*-Tetrahydropyran-2-yl Ether 10 with Sodium Borohydride. a) Preparation of 10: A mixture of *p*-toluenesulfonic acid (20 mg) and dienoic ester **8** (357 mg) in CH_2Cl_2 (2 ml) was stirred for 5 min; 2*H*-3,4-dihydropyran (276 mg) was then added into the stirred solution. After stirring for 18 h the reaction mixture was extracted with CH_2Cl_2, and the extract washed with a saturated aqueous $NaHCO_3$ and water. The usual workup gave a colorless oily product **10** (430 mg, 93%): IR (film) 1670, 1610, 1240, 1010, 950 cm^{-1}.

b) Reduction with $NaBH_4$: Into a stirred solution of the above-mentioned ester **10** (240 mg) in MeOH (5 ml) was added $NaBH_4$ (122 mg) over a 5 min period. After stirring for 2 h, the reaction mixture was adjusted to pH 2; stirring was then continued for additional 2 h. The usual workup gave a crude product (163 mg, quantitative yield), which was chromatographed on silica gel (20 g) with benzene-ethyl acetate (15 : 1) to afford the less polar isomer **9b** (46 mg, 28%) and the polar isomer **9a** (109 mg, 66%).

3β(eq)-Hydroxyepieremophilenolide (9a): Mp 167.0—168.0 °C as colorless needles; $[\alpha]_D^{27}$ −157° (*c* 0.99, $CHCl_3$); UV (MeOH) 217.5 nm (ε 5600); CD (*c* 4.010×10^{-3}, MeOH, 22 °C) $[\theta]_{253}$ +350; IR ($CHCl_3$) 3600, 3450 (OH), 1735, 1680, 1095 cm^{-1} (α,β-unsaturated γ-lactone); ^1H NMR ($CDCl_3$) δ=4.80 (br m, $W_{1/2}$=15.8 Hz, 8α-H), 4.10 (ddd, *J*=5.5, 5.5, 11 Hz, 3α-H), 2.78 (d, *J*=14.5 Hz, 6α-H), 1.79 (t, *J*=1.6 Hz, 13-Me), 0.97 (d, *J*=7 Hz, 14-Me), 0.85 (s, 15-Me); ^{13}C NMR (Table 2).

Found: C, 71.82; H, 9.19%. Calcd for $C_{15}H_{22}O_3$: C, 71.97; H, 8.86%.

3β(ax)-Hydroxyereemophilenolide (9b): Mp 169.5—170.5 °C as colorless needles; $[\alpha]_D^{27}$ +196° (*c* 1.04, $CHCl_3$); UV (MeOH) 217.5 nm (ε 15200); CD (*c* 4.140×10^{-3}, MeOH, 22 °C) $[\theta]_{248}$ +10200; IR ($CHCl_3$) 3600, 3470 (OH), 1740, 1690, 1095 cm^{-1} (α,β-unsaturated γ-lactone); ^1H NMR ($CDCl_3$) δ=4.72 (m, *W*1/2=18 Hz, 8β-H), 3.81 (ddd, *J*=4, 4, 5 Hz, 3α-H), 2.89 (d, *J*=14.6 Hz, 6α-H), 1.80 (t, *J*=1.8 Hz, 13-Me), 1.29 (s, 15-Me), 1.01 (d, *J*=6.8 Hz, 14-Me); ^{13}C NMR (Table 2).

Found: C, 72.01; H, 8.89%. Calcd for $C_{15}H_{22}O_3$: C, 71.97; H, 8.86%.

Oxidation of 3β(eq)-Hydroxyepieremophilenolide (9a). a) Jones' Oxidation: Jones' reagent (0.8 ml) was added into a stirred solution of **9a** (150 mg) in acetone (3 ml) over a period of 5 min under ice cooling. After stirring for additional 10 min at room temperature, the excess reagent was decomposed with MeOH and the reaction mixture extracted with ethyl acetate. Working up as usual gave a crude crystalline product (114 mg, quantitatively), mp 130.5—132.5 °C, which showed the presence of a pair of epimers concerning the configuration of 14-methyl in its ^1H NMR spectrum (δ=0.91 and 1.03, each s, 15-Me; 1.06 and 1.20, each d, *J*=6.5 Hz, 14-Me). Recrystallization from ethyl acetate gave a pure specimen of 3-oxoepiermophilenolide (**11a**), mp 131.5—132.5 °C (55 mg, 37%).

b) PDC (Pyridinium Dichromate) Oxidation. PDC (1.0 g) was gradually added into a stirred solution of **9a** (118 mg) in CH_2Cl_2 (20 ml). After stirring for additional 2 h, the reaction mixture was shaken with Celite (5 g) and filtered. Evaporation of the filtrate in vacuo gave **11a** (109 mg, 93%).

3-Oxoepieremophilenolide (11a): Mp 131.5—132.5 °C, colorless needles (ethyl acetate-diisopropyl ether); $[\alpha]_D^{26}$ −157° (*c* 1.08, $CHCl_3$); UV (MeOH) 224 nm (ε 9000); CD (c 3.670×10^{-3}, MeOH, 22 °C) $[\theta]_{241}$ −655, $[\theta]_{288}$ −3410; IR ($CHCl_3$) 1740, 1685 (α,β-unsaturated γ-lactone), 1710 cm^{-1} (ketone); ^1H NMR ($CDCl_3$) δ=4.82 (br m, $W_{1/2}$=14 Hz, 8α-H), 1.79 (d, *J*=1.8 Hz, 13-Me), 1.20 (d, *J*=6.5 Hz, 14-Me), 0.89 (s, 15-Me). ^{13}C NMR (Table 2).

Found: C, 72.44; H, 8.13%. Calcd for $C_{15}H_{20}O_3$: C, 72.55; H, 8.12%.

Oxidation of 3β(ax)-Hydroxyeremophilenolide 9b. a) Jones' Oxidation. Jones' reagent (1 ml) was added into a stirred solution of **9b** (100 mg) in acetone (2 ml) over a period of 5 min under ice cooling. After stirring for additional 30 min, the reaction mixture was worked up in a similar manner to that mentioned above, giving a crude crystalline product (101 mg, quantitatively), which was recrystallized from ethyl acetate-diisopropyl ether to afford 3-oxoeremophilenolide (**11b**) (126 mg, 95.5%).

b) PDC Oxidation. PDC (1.8 g) was gradually added into a solution of **9b** (153 mg) in CH_2Cl_2 (20 ml) at room temperature. After stirring for additional 2.5 h, the mixture was worked up in a similar manner as to that mentioned above, giving **11b** (148 mg, 97.5%).

3-Oxoeremophilenolide (11b). Mp 155.5—156.5 °C, colorless needles (ethyl acetate-diisopropyl ether); $[\alpha]_D^{26}$ +154° (*c* 0.99, $CHCl_3$); UV (MeOH) 224 nm (ε 11800); CD (*c* 4.301×10^{-3} MeOH, 22 °C) $[\theta]_{245}$ +6790, $[\theta]_{284}$ −10600; IR ($CHCl_3$) 1740, 1695, 1205 (α,β-unsaturated γ-lactone), 1705 cm^{-1} (ketone); ^1H NMR ($CDCl_3$) δ=4.87 (br m, $W_{1/2}$=15.2 Hz, 8β-H), 2.88 (d, *J*=14.0 Hz, 6α-H), 1.83 (t, *J*=1.3 Hz, 13-Me), 1.00 (s, 15-Me) , 0 96 (d, *J*=7 Hz, 14-Me); ^{13}C NMR (Table 2).

Found: C, 72.39; H, 8.14%. Calcd for $C_{15}H_{20}O_3$: C, 72.55; H, 8.12%.

Reduction of 3-Oxoepieremophilenolide (11a) via Ethylene Dithioacetal 12a. Ten drops of BF_3-diethyl ether (1/1) were added into a stirred solution of **11a** (55 mg) in 1,2-ethanedithiol (0.5 ml) under ice-cooling. After stirring for 6 h at room temperature and the addition of MeOH (5 drops), the reaction mixture was concentrated in vacuo, diluted with water, and then extracted with ethyl acetate. The usual workup gave an oily product (75 mg, quantitatively), which was crystallized from ethyl acetate-light petroleum to afford ethylene dithioacetal **12a**, mp 129.5—131.5 °C, as colorless needles; $[\alpha]_D^{26}$ −157° (*c* 1.20, $CHCl_3$); IR ($CHCl_3$) 1742, 1682, 1096, 1036 cm^{-1}; ^1H NMR ($CDCl_3$) δ=4.80 (m, $W_{1/2}$=14 Hz, 8α-H), 3.4—3.1 (m, acetal methylene), 1.79 (t, *J*=1.5 Hz, 13-Me), 1.31 (d, *J*=6.8 Hz, 14-Me), 0.91 (s, 15-Me)

A suspension of dithioacetal **12a** (153 mg) and Raney nickel (500 mg) in ethanol (10 ml) was refluxed for 3 h and then filtered. The filtrate was concentrated in vacuo to leave a colorless oil (110 mg, 90%). Purification by PTLC (benzene-ethyl acetate, 30 : 1) followed by recrystallization from pentane gave epieremophilenolide (**13a**) (32 mg, 26%).

Epieremophilenolide (13a): Mp 86.0—86.5 °C, colorless prisms; $[\alpha]_D^{26}$ −127° (*c* 1.00, $CHCl_3$); CD (*c* 4.22×10^{-3}, MeOH, 22 °C) $[\theta]_{248}$ −1800; IR ($CHCl_3$) 1750, 1675, 1080 cm^{-1} (α,β-unsaturated γ-lactone); ^1H NMR ($CDCl_3$) δ=4.82 (br m, $W_{1/2}$=13.6 Hz, 8α-H), 1.80 (t, *J*=1.5 Hz, 13-Me), 0.92 (d, *J*=6.6 Hz, 14-Me), 0.88 (s, 15-Me); ^{13}C NMR (Table 2).

Found: C, 76.86; H, 9.52%. Calcd for $C_{15}H_{22}O_2$: C,76.88; H, 9.46%.

Reduction of 3-Oxoepieremophilenolide (11b) via Eth-

ylene Dithioacetal 12b. The 3-ketone **11b** (54 mg) was treated with 1,2-ethanedithiol (0.5 ml) and BF_3-diethyl ether (1/1) (7 drops), as described above. A similar type workup gave a crude product (64 mg, 90%), which was crystallized from ethyl acetate as colorless needles to afford the dithioacetal **12b**, mp 195.5—196.5 °C, $[\alpha]_D^{22}$ +133° (*c* 1.0, $CHCl_3$); IR ($CHCl_3$) 1735, 1685, 1090 cm^{-1} (α,β-unsaturated γ-lactone); ^1H NMR ($CDCl_3$) δ=4.65 (br m, $W_{1/2}$=13.3 Hz, 8β-H), 3.5—3.0 (m, acetal methylene), 1.82 (t, *J*=1.4 Hz, 13-Me), 1.20 (s, 15-Me), 1.16 (d, *J*=5.7 Hz, 14-Me).

The dithioacetal **12b** (50 mg) was treated with Raney nickel (250 mg) in ethanol (5 ml) in a similar manner as that stated above to give an oily product (34 mg, 94%), which was crystallized from diisopropyl ether or light petroleum to afford eremophilenolide (**13b**).

Eremophilenolide (13b): Mp 123.5—124.5 °C, colorless needles; $[\alpha]_D^{21}$ +163° (*c* 1.00, $CHCl_3$); UV (MeOH) 224 nm (ε 13500); CD (*c* 8.74×10^{-3}, MeOH, 22 °C) $[\theta]_{248}$ +7950; IR ($CHCl_3$) 1755, 1690 cm^{-1} (α,β-unsaturated lactone); ^1H NMR ($CDCl_3$) δ=4.67 (br m, $W_{1/2}$=16.5 Hz, 8β-H), 2.90 (d, *J*=14.5 Hz, 6α-H), 1.80 (t, *J*=1.4 Hz, 13-Me), 1.04 (s, 15-Me), 0.80 (d, *J*=5.9 Hz, 14-Me); ^{13}C NMR (Table 2). This lactone was found to be identical with the natural specimen by a comparison of the IR and ^1H NMR spectra, and by a mixed-melting point determination.

Tosylation of 3β(eq)-Hydroxyepieremophilenolide (9a). Into a solution of **9a** (55 mg) in pyridine (1.5 ml) was added tosyl chloride (200 mg) at −5 °C; the mixture was left for 24 h at room temperature. The usual workup gave a crystalline product (75 mg, 84.4%), which was recrystallized from ethyl acetate-light petroleum to afford the tosylate **14a** as colorless leaflets, mp 156.5—158.0 °C (decomp); IR ($CHCl_3$) 1740, 1685 (α,β-unsaturated lactone), 1190, 1180, 1040, 885 cm^{-1} (tosylate); ^1H NMR ($CDCl_3$) δ=7.85—7.25 (q, aromatic 4H), 4.83 (ddd, *J*=5.5, 5.5, 11.5 Hz, 3α-H), 2.46 (s, tosyl Me), 1.76 (t, *J*=1.5 Hz, 13-Me), 0.96 (d, *J*=7.2 Hz, 14-Me), 0.80 (s, 15-Me).

Found: C, 65.16; H, 7.19%. Calcd for $C_{22}H_{28}O_5S$: C, 65.32; H, 6.98%.

Treatment of Tosylate 14a with Sodium Iodide. A suspension of **14a** (85 mg) and NaI (300 mg) in dry acetone (3 ml) was stirred for 5 min at room temperature and then left for 1 week. The usual workup gave a crystalline product (40 mg, 82%), which was crystallized from ethyl acetate-light petroleum to afford 3,4-dehydroepieremophilenolide (**15a**).

3,4-Dehydroepieremophilenolide (15a): Mp 134.0—135.5 °C as colorless leaflets; IR ($CHCl_3$) 1750, 1680, 1090 cm^{-1}; ^1H NMR ($CDCl_3$) δ=5.34 (br s, 3-H), 4.71 (br m, $W_{1/2}$= 15.2 Hz, 8α-H), 1.73 (t, *J*=1.7 Hz, 13-Me), 1.63 (d, *J*=1.3 Hz, 14-Me), 0.89 (s, 15-Me); ^{13}C NMR ($CDCl_3$) δ=25.7 (t, 1-C), 26.1 (t, 2-C), 122.6 (d, 3-C), 139.6 (s, 4-C), 40.8 (s, 5-C), 36.7 (t, 6-C), 160.8 (s, 7-C), 77.8 (d, 8-C), 40.4 (t, 9-C), 36.7 (d, 10-C), 121.0 (s, 11-C), 174.5 (s, 12-C), 7.9 (q, 13-C), 18.6 (q, 14-C), 22.7 (q, 15-C).

Found: C, 77.29; H, 8.97%. Calcd for $C_{15}H_{20}O_2$: C, 77.55; H, 8.68%.

Mesylation of 9a. Methanesulfonyl chloride (1 ml) was added into a solution of **9a** (134 mg) in pyridine (1 ml) at 0 °C; the mixture was left for 15 h. The usual workup gave **15a** (116 mg, 93%), which was crystallized from ethyl acetate-light petroleum as colorless leaflets, mp 134.0—135.0 °C. This compound was identical in all respects to the above-mentioned sample **15a** derived by tosylation of **9a**, followed by treatment with NaI.

Hydrogenation of 15a. Compound **15a** (67 mg) in ethanol (6 ml) was hydrogenated over 10% Pd-C (35 mg) for 1 h at room temperature. The filtrate was evaporated in vacuo to leave a crystalline product (65 mg, 96%), which was recrystallized from pentane to afford epieremophilenolide (**13a**) as colorless prisms, mp 84.0—85.0 °C. This compound was identical to the above-mentioned sample **13a**, transformed from **11a** via dithioacetal **12a** by a mixed-melting-point determination and a comparison of the IR and ^1H NMR spectra.

Mesylation of 9b. Methanesulfonyl chloride (1 ml) was added into a solution of **9b** (163 mg) in pyridine (1 ml) over a period of 2 min at 0 °C, and then left at room temperature for 14 h. The usual workup gave 3,4-dehydroeremophilenolide (**15b**) (137 mg, 91%), which was crystallized from ethyl acetate-light petroleum.

3,4-Dehydroeremophilenolide (15b): Mp 138.9—139.5 °C as colorless needles; IR ($CHCl_3$) 1755, 1685, 1335, 1090, 755 cm^{-1}; ^1H NMR ($CDCl_3$) δ=5.23 (br s, 3-H), 4.61 (br m, $W_{1/2}$= 16.3 Hz, 8β-H), 3.03 (d, *J*=14 Hz, 6α-H), 1.83 (d, *J*=1.3 Hz, 13-Me), 1.60 (d, *J*=1.1 Hz, 14-Me), 1.24 (s, 15-Me); ^{13}C NMR ($CDCl_3$) δ=23.1 (t, 1-C), 21.5 (t, 2-C), 122.5 (d, 3-C), 135.8 (s, 4-C), 41.3 (s, 5-C), 35.7 (t, 6-C), 160.6 (s, 7-C) , 80.2 (d, 8-C), 34.8 (t, 9-C), 38.6 (d, 10-C), 119.2 (s, 11-C), 174.9 (s, 12-C), 8.7 (q, 13-C), 19.5 (q, 14-C), 25.7 (q, 15-C).

Hydrogenation of 15b. A solution of **15b** (85 mg) in EtOH (7 ml) was hydrogenated with 10% Pd-C (53 mg) for 45 min. The filtrate was evaporated to give a crude eremophilenolide (**13b**) (85 mg, 99%), which was crystallized from light petroleum as colorless needles, mp 123.0—124.0 °C. This compound was identical in all respects with the natural specimen by a mixed-melting point determination, and by a comparison of the IR and ^1H NMR spectra.

Reduction of 3-Oxoepieremophilenolide (11a) with Sodium Borohydride. A solution of **11a** (51 mg) in MeOH (5 ml) was added into a solution of $NaBH_4$ (163 mg) in MeOH (2 ml) over a 3 min period at room temperature. After stirring for additional 35 min and acidification with 0.1 M HCl, the mixture was extracted with ether. The usual workup gave a reduction product (52 mg, quantitatively), which showed 2 spots on TLC (R_f 0.29 and 0.43; benzene-ethyl acetate 2:1). The product was chromatographed on silica gel (5 g) with benzene-ethyl acetate (5:1) to 3α(*ax*)-hydroxyepieremophilenolide (**16a**) (R_f 0.43, 29 mg, 56.3%) and **9a** (R_f 0.29, 19 mg, 36.9%). Both were crystallized from ethyl acetate-light petroleum; the polar product, mp 167.0—168.0 °C, was identified as **9a** (described above) by a mixed-melting point determination and a comparison of the spectral data.

3α(ax)-Hydroxyepieremophilenolide (16a): Mp 138.5—139.5 °C, as colorless prisms; $[\alpha]_D^{24}$ −138° (*c* 0.98, $CHCl_3$); CD (*c* 4.522×10^{-3}, MeOH, 22 °C) $[\theta]_{248}$ −150; IR ($CHCl_3$) 3450 (OH), 1745, 1680 cm^{-1} (α,β-unsaturated lactone); ^1H NMR ($CDCl_3$) δ=4.88 (br t, *J*=9.7 Hz, 8α-H), 3.97 (ddd, *J*=3, 3, 3 Hz, 3β-H), 3.70 (d, *J*=14.5 Hz, 6α-H), 2.16 (d, *J*=14.5 Hz, 6β-H), 1.78 (t, *J*=1.5 Hz, 13-Me), 0.95 (d, *J*=7.3 Hz, 14-Me), 0.80 (s, 15-Me); ^{13}C NMR (Table 2).

Found: C, 71.95; H, 8.71%. Calcd for $C_{15}H_{22}O_3$: C, 71.97; H, 8.86%.

Reduction of 3-Oxoepieremophilenolide (11b) with Sodium Borohydride. A solution of the ketone **11b** (152 mg) in MeOH (4 ml) was added into a stirred solution of

$NaBH_4$ (193 mg) in MeOH (5 ml) over a 10 min period at room temperature. After stirring for an additional 30 min, the mixture was acidified with 0.1 M HCl and extracted with ether. The usual workup gave a crude product (135 mg, 90%), which showed 2 spots on TLC (R_f 0.60 and 0.45; benzene-ethyl acetate 2:1). The product was chromatographed on silica gel (12 g) by elution with benzene-ethyl acetate (10:1) to give a less polar compound (R_f 0.60, 120 mg, 80%), which was crystallized from ethyl acetate-diisopropyl ether to afford **9b**, mp 169.5—170.5 °C, as colorless needles. This compound was identified as 3β(ax)-hydroxyeremophilenolide (**9b**), as described above. Further elution with the same solvent gave a polar compound, 3α(eq)-hydroxyeremophilenolide (**16b**) (R_f 0.45, 15 mg, 10%).

3α(eq)-Hydroxyeremophilenolide (16b): Mp 158.0—159.0 °C, colorless needles (ethyl acetate-light petroleum); $[\alpha]_D^{24}$ +214° (*c* 1.12, $CHCl_3$); CD (*c* 4.312×10⁻³, MeOH, 22 °C) $[\theta]_{252}$ +1250; IR ($CHCl_3$) 3440 (OH), 1745, 1690 cm^{-1} (α,β-unsaturated lactone); ^1H NMR ($CDCl_3$) δ=4.70 (br m, 8β-H), 3.61 (ddd, *J*=5, 10.3, 10.3 Hz, 3β-H), 2.90 (d, *J*=14.6 Hz, 6α-H), 1.81 (t, *J*=1.5 Hz, 13-Me), 1.05 (s, 15-Me), 1.01 (d, *J*=8.5 Hz, 14-Me); ^{13}C NMR (Table 2).

Found: C, 71.67; H, 9.04%. Calcd for $C_{15}H_{22}O_3$: C, 71.97; H, 8.86%.

Preparation of Eremophilenolide (13b) from the Natural 6β-Hydroxyeremophilenolide (17b). A 2 M KOH-MeOH solution (4 ml) was added into a solution of natural **17b** (300 mg) in MeOH (3 ml); the mixture was left overnight. After removing the solvent in vacuo and dilution with water, the solution was acidified with aqueous 10% H_2SO_4 and extracted with ether. Without isolation of the free acid, the ethereal extract was treated with CH_2N_2 in diethyl ether. The usual workup gave an oil (302 mg, 95%), which was purified by vacuum distillation to furnish an enoic ester **18** as a colorless oil (263 mg), bp 116—118 °C/0.3 mmHg (40 Pa); $[\alpha]_D^{25}$ +15.5° (*c* 0.99, $CHCl_3$); UV (MeOH) 238 nm (ε 14300); IR (film) 1730, 1670, 1635, 1240 cm^{-1}; ^1H NMR ($CDCl_3$) δ=6.63 (br s, 6-H), 3.65 (s, OMe), 1.27 (d, *J*=7.2 Hz, 13-Me), 1.12 (s, 15-Me), 0.91 (d, *J*=6.5 Hz, 14-Me); ^{13}C NMR ($CDCl_3$) δ=20.4 (t, 1-C), 27.0 (t, 2-C), 30.2 (t, 3-C), 36.1 (d, 4-C), 38.9 (s, 5-C), 156.4 (d, 6-C), 136.6 (s, 7-C), 198.4 (s, 8-C), 39.4 (t, 9-C), 37.9 (d, 10-C), 38.2 (d, 11-C), 175.0 (s, 12-C), 16.5 (q, 13-C), 15.8 (q, 14-C), 20.8 (q, 15-C), 51.8 (q, OMe).

A solution of $NaBH_4$ (98 mg) in MeOH (6 ml) was added into a solution of the ester **18** (267 mg) in MeOH (3 ml) and left at room temperature for 4 h to deposit a crystalline product. The usual workup gave crude crystals (213 mg, 90%). Recrystallization from light petroleum furnished eremophilenolide (**13b**, 87 mg) as colorless needles, mp 123.5—124.5 °C. This compound was identical in all respects with the natural specimen as well as the above-mentioned synthesized **13b**.

Reduction of Ester 22 with Sodium Borohydride. a) Preparation of Ester 22: Dienoic acid **21**[1,2] (323 mg) was subjected to esterification in a similar method as that used in the preparation of ester **8** to furnish ester **22** as an oily product (273 mg, 80%), which was purified by vacuum distillation, bp 100—120 °C (bath temperature)/10^{-2} mmHg (2.7 Pa); $[\alpha]_D^{23}$ +16.5° (*c* 1.24, $CHCl_3$); IR (film) 1725, 1680, 1620, 1200, 1150, 1050, 945, 930 cm^{-1}; ^1H NMR ($CDCl_3$) δ=6.78 (s, 6-H), 6.21 (d, *J*=1.5 Hz, 13-H), 5.65 (d, *J*=1.3 Hz, 13-H), 3.73 (s, $COOCH_3$), 2.75 (dd, *J*=17, 11 Hz, 9α-H), 1.16 (s, 15-Me), 0.94 (d, *J*=6.6 Hz, 14-Me).

b) Reduction of Ester 22: Into a solution of ester **22** (231 mg) in MeOH (4 ml) was added a solution of $NaBH_4$ (91 mg) in MeOH (3.5 ml) and left at room temperature overnight. Working up as mentioned above furnished quantitatively crude crystals (202 mg). Recrystallization from light petroleum gave eremophilenolide (**13b**), mp 123.5—124.0 °C. This compound was identical with the natural and synthetic samples in all respects.

References

1) K. Naya, R. Kanazawa, and M. Sawada, *Bull. Chem. Soc. Jpn.*, **48**, 3220 (1975).

2) K. Naya, N. Nogi, Y. Makiyama, H. Takashina, and T. Imagawa, *Bull. Chem. Soc. Jpn.*, **50**, 3002 (1977).

3) K. Naya, T. Matsuura, M. Makiyama, and M. Tsumura, *Heterocycles*, **10**, 177 (1978).

4) N. H. Fischer, E. J. Olivier, and H. D. Fischer, "Progress in the Chemistry of Organic Natural Products," ed by W. Herz and G. W. Kirby, Springer-Verlag, Wien (1979), Vol. 38, pp. 257—264.

5) L. Novotný, V. Herout, and F. Šorm, *Tetrahedron Lett.*, **1961**, 697; L. Novotný, J. Jizba, V. Herout, F. Šorm, L. H. Zalkow, S. Hu, and C. Djerassi, *Tetrahedron*, **19**, 1101 (1963); L. Novotný, V. Herout, and F. Šorm, *Collect. Czech. Chem. Commun.*, **29**, 2189 (1964); K. Moriyama and T. Takahashi, *Chem. Pharm. Bull.*, **24**, 360 (1976).

6) K. Ito, T. Iida, and T. Funatani, *Yakugaku Zasshi*, **99**, 349 (1979); K. Sugawa, K. Hayashi, and H. Mitsuhashi, *Phytochemistry*, **24**, 1531 (1985).

7) E. Piers and M. B. Geraghty, *Can. J. Chem.*, **51**, 2166 (1973); I. Nagakura, S. Maeda, M. Ueno, M. Funamizu, and Y. Kitahara, *Chem. Lett.*, **1975**, 1143.

8) In our recent experiment, the photosensitized oxygenation and the following acetylation of petasalbin (6β-hydroxyfuranoeremophilane)[1] (452 mg) gave 6β-acetoxy-8β-methoxyeremophilenolide (296 mg) and 6β-acetoxy-8α-methoxyepieremophilenolide (289 mg). In the previous paper, [Ref. 2, p. 3005], furanoeremophilane furnished isomeric 8α- (181 mg) and 8β-methoxyhydroperoxides (167 mg), and 8α-methoxylactone (130 mg) and 8β-isomer (143 mg) by the photooxygenation and the following acetylation.

9) K. Naya, M. Nakagawa, M. Hayashi, K. Tsuji, and M. Naito, *Tetrahedron Lett.*, **1971**, 2961.

10) K. Naya, Y. Makiyama, T. Matsuura, N. Ii, H. Nagano, and T. Takahashi, *Chem. Lett.*, **1978**, 301.

11) N. S. Bhacca and D. H. Williams, "Application of NMR Spectroscopy in Organic Chemistry, Illustration from the Steroid Field," Prentice-Hall, San Francisco (1964), p. 110.

12) The relations of melting points and absorptive activities in the paired lactones were not in accord with those expected on the basis of our proposed classification procedure in Refs. 1 and 2. This may be accounted for based on the steric compression around the oxygenated functions at C-3.

13) L. M. Jackman and S. Sternhell, "Application of NMR Spectroscopy in Organic Chemistry," Pergamon Press, Oxford (1969), p. 240.

14) A. C. Huttric, J. B. Carr, W. F. Trager, and B. J. Nist, *Tetrahedron*, **19**, 2145 (1963); A. Hassner and C. Heathcock, *J. Org. Chem.*, **29**, 1350 (1964).

15) E. L. Eliel, N. L. Allinger, S. J. Angyal, and G. A.

Morrison, "Conformational Analysis," John Wiley & Sons, New York (1965), Chap. 2, p. 71.

16) A. Moscowitz, E. Charney, V. Weiss, and H. Ziffer, *J. Am. Chem. Soc.*, **83**, 466 (1961); C. Djerassi, R. Records, E. Bunnenberg, K. Mislow, and A. Moscowitz, *ibid.*, **84**, 870 (1962).

17) H. Beierbeck, J. K. Saunders, and J. W. ApSimon, *Can. J. Chem.*, **55**, 2813 (1977).

18) D. K. Dalling and D. M. Grant, *J. Am. Chem. Soc.*, **89**, 6612 (1967); *ibid.*, **94**, 5318 (1972).

19) D. K. Dalling, D. M. Grant, and E. G. Paul, *J. Am. Chem. Soc.*, **95**, 3718 (1973).

Syntheses and Properties of *N*-Fluoropyridinium Salts

Teruo UMEMOTO,* Kikuko HARASAWA, Ginjiro TOMIZAWA, Kosuke KAWADA,† and Kyoichi TOMITA†
Sagami Chemical Research Center, Nishi-Ohnuma 4-4-1, Sagamihara, Kanagawa 229
(Received July 18, 1990)

Various stable *N*-fluoropyridinium salts with a non- or weakly nucleophilic counter anion such as TfO^-, FSO_3^-, BF_4^-, SbF_6^-, ClO_4^-, $CH_3SO_3^-$ etc., or with an electron-donating or -withdrawing substituent(s) on the pyridine ring were synthesized and their properties investigated. *N*-Fluoropyridinium-2-sulfonates, *N*-fluoroquinolinium triflate, and highly hindered *N*-fluoro-2,6-di-*t*-butylpyridinium salts were also synthesized. They were synthesized by counter anion displacement reactions of unstable pyridine-F_2 compounds, fluorination of salts of pyridines with protonic acids or silyl esters with F_2, and/or fluorination of Lewis acid complexes of pyridines. The scope of each method was examined in detail. Each of the *N*-fluoropyridinium salts was assigned as the first stable 1 : 1 salt structure of the pyridine nucleus and halogen atom on the basis of the spectral and elemental analyses. The stability depended on the nucleophilicity or basicity of the counter anions and electronic nature or position of the ring substituents. These results and NMR analyses clearly showed the unstable pyridine-F_2 compounds to have *N*-fluoropyridinium fluoride salt structure. Some *N*-fluoropyridinium triflates were hydrolyzed and the products were examined, suggesting a unique hydrolysis mechanism.

Although the reactions of pyridine and many substituted pyridines with Cl_2, Br_2, or I_2, producing molecular complexes with linear nitrogen-halogen-halogen atom structure, have been examined extensively, only limited attention has been directed to those of pyridines with molecular fluorine (F_2).[1] F_2 differes greatly from the other halogens[2] and so consequently, the products obtained from its reaction should be of considerable interest.

Simons first found that liquid pyridine smoothly and completely absorbs F_2 and when absorption is conducted at −40 °C, a dark brown solid separates from the liquid, which decomposes on warming to 0 °C.[3] He described that the thermally unstable solid was apparently a molecular complex between pyridine and F_2, $C_5H_5N \cdot F_2$.[3]

Meinert noted a solid, isolated by bubbling F_2 diluted with N_2 into a solution of pyridine in $CFCl_3$ at −80 °C followed by filtering at low temperature, to decompose violently above −2 °C.[4] He considered this solid to be a pyridine-F_2 compound with polar character. However, no spectral or other data on the structure of the pyridine-F_2 compound are presently not available, probably due to its explosive nature.

The authors found unstable pyridine-F_2 compounds to smoothly undergo counter anion displacement reactions with nonnucleophilic anions to give stable *N*-fluoropyridinium salts.[5] It was also found that insertion reactions of F_2 to salts or complexes of pyridines with protonic acids, silyl esters, or Lewis acids gave the *N*-fluoropyridinium salts. In this paper, syntheses of various *N*-fluoropyridinium salts by different methods and their properties are described in detail.

Experimental

General. Melting points were uncorrected. ^1H NMR spectra were measured on a Varian EM 390 or XL-100 NMR spectrometer or a Bruker AM-400 NMR spectrometer. ^{19}F NMR spectra were obtained on a Hitachi R-20B NMR spectrometer and the chemical shifts were given in ppm downfield from $CFCl_3$ as an internal standard. Both ^1H and ^{19}F NMR spectra were taken by using CD_3CN solvent, unless otherwise noted. IR spectra were measured on a JASCO A-202 diffraction grating infrared spectrometer. Mass spectra were recorded on a Hitachi RMU-6MG mass spectrometer at 70 eV or a Hitachi M-80A mass spectrometer by EI (electron impact ionization) method or SIMS (secondary ion mass spectrometry) method. Unless otherwise noted, the data by EI method are given.

Materials. A 20% F_2–80% N_2 cylinder was purchased from Kanto Denka Kagaku Company (Japan). Since the content of HF in the fluorine was very low (0.2—0.3%), it was used without a NaF trap. 3-Chloro-5-trifluoromethylpyridine and 3,5-bis(trifluoromethyl)pyridine were given by Ishihara Sangyo Company (Japan). 2-[(1*R*,3*R*,4*S*)-Menthyloxy]pyridine (bp 112 °C/0.2 mmHg, 1 mmHg=133.322 Pa, $[\alpha]_D^{20}=-110.7$ (c=0.994, $CHCl_3$)) was prepared by treatment of 2-chloropyridine with (−)-menthol by the action of NaH in tetrahydrofuran (THF) under reflux for 19 h. 2-(Fluoromethyl)-4,6-dimethylpyridine was prepared from 2,4,6-trimethylpyridine by oxidation with 35% H_2O_2 in acetic acid, rearrangement reaction with Ac_2O, alkaline hydrolysis, and fluorination with (diethylamino)sulfur trifluoride. 6-Chloropyridine-2-sulfonic acid was prepared by treatment of 2,6-dichloropyridine with sodium sulfite. Dry CH_3CN was made by distillation over CaH_2 and used immediately. Other solvents used were dried by usual methods and stored over molecular sieves.

Synthesis of *N*-Fluoropyridinium Salts 1—46. [CAUTION!]. Since F_2 is a highly oxidizing and toxic gas, the experimenter should familiarize him- or herself with the precautions necessary for the safe handling of F_2.[6] The use of diluted F_2 in an inert gas (N_2 or Ne) is considerably safer than pure F_2.

Apparatus: As shown in Fig 1, the apparatus used for the fluorination consisted of a 20% F_2–80% N_2 cylinder, a N_2 cylinder, two flow meters (Hastings Mass Flowmeters Model CST), a Pyrex®-glass reactor, and valves made of

† From Onoda Cement Company.

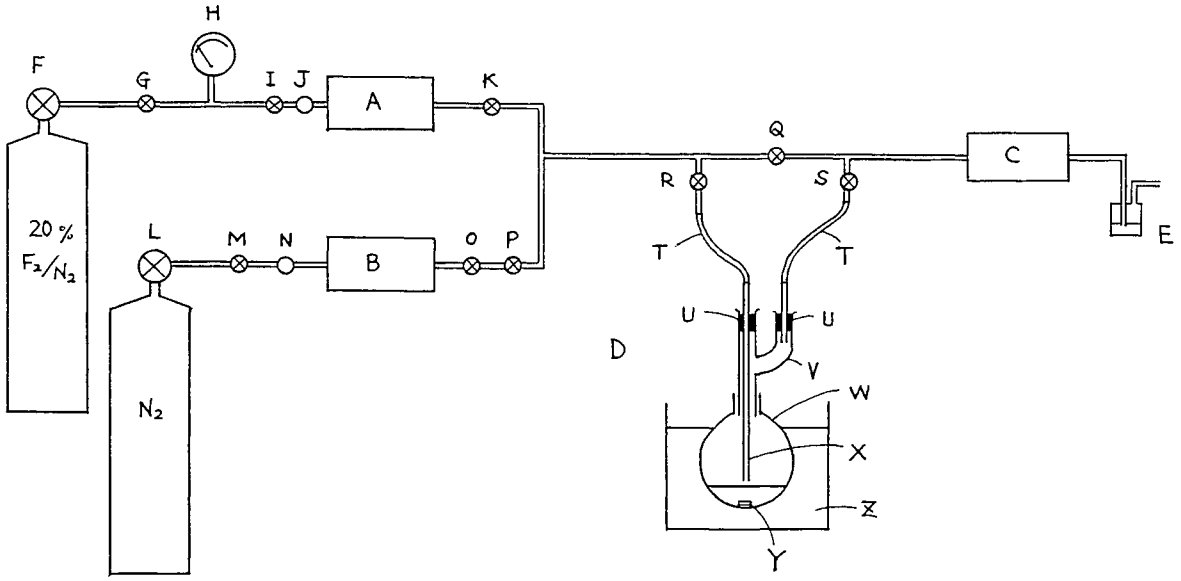

Fig. 1. Apparatus for fluorination.
A: A flow meter (Hastings Mass Flowmeter Model CST-M). B: A flow meter (Hastings Mass Flowmeter Model CST). C: An alumina trap. D: A reactor. E: A bubble counter containing perfluorotributylamine. F: A pressure regulator for fluorine (Takachiho F_2 Regulator Model 7630H). G,I, K,O,P: Valves made of stainless steel. H: A pressure gauge made of stainless steel. J,N: Filters made of stainless steel. L: A pressure regulator for nitrogen. M,Q,R,S: Valves made of brass. T: A Viton® tube. U: A Teflon® cork. V: An adaptor made of Pyrex®-glass. W: A round-bottomed flask made of Pyrex®-glass. X: A Pyrex®-glass tube. Y: A Teflon®-coated stirring bar. Z: A bath of −40 °C.

stainless steel or brass. The cylinders, the flow meters, and the valves were connected with stainless steel or copper tubes. The 20% F_2-N_2 cylinder was equipped with a pressure regulator (Takachiho F_2 Regulator Model 7630H) that was designed for fluorine service. The glass reactor was connected to the outlet of further diluted F_2 (10% F_2-N_2) by using a Viton® tube. The gas outlet of the reactor was connected to a granular alumina trap to consume the F_2 gas. The designed concentration of F_2 in N_2 and the flow rates of a F_2-N_2 mixture gas were adjusted by the flow meters.

Method A (a two-step procedure): **General Procedure;** a 50-mL reaction flask was charged with 3 mmol of a pyridine and 6 mL of dry CH_3CN. The system was purged with N_2 and the reaction mixture was immersed in a cooling bath of −40 °C. A 10% F_2-90% N_2 mixture gas was introduced at a flow rate of 30 mL min^{-1} just above the surface of the rapidly stirred solution. Total amount of F_2 used was 9 mmol. After the flow of F_2 was stopped, N_2 only was flowed through the system at rate of 15 mL min^{-1} for 30 min while keeping the reaction mixture at −40 °C. After that, 3 mmol of TfOH (a reactant shown in Tables 1 and 2) was added into the reaction mixture and it was stirred for 1 h at −40 °C. The post-treatment for *N*-fluoropyridinium triflate (**1a**) was as follows; 50 mL of diethyl ether (Et_2O) was added into the reaction mixture and warmed to room temperature. The resulting solid was collected by filteration to give a solid of 0.306 g, which was sufficiently washed with 1 ml of dry ethyl acetate (AcOEt) to give 0.242 g (33%) of pure **1a**.

Method B (a one-step procedure): **General Procedure;** a solution of 3 mmol of a pyridine, 3 mmol of NaOTf (a reactant shown in Tables 1 and 2), and 6 mL of dry CH_3CN was fluorinated in the same manner as described in Method A. The reaction mixture was then warmed to room temperature, filtered through Celite to remove NaF formed, and evaporated up to dryness at room temperature. The resulting solid was washed with dry AcOEt to give 0.554 g (75%) of **1a**. Analytically pure crystals were obtained by recrystallization from CH_3CN-AcOEt at room temperature. When KOTf was used in place of NaOTf, 12 mL of dry CH_3CN was used as a solvent.

Method C: General Procedure; a solution of a pyridinium hydrogen salt or a *N*-silylpyridinium salt which was in situ prepared by mixing 3 mmol of a pyridine and 3 mmol of a protonic acid or a silyl ester (a reactant shown in Tables 1 and 2) in 6 mL of dry CH_3CN, was treated with 10% F_2-N_2 at −40 °C in the same manner as described in Method A (CAUTION!; a 2% F_2-98% N_2 mixture gas should be used for fluorination of *N*-trimethylsilylpyridinium triflates). The post-treatment for **1a** was as follows; the reaction solution was completely evaporated up to dryness at room temperature and the residue was washed with dry AcOEt to give pure crystals of **1a**.

Method D: General Procedure; a solution of a pyridine-Lewis acid complex, which was in situ prepared by mixing 3 mmol of a pyridine and 3 mmol of a Lewis acid (a reactant shown in Tables 1 and 2) in 6 mL of dry CH_3CN, was treated with 10% F_2-N_2 at −40 °C in the same manner as described in Method A. The reaction mixture was warmed to room temperature and evaporated up to dryness at room temperature. For **29b**, the residue was crystrallized from CH_3CN-Et_2O, giving 79% of **29b**.

Tables 1 and 2 summarize the results. Melting points, spectral data, and elemental analyses of the *N*-fluoropyridinium salts synthesized by the above methods are shown below. Their ^{19}F NMR data will be shown and discussed elsewhere.

***N*-Fluoropyridinium Triflate (1a):** Mp 185—187 °C (recrystallization solvent CH_3CN-Et_2O); ^{19}F NMR δ=48.8 (1F, bs, NF), −77.6 (3F, s, CF_3); ^1H NMR δ=8.32 (2H, dt, $J_{3\text{-H-F}}$=4.8 Hz, $J_{3\text{-H-2-H}}$=$J_{3\text{-H-4-H}}$=7.0 Hz, 3-H), 8.77 (1H, dt, $J_{4\text{-H-F}}$=2.0 Hz, $J_{4\text{-H-3-H}}$=7.0 Hz, 4-H) , 9.33 (2H, dd, $J_{2\text{-H-F}}$= 16.0 Hz, $J_{2\text{-H-3-H}}$=7.0 Hz, 2-H); MS *m/z* 227 (M^+−HF), (SIMS method) 98 (M^+−OTf). Found: C, 29.17; H, 1.99; N, 5.66; F, 30.49; S, 13.21%. Calcd for $C_6H_5F_4NO_3S$: C, 29.16; H, 2.04; N, 5.67; F, 30.75; S, 12.97%.

***N*-Fluoropyridinium Fluorosulfate (1b):** Mp 120—125 °C (CH_3CN-Et_2O); MS *m/z* 177 (M^+−HF). Anal. ($C_5H_5F_2NO_3S$) C, H, N.

***N*-Fluoropyridinium Methanesulfonate (1c):** Mp 140—142 °C; MS *m/z* 173 (M^+−HF). Anal. ($C_6H_8FNO_3S$), C, H, N.

***N*-Fluoropyridinium Trichloromethanesulfonate (1d):** Mp 205.5—207 °C (with decomp) (CH_3CN); MS *m/z* 277, 275 (M^+−HF). Anal. ($C_6H_5Cl_3FNO_3S$) C, H, N.

***N*-Fluoropyridinium Nonafluorobutanesulfonate (1e):** Mp 111—112 °C (AcOEt-Et_2O); MS *m/z* 377 (M^+−HF). Anal. ($C_9H_4F_{10}NO_3S$) C, H, N.

***N*-Fluoropyridinium Tetrafluoroborate (1f):** Mp 196.8—198 °C (CH_3CN-AcOEt, or CH_3CN); MS *m/z* 104. Anal. ($C_5H_5BF_5N$) C, H, N.

***N*-Fluoropyridinium Hexafluorophosphate (1g):** Decomp 202 °C (THF); MS *m/z* 174, 172, 107, 97. Anal. ($C_5H_5F_7NP$) C, H, N.

***N*-Fluoropyridinium Hexafluoroarsenate (1h):** Decomp 230 °C (CH_3CN-Et_2O); MS *m/z* 97. Anal ($C_5H_5F_7NAs$) C, H, N.

***N*-Fluoropyridinium Hexafluoroantimonate (1i):** Decomp 293 °C (CH_3CN-Et_2O); MS *m/z* 278, 276. Anal. ($C_5H_5F_7NSb$) C, H, N.

***N*-Fluoropyridinium Perchlorate (1j):** Mp 225—227.5 °C (with decomp) (CH_3CN); MS *m/z* 156, 155, 97, 79. Anal. ($C_5H_5ClFNO_4$) C, H, N.

***N*-Fluoro-2-methylpyridinium Triflate (2):** Mp 119.5—120.5 °C (CH_3CN-Et_2O); ^1H NMR δ=2.90 (3H, d, J_{H-F}=4.5 Hz, CH_3), 9.23 (1H, dd, *J*=15.0, 7.5 Hz, 6-H).

***N*-Fluoro-3-methylpyridinium Triflate (3):** Oil; ^1H NMR δ=2.55 (3H, s, CH_3); MS *m/z* 241 (M^+−HF). Anal. ($C_7H_7F_4NO_3S$) C, H, N.

***N*-Fluoro-4-methylpyridinium Triflate (4):** Mp 84—88 °C (AcOEt); ^1H NMR δ=2.70 (3H, s, CH_3); MS *m/z* 241 (M^+−HF). Anal. ($C_7H_7F_4NO_3S$) C, H, N.

***N*-Fluoro-2,6-dimethylpyridinium Triflate (5):** Mp 126—128 °C (CH_3CN-THF); ^1H NMR δ=2.83 (6H, d, J_{H-F}=4.8 Hz, CH_3); MS *m/z* 255 (M^+−HF). Anal. ($C_8H_9F_4NO_3S$) C, H, N.

***N*-Fluoro-3,5-dimethylpyridinium Triflate (6):** Mp 51—54 °C (CH_2Cl_2); ^1H NMR δ=2.57 (6H, s, CH_3), 9.02 (2H, d, *J*=16.5 Hz, 2-H); MS *m/z* 255 (M^+−HF). Anal. ($C_8H_9F_4NO_3S$) C, H, N.

***N*-Fluoro-2,4,6-trimethylpyridinium Triflate (7a):** Mp 168—170 °C (CH_3CN-Et_2O); ^1H NMR δ=2.58 (3H, s, 4-CH_3), 2.75 (6H, d, J_{H-F}=3.5 Hz, 2-CH_3), 7.73 (2H, d, *J*=6.5 Hz, 3-H); MS *m/z* 269 (M^+−HF), (SIMS method) 288 (M^+−1), 140 (M^+−OTf). Anal. ($C_9H_{11}F_4NO_3S$) C, H, N.

***N*-Fluoro-2,4,6-trimethylpyridinium Fluorosulfate (7b):** Mp 162—164 °C (with decomp) (CH_3CN-Et_2O). Anal. ($C_8H_{11}F_2NO_3S$) C, N, H.

***N*-Fluoro-2,4,6-trimethylpyridinium (+)-10-Camphorsulfonate (7c):** Mp 135—136.5 °C (CH_3CN-AcOEt); $[\alpha]_D^{22}$=29.51 (*c*=0.664, CH_3CN); ^1H NMR δ=0.80 (3H, s, CH_3), 1.10 (3H, s, CH_3), 2.57 (3H, s, 4-CH_3), 2.78 (6H, d, *J*=4.5 Hz, 2-CH_3), 7.77 (2H, d, *J*=6.0 Hz, 3-H); MS (SIMS method) *m/z* 140 (M^+−OTf). Anal. ($C_{18}H_{26}FNO_4S$) C, H, N.

***N*-Fluoro-2,4,6-trimethylpyridinium Tetrafluoroborate (7d):** Mp 215—217 °C (with decomp) (CH_3CN-Et_2O); MS (SIMS method) *m/z* 228 (M^+−1), 140 (M^+−BF_4). Anal. ($C_8H_{11}BF_5N$) C, H, N.

***N*-Fluoro-2,3,5,6-tetramethylpyridinium Triflate (8):** Mp 136—138 °C (CH_2Cl_2-Et_2O); ^1H NMR δ=2.45 (6H, s, 3-CH_3), 2.68 (6H, d, J_{H-F}=4.5 Hz, 2-CH_3), 8.05 (1H, s, 4-H); MS *m/z* 283 (M^+−HF). Anal. ($C_{10}H_{13}F_4NO_3S$) C, H, N.

***N*-Fluoro-2,3,4,5,6-pentamethylpyridinium Triflate (9):** Mp 97—97.5 °C (CH_2Cl_2-Et_2O); ^1H NMR δ=2.10 (6H, s, 3-CH_3), 2.35 (3H, s, 4-CH_3), 2.73 (6H, d, J_{H-F}=4.5 Hz, 2-CH_3); MS *m/z* 168 (M^+−OTf). Anal. ($C_{11}H_{15}F_4NO_3S$) C, H, N.

***N*-Fluoro-4-*t*-butylpyridinium Triflate (10):** Mp 116—118 °C (CH_3CN-Et_2O); ^1H NMR δ=1.42 (9H, s, *t*-Bu); MS *m/z* 268 (M^+−HF). Anal. ($C_{10}H_{13}F_4NO_3S$) C, H, N.

***N*-Fluoro-2,6-di-*t*-butylpyridinium Triflate (11):** Mp 112—114 °C (CH_2Cl_2-Et_2O); ^1H NMR δ=1.59 (18H, d, J_{H-F}=2.0 Hz, 2×*t*-Bu); MS *m/z* 210 (M^+−OTf). Anal. ($C_{14}H_{21}F_4NO_3S$) C, H, N.

***N*-Fluoro-2,4,6-tri-*t*-butylpyridinium Triflate (12):** Mp 238—239 °C (with decomp) (CH_2Cl_2-Et_2O); ^1H NMR δ=1.43 (9H, s, 4-*t*-Bu), 1.58 (18H, d, J_{H-F}=1.5 Hz, 2,6-*t*-Bu), 7.82 (2H, d, *J*=7.5 Hz, 3-H); MS *m/z* 266 (M^+−OTf). Anal. ($C_{18}H_{29}F_4NO_3S$) C, H, N.

***N*-Fluoro-2,6-di-*t*-butyl-4-methylpyridinium Triflate (13):** Mp 158—159 °C (CH_2Cl_2-Et_2O); ^1H NMR δ=1.55 (18H, d, *J*=2.0 Hz, 2,6-*t*-Bu), 2.63 (3H, s, CH_3), 7.83 (2H, d *J*=7.5 Hz, 3-H); MS *m/z* 224 (M^+−OTf). Anal. ($C_{15}H_{23}F_4NO_3S$) C, H, N.

***N*-Fluoro-1,2,3,4,5,6,7,8-octahydroacridinium Triflate (14):** Mp 150—152 °C (CH_2Cl_2-Et_2O); ^1H NMR δ=8.02 (1H, s, 4-H); MS *m/z* 206 (M^+−OTf). Anal. ($C_{14}H_{17}F_4NO_3S$) C, H, N.

***N*-Fluoro-2,6-bis(methoxymethyl)pyridinium Triflate (15):** Mp 56—58 °C (CH_2Cl_2-Et_2O); ^1H NMR δ=3.58 (6H, s, CH_3), 4.78 (4H, s, CH_3); MS *m/z* 186 (M^+−OTf). Anal. ($C_{10}H_{13}F_4NO_3S$) C, H, N.

***N*-Fluoro-2,4,6-tris(methoxymethyl)pyridinium Triflate (16):** Crystalline solid; ^1H NMR ($CDCl_3$) δ=3.50 (3H, s, 4-OMe), 3.57 (6H, s, 2, 6-OMe), 4.72 (2H, bs, 4-CH_2), 4.95 (4H, bs, 2, 6-CH_2), 7.95 (2H, d, J_{H-F}=6.0 Hz, 3, 5-H); MS *m/z* 230 (M^+−OTf).

***N*-Fluoro-2-(benzoyloxymethyl)pyridinium Triflate (17):** Mp 94—96 °C (AcOEt); ^1H NMR δ=5.82 (2H, d, J_{H-F}=1.5 Hz, CH_2O), 9.28 (1H, dd, *J*=16.5, 7.5 Hz, 6-H); MS *m/z* 361 (M^+−HF). Anal. ($C_{13}H_9F_4NO_5S$) C, H, N.

***N*-Fluoro-2,6-bis(acetoxymethyl)pyridinium Triflate (18):** Mp 125—127 °C (AcOEt-Et_2O); ^1H NMR δ=2.17 (6H, s, CH_3), 5.56 (4H, d, J_{H-F}=3.0 Hz, CH_3); IR (Nujol on NaCl) 1765 cm^{-1} (CO); MS *m/z* 271 (M^+−OTf). Anal. ($C_{12}H_{13}F_4NO_7S$) C, H, N.

***N*-Fluoro-2-fluoromethyl-4,6-dimethylpyridinium Triflate (19):** Mp 160—162 °C (CH_3CN-Et_2O); ^1H NMR δ=2.62 (3H, s, 4-CH_3), 2.80 (3H, d, J_{H-F}=4 Hz, 2-CH_3), 5.81 (2H, dd, J_{H-F}=45 Hz, J_{H-NF}=1 Hz, CH_2); MS *m/z* 258 (M^+−HF). Anal. ($C_9H_{10}F_5NO_3S$) C, H, N.

***N*-Fluoro-2-methoxypyridinium Triflate (20):** Mp 95—96 °C (CH_3CN-Et_2O); ^1H NMR δ=4.38 (3H, s, CH_3); MS *m/z* 128 (M^+−OTf), 113 (M^+−OTf−Me), (SIMS method) 128 (M^+−OTf). Anal. ($C_7H_7F_4NO_4S$) C, H, N.

***N*-Fluoro-3-methoxypyridinium Triflate (21):** Oil; ^{1}H NMR δ=4.07 (3H, s, CH_3); MS *m/z* 257 (M^+−OTf).

***N*-Fluoro-4-methoxypyridinium Triflate (22):** Mp 32 °C (AcOEt-Et_2O); ^{1}H NMR δ=4.12 (3H, s, CH_3); MS *m/z* 257 (M^+−HF). Anal. ($C_7H_7F_4NO_4S$) C, H, N.

***N*-Fluoro-2-[(1*R*,3*R*,4*S*)-menthyloxy]pyridinium Triflate (23):** Mp 111—111.5 °C (with decomp) (CH_2Cl_2-Et_2O); $[\alpha]_D^{20}$=−77.7 (*c*=4.16, $CHCl_3$); ^{1}H NMR δ=0.83 (3H, d, *J*=6.6 Hz, CH_3), 0.98 (6H, d, *J*=6.6 Hz, CH_3), 4.93 (1H, td, *J*=9.6, 4.5 Hz, CH-O), 7.52 (1H, m, 5-H), 7.89 (1H, td, *J*=9.0, 1.5 Hz, 3-H), 8.45 (1H, ddd, *J*=9.0, 7.8, 1.5 Hz, 4-H), 8.83 (1H, ddd, *J*=17.4, 7.8, 1.5 Hz, 6-H); MS (SIMS method) *m/z* 252 (M^+−OTf). Anal.($C_{16}H_{23}F_4NO_4S$) C, H, N.

***N*-Fluoro-4-phenylpyridinium Triflate (24):** Mp 130.5—132.5 °C (CH_3CN-Et_2O); ^{1}H NMR δ=7.64 (3H, m, 3′-H, 4′-H), 7.90 (2H, m, 2′-H); MS *m/z* 303 (M^+−HF). Anal. ($C_{12}H_9F_4NO_3S$) C, H, N.

***N*-Fluoro-2-fluoropyridinium Triflate (1:1 salt with LiOTf) (25):** Decomp ca. 145 °C (in a sealed tube) (CH_3CN-Et_2O); ^{1}H NMR δ=9.25 (1H, m, 6-H). Anal. ($C_7H_4F_8LiNO_6S_2$) C, H, N.

***N*-Fluoro-2-chloropyridinium Triflate (26):** Mp 149—151 °C (AcOEt); ^{1}H NMR δ=9.42 (1H, ddd, *J*=16.0, 6.7, 1.5 Hz, 6-H); MS *m/z* 263, 261 (M^+−HF), (SIMS method) 134, 132 (M^+−OTf). Anal. ($C_6H_4ClF_4NO_3S$) C, H, N.

***N*-Fluoro-3-chloropyridinium Triflate (27):** MP 108—109 °C (CH_3CN-CH_2Cl_2); ^{1}H NMR δ=9.60 (1H, ddd, *J*=14.5, 2.5, 1.8 Hz, 2-H); MS *m/z* 263, 261 (M^+−HF). Anal. ($C_6H_4ClF_4NO_3S$) C, H, N.

***N*-Fluoro-2,6-dichloropyridinium Triflate (28):** Mp 151—153 °C (CH_3CN-Et_2O) (mp 126 °C was indicated by thermometric analysis conducted by Dr. Takao Iida of Onoda Cement Co.); MS *m/z* 169, 167, 165 (M^+−HOTf), 151, 149, 147 (M^+−OTf−F). Anal. ($C_6H_3Cl_2F_4NO_3S$) C, H, N.

***N*-Fluoro-3,5-dichloropyridinium Triflate (29a):** Mp (in a sealed tube) 118.5—121 °C (CH_3CN-Et_2O); ^{1}H NMR δ=9.61 (2H, dd, *J*=14.0, 1.8 Hz, 2-H); MS *m/z* 299, 297, 295 (M^+−HF), (SIMS method) 166 (M^+−OTf). Anal. ($C_6H_3Cl_2F_4NO_3S$) C, H, N.

***N*-Fluoro-3,5-dichloropyridinium Tetrafluoroborate (29b):** Mp 208—209 °C (CH_3CN-Et_2O); MS *m/z* 169, 167, 165 (M^+−HBF_4). Anal. ($C_5H_3BCl_2F_5N$) C, H, N.

***N*-Fluoropentachloropyridinium Triflate (30a):** Mp 122—123 °C (CH_3CN); MS *m/z* 274, 272, 270, 268 (M^+−OTf). Anal. ($C_6Cl_5F_4NO_3S$) C, H, N.

***N*-Fluoropentachloropyridinium Tetrafluoroborate (30b):** Mp (in a sealed tube) 198—200 °C (CF_3COOH-AcOEt); MS *m/z* 293, 291, 289, 287 (M^+−BF_3). Anal. ($C_5BCl_5F_5N$) C, H, N.

***N*-Fluoro-3-chloro-5-(trifluoromethyl)pyridinium Triflate (31):** Mp 105—108 °C (THF-CH_2Cl_2); ^{1}H NMR δ=9.95 (2H, dm, J_{H-F}=14 Hz, 2-H, 6-H); MS *m/z* 343, 341, 199 (M^+−F−Tf), 197 (M^+−F−Tf). Anal. ($C_7H_3ClF_7NO_3S$) C, H, N.

***N*-Fluoro-3,5-bis(trifluoromethyl)pyridinium Triflate (32):** Mp 193—195 °C (CH_3CN-Et_2O); ^{1}H NMR δ=10.19 (2H, d, *J*=13.5 Hz, 2-H); MS *m/z* 375, 363 (M^+−HF). Anal. ($C_8H_3F_{10}NO_3S$) C, H, N.

***N*-Fluoro-3-acetoxypyridinium Triflate (33):** Mp 111.5—112.5 °C (CH_3CN-Et_2O); ^{1}H NMR δ=9.46 (1H, dm, *J*=16.0 Hz, 2-H); IR (Nujol on NaCl) 1780 cm^{-1} (CO); MS *m/z* 243, 187, 186, 137, 135, 113, (SIMS method) 156 (M^+−OTf). Anal. ($C_8H_7F_4NO_5S$) C, H, N.

***N*-Fluoro-2-(methoxycarbonyl)pyridinium Triflate (34):** Mp 115—166 °C (CH_3CN-Et_2O); ^{1}H NMR δ=4.16 (1H, s, CH_3); IR (Nujol on NaCl) 1740 cm^{-1} (CO); MS *m/z* 137, 107, 79, 78. Anal. ($C_8H_7F_4NO_5S$) C, H, N.

***N*-Fluoro-3-(ethoxycarbonyl)pyridinium Triflate (35):** Mp 115—116 °C (THF-CH_2Cl_2); ^{1}H NMR δ=1.42 (3H, t, *J*=7.0 Hz, CH_3), 5.52 (2H, q, *J*=7.0 Hz, CH_2); IR (Nujol on NaCl) 1735 cm^{-1} (CO); MS *m/z* 299 (M^+−HF). Anal. ($C_8H_7F_4NO_5S$) C, H, N.

***N*-Fluoro-4-(methoxycarbonyl)pyridinium Triflate (36):** Solid (recrystallization failed); ^{1}H NMR δ=4.07 (3H, s, CH_3); IR (Nujol on NaCl) 1740 cm^{-1} (CO).

***N*-Fluoro-2,6-bis(methoxycarbonyl)pyridinium Triflate (37):** Mp 140—143 °C (CH_3CN-Et_2O); ^{1}H NMR δ=4.13 (6H, s, CH_3), IR (Nujol on NaCl) 1770 cm^{-1} (CO); MS *m/z* 227, 137, 69, 59. Anal. ($C_{10}H_9F_4NO_7S$) C, H, N.

***N*-Fluoro-3,5-bis(methoxycarbonyl)pyridinium Triflate (38):** Mp 144—147 °C (CH_3CN-Et_2O); ^{1}H NMR δ=4.08 (6H, s, CH_3); IR (Nujol on NaCl) 1760 cm^{-1} (CO); MS *m/z* 343 (M^+−HF). Anal. ($C_{10}H_9F_4NO_7S$) C, H, N.

***N*-Fluoro-2,4,6-tris(methoxycarbonyl)pyridinium Triflate (1:1 Salt with LiOTf) (39):** Decomp ca. 145 °C (CH_3CN-Et_2O); ^{1}H NMR δ=4.05 (3H, s, 4-CH_3), 4.12 (6H, s, 2-CH_3); IR (Nujol on NaCl) 1780 (CO), 1750 (CO) cm^{-1}. Anal. ($C_{13}H_{11}F_7LiNO_{12}S_2$) C, H, N.

***N*-Fluoro-2-acetylpyridinium Triflate (40):** Mp 151—152 °C (CH_3CN-Et_2O); ^{1}H NMR δ=2.77 (3H, s, CH_3).

***N*-Fluoro-4-acetylpyridinium Triflate (41):** Pale yellow oil; ^{1}H NMR δ=2.72 (3H, s, CH_3); IR (Nujol on NaCl) 1715 cm^{-1} (CO); MS *m/z* 269 (M^+−HF).

***N*-Fluoro-2-cyanopyridinium Tetrafluoroborate (42):** Mp 114—116 °C (CH_3CN-AcOEt); ^{1}H NMR δ=9.58 (1H, dd, *J*=15, 6 Hz, 6-H); MS *m/z* 122 (M^+−HBF_4), 95, 49, (SIMS method) 195, 121, 93, 75, 57. Anal. ($C_6H_4BF_5N_2$) C, H, N.

***N*-Fluoro-3-cyanopyridinium Triflate (43):** Mp 63—67 °C (AcOEt); ^{1}H NMR δ=9.88 (1H, ddd, *J*=13.5, 2.5, 1.4 Hz, 2-H); IR (Nujol on NaCl) 2255 cm^{-1} (CN); MS *m/z* 252 (M^+−HF). Anal. ($C_7H_4F_4N_2O_3S$) C, H, N.

***N*-Fluoro-4-cyanopyridinium Triflate (44):** Mp 137—140 °C (CH_3CN-Et_2O); ^{1}H NMR δ=9.52 (2H, dd, *J*=14, 7 Hz, 2-H); MS *m/z* 252 (M^+−HF). Anal. ($C_7H_4F_4N_2O_3S$) C, H, N.

***N*-Fluoro-2,6-dicyanopyridinium Triflate (45):** Mp (in a sealed tube) 123—132 °C (with decomp) (CH_3CN-Et_2O); ^{1}H NMR δ=9.02 (3H, m, 3-H, 4-H); IR (Nujol on NaCl) 2260 cm^{-1} (CN); MS *m/z* 147, 129. Anal. ($C_8H_3F_4N_3O_3S$) C, H, N.

***N*-Fluoro-4-nitropyridinium Triflate (46):** Mp (in a sealed tube) 55—59 °C (AcOEt-Et_2O); ^{1}H NMR δ=9.68 (2H, dd, *J*=13, 7.5 Hz, 2-H); IR (Nujol on NaCl) 1555, 1355 cm^{-1} (NO_2); MS *m/z* 272 (M^+−HF). Anal. ($C_6H_4F_2N_2O_5S$) C, H, N.

Synthesis of *N*-Fluoroquinolinium Triflate (49). This salt was prepared in 16% yield according to Method B. Mp (in a sealed tube) 144—154 °C (with decomp) (CH_3CN-AcOEt); ^{1}H NMR δ=9.28 (1H, d, $J_{4-H-3-H}$=8 Hz, 4-H), 9.69 (1H, dd, J_{2-H-F}=18 Hz, $J_{2-H-3-H}$=7 Hz, 2-H); MS *m/z* 277 (M^+−HF), (SIMS method) 148 (M^+−OTf). Anal. ($C_{10}H_7F_4NO_3S$) C, H, N.

Synthesis of *N*-Fluoropyridinium-2-sulfonates 52 and 53. Typical Procedure; a mixture of 0.209 g (1.08 mmol) of 6-chloro-2-pyridinesulfonic acid in 2.1 mL of H_2O-CH_3CN

(1/20 v/v) was fluorinated at −25 °C in a similar manner as Method A. Total amount of F_2 was 3.24 mmol. After the fluorination, 25 mL of THF was added into the reaction mixture at −25 °C under stirring and it was warmed to room temperature. The resulting crystals were collected by filtration and dried to give 0.177 g (77%) of *N*-fluoro-6-chloropyridinium-2-sulfonate (**53**). Analytically pure crystals were obtained by the recrystallization from CH_3CN-Et_2O.

***N*-Fluoropyridinium-2-sulfonate (52):** 81%; Decomp 232—235 °C (CH_3CN); ^1H NMR (400 MHz) δ=9.04 (1H, ddd, J=14.5, 7.0, 1 Hz, 6-H); MS m/z 177 (M^+). Anal. ($C_5H_4FNO_3S$) C, H, N.

***N*-Fluoro-6-chloropyridinium-2-sulfonate (53):** 77%; Mp 171—173 °C (CH_3CN-Et_2O); MS m/z 112 (M^+−F−SO_3). Anal. ($C_5H_3ClFNO_3S$) C, H, N.

Hydrolysis of *N*-Fluoropyridinium Salts 1a, 28, 29a, 30a, and 49. A *N*-fluoropyridinium salt was added into a stirred water at room temperature. The amount of water used was ca. 2 mL to 1 mmol of a *N*-fluoropyridinium salt and 5.2 mmol of **1a**, 1.6 mmol of **28**, 5.3 mmol of **29a**, 4 mmol of **30a**, and 0.34 mmol of **49** were used for the hydrolysis experiments. The reaction mixture was stirred at room temperature for 14 d (**1a**), 6 h (**28**), ca. 10 min (**29a**), 0.5 h (**30a**), and ca. 10 min (**49**) and then neutralized to pH 7 with $NaHCO_3$. The hydrolysis products were isolated by usual post-treatments. The results are described in Result section. The structural assignment of the products was carried out by analyzing their spectral data. 2-Pyridinol and 2-quinolinol were in agreement with authentic samples. The data of other products are shown in the following.

3,5-Dichloro-2-pyridinol (56): ^1H NMR δ=7.42 (1H, d, J=3.0 Hz, 4 or 5-H), 7.61 (1H, d, J=3.0 Hz, 4 or 5-H); IR (KBr) 3100 (NH), 1695 cm^{-1} (CO); MS m/z 167, 165, 163 (M^+).

***N*-Fluoro-6-chloro-2-pyridone (57):** Mp 74 °C; ^{19}F NMR ($CDCl_3$) δ=−44.6 (s, NF); ^1H NMR ($CDCl_3$) δ=6.26 (1H, ddd, J=7.5, 4.5, 2.0 Hz, 3-H), 6.66 (1H, ddd, J=9.5, 8.0, 2.0 Hz, 5-H), 7.26 (1H, dd, J=9.5, 7.5 Hz, 4-H); IR (KBr) 1680 cm^{-1} (CO); MS m/z 149, 147 (M^+). Anal. (C_5H_3ClFNO) C, H, N.

2,6-Dichloro-4-pyridinol (58): ^1H NMR ($CDCl_3$) δ=6.79 (s); IR (KBr) 3100—3000 cm^{-1} (OH); MS m/z 167, 165, 163 (M^+).

***N*-Fluoro-3,4,5,6-tetrachloro-2-pyridone (59):** Mp 102—104 °C (CCl_4); ^{19}F NMR ($CDCl_3$) δ=−33.0 (s, NF); IR (Nujol on NaCl) 1680 cm^{-1} (CO); MS m/z 255, 253, 251, 249 (M^+). Anal. (C_5Cl_4FNO) C, H, N.

Alkaline Hydrolysis of *N*-Fluoropyridinium Triflate (1a). Into a stirred solution of 10 mL of aq KOH (1 mol dm^{-3}) was by portions added 1.29 g (5.21 mmol) of **1a**. After 2 h, the reaction mixture was neutralized to pH 7 with $NaHCO_3$ and extracted with CH_2Cl_2. GC and GC-Mass analyses of the organic layer showed that 2-pyridyl triflate and 2-fluoropyridine were produced in 0.5 and 0.6% yields, respectively. A column (2 m×2 mm) packed with PEG-6000 (15%) on Uniport B was used for the GC analysis. The post-treatment of the organic layer gave 0.246 g (50%) of 2-pyridinol.

Alkaline Hydrolysis of *N*-Fluoro-2,4,6-trimethylpyridinium Triflate (7a). Into a stirred solution of 10 mL of aq KOH (2.9 mol dm^{-3}) was by portions added 1.48 g (5.11 mmol) of **7a**. An exothermic reaction occurred. After it ceased, the usual post-treatment was carried out to give 170 mg (24%) of 2-hydroxymethyl-4,6-dimethylpyridine (**54**) and 166 mg (23%) of 2-fluoromethyl-4,6-dimethylpyridine (**55**). Spectral data of **54** and **55** were in agreement with those of each authentic sample.

Reaction of *N*-Fluoro-2,4,6-trimethylpyridinium Triflate (7a) with Triethylamine or Sodium Hydride. Into a stirred solution of 1 mmol of triethylamine or sodium hydride (50% in oil) in 2 mL of a dry solvent was added 0.289 g (1 mmol) of **7a** at room temperature under argon atmosphere. After 10 min., the reaction mixture was analyzed by ^{19}F NMR. The results are described in Result section. The assignment of product **60** was carried out by the spectral analysis of the isolated product.

3-Fluoro-2,4,6-trimethylpyridine (60): Oil; ^{19}F NMR ($CDCl_3$) δ=−137.1 (bs); ^1H NMR ($CDCl_3$) δ=2.24 (3H, d, J=1.5 Hz, 4-CH_3), 2.45 (3 H, d, J=0.5 Hz, 6-CH_3), 2.46 (3H, d, J=3.2 Hz, 2-CH_3), 6.82 (1H, d, J=5.3 Hz, 4-H); IR (neat) 2940, 1620, 1470, 1230, 1215, 1160, 1025, 928, 860, 755 cm^{-1}. Found: m/z 139.0780 (M^+). Calcd for $C_8H_{10}FN$: M, 139.0796.

Thermal Stability. The sample was heated in a NMR tube under air in an oil bath of which temperature was set and monitored by ^{19}F NMR.

Results

Syntheses of *N*-Fluoropyridinium Salts. Various *N*-fluoropyridinium salts **1**—**46** were synthesized in varying yields as follows; by the fluorination of a pyridine and subsequent acid, metal salt of an acid, silyl ester, or Lewis acid treatment (Method A), fluorina-

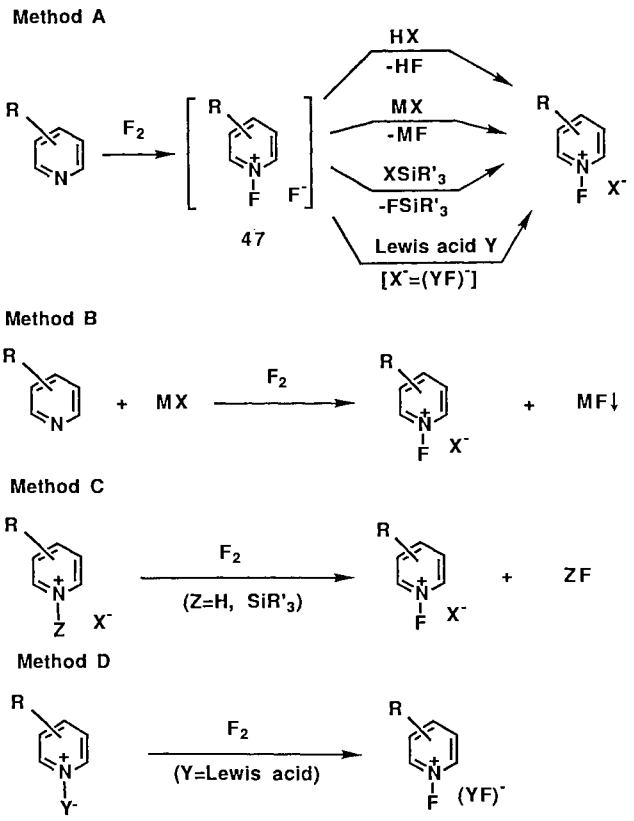

Scheme 1.

Table 1. Syntheses of *N*-Fluoropyridinium Salts **1** with a Different Counter Anion

Run			Method[a]	Reactant	Yield of **1**[b] / %
1	X=OTf	**1a**	B	LiOTf	87
2	X=OTf	**1a**	B	NaOTf	75
3	X=OTf	**1a**	B	KOTf	63
4	X=OTf	**1a**	C	TfOH	66
5	X=OTf	**1a**	C[c]	TfOH	96
6	X=OTf	**1a**	A	TfOH	33
7	X=OTf	**1a**	A[d]	NaOTf	32
8	X=OTf	**1a**	A	$TfOSiMe_3$	29
9	X=OTf	**1a**	C	$TfOSiMe_3$	40
10	$X=OSO_2F$	**1b**	A	FSO_3H	45
11	$X=OSO_2CH_3$	**1c**	C[e]	CH_3SO_3H	79
12	$X=OSO_2CH_3$	**1c**	C	$CH_3SO_3SiMe_3$	42
13	$X=OSO_2CCl_3$	**1d**	B	CCl_3SO_3Na	83
14	$X=OSO_2C_4F_9{}^n$	**1e**	B	n-$C_4F_9SO_3Na$	87
15	$X=BF_4$	**1f**	B	$NaBF_4$	78
16	$X=BF_4$	**1f**	A	$BF_3 \cdot OEt_2$	33
17	$X=PF_6$	**1g**	B	$NaPF_6$	83
18	$X=AsF_6$	**1h**	B	$NaAsF_6$	66
19	$X=SbF_6$	**1i**	B	$NaSbF_6$	85
20	$X=SbF_6$	**1i**	B	$LiSbF_6$	93
21	$X=SbF_6$	**1i**	A	SbF_5	35
22	$X=ClO_4$	**1j**	B	$NaClO_4$	69

a) See Experimental Section. The fluorination was conducted in CH_3CN at −40 °C unless otherwise noted. b) Isolated yields. c) The fluorination was carried out at −20 °C. d) In place of CH_3CN, $CFCl_3$ was used as a solvent in the first fluorination step which was carried out at −78 °C. The solvent of the second step at −40 °C was a 1 : 2 mixture of $CFCl_3$ and CH_3CN. e) The fluorination was carried out at −20 °C by using H_2O-CH_3CN (1/20) solvent. The post-treatment for **1c** was as follows; a large amount of THF was added to the reaction mixture cooled at −20 °C and the resulting precipitates of **1c** was collected by filtration.

tion of a mixture of a pyridine and metal salt of an acid (Method B), fluorination of a pyridinium hydrogen salt or a *N*-silylpyridinium salt (Method C), or fluorination of a pyridine-Lewis acid complex (Method D), as outlined in Scheme 1. The results are summarized in Tables 1 and 2.

According to Method A, the first treatment of pyridine in CH_3CN with 10% F_2-N_2 mixture gas at −40 °C and successive treatment with TfOH (Tf=CF_3SO_2), fluorosulfuric acid, trimethylsilyl triflate, $BF_3 \cdot OEt_2$, or SbF_5 gave the corresponding N-fluoropyridinium salts **1** in 29—45% yields. In case of a more basic pyridine, 2,4,6-trimethylpyridine, the first fluorination step was conducted in the presence of a 4—10 equivalent amount of NaF added as a HF trapping agent (modified Method A) to lessen the formation of 2,4,6-trimethylpyridinium hydrogen triflate (**48**).

Method B, a one-step procedure, afforded good yields of *N*-fluoropyridinium salts. Thus a mixture of pyridine and metal salt of a strong acid such as NaOTf, CCl_3SO_3Na, $NaBF_4$, n-$C_4F_9SO_3Na$, $NaPF_6$, $NaAsF_6$ etc. in CH_3CN was treated with 10% F_2-N_2 mixture gas at −40 °C to produce *N*-fluoropyridinium salt **1** in 63—93% yields, as shown in Table 1. As fluorination proceeded, metal fluoride appeared gradually in the form of precipitates. Table 2 shows that by Method B, the synthesis of a large number of *N*-fluoropyridinium salts possessing an electron-donating or -withdrawing atom(s) or group(s) on the pyridine ring can be effectively carried out using substituted pyridines.

In the Method B fluorination of pyridine, LiOTf, NaOTf, and KOTf were used to obtain 87, 75, and 62% yields of *N*-fluoropyridinium triflate (**1a**), respec-

Table 2. Syntheses of a Variety of Substituted *N*-Fluoropyridinium Salts **2**—**46**

Run	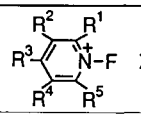							Method[c]	Reactant	Yield[d] / %
	No.[a]	X[b]	R^1	R^2	R^3	R^4	R^5			
1	**2**	OTf	Me	H	H	H	H	B	NaOTf	60
2	**3**	OTf	H	Me	H	H	H	B	NaOTf	—[e]
3	**4**	OTf	H	H	Me	H	H	B[f]	NaOTf	90
4	**5**	OTf	Me	H	H	H	Me	B	NaOTf	69
5	**6**	OTf	H	Me	H	Me	H	A[g]	NaOTf	60
6	**7a**	OTf	Me	H	Me	H	Me	B	LiOTf	22
7	**7b**	OSO_2F	Me	H	Me	H	Me	A	FSO_3H	56[h]
8	**7c**	OSO_2Camph	Me	H	Me	H	Me	A[f]	$NaOSO_2$Camph[i]	50
9	**7d**	BF_4	Me	H	Me	H	Me	B[f]	$NaBF_4$	70
10	**8**	OTf	Me	Me	H	Me	Me	B[f]	NaOTf	9
11	**9**	OTf	Me	Me	Me	Me	Me	B[f]	NaOTf	12
12	**10**	OTf	H	H	*t*-Bu	H	H	B[f]	NaOTf	86
13	**11**	OTf	*t*-Bu	H	H	H	*t*-Bu	B[f]	NaOTf	12
14	**12**	OTf	*t*-Bu	H	*t*-Bu	H	*t*-Bu	B[f]	NaOTf	1.3
15	**13**	OTf	*t*-Bu	H	Me	H	*t*-Bu	B[f]	NaOTf	5
16	**14**	OTf	$-(CH_2)_4-$		H	$-(CH_2)_4-$		B	KOTf	48
17	**15**	OTf	CH_2OMe	H	H	H	CH_2OMe	B	NaOTf	85
18	**16**	OTf	CH_2OMe	H	CH_2OMe	H	CH_2OMe	B	NaOTf	73
19	**17**	OTf	CH_2OCOPh	H	H	H	H	B	NaOTf	84

Table 2. (Continued)

Run	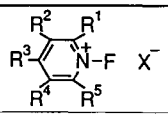						Method[c]	Reactant	Yield[d]
	No.[a]	X[b]	R^1	R^2	R^3	R^4	R^5			%
20	**18**	OTf	CH_2OAc	H	H	H	CH_2OAc	B	NaOTf	74
21	**19**	OTf	CH_2F	H	Me	H	Me	B	KOTf	75
22	**20**	OTf	OMe	H	H	H	H	B	NaOTf	73
23	**21**	OTf	H	OMe	H	H	H	B[f]	NaOTf	62
24	**22**	OTf	H	H	OMe	H	H	B[f]	NaOTf	87
25	**23**	OTf	OMenth[i]	H	H	H	H	B	NaOTf	57
26	**24**	OTf	H	H	Ph	H	H	B	NaOTf	41
27	**25**	OTf	F	H	H	H	H	B	LiOTf	23[k]
28	**26**	OTf	Cl	H	H	H	H	B	NaOTf	71
29	**27**	OTf	H	Cl	H	H	H	C	$TfOSiMe_3$	79
30	**28**	OTf	Cl	H	H	H	Cl	B[l]	LiOTf	38
31	**28**	OTf	Cl	H	H	H	Cl	C[m]	TfOH	62
32	**28**	OTf	Cl	H	H	H	Cl	C	TfOH	56
33	**29a**	OTf	H	Cl	H	Cl	H	B	LiOTf	77
34	**29a**	OTf	H	Cl	H	Cl	H	B	NaOTf	27
35	**29b**	BF_4	H	Cl	H	Cl	H	D	$BF_3 \cdot OEt_2$	79
36	**30a**	OTf	Cl	Cl	Cl	Cl	Cl	C[n]	TfOH	85
37	**30a**	OTf	Cl	Cl	Cl	Cl	Cl	C	TfOH	32
38	**30b**	BF_4	Cl	Cl	Cl	Cl	Cl	D[n]	BF_3	87
39	**31**	OTf	H	Cl	H	CF_3	H	C	$TfOSiMe_3$	71
40	**31**	OTf	H	Cl	H	CF_3	H	C	$TfOSiMe_2Ph$	71
41	**32**	OTf	H	CF_3	H	CF_3	H	C	$TfOSiMe_3$	68
42	**33**	OTf	H	OAc	H	H	H	B	NaOTf	90
43	**34**	OTf	COOMe	H	H	H	H	C	$TfOSiMe_3$	86
44	**35**	OTf	H	COOEt	H	H	H	C	$TfOSiMe_3$	69
45	**36**	OTf	H	H	COOMe	H	H	C	$TfOSiMe_3$	—[e]
46	**37**	OTf	COOMe	H	H	H	COOMe	B	NaOTf	72
47	**37**	OTf	COOMe	H	H	H	COOMe	B	LiOTf	78
48	**38**	OTf	H	COOMe	H	COOMe	H	C	$TfOSiMe_3$	60
49	**39**	OTf	COOMe	H	COOMe	H	COOMe	B	LiOTf	15[k]
50	**40**	OTf	$COCH_3$	H	H	H	H	B	NaOTf	72
51	**41**	OTf	H	H	$COCH_3$	H	H	B	LiOTf	96
52	**42**	BF_4	CN	H	H	H	H	B	$LiBF_4$	78
53	**43**	OTf	H	CN	H	H	H	B	LiOTf	84
54	**44**	OTf	H	H	CN	H	H	B	LiOTf	94
55	**45**	OTf	CN	H	H	H	CN	B	LiOTf	50
56	**46**	OTf	H	H	NO_2	H	H	B	LiOTf	86

a) Compound numbers. b) Counter anion part of *N*-fluoropyridinium salts. c) See Experimental Section. Fluorination was conducted in CH_3CN at −40 °C unless otherwise noted. d) Isolated yields. e) Good yields. f) Modified Method using added NaF. g) This reaction was carried out in the similar manner as Run 7 in Table 1. Thus, $CFCl_3$ was used as a solvent in the first fluorination step. h) A crude yield. i) Sodium (+)-10-camphorsulfonate. j) (1*R*,3*R*,4*S*)-Menthyloxy group. k) Products were isolated as 1 : 1 salts with LiOTf. l) This reaction was carried out in dry propionitrile solvent at −60 °C. m) This reaction was carried out in dry propionitrile at −78 °C. n) Fluorination with 20% F_2-N_2 was conducted in CF_3COOH at room temperature (ca. 10 °C).

tively. With 2,4,6-trimethylpyridine, LiOTf gave only a 22% yield of *N*-fluoro-2,4,6-trimethylpyridinium triflate (**7a**). In this reaction, two by-products, **48** (26%) and *N*-fluoro-2-fluoromethyl-4,6-dimethylpyridinium triflate (**19**) (5%) were found. As seen in Table 3, the yield of **7a** depended on the nature of metal triflate used, and KOTf greatly increased **7a** and decreased the by-product **48**. Salt **7a** was obtained in highest yield and **48** suppressed completely by KOTf in H_2O-CH_3CN (1/100) solvent. No significant change was noted in the yields of **19**. Runs 5 and 6 in Table 3 show better yields of **7a** by modified Method B in which the fluorination was conducted in the presence of a 4—10 equivalent amount of NaF added. Salt **7a** could be separated easily from **48** by recrystallization, though its complete separation from **19** was difficult.

Pure *N*-fluoro-2,3,5,6-tetramethylpyridinium triflate (**8**) and -pentamethylpyridinium triflate (**9**) were isolated in very low yields by the modified Method B. Considerable amounts of the corresponding pyridinium hydrogen salts were formed in these reactions.

Table 3. Reaction Conditions for Preparation of *N*-Fluoro-2,4,6-trimethylpyridinium Triflate (**7a**)

Run	Method[a]	MOTf	Solv.	Additive[b]	Yield[c]/%		
					7a	**48**	**19**
1	B	LiOTf	CH_3CN	—	22	26	5
2	B	NaOTf	CH_3CN	—	39	23	7
3	B	KOTf	CH_3CN	—	71	5	8
4	B	KOTf	H_2O-CH_3CN(1/100)	—	81	0	7
5	B[d]	NaOTf	CH_3CN	NaF(4 equiv)	52	20	9
6	B[d]	NaOTf	CH_3CN	NaF(10 equiv)	57	15	8

a) See Experimental Section. b) Figures in parentheses mean equivalent amounts of NaF based on 2,4,6-trimethylpyridine. c) Yields of **7a** were isolated yields. The yields of **48** and **19** were determined by ^1H NMR of the crude reaction products, based on the isolated yields of **7a**. d) This method was specified as modified Method B.

Highly hindered pyridines, 2,6-di-*t*-butylpyridine and its derivatives were fluorinated according to the modified Method B to give *N*-fluoro-2,6-di-*t*-butylpyridinium triflate (**11**), *N*-fluoro-2,4,6-tri-*t*-butylpyridinium triflate (**12**), and *N*-fluoro-2,6-di-*t*-butyl-4-methylpyridinium triflate (**13**). The yields, however, were quite low. During the reactions, the corresponding pyridinium hydrogen salts and tars were also formed. The separation of these pure *N*-fluoro salts from the protonated pyridinium salts was successfully carried out by treatment of a CH_2Cl_2 solution of the mixture with aq $NaHCO_3$ followed by recrystallization. Method B using KOTf in the aq CH_3CN solvent improved the yields only to a very slight extent.

The yields of *N*-fluoropyridinium salts possessing an electron-withdrawing ring-substituent(s) by Method B varied depending on the metal salts used, or on the nature, ring-position and number of substituents. Apparently, lithium salts give better yields than sodium or potassium salts. *N*-Fluoro-3,5-dichloropyridinium triflate (**29a**) was obtained in 77% yield using LiOTf, but in 22% yield by NaOTf. Isomeric *N*-fluoro-2,6-dichloropyridinium triflate (**28**) was prepared in only a 38% yield by LiOTf.

As the pyridine nitrogens became weak in basicity, efficiency of the fluorination decreased. When 2,4,6-tris(methoxycarbonyl)pyridine and 2-fluoropyridine were fluorinated by Method B using LiOTf, *N*-fluoro-2,4,6-tris(methoxycarbonyl)pyridinium triflate (**39**) and *N*-fluoro-2-fluoropyridinium triflate (**25**) were isolated in low yields as 1 : 1 crystals with unreacted LiOTf.

Method C fluorination of salts of pyridine, 2,6-dichloropyridine, and pentachloropyridine with triflic acid gave **1a** (66%), **28** (56—62%), and *N*-fluoropentachloropyridinium triflate (**30a**) (32%), respectively, while the corresponding salt **48** of 2,4,6-trimethylpyridine failed to produce **7a** under the same conditions. In the latter case, a large amount of the starting **48** was found to remain. The yield of **1a** was improved by the fluorination at elevated temperature and was high at −20 °C (96%, Run 5 in Table 1). The fluorination of the salt of extremely low basic pentachloropyridine was most efficiently carried out at room temperature using trifluoroacetic acid as a solvent to obtain **30a** in 85% yield.

By Method C, the reaction of *N*-(trimethylsilyl)-pyridinium triflate, easily obtained from pyridine and trimethylsilyl triflate, with F_2 in CH_3CN at −40 °C led to the formation of **1a** in 40% yield. In this reaction, trimethylsilyl fluoride, as another product, was detected by ^{19}F NMR of the reaction mixture. As can be seen from Table 2, Method C is suitable for pyridine itself or pyridines possessing an electron-withdrawing substituent(s). A pyridinium salt with the electron-donating groups, *N*-trimethylsilyl-2,4,6-trimethylpyridinium triflate did not produce **7a** under the same reaction conditions.

Care must be taken when fluorinating *N*-(trimethylsilyl)pyridinium salts. When the very dilute 2% F_2-N_2 was used for the fluorination, there was no *explosion* while at 5% or more, there ensued a violent gas-phase reaction. This may possibly have resulted from a gas-phase reaction of the volatile by-product, trimethylsilyl fluoride, with F_2, since no *violent reaction* occurred with *N*-(dimethylphenylsilyl)pyridinium triflate by which nonvolatile dimethylphenylsilyl fluoride was produced as the by-product (Run 40 in Table 2).

Method D fluorination of a BF_3 complex of 3,5-dichloropyridine formed tetrafluoroborate **29b** in 79% yield while only a trace of **1f** could be formed from pyridine-BF_3 complex under the same conditions. *N*-Fluoropentachloropyridinium tetrafluoroborate (**30b**) was synthesized in 87% yield by Method D fluorination with 20% F_2-N_2 in trifluoroacetic acid at room temperature.

N-Fluoropyridinium trifluoroacetate, regarded as a salt with a weakly nucleophilic counter anion, was produced by Method A using sodium trifluoroacetate or trimethylsilyl trifluoroacetate. The pure salt could not be obtained owing to its failure to be crystallized. The ^1H NMR of the crude product was in good agreement with that of the *N*-fluoropyridinium moiety of **1a** and ^{19}F NMR showed an N-F peak at δ=48.4. *N*-Fluoropyridinium methanesulfonate

(**1c**), a salt with another weakly nucleophilic counter anion, was isolated in good yield according to Method C (Runs 11 and 12 in Table 1). The synthesis of *N*-fluoropyridinium acetate, a salt possessing a considerably strongly nucleophilic counter anion, was attempted by Method B using sodium acetate (NaOAc). Treatment of an equimolar mixture of pyridine and NaOAc in CH_3CN with 10% F_2-N_2 at −40 °C produced new precipitates, probably NaF, but the reaction mixture immediately became dark on rising to room temperature. *N*-Fluoropyridinium acetate may thus possibly be present at low temperature but decomposes with its increase.

A higher homologue of pyridinium salts, *N*-fluoroquinolinium triflate (**49**), was synthesized in 16% yield by Method B using NaOTf. The low yield obtained may possibly have been due to the considerably low stability of **49** toward moisture.

N-Fluoropyridinium-2-sulfonate (**52**) and *N*-fluoro-6-chloropyridinium-2-sulfonate (**53**), counter anion-bound salts, were synthesized as stable crystals in 81 and 77% yields by treating 2-pyridinesulfonic acid (**50**) and 6-chloro-2-pyridinesulfonic acid (**51**) with 10% F_2-N_2 in H_2O-CH_3CN (1/20) solution at −25 °C, respectively.

Hydrolysis Experiment. *N*-Fluoropyridinium salt **1a** was dissolved in water and decomposed very slowly at room temperature. When a solution of **1a** in water stood for 14 days at room temperature, **1a** decomposed completely to give 2-pyridinol in 66% yield. The half decay for its decomposition in heavy water at room temperature was 13 days. Its hydrolysis was accelerated by alkali. Salt **1a** was thus readily hydrolyzed with aq KOH solution at room temperature. GC and GC-Mass analyses of a reaction mixture showed traces of 2-pyridyl triflate (0.5%) and 2-fluoropyridine (0.6%) to form in addition to 2-pyridinol which was isolated in 50% yield.

2,4,6-Trimethyl salt **7a** dissolved in water without decomposing. It remained intact after 30 days at room temperature in heavy water, but decomposed immediately with aq KOH solution to give 2-(hydroxymethyl)-4,6-dimethylpyridine (**54**) and 2-(fluoromethyl)-4,6-dimethylpyridine (**55**) in 24 and 23% yields, respectively. Treatment of **7a** with triethylamine in CH_2Cl_2 and THF afforded a new fluoro product, 3-fluoro-2,4,6-trimethylpyridine (**60**), in addition to **55** in total 62 and 63% yields, respectively. The ratios of **55**/**60** were 2/1 in CH_2Cl_2 and 1/1 in THF. The treatment with NaH in CH_2Cl_2 gave **55**/**60**=8/1 (total yield; 60%).

In water, 3,5-dichloro salt **29a** decomposed immediately and exothermally to give 3,5-dichloro-2-pyridinol (**56**) in 82% yield. 2,6-Dichloro salt **28** decomposed slowly in water, compared to **29a**, to give *N*-fluoro-6-chloro-2-pyridone (**57**) and 2,6-dichloro-4-pyridinol (**58**) in 35 and 7% yields, respectively. Pentachloro salt **30a** decomposed rapidly in water, affording *N*-fluoro-3,4,5,6-tetrachloro-2-pyridone (**59**) in 62% yield. *N*-Fluoroquinolinium salt **49** decomposed immediately in water, so that 2-hydroxyquinoline was obtained in 68% yield.

Thermal Stability. *N*-Fluoropyridinium salts with nonnucleophilic counter anions are generally stable crystals with high melting points. *N*-Fluoropyridinium salt **1a** and 2,4,6-trimethyl salt **7a** remained intact after 5 h at 150 °C, but melted and decomposed within a few minutes at 190 °C. 3,5-Dichloro salt **29a** remained spectroscopically intact after 6 h at 100 °C, though its crystals turned pale brown. Salt **29a**, however, melted and decomposed in less 1 min at 190 °C and in ca. 45 min at 150 °C. These salts may thus be considered to retain their stability for prolonged periods at temperatures less than their melting points, but decompose rapidly or slowly above their melting points.

Solubility. *N*-Fluoropyridinium salts in most cases are freely soluble in polar solvents such as acetonitrile, but insoluble or sparingly soluble in nonpolar organic solvents. The solubilities of *N*-fluoropyridinium triflate **1a**, tetrafluoroborate **1f**, hexafluoroantimonate **1i**, and perchlorate **1j** in CH_2Cl_2 are 0.63, 0.05, 0.09, and 0.035 mg cm^{-3}, respectively. Thus, triflate **1a** has relatively high solubility in this series. Salts having bulky ring-substituents or counter anions such as **10, 11, 12, 14, 15, 16, 18, 23,** or **7c** are soluble in CH_2Cl_2. The solubility of **1a** in THF is 1.71 mg cm^{-3}.

Discussion

Syntheses of *N*-Fluoropyridinium Salts. The pyridine-F_2 compounds produced with pyridine or substituted pyridines and F_2 smoothly underwent the counter anion displacement reactions to give stable *N*-fluoropyridinium salts. They also reacted smoothly with Lewis acids to give *N*-fluoropyridinium salts. The products were determined to have completely ionic structures on the basis of their spectral and elemental analyses. From these results, it appears quite likely that unstable pyridine-F_2 compounds have the *N*-fluoropyridinium fluoride salt structure **47**, which is in agreement with the fact that fluorine atoms have extremely poor two-coordinating ability.[7]

At room temperature, the ^1H NMR spectrum of a homogeneous CH_3CN solution prepared by treating pyridine with 10% F_2-N_2 in CH_3CN at −40 °C, was totally consistent with that of *N*-fluoropyridinium salts. Its ^{19}F NMR showed two peaks at 48.2 and −175 ppm (strong peak), these corresponding to the N-F chemical shifts of the *N*-fluoropyridinium salts and F^- or HF, respectively. An unidentified small peak at 57.4 ppm, however, was also detected. In a concentrated solution, some other small peaks were noted in the range of −63—−100 ppm. Subsequent cooling of the CH_3CN solution to −40 °C followed by treatment with $BF_3 \cdot OEt_2$ gave tetrafluoroborate **1f** in

31% yield, which was the same as that (33%) obtained while keeping the reaction mixture at −40 °C during the treatment.

Since F^- forms a tight hydrogen bond with HF, the pyridine-F_2 compound may quite likely be present as *N*-fluoropyridinium fluoride stabilized by HF, in the form as $[C_5H_5N\text{-}F]^+F^-(HF)_n$. A large part of this compound remained intact in the solution even after standing for 11 days at room temperature.

A comparison of the HF-stabilized salt with the explosive pyridine-F_2 solid, as reported by Meinert,[4] was considered pertinent to the present study. The unstable solid also gave triflate **1a** (32%) and NaF on treatment with NaOTf at low temperature (Run 7 in Table 1). It is thus evident from these data that the unstable solid is *N*-fluoropyridinium fluoride not stabilized by HF, which is most likely formed by immediate precipitation and without the formation of HF as a by-product due to the use of $CFCl_3$ as a solvent inactive toward F_2 under such reaction conditions.

Quantitative ^{19}F NMR analysis indicated the HF-stabilized *N*-fluoropyridinium fluoride to be formed in about a 45% yield, based on the starting pyridine. HF may have been produced by decomposition of the unstable *N*-fluoropyridinium fluoride formed at the first stage and by side-reactions brought about by the extremely reactive F_2. The decomposition reaction would explain well why one-step Method B, in which the unstable *N*-fluoropyridinium fluoride during its formation can immediately react with metal salts of acids, gave good yields of *N*-fluoropyridinium triflates and other salts, while the two-step Method A gave only low yields.

By Method B, in which metal triflates are used, the yield of **1a** increased from 62% to 75% to 87% in the order, KOTf<NaOTf<LiOTf. As noted in the preparation of 3,5-dichloro salt **29a**, the effect of the lithium salt was great in the fluorination of pyridines having electron-withdrawing substituents particularly at β- or γ-positions. It was shown in the related study that *N*-fluoropyridinium salts having an acidic α-proton(s) undergo novel base-initiated decomposition and that even KF causes the decomposition of **1a**, though at a slow rate.[8] The results of the hydrolysis experiments indicated decompostion to occur more easily with *N*-fluoropyridinium salts possessing electron-withdrawing substituents which made the α-proton more acidic. Method B gives metal fluoride as another product as fluorination proceeds. Since their reactivity as a base should decrease in the order of KF>NaF>LiF, the high yields obtained with LiOTf may be attributed to extremely low reactivity of LiF; LiF does not actually decompose any of the formed *N*-fluoropyridinium salts.

To the contrary, in the fluorination of 2,4,6-trimethylpyridine, the yield of product **7a** decreased from 71% to 39% and then to 22% as the metal triflate varied from KOTf to NaOTf and to LiOTf, as shown in Table 3. This may be explained by the decreasing order (KF>NaF>LiF) of the HF-trapping ability of resulting metal fluorides, which can suppress the formation of the by-product **48**. That KOTf in aq CH_3CN completely inhibited **48** is due to the fact that water can act as an additional HF-trapping agent. The effect of NaF as an additive in modified Methods A and B also supports this mechanism. The by-product **19** may be produced by further fluorination of decomposition product **55**, which was shown to form on treatment of **7a** with a base.

N-Fluoropyridinium salts could also be synthesized by insertion reactions of F_2 to proton or silyl salts or Lewis acid-complexes of some pyridines. Thus, pyridinium hydrogen triflate (**63**) and 2,6-dichloro- and pentachloropyridinium hydrogen triflates (**64**) and (**65**) were inserted by F_2 at their N^+-H bonds in CH_3CN at −40 °C to give salts **1a**, **28**, and **30a**, respectively. However, the same treatment of salt **48** of 2,4,6-trimethylpyridine failed to provide **7a**. 3,5-Dichloropyridine-BF_3 complex (**66**) gave a good yield of **29b**, but pyridine-BF_3 complex only a trace of **1f**. It would thus follow that the successful fluorine insertion to N^+-H or N^+-BF_3^- bonds of **63**—**66** is due to their relatively weak bonding. Similarly, the insertion reaction of F_2 into N^+-Si bonds depends on the strength of N^+-Si bonding. The reaction thus proceeded well in the case of the *N*-trimethylsilyl salts of pyridine itself or lower basic pyridine derivatives, while the corresponding silyl salt of more basic 2,4,6-trimethylpyridine did not give **7a** under the same conditions.

In regard to steric hindrance, it should be of considerable interest to fluorinate highly hindered pyridines such as 2,6-di-*t*-butylpyridine and its analogues. Such hindered pyridines react with protonic acid but not with other electrophiles such as BF_3 or methyl iodide by conventional procedure due to steric hindrance between the bulky groups and reactants. They react with methyl iodide or methyl fluorosulfate only under very high pressure of 5000—6000 atm at 90 °C to give stable *N*-methylpyridinium salts.[9] Since van der Waal's radius of fluorine atom (1.47 Å) is close to that of a hydrogen atom (1.20 Å), fluorine should be capable of penetrating into a hindered nitrogen site, as it does in the case of a hydrogen atom.

By the modified Method B, the expected *N*-fluoro-2,6-di-*t*-butyl salts **11**, **12**, and **13** could be obtained along with large amounts of the corresponding pyridinium hydrogen triflates. These *N*-fluoro salts are stable crystals with high melting points, and not sensitive to moisture.

Thus, except for the hydrogen atom, fluorine is the first atom to be inserted into highly crowded nitrogen sites at atmospheric pressure. It is thus clear that, in contrast to the chlorine atom, fluorine atom is capable of substituting all or any hydrogen atom in compounds even though greatly hindered.

Structures and Properties of *N*-Fluoropyridinium Salts. The halogen cations, Cl^+, Br^+, and I^+, have a strong tendency toward two coordination.[10] They thus combine with pyridine or its derivatives to form two kinds of compounds, depending on the nature of the counter anions. One is ionic 2 : 1 salts of pyridine nucleus (Py) and the halogen atom (X) with noncoordinating counter anions such as ClO_4^- or SbF_6^-, as shown by $[Py_2X]^+ClO_4^-$ or SbF_6^-. The other is 1 : 1 covalent molecular complexes with strongly coordinating anions such as carboxylate anions, PyXOCOR.[11] Moderate counter anions such as NO_3^- form both types of compounds, $[Py_2X]^+NO_3^-$ and $PyXONO_2$.

All synthesized *N*-fluoropyridinium compounds possessing non- or weakly coordinating counter anions are concluded to possess completely ionic 1 : 1 structures, $[PyF]^+Y^-$ (Y^-; counter anion). The ease of formation and high stability of 1 : 1 salts contrast sharply with other halogens having the two-coordination form. The reason for this must surely be the low polarizability or lack of d-orbitals of the fluorine atom, or the great difficulty of positive fluorine F^+ formation.[2]

N-Fluoropyridinium fluoride is an unstable solid with an explosive nature, while *N*-fluoropyridinium salts possessing nonnucleophilic counter anions are stable crystals with high melting points. *N*-Fluoropyridinium methanesulfonate (**1c**), a salt having a weakly nucleophilic counter anion, is also stable crystals which melt at 140—142 °C. *N*-Fluoropyridinium trifluoroacetate is also stable at room temperature though its pure salt could not be isolated in the present study. But *N*-fluoropyridinium acetate, a salt having a strongly coordinating or considerably nucleophilic counter anion, was shown by the present data to decompose at room temperature. The stability of *N*-fluoro salts thus clearly depends on the basicity or nucleophilicity of the counter anions. Salts **1** with nonnucleophilic counter anions except for $^-OSO_2F$ are nonhygroscopic crystals.

Electron-withdrawing substituents on the pyridine ring lessen the stability of *N*-fluoropyridinium salts. Particularly 2-fluoro salt **25** and 2,6-dicyano salt **45** were sensitive to moisture. Hydrolysis experiments have afforded some further evidence. The hydrolysis of **1a** in water proceeded quite slowly while that of 3,5-dichloro salt **29a**, rapidly to give 2-pyridinol **56**. Its isomer, 2,6-dichloro salt **28**, was hydrolyzed somewhat slowly, giving other types of hydrolysis products, *N*-fluoro-2-pyridone **57** and 4-pyridinol **58**. Thus, the activating effect of a chlorine atom is outstanding, as is also the blocking effect of an α-chlorine atom. The latter effect suffices to explain why **28** is more stable than **29a** in air in spite of more activation of the N–F moiety of **28**. It should be clear now that, although extremely activated, pentachloro salts **30a** and **30b**, in which all positions are blocked, still possess relatively high stability.

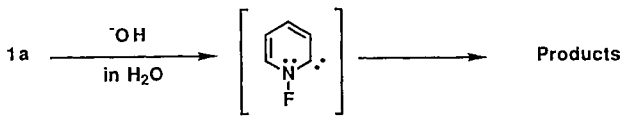

67

Scheme 2.

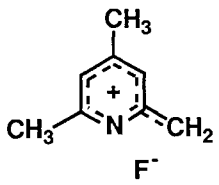

69

Fig. 2.

The hydrolysis of *N*-fluoropyridinium salts contrasts sharply with that of other pyridinium salts having electron-withdrawing groups at the nitrogen sites. *N*-Cyano, -nitro, -nitroso and -(2,4-dinitrophenyl)pyridinium salts and pyridine–SO_3 complex have all been shown to undergo ring opening reaction by alkaline hydrolysis, giving glutaconaldehyde or its derivatives.[14] The mechanism of this is said to be the addition of a hydroxide anion to the α-position. This marked difference may possibly arise from the very different reaction mechanism of *N*-fluoropyridinium salts. As indicated in the related study, *N*-fluoropyridinium salts react with a base to generate a unique carbene **67** (Scheme 2).[8] The detection of traces of 2-pyridyl triflate and 2-fluoropyridine in the alkaline hydrolysis of **1a** supports this mechanism. In the hydrolysis in water, H_2O may serve as a base.

Treatment of **7a** with aq alkaline solution and with a base in an organic solvent afforded different types of products, **54**, **55**, or **60**. They can be explained by an ion pair intermediate **69** (Fig. 2) resulting from deprotonation of **7a**, similar to those for rearrangement reactions of 2- and 4-methylpyridine *N*-oxides.[15]

Conclusions

N-Fluoropyridinium salts provide a new chemistry of pyridine–halogen compounds. Their syntheses can be conducted by counter anion displacement reactions of unstable *N*-fluoropyridinium fluorides and/or insertion reactions of F_2 with salts or complexes of pyridines with protonic acids, silyl esters, and Lewis acids. Their structures and stability characterization, and hydrolysis experiments indicate unique characters of fluorine. The results of this study demonstrate the presence of a new interesting pyridinium salt system based on the superlative nature of fluorine and thus extend the concept of pyridine and fluorine chemistry.

The authors thank Mr. Shinji Fukami (from Onoda Cement Company) for his technical assistance.

References

1) a) M. M. Boudakian, "The Chemistry of Heterocyclic Compounds, Pyridine and Its Derivatives," ed by R. A. Abramovitch, John Wiley & Sons, Inc., New York (1974), Vol. 14, Supplement Part Two, Chap. VI, pp 416—419. b) C. Reid and R. S. Mulliken, *J. Am. Chem. Soc.*, **76**, 3869 (1954). c) O. Hassel, *Proc. Chem. Soc.*, **1957**, 250.

2) W. A. Sheppard and C. M. Sharts, "Organic Fluorine Chemistry," W. A. Benjamin, Inc., New York (1969), pp. 1—17.

3) J. H. Simons, "Fluorine Chemistry," ed by J. H. Simons, Academic Press Inc., New York (1950), Vol. 1, pp. 420—421.

4) H. Meinert, *Z. Chem.*, **5**, 64 (1965).

5) T. Umemoto and K. Tomita, *Tetrahedron Lett.*, **27**, 3271 (1986).

6) "Inorganic Syntheses," ed by J. M. Shreeve, John Wiley & Sons, Inc., New York (1986), Vol. 24, Chap. 1, pp. 22—27.

7) B. E. Smart, "Supplement D, The Chemistry of Halides, Pseudo-Halides and Azides," ed by S. Patai and Z. Rappoport, John Wiley & Sons, New York (1983), Part 1, pp. 616—618.

8) a) T. Umemoto and G. Tomizawa, *Tetrahedron Lett.*, **28**, 2705 (1987). b) T. Umemoto and G. Tomizawa, *J. Org. Chem.*, **54**, 1726 (1989).

9) Y. Okamoto and K. I. Lee, *J. Am. Chem. Soc.*, **97**, 4015 (1975).

10) A. J. Downs and C. J. Adams, "Comprehensive Inorganic Chemistry," ed by J. C. Bailar, H. J. Elmeleus, S. R. Nyholm, and A. F. Trotman-Dickenson, Pergamon Press, Oxford (1973), Supplement Part 2, Vol. 14, pp. 416—420.

11) Recently A. Vervoglis et al. suggested a completely ionic structure for PyIOCOAr, since the carbonyl absorptions (1660—1690 cm^{-1}) were typical of carboxylate ions.[12] However, Zingaro et al. treated of absorption bands in the 950—1100 cm^{-1} region of many pyridine coordinated iodine compounds and revealed that $PyIOCOCH_3$ or PyIOCOPh has a small polar character.[13]

12) O. Menkisoglou-Spyroudi and A. Varvoglis, *J. Chem. Soc., Perkin Trans. 1*, **1986**, 795.

13) R. A. Zingaro and W. E. Tolberg, *J. Am. Chem. Soc.*, **81**, 1353 (1959).

14) a) E. N. Shaw, "The Chemistry of Heterocyclic Compounds, Pyridine and Its Derivatives, Part Two," ed by E. Klingsberg, Interscience Publishers, Inc., New York (1961), Chap, III, pp. 58—63. b) G. A. Olah, J. A. Olah, and N. A. Overchuk, J. Org. Chem., **30**, 3373 (1965).

15) R. A. Abramovitch and M. S. Elizabeth, "The Chemistry of Heterocyclic Compounds, Pyridine and Its Derivatives," ed by R. A. Abramovitch, John Wiley & Sons, Inc., New York (1974), Vol. 14, Supplement Part Two, Chap. IV, pp. 129—146.

Preparation, Stability, and Compositions of the Crystals of Reduced Riboflavins

Matsue EBITANI,* Hiroshi KASHIWAGI,† Masami INOUE,* and Keiichi NISHIBE
Faculty of Engineering, Toyama University, Gofuku, Toyama 930
†Faculty of Pharmaceutical Sciences, Toyama Medical and Pharmaceutical University, Sugitani, Toyama 930-01
(Received October 29, 1990)

Green crystals were obtained after a reduction of riboflavin (RF) with $Na_2S_2O_4$. These crystals were gradually oxidized to RF when stored in air, even at −10°C. The emission spectra and X-ray powder diffraction analyses of the green crystals clearly showed different patterns from those of RF. The ESR spectra and number of the reduced species determined by the titration with $KMnO_4$ supported the formation of an RF-flavosemiquinone radical (1 : 1) complex. Reduced riboflavin tetrabutyrate prepared according to the same procedure was too unstable for dioxygen to obtain spectroscopic data.

The biochemical activities of riboflavin (RF), vitamin B_2, have long attracted attention, for example, as a precursor of flavin adenine dinucleotide, which has an important role as a coenzyme for the flavoproteins.[1] Although the reduced species of RF were unstable, the presence of flavosemiquinone radicals (RFH) was confirmed with electron spin resonance (ESR) and UV spectroscopy.[2] Further, the in situ reduction of RF with $Na_2S_2O_4$ or $SnCl_2$ in an aqueous solution has resulted in some spectra of mixtures of reduced riboflavins involving RFH, which may be produced according to the equilibrium scheme shown in Chart 1.[2] Unstable RFH, once prepared, was easily oxidized again to RF by exposure to air.[3]

The authors first separated a mixture of RF and RFH as fine green crystals out of a solution of RF reduced with $Na_2S_2O_4$. The stability of the crystals in air was studied quantitatively by reflection spectroscopy. For the separated crystals infrared (IR) and ESR spectra, as well as X-ray powder diffraction patterns, were measured, providing the composition of the green crystals. The same procedures were also applied to riboflavin tetrabutyrate (RTB)[4] to give reduced riboflavin tetrabutyrate (RTBH).

Therefore, the preparation, stability, and composition of RFH and RTBH in the crystals could be described from both chemical and spectroscopic standpoints.

Experimental

Preparation of RFH. RF (5.0 g) was dissolved in boiling water (3 l). Insoluble powdery materials were removed by filtration. To the solution, cooled at 60 °C, was added $Na_2S_2O_4$ (0.9 g). Within a few minutes a separated dark solid changed to green. The reaction solution was kept in an ice bath for 3 h. Fine crystals which precipitated were separated and washed twice with ice-cold water. Finally, the crystals were washed with ethanol and dried at 60 °C for 24 h under reduced pressure (130 Pa). Dark-green fine needles (ca. 0.1 mm long, yield. 2.89 g) were obtained.

Preparation of RTB. Crude RTB prepared from *n*-butyric acid, pyridine, $POCl_3$, and RF by heating at 70—75 °C for 5 h was recrystallized from 85% MeOH.

Preparation of RTBH. RTB (5.0 g) was dissolved in hot MeOH-H_2O (45 : 55) (2.1 l). To the solution, kept at 60 °C, was added $Na_2S_2O_4$ (0.5 g). After the solution was cooled in an ice bath for 3 h, precipitated green crystals were collected by filtration, washed twice with water, and then dried at 60 °C for 12 h under reduced pressure. Yield 4.3 g. Mp 148.2 °C.

Oxidation of RFH or RTBH with $KMnO_4$. Fine crystals (0.3 g) prepared by the reduction of RF were dispersed in 1% H_2SO_4 (100 ml). The solution was titrated with 2×10^{-3} mol dm^{-3} $KMnO_4$ under magnetic stirring. The end point of titration was determined potentiometrically with an $HgCl_2$-Pt electrode as a standard half cell.

Freshly prepared RTBH (500 mg) was dissolved in acetic acid (50 ml). To the solution was added 10% H_2SO_4 (10 ml) and water (40 ml). Then, RTBH was titrated with 2×10^{-3}

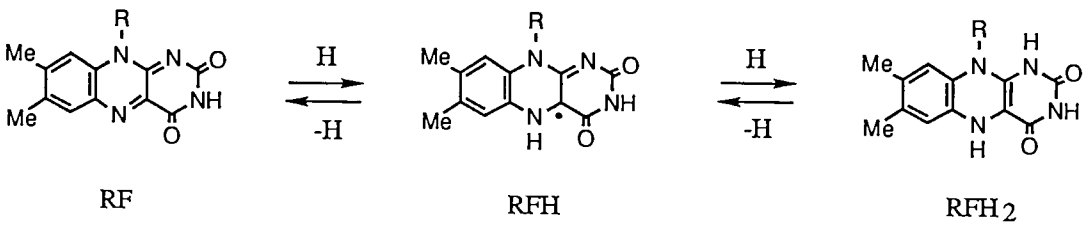

RF RFH RFH_2

R=ribityl

Chart 1.

mol dm^{-3} $KMnO_4$.

Emission Spectra Measurement. Emission spectra were recorded on a Shimadzu RF-502 type spectrophotometer. Powdery samples were packed in a holder and measured under the following conditions: Excitation slit, 15 nm; emission slit 2.2 nm; excitation wavelength, 370 nm.

X-Ray Powder. Diffraction Measurement. An X-ray powder diffraction analysis was carried out using an X-ray diffractometer (Geigerflex D-8C, Rigaku Co.). The conditions were: Target, Cu; filter, Ni; voltage, 30 kV; current, 20 mA; time constant, 1 s; sweep, 2° min^{-1}; divergency slit, 1°; receiving slit, 0.4 mm; detector, Geiger Müller counter.

ESR Measurement. ESR spectra were recorded on a JES-FE3X type spectrometer (X band, 100 kHz modulation). The conditions were: Power, 20 mW; modulation amplitude, 0.63 mT; scan rate, 3.125 mT min^{-1}; time constant, 1 s; gain, 2×1000.

Reflection Spectra Measurement. Reflection spectra were recorded on a Hitachi 228 A type spectrometer equipped with a spherically integrated reflection apparatus (150 mm i.d.). Fine crystals were packed in a dark cell and covered with a glass plate.

IR Spectra Measurement. IR spectra were recorded on a Hitachi 260-50 type spectrometer after preparing KBr tablets by mixing powdery samples (2 mg) with KBr powder (200 mg) and compressing the mixture.

Results and Discussion

The Stability of Reduced RF and Reduced RTB. Fine dark-green needles obtained by the reduction of RF with $Na_2S_2O_4$ were gradually oxidized by exposure to the air.

The color of the crystals changed from green to yellow according to the progress of oxidation. The time courses in the oxidation of the crystals of reduced RF and RTB in air were traced with the reflection spectra.

As shown in Fig. 1, a crystal of reduced RF stored at room temperature was rapidly oxidized into RF during 10 d, followed by slow oxidation. Reduced RF stored at −10 °C also oxidized into RF, although the rate was slower than that at room temperature. The oxidation rate of reduced RTB was twice as fast as that of reduced RF.

Since an RTBH molecule possesses considerably large substituent groups, the average distance between two isoalloxazine rings in a crystal of RTBH may be greater than that in a crystal of RFH. Then, the overlap of the orbitals of the unpaired electron with those of π-electrons on other isoalloxazine rings for RTBH crystal may be smaller than that for the RFH crystal. Therefore, the instability of RTBH crystal against oxidation may be ascribed to delocalization of unpaired electrons over aromatic rings in the crystal.

The nuclear magnetic resonance and high-performance liquid chromatography analysis of a diluted solution of the fine needles failed, since fast oxidation took place to give RF exclusively. Also, an elemental analysis could not be carried out due to an increase in weight during the weighing operation.

IR Spectra. The IR spectra of the fine needles of reduced RF in KBr tablets were obtained and compared with those of RF. A strong, wide spectral band of RFH observed at 3400 cm^{-1} could be assigned to newly formed NH groups. The spectral bands of amide groups of RF at 1736 and 1650 cm^{-1} were spread and duplicated to make one broad band at 1635 cm^{-1}. On the other hand, the IR spectrum of reduced RTB

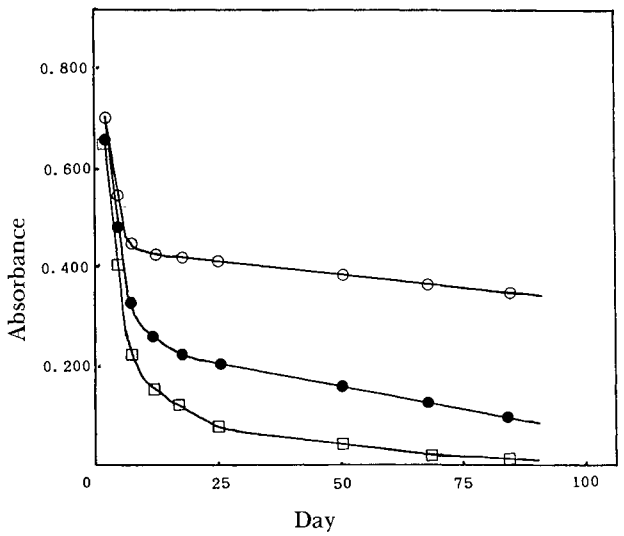

Fig. 1. Decrease in the intensity of reflection spectra of the crystals of reduced RF and reduced RTB in the air.
○: Reduced RF stored at −10 °C,
●: Reduced RF stored at room temperatures,
□: Reduced RTB stored at room temperatures.

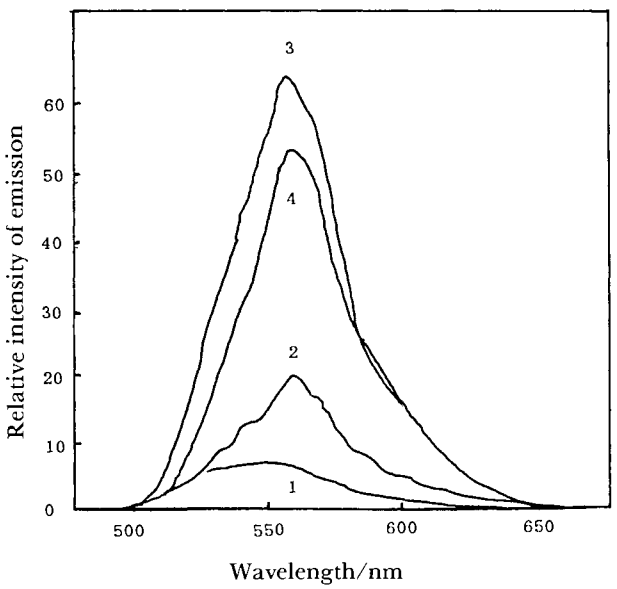

Fig. 2. Emission spectra of the green crystals of reduced RF when oxidized with air or a 2×10^{-3} mol dm^{-3} $KMnO_4$ solution.
1: Reduced RF, 2: Oxidized with air, 3: Oxidized with $KMnO_4$, 4: RF.

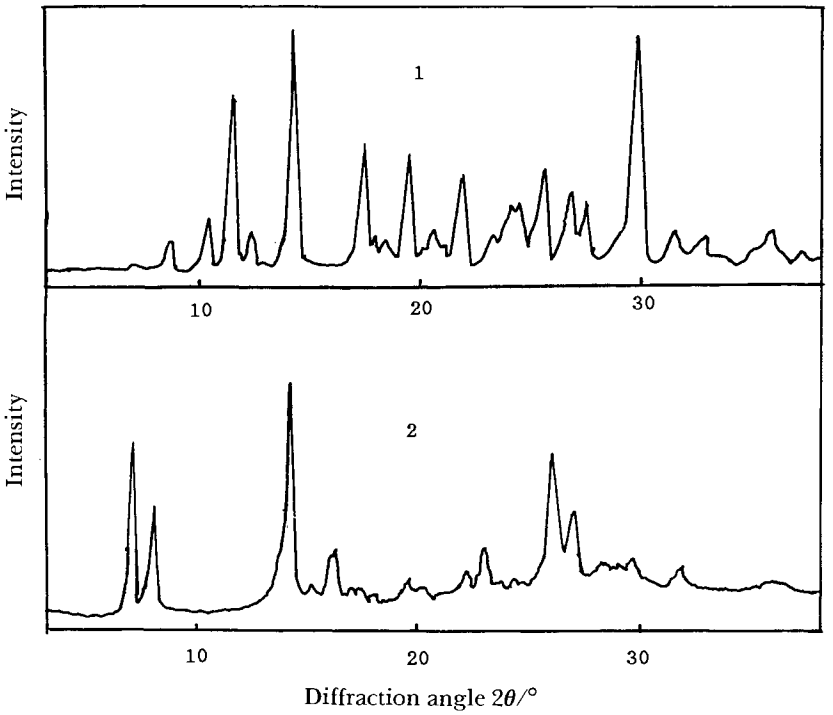

Fig. 3. X-Ray diffraction patterns of the green crystals of reduced RF and orange crystals of RF.
1: RF, 2: Reduced RF.

crystals was the same as that of RTB, suggesting a fast oxidation of the crystal during the preparation of KBr tablets.

Emission Spectra. The emission spectra of crystals of reduced RF and RTB are shown in Fig. 2. The spectral intensity for reduced RF just after preparation is very weak, whereas that for RF is strong. When the crystals of reduced RF dispersed in water came into contact with oxygen by bubbling through air at room temperature, the spectral intensity gradually approached that of RF. Oxidation with a $KMnO_4$ solution (2×10^{-3} mol cm^{-3}) increased the peak intensity for the reduced RF to that of RF. The same tendency was also observed for reduced RTB, except that the oxidation rate with air was faster than reduced RF.

X-Ray Diffraction of Powders. An X-ray powder analysis was carried out for reduced RF. As shown in Fig. 3, the diffraction pattern clearly differed from that of RF. No peaks from RF were observed. The X-ray diffractogram of reduced RF was rather simple and the number of peaks was smaller than those of RF. Sharp peaks were spread from $2\theta=10°$ to 50°, suggesting the presence of well crystallized solids. The relative intensities of peaks as low as at 7.0° and 8.0° were very strong in reduced RF. These facts suggest that RF and RFH produced new structures. The crystals of reduced RTB were unstable in air. The patterns of the X-ray spectra taken after 3 d were almost the same as those of yellow RTB crystals.

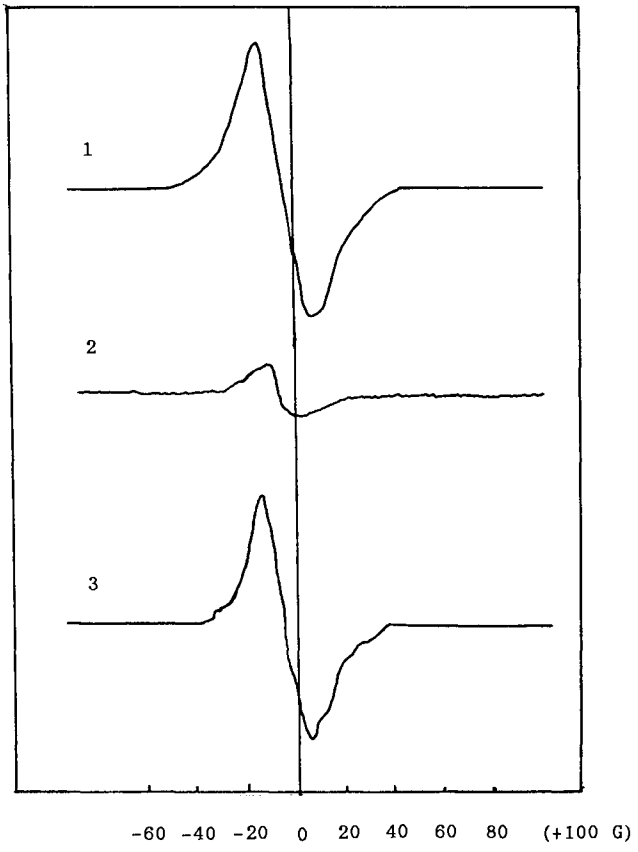

Fig. 4. ESR spectra of the crystals of reduced RF and reduced RTB in the solid state.
1: Reduced RF, 2: RF, 3: Reduced RTB.

ESR Spectra. A solid RF showed weak ESR signals. On the other hand, orange RTB crystals gave no ESR signals.[5] In contrast, the crystals of RFH and RTBH gave strong signals at $g=2.005$ (Fig. 4). The half-width for reduced RF or RTB was 2.278 or 1.964 mT, respectively. Well-resolved hyperfine structures were observed for the latter. The intensities of signals for reduced RF was 5.8-times stronger than that of reduced RTB. These results suggest that the reduced RF crystals contained flavosemiquinone radicals.

Composition of the Crystals of Reduced Riboflavins. The quantitative oxidation of freshly prepared crystals of reduced RF with $KMnO_4$ showed that the molar ratio (RF : RFH) was 47.1 : 52.9. The purity of RF after oxidation was 99.7%. On the other hand, the molar ratio of RTB : RTBH was 86.9 : 13.1. To explain these results, two possible cases were considered. In the first case, a mixture or a complex of RF-RFH (1 : 1) formed a quasi-stable species. The other case involved the formation of a mixture or a complex of RF-RFH_2 (3 : 1). X-Ray powder patterns of RFH contained no peaks from orange RF crystals. The intensity of the emission spectra of the crystals of reduced RF was approximately nil, while those of RF crystals were strong when excited at 370 nm. Furthermore, the ESR spectra showed the presence of radical species in the crystals of reduced RF. When RF was hydrogenated, the color of crystals changed from orange to dark green, and then faded to pale green.

All of these results suggest that unstable RFH_2 formed during the first stage of reduction was quickly oxidized into an RF-RFH (1 : 1) complex followed by successive oxidation to give RF in an oxidative atmosphere.

References

1) H. Beinert, *J. Am. Chem. Soc.*, **78**, 5323 (1956).

2) F. Muller, *Free Radicals Biol. Med.*, **3**, 215 (1987).

3) "Explanation to Japanese Pharmacopoeia XI," ed by Nihon Kouteisho Kyoukai, Hirokawa, Tokyo (1986), p. C-1659.

4) "Nippon Yakkyokuhogai Iyakuhin Seibun Kikaku," ed by Koseisho Yakumukyoku, Yakugyo Jiho, Tokyo (1986), p. 1122.

5) One of the authors prepared three types of RTB crysals, A (orange), B (brown), and C (yellow) types, respectively. Among those, RTB B, recrystallized from *i*-PrOH, gave a strong ESR signal ($g=2.006$); M. Ebitani, *Yakugaku Zasshi*, **107**, 338 (1987).

 © 1991 The Chemical Society of Japan Bull. Chem. Soc. Jpn., 64, 1097—1107 (1991)

Manganese(III) or Cobalt(III)-Mediated Oxidative Radical Reactions of Terminal Dienes. One-Pot Synthesis of Bis(dihydrofuran)s

Hiroshi NISHINO,* Tomoaki YOSHIDA, and Kazu KUROSAWA
Department of Chemistry, Faculty of Science, Kumamoto University,
Kurokami 2-39-1, Kumamoto 860
(Received October 31, 1990)

The reactions of terminal dienes such as 1,4-pentadienes and 1,5-hexadienes with tris(2,4-pentanedionato)-manganese(III) ([Mn(acac)$_3$]) gave α,ω-bis(dihydrofuryl)alkanes (abbreviated bis(dihydrofuran)s, hereafter) in good yields. The reactions with tris(2,4-pentanedionato)cobalt(III) ([Co(acac)$_3$]) instead of [Mn(acac)$_3$] yielded the same bis(dihydrofuran)s quantitatively. The dienes also reacted with ethyl 3-oxobutanoate in the presence of manganese(III) acetate ([Mn(OAc)$_3$]) or cobalt(III) acetate ([Co(OAc)$_3$]) to produce the corresponding bis(dihydrofuran)s. The reactions of 1,3-butadienes with the manganese(III) or cobalt(III) complexes afforded only mono(dihydrofuran)s and oxidative rearrangement products, but the corresponding bis(dihydrofuran)s were not formed. The reaction of 1,5-hexadienes with ethyl hydrogen malonate in the presence of [Mn(OAc)$_3$] did not give bis-annulated products, but mono(γ-lactone)s in moderate yields. The synthetic applications and limitations of the bis(dihydrofuran)s formation are discussed.

Recently, one of the most interesting synthetic methods in organic chemistry was reported. That is the technique involving the intermolecular or intramolecular cyclization reaction of alkenes or alkynes using metal compounds, such as palladium, nickel, cobalt, ruthenium, manganese, chromium, and so on.[1] Especially, we are very interested in the intermolecular or intramolecular radical cyclization reaction using manganese(III) or cobalt(III) complexes.[1c] Previously we reported the oxidation of alkenes with malonic acid in the presence of manganese(III) acetate[2] which was simply abbreviated [Mn(OAc)$_3$].[3] This reaction gave 2,7-dioxaspiro[4.4]nonane-1,6-diones in high yields, although we could not control their stereochemistry at the C-3 and C-8 carbons. Similar reactions with malonic acid derivatives, such as methylmalonic acid, bromomalonic acid, chloromalonic acid, and ethyl hydrogen malonate, yielded the corresponding 2-carboxy-4-butanolides and/or 2-buten-4-olides in good yields.[5] Using malonamide or 2-cyanoacetamide instead of malonic acid in these oxidation reactions afforded not only 2-buten-4-olides, but also 1,5-dihydro-2*H*-pyrrol-2-ones in moderate yields.[6,7] Fristad,[8] Snider,[9] Corey,[10] and Citterio[11] also reported the manganese(III)-mediated inter- or intra-molecular radical cyclization reactions. In connection with the oxidative inter- or intramolecular cyclization reaction using [Mn(OAc)$_3$], we noticed that the ligand-exchange reaction of the manganese(III) complex occurred easily in acetic acid and the corresponding ligand radicals were readily formed.[12] Then, we discovered the facile synthesis of dihydrofurans using tris(2,4-pentanedionato)-manganese(III) ([Mn(acac)$_3$]).[12a] It was also shown that tris(2,4-pentanedionato)cobalt(III) ([Co(acac)$_3$]) had a similar role in acetic acid.[12c] Heiba and Dessau reported that the reaction of styrene with ethyl 3-oxobutanoate in the presence of [Mn(OAc)$_3$] also gave the corresponding dihydrofuran in 57% yield.[13] Corey applied these methods to enol ethers and obtained 2-alkoxy-2,3-dihydrofurans which were transformed to fused or spiro 2-cyclopentenones or converted to the corresponding furans in good yields.[14] However, any attempts to get α,ω-bis(dihydrofuryl)alkanes (abbreviated bis(dihydrofuran)s, hereafter), which might have either an antibiotic nature or bioactive character[15] or might be used as a starting material for the synthesis of many kinds of natural products containing furan rings,[16] were not accomplished by taking advantage of the ligand-exchange process of the manganese(III) or cobalt(III) complexes. We describe in this paper the one-pot synthesis of bis(dihydrofuran)s using Mn(III)- or Co(III)-promoted annulation.

Results

Reaction of Dienes with [Mn(acac)$_3$] or [Co(acac)$_3$]. We used 1,3-butadienes (**1a—e**), 1,4-pentadienes (**1f—h**), and 1,5-hexadienes (**1i—l**) as a substrate (Fig. 1). The reaction of **1a** with [Mn(acac)$_3$] was carried out in the molar ratio from 1 : 4 to 1 : 10 in boiling acetic acid until the oxidant was consumed completely, which gave only 4-ethenyl-4,5-dihydrofuran (**3a**) and 3-acetyl-4-hydroxy-3-hexene-2,5-dione (**5**) in the yields shown in Table 1. An expected bis(dihydrofuran), however, was not formed. The reaction of **1b—e** with [Mn(acac)$_3$] also gave only mono(dihydrofuran)s (**3b**,c and **4d**,e) and the dione (**5**). The results for the reaction of **1d** and **1e** were similar to Hanafusa's work.[17] The 1,4-pentadiene (**1f**) reacted with [Mn(acac)$_3$] to afford the expected bis(dihydrofuran) (**2f**) in moderate yield, although mono(dihydrofuran) (**3f**) was also formed together with **2f** in the reaction at a lower oxidant/substrate ratio (Table 1, Entry 11). The same type of products were obtained from the reactions of **1g** and **1h** (Table 1, Entries 14 and 16). Similar reactions of 1,5-hexadienes (**1i—l**) with

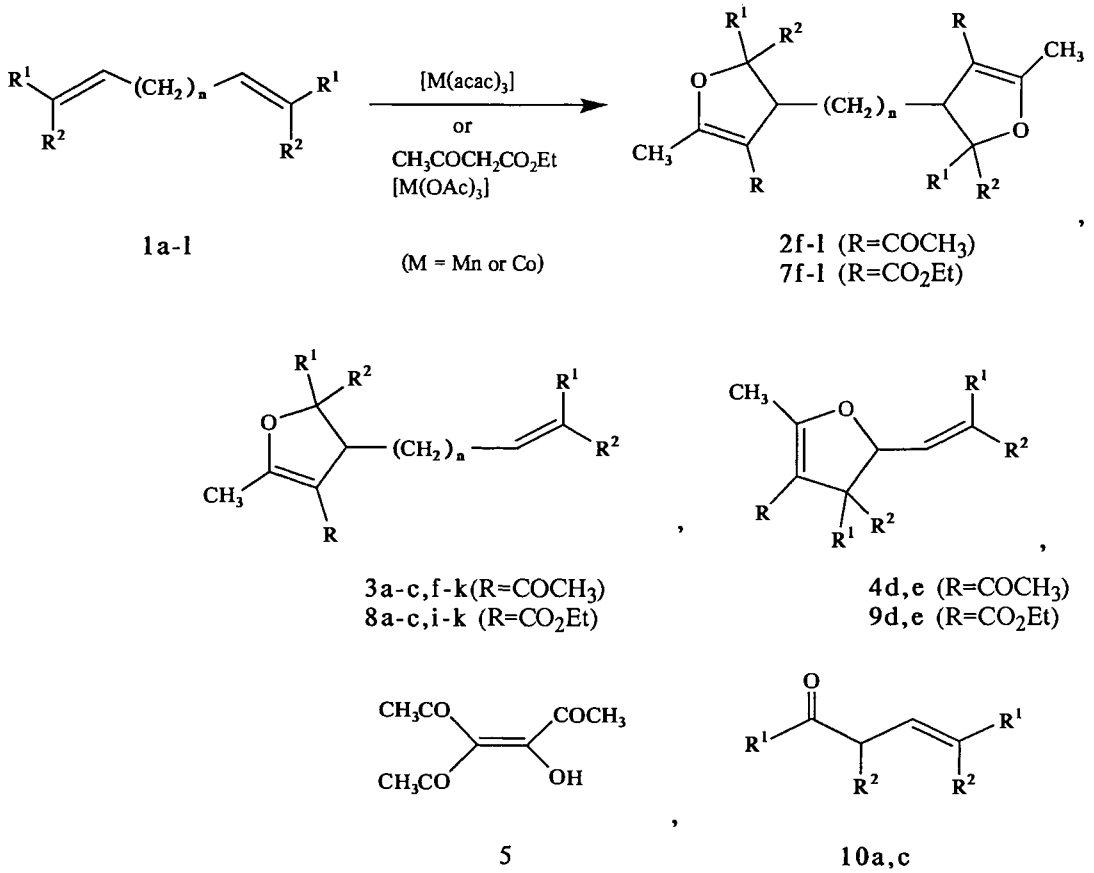

a : n=0, R^1=R^2=Ph
b : n=0, R^1=R^2=4-ClC_6H_4
c : n=0, R^1=R^2=4-MeC_6H_4
d : n=0, R^1=Ph, R^2=H
e : n=0, R^1=R^2=Me
f : n=1, R^1=R^2=Ph
g : n=1, R^1=R^2=4-ClC_6H_4
h : n=1, R^1=R^2=4-MeC_6H_4
i : n=2, R^1=R^2=Ph
j : n=2, R^1=R^2=4-ClC_6H_4
k : n=2, R^1=R^2=4-MeC_6H_4
l : n=2, R^1=R^2=4-$MeOC_6H_4$

Fig. 1.

[Mn(acac)3] gave the expected bis(dihydrofuran)s (**2i—k**) in good yields except for **2l** (Table 1).

The reaction using [Co(acac)3] instead of [Mn(acac)3] resulted in an increased yield of the bis(dihydrofuran). Especially, bis(dihydrofuran)s (**2i—l**) were obtained quantitatively. However, the yield of mono(dihydrofuran)s (**3a—c**, **4e**) was not improved in the oxidation of **1a—e**.

Reaction of Dienes with Ethyl 3-Oxobutanoate in the Presence of Manganese(III) Acetate or Cobalt(III) Acetate. The dienes (**1a—l**) were oxidized with [Mn(OAc)3] in the presence of ethyl 3-oxobutanoate under various reaction conditions. The results are shown in Table 2. When **1f—l** were used during this reaction, the corresponding bis(dihydrofuran)s (**7f—l**) were produced in good to moderate yields. However, we could not obtain any bis(dihydrofuran)s in the case of 1,3-butadienes (**1a—e**), but only ethenyl-substituted dihydrofurans (**8a—c**, and **9d,e**) together with oxidative rearrangement products (**10a,c**). On the other hand, the reaction of 1,5-hexadienes (**1i—l**) with cobalt(III) acetate ([Co(OAc)3])[18] gave both bis(dihydrofuran)s (**7i—l**) and mono(dihydrofuran)s (**8i—k**). The product yields of the reactions by [Co(OAc)3], however, were lower than those of the reactions employing [Mn(OAc)3].

Reactions of 1,5-Hexadienes (1i—l) with Ethyl Hydrogen Malonate in the Presence of [Mn(OAc)3]. It was reported that the reaction of 1-heptene with diethyl malonate in the presence of [Mn(OAc)3]/[Cu(OAc)2] afforded heptylmalonate.[20] However, intramolecular cyclization did not occur under the reaction conditions. Fristad examined the reaction of 1,5-hexadienes with malonic acid and obtained 2,7-dioxacyclopenta[*c*]pentalene-1,8-diones in low yields.[8a] So the reaction of **1i—l** with ethyl hydrogen malonate in the presence of [Mn(OAc)3] was examined in order to get bis-annulated lactone and compare this

Table 1. Reaction of Terminal Dienes (**1a**—**l**) with [M(acac)$_3$] (M=Mn, Co) in Boiling Acetic Acid

Entry	Diene	Oxidant	Molar ratio[a]	Reaction time[b] / min	Product (yield/%)[c]			Recovered diene / %
1	**1a**	[Mn(acac)$_3$]	1:4	2	**3a**(19)		**5**(42)	78
2			1:10	3	**3a**(35)		**5**(46)	56
3		[Co(acac)$_3$]	1:6	120	**3a**(42)			56
4	**1b**	[Mn(acac)$_3$]	1:10	2	**3b**(30)		**5**(48)	69
5		[Co(acac)$_3$]	1:6	120	**3b**(21)			73
6	**1c**	[Mn(acac)$_3$]	1:6	2	**3c**(38)		**5**(40)	36
7		[Co(acac)$_3$]	1:6	120	**3c**(56)			26
8	**1d**	[Mn(acac)$_3$]	1:2	1		**4d**(85)		6
9	**1e**	[Mn(acac)$_3$]	1:8	2		**4e**(72)	**5**(33)	
10		[Co(acac)$_3$]	1:1	42		**4e**(20)		
11	**1f**	[Mn(acac)$_3$]	1:4	1	**2f**(13)	**3f**(12)	**5**(17)	
12			1:10	2	**2f**(48)		**5**(22)	
13		[Co(acac)$_3$]	1:10	150	**2f**(70)			
14	**1g**	[Mn(acac)$_3$]	1:10	2	**2g**(23)	**3g**(22)	**5**(29)	24
15		[Co(acac)$_3$]	1:10	150	**2g**(47)			
16	**1h**	[Mn(acac)$_3$]	1:8	2	**2h**(71)	**3h**(11)	**5**(25)	
17		[Co(acac)$_3$]	1:10	150	**2h**(78)	**3h**(18)		
18	**1i**	[Mn(acac)$_3$]	1:10	3	**2i**(71)	**3i**(17)	**5**(31)	4
19		[Co(acac)$_3$]	1:6	90	**2i**(92)			
20	**1j**	[Mn(acac)$_3$]	1:10	2	**2j**(46)	**3j**(24)	**5**(28)	16
21		[Co(acac)$_3$]	1:10	150	**2j**(91)			
22	**1k**	[Mn(acac)$_3$]	1:2	1	**2k**(29)	**3k**(39)		30
23			1:10	2	**2k**(98)			
24		[Co(acac)$_3$]	1:10	150	**2k**(92)			
25	**1l**	[Mn(acac)$_3$]	1:8	2	**2l**(29)		**5**(15) **6**(45)	
26		[Co(acac)$_3$]	1:10	150	**2l**(91)			

a) Diene: [M(acac)$_3$]. b) The reaction time shows consumption time of each oxidant. c) The yield based on the diene added except for the yield of product (**5**) which was calculated by [Mn(acac)$_3$] added.

Table 2. Reactions of Terminal Dienes (**1a**—**l**) with Ethyl 3-Oxobutanoate in the Presence of [M(OAc)$_3$] (M=Mn, Co)[a]

Entry	Diene	Oxidant	Molar ratio[b]	Reaction time[c] / min	Product (yield/%)[d]				
1	**1a**	[Mn(OAc)$_3$]	1:4:6	5			**8a**(46)		**10a**(12)
2[e]	**1b**		1:4:6	7			**8b**(29)		
3	**1c**		1:2:4	3			**8c**(11)		**10c**(72)
4[f]	**1d**		1:1:2	1				**9d**(49)	
5	**1e**		1:2:4	4				**9e**(57)	
6	**1f**		1:4:6	4		**7f**(22)			
7	**1g**		1:6:8	8		**7g**(17)			
8	**1h**		1:6:8	8		**7h**(14)			
9	**1i**		1:6:8	6		**7i**(89)			
10		[Co(OAc)$_3$]	1:6:8	180		**7i**(61)	**8i**(38)		
11	**1j**	[Mn(OAc)$_3$]	1:6:8	4		**7j**(71)			
12		[Co(OAc)$_3$]	1:6:8	150		**7j**(43)	**8j**(50)		
13	**1k**	[Mn(OAc)$_3$]	1:5:7	9		**7k**(79)			
14		[Co(OAc)$_3$]	1:6:8	90		**7k**(69)	**8k**(23)		
15	**1l**	[Mn(OAc)$_3$]	1:5:7	4	**6**(11)	**7l**(62)			
16		[Co(OAc)$_3$]	1:6:8	120		**7l**(trace)			

a) The reactions were carried out in acetic acid at reflux temperature until the each oxidant was consumed completely. b) Diene: $CH_3COCH_2CO_2Et$: [M(OAc)$_3$]. c) The reaction time shows consumption time of each oxidant. d) The yield based on the diene added. e) The diene (**1b**) was recovered (14%). f) The diene (**1d**) was recovered (17%).

reaction with the bis(dihydrofuran) formation reaction previously mentioned. The 1,5-hexadienes (**1i**—**l**) and ethyl hydrogen malonate were oxidized with [Mn(OAc)$_3$] in boiling acetic acid to yield 3-(3-butenyl)-2-buten-4-olides (**11i**—**l**). The results are shown in Table 3.

Table 3. Reactions of Terminal Dienes (**1i—l**) with Ethyl Hydrogen Malonate in the Presence of [Mn(OAc)$_3$][a)]

Entry	Diene	Molar ratio[b)]	Reaction time[c)] / min	Product (yield/%)[d)]	Recovered diene / %
1	**1i**	1:4:5	1	**11i**(81)	11
2	**1j**	1:4:5	2	**11j**(65)	
3	**1k**	1:4:5	6	**11k**(47)	9
4	**1l**	1:6:7	1	**11l**(33)	

a) The reactions were carried out in acetic acid at reflux temperature until the oxidant was consumed completely. b) Diene: Ethyl hydrogen malonate: [Mn(OAc)$_3$]. c) The reaction time shows consumption time of the oxidant. d) The yield based on the diene added.

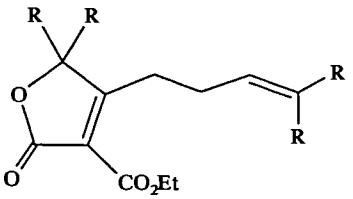

11i-l

i : R=Ph
j : R=4-ClC$_6$H$_4$
k: R=4-MeC$_6$H$_4$
l : R=4-MeOC$_6$H$_4$

Fig. 2.

Discussion

We reported the reaction mechanism for the formation of the dihydrofuran ring involving diacetylmethyl radical, ·CH(COCH$_3$)$_2$, which was produced by the thermolysis of [Mn(acac)$_3$] or [Co(acac)$_3$] in boiling acetic acid.[12a)] Therefore, the formation of bis(dihydrofuran)s (**2f—l**) using [Mn(acac)$_3$] or [Co(acac)$_3$] could be also explained by an akin mechanism previously discussed. The reactions of 1,4-pentadienes (**1f—h**) and 1,5-hexadienes (**1i—l**) with [Mn(acac)$_3$] or [Co(acac)$_3$] gave expected **2f—l** in good yields. However, it was very difficult to get the corresponding bis(dihydrofuran)s by the reaction of 1,3-butadienes (**1a—e**), and considerable amounts of **1a—c** were recovered even for the reactions at a high oxidant/substrate ratio after completion of the reaction. This was considered to be due to the bulky diacetylmethyl radicals not being able to attack the other sterically crowded double bond after forming one dihydrofuran ring in the 1,3-butadiene molecule, because **1a—c** have two pairs of aryl groups at the terminal carbons and the carbon chain (n=0) was very short. Therefore, only mono(dihydrofuran)s (**3a—c** and **4d,e**) were obtained from the reaction of **1a—e**. The generation of isomeric ring systems of **3a—c** and **4d,e** is due to the stability of the intermediate radical (**I** and **II**), that is to say, the benzyl type radical **I** formed from **1a—c** was stabilized by two aryl groups (R^1=R^2=aryl) and the allyl type radical **II** produced from **1d** and **1e** was stabilized by allyl conjugation (Fig. 3). For the reaction of 1,4-pentadienes (**1f—h**) using [Co(acac)$_3$] the yield of **2f—h** was slightly better than that using [Mn(acac)$_3$]. However, the yield of **2g** was low in both cases since the corresponding benzyl radical, e.g., radical **I** was destabilazed by the inductive effect of chloro-substituent on the aryl ring. The reaction of 1,5-hexadienes (**1i—l**) with [Co(acac)$_3$] gave **2i—l** quantitatively and no effect of substituents was

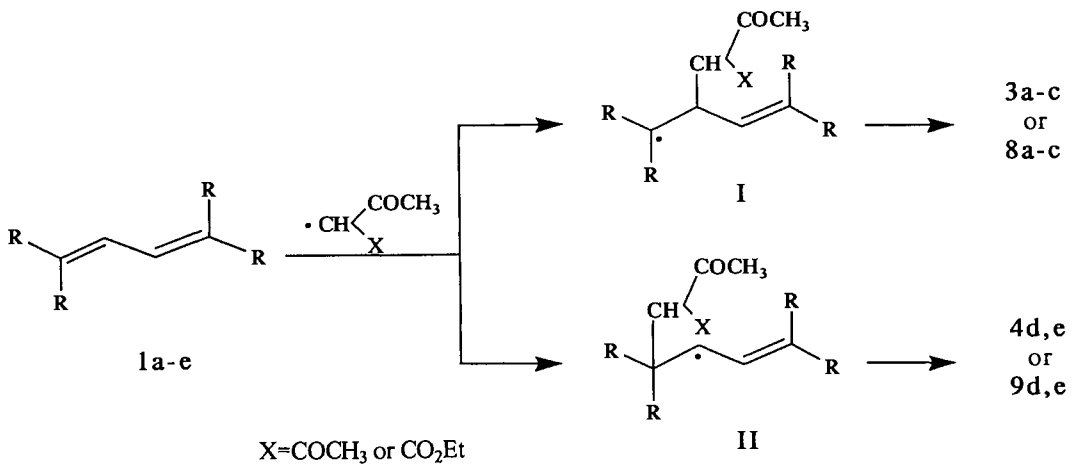

Fig. 3.

observed. On the other hand, **2l** was obtained in poor yield when [Mn(acac)$_3$] was used. This result clearly showed that the electron-transfer from **1l** to Mn(III), generally observed during the oxidation with metal compounds,[1c,21] occurred predominantly since the electron-donating effect of the methoxyl group on the aromatic ring lowered the ionization potential of **1l**.[6,22-24] Actually 4,4′-dimethoxybenzophenone (**6**), which was a typical product via the electron-transfer reaction process, was obtained as the main product (Table 1, Entry 25).

In order to explain the fact that [Co(acac)$_3$] was superior to [Mn(acac)$_3$] for the formation of dihydrofuran ring, we propose the mechanism via the complex formation between [Co(acac)$_3$] and diene. The nature of the complex could be either π- or σ-complex,[25-28] but it is not clear at present moment. Then the oxidation of the complex (**A**) with Co(III) would give rise to mono(dihydrofuran) (**3**). The similar reaction of **3** with [Co(acac)$_3$] was repeated to yield bis(dihydrofuran) (**2**). The reaction mechanism is briefly shown in Scheme 1. On the other hand, it was considered that [Mn(acac)$_3$] could not make a complex (e.g., either π-complex or σ-complex) with the terminal diene or the interaction between [Mn(acac)$_3$] and the diene was very weak. Accordingly, the diacetylmethyl radical has roughly two chances for coupling reactions; one is the coupling between the diene and diacetylmethyl radical and the other is a bimolecular radical coupling of the diacetylmethyl radical itself. In fact, the by-product (**5**), which is usually formed in the [Mn(acac)$_3$]-AcOH oxidation system, was obtained in all of the reactions with [Mn(acac)$_3$] regardless of these substrates.[22] The formation mechanism of **5** via the bimolecular radical coupling of diacetylmethyl radical will be discussed elsewhere.[12c]

Similar results for the synthesis of bis(dihydrofuran)s were obtained by the reaction of dienes (**1a—l**) with ethyl 3-oxobutanoate in the presence of [Mn(OAc)$_3$] or [Co(OAc)$_3$]. In the case of **1i—l**, however, the product yields using [Co(OAc)$_3$] were lower than those using [Mn(OAc)$_3$]. This can be ascribed to the different behavior of [Mn(OAc)$_3$] and [Co(OAc)$_3$] in the reaction system. In other words, if ethyl 3-oxobutanoate radical, ·CH(COCH$_3$)CO$_2$Et, is formed during the ligand-exchange reaction between metal acetate and the oxobutanoate,[8a,29] the ligand-exchange reaction between [Mn(OAc)$_3$] and the oxobutanoate must be much faster than that between [Co(OAc)$_3$] and the oxobutanoate. Therefore, the reaction of **1i—l** in the presence of [Mn(OAc)$_3$] gave the corresponding bis(dihydrofuran)s (**7i—l**) in good yields for much shorter reaction time (4—9 min). On the other hand, it must need much longer reaction time (90—180 min) for the consumption of

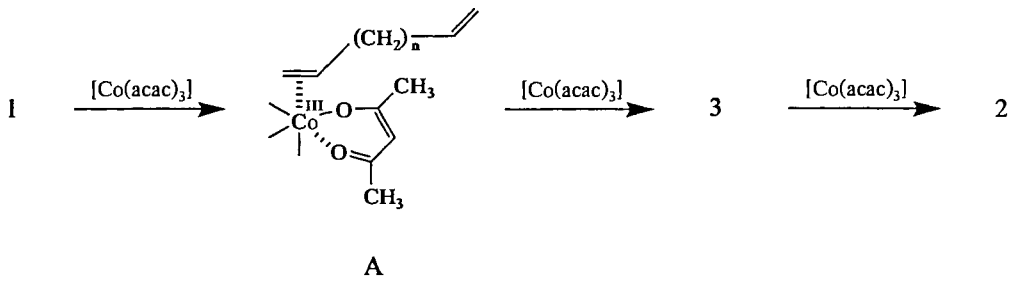

A

Scheme 1.

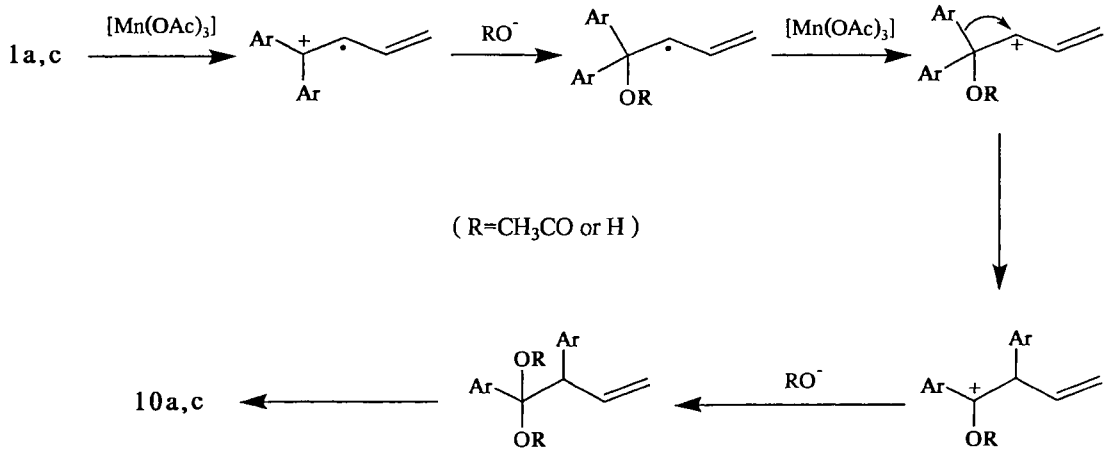

Scheme 2.

[$Co(OAc)_3$] since the ligand-exchange reaction between [$Co(OAc)_3$] and the oxobutanoate is much slower, although Co(III) is a stronger oxidant than Mn(III) according to the comparison with the standard potential ($E°$) of single electrode.[30] Thus, it is considered that the yields of **7i—l** are lower than those using [$Mn(OAc)_3$] since the ligand-exchange reaction between [$Co(OAc)_3$] and the oxobutanoate competes with other side-reactions such as oxidative decarboxylation of solvent.[31] It is noteworthy that the reactions of **1a** and **1c** with [$Mn(OAc)_3$] gave oxidative rearrangement products (**10a** and **10c**) along with mono(dihydrofuran)s (**8a** and **8c**). This rearrangement is presumed to occur via the oxidation through the electron-transfer process regardless of the presence of ethyl 3-oxobutanoate (Scheme 2). Furthermore, it was confirmed that the rearrangement occurred intramolecularly according to the result for the cross-over experiment (see Experimental).

It is not clear why no bis-annulated compound was formed in the reaction with ethyl hydrogen malonate. Even if the molar ratio of **1i**:ethyl hydrogen malonate:[$Mn(OAc)_3$] was increased up to 1:6:7, the corresponding bis-annulated lactone was not isolated and an intractable mixture was obtained (see Experimental). Probably, **11i** was simply oxidized with [$Mn(OAc)_3$] to give a complex mixture before the second attack of $\cdot CH(CO_2Et)CO_2H$ radical to **11i**, or ethyl hydrogen malonate itself was also oxidized to decomposition (the decomposed products were not checked).

In conclusion, [$Co(acac)_3$] has a higher selectivity for the formation of bis(dihydrofuran)s than [$Mn(acac)_3$]. [$Mn(OAc)_3$] is better than [$Co(OAc)_3$] for the production of bis(dihydrofuran)s in the presence of ethyl 3-oxobutanoate under present reaction conditions. In addition, the terminal dienes, which have longer carbon chains than 1,3-butadienes, are advantageous for the synthesis of bis-annulated compounds. We firmly believe that the synthesis of bis(dihydrofuran)s utilizing the present method is important since bis(dihydrofuran)s can be converted to the corresponding bis(furan)s and bis(tetrahydrofuran)s.

Experimental

Instrumentation. ^1H NMR spectra were measured in chloroform-*d* on either a JEOL JNM-PMX60SI or a JEOL FX90Q spectrometer. Chemical shifts are reported in ppm downfield from an intermal TMS standard. Infrared spectra were recorded in chloroform on a JASCO A-102 infrared spectrometer. The IR spectral data are expressed in cm^{-1}. Mass spectra were measured on either a JEOL JMS-01SG-2, JMS-DX303HF, or a Finnigan 6000 GC/MS mass spectrometer at 70 eV of ionization energy. All melting points were determined with a Yanaco MP-J3 micromelting point apparatus (Yanagimoto) and were uncorrected. Elemental analyses were performed by the Elemental Analysis Center, Faculty of Science, Kyushu University.

Materials. Tris(2,4-pentanedionato)manganese(III),[32] manganese(III) acetate,[33] and cobalt(III) acetate[19] were prepared according to methods previously described. Tris(2,4-pentanedionato)cobalt(III) (Wako) was used as received. 1,3-Butadienes (**1a—c**) were prepared by dehydration of the corresponding diols which were synthesized from diethyl succinate (Nacalai) and the corresponding phenylmagnesium bromide. 1,1,4,4-Tetraphenyl-1,3-butadiene (**1a**): Yellow microcrystals (from benzene), mp 195—197 °C (lit,[34] mp 192—193 °C). 1,1,4,4-Tetrakis(4-chlorophenyl)-1,3-butadiene (**1b**): Yellow needles (from benzene), mp 240—242 °C (lit,[35] mp 244 °C). 1,1,4,4-Tetrakis(4-methylphenyl)-1,3-butadiene (**1c**): Pale yellow needles (from acetic acid), mp 251—253 °C (lit,[36] mp 248—250 °C). 1,4-Diphenyl-1,3-butadiene (**1d**) (Aldrich) and 2,5-dimethyl-2,4-hexadiene (**1e**) (Aldrich) were used as received. 1,4-Pentadienes (**1f—h**) were prepared from diethyl glutarate (Tokyokasei) and the corresponding phenylmagnesium bromide according to the similar reaction previously mentioned. 1,1,5,5-Tetraphenyl-1,4-pentadiene (**1f**): Orange liquid; IR 1656 (C=C); ^1H NMR δ=2.80—3.17 (2H, m, $-CH_2-$), 5.90—6.25 (2H, m, 2×=CH-), and 6.90—7.70 (20H, m, 4×Ph). 1,1,5,5-Tetrakis(4-chlorophenyl)-1,4-pentadiene (**1g**): Yellow liquid; IR 1650 (C=C); ^1H NMR δ=2.67—3.13 (2H, m, $-CH_2-$), 5.83—6.23 (2H, m, 2×=CH-), and 6.77—7.78 (16H, m, arom. H). 1,1,5,5-Tetrakis(4-methylphenyl)-1,4-pentadiene (**1h**): Pale yellow microcrystals (from benzene-petroleum ether), mp 94—96 °C; IR 1665 (C=C); ^1H NMR δ=2.30 (6H, s, 2×Me), 2.34 (6H, s, 2×Me), 2.78—3.13 (2H, m, $-CH_2-$), 5.88—6.22 (2H, m, 2×=CH-), and 6.93—7.22 (16H, m, arom.H). 1,1,6,6-Tetraphenyl-1,5-hexadiene (**1i**) was prepared from 1,4-dibromobutane (Wako) and benzophenone (Wako) according to the procedure previously described: Colorless needles (from ethyl acetate-ethanol), mp 101—102 °C (lit,[37] mp 108—109 °C). Other 1,5-hexadienes (**1j—l**) were prepared from diethyl adipate (Nacalai) and the corresponding phenylmagnesium bromide. 1,1,6,6-Tetrakis(4-chlorophenyl)-1,5-hexadiene (**1j**): Colorless microcrystals (from ethyl acetate-ethanol), mp 177—179 °C; IR 1669 (C=C); ^1H NMR δ=2.12—2.33 (4H, m, 2×$-CH_2-$), 5.83—6.20 (2H, m, 2×CH-), and 6.90—7.60 (16H, m, arom.H). 1,1,6,6-Tetrakis(4-methylphenyl)-1,5-hexadiene (**1k**): Colorless microcrystals (from benzene-hexane), mp 134—136 °C; IR 1660 (C=C); ^1H NMR δ=2.11—2.29 (4H, m, 2×$-CH_2-$), 2.31 (6H, s, 2×Me), 2.39 (6H, s, 2×Me), 5.94—6.23 (2H, m, 2×=CH-), and 6.91—7.58 (16H, m, arom.H). 1,1,6,6-Tetrakis(4-methoxyphenyl)-1,5-hexadiene (**1l**): Yellow-green needles (from ether), mp 106—107 °C (lit,[38] mp 108 °C). Ethyl 3-oxobutanoate (Wako) was used as received. Ethyl hydrogen malonate was prepared from diethyl malonate (Wako) according to the literature:[39] Colorless liquid, bp_{19} 145 °C (lit,[39] bp_{21} 147 °C).

Reaction of Terminal Dienes with [Mn(acac)$_3$]. The typical procedure for the reaction of terminal dienes with [$Mn(acac)_3$] was as follows. To a heated solution of a terminal diene (0.5—1.0 mmol) in acetic acid (30 cm^3), [$Mn(acac)_3$] was added. The mixture was heated under reflux until the opaque dark brown color turned a clear yellow. The solvent was removed in vacuo and the residue was triturated with 2M (1M=1 mol dm^{-3}) HCl (30 cm^3), followed by extraction with chloroform. The chloroform extract was concentrated and the residue was separated on TLC (either Wakogel B-10 or Kieselgel 60G) with chloro-

form as the developing solvent. The yields are summarized in Table 1.

Reaction Products. 3-Acetyl-2-methyl-4-(2,2-diphenylethenyl)-5,5-diphenyl-4,5-dihydrofuran (3a): Yellow liquid; IR 1662 (C=O); ^{1}H NMR δ=2.21 (3H, s, COMe), 2.37 (3H, s, Me), 4.81 (1H, d, J=11.0 Hz, >CH-), 5.44 (1H, d, J=11.0 Hz, =CH-), and 6.54—7.79 (20H, m, 4×Ph); MS m/z (rel intensity) 456 (M^+, 44), 414 (60), 289 (58), 231 (65), 215 (81), 165 (100), and 105 (50). Found: m/z 456.2098. Calcd for $C_{33}H_{28}O_2$: M, 456.2089.

3-Acetyl-4-[2,2-bis(4-chlorophenyl)ethenyl]-5,5-bis(4-chlorophenyl)-2-methyl-4,5-dihydrofuran (3b): Yellow liquid; IR 1664 (C=O); ^{1}H NMR δ=2.27 (3H, s, COMe), 2.38 (3H, s, Me), 4.75 (1H, d, J=11.0 Hz, >CH-), 5.37 (1H, d J=11.0 Hz, =CH-), and 6.47—7.57 (16H, m, arom.H); MS m/z (rel intensity) 594 (M^+, 34), 592 (M^+, 26), 552 (75), 550 (60), 534 (56), 532 (44), 357 (26), 315 (18), 299 (33), 277 (37), 264 (26), 251 (36), 235 (26), 199 (41), 165 (13), 139 (56), and 111 (12). Found: m/z 594.0499; 592.0529. Calcd for $C_{33}H_{24}O_2{}^{35}Cl_3{}^{37}Cl$; $C_{33}H_{24}O_2{}^{35}Cl_4$: M, 594.0506; 592.0530.

3-Acetyl-4-[2,2-bis(4-methylphenyl)ethenyl]-5,5-bis(4-methylphenyl)-2-methyl-4,5-dihydrofuran (3c): Yellow liquid; IR 1661 (C=O); ^{1}H NMR δ=2.18 (3H, s, Me), 2.22 (6H, s, 2×Me), 2.25 (3H, s, Me), 2.35 (3H, s, Me), 2.42 (3H, s, Me), 4.76 (1H, d, J=11.0 Hz, >CH-), 5.12 (1H, d, J=11.0 Hz, =CH-), and 6.51—7.40 (16H, m, arom.H); MS m/z (rel intensity) 512 (M^+, 55), 469 (100), 452 (96), 317 (31), 219 (32), and 195 (49). Found: m/z 512.2707. Calcd for $C_{37}H_{36}O_2$: M, 512.2715.

3-Acetyl-2-methyl-5-[(*E*)-2-phenylethenyl]-4-phenyl-4,5-dihydrofuran (4d): Colorless needles (from methanol), mp 101—103 °C; IR 1663 (C=O); ^{1}H NMR δ=1.86 (3H, s, COMe), 2.38 (3H, d, J=1.8 Hz, Me), 4.18 (1H, dq, J=6 and 1.8 Hz, H-4), 4.91 (1H, t, J=6 Hz, H-5), 6.23 (1H, dd, J=6 and 16 Hz, =CH-), 6.55 (1H, d, J=16 Hz, =CH-), and 6.85—7.55 (10H, m, arom.H). Found: C, 82.76; H, 6.57%. Calcd for $C_{21}H_{20}O_2$: C, 82.86; H, 6.57%.

3-Acetyl-5-(2-methyl-1-propenyl)-2,4,4-trimethyl-4,5-dihydrofuran (4e): Yellow liquid; IR 1655 (C=O); ^{1}H NMR δ=1.07 (3H, s, Me), 1.25 (3H, s, Me), 1.68 (3H, d, J=1.2 Hz, Me), 1.76 (3H, d, J=1.2 Hz, Me), 2.19 (3H, s, Me), 2.26 (3H, s, Me), 4.75 (1H, d, J=10 Hz, >CH-), and 5.38 (1H, br.d, J=10 Hz, =CH-); MS m/z (rel intensity) 209 (100), 208 (M^+, 9), 197 (6), 181 (36), 155 (13), 110 (10), and 83 (3). Found: m/z 208.1443. Calcd for $C_{13}H_{20}O_2$: M, 208.1463.

3-Acetyl-4-hydroxy-3-hexene-2,5-dione (5): Colorless prisms (from benzene), mp 113—114 °C (lit,[22] mp 115—116 °C).

Bis(4-acetyl-5-methyl-2,2-diphenyl-2,3-dihydro-3-furyl)methane (2f): Yellow liquid; IR 1679 (C=O); ^{1}H NMR δ=1.65—1.76 (2H, m, -CH_2-), 2.12 (6H, s, 2×COMe), 2.18 (6H, s, 2×Me), 4.1 (2H, br.t, J=6 Hz, 2×>CH-), and 6.70—7.93 (20H, m, arom.H); MS m/z (rel intensity) 568 (M^+, 15), 468 (10), 401 (5), 290 (100), 277 (53), 235 (10), 191 (10), 167 (15), and 91 (8). Found: m/z 568.2626. Calcd for $C_{39}H_{36}O_4$: M, 568.2614.

3-Acetyl-2-methyl-4-(3,3-diphenyl-2-propenyl)-5,5-diphenyl-4,5-dihydrofuran (3f): Yellow liquid; IR 1663 (C=O); ^{1}H NMR δ=2.01 (3H, s, COMe), 2.08—2.17 (2H, m, -CH_2-), 2.25 (3H, s, Me), 4.03 (1H, br.t, J=6.0 Hz, >CH-), 5.70 (1H, t, J=8.0 Hz, =CH-), and 6.72—7.86 (20H, m, arom.H); MS m/z (rel intensity) 471 (100), 470 (M^+, 4), 458 (7), 337 (32), 227 (29), 183 (26), and 105 (7). Found: m/z 470.2236. Calcd for $C_{34}H_{30}O_2$: M, 470.2246.

Bis[4-acetyl-2,2-bis(4-chlorophenyl)-5-methyl-2,3-dihydro-3-furyl]methane (2g): Yellow liquid; IR 1660 (C=O); ^{1}H NMR δ=0.80—1.08 (2H, m, -CH_2-), 2.10 (6H, s, 2×COMe), 2.27 (7H, s, 2×Me), 4.0—4.3 (2H, m, >CH-), and 6.87—7.67 (16H, m, arom.H); MS m/z (rel intensity) 706 (M^+, 3), 704 (M^+, 2), 606 (5), 604 (4), 509 (3), 507 (2), 358 (64), 345 (31), 316 (7), 235 (12), 199 (9), and 139 (8). Found: m/z 704.1011. Calcd for $C_{39}H_{32}O_4{}^{35}Cl_4$: M, 704.1055.

3-Acetyl-4-[3,3-bis(4-chlorophenyl)-2-propenyl]-5,5-bis(4-chlorophenyl)-2-methyl-4,5-dihydrofuran (3g): Yellow liquid; IR 1697 (C=O); ^{1}H NMR δ=1.72—1.97 (2H, m, -CH_2-), 2.10 (3H, s, COMe), 2.22 (3H, s, Me), 3.70—4.18 (1H, m, >CH-), 5.5—5.8 (1H, m, =CH-), and 6.61—7.50 (16H, m, arom.H); MS m/z (rel intensity) 608, (M^+, 4), 606 (M^+, 3), 565 (35), 563 (26), 509 (18), 507 (15), 371 (13), 345 (60), 261 (17), 235 (36), and 139 (18). Found: m/z 608.0678; 606.0660. Calcd for $C_{34}H_{26}O_2{}^{35}Cl_3{}^{37}Cl$; $C_{34}H_{26}O_2{}^{35}Cl_4$: M, 608.0657; 606.0687.

Bis[4-acetyl-2,2-bis(4-methylphenyl)-5-methyl-2,3-dihydro-3-furyl]methane (2h): Yellow liquid; IR 1715 (C=O); ^{1}H NMR δ=0.75—1.40 (2H, m, -CH_2-), 2.17 (6H, s, 2×Me), 2.19 (6H, s, 2×Me), 2.23 (6H, s, 2×Me), 2.31 (6H, s, 2×Me), 3.65 (2H, br.t, J=7.0 Hz, 2×>CH-), and 6.77—7.47 (16H, m, arom.H); MS m/z (rel intensity) 624 (M^+, 65), 523 (5), 480 (3), 428 (4), 368 (3), 317 (65), 263 (17), 219 (28), 195 (40), 179 (25), and 105 (16). Found: m/z 624.3204. Calcd for $C_{43}H_{44}O_4$: M, 624.3240.

3-Acetyl-4-[3,3-bis(4-methylphenyl)-2-propenyl]-5,5-bis(4-methylphenyl)-2-methyl-4,5-dihydrofuran (3h); Yellow liquid; IR 1662 (C=O); ^{1}H NMR δ=1.99 (2H, m, -CH_2-), 2.27 (12H, s, 3×Me), 2.33 (6H, s, 2×Me), 3.93 (1H, br.t, J=6 Hz, >CH-), 5.55 (1H, t, J=7 Hz, =CH-), and 6.67—7.48 (16H, m, arom.H); MS m/z (rel intensity) 526 (M^+, 60), 482 (5), 426 (10), 346 (15), 304 (100), 284 (22), 262 (43), 221 (100), 195 (91), 179 (35), 119 (62), and 91 (32). Found: m/z 526.2902. Calcd for $C_{38}H_{38}O_2$: M, 526.2872.

1,2-Bis(4-acetyl-5-methyl-2,2-diphenyl-2,3-dihydro-3-furyl)ethane (2i): Yellow microcrystals (from benzene-petroleum ether), mp 220—222 °C; IR 1662 (C=O); ^{1}H NMR δ=0.78—1.01 (4H, m, 2×-CH_2-), 1.97 (6H, s, 2×COMe), 2.07 (6H, 2×Me), 3.30.—3.60 (2H, m, 2×>CH-), and 6.78—7.42 (20H, m, 4×Ph). Found: C, 82.31; H, 6.60%. Calcd for $C_{40}H_{38}O_4$: C, 82.44; H, 6.57%.

3-Acetyl-2-methyl-4-(4,4-diphenyl-3-butenyl)-5,5-diphenyl-4,5-dihydrofuran (3i): Colorless microcrystals (from benzene-petroleum ether), mp 109—110 °C; IR 1663 (C=O); ^{1}H NMR δ=1.35—1.78 (4H, m, 2×-CH_2-), 2.15 (3H, s, COMe), 2.19 (3H, s, Me), 3.68—3.95 (1H, m, >CH-), 5.57—5.88 (1H, m, =CH-), and 6.63—7.53 (20H, m, 4×Ph). Found: C, 86.55; H, 6.70%. Calcd for $C_{35}H_{32}O_2$: C, 86.74; H, 6.66%.

1,2-Bis[4-acetyl-2,2-bis(4-chlorophenyl)-5-methyl-2,3-dihydro-3-furyl]ethane (2j): Yellow microcrystals (from benzene-petroleum ether), mp 252—253 °C; IR 1665 (C=O); ^{1}H NMR δ=0.72—1.13 (4H, m, 2×-CH_2-), 2.15 (6H, s, 2×COMe), 2.18 (6H, s, 2×Me), 3.35—3.57 (2H, m, 2×>CH-), and 6.95—7.72 (16H, m, arom.H); MS m/z (rel intensity) 720 (M^+, 13), 718 (M^+, 10), 620 (23), 618 (17), 483 (8), 423 (4), 372 (60), 346 (32), 329 (18), 261 (15), 235 (26), 199 (20), and 125 (10). Found: m/z 720.1184; 718.1193. Calcd for $C_{40}H_{34}O_4{}^{35}Cl_3{}^{37}Cl$; $C_{40}H_{34}O_4{}^{35}Cl_4$: M, 720.1189; 718.1212.

3-Acetyl-4-[4,4-bis(4-chlorophenyl)-3-butenyl]-5,5-bis(4-chlorophenyl)-2-methyl-4,5-dihydrofuran (3j): Yellow microcrystals (from benzene-petroleum ether), mp 174—176 °C; IR 1665 (C=O); ^{1}H NMR δ=1.23—1.80 (4H, m, 2×-CH_2-), 2.23 (6H, s, COMe and Me), 3.67—3.97 (1H, m, >CH-), 5.73—6.07 (1H, m, =CH-), and 6.83—7.60 (16H, m, arom.H). Found: C, 67.58; H, 4.49%. Calcd for $C_{35}H_{28}O_2Cl_4$: C, 67.54; H, 4.53%.

1,2-Bis[4-acetyl-2,2-bis(4-methylphenyl)-5-methyl-2,3-dihydro-3-furyl]ethane (2k): Yellow liquid; IR 1665 (C=O); ^{1}H NMR δ=0.82—1.05 (4H, m, 2×-CH_2-), 1.96 (6H, s, 2×Me), 2.06 (6H, s, 2×Me), 2.22 (6H, s, 2×Me), 2.31 (6H, s, 2×Me), 3.25—3.57 (2H, m, 2×>CH-), and 6.77—7.35 (16H, m, arom.H); MS *m/z* (rel intensity) 638 (M^+, 50), 537 (27), 442 (15), 331 (90), 305 (66), 288 (37), 262 (46), 219 (63), 195 (100), 179 (81), 105 (80), and 91 (30). Found: *m/z* 638.3388. Calcd for $C_{44}H_{46}O_4$: M, 638.3396.

3-Acetyl-4-[4,4-bis(4-methylphenyl)-3-butenyl]-5,5-bis(4-methylphenyl)-2-methyl-4,5-dihydrofuran (3k): Yellow liquid; IR 1660 (C=O); ^{1}H NMR δ=1.12—1.85 (4H, m, 2×-CH_2-), 2.17 (3H, s, Me), 2.22 (3H, s, Me), 2.29 (9H, s, 3×Me), 2.38 (3H, s, Me), 3.68—3.98 (1H, m, >CH-), 5.58—5.88 (1H, m, =CH-), and 6.78—7.48 (16H, m, arom.H); MS *m/z* (rel intensity) 540 (M^+, 18), 306 (100), 263 (22), 234 (81), 219 (31), 195 (17), 105 (15). Found: *m/z* 540.3031. Calcd for $C_{39}H_{40}O_2$: M, 540.3028.

1,2-Bis[4-acetyl-2,2-bis(4-methoxyphenyl)-5-methyl-2,3-dihydro-3-furyl]ethane (2l): Yellow liquid; IR 1665 (C=O); ^{1}H NMR δ=0.71—1.18 (4H, m, 2×-CH_2-), 2.09 (6H,s, 2×Me), 2.13 (6H, s, 2×Me), 3.34—3.64 (2H, m, 2×>CH-), 3.76 (6H, s, 2×OMe), 3.83 (3H, s, OMe), 3.86 (3H, s, OMe), and 6.51—7.96 (16H, m, arom.H); MS *m/z* (rel intensity) 702 (M^+, 25), 602 (6), 475 (10), 364 (72), 338 (100), 227 (52), 211 (15), and 135 (23). Found: *m/z* 702.3201. Calcd for $C_{44}H_{46}O_8$: M, 702.3193.

4,4′-Dimethoxybenzophenone (6): Yellow needles (from ethanol), mp 140—141 °C (lit,[40] mp 144 °C)

Reaction of Terminal Dienes with [Co(acac)$_3$]. In order to determine the optimum reaction conditions for the formation of bis(dihydrofuran), the reactions were examined using diene (**1i**) changing molar ratio, solvent, and reaction temperature. The effect of additive was also tested. When **1i** was allowed to react with [Co(acac)$_3$] at the molar ratio of 1 : 6 in acetic acid at the reflux temperature, the best yield of **2i** was obtained. The reaction predominantly gave **2i** irrespective of the presence of an active methylene compound such as malonic acid, malonamide, and diethyl malonate. The results are shown in Table 4. Accordingly, the reaction with [Co(acac)$_3$] was conducted as follows. To a heated solution of a terminal diene (0.5—1.0 mmol) in acetic acid (30 cm^3), [Co(acac)$_3$] was added. The mixture was heated under reflux until its dark green solution turned pink. The solvent was evaporated in vacuo and the residue was triturated with 2M HCl (30 cm^3), followed by extraction with chloroform. The chloroform was removed in vacuo and the product residue was separated on TLC with chloroform as the developing solvent. The yields are summarized in Table 1.

Reaction of Terminal Dienes with Ethyl 3-Oxobutanoate in the Presence of [Mn(OAc)$_3$]. To a heated solution of a diene (0.5—1.0 mmol) and ethyl 3-oxobutanoate in acetic acid (30 cm^3), [Mn(OAc)$_3$] was added. The mixture was heated under reflux until its dark-brown color turned clear yellow. The solvent was removed and the residue was treated with the same work-up previously mentioned. The results are shown in Table 2.

3-Ethoxycarbonyl-2-methyl-4-(2,2-diphenylethenyl)-5,5-diphenyl-4,5-dihydrofuran (8a): Colorless microcrystals (from ethyl acetate-ehanol), mp 133—134 °C; IR 1686 (C=O); ^{1}H NMR δ=1.24 (3H, t, J=7.0 Hz, Me), 2.39 (3H, s, Me), 4.18 (2H, q, J=7.0 Hz, -CH_2-), 4.92 (1H, br.d, J=11.0 Hz, >CH-), 5.44 (1H, d, J=11.0 Hz, =CH-), and 6.54—7.91 (20H, m, 4×Ph). Found: C, 83.90; H, 6.16%. Calcd for $C_{34}H_{30}O_3$: C, 83.92; H, 6.21%.

1,2,4,4-Tetraphenyl-3-butene-1-one (10a):[41] Yellow liquid; IR 1679 (C=O); ^{1}H NMR δ=5.35 (1H, d, J=10.0 Hz, >CH-), 6.69 (1H, d, J=10.0 Hz, =CH-), and 6.89—7.85 (20H, m, arom.H); MS *m/z* (rel intensity) 374 (M^+, 1), 345 (13), 269 (100), 191 (43), 105 (45), and 91 (13).

4-[2,2-Bis(4-chlorophenyl)ethenyl]-5,5-bis(4-chlorophenyl)-3-ethoxycarbonyl-2-methyl-4,5-dihydrofuran (8b): Colorless prisms (from ethyl acetate-ethanol), mp 181—182 °C; IR 1686 (C=O); ^{1}H NMR δ=1.27 (3H, t, J=7.0 Hz, Me), 2.33 (3H, s, Me), 4.16 (2H, q, J=7.0 Hz, -CH_2-), 4.66 (1H, br.d, J=11.0 Hz, >CH-), 5.26 (1H, d, J=11.0 Hz, =CH-), and 6.36—7.78 (16H, m, arom.H). Found: C, 65.41; H, 4.25%. Calcd for $C_{34}H_{26}O_3Cl_4$: C, 65.40; H, 4.20%.

3-Ethoxycarbonyl-4-[2,2-bis(4-methylphenyl)ethenyl]-

Table 4. Reaction of 1,1,6,6-Tetraphenyl-1,5-hexadiene (**1i**) with [Co(acac)$_3$]

Entry	Solvent	Additive	Molar ratio[a]	Reaction time[b]	Recovered **1i**	Product (yield/%)[c]	
				h	%	**2i**	**3i**
1	Acetic acid	None	1:0:4	1.5		59	18
2		None	1:0:6	1.5		92	
3		None	1:0:8	1.5		88	
4[d]		None	1:0:6	16		68	
5	Propanoic acid	None	1:0:6	2.5	10	12	25
6	2,4-Pentanedione	None	1:0:6	24	85		
7	Benzene	None	1:0:6	24	93		
8	Acetic acid	$CH_2(CO_2H)_2$	1:6:8	0.7		79	
9		$CH_2(CONH_2)_2$	1:6:8	0.7		51	23
10		$CH_2(CO_2Et)_2$	1:6:8	1.0		46	
11		Ac_2O	1:10:6	2.0		80	15

a) **1i**: Additive: [Co(acac)$_3$]. b) The reaction time shows consumption time of the oxidant. c) The yield based on **1i** added. d) The reaction was carried out at 100 °C.

5,5-bis(4-methylphenyl)-2-methyl-4,5-dihydrofuran (8c): Colorless needles (from ethanol), mp 133—135 °C; IR 1687 (C=O); ^{1}H NMR δ=1.23 (3H, t, J=7.0 Hz, Me), 2.19 (6H, s, 2×Me), 2.29 (6H, s, 2×Me), 2.42 (3H, s, Me), 4.11 (2H, q, J=7.0 Hz, -CH_2-), 4.71 (1H, br. d, J=11.0 Hz, >CH-), 5.21 (1H, d, J=11.0 Hz, =CH-), and 6.29—7.52 (16H, m, arom.H). Found: C, 84.05; H, 7.01%. Calcd for $C_{38}H_{38}O_3$: C, 84.10; H, 7.06%.

1,2,4,4-Tetrakis(4-methylphenyl)-3-butene-1-one (10c): Colorless needles (from ethyl acetate-ethanol), mp 130—131 °C; IR 1675 (C=O); ^{1}H NMR δ=2.27 (6H, s, 2×Me), 2.31 (3H, s, Me), 2.39 (3H, s, Me), 5.36 (1H, d, J=10.0 Hz, >CH-), 6.58 (1H, d, J=10.0 Hz, =CH-), and 6.87—7.80 (16H, m, arom.H); MS m/z (rel intensity) 430 (M^+, 1), 311 (100), 219 (33), 203 (3), 119 (6), and 91 (4). Found: C, 89.34; H, 7.03%. Calcd for $C_{32}H_{30}O$: C, 89.26; H, 7.02%.

3-Ethoxycarbonyl-2-methyl-5-[(*E*)-2-phenylethenyl]-4-phenyl-4,5-dihydrofuran (9d): Yellow liquid; IR 1693 (C=O); ^{1}H NMR δ=0.95 (3H, t, J=7.0 Hz, Me), 2.33 (3H, d, J=2.0 Hz, Me), 3.91 (2H, q, J=7.0 Hz, -CH_2-), 4.12 (1H, q, J=2.0 Hz, >CH-), 4.90 (1H, t, J=6.0 Hz, >CH-O-), 6.15 (1H, dd, J=6.0 and 16.0 Hz, =CH-), 6.48 (1H, d, J=16.0 Hz, =CH-), and 6.88—7.45 (10H, m, 2×Ph); MS m/z (rel intensity) 334 (M^+, 84), 305 (3), 292 (66), 279 (17), 260 (14), 245 (100), 231 (28), 217 (78), 202 (28), 180 (30), 167 (18), 149 (30), 115 (25), and 105 (50). Found: m/z 334.1541. Calcd for $C_{22}H_{22}O_3$: M, 334.1569.

3-Ethoxycarbonyl-2,4,4-trimethyl-5-(2-methyl-1-propenyl)-4,5-dihydrofuran (9e): Colorless liquid; IR 1678 (C=O); ^{1}H NMR δ=1.00 (3H, s, Me), 1.19 (3H, s, Me), 1.26 (3H, t, J=7.0 Hz, Me), 1.72 (3H, d, J=1.7 Hz, Me), 1.81 (3H, d, J=1.7 Hz, Me), 2.09 (3H, s, Me), 4.11 (2H, q, J=7.0 Hz, -CH_2-), 4.66 (1H, d, J=10.0 Hz, >CH-), and 5.27 (1H, br.d, J=10.0 Hz, =CH-); MS m/z (rel intensity) 238 (M^+, 59), 223 (100), 195 (67), 149 (73), 121 (88), and 107 (26). Found: m/z 238.1576. Cacld for $C_{14}H_{22}O_3$: M, 238.1569.

Bis(4-ethoxycarbonyl-5-methyl-2,2-diphenyl-2,3-dihydro-3-furyl)methane (7f): Yellow liquid; IR 1685 (C=O); ^{1}H NMR δ=0.71—1.09 (2H, m, -CH_2-), 1.24 (6H, t, J=7.0 Hz, 2×Me), 2.12 (6H, s, 2×Me), 3.38—3.88 (2H, m, 2× >CH-), 4.15 (4H, q, J=7.0 Hz, 2×-CH_2-), and 6.68—7.84 (20H, m, 4×Ph); MS m/z (rel intensity) 628 (M^+, 1), 583 (3), 320 (100), 278 (24), 191 (27), and 105 (21). Found: m/z 628.2833. Calcd for $C_{41}H_{40}O_6$: M, 628.2825.

Bis[2,2-bis(4-chlorophenyl)-4-ethoxycarbonyl-5-methyl-2,3-dihydro-3-furyl]methane (7g): Yellow liquid; IR 1681 (C=O); ^{1}H NMR δ=0.69—1.12 (2H, m, -CH_2-), 1.26 (6H, t, J=7.0 Hz, 2×Me), 2.15 (6H, s, 2×Me), 3.19—3.66 (2H, m, 2×>CH-), 4.18 (4H, q, J= 7.0 Hz, 2×-CH_2-), and 6.76—7.69 (16H, m, arom.H); MS m/z (rel intensity) 766 (M^+, 2), 764 (M^+, 1), 634 (3), 632 (2), 388 (100), 346 (16), 302 (12), 259 (10), 199 (12), 167 (22), 149 (50), and 113 (7). Found: m/z 766.1257; 764.1323. Calcd for $C_{41}H_{36}O_6{}^{35}Cl_3{}^{37}Cl$; $C_{41}H_{36}O_6{}^{35}Cl_4$: M, 766.1244; 764.1266.

Bis[4-ethoxycarbonyl-2,2-bis(4-methylphenyl)-5-methyl-2,3-dihydro-3-furyl]methane (7h): Yellow liquid; IR 1687 (C=O); ^{1}H NMR δ=0.73—1.46 (2H, m, -CH_2-), 1.23 (6H, t, J=7.0 Hz, 2×Me), 2.19 (6H, s, 2×Me), 2.29 (6H, s, 2×Me), 2.42 (6H, s, 2×Me), 3.61—3.70 (2H, m, 2×>CH-), 4.11 (4H, q, J=7.0 Hz, 2×-CH_2-), and 6.60—7.53 (16H, m, arom.H); MS m/z (rel intensity) 684 (M^+, 1), 639 (3), 348 (100), 306 (27), 261 (10), and 195 (5). Found: m/z 684.3441. Calcd for $C_{45}H_{48}O_6$: M, 684.3451.

1,2-Bis(4-ethoxycarbonyl-5-methyl-2,2-diphenyl-2,3-dihydro-3-furyl)ethane (7i): Colorless microcrystals (from ethyl acetate/ethanol), mp 162—164 °C; IR 1690 (C=O); ^{1}H NMR δ=0.84—1.11 (4H, m, 2×-CH_2-), 1.20 (6H, t, J=7.0 Hz, 2×Me), 2.09 (6H, s, 2×Me), 3.33—3.71 (2H, m, 2× >CH-), 4.09 (4H, q, J=7.0 Hz, 2×-CH_2-), and 6.98—7.61 (20H, m, 4×Ph); MS m/z (rel intensity) 642 (M^+, 5), 596 (8), 550 (5), 512 (47), 466 (8), 429 (7), 383 (8), 334 (37), 307 (16), 245 (17), 193 (17), 149 (13), and 105 (30). Found: C, 78.37; H, 6.53%; m/z 642.2990. Calcd for $C_{42}H_{42}O_6$: C, 78.48; H, 6.59%; M, 642.2982.

1,2-Bis[2,2-bis(4-chlorophenyl)-4-ethoxycarbonyl-5-methyl-2,3-dihydro-3-furyl]ethane (7j): Colorless microcrystals (from benzene-petroleum ether), mp 103—105 °C; IR 1686 (C=O); ^{1}H NMR δ=0.82—1.09 (4H, m, 2×-CH_2-), 1.12 (6H, t, J=7.0 Hz, 2×Me), 2.11 (6H, s, 2×Me), 3.19—3.49 (2H, m, 2×>CH-), 4.07 (4H, q, J=7.0 Hz, 2×-CH_2-), and 6.89—7.42 (16H, m, arom.H); MS m/z (rel intensity) 780 (M^+, 4), 778 (M^+, 3), 734 (15), 732 (10), 688 (6), 686 (4), 650 (50), 648 (40), 604 (7), 602 (4), 543 (2), 497 (12), 451 (10), 402 (100), 375 (24), 356 (20), 261 (22), 235 (18), 199 (26), 165 (6), and 139 (15). Found: m/z 780.1308; 778.1379. Calcd for $C_{42}H_{38}O_6{}^{35}Cl_3{}^{37}Cl$; $C_{42}H_{38}O_6{}^{35}Cl_4$: M, 780.1401; 778.1423.

1,2-Bis[4-ethoxycarbonyl-2,2-bis(4-methylphenyl)-5-methyl-2,3-dihydro-3-furyl]ethane (7k): Colorless needles (from ethyl acetate-ethanol), mp 161—163 °C; IR 1683 (C=O); ^{1}H NMR δ=0.70—1.06 (4H, m, 2×-CH_2-), 1.23 (6H, t, J=7.0 Hz, 2×Me), 2.07 (6H, s, 2×Me), 2.28 (6H, s, 2×Me), 2.34 (6H, s, 2×Me), 3.19—3.49 (2H, m, 2×>CH-), 4.02 (4H, q, J=7.0 Hz, 2×-CH_2-), and 6.81—7.33 (16H, m, arom.H). Found: C, 79.06; H, 7.18%. Calcd for $C_{46}H_{50}O_6$: C, 79.05; H, 7.21%.

1,2-Bis[4-ethoxycarbonyl-2,2-bis(4-methoxyphenyl)-5-methyl-2,3-dihydro-3-furyl]ethane (7l): Colorless microcrystals (from benzene-petroleum ether), mp 97—98 °C; IR 1686 (C=O); ^{1}H NMR δ=0.85—1.08 (4H, m, 2×-CH_2-), 1.23 (6H, t, J=7.0 Hz, 2×Me), 2.08 (6H, s, 2×Me), 3.18—3.48 (2H, m, 2×>CH-), 3.74 (6H, s, 2×OMe), 3.81 (6H, s, 2×OMe), 4.07 (4H, q, J=7.0 Hz, 2×-CH_2-), and 6.58—7.38 (16H, m, arom.H); MS m/z (rel intensity) 762 (M^+, 24), 716 (6), 674 (9), 652 (18), 632 (70), 606 (18), 586 (13), 562 (7), 535 (15), 498 (24), 443 (5), 394 (100), 348 (47), 293 (38), 253 (35), 227 (66), 211 (22), 165 (7), and 135 (24). Found: m/z 762.3378. Calcd for $C_{46}H_{50}O_{10}$: M, 762.3404.

Reaction of Terminal Dienes with Ethyl 3-Oxobutanoate in the Presence of [Co(OAc)$_3$]. A mixture of a diene (0.5 mmol) and ethyl 3-oxobutanoate (3 mmol) was heated under reflux in acetic acid (30 cm^3) and then [Co(OAc)$_3$] (4 mmol) was added. The mixture was continued to be heated under reflux until a dark green color turned pink. On cooling, the solvent was removed in vacuo and the residue was treated by the procedure previously described. The products and their yields are shown in Table 3.

3-Ethoxycarbonyl-2-methyl-4-(4,4-diphenyl-3-butenyl)-5,5-diphenyl-4,5-dihydrofuran (8i): Colorless needles (from ethyl acetate-ethanol), mp 113—114 °C; IR 1683 (C=O); ^{1}H NMR δ=1.20 (3H, t, J=7.0 Hz, Me), 1.39—1.99 (4H, m, 2×-CH_2-), 2.20 (3H, s, Me), 3.77 (1H, br.t, J=5.0 Hz, >CH-), 4.07 (2H, q, J=7.0 Hz, -CH_2-), 5.73 (1H t, J=7.0 Hz, =CH-), and 6.82—7.52 (20H, m, 4×Ph). Found: C, 84.17; H, 6.66%. Calcd for $C_{36}H_{34}O_3$: C, 84.01; H, 6.66%.

4-[4,4-Bis(4-chlorophenyl)-3-butenyl]-5,5-bis(4-chlorophenyl)-3-ethoxycarbonyl-2-methyl-4,5-dihydrofuran (8j):

Yellow liquid; IR 1684 (C=O); ^{1}H NMR δ=1.24 (3H, t, J=7.0 Hz, Me), 1.47—1.91 (4H, m, 2×-CH_2-), 2.20 (3H, s, Me), 3.70 (1H, br.t, J=5.0 Hz, >CH-), 4.14 (2H, q, J=7.0 Hz, -CH_2-), 5.77 (1H, t, J=7.0 Hz, =CH-), and 6.81—7.84 (16H, m, arom.H); MS m/z (rel intensity) 652 (M^+, 8), 650 (M^+, 6), 561 (3), 559 (2), 522 (3), 520 (2), 389 (10), 343 (27), 301 (8), 274 (100), 239 (77), 199 (26), 165 (16), and 125 (22). Found: m/z 652.0901; 650.0922. Calcd for $C_{36}H_{30}O_3{}^{35}Cl_3{}^{37}Cl$; $C_{36}H_{30}O_3{}^{35}Cl_4$: M, 652.0926; 650.0949.

3-Ethoxycarbonyl-4-[4,4-bis(4-methylphenyl)-3-butenyl]-5,5-bis(4-methylphenyl)-2-methyl-4,5-dihydrofuran (8k): Yellow liquid; IR 1685 (C=O); ^{1}H NMR δ=1.22 (3H, t, J=7.0 Hz, Me), 1.44—1.87 (4H, m, 2×-CH_2-), 2.22 (3H, s, Me), 2.26 (3H, s, Me), 2.29 (6H, s, 2×Me), 2.37 (3H, s, Me), 3.77 (1H, br.t, J=6.0 Hz, >CH-), 4.12 (2H, q, J=7.0 Hz, -CH_2-), 5.72 (1H, t, J=7.0 Hz, =CH-), and 6.77—7.47 (16H, m, arom. H); MS m/z (rel intensity) 570 (M^+, 10), 525 (4), 440 (3), 391 (3), 349 (10), 335 (5), 303 (20), 290 (15), 275 (7), 261 (10), 234 (100), 219 (45), 195 (14), 143 (6), 129 (12), and 105 (18). Found: m/z 570.3125. Calcd for $C_{40}H_{42}O_3$: M, 570.3134.

Reactions of Terminal Dienes (1i—l) with Ethyl Hydrogen Malonate in the Presence of [Mn(OAc)$_3$]. A mixture of a diene (0.5—1.0 mmol) and ethyl hydrogen malonate was heated under reflux in acetic acid (30 cm^3) and then [Mn(OAc)$_3$] was added. The mixture was continued to be heated under reflux until a dark-brown color turned clear yellow. After removal of the solvent, the residue was triturated with 2M HCl (30 cm^3). The aqueous solution was extracted with chloroform and separated on TLC. The product and its yield are shown in Table 3.

2-Ethoxycarbonyl-3-(4,4-diphenyl-3-butenyl)-4,4-diphenyl-2-buten-4-olide (11i): Colorless microcrystals (from methanol), mp 181—183 °C; IR 1785 and 1730 (C=O); ^{1}H NMR δ=0.47 (3H, t, J=7.0 Hz, Me), 1.09—1.92 (2H, m, -CH_2-), 2.26—2.96 (2H, m, -CH_2-), 4.28 (2H, q, J=7.0 Hz -CH_2-), and 6.89—7.69 (21H, m, =CH- and 4×Ph); MS m/z (rel intensity) 514 (M^+, 65), 496 (28), 470 (57), 450 (20), 424 (40), 397 (46), 303 (29), 275 (50), 259 (30), 229 (35), 215 (42), 193 (100), 167 (60), 115 (30), and 105 (62). Found: C, 81.48; H, 5.88%. Calcd for $C_{35}H_{30}O_4$: C, 81.69; H, 5.88%.

The reaction of **1i** with ethyl hydrogen malonate in the presence of [Mn(OAc)$_3$] at the molar ratio of 1:6:7 under the similar reaction conditions was completed for 10 min to give a complex mixture, from which **11i** (46%) was obtained as an only isolable product.

3-[4,4-Bis(4-chlorophenyl)-3-butenyl]-4,4-bis(4-chlorophenyl)-2-ethoxycarbonyl-2-buten-4-olide (11j): Colorless needles (from ethyl acetate-ethanol), mp 195—197 °C; IR 1775 and 1730 (C=O); ^{1}H NMR δ=0.57 (3H, t, J=7.0 Hz, Me), 1.09—3.15 (4H, m, 2×-CH_2-), 4.18 (2H, q, J=7.0 Hz, -CH_2-), and 6.88—7.85 (17H, m, =CH- and arom.H); MS m/z (rel intensity) 652 (M^+, 45), 650 (M^+, 33), 634 (37), 632 (27), 606 (59), 604 (31), 588 (19), 586 (14), 535 (26), 533 (22), 490 (8), 437 (9), 389 (35), 372 (20), 343 (75), 261 (100), 235 (37), 202 (15), 165 (20), and 139 (55). Found: m/z 652.0586; 650.0585. Calcd for $C_{35}H_{26}O_4{}^{35}Cl_3{}^{37}Cl$; $C_{35}H_{26}O_4{}^{35}Cl_4$: M, 652.0556; 650.0585.

2-Ethoxycarbonyl-3-[4,4-bis(4-methylphenyl)-3-butenyl]-4,4-bis(4-methylphenyl)-2-buten-4-olide (11k): Colorless needles (from methanol), mp 155—157 °C; IR 1781 and 1729 (C=O); ^{1}H NMR δ=0.50 (3H, t, J=7.0 Hz, Me), 0.72—3.13 (4H, m, 2×-CH_2-), 2.19 (6H, s, 2×Me), 2.26 (6H, s, 2×Me), 4.15 (2H, q, J=7.0 Hz, -CH_2-), and 6.77—7.85 (17H, m, =CH- and arom.H); MS m/z (rel intensity) 570 (M^+, 38), 552 (17), 526 (54), 506 (13), 480 (40), 453 (53), 375 (11), 349 (22), 332 (15), 305 (39), 287 (12), 257 (16), 243 (21), 221 (100), 195 (38), 165 (13), and 119 (33). Found: m/z 570.2776. Calcd for $C_{39}H_{38}O_4$: M, 570.2770.

2-Ethoxycarbonyl-3-[4,4-bis(4-methoxyphenyl)-3-butenyl]-4,4-bis(4-methoxyphenyl)2-buten-4-olide (11l): Colorless needles (from benzene-petroleum ether), mp 143—144 °C; IR 1780 and 1729 (C=O); ^{1}H NMR δ=0.55 (3H t, J=7.0 Hz, Me), 1.40—1.83 (2H, m, -CH_2-), 2.27—2.97 (2H, m, -CH_2-), 3.67 (6H, s, 2×OMe), 3.72 (6H, s, 2×OMe), 4.17 (2H, q, J=7.0 Hz, -CH_2-), and 6.51—7.57 (17H, m, =CH- and arom.H). Found: C, 73.54; H, 6.00%. Calcd for $C_{39}H_{38}O_8$: C, 73.80; H, 6.04%.

Cross-Over Experiment for the Formation of Rearrangement Product. The butadienes **1a** (185.4 mg; 0.5 mmol) and **1c** (203.2 mg; 0.5 mmol) were dissolved in acetic acid (30 cm^3) upon heating and then [Mn(OAc)$_3$] (742.6 mg; 1 mmol=3 equivalents) was added. The mixture was heated under reflux until the dark Mn(III) ion completely disappeared (15 min). The solvent was removed in vacuo and the residue was worked up by the same procedure previously mentioned. After TLC separation, the oxidative rearrangement products **10a** (61.5 mg; 33%) and **10c** (173.4 mg; 81%) were obtained and **1a** (85.7 mg; 46%) was recovered. No cross-over compound was isolated.

We are grateful for the financial support of this work by a Grant-in-Aid for Encouragement of Young Scientists No. 62740301 from the Ministry of Education, Science and Culture. The authors wish to thank Dr. Terry Marriott of the Department of Chemistry, Rice University, Houston, Texas, U.S.A., for his measurement of high-resolution mass spectra. We also acknowledge Mr. Yasunori Sudoh of the Taiho Pharmaceutical Co., Inc., Tokushima, for his arrangement of the measurements of high-resolution mass spectra.

References

1) a) L. S. Liebeskind, "Advances in Metal-Organic Chemistry," Vol. 1 (1989), JAI Press (1988). b) P. A. Chaloner, "Handbook of Coordination Catalysis in Organic Chemistry," Butterworths (1986). c) W. J. Mijs and C. R. H. I. de Jonge, "Organic Syntheses by Oxidation with Metal Compounds," Plenum Press (1986).

2) N. Ito, H. Nishino, and K. Kurosawa, *Bull. Chem. Soc. Jpn.*, **56**, 3527 (1983).

3) The structure of manganese(III) acetate has been stated as an oxygen-centered triangle structure.[4] Although the chemical constitution comes close to [Mn(OAc)$_3$]·2H$_2$O,[1c] the exact structure has not yet been clarified.

4) F. A. Cotton and G. Wilkinson, "Advanced Inorganic Chemistry," 5th ed, John Wiley & Sons (1988).

5) N. Fujimoto, H. Nishino, and K. Kurosawa, *Bull. Chem. Soc. Jpn.*, **59**, 3161 (1986).

6) H. Nishino, *Bull. Chem. Soc. Jpn.*, **58**, 217 (1985).

7) H. Sato, H. Nishino, and K. Kurosawa, *Bull. Chem. Soc. Jpn.*, **60**, 1753 (1987).

8) a) W. E. Fristad and S. S. Hershberger, *J. Org. Chem.*,

50, 1026 (1985). b) W. E. Fristad, J. R. Peterson, and A. B. Ernst, *J. Org. Chem.*, **50**, 3143 (1985); F. Z. Yang, M. K. Trost, and W. E. Fristad, *Tetrahedron Lett.*, **28**, 1493 (1987).

9) B. B. Snider and J. J. Patricia, *J. Org. Chem.*, **54**, 38 (1989), and references cited therein.

10) E. J. Corey and M. Kang, *J. Am. Chem. Soc.*, **106**, 5384 (1984).

11) A. Citterio, D. Fancelli, C. Finzi, L. Pesce, and R. Santi, *J. Org. Chem.*, **54**, 2713 (1989).

12) a) H. Nishino, *Bull. Chem. Soc. Jpn.*, **58**, 1922 (1985). b) S. Tategami, T. Yamada, H. Nishino, J. D. Korp, and K. Kurosawa, *Tetrahedron Lett.*, **31**, 6371 (1990). c) H. Nishino, S. Tategami, T. Yamada, J. D. Korp, and K. Kurosawa, *Bull. Chem. Soc. Jpn.*, **64**, (1991), (in press).

13) E. I. Heiba and R. M. Dessau, *J. Org. Chem.*, **39**, 3456 (1974).

14) E. J. Corey and A. K. Ghosh, *Chem. Lett.*, **1987**, 223; *Tetrahedron Lett.*, **28**, 175 (1987).

15) a) S. D. Jolad, J. J. Hoffmann, K. H. Schram, J. R. Cole, M. S. Tempesta, G. R. Kriek, and R. B. Bates, *J. Org. Chem.*, **47**, 3151 (1982). b) S. D. Jolad, J. J. Hoffmann, J. R. Cole, C. E. Barry, R. B. Bates, G. S. Linz, and W. A. Konig, *J. Nat. Prod.*, **48**, 644 (1985). c) T. T. Dabrah and A. T. Sneden, *Phytochemistry*, **23**, 2013 (1984). d) T. T. Dabrah and A. T. Sneden, *J. Nat. Prod.*, **47**, 652 (1984). e) J. K. Rupprecht, C. J. Chang, J. M. Cassady, J. L. McLaughlin, K. L. Mikolajczak, and D. Weisleder, *Heterocycles*, **24**, 1197 (1986). f) D. Cortes, J. L. Rios, A. Villar, and S. Valverde, *Tetrahedron Lett*, **25**, 3199 (1984). g) T. R. Hoye and J. C. Suhadolnik, *J. Am. Chem. Soc.*, **109**, 4402 (1987).

16) a) U. Schmidt, J. Gombos, E. Haslinger, and H. Zak, *Chem. Ber.*, **109**, 2628 (1976). b) E. J. Corey and X-M. Cheng, "The Logic of Chemical Synthesis," John Wiley & Sons (1989).

17) K. Ohkata, T. Isako, and T. Hanafusa, *Chem. Ind. (London)*, **15**, 274 (1978).

18) The structure of cobalt(III) acetate has also been said to be an oxo-centered structure.[4] However, it might be a Co(III)-Co(II) mixed valence oxygen-centered complex.[19]

19) J. Hanotier, Ph. Camerman, M. Hanotier-Bridoux, and P. de Radzitzky, *J. Chem. Soc., Perkin Trans. 2*, **1972**, 2247.

20) G. I. Nikishin, M. G. Vinogradov, and T. M. Fedorova, *J. Chem. Soc., Chem. Commun.*, **1973**, 693.

21) R. A. Sheldon and J. K. Kochi, "Metal-Catalyzed Oxidations of Organic Compounds," Academic Press (1981).

22) H. Nishino, *Bull. Chem. Soc. Jpn.*, **59**, 1733 (1986).

23) W. E. Fristad and J. R. Peterson, *J. Org. Chem.*, **50**, 10 (1985); W. E. Fristad, J. R. Peterson, A. B. Ernst, and G. B. Urbi, *Tetrahedron*, **42**, 3429 (1986).

24) J. A. Norman, C. B. Thomas, and M. J. Burrow, *J. Chem. Soc., Perkin Trans. 1*, **1985**, 1087.

25) M. Hirano and T. Morimoto, *J. Chem. Soc., Perkin Trans. 2*, **1984**, 1033.

26) A. J. Pearson, "Metallo-Organic Chemistry," John Wiley & Sons (1985).

27) B. B. Snider, J. J. Patricia, and S. A. Kates, *J. Org. Chem.*, **53**, 2137 (1988).

28) K. Narasaka, N. Miyoshi, K. Iwakura, and T. Okauchi, *Chem. Lett.*, **1989**, 2169.

29) M. E. Kurz, V. Baru, and P-N, Nguyen, *J. Org. Chem.*, **49**, 1603 (1984).

30) J. A. Dean, "Lange's Handbook of Chemistry," 13th ed, McGraw-Hill (1985), pp. 6-8—6-12.

31) S. S. Lande and J. K. Kochi, *J. Am. Chem. Soc.*, **90**, 5196 (1968).

32) M. N. Bhattacharjee, M. K. Chaudhuri, and D. T. Khathing, *J. Chem. Soc., Dalton Trans.*, **1982**, 669.

33) E. I. Heiba, R. M. Dessau, and W. J. Koehl, Jr., *J. Am. Chem. Soc.*, **91**, 138 (1969).

34) Y. Zalkind and A. Krugrov, *J. Russ. Phys. Chem. Soc.*, **68**, 803 (1929); *Chem. Abstr.*, **23**, 4679 (1929).

35) W. Tadros, *J. Chem. Soc.*, **1954**, 2966.

36) W. Tadros, A. B. Sakla, and Y. Akhookh, *J. Chem. Soc.*, **1956**, 2701.

37) K. H. Baner and H. Herzog, *J. Prakt. Chem.*, **147**, 4 (1936); *Chem. Abstr.*, **31**, 387 (1937).

38) E. Buchta and H. Weidinger, *Justus Liebigs Ann. Chem.*, **580**, 83 (1953); *Chem. Abstr.*, **48**, 3938 (1954).

39) F. Marguery, *Bull. Soc. Chim. Fr.*, **33**, 544 (1905).

40) M. Bösler, *Ber.*, **14**, 328 (1881).

41) R. E. Lutz, R. G. Bass, and D. W. Boykin, *J. Org. Chem.*, **29**, 3660 (1964).

Reactions of α,β-Unsaturated Ketone Acetals with Trimethylsilyl Cyanide and Trimethylsilyl Sulfides

Tsunehiko SOGA, Haruhiro TAKENOSHITA, Masaaki YAMADA, Jeng S. HAN, and Teruaki MUKAIYAMA*
Department of Applied Chemistry, Faculty of Science, Science University of Tokyo,
Kagurazaka, Shinjuku-ku, Tokyo 162
(Received November 8, 1990)

In the presence of a catalytic amount of trityl perchlorate, trimethylsilyl cyanide reacts with the dimethyl acetals of chalcone derivatives, with simultaneous double bond isomerization, to yield γ-methoxy-α,β-unsaturated carbonitriles. Trimethylsilyl sulfides react with dimethyl acetals derived from α,β-unsaturated ketones to yield 1,3-bis(alkylthio)propene derivatives under similar conditions.

In recent years, various reactions between acetals and a silylated nucleophile such as trimethylsilyl cyanide (TMS-CN),[1] silyl enol ethers,[2] ketene silyl acetals,[2] or allyltrimethylsilane[3] have been developed employing several efficient catalysts or promoters. Concerning the reaction of acetals derived from α,β-unsaturated ketones with silyl enol ethers, it was shown that either the Michael product or the β-alkoxy ketone was obtained, and that regioselectivity depends mostly on the reaction conditions.[4] It was also reported that a Lewis acid catalyst such as $SnCl_4$ or $BF_3 \cdot Et_2O$ promotes the reaction of acetals with TMS-CN and, in the case of the reaction of acetals derived from α,β-unsaturated ketones with TMS-CN, α-methoxy carbonitriles are obtained as major products.[1]

Recently, we have reported that, in the presence of a catalytic amount of transition metal salts such as $NiCl_2$, $CoCl_2$, or di-μ-chloro-bis(1,5-cyclooctadiene)-dirhodium ([Rh(COD)Cl]$_2$), TMS-CN reacts readily with various acetals under mild conditions.[5] During subsequent experiments, an interesting observation was made concerning the reaction of dimethyl acetals derived from α,β-unsaturated ketones: in the presence of 2 mol% of [Rh(COD)Cl]$_2$, TMS-CN reacts with (*E*)-chalcone dimethyl acetal to yield (*E*)-2-methoxy-2,4-diphenyl-3-butenenitrile, a normal cyanation product along with its isomerized product. The present study was initiated to examine in detail the reaction conditions required and the mechanism of this reaction in forming predominantly the isomerized product (*Z*)-4-methoxy-2,4-diphenyl-2-butenenitrile, briefly reported in preliminary communications.[6] This report describes in full the results of our investigation of the above reaction, and of a similar reaction employing another silylated nucleophile, trimethylsilyl sulfide, and of the reaction of the isomerized products thus obtained with several silylated nucleophiles.

Results and Discussion

Cyanation of Chalcone Dimethyl Acetal. We have already reported that when (*E*)-chalcone dimethyl acetal (**1**) was allowed to react with TMS-CN in the presence of 2 mol% of $CoCl_2$ in CH_2Cl_2 at room temperature for 18 h, (*E*)-2-methoxy-2,4-diphenyl-3-butenenitrile (**2**) was obtained in 99% yield.[5] On the other hand, **2** and its isomerized compound (**3**) were obtained in 89% yield when the above reaction was carried out in the presence of 2 mol% of [Rh(COD)Cl]$_2$ in CH_2Cl_2 at room temperature for 40 h (**2**:**3**=20:80, Scheme 1).[6] The structure of the above compound **3** was determined, mainly by ^{1}H and ^{13}C NMR measurement, to be (*Z*)-4-methoxy-2,4-diphenyl-2-butenenitrile as shown in Fig. 1. Concerning the geometry of the double bond in **3**, only one isomer was observed by ^{1}H and ^{13}C NMR measurement and we considered that it had the *Z*-configuration on the basis of the value of the coupling constant between the 1-position carbon and the 3-position proton ($^3J_{C1,H3}$=13.9 Hz) as measured by

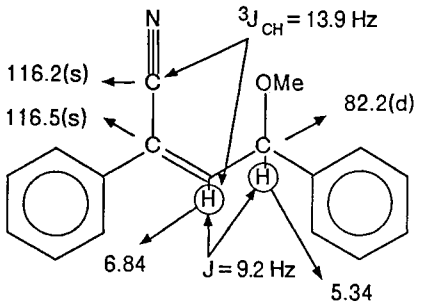

Fig. 1.

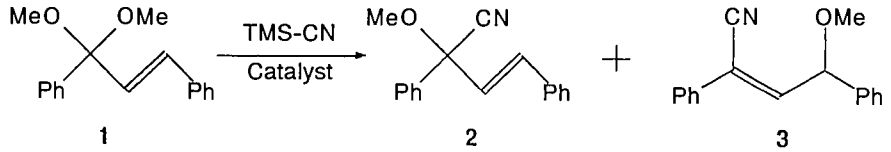

1 2 3

Scheme 1.

Table 1. Examination of Catalysts and Solvents[a]

Entry	Catalyst[b]	Solvent	Time/h	Yield/%	Ratio of 2:3[c]
1[d]	$[Rh(COD)Cl]_2$	CH_2Cl_2	5	86	100: 0
2[d]	$[Rh(COD)Cl]_2$	CH_2Cl_2	10	83	64: 36
3[d]	$[Rh(COD)Cl]_2$	CH_2Cl_2	40	89	20: 80
4[d]	$[Rh(COD)Cl]_2$	CH_3CN	5	86	39: 61
5[d]	$[Rh(COD)Cl]_2$	CH_3CN	20	85	0:100
6	$NiCl_2$	CH_3CN	20	64	100: 0
7	$CoCl_2$	CH_3CN	20	83	81: 19
8	$Pd(acac)_2$	CH_3CN	20	77	100: 0
9	$Pd(OAc)_2$	CH_3CN	20	95	100: 0
10	$SnCl_2$	CH_3CN	3	98	96: 4
11	$BF_3 \cdot Et_2O$	CH_3CN	3	98	100: 0
12	$SnCl_4$	CH_3CN	3	Quant.	24: 76
13[e]	$AlCl_3$	CH_3CN	3	76	100: 0
14	$TiCl_4$	CH_3CN	3	97	88: 12
15	Ph_3CClO_4	CH_3CN	3	92	0:100
16	Ph_3CCl–$SnCl_2$[8]	CH_3CN	15	86	0:100
17	TMSCl–$SnCl_2$[9]	CH_3CN	15	85	0:100

a) Reactions were carried out using 1.5 equiv of TMS-CN at room temperature. b) Five mol% of catalyst was used except for Entries 1—5 and 13. c) Determined by ^1H NMR measurement. d) Two mol% of catalyst was used. e) Twenty-five mol% of catalyst was used.

Table 2. Isomerization from Isolated 2 to 3[a]

Entry	Reagent	Time/h	Ratio of 2:3[b]	Isolated yield of 3/%
1	Ph_3CClO_4 (5 mol%)	18	100: 0	—
2	Ph_3CClO_4 (5 mol%)–TMSOMe (2 equiv)	3	0:100	96
3	$SbCl_5$ (5 mol%)	3	8: 92	87
4	$SbCl_5$ (5 mol%)–TMSOMe (1.5 equiv)	1.5	0:100	83

a) Reactions were carried out in CH_3CN at room temperature. b) Determined by ^1H NMR measurement.

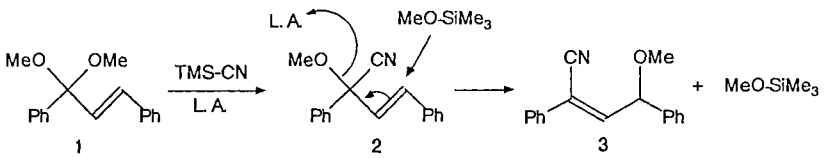

Scheme 2.

^{13}C NMR measurement (gated method).[7] In addition, the steric effect of the C2-phenyl group supports the above conclusion.

After experimentation with various reaction conditions, taking acetal **1** as a model substrate, it was found that **3** was obtained in good yield when the reaction was carried out in CH_3CN with the use of $[Rh(COD)Cl]_2$ or trityl perchlorate (Ph_3CClO_4) as catalyst (see Table 1).

Table 1 shows that, in the initial stage of the present reaction (after 5 h in CH_2Cl_2), cyanation gave only **2**, which in turn was isomerized to **3** when the mixture was kept standing for a long time. After a trial of various solvents, it was shown that CH_3CN is the best solvent, and isomerization from **2** to **3** was achieved within 20 h by using $[Rh(COD)Cl]_2$ as a catalyst. Isomerization proceeded slowly when such transition metal salts as $NiCl_2$, $CoCl_2$, $Pd(acac)_2$, or $Pd(OAc)_2$ was used as the catalyst. Very rapid isomerization took place when Ph_3CClO_4 was used, but the process was slower in the presence of generally known strong Lewis acids such as $BF_3 \cdot Et_2O$ and $AlCl_3$.

Concerning the mechanism of the isomerization, it is reasonable to consider that **3** was produced by the following reaction (Scheme 2). Trimethylsilyl methoxide (TMS-OMe), formed by the reaction of **1** with TMS-CN, would attack the 4-position carbon of **2** in the presence of a catalyst to result in the formation of a conjugated nitrile **3**.

Isomerization of isolated **2** to **3** was tried under various conditions (Table 2) and it was found that the isomerization did not occur in the presence of a catalytic amount of Ph_3CClO_4 alone, but was completed within 3 h in the presence of both 5 mol% of Ph_3CClO_4

Table 3. Reactions of Dimethyl Acetals of Chalcone Derivatives with TMS-CN[a]

Entry	Ar^1	Ar^2	Time/h	Yield/%	Ratio of **5** : **6**[b]
1	Ph	Ph	3	92	0 : 100
2	*p*-Me-C_6H_4	Ph	5	98	0 : 100
3	*p*-MeO-C_6H_4	Ph	8	81	0 : 100
4	*p*-NO_2-C_6H_4	Ph	5	Quant.	82 : 18
5	*p*-NO_2-C_6H_4	Ph	20	91	53 : 47
6	Ph	*p*-NO_2-C_6H_4	5	42	100 : 0
7	Ph	*p*-NO_2-C_6H_4	20	97	81 : 19
8	Ph	1-Naphthyl	20	73	47 : 53
9	Ph	2-Naphthyl	15	67	0 : 100
10	*p*-MeO-C_6H_4	*p*-NO_2-C_6H_4	20	94	0 : 100

a) Reactions were carried out using 1.5 equiv of TMS-CN and 5 mol% of Ph_3CClO_4 in CH_3CN at room temperature. b) Determined by ^1H NMR measurement.

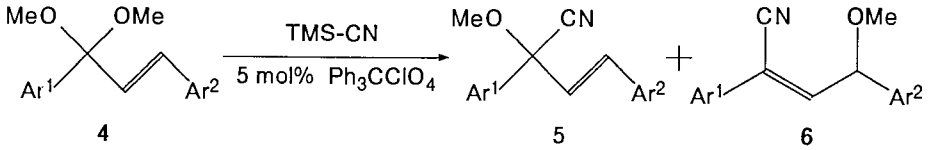

Scheme 3.

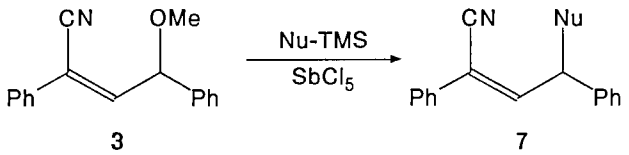

Scheme 4.

Table 4. Reactions of **3** with Various Silylated Nucleophiles[a]

Entry	Nucleophile	Temp/°C	Yield/%
1	$^tBuC(OSiMe_3)=CH_2$	−78	96
2	$PhC(OSiMe_3)=CH_2$	−78	76
3	$CH_2=CHCH_2SiMe_3$	0	64[b]
4	TMS-CN	−23	87

a) Reactions were carried out using 1.5—1.8 equiv of nucleophiles and 1.1 equiv of $SbCl_5$ in CH_2Cl_2 for 1 h. b) Starting material **3** was recovered in 22%.

and 2 equiv of TMS-OMe. This result supported the validity of the above-described mechanism of the isomerization. With the use of $SbCl_5$ catalyst, a stronger Lewis acid, the isomerization took place even in the absence of TMS-OMe.

Similar reactions of various acetals of substituted chalcone derivatives with TMS-CN were tried in the presence of a catalytic amount of Ph_3CClO_4 (Scheme 3, Table 3). It is important to note, in these reactions, that the electronic effect of substituents contained in the aromatic rings of chalcone derivatives influences in the rate of isomerization. On the other hand, compounds having one or both of the phenyl groups in chalcone substituted with non-aromatic groups could be cyanated with TMS-CN to yield α-methoxy carbonitriles, but were not isomerized to γ-methoxy-α,β-unsaturated carbonitriles at all under similar conditions.

Concerning the utility of the isomerized compound **3** in the synthesis, it is thought that substitution by silylated nucleophiles at the allyl ether position[10] is possible in addition to the commonly known reactions of an α,β-unsaturated carbonitrile (Scheme 4). The reactions of **3** with several silylated nucleophiles under promotion by $SbCl_5$ are demonstrated in Table 4.

Reaction of Acetals Derived from α,β-Unsaturated Ketones with Trimethylsilyl Sulfide. In order to extend the scope of the above reaction, trimethylsilyl sulfide was employed as a silylated nucleophile instead of TMS-CN. It is well known that, in the presence of a catalytic amount of ZnI_2, aldehydes or ketones including α,β-unsaturated ketones react with trimethylsilyl sulfide to give the corresponding dithioacetals.[11] However, there have been few reports on the reaction of α,β-unsaturated ketone acetals with trimethylsilyl sulfide; for example, $AlCl_3$ promotes the above reaction to give 3-methoxyallyl sulfides or dithioacetals.[12] Firstly, acetal compound **1** was allowed to react with 2 equiv of phenylthiotrimethylsilane (PhS-TMS) in the presence of a catalytic amount of Ph_3CClO_4 in CH_3CN. It was found that 1,3-diphenyl-1,3-bis(phenylthio)-1-propene (**8**) (a mixture of *E*- and *Z*-isomers, 1 : 4), formed by isomerization of double bond, and 1,3-diphenyl-3-phenylthio-1-propanone (**9**), the Michael adduct, were obtained in 60 and 34% yields, respectively (Scheme 5). The dithioacetal of chalcone was not isolated under the above conditions.

In order to increase the yield of the desired **8**, various reaction conditions (catalyst, solvent, temperature)

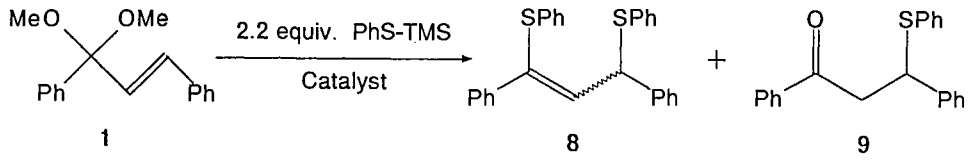

Scheme 5.

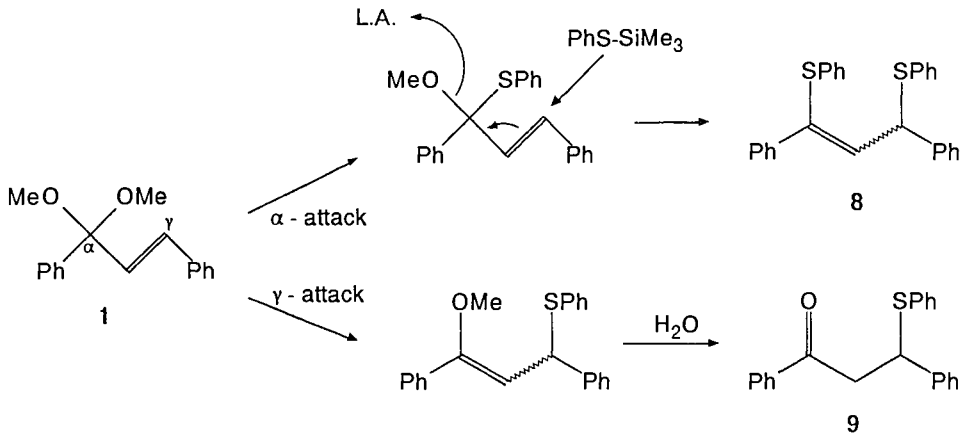

Scheme 6.

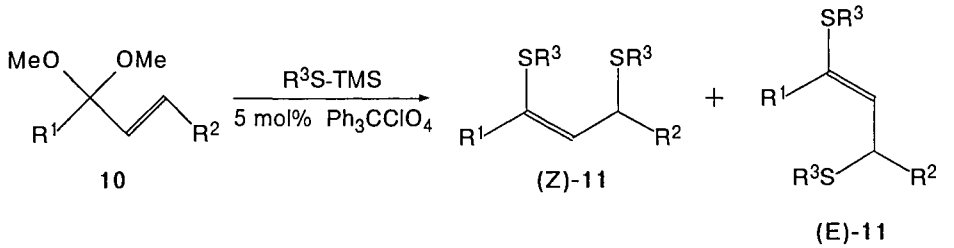

Scheme 7.

Table 5. Examination of Catalyst, Solvent, and Temperature[a)]

Entry	Catalyst	Solvent	Temp/°C	Yield/%	Ratio of **8**:**9**[b)]
1	$SnCl_4$	CH_3CN	R.T.	Quant.	70: 30
2	$SnCl_4$	CH_3CN	60	89	83: 17
3	$TiCl_4$	CH_3CN	R.T.	71	0:100
4	$TiCl_4$	CH_3CN	60	87	0:100
5	$EtAlCl_2$	CH_3CN	R.T.	98	76: 24
6[c)]	Ph_3CClO_4	CH_2Cl_2	−78	99	15: 85
7	Ph_3CClO_4	CH_2Cl_2	R.T.	Quant.	61: 39
8	Ph_3CClO_4	CH_3CN	R.T.	94	64: 36
9	Ph_3CClO_4	CH_3CN	60	Quant.	88: 12
10	Ph_3CClO_4	Toluene	60	84	100: 0
11	Ph_3CClO_4	Benzene	60	98	100: 0

a) Reactions were carried out using 2.2 equiv of PhS-TMS and 5 mol% of catalyst for 3 h except for Entry 6. b) Determined by preparative TLC (silica gel). Ratio of *E*:Z in **8** was 1:9—3:7 (determined by ^1H MMR measurement). c) Reaction time was 8 h.

were examined (Table 5), and the ratio of **8** to **9** was found to be increased by raising the reaction temperature. Eventually **8** was obtained in good yield without the accompanying by-product **9** when the reaction was carried out using 5 mol% of Ph_3CClO_4 in benzene or toluene at 60 °C (Entries 10 and 11). On the other hand, the Michael adduct **9**, was obtained mainly when the reaction was carried out at −78 °C (Entry 6). In this reaction, PhS-TMS could attack either on the α- or the γ-position of acetal **1** (Scheme 6). In the former possibility, 3-methoxy-3-phenylthio-1-propene would be formed and be attacked by one more PhS-

Table 6. Reactions of α,β-Unsaturated Ketone Acetals with Trimethylsilyl Sulfide[a)]

Entry		Substrate		Sulfide	Yield of	Ratio of
		R^1	R^2	R^3	**11**/%	$E:Z$[b)]
1	**10a**	Ph	Ph	Ph	96	12: 88
2	**10a**	Ph	Ph	Et	96	23: 77
3	**10b**	^{t}Bu	Ph	Ph	93	0:100
4	**10b**	^{t}Bu	Ph	Et	77	0:100
5	**10c**	Ph	^{t}Bu	Ph	99	59: 41
6	**10c**	Ph	^{t}Bu	Et	69	4: 96
7	**10d**	Ph	COOMe	Ph	87	25: 75
8	**10d**	Ph	COOMe	Et	77	25: 75
9	**10e**	p-NO_2-C_6H_4	p-MeO-C_6H_4	Et	65	15: 85
10	**10f**	Me	COOMe	Ph	77	38: 62

a) Reactions were carried out using 2.2—2.4 equiv of sulfide and 5 mol% of Ph_3CClO_4 in benzene at 60 °C for 0.5—2 h. b) Determined by ^{1}H NMR measurement.

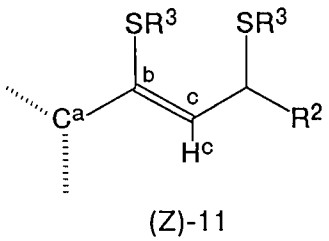

(Z)-11

Fig. 2.

TMS only at the γ-position because of steric hindrance which would result in the formation of isomerized compound **8**. In the latter, the 1-methoxy-3-phenylthio-1-propene formed would not react further, so that the Michael adduct **9**, would be obtained after quenching with water.

Next, similar reactions of various acetals of α,β-unsaturated ketones with PhS-TMS or EtS-TMS were tried in the presence of a catalytic amount of Ph_3CClO_4 in benzene at 60 °C (Scheme 7, Table 6). Isomerized compound **11** was obtained under the above conditions and the ratio between (*E*)-**11** and (*Z*)-**11** was influenced by the structure of **10**. The geometries of the double bond in **11** are considered to be as follows: (1) in Entries 1, 2, and 5—9, the isomer in which an olefinic proton (H^c in Fig. 2) occurs in a lower field on ^{1}H NMR measurement was considered to be a *Z*-isomer; (2) in Entries 3 and 4, only one isomer was obtained and it was thought to be a *Z*-isomer because of the steric hindrance of the ^{t}Bu group; (3) in Entries 9 and 10, the isomer in which a signal of a carbon atom bonded to the double bond (C^a in Fig. 2) occurs in a lower field on ^{13}C NMR measurement suggested the *Z*-configuration.

It is interesting to note that the compounds **10b—d**, and **10f**, which have a *t*-butyl or methoxycarbonyl group instead of a phenyl group in the chalcone (and which could be cyanated with TMS-CN to yield α-methoxy carbonitriles, but were not isomerized to γ-methoxy-α,β-unsaturated carbonitriles at all under conditions similar to those mentioned in the previous section), were also readily converted to the corresponding isomerized products **11**. On the other hand, when these acetals were treated with 1,3-bis(trimethylsilylthio)propane under similar conditions (Scheme 8), it was found that only dithiane **12** was obtained from **10a**, and the mixtures of **12** and 1,5-dithia-2-cyclooctene derivative **13** were obtained from **10b** or **10c** (Table 7).

In relation to the utility of the isomerized compounds **11**, it was considered that allyl sulfides could

Table 7. Reactions of α,β-Unsaturated Ketone Acetals with $Me_3SiS(CH_2)_3SSiMe_3$[a)]

Entry	R^1	R^2	Yield/%	Ratio of **12**:**13**[b)]
1	Ph	Ph	70	100: 0
2	^{t}Bu	Ph	87	56:44
3	Ph	^{t}Bu	72	43:57

a) Reactions were carried out using 1.1 equiv of sulfide and 5 mol% of Ph_3CClO_4 in benzene at 60 °C for 2—3 h. b) Determined by ^{1}H MMR measurement.

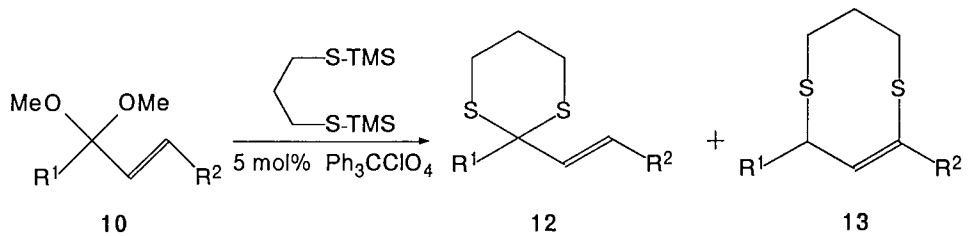

10 12 13

Scheme 8.

Table 8. Reactions of (**Z**)-**11** with Various Silylated Nucleophiles[a)]

Entry	R^1	R^2	Nucleophile	Temp/°C	Yield/%
1	^{t}Bu	Ph	^{t}BuC(OSiMe$_3$)=CH$_2$	0	84
2	^{t}Bu	Ph	PhC(OSiMe$_3$)=CH$_2$	0	72
3	^{t}Bu	Ph	Et$_3$SiH	0	74
4	^{t}Bu	Ph	CH$_2$=CHCH$_2$SiMe$_3$	R.T.	74
5	Ph	Ph	^{t}BuC(OSiMe$_3$)=CH$_2$	0	92
6	Ph	Ph	PhC(OSiMe$_3$)=CH$_2$	0	97
7	Ph	Ph	Et$_3$SiH	0	69
8	Ph	COOMe	PhC(OSiMe$_3$)=CH$_2$	R.T.	54

a) Reactions were carried out using 1.5—1.8 equiv of nucleophile and 1.1 equiv of $SnCl_4$ in CH_2Cl_2 for 0.5—1 h.

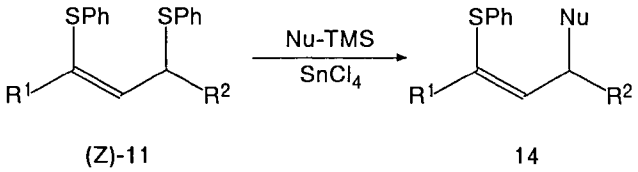

(Z)-11 14

Scheme 9.

be activated toward silylated nucleophiles by means of a Lewis acid. It is already known that dithioacetals reacted with silyl enol ethers in the presence of Ph_3CBF_4[13)] and that the allylic methoxyl group of **3** is replaced by silylated nucleophiles in the presence of $SbCl_5$, as mentioned in the previous section. Substitution at the 3-position of **11** with several silylated nucleophiles (Scheme 9) was therefore tried and it was found that $SnCl_4$, promotes the reaction of **11** with the silylated nucleophiles, as shown in Table 8.

In conclusion, it is noted that in the presence of a catalytic amount of Ph_3CClO_4, TMS-CN reacts with dimethyl acetals derived from chalcone derivatives, with simultaneous double bond isomerization, to yield γ-methoxy-α,β-unsaturated carbonitriles; and trimethylsilyl sulfides react with dimethyl acetals derived from α,β-unsaturated ketones to yield 1,3-bis(alkylthio)propene derivatives under similar conditions.

This type of reaction accompanying isomerization of a double bond opens up new possibilities, especially in the synthesis of olefin derivatives.

Experimental

All melting points were uncorrected. The IR spectra were determined on a Hitachi 270-30 or JASCO IRA-2 spectrometer. The NMR spectra were recorded with a Hitachi R-24B, a JEOL FX90Q, a JEOL GSX-400 or a JEOL GSX-500 spectrometer in $CDCl_3$ with tetramethylsilane as an internal standard. The mass spectra were taken on a JEOL JMS-HX110 or a JEOL JMS-D300. Dichloromethane and acetonitrile were distilled from P_2O_5, and then distilled from CaH_2 and stored over Molecular Sieves. Benzene and toluene were dried over $CaCl_2$, then distilled from P_2O_5 and stored over Molecular Sieves. Purification of products was performed by column chromatography on silica gel (Merck, Art. 7734 Kieselgel 60) or preparative TLC on silica gel (Wakogel B-5F).

Dimethyl acetals were prepared by transacetalization of the corresponding ketones with trimethyl orthoformate in the presence of *p*-TsOH·H_2O, and purified by distillation or recrystallization. Trimethylsilyl cyanide, allyltrimethylsilane, and triethylsilane were purified by distillation. Trimethylsilyl sulfides were prepared by silylation of the corresponding lithium salts of mercaptans. Silyl enol ethers were prepared by silylation of the corresponding enolates of ketones, and purified by distillation.

Preparation of γ-Methoxy-α,β-unsaturated Carbonitriles (6) (Table 3). A typical reaction procedure is described for (*E*)-chalcone dimethyl acetal (**1**) with TMS-CN by the use of Ph_3CClO_4, as a catalyst (Entry 1): In an argon atmosphere, Ph_3CClO_4 (3.4 mg, 0.01 mmol) and TMS-CN (34.7 mg, 0.350 mmol) were stirred in acetonitrile (3 ml) at room temperature for 15 min, and to the mixture was added (*E*)-chalcone dimethyl acetal (52.9 mg, 0.208 mmol) in acetonitrile (1 ml). The reaction mixture was stirred for 3 h at room temperature, then quenched with pH 7 phosphate buffer. The organic materials were extracted with ethyl acetate and the combined extract was dried over Na_2SO_4. After evaporation of the solvent, the residue was purified by preparative TLC (silica gel, hexane : AcOEt=5 : 1) to afford (*Z*)-4-methoxy-2,4-diphenyl-2-butenenitrile (**3**) (47.9 mg, 0.192 mmol, 92%). IR (neat) 2220, 1495, 1450, 1085, 755, 690 cm^{-1}; ^{1}H NMR δ=3.43 (3H, s), 5.34 (1H, d, *J*=9.2 Hz), 6.84 (1H, d, *J*=9.2 Hz), 7.3—7.6 (10H, m); ^{13}C NMR δ=56.8 (q), 82.2 (d), 116.2 (s), 116.5 (s), 126.0 (d), 126.6 (d), 128.6 (d), 129.0 (d and d, 2C), 129.7 (d), 132.3 (s), 139.1 (s), 144.9 (d); MS *m/z* 249 (M$^+$), 217, 140, 121, 105. Found: *m/z* 249.1124. Calcd for $C_{17}H_{15}NO$: M, 249.1154.

In Entries 4 and 5, the isomerization from **5** to **6** was not achieved completely, and pure **6** was obtained by preparative TLC. Other analytical data of **6** follow.

(Z)-4-Methoxy-2-(4-methylphenyl)-4-phenyl-2-butenenitrile (Entry 2). IR (neat) 2220, 1450, 1085, 750 cm^{-1}; ^{1}H NMR δ=2.35 (3H, s), 3.43 (3H, s), 5.33 (1H, d, *J*=9.2 Hz), 6.79 (1H, d, *J*=9.2 Hz), 7.18 (2H, d, *J*=8.3 Hz), 7.3—7.5 (7H, m); ^{13}C NMR δ=21.2 (q), 56.8 (q), 82.1 (d), 116.3 (s), 116.4 (s), 125.8 (d), 126.5 (d), 128.5 (d), 128.9 (d), 129.3 (s), 129.7 (d), 139.2 (s), 139.9 (s), 143.7 (d); MS, *m/z* 263 (M$^+$), 248, 231, 216. Found: *m/z* 263.1304. Calcd for $C_{18}H_{17}NO$: M, 263.1310.

(Z)-4-Methoxy-2-(4-methoxyphenyl)-4-phenyl-2-butenenitrile (Entry 3). IR (neat) 2210, 1605, 1515, 1255, 1180, 1085 cm^{-1}; ^{1}H NMR δ=3.43 (3H, s), 3.81 (3H, s), 5.32 (1H, d, *J*=9.2 Hz), 6.70 (1H, d, *J*=9.2 Hz), 6.89 (2H, d, *J*=8.2 Hz), 7.3—7.5 (7H,

m); ^{13}C NMR δ=55.4 (q), 56.7 (q), 82.2 (d), 114.4 (d), 116.1 (s), 116.4 (s), 124.8 (s), 126.5 (d), 127.4 (d), 128.5 (d), 128.9 (d), 139.4 (s), 142.5 (d), 160.7 (s); MS m/z 279 (M^+), 264, 248, 176. Found: m/z 279.1263. Calcd for $C_{18}H_{17}NO_2$: M, 279.1259.

(*Z*)-4-Methoxy-2-(4-nitrophenyl)-4-phenyl-2-butenenitrile (Entry 4). Mp 110—112 °C; IR (KBr) 2220, 1600, 1515, 1340, 1120, 1095, 855, 750 cm^{-1}; ^{1}H NMR δ=3.43 (3H, s),5.35 (1H, d, J=9.2 Hz), 7.03 (1H, d, J=9.2 Hz), 7.35—7.5 (5H, m), 7.72 (2H, d, J=9.2 Hz), 8.25 (2H, d, J=9.2 Hz); ^{13}C NMR δ=56.9 (q), 82.2 (d), 114.3 (s), 115.3 (s), 124.3 (d), 126.7 (d), 126.9 (d), 129.0 (d), 129.2 (d), 138.3 (s), 148.3 (s), 148.9 (d); MS m/z 294 (M^+), 279, 263, 217. Found: C, 69.25; H, 4.76; N, 9.56%. Calcd for $C_{17}H_{14}N_2O_3$: C, 69.38; H, 4.79; N, 9.52%.

(*Z*)-4-Methoxy-4-(4-nitrophenyl)-2-phenyl-2-butenenitrile (Entry 5). IR (neat) 2200, 1605, 1595, 1525, 1350, 1080 cm^{-1}; ^{1}H NMR δ=3.49 (3H, s), 5.46 (1H, d, J=9.2 Hz), 6.74 (1H, d, J=9.2 Hz), 7.41 (3H, m), 7.56 (2H, m), 7.66 (2H, d, J=9.2 Hz), 8.26 (2H, d, J=8.2 Hz); ^{13}C NMR δ=57.2 (q), 81.1 (d), 116.0 (s), 118.1 (s), 124.2 (d), 126.1 (d), 127.3 (d), 129.2 (d), 130.2 (d), 131.7 (s), 143.1 (d), 146.2 (s), 148.0 (s); MS m/z 294 (M^+), 277, 262, 247, 217. Found: m/z 294.1001. Calcd for $C_{17}H_{14}N_2O_3$: M, 294.1004.

(*Z*)-4-Methoxy-4-(1-naphthyl)-2-phenyl-2-butenenitrile (Entry 6). IR (neat) 2210, 1600, 1510, 1450, 1085, 780, 760 cm^{-1}; ^{1}H NMR δ=3.50 (3H, s), 5.93 (1H, d, J=9.2 Hz), 7.06 (1H, d, J=9.2 Hz), 7.35 (3H, m), 7.5—7.6 (5H, m), 7.73 (1H, d, J=7.3 Hz), 7.85 (1H, d, J=8.3 Hz), 7.89 (1H, d, J=8.3 Hz), 8.36 (1H, d, J=8.3 Hz); ^{13}C NMR δ=56.9 (q), 80.6 (d), 116.2 (s), 117.2 (s), 123.6 (d), 125.5 (d), 125.6 (d), 126.0 (d), 126.1 (d), 126.8 (d), 129.0 (d and d, 2C), 129.3 (d), 129.7 (d), 130.8 (s), 132.3 (s), 134.1 (s), 134.7 (s), 144.2 (d); MS m/z 299 (M^+), 284, 267, 241, 155. Found: m/z 299.1280. Calcd for $C_{21}H_{17}NO$: M, 299.1310.

(*Z*)-4-Methoxy-4-(2-naphthyl)-2-phenyl-2-butenenitrile (Entry 7). IR (neat) 2210, 1600, 1450, 1080, 750 cm^{-1}; ^{1}H NMR δ=3.48 (3H, s), 5.51 (1H, d, J=9.2 Hz), 6.92 (1H, d, J=9.2 Hz), 7.3—7.6 (8H, m) , 7.8—7.9 (3H, m), 7.95 (1H, s); ^{13}C NMR δ=56.9 (q), 82.3 (d), 116.3 (s), 116.6 (s), 124.0 (d), 125.9 (d), 126.0 (d), 126.4 (d), 126.5 (d), 127.8 (d), 128.1 (d), 129.0 (d and d, 2C), 129.7 (d), 132.3 (s), 133.4 (s), 136.4 (s), 144.7 (d); MS m/z 299 (M^+), 284, 268, 241, 155. Found: m/z 299.1306. Calcd for $C_{21}H_{17}NO$: M, 299.1310.

(*Z*)-4-Methoxy-2-(4-methoxyphenyl)-4-(4-nitrophenyl)-2-butenenitrile (Entry 8). IR (neat) 2200, 1605, 1515, 1350, 1250, 1180, 825 cm^{-1}; ^{1}H NMR δ=3.48 (3H, s), 3.83 (3H, s), 5.43 (1H, d, J=9.2 Hz), 6.59 (1H, d, J=9.2 Hz), 6.92 (2H, d, J=9.2 Hz), 7.50 (2H, d, J=8.3 Hz), 7.65 (2H, d, J=9.2 Hz), 8.25 (2H, d, J=8.3 Hz); ^{13}C NMR δ=55.5 (q), 57.1 (q), 81.2 (d), 114.5 (d), 116.1 (5), 117.7 (s), 124.2 (d), 127.2 (d), 127.5 (d), 140.5 (d), 146.5 (s), 147.9 (s), 161.1 (s); MS m/z 324 (M^+), 307, 293, 150. Found: m/z 324.1112. Calcd for $C_{18}H_{16}N_2O_4$: M, 324.1110.

The α-methoxy carbonitrile **5** corresponding to **6** was obtained by the reaction of the corresponding acetal **4** and TMS-CN (1.5 equiv) in the presence of 2 mol% of $CoCl_2$ in CH_2Cl_2.[5a] ^{1}H and ^{13}C NMR data of **5** follow.

(*E*)-2-Methoxy-2,4-diphenyl-3-butenenitrile (Entry 1). ^{1}H NMR δ=3.47 (3H, s), 6.18 (1H, d, J=15.6 Hz), 7.01 (1H, d, J=15.6 Hz), 7.3—7.5 (8H, m), 7.59 (2H, m); ^{13}C NMR δ=53.9 (q), 81.2 (s), 117.2 (s), 126.1 (d), 127.1 (d and d, 2C), 128.8 (d), 128.9 (d), 129.0 (d), 129.3 (d), 133.5 (d), 135.0 (s), 137.4 (s).

(*E*)-2-Methoxy-2-(4-methylphenyl)-4-phenyl-3-butenenitrile (Entry 2). ^{1}H NMR δ=2.37 (3H, s), 3.45 (3H, s), 6.18 (1H, d, J=15.6 Hz), 6.98 (1H, d, J=15.6 Hz), 7.23 (2H, d, J=7.3 Hz), 7.3 (3H, m), 7.41 (2H, d, J=7.3 Hz), 7.46 (2H, d, J=8.3 Hz); ^{13}C NMR δ=21.1 (q), 53.8 (q), 81.1 (s), 117.3 (s), 126.0 (d), 127.1 (d), 127.2 (d), 128.7 (d), 128.8 (d), 129.6 (d), 133.3 (d), 134.4 (s), 135.0 (s), 139.3 (s).

(*E*)-2-Methoxy-2-(4-methoxyphenyl)-4-phenyl-3-butenenitrile (Entry 3). ^{1}H NMR δ=3.44 (3H, s), 3.83 (3H, s), 6.18 (1H, d, J=15.6 Hz), 6.94 (2H, d, J=9.2 Hz), 6.97 (1H, d, J=16 Hz), 7.28—7.36 (3H, m), 7.41 (2H, m), 7.50 (2H, d, J=9.2 Hz); ^{13}C NMR δ=53.8 (q), 55.4 (q), 80.7 (s), 114.3 (d), 117.3 (s), 127.1 (d), 127.2 (d), 127.5 (d), 128.8 (d and d, 2C), 129.3 (s), 133.3 (d), 135.0 (s), 160.3 (s).

(*E*)-2-Methoxy-2-(4-nitrophenyl)-4-phenyl-3-butenenitrile (Entry 4). ^{1}H NMR δ=3.54 (3H, s), 6.07 (1H, d, J=15.6 Hz), 7.11 (1H, d, J=15.6 Hz), 7.3—7.45 (5H, m), 7.79 (2H, d, J=8.3 Hz), 8.29 (2H, d, J=8.3 Hz); ^{13}C NMR δ=54.2 (q), 80.6 (s), 116.3 (s), 124.2 (d), 125.4 (d), 127.1 (d), 127.2 (d), 128.9 (d), 129.4 (d), 134.3 (s), 135.2 (d), 144.5 (s), 148.4 (s).

(*E*)-2-Methoxy-4-(4-nitrophenyl)-2-phenyl-3-butenenitrile (Entry 5). ^{1}H NMR δ=3.47 (3H, s), 6.36 (1H, d, J=16.5 Hz), 7.05 (1H, d, J=15.6 Hz), 7.4—7.6 (7H, m), 8.20 (2H, d, J=9.2 Hz); ^{13}C NMR δ=54.1 (q), 81.0 (s), 116.7 (s), 124.1 (d), 126.1 (d), 127.8 (d), 129.2 (d), 129.7 (d), 130.7 (d), 131.7 (d), 136.3 (s), 141.3 (s), 147.7 (s).

(*E*)-2-Methoxy-4-(1-naphthyl)-2-phenyl-3-butenenitrile (Entry 6). ^{1}H NMR δ=3.54 (3H, s), 6.24 (1H, d, J=15.6 Hz), 7.4—7.9 (12H, m), 8.10 (1H, d, J=8.3 Hz); ^{13}C NMR δ=54.0 (q), 81.3 (s), 117.3 (s), 123.5 (d), 124.4 (d), 125.5 (d), 126.1 (d and d, 2C), 126.6 (d), 128.6 (d), 129.0 (d), 129.1 (d), 129.4 (d), 130.1 (d), 130.9 (d), 131.2 (s), 132.7 (s), 133.6 (s), 137.3 (s).

(*E*)-2-Methoxy-4-(2-naphthyl)-2-phenyl-3-butenenitrile (Entry 7). ^{1}H NMR δ=3.50 (3H, s), 6.30 (1H, d, J=16.5 Hz), 7.16 (1H, d, J=15.6 Hz), 7.4—7.5 (5H, m), 7.56 (1H, m), 7.62 (2H, m), 7.80 (4H, m); ^{13}C NMR δ=54.0 (q), 81.3 (s), 117.2 (s), 123.4 (d), 126.1 (d), 127.3 (d), 127.7 (d), 127.9 (d), 128.2 (d), 128.5 (d), 129.0 (d), 129.3 (d), 132.4 (s), 133.4 (s), 133.5 (s), 133.6 (d), 137.4 (s).

(*E*)-2-Methoxy-2-(4-methoxyphenyl)-4-(4-nitrophenyl)-3-butenenitrile (Entry 8). ^{1}H NMR δ=3.43 (3H, s), 3.84 (3H, s), 6.37 (1H, d, J=16.5 Hz), 6.97 (2H, d, J=9.2 Hz), 7.02 (1H, d, J=16.5 Hz), 7.49 (2H, d, J=9.2 Hz), 7.55 (2H, d, J=9.2 Hz), 8.19 (2H, d, J=9.2 Hz); ^{13}C NMR δ=54.0 (q), 55.4 (q), 80.5 (s), 114.5 (d), 116.8 (s), 124.1 (d), 127.6 (d), 127.7 (d), 128.1 (s), 130.4 (d), 131.9 (d), 141.4 (s), 147.7 (s), 160.6 (s).

Isomerization from Isolated 2 to 3. The following is a description of a typical procedure for isomerization in the presence of Ph_3CClO_4 and TMS-OMe (Entry 2): In an argon atmosphere, Ph_3CClO_4 (3.2 mg, 0.009 mmol) and TMS-OMe (42.7 mg, 0.410 mmol) were stirred in CH_3CN (2 ml) for 10 min at room temperature, and then (*E*)-2-methoxy-2,4-diphenyl-3-butenenitrile (**2**) (47.8 mg, 0.192 mmol) in CH_3CN (1 ml) was added. The reaction mixture was stirred for 3 h at room temperature and quenched with an aqueous solution of $NaHCO_3$. The organic materials were extracted with ethyl acetate and the combined extract was dried over Na_2SO_4. After evaporation of the solvent, the residue was purified by preparative TLC (silica gel, hexane : AcOEt=7 : 1) to afford (*Z*)-4-methoxy-2,4-diphenyl-2-butenenitrile (**3**) (46.1 mg, 0.185 mmol, 96%).

Reaction of 3 with Silylated Nucleophiles (Table 4). A typical procedure for the reaction of **3** with trimethylsilyl enol ether of *t*-butyl methyl ketone (Entry 1) follows: In an argon atmosphere, (*Z*)-4-methoxy-2,4-diphenyl-2-butenenitrile

(**3**) (49.1 mg, 0.197 mmol) and the trimethylsilyl enol ether of *t*-butyl methyl ketone (57.0 mg, 0.331 mmol) were dissolved in CH_2Cl_2 (2 ml). The solution was cooled to −78 °C, and 0.5 M $SbCl_5$ solution (1 M=1 mol dm^{-3}) in CH_2Cl_2 (0.44 ml, 0.22 mmol) was added. The reaction mixture was stirred for 1 h at −78 °C and quenched with an aqueous solution of $NaHCO_3$. The organic materials were extracted with CH_2Cl_2 and the combined extract was dried over Na_2SO_4. After evaporation of the solvent, the residue was purified by preparative TLC (silica gel, hexane : AcOEt=5 : 1) to afford (*Z*)-7,7-dimethyl-6-oxo-2,4-diphenyl-2-octenenitrile (59.9 mg, 0.189 mmol, 96%); mp 101—103 °C; IR (KBr) 2220, 1700, 1475, 1455, 1070, 760, 695 cm^{-1}; ^{1}H NMR δ=1.03 (9H, s), 2.98 (2H, m), 4.4 (1H, m), 6.82 (1H, d, *J*=10 Hz), 7.2 (10H, m). Found: C, 83.03; H, 7.51; N, 4.37%. Calcd for $C_{22}H_{23}NO$: C, 83.24; H, 7.30; N, 4.41%.

Other analytical data are presented below.

(*Z*)-6-Oxo-2,4,6-triphenyl-2-hexenenitrile (Entry 2). Mp 117—118 °C; IR (KBr) 2220, 1750, 1450, 1210, 750, 690 cm^{-1}; ^{1}H NMR δ=3.52 (2H, d, *J*=7 Hz), 4.70 (1H, dt, *J*=10 Hz, 7 Hz), 6.80 (1H, d, *J*=10 Hz), 7.1—7.4 (8H, m), 7.77 (2H, m) Found: C, 85.20; H, 5.93; N, 4.10%. Calcd for $C_{24}H_{19}NO$: C, 85.43; H, 5.68; N, 4.15%.

(*Z*)-2,4-Diphenyl-2,6-heptadienenitrile (Entry 3). IR (neat) 2210, 1640, 1600, 1495, 1450, 915, 755, 695 cm^{-1}; ^{1}H NMR δ=2.55 (2H, t, *J*=7 Hz), 3.99 (1H, dt, *J*=10 Hz, 7 Hz), 4.8—5.1 (2H, m), 5.5 (1H, m), 6.58 (1H, d, *J*=10 Hz), 7.1 (10H, m); MS *m*/*z* 259 (M$^+$), 218, 191. Found: *m*/*z* 259.1335. Calcd for $C_{19}H_{17}N$: M, 259.1361.

(*Z*)-2,4-Diphenyl-2-pentene-1,5-dinitrile (Entry 4). IR (neat) 2230, 2210, 1600, 1495, 1450, 755, 690 cm^{-1}; ^{1}H NMR δ=5.00 (1H, d, *J*=10 Hz), 6.55 (1H, d, *J*=10 Hz), 7.2 (10H, m).

Reaction of α,β-Unsaturated Ketone Acetals with Trimethylsilyl Sulfides (Table 6). A typical procedure for the reaction of (*E*)-chalcone dimethyl acetal **1** with PhS-TMS (Entry 1) was as follows.

In an argon atmosphere, Ph_3CClO_4 (5.4 mg, 0.016 mmol) was suspended in benzene (1 ml), to which was added PhS-TMS (135.0 mg, 0.740 mmol) in benzene (1 ml). The reaction mixture was heated to 60 °C and stirred for 30 min, and (*E*)-chalcone dimethyl acetal (79.7 mg, 0.314 mmol) in benzene (1 ml) was then added over a 5 min period. The reaction mixture was stirred for 3 h at 60 °C and quenched with aqueous $NaHCO_3$ solution. The organic materials were extracted with ethyl acetate and the combined extract was dried over Na_2SO_4. After evaporation of the solvent, the residue was purified by preparative TLC (silica gel, hexane : ether=93 : 7) to afford 1,3-diphenyl-1,3-bis (phenylthio)propene (123.8 mg, 0.302 mmol, 96%) as a mixture of *E*- and *Z*-isomer (*E* : *Z*=12 : 88). Pure *Z*-isomer was obtained by recrystallization from ethanol (90.1 mg).

***Z*-Isomer:** Mp 103—105 °C; IR (KBr) 1580, 1480, 1440, 750, 735, 695 cm^{-1}; ^{1}H NMR δ=5.85 (1H, d, *J*=10.1 Hz), 6.59 (1H, d, *J*=10.1 Hz), 6.8—7.55 (20H, m); ^{13}C NMR δ=53.3 (d), 125.8 (d), 127.6 (d), 127.8 (d), 127.9 (d), 128.0 (d), 128.1 (d), 128.5 (d), 128.8 (d), 128.9 (d), 129.2 (d), 133.7 (d), 134.2 (s), 134.5 (s), 135.8 (s), 137.2 (d), 139.2 (s), 139.8 (s); MS *m*/*z* 410 (M$^+$), 301. Found: C, 79.28; H, 5.23; S, 15.63%. Calcd for $C_{27}H_{22}S_2$: C, 78.98; H, 5.40; S, 15.62%.

***E*-Isomer:** ^{1}H NMR δ=4.90 (1H, d, *J*=11.0 Hz), 6.13 (1H, d, *J*=11.0 Hz), 7.00 (2H, m), 7.15—7.35 (18H, m); ^{13}C NMR δ=52.7 (d), 127.4 (d), 127.5 (d), 127.7 (d), 127.9 (d), 128.7 (d), 128.9 (d), 129.3 (d), 130.3 (d), 132.4 (d), 133.3 (s), 134.0 (d), 136.8 (s), 137.8 (s), 139.9 (s).

Other analytical data are shown below.

1,3-Bis(ethylthio)-1,3-diphenylpropene. (*E* : *Z*=23 : 77, mixture) (Entry 2). IR (neat) 1600, 1495, 1450, 1255, 820 cm^{-1}; ^{1}H NMR δ=1.02 and 1.06 (3H, 23 : 77, t, *J*=7.3 Hz), 1.18 and 1.31 (3H, 23 : 77, t, *J*=7.3 Hz), 2.33 and 2.40 (2H, 23 : 77, q, *J*=7.3 Hz), 2.5 (2H,m), 4.57 (0.23×1H, d, *J*=10.8 Hz), 5.47 (0.77×1H, d, *J*=9.8 Hz), 6.03 (0.23×1H, d, *J*=10.7 Hz), 6.23 (0.77×1H, d, *J*=9.8 Hz), 7.2—7.55 (10H, m); ^{13}C NMR δ=14.1 (q, *E*), 14.5 (q, *E*), 15.0 (q, *Z*), 15.1 (q, *Z*), 25.4 (t, *E*), 25.5 (t, *Z*), 26.0 (t, *E*), 26.4 (t, *Z*), 47.8 (d, *E*), 48.3 (d, *Z*), 127.2 (d, *Z*), 127.8 (d, *Z*), 128.0 (d, *Z*), 128.3 (d, *Z*), 128.7 (d, *Z*), 129.3 (d, *Z*), 135.0 (d, *Z*), 137.3 (s, *Z*), 139.4 (s, *Z*), 140.9 (s, *Z*), 141.0 (s, *E*); MS *m*/*z* 314 (M$^+$), 286, 270, 253. Found: *m*/*z* 253.1022. Calcd for $C_{17}H_{17}S$: M−SEt, 253.1051.

(*Z*)-4,4-Dimethyl-1-phenyl-1,3-bis(phenylthio)-2-pentene (Entry 3). Mp 105—108 °C; IR (KBr) 1580, 1480, 1440, 740, 690 cm^{-1}; ^{1}H NMR δ=1.04 (9H, s), 5.46 (1H, d, *J*=10.1 Hz), 6.47 (1H, d, *J*=10.1 Hz), 6.8—7.5 (15H, m); ^{13}C NMR δ=29.4 (q), 39.6 (s), 53.3 (d), 124.8 (d), 126.7 (d), 127.3 (d), 127.7 (d), 128.0 (d), 128.4 (d), 128.6 (d and d, 2C), 133.9 (s), 134.1 (d), 135.8 (d), 137.9 (s), 139.5 (s), 143.6 (s); MS *m*/*z* 390 (M$^+$), 281. Found: C, 77.00; H, 6.57; S, 16.11%. Calcd for $C_{25}H_{26}S_2$: C, 76.87; H, 6.71; S, 16.42%.

(*Z*)-1,3-Bis(ethylthio)-4,4-dimethyl-1-phenyl-2-pentene (Entry 4). IR (neat) 1600, 1455, 1265, 690 cm^{-1}; ^{1}H NMR δ=1.18 (3H, t, *J*=7.3 Hz), 1.19 (9H, s), 1.26 (3H, t, *J*=7.3 Hz), 2.35—2.65 (4H,m), 5.41 (1H, d, *J*=10.2 Hz), 6.20 (1H, d, *J*=10.2 Hz), 7.2—7.45 (5H, m); ^{13}C NMR δ=14.8 (q), 15.1 (q), 25.5 (t), 29.5 (q), 31.9 (t), 39.6 (s), 48.7 (d), 127.1 (d), 127.8 (d), 128.6 (d), 133.3 (d), 141.0 (s), 147.3 (s); MS *m*/*z* 294 (M$^+$), 278, 233,210. Found: *m*/*z* 294.1482. Calcd for $C_{17}H_{26}S_2$: M, 294.1476.

4,4-Dimethyl-1-phenyl-1,3-bis(phenylthio)-1-pentene (*E* : *Z*= 59 : 41, mixture) (Entry 5). IR (neat) 1580, 1480, 1440, 1370, 1025, 740, 690 cm^{-1}; ^{1}H NMR δ=1.03 and 1.17 (9H, 59 : 41, s), 3.45 (0.59×1H, d, *J*=11.0 Hz), 4.51 (0.41×1H, d, *J*=11.0 Hz), 6.02 (0.59×1H, d, *J*=11.0 Hz), 6.29 (0.41×1H, d, *J*=10.1 Hz), 6.5—7.55 (15H, m); ^{13}C NMR δ=28.0 (q, *E*), 28.1 (q, *Z*), 35.5 (s, *E*), 36.0 (s, *Z*), 61.2 (d, *Z*), 61.4 (d, *E*), 125.6 (d), 126.7 (d), 127.2 (d), 127.5 (d), 127.7 (d), 127.9 (d), 128.0 (d), 128.3 (d), 128.7 (d), 128.8 (d), 128.9 (d), 129.2 (d), 129.3 (d), 130.0 (d) , 131.9 (d) , 132.1 (d), 133.7 (d and s, 2C), 134.2 (d), 134.5 (s), 134.6 (s), 134.8 (s), 135.6 (s), 135.7 (d), 135.9 (s), 136.7 (d), 137.0 (s), 139.5 (s); MS *m*/*z* 390 (M$^+$), 333, 281. Found: *m*/*z* 281.1361. Calcd for $C_{19}H_{21}S$: M−SPh, 281.1364.

1,3-Bis(ethylthio)-4,4-dimethyl-1-phenyl-1-pentene (*E* : *Z*= 4 : 96, mixture) (Entry 6). IR (neat) 1450, 1370, 1260, 700 cm^{-1}; ^{1}H NMR δ=1.05 (12H, s and t, *J*=7 Hz), 1.30 (3H, t, *J*=7 Hz), 2.37 (2H, q, *J*=7 Hz), 2.53 (2H, m), 3.22 (0.04×1H, d, *J*=11.2 Hz), 4.05 (0.96×1H, d, *J*=10.8 Hz), 5.87 (0.04×1H, d, *J*=11.2 Hz), 5.97 (0.96×1H, d, *J*=10.7 Hz), 7.2—7.4 (3H, m), 7.53 (2H, m); ^{13}C NMR (*Z*-isomer) δ=15.1 (q), 15.4 (q), 24.9 (t), 26.3 (t), 28.0 (q), 35.3 (s), 55.7 (d), 127.7 (d), 128.0 (d), 128.3 (d), 134.8 (d), 136.9 (s), 139.9 (s); MS *m*/*z* 294 (M$^+$), 237, 233. Found: *m*/*z* 294.1483. Calcd for $C_{17}H_{26}S_2$: M, 294.1476.

Methyl 4-Phenyl-2,4-bis(phenylthio)-3-butenoate (*E* : *Z*= 25 : 75, mixture) (Entry 7). Pure *Z*-isomer was obtained by recrystallization from ethanol.

***Z*-Isomer:** Mp 74—75 °C; IR (KBr) 1735, 1440, 1325, 1290, 1150, 750, 690 cm^{-1}; ^{1}H NMR δ=3.72 (3H, s), 5.35 (1H, d, *J*=9.8 Hz), 6.39 (1H, d, *J*=9.8 Hz), 6.9—7.1 (5H, m), 7.2 (3H, m), 7.3 (3H, m), 7.4 (2H, m), 7.6 (2H, m); ^{13}C NMR

δ=51.4 (d), 52.7 (q), 126.2 (d), 128.0 (d), 128.2 (d), 128.4 (d), 128.6 (d), 128.7 (d), 129.1 (d), 129.6 (d), 130.5 (d), 132.0 (s), 134.1 (s), 134.6 (d), 138.7 (s), 139.2 (s), 170.3 (s); MS *m/z* 294 (M^+), 237, 233. Found: C, 70.14; H, 5.19; S, 16.23%. Calcd for $C_{23}H_{20}O_2S_2$: C, 70.38; H, 5.14; S, 16.34%.

***E*-Isomer:** ^{1}H NMR δ=3.66 (3H, s), 4.40 (1H, d, *J*=10.7 Hz), 5.75 (1H, d, *J*=10.7 Hz), 6.9—7.6 (15H, m); ^{13}C NMR δ=50.8 (d), 52.5 (q), 122.2 (d), 127.5 (d), 128.0 (d), 128.4 (d), 128.5 (d), 128.9 (d), 129.2 (d), 131.7 (s), 132.3 (s), 133.1 (d), 136.2 (s), 141.9 (s), 170.2 (s).

Methyl 2,4-Bis(ethylthio)-4-phenyl-3-butenoate (*E*:*Z*=25:75, mixture) (Entry 8). IR (neat) 1735, 1450, 1265, 1155, 760, 700 cm^{-1}; ^{1}H NMR δ=1.06 and 1 08 (3H, 75:25, t, *J*=7 Hz), 1.23 and 1.32 (3H, 25:75, t, *J*=7.3 Hz), 2.41 (0.75×2H, q, *J*=7.3 Hz), 2.50 (0.25×2H, m), 2.60 and 2.71 (2H, 25:75, m), 3.74 and 3.77 (3H, 25:75, s), 4.09 (0.25×1H, d, *J*=10.1 Hz), 4.94 (0.75×1H, d, *J*=10.1 Hz), 5.79 (0.25×1H, d, *J*=11.0 Hz), 6.17 (0.75×1H, d, *J*=9.2 Hz), 7.3—7.55 (5H, m); ^{13}C NMR δ=13.8 (q, *E*), 14.4 (q, *E*), 14.7 (q, *Z*), 15.1 (q, *Z*), 25.2 (t, *E*), 25.5 (t, *Z*), 26.1 (t, *E*), 26.5 (t, *Z*), 45.9 (q, *E*), 46.3 (q, *Z*), 52.5 (d, *E*), 52.6 (d, *Z*), 128.1 (d, *Z*), 128.3 (d, *Z*), 128.4 (d and d, 2C, *Z*), 129.2 (d, *E*), 136.8 (s, *E*), 139.0 (s, *Z*), 140.5 (s, *Z*), 141.0 (s, *E*), 171.0 (s, *E*), 171.3 (s, *Z*); MS *m/z* 296 (M^+), 264, 235, 175. Found: *m/z* 296.0911. Calcd for $C_{15}H_{20}O_2S_2$: M, 296.0905.

1,3-Bis(ethylthio)-3-(4-methoxyphenyl)-1-(4-nitrophenyl)-propene (*E*:*Z*=15:85, mixture) (Entry 9). IR (neat) 1595, 1515, 1455, 1345, 1245, 1175, 1110, 1030, 850, 750 cm^{-1}; ^{1}H NMR δ=1.04 and 1.09 (3H, 15:85, t, *J*=7.3 Hz), 1.20 and 1.31 (3H, 15:85, t, *J*=7.3 Hz), 2.29 and 2.41 (2H, 15:85, q, *J*=7 Hz), 2.54 (2H, m), 3.79 (3H, s), 4.42 (0.15×1H, d, *J*=10.7 Hz), 5.43 (0.85×1H, d, *J*=10.3 Hz), 6.16 (0.15×1H, d, *J*=10.8 Hz), 6.37 (0.85×1H, d, *J*=9.8 Hz), 6.88 (2H, d, *J*=8 Hz), 7.23 and 7.35 (2H, 15:85, d, *J*=8 Hz), 7.56 and 7.70 (2H, 15:85, d, *J*=8 Hz), 8.20 and 8.24 (2H, 85:15, d, *J*=8 Hz); ^{13}C NMR (*Z*-isomer) δ=15.0 (q), 15.1 (q), 25.6 (t), 26.7 (t), 47.8 (d), 55.3 (q), 114.2 (d), 123.8 (d), 128.7 (d), 128.9 (d), 132.2 (s), 134.7 (s), 139.0 (d), 146.2 (s), 147.3 (s), 158.9 (s); (*E*-isomer) δ=14.1 (q), 14.5 (q), 25.4 (t), 26.2 (t), 47.3 (d), 55.3 (q), 114.3 (d), 123.6 (d), 128.6 (d), 128.9 (d), 132.2 (s), 134.5 (s), 139.0 (d), 144.4 (s), 147.5 (s), 158.9 (s); MS *m/z* 389 (M^+), 328. Found: *m/z* 328.1015. Calcd for $C_{18}H_{18}NO_3S$: M−SEt, 328.1008.

Methyl 2,4-Bis(phenylthio)-3-pentenoate (*E*:*Z*=38:62, mixture) (Entry 10). IR (neat) 1735, 1477, 1440, 1155, 745, 690 cm^{-1}; ^{1}H NMR δ=1.74 and 1.89 (3H, 38:62, s), 3.67 and 3.69 (3H, 38;62, s), 4.54 (0.38×1H, d, *J*=9.8 Hz), 5.13 (0.62×1H, d, *J*=9.8 Hz), 5.65 (0.38×1H, d, *J*=10.3 Hz), 5.90 (0.62×1H, d, *J*=9.8 Hz), 7.2—7.6 (10H, m); ^{13}C NMR δ=17.4 (q, *E*), 24.0 (q, *Z*), 50.4 (d, *E*), 50.6 (d, *Z*), 52.5 (q, *Z*), 52.6 (q, *E*), 122.7 (d), 126.6 (d), 127.3 (d), 127.8 (d), 128.4 (d), 128.7 (d), 128.9 (d), 129.1 (d), 130.4 (d), 132.1 (s), 132.4 (s), 132.5 (s), 132.7 (d), 132.8 (s), 134.1 (d), 134.7 (d), 136.1 (s), 136.9 (s), 137.2 (d), 170.2 (s, *E*) , 173.8 (s, *Z*); MS *m/z* 330 (M^+), 314, 238, 206. Found: *m/z* 206.0386. Calcd for $C_{11}H_{10}O_2S$: M−SPh−Me, 206.0402.

Reaction of α,β-Unsaturated Ketone Acetals with 1,3-Bis(trimethylsilylthio)propane (Table 7). Reactions were carried out in a manner similar to that described for compounds **8**, using 1.1 equiv of 1,3-bis(trimethylsilylthio)-propane. Analytical data are listed below.

(*E*)-2-Phenyl-2-styryl-1,3-dithiane[14] (Entry 1). IR (KBr) 1595, 1495, 1480, 1445, 1410, 1275, 745, 730, 695 cm^{-1}; ^{1}H NMR δ=1.7—2.2 (2H, m), 2.4—3.2 (4H, m), 6.27 (1H, d, *J*=16 Hz), 6.61 (1H, d, *J*=16 Hz), 6.9—7.4 (8H, m), 7.6—7.8 (2H, m); MS *m/z* 298 (M^+), 223, 191. Found: *m/z* 298.0854. Calcd for $C_{18}H_{18}S_2$: M, 298.0850.

(*E*)-2-*t*-Butyl-2-styryl-1,3-dithiane[15] **and 2-*t*-Butyl-4-phenyl-1,5-dithia-2-cyclooctene** (56:44, mixture) (Entry 2). ^{1}H NMR δ=1.18 (0.56×9H, s), 1.22 (0.44×9H, s), 1.7—2.2 (2H, m), 2.5—3.0 (4H, m), 5.62 (0.44×1H, d, *J*=10 Hz), 6.14 (0.44×1H, d, *J*=10 Hz), 6.35 (0.56×1H, d, *J*=16 Hz), 6.80 (0.56×1H, d, *J*=16 Hz), 7.2—7.5 (5H, m); ^{13}C NMR δ=25.3 (t), 26.0 (q), 27.3 (t), 29.5 (q), 30.3 (t), 35.2 (t), 37.1 (t), 40.0 (s), 40.3 (s), 48.0 (d), 65.7 (s), 126.5 (d), 127.4 (d), 127.7 (d), 128.0 (d), 128.6 (d), 131.4 (d), 133.0 (d), 135.2 (d), 136.7 (s), 140.1 (s), 145.5 (s).

(*E*)-2-(3,3-Dimethyl-1-butenyl)-2-phenyl-1,3-dithiane and 4-*t*-Butyl-2-phenyl-1,5-dithia-2-cyclooctene (43:57, mixture) (Entry 3). ^{1}H NMR δ=1.09 (9H, s), 1.9—2.1 (2H, m), 2.4—3.0 (4H, m), 4.53 (0.57×1H, d, *J*=11 Hz), 5.61 (0.43×1H, d, *J*=16 Hz), 5.84 (0.43×1H, d, *J*=16 Hz), 6.43 (0.57×1H, d, *J*=11 Hz), 7.2—7.4 (3H, m), 7.68 (0.57×2H, m), 7.77 (0.43×2H, m); ^{13}C NMR δ=24.7 (t), 28.1 (q), 28.6 (t), 29.3 (t), 29.8 (q), 33.3 (s), 33.9 (s), 34.9 (t), 35.2 (t), 56.3 (d), 58.6 (s), 127.0 (d), 127.7 (d), 127.8 (d), 128.3 (d and d, 2C), 128.5 (d), 134.3 (s), 136.5 (d), 140.8 (s), 142.0 (s), 146.6 (d).

Reactions of 11 with Silylated Nucleophiles (Table 8). The following is a typical reaction procedure for (*Z*)-4,4-dimethyl-1-phenyl-1,3-bis(phenylthio)-2-pentene (**11**) (R^1=^{t}Bu, R^2=Ph) with the trimethylsilyl enol ether of *t*-butyl methyl ketone (Entry 1): In an argon atmosphere, **11** (R^1=^{t}Bu, R^2=Ph) (52.3 mg, 0.134 mmol) and the trimethylsilyl enol ether of *t*-butyl methyl ketone (39.6 mg, 0.230 mmol) were dissolved in CH_2Cl_2 (2 ml), to which was added 1.0 M $SnCl_4$ solution in CH_2Cl_2 (0.15 ml, 0.15 mmol) at 0 °C. The reaction mixture was stirred for 1 h at 0 °C and quenched with aqueous $NaHCO_3$ solution. The organic materials were extracted with CH_2Cl_2 and the combined extract was dried over Na_2SO_4. After evaporation of the solvent, the residue was purified by preparative TLC (silica gel, hexane:AcOEt=96:4) to afford (*Z*)-2,2,8,8-tetramethyl-5-phenyl-7-phenylthio-6-nonen-3-one (42.7 mg, 0.112 mmol, 84%). IR (neat) 1710, 1580, 1480, 1365, 1070, 740, 700 cm^{-1}; ^{1}H NMR δ=0.98 (9H, s), 1.15 (9H, s), 2.65 (1H, dd, *J*=17 Hz, 6 Hz), 2.95 (1H, dd, *J*=17 Hz, 8 Hz), 4.43 (1H, m), 6.36 (1H, d, *J*=9 Hz), 7.0—7.3 (10H, m); MS *m/z* 380 (M^+), 281, 271. Found: *m/z* 380.2170. Calcd for $C_{25}H_{32}OS$: M, 380.2174.

Other analytical data follow.

(*Z*)-6,6-Dimethyl-1,3-diphenyl-5-phenylthio-4-hepten-1-one (Entry 2). IR (neat) 1705, 1495, 1480, 1440, 1070, 755, 740, 700 cm^{-1}; ^{1}H NMR δ=1.08 (9H, s), 2.95 (1H, dd, *J*=17 Hz, 8 Hz), 3.10 (1H, dd, *J*=17 Hz, 7 Hz), 4.85 (1H, m), 6.42 (1H, d, *J*=10 Hz), 6.95—7.5 (15H, m); MS *m/z* 400 (M^+), 301, 291. Found: *m/z* 400.1850. Calcd for $C_{27}H_{28}OS$: M, 400.1861.

(*Z*)-4,4-Dimethyl-1-phenyl-3-phenylthio-2-pentene (Entry 3). IR (neat) 1580, 1480, 1455, 1440, 1025, 735, 700 cm^{-1}; ^{1}H NMR δ=1.20 (9H, s), 3.54 (2H, d, *J*=7 Hz), 6.33 (1H, t, *J*=7 Hz), 7.0—7.5 (10H, m); MS *m/z* 282 (M^+), 255. Found: *m/z* 282.1433. Calcd for $C_{19}H_{22}S$: M, 282.1442.

(*Z*)-7,7-Dimethyl-4-phenyl-6-phenylthio-1,5-octadiene (Entry 4). IR (neat) 1640, 1580, 1480, 1440, 735, 700 cm^{-1}; ^{1}H NMR δ=1.19 (9H, s), 2.41 (2H, m), 3.95 (1H, m), 4.92 (2H, m), 5.61 (1H, m), 6.35 (1H, d, *J*=10 Hz), 7.0—7.6 (10H, m); MS *m/z* 322 (M^+), 281, 171. Found: *m/z* 322.1728. Calcd for $C_{22}H_{26}S$: M, 322.1755.

(Z)-2,2-Dimethyl-5,7-diphenyl-7-phenylthio-6-hepten-3-one (Entry 5). IR (neat) 1710, 1490, 1480, 1455, 1070, 760, 740, 700 cm^{-1}; ^1H NMR δ=1.07 (9H, s), 2.89 (1H, dd, J=17 Hz, 7 Hz), 3.13 (1H, dd, J=17 Hz, 7 Hz), 4.85 (1H, m), 6.42 (1H, d, J=9 Hz), 7.0—7.5 (15H, m); MS m/z 400 (M^+), 301, 291. Found: m/z 400.1884. Calcd for $C_{27}H_{28}OS$: M, 400.1861.

1,3,5-Triphenyl-5-phenylthio-4-penten-1-one (mixture of *E,Z*-isomer, 34:66) (Entry 6). IR (neat) 1685, 1600, 1580, 1490, 1480, 1450, 740, 700 cm^{-1}; ^1H NMR δ=3.29 (0.34×2H, d, J=7 Hz), 3.46 (0.66×1H, dd, J=16 Hz, 8 Hz), 3.56 (0.66×1H, dd, J=16 Hz, 7 Hz), 4.20 (0.34×1H, dt, J=10 Hz, 7 Hz), 5.01 (0.66×1H, m), 6.16 (0.34×1H, d, J=11 Hz), 6.48 (0.66×1H, d, J=10 Hz), 6.9—8.0 (20H, m); MS m/z 420 (M^+), 311, 301. Found: m/z 420.1541. Calcd for $C_{29}H_{24}OS$: M, 420.1548.

(Z)-1,3-Diphenyl-1-phenylthio-1-propene (Entry 7). IR (neat) 1580, 1490, 1480, 1455, 1025, 760, 740, 695 cm^{-1}; ^1H NMR δ=3.91 (2H, d, J=7 Hz), 6.55 (1H, t, J=7 Hz), 7.0—7.6 (15H, m); MS m/z 302 (M^+), 218, 193. Found: m/z 302.1125. Calcd for $C_{21}H_{18}S$: M, 302.1129.

Methyl (Z)-4-Phenyl-2-phenacyl-4-phenylthio-3-butenoate (Entry 8). IR (neat) 1735, 1685, 1450, 1215, 740, 690 cm^{-1}; ^1H NMR δ=3.35 (1H, dd, J=18 Hz, 6 Hz), 3.68 (1H, dd, J=18 Hz, 7 Hz), 3.74 (3H, s), 4.62 (1H, m), 6.46 (1H, d, J=9 Hz), 7.0—8.0 (15H, m); MS m/z 402 (M^+), 370, 293, 261. Found: m/z 402.1281. Calcd for $C_{25}H_{22}O_3S$: M, 402.1290.

References

1) For examples, D. A. Evans, G. L. Carroll, and L. K. Truesdale, *J. Org. Chem.*, **39**, 914 (1974); R. Noyori, S. Murata, and M. Suzuki, *Tetrahedron*, **37**, 3899 (1981); K. Utimoto, Y. Wakabayashi, Y. Shishiyama, M. Inoue, and H. Nozaki, *Tetrahedron Lett.*, **22**, 4279 (1981); K. Utimoto, Y. Wakabayashi, T. Horiie, M. Inoue, Y. Shishiyama, M. Obayashi, and H. Nozaki, *Tetrahedron*, **39**, 967 (1983).

2) For examples, T. Mukaiyama and M. Hayashi, *Chem. Lett.*, **1974**, 15; K. Saigo, M. Osaki, and T. Mukaiyama, *ibid.*, **1976**, 769; T. Sato, M. Arai, and I. Kuwajima, *J. Am. Chem. Soc.*, **99**, 5827 (1977); S. Murata, M. Suzuki, and R. Noyori, *ibid.*, **102**, 3248 (1980); T. Mukaiyama, S. Kobayashi, and M. Murakami, *Chem. Lett.*, **1984**, 1759.

3) For examples, A. Hosomi, M. Endo, and H. Sakurai, *Chem. Lett.*, **1976**, 941; T. Tsunoda, M. Suzuki, and R. Noyori, *Tetrahedron Lett.*, **21**, 71 (1980); H. Sakurai, K. Sasaki, and A. Hosomi, *Tetrahedron Lett.*, **22**, 745 (1981); T. Mukaiyama, H. Nagaoka, M. Murakami, and M. Ohshima, *Chem. Lett.*, **1985**, 977.

4) For examples, T. Mukaiyama and A. Ishida, *Chem. Lett.*, **1975**, 1201; K. Narasaka, K. Soai, Y. Aikawa, and T. Mukaiyama, *Bull. Chem. Soc. Jpn.*, **49**, 779 (1976).

5) a) T. Mukaiyama, T. Soga, and H. Takenoshita, *Chem. Lett.*, **1989**, 997; b) T. Mukaiyama, T. Soga, and H. Takenoshita, *ibid.*, **1989**, 1273.

6) T. Mukaiyama, H. Takenoshita, M. Yamada, and T. Soga, *Chem. Lett.*, **1990**, 229; T. Mukaiyama, H. Takenoshita, M. Yamada, and T. Soga, *ibid.*, **1990**, 1259.

7) U. Vogeli and W. von Philipsborn, *Org. Magn. Reson.*, **7**, 617 (1975).

8) T. Mukaiyama, S. Kobayashi, M. Tamura, and Y. Sagawa, *Chem. Lett.*, **1987**, 491.

9) N. Iwasawa and T. Mukaiyama, *Chem. Lett.*, **1987**, 1463.

10) T. Mukaiyama, H. Nagaoka, M. Ohshima, and M. Murakami, *Chem. Lett.*, **1986**, 1009; M. Murakami, T. Kato, and T. Mukaiyama, *ibid.*, **1987**, 1167.

11) D. A. Evans, L. K. Truesdale, K. G. Grimm, and S. L. Nesbitt, *J. Am. Chem. Soc.*, **99**, 5509 (1977).

12) T. Mukaiyama, T. Takeda, and K. Atsumi, *Chem. Lett.*, **1974**, 1013.

13) M. Ohshima, M. Murakami, and T. Mukaiyama, *Chem. Lett.*, **1985**, 1871.

14) D. Ghiringhell, *Synthesis*, **1982**, 580.

15) A. E. Davey, A. F. Parsons, and R. J. K. Taylor, *J. Chem. Soc., Perkin Trans. 1*, **1989**, 1853.

Nucleophilic Displacement Catalyzed by Transition Metal. IX.[1] $[Pd_2(dba)_3]\cdot CHCl_3$–DPPF Catalyzed Cyanation of Aryl Halides and Aryl Triflates

Kentaro TAKAGI,* Ken SASAKI,† and Yasumasa SAKAKIBARA†
College of Liberal Arts and Science, Okayama University, Tsushima, Okayama 700
†Department of Polymer Science and Engineering, Kyoto Institute of Technology, Kyoto 606
(Received November 17, 1990)

A catalyst system comprising $[Pd_2(dba)_3]\cdot CHCl_3$ and DPPF was proved to be efficient for the cyanation of aryl iodides and aryl triflates with KCN. The reactivities of aryl substrates decreased in the order ArI>ArOTf>ArBr.

Although a nucleophilic displacement of nonactivated aryl halides with alkali metal cyanides does not take place under conventional conditions, some transition metals like Ni, Pd, and Co induce a reaction through activation of the sp^2 carbon–halogen bonds of the substrates.[2] Regarding the Pd catalyst, $Pd(PPh_3)_4$ and Pd(II) salts, such as $Pd(OAc)_2$, are hitherto known to be active for catalytic cyanation.[3] The former is one of the most extensively used complexes in a variety of transition metal-catalyzed reactions,[4] although its efficiency toward the cyanation is not satisfactory. Several modifications of this method have thus appeared, in which cyanation was accelerated by adding crown ethers as co-catalysts[5] or by using Me_3SiCN[6] or NaCN impregnated on alumina[7] as a cyanide source. Another possible modification, i.e., tuning the reactivity of Pd(0) by controlling the ligating species, has not been explored for this important transformation.[8] In this paper we report that an alternation of the ligand from conventional PPh_3 to 1,1′-bis(diphenylphosphino)ferrocene (DPPF) improves the catalytic efficiency of Pd(0) to a great extent, thereby providing a convenient method for the preparation of aryl cyanides from not only aryl

Table 1. Effect of Solvents and/or Ligands for the Pd(0)-Catalyzed Cyanation of Iodobenzene[a]

Run	Solvent	Ligand (Molar ratio of Ligand/$[Pd_2(dba)_3]\cdot CHCl_3$)	Time / h	Yield[b] / %
1	NMP	—	5	40
2	Acetone	—	5	22
3	THF	—	5	8
4	DMF[c]	—	5	<1
5	Acetonitrile	—	5	<1
6	Toluene	—	5	<1
7	Methanol	—	5	<1
8	NMP	DPPF (2)	2	96
9	NMP	DPPF (4)	1	98
10	NMP	DPPF (6)	2	98
11	Acetone	DPPF (4)	5	96
12	THF	DPPF (4)	5	34
13	NMP	$P(o\text{-Tol})_3$[d] (8)	5	79
14	NMP	DPPP (4)	5	5
15	NMP	PPh_3 (8)	5	<1
16[e]	NMP	PPh_3	5	<1
17	NMP	PBu_3 (8)	5	<1
18	NMP	$P(OPr^i)_3$ (8)	5	<1
19	NMP	PHEN (4)	5	<1
20	NMP	bpy (4)	5	<1
21[f]	NMP	DPPF (4)	12	95
22[f,g]	NMP	DPPF (4)	2	96
23[h]	NMP	DPPF (4)	12	12

a) In the presence of 1 mmol of iodobenzene, 2 mmol of KCN, 0.005 mmol of $[Pd_2(dba)_3]\cdot CHCl_3$, and 0.01—0.04 mmol of ligand in 0.5 cm^3 of the solvent at 60 °C under nitrogen unless otherwise noted. b) Yields were determined by GLC using an internal standard. c) *N*,*N*-Dimethylformamide. d) Tri-*o*-tolylphosphine. e) $Pd(PPh_3)_4$ was used in the place of $[Pd_2(dba)_3]\cdot CHCl_3$ and ligand. f) This run was carried out at 40 °C. g) This run was carried out by a successive procedure. h) Bromobenzene was used in the place of iodobenzene.

iodides, but also aryl triflates:[9]

$$ArX + KCN \xrightarrow[X=I \text{ or } OTf]{\text{"Pd(0)-DPPF"}} ArCN + KX$$

Results and Discussion

Cyanation of Aryl Iodides. At the beginning, the reaction of iodobenzene with KCN was studied using tris(dibenzylideneacetone)dipalladium(0)-chloroform (1/1) ([Pd2(dba)3]·CHCl3; dba=dibenzylideneacetone), a commercially available, air-stable zerovalent palladium possessing substitution-labile ligands,[10] as a catalyst precursor to investigate the effect of ligands and solvents on the progress of the Pd(0)-catalyzed cyanation (Table 1). Even in the absence of supporting ligands, the catalytic reaction took place in 1-methyl-2-pyrrolidinone (NMP), acetone, and tetrahydrofuran (THF), but stopped before it reached completion. Although such additives as PPh_3, PBu_3, 1,3-bis(diphenylphosphino)propane (DPPP), triisopropyl phosphite ($P(OPr^i)_3$), 1,10-phenanthroline (PHEN), and 2,2'-bipyridyl (bpy) lowered the catalytic activity of Pd(0), DPPF raised it reversely.[11] Thus, a clean reaction of iodobenzene with KCN proceeded in NMP or acetone at 60 °C by the catalysis of [Pd2(dba)3]·CHCl3 and DPPF to afford benzonitrile in excellent yield. The present catalyst system is far more reactive than the conventional $Pd(PPh_3)_4$, as exemplified by Runs 9, 15, and 16. The same reaction took place at a lower temperature of 40 °C, as well. In the presence of this catalyst system, a variety of aryl iodides readily underwent cyanation with KCN: substituents like alkyl, alkoxy, acyl, alkoxycarbonyl, and chloro and one attached on the ortho position to iodo-leaving group did not interfere with the progress of cyanation (Table 2). Bromobenzene, however, was ascertained to be far less reactive than aryl iodides for cyanation. It is to be noted that the manner of operation influences the progress of the reaction to a great extent. That is, a simple procedure (see Experimental) required prolonged heating to complete the reaction, compared with a successive procedure: [Pd2(dba)3]·CHCl3, DPPF, and a solvent were mixed at room temperature before the substrate and KCN were added successively; entire mixture was then heated to the cited temperature (Tables 1 and 3).[12] For the sake of convenience, however, the former procedure was adopted for all runs, except otherwise noted.

Cyanation of Aryl Triflates. The catalytic cyanation of phenolic oxygen was examined next. There has hitherto been no convenient way to convert the hydroxyl group into a cyano group, mainly because of a difficult nucleophilic displacement at the sp^2 carbon atoms.[14] In view of the facts that 1) aryl triflates are prepared readily from phenols[15] and 2) their carbon-oxygen bonds are cleaved by transition metals to form the oxidative adducts,[16] the application of our Pd(0)-catalyzed cyanation to aryl triflates looks promising as an approach to this problem. Recently, a reaction of vinyl triflates with LiCN was attempted in the presence of catalytic amounts of $Pd(PPh_3)_4$ and 12-crown-4.[17] As shown in Table 3, with the aid of the catalyst system comprising [Pd2(dba)3]·CHCl3 and DPPF, aryl triflates readily underwent a reaction with KCN to afford the corresponding aryl cyanides in good yields:

Table 2. Cyanation of Aryl Iodides[a]

Run	R-C6H4-I R	Time h	Yield[b] %
24	*p*-$COCH_3$	2	94
25	*p*-Cl	2	93
26	*p*-CH_3	4	94
27[c]	*p*-OCH_3	1	92
28	*m*-CO_2CH_3	2	96
29	*o*-CO_2CH_3	8	93
30	*o*-CH_3	4	87

a) In the presence of 1 mmol of aryl iodide, 2 mmol of KCN, 0.005 mmol of [Pd2(dba)3]·CHCl3, and 0.02 mmol of DPPF in 0.5 cm^3 of NMP at 60 °C under nitrogen. b) Isolated yield. c) This run was carried out at 80 °C.

Table 3. Cyanation of Aryl Triflates[a]

Run	Aryl Triflate R-C6H4-OTf R	Time h	Yield[b] %
31	H	8	(94)
32[c]	H	30	(96)
33[c,d]	H	8	(93)
34	*p*-$COCH_3$	3	92
35	*p*-Cl	3	(94)
36	*p*-CH_3	25	87
37	*p*-CN	2	95
38	*p*-CO_2CH_3	3	94
39	*p*-NO_2	2	90
40	*p*-C_6H_5	8	92
41	*p*-OCH_3	25	(45)[e]
42	*p*-$NHCOCH_3$	25	(35)[f]
43	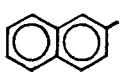	4	91
44	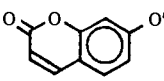	2	98
45	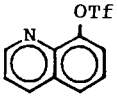	2	95

a) In the presence of 1 mmol of aryl triflate, 2 mmol of KCN, 0.02 mmol of [Pd2(dba)3]·CHCl3, and 0.08 mmol of DPPF in 0.5 cm^3 of NMP at 60 °C under nitrogen. b) Isolated yield. Yield in parentheses were determined by GLC. c) This run was carried out using 0.005 mmol of [Pd2(dba)3]·CHCl3 and 0.02 mmol of DPPF. d) This run was carried out by a successive procedure. e) The conversion was 50%. f) The conversion was 48%.

alkyl, aryl, chloro, acyl, alkoxycarbonyl, cyano, or nitro substituent but also 2-naphthyl, 2-oxo-2*H*-benzopyran-7-yl, or 8-quinolyl did not interfere with the progress of cyanation. Electron-donating groups, like alkoxyl and acylamino, however, retarded the reaction, so that the catalytic reaction did not reach completion, even after long heating.

The order of reactivity of aryl substrates in the present Pd(0)-catalyzed cyanation is ArI>ArOTf>ArBr>ArCl. For the closely related Pd(0)-catalyzed cross-coupling with organostannanes, however, a different order (ArI>ArBr>ArOTf>ArCl) had been reported.[18]

At present, the reason why the DPPF-ligand works so well is not clear. Recent papers describe the efficiency of chelation with diphosphorus ligands in the Pd(0)-catalyzed carbonylation of aryl halides.[19] In our case, the cyanide anion, although absolutely neccesary as a reagent, has an inhibitory action on the catalyst; it is capable of binding to Pd(0) too strongly to render the catalyst inactive.[2,3,8,13] Therefore, ligands which can appropriately protect the palladium center from an attack of the free cyanide anion might be desirable.

In conclusion, a catalyst system comprising $[Pd_2(dba)_3]\cdot CHCl_3$ and DPPF was found to be effective for the cyanation of various aryl iodides and aryl triflates with KCN. The facile procedure adopted, owing to the stability of the catalyst precursor and the convenience of the batch method, also makes this catalytic reaction attractive as a new synthetic method of aryl cyanides.

Experimental

$[Pd_2(dba)_3]\cdot CHCl_3$ was utilized as obtained from Kanto Chemical Co. KCN was recrystallized from water and dried under reduced pressure (at ca. 300 °C) prior to use. The solvents were distilled and dried over Molecular Sieves. Aryl triflates were prepared according to a procedure described in the literature.[15] The other materials were commercial products and were used without further purification. A Hitachi 160 gas chromatograph was used for the GLC analysis. The ^1H NMR spectra were obtained on a JEOL FX90A spectrometer, using Me_4Si as the internal standard. The IR spectra were recorded on a Hitachi 260-10 spectrometer.

General Procedure for Cyanation. Preparation of *p*-Chlorobenzonitrile: To the dry KCN (139 mg, 2.0 mmol), $[Pd_2(dba)_3]\cdot CHCl_3$ (5.2 mg, 0.005 mmol), DPPF (11.1 mg, 0.02 mmol), *p*-chloroiodobenzene (238 mg, 1.0 mmol), and NMP (0.5 cm^3) were added, evacuated, flushed with nitrogen, and kept at 60 °C with stirring for 2 h. The resulting mixture was chromatographed on a silica-gel column using hexane-ethyl acetate as an eluent, affording 129 mg of *p*-chlorobenzonitrile (93%). Mp 90—91 °C (lit,[20] 90 °C); IR 2220 cm^{-1}; ^1H NMR ($CDCl_3$) δ=7.3—7.5 (m, 4H).

***p*-Cyanoacetophenone:** Mp 56.5—57 °C (lit,[21] 60—61 °C); IR 1680, 2210 cm^{-1}; ^1H NMR ($CDCl_3$) δ=2.7 (s, 3H), 7.8 (d, J=8.0 Hz, 2H), 8.1 (d, J=8.0 Hz, 2H).

***p*-Cyanotoluene:** Mp 25. 5—27.5 °C (lit,[22] 27—28 °C); IR 2220 cm^{-1}; ^1H NMR ($CDCl_3$) δ=2.4 (s, 3H), 7.3 (d, J=8.0 Hz, 2H), 7.5 (d, J=8.0 Hz, 2H).

***p*-Cyanoanisole:** Mp 56—56.5 °C (lit,[23] 59 °C); IR 1020, 1260, 2220 cm^{-1}; ^1H NMR ($CDCl_3$) δ=3.8 (s, 3H), 7.0 (d, J=9.0 Hz, 2H), 7.6 (d, J=9.0 Hz, 2H).

Methyl *m*-Cyanobenzoate: Mp 58.5—59 °C (lit,[24] 65 °C); IR 1290, 1720, 2220 cm^{-1}; ^1H NMR ($CDCl_3$) δ=4.0 (s, 3H), 7.4—7.9 (m, 2H), 8.2—8.4 (m, 2H).

Methyl *o*-Cyanobenzoate: Mp 48.5—49 °C (lit,[25] 50—51 °C); IR 1270, 1720, 2210 cm^{-1}; ^1H NMR ($CDCl_3$) δ=4.0 (s, 3H), 7.6—7.8 (m, 3H), 8.1—8.2 (m, 1H).

***o*-Cyanotoluene:** IR 2220 cm^{-1}; ^1H NMR ($CDCl_3$) δ=2.5 (s, 3H), 7.2—7.6 (m, 4H).

1,4-Dicyanobenzene: Mp 221—222 °C (lit,[26] 221—222.5 °C); IR 2240 cm^{-1}; ^1H NMR ($CDCl_3$) δ=7.8 (s, 4H).

Methyl *p*-Cyanobenzoate: Mp 67—68 °C (lit,[27] 62 °C); IR 1280, 1745, 2235 cm^{-1}; ^1H NMR ($CDCl_3$) δ=4.0 (s, 3H), 7.8 (d, J=8.7 Hz, 2H), 8.2 (d, J=8.6 Hz, 2H).

***p*-Cyanonitrobenzene:** Mp 147—149 °C (lit,[26] 148—149 °C); IR 1350, 1530, 2240 cm^{-1}; ^1H NMR ($CDCl_3$) δ=7.9 (d, J=8.8 Hz, 2H), 8.4 (d, J=8.8 Hz, 2H).

1,1'-Biphenyl-4-carbonitrile: Mp 87.5—88 °C (lit,[28] 86—86.5 °C); IR 2230 cm^{-1}; ^1H NMR ($CDCl_3$) δ=7.4—7.8 (m, 9H).

2-Cyanonaphthalene: Mp 67.5—68 °C (lit,[29] 65—66 °C); IR 2230 cm^{-1}; ^1H NMR ($CDCl_3$) δ=7.6—7.7 (m, 3H), 7.9—8.0 (m, 3H), 8.25 (s, 1H).

7-Cyanocoumarin: Mp 229—230 °C; IR 1620, 1730, 2240 cm^{-1}; ^1H NMR ($CDCl_3$) δ=6.6 (d, J=9.6 Hz, 1H), 7.6 (m, 3H), 7.7 (d, J=9.7 Hz, 1H); Calcd for $C_{10}H_5NO_2$: C, 70.18; H, 2.94; N, 8.18%. Found: C, 70.09; H, 3.00; N, 8.10%.

8-Cyanoquinoline: Mp 83—83.5 °C (lit,[30] 82—83.5 °C); IR 2230 cm^{-1}; ^1H NMR ($CDCl_3$) δ=7.5—7.7 (m, 2H), 8.0—8.4 (m, 3H), 9.1—9.2 (m, 1H).

References

1) Part VIII: K. Takagi and Y. Sakakibara, *Chem. Lett.*, **1989**, 1957.

2) G. P. Ellis and T. M. Romney-Alexander, *Chem. Rev.*, **87**, 779 (1987).

3) K. Takagi, T. Okamoto, Y. Sakakibara, and S. Oka, *Chem. Lett.*, **1973**, 471; K. Takagi, T. Okamoto, Y. Sakakibara, A. Ohno, S. Oka, and N. Hayama, *Bull. Chem. Soc. Jpn.*, **48**, 3298 (1975).

4) R. F. Heck, "Palladium Reagents in Organic Synthesis," Academic Press, New York (1985).

5) H. Prochazka and M. Siroky, *Coll. Czech. Chem. Commun.*, **48**, 1765 (1983); N. Sato and M. Suzuki, *J. Heterocycl. Chem.*, **24**, 1371 (1987).

6) N. Chatani and T. Hanafusa, *J. Org. Chem.*, **51**, 4714 (1986).

7) J. R. Dalton and S. L. Regen, *J. Org. Chem.*, **44**, 4443 (1979); W. Oppolzer and D. A. Roberts, *Helv. Chim. Acta*, **63**, 1703 (1980).

8) The application of a reducing potential increased in the catalytic activity of $Pd(PPh_3)_4$ for the aryl cyanation: J. B. Davison, P. J. Peerce-Landers, and R. J. Jasinski, *J. Electrochem. Soc.*, **130**, 1862 (1983).

9) For a preliminary communication on a portion of this work, see K. Takagi and Y. Sakakibara, *Chem. Lett.*, **1989**, 1957.

10) For the exchange of the dba ligand with phosphorus ligands, see for example: T. Ukai, H. Kawazura, Y. Ishii, J. J. Bonnet, and J. A. Ibers, *J. Organomet. Chem.*, **65**, 253 (1974); L. Y. Ukhin and N. A. Dolgopolova, *Zh. Obshch. Khim.*, **53**, 703 (1983); G. K. Anderson and R. Kumar, *Inorg. Chim. Acta*, **97**, L21 (1985); S. Park, D. Hedden, A. L. Rheingold, and D. M. Roundhill, *Organometallics*, **5**, 1305 (1986); C. L. Lee, Y. P. Yand, S. J. Rettig, B. R. James, D. A. Nelson, and M. A. Lilga, *ibid.*, **5**, 2220 (1986).

11) Precedents where ligands play an important role in determing the reaction course or the catalytic activity of [$Pd_2(dba)_3$]·$CHCl_3$-assisted or catalyzed reactions. See for example: B. M. Trost and A. R. Sudhakan, *J. Am. Chem. Soc.*, **109**, 3792 (1987); B. Seddig and J. Alm, *J. Prak. Chem.*, **329**, 711 (1987).

12) This observation is not unexpected since the cyanide anion plays an inhibitory action on the palladium catalyst.[2,3,8,13]

13) Y. Sakakibara, F. Okuda, A. Shimobayashi, K. Kirino, M. Sakai, N. Uchino, and K. Takagi, *Bull. Chem. Soc. Jpn.*, **61**, 1985 (1988).

14) B. R. Castro, *Org. React.*, **29**, 1 (1983).

15) P. J. Stang, M. Hanack, and L. R. Subramanian, *Synthesis*, **1982**, 85.

16) W. J. Scott and J. E. McMurry, *Acc. Chem. Res.*, **21**, 47 (1988).

17) E. Piers and F. F. Fleming, *J. Chem. Soc., Chem. Commun.*, **1989**, 756.

18) A. M. Echavarren and J. K. Stille, *J. Am. Chem. Soc.*, **109**, 5478 (1987); G. Martorell, A. Garcia-Raso, and J. M. Saa, *Tetrahedron Lett.*, **31**, 2357 (1990).

19) Y. Ben-David, M. Portnoy, and D. Milstein, *J. Am. Chem. Soc.*, **111**, 8742 (1989); *idem.*, *J. Chem. Soc., Chem. Commun.*, **1989**, 1816.

20) M. L. van Scherpenzeel, *Recl. Trav. Chim. Pays-Bas*, **16**, 113 (1897).

21) F. Ahrens, *Ber.*, **20**, 2952 (1887).

22) K. Gasiorowski and V. Merz, *Ber.*, **18**, 1001 (1885).

23) W. Reinders and W. E. Ringer, *Recl. Trav. Chim. Pays-Bas*, **18**, 326 (1899).

24) W. Boromme, *Ber.*, **20**, 524 (1887).

25) S. Hoogewerff and W. A. van Dorp, *Recl. Trav. Chim. Pays-Bas*, **11**, 84 (1892).

26) I. E. Coop and L. E. Sutton, *J. Chem. Soc.*, **1938**, 1269.

27) K. H. Slotta and R. Kethur, *Ber.*, **71**, 335 (1938).

28) K. B. Everard, L. Kumar, and L. E. Sutton, *J. Chem. Soc.*, **1951**, 2807.

29) J. F. Norris and A. J. Klemka, *J. Am. Chem. Soc.*, **62**, 1432 (1940).

30) L. F. Fieser and E. B. Hershberg, *J. Am. Chem. Soc.*, **62**, 1640 (1940).

Stereoselective Synthesis of (*E*)- and (*Z*)-2-Alkenyltrimethylsilanes from 1,2-Epoxy-1,3-bis(trimethylsilyl)propane[1)]

Nobujiro SHIMIZU,* Sachiko IMAZU, Fumihiro SHIBATA, and Yuho TSUNO
Department of Chemistry, Faculty of Science, Kyushu University,
Hakozaki, Higashi-ku, Fukuoka 812
(Received November 20, 1990)

Stereoselective synthesis of various (*E*)- and (*Z*)-2-alkenyltrimethylsilanes ($RCH{=}CHCH_2SiMe_3$; R=Me, Et, *n*-Bu, *i*-Pr, *c*-hexyl, *t*-butyl, and phenyl) has been accomplished by a reaction of 1,2-epoxy-1,3-bis(trimethylsilyl)propane with Grignard reagents (RMgX) followed by subsequent Peterson olefination reactions of resulting 1,2-bis(trimethylsilyl)-3-alkanols [$RCH(OH)CH(SiMe_3)CH_2SiMe_3$]; the acid ($BF_3OEt_2$ or $HClO_4$)-catalyzed olefination yields the (*E*)-isomer, while the base (KH or NaH)-induced olefination yields the (*Z*)-isomer in more than 95% stereochemical purity in most cases.

The chemistry of allylsilanes has received continuing synthetic and mechanistic interests.[2,3)] Synthetic methods for acyclic allylsilanes include coupling reactions between allyl-metal species and halosilanes,[4,5)] between silyl-metal species and allyl halides,[6)] or between allyl methyl ethers and halosilanes with the aid of sodium,[7)] Wittig condensation of 2-trimethylsilylethylidenetriphenylphosphorane with carbonyl compounds,[8)] hydrosilylation or reductive silylation of 1,3-dienes,[9)] a Ramberg-Backlund olefination,[10,11)] and transition metal-catalyzed reaction between allylic halides and disilanes.[12)] These methods are generally nonstereospecific and give a mixture of stereoisomers which are usually not readily separable from each other. Furthermore, some of these methods are not regiospecific. During the course of our study on the ene reactions of allylsilanes,[13,14)] we needed a series of (*E*)- and (*Z*)-2-alkenylsilanes in high stereochemical purity. 2-Alkenylsilanes may be prepared stereoselectively from 1-alkynes via hydroboration[15)] and from vinyl triflates via palladium-catalyzed coupling with tris(trimethylsilylmethyl)aluminum.[16)] We describe here a new stereoselective method for (*E*)- and (*Z*)-2-alkenyltrimethylsilanes (**2**) via a Grignard reaction of *trans*-1,2-epoxy-1,3-bis(trimethylsilyl)propane (**1**) followed by the Peterson olefination reaction.[17)]

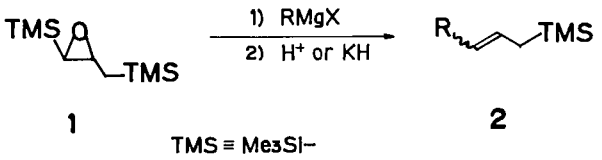

Results and Discussion

The requisite oxirane **1** was obtained in 84% yield by epoxidation of (*E*)-1,3-bis(trimethylsilyl)propene (**3**) with *m*-chloroperbenzoic acid in dichloromethane at −15 °C. The oxirane was labile and decomposed to 3-trimethylsilylpropanal (**4**) on exposure to acids; however, it could be stored for years in a refrigerator without appreciable decomposition. The precursory olefin **3** can be prepared from allyltrimethylsilane,[18)] but we prepared it more conveniently in 74% yield from 1,3-dichloropropene by in situ coupling with chlorotrimethylsilane with the aid of magnesium in THF under reflux. Although commercial 1,3-dichloropropene was a mixture of (*E*) and (*Z*) isomers in the ratio 45 : 55, the coupling reaction led to almost stereospecific formation of (*E*)-**3**. This arose from the silylation via double rearrangement of the allylic double bonds. The first silylation yields (1-chloroallyl)trimethylsilane (**5**) and the subsequent silylation occurs at the 3-position of allyl group to give (*E*)-**3** from steric reason. Indeed, a controlled reaction afforded **5** in good yield.[19)]

Lithium dibutylcuprate(I) reacted relatively slowly with **1** in ether at −40 °C affording 1,3-bis(trimethylsilyl)-2-heptanol (**6**) together with a small amount of its trimethylsilyl ether **7** in a combined 75% yield, the products of the anticipated α cleavage.[20)] A sodium hydride-induced olefination of the resulting alcohol stereoselectively gave [(*E*)-2-heptenyl]-trimethylsilane [**2c**, (*E*)/(*Z*)=98/2] consistent with syn-elimination[21)] from a configuration shown in **6**. On the other hand, a BF_3OEt_2-catalyzed olefination of **6** proceeded without significant stereoselectivity yielding a 48 : 52 mixture of the (*E*) and (*Z*) isomers in 88% yield. This is presumably due to the steric strain imposed on the anti-oriented transition state. The regiochemistry of this olefination reaction is worth

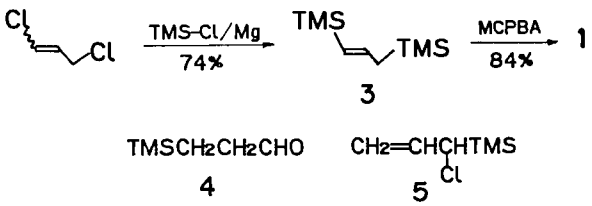

Scheme 1.

stating. Predominant (>95%) formation of **2c** instead of its regioisomer **8** indicates that the internal $SiMe_3$ is more reactive than the terminal one either in the acid-catalyzed or base-induced reaction. Stability of the producing alkenes appears to play a dominant role in the regiocontrol.

The oxirane **1** smoothly reacted with alkyl and phenyl Grignard reagents (RMgX) in ether at room temperature to give 1,2-bis(trimethylsilyl)-3-alkanols **10a—g** in good yields except for the reaction with *t*-butylmagnesium bromide, as shown in Table 1 which includes the results of the subsequent olefination reactions as well. The reaction obviously involves an initial skeletal rearrangement of **1** to 2,3-bis(trimethylsilyl)propanal (**9**) probably effected by magnesium halides,[22] as shown in Scheme 3. The acid-catalyzed olefination of **10** by use of BF_3OEt_2 or 70% perchloric acid gave the (*E*) isomer of 2-alkenyltrimethylsilanes (**2a—g**), while the sodium hydride- or potassium hydride-induced reaction afforded the (*Z*) isomer with more than 97% stereoselectivity in most cases. These stereochemical results indicate that the alcohol **10** was formed in high diastereomeric purity almost as a single diastereomer of a configuration shown in **10**. The structure of the alcohol is predictable from the Cram's rule[23] if we assume that $SiMe_3$ is larger than CH_2SiMe_3. Relatively low stereoselectivities in the olefination of the alcohol **10a** are presumably attributed to contamination of an alternative diastereoisomer of **10a**. The reaction between **1** and *t*-butylmagnesium bromide

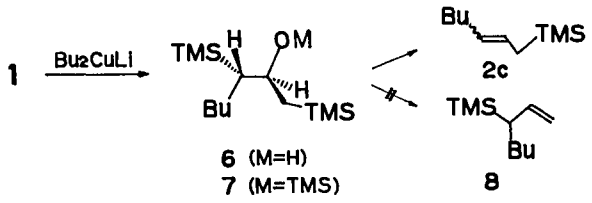

Scheme 2.

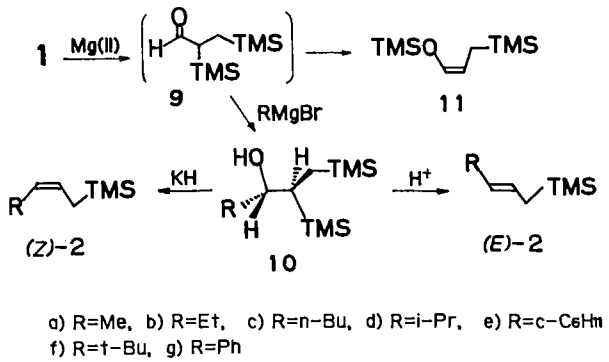

Scheme 3.

Table 1. Reaction of **1** with Grignard Reagents and Subsequent Olefination

Reaction of **1**			Olefination		
Reagent	product	Yield[a]/%	Conditions[b]	Product [(*E*)/(*Z*)]	Yield[a]/%
MeMgI	**10a**	89,97[c]	A[d]	**2a** (94/6)	92[c]
			D	**2a** (11/89)	58[c]
EtMgBr	**10b**	88	A	**2b** (97/3)	71
			B[e]	**2b** (97/3)	86
			C	**2b** (2/98)	76
n-BuMgBr	**10c**	85	A	**2c** (97/3)	90
			B	**2c** (95/5)	92
			C	**2c** (2/98)	85
			D	**2c** (2/98)	73[c]
i-PrMgCl	**10d**	87,94[c]	A	**2d** (98/2)	92[c]
			B	**2d** (98/2)	81
			C	**2d** (2/98)	62
			D	**2d** (2/98)	45[c]
c-C_6H_{11}MgCl	**10e**	86	A[d]	**2e** (98/2)	96
			D	**2e** (2/98)	55
t-BuMgBr	**10f**	10[c]	A	**2f** (98/2)	75[c]
			B	**2f** (98/2)	53
			C	**2f** (2/98)	43
			D	**2f** (2/98)	50[c]
PhMgBr	**10g**	92	A[f]	**2g** (98/2)	88
			B[g]	**2g** (98/2)	65
			C[d,g]	**2g** (9/91)	55
			D[h]	**2g** (6/94)	94[c]

a) Isolated yield unless otherwise noted. b) Reaction conditions are as follows: (A) with ca. 1 equiv BF_3OEt_2 at 0 °C for 30 min in ether; (B) with 3 equiv 70% $HClO_4$ at 0 °C for 30 min in ether; (C) with 2 equiv KH in THF under reflux for 30 min; (D) with 2 equiv NaH in 1,2-dimethoxyethane under reflux for 3—5 h. c) GLC yield. d) At room temperature. e) Reflux for 90 min. f) Stirred for 15 min. g) Stirred for 5 min. h) Reflux for 20 min.

gave the alcohol **10f** in only 10% yield; the major reaction in this case was the formation of (*Z*)-1-trimethylsiloxy-3-trimethylsilyl-1-propene (**11**) which was isolated in 72% yield, indicating that **9** decayed to **11** more rapidly than it reacted with the bulky Grignard reagent.

The stereochemistry of **2a—g** was deduced from IR spectra. The (*E*) and (*Z*) stereoisomers of **2a—g** appeared on GLC at different retention times and exhibited the C=C stretching vibration at different wavenumbers; one showed an absorption near 1660 cm^{-1} together with a strong out-of-plane deformation band near 960 cm^{-1}, while the other showed an absorption near 1645 cm^{-1} together with a weak band near 720 cm^{-1} but no significant band near 960 cm^{-1}. These differences in the IR spectra allow us to assign the former to the (*E*) and the latter to the (*Z*) isomers, respectively.[24] Both (*E*) and (*Z*) stereoisomers exhibited very complicated NMR spectra for olefinic protons which were not readily resolvable except for (*Z*)-**2g**.

The oxidation of the alcohols **10** to the corresponding ketones **12** and the subsequent Grignard reaction followed by olefination may provide a stereoselective route to (3,3-disubstituted allyl)trimethylsilanes. This was exemplified by preparation of (*E*) and (*Z*) isomers of (3-phenyl-2-butenyl)trimethylsilanes (**14a**; R=CH_3) from **10a** via a ketone **12a** and an alcohol **13a**, as shown in Scheme 4. The BF_3OEt_2-catalyzed reaction almost stereospecifically gave (*Z*)-**14a** in 92% yield, while the NaH-induced reaction did (*E*)-**14a** in 78% yield. The stereochemical assignment for **14a** was deduced from the NMR analysis and from the fact that **13a** gave (*E*)-2-phenyl-2-butene instead of **14a** on prolonged treatment with NaH. The stereochemical results suggest that PhMgBr added to the ketone **12a** exclusively in an anti-Cram fashion.

In connection with the stereoselective preparation of allylsilanes from **1**, we briefly examined reactions of a related oxirane **15**. Reaction with (n-Bu)$_2$CuLi gave an expected alcohol **16** which on treatment with perchloric acid and with KH respectively gave (*Z*)- and (*E*)-2-hepten-1-ol (**17**) almost in a stereospecific

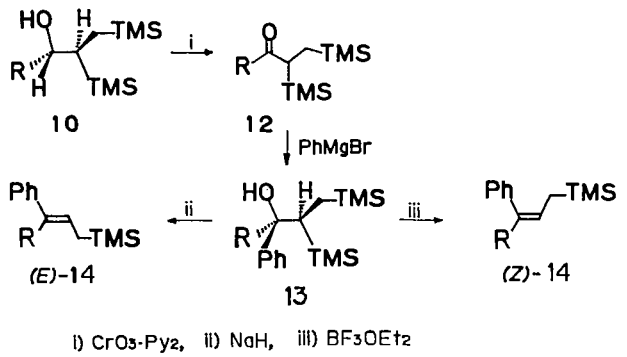

Scheme 4.

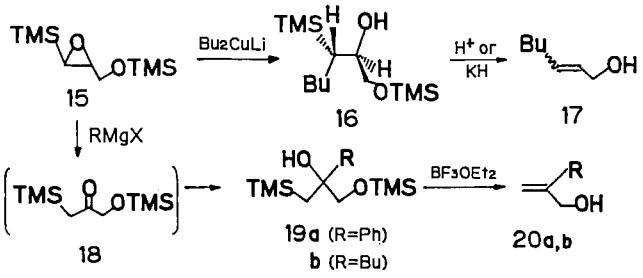

Scheme 5.

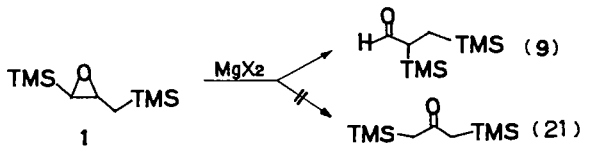

Scheme 6.

manner in each case. On the other hand, phenylmagnesium bromide reacted with **15** yielding 2-phenyl-1-trimethylsiloxy-3-trimethylsilyl-2-propanol (**19**), which on treatment with BF_3OEt_2 afforded 2-phenylallyl alcohol (**20a**) in 91% yield. Similarly, reaction with butylmagnesium bromide and subsequent olefination gave 2-butylallyl alcohol (**20b**). The formation of the alcohol **19** indicates an initial rearrangement of **15** to 1-trimethylsiloxy-3-trimethylsilyl-2-propanone (**18**), as shown in Scheme 5.

Magnesium halide-induced rearrangement of 1-silyl-1,2-epoxyalkanes generally gives 1-silyl-2-alkanones instead of 2-silylalkanals via a regioselective ring-opening through the α-cleavage followed by migration of hydrogen rather than alkyl groups.[25] In addition, a group *cis* to silicon is in general more labile than the corresponding *trans* group.[26] This was indeed true for the oxirane **16**. Accordingly, the magnesium halide-induced rearrangement of **1** might produce 1,3-bis(trimethylsilyl)-2-propanone (**21**) instead of the aldehyde **9**. The absence of **21** suggests either a large migratory aptitude for CH_2SiMe_3 as compared to hydrogen or the selective β ring-opening followed by a 1,2-$SiMe_3$ shift, although we have no compelling evidence for the latter pathway.

Experimental

IR spectra were recorded on a Hitachi 260-10 spectrophotometer. NMR spectra were recorded on a Hiatachi R-600 (60 MHz) spectrometer in carbon tetrachloride using TMS as internal standard except otherwise noted. Mass spectra were recorded on a Hiatchi M-60 mass spectrometer. UV spectra were recorded on a Hitachi 220A spectrophotometer. Analytical and preparative GLC were performed on a Hitachi 163 gas chromatograph equipped with the following columns: (A): 4 mm×25% Apiezon Grease L on Chamelite CK, (B): 4 mm×3 m; 25% Silicone oil SE-30 on Chromosorb W (A.W), and (C): 4 mm×2 m; 25% Silicone DC 550 on

Chromosorb W (A.W), and DMCS.

1,3-Bis(trimethylsilyl)propene (3). To a mixture of chlorotrimethylsilane (49 g) and magnesium (30 g) in THF (100 cm^3) heated to ca. 60 °C was added dropwise a mixture of 1,3-dichloropropene (50 g) and chlorotrimethylsilane (49 g) in THF (200 cm^3) over a period of 8 h at such a rate as to maintain gentle reflux. After completion of the addition, the mixture was stirred for 2 h under reflux and was allowed to cool to room temperature. Hexane (500 cm^3) was then added and inorganic material was filtered off. The filtrate was washed with water, with 10% aq NaOH, and with water, and dried over $MgSO_4$. Fractionation using an efficient column gave 62 g (74%) of 1,3-bis(trimethylsilyl)propene, bp 68—69 °C (20 Torr; 1 Torr=133.3 Pa) [lit,[18a] bp 171 °C].

1,2-Epoxy-1,3-bis(trimethylsilyl)propane (1). To a stirred mixture of *m*-chloroperbenzoic acid (85% purity, 25 g) in dichloromethane (100 cm^3) cooled to −15 °C was added **3** (21 g, 0.113 mol) over a period of 10 min and the mixture was stirred for 3 h at that temperature. Pentane (100 cm^3) was added and a solid was removed by filtration. The solid was washed with pentane and the combined pentane solution was washed three times with every 15 cm^3 of 10% cold aq NaOH, with cold water, and dried over $MgSO_4$. Solvent was removed on a rotary evaporator and the residual oil was distilled to give 19 g (83%) of **1** as a colorless oil: Bp 69—70 °C (9 Torr); IR (neat) 1255, 1185, 870, 840 cm^{-1}; ^1H NMR δ=0.03 (9H, s), 0.05 (9H, s), 0.58 (1H, double d, J=14 and 7.5 Hz), 1.15 (1H, double d, J=14 and 5.5 Hz), 1.71 (1H, d, J=3.2 Hz), 2.62 (1H, m). Found: C, 53.18; H, 10.71%. Calcd for $C_9H_{22}OSi_2$: C, 53.41; H, 10.96%. Acidic workup should be avoided; in a separate experiment, washing a crude pentane solution with 10% aq HCl led to the formation of 3-trimethylsilylpropanal (**4**, 51%) instead: Bp 90—91 °C (118 Torr); IR (neat) 1730, 1250, 860, 840 cm^{-1}; ^1H NMR δ=0.0 (9H, 5), 0.58—0.90 (2H, m), 2.29 (1H, t (J=8.5 Hz) of d (J=1.5 Hz)), 9.60 (1H, t, J=1.5 Hz).

Reaction of 1 with Lithium Dibutylcuprate(1). To a solution of Bu_2CuLi prepared from BuLi (1.73 mol dm^{-3} in hexane, 12 cm^3) and CuI (1.9 g) in ether (20 cm^3) cooled to −78 °C was added the oxirane **1** (1.01 g, 5.0 mmol) and the mixture was stirred for 1 d at ca. −40 °C. Usual workup gave an oil (1.1 g), bp 105—110 °C (7 Torr), which was shown to be a mixture of 1,3-bis(trimethylsilyl)-2-heptanol (**6**) and its trimethylsilyl ether **7** in the ratio 8 : 1.

6: IR 3480 (broad), 1255, 855, 840 cm^{-1}; ^1H NMR δ=0.0 (18H, s), 0.5—1.0 (6H, m), 1.0—1.5 (6H, m), 1.8 (1H, disappeared on addition of D_2O), 3.8 (1H, broad m). Found: C; H, 12.39%. Calcd for $C_{13}H_{32}OSi_2$: C, 59.24; H, 12.24%.

7: IR 1255, 1030, 850, 835 cm^{-1}; ^1H NMR δ=0.0 (18H, s), 0.06 (9H, s), 0.5—1.0 (6H, m), 1.0—1.4 (6H, m), 4.05 (1H, t (J=7 Hz) of d (J=1.5 Hz)).

Preparation of 1,2-Bis(trimethylsilyl)-3-alkanols 10. General Procedure. A small portion (ca. 1 cm^3) of a solution of the oxirane **1** (5.05 g, 25 mmol) in ether (5 cm^3) was added to a solution of a Grignard reagent (30 mmol) in ether (25 cm^3) at room temperature. After an exothermic reaction had commenced, the rest of the epoxide solution was added over a period of 10 min and the resulting mixture was stirred for 1 h at ambient temperature. The mixture was cooled to 0 °C and aq ammonium chloride was added. Organic layer was separated, washed with aq $NaHCO_3$, and dried over $MgSO_4$. A crude product was purified by distillation or by column chromatography over alumina.

3,4-Bis(trimethylsilyl)-2-butanol (10a): Bp 110—111 °C (27 Torr): IR 3420, 1250, 1110, 1080, 850, 840 cm^{-1}; ^1H NMR δ=−0.02 (18H, s), 0.4—1.2 (3H, m), 1.09 (3H, d, J=6.5 Hz), 1.52 (1H, broad s, disappeared on addition of D_2O), 3.86 (1H, q (J=6.5 Hz) of d (J=4.5 Hz)). Found: C, 55.10; H, 12.21%. Calcd for $C_{10}H_{26}OSi_2$: C, 54.98; H, 12.00%.

1,2-Bis(trimethylsilyl)-3-pentanol (10b): Bp 87—88 °C (4 Torr); IR 3475, 1250, 840 cm^{-1}; ^1H NMR δ=0.0 (9H, s), 0.02 (9H, s), 0.51 (2H, d, J=5.4 Hz), 0.81—1.04 (4H, m), 1.43 (3H, m including OH proton), 3.61 (1H, m).

1,2-Bis(trimethylsilyl)-3-heptanol (10c): Bp 89—90 °C (1 Torr); IR 3480, 1250, 1020, 990, 840 cm^{-1}; ^1H NMR ($CDCl_3$) δ=0.0 (9H, s), 0.03 (9H, s), 0.44—0.55 (2H, m), 0.81—0.97 (3H, m), 1.38 (8H, m), 3.71 (1H, m). Found: C, 59.21; H, 12.35%. Found: $C_{13}H_{32}OSi_2$: C, 59.24; H, 12.24%.

4-Methyl-1,2-bis(trimethylsilyl)-3-pentanol (10d): Bp 86—87 °C (3 Torr) IR 3500, 1250, 1000, 840 cm^{-1}; ^1H NMR δ=0.0 (18H, s), 0.4—0.6 (2H, m), 0.80 (3H, d, J=7 Hz), 0.87 (3H, d, J=7 Hz), 0.7—1.3 (1H, m), 1.60 (2H, m, including OH proton), 3.19 (1H, m). Found: C, 58.35; H, 12.25%. Calcd for $C_{12}H_{30}OSi_2$: C, 58.47; H, 12.27%.

1-Cyclohexyl-2,3-bis(trimethylsilyl)-1-propanol (10e): After purification by column chromatography: IR 3490, 1250, 995, 840 cm^{-1}; ^1H NMR δ=0.0 (18H, s), 0.53 (2H, m), 0.7—2.05 (13H, m), 3.22 (1H, broad m).

4,4-Dimethyl-1,2-bis(trimethylsilyl)-3-pentanol (10f): IR 3600, 1250, 1055, 1000, 840 cm^{-1}; ^1H NMR δ=0.0 (9H, s), 0.04 (9H, s), 0.86 (9H, s), 0.3—1.3 (3H, m), 3.43 (1H, d, J=10.5 Nz).

1-Trimethylsiloxy-3-trimethylsilyl-1-propene (11): Bp 65—66 °C (22 Torr); IR 1645, 1250, 1155, 1090, 860, 840 cm^{-1}; ^1H NMR δ=0.0 (9H, s), 0.19 (9H, s), 1.37 (2H, double d, J=8.4 and 1.5 Hz), 4.35 (1H, d (J=8.4 Hz) of t (J=5.6 Hz)), 6.02 (1H, broad d, J=5.6 Hz).

1-Phenyl-2,3-bis(trimethylsilyl)-1-propanol (10g): IR 3460, 1255, 1050, 1010, 860, 840, 760, 700 cm^{-1}; ^1H NMR δ=−0.18 (9H, s), −0.15 (9H, s), 0.58 (2H, m), 0.94—1.21 (1H, m), 1.37 (1H, d, J=3.6 Hz, disappeared on addition of D_2O), 4.68 (1H, double d, J=6.6 and 3.6 Hz), 7.22 (5H, almost s). Found: C, 64.48; H, 10.25%. Calcd for $C_{15}H_{28}OSi_2$: C, 64.23; H, 10.16%.

Preparation of 2-Alkenyltrimethylsilanes 2. 1,2-Bis(trimethylsilyl)-3-alkanols (**10**) were olefinated by the following methods under conditions listed in Table 1. Crude product obtained after workup was purified by distillation or by column chromatography.

Procedure A. To a stirred solution of an alcohol **10** (10 mmol) in ether (25 cm^3) cooled to 0 °C was added 0.6 ml of fresh boron trifluoride–diethyl ether. The mixture was stirred for 30 min at 0 °C. Aq 10% NaOH solution was added and organic layer was separated, washed with saturated aq NaCl and dried ($MgSO_4$).

Procedure B. Procedure was the same as the Procedure A except for the use of 70% perchloric acid (0.25 g per 10 mmol of **10**) instead of boron trifluoride–diethyl ether.

Procedure C. Potassium hydride (3.2 g, ca. 25% slurry in oil) was washed three times with pentane, dried under argon, and was weighed. To the residue (ca. 0.8 g) was added THF (10 cm^3) followed by addition of an alcohol **10** (10 mmol) in THF (2 cm^3) at 0 °C. After evolution of gas had ceased, the mixture was heated under reflux for 15 to 30 min.

Procedure D. Sodium hydride (0.87 g, 55% dispersion in

oil, ca. 20 mmol) was washed three times with hexane and dried under argon. To the residue was added a solution of an alcohol **10** (10 mmol) in 1,2-dimethoxyethane (10 cm³) at room temperature and the mixture was stirred under reflux for 3 to 5 h.

2-Butenyl(trimethyl)silane (2a): IR and NMR spectra of (*E*) and (*Z*) isomers [GLC retention time t_R (Column B, 60 °C): 16.4 and 19.6 min, respectively] were identical to those reported.[27]

2-Pentenyl(trimethyl)silane (2b): (*E*)-**2b**: Bp 73 °C (100 Torr) ; IR 1660, 1250, 960, 845, 690 cm⁻¹ ^{1}H NMR δ=−0.04 (9H, s), 0.93 (3H, t, J=7.8 Hz), 1.29—1.39 (2H, m), 1.66—2.20 (2H, m), 5.16—5.35 (2H, m); MS m/z 142 (M^+, 13), 73 (100).

(*Z*)-**2b**: Bp 76—77 °C (98 Torr); IR 1640, 1250, 850, 720 cm⁻¹; ^{1}H NMR δ=−0.01 (9H, s), 0.92 (3H, t, J=7.2 Hz), 1.34—1.46 (2H, m), 1.60—2.22 (2H, m), 5.12—5.35 (2H, m); MS m/z 142 (M^+, 10), 73 (100).

Retention times for (*E*)-**2b** and (*Z*)-**2b** were 16.2 and 19.4 min, respectively (Column A, 100 °C).

2-Heptenyl(trimethyl)silane (2c): (*E*)-**2c**: Bp 102—103 °C (58 Torr); IR 1660, 1250, 960, 850, 690 cm⁻¹; ^{1}H NMR δ=0.0 (9H, s), 0.90 (3H, m), 1.28—1.43 (6H, m), 1.94—2.02 (2H, m), 5.21—5.42 (2H, m); MS m/z 170 (M^+, 8), 73 (100).

(*Z*)-**2c**: Bp 104—105 °C (55 Torr): IR 1640, 1250, 850, 720 cm⁻¹; ^{1}H NMR δ=0.02 (9H, s), 0.91 (3H, m), 1.12—1.6 (6H, m), 1.8—2.15 (2H, m), 4.95—5.6 (2H, m); MS m/z 170 (M^+, 6), 73 (100).

Retention times for (*E*)-**2c** and (*Z*)-**2c** were 23.6 and 25.6 min, respectively (Column B, 100 °C).

Trimethyl(4-methyl-2-pentenyl)silane (2d): (*E*)-**2d**: Bp 76—77 °C (66 Torr); IR 1660, 1250, 1155, 1020, 960, 855, 840 cm⁻¹; ^{1}H NMR δ=−0.04 (9H, s), 0.91 (6H, d, J=8.4 Hz), 1.31 (2H, d, J=6 Hz), 2.15 (1H, m), 4.87—5.32 (2H, m); MS m/z 156 (M^+, 6), 73 (100).

(*Z*)-**2d**: Bp 79—80 °C (65 Torr); IR 1645, 1250, 1150, 855, 840, 730 cm⁻¹; ^{1}H NMR δ=0.0 (9H, s), 0.91 (6H, d, J=6.4 Hz), 1.42 (2H, d, J=7.2 Hz), 2.5 (1H, m), 4.83—5.24 (2H, m); MS m/z 156 (M^+, 5), 73 (100).

Retention times for (*E*)-**2d** and (*Z*)-**2d** were 15.5 and 16.0 min, respectively (Column B, 100 °C).

(3-Cyclohexylallyl)trimethylsilane (2e): (*E*)-**2e**: IR 1660, 1250, 1155, 960, 850 cm⁻¹; ^{1}H NMR δ=−0.03 (9H, s), 0.6—2.3 (13H, m), 4.91—5.51 (2H, m); MS m/z 196 (m/z 4), 73 (100).

(*Z*)-**2e**: IR 1645, 1250, 1150, 850, 725 cm⁻¹; ^{1}H NMR 0.0 (9H, s), 0.6—2.5 (13H, m), 4.85—5.5 (2H, m). MS m/z 196 (M^+, 8), 73 (100).

Retention times for (*E*)-**2e** and (*Z*)-**2e** were 49.6 and 45.4 min, respectively (Column B, 120 °C).

(4,4-Dimethyl-2-pentenyl)trimethylsilane (2f): (*E*)-**2f**: IR 1250, 1155, 970, 850, 840 cm⁻¹; ^{1}H NMR δ=−0.04 (9H, s), 0.95 (9H, s), 1.30 (2H, m), 5.22 (2H, m); MS m/z 170 (M^+, 9), 73 (100).

(*Z*)-**2f**: IR 1645, 1250, 1150, 850, 720 cm⁻¹; ^{1}H NMR δ=0.0 (9H, s), 1.06 (9H, s), 1.56 (2H, m), 4.9—5.2 (2H, m); MS m/z 170 (M^+, 8), 73 (100).

Retention times for (*E*) and (*Z*)-**2f** were 2.6 and 2.0 min respectively (Column C, 150 °C).

(3-Phenylallyl)trimethylsilane (2g): (*E*)-**2g**: Bp 70—71 °C (2 Torr); IR 1640, 1250, 1140, 1020, 960, 855, 730, 680 cm⁻¹; ^{1}H NMR 0.04 (9H, s), 1.62 (2H, m), 6.02—6.30 (2H, m), 7.08—7.32 (5H, m). Found: C, 75.61; H, 9.52%. Calcd for $C_{12}H_{18}Si$: C, 75.72; H, 9.53%.

(*Z*)-**2g**: Bp 62—63 °C (2 Torr); IR 1630, 1250, 1145, 860, 840, 760, 720, 690 cm⁻¹; ^{1}H NMR δ=0.0 (9H, s), 1.76 (2H, double d, J=9.0 and 1.2 Hz), 5.61 (1H, d (J=11.7 Hz) of t (J=8.6 Hz)), 6.26 (1H, d, J=12 Hz), 7.18 (5H, m). Found: C, 75.70; H, 9.42%. Calcd for $C_{12}H_{18}Si$: C; 75.72; H, 9.53.

Retention times for (*E*)-**2g** and (*Z*)-**2g** were 12.8 and 10.8 min, respectively (Column C, 180 °C).

Olefination of 6. Treatment of **6** (260 mg) with BF_3OEt_2 in the Procedure A gave 149 mg (88%) of **2c** (*E*/*Z*=48 : 52). Treatment of **6** (260 mg) with NaH in the Procedure D (reflux, 5 h) gave 127 mg (75%) of (*Z*)-**2c**. A small amount (ca. 5%) of an unidentified compound, which would probably be (1-butylallyl)trimethylsilane (**8**), was also formed in both cases.

Oxidation of 10a. To a solution of $CrO_3 \cdot Py_2$ (3.7 g) in dichloromethane (40 cm³) was added a solution of **10a** (1.03 g) in dichloromethane (5 cm³) at room temperature and stirred for 15 min at ambient temperature. A crude oil obtained after workup was subjected to bulb-to-bulb distillation (ca. 80 °C at 6 Torr) to give 680 mg (70%) of 3,4-bis(trimethylsilyl)-2-butanone (**12a**): IR 1690, 1250, 1085, 840 cm⁻¹; ^{1}H NMR δ=−0.06 (9H, s), 0.06 (9H, s), 0.35 (1H, double d, J=15 and 1.2 Hz), 1.28 (1H, double d, J=15 and 1.2 Hz), 1.99 (3H, s), 2.34 (1H, d, J=12 Hz).

Reaction of 12a with Phenylmagnesium Bromide and Subsequent Olefination. To a solution of phenylmagnesium bromide (5 mmol) in ether (15 cm³) was added **12a** (680 mg) in ether (2 cm²) at room temperature and the mixture was stirred for 1 h at ambient temperature. A crude oil obtained after workup was subjected to column chromatography over alumina eluting with 5% ether in hexane containing 1% methanol gave 497 mg (51%) of 2-phenyl-3,4-bis(trimethylsilyl)-2-butanol (**13a**): IR 3500, 1600, 1250, 840, 760, 695 cm⁻¹; ^{1}H NMR δ=−0.15 (9H, s), −0.09 (9H, s), 1.49 (3H, s), 7.26 (5H, m). Treatment of **13a** (110 mg) with BF_3OEt_2 in the olefination Procedure A (0 °C, 15 min) gave 70 mg (92%) of (*Z*)-(3-phenyl-2-butenyl)trimethylsilane (**14a**) after purification by column chromatography: IR 1600, 1250, 855, 840, 760, 695 cm⁻¹; ^{1}H NMR δ=−0.06 (9H, s), 1.37 (2H, broad d, J=8.0 Hz), 1.99 (3H, s), 5.42 (1H, t, J=8 Hz), 6.9—7.3 (5H, m). Treatment of **13a** (240 mg) with NaH in the Procedure D (reflux, 2 h) gave 94 mg (88%) of (*E*)-2-phenyl-2-butene. ^{1}H NMR 1.77 (3H, d, J=7 Hz), 1.99 (3H, s), 5.77 (1H, broad q, J=7 Hz), 7.18 (5H, m). The same treatment of **13a** (70 mg) under reflux for 15 min gave 38 mg (78%) of (*E*)-**14a** after purification by column chromatography: IR 1640, 1250, 850, 750, 690 cm⁻¹; ^{1}H NMR δ=0.06 (9H, s), 1.62 (2H, d, J=9.0 Hz), 1.95 (3H, s), 5.77 (1H, t, J=9 Hz), 7.0—7.25 (5H, m).

Preparation of 1,2-Epoxyl-3-trimethylsiloxy-1-trimethylsilylpropane (15). To a cold mixture of *m*-chloroperbenzoic acid (7.0 g, 85% purity) in dichloromethane (50 cm³) was added a solution of [(*E*)-3-trimethylsilyl-2-propenoxy]trimethylsilane (6.0 g) in dichloromethane (10 cm³) over a period of 15 min at 0 °C. Usual workup gave 5.3 g (71%) the oxirane *trans*-**15**: Bp 94—95 °C (17 Torr); IR 1255, 1145, 1100, 1020, 860, 840 cm⁻¹; ^{1}H NMR δ=0.05 (9H, s), 0.09 (9H, s), 1.90 (1H, d, J=3.5 Hz), 2.77 (1H, m), 3.50 (1H, double d, J=11.7 and 4.5 Hz), 3.70 (1H, double d, J=11.7 and 3.9 Hz). Found: C, 49.21; H, 10.01%. Calcd for $C_9H_{22}O_2Si_2$: C, 49.49; H, 10.15%.

Reaction of 15 with Lithium Dibutylcuprate(I) and Subsequent Olefination. To a solution of $(n\text{-Bu})_2$CuLi prepared from BuLi (34.5 mmol, 1.7 mol dm⁻³ in hexane) and

CuI (3.23 g) in ether (25 cm³) was added a solution of **15** (1.5 g, 6.9 mmol) in ether (2 cm³) at −40 °C and the mixture was stirred for 1.5 h at −40 °C. Workup followed by bulb-to-bulb distillation (ca. 130 °C at 17 Torr) gave 1.50 g (80%) of 1-trimethylsiloxy-3-trimethylsilyl-2-heptanol (**16**): IR 3480, 1255, 1105, 1085, 870, 845 cm⁻¹; ¹H NMR δ=0.03 (9H, s), 0.12 (9H, s), 0.6—1.6 (10H, m), 2.19 (1H, broad s, disappeared on addition of D_2O), 3.2—3.9 (3H, m). Treatment of **16** (275 mg) with 70% $HClO_4$ in the Procedure B (0 °C, 30 min) gave 135 mg (90%) of a mixture of (*Z*)-2-hepten-1-ol (**17**) [IR 1660, 1250, 990, 875, 840, 740 cm⁻¹; ¹H NMR 0.07 (9H, s), 0.91 (3H, m), 1.15—1.65 (4H, m), 2.0 (2H, m), 3.92—4.19 (2H, m), 5.24—5.56 (2H, m)] and its trimethylsilyl ether [IR 3320, 1660, 1020 cm⁻¹; ¹H NMR δ=0.7—1.7 (7H, m), 1.8—2.3 (2H, m), 4.06 (2H, broad d, *J*=4.5 Hz), 5.3—6.8 (2H, m)] in the ratio 1:1. Treatment of **16** (413 mg) with KH in the olefination Procedure C (reflux, 2 h) gave 229 mg (81%) of (*E*)-2-heptenoxytrimethylsilane: IR 1675, 1250, 1100, 1055, 970, 870, 840 cm⁻¹; ¹H NMR δ=0.07 (9H, s), 0.91 (3H, m), 1.1—1.6 (4H, m), 2.0 (2H, m), 3.95 (2H, m), 5.48 (2H, m). On treatment with methanol, this compound gave (*E*)-**17** quantitatively: IR 3330, 1675, 1085, 1000, 970 cm⁻¹; ¹H NMR δ=0.91 (3H, m), 1.1—1.6 (5H, m), 2.0 (2H, m), 3.95 (2H, m), 5.57 (2H, m).

Reaction of 15 with Phenylmagnesium Bromide and Subsequent Olefination. To a stirred solution of phenylmagnesium bromide (10 mmol) in ether (25 cm³) was added a solution of **15** (1.03 g) in ether (2 cm³) at room temperature and the mixture was stirred for 4 h under reflux. Usual workup gave 857 mg (62%) of 2-phenyl-1-trimethylsiloxy-3-trimethylsilyl-2-propanol (**19a**) after purification by bulb-to-bulb distillation (ca. 120 °C at 6 Torr): IR 3550, 1600, 1250, 1090, 850, 840, 750, 695 cm⁻¹; ¹H NMR δ=−0.20 (9H, s), 0.0 (9H, s), 1.08 (d, *J*=14.5 Hz), 1.24 (1H, d, *J*=14.5 Hz), 2.73 (1H, s, disappeared on addition of D_2O), 3.51 (2H, s), 7.29 (5H, m). Treatment of **19a** (312 mg) with BF_3OEt_2 in the olefination Procedure A (room temperature, 30 min) gave 195 mg (91%) of a mixture of 2-phenylallyl alcohol (**20a**) and its trimethylsilyl ether in the ratio 55:45 after purification by bulb-to-bulb distillation (ca. 120 °C at 35 Torr). Treatment of the mixture with methanol containing a small amount of potassium carbonate cleanly gave **20a**: ¹H NMR δ=2.56 (1H, s, disappeared on addition of D_2O), 4.34 (2H, s), 5.24 (1H, broad s), 5.34 (1H, broad s), 7.26 (5H, m).

Reaction of 15 with Butylmagnesium Bromide and Subsequent Olefination. To a solution of *n*-BuMgBr (6.5 mmol) in ether (25 cm³) was added a solution of **15** (722 mg) in ether (2 cm³) and the mixture was stirred for 5 h under reflux. Workup followed by bulb-to-bulb distillation gave 550 mg (61%) of 1-trimethylsiloxy-2-(trimethylsilylmethyl)-2-hexanol (**19b**): IR 3430, 1250, 1090, 860, 840 cm⁻¹; ¹H NMR δ=0.03 (9H, s), 0.11 (9H, s), 0.65—1.7 (12H, m), 3.28 (2H, s). Treatment of **19b** (270 mg) with BF_3OEt_2 in the Procedure A (room temperature, 15 min) gave 51 mg (45%) of 2-butylallyl alcohol (**20b**) after treatment with methanol: ¹H NMR δ=0.6—1.7 (8H, m), 1.7—2.2 (2H, m), 3.94 (2H, s), 4.77 (1H, s), 4.92 (1H, s).

References

1) Preliminary report; N. Shimizu, F. Shibata, and Y. Tsuno, *Chem. Lett.*, **1985**, 1593.

2) W. P. Weber, "Slicon Reagents for Organic Synthesis," Springer-Verlag, Berlin (1983); E. W. Colvin, "Silicon in Organic Synthesis," Butterworths, London (1981).

3) S. D. Kahn, C. F. Pau, A. R. Chamberlin, and W. J. Hehre, *J. Am. Chem. Soc.*, **109**, 650 (1987); G. Wickam and W. J. Kitching, *J. Org. Chem.*, **48**, 612 (1983); I. Fleming and N. K. Terrett, *J. Organomet. Chem.*, **264**, 99 (1984); T. Hayashi, M. Konoishi, H. Ito, and M. Kumada, *J. Am. Chem. Soc.*, **104**, 4962 (1982); T. Hayashi, M. Konishi, and M. Kumada, *ibid.*, **104**, 4963 (1982).

4) L. H. Sommer, J. Tylor, and F. C. Whitemore, *J. Am. Chem. Soc.*, **70**, 2872 (1948); T. H. Chan and I. Flemming, *Synthesis*, **1979**, 761.

5) D. Seyferth, K. R. Wursthorn, and R. E. Mammarella, *J. Org. Chem.*, **42**, 3104 (1977); E. M. Tchiroukhine and P. Cadiot, *J. Organomet. Chem.*, **121**, 155 (1976).

6) I. Fleming and A. D. Thomas, *J. Chem. Soc., Chem. Commun.*, **1985**, 411; J. G. Smith, S. E. Drozda, S. P. Petraglia, N. R. Quinn, E. M. Rice, B. S. Traylor, and M. Viswanathan, *J. Org. Chem.*, **49**, 4114 (1984); B. M. Trost and D. M. T. Chan, *J. Am. Chem. Soc.*, **104**, 3733 (1982).

7) D. Tzeng and W. P. Weber, *J. Org. Chem.*, **46**, 265 (1981).

8) I. Fleming and I. Paterson, *Synthesis*, **1979**, 446; D. Seyferth, K. R. Wursthorn, T. F. O. Lim, and D. J. Sepelak, *J. Organomet. Chem.*, **181**, 293 (1979); D. Seyferth, K. R. Wursthorn, and R. E. Mammarella, *J. Org. Chem.*, **42**, 3104 (1977).

9) H. Watanabe, M. Kobayashi, K. Higuchi, and Y. Nagai, *J. Organomet. Chem.*, **186**, 51 (1980); Y. Tsuji, M. Hara, and K. Ohno, *Tetrahedron*, **30**, 2143 (1974).

10) M. G. Ranasinghe and P. L. Fuchs, *J. Am. Chem. Soc.*, **111**, 779 (1989).

11) C.-N. Hsiao and H. Shechter, *Tetrahedron Lett.*, **23**, 1963 (1982).

12) R. Calas, J. Dunogues, G. Deleris, and N. Duffaut, *J. Organomet. Chem.*, **225**, 117 (1982); H. Matsumoto, T. Yako, S. Nagashima, T. Motogi, and Y. Nagai, *ibid.*, **148**, 97 (1978).

13) N. Shimizu, F. Shibata, S. Imazu, and Y. Tsuno, *Chem. Lett.*, **1987**, 1071.

14) S. Imazu, N. Shimizu, and Y. Tsuno, *Chem. Lett.*, **1990**, 1845.

15) H. Yatagi, Y. Yamamoto, and K. Maruyama, *J. Am. Chem. Soc.*, **102**, 4548 (1980).

16) M. G. Saulnier, J. F. Kadow, M. M. Tun, D. R. Langley, and D. M. Vyas, *J. Am. Chem.*, **111**, 8320 (1989).

17) D. J. Peterson, *J. Org. Chem.*, **33**, 780 (1968).

18) a) J. Dunogues, R. Calas, N. Ardoin, and C. Biran, *J. Organomet. Chem.*, **32**, C31 (1971); b) R. Corriu and J. Massee, *ibid.*, **57**, C5 (1973); c) H. O. House, P. C. Gaa, J. H. C. Lee, and D. VanDerveer, *J. Org. Chem.*, **48**, 1670 (1983).

19) N. Shimizu, F. Shibata, and Y. Tsuno, *Bull. Chem. Soc. Jpn.*, **57**, 3017 (1984).

20) P. F. Hudrlik, D. Peterson, and R. J. Rona, *J. Org. Chem.*, **40**, 2263 (1975).

21) P. F. Hudrlik and D. Peterson, *J. Am. Chem. Soc.*, **97**, 1464 (1975).

22) P. F. Hudrlik, R. N. Misra, G. P. Withers, A. M. Hudrlik, R. J. Rona, and J. P. Arcoleo, *Tetrahedron Lett.*, **1976**, 1453.

23) D. J. Cram and F. A. A. Elhafez, *J. Am. Chem. Soc.*, **74**, 5828 (1952).

24) L. J. Bellamy, "The Infra-Red Spectra of Complex Molecules," John Wiley & Sons, New York (1966).
25) P. F. Hudrlik, A. M. Hudrlik, R. N. Misra, D. Peterson, G. P. Withers, and A. K. Kulkarni, *J. Org. Chem.*, **45**, 4444 (1980).
26) M. Obayashi, K. Utimoto, and H. Nozaki, *Tetrahedron Lett.*, **1977**, 1807; *idem.*, *Bull. Chem. Soc. Jpn.*, **52**, 2646 (1979).
27) D. Seyferth, T. F. Jula, H. Dertouzos, and M. Pereyre, *J. Organomet. Chem.*, **11**, 63 (1968).

A Novel Synthesis of Methylenecyclopropane Spiro-Linked with Cycloalkanes via a Cyclization of Allylic Epoxides and Its Application to a Synthesis of Fused 3-Methylfurans[1)]

Tsuyoshi SATOH, Yasushi KAWASE, and Koji YAMAKAWA*
Faculty of Pharmaceutical Sciences, Science University of Tokyo,
Ichigaya-funagawara-machi, Shinjuku-ku, Tokyo 162
(Received November 26, 1990)

Ring closure of allylic epoxides derived from 1-chloroalkyl phenyl sulfoxides and cyclic ketones with lithium diisopropylamide (LDA) in 3-Exo-Tet mode gave spiro-linked methylenecyclopropanes having a hydroxyl group in good yields. Oxidation of these compounds gave ketones, which were then treated with *p*-toluenesulfonic acid in 1,4-dioxane or DMSO at 100 °C to give fused 3-methylfurans in good overall yields. This procedure was applied to a synthesis of menthofuran from 4-methylcyclohexanone.

Intramolecular nucleophilic ring-opening of epoxides with carbanions is one of the most useful reactions for the synthesis of carbocyclic compounds.[2)] We recently reported a new procedure for the synthesis of highly functionalized cyclohexane derivatives from ketones via epoxy sulfone cyclization.[3)] As shown in Scheme 1, treatment of the epoxy sulfone **1a** with LDA, a cyclization in 6-Endo-Tet mode[4)] took place to afford the cyclized product **2** in high yields (path a). In the study we found that treatment of **1b** with LDA did not give the 14-membered cyclized product **2b** but, instead, gave methylenecyclopropane **3** in moderate yield (path b). Clearly, from this case, the 3-Exo-Tet type reaction was shown to be easier than 14-Endo-Tet cyclization.

In this paper we would like to report in detail a novel method for the synthesis of spiro-linked methylenecyclopropanes **8** from cyclic ketones **4** and 1-chloroalkyl phenyl sulfoxides **5** through α,β-epoxy sulfoxides **7** (Scheme 2).[5)] We also report the two-step conversion of the methylenecyclopropanes **8** to cycloalkane-fused 3-methylfurans **10** via ketones **9**.

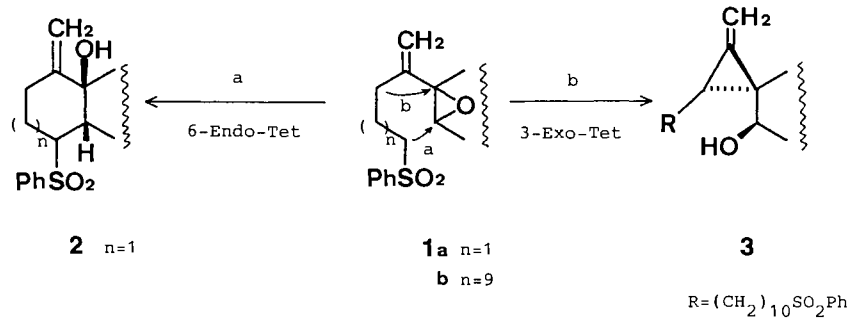

Scheme 1.

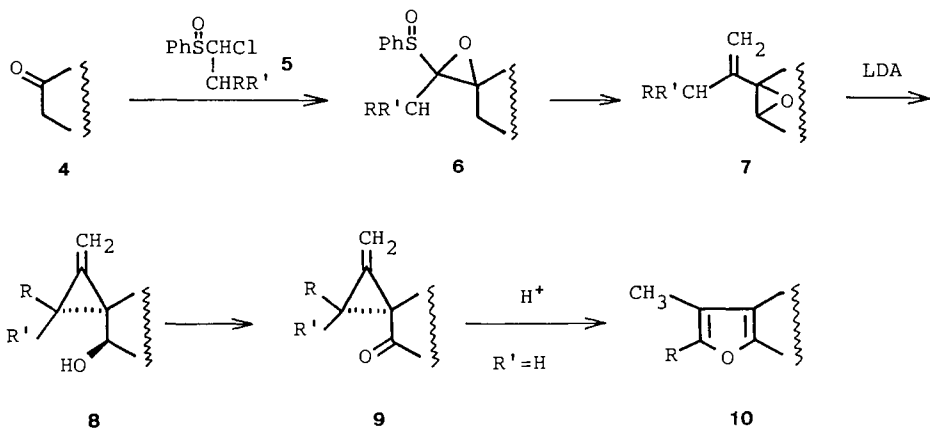

Scheme 2.

Results and Discussion

A Synthesis of Methylenecyclopropane Spiro-Linked with Cycloalkanes. Cyclopropanes are quite interesting compounds in synthetic organic chemistry and their chemistries have extensively been studied.[6] However, methylene-substituted cyclopropanes show somewhat different properties owing to their highly strained nature.[7] Some methods for the synthesis of methylenecyclopropanes and the use of these compounds in organic synthesis have been reported.[8] In perticular, the use of methylenecyclopropanes as a

Table 1. Synthesis of Methylenecyclopropane Spiro-Linked with Cycloalkanes from Cyclic Ketones and 1-Chloroalkyl Phenyl Sulfoxide **5**

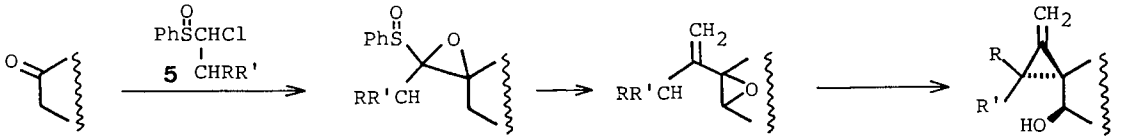

Entry	Ketone	R	R′	Allylic epoxide (Yield/%)[a]	Methylenecyclopropane (Yield/%)[b]
1		H	H	**14** (70)	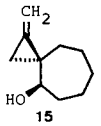 **15** (88)
2		Et	H	**16** (74)	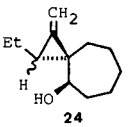 **24** (89)[c]
3		Ph	H	**17** (43)	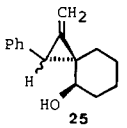 **25** (99)[c]
4		Et	H	**18** (57)	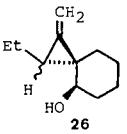 **26** (83)[c]
5		-$(CH_2)_5$-		**19** (57)	— (0)[d]
6		$CH_3(CH_2)_5$	H	**20** (70)	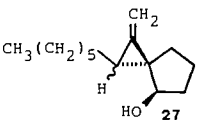 **27** (91)[e]
7	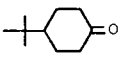	H	H	**21** (50)	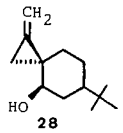 **28** (93)[c]
8	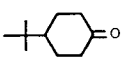	Et	H	**22** (51)	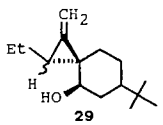 **29** (91)[c]
9	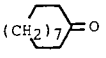	H	H	**23** (62)	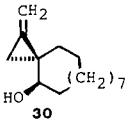 **30** (94)

a) The overall yield from the α,β-epoxy sulfoxides **6**. Isolated yield. b) The yield in the cyclization step. Isolated yield. c) Inseparable diastereomeric mixture. d) No reaction was observed. e) Separable diastereomeric mixture (ratio about 2 : 1).

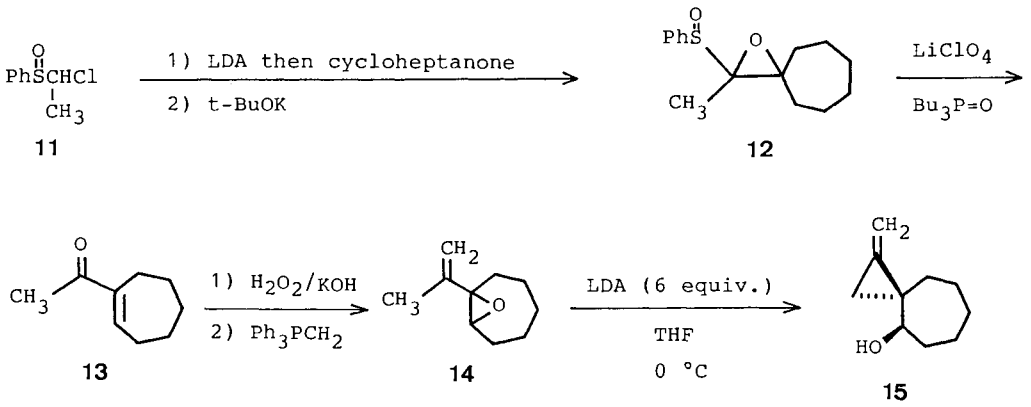

Scheme 3.

precursor for trimethylenemethanes has been known.[7] However, to the best of our knowledge, no report on the synthesis of methylenecyclopropane spiro-linked with cycloalkanes has appeared so far. Here we report a novel synthesis of spiro-linked methylenecyclopropanes; the synthesis of (3*R**,4*S**)-1-methylenespiro[2.6]nonan-4-ol **15** as an example (Scheme 3).

α,β-Epoxy sulfoxide **12** was easily prepared in quantitative yield from 1-chloroethyl phenyl sulfoxide **11** and cycloheptanone through a chloro alcohol. Heating **12** with lithium perchlorate trihydrate in refluxing toluene in the presence of tributylphosphine oxide afforded enone **13** in 85% yield.[9] Epoxidation of **13** was carried out with alkaline hydrogen peroxide in methanol to give the epoxy ketone, which was then treated with methylenetriphenylphosphorane in THF to afford the allylic epoxide **14** in 91% overall yield. Cyclization of **14** to methylenecyclopropane took place cleanly with six equivalents of LDA at 0 °C for 4 h to afford **15** in 84% yield.

The structure of **15** was determined by ^{13}C NMR and IR. In ^{13}C NMR the chemical shift observed (δ=16.3, 102.6, 140.4) was characteristic of methylenecyclopropanes.[10] IR spectrum of **15** showed 3450 cm^{-1} (OH) and the characteristic vibration due to carbon-carbon double bond of methylenecyclopropanes (1760 cm^{-1}).[11] The stereochemistry of **15** was tentatively assigned on the basis of the mechanistic consideration of cyclization of **14**. Representative examples for the synthesis of spiro-linked methylenecyclopropanes from various cyclic ketones and 1-chloroalkyl phenyl sulfoxides are summarized in Table 1.

As shown in Table 1, this procedure can be applied to the synthesis of spiro-linked methylenecyclopropane or its 2-substituted derivatives. Spiro derivatives of 1-methylene-2-alkyl(or phenyl)cyclopropanes were obtained as an inseparable diastereomeric mixture with respect to the asymmetric carbon of the cyclopropane ring. The cyclization of the allylic epoxide **17** having phenyl group took place quite smoothly (the reaction was completed within 1 h) giving **25** in quantitative yield (Entry 3). This result implies that the rate of the cyclization is dependent on the acidity of the allylic hydrogen. α-(Secondary alkyl)-substituted allylic epoxide **19** did not cyclize (Entry 5).

Application of the Method to the Synthesis of Fused 3-Methylfurans. It has been known that cyclopropanes in conjugation with imines undergo acid-catalyzed thermal rearrangement to afford pyrrolines.[12] Analogous with this reaction, it was anticipated that the methylenecyclopropanes in conjugation with the carbonyl group would be rearranged to methylenedihydrofurans or 3-methylfurans. In continuation of our studies with spiro-linked methylenecyclopropanes **8**, we planned to synthesize 3-methylfurans **10**, which are widely found in natural products, especially in sesquiterpenes,[13] through the methylenecyclopropane ketones **9**.[14]

Methylenecyclopropane **28** (see Table 1) was oxidized under the Swern's conditions to give methylenecyclopropane conjugated with ketone **31** in 90% yield. This ketone was quite stable under heating (in refluxing toluene for 2 h, no reaction was observed); however, with 0.3 equivalents of *p*-toluenesulfonic acid it gave the desired 3-methylfuran **34** (see Table 2) in 65% yield. Heating **31** with one equivalent of *p*-toluenesulfonic acid at 100 °C for 2 h was found to be the optimum conditions giving **34** in 84% yield. In this reaction, DMSO was similarly effective as the solvent.

Synthesis of fused 3-methylfurans from methylenecyclopropanes through the ketones is summarized in Table 2. As shown in the table, 1-ethyl-2-methylenecyclopropane **29** gave 2-ethyl-3-methylfuran **35** in a yield similar to that of another example (Entry 2). The rate of the rearrangement was not affected by the size of the ring spiro-linked with cyclopropane (Entry 3).

Scheme 4 shows a synthesis of menthofuran **42**[15] from 4-methylcyclohexanone by the method described above. The α,β-epoxy sulfoxide **37** was synthesized from commercially available 4-methylcyclohexanone in 91% overall yield. Treatment of **37** with $LiClO_4$ gave the enone **38**, which was then epoxidized and

Table 2. Synthesis of Fused 3-Methylfurans **10** from Methylenecyclopropanes **8** through Ketones **9**

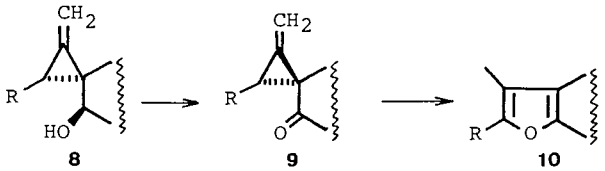

Entry	Methylene-cyclopropane	Ketone (Yield/%)	Solvent[a] (Time)	3-Methylfuran (Yield/%)
1	**28**	**31** (90)	dioxane (2 h)	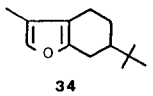 **34** (84)
2	**29**	**32** (83)	dioxane (3 h)	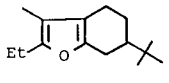 **35** (58)
3	**30**	**33** (99)	DMSO (3 h)	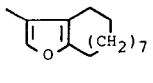 **36** (62)

a) All reactions were carried out at 100 °C with one equivalent of *p*-toluenesulfonic acid.

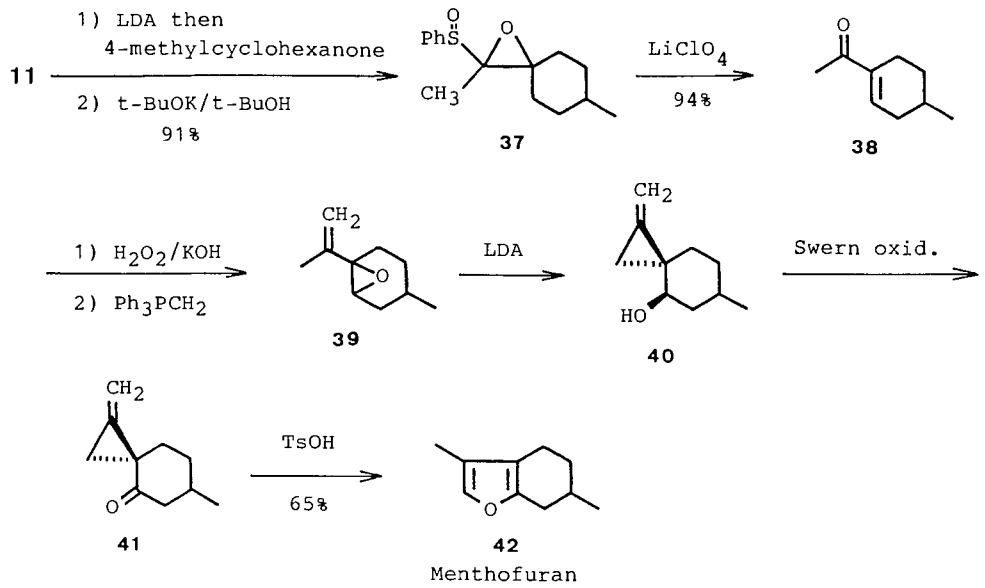

Scheme 4.

methylenated to afford allylic epoxide **39** in good overall yield as a diastereomeric mixture. The cyclization took place smoothly with LDA to give methylenecyclopropane **40** (87%), which was then oxidized to give the ketone **41** in 85% yield. The rearrangement of **41** with one equivalent of *p*-toluenesulfonic acid in DMSO at 100 °C for 2 h gave menthofuran **42** (65% yield), which was identical (IR, NMR, and MS) with the authentic sample.

In conclusion, a novel synthesis of methylenecyclopropane spiro-linked with cycloalkanes and their application to fused 3-methylfurans were achieved. We believe that this study will be of value to explore further the chemistry of methylenecyclopropanes.

Experimental

All melting points are uncorrected. ^{1}H NMR and ^{13}C NMR spectra were measured in a $CDCl_3$ solution with a JEOL FX-100 spectrometer. Electron-impact mass spectra (MS) were obtained at 70 eV by direct insertion. Silica gel BW-127 ZH (Fuji-Devison) containing 2% fluorescence reagent 254 and quartz column were used for column chromatography, and the products having UV absorption were detected by UV irradiation. In experiment requiring dry solvents, THF was distilled from benzophenone ketyl; diisopropylamine, toluene, and DMSO were dried over CaH_2 and distilled. All new compounds, especially oily products, did not give acceptable data for combustion analysis; however, the purity of all the title compounds was judged to be over

95% by ^{1}H NMR spectral determination and chromatographic analyses.

2′-Methyl-2′-(phenylsulfinyl)spiro[cycloheptane-1,1′-oxirane] (12). A solution of **11** (1.02 g; 5.43 mmol) in 3 ml of dry THF was added dropwise to a stirring solution of LDA (6.25 mmol) in dry THF at −60 °C under N_2. The mixture was stirred for 15 min, then cycloheptanone (6.25 mmol) was added. After 5 min the reaction was quenched with saturated aqueous NH_4Cl. The whole was extracted with ether-benzene and after the usual workup the product was purified by silica-gel column chromatography to give 1.61 g (98%) of adduct. *t*-BuOK (6.24 mmol) was added to a solution of the adduct in a mixture of *t*-BuOH-THF (3 : 1, 40 ml) and the solution was stirred at room temperature for 10 min, and then the reaction was quenched with powdered NH_4Cl. The organic solvent was evaporated and the residue was extracted with ether-benzene. The usual workup gave **12** (1.49 g; 92%) as a colorless oil. IR (neat) 1080, 1050 (SO) cm^{-1}; ^{1}H NMR δ=1.32 (3H, s), 1.4—2.0 (10H, m), 2.29 (2H, m), 7.4—7.7 (5H, m); MS *m/z* (%) 139 ([M−PhSO]$^+$ 45), 126 (46), 43 (100).

1-Acetylcycloheptene (13). A mixture of **12** (1.08 g; 4.08 mmol), $LiClO_4 \cdot 3H_2O$ (4.9 mmol), and *n*-Bu_3PO (4.1 mmol) in 40 ml of toluene was refluxed under N_2 for 45 min. The reaction mixture was diluted with benzene and was washed with water. The usual workup followed by silica-gel column chromatography gave 482 mg (85%) of the enone **13** as a colorless oil. IR (neat) 1670 (CO), 1640 cm^{-1}; ^{1}H NMR δ=1.3—1.9 (6H, m) , 2.2—2.56 (4H, m), 2.30 (3H, s), 7.05 (1H, t, *J*=6 Hz); MS *m/z* (%) 138 (M$^+$, 50), 123 (58), 95 (87), 43 (100). Found: *m/z* 138.1037. Calcd for $C_9H_{14}O$: M, 138.1043.

1-Isopropenyl-1,2-epoxycycloheptane (14). To a solution of **13** (470 mg; 3.4 mmol) in 15 ml of MeOH was added 30% H_2O_2 (1.74 ml) and 6 equiv KOH (1.02 mmol). The reaction mixture was stirred at room temperature for 3 h, then the mixture was diluted with water and the whole was extracted with CH_2Cl_2. The usual workup followed by silica-gel column chromatography afforded the epoxide 482 mg (94%) as a colorless oil; IR (neat) 1710 (CO) cm^{-1}; ^{1}H NMR δ=2.03 (3H, s), 3.22 (1H, t, *J*=6 Hz). To a mixture of methyltriphenylphosphonium iodide (1.69 g; 4.19 mmol) and *t*-BuOK (4.19 mmol) in a flame-dried flask was added 8 ml of dry THF and the yellow suspension was stirred at room temperature for 15 min. To this mixture was added a solution of the epoxide (415 mg; 2.7 mmol) and then, the reaction mixture was stirred for 30 min. The reaction was quenched with saturated aqueous NH_4Cl; then the whole was extracted with ether. The usual workup followed by silica-gel column chromatography gave **14** (409 mg; 99%) as a colorless oil. IR (neat) 1655 (C=C) cm^{-1}; ^{1}H NMR δ=1.2—2.3 (10H, m), 1.76 (3H, t, *J*=1 Hz), 2.98 (1H, t, *J*=6 Hz), 4.81 (1H, m), 4.94 (1H, m); MS *m/z* (%) 152 (M$^+$, 32), 123 (63), 109 (48), 81 (100). Found: *m/z* 152.1195. Calcd for $C_{10}H_{16}O$: M, 152.1199.

(3*R,4*S**)-1-Methylenespiro[2.6]nonan-4-ol (15).** A solution of **14** (41 mg; 0.27 mmol) in 1 ml of dry THF was added to a stirring solution of LDA (1.62 mmol) in 3 ml of dry THF at −60 °C under N_2. The mixture was stirred at −60 °C for 10 min and then at 0 °C for 4 h. The reaction was quenched with saturated aqueous NH_4Cl and the whole was extracted with ether. The usual workup followed by silica-gel column chromatography gave **15** (36 mg; 88%) as a colorless oil. IR (neat) 3450 (OH), 1760 (C=C) cm^{-1}; ^{1}H NMR δ=0.8—2.3 (13H, m), 3.38 (3H, t, *J*=6 Hz), 5.37 (1H, m), 5.49 (1H, m); ^{13}C NMR δ=16.33, 22.27, 26.66, 29.34, 30.56, 30.70, 35.82, 76.32, 102.64, 140.41; MS *m/z* (%) 152 (M$^+$, 0.5), 151 (3.5), 123 (34), 109 (91), 81 (100). Found: *m/z* 152.1197. Calcd for $C_{10}H_{16}O$: M, 152.1199.

Allylic Epoxide (16—23). These allylic epoxides were synthesized from cyclic ketones and 1-chloroalkyl phenyl sulfoxides in a similar way as described for **14**.

2-(1,2-Epoxycycloheptyl)-1-pentene (16). Colorless oil; IR (neat) 1660 cm^{-1}; ^{1}H NMR δ=0.92 (3H, t, *J*=7 Hz), 1.0—1.7 (8H, m), 1,7—2.2 (6H, m), 2.90 (1H, t, *J*=5 Hz), 4.76 (1H, m), 4.98 (1H, m); MS *m/z* (%) 180 (M$^+$, 10), 151 (100), 137 (23). Found: *m/z* 180.1520. Calcd for $C_{12}H_{20}O$: M, 180.1514.

2-(1,2-Epoxycyclohexyl)-3-phenylpropene (17). Colorless oil; IR (neat) 1640 cm^{-1}; ^{1}H NMR δ=0.8—2.1 (8H, m), 2.76 (1H, m), 3.42 (2H, bs), 4.80 (1H, m), 5.15 (1H, m), 7.18 (5H, m); MS *m/z* (%) 214 (M$^+$, 33), 185 (21), 129 (78), 91 (100). Found: *m/z* 214.1353. Calcd for $C_{15}H_{18}O$: M, 214.1355.

2-(1,2-Epoxycyclohexyl)-1-pentene (18). Colorless oil; IR (neat) 1650 cm^{-1}; ^{1}H NMR δ=0.91 (3H, t, *J*=7 Hz), 1.1—2.2 (12H, m), 2.93 (1H, m), 4.80 (1H, m), 5.02 (1H, m); MS *m/z* (%) 166 (M$^+$, 22), 137 (100), 123 (82). Found: *m/z* 166.1357. Calcd for $C_{11}H_{18}O$: M, 166.1357.

1-Cyclohexyl-1-(1,2-epoxycyclohexyl)ethylene (19). Colorless oil; IR (neat) 1620 cm^{-1}; ^{1}H NMR δ=0.8—2.2 (19H, m), 2.88 (1H, m), 4.79 (1H, m), 5.04 (1H, m); MS *m/z* (%) 206 (M$^+$, 39), 191 (8), 177 (13), 163 (100). Found: *m/z* 206.1664. Calcd for $C_{14}H_{22}O$: M, 206.1669.

2-(1,2-Epoxycyclopentyl)-1-nonene (20). Colorless oil; IR (neat) 1650 cm^{-1}; ^{1}H NMR δ=0.87 (3H, t, *J*=7 Hz), 1.0—2.1 (21H, m), 3.38 (1H, s), 4.97 (1H, m), 5.15 (1H, m); MS *m/z* (%) 208 (M$^+$, 40), 179 (10), 151 (26), 124 (100). Found: *m/z* 208.1831. Calcd for $C_{14}H_{24}O$: M, 208.1826.

2-(1,2-Epoxy-4-*t*-butylcyclohexyl)propene (21). Colorless oil; IR (neat) 1650 cm^{-1}; ^{1}H NMR δ=0.84 (9H, s), 1.0—2.3 (7H, m), 1.76 (3H, m), 3.10 (1H, bs), 4.79 (1H, m), 4.94 (1H, m); MS *m/z* (%) 194 (M$^+$, 48), 179 (25), 165 (5), 137 (82), 41 (100). Found: *m/z* 194.1669. Calcd for $C_{13}H_{22}O$: M, 194.1669.

2-(1,2-Epoxy-4-*t*-butylcyclohexyl)-1-pentene (22). Colorless oil; IR (neat) 1650 cm^{-1}; ^{1}H NMR δ=0.86 (9H, s), 0.92 (3H, t, *J*=7 Hz), 1.2—2.3 (11H, m), 3.03 (3H, bs), 4.78 (1H, m), 4.99 (1H, m); MS *m/z* (%) 222 (M$^+$, 3), 207 (6), 193 (67), 165 (74), 57 (100). Found: *m/z* 222.1985. Calcd for $C_{15}H_{26}O$: M, 222.1982.

2-(1,2-Epoxycyclododecyl)propen (23). Colorless oil; IR (neat) 1655 cm^{-1}; ^{1}H NMR δ=1.0—1.9 (20H, m), 1.89 (3H, t, *J*=1 Hz), 3.00 (1H, m), 4.85 (1H, m), 4.92 (1H, m); MS *m/z* (%) 222 (M$^+$, 25), 179 (5), 151 (6), 123 (15), 41 (100). Found: *m/z* 222.1980. Calcd for $C_{15}H_{26}O$: M, 222.1982.

Methylenecyclopropane (24—30). These methylenecyclopropanes were synthesized from the corresponding allylic epoxides in a similar way as described for **15**.

(3*R,4*S**)-2-Ethyl-1-methylenespiro[2.6]nonan-4-ol (24).** Colorless oil; IR (neat) 3425 (OH), 1745 (C=C) cm^{-1}; ^{1}H NMR δ=0.8—1.2 (4H, m), 1.2—2.2 (12H, m), 3.40 (1H, m), 5.38 (2H, m); MS *m/z* (%) 180 (M$^+$, 1), 151 (96), 137 (97), 81 (100). Found: *m/z* 180.1514. Calcd for $C_{12}H_{20}O$: M, 180.1513.

(3*R,4*S**)-1-Methylene-2-phenylspiro[2.5]octan-4-ol (25).** Colorless oil; IR (neat) 3420 (OH), 1740 (C=C) cm^{-1};

^{1}H NMR δ=0.8—2.3 (9H, m), 2.90 (1H, m), 3.60 (3/4H, m), 3.84 (1/4H, m), 5.68 (2H, m), 7.0—7.6 (5H, m); MS *m/z* (%) 214 (M^+, 58), 196 (81), 185 (99), 171 (88), 115 (100). Found: *m/z* 214.1359. Calcd for $C_{15}H_{18}O$: M, 214.1356.

(3*R,4*S**)-2-Ethyl-1-methylenespiro[2.5]octan-4-ol (26).** Colorless oil; IR (neat) 3410 (OH), 1750 (C=C) cm^{-1}; ^{1}H NMR δ=0.8—1.1 (4H, m), 1.1—2.3 (11H, m), 3.40 (1H, m), 5.36 (2H, s); MS *m/z* (%) 166 (M^+, 0.6), 151 (14), 137 (100). Found: *m/z* 166.1378. Calcd for $C_{11}H_{18}O$: M, 166.1357.

(3*R,4*S**)-2-Hexyl-1-methylenespiro[2.4]heptan-4-ol (27).** Separable two diastereomeric mixture. Clearly separated more polar isomer is reported. Colorless oil; IR (neat) 3420 (OH), 1755 (C=C) cm^{-1}; ^{1}H NMR δ=0.88 (3H, t, *J*=7 Hz), 1.0—2.1 (18H, m), 3.72 (1H, m), 5.39 (2H, bs).

(3*R,4*S**)-6-*t*-Butyl-1-methylenespiro[2.5]octan-4-ol (28).** Colorless crystals; mp 88—96 °C (AcOEt-hexane); IR (KBr) 3430 (OH), 1740 (C=C); ^{1}H NMR δ=0.88 (9H, s), 0.9—2.2 (9H, m), 3.25 (1H, bs), 5.31 (1H, m), 5.45 (1H, m); MS *m/z* (%) 191 (M^+, 1), 137 (75), 109 (100). Found: *m/z* 194.1663. Calcd for $C_{13}H_{22}O$: M, 194.1668.

(3*R,4*S**)-6-*t*-Butyl-2-ethyl-1-methylenespiro[2.5]octan-4-ol (29).** Colorless oil; IR (neat) 3420 (OH), 1755 (C=C) cm^{-1}; ^{1}H NMR δ=0.88 (9H, s), 0.9—2.1 (13H, m), 3.22 (1H, m), 5.29 (1H, m), 5.33 (1H, m); MS *m/z* (%) 222 (M^+, 33), 207 (16), 193 (60), 165 (70), 123 (66), 41 (100). Found: *m/z* 222.1982. Calcd for $C_{15}H_{26}O$: M, 222.1982.

(3*R,4*S**)-1-Methylenespiro[2.11]tetradecan-4-ol (30).** Colorless crystals; mp 64—65 °C (AcOEt-hexane); IR (KBr) 3370 (OH), 1755 (C=C) cm^{-1}; ^{1}H NMR δ=0.8—1.0 (2H, m), 1.0—2.1 (20H, m), 3.80 (1H, m), 5.37 (2H, m); Anal. Calcd for $C_{15}H_{26}O$: C, 81.08; H, 11.70%. Found: C, 81.17; H, 11.69%.

6-*t*-Butyl-1-methylenespiro[2.5]octan-4-one (31). DMSO (0.4 ml) was added dropwise to a solution of oxalyl dichloride (0.25 ml) in 8 ml of dry CH_2Cl_2 at −60 °C with stirring. The mixture was stirred for 2 min at −60 °C, then a solution of **28** (369 mg; 1.9 mmol) in 2 ml of CH_2Cl_2 was added and the mixture was stirred for 15 min. Et_3N (1.33 ml) was added to the reaction mixture and it was allowed to warm to room temperature. Water (5 ml) was added and the whole was extracted with CH_2Cl_2. The organic layer was washed successively with 5% HCl, saturated aqueous $NaHCO_3$, and saturated brine. The usual workup followed by silica-gel column chromatography gave **31** (332 mg; 90%) as a colorless oil. IR (neat) 1690 (CO) cm^{-1}; ^{1}H NMR δ=0.91 (9H, s), 1.2—2.7 (9H, m), 5.44 (2H, m); MS *m/z* (%) 192 (M^+, 41), 149 (6), 135 (20), 108 (61), 41 (100). Found: *m/z* 192.1513. Calcd for $C_{13}H_{20}O$: M, 192.1513.

6-*t*-Butyl-2-ethyl-1-methylenespiro[2.5]octan-4-one (32). Colorless oil; IR (neat) 1695 (CO) cm^{-1}; ^{1}H NMR δ=0.90 (9H, s), 1.04 (3H, t, *J*=7 Hz), 1.2—2.7 (10H, m), 5.28 (1H, d, *J*=2 Hz), 5.38 (1H, d, *J*=2 Hz); MS *m/z* (%) 220 (M^+, 24), 205 (51), 192 (56), 108 (100). Found: *m/z* 220.1824. Calcd for $C_{15}H_{24}O$: M, 220.1825.

1-Methylenespiro[2.11]tetradecan-4-one (33). Colorless oil; IR (neat) 1700 (CO) cm^{-1}; ^{1}H NMR δ=1.1—2.6 (22H, m), 5.44 (1H, m), 5.51 (1H, m); MS *m/z* (%) 220 (M^+, 14), 205 (30), 177 (63), 163 (67), 79 (100). Found: *m/z* 220.1827. Calcd for $C_{15}H_{24}O$: M, 220.1825.

Cycloalkane-Fused 3-Methylfurans (34—36). A solution of ketone **31** (63 mg; 0.33 mmol) and *p*-TsOH·H_2O (0.33 mmol) in 5 ml of 1,4-dioxane was refluxed under N_2 for 3 h. The reaction mixture was cooled, then saturated aqueous $NaHCO_3$ was added. The whole mixture was extracted with ether, and the usual workup followed by silica-gel column chromatography gave 6-*t*-butyl-3-methyl-4,5,6,7-tetrahydrobenzofuran **34** (53 mg; 84%) as a colorless oil. IR (neat) 1645, 1565 cm^{-1}; ^{1}H NMR δ=0.94 (9H, s), 1.1—2.8 (7H, m), 1.90 (3H, d, *J*=1 Hz), 7.00 (1H, m); MS *m/z* (%) 192 (M^+, 35), 177 (5), 135 (8), 108 (100). Found: *m/z* 192.1513. Calcd for $C_{13}H_{20}O$: M, 192.1513. 3-Methylfuran derivative **35**: Colorless oil; IR (neat) 1665, 1610 cm^{-1}; ^{1}H NMR δ=0.93 (9H, s), 1.16 (3H, t, *J*=7 Hz), 1.83 (3H, s), 2.53 (2H, q, *J*=7 Hz); MS *m/z* (%) 192 (M^+, 34), 135 (8), 108 (100). Found: *m/z* 192.1513: Calcd for $C_{13}H_{20}O$: M, 192.1513. 3-Methylfuran derivative **36**: Colorless oil; IR (neat) 1635, 1570 cm^{-1}; ^{1}H NMR δ=1.0—2.0 (16H, m), 1.93 (3H, d, *J*=1 Hz), 2.35 (2H, t, *J*=7 Hz), 2.54 (2H, t, *J*=7 Hz) 7.02 (1H, m); MS *m/z* (%) 220 (M^+, 92), 205 (35), 109 (100). Found: *m/z* 220.1827. Calcd for $C_{15}H_{24}O$: M, 220.1826.

A Synthesis of (±)-Menthofuran (42). (±)-Menthofuran **42** was synthesized starting from **11** and 4-methylcyclohexanone in a similar way as described above. Spectral data of the intermediates **37—41** are recorded as follows. α,β-Epoxy sulfoxide **37** (91% yield from **11**): Colorless oil; IR (neat) 1090, 1050 (SO) cm^{-1}; ^{1}H NMR δ=0.98 (3H, d, *J*=6 Hz), 1.29 (3H, s), 7.4—7.7 (5H, m); MS *m/z* (%) 264 (M^+, trace), 139 (40), 43 (100). Found: *m/z* 264.1174. Calcd for $C_{15}H_{20}O_2S$: M, 264.1182. Enone **38** (94% yield from **37**): Colorless oil; IR (neat) 1670 (CO), 1645 cm^{-1}; ^{1}H NMR δ=0.98 (3H, d, *J*=6 Hz), 2.27 (3H, s), 6.82 (1H, m); MS *m/z* (%) 138 (M^+, 81), 123 (93), 95 (88), 43 (100). Found: *m/z* 138.1044. Calcd for $C_9H_{14}O$: M, 138.1044. Epoxide **39** (69% from **38**): Colorless oil; IR (neat) 1650 cm^{-1}; ^{1}H NMR δ=0.88 (3H, d, *J*=6 Hz), 1.76 (3H, m), 3.03 (1H, m), 4.82 (1H, m), 4.96 (1H, m); MS *m/z* (%) 152 (M^+, 82), 137 (75), 41 (100). Found: *m/z* 152.1195. Calcd for $C_{10}H_{16}O$: M, 152.1199. Methylenecyclopropane **40** (87% yield from **39**): Colorless oil; IR (neat) 3370 (OH), 1745 (C=C) cm^{-1}; ^{1}H NMR δ=0.92 (3H, d, *J*=7 Hz), 0.9—2.3 (9H, m), 3.23 (1H, bs), 5.31 (1H, m), 5.45 (1H, m); MS *m/z* (%) 152 (M^+, 1), 151 (3), 137 (20), 123 (100). Found: *m/z* 152.1203. Calcd for $C_{10}H_{16}O$: M, 152.1200. Ketone **41** (85% yield from **40**): Colorless oil; IR (neat) 1705 (CO) cm^{-1}; ^{1}H NMR δ=1.05 (3H, d, *J*=6 Hz), 1.2—2.6 (9H, m), 5.40 (2H, m); MS *m/z* (%) 150 (M^+, 22), 121 (4), 108 (52), 79 (92), 39 (100). Found: *m/z* 150.1051. Calcd for $C_{10}H_{14}O$: M, 150.1044.

This work was supported by a Grant-in-Aid for Scientific Research No. 01571168 from the Ministry of Education, Science and Culture which is gratefully acknowledged.

References

1) α,β-Epoxy sulfoxides as useful intermediates in organic synthesis. 27. Part 26: T. Satoh, J. Shishikura, and K. Yamakawa, *Chem. Pharm. Bull.*, **38**, 1798 (1990).

2) G. Stork, L. D. Cama, and D. R. Coulson, *J. Am. Chem. Soc.*, **96**, 5268 (1974); G. Stork and J. F. Cohen, *ibid.*, **96**, 5270 (1974); A. S. Rao, *Tetrahedron*, **39**, 2323 (1983); J. G. Smith, *Synthesis*, **1984**, 629; J. H. Babler, *J. Org. Chem.*, **52**, 4614 (1987); G. Procter, A. T. Russell, P. J. Murphy, T. S. Tan, and A. N. Mather, *Tetrahedron*, **44**, 3953 (1988).

3) T. Satoh, Y. Kawase, and K. Yamakawa, *J. Org. Chem.*, **55**, 3962 (1990).

4) J. E. Baldwin, *J. Chem. Soc., Chem. Comm.*, **1976**,

734.

5) Preliminary communication of this study: T. Satoh, Y. Kawase, and K. Yamakawa, *Tetrahedron Lett.*, **31**, 3609 (1990).

6) For a recent review: H. N. C. Wong, M-Y. Hon, C-W. Tse, and Y-C. Yip, *Chem. Rev.*, **89**, 165 (1989).

7) P. Dowd, *Acc. Chem. Res.*, **5**, 242 (1972); J. A. Berson, *ibid.*, **11**, 446 (1978); W. E. Billups, M. H. Haley, and G-A. Lee, *Chem. Rev.*, **89**, 1147 (1989); B. Halton, *ibid.*, **89**, 1161 (1989); J. F. Liebman, *ibid.*, **89**, 1225 (1989).

8) For recent reports: R. Noyori, M. Yamakawa, and H. Takaya, *Tetrahedron Lett.*, **1978**, 4823; P. Binger and M. H. Buch, *Top. Curr. Chem.*, **135**, 77 (1987); T. Cohen, S-H Jung, M. L. Romberger, and D. W. McCullough, *Tetrahedron Lett.*, **29**, 25 (1988); D. W. McCullough and T. Cohen, *ibid.*, **29**, 27 (1988); J. A. Stafford and J. E. McMurry, *ibid.*, **29**, 2531 (1988); N. Chatani, T. Takeyasu, and T. Hanafusa, *ibid.*, **29**, 3979 (1988); S. A. Bapuji, W. B. Motherwell, and M. Shipmann, *ibid.*, **30**, 7107 (1989); W. A. Donaldson, J. Wang, V. G. Cepa, and J. D. Suson, *J. Org. Chem.*, **54**, 6056 (1989); P. Binger, A. Freund, and P. Wedemann, *Tetrahedron*, **45**, 2887 (1989); W. A. Smit, S. L. Kireev, O. M. Nefedov, and V. A. Tarasov, *Tetrahedron Lett.*, **30**, 4021 (1989); M. Lai and H. Liu, *J. Am. Chem. Soc.*, **112**, 4034 (1990); F. M. Cordero, A. Brandi, C. Querci, A. Goti, F. D. Sarlo, and A. Guarna, *J. Org. Chem.*, **55**, 1762 (1990); W. A. Donaldson, J. T. North, J. A. Gruetzmacher, M. Finley, and D. J. Stepuszek, *Tetrahedron*, **46**, 2263 (1990); W. A. Donaldson, D. J. Stepuszek, and J. A. Gruetzmacher, *ibid.*, **46**, 2273 (1990).

9) T. Satoh, M. Itoh, T. Ohara, and K. Yamakawa, *Bull. Chem. Soc. Jpn.*, **60**, 1839 (1987).

10) H-O. Kalinowski, S. Berger, and S. Braun, "Carbon-13 NMR Spectroscopy," John Wiley and Sons, New York (1988), pp. 118—139.

11) R. M. Silverstein, G. C. Bassler, and T. C. Morrill, "Spectrometric Identification of Organic Compounds," 4th ed, John Wiley and Sons, New York (1981), p. 109. The absorption frequency of external exocyclic-olefinic bond of methylenecyclopropane shows 1781 cm^{-1}.

12) R. V. Stevens, M. C. Ellis, and M. P. Wentland, *J. Am. Chem. Soc.*, **90**, 5576 (1968).

13) T. K. Devon and A. I. Scott, "Handbook of Naturally Occurring Compounds," Academic Press, New York (1972), Vol, II.

14) Some methods for a synthesis of 3-methylfurans from ketones: H. Hagiwara, H. Uda, and T. Kodama, *J. Chem. Soc., Perkin Trans. 1*, **1980**, 963; M. Aso, M. Sakamoto, N. Urakawa, and K. Kanematsu, *Heterocycles*, **31**, 1003 (1990).

15) T. Sato, M. Tada, and T. Takahashi, *Bull. Chem. Soc. Jpn.*, **52**, 3129 (1979).

Conformation in Solution of the Fully Toxic Domain of Heat-Stable Enterotoxin (ST_p) Produced by Enterotoxigenic *Escherichia coli*[1)]

Hiroshi Ozaki,* Hirokazu Kubota, Takashi Sato, Yuji Hidaka, Haruhiko Tamaoki, Yuji Kobayashi, Yoshimasa Kyogoku, Takashi Sugimura,† Akira Tai,† and Yasutsugu Shimonishi
Institute for Protein Research, Osaka University, Yamada-oka 3-2, Suita, Osaka 565
†Faculty of Science, Himeji Institute of Technology, 2167 Shosha, Himeji, Hyogo 671-22
(Received November 27, 1990)

Heat-stable enterotoxin (ST_p) produced by a porcine strain of enterotoxigenic *Escherichia coli* is a peptide of 18 amino acid residues. The full toxicity is generated by a core peptide of 13 amino acids from residue 5 to 17 ($ST_p(5—17)$). Detailed conformational analysis of $ST_p(5—17)$ was performed by NMR spectroscopy and distance geometry calculations. The tertiary structure of $ST_p(5—17)$ was found to have a right-handed spiral fold throughout the whole molecule which was stabilized by the network of disulfide linkages and hydrogen bonds. This folding pattern was demonstrated in both organic and aqueous solutions.

Enterotoxigenic *E. coli* elaborates two kinds of heat-stable enterotoxins (named ST_p and ST_h) with 18 and 19 amino acid residues respectively, which are responsible for acute diarrhea in infants and domestic animals.[2-5)] The ST acts on ST-sensitive cells in the intestine to stimulate guanylate cyclase and to increase the level of cyclic GMP in the cells, resulting in fluid secretion from the intestinal epithelial cells.[6-9)] Recently, a selective and high-affinity binding protein(s) for ST on rat intestinal cell membranes has been identified and membrane bound guanylate cyclase has been suggested to be bound to, or present near this protein(s).[10-12)] The initial step in the biological reaction of ST is the formation of an ST-protein(s) complex. However, details of this step are not yet fully understood. For understanding the molecular basis of the interaction of ST with its receptor protein(s) and the role of amino acid residues of ST in generation of its toxicity, an important problem is to elucidate the molecular conformation of ST and to identify the part(s) of the ST molecule recognized by its receptor protein(s).

Our recent studies demonstrated that the full enterotoxigenic activities of ST_p and ST_h are generated by toxic domains (abbreviated as $ST_p(5—17)$ and $ST_h(6—18)$, respectively) consisting of 13 amino acid residues (boxed by a broken line in Fig. 1).[1)] These findings imply that this domain includes the site(s) for recognition of ST by its receptor protein(s) on the intestinal cell membrane.[13,14)] The conformation of the toxic domain of ST_h in solution was initially studied by us[15)] and by Gariepy et al.[16)] by ^1H NMR spectroscopy and distance geometry calculations. Both studies provided useful information on the conformation of the peptide backbone of the toxic domain of ST_h. However, the structure of the whole molecule could not be refined, because an efficient nuclear Overhauser effect (NOE) could not be observed and the exact disulfide pairings in ST were not known at that time. Thus, the conformation of ST in solution is still uncertain.

In this work, we investigated the conformation in solution of $ST_p(5—17)$, the toxic domain of ST_p, which differs from $ST_h(6—18)$ in only one amino acid residue, by ^1H NMR spectroscopy and distance geometry algorithm analysis.[15,17,18)] $ST_p(5—17)$ rather than $ST_h(6—18)$ was chosen for confomational study of ST, because ST_p is found more often than ST_h. In an organic solvent, $ST_p(5—17)$ was shown to have a spatial structure with a right-handed spiral stabilized by three intramolecular disulfide linkages and hydrogen bondings, and its structure in an aqueous solution

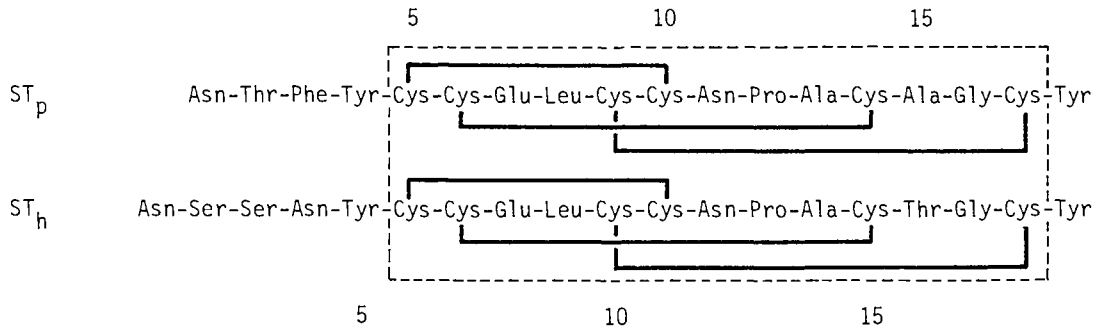

Fig. 1. Amino acid sequences and disulfide linkages of heat-stable enterotoxins (ST_p[5)] and ST_h[4,14)]) of enterotoxigenic *E. coli*.

was suggested to be almost the same. The conformation of $ST_p(5—17)$ elucidated here should be useful for understanding the molecular interaction of ST and its binding protein(s), which proceeds in an aqueous environment, and for examining the conformation-function relationship of the peptide.

Results and Discussion

Resonance Assignment: The ^1H NMR spectrum of

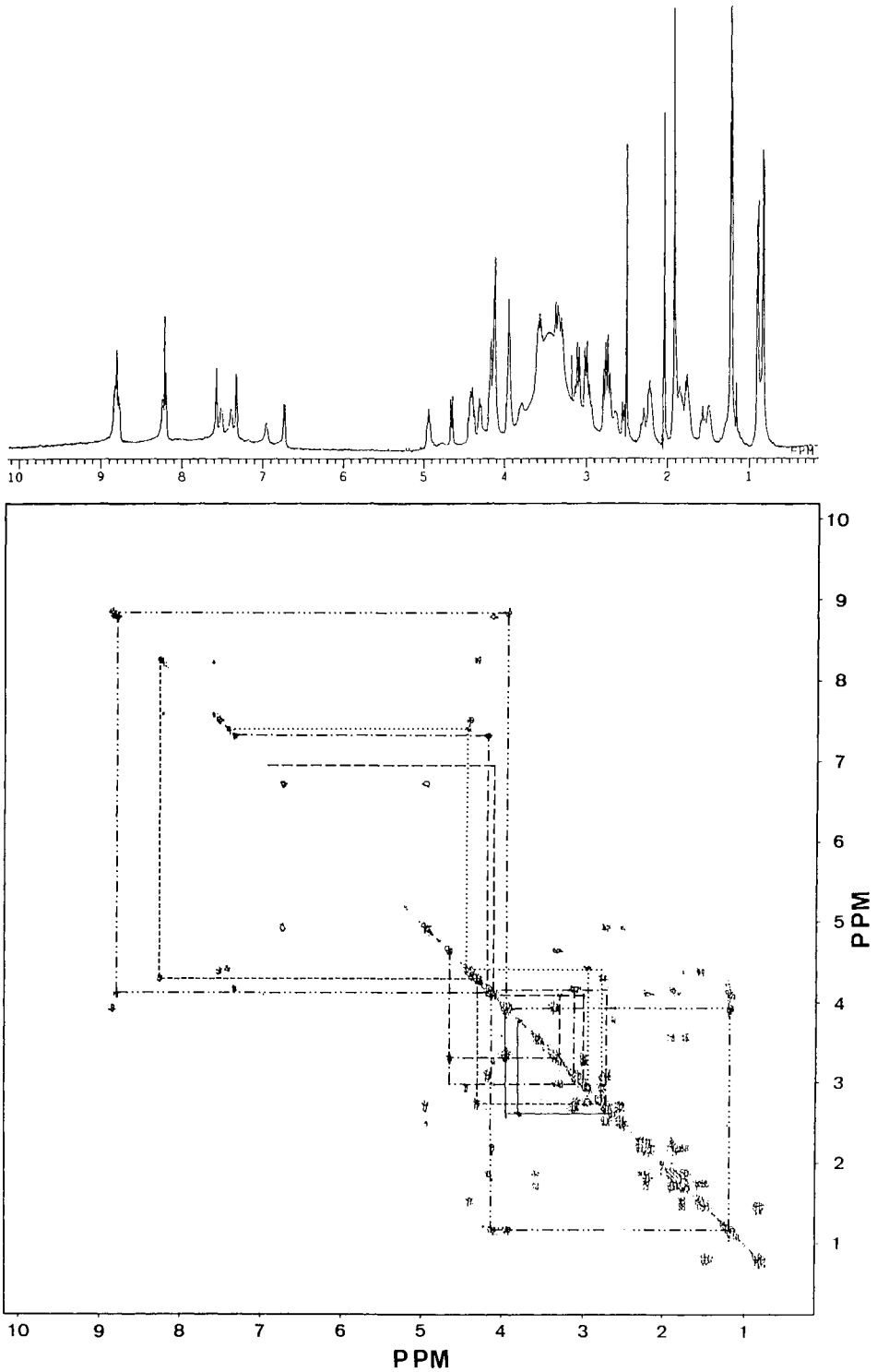

Fig. 2. DQF-COSY spectrum of ST_p (5—17) at 10 °C in DMSO-d_6/CH_3CN-d_3 (v/v, 85/15). Spin systems for six Cys and two Ala residues are indicated: Cys^5 (——), Cys^6 (– · –), Cys^9 (------), Cys^{10} (— —), Cys^{14} (— · —), Cys^{17} (·····), Ala^{13} (— · · —), and Ala^{15} (— ··· —).

ST_p(5—17) was measured in a mixture of DMSO-d_6 and CH_3CN-d_3, as used in ^1H NMR spectroscopy of ST_h(6—19).[15] Peak and sequential assignment were achieved by analyzing spin systems of constituent amino acid residues. These were examined by through-bond connectivities in the DQF-COSY spectrum of ST_p(5—17) and sequential NOE connectivities between the NH proton of an amino acid residue (i+1) and the protons of the $C_\alpha H$, NH and $C_\beta H$ of the neighboring residue (i) according to the procedures described in Refs. 19 and 20, respectively.

Figures 2 and 3 show the DQF-COSY spectrum of the peptide and its NOESY spectrum in the $C_\alpha H$-NH cross peak region, respectively. The chemical shifts of all the constituent amino acid residues of ST_p(5—17) were assigned except for those of Cys^5 and Cys^6. These protons were assigned by comparison of the 1D spectrum of ST_p(5—17) with that of [β,β-d_2-Cys^5]ST_p(5—17), in which two protons on the C_β of Cys^5 were replaced by deuterium, as shown in Fig. 4. However, no sequential connectivity was detected between Cys^5 and Cys^6 or between Cys^6 and Glu^7 in the N-terminal segment Cys^5-Cys^6-Glu^7, because the NH protons were exchanged quickly with protons from a trace of water contaminating the solvent and so the NH protons of Cys^5 and Cys^6 could not be observed in the spectrum and the peak of the NH proton of Glu^7 became broad. The connectivities in the sequence from Asn^{11} to Ala^{13} were confirmed by through space NOEs between the $C_\alpha H$ of Asn^{11} and the $C_\delta H$ of Pro^{12} and between the $C_\delta H$ and $C_\gamma H$ of Pro^{12} and the NH of Ala^{13}, although Asn^{11} could not be connected to Pro^{12} by sequential NOE connectivities. The presence of the former NOE indicated that the peptide bond between Asn^{11} and Pro^{12} had the trans configuration, and this was confirmed by construction of a molecular model. Table 1 summarizes the resonance assignment of ST_p(5—17).

The resonance assignments of the four Cys residues at positions of 5, 6, 9, and 10 in ST_p(5—17) (corresponding to 6, 7, 10, and 11 in ST_h) were essential to provide the distance information in the N-terminal region, as discussed later, because all long-range NOEs observed in the region from Cys^5 to Cys^{10} were derived from the protons of these four Cys residues, as summarized in Table 2. In a previous study of ST_h(6—19),[16] the spin systems of these four Cys were not assigned, because no sequential NOEs in the sequence containing these amino acid residues were detected as the peptide was examined in aqueous

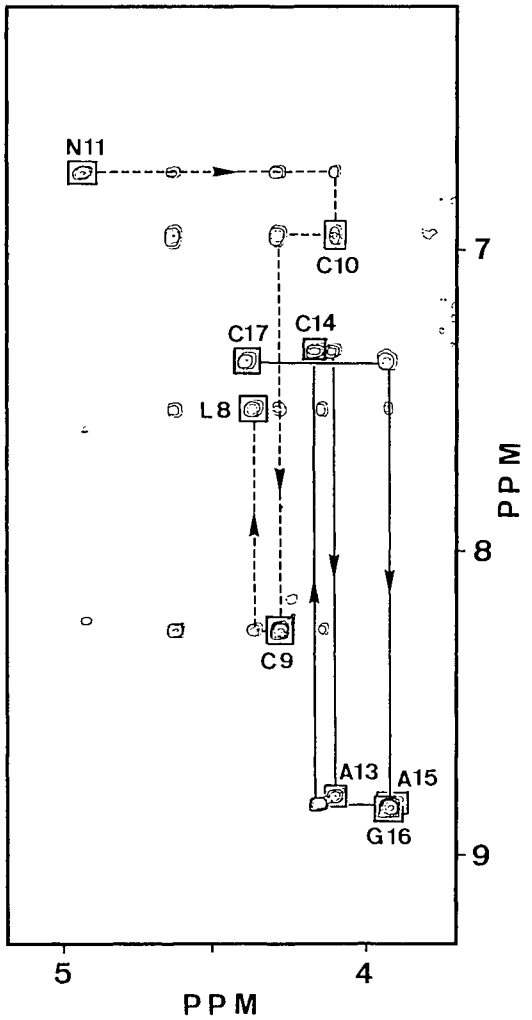

Fig. 3. NOESY spectrum of ST_p (5—17) in the $C_\alpha H$-NH NOE cross peak region. Sequential assignments of segments 8—11 (----) and 13—17 (——) are indicated by arrows according to the direction of the assignment. COSY cross peak positions for each residue are indicated by boxes.

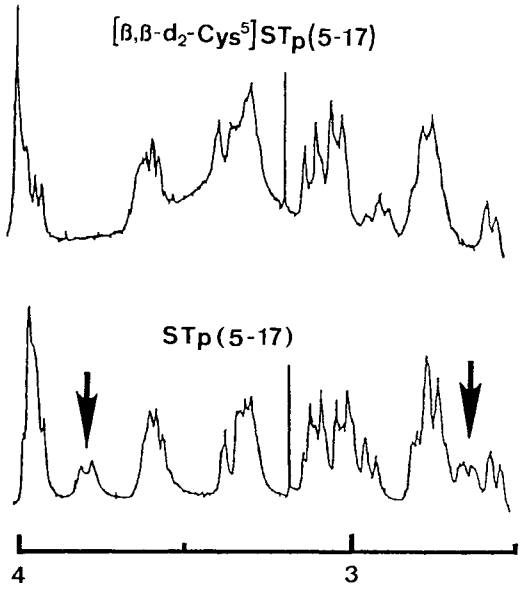

Fig. 4. 1D ^1H NMR spectra of ST_p (5—17) and [β,β-d_2-Cys^5]ST_p (5—17) in DMSO-d_6/CH_3CN-d_3 (v/v, 85/15). The peaks of $C_\beta H$ protons of Cys^5 are indicated by arrows.

Table 1. Resonance Assignment of ST_p (5-17) in DMSO-d_6/CH_3CN-d_3 (85/15)[a]

Residue	Chemical shift/ppm					
	NH	$C_\alpha H$	$C_\beta H$	$C_\gamma H$	$C_\delta H$	β-$CONH_2$
Cys^5	—	3.95	3.80, 2.65			
Cys^6	—	4.65	3.01, 3.34			
		(4.88)	(3.06, 3.58)			
Glu^7	10.33	4.17	1.91—1.94	2.30		
	(9.66)	(4.35)	(2.16)	(2.46, 2.67)		
Leu^8	7.51	4.39	1.58, 1.78	1.48	0.82, 0.90	
	(7.38)	(4.69)	(1.59, 1.86)	(1.51)	(0.89, 0.94)	
Cys^9	8.22	4.31	2.77, 3.09			
	(8.35)	(4.41)	(2.91, 3.27)			
Cys^{10}	6.95	4.11	3.00, 3.30			
		(4.50)	(3.32, 3.51)			
Asn^{11}	6.73	4.94	2.55, 2.73			7.58, 8.20
	(7.12)	(5.16)	(2.79, 2.87)			(7.12, 7.90)
Pro^{12}		4.13	1.85, 2.22	1.74, 1.91	3.59	
		(4.34)	(1.99, 2.35)	(2.00)	(3.75)	
Ala^{13}	8.78	4.13	1.21			
	(8.49)	(4.32)	(1.37)			
Cys^{14}	7.32	4.17	2.70, 3.10			
	(7.70)	(4.37)	(3.14—3.16)			
Ala^{15}	8.81	3.94	1.20			
	(8.71)	(4.21)	(1.41)			
Gly^{16}	8.84	3.38, 3.96				
	(8.87)	(3.80, 4.11)				
Cys^{17}	7.34	4.42	2.77, 2.94			
	(7.63)	(4.81)	(2.98, 3.14)			

a) Values in parentheses indicate chemical shifts (ppm) in H_2O/D_2O (80/20) at 17°C and pH 5.6. Chemical shifts are shown with reference to internal tetramethylsilane in DMSO-d_6/CH_3CN-d_3 (85/15) and sodium 3-(trimethylsilyl)-1-propanesulfonate in H_2O/D_2O (8/2).

Table 2. Input Distance Constraints (in Å) for the Distance Geometry Calculations on ST_p (5—17)

Proton pair[1]				Upper limit of distance[2]/Å		Proton pair[1]				Upper limit of distance[2]/Å	
				in DMSO[3]	in H_2O[4]					in DMSO[3]	in H_2O[4]
Cys^5	$C_\alpha H$	Cys^{10}	$C_\beta P$	5.0[a]			NH	Asn^{11}	NH	3.5	
Cys^6	$C_\alpha H$	Leu^8	NH	3.5			NH	Cys^{10}	$C_\beta P$	4.1[b]	
	$C_\alpha H$	Cys^9	$C_\alpha H$	3.5	(4.0)	Asn^{11}	$C_\alpha H$	Ala^{13}	NH	4.0	
	$C_\alpha H$	Cys^9	NH	3.5			$C_\alpha H$	Pro^{12}	$C_\delta P$	3.5[a]	4.0[a]
	$C_\alpha H$	Cys^{10}	NH	3.5			NH	Cys^{14}	NH	4.0	
	$C_\alpha H$	Asn^{11}	NH	3.5	(4.0)		$C_\beta P$	Ala^{13}	NH		(5.0[a])
	$C_\alpha H$	Cys^{14}	$C_\beta P$	4.5[a]	(5.0[a])		NH	Asn^{11}	$C_\beta P$	4.1[b]	4.1[b]
Glu^7	$C_\alpha H$	Leu^8	NH	3.5		Pro^{12}	$C_\gamma P$	Ala^{13}	NH	4.5[a]	4.5[a]
	NH	Leu^8	NH	4.0	4.0		$C_\delta P$	Ala^{13}	NH	4.5[a]	4.5[a]
	$C_\beta P$	Leu^8	NH	5.0[a]			$C_\alpha H$	Cys^{17}	$C_\beta P$	5.0[a]	
	NH	Glu^7	$C_\beta P$		4.1[b]	Ala^{13}	$C_\alpha H$	Cys^{14}	NH	3.0	(4.0)
Leu^8	$C_\alpha H$	Leu^8	$C_\delta Q$	4.7[c]	4.7[c]		$C_\beta M$	Cys^{14}	NH	4.5[a]	(5.0[a])
	$C_\alpha H$	Leu^8	$C_\gamma H$	3.5			NH	Cys^{14}	NH	3.0	3.0
	NH	Leu^8	$C_\beta P$	4.1[b]	4.6[b]		NH	Ala^{13}	$C_\beta M$	3.6[b]	3.6[b]
	$C_\alpha H$	Cys^9	NH	3.5	4.0	Cys^{14}	$C_\alpha H$	Ala^{15}	NH	3.0	2.5
	NH	Cys^9	$C_\alpha H$	4.0			$C_\beta P$	Ala^{15}	NH	4.5[a]	4.5[a]
	NH	Cys^9	NH	3.0	3.5		NH	Cys^{14}	$C_\beta P$	3.6[b]	3.1[b]
	NH	Cys^{10}	NH	3.5		Ala^{15}	$C_\alpha H$	Gly^{16}	NH	3.0	2.5
Cys^9	$C_\alpha H$	Asn^{11}	NH	3.5	3.5		$C_\beta M$	Gly^{16}	NH		4.5[a]
	$C_\alpha H$	Cys^{10}	NH	3.5			NH	Ala^{15}	$C_\beta M$	3.6[b]	3.6[b]
	NH	Cys^{10}	NH	3.5			$C_\alpha H$	Cys^{17}	NH		4.0
	NH	Cys^9	$C_\beta P$	4.6[b]		Gly^{16}	$C_\alpha P$	Cys^{17}	NH	4.5[a]	4.5[a]
Cys^{10}	$C_\alpha H$	Asn^{11}	NH	3.5	4.0		NH	Cys^{17}	NH	3.5	3.5
	$C_\beta P$	Asn^{11}	NH	5.0[a]		Cys^{17}	NH	Cys^{17}	$C_\beta P$	4.1[b]	3.6[b]

1) P and M indicate pseudoatoms of methylene (including β-amido) and methyl protons, respectively. The pseudo position for methyl protons of leucine is Q in Ref. 25. 2) Upper limit of interatomic distances containing pseudoatoms include their corrections of a 1.0, b 0.6, and c 1.7 Å. 3) NOE cross peaks were collected from NOESY spectra in DMS0-d_6/CH_3CN-d_3 (85/15) at 10 °C. 4) NOE cross peaks were collected from NOESY spectra in H_2O/D_2O (80/20) at pH 5.6 and 17 °C. All these NOEs were also observed at 5 °C. Values in parentheses indicate upper constraints for NOEs detected only at 5 °C.

conditions. This was probably the reason for lack of the distance information in the N-terminal region, resulting in uncertainty about the conformation of $ST_h(6—19)$.

The ^1H NMR spectrum of $ST_p(5—17)$ was also measured in aqueous solution to obtain information about the conformation of the peptide in an aqueous environment. Chemical shifts were assigned by two procedures: sequential assignment as described above, and assignment of the NH and $C_\alpha H$ protons derived by titration of the peptide in DMSO-d_6/CH_3CN-d_3 with H_2O. Results on resonance assignment are listed in Table 1.

Folding Pattern of $ST_p(5—17)$: The data on interatomic distance constraints obtained from NOEs are summarized in Table 2. The folding pattern of the peptide backbone of $ST_p(5—17)$ was calculated from these data and disulfide pairings by distance geometry algorithm analysis.[15] Thirty calculations were performed using different random initial structures. The value of the target function (T-value)[15,17] should be zero if a calculated structure satisfies all constraints. Therefore, T-values were used for evaluating the calculated structures. In addition, the compatibility of the interatomic distances in the calculated structures with the input data was examined by checking individual NOE distance constraint violations. For non-bonded contact, 0.1 Å was an acceptable allowance within the range of possible contacts between two atoms. Among the 30 calculated structures, 14 exhibited no individual violations or non-bonded contacts of more than 0.1 Å. All these structures had T-values of less than 0.1. The convergency of these structures was estimated by calculating the RMSDs between these structures, because the average RMSD of calculated structures with the same folding pattern fell within 2.8 Å, as seen in Table 3. The averaged RMSD was 1.80 Å for atoms in the peptide backbone. All these structures showed the same folding pattern, as seen in Fig. 5(R).

For conformational analysis by distance geometry calculation, sufficient distance information is required to define the correct folding pattern of the peptide backbone.[21] In previous conformational studies of ST, its unique conformation could not be determined because of lack of sufficiently useful NOE data, as described above.[15,16] The question arose of how much interatomic distance information was necessary for defining the conformation of the ST molecule. Therefore, we examined the relationship between the amount and kind of distance information and the folding patterns of the calculated structures, as summarized in Table 3. Thirty calculations were carried out for all cases and T-values were used to evaluate the folding patterns of calculated structures. When the distance information was only that for disulfide pairings, the structure ($T<0.1$) were roughly classified into five folding patterns by viewing the folding patterns obtained by computer graphics; (1) a right-handed spiral fold (R), (2) a left-handed spiral fold (L), (3) R in the N-terminal region end L in the C-terminal region (RML), (4) L in the N-terminal and R in the C-terminal (LMR). and (5) a fold in which the N-terminal portion passes through the loop formed in the central region (C). These folding patterns are drawn as ribbon models in Fig. 5. Examination of the folding pattern of the peptide using intra-residual and sequentially connected NOEs and disulfide pairings excluded two folding patterns (LMR and C) and revealed three folding patterns (R, L and RML). By

Table 3. Amount of Distance Constraints Used and Fold Patterns of Calculated Structures

Constraints used	Number of conformers (x/n)	Total RMSD Å	Type of fold pattern[a]	RMSD in fold type Å
S-S	24/30	3.63	R (8)	2.10
			L (5)	2.40
			RML (3)	1.81
			LMR (3)	2.80
			C (5)	1.87
S-S + Short-range NOEs	9/30	3.50	R (3)	2.20
			L (4)	2.02
			RML (2)	1.90
S-S + All NOEs	14/30	1.80	R (14)	1.80
All NOEs	12/30	1.62	R (12)	1.62

a) R, right-handed spiral fold pattern; L, left-handed spiral fold pattern; RML, R in the N-terminal region and L in the C-terminal region; LMR, L in the N-terminal region and R in the C-terminal region; C, the peptide backbone passes through the loop formed by disulfide linkages. Values in parentheses indicate numbers of conformers to the respective folding patterns.

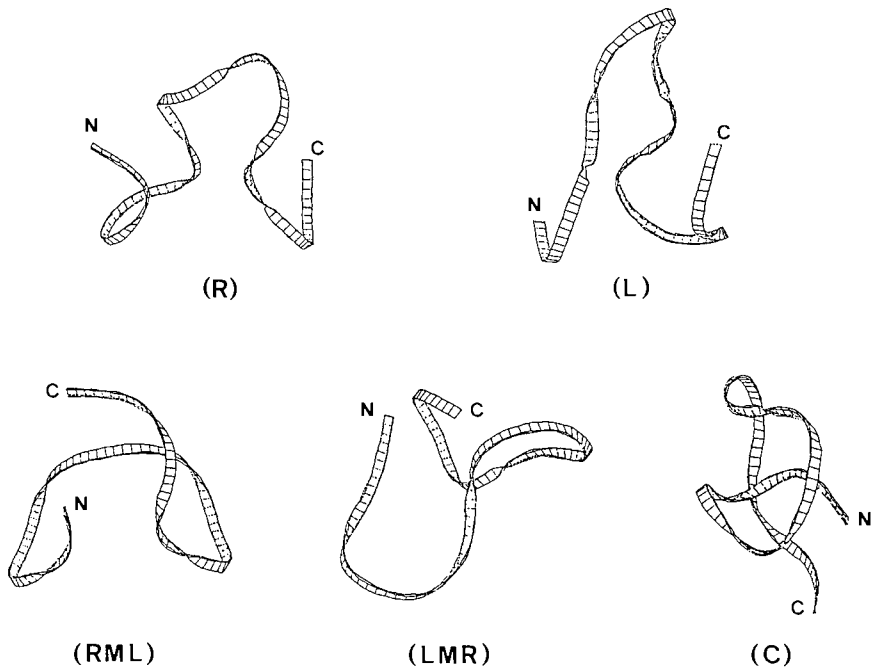

Fig. 5. Typical folding patterns of R, L, RML, LMR and C in Table 3. When the amounts of distance information were not sufficient, the single fold pattern could not be defined. The fold patterns of the peptide backbone are shown as ribbon models.

use of the distance information of all NOEs, all structures ($T<0.1$) gave the R-folding pattern. These results indicated that the distance information of NOEs shown in Table 2, especially the inter-residual NOE set, was indispensable for defining the folding pattern of $ST_p(5—17)$.

During the process of these calculations the possibility was suggested that disulfide pairings can be determined using only the distance information of NOEs, even if the positions of disulfide linkages are not known. Since $ST_p(5—17)$ contains six Cys residues, there are 15 possible combinations of disulfide linkages. Of these combinations, the disulfide pairings that satisfied the constraints of NOEs were searched; that is, the correct disulfide pairings should not affect the violation of NOE constraints and the structure of the peptide with $T<0.1$ should be obtained in the calculation using the distance information of NOE and a given combination of disulfide linkages as well as only the distance information of NOEs. Ten calculations were carried out using random initial structures for each combination of disulfide linkages. In each case, the structure with $T<0.1$ was obtained with only one combination of disulfide linkages, which was the same as that determined chemically.[14] This result demonstrates that with a sufficient amount of distance information, not only the unique folding pattern of $ST_p(5—17)$ but also its disulfide pairings can be determined. These processes may be useful not only for calculation of the folding pattern of ST, but also for determination of disulfide linkages in natural ST and synthetic ST analogs in which the disulfide pairings are unknown, if a NOE set such as that in Table 2, and especially inter-residual NOEs, can be obtained.

The distance constraints from NOEs of $ST_p(5—17)$ in aqueous solution are also summarized in Table 2. Almost all NOEs in an aqueous solvent were the same as those in an organic solvent, although only about 40% of the NOEs of the N-terminal region of the peptide observed in an organic solvent were detected in an aqueous solvent. From twenty calculations using constraints of disulfide linkages and NOEs in an aqueous solvent (Table 2), eight structures ($T<0.1$) were obtained and they all exhibited the R-folding pattern (not shown). Their average RMSD was 1.98 Å for backbone atoms. This result demonstrated that the folding pattern of $ST_p(5—17)$ was the same in an organic solvent as in an aqueous solvent.

Refinement of Tertiary Structure of $ST_p(5—17)$: From an H-D exchange experiment (not shown) five NH protons of Cys^9, Asn^{11}, Ala^{13}, Cys^{14}, and Cys^{17} were found to show slow H-D exchange, although four amide protons of Asn^{12}, Ala^{14}, Cys^{15}, and Cys^{18} of ST_h (corresponding to Asn^{11}, Ala^{13}, Cys^{14}, and Cys^{17}, respectively, in ST_p) were reported to be involved in hydrogen bondings in Ref. 16. The signals of these NH protons were still observed in the spectrum 6.5 h after addition of 500 μl of D_2O to the peptide solution in 500 μl of DMSO-d_6/CH_3CN-d_3 (v/v, 85/15). The NH proton of Cys^{17} was most labile among these protons. Taking account of the size of $ST_p(5—17)$,

these NH protons with slow H-D exchangeability were assumed to be involved in hydrogen bondings. The most plausible CO groups forming hydrogen bonds with these NH groups were searched according to the following criteria: (1) Structures with $T<0.1$ should be obtained for the correct pairing of a given NH and CO, because additional information on a hydrogen bonding does not increase interatomic distance violations. (2) Hydrogen bonding pairs with an angle ∠N-O-C of 100° to 140° are expected to be present in the tertiary structure of the peptide, because in the molecular structure of an analog of ST_p ([Mpr^5]ST_p(5—17)) the angles ∠N-O-C for all intramolecular hydrogen bonds are in this range.[22] (3) The NH protons may be hydrogen-bonded with the CO oxygens in the same loops, as seen in the folding pattern of ST_p(5—17) in Fig. 5(R). Furthermore, upper and lower constraints of 2.5 Å and 2.0 Å, respectively, were input into the calculation as the distance of the hydrogen bonding between an NH proton and a CO oxygen. Ten calculations were carried out from different random initial structures in all cases using the distance constraints of NOEs that were obtained from the measurement of ST_p(5—17) in an organic solvent (Table 2).

First we examined the hydrogen bonding of the NH proton of Cys^9 with either the CO group of Cys^5 or Cys^6 or Glu^7 in the segment from Cys^5 to Cys^{10} in the first loop from the N-terminus, as depicted in Fig. 5(R). Structures with $T<0.1$ were obtained for the CO groups of both Cys^5 and Cys^6 and the values of ∠N-O-C were 73°±6° and 100°±0.5° for Cys^5 and Cys^6, respectively. According to the second criterion described above, the acceptor of the NH proton of Cys^9 was concluded to be the CO group of Cys^6. Similarly, the acceptors of the NH protons of Cys^{14} and Cys^{17} in the segments from Cys^{10} to Cys^{14} and from Cys^{14} to Cys^{17} in the second and third loop, respectively, in Fig. 5(R) were examined and determined to be the CO of Asn^{11} and the CO of Cys^{14}, respectively. The CPK-model constructed from the calculated structures at this stage suggested that the acceptor in the hydrogen bonding with the NH proton of Asn^{11} was the CO group of Cys^5 or Cys^9. The CO of Cys^5 gave structures with $T<0.1$, while the CO of Cys^9 did not. However, the hydrogen bonding of the NH of Asn^{11} to the CO of Cys^5 was excluded by the second criterion. The NH proton of Asn^{11} might be present close to the CO of Cys^5 in the interior of the molecule. Finally, the acceptor for the NH of Ala^{13} was concluded to be the β-CO of Asn^{11}, because only this CO can be present in the space where the NH of Ala^{13} can interact. This type of hydrogen bonding between the side-chain and the main-chain has been reported.[23] These results (in Table 4) indicate that the hydrogen bondings were between the NH of Cys^9 and the CO of the Cys^6, the NH of Cys^{14} and the CO of Asn^{11}, the NH of Cys^{17} and the CO of Cys^{14}, and the NH of Ala^{13} and the β-CO of Asn^{11}.

Table 4. Pairing of Hydrogen Bonds and Bond Angles (∠N-O-C) in Calculated Structures

	Pairing of hydrogen bonds		Number of structures ($T<0.1$)	r^d (∠N-O-C)
	NH	CO		
1	Cys^9	Cys^5	3	73±6
		Cys^6	2	100±0.5
		Glu^7	0	
2[a]	Cys^{14}	Cys^{10}	0	
		Asn^{11}	2	113±0.5
		Pro^{12}	0	
		Gly^{16}	0	
3[b]	Cys^{17}	Ala^{13}	0	
		Cys^{14}	2	102+0.5
		Ala^{15}	2	83±2
4[c]	Asn$_{11}$	Cys^5	3	164±8
		Cys^9	0	
5[c]	Ala^{13}	Asn^{11}(β-CO)	2	117±1

Information on disulfide bonds and all NOEs were used for all calculations. a, b, and c: additional information on hydrogen bonds was used: a, the NH of Cys^9 and the CO of Cys^6; b, a and the NH of Cys^{14} and the CO of Asn^{11}; c, b and the NH of Cys^{17} and the CO of Cys^{14}. d: Averaged angles of ∠N-O-C under consideration are shown in degrees.

Thirty calculations were carried out using constraints from three disulfide bonds, all NOEs and the four hydrogen bonds determined above. Seven structures ($T<0.1$) were obtained and the average RMSD between them was 1.13 Å for all backbone atoms. Thus, the RMSD was further improved by using additional information of hydrogen bondings. Four structures with similar low T-values were superimposed on the structure with the lowest T-value, as shown in Fig. 6.

The tertiary structure of ST_p(5—17) had a right-handed spiral fold throughout the whole molecule with three loops along this spiral. The first loop (Cys^5-Cys^{10}) was fixed by the disulfide bond between Cys^5 and Cys^{10} and the hydrogen bond between the NH of Cys^9 and the CO of Cys^6. The second loop (Cys^{10}-Cys^{14}) was stabilized by the two disulfide bonds between Cys^5 and Cys^{10} and Cys^6 and Cys^{14} and the two hydrogen bonds between the NH of Cys^{14} and the CO of Asn^{11} and the NH of Ala^{13} and the β-CO of Asn^{11}. The third loop (Cys^{14}-Cys^{17}) was stabilized by the two disulfide bonds between Cys^6 and Cys^{14} and Cys^9 and Cys^{17} and the hydrogen bond between the NH of Cys^{17} and the CO of Cys^{14}. The formation and stabilization of the β-turn in each loop were attributed to the hydrogen bonds between the backbone atoms. Thus, the spatial structure of ST_p(5—17) was strongly stabilized by the network of disulfide and hydrogen bonds.

Comparison of the Conformations of ST_p(5—17) in Solution and the Solid State: Recently we determined the molecular structure of an analog of ST_p(5—

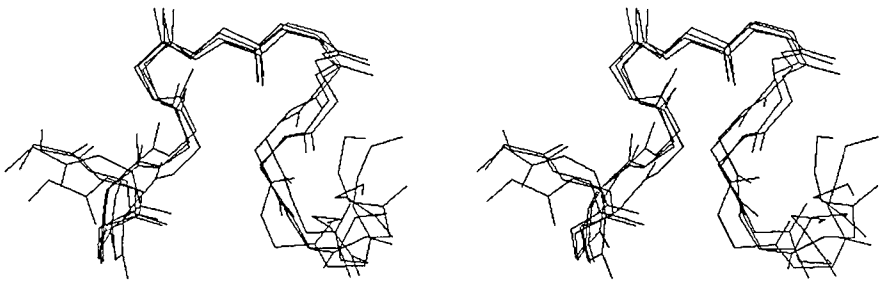

Fig. 6. Stereo view of backbone structures of ST_p (5—17) superimposed to give the minimum averaged RMSD. The all structures exhibited violations of less than 0.1 Å.

17) in which Cys was replaced by Mpr at position 5 ([Mpr^5]ST_p(5—17)).[22] We compared the structure of ST_p(5—17) in solution with that of [Mpr^5]ST_p(5—17) in the solid state, because [Mpr^5]ST_p(5—17) lacks only the N-terminal NH_2-group of ST_p(5—17) and therefore the structure of this Mpr^5-derivative should be very similar to that of ST_p(5—17). The backbone structure of ST_p(5—17) was superimposed on that of [Mpr^5]ST_p(5—17) in the solid state, as shown in Fig. 7. The two structures had the same folding pattern. Four intramolecular hydrogen bonds and three β-turns in the structure of ST_p(5—17) in solution have also been observed in the solid structure of [Mpr^5]ST_p(5—17). The common folding pattern and secondary structure in solution and the solid states might be caused by the tight stabilization by the net work of disulfide and hydrogen bonds. The RMSD values for backbone atoms in the first, second, and third loops were 0.92, 0.45, and 0.76 Å, respectively. The second loop had the smallest RMSD value and fitted extremely well to that in the solid state, implying that this region is scarcely perturbed in solution. The slightly larger deviations of the first and third loops of the structure in solution from those in the solid state might be due to fluctuations in these loops.

In conclusion, the toxic domain of ST_p in solution could be defined by ^{1}H NMR spectroscopy and distance geometry calculations. The conformation of ST_p(5—17) in solution was almost the same as that of [Mpr^5]ST_p(5—17) in the solid state, indicating that the toxic domain of ST_p has a stable conformation with low perturbation in solution. The present finding should be useful for understanding the part(s) of ST_p recognized by its receptor protein(s) and for conformational analyses of analogs of ST_p and its conformation-activity relationship.

Experimental

Boc-amino acids were purchased from the Peptide Institute Inc. (Minoh, Osaka). Deuterated solvents, DMSO-d_6 (99.96%), CH_3CN-d_3 (99.6%), and D_2O (99.95%), were obtained from CEA (Commissariat a L'Energie Atomique, Cedex, France). All other reagents were commercial products and were purified further before use in analytical

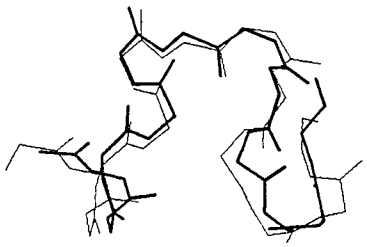

Fig. 7. Comparison of the backbone structure of ST_p (5—17) in solution (——) with that of [Mpr^5]ST_p (5—17) in the solid state (——).

experiments.

Syntheses of ST_p(5—17) and [β,β-d_2-Cys^5]ST_p(5—17): ST_p(5—17) was synthesized by the solid-phase method.[14] [β,β-d_2-Cys^5]ST_p(5—17) was prepared by the same procedure as ST_p(5—17), except for the use of Boc-β,β-d_2-Cys(MeBzl) at position 5 in the sequence of ST_p instead of Boc-Cys-(MeBzl). The synthesis of Boc-β,β-d_2-Cys(MeBzl) was described previously.[24]

NMR Spectroscopy: 2D ^{1}H NMR spectra were measured in DMSO-d_6/CH_3CN-d_3 (v/v, 85/15) (8 mmol dm^{-3}) at 10 °C and in H_2O/D_2O (2.4 mmol dm^{-3}) at 3—20 °C in a JEOL GX-500 spectrometer. DMSO-d_6/CH_3CN-d_3 was chosen as solvent, because ST_p(5—17) was soluble in DMSO but was gradually destroyed under the conditions for ^{1}H NMR measurement, while ST_p(5—17) was stable in CH_3CN but not soluble enough in this solvent. 2D DQF-COSY and NOESY were performed in the phase-sensitive detection mode by the four-quadrant method.[25] Chemical shifts were measured relative to the methyl resonance of tetramethylsilane added as an internal standard. For NOESY in an organic solvent, a mixing time of 150 ms was adopted, because it was short enough to exclude the effects of spin diffusion and coherent magnetization transfer.[15] NOESY spectra in an aqueous solvent were recorded with mixing times of 100, 150, and 300 ms. From evaluation of secondary effects, NOEs for distance geometry calculation were collected from the NOESY spectra recorded with a mixing time of 150 ms. The sizes of the time domain data were 2K or 4K points for the t_2 direction and 256 points for the t_1 direction. The data size was zero-filled once or twice in the t_1 direction.

The H-D exchange experiment was performed by addition of D_2O to a sample solution in DMSO-d_6/CH_3CN-d_3. The time course of change in 1D spectra of this sample was

recorded in a JEOL GX-400 at 22 °C.

Distance Constraints: The intensities of the NOE peaks were translated into the coresponding interatomic distances based on the relation, NOE intensity $\propto 1/r^6$.[18] The aptitude of the interpretation method was discussed in a previous paper.[15,18] The intensity of NOE was evaluated from the number of lines in contour plots of the NOESY spectra of the peptide, and the intensity of the strongest NOE between two C_β protons of Cys was used as a standard intensity for the distance 1.75 Å. The relative intensities with 7—5, 4—3, 2 and 1 contour lines were estimated to be 2.5, 3.0, 3.5, and 4.0 Å, respectively. These values were used as the upper distance constraints. The lower distance constraints were assumed to be the sums of the core radii of the two protons, i.e., 2.0 Å. Information of three disulfide linkages provided an additional distance constraint of 2.04 Å on the S^i-S^j bond (where S^i and S^j are the sulfur atoms of Cys^i and Cys^j residues, which are linked by a disulfide bond) and 3.05 Å on the S^i-$C_\beta{}^j$ and S^j-$C_\beta{}^i$ distances across the disulfide bridge.[26] Since the dihedral angles χ_3 (C_β-S-S-C_β) of disulfide bonds in all proteins observed by high resolution X-ray crystallography are approximately $\pm 90° \pm 10°$,[27] this value of χ_3 was defined by a distance constraint of 3.86 Å on the $C_\beta{}^i$-$C_\beta{}^j$ distance.

Since protons on a methylene or methyl group could not be assigned stereospecifically, these protons were replaced by pseudoatoms as reference points by the method suggested by Wüthrich and his associates.[28]

Distance Geometry Calculations: The distance geometry program DADAS[15,17] was used to construct the tertiary structure of $ST_p(5—17)$. DADAS defines the target function (T) as an error function consisting of the square sum of the differences between atomic distances in calculated structures and the input distance constraints. The initial structure is constructed by generating the random values for dihedral angles. Then T is minimized by the algorism working in the dihedral angle space.[15,17] Calculations were performed with ACOS S2020 and SX-2N computers at the Computer Center of Osaka University. The computed structures were visualized and analyzed using a computer graphics program VENUS at the Research Center for Protein Engineering, Institute for Protein Research, Osaka University.

This work was supported in part by a Grant-in-Aid from the Ministry of Education, Science and Culture. We are indebted to Mrs. Kazuko Kawaguchi for preparation of the manuscript.

References

1) Presented partly in "Peptide Chemistry 1988," (Proceedings of the 26th Symposium on Peptide Chemistry), ed by M. Ueki, pp. 179—182. The abbreviations used in this paper are those recommended by the IUPAC-IUB [*J. Biol. Chem.*, **261**, 1 (1986)]. Additional abbreviations are: *E. coli*, *Escherichia coli*; DMSO, dimethyl sulfoxide; 1D and 2D, one and two dimensional, respectively; DQF, double quantum filtered; COSY, correlated spectroscopy; NOE, nuclear Overhauser enhancement; NOESY, NOE spectroscopy; RMSD, root mean square distance; Mpr, 3-mercaptopropionic acid; MeBzl, 4-methylbenzyl.

2) H. W. Smith and C. L. Gyles, *J. Med. Microbiol.*, **3**, 387 (1970).

3) R. N. Greenberg and R. L. Guerrant, *Pharmacol. Ther.*, **13**, 507 (1981).

4) S. Aimoto, T. Takao, Y. Shimonishi, S. Hara, T. Takeda, Y. Takeda, and T. Miwatani, *Eur. J. Biochem.*, **129**, 257 (1982).

5) T. Takao, T. Hitouji, S. Aimoto, Y. Shimonishi, S. Hara, T. Takeda, Y. Takeda, and T. Miwatani, *FEBS Lett.*, **152**, 1 (1983); M. R. Thompson and R. A. Giannella, *Infect. Immun.*, **47**, 834 (1985).

6) M. Field, L. H. Graf, Jr., W. J. Laird, and P. L. Smith, *Proc. Natl. Acad. Sci. U.S.A.*, **75**, 2800 (1978).

7) J. M. Hughes, F. Murad, B. Chang, and R. L. Guerrant, *Nature*, **271**, 755 (1978).

8) P. M. Newsome, M. N. Burgess, and N. A. Mullan, *Infect. Immun.*, **22**, 290 (1978).

9) M. C. Rao, S. A. Orellana, M. Field, D. C. Robertson, and R. L. Guerrant, *Infect. Immun.*, **33**, 165 (1981).

10) S. A. Waldman, T. Kuno, Y. Kamisaki, L. Y. Chang, J. Gariepy, P. O'Hanley, G. K. Schoolnik, and F. Murad, *Infect. Immun.*, **51**, 320 (1986).

11) J. Gariepy, A. K. Judd, and G. K. Schoolnik, *Proc. Natl. Acad. Sci. U.S.A.*, **84**, 8907 (1987).

12) T. Hirayama, Y. Oku, Y. Takeda, N. Iwata, S. Aimoto, and Y. Shimonishi, "Advances in Cholera and Related Diarrheas," ed by R. B. Sack and Y. Zinnaka, **1990**, Vol. 7. p. 105.

13) S. Yoshimura, H. Ikemura, H. Watanabe, S. Aimoto, Y. Shimonishi, S. Hara, T. Takeda, T. Miwatani, and Y. Takeda, *FEBS Lett.*, **181**, 138 (1985).

14) Y. Shimonishi, Y. Hidaka, M. Koizumi, M. Hane, S. Aimoto, T. Takeda, T. Miwatani, and Y. Takeda, *FEBS Lett.*, **215**, 165 (1987).

15) T. Ohkubo, Y. Kobayashi, Y. Shimonishi, Y. Kyogoku, W. Braun, and N. Gō, *Biopolymers*, **25**, S123 (1986).

16) J. Gariepy, A. Lane, F. Frayman, D. Wilbur, W. Robien, G. K. Schoolnik, and O. Jardetzky, *Biochemistry*, **25**, 7854 (1986).

17) W. Braun and N. Gō, *J. Mol. Biol.*, **186**, 611 (1985).

18) W. Braun, C. Bösch, L. R. Brown, N. Gō, and K. Wüthrich, *Biochim. Biophys. Acta*, **667**, 377 (1981).

19) G. M. Clore and A. M. Gronenborn, *Protein Eng.*, **1**, 275 (1987).

20) M. Billeter, W. Braun, and K. Wüthrich, *J. Mol. Biol.*, **155**, 321 (1982).

21) W. J. Metzler, D. R. Hare, and A. Pardi, *Biochemistry*, **28**, 7045 (1989).

22) H. Ozaki, T. Sato, H. Kubota, Y. Hata, Y. Katsube, and Y. Shimonishi, *J. Biol. Chem.*, in press (1991).

23) M. Marraud, S. Premilat, and A. Aubry, "Peptides," (Proceedings of the 11th American Peptide Symposium), ed by J. E. Rivier and G. R. Marshall, (1990) p. 535.

24) Y. Hidaka and Y. Shimonishi, *Bull. Chem. Soc. Jpn.*, **62**, 1986 (1989).

25) D. J. States, R. A. Haberkorn, and D. J. Reuben, *J. Magn. Reson.*, **48**, 286 (1982).

26) G. Nemethy, M. S. Pottle, and H. A. Scheraga, *J. Phys. Chem.*, **87**, 1883 (1983).

27) J. S. Richardson, *Adv. Protein Chem.*, **34**, 167 (1981).

28) K. Wüthrich, M. Billeter, and W. Braun, *J. Mol. Biol.*, **169**, 949 (1983).

Rates and Mechanism for the Solvolyses of 2,2-Dimethyl-2-sila-1-indanyl Bromide and α-Trialkylsilylbenzyl *p*-Toluenesulfonates. α-Silicon Effect on the Stability of Benzylic Cations in Solution

Nobujiro SHIMIZU,* Erika OSAJIMA, and Yuho TSUNO
Department of Chemistry, Faculty of Science, Kyushu University,
Hakozaki, Higashi-ku, Fukuoka 812
(Received November 29, 1990)

α-Silicon effect on the benzylic solvolysis has been investigated. The solvolysis of 2,2-dimethyl-2-sila-1-indanyl bromide in aq acetone exhibits a linear response to the solvent ionizing power Y_{Br} with a slope m close to unity (m=0.93) and gives the corresponding alcohol without skeletal rearrangement indicative of a k_c mechanism; it solvolyzes 4.98×10^2 times less rapidly than a carbon reference, 2,2-dimethyl-1-indanyl bromide, in 60% aq acetone at 25 °C suggesting that solvolytic generation of the α-silylated benzylic cation is electronically about 4 kcal mol^{-1} less favorable than that of the corresponding α-alkylated benzylic cation. A more pronounced rate-retardation of 1.65×10^4 by an α-$SiMe_3$ group relative to Me is observed in the solvolysis of an open benzylic system due to the additional steric effect. Mechanism for the solvolysis of α-trialkylsilylbenzyl *p*-toluenesulfonates including $SiMe_3$, $SiEt_3$, and Si(*t*-Bu)Me_2 groups has been also examined on the basis of the solvent effect, salt effect, and ethanol/water selectivity as well as product analysis; a k_c mechanism including a product forming step via preferential front side solvent attack is suggested.

The effect of silicon on the stability of adjacent carbocations has been the subjects of recent theoretical and mechanistic interests.[1] During the course of our study on the mechanism of solvolysis of α-disilanylbenzyl halides, we needed precise estimation for the α-silicon effect relative to carbon on the ionization of benzylic derivatives.[2] While strong electron-releasing property of β-silicon has been verified experimentally[3] as well as theoretically,[4] the effects of α-silicon are rather puzzling. A trimethylsilyl group, the most commonly used silyl group, sometimes acts as a weak electron-accepting group contrary to a low electronegativity of silicon.[5] Theoretical study suggests that a carbocation $SiH_3CH_2^+$ is 17 kcal mol^{-1} more stable than methyl cation but 17 kcal mol^{-1} less stable than ethyl cation.[4b] Experimental results are, however, diverse. For example, $SiMe_3$ relative to methyl accelerates the solvolysis of vinyl triflates,[6] while replacement of one of methyl groups in *t*-butyl bromide with $SiMe_3$ results in a marked rate retardation.[7] On the other hand, $SiMe_3$ exerts essentially the same effect as methyl in the solvolysis of 2-adamantyl derivatives.[8] A deactivating effect of $SiMe_3$ has been also reported in the benzylic solvolysis but the data are not quantitative.[9] These diverse results on the α-silicon effect arise in part from the steric effect which varies with the system and hence is difficult to estimate precisely. The $SiMe_3$ group is undoubtedly a bulky group as compared to methyl, although it is considered to be significantly smaller in its effective size than *t*-butyl.[10,11] Since the solvolysis of α-alkylbenzyl derivatives is susceptible to steric effect of the α-alkyl groups,[12,13] a direct comparison between the solvolysis rates for α-$SiMe_3$- and α-alkylbenzyl derivatives may not provide a reasonable estimation for the α-silicon effect relative to carbon on the stability of adjacent benzylic cations. In order to minimize the steric effect, we selected the solvolysis of 2,2-dimethyl-2-sila-1-indanyl bromide (**1a-Br**) and compared its solvolysis rates with those of a carbon reference, 2,2-dimethyl-1-indanyl bromide (**1b-Br**). Since the two substrates undergo the same structural change during the ionization, rate ratios between the two substrates would be attributable primarily to the difference in stability of the corresponding cations in solution. This paper also deals with the mechanism of the solvolysis of α-trialkylsilylbenzyl derivatives (**2a—c**) on the basis of the Winstein-Grunwald solvent analysis,[14] salt effect, ethanol/water selectivity, and product analysis.

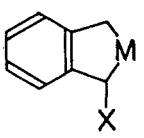

1a: M=SiMe2
1b: M=CMe2
1c: M=CH2

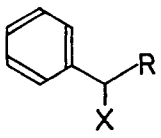

2a: R=SiMe3
2b: R=SiEt3
2c: R=SiMe2(t-Bu)
3a: R=Me
3b: R=CMe3

Results

1a-Br was prepared by halogenation of 2,2-dimethyl-2-silaindane with *N*-bromosuccinimide. α-Trimethylsilyl-, α-triethylsilyl-, and α-*t*-butyldimethylsilylbenzyl *p*-toluenesulfonates (**2a-OTs**, **2b-OTs**, and **2c-OTs**) were prepared by treatment of the corresponding benzyl trialkylsilyl ethers with *s*-butyllithium followed by addition of *p*-toluenesulfonyl chloride.

Table 1. Rate Constants for Solvolysis of **1**—**3** at 25.0±0.05 °C

Solvent[b]	$k\times10^5/s^{-1}$ [a]						
	1a-Br	**1b-Br**	**2a-Br**	**3a-Br**	**2a-OTs**	**2b-OTs**	**2c-OTs**
EtOH		6.70[c]			4.91, 4.96[c]	1.80	0.809[c]
90E					17.7	7.71	4.97
80E	1.00[c]	354			40.6	19.7	15.6
70E					78.4	45.5	37.5
60E					199	101	91.4
50E	32.8[c]				504, 513[c]	237	216
40E	162[c]				1790	829	791
80A		55.5			3.56	1.98	1.76
70A	0.642	373		12.6	14.1	8.33	7.41
60A	3.17	1580		50.9	49.8	36.5	31.5
50A	14.4			233	212[d]	130	114[d]
40A	81.0			876	866	598	601[d]
30A	372		0.102[c]	3100	4130		2470[d]
97T	223[c]		0.0313[e,f]	515, 518[c]	2064[d]	3050[d]	3820[d]
80T				893	2090[d]	2820[d]	3440[d]
50T	302[c]						3860[d]
40T					3730[d]	3810[d]	4570[d]

a) $k_{UV(acridine)}$ determined by measuring increase in an acid generated as its acridinium ion except otherwise noted. b) E: ethanol/water (v/v), A: acetone/water (v/v), and T: TFE/water (v/v) mixtures except for 97T which is a 97/3 (w/w) TFE/water mixture. c) k_{UV} determined by measuring decrease in a reactant. d) Average of duplicate runs. e) Conductimetric rate. f) Extrapolated: $k=(4.76\pm0.003)\times10^{-6}$ and $(4.89\pm0.001)\times10^{-5}$ s^{-1} at 50.0 and 75.0 °C, respectively; $\Delta H^{\ddagger}_{298}=20.2$ kcal mol^{-1} and $\Delta S^{\ddagger}_{298}=-20.3$ cal K^{-1} mol^{-1}.

Table 2. α-Silicon Effect on the Solvolysis Rates for Benzyl and 1-Indanyl Derivatives

Solvent	$10^5k/s^{-1}$ [a]				Ratio $k(1)/k(2)$
	Substrate (1)		Substrate (2)		
60A	**1a-Br:** 3.17	**1b-Br:**	1580		2.01×10^{-3}
70A	0.642		373		2.26×10^{-3}
80E	1.00		354		2.82×10^{-3}
97T	**2a-Br:** 0.0313	**3a-Br:**	515		6.06×10^{-5}
30A	0.102		3100		3.30×10^{-5}
97T	**2a-OTs:** 2060	**3b-OTs:**	1348[b]		1.53
60A	49.8		24.9[b]		2.00

a) At 25 °C. b) Rata data were taken from Ref. 30.

Table 3. Comparison of Solvolysis Rates between Benzyl and 1-Indanyl Derivatives[a]

Solvent	$10^5k/s^{-1}$				Ratio $k(1)/k(2)$
	Indanyl (1)		Benzyl (2)		
97T	**1a-Br:** 223	**2a-Br:**	0.0313		7130
30A	372		0.102		3650
EtOH	**1b-Cl:** 2.93[b]	**3b-Cl:**	0.0000217[c]		13500
EtOH	**1c-Cl:** 15.1[b]	**3a-Cl:**	0.0216[d]		700

a) At 25 °C. b) Ref. 14. c) Estimated from the rate constant in 80% aq ethanol (Ref. 12) and a k_{EtOH}/k_{80E} rate ratio of 0.021 for **3a-Cl**. d) A. H. Fainberg and S. Winstein, *J. Am. Chem. Soc.*, **79**, 1597 (1957).

Solvolyses were followed spectrophotometrically by measuring decrease in a reactant or increase in a liberated acid as its acridinium salt for $(0.2—2)\times10^{-4}$ M solutions (1 M=1 mol dm^{-3}). In the latter case, the solvolysis was monitored by a 402.5 nm light in the presence of 2—3 equiv acridine and $(5—10)\times10^{-5}$ M of acridinium *p*-toluenesulfonate. The initial addition of the acridinium salt was necessary to assure linear response of absorbance to the concentration of the produced acid. In several cases, the solvolysis were followed conductimetrically. In most cases, the solvolyses followed excellent first-order kinetics over a range of 3 to 4 half-lives (correlation coefficient $R>0.9999$) giving rate constants within ±3% reproducibility. Table 1 shows solvolysis rates for **1**, **2**, and α-methylbenzyl bromide (**3a-Br**) in various solvents including 30/70 to 80/20 (v/v) acetone/water (A-series), 40/60 to 100/0 (v/v) ethanol/water (E-series),

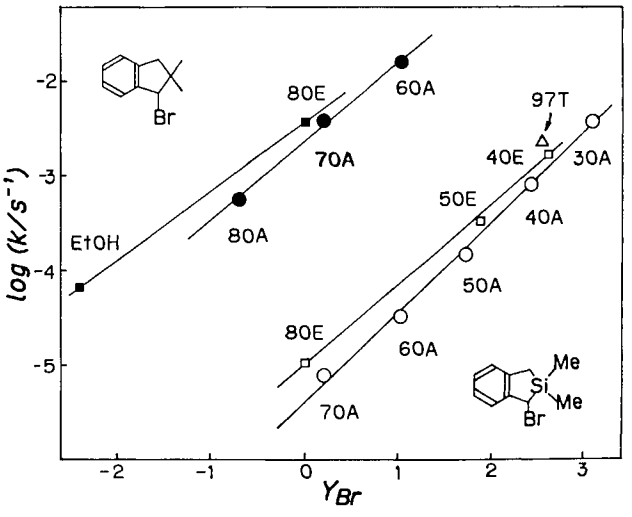

Fig. 1. Plots of log *k* for solvolyses of **1a-Br** (bottom) and **1b-Br** (top) vs. Y_{Br}.

Table 4. Grunwald-Winstein Analysis for the Solvolysis of **1** and **2**

Substrate	m[a]		Rate-increment[b]		
	For aq acetone	For all solvents	EtOH	80E	97Tw
1a-Br	0.93 (n=5, R=0.997)	0.91 (n=9, R=0.986)	0.38	0.37	
1b-Br	0.84 (n=3, R=0.998)	0.70 (n=5, R=0.991)	0.49	0.19	
2a-OTs	0.91 (n=6, R=0.993)	0.81 (n=16, R=0.979)	0.95	0.26	0.29
2b-OTs	0.92 (n=5, R=0.999)	0.90 (n=15, R=0.971)	0.72	0.15	0.64
2c-OTs	0.94 (n=6, R=0.999)	0.99 (n=18, R=0.979)	0.46	0.10	0.76

a) Based on Y_{Br} (Ref. 15) and Y_{OTs} (Ref. 16) for bromides and p-toluenesulfonates, respectively. b) Deviations from the acetone correlation line in log k unit.

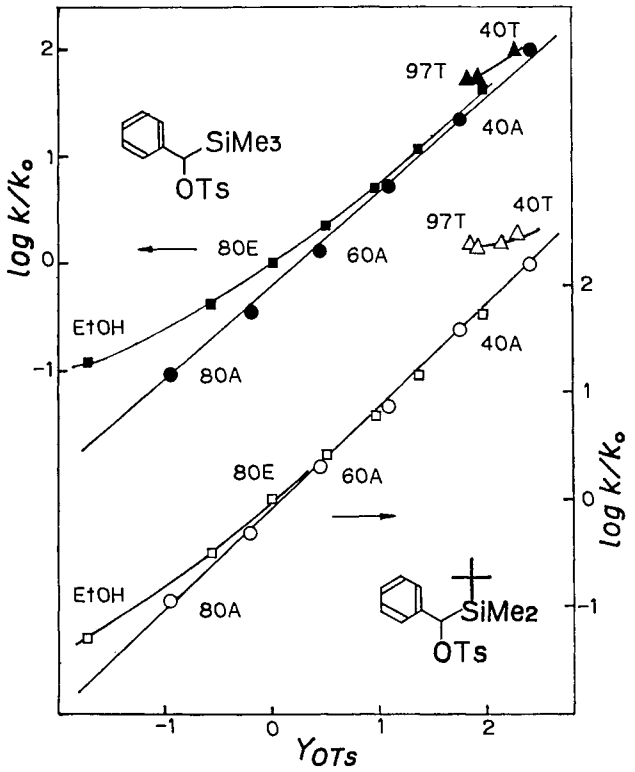

Fig. 2. Plots of log k for solvolyses of **2a-OTs** (top) and **2c-OTs** (bottom) vs. Y_{OTs}.

Table 5. Salt Effects on Hydrolysis of **2a-OTs** and **2c-OTs**[a]

Substrate	Salt	[Salt]/M	$10^5k/s^{-1}$[b,c]	k_{rel}
2a-OTs	None		212	1.00
	NaOTs	0.100	203	0.95
		0.300	177	0.84
	NaCl	0.100	206	0.97
		0.300	186	0.88
	$LiClO_4$	0.101	240	1.13
		0.321	318	1.45
2c-OTs	None		114	1.00
	NaOTs	0.100	103	0.91
		0.300	94.9	0.84
	NaCl	0.100	108	0.95
		0.300	94.7	0.83
	$LiClO_4$	0.101	131	1.15
		0.321	184	1.62

a) In 50% acetone/water (v/v) at 25 °C. b) Average of duplicate runs. c) $k_{UV(acridine)}$; [reactant]=1.0×10^{-4} M, [acridine]=3.0×10^{-4} M, and [acridinium p-toluenesulfonate]=1×10^{-4} M.

Table 6. Products, Selectivity, and Rate Increment in the Solvolysis of **2a-OTs** in aq Ethanol

Solvent	Products[a]		Selectivity[b]	Rate-increment
	2a-OH	**2a-OEt**	k_W/k_E	k_{obsd}/k_{calcd}[c]
EtOH	0%	100%		6.89
90E	36.9%	63.1%	1.62	2.34
80E	55.9%	45.1%	1.53	1.51
50E	82.1%	17.9%	1.42	0.92
40E	86.1%	13.9%	1.28	1.06

a) Determined by GLC. b) Defined by k_W/k_E=[**2a-OH**][EtOH]/[**2a-OEt**][H_2O]. c) The k_{calcd} is the rate constant expected from the mY correlation line observed for aq acetone: log k_{calcd}=0.915Y_{OTs}−3.648.

and 40/60 to 80/20 (v/v) and 97/3 (w/w) 2,2,2-trifluoroethanol (TFE)/water (T-series) binary solvent mixtures at 25 °C. The α-silicon effects on the solvolysis rates in 1-indanyl and benzyl systems are summarized in Table 2. Marked deactivation effects of α-silicon are apparent in both cases. Table 3 shows a comparison of the solvolysis rates between 1-indanyl and benzylic derivatives. Obviously, the indanyl system solvolyzes much more rapidly than the corresponding benzyl system. Figure 1 illustrates the dependence of solvolysis rates on the solvent ionizing power Y_{Br}[15] for the solvolyses of **1a-Br** and **1b-Br**. Since α-trimethylsilylbenzyl bromide (**2a-Br**) solvolyzed at inconveniently slow rates, we examined the solvent effect on the ionization of α-silylbenzyl derivatives by using α-trialkylsilylbenzyl p-toluenesulfonates **2a-OTs**—**2c-OTs**. Figure 2 represents the solvent dependence of the solvolyses of **2a-OTs** and **2c-OTs** on Y_{OTs}.[16] Table 4 summarizes the results of solvent mY analysis[14] for **1** and **2**. Table 5 shows salt effects on the solvolyses of **2a-OTs** and **2c-OTs**.

Hydrolysis of **1a-Br** in 50% aq acetone cleanly gave the corresponding alcohol **1a-OH**. Similarly, **1b-Br** gave 2,2-dimethyl-1-indanol as a single product on hydrolysis in 80% aq acetone. Solvolytic reactions of **2a-OTs** and **2c-OTs** with TFE, ethanol, and aq acetone cleanly gave the corresponding ethers (**2-OTFE**

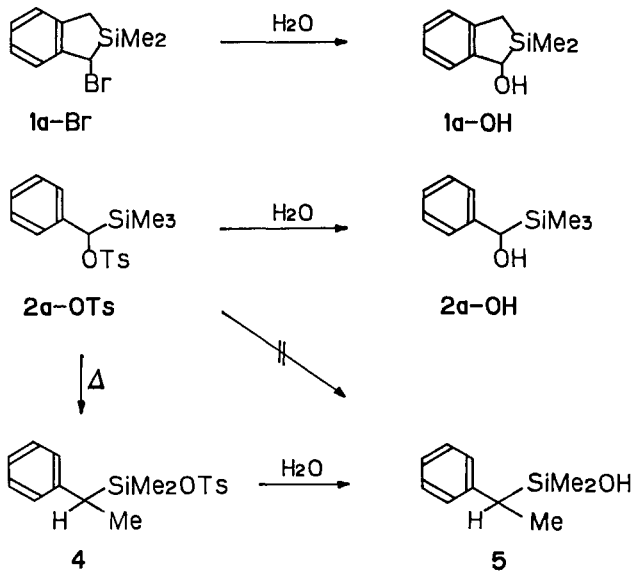

and **2-OEt**) or alcohols (**2-OH**) without skeletal rearrangement in contrast to the fact that the solvolysis of 2-trimethylsilyl-2-adamantyl *p*-nitrobenzoate involves an extensive 1,2-methyl shift from the silicon to the carbenium carbon.[17] Thermally, however, **2a-OTs** rearranged to a silyl *p*-toluenesulfonate **4**, which on hydrolysis gave a rearranged alcohol **5**.[18] Product analysis for the solvolysis of **2a-OTs** in ethanol-water binary solvent mixtures was given in Table 6 which includes selectivity, $S=k_W/k_E$, defined by Eq. 1 where k_W and k_E are the rate constants for nucleophilic attack of water and ethanol respectively in the product forming step, [**2-OH**]/[**2-OEt**] is the product ratio determined by GLC analysis, and [EtOH]/[H_2O] is the molar ratio of ethanol to water in binary solvent mixtures.

$$S=k_W/k_E=[\textbf{2-OH}][EtOH]/[\textbf{2-OEt}][H_2O] \quad (1)$$

Discussion

Table 2 shows a marked rate retardation of (1.6—3.0)×10^4 by an α-$SiMe_3$ group relative to methyl in the benzylic solvolysis. A different situation, however, arises when *t*-butyl is selected as an alkyl reference; k(**2a-OTs**)/k(**3b-OTs**) rate ratios suggest the effect of $SiMe_3$ to be comparable to that of *t*-butyl. These results in the benzylic solvolysis contrast to the α-silicon effect in the 2-adamantyl solvolysis where the rates are in the order $k(\alpha\text{-SiMe}_3):k(\alpha\text{-Me}):k(\alpha\text{-}t\text{-Bu})$=ca. $1:1.0:10^5$.[8,19] The discrepancy of the α-silicon effect between the two systems is undoubtedly associated with the steric effect. Whereas a bulky α-alkyl group facilitates the 2-adamantyl solvolysis,[19] it retards the rate of solvolysis of benzyl derivatives.[12,13] The steric rate retardation in the latter system results partly from steric strain imposed on the benzylic cations in which the α-alkyl group is coplanar to the phenyl ring or nearly so and partly from steric hindrance to solvation in the transition state. We have found a rather simple relation between the solvolysis rates of α-alkylbenzyl chlorides (PhCHRCl; R=Me, Et, *i*-Pr, and *t*-Bu) reported by Baddeley and coworkers[12] and a steric parameter *A*-value[11a] (free energy difference between axial and equatorial conformers in mono-substituted cyclohexanes) represented by Eq. 2 where k_R and k_{Me} are the rate constants for α-R and α-methylbenzyl chlorides, and A_R and A_{Me} are *A* values for R and methyl groups respectively. This relationship suggests the α-alkyl effect to be largely steric in the benzylic solvolysis, although this steric rate-retardation effect seems to be complicated by an opposing rate-acceleration effect arising from the release of B-strain for a bulky group larger than *t*-Bu.[12] If an *A* value of 2.5 is used for $SiMe_3$,[10a] a

$$\log k_R/k_{Me}=1.73\,(A_R-A_{Me})^{1/3} \quad (2)$$
(R = Me, Et, *i*-Pr, *t*-Bu; $R=0.999$)

rate retardation by the steric effect of $SiMe_3$ can be estimated to be by a factor of 40 relative to methyl. Obviously, the steric effect alone is insufficient to account for the observed low reactivity of **2a-Br**. Provided the observed k(**3a-Br**)/k(**2a-Br**) rate ratio includes a steric rate retardation of 40 by $SiMe_3$, a rate ratio of (4—8)×10^2 of the total rate difference should be ascribed to the electronic deactivation effect of $SiMe_3$ relative to methyl on the ionization step. In connection with this, α-silicon effect on the solvolysis of the indanyl system is informative. Table 2 shows that the replacement of a C_2 group from CMe_2 to $SiMe_2$ results in a rate retardation by a factor of (3—5)×10^2. A high sensitivity (m) to the solvent ionizing power Y_{Br}, i.e., m=0.93 for aq acetone (Fig. 1 and Table 3), together with the clean formation of the hydrolysis product without skeletal rearrangement is indicative of k_c mechanism for **1a-Br**. Since **1a-Br** and **1b-Br** are structurally close to each other and undergo practically the same structural change during the ionization, the difference in electronic effects between the $SiMe_2$ and the CMe_2 groups must be primarily responsible for the rate difference between the two substrates. The fact that the ethanolysis of **1b-Cl** proceeds ca. 50 times less rapidly than that of **1c-Cl**[20] implies small steric effect to be still operative in the indanyl system probably due to the steric hindrance to solvation in the transition state. Since $SiMe_2$ must have a small effective size as compared to CMe_2,[10a] a slightly more pronounced α-silicon effect than the observed k(**1b-Br**)/k(**1a-Br**) rate ratio would result, if the steric effect is taken into consideration. It is thus concluded that in solution, the α-silicon group destabilizes the adjacent benzylic cation by about 4 kcal mol^{-1} relative to the corresponding carbon group. This is in agreement with the theoretical study.[1,4b] A similar α-silicon effect of $SiMe_3$ relative to *t*-Bu has been reported in the formation of α-

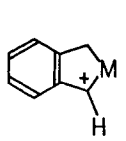
6

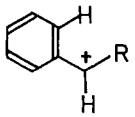
7

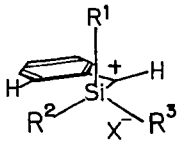
8

methoxycarbenium ions via acid-catalyzed hydrolysis of vinyl ethers.[21] The above conclusion also provides a major reason for the markedly low reactivity of **2a-Br** as compared to **3a-Br** compatible with the discussion mentioned earlier.

Table 3 indicates that indanyl derivatives solvolyze 10^2 to 10^4 times as rapidly as the corresponding benzyl derivatives. Major factors attributable to the rate differences between the two systems include ortho-alkyl effect and difference in conformational requirements of the corresponding cations **6** and **7**. The ortho effect can be estimated from the substituent effect. Provided ρ value is around -5 for the solvolysis of α-alkylbenzyl derivatives[22] and the electronic effect of *o*-alkyls is comparable to *p*-Me ($\sigma^+=-0.31$), *o*-alkylation would lead to a rate acceleration of about 40. Apparently, the *ortho*-effect alone does not explain the observed large rate differences, particularly those between **1a-Br** and **2a-Br**, and between **1b-Cl** and **3b-Cl**, even if we consider anticipated difference in inductive effect between *o*- and *p*-alkyls. Conformational factor must be the chief reason for the rate difference in these cases. 1-Indanyl derivatives ionize probably without significant increase in steric strain yielding the corresponding cations **6** which can receive the maximal resonance stabilization from the aromatic ring, while the formation of planar α-alkylbenzyl cations **7** must involve substantial steric strain because of proximity of *ortho* hydrogens to the α-alkyl group. The k(indanyl)/k(benzyl) rate ratios increase with increasing steric size of the α-groups in the order k(**1b**)/k(**3b**)>k(**1a**)/k(**2a**)>k(**1c**)/k(**3a**); this arises from the fact that the benzylic solvolysis is more sensitive to the steric effect than the indanyl solvolysis.[12,20]

The solvolyses of α-trialkylsilylbenzyl *p*-toluenesufonates **2-OTs** in A, E, and T solvent series do not show a single linear response to the solvolysis of the reference compound, 2-adamantyl *p*-toluenesulfonate, as shown in Fig. 2. Similarly, the solvolysis of **1a-Br** exhibits a diverging response to the solvent ionizing power Y_{Br} for the three solvent series. It should be noted, however, that each substrate shows a straight line with a slope m close to unity (m>0.9) for acetone/water mixtures which are nearly isonucleophilic in a wide range of water contents (Table 4). The high m values together with the absence of skeletal rearrangement during the solvolysis are indicative of the k_c mechanism for these α-silyl substrates. Lithium perchlorate showed normal salt effect on the solvolyses of **2a-OTs** and **2c-OTs**, as shown in Table 5. On the other hand, addition of sodium *p*-toluenesulfonate significantly retarded the solvolysis rate. It is questionable, however, whether this is the common ion effect because external chloride ion also caused a similar rate depression. We do not understand the origin for these rate depression quite well but intervention of the free cation is unlikely because of the following observation on product selectivity. The solvolysis through the free cation is considered to exhibit normal water/ethanol selectivity ($S=k_W/k_E<1$), as has been demonstrated by the solvolysis of diphenylmethyl chloride, e.g., S=0.36 in 80% aq ethanol.[23] **2a-OTs**, however, exhibited small but negative selectivities (S=1.28—1.65) in the solvolysis in 40% to 90% aq ethanol (Table 6). Interestingly, these selectivities are rather close to those observed in the 1- and 2-adamantyl solvolyses (s=1.6—2.2) which include a product formation step exclusively from the solvent-separated ion pair through the front side solvent attack.[24-26] One explanation for the negative selectivity in the present case is to assume a restricted conformation **8** for an intermediate ion pair. It is likely that during the ionization, one of alkyl groups of the α-trialkylsilyl group, probably the largest group of the three alkyls, takes the anti position to the leaving group to minimize the steric interaction between ortho hydrogens and the alkyl groups on the silicon. Such a conformation interferes with solvent attack from the rear side; hence, the product formation would preferentially occur from the front side.

It is worth stating a diverging mY plot pattern for **2-OTs** shown in Fig. 2. Both E- and T-series deviate substantially above the aq acetone line. The deviations for three typical solvents, ethanol, 80E, and 97T, are listed in Table 4 as rate-increments defined by log k_{obsd}/k_{calcd} where k_{obsd} and k_{calcd} are the rate constants observed and calculated from the acetone correlation line, respectively. The rate-increment for ethanol decreases with increasing steric size of the α-silyl group in the order $SiMe_3$, $SiEt_3$, and $SiMe_2$(*t*-Bu), while the rate-increment for 97T increases in this order. Although k_Δ processes often encounter diverging mY plot patterns,[27] the absence of the skeletal rearrangement in the present case eliminates such a possibility. Since α-silicon enhances S_N2 reactivity,[28] the upward deviation for E solvents seems to suggest nucleophilic solvent assistance; however, this is not the case either. Such solvent interaction would lead to downward deviations for T solvents which are much less nucleophilic than aq acetone, clearly against the observation. In fact, the mY correlation for the solvolysis of **2c-OTs** in the A, E, and T solvents was not improved at all by application of the extended Winstein-Grunwald equation[29] which includes a solvent nucleophilicity term. A diverging mY plot is not confined to the present α-silylbenzyl derivatives. α-Alkylbenzyl derivatives, for example, **3a-Cl** and **3b-OTs**, have been shown to exhibit diverging patterns as

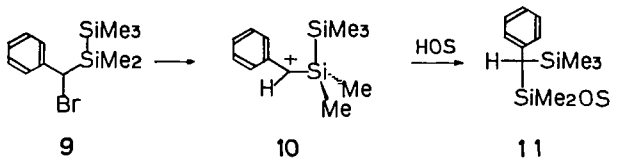

9 10 11

well.[22,30] Interestingly, α-(pentamethyldisilanyl)benzyl bromide (**9**), structurally close to **2c-OTs**, exhibits a very similar mY pattern to that for **2c-OTs**.[2] The bromide **9** has been classified as a k_c substrate solvolyzing via α-(pentamethyldisilanyl)benzyl cation **10** despite the fact that it solvolyzes 2×10^5 times more rapidly than the corresponding α-silyl substrate, **2a-Br**, and cleanly gives 1,2-$SiMe_3$ rearranged solvolysis products **11**.[2] Thus, the diverging mY plot does not necessarily mean a mechanistic shift from the k_c solvolysis. Different responses to the solvent ionizing power between adamantyl derivatives and the present α-silylbenzyl substrates are presumably responsible for the apparent diverging solvent effect. Nevertheless, the decreasing deviation for E-solvents with increasing steric hindrance of the α-silyl groups appears to suggest unattested rear side solvent interaction. The fact that the k_W/k_E ratios increase with increasing rate-increment suggest this interaction to be purely kinetic and different from the k_s process; if the rate-increments of E-solvents are related with the k_s interaction, the k_W/k_E ratios should decrease with increasing ethanol content of the E-solvents against the observation.

Experimental

IR spectra were recorded on a Hitachi R-215 spectrophotometer. NMR spectra were recorded on a Hitachi R-20B spectrometer. GLC were performed with a Hitachi 163 gas chromatograph by using glass columns (6 mm×1.5, and 2.0 m) packed with 10% Silicone oil SE-30 on Chamelite CS or 25% Apiezon Grease L on Chromosorb W.

2,2-Dimethyl-2-sila-1-indanyl Bromide (1a—Br). Into a mixture of Mg (6.10 g) and HMPA (20 cm³) in THF (75 cm³) was added slowly a solution of α,α′-dichloro-*o*-xylene (20.0 g 0.114 mol) and dichlorodimethylsilane (16.2 g, 0.126 mol) in THF (50 cm³) during a period of 8 h at ambient temperature. The mixture was stirred overnight at ambient temperature, heated under reflux for 3 h, and worked up. A crude oil was fractionated to give 2,2-dimethyl-2-silaindane (14.5 g), bp 100.5—101 °C (2.9 kPa). The product was heated with *N*-bromosuccinimide (14.3 g) and benzoyl peroxide (160 mg) in carbon tetrachloride (150 cm³) for 1.5 h. Solvent was removed on a rotary evaporator. The residue was washed with pentane and filtered. The filtrate was evaporated and the remaining oil was fractionated using a spinning band column to give **1a-Br** as a colorless oil (11.5 g, 59%); bp 62—63 °C (0.13 kPa); UV (95% EtOH) 235 (log ε=3.76), 275 (3.27); ^{1}H NMR (CCl_4) δ=0.13 (3H, s), 0.48 (3H, s), 1.91 (1H, d J=16.2 Hz), 2.19 (1H, d, J=16.2 Hz), 4.31 (1H, s), 6.9—7.5 (4H, m). Found: C, 49.82; H, 5.44%. Calcd for $C_{10}H_{13}BrSi$: C, 49.80; H, 5.43%.

2,2-Dimethyl-1-indanyl Bromide (1b—Br). To a solution of LDA (0.21 mol) in ether (200 cmm³) was added ethyl isobutyrate (21.8 g) over a period of 15 min at −78 °C and the mixture was stirred for 30 min at −78 °C. Benzyl bromide (30.5 g) was added and the mixture was heated under reflux for 2 d. Usual workup gave 2,2-dimethyl-3-phenylpropionic acid (22 g), which was converted into the acyl chloride by treatment with thionyl chloride. The crude acyl chloride was added to a mixture of $AlCl_3$ (15.7 g) in carbon disulfide (80 cm³) and the resulting mixture was heated under reflux for 30 min. Workup gave 16.2 g of 2,2-dimethyl-1-indanone which on treatment with $LiAlH_4$ (2.0 g) gave 2,2-dimethyl-1-indanol (11.6 g); mp 55—56 °C [lit,[20] mp 56—57 °C]. The alcohol (2.9 g) was dissolved in ether (25 cm³) and dry hydrogen bromide was bubbled into the solution for 30 min at ambient temperature. A crude oil obtained after workup was distilled to give **1b-Br** (3.0 g), bp 69—70 °C (0.27 kPa); NMR (CCl_4) δ=1.17 (3H, s), 1.28 (3H,s), 2.62 (1H, d, J=14.4 Hz), 2.89 (1H, d, J=14.4 Hz), 5.05 (1H, s), 7.04—7.4 (m, 4H). Found: C, 58.83; H, 5.76%. Calcd for $C_{11}H_{13}Br$: C, 58.69; H, 5.82%.

α-Trimethylsilylbenzyl Bromide (2a—Br). Into a cold (−78 °C) stirred mixture of LDA (16 mmol) and chlorotrimethylsilane (2.2 cm³) in THF (20 cm³) was added benzyl bromide (2.4 g) in THF (20 cm³) at −78 °C and the mixture was stirred overnight at −78 °C. Usual workup gave **2a-Br** (3.0 g, 87%), bp 100—101 °C (0.5 kPa) [lit,[9] bp 98 °C (0.5 kPa)].

α-Trimethylsilylbenzyl *p*-Toluenesulfonate (2a-OTs). Into a cold (−78 °C) solution of benzyl trimethylsilyl ether (1.8 g) in THF (25 cm³) was added *s*-BuLi (1.3 M in cyclohexane, 10 cm³) and the mixture was stirred at −78 °C for 4 h. Then, *p*-toluenesulfonyl chloride (1.9 g) in ether (15 cm³) was added and the mixture was allowed to worm to ca. 0 °C. The mixture was stirred for 1 h at 0 °C and worked up. Crude product was recrystallized from hexane to give **2a-OTs** (2.2 g, 66%); mp 103—104 °C; IR (Nujol) 1600, 1355, 1250, 1095, 925, 910, 860, 850, 825, 800 cm⁻¹; ^{1}H NMR ($CDCl_3$) δ=0.01 (9H, s), 2.33 (3H, s), 5.27 (1H, s), 6.8—7.3 (5H, m), 7.21 and 7.59 (4H, A_2B_2, J=7.8 Hz). Found: C, 61.05; H, 6.54%. Calcd for $C_{17}H_{22}O_3SSi$: C, 61.05; H, 6.64%.

α-Triethylsilylbenzyl *p*-Toluenesulfonate (2b-OTs). In the same procedure described for the preparation of **2a-OTs**, benzyl triethylsilyl ether (2.2 g) was converted into **2b-OTs** (2.06 g, 55%); mp 32.8—33.5 °C; ^{1}H NMR (CCl_4) δ=0.3—1.2 (15H, m), 2.30 (3H, s), 5.35 (1H, 6.8—7.15 (5H, m), 6.99 and 7.46 (4H, A_2B_2, J=7.8 Hz). Found: C, 63.70; H, 7.42%. Calcd for $C_{20}H_{28}O_3SSi$: C, 63.79; H, 7.50%.

α-*t*-Butyldimethylsilylbenzyl *p*-Toluenesulfonate (2c-OTs). In the same procedure described for the preparation of **2a-OTs**, benzyl *t*-butyldimethylsilyl ether (2.2 g) was converted into **2c-OTs** (2.1 g, 55 %); mp 93—94 °C; ^{1}H NMR ($CDCl_3$) δ=−0.20 (3H, s), 0.06 (3H, s), 0.93 (9H, s), 2.28 (3H, s), 5.42 (1H, s), 6.8—7.1 (7H, m), 7.41 (2H, d, J=7.8 Hz). Found: C, 63.88; H, 7.50%. Calcd for $C_{20}H_{28}O_3SSi$: C, 63.79; H, 7.50%.

Solvents. Ethanol was distilled twice over sufficient amounts of magnesium ethoxide. Acetone was refluxed with potassium permanganate and the distillate was dried over potassium carbonate and fractionated. 2,2,2-Trifluoroethanol was dried over Molecular Sieve 4A for a week and distilled over sodium carbonate.

Kinetics. Solvolysis rates were measured in most cases spectrophotometrically by use of a Hitachi 220A spectro-

photometer equipped with a programmed data printer. Solvolyses were followed by measuring either decrease in a reactant at an appropriate wavelength [253 (**1a-Br**), 240 (**1b-Br**), 235 (**2a-OTs**), 240 (**2b-OTs** and **2c-OTs**), and 231 nm (**3a-Br**)] or increase in a liberated acid as its acridinium ion at 402.5 nm by using $(0.2—2)\times10^{-4}$ M solutions. In the latter method, each sample solution contained a reactant, 2—3 equiv acridine, and $(0.5—1)\times10^{-4}$ M of acridinium *p*-toluenesulfonate. In the absence of the acridinium salt, the first-order plot exhibited a curve for the initial ca. 25% reaction because of non-linear response of the absorbance to the concentration of the acridium ion below 10^{-5} M. For rapid reactions ($k>10^{-2}s^{-1}$), 1 μl of a stock solution (ca. 0.3 M) of a reactant in acetonitrile was added to a given solvent (3 cm^3) which had been maintained at 25 °C in a UV cell and the reaction was immediately followed after short mixing effected by mechanical stirring or bubbling nitrogen through a syringe needle. In several cases, the rates were determined conductimetrically by using a TOA CM-50AT conductivity meter for $(5—10)\times10^{-4}$ M solutions.

Product Analysis. The following products were isolated and characterized from reactions carried out in TFE, ethanol, and aq acetone in the presence of equivalent amounts of 2,6-dimethylpyridine. The reactions in these solvents gave a single product shown below in each case.

Solvolysis in 2,2,2-Trifluoroethanol: 2a-OTFE (93% yield): IR 1600, 1280, 1250, 1150, 1110, 980, 870, 845, 750, 700 cm^{-1}; ^1H NMR (CCl_4) δ=0.0 (9H, s), 3.69 (2H, m), 4.20 (1H, 5), 6.92—7.42 (5H, m). Found: C, 54.86; H, 6.33%. Calcd for $C_{12}H_{17}F_3OSi$: C, 54.94; H, 6.53%. **2c-OTFE** (100% yield): IR 1600, 1285, 1270, 1160, 1110, 980, 840, 800, 760 cm^{-1}; ^1H NMR (CCl_4) δ=−0.24 (3H, s) , 0.0 (3H, s) , 0.95 (9H, s) , 3.65 (2H, m), 4.37 (1H, s), 6.9—7.3 (5H, m). Found: C, 59.01; H, 7.51%. Calcd for $C_{15}H_{23}F_3OSi$: C, 59.18; H, 7.62%.

Sovolysis in Ethanol: 2a-OEt (91% yield): IR 1600, 1250, 1150, 1085, 1070, 865, 840, 745, 730 cm^{-1}; ^1H NMR (CCl_4) δ=−0.06 (9H, s), 1.15 (3H, t, J=6.8 Hz), 3.37 (2H, m), 3.96 (1H, s), 6.9—7.3 (5H, m). Found: C, 69.08; H, 9.63%. Calcd for $C_{12}H_{20}OSi$: C, 69.18; H, 9.68%.

Solvolysis in 50% aq Acetone. 1a-OH (87% yield): IR 3360, 1250, 1030, 940, 840, 820 cm^{-1}; ^1H NMR (CCl_4) δ=0.19 (3H, s), 0.22 (3H, s), 1.90 (1H, d, J=16.8 Hz), 2.05 (1H, d, J=16.8 Hz), 4.43 (1H, s), 6.9—7.5 (4H, m). Found: C, 67.09; H, 7.68%. Calcd for $C_{10}H_{14}OSi$: C, 67.36; H, 7.91%. **1b-OH** (88% yield; from the reaction of **1b-Br** in 80% aq acetone). **2a-OH** (94% yield): IR 3410, 1600, 1250, 1000, 860, 840, 745, 695 cm^{-1}; ^1H NMR ($CDCl_3$) δ=0.03 (9H, s), 4.53 (1H, s), 1.75 (IN, OH), 7.25 (5H, m). **2c-OH** (95% yield): ^1H NMR (CCl_4) δ=−0.23 (3H, s), −0.04 (3H, s), 0.95 (9H, s), 4.59 (1H, s), 7.15 (5H, almost s). Found: C, 70.20; H, 9.81%. Calcd for $C_{13}H_{22}OSi$: C, 70.21; H, 9.97%.

Water/Ethanol Selectivity. After completion of solvolysis of **2a-OTs** in aq ethanol in the presence of 1 equiv of 2,6-dimethylpyridine, the mixture was concentrated, extracted with benzene, and dried. Benzene was evaporated and the residual oil was directly analyzed by GLC (AGL, 170 °C, retention time; 10.4 and 15.2 min for **2a-OEt** and **2a-OH**, respectively).

Thermal Rearrangement of 2a-OTs. 2a-OTs (350 mg) was heated to 150 °C for 30 min in a glass ampoule. ^1H NMR analysis indicated the formation of two products in the ratio 2 : 1. The more abundant product was assigned to (1-phenylethyl)dimethylsilyl *p*-toluenesulfonate (**4**): ^1H NMR (CCl_4) δ=0.35 (6H, s), 1.40 (3H, d, J=7.2 Hz), 2.40 (3H, s), 6.8—7.8 (9H, m). A benzylic proton coalesces in the methyl peak of the tosyl group. The crude product was dissolved in ether, washed with aq sodium carbonate, and dried. Solvent was removed and the residual oil was subjected to column chromatography over silica gel. Elution with 1% methanol in benzene gave (1-phenylethyl)-dimethylsilanol (**5**) (80 mg): IR 3300, 1600, 1250, 840 cm^{-1}; ^1H NMR δ=0.0 (6H, s), 1.33 (3H, d, J=7.2 Hz), 1.61 (1H, disappeared on addition of D_2O), 2.12 (1H, m), 6.8—7.3 (5H, m).

The present work was supported by a Grant-in-Aid for Scientific Research No. 01470025 from the Ministry of Education, Science and Culture.

References

1) a) Y. Apeloig, "The Chemistry of Organic Silicon Compounds," ed by S. Patai and Z. Rappoport, John Wiley & Sons, Chichester (1989), Part 1, Chap.2; b) A. R. Bassindale and P. G. Taylor, *ibid.*, Part 2, Chap. 14; c) V. J. Shiner, Jr. and M. W. Ensinger, *J. Am. Chem. Soc.*, **108**, 842 (1986).

2) N. Shimizu, C. Kinoshita, E. Osajima, and Y. Tsuno, *Chem. Lett.*, **1990**, 1937.

3) a) J. B. Lambert, G. Wang, R. B. Finzel, and D. H. Teramura, *J. Am. Chem. Soc.*, **109**, 7838 (1987); b) X. Li and J. A. Stone, *ibid.*, **111**, 5586 (1989); c) D. J. Hajdasz and R. R. Squires, *J. Chem. Soc., Chem. Commun.*, **1988**, 1212.

4) a) M. R. Ibrahim and W. L. Jorgensen, *J. Am Chem. Soc.*, **111**, 819 (1989); b) S. G. Wierschke, J. Chandrasekhar, and W. L. Jorgensen, *ibid.*, **107**, 1496 (1985); c) Y. Apeloig, M. Karme, A. Stanger, H. Schwarz, T. Drewellow, and G. Czekay, *J. Chem. Soc., Chem. Commun.*, 989 (1987).

5) a) M. A. Cook, C. Eaborn, and D. R. M. Walton, *J. Organomet. Chem.*, **23**, 85 (1970); b) H. Bock, G. Brahler, G. Fritz, and E. Matern, *Angew. Chem., Int. Ed. Engl.*, **15**, 699 (1976); c) R. A. Benkeser and H. R. Krysiak, *J. Am. Chem. Soc.*, **75**, 2421 (1953).

6) M. D. Schiavelli, D. M. Jung, A. K. Vaden, P. J. Stang, T. E. Fisk, and D. S. Morrison, *J. Org. Chem.*, **46**, 92 (1981).

7) F. K. Cartledge and J. P. Jones, *Tetrahedron Lett.*, **1971**, 2193; *idem., J. Organomet. Chem.*, **67**, 379 (1974).

8) Y. Apeloig and A. Stanger, *J. Am. Chem. Soc.*, **107**, 2806 (1985).

9) M. A. Cook, C. Eaborn, and R. M. Walton, *J. Organomet. Chem.*, **29**, 389 (1971).

10) a) W. Kitching, H. A. Olszonwy, G. M. Drew, and W. Adcock, *J. Org. Chem.*, **47**, 5153 (1982); b) R. J. Quellette, D. Baron, J. Stolfo, A. Rosenblum, and P. Weber., *Tetrahedron*, **28**, 2163 (1978).

11) a) J. A. Hirsch, *Top. Stereochem.*, **1**, 199 (1967); b) S. H. Onger and C. Hansch, *Progr. Phys. Org. Chem.*, **12**, 91 (1976).

12) G. Baddeley, J. Chadwick, and H. T. Taylor, *J. Chem. Soc.*, **1954**, 2405.

13) H. Tanida and H. Matsumura, *J. Am Chem. Soc.*, **95**, 1586 (1972).

14) E. Grunwald and S. Winstein, *J. Am. Chem. Soc.*, **70**, 846 (1948).

15) T. W. Bentley and G. E. Carter, *J. Am. Chem. Soc.*, **104**, 5741 (1982).
16) F. L. Schadt, T. W. Bentley, and P. v. R. Schleyer, *J. Am. Chem Soc.*, **98**, 7667 (1976); M. Fujio, M. Goto, K. Funatsu, Y. Tsuji, S. Ouchi, and Y. Tsuno, *Mem. Fac. Sci., Kyushu Univ., Ser. C*, **16**(**1**), 85 (1987).
17) Y. Apeloig and A. Stanger, *J. Am. Chem. Soc.*, **109**, 272 (1987).
18) A. R. Bassindale, A. G. Brook, P. F. Jones, and J. M. Lennon, *Can. J. Chem.*, **53**, 332 (1975).
19) J. L. Fry, E. M. Engle, and P. v. R. Schleyer, *J. Am. Chem. Soc.*, **94**, 4628 (1972).
20) G. Baddeley, J. W. Rasburn, and R. Rose, *J. Chem. Soc.*, **1958**, 3168.
21) J. A. Soderquist and A. Hassner, *Tetrahedron Lett.*, **29**, 1899 (1988).
22) a) S. Usui, Y. Shibuya, T. Adachi, M. Fujio, and Y. Tsuno, *Mem. Fac. Sci., Kyushu Univ., Ser. C*, **14**(**2**), 355 (1984); b) Y. Tsuno, Y. Kusuyama, M. Sawada, T. Fujii, and Y. Yukawa, *Bull. Chem. Soc. Jpn.*, **48**, 3337 (1975).
23) Y. Karton and A. Pross, *J. Chem. Soc., Perkin Trans. 2*, **1977**, 1860.
24) Y. Karton and A. Pross, *J. Chem. Soc. Perkin Trans. 2*, **1978**, 595.
25) J. M. Harris, A. Becker, J. F. Fagan, and F. A. Walden, *J. Am. Chem. Soc.*, **96**, 4484 (1974).
26) J. Kaspi and Z. Rappoport, *J. Am. Chem. Soc.*, **102**, 3829 (1980).
27) a) D. D. Roberts, *J. Org. Chem.*, **49**, 2521 (1984); b) D. J. Raber, W. C. Neal, Jr., M. D. Dukes, J. M. Harris, and D. L. Mount, *J. Am. Chem. Soc.*, **100**, 8137 (1978).
28) P. J. Stang, M. Ladika, Y. Apeloig, A. Stanger, M. D. Schiavelli, and M. Hughey, *J. Am. Chem. Soc.*, **102**, 6852 (1982).
29) F. L. Schadt, T. W. Bentley, and P. v. R. Schleyer, *J. Am. Chem. Soc.*, **98**, 7667 (1976).
30) Y. Tsuji, M. Fujio, and Y. Tsuno, *Mem. Fac. Sci., Kyushu University, Ser. C*, **17**(**2**), 281 (1989); **17**(**1**), 139 (1989).

Small-Angle X-Ray Scattering Study of Cytochrome Oxidase from Beef Heart and Its Complex with Cytochrome *c* Using Contrast Variation Method

Yukio MORIMOTO,*,† Mamoru SATO, Tatsuhisa KATO, Nobuo TANAKA,††
Yukiteru KATSUBE, Masashi TANAKA,††† and Takayuki OZAWA†††
Institute for Protein Research, Osaka University, Suita, Osaka 565
†††Faculty of Medicine, University of Nagoya, Tsurumai, Nagoya 466
(Received September 5, 1990)

The structure of cytochrome oxidase from beef heart and its complex with cytochrome *c* were investigated in solution by X-ray small-angle scattering. The contrast variation method was applied to the present analysis. The radii of gyration and maximum dimensions were estimated to be 54 and 165 Å for the cytochrome oxidase and 56 and 165 Å for the complex, respectively. A model of the dimer was constructed so as to interpret the X-ray scattering data well. It was concluded that cytochrome *c* is bound to the hydrophilic surface of the enzyme near the edges of the ellipsoidal molecule, and that detergent molecules exist on the surface of the central parts of the enzyme.

Cytochrome oxidase (ferrocytochrome *c*: oxygen oxidoreductase EC 1.9.3.1) is the terminal component of the electron-transfer chain in the mitochondrial inner membrane of eukaryotes. It catalyzes an electron transfer from ferrocytochrome *c* to molecular oxygen and plays an important role as an energy transducer for ATP synthesis. Many biological and physicochemical studies have been undertaken concerning mitochondrial enzymes.[1] In spite of these extensive studies, no structural evidence concerning its precise subunit composition or the locations of the prosthetic groups has been established. For cytochrome oxidase isolated from beef heart, although the number of subunits and the specific heme *a* and copper contents have been reported in many papers, the results show wide variations.

A small-angle X-ray scattering (SAXS) technique followed by a contrast variation method is useful for investigating the protein structure in solution, even though the structure can not be determined accurately. The enzyme is highly hydrophobic and makes a complex with a large number of detergent molecules, forming a micelle in solution. The relative location of each component is detected by the contrast variation method of small-angle X-ray scattering from a solution in which the electron density is close to those the protein or detergent molecules, utilizing the fact that the mean electron density of the detergent micelle is significantly lower than that of the protein.

In the present work, the molecular structures of the cytochrome oxidase from beef heart and its complex with cytochrome *c* was studied using small-angle X-ray scattering. The binding sites of the detergent molecules and cytochrome *c* in the complex are discussed.

† Present address: Faculty of Science, Himeji Institute of Technology, Shosha, Himeji 671-22.
†† Present address: Faculty of Bioscience and Biotechnology, Tokyo Institute of Technology, Yokohama 227.

Experimental

Preparation of Samples. Cytochrome oxidase was isolated from beef heart mitochondria according to a method of Fowler et al.,[2] and was refractionated with ammonium sulfate in the presence of 1% cholate by a method of Tzagoloff and MacLennan.[3] The fractionated cytochrome oxidase was further purified by hydrophobic chromatography on phenyl-Sepharose CL-4B[4] and affinity chromatography on cytochrome *c*-Sepharose 4B.[5,6] The purified enzyme was finally applied on Sephacryl S-300 equilibrated with 10 mM Tris-HCl buffer, pH 7.5, containing 0.1% Triton X-100 and 0.1 M NaCl (1 M=1 mol dm^{-3}). An enzyme-cytochrome *c* complex was prepared by adding cytochrome *c* purified by a method of Hagihara et al.[7] to an enzyme solution in heme *c*: a heme *a* ratio of 1 : 2 (1 : 1 mol/mol) and an excess of cytochrome *c* was removed by gel filtration on a Sephadex G-75. The heme *a* concentration was determined from a difference spectrum of oxidase reduced with $Na_2S_2O_4$ using a millimolar extinction coefficient of $\Delta\varepsilon_{605-630}$=16.5 mM^{-1}cm^{-1}.[8] The protein concentration was determined by the biuret method.[9]

The electron densities of the X-ray scatterers were calculated from the number of electrons and the partial specific volumes of the enzyme, bound detergent, and cytochrome *c*. The partial specific volume of the enzyme was calculated to be a weighted mean of those of the enzyme and the bound detergent.[10] The amount of detergent molecules was estimated by gel filtration on Sephacryl S-300.[11] The difference in absorption at 280 nm between an enzyme bound with Triton X-100 and that with cholate resulted in 180 molecules of Triton X-100/heme aa_3. To realize a wide range of electron density of the solvent, sucrose, which exhibits a high electron density, was added to a concentrated protein solution so that the protein concentration could be maintained at 0.5% (w/v). A buffer solution containing the detergent was also prepared under the same conditions as that for the protein solution. Contrast variation measurements were carried out in 0.0, 5.0, 10.0, 18.5, 22.0, 30.7, 36.3, 40.0, 45.0, and 50.0% (w/w) sucrose concentrations, corresponding to averaged electron densities of 0.334, 0.341, 0.348, 0.359, 0.363, 0.377, 0.385, 0.391, 0.400, 0.408 e Å^{-3}.

Small-Angle X-Ray Scattering. The X-ray source was a

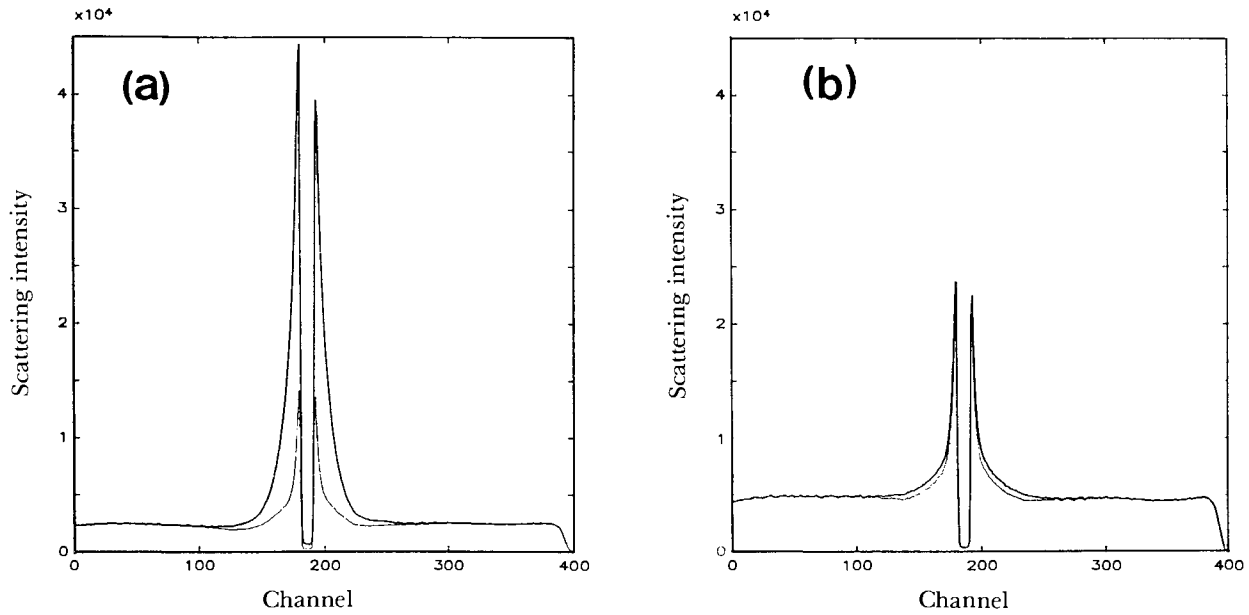

Fig. 1. Typical scattering intensity profiles of cytochrome oxidase solutions containing (a) 0% sucrose and (b) 30.7% sucrose (thick line) and those of the respective cytochrome oxidase free solutions for background intensity subtraction (thin line).

0.4×8 mm spot on the copper anode of a Phillips fine-focus X-ray tube, which was operated at 40 kV-30 mA with a Rigaku Denki D9C X-ray generator. The spot was foreshortened to 0.04×8 mm at a glancing angle of 6°. Ni-filtered X-rays were reflected and focused by a nickel-coated glass mirror (20×60×5 mm), and then introduced to a sample solution through two kinds of limiting slits: the first slit was located behind a mirror holder in order to collimate reflected X-rays; the other one was located in front of a sample holder and was used to reduce parasitic scattering from the edge of the first slit. The scattered X-rays were recorded with a one-dimensional position-sensitive proportional counter (delay-line type) over a scattering range of 4.0×10^{-3} to 7.7×10^{-3} rad. The counter length was 50 mm and was divided into 512 channels on a multichannel analyzer. The sample-to-counter distance was 305 mm. The path between the sample holder and the counter was evacuated in order to eliminate any air scattering. A sample solution was introduced into a 1.0 mϕ thin-walled quartz capillary by an injector incorporated into the sample holder. All X-ray measurements were performed at 5±0.1 °C.

Figure 1 shows typical scattering intensity profiles of cytochrome oxidase and cytochrome oxidase free solutions on a multichannel analyzer. The scattering intensities recorded on both sides of the primary beam were averaged at equivalent points after subtracting background intensities. The center of the primary beam (zero-angle scattering) was adjusted around the center of the quartz capillary, and then refined so as to realize the best coincidence of the scattering intensities at equivalent points. After averaging, an iterative method by O. Glatter[12] was applied in order to deconvolute the slit effects: the beam size, the counter width along the longitudinal axis, and the beam divergent effect. Data smoothing, which was free from random error, was also carried out using the program.

The radius of gyration, R_g, was calculated from both Guinier plots[13] of the scattering intensity data, $I(\boldsymbol{h})$, in a smaller-angle scattering region, and from an integration of the distance distribution function, $P(\boldsymbol{r})$, which (multiplied by 4π) represents for homologous particles (X-ray scatterers) the number of distances within the particle and is obtained from a Fourier transformation of $I(\boldsymbol{h})$ using the following equation:

$$P(\boldsymbol{r}) = 1/2\pi^2 \left(\int_0^\infty I(\boldsymbol{h}) \cdot \boldsymbol{hr} \cdot \sin(\boldsymbol{hr})\, d\boldsymbol{h}\right) \quad (1)$$

$h = 4\pi \sin\theta/\lambda$, 2θ; scattering angle
λ; wavelength

The $P(\boldsymbol{r})$ function was also utilized in order to estimate the maximum dimension of the X-ray scatterer from a distance r, where $P(\boldsymbol{r})$ decreases to zero. The model was constructed by assemblies of spheres to fit the calculated $P(\boldsymbol{r})$ functions to the observed ones.

Results

Table 1 summarizes the R_g and D_{max} obtained in various sucrose concentrations. The R_gs of the enzyme are smaller than that of the complex with cytochrome *c* in all sucrose concentrations, though the D_{max}s are the same as each other in cases (a), (b), and (c). The increase of R_g in the complex indicates that cytochrome *c* is not buried inside but, rather, far from the center of the enzyme. However, cytochrome *c* should not be outside of the enzyme, judging from the equivalent D_{max}. The dimeric enzyme is assumed to bind two molecules of cytochrome *c* symmetrically, and the radius of gyration of the complex is calculated using the radius and molecular weight (R_{g1} and m_1 for oxidase and R_{g2} and m_2 for cytochrome *c*), as well as the distance (X) between the two molecules, as

Table 1. Radius of Gyration(R_g) and Maximum Dimension(D_{max}) of the Cytochrome Oxidase and its Complex with Cytochrome c[a)]

Sample	Sucrose concn	Complex with cytochrome c			Cytochrome oxidase		
		R_g[b)]	R_{g_A}[c)]	D_{max}[d)]	R_g	R_{g_A}	D_{max}
	%	Å	Å	Å	Å	Å	Å
(a)	0.0	55.5(1)	55(1)	165(8)	53.8(1)	54(1)	165(8)
(b)	5.0	55.4(1)	54	160	53.5(2)	54	161
(c)	10.0	55.7(2)	55	156	52.3(4)	52	152
(d)	18.5	55.2(2)	54	156	49.7(2)	49	141
(e)	22.0	54(2)	53(2)	147(6)	48.2(2)	49(2)	149(6)
(f)	30.7	41.4(3)	44	140	35.2(2)	36	135
(g)	36.3	18.3(1)	29(2)		—	—	
(h)	40.0	—[e)]	—		—	—	
(i)	45.0	17.6(1)	13		—	—	
(j)	50.0	28.7(1)	28(2)		—	—	

a) Standard deviations are in parenthesis. b) Radius of gyration calculated from Guinier plot. c) Radius of gyration calculated from distance distribution function. d) Maximum dimension. e) Not detected.

follows:

$$R_g^2(\text{complex}) = (m_1 R_{g1}^2 + 2m_2 R_{g2}^2 + 2m_2 X^2)/(m_1 + 2m_2). \quad (2)$$

By using m_1=260000, m_2=13000, R_{g1}=53.5 Å, R_{g2}=12 Å, R_g(complex)=55.1 Å, X was calculated to be 68 Å, which is less than half of D_{max} by 12 Å. This also indicates that cytochrome c is not deeply buried in the enzyme, but clings to it, since half of the D_{max} of cytochrome c has been estimated to be about 17 Å from a crystal-structure analysis.

The scattering of an X-ray from a particle depends on the difference in the electron density between the particle and the solvent, as follows:[14)]

$$I(\boldsymbol{h}) = \Delta\rho^2 I_v(\boldsymbol{h}) + \Delta\rho I_{vf}(\boldsymbol{h}) + I_f(\boldsymbol{h}), \quad (3)$$

where $\Delta\rho$ is the difference between the averaged electron density between the particle and solvent ($\Delta\rho = \rho_{scatterer} - \rho_{solvent}$), I_v is a shape function of the particle, I_f is from the internal structure of the particle, and I_{vf} is a correlation term between the shape and internal structure of the particle, respectively. The I_v mainly contributes to $I(\boldsymbol{h})$, and the latter two term are quite weak, except for $\Delta\rho$=0. In the present case, a large number of detergent molecules are bound to the hydrophobic surface of the enzyme as a micelle. The averaged electron density of the micelle of Triton X-100 (0.363 e Å^{-3}) was lower than that of the protein, though both were higher than that of 0.1% Triton X-100 solution (pH 7.5, 10 mM Tris-HCl). The square root of the zero-angle scattering intensity, $\sqrt{I(0)}$, was plotted against the electron density of the solvent. In the equation, the I_{vf} and I_f terms are zero at $\boldsymbol{h}$=0, since the average of the internal variation of the structure is zero, and $I(0)$ against the electron density plot may be linear if I_v is not changed; that is, a invariant volume hypothesis[15)] is valid. In Fig. 2, both plots of the enzyme and enzyme-cytochrome c complex revealed excellent linearity to ascertain that the enzyme does not react with sucrose. From this plot, the averaged electron density of the particle was derived to be 0.38 e Å^{-3} at $I(0)$=0, which is in good agreement with the calculated value of the detergent-bound enzyme.

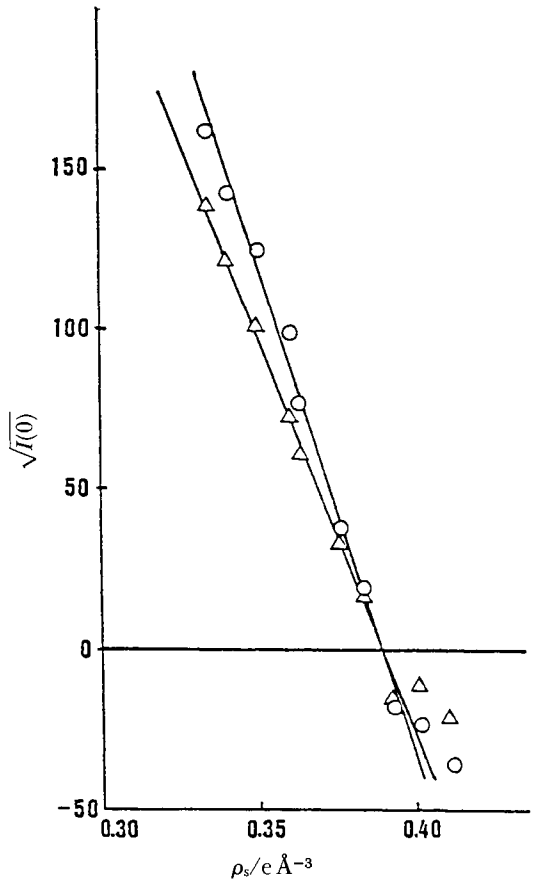

Fig. 2. Relationship between $\sqrt{I(0)}$ and the electron density of a solvent, ρ_s; (△): cytochrome oxidase; (○): cytochrome oxidase -cytochrome c complex.

The distance distribution function, $P(\boldsymbol{r})$, was utilized in the present structural study. As shown in

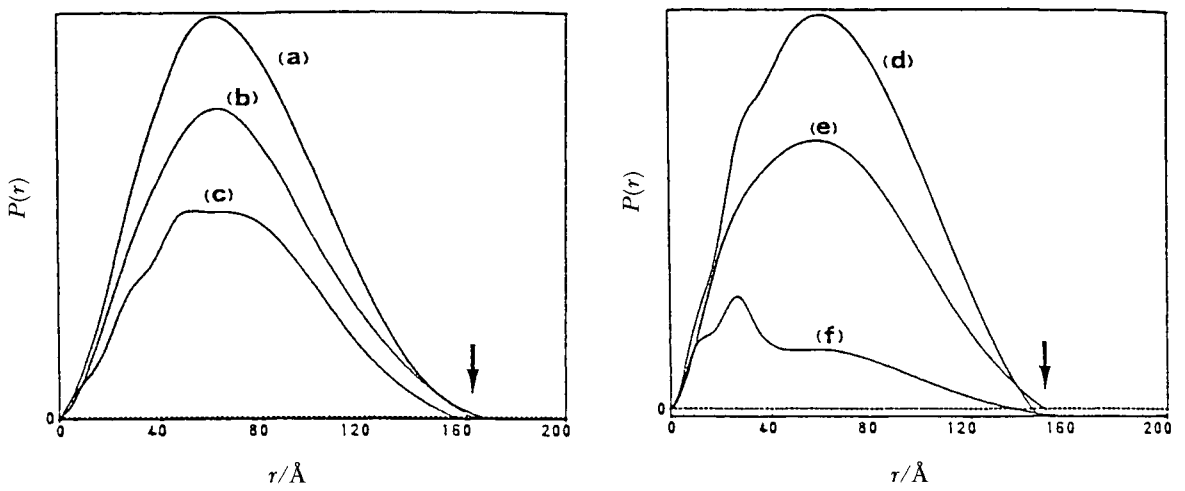

Fig. 3. Distance distribution functions $P(r)$'s for cytochrome oxidase in various sucrose concentrations; ((a) to (f)) correspond to those of Table 1. Arrows indicate the maximum dimension of the enzyme particle.

Fig. 3, the single broad profile of the $P(r)$'s trended to express an undulating character with an increase in the electron density of the solvent. However, the function at the highest sucrose concentration ((f) in Fig. 3) represented a single profile similar to those in the lower sucrose concentration (a)—(c). This behavior suggests that the enzyme comprises different electron-density regions (detergent and protein) separately. When the averaged electron density of the solvent was matched with the detergent, the protein was visible and the detergent invisible ((e) in Fig. 3). The I_f and I_{vf} terms of the protein moiety could be neglected, since the data observed in the present analysis was within a 20 Å resolution, which was too low to show any fine variations of the electron density in one molecule. The electron density of the solvent matched that of the protein erases the part of the protein. The intermediate gives a positive protein and a negative detergent to the $P(r)$ function ((f) in Fig.3).

The SAXS profile was compared with some theoretical intensity curves for various eccentricities. As drawn in Fig. 4, the curve of an ellipsoid with an eccentricity of 2.0 expressed good coincidence with the observed profile in the small-angle region ($2\theta < 14 \times 10^{-3}$ rad). Disagreement of the observed profile at slightly high angles was caused by deviations from a uniform electron density within a prolate ellipsoid model. A molecular model was simulated as assemblies of spheres with a radius of 12 Å, half of the resolution of the observed data, where the electron density of the polypeptide moiety was 0.408 e Å^{-3}, and that of the detergent was 0.363 e Å^{-3}. At first, 56 spheres were gathered in a prolate ellipsoid whose axes were 30, 30, and 50 Å. Spheres as detergent molecules were located around the side surface of the model. The model was refined so as to relate the

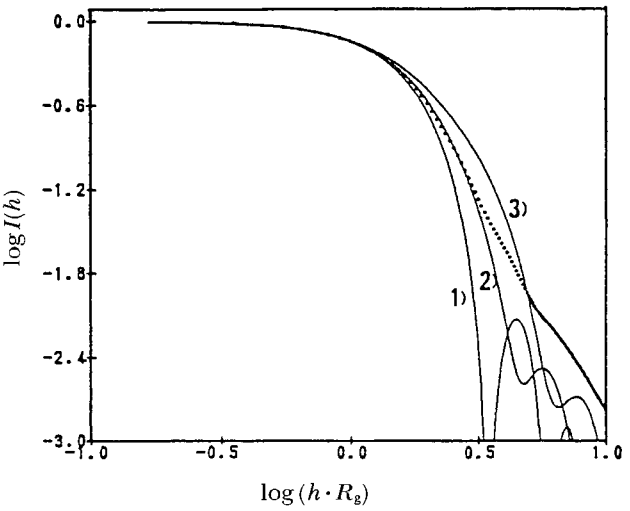

Fig. 4. Log I-log (hR_g) plot of scattering intensities of the cytochrome oxidase in 0% sucrose concentration. Superimposed are the logarithms of the theoretical scattering intensity function (solid line) of the prolate ellipsoids with eccentricities, ω of 1) ω=1.0 (sphere), 2) ω=2.0, and 3) ω=3.0.

calculated scattering data with the observed data, step by step, by the addition of a new sphere and/or the removal of a sphere. The final model comprised 74 spheres, in which 30 were designated as bound-detergent molecules. It should be noted that the relative orientation of individual spheres is not biochemically significant, that is, they do not represent the position of enzyme subunits, but only express a domain having a certain value of electron density. Spheres used as detergent molecules were located around the side surface of the model. Two spheres of cytochrome c were also combined so as to satisfy the distance derived from the complex experiments. The

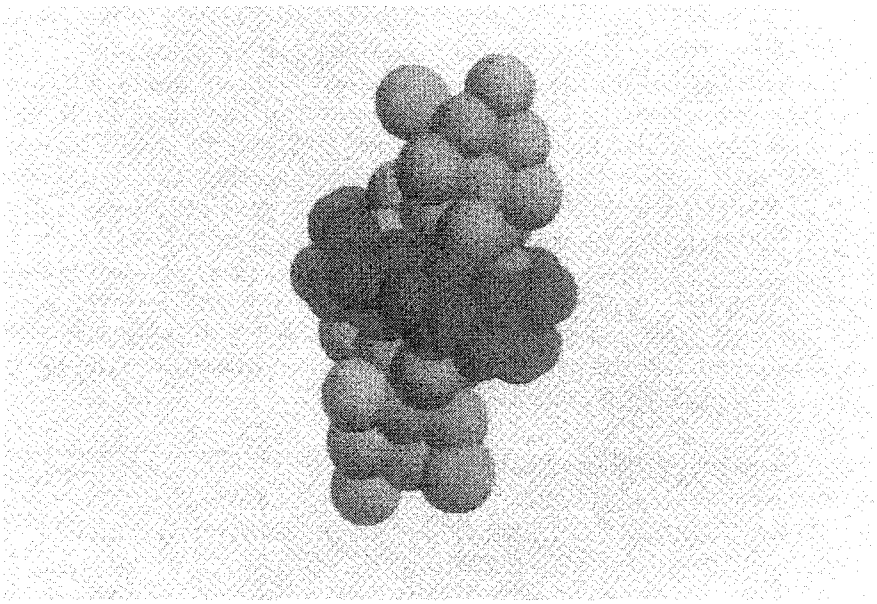

Fig. 5. Proposed dimeric structure of cytochrome oxidase complexed with cytochrome *c* drawn as a sphere model; central dark spheres, Triton X-100; slightly dark two spheres, cytochrome *c*; others, cytochrome oxidase. The size of spheres for proteins or detergents is not real one, but the spheres are used to depict the positions of their components.

consensus model shown in Fig. 5 shows two monomers in contact with each other by a relation of twofold symmetry and reproduced the structural parameters obtained in the present study, qualitatively. Hydrophobic part of the enzyme was protected by detergents, which seems to be likely in the lipid-bilayer in mitochondrial membrane, while hydrophilic part or cytochrome *c* binding site is far from each other.

Discussion

The maximum dimension of the enzyme under the highest contrast was clarified to be 165 Å, and its volume 650000 Å^3. From an electron microscopic study,[16] the span of the Y-shaped cytochrome oxidase monomer was about 70—80 Å in the mitochondrial membrane. These facts suggest that the enzyme exists as a dimer in a solution containing 0.1% Triton X-100. The enzyme, therefore, as the prolate ellipsoidal form derived from Fig. 4, comprises the connection of two identical monomers so as to contact with each Y-head. The force of this connection is considered to be a hydrophobic interaction of each subunit. This dimeric form is consistent with an ultracentrifugation study in the presence of 0.1% Triton X-100.

The values of maximum dimensions at various electron-density levels reveal an aspect of the binding

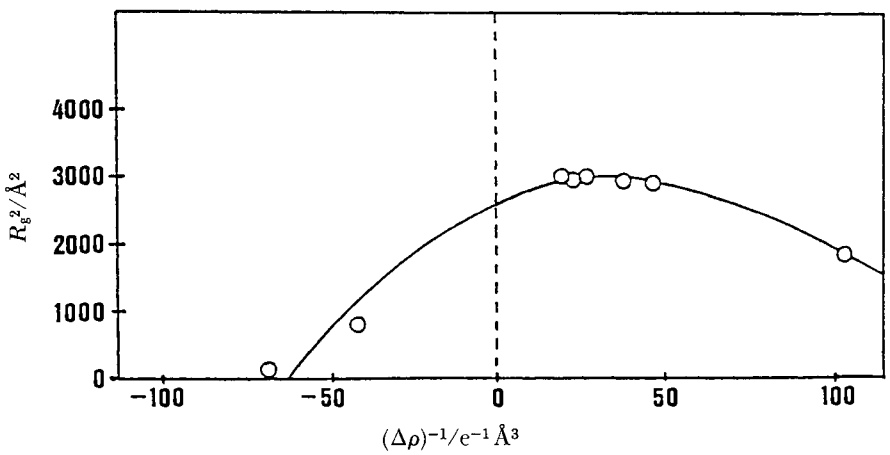

Fig. 6. Relationship between R_g^2 and $1/\Delta\rho$ (Stuhrmann plot) of cytochrome oxidase-cytochrome *c* complex.

site of detergents. A D_{max} of 165 Å under highest contrast exhibits no significant change below sucrose concentrations of 22%, whose electron density is close to that of the bound detergent micelle. This indicates that the enzyme binds the detergent molecules at the sites where its longest span is not varied. Judging from a negative quadratic character of the R_g^2—$1/\Delta\rho$ plot depicted in Fig. 6, the enzyme comprises an electron-dense region in its core and an electron-sparse region at its surface.[14] From these results it may be concluded that the detergent molecules are bound to the side surface of the ellipsoidal dimer, where the Y-heads of two monomers interact with each other by the hydrophobic characters.

A model construction based on the obtained molecular parameters and other structural information[1,16,17] definitely express the characteristics of the enzyme in solution. A preliminary structure analysis shows that the overall structure of the enzyme can be approximated by a prolate ellipsoid with an eccentricity of 2.0. An ellipsoidal model comprising 74 spheres shows that two monomers contact each other through a twofold symmetry. The hydrophobic part of the enzyme is protected by detergents, which seems to be likely in the lipid-bilayer in a mitochondrial membrane, while the hydrophilic part or the cytochrome *c* binding site is far from each other. From these results, the monomer model is consistent with the fact that the molecule passes through the mitochondrial membrane perpendicularly.[16]

The enzyme involves a variety of dense electron regions which are beyond the resolution of the data. Although in the small-angle region the scattering profile calculated according to the rigid body of uniform electron density agreed well with that observed, the consistency between that observed and calculated was worse at the higher-angle region, as is shown in Fig.4. The depicted model, which has two kinds of electron density levels in the ellipsoidal body, decreased the discrepancy, as shown in Fig.7. This feature of the enzyme is also enforced by the effects of contrast on the $P(r)$ function. The calculated $P(r)$s in various contrasts are qualitatively consistent with those of experiments (Fig. 8), from which it may be concluded that the model was constructed correctly. However, the fact that the model is the one which reasonably describes the results from the present study should be noted.

Although there were some errors in X-ray experiments, within the error the present model qualitatively expresses the character of the enzyme in solution, and describes not only the shape of the enzyme

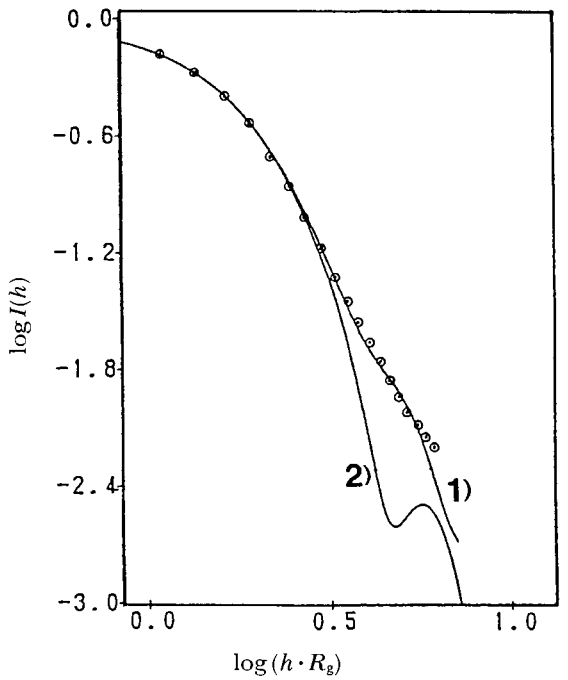

Fig. 7. Log$I$-log (hR_g) plot of the observed scattering intensity. Superimposed are the logarithms of the theoretical scattering intensity functions of a final sphere model: 1) and a preliminary ellipsoidal model with eccentricity of 2.0 : 2).

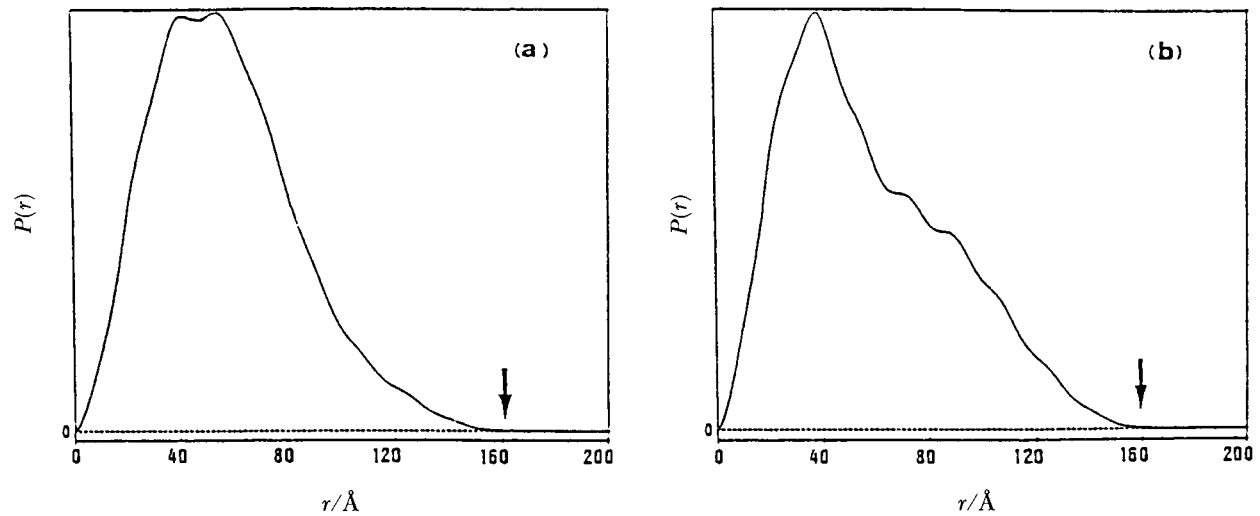

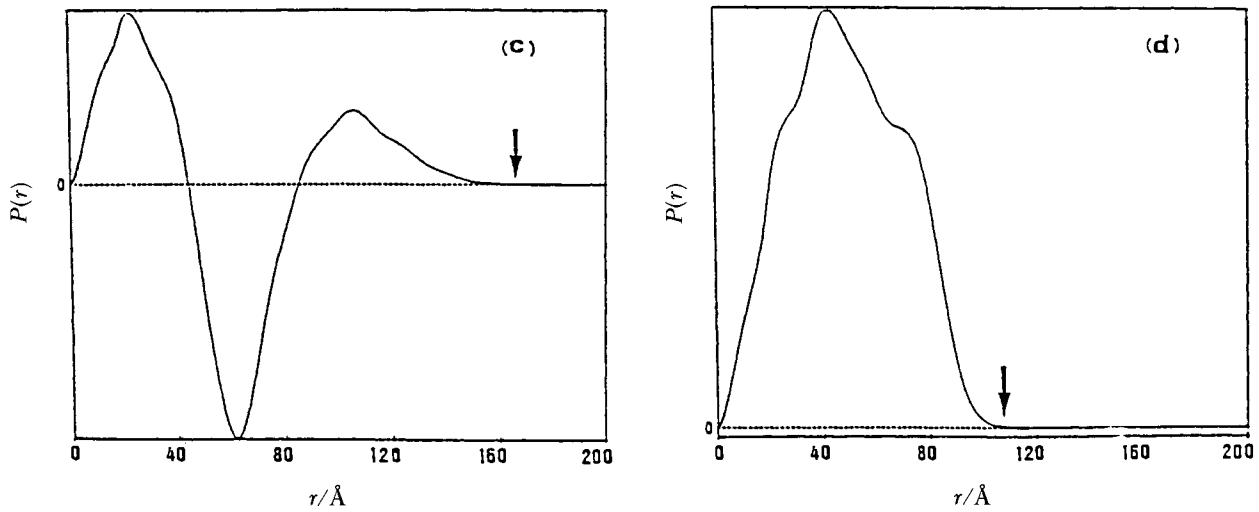

Fig. 8. Distance distribution functions $P(r)$'s for the final sphere model; (a), 0% sucrose; (b), 22% sucrose; (c), 36.3% sucrose; (d), 50% sucrose. Arrows indicate the maximum dimensions.

but also the location of the bound detergent and cytochrome *c*. Judging from only the proposed model, the molecule comprises a hydrophobic central core with detergent molecules and hydrophilic edge regions. Hydrophilic cytochrome *c* is expected to bind to the edge of the oxidase due to the electrostatic character, as discussed and established in our previous paper.[17] The limits of resolution and simulation, however, restrain any detailed modeling of the enzyme. To overcome this problem, high-angle scattering measurements or a crystal structure analysis is indispensable.

One of the authors (Yukio Morimoto) wishes to express his gratitude to Professor Noritake Yasuoka and Dr. Yoshiki Higuchi of Himeji Institute of Technology for their encouragement and to Emeritus Professor Masao Kakudo of Osaka University for variable discussion and encouragement throughout this study.

References

1) T. Ozawa, "Transport and Bioenergetics in Biomembranes," ed by R. Sato and Y. Kagawa, Japan Scientific Societies Press, Tokyo (1982).

2) L. R. Fowler, S. H. Richardson, and Y. Hatefi, *Biochim. Biophys. Acta*, **64**, 170 (1962).

3) A. Tzagoloff and D. H. MacLennan, *Biochim. Biophys. Acta*, **99**, 476 (1965).

4) T. Ozawa, M. Tada, and H. Suzuki, "Cytochrome Oxidase," ed by T. E. King, Y. Orii, B. Chance, and K. Okunuki, Elsevier (North-Holland), Amsterdam (1979).

5) T. Ozawa, M. Okumura, and K. Yagi, *Biochem. Biophys. Res. Commun.*, **65**, 1102 (1975).

6) T. Ozawa, H. Suzuki, and M. Tanaka, *Proc. Natl. Acad. Sci. U.S.A.*, **77**, 928 (1980).

7) B. Hagihara, I. Norikawa, I. Sekuzu, and K. Okunuki, *J. Biochem.*, **45**, 551 (1958).

8) T. Yonetani, *J. Biol. Chem.*, **236**, 1680 (1961).

9) A. G. Gornall, C. J. Bardawill, and M. M. David, *J. Biol. Chem.*, **177**, 751 (1949).

10) C. Tanford, Y. Nozaki, J. A. Reynolds, and S. Makino, *Biochemistry*, **13**, 2369 (1974).

11) N. C. Robinson and R. A. Capaldi, *Biochemistry*, **16**, 375 (1977).

12) O. Glatter, *J. Appl. Cryst.*, **7**, 147 (1974).

13) A. Guinier and G. Fournet, "Small Angle Scattering of X-Ray," John Wiley and Sons, New York (1965).

14) H. B. Stuhrmann and R. G. Kirste, *Z. Phys. Chemi. (Frankfurt)*, **46**, 247 (1965).

15) L. Luzzati, A. Tardieu, L. Mateu, and H. B. Stuhrmann, *J. Mol. Biol.*, **101**, 115 (1976).

16) R. Henderson, R. A. Capaldi, and J. S. Leigh, *J. Mol. Biol.*, **112**, 631 (1977).

17) M. Sato, M. Kato, N. Kasai, Y. Hata, N. Tanaka, M. Kakudo, M. Tanaka, and T. Ozawa, *Biochem. Int.*, **5**, 595 (1982).

Oxygen Effect on Photocatalytic Reaction of Ethanol over Some Titanium Dioxide Photocatalysts

Kozo Iseda
Government Industrial Research Institute, Nagoya, Hirate-cho, Kita-ku, Nagoya 462
(Received September 25, 1990)

The suspensions of four kinds of TiO_2 photocatalysts in ethanol have been studied under ultraviolet light in an atmosphere of Ar, air, or O_2 at 25 °C. The main products were acetaldehyde, acetaldehyde diethyl acetal (acetal), acetic acid, water, ethylene, methane, carbon dioxide, and hydrogen. Acetaldehyde and acetal were abundantly produced in all of the products. The formation of all of the products under O_2 was more efficient than those under Ar and air. The photochemical activity of each TiO_2 is stronger than that of either Ti_2O_3 or TiO.

Photocatalytic H_2 evolution from ethanol over Pt/TiO_2 catalysts has frequently been reported;[1-6] CH_3CHO,[1,2,4,5] acetal,[2] and acetic acid[1] are major photocatalytic products. However, no instance has yet been reported concerning a quantitative photocatalytic formation on all products from ethanol using various TiO_2 catalysts.

Because the catalytic activity of TiO_2 is presumed to be caused by active oxygen liberated from TiO_2,[7] the activity is decreased by a reduction of the catalyst, itself, due to light illumination;[7] no report, however, has demonstrated the influence of such a decrease in the activity on all products from ethanol, except that regarding the evolution of C_2H_4 and H_2 by the author.[8] To determine the catalytic activity of TiO_2, itself, becomes difficult if Pt is deposited on TiO_2, since the reduction of TiO_2 is depressed by Pt.[9] Therefore, this work was undertaken with only TiO_2, without Pt, and studied in detail regarding effects due to the reactivation of TiO_2 with O_2 on all of the products formed from C_2H_5OH by a comparison of the results from blank tests under Ar, air, or O_2 atmospheres, and that with the TiO_2 under each atmosphere. Furthermore, a comparison was made with that involving TiO_2 as well as Ti_2O_3 or TiO.

Experimental

Photocatalysts. The TiO_2, Ti_2O_3, and TiO used were the same as that described previously.[8] Commercial Ti_2O_3 and TiO used were 99.9%, 300 mesh, Furuuchi Chemical Co., Ltd., respectively.

Ethanol. In the same manner as described in a previous paper,[8] the commercial C_2H_5OH (99.5%, special grade, Katayama Chemical Co., Ltd.) used was purified by distillation after drying over CaO.

Reaction Procedure. The experimental conditions were similar to those published previously.[8] The water tank used was a Riko RH400-10W photochemical reactor. After illumination, the reaction tube was immediately transferred to a beaker containing ice-water and was kept for about 15 min in a refrigerator. This is because the CH_3CHO produced should be kept in the dark while in the liquid-phase as much as possible. A blank test for a mixture of CH_3CHO (0.2 ml) and H_2O (1.8 ml) or that of CH_3CHO (0.2 ml) and C_2H_5OH (1.8 ml) was carried out under an Ar atmosphere without any catalyst in a similar manner as in a previous study.[10]

Analysis. The analytical conditions were also similar to those run in a previous study.[8] A Shimadzu GC-8A gas chromatograph (activated charcoal, 60—80 mesh) was used for the analysis of gaseous products. All liquid products, except for acetic acid, were analyzed using a Shimadzu GC-4B gas chromatograph (PEG-6000 10%, Flusin P, 30—60 mesh). Subsequently, acetic acid was analyzed by a Perkin-Elmer 900 gas chromatograph (PEG-6000 10%, Flusin P, 30—60 mesh, 2 mmϕ×1.8 m glass column, 140 °C, N_2 carrier, FID). In this experiment, the yields of all products with TiO_2, Ti_2O_3, and TiO include that of a blank test under each atmosphere (Figs. 1,2, and 10).

Results and Discussion

Figures 1 and 2 show the formation of liquid products and that of gaseous products from ethanol versus the illumination time observed for a blank test under an Ar or air atmosphere, respectively. Because CH_3CHO and H_2 are produced during the initial illumination, the first reaction of ethanol proceeds as follows:[1]

$$C_2H_5OH \xrightarrow{h\nu} CH_3CHO + H_2 \quad \Delta G^\circ = 41.0 \text{ kJ mol}^{-1}. \quad (1)$$

This result is particularly important in view of the fact that ethanol fails to undergo any reaction; this is because of its absorption maximum at 174 nm[11] under UV light, since Pyrex glass does not pass UV light below about 230 nm. The cause of the reaction described in Eq. 1 is most likely to be due to slight substances having photosensitive action dissolved in ethanol from the natural rubber liner; natural rubber usually contains small amounts of other additive impurities. Once CH_3CHO forms, it serves as a sensitizer, since it has an absorption maximum at 293 nm[12] in its ultraviolet spectrum, and Pyrex glass passes about 40% of the UV light at a wavelength of 290 nm. Accordingly, some of the products shown in Figs. 1 and 2 were slightly produced without TiO_2. Acetal and CH_3COOH were not detected at for illumi-

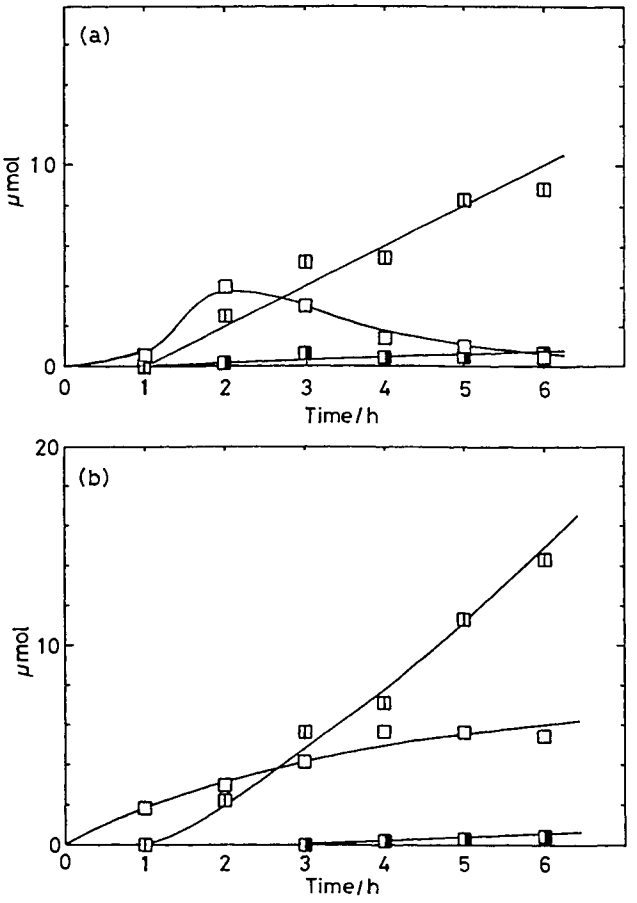

Fig. 1. Formation of liquid products from 2.0 ml ethanol vs. illumination time for a blank test without any TiO_2 under Ar (a) or air (b) atmosphere. □: acetaldehyde, ▥: acetaldehyde diethyl acetal (acetal), ◨: acetic acid.

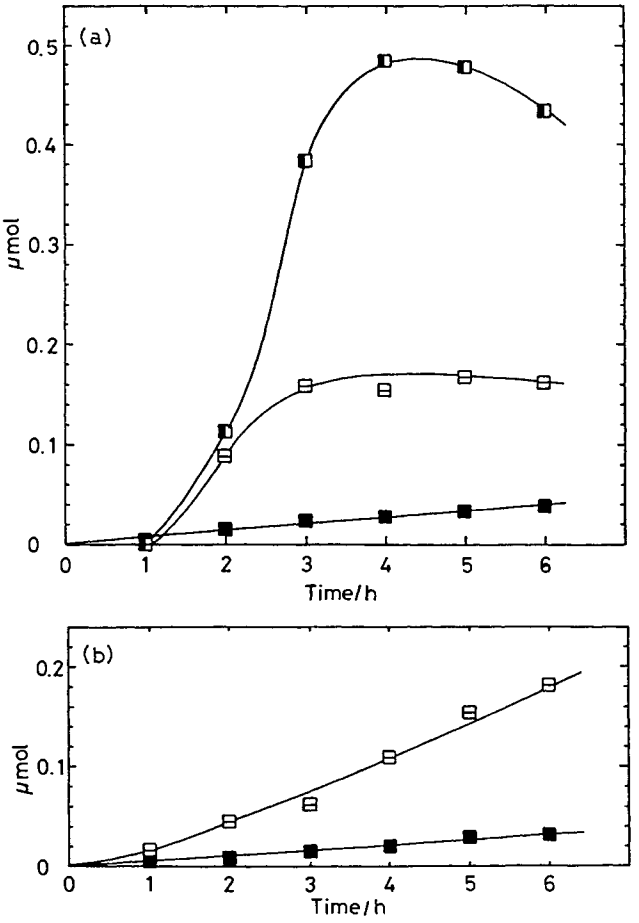

Fig. 2. Evolution of gaseous products from 2.0 ml ethanol vs. illumination time for a blank test without any TiO_2 under Ar (a) or air (b) atmosphere. ◧: CH_4, ⊟: CO_2, ■: H_2.

nation times less than 1 h, and therefore appear to be formed in the following way:

$$CH_3CHO + 2\,C_2H_5OH \xrightarrow{h\nu} CH_3CH(OC_2H_5)_2 + H_2O. \quad (2)$$

Actually, this reaction was confirmed by the formation of acetal and H_2O from a mixture of CH_3CHO (0.2 ml) and C_2H_2OH (1.8 ml) under an Ar atmosphere without TiO_2. Acetic acid is formed as proposed by Sakata and Kawai,[1]

$$CH_3CHO + H_2O \xrightarrow{h\nu} CH_3COOH + H_2 \qquad \Delta G^\circ = -18.9\ \mathrm{kJ\,mol^{-1}}. \quad (3)$$

The formation of CH_3COOH and H_2 was also observed in a mixture of CH_3CHO (0.2 ml) and H_2O (1.8 ml) under Ar. In addition, CH_4 and CO_2 from Eq. 4, shown later, were evolved. The H_2O in Eq. 3 is contained as a small amount of impurity in ethanol and is provided by Eq. 2 as well as by the oxidation of C_2H_5OH by O_2 under an air atmosphere.[8] Actually, H_2O formation under air was more than that under an Ar atmosphere.

No evolution of CH_4 and CO_2 was detected for illumination times less than 1 h under Ar. This is because the decomposition of CH_3COOH gives an evolution of CH_4 and CO_2, as reported by Kraeutler and Bard,[13] and no CH_3COOH was formed during the initial stage.

$$CH_3COOH \xrightarrow{h\nu} CH_4 + CO_2 \quad \Delta G^\circ = -55.8\ \mathrm{kJ\,mol^{-1}}. \quad (4)$$

By the way, in spite of the formation of CH_3COOH and CO_2 under air, no CH_4 was detected. One possible reason for no CH_4 evolution involves the oxidation of CH_4 by O_2 in air.

Figure 3 shows the formation of CH_3CHO from ethanol versus the illumination time observed for four TiO_2 catalysts under an atmosphere of Ar and that of air. Because of the higher yield with each TiO_2, compared to the yield of the blank test, all of the TiO_2 contributes to the formation of CH_3CHO. Acetaldehyde is also formed by the reduction of TiO_2, itself, as shown in Eq. 5 for the following reason. Buss and co-workers proposed the formation of Ti_2O_3 through a color change of the illuminated TiO_2 in normal

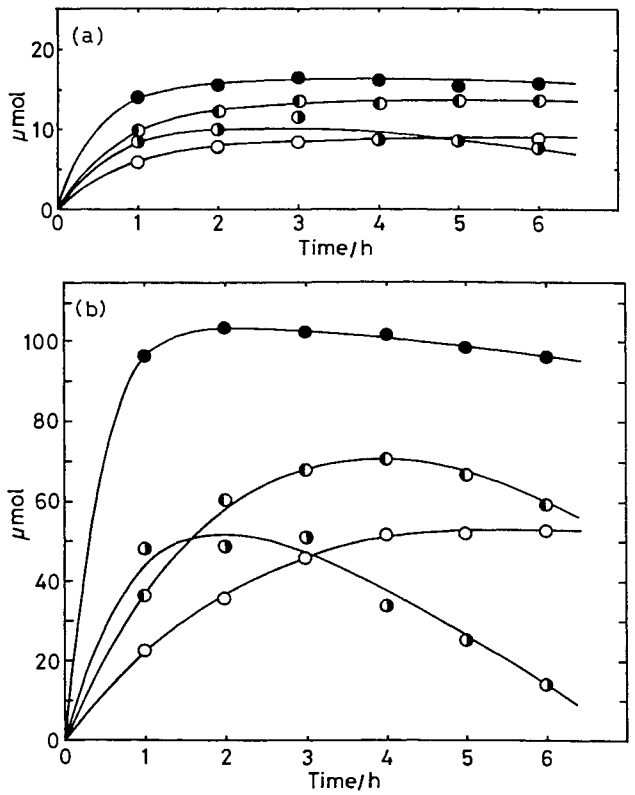

Fig. 3. Formation of acetaldehyde vs. illumination time for suspensions of 30 mg TiO_2 in 2.0 ml ethanol under Ar (a) or air (b) atmosphere. ○: anatase (Aldrich), ◑: rutile (Aldrich), ◐: rutile (Furuuchi), ●: P-25 (Nippon Aerosil).

primary alcohols.[14] Nishimotol et al. demonstrated the cause for the color change by which Ti_2O_3 is formed by a reduction of TiO_2 with 2-propanol.[9] Judging from these two reports, the color change of illuminated TiO_2 in the present work is considered to be caused by a partial formation of Ti_2O_3 due to the reduction of TiO_2 with ethanol,

$$C_2H_5OH + 2\,TiO_2 \xrightarrow{h\nu} CH_3CHO + Ti_2O_3 + H_2O. \quad (5)$$

The molar quantities of TiO_2 required to react with 2.0 ml (343×10^2 μmol) of ethanol are 686×10^2 μmol, as can be seen from Eq. 5. However, 30 mg (375 μmol) of TiO_2 is about 1/200 of the value of μmol required to react with 2.0 ml of ethanol. Therefore, the TiO_2 may be further reduced with a large excess of the ethanol,

$$C_2H_5OH + TiO_2 \xrightarrow{h\nu} CH_3CHO + TiO + H_2O. \quad (6)$$

If only gaseous O_2 in the reaction tube contributed to the formation for CH_3CHO, the ratio of CH_3CHO formation under Ar to that under air in a blank test should be the same as that with TiO_2. However, the formation of CH_3CHO with most TiO_2 catalysts under air is above about 5-times that under Ar, while its formation in a blank test under air is approxi-

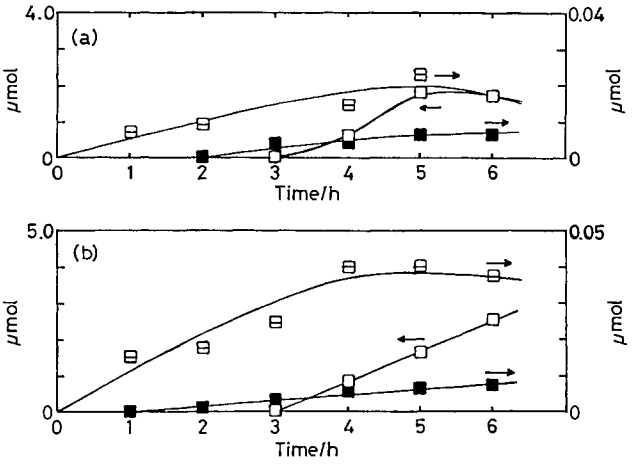

Fig. 4. Formation of products vs. illumination time for suspension of 30 mg Ti_2O_3 in 2.0 ml ethanol under Ar (a) or air (b) atmosphere. □: acetaldehyde, ⊟ CO_2, ■: H_2.

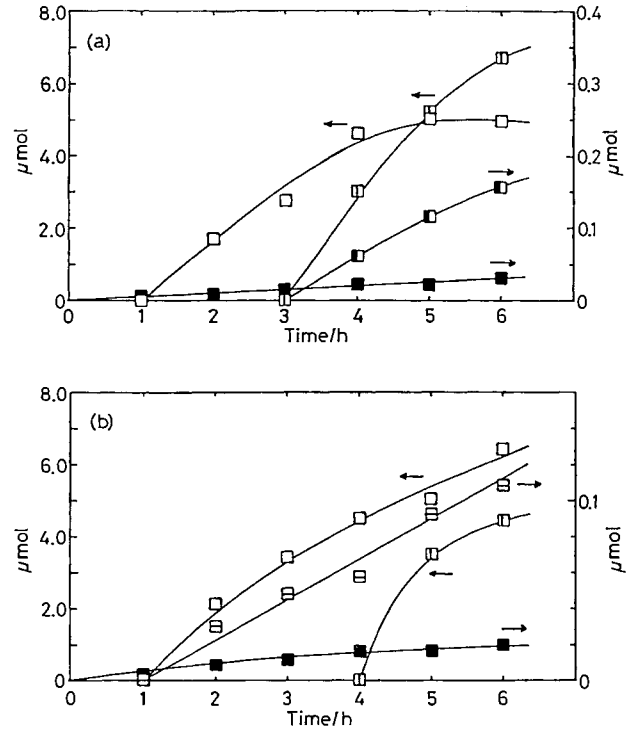

Fig. 5. Formation of products vs. illumination time for suspension of 30 mg TiO in 2.0 ml ethanol under Ar (a) or air (b) atmosphere. □: acetaldehyde, ◫: acetal, ◧: CH_4, ⊟: CO_2, ■: H_2.

mately twice that under Ar. Such a difference between the ratio with the TiO_2 and that in the blank test is remarkably observed for other products, as shown later, since the yields of the other products under Ar in the blank test are roughly the same as those under air, in contrast to the larger difference in the yields with the TiO_2 than the result for CH_3CHO. Consequently, the active O_2 from the reoxidized

TiO_2[7] by O_2 in air seems to be the reason for the higher yield of CH_3CHO under air than that under Ar. If this assumption were correct, the color change[9,14] due to the reduction of TiO_2 observed under air should be much less than that under Ar; further, O_2 in the reaction tube must be decreased, and water must be formed. In fact, these three observations were obtained. To make sure of this estimate, we tried to produce CH_3CHO with Ti_2O_3 or TiO corresponding to the reduction product of TiO_2; these two catalysts gave much fewer products, as shown in Figs. 4 and 5, respectively. Accordingly, the retarding photochemical reduction of TiO_2 under an air atmosphere led to much CH_3CHO formation.

Figure 6 shows the formation of acetal. Under Ar, in spite of the higher yield of CH_3CHO with P-25 and rutile (Furuuchi), compared to the rutile (Aldrich), these two TiO_2 gave no acetal. Although there was no large difference between the yield of CH_3CHO with rutile (Aldrich) and that with anatase, the anatase yielded no acetal. It is therefore evident that these three TiO_2 of P-25, rutile (Furuuchi), and anatase did not catalyze the formation of acetal under Ar.

In the case of an air atmosphere, all of the TiO_2, except for anatase, gave more acetal than that under Ar. That only anatase gave no acetal is interesting, since this TiO_2 produces CH_3CHO.

Figure 7 shows the formation of CH_3COOH. The water in Eq. 3 required to produce CH_3COOH is further supplied from Eqs. 5 and 6, and the evolution of C_2H_4 from C_2H_5OH,[8,10] besides being available from only a small amount of H_2O in ethanol and H_2O from Eq. 2.

In spite of no large difference in the yield of CH_3CHO (Fig. 3, under Ar), no CH_3COOH can be detected on both rutiles (Aldrich and Furuuchi) and P-25 in Ar. However, it seems reasonable to assume that these three TiO_2 may also produce in practice CH_3COOH, due to CH_4 and CO_2 formation in Eq. 4 from the CH_3COOH formed with all of the TiO_2 tested (as is shown later). Each yield of their CH_3COOH, however, seems to be much less than the yield with anatase, and such a minor CH_3COOH is almost consumed during the evolution of CH_4 and CO_2, accordingly to Eq. 4. If a slight amount of CH_3COOH exists in the reaction solution after decomposition to CH_4 and CO_2, it is almost adsorbed on the surface of the analysis path of the gas chromatograph because of the high adsorptive property of the acid. The more rapid decomposition rate of CH_3COOH with both rutiles and P-25 than anatase may have also been a cause for no detection of the acid.

All of the TiO_2 in an air atmosphere catalyzes the formation of CH_3COOH and gives much more CH_3COOH than that under Ar. Anatase did not give as much CH_3CHO as that shown in Fig. 3, but never-

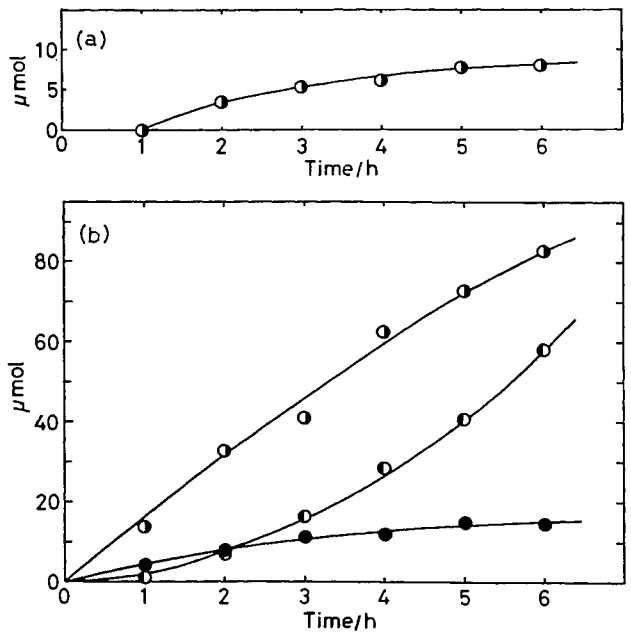

Fig. 6. Formation of acetal vs. illumination time for suspensions of 30 mg TiO_2 in 2.0 ml ethanol under Ar (a) or air (b) atmosphere. ◑: rutile (Aldrich), ◐: rutile (Furuuchi), ●: P-25 (Nippon Aerosil).

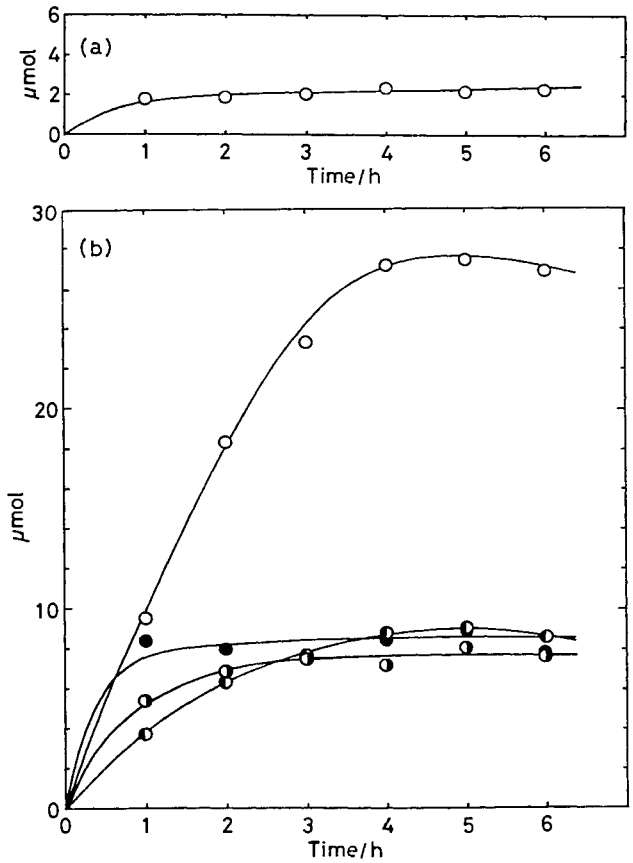

Fig. 7. Formation of acetic acid vs. illumination time for suspensions of 30 mg TiO_2 in 2.0 ml ethanol under Ar (a) or air (b) atmosphere. ○: anatase (Aldrich), ◑: rutile (Aldrich), ◐: rutile (Furuuchi), ●: P-25 (Nippon Aerosil).

theless showed a much higher CH_3COOH yield than did the other TiO_2 catalysts. This is because only anatase did not give acetal (Fig. 6), which is produced from CH_3CHO, as shown in Eq. 2. That is to say, because CH_3CHO with anatase produced CH_3COOH without being used up in the formation of acetal, the anatase could give the greatest CH_3COOH yield.

Figure 8 shows the evolution of CH_4. In the case of an Ar atmosphere, since no evolution of CH_4 took place in the blank test during the initial time, all of the TiO_2 catalyzed evolving CH_4 at that time. However, since the yield of CH_4 was much less than that in the blank test, oxidation of the CH_4 by the O_2 released from TiO_2 seems to be the reason for this result.

All of the TiO_2 under an air atmosphere catalyzed the evolution of CH_4, since no CH_4 evolved in a blank test under air. The result that CH_4 evolution under air is more than that under Ar is consistent with a similar data observed regarding CH_3COOH formation, since CH_4 evolves from CH_3COOH.

Figure 9 shows the evolution of CO_2. All of the TiO_2 gives much more CO_2 under air than that under an Ar atmosphere, because CH_3COOH formation under air is much higher than that under Ar.

Because the evolution of H_2 and C_2H_2 under Ar and air had been previously reported,[8,10] it was omitted.

As described above, air has been found to be effective for the formation of all products; to prove such an effect, further experiments were performed under an O_2 atmosphere.

Figure 10 shows the formation of products from ethanol observed for a blank test under an O_2 atmosphere. Although trace amounts of CH_3COOH and CH_4 were detected, no C_2H_4 evolved. Only the yield of CO_2 was more than that under air (Fig. 2).

Figure 11 shows the formation of liquid products from ethanol versus the illumination time observed for the TiO_2 (rutile, Furuuchi) under an atmosphere of O_2. All of the products were formed in greater quantities than those under air.

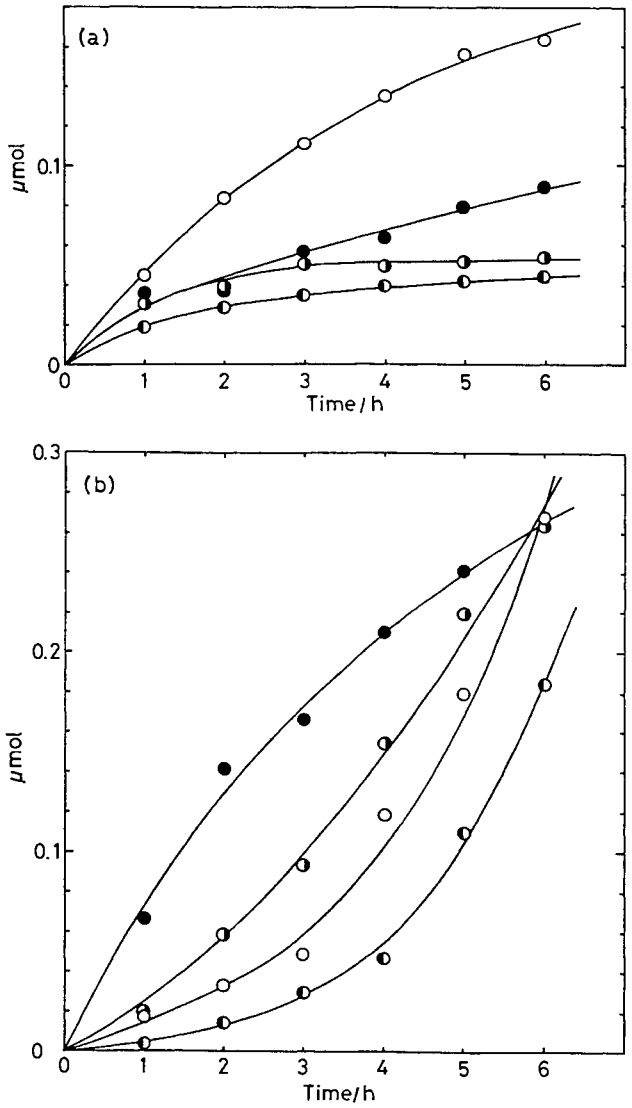

Fig. 8. Evolution of CH_4 vs. illumination time for suspensions of 30 mg TiO_2 in 2.0 ml ethanol under Ar (a) or air (b) atmosphere. ○: anatase (Aldrich), ◑: rutile (Aldrich), ◐: rutile (Furuuchi), ●: P-25 (Nippon Aerosil).

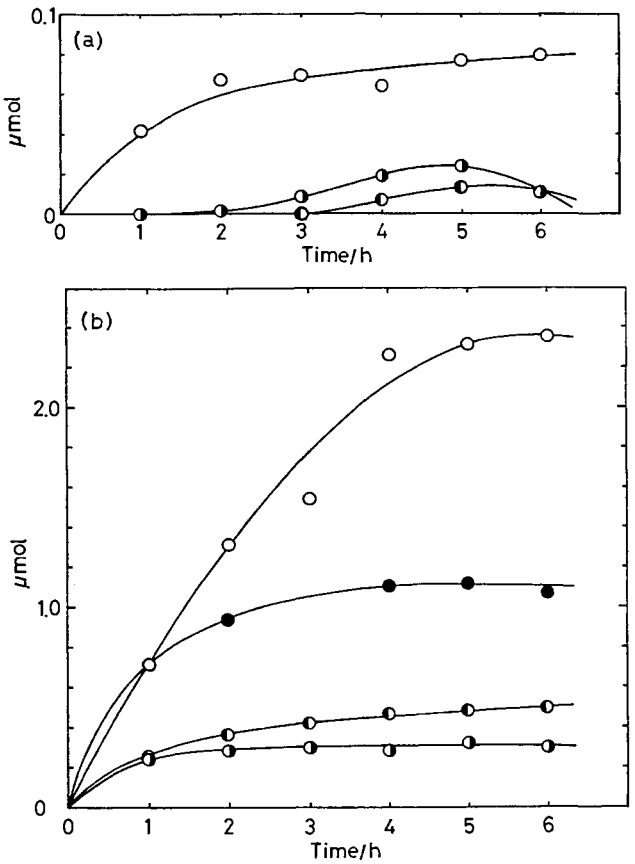

Fig. 9. Evolution of CO_2 vs. illumination time for suspensions of 30 mg TiO_2 in 2.0 ml ethanol under Ar (a) or air (b) atmosphere. ○: anatase (Aldrich), ◑: rutile (Aldrich), ◐: rutile (Furuuchi), ●: P-25 (Nippon Aerosil).

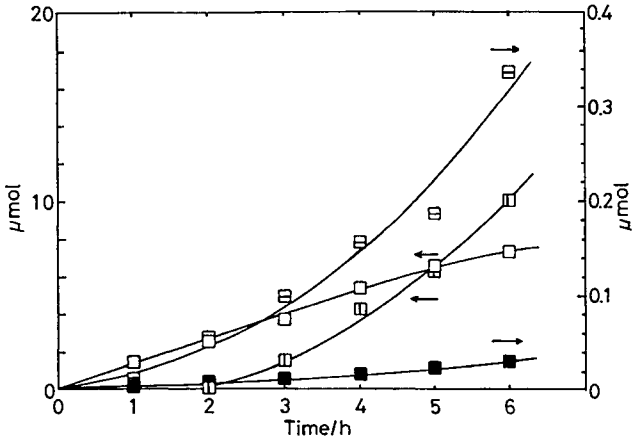

Fig. 10. Formation of products from 2.0 ml ethanol vs. illumination time for a blank test without any TiO_2 under O_2 atmosphere. □: acetaldehyde, ⊡: acetaldehyde diethyl acetal (acetal), ⊟: CO_2, ■: H_2.

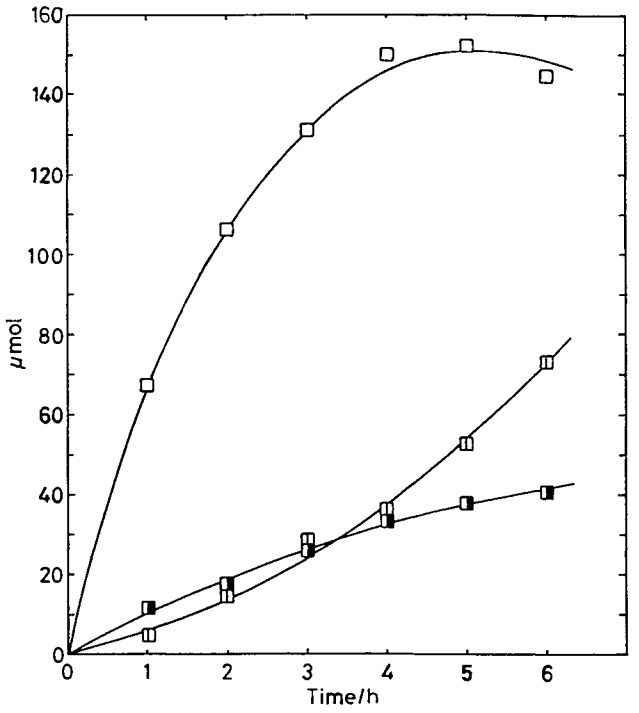

Fig. 11. Formation of liquid products vs. illumination time for suspension of 30 mg TiO_2 (rutile, Furuuchi) in 2.0 ml ethanol under O_2. □: acetaldehyde, ⊡: acetaldehyde diethyl acetal (acetal), ◨: acetic acid.

Figure 12 shows the formation of gaseous products with TiO_2 (rutile, Furuuchi) under O_2. All of the gaseous products, except for CH_4, were formed in greater quantities than those under an air atmosphere. One possible reason why only CH_4 evolution is less than that under air is as given below. In a blank test, no CH_4 was formed under O_2 and air, although it was evolved under Ar. Judging from

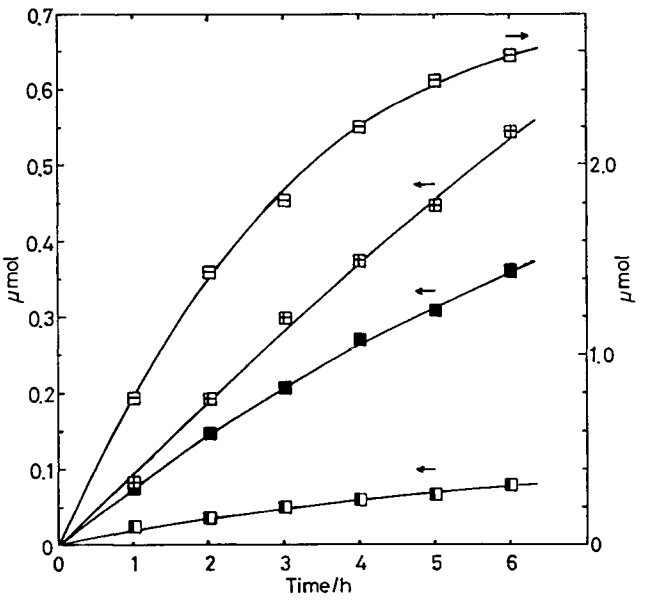

Fig. 12. Evolution of gaseous products vs. illumination time for suspension of 30 mg TiO_2 (rutile, Furuuchi) in 2.0 ml ethanol under O_2. ⊞: C_2H_4, ◧: CH_4, ⊟: CO_2, ■: H_2.

these results, even if CH_4 evolved more than that under air, it was further oxidized by excess O_2 in the reaction tube. The fact that the CO_2 yield was about 5-times that under air supports this assumption.

The yield of C_2H_4 vs. the illumination time is approximately linear, while under air it gave a downward curvature.[8] The reason for such a high activity of TiO_2 is a smaller reduction of part of the TiO_2 than that under air. Actually, no color change[9,14] due to a reduction of TiO_2 was observed, in contrast to the result under air.

The differences among the yields regarding products with TiO_2 under Ar, air, and O_2 was much larger than that in blank tests under these three atmospheres; the yields with TiO_2 increased in the order Ar $<$ air $<$ O_2 atmosphere. Consequently, it has become apparent that active O_2 from reoxidized TiO_2 by O_2 in the reaction tube has a considerably greater effect on the photolysis of ethanol with TiO_2 than does gaseous O_2 present in the reaction tube.

References

1) T. Sakata and T. Kawai, *Chem. Phys. Lett.*, **80**, 341 (1981).

2) P. Pichat, J.-M. Herrmann, J. Disdier, H. Courbon, and M-N. Mozzanega, *Nouv. J. Chim.*, **5**, 627 (1981).

3) E. Borgarello and E. Pelizzetti, *Chim. Ind. (Milan)*, **65**, 474 (1983).

4) M. Kawai, T. Kawai, S. Naito, and K. Tamaru, *Chem. Phys. Lett.*, **110**, 58 (1984).

5) S. Nishimoto, B. Ohtani, and T. Kagiya, *J. Chem. Soc., Faraday Trans. 1*, **81**, 2467 (1985).

6) A. Hamano and S. Matsuo, *Kenkyu Hokoku-Sasebo*

Kogyo Koto Senmon Gakko, **23**, 49 (1986).
7) G. F. Huttig, *Kolloid Z.*, **106**, 166 (1944); S. Kato and F. Masuo, *Kogyo Kagaku Zasshi*, **67**, 1136 (1964).
8) K. Iseda, *Chem. Express*, **5**, 729 (1990).
9) S. Nishimoto, B. Ohtani, A. Sakamoto, and T. Kagiya, *Nippon Kagaku Kaishi*, **2**, 246 (1984).
10) K. Iseda, *Chem. Express*, **5**, 209 (1990).
11) H. Tsubomura, K. Kimura, K. Kaya, J. Tanaka, and S. Nagakura, *Bull. Chem. Soc. Jpn.*, **37**, 417 (1964).
12) S. Patai, "The Chemistry of the Carbonyl Group," Interscience Publishers, London (1966), p. 828.
13) B. Kraeutler and A. J. Bard, *J. Am. Chem. Soc.*, **100**, 2239 (1978).
14) A. D. Buss, M. A. Malati, and R. Atkinson, *J. Oil Col. Chem. Assoc.*, **59**, 369 (1976).

Electrochromism of Octacyanophthalocyanine Thin Film. Investigation by Means of in situ Visible and Raman Spectroscopies

Kimiya TAKESHITA, Yuko AOYAMA, and Michio ASHIDA*
Department of Industrial Chemistry, Faculty of Engineering, Kobe University, Nada, Kobe 657
(Received October 3, 1990)

The electrochromism of an octacyanophthalocyanine ($H_2Pc(CN)_8$) thin film was investigated by in situ visible and Raman spectroscopies in acid and alkaline electrolytes. A new absorption band was observed in the range 700—900 nm of the visible spectra during a reduction of the film. The absorbance reached a constant value at 2 F mol^{-1} of the cathodic electricity in an alkaline electrolyte. The Raman spectra showed a spectral change in the vibration range which is attributed to the macrocycle and the isoindole moiety; hence, the reduction seems to occur in the azaporphyrin ring. From both the visible and Raman spectra, it was revealed that $H_2Pc(CN)_8$ was protonated at the nitrogens in positions 6,13,20,27 by electrochemical reduction. The protonated $H_2Pc(CN)_8$ shows absorption in the near-infrared region in both acid and alkaline electrolytes. The mechanism for the formation of protonated $H_2Pc(CN)_8$ is considered to be analogous to that of hydrogen evolution in alkaline electrolytes. Both the visible and Raman spectra were reversible during reoxidation.

(Phthalocyaninato)metals (MPcs) are composed of a tetraazaporphyrin ring; their structures are analogous to porphyrins, which are important functional compounds found in nature. On account of both chemical and thermal stability, CuPc has been used for a long time as a blue pigment. Recently, MPcs have attracted a good deal of attention as new functional materials, such as catalysts,[1] semiconductors,[2-4] and photoconductors.[5-8] A redox state of MPcs plays an important role in their properties. The electrochromism of MPcs caused by the redox reaction has attracted attention regarding applications in display devices. Since Nicholson and co-workers investigated the electrochromism of lutetium diphthalocyanine films,[9] several other groups have reported results for rare-earth diphthalocyanine.[10-12] Single-ring MPcs (M=Fe, Co, Ni, Cu, Zn, and Mg) films also show electrochromism in the oxidized state.[13,14] In these electrochromic processes, a charge-compensating anion for MPc cation formed by electrolysis usually penetrates into the film from an electrolyte. The charge-compensating anion can be considered to be a dopant to MPcs. According to Marks and co-workers as well as Orr and Dahlberg,[15,16] carefully designed, doped phthalocyanines can show metallic conductivity. Furthermore, modified electrodes with MPcs show catalytic activity induced by the electrochemical redox reaction of MPcs.[17,18] It therefore seems to be useful to investigate the electrochromism of MPc films precisely.

We have recently reported that (Octacyanophthalocyaninato)metal ($MPc(CN)_8$) is synthesized from tetracyanobenzene (TCNB) vapor on metal or alkaline halide substrates.[19] Wöhrle and co-workers have reported that thin films of $MPc(CN)_8$ (M=2H, Cu, Zn) show stable electrochromic redox behavior at the reduced state in an aqueous electrolyte.[20] The eight cyano groups of the molecule play an important role in the redox behavior of $MPc(CN)_8$. According to Louati and co-workers,[21] half-wave potentials of the reduction wave of $MPc(CN)_8$ in *N,N*-dimethylformamide (DMF) shifted to the anodic direction by 0.5—1.0 V, as compared with those of MPcs. This finding indicates that $MPc(CN)_8$ is reduced more easily than MPcs. They mentioned that the property of $MPc(CN)_8$ is very close to an organic electron acceptor, such as tetracyanoquinodimethane (TCNQ).

The redox state of MPcs has generally been investigated using an electrochemical method in company with a spectroscopic type. In most studies, in situ electronic transition spectra have also been reported with electrochemical results. In the case of MPc films, however, the electronic transition spectra may not be used to investigate the electrochromism, since the electronic spectra of MPcs depend on their crystal structures. The change in the spectra is caused not only by electrochemical reactions, but also by a structure change due to the solvent.[22] The possibility of an alternation in the molecular packing or crystalline structure has also been recognized for the electrochromism of MPcs by Kahl and co-workers.[14] This suggests that an investigation of the vibrational spectra should be carried out at the same time. The vibrational spectra during electrochromism of an MgPc film were only reported by Kahl and co-workers.[14] Unfortunately, Wöhrle and co-workers have not reported any in situ electronic and vibrational spectra of $H_2Pc(CN)_8$ film during electrochromism.[20]

In this work, we found a new absorption band in the near-infrared (NIR) region during the electrochromism of $H_2Pc(CN)_8$ films in aqueous electrolytes, and investigated the electrochromism with electronic transition and vibrational spectroscopies.

Experimental

$H_2Pc(CN)_8$ was synthesized following the method of

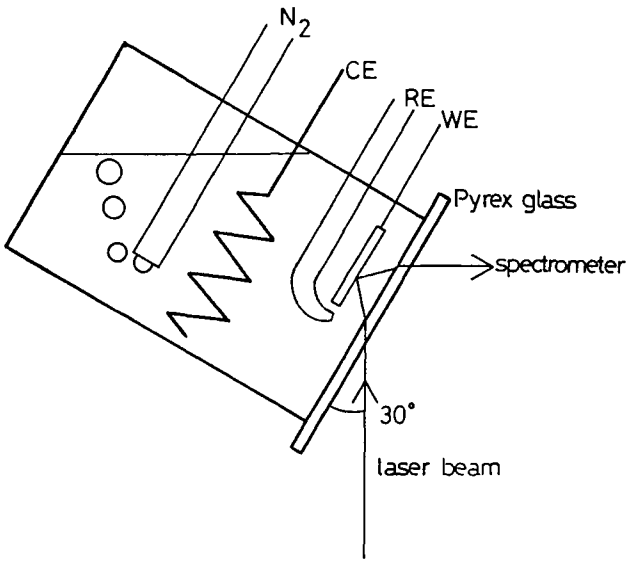

Fig. 1. Experimental setup for in situ Raman spectroscopy of thin film $H_2Pc(CN)_8$ electrodes.

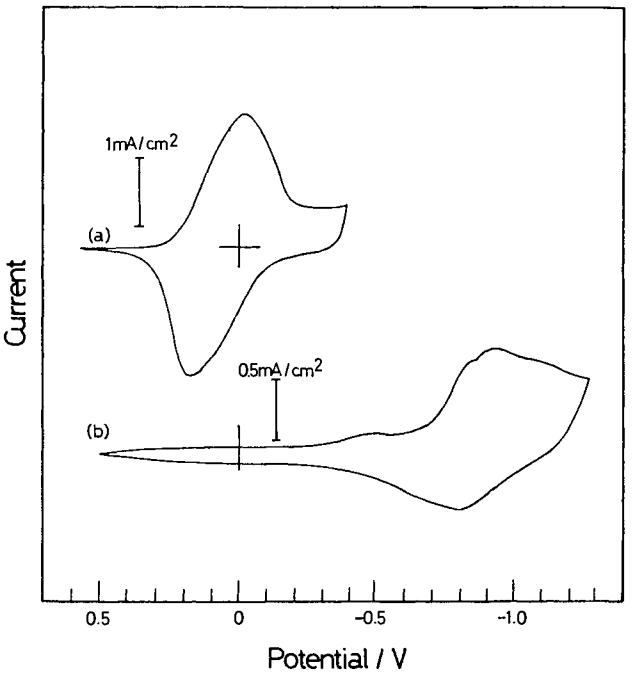

Fig. 2. Stable cyclic voltammograms of $H_2Pc(CN)_8$ films in 1 M HCl (a) and 0.1 M KOH/1 M KCl (b). Thichness of the film are 670 nm (a) and 580 nm (b), respectively. Scan rate 40 mV s^{-1}.

Wöhrle and co-workers,[23] and was purified by column chromatography with silica gel and DMF. $H_2Pc(CN)_8$ was dissolved into DMF and was cast onto an ITO (tin doped indium oxide coated glass) for an optical transparent electrode. The film on ITO was dried in vacuum at 373 K. The amount of $H_2Pc(CN)_8$ on ITO was estimated to be about 10^{-7} mol from the specific gravity of the bulk material (1.49 g cm^{-3}) and the cross section of the film by a direct observation with a scanning electron microscope.

A copper lead wire was attached with silver paste to the ITO, which was used as a working electrode. They were covered with epoxy resin to adjust the electrode area of 1 cm^2. All electrochemical measurements were carried out under an N_2 atmosphere at 298 K with a Hokuto Denko HA-301 potentio/galvanostat and a Hokuto Denko HB-104 potential sweeper. A working electrode, a Ag/AgCl reference electrode and a Pt wire counter electrode were set in an electrochemical cell with quartz windows for optical measurements. Visible spectra of the film in the cell were measured under electrolysis with a Shimadzu UV-240 spectrometer. In the case of potentiostatic electrolysis, visible spectra were recorded when the current reached a stationary state after about 15 min from an application of the potential. The transient time was controlled to be about 30 s in order to avoid any influence of convection and an electric double layer during the galvanostatic electrolysis.

A cell for in situ Raman spectroscopy was shown in Fig. 1. A Raman measurement was made using a Spex Ramalog 5 Raman spectrometer controlled by an NEC PC-9801VM personal computer. An NEC GLS-3300 Ar^+ laser was used as an excitation source. The light power at the sample point was less than 30 mW. The spectral slit width of the spectrometer was set at 4 cm^{-1}.

Results and Discussion

Stable cyclic voltammograms of $H_2Pc(CN)_8$ films on ITO are shown in Fig. 2. In the cathodic scan from the potential of 0.6 V to −0.4 V vs. Ag/AgCl in 1 M HCl (1 M=1 mol dm^{-3}), the film turned from green to blue at ca. 0 V and from blue to purple at ca. −0.2 V. In the reversal scan, the film turned from purple to blue at ca. 0.2 V and from blue to green at about 0.4 V. In a cathodic scan from 0 V to −1.22 V in 0.1 M KOH/1 M KCl, the film turned from green to blue at ca. −0.7 V and from blue to purple at ca. −0.8 V. In the reversal scan, the film turned from purple to blue at ca. −0.7 V and from blue to green at ca. −0.5 V.

The electrochemistry of an $H_2Pc(CN)_8$ film on the Au electrode was intensively investigated by Wöhrle and co-workers.[20] They mentioned that $H_2Pc(CN)_8$ films showed stable electrochromism during reduction in an acid electrolyte, as follows:

$$H_2Pc(CN)_8 + ne^- + nH^+ \longrightarrow H_2Pc(CN)_8^{n-} \cdot nH^+ \ (n=1—3).$$

The cyclic voltammogram of the film showed two reduction peaks; the first and second reduction peaks of the films were 81 and 20 mV vs. Ag/AgCl in 1 M HCl, respectively. On the other hand, the first and second reduction peaks of the films were −756 and −866 mV in 0.1 M KOH/1 M KCl, respectively. They suggested on the basis of those results that the rate-determining step in alkaline electrolytes was the transport of charge-compensating cations in the redox process of $H_2Pc(CN)_8$ film. They did not, however, mention the mechanism of the redox process in an alkaline electrolyte. Although the $H_2Pc(CN)_8$ film on Au electrode showed two distinctive reduction

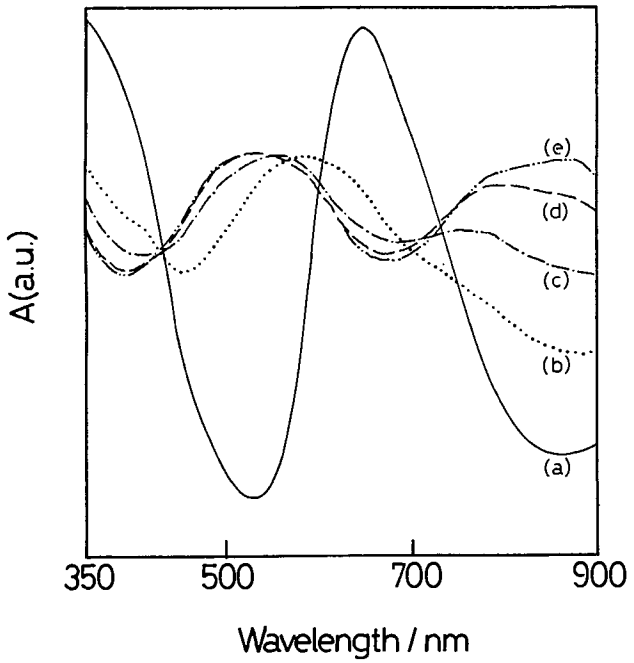

Fig. 3. In situ visible spectra of $H_2Pc(CN)_8$ films in 1 M HCl: original film (a) and films reduced at 0.025 V (b), −0.05 V (c), −0.175 V (d), and −0.4 V (e).

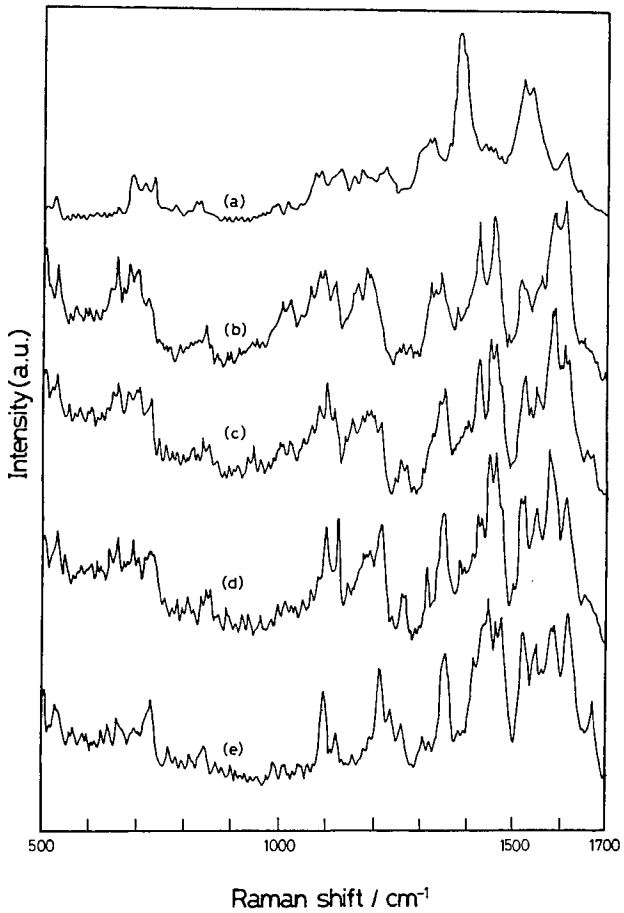

Fig. 4. In situ Raman spectra of $H_2Pc(CN)_8$ films in 1 M HCl: original film (a) and films reduced at 0.025 V (b), −0.05 V (c), −0.175 V (d), and −0.4 V (e). λ_{exc}=514.5 nm.

peaks in the cyclic voltammogram, the $H_2Pc(CN)_8$ film on ITO showed one reduction peak. This may be attributed to a complicated characteristic of a semiconductive ITO electrode.

In Situ Spectra in Acid Electrolyte. In situ visible spectra of $H_2Pc(CN)_8$ films during potentiostatic electrolysis in 1 M HCl are shown in Fig. 3. With the progress of reduction, the absorption peak at 640 nm shifted to a lower wavelength, and a new absorption appeared in the NIR region. When the film was reduced at −0.05 V, the new absorption had a peak at 760 nm; at −0.4 V the absorption had two peaks at 760 nm and 880 nm. During the reduction, the film turned from green to blue at 0.025 V and to violet at −0.4 V. According to Gaspard and co-workers,[24] the Pc protonated at the nitrogen atoms in positions 6,13,20,27 showed absorption in the NIR region; successive protonation of Pc shifted the NIR absorption to a higher wavelength. Therefore, NIR absorption may be attributed to protonated Pcs. The additional absorption appearing at 880 nm suggests further protonation.

In situ Raman spectra of $H_2Pc(CN)_8$ films during potentiostatic electrolysis in 1 M HCl are shown in Fig. 4. Because the film had absorption at the wavelength of the light source (514.5 nm) under electrolysis, the Raman spectra were affected by a resonance Raman effect. The relative intensity of the Raman scattering was compared with that at 531 cm^{-1}, since the intensity at 531 cm^{-1} was changed little by the electrolysis. Fluorescence could be neglected in the Raman spectra as a result of measurements at a different exciting wavelength. The main bands of the Raman spectra were assigned on a basis of those of H_2Pc reported by Aroca and co-workers,[25] since the Raman spectra of $H_2Pc(CN)_8$ have not been reported. The Raman bands are classified into several groups. The Raman band at 1250—1600 cm^{-1} can be mainly attributed to C=C and C=N stretching in the isoindole moieties. In this range, the original film of $H_2Pc(CN)_8$ shown in Fig. 4(a) has peaks at 1391, 1510, 1527, and 1602 cm^{-1}. The second band at 650—800 cm^{-1} is mainly attributed to macrocycle vibration. When the film was reduced at 0.025 V, the peaks at 1391, 1510, and 1527 cm^{-1} disappeared and new peaks appeared at 1423 and 1455 cm^{-1}. The band at 650—800 cm^{-1} changed at the same potential. The result indicated that the isoindole moiety was strongly affected by reduction and that the azaporphyrin ring was distorted by the electrolysis. The same tendency was observed in the oxidation of MgPc film.[14] This finding coincided with the result of Louati and co-workers, in which the redox reaction of $H_2Pc(CN)_8$ took place on the azaporphyrin ring in the DMF solution.[21]

Many strong bands appeared at 1500—1700 cm^{-1} under the electrochemical reduction. According to Sugimoto,[26] phlorin, which is a protonated porphyrins at the *meso* position, has electronic transitions in the NIR region and vibrational modes at 1500—1700 cm^{-1}. By a comparison with the spectra of phlorin, the absorption in the NIR region and the band at 1500—1700 cm^{-1} in the Raman spectra may be attributed to the protonated $H_2Pc(CN)_8$ in the reduced film.

In Situ Spectra in Alkaline Electrolyte. The in situ visible spectra of $H_2Pc(CN)_8$ films during potentiostatic electrolysis in 0.1 M KOH/1 M KCl are shown in Fig. 5. The film turned from green to blue at −0.85 V, and to purple at −0.97 V. As the films were reduced under a more negative potential, the Q-band shifted to a lower wavelength, as in the case in 1 M HCl, and a new absorption peak appeared only at 880 nm. The dependence of the absorption of $H_2Pc(CN)_8$ films on the potential during potentiostatic electrolysis in 0.1 M KOH/1 M KCl is shown in Fig. 6(a). The absorbancies were normalized by absorbance at 640 nm of the original film. The absorbance at 640 nm decreased and that at 530 nm increased at −0.6 V, while that at 880 nm increased at −0.7 V. The change of absorbancies at 640 and 530 nm before the appearance of absorbance at 880 nm indicates that a two-step electrochemical reaction takes place depending on the potential. The dependence of the absorption of $H_2Pc(CN)_8$ films on charge during galvanostatic electrolysis in 0.1 M KOH/1 M KCl is shown in Fig. 6(b). The absorbance at 640 nm gradually decreased and reached a constant value at about 2 F mol^{-1}. The absorbance at 880 nm increased linealy with charge to 1 F mol^{-1} and increased quickly to a plateau which was saturated at about 2 F mol^{-1}. These findings seem to lead to the conclusion that the NIR absorption of the film in 0.1 M KOH/1 M KCl is attributed to $[H_2Pc(CN)_8]^{2-}$. The new absorption in 0.1 M KOH/1 M KCl, however, could not be attributed to $[H_2Pc(CN)_8]^{2-}$, itself, because $[H_2Pc(CN)_8]^{2-}$ does not show any absorption in the NIR region in the DMF solution.[18] To explain the absorption in the NIR region in more detail, the Raman spectra of $H_2Pc(CN)_8$ film is discussed.

The in situ Raman spectra of $H_2Pc(CN)_8$ films during potentiostatic electrolysis in 0.1 M KOH/1 M KCl are shown in Fig. 7. When the film was reduced over −0.62 V, the spectrum coincided with that of the original film. At −0.85 V the band at 650—800 cm^{-1} changed and the peak at 1391 cm^{-1} disappeared as well as in the case of 1 M HCl. The band at 1000—1500 cm^{-1} changed to a different type from that in 1 M HCl. These results indicate that the azaporphyrin ring was affected by electrolysis in alkaline electrolyte, as well as in acid electrolyte and that the charge-compensating cation in the film affected the Raman

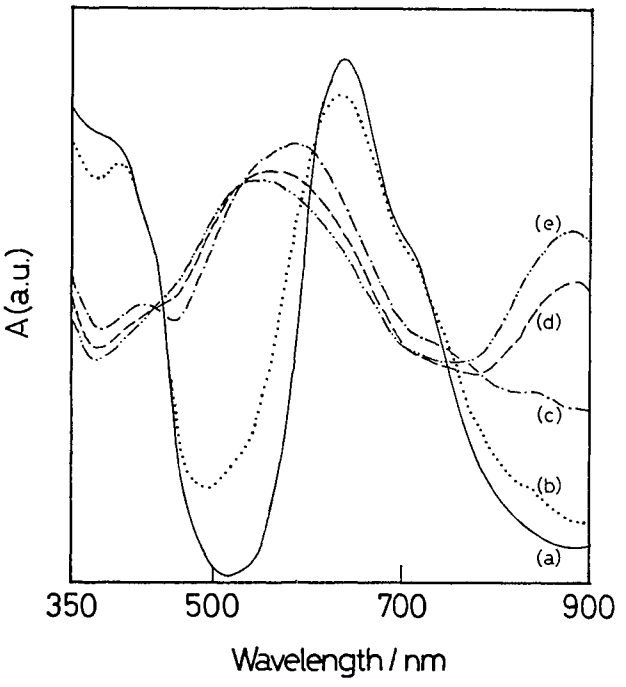

Fig. 5. In situ visible spectra of $H_2Pc(CN)_8$ films in 0.1 M KOH/1 M KCl: original film (a) and films reduced at −0.62 V (b), −0.85 V (c), −0.97 V (d), and −1.22 V (e).

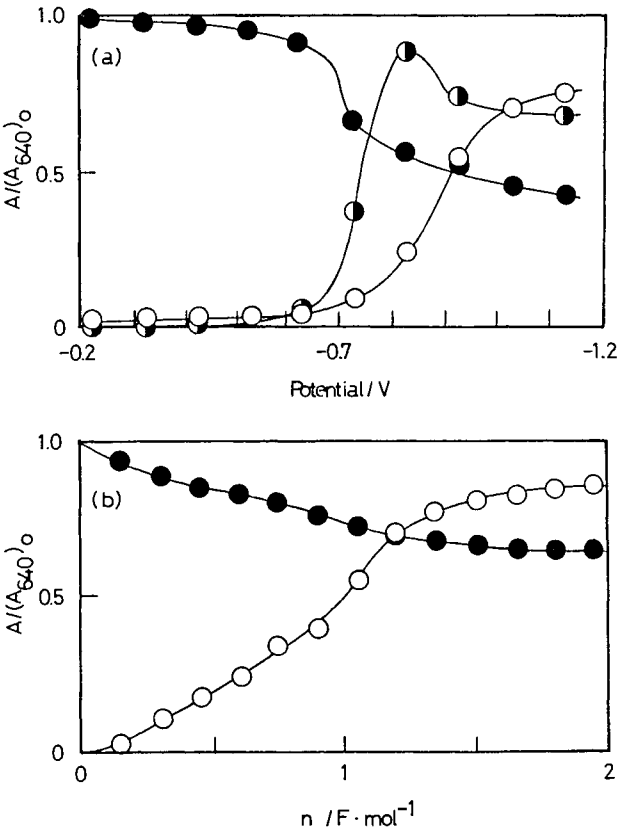

Fig. 6. Dependence of absorbancies of $H_2Pc(CN)_8$ films on potential (a) and charge (b) of the electrolysis in 0.1 M KOH/1 M KCl: ○; at 880 nm, ●; at 640 nm, ◑; at 530 nm.

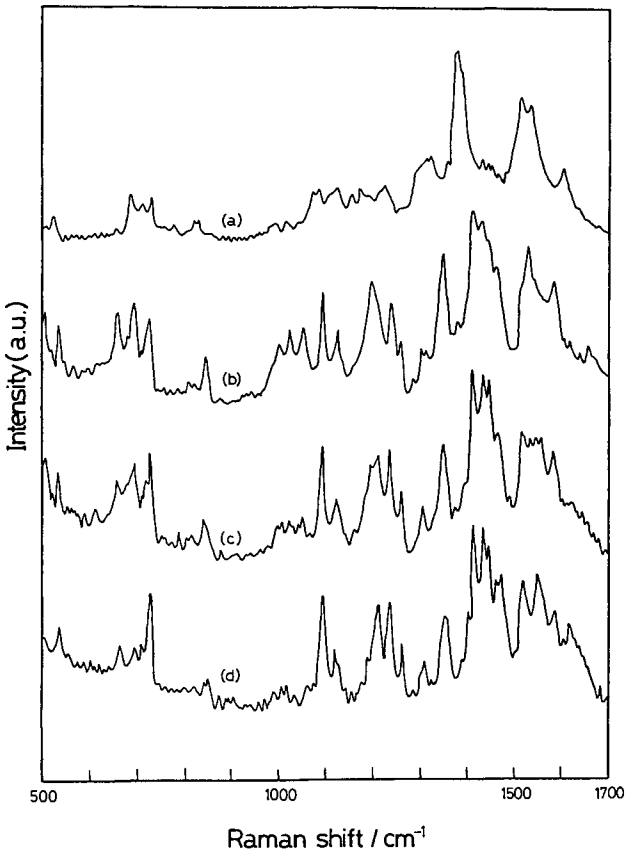

Fig. 7. In situ Raman spectra of $H_2Pc(CN)_8$ films in 0.1 M KOH/1 M KCl: original film and films reduced at −0.62 V (a), −0.85 V (b), 0.97 V (c), and −1.22 V (d). λ_{exc}=514.5 nm.

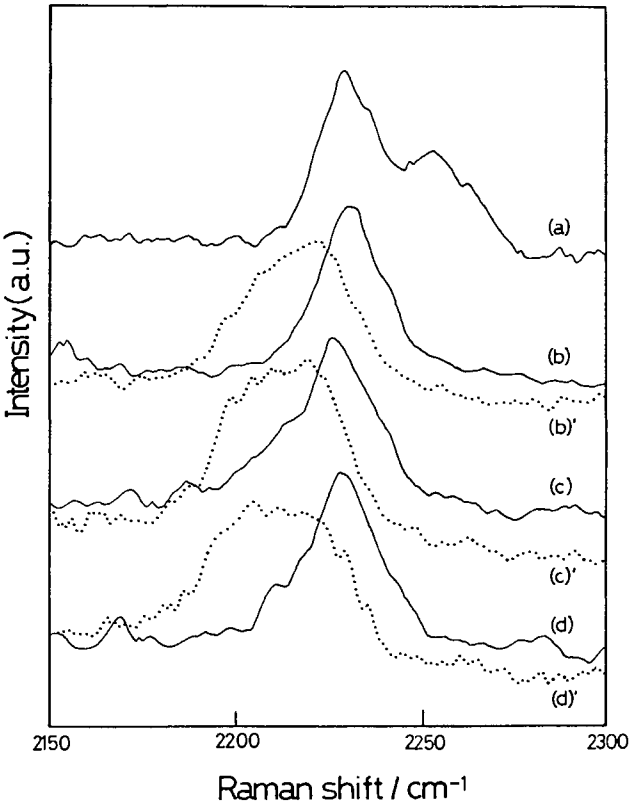

Fig. 8. In situ Raman spectra in C≡N stretching region of $H_2Pc(CN)_8$ films: original film (a), films reduced in 1 M HCl at 0.025 V (b), −0.05 V (c), and −0.4 V (d), and films reduced in 0.1 M KOH/1 M KCl at −0.85 V (b)', −0.97 V (c)', and −1.22 V (d)'. λ_{exc}=514.5 nm.

spectra of the reduced $H_2Pc(CN)_8$. At a potential between −0.97 and −1.22 V, many bands appeared at 1500—1700 cm^{-1}. In consideration of the absorption in the NIR region and for the bands at 1500—1700 cm^{-1}, it seems that $H_2Pc(CN)_8$ is protonated by electrolysis at the potential in 0.1 M KOH/1 M KCl.

From these results, the mechanism of elctrochemical reduction of $H_2Pc(CN)_8$ film in 0.1 M KOH/1 M KCl may be written as follows:

$$H_2Pc(CN)_8 + K^+ + e^- \longrightarrow [H_2Pc(CN)_8]^- \cdot K^+ \quad (1)$$

and

$$[H_2Pc(CN)_8]^- \cdot K^+ + H_2O + e^- \longrightarrow [H_2Pc(CN)_8\text{-}H]^- \cdot K^+ + OH^- \quad (2)$$

Reaction (1) takes place at −0.6 V. At −0.7 V, Reaction (2) produces a protonated $H_2Pc(CN)_8$ anion ($[H_2Pc(CN)_8\text{-}H]^-$) which has absorption in the NIR region. Reaction (1) may be the rate-determining step, since the diffusion of K^+ into the film has been found to be the rate determining step.[20] Reaction (2) is analogous to that of hydrogen evolution in alkaline electrolytes ($2H_2O+2e^- \rightarrow H_2+2OH^-$). The same reaction process occurred in the electrochemical reduction of zinc tetraphenylporphyrin (ZnTPP).[27] In that case, ZnTPP in a DMF solution which contained protic solvent was reduced to $[ZnTPP]^{2-}$, followed by rapid protonation to form a phlorin anion ($[ZnTPP\text{-}H]^-$) which showed absorption in the NIR region. Generally, porphyrin and phthalocyanine have quiet similar electrochemical reactivity and overall redox mechanisms. It therefore seems that such a proposed mechanism of electrochemical reduction is reasonable for the $H_2Pc(CN)_8$ film in an alkaline electrolyte.

C≡N Stretching Vibration. Figure 8 shows the C≡N stretching of $H_2Pc(CN)_8$ films on ITO during potentiostaic electrolysis in 1 M HCl and 0.1 M KOH/1 M KCl. The phthalocyanine films showed two C≡N stretching peaks at 2228 and 2253 cm^{-1}, and a doublet band turned to a singlet in this type of electrolysis. The peak of the singlet band shifted slightly in 1 M HCl during the electrolysis. On the other hand, the band in 0.1 M KOH/1 M KCl shifted to the shorter wavenumber direction by about 50 cm^{-1}, indicating that the charge compensating cation affected the electrochemical reaction of $H_2Pc(CN)_8$ film. In the case of TCNQ films reduced by alkaline metals, C≡N stretchings of TCNQ shifted by about 100 cm^{-1} to a shorter wavenumber.[28] The C≡N stretchings of TCNQ shifted to a shorter wavenumber by electrolysis

to the TCNQ anion in an acetonitrile solution.[29] These findings indicated that the C≡N stretchings of TCNQ were strongly affected by the reduction of TCNQ and the formation of the anion. It is interesting that the C≡N stretchings of the $H_2Pc(CN)_8$ films show a smaller shift than that of TCNQ. For $H_2Pc(CN)_8$, Louati and co-workers mentioned from their electrochemical results that the eight electron-withdrawn cyano groups of $H_2Pc(CN)_8$ interacted indirectly with the conjugated π electron system of the azaporphyrin ring.[21] The reduction of the conjugated π system of $H_2Pc(CN)_8$ probably affects to the cyano group in a weaker way than does that of TCNQ. It therefore seems that the C≡N stretchings of $H_2Pc(CN)_8$ shift less than those of TCNQ by electrochemical reduction.

Spectral Reversibility of $H_2Pc(CN)_8$ Film. The visible and Raman spectra of the film were reversible in the reoxidation process in those electrolytes. When the circuit was opened after the film was completely reduced in the violet state, the film gradually turned to blue during about 10 min, and returned to green after about 30 min. When the film was completely reduced at the violet state and placed into water, it returned to green immediately. The visible and Raman spectra of the film coincided with those of the original film. We have reported that $MPc(CN)_8$ can be synthesized on metal and alkaline halide surfaces, forming a film of an $MPc(CN)_8$-M complex crystal on the substrate. It is expected that $MPc(CN)_8$ in the $MPc(CN)_8$-M film is reduced by an electrochemical reaction and that the electrochromic property of the film is different from that of the $H_2Pc(CN)_8$ film. We are now investigating the electrochromic properties of $MPc(CN)_8$-M films.

References

1) F. H. Moser and A. L. Thomas, "The Phthalocyanines," CRC Press, Boca Raton, Fl (1983), Vol. 1 and 2.

2) A. Giraudeau, F. R. F. Fan, and A. J. Bard, *J. Am. Chem. Soc.*, **102**, 5137 (1980).

3) C. J. Schramm, R. P. Scaringe, D. R. Stojakovic, B. M. Hoffman, J. A. Ibers, and T. J. Marks, *J. Am. Chem. Soc.*, **102**, 1551 (1983).

4) B. N. Diel, T. Inabe, J. W. Lyding, K. F. Schoch, C. R. Kannewurf, and T. J. Marks, *J. Am. Chem. Soc.*, **105**, 1551 (1983).

5) Z. D.Popovic and J. H. Sharps, *J. Chem. Phys.*, **66**, 5076 (1977).

6) E. R. Menzel and R. O. Loutfy, *Chem. Phys. Lett.*, **72**, 522 (1980).

7) R. O. Loutfy, J. H. Sharps, C. K. Hsiao, and R. Ho, *J. Appl. Phys.*, **52**, 5218 (1981).

8) R. O. Loutfy and L. F. McIntyre, *Can. J. Chem.*, **61**, 73 (1983).

9) M. M. Nicholson and F. A. Pizzarello, *J. Electrochem. Soc.*, **126**, 1490 (1979).

10) M. Yamana, *Oyo Butsuri*, **48**, 441 (1979).

11) D. Walton, B. Ely, and G. Elliott, *J. Electrochem. Soc.*, **128**, 2479 (1981).

12) L. G. Tomilova, E. V. Chernykh, N. T. Ioffe, and E. A. Luk'yanets, *Zh. Obshch. Khim.*, **53**, 2594 (1983).

13) J. M. Green and L. R. Faulkner, *J. Am. Chem. Soc.*, **105**, 2950 (1983).

14) J. L. Kahl, L. R. Faulkner, K. Dwarakanath, and H. Tachikawa, *J. Am. Chem. Soc.*, **108**, 5434 (1986).

15) T. Inabe, T. J. Marks, R. L. Burton, I. W. Lyding, W. J. McCarthy, C. R. Kannenwurf, G. M. Reisner, and F. H. Harbstein, *Solid State Commun.*, **54**, 501 (1985).

16) W. A. Orr and S. C. Dahlberg, *J. Am. Chem. Soc.*, **101**, 2875 (1979).

17) R. Jasinski, *Nature*, **201**, 1212 (1964).

18) J. Zagal, R. K. Sen, and E. Yeager, *J. Electroanal. Chem., Interfacial Electrochem.*, **83**, 207 (1977).

19) M. Ashida, Y. Ueda, H. Yanagi, and K. Sayo, *J. Poly. Sci., Part A: Poly. Chem.*, **27**, 3883 (1989).

20) B. Schumann, D. Wöhrle, and N. I. Jaeger, *J. Electrochem. Soc.*, **132**, 2144 (1985).

21) A. Louati, M. El Meray, J. J. Andre, J. Simon, K. M. Kadish, M. Gross, and A. Giraudeau, *Inorg. Chem.*, **24**, 1175 (1985).

22) A. M. Hor and R. O. Loutfy, *Thin Solid Films*, **106**, 291 (1983).

23) D. Wöhrle, G. Meyer, and B. Wahl, *Makromol. Chem.*, **181**, 2127 (1979).

24) S. Gaspard, M. Verdaguer, and R. Viovy, *J. Chem. Res. (s)*, 271 (**1979**).

25) R. Aroca and D. P. DiLella, *J. Phys. Chem. Solids*, **43**, 707 (1982).

26) H. Sugimoto, *J. Chem. Soc., Dalton Trans.*, **1982**, 1169.

27) J. G. Lanese and G. S. Wilson, *J. Electrochem. Soc.*, **119**, 1040 (1972).

28) M. S. Khatkale and J. P. Devlin, *J. Chem. Phys.*, **70**, 1851 (1979).

29) P. A. Klowers and G. Mamantov, *Anal. Chem.*, **61**, 190 (1989).

Reaction Mechanism for Ozone Oxidation of Polyethylene as Studied by ESR and IR Spectroscopies

Jun YAMAUCHI,* Akiyoshi YAMAOKA,† Kunji IKEMOTO,† and Tetsuji MATSUI††
College of Liberal Arts and Sciences, Kyoto University, Kyoto 606
†Himeji Institute of Technology, Shosha, Himeji 671-22
††Kobe City College of Technology, Gakuen Higashimachi, Nishi-ku, Kobe 655-21
(Received October 8, 1990)

In a previous study of graft copolymerization of methyl methacrylate onto polyethylene oxidized with ozone, we clarified that ozone-oxidation reactions produce peroxyl radicals in polyethylene and that the graft copolymerization is assumed to start upon heating, through the decomposition of hydroperoxides which are converted from the peroxyl radicals. A series of reaction processes proposed for the ozone oxidation were examined from the viewpoint of the reaction rate. The time-dependent content of the peroxyl radicals was pursued by observing in situ ESR; the initial evolution rate of the peroxyl radicals and the decay rate after the ozone-stop were discussed on the basis of the proposed ozone-oxidation mechanism, leading to a good agreement between the experiment and theory. The amounts of hydroperoxide and carbonyl species determined from iodometry and the IR spectra, respectively, were also discussed with regard to the oxidation time, showing reasonable linear dependences.

Many investigations regarding polymer degradation have been reported.[1] Free-radical species in polyethylene and polypropylene irradiated by UV light or γ-rays have also been extensively discussed, and a reaction mechanism involving those radical species proposed.[2-10] On the other hand, we recently found that the ozone oxidation of polyethylene is very effective for its graft copolymerization with methyl methacrylate.[11] The influence of the ozone-oxidation and polymerization times on the total conversion, degree of grafting, and graft efficiency were discussed in detail, and the molecular weight of branch polymers estimated. This graft copolymerization can be initiated by active species on polymers introduced by means of ozone oxidation. Making use of ESR spectroscopy, the active species were determined to be peroxyl radicals, as in the case of polypropylene.[12]

The reaction mechanism for the ozone oxidation of polyethylene was presumed in a previous study,[11] based on the detected species in oxidation reactions, such as the peroxyl radical and hydroperoxide. In order to examine the proposed reaction mechanism from the view-point of the reaction rate, we performed in situ ESR measurements and pursued the time-dependent contents of the peroxyl radicals during the initial reaction stage and after stopping the ozone flow (ozone-stop). In addition, the hydroperoxide product was determined from iodometry, and the final inert products were also checked by the IR spectra. The amounts of these products depended on the oxidation time, and were examined on the basis of the proposed reaction mechanism.

Experimental

Polyethylene samples were purchased from Sumitomo Seika Co., Ltd.; 80—100 mesh of low-density type, 0.918 g cm^{-3}, mp 105-111 °C, and molecular weight 4.84×10^4. Polyethylene fibers were obtained from Daiwa Boseki Co., Ltd.; density 0.955—0.961, mp 125—130 °C. Polyethylene films were made by pressing the above-mentioned polyethylene powder at a temperature of 140 °C and a pressure of 10 kg cm^{-2}.

Ozone was produced in a silently discharged oxygen flow (concentration ca. 30 g m^{-3}) and then introduced to a sample tube set in the ESR cavity. For IR measurements polyethylene films were exposed to ozone flow for a prescribed time.

ESR measurements were carried out using a JEOL X-band spectrometer (ME-3X type) with 100-kHz field modulation. Polyethylene fibers of 100—200 mg weight in a quartz glass tube were set inside the ESR cavity and an ozone stream was directly introduced. The decay rate after stopping the ozone was so rapid that the spectral intensity could not be calculated by integration, and was pursued by sitting on the ESR signal; the peak heights were plotted.

The IR spectra were measured for both untreated polyethylene and ozone-exposed polyethylene films using a Shimadzu IR spectrometer (IR-27G type). The absorption intensity was calculated by the usual base-line method.

A determination of hydroperoxide was made according to Chien's method.[13] Details have been described in the literature;[11] data involving the concentration of hydroperoxide vs. the oxidation time were utilized for a rate-process analysis.

Results

The ESR spectrum of polyethylene during ozone oxidation consists of one absorption line with g=2.015 and a line width of ca. 2.4 mT. The radical species was identified as being peroxyl radicals ROO·, as was discussed in a previous paper.[11] The spectral intensities of the ESR spectra during ozone oxidation, as well as after stopping ozone flow, are depicted in Fig. 1, which shows a gradual growth of the radical species for ca. 10 min, then reaching a plateau (a stationary radical concentration). After stopping the ozone flow the intensity decreased rapidly, becoming

very weak after ca. 6 min.

The IR spectra shown in Fig. 2 indicate spectral variations with the ozone oxidation time. The spectra are almost the same as those reported earlier.[7,8] The absorption band at 1710 cm^{-1} can be assigned to a streching vibration of carbonyl groups (C=O) and those at 3400 and 3200 cm^{-1} to that of OH groups. The increased absorption by ozone oxidation can also be seen in the area of 900—1400 cm^{-1}, probably due to other vibration modes of the C=O and OH groups. From these spectral variations, a relationship between the oxidation time and the optical density of the carbonyls (Fig. 3) was obtained, showing a good linear dependence of the C=O content on the oxidation time.

In our spectra the absorption at 3555 cm^{-1}, which was assigned to hydroperoxide by Luongo,[8] was not observed. This discrepancy may be attributed to the treated temperatures, that is, room temperature in our case, as compared to 120 or 145 °C in Luongo's experiment. We determined the content of the hydroperoxide by iodometry, the result of which was reported in a previous paper.[11] Like the C=O content, the hydroperoxide concentration increases linearly with the

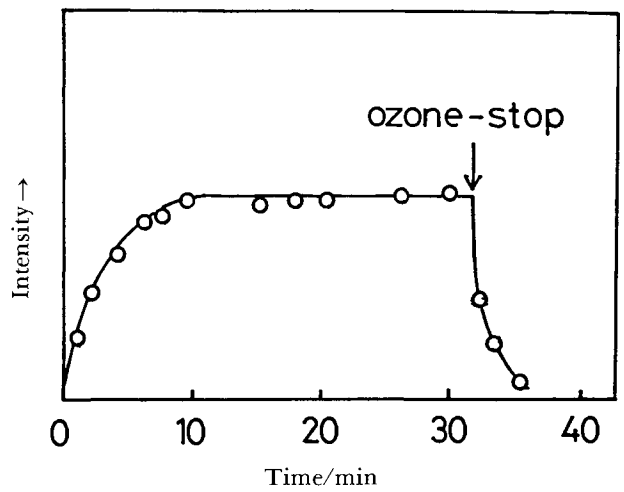

Fig. 1. Variation of the ESR spectral intensities of polyethylene with the ozone-oxidation time and after the ozone-stop.

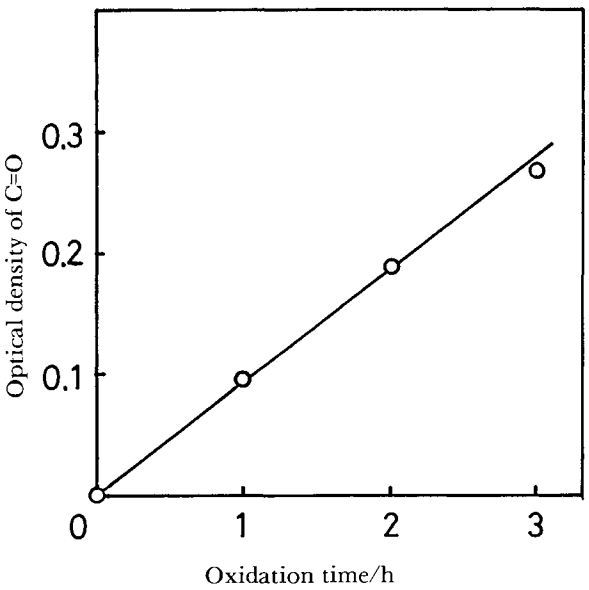

Fig. 3. Relationship between the oxidation time and the optical density of carbonyl groups in polyethylene oxidized with ozone.

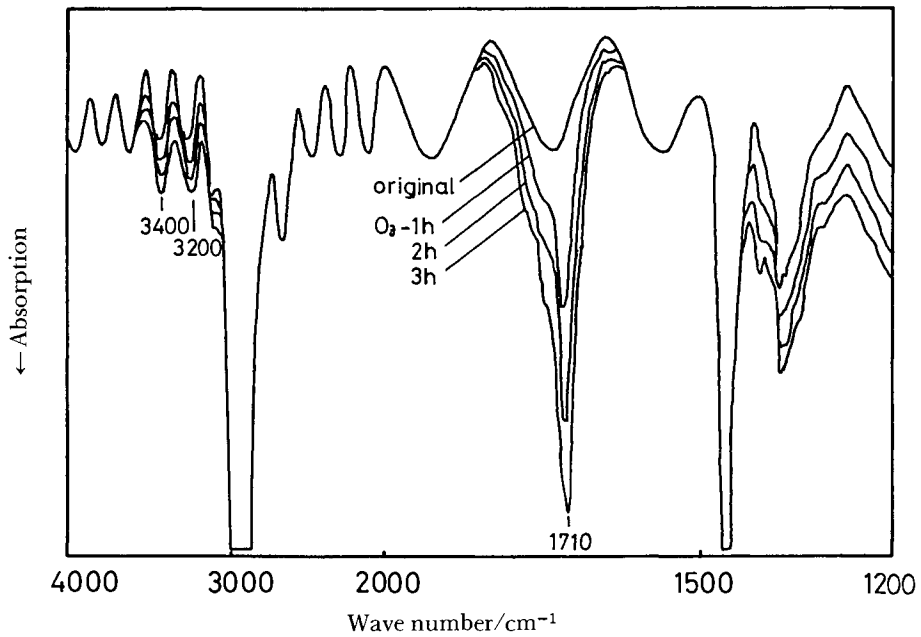

Fig. 2. Variation of the IR spectra of polyethylene with the ozone-oxidation time.

ozone oxidation time.

Discussion

Ozone-Oxidation Mechanism. The presumed ozone-oxidation mechanism[11] is first summarized as follows. An atomic oxygen arising from ozone decomposition attacks polymers, producing carbon and hydroxyl radicals. The carbon radical reacts almost immediately with an oxygen molecule, giving a peroxyl radical:

$$O_3 \longrightarrow O_2 + (O) \tag{1}$$

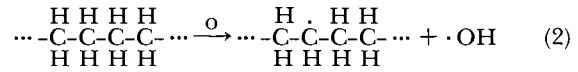

(2)

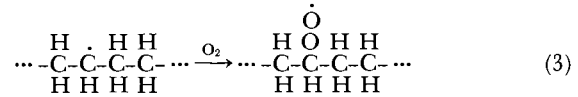

(3)

A part of the peroxyl radicals, thus produced, gives hydroperoxide by pulling out a hydrogen atom from polyethylene:

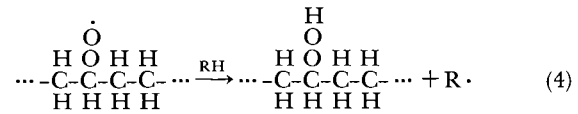

(4)

Another part of the peroxyl radicals gives inert substances, such as ketone and alcohol by recombination:

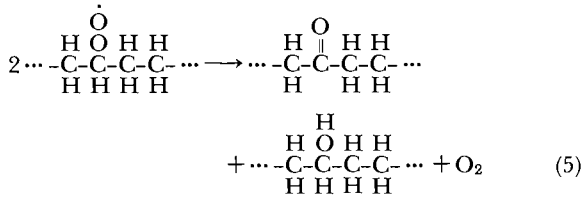

(5)

The O-O bond of the hydroperoxide given in reaction (4) is broken by heating:

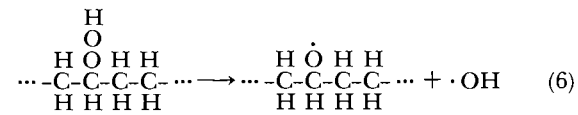

(6)

The alkoxyl and hydroxyl radicals, thus obtained, are presumed to initiate polymerization as active sites and to give graft copolymers and homopolymers, respectively.

Rate-Process Analyses. For simplicity, the following rate processes are taken into consideration. Reactions (2) and (3) can be expected to take place almost concurrently; that is,

$$RH + O_3 \xrightarrow{k_1} ROO\cdot + \cdot OH. \tag{7}$$

The rate constants in reaction (4) and the following chain reaction are set to be k_2 and k_3, respectively:

$$ROO\cdot + RH \xrightarrow{k_2} ROOH + R\cdot \tag{8}$$

and

$$R\cdot + O_2 \xrightarrow{k_3} ROO\cdot. \tag{9}$$

The chain reaction is terminated as in reaction (5):

$$2ROO\cdot \xrightarrow{k_4} \text{inert products.} \tag{10}$$

We assume a steady state of R· in reactions (8) and (9). Then, the production rate of ROO· is obtained as

$$\frac{d[ROO\cdot]}{dt} = k_1[RH][O_3] - k_4[ROO\cdot]^2. \tag{11}$$

Here, we use two parameters, $I = k_1[RH][O_3]$ and $K = (I/k_4)^{1/2}$, and then obtain a solution of the Eq. 11 as[14]

$$\ln \frac{K + [ROO\cdot]}{K - [ROO\cdot]} = \frac{2I}{K} t \tag{12}$$

or

$$[ROO\cdot] = \frac{e^{(2I/K)t} - 1}{e^{(2I/K)t} + 1} \times K. \tag{13}$$

One can see that the saturated concentration of product ROO· is given by the parameter K, where

$$[ROO\cdot]_s = K = (I/k_4)^{1/2}. \tag{14}$$

If we assume a small concentration of intermediate R·, as compared to that of ROO·, the observed ESR intensity becomes proportional to the concentration of ROO·.[15]

Figure 4 shows the time-dependent ESR intensities in the form

$$\ln\{([ROO\cdot]_s + [ROO\cdot])/([ROO\cdot]_s - [ROO\cdot])\},$$

which was calculated from the observed ESR intensity and the saturated value given in Fig. 1. A good linear correlation with the oxidation time given in Fig. 4 is

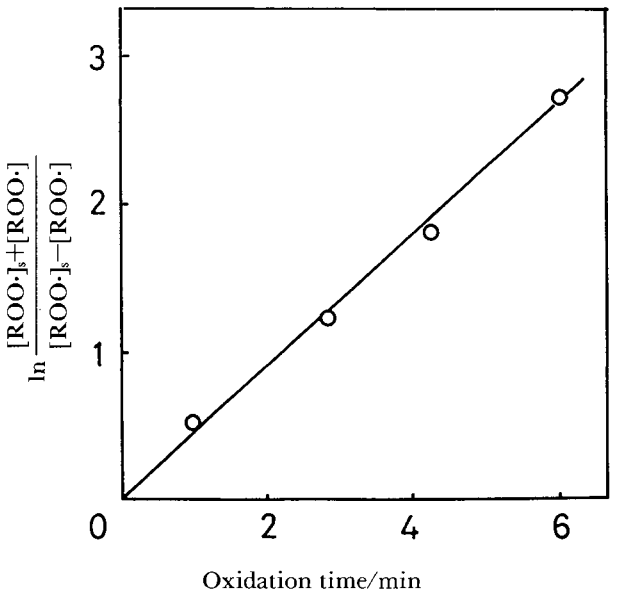

Fig. 4. Plot of $\ln\{([ROO\cdot]_s + [ROO\cdot])/([ROO\cdot]_s - [ROO\cdot])\}$ against ozone-oxidation time.

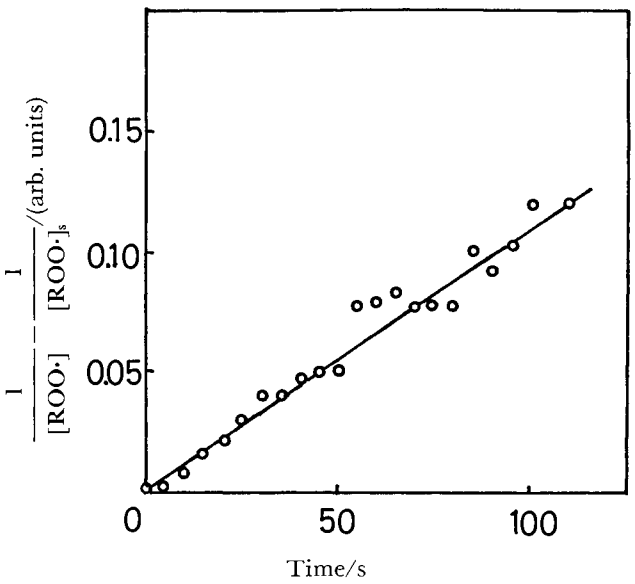

Fig. 5. Plot of $1/[ROO\cdot]-1/[ROO\cdot]_s$ against time after the ozone-stop.

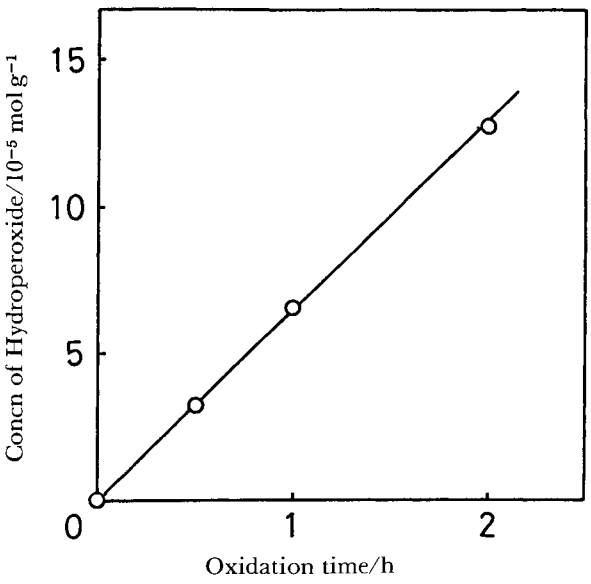

Fig. 6. Relationship between oxidation time and concentration of hydroperoxide in polyethylene oxidized with ozone.

indicative of the validity of Eqs. 12 or 13.

After stopping the ozone flow, the decomposition of ROO· can be expressed by Eq. 10, giving

$$\frac{1}{[ROO\cdot]}-\frac{1}{[ROO\cdot]_s}=k_4t. \tag{15}$$

Using this equation, the decay process is plotted in Fig. 5, which also exhibits a linear time dependence of $1/[ROO\cdot]-1/[ROO\cdot]_s$, supporting Eq. 15.

Products of Hydroperoxide and Ketone. In order to obtain more evidence for the ozone-oxidation mechanism we measured the amounts of products, such as hydroperoxide and ketone, depending on the ozone-oxidation time. From Eq. 8,

$$\frac{d[ROOH]}{dt}=k_2[ROO\cdot][RH]. \tag{16}$$

Here, we use the saturated value, $[ROO\cdot]_s$, for $[ROO\cdot]$ in the case of a longer oxidation time than 10 min. Then, [ROOH] becomes proportional to time:

$$\begin{aligned}[ROOH]&=k_2[ROO\cdot][RH]t\\&=k_2k_1^{1/2}k_4^{-1/2}[RH]^{3/2}[O_3]^{1/2}t.\end{aligned} \tag{17}$$

The iodometry disclosed the content of hydroperoxide, as shown in Fig. 6.[11] It is concluded that hydroperoxide is increasingly yielded with the oxidation time, as is predicted by Eq. 8. This is compatible with reactions (1)—(4).

One of the inert products in reaction (5), the ketone, can be monitored from the IR spectra (Fig. 2). From Eq. 10,

$$\frac{d[C{=}O]}{dt}=k_4[ROO\cdot]^2. \tag{18}$$

Here, we again discuss the process after the saturation of ROO·; Eq. 18 then becomes

$$\frac{d[C{=}O]}{dt}=k_4[ROO\cdot]_s^2. \tag{19}$$

Since $[ROO\cdot]_s$ can be replaced by $(Ik_4)^{1/2}$ from Eq. 14 we obtain

$$[C{=}O]=It. \tag{20}$$

The optical density of the C=O groups in the IR spectra for the various oxidized polyethylenes again shows a linear relation with the oxidation time, as in Fig. 3, indicating the decomposition process of ROO·, like Eqs. 5 or 10.

In this paper concerning the ozone oxidation of polyethylene we pursued the time-dependent radical species ROO· by ESR spectroscopy; the influence of the oxidation time upon such products as hydroperoxide and ketone were clarified by iodometry and IR spectroscopy, respectively. The radical evolution in the initial stage and the radical decay after stopping ozone flow were kinetically analyzed on the basis of several assumptions, affording supporting evidence concerning the reaction mechanism involved in reactions (1)—(5).

The final product, hydroperoxide, which is useful for graft-copolymerization, has a reasonable linear dependence on the oxidation time; the inert product, the ketone, which arises from the decomposition of ROO·, shows the same dependence on the oxidation time. These two findings also support the proposed oxidation mechanism.

References

1) W. Scnabel, "Polymer Degradation-Principles and

Practical Application," Hanser, Munchen (1981); Z. Osawa, "Degradation and Stabilization of Polymers," ed by H. H. G. Jellinek, Elsvier, Amsterdam (1983).

2) S. Ohnishi, S. Sugimoto, and I. Nitta, *J. Polym. Sci., Part A*, **11**, 605, 625 (1963).

3) A. V. Tobolsky, P. M. Norling, N. H. Frick, and H. Yu, *J. Am. Chem. Soc.*, **86**, 3925 (1964).

4) J. C. W. Chien and C. R. Boss, *J. Polym. Sci.*, **5**, 3091 (1967).

5) Z. Kuri, H. Ueda, and S. Shida, *J. Chem. Phys.*, **32**, 371 (1960).

6) E. J. Lawton, J. S. Balmit, and R. S. Powell, *J. Chem. Phys.*, **33**, 395 (1960).

7) M. Imoto, T. Ohtsu, and K. Yamada, *Kogyokagaku Zassi*, **65**, 1875 (1962).

8) J. P. Luongo, *J. Polym. Sci.*, **42**, 139 (1960).

9) S. Shimada, Y. Hori, and H. Kashiwabara, *Macromolecules*, **18**, 170 (1985).

10) D. J. Carlsson, C. J. B. Dobbin, and D. M. Wiles, *Macromolecules*, **18**, 1791, 2092 (1985).

11) A. Yamaoka, K. Ikemoto, T. Matsui, and J. Yamauchi, *Nippon Kagaku Kaishi*, **1989**, 1919; J. Yamauchi, A. Yamaoka, K. Ikemoto, and T. Matsui, *J. Appl. Polym. Sci.*, in press.

12) J. Yamauchi, K. Ikemoto, and A. Yamaoka, *Makromol. Chem.*, **178**, 2483 (1977).

13) J. C. W. Chien, E. J. Vanderberg, and H. Jabloner, *J. Polym. Sci., Part A-1*, **6**, 381 (1968).

14) In the present rate analyses we assumed a constant ozone concentration [O_3] and vast excess of RH.

15) In the case of $k_3 \gg k_2$ this assumption may be plausible. Even if this is not the case, in the steady state approximation about R·, [R·] is related to [ROO·] so that the ESR intensity due to R· and ROO· is eventually proportional to [ROO·].

An Ab Initio Molecular Orbital Study on Twisting in Silyl-Substituted Ethylene Cation Radicals

Ohgi TAKAHASHI, Kenji MORIHASHI, and Osamu KIKUCHI*
Department of Chemistry, University of Tsukuba, Tsukuba 305
(Received October 29, 1990)

Twisting in two silyl-substituted ethylene cation radicals, the cation radicals of vinylsilane (**1**) and vinylidenebissilane (**2**), were investigated by ab initio UHF calculations with the 3-21G and 3-21G(*) basis sets. Both $\mathbf{1}^{+\cdot}$ and $\mathbf{2}^{+\cdot}$ were found to have twisted equilibrium structures, the twist angle being 29° and 42°, respectively. The planarization barriers evaluated for $\mathbf{1}^{+\cdot}$ and $\mathbf{2}^{+\cdot}$ are about 1 and 7 kcal mol^{-1}, respectively. The planar and 90°-twisted forms of $\mathbf{2}^{+\cdot}$ have comparable energies. The hyperconjugation of the C-Si bonds is reflected in the calculated molecular structures.

The possibility of twisting in olefin cation radicals has attracted considerable attention.[1,2] However, it was recently concluded, based on semiempirical UHF/AM1 calculations of hyperfine coupling constants for some alkyl-substituted ethylene cation radicals, that the only olefin cation radicals with a twisted structure are the ethylene cation radical, itself, and a series of trimethylsilyl-substituted ethylene cation radicals.[1] These cation radicals benefit from hyperconjugation of C-H or C-Si bonds, which stabilizes the positive charge, by twisting around the C-C bond. The ethylene cation radical was experimentally found to be twisted by about 25° in the gas phase with a planarization barrier of only 0.7—0.8 kcal mol^{-1} (1 cal=4.184 J);[3] considerable twisting in trimethylsilyl-substituted ethylene cation radicals was suggested based on their ESR spectra by Sakurai et al.[4] and Symons et al.[5] Consequently, the trimethylsilyl-substituted ethylene cation radicals are the only olefin cation radicals which have shown any marked twisted structure so far.

Stabilization of a positive charge center by β-C-Si bonds is now well recognized.[6] This stabilizing effect is orientation-dependent, since the β-C-Si bond interacts with the positive charge center hyperconjugatively.[6,7] Hence, the twist angle in silyl-substituted ethylene cation radicals may be determined by a compromize between the breaking of a one-electron π-bond and hyperconjugative stabilization of the positive charge. Although the hyperfine coupling constants of olefinic protons can be a good measure of the degree of twisting (as discussed in Refs. 4 and 5), a theoretical evaluation of the potential energy surface may be also desirable. This note reports the first ab initio level of calculations concerning the twisting in silyl-substituted ethylene cation radicals. Vinylsilane (**1**) and vinylidenebissilane (**2**) were selected as model compounds for a calculation, and the 3-21G[8] and 3-21G(*)[9] basis sets and UHF formalism were employed. The latter basis set includes d-type polarization functions on silicon atoms.

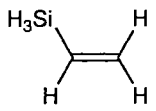

1

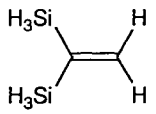

2

Results and Discussion

Vinylsilane Cation Radical ($\mathbf{1}^{+\cdot}$). The structures for the planar, twisted, and 90°-twisted forms were all optimized with the 3-21G and 3-21G(*) basis sets.

Table 1. Calculated Total Energies (a.u.) and Relative Energies (kcal mol^{-1}, in Parentheses) of Vinylsilane Cation Radical ($\mathbf{1}^{+\cdot}$)

Form	Symmetry	State	3-21G//3-21G	3-21G(*)//3-21G	3-21G(*)//3-21G(*)
Planar	$C_s(syn)$[a]	$^2A''$	−365.83405(1.3)	−365.92949(1.3)	−365.92992(1.2)
	$C_s(anti)$[b]	$^2A''$	−365.83323(1.8)	−365.92867(1.8)	−365.92911(1.7)
Twisted	C_1[c]	^2A	−365.83616(0)	−365.93150(0)	−365.93190(0)
	C_1[d]	^2A	−365.83627(−0.06)	−365.93156(−0.04)	−365.93201(−0.07)
90°-Twisted	$C_s(syn)$	$^2A''$	−365.80929(16.9)	−365.90344(17.6)	−365.90403(17.5)
	$C_s(anti)$	$^2A''$	−365.80958(16.7)	−365.90376(17.4)	−365.90427(17.3)
	$C_s(syn)$	$^2A'$	−365.79801(23.9)	−365.89364(23.7)	−365.89412(23.7)
	$C_s(anti)$	$^2A'$	−365.79805(23.9)	−365.89364(23.7)	−365.89415(23.7)

a) One Si-H bond is synperiplanar to the C-C bond. b) One Si-H bond is antiperiplanar to the C-C bond. c) Planarity was assumed around the carbon atoms. d) No constraint was imposed.

Table 2. Structural Parameters of Vinylsilane Cation Radical ($1^{+\cdot}$) Obtained by UHF/3-21G and UHF/3-21G(*) (in Parentheses) Calculations[a]

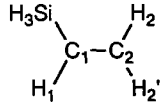

	C_s planar (*syn*)[b]	C_1 twisted[c]	C_s 90°-twisted (*anti*)[d]
Bond lengths			
C_1-C_2	1.412(1.415)	1.384(1.386)	1.368(1.373)
C_1-Si	1.974(1.943)	1.988(1.958)	2.047(1.996)
C_1-H_1	1.080(1.081)	1.082(1.082)	1.078(1.081)
C_2-H_2	1.074(1.074)	1.076(1.076)	1.082(1.082)
C_2-H_2'	1.075(1.074)	1.077(1.077)	1.082(1.082)
Si-H(1)	1.472(1.460)	1.472(1.460)	1.472(1.462)
Si-H(2)	1.474(1.463)	1.474(1.463)	1.466(1.457)
Si-H(3)	1.474(1.463)	1.472(1.460)	1.472(1.462)
Bond angles			
C_2C_1Si	125.6(125.5)	125.4(125.1)	115.7(118.5)
$C_2C_1H_1$	115.9(116.1)	117.8(117.9)	130.2(127.4)
$C_1C_2H_2$	121.0(120.9)	121.5(121.5)	121.7(121.7)
$C_1C_2H_2'$	121.5(121.4)	121.2(121.3)	121.7(121.7)
C_1SiH(1)	105.0(105.2)	104.9(105.3)	104.9(105.2)
C_1SiH(2)	103.6(103.3)	102.4(101.9)	100.4(101.4)
C_1SiH(3)	103.6(103.3)	103.7(103.8)	104.9(105.2)
Dihedral angles			
$SiC_1C_2H_2$[e]	0.(0.)	29.3(29.5)	90.(90.)
C_2C_1SiH(1)	0.(0.)	−0.4(−0.6)	−59.9(−59.8)
C_2C_1SiH(2)	−120.4(−120.4)	−120.4(−120.4)	180.(180.)
C_2C_1SiH(3)	120.4(120.4)	120.4(120.3)	59.9(59.8)

a) Bond lengths are in Å and angles are in degrees. b) One Si-H bond is synperiplanar to the C-C bond. c) The planar carbons were assumed. d) One Si-H bond is antiperiplanar to the C-C bond. e) The twist angle around the C-C bond.

The calculated energies are shown in Table 1, and the structures in Table 2.

The structure for the planar form was optimized assuming C_s symmetry. Two conformations of the silyl group are possible. In the "*syn*" conformation, one Si-H bond is synperiplanar to the C-C bond, while one Si-H bond is antiperiplanar to the C-C bond in the "*anti*" conformation. The *syn* conformation was calculated to be more stable than the *anti* conformation by 0.5 kcal mol^{-1}, and was found to be the most favorable conformation.

Twisting of the planar cation radical around the C-C bond lowered the energy, and the structure of the twisted form was optimized assuming sp^2 hybridization (planarity) of the carbon atoms (Without this constraint, the energy was lowered by 0.06—0.07 kcal mol^{-1}). The twist angles at the 3-21G and 3-21G(*) optimized structures are 29.3° and 29.5°, respectively. The energy of the twisted form is lower than that of the planar form by 1.2—1.3 kcal mol^{-1}.

The structure of the 90°-twisted form was optimized assuming C_s symmetry. The *anti* conformation of the silyl group was slightly (0.2 kcal mol^{-1}) favored, and was found to be the most favorable. The energy of the 90°-twisted form is higher in energy than that of the twisted equilibrium structure by about 17 kcal mol^{-1}. The ground state of the 90°-twisted form is the

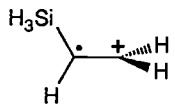

$^2A''$

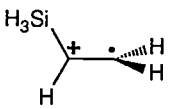

$^2A'$

$^2A''$ state, which is formally regarded as being a "silylmethyl radical+methyl cation." The energy and structure of the $^2A'$ state, which is regarded as "silylmethyl cation+methyl radical," were also calculated. The $^2A'$ cation radical is higher in energy than the $^2A''$ cation radical by 6—7 kcal mol^{-1}. This result is in contrast to that for the methyl analogue, the propene cation radical.[10] The preference of the $^2A''$ state in $1^{+\cdot}$ is apparently due to a hyperconjugative stabilization of the positive charge by the C-Si bond; in the propene cation radical, the α-methyl group stabilizes the positive charge of the $^2A'$ state.

In summary, $1^{+\cdot}$ is twisted by about 29°, the planarization barrier is about 1 kcal mol^{-1}, and the barrier to rotation through the 90°-twisted form is about 17 kcal mol^{-1}.

Vinylidenebissilane Cation Radical ($2^{+\cdot}$). The structures for the planar, twisted, and 90°-twisted forms of $2^{+\cdot}$ were optimized only with the 3-21G basis set, while the energies were also evaluated with the 3-

21G(*) basis set in some cases, because for $\mathbf{1}^{+\cdot}$, both the 3-21G and 3-21G(*) basis sets gave similar structures, except that the latter gave slightly (0.03—0.05 Å) shorter C-Si bonds, and the 3-21G(*)//3-21G(*), 3-21G(*)//3-21G, and 3-21G//3-21G levels of the calculation all gave very similar results regarding the relative energies (See Tables 1 and 2). The results for $\mathbf{2}^{+\cdot}$ are shown in Tables 3 and 4.

The structure of the planar form was optimized assuming C_{2v} symmetry. The *syn* conformation of the silyl groups was favored by about 1 kcal mol^{-1}. The potential energy surface was found to be very flat against silyl-group rotation in the vicinity of the *syn* conformation.

Twisting of the planar cation radical lowered the energy, and the structure of the twisted form was optimized assuming C_2 symmetry. The twist angle at the optimized structure is 42.4°, which is quite large as an olefin cation radical. The energy of the twisted form is lower than that of the planar form by 7—8 kcal mol^{-1}.

The structure of the 90°-twisted form was optimized first assuming C_{2v} symmetry. The *anti* conformation was slightly more stable (0.3 kcal mol^{-1}) than the *syn* conformation. When a C_2 symmetry was assumed, however, the energy was further lowered by about 0.2 kcal mol^{-1}. The energy of the 90°-twisted form is higher than that of the twisted equilibrium structure by 8—8.5 kcal mol^{-1}. As expected, the ground state of the 90°-twisted form corresponds to "disilyl-

Table 3. Calculated Total Energies (a.u.) and Relative Energies (kcal mol^{-1}, in Parentheses) of Vinylidenebissilane Cation Radical ($\mathbf{2}^{+\cdot}$)

Form	Symmetry	State	3-21G//3-21G	3-21G(*)//3-21G
Planar	C_{2v}(*syn*)[a]	$^2B_1$	−654.39321(7.4)	−654.58321(7.6)
	C_{2v}(*anti*)[b]	$^2B_1$	−654.39158(8.5)	—
Twisted	C_2	^2B	−654.40508(0)	−654.59534(0)
90°-Twisted	C_{2v}(*syn*)	$^2B_1$	−654.39151(8.5)	—
	C_{2v}(*anti*)	$^2B_1$	−654.39199(8.2)	−654.58222(8.2)
	C_2	^2B	−654.39235(8.0)	—
	C_{2v}(*syn*)	$^2B_2$	−654.36337(26.2)	—
	C_{2v}(*anti*)	$^2B_2$	−654.36420(25.6)	—

a) One Si-H bond is synperiplanar to the C-C bond. b) One Si-H bond is antiperiplanar to the C-C bond.

Table 4. Structural Parameters of Vinylidenebissilane Cation Radical ($\mathbf{2}^{+\cdot}$) Obtained by UHF/3-21G Calculation[a]

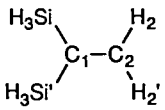

	C_{2v} planar (*syn*)[b]	C_2 twisted	C_2 90°-twisted
Bond lengths			
C_1-C_2	1.421	1.354	1.353
C_1-Si	1.974	1.994	1.998
C_2-H_2	1.075	1.079	1.082
Si-H(1)	1.474	1.474	1.472
Si-H(2)	1.476	1.473	1.471
Si-H(3)	1.476	1.473	1.474
Bond angles			
C_2C_1Si	119.9	121.9	123.0
$C_1C_2H_2$	121.7	121.9	121.9
$C_1SiH(1)$	106.2	104.8	106.0
$C_1SiH(2)$	104.3	104.9	104.1
$C_1SiH(3)$	104.3	103.6	103.9
Dihedral angles			
$SiC_1C_2H_2$[c]	0.	42.4	90.
$C_2C_1SiH(1)$	0.	−23.4	−30.0
$C_2C_1SiH(2)$	−120.6	−144.2	−150.3
$C_2C_1SiH(3)$	120.6	96.5	90.2

a) Bond lengths are in Å and angles are in degrees. b) One Si-H bond is synperiplanar to the C-C bond. c) The twist angle around the C-C bond.

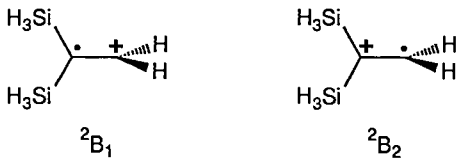

methyl radical+methyl cation" (the $^2B_1$ state in the C_{2v} cases). Another state, the $^2B_2$ state of the C_{2v} 90°-twisted form ("disilylmethyl cation+methyl radical") was also investigated, and was found to be higher in energy than the $^2B_1$ state by 17—18 kcal mol^{-1}. The energy difference between the two states is considerably larger than that between the $^2A''$ and $^2A'$ states of the C_s 90°-twisted form of $1^{+\cdot}$, and is also in contrast to that for the methyl analogue, 2-methylpropene cation radical.[11]

In summary, $2^{+\cdot}$ is twisted by about 42°, the planarization barrier is about 7 kcal mol^{-1}, and the barrier to rotation through the 90°-twisted form is about 8 kcal mol^{-1}. It should be noted that the planar and 90°-twisted forms have comparable energies.

Hyperconjugation of C-Si Bonds. As mentioned in the introduction part, the twisted equilibrium structures of $1^{+\cdot}$ and $2^{+\cdot}$ can be attributed to the hyperconjugative stabilization of the positive charge by the C-Si bond(s). The hyperconjugation effect of the C-Si bond(s) should be maximized at the 90°-twisted form where the overlap between the "vacant" p_π orbital of the carbon atom of $-CH_2$ and the C-Si σ orbital(s) becomes maximum, while the π conjugation between the two carbon atoms is maximized at the planar form. These two competing factors are considered to determine the degree of the twisting. Indeed, $2^{+\cdot}$ which has two silyl groups is more twisted and stabilized by twisting than $1^{+\cdot}$.

The hyperconjugation of the C-Si bond(s) is well reflected in the shape of the LUMO[12] of the 90°-twisted $^2A''$ state of $1^{+\cdot}$ and the 90°-twisted $^2B_1$ state of $2^{+\cdot}$, which are essentially the p_π orbitals of the carbon atom of the $-CH_2$ fragment combined out-of-phase with the C-Si σ orbital(s) (See Fig. 1).[13]

The hyperconjugation is also reflected in the calculated molecular structures. In Table 5, the C-C and C-Si bond lengths and the C-C-Si bond angle at several twist angles are shown (other structural parameters were optimized). As the twist angle is increased, the C-C bond becomes shorter (up to 60°),[14]

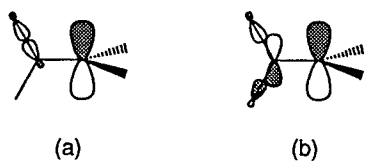

Fig. 1. Schematic representation of the LUMO's of (a) C_s 90°-twisted $^2A''$ state of $1^{+\cdot}$, and (b) C_{2v} 90°-twisted $^2B_1$ state of $2^{+\cdot}$.

Table 5. UHF/3-21G Optimized Values of the C-C and C-Si Bond Lengths and C-C-Si Bond Angle in $1^{+\cdot}$ and $2^{+\cdot}$ for Various Values of the Twist Angle Around the C-C Bond

	Twist angle[a]	R(C-C)[b]	R(C-Si)[c]	∠CCSi[d]
$1^{+\cdot}$	0.0	1.412	1.974	125.6
	29.3	1.384	1.988	125.4
	60.0	1.364	2.009	123.7
	90.0	1.368	2.047	115.7
$2^{+\cdot}$	0.0	1.421	1.974	119.9
	30.0	1.364	1.992	121.8
	42.4	1.354	1.994	121.9
	60.0	1.348	1.995	122.4
	90.0	1.353	1.998	123.0

a) In degrees. b) The C-C bond length in Å. c) The C-Si bond length in Å. d) The C-C-Si bond angle in degrees.

while the C-Si bond(s) becomes longer. Considering the following resonance, this trend is attributable to increasing C-Si hyperconjugation.

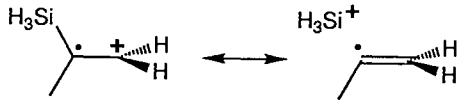

The change in the C-C-Si bond angle in $1^{+\cdot}$, which decreases as the twist angle is increased, is also attributable to increasing C-Si hyperconjugation. For $2^{+\cdot}$, however, the C-C-Si bond angle unexpectedly increases as the twist angle is increased; the reason for this is not clear.

It should be noted that silyl-substituted ethylene cation radicals are largely twisted by the electronic factor without any steric hindrance, because the trimethylsilyl groups were replaced by the silyl groups in the present calculations.

Orbital Mixing upon Twisting. In the above discussion, the preference of the twisted structures in $1^{+\cdot}$ and $2^{+\cdot}$ was interpreted using the hyperconjugation concept. Here, we see the same thing from a different point of view; we predict twisted equilibrium structures from the MO's of the planar form.

The HOMO ($3b_1$) and NHOMO ($8b_2$) of the neutral

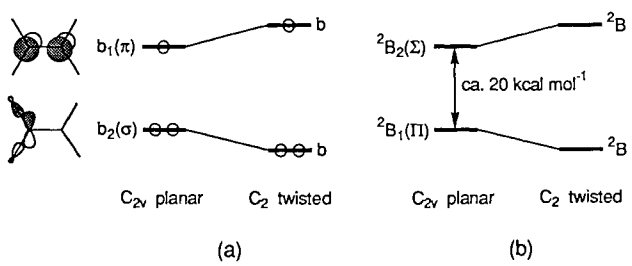

Fig. 2. σ-π Mixing upon twisting of the C_{2v} planar form of $2^{+\cdot}$: (a) Orbital description. (b) State description.

2 (C_{2v} planar) are energetically close to each other;[16] the HOMO is associated with the C-C π bond, while the NHOMO with the two C-Si bonds (Fig. 2). Upon twisting of the molecule around the C-C bond, these two orbitals come to have the same symmetry and mix with each other. This orbital mixing leads to stabilization in the case of the cation radical, as shown in Fig. 2. If we use "state description" instead of "orbital description", the $^2B_1$ (Π) and $^2B_2$ (Σ) states of the C_{2v} planar $\mathbf{2}^{+\cdot}$ interact with each other upon twisting to lower the ground state energy (Fig. 2).[17]

A similar discussion is also valid for $\mathbf{1}^{+\cdot}$. In this case, however, the energy difference between the 3a″ (π) and 13a′ (σ) orbitals (or the $^2A''$ (Π) and $^2A'$ (Σ) states) of the C_s planar form is larger than in **2**,[18] and the interaction of the two orbitals (or states) is weak. This results in smaller stabilization upon twisting.

References

1) T. Clark and S. F. Nelsen, *J. Am. Chem. Soc.*, **110**, 868 (1988).

2) K. Morihashi, H. Kometani, O. Takahashi, H. Togo, and O. Kikuchi, *J. Chem. Soc., Chem. Commun.*, **1989**, 1473.

3) A. J. Merer and L. Schoonveld, *Can. J. Phys.*, **47**, 1731 (1969); H. Köppel, W. Domcke, L. S. Cederbaum, and W. von Niessen, *J. Chem. Phys.*, **69**, 4252 (1978).

4) M. Kira, H. Nakazawa, and H. Sakurai, *J. Am. Chem. Soc.*, **105**, 6983 (1983).

5) G. W. Eastland, Y. Kurita, and M. C. R. Symons, *J. Chem. Soc., Perkin Trans. 2*, **1984**, 1843.

6) Review: J. B. Lambert, *Tetrahedron*, **46**, 2677 (1990).

7) S. G. Wierschke, J. Chandrasekhar, and W. L. Jorgensen, *J. Am. Chem. Soc.*, **107**, 1496 (1985).

8) J. S. Binkley, J. A. Pople, and W. J. Hehre, *J. Am. Chem. Soc.*, **102**, 939 (1980); M. S. Gordon, J. S. Binkley, J. A. Pople, W. J. Pietro, and W. J. Hehre, *J. Am. Chem. Soc.*, **104**, 2797 (1982).

9) W. J. Pietro, M. M. Francl, W. J. Hehre, D. J. DeFrees, J. A. Pople, and J. S. Binkley, *J. Am. Chem. Soc.*, **104**, 5039 (1982).

10) UHF/3-21G calculations have shown that the 90°-twisted $^2A'$ state of the propene cation radical is more stable than the $^2A''$ state by about 16 kcal mol^{-1}.

11) UHF/3-21G calculations have shown that the 90°-twisted $^2B_2$ state of the 2-methylpropene cation radical is more stable than the $^2B_1$ state by about 28 kcal mol^{-1}.

12) The UHF LUMO of the 90°-twisted $^2A''$ state of $\mathbf{1}^{+\cdot}$ and the 90°-twisted $^2B_1$ state of $\mathbf{2}^{+\cdot}$ do not correspond to the SOMO in the RHF case, but to the RHF LUMO. This phenomenon seems to be characteristic of cation radicals in which the positive charge and unpaired electron are separated in different regions. The UHF result is quite natural in view of the most important valence-bond structure.

13) Since the LUMO is not occupied, it has no direct concern with stabilization of the cation radical. Nevertheless, its characteristic shape may be regarded as being a reflection of the hyperconjugation in which the cation center is partially filled by a flow of electrons associated with the C-Si bond(s); the relavent occupied MO, an in-phase combination of the p_π orbital of the carbon atom and the C-Si σ orbital(s), is less apparent due to other mixing. See also Ref. 7.

14) The ethylene cation radical itself also seems to show a similar trend. See Ref. 15.

15) N. C. Handy, R. H. Nobes, and H.-J. Werner, *Chem. Phys. Lett.*, **110**, 459 (1984); H. Ichikawa, Y. Ebisawa, and A. Shigihara, *Bull. Chem. Soc. Jpn.*, **58**, 3619 (1985).

16) The orbital energies (3-21G) are −11.18 eV (HOMO) and −10.45 eV (NHOMO). The difference is 0.73 eV.

17) The energy of the $^2B_2$ (Σ) state calculated at the geometry for the $^2B_1$ (Π) state is −654.36133 a.u. and higher than the Π state by 20.0 kcal mol^{-1} (3-21G).

18) The orbital energies (3-21G) of the HOMO (3a″) and NHOMO (13a′) of **1** (C_s planar) are −10.38 eV and −12.09 eV, respectively (The difference is 1.70 eV), while the energy of the $^2A'$ (Σ) state of $\mathbf{1}^{+\cdot}$ calculated at the geometry for the $^2A''$ (Π) state is −365.76545 a.u. and higher than the Π state by 43.0 kcal mol^{-1} (3-21G).

Structural Study of Optical Resolution. XV. Chiral Discrimination of the Facial Isomer of the Tris((*R,S*)-1,2-cyclohexanediamine)cobalt(III) Cation with (*R,R*)-Tartrate Anion

Tsutomu MIZUTA, Kazuo TOSHITANI, and Katsuhiko MIYOSHI*
Department of Chemistry, Faculty of Science, Hiroshima University,
1-1-89 Higashi-senda-machi, Naka-ku, Hiroshima 730
(Received October 18, 1990)

Crystal structures of the two diastereomeric salts of the title *Δ* complex cation with (*R,R*)-tartrate anion, *Δ-fac*-[Co(*R,S*-chxn)$_3$](ClO$_4$)(d-tart)·*m*H$_2$O (**1**) and *Δ-fac*-[Co(*R,S*-chxn)$_3$]Cl(d-tart)·*n*H$_2$O (**2**) (*R,S*-chxn=(*R,S*)-1,2-cyclohexanediamine and d-tart=dextro-rotatory (*R,R*)-tartrate dianion), have been determined by single crystal X-ray diffraction techniques. The former crystal **1** is orthorhombic with the space group $P22_12_1$, a=12.358(3), b=22.094(5), c=32.770(7) Å, and Z=12, while the latter **2** is trigonal with the space group $P3_121$, a=15.367(7), c=26.208(4) Å, and Z=6. In **1** are found two similar face-to-face contact modes in both of which the d-tart^{2-} ion directs its four almost coplanar O atoms to the complex along the C_3 axis, and three of them, two alcoholic and one carboxylic, are triply hydrogen-bonded to the three N-H protons on one of the triangular faces of the *Δ* complex denoted as the *Δ-cis* RRR face, where R stands for the chirality of the carbon atom adjacent to the N-H group hydrogen-bonded to the d-tart^{2-} ion. The other triangular face of the complex denoted as the *Δ-cis* SSS face is so crowded that only two O atoms of the d-tart^{2-} ion are hydrogen-bonded to the face. In **2** is found one face-to-face contact mode in which the d-tart^{2-} ion approaches the *Δ* complex similarly, but the three O atoms are each placed midway between two of the three N-H protons on the triangular *Δ-cis RRR* face to form three bifurcated hydrogen bonds to them, and the d-tart^{2-} ion tactfully avoids the steric repulsion marginally by inclining its molecular plane a little relative to the triangular face at the least expense of the multiple hydrogen bonds to the face. Based on the assumption that the face-to-face contact mode found in **2** is the most probable interaction mode conceivable in solution, the elution order and separation factor obtained by ion-exchange chromatography for some related [Co(chxn)$_3$]$^{3+}$ complexes are rationally interpreted.

It is well-known that naturally occurring dextro-rotatory (*R,R*)-tartrate anion (abbreviated as d-tart^{2-} hereafter) serves as an effective resolving agent for many chiral metal-amine complex cations, and several studies have been reported on the mechanisms by which the d-tart^{2-} anion discriminates the chirality of these complexes in solution and in the solid state.[1,2] In the preceding paper of this series,[3] a crystal structure analysis has been carried out on a pair of diastereomeric salts of the *lel*$_3$-[Co(*trans*-chxn)$_3$]$^{3+}$ complex (chxn=1,2-cyclohexanediamine) with d-tart^{2-} and Cl$^-$ ions. It has been found there that the d-tart^{2-} anion makes a favorable face-to-face contact with the *Δ-lel*$_3$-[Co(*trans*-chxn)$_3$]$^{3+}$ complex through multiple hydrogen bonds to the three N-H protons on one of the two triangular faces along the C_3 axis. In the *Δ-lel*$_3$-[Co(*trans*-chxn)$_3$]$^{3+}$ complex salt, on the other hand, the d-tart^{2-} ion is forced to rotate its distal carboxylate group when it makes a similar face-to-face contact, because one of the bulky chxn ligands of the *Δ* complex would otherwise impose a severe steric repulsion on the carboxylate group. These observations indicate that the *Δ* complex has two favorable triangular faces which allow a smooth access of the d-tart^{2-} ion along the C_3 axis. These faces are denoted here as the *Δ-trans* SSS face (Fig. 1), where S stands for the chirality of the carbon atom adjacent to the N-H group hydrogen-bonded to the d-tart^{2-} ion. In contrast, the two *Δ-trans* RRR faces (Fig. 1) possessed by the *Δ* complex serve only as a "less-favorable" interaction site, as mentioned above. In this way, highly efficient chiral discrimination attained in these systems has been reasonably interpreted in terms of the steric repulsion expected stereoselectively between the distal carboxylate group and one of the chxn ligands on the *Δ* complex.

Ab initio MO calculations performed on d-tart^{2-} ion[3] have revealed that the rotation of the carboxylate group leads to a substantial destabilization of isolated d-tart^{2-} ion, which is fully compensated in the *Δ-lel*$_3$-[Co(*trans*-chxn)$_3$]$^{3+}$ complex salt, by the multiple hydrogen bonds not only to the triangular face of the

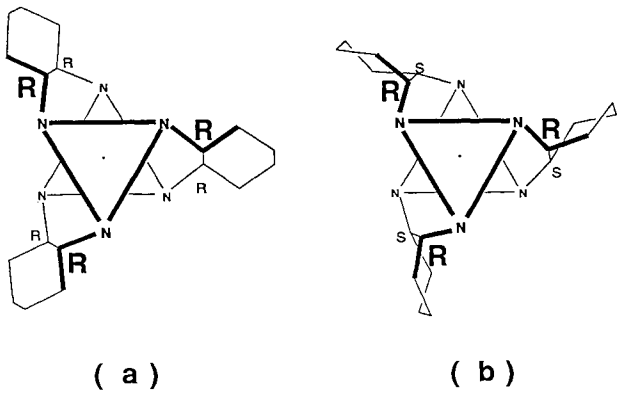

Fig. 1. A schematic presentation of the *Δ-trans* RRR face (a) and the *Δ-cis* RRR face (b). The *Δ-trans* SSS and *Δ-cis* SSS faces are enantiomeric to (a) and (b), respectively, and the *Δ-cis SSS* face is on the opposite side of the *Δ-cis* RRR face in (b) and is enantiomeric to the *Δ-cis* RRR face.

complex but also to another neighboring *Δ* complex. However, d-tart^{2-} ion does not readily assume such an unstable conformation, particularly in solution where another neighboring complex is absent to support the conformational change. Therefore, d-tart^{2-} ion has to adopt a contact mode different from that found in the *Δ* complex salt, when it makes a face-to-face contact in solution with the "less-favorable" *Δ-trans* RRR face of the *Δ* complex. In the present study, X-ray crystal analyses have been made on the two salts with d-tart^{2-} ion of the *Δ-fac*-[Co(*cis*-chxn)$_3$]$^{3+}$ complex which has one triangular *Δ-cis* RRR face (Fig. 1) similar to the "less-favorable" *Δ-trans* RRR face of the *Δ-lel*$_3$-[Co(*trans*-chxn)$_3$]$^{3+}$ complex, in addition to one *Δ-cis* SSS face (Fig. 1), in a hope to search for another interaction mode by which d-tart^{2-} ion makes a face-to-face contact with the "less-favorable" face of these *Δ* complexes having bulky chxn ligands.

Experimental

X-Ray Structure Analysis. *Δ-fac*-[Co(*cis*-chxn)$_3$](ClO$_4$)(d-tart)·mH$_2$O (**1**) formed on mixing *Δ-fac*-[Co(*cis*-chxn)$_3$](ClO$_4$)$_3$[4] with sodium d-tartrate in water, was dissolved in water, and orange crystals were grown by slow evaporation. Orange crystals of *Δ-fac*-[Co(*cis*-chxn)$_3$]Cl(d-tart)·nH$_2$O (**2**) were obtained in a similar manner starting with the corresponding chloride salt.[4] X-Ray data collection was carried out on a Syntex R3 and a Rigaku AFC5 diffractometer for **1** and **2**, respectively with graphite-monochromated Mo$K\alpha$ radiation. The crystal data are summarized in Table 1. The structures were solved by the same procedures as applied previously.[3] The number m and the positions of water molecules present in **1** were not precisely determined because some of them were disordered. The crystal **2** was not big enough to collect ample reflections with $|F_o|>3\sigma(F_o)$, so that the R value was converged only to 9.5%, and since some water molecules were also disordered, they were not unambiguously allocated and counted. However, the molecular structures thus derived were proved to be reasonable both in **1** and **2**, and the accompanying uncertainties had no practical influence on the validity of our discussions described below. With the coordinates of the non-hydrogen atoms thus determined, all hydrogen atoms, except those of water molecules and hydroxyl groups, were assigned idealized positions on the basis of a bond length of 1.09 Å and 1.00 Å for each C–H and N–H bonds, respectively, and a tetrahedral angle around each carbon and nitrogen atoms.

All the computations were done on a HITAC M-680H computer using the programs UNICS-III[5] and ORTEP.[6]

Chromatographic Separation. A racemic mixture of *fac*-[Co(*cis*-chxn)$_3$]$^{3+}$ and its related complexes[4,7] were absorbed on an SP-Sephadex ion-exchange column and were eluted with aqueous 0.2 mol dm^{-3} sodium d-tartrate. Experimental conditions used were the same as described previously.[3] Elution orders and conventional separation factors were determined as before by monitoring the absorption and circular dichroism spectra of the effluents.[4,7]

Results and Discussion

X-Ray Crystallography. All the allocated atomic coordinates in *Δ-fac*-[Co(*cis*-chxn)$_3$](ClO$_4$)(d-tart)·mH$_2$O (**1**) and *Δ-fac*-[Co(*cis*-chxn)$_3$]Cl(d-tart)·nH$_2$O (**2**) except for hydrogen atoms are given in Tables 2 and 3, respectively.[8] The bond distances and angles of the composite ions in both crystals are found to be fairly reasonable and they are deposited as Document No. 9108 at the Office of the Editor of Bull. Chem. Soc. Jpn.[8] The numbering schemes adopted for the respective atoms are those given in several figures that follow.

In the former crystal **1**, the asymmetric unit is composed of three sets each of which is represented as *Δ-fac*-[Co(*cis*-chxn)$_3$](ClO$_4$)(d-tart)·mH$_2$O, each complex cation directs its C$_3$ axis almost parallel to the c-axis of the unit cell, and each d-tart^{2-} ion is sandwiched between the two complex cations. In the

Table 1. Crystallographic Data

Crystal	**1**	**2**
Formula	$C_{18}H_{42}N_6Co$, $C_4H_4O_6\cdot ClO_4\cdot H_2O$[a]	$C_{18}H_{42}N_6Co$, $C_4H_4O_6\cdot Cl\cdot 2.75H_2O$[a]
a/Å	12.358(3)	15.367(7)
b/Å	22.094(5)	
c/Å	32.770(7)	26.208(4)
V/Å^3	8948(4)	5357(4)
Z	12	6
Space group	$P2\,2_12_1$	$P3_12\,1$
T/°C	20	20
λ/Å	0.71069	0.71069
ρ calcd/g cm^{-3}[b]	1.486	1.183
ρ obsd/g cm^{-3}	1.469	1.330
μ (Mo $K\alpha$)/cm^{-1}[b]	7.255	5.988
R[c]	0.088	0.095
R_w[d]	0.077	0.109

a) Numbers of water molecules that could be located on a difference map and could be refined. b) Values based on the above tentative formulae. c) $R=\sum(||F_o|-|F_c||)/\sum|F_o|$. d) $R_w=[\sum w(|F_o|-|F_c|)^2/\sum w(F_o)^2]^{1/2}$.

Table 2. Atomic Coordinates ($\times 10^4$) and Equivalent Temperature Factors for Non-Hydrogen Atoms in Δ-*fac*-[Co(*cis*-chxn)$_3$](ClO$_4$)(d-tart)·mH$_2$O (**1**)

Atom	x	y	z	B_{eq}[a)]/Å^2	Atom	x	y	z	B_{eq}[a)]/Å^2
CoA	5966(1)	3193(1)	4349(0)	2.7	C16B	10955(11)	4599(6)	7196(5)	4.6
N1A	4705(8)	2939(4)	4685(3)	2.8	C17B	9923(12)	4662(5)	6945(4)	4.0
N2A	4891(7)	3674(4)	4026(3)	2.4	C18B	8879(12)	4424(5)	7142(4)	3.7
N3A	6318(9)	3875(5)	4737(3)	3.7	C19B	5792(11)	2647(5)	5776(4)	3.3
N4A	7134(8)	3536(4)	4005(3)	2.9	C20B	6858(10)	2554(6)	6022(3)	3.4
N5A	6963(8)	2658(5)	4655(3)	3.2	C21B	7641(10)	3081(5)	6003(4)	3.2
N6A	5751(8)	2486(5)	3975(3)	3.8	C22B	8753(12)	2844(6)	6147(3)	3.5
C1A	3700(10)	3268(6)	4547(3)	3.0	O1B	5924(7)	2825(4)	5411(2)	4.2
C2A	3471(10)	3860(6)	4790(4)	3.1	O2B	4945(7)	2502(4)	5945(3)	4.6
C3A	2465(11)	4181(6)	4641(4)	3.7	O3B	6560(9)	2455(5)	6440(3)	5.8
C4A	2626(11)	4331(6)	4176(4)	4.5	O4B	7345(8)	3579(4)	6261(2)	4.3
C5A	2872(12)	3789(6)	3929(4)	4.1	O5B	9087(8)	2946(4)	6493(2)	4.0
C6A	3816(10)	3399(6)	4099(3)	3.2	O6B	9287(7)	2564(4)	5882(3)	4.7
C7A	7230(11)	4259(6)	4573(4)	3.4	ClB	5248(3)	4506(2)	5771(1)	4.5
C8A	8295(10)	4096(7)	4762(4)	4.3	O7B	4458(10)	4047(5)	5770(4)	8.5
C9A	9250(11)	4449(7)	4580(4)	4.7	O8B	6302(10)	4252(5)	5662(3)	8.5
C10A	9268(12)	4376(7)	4117(4)	5.2	O9B	5007(9)	4977(6)	5479(4)	9.8
C11A	8173(12)	4505(6)	3910(4)	4.4	O10B	5356(12)	4760(6)	6152(4)	10.9
C12A	7240(11)	4188(5)	4098(4)	3.5	CoC	7898(1)	3384(1)	10900(1)	3.0
C13A	7067(12)	2031(5)	4443(4)	3.8	N1C	7213(8)	4030(4)	10579(3)	3.3
C14A	6354(13)	1578(6)	4663(4)	4.3	N2C	6680(9)	3490(5)	11281(3)	3.8
C15A	6436(16)	966(6)	4435(5)	6.7	N3C	7084(8)	2763(4)	10580(3)	2.8
C16A	6041(15)	1052(6)	3986(4)	5.7	N4G	8462(9)	2666(5)	11229(3)	3.6
C17A	6743(16)	1514(7)	3760(5)	7.0	N5C	9145(8)	3369(5)	10521(3)	3.4
C18A	6801(11)	2139(6)	4004(4)	3.9	N6C	8783(8)	3974(4)	11214(3)	3.0
C19A	6418(10)	4497(6)	2732(4)	3.3	C1C	6201(11)	4271(6)	10766(4)	4.2
C20A	5522(10)	4019(5)	2849(3)	2.2	C2C	5154(12)	3991(6)	10589(4)	4.3
C21A	6012(10)	3391(5)	2847(3)	2.7	C3C	4169(12)	4201(6)	10811(5)	5.5
C22A	5040(10)	2935(5)	2898(3)	2.0	C4C	4227(12)	4051(7)	11274(5)	5.8
O1A	6791(8)	4459(4)	2384(3)	5.1	C5C	5282(11)	4283(6)	11480(4)	4.0
O2A	6618(7)	4904(4)	2988(3)	4.1	C6C	6309(12)	4163(6)	11237(4)	3.8
O3A	5144(7)	4173(3)	3241(2)	3.6	C7C	7376(11)	2122(5)	10701(4)	3.8
O4A	6797(7)	3335(4)	3160(2)	3.5	C8C	8321(11)	1872(6)	10452(4)	3.8
O5A	4838(7)	2710(4)	3226(2)	3.6	C9C	8539(13)	1229(6)	10586(4)	4.2
O6A	4515(7)	2861(4)	2572(3)	3.7	C10C	8888(13)	1211(6)	11054(5)	5.2
ClA	8236(3)	2253(2)	2535(1)	5.2	C11C	8029(13)	1543(6)	11320(4)	5.1
O7A	7319(11)	2082(6)	2738(5)	11.0	C12C	7617(11)	2148(5)	11159(4)	3.3
O8A	8554(9)	2837(4)	2693(4)	7.6	C13C	10069(11)	3765(6)	10658(4)	3.5
O9A	9059(9)	1842(5)	2564(5)	12.6	C14C	10069(11)	4353(6)	10428(4)	4.0
O10A	7835(16)	2330(6)	2122(4)	14.1	C15C	10994(12)	4729(6)	10595(4)	5.2
CoB	7629(1)	3501(1)	7511(0)	2.1	C16C	10755(14)	4885(6)	11066(5)	6.1
N1B	8604(8)	3079(4)	7903(3)	2.4	C17C	10762(12)	4274(6)	11292(4)	4.1
N2B	7512(8)	2705(4)	7238(2)	2.1	C18C	9935(11)	3838(6)	11128(4)	3.4
N3B	6366(7)	3354(4)	7877(3)	2.4	C19C	7945(13)	4464(8)	8955(5)	6.4
N4B	6554(8)	3824(4)	7113(3)	2.5	C20C	8195(13)	3767(6)	8967(4)	4.2
N5B	7851(8)	4310(4)	7787(3)	2.9	C21C	8016(11)	3467(6)	9389(4)	3.6
N6B	8836(8)	3730(4)	7143(3)	2.8	C22C	6843(11)	3309(6)	9483(4)	3.7
C1B	8765(10)	2402(5)	7796(3)	2.9	O1C	7804(12)	4685(5)	8638(3)	9.5
C2B	7934(12)	2003(5)	8034(3)	3.6	O2C	7969(10)	4742(5)	9293(3)	8.1
C3B	8039(13)	1331(6)	7868(4)	4.6	O3C	7594(8)	3470(4)	8661(2)	5.1
C4B	7761(12)	1337(5)	7402(4)	3.8	O4C	8519(9)	3803(5)	9690(3)	6.2
C5B	8517(12)	1718(5)	7161(4)	3.6	O5C	6524(9)	3326(4)	9846(3)	5.8
C6B	8555(10)	2366(5)	7317(3)	2.3	O6C	6260(8)	3116(4)	9196(3)	5.4
C7B	5352(9)	3565(5)	7689(4)	2.6	ClC	212(5)	2398(3)	8935(2)	10.8
C8B	4996(11)	4216(5)	7827(4)	4.0	O7C	776(12)	2216(6)	9278(4)	12.3
C9B	3968(11)	4419(6)	7615(5)	4.4	O8C	−843(10)	2268(8)	8974(7)	19.0
C10B	4178(11)	4440(6)	7145(5)	5.2	O9C	399(16)	3030(6)	8867(7)	19.8
C11B	4509(12)	3793(7)	6981(5)	5.2	O10C	753(19)	1985(9)	8598(6)	21.4
C12B	5491(10)	3556(6)	7214(3)	3.1	OW1	8198(10)	3730(5)	2026(3)	7.7
C13B	8821(9)	4614(5)	7596(3)	2.4	OW2	5610(10)	2783(6)	1866(3)	8.4
C14B	9835(10)	4507(6)	7827(4)	3.3	OW3	974(14)	2535(9)	53(4)	15.3
C15B	10784(11)	4814(7)	7643(5)	4.9					

a) $B_{eq}=4/3\{\sum_i\sum_j \beta_{ij}\boldsymbol{a}_i\boldsymbol{a}_j\}$.

Table 3. Atomic Coordinates ($\times 10^4$) and Equivalent Temperature Factors for Non-Hydrogen Atoms in *Δ-fac*-[(Co(*cis*-chxn)$_3$]Cl(d-tart)·nH$_2$O (**2**)

Atom	x	y	z	B_{eq}/Å^2
Co	3593(2)	5155(2)	2145(1)	2.7
N1	3800(13)	4626(13)	1502(5)	3.0
N2	5050(13)	6030(12)	2125(6)	3.0
N3	3350(16)	6151(17)	1771(6)	4.5
N4	3531(13)	5834(13)	2762(6)	3.1
N5	2141(13)	4184(14)	2182(6)	3.3
N6	3700(13)	4146(14)	2539(5)	2.6
C1	4820(18)	5110(18)	1319(7)	3.2
C2	5081(19)	5960(20)	931(8)	4.5
C3	6186(19)	6466(19)	773(8)	5.1
C4	6861(17)	6979(17)	1230(9)	4.3
C5	6560(15)	6111(18)	1674(9)	4.1
C6	5460(17)	5466(18)	1790(8)	3.6
C7	3256(19)	6867(20)	2128(9)	4.4
C8	2179(21)	6503(21)	2180(8)	5.1
C9	2005(20)	7169(21)	2619(10)	6.0
C10	2541(20)	7187(19)	3132(8)	5.2
C11	3629(20)	7487(19)	3051(8)	4.8
C12	3814(17)	6931(18)	2621(8)	3.8
C13	1923(19)	3249(18)	2453(7)	4.0
C14	1745(22)	2411(20)	2088(10)	6.7
C15	1703(30)	1539(21)	2393(11)	10.6
C16	2608(25)	1751(22)	2732(10)	7.7
C17	2676(22)	2567(25)	3043(10)	6.7
C18	2761(20)	3507(18)	2792(8)	4.7
C19	5564(21)	7294(22)	4098(9)	5.8
C20	5955(20)	6839(20)	3698(9)	5.2
C21	5429(19)	5694(18)	3718(8)	4.1
C22	6063(19)	5395(17)	3361(7)	4.0
O1	5405(17)	6879(17)	4538(6)	8.2
O2	5402(24)	7932(22)	3975(7)	12.4
O3	5897(15)	7161(15)	3199(6)	6.7
O4	4406(12)	5264(14)	3571(5)	5.1
O5	5713(12)	5044(12)	2944(4)	4.1
O6	6841(12)	5499(13)	3565(5)	4.7
Cl	5592(6)	8389(6)	1638(3)	7.3
OW1	3386(27)	7656(18)	905(7)	15.2
OW2	1353(21)	6973(18)	893(8)	13.2
OW3[a)]	3283(36)	2358(38)	637(14)	10.2
OW4[a,b)]	0(0)	3188(58)	1667(0)	13.3

a) The probability was treated as half. b) Lies on a C_2 symmetry element.

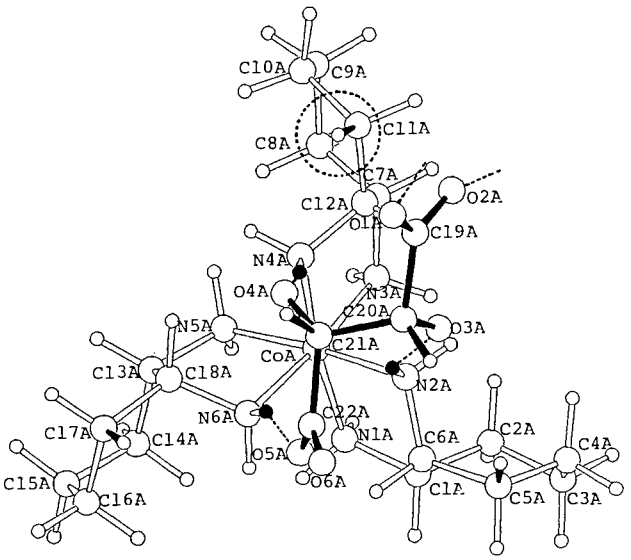

Fig. 2. One face-to-face contact mode of d-tart^{2-} ion with the triangular *Δ-cis* RRR face found in **1** as viewed down the C_3 axis.

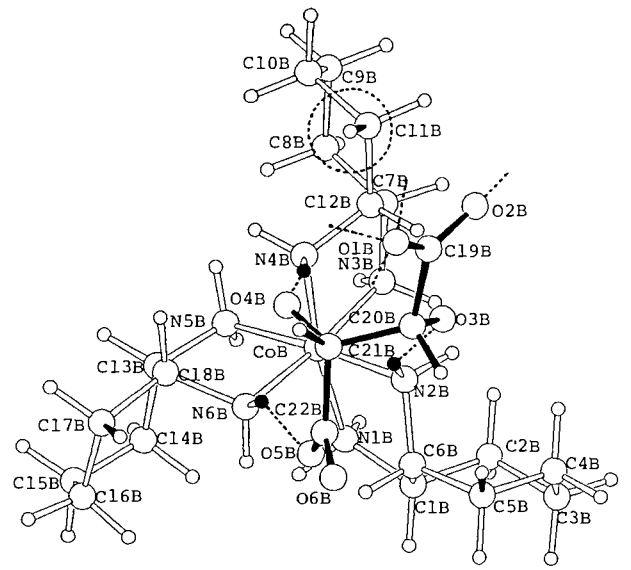

Fig. 3. The other face-to-face contact mode of d-tart^{2-} ion with the triangular *Δ-cis* RRR face found in **1** as viewed down the C_3 axis.

latter crystal **2**, on the other hand, the asymmetric unit is represented simply as *Δ-fac*-[Co(*cis*-chxn)$_3$]Cl(d-tart)·nH$_2$O, in which the complex cation is arranged such that its C_3 axis makes an angle of ca. 52° to the 3_1 screw axis (c-axis), and each d-tart^{2-} ion connects the two complex cations in a different fashion from those found in **1**. That is, the two crystals **1** and **2** are completely different not only in the space group and lattice constants (Table 1) but also in the packing mode. Consequently, it is almost impossible to compare the two crystals even qualitatively with respect to the counter ion effect on the interaction mode of the complex cation with the d-tart^{2-} ion. However, since similar contact modes between the complex and the d-tart^{2-} ions are found in common in **1** and **2**, which we have so far asserted to play a key role in the chiral discrimination, we focus our attention exclusively on these contact modes in the following.

Contact Modes in 1. The two similar face-to-face contact modes found in **1** are shown in Figs. 2 and 3 in both of which the *Δ-fac*-[Co(*cis*-chxn)$_3$]$^{3+}$ complex cation assumes a *lel*$_3$ conformation[4)] and the d-tart^{2-} anion, a normal one usually found.[3)] Consequently, the three N–H protons on each of the two triangular faces[9)] of the complex are disposed almost parallel to the C_3 axis like those of the *lel*$_3$-[Co(*trans*-chxn)$_3$]$^{3+}$ complex.[3)] It appears that conformationally labile metal complexes with three five-membered diamine

chelates assume preferentially a *lel*$_3$ conformation when they form salts with d-tart^{2-} ion or other hydrogen-bonding anions.[10,11]

The two contact modes found in **1** are surprisingly similar to each other; the d-tart^{2-} ion directs its four O atoms (O2, O3, O4, and O5) to the *Δ* complex along the C_3 axis, with three of them (O3, O4, and O5) each hydrogen-bonded to each of the three N-H protons on the "less-favorable" triangular *Δ-cis* RRR face of the complex. However, these contact modes are apparently different from those found in the *Δ-lel*$_3$-[Co(en)$_3$]$^{3+}$ (en=1,2-ethanediamine) and *Δ-lel*$_3$-[Co(*trans*-chxn)$_3$]$^{3+}$ salts.[3,12] In the former salt, the d-tart^{2-} ion comes close to the complex along the C_3 axis and the three O atoms each lie midway between two of the three N-H protons on the triangular face to form three bifurcated hydrogen bonds to them; the d-tart^{2-} ion enjoys up to six hydrogen bonds to the complex without feeling any appreciable steric repulsion from the small en chelates (Table 4). Thus, this contact mode is considered close to an ideal one for the d-tart^{2-} ion coming to the triangular face, and it is adopted with the *Δ-lel*$_3$-[Co(en)$_3$]$^{3+}$ as well.[13] In the *Δ-lel*$_3$-[Co(*trans*-chxn)$_3$]$^{3+}$ salt, the three O atoms of the d-tart^{2-} ion are similarly hydrogen-bonded to one of the "less-favorable" *Δ-trans* RRR faces of the complex, but the distal carboxylate group is greatly rotated to avoid the steric repulsion from the C-H proton on one of the bulky chxn ligands; the multiple hydrogen bonds to the complex are almost fully retained at the expense of the conformational energy (Table 4).[3]

In the present crystal, on the other hand, the d-tart^{2-} ion avoids a similar steric repulsion from the "less-favorable" *Δ-cis* RRR face at the expense of the multiple hydrogen bonds to the complex. That is, the d-tart^{2-} ion approaches the complex along the C_3 axis as usual but it rotates itself clockwise as a whole relative to the complex to avoid the repulsion from the C-H proton marked with a broken circle on the chxn ligand (Figs. 2 and 3), and the number of the hydrogen bonds formed is accordingly reduced from six virtually to three. However, the remaining three hydrogen bonds (O3··H-N2, O4··H-N4, and O5··H-N6) are fairly improved with respect to length and angle (Table 4), and the distal carboxylate group is placed such that its two O atoms (O1 and O2) form intimate hydrogen bonds to the N-H group(s) of other neighboring complexes in the *Δ-fac*-[Co(*cis*-chxn)$_3$](ClO$_4$)(d-tart)·*m*H$_2$O (**1**), as shown by dotted lines in Figs. 2 and 3. In this respect, the hydrogen-bonding scheme found in the present crystal is similar to that found in the *Δ-ob*$_3$-[Co(*trans*-chxn)$_3$]$^{3+}$ salt where all of the three N-H groups are oblique to the C_3 axis, so that practically only three but linear hydrogen bonds are formed to them.[11] The hydrogen bonds associated with these face-to-face contact modes are all compared numerically in Table 4.

The other triangular face of the *Δ-fac*-[Co(*cis*-chxn)$_3$]$^{3+}$ denoted as the *Δ-cis* SSS face, is depicted in Fig. 4a. It is seen there that the three C-H protons marked with broken circles on the chxn ligands are

Table 4. Comparison of Hydrogen-Bond Distances and Angles in Some Face-to-Face Contacts

Acceptor Donor	O3 H1N2	O3 H1N4	O4 H1N4	O4 H1N6	O5 H1N6	O5 H1N2
			Distances of O···H/Å			
(**1**)-A[a]	1.97	3.11	1.84	2.75	1.81	2.68
(**1**)-B[b]	2.06	3.13	2.01	2.58	1.90	2.58
(**2**)[c]	2.33	2.61	1.94	2.30	2.01	2.38
Δ-lel$_3$[d]	2.94	1.98	2.32	2.07	2.10	2.02
Δ-en$_3$[e]	2.33	2.26	2.22	2.14	2.21	2.14
Δ-ob$_3$[f]	2.03	3.00	2.11	2.47	1.92	2.52
			Distances of O···N/Å			
(**1**)-A	2.82	3.78	2.83	3.51	2.75	3.38
(**1**)-B	2.92	3.74	3.01	3.45	2.76	3.17
(**2**)	3.22	3.36	2.87	3.10	2.89	3.08
Δ-lel$_3$	3.72	2.93	3.12	2.97	3.04	3.01
Δ-en$_3$	3.08	3.10	3.07	2.99	2.99	2.96
Δ-ob$_3$	3.02	3.29	3.05	3.10	2.88	2.84
			Angles of O···H-N/°			
(**1**)-A	141	126	172	133	155	127
(**1**)-B	144	127	172	144	143	118
(**2**)	149	131	154	135	145	126
Δ-lel$_3$	128	144	130	137	142	150
Δ-en$_3$	138	141	141	133	133	138
Δ-ob$_3$	168	98	157	120	162	93

a) The mode in Fig. 2. b) The mode in Fig. 3. c) The mode in Fig. 6. d) *Δ-lel*$_3$-[Co(*trans*-chxn)$_3$]Cl(d-tart)·2H$_2$O in Ref. 3. e) *Δ-lel*$_3$-[Co(en)$_3$]$_2$(d-tart)$_3$·11.5H$_2$O in Ref. 12. f) *Δ-ob*$_3$-[Co(*trans*-chxn)$_3$]Cl(d-tart)·3.5H$_2$O in Ref. 11.

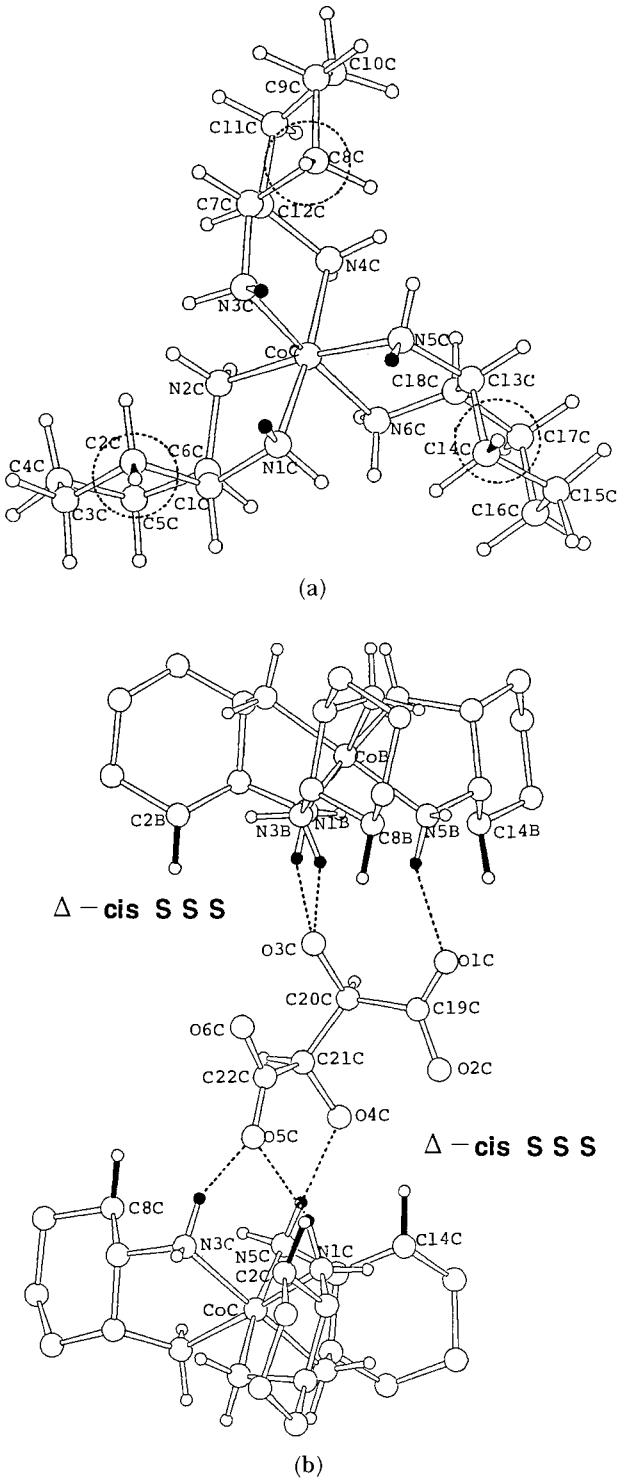

Fig. 4. The structure of the triangular *Δ-cis* SSS face (a) and the contact mode of d-tart^{2-} ion with the face (b). Most of the C-H protons are eliminated for clarity in (b).

disposed so closely to the N-H protons that any of them necessarily serves as an obstacle to the d-tart^{2-} ion when it makes a face-to-face contact with the face. The contact mode of the *Δ-cis* SSS face actually found in **1** is shown in Fig. 4b where the d-tart^{2-} anion is sandwiched between the two *Δ-fac*-[Co(*cis*-chxn)$_3$]$^{3+}$ complex cations, and only two O atoms, one carboxylic and one alcoholic, of the d-tart^{2-} ion are involved in the hydrogen bonding to the respective *Δ-cis* SSS face. Thus, the *Δ-cis* SSS face does not serve as an interaction site for the face-to-face contact, as supposed in Fig. 4a.

Since the *Λ-cis* RRR face enantiomeric to the *Δ-cis* SSS face depicted in Fig. 4a, is naturally crowded, it follows that the *Λ-fac*-[Co(*cis*-chxn)$_3$]$^{3+}$ complex has practically only one favorable triangular face available for the face-to-face contact, i.e., the *Λ-cis* SSS face similar in structure to the favorable *Λ-trans* SSS face of the *Λ-lel*$_3$-[Co(*trans*-chxn)$_3$]$^{3+}$ complex.

It is additionally noteworthy in Fig. 4b that the d-tart^{2-} ion sandwiched between the two *Δ-cis* SSS faces assumes a conformation appreciably different from a usual one; the torsion angle ϕ of the $^{-}$OOC-C-C-COO^{-} group is 81.5°, whereas it is around 180°, i.e., the two COO^{-} groups are trans to each other, in a usual conformer. To demonstrate how the observed angle of 81.5° is surprisingly unusual, the distribution of the torsion angle ϕ is shown in Fig. 5 for d-tart^{2-} and d-tartH^{-} ions in their simple salts[14] and diastereomeric salts with tris(diamine)-metal complexes.[3,15,16] The conformer found here is probably the first example in which the two COO^{-} groups are in gauche positions.

Contact Modes in 2. In Fig. 6 is shown a face-to-face contact mode found in **2**, where the *Δ-fac*-[Co(*cis*-chxn)$_3$]$^{3+}$ takes a *lel*$_3$ conformation and the d-tart^{2-} ion, a usual one as in **1**, and the triangular face used is naturally the *Δ-cis* RRR face. It is evident that the contact mode bears a close resemblance to the ideal one found in the *Δ-lel*$_3$-[Co(en)$_3$]$^{3+}$ salt;[3,12] the three O atoms of the d-tart^{2-} ion are each placed almost midway between two of the three N-H protons on the triangular face and are involved in the three bifurcated hydrogen bonds to them. The hydrogen bonds pertinent to the present face-to-face contact mode found in **2** are summarized also in Table 4.

A glance of Fig. 6a might lead us to suppose that the distal carboxylate group closely approaches one of the chxn ligands to suffer a severe steric repulsion from the C-H proton marked with a broken circle. However, if the contact mode is viewed normal to the C$_3$ axis (Fig. 6b), it is confirmed that the d-tart^{2-} ion avoids the repulsion by inclining the plane consisting of the three O atoms a little relative to the "less-favorable" *Δ-cis* RRR face of the complex. As a result, the nearest O2 atom of the distal carboxylate group is placed ca. 2.49 Å apart from the C-H proton to avoid the repulsion marginally, and some of the multiple hydrogen bonds are obliged to be somewhat longer[17] than the corresponding hydrogen bonds formed in the *Δ-lel*$_3$-[Co(en)$_3$]$^{3+}$ salt (Table 4). For example, the O3··H-N4 bond distance is 2.61 Å in Fig. 6, while the corresponding distance is 2.26 Å in the *Δ-*

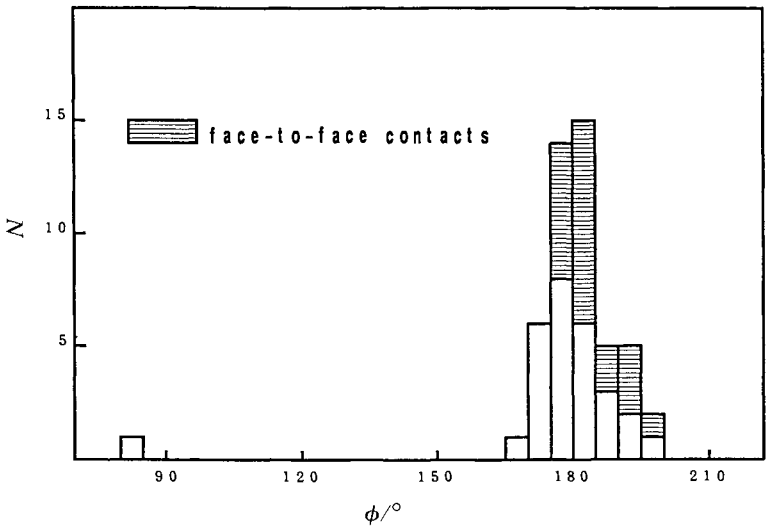

Fig. 5. The distribution of the $^{-}$OOC-C-C-COO^{-} torsion angle (ϕ) in some salts of d-tart^{2-} and d-tartH^{-} ions.

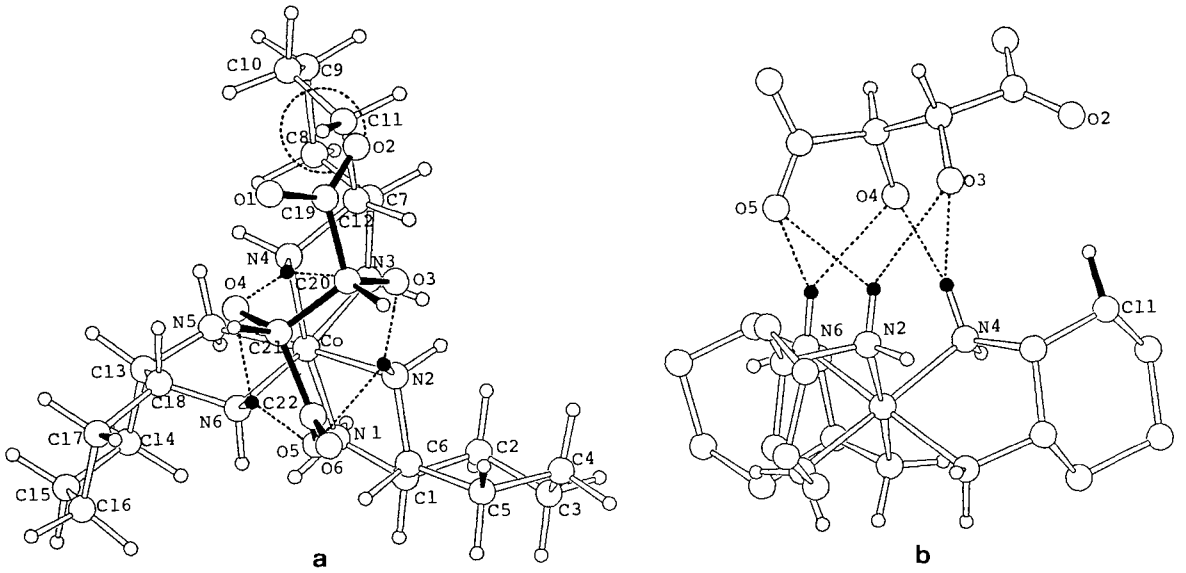

Fig. 6. The face-to-face contact mode of d-tart^{2-} ion with the triangular *Δ-cis* RRR face found in **2** as viewed down (a) and normal to (b) the C_3 axis. Most of the C-H protons are eliminated for clarity in (b).

lel$_3$-[Co(en)$_3$]$^{3+}$ salt.[12] Instead, the distal carboxylate group is in a position to form multiple hydrogen bonds to the triangular *Δ-cis* SSS face of another neighboring complex cation in the *Δ-fac*-[Co(*cis*-chxn)$_3$]Cl(d-tart)·nH$_2$O (**2**) (vide infra).

The other triangular face of the *Δ* complex denoted as the *Δ-cis* SSS face is so crowded as mentioned in Fig. 4a, that it may accommodate only two O atoms of the d-tart^{2-} ion coming to the face in **2**. The contact mode of the *Δ-cis* SSS face actually found in **2** is shown in Fig. 7, where the two O atoms (O1 and O2) of the distal carboxylate group are hydrogen-bonded to the face, as expected, and the remaining three O atoms (O3, O4, and O5) are involved in the face-to-face contact with the "less-favorable" *Δ-cis* RRR face of another neighboring *Δ* complex.[18] Thus, this *Δ-cis* SSS face is again proved to be of no use for the face-to-face contact, probably in solution as well.

We assume here that the face-to-face contact mode found in **2** and shown in Fig. 6 is the one in which the d-tart^{2-} ion avoids the steric repulsion tactfully at the least expense of the multiple hydrogen bonds to the "less-favorable" *Δ-cis* RRR face without any disadvantageous conformational change, and that it is the most probable interaction mode conceivable in solution where another neighboring complex is absent to assist the conformational change. In addition, this contact mode will be adopted in solution by the *Δ-lel*$_3$-

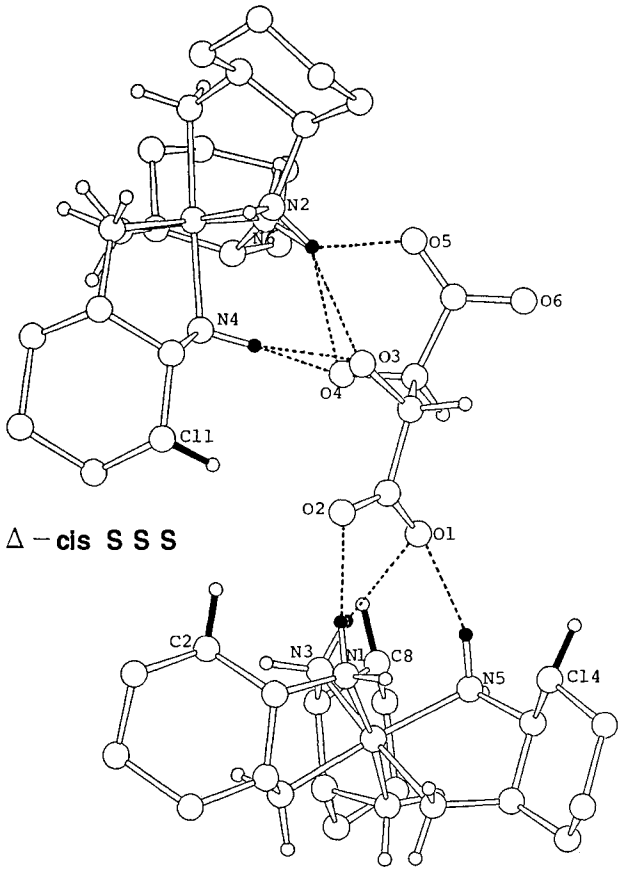

Fig. 7. The contact mode of d-tart^{2-} ion with the triangular *Δ-cis* SSS face found in **2**. Most of the C–H protons are eliminated for clarity.

[Co(*trans*-chxn)$_3$]$^{3+}$ complex as well, since the complex has two "less-favorable" *Δ-trans* RRR faces similar to the *Δ-cis* RRR face. These assumptions are indirectly supported by the results of the chromatographic separation of some related complexes, which will be described in the next section. It goes without saying that the *Δ-cis* SSS and *Λ-cis* RRR faces are neglected in counting the interaction sites available for the face-to-face contact with d-tart^{2-} ion even in solution, because these faces are heavily crowded as seen in Fig. 4a.

Elution Order in Chromatography. The chromatographic separation was carried out for some [Co(chxn)$_3$]$^{3+}$ complexes on an SP-Sephadex ion-exchange column with aqueous sodium d-tartrate (0.2 mol dm^{-3}) as an eluent. The elution order obtained is *Λ-lel*$_3$-[Co(*trans*-chxn)$_3$]$^{3+}$ ≫ *Λ-fac*-[Co(*cis*-chxn)$_3$]$^{3+}$ ≫ *Δ-lel*$_3$-[Co(*trans*-chxn)$_3$]$^{3+}$ > *Δ-fac*-[Co(*cis*-chxn)$_3$]$^{3+}$ > *Λ-ob*$_3$-[Co(*trans*-chxn)$_3$]$^{3+}$ ≫ *Δ-ob*$_3$-[Co(*trans*-chxn)$_3$]$^{3+}$, and the conventional separation factor[3] for an enantiomeric pair is 1.57 for *lel*$_3$-[Co(*trans*-chxn)$_3$]$^{3+}$, 1.37 for *fac*-[Co(*cis*-chxn)$_3$]$^{3+}$, and 1.39 for *ob*$_3$-[Co(*trans*-chxn)$_3$]$^{3+}$ (cf. 1.18 for [Co(en)$_3$]$^{3+}$ and 1.33 for *mer*-[Co(*cis*-chxn)$_3$]$^{3+}$). No practical separation of these complexes was attained with aqueous sodium chloride as an eluent, the [Co(*cis*-chxn)$_3$]$^{3+}$ complexes coming out slightly late.

It is notable that the *Δ-fac*-[Co(*cis*-chxn)$_3$]$^{3+}$ is eluted faster than the *Λ-ob*$_3$-[Co(*trans*-chxn)$_3$]$^{3+}$, though the latter complex has two triangular faces available for the three linear hydrogen bonds with d-tart^{2-} ion.[11] If the *Δ-fac*-[Co(*cis*-chxn)$_3$]$^{3+}$ should adopt in solution the contact mode shown in Fig. 2 or 3 where only three linear hydrogen bonds are formed, the *Λ-ob*$_3$-[Co(*trans*-chxn)$_3$]$^{3+}$ should be eluted faster. Therefore, the *Δ-fac*-[Co(*cis*-chxn)$_3$]$^{3+}$ as well as the *Δ-lel*$_3$-[Co(*trans*-chxn)$_3$]$^{3+}$ adopts in solution preferentially the contact mode shown in Fig. 6 where six hydrogen bonds, though some are somewhat long,[17] are formed.

Finally, the elution order and separation factors obtained are interpreted. First of all, the *Λ-lel*$_3$-[Co(*trans*-chxn)$_3$]$^{3+}$ has two equivalent triangular faces (*Λ-trans* SSS) which allow a smooth access of d-tart^{2-} ion along the C_3 axis, and thus it should be eluted the fastest. The *Λ-fac*-[Co(*cis*-chxn)$_3$]$^{3+}$ has one such favorable face (*Λ-cis* SSS) and is eluted the second. Though no such favorable face is present in either the *Δ-lel*$_3$-[Co(*trans*-chxn)$_3$]$^{3+}$ or the *Δ-fac*-[Co(*cis*-chxn)$_3$]$^{3+}$, the former has two "less-favorable" faces (*Δ-trans* RRR) to which the d-tart^{2-} ion forms six but somewhat long hydrogen bonds and the latter has one such face (*Δ-cis* RRR). Consequently, they should be eluted the next in this order. The fact that the *Δ-fac*-[Co(*cis*-chxn)$_3$]$^{3+}$ is eluted faster than the *Λ-ob*$_3$-[Co(*trans*-chxn)$_3$]$^{3+}$ which has two equivalent triangular faces available for the three linear hydrogen bonds with d-tart^{2-} ion, suggests that d-tart^{2-} ion interacts more strongly with these tris(diamine)cobalt(III) complexes when more hydrogen bonds are formed to them rather than when fewer but more linear hydrogen bonds are formed.[11,19,20] In this way, the elution order obtained is readily interpreted in terms of the number of available interaction sites counted above and the number of hydrogen bonds formed there, consistent with the proposals offered by Searle[21] and Sakakibara et al.[22] Consequently, it is concluded that the face-to-face contact mode found in **2** and shown in Fig. 6 but not in Fig. 2 or 3 is the one which is adopted in solution by both *Δ*-[Co(*trans*-chxn)$_3$]$^{3+}$ and *Δ-fac*-[Co(*cis*-chxn)$_3$]$^{3+}$ complexes; the "less-favorable" *Δ-trans* RRR or *Δ-cis* RRR face is preferentially utilized for the association with the d-tart^{2-} ion.

Since the magnitude of the separation factor has been already discussed for the *lel*$_3$ and *ob*$_3$-[Co(*trans*-chxn)$_3$]$^{3+}$ complexes,[3] it needs to examine only for the *fac*-[Co(*cis*-chxn)$_3$]$^{3+}$. The conventional separation factor estimated for this complex is 1.37, which is considerably lower than 1.57 estimated for the *lel*$_3$-[Co(*trans*-chxn)$_3$]$^{3+}$. This is apparently because the *Λ-fac*-[Co(*cis*-chxn)$_3$]$^{3+}$ has one favorable *Λ-cis* SSS face and one useless *Λ-cis* RRR faces but the enantio-

mer has one "less-favorable" *Δ-cis* RRR and one useless *Δ-cis* SSS faces, whereas the *Λ-lel*$_3$-[Co(*trans*-chxn)$_3$]$^{3+}$ has as many as two favorable *Λ-trans* SSS faces but the enantiomer has two "less-favorable" *Δ-trans* RRR faces only. That is, the *Δ-lel*$_3$-[Co(*trans*-chxn)$_3$]$^{3+}$ is more handicapped with respect to the number of the available interaction sites than the *Δ-fac*-[Co(*cis*-chxn)$_3$]$^{3+}$ is, relative to the respective enantiomer.

References

1) Y. Yoshikawa and K. Yamasaki, *Coord. Chem. Rev.*, **28**, 205 (1975).

2) H. Yoneda, *J. Chromatogr.*, **313**, 59 (1984).

3) Part 14 of this series; T. Mizuta, K. Toshitani, K. Miyoshi, and H. Yoneda, *Inorg. Chem.*, **29**, 3020 (1990).

4) H. Toftlund and T. Laier, *Acta Chem. Scand., Ser. A*, **31**, 651 (1977).

5) T. Ashida, "The Universal Crystallographic Computation Program System," ed by T. Sakurai, The Crystallographic Society of Japan, Tokyo (1979).

6) C. K. Johnson, *Oak Ridge Nat. Lab.*, [Rep.] ORNL (U.S.), 3794 (1976).

7) S. E. Harnung, B. S. Sorensen, I. Creaser, H. Maegaard, U. Pfenninger, and C. E. Schaffer, *Inorg. Chem.*, **15**, 212 (1976); P. Osvath and A. G. Lappin, *Inorg. Chem.*, **26**, 195 (1987).

8) Tables of a full listing of crystallographic data, coordinates of hydrogen atoms, bond lengths and angles, hydrogen bond distances and angles, anisotropic thermal parameters of non-hydrogen atoms, and observed and calculated structure factors are kept as Document No. 9108 at the Office of the Editor of Bull. Chem. Soc. Jpn.

9) The three N-H protons on the *Δ-cis* RRR face are certainly disposed almost parallel to the C_3 axis (Fig. 2 or 3), whereas those on the opposite face (*Δ-cis* SSS) are faintly oblique to the C_3 axis (Fig. 4a), though the *Δ* complex itself assumes a *lel*$_3$ conformation.

10) R. E. Cramer and J. T. Huneke, *Inorg. Chem.*, **17**, 365 (1978).

11) T. Mizuta, K. Toshitani, and K. Miyoshi, *Inorg. Chem.*, in press.

12) T. Mizuta, T. Tada, Y. Kushi, and H. Yoneda, *Inorg. Chem.*, **27**, 3836 (1988).

13) Y. Kushi, M. Kuramoto, and H. Yoneda, *Chem. Lett.*, **1976**, 135.

14) Data on the torsion angle (ϕ) were taken from the Cambridge Crystallographic Data File (CCDF) up to 1986. The criterion for accepting an entry from the CCDF was that no atom heavier than calcium should be present in the structure.

15) T. Mizuta, H. Yoneda, and Y. Kushi, *Inorg. Chim. Acta*, **132**, 11 (1987).

16) T. Mizuta and K. Miyoshi, submitted.

17) Some of the multiple hydrogen bonds in **2** are certainly longer but others are slightly shorter than the corresponding hydrogen bonds in the *Δ-lel*$_3$-[Co(en)$_3$]$^{3+}$ salt. However, the overall hydrogen-bonding interaction is definitely weaker in **2**, as judged from the bond lengths and angles (Table 4).

18) It is interesting to note that a contact mode similar to that shown in Fig. 7 has been found in the *rac*-[Ni(en)$_3$](*rac*-tart)·H_2O salt,[15] where the three N-H protons on the triangular face of the *Δ*(*Λ*) complex are hydrogen-bonded to the distal carboxylate group of the d(l)-tart^{2-} ion, the remaining three O atoms of which are making a usual face-to-face contact with the triangular face of the neighboring *Λ*(*Δ*) complex.

19) I. Bernal, J. D. Korp, and I. Creaser, *Aust. J. Chem.*, **37**, 2365 (1984).

20) R. Taylor and O. Kennard, *Acc. Chem. Res.*, **17**, 320 (1984).

21) G. H. Searle, *Aust. J. Chem.*, **30**, 2625 (1977).

22) K. Sakakibara, Y. Yoshikawa, and H. Yamatera, *Bull. Chem. Soc. Jpn.*, **52**, 2725 (1979).

Redox Potential of Fe_4S_4 Cluster in Hydrophobic and Hydrophilic Spheres

Koji TANAKA* and Satoshi TANAKA†
Institute for Molecular Science, Myodaiji, Okazaki 444
†Department of Applied Chemistry, Faculty of Engineering, Osaka University, Suita, Osaka 565
(Received November 13, 1990)

The redox behavior of the $[Fe_4S_4(SC_6H_4Bu^t(p\text{-}))_4]^{2-/3-}$ couple was examined not only in a CH_2Cl_2 solution of a CH_2Cl_2/H_2O two phase system but also in the absence and presence of Triton X-100 in H_2O to elucidate the solvent effect of water on the redox potential of the cluster. Protonation of $[Fe_4S_4(SC_6H_4Bu^t(p\text{-}))_4]^{3-}$ takes place in those media, and protonated and unprotonated clusters exist as an equilibrium mixture. Although the redox potential of the cluster is hardly affected by the pK_a value, it is largely influenced by a thickness of $[Fe_4S_4(SC_6H_4Bu^t(p\text{-}))_4]^{2-}$ adsorbed on a surface of an electrode in water. The $E_{1/2}$ value of the cluster in a near monomolecular layer on the electrode exhibits a pronounced anodic shift compared with that in CH_2Cl_2 and falls in the range of that of 4Fe- and 8Fe-ferredoxins. On the other hand, the cluster in the multimolecular layer does not show such an anodic shift of the $E_{1/2}$ value in water.

A variety of Fe_4S_4 clusters have been prepared[1] as a model of the active center of iron-sulfur proteins, which play key roles as electron-transfer catalysts in various biological redox reactions such as photosynthesis,[2] N_2-fixation,[3] NO_3^- reduction.[4] The redox potentials of synthetic Fe_4S_4 clusters in organic solvents obey the Hammet σ_p and Taft σ^* values of terminal thiolate ligands.[5] Water, however, gives a serious effect on the redox potentials of the clusters, since water soluble Fe_4S_4 clusters in the presence of excess of free thiolate ligands (due to an instability of water soluble Fe_4S_4 clusters in water) show a positive potential shift of the redox potentials by 250—400 mV in water compared with those in organic solvents.[6] A positive potential shift of $E_{1/2}$ (60—120 mV) of *Clostridium pasteurianum* ferredoxin in H_2O containing of 0—40 vol% Me_2SO_4, where the protein adopts its normal tertiary structure, compared with a synthetic Fe_4S_4 cluster ligated with cysteine in the same medium, therefore, has been ascribed to the tertiary structure of proteins.[6] We have reported that synthetic Fe_4S_4 clusters are protected from hydrolysis in aqueous lecithin vesicle[7] and micellar solutions,[8] and the redox potentials of the clusters in those media are essentially consistent with those of 4Fe- and 8Fe-ferredoxins. The redox potentials of synthetic Fe_4S_4 clusters as well as ferredoxins, therefore, are considered to be largely influenced by hydrophobic spheres in water. To elucidate the effect of hydrophobic spheres on the redox potential of a Fe_4S_4 cluster in water, the redox behavior of $(Bu_4N)_2[Fe_4S_4(SC_6H_4Bu^t(p\text{-}))_4]$ was examined not only in a CH_2Cl_2 solution of a CH_2Cl_2/H_2O two phase system but also in the absence and presence of Triton X-100 micellar solution using a glassy carbon and an Hg electrode.

Experimental

General Procedure and Materials. All manipulations were carried out under N_2 atmosphere. Commercially available guaranteed reagent grade of *p*- *t*-butylbenezenethiol was used without further purification. $(Bu_4N)_2[Fe_4S_4(SC_6H_4Bu^t(p\text{-}))_4]$ was prepared according to the literature.[9]

Cyclic Voltammetry of the Cluster in a CH_2Cl_2/H_2O Two Phase System. An aqueous H_3PO_4-NaOH buffer (0.1 mol dm^{-3}, 20 cm^3) solution containing Bu_4NBr (1.8 mmol) was poured in a CH_2Cl_2 solution (20 cm^3) containing $(Bu_4N)_2[Fe_4S_4(SC_6H_4Bu^t(p\text{-}))_4]$ (20 mg, 12 μmol) and Bu_4NBr (0.6 g, 1.8 mmol), and the mixture was stirred by bubbling N_2 for several minutes. Then, the cell was allowed to stand until the CH_2Cl_2 and H_2O phases were completely separated. The pH of the H_2O phase was adjusted by addition of a small amount of either aqueous NaOH or H_3PO_4 solution (0.1 mol dm^{-3}) to the H_2O phase, followed by stirring the mixture by the same method, and measured with a Toa Electronics pH meter HM-7B. The cyclic voltammograms of $(Bu_4N)_2[Fe_4S_4(SC_6H_4Bu^t(p\text{-}))_4]$ dissolved in the CH_2Cl_2 phase and adsorbed on a surface of Hg were obtained by using a Yanaco glassy carbon disk electrode GC-2p and Metrohm hanging mercury drop electrode, respectively. When the HMDE was used as a working electrode, voltage scan was started after the surface of a mercury drop (0.0187 cm^2) had been exposed to the aqueous phase. The working electrode, a Pt auxiliary electrode, and a luggin capillary of a reference electrode were immersed into the same phase either a CH_2Cl_2 or H_2O phase.

Solubilization of the Cluster in an Aqueous Triton X-100 Micellar Solution. A DMF (1.0 cm^3) solution of $(Bu_4N)_2[Fe_4S_4(SC_6H_4Bu^t(p\text{-}))_4]$ (12 μmol) was added to a stirred aqueous solution (25 cm^3, pH 6—10) containing NaOH-H_3PO_4 (0.1 mol dm^{-3}) and Triton X-100 (0.05 mol dm^{-3}).

Preparation of a Cluster Modified Glassy Carbon and Hg Amalgamated Au Plate Electrode. A given amount of a CH_3CN solution of $(Bu_4N)_2[Fe_4S_4(SC_6H_4Bu^t(p\text{-}))_4]$ (1.0 mmol dm^{-3}) was dropped to the surface of a glassy carbon[10] or an Hg amalgamated Au plate (1.0 cm^3) by syringe techniques, and then dried under N_2 atmosphere.

Results and Discussion

Redox Behavior of $[Fe_4S_4(SC_6H_4Bu^t(p\text{-}))_4]^{2-}$ in CH_2Cl_2/H_2O Two Phase System. The cyclic voltammogram (CV) of $(Bu_4N)_2[Fe_4S_4(SC_6H_4Bu^t(p\text{-}))_4]$ using a glassy carbon disk electrode (GC) shows a cathodic

and an anodic wave of the (2−/3−) redox couple at E_{pc}=−1.03 and E_{pa}=−0.90 V vs. SCE at a sweep rate 10 mV s^{-1} in dry CH_2Cl_2. Those redox waves are also observed at E_{pc}=−0.97 and E_{pa}=−0.89 V in a CH_2Cl_2 solution of a CH_2Cl_2/H_2O (pH=10.06) two phase system (Fig. 1a). Thus, H_2O in the CH_2Cl_2 phase causes a slight potential shift of the $[Fe_4S_4(SC_6H_4Bu^t(p\text{-}))_4]^{2-/3-}$ redox couple. The peak currents of those redox waves in the wet CH_2Cl_2 phase were proportional to one-half order with respect to the sweep rate in the range of 10—300 mV s^{-1}. In addition, the electronic absorption spectrum of $(Bu_4N)_2[Fe_4S_4(SC_6H_4Bu^t(p\text{-}))_4]$ in wet CH_2Cl_2 did not show an appreciable change for 4 h. These results indicate that $[Fe_4S_4(SC_6H_4Bu^t(p\text{-}))_4]^{2-}$ stably exists in wet CH_2Cl_2 and undergoes a redox reaction in that medium. The redox potentials of Fe_4S_4 clusters solubilized in aqueous micellar solutions have been shown to be largely controlled by proton concentrations in bulk water.[8] The proton concentration in the CH_2Cl_2 phase of the CH_2Cl_2/H_2O system may also be equilibriated with that in the H_2O phase, as similar to the equilibrium between hydrophobic spheres of micelles and bulk water. Figure 2 shows the $E_{1/2}$ value ($E_{1/2}=(E_{pa}+E_{pc})/2$) of the $[Fe_4S_4(SC_6H_4Bu^t(p\text{-}))_4]^{2-/3-}$ couple in the CH_2Cl_2 solution of the CH_2Cl_2/H_2O system at a sweep rate 10 mV s^{-1} at various pH of the H_2O phase. The $E_{1/2}$ value of the cluster in the CH_2Cl_2 solution is independent on pH of the H_2O phase in the pH range higher than 7.0, while shifted by −60 mV pH^{-1} in the pH lower than 7.0. This result clearly indicates that one proton participates in the $[Fe_4S_4(SC_6H_4Bu^t(p\text{-}))_4]^{2-/3-}$ redox reaction[7,8] in the CH_2Cl_2 solution when pH of the H_2O phase is lower than 7.0, and protonated and unprotonated $[Fe_4S_4(SC_6H_4Bu^t(p\text{-}))_4]^{3-}$ exist as an equilibrium mixture. The break point at pH 7.0 in the plot of $E_{1/2}$ vs. pH (○ in Fig. 2), therefore, may be associated with an apparent proton dissociation constant (pK_a') of protonated $[Fe_4S_4(SC_6H_4Bu^t(p\text{-}))_4]^{3-}$. Despite a significant difference in the proton concentrations between the CH_2Cl_2 and H_2O phases of the CH_2Cl_2/H_2O system, the present pK_a'=7.0 still falls in the pK_a range of iron-sulfur proteins reported so far (pK_a=6.8—8.9).[11]

An Hg electrode has been used for the measurement of the redox potential of iron-sulfur proteins by taking advantage of a strong affinity of sulfur for Hg.[12] Otherwise, a direct electron transfer between the Fe_4S_4 cores and an electrode is strongly inhibited by an adsorption of polypeptide chains on the electrode. The CV of $[Fe_4S_4(SC_6H_4Bu^t(p\text{-}))_4]^{2-}$ in the CH_2Cl_2 solution of the CH_2Cl_2/H_2O system using a hanging mercury drop electrode (HMDE) exhibited a very strong cathodic current of the $[Fe_4S_4(SC_6H_4Bu^t(p\text{-}))_4]^{2-/3-}$ redox couple maybe due to a strong adsorption of the cluster on the surface of the HMDE, and the anodic and cathodic peak potentials of the redox couple were not determined correctly. To decrease the amount of the cluster adsorbed on the Hg surface, the HMDE was drawn up to the H_2O phase from the CH_2Cl_2 solution of $(Bu_4N)_2[Fe_4S_4$-

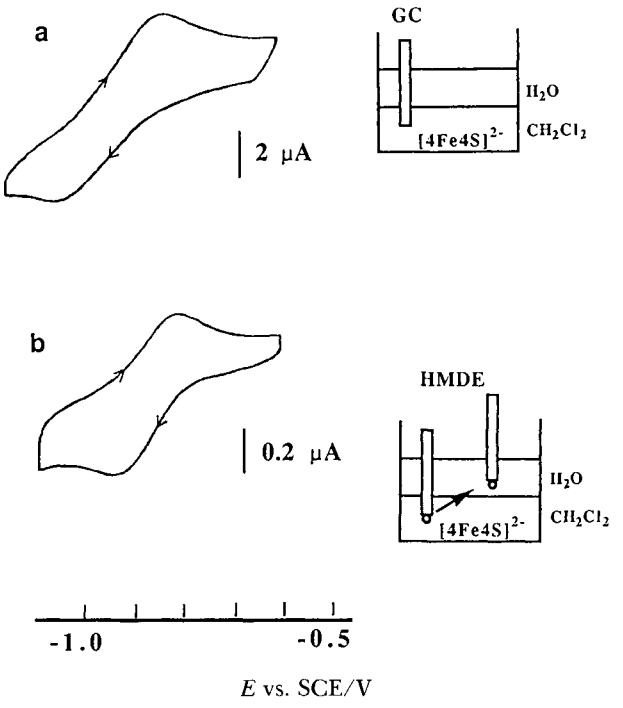

Fig. 1. Cyclic voltammograms of $[Fe_4S_4(SC_6H_4Bu^t(p\text{-}))_4]^{2-}$ using a glassy carbon electrode in a CH_2Cl_2 solution (a) and an HMDE in an H_2O phase (b) of the CH_2Cl_2/H_2O (pH 10.06) system; sweep rate 10 mV s^{-1}.

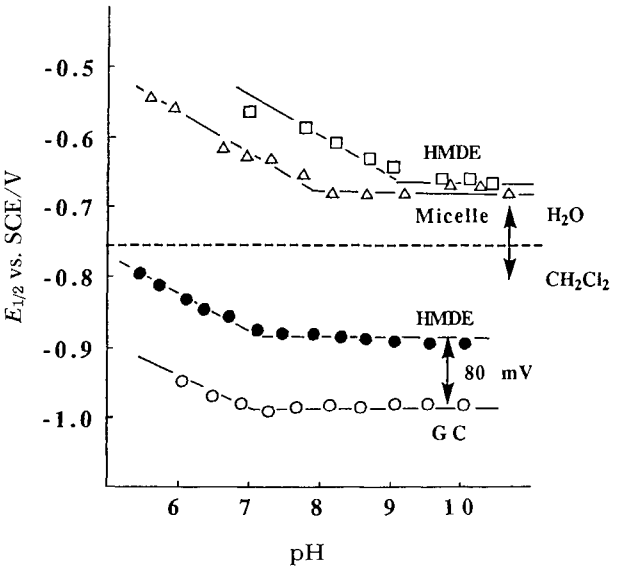

Fig. 2. $E_{1/2}$ values of the $[Fe_4S_4(SC_6H_4Bu^t(p\text{-}))_4]^{2-/3-}$ redox couple in the CH_2Cl_2 solution of the CH_2Cl_2/H_2O system using GC (○) and HMDE (●), and in the absence (□) and presence of Triton X-100 (△) using HMDE.

$(SC_6H_4Bu^t(p\text{-}))_4]$ after dipping the top end of the electrode in the CH_2Cl_2 phase for less than one minute. Even after this procedure, the surface of the HMDE placed in the H_2O phase was covered with a drop of the CH_2Cl_2 solution of $(Bu_4N)_2[Fe_4S_4(SC_6H_4Bu^t(p\text{-}))_4]$. The CV of $[Fe_4S_4(SC_6H_4Bu^t(p\text{-}))_4]^{2-}$ in the CH_2Cl_2 drop in H_2O (pH=10.06) is depicted in Fig. 1b, which shows the (2−/3−) redox couple at E_{pc}=−0.93 and E_{pa}=−0.82 V at a sweep rate 10 mV s^{-1} (Fig. 1b). The $E_{1/2}$ value of the cluster in the CH_2Cl_2 drop on the HMDE against pH are also plotted in Fig. 2 (●). The $E_{1/2}$ value of the cluster in the CH_2Cl_2 drop on the HMDE in the H_2O phase is shifted to a positive potential by 80 mV compared with that determined by a GC electrode in the CH_2Cl_2 phase (○ and ● in Fig. 2). The 80 mV difference in two lines may result from an adsorption of $[Fe_4S_4(SC_6H_4Bu^t(p\text{-}))_4]^{2-}$ on an Hg electrode, since an $E_{1/2}$ value of a synthetic Fe_4S_4 cluster undergoes a positive potential shift by 80 mV due to an adsorption on a surface of an Hg electrode.[7] Taking account of the adsorption energy of $[Fe_4S_4(SC_6H_4Bu^t(p\text{-}))_4]^{2-}$ on Hg, the redox potential of the cluster in the CH_2Cl_2 drop in the H_2O phase may be essentially unchanged that in wet CH_2Cl_2. Furthermore, an agreement of the break points (pK_a') of the plots of pH vs. $E_{1/2}$ in the CH_2Cl_2 drop on the HMDE with that in the CH_2Cl_2 phase (○ and ● in Fig. 2) indicates that the proton concentration in the bulk CH_2Cl_2 phase is maintained in the CH_2Cl_2 drop on the HMDE in the H_2O phase.

Redox Reaction in Aqueous Phases. As described above, one proton participates in the $[Fe_4S_4(SC_6H_4Bu^t(p\text{-}))_4]^{2-/3-}$ redox reaction in the CH_2Cl_2 solution of the CH_2Cl_2/H_2O system, and protonated and unprotonated $[Fe_4S_4(SC_6H_4Bu^t(p\text{-}))_4]^{3-}$ exists as an equilibrium mixture. Comparison of the pK_a value of the protonated $[Fe_4S_4(SC_6H_4Bu^t(p\text{-}))_4]^{3-}$ in wet CH_2Cl_2 with that in an aqueous micellar solution may afford an information about the solvent effect of water on the redox potential of the cluster. As an adsorption of the surfactant on a GC electrode[13] inhibited the electron transfer to $(Bu_4N)_2[Fe_4S_4(SC_6H_4Bu^t(p\text{-}))_4]$ in an aqueous Triton X-100 micellar solution, the CV of the aqueous micellar solution of $(Bu_4N)_2[Fe_4S_4(SC_6H_4Bu^t(p\text{-}))_4]$ was obtained by using HMDE, as depicted in Fig. 3a. Two cathodic waves (E_{pc}=−0.84 and −0.69 V) and one anodic wave (E_{pa}=−0.64 V) were observed at pH 10.20 in the initial scan. The strong cathodic waves compared with the anodic one are indicative of the stronger adsorption of the (2−) state of the cluster on a surface of an Hg electrode than the (3−) one.[7,8] In the following sweep, the −0.84 V cathodic wave almost disappears, while the −0.69 V cathodic wave remains at the same potential with decreasing the peak current. In the micellar solution, the coulombs consumed in the cathodic wave are proportional to the number of the clusters adsorbed on the Hg electrode, since only the

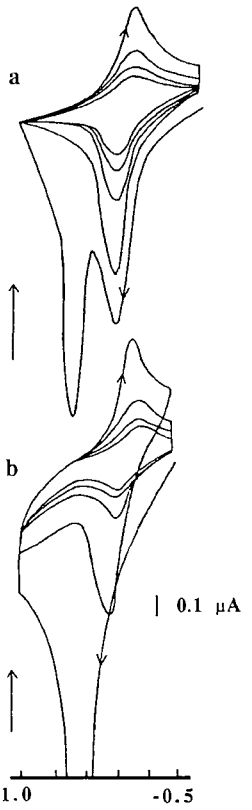

Fig. 3. Multi-sweep cyclic voltammograms of $[Fe_4S_4(SC_6H_4Bu^t(p\text{-}))_4]^{2-}$ in an aqueous Triton X-100 micellar solution at pH 10.20 (a), and of [4Fe4S]/HMDE in H_2O at pH 10.00 (b); sweep rate 10 mV s^{-1}.

cluster adsorbed on the Hg electrode undergoes the one-electron redox reaction. Although the exact area of the −0.83 V cathodic wave in the initial scan could not be determined due to overlap with the −0.69 V cathodic wave, the surface concentration of $[Fe_4S_4(SC_6H_4Bu^t(p\text{-}))_4]^{2-}$ on the HMDE in the second potential sweep could be evaluated from the area of the −0.69 V cathodic wave. On the basis of the surface area of the HMDE (0.0187 cm^2), the surface concentration of the cluster calculated from the wave was 2.9×10^{-10} mol cm^{-2}. This value is somewhat larger than the surface concentration of the monomolecular layer of $[Fe_4S_4(SC_6H_4C_8H_{17}{}^n(p\text{-}))_4]^{2-}$ adsorbed on an Hg electrode (1.6×10^{-10} mol cm^{-2}).[7] The strong −0.83 V cathodic wave observed only in the initial scan, therefore, may be assigned to the redox couple resulting from a multimolecular adsorption of the cluster on the HMDE. The disappearance of the −0.83 V cathodic wave in the second sweep, therefore, may be caused by desorption of $[Fe_4S_4(SC_6H_4Bu^t(p\text{-}))_4]^{3-}$ due to not only a stronger coulomb repulsion of the neighboring (3−) state of the clusters but also a migration of the counter ion into the multimolecular layer of the cluster formed on a fluid Hg surface to

maintain the charge neutrality (vide infra). The $E_{1/2}$ value of the cluster adsorbed on the HMDE in aqueous Triton X-100 micellar solutions, therefore, was employed after both E_{pc} and E_{pa} values become constant in the multiscanning CV (usually the third or fourth sweep). The plot of $E_{1/2}$ of the cluster vs. pH of the aqueous micellar solution (△ in Fig. 2) also clearly shows the break point at pH 7.8 due to the pK_a of the protonated $[Fe_4S_4(SC_6H_4Bu^t(p\text{-}))_4]^{3-}$. The shift of the p$K_a$ 7.8 in the micellar solution from 7.0 in wet CH_2Cl_2 suggests that protonation of the cluster in the former takes place more easily than in the latter. It is also worthy to note that the $E_{1/2}$ value in the aqueous micellar solution is shifted to positive potentials about by 200 mV compared with that in the CH_2Cl_2 solution, and falls in the range of the redox potentials of 4Fe- and 8Fe-ferredoxins (−0.52 to −0.73 V vs. SCE around pH 7.0).[6]

The redox behavior of the cluster on the HMDE was measured in the absence of Triton X-100 to elucidate the effects of hydrophobic spheres of micelles on the redox potential of the cluster in H_2O. The present cluster is not soluble in H_2O. A cluster modified HMDE ([4Fe4S]/HMDE), therefore, was prepared by dipping the HMDE in a dry CH_2Cl_2 solution of $(Bu_4N)_2[Fe_4S_4(SC_6H_4Bu^t(p\text{-}))_4]$ (0.40 mmol dm^{-3}) for less than one minute, followed by drying under N_2 stream. The [4Fe4S]/HMDE displays a very strong cathodic wave at E_{pc}=−0.83 V and an anodic wave at E_{pc}=−0.64 V in the initial scan in H_2O at pH 10.00 (Fig. 3b). As similar to the aqueous micellar solution, the −0.83 V cathodic wave disappears in the second scan, and a new cathodic wave is observed at −0.70 V with the surface concentration of 2.6×10^{-10} mol cm^{-2}. Thus, the very strong −0.83 V cathodic wave in the first scan is assigned to the multimolecular adsorption of the cluster on the Hg electrode. After the second potential sweep, the −0.70 V cathodic wave was slightly shifted to positive potentials with decreasing the peak current, and finally the constant value $E_{1/2}$=−0.65 V (E_{pc}=−0.66 V and E_{pa}=−0.63 V) was obtained. This result also indicates that the peak potential of the (2−/3−) redox couple is dependent on the thickness of the cluster adsorbed on the electrode (or the amount of the cluster adsorbed) and becomes a constant value when the thickness of the adsorbed cluster approaches to a monomolecular layer. The plot of the $E_{1/2}$ obtained after the constant value in H_2O against pH shows the pK_a 8.9, as depicted in Fig. 2 (□). Despite the difference in the pK_a of the cluster in the absence (8.9) and presence of the surfactant (7.8) in H_2O, the $E_{1/2}$ values at higher pH than their pK_a values are essentially consistent with each other (□ and △ in Fig. 2). This result indicates that hydrophobic spheres of micelles hardly affect the redox potential of the Fe_4S_4 cluster on an Hg electrode in H_2O.

Redox Reaction in Multi-Adsorption Layer in H_2O. We have reported that a $(Bu_4N)_3[Mo_2Fe_6S_8(SPh)_9]$ modified glassy carbon plate stably undergoes a redox reaction without desorption from the GG plate in water.[10] In accordance with this, the $(Bu_4N)_2[Fe_4S_4(SC_6H_4Bu^t(p\text{-}))_4]$ (1×10^{-8}mol) modified GC plate ([4Fe4S]/GC, 1.0 cm^2) also shows a cathodic and anodic wave at E_{pc}=−1.14 and E_{pa}=−0.87 V in water at pH 10.04 (Fig. 4a). A strong cathodic current at potentials more negative than −1.2 V comes from H_2 evolution catalyzed by the reduced cluster,[10,14] and the pattern was unchanged in the multi-sweep CV for 30 min.[15] Although the peak separation between the cathodic and anodic waves of the [4Fe4S]/GC is fairly large compared with that of the [4Fe4S]/HMDE,[16] the $E_{1/2}$ value (−1.02 V vs. SCE) of the [4Fe4S]/GC at pH 10.04 is close to that in a dry CH_2Cl_2 solution obtained by a GC disk electrode rather than that of [4Fe4S]/HMDE in H_2O. Thus, the redox potential of $(Bu_4N)_2[Fe_4S_4(SC_6H_4Bu^t(p\text{-}))_4]$ aggregated on the GC plate[17] does not undergo a positive potential shift by water. This is quite contrast to the $E_{1/2}$ value of the monomolecular layer of the [4Fe4S]/HMDE in water at pH 10.0 (□ in Fig. 2). To compare the redox behavior of $[Fe_4S_4(SC_6H_4Bu^t(p\text{-}))_4]^{2-}$ modified GC plate with an Hg electrode in H_2O, a cluster modified Hg amalgamated Au plate electrode ([4Fe4S]/HgAu) was prepared by addition of CH_3CN solution of $(Bu_4N)_2[Fe_4S_4(SC_6H_4Bu^t(p\text{-}))_4]$ on the surface of an Hg amalgamated Au plate (1×10^{-8} mol, 1.0 cm^2),[17] followed by drying under N_2 atmosphere. The [4Fe4S]/HgAu exhibits a cathodic and an anodic waves at

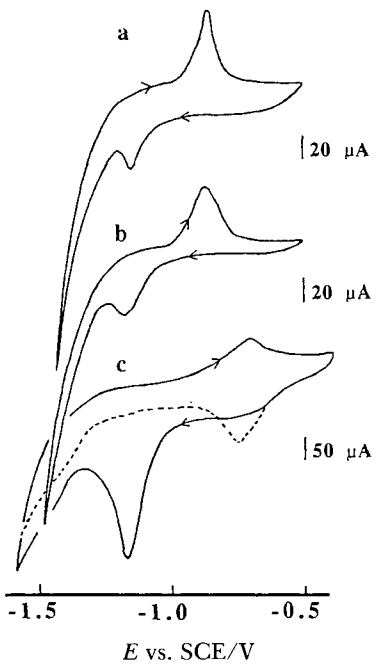

Fig. 4. Cyclic voltammograms of [4Fe4S]/GC at 10 mV s^{-1} (a) in H_2O (pH 10.04), and [4Fe4S]/HgAu at 10 mV s^{-1} (b) and 100 mV s^{-1} (c) in H_2O (pH 10.06); a dotted line is the second potential sweep.

E_{pc}=−1.16 and E_{pa}=−0.87 V at the sweep rate 10 mV s^{-1} in H_2O at pH 10.06 (Fig. 4b). The amounts of the cluster calculated from the areas of the −1.16 V cathodic and the −0.87 anodic waves were 2.9×10^{-9} and 5.6×10^{-9} mol, respectively. The decrease in the coulombs consumed in the cathodic wave compared with that in the anodic one may be due to subsequent H_2 evolution catalyzed by the reduced cluster. Despite the disagreement of the peak currents of those waves, the peak potentials are almost completely consistent with those of the [4Fe4S]/GC at the same pH. On the other hand, the CV of the [4Fe4S]/HgAu affords a quite different pattern, when the sweep rate is increased to 100 mV s^{-1}; a strong cathodic wave and an anodic one are observed at E_{pc}=−1.16 and E_{pa}=−0.70 V in the initial potential sweep (a solid line in Fig. 4c). In the following potential sweep, the −1.16 V cathodic wave completely disappears, and a new cathodic wave appears at −0.76 V (a dotted line in Fig. 4c). It should be noticed that the redox waves at E_{pc}=−0.76 V and the E_{pa}=−0.70 V, which are observed in the second sweep, are close to those of the monomolecular layer of [4Fe4S]/HMDE. The marked difference in the CV of the voltage scanning at 10 and 100 mV s^{-1} may be explained by desorption of the cluster from the multimolecular layer on the surface of HgAu plate; the charge neutrality of the multimolecular layer of the cluster on the HgAu plate is maintained by the transport of the counter ion into and out of the contacting aqueous phase, so that a rapid transport of counter ion into the multimolecular layer of the cluster accelerates the detachment of the cluster from the layer to form a near monomolecular layer on the HgAu electrode. In accordance with this assumption that the amounts of the cluster on the HgAu plate[18] were determined as 5.6×10^{-9} and 5.4×10^{-10} mol from the areas of the −0.87 anodic wave of Fig. 4b (10 mV s^{-1}) and the −0.70 V one of Fig. 4c (100 mV s^{-1}), respectively.

The $E_{1/2}$ value of the near monomolecular layer of [4Fe4S]/HMDE and [4Fe4S]/HgAu is shifted to positive potentials in water, while that of the multimolecular layer of [4Fe4S]/HgAu and [4Fe4S]/GC in water is very close to the value in CH_2Cl_2. Thus, the influence of water on the redox potential of the Fe_4S_4 cluster in the multi- and monomolecular layer is quite different from each other. As similar to the monomolecular layer in H_2O, the redox potential of the cluster contacting with the H_2O phase (near the surface of the multimolecular layer) would undergo a pronounced solvent effect by water. On the other hand, a hydrophobicity of the terminal ligand $SC_6H_4Bu^t(p\text{-})$ of the Fe_4S_4 cluster may depress penetration of bulk water into the multimolecular layer, so that the redox potential of the cluster contacting electrode (at the bottom of the multimolecular layer) may be isolated from bulk water. This assumption suggests that the redox potential of the cluster in the multimolecular layer is largely dependent on the distance from the aqueous phase. The redox reaction of the cluster in the multimolecular layer may be caused by an electron self-exchange between neighboring oxidized and reduced clusters. In addition, the electron transfer between the electrode and the cluster takes place only in the first layer of the adsorption layer (contacted with the electrode), and then the electron is transferred successively to the surface of the multimolecular layer (Fig. 5a). Accordingly, the electrode can detect only the redox potential of the cluster contacted with the electrode. In harmony with this, a multisweep CV of the cluster of the multimolecular adsorption on Hg electrodes displays a positive potential shift of the $E_{1/2}$ value with decreasing the peak current by gradual desorption of the cluster, and reaches a constant value at the near monomolecular layer (Fig. 5b). The fact that the $E_{1/2}$ value of the multimolecular layer of the [4Fe4S]/GC and [4Fe4S]/HgAu in H_2O is close to that in a CH_2Cl_2 solution suggests that the effect of the aggregate of the cluster on the redox potential is essentially same as that of an organic solvent. It is, therefore, concluded that hydrophobic spheres around the Fe_4S_4 core in water do not cause an anodic shift of the redox potential of the cluster.

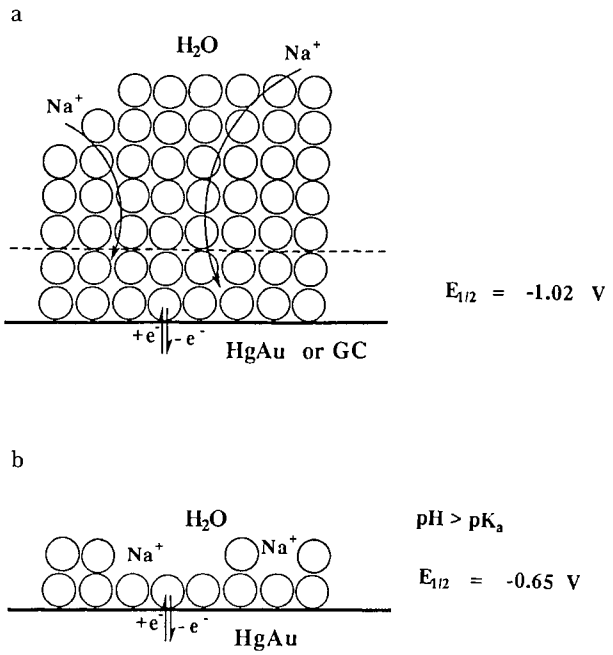

Fig. 5. Redox of Fe_4S_4 cluster in a multimolecular (a) and near monomolecular layer (b) on an HgAu electrode.

References

1) R. H. Holm, "Ion-Sulfur Proteins," ed by T. G. Spiro, John Wiley & Sons, New York (1982), Vol. IV, p. 1—66.

2) D. C. Yoch, D. I. Arnon, and W. V. Sweeney, *J. Biol.*

Chem., **250**, 8330 (1975); H. Hiura, T. Kakuno, J. Yamashita, H. Matsubara, and T. Horio, *J. Biochem.*, **89**, 1787 (1981); K. T. S. Shanmugan, D. B. Buchanan, and D. E. Arnon, *Biochim. Biophys. Acta*, **256**, 477 (1972).

3) B. E. Smith, D. J. Lowe, and R. C. Bay, *Biochem. J.*, **137**, 169 (1974); M. Tanaka, M. Haniu, K. T. Yasunobu, and L. E. Mortenson, *J. Biol. Chem.*, **252**, 7093 (1977); V. Sunderson and F. M. Ausubel, *J. Biol. Chem.*, **256**, 2808 (1981).

4) K. M. Weber and M. Mevarech, *Arch. Biochem. Biophys.*, **186**, 60 (1978); S. Seki, M. Hagiwara, K. Kudo, and M. Ishimoto, *J. Biochem.*, **85**, 833 (1979).

5) B. V. Depamphilis, B. A. Averill, T. Herskovitz, L. Que, and R. H. Holm, *J. Am. Chem. Soc.*, **96**, 4159 (1974).

6) C. L. Hill, J. Renaud, R. H. Holm, and L. E. Mortenson, *J. Am. Chem. Soc.*, **99**, 2549 (1977).

7) K. Tanaka, M. Masanaga, and T. Tanaka, *J. Am. Chem. Soc.*, **108**, 5448 (1986).

8) K. Tanaka, T. Tanaka, and I. Kawafune, *Inorg. Chem.*, **23**, 517 (1984); K. Tanaka, M. Moriya, and T. Tanaka, *ibid.*, **25**, 835 (1986).

9) M. Nakamoto, K. Tanaka, and T. Tanaka, *Bull. Chem. Soc. Jpn.*, **61**, 4099 (1988).

10) S. Kuwabata, K. Tanaka, and T. Tanaka, *Inorg. Chem.*, **25**, 1691 (1986).

11) R. S. Maglizzo, B. A. Mclntosh, and W. D. Sweeney, *J. Biol. Chem.*, **257**, 3506 (1982); D. B. Knaff and R. Malkin, *Arch. Biochem. Biophys.*, **159**, 555 (1973); R. Malkin and A. Bearden, *J. Biochim. Biophys. Acta*, **505**, 147 (1978).

12) T. Ikeda, K. Toriyama, and M. Senda, *Bull. Chem. Soc. Jpn.*, **52**, 1937 (1979); R. Parsons and P. C. Symons, *Trans. Faraday Soc.*, **64**, 1077 (1968); N. Kobayashi, A. Osawa, K. Shimizu, Y. Hayashi, H. Kimoto, and T. Fujisawa, *J. Polym. Sci., Polym. Lett. Ed.*, **15**, 137 (1977); P. J. Peerce and F. C. Arnon, *J. Electroanal. Chem. Interfacial Electrochem.*, **105**, 317 (1979).

13) Z. Kozarac and B. Cosovic, *Bioelectrochem. Bioenerg.*, **12**, 353 (1984); B. Cosovic, N. Batina, and Z. Kozarac., *J. Electroanal. Chem.*, **113**, 239 (1980); L. Pospisil, J. Kuta, E. Muller, and H.-D. Dorfler, *J. Electroanal. Chem.*, **106**, 359 (1980); E. Muller, H. Emons, and H.-D. Dorfler, *Bioelectrochem. Bioenerg.*, **10**, 279 (1983).

14) T. Yamamura, G. Christou, and R. H. Holm, *Inorg. Chem.*, **22**, 939 (1983).

15) The fast desorption of $[Fe_4S_4(SC_6H_4Bu^t(p\text{-}))_4]^{2-}$ from the multimolecular layer on the [4Fe4S]/HMDE compared with that from the [4Fe4S]/GC may be due to a fluidity of the surface of an Hg. On the other hand, a strong affinity of sulfur for Hg stabilizes the monomolecular layer on the Hg electrode.

16) Peak separation of an adsorbed species becomes an increase with decreasing the electron transfer of the electrode and the adsorbed species. The configurational change between oxidized and reduced cluster adsorbed on the GC plate may, therefore, be slower than that on an Hg electrode.

17) When the cluster in a CH_3CN solution was solidified on the GC and HgAu plate under N_2, the cluster is not homogeneously distributed over the surface of those electrode.

18) The surface of the HgAu plate is not as smooth as that of the HMDE. So, the surface area of the HgAu plate is considered to be fairly larger than 1.0 cm^2.

Solvation and Ionic Association of (1*R*,4*S*,8*R*,11*S*)-1,4,8,11-Tetramethyl-1,4,8,11-tetraazacyclotetradecanenickel(II) Perchlorate in Mixed Solvents of *N,N*-Dimethylformamide and *N,N*-Dimethylacetamide with Nitrobenzene and 1,2-Dichloroethane

Takashi YOKOYAMA, Etsuro IWAMOTO, and Takahiro KUMAMARU*
Department of Chemistry, Faculty of Science, Hiroshima University, Hiroshima 730
(Received November 30, 1990)

The conductances of $[NiL]^{2+}$ ($[NiL]^{2+}$=(1*R*,4*S*,8*R*,11*S*)-1,4,8,11-tetramethyl-1,4,8,11-tetraazacyclotetradecanenickel(II)) have been measured in *N,N*-dimethylformamide (DMF)-1,2-dichloroethane (DCE), and *N,N*-dimethylacetamide (DMA)-DCE, and iso-relative permittivity mixtures DMF-nitrobenzene (NB), DMA-NB, and DMF-DMA at 25 °C. The first ionic association constant of $[NiL]^{2+}$ with the perchlorate ion in the mixtures with NB decreases with increasing fraction of both DMF and DMA, although DMF is coordinated to $[NiL]^{2+}$ and DMA is not, this showing that DMA as well as DMF in NB selectively solvates the axial coordination site of $[NiL]^{2+}$ to change from contact ion pairs to solvent-separated ion pairs. Bulky and delocalized negative pole of NB of which the dipole moment is larger than that of DMF and DMA results in a weak ion-dipole interaction, leading to a larger degree of ionic association. Ionic association was discussed from the viewpoint of steric hindrance and ion-dipole interactions.

The title metal chelate ($[NiL]^{2+}$=(1*R*,4*S*,8*R*,11*S*)-1,4,8,11-tetramethyl-1,4,8,11-tetraazacyclotetradecanenickel(II)) cation exists in solutions as an equilibrium mixture of a red, square species and a green, square-pyramidal species according to the reaction

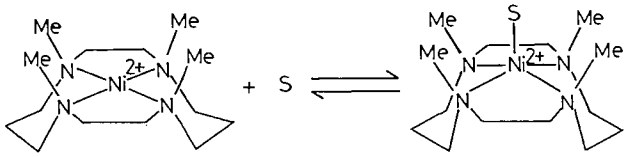

Reaction (1)

where S is a basic solvent.[1-6] In our previous work,[7] it was found that although *N,N*-dimethylformamide (DMF), *N,N*-diethylformamide, formamide, and *N*-methylformamide were coordinated to $[NiL]^{2+}$, *N,N*-dimethylacetamide (DMA), *N,N*-dimethylpropionamide, and *N,N*-diethylacetamide were not coordinated to the square complex, in spite of these solvents having nearly the same basicity. This was explained by steric hindrance between -CO-Me of the DMA, and four -N-Me and methylene groups of L. This led us to inquire as to whether solvation effects of non-coordinating DMA molecules on ionic association of $[NiL]^{2+}$ is different from that of coordinating DMF. 1,2-Dichloroethane (DCE) of a low relative permittivity (10.36) and nitrobenzene (NB) which has nearly the same relative permittivity (34.82) as the amides were used as diluents.

Experimental

NB, DMF, and DMA were purified as described previously.[7] DCE (reagent grade, Wako Pure Chemical Industries Ltd.) was purified by fractional distillation under reduced pressure through a 1.2-m column and left into molecular sieves 4A for a week.

$[NiL](ClO_4)_2$, $[NiL(N_3)]ClO_4$, where N_3 is the azide ion, butyltriisopentylammonium tetraphenylborate (i-Pent)$_3$BuNBPh$_4$, and butyltriisopentylammonium perchlorate (i-Pent)$_3$BuNClO$_4$ were prepared by the published method.[1,8,9] The purities of all the complexes were confirmed by the elemental analysis.

The instrumentation and the procedure used for measurements of conductances, viscosities, relative permittivities,

Table 1. Solvent Properties of Mixed Solvents of DMA and DMF with DCE at 25 °C

X_{DMA}	ε	η / cp	d / g cm^{-3}	X_{DMF}	ε	η / cp	d / g cm^{-3}
0.000	10.36	0.787	1.2458	0.000	10.36	0.787	1.2458
0.228	17.8	0.858	1.1642				
0.368	22.0	0.900	1.1184				
0.431	23.7	0.914	1.0981	0.443	24.4	0.854	1.1122
0.526	27.0	0.932	1.0696	0.576	28.3	0.858	1.0722
0.630	29.5	0.944	1.0380				
0.728	32.6	0.949	1.0098	0.759	32.6	0.845	1.0170
1.000	37.78	0.919	0.9366	1.000	36.71	0.802	0.9433

Table 2. Solvent Properties of Mixed Solvents of DMA and DMF with NB at 25 °C

X_{DMA}	ε	η / cp	d / g cm^{-3}	X_{DMF}	ε	η / cp	d / g cm^{-3}
0.000	34.82	1.8415	1.1986	0.000	34.82	1.8415	1.1986
0.139	35.7	1.722	1.1651	0.158	35.5	1.675	1.1669
0.319	36.2	1.562	1.1206	0.360	36.0	1.462	1.1231
0.586	36.7	1.312	1.0516	0.627	36.8	1.175	1.0567
0.809	37.3	1.093	0.9900	0.837	37.1	0.959	0.9968
0.926	37.7	0.993	0.9574	0.938	37.1	0.908	0.9644
1.000	37.78	0.919	0.9366	1.000	36.71	0.802	0.9433

Table 3. Solvent Properties of Mixed Solvents of DMA with DMF at 25 °C

X_{DMF}	ε	η / cp	d / g cm^{-3}
0.000	37.78	0.919	0.9365
0.340	36.6	0.890	0.9387
0.544	36.6	0.864	0.9403
0.735	36.6	0.838	0.9418
0.873	36.6	0.817	0.9428
0.955	36.6	0.807	0.9435
1.000	36.71	0.802	0.9439

and spectra were described previously.[7] The relative permittivities (ε), viscosities (η), and densities (d) of the solvent mixtures used for analyses were given in Tables 1 to 3. The specific conductances (S cm^{-1}) of the solvents are 2.2×10^{-8}—2.9×10^{-7} for NB-DMA mixtures, 2.1×10^{-8}—3.4×10^{-7} for NB-DMF, 1.8×10^{-7}—9.3×10^{-7} for DCE-DMA, 2.0×10^{-7}—9.2×10^{-7} for DCE-DMF, and 1.2×10^{-7}—4.0×10^{-7} for DMF-DMA. All solutions were prepared by weight. Densities were measured by using an Anton Paar model DMA 02D digital density meter at 25±0.002 °C.

Results and Discussion

Conductances for $[NiL](ClO_4)_2$ and $[NiL(N_3)]ClO_4$ were measured at seven to ten concentrations ranging from 1×10^{-4} to 4×10^{-3} mol dm^{-3} in each system. Typical molar conductances measured in the DMA-NB system which of nearly the same relative permittivity are shown in Fig. 1. To analyze conductance data for the 2-1 type of electrolyte the limiting molar conductance for ClO_4^- must be evaluated. In this work, $(i\text{-Pent})_3BuNBPh_4$ was used as a reference electrolyte (i.e. assuming $\lambda_0[(i\text{-Pent})_3BuN^+]=\lambda_0(BPh_4^-)$].[9] The conductances for $(i\text{-Pent})_3BuNBPh_4$ and $(i\text{-Pent})_3BuNClO_4$ in each mixture were measured at 25 °C and analyzed by the Fuoss-Hsia conductance equation for symmetrical electrolytes in the form[10,11]

$$\Lambda=\Lambda_0-S(C\gamma)^{1/2}+EC\gamma\log C\gamma+JC\gamma+J_2(C\gamma)^{3/2}-K_aC\gamma f^2$$

for associated electrolytes, where the coefficients S, E, J, and J_2 have the usual meanings[12] and the relative permittivity and viscosity of solvents were used to calculate these coefficients. The symbol γ is the fraction of solute present as unpaired ions,

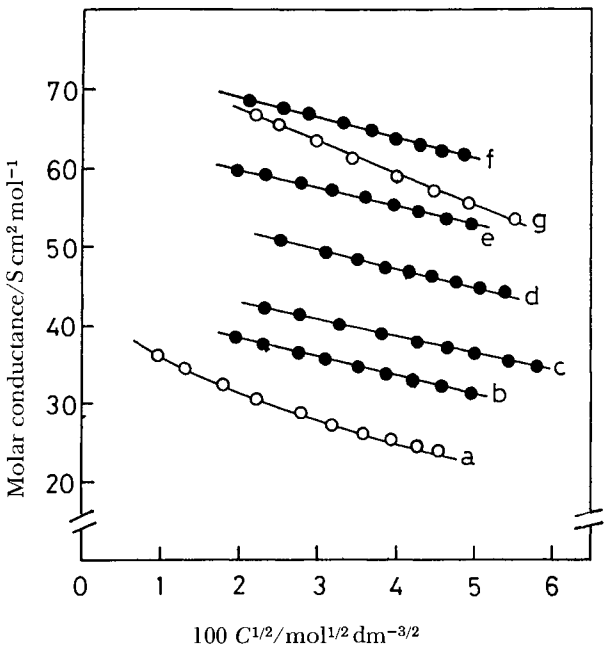

Fig. 1. Plots of molar conductivities of $1/2[NiL](ClO_4)_2$ against the square root of the concentration in DMA-NB mixtures at 25 °C. DMA fraction: a, 0.00; b, 0.14; c, 0.32; d, 0.59; e, 0.81; f, 0.93; g, 1.00.

Λ_0 and Λ are the limiting molar conductance and molar conductance, respectively, and f is the mean ionic activity coefficient on the molarity scale which was evaluated from molality by using the density of solutions. The equation is the form

$$\Lambda=\Lambda_0-SC^{1/2}+EC\log C+JC+J_2C^{3/2}$$

in the cases where association is negligible. For most of the systems the analyses yielded plots of σ against ion distance parameter a with double minimum where is the standard deviation of the individual N points calculated using the expression

$$\sigma=[\Sigma(\Lambda_{obs}-\Lambda_{calc})^2/(N-3)]^{1/2}$$

Tables 4 to 6 give compilation of the values of Λ_0, K_{a1}, and σ corresponding to the minimum at larger a values: Λ_0 and σ are almost the same as those corresponding to the minimum at smaller a values, but K_a is a little larger.

Table 4. Conductance Parameters for $(i\text{-Pent})_3BuNClO_4$, $[NiL](ClO_4)_2$, and $[NiL(N_3)]ClO_4$ in Mixed Solvents of DMA and DMF with DCE at 25 °C

(a) DMA–DCE

X_{DMA}	$(i\text{-Pent})_3BuNBPh_4$			$(i\text{-Pent})_3BuNClO_4$			$\lambda_0(ClO_4^-)$	$[NiL](ClO_4)_2$		$[NiL(N_3)]ClO_4$		
	Λ_0 / S cm² mol⁻¹	K_a / dm³ mol⁻¹	σ	Λ_0 / S cm² mol⁻¹	K_a / dm³ mol⁻¹	σ	/ S cm² mol⁻¹	Λ_0 / S cm² mol⁻¹	K_{a_1} / dm³ mol⁻¹	Λ_0 / S cm² mol⁻¹	K_a / dm³ mol⁻¹	σ
0.228	44.00±0.04	151±1	0.012	59.46±0.06	226±1	0.013	37.46	59.19±1.50	1120±300			
0.368	41.99±0.04	68±1	0.017	58.36±0.05	97±1	0.018	37.36	65.58±0.08	392±10			
0.431	41.70±0.03	57±1	0.016	58.31±0.08	73±3	0.039	37.46	68.62±0.11	496±12	58.16±0.52	112±2	0.023
0.526	41.02±0.04	34±1	0.010	58.02±0.13	53±2	0.072	37.51	70.44±0.05	247±4			
0.630	40.64±0.03	29±1	0.016	58.59±0.07	37±1	0.014	38.27	70.31±0.02	52±1			
0.728	40.43±0.04	23±1	0.035	59.65±0.03	28±1	0.007	39.43	71.86±0.03	31±1	59.54±0.10	34±1	0.028
1.000	41.50±0.03	14±1	0.027	64.20±0.05	16±2	0.10	43.5[a]	74.79±0.53	0	64.68±0.17[a]	20±2[a]	0.10[a]

(b) DMF–DCE

X_{DMF}	$(i\text{-Pent})_3BuNBPh_4$			$(i\text{-Pent})_3BuNClO_4$			$\lambda_0(ClO_4^-)$	$[NiL](ClO_4)_2$		$[NiL(N_3)]ClO_4$		
	Λ_0 / S cm² mol⁻¹	K_a / dm³ mol⁻¹	σ	Λ_0 / S cm² mol⁻¹	K_a / dm³ mol⁻¹	σ	/ S cm² mol⁻¹	Λ_0 / S cm² mol⁻¹	K_{a_1} / dm³ mol⁻¹	Λ_0 / S cm² mol⁻¹	K_a / dm³ mol⁻¹	σ
0.443	45.06±0.10	54±2	0.065	64.11±0.07	70±7	0.035	41.58	74.79±0.07	424±7	63.49±0.09	98±2	0.047
0.576	44.93±0.09	31±2	0.053	66.09±0.25	30±4	0.049	43.62	77.11±0.25	78±18			
0.759	46.42±0.03	22±2	0.014	69.71±0.04	23±2	0.024	46.50	83.87±0.06	30±3	69.65±0.06	38±1	0.032
1.000	49.27±0.12	20±1	0.06	76.34±0.15	23±2	0.14	51.7[a]	93.70±0.03	6±1	76.64±0.25	26±3	0.13

a) Ref. 7.

Table 5. Conductance Parameters for (i-Pent)$_3$BuNBPh$_4$, (i-Pent)$_3$BuNClO$_4$, and [NiL](ClO$_4$)$_2$ in Mixed Solvents of DMA and DMF with NB at 25 °C

(a) DMA-NB

X_{DMA}	(i-Pent)$_3$BuNBPh$_4$			(i-Pent)$_3$BuNClO$_4$			$\lambda_0(ClO_4^-)$	[NiL](ClO$_4$)$_2$	
	Λ_0	K_a	σ	Λ_0	K_a	σ		Λ_0	K_{a_1}
	S cm^2 mol^{-1}	dm^3 mol^{-1}		S cm^2 mol^{-1}	dm^3 mol^{-1}		S cm^2 mol^{-1}	S cm^2 mol^{-1}	dm^3 mol^{-1}
0.000	21.25[b]	0[b]	0.014[b]	31.72[b]	0[b]	0.030[b]	21.1[a]	39.2[a]	1190[a]
0.139	22.73±0.03	13±2	0.014	33.91±0.03	31±1	0.014	22.54	42.35±0.04	216±4
0.319	25.21±0.04	17±1	0.028	37.56±0.04	28±2	0.028	24.95	46.59±0.06	99±4
0.586	29.89±0.03	23±1	0.007	44.87±0.02	20±3	0.007	29.92	55.76±0.01	48±1
0.809	35.34±0.06	17±1	0.029	53.79±0.05	22±1	0.020	36.12	66.91±0.04	30±2
0.926	38.68±0.12	15±2	0.065	59.81±0.06	18±9	0.028	40.48	74.19±0.04	17±1
1.000	41.50±0.03	14±1	0.027	64.20±0.05	16±2	0.10	43.5[a]	74.79±0.53	0

(b) DMF-NB

X_{DMF}	(i-Pent)$_3$BuNBPh$_4$			(i-Pent)$_3$BuNClO$_4$			$\lambda_0(ClO_4^-)$	[NiL](ClO$_4$)$_2$	
	Λ_0	K_a	σ	Λ_0	K_a	σ		Λ_0	K_{a_1}
	S cm^2 mol^{-1}	dm^3 mol^{-1}		S cm^2 mol^{-1}	dm^3 mol^{-1}		S cm^2 mol^{-1}	S cm^2 mol^{-1}	dm^3 mol^{-1}
0.000	21.25[b]	0[b]	0.014[b]	31.72[b]	0[b]	0.030[b]	21.1[a]	39.2[a]	1190[a]
0.158	23.82±0.05	21±1	0.025	35.65±0.09	32±5	0.044	23.75	44.26±0.06	218±6
0.360	27.16±0.13	11±7	0.066	41.37±0.02	27±1	0.011	27.80	51.24±0.05	109±3
0.627	34.04±0.03	19±1	0.007	51.92±0.03	24±2	0.013	34.90	64.28±0.02	51±1
0.837	41.91±0.03	18±1	0.014	63.60±0.14	15±5	0.060	42.65	78.37±0.21	28±7
0.938	45.84±0.10	20±1	0.052	71.01±0.09	24±1	0.034	48.09	84.26±0.03	13±1
1.000	49.27±0.12	20±1	0.065	76.34±0.15	23±2	0.14	51.7[a]	93.70±0.03	6±1

a) Ref. 7. b) Ref. 14.

Conductances for [NiL](ClO$_4$)$_2$ were analyzed using the Fuoss-Edelson technique for unsymmetrical electrolytes.[13] This method consists of evaluating Λ_0 and the first association constant K_{a1} for 2-1 electrolytes with some approximations, such as $\lambda_0(MX^+)=0.5\lambda_0(1/2M^{2+})$ and the second association constant $K_{a2}=0$. Typical Fuoss-Edelson plots of Λ^* against X for DMA-NB solution are shown in Fig. 2, where

$$\Lambda^*=\Lambda F,\ X=C'\Lambda^*(\Lambda^*-\Lambda_0/2),\ C'=2Cf$$

and

$$\Lambda^*=\Lambda_0-(K_{a1}/\Lambda_0)X$$

The function F is given as

$$F=[1/(1+\lambda_0(1/2M^{2+})/2\Lambda_0)][1/\{1-S_{2:1}(2I)^{1/2}/\Lambda_0\}+\lambda_0(1/2M^{2+})/2\Lambda]\Lambda/\Lambda_0$$

where $S_{2:1}$ is the Onsager conductance coefficient for a 2-1 electrolyte and I is the ionic strength. Good linear relations for the plots were obtained. The first association constant K_{a1} is obtained from the negative product of the slope and intercept of the curve. The results obtained for DMA-DCE, DMF-DCE, DMA-NB, DMF-NB, and DMA-DMF binary mixture systems are given in Tables 4 to 6. The extended Jenkins-Monk method[14] was also used to evaluate the second association constants K_{a2} and it was found that

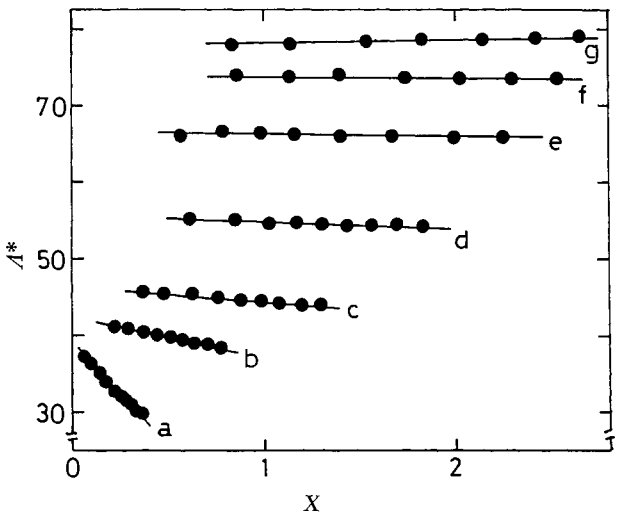

Fig. 2. Fuoss-Edelson plots for [NiL](ClO$_4$)$_2$ in DMA-NB mixtures at 25 °C. DMA fraction: a, 0.00; b, 0.14; c, 0.32; d, 0.59; e, 0.81; f, 0.93; g, 1.00.

in most cases the K_{a2} values are negligibly small so that neglecting K_{a2} is not serious for evaluating K_{a1}. For example, in NB, where the salts used are most associative, the extended Jenkins-Monk method gave the values of $K_{a1}=1190$ and $K_{a2}=12$[7] and the analysis of conductances on neglecting the K_{a2} value gave the

Table 6. Conductance Parameters for (i-Pent)$_3$BuNBPh$_4$, (i-Pent)$_3$BuNClO$_4$, [NiL](ClO$_4$)$_2$, and [NiL(N$_3$)]ClO$_4$ in Mixed Solvents of DMA with DMF at 25 °C

DMF-DMA	(i-Pent)$_3$BuNBPh$_4$			(i-Pent)$_3$BuNClO$_4$			λ_0(ClO$_4^-$)	[NiL](ClO$_4$)$_2$			[NiL(N$_3$)]ClO$_4$		
X_{DMF}	Λ_0	K_a	σ	Λ_0	K_a	σ		Λ_0	K_{a_1}		Λ_0	K_a	σ
	S cm^2 mol^{-1}	dm^3 mol^{-1}		S cm^2 mol^{-1}	dm^3 mol^{-1}		S cm^2 mol^{-1}	S cm^2 mol^{-1}	dm^3 mol^{-1}		S cm^2 mol^{-1}	dm^3 mol^{-1}	
0.000	41.50±0.03	14±1	0.027	64.20±0.05	16±2	0.10	43.5	74.79±0.53	0		64.68±0.17[a]	20±2[a]	0.10[a]
0.340	43.52±0.01	19±1	0.0049	66.85±0.04	21±1	0.014	45.08	82.52±0.06	0±1		67.34±0.10	24±1	0.033
0.544	44.91±0.10	16±2	0.048	68.83±0.06	19±1	0.025	46.38	85.24±0.08	1±3				
0.735	46.93±0.31	12±6	0.066	71.85±0.10	11±2	0.016	48.38	88.98±0.04	10±1		72.13±0.13	25±1	0.024
0.873	48.11±0.05	18±3	0.025	73.91±0.10	21±1	0.035	49.86	91.72±0.03	15±2				
0.955	48.56±0.03	16±1	0.011	75.05±0.16	19±3	0.059	50.77	93.21±0.03	13±1				
1.000	49.27±0.12	20±1	0.065	76.34±0.15	23±2	0.14	51.7	93.70±0.03	6±1		76.64±0.25	26±3	0.13

a) Ref. 7.

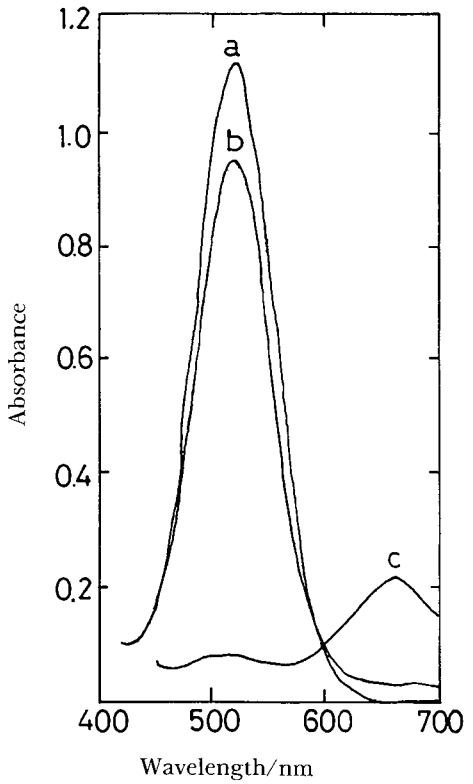

Fig. 3. Visible absorption spectra for [NiL](ClO$_4$)$_2$ (1.0×10^{-3} mol dm^{-3}) in (a) NB, (b) DMA, and (c) DMF at 25 °C.

value of K_{a_1}=1200.

The visible spectra of [NiL]$^{2+}$ in NB, DMF, and DMA are shown in Fig. 3. The absorption peaks at 519 nm in DMA and NB, and 503 nm in DMF are assigned to the square species and those at 660 and 400 nm in DMF are assigned to the square pyramidal species. There is no change in spectra of [NiL]$^{2+}$ in those solvents over 40 h at 25 °C. Therefore, the isomerization of [NiL]$^{2+}$ can be neglected. These spectra clearly show that NB and DMA are not coordinated to the [NiL]$^{2+}$ cation but DMF is done. DCE of a very low basicity is not coordinated.

Thus, there is a clear difference in coordination behavior between DMA and DMF, but the K_{a_1} values obtained for DMA are almost the same as those for DMF in all the mixed solvents. In the relative permittivity-changing media (DMF- and DMA-DCE) the logarithms of K_{a_1} were plotted against the reciprocal of relative permittivity in Fig. 4. Solid and broken lines show the association constants for the 1-1 and 2-1 types of salts, repectively, calculated by the Bjerrum association theory[15] with various ionic size parameters. When the ionic radius of ClO$_4^-$ is 0.236 nm, the Ni-ClO$_4^-$ distance is more than 0.31 nm. The salts of (i-Pent)$_3$BuN$^+$ and [NiL(N$_3$)]$^+$ give the K_a values expected from the electrostatic theory. However, the K_{a_1} values for [NiL]$^{2+}$ are much less than those expected from the Bjerrum calculation with a

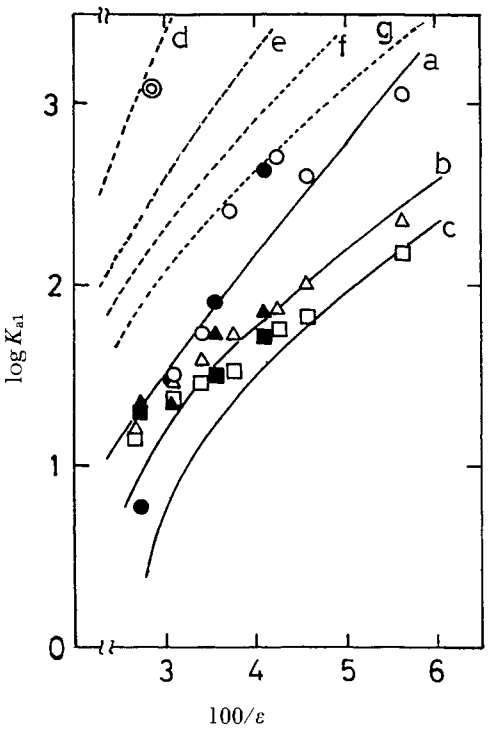

Fig. 4. The dependence of K_{a1} and K_a on the relative permittivity. ●, DMF-DCE; ○, DMA-DCE; ◎, NB for $[NiL](ClO_4)_2$; ▲, DMF-DCE; △, DMA-DCE for $(i\text{-Pent})_3BuNClO_4$; ■, DMF-DCE; □, DMA-DCE for $(i\text{-Pent})_3BuNBPh_4$. Solid and broken lines show the values calculated for 1-1 and 2-1 types of electrolytes, respectively, at 25 °C. Ionic size parameter in nm: a, 0.3; b, 0.5; c, 0.7; d, 0.3; e, 0.5; f, 0.7; g, 1.0.

range of 0.3 to 1.0 nm of a parameter which are reasonable for $[NiL]^{2+}$-ClO_4^- association. On the contrary, NB gives a much greater K_{a1} value which corresponds to an ionic distance parameter of 0.32 nm for the Bjerrum equation. It is interesting that when DMF and DMA are added to NB, the K_{a1} value decreases with increasing fraction of DMF and DMA in spite of nearly the same relative permittivity of the mixed solvents. This means that since DMF is bonded to the nickel on the same side as the four methyl groups, the site of ion pairing is mainly the axial pocket in the second coordination sphere surrounded by the four nitrogen substituents, and the axially associated perchlorate ions are easily displaced by the basic solvent. Furthermore, a similar K_{a1}-decreasing effect of non-coordinating DMA indicates that the perchlorate ion associated is easily displaced by DMA through ion-dipole interactions between $[NiL]^{2+}$ and DMA. The large K_{a1} values in NB suggests that the contact ion pair is possibly formed, considering that the K_{a1} value of the octahedral complex, $[Fe(phen)_3](ClO_4)_2$ (phen=1,10-phenanthroline), of the same 2-1 electrolyte as $[NiL](ClO_4)_2$ is only 39 $dm^3\,mol^{-1}$ in NB,[14] although the dipole moment of NB (μ=4.2 Debye) is larger than that of DMF (μ=3.86) and DMA (μ=3.81). This results from a weaker ion-dipole interaction because of the delocalized negative pole on the oxygen atoms and steric hindrance of nitro group for NB, leading to more degree of ionic association. Although the ion-pair formation constants between $[NiL]^{2+}$ and the perchlorate ion in NB is

Table 7. Stokes Radii r_s/nm for ClO_4^-, $[NiL]^{2+}$, and $[NiL(N_3)]^+$ in Various Binary Mixed Solvents at 25 °C

(a) with DCE

X_{DMF}	$r_s(ClO_4^-)$	$r_s([NiL]^{2+})$	$r_s([NiL(N_3)]^+)$	X_{DMA}	$r_s(ClO_4^-)$	$r_s([NiL]^{2+})$	$r_s([NiL(N_3)]^+)$
	nm	nm	nm		nm	nm	nm
				0.228	0.26	0.88	
				0.368	0.24	0.65	
0.443	0.23	0.58	0.44	0.431	0.24	0.58	0.43
0.576	0.22	0.57		0.526	0.24	0.53	
				0.630	0.23	0.54	
0.759	0.21	0.52	0.42	0.728	0.22	0.53	0.43
1.000	0.20	0.49	0.41	1.000	0.21	0.57	0.42

(b) with NB

X_{DMF}	$r_s(ClO_4^-)$	$r_s([NiL]^{2+})$	X_{DMA}	$r_s(ClO_4^-)$	$r_s([NiL]^{2+})$
	nm	nm		nm	nm
0.000	0.21	0.49	0.000	0.21	0.49
0.158	0.21	0.48	0.139	0.21	0.48
0.360	0.20	0.48	0.319	0.21	0.49
0.627	0.20	0.48	0.586	0.21	0.48
0.837	0.20	0.48	0.809	0.21	0.49
0.938	0.19	0.50	0.926	0.20	0.49
1.000	0.20	0.49	1.000	0.21	0.57

(c) with DMA

X_{DMF}	$r_s(ClO_4^-)$	$r_s([NiL]^{2+})$	$r_s([NiL(N_3)]^+)$
	nm	nm	nm
0.000	0.21	0.57	0.42
0.340	0.20	0.49	0.41
0.544	0.21	0.49	
0.735	0.20	0.48	0.41
0.873	0.20	0.48	
0.955	0.20	0.48	
1.000	0.20	0.49	0.41

larger than in DMA, the absorbance of $[NiL]^{2+}$ at 520 nm in NB is larger than that in DMA. This means the outer-sphere interaction of the perchlorate ion with $[NiL]^{2+}$. The localized negative pole on the oxygen atom of DMA[16,17] can be so close to the central nickel that the contact ion-pair cannot be formed.

The K_{a1} values of $[NiL]^{2+}$ in DMF-DMA mixtures are a little less than the K_a values of $[NiL(N_3)]^+$, showing that the double charge for $[NiL]^{2+}$ interacts more strongly with the DMA dipole than with the perchlorate ion, compared with the case for $[NiL(N_3)]^+$.

Table 7 shows the Stokes radii r_s for ClO_4^-, $[NiL]^{2+}$, and $[NiL(N_3)]^+$ ions in all the media used, where

$$r_s = 0.82|z|/\lambda_0\eta$$

and z is the charge of ions. The r_s values in each medium are almost constant except for the DCE systems of a lower relative permittivity, and the r_s values of $[NiL]^{2+}$ are larger than those of $[NiL(N_3)]^+$ in all the mixed solvents. This is compatible with strong solvation by DMA as well as DMF.

Conclusion

The main site of ion pairing for $[NiL]^{2+}$ is the axial pocket surrounded by the four *N*-methyl groups. DMA preferentially solvates the axial pocket by an ion-dipole interaction without a chemical bond between the central nickel and the oxygen atom of DMA, although DMF solvates by the chemical bond. The solvent-separated ion pair is formed in both DMA and DMF, but the contact ion pair is formed in NB.

This work was supported by a Grant-in-Aid for Scientific Research No. 61134043 from the Ministry of Education, Science and Culture.

References

1) E. K. Barefield and F. Wagner, *Inorg. Chem.*, **12**, 2435 (1973).
2) I. S. Crick and P. A. Tregloan, *Inorg. Chim. Acta*, **142**, 291 (1988).
3) A. Anichini, L. Fabbrizzi, P. Paoletti, and R. M. Clay, *Inorg. Chim. Acta Lett.*, **24**, 21 (1977).
4) N. Herron and P. Moore, *Inorg. Chim. Acta*, **36**, 89 (1979).
5) P. Moore, J. Sacchinidis, and G. R. Willey, *J. Chem. Soc., Dalton Trans.*, **1984**, 1323.
6) K. E. Newman, *Inorg. Chim. Acta Lett.*, **89**, 3 (1984).
7) E. Iwamoto, T. Yokoyama, S. Yamasaki, T. Yabe, T. Kumamaru, and Y. Yamamoto, *J. Chem. Soc., Dalton Trans.*, **1988**, 1935.
8) E. K. Barefield, F. Wagner, A. W. Herlinger, and A. R. Dahl, *Inorg. Syn.*, **16**, 220 (1975).
9) M. A. Coplan and R. M. Fuoss, *J. Phys. Chem.*, **68**, 1177 (1964).
10) R. M. Fuoss and K. L. Hsia, *Proc. Natl. Acad. Sci., U.S.A.*, **57**, 1550 (1967).
11) R. Fernández-Prini, *Trans. Faraday Soc.*, **65**, 3311 (1969).
12) R. M. Fuoss and F. Accasina, "Electrolytic Conductance," Interscience Publishers, Inc., New York (1959).
13) R. M. Fuoss and D. Edelson, *J. Am. Chem. Soc.*, **73**, 269 (1951).
14) E. Iwamoto, S. Monya, and Y. Yamamoto, *J. Chem. Soc., Faraday Trans. 1*, **79**, 625 (1983).
15) N. K. Bjerrum, *Danske Vidensk. Selk*, No. 9, 7 (1926).
16) J. F. Yan, F. A. Momany, R. Hoffmann, and H. A. Scheraga, *J. Phys. Chem.*, **74**, 420 (1970).
17) S. Itoh and H. Ohtaki, *Z. Naturforsch., A*, **42**, 858 (1987).

ESR and Magnetic Susceptibility Studies on High-Spin Tetrahedral Cobalt(II)-Thiolate Complexes: An Approach to Rubredoxin-Type Active Sites

Kouichi FUKUI, Hiroaki OHYA-NISHIGUCHI,* and Noboru HIROTA
Department of Chemistry, Faculty of Science, Kyoto University, Sakyo-ku, Kyoto 606
(Received December 3, 1990)

Magnetic susceptibility and ESR studies on high-spin (S=3/2) tetrahedral cobalt(II)-thiolate complexes were performed for $A_2[Co(SPh)_4]$; A=Me_4N (**1a**), Et_4N (**1b**), Ph_4P (**1c**) and $(Et_4N)_2[Co(SR)_4]$; R=C_6H_4-*p*-Me (**2**), C_6H_4-*p*-Cl (**3**), C_6F_5 (**4**). It was found that the magnitude of zero-field splitting and the anisotropy of g-factor are exceptionally large for **1c** as $D\approx-100\,cm^{-1}$, $E\approx0$, $g_x\approx g_y<g_z$. This parameter set shows that $Co(SPh)_4^{2-}$ in **1c** is strongly affected by an axial distortion. On the contrary, a rhombic distortion with moderate magnitude was found for **1a** (D^*=6.5 cm^{-1}, E/D=−0.21) and **1b** (D^*=5.0 cm^{-1}, E/D=0.19). The results for the other compounds are D^*=7.0 cm^{-1}, E/D=0.14 for **2**, D^*=12 cm^{-1}, E/D=0.10 for **3**, and D^*=2.0 cm^{-1}, E/D=0.02 for **4**. Attempts were made to correlate the magnetic properties and the coordination geometry for **1a—c** by use of available X-ray data. As a result, the importance of the orientation of the thiolate ligands was confirmed.

Cobalt is an important element in bioinoganic chemistry because the Co(II) ion is frequently employed as a spectroscopic probe in metal-exchange studies of metalloproteins.[1-6] The advantage of Co(II) is derived from the sensitivity of its d-d absorptions,[7] effective magnetic moment (μ_{eff}),[8] and zero-field splitting (zfs)[9] to coordination environment around the metal ion. It has been also pointed out that the ESR spectra of high-spin Co(II) complexes are susceptible even to slight change and/or distortion of the geometry.[10-15] Many Co(II)-substituted metalloproteins, therefore, have been prepared in order to elucidate their active-site geometries with or without substrate/inhibitor by using UV-visible, MCD,[1,3,4] and ESR spectroscopies.[2-6]

Rubredoxin, which is the simplest iron-sulfur protein, contains a $Fe(SCys)_4$ site relevant to its electron-transfer function.[16] In the $Fe(SCys)_4$ site, four thiolate anions from cysteine residues are ligated to an Fe ion in a distorted tetrahedral arrangement.[17,18] Of paticular interest have been the geometric effects on the electron-transfer properties of this site. Previous molecular orbital (MO) calculations for simple models, $Fe(SR)_4^{-/2-}$ (R=H, CH_3), suggest that the most important geometric factor in the active site is the orientation of the thiolate ligands, rather than the tetragonal compression/elongation of the FeS_4 tetrahedron.[19,20] However, in the studies of synthetic models exemplified by $Fe(SPh)_4^{2-}$, the interest has been rather focused on the tetragonal distortion. In view of the sensitivity of Co(II) to coordination environment, model studies of cobalt thiolates are expected to provide valuable information concerning the relationship(s) between thiolate orientation (or other geometric factors) and electronic structure in metal thiolates. For this reason, we have chosen cobalt thiolates as a target of the present work.

The stereochemistry of metal-benzenethiolate complexes, $M(SPh)_4^{-/2-}$, is now well characterized through extensive X-ray studies of different metal analogs with different counter ions.[21-27] It was pointed out by Coucouvanis et al.[22] and, more explicitly, by Koch et al.,[23] that only two conformations are possible for the overall orientation of the benzenethiolates (Fig.1): One conformation is found in $(Ph_4P)_2[M^{II}(SPh)_4]$ (M=Co, Fe, Zn, etc.).[21,22] Their S'-M-S-C tortion angles are all ca. 0° or 180°, forming a D_{2d} geometry in the idealized case. The other is found in

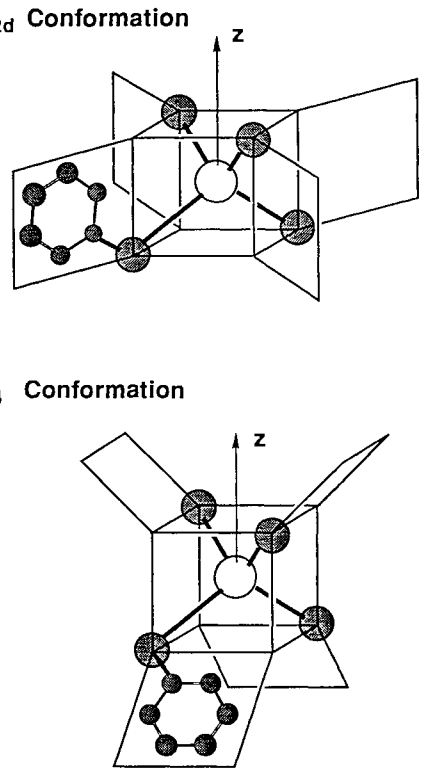

Fig. 1. Schematic drawings of the two idealized conformations for the thiolate-orientation in $M(SPh)_4^{-/2-}$. The phenyl rings lie in the planes standing on edges of the cubes.

$(Et_4N)[Fe^{III}(SPh)_4]$,[23] $(Me_4N)_2[M^{II}(SPh)_4]$ (M=Mn,[24] Zn[25]) and $(Et_4N)_2[M^{II}(SPh)_4]$ (M=Ni,[26] Fe (Fig. 8 in Ref. 22)). In these complexes, two of the four thiolates are rotated by ca. ±120° about the respective M-S bonds from the positions in the D_{2d} conformation. The overall symmetry is S_4 in the idealized case. Such conformational constraint is due to a combined effect of the sulfur p_π-phenyl π interactions and the ortho phenyl hydrogen-sulfur-metal interactions.[22] The active-site geometry of rubredoxin has been classified to the D_{2d} conformation,[17,18] though two of the thiolates are rotated by ca. 30° from the idealized positions.[20]

In the present paper, we report the ESR and magnetic susceptibility results of $A_2[Co(SPh)_4]$; A=Me_4N (**1a**), Et_4N (**1b**), Ph_4P (**1c**) and $(Et_4N)_2[Co(SR)_4]$; R=C_6H_4-*p*-Me (**2**), C_6H_4-*p*-Cl (**3**), C_6F_5 (**4**). Their magnetic properties (*g*-values and zfs parameters) are examined closely. The electronic structures of **1a**—**1c** are discussed based on their zfs and above-described conformational properties.

Experimental

Materials. Acetonitrile was distilled over CaH_2 and stored over molecular sieves 4A. The other reagents were used as purchased. The compounds $A_2[Co(SR)_4]$ were prepared according to a modified Dance's method[27] in vacuo or under dinitrogen atmosphere. They were obtained as emerald-green microcrystals except that **4** as blue-green powder. Their Zn analogs were prepared similarly. Magnetically diluted Zn-doped samples were obtained by recrystallization from an acetonitrile solution containing one of the Co compounds and its Zn analog in a mole ratio of Co/Zn=1% or 10%.

$A_2[Co(SPh)_4]$; A=Me_4N (1a), A=Et_4N (1b), A=Ph_4P (1c). The UV-visible spectra in CH_3CN agree well with those reported previously.[27] ^1H NMR (CD_3CN) δ=16.9 (2,m-H), −23.7 (1,p-H).[28] For **1c**, Found: C, 73.14; H, 5.02; P, 5.19%. Calcd for $CoS_4C_{72}H_{60}P_2$: C, 73.64; H, 5.15; P, 5.27%.

$(Et_4N)_2[Co(SC_6H_4$-*p*-Me$)_4]$ (2). ^1H NMR (CD_3CN) δ= 17.1 (2,m-H), 27.0 (3,p-Me). Found: C, 64.02; H, 8.52; N, 3.28%. Calcd for $CoS_4C_{44}H_{68}N_2$: C, 65.07; H, 8.44; N, 3.45%.

$(Et_4N)_2[Co(SC_6H_4$-*p*-Cl$)_4]$ (3). ^1H NMR (CD_3CN) δ=17.9 (2,m-H). Found: C, 53.05; H, 6.30; N, 3.07; Cl, 15.73%. Calcd for $CoS_4C_{40}H_{56}N_2Cl_4$: C, 53.73; H, 6.31; N, 3.13; Cl, 15.87%.

$(Et_4N)_2[Co(SC_6F_5)_4]$ (4). This compound is unstable to heat, so that the temperature should be kept below 30 °C during the synthesis and stored in a refrigerator.[29] Found: C, 41.10; H, 3.61; N, 2.41; F, 32.93%. Calcd for $CoS_4C_{40}H_{40}N_2F_{20}$: C, 43.05; H, 3.59; N, 2.51; F, 34.08%.

Measurements. ESR spectra were recorded on a JEOL FE-3X spectrometer equipped with an Air Product Model LTR-3-110 Heil-Tran liquid-helium-transferring refrigerator. The microwave frequency (X-band, 9 GHz) was measured with a Takeda Riken TR5211 frequency counter. Cr(III) in MgO was used as a calibrant of the magnetic field. For the ESR measurements, each compound was examined in three forms; magnetically undiluted neat powder, magnetically diluted Zn-doped powder, and frozen MeCN solution. Magnetic susceptibility measurements were performed on a Faraday-type susceptometer over a temperature range of 1.5 K to room temperature at a magnetic field of 700 mT. Neat powder samples were used for the measurements. The temperature was measured with a thermocouple and a Ge resistor, and the magnetic field with a Hall probe. The calibrations of the temperature and the field-gradient were made using $KCr(SO_4)_2\cdot 12H_2O$ and $HgCo(NCS)_4$, respectively. Temperature-independent magnetism and μ_{eff} at room temperature, μ_{eff}(R.T.), were estimated from the least-squares fit of the data in a high-temperature region (typically 100K—room temperature) to the Curie law.

Results and Analyses

Magnetic Susceptibility. In the second column of Table 1 are listed the μ_{eff}(R.T.) values, which are all within the range for high-spin Co(II) complexes (S=3/2).[8] It is notable here that the μ_{eff}(R.T.) value of **1c** (5.0 BM) is significantly larger than the others (4.1—4.4 BM). This result, together with those given later, shows that the magnetic properties of **1c** are exceptional.

The susceptibility data of **3** and **4** are representatively shown in Fig. 2 as a μ_{eff} vs. T plot. The decrease of μ_{eff} at lower temperatures is attributed to thermal depopulation of the upper partner of the zero-field split levels (upper Kramers doublet). Similar temperature dependence was found for **1a**, **1b**, and **2**. The susceptibility data of **1c** is presented in Fig. 3, where a gradual decrease of μ_{eff} occurs over a wide temperature range. Although this magnetic behavior is unusual for a mononuclear complex, the ESR results of **1c** show that no exchange interaction exists between the Co ions (vide infra).

We have analyzed the variable-temperature susceptibility data by using the S=3/2 spin Hamiltonian;

$$H = D(S_z^2 - 5/4) + E(S_x^2 - S_y^2) + \sum \mu g_p S_p H_p \qquad (1)$$

Here D and E denote the conventional zfs parameters and g_p (p=x,y,z) the principal p-component of the g-tensor. Some remarks should be made about the notations: (1) We take $E \geq 0$ throughout this paper, so that the sign of the rhombicity parameter (E/D)

Table 1. Results from the Variable-Temperature Magnetic Susceptibility Measurements

Compounds	μ_{eff}/BM[a]	D^*/cm^{-1}[b]	g_{av}
$(Me_4N)_2[Co(SPh)_4]$ (**1a**)	4.3	6.5	2.22
$(Et_4N)_2[Co(SPh)_4]$ (**1b**)	4.4	5.0	2.27
$(Ph_4P)_2[Co(SPh)_4]$ (**1c**)[c]	5.0	100±30	$g_{x,y}$=2.25, g_z=3.13
$(Et_4N)_2[Co(SC_6H_4$-*p*-Me$)_4]$ (**2**)	4.1	7.0	2.12
$(Et_4N)_2[Co(SC_6H_4$-*p*-Cl$)_4]$ (**3**)	4.2	12±1	2.17
$(Et_4N)_2[Co(SC_6F_5)_4]$ (**4**)	4.3	2.0	2.22

a) Room-temperature values. b) The estimated errors are ±0.5 cm^{-1} when not indicated. c) Analyzed in terms of anisotropic *g*-factor.

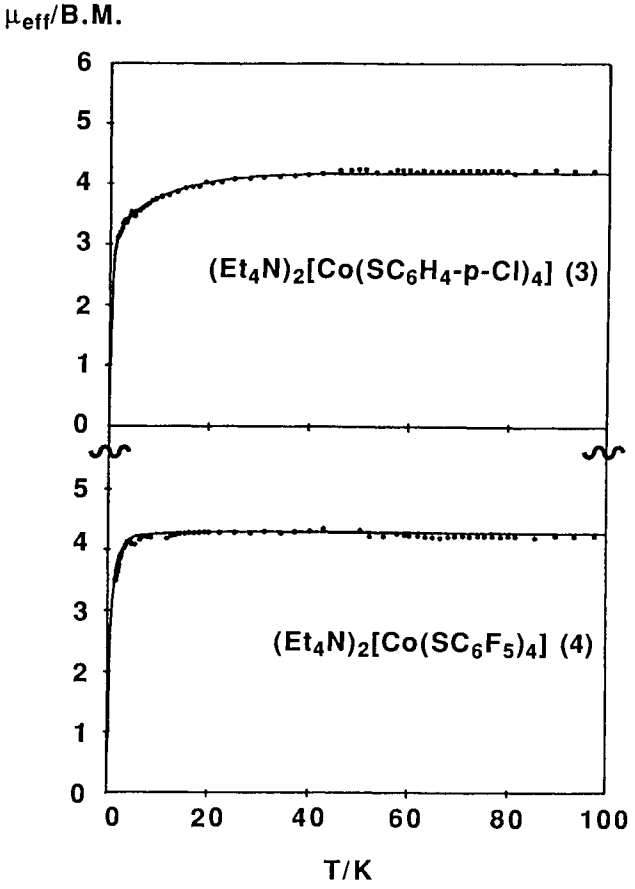

Fig. 2. Temperature dependence of μ_{eff} obtained from the neat powder samples of $(Et_4N)_2[Co(SC_6H_4$-p-$Cl)_4]$ (**3**) and $(Et_4N)_2[Co(SC_6F_5)_4]$ (**4**). The solid curves represent the theoretical fits.

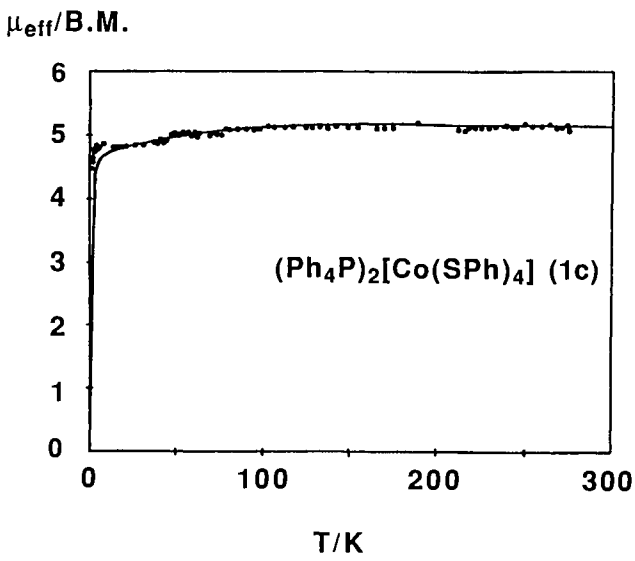

Fig. 3. Temperature dependence of μ_{eff} obtained from the neat powder sample of $(Ph_4P)_2[Co(SPh)_4]$ (**1c**). The solid curve represents the theoretical fit, where $D=-100$ cm^{-1}, $g_x=g_y=2.25$, $g_z=3.13$.

always corresponds to that of D. (2) We distinguish g_p from g'_p ($p=x,y,z$; or $p=1,2,3$). g'_p is used to represent the resonant position of an ESR signal feature. The two parameters, g_p and g'_p, can be connected analytically when the Zeeman term in Eq. 1 is treated as a perturbation.[15]

The anisotropy of g-factor is usually small in tetrahedral high-spin Co(II) complexes.[10-15,30] Thus, in analyzing the susceptibility data, we first assumed that g-factor is isotropic ($g_x=g_y=g_z=g_{av}$). It is important to note that, in this case, variation of E/D has practically no effects on spatially-averaged μ_{eff}. Furthermore, g_{av} is directly connected with μ_{eff}(R.T.) as

$$\mu_{eff}(\text{R.T.})=(15/4)^{1/2}g_{av}. \quad (2)$$

Hence we had only one parameter, $D^*=(D^2+3E^2)^{1/2}$, to be varied in the fitting. For **1a**, **1b**, and **2**—**4**, the best-fit curves obtained in this manner reproduce the experimental data quite satisfactorily, as shown in Fig. 2 for **3** and **4** representatively. The D^* and g_{av} values obtained for these compounds are shown in Table 1. For **1c**, however, we were not able to obtain any reasonable fits when an isotropic g-factor was assumed. The temperature-dependence behavior of μ_{eff} of **1c**, which is presented in Fig. 3, indicates that the D^* value is anomalously large, being on the order of 100 cm^{-1}. Since large zfs implies large g-anisotropy, we should go into the case of anisotropic g-factor. Hence we subsequently assumed the axial case ($E=0$, $g_x=g_y\neq g_z$). This assumption can be justified by the X-ray data showing an approximate D_{2d} structure for $Co(SPh)_4^{2-}$ of **1c**.[21] The ESR results of **1c** also suggest $E\approx 0$, as described in Discussion. The best fit for the axial case was achieved with $D=-100\pm30$ cm^{-1}, $g_x=g_y=2.25$, and $g_z=3.13$ (Fig. 3). This parameter set has a few notable features: (1) D is negative in sign and anomalously large in magnitude. The fits using positive D were always poor, and resulted in unreasonable values (i.e. $g_z=0$) at best. (2) g_z is very large while g_x and g_y are comparable to g_{av} of the other compounds. (3) The relation; g_x, $g_y<g_z$, is consistent with the negative sign of D, and its large anisotropy also with the large magnitude of D. Finally attempted were the analyses including rhombicity ($E\neq0$, $g_x\neq g_y$), where, unfortunately, we were not able to determine the best fit uniquely. Although many sets of parameters gave comparably good fits in this case, the above features still held for the sets. Consequently the above features must exist in the magnetic properties of **1c**.

ESR. It was found that the neat powder samples commonly exhibit broad ESR spectra even at 4.2 K. These results are due to dipolar interactions among neighboring Co ions. The dipolar interactions, as well as intermolecular exchange interactions, can be reduced by doping the compounds in diamagnetic crystals. Sharpened spectra were thus obtained from

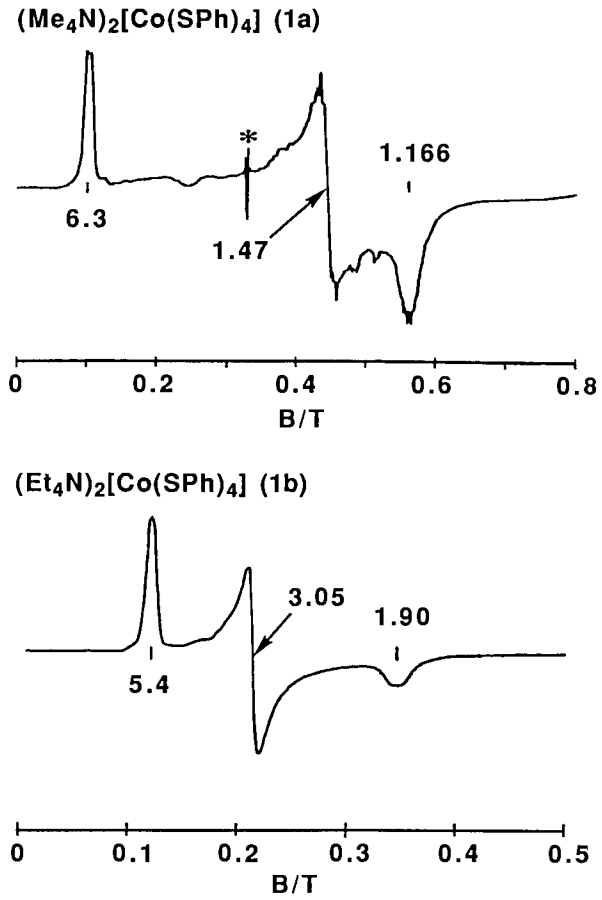

Fig. 4. ESR spectra of the Zn-doped powder samples (Co/Zn=1%) of $(Me_4N)_2[Co(SPh)_4]$ (**1a**) and $(Et_4N)_2[Co(SPh)_4]$ (**1b**) measured at 4.2 K. The signals marked with * are from a radical impurity and Cr(III) in MgO used as a g-value marker.

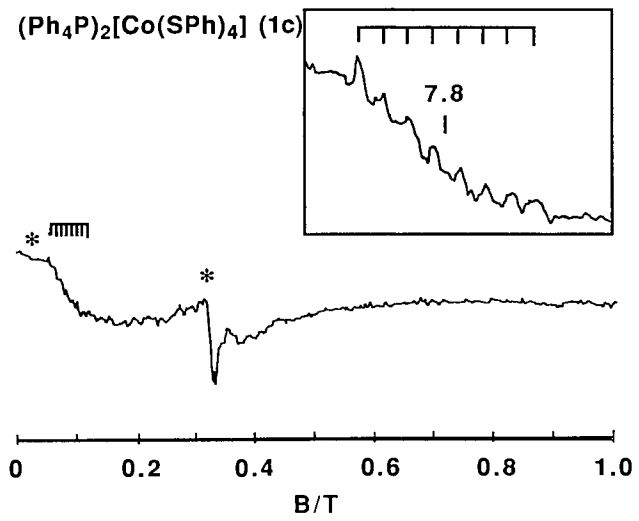

Fig. 5. ESR spectrum of the Zn-doped powder sample (Co/Zn=10%) of $(Ph_4P)_2[Co(SPh)_4]$ (**1c**): Conditions Temperature, 4.2 K; Sample amount, 30 μmol; Power 1 mW; Amplitude, 1.25×1000; Modulation, 10 G at 100 kHz. The signals marked with * are due to impurities. The g'=7.8 signal is enlarged in the inset.

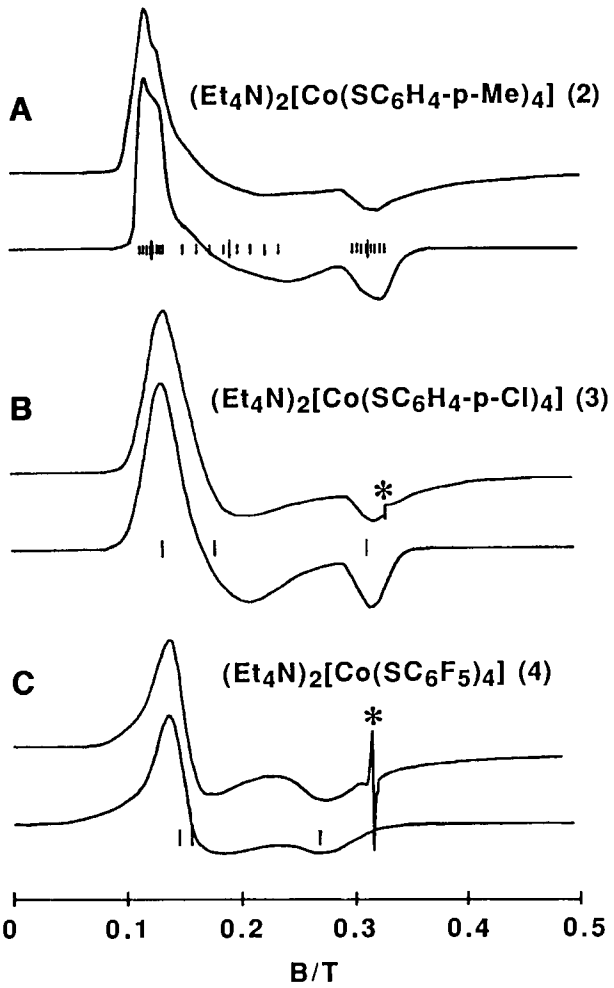

Fig. 6. ESR spectra of the Zn-doped powder samples (Co/Zn=1%) of $(Et_4N)_2[Co(SC_6H_4\text{-}p\text{-}Me)_4]$ (**2**), $(Et_4N)_2[Co(SC_6H_4\text{-}p\text{-}Cl)_4]$ (**3**), and $(Et_4N)_2[Co(SC_6F_5)_4]$ (**4**) obtained at 4.2 K. The lower spectrum for each is the result from the computer simulation. The signals marked with * are from Cr(III) in MgO (B) and from a radical impurity (C).

the Zn-doped samples as shown in Fig. 4 for **1a** and **1b**, in Fig. 5 for **1c**, and in Fig. 6 for **2**—**4**. The sharpening of the spectra was especially drastic for **1a** and **1b**. The principal g'-values obtained from the Zn-doped spectra are summarized in Table 2. For **1b**, **1c**, and **2**—**4**, the Zn-doped powder spectra are practically identical with the corresponding neat powder spectra excepting the difference in line width. This suggests that the geometric distortions are not altered appreciably by the Zn-doping. (Especially **1c** is known to be isomorphous and isostructural to the Zn analog.[21]) For **1a**, however, the two spectra are slightly different, although this difference does not seem to be so important.[31] Thus in the two states the geometric distortions of **1a** are not exactly the same, but still essentially similar.

In the Zn-doped spectrum of **1a**, each signal feature contains a partially resolved hyperfine structure due to

Table 2. Results from the ESR Measurements of the Zn-Doped Powder Samples at 4.2 K

Compounds	g′-Values			hfcc/mT[a]			E/D[b]	g_{av}
	g'_1	g'_2	g'_3	A_1	A_2	A_3		
$(Me_4N)_2[Co(SPh)_4]$ (**1a**)	6.3	1.47	1.166	0.8	4.0	4.4	−0.21	2.19
$(Et_4N)_2[Co(SPh)_4]$ (**1b**)	5.4	3.05	1.90			2*	0.19	2.16
$(Ph_4P)_2[Co(SPh)_4]$ (**1c**)	7.8[c]			9.2[c]			−0	
$(Et_4N)_2[Co(SC_6H_4\text{-}p\text{-}Me)_4]$ (**2**)	5.1	3.3	2.04	3*	12*	4*	0.14	2.14
$(Et_4N)_2[Co(SC_6H_4\text{-}p\text{-}Cl)_4]$ (**3**)	4.8	3.6	2.08				0.10	2.12
$(Et_4N)_2[Co(SC_6F_5)_4]$ (**4**)	4.3	4.0	2.35				0.02	2.11

a) The values marked with * are from the simulations. b) The estimated errors are about ±0.02. The negative sign means negative D value. c) Very weak.

^{59}Co (I=7/2). The coupling constants are A/mT=0.8 at g'=6.3, 4.0 at g'=1.47, and 4.4 at g'=1.166. As for **1b**, we did not observe any resolved hyperfine splittings. However, the line shape of the g'=1.90 feature is indicative of unresolved structure of A≈2 mT (Fig. 4).

No apparent ESR signals were obtained from **1c** despite that we measured some forms of samples from different sources each. Both the Zn-doped (Co/Zn=10%) and the neat powder samples of **1c** exhibit only an incomplete and extremely weak signal up to 1.0 T even at 4.2 K. This signal is centered at g'=7.8 with a resolved hyperfine structure of A=9.2 mT, although the signal was too weak to be detected clearly (Fig. 5). Under the same conditions, the low-field components of the other compounds gave 100—1000 times the intensity of the g'=7.8 signal. No signal has been obtained from the Co/Zn=1% sample, which is however consistent with the extraordinary weakness of the g'=7.8 signal. Although uncertainty remains as to whether the g'=7.8 signal is attributable to **1c**, it is at least clear that the ESR signal of this compound is extremely weak or even can not be observed. Weakness (or absence) of ESR signals is often attributed to intermolecular exchange interaction. However, the fact that weak (or no) signal is invariably observed from the three different forms shows that this is not the case. Additionally, the crystallographic data of the X-ray isomorphous Fe analog show that the nearest-neighboring metal ion sites are separated sufficiently by 10 Å. The origin of the weakness is discussed later.

The ESR spectra of Zn-doped **2**, **3**, and **4** are relatively broad, so that we simulated the spectra to estimate the principal g'-values (Fig. 6). The simulations are based on the S'=1/2 effective spin Hamiltonian using the gaussian-type lineshape function.[5] The compound **2** gives a characteristic signal shape from 0.1 to 0.2 T. This shape can only be reproduced when a fairly large but unresolved hyperfine splitting is assigned to the principal g'=3.3 component. On the other hand, the spectra of **3** and **4** show no evidence for hyperfine splittings, so that hyperfine interaction was neglected in the simulations of these spectra.

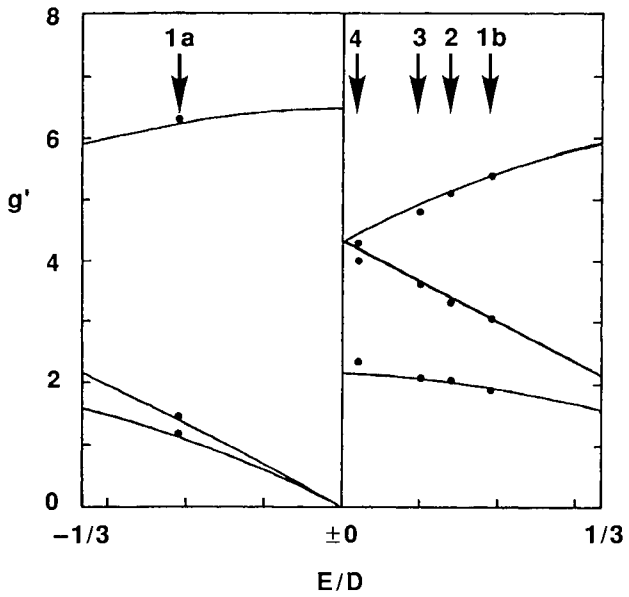

Fig. 7. Theoretical curves of g'-values versus E/D accompanied by the experimental results from the Zn-doped powder samples.

In contrast to the low-temperature behavior of μ_{eff}, g'_p does not depend on D^* but only on g_p and E/D when $D^* \gg h\nu$=0.3 cm^{-1}. The variation of g'_p vs. E/D is graphed in Fig. 7 for the transition within the lower Kramers doublet, together with the experimental values from the Zn-doped powder spectra. Since the intensities of the observed signals all decrease with increasing temperatures above 4.2 K, the signals are assigned to arise from the lower doublets. Based on these assignments and approximation of isotropic g-factor, we have estimated E/D and g_{av} (Table 2). These g_{av} values are in good agreement with those obtained from the susceptibility results.

The ESR spectra obtained from the frozen solution samples are less informative. All the compounds including **1c** exhibit similar spectra, which consist of broad features at g'≈4 and ≈2. However, the observation of such broad spectra is not surprising. In solution, no uniformity is anticipated among the conformations or distortions of the complexes, to which the ESR spectrum is sensitive as typically demon-

strated by the powder spectra of **1a—c**.

Discussion

Magnetic Properties of 1c. We have estimated the zfs parameters, D^* and E/D, from the susceptibility and ESR results, respectively, for **1a**, **1b**, and **2—4**. For **1c**, while it is now clear from the susceptibility data that $D^*\approx 100$ cm^{-1} and $D<0$, E/D still remains ambiguous. The ESR signals from the powder samples of **1c** are always too weak to allow a definite estimate of E/D. However, the extraordinary weakness is indicative of a negligibly small E value. When $E/D=-0$ (here '-0' means $E=0$ and $D<0$ simultaneously), the lower Kramers doublet consists of pure $S_z=\pm 3/2$ states. Then the transition within this doublet is forbidden and no (or very weak) ESR signal is expected. Indeed the transition within the upper doublet is alternatively allowed, but large zfs as in **1c** makes it difficult to detect this transition because of insufficient thermal distribution to this doublet. A literature example for this situation is bis(*N*-*t*-butylpyrrolecarbaldimino)cobalt(II),[13,15] which was reported to be ESR silent and assigned as $E/D=-0$. On the other hand, when E is not negligible, the ground $S_z=\pm 3/2$ states are mixed with the $S_z=\pm 1/2$ ones and, hence the transition gains some intensity. This is the very case for Zn-doped **1a** ($E/D=-0.21$), which exhibits enough intense ESR spectrum. We therefore conclude that $E/D=-0$ is most likely for **1c**. We also point out that the g'_z value predicted for $E/D=-0$ ($g'_z=3g_z=9.4$) can be compared with the observed value of $g'=7.8$.

g-Factor. For high-spin tetrahedral Co(II) complexes, the deviation of g-values from the free-electron value arises mainly from the interaction between the ground $^4A_2$ and the lowest excited $^4T_2$ states through the spin-orbit coupling. Thus g_{av} is expressed as[30]

$$g_{av}\approx 2-8k^2\lambda_0/\Delta_t, \qquad (3)$$

where k represents the orbital-reduction factor, λ_0 the spin-orbit coupling constant for the free ion (-178 cm^{-1}), and Δ_t the energy separation between the e and t_2 orbitals (4030 cm^{-1}).[32] By using the most reliable values of $g_{av}=2.16$—2.19, which are from the ESR results of Zn-doped **1a** and **1b**, we obtain $k=0.67$—0.73. This k value is remarkably small compared with those of other tetrahedral Co(II) complexes; for example, $k=0.8$ for a CoN_4 chromophore,[14] $k=0.9$ for a CoO_4 chromophore,[33] and $k=0.92$ for $CoCl_4^{2-}$.[34] This remarkable reduction of k, together with that of the Racah parameter B,[32] shows a highly covalent character of the Co-S bondings. Such high covalency was also reported for Fe-S bondings.[35]

The remarkable g-anisotropy in **1c**, together with the large zfs, suggests that the electronic structure is deviated extremely from that under T_d symmetry. This deviation must contain a remarkably low excitation energy of the z-component of $^4T_2$, as is evident from the large g_z value. This excitation energy could be estimated by using a modified version of Eq. 3 if the obtained g-values were sufficiently reliable. However, unfortunately, the g-values of **1c** are less reliable because they were obtained only from powder susceptibility data. Further ESR and susceptibility studies on **1c** are now in progress by using single crystals.

ZFS Parameters. Previously Makinen et al.[9] reported that D^* can be a good measure of the coordination number for high-spin Co(II) complexes: The D^* value should be in the range of 0—6.5 cm^{-1} for tetrahedral ones, 10—25 cm^{-1} for pentacoordinate ones, and larger than 25 cm^{-1} for octahedral ones. If we followed this criterion, we could assign **3** as a pentacoordinate complex, and **1c** as an octahedral one. However, these assignments are unreasonable, contradicting the X-ray data which undoubtedly show a tetrahedral geometry for **1c**. As has been pointed out elsewhere,[5] the criterion by Makinen et al. is not so strict. This is because the complexes which they treated are rather simple and possess mild distortions in the coordination geometries.

Interestingly, the D^* values of **1a**, **1b**, and **2**, though they are much smaller than that of **1c**, can be presumed to be *large* (when compared with simple complexes) according to the criterion. It is of great interest to examine whether the *large* D^* values can be interpreted in terms of the tetragonal compression/elongation, which has been supposed to be an important geometric factor in metal-thiolate complexes.[21—27] There have been several theoretical studies concerning the relationship between zfs and the magnitude of the tetragonal distortion. For example, according to the equation given by Fukui et al. (Eq. 25 in Ref. 36), the contribution to D from the tetragonal distortion, D_{tet}, for the CoS_4 cores is expressed as

$$D_{tet}/\text{cm}^{-1}\approx 0.57(\theta/\text{deg}-109.47). \qquad (4)$$

Here we have used $\Delta_t=4030$ cm^{-1}, $\lambda=k\lambda_0\approx -125$ cm^{-1}. θ is the S-Co-S′ angle whose bisector coincides with the tetragonal axis. Equation 4 shows that, as θ varies in a range plausible for the CoS_4 cores (95°—120°),[21] the D_{tet} value varies from -8 to 6 cm^{-1}. Thus, for **1a**, **1b**, and **2**, it seems reasonable to attribute the *large* zfs (in the sense of Makinen's criterion) to large tetragonal distortion of the CoS_4 core. This situation further leads to another important conclusion that the zfs in **1c** is too large to be interpreted in terms of the tetragonal distortion.

Magnetic Properties and Thiolate Orientation. Since **1a**, **1b**, and **1c** have the identical anion complex, the wide variety among their magnetic properties provides a good example for the sensitivity of Co(II) complexes to changes in coordination environment. This wide variety also provides an opportunity to investigate the relationship between the geometric distortion and the electronic structure in metal-thio-

late complexes. The X-ray molecular structure of **1c** was reported previously, showing the D_{2d} conformation for the overall orientation of the SPh^- ligands (Fig. 1).[21] Although no X-ray data are available for the other compounds, the Zn analog of **1a**, $(Me_4N)_2[Zn(SPh)_4]$ (**5**), has been studied by X-ray crystallography.[25] Because the ESR spectrum of Zn-doped **1a** is reasonably sharp, **1a** is expected to have the same geometry as **5** at least in the Zn-doped sample. It is known that **5** has the S_4 conformation for the overall thiolate orientation (Fig. 1). Notably the S-M-S′ angles are very similar between **1c** and **5**. The observation of the remarkably different magnetic properties between **1c** and Zn-doped **1a**, therefore, confirms the importance of the thiolate orientation in metal-thiolate complexes.

In the D_{2d} conformation, the phenyl rings lie in the same direction with respect to the z-axis. Thus the sulfur p_π-orbitals, which are in conjugation with the corresponding phenyl π-orbitals, are all perpendicular to the z-axis. This coordination mode will produce a strong axial ligand field and, hence give large and axial zfs. This expectation is consistent with the observed zfs for **1c**. In the S_4 conformation, on the other hand, the sulfur p_π-orbitals are no more in phase, or interact with a specific metal d-orbital. Little contribution is therefore expected toward zfs from the ligand field due to the sulfur p_π-orbltals. This explains the relatively small D^* value of **1a**.[37] It seems from Eq. 4 that zfs under the S_4 conformation is rather dominated by the tetragonal distortion and some rhombic distortion, where the latter breaks the strict S_4 symmetry and generates the E parameter. Similar explanation can be adopted to the zfs of **1b**, whose Fe(II)[22] and Ni(II)[26] analogs also have the S_4 conformation.

Based on the above consideration, we infer that **2**, **3**, and **4** have the S_4 conformation because their D^* values are rather small.[38] The slightly larger D^* value of **3** is probably due to a minor difference in the thiolate orientation. Here it is worth noting that the ortho-substitutions in **4** may lead to another type of thiolate conformation as found in Fe(2,3,5,6-tetramethylbenzenethiolate)$_4^-$. In this complex, steric hindrance due to the ortho methyl groups prevents the Fe-S-C and phenyl-ring planes from being coplanar. They are rather perpendicular to each other, though the overall geometry retains S_4 symmetry.[39] Recently the electronic structure of this complex was examined closely.[35]

Finally we turn our attention to the active-site geometry of rubredoxin. The ESR spectrum of oxidized rubredoxin is featured by an isotropic $g'=4.3$ feature,[40] which is indicative of an extremely rhombic geometry ($E/D=1/3$) around the Fe ion. Interestingly, nearly extreme rhombicity is found in the zfs of **1a** and **1b** (See Table 2). At the moment it is not clear whether the extreme rhombicity is only an accidental phenomenon or not. Nevertheless, it is notable that the appearance of the extreme rhombicity is not consistent with the D_{2d} conformation proposed so far for the active-site geometry of rubredoxin. This situation implies the importance of the seemingly irrelevant distortion; the rotations of two thiolates by ca. 30° from the idealized positions. The importance of this distortion was previously pointed out by Ueyama et al. from extended Hückel MO calculations.[20] Unfortunately it seems that neither ESR nor magnetic susceptibility study has been performed for Co(II)-substituted rubredoxin, though the Co(II)-substitution has been accomplished.[1] However, the present work arouses the interest in the magnetic properties of Co(II)-substituted rubredoxin, and other Co(II)-substituted metalloproteins possessing rubredoxin-type active sites. Such metal-exchange approaches will provide further insight into the geometric effects on the electronic structure and the electron-transfer properties of the sites.

We thank Dr. Ryuichi Imamura for the measurements of the NMR spectra. This work is partially supported by the Grant-in-Aid for Sientific Research No. 01470050 from the Ministry of Education, Science and Culture.

References

1) S. W. May and J.-Y. Kuo, *Biochemistry*, **17**, 3333 (1978).
2) L. C. Kuo and M. W. Makinen, *J. Am. Chem. Soc.*, **107**, 5255 (1985).
3) R. Bicknell, A. Schäffer, S. G. Waley, and D. S. Auld, *Biochemistry*, **25**, 7208 (1986).
4) M. Good and M. Vask, *Biochemistry*, **25**, 3328 (1986).
5) R. A. Martinelli, G. R. Hanson, J. S. Thompson, B. Holmquist, J. R. Pilbrow, D. S. Auld, and B. L. Vallee, *Biochemistry*, **28**, 2251 (1989). References concerning the theoretical foundation of the ESR simulation are cited therein. The difference between their simulation and ours is that theirs includes the M_I dependence of line widths while ours not
6) S. Dahlin, B. Reinhammar, and Ånström, *Biochemistry*, **28**, 7224 (1989).
7) W. D. Behnke and B. L. Vallee, *Proc. Natl. Acad. Sci. U.S.A.*, **69**, 2442 (1972).
8) L. Sacconi and R. Morassi, *J. Chem. Soc. A*, **1970**, 575.
9) M. W. Makinen, L. C. Kuo, M. B. Yim, G. B. Wells, J. M. Fukuyama, and J. E. Kim, *J. Am. Chem. Soc.*, **107**, 5245 (1985).
10) L. J. Guggenberger, C. T. Prewitt, P. Meakin, S. Trofimenko, and J. P. Jesson, *Inorg. Chem.*, **12**, 508 (1973).
11) A. Bencini and D. Gatteschi, *Inorg. Chem.*, **16**, 2141 (1977).
12) A. Bencini, C. Benelli, D. Gatteschi, and C. Zanchini, *Inorg. Chem.*, **18**, 2137 (1979); *ibid.*, **18**, 2526 (1979); *ibid.*, **19**, 1301 (1980); *ibid.*, **19**, 3839 (1980).
13) A. Bencini and D. Gatteschi, *Transition Met. Chem. (N.Y.)*, **8**, 1 (1982).
14) L. Banci, C. Benelli, D. Gatteschi, and F. Mani, *Inorg.*

Chem., **21**, 1133 (1982).
15) H. Drulis, K. Dyrek, K. P. Hoffmann, S. K. Hoffmann, and A. Weselucha-Birczynska, *Inorg. Chem.*, **14**, 4009 (1985).
16) A. J. Thomson, "Metallproteins," Part 1, ed by P. M. Harrison, Macmillan Press, Hampshire (1985).
17) K. D. Watenpaugh, L. C. Sieker, and L. H. Jensen, *J. Mol. Biol.*, **131**, 509 (1979).
18) M. Frey, L. Sieker, F. Paya, R. Haser, M. Bruschi, G. Pepe, and J. LeGall, *J. Mol. Biol.*, **197**, 525 (1987).
19) R. A. Bair and W. A. Goddard III, *J. Am. Chem. Soc.*, **100**, 5669 (1978); L. Noodleman, J. G. Norman, Jr., J. H. Osborne, A. Aizman, and D. A. Case, *J. Am Chem. Soc.*, **107**, 3418 (1985).
20) N. Ueyama, T. Sugawara, K. Tatsumi, and A. Nakamura, *Inorg. Chem.*, **26**, 1978 (1987).
21) D. Swenson, N. C. Baenzigar, and D. Coucouvanis, *J. Am. Chem. Soc.*, **100**, 1932 (1978).
22) D. Coucouvanis, D. Swenson, N. C. Baenzigar, C. Murphy, D. G. Holah, N. Sfarnas, A. Simopoulos, and A. Kostikas, *J. Am. Chem. Soc.*, **103**, 3350 (1981).
23) S. A. Koch, L. E. Maelia, and M. Millar, *J. Am. Chem. Soc.*, **105**, 5944 (1983).
24) T. Sugawara, N. Ueyama, A. Nakamura, and N. Yasuoka, The 39th Symposium on Coordination Chemistry of Japan, Mito, 1989, Abstr., No. 3D05, p. 671.
25) N. Ueyama, T. Sugawara, N. Sasaki, A. Nakamura, S. Yamashita, Y. Wakatsuki, H. Yamazaki, and N. Yasuoka, *Inorg. Chem.*, **27**, 741 (1988).
26) T. Yamamura, H. Miyamae, Y. Katayama, and Y. Sasaki, *Chem. Lett.*, **1985**, 269.
27) I. G. Dance, *J. Am. Chem, Soc.*, **101**, 6264 (1979).
28) a) The signs are positive for the chemical shifts downfield of Me_4Si peak, and are negative for those upfield. b) Unfortunately no ortho-hydrogen peaks were observed in a range of −30—30 ppm. For $Fe(SPh)_4^{2-}$, the *o*-H peak is very broad because of the vicinity to the paramagnetic Fe ion. Thus it is likely that the *o*-H peaks of the cobalt thiolates are also broad and difficult to detect. (K. S. Hagen, J. G. Reynolds, and R. H. Holm, *J. Am. Chem. Soc.*, **103**, 4054 (1981)).
29) B. A. Averill, T. Herskovitz, R. H. Holm, and J. A. Ibers, *J. Am. Chem. Soc.*, **95**, 3523 (1973).
30) J. S. Griffith, "The Theory of Transition Metal Ions," Cambridge University Press, Cambridge (1961).
31) The neat powder sample of **1a** exhibits broad features at $g_1' \approx 6$, $g_2' \approx g_3' \approx 2$ ($E/D \approx 1/3$). It is known that an exact isomorphism does not occur between **1a**[27] and its Zn analog.[25]
32) R. W. Lane, J. A. Ibers, R. B. Frankel, G. C. Papaefthymiou, and R. H. Holm, *J. Am. Soc.*, **99**, 84 (1977).
33) K. Kojima, J. Matsuda, N. Kojima, T. Ban, and I. Tsujikawa, *Bull. Chem. Soc. Jpn.*, **60**, 3213 (1987).
34) W. DeW. Horrocks, Jr. and D. A. Burlone, *J.Am. Chem. Soc.*, **98**, 6512 (1976).
35) J. C. Deaton, M. S. Gebhard, S. A. Koch, M. Millar, and E. I. Solomon, *J. Am. Chem. Soc.*, **110**, 6241 (1988); M. S. Gebhard, J. C. Deaton, S. A. Koch, M. Millar, and E. I. Solomon, *ibid.*, **112**, 2217 (1990).
36) K. Fukui, H. Ohya-Nishiguchi, and N. Hirota, *Mol. Phys.*, **71**, 1269 (1990).
37) Stricktly speaking, the D^* value of Zn-doped **1a** is not known. However, the ESR spectrum of the Zn-doped powder sample was well analyzed by using isotropic *g*-factor. This fact indicates that the D^* value is not so large, either.
38) A preliminary single crystal X-ray analysis of **3** confirms the S_4 conformation for this compound: $(Et_4N)_2[Co(SC_6H_4\text{-}p\text{-}Cl)_4]$; $P2_1/c$, a=12.388, b=12.251, c=59.850 Å, β=95.85°, V=9035.9 Å^3, Z=8. The complete structure determination, however, has been hampered because the lattice parameter c is too large. We thank Dr. Hideki Masuda (Institute for Molecular Science) for the X-ray analysis.
39) M. Millar, J. F. Lee, S. A. Koch, and R. Fikar, *Inorg. Chem.*, **21**, 4105 (1982).
40) K. K. Rao, M. C. Evans, R. Cammack, D. O. Hall, C. L. Thompson, P. J. Jackson, and C. E. Johnson, *Biochem. J.*, **129**, 1063 (1972).

Synthesis of Strapped, Dimeric, and Trimeric Porphyrins Based on Intramolecular Macrocyclization Reactions

Atsuhiro Osuka, Fumikazu Kobayashi, and Kazuhiro Maruyama*
Department of Chemistry, Faculty of Science, Kyoto University, Kyoto 606
(Received November 2, 1990)

Strapped porphyrins were prepared directly by the acid-catalyzed condensation reaction of 3,3′-diethyl-4,4′-dimethyl-2,2′-dipyrrylmethane and methylenedioxy bridged dialdehydes having a strap linkage longer than 7 atoms. Dimeric and trimeric porphyrins with coplanar and orthogonal (T-shape) geometries were also synthesized in good yields as an application of this method. In the strapped porphyrins, the distortion of porphyrin ring increases systematically on shortening the strap linkage, which is confirmed by their ^{1}H NMR data, red shifted absorption, and fluorescence spectra. In the coplanar dimeric and trimeric porphyrins, the electronic interactions between the porphyrins were distinctly observed, while in the orthogonal "T-shaped" dimers and "H-shaped" trimers, appreciable electronic interactions were not observed.

Important roles of porphyrins and their analogous tetrapyrroles as well as their aggregates in biological proceses such as aspiration, metabolism, and photosynthesis have stimulated the development of a wide range of synthetic porphyrin model compounds in recent years.[1] Among them, 5,15-diaryloctaalkylporphyrin is an useful unit for the model construction because of their easy preparation, high symmetry, and thermal stabillity of atropisomers.[2-4] Synthesis of these porphyrins from 5,5′-unsubstituted dipyrromethane and aromatic aldehydes was first reported by Ogoshi et al.[2] and later modified by Gunter and Mander[3] and Young and Chang.[4] Recently we have found the improved conditions (CCl_3CO_2H/CH_3CN) for the synthesis of these porphyrins[5] and applied them to the synthesis of conformationally restricted oligomeric porphyrins.[6]

Described herein is the direct synthesis of strapped porphyrins from the dialdehydes as well as the synthesis of a novel class of dimeric and trimeric porphyrins based on our improved method.[7,8]

In relation to the importance of porphyrin ring-distortion in biological functions of hemoproteins and photosynthetic pigments, considerable attention has been focused on the synthesis and characterization of permanently distorted porphyrins.[9] One of important issues is the details of how the distortions of the macrocyclic ring influence their electronic and optical properties. Theoretical calculations on the effects of nonplanarity indicate that the highest occupied molecular orbital should be destabilized with respect to the lowest unoccupied molecular orbital, resulting in a red shift of the first visible absorption band.[9] Extremely short-chain-strapped porphyrins are very simple and useful model for this purpose.[10] While the dimeric and trimeric porphyrins synthesized here have rather restricted coplanar and orthogonal geometries and thus are promising models for studies on the geometry dependence of photoinduced excitation energy-transfer and electron-transfer processes.[11]

Results and Discussion

Synthesis of Strapped Porphyrins. Strapped porphyrins synthesized here are 5,15-diphenyl-2,8,12,18-tetraethyl-3,7,13,17-tetramethylporphine derivatives in which ortho positions of the *meso*-phenyl groups are bridged by a methylenedioxy chain with chain length longer than 7 atoms.[12] General procedure is as follows: 3,3′-diethyl-4,4′-dimethyl-2,2′-dipyrrylmethane **1**[13] (100 mg, 0.43 mmol) and the dialdehyde **2** (0.22 mmol) were dissolved or suspended in dry acetonitrile under N_2, and to this mixture a catalytic amount of trichloroacetic acid (10 mg) was added.[5] After standing at room temperature for about 5 h, *p*-chloranil (0.3 g, 1.2 mmol) in dry tetrahydrofuran (THF, 10 ml) was added and the mixture was stirred overnight. Porphyrin product was separated on alumima column (activity III) using CH_2Cl_2 as eluent, and recrystallized from CH_2Cl_2–methanol (Table 1). The cyclization yields were found to be dependent on the concentrations of the reactants (Table 1, Runs 1—4). The highest yield (15%) was obtained at [**1**]= 0.02 M (1 M=1 mol dm^{-3}). At high concentrations [**1**]>0.05 M, the formation of the dark blue insoluble

Table 1.

Run	Dialdehyde	Chain length of X	Concn of **1**/M	Product	Yield/%
1	**2a**	7	0.05	**3a**	6
2	**2a**	7	0.03	**3a**	13
3	**2a**	7	0.02	**3a**	15
4	**2a**	7	0.01	**3a**	Trace
5	**2b**	12	0.02	**3b**	21
6	**2c**	8	0.02	**3c**	25
7	**2d**	6	0.02	**4d**	5
8	**2e**	5	0.02	**4e**	2
9	**2f**	14	0.02	**3f**	33
10	**2g**	8	0.02	**3g**	54
11	**2h**	8	0.03	**3h**	61
12	**2i**	8	0.02	**3i**	25
13	**2j**	8	0.02	**4j**	Trace

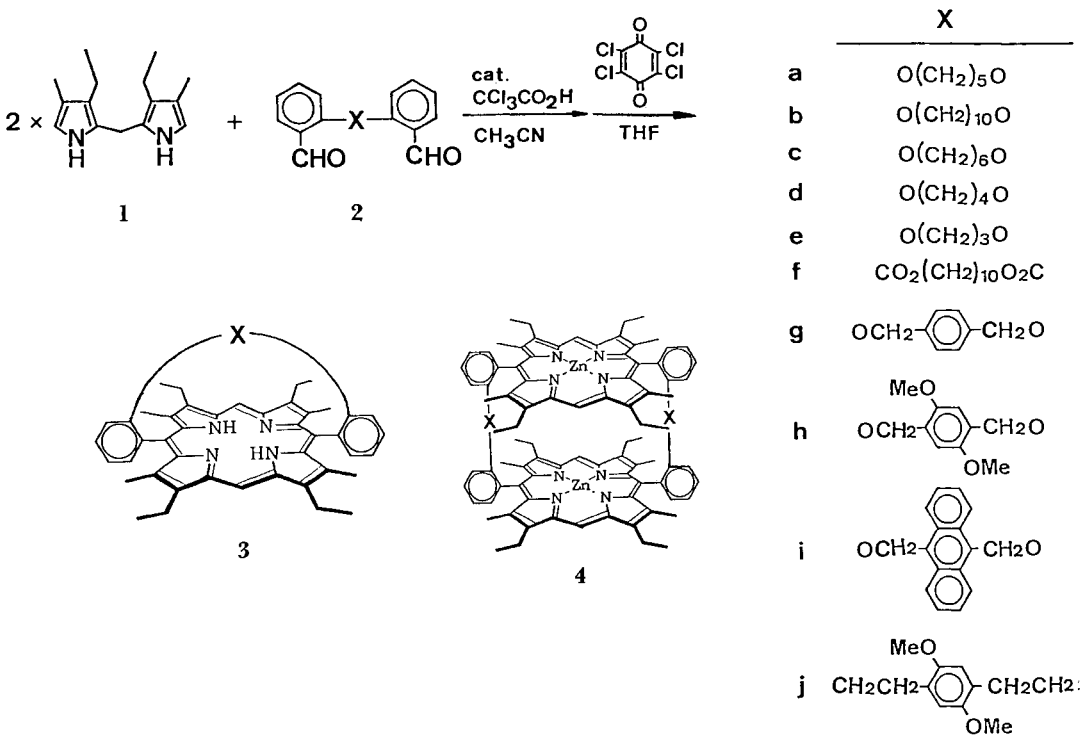

Scheme 1.

solids took place predominantly, while at low concentrations [**1**]<0.01 M, the yield decreased significantly. In the cases of dialdehydes **2d** and **2e**, the corresponding strapped porphyrins were no longer formed but instead face-to-face porphyrin dimers **4d** and **4e** were obtained in 5% and 2%, respectively (Table 1, Runs 7, 8). Although the yields of **4d** and **4e** are not so high, this reaction will be useful for the preparation of porphyrin dimers of this type in view of its simple manipulation, easy separation, and direct synthesis from easily available starting materials. Of dialdehydes (**2k**, **2m**, and **2n**), only **2n** gave dimeric porphyrin **4n** in 2% yield (Scheme 2). This may be ascribed to more conformational flexibility or less steric hindrance of **2n** compared with **2k** and **2m**.

Strapped porphyrins **3g** and **3h**, in which the strap linkage contains an aromatic ring, were also prepared by this procedure in high yields (Table 1, Runs 10, 11). From the CPK (Corey-Pauling-Koltun) models, it is suggested that the porphyrin ring of **3g** and **3h** is

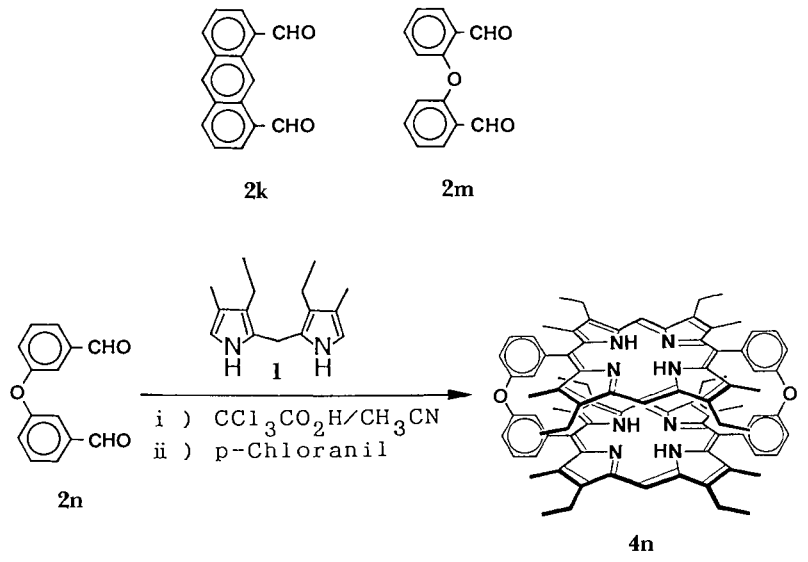

Scheme 2.

forced to be distorted due to the short *p*-xylylene linkages. However, the *p*-xylylene linkages are best-fitted in length for its porphyrinogen precursor. Probably this situation may account for the high yields of **3g** and **3h**. In the dialdehyde **2i**, *syn-anti* isomers exist due to the steric hindrance around 9,10-positions of the anthracene ring, and only the *syn* isomer seemed to adopt the preferred geometry for the porphyrinogen intermediate. Thus the yield of **3i** was lower than **3g**. The dialdehyde **2j**, which has the same number of chain atoms as **2g** and **2h**, gave no strapped porphyrin (Table 1, Run 13), presumably due to the more crowded steric hindrance around the methylene.

Synthesis of Dimeric and Trimeric Porphyrins. For the synthesis of the porphyrin trimer **9**, 5,15-bis(2,6-dimethoxyphenyl)etioporphyrin II (**5**)[5] was used as a precursor. Demethylation with BBr_3 gave the tetrahydroxy porphyrin **6** and then four hydroxyl groups were alkylated with 3-(aryloxy)propyl iodide **12** in refluxing acetone containing K_2CO_3 to give a both-face modified porphyrin **7** (43%). The iodide **12** was prepared in 3 steps from salicylaldehyde in a overall yield of 78% (Scheme 3). The acetal groups were hydrolyzed under acidic conditions[14] to give porphyrin tetraaldehyde **8**(H_2) (92%). We first tried the reaction of free-base porphyrin **8**(H_2) with dipyrrylmethane **1**, which resulted in the formation of the porphyrin trimer **9**(H_6) (*m/z* 2180.5, M^+) in rather poor yields (<10%). In contrast, the yield of the trimer **9**(H_4Zn) was markedly improved (35%) by the use of the zinc complex **8**(**Zn**) as the starting porphyrin (**9**(H_4Zn). Found: *m/z* 2244.120. Calcd for $C_{144}H_{153}N_{12}O_8Zn$: M+H, 2244. 126).

Face-to-face dimeric porphyrin **4e** was alternatively synthesized from the porphyrin dialdehyde (**15**) in a similar manner. Isomerically pure porphyrin dialdehyde **15** was prepared from *p*-xylylene-strapped porphyrin **3g** by the same procedure as **8**. The porphyrin dialdehyde **15**(**Zn**) was treated with dipyrrylmethane **1** in acetonitrile in the presence of trichloroacetic acid followed by oxidation with *p*-chloranil to give the porphyrin dimer **4e**(H_2Zn) in 56% yield as a mono-zinc complex. (Scheme 4).

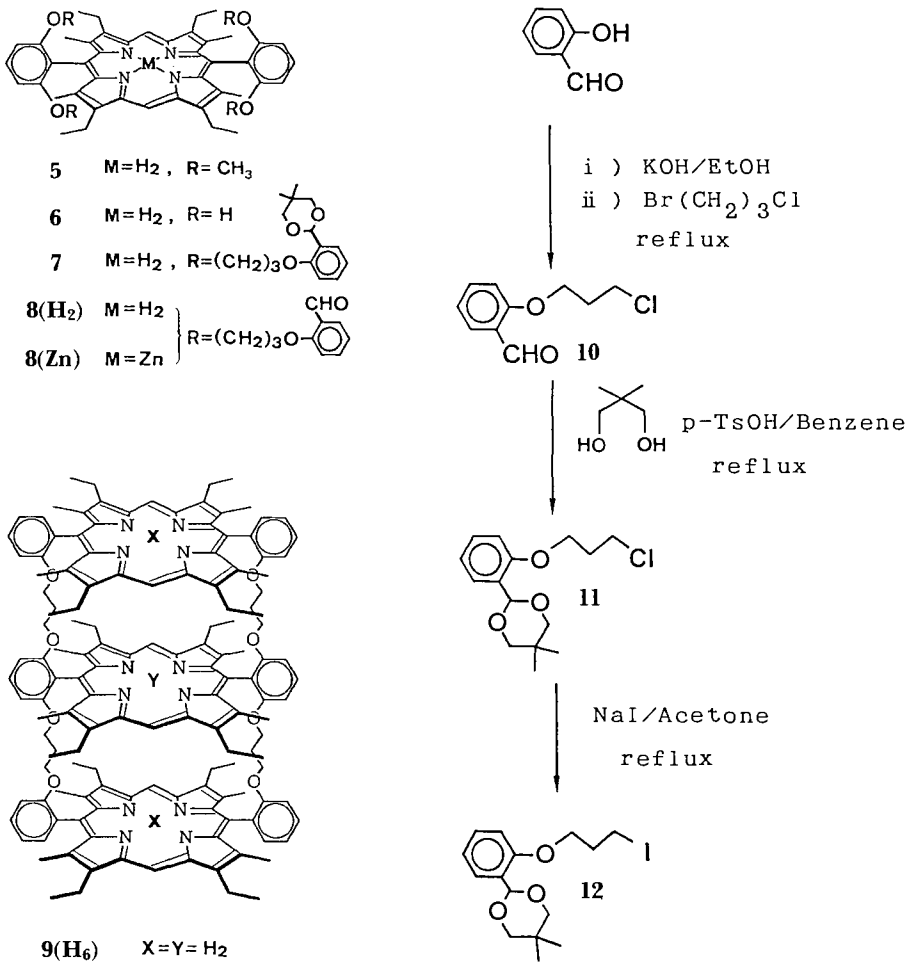

Scheme 3.

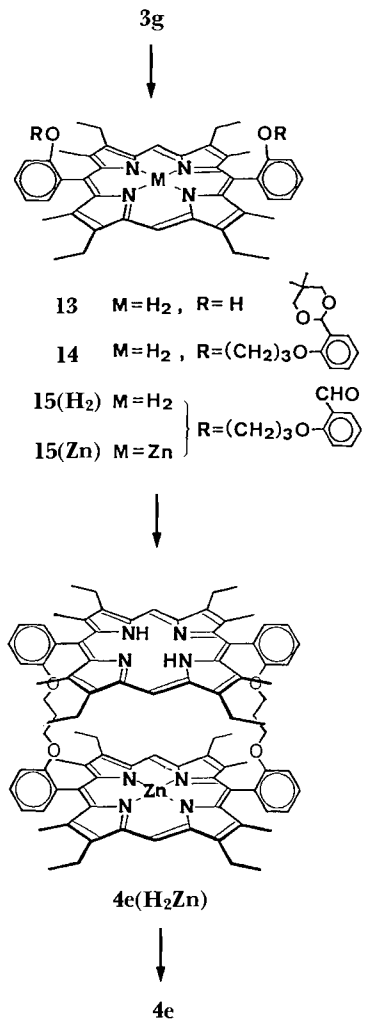

Scheme 4.

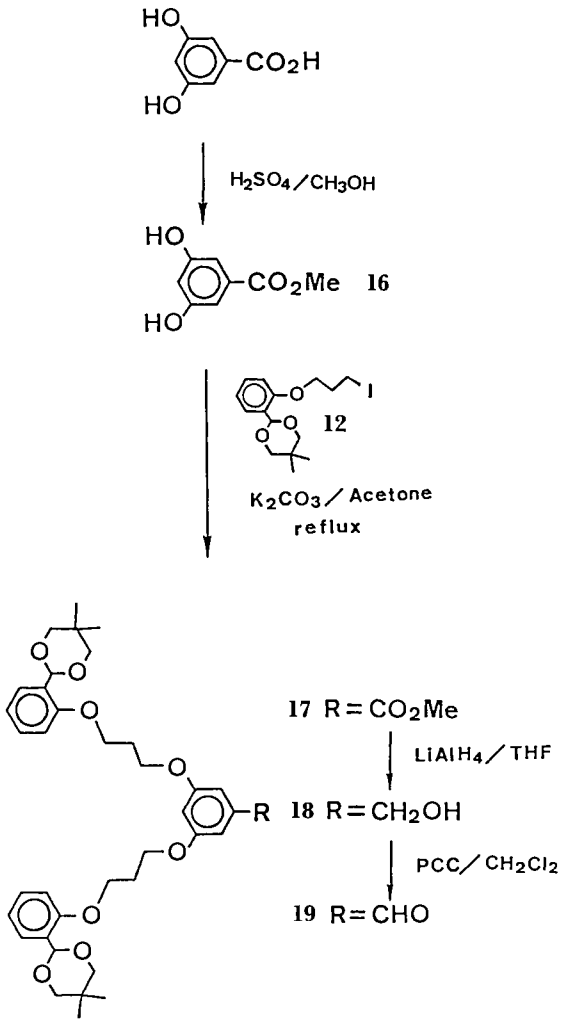

Scheme 5.

Table 2. ^{1}H NMR Chemical Shift of the Strapped Porphyrins in $CDCl_3$

Compound	δ/ppm				
	meso-H	*o*-H	β-CH_3	NH	X
3f	10.16	8.37	2.45	−2.19	3.31, −0.28, −0.83, −1.05, −1.18
3b	10.16	8.25	2.56	−2.33	3.68, 0.55, −0.94, −0.94, −1.69
3c	9.93	8.87	2.60	−1.70	2.29, −1.85, −2.85
3a	9.79	8.94	2.61	−1.27	0.96, −1.70, −3.49
3g	9.74	8.95	2.62	−1.36	2.92 (s, OCH_2), 3.42 (s, Ar-H)
3h	9.76	8.93	2.72, 2.57	−2.52	3.47, 2.44 (d, d, J=13Hz, OCH_2) 3.50 (s, Ar-H), 1.86 (s, OCH_3)
3i	9.39	8.91	2.66	−2.41	4.68 (s, OCH_2) 6.34, 6.11 (m, m, An-H)
28	10.22	8.08	2.48	−2.40	

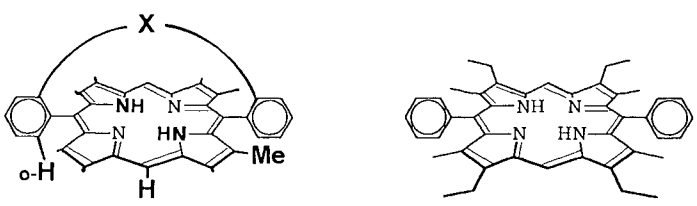

28

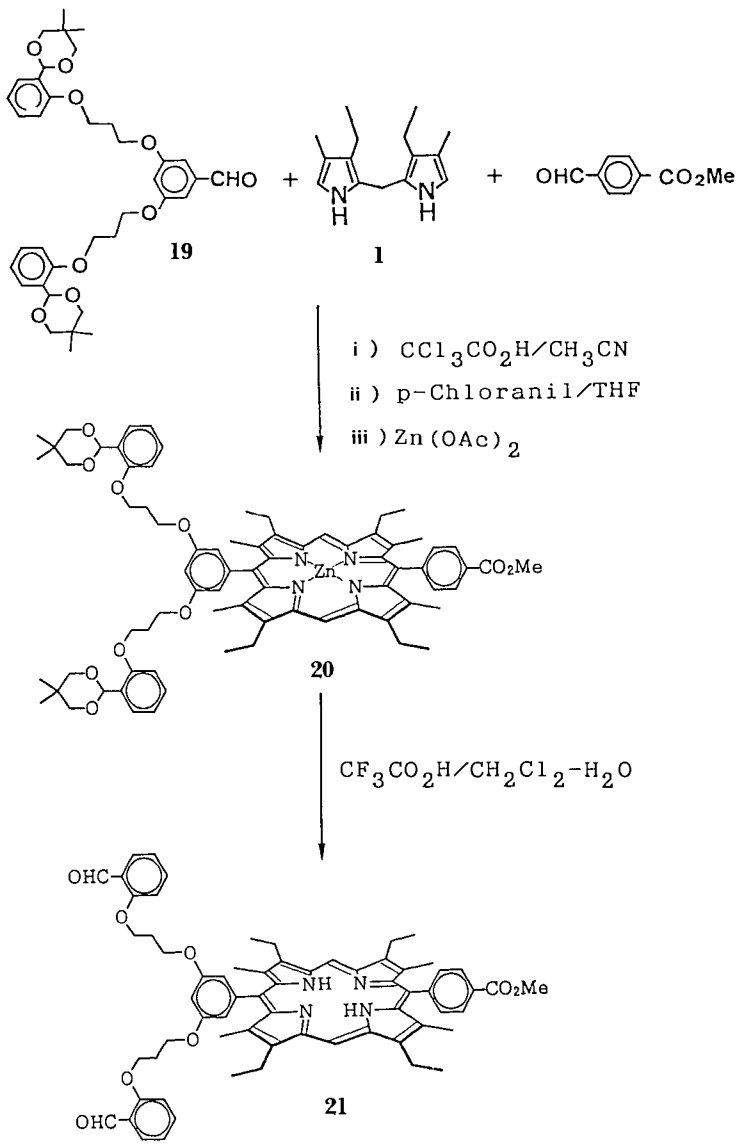

Scheme 6.

The "T-shaped" porphyrin dimers **22**(H_4) and **22**(H_2Zn) were also prepared from porphyrin dialdehydes **21**(H_2) and **21**(**Zn**) in 54% and 33% yield, respectively. (Scheme 5—7).

The "H-shaped" porphyrin trimer **27** was prepared in a different strategy. The strapped porphyrin **24** was first prepared from the corresponding dialdehyde **23** in 41% yield. The ester group on the strap chain was converted into the formyl group by reduction with $LiAlH_4$ followed by oxidation with activated MnO_2 in refluxing chloroform in a overall 82% yield.[15] The strapped porphyrin **26** thus prepared was treated with dipyrrylmethane **1** to give "H-shaped" porphyrin trimer **27**(H_6) in 59% yield (*m/z* 2181.6, $M+H^+$).[6] (Scheme 8).

Ring Distortion of Strapped Porphyrins. ^{1}H NMR and UV-vis Spectra. In their ^{1}H NMR spectra of methylene chain strapped porphyrins (**3a**, **3b**, **3c**, and **3f**), the methylene protons of the strap was significantly upfield shifted in accord with these protons lying above the porphyrin plane (Table 2). On shortening the methylene strap, the ring current effect for the *meso*-H and NH protons decreased systematically presumably due to the ring distortion from planarity. In addition, the ortho protons of the *meso*-phenyl groups were downfield shifted in **3a** and **3c**, suggesting that the phenyl rings are tipped in such a way to place the ortho phenyl protons moving closely into the deshielding field of the porphyrin ring current (Table 2, Fig. 1). Soret and Q-bands of the strapped porphyrins were also red-shifted on shortening the methylene chains, showing the significant perturbations of the π orbitals (Table 3).[9,16]

Similar tendency was observed in the xylene-strapped porpyrins **3g** and **3h**, in which the meso protons were upfield shifted and the ortho phenyl

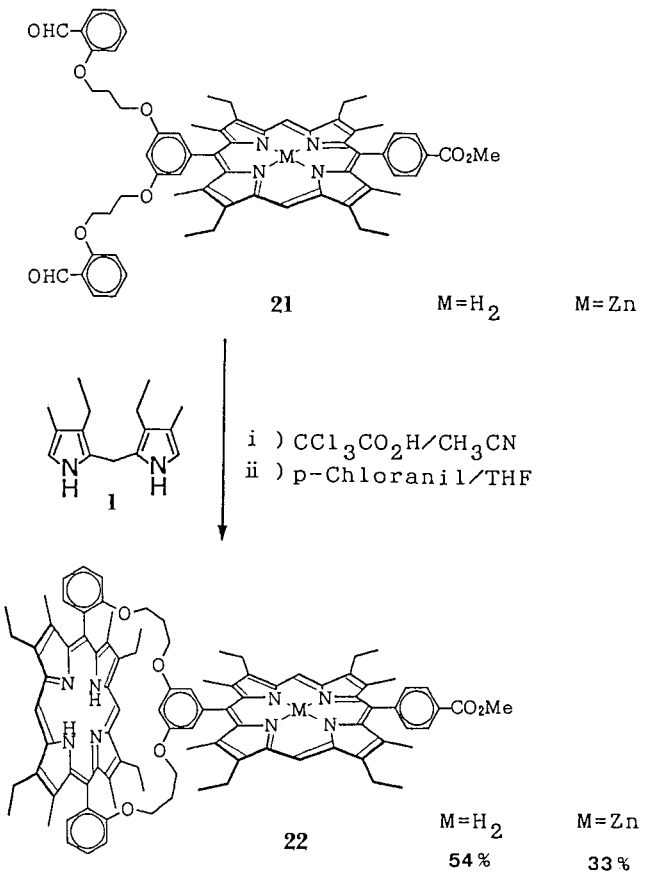

Scheme 7.

protons were downfield shifted in the ^{1}H NMR spectra (Table 2) and the Soret and Q-bands were 7—17 nm red shifted with respect to the reference porphyrin **28** (Table 3). There exist some conformational differences caused by the methoxyl groups on the xylene moiety between **3g** and **3h**. The aromatic protons of the xylene strap appeared as a singlet at 3.47 ppm for **3g** and 3.50 ppm for **3h**, respectively. But the NH protons of **3g** appeared at −1.36 ppm, while those of **3h** appeared at −2.52 ppm due to the ring current shielding of the xylene cap, indicating that the dimethoxyxylene cap of **3h** was restricted to have a parallel geometry to the porphyrin ring. In accord with this consideration, the benzyl protons of **3h** were observed

Table 3. Absorption Maxima (nm) of the Strapped Porphyrins in CH_2Cl_2

Compound	Free-base		Zinc complex	
	Soret	Q-bands	Soret	Q-bands
3f	411	509 541 580 629	412	540 574
3b	409	507 539 575 629	410	538 574
3c	412	510 543 579 632	413	541 577
3a	417	516 552 587 637	420	550 585
3g	415	514 550 584 637	419	546 579
3h	417	514 550 585 639	419	546 582
3i	422	517 551 588 640	422	550 582
28	407	507 536 574 622	409	537 573

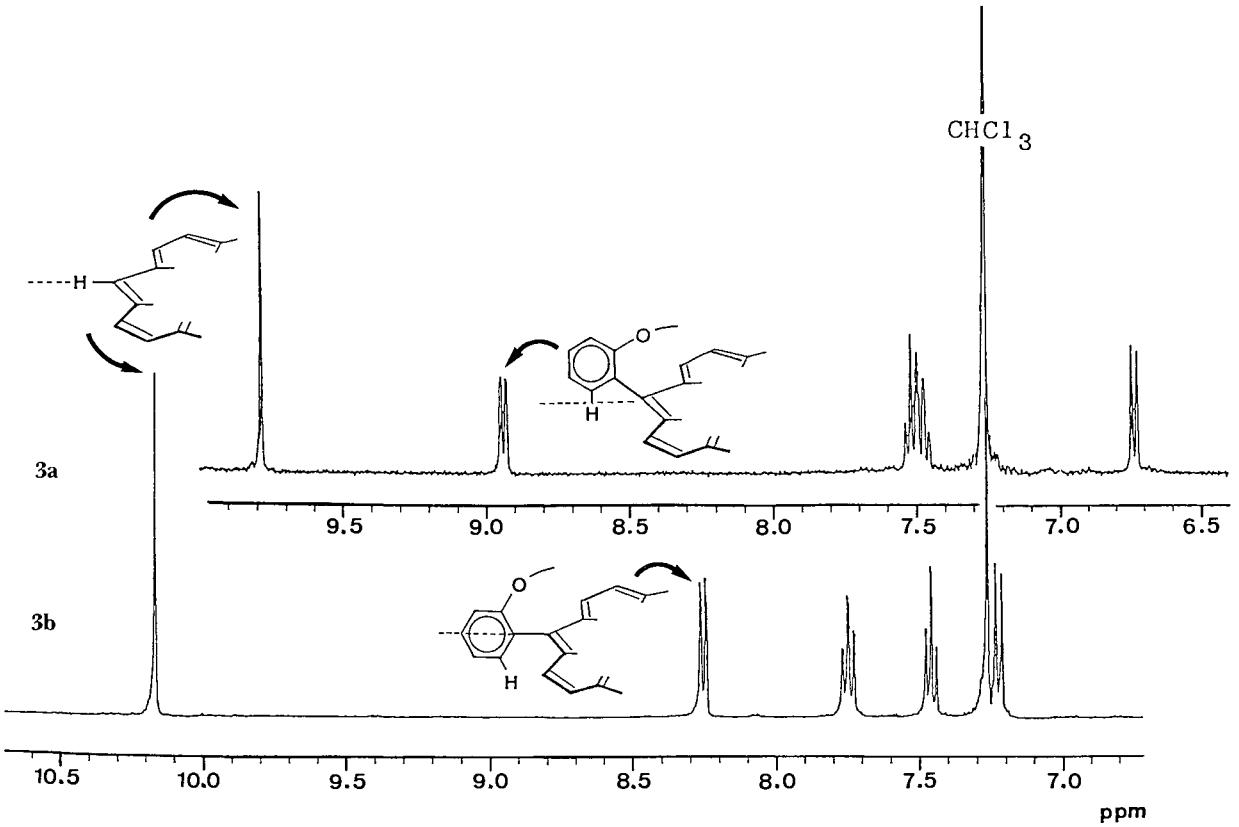

Fig. 1. ^{1}H NMR spectra of strapped porphyrins **3a** and **3b** in $CDCl_3$.

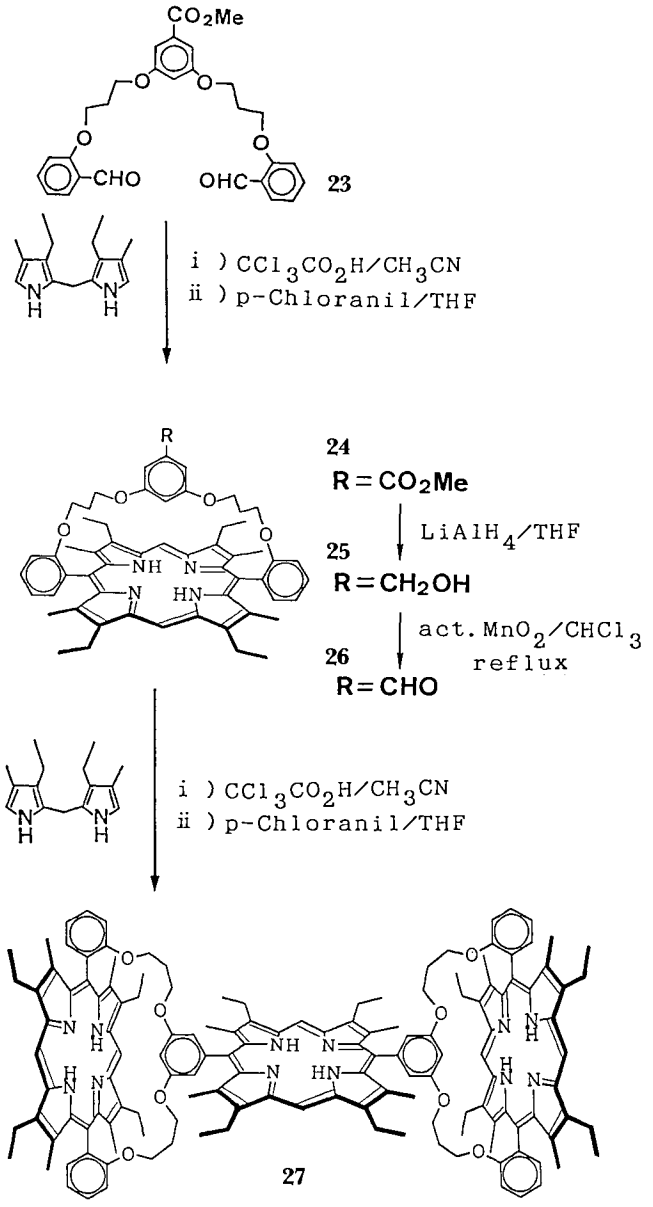

Scheme 8.

as two doublets (3.47 and 2.44 ppm, J=13 Hz). In addition, β-methyl and β-ethyl signals separated to two signals in **3h**, one on the same side with methoxyl groups and the other not. In the case of **3i**, the large anthracene ring was forced to have a parallel geometry to the porphyrin ring, and thus the NH and *meso*-H protons of **3i** appeaed at −2.41 ppm and 9.39 ppm, respectively; both of them were upfield shifted by the ring current shielding of the anthracene cap (Table 2).

Fluorescence Spectra. Fluorescence spectra of the methylene-chain-strapped porphyrins also showed systematic changes. Emission maxima were shifted to the longer wavelength on shortening the strap linkage and the fluorescence quantum yield and fluorescence lifetime were reduced by the ring distortion. The red shift of the emission maxima was in line with those observed in their UV-vis spectra. In addition, a new peak between the two peaks appeared in the free-base porphyrins and this center peak merged with the preceding peak in **3a** and **3c**. (Fig. 2, Table 4). On the other hand, no decrease of the fluorescence intensity and lifetime was observed in the xylylene-strapped porphyrins **3g** and **3h** (Table 4). This difference is presumably due to the difference of the conformational flexibility of the porphyrin ring. The porphyrin ring was distorted in **3g** and **3h** as well as **3a**, but the molecular motion should be restricted in **3g** and **3h** due to the rigid *p*-xylylene linkage.

Table 4. Fluorescence Spectral Data[a)]

Compd	λ em/nm	Φ f, rel[b)]	τ/ns
Free base			
3f	631 658 698	1.0	9.3
3b	630 659 695	1.0	c)
3c	639 654 697	0.9	ca. 8.5
3a	650 711	0.6	5.9
3g	643 707	1.0	9.5
3h	641 706	1.0	c)
Zinc complex			
3f(Zn)	580 637	1.0	1.6
3b(Zn)	578 632	1.0	c)
3c(Zn)	590 636	0.8	c)
3a(Zn)	605 655	0.6	1.2
3g(Zn)	597 654	1.0	1.6
3h(Zn)	595 650	1.0	c)

a) Measured in CH_2Cl_2 solution. b) Relative fluorescence intensities with respect to **3f**; excitation at Soret wavelength. c) Not measured.

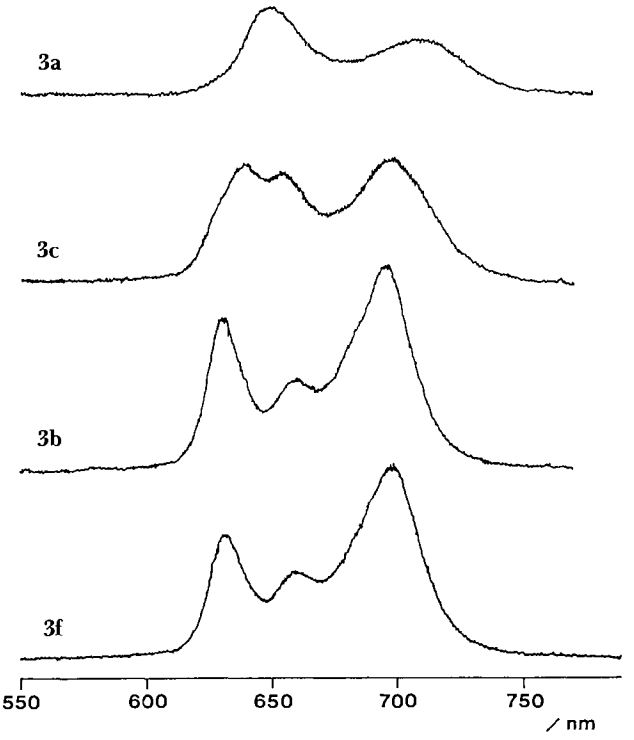

Fig. 2. Fluorescence spectra of strapped porphyrins.

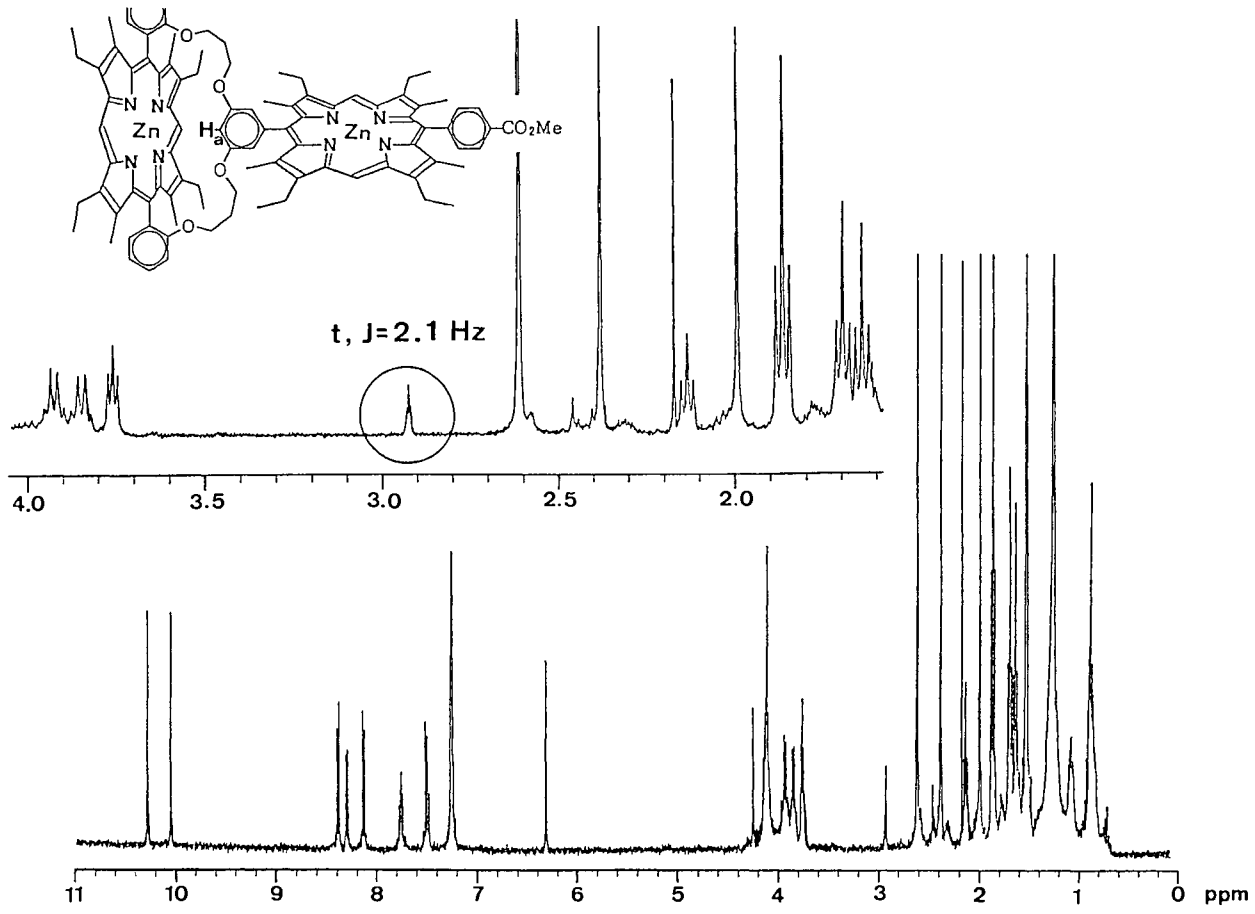

Fig. 3. ^{1}H NMR spectrum of "T-shaped" dimeric porphyrin **22**(Zn_2) in $CDCl_3$.

Table 5. UV-vis Spectra of Dimeric and Trimeric Porphyrins in CH_2Cl_2

Compd	λ_{max}/nm	
	Soret	Q-bands
4d	408	538 574
4e	405	538 574
9(Zn_3)	404	539 576
22(Zn_2)	411	540 574
27(Zn_3)	411	539 574
28(Zn)[a]	409	538 574

a) Zinc 5,15-diphenyletioporphyrin II was used as a reference porphyrin.

UV-vis and ^{1}H NMR Spectra of Dimeric and Trimeric Porphyrins. The stacked type porphyrins **4e** and **9**(Zn_3) showed blue-shifted Soret band similar to the other face-to-face dimeric porphyrins,[1,6] while the UV-vis spectra of **22**(Zn_2) and **27**(Zn_3) were almost unchanged with respect to the monomeric porphyrin **28** indicating that the ground state interactions between the porphyrins were small in the orthogonal geometries. (Table 5).

The unique geometries of "T-shaped" dimer **22** and "H-shaped" trimer **27** were characterized by their

Table 6. Chemical Shifts of H_a

Compd	δ
22(H_4)	3.01
22(H_2Zn)	3.03
22(Zn_2)	2.93
27(H_6)	2.97
27(Zn_3)	2.92
21	6.94
21(Zn)	6.95

^{1}H NMR spectra. The inside aromatic protons (H_a, designated in Table 6) appeared at ca. 3 ppm region due to the strong shielding effect of porphyrin ring current. The distance between the H_a and the porphyrin plane was estimated to be 4.1 Å in **22** on the basis of the porphyrin ring current model,[17] then the center-to-center distance between two porphyrin rings was estimated to be 12.8 Å, which was in good agreement with those estimated from Corey-Pauling-Koltun (CPK) molecular models (12.5—13 Å for **22** and **27**).

In summary, the acid-catalyzed intramolecular macrocyclization reaction is particularly useful for the synthesis of strapped porphyrins as well as dimeric and trimeric porphyrins. Use of *o*-alkoxybenzaldehydes as the starting material is also useful for model construction because of their easy preparation, high yield of the porphyrin, sufficient stability of the ether linkage, and the possible separation of the porphyrin atropisomers. Strapped porphyrins synthesized here showed systematic increase of ring distortion on shortening the strap linkage, while "T-shaped" dimeric porphyrins and "H-shaped" trimeric porphyrins had unique geometries. In these dimeric and trimeric porphyrins, there exists no direct π-π conjugation between porphyrin rings, rendering through-bond interactions to be negligibly small. Therefore, these models would be quite useful for studies on through-space electron-transfer process.

Experimental

The ^{1}H NMR spectra were recorded at 400 MHz on a JEOL JNM-GX-400 spectrometer, with tetramethylsilane or $CHCl_3$ as internal reference. All ^{1}H NMR spectra were measured in $CDCl_3$ solution. Mass spectra were recorded on a JEOL JMS-DX-300 instrument (EI, 3 kV). Fast atom bombardment mass spectra were recorded on a JEOL JMS-HX-110 (10 kV) or a JEOL JMS-DX-300 (1.5 kV) with *m*-nitrobenzyl alcohol as the matrix. High-resolution mass spectra of porphyrins were obtained on a JEOL JMS-HX-110 (10 kV) with polyethylene glycol as a standard. UV-vis spectra were recorded in dichloromethane on a Shimadzu UV-200 and a Shimadzu UV-3000 spectrophotometer. Steady-state fluorescence spectra were recorded by using a Shimadzu RF-502a spectrofluorometer. Fluorescence lifetimes were measured on a Horiba NAES 1100. Flash column chromatography was carried out using Wakogel FC-40 or Merck Kieselgel 60HF254 Art. 7739.

Anhydrous acetonitrile was distilled from diphosphorus pentaoxide and stored with Molecular Sieves 3A. Anhydrous acetone was distilled and dried over anhydrous calcium sulfate.

Unless otherwise stated all reactions were performed under an atmosphere of dry nitrogen. All organic extracts were dried over anhydrous sodium sulfate.

Preparation of the Dialdehyde Derivatives. Dialdehydes **2a**, **2b**, **2c**, **2d**, **2e**, **2g**, **2h** and **2i** were prepared according to the published procedure.[10a,18]

C3 Dialdehyde 2e. Colorless needles; mp 94—96 °C; ^{1}H NMR ($CDCl_3$) δ=10.50 (2H, s, CHO), 7.83+7.55+7.03 (2H+2H+4H, dd+m+m, Ar-H), 4.33 (4H, t, OCH_2), 2.43 (2H, m, $OCH_2C\underline{H}_2$). MS(EI) Found: *m/z* 284.1060. Calcd for $C_{17}H_{16}O_4$: M, 284.1049.

XY Dialdehyde 2g. Colorless needles; mp 191 °C. Found: C, 76.01; H, 5.08%. Calcd for $C_{22}H_{18}O_4$: C, 76.28; H, 5.24%. ^{1}H NMR ($CDCl_3$) δ=10.56 (2H, s, CHO), 7.87+7.55+7.49+7.07 (2H+2H+4H+4H, dd+m+s+m, Ar-H), 5.22 (4H, s, OCH_2). MS(EI) *m/z* 346 (M^+), 328 ($M-H_2O$).

XY(OMe)$_2$ Dialdehyde 2h. Dialdehyde **2h** was prepared from 2,5-bis(chloromethyl)-1,4-dimethoxybenzene.[19] Colorless needles; mp 193—5 °C. Found: C, 70.68; H, 5.49%. Caicd for $C_{24}H_{22}O_6$: C, 70.92; H, 5.46%. ^{1}H NMR ($CDCl_3$) δ=10.57 (2H, s, CHO), 7.86+7.56+7.12+7.12+7.06 (each 2H, dd+m+s+d+t, Ar-H), 5.24 (4H, s, OCH_2), 3.84 (6H, s, CH_3). MS(EI) *m/z* 406 (M^+).

AN Dialdehyde 2i. Dialdehyde **2i** was prepared from 9,10-bis(chloromethyl)anthracene.[20] Yellow solid; mp> 190 °C. Found: C, 80.74; H, 5.26%. Calcd for $C_{30}H_{22}O_4$: C, 80.70; H, 4.97%. ^{1}H NMR ($CDCl_3$) δ=10.25 (2H, s, CHO), 8.38+7.60 (4H+4H, m+m, An-H), 7.90+7.70+7.47+7.14 (each 2H, dd+m+d+t, Ar-H), 6.15 (4H, s, OCH_2).

C$_{10}$-Diester Dialdehyde 2f. 1,10-dibromodecane (0.43 g, 1.4 mmol) and 2-formylbenzoic acid (0.50 g, 3.3 mmol) was dissolved in dry acetone (10 ml). Anhydrous potassium carbonate (0.32 g, 2.3 mmol) was added and the mixture was refluxed overnight. After cooling, water (10 ml) was added and acetone was evaporated. The precipitated white solid was filtered, washed with water, and dried. (0.50 g, 1.1 mmol, 80%) mp 73—5 °C. Found: C, 69.52; H, 6.82%. Calcd for $C_{26}H_{30}O_6 \cdot 1/2H_2O$: C, 69.78; H, 6.98%. ^{1}H NMR ($CDCl_3$) δ=10.61 (2H, s, CHO), 7.94+7.63 (4H+4H, m+m, Ar-H), 4.37 (4H, t, OCH_2), 1.76+1.40+1.32 (4H+4H+8H, m+br+br, $OCH_2(C\underline{H}_2)_8CH_2O$). MS(FAB) *m/z* 439 ($M+H^+$).

2,5-Bis[2-(2-formylphenyl)ethyl]-1,4-dimethoxybenzene 2j. 2,5-Bis[2-[2-(methoxycarbonyl)phenyl]ethyl]-1,4-dimethoxybenzene was obtained from 2,5-dimethoxy-1,4-benzenedicarbaldehyde[21] according to the published procedure.[22] (2 steps 46%) The dimethyl ester was converted into the dialdehyde **2j** by lithium aluminium hydride reduction (94%) followed by oxidation with activated MnO_2 (61%) according to the usual procedure. **2j**: Pale yellow needles; mp 142—144 °C. ^{1}H NMR ($CDCl_3$) δ=10.29 (2H, s, CHO), 7.85+7.50+7.35+7.25+6.54 (each 2H, d+t+t+d+s, Ar-H), 3.70 (6H, s, CH_3), 3.26+2.88 (4H+4H, m+m, CH_2CH_2). MS (EI) Found: *m/z* 402.1833. Calcd for $C_{26}H_{26}O_4$: M, 402.1831.

2,2′-Oxybis(benzaldehyde) 2m. To the solution of diphenyl ether (1.0 ml) in dry ether (15 ml), butyllithium (1.6 M solution in hexanes, 12 ml) was added dropwise at 0 °C and the mixture was stirred at room temperature for 2 d.[23] *N,N*-dimethylformamide (3.0 ml) was added dropwise at 0 °C and the solution was stirred for 8 h. The mixture poured into the water, acidified with hydrochloric acid, and extracted with ethyl acetate. The organic layer was washed twice with water, dried, and evaporated. The residue was purified by column chromatography (silica gel, benzene) to give colorless crystals. (0.61 g, 43%) mp 74 °C. Found: C, 74.47; H, 4.53%. Calcd for $C_{14}H_{10}O_3$: C, 74.33; H, 4.46%. ^{1}H NMR ($CDCl_3$) δ=10.50 (2H, s, CHO), 7.99+7.58+7.29+6.94 (each 2 H, dd+m+t+d, Ar-H). MS(EI) *m/z* 226 (M^+).

3,3′-Oxybis(benzaldehyde) 2n. 3-Hydroxybenzaldehyde

(5.0 g, 41 mmol), 3-bromobenzaldehyde (5.0 g, 27 mmol), copper (II) oxide (2.9 g) and potassium carbonate (2.8 g) were dissolved in dry pyridine (30 ml) and the solution was refluxed for 20 h.[24] The same work up procedure as described above was carried out to give colorless oil (2.9 g, 47%). Found: C, 74.15; H, 4.32%. Calcd for $C_{14}H_{10}O_3$: C, 74.33; H, 4.46%. ^{1}H NMR ($CDCl_3$) δ=9.98 (2H, s, CHO), 7.67+7.56+7.50+7.32 (each 2H, m+t+m+m, Ar-H). MS (EI) m/z 226 (M^+).

General Procedure for the Synthesis of Strapped Porphyrins. 3,3′-Diethyl-4,4′-dimethyl-2,2′-dipyrrylmethane (**1**)[13] (100 mg, 0.43 mmol) and the dialdehyde **2** (0.22 mmol) were dissolved or suspended in dry acetonitrile (20 ml) under N_2, and to this mixture a catalytic amount of trichloroacetic acid (10 mg) was added. After standing at room temperature for about 5 h, *p*-chloranil (0.3 g, 1.2 mmol) in dry tetrahydrofuran (THF, 10 ml) was added and the mixture was stirred overnight. Porphyrin product was separated on alumina column (activity III) eluting with CH_2Cl_2, and recrystallized from CH_2Cl_2–methanol. Yields are listed in Table 1.

C5 Strapped Porphyrin 3a. ^{1}H NMR ($CDCl_3$) δ=9.79 (2H, s, meso-H), 8.94+7.50+6.73 (2H+4H+2H, dd+m+d, ArH), 3.98+3.82 (4H+4H, m+m, Et), 2.60 (12H, s, Me), 1.70 (12H, t, Et), 0.96+−1.73+−3.49 (4H+4H+2H, t+m+m, $O(C\underline{H}_2)_5O$), −1.27 (2H, br, NH). MS(FAB) Found: m/z 731.4333. Calcd for $C_{49}H_{55}N_4O_2$: M+H, 731.4325.

C10 Strapped Porphyrin 3b. ^{1}H NMR ($CDCl_3$) δ=10.16 (2H, s, *meso*-H), 8.25+7.75+7.46+7.22 (each 2H, dd+m+m+d, ArH), 4.02 (8H, m, Et), 3.68 (4H, t, OCH_2), 2.56 (12H, s, Me), 1.81 (12H, t, Et), 0.55+−0.94+−1.69 (4H+8H+4H, m+m+m, $OCH_2(C\underline{H}_2)_8CH_2O$, −2.33 (2H, br, NH). MS(FAB) m/z 918 ($M+H^+$).

C6 Strapped Porphyrin 3c. ^{1}H NMR ($CDCl_3$) δ=9.93 (2H, s, *meso*-H), 8.87+7.56+6.85 (2H+4H+2H, dd+m+dd, ArH), 4.00+3.89 (4H+4H, m+m, Et), 2.60 (12H, s, Me), 2.29 (4H, t, OCH_2), 1.72 (12H, t, Et), −1.70 (2H, br, NH), −1.85+−2.85 (4H+4H, br+br, $OCH_2(C\underline{H}_2)_4CH_2O$). MS (FAB) Found: m/z 745.4481. Calcd for $C_{50}H_{57}N_4O_2$: M+H, 745.4482.

XY Strapped Porphyrin 3g. ^{1}H NMR ($CDCl_3$) δ=9.74 (2H, s, *meso*-H), 8.95+7.54+6.67 (2H+4H+2H, dd+m+d, ArH), 3.89+3.77 (4H+4H, m+m, Et), 3.42 (4H, s, C_6H_4), 2.92 (4H, s, OCH_2), 2.62 (12H, s, Me), 1.63 (12H, t, Et), −1.36 (2H, br, NH). MS (FAB) Found: m/z 765.4149. Calcd for $C_{52}H_{53}N_4O_2$: M+H, 765.4169.

XY(OMe)$_2$ Strapped Porphyrin 3h. ^{1}H NMR ($CDCl_3$) δ=9.76 (2H, s, *meso*-H), 8.93+7.64+7.07 (2H+4H+2H, dd+m+d, ArH), 3.91 (8H, m, Et), 3.50 (2H, s, $C_6H_2(OMe)_2$), 3.47+2.44 (2H+2H, d+d, J=13 Hz, OCH_2), 2.72+2.57 (6H+6H, s+s, Me), 1.86 (6H, s, OCH_3), 1.82+1.75 (6H+6H, t+t, Et), −2.52 (2H, br, NH). MS (FAB) Found: m/z 825.4351. Calcd for $C_{54}H_{57}N_4O_4$: M+H, 825.4380.

AN Strapped Porphyrin 3i. ^{1}H NMR ($CDCl_3$) δ=9.39 (2H, s, *meso*-H), 8.91+7.67+7.53+6.98 (each 2H, dd+m+t+d, ArH), 6.34+6.11 (4H+4H, m+m, An-H), 4.68 (4H, s, OCH_2), 3.87+3.73 (4H+4H, m+m, Et), 2.66 (12H, s, Me), 1.66 (12H, t, Et), −2.41 (2H, br, NH). MS (FAB) m/z 865 ($M+H^+$).

C10-Diester Strapped Porphyrin 3f. ^{1}H NMR ($CDCl_3$) δ=10.16 (2H, s, *meso*-H), 8.37+7.8 (8H, m, Ar-H), 3.99 (8H, m, Et), 3.31 (4H, t, OCH_2), 2.45 (12H, s, Me), 1.77 (12H, t, Et), −0.28+−0.83+−1.05+−1.18 (each 4H, m+m+br+br, $OCH_2(C\underline{H}_2)_8CH_2O$), −2.19 (2H, br, NH). MS (FAB) Found: m/z 857.5002. Calcd for $C_{56}H_{65}N_4O_4$: M+H, 857.5006.

C4 Dimer 4d. The ^{1}H NMR spectrum of bis-zinc dimer **4d** was broadened and complicated at ambient temperatures. On heating the sample to 100 °C in 1,1,2,2-tetrachloroethane-d_2, the spectrum became sharp and the peak assignment was achieved. **4d**: ^{1}H NMR ($CDCl_2CDCl_2$, at 100 °C) δ=9.67 (s, *meso*-H), 7.64, 7.25—7.14 (each m, Ar-H), 3.73 (m, Et), 3.42 (br, OCH_2), 2.31 (s, Me), 1.56 (t, Et), 0.49 (br, $OCH_2C\underline{H}_2$. MS (FAB) m/z 1558—1563 (M^+). UV-vis (CH_2Cl_2) 408, 538, 575 nm.

C3 Dimer 4e. ^{1}H NMR ($CDCl_3$) δ=9.63 (s, *meso*-H), 7.66+7.41+7.17 (m+m+m, ArH), 3.74(m, Et), 2.25 (s, Me), 1.5 (m, Et). MS (FAB) m/z 1530—1535 (M^+). UV-vis (CH_2Cl_2) 405, 538, 574 nm.

***m*-Oxy Dimer 4n.** ^{1}H NMR ($CDCl_3$) δ=9.46+8.22 (s+s, *meso*-H), 8.12+7.7+7 50 (dd+m+t, ArH), 3.63 (m, Et), 2.17 (s, Me), 1.45 (t, Et). MS (FAB) m/z 1290 ($M+H^+$). UV-vis (CH_2Cl_2) 403, 509, 541, 576, 626 nm.

Preparation of the Iodide 12. 2-(3-Chloropropoxy)-benzaldehyde 10. Salicylaldehyde (4.2 ml, 40 mmol) was added to a solution of potassium hydroxide (85%, 2.6 g, 40 mmol) in ethanol (40 ml) and then 1-bromo-3-chloropropane (4.5 ml, 46 mmol) was added. The mixture was heated under reflux for 10 h and then cooled to 0 °C. The precipitate was filtered off and the filtrate was evaporated. The residue was dissolved in CH_2Cl_2, washed with water, dried and evaporated. Remaining salicylaldehyde and 1-bromo-3-chloropropane were distilled off under reduced pressure to leave colorless oil (7.8 g, 39 mmol, 97%). ^{1}H NMR ($CDCl_3$) δ=10.49 (1H, s, CHO), 7.84+7.55+7.03 (1H+1H+2H, dd+m+m, Ar-H), 4.26+3.38+2.30 (2H+2H+2H, t+t+m, O $(C\underline{H}_2)_3Cl$). MS (FAB) m/z 199 ($M+H^+$).

2-(3-Chloropropoxy)-1-(5,5′-dimethyl-1,3-dioxan-2-yl)-benzene 11. The aldehyde **10** (7.8 g, 39 mmol), 2,2-dimethyl-1,3-propanediol (5.0 g, 48 mmol), and *p*-toluenesulfonic acid monohydrate (0.3 g) were dissolved in benzene (80 ml), and the mixture was heated under reflux. Water was removed using a Dien-Stark apparatus. After 7 h, the mixture was cooled and the organic layer was washed with aqueous sodium hydrogencarbonate, with water, and then evaporated. The residue was purified on silica gel (eluting with benzene–ether) to give colorless oil (9.7 g, 34 mmol, 87%). ^{1}H NMR ($CDCl_3$) δ=7.65+7.29+7.01+6.89 (each 1H, dd+m+t+d, Ar-H), 5.74 (1H, s, ArCH), 4.15 (2H, t, $OC\underline{H}_2CH_2$), 3.76 (4H, m, $OC\underline{H}_2$+$C\underline{H}_2Cl$), 3.66 (2H, d, $OC\underline{H}_2$), 2.26 (2H, m, $C\underline{H}_2CH_2Cl$), 1.32+0.80 (3H+3H, s+s, Me). MS (FAB) m/z 285 ($M+H^+$).

2-(3-Iodopropoxy)-1-(5,5′-dimethyl-1,3-dioxan-2-yl)-benzene 12. The chloride **11** (14.2 g, 50 mmol) and sodium iodide (15 g, 0.1 mol) were dissolved in dry acetone (100 ml) and the mixture was refluxed overnight. After cooling, the precipitate was filtered off and the filtrate was evaporated. The residue was dissolved in CH_2Cl_2, washed with aqueous sodium thiosulfate, with water, dried and evaporated to leave pale yellow oil (17.2 g, 46 mmol, 92%). ^{1}H NMR ($CDCl_3$) δ=7.65+7.29+7.01+6.88 (each 1H, dd+m+t+d, Ar-H), 5.73 (1H, s, ArCH), 4.08 (2H, t, $OC\underline{H}_2CH_2$), 3.76+3.66 (2H+2H, d+d, OCH_2), 3.38+2.30 (2H+2H, t+m, $C\underline{H}_2$-$C\underline{H}_2I$), 1.32+0.80 (3H+3H, s+s, Me). MS (EI) Found: m/z 376.0538. Calcd for $C_{15}H_{21}IO_3$: M, 376.0534.

Synthesis of Trimeric Porphyrin 9. 5,15-Bis(2,6-dihy-

droxyphenyl)etioporphyrin II (6). 5,15-Bis(2,6-dimethoxyphenyl)etioporphyrin II (**5**)[5] (158 mg, 0.21 mmol) in dry CH_2Cl_2 (30 ml) was treated with BBr_3 (0.3 ml) at −78 °C. The mixture was gradually warmed to room temperature and stirred overnight. The mixture was poured into water and extracted with CH_2Cl_2 and then with ethyl acetate. The extract was washed with aqueous sodium hydrogencarbonate, with water, and then evaporated. Recrystallization from CH_2Cl_2–hexane gave purple microcrystals (145 mg, 0.21 mmol, 99%). ^{1}H NMR ($CDCl_3$) δ=10.31 (2H, s, *meso*-H), 7.64+7.00 (2H+4H, t+d, ArH), 4.66(4H, br, OH), 4.05 (8H, q, Et), 2.78 (12H, s, Me), 1.80 (12H, t, Et). MS (FAB) *m/z* 695 ($M+H^+$).

Porphyrin Tetraacetal 7. 5,15-Bis(2,6-dihydroxyphenyl)-etioporphyrin II (**6**, 135 mg, 0.19 mmol), the iodide **12** (2.85 g, 7.6 mmol), and anhydrous potassium carbonate (1.0 g) were dissolved in dry acetone (90 ml) and refluxed for 2 d. After cooling, acetone was evaporated and the residue was dissolved in CH_2Cl_2, washed with water, dried and evaporated. Porphyrin **7** was separated by flash column chromatography (silica gel, CH_2Cl_2) and then recrystallized from CH_2Cl_2–methanol to give purple crystals (140 mg, 0.083 mmol, 44%). ^{1}H NMR ($CDCl_3$) δ=10.06 (2H, s, *meso*-H), 7.72+7.04 (2H+4H, t+d, C_6H_3), 7.43+6.69+6.48 (4H+4H+8H, dd+t+m, C_6H_4), 5.50 (4H, s, ArCH), 4.08+2.82+1.38 (each 8H, t+t+m, $O(C\underline{H}_2)_3O$), 3.82 (8H, q, Et), 3.65+3.51 (8H+8H, d+d, OCH_2), 2.60 (12H, s, β-Me), 1.65 (12H, t, Et), 1.24+0.72 (12H+12H, s+s, acetal-Me), −2.23 (2H, br, NH). MS (FAB) *m/z* 1688 ($M+H^+$).

Porphyrin Tetraaldehyde 8. To a solution of the porphyrin **7** (100 mg, 0.059 mmol) in CH_2Cl_2 (30 ml), trifluoroacetic acid (5 ml) and water (5 ml) were added and the mixture was stirred for 8 h.[14] The mixture was poured into water and extracted with CH_2Cl_2. The extract was washed with aqueous sodium hydrogen carbonate, with water, dried and evaporated. Porphyrin **8** was purified on silica gel (CH_2Cl_2–1% methanol) and recrystallized from CH_2Cl_2–methanol to give purple crystals (**8**(H_2), 74 mg, 0.055 mmol, 92%). ^{1}H NMR ($CDCl_3$) δ=9.98 (4H, s, CHO), 9.96 (2H, s, *meso*-H), 7.78+7.09 (2H+4H, t+d, C_6H_3), 7.29+6.21+5.35+4.18 (each 4H, dd+t+m+d, C_6H_4), 4.12+2.38+1.44 (each 8H, t+t+m, $O(C\underline{H}_2)_3O$), 3.75 (8H, q, Et), 2.60 (12H, s, Me), 1.59 (12H, t, Et), −2.26 (2H, br, NH). MS (FAB) Found: *m/z* 1343.616. Calcd for $C_{84}H_{87}N_4O_{12}$: M+H, 1343.632.

8(Zn): ^{1}H NMR ($CDCl_3$) δ=9.93(2H, s, *meso*-H), 9.39 (4H, s, CHO), 7.79+7.12 (2H+4H, t+d, C_6H_3), 6.89+6.00+5.29+3.95 (each 4H, dd+t+m+d, C_6H_4), 4.12+2.25+1.46 (each 8H, t+t+m, $O(C\underline{H}_2)_3O$), 3.82 (8H, q, Et), 2.61 (12H, s, Me), 1.65 (12H, t, Et). MS (FAB) *m/z* 1404—1409 (M^+).

Trimeric Porphyrin 9. The porphyrin tetraaldehyde **8(Zn)** (14.8 mg, 0.0105 mmol) and dipyrrylmethane **1** (12. 8 mg, 0.056 mmol) were dissolved in dry acetonitrile (10 ml) containing trichloroacetic acid (3.8 mg, 0.023 mmol) and the mixture was stirred for 12 h. *p*-Chloranil (50 mg) in THF (5 ml) was added and stirring was continued overnight. Solvent was evaporated. Trimeric porphyrin **9(H_4Zn)** was separated on alumina (activity III, eluting with CH_2Cl_2) and then on silica gel (CH_2Cl_2–2% methanol). (8.3 mg, 0.0037 mmol, 35%).

9(H_4Zn): ^{1}H NMR ($CDCl_3$) δ=9.58+9.17 (4H+2H, s+s, *meso*-H), 3.63+3.48 (m, Et), 2.19+2.07 (s+s, Me), 1.41+1.30 (t+t, Et). MS (FAB) Found: *m/z* 2244.120. Calcd for the highest peak of $C_{144}H_{153}N_{12}O_8Zn$: M+H, 2244.126 (CsI was used as a standard).

9(Zn_3): ^{1}H NMR ($CDCl_3$) δ=9.56+9.15 (4H+2H, s+s, *meso*-H), 7.62+7.55+7.43+7.15+7.08+6.72 (m, ArH), 3.63+3.45 (m, Et), 2.17+2.06 (s+s, Me), 1.42+1.30 (t+t, Et). MS (FAB) *m/z* 2364—2375 (M^+).

Stepwise Synthesis of Dimeric Porphyrin 4e. α,α-5,15-Bis(2-hydroxyphenyl)etioporphyrin II (13). Strapped porphyrin **3g** (505 mg, 0.66 mmol) was treated with BBr_3 (1 ml) by the same procedure as **6** to give purple microcrystals (400 mg, 0.60 mmol, 91%). ^{1}H NMR ($CDCl_3$) δ=10.26 (2H, s, *meso*-H), 7.75+7.36+7.28 (2H+4H+2H, t+m+m, ArH), 5.6 (2H, br, OH), 4.04 (8H, m, Et), 2.66 (12H, s, Me), 1.81 (12H, t, Et). MS (FAB) *m/z* 663 ($M+H^+$).

Porphyrin Diacetal 14. Porphyrin diacetal **14** was prepared from the porphyrin **13** (200 mg, 0.30 mmol) and the iodide **12** (1.9 g, 5.0 mmol) by the same procedure as **7**. (187 mg, 0.16 mmol, 54%). ^{1}H NMR ($CDCl_3$) δ=10.15 (2H, s, *meso*-H), 7.77+7.46+7.35+6.75+6.56+5.56 (4H+2H+4H+2H+2H+2H, m+dd+m+t+m+d, ArH), 5.53 (2H, s, ArCH), 4.21+2.97+1.56 (each 4H, t+t+m, $O(C\underline{H}_2)_3O$), 3.96+ 3.85 (4H+4H, m+m, Et), 3.66+3.52 (4H+4H, d+d, OCH_2), 2.53 (12H, s β-Me), 1.72 (12H, t, Et), 1.25+0.72 (6H+6H, s+s, acetal-Me), −2.36 (2H, br, NH). MS (FAB) *m/z* 1160 ($M+H^+$).

Porphyrin Dialdehyde 15. The porphyrin diacetal **14** was hydrolyzed by the same procedure as **8**.

15(H_2): ^{1}H NMR ($CDCl_3$) δ=10.11+10.10 (4H, s+s, CHO+*meso*-H), 7.81+7.39+6.38+5.83+4.71 (4H+6H+2H+2H+2H, m+m+t+m+d, ArH), 4.22+2. 68+1.79 (each 4H, t+t+m, $O(C\underline{H}_2)_3O$), 3.91+3.84 (4H+4H, m+m, Et), 2.52 (12H, s, Me), 1.69 (12H, t, Et), −2.37 (2H, br, NH). MS (FAB) *m/z* 987 ($M+H^+$).

15(Zn): ^{1}H NMR ($CDCl_3$) δ=10.06 (2H, s, *meso*-H), 9.50 (2H, s, CHO), 7.80+7.39+6.95+6.10+5.72+4.55 (4H+4H+2H+2H+2H+2H, m+m+dd+t+m+d, ArH), 4.23+2.61+1.61 (each 4H, t+t+m, $O(C\underline{H}_2)_3O$), 4.1—3.8 (8H, m, Et), 2.52 (12H, s, Me), 1.72 (12H, t, Et). MS (FAB) *m/z* 1048—1052 (M^+).

Face-to-Face Dimeric Porphyrin 4e. The porphyrin dialdehyde **15(Zn)** (30.1 mg, 0.029 mmol) was treated with dipyrrylmethane **1** (16 mg, 0.069 mmol) in acetonitrile (6.8 ml) in the presence of trichloroacetic acid (6 mg) followed by oxidation with *p*-chloranil (75 mg) in a similar manner as **9(H_4Zn)** to give the porphyrin dimer **4e(H_2Zn)** (24 mg, 0.016 mmol, 56%). The bis-zinc complex (**4e**) was identical with that prepared in a one-pot procedure.

4e(H_2Zn): MS (FAB) *m/z* 1468—1472 (M^+).

Synthesis of the Aldehyde 19. Methyl 3,5-Bis[3-[2-(5,5-dimethyl-1,3-dioxan-2-yl)phenoxy]propoxy]benzoate 17. Methyl 3,5-dihydroxybenzoate (**16**, 1.50 g, 8.9 mmol), the iodide **12** (7.61 g, 20 mmol), and anhydrous potassium carbonate (1.4 g) were dissolved in dry acetone (60 ml) and refluxed for 2 d. After cooling, acetone was evaporated and the residue was dissolved in CH_2Cl_2, washed with water, dried and evaporated. The methyl ester **17** was purified on silica gel eluting with CH_2Cl_2. Colorless oil (5.0 g, 7.5 mmol, 83%). ^{1}H NMR ($CDCl_3$) δ=7.64+7.27+7.21+7.00+6.88+6.67 (2H+2H+2H+2H+2H+1H,dd+m+d+m+dd+t, ArH), 5.74 (2H, s, ArCH), 4.2+2.28 (8H+4H, m+m, $O(C\underline{H}_2)_3O$), 3.88 (3H, s, OMe), 3.73+3.61 (4H+4H, d+d, OCH_2), 1.29+0.75 (6H+6H, s+s, acetal-Me) MS (FAB) *m/z* 665 ($M+H^+$).

3,5-Bis[3-[2-(5,5-dimethyl-1,3-dioxan-2-yl)phenoxy]-propoxy]benzyl Alcohol 18. The methyl ester **17** (5.0 g, 7.5

mmol) was treated with $LiAlH_4$ (0.56 g) in dry THF (100 ml) at room temperature. The benzyl alcohol **18** was purified on silica gel eluting with CH_2Cl_2. White Solids (3.7 g, 5.8 mmol, 77%). ^1H NMR ($CDCl_3$) δ=7.65+7.28+6.99+6.87+6.51+6.41 (2H+2H+2H+2H+2H+1H, dd+t+t+d+d+t, ArH), 5.74 (2H, s, ArCH), 4.49 (2H, d, $C\underline{H}_2OH$), 4.17+2.26 (8H+4H, t+m, $O(C\underline{H}_2)_3O$), 3.72+3.62 (4H+4H, d+d, OCH_2), 1.88 (1H, t, OH), 1.30+0.76 (6H+6H, s+s, Me). MS (FAB) m/z 637 ($M+H^+$).

3,5-Bis[3-[2-(5,5′-dimethyl-1,3-dioxan-2-yl)phenoxy]-propoxy]benzaldehyde 19. To a suspension of pyridinium chlorochromate (PCC, 0.33 g, 1.5 mmol) and anhydrous sodium acetate (35 mg, 0.42 mmol) in dry CH_2Cl_2, a solution of the benzyl alcohol **18** (0.54 g, 0.85 mmol) in CH_2Cl_2 (25 ml) was added in one portion. After stirring for 2 h, ether (50 ml) was added and the liquid phase was separated by decantation. The residual gummy solids were washed with ether, and the combined liquid phase was passed through a Florisil short column. Evaporation of solvent gave viscous oil (0.47 g, 0.74 mmol, 87%). ^1H NMR ($CDCl_3$) δ=9.87 (1H, s, CHO), 7.65+7.28+7.03+7.00+6.89+6.73 (2H+2H+2H+2H+2H+1H, dd+m+d+m+dd+t, ArH), 5.74 (2H, s, ArCH), 4.20+2.29 (8H+4H, m+m, $O(C\underline{H}_2)_3O$), 3.72+3.61 (4H+4H, d+d, OCH_2), 1.29+0.75 (6H+6H, s+s, Me). MS (FAB) m/z 635 ($M+H^+$).

Synthesis of the "T-Shaped" Dimeric Porphyrin 22. Porphyrin 20. The aldehyde **19** (250 mg, 0.39 mmol), methyl 4-formylbenzoate (128 mg, 0.78 mmol), and dipyrrylmethane **1** (271 mg, 1.18 mmol) were dissolved in dry acetonitrile (22 ml) containing trichloroacetic acid (32 mg, 0.2 mmol) and the mixture was stirred for 15 h. *p*-Chloranil (0.8 g) dissolved in THF (30 ml) was added and stirring was continued overnight. Solvent was evaporated and the residue was purified on alumina (activity III, CH_2Cl_2). The resulting porphyrins were converted to the zinc complexes ($Zn(OAc)_2$ in CH_2Cl_2–methanol) and separated by flash column chromatography (silica gel, CH_2Cl_2).

20: Red crystals (220 mg, 0.17 mmol, 44% based on **19**). ^1H NMR ($CDCl_3$) δ=10.20 (2H, s, *meso*-H), 8.84+8.21 (2H+2H, d+d, $C_6\underline{H}_4CO_2Me$), 7.59+7.30+7.25+6.96+6.91 (2H+2H+2H+3H+2H, dd+d+m+m+d, ArH), 5.71 (2H, s, ArCH), 4.34+4.24+2.35 (each 4H, t+t+m, $O(C\underline{H}_2)_3O$), 4.13 (3H, s, OMe), 4.01 (8H, m, Et), 3.59+3.51 (4H+4H, d+d, OCH_2), 2.67+2.44 (6H+6H, s+s, β-Me), 1.77 (12H, t, Et), 1.17+0.48 (6H+6H, s+s, acetal-Me). MS (FAB) m/z 1278—1284 (M^+).

Porphyrin Dialdehyde 21. The acetal groups were hydrolyzed under acidic conditions[14] as described for **8** to give porphyrin dialdehyde **21(H)** (99%).

21(H_2): Purple crystals; mp 105—107 °C. ^1H NMR ($CDCl_3$) δ=10.52 (2H, s, CHO), 10.24 (2H, s, *meso*-H), 8.44+8.19 (2H+2H, d+d, $C_6\underline{H}_4CO_2Me$), 7.80+7.51+7.04+6.99 (each 2H, dd+m+d+t, $C_6\underline{H}_4CHO$), 7.28+6.94 (2H+1H, d+t, C_6H_3), 4.36+2.41 (8H+4H, t+t+m, $O(C\underline{H}_2)_3O$), 4.13 (3H, s, OMe), 4.02 (8H, m, Et), 2.60+2.47 (6H+6H, s+s, β-Me), 1.77 (12H, m, Et), −2.44 (2H, br, NH). MS (FAB) m/z 1045 ($M+H^+$).

21(Zn): Red crystals. ^1H NMR ($CDCl_3$) δ=10.34 (2H, s, CHO), 10.20 (2H, s, *meso*-H), 8.44+8.21 (2H+2H, d+d, $C_6\underline{H}_4CO_2Me$), 7.72+7.49+7.01+6.96 (each 2H, dd+m+d+t, $C_6\underline{H}_4CHO$), 7.31+6.95 (2H+1H, d+t, C_6H_3), 4.34+2.40 (8H+4H, t+t+m, $O(C\underline{H}_2)_3O$), 4.13 (3H, s, OMe), 4.01 (8H, m, Et), 2.63+2.44 (6H+6H, s+s, β-Me), 1.77 (12H, m, Et). MS(FAB) m/z 1106—1110 (M^+).

"T-Shaped" Dimeric Porphyrin 22. The porphyrin dialdehyde **21(H_2)** (110 mg, 0.105 mmol) and dipyrrylmethane **1** (58.5 mg, 0.25 mmol) were dissolved in dry acetonitrile (40 ml). Trichloroacetic acid (41 mg, 0.25 mmol) dissolved in dry acetonitrile (1.4 ml) was added and the mixture was stirred for 10 h. *p*-Chloranil (0.18 g) in THF (7 ml) was added and stirring was continued overnight. Solvent was evaporated and the residue was purified on alumina (activity III, CH_2Cl_2), then on silica gel (CH_2Cl_2–2% methanol) and recrystallized from CH_2Cl_2–methanol to give purple microcrystals (82.5 mg, 0.056 mmol, 54%).

22(H_4): Mp >270 °C (decomp). ^1H NMR ($CDCl_3$) δ=10.30+10.10 (2H+2H, s+s, *meso*-H), 8.40+8.13 (2H+2H, d+d, $C_6\underline{H}_4CO_2Me$), 8.32+7.76+7.50+7.2 (each 2H, dd+m+t+d, $C_6\underline{H}_4O$), 6.36+3.01 (2H+1H, d+t, J=2.4 Hz, C_6H_3), 4.12+3.94+3.87 (8H+4H+4H, m+m+m, Et), 4.11 (3H, s, OMe), 3.77+1.98+1.09 (each 4H, t+t+m, $O(C\underline{H}_2)_3O$), 2.63+2.41+2.06 (12H+6H+6H, s+s+s, β-Me), 1.87+1.70+1.65 (12H+6H+6H, t+t+t, Et); −2.10+−2.59+ −2.71 (2H+1H+1H, br, NH). MS (FAB) Found: m/z 1463.802. Calcd for $C_{90}H_{103}N_8O_6$: M+H, 1463.800.

The porphyrin dialdehyde **21(Zn)** (14. 4 mg, 0.013 mmol) was treated with dipyrrylmethane **1** (6.7 mg, 0.029 mmol) in the presence of trichloroacetic acid (2 mg, 0.012 mmol) in dry acetonitrile (3.5 ml) as described above to give a monozinc complex **22(H_2Zn)** (6.6 mg, 0.0043 mmol, 33%).

22(H_2Zn): Red crystals. ^1H NMR ($CDCl_3$) δ=10.31+10.06 (2H+2H, s+s, *meso*-H), 8.40+8.14 (2H+2H, d+d, $C_4\underline{H}_6CO_2Me$), 8.32+7.76+7.50+7.2 (each 2H, dd+m+t+d, $C_6\underline{H}_4O$), 6.37+3.03 (2H+1H, d+t, J=2.4 Hz, C_6H_3), 4.11 (3H, s, OMe), 4.11+3.92+3.85 (8H+4H+4H, m+m+m, Et), 3.77+1.77+1.08 (each 4H, t+t+m, $O(C\underline{H}_2)_3O$), 2.63+2.38+2.02 (12H+6H+6H, s+s+s, β-Me), 1.87+1.70+1.65 (12H+6H+6H, t+t+t, Et), −2.10 (2H, br, NH.) MS (FAB) m/z 1525—1530 (M^+).

Synthesis of the "H-Shaped" Porphyrin Trimer 27. Dialdehyde 23. The diacetal **17** was hydrolyzed by the same procedure as **8** to give dialdehyde **23**.

White crystals; mp 127 °C. Found: C, 67.81; H, 5.85%. Calcd for $C_{28}H_{26}O_8$: C, 68.28; H, 5.73%. ^1H NMR ($CDCl_3$) δ=10.51 (2H, s, CHO), 7.82+7.53+7.19+7.02+6.66 (2H+2H+2H+4H+1H, dd+m+d+m+t, ArH), 4.29+4.21+2.34 (each 4H, t+t+m, $O(C\underline{H}_2)_3O$), 3.89 (3H, s, Me). IR (KBr) 1705 and 1680 cm^{-1} (C=O). MS(FAB) m/z 493 ($M+H^+$).

Strapped Porphyrin 24. The strapped porphyrin **24** was prepared from the dialdehyde **23** in 41% yield. ^1H NMR ($CDCl_3$) δ=9.88 (2H, s, *meso*-H), 8.21+7.78+7.48+7.34 (each 2H, dd+m+t+d, $C_6\underline{H}_4O$), 6.54+2.99 (2H+1H, d+t, J=2 Hz, $C_6\underline{H}_3CO_2Me$), 4.06 (3H, s, OMe), 4.01—3.82 (12H, m, Et+$OC\underline{H}_2$), 2.57 (12H, s, β-Me), 1.75 (12H, t, Et), 1.56+1.22 (4H+4H, t+m, $OC\underline{H}_2C\underline{H}_2$), −2.51 (2H, br, NH). IR (KBr) 1718 cm^{-1} (C=O). MS (FAB) m/z 911 ($M+H^+$).

Strapped Porphyrin 25. The strapped porphyrin **24** (204 mg, 0.22 mmol) was treated with $LiAlH_4$ (120 mg, 3.2 mmol) in dry THF (80 ml) at room temperature for 4 h. The strapped porphyrin **25** was purified by flash column chromatography (silica gel, CH_2Cl_2) and recrystallized from CH_2Cl_2–methanol (196 mg, 0.22 mmol, 99%). ^1H NMR ($CDCl_3$) δ=9.95 (2H, s, *meso*-H), 8.24+7.78+7.48+7.33 (each 2H, dd+m+t+d, $C_6\underline{H}_4O$), 5.43+2.99 (2H+1H, d+t, J=2 Hz, $C_6\underline{H}_3$), 4.00—3.86 (12H, m, Et+$OC\underline{H}_2$), 3.79 (2H, br, $C\underline{H}_2OH$), 2.56 (12H, s, Me), 1.76 (12H, t, Et), 1.58+1.24

(4H+4H, t+m, $OC\underline{H}_2C\underline{H}_2$), −2.49 (2H, br, NH). MS (FAB) m/z 883 ($M+H^+$).

Strapped Porphyrin 26. To a suspension of activated MnO_2 (1.2 g) in $CHCl_3$ (methanol free, 15 ml), a solution of the strapped porphyrin **25** (196 mg, 0.22 mmol) in $CHCl_3$ (methanol free, 70 ml) was added dropwise and the mixture was refluxed for 2 d.[15] Solid material was filtered off, washed with $CHCl_3$ and the filtrate was evaporated. The residue was recrystallized from CH_2Cl_2–methanol to give purple microcrystals (162 mg, 0.18 mmol, 83%). ^1H NMR ($CDCl_3$) δ=9.88 (2H, s, *meso*-H), 9.61 (1H, s, CHO), 8.17+7.78+7.47+7.35 (each 2H, dd+m+t+d, $C_6\underline{H}_4O$), 6.02+3.22 (2H+1H,d+t, J=2 Hz, C_6H_3CHO, 4.0—3.8 (12H, m, Et+$OC\underline{H}_2$), 2.56 (12H, s, β-Me), 1.75 (12H, t, Et), 1.71+1.26 (4H+4H, t+m, $OC\underline{H}_2C\underline{H}_2$), −2.57 (2H, br, NH). IR (KBr) 1700 cm^{-1} (C=O). MS (FAB) m/z 881 ($M+H^+$).

"H-Shaped" Trimeric Porphyrin 27. The strapped porphyrin **26** was treated with dipyrrylmethane **1** to give "H-shaped" trimeric porphyrin **27(H$_6$)** in 59% yield.[6] Purple crystals; mp >300 °C. ^1H NMR ($CDCl_3$) δ=10.28+9.95 (4H+2H, s+s, *meso*-H), 8.31+7.75+7.49+7.25 (each 2H, dd+m+t+d, $C_6\underline{H}_4O$), 6.30+2.97 (4H+2H, d+t, J=2. 4 Hz, C_6H_3), 4.09+3.79 (8H+8H, m+m, Et), 3.74+1.95+1.06 (each 4H, t+t+m, $O(C\underline{H}_2)_3O$), 2.61+2.00 (12H+12H, s+s, Me), 1.84+1.57 (12H+12H, t+t, Et), −2.14+−2.91 (4H+2H, br+br, NH). MS (FAB) m/z 2181.6 ($M+H^+$).

This work was partially supported by the Grant-in-Aid for Scientific Research No. 02102005 from the Ministry of Education, Science and Culture and Nissan Science Foundation, and Kurata Research Grant. We thank Professor I. Yamashina of Kyoto Industrial University for measurement of high-resolution mass spectra.

References

1) D. Dolphin, J. Hiom, and J. B. Paine III, *Heterocycles*, **16**, 417 (1981); S. S. Eaton, G. R. Eaton, and C. K. Chang, *J. Am. Chem. Soc.*, **107**, 3177 (1985); J. L. Sessler, M. R. Johnson, T. Y. Lin, and S. E. Creager, *J. Am. Chem. Soc.*, **110**, 3659 (1988); A. Osuka and K. Maruyama, *J. Am. Chem. Soc.*, **110**, 4454 (1988), and references cited in these publications.

2) H. Ogoshi, H. Sugimoto, T. Nishiguchi, T. Watanabe, Y. Matsuda, and Z. Yoshida, *Chem. Lett.*, **1978**, 29.

3) M. J. Gunter and L. N. Mander, *J. Org. Chem.*, **46**, 4792 (1981).

4) R. Young and C. K. Chang, *J. Am. Chem. Soc.*, **107**, 898 (1985).

5) A. Osuka, T. Nagata, F. Kobayashi, and K. Maruyama, *J. Heterocycl. Chem.*, **27**, 1657 (1990).

6) T. Nagata, A. Osuka, and K. Maruyama, *J. Am. Chem. Soc.*, **112**, 3054 (1990).

7) A. Osuka, F. Kobayashi, T. Nagata, and K. Maruyama, *Chem. Lett.*, **1990**, 287.

8) A. Osuka, F. Kobayashi, and K. Maruyama, *Chem. Lett.*, **1990**, 1521.

9) K. M. Barkigia, L. Chantranupong, K. M. Smith, and J. Fajer, *J. Am. Chem. Soc.*, **110**, 7566 (1988); B. Evans, K. M. Smith, and J. H. Fuhrhop, *Tetrahedron Lett.*, **1977**, 443.

10) a) U. Simonis, F. A. Walker, P. L. Lee, B. J. Hanquet, D. J. Meyerhoff, and W. R. Scheidt, *J. Am. Chem. Soc.*, **109**, 2659 (1987); b) T. P. Wijesekera, J. B. Paine III, D. Dolphin, F. W. B. Einstein, and T. Jones, *ibid.*, **105**, 6747 (1983).

11) M. R. Wasielewski, "Distance Dependence of Electron Transfer Reactions," in "Photoinduced Electron Transfer," ed by M. A. Fox and M. Chanon, Elesevier, Amsterdam (1988), Part A, Chap. 1.4, pp.161—206.

12) A stepwise synthesis for this type of strapped porphyrin was reported: J. E. Baldwin, M. J. Crossley, T. Klose, E. A. O'rear III, and M. K. Peters, *Tetrahedron*, **38**, 27 (1982).

13) P. S. Clezy and A. W. Nichol, *Aust. J. Chem.*, **11**, 1835 (1965).

14) J. S. Lindsey, P. A. Brown, and D. A. Siesel, *Tetrahedron*, **1989**, 4845.

15) I. Tabushi, S. Kugimiya, M. G. Kinnaird, and T. Sasaki, *J. Am. Chem. Soc.*, **107**, 4192 (1985).

16) The red shifts of Soret and Q-bands in distorted porphyrins were reported in Ref. 10.

17) R. J. Abraham, S. C. M. Fell, and K. M. Smith, *Org. Magn. Reson.*, **9**, 367 (1977).

18) M. Momenteau et al., *J. Chem. Soc., Perkin Trans. 1*, **1983**, 189.

19) J. H. Wood and R. E. Gibson, *J. Am. Chem. Soc.*, **71**, 393 (1949).

20) M. W. Miller, R. W. Amidon, and P. O. Tawney, *J. Am. Chem. Soc.*, **77**, 2845 (1955).

21) S. J. Angyal, P. J. Morris, J. R. Tetaz, and J. G. Wilson, *J. Chem. Soc.*, **1950**, 2141.

22) T. W. Campbell and R. N. McDonald, *J. Org. Chem.*, **24**, 1426 (1959).

23) K. Oita and H. Gilman, *J. Am. Chem. Soc.*, **79**, 339 (1957).

24) M. Kodama, Y. Shinobara, K. Matsumura, and H. Sumitomo, *Tetrahedron Lett.*, **1985**, 877.

Color Change of (*E*)-2,3-Bis(2,3,4,5,6-Pentafluorophenyl)-3-[2,3,5,6-tetrafluoro-4-(cyanomethyl)phenyl]acrylonitrile by the Addition of Amines

Yasuhide NAKAYAMA,* Kazuo INUKAI, Koichiro HAYASHI, and Masahiro IRIE*,†
The Institute of Scientific and Industrial Research, Osaka University, Mihogaoka 8-1, Ibaraki, Osaka 567
†Institute of Advanced Material Study, Kyushu University, Kasuga-Koen 6-1, Kasuga, Fukuoka 816
(Received November 9, 1990)

(*E*)-2,3-Bis(2,3,4,5,6-pentafluorophenyl)-3-[2,3,5,6-tetrafluoro-4-(cyanomethyl)phenyl]acrylonitrile (**3E**) was synthesized. A benzene solution of **3E** turns into a brilliant red color by the addition of aliphatic amines. The coloration mechanism is studied by optical absorption, conductivity and product analyses. It has become apparent that ion-pair formations between **3E** and the amines by proton transfer reactions are responsible for the coloration. Structural requirements of the amines for the ion-pair formation are discussed.

Molecular complexes of macrocyclic polyethers have been utilized in various directions, such as selective extraction, separation and transport of guest molecules, phase transfer catalyses or models of vital systems.[1-6] In spite of such explosive development of host-guest complexes, much less attention has been paid to ion-pair complexes.[7,8]

The ion-pair formation in less polar solvents via an intermolecular proton transfer is also expected to be useful for recognition of ionizable molecules, such as amines. In the present study, we studied structural requirements for the ion-pair formation by using (*E*)-2,3-bis(2,3,4,5,6-pentafluorophenyl)-3-[2,3,5,6-tetrafluoro-4-(cyanomethyl)phenyl]acrylonitrile (**3E**) as a proton donating molecule. The compound **3E** formed ion-pair complexes with various amines in organic solvents along with a brilliant red coloration. The ion-pair formation depends on the structure of the amines and the nature of the solvents. The association constants (K_a) for the formation of ion-pair complexes between **3E** and various amines have been determined to reveal what factors control the complex formation.

Results and Discussion

Synthesis. (*E*)-2,3-Bis(2,3,4,5,6-pentafluorophenyl)-3-[2,3,5,6-tetrafluoro-4-(cyanomethyl)phenyl]acrylonitrile **3E** was prepared by a self-coupling reaction of two 2,3,4,5,6-pentafluoro-1-(cyanomethyl)benzenes (**1**) followed by replacement of a cyano group by another molecule of **1**. The reaction process is presumed as follows.[9,10]

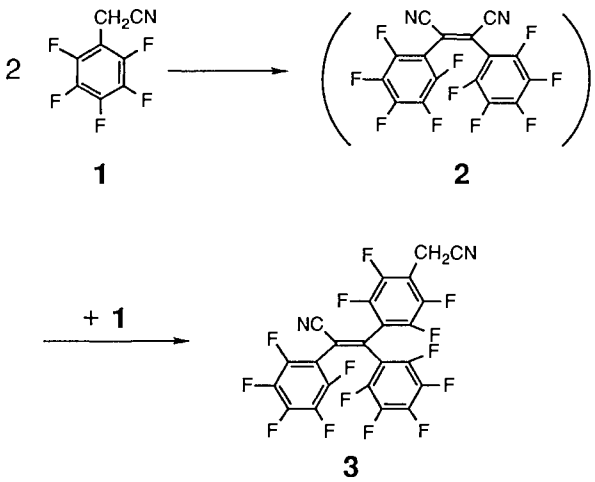

Scheme 1.

Isolation of the intermediate **2** was failed. The self coupling product **2** and the active fluorine atom at 4 position of **1** is considered to react easily each other to produce **3**.[11,12] Compound **3** was a chief product and a very small amount of by-product was prepared by further replacement of a cyano group of **3** by another molecule of **1**.[22] Compound **3** was obtained as a mixture of *E*/*Z* isomer whose assignment was performed based on ^{19}F NMR spectra. The mixture was dissolved in benzene and exposed to ultraviolet light (280 nm). The *Z* form was efficiently converted to *E* form by the irradiation. The *E* form was isolated by high-performance liquid chromatography and purified by recrystallization from a benzene-hexane mixture. The structure of the product was determined on the basis of mass spectra, NMR spectra, and material analysis whose data are presented in the experimental section. This material was used for further experiments.

Formation of Ion-Pair Complexes and Absorption Spectral Changes. The absorption spectra of (*E*)-2,3-bis(2,3,4,5-pentafluorophenyl)-3-[2,3,5,6-tetrafluoro-4-(cyanomethyl)phenyl]acrylonitrile (**3E**) in 300—650 nm region were measured at 20 °C in benzene solution in the absence and presence of various amines.

Figure 1 shows a typical absorption spectral change of a dilute benzene solution of **3E** ($[\mathbf{3E}]_0=3.4\times10^{-5}$ mol dm^{-3}) by the addition of Et_2NH. The benzene solution turns red in the presence of small amount of Et_2NH. An absorption maxima is observed at about 500 nm. The maximum gradually shifts to 503 nm with increasing the amount of Et_2NH.[13,14] An isosbestic point is observed at 305 nm in the absorption spectrum.

The absorption spectrum maintained a constant

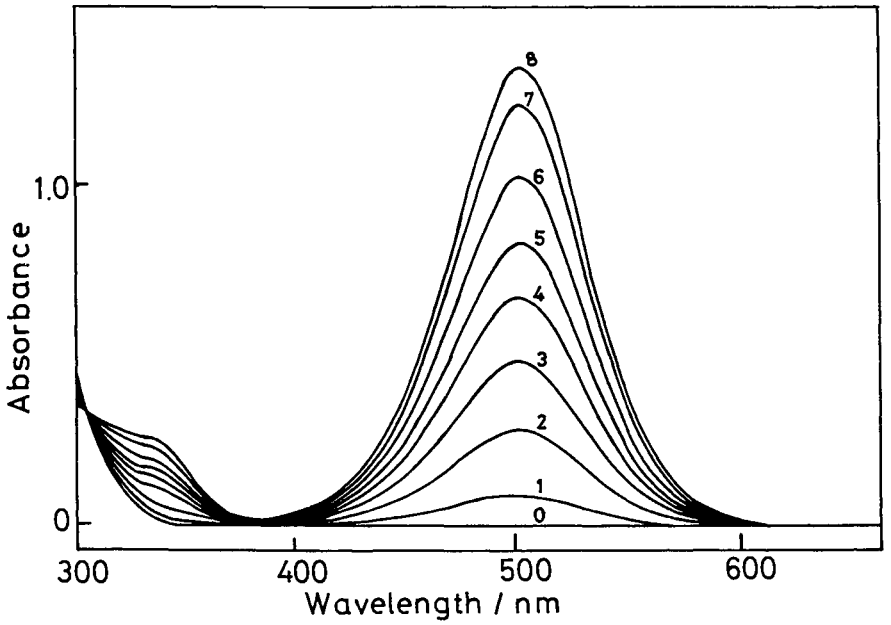

Fig. 1. Absorption spectral change of the benzene solution of **3E** (3.4×10^{-5} mol dm^{-3}) by the addition of Et_2NH.
[Et_2NH]: (0) 0, (1) 3.4×10^{-2}, (2) 6.8×10^{-2}, (3) 1.0×10^{-1}, (4) 1.4×10^{-1}, (5) 1.7×10^{-1}, (6) 2.4×10^{-1}, (7) 3.4×10^{-1}, and (8) 5.1×10^{-1} mol dm^{-3}.

intensity, so far the solution being stored in the dark at room temperature. The addition of H^+ (H_2SO_4, HCl) to the reaction mixture decreased the absorption intensity and the initial colorless solution was obtained. The absorption spectrum of 2,3,4,5,6-pentafluoro-1-(cyanomethyl)benzene (**1**) was not affected by the addition of amines. These results suggest that the absorption observed at around 500 nm is ascribable to the ion-pair complex of **3E** with the amine by proton transfer, as shown right.

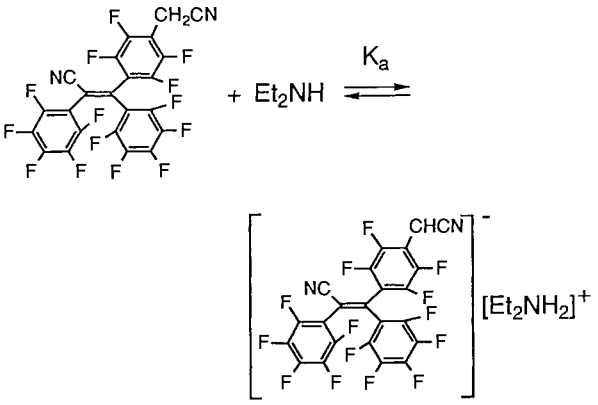

Bazavluk et al.[8] reported a similar ion-pair formation for heptafluoro-2-naphthol and aliphatic amines system in undecane.

Table 1. Association Constants, Molar Absorption Coefficients and Absorption Maxima of the Complexes of **3E** with Amines in Benzene Solution

Entry	Amine	K_a	$10^4\varepsilon$	λ_{max}
		mol dm^{-3}	$dm^3\,mol^{-1}\,cm^{-1}$	nm
1	*n*-$PrNH_2$	10.0	4.2	509
2	*n*-$BuNH_2$	7.8	4.3	509
3	Cyclohexylamine	11.1	4.5	507
4	Et_2NH	22.0	4.2	501
5	*n*-Pr_2NH	4.0	4.5	499
6	*i*-Pr_2NH	6.8	4.5	501
7	*n*-Bu_2NH	4.3	4.4	496
8	Et_3N	3.4	3.8	496
9	Aniline	c)	c)	c)
10	Pyridine	c)	c)	c)
11	Et_2NH[a]	30.0	4.7	510
12	Et_2NH[b]	13.6	4.7	502
13	*n*-Pr_2NH[a]	13.4	4.8	510

a) In CH_2Cl_2. b) In hexane. c) Not observed.

Association Constants Measurements. The association constants and the molar absorption coefficients of the complexes of **3E** with various amines ($[\mathbf{3E}]_0 = 2.2\times10^{-5}$ mol dm^{-3}) are shown in Table 1. These values were determined by using the UV-vis spectrophotometric method.[15,16]

Table 1 also gives the position of the absorption peaks for the ion-pair complexes of **3E** and various amines.

With some exceptions K_a values increases with increasing λ_{max} and exhibit approximately linear relationships.

Aromatic amines, such as aniline and pyridine do not make ion-pair complexes with **3E**. This is possibly due to the low basicity. The association constant has a tendency to decrease in the order: primary > secondary > tertiary amines. This order agrees with the observation for the charge transfer complex formations.[17,18] Primary amines, n-$PrNH_2$ and n-$BuNH_2$, have large association constants, which are around twice the corresponding secondary amines. Among the secondary amines, Et_2NH has an extraordinary large association value, which is 5 times larger than the values of n-Pr_2NH and n-Bu_2NH. A simple steric hindrance explanation[19,20] that large alkyl groups prohibit the close approach of the amines to **3E** can not be applied to the present system, because the large association constant is observed for cyclohexylamine and the value of Et_3N is close to the values of n-Pr_2NH and n-Bu_2NH. The large value for Et_2NH and cyclohexylamine suggests that **3E** has a site which recognizes the difference in the shape between cyclohexylamine and n-Pr_2NH, and the site favorably accepts Et_2NH. Such a steric requirement to allow close approach is considered to play an important role in the proton transfer process.

The association value is also dependent on the solvent polarity. The value increases with the increases in the solvent polarity. It is worthwhile to note that along with the increases in the association constants the difference in the values between Et_2NH and n-Pr_2NH decreases in polar CH_2Cl_2. In polar solvents, large stabilization in the ion-pair states possibly diminishes the energy barrier difference in the recognition process.

Coloration Mechanism. In order to confirm the ion-pair mechanism for the coloration, we measured conductivity[21] of CH_2Cl_2 solution containing **3E** and Et_2NH.

Figure 2 shows the conductivity change of a dilute CH_2Cl_2 solution of **3E** by the addition of Et_2NH (a) and the change of the optical density at λ_{max} (510 nm) of the same solution (b). Addition of Et_2NH increased the absorption intensity along with the increases in the conductivity. Although slight increase in the conductivity is observed even in the absence of **3E**, the value is much smaller than the value in the presence of **3E**. Both the conductivity value and the intensity of

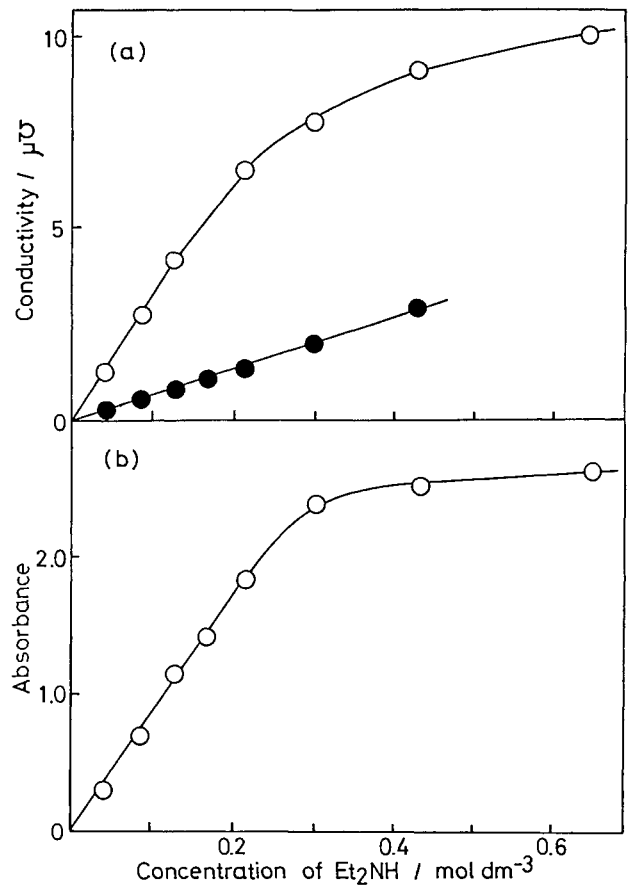

Fig. 2. (a) Conductivity change of **3E**-Et_2NH system in CH_2Cl_2.
(○), with **3E** (4.3×10^{-5} mol dm^{-3}); (●), without **3E**.
(b) Absorption intensity change of **3E**-Et_2NH system in CH_2Cl_2 at 510 nm.

the absorbance showed a saturation behavior above 0.3 mol dm^{-3} of amine. The good correlation between the conductivity and the absorption intensity clearly indicates that the coloration is due to the formation of ion-pair between **3E** and the amine.

Product analysis also supported the ion-pair formation. The colored form was quenched in CH_2Cl_2 by deuterium chloride and then **3E** was analyzed. One of the cyano methyl protons of **3E** was found to be replaced by a deuterium atom.[22] Addition of deuterium chloride to a colorless benzene solution of **3E** does not led to the exchange reaction of a deuterium and proton atom.[22] These are unambiguous evidence that a proton is transferred from CH_2CN group of **3E** to the amine in the formation of ion-pair complex.[23-25]

The compound **3E** also interacts with many compounds with basic nature to produce red colored solutions, such as ethers, THF, or alcohols. When **3E** in solid state was placed in the THF vapor, the solid turned to red. By evacuating THF from the solid, the solid again returned to colorless state. It was possible to repeat the coloration/decoloration cycles many

times.

Experimental

IR spectra were measured with a Shimadzu IR-408 spectrophotometer. ^{1}H NMR spectra (360 MHz) and ^{13}C NMR spectra (91 MHz) were recorded in $CDCl_3$ with a Bruker WN-360 instrument. All chemical shifts are reported in parts per million (δ) downfield from internal tetramethylsilane. ^{19}F NMR were recorded on a Bruker WN-360 instrument at 339 MHz and are reported in ppm from internal trichlorofluoromethane. Mass spectra and elemental analyses were performed in the Material Analysis Center of Osaka University. HPLC analysis was performed on a JASCO 800 system. Absorption spectra were measured with a Shimadzu MPS-200 instrument. Photoisomerization was performed by a mercury lamp (Ushio, 1 kW), associated with a monochrometer (Jobin Yvon H10-UV) and filters (agueous solution of $CuSO_4$ and Toshiba UV-28 glass filter), as a light source. Ion-pair complex formation constants (association constant) (K_a) were determined by using the UV-vis spectrophotometric method.[15,16] K_a and molar absorption coefficients (ε) of the complexes are obtained from the plots of $[\mathbf{3E}]_0[\mathbf{Amine}]_0/OD$ values vs $[\mathbf{Amine}]_0$ values.

$$\frac{l[\mathbf{3E}]_0[\mathbf{Amine}]_0}{OD}=\frac{1}{\varepsilon}[\mathbf{Amine}]_0+\frac{1}{\varepsilon K_a}$$

In the equation, OD is the optical density of the solution and l is the cell width (1 cm). Conductivities were measured at 20 °C using a autobalance universal bridge (WAYNE KERR B642). The solvent was CH_2Cl_2 which was dried with phosphorus pentoxide and distilled from potassium carbonate.

Reversible coloration of **3E** in solid state with THF was performed as follows. Compound **3E** adsorbed on the surface of a silica-gel plate was placed in the THF vapor until the red color was attained. The coloration time was less than few second. Then, upon the adsorbed THF gas was released by heated weakly, the red color disappeared and initial colorless **3E** was restored. It also took less than few second. The coloration/decoloration cycles was repeated.

Materials. All amines were obtained commercially and were purified by distillation.

2,3,4,5,6-Pentafluoro-1-(Cyanomethyl)benzene (1).[26,27] NaCN (9.2 g, 0 19 mol) and tetrabutylammonium chloride (0.108 g, 0.39 mmol) was dissolved in 32.8 mL of water. To this solution was added 2,3,4,5,6-pentafluoro-1-(bromomethyl)benzene (10.0 g, 38 mmol) in 32.8 mL of THF, and stirred for 10 min. The reaction mixture was poured into water and then the product was extracted with ether. Removal of the ether and distillation of the residual under vacuum gave 5.0 g of 2,3,4,5,6-pentafluoro-1-(cyanomethyl)-benzene. 63% yield; bp 101 °C; ^{1}H NMR ($CDCl_3$) δ=3.71 (s); ^{13}C NMR ($CDCl_3$) δ=104.17—104.69, 114.38, 135.70—136.21, 139.50—139.85, 143.03—143.55, 146.83—146.94; ^{19}F NMR ($CDCl_3$) δ=−160.73 (m, 2F), −152.51 (m, 1F), −141.65 (m, 2F); IR (KBr) 2260 cm^{-1} (-CN). MS (EI) m/z (rel intensity) 207 (M^+, 100), 188 (M^+−F, 35), 181 (M^+−CN, 28). Found: C, 46.40; H, 0.97; N, 6.76; F, 45.87%. Calcd for $C_8H_2N_1F_5$: C, 46.64; H, 0.87; N, 6.52; F, 45.75%.

(*E*)-2,3-Bis(2,3,4,5,6-Pentafluorophenyl)-3-[2,3,5,6-tetrafluoro-4-(cyanomethyl)phenyl]acrylonitrile (3E).[9,10] To 2.9 mL of 50% NaOH aqueous solution containing tetrabutylammonium bromide (0.195 g, 0.6 mmol) was added, over a period 0.5 h a mixture of 2,3,4,5,6-pentafluoro-1-(cyanomethyl)benzene (**1**) 3 g (14.5 mmol) and CCl_4 2.25 mL (23.3 mmol) at 40 °C. The solution was stirred for 1.5 h at 45 °C. Then, the reaction mixture was poured into water. The aqueous solution was extracted with $CHCl_3$, and the organic phase was dried over $MgSO_4$. After the solvent was removed, the mixture of *E* and *Z* forms of 2,3-Bis[2,3,4,5,6-pentafluorophenyl]-3-[2,3,5,6-tetrafluoro-4-(cyanomethyl)-phenyl]acrylonitrile was obtained in 4.7% yield by column chromatography on silica gel using THF/hexane (1 : 1) and then benzene as the eluting solvent. The *Z*/*E* mixture was dissolved in benzene and exposed to ultraviolet light (280 um). The *Z* form converted to *E* form by the irradiation. The *E* form (**3E**) was separated by HPLC[28] and then purified by recrystallization from a benzene–hexane mixture. The compound **3E** was obtained in 4% yield; mp 135 °C; ^{1}H NMR ($CDCl_3$) δ=5.83 (s); ^{19}F NMR ($CDCl_3$)[29] δ=159.60 (m, 2F), −159.28 (m, 2F), −149.84 (m, 1F), −148.90 (m, 1F), −139.75 (m, 2F), −139.46 (m, 2F), −138.80 (m, 2F), −134.18 (m, 2F). MS (EI) m/z (rel intensity) 572 (M^+, 100), 405 (M^+−C_6F_5, 14); IR (KBr) 2240 cm^{-1} (-CN). Found: C, 48.02; H, 0.52; N, 4.94%, Calcd for $C_{23}H_2N_2F_{14}$: C, 48.27: H, 0.35; N, 4.90; F, 46.48%.

References

1) R. M. Izatt and J. J. Christensen, Academic Press, New York (1978), p. 1.

2) F. Voegtle, *Top. Curr. Chem.*, **98**, 1 (1981) and **101**, 1 (1982).

3) M. Hiraoka, "Crown Compounds," Elsevier, New York (1982), p. 1.

4) G. W. Gokel and S. H. Korzeniowski, "Macrocyclic Polyether Synthsis," Spring-Verlag, New York (1982), p. 1.

5) F. Voegtle and E. Weber, *Top. Curr. Chem.*, **121**, 1 (1984).

6) R. M. Izatt, J. S. Bradshow, S. A. Nielsen, J. D. Lamb, J. J. Christensen, and D. Sen, *Chem. Rev.*, **85**, 271 (1985).

7) T. K. Pal, G. K. Mallik, T. Ganguly, and S. B. Banerjee, *Bull. Chem. Soc. Jpn.*, **62**, 3315 (1989).

8) Y. A. Bazavluk, A. N. Delnov, and G. S. Denisov, *Zh. Prikl. Spektrosk.*, **48**, 799 (1988).

9) M. Irie and M. Mohri, *J. Org. Chem.*, **53**, 803 (1988).

10) Y. Nakayama, K. Hayashi, and M. Irie, *J. Org. Chem.*, **55**, 2592 (1990).

11) J. M. Birchall and R. N. Haszeldine, *J. Chem. Soc.*, **1961**, 3719.

12) M. Zupan and B. Sket, *Isr. J. Chem.*, **17**, 92 (1978).

13) J. A. Riddic and W. B. Bunger, "Organic Solvents. Techniques of Chemistry," 3rd ed, Wily-Interscience, New York, (1970), Vol. II.

14) H. Fujiwara, T. Takaba, Y. Yamazaki, and Y. Sasaki, *J. Chem. Soc., Faraday Trans. 1*, **75**, 79 (1979).

15) L. Forlani and P. E. Todesco, *J. Chem. Soc., Perkin Trans. 2*, **1980**, 313.

16) R. Foster, "Organic Charge-Transfer Complexes," Academic Press, London (1969).

17) R. Foster, *J. Chem. Soc.*, **1960**, 1075.

18) O. D. Bonner and G. B. Woolsey, *Tetrahedron*, **24**, 3625 (1968).

19) J. O. Singh, J. D. Anunziata, and J. J. Silber, *Can. J. Chem.*, **63**, 903 (1985).

20) A. S. N. Murthy and A. P. Bhardwaj, *J. Chem. Soc., Faraday Trans. 2*, **78**, 1811 (1982).
21) M. F. Mayahi and H. A. Hussain, *J. Indian Chem. Soc., L*, **1973**, 34.
22) The determination was performed by mass spectra.
23) S. Bruckenstein and A. Saito, *J. Am. Chem. Soc.*, **87**, 698 (1965).
24) E. A. Yerger and G. M. Barrow, *J. Am. Chem. Soc.*, **77**, 4474 (1955).
25) G. M. Barrow, *J. Am. Chem. Soc.*, **78**, 5802 (1956).
26) K. Fukunaga, *Yuki Gosei Kagaku Kyokai Shi*, **33**, 774 (1975).
27) R. Filler and S. M. Woods, *Org. Synth.*, **57**, 80 (1977).
28) Conditions of HPLC analysis is as follows: Column JASCO Fine SIL (silica gel) 4.6×250 mm for analytical purposes: Elution, benzene: Flow rate, 1 mL: retention time: **3E**, 4.3 min and **3Z**, 5.3 min: Column JASCO Fine SIL (silica gel) 10.0×250 mm for preparative purposes.
29) **3Z**, ^{19}F NMR ($CDCl_3$), δ=−159.25 (m, 2F), −159.10 (m, 2F), −149.60 (m, 1F), −147.96 (m, 1F), −140.05 (m, 2F), −138.37 (m, 2F) −138.12 (m, 2F), −135.78 (m, 2F).

Polymerization Mechanism of Styrene Initiated by 2,2-Bis(*t*-butyldioxy)alkanes

Yasumasa WATANABE, Hideyo ISHIGAKI, Hiroshi OKADA, and Shuji SUYAMA*
Chemicals and Explosives Research Laboratory, Nippon Oil & Fats Co.,
Taketoyo-cho, Chita-gun, Aichi 470-23
(Received November 20, 1990)

The radical polymerization mechanism of styrene initiated by 2,2-bis(*t*-butyldioxy)alkanes (**1**) has been studied in benzene. The decomposition products of **1** are acetone, alkyl methyl ketone, *t*-butyl alcohol, and *t*-butyl peracetate. Styrene monomer converts to polystyrene along with styrene oxide. The peroxides **1** cleave homolytically at one of dioxy bonds to yield intermediate alkoxyl radicals with α-*t*-butyldioxyl group, which undergo β-scission to afford *t*-butyldioxyl or alkyl radicals. The resulting *t*-butyldioxyl radical reacts with styrene to form 2-(*t*-butyldioxy)-1-phenylethyl radical, which decomposes subsequently to styrene oxide and *t*-butoxyl radical via γ-scission. Alternatively, a part of *t*-butyldioxyl radical adds to styrene to afford polystyrene containing dioxy bond.

gem-Bis(*t*-alkyldioxy)alkanes can be used as excellent free radical initiators for polymerization of styrene. But only a few studies have been reported on the mechanism of polymerization using them.

Yenal'ev and co-workers[1,2] studied the polymerization of styrene with *gem*-bis(*t*-alkyldioxy)alkanes. Interestingly, they found that parts of polystyrene molecules possessed dioxyl group. It was concluded that the initial decomposition of the peroxides occurred at one of dioxy bonds (Eq. 1) rather than the synchronous two bond scission (Eq. 2), and suggested that the polystyrene molecules containing dioxyl groups were produced by the addition of the alkoxyl radical having dioxyl group to styrene. However, the detailed polymerization mechanism has not been clear.

$$\mathrm{ROOMOOR} \longrightarrow \mathrm{RO}\cdot + \cdot\mathrm{OMOOR} \quad (1)$$

$$\mathrm{ROOMOOR} \longrightarrow 2\mathrm{RO}\cdot + \cdot\mathrm{OMO}\cdot \quad (2)$$

Recently we have reported on the mechanism of thermal decomposition of 2,2-bis(*t*-butyldioxy)alkanes (**1**) in diphenylmethane or cumene.[3,4] The results have shown that the peroxides cleave homolytically at one of dioxy bonds to yield *t*-butoxyl and intermediate alkoxyl radicals (**2**) with α-*t*-butyldioxyl group (Eq. 3), which undergo β-scission to afford *t*-butyldioxyl or alkyl radicals.

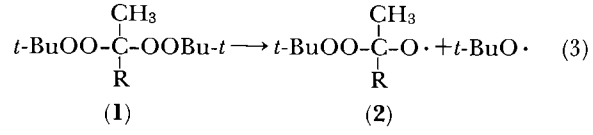

(3)

(**1**) (**2**)

(**1a**): R=CH_3, (**1b**): R=CH_2-CH_3, (**1c**) R=$CH(CH_3)_2$

In the polymerization of styrene using **1**, if the addition reaction of **2** to styrene occurs much faster than the β-scission of **2**, the polymer radical with *t*-butyldioxyl end group would be formed as suggested by Yenal'ev and co-workers (Eq. 4). The terminal dioxyl group of the resulting polymer would further

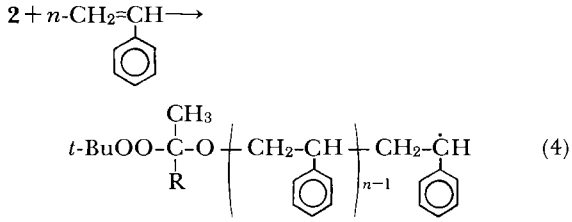

(4)

cleave at O–O bond and reinitiate the polymerization of styrene, i.e., the peroxides **1** would act as bifunctional initiators. Alternatively, if the β-scission of **2** occurs much faster than the addition of **2** to styrene, radicals generated by β-scission of **2** would initiate the polymerization of styrene.

In the present paper we report the study on the polymerization of styrene using 2,2-bis(*t*-butyldioxy)-alkanes **1** in order to elucidate the initiation mechanism forcusing on the facile β-scission of radicals from **2**.

Experimental

GLC analysis was performed with a Shimadzu GC-9A gas chromatograph with a flame ionization detector by using a 15 m flexible fused silica capillary column (0.53 mm in diameter) coated with silicone OV-1. A Shimadzu Chromatopac C-R6A integrator was used for quantitative analysis. Mass spectra were obtained on a JEOL JMS-DX300 mass spectrometer at 70 eV under electron impact condition. GPC analysis was accomplished on a Shimadzu CTO-6A equipped with a Shimadzu RID-6A using THF as the eluent. Two columns, a Shodex KF-80M (60 cm) and a Shimadzu HSG-10S (60 cm) were connected in series. The calibration curve was made using standard samples of polystyrene.

Materials. 2,2-Bis(*t*-butyldioxy)alkanes were prepared by the methods previously described.[4] The purities of peroxides were over 97.0% by iodometric titration or GLC analysis. Styrene was washed with 2% aqueous sodium hydroxide and water, dried over anhydrous $MgSO_4$, and distilled under reduced pressure. Cumene was purified by distillation after washing with concentrated sulfuric acid.

Polymerization and Thermolysis. Radical polymeriza-

tions of styrene with peroxides were carried out in a sealed-glass ampoule in benzene at 110 °C. After polymerization for a given time, the molecular weight of polystyrene was determined by GPC analysis and reaction products were analyzed by GLC and/or GC-MS in comparison with authentic samples.

Thermolyses of **1** were carried out in cumene under the same conditions as those of polymerization, and reaction products were analyzed by GLC and/or GC-MS.

Determination of Active Oxygen. After polymerization, the content of the ampoule was poured into large amount of methyl alcohol to isolate the polymer. The resulting polymer was purified by two reprecipitations with methyl alcohol and dried in vacuum at room temperature to constant weight. A weighed amount of the purified polystyrene was added to isopropyl alcohol containing acetic acid, sodium carbonate, and potassium iodide. After boiled for 5 min, 36% hydrochloric acid was added to the mixture and boiled further for 3 min. Then the liberated iodine was titrated with aqueous sodium thiosulfate solution.

Results and Discussion

The thermal decomposition of **1** was carried out in cumene under nitrogen. The products obtained by the decomposition were acetone, alkyl methyl ketone, *t*-butyl alcohol, *t*-butyl hydroperoxide, *t*-butyl peracetate (**3**), *t*-butyl 1-methyl-1-phenylethyl peroxide, and 2,3-dimethyl-2,3-diphenylbutane (Table 1A). A likely scheme leading to the products in cumene is shown by following equations. Here, R'H denotes cumene

$$2 \longrightarrow \underset{(\mathbf{3})}{CH_3\text{-}C(=O)OBu\text{-}t} + R\cdot \quad (5)$$

$$2 \longrightarrow CH_3\text{-}\overset{O}{\overset{\|}{C}}\text{-}CH_3 + t\text{-}BuOO\cdot \quad (6)$$

$$t\text{-}BuO\cdot + R'H \longrightarrow t\text{-}BuOH + R'\cdot \quad (7)$$

$$t\text{-}BuO\cdot \longrightarrow CH_3\text{-}\overset{O}{\overset{\|}{C}}\text{-}CH_3 + CH_3\cdot \quad (8)$$

$$t\text{-}BuOO\cdot + R'H \longrightarrow t\text{-}BuOOH + R'\cdot \quad (9)$$

$$t\text{-}BuOO\cdot + R'\cdot \longrightarrow t\text{-}BuOOR' \quad (10)$$

$$R'\cdot + R'\cdot \longrightarrow R'\text{-}R' \quad (11)$$

and R'-R' is 2,3-dimethyl-2,3-diphenylbutane. As shown in Eq. 3, the O-O homolysis of **1** produces *t*-butoxyl radical and 1-*t*-butyldioxy-1-methylalkoxyl radical (**2**). The resulting alkoxyl radical **2** undergoes β-scission to afford *t*-butyl peracetate (**3**) and alkyl methyl ketone (Eqs. 5 and 6). *t*-Butyl alcohol and acetone are formed by a hydrogen abstraction of *t*-BuO· from solvent cumene (Eq. 7) and scission of methyl radical from *t*-BuO· (Eq. 8). *t*-BuOO· generated by Eq. 6 undergoes a hydrogen abstraction to afford *t*-BuOOH (Eq. 9) or a coupling reaction with R'· to afford *t*-BuOOR' (Eq. 10). Another coupling reaction of R'· affords R'-R' (Eq. 11).

It is noted that the yield of **3** in cumene changes dramatically with the structure of **1** (i.e., **1a** $\ll$ **1b** $\lesssim$ **1c**). As shown by the previous report,[4] this result can be explained by the difference in elimination rates of alkyl radicals from **2** (i.e., Me < Et < *i*-Pr).

The polymerization of styrene using **1** was carried out in benzene. The liquid products in the reaction were acetone, alkyl methyl ketone, *t*-butyl alcohol, **3**, and styrene oxide (Table 1B). It is worth to note that the yields of **3** obtained in the polymerization of styrene are very close to those obtained in cumene. The result indicates that the addition reaction of **2** to styrene (Eq. 4) is negligibly slow in comparison with the scission reaction of **2**. If Eq. 4 occurs faster than Eq. 5 or 6, the yields of **3** formed in the styrene polymerization shoud be reduced appreciably compared to those of **3** formed in cumene.

The difficulty in addition reaction of **2** to styrene is quite interesting since the analogous alkoxyl radical, *t*-BuO·, is well known to react with styrene easily. For example, Solomon and co-workers[5] showed that the relative rate of β-scission of *t*-BuO· vs. addition reaction to styrene in benzene at 60 °C was 0.11, revealing the facile addition reaction. The difference in reactivity between *t*-BuO· and **2** is explained mainly

Table 1. Products on Decomposition of **1**[a]

Peroxide	Product yield[b]/%							
	Me_2CO	RCOMe	*t*-BuOH	*t*-BuOOH	$MeCO_3Bu$-*t*	*t*-BuOOR'	R'-R'	Epoxide[c]
	A) Decomposition in cumene							
1a	44	[d]	51	19	16	46	44	
1b	30	7	56	<1	61	9	82	
1c	35	3	71	<1	70	2	73	
	B) Decomposition in styrene/benzene[e]							
1a	67	[d]	18	<1	17			21
1b	25	8	17	<1	66			2
1c	29	1	28	<1	69			2

a) Decomposition was carried out at 110 °C. Initial concentration: $[\mathbf{1}]_0$=0.1 mol dm^{-3}. Reaction time: **1a**, 4 h; **1b**, 2 h; **1c**, 1 h. b) Yields of products: [(moles of prducts)/(moles of **1** consumed)]×100. The conversion of **1** was 30—40%. R: **1a**=CH_3, **1b**=CH_2-CH_3, **1c**=$CH(CH_3)_2$. Me=CH_3, R'=$C_6H_5C(CH_3)_2$. c) Styrene oxide. d) RCOMe=Me_2CO. e) Styrene/benzene=50 v/v%.

on the basis of the difference in scission rates of radicals from alkoxyl radical. We have recently shown that relative rates of β-scission of radicals from **2** in cumene at 100 °C are isopropyl : ethyl : *t*-butyldioxyl : methyl=133 : 33 : 7 : 1.[4] This result indicates that the β-scission reaction of **2** occurs much faster than that of *t*-BuO· having only methyl groups.

Considerable amounts of acetone and *t*-butyl alcohol were obtained even in styrene/benzene, e.g., for the case of **1b**, the yields were 25% and 17%, respectively. The result indicates that β-scission and hydrogen abstraction reactions of *t*-BuO· occur comparably to the addition reaction of *t*-BuO· to styrene under the present conditions (i.e., at 110 °C). Here, polystyrene produced in the polymerization may be considered as a hydrogen donor. Niki and Kamiya[6] reported the reactivity of polystyrene toward *t*-BuO· and showed that an appreciable amount of *t*-butyl alcohol was obtained by the hydrogen abstraction from polystyrene at relatively high temperature (125 °C). Peroxides **1** are also considered as hydrogen donors. But we have previously showed that the induced decomposition of **1** is negligible in diphenylmethane[3] or cumene.[4] It suggests that the hydrogen abstraction from **1** by *t*-BuO· is a minor reaction, if any, under these conditions.

Interestingly, appreciable amount of styrene oxide (21%) was obtained in the polymerization of styrene with **1a**. The formation mechanism of styrene oxide can be explained by radical epoxidation of styrene by dioxyl radical:[7] *t*-BuO· adds to styrene to produce 2-(*t*-butyldioxy)-1-phenylethyl radical (Eq. 12), which decomposes subsequently to styrene oxide and *t*-BuO· by γ-scission process (Eq. 13). The mechanism is

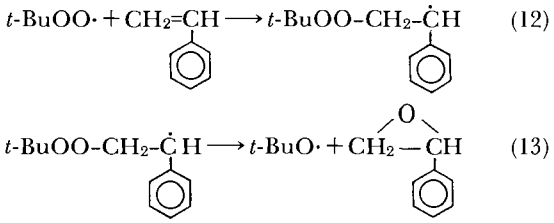

(12)

(13)

suppproted by the dependence of the yield of styrene oxide on the amount of *t*-BuOO· generated from the decomposition of **1**. *t*-BuOO· is a precursor for *t*-BuOOH and *t*-BuOOR'as shown by Eqs. 9 and 10; therefore the total yield of *t*-BuOOH and *t*-BuOOR' on the decomposition in cumene roughly coincides with that of *t*-BuOO· generated from the decomposition of **1** (i.e., 65% for **1a** and <10% for **1b** and **1c**). The significant *t*-BuOO· scission process for **1a** can contribute to the styrene oxide formation.

There is a difference between the total amount of *t*-BuOO· generated from β-scission of **2a** (65%) and the amount of *t*-BuOO· consumed by styrene oxide formation (21%). It can be assumed that the residual *t*-BuOO· (44%) would mainly initiate the polymerization of styrene, resulting in the production of polystyrene containing *t*-butyldioxyl group at the polymer end (Eq. 14).

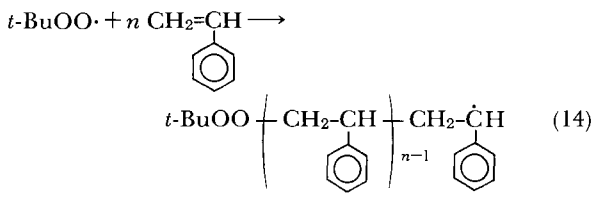

(14)

Table 2. Characteristics of Polystyrenes[a]

Peroxide	Yield of polystyrene/%	$\overline{M}_n \times 10^4$	Active oxygen[b]/%	Active polymer[c]/%
1a	94	1.4	0.052	46
1b	91	1.2	<0.005	<4
1c	82	1.1	<0.005	<3

a) Polystyrenes were obtained by the same condition as footnote a in Table 1. b) [16×(number of O-O in a polystyrene molecule)/(molecular weight of polystyrene)]×100. See experimental section for the detection. c) Proportion of polystyrene molecules having a dioxy bond: Active oxygen(%)×M_n/16.

The characteristics of polystyrenes obtained by the polymerization with **1** are given in Table 2. The molecular weight ($\overline{M}_n$) of each polystyrene was about 10000. Interestingly, active oxygen (0.052%) was found to be contained in polystyrene obtained with **1a** by iodometric titration; however we could not detect it in polystyrenes obtained with **1b** and **1c** (<0.005%). The detection of active oxygen is an important evidence indicating the existence of dioxy bond. From the values of active oxygen and molecular weight, we can estimate the proportion of polystyrene molecules containing a dioxy bond. For the case of **1a**, it was found that about half of polystyrene molecules had a dioxy bond (Table 2). In analogy with the styrene oxide formation, the amount of active oxygen in polystyrene is consistent with that of *t*-BuOO· generated from **1**. The considerable generation of *t*-BuOO· for **1a** is responsible for the production of the polystyrene containing dioxy bond as shown in Eq. 14.

Yenal'ev and co-workers[1] reported that the polystyrene obtained by the polymerization with gem-bis(*t*-pentyldioxy)alkanes contained dioxyl group. From the results, they suggested that the polystyrene was given by the reaction of alkoxyl radical having α-dioxyl group with styrene. However, our detailed investigation on polymerization mechanism with **1** rules out the possibility of Eq. 4 and leads to the conclusion that *t*-BuOO· eliminated from **2** contributes to the production of active polystyrene. It is attractive that the polymer containing dioxyl group can be obtained easily by the use of **1a** because such active polymer gives the possibility to be applied to the syntheses of block polymers.

References

1) V. D. Yenal'ev, V. V. Zaitseva, Yu. S. Sadovskii, T. N.

Sadovskaya, and Z. F. Nazarova, *Vysokomol. Soedin. (Engl. Transl.)*, **7**, 275 (1965).

2) V. V. Zaitseva, V. D. Yenal'ev, and A. I. Yurzhenko, *Vysokomol. Soedin.Ser. A, (Engl. Transl.)*, **9**, 1958 (1967).

3) T. Komai and S. Suyama, *Bull. Chem. Soc. Jpn.*, **58**, 3045 (1985).

4) S. Suyama, Y. Watanabe, and Y. Sawaki, *Bull. Chem. Soc. Jpn.*, **63**, 716 (1990).

5) D. Bednarek, G. Moad, E. Rizzardo, and D. H. Solomon, *Macromolecules*, **21**, 1522 (1988).

6) E. Niki and Y. Kamiya, *J. Org. Chem.*, **38**, 1403 (1973); E. Niki and Y. Kamiya, *J. Chem. Soc., Perkin Trans. 2*, **1975**, 1221.

7) F. R. Mayo, *J. Am. Chem. Soc.*, **80**, 2465 (1958); C. Walling and L. Heaton, *ibid.*, **87**, 38 (1965).

Metal Ion Dependent Site Selective Cleavage of P-O-S Linkage in the Methanolysis of Phenyl Phosphatosulfate

Toshio EIKI* and Waichiro TAGAKI†
Department of Chemistry, Faculty of Technology, Gunma University, Kiryu, Gunma 376
†Department of Bioapplied Chemistry, Faculty of Engineering, Osaka City University, Sugimoto 3-3-138, Sumiyoshi-ku, Osaka 558
(Received December 13, 1990)

Effects of various metal ions on the methanolysis of phenyl phosphatosulfate having P-O-S linkage were investigated. Metal ions examined were found to be divided into two different groups in the manner of cleavage of P-O-S linkage: Mg^{2+}, Cr^{3+}, Cu^{2+}, Mn^{2+}, and Ca^{2+} with larger ionic radii catalyzed the selective P-O bond cleavage, while Be^{2+}, Al^{3+}, Fe^{2+}, and Zn^{2+} with smaller ionic radii promoted the selective S-O bond cleavage. Such selectivity was discussed in terms of the difference in the mechanisms of P-O and S-O bond cleavage.

In the biological sulfur metabolism, the key intermediates are 3′-phosphoadenosine-5′-phosphosulfate (PAPS) and adenosine-5′-phosphosulfate (APS).[1-9] Both intermediates have a P-O-S linkage as the reactive bond. The enzymes catalyzing the cleavage of this P-O-S bond require a metal ion as the essential cofactor. For example, Mg^{2+} is known to be an essential cofactor for the enzymes catalyzing the sulfuryl group transfer from PAPS to numerous acceptors such as polysaccharides, phenols, steroids, and other nucleophiles.[1-5] For such reactions to occur, the S-O bond must be selectively cleaved. It is also known that an APS reductase contains a non-heme iron with an FAD coenzyme.[4,9] Here again, the S-O bond must be selectively cleaved. On the contrary, it was suggested that the enzyme-catalyzed hydrolysis of PAPS occurs with the selective P-O bond cleavage in the presence of Mn^{2+} or Co^{2+}.[3,6] Yet much remains to be clarified as to the mechanism of metal-ion catalysis, in particular as to the question how a metal ion affects the rate and the selectivity in the cleavage of the S-O vs. P-O bond of P-O-S linkage.

In our previous model studies, Mg^{2+} was found to enhance the rate of acid-catalyzed hydrolysis of phenyl phosphatosulfate (PPS) and suggested to cause the selective S-O bond cleavage.[10-12] On the other hand, the same Mg^{2+} was observed to catalyze the selective P-O bond cleavage with amine nucleophiles at neutral pH.[13,14] More explicitly, it was disclosed that metal ions such as Mg^{2+} and Zn^{2+} catalyze the attack of a nucleophile on the phosphorus of 2-pyridyl phosphonosulfate to result in the selective P-O bond cleavage at neutral pH.[15] Although this mysterious gap between the effects of Mg^{2+} on the model and enzyme reactions has remained unfilled, we reported previously that there are two different groups of metal ions which promote the selective cleavage of either the S-O or the P-O bond of PPS and the selectivity appears to depend on the ionic radii of the metal ions.[17] However, things are not so simple that Zn^{2+} has now been found to promote the selective S-O bond cleavage in the methanolysis, contrary to the expected selective P-O bond cleavage based on the ionic radius. With this additional finding, we describe herein the full account of the previous communication[16,17] on the metal ion-dependent site selective cleavage of P-O-S linkage in the methanolysis of PPS.

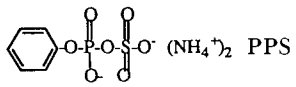

Experimental

Materials and Methods. UV and visible spectra were recorded on a Shimadzu UV-200 spectrophotometer and NMR spectra with a Varian A-60 spectrometer. pH was measured with a Hitachi-Horiba F-7DE pH meter. Water used for kinetics was purified by treating deionized water with $KMnO_4$ followed by double distillation. Buffer and other reagents for analysis were obtained from commercial sources as extra pure reagents. Metal salts used were of analytical grade. Organic solvents, *N*-ethylmorpholine and *N*,*N*-diethylaniline were distilled before use according to the standard procedures.

The diammonium salt of PPS was prepared by the reaction of phenyl phosphate with DMF-SO_3 complex in DMF at room temperature according to our method.[18] Bis(triethylammonium) salt of PPS used for the sulfonation of *N*,*N*-diethylaniline was prepared as follows. An excess of triethylamine was added to the methanol solution of diammonium salt of PPS and the exchanged NH_3 was removed by evaporation under reduced pressure to give an oily residue which was recrystallized from a methanol/ether mixed solvent. Anal. Calcd. for $C_{18}H_{37}O_7N_2PS$: C, 47.39; H, 8.11; N, 6.13%. Found: C, 46.94; H, 8.11; N,6.08%.

Alcoholyses. Although the methods of kinetics and product analyses were essentially the same as those reported previously,[13-15,18] the details are now described below.

a) Kinetics. In ampoules, the reaction was carried out in a mixed solvent of DMF-methanol (1 : 1, v/v) containing the diammonium salt of PPS (1.0×10^{-2} mol dm^{-3}), a metal ion (0—0.1 mol dm^{-3}), and *N*-ethylmorpholine (0.55 mol dm^{-3}) at 55 °C. The rate was determined by quenching two samples at appropriate time intervals: one for the monitor of

inorganic sulfate released by colorimetric barium chloranilate or barium chromate method, and the other for the monitor of phenyl phosphate and methyl phenyl phosphate formed by the UV method described below.

b) Product Analysis. Amounts of the liberated inorganic sulfate was determined colorimetrically as mentioned above and the amounts of phosphates formed were determined on the basis of UV absorption intensity. Constants employed for the analyses are listed in Table 1.

(i) UV Method. Two methods were employed. In one method, a reaction mixture (0.5 ml) was mixed with 1 mol dm^{-3} NaOH (0.5 ml) and water (4 ml), and the resulting metal hydroxide precipitate was removed by centrifuge, and the supernatant was subjected to UV analysis (for Be^{2+}, Al^{3+}, Fe^{3+}, Zn^{2+}, Mg^{2+}, Mn^{2+}, and Ca^{2+}). In the other method, a reaction mixture (0.5 ml) was mixed with 0.2 mol dm^{-3} Na_2HPO_4 (4.5 ml), and the precipitated metal ion salt of orthophosphate was removed by centrifuge, and the supernatant was subjected to the UV analysis (for Be^{2+}, Al^{3+}, Fe^{3+}, Zn^{2+}, Cr^{2+}, and Cu^{2+}). The two methods gave the same results.

(ii) NMR Method. (ii-a). For the competitive solvolysis by methanol and 2-propanol (Be^{2+}, Al^{3+}, Fe^{3+}, and Zn^{2+}): A reaction mixture (50 ml) consisting of PPS $(NH_4^+)_2$ (1×10^{-2} mol dm^{-3}), *N*-ethylmorpholine (0.55 mol dm^{-3}), and a metal ion (3×10^{-2} mol dm^{-3}) in a mixed solvent of methanol, 2-propanol, and DMF was kept for ten half-lives at 55 °C. Then the reaction mixture was concentrated to remove the solvent, and the residual oil was dissolved in water (3 ml), and to this was added 0.2 mol dm^{-3} Na_2HPO_4 (10 ml) and 1 mol dm^{-3} NaOH (2 ml). The resulting precipitate of metal ion salt of orthophosphate was separated from the supernatant by centrifuge and washed with water. The combined supernatant and the washings were concentrated to give a solid residue, and the residue was washed with ether to remove remaining *N*-ethylmorpholine. Dried final residue was dissolved in D_2O and subjected to the NMR analysis.

(ii-b). For the cases of Mg^{2+} and Ca^{2+}: A reaction mixture consisting of PPS $(NH_4^+)_2$ (1×10^{-2} mol dm^{-3}), *N*-ethylmorpholine (0.55 mol dm^{-3}), and a metal ion (5×10^{-2} mol dm^{-3}) in a mixed solvent of methanol and DMF (1 : 1, v/v %) was concentrated and the residual oil was dissolved in water (5 ml) and mixed with 0.5 mol dm^{-3} NaOH (5 ml). The metal hydroxide was separated from the supernatant by centrifuge and the precipitate was washed with 0.5 mol dm^{-3} NaOH (5 ml). The combined supernatant and the washings were treated as in the above procedure for the NMR analysis.

(ii-c). For the case of Cu^{2+}: A similar reaction mixture ($Cu^{2+}=2\times10^{-2}$ mol dm^{-3}) was concentrated to give a residual oil, and this was dissolved in 1 mol dm^{-3} HCl (20 ml). To the HCl solution was introduced H_2S gas and the copper sulfide was removed by filtration. The filtrate was treated with active carbon and the colorless filtrate was concentrated after pH adjustment (pH 11). The dried residue was subjected to the NMR analysis as mentioned above.

(iii) HPLC Method (for the reactions of Mg^{2+}, Cu^{2+}, Cr^{3+}, and Mn^{2+}): The column and the elution solvent were YANACO PELAX and 20% H_2O–80% CH_3OH, respectively. A kinetic reaction mixture (0.5 ml) was mixed with 1 mol dm^{-3} NaOH (0.5 ml) and water (4 ml), and the metal hydroxide was removed by centrifuge, and the supernatant was subjected to the NMR analysis.

(iv) Paper Chromatography. Both a raw reaction mixture and the final NMR sample were analyzed. In all the cases, only a single spot corresponding to either methyl phenyl phosphate (MPP), phenyl isopropyl phosphate or phenyl phosphate (PP) was detected.

Sulfonation. Ammonium *p*-(diethylamino)benzenesulfonate used as the authentic sample was prepared by the reaction of *N*,*N*-diethylaniline (3 ml, 19.2 mmoles) with DMF–SO_3 complex (9.6 mmoles) in DMF (6 ml). The reaction mixture was left for 10 h at ambient temperature and quenched with an excess of NH_3 in methanol. The product was precipitated by the addition of ether and recrystallized from methanol–ether. Anal. Calcd. for $C_{10}H_{18}O_3N_2S$: C, 48.79; H, 7.31; N, 11.37%. Found: C, 48.76; H, 7.36; N, 11.37%. Mp. 168—170 °C. UV (see Tables 1).

The $AlCl_3$-promoted sulfonation was conducted by the reaction of bis(triethylammonium) PPS (200 mg, 0.43 mmoles) with *N*,*N*-diethylaniline (4 ml, 25.7 mmoles) in the presence of anhydrous $AlCl_3$ (70.6 mg, 0.53 mmoles) in dry acetonitrile solvent (3 ml) at ambient temperature for 45 h. The product, ammonium *p*-(diethylamino)benzenesulfonate, was obtained in a quantitative yield by treating the reaction mixture according to the above procedure, and identified by comparing UV, ^1H NMR, and IR spectra with those of the authentic sample.

Results

Metal Ion Effects in the Methanolysis. (a) Product Analysis. Methanolysis of diammonium PPS (1×10^{-2} mol dm^{-3}) was carried out in a mixed solvent of methanol and DMF (1 : 1, v/v) under basic conditions containing *N*-ethylmorpholine (0.55 mol dm^{-3}) at

Table 1. Analytical Data for the Product Analyses

Salts	UV data[a]		^1H NMR[b]		R_f[c]
	λ_{max}/nm	(ε)	δ CH_3	δ CH	
Phenyl phosphatosulfate (PPS)	262	(440)	—	—	0.65
Methyl phenyl phosphate (MPP)	262	(580)	3.74 (d)	—	0.85
Phenyl phosphate (PP)	267	(740)	—	—	0.48
Methyl sulfate (MS)	—		3.80	—	—
Isopropyl sulfate (PS)	—		1.28 (d)	4.63 (m)	—
p-(Diethylamino)benzenesulfonate	278	(22700)	—	—	

a) In 0.1 equiv NaOH. b) In D_2O and from sodium 2,2-dimethyl-2-silapentane-5-sulfonate.
c) Toyo Filter Paper, No. 50; PrOH–NH_3(28%)–H_2O (6 : 3 : 1, v/v).

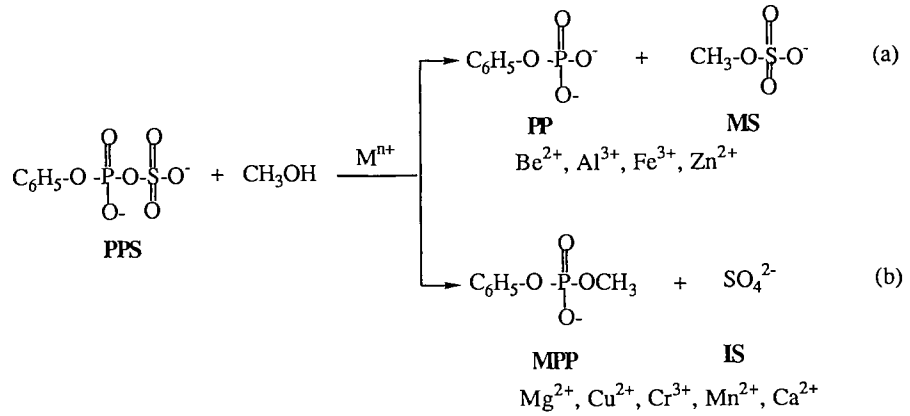

Scheme 1.

55 °C. Previously, *N*-ethylmorpholine was confirmed to be unreactive toward PPS either in the presence or absence of a metal ion examined.[10,13] The reaction was very slow in the absence of a metal ion. All metal ions tested in this study enhanced the rate of reaction. Fortunately, the product analyses described in the experimental section could be performed readily and quantitatively. The reason for the ease of analyses was first due to the simplicity of the products because of the site-selective S-O or P-O bond cleavage of P-O-S linkage. The second was due to the ease of quantitative analyses of the methylated products based on the ^{1}H NMR signals of methyl protons (Table 1) as well as their HPLC analysis. The results are summarized in Scheme 1. Scheme 1 indicates that the metal ions are divided into two different groups in the selectivity of bond cleavage. That is, Be^{2+}, Al^{3+}, Fe^{3+}, and Zn^{2+} promoted an exclusive S-O bond cleavage to form phenyl phosphate (PP) and methyl sulfate (MS) in quantitative yields, whereas Mg^{2+}, Cu^{2+}, Cr^{3+} Mn^{2+}, and Ca^{2+} catalyzed an exclusive P-O bond cleavage to form methyl phenyl phosphate (MPP) and inorganic sulfate (IS) in quantitative yields. The metal ions were used as the chlorides containing hydrated water, but the results obtained with the hydrated metal ions were essentially the same as those obtained with anhydrous metal ions. The counterions of the metal ions such as chloride, nitrate, or perchlorate did not affect the selectivity.

(b) Kinetics. The pseudo-first-order rate constants (k_{obsd}) were obtained by following spectrophotometrically the formation of either one of PP, MPP, or IS.[13,18] In the P-O bond cleavage to form MPP and IS, the metal ions performed as catalysts, i.e. a good peudo-first-order rate constants were obtained regardless of using an excess of substrate or a metal ion over the other. However, in the S-O bond cleavage to form PP and MS, precipitation occurred owing to the formation of a strongly bound PP-metal ion complex in the absence of DMF. This was one of the reasons to use DMF for a component of the mixed solvent. Thus, in the S-O bond cleavage, the rates were of pseudo-first-order in the presence of an excess of a metal ion over the substrate PPS in the mixed solvent, but under reversed conditions of an excess of PPS over a metal ion, burst kinetics were observed, i.e. an initial fast reaction followed by the slow production of PP, as exemplified in Fig. 1 (lower two curves). Most kinetics were carried out with metal ion concentrations below 0.03 mol dm^{-3}. Within this concentration range, the k_{obsd} values were first-order with respect to the metal ion concentration to give second-order rate constants, k_2(S-O) and k_2(P-O) as listed in Table 2. However, at higher metal ion concentrations, saturation kinetics were observed as shown in Fig. 2 for the three representative metal ions, Zn^{2+}, Mg^{2+}, and Ca^{2+}. The saturation curves in Fig. 2 seem to be accounted for by

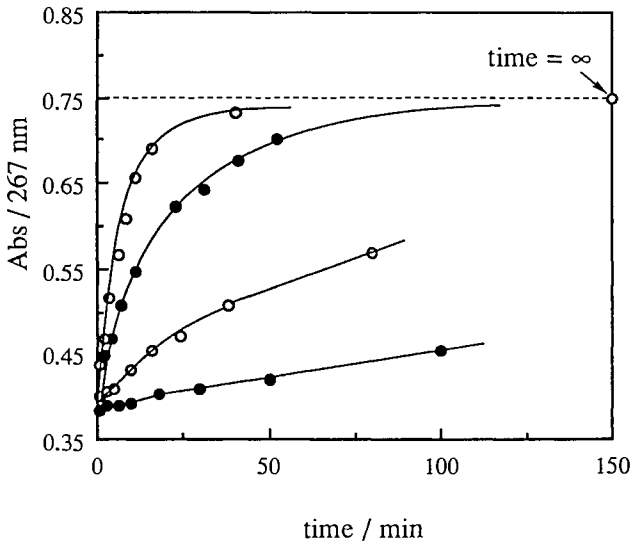

Fig. 1. Absorbance change vs. reaction time in the Zn^{2+} promoted methanolysis of PPS (1×10^{-2} mol dm^{-3}) in MeOH-DMF (1 : 1, v/v) at 55 °C: Zn^{2+} concentration (mol dm^{-3}) from the top, 1×10^{-1}, 3×10^{-2}, 1×10^{-2}, 5×10^{-3}.

Table 2. The Second Order Rate Constants, k_2(S-O) and k_2(P-O), and Ionic Radii of the Metal Ions

Metal ion	Ionic radii[a]/Å	k_2(S-O) or k_2(P-O)/mol^{-1} dm^3 s^{-1}
Be^{2+}	0.3	1.40×10^{-2}
Al^{3+}	0.53	9.56×10^{-2}
Fe^{3+}	0.63	3.33×10^{-2}
Zn^{2+}	0.74	2.45×10^{-2}
Mg^{2+}	0.71	1.31×10^{-3}
Cu^{3+}	0.71	3.51×10^{-2}
Cr^{3+}	0.76	5.80×10^{-2}
Mn^{2+}	0.8	4.13×10^{-3}
Ca^{2+}	1.14	2.81×10^{-4}

a) Ref. 20.

Table 3. Kinetic Parameters for the Metal Ion Catalyzed and/or Promoted Methanolysis[a]

Metal ion[b]	k_m/s^{-1}	K/mol^{-1} dm^3	$k_mK/(1+K[S]_T)$/mol^{-1} dm^3 s^{-1}
Zn^{2+}	8.33×10^{-3}	3.03	2.45×10^{-2}
Mg^{2+}	2.60×10^{-5}	102	1.31×10^{-3}
Ca^{2+}	1.01×10^{-5}	38.6	2.81×10^{-4}

a) Based on the data shown in Fig. 2: [PPS]=1.0×10^{-2} mol dm^{-3}, [*N*-ethylmorpholine]=0.55 mol dm^{-3} in CH_3OH/DMF (1 : 1, v/v), 55 °C. b) Chloride.

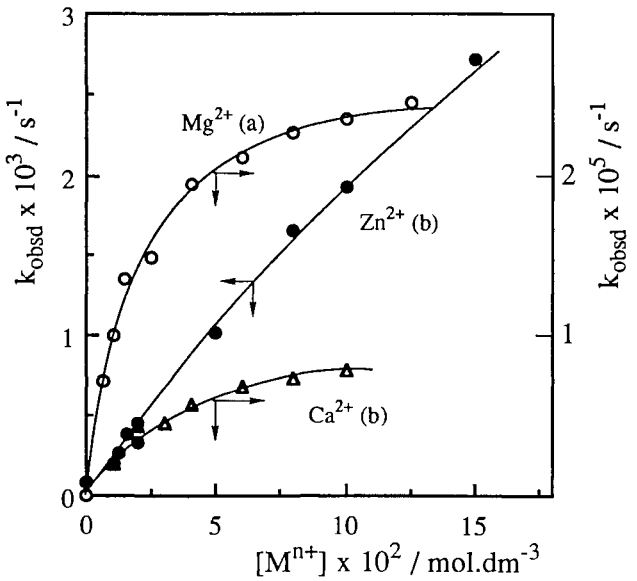

Fig. 2. Plots of k_{obsd} vs. metal ion concentration (see text for the kinetic conditions and the methods): a, SO_4^{2-} method; b, UV method.

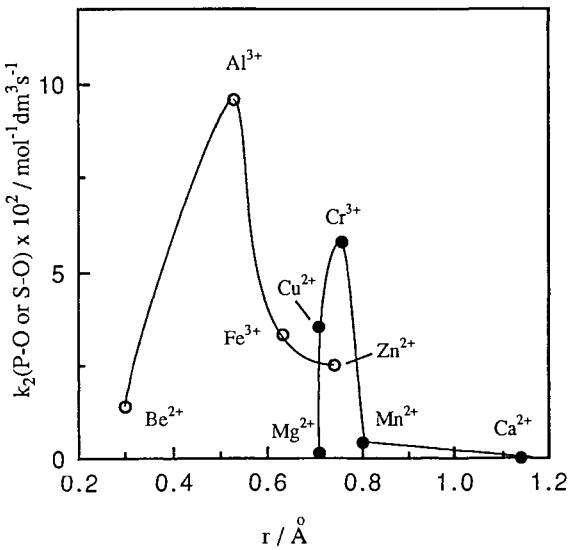

Fig. 3. Plots of the second-order rate constants vs. ionic radii of the metal ions: ○ k_2(S-O); ● k_2(P-O).

$$M+S \underset{}{\overset{K}{\rightleftarrows}} C \xrightarrow{k_m} \text{products} \qquad (1)$$
$$\qquad\qquad \downarrow k_0$$

$$k_{obsd}=k_0+\frac{(k_m-k_0)K[M]_T}{1+K[M]_T+K[S]_T\left(1-\dfrac{k_{obsd}-k_0}{k_m-k_0}\right)} \qquad (2)$$

assuming the preequilibrium formation of a 1 : 1 complex (C) of the substrate (S) and metal ion (M) on the basis of Eq. 1. Eq. 2 is formulated in accordance with Eq. 1,[15,19] where $[M]_T$ and $[S]_T$ are the initial stoichiometric concentration of metal ion and substrate, respectively, k_o and k_m are the rate constants for the methanolyses of the metal-free and metal-coordinated substrate, respectively, and K stands for the formation constant for the 1 : 1 complex (C). In practice, the k_0 value was negligibly small and could be neglected in the rate calculation. The calculated curves in Fig. 2 are obtained by Eq. 2, using the evaluated K and k_m values given in Table 3, where the $k_mK/(1+K[S]_T)$ values in the last column correspond to the above mentioned k_2 values. Table 3 indicates that the k_m value for the Zn^{2+}-promoted S-O bond cleavage is 320- and 824-fold larger than those for the Mg^{2+} and

Ca^{2+} catalyzed P-O bond cleavage, respectively. It is interesting to note that the K value for Mg^{2+} with PPS in the present mixed solvent is much larger than that in water reported previously (K=1.19 $mol^{-1}dm^3$, pH 7.9, 55 °C),[14] suggesting for a strong solvation (hydration) to inhibit Mg^{2+} from complexation with PPS in water.

(c) The k_2 Values vs. Ionic Radii of the Metal Ions. In Fig. 3 are shown the k_2 values in Table 2 as a function of ionic radii of the metal ions.[20] The figure shows that the ionic radii of the metal ions which promote the O-S bond cleavage are shorter than those of the metal ions which catalyze the P-O bond cleavage, although Zn^{2+} appears to be an exception. It is interesting to note that there are two maxima in the vicinity of 0.53 and 0.75 Å corresponding to the S-O and P-O bond cleavage, respectively. These observations suggest that the ionic radius of a metal ion is a key factor for both selectivity and rate enhancement of the bond cleavage.

(d) Effect of Methanol Concentration on the Rates. The results are shown in Fig. 4 for the Al^{3+}-promoted S-O bond cleavage and the Mg^{2+} catalyzed P-O bond cleavage. Fig. 4 shows that the k_2 values of Mg^{2+} increase linearly with increasing methanol concentration, but those of Al^{3+} tend to be saturated with increasing methanol concentration. Since methanol is the nucleophile, it is no wonder that the rate is linear to the concentration of nucleophile if the rate-limiting step is the attacking of nucleophile. However, the rate is presumed to be indifferent to the methanol concentration if the rate-limiting step is the unimolecular cleavage of the terminal S-O bond. This argument may be too simple, because the increasing of methanol concentration should affect the rate through the change of solvent property, perhaps nonlinearly. Nevertheless, the linearlity in the case of Mg^{2+} suggests that the attacking of methanol on phosphorus to cleave the P-O bond is the rate-limiting step. In the case of Al^{3+} the situation seems to be more complex, but the data appear to support unimolecular process, at least at higher methanol concentration.

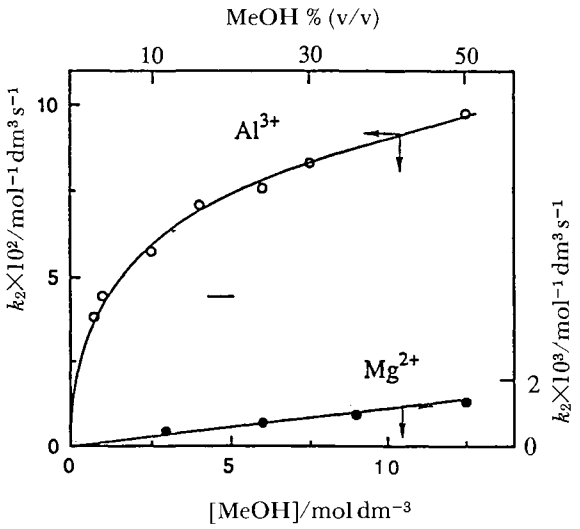

Fig. 4. Dependency of k_2 on methanol concentration in DMF.

(e) Alcoholysis by Methanol vs. 2-Propanol. The metal ions, Be^{2+}, Al^{3+}, Fe^{3+}, and Zn^{2+} were also found to promote the S-O bond cleavage of PPS in the alcoholysis by 2-propanol to give PP and isopropyl sulfate (PS) in quantitative yields. The k_2 value for the Al^{3+}-promoted alcoholysis by 2-propanol in a mixed solvent of 2-propanol and DMF (1 : 1, v/v%) at 55 °C was 1.3 times smaller than that of the corresponding methanolysis. In the case of Mg^{2+}, neither phenyl isopropyl phosphate (P-O bond cleavage) nor isopropyl sulfate (S-O bond cleavage) was obtained, but the detected products were only PP and IS, presumably due to the hydrolysis by a trace of water. In the case of Ca^{2+}, the expected phenyl isopropyl phosphate could be detected after a prolonged reaction as in the methanolysis due to the P-O bond cleavage. Thus, there seemed to be a severe steric hindrance to the attack of 2-propanol on the phosphorus to result in the P-O bond cleavage, whereas such steric hindrance seemed to be less important in the S-O bond cleavage.

In order to obtain more information, the competitive alcoholysis by methanol vs. 2-propanol was examined in the mixed solvents of methanol and 2-propanol in DMF, in the presence of either one of

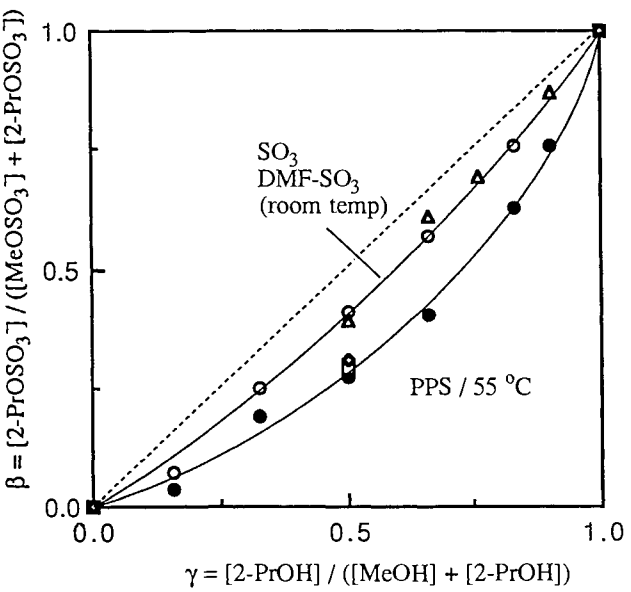

Fig. 5. Competitive solvolyses of PPS, SO_3, and DMF-SO_3 in the mixed solvents of MeOH, i-PrOH, and DMF: concentrations(mol dm^{-3}), [MeOH]+[2PrOH]=6.0, [N-ethylmorpholine]= 0.55, ○ [SO_3]=0.15—1.0×10^{-2}, △ [DMF-SO_3]= 1.6×10^{-2}, [PPS]=1.0×10^{-2} ([Be^{2+}]=3.0×10^{-2} (□), [Al^{3+}]=2.5×10^{-2} (●), [Fe^{3+}]=2.5×10^{-2} (□), [Zn^{2+}]= 2.8×10^{-2} (◇)).

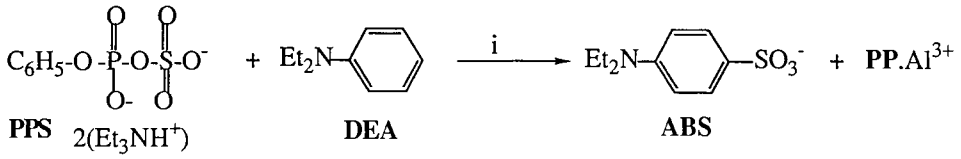

Scheme 2. Reagents: i, $AlCl_3$ in CH_3CN; room temp.

Be^{2+}, Al^{3+}, Fe^{3+}, or Zn^{2+}. The substrates examined were SO_3 and DMF-SO_3 in the absence of a metal ion, and PPS in the presence of a metal ion. The former two may be the same, because their difference was only in that whether SO_3 gas was introduced into a mixed solvent of methanol, 2-propanol and DMF or a mixture of methanol and 2-propanol was mixed with a DMF-SO_3 solution prepared prior to the mixing. The results are shown in Fig. 5. In Fig. 5, the diagonal straight line would be expected if methanol and 2-propanol are equally reactive. The observed line in the absence of a metal ion indicates that methanol is slightly more active than 2-propanol. Namely it shows that the product ratio was PS : MS=1 : 1.5 (β=0.4) when a mixture of equal amount of methanol and 2-propanol (γ=0.5) was used. The solid line was observed for the reaction of PPS in the presence of a metal ion. The four metal ions gave almost the same results in product ratio. When γ=0.5, the observed β value was about 0.3 for each metal ion, corresponding to a ratio of PS : MS=1 : 3. These results indicate that although there is a sizable difference in reactivity between methanol and 2-propanol, it is much less in the S-O bond cleavage than in the above mentioned P-O bond cleavage.

Sulfonation. The different behavior of the two groups of the metal ions was further manifested in the reaction of PPS with *N*,*N*-diethylaniline (DEA) in the presence of Al^{3+} or Mg^{2+} as a representative of each group of the metal ions. In acetonitrile, PPS (bis(triethylammonium) salt) and DEA did not react at room temperature irrespective of the presence or absence of Mg^{2+}. By contrast, Al^{3+} readily promoted the reaction to give *p*-(diethylamino)benzenesulfonate and PP in quantitative yields as shown in Scheme 2.

Discussion

The rate of Mg^{2+}-catalyzed methanolysis of PPS (k_2(P-O)) was first-order with respect to the methanol concentration (Fig. 4), suggesting the rate-limiting nucleophilic attack of methanol on phosphorus of PPS. This is in accordance with our previous observation that in aqueous media Mg^{2+} catalyzes the nucleophilic attack of primary and secondary amines on phosphorus of PPS to give the corresponding phosphoramidates and IS, but the reaction does not occur with a sterically crowded amine such as *N*-ethylmorpholine and 2,6-lutidine irrespective of the presence or absence of Mg^{2+}.[10,13]

The dependency of rates of Al^{3+}-promoted methanolysis (k_2(S-O)) on the methanol concentration (Fig. 4) was quite different from that mentioned above. The rates tended to become independent of methanol concentration at higher concentration. The two different pathways can be conceivable for the S-O bond cleavage: (1) the unimolecular elimination of sulfur trioxide (SO_3) or its solvated species, and (2) the bimolecular nucleophilic attack of methanol on sulfur as in the case of above mentioned phosphorus attack. However, the latter possibility seems to be unlikely on the following grounds in addition to the above concentration effect. As shown in Fig. 5, the difference between the rates for methanol and 2-propanol is rather small in the S-O bond cleavage as compared to a large difference in the case of P-O bond cleavage, suggesting the formation of a very reactive species, i.e. SO_3 in the former case. Further supporting evidence is the Al^{3+}-promoted sulfonation of DEA with PPS in acetonitrile, where SO_3 is likely generated as the reactive sulfonating agent.

As discussed above, the P-O and S-O bond cleavage appear to occur with different mechanisms. Then, what is the role of a metal ion? The answer seems to be partly obtained by examining the data in Fig. 3 which shows the correlation of k_2 values with the ionic radii of the metal ions. Fig. 3 shows two rate maxima corresponding to the two different groups of metal ions which either catalyze the P-O or promote the S-O bond cleavage of PPS. The ionic radius of the metal ion to give the former rate maximum is in the vicinity of 0.75 Å. Quite interestingly the same ionic radius for the rate maximum was also reported by Benkovic et al. for the divalent metal ion-catalyzed hydrolysis of lactic acid *O*-phenyl phosphate, and it was suggested that the role of metal ion is to facilitate the formation of phosphorus(V)intermediate (**1** or **2**) which then rapidly decomposes to the products.[21]

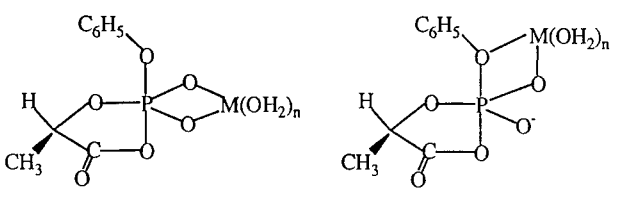

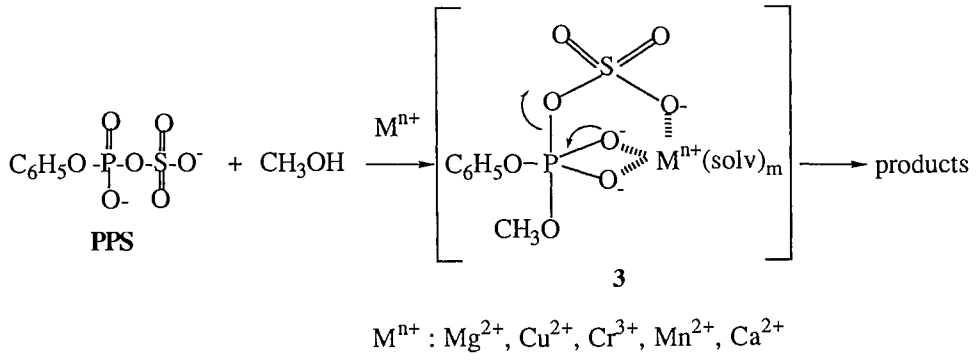

Scheme 3. A postulated pentacovalent phosphorus intermediate in a metal ion catalyzed methanolysis of PPS to give P-O bond cleavage.

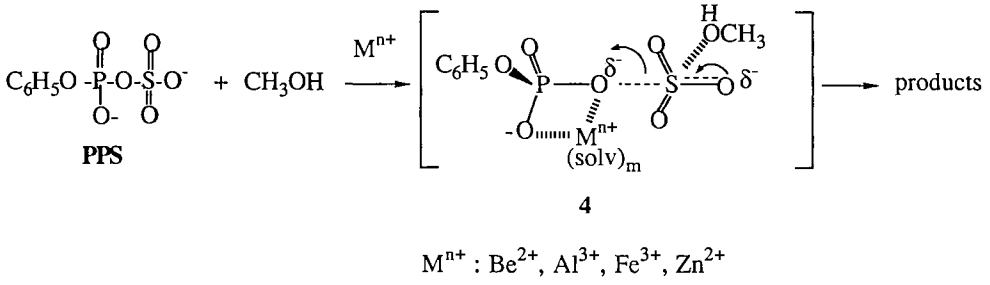

Scheme 4. Proposed transition state involving solvated sulfur trioxide.

The correlation with ionic radius suggests the importance of bidentate coordination with strict geometrical requirements as in **1** or **2**. Similar phosphorus(V) intermediate (**3**) can also be considered for the present metal ion-catalyzed P-O bond cleavage as illustrated in Scheme 3. In the structure **3**, a metal ion occupies a basal position and is chelated with two anionic oxygen ligands to form a four-membered cyclic complex. The metal ion is also assumed to form an ionic bond with sulfate oxygen ion. It is important to notice that the bond angle of the chelating $\angle^{-}O\text{-}P\text{-}O^{-}$ is 120°, the same as that of **1** but different from that of 90° in **2**. As discussed below, the relationship between the metal ion radius and the bond angle of a bidentate ligand seems to be of key importance in determining the selectivity in the P-O and S-O bond cleavage.

In the case of the S-O bond cleavage, Fig. 3 shows that the ionic radius of a metal ion to give the rate maximum is in the vicinity of 0.53 Å, much shorter than 0.75 Å in the case of P-O bond cleavage. A shorter ionic radius suggests a smaller bond angle for the bidentate chelation, and it led us to consider **4** in Scheme 4 as a possible transition state structure. In **4** is assumed a solvent assisted unimolecular S-O bond cleavage which is consistent with the above mentioned results (Figs. 4, 5 and Scheme 2). It is important to notice in **4** that a metal ion assists the S-O bond cleavage by chelating with two anionic oxygen ligands of the leaving phosphoryloxy group, in which the $\angle^{-}O\text{-}P\text{-}O^{\delta-}$ bond angle is near 109.5°, much smaller than the above 120° in the P-O bond cleavage.

The Zn^{2+} which promotes the selective S-O bond cleavage appears to be an exception from the consideration of ionic radius alone, since our previous studies demonstrated that in aqueous media Zn^{2+} always catalyzes the P-O bond cleavage, e.g. in the aminolysis of PPS,[10,13] in the 2-pyridinecarbaldehyde oxime-catalyzed hydrolysis of PPS,[10,22] and in the hydrolysis of 2-pyridyl phosphonosulfate.[15] It is known that Be^{2+} and Al^{3+} with smaller ionic radii, or Zn^{2+} and Fe^{3+} with the electron configuration of $3d^{10}$ and $3d^{5}$, respectively favor tetrahedral coordination.[23] On the other hand, metal ions such as Mg^{2+}, Cu^{2+}, Cr^{3+}, Mn^{2+}, and Ca^{2+} favor octahedral coordination. Thus, it is conceivable that the change in selectivity of Zn^{2+} from the P-O in water to the S-O bond cleavage in methanol is due to the change of solvation in the metal ion-substrate complex which affects the type of coordination, i.e. tetrahedral in methanol but octahedral coordination in water.

Finally, it is considered in general that the effective charge of metal ion is important for an electrophilic catalysis as in the present case. For this point, the above mentioned results are not conclusive, since the difference in k_2 values is rather small between Fe^{3+} and Zn^{2+} or between Cr^{3+} and Cu^{2+}. It is conceibable that the solvation to reduce effective charge is stronger for a trivalent metal ion than for a divalent metal ion, resulting in a smaller difference in their reactivities.

Much remains to be clarified as to the mechanism of

metal ion catalysis in the reactions of P-O-S linkage, as seen in the dual behavior of Zn^{2+}. Moreover, a mysterious gap between the selectivity of Mg^{2+} in the P-O-S bond cleavage in enzyme and model reactions has still remain unsolved. Nevertheless, it is important to notice that there is a certain correlation between the ionic radii of metal ions and the selectivity in the P-O-S bond cleavage.

We are much indebted to Messrs T. Ogihara and A. Kato, and Miss F. Arai who carried out the early part of this study.

References

1) D. E. Metzler, "Biochemistry," Academic Press, New York (1977), pp. 395, 611—615, and 636.
2) F. Lipmann, *Science*, **128**, 575 (1958).
3) A. B. Roy, *Adv. Enzymol.*, **22**, 205 (1960).
4) H. D. Peck, Jr., in "The Enzymes," 3rd ed, ed by P. D. Boyer, Academic Press, New York (1974), Vol. 10, Chapt. 21, pp. 61.
5) A. B. Roy and P. A. Trudinger, "The Biochemistry of Inorganic Compounds of Sulfur," Cambridge Univ. Press, London and New York (1970).
6) A. B. Roy, "The Enzymes," 3rd ed, ed by P. D. Boyer, Academic Press, New York (1971), Vol. 5, Chapt. 1, pp. 1.
7) R. E. Dickerson and R. Timkovich, in "The Enzymes," 3rd ed, ed by P. D. Boyer, Academic Press, New York (1975), Vol. 11, pp. 397—547.
8) D. V. DerVartanian and J. LeGall, *BBA*, **346**, 79 (1974).
9) H. D. Peck, Jr., R. Bramlett, and D. V. DerVartanian, *Z. Naturforsch., B*, **27**, 1084 (1972).
10) W. Tagaki and T. Eiki, *Adv. Chem. Ser.*, **191**, 409 (1980).
11) W. Tagaki, Y. Asai, and T. Eiki, *J. Am. Chem. Soc.*, **95**, 3037 (1973).
12) T. Eiki, Y. Asai, and W. Tagaki, *Bull. Chem. Soc. Jpn.*, **55**, 1097 (1982).
13) T. Eiki, K. Tomuro, S. Aoshima, M. Suda, and W. Tagaki, *Nippon Kagaku-Kaishi*, **1980**,454.
14) T. Eiki and W. Tagaki, *Bull. Chem. Soc. Jpn.*, **55**, 1102 (1982).
15) T. Eiki, T. Horiguchi, M. Ono, S. Kawada, and W. Tagaki, *J. Am. Chem. Soc.*, **104**, 1986 (1982).
16) T. Eiki and W. Tagaki, *Chem. Lett.*, **1981**, 1465.
17) T. Eiki, T. Ogihara, A. Kato, F. Arai, and W. Tagaki, *J. Chem. Soc., Chem. Commun.*, **1985**, 49.
18) W. Tagaki, T. Eiki, and I. Tanaka, *Bull. Chem. Soc. Jpn.*, **44**, 1139 (1971).
19) S. J. Benkovic and L. Dunikoski, *J. Am. Chem. Soc.*, **93**, 1526 (1971).
20) R. D. Shannon, *Acta Crystallogr., Sect. A*, **32**, 751 (1976).
21) J. J. Steffens, I. J. Siewers, and S. J. Benkovic, *Biochemistry*, **14**, 2431 (1975).
22) K. Tomuro, Thesis, Gunma University, Kiryu, 1976.
23) R. P. Houghton, "Metal Complexes in Organic Chemisty," Cambridge Univ. Press, London, New Yord and Melbourne (1979).

1 : 1 Adduct Ion Formation of Permethylated Monosaccharides with Organic Cations in FAB Mass Spectrometry[1)]

Masami SAWADA,* Li OUYANG, Yoshio TAKAI, Hitoshi YAMADA, Motohiro SHIZUMA, Takeshi KINOSHITA,† Tomoko MOCHIZUKI,† and Terukiyo HANAFUSA
Material Analysis Center, The Institute of Scientific and Industrial Research, Osaka University, 8-1, Mihogaoka, Ibaraki, Osaka 567
†Analytical and Metabolic Research Laboratories, Sankyo Co., Ltd., Hiromachi, Shinagawa-ku, Tokyo 140
(Received December 17, 1990)

The 1 : 1 adduct ion formation between a series of permethylated monosaccharides (M; $\mathbf{I_a}$—$\mathbf{I_h}$) and an organic or a metallic cation (A^+) has been examined in quantitative FAB mass spectrometry. In a careful comparison under the same FABMS conditions, the relative $(M+A)^+$ peak intensities increase in the following order of the monosaccharides, and further increase at nearly the same extents in spite of using three different cations such as octylammonium, (methoxycarbonyl)methylammonium, and potassium ions:

$$\beta\text{-Glc} < \alpha\text{-Glc} < \alpha\text{-Gal} < \beta\text{-Gal} \leq \alpha\text{-Man} < \beta\text{-Man} < \alpha\text{-Tal} < \beta\text{-Tal}.$$

The order and cation-independency clearly indicate the OCH_3 configurational effects of M on $(M+A)^+$ adduct ion formation. The findings can be interpreted in terms of multisite electrostatic interaction of oxygens with the cation. Coupled with the results of gas-phase behavior by FABMS/MS(CAD), solution behavior by ^1H NMR, and model calculations by MNDO, the characteristic structure of the 1 : 1 adduct ion is deduced as host-guest type association between permethylated monosaccharides and cationic species in particular cases, at least β-Tal and α-Tal cases.

Elucidation of stereochemical effects of organic compounds on mass spectra has been a challenging problem for a long time. Much attention has been paid to this problem on the basis of fragmentation patterns in EIMS (electron impact mass spectrometry)[2)] or peak intensities of quasi-molecular ions in CIMS (chemical ionization mass spectrometry),[3,4)] etc.[5)] Recently, Puzo et al. reported epimer-identification of underivatized monosaccharides with metallic cations in FAB/MIKES (Fast Atom Bombardment)/(Mass Analyzed Ion Kinetic Energy Spectroscopy).[6)] However, there are almost no systematic studies concerning stereochemical effects on conventional FABMS.[7-12)] We now focus our attention on the structural factors which promote the 1 : 1 adduct ion formation in quantitative FABMS.

In the present study, permethylated monosaccharides, $\mathbf{I_a}$—$\mathbf{I_h}$ (family **I**), are chosen as the substrates (M), and compared with monomethylated monosaccharides, $\mathbf{II_a}$—$\mathbf{II_h}$ (family **II**), as the references.[13)] The permethylated monosaccharides can avoid the effects of intramolecular hydrogen bonding of M,[14)] and further intermoleculer hydrogen bonding of M with matrix (for example, glycerol; G).[15)] The monomethylated monosaccharides can prevent α, β isomerization during the preparation of sample solutions of M.

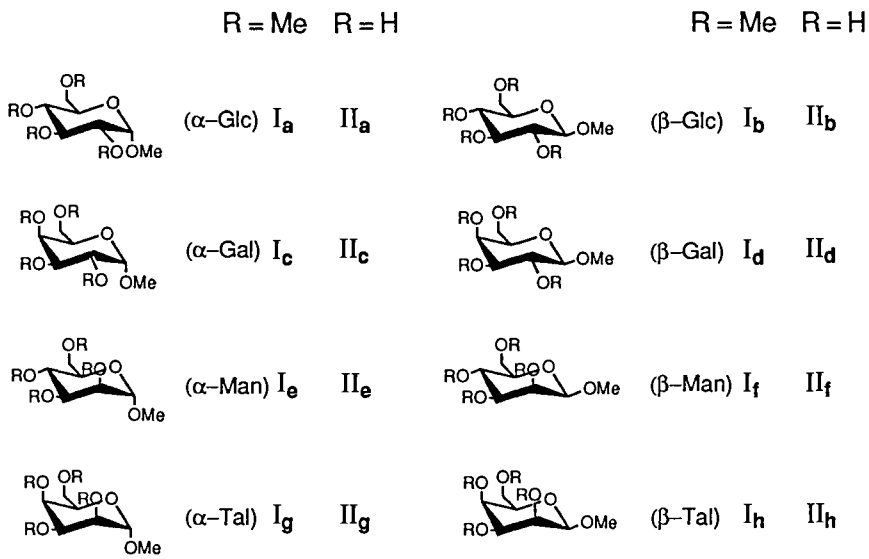

Chart 1.

Complexations of metallic cations with underivatized monosaccharides were extensively studied by Angyal et al. mainly on the basis of ^{1}H NMR and X-ray crystal data, where importance of axial-equatorial-axial arrangement of three sequential OH groups was explored for strong 1 : 1 complexation.[16] This paper describes primarily the stereochemical effects of permethylated monosaccharides (M) on $(M+A)^+$ adduct ion formation with organic cations (A^+) in conventional FABMS, and deduces the structure as host-guest type association in particular cases.[17–19]

Results

Selection of Cations. Table 1 shows the results of qualitative FABMS experiments for searching good cations (A^+), where $\mathbf{I}_f$ (β-Man) is fixed as a common substrate (M). From the relative intensity values, ($I[M+A]^+/I[M+1]^+$), it was found that primary and secondary alkylammonium ions with relatively long alkyl chains, and metallic cations with one positive charge, are suitable for generating abundant $(M+A)^+$ adduct ions. Figure 1 is a typical example of a FAB mass spectrum for the case of adding octylammonium ion salt.

Selectivity of Permethylated Monosaccharides. Based on the data in Table 1, octylammonium (A_1^+), (methoxycarbonyl)methylammonium, $CH_3OCOCH_2NH_3^+$ (A_2^+), and potassium ions (A_3^+) were chosen as better cationic species in the present quantitative

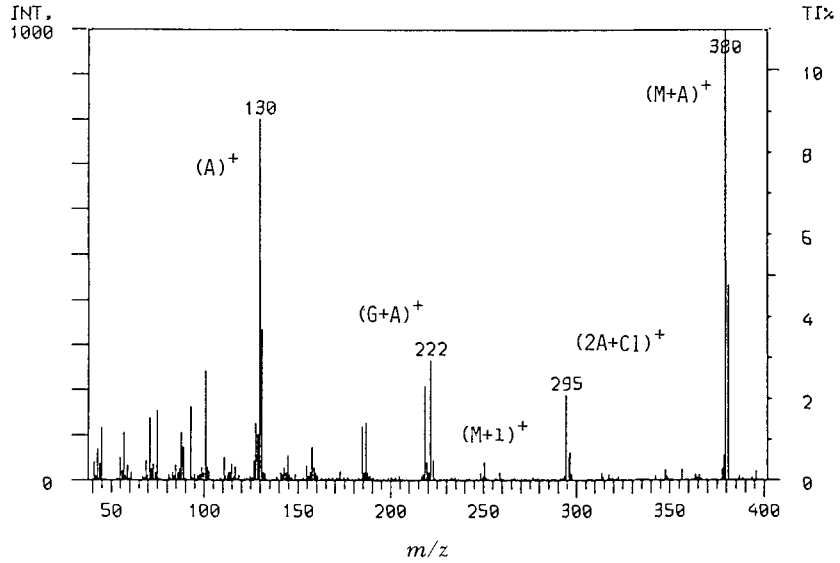

Fig. 1. A FAB mass spectrum of M with A^+X^- (glycerol matrix): M=$\mathbf{I}_f$ (β-Man), A^+X^-=n-$C_8H_{17}NH_3^+Cl^-$ (M: A^+X^-=1 : 1).

Table 1. Search Experiments for Good Additives by Using FABMS (Glycerol Matrix)

additive A^+X^-	Molar ratio $A^+ : M^{a)}$	Relative peak intensity $I[M+A]^{+b)}$
$CH_3CH_2NH_3^+Cl^-$	1 : 1	16
$CH_3(CH_2)_3NH_3^+Cl^-$	1 : 1	68 (3)
$CH_3(CH_2)_7NH_3^+Cl^-$	1 : 1	>1000 (40)
$CH_3(CH_2)_9NH_3^+Cl^-$	1 : 1	>1000 (36)
$PhCH_2CH_2NH_3^+Cl^-$	2 : 1	59 (4)
$PhCH_2CH_2NH_2^+(CH_3)Cl^-$	2 : 1	47 (4)
$PhCH_2NH^+(CH_3)_2Cl^-$	2 : 1	8 (<1)
$CH_3OCOCH_2NH_3^+Cl^-$	2 : 1	68
$NH_4^+Cl^-$	5 : 1	36
$HOOCCH_2CH_2CH(COOH)NH_3^+Cl^-$	1 : 1	2
$CH_3CH(CH_3)CH(COO^-)NH_3^+$	1 : 1	9
Na^+Cl^-	2 : 1	29
K^+Cl^-	2 : 1	280
Rb^+Cl^-	2 : 1	240
Cs^+Cl^-	2 : 1	170
Ag^+Cl^-	5 : 1	26

a) M=$\mathbf{I}_f$. b) Normalized to $I[M+1]^+$=10. In parenthesis, neutral amine was used as an additive compound.

study. Affinities of a series of permethylated monosaccharides (family **I**) toward the cation were determined by measuring relative peak intensities of the relevant $(M+A)^+$ adduct ions. Internal standard technique was employed for quantitative measurements so as to get highly reliable peak intensity data in FABMS.[20-22] Deuterated monosaccharide, $\mathbf{I}_e$-d_{12} (methyl tetra-*O*-methyl-d_{12}-α-D-mannoside), was used as an internal standard (R), and competitive conditions[23] where an equimolar amount of M and R was included in a matrix (glycerol) were employed. The relative peak intensity value, $I(M+A)^+/I(R+A)^+$, was taken as a measure of $(M+A)^+$ adduct ion formation. It should be noted here that measuring conditions of a mass spectrometer and concentration conditions of all sample solutions were kept constant throughout the experiments of getting a set of relative peak intensity values.

Different affinities were observed for the set of monosaccharides. By contrast, they were very close to each other for the three sets of cations (A_1^+, A_2^+, and A_3^+; Table 2). The $(M+A)^+$ peak of $\mathbf{I}_h$ (β-Tal) was almost 100 times more intense than that of $\mathbf{I}_b$ (β-Glc). The characteristic ordering of the resulting relative affinities is, β-Tal>α-Tal>β-Man>α-Man≥β-Gal>α-Gal>α-Glc>β-Glc. This indicates that the relative peak intensities of $(M+A)^+$ ions are strongly related with the configuration of the OCH_3 groups in the family **I**.

Table 2. Relative Peak Intensities of $(M+A)^+$ Adduct Ions for Permethylated Monosaccharides in FABMS (Glycerol Matrix)

Monosaccharide M (R)[a]	$I[M+A]^+/I[R+A]^+$ value		
	(A_1^+)[b]	(A_2^+)[c]	(A_3^+)[d]
$\mathbf{I}_a$	0.4	0.5	0.5
$\mathbf{I}_b$	0.3	0.3	0.2
$\mathbf{I}_c$	0.6	0.8	0.7
$\mathbf{I}_d$	1.0	0.9	1.0
$\mathbf{I}_e$ ($\mathbf{I}_e$-d_{12})	1.0	1.0	1.0
$\mathbf{I}_f$	5.8	4.2	3.7
$\mathbf{I}_g$	9.0	6.1	12
$\mathbf{I}_h$	36	22	18

a) R=$\mathbf{I}_e$-d_{12} (α-Man-d_{12}). See text. b) $A_1^+X^-$=CH_3-$(CH_2)_7NH_3^+Cl^-$. c) $A_2^+X^-$=$CH_3OCOCH_2NH_3^+Cl^-$. d) $A_3^+X^-$=K^+Cl^-.

Selectivity of Monomethylated Monosaccharides. Affinities of a series of monomethylated monosaccharides (family **II**) toward the cation were determined by the same method as that mentioned above (Table 3). Here, methyl-d_3 α-D-glucopyranoside ($\mathbf{II}_a$-d_3) was employed as an internal standard (R). As seen in the FABMS columns of Table 3, the differences in affinities toward each cation largely diminished or disappeared. For example, the $(M+A)^+$ peak of $\mathbf{II}_h$ (β-Tal) was at most 2—5 times more intense than that of $\mathbf{II}_a$ (α-Glc), being in marked contrast to a much larger selectivity of the family **I**.

$(M+A)^+$ Adduct Ions Detected by FABMS/MS(CAD). FABMS/MS (mass spectrometry/mass spectrometry) is useful to know purely gas-phase ion phenomena. MS/MS operating principle is (1) a selected ion is directed into a second mass spectrometer, and (2) the ion (precursor ion) is decomposed typically by argon collision, and (3) the resulting fragment ions are analyzed.[24] The MS/MS has been a rapidly growing technique for studying the order of relative binding energies,[25] and for analysing organic ions in the gas-phase.[31] Our precursor ions used were Puzo's three component ions,[6a] $(M+K+DEA)^+$ (m/z 338), which were composed of the family **II**, K^+, and diethanolamine (DEA) (Chart 2).

Relative area intensities of the $(M+K)^+$ adduct ions (m/z 233) to the reference one $(DEA+K)^+$ (m/z 144) were measured under the same experimental conditions,[26] and tabulated in the FABMS/MS column of Table 3. The present FABMS/MS area intensity data

Table 3. Relative Peak Intensities of $(M+A)^+$ Adduct Ions for Monomethylated Monosaccharides in FABMS

M (R)[a]	$I[M+A]^+/I[R+A]^+$ FABMS				$A[M+A]^+/A[R+A]^+$	
					FABMS/MS	FAB/MIKES
	(A_4^+)[b] (G)[e]	(A_2^+)[c] (G)[e]	(A_3^+)[d] (G)[e]	(A_3^+)[d] (DEA)[f]	(A_3^+)[d] (DEA)[f]	(A_3^+)[d] (DEA)[f]
$\mathbf{II}_a$ ($\mathbf{II}_a$-d_{12})	1.0	1.0	1.0	0.3	0.9	(0.2)[h]
$\mathbf{II}_b$	0.8		1.0	0.3	0.9	
$\mathbf{II}_c$	0.9			0.4	1.3	(0.7)[h]
$\mathbf{II}_d$	1.2			0.8	2.1	
$\mathbf{II}_e$	1.5	1.8	2.5	1.0[g]	1.5	(1.0)[h]
$\mathbf{II}_f$	1.7				3.6	
$\mathbf{II}_g$	1.6	1.7	1.8	1.3	3.7	(3.7)[h]
$\mathbf{II}_h$	2.0	1.8	2.2	1.6	4.8	

a) R=$\mathbf{II}_a$-d_3 (α-Glc-d_3). See text. b) $A_4^+X^-$=$PhCH_2CH_2NH_3^+Cl^-$. c) $A_2^+X^-$=CH_3-$OCOCH_2NH_3^+Cl^-$. d) $A_3^+X^-$=K^+Cl^-. e) Glycerol matrix. f) Diethanolamine matrix. g) As an internal standard (R), $\mathbf{II}_e$-d_3 (α-Man-d_3) was used. h) Anomers for underivatized monosaccharides were not differentiated.[6a]

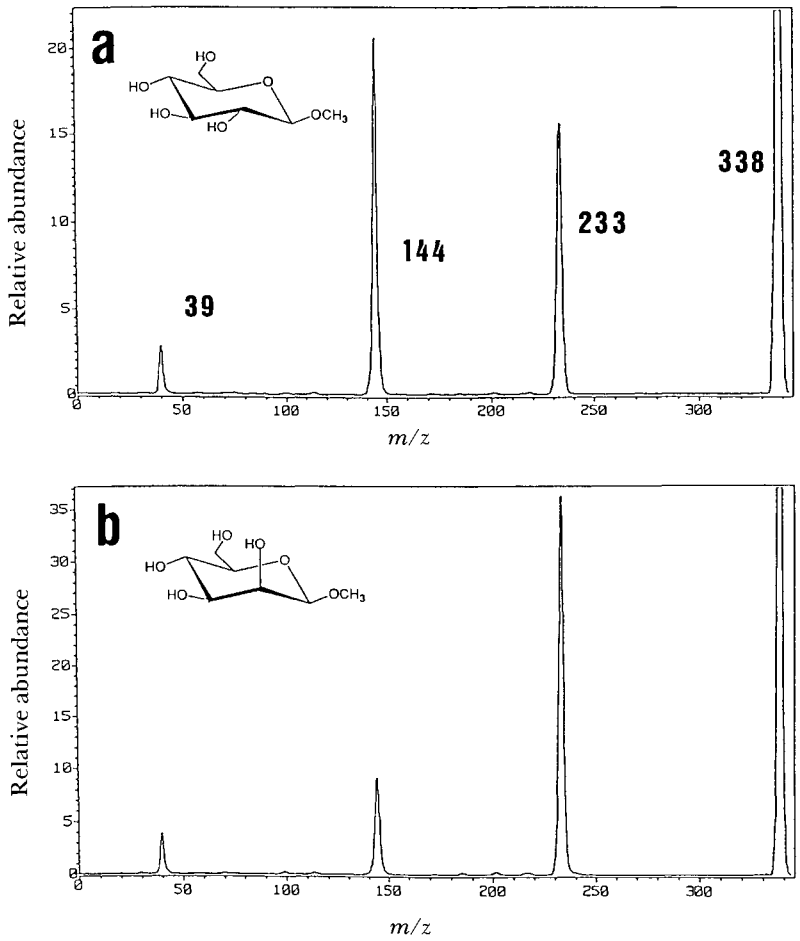

Fig. 2. FABMS/MS (CAD) spectra of the precursor ion $(M+K+DEA)^+$; *m/z* 338. (a) M=**II**$_b$ (β-Glc), (b) M=**II**$_f$ (β-Man).

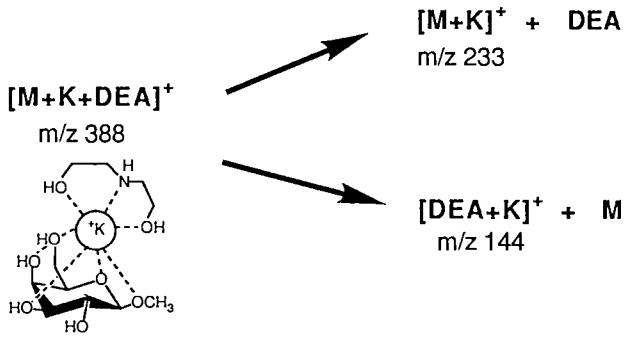

Chart 2.

via CAD (collisionally activated decomposition) process are consistent with earlier FAB/MIKES data via unimolecular decomposition process.[6a] The resulting ordering of the binding energies for $(M+K)^+$ adduct ions is, β-Tal>α-Tal>β-Man>-β-Gal>α-Man>α-Gal>α-Glc=β-Glc, which is in good agreement with the affinity ordering of the family **I** in FABMS.

$(M+A)^+$ Adduct Ions Supported by ^{1}H NMR. ^{1}H NMR experiments were carried out to see if the $(M+A)^+$ adduct ions between the family **I** and organic cations in solution can be detected or if existence of equilibrium (Eq. 1) can be established by means of diamagnetic induced chemical shifts (ICS).[16,27] Because of solubility problems of the alkylammonium ion salts employed, acetonitrile-d_3 was utilized as a solvent.

$$M + A^+ \rightleftarrows (M+A)^+ \quad (1)$$

Typical ^{1}H NMR spectra before and after addition of 2-phenylethylammonium hexafluorophosphate ($A_4^+PF_6^-$) are compared in Fig. 3 ([M]=0.014 M, $[A_4^+PF_6^-]$=0.008 M). Here, M is **I**$_h$ (β-Tal), because it gave the highest $(M+A)^+$ peak in Table 2. Position-dependent ICS was clearly observed after the addition. That is, (1) the broad ammonium proton signal moves to a downfield direction to the greatest extent (ca. 0.15 ppm), (2) the monosaccharide ring proton signals also undergo downfield shifts to different extents, and (3) some of methyl proton signals (around δ=3.4) show downfield shifts. These observations in both sides of A^+ and M suggest that $(M+A)^+$ adduct ion formation is in an fast equilibrium on the NMR time scale, and that apparent ICS

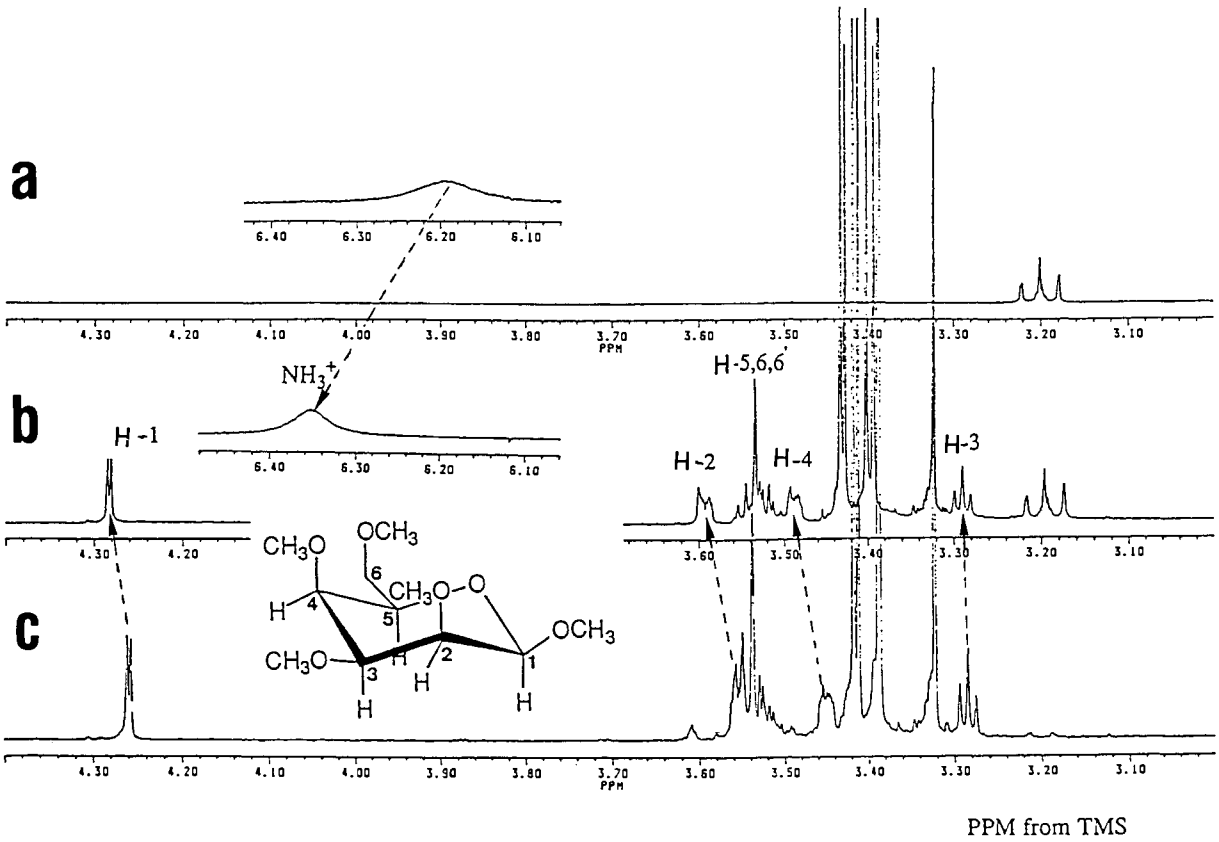

Fig. 3. ^{1}H NMR spectra (360 MHz) of M before and after an addition of A^+X^- in CD_3CN: M=$\mathbf{I_h}$ (β-Tal), A^+X^-=$PhCH_2CH_2NH_3^+PF_6^-$. A solution of (a) A^+X^-, (b) M+A^+X^-, or (c) M.

values reflect weighted averages of the existing M (or A^+) and $(M+A)^+$ species.

(a) Equilibrium Constant in Solution: From the concentration-dependent ICS of the ammonium proton signal, the equilibrium constant (K_s for Eq. 1) could be determined by using a Benesi-Hildebrand equation.[28] The K_s for $(M+A)^+$ adduct ion formation between $\mathbf{I_h}$ and 2-phenylethylammonium ion ($A_4^+PF_6^-$) is estimated to be 9 M^{-1} at 30 °C in CD_3CN ([M]/[$A_4^+PF_6^-$]=10—23, [$A_4^+PF_6^-$]$_{fix}$=0.0045 M, ICS range=113—195 Hz).[29,30]

(b) Position-Dependent Induced Chemical Shifts in Solution: ICS values for different pairs of M and A^+X^- in CD_3CN could be determined by using ^{1}H NMR. Spectral assignment was done by irradiation techniques and in light of the reported assignments.[32] In spite of different cationic species such as 2-phenylethylammonium, ammonium, and potassium ions, similar ICS patterns of M were observed for $\mathbf{I_h}$: that is, (1) the ICS ordering for the ring protons is H_2=H_4>H_1>H_3, (2) three of five methyl proton signals show more downfield shifts than the others (not assigned).

Compared with the results for $\mathbf{I_h}$, those for $\mathbf{I_g}$ are characterized by the decrease of the H_1 ICS value, and the decrease of the number of more downfield methyl proton signsls. On the other hand, $\mathbf{I_f}$ seems to give nearly isotropic shift pattern, and $\mathbf{I_a}$ shows no NMR changes to detectable extents. These position-dependent ICS data are deposited as Document No. 9109 at the office of Bull. Chem. Soc. Jpn.

MNDO Calculations of Model Systems. MNDO optimized structures were obtained by using the simplest model system, where Li^+ was used instead of K^+ (or RNH_3^+) to elucidate the essential complexation sites and relative binding energies of M toward the cation in the gas-phase. As schematically shown in Chart 3, in the cases of $(M+A)^+$ ions for $\mathbf{I_h}$ and $\mathbf{I_g}$, the cationic centers are located at almost equal distance (2.3 Å±0.1) from the three oxygens of the O-2, O-4, and the ring-O.[33] The distance corresponds to a sum of oxygen Van der Waals radius (1.6 Å) and Li^+ radius (0.6 Å).

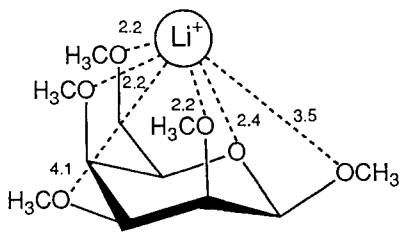

Chart 3.

Discussion

Relative Peak Intensity in FABMS vs. Gas-Phase Stability for $(M+A)^+$ Adduct Ion Formation. An illustration of the importance of gas-phase phenomena for the relative peak intensities in FABMS is shown in Fig. 4. The results are similar to those of Kebarle et al.[34,35] Here, the logarithm of the relative peak intensity, $\log[I(M+K)^+/I(R+K)^+]$, for the family **I** is plotted against that of the corresponding relative area intensity, $\log[A(M+K)^+/A(R+K)^+]$, in FABMS/MS (CAD). The latter quantities are taken as a reference measure of the relative stabilities (relative binding energies) of the relevant $(M+K)^+$ ions in the gas-phase.

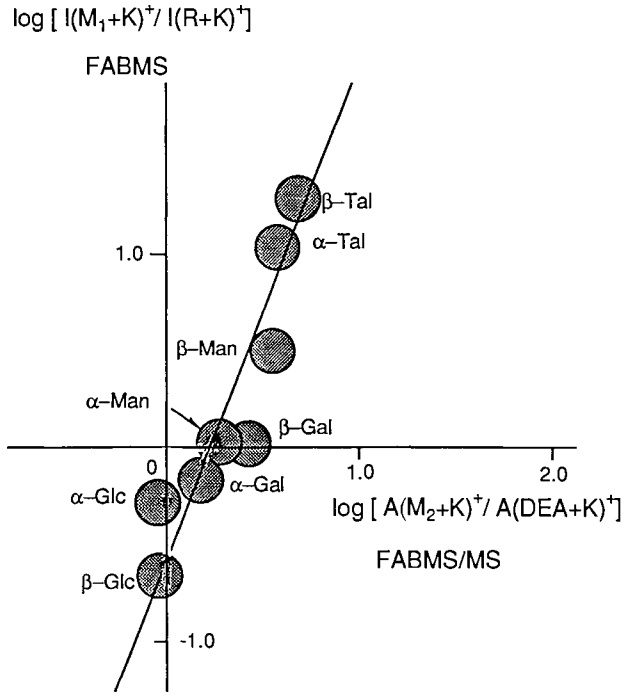

Fig. 4. Relative $(M_1+K)^+$ peak intensity data on FABMS are plotted against relative $(M_2+K)^+$ area intensity data on FABMS/MS(CAD). M_1 is the family **I**, and M_2 is the family **II**.

A good correlation is observed for the family **I**, but not clearly observed for the family **II** because of a narrow range of the relative peak intensities (not shown). This illustrates that the relative peak intensities of the family **I** in FABMS reflect characteristically the relative stabilities of $(M+A)^+$ ions in the gas-phase.[23–25] Recently, there has appeared the other aspect that relative peak intensities in FABMS reflect just solution phenomena on the basis of the results for 18-crown-6 complexations,[20,36] etc.[37] Unfortunately, we can not estimate the K_s values in solution except for $\mathbf{I}_h$. They are too small to be estimated for the entire series of the family **I** by ^{1}H NMR ICS methods.[29] Therefore, there still remains the possibility that the gas-phase stability is essentially parallel to the solution-phase stabilities for $(M+A)^+$ ions of the family **I**. In the family **II**, intramolecular hydrogen bonding toward transannually located oxygens may mask such selective complexations. One of the relevant examples has been seen in the complexation of a modified crown ether.[14]

The demonstration that the family **I**, compared with the family **II**, shows much larger selectivity toward an organic (or metallic) cation is practically important for wider applications of FABMS. Permethylation of saccharides would also provide the increase of electron densities on the oxygen atoms for good complexation. The finding of such a larger selectivity will open a new practical approach that the relative stabilities of saccharide-cation adduct ions can

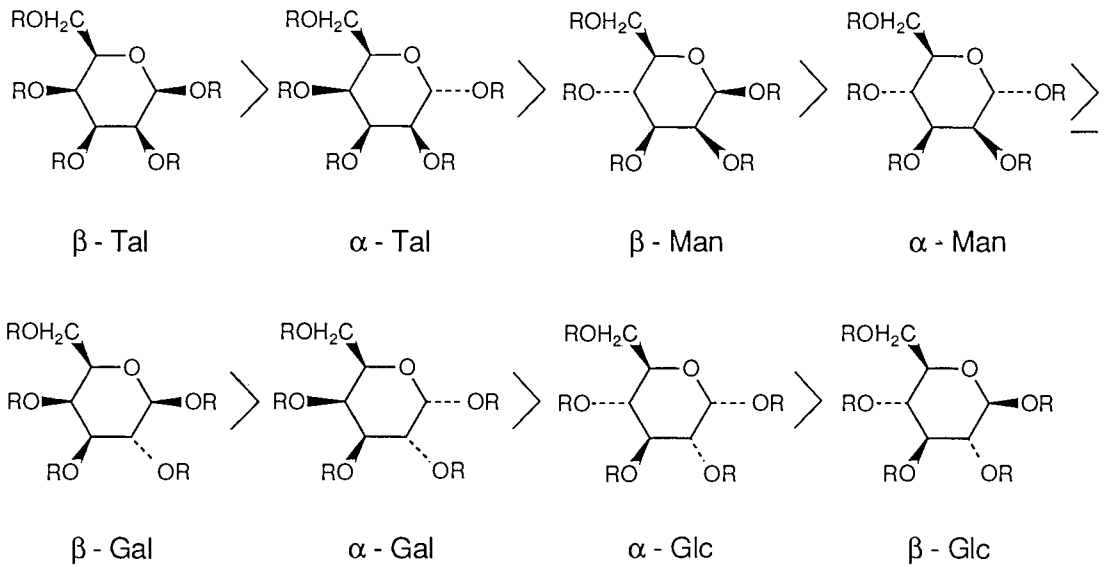

Chart 4.

Table 4. Effects of Alkylammonium Ions on Relative Peak Intensities in FABMS (Glycerol Matrix)

Substrate M	Relative peak intensity			
	$[M+A_1]^{+}$ a)	$[M+A_2]^{+}$ b)	$[M+A_3]^{+}$ c)	$[R+1]^{+}$ d)
I$_f$ (β-Man)	32	23	5	100
I$_h$ (β-Tal)	120	69	8	100
15-crown-5	120	12	—	100
18-crown-6	400	8	—	100

a) $A_1^+X^-$=$PhCH_2CH_2NH_3^+Cl^-$. b) $A_2^+X^-$=$PhCH_2NH_2^+(CH_3)Cl^-$. c) $A_3^+X^-$=$PhCH_2NH^+(CH_3)_2Cl^-$. d) R^+X^-=$(n\text{-}C_4H_9)_4N^+Cl^-$ (internal reference).

be easily judged by the corresponding relative peak intensities in conventional FABMS, (1) if saccharides are permethylated or more generally peralkylated, and (2) if FABMS is applied to a proper stereoisomeric series of saccharides in a careful comparison.

Stereochemical Effects of Permethylated Monosaccharides on $(M+A)^+$ Peak Intenstities. It is obviously found from Table 2 that the relative $(M+A)^+$ peak intensities for the family **I** show a close relationship with the configuration effect of the CH_3O groups included. The ordering is pictured by using Mills formulae (Chart 4). From the comparison among epimers, the more CH_3O groups are located on the same side, the larger the $(M+A)^+$ ion peak is. From the comparison between anomers, the $(M+A)^+$ ion peak for β-anomer is essentially larger than that for α-one.

Let us consider a series of β-anomers for the pyranose set. Here, the O-1, O-3, O-6, and the ring-O are common in the series. In the case of the highest peak-intensity (β-Tal), the monosaccharide has two upward axial oxygens (O-2, O-4). In the case of middle one (β-Man or β-Gal), M has one upword axial oxygen (O-2 or O-4, respectively). In the lowest case (β-Glc), there is no upward axial oxygen. These characteristics are consistent with the fact that the upward axial oxygen is very effective for stabilizing $(M+A)^+$ adduct ions. Further, the β-anomer preference is also consistent with the fact that the upward equatrial oxygen has also a contribution for stabilizing $(M+A)^+$ ions somewhat less than the upward axial one. These findings are in good agreement with some MNDO predictions of the model systems. The intensity difference of β-Man from β-Gal informs that the axial O-2 can act more effectively for stabilization than the axial O-4.

The affinity ordering of different permethylated monosaccharides for the cation by generating $(M+A)^+$ ions can be reasonably interpreted in terms of multisite electrostatic interaction for effective binding.[38,39] The cooperative multisite binding is one of the main interaction mechanisms for the well-known crown ether-cation complexation.[38] A complexation site of the organic (or metallic) cation can be deduced from MNDO model calculations, at least for the cases of **I**$_h$ and **I**$_g$, where the cationic centers are located at nearly equal distance from the O-2, O-4, and the ring-O: that is, the Li^+ cation stands in contact with the three oxygens.[33]

^1H NMR ICS data also support this type of structures with organic (or metallic) cations. The picture is just consistent with the host-guest type association, as seen, for example, in the crystal structure of the complex between benzo-15-crown-5 and Ca^{2+} ion.[40] On the other hand, a different complexation site in the complex between epi-inositol and La^{3+} (D_2O) has been reported.[16] The ^1H NMR limiting shift values[16c,41] of H-3 are completely different each other, supporting the different complexation sites with cations between the two complexes in solutions.

Affinities toward primary, secondary, and tertiary alkylammonium ions are informative (Table 4). In the case of crown ethers (18C6, 15C5), the primary alkylammonium ion provides the highest $(M+A)^+$ peak, and the tertiary one shows no $(M+A)^+$ peak. The affinity ordering (prim.≫sec.≫tert.) is corresponding to the number of ^+N-H hydrogen atoms which can exert hydrogen bondings with host oxygens. Similarly, in the case of the permethylated monosaccharides (β-Tal, β-Man), the ordering is prim.>sec.>tert. Hydrogen bonding between the permethylated monosaccharide and alkylammonium ion may be effective to lesser extents in these complexations.

Experimental

General. ^1H NMR spectra were determined on a Bruker AM360 spectrometer. Chemical shifts are given in units in ppm relative to TMS as an internal standard (δ=0). Liquid column chromatography was carried out on a Yamazen LC apparatus using a column (50×1.5 cm) packed with Merck LiChroprep Si 60 (0.025—0.040 mm) under medium-pressure (1.5—2 kg cm^{-2}, flow rate 1.5 mL min^{-1}); 1:1 hexane/ethyl acetate was used as a typical eluent. For separation of aldopyranose/aldofuranose or its anomer derivative, a fraction collector (Gilson model 203) was employed with continuous TLC checking or RI monitoring (Yamazen, RI-31). The TLC checking was carried out on a piece (size 10×2. 5 cm) of Merck Kieselgel 60 F_{254} sheet. The TLC plates were sprayed with an 10% aqueous H_2SO_4 solution containing 1% $Ce(SO_4)_2$, and then heated on a hot plate until the spots become visible in blown (2—3 min).

Gas chromatography was performed on a Shimadzu GC-

9A instrument using a conventional glass column packed with Silicone OV 17/Chromosorb W or SE 30 (detection by FID mode, data reduction by C-R5A chromatopac). IR spectra were measured with a Hitachi 345 IR or an Analect RFX65 FTIR spectrometer. Mass spectra were recorded with a JEOL DX300 instrument under FAB and/or EI mode. MS/MS spectra were obtained with a JEOL JMS-HX100 instrument having E/B/E-type operation.[26]

Purity of the materials prepared was verified by ^{1}H NMR, EIMS, FABMS, and FTIR spectra. These spectra of the family **I** and the family **II** have been stored in the total computer system designated as 'TASMAC', ISIR, Osaka Univ.[43]

Materials. KF–alumina reagent was prepared according to the published procedure by Ando et al.[44] Alumina (Al_2O_3, Merck Aluminiumoxid 90 aktiv, neutral, 70—230 mesh, 60 g) was poured into an aqueous solution (70 ml) of KF (40 g) and fully shaked and stirred. After then, the water was removed at 50—60 °C with a rotary evaporator in vacuo. The impregnated alumina was further dried in a vacuum oven (15—20 mmHg) for 7 h at 70—80 °C (yield 102 g).

General Preparation of Permethylated Monosaccharides (family I). The respective methyl α- or β-D-aldopyranoside (0.20 g, 1.0 mmol) was mixed with methyl iodide (0.5 mL, ca. 8 mmol), and KF–alumina reagent (2.75 g, ca. 20 mmol) in acetonitrile (20 ml), and magnetically stirred in a teflon sealed tube at room temperature for 2 or 3 d (tetramethylation). The solid material was filtered off and washed several times with acetonitrile. The combined acetonitrile solution was evaporated in vacuo to dryness. The residue was dissolved into chloroform, washed with water, and filtered. Purification by liquid column chromatography usually at atmospheric pressure using Merck Kieselgel 60 (0.040—0.063 mm (230—400 mesh), 15 cm or 50 cm column length, 1 : 1 hexane/ethyl acetate or 5 : 5 : 1 hexane/ethyl acetate/methanol eluent) gave the corresponding methyl tetra-*O*-methyl-D-aldopyranoside (family **I**) in a yield of 70—80% as a ^{1}H NMR pure sample. Examples of starting materials are methyl α-D-glucoside (Wako),[45] methyl β-D-glucoside (Wako),[45] methyl α-D-galactoside (Nakalai), methyl β-D-galactoside (Sigma), methyl α-D-mannopyranoside,[46] methyl α-D-talopyranoside,[47] methyl α-D-ribofuranoside, and methyl β-D-ribofuranoside.[47,48]

In the case of pentamethyl β-D-mannopyranoside ($\mathbf{I}_f$) or pentamethyl β-D-talopyranoside ($\mathbf{I}_h$), the corresponding underivatized D-aldose commercially available was directly methylated (pentamethylation) with KF–alumina reagent by the same method as described before and then, the desired permethylated derivative was separated from a mixture of aldopyranosides and aldofuranosides by using medium-pressure liquid column chromatography (see below).

Preparation of Methyl Tetra-*O*-methyl-β-D-mannopyranoside ($\mathbf{I}_f$). A mixture of D-mannose (Wako. 0.20 g), methyl iodide (0.5 ml), and KF–alumina reagent (2.75 g) in acetonitrile (30 mL) was magnetically stirred at room temperature for a prolonged period (7 d, pentamethylation). After filteration and evaporation, the products were dissolved into chloroform, washed with water. The solution was filtered and evaporated to dryness. TLC analyses showed four major spots suggesting four stereoisomers. By using medium-pressure liquid column chromatography with an eluent of 5 : 5 : 1 hexane/ethyl acetate/methanol (v/v), the fraction showing R_f value of 0.38 (the fourth spot from top) was collected as the major one. The ^{1}H NMR[32] and mass spectral data indicated the product being the desired $\mathbf{I}_f$ (40% yield); ^{1}H NMR ($CDCl_3$) δ=4.29 (d, 1H $J_{1,2}$=0.8 Hz, C_1-H), 3.69 (dd. 1H, $J_{6,6'}$=9.1 Hz, C_6-H), 3.67 (dd, 1H, $J_{2,3}$=3.2 Hz, C_2-H), 3.60 (dd, 1H, $J_{5,6'}$=5.6 Hz, $C_{6'}$-H), 3.35 (t, 1H, $J_{4,5}$=9.5 Hz, C_4-H), 3.29 (octet. 1H, $J_{5,6}$=2.0 Hz, C_5-H), 3.19 (dd, 1H, $J_{3,4}$=8.7 Hz, C_3-H), 3.618, 3.520, 3.518, 3.493, 3.407 (s, 15H, OMe).

Preparation of Methyl Tetra-*O*-methyl-β-D-talopyranoside ($\mathbf{I}_h$). $\mathbf{I}_h$ was prepared by the analogous way mentioned above. Direct pentamethylation of D-talose (Sigma, 0.20 g) gave four TLC spots. Three major materials could be separated. Among them, the fractions showing R_f value of 0.17 (the fourth from top) was collected as the major one (eluent 1 : 1 hexane/ethyl acetate or 5 : 5 : 1 hexane/ethyl acetate/methanol). The product was the desired $\mathbf{I}_h$ on the basis of ^{1}H NMR and mass spectral data (60 mg, 22% yield); ^{1}H NMR ($CDCl_3$) δ=4.33 (d, 1H, $J_{1,2}$=1.6 Hz, C_1-H), 3.75—3.70 (m, 2H), 3.63—3.54 (m, 3H), 3.265 (t, 1H, J=3.17 Hz), 3.593, 3.522, 3.507, 3.485, 3.404. In this pentamethylation process, *N*-methylacetamide was detected as a by-product (^{1}H NMR, IR, and GC analyses).

Quantitative FABMS Measurements. FAB mass spectra were obtained by using argon as the bombarding atom, with a beam energy of 6 keV. A stainless steel probe-tip was employed in each case. Mass conversion was carried out off-line on the basis of perfuruoro kerosene (PFK) calibration. In order to get higher reproducibility on peak intensity data, all the FAB spectra by quantitative measurements were averaged from at least 10 scans (1 scan=4 s) using a JMA-3100 data system.[22]

A typical preparation of sample solution is as the following. (1) The respective permethylated monosaccharide (16 μL) was dissolved into methanol (1 mL) (17.6 mg mL^{-1}; 0.07 M). (2) (Methoxycarbonyl)methylammonium chloride (0.88 g) was dissolved into methanol (10 mL) (8.8 mg mL^{-1}, 0.7 M). (3) Methyl tetra-*O*-methyl-d_{12}-α-D-mannopyranoside ($\mathbf{I}_f$-d_{12}) as an internal standard was dissolved into a mixture of glycerol and methanol (3/1 v/v) (1.0 ml; 0.07 M). The above three solutions were mixed: 10 μL of the solution (1) +10 μL of the solution (2) +20 μL of the solution (3). After mixing well with a vibrater, 1.5 μL of the resulted solution was deposited on a probe-tip as a sample solution for quantitative measurements on positive ion FABMS. This corresponded the molar concentration ratio of each monosaccharide (M) to the internal standard (R) to be 1 : 1.

In the case of octylammonium ion series, octylammonium chloride (0.12 g) was dissolved into methanol (10 mL), (0.07 M), and it was used as the solution (2) in the above series mentioned.

The probe-tip was placed in the ion source and ca. 2 min were allowed for the source vacuum to settle (5×10^{-6} Torr, 1 Torr=133.322 Pa), and the Ar atom gun was turned on. After a further 1 min, FAB spectra were recorded. At an accelerating voltage of 3 kV, the mass range *m/z* 200—400 was scanned in 3 s scan cycle time. Thirty successive spectra of each sample solution were acquired and the 10 scans between 10 and 20 were summed to get the quantitative spectra for the family **I** or the 10 scans between 15 to 25 for the family **II**. The relative abundance at the required *m/z* values was measured and averaged over the 3 runs, and

compared with the data of other monosaccharides after normalization to the constant abundance of the internal standard (R).[20]

MNDO Calculations. Calculations of geometries and energies for the $(M+A)^+$ ion composed of $\mathbf{I}_h$ (or $\mathbf{I}_g$, $\mathbf{I}_f$) and Li^+ were carried out on a FACOM S3500 superminicomputer (ANCHOR in TASMAC system)[43] by using MNDO molecular orbital methods.[49] The geometries and energies were obtained from the standard DFP optimization procedures. For example, for obtaining an initial geometry of $\mathbf{I}_h$, crystal structure data of underivatized α-D-talose were employed.[50]

We are grateful to Mr. Takanori Tanaka and Mrs. Fusako Fukuda for the measurements of FTIR spectra and the elemental microanalyses at Material Analysis Center, ISIR, Osaka University.

References

1) Preliminary accounts of this work: a) M. Sawada, L. Ouyang, Y. Takai, H. Yamada, and T. Hanafusa, *Chem. Lett.*, **1989**, 1743; b) M. Sawada, L. Ouyang, Y. Takai, H. Yamada, T. Hanafusa, T. Kinoshita, and T. Mochizuki, *Chem. Lett.*, **1990**, 1361.

2) M. Green, *Pure Appl. Chem.*, **50**, 185 (1978).

3) A. G. Harrison, "Chemical Ionization Mass Spectrometry," CRC Press, Inc., Florida (1983), Chaps. 5 and 6.

4) T. Murata, *Bunseki Kagaku*, **34**, 414 (1985).

5) J. R. J. Pare, K. Jankowski, and J. W. Apsimon, *Adv. Heterocycl. Chem.*, **42**, 335 (1987).

6) a) G. Puzo, J.-J. Fournie, and J.-C. Prome, *Anal. Chem.*, **57**, 892 (1985); b) G. Puzo, J.-C. Prome, and J.-J. Fournie, *Carbohydr. Res.*, **140**, 131 (1985); c) J.-J. Fournie and G. Puzo, *Anal. Chem.*, **57**, 2287 (1985).

7) a) M. Barber, R. S. Bordoli, R. D. Sedgwick, and A. N. Tyler, *Nature*, **293**, 270 (1981); b) M. Barber, R. S. Bordoli, R. D. Sedgwick, and A. N. Tyler, *J. Chem. Soc., Chem. Commun.*, **1981**, 325; c) M. Barber, R. S. Bordoli, G. J. Elliott, R. D. Sedgwick, and A. N. Tyler, *Anal. Chem.*, **54**, 645A (1982).

8) a) D. H. Williams, C. Bradley, G. Bojesen, S. Santikarn, and L. C. E. Taylor, *J. Am. Chem. Soc.*, **103**, 5700 (1981); b) K. L. Rinehart, *Science*, **218**, 254 (1982).

9) a) C. Fenselau, "Ion Formation from Organic Solids," ed by A. Benninghoven, Springer-Verlag, Berlin (1983), p. 90; b) C. Fenselau and R. J. Cotter, *Chem. Rev.*, **87**, 501 (1987).

10) J. A. Leary and S. F. Pedersen, *J. Org. Chem.*, **54**, 5650 (1989).

11) S. S. Wong, F. W. Rollgen, I. Manz, and M. Przybylski, *Biomed. Mass Spectrom.*, **12**, 43 (1986).

12) K. Harada, M. Suzuki, and H. Kambara, *Org. Mass Spectrom.*, **17**, 386 (1982).

13) The compounds used here are known to take Cl conformation. For example, S. J. Angyal and K. Dawes, *Aust. J. Chem.* **21**, 2747 (1968).

14) K. E. Koenig, R. C. Helgeson, and D. J. Cram, *J. Am. Chem. Soc.*, **98**, 4018 (1976).

15) Y. Aoyama, Y. Tanaka, and S. Sugahara, *J. Am. Chem. Soc.*, **111**, 5397 (1989).

16) a) S. J. Angyal, *Adv. Carbohydr. Chem. Biochem.*, **47**, 1 (1989); b) S. J. Angyal, *Chem. Soc. Rev.*, **9**, 415 (1980); c) $\Delta\delta_{limiting}=\Delta\delta_{obsd}(2\,K_s\,[M]_0)/[(4\,[M]_0K_s^2+1)^{1/2}-1]$.

17) a) F. Vogtel and E. Weber, "The Chemistry of Ethers, Crown Ethers, Hydroxy Groups, and their Sulphur Analogues," Part 1, ed by S. Patai, John Wiley, New York (1980), Chap. 2; b) H. K. Frensdorff, *J. Am. Chem. Soc.*, **93**, 600 (1970); c) R. M. Izatt, N. E. Izatt, B. E. Rossiter, J. J. Christensen, and B. L. Haymore, *Science*, **199**, 994 (1978).

18) D. J. Cram, *Angew. Chem., Int., Ed. Engl.*, **27**, 1009 (1988).

19) E. Weber and F. Vogtel, "Host Guest Complex Chemistry I," ed by F. Vogtel, Springer-Verlag, Berlin (1981), Chap. 1.

20) a) R. A. W. Johnstone and M. E. Rose, *J. Chem. Soc., Chem. Commun.*, **1983**, 1268; b) R. A. W. Johnstone, I. A. S. Lewis, and M. E. Rose, *Tetrahedron*, **39**, 1597 (1983); c) R. A. W. Johnstone and I. A. S. Lewis, *Int. J. Mass Spectrom. Ion Phys.*, **46**, 451 (1983).

21) R. M. Caprioli, *Anal. Chem.*, **55**, 2387 (1983).

22) M. Sawada, H. Yamada, Y. Furukawa, C. Chang, F. Fukuda, T. Tanaka, Y. Takai, T. Hanafusa, and S. Misumi, *Nippon Kagaku Kaishi*, **1986**, 560.

23) J. A. Sunner, A. Morales, and P. Kebarle, *Anal. Chem.*, **59**, 1378 (1987).

24) For example, a) F. W. McLafferty, *Acc. Chem. Res.*, **1980**, 33; b) F. W. McLafferty, *Science*, **214**, 280 (1981); c) R. P. Grese, R. L. Cerny, and M. L. Gross, *J. Am. Chem. Soc.*, **111**, 2835 (1989).

25) a) R. G. Cooks and T. L. Kruger, *J. Am. Chem, Soc.*, **99**, 1279 (1977); b) S. A. McLuckey, D. Cameron, and R. G. Cooks, *J. Am. Chem. Soc.*, **103**, 1313 (1981); c) S. A. McLuckey, A. E. Schoen, and R. G. Cooks, *J. Am. Chem, Soc.*, **104**, 848 (1982); d) G. Bojesen, *J. Chem. Soc., Chem. Commun.*, **1986**, 244; e) G. Bojesen, *J. Am. Chem. Soc.*, **109**, 5557 (1987).

26) T. Kinoshita, T. Nakamura, and H. Nagaki, *Nippon Kagaku Kaishi*, **1986**, 1665.

27) For example, a) M. L. Martin, G. J. Martin, and J.-J. Delpuech, "Practical NMR Spectroscopy," Heyden, London (1980), Chap. 10; b) R. J. Abraham and P. Loftus, "Proton and Carbon-13 NMR Spectroscopy. An Integrated Approach," Heyden, London (1978), Chap. 7.

28) a) H. A. Benesi and J. H. Hildebrand, *J. Am. Chem. Soc.*, **71**, 2703 (1947); b) S. J. Hu, E. Goldberg, and S. I. Miller, *Org. Magn. Reson.*, **4**, 683 (1972); c) $(\delta_i-\delta_A)^{-1}=[K_sM_i(\delta_C-\delta_A)]^{-1}+(\delta_C-\delta_A)^{-1}$.

29) The K_s for $\mathbf{I}_e$ (α-Man) with $A_4^+PF_6^-$ was also estimated to be ca. 3 M^{-1} (in CD_3CN, at 30 °C), but less reliable because of a narrow ICS range (ICS range=24—68 Hz, $[M]/[A^+X^-]$=9—46, $[A^+X^-]_{fix_h}$=0.015 M).

30) For example, the K_s for complex between α-allopyranose and Ca^{2+} in D_2O is ca. 4.[16a,31] The K_s between 18-crown-6 and NH_4^+ (K^+) in MeOH is 1.9×10^4 (1.3×10^6).[17b,c]

31) S. J. Angyal and K. P. Davies, *J. Chem. Soc., Chem. Commun.*, **1971**, 500.

32) a) J. Haverkamp, M. J. A. de Bie, and J. F. G. Vliegenthart, *Carbohydr. Res.* **39**, 201 (1975); b) J. Haverkamp, J. P. C. M. van Dongen, and J. F. G. Vliegenthart, *Carbohydr. Res.*, **33**, 319 (1974); c) J. Haverkamp, J. P. C. M. van Dongen, and J. F. G. Vliegenthart, *Tetrahedron*, **29**, 3431 (1973).

33) In the case of $\mathbf{I}_f$ the Li^+ cation is located at 2.2 Å from the three oxygen atoms of the O-1, O-2, and the ring-O. From the binding energies (stabilization energies) calculated

for the reaction $(M+Li^+ \rightarrow (M+Li)^+)$, the ordering of the entalpy change is $\mathbf{I_h}$ ($|-67|$ kcal mol^{-1})>$\mathbf{I_g}$ ($|-66|$)>$\mathbf{I_f}$ ($|-50|$), indicating a MNDO support of the corresponding affinity ordering obtained in FABMS.

34) J. A. Sunner, R. Kulatunga, and P. Kebarle, *Anal. Chem.*, **58**, 2009 (1986).

35) J. A. Sunner, R. Kulatunga, and P. Kebarle, *Anal. Chem.*, **58**, 1312 (1986).

36) G. Bonas, C. Bosso, and M. R. Vignon, *Rapid Commun. Mass Spectrom.*, **2**, 88 (1988).

37) R. M. Caprioli, "Mass Spectrometry in Biological Research," ed by S. Gaskell, John Wiley, New York (1986), p. 41.

38) J. M. Timko, S. S. Moore, D. M. Walba, P. C. Hiberty, and D. J. Cram, *J. Am. Chem. Soc.*, **99**, 4207 (1977).

39) R. W. Taft and R. D. Topsom, *Prog. Phys. Org. Chem.*, **16**, 1 (1987).

40) J. D. J. Owen, *J. Chem. Soc., Dalton Trans.*, **1978**, 1418.

41) The limiting shift values (ppm) of the adduct ion between $\mathbf{I_h}$ and A_4^+ in CD_3CN are 0.29 (H-1), 0.56 (H-2), 0.07 (H-3), 0.49 (H-4), 0.20, 0.20, 0.17, 0.09, 0.02 ($5\times CH_3$). A Buckingham treatment can reproduce only the ICS ordering.[42]

42) A. D. Buckingham, *Can. J. Chem.*, **38**, 300 (1960).

43) For example, M. Sawada, *Chemistry*, **42**, 300 (1987).

44) T. Ando, J. Yamawaki, T. Kawate, S. Sumi, and T. Hanafusa, *Bull. Chem. Soc. Jpn.*, **55**, 2504 (1982).

45) *Org. Synth.*, Col. Vol. 1, 364 (1941).

46) a) H. G. Bott, W. N. Haworth, E. L. Hirst, and R. S. Tipson, *J. Chem. Soc.*, **1930**, 2653; b) *Chem. Abstr.*, **25**, 1222 (1931).

47) S. J. Angyal, C. L. Bodkin, and F. W. Parrish, *Aust. J. Chem.*, **28**, 1541 (1975).

48) P. Heath, J. Mann, E. B. Walsh, and A. H. Wadsworth, *J. Chem. Soc., Perkin Trans. 1*, **1983**, 2675.

49) a) M. J. S. Dewar and W. J. J. Thiel, *J. Am. Chem. Soc.*, **99**, 4899 (1977); b) W. J. J. Thiel, *J. Am. Chem. Soc.*, **103**, 1413 (1981); c) T. Clark, "A Handbook of Computational Chemistry: a Practical Guide to Chemical Structure," John Wiley, New York (1985), Chap. 4; d) Original MNDOC and MNDO programs were obtained through QCPE, Indiana Univ.

50) P. J. Ohanessi Avenel, J. A. Kanters, and D. Smits, *Acta Crystallogr., Sect. B*, **33**, 1063 (1977).

Effect of a Hydrogen Pretreatment on the Mechanism of Deuterium Addition and Exchange of Propene over Ni-Cu Alloy Catalysts

Shuichi NAITO* and Mitsutoshi TANIMOTO†
Research Centre for Spectrochemistry, Faculty of Science, The University of Tokyo, Hongo, Bunkyo-ku, Tokyo 113
†Department of Chemistry, Faculty of Science, Shizuoka University, 836 Ohya, Shizuoka 422
(Received August 30, 1990)

The effects of a hydrogen pretreatment on the activity and reaction intermediate in a C_3H_6–D_2 reaction over a Ni-Cu alloy as well as Ni metal catalysts were investigated in detail by applying an isotope tracer technique. Ni metal and Ni-rich alloy catalysts, cooled down to the reaction temperature under a hydrogen atmosphere (D-surface), exhibited low activity compared to that of a surface evacuated before cooling (E-surface). For Cu-rich alloy catalysts, however, the E-surface exhibited a lower activity and a higher activation energy than did the D-surface. A comparison of the TPD spectra of adsorbed hydrogen with the dependence of the activity upon the evacuation temperature suggests that strongly adsorbed hydrogen retards the reaction over Ni and Ni-rich alloy catalysts at lower temperature. Microwave spectroscopic analysis demonstrated that the reaction intermediates over D- and E-surfaces of Cu-rich alloy catalysts were similar to those over Cu and Ni metals, respectively. This result suggests that a hydrogen pretreatment of Cu-rich alloys forms a specific surface structure which is destroyed by evacuation at elevated temperatures.

Bimetallic alloy systems comprising an active group-VIII metal and an inactive group-IB metal have extensively been investigated, since they allow one to study the role of the "geometric, or ensemble, effect" as well as the "electronic, or ligand, effect" in alloy catalysts.[1-3] Among them, a nickel-copper alloy system has received particular attention from the viewpoint of both the surface structure and the catalytic behavior in hydrogen exchange,[4-6] hydrogenation,[7-12] hydrogenolysis[13] or dehydrogenation[14] of various hydrocarbons. Analyses of its surface composition by various methods, such as selective chemisorption,[15,16] work function change,[17-19] and AES (Auger Electron Spectroscopy) measurements,[20,21] have disclosed a considerable enrichment of copper on the surface, which is inactive for the reactions mentioned above. Accordingly, the dilution effect of active metal ensembles by inactive atoms would be significantly pronounced in these systems (ensemble effect). In fact, it is well known that reactions involving C-C bond fission or formation are suppressed much more efficiently by alloying than reactions involving C-H bonds on this catalyst.[1,4,6,13] The situation is somewhat different in the case of the hydrogenation reaction, which proceeds at a much lower temperature than does hydrogenolysis or dehydrogenation.

Best and Russell[7] examined the hydrogenation of ethene over Ni-Cu alloy catalysts of various composition and observed several orders of magnitude higher activity in the copper-rich range than over a pure Ni catalyst. Hall and Emmett[8] reported a remarkable dependence of the activity for this reaction upon the pretreatment over Ni-Cu alloy catalysts as well as pure Ni catalysts. When the catalysts were evacuated at the temperature at which the reduction had been carried out, and then cooled in vacuo or in flowing helium, the activity decreased as the copper content of the catalyst increased. On the other hand, if the catalysts were cooled in a hydrogen atmosphere the activity showed two maxima at around 30 and 70 atm% of copper in the alloy composition.[9] Hall and Hassell further demonstrated that these results could be explained in terms of a promotion effect of strongly adsorbed hydrogen on the hydrogenation rate over alloy catalysts and a suppression effect over pure Ni metal.[10] To clarify the intrinsic nature of this effect, it is obviously necessary to study changes not only in the reaction rates, but also in the reaction mechanism by these pretreatments.

Deuterium addition and exchange of propene (C_3H_6–D_2 reaction) would be an excellent probe reaction for this purpose, since it enables one to investigate the fine structure of the reaction mechanism by applying microwave spectroscopy.[22] The temporal changes in the isotope distribution in monodeuteriopropene formed during the reaction can be followed. We have examined the effect of a pretreatment on the C_3H_6–D_2 reaction over Ni-Cu alloy catalysts of various compositions and found the same phenomena as in the case of the C_2H_4–H_2 reaction. Moreover, the relative activity of the reaction intermediates, propyl and isopropyl adsorbed species, was demonstrated to change with the manner of pretreatment, as well as the surface composition of Ni and Cu. In the present paper we describe in detail the experimental results and discuss in depth possible features of this effect.

Experimental

Catalyst Preparation. Powders of Ni-Cu alloy and pure metals (Ni and Cu) were prepared by carefully reducing the corresponding oxide powders according to a method described in the literature.[15] First of all, carbonate powders were coprecipitated by adding aqueous nitrate solutions ($Ni(NO_3)_2 \cdot 6H_2O$ and $Cu(NO_3)_2 \cdot 3H_2O$; Wako Chemicals,

spec. pure) dropwise to aqueous NH_4HCO_3 solutions (Wako Chemicals, spec. pure) with vigorous stirring. The precipitates were filtered, washed thoroughly with distilled water, dried, and calcined in air at 673 K for 2 h. The oxide powders were placed in an U-shaped reactor and reduced with flowing hydrogen by increasing the temperature very slowly from 298 to 773 K (within about 12 h) and then maintaining that temperature for 20 h. The bulk composition of the alloys employed were 0.5, 25, 60, and 90 atom% of copper.

Catalyst Characterizations. The surface areas and surface compositions in alloy catalysts were determined by N_2 physisorption at its normal boiling point and H_2 chemisorption at room temperature. About a one-order-of-magnitude larger amount of the catalysts (10—15 g) than that used for the catalytic reaction were employed in order to obtain precise values for adsorption experiments. Before measurements, the catalysts were reduced with H_2 at 623 K for 2 h and then evacuated at the same temperature for 0.5 h in a volumetric apparatus (base pressure was 1×10^{-3} Pa). The crosssectional areas of the N_2 molecule and the H atom were assumed to be 16.2 and 6.45 Å^2, respectively. Hydrogen was chemisorbed at room temperature in order to obtain total uptake. The catalyst was then evacuated under vacuum for 30 min at room temperature. Readsorption measurements were carried out in order to determine the amount of weakly adsorbed hydrogen. The amount of strongly adsorbed hydrogen was determined from the difference between these two values. The surface area of this strongly adsorbed hydrogen was assumed to correspond to that of surface Ni. Comparing this with the total surface area obtained by the BET method, the surface compositions of Ni and Cu could be estimated. The obtained results were as follows: 0.5 mol% bulk Cu=0.55 surface Cu, 25 mol% bulk Cu=0.77 surface Cu, 60 mol% bulk Cu=0.78 surface Cu, 90 mol% bulk Cu=0.91 surface Cu. These surface compositions were qualitatively confirmed by XPS (X-ray photoelectron spectroscopy) analysis (ESCALAB 5). The formation of a monophase homogeneous alloy was confirmed by observing their characteristic X-ray diffraction pattern. The lattice constants of alloy powders obtained were consistent with Vegard's law: Ni=3.52 Å, Ni-Cu(0.5)=3.52 Å, Ni-Cu(25)=3.54 Å, Ni-Cu(60)=3.58 Å, Ni-Cu(90)=3.60 Å, and Cu=3.61 Å.

Reaction Procedure, Detection Method, and TPD Procedure. H_2 and D_2 gases from commercial cylinders were purified by circulating over a heated palladium black catalyst to remove trace amount of oxygen. C_3H_6 purchased from Takachiho Kagaku K.K. was purified by a freeze-thaw cycle. The C_3H_6-D_2 reaction was carried out in a closed gas circulation system (total volume: 310 cm^3). Before each run the catalyst was freshly reduced by D_2 at 473 K for 2 h. For a reaction over a deuterium pretreated surface (D-surface), the catalyst was cooled to the reaction temperature without evacuating deuterium gas. For a reaction over an evacuated surface (E-surface), the catalyst was evacuated at 473 K for 1 h and then cooled down to the reaction temperature under vacuum. A certain amount of the C_3H_6-D_2 mixture was introduced into the system and the reaction started. The reaction temperature was maintained with suitable slush bathes.

At certain intervals during the reaction, a few percent of the circulating gas was sampled and analyzed. The composition of the gas was determined by gas chromatography (alumina column, He carrier). The deuterium contents in the exchanged propene and formed propane were determined with a mass spectrometer (Hitachi, RMU-6MG) using ionization voltages of 12 and 15 eV, respectively. The location of the deuterium atom in mono- and dideuteriopropene was determined by recording the microwave absorption line (1_{01}—0_{00} rotational transition) characteristic of each isotopic species. The notation for isotopic isomers in monodeuteriopropene is:

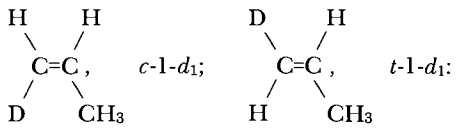

CH_2=CD-CH_3, 2-d_1. CH_2=CH-CH_2D, 3-d_1.

TPD (Temperature programmed desorption) experiments were carried out in a separate UHV apparatus (base pressure: 1×10^{-7} Pa), equipped with a mass spectrometer (UTI 100). The heating part was made of a quartz cell, in which about 10 mg of catalyst was placed. The heating rate was set to 15 K min^{-1}.

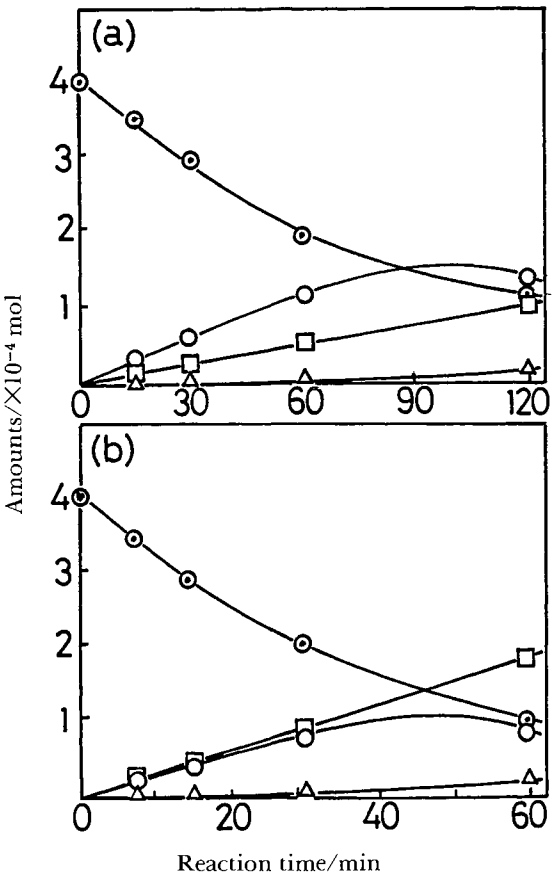

Fig. 1. Time courses of C_3H_6-D_2 reaction (D-surface) over (a) Ni metal at 210 K and (b) Ni-Cu(25) at 180 K.
p_{D_2}=6.7 kPa, $p_{C_3H_6}$=2.0 kPa, Catalysts=1 g.
⊙: Propene-d_0, ○: Propene-d_1, △: Propene-d_2, □: Propane.

Results

Kinetics of C_3H_6-D_2 Reaction over D-Surfaces. When a mixture of D_2 (6.7 kPa) and C_3H_6 (2.0 kPa) was introduced over D-surfaces of Ni and Ni-Cu alloy catalysts at 170—220 K, both deuterium addition and exchange reaction took place simultaneously. The D-surface was prepared by D_2 reduction at 473 K or 2 h, followed by cooling down to the reaction temperature without evacuation. Typical time courses of the reaction over Ni metal and Ni-Cu(25) (25 mol% bulk Cu) catalysts are shown in Fig. 1. In the case of Ni metal (Fig. 1(a)), the main product in the exchange process was C_3H_5D (propene-d_1), the formation rate of which was twice as fast as that of propane. During a later stage of the reaction, $C_3H_4D_2$ (propene-d_2) was detected, suggesting a successive reaction in the exchange process. The reaction over Ni-Cu(25) was nearly two orders of magnitude faster than that over Ni metal (Fig. 1(b)). The time course was similar to that over Ni, except that C_3H_5D and propane were formed in comparable amounts. The reaction behavior of other catalysts could be divided into these two categories: Ni-Cu(0.5) alloy was similar to Ni metal; Ni-Cu(60) and (90) alloys were similar to Ni-Cu(25).

The temperature dependence of the turnover frequency (TOF) of propane formation over various catalysts is displayed in Fig. 2. The TOF was estimated assuming that only the surface Ni atoms are active for this reaction. The activity for propane formation decreased in the following order: Ni-Cu(60)≈Ni-Cu(25)>Ni-Cu(90)>Ni-Cu(0.5)<Ni metal. The activation energies of the reaction were also classified into two categories. Ni-Cu(0.5) catalyst exhibited an activation energy (41 kJ mo^{-1}) similar to that of Ni metal (39 kJ mol^{-1}). The activation energy considerably decreased by alloying, and the same value (31 kJ mol^{-1}) was observed for Ni-Cu(25), (60), and (90) alloy catalysts.

The pressure dependence of the turnover frequency for propane formation over Ni and Ni-Cu(25) catalysts is demonstrated in Fig. 3. Over a Ni catalyst the reaction orders for the partial pressures of hydrogen and propene were 0.37 and 0.07, respectively. Upon alloying, they decreased as follows: 0.45 for the partial pressure of hydrogen and −0.15 for propene; this suggests an increase in the adsorption strength of propene by alloying.

Kinetics of C_3H_6-D_2 Reaction over E-Surfaces. Figure 4 demonstrates the temperature dependence of propane formation over the E-surfaces of Ni and Ni-Cu alloy catalysts. The E-surfaces were prepared by D_2 reduction at 473 K, followed by evacuation at the same temperature for 1 h. It was recognized that this evacuation treatment drastically accelerates the propane formation rate over both Ni and Ni-Cu(0.5) catalysts, although their activation energies did not change at all. The situation was completely different over

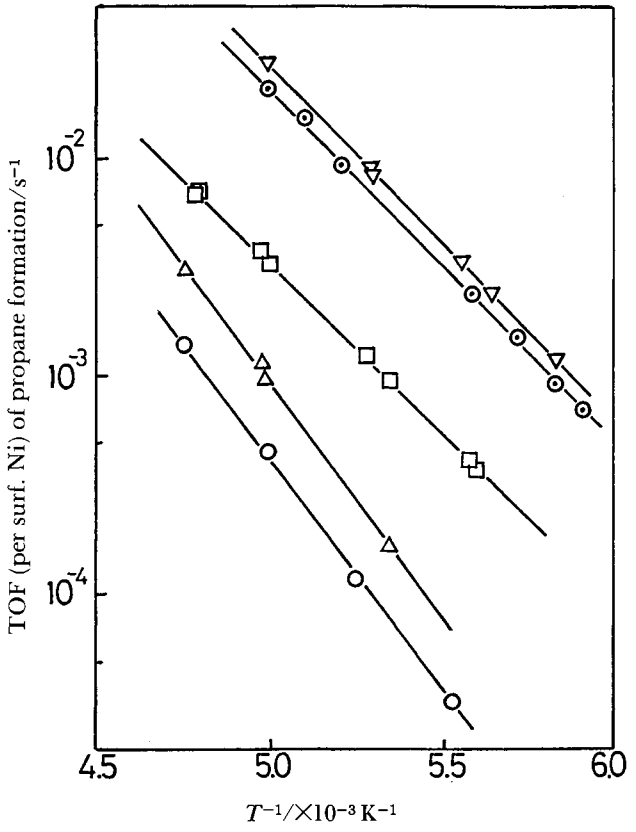

Fig. 2. Temperature dependence of TOF of propane formation (D-surface) over various catalysts.
p_{D_2}=6.7 kPa, $p_{C_3H_6}$=2.0 kPa, Catalyst=1 g.
○: Ni, △: Ni-Cu(0.5), ⊙: Ni-Cu(25), ▽: Ni-Cu(60), □: Ni-Cu(90).

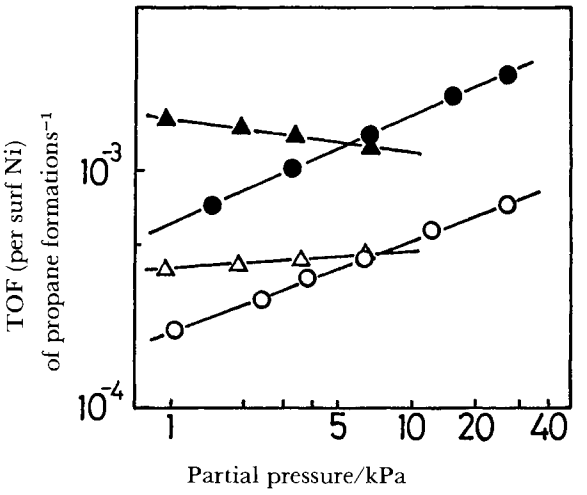

Fig. 3. Pressure dependence of TOF of propane formation (D-surface) over (a) Ni metal at 210 K (open symbols), and (b) Ni-Cu(25) alloy catalyst at 180 K (closed symbols).
○●: Dependence of H_2 partial pressure ($p_{C_3H_6}$=3.3 kPa, constant). △▲: Dependence of C_3H_6 partial pressure (p_{H_2}=6.7 kPa, constant).

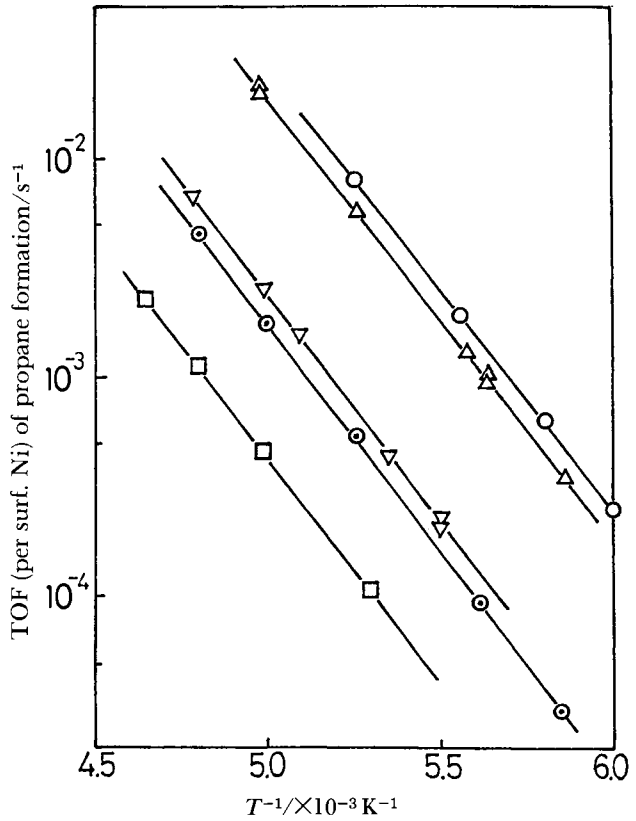

Fig. 4. Temperature dependence of TOF of propane formation (E-surface) over various catalysts.
p_{D_2}=6.7 kPa, p_{D_2}=2.0 kPa, Catalyst=1 g.
○: Ni, △: Ni-Cu(0.5), ⊙: Ni-Cu(25), ▽: Ni-Cu(60).
□: Ni-Cu(90).

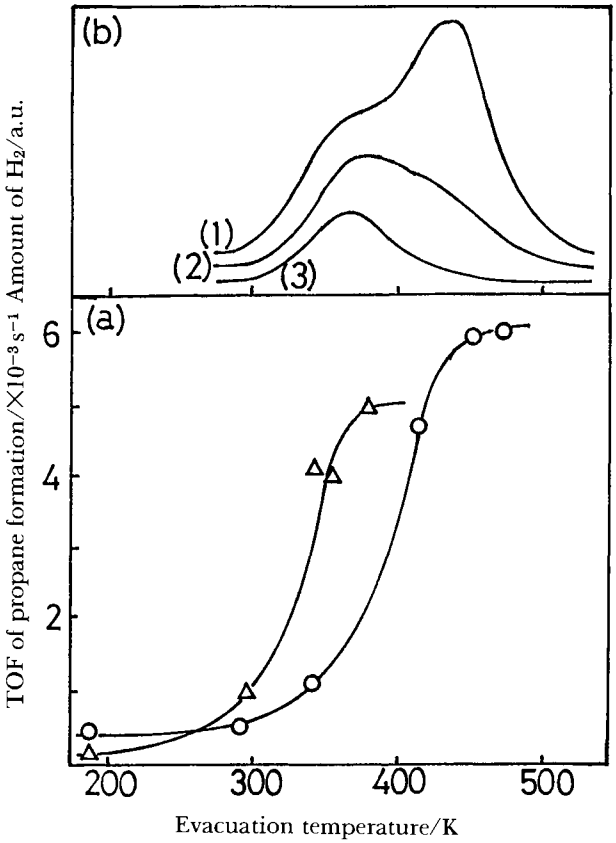

Fig. 5. (a) Effect of evacuation temperature on TOF of propane formation over Ni metal at 190 K, and over Ni-Cu(0.5) catalyst at 210 K.
p_{D_2}=6.7 kPa, $p_{C_3H_6}$=2.0 kPa, Catalyst=1 g.
○: Ni, △: Ni-Cu(0.5).
(b) TPD spectra of adsorbed H(a) over various catalysts.
(1) Ni, (2) Ni-Cu(0.5), (3) Ni-Cu(25).
Adsorption temperature=273 K for 1 h. (p_{H_2}=6.7 kPa).

other alloy catalysts: the rate decreased more than one order of magnitude with an increase in the activation energy to 40 kJ mol^{-1} for Ni-Cu(25), (60), and (90) catalysts.

To investigate the relation between the D- and E-surfaces of Ni and Ni-Cu(0.5) catalysts, the effect of the evacuation temperature upon the rate of propane formation was examined, as summarized in Fig. 5(a). After reduction by D_2 at 623 K for 2 h, the catalyst was evacuated for 1 h at various temperatures from 190 to 623 K and then cooled down to the reaction temperature (190 K for Ni and 210 K for Ni-Cu(5)), before C_3H_6-D_2 reaction was carried out. In the case of the Ni catalyst, the rate gradually increased as the evacuation temperature was increased, and reached a plateau activity at around 450 K. Over a Ni-Cu(0.5) catalyst, this plateau temperature was considerably lowered (360 K). Fig. 5(b) demonstrates the TPD spectra of adsorbed hydrogen over pure Ni, Ni-Cu(0.5) and Ni-Cu(25) alloy catalysts. The adsorption was carried out at 273 K for 1 h (P_{H_2}=6.7 kPa). After evacuation up to 10^{-7} Pa, the catalyst was heated at a rate of 15 K min^{-1}. Two maximum peaks were observed in the case of Ni. The higher temperature peak was considerably diminished and disappeared in the Ni-Cu(25) catalyst.

Microwave Spectroscopic Study of C_3H_6-D_2 Reaction. It has been well established that deuterium addition and exchange processes in the C_3H_6-D_2 reaction over Ni and Cu metal catalysts proceed through common σ-alkyl intermediates: propyl and isopropyl adsorbed species (associative mechanism).[23,24] The situation seemed to be identical over Ni-Cu alloy catalysts in the present study, because the rates of both addition and exchange processes exhibited similar temperature dependences, indicating equal activation energies. Moreover, the rate of the hydrogen exchange in the C_3H_6-C_3D_6 reaction, which should proceed via a dissociative mechanism, was more than two orders of magnitudes slower than that in the C_3H_6-D_2 reaction. Consequently, it is evident that hydrogen exchange in the C_3H_6-D_2 reaction over alloy catalysts takes place via a reverse process of the σ-alkyl intermediate formation, as in Ni and Cu catalysts.

The isotopic distributions of formed propane over

Table 1. Isotopic Distribution of Propane and Propene-d_2 in C_3H_6-D_2 Reaction over D-Surfaces of Various Catalysts

Catalysts	Ni	Ni-Cu (0.5)	Ni-Cu (25)	Cu
Reac. Temp	190	190	180	263
Reac. Time/min	60	60	120	600
Conversion	0.41	0.45	0.32	0.35
C_3H_8	0.33	0.30	0.05	0.04
C_3H_7D	0.28	0.29	0.26	0.25
$C_3H_6D_2$	0.29	0.32	0.55	0.58
$C_3H_5D_3$	0.09	0.09	0.11	0.12
$C_3H_4D_4$	0.01	0.01	0.02	0.02
$C_3H_3D_5$-C_3D_8	0.00	0.00	0.00	0.00
CD_2=CH-CH_3	0.03	0.04	0.06	0.07
CHD=CD-CH_3	0.85	0.85	0.80	0.79
CHD=CH-CH_2D	0.01	0.00	0.03	0.02
CH_2=CD-CH_2D	0.12	0.12	0.11	0.12
CH_2=CH-CHD_2	0.00	0.00	0.00	0.00

these catalysts are summarized in Table 1. Propane-d_2 was the main product over Cu (24), whereas comparable amounts of propane-d_0, -d_1, and -d_2 were formed over Ni catalyst.[23] The latter phenomenon corresponds well to the first observation by Turkevich et al.[25] that C_2H_6 was mainly formed during the initial stage of the C_2H_4-D_2 reaction over Ni, which was reasonably explained by an associative mechanism.[26]

The relative reactivity of propyl and isopropyl intermediates can be estimated by observing the isotopic distribution of monodeuteriopropene formed in the exchange process of the C_3H_6-D_2 reaction. Microwave spectroscopic results over the D-surface are summarized in Figs. 6 and 7. Over a Ni catalyst (Fig. 6(a)) more than 90% of the exchanged products was propene-2-d_1, which would be formed through a propyl adsorbed intermediate. The remainder of the products were equal amounts of propene *cis*- and *trans*-1-d_1 with a small amount of propene-3-d_1. This result suggests that the isopropyl species is adsorbed in a distorted manner, so that hydrogen exchange takes place mainly on the C_1 carbon of the double bond. On the other hand, over a Cu catalyst (Fig.6(b)), the proportion of propene-2-d_1 decreased from 93 to 73%, with an increase of *cis*- and *trans*-1-d_1. As on the Ni catalyst, the amount of propene-3-d_1 was slight during the reaction, suggesting a sterically distorted adsorption of the isopropyl intermediate. Figure 7 demonstrates the isotopic distribution pattern in the case of Ni-Cu(0.5) and (25) catalysts. This pattern is quite similar to that of Ni metal in the case of a Ni-Cu(0.5) catalyst (Fig. 7(a)), whereas it resembles that of Cu metal in the case of a Ni-Cu(25) catalyst (Fig. 7(b)).

The closed symbols in the figures represent data for

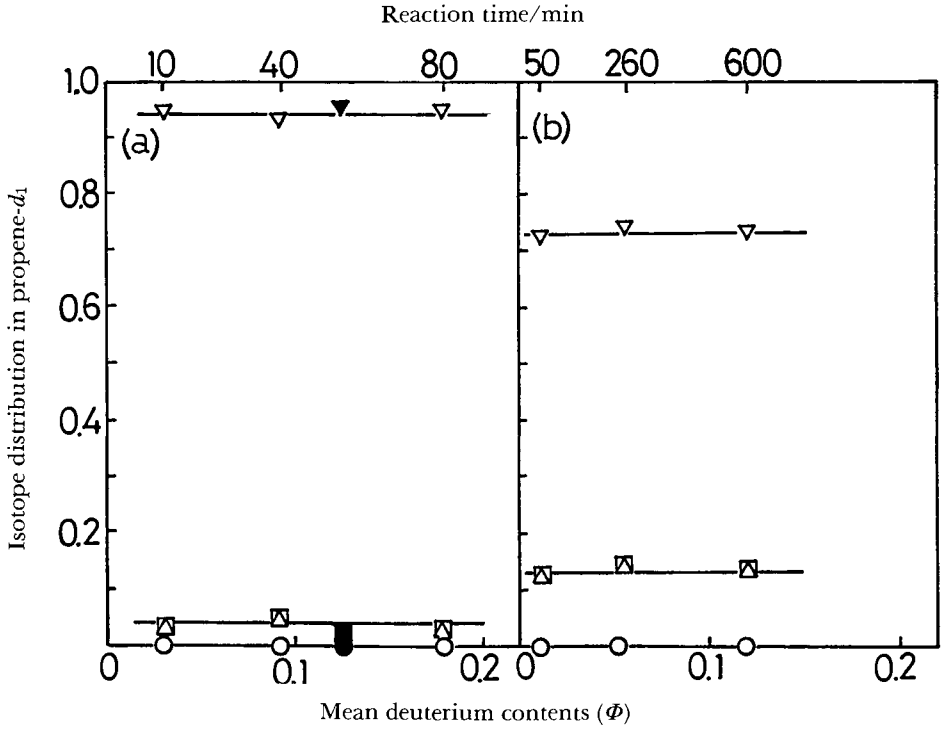

Fig. 6. Time course of the isotopic distribution in monodeuteriopropene during C_3H_6-D_2 reaction over (a) Ni metal at 200 K, and (b) Cu metal at 263 K. p_{D_2}=6.7 kPa, $p_{C_3H_6}$=2.0 kPa, Catalyst=1 g. Open symbols: over D-surfaces, closed symbols: over E-surfaces.
□■: *c*-1-d_1, △▲: *t*-1-d_1, ▽▼: 2-d_1, ○●: 3-d_1.

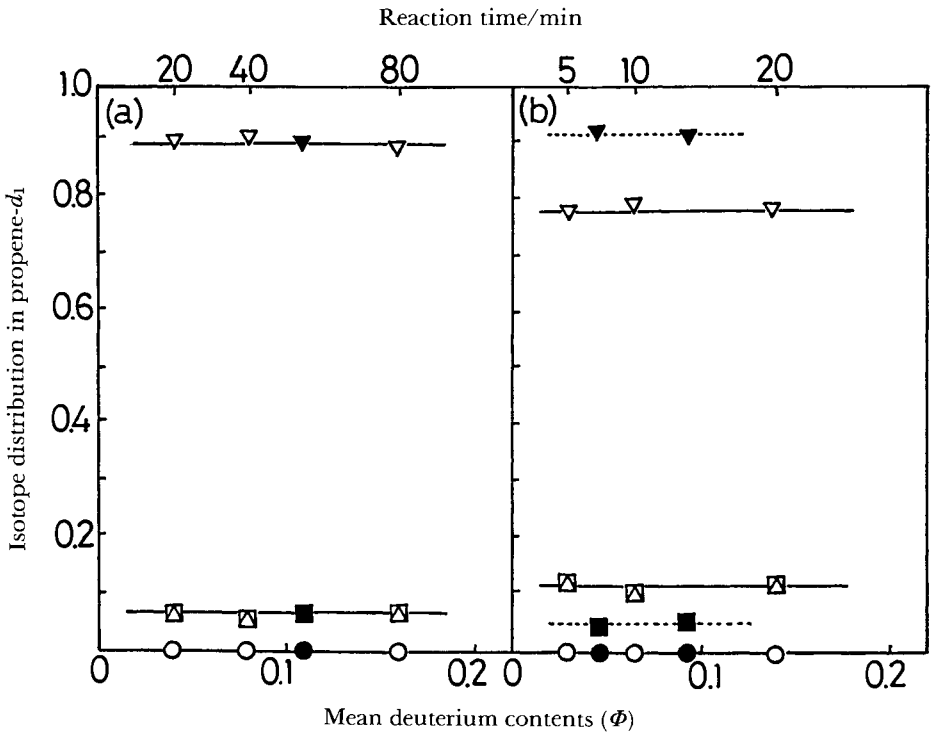

Fig. 7. Time course of the isotopic distribution of monodeuteriopropene during C_3H_6-D_2 reaction over (a) Ni-Cu(0.5) alloy at 190 K, and (b) Ni-Cu(25) alloy at 180 K.
p_{D_2}=6.7 kPa, p_{D_2}=2.0 kPa, Catalyst=1 g. Open symbols: D-surfaces, closed symbols: E-surfaces.
□■: c-1-d_1, △▲: t-1-d_1, ▽▼: 2-d_1, ○●: 3-d_1.

the corresponding E-surfaces. The time-course curves on the E-surface do not differ from those on the D-surfaces in the case of Ni and Ni-Cu(0.5) catalysts, whereas a clear difference can be seen for the Ni-Cu(25) catalyst. Its pattern resembles that on pure Ni metal. Similar results were observed in the cases of Ni-Cu(60) and (90) catalysts.

The results of a microwave spectroscopic analysis of propene-d_2 over D-surfaces of these catalysts are summarized in Table 1. The main d_2-product was propene-1,2-d_2, which can be reasonably explained by a successive reaction in the exchange process; dideuteriopropene may be formed by a repetitive exchange of monodeuteriopropene through σ-alkyl intermediates.

Discussion

It is well known that the surface composition of alloy catalysts is different from the bulk composition.[2,3] In the case of a Ni-Cu alloy, segregation and enrichment of copper on the surface is demonstrated by various methods.[15-21] In the present study, a hydrogen treatment at 773 K realized homogenization of alloys, which was confirmed by their characteristic X-ray diffraction patterns, as described in the experimental section. The surface compositions of alloys were determined by hydrogen chemisorption at room

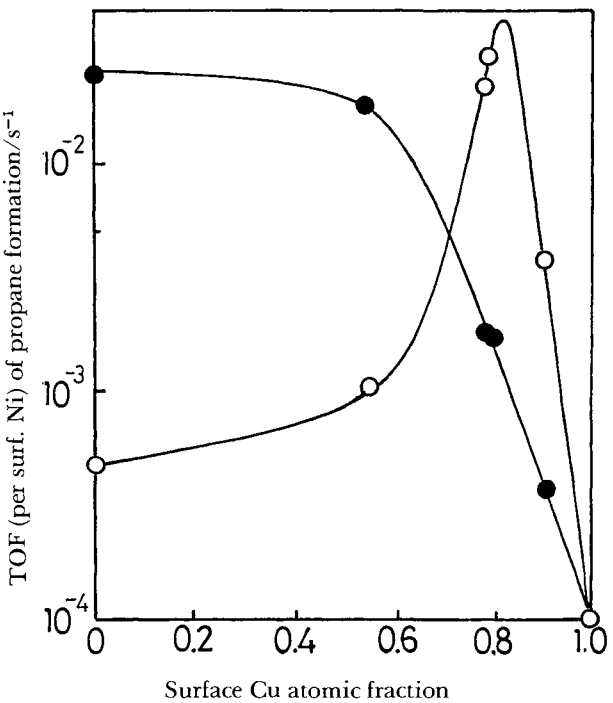

Fig. 8. Dependence of TOF of propane formation at 200 K upon the surface Cu atomic fraction.
○: D-surfaces, ●: E-surfaces:

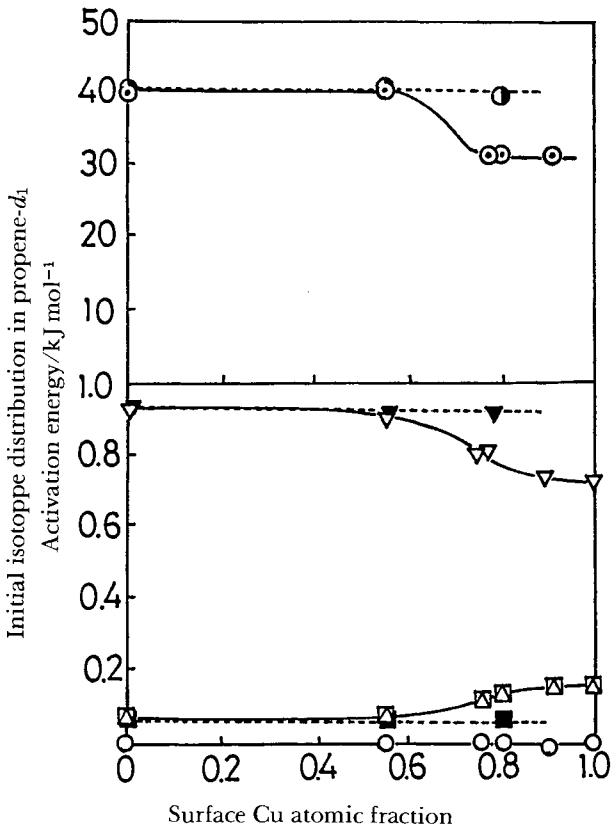

Fig. 9. Dependence of (a) the initial isotopic distribution of monodeuteriopropene and (b) activation energy upon the surface Cu atomic fraction.
Open symbols: D-surfaces, closed symbols: E-surfaces.
□■: c-1-d_1, △▲: t-1-d_1, ▽▼: 2-d_1, ○●: 3-d_1, ⊙◑: Activation energy.

temperature, under the assumption that strong adsorption of hydrogen occurs only on surface nickel atoms. Since adsorption was measured after evacuation at 623 K, the estimated values should correspond to the surface composition of the E-surfaces. It is impossible to determine the surface composition of the D-surfaces by this method. We therefore assumed that the number of surface Ni atoms does not change upon evacuation of hydrogen gas and the surface composition of E-surfaces was used to estimate the TOF over the D-surfaces.

Figure 8 demonstrates the change in the TOF of propane formation (estimated from Figs. 2 and 4) over D- and E-surfaces against surface copper atomic fractions. The catalytic behavior can be divided into two parts, the boundary being at around 60% of surface copper fraction. Over pure Ni and Ni-Cu(0.5) catalysts (nickel-rich alloy catalyst), the activity of the E-surface is much higher than that of the D-surface. The situation is opposite over Ni-Cu(25), (60), and (90) catalysts (copper-rich alloy catalyst); the D-surface is much more active than is the E- surface. Figure 9 summarizes the change in the initial isotope distribution pattern of monodeuteriopropene formed during a C_3H_6-D_2 reaction, as well as the activation energy of propane formation against surface copper atomic fractions. A similar change in the catalytic behavior was observed at around 60% of the surface copper atomic fraction. Over D-surfaces of nickel rich alloy catalysts, the isotopic distribution pattern as well as the activation energy were similar to those of Ni metal, itself. Over D-surfaces of copper-rich alloy catalysts, the distribution pattern considerably changed and became similar to that of Cu metal. On the other hand, over E-surfaces such changes were not observed even in the copper-rich alloy regions, and isotopic distribution pattern as well as activation energy remained similar to those of Ni metal.

The activity decrease over D-surfaces of Ni and Ni-rich alloy catalyst may be explained by an inhibition effect caused by strongly adsorbed hydrogen at lower temperatures. The existence of such strongly adsorbed hydrogen has been observed in TPD experiments of adsorbed hydrogen over a Ni surface.[16,27,28] Three desorption peaks have been reported in the literature, whose maxima are at temperatures β_1=250 K, β_2=329 K and α=370 K.

We also examined the TPD spectra of H_2 on catalysts employed in this study, displayed in Fig. 5(b). Only two peaks were observed, corresponding to β_2 and α, whose peak maxima shifted by about 50 K to higher temperatures than those reported in the literature. Can be seen from the spectra, the amount of strongly adsorbed hydrogen drastically decreased as the surface copper composition increased in the alloy catalysts. By comparing Figs. 5(a) and (b) it was realized that the hydrogen desorption temperature corresponds well to the temperature of steeply increasing catalytic activity. Accordingly, it is reasonable to suppose that α hydrogen may be responsible for the inhibition of hydrogenation of propene at lower temperatures. Because of the lack of this α hydrogen peak, such inhibition does not occur in Cu-rich alloy catalysts. During a C_3H_6-D_2 reaction over the E-surface at lower temperatures, no drastic decrease in the reaction rate was observed, indicating a slow rate of α hydrogen adsorption at low temperatures. Moreover, the results of a pressure-dependence study indicate that the surface was mostly covered by adsorbed propene during the reaction, which also retards the adsorption rate of α hydrogen. However, once the E-surface was exposed to hydrogen at room temperature, the reaction rate at lower temperatures was considerably reduced, which is consistent with the above-mentioned consideration.

Another interesting point regarding these systems is the high activity of the D-surface in the case of Cu-rich alloy catalysts. Hall suggested that the catalytic activity of the surface alloy phase is increased by enrichment with Ni.[29] The present microwave spectroscopic investigation, however, clearly demonstrated that the structure of the reaction intermediate is sim-

ilar to that on Cu metal. Accordingly, the hydrogen treatment effect is not ascribed to surface-enriched Ni alone, but to some novel sites involving both Cu and Ni atoms. Such an effect was really observed only on the Cu-rich alloy surface, where every surface Ni atom might be surrounded by surface Cu atoms. A marked decrease in the activity over the E-surface suggests that evacuation at higher temperatures causes a reconstruction of the pertinent surface structure.

References

1) J. H. Sinfelt, *Acc. Chem. Res.*, **10**, 15 (1977).
2) V. Ponec, *Catal. Res. Sci. Eng.*, **11**, 41 (1975).
3) W. M. H. Sachtler and R. A. Van Santen, "Adv. in Catalysis," Academic Press, New York (1977), Vol. 26, p. 69.
4) V. Ponec and W. M. H. Sachtler, *J. Catal.*, **24**, 250 (1977).
5) J. M. Beelen, V. Ponec, and W. M. H. Sachtler, *J. Catal.*, **28**, 376 (1973).
6) A. Roberti, V. Ponec, and W. M. H. Sachtler, *J. Catal.*, **28**, 381 (1973).
7) R. J. Best and W. W. Russell, *J. Am. Chem. Soc.*, **76**, 838 (1954).
8) W. K. Hall and P. H. Emmett, *J. Phys. Chem.*, **63**, 1102 (1959).
9) M. K. Gharpurey and P. H. Emmett, *J. Phys. Chem.*, **65**, 1182 (1961).
10)) W. K. Hall and J. A. Hassell, *J. Phys. Chem.*, **67**, 636 (1963)
11) J. S. Campbell and P. H. Emmett, *J. Catal.*, **7**, 252 (1967).
12) T. Takeuchi, Y. Tezuka, and O. Takayasu, *J. Catal.*, **14**, 126 (1969).
13) H. C. De Jongste and V. Ponec, *J. Catal.*, **63**, 389 (1980).
14) E. M. Silverman and R. J. Madix, *J. Catal.*, **56**, 349 (1979).
15) E. Iglesia and M. Boudart, *J. Catal.*, **81**, 204 (1983).
16) M. I. Chen, C. T. Cheng, and C. T. Yen, *J. Catal.*, **95**, 346 (1985).
17) W. M. H. Sachtler and G. J. H. Dorgelo, *J. Catal.*, **4**, 654 (1975)
18) W. M. H. Sachtler and R. Jongepier, *J. Catal.*, **4**, 665 (1965)
19) P. E. C. Franken and V. Ponec, *J. Catal.*, **42**, 398 (1976).
20) Y. Takasu and H. Shimizu, *J. Catal.*, **42**, 479 (1973).
21) C. R. Helms, *J. Catal.*, **36**, 114 (1975).
22) S. Naito and M. Tanimoto, *J. Catal.*, **102**, 377 (1986).
23) S. Naito and M. Tanimoto, *J. Chem. Soc., Faraday Trans. 1*, **83**, 2475 (1987).
24) S. Naito and M. Tanimoto, *J. Catal.*, **119**, 300 (1989).
25) J. Turkevich, F. Bonner, D. O. Schissler, and P. Irsa, *Discuss. Faraday Soc.*, **8**, 352 (1950).
26) T. Keii, *J. Chem. Phys.*, **22**, 144 (1954).
27) K. Y. Yu, D. T. Ling, and W. E. Spicer, *J. Catal.*, **44**, 373 (1976).
28) E. M. Silverman, R. J. Madix, and P. Delreu, *Surf. Sci.*, **109**, 127 (1981).
29) W. K. Hall, *J. Catal.*, **6**, 314 (1966).

Application of the SPE Method to Organic Electrochemistry. XII. Lead Dioxide as a Mediator for Electrooxidation of Cinnamyl Alcohol on Pt-Nafion

Zhen CHEN, Zempachi OGUMI,* and Zen-ichiro TAKEHARA
Department of Industrial Chemistry, Faculty of Engineering, Kyoto University, Sakyo-ku, Kyoto 606
(Received October 8, 1990)

Lead dioxide was examined as a mediator to oxidize cinnamyl alcohol on Pt-Nafion, and was compared with manganese dioxide. Lead dioxide was deposited into Pt-Nafion. The current efficiency for the formation of cinnamaldehyde reached 65% at room temperature, slightly lower than that in the case of using manganese dioxide. The production of cinnamic acid was more remarkable on Pb,Pt-Nafion than on Mn,Pt-Nafion because of the higher oxidation potential of the former. The mediatory action of both oxides was examined and compared with the activity in chemical oxidation using oxides produced separately. The oxidation of cinnamyl alcohol by lead dioxide was faster than that by manganese dioxide. Their mediatory action reflected their chemical activity for the oxidation.

Due to an inherently high oxidation potential[1,2] of the hydroxyl group, a variety of indirect procedures utilizing appropriate organic and inorganic chemicals as mediators have been devised for oxidizing the group.[3-6] We have reported in previous papers[7,8] that in a system comprising solid polymer electrolyte (SPE) electrolyzers, with Nafion as an SPE material, manganese dioxide deposited into Pt-Nafion behaves as a mediator and enhances the reaction selectivity of alcohol to the corresponding aldehyde.

As known, PbO_2 is widely used in practical rechargeable lead-acid batteries due to its high electrochemical reversibility and high oxidation potential under acidic conditions. These properties are attractive for use as an oxidizing reagent of organic substances. In the present study lead dioxide was focused as a mediator for indirect oxidation of cinnamyl alcohol using an SPE composite electrode prepared by depositing a porous platinum layer on Nafion, Pt-Nafion.[9] It was reported in our previous papers that Mn, Pt-Nafion prepared by incorporating manganese dioxide into Pt-Nafion as a mediator behaved as a good electrode for the selective oxidation of cinnamyl alcohol to cinnamaldehyde, while leaving C=C unchanged.[7] The activity and reaction selectivity of Pb,Pt-Nafion were compared with Mn,Pt-Nafion.

Since the oxidation of cinnamyl alcohol by a metal-oxide mediatory system involves an irreversible catalytic reaction following a reversible charge-transfer reaction producing reactive oxides on the anode, the chemical reactions between oxides (PbO_2 and MnO_2) and cinnamyl alcohol were also investigated in order to improve our understanding of the reaction systems.

Experimental

Electrochemical Oxidation. Pt-Nafion composite electrodes were prepared by an electroless deposition of a porous platinum layer on Nafion 417.[9] After platinum deposition, the Pt-Nafion was immersed in 1 mol dm^{-3} H_2SO_4 for more than 2 h in order to exchange the counter ion for H^+. This H^+-type Pt-Nafion was then immersed in a 0.5 mol dm^{-3} $Pb(NO_3)_2$ aqueous solution for more than 8 h in order to incorporate Pb^{2+} into Pt-Nafion. An electrolytic cell equipped with Pb,Pt-Nafion was described previously.[7] The effective geometric surface area of the anode was found to be 3.14 cm^2. The volumes of the working electrode (anodic) and the counter electrode (cathodic) compartments (WEC and CEC) were 6.5 cm^3 and 16 cm^3, respectively. The electrode potential was set vs. the Ag/AgCl reference electrode via a Luggin capillary inserted in a CEC using a potentio/galvanostat (Hokuto Denko HA-301). In all cases, the set potential was not corrected for both the junction potential at the interface between Nafion and the contacting solution and a fairly large ohmic drop through the Nafion.

Tetrahydrofuran (THF) was selected as a solvent. The concentration of cinnamyl alcohol was fixed at 50 vol% in THF. In order to suppress any dissolving out of Pb^{2+} into a CEC from Pt-Nafion, 0.05 mol dm^{-3} $Pb(NO_3)_2$ was added to a CEC containing 0.05 mol dm^{-3} HNO_3 during electrolysis.

Electrolysis was carried out using a conventional potentio/galvanostatic electrolysis set-up at 25 °C, except for those cases specified. The experimental details were identical to those described in a previous paper.[10]

Chemical Reactions. Electrolytic manganese dioxide (EMD) was donated by Mitsui Mining and Smelting Co., Ltd. Because of the low chemical activity of commercially available lead dioxide, freshly prepared lead dioxide was utilized for chemical reactions.[11] The fresh, active lead dioxide was prepared by decomposition of lead tetraacetate.[12] Then, 50 g of lead tetraacetate was added to 500 cm^3 of water under stirring. It decomposed to brown lead dioxide precipitates. The crude lead dioxide was washed with 100 cm^3 of water 4 times and filtered under suction, followed by washing with 50 cm^3 of acetone 4 times. The yield of a dark-brown powder of lead dioxide was about 20 g. Cinnamyl alcohol (0.2 g) was stirred with a suspension of excess amount of EMD (0.5 g) or PbO_2 (2 g) in acetone (50 cm^3) or in acetone (50 cm^3) containing 0.4 mol dm^{-3} sulfuric acid and 4% water at a fixed temperature.

Analysis. The products were analyzed by an HPLC device (Hitachi 638-30) equipped with a Synchropak SCD 100 column. 4-Nitrotoluene was selected as an internal

standard.

Results and Discussion

Electrochemical Behaviors of Pb,Pt-Nafion. In order to examine the electrochemical behaviors of a lead redox couple in Pt-Nafion, cyclic voltammetry measurements were conducted. The cyclic voltammogram on Pb,Pt-Nafion in 0.05 mol dm^{-3} HNO_3 in a CEC (curve a of Fig. 1) was compared with that on Mn,Pt-Nafion in 0.025 mol dm^{-3} H_2SO_4 in a CEC (curve b of Fig.1). Ar gas was filled in a WEC in both cases. An anodic plateau (E_{ap}=1.42 V) and a cathodic peak (E_{cp}=1.22 V) appear on curve a. The peak separation was fairly large (200 mV) because of an uncorrected ohmic drop caused by the low conductivity of Nafion. This peak and plateau correspond to a reduction and oxidation of the lead redox couple. Oxygen evolution began at a potential close to lead dioxide formation (E>1.50V), according to curve a. Although the deposition of lead dioxide on Pt-Nafion enhanced the oxygen overvoltage, this enhancement was not as large as was expected. On the other hand, Mn,Pt-Nafion gave a better-defined cyclic voltammogram, although the peak separation was still large. Pb,Pt-Nafion gave higher redox peaks, by about 200 mV, than Mn,Pt-Nafion, as was expected from their standard redox potentials reported (1.45 V and 1.23 V vs. NHE, respectively).

Figure 2 shows anodic polarization curves under quasi-steady state conditions for Pb,Pt-Nafion (curve a,c), which were compared with those for Mn,Pt-Nafion (curve b,d). The electrode potentials for Pb,Pt-Nafion were higher than those for Mn,Pt-Nafion in two systems: with (curve a,b) and without (curve c,d) cinnamyl alcohol in a WEC. Even in the presence of alcohol, the potentials of both electrodes were kept low at current densities lower than 2 mA cm^{-2}. This was ascribed to the proceeding of mediatory oxidation processes on both electrodes: the primary electrode reaction involved the oxidation of two metal ions regenerated by reactions of the metal oxides with the alcohol in a low-current density region.

$$Pb^{2+} + 2H_2O = PbO_2 + 4H^+ + 2e^- \quad 1.45 \text{ V vs. NHE} \quad (1)$$

$$Mn^{2+} + 2H_2O = MnO_2 + 4H^+ + 2e^- \quad 1.23 \text{ V vs. NHE} \quad (2)$$

$$C_6H_5CH{=}CHCH_2OH + MO_2 + 2H^+ =$$

$$\text{(acidic)} \quad C_6H_5CH{=}CHCHO + M^2 + 2H_2O \quad (3)$$

$$C_6H_5CH{=}CHCH_2OH + MO_2 =$$

$$\text{(neutral or basic)} \quad C_6H_5CH{=}CHCHO + M(OH)_2 \quad (4)$$

(M=Pb or Mn)

On the other hand, when electrolytic current density exceeded 2 mA cm^{-2}, the anodic potential gradually shifted to the positive direction and reached the value for oxygen evolution on both electrodes. Gas evolution was observed on both electrodes at high current densities. The potential for oxygen evolution was higher on both electrodes in the presence of alcohol (a,b) than in its absence (c,d). This might be caused by a poisoning of the electrodes by by-products from the substrate or solvents which were not detected, though, in HPLC analysis. The by-products might decrease the ionic conductivity of Nafion and enhance the uncorrected ohmic drop. This poisoning was also suggested by a potential change during electrolysis. As shown in Fig. 3, the anode potential of Pb,Pt-Nafion gradually increased, even at a current density

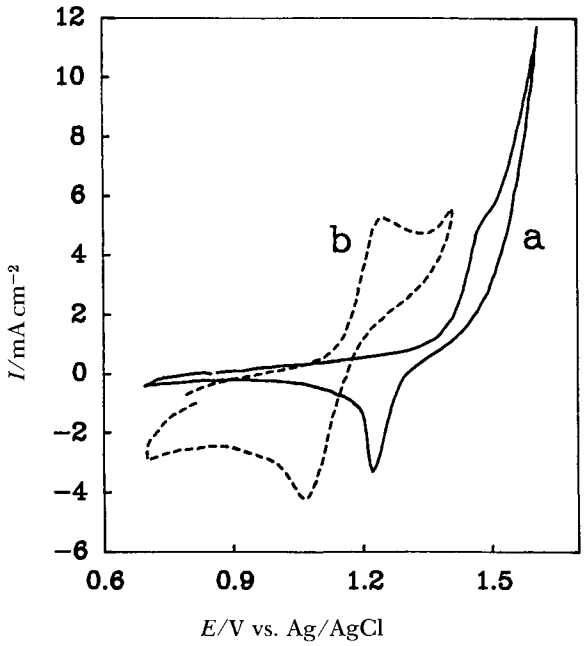

Fig. 1. Cyclic voltammograms (a); on Pb,Pt-Nafion, 0.05 mol dm^{-3} HNO_3 in CEC, (b); on Mn,Pt-Nafion, 0.025 mol dm^{-3} H_2SO_4 in CEC, W.E.C: Ar, at 10 mV s^{-1}.

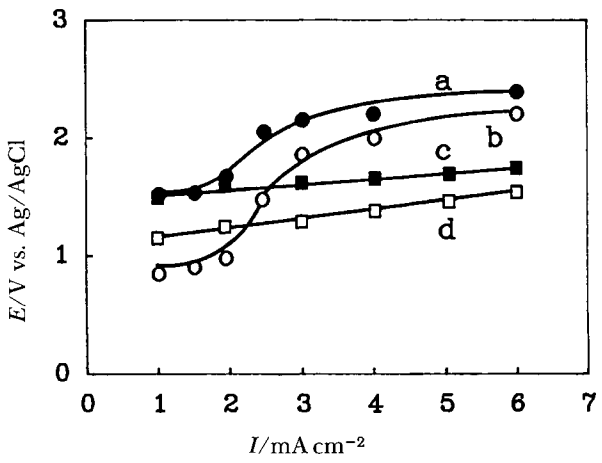

Fig. 2. Steady state polarization curves on Pb,Pt-Nafion (a, c) and Mn,Pt-Nafion (b, d).
Solutions in CEC were the same as in Fig. 1.
a, b: cinnamyl alcohol 50% in THF in WEC. c, d: Ar in WEC.

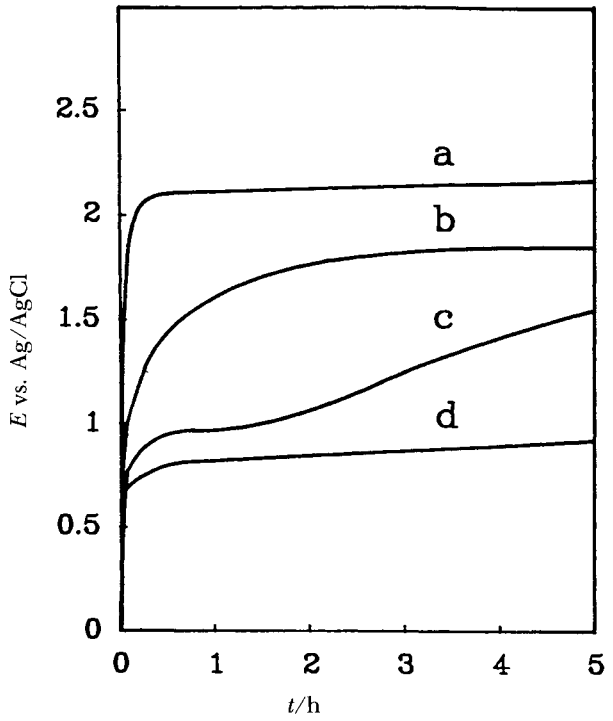

Fig. 3. Potential changes during electrolysis on Pb,Pt-Nafion under galvanostatic electrolysis conditions in cinnamyl alcohol 50% in THF in WEC at 25 °C.
a: 4, b: 3, c: 2, d: 1 mA cm^{-2}.

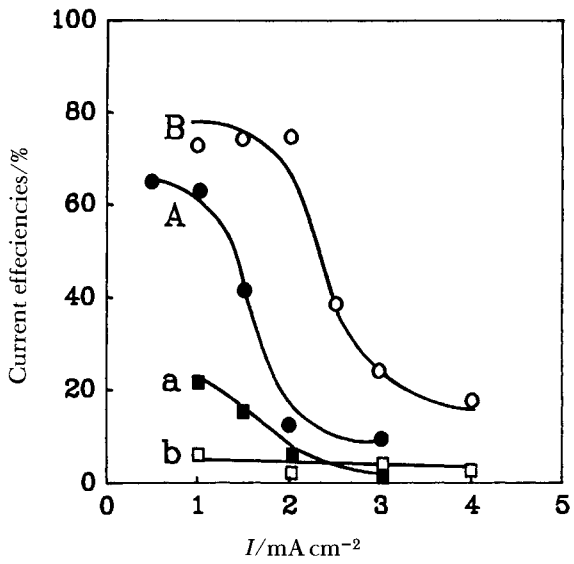

Fig. 4. Current efficiencies of cinnamaldehyde (A, B) and cinnamic acid (a, b) under galvanostatic electrolysis conditions in cinnamyl alcohol 50% in THF in WEC on Mn,Pt-Nafion (B, b) and Pb,Pt-Nafion (A, a).

as low as 2 mA cm^{-2}, and reached the potential necessary for oxygen evolution, although its change was very slow at a very low current density of 1 mA cm^{-2}. A similar potential change was also observed for Mn,Pt-Nafion. In addition to the above-mentioned reasons, it was reported that the ionic conductivity of Nafion was remarkably decreased in some organic solvents.[13]

Galvanostatic Oxidation of Cinnamyl Alcohol. As reported in a previous paper,[7] the reaction selectivity for aldehyde formation was remarkably enhanced by the incorporation of a manganese redox couple into Pt-Nafion. The current efficiency of the oxidation of cinnamyl alcohol using Pb,Pt-Nafion was examined under galvanostatic electrolysis conditions. The results are given in Fig. 4 (curves A and a), together with the results using Mn,Pt-Nafion (curves B and b). At low current densities, cinnamaldehyde was produced in high current efficiency (A), which, however, slightly lower than that on Mn,Pt-Nafion (B). On the other hand, the efficiency of cinnamic acid production on Pb,Pt-Nafion (a) was higher at low current densities than that on Mn,Pt-Nafion (b). On both composite electrodes the current efficiency for aldehyde formation decreased upon increasing the current density, although the decrease began at a lower current density on Pb,Pt-Nafion (A) than that on Mn,Pt-Nafion (B). On the former electrode acid production reached 20% at a low current density and then decreased with an increase in the current density; however, it was low, and almost unchanged, on the latter electrode. The rapid decrease in the current efficiencies on the former should be ascribed to easier oxygen evolution since the potential of oxygen evolution was closer to that of lead dioxide formation than on the latter electrode (Fig. 1). The higher efficiency of acid formation on Pb,Pt-Nafion than that on Mn,Pt-Nafion should be ascribed to the more positive potential of lead dioxide (ca. 200 mV) than that of manganese dioxide.

Since no organic by-product was detected on HPLC and gas chromatography analyses, only oxygen evolution was considered to exist as a side reaction.

Oxidation was also affected by the electrolysis temperature. As shown in Fig. 5, the current efficiencies of aldehyde formation increased upon increasing the temperature on both Mn,Pt-Nafion and Pb,Pt-Nafion at 1.5 mA cm^{-2}. At high temperature the reaction between mediator oxides and the alcohol became faster and the mediatory reaction proceeded more smoothly. Thus, the current efficiency of aldehyde formation increased on both electrodes upon increasing the temperature. The current efficiency of cinnamic acid formation increased on Pb,Pt-Nafion with a temperature increase, whereas on Mn,Pt-Nafion it remained almost unchanged with a temperature change, while maintaining a low value. This result suggests that a high potential is necessary for the oxidation of the alcohol to the corresponding acid, and that the potential of MnO_2 was not sufficiently high to oxidize the alcohol to acid. N.L. Weinberg

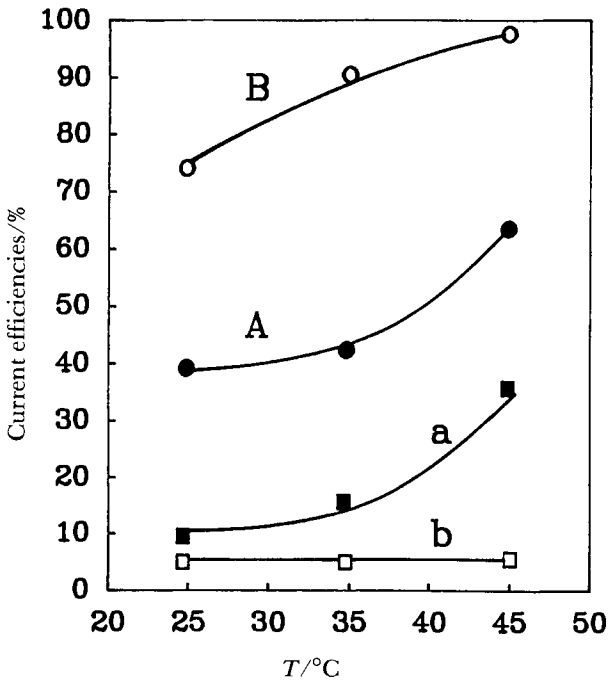

Fig. 5. Dependencies of current efficiencies on electrolysis temperature at 1.5 mA cm^{-2}. Mediator: PbO_2 (A and a), MnO_2 (B and b). Cinnamaldehyde (A and B), cinnamic acid (a and b).

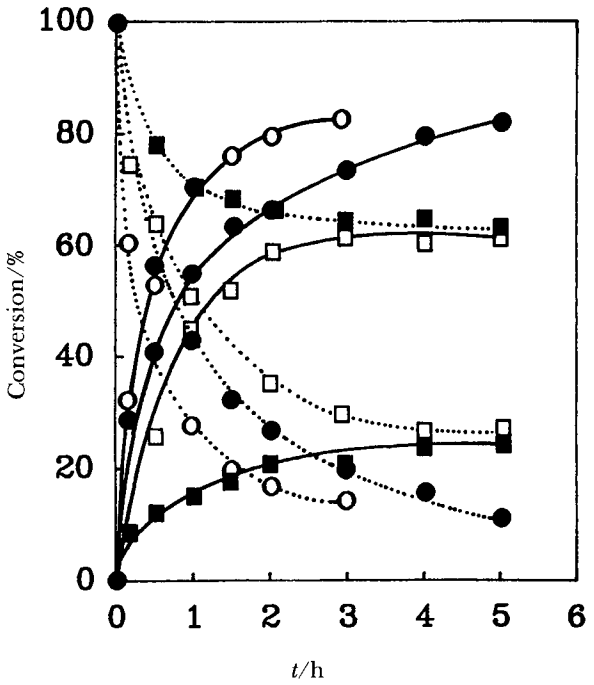

Fig. 6. Oxidation of cinnamyl alcohol by MnO_2 in neat THF (○), acetone (●), benzene (□), and acetic acid (■) at 22 °C. (——): cinnamaldehyde, (------): remaining cinnamyl alcohol.

reported that the half-wave potential for the oxidation of cinnamyl alcohol to cinnamaldehyde was 1.36 V, and that of cinnamaldehyde to cinnamic acid 1.77 V (vs. Ag/0.1 mol dm^{-3} Ag^+) in a CH_3CN-$NaClO_4$ solution system.[1,2] The potential difference between two oxidation steps is about 0.4 V. The above-mentioned potential values can not be directly compared with those in the present system since the electrodes, solvents, and reference electrodes are different. However, judging from the results described above, MnO_2 can oxidize the cinnamyl alcohol to cinnamaldehyde, but can not do so to cinnamic acid. On the other hand, the oxidation potential of PbO_2 is more positive by ca. 0.2 V than that of MnO_2, and it is sufficiently high to oxidize the alcohol to acid.

Chemical Reactions. The electrochemical oxidation of cinnamyl alcohol proceeds via consecutive reactions: electrochemical formation of oxides (Eqs. 1 and 2) is followed by their reaction with alcohol (Eqs. 3 and 4). It is not clear yet which of the reaction steps is rate-determining. We have examined the activation energy of anodic oxidation using Mn,Pt-Nafion. The value was 12.1 kcal mol^{-1}, higher than the value for the anodic formation of MnO_2 from Mn^{2+} on Pt (9.2 kcal mol^{-1}).[14] This result suggests that the reaction step of Eq. 3 or 4 is slower than the electrode reaction and following chemical reactions seem to be important in the mediatory systems. From this point of view, the chemical reactions of the oxides with cinnamyl alcohol were examined.

For electrochemical systems, THF was selected as a solvent, which was stable and did not remarkably swell Nafion. Some solvents were examined for possible use as a solvent for the chemical oxidation of cinnamyl alcohol by MnO_2. As shown in Fig. 6, THF gave the highest oxidation rate among the solvents examined. In all cases using neat solvents, no other product beside cinnamaldehyde was detected during HPLC analysis, while in electrochemical reaction systems acetone gave some unidentified by-products together with cinnamic acid. Since the reaction rate in THF was too high to examine the reaction in detail, acetone was selected as a solvent for the chemical oxidation.

The oxidation of cinnamyl alcohol by PbO_2 was examined in neat acetone. As shown in Fig. 7, the oxidation rate was faster than that by MnO_2. While only a trace amount of cinnamic acid was formed at 25 °C, a significant amount of the acid was formed at 40 °C.

The influence of the water content and acidity is easily inferred from Eqs. 1 to 4.[8] The influence of the water content on the oxidation is exhibited in Fig. 8. The reaction rate decreased with an increase in the water content, since the oxidation potential decreased with increasing water content, as can be expected from Eqs. 1 and 2. In the presence of water cinnamic acid was formed.

$$C_6H_5CH{=}CHCHO + MnO_2 + H_2O = C_6H_5CH{=}CHCOOH + Mn(OH)_2 \quad (5)$$

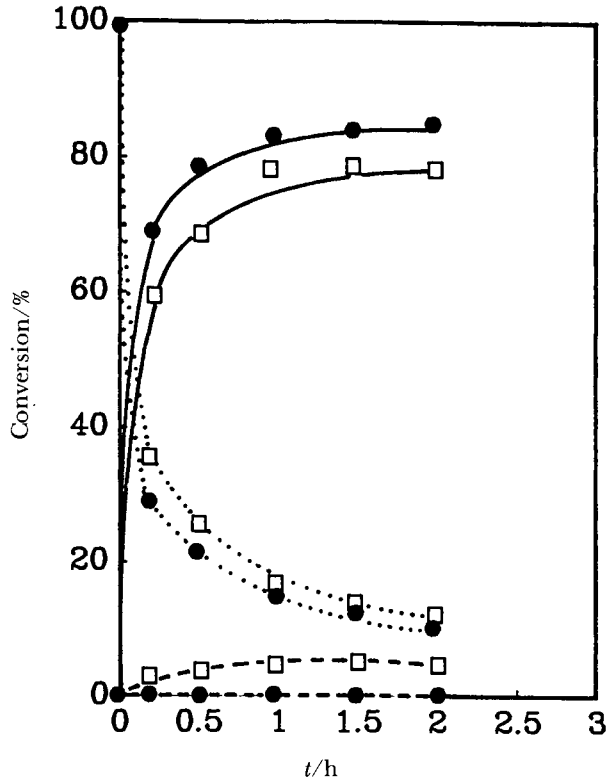

Fig. 7. Oxidation of cinnamyl alcohol by PbO_2 in neat acetone at 25 °C (●) and 40 °C (□). (——): cinnamaldehyde, (----): cinnamic acid, (.....): remaining cinnamyl alcohol.

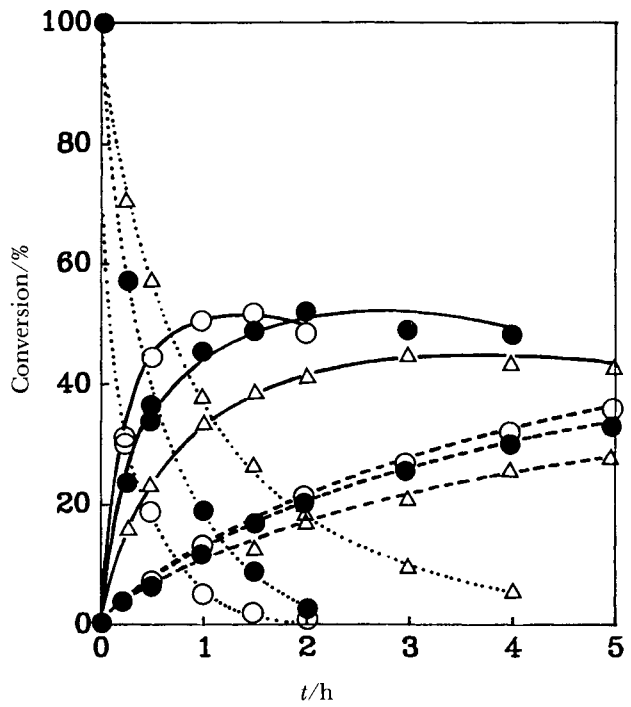

Fig. 8. Influence of water content in acetone on the oxidation of cinnamyl alcohol by MnO_2 at 22 °C. (.....): remaining alcohol, (——): cinnamaldehyde, (----): cinnamic acid. Water content: ○: 4%, ●: 6%, △: 8%.

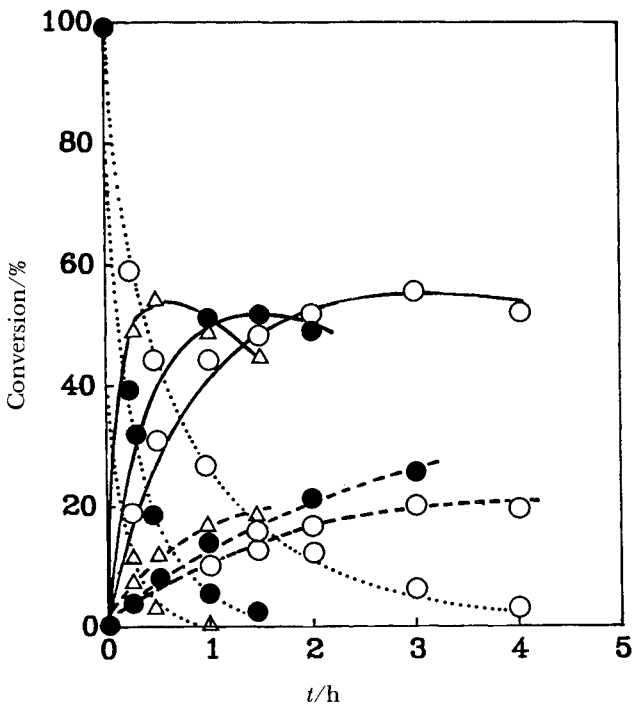

Fig. 9. Dependencies of conversion on sulfuric acidic concentration in acetone containing 4% of water by MnO_2 at 22 °C. (.....): remaining alcohol, (——): cinnamaldehyde, (----): cinnamic acid. H_2SO_4 (mol dm^{-3}), △: 0.65, ●: 0.43, ○: 0.22.

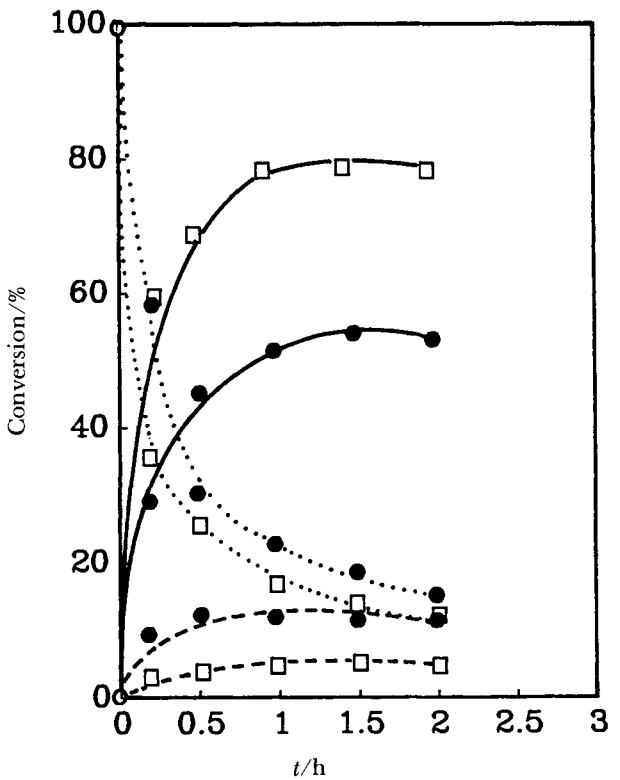

Fig. 10. Reactions of cinnamyl alcohol with PbO_2 at 40 °C in acetone containing 4% water and 0.43 mol dm^{-3} H_2SO_4 (●) and in neat acetone (□). (.....): remaining alcohol, (——): cinnamaldehyde, (----): cinnamic acid.

In the absence of water the aldehyde can not be oxidized by MnO_2. The decrease in acid formation upon increasing the water content can also be ascribed to a decrease in the oxidation potential. These results suggest the existence of an optimum water content.

An increase in the sulfuric acid concentration at a fixed water content of 4% increased the reaction rate as well as acid formation, as shown in Fig. 9. It is easily deduced from Eqs. 1 and 2 that an increase in acidity enhances the oxidation potential of MnO_2, and that this high oxidation potential enhances the reaction rate and acid formation.

Similar influences of the acid concentration were observed in the oxidation of cinnamyl alcohol by PbO_2. As is shown in Fig. 10, its oxidation rate was increased by the addition of sulfuric acid. However, this increase was due to its oxidation to cinnamic acid, and even a slight decrease in the current efficiency of the aldehyde formation was observed. Thereafter, the reaction selectivity to the aldehyde was decreased.

An increase in the acid concentration also accelerates the reaction rate of Eq. 3. The increased oxidation potential of oxides with an increase in a solution acidity, as well as the increased oxidation rate of Eq. 3, additively enhance the oxidation rate, though the contribution from the former seems to be larger at the low acid concentration examined here than that from the latter.

As expected, the increase in the reaction temperature enhanced the reaction rate of both aldehyde and acid formation, as shown in Fig. 11.

Figure 12 shows the difference between MnO_2 and PbO_2 in acetone at 40 °C. PbO_2 gave a greater oxidation rate than did MnO_2. Although cinnamic acid was not formed using MnO_2 (Fig. 6), it was formed using PbO_2. The higher oxidation potential of PbO_2 than MnO_2 explains the results.

It is not easy to determine the conditions surrounding an active site of Pt-Nafion, since Nafion is a strong acid-type cation-exchange membrane and its acidity is considered to correspond to 1—3 mol dm^{-3} H_2SO_4 under aqueous conditions. At the reaction site for the present mediatory electrochemical oxidation, a solvent, THF, is mixed with water, both of which exist in WEC and CEC, respectively. This mixing makes substrate transportation to the reaction site easy.[8] Although the acidity might be decreased by mixing, it may be considered that the reaction site on Pt-Nafion is an aqueous mixture and is fairly acidic. Under these conditions oxidation of the alcohol by two oxides must be rapid enough to supply M^{2+} ions to the electrode by the regeneration reaction (Eq. 3). The critical current density, above which the regeneration rate of Mn^{2+} can not follow up its consumption by a charge-transfer reaction on the anode, was about 2 mA cm^{-2}; this value was dependent on many factors, such as deposition conditions of platinum, the amount of metal oxide incorporated into Pt-

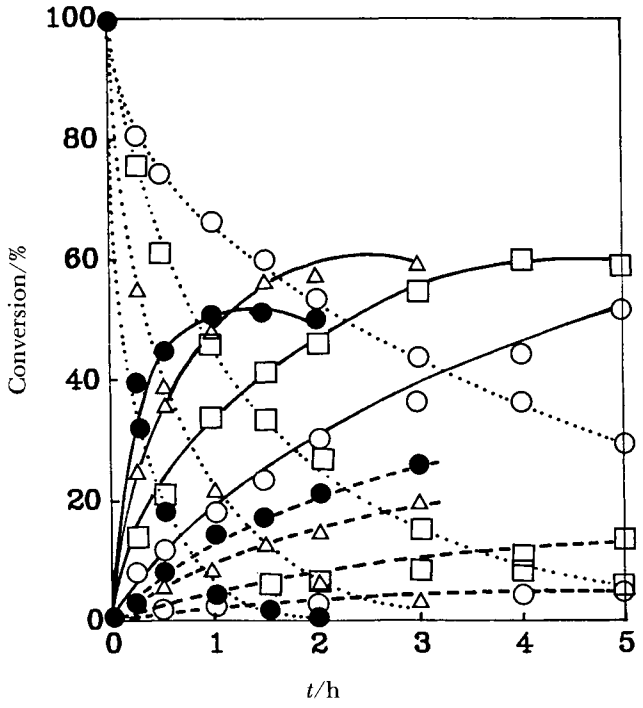

Fig. 11. Influence of temperature on conversion in acetone containing 4% water and 0.43 mol dm^{-3} H_2SO_4 by MnO_2.
(·····): remaining alcohol, (——): cinnamaldehyde, (----): cinnamic acid formation.
Temperature (°C): ○: 10, □: 20, △: 30, ●: 40.

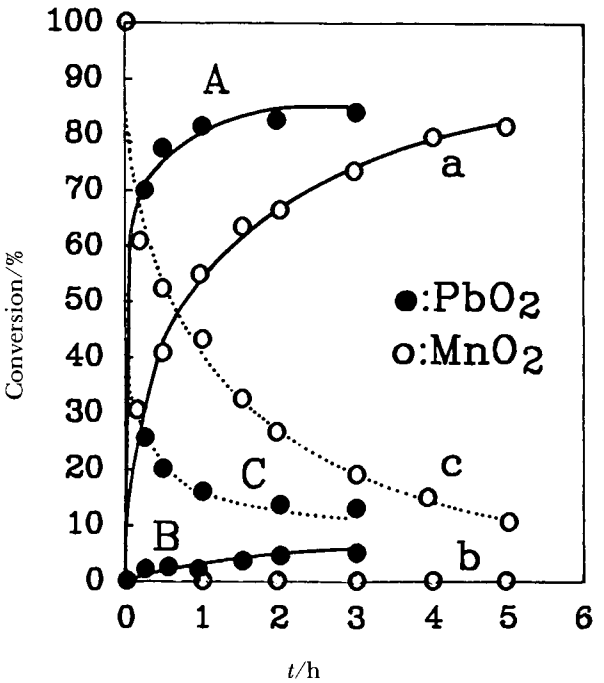

Fig. 12. Oxidation of cinnamyl alcohol in neat acetone by PbO_2 (A, B, C) and MnO_2 (a, b, c) at 40 °C.
A and a: cinnamaldehyde, B and b: cinnamic acid, C and c: remaining cinnamyl alcohol.

Nafion, solvent composition, and temperature.

The results obtained for the mediatory electrochemical oxidation, that cinnamic acid production is more remarkable on Pb,Pt-Nafion than that on Mn,Pt-Nafion, were coincident with the results obtained through chemical oxidation.

References

1) N. L. Weinberg, "Technique of Electroorganic Synthesis," ed by N.L. Weinberg, John Wiley, New York (1974), Part II, pp. 733.

2) H. Lund, *Acta Chem. Scand.*, **11**, 491 (1957).

3) T. Shono, Y. Matsumura, J. Hayashi, and M. Mizoguchi, *Tetrahedron Lett.*, **2**, 1658 (1979).

4) S. Torii, T. Inokuchi, and T. Sugiura, *J. Org. Chem.*, **51**, 161 (1986).

5) T. Shono, Y. Matsumura, M. Mizoguchi, and J. Hayashi, *Tetrahedron Lett.*, **40**, 3861 (1979).

6) T. Shono, Y. Matsumura, J. Hayashi, and M. Mizoguchi, *Tetrahedron Lett.*, **21**, 1867 (1980).

7) Z. Ogumi, T. Mizoe, Z. Chen, and Z. Takehara, *Bull. Chem. Soc. Jpn.*, **63**, 3365 (1990).

8) Z. Chen, Z. Ogumi, T. Mizoe, and Z. Takehara, *Bull. Chem. Soc. Jpn.*, **64**, 537 (1991).

9) Z. Ogumi and Z. Takehara, *Denki Kagaku*, **52**, 70 (1984).

10) Z. Ogumi, H. Yamashita, K. Nishio, Z. Takehara, and S. Yoshizawa, *Denki Kagaku*, **52**, 180 (1984).

11) R. Adams and R.A. Wankel, *J. Am. Chem. Soc.*, **73**, 2219 (1951).

12) R. Kuhn and I. Hammer, *Chem. Ber.*, **83**, 413 (1950).

13) R. S. Yeo and H. L. Yeager, "Modern Aspect of Electrochemistry," ed by B. E. Conway, R. E. White, and J. O'M. Bockris, Plenum, New York (1985), Vol. 16, pp. 437.

14) M. Sugimori and T. Sekine, *Denki Kagaku*, **37**, 63 (1969).

Photokilling of Malignant Cells with Ultrafine TiO_2 Powder

Ruxiong CAI, Kazuhito HASHIMOTO, Kiminori ITOH,† Yoshinobu KUBOTA,†† and Akira FUJISHIMA*
Department of Synthetic Chemistry, The University of Tokyo, Hongo, Bunkyo-ku, Tokyo 113
†Institute of Environmental Science and Technology, Yokohama National University, Tokiwadai, Hodogaya-ku, Yokohama 240
††Faculty of Medicine, Yokohama City University, Fukuura, Kanazawa-ku, Yokohama 236
(Received October 18, 1990)

Photo-irradiated TiO_2 particles drive various chemical reactions due to their strong oxidation and reduction ability. This effect is applied in order to kill malignant HeLa cells with TiO_2 particles. During 10-min UV irradiation periods, HeLa cells were completely killed in the presence of TiO_2 (100 $\mu g\,cm^{-3}$). However, without irradiation these particles showed little cytotoxicity up to 360 $\mu g\,cm^{-3}$. It is concluded that the cells were killed by hydroxyl ($OH\cdot$) and perhydroxyl ($HO_2\cdot$) radicals produced from water by the irradiated TiO_2 particles, and also that the cells were directly oxidized by photogenerated holes in TiO_2. The distribution of TiO_2 powders in the cells was observed using a transmission electron microscope. The TiO_2 powder existed not only on the cell membrane, but also in the cytoplasm. Thus, the cells were damaged by photoexcited TiO_2 not only from the cell membrane, but also from the inside of cytoplasm. Finally, the application of this malignant cell photokilling effect to photodynamic therapy is discussed.

When a TiO_2 semiconductor absorbs light with energy greater than its band gap, electrons in the valence band are excited to the conduction band, creating electron-hole pairs and causing various chemical reactions. Photochemical reactions using TiO_2 powders are therefore being studied for solar energy conversion applications,[1-2] and photo-organic synthesis research,[3-5] Few studies, however, have investigated biochemical reactions using the semiconductor photoeffect. Matsunaga et al. reported the photocatalytic sterilization using TiO_2 powder. In their system, microbial (*Escherichia coli*) cells were killed by photocatalytic reaction.[6] The present study proposes applying heterogeneous photocatalysis with TiO_2 dispersion to a biochemical reaction in order to "photo-kill" cancer cells.

It was previously reported that HeLa cells could be photoelectrochemically killed on a TiO_2 electrode.[7] In this system, HeLa cells were cultured on TiO_2 electrode surface, and the electrode was anodically polarized under UV-irradiation. Photoexcited TiO_2 anode has a strong oxidation power, so that the cells on the electrode are damaged from the cell membrane.

Instead of using an electrode, the present study uses small TiO_2 particles which function as a "short-circuit," photoelectrochemical cell. In this "particulate system," both photogenerated electrons and holes reach the surface, thus oxidation and reduction are induced on the surface. Additionally these particulate suspensions yield a large interfacial surface area in small volumes. The ability of a photochemical reaction using particulate TiO_2 becomes higher when the size of particles becomes smaller,[8] allowing the particles to be easily incorporated into the cells. Therefore this method is easier to apply than the electrode method. The effects of small photoexcited TiO_2 particles on cells is an attractive investigation area because it is expected that the small particles are incorporated inside the cell, and the particulate reaction with the cellular components can more effectively proceed as compared to the electrode method.

In the present study, the cytotoxicity of ultrafine TiO_2 powder and the effect of photoexcited TiO_2 particles on malignant cells were investigated. Distribution of TiO_2 particles in the cells was also examined with a transmission electron microscope (TEM), and a cyclic voltammogram technique was applied to get electrochemical information. The possibility to apply this photocatalytic reaction to photodynamic therapy is also discussed.

Materials and Methods

TiO_2 Powder: TiO_2 particles (anatase, p-25; Nippon-Aerosil Co., Tokyo, Japan) with an average size of 300 Å in diameter were used. The particles were ultra-sonically dispersed in water, then sterilized using autoclave. During sterilization the TiO_2 particles aggregated and could not be sonically dispersed, thus they were removed by centrifugation, and the small aggregates were then collected. The average size of TiO_2 aggregates in the suspension, observed by a scannig electron microscope (SEM) [JSM-840, JEOL., Tokyo, Japan], depended on the centrifugal acceleration, with the TiO_2 suspension quantity being measured with combustion analysis. The optimum acceleration was chosen to be 1600×g in the present experiment. This will be discussed later. A minimum essential medium (MEM, Gibco) solution (5×MEM) and 10% fetal bovine serum were added to the ultrafine TiO_2 aqueous suspension to prepare a MEM solution containing TiO_2 (MEM-TiO_2 solution), which was used to investigate both the photokilling ability (with irradiation) and the cytotoxicity (no irradiation) of HeLa cells.

Cell Lines and Antitumor Activity of the TiO_2 Powder: The HeLa cells were cultured in an MEM solution supplemented with 10% fetal calf serum in a humidified incubator with an atmosphere of 5% CO_2 in air at 37 °C.

The antitumor activity of the ultrafine TiO_2 aggregates

was evaluated with a colony forming assay (plating efficiency: 80—85%). The cells were plated in 60 mm petri dishes (Becton-Dickinson Co.), and after incubated for 24 h at 37 °C in 5% CO_2 allow cell attachment, the old MEM solution was replaced with an MEM-TiO_2 solution. The cells were then incubated for 24 h, the solution was removed, and the cells were washed twice with a Hanks' balanced salt solution (Gibco). A TiO_2-free medium was finally added to the cells and the prepared cells were irradiated with a 500-W high pressure Hg lamp (USHIO Co., Tokyo, Japan) at room temperature. For the visible light experiments a sharp cut-off filter (L-44, Kenko Co., Tokyo, Japan) was used to get a light wavelength greater than 440 nm. For the UV light experiments a UV pass filter (UV-D2, TOSHIBA Co., Tokyo, Japan) was used to get a light wavelength between 300—400 nm. After culturing again for 10 days, the colonies were fixed with 70% methanol, stained with a 5% Giemsa solution, and then counted. In cytotoxicity experiment, cultures without drug in dark were used as controls. In irradiation experiment, cultures exposured to the various drugs as described above but not exposured to light were used as controls in irradiation experiments. Each experiment was done using three dishes at the same time and under the same conditions. Then those three data were averaged. Moreover, those experiments were repeated 3 to 4 times. The error bars in the figures represent the maximum and minimum value at each experiment. During the irradiation a water filter was used to remove infrared radiation, and light doses were measured by a photodiode.

Transmission Electron Microscope Measurement: HeLa cells were incubated in an MEM-TiO_2 (TiO_2=100 $\mu g\,cm^{-3}$) solution for 24 h, and then were collected and immediately fixed using a 2.5% glutaraldehyde solution at 4 °C. In some experiments, TiO_2 aggregates whose size was smaller than 0.22 μm were used. This small aggregates were obtained by filterating the centrifugated TiO_2 solution with a 0.22 μm milipore filter. After 2 h the cells were fixed again with a 2% osmium tetraoxide, then dehydrated by gradually increasing the concentration of alcohol, and embedded in synthetic resin (EPON 812). Semi-thin (2 μm) sections of the cell were stained with methylene blue, which were then made into ultrathin sections (0.05—0.1 μm) by using a Reihert ultramicrotome and a diamond knife, and then double stained with uranyl acetate and lead(II) citrate. Finally, distribution of the ultrafine TiO_2 particles in the cells was observed with a Hitachi H-7000 (75 kV) TEM.

Electrochemical Measurements: Cyclic voltammograms were taken using a slightly modified three-electrode system.[9] A graphite electrode, polished before each run (0.4 cm^2 surface area), a counter electrode (platinum wire), and a reference electrode (saturated calomel electrode: SCE) were fitted into the top of a glass vessel (25 cm^3 capacity). A sufficient number of HeLa cells were first dropped on the membrane filter while applying a slight suction, and were retained on the membrane filter surface. This filter was attached to the surface of the graphite electrode, which was then inserted into phosphate buffered saline [PBS] (pH 7.0, 15 cm^3) to get the cyclic voltammograms, obtained by using a potentiostat (Toho Technical Research Co., Tokyo, Japan; Model UFB-4), function generator (Hokuto Denko Co., Tokyo, Japan; Model HB-III), and X-Y recorder (Riken Denshi Co., Tokyo, Japan; Model F-5c).

Results and Discussion

Cytotoxicity of TiO_2: Investigation of the cytotoxicity of a drug, without irradiation, is important before it can be used as a photodrug, i.e., antitumor drugs used in PDT are required to be almost nontoxic, and yet have a high photokilling ability under irradiation.

The initial TiO_2 particles had an average size of 300 Å in diameter, and since hydroxyl groups (-OH) exist at the surface of the particles,[10] the hydrogen bond between the hydroxyl groups is formed in the aqueous solution, resulting in aggregation of the particles. Figure la shows an SEM image of the particles in the suspension. The average size of the aggregated TiO_2 was much larger (20 μm) than that of the initial ones. It was found that such large aggregated TiO_2 particles showed a high cytotoxicity to the cells. This is probably because they deposit and covered the

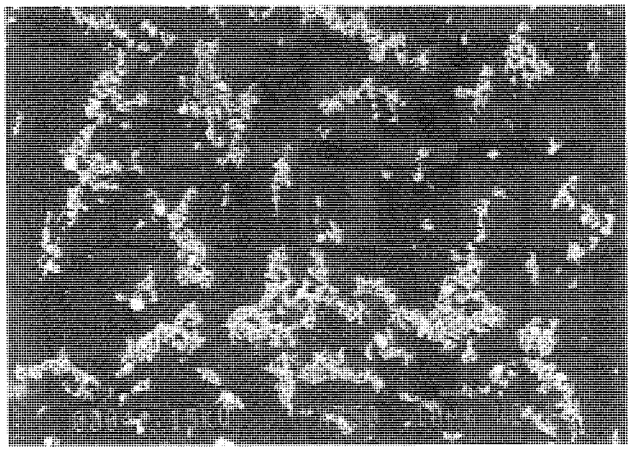

(a)

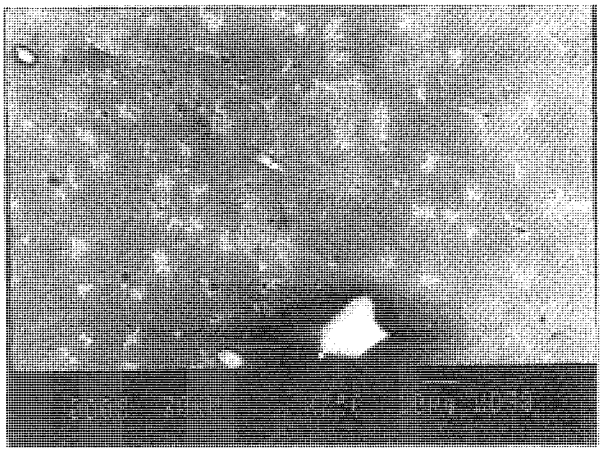

(b)

Fig. 1. SEM pictures of TiO_2 particles
(a) without centrifugation, (b) after centrifugation at 1600×g.

cells. However, the large aggregated particles can be removed by centrifugation and small aggregates in the suspension can be obtained. The size of TiO_2 aggregates depended on the centrifugal acceleration. Smaller TiO_2 aggregated can be obtained using a higher acceleration. However, if the acceleration was too high, the concentration of TiO_2 in the suspension decreased, therefore the optimum acceleration was chosen to be 1600×g, with the size of the TiO_2 particles being in the range of 0.03—10 μm (Fig 1b), much smaller than the size of HeLa cells (50 μm).

When HeLa cells were incubated in an MEM-TiO_2 for 24 h (without irradiation), the surviving fraction of the cells with respect to the amount of TiO_2 powder is shown in Fig. 2. The surviving fraction was greater than 90% when the concentration of MEM-TiO_2 reached 360 μg cm^{-3}, and it is subsequently concluded that the small TiO_2 particles showed little cytotoxicity without irradiation.

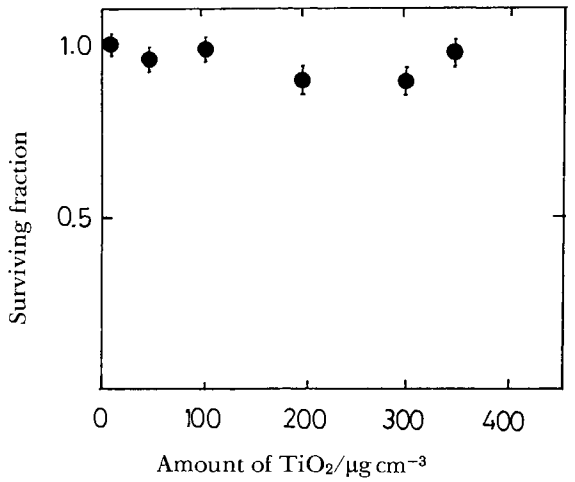

Fig. 2. After HeLa cells were incubated with an MEM-TiO_2 solution for 24 h without irradiation, the surviving fraction of HeLa cells is shown as a function of the amount of ultrafine TiO_2 particles.

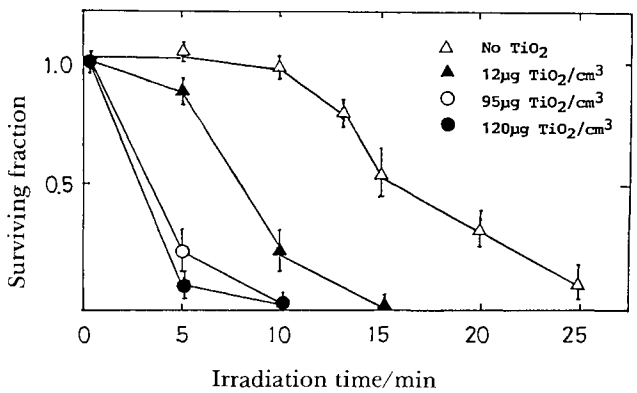

Fig. 3. Surviving fraction of HeLa cells as a function of unfiltered irradiation light in the presence of different concentrations of MEM-TiO_2 solutions.

Photokilling of Cells Using TiO_2 Powders: The irradiation effects when TiO_2 is not used are shown in Fig. 3, with the surviving fraction of HeLa cells given as a function of the unfiltered light irradiation time. The 500-W Hg lamp emitted a relatively strong UV light, thus a significant number of cells were killed after a 25 min exposure, whereas after a 10 min exposure, more than 90% of the cells remained alive.

When TiO_2 was added, the HeLa cells were killed at a much higher rate as shown in Fig. 3. Notice when the amount of TiO_2 was 12 μg cm^{-3}, 20% of the cells were killed after 5 min of irradiation, and also that when the amount of TiO_2 was 95 μg cm^{-3} and 120 μg cm^{-3}, 75% and 90% of the cells were respectively killed. The ultrafine TiO_2 particles showed little cytoxicity at 100 μg cm^{-3}, Therefore, it is concluded that under irradiation the ultrafine TiO_2 particles can actively kill the cells.

When the cultured cells are exposed to the white light from the 500-W Hg lamp, the semiconductor TiO_2 absorbs only the light whose energy is larger than its band gap (the TiO_2 band gap is 3 eV, corresponding to a wavelength of 410 nm). In order to prove whether the cell death was caused by a photo process or a thermal process, the following experiments were done. First the temperature increse of MEM-TiO_2 caused by the light irradiation was measured. The result is shown in Fig.4. In the beginning, it was 27 °C, and was raised up to about 36 °C after 30 min irradiation. However, that temperature was lower than that at culture environment (37 °C). Therefore it is reasonable to expect that such a temperature increase does not affect on the cell. Actually it was reported that the thermal effect is observed at the temperature is higher than 41 °C.[11] Next, a sharp cut-off filter (L-44) was inserted between the Hg lamp and the cells, allowing only light with wavelength larger than 440 nm to irradiate. Figure 5 shows that even after a 25 min irradiation more than 90% of the

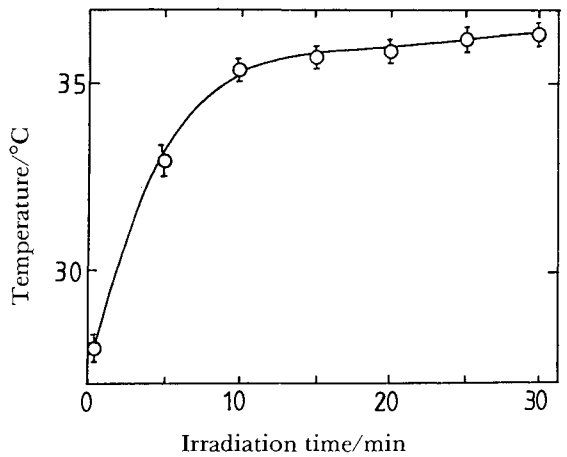

Fig. 4. Temperature increase of MEM as a function of irradiation (white light) time.

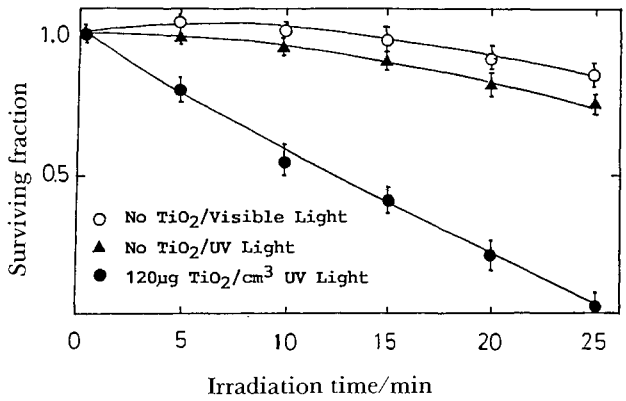

Fig. 5. Surviving fraction of HeLa cells as a function of visible light and UV irradiation with no TiO_2, and UV light irradiation with TiO_2. An MEM-TiO_2 solution (120 $\mu g\,cm^{-3}$) was added to the HeLa cells for 24 h before the UV irradiation.

cells were alive. It indicated that light with wavelength larger than 440 nm do not cause the photokilling effect. Finally, a UV-D2 filter was then used so that only light with wavelength between 300—400 nm irradiated. After a 25 min irradiation (TiO_2=120 $\mu g\,cm^{-3}$) all cells were completely killed, whereas in the absence of TiO_2 more than 85% of the cells remained alive. These results clearly show that the cell death in the presence of TiO_2 is caused by a photoeffect, not a thermal effect.

Distribution of TiO_2 Powder in the Cell: After the cells were incubated with MEM-TiO_2 (TiO_2=100 $\mu g\,cm^{-3}$) for 24 h, the TiO_2 distribution was observed with the TEM as shown in Fig. 6. TiO_2 particles were found on the cell membrane and in the cytoplasm, but not in the nuclei of the cells.

Cells can incorporate small particles by the process of phagocytosis, thus it can be resonably assumed that the same process takes place when the MEM-TiO_2 solution was added to the cells.

Moreover, it was found that the TiO_2 in the cytoplasm was gathered forming larger aggregates. This was concluded by the following experiment. That is, when TiO_2 aggregates whose size was smaller than 0.22 μm were incorporated, much larger aggregates (1.5 μm) were observed in the cytoplasm as shown in Fig. 7.

The observation that TiO_2 exist not only on the cell membrane, but also in the cytoplasm is very important to consider the reason why the present system effectively kill the cells. The organs in the cell were also damaged by the TiO_2. This point is quite different from the mechanism of TiO_2 electrode system. In the latter system, only the cell membrane is damaged by photoexcited TiO_2.

Reaction Mechanism: Two different photochemical processes are proposed which kill the HeLa cells in the present system. The first is the direct reaction between photoexcited TiO_2 and the cells. It is well known that the photoexcited TiO_2 is a strong oxi-

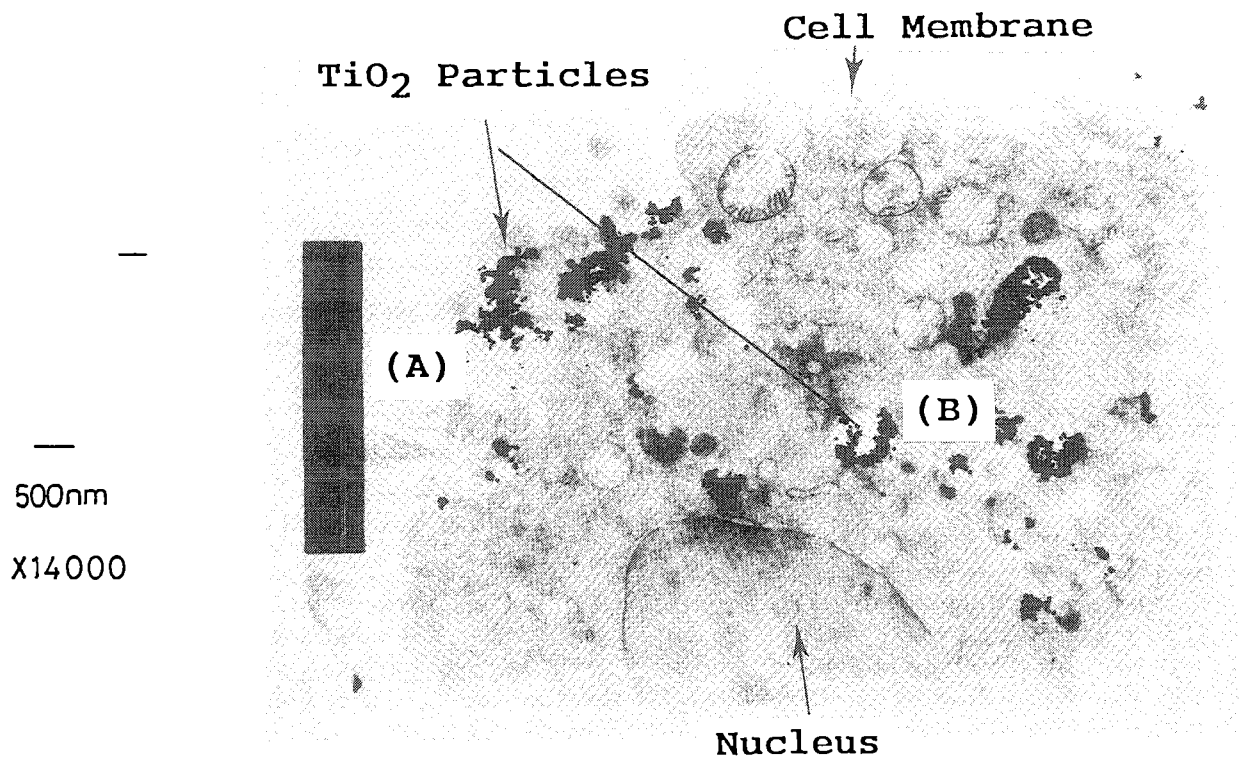

Fig. 6. TEM picture of HeLa cells after the TiO_2-MEM (TiO_2=100 $\mu g\,cm^{-3}$) solution was added to the cells for 24 h. TiO_2 aggregates were found on the cell membrane (A), and in the cytoplasm (B).

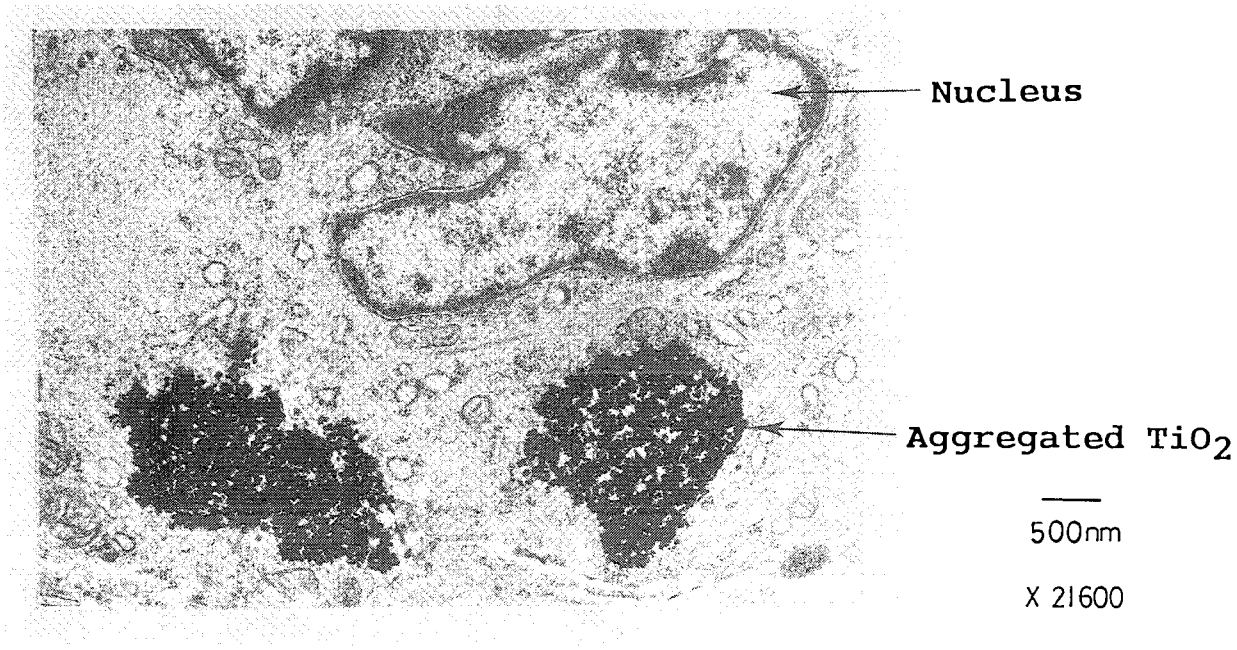

Fig. 7. TEM picture of HeLa cells after the ultrafine TiO_2 (0.03—0.22 μm) was added to the cells for 24 h. The TiO_2 particles was obtained using 0.22 μm milipore filter.

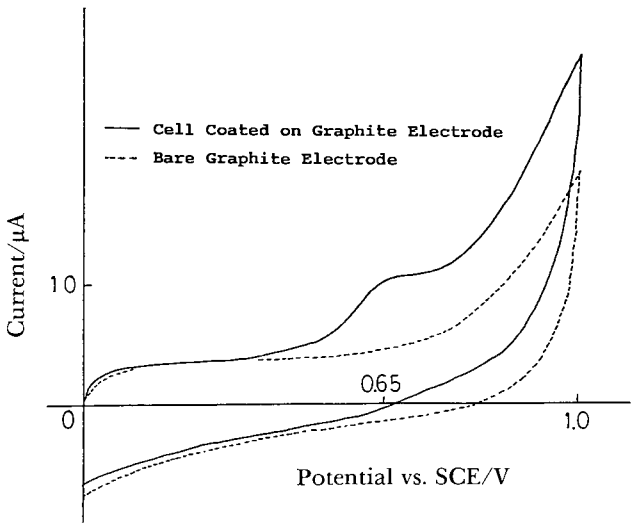

Fig. 8. Cyclic voltammogram of (——) a graphite electrode coated with HeLa cells and (----) a bare graphite electrode, in a 0.1 M phosphate buffer (pH 7.0). 1 M=1 mol dm^{-3}.

dizer.[12] Therefore it is expected that the cells are directly oxidized by the holes formed in the valence band. In order to determine the oxidation potential of the HeLa cells, we measured cyclic voltammograms of the cells adsorbed on a graphite working electrode in the potential range of 0 to 1.0 V vs. SCE in PBS (pH 7.0) solution (See Fig. 8). An anodic peak appeared at 0.65 V vs. SCE in the first positive forward direction scan, with peak intensity increasing as the number of HeLa cells increases on the electrode. However, no corresponding reduction peak was observed during the negative backwards direction scan, indicating that the HeLa cell oxidation process occurred in the potential range of 0.65 V vs. SCE. Since the energy level of valence band edge of TiO_2 is reported to be 2.4 V vs. SCE at pH 7,[12] it is reasonable to assume that the photogenerated holes in TiO_2 can oxidize the cells.

The other proposed process is the indirect reaction between photoexcited TiO_2 and the cells. Hydroxyl radicals ($OH\cdot$) and/or perhydroxy radicals ($HO_2\cdot$) are first created from water. When the photogenerated holes react with water, $OH\cdot$ radicals are produced.[13]

$$(TiO_2) + h\nu(>3\ eV) \rightarrow h^+ + e^- \quad (1)$$

$$H_2O + h^+ \rightarrow OH\cdot + H^+ \quad (2)$$

Additionally, in the presence of oxygen in water, it is reported that both $HO_2\cdot$ and $OH\cdot$ radicals are formed as follows.[13]

$$H^+ + e^- \rightarrow H\cdot \quad (3)$$

$$O_2 + e^- \rightarrow O_2^{-\cdot} \xrightarrow{H\cdot} HO_2^- \quad (4)$$

$$HO_2^- + h^+ \rightarrow HO_2\cdot \quad (5)$$

$$2HO_2\cdot \rightarrow O_2 + H_2O_2 \xrightarrow{O_2^{-\cdot}} OH\cdot + OH^- + O_2 \quad (6)$$

Those radicals may attack the cell membrane and cellular components, and oxidation-reduction substances which are important for producing ATP in a HeLa cell such as reduced glutathione (GSH), reduced nicotinamide adenine dinucleotide(NADH), coenzyme A (CoA), flavin adenine dinucleotide ($FADH_2$), may react with these radicals. The cell will die if these substrates are either depleted or exhausted. Preliminary experiments confirmed that in the presence

of cystein and catalase, respectively scavengers of OH· and H_2O_2, the surviving fraction significantly recovered.

Application of Photocatalytic Reaction of TiO_2 to Photodynamic Therapy: Research on light absorbing anti-cancer drugs is studied in biological systems, with these drugs being exposed to UV or visible light.[14-16] Extensive clinical trials have been performed using HpD as a PDT sensitizer because it is selectively localized in tumors. Further improvement of PDT can be envisaged through the use of more efficient photosensitizers.

In the HpD system two different mechanisms have been found that cause cell damage i.e., the sensitizer molecules excited in the lowest triplet state react directly with biological substrates,[17-18] and the photogenerated triplet state of the sensitizer transfers energy to oxygen to produce singlet molecular oxygen which damages cells by reacting with various biological substrates.[19-20] These two mechanisms are based on photochemical reactions, however, hyperthermal processes are also believed to photokill the tumor cells during irradiation.[21]

In the present system HeLa cells were definitely killed by a photochemical reaction and not by hypothermal effects. This large photokilling ability may be applied to PDT because the TiO_2 particles could be injected into the tumor, irradiated by UV light by laser fiber, thus destroying the tumor.

The UV light is strongly absorbed by patient's body, so the present system may not be useful for PDT of tumor formed in deep part of body. For a tumor formed near skin, such as skin tumor, however, this strong photoeffect may be useful. Compared to the conventional PDT of tumor using HpD, the present system has an advantage that cancer cell can be killed by a rather weak light intensity. We are now applying this method to animal experiment, i.e., bladder tumor of rat.

However, photoexcited TiO_2 has a very strong oxidation power and TiO_2 particles are incorporated not only by cancer cells but also by normal cells. Therefore, if UV light is irradiated uniformly, both the cancer cells and the normal cells are killed. This problem can be solved by focusing the light only on the tumor. Such a site selectivity is one of the superior characteristics of photodynamic therapy.

The other method to kill only the cancer cell is to bind TiO_2 particles to an HpD, causing them to be selectively localized in tumor, and thereby selectively killing the tumor during irradiation. In this case, the tumor formed not only near skin, but also near the surface of the organ, e.g. bladder, stomach, lung, can be killed by using strong photoeffect of TiO_2.

One of the authors (R. Cai) would like to express his gratitude to President H. Komiya of Bionics Co. for his financial support.

References

1) T. Inoue, A. Fujishima, S. Konishi, and K. Honda, *Nature*, **277**, 637 (1979).
2) E. Borgarello, J. Kiwi, E. Pelizzetti, N. Visca, and N. Gratzel, *J. Am. Chem. Soc.*, **103**, 6324 (1981).
3) N. Fujihira, Y. Satoh, and T. Osa, *Nature*, **293**, 206 (1981).
4) J. Onoe and T. Kawai, *J. Chem. Soc., Chem. Commun.*, **401**, 1480 (1987).
5) T. Kawai and T. Sakata, *Nature*, **268**, 474 (1980).
6) T. Matsunaga, R. Tomoda, T. Nakajima, N. Nakamura, and T. Komine, *Appl. Environ. Microbiol.*, **42**, 1330 (1988).
7) A. Fujishima, J. Ootsuki, T. Yamashita, and S. Hayakawa, *Photomed. Photobiol.*, **8**, 45 (1986).
8) N. Anpo, T. Shima, S. Kodama, and Y. Kubokawa, *J. Am. Chem. Soc.*, **91**, 4305 (1987).
9) T. Matsunaga and Y. Namba, *Anal. Chem.*, **56**, 798 (1984).
10) T. Morimoto, N. Nagao, and F. Tokuda, *J. Phys. Chem.*, **73**, 243 (1969).
11) J. A. Dickson, "Selective Heat Sensitivity of Cancer Cells," Springer-Verlag, Berlin, Heidelberg, New York (1977), p. 43.
12) H. Gerischer, "Solar Energy Conversion," Topics in Applied Physics, ed by B. O. Seraphin, Springer-Verlag, West Berlin (1979), Vol. 31.
13) I. Izumi, I. W. W. Dunn, K. O. Wilbourn, F. F. Fan, and A. J. Bard, *J. Phys. Chem.*, **84**, 3207 (1980).
14) T. Dougherty, *Photochem. Photobiol.*, **45**, 879 (1987).
15) J. Moan, *Photochem. Photobiol.*, **43**, 681 (1986).
16) D. Kessel, *Photochem. Photobiol.*, **39**, 851 (1984).
17) K. Lee See, I.J. Forbes, and W. H. Betts, *Photochem. Photobiol.*, **39**, 631 (1984).
18) G. R. Buettner and M. J. Need, *Cancer Lett.*, **25**, 297 (1985).
19) A. Blum and L. I. Grossweiner, *Photochem. Photobiol.*, **41**, 27 (1985).
20) B. W. Hender and A. C. Miller, *Rad. Res.*, **108**, 196 (1986).
21) T. S. Mang and T. J. Dougherty, *Photochem. Photobiol.*, **42**, 533 (1985).

Effect of Ether Oxygen on Proton Transfer and Aggregation Reactions of Amines in Water by Ultrasonic Absorption Method

Sadakatsu NISHIKAWA,* Hiroshi HARAGUCHI, and Yasuyo FUKUYAMA
Department of Chemistry, Faculty of Science and Engineering, Saga University, Saga 840
(Received October 25, 1990)

Ultrasonic absorption coefficients in the frequency range from 6.5 to 220 MHz have been measured in aqueous solutions of 3-ethoxy- and 3-butoxypropylamine as functions of their concentrations along with the sound velocity at 2.5 MHz and the density. In a 3-ethoxypropylamine solution, only one relaxational absorption has been observed up to 3.0 mol dm^{-3}. The cause has been clarified to be due to a proton-transfer reaction of the amine from the concentration dependences of the relaxation frequency and the relaxational amplitude. The rate and thermodynamic parameters have been determined and reasonable values have been obtained as a diffusion-controlled reaction. In the solution of 3-butoxypropylamine, another relaxation process in addition to that due to the proton-transfer reaction has been observed in the concentrations of more than 0.5 mol dm^{-3}. This relaxation process has been attributed to a perturbation associated with an aggregation reaction, $4A \longleftrightarrow A_4$, from the concentration dependences of the relaxation frequency and the relaxational amplitude of the absorption. The rate and thermodynamic constants for the proton-transfer and aggregation reactions have been determined. It has been found from a comparison of the results for the two solutions and others reported previously that the introduction of ether oxygen into amine molecules has little influence on the proton-transfer reaction, but prevents the formation of aggregates due to the hydrophobic interaction. It has also been seen from the results of 3-butoxypropylamine solutions that the butoxyl group has a fairly high ability of hydrophobic interaction and that nonionized molecules form aggregates in the aqueous solution.

The dynamic properties of aqueous solutions of various alkylamines have been clarified so far by measurements of the ultrasonic absorption coefficients in a pulse frequency range from 6.5 to 220 MHz.[1-4] One of the characteristic properties regarding absorption is the observation of a relaxation process due to a proton-transfer reaction. This process has been found in many aqueous and nonaqueous solutions of amines, phenols and benzoic acids in a similar frequency range.[5-9] It is generally expressed for amine solutions as $R\text{-}NH_3^+ + OH^- \leftrightarrow R\text{-}NH_3^+ \cdots OH^- \leftrightarrow R\text{-}NH_2 + H_2O$. In addition, we have proposed from a detailed analysis of the absorption data[3] that the cause of the relaxational absorption observed in the pulse frequency range is only due to the first step though the intermediate of the above mentioned reaction is important. The effect of the second step on absorption is negligibly small. The importance of the proton-transfer reaction mechanisms in biological systems is stressed,[10] and a detailed dynamical interpretation for the process is desired in relation to both the solute structure and kinetics.

When the hydrophobicity of amine molecule increases, such as butyl-[1] and pentylamine,[2,4] another relaxational absorption appears in a slightly lower frequency range, although the position of the relaxation frequency depends on the structure of the solutes. We have predicted that the relaxation process is related to the molecular aggregation of the nonionized amine molecules, and that such aggregates have a relatively small aggregation number. This phenomenon begins remarkably with the solution of butylamines for monoalkylamines, and it is characterized by the so-called Peak Sound Absorption Concentration. This was originally discussed by Barfield and Schneider[11] regarding an aqueous solution of diethylamine in relation to the solute and solvent interaction. However, it is very dependent of the hydrophobicity of solute molecules. If an ether oxygen is introduced to the alkyl group of an amine molecule, it is expected that the hydrophobicity would decrease and that the dynamic characters of the solutions might be changed. It is desired to dynamically elucidate how the ether oxygen affects the balance of the hydrophobicity and hydrophilicity of amine molecules. In order to observe the above speculation, we chose the two solutes, 3-butoxypropylamine and 3-ethoxypropylamine, and the ultrasonic absorption coefficients were measured as functions of both the frequency and concentration. The results are reported in this paper.

Experimental

Chemical: 3-Butoxypropylamine and 3-ethoxypropylamine were purchased from Wako Pure Chemicals. The former was distilled at normal pressure. The latter was used without further purification, since the gas-chromatographic data indicated the purity to be more than 99%. The solvent water was distilled twice and highly pure N_2 gas was passed for about 10 min with boiling. The desired aqueous solutions were made by weight and by dilution for the dilute solutions.

Apparatus: The ultrasonic absorption coefficient was measured by a pulse method in the frequency range from 6.5 to 220 MHz. Detail of the measurement procedure are described elsewhere.[12] The frequency dependence of the absorption coefficient has been analyzed by a Debye-type relaxational equation as

$$\alpha/f^2=\sum_i A_i/[1+(f/f_{ri})^2]+B \quad (1)$$

and

$$\mu=(\alpha/f^2-B)fc=\sum_i A_i fc/[1+(f/f_{ri})^2], \quad (1')$$

where α is the absorption coefficient, f the frequency, A_i the relaxational absorption amplitude for the i-th process, f_{ri} the relaxation frequency, μ the absorption per wave length, c the sound velocity and B includes the residual and classical absorptions. The ultrasonic parameters were determined by a nonlinear least mean-squares computer program, which is also described elsewhere.[12] The sound velocity was measured by an interferometer at 2.5 MHz. These ultrasonic cells were immersed in a water bath maintained at a constant temperature within ±0.002 °C. All the solutions were isolated from the air by circulating dry N_2 gas onto the solutions in the cells in order to maintain a constant hydroxide concentration. The solution density was measured using a conventional Ostwald-type pycnometer, of which the volume was about 5 cm³. The solution pH's were determined by Hitachi-Horiba pH meter and the Towa Denpa HM-60S pH meter. All measurements were carried out at 25 °C.

Results

Figures 1 and 2 show the representative ultrasonic absorption spectra in aqueous solutions of 3-butoxypropylamine and 3-ethoxypropylamine at various concentrations, respectively. The solid curves in the figures indicate the calculated values by Eqs. 1 and 1′ when i=1. The detailed procedure for judging if the spectrum is due to a single relaxational process or not is described elsewhere.[13] The fitnesses between the experimental and theoretical values might look as if a single relaxational process was observed. However, small deviations at a lower frequency range were found at concentrations at around 0.6—1.2 mol dm⁻³ of 3-butoxypropylamine. The concentration

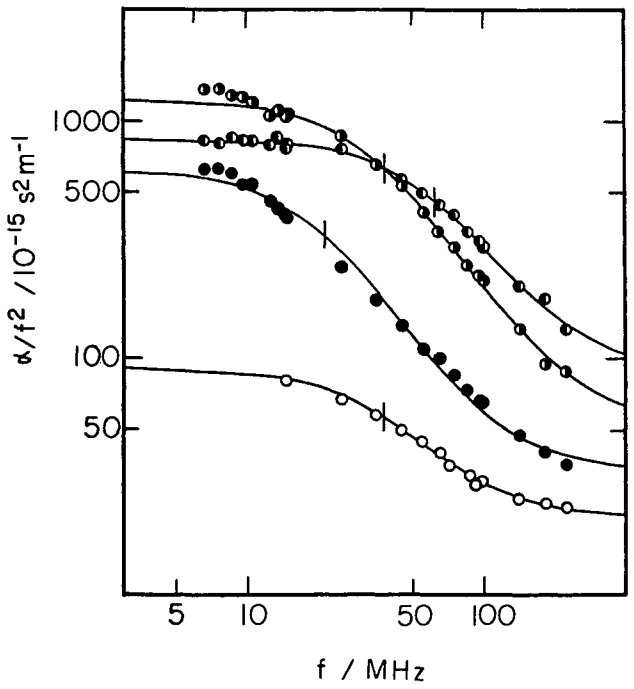

Fig. 1. The representative ultrasonic absorption spectra in aqueous solution of 3-butoxypropylamine at 25 °C.
○: 0.148 mol dm⁻³, ●: 0.606 mol dm⁻³, ◑: 1.212 mol dm⁻³, ◐: 1.798 mol dm⁻³.

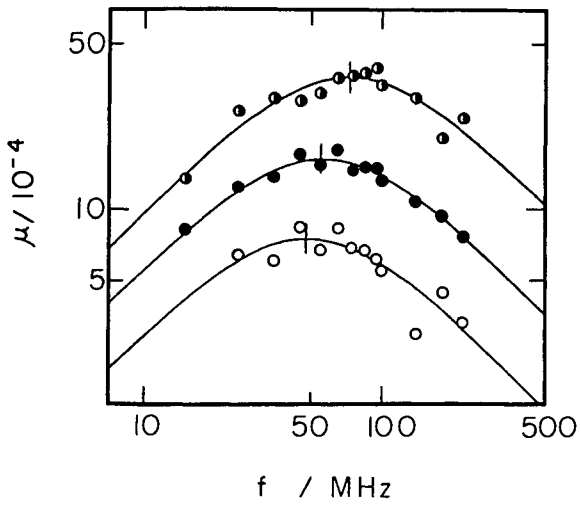

Fig. 2. The representative ultrasonic absorption spectra in aqueous solution of 3-ethoxypropylamine at 25 °C.
○: 0.0489 mol dm⁻³, ●: 0.127 mol dm⁻³, ◑: 3.028 mol dm⁻³.

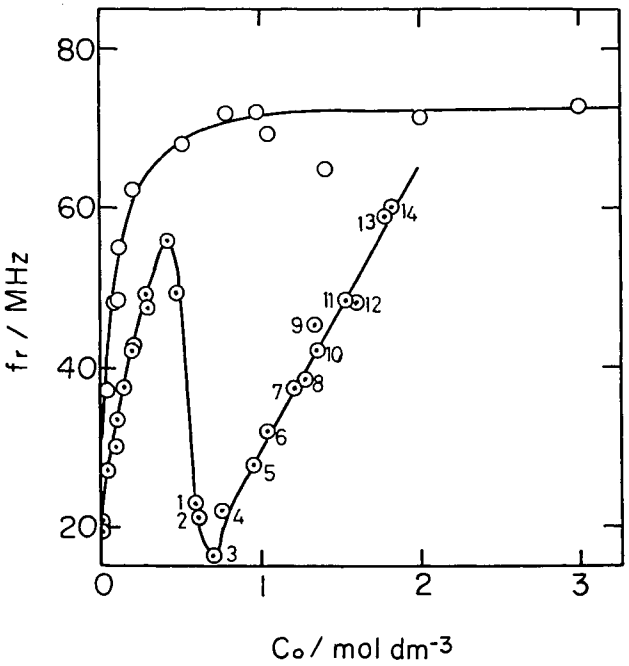

Fig. 3. Concentration dependence of the apparent relaxation frequency for aqueous solutions of 3-ethoxypropylamine (○) and 3-butoxypropylamine (◉).

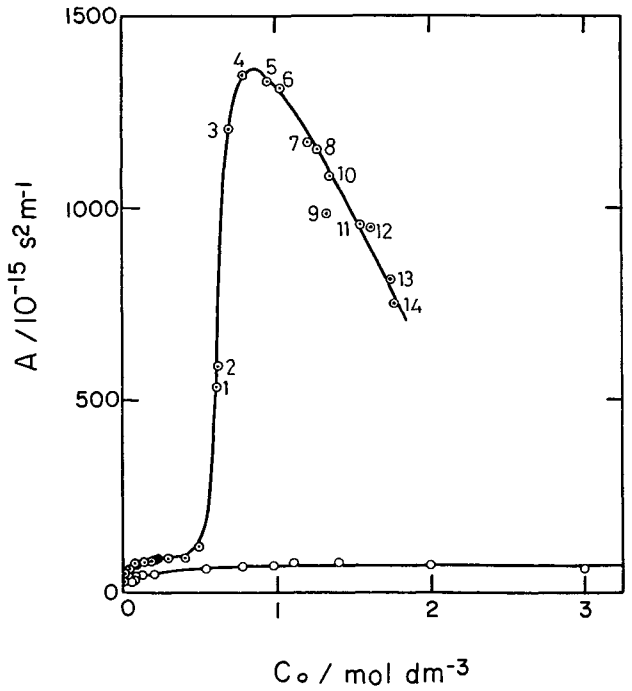

Fig. 4. Concentration dependence of the apparent amplitude of the relaxational absorption for aqueous solutions of 3-ethoxypropylamine (O) and 3-butoxypropylamine (⊙).

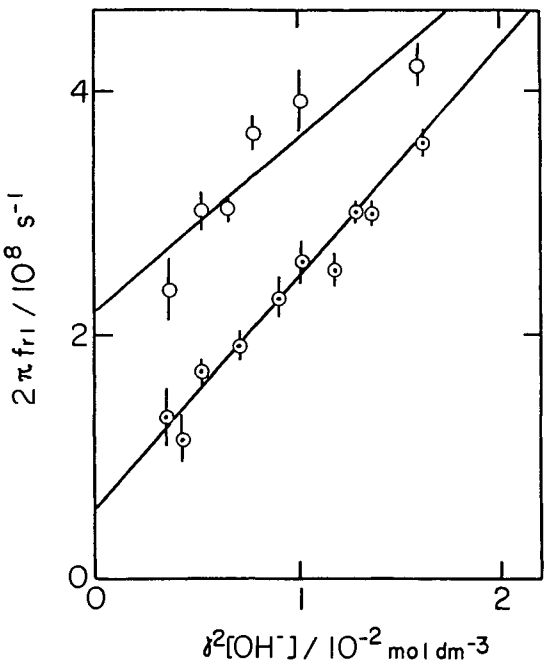

Fig. 5. The plots of the relaxation frequency, f_{r1} $\gamma^2[OH^-]$ for aqueous solutions of 3-ethoxypropylamine (O) and 3-butoxypropylamine (⊙).

dependences of the relaxation frequency and the relaxational amplitude, thus calculated, are presented in Figs. 3 and 4 for both solutions. The obtained ultrasonic absorption coefficients as a function of the frequency (12 concentrations for 3-ethoxypropylamine solution and 26 concentrations for 3-butoxypropylamine) and the ultrasonic parameters including the probable errors as a function of concentration are available upon request to one of the authors, S. N. As can be seen in Fig. 3, the relaxation frequency for the solutions of 3-ethoxypropylamine increases monotonously with the analytical concentration, C_o, and tends to reach a plateau at more than 1 mol dm^{-3}. The relaxational amplitude also increases and shows a plateau at more than 0.5 mol dm^{-3} (Fig. 4). On the other hand, in the solutions of 3-butoxypropylamine, the relaxation frequency indicates a discontinuous trend regarding the concentration. The relaxational amplitude shows a similar dependence at less than 0.4 mol dm^{-3}, as that for 3-ethoxypropylamine, and increases dramatically at more than 0.4 mol dm^{-3}. It then goes through a maximum at 0.8 mol dm^{-3}. The smooth changes of the relaxation frequency and the relaxation amplitude for 3-ethoxypropylamine seem to suggest that a perturbation of only one equilibrium is the cause of relaxational absorption. On the other hand, the curious dependences of the ultrasonic parameters in 3-butoxypropylamine may indicate that another cause of the absorption also exists in concentrations of more than 0.5 mol dm^{-3}. However, the dependences of the ultrasonic parameters on the analytical concentration at a low concentration range of less than 0.6 mol dm^{-3} for the 3-ethoxypropylamine solution and 0.4 mol dm^{-3} for the 3-butoxypropylamine solution are similar. We therefore first tried to analyze the results at these concentration ranges.

Such dependences of the ultrasonic parameters are characteristic of a perturbation of an equilibrium associated with the proton-transfer reaction of amine. It is generally described by

$$R\text{-}NH_3^+ + OH^- \underset{k_{21}}{\overset{k_{12}}{\longleftrightarrow}} R\text{-}NH_3^+\cdots OH^- \underset{k_{32}}{\overset{k_{23}}{\longleftrightarrow}} R\text{-}NH_2 + H_2O, \quad (2)$$

where k_{ij} is the rate constant for each step. The relation between the relaxation frequency and the concentrations of the reactants is given by the following equation on the assumption that the effect of the second step on the first one is either small or negligible:

$$2\pi f_{r1} = 2k_{12}\gamma^2[OH^-] + k_{21}, \quad (3)$$

where γ is the activity coefficient, which can be estimated by the Davis equations,[14] subscript 1 for the relaxation frequency is indicated in order to distinguish the other process shown next. Figure 5 shows plots of $2\pi f_{r1}$ vs. $\gamma^2[OH^-]$ for the two solutions, the slope and intercept of which provide the forward and backward rate constants. It should be noticed that the intercept is not close to zero. The rate constants, thus obtained, are listed in Table 1.

Table 1. The Kinetic and Thermodynamic Constants for the Proton-Transfer Reaction in Aqueous Solutions of 3-Ethoxypropylamine and 3-Butoxypropylamine at 25 °C

Solute	$10^{-10}\,k_{12}$	$10^{-8}\,k_{21}$	K_{23}	$10^{4}\,K_b$	$10^{6}\,\Delta V_1$
	$mol^{-1}\,dm^3\,s^{-1}$	s^{-1}		$mol\,dm^{-3}$	$m^3\,mol^{-1}$
3-Ethoxypropylamine	1.2±0.2	2.3±0.2	0.0068	1.3±0.4[a] (1.4±0.6)[b]	30
3-Butoxypropylamine	1.8±0.1	0.57±0.08	0.066	2.0±0.5[a] (2.0±0.5)[b]	21

a) Estimated values from the relation, $K_b=\gamma^2[OH^-]^2/(C_o-[OH^-])$. b) The equilibrium constant was determined by the relation between the analytical concentration and the relaxation frequency (Eq. 12 given in Ref. 3). c) All of the rate and thermodynamic constants in this table were determined in the concentration range less than 0.5 mol dm^{-3}.

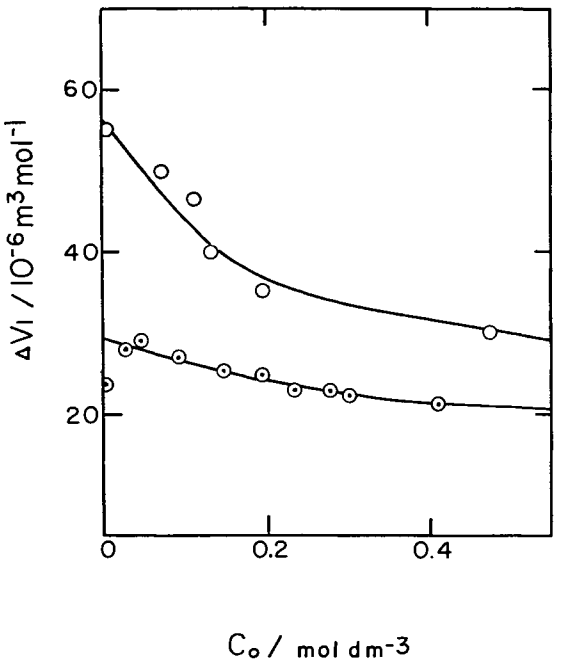

Fig. 6. The concentration dependence of the standard volume change of the proton-transfer reaction for 3-ethoxypropylamine (○) and 3-butoxypropylamine (⊙).

For the proton-transfer reaction it is possible to estimate the concentration dependence of the maximum excess absorption per wave length, μ_{m1}, by

$$\mu_{m1}=0.5\,A_1 f_{r1} c=\pi\rho c^2\Gamma_1\,(\Delta V_1)^2/2RT, \quad (4)$$

where ρ is the solution density, ΔV_1 the standard volume change of the reaction and $\Gamma_1=\{2/[OH^-]+1/[R\text{-}NH_3^+\cdots OH^-]+2\partial \ln \gamma/\partial[OH^-]\}^{-1}$. Using the above relation, the volume change has been determined and the results are shown in Fig. 6. Usually, the standard volume change of the reaction has been considered to be concentration independent. However, as can be seen in this figure, it seems to be dependent on the concentration for both solutions. This trend has also been found by Atkinson et al.[16] for an aqueous solution of *t*-butylamine. A detailed analysis by the present authors[15] also shows that the dependence is quite large in relatively dilute solutions, and that it reaches a constant value with increasing concentration. The values which seem to have become constant are listed in Table 1. In these analyses, the ultrasonic absorption results in relatively concentrated solutions were not used, and those in the concentration range of less than 0.5 mol dm^{-3} were taken. The reason will be considered in the discussion section. The equilibrium constant, K_b, for hydrolysis may provide useful information concerning a clarification of the proton-transfer reaction mechanisms. Unfortunately, it has not been previously reported for these aqueous solutions. It has therefore been estimated by the relation $K_b=\gamma^2[OH^-]^2/(C_o-[OH^-])$, where $C_o=[R\text{-}NH_3^+]+[R\text{-}NH_2]+[R\text{-}NH_3^+\cdots OH^-]$. They are also listed in Table 1. It is seen that the equilibrium constants, K_b, are far apart from the ratio of the forward and backward rate constant, k_{21}/k_{12}.

Secondly, we analyze the absorption mechanism observed in the relatively concentrated solution of 3-butoxypropylamine. A different relaxation process is considered to be observed in the solution from the profile of the ultrasonic parameters, as can be seen in Figs. 3 and 4. The relaxational amplitude goes through a maximum, the so-called Peak Sound Absorption Concentration. Similar dependences of the relaxation frequency and the relaxational amplitude on the concentration were observed in the solutions of various butylamines and pentylamines.[1,2,4] Therefore, we have considered that the same reaction may proceed in solution of 3-butoxypropylamine. However, the proton-transfer reaction is also expected to proceed in the solution; then, the values of α/f^2 due to the proton-transfer reaction should be subtracted from the experimental values. In order to carry out this procedure correctly it is appropriate to express the concentration dependences of the pH, the sound velocity and the solution density by proper functions of the analytical concentration. These experimental values were fitted to appropriate polynomials in order to minimize the standard deviations by a least-mean

squares method. They are as follows:

$$pH = 0.28248C_o^{1/2} + 12.037 \quad (0.596—1.902\ \text{mol dm}^{-3}),$$

$$c = 1495.12 + 139.557C_o - 110.401C_o^2 + 24.8807C_o^3 \quad (0—1.8\ \text{mol dm}^{-3}),$$

and

$$\rho = 0.99727 - 3.6015\times10^{-2}\,C_o + 2.5046\times10^{-2}\,C_o^2 - 8.5832\times10^{-3}\,C_o^3 \quad (0—1.8\ \text{mol dm}^{-3}),$$

where the values indicated in the parentheses are the concentration ranges within which the above equations are applicable. Also, the relaxation frequency and the relaxational amplitude at any concentration can be speculated by Eqs. 3 and 4 for the proton-transfer reaction. It is then possible to calculate $(\alpha/f^2)_{\text{residual}}$ which is the residual absorption subtracted those due to the proton-transfer reaction from the experimental values. The residual absorptions were again analyzed by the single relaxational equation; and it was found that they could be reasonably fit to the theoretical curves. The calculated ultrasonic absorption parameters are shown in Figs. 7 and 8; the numbers which correspond to the data are shown in Figs. 3 and 4. As can be seen, the relaxational amplitude are close to those values given in Fig. 4, but are slightly larger, and the increment at a concentration around 0.6 mol dm^{-3} becomes steeper. The relaxation frequencies shift to a slightly lower frequency and tend to increase monotonously, as can be seen in Fig. 7. These results indicate that the absorption is much larger than that due to the proton-transfer reaction. The cause of the residual relaxational absorption is considered to be due to an aggregation reaction associated with the hydrophobicity of the nonionized amine molecules since the relaxation process disappears when the solution pH decreases, it is not found in 3-ethoxypropylamine aqueous solution, and it is not observed when organic solvents are used. In general, although the aggregation reaction may proceed through a stepwise process,[19] we simply assume that it is given by the following formula for a reaction with a small aggregation number:

$$n\,A \underset{k_{43}}{\overset{k_{34}}{\longleftrightarrow}} A_n. \tag{5}$$

The relation between the relaxation frequency, f_{r2}, and the reactant concentration is derived as[1]

$$2\pi f_{r2} = n^2 k_{34}[A]^{n-1} + k_{43} \tag{6}$$

where subscript 2 for the relaxation frequency is used in order to distinguish that for the proton-transfer reaction and n, the aggregation number. In order to analyze the concentration dependence of the ultrasonic parameters, the concentration of the nonionized monomer molecules is necessary. It may be a good approximation that the equilibrium constant of the hydrolysis, defined as $K_b = \gamma^2[OH^-][R\text{-}NH_3^+]/([R\text{-}$

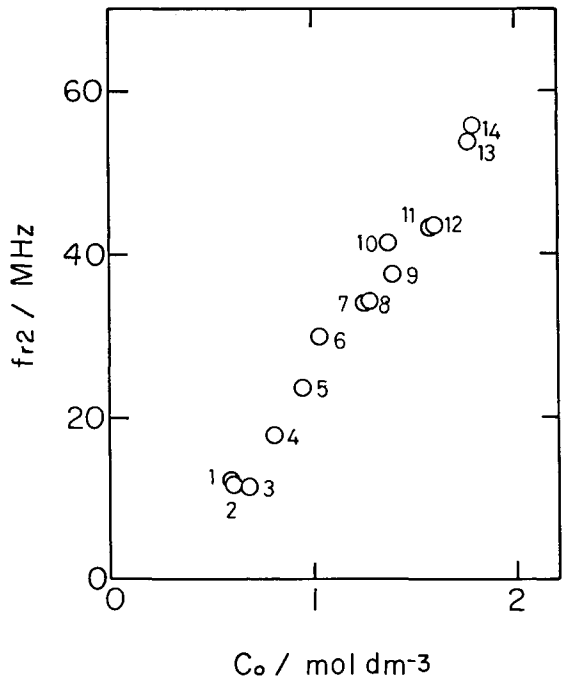

Fig. 7. The concentration dependence of the relaxation frequency, f_{r2}, calculated from the residual absorption for aqueous solution of 3-butoxypropylamine.

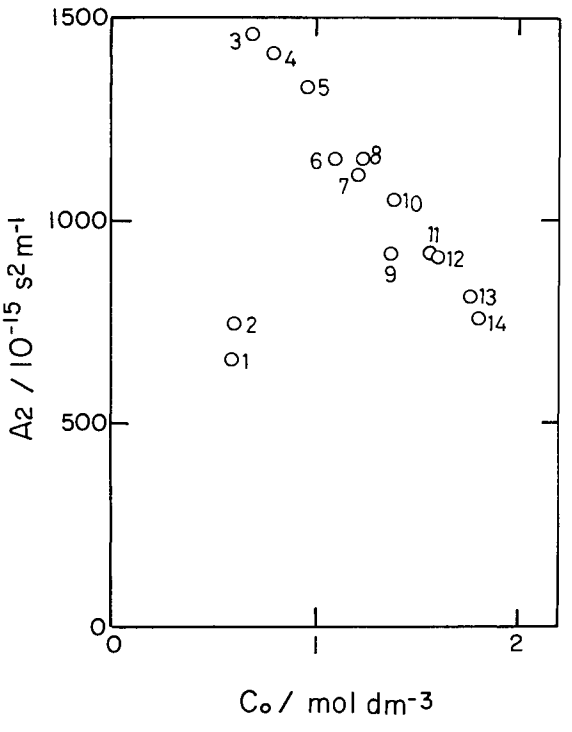

Fig. 8. The concentration dependence of the amplitude of the relaxational absorption, A_2, calculated from the residual absorption for aqueous solution of 3-butoxypropylamine.

$NH_3^+\cdots OH^-]+[R\text{-}NH_2]$), is still held in a slightly concentrated solution. The equilibrium constants for the first and second step in Eq. 2, $K_{12}=k_{21}/k_{12}=\gamma^2[OH^-]^2/[R\text{-}NH_3^+\cdots OH^-]$ and $K_{23}=k_{32}/k_{23}=[R\text{-}NH_3^+\cdots OH^-]/[R\text{-}NH_2]$ may be also defined. Then, Eq. 6 can be arranged as

$$2\pi f_{r2}=n^2(\gamma^2[OH^-]^2)^{n-1}\,k_{34}(1/K_b-1/K_{12})^{n-1}+k_{43}. \quad (7)$$

The aggregation number, n, was changed so as to obtain a least error of plots of $2\pi f_{r2}$ vs. $(\gamma^2[OH^-]^2)^{n-1}$. When $n=3$ the intercept of the plots gave a negative value. By giving more than 4 for the aggregation number, the error is increased. We thus took the aggregation number to be four. Figure 9 shows plots of $2\pi f_{r2}$ vs. $(\gamma^2[OH^-]^2)^3$, which give the backward rate constant, k_{43}, from the intercept to be $(5.7\pm0.8)\times10^7\ s^{-1}$ and the product of the rate and equilibrium constants from the slope. Equation 6 is also arranged using the total concentration of the reactants under consideration, C_o', as

$$2\pi f_{r2}=k_{43}\,nC_o'(\gamma^2[OH^-]^2)^{-1}\,(1/K_b-1/K_{12})^{-1}+(1-n)k_{43}, \quad (8)$$

where

$$C_o'=C_o-[R\text{-}NH_3^+]-[R\text{-}NH_3^+\cdots OH^-]$$
$$=[R\text{-}NH_2]+n[(R\text{-}NH_2)_n].$$

Figure 10 shows plots using Eq. 8 when $n=4$. The obtained backward rate constant, k_{43}, was $(12\pm1)\times10^7\ s^{-1}$ from the intercept, the plots of which gave a better linearity with smaller probable errors. It is therefore shown in Table 2. It seems to be close to that value obtained by Eq. 7. The equilibrium constant, K_b, was thus estimated to be $(3.8\pm0.2)\times10^{-4}$ mol dm^{-3} using the slope and intercept values of linear plots of Eq. 8, since the equilibrium constant, K_{12}, is obtained from the results concerning the proton-transfer reaction. As a result, going back to Eq. 7, it is possible to obtain the forward rate constant, k_{34}, from the slope of the linear plots; it is also shown in Table 2.

The maximum excess absorption per wave length for this process is derived as[1]

$$\mu_{m2}=\pi\,\rho c^2\,k_{34}[A]^n\,\tau\,(\Delta V_2)^2/2RT, \quad (9)$$

where the volume relaxation has been assumed for the above process and $\tau=(2\pi f_{r2})^{-1}$. Once the rate con-

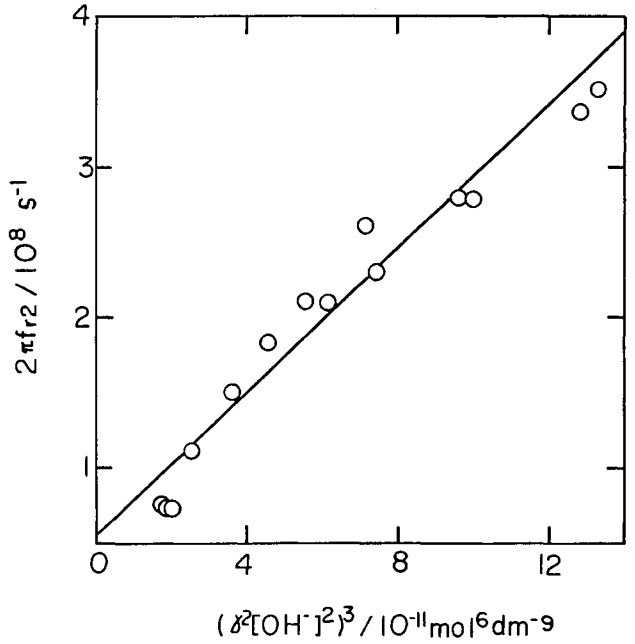

Fig. 9. The plots of $2\pi f_{r2}$ vs. $(\gamma^2[OH^-]^2)^3$ for aqueous solution of 3-butoxypropylamine.

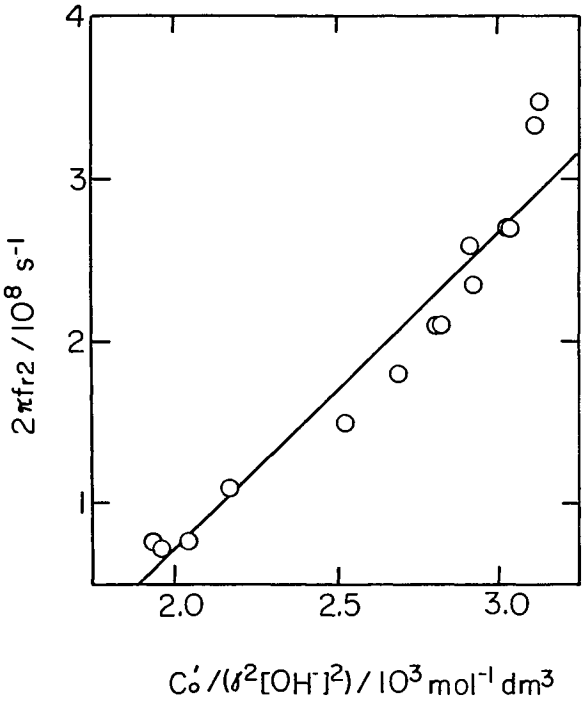

Fig. 10. The plots of $2\pi f_{r2}$ vs. $C_o'/(\gamma^2[OH^-]^2)$ for aqueous solution of 3-butoxypropylamine.

Table 2. Rate and Thermodynamic Parameters for the Aggregation Reactions at 25 °C

Solute	n	$10^{-6}\,k_{34}$ $(mol^{-1}\,dm^3)^{n-1}\,s^{-1}$	$10^{-7}\,k_{43}$ s^{-1}	$10^6\,\Delta V_2$ $m^3\,mol^{-1}$	Reference
Butylamine	4	2.2	9.0	14	(1)
3-Butoxypropylamine	4	12	12	21	This work
Pentylamine	5	4.7	3.0	17	(2)

stants, k_{34} and k_{43}, are obtained, the monomer concentration is available. Using the experimental τ values, then, the volume change of the reaction has been estimated, and is given in Table 2.

Discussion

The results of the proton-transfer reaction are first discussed. The forward rate constants, k_{12}, for both solutions are reasonable as a diffusion-controlled reaction.[17] However, the ratio of the forward and backward rate constants, k_{21}/k_{12}, is far apart from the equilibrium constant, K_b, for the hydrolysis, as can be seen in Table 1. Similar results have been obtained in other amine solutions.[3,4,14] The coupling effect of the faster process on the slower one is usually taken into account in order to interpret such phenomena. However, as has been reported in a previous paper,[3] it is rather reasonable that the perturbation of the first step in Eq. 2 is the cause of the observed relaxation and the second step is too fast to affect on the first step. Furthermore, our analytical procedure[3] using the relation between the relaxation frequency and the analytical concentration (Eq. 12 in Ref. 3) has given the reasonable equilibrium constants, K_b, as is shown in Table 1. Another equilibrium constant, K_{23}, was estimated to be less than unity from the relation, $K_b=K_{12}/(1+K_{23}^{-1})$ where the K_b value estimated by the static procedure (listed in Table 1) was used. These results show that the concentration of the intermediate is very small compared with that of R-NH_2. This means that the second step may correspond to a intramolecular proton-transfer and that the intermediate is not very stable. It is expected that this process is too fast to be observed by the time range under study. As can be seen in Table 1, the forward rate constant, k_{12}, is not much affected, even if the structures of amine molecules are different. This means that the most effective term in the reaction includes the diffusion of hyrdoxyl ions in aqueous media. Although only data for relatively dilute solutions of both solutions are used to obtain the proton-transfer reaction rate constants, the same ultrasonic relaxational absorption due to the reaction can be observed in concentrated solutions of 3-ethoxypropylamine (Fig. 3). The relaxation frequencies obtained (more than 0.6 mol dm^{-3}) are lower than those expected from the calculated values (around 100 MHz) using Eq. 2. This might be because a solute-solute interaction, such as the interaction due to hydrogen bonding, interrupts the proton-transfer reaction. However, the aggregates associated with the hydrophobicity of the solute (discussed next) may not exist in solution of 3-ethoxypropylamine. Another possibility may be due to an alternation of the solvent water structure by the addition of an amine at the high-concentration range.

It is not very clear why the volume change of the reaction is dependent on the concentrations of both solutions. One of the reasons might be that the approximation of the volume relaxation for the proton-transfer reaction is not appropriate. If it includes a thermal-relaxation term, the volume change, ΔV_1, should be expressed as $\Delta V_1=\Delta V_{real}-\alpha_p\Delta H/\rho C_p$, were α_p is the thermal expansion coefficient, ΔH the standard enthalpy change of the reaction, and C_p the specific heat at constant pressure. However, without this experimental information concerning α_p and C_p, no definite conclusion can be given at this stage.

Next, the absorption mechanism observed in a relatively concentrated solution of 3-butoxypropylamine is discussed. The difference in the absorption characters from those in solution of 3-ethoxypropylamine can clearly be seen in the profiles given in Figs. 3 and 4; that is, the relaxational amplitude increases steeply and goes through a maximum. Although the original ultrasonic absorption spectra look like those due to single relaxational absorption, as was analyzed in a previous section, the spectra associated with two relaxation processes are considered to be superimposed since the relaxational amplitude due to the proton-transfer reaction is much smaller than that newly observed in the relatively concentrated solution, and the respective relaxation frequencies are not very far apart. Ideally, two relaxation processes should be distinguished by the double relaxational equation (i=2 in Eq. 1) using the observed values of the absorp-

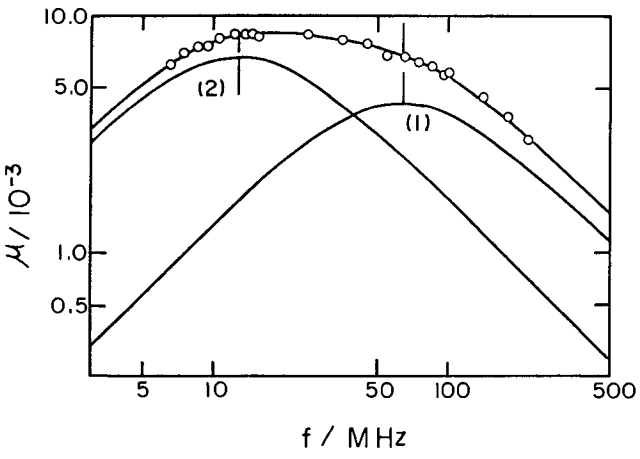

Fig. 11. The spectrum analyzed by the double relaxational equation for 3-butoxypropylamine at 0.605 mol dm^{-3}. The calculated parameters are f_{r1}=(64.4±5.5) MHz, A_1=(88.5±10.5)×10^{-15} s^2m^{-1}, f_{r2}=(12.7±0.6) MHz, A_2=(690.8±16.1)×10^{-15} s^2m^{-1} and B=(27.2±0.8)×10^{-15} s^2m^{-1}. The parameters obtained by the extrapolation by Eqs. 3 and 4 are f_{r1}=79.8 MHz and A_1=90.3×10^{-15} s^2m^{-1} and those calculated by the procedure shown in result section are f_{r2}=11.7 MHz, A_2=745.5×10^{-15} s^2m^{-1} and B=22.3×10^{-15} s^2m^{-1}.
(1): The absorption due to the proton transfer reaction and (2): That due to the aggregation reaction.

tion coefficients. Then, applying the double relaxational equation to the data at more than 0.5 mol dm^{-3}, unrealistic ultrasonic parameters were obtained (e.g. negative ultrasonic parameters and the larger probable errors than the most probable values), except those at 0.596 and 0.605 mol dm^{-3} These data correspond to those indicated by the number, 1 and 2, in Figs. 3 and 4. At these limited concentrations, the relaxation amplitudes are not very much larger and the relaxation frequencies are still quite far apart from that due to the proton transfer. Also, the deviations from the calculated values in the original spectra have been found, as can be seen in Fig. 1. Figure 11 shows one of the spectra calculated by the double relaxational equation at such intermediate concentrations. Thus, the calculated ultrasonic parameters at these two concentrations are very close to those determined in the previous section. These calculations indicate that the superimposed spectra are observed at more than 0.65 mol dm^{-3}. The subtraction procedure used to obtain the ultrasonic parameters given in the previous section seems to be appropriate.

Even if the ether oxygen, which produces hydrophilic activity, is introduced to the molecule, the butyl group seems to play fairly the rule as the hydrophobic interaction. Thus, a small aggregate exists in aqueous media. It should be noticed that the equilibrium constant, K_b, estimated from the aggregation reaction given by Eq. 8, (K_b=3.8×10^{-4} mol dm^{-3}) seems to be close to that obtained in the lower concentration range listed in Table 1. This also supports the idea that the cause of the relaxational absorption is due to reaction associated with aggregates of the nonionized amine molecules. The slightly larger value may be due to a solute-solute interaction, such as a hydrogen-bonding interaction in the relatively concentrated solutions. The aggregation number is close to that in a solution of pentyl or butylamine. This might mean that the activity of the hydrophobicity is close to that of the alkylamines, which have five or four carbon atoms. We speculate that the propyl group has a border activity regarding hydrophobicity to form the aggregate. This is also considered to be true from the fact that the relaxation associated with the aggregation reaction is observed in an aqueous solution of propyl alcohol,[18] although it is not found in a aqueous solution of propylamine. The hydroxyl group may be considered to be less hydrophilic than the amino group. This is also recognized from the solubility difference between the butyl alcohol and butylamine in water. It is interesting to compare the ultrasonic results with those in solutions of pentylamine and butylamine,[1,2] which have previously been reported and are also shown in Table 2. The position of the peak sound absorption concentration in the present solution is lower than that of butylamine. The relaxational amplitude is larger than that of butylamine. These differences seem to indicate that the hydrophobicity of 3-butoxypropylamine is slightly larger than butylamine. This comparison may indicate that the propyl group bonded with the ether oxygen has a slightly the hydrophobic character, which increases the hydrophobicity of the entire molecule. A similar comparison between 3-butoxypropylamine and pentylamine shows that the former is less hydrophobic than the latter. It can then be easily understood why such aggregate is not formed in solution of 3-ethoxypropylamine. Either the ethyl group is too small to form an aggregate through a hydrophobic interaction, or the ether oxygen acts as the hydrophilicity, thus preventing the formation of an aggregate by the hydrophobic interaction.

Finally, it may be meaningful to indicate that the concentration dependence of the relaxation frequency for the aggregation reaction (Eq. 8 used in this study) is very similar to that proposed theoretically by Teubner[19] and widely used.[20,21] That is, the relaxation frequency is proportional to C_0'/[A] in both treatments, even though the former corresponds to a variance of the size distribution of unity and $k_{43}n$ is k^-/m when k^- is the mean of the dissociation rate constant and m is the mean aggregation number.

Although the two relaxation processes due to both proton-transfer and aggregation reactions were observed in the same ultrasonic frequency range in the present study, the coupling effect of the two reactions may be ignored since a very fast intramolecular reaction proceeds between the above-two reactions under consideration.

This work was partly supported by a Grant-in-Aid for Scientific Research No. 02640350 from the Ministry of Education, Science and Culture.

References

1) S. Nishikawa and T. Yasunaga, *Bull. Chem. Soc. Jpn.*, **46**, 1098 (1973).
2) S. Nishikawa, T. Yasunaga, and K. Takahashi, *Bull. Chem. Soc. Jpn.*, **46**, 2992 (1973).
3) Y. Yoshida and S. Nishikawa, *Bull. Chem. Soc. Jpn.*, **59**, 1941 (1986).
4) S. Nishikawa, Y. Yoshida, and A. Nakano, *Bull. Chem. Soc. Jpn.*, **61**, 2731 (1986).
5) K. Applegate, L. J. Slutsky, and R. C. Parker, *J. Am. Chem. Soc.*, **90**, 6909 (1968).
6) R. D. white, L. J. Slutsky, and S. Pattison, *J. Phys. Chem.*, **75**, 161 (1971).
7) R. D. White and L. J. Slutsky, *J. Phys. Chem.*, **76**, 1327 (1972).
8) L. W. Dickson, H. Nomura, R. E. Berrall, T. Suzuki, and S. Kato, *J. Phys. Chem.*, **85**, 2273 (1981).
9) R. J. Adamic, B. A. Lloyd, E. M. Eyring, S. Petrucci, and R. A. Bartsh, *J. Phys. Chem.*, **90**, 1659 (1986).
10) R. A. Copeland and S. I. Chan, *Annu. Rev. Phys. Chem.*, **40**, 671 (1989).
11) R. N. Barfield and W. G. Schneider, *J. Chem. Phys.*, **31**, 488 (1959).

12) S. Nishikawa and K. Kotegawa, *J. Phys. Chem.*, **89**, 2896 (1985).
13) S. Nishikawa and F. Matsuo, *J. Phys. Chem.*, **95**, 437 (1991).
14) C. W. Davis, "Ion Association," Butterworth, London (1962).
15) S. Nishikawa and Y. Harano, *J. Phys. Chem.*, **93**, 7152 (1989).
16) G. Atkinson, M. M. Emara, H. Endo, and B. L. Atkinson, *J. Phys. Chem.*, **84**, 259 (1980).
17) M. Eigen and L. DeMaeyer, "Technique of Organic Chemistry," ed by A. Weissberger, Jr., Wiley, New York, N. Y. (1961), Vol. VIII, Part 2.
18) S. Nishikawa, M. Mashima, and T. Yasunaga, *Bull. Chem. Soc. Jpn.*, **48**, 661 (1975).
19) M. Teubner, *J. Phys. Chem.*, **83**, 2917 (1979).
20) S. Kato, H. Nomura, H. Honda, R. Zielinski, and S. Ikeda, *J. Phys. Chem.*, **92**, 2305 (1988).
21) R. Zana and B. Michels, *J. Phys. Chem.*, **93**, 2643 (1989).

Small-Angle X-Ray Scattering Study on Sol-Gel Transition of Mixtures of Colloidal Silica and Organic Polymer

Hideki MATSUOKA, Sheng-rong CHEN, Hiroshi ISHII, Norio ISE,*
Kazuki NAKANISHI,† and Naohiro SOGA†
Department of Polymer Chemistry, Kyoto University, Kyoto 606
†Department of Industrial Chemistry, Kyoto University, Kyoto 606
(Received November 2, 1990)

Sol-gel transition of mixtures of colloidal silica-water soluble organic polymer (sodium polystyrenesulfonate) has been investigated by the small-angle X-ray scattering technique. With proceeding gelation, an increase of the intensity at small-angle regions was observed and the values of radius of gyration (R_g) were estimated by the Guinier method. The addition of polymer increased the initial increase of R_g with gelation, i.e., sol-gel transition was accelerated by the presence of the polymer. This observation is not in contradiction to the prediction of micro-phase separation into silica-rich phase and polymer-rich phase proposed by Nakanishi and Soga. The fractal analyses predicted that the geometrical structure of the gel finally formed is similar to those of random coil linear polymer and swollen branched polymer.

The sol-gel route to glass or ceramic materials is attracting increasing attention. The main advantage of this method is that the materials can be made at fairly low temperatures compared with conventional methods.[1] For the alkoxy-derived silica system, the sol-gel reaction has been suggested to consist of two steps, i.e., the formation of primary silica particles by hydrolysis of alkyl silicate by water and the gel-network formation by aggregation of primary particles.[2] The structure and properties of the gel-derived materials have been investigated by electron microscopy (EM),[3] BET method,[4] etc. while its mechanism has been studied by Raman scattering,[5] NMR,[6] and so on. Dynamical properties of sol-gel transition of tetramethoxysilane have been well-investigated by a variety of experimental techniques.[7] Very recently, Nakanishi and Soga have found by EM that the glass finally obtained by the sol-gel method from mixtures of alkylsilicate and organic polymer has an interconnected porous structure in the micron-range.[8] The production of glass materials with well-controlled porosity (in size and in its fraction) would have immeasurable value in materials science. The mechanism producing the porous structure has been considered to be microphase separation in the sol-gel system: silica-rich phases and polymer-rich phases are formed in the system whose size determines that of porosity.[8] Porous structures of the glass finally obtained are clearly seen by EM. In addition, the same kind of porous gel can be obtained when colloidal silica is used as a silica source.[8b] However, the mechanism and the structural change in sol-gel process for such systems are not yet clear. In this study, we applied the small-angle X-ray scattering (SAXS) technique to investigate the sol-gel process (from reaction mixture to wet gel with coexistence of an organic, water-soluble polymer). In this study, we used colloidal silica dispersion as a reaction material instead of alkyl silicate, since we can observe only the second step (aggregation of primary silica particles to form gel network). The SAXS technique has been shown recently to be useful[9] to investigate the sol-gel process and the fractal structure[10] of the gel formed.

Experimental

Colloidal silica used was SNOWTEX S kindly supplied by Nissan Chemical Co. (Tokyo, Japan). The diameter was found to be 6.65 nm by the Guinier method.[11] The mother suspension was dialyzed against 10^{-4} NaOH solution to avoid aggregation until the NaOH solution shows a constant conductivity. The conductivity was checked by a Wayne-Kerr Auto Balance Precision Bridge (Model B331, Surry, England) with a glass conductivity cell with platinum electrodes. The organic polymer used was sodium polystyrenesulfonate (NaPSS) purchased from Pressure Chemical Co. (Pittsburgh, PA) whose molecular weight was 88000 by the supplier. NaPSS was also purified by dialysis against high quality Milli-Q water. The end point of dialysis was also determined by the conductivity method. The dialysis tube used both for colloidal silica and NaPSS was made by Union Carbide Corp. (Chicago, IL). The water used for sample preparation and for dialysis was obtained by the Milli-Q system (Millipore, Bedford, MA).

The SAXS apparatus used was made by Rigaku Corporation (Tokyo, Japan) the details of which have been described fully elsewhere.[12] Since our SAXS system has a position sensitive proportional counter (PSPC), no angle-scanning is necessary. This enabled us to perform time-resolved measurements. The power of the X-ray generator was chosen to be 40 kV—100 mA because the strong scattering from the gel formed at high power condition is out of dynamic range of the detector. We used a Mark glass capillary (Diameter: 1.5 mm) as a SAXS cell. The SAXS cell was thermostatted at about 30 °C during measurements by circulating water from a temperature-controlled bath (Model K2R, Neslab, Newington, NH). The data obtained were corrected for slit smearing by Lake's method. The preparation of reaction mixture was as follows: an NaPSS solution at various concentrations was added into a purified colloidal silica suspension (4.0 vol%). An NaCl solution (0.2 M, M=mol dm^{-3})

Table 1. Component of Colloidal Silica-NaPSS Mixtures

[Silica]/vol%	[NaCl]/M	[NaPSS]/g dm^{-3}
4.0	0.2	0.0
4.0	0.2	0.1
4.0	0.2	0.5
4.0	0.2	1.0
4.0	0.2	2.0
4.0	0.2	6.0
4.0	0.2	12.0

Table 2. Component of Colloidal Silica and NapTS Mixtures

[Silica]/vol%	[NaCl]/M	[NapTS]/g dm^{-3}	[NapTS]/M
4.0	0.2	0.095	4.9×10^{-3}
4.0	0.2	0.94	4.8×10^{-2}
4.0	0.2	6.0	3.1×10^{-1}

was then added into the mixture to trigger gelation. Table 1 shows the composition of reaction mixtures at the onset of the reaction.

We used sodium *p*-toluenesulfonate (NapTS, Wako Chemicals Co., Osaka, Japan) as a monomer analog of NaPSS. The purification of NapTS was kindly done by Mr. Naoki Tanaka of our laboratory by recrystallization. Table 2 shows the compositions of NapTS systems. The concentrations of NapTS were determined to be comparable to the monomer concentration of NaPSS systems.

Results

Figure 1 shows the SAXS curves for a colloidal silica-NaPSS mixture at various gelation times. The time when salt solution was added into the system was defined as the gelation time zero. The abscissa q is the scattering vector ($q=4\pi\sin\theta/\lambda$, 2θ: scattering angle, λ: wavelength of X-ray (1.542 Å) and the ordinate is the relative intensity of scattered X-rays. It is clear that, with proceeding gelation, the intensity at very small-angle regions increases remarkably.

Figure 2 shows a comparison of the scattering behavior at three different NaPSS concentrations. The increase of scattered intensity at small-angle regions becomes significant and is rapid for higher NaPSS concentration systems.

Figure 3 shows a similar comparison for the NapTS systems. There was no significant difference at various concentrations.

Discussion

Guinier Analyses of Small-Angle Regions. In the small-angle regions called Guinier region, the scattering behavior follows a well-known Guinier law:[11]

$$I(q)=N\exp[(-1/3)\,R_g^2\,q^2] \qquad (1)$$

where R_g is the apparent radius of gyration of scatterer and N a constant depending on the apparatus and the concentration. In $\ln I(q)$ vs. q^2 plot (Guinier

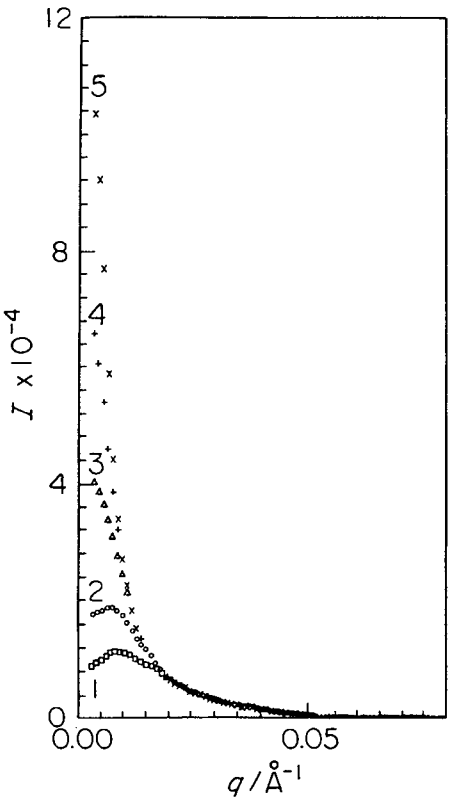

Fig. 1. Small-angle X-ray scattering (SAXS) curves for the gelation of a colloidal silica-NaPSS mixture. [silica]=4.0 vol%; [NaPSS]=1.0 g dm^{-3}; [NaCl]=0.2 M. Time/h: 1) 0.42, 2) 2.92, 3) 5.42, 4) 9.42, 5) 23.

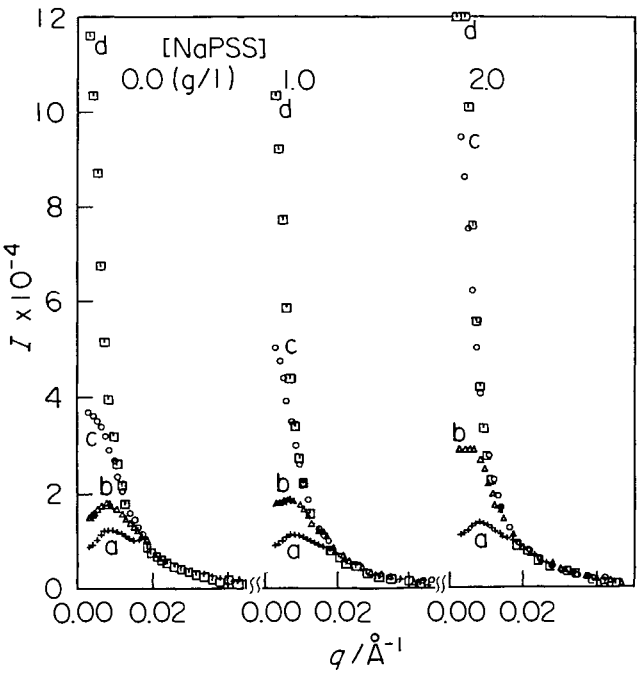

Fig. 2. Comparison of SAXS curves for gelation of colloidal silica at different NaPSS concentrations. [silica]=4.0 vol%; [NaCl]=0.2 M; Gelation time/h: a) 0.42, b) 2.9, c) 6.3, d) 20.

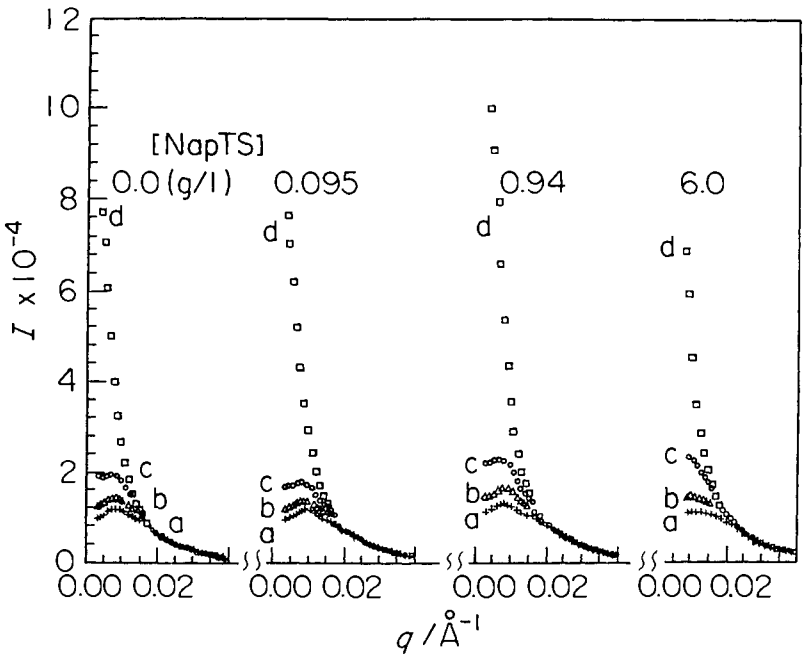

Fig. 3. SAXS curves for gelation of colloidal silica at different NapTS concentrations. [silica]=4.0 vol%; [NaCl]=0.2 M; Gelation time/h: a) 0.42, b) 2.9, c) 6.3, d) 23.

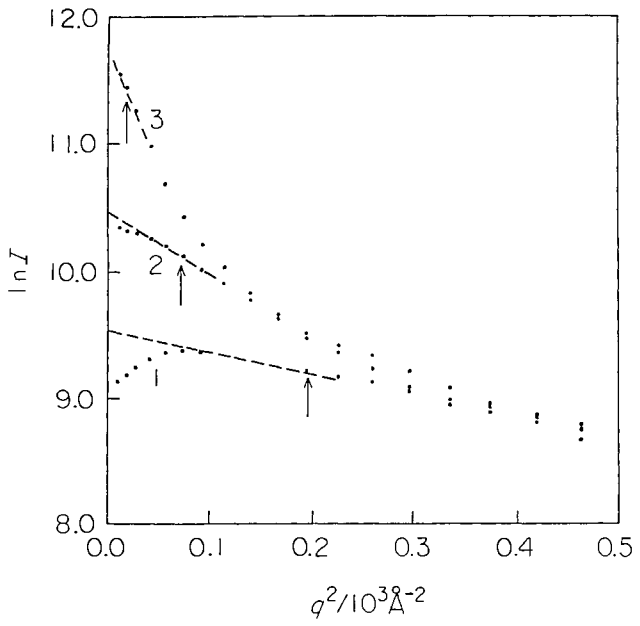

Fig. 4. Guinier plots for the gelation of a colloidal silica-NaPSS mixture. [silica]=4.0 vol%; [NaPSS]=1.0 g dm^{-3}; [NaCl]=0.2 M; Gelation time/h: 1) 0.42, 2) 4.6, 3) 23. The arrows mean the limit of Guinier region for the R_g values obtained from the slope of the straight line.

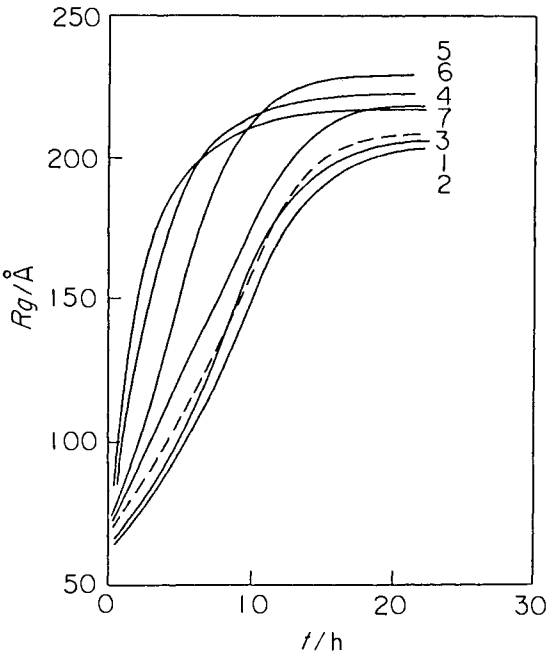

Fig. 5. Changes of the radii of gyration with gelation of colloidal silica dispersion at different NaPSS concentrations. [silica]=4.0 vol%; [NaCl]=0.2 M; [NaPSS]: 1) 0.0, 2) 0.1, 3) 0.5, 4) 1.0, 5) 2.0, 6) 6.0, 7) 12.0 g dm^{-3}.

plot), a linearity should appear in this region and R_g can be calculated from the slope of the straight line. Figure 4 shows typical examples of the Guinier plots, and the R_g values thus obtained are plotted against gelation time in Fig. 5 for different NaPSS concentrations. In general, the R_g value increased rapidly with proceeding gelation and reached constant values. The larger the NaPSS concentration, the steeper and faster the initial increase of R_g value. This tendency can be explained by invoking the concept of phase

separation proposed by Nakanishi and Soga:[8] When a microphase separation occurs, silica-rich phases and polymer-rich phases are formed. The sol-gel process, i.e. aggregation of silica particles occurs in silica-rich phase in which the silica concentration is larger than the average concentration. Due to the higher silica concentration, the aggregation process and hence the sol-gel process is accelerated. A similar phase separation phenomenon has recently been reported by Furusawa et al. for a mixture of polystyrene-based polymer latex and NaPSS systems.[13]

Another possible interpretation of the acceleration phenomena described above may be adsorption of polymer: one linear polymer molecule adsorbed on surfaces of two or more silica particles bringing the particles closer and hence accelerate the aggregation reaction (enhanced collision). This phenomenon is called a bridging effect.[14] However, for our systems, the surface of the silica particles are negatively charged under these conditions (pH=8.9) and NaPSS is, of course, anionic. Adsorption of anionic polymer on negatively charged surface would be implausible due to the electrostatic repulsive interaction between them. In fact, Furusawa et al. reported that no adsorption occurred between NaPSS and polystyrene based, negatively charged polymer latex particle although these two consisted of the same material.[13]

If simple ionic salt is added into the system, the gelation process may be accelerated by the shielding effect of the salt; ionic impurities in the medium reduce the electrostatic repulsive interaction between silica particles, making the contact of the particles easier. Since NaPSS is also ionic, it may act as an ionic impurities and have a shielding effect. However, for our systems, the amount of NaPSS is 0.06 M at maximum, which can be considered to be much smaller than that of simple salt (NaCl, 0.2 M). Moreover, the results for NapTS systems (Fig. 6) clearly rule out this possibility. When compared at the same "monomer" concentration NapTS had nearly no acceleration effect (only at a NapTS concentration of 6.0 g dm^{-3} NapTS, a slight acceleration effect may be seen). Thus it is probable that the acceleration is due to a microphase separation, although the exact mechanism of separation phenomena is not clear at this stage. Further detailed experiments with polymers of various molecular weights are now in progress, and the results will be described in a forthcoming paper.

A few words are necessary on the physical meaning of R_g value. It would be highly possible that, just at the start point of gelation, R_g means the mean size of the colloidal silica particle and that, at the early stage of the reaction, R_g reflects the average size of small (isolated) aggregates of silica particles. However, at a certain point in the middle or late stages of the reaction, a cross-linking reaction should occur to form gel network. Hence, at least, at the final stage of the reaction, R_g should reflect the size of the network (or a correlation length of the network), or the size of "hole" in the network when we take into account the famous Babinet principle in optics.[15] Brinker et al.[16] proposed an interpretation of the meaning of R_g value for both cases of acid and base-catalyzed sol-gel transitions of tetraethoxysilane (TEOS) by a dilution technique. They claimed that the R_g for these two cases should be different; only for the acid case, an increase of R_g by dilution was observable indicating that R_g reflected the network size, while negligibly small changes of R_g for the base case indicated R_g to reflect the mean size of aggregates. However, since the possibility of swelling of the gel by dilution should be taken into account, their proposal of the interpretation might not be universal. For our case, what R_g means is not very clear at this stage. However, we can say that the size of aggregate, the network size, and the phase size in the system if a phase separation occurs, are important factors influencing R_g value.

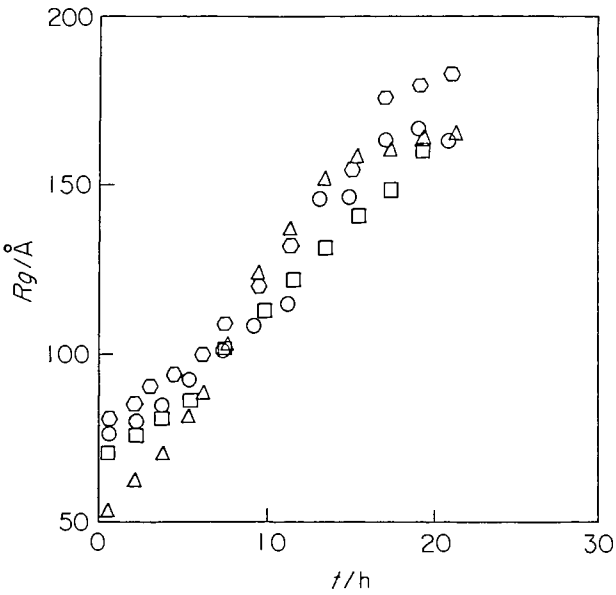

Fig. 6. Changes of radii of gyration with gelation of colloidal silica dispersion at different NapTS concentrations. [silica]=4.0 vol%; [NaCl]=0.2 M; [NapTS]: ○: 0.0, □: 0.095, ○: 0.94, △: 6.0 g dm^{-3}.

Fractal Analyses at the Middle and Large Angle Regions. In relatively higher angle regions, it is well-known that the scattering behavior follows a power law,[17] namely

$$I(q) \propto q^{-\alpha} \tag{2}$$

Hence, the double logarithmic plot of $I(q)$ and q (Porod plot) shows linearity and its slope α is called the Porod slope. When $3 < \alpha \leqslant 4$ holds, α reflects the geometrical structure of the surface of the scatterer and α can be related to the surface fractal dimension D_s by $D_s = 6 - \alpha$.[9] When the surface is perfectly smooth, α

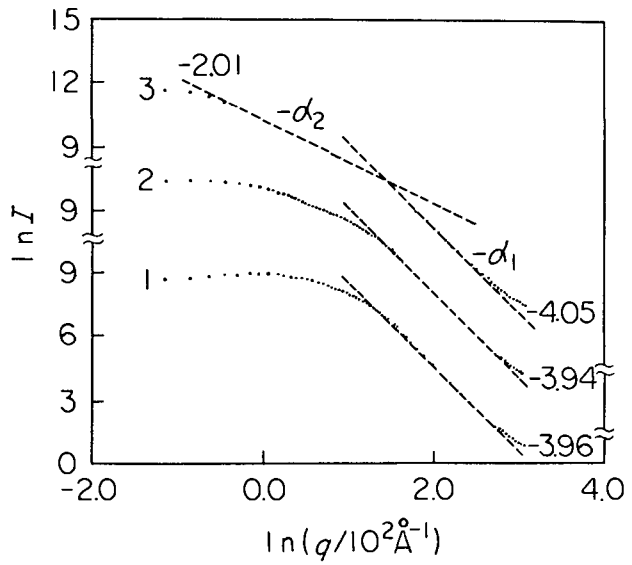

Fig. 7. Porod plots for the gelation of a colloidal silica-NaPSS mixture. [silica]=4.0 vol%; [NaPSS]=1.0 g dm^{-3}; [NaCl]=0.2 M; Gelation time/h: 1) 0.42, 2) 4.6, 3) 23.

should be equal to 4, and this relation had been well-known as a Porod law[18] much before Mandelbrot proposed the concept of fractal.[10] When α is less than or equal to 3, α reflects the geometrical structure of the scatterer itself and α can be related to the volume fractal dimension D_v by $\alpha=D_v$.[9] For both cases, the q range, in which the linearity holds, depends on the dimension of the scatterer which has a fractal character.

Figure 7 shows examples of the Porod plot at three different gelation times. At any gelation time, an excellent linearity is seen at relatively high angle regions. For middle angle region, no linearity is observed at the early stage of the reaction. But as gelation proceeds, linearity appears and at the end of the gelation also excellent linearity holds. The Porod slopes thus obtained for both large (α_1) and middle (α_2) regions are summarized in Table 3. The average radius of the units of the structure, R_u and a correlation length of the gel, R_c obtained from a low q-limit of the linearity for α_1 and α_2, respectively, are also shown in Table 3. The average values of α_1 and α_2 were 4.02 and 1.98, respectively. As mentioned above, it is most reasonable to conclude that α_1 and α_2 reflect the surface and the geometrical structure of the scatterer, respectively. Since the linearity whose slope gives α_1 is already observed at the early stage of the gelation, α_1 reflects the surface structure of colloidal silica particles. The result that R_u values are smaller than the radius of the silica particle corroborates our interpretation. $\alpha_1=4$ means that its surface is smooth (Porod law). The α_2 value, about 2, means the geometrical (fractal) structure of aggregates of primary particles and/or of the gel network formed.

Table 3. Properties of Gels of Colloidal Silica-NaPSS Mixtures

[NaPSS]	Porod slope		Average radius	Correlation
g dm^{-3}	α_1	α_2	R_u/Å	length R_c/Å
0.0	3.99	1.94	24.7	168
0.1	4.02	1.94	25.2	143
0.5	4.00	1.95	25.7	144
1.0	4.05	2.01	23.7	168
2.0	4.06	2.01	22.5	172
6.0	4.01	2.02	23.5	179

[Silica]=4.0 vol%, [NaCl]=0.2 M. $R_u=1/q_u$: q_u is the q value at the crossover point of two straight lines for α_1 and α_2. $R_c=1/q_c$: q_c is the low-q limit of the linearity for α_2.

Since the linearity for α_2 is observed in the angular range between those for the Guinier region and for α_1 linearity, it may be most reasonable to conclude that α_2 reflects the geometrical structure of silica aggregate if R_g reflects the size of the gel network. According to Schaefer,[19] the slope of -2 may be obtained for α at least two geometrical structures, a linear polymer (random coil) and swollen branched polymer. Hence, the structure of the aggregates and/or gel network observed in the present work would be very similar to those of linear polymer or swollen branched polymer, although it is not clear which is correct at the moment. We also observed that the α_2 value increases with increasing polymer concentration, although very slightly. This may reflect the possibility of the control of gel structure by addition of polymer. However, since the change is small, experiments in a much larger polymer concentration range and with other polymers are necessary for further detailed discussion and for study on the relation to the porous structure of final materials, and now are in progress.

Conclusion

Sol-gel transition of a colloidal silica suspension was accelerated by addition of water soluble polymer (NaPSS in this study). This acceleration may have been due to microphase separation between the colloidal silica and polymer, which is not in contradiction with the model proposed by Soga and Nakanishi. The geometrical structure of the gel formed had a fractal nature, and its (volume) fractal dimension was about 2, which is very close to those of linear polymer and swollen linear polymer. The fractal dimension of the gel was slightly affected by the concentration of the coexisting polymer, which makes it feasible to control a gel structure by addition of polymer.

Our sincere gratitude goes to Messrs. K. Tanimoto and S. Ozora, Nissan Chemicals Co., who kindly donated samples. We thank Mr. Naoki Tanaka of our laboratory for the purification of NapTS. This

study was partly supported by Asahi Glass Foundation, to which our sincere gratitudes are due.

References

1) S. Sakka, *J. Non-Cryst. Solids*, **48**, 31 (1982).
2) R. Iler, "The Chemistry of Silica," Wiley, New York (1979), Chap. 3, p. 172.
3) C. J. Brinker, K. D. Keefer, D. W. Schaefer, and C. S. Ashley, *J. Non-Cryst. Solids*, **48**, 47 (1982).
4) N. Soga and K. Nakanishi, *J. Non-Cryst. Solids*, **100**, 399 (1988).
5) V. Gottardi et al., *J. Non-Cryst. Solids*, **63**, 71 (1984).
6) T. W. Zerda, I. Artaki, and J. Jonas, *J. Non-Cryst. Solids*, **81**, 365 (1986).
7) R. Winter, D. W. Hua, X. Song, W.Mantulin, and J. Jonas, *J. Phys. Chem.*, **94**, 2706 (1990).
8) a) K. Nakanishi and N. Soga, *J. Chem. Phys.*, submitted; b) S. Motowaki, K. Nakanishi, and N. Soga, Proceedings of 3rd Autumn Symposium of Ceramic Society Jpn. (Kanazawa).
9) D. W. Schaefer, *Science*, **243**, 1023 (1989); P. W. Schmidts, "Use of Scattering to Determine the Fractal Dimension," in "The Fractal Approach to Heterogeneous Chemistry—Surfaces, Colloids, Polymers," ed by D. Avnir, John Wiley & Sons, New York (1989), Chap. 2.2, p.67.
10) B. B. Mandelbrot, "The Fractal Geometry of Nature," W. H. Freeman and Co., New York (1983).
11) A. Guinier and G. Fournet, "Small-Angle Scattering of X-Rays," Wiley, New York (1955), Chap. 2.
12) N. Ise et al., *J. Chem. Phys.*, **81**, 3294 (1984).
13) K. Furusawa et al., "Proceedings of 42th Meeting of Division of Colloid and Surface Chemistry of the Chemical Society of Japan, 1989, Abstr., p. 336.
14) G. J. Fleer and J. Lyklema, *J. Coll. Interface Sci.*, **46**, 1 (1974).
15) O. Kratky and O. Glatter, "Small-Angle X-Ray Scattering," Academic Press, New York (1982), Chap. 2.
16) C. J. Brinker, K. D. Keefer, D. W. Schaefer, R. A. Assink, B. D. Kay, and C. S. Ashley, *J. Non-Cryst. Solids*, **63**, 45 (1984).
17) D. W. Schaefer and K. D. Keefer, *Phys. Rev. Lett.*, **53**, 1383 (1984).
18) G. Porod, *Kolloid-Z.*, **124**, 83 (1951).
19) D. W. Schaefer, K. D. Keefer, J. H. Anbert, and P. B. Rand, "Structure of Porous Materials: Silica Aerogels and Organic Foams,"in "Science of Ceramic Chemical Processing," ed by L. L. Hench and D. R. Ulrich, John Wiley & Sons, New York (1986), p. 140.

 © 1991 The Chemical Society of Japan Bull. Chem. Soc. Jpn., 64, 1289—1293 (1991)

Mössbauer Emission Study of Recoil ^{119}Sb and ^{119m}Te Atoms after Nuclear Decays and Reactions in SnS and SnSe

Shizuko Ambe and Fumitoshi Ambe*
The Institute of Physical and Chemical Research (RIKEN), Wako-shi, Saitama 351-01
(Received December 4, 1990)

The chemical fates of ^{119}Sb and ^{119m}Te recoil atoms after p- and α-reactions in SnS and SnSe were studied by Mössbauer emission spectroscopy. The ^{120}SnS and ^{120}SnSe samples irradiated with protons gave a partly resolved asymmetric doublet ascribable to ^{119}Sn at the Sn site of the matrices. The α-irradiated ^{117}SnS and ^{117}SnSe samples gave emission spectra, drastically different from those of p-irradiated ^{120}SnS and ^{120}SnSe as well as that of α-irradiated ^{120}SnTe. The spectra are decomposable into three lines which are hardly assignable to any known chemical species of Sn and S or Se. Two of the lines are assigned to a doublet of divalent ^{119}Sn in the Sn site of SnS or SnSe with a nearby defect on the basis of their behavior on thermal annealing. The other line is ascribed to tetravalent ^{119}Sn in a defect structure.

The defect structures created in metals, semiconductors, and chemical compounds by energetic atoms have been extensively studied by hyperfine techniques.[1-10] However, the physical and chemical factors determining the final states of the atoms are not yet fully understood, especially concerning the last matrices. We previously reported a Mössbauer spectroscopic investigation of the ^{119}Sn atoms produced by nuclear-reaction and decay sequences (^{120}Sn(p,2n)^{119}Sb $\xrightarrow{EC}$ ^{119}Sn and ^{117}Sn(α,2n)^{119m}Te $\xrightarrow{EC}$ ^{119}Sb $\xrightarrow{EC}$ ^{119}Sn) in SnTe.[11,12] In the matrix, the recoil ^{119}Sb atoms were found to be stabilized at both the Sn and Te sites.

In the present work, a similar investigation of the recoil atoms produced by nuclear reactions and decays in SnS and SnSe is described.[13] Although the results concerning SnS and SnSe were similar to each other, they were drastically different from that on SnTe. The ^{119}Sn atoms arising from ^{119}Sb atoms produced by the proton reaction were found exclusively at the Sn sites of SnS and SnSe, while those from ^{119m}Te after the α-reaction were found in defect states not observed in SnTe. The results are discussed in terms of the chemical properties of both the recoil atoms and the matrices.

Experimental

Tin isotopes enriched in ^{120}Sn or in ^{117}Sn and consequently depleted in ^{119}Sn (^{120}Sn 98.39% and ^{119}Sn 0.39% or ^{117}Sn 89.2% and ^{119}Sn 1.12%) were used for the preparation of both SnS and SnSe samples in order to reduce the resonant self-absorption of Mössbauer γ-rays in the samples. Crystalline ^{120}SnS and ^{117}SnS were prepared by the vacuum sublimation of amorphous tin sulfide, obtained by a reaction of H_2S gas on tin(II) ions in an aqueous solution. The samples of ^{120}SnSe and ^{117}SnSe were prepared by fusing a stoichiometric mixture of ^{120}Sn or ^{117}Sn metal with selenium under an Ar stream. The samples were examined by powder X-ray pattern and Mössbauer absorption measurements on the ^{119}Sn contained in them by a minute fraction.

Sample powder (50—100 mg cm^{-2}) pressed onto an aluminum plate was irradiated in a target chamber filled with flowing helium gas with 15-MeV protons or 32-MeV α-particles accelerated by the RIKEN 160 cm cyclotron. In the case of protons, irradiation with a beam of about 2.5 μA cm^{-2} was continued for several hours. For α-particles, the corresponding values were 0.5—0.6 μA cm^{-2} and 10—12 h. The targets were thin enough to let the bombarding particles pass through them, so that the intense energy dissipation of the particles near the end of their tracks did not occur in the samples, but in the aluminum backing. The backside of the aluminum plate was cooled directly with water during irradiation. After irradiation the samples were left standing at ambient temperature for 10—20 h, allowing short-lived nuclides to decay. Although neither the bulk temperature of the samples during irradiation nor the local temperature of the end point of the energetic recoil atoms were measurable, the effects of thermal annealing showed that the bulk temperature were less than 100 °C, and that the effect of local heating along the track of the recoil atoms was not serious, if any. The Mössbauer absorption spectra of the irradiated samples showed no trace of radiation damage. Annealing and fusion of the irradiated samples were carried out under an Ar atmosphere.

The Mössbauer emission spectra of the samples were measured against a $BaSnO_3$ (0.9 mg ^{119}Sn cm^{-2}) absorber, both being kept at liquid-nitrogen temperature. Measurements of the α-irradiated samples were performed after radioactive equilibrium had been attained between ^{119m}Te and ^{119}Sb. The spectra were least-squares fitted with lines of a Lorentzian shape using a FACOM M380 computer in our institute.

Results

The obtained emission Mössbauer spectra are shown in Figs. 1—5. The results of fitting are summarized in Table 1. The isomer shift is given relative to $BaSnO_3$ at room temperature.

The ^{119}Sn atoms produced in ^{120}SnS and ^{120}SnSe irradiated with protons gave a partly resolved asymmetric doublet, as can be seen in Figs. 1(A) and (B).

The emission spectra of ^{119}Sn in α-irradiated ^{117}SnS and ^{117}SnSe were complex (Figs. 2(A) and 3(A)), being completely different from those of p-irradiated ^{120}SnS and ^{120}SnSe sources. They were decomposable into

Table 1. Mössbauer Parameters of ^{119}Sn Arising from ^{119}Sb and ^{119m}Te in p- and α-Irradiated SnS and SnSe at Liquid Nitrogen Temperature. Errors for the Isomer Shift and Quadrupole Splitting are Estimated to be 0.05—0.1 mm s^{-1} for Large Peaks and 0.1—0.2 mm s^{-1} for Small Ones.

Samples	Annealing[a)]	Isomer[b)] shift	Quadrupole splitting	Relative area
		mm s^{-1}	mm s^{-1}	%
p-Irradiated ^{120}SnS	None	3.11	0.94	100
α-Irradiated ^{117}SnS	None	0.84		20
		3.10	1.66	80
	100 °C, 1 h	0.95		23
		3.18	1.55	77
	200 °C, 1 h	1.10		23
		3.27	1.22	77
	600 °C, 1 h	3.13	0.93	100
p-Irradiated ^{120}SnSe	None	3.27	0.79	100
α-Irradiated ^{117}SnSe	None	0.89		30
		3.16	1.73	70
	100 °C, 1 h	0.91		28
		3.18	1.50	72
	200 °C, 1 h	0.91		4
		3.04	1.10	96
	600 °C, 1 h	3.21	0.83	100

a) In an Ar stream. b) Relative to $BaSnO_3$ at room temperature.

three Lorentzian lines (designated as Line 1, 2, and 3 from the left to the right). Remarkable changes in the position and in the relative intensities of each line were observed upon thermal annealing of the irradiated samples, as can be seen in Figs. 2(B)—(D) and 3(B)—(D). In both cases of ^{117}SnS and ^{117}SnSe, Line 1 completely vanished upon annealing at 600 °C. Upon elevating the annealing temperature, the relative intensities of Lines 2 and 3 increased in parallel and the two lines shifted closer to each other, their

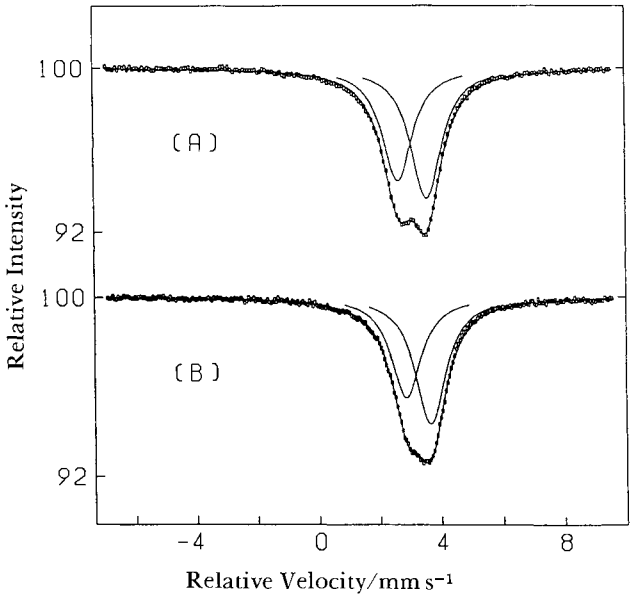

Fig. 1. Mössbauer emission spectra of ^{119}Sb→^{119}Sn in p-irradiated (A) ^{120}SnS and (B) ^{120}SnSe (measurement at liquid nitrogen temperature).

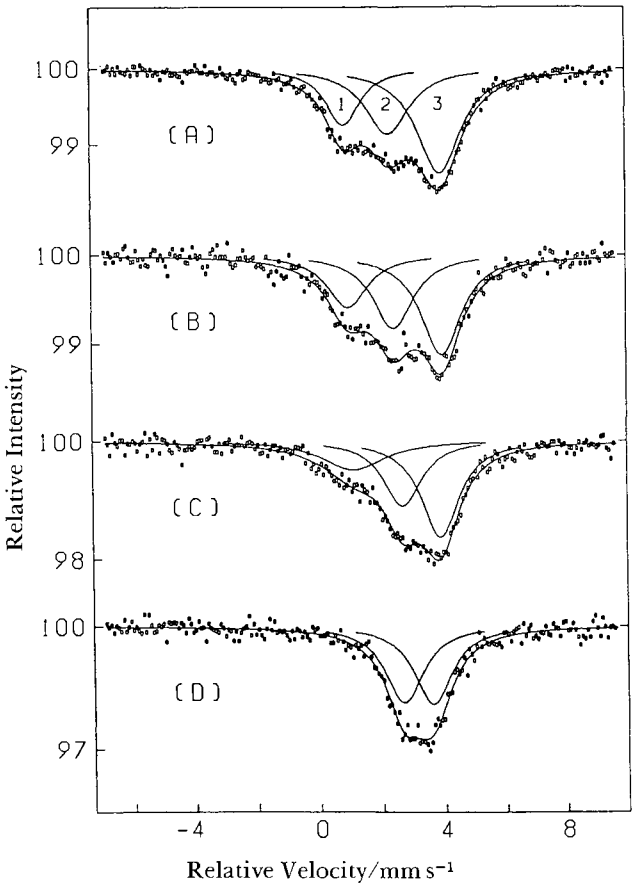

Fig. 2. Mössbauer emission spectra of ^{119m}Te→^{119}Sb→^{119}Sn in α-irradiated ^{117}SnS (measurement at liquid nitrogen temperature). (A) As irradiated, (B) after 1 h annealing at 100 °C, (C) after 1 h annealing at 200 °C, and (D) after 1 h annealing at 600 °C.

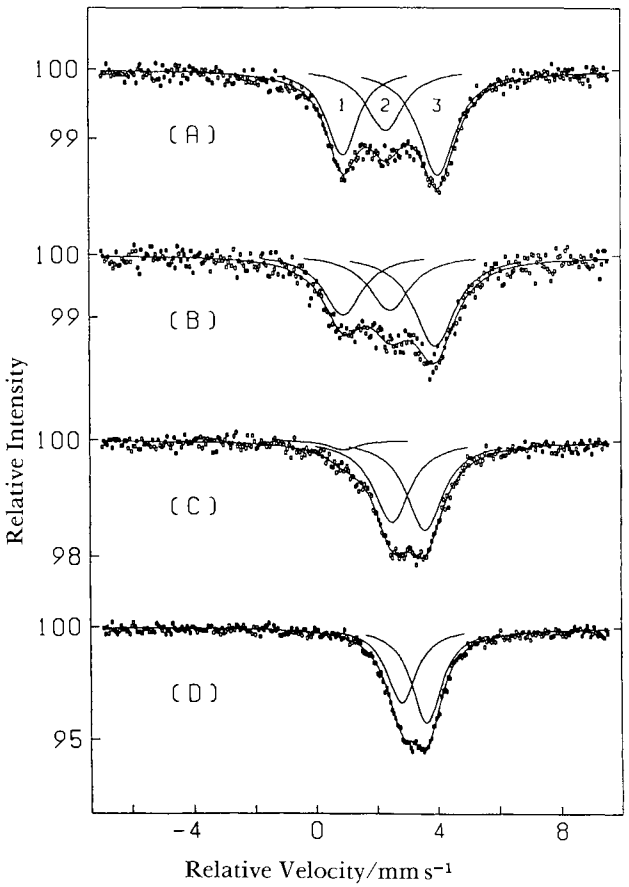

Fig. 3. Mössbauer emission spectra of ^{119m}Te→ ^{119}Sb→^{119}Sn in α-irradiated ^{117}SnSe (measurement at liquid nitrogen temperature). (A) As irradiated, (B) after 1 h annealing at 100 °C, (C) after 1 h annealing at 200 °C, and (D) after 1 h annealing at 600 °C.

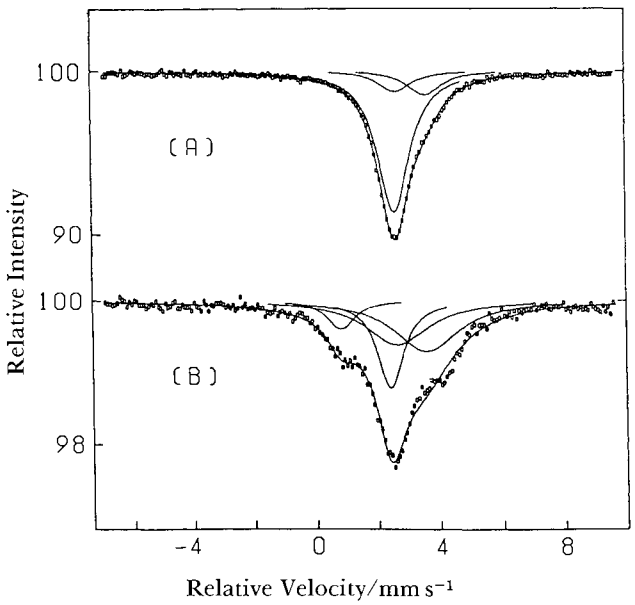

Fig. 4. Mössbauer emission spectra of SnS samples fused and recrystallized with additional 3 at. % ^{120}Sn or ^{117}Sn metal after p- or α-irradiation (measurement at liquid nitrogen temperature). (A) ^{120}Sn$_{1.03}$S(^{119}Sb), (B) ^{117}Sn$_{1.03}$S(^{119m}Te).

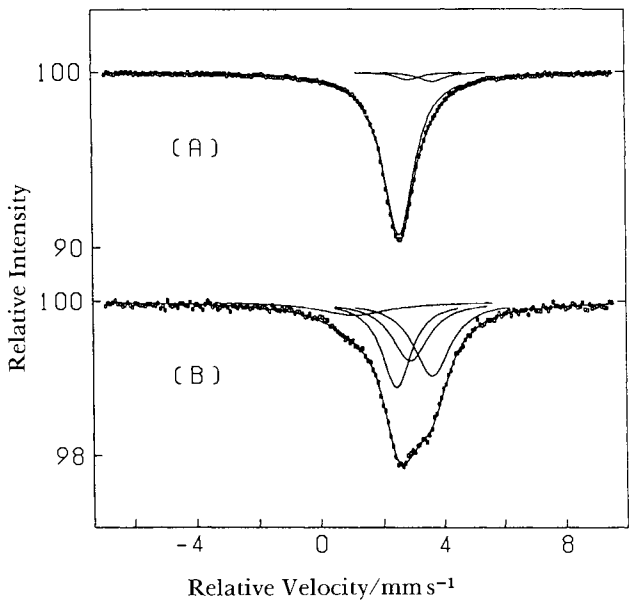

Fig. 5. Mössbauer emission spectra of SnSe samples fused and recrystallized with additional 3 at. % ^{120}Sn or ^{117}Sn metal after p- or α-irradiation (measurement at liquid nitrogen temperature). (A) ^{120}Sn$_{1.03}$Se(^{119}Sb), (B) ^{117}Sn$_{1.03}$Se(^{119m}Te).

centers and widths remaining almost unchanged.

The emission spectra of stoichiometric ^{117}SnS and ^{117}SnSe samples fused and recrystallized after α-irradiation gave spectra similar to those of p-irradiated samples. Figure 4 shows the spectra of ^{120}SnS and ^{117}SnS fused and recrystallized with an additional 3 at. % ^{120}Sn or ^{117}Sn metal after p- or α-irradiation. The samples are designated as ^{120}Sn$_{1.03}$S(^{119}Sb) and ^{117}Sn$_{1.03}$S(^{119m}Te), though their X-ray patterns show that they are not single phase and contain a small amount of β-Sn. The spectra of similarly obtained ^{120}Sn$_{1.03}$Se(^{119}Sb) and ^{117}Sn$_{1.03}$Se-(^{119m}Te) are shown in Fig. 5.

Discussion

Both SnS and SnSe have a rhombically distorted NaCl-type crystal structure (*Pnma*-D_{2h}^{16}). The nuclear reactions and decay sequences studied in this work are:

$$^{120}\text{Sn(p,2n)}^{119}\text{Sb} \xrightarrow{\text{EC}} {}^{119}\text{Sn}^* \longrightarrow {}^{119}\text{Sn}$$

and

$$^{117}\text{Sn}(\alpha,2n)^{119m}\text{Te} \xrightarrow{\text{EC}} {}^{119}\text{Sb} \xrightarrow{\text{EC}} {}^{119}\text{Sn}^* \longrightarrow {}^{119}\text{Sn}.$$

Here, ^{119}Sn* signifies ^{119}Sn in the nuclear first excited state (Mössbauer level).

The p- and α-reactions impart the ^{119}Sb and ^{119m}Te atoms with a recoil energy that is sufficient for their displacement from the sites of the target atoms. In the following EC decay of ^{119m}Te to ^{119}Sb, the neutrino emitted from the nucleus imparts on the atom a recoil energy amounting to 24 eV. The γ-quanta emitted in cascades give recoil energies up to a maximum

value of 20 eV. Assuming that these particles are emitted isotropically, the total recoil energy is estimated to have a distribution with a minimum below the displacement energy, E_d (roughly 25 eV for metals[14]) and somewhat smaller for compounds), and a maximum exceeding it. Therefore, a part of the ^{119}Sb atoms are expected to be displaced from the site of ^{119m}Te as a result of the decay; the others remain in the original site of ^{119m}Te. This was experimentally demonstrated in our previous study on Sn^{119m}Te and $Sb_2{}^{119m}Te_3$ samples.[11] On the other hand, the recoil energy of the EC decay of ^{119}Sb is estimated to be 1.5 eV. Since it is smaller than the displacement energy in a solid, the ^{119}Sn atoms arising from ^{119}Sb remain in the position of the ^{119}Sb atoms after the decay.

We attribute the doublets observed for p-irradiated ^{120}SnS and ^{120}SnSe (Figs. 1(A) and (B)) to ^{119}Sn at normal Sn sites of the matrices on the basis of the similarity of their Mössbauer parameters to those of normal tin atoms in SnS and SnSe observed by conventional Mössbauer absorption measurements on the compounds.[15,16] It is concluded from the observation that the energetic ^{119}Sb atoms produced by the proton reaction are exclusively stabilized at the scarcely perturbed Sn sites of SnS and SnSe, since the recoil energy of the EC decay of ^{119}Sb is smaller than the displacement energy in solid, as described above. Namely, in the last stage of recoil the ^{119}Sb atoms replace an Sn atom in the matrix and the Sn atom is displaced to a position at which the resulting defect structure does not affect the Mössbauer parameters of ^{119}Sn arising from ^{119}Sb. This forms a contrast to the case of ^{120}SnTe, in which ^{119}Sb atoms occupy both the Sn and Te sites after the p-reaction.

The results on α-irradiated samples show that the effect of the α-reaction and the EC decay is entirely different from that of the p-reaction. Lines 1—3 observed for α-irradiated ^{117}SnS and ^{117}SnSe (Figs. 2(A) and 3(A)) can be hardly assigned to known chemical species of Sn having S or Se ligands. On the basis of the isomer shift, Line 1 is assigned to $^{119}Sn^{4+}$ ions accompanied by a nearby defect. The behavior of Lines 2 and 3 upon annealing suggests that they are correlated. After 1 h of annealing at 600 °C, the lines turned out to be a quadrupole doublet assignable to ^{119}Sn at the normal Sn site of SnS or SnSe (Figs. 2(D) and 3(D)). Therefore, Lines 2 and 3 in Figs. 2(A) and 3(A) are ascribed to a quadrupole doublet of ^{119}Sn at Sn site of SnS or SnSe accompanied by a certain defect. Since the isomer shift is virtually the same as that of normal tin atoms in SnS or SnSe, the number of sulfide or selenide ions in the first coordination sphere is not considered to be different from that of normal Sn in SnS or SnSe. The distortion in the first coordination sphere or the defect in the second or further coordination sphere is most probable.

It is to be noted here that the effects of annealing were observed not on ^{119}Sb, but on ^{119m}Te in the experiment described above, since the annealed samples were measured after the ^{119}Sb subjected to annealing had decayed and a radioactive equilibrium between ^{119m}Te and ^{119}Sb had been attained. As described above, the ^{117}SnS and ^{117}SnSe samples fused and recrystallized after irradiation showed no trace of defect structures. Those with chemically doped ^{119m}Te also gave similar results. It is evident from these observations that the defect structures are not the result of the EC decay of ^{119m}Te, but of the α-reaction.

In the thoroughly annealed, fused, and chemically doped samples ^{119m}Te are considered to be at the S or Se site on the basis of a similarity in the chemical properties of the elements. A part of ^{119}Sb atoms arising from ^{119m}Te are displaced from the site due to recoil associated with EC decay. For the rest of ^{119}Sb, although the recoil energy is insufficient for any displacement, the S or Se site is much less favorable for ^{119}Sb than the Sn site with regard to its chemical nature. Namely, the physical and chemical properties of Sb are much closer to that of Sn than to S or Se. Consequently, all of the ^{119}Sb atoms are stabilized at only the Sn site. On the other hand, the properties of Sb lie just in the middle of those of the components of the matrix in the case of SnTe. This enables stabilization of Sb in both sites.

Computer simulations on metal showed that a recoil atom of the same element as the matrix most frequently replaces a lattice atom in the final stage of its energy dissipation and are stabilized at the substitutional site.[17-19] On the other hand, it has been shown that implanted iron atoms tend to occupy interstitial sites in metals having large atomic volumes.[2] In case of ^{119}Sb after the p-reaction, the recoil atom is considered to replace mainly a ^{120}Sn atom, which has a mass close to that of ^{119}Sb and rests at the site. Moreover, the experimental results described above show that the ^{119}Sb atoms stopped at the S or Se site or at an interstitial site move to an Sn site which is chemically much more favorable for them than the S or Se site.

From only a kinematical point of view, the ^{119m}Te recoil atoms are considered to dominantly replace ^{117}Sn in the SnS or SnSe matrix. However, the Sn site is not favorable for ^{119m}Te and a certain metastable defect structure including the surrounding S or Se atoms are formed. This structure is considered to be partly preserved, even after the decay of ^{119m}Te, and to be reflected in the spectra of α-irradiated ^{117}SnS and ^{117}SnSe before annealing (Figs. 2(A) and 3(A)).

Measurements on the SnS and SnSe samples fused and recrystallized with 3 at. % Sn metal were undertaken in order to determine whether stabilization of diluted ^{119}Sb at the S and Se sites is not allowed at all in SnS and SnSe. The SnS or SnSe phase in the samples is considered to be saturated with Sn. This is considered to be a condition promoting ^{119}Sb to the S or Se site based on the result on SnTe.[12] Besides

the doublet of SnS or SnSe, a dominant line with an isomer shift of 2.56±0.03 mm s^{-1} was found in the spectra of $^{120}Sn_{1.03}S(^{119}Sb)$ and $^{120}Sn_{1.03}Se(^{119}Sb)$ samples (Figs. 4(A) and 5(A)). Since the isomer shift is in good agreement with that of β-Sn,[20] this line is assigned to ^{119}Sn arising from ^{119}Sb dissolved in the β-Sn phase of the samples. The large relative intensity of the line shows that ^{119}Sb is much more soluble in β-Sn than in SnS or SnSe. In the $^{117}Sn_{1.03}S(^{119m}Te)$ and $^{117}Sn_{1.03}Se(^{119m}Te)$ samples (Figs. 4(B) and 5(B)), the relative intensity of the peak due to β-Sn is much smaller than in $^{120}Sn_{1.03}S(^{119}Sb)$ and $^{120}Sn_{1.03}Se(^{119}Sb)$. The origin of this large difference is ascribed to the higher solubility of ^{119m}Te, than that of ^{119}Sb, in SnS and SnSe which have a homologous element of Te as a component. The lines with isomer shifts of 0.82 and 1.07 observed for the $^{117}Sn_{1.03}S(^{119m}Te)$ and $^{117}Sn_{1.03}Se(^{119m}Te)$ samples are attributed to the Sn^{4+} species, the origin of which is not understood. They may be the same species as those observed in α-irradiated ^{117}SnS and $^{117}SnSe$. In any case, we conclude that no line ascribable to ^{119}Sn at S or Se site of the matrices has been identified in the specta of samples fused with excess Sn metal,although the possibility is not denied that one is hidden in the large peak due to ^{119}Sb in β-Sn.

The authors are thankful to the staff of the RIKEN 160 cm cyclotron for many irradiation runs and also to Mr. Y. Iimura for X-ray powder pattern measurements.

References

1) G. Weyer, *Hyperfine Interact.*, **27**, 249 (1986).
2) M. Menningen, R. Sielemann, G. Vogl, Y. Yoshida, K. Bonde-Nielsen, and G. Weyer, *Hyperfine Interact.*, **35**, 807 (1987).
3) G. Weyer, *Hyperfine Interact.*, **43**, 187 (1988).
4) J. A. Sawicki and B. D. Sawicka, *Nucl. Instrum. Methods, Phys. Res., Sect. B*, **46**, 38 (1990).
5) S. Laubach, P. Schwalbach, M. Hartick, E. Kankeleit, B. Keck, and R. Sielemann, *Hyperfine Interact.*, **53**, 75 (1990).
6) H. Bemelmans, G. Borghs, and G. Langouche, *Hyperfine Interact.*, **56**, 1553 (1990).
7) H. Binczycka, G. Marest, N. Moncoffre, and J. Stanek, *Hyperfine Interact.*, **56**, 1557 (1990).
8) D. Mo, G. L. Zhang, Z. N. Liang, and L. Niesen, *Hyperfine Interact.*, **56**, 1621 (1990).
9) G. L. Zhang, D. Mo, Z. N. Liang, and L. Niesen, *Hyperfine Interact.*, **56**, 1661 (1990).
10) P. Zhang, L. Urhahn, I. Dézsi, A. Vantomme, and G. Langouche, *Hyperfine Interact.*, **56**, 1667 (1990).
11) F. Ambe and S. Ambe, *J. Chem. Phys.*, **73**, 2029 (1980).
12) F. Ambe and S. Ambe, *J. Chem. Phys.*, **75**, 2463 (1981).
13) Partly presented at the Intern. Conf. on the Appl. of the Mössbauer Effect, Crayton, 1987.
14) F. Seitz, in "Solid State Physics," ed by F. Seitz and D. Turnbull, Academic, New York (1956), Vol. 2, p. 305.
15) J. D. Donaldson and B. J. Senior, *J. Inorg. Nucl. Chem.*, **31**, 881 (1969).
16) V. Fano and I. Ortalli, *J. Chem. Phys.*, **61**, 5017 (1974).
17) J. B. Gibson, A. N. Goland, M. Milgram, and G. H. Vineyard, *Phys. Rev.*, **120**, 1229 (1960).
18) C. Erginsoy, G. H. Vineyard, and A. Englert, *Phys. Rev. A*, **133**, 595 (1964).
19) C. Erginsoy, G. H. Vineyard, and A. Shimizu, *Phys. Rev, A*, **139**, 118 (1965).
20) N. N. Greenwood and T. C. Gibb, "Mössbauer Spectroscopy," Chapman and Hall, London (1971), p. 374.

Dynamical Characterization in Aqueous Solutions of 3-Methoxy- and 3-Ethoxy-1-propanol by Ultrasonic Methods

Sadakatsu NISHIKAWA* and Masayuki UEDA
Department of Chemistry, Faculty of Science and Engineering, Saga University, Saga 840
(Received November 17, 1990)

3-Methoxy-1-propanol and 3-ethoxy-1-propanol were synthesized through potassium propoxide from 1,3-propanediol. Ultrasonic absorptions in their aqueous solutions were measured in the frequency range from 8.5 to 220 MHz as functions of their concentrations along with the sound velocity and density. In a solution of 3-ethoxy-1-propanol, a single relaxational absorption was observed; the cause was attributed to a perturbation of an equilibrium as $AB \leftrightarrow A + B$, where AB represents the solute-solvent complex, A the solute and B the solvent molecules. On the other hand, no relaxational absorption was observed in a 3-methoxy-1-propanol solution up to 4 mol dm^{-3}. The thermodynamic and the kinetic parameters were evaluated for the above-mentioned process from the concentration dependences of the ultrasonic parameters in a 3-ethoxy-1-propanol solution. From evidence concerning the appearance and disappearance of ultrasonic relaxational absorption and comparisons of the rate and thermodynamic constants in aqueous solutions of various alcohols, the alternation of the water structure affected by the addition of the solutes is discussed in connection with the solute structures. The methoxyl group was explicitly found to act as a water structure breaker and the ethoxyl group to do so slightly.

It has been well-known that the addition of a nonelectrolyte into water leads to a water structural change.[1] Recent small-angle X-ray scattering studies[2] in aqueous solutions of nonelectrolytes have provided information about the microscopic properties, and it has been reported that quite large changes of the water structure are caused by the addition of such alcohols, as 2-methyl-2-propanol and 1-propanol and 2-propanol. However, the structural and dynamical properties in the solutions still seem to be beyond our understanding, especially in the concentrated solutions. Ultrasonic absorption methods[3] which provide rather macroscopic or phenomenological properties have been widely used to investigate such concentrated solution properties. From the results of sound absorption in some nonelectrolyte aqueous solutions, the solutes of which have hydroxyl groups,[4,5] we have shown that the cause of ultrasonic absorption is due to a solute-solvent interaction, and have speculated that the methoxyl group acts as a water structure breaker and that the propoxyl group acts as a promoter. Through an investigation of aqueous solutions concerning alcohols with an oxyethylene group,[6] we have predicted that the group has a small breaking effect on the water structure. In 1-propanol aqueous solutions, furthermore, another relaxation process was observed, which was responsible for the hydrophobic interaction of solute molecules. Under these circumstances, it is desired to determine how the ethoxyl group affects the water structure. Another purpose of this study is to observe dynamically whether the methoxyl group causes the hydrophobicity of the molecule to decrease when it is introduced to a molecule with quite high hydrophobicity.

Experimental

The chemicals for 3-methoxy-1-propanol and 3-ethoxy-1-propanol synthesis, 1,3-propanediol, anhydrous potassium carbonate, methyl iodide, and ethyl bromide were purchased from Wako Pure Chemical Co. The desired alcohols were obtained through potassium propoxide. The boiling points were 152 °C for 3-methoxy-1-propanol and 161 °C for 3-ethoxy-1-propanol. Identifications of the synthesized compounds were confirmed by their ^{1}H NMR spectra; the purities were verified by a gas chromatographic method to be more than 96% and the water contents in the synthesized compounds were checked by Karl Fischer method to be less than 2.5%.

The ultrasonic absorption coefficient was measured by a pulse method in the frequency range from 8.5 to 220 MHz. The detail procedure for the absorption measurement is described elsewhere.[7] The sound velocity was measured using an interferometer operated at 2.5 MHz. The cells for the absorption coefficient and the sound velocity measurements were immersed in a water bath controlled within ±0.002 °C. The density was measured by a standard pycnometer, the volume of which was about 5.5 cm^3. All measurements were carried out at 25 °C.

Results and Discussion

There are several procedures to interpret the ultrasonic absorption: analysis of the concentration dependence, frequency dependence, and temperature dependence of the absorption.[8] The experimental absorption coefficients in this study were obtained as functions of the solute concentration and the frequency. In order to obtain the dynamic characteristics in solutions, the analysis of the frequency dependence may provide useful information. A Debye-type equation is well used and is associated with a perturbation of chemical equilibrium, although an analyti-

cal equation for the absorption spectra was still developed.[9] For a single relaxational process, the absorption spectrum is fitted by the following equation:

$$\alpha/f^2 = A/(1+(f/f_r)^2)+B. \quad (1)$$

Here, α is the absorption coefficient, f the frequency, A the amplitude of the relaxational absorption, B the background absorption and f_r the relaxation frequency. The procedures for determining the ultrasonic parameters and for judging whether the spectrum is due to single relaxational absorption or not are described elsewhere.[7,10] Figure 1 shows representative ultrasonic absorption spectra in aqueous solutions of 3-methoxy-1-propanol and 3-ethoxy-1-propanol. A clear frequency dependence of α/f^2 was found for the latter solution, but no dependence was found for the former solution. The frequency-dependent experimental data were analyzed in terms of Eq. 1 by using a nonlinear least-mean-squares method. As can be seen in the figure, the experimental data are well-fitted to the single relaxational curves. The values of $[(\alpha/f^2)_{exp}-(\alpha/f^2)_{cal})]/(\alpha/f^2)_{exp}$ at all frequencies measured were less than ± 0.1, where subscripts *exp* and *cal* indicate those of the experiment and calculation, respectively. The calculated ultrasonic parameters are listed in Table 1 along with the solution density and sound velocity values. Complete sets of the absorption coefficient as functions of the concentration and frequency are available upon request to one of authors (S. N.). Figure 2 shows the concentration dependence of the relaxation frequency for the 3-ethoxy-1-propanol solution. Figure 3 represents the results regarding the amplitude of the relaxational absorption and the background absorption. Because no relaxational absorption was

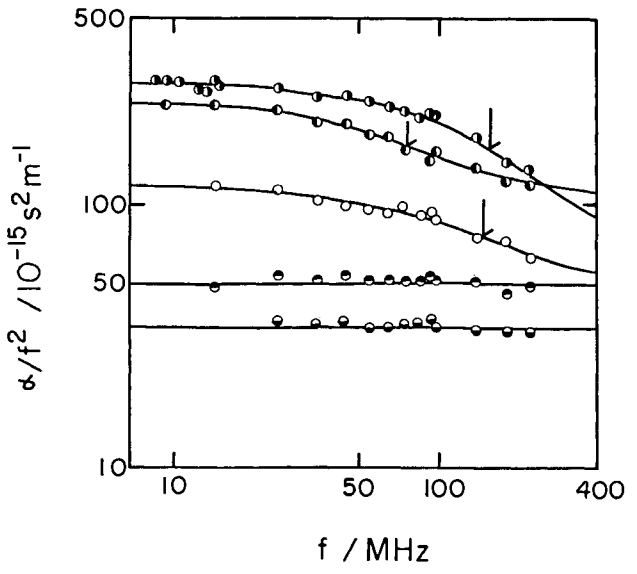

Fig. 1. The representative ultrasonic absorption spectra in aqueous solutions of 3-methoxy-1-propanol and 3-ethoxy-1-propanol at 25 °C. ◓: 3.91 mol dm^{-3} and ◒: 3.00 mol dm^{-3} 3-methoxy-1-propanol, ○: 3.00 mol dm^{-3}, ◐: 4.01 mol dm^{-3} and ◑: 6.00 mol dm^{-3} 3-ethoxy-1-propanol.

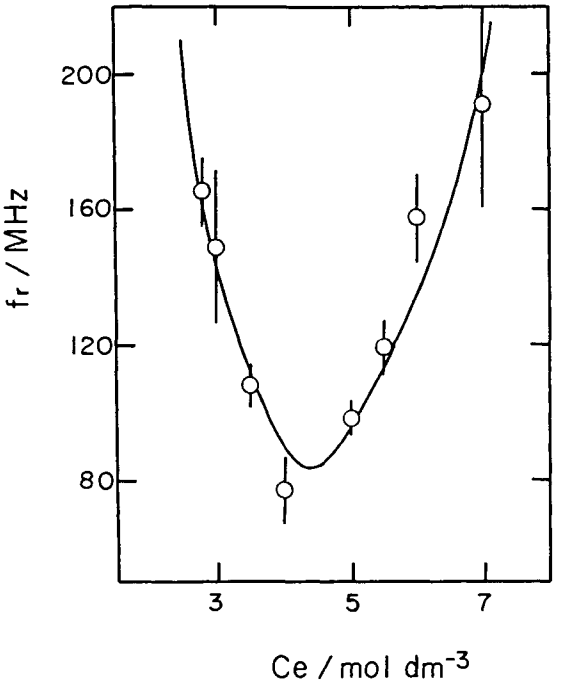

Fig. 2. The concentration dependence of the relaxation frequency for 3-ethoxy-1-propanol solution at 25 °C.

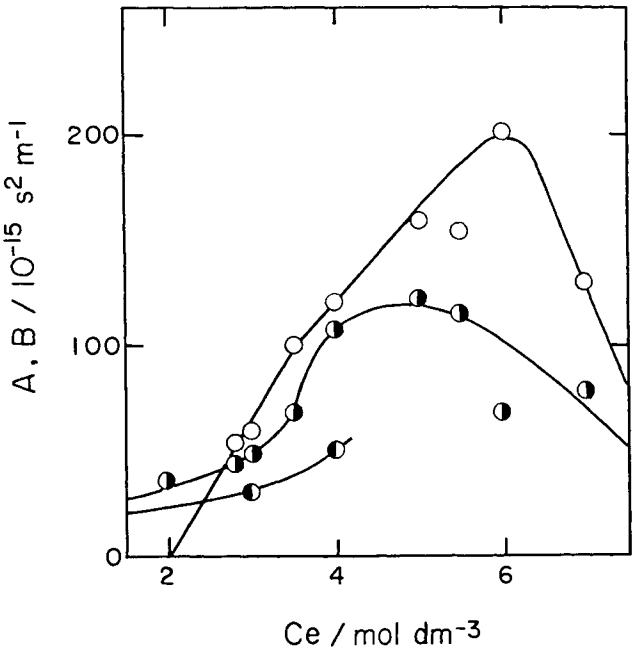

Fig. 3. The concentration dependences of the amplitude of the relaxational absorption and back ground absorption. ○: A for 3-ethoxy-1-propanol, ◑: B for 3-ethoxy-1-propanol ◐: B for 3-methoxy-1-propanol solutions.

Table 1. Ultrasonic Parameters and Density for Aqueous Solution of 3-Ethoxy-1-propanol at 25 °C

C_e	A	B	f_r	c	ρ
mol dm^{-3}	10^{-15} s^2 m^{-1}		MHz	m s^{-1}	kg dm^{-3}
1.00	—	—	—	1562.3	0.9951
2.00	—	—	—	1608.4	0.9933
2.50	—	—	—	1624.5	0.9927
2.80	54.6±1.8	43.1±2.4	165.8±10.9	1629.7	0.9925
3.00	58.1±3.9	47.9±5.5	149.3±24.0	1631.7	0.9923
3.50	100.5±2.5	67.8±2.5	108.9±7.0	1627.6	0.9915
4.01	119.0±9.8	108.4±3.5	76.6±10.0	1612.0	0.9843
5.00	159.6±4.0	123.8±3.0	98.8±5.5	1588.5	0.9814
5.50	154.8±3.8	115.2±4.6	119.8±8.1	1568.7	0.9765
6.00	201.3±8.0	69.6±10.7	157.9±13.1	1547.5	0.9716
7.00	131.2±18.1	79.5±20.3	191.3±30.2	1491.3	0.9601

Table 2. Rate and Thermodynamic Parameters in Aqueous Solutions of 3-Ethoxy-1-propanol and 1-Propanol at 25 °C

Alcohol	k_{21}	K_{12}	β
	10^8 mol^{-1} dm^3 s^{-1}	mol dm^{-3}	
1-Propanol	0.51±0.05	4.5±1.0	0.141±0.013
3-Ethoxy-1-propanol	2.41±0.12	0.27±0.07	0.159±0.004

observed in the 3-methoxy-1-propanol solution within the measured frequency range, the background absorption is only indicated in the same figure.

The sound velocity also goes through a maximum, as can be seen in Table 1. The phenomenon of the peak sound velocity as being a function of the concentration is also a characteristic of aqueous solutions of alcohols, along with the peak sound absorption concentration.

The characteristic phenomena associated with the observed relaxation are that the relaxation frequency goes through a minimum and that the amplitude of the relaxational absorption goes through a maximum. These trends are not interpreted by reaction models only associated with the solutes in the solution. Under these experimental facts, we have proposed the following reaction mechanism for interpreting the relaxational absorption.[4] That is, the solute may interact with solvent water and they form the complex, presumably, due to their hydrogen-bonding ability.

$$AB \underset{k_{21}}{\overset{k_{12}}{\longleftrightarrow}} A+B \qquad (2)$$

where AB is the complex formed by alcohol and water and A the solute molecules. Attention should be paid to the notation, B, which represents non-hydrogen-bonded water molecules, or less-structured water molecules; we assume that such reactants, B, can only participate in the reaction described by Eq 2. Under this assumption, the relation between the analytical concentrations and the relaxation frequency is derived as[5]

$$2\pi f_r = k_{21}\{(C_e-\beta C_w+K_{12})^2+4\beta C_w K_{12}\}^{1/2} \qquad (3)$$

where k_{ij} is the rate constant, C_e and C_w the analytical concentration of alcohol and water, respectively, and β the fraction of non-hydrogen-bonded water; K_{12} is defined as $K_{12}=k_{12}/k_{21}$. The three parameters, k_{21}, β and K_{12}, in Eq. 3 are determined in order to give the best agreement with the experimental data, by means of a nonlinear least-mean-squares. The solid curve in Fig. 2 was calculated from the variation of the concentration. The determined rate and thermodynamic constants are listed in Table 2, along with those for a 1-propanol solution for a comparison.

In order to confirm the cause of relaxational absorption, the concentration dependence of the amplitude of the relaxational absorption should also be analyzed. In ultrasonic studies, the maximum excess absorption per wave length, μ_{max}, is usually considered. For the reaction under consideration, it is given

$$\mu_{max} = 0.5\, A f_r c = (\pi\rho c^2\Gamma/2RT)(\Delta V-\alpha_p\Delta H/\rho C_p)^2, \qquad (4)$$

where ρ is the solution density, ΔV the standard volume change of the reaction, ΔH the standard enthalpy change of the reaction, C_p the specific heat at the constant pressure, α_p the thermal expansion coefficient, and Γ the concentration term given by $\Gamma=\{[AB]^{-1}+[A]^{-1}+[B]^{-1}-([AB]+[A]+[B])^{-1}\}^{-1}$. In order to grasp the precise variation of μ_{max} on the analytical concentration, the values of the specific heat and the thermal expansion coefficient are desired. Without these values, we reluctantly compare the experimental values of μ_{max} with $\rho c^2\Gamma$, which is the most controlling term to μ_{max}. Figure 4 indicates the concentration dependences of μ_{max} and $\rho c^2\Gamma$.

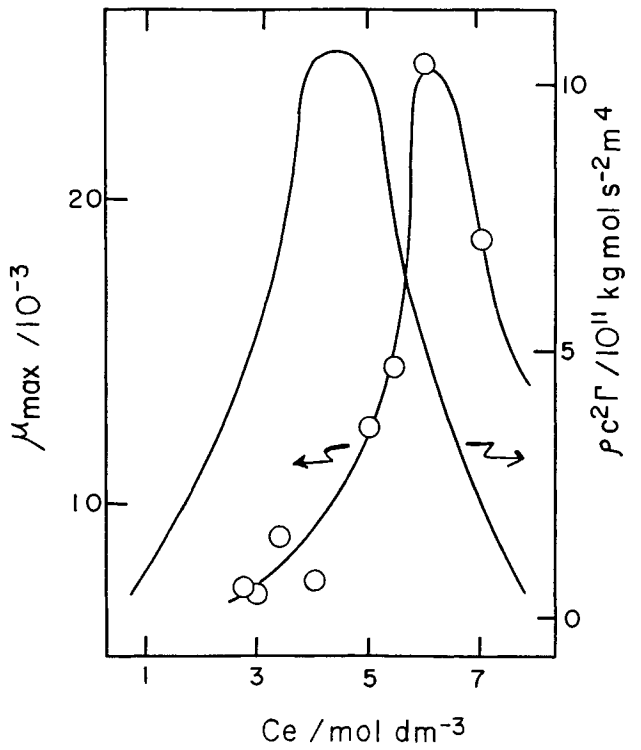

Fig. 4. The comparison of the μ_{max} and $\rho c^2\Gamma$ for 3-ethoxy-1-propanol solution.

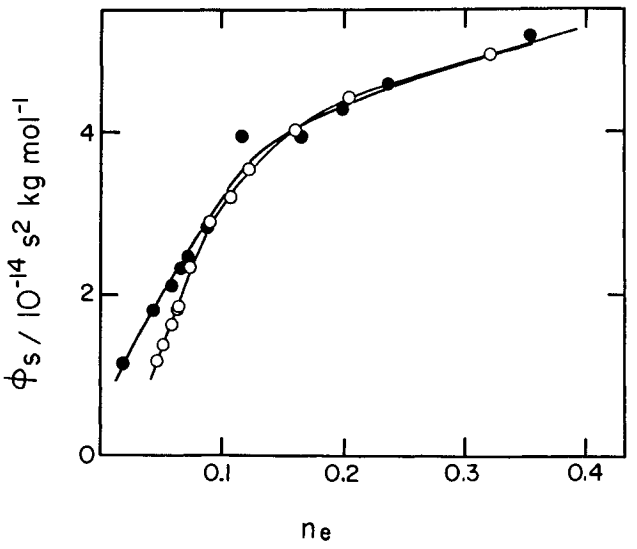

Fig. 5. The apparent molar compressibility for 3-ethoxy-1-propanol (○) and 1-propanol (●) solutions as a function of alcohol mole fraction, n_e at 25 °C.

Though the peak positions are slightly different, the trends seem to be similar, which supports our analysis.

The relaxational absorption in aqueous solutions of alcohols is very sensitive to the hydrophobicity of alcohol molecules. In a solution of methanol, relaxational absorption at room temperature is reported to be observed over a frequency range of more than 500 MHz;[11] in the solution of ethanol it is found at around 300 MHz[12,13] and in that of 1-propanol it exists in a range less than 100 MHz.[5,14,15] Madigosky and et al.[15] have reported the absorption coefficients far below 100 kHz in a solution of 1-propanol, and have preferred to analyze the absorption using fluctuation theories. In this type solution, the absorption coefficient divided by the square of the frequency increases upon decreasing the frequency far below the MHz frequency range. However, in a solution of 2-propanol, the values are almost frequency independent below 10 MHz.[16] As can be seen in Fig. 1, the dependence of α/f^2 in the solution of 3-ethoxy-1-propanol is too small below 10 MHz and the absorption spectrum can be well-analyzed by the Debye-type single relaxational equation. Following our experimental results, we have considered that the absorption is very dependent on the structure of the alcohols, especially on the hydrophobic group. Our analytical results also indicate that the water structure is considered to be altered, depending upon the change in the solute hydrophobicity. As is shown in the present study, no relaxational absorption is observed in the solution of 3-methoxy-1-propanol in the pulse frequency range, and the single relaxational absorption is found in the solution of 3-ethoxy-1-propanol. The cause of the relaxational absorption is reasonably analyzed by a model associated with the interaction between the solute and the solvent; the relaxation process also reflects a change in the ratio of the hydrogen-bonded water and non-hydrogen-bonded water. It is, therefore, interesting to compare the result for the aqueous solution of 3-ethoxy-1-propanol with that of the 1-propanol solution. As can be seen in Table 2, the β value for 1-propanol solution is slightly smaller than that for 3-ethoxy-1-propanol, which means that the introduction of the ethoxyl group makes the hydrophobicity of 1-propanol decrease. The same decreasing trend of the β value has been observed in solutions of alcohols with oxyethylene groups, although the magnitude of the β change is smaller than that for the ethoxyl group.[6] One way to estimate the strength of hydrophobicity is to determine the concentration dependence of the apparent molar compressibility, Φ_s. This method is used by Desnoyers and his co-worker,[17] and is calculated by

$$\Phi_s = \kappa_s\Phi_v + (\kappa_s - \kappa_w)/m\rho_0, \quad (5)$$

where κ_s is the adiabatic compressibility of the solution, κ_w that of solvent, Φ_v the apparent molar volume, ρ_0 the solvent density and m the molality which is converted from the molarity using the solution density. The sharper is the profile of the dependence, the greater is the hydrophobicity. Figure 5 indicates a comparison of the two solutions of 1-propanol and 3-

ethoxy-1-propanol as a function of mole fraction. The latter solution shows a broader dependence than does the former, the result of which is consistent with that obtained from the above-mentioned absorption data. It should be noticed that another relaxation process associated with molecular aggregation through a hydrophobic interaction is observed in the solution of 1-propanol, in addition to absorption due to a solute-solvent interaction. The former absorption disappears when the ethoxyl group is involved. This is because the ether oxygen may prevent the formation of an aggregate in an aqueous solution, and because of a decrease in the hydrophobicity. The small change in the molecular structure of alcohols provides a quite large change in the structure of water. This is clearly seen by comparing the results for the 3-ethoxy-1-propanol solution with that for a 2-propoxyethanol solution,[18] in which the single relaxational absorption due to a solute solvent interaction is found and the β value is 0.10. In general, the ultrasonic relaxational absorption associated with the solute solvent interaction would appear in the MHz frequency region when the sizes of the alcohols are order of propanols or butanols. Upon decreasing the hydrophobicity, the relaxation frequency increases to more than 100 MHz. However, in the solution of 3-methoxy-1-propanol, no relaxational absorption is observed, although the relaxation is found in the solution of 1-methoxy-2-propanol.[3] According to the studies reported so far, 2-propanol has less hydrophobic activity than does 1-propanol. The introduction of a methoxyl group seems to cause the relaxation process to shift to a higher frequency range. It might then be considered that 1-methoxy-2-propanol is less hydrophobic than 3-methoxyl-1-propanol. However, the disappearance of relaxation in the latter solution is speculated since intramolecular hydrogen boning might be plausible in 3-methoxyl-1-propanol, and the total hydrophobic activity of the molecule might decrease. We expect that the hydrophobic and hydrophilic balance of 3-methoxy-1-propanol is close to or less than ethanol, and that the relaxational absorption may appear at more than 200 MHz.

The authors are indebted to organic chemist, Assistant Professor H. Horimoto in the Chemistry Department, for guiding us in the synthesis of the used compounds. This work was partly supported by a Grand-in-aid for Scientific Research on Priority Area of "Molecular Approaches to Non-equilibrium Processes in Solution in 1990" (No. 02640350) from the Ministry of Education, Science and Culture.

References

1) F. Frank and D. J. Eves, *Q. Rev., Chem. Soc.*, **20**, 1 (1966).
2) K. Nishikawa and T. Iijima, *J. Phys. Chem.*, **94**, 6227 (1990); H. Hayashi, K. Nishikawa, and T. Iijima, *J. Phys. Chem.*, **94**, 8334 (1990).
3) M. P. Mason, "Physical Acoustics," Academic Press, New York (1965).
4) S. Nishikawa, Y. Moritsubo, F. Matsuo, and Y. Endo, *Bull. Chem. Soc. Jpn.*, **63**, 26 (1990).
5) S. Nishikawa, M. Mashima, and T. Yasunaga, *Bull. Chem. Soc. Jpn.*, **48**, 661 (1975).
6) S. Nishikawa and R. Shinohara, *J. Soln. Chem.*, **15**, 221 (1986).
7) S. Nishikawa and K. Kotegawa, *J. Phys. Chem.*, **89**, 2896 (1985).
8) M. J. Blandamer, "Chemical Ultrasonics," Academic Press, New York (1973).
9) H. Endo, *J. Chem. Phys.*, **92**, 1986 (1990).
10) S. Nishikawa and F. Matsuo, *J. Phys. Chem.*, **95**, 437 (1991).
11) J. Emery and S. Gasse, *Acustica*, **43**, 205 (1979).
12) K. Takagi and K. Negishi, *Jpn. J. Appl. Phys.*, **14**, 953 (1975).
13) S. G. Bruun, P. Sorensen, and A. Hvidt, *Acta Chem. Scand., Ser. A*, **28**, 1047 (1974).
14) M. J. Blandamer, N. J. Hidden, M. C. R. Symons, and N. C. Treloar, *Trans. Faraday Soc.*, **64**, 3242 (1968).
15) W. M. Madigosky and R. W. Warfield, *J. Chem. Phys.*, **86**, 1491 (1987).
16) S. Nishikawa, M. Mashima, and T. Yasunaga, *Bull. Chem. Soc. Jpn.*, **49**, 1413 (1976).
17) J. Lara and J. E. Desnoyers, *J. Soln. Chem.*, **10**, 465 (1981).
18) S. Nishikawa, Y. Yamashita, and M. Mashima, *Bull. Chem. Soc. Jpn.*, **55**, 1 (1982).

Molecular Motion and Phase Changes in Long Chain Solid Normal Alkanes as Studied by ^1H and ^{13}C NMR

Takahiro UEDA, Sadamu TAKEDA, Nobuo NAKAMURA,* and Hideaki CHIHARA
Department of Chemistry, Faculty of Science, Osaka University, Toyonaka, Osaka 560
(Received December 18, 1990)

Proton spin-lattice and dipolar relaxation times and ^{13}C CP/MAS NMR spectra were measured on crystalline samples of n-$C_{50}H_{102}$ and long chain normal alkanes (n-alkanes) with average molecular weight of 595, 1214, and 2305 in order to characterize the static and dynamic molecular structures in the solid state. The ^{13}C CP/MAS spectra indicate that the molecules take all-trans conformation in the orthorhombic unit cell and do not undergo any discernible change on annealing and/or quenching of specimens. On the other hand, the T_{1d} in each material assumes a deep and clear minimum value in the orthorhombic phase; this relaxation process was unambiguously assigned to the molecular uniaxial reorientation about the long chain axis. There is a linear relation between the activation energy and the reciprocal of the chain length. In the case of n-$C_{50}H_{102}$ a solid state phase transition was found at 351 K. The T_{1d} in the high temperature phase led to extremely high activation energy, 150 kJ mol^{-1}, which may be attributable to molecular self-diffusion or other motion accompanying drastic change in the molecular structure.

Normal alkanes, n-C_nH_{2n+2}, crystallize generally in an orthorhombic unit cell in which molecules assume the all-trans conformation and arrange the molecules parallel to each other.[1] Short n-alkanes with carbon atoms less than 50 undergo so-called "rotational phase transition" into the high temperature phase in which molecules rotate about the long axis.[2] The mechanism of this kind of phase transition has been studied extensively in relation to molecular motion as well as the well-known odd-even effect.[3] Long-chain n-alkanes are situated between the short n-alkanes and polyethylene and possess on the one hand some common characteristics to short n-alkanes, and on the other to polyethylene. Indeed, Whiting and others[4] succeeded in the synthesis of pure long-chain n-alkanes with the number of carbons from 102 to 390 and they also found very interesting fact that the partial chain-folding occurs for the n-alkanes with the carbon number of 150 and more but not for that with 102 carbons.

Thus, the studies of structure and dynamics of long-chain n-alkanes are promising and would provide useful clue to studying variety of physical properties as well as structure of polyethylene and other complex polymers from the molecular point of view. However, although numerous thermodynamic studies have been done on high molecular weight n-alkanes,[5] there have been reported very few works on rigorous characterizations, microscopic structure, and molecular dynamical nature for these substances.

In the present work, we attempted to study long-chain n-alkanes from the molecular point of view and conducted experimental works on the phase characterization and molecular structure by differential scanning calorimetry (DSC) and solid state high resolution ^{13}C NMR and on the molecular dynamical structure by proton nuclear magnetic relaxation measurements. This paper presents the results of these experiments and discuss the possibility of very slow molecular motion in "hard" crystalline state.

Experimental

Powdered specimens of linear polyethylene (PE) with M_w of 595, 1214, and 2305 (M_w/M_n=1.11, 1.20, and 1.14, respectively) which were crystallized from o-dichlorobenzene solution were obtained from Scientific Polymer Products, Inc. (U.S.A.), and were used as received. Even numbered n-alkane, pentacontane (n-$C_{50}H_{102}$), was obtained from Tokyo Kasei Co. in the best commercially available quality (Purity >99%) and was also used without further purification. For proton spin-lattice relaxation time T_1 and dipolar relaxation time T_{1d} measurements, these samples were sealed into ampoules with He exchange gas after being pumped overnight at room temperature.

All NMR measurements were carried out with a Bruker Model MSL-200 spectrometer operating at the Larmor frequencies 200.13 MHz and 50.32 MHz for proton and carbon, respectively. The proton line shape was determined by the Fourier transform of the solid echo.[6]

Measurements of the proton spin-lattice relaxation time, T_1, were made using "solid echo" method which consists of $90°_x$—τ—$90°_y$—$90°_x$ three pulse sequence.[6] Typical interval between the second and third pulses was chosen to be 10—15 μs. Measurements of the proton dipolar relaxation time, T_{1d}, were made using the three pulse Jeener-Broekaert $90°_x$—$45°_y$—τ—$45°_x$ sequence.[7] The interval between 90° and phase-shifted 45° pulses was 8—10 μs. The recovery of the magnetization in each specimen was exponential within the experimental error. The experimental errors for the T_1 and T_{1d} were estimated to be within 5% and 10%, respectively.

^{13}C CP/MAS NMR spectra were recorded with the spectrometer described above. The applied cross-polarization time was 1 ms followed by the ^{13}C detection period during which the proton decoupling field was maintained. MAS (magic angle spinning) was carried out at a rate of 1.5—3 kHz with a double bearing type rotor made of zirconia whose volume was about 0.7 cm^3. In the present work, the

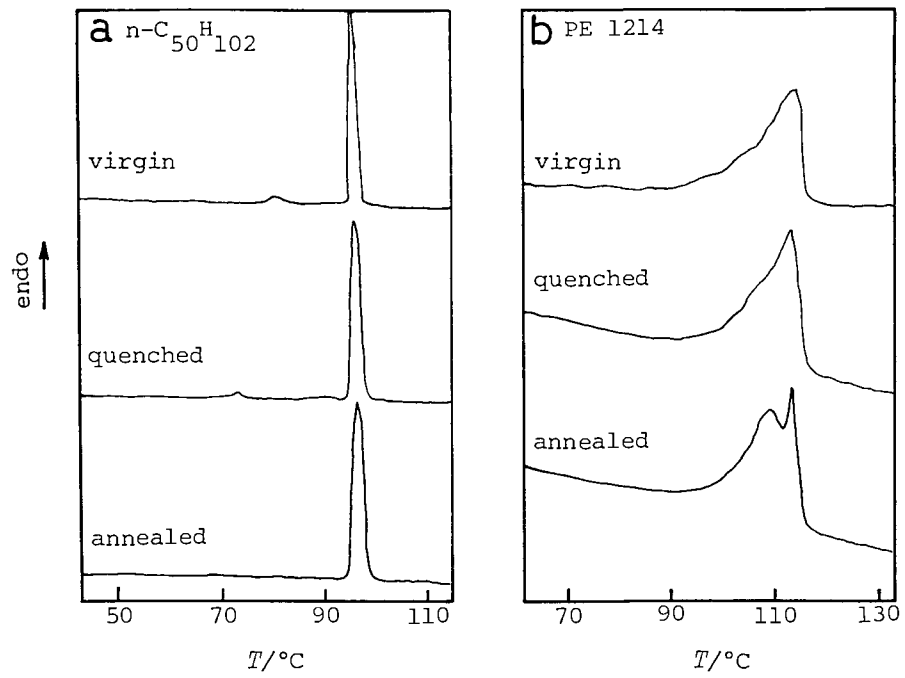

Fig. 1. Differential calorimetric scans for virgin (recrystallized from solution), quenched from the melt, and annealed specimens of n-$C_{50}H_{102}$ (a) and PE 1214 (b).

^{13}C chemical shifts relative to TMS were determined from the CO line (176.46 ppm) of solid glycine.

For all experiments, the temperature control was achieved by Bruker variable temperature unit VT-1000. The melting points and solid state phase transition points of all samples were determined by means of Shimadzu DT-30B differential scanning calorimeter with a heating rate of 5 K min^{-1}. X-Ray diffraction powder patterns were measured by means of RAD-RC type, fully automatic, X-ray diffractometer (Rigaku electronics Inc.).

Results and Discussion

X-ray diffraction powder patterns of all the specimens consisted of sharp reflections which can be indexed to the orthorhombic unit cell corresponding to ordinary polyethylene crystal and weak halo components were discerned, indicating that each specimen can be regarded as good crystals with negligible amount of amorphous components.

Melting points, probable transition points determined by DSC measurements, and crystallinity estimated by proton line shape analysis are listed in Table 1; DSC curves for n-$C_{50}H_{102}$ and PE 1214 are shown in Fig. 1(a) and (b) as typical examples.

The virgin and quenched# samples of n-$C_{50}H_{102}$ undergo solid state phase transition just below the melting point, while the annealed# sample gives no evidence of phase transition. The melting of PE 1214 begins near 363 K as shown in Fig. 1(b) due probably to the melting of the amorphous part, suggesting that even negligible amount of amorphous part causes premelting phenomenon in long chain alkane.[8] The proton spectrum in each substance consists of a narrow and a broad components due obviously to an amorphous part and the rigid crystalline part, respectively, in the specimen. Two components were approximated by a narrow Lorentzian peak and the

Table 1. The Melting Points, the Phase Transition Points Determined by DSC, and Crystallinity for the n-Alkane Specimens with Different Thermal Histories

Sample	Treatment	Melting point/K	Transition point/K	Crystallinity %
n-$C_{50}H_{102}$	Virgin	366	351[a]	
	Annealed	366	—	
	Quenched	366	343, 361[a]	
PE 595	Virgin	—		
	Annealed	330		91
	Quenched	330		
PE 1214	Virgin	376		
	Annealed	380	369[b]	95
	Quenched	376	368[b]	
PE 2305	Virgin	391		
	Annealed	392	386[b]	98
	Quenched	393	386[b]	

a) Rotational phase transition for n-alkane. b) Peak or shoulder of the melting curve which was assigned to the permelting of the amorphous part.

Virgin sample was obtained by crystallization from solvent, quenched one by rapid solidification of the melt, and annealed one by slow cooling of the melt.

Pake doublet with an appreciable line broadening (Gaussian) and the whole spectrum was simulated by changing the composition. The result led directly to the crystallinity listed in Table 1. In the case of n-$C_{50}H_{102}$ no narrow component was observed, indicating that the material is pure crystal.

Carbon-13 CP/MAS NMR Spectra. Fig. 2(a) shows the ^{13}C CP/MAS NMR spectrum of n-$C_{50}H_{102}$ at room temperature. The spectrum of n-$C_{50}H_{102}$ consists of four sharp peaks which can be assigned according to Van der Hart[9] to, from the high field side downward, the methyl carbon, the α-methylene carbon bonded to the methyl carbon, inner carbons with trans zig-zag conformation, and the β-methylene carbon bonded to α-carbon, respectively. The signal with star is the spinning side band of the strongest signal due to inner carbons.

The facts that the inner carbon line is very sharp and located at a lower field than α-methylene peak by 8 ppm show obviously that the linear chain molecules have the all-trans conformation in the orthorhombic unit cell,[9] and moreover, the specimen contains only negligible amounts of amorphous part. The spectrum of PE 1214 shown in Fig. 2(b) consists also of four peaks the location of which are almost the same as in n-$C_{50}H_{102}$. The line width of each peak is about twice as large as in n-$C_{50}H_{102}$ due probably to a slight disorder in the molecular arrangement associated with the molecular weight distribution. Then, the spectrum of this material shows that the molecules take the all-trans conformation. The fraction of the gauche form,[10] if any, is estimated to be less than 1% and that of amorphous part is negligibly small as shown in Table 1. We did not see any change in the spectrum due to quenching and/or annealing of specimen.

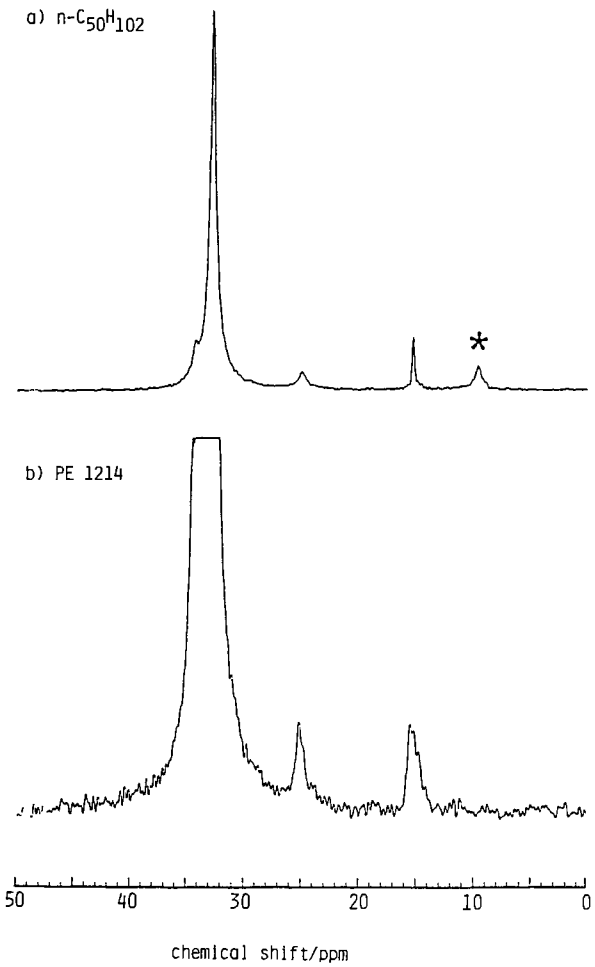

Fig. 2. ^{13}C CP/MAS NMR spectra of n-$C_{50}H_{102}$ (a) and PE 1214 (b) at room temperature. The sign (*) is the spinning side band.

As to the temperature dependence of the spectra only a slight narrowing of the methyl carbon signal on heating were observed for both quenched and annealed specimens due probably to the rapid rotation of the methyl group. The α-methylene and the inner carbon line widths did not show any significant temperature dependence.

Other substances, PE 595 and PE 2305, gave similar spectra to that of PE 1214 although the line width increases slightly with the chain length. It is therefore concluded that all the materials examined here have extremely high crystallinity (see in Table 1) and the molecules assume all-trans conformation; there is no evidence of wrong, gauche conformation nor chain-folding.[10]

Proton Spin Lattice and Dipolar Relaxation Times. n-Alkanes or linear polyethylenes consist of long $-CH_2-$ chain and terminal CH_3 groups. These different groups contribute to the proton relaxation in a different manner from each other. Therefore, the experimental relaxation rates due to these two groups under the condition that the spin temperature is established over the whole spin system, are given by

$$\frac{1}{T_1}=\frac{1}{n}\left(\frac{n(CH_2)}{T_1(CH_2)}+\frac{n(CH_3)}{T_1(CH_3)}\right), \tag{1}$$

and

$$\frac{1}{T_{1d}}=\frac{1}{n}\left(\frac{n(CH_2)}{T_{1d}(CH_2)}+\frac{n(CH_3)}{T_{1d}(CH_3)}\right), \tag{2}$$

where n is the total number of protons in the specimen and $n(CH_2)$ and $n(CH_3)$ are those in the methylene and methyl groups, respectively. In the present specimens the condition that $n(CH_2)\gg n(CH_3)$ holds and moreover, both $T_1(CH_3)$ and $T_{1d}(CH_3)$ are very long because of very rapid internal rotation of CH_3 groups. Hence we can ignore the second terms of Eqs. 1 and 2, and so the relaxation rates can be interpreted in terms of the dipolar relaxation due to the motion of the methylene groups. In such a case the relaxation process is described by a single correlation time τ_c of the motion of CH_2 segments and, under the "weak collision limit",[11] T_1 and T_{1d} are given by

$$\frac{1}{T_1}=K\left[\frac{\tau_c}{1+\omega_0^2\tau_c^2}+\frac{4\tau_c}{1+4\omega_0^2\tau_c^2}\right], \quad (3)$$

and

$$\frac{1}{T_{1d}}=\frac{K}{2}\left[\frac{5\tau_c}{1+\omega_0^2\tau_c^2}+\frac{2\tau_c}{1+4\omega_0^2\tau_c^2}+\frac{3\tau_c}{1+4\omega_d^2\tau_c^2}\right], \quad (4)$$

where K represents the strength of the dipolar interaction; in the case of a two-spin system such as CH_2 segment $K\sim(9/40)\ \gamma^4\hbar^2/r^6$ where r is the distance between two protons and γ the proton gyomagnetic ratio, ω_0 is the Larmor frequency and $\omega_d\sim K^{1/2}$ the local field in the frequency unit. When the chain undergoes reorientation about its long axis, the intramolecular interaction between CH_2 segment brings about $\omega_d/2\pi\sim1.3\times10^4$ Hz. If the motion is limited to some local motion such as conformational change or kink diffusion,[12] ω_d should be much smaller.

Figure 3 shows the temperature dependence of T_1 and T_{1d} for PE 1214 between room temperature and the melting point. It shows that each of T_1 and T_{1d} for the virgin sample measured in the heating direction coincides with the result which was observed on cooling from the melt. The fact that T_1 does not vary appreciably with temperature suggests that a trace of some paramagnetic impurity governs the Zeeman spin lattice relaxation. The T_1 in PE 595 and PE 2305 behaves similarly. On the other hand, T_{1d} varies

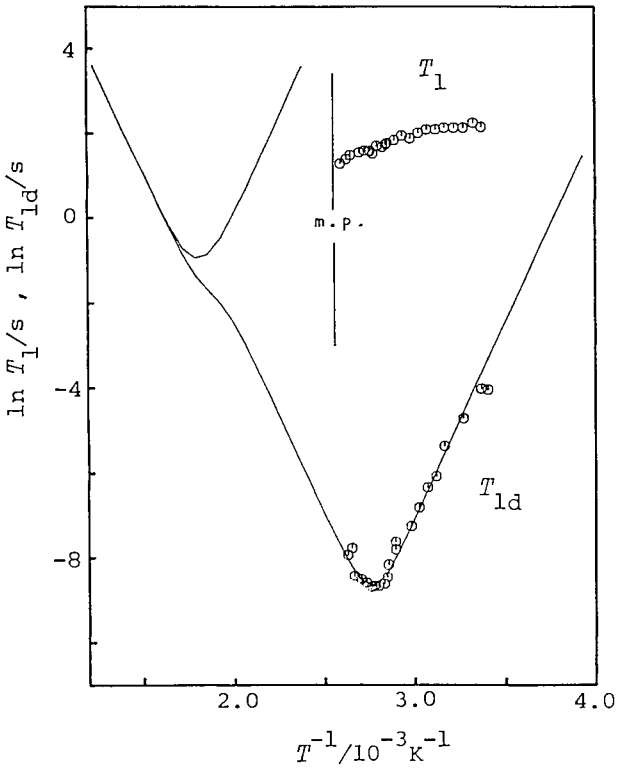

Fig. 3. Temperature dependence of proton spin lattice relaxation time (T_1) and dipolar relaxation time (T_{1d}) in PE 1214 at 200 MHz. The solid lines indicate the calculated T_1 and T_{1d} with Eqs. 4 and 5 and with the parameters listed in Table 2.

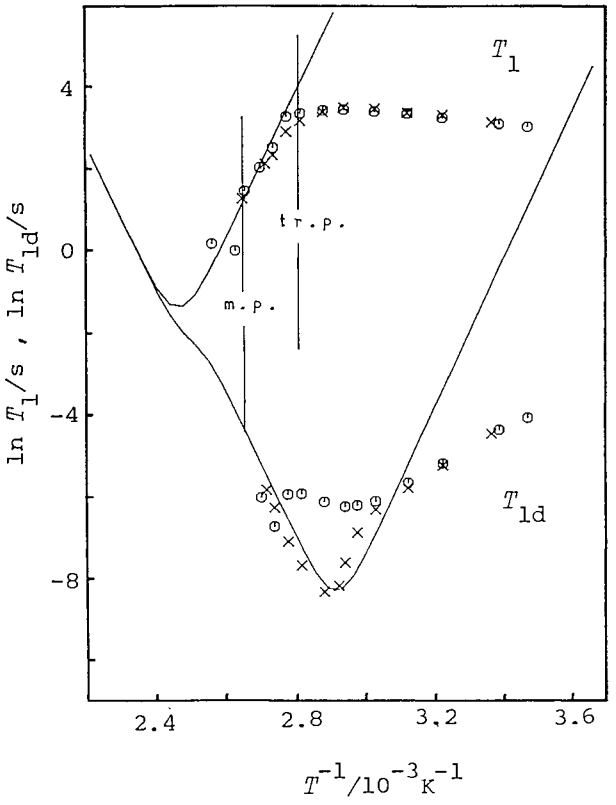

Fig. 4. Temperature dependence of proton spin lattice relaxation time (T_1) and dipolar relaxation time (T_{1d}) in n-$C_{50}H_{102}$ at 200 MHz; heating (O), cooling (X). The solid lines indicate the calculated T_1 and T_{1d} with Eqs. 4 and 5 and with the parameters listed in Table 2.

Table 2. The Temperature of T_{1d} Minimum, the Activation Parameters, and Strength of the Dipolar Field for Each Substance

Sample	T_{min}/K	E_a/kJ mol^{-1}	τ_0/s	K/s^{-2}	$(\omega_d/2\pi)$kHz
n-$C_{50}H_{102}$	340	42.0	2.3×10^{-12}	1.1×10^{8}	13
	344	150	2.3×10^{-29}	3.5×10^{9}	51
PE 595	286	31.0	7×10^{-12}	8.6×10^{8}	29
PE 1214	360	77.0	2.6×10^{-17}	2.3×10^{9}	23
PE 2305	365	85.0	2.4×10^{-18}	1.25×10^{9}	23

with temperature as expected from the usual BPP theory, Eq. 4, and assumes a minimum value at the temperature as listed in Table 2. Hence Eq. 4 was attempted to fit the experimental data in Fig. 3 assuming the Arrhenius activation process,

$$\tau_c = \tau_0 \exp(E_a/RT), \quad (5)$$

for molecular motion, and the resulting values together with those for PE 595 and PE 2305 are recorded in Table 2.

In the case of n-$C_{50}H_{102}$ the T_1 and the T_{1d} show novel temperature dependence as shown in Fig. 4. The T_1 does not change appreciably on heating up to the transition at 351 K but decreases very sharply above the transition point. This behavior of T_1 was reproduced in the cooling direction. On the other hand the T_{1d} decreases on heating and assumes a minimum value, 20 ms, at 340 K, then increases as the transition point is reached, where a sudden decrease of T_{1d} occurs. However, on cooling from the high temperature phase T_{1d} decreases remarkably, assumes a deep minimum value of 270 μs at 344 K, then increases dramatically on further cooling down to 328 K. Below 328 K the value of T_{1d} settles into that determined in the heating direction. The peculiar behavior of T_{1d} on cooling can be accounted for by reference to the results of DSC on this compound: The high temperature phase (HTP) can be easily supercooled. In our NMR experiment it remains down to about 344 K on cooling and so the T_{1d} measured between the melting point and 344 K is attributed to that in the HTP. Between 344 K and about 333 K the phase transition to the low temperature phase (LTP) sets in so that the apparent T_{1d} in this temperature region is the weighted average of the T_{1d} of the HTP and LTP. Since the T_{1d} in the HTP in this temperature range is very short but that in the LTP is significantly longer, the measured T_{1d} goes up dramatically as the phase transformation proceeds from the HTP to the LTP.

For the sake of data analysis, T_{1d} measured on heating was used for the molecular motion in the LTP, and T_{1d} measured between the melting point and 344 K on cooling was used for the HTP. For the LTP the value of ω_d can be accounted for by the model that all CH_2 segments are undergoing the rotation or reorientation about the long chain axis simultaneously. The results of the analysis by the above mentioned procedure are listed in Table 2. The activation energy, 42 kJ mol^{-1}, obtained here for the LTP may be compared with a value of 40 kJ mol^{-1} which was calculated for infinite chain model at 400 K by means of molecular dynamics simulation by Ryckaert and Klein.[13]

On the other hand, very large values of E_a and ω_d in the HTP cannot be fitted to the uniaxial reorientation model. Generally, short n-alkanes with carbon number smaller than 44 undergo "rotational transition" in which the molecular rotation about its long axis is excited in the high temperature rotational phase.[12] In the case of n-$C_{50}H_{102}$ it is suggested that the molecular reorientation or rotation is excited to some extent in the HTP as in other shorter n-alkanes; however, as mentioned above such a local molecular motion cannot account for the extremely large E_a and ω_d. It is therefore considered that some other motion such as molecular translational self-diffusion or drastic and dynamic change of molecular shape occurs

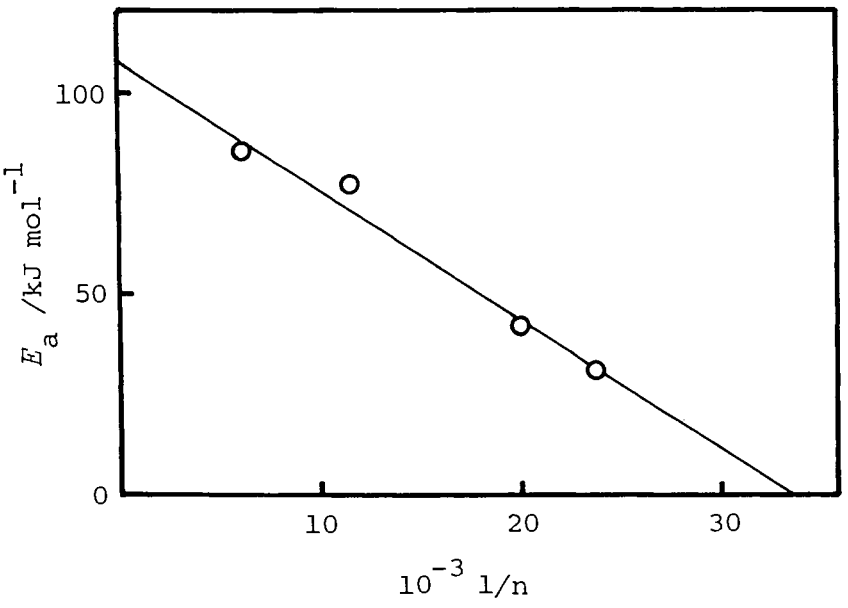

Fig. 5. The plot of E_a against the reciprocal of the number of carbons ($1/n$) in the single molecular chain.

above the transition point.[14]

Figure 5 plots the activation energy E_a for the chain reorientation against the reciprocal of the number of carbons in the single molecular chain. This plot gives a straight line, suggesting that the E_a is not proportional to the number of CH_2 segments but instead approaches a limiting value, 100—110 kJ mol^{-1}, as n increases. This tendency of E_a resembles the chain length dependence of the melting point of long n-alkanes[1-3] that the melting point approaches a limiting value, about 410 K, as n increases. These facts seem to indicate that there exists some close correlation between the activation process of molecular rotation or reorientation about the long axis and the melting phenomenon.

The activation process in the low molecular weight n-alkanes cannot be predicted from Fig. 5 because the assumption of the straight line in this figure leads to the zero activation energy at $n \approx 30$; this means that the orthorhombic structure is not stable for $n < 30$. However odd-numbered n-alkanes with 9 carbons or more crystallize in the orthorhombic unit cell actually.[1] We need the activation energy for short n-alkanes in order to discuss this point in greater detail but only few E_a data have been reported so far[14] for which some ambiguity about the assignment of the relaxation data remains.

The present work was partially supported by Grand-in-Aid for Scientific Research No. 61430006 from the Ministry of Education, Science and Culture. We are also grateful to Asahi Chemical Industry Co., Ltd. for partial financial support.

References

1) For example: a) A. Müller, *Proc. R. Soc. London, Ser. A*, **127**, 417 (1930); b) A. Müller and K. Lonsdale, *Acta Crystallogr.*, **1**, 129 (1948); c) M. G. Broadhurst, *J. Res. Natl. Bur. Stand., Sect. A*, **66**, 241 (1962).

2) a) J. Doucet, I. Denicolo, A. Craievich, and A. Collet, *J. Chem. Phys.*, **75**, 5125 (1981); b) G. Ungar, *J. Phys. Chem.*, **87**, 689 (1983).

3) N. G. Parsonage and L. A. K. Staveley, "Disorder in Crystals," Oxford University Press, Oxford (1978).

4) G. Ungar, J. Stejny, A. Keller, I. C. Bidd, and M. C. Whiting, *Science*, **229**, 386 (1985).

5) a) G. M. Stack, L. Mandelkern, C. Kröhnke, and G. Wegner, *Macromolecules*, **22**, 4351 (1989); b) J. D. Hoffman, *Polym. Commun.*, **27**, 39 (1986).

6) J. G. Powles and J. H. Strange, *Proc. Phys. Soc., London*, **82**, 6 (1963).

7) J. Jeener and P. Broekaert, *Phys. Rev.*, **157**, 232 (1967).

8) a) Y. Kim, H. L. Strauss, and R. G. Snyder, *J. Phys. Chem.*, **93**, 485 (1989); b) **93**, 7520 (1989).

9) D. L. Van der Hart, *J. Magn. Reson.*, **44**, 117 (1981).

10) I. Ando, T. Yamanobe, T. Sorita, T. Komoto, H. Sato, K. Deguchi, and M. Imanari, *Macromolecules*, **17**, 1955 (1984).

11) R. Van Steenwinkel, *Z. Naturforsch. A*, **24**, 1526 (1969).

12) a) W. Pechhold, *Kolloid Z. u. Z. Polym.*, **228**, 1 (1968); b) R. Kimmich, *Colloid Polym. Sci.*, **252**, 786 (1974).

13) J.-P. Ryckaert and M. L. Klein, *J. Chem. Phys.*, **85**, 1613 (1986).

14) M. Stohrer and F. Noack, *J. Chem. Phys.*, **67**, 3729 (1977).

Electrode Kinetics of the $[Fe(CN)_6]^{4-/3-}$ Complex Confined in Cationic Perfluoropolymer Films on Electrode Surfaces

Takeyoshi OKAJIMA,† Takeo OHSAKA,†† and Noboru OYAMA*
Department of Applied Chemistry, Tokyo University of Agriculture and Technology, 2-24-16 Nakamachi, Koganei, Tokyo 184
†Department of Industrial Chemistry, College of Science and Technology, Nihon University, 1-8-14 Kanda-surugadai, Tokyo 101
††Department of Electronic Chemistry, Graduate School at Nagatsuta, Tokyo Institute of Technology, 4259 Nagatsuta, Midori-ku, Yokohama 227
(Received December 27, 1990)

A heterogeneous electron-transfer process of the $[Fe(CN)_6]^{4-/3-}$ complex confined electrostatically in cationic perfluoropolymer (CPFP) films on graphite electrodes and a homogeneous charge-transport process within the films were examined by potential-step methods. The relevant kinetic parameters (i.e., standard rate constant; k°/cm s^{-1} and transfer coefficient; α) of the heterogeneous electron-transfer process and the apparent diffusion coefficient (D_{app}/cm^2 s^{-1}) of the homogeneous charge-transport process within the films were evaluated at various concentrations (C°) of the complex within the film. The values of D_{app} and k° slightly decreased with an increase in C°. The value of α was independent of C° (cathodic transfer coefficient, α_c=0.20, anodic transfer coefficient; α_a=0.80). The values of k°, α, and D_{app} were compared with those obtained previously for protonated poly(4-vinylpyridine) ($PVPH^+$)-$[Fe(CN)_6]^{4-/3-}$ system and poly(*N*,*N*-dimethylaniline) (PDMA)-$[Fe(CN)_6]^{4-/3-}$ system. It was found that k°, α_c, and D_{app} decrease, depending on the polymer film in which the complex is confined, in the following order: for D_{app} and k°, $PVPH^+$>PDMA>CPFP and for α_c, $PVPH^+\approx$PDMA>CPFP.

Thus far several polyelectrolytes (e.g., Nafion and protonated poly(4-vinylpyridine), shown in Fig. 1) have been used as an "electrode modifier" in the field of polymer-modified electrodes.[1-5] A number of papers dealing with Nafion film-coated electrodes have been reported since it was found that Nafion, which has the structure consisting of hydrophobic and hydrophilic domains,[6] could be used as an electrode modifier, because of its chemical stability and stable adhesion onto electrode surfaces.[6-21] A perfluoropolycarboxylic acid (PFPC) has also been used as electrode modifier.[5,22]

More recently, a new cationic perfluoropolymer membrane (CPFP, Fig. 1) has been produced by Tosoh Co., Ltd. This is a new cationic anion-exchange membrane with quaternary ammonium groups, in contrast to Nafion and PFPC which are anionic cation-exchange membranes with sulfonyl and carboxyl groups, respectively. In recent papers,[23-25] we have reported the preparation and the

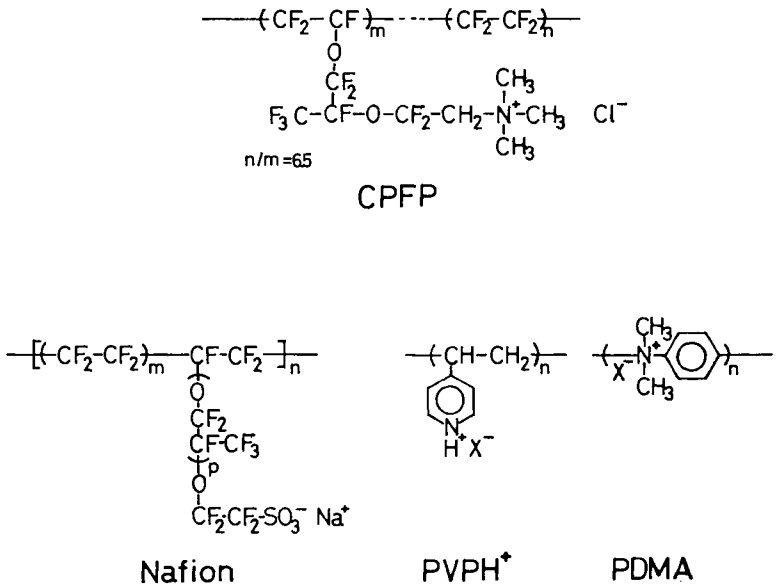

Fig. 1. Structures of cationic perfluolopolymer (CPFP), protonated poly(4-vinylpyridine) ($PVPH^+$), poly(*N*,*N*-dimethylaniline) (PDMA), and Nafion.

basic properties of the CPFP film as an electrode modifier and the charge-transport process within the film in which anionic Alizarine Red S dye is confined electrostatically as electroactive species.

In this work, we aim to examine the kinetics of the heterogeneous electron-transfer process of $[Fe(CN)_6]^{4-/3-}$ complex confined electrostatically in CPFP film on graphite electrode surfaces and the homogeneous charge-transport process within the film. The relevant kinetic parameters (standard rate constant: k°/cm s^{-1}, anodic and cathodic transfer coefficients: α_a and α_c) of the electrode reaction and apparent diffusion coefficient (D_{app}/cm^2 s^{-1}) of the homogeneous charge-transport process within the film are evaluated at various concentrations of the complex within the film. Further, the obtained values of k°,α_c, and D_{app} will be compared with those obtained previously for protonated poly(4-vinylpyridine) ($PVPH^+$)-$[Fe(CN)_6]^{4-/3-}$ system[26] and poly(*N*,*N*-dimethylaniline) (PDMA)-$[Fe(CN)_6]^{4-/3-}$ system.[27]

Experimental

Materials. CPFP membrane specimen was a gift of Tosoh Co., Ltd. Trifluoroacetic acid and sodium trifluoroacetate (Aldrich) used as supporting electrolytes and $K_3[Fe(CN)_6]$ (Merck) were of reagent grade and were used as received.

Basal-plane pyrolytic graphite (BPG) (Union Carbide Co.) was used as a working electrode material. The BPG disk electrodes were prepared and mounted into a glass tube with a heat-shrinkable polyolefin tube. The exposed area of these electrodes was 0.194 cm^2. Before use of electrodes, they were cut with a scalpel and their fresh surfaces were exposed. Aqueous solutions were prepared from doubly distilled water. Other chemicals were of reagent grade.

Preparation of CPFP Film-Coated Electrodes. The stock solution of CPFP, which was prepared as reported previously,[23] was diluted twice with $H_2O/C_2H_5OH/2$-C_3H_7OH(1/1/1(volume ratio)) mixed solvent. Then, the concentration of CPFP in the diluted stock solution was 10.5 mg ml^{-1}. For the preparation of CPFP film-coated electrodes, aliquots (usually 4 μl) of the diluted stock solution were spread by a microsyringe on the freshly cleaved disk surface of BPG electrode, and then were air-dried to remove the solvent at room temperature.

Measurement of the Film Thickness. The film thickness was measured as follows. The glass slide (ca. 1 cm×1 cm) was coated with silicone film (PRX 305-Clear, Toray Silicone Co., Ltd.), keeping a portion of ca. 0.20 cm^2 uncoated. Aliquots of the CPFP stock solution were spread with a microsyringe on the uncoated portion of the glass slide, and they were dried. After that, the silicone film was stripped. With a Surfcom 550A (Surface texture measuring instruments, Tokyo Seimitsu Co., Ltd.), the average difference between the surface profile of the glass slide and that of the CPFP film was measured. As seen from the inset in Fig. 2 this difference was taken as a film thickness under the dry state. After the glass slide which was used to measure the film thickness under the dry state was soaked overnight in a supporting electrolyte aqueous solution (0.2 M $CF_3COONa+CF_3COOH$, pH 1.0, 1 M=1 mol dm^{-3}) and water on the CPFP film was removed, the film thickness was measured again as that under the wet state. The clear difference between the film thicknesses under the dry and wet states was not observed, and thus the film thickness under the wet state was regarded as equal to that under the dry state within experimental errors. Figure 2 shows a linear plot of the film thickness under the dry state (μm in unit) vs. the coverage of the CPFP stock solution (μl in unit). The film thickness on the CPFP film-coated electrode, which was used to examine the kinetics of charge-transfer reaction, was estimated to be ca 1.0×10^{-4} cm from this linear relationship.

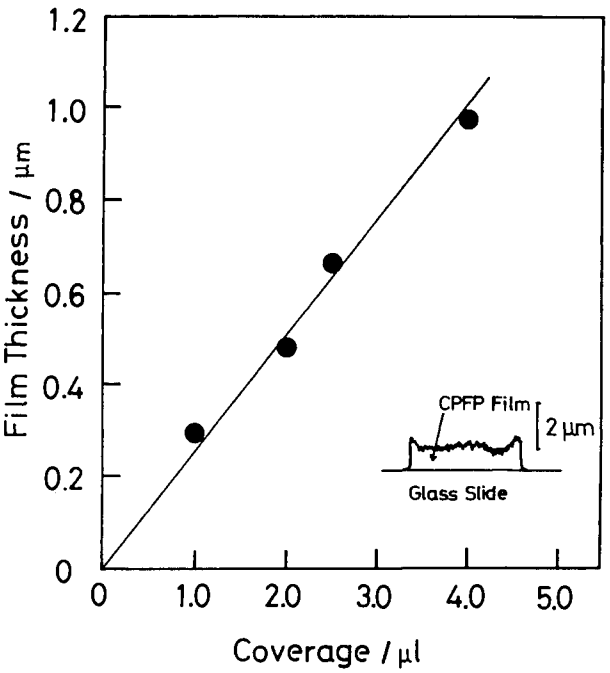

Fig. 2. Correlation between film thickness of CPFP and its coverage.
The coverage means the amount of the CPFP stock solution (see Experimental section) put and solvent-evaporated on the slide glass of a known area. The inset shows a typical vertical sectional profile of the CPFP film prepared on slide glass.

Apparatus and Procedures. The same standard three-electrochemical cell and electrode assembly as described previously were used in this work.[37] Electrode potentials were measured and are quoted with respect to a sodium chloride saturated calomel electrode (SSCE).

For cyclic voltammetry, potential-step chronoamperometry, potential-step chronocoulometry, and normal pulse voltammetry, the same instruments as described previously were used.[26,27] In potential-step chronoamperometric and chronocoulometric experiments, the electrode potentials were stepped from 0.8 to −0.2 V vs. SSCE for the reduction and from −0.2 to 0.8 V vs. SSCE for the oxidation. Then, the time of pulsed electrolysis was 40 ms for each case. In normal pulse voltammetric experiments, the electrode potentials were stepped from 0.8 V vs. SSCE for the reduction and from −0.2 V vs. SSCE for the oxidation, and then the height of pulsed wave was increased with 10 mV after each waiting period (usually 30—60 s). Currents were

sampled in the range from 2 to 24 ms. A positive feedback circuit was used to compensate IR drop of applied voltage resulting from the resistances of the solution and the coating films.

The kinetic measurements were carried out in 0.2 M $CF_3COONa+CF_3COOH$ aqueous solutions (pH 1.0) containing $[Fe(CN)_6]^{3-}$ in the concentration range from 10^{-5} to 10^{-4} M to keep its concentration within the film a given constant value.

The surface concentration (Γ/mol cm^{-2}) of $[Fe(CN)_6]^{4-/3-}$ within the CPFP film was estimated from graphical integration of the cyclic voltammogram, which was obtained at slow potential sweep rates (2—5 mV s^{-1}), with correction of background current for the oxidation and reduction. After substituting dissolved oxygen in a solution with a purified nitrogen gas, all electrochemical measurements were carried out under an atmosphere of nitrogen gas at room temperature.

The temperature dependence of formal potential ($E^{\circ\prime}$) was examined using a "non-isothermal electrochemical cell"[31,32] having a thermally jacketed compartment for the working and counter electrodes and a separate compartment for the reference electrode which was connected to the cell with a 3 M NH_4Cl salt bridge. The reference electrode was maintained at a fixed temperature (25±0.2 °C). The temperature of the cell was varied in the range of 3—37 °C. The values of $E^{\circ\prime}$ were estimated as the average of the anodic and cathodic peak potentials of the cyclic voltammograms.

Results

Cyclic Voltammetry. The cyclic voltammetric experiments were performed with the CPFP-film coated and naked BPG electrodes in a 0.2 M $CF_3COONa+CF_3COOH$ aqueous solution (pH 1.0) containing 0.2 mM $[Fe(CN)_6]^{3-}$. When the CPFP-film coated BPG electrode was immersed into the solution, the anodic and cathodic peak currents (i_p^a and i_p^c) of the cyclic voltammogram gradually increased as the electrode potential was scanned repeatedly between 0.8 and −0.2 V vs. SSCE. After about an hour, as shown in Fig. 3(A), these peak currents indicated constant values, and the steady-state cyclic voltammogram was obtained. In this case, the values of i_p were about 10 times as large as those obtained at the naked BPG electrode in the same solution as used in Fig. 3(A). Then, C° was ca. 0.15 M and was by a factor of about 750 larger than the concentration (0.2 mM) of $[Fe(CN)_6]^{3-}$ in the bulk solution.

Further, the formal redox potential ($E^{\circ\prime}$=0.310 V vs. SSCE) of $[Fe(CN)_6]^{4-/3-}$ couple confined in the CPFP film was different from that (0.367 V vs. SSCE) of the same couple in the bulk solution. This indicates that the environment around the redox couple within the film is different from that in the bulk solution. In this case, it may be presumed that the oxidized half of the redox couple exists within the film more stably than in the bulk solution and/or the reduced one exists in the bulk solution more stably than within the bulk. When the CPFP film-coated electrode used in Fig. 3(A) was transferred into the supporting electrolytic solution containing no $[Fe(CN)_6]^{3-}$, i_p gradually decreased, suggesting the releasing of the complex into the bulk solution. However, when this electrode was re-transferred into the same solution as used in (A), i_p increased and the same cyclic voltammograms as shown in (A) were obtained. From this fact, it is obvious that the CPFP film stably adsorbed on the electrode surfaces. Further, it has previously been demonstrated that two kinds of anionic metal complexes can be simultaneously concentrated into the CPFP film.[23]

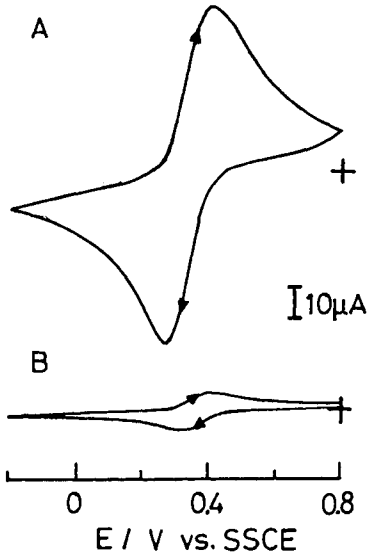

Fig. 3. (A) Steady-state cyclic voltammogram obtained for CPFP film-coated BPG electrode in 0.2 M CF_3COONa aqueous solution (pH 1.0) containing 0.2 mM $[Fe(CN)_6]^{3-}$. Thickness of CPFP film: 3.0×10^{-4} cm. Surface concentration (Γ) of quaternized ammonium site in CPFP film: 5.2×10^{-7} mol cm^{-2} (volume concentration: 1.7 M). (B) Cyclic voltammogram obtained for bare BPG electrode in the same solution as that used in A. In both cases, potential scan rate: 50 mV s^{-1}.

As described above, the overall electrode process at the CPFP film-coated electrode consists of two processes. One is the heterogeneous electron-transfer reaction which is characterized by standard rate constant (k°) and transfer coefficient (α). The other is the homogeneous charge-transport reaction which is characterized by apparent diffusion coefficient (D_{app}). These reactions were quantitatively examined with electrochemical pulse methods, as shown below.

Potential-Step Chronoamperometry (PSCA) and Chronocoulometry (PSCC). The curves A-1 and B-1 shown in Fig. 4 show current-time and coulomb-time responses, respectively, which were obtained with PSCA and PSCC for the reduction of $[Fe(CN)_6]^{3-}$ incorporated into the CPFP film on the electrode. In these figures, the dashed lines show the data of blank experiments obtained at the $[Fe(CN)_6]^{3-}$-free CPFP

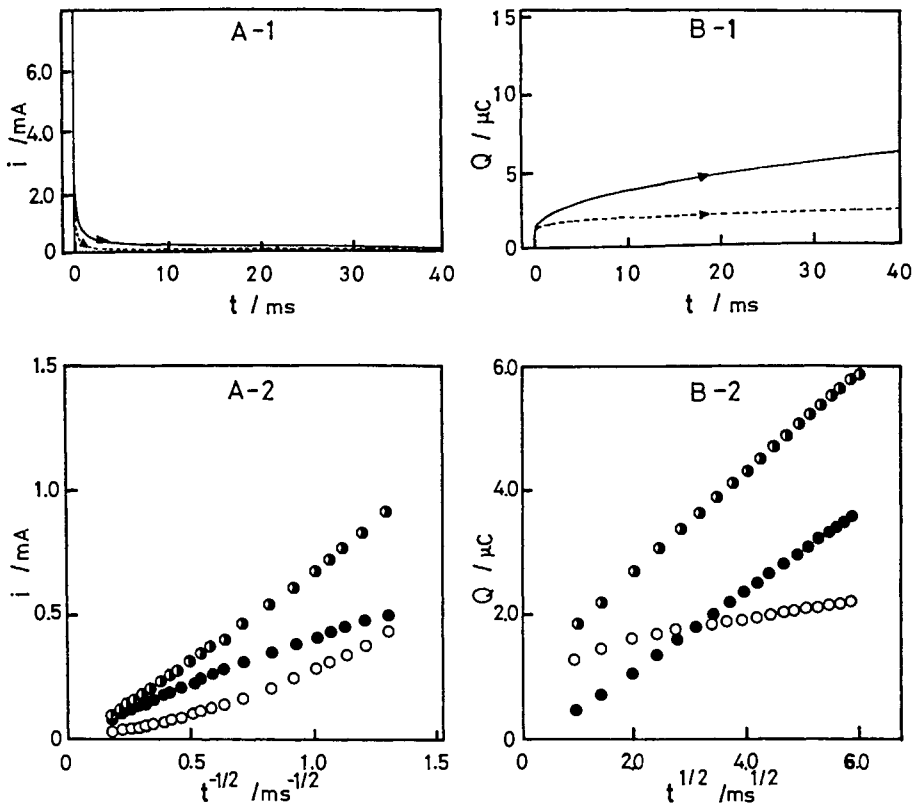

Fig. 4. Typical potential-step (A-1) chronoamperometric and (B-1) chronocoulometric responses for the reduction of $[Fe(CN)_6]^{3-}$ complex confined in the CPFP film on BPG electrode in 0.2 M CF_3COONa solution (pH 1.0). A-2 and B-2 represent chronoamperometric and chronocoulometric Cottrell plots for the data shown in A-1 and B-1, respectively. The dashed lines correspond to the background current responses obtained at the CPFP film (containing no $[Fe(CN)_6]^{3-}$)-coated BPG electrode in 0.2 M CF_3COONa solution (pH 1.0). Open and half-solid circles correspond to the dashed and solid lines in A-1 and B-1, respectively, and solid circles represent the background-current-corrected response.

film-coated electrodes. In these measurements the potential was stepped from 0.8 to −0.2 V vs. SSCE, and the time of pulsed electrolysis was 40 ms. Within this time window, a thickness of diffusion layer, which can be estimated to be ca. $(1—2)\times10^{-5}$ cm based on the D_{app} values obtained (shown below), is much thinner than the film thickness (1.0×10^{-4} cm). Therefore, the homogeneous charge-transport reaction can be regarded as a semi-infinite diffusion. The Cottrell equation and its integrated form were used to analyze the obtained curves.[28]

The plots A-2 and B-2 in Fig. 4 show the Cottrell plots for the data of A-1 and B-1, respectively. The values of D_{app} were estimated from the slopes of the plots which were corrected with the data of blank experiments for A-1 and B-1. The obtained values of

Table 1. Kinetic Parameters of the Heterogeneous Electron-Transfer Process at the Electrode/Film Interfaces and the Homogeneous Charge-Transport Process in the Films for the $[Fe(CN)_6]^{3-/4-}$/CPFP Film-Coated BPG Electrode System[a]

Film	Electrode process[b]	$C°$/M	D_{app}/cm^2 s^{-1}	$k°$/cm s^{-1}	α_a,α_c[c]
CPFP	Ox	8.9×10^{-2}	1.2×10^{-9}	$(5.4\pm2.0)\times10^{-5}$	0.80±0.02
CPFP	Red	3.2×10^{-2}	2.4×10^{-9}	$(7.6\pm1.7)\times10^{-5}$	0.20±0.03
CPFP	Red	1.0×10^{-1}	1.8×10^{-9}	$(6.7\pm1.6)\times10^{-5}$	0.21±0.03
PDMA[d]	Red	1.2×10^{-1}	5.0×10^{-9}	1.2×10^{-4}	0.30±0.03
$PVPH^{+}$[e]	Red	1.1×10^{-1}	2.5×10^{-8}	1.0×10^{-3}	0.30

a) Supporting electrolyte: 0.2 M $CF_3COONa+CF_3COOH$ (pH=1.0). b) Ox: oxidation process; Red: reduction process. c) α_a: anodic transfer coefficient, α_c: cathodic transfer coefficient. d) Ref. 27. e) Ref. 26.

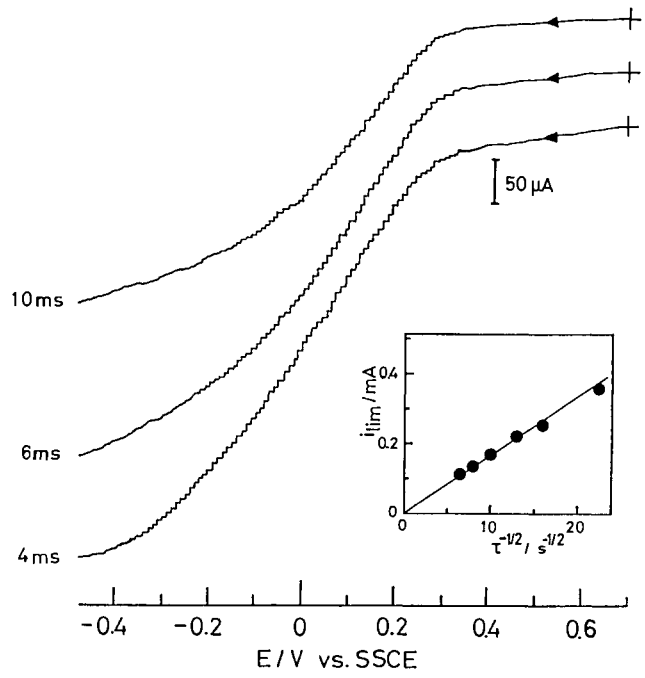

Fig. 5. Typical normal pulse voltammograms for the reduction of $[Fe(CN)_6]^{3-}$ complex confined in the CPFP film on BPG electrode in 0.2 M CF_3COONa solution (pH 1.0) containing 1.0×10^{-5} M $[Fe(CN)_6]^{3-}$. Concentration of $[Fe(CN)_6]^{3-}$ complex confined in the film: 3.2×10^{-2} M. The dashed lines show the background current responses. The inset shows a typical normal pulse voltammetric Cottrell plot of limiting current, i_{lim}, vs. (sampling time)$^{-1/2}$, $\tau^{-1/2}$.

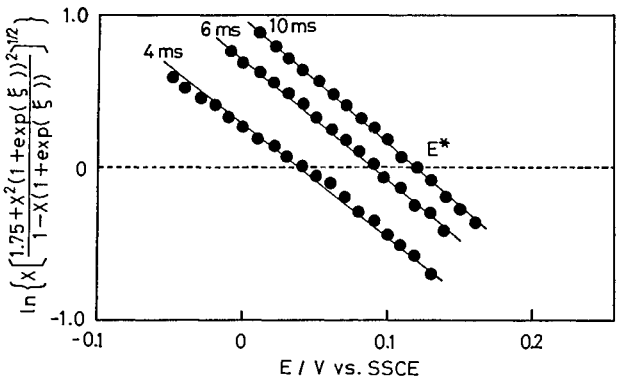

Fig. 6. Modified log-plots for the normal pulse voltammograms shown in Fig. 5. Sampling times are indicated on each straight line.

D_{app} are shown in Fig. 7.

Normal Pulse Voltammetry. Figure 5 shows typical normal pulse voltammograms obtained for the reduction of $[Fe(CN)_6]^{3-}$ confined in the CPFP film at various sampling times (τ/ms). At sufficiently negative applied potentials, the limiting currents (i_{lim}) were obtained. The dependence of the limiting currents (i_{lim}) of these normal pulse voltammograms on τ was examined. As shown in the inset of Fig. 5, i_{lim} was plotted against $\tau^{-1/2}$. This plot gave a straight line and passed through the origin. From this fact, it was found that the homogeneous charge-transport reaction within the film was controlled by diffusion and obeyed Fick's law.[26-28] The values of D_{app}, obtained from the slopes of such linear plots, are shown in Fig. 7 and Table 1. Further, the kinetic parameters (i.e., k° and α) of the heterogeneous electron-transfer reaction were estimated from the conventional analysis of the rising part of each normal pulse voltammogram.[26,27,29] Figure 6 shows the modified log-plots of $\ln(x[\{1.75+x^2(1+\exp(\xi))^2\}/\{1-x(1+\exp(\xi))\}]^{1/2})$ vs. E for each voltammogram shown in Fig. 5, where x is the ratio of the current at potential E to the limiting

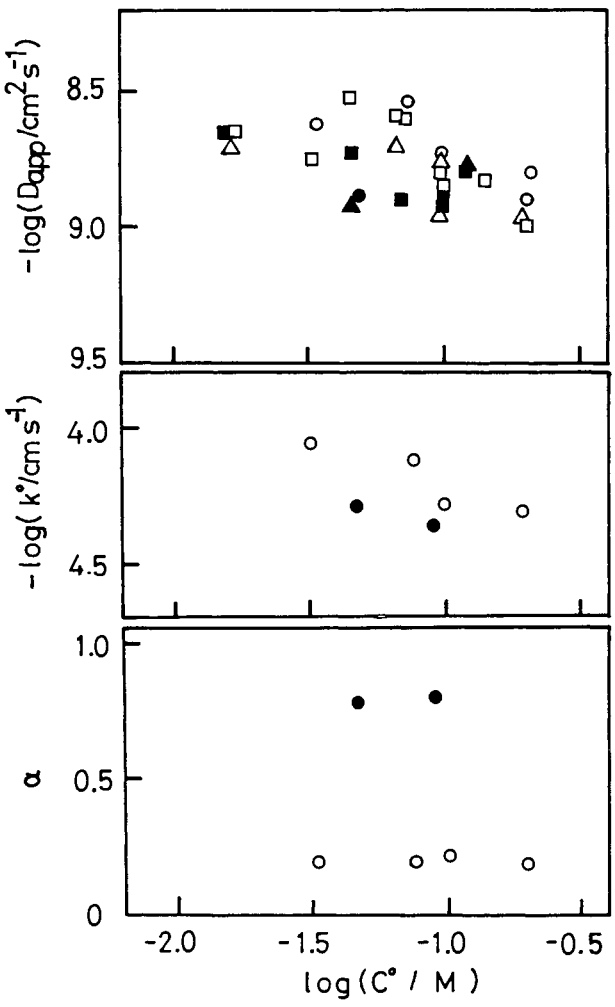

Fig. 7. Dependences of D_{app}, k°, and α on C°. Thickness of CPFP film: 1.0×10^{-4} cm. Supporting electrolyte: 0.2 M CF_3COONa+CF_3COOH (pH 1.0). C° denotes the volume concentration of $[Fe(CN)_6]^{3-}$ (or $[Fe(CN)_6]^{4-}$) complex confined in CPFP film. The data shown by squares, triangles, and circles were obtained by PSCA, PSCC, and NPV, respectively. Solid and open symbols correspond to the anodic and cathodic processes, respectively.

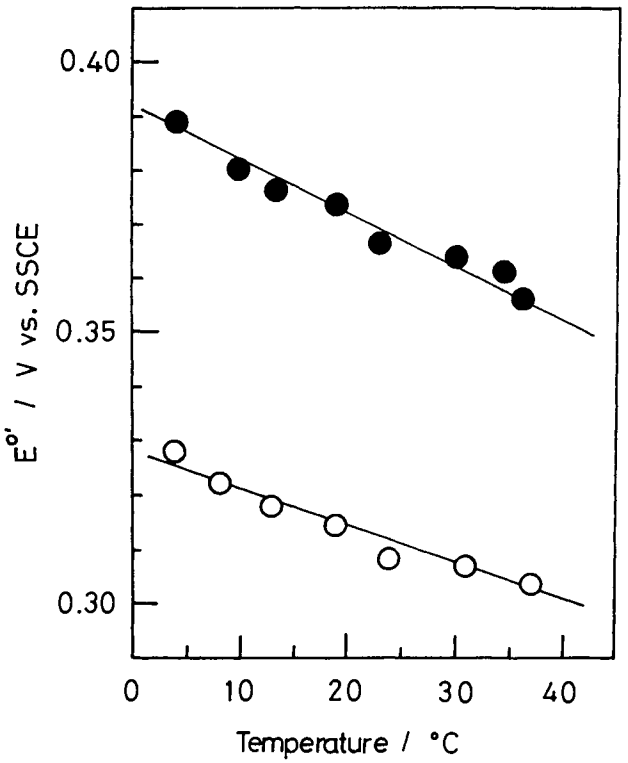

Fig. 8. Temperature dependences of formal potential ($E^{\circ\prime}$) of $[Fe(CN)_6]^{4-/3-}$ redox couple confined in the CPFP film and dissolved in 0.2 M CF_3COONa solution. Solution composition: 0.2 M CF_3COONa+CF_3COOH (pH 1.0) $+1.0\times10^{-5}$ M $[Fe(CN)_6]^{3-}$. Thickness of CPFP film: 1.0×10^{-4} cm, (●) at bare BPG electrode, (○) at CPFP film-coated electrode.

diffusion current expressed by the Cottrell equation[26,27,29] and ξ is the dimensionless parameter expressed as $\{(nF/RT)(E-E^{r}_{1/2})\}$ ($E^{r}_{1/2}$: the reversible half-wave potential, n: the number of electrons involved in the heterogeneous electron-transfer reaction, F: the Faraday constant, R: the gas constant, T: the absolute temperature). The plots gave the straight lines with the almost same slope at different sampling times. The transfer coefficient (α) was determined from the slopes of the plots in Fig. 6, and the standard rate constant (k°) was determined from the difference between the reversible half-wave potential ($E^{r}_{1/2}$) and the intercept potential (E^{*}) on the potential axis.[29] The obtained values of k° and α are shown in Fig. 7 and Table 1.

Figure 8 shows the temperature (T) dependence of the formal potential ($E^{\circ\prime}$) for the $[Fe(CN)_6]^{4-/3-}$ couple confined in the CPFP film and dissolved in solution. The linear relationships between $E^{\circ\prime}$ and T were obtained and thus the reaction entropy differences (ΔS°_{rc}) for the couple were estimated by using the equation:[31,32]

$$\Delta S^{\circ}_{rc} = S^{\circ}_{red} - S^{\circ}_{ox} = F\left(\frac{dE^{\circ\prime}}{dT}\right) \quad (1)$$

where S°_{red} and S°_{ox} are absolute ionic entropies of the reduced and oxidized halves of the redox couple and F is the Faraday constant. The ΔS°_{rc} values were estimated to be -24 ± 2 and -14 ± 2 cal mol^{-1} K^{-1} for the bulk solution (0.2 M CF_3COONa+CF_3COOH, pH 1.0) and the CPFP film, respectively.

Discussion

Figure 7 shows dependence of D_{app} on C°. When C° was increased from 0.01 to 0.2 M, D_{app} slightly decreased from 2.3×10^{-9} cm^2 s^{-1} to 1.2×10^{-9} cm^2 s^{-1}. As shown in Fig. 1, the structure of CPFP consists of the hydrophobic perfluorocarbon chain and ether-bond part and the hydrophilic quaternary ammonium sites, and the former occupies most of the structure. From this fact, it is assumed that the CPFP film as well as Nafion film[6,10,30] may have the domain structure which consists of the hydrophobic and hydrophilic parts in a solvent-swollen state, and that three-dimensional micro channels of the quaternary ammonium ion sites may exist within the CPFP film. Therefore, $[Fe(CN)_6]^{3-}$ (or $[Fe(CN)_6]^{4-}$) may diffuse within such channels with an electrostatic interaction with positively charged sites of the CPFP film and a hydrophobic interaction with the hydrophobic domain.[10,12,30] The fact that D_{app} slightly decreased with an increase in C° may be explained by an electrostatic cross-linking[1-5,7,10,11,14,15,22-27,33-39] of the polyelectrolyte coatings occurring when the multiply charged electroactive species are incorporated into organic polyelectrolyte coatings having the opposite charge, because the electrostatic cross-linking of the film hinders the physical diffusion of electroactive species itself and the motion of counterions associated with the redox reaction, which occurs to keep a charge neutrality.

If an electrostatic cross-linking which is often observed in a well-swollen film (e.g., $PVPH^+$ film) occurs, it could be expected that D_{app} largely decreases with an increase in C°.[26,38,39] However, in the case of the CPFP film, the dependence of D_{app} on C° is small. The CPFP film contains a far more hydrophobic domain compared to the $PVPH^+$ film. The distance between the positively charged sites was calculated to be 3—8 and 19—23 Å for the $PVPH^+$ film and the CPFP film, respectively by assuming a simple cubic lattice model for the statistical distribution of ammonium or pyridinium sites in these films. Therefore, the smaller effect of the electrostatic cross-linking in the CPFP film compared to the $PVPH^+$ film can be ascribed to the lower degree of swelling of this film, as supported by the experimental result that the thickness of a given film under the wet state is almost the same as that under the dry state.

The C° dependence of D_{app} may also be thought to reflect a single-file diffusion effect,[10,11,22,40] because $[Fe(CN)_6]^{4-}$ (or $[Fe(CN)_6]^{3-}$) ions which must move

between more or less fixed sites within the CPFP matrix are considered to have their rate of motion limited by the decreasing availability of sites as C° increases.

In Fig. 7 are also shown the dependences of k° and α on C°. The dependence of k° on C° is similar to that of D_{app} on C°, and k° slightly decreases when C° is increased. In contrast, α is almost independent of C°, and α values of anodic and cathodic processes (α_a and α_c) are ca. 0.80 and ca. 0.20, respectively. In addition, the sum of α_a and α_c is ca. 1.0, indicating that the anodic and cathodic reactions occur by way of the same activated state.[44]

The values of D_{app}, k°, and α_c obtained for the CPFP-$[Fe(CN)_6]^{3-}$ system are compared with those obtained previously for $PVPH^+$-$[Fe(CN)_6]^{3-}$ system[26] and PDMA-$[Fe(CN)_6]^{3-}$ system[27] (Table 1). At almost the same concentration of $[Fe(CN)_6]^{3-}$ in the films, the values of D_{app} and k° decrease in the following order; $PVPH^+$ film system>PDMA film system> CPFP film system. For example, when C° is (1.0—1.2)$\times 10^{-1}$ M, the D_{app} for the CPFP film is about 1/3 and 1/13 of those for the PDMA and $PVPH^+$ films,[26,27] respectively. This may be ascribed to a different extent of the electrostatic cross-linking of these films by $[Fe(CN)_6]^{3-}$ (and $[Fe(CN)_6]^{4-}$) ions which is considered to originate from their different morphologies in the solvent-swollen states. The α_c value for the CPFP film system is ca. 0.2 and is smaller than those (0.30) for the $PVPH^+$ film and PDMA film systems.[26,27] Such different α_c values for different film systems may reflect the different reaction positions of $[Fe(CN)_6]^{4-/3-}$ complex (e.g., with respect to the outer Helmholtz plane) in the transition state of the electron-transfer reaction and/or the existence of the potential-independent chemical reaction preceeding the electron-transfer reaction proper.[14,41-44]

The reaction entropy ΔS°_{rc} is an important parameter in considering the factors influencing the kinetics of electron-transfer process, since it provides a sensitive monitor of the changes in solvent polarization that are necessary in order for electron transfer to occur. The negative value (-24 ± 2 cal mol^{-1} K^{-1}) was obtained for the $[Fe(CN)_6]^{4-/3-}$ couple dissolved in 0.2 M CF_3COONa+CF_3COOH solution (pH 1.0) in qualitative agreement with the expectation from an electrostatic treatment such as the Born model.[31,32] Assuming that the equivalent radii of $[Fe(CN)_6]^{3-}$ and $[Fe(CN)_6]^{4-}$ are 2 and 2.5 Å, respectively, ΔS°_{rc} is roughly estimated to be -19 cal mol^{-1} K^{-1}.[32] In the case of the $[Fe(CN)_6]^{4-/3-}$ couple confined in the CPFP film, the negative ΔS°_{rc} (-14 ± 2 cal mol^{-1} K^{-1}) was also obtained, but its value is more positive compared to that for the solution-phase $[Fe(CN)_6]^{4-/3-}$ couple. This fact suggests that the degree of the entropy in the oxidized form is smaller in the CPFP film than in the bulk solution and/or the degree of the entropy in the reduced form is larger in the film than in the solution. In other words, $[Fe(CN)_6]^{3-}$ (or $[Fe(CN)_6]^{4-}$) ions seem to interact more strongly (or weakly) with their surroundings within the CPFP film matrix than in the solution.

The present work was partially supported by a Grant-in-Aid for Scientific Research No. 01470064 from the Ministry of Education, Science and Culture. The authors express their appreciations to Tosoh Co., Ltd. for providing CPFP membranes.

References

1) N. Oyama and F. C. Anson, *J. Electrochem. Soc.*, **127**, 247 (1980).
2) N. Oyama, T. Shimomura, K. Shigehara, and F. C. Anson, *J. Electroanal. Chem.*, **112**, 271 (1980).
3) F. C. Anson, J. M. Savéant, and K. Shigehara, *J. Am. Chem. Soc.*, **105**, 1096 (1983).
4) I. Rubinstein and A. J. Bard, *J. Am. Chem. Soc.*, **102**, 6642 (1980).
5) Y. M. Tsou and F. C. Anson, *J. Electrochem. Soc.*, **131**, 595 (1984).
6) H. L. Yeager and A. Steck, *J. Electrochem. Soc.*, **128**, 1880 (1981).
7) H. S. White, J. Leddy, and A. J. Bard, *J. Am. Chem. Soc.*, **104**, 4811 (1982).
8) T. P. Henning, H. S. White, and A. J. Bard, *J. Am. Chem. Soc.*, **104**, 5862 (1982).
9) D. A. Buttry and F. C. Anson, *J. Am. Chem. Soc.*, **104**, 4824 (1982).
10) D. A. Buttry and F. C. Anson, *J. Am. Chem. Soc.*, **105**, 685 (1983).
11) Y. M. Tsou and F. C. Anson, *J. Phys. Chem.*, **89**, 3818 (1985).
12) C. R. Martin and K. A. Dollard, *J. Electroanal. Chem.*, **159**, 127 (1983).
13) N. Oyama, T. Ohsaka, K. Sato, and H. Yamamoto, *Anal. Chem.*, **55**, 1431 (1983).
14) T. Ohsaka, H. Yamamoto, M. Kaneko, A. Yamada, M. Nakamura, S. Nakamura, and N. Oyama, *Bull. Chem. Soc. Jpn.*, **57**, 1844 (1984).
15) T. Ohsaka, N. Oyama, K. Sato, and H. Matsuda, *J. Electrochem. Soc.*, **132**, 1871 (1985).
16) I. Rubinstein, *J. Electroanal. Chem.*, **188**, 227 (1985).
17) C. M. Elliott and J. G. Redepenning, *J. Electroanal. Chem.*, **181**, 137 (1984).
18) Z. Lu and S. Dong, *J. Chem. Soc., Faraday Trans. 1*, **84**, 2979 (1988).
19) D. W. DeWulf and A. J. Bard, *J. Electrochem. Soc.*, **135**, 1977 (1988).
20) Z. Ogumi, T. Mizoe, and Z. Takehara, *Bull. Chem. Soc. Jpn.*, **61**, 4183 (1988).
21) K. Uosaki, J. Wang, and H. Kita, *J. Electroanal. Chem.*, **273**, 275 (1989).
22) N. Oyama, T. Ohsaka, T. Ushirogouchi, S. Sanpei, and S. Nakamura, *Bull. Chem. Soc. Jpn.*, **61**, 3103 (1988).
23) N. Oyama, T. Ohsaka, and T. Okajima, *Anal. Chem.*, **54**, 979 (1986).
24) T. Ohsaka, Y. Takahira, O. Hatozaki, and N. Oyama, *Bull. Chem. Soc. Jpn.*, **62**, 1023 (1989).
25) T. Ohsaka, Y. Takahira, S. Nakamura, and N. Oyama,

J. Electroanal. Chem., **247**, 339 (1988).
26) N. Oyama, T. Ohsaka, M. Kaneko, K. Sato, and H. Matsuda, *J. Am. Chem. Soc.*, **105**, 6003 (1983).
27) T. Ohsaka, T. Okajima, and N. Oyama, *J. Electroanal. Chem.*, **215**, 191 (1986).
28) A. J. Bard and L. Faulkner, "Electrochemical Methods," Wiley, New York, N.Y. (1985), Chap. 5.
29) H. Matsuda, *Bull. Chem. Soc. Jpn.*, **53**, 3439 (1980).
30) I. Rubinstein, J. Rishpon, and S. Gottesfeld, *J. Electrochem. Soc.*, **133**, 729 (1986).
31) E. L. Yee, R. J. Çave, K. L. Guyer, P. D. Tyma, and M. J. Weaver, *J. Am. Chem. Soc.*, **101**, 1113 (1979).
32) T. Ohsaka, H. Yamamoto, and N. Oyama, *J. Phys. Chem.*, **91**, 3775 (1987).
33) P. Daum, J. R. Lenhard, D. Rolison, and R. W. Murray, *J. Am. Chem. Soc.*, **102**, 4649 (1980).
34) J. Facci and R. W. Murray, *J. Electroanal. Chem.*, **152**, 97 (1983).
35) N. Oyama and F. C. Anson, *J. Electrochem. Soc.*, **127**, 640 (1980).
36) N. Oyama and F. C. Anson, *Anal. Chem.*, **52**, 1192 (1980).
37) F. C. Anson, T. Ohsaka, and J. M. Saveant, *J. Phys. Chem.*, **87**, 640 (1983).
38) N. Oyama, S. Yamaguchi, Y. Nishiki, K. Tokuda, H. Matsuda, and F. C. Anson, *J. Electroanal. Chem.*, **139**, 371 (1982).
39) K. Sato, S. Yamaguchi, H. Matsuda, T. Ohsaka, and N. Oyama, *Bull. Chem. Soc. Jpn.*, **56**, 2004 (1983).
40) K. Heckmann, "Biomembranes," ed by A. L. Manson, Plenum Press, New York (1972), Vol. 3, p. 127.
41) N. Oyama, T. Ohsaka, and T. Ushirogouchi, *J. Phys. Chem.*, **88**, 5274 (1984).
42) M. J. Weaver, *J. Phys. Chem.*, **83**, 1748 (1979).
43) W. R. Fawcett, *J. Electroanal. Chem.*, **22**, 19 (1969).
44) R. Tamamushi, "Denki Kagaku," Tokyo Kagaku Dojin, Tokyo (1967), Chap. 5.

Electrochemical Formation of 11-Molybdophosphate Anion at the Nitrobenzene/Water Interface and Its Applicability to the Determination of Orthophosphate Ion

Toshiyuki OSAKAI,* Sadayuki HIMENO, and Atsuyoshi SAITO
Department of Chemistry, College of Liberal Arts, Kobe University, Nada-ku, Kobe 657
(Received October 29, 1990)

Transfer of the hexamolybdate ion, $Mo_6O_{19}^{2-}$, at the nitrobenzene(NB)/water(W) interface was studied by ion-transfer voltammetry. The $Mo_6O_{19}^{2-}$ ion decomposed immediately after being transfered from NB to W. In the presence of orthophosphate ions in the weakly acidic W phase (pH 3.1), molybdophosphate anions, i.e. $[H_3PMo_{11}O_{39}]^{4-}$, were formed at the interface. A well-defined voltammetric wave due to the transfer of complex anions from W to NB was observed; the peak current was proportional to the bulk concentration of orthophosphate ions. Thus, the NB/W interface containing $Mo_6O_{19}^{2-}$ in NB can function as an ion-selective electrode surface for a voltammetric determination of orthophosphate ions.

Much attention is presently being paid to a new voltammetric method for the determination of ions with a polarizable oil/water interface.[1-4] Previously, one of the authors (T.O.) and co-workers developed oil/water interfaces which function as voltammetric (or amperometric) ion-selective electrode (ISE)-surfaces for several cations, including: Na^+, K^+, and NH_4^+.[5] Some of these ISE's were further applied to the design of amperometric chemical sensors for ammonia,[6] urea,[7] and volatile amines.[8] Most of the ISE's and sensors, however, are based upon the cation selectivity of crown ethers.

In our recent studies,[9,10] the transfer of heteropolyanions at the NB/W interface was investigated by ion-transfer voltammetry.[1-4] As already described,[9,10] such voltammetric studies shed light on the mechanisms of extraction processes of heteropolyacids. Still, it should be noted that another important objective of the studies is to develop oil/water interfaces which serve as ISE-surfaces for a voltammetric determination of such oxoanions as orthophosphate and silicate ions.

In parallel with the above-mentioned studies concerning the phase transfer of heteropolyanions, we have investigated electrode reactions of heteropoly- and isopolymolybdate anions.[11-13] In a previous study[13] we elucidated that the hexamolybdate ion, $Mo_6O_{19}^{2-}$, is partially electroreduced to decompose rapidly to Mo(V) and Mo(VI) in acidic aqueous-organic media. On the basis of this electrode reaction, the formation of a certain blue (reduced) heteropoly complex(es) can be electrochemically controlled. As an example of the application, we reported on a voltammetric method for the determination of the sulfate ion as the blue molybdosulfate complex.[12]

In this study, it has been found that when $Mo_6O_{19}^{2-}$ transfers across a nitrobenzene(NB)/water(W) interface from NB to W, it decomposes rapidly to some Mo(VI) species. In the presence of orthophosphate ions in W, a yellow (oxidized) heteropoly complex is formed at the interface. The present paper describes the principle of a new method for the voltammetric determination of orthophosphate ions based on such an electrochemical formation of this yellow complex at the NB/W interface.

Experimental

Electrochemical Measurements. Since a large current due to the transfer of $Mo_6O_{19}^{2-}$ flows through the interface, a three-electrode cell (Fig. 1) was used instead of the two-electrode cell previously used.[9] The cell system was supplemented with an Ag/AgCl electrode (F) as the reference

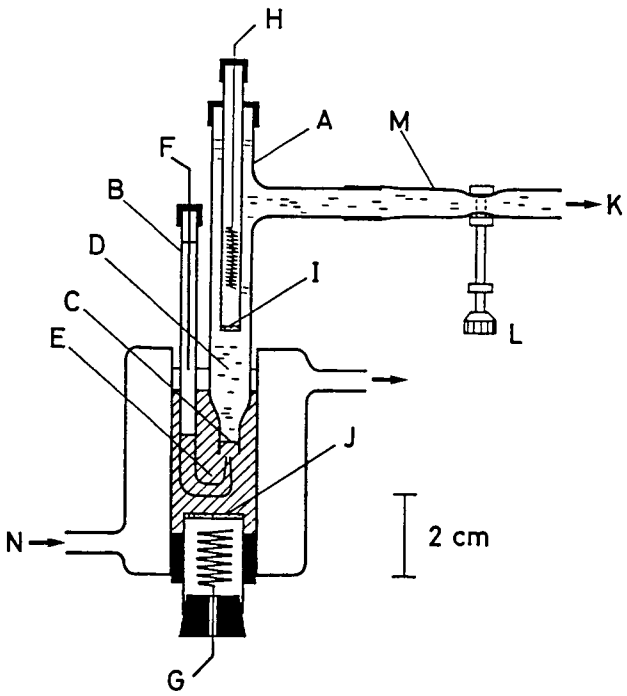

Fig. 1. Diagram of the three-electrode cell. A, glass tube; B, Luggin capillary; C, test interface (0.127 cm^2); D, water phase; E, oil phase; F, G, and H, Ag/AgCl electrodes; I and J, glass sinters; K, to solution reservoir; L, screw cock for the interface adjustment; M, silicone tube; N, thermostated water (25±0.1 °C).

electrode, which was connected to the NB phase close to the test interface (C) through a Luggin capillary (B). The Ag/AgCl electrodes (F and G) were immersed in 0.1 M (1 M=1 mol dm^{-3}) tetrabutylammonium chloride (TBACl) aqueous solutions, while the Ag/AgCl electrode (H) was immersed in a 0.5 M $MgCl_2$ aqueous solution separated from the W phase by means of a glass sinter (I). Accordingly, the electrochemical cell can be expressed as

	I	II		
Ag/AgCl (F or G)	0.1 M TBACl (W)	0.1 M TBATPB a mM $(TBA)_2Mo_6O_{19}$ (NB)		
	III	IV		
	0.5 M $MgCl_2$+buffer ($+b$ mM KH_2PO_4) (W)	0.5 M $MgCl_2$ (W)	AgCl/Ag. (H)	(A)

Here, TBATPB stands for tetrabutylammonium tetraphenylborate. The pH of phase-III was adjusted with a CH_3COOH-$(CH_3COO)_2Mg$ buffer ($[CH_3COO^-]$=0.1 M) or HCl (at pH<3). The potential difference (E) between the metal phases of electrodes F and H was controlled by a programmable function generator (Hokuto Denko Model HB-105) through a laboratory-made potentiostat. The solution resistance between the tip of the Luggin capillary and electrode H was compensated for by positive feedback. The current flowing through the test interface was detected by means of Ag/AgCl electrodes G and H with large surface areas (ca. 15 and ca. 10 cm^2, respectively), and the cyclic voltammograms were recorded with an X-Y pen recorder (Yokogawa Model 3023), unless otherwise noted.

Chemicals. The $(TBA)_2Mo_6O_{19}$ salt was prepared as described previously.[13,14] Other chemicals, except for $(TBA)_4[H_3PMo_{11}O_{39}]$ (see below), were described in the previous paper.[9]

The $(TBA)_4[H_3PMo_{11}O_{39}]$ salt was prepared according to the following procedure: To a stirred aqueous solution containing 120 mM $Na_2MoO_4\cdot 2H_2O$ and 10 mM $Na_2HPO_4\cdot 12H_2O$, concd HCl was added dropwise until the pH became 3.1. The addition of solid TBABr produced yellow precipitates. These precipitates were collected by filtration, washed several times with acetone to remove any TBA^+-salt of the Keggin anion $(TBA)_3[PMo_{12}O_{40}]$ (yellow) formed simultaneously, and then dried at 50 °C. The results of an elemental analysis for the resulting pale-yellow salt are as follows. Found: Mo, 39.12; P, 1.14; C, 28.75; H, 5.50; N, 2.09%. Calcd for $(TBA)_4[H_3PMo_{11}O_{39}]$: Mo, 39.33; P, 1.15; C, 28.65; H, 5.52; N, 2.08%. In the TG-DTA, the evolution of water was not observed up to 120 °C.

Figure 2(a) shows the IR spectrum of $(TBA)_4[H_3PMo_{11}O_{39}]$, which was recorded with a Hitachi Model 270-30 spectrophotometer. The spectrum is characterized by absorption bands at 1081, 1041, 936, 863, 821, and 762 cm^{-1}. For a comparison, Fig. 2(b) shows the IR spectrum of the TBA^+-salt of the Keggin anion, $(TBA)_3[PMo_{12}O_{40}]$, prepared according to a reported method.[15] The strong band at 1062 cm^{-1} for the Keggin anion, which can be assigned to the asymmetric stretch of the PO_4 group, splits into two bands at 1081 and 1041 cm^{-1} for $[H_3PMo_{11}O_{39}]^{4-}$. A similar splitting has been reported for the 11-tungstophosphate anion.[16-18] Rocchiccioli-Deltcheff and Thouvenot[18] reported corresponding bands at 1060 and 1010 cm^{-1} for the NH_4^+-salt of the 11-molybdophosphate anion. However, it should be noted that the crystal $Na_3H_6Mo_9PO_{34}(H_2O)_x$ prepared according to Strandberg's method[19] gave the same two bands at 1061 and 1009 cm^{-1}.

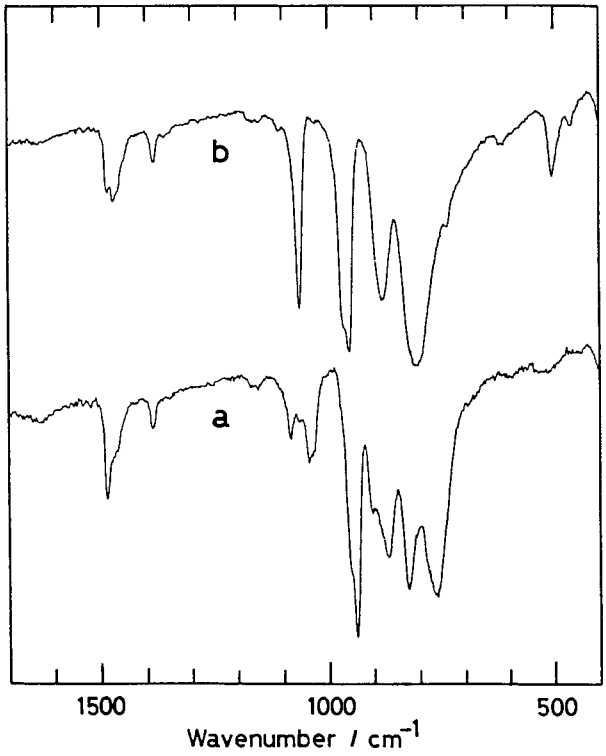

Fig. 2. IR spectra of (a) $(TBA)_4[H_3PMo_{11}O_{39}]$ and (b) $(TBA)_3[PMo_{12}O_{40}]$ in the KBr pellets.

From the above results it may be concluded that the $[H_3PMo_{11}O_{39}]^{4-}$ anion is a so-called "lacunary" derivative of the Keggin structure.[20]

Results and Discussion

Phase Transfer of $Mo_6O_{19}^{2-}$. Figure 3 shows cyclic voltammograms recorded at various scan rates when the NB phase contained 0.2 mM $Mo_6O_{19}^{2-}$ (note that orthophosphate ion was absent in this case).

At high scan rates (1.0—5.0 V s^{-1}), a typical wave with a pair of anodic (positive-current) and cathodic (negative-current) peaks was obtained, as represented by voltammogram (1). The anodic and cathodic peaks correspond, respectively, to the transfer of $Mo_6O_{19}^{2-}$ from NB to W and its transfer back to NB. Both the anodic and cathodic peak potentials, E_{pa} and E_{pc}, were almost independent of the pH of the W phase in the range 1.5 to 5.0. The midpoint potential, E_{mid} ($\equiv(E_{pa}+E_{pc})/2$=0.387±0.002 V), may be taken as a reversible half-wave potential, $E_{1/2}^{r}$, from which the standard potential difference, $\Delta_{NB}^{W}\phi^{\ominus}$, and the standard Gibbs energy, $\Delta G_{tr}^{\ominus,NB\to W}$, for the $Mo_6O_{19}^{2-}$ transfer were determined to be 0.164 V and 32 kJ mol^{-1}, in a similar manner as described previously.[9]

At lower scan rates ($\leq$0.2 V s^{-1}), the cyclic voltammogram showed an irreversible behavior. As can be

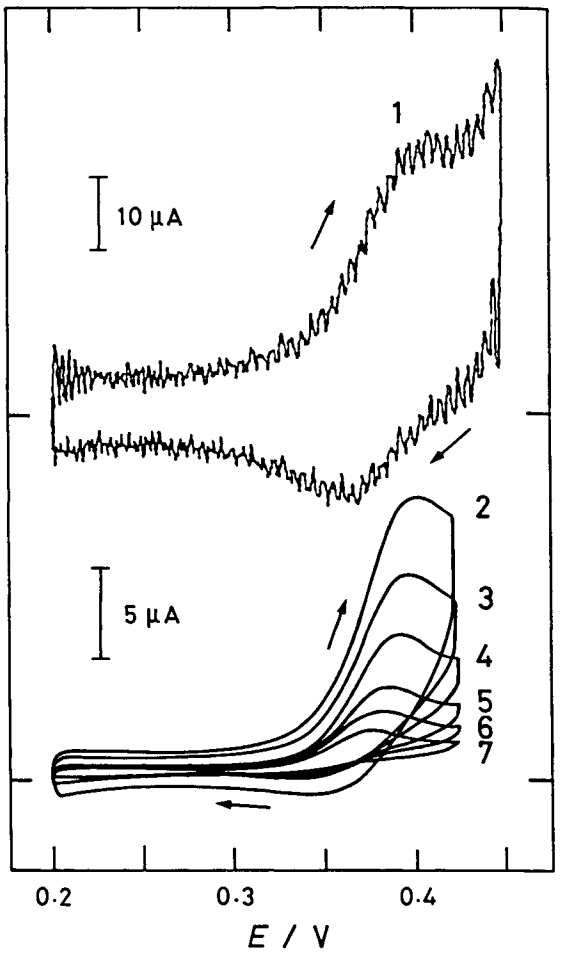

Fig. 3. Cyclic voltammograms of the transfer of $Mo_6O_{19}^{2-}$ at the NB/W (pH 3.1) interface. The NB phase contained 0.2 mM $(TBA)_2Mo_6O_{19}$. Scan rate: (1) 1.0; (2) 0.2; (3) 0.1; (4) 0.05; (5) 0.02; (6) 0.01; (7) 0.005 V s^{-1}. Voltammogram (1) was recorded with a transient recorder (Yokogawa Model 3655) instead of an X-Y pen recorder.

seen in voltammograms (2)—(7) in Fig. 3, no distinct cathodic peak due to the transfer of $Mo_6O_{19}^{2-}$ back to NB was observed, clearly showing that the anion decomposed rapidly in the W phase. This result is in line with the previous observations, that $Mo_6O_{19}^{2-}$ could be hardly detected in aqueous solutions; the anion was stabilized by the addition of certain water-miscible organic solvents.[13,14] Thus, the present ion-transfer process can be represented by

$$Mo_6O_{19}^{2-}(NB) \rightleftarrows Mo_6O_{19}^{2-}(W) \quad (1)$$

and

$$Mo_6O_{19}^{2-}(W) \xrightarrow{k_d} Mo(VI)(W). \quad (2)$$

To this system we can apply the theory of stationary electrode voltammetry[21] for a reversible charge transfer followed by an irreversible chemical reaction. According to the theory, it follows that E_{pa} is given by

$$E_{pa} = E^r_{1/2} - 0.780\,(RT/zF) + (RT/2zF)\ln[k_d(RT/|z|F)/v], \quad (3)$$

where k_d is the first-order rate constant of the decomposition reaction (Eq. 2), v the scan rate, and z the ionic valence (here, $z=-2$). R, T, and F have their usual meanings. In accord with Eq. 3, E_{pa} shifted toward positive potentials by about 18 mV for a ten-fold increase in v. The value of 18 mV is close to the theoretical value of 15 mV ($=-2.303(RT/2zF)$) at 25 °C. Using Eq. 3 and the $E^r_{1/2}$-value of 0.387 V, k_d was estimated to be 12±3 s^{-1} (at pH 3.1).

Electrochemical Formation of a Molybdophosphate Anion. From the above results, we expected that when such an oxoanion as the orthophosphate ion is present in the W phase, the transfer of $Mo_6O_{19}^{2-}$ from NB to W would be followed by the formation of a heteropoly complex at the interface. In Fig. 4, the dashed line indicates the cyclic voltammogram

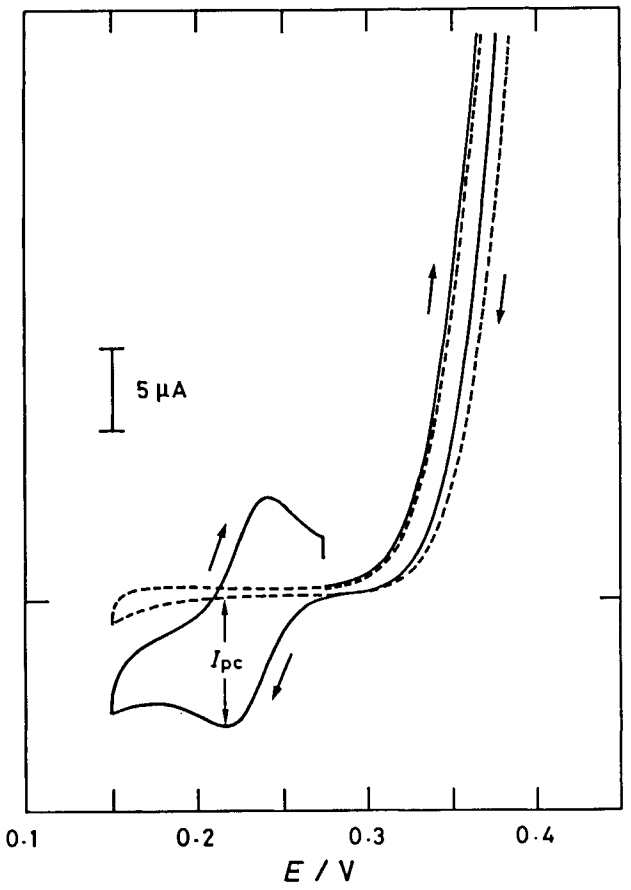

Fig. 4. Cyclic voltammograms of the transfer of $Mo_6O_{19}^{2-}$ at the NB/W interface in the presence (——) and absence (----) of 0.2 mM orthophosphate ion in the W phase (pH 3.1). The NB phase contained 5.0 mM $(TBA)_2Mo_6O_{19}$. The potential sweep was applied from 0.275 to 0.40 V in the anodic direction, followed by the cathodic to 0.15 V, then the anodic back to the initial potential. The potential-holding period at 0.40 V was 0 s in this case. Scan rate: 0.02 V s^{-1}.

obtained when $Mo_6O_{19}^{2-}$ was added in NB in a higher concentration (5.0 mM). On the initial anodic scan from 0.275 to 0.40 V, a large current due to $Mo_6O_{19}^{2-}$ transfer from NB to W was observed. As mentioned above, the anodic current was not followed by a cathodic current because of the rapid decomposition of $Mo_6O_{19}^{2-}$ in W. In the presence of orthophosphate ions in the W phase, however, a well-developed cathodic peak appeared at around 0.22 V on the succeeding cathodic scan, as shown by the solid line in Fig. 4. The cathodic peak was followed by an anodic peak at around 0.24 V. Obviously, these cathodic and anodic peaks were due to a phase transfer of certain molybdophosphate anions formed in the W phase in the vicinity of the interface. As the pH was raised, the wave shifted to negative potentials with a current change. In the following experiments, the pH was set at 3.1 so as to obtain the wave at a preferable potential, as shown in Fig. 4. Under these conditions, the cathodic peak current, i_{pc}, was proportional to the bulk concentration of orthophosphate ions in the range from 0.02 to 0.3 mM (shown in Fig. 5 by open circles). At concentrations higher than 0.3 mM, the cathodic current no longer increased, possibly because of a deficiency of Mo(VI). In this higher concentration range, the reproducibility of the currents was also poor. However, when the initial anodic scan was stopped at a switching potential of 0.40 V for a definite time, the lineality of the concentration dependence of i_{pc}, as well as the reproducibility, was much improved. At a potential-holding period of 60 s, i_{pc} was linear to the orthophosphate-ion concentration up to 0.5 mM (shown in Fig. 5 by full circles). In the lower concentration range (<0.3 mM), i_{pc} was virtually independent of the potential-holding period, indicating that the current was controlled only by the diffusion of orthophosphate ions to the interface.

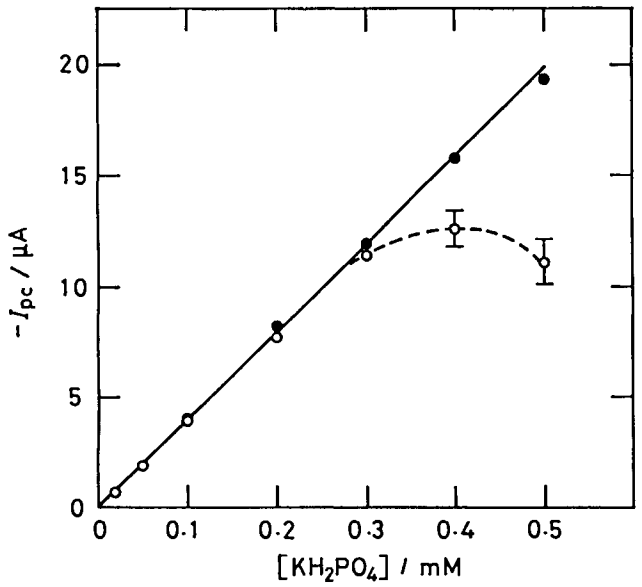

Fig. 5. Dependence of i_{pc} on the bulk concentration of orthophosphate ions added to the W phase. The potential-holding period: (○) 0; (●) 60 s.

These results clearly show that an NB/W interface containing $Mo_6O_{19}^{2-}$ in NB may function as a voltammetric ISE-surface for orthophosphate ions. An investigation is now in progress to develop a voltammetric sensor for practical uses based on such an oil/water interface.

Identification of the Heteropolyanion Formed at the Interface. For this purpose, a molybdophosphate anion formed at pH 3.1 in the aqueous molybdate solution was isolated as a TBA^+-salt, i.e. $(TBA)_4[H_3PMo_{11}O_{39}]$, as mentioned in the experimental section. By adding the salt to the NB phase, where the heteropoly complex was stable, a well-defined voltammogram for the phase transfer of the lacunary anion was observed at the same position as that in Fig. 4 (see Fig. 6). This shows that the heteropoly species formed predominantly as a result of the $Mo_6O_{19}^{2-}$ transfer was the lacunary anion. It should be stressed that the wave in Fig. 4 can never be assigned to the Keggin anion, $[PMo_{12}O_{40}]^{3-}$, whose ion-transfer potential was quite positive ($E_{1/2}^r$=0.475 V).[10]

In the voltammograms shown in Fig. 6, the anodic and cathodic peaks correspond to the transfer of anions from NB to W and their transfer back to NB,

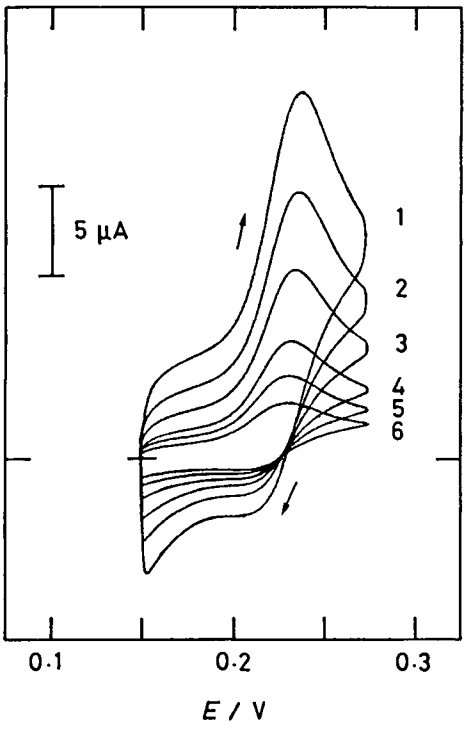

Fig. 6. Cyclic voltammograms of the transfer of $[H_3PMo_{11}O_{39}]^{4-}$ at the NB/W (pH 3.1) interface. The NB phase contained 0.18 mM $(TBA)_4[H_3PMo_{11}O_{39}]$. Scan rate: (1) 0.2; (2) 0.1; (3) 0.05; (4) 0.02; (5) 0.01; (6) 0.005 V s^{-1}.

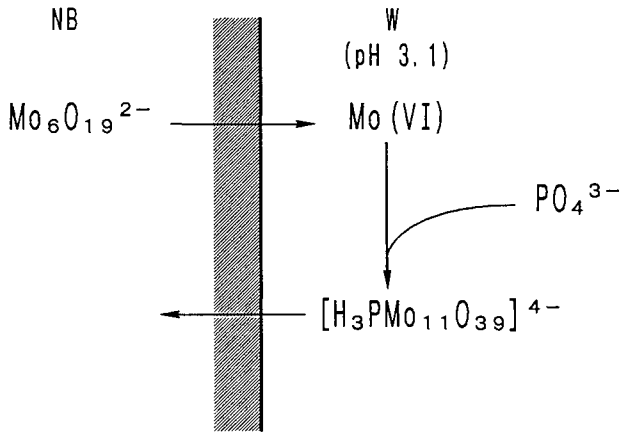

Fig. 7. Illustration of the electrochemical formation of a molybdophosphate anion at the NB/W interface. The succeeding transfer of the resulting $[H_3PMo_{11}O_{39}]^{4-}$ ion from W to NB can be utilized for the voltammetric determination of orthosphosphate ions in W.

respectively. Compared with the anodic peak currents, the cathodic ones were small, particularly at lower scan rates. This shows that the complex anions decomposed partially in the W phase, even at pH 3.1. Accordingly, the same theory[21] as that for $Mo_6O_{19}^{3-}$ transfer may be applied to this ion-transfer process. The slope (8 mV) of the E_{pa} vs. $\log v$ plot at pH 3.1 was close to the theoretical slope (7.4 mV) for $z=-4$. This suggested that the lacunary anion transferred across the interface as the tetravalent anion, i.e. $[H_3PMo_{11}O_{39}]^{4-}$ under these conditions.

Finally, the electrochemical formation of molybdophosphate anions at the NB/W interface may be illustrated graphically in Fig. 7. We would like to add that the present interface system possibly serves as a powerful tool for studying the dynamics of the heteropolyanion formation in aqueous solutions.

We would like to thank Dr. Toshitaka Hori of Kyoto University for his helpful suggestions. The present work was partially supported by a Grant-in-Aid for Scientific Research No. 2740292 from the Ministry of Education, Science and Culture.

References

1) J. Koryta, *Electrochim. Acta*, **24**, 293 (1979); *ibid.*, **29**, 445 (1984); *ibid.*, **33**, 189 (1988).
2) E. Wang and Z. Sun, *Trends Anal. Chem.*, **7**, 99 (1988).
3) T. Osakai, *Kagaku To Kogyo*, **43**, 184 (1990).
4) M. Senda, T. Kakiuchi, and T. Osakai, *Electrochim. Acta*, **36**, 253 (1991).
5) M. Senda, T. Osakai, T. Kakutani, and T. Kakiuchi, *Nippon Kagaku Kaishi*, **1986**, 956.
6) T. Osakai, T. Kakutani, and M. Senda, *Anal. Sci.*, **3**, 521 (1987).
7) T. Osakai, T. Kakutani, and M. Senda, *Anal. Sci.*, **4**, 529 (1988).
8) Y. Yamamoto, T. Nuno, T. Osakai, and M. Senda, *Bunseki Kagaku*, **38**, 589 (1989).
9) T. Osakai, S. Himeno, and A. Saito, *Anal. Sci.*, **5**, 771 (1989).
10) T. Osakai, S. Himeno, and A. Saito, *J. Electroanal. Chem. Interfacial Electrochem.*, in press.
11) S. Himeno, T. Osakai, and A. Saito, *Bull. Chem. Soc. Jpn.*, **62**, 1335 (1989).
12) T. Osakai, S. Himeno, A. Saito, and T. Hori, *J. Electroanal. Chem. Interfacial Electrochem.*, **278**, 217 (1990).
13) T. Osakai, S. Himeno, A. Saito, and T. Hori, *J. Electroanal. Chem. Interfacial Electrochem.*, **285**, 209 (1990).
14) S. Himeno, N. Ishii, M. Hasegawa, A. Saito, and T. Hori, *Inorg. Chim. Acta*, **131**, 11 (1987).
15) C. Sanchez, J. Livage, J. P. Launay, M. Fournier, and Y. Jeannin, *J. Am. Chem. Soc.*, **104**, 3194 (1982).
16) R. D. Peacock and T. J. R. Weakley, *J. Chem. Soc. A*, **1971**, 1836.
17) F. Zonnevijlle, C. M. Tourné, and G. F. Tourné, *Inorg. Chem.*, **21**, 2742 (1982).
18) C. Rocchiccioli-Deltcheff and R. Thouvenot, *J. Chem. Res. (S)*, **1977**, 46; *J. Chem. Res. (M)*, **1977**, 0549.
19) R. Strandberg, *Acta Chem. Scand., Ser. A*, **28**, 217 (1974).
20) M. T. Pope, "Heteropoly and Isopoly Oxometalates," Springer-Verlag, Berlin (1983), Chap. 4.
21) R. S. Nicholson and I. Shain, *Anal. Chem.*, **36**, 706 (1964).

 © 1991 The Chemical Society of Japan Bull. Chem. Soc. Jpn., 64, 1318—1324 (1991)

Preparation and Characterization of Optically Active Quadridentate Schiff Base-Titanium(IV) Complexes and the Catalytic Properties of These Complexes on Asymmetric Oxidation of Methyl Phenyl Sulfide with Organic Hydroperoxides

Caori SASAKI, Kiyohiko NAKAJIMA,† Masaaki KOJIMA,*,†† and Junnosuke FUJITA
Department of Chemistry, Faculty of Science, Nagoya University, Chikusa-ku, Nagoya 464-01
†Coordination Chemistry Laboratories, Institute for Molecular Science, Myodaiji, Okazaki 444
(Received December 1, 1990)

Titanium(IV) complexes, [TiCl(Schiff base)]$_2$O, with quadridentate Schiff base ligands derived from optically active 1,2-diamines and salicylaldehyde were prepared by treating $TiCl_4$ with an equimolar amount of the Schiff base ligand in wet pyridine. The complexes were characterized by their ^{13}C NMR, absorption, and circular dichroism spectra, and conductivity measurements. The complexes in dichloromethane take a μ-oxo dinuclear structure, and in methanol the complexes break up into a mononuclear species, [Ti(OMe)(MeOH)-(Schiff base)]Cl. The complexes catalyze the asymmetric oxidation of methyl phenyl sulfide into the sulfoxide with organic hydroperoxides; the highest enantiomeric excess (ee) was ca. 60%. The kinetics conform to a rate law which is first order in the concentration of each sulfide, hydroperoxide, and complex catalyst.

Optically active sulfoxides are attracting considerable attention in the asymmetric synthesis of organic compounds.[1] An efficient asymmetric oxidation of prochiral organic sulfides into optically active sulfoxides has been reported, using a modified Sharpless reagent (Ti(OPr^i)$_4$/diethyl (*R*,*R*)-tartrate/Bu^{t}OOH) for asymmetric epoxidation.[2,3] We have succeeded in a similar asymmetric oxidation of sulfides with organic hydroperoxides catalyzed by oxovanadium(IV) complexes containing quadridentate Schiff base ligands derived from optically active 1,2-diamines and salicylaldehyde or its derivatives.[4] Thus, it is interesting to study the catalytic properties of titanium(IV) analogs.

Here, we report the preparation and characterization of optically active quadridentate Schiff base-titanium(IV) complexes, and the asymmetric oxidation of methyl phenyl sulfide with organic hydroperoxides catalyzed by these complexes. A part of this study has been reported briefly.[5]

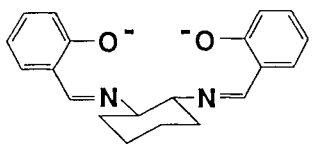

sal-(*RR*)-chxn

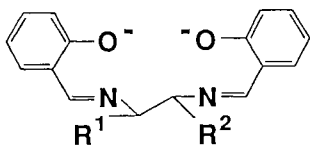

R^1=CH_3 , R^2=H ; sal-(*R*)-pn

R^1=R^2=C_6H_5 ; sal-(*RR*)-stien

Experimental

(*R*)-1,2-Propanediamine ((*R*)-pn), (*R*,*R*)-1,2-cyclohexanediamine ((*RR*)-chxn), and (*R*,*R*)-1,2-diphenylethylenediamine ((*RR*)-stien) were prepared by the published methods[6,7,8]

(*R*)-pn: $[\alpha]_D$ −11.0° (*c* 1.6, H_2O); lit, $[\alpha]_D$ −11.0° (c 2.5, H_2O).[6]

(*RR*)-chxn: $[\alpha]_D$ −42.1° (*c* 2.0, CH_3OH); lit, $[\alpha]_D$ −44.1° (c 3.0, CH_3OH).[7]

(*RR*)-stien: $[\alpha]_D$ +104° (*c* 0.57, CH_3OH); lit, $[\alpha]_D$ +106.9° (c 1.07, CH_3OH).[8]

Schiff bases were prepared by the methods of Gullotti et al.[9]

Preparation of [TiCl(Schiff Base)]$_2$O (Schiff Base=sal-(*R*)-pn, sal-(*RR*)-chxn, sal-(*RR*)-stien). These complexes were prepared by a similar method, and a representative procedure is given for [TiCl(sal-(*R*)-pn)]$_2$O.

To a pyridine solution (5 cm^3) of H$_2${sal-(*R*)-pn} (0.56 g, 2 mmol) was added $TiCl_4$ (0.38 g, 2 mmol) with stirring. The resulting orange solution was cooled in an ice-bath to yield an orange precipitate. It was collected by filtration, and recrystallized from dichloromethane by the addition of acetone. Yield: 0.41 g (56%). Found: C, 54.91; H, 4.55; N, 7.30%. Calcd for $C_{34}H_{32}N_4Cl_2O_5Ti_2$: C, 54.94: H, 4.34; N, 7.54%. Found: C, 58.79; H, 5.49; N, 6.05%. Calcd for [TiCl(sal-(*RR*)-chxn)]$_2$O·2$(CH_3)_2CO$=$C_{40}H_{40}N_4Cl_2O_5Ti_2$·2$C_3H_6O$: C, 58.80; H, 5.58; N, 5.96%. $^{13}C\{^1H\}$ NMR ($CDCl_3$) δ=24.4, 24.5, 28.8, 28.9, 67.2, 67.7, 115.8, 116.4, 119.8, 120.0, 123.4, 124.0, 134.5, 135.1, 135.2, 135.3, 157.9, 158.7, 162.2, and 162.4. $^{13}C\{^1H\}$ NMR (CD_3OD) δ=25.3, 30.1, 70.1, 117.5, 121.9, 124.3, 136.5, 137.8, 163.6, and 164.0. Found: C, 65.75; H, 4.43; N, 5.85%. Calcd for [TiCl(sal-(*RR*)-stien)]$_2$O =$C_{56}H_{44}N_4Cl_2O_5Ti_2$: C, 65.97; H, 4.35; N, 5.49%.

Oxidation of Methyl Phenyl Sulfide by Organic Hydroperoxides with a Catalytic Amount of Schiff Base-Titanium(IV) Complexes. A typical run was performed as

†† Present address: Department of Chemistry, Faculty of Science, Okayama University, Tsushima, Okayama 700.

follows: A methanol solution (20 cm^3) containing [TiCl(sal-(*RR*)-chxn)]$_2$O·2$(CH_3)_2CO$ (7.5×10^{-5} mol) and triphenylmethyl hydroperoxide (1.5×10^{-3} mol) was cooled to 0 °C. Methyl phenyl sulfide (1.5×10^{-3} mol) was added and the mixture was kept at 0 °C for 110 h. The solvent was removed under reduced pressure, and the residue was extracted with diethyl ether, which was evaporated under reduced pressure. From the resulting oil, methyl phenyl sulfoxide was isolated and purified by column chromatography on silica gel (eluent: cyclohexane-ethyl acetate (1 : 1 v/v)). Yield: 87%. The enantiomeric excess (ee) was determined on the basis of the reported optical rotation of the pure enantiomer;[10] $[\alpha]_D$ +79.7° (*c* 1.9, CH_3OH); 53% ee (*R*).

The progress of the reaction could be checked by high-performance liquid chromatography. Portions of the reaction mixture were withdrawn at intervals and then chromatographed (sample volume, 1—4×10^{-3} cm^3) with a column of Develosil ODS-5 (Nomura Chemical Co., Ltd., ϕ 0.46 cm×25 cm; eluent, acetonitrile-water (6 : 4 v/v)) or JASCO Fine Pack C18S (ϕ 0.46 cm×15 cm; eluent, acetonitrile-water (9 : 1 v/v)). Chromatography was carried out with a JASCO Tri Rotar V system and the components were detected with a JASCO UVIDEC 100 IV spectrophotometric detector at 260 nm. The amounts of sulfide, sulfoxide, and sulfone were determined from the absorption spectra of the collected fractions or by paper cut-outs matching the bands in the elution curve, while taking the molar absorption coefficients into consideration. The ee was determined from the circular dichroism (CD) spectrum of the fraction containing the sulfoxide on the basis of $\Delta\varepsilon_{237}$=+13.9 for the pure (*R*)-isomer.[4]

Kinetics Studies. The kinetics of the oxidation reactions was studied by high-performance liquid chromatography as described above. Since triphenylmethyl hydroperoxide is rather unstable, we used stable 1-methyl-1-phenylethyl hydroperoxide as the oxidant. All reactions were carried out under pseudo-first-order reaction conditions.

Spectroscopic Measurements. $^{13}C\{^1H\}$ NMR spectra were recorded on a JEOL GX-400 spectrometer using TMS as an internal reference. Optical rotations were measured with a JASCO DIP 4 polarimeter. Absorption and CD spectra were recorded on a Hitachi U-3400 spectrophotometer and a JASCO J-40CS spectropolarimeter, respectively. Conductivity measurements were carried out with a Toa CM-6A conductivity meter.

Results and Discussion

Preparation, Characterization, and Structure of the Schiff Base-Titanium(IV) Complexes. [TiCl(SB)]$_2$O (SB=Schiff base) was prepared by treating $TiCl_4$ with an equimolar amount of the Schiff base ligand in wet pyridine (water content≧0.4%). Although several titanium(IV) complexes with quadridentate Schiff base ligands have been prepared in the same way, they have been formulated differently.[11,12], Thus, the structure was determined by X-ray analysis on the sal-(*RR*)-chxn complex (Fig. 1); the details have been reported in a separate paper.[13] The structure shows a μ-oxo ligand bridging two TiCl(sal-(*RR*)-chxn) units. It is to be noted that [$TiCl_2$(SB)] is formed instead of [TiCl(SB)]$_2$O when the reaction is carried out in anhydrous solvents. The bridging oxygen atom seems to come from water in wet pyridine (Scheme 1).

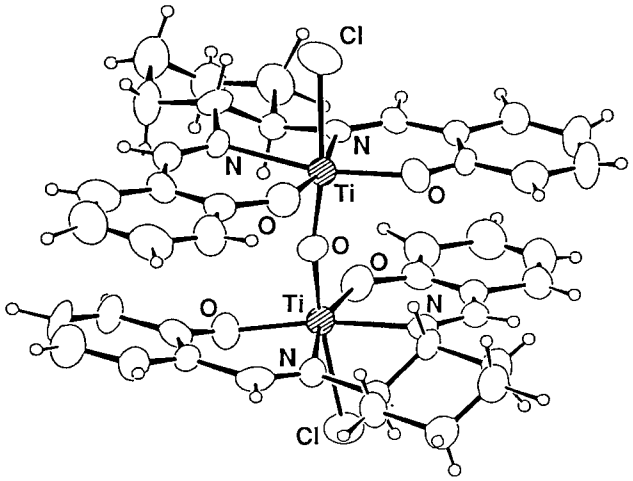

Fig. 1. An ORTEP drawing of [TiCl(sal-(*RR*)-chxn)]$_2$O.

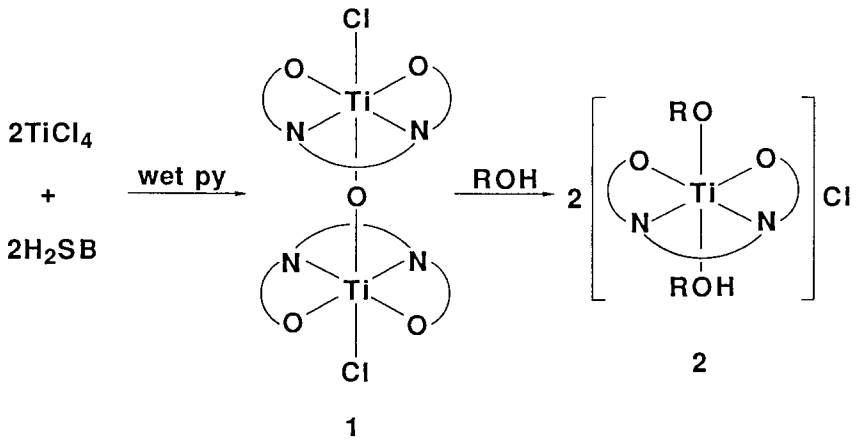

Scheme 1.

Very recently, Mozzanti et al.[14] have reported a μ-oxo dinuclear complex, [TiCl(acen)]$_2$O (acen=*N*,*N*′-ethylenebis(4-imino-2-penten-2-olate), the structure of which is very similar to that of [TiCl(sal-(*RR*)-chxn)]$_2$O.

Conductivity measurement reveals that [TiCl(sal-(*RR*)-chxn)]$_2$O is a non-electrolyte in dichloromethane, and the $^{13}C\{^1H\}$ NMR spectrum of the complex in CD_2Cl_2 shows 20 signals as expected for the crystal structure. On the other hand, the $^{13}C\{^1H\}$ NMR spectrum in CD_3OD shows only 10 signals, suggesting that the complex breaks up into a mononuclear one with a C_2 axis. The molar conductivity of 64 S cm^2 mol^{-1} in methanol calculated on the basis of the mononuclear complex, is in the range expected for a 1:1 electrolyte.[15] The most probable structure in methanol will be **2** in Scheme 1. Since protons migrate quickly on the NMR time scale, a coordinated methanol molecule and a methoxide ion will be indistinguishable by NMR (pseudo C_2). The absorption spectrum of [TiCl(sal-(*RR*)-chxn)]$_2$O in dichloromethane is quite different from those in methanol, ethanol, or 1-propanol, the spectra in alcohols being similar to each other (Fig. 2). Conductivities in ethanol (28 S cm^2 mol^{-1}) and 1-propanol (12 S cm^2 mol^{-1}) also suggest structure **2** in these solvents.

Figure 3 shows the CD spectra of [TiCl(sal-(*RR*)-chxn)]$_2$O in dichloromethane, methanol, ethanol, and 1-propanol. Here, again, the spectral pattern in

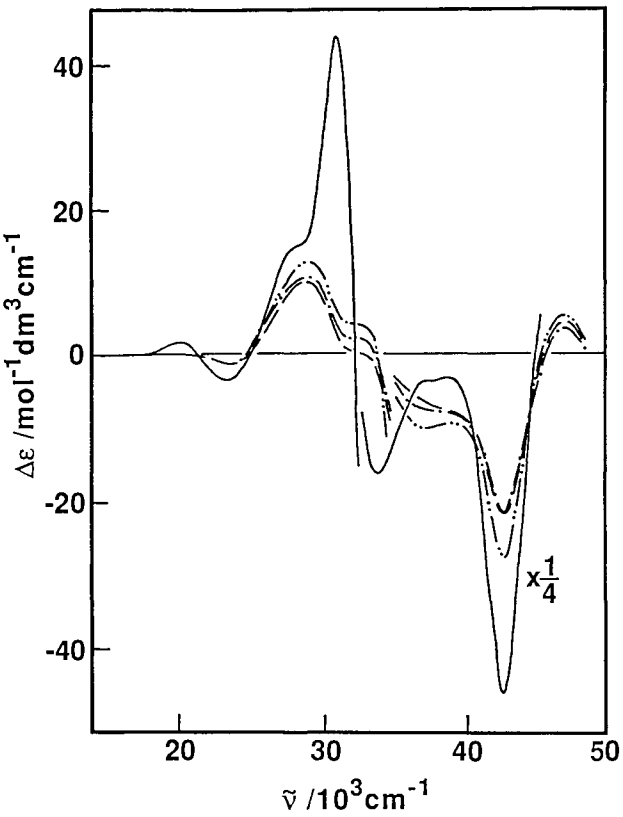

Fig. 3. CD spectra of [TiCl(sal-(*RR*)-chxn)]$_2$O in dichloromethane (——), methanol (— —), ethanol (— · —), and 1-propanol (— ·· —).

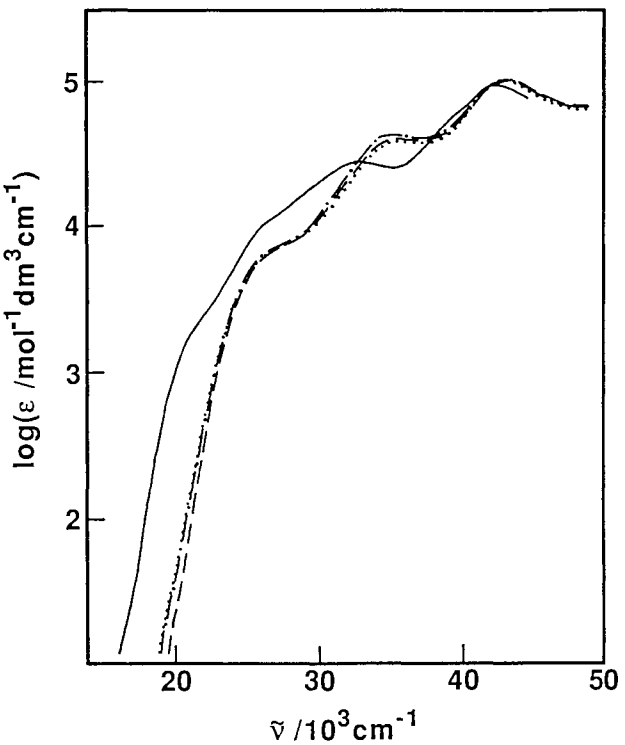

Fig. 2. Absorption spectra of [TiCl(sal-(*RR*)-chxn)]$_2$O in dichloromethane (——), methanol (— —), ethanol (— · —), and 1-propanol (·····).

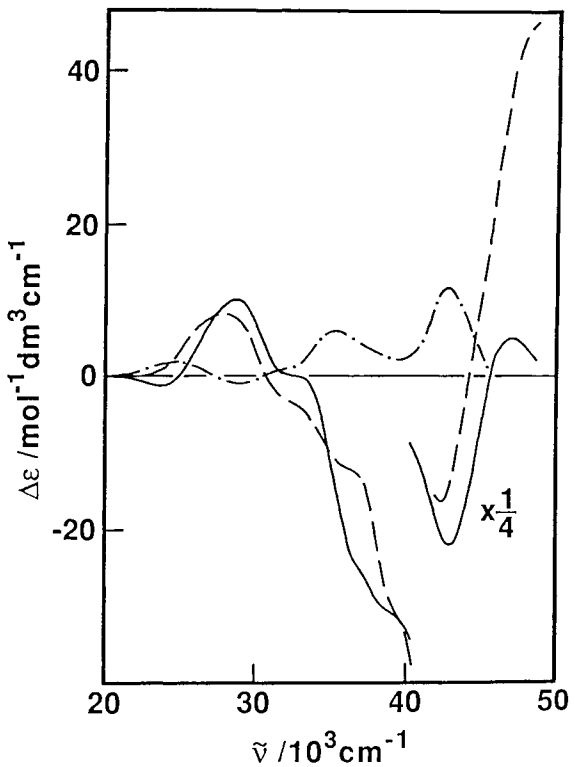

Fig. 4. CD spectra of [TiCl(SB)]$_2$O in methanol, SB=sal-(*RR*)-chxn (——), sal-(*RR*)-stien (— —), and sal-(*R*)-pn (— · —).

Table 1. Rates of Oxidation of Methyl Phenyl Sulfide by 1-Methyl-1-phenylethyl Hydroperoxide in Methanol at 40 °C

$[Cat]_0/M$[b]	$[RO_2H]_0/M$	$k_{1(obs)}/s^{-1}$[c]	$k_{2(obs)}$[d] $M^{-1}s^{-1}$	$k_{2(obs)}-k_{2(uncat)}$ $M^{-1}s^{-1}$	$k_{3(cat)}$[e] $M^{-2}s^{-1}$
7.5×10^{-3}	0.75	2.34×10^{-4}	3.12×10^{-4}	2.92×10^{-4}	3.9×10^{-2}
7.5×10^{-3}	1.5	5.17×10^{-4}	3.45×10^{-4}	3.25×10^{-4}	4.3×10^{-2}
7.5×10^{-3}	2.25	8.36×10^{-4}	3.71×10^{-4}	3.51×10^{-4}	4.7×10^{-2}
3.75×10^{-3}	0.75	1.09×10^{-4}	1.45×10^{-4}	1.25×10^{-4}	3.3×10^{-2}
1.88×10^{-2}	0.75	5.14×10^{-4}	6.86×10^{-4}	6.66×10^{-4}	3.6×10^{-2}
3.75×10^{-2}	0.75	9.92×10^{-4}	1.32×10^{-3}	1.30×10^{-3}	3.5×10^{-2}

$[Cat]_0/M$[b]	$[RO_2H]_0/M$	$k_{1(uncat)}=k_{1(obs)}$[c]	$k_{2(uncat)}$[d] $M^{-1}s^{-1}$
0	0.75	1.47×10^{-5}	1.96×10^{-5}

a) In all runs $[S]_0$ was 7.5×10^{-2} M. b) $[Cat]_0$ denotes the initial concentration of the titanium(IV) complex catalyst calculated as the mononuclear species. c) $k_{1(obs)}$ and $k_{1(uncat)}$ were obtained from the slope of the plot of $\log([S]_t/[S]_0)$ vs. time. d) $k_{2(obs)}$ and $k_{2(uncat)}$ were estimated as $k_{1(obs)}/[RO_2H]_0$ and $k_{1(uncat)}/[RO_2H]_0$, respectively. e) $k_{3(cat)}$ was estimated as $(k_{2(obs)}-k_{2(uncat)})/[Cat]_0$.

dichloromethane is quite different from those in alcohols. Figure 4 compares the CD spectra of the titanium(IV) complexes of sal-(*RR*)-chxn, sal-(*RR*)-stien, and sal-(*R*)-pn in methanol. The sal-(*RR*)-stien complex has a CD spectrum similar to that of the sal-(*RR*)-chxn complex. The central chelate ring of sal-(*RR*)-chxn is locked in a λ gauche conformation. The similarity in CD spectra between the two complexes, sal-(*R*)-stien and sal-(*RR*)-chxn, suggests that the sal-(*RR*)-stien complex also takes a λ gauche conformation. Examination of a molecular model indicates that the steric interaction between the phenyl groups and the axial ligands is very severe in the sal-(*RR*)-stien complex when the phenyl groups take axial positions, and the chelate should take the λ form stereoselectively. The CD spectral pattern of the sal-(*R*)-pn complex is almost a mirror image of the others, despite the fact that all parent diamines have the same absolute configuration. The intensity of the sal-(*R*)-pn complex is small compared with the others. Probably the greater part of the sal-(*R*)-pn complex in methanol takes a δ gauche conformation to reduce the steric interaction between the hydrogen on the azomethine carbon and the pn methyl group; the complex will be in an equilibrium mixture of the conformational isomers (δ and λ) with a small preference of the δ form. Similar relationships among the CD spectra have been reported for the corresponding oxovanadium(IV) complexes, VO(sal-(*SS*)-chxn), VO(sal-(*SS*)-stien), and VO(sal-(*S*)-pn).[16]

Oxidation of Methyl Phenyl Sulfide. The $[TiCl(SB)]_2O$ complexes catalyze the oxidation of methyl phenyl sulfide by organic hydroperoxides. Since organic hydroperoxides themselves oxidize sulfides in the absence of any added catalyst, the entire oxidation process must be the result of two independent pathways, catalyzed and uncatalyzed. Uncatalyzed oxidation is known to be first order both in the sulfide concentration ([S]) and in the hydroperoxide concentration ($[RO_2H]$), $R=k_{2(uncat)}[S][RO_2H]$.[17] In the absence of the complex catalyst, the oxidation of methyl phenyl sulfide by 1-methyl-1-phenylethyl hydroperoxide (CHP) was performed in methanol at 40 °C with the hydroperoxide in large excess over the sulfide. Pseudo-first-order behavior was observed, and the second-order rate constant ($k_{2(uncat)}$) for the uncatalyzed oxidation was calculated as $k_{1(uncat)}/[RO_2H]_0$; the result is given in Table 1.

In the presence of a complex catalyst, the rate law can be written as

$$-d[S]/dt = k_{2(uncat)}[S][RO_2H] + k_{3(cat)}[Cat]^p[RO_2H]^q[S]^r. \quad (1)$$

The first term on the right represents the uncatalyzed oxidation, while the second term the catalyzed one. Figure 5(a) shows the reaction profile for the oxidation of methyl phenyl sulfide (7.5×10^{-2} M, 1 M=1 mol dm^{-3}) with large excess CHP (7.5×10^{-1} M) in methanol in the presence of $[TiCl(sal\text{-}(RR)\text{-}chxn)]_2O$ (3.75×10^{-3} M) at 40 °C. The formation of the sulfone and the decomposition of the catalyst were negligibly small during the reaction. A plot of $\log([S]_t/[S]_0)$ vs. time gave a straight line for at least three half-lives (Fig. 5(b)); the pseudo-first-order rate constant ($k_{1(obs)}$) is given in Table 1. Table 1 also shows that at reasonable catalyst concentrations the complex-catalyzed reaction proceeds much faster than does uncatalyzed oxidation. In order to determine the order in CHP, we studied the oxidation with different $[RO_2H]_0$. The data in Table 1 suggest that $q=1$. Thus, Eq. 1 reduces to Eq. 2 under the conditions given in Table 1.

$$\begin{aligned} -d[S]/dt &= (k_{2(uncat)} + k_{3(cat)}[Cat]^p)[RO_2H][S] \\ &= k_{2(obs)}[RO_2H][S] \\ &= k_{1(obs)}[S] \end{aligned} \quad (2)$$

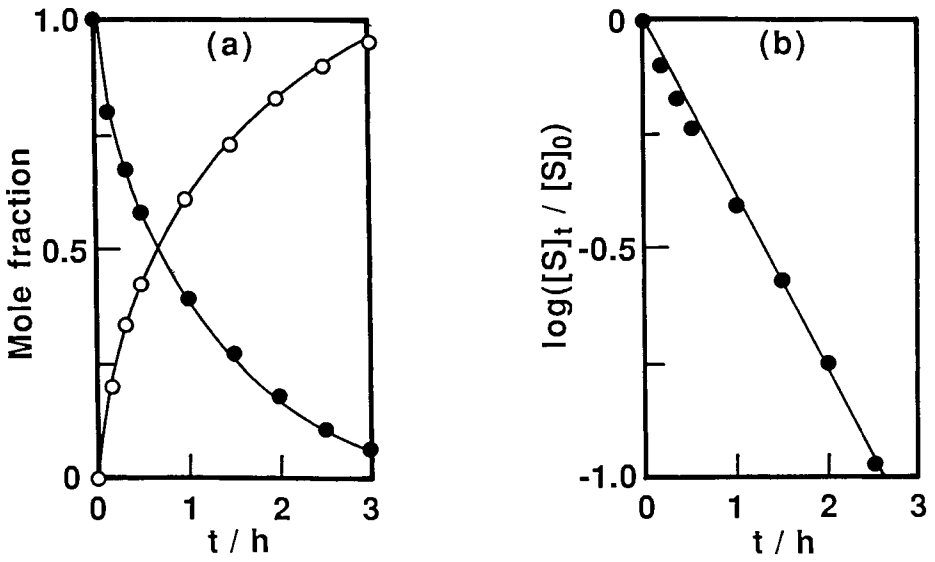

Fig. 5. Oxidation of methyl phenyl sulfide (7.5×10^{-2} M) by 1-methyl-1-phenylethyl hydroperoxide (7.5×10^{-1} M) with the [TiCl(sal-(*RR*)-chxn)]$_2$O (3.75×10^{-3} M) catalyst in methanol at 40 °C. (a) Reaction profile: ●, sulfide; ○, sulfoxide, and (b) the plot of $\log([S]_t/[S]_0)$ vs. reaction time. [S]=sulfide concentration.

At constant CHP and MeSPh initial concentrations, the rates increase upon increasing the catalyst concentration (Table 1). A $\log(k_{2(obs)}-k_{2(uncat)})$-$\log[Cat]_0$ plot gives a slope of 0.95, indicating that the order in the catalyst is unity ($p=1$). Hence, the catalytic third-order rate constant, $k_{3(cat)}=(k_{2(obs)}-k_{2(uncat)})/[Cat]$, could be estimated to be 3.9×10^{-2} $M^{-2}s^{-1}$. The first-order dependence on sulfide, hydroperoxide, and titanium catalyst implies that one molecule of each reactant is involved in the transition state of the rate-determining step. Since the probability of a trimolecular collision would be extremely small, two of the components must have interacted at a prior stage. Neither the addition of CHP nor methyl phenyl sulfide in moderate excess had any effect on the absorption and CD spectra of [TiCl(sal-(*RR*)-chxn)]$_2$O. However, an appreciable CD change was observed upon the addition of a large excess of dibutyl sulfide, which is considered to be a stronger ligand than methyl phenyl sulfide. Coordination of sulfides to Ti(IV) is not an unlikely process, and various titanium complexes with sulfide ligands have been identified.[18,19] We therefore suggest that the mechanism of oxidation involves an external attack by CHP on the coordinated sulfide, as proposed by Colombo et al.[20]

Several optically active Schiff base-titanium(IV) complex catalysts, solvents, and peroxides were used for the asymmetric oxidation of methyl phenyl sulfide; the results are given in Table 2.

Among the four organic hydroperoxides that we used, triphenylmethyl hydroperoxide (THP) gave higher ee's than did the others; the results may be associated with a steric effect of the phenyl groups in THP. In asymmetric catalytic reactions the importance of the orientation of the phenyl groups has been pointed out.[21,22] Recently, it has been reported that a similar oxidation of MeSPh with H_2O_2 catalyzed by titanium(IV) complexes containing optically active Schiff base ligands, such as sal-(*SS*)-chxn, led to low ee's (<20%) of the sulfoxide, the structures of the complexes being not described clearly.[20] The low ee's may result from the use of H_2O_2 in EtOH-H_2O.

Lowering of the temperature results in an enhancement in the enantioselectivity. However, as the temperature is lowered the reactivity decreases, and it takes an extremely long reaction time to oxidize the sulfide below 0 °C. We thus studied most of the oxidation at 0 °C by THP.

The ee shows a remarkable solvent dependence (Table 2); enantioselectivity decreases in the order MeOH>CH_2Cl_2>EtOH>PrOH in the oxidation of MeSPh by THP with the [TiCl(sal-(*RR*)-chxn)]$_2$O catalyst. The results may be partly attributed to a difference in the structure of the complex catalyst in solution. The complex has a dinuclear structure in CH_2Cl_2, while in alcohols it breaks up into a mononuclear species (vide supra). The difference in ee among the alcohols seems to be related to the different reactivities of the catalyst. For example, the oxidation of the sulfide in MeOH for 19 h and in EtOH for 110 h gave the sulfoxide in 73% (58% ee, Entry 6) and 61% (18% ee, Entry 18), respectively, while the same reaction in PrOH took as long as 240 h to yield the sulfoxide in 74% (ca. 0% ee, Entry 19). The oxidation of the sulfide is the result of the catalyzed and uncatalyzed pathways, and chiral discrimination occurs only

Table 2. Asymmetric Oxidation of Methyl Phenyl Sulfide to the Sulfoxide Catalyzed by the Titanium(IV) Complexes

Entry	Peroxide[a]	$[TiCl(SB)]_2O$ SB	[Ti]:[O]:[S][b]	Solvent	Temp/°C	Time/h	Yield/%[c]	ee/%[d] (config.)
1	THP	sal-(*RR*)-chxn	0.25:20:10	MeOH	0	15	58	43 (*R*)
2	THP	sal-(*RR*)-chxn	0.25:20:10	MeOH	0	70	81[e]	46 (*R*)
3	THP	sal-(*RR*)-chxn	0.5:20:10	MeOH	0	14	75	56 (*R*)
4	THP	sal-(*RR*)-chxn	0.5:20:10	MeOH	0	70	54[f]	58 (*R*)
5	THP	sal-(*RR*)-chxn	1:20:10	MeOH	0	15	98	62 (*R*)
6	THP	sal-(*RR*)-chxn	1:11:10	MeOH	0	19	73	58 (*R*)
7	THP	sal-(*RR*)-chxn	1:11:10	MeOH	0	44	98	61 (*R*)
8	THP	sal-(*RR*)-chxn	2:11:10	MeOH	0	16	89	63 (*R*)
9	THP	sal-(*RR*)-chxn	4:11:10	MeOH	0	1.5	42	58 (*R*)
10	THP	sal-(*RR*)-chxn	4:11:10	MeOH	0	3	59	60 (*R*)
11	THP	sal-(*RR*)-chxn	4:11:10	MeOH	0	7	77	62 (*R*)
12	THP	sal-(*RR*)-chxn	4:11:10	MeOH	0	9	84	58 (*R*)
13	THP	sal-(*RR*)-chxn	4:11:10	MeOH	0	15	95[g]	61 (*R*)
14	THP	sal-(*RR*)-chxn	1:10:10	MeOH	40	20	86[h]	22 (*R*)
15	THP	sal-(*RR*)-chxn	1:10:10	MeOH	20	70	86[h]	48 (*R*)
16	THP	sal-(*RR*)-chxn	1:10:10	CH_2Cl_2	20	64	60[h]	12 (*R*)
17	THP	sal-(*RR*)-chxn	1:10:10	CH_2Cl_2	0	170	46[h]	26 (*R*)
18	THP	sal-(*RR*)-chxn	1:10:10	EtOH	0	110	61[h]	18 (*R*)
19	THP	sal-(*RR*)-chxn	1:10:10	PrOH	0	240	74[h]	ca. 0
20	TBHP	sal-(*RR*)-chxn	1:10:10	CH_2Cl_2	0	144	61[h]	8 (*R*)
21	TMBHP	sal-(*RR*)-chxn	1:10:10	CH_2Cl_2	0	141	68[h]	12 (*R*)
22	CHP	sal-(*RR*)-chxn	1:10:10	CH_2Cl_2	0	170	32[h]	19 (*R*)
23	THP	sal-(*RR*)-stien	0.2:10:10	MeOH	0	71	95[h]	14 (*R*)
24	THP	sal-(*R*)-pn	0.2:10:10	MeOH	0	65	83[h]	9 (*S*)
25	THP	—	0:11:10	MeOH	0	19	16	—
26	THP	—	0:11:10	MeOH	0	46	38	—
27	THP	—	0:20:10	MeOH	0	15	30	—
28	THP	—	0:20:10	MeOH	0	70	66	—

a) Peroxide: THP, triphenylmethyl hydroperoxide; TBHP, *t*-butyl hydroperoxide; TMBHP, 1,1,3,3-tetramethylbutyl hydroperoxide; CHP, 1-methyl-1-phenylethyl hydroperoxide. b) [Ti]:[O]:[S] denotes molar ratio of $[TiCl(SB)]_2O$ (calculated as the mononuclear species):organic hydroperoxide:methyl phenyl sulfide (8.0×10^{-2} M). c) Analyzed by high-performance liquid chromatography unless otherwise stated. d) Based on the CD spectral data or the optical rotation of the pure enantiomer (see Experimental). e) In addition there is 12% sulfone. f) In addition there is 36% sulfone. g) In addition there is 5% sulfone. h) Isolated yield, based on the sulfide.

in the former. Hence, the ee becomes lower as the reactivity of the catalyst decreases. The greater part of the oxidation in PrOH may result from the uncatalyzed process. The solvent plays an important role in the present catalyzed reaction. Entries 25—28 show that the uncatalyzed oxidation of the sulfide with THP proceeds rather fast, even in MeOH; we therefore carried out the oxidation with different catalyst concentrations in order to estimate the contribution of the uncatalyzed pathway to the entire oxidation. At reasonably high catalyst concentrations, [Ti]/[S]>0.05, the ee stayed almost constant (ca. 60% ee), suggesting that the catalyzed process dominates the uncatalyzed one under these conditions. The ee did not change appreciably during the oxidation.

The complex catalysts containing an (*RR*)-chxn moiety or an (*RR*)-stien moiety gave the (*R*)-sulfoxide, while that containing an (*R*)-pn moiety gave the (*S*)-sulfoxide (Entry 24). These results can be understood if we assume that the catalytically active species has a conformational chirality similar to that of the added complex. As described before, the central chelate rings of the sal-(*RR*)-chxn and sal-(*RR*)-stien complexes take a λ gauche conformation. On the other hand, $[TiCl(sal\text{-}(R)\text{-}pn)]_2O$ in solution is suggested to be an equilibrium mixture of the conformational isomers (δ and λ) with a small preference of the δ form. Such a difference in conformational chirality among the complexes should be responsible for the enantioselectivity. It should be noted that oxovanadium(IV) complex catalysts give the antipode in a similar oxidation; for example, VO(sal-(*RR*)-chxn) gives the (*S*)-sulfoxide. Although the reason is not clear it may be related to a difference in mechanism between the two systems. As described above, we suggested coordination of sulfur to titanium prior to oxidation. Prochiral sulfides become chiral upon coordination, and chiral induction occurs at this stage. On the other hand, in a similar reaction with the VO(SB) complex catalyst, the catalytically active species was suggested to be a vanadium peroxide complex and the activated peroxide will oxidize sulfides.[4]

The present work was partially supported by the Grant-in-Aid for Scientific Research Nos. 61430013 and 02740307 from the Ministry of Education, Science and Culture.

References

1) For example, G. Solladié, *Synthesis*, **1981**, 185.
2) P. Pitchen and H. B. Kagan, *Tetrahedron Lett.*, **1984**, 1049; P. Pitchen, M. Deshmukh, E. Duñach, and H. B. Kagan, *J. Am. Chem. Soc.*, **106**, 8188 (1984); H. B. Kagan, E. Duñach, C. Nemecek, P. Pitchen, O. Samuel, and S. Zhao, *Pure Appl. Chem.*, **57**, 1911 (1985); E. Duñach and H. B. Kagan, *Nouv. J. Chim.*, **9**, 1 (1985); S. H. Zhao, O. Samuel, and H. B. Kagan, *Tetrahedron*, **43**, 5135 (1987).
3) F. Di Furia, G. Modena, and R. Seraglia, *Synthesis*, **1984**, 325.
4) K. Nakajima, K. Kojima, M. Kojima, and J. Fujita, *Bull. Chem. Soc. Jpn.*, **63**, 2620 (1990).
5) K. Nakajima, C. Sasaki, M. Kojima, T. Aoyama, S. Ohba, Y. Saito, and J. Fujita, *Chem. Lett.*, **1987**, 2189.
6) F. P. Dwyer, F. L. Garvan, and A. Shulman, *J. Am. Chem. Soc.*, **81**, 290 (1959) and "Shin-Zikken Kagaku Koza," Maruzen, Tokyo (1977), Vol. 8, p. 1429.
7) R. G. Asperger and C. F. Liu, *Inorg. Chem.*, **4**, 1429 (1965).
8) K. Saigo, N. Kubota, S. Takebayashi, and M. Hasegawa, *Bull. Chem. Soc. Jpn.*, **59**, 931 (1986).
9) M. Gullotti, A. Pasini, P. Fantucci, R. Ugo, and R. D. Gillard, *Gazz. Chim. Ital.*, **102**, 855 (1972).
10) J. Jacobus and K. Mislow, *J. Am. Chem. Soc.*, **89**, 5228 (1967).
11) P. Pfeiffer and H. Thielert, *Chem. Ber.*, **71**, 119 (1938).
12) M. Gullotti and A. Pasini, *Inorg. Chim. Acta*, **15**, 129 (1975).
13) T. Aoyama, S. Ohba, Y. Saito, C. Sasaki, M. Kojima, J. Fujita, and K. Nakajima, *Acta Cryst., Sect. C*, **44**, 1309 (1988).
14) M. Mazzanti, J.-M. Rosset, C. Floriani, A. Chiesi-Villa, and C. Guastini, *J. Chem. Soc., Dalton Trans.*, **1989**, 953.
15) W. J. Geary, *Coord. Chem. Rev.*, **7**, 81 (1971).
16) A. Pasini, M. Gullotti, and R. Ugo, *J. Chem. Soc., Dalton Trans.*, **1977**, 346.
17) G. Modena, *Gazzetta*, **89**, 834 (1959); M. A. P. Dankleff, R. Curci, J. O. Edwards, and H.-Y. Pyun, *J. Am. Chem. Soc.*, **90**, 3209 (1968).
18) O. Bortolini, F. Di Furia, and G. Modena, *J. Mol. Catal.*, **16**, 61 (1983); O. Bortolini, C. Campello, F. Di Furia, and G. Modena, *J. Mol. Catal.*, **14**, 63 (1982).
19) G. W. A. Fowles, D. A. Rice, and J. D. Wilkins, *J. Chem. Soc. A*, **1971**, 1920.
20) A. Colombo, G. Marturano, and A. Pasini, *Gazz. Chim. Ital.*, **116**, 35 (1986).
21) B. Bosnich and N. K. Roberts, *Adv. Chem. Ser.*, **196**, 337 (1982).
22) J. M. Hawkins and K. B. Sharpless, *Tetrahedron Lett.*, **28**, 2825 (1987).

On the Reaction of (Vinylimino)phosphoranes. Part 17.[1] Preparation of *N*-Vinylcarbodiimides and Their [4+2] Cycloaddition with Several Dienophiles to Give Pyridine Ring System[2]

Makoto NITTA,* Hironobu SOEDA, Shinya KOYAMA, and Yukio IINO
Department of Chemistry, School of Science and Engineering, Waseda University, Shinjuku-ku, Tokyo 169
(Received November 14, 1990)

The aza-Wittig reaction of (vinylimino)triphenylphosphorane and its several derivatives was examined to give *N*-phenyl-*N'*-vinylcarbodiimide and its derivatives, all of which underwent a [4+2] cycloaddition reaction with electron-rich dienophiles (enamines) and/or electron-deficient dienophiles (activated acetylenes), resulting in the formation of a pyridine ring system. The regioselectivity of the cycloaddition reaction could be rationalized on the basis of a frontier orbital consideration.

The [4+2] cycloaddition reaction of azadiene has proved to be one of the most powerful methods for the synthesis of six-membered nitrogen heterocycles.[3] Thus, the development of a new azadiene should provide a convenient way to produce heterocycles containing a pyridine ring. During the last decade, the synthesis and reaction of acyclic 2-aza-1,3-butadiene **1** have been studied extensively. For example, the [4+2] cycloaddition reaction of a 2-aza-1,3-butadiene (**1A**) having an electron-donating substituent, such as an amino[4-6] or silyloxy[7] group, with electron deficient dienophiles has been successfully examined; the reactivity and regioselectivity of the reaction have been rationalized on the basis of the frontier orbital treatment.[6] A compound of type (**1B**), which has an alkyl or aryl substituent, has been demonstrated to undergo [4+2] cycloaddition with both hetero-dienophiles[8,9] and electron-deficient dienophiles.[9,10] Furthermore, a 2-aza-1,3-butadiene (**1C**) having an electron-withdrawing substituent[11] has also been clarified to undergo a [4+2] cycloaddition reaction with enamines.[12] A few examples of C=C-conjugated carbodiimide, which also has a 2-aza-1,3-butadiene unit, has been known[13-15] and intermolecular cycloaddition with tetracyanoethylene[13] and intramolecular cyclization[14] has been reported.

We have recently demonstrated a simple preparation method of various (vinylimino)phosphoranes, which were found to react with α-bromo ketones, α,β-unsaturated ketones, and tropone derivatives in an enamine alkylation process followed by aza-Wittig reaction to provide convenient routes to pyrroles,[16,17] pyridines,[18] [*n*](2,4)pyridinophanes (*n*=6—9),[19] and 1-azaazulenes.[20] As part of a series of studies on (vinylimino)phosphoranes and related compounds, we examined the aza-Wittig reaction of (vinylimino)-phosphoranes with phenyl isocyanate to give C=C-conjugated carbodiimide derivatives, which undergo a [4+2] cycloaddition reaction with several dienophiles to give a pyridine ring system.

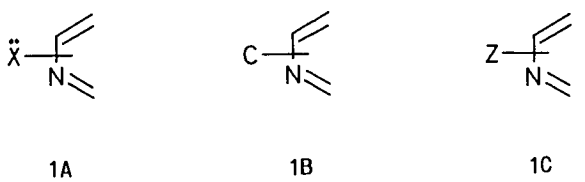

Fig. 1.

Results and Discussion

Preparation and [4+2] Cycloaddition Reaction of *N*-Phenyl-*N'*-vinylcarbodiimide and Its Derivatives. *N*-Vinyl-, *N*-(1-phenylvinyl)-, *N*-(1,3,5-cycloheptatrienyl)-, and *N*-(3-oxo-1-cyclohexenyl)-substituted carbodiimides (**6**), (**7**), (**8**), and (**9**), were prepared by the aza-Wittig reaction of phenyl isocyanate with the corresponding (vinylimino)triphenylphosphorane (**2**) and its derivatives **3**—**5** (Scheme 1). Compounds **6**—**8** could be purified by column chromatography on silica gel, and the structural assignment was based on high-resolution mass, IR, and ^{1}H NMR spectral data.

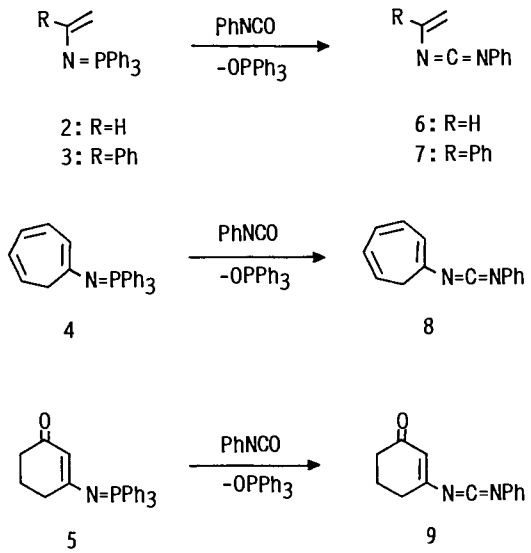

Scheme 1.

Table 1. Results for the Reaction of **6** or **7** with Enamines **10a—c** or **13a,b**[a]

Entry	Compound	Enamine	Solvent	Product	Yield/%
1	**6**	**10a**	PhMe	**12a**	9
2	**7**	**10a**	PhBr	**15a**	41
3	**7**	**10a**	DMF[b]	**15a**	33
4	**7**	**10b**	PhBr	**15b**	34
5	**7**	**10c**	PhBr	**15c**	30
6	**7**	**13a**	PhBr	**15a**	38
7	**7**	**13b**	PhBr	**15b**	39

a) Reactions were carried out under refluxing for 0.5 h. b) Denote *N*,*N*-dimethylformamide.

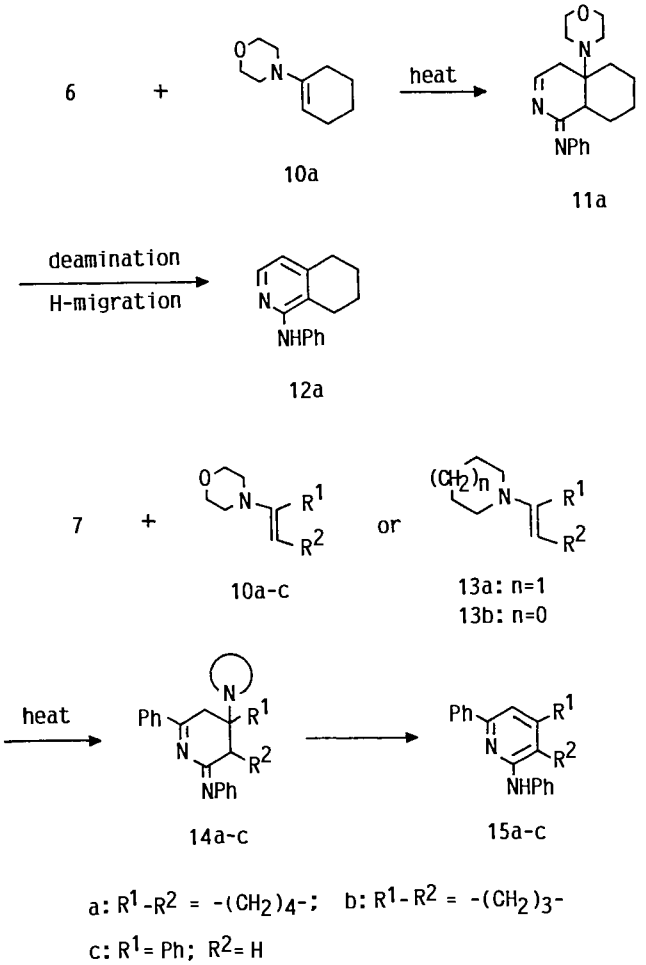

Scheme 2.

Compound **9** was unstable and decomposed through chromatography on silica gel, and the structural proof for **9** was not obtained from the ^{1}H NMR spectrum of crude **9**. Thus, the reaction was conveniently carried out using a one-pot procedure without isolating **9**.

A thermal reaction of **6** with enamine **10a** was carried out in toluene to give an isoquinoline derivative **12a** in low yield (Scheme 2, Table 1, Enty 1). Similarly, reactions of **7** with enamines **10a—c** and **13a,b** were carried out in bromobenzene under refluxing to give isoquinoline derivatives **15a,b** and pyridine derivative **15c** in modest yields (Scheme 2). The results are also summarized in Table 1 (Entries 2—7). Neither the yields of the products nor the reaction time was dependent on the amine moiety of the enamines (Entries 7 and 8). Furthermore, no drastic change in the reaction time and yield of the product was observed, even in a polar solvent (DMF) (Entry 3). Thus, the reaction seemed to proceed via a concerted [4+2] cycloaddition rather than an ionic process. Furthermore, enamines from cycloalkanones, **10a,b**, resulted in higher yields of the products, as compared to that of **10c**.

Each of the ^{1}H NMR spectra of the new compounds **12a** and **15a,b** showed, besides signals for the aromatic ring, characteristic signals for the alicyclic methylene chain. The assignment of the signals are summarized in the Experimental section. Furthermore, the structure of **15c** was deduced on the basis of the spectral data, the ^{1}H NMR spectrum of which showed a pair of doublets at δ=7.02 and δ=7.42 (J=1.1 Hz, meta-coupled), thus, **15c** could be differentiated from the other regioisomer, 2-phenylamino-3,6-diphenylpyridine (**23**), which exhibited a signal at δ=7.34 (J=7.7 Hz, ortho-coupled) (vide infra). Thus, in the formation of compounds **12a**, **15a—c** is postulated to proceed through intermediates **11a** and **14a—c**, all of which undergo hydrogen migration and subsequent deamination. The regioselectivity of the enamine addition process giving **11a** or **14a—c** is suggested by the formation of **15c**, as well as with frontier molecular orbital consideration (vide infra).

The reaction of the carbodiimide **8** with enamines **10a—c** were examined in bromobenzene under refluxing to give a mixture of 9*H*-cyclohepta[*b*]pyridine (**17a—c**) and 7*H*-cyclohepta[*b*]pyridine (**18a—c**) derivatives (Scheme 3). Compounds **18a—c** are possibly derived from base catalyzed isomerization of **17a—c**,

Table 2. Results for the Reaction of **8** with Enamines **10a—c** to Give **17a—c** and **18a—c**[a]

Enamine	Product yield/%	Molar ratio of **17**/**18**
10a	47	1.85
10b	61	0.33
10c	48	1.50

a) Reactions were carried out in bromobenzene under refluxing for 0.5 h.

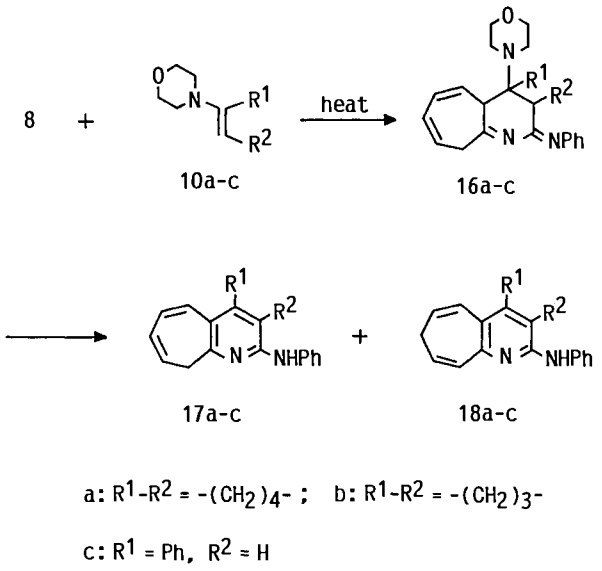

Scheme 3.

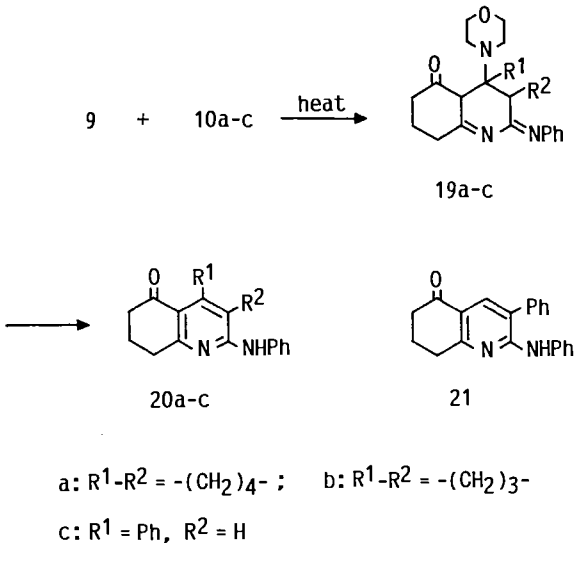

Scheme 4.

respectively. The results are summarized in Table 2. The spectral data of the new compounds were consistent with the proposed structures (Experimental). Each of the ^{1}H NMR spectra of the mixtures showed, in addition to signals for the substituted pyridine ring and phenyl group, characteristic signals for the cycloheptatriene ring and annulated methylene chain.[18]

The methylene signal of the cycloheptatriene moiety of **17a—c** appears around δ=2.4 as a triplet, and that of **18a—c** appears around δ=3.2, which is typical for 9*H*-cyclohepta[*b*]pyridines.[18] Thus, the ratio (**17**/**18**) was estimated by using these signals (Experimental). The regiochemistry of the enamine addition process giving intermediate **16a—c** was postulated as depicted in Scheme 3 by assuming a similarity to the reaction of **7**. Although the position of a phenyl group on the pyridine ring of **17c** and **18c** is unclear from the ^{1}H NMR spectrum, the structures of **17c** and **18c** have been tentatively assigned by assuming a mechanistic similarity (vide infra) to the reaction of **7** with enamine **10c**.

The reaction of the carbodiimide **9**, which could not be isolated in its pure form, with enamines **10a—c** were also examined in a one-pot procedure to give ring-annulated pyridine derivatives (Scheme 4). After a solution of iminotriphenylphosphorane **5** was reacted with phenyl isocyanate in bromobenzene at room temperature, the enamines **10a—c** were added to the solution. The mixtures were then heated under reflux to give **20a—c**. The results are summarized in Table 3. The structures of the new compounds **20a,b** were easily assigned on the basis of the spectral data. However, compound **20c** could not be differentiated from the other regioisomer **21** by spectral data. Therefore, **20c** was tentatively assigned by assuming a mechanistic similarity (vide infra) to the reaction of **7** with enamine **10c**.

On the other hand, the cycloaddition reaction of **7** with phenylacetylene in bromobenzene under refluxing for 3 h resulted in the formation of a pair of regioisomers, **23** and **15c**, in 5 and 2% yields, respectively (Scheme 5). This reaction was not regioselec-

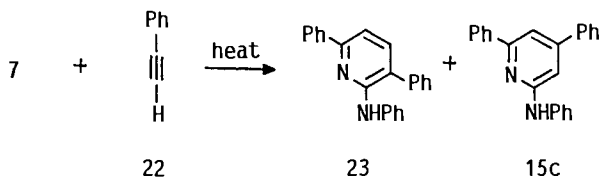

Scheme 5.

Table 3. Results for the Reaction of **9** with Enamines **10a—c** to Give **20a—c**[a]

Enamine	Product yield/%
10a	49
10b	50
10c	42

a) Reactions were carried out in bromobenzene under refluxing for 3 h.

Table 4. Results for the Reaction of **6** or **7** with Activated Acetylenes **24a—c** to Give **26a** or **28a—c**[a]

Compound	Acetylene **24**	Reaction time/h	Product yield/%
6	**24a**	72	20
7	**24a**	8	24
7	**24b**	20	22
7	**24c**	9	28

a) Reactions were carried out in bromobenzene under refluxing.

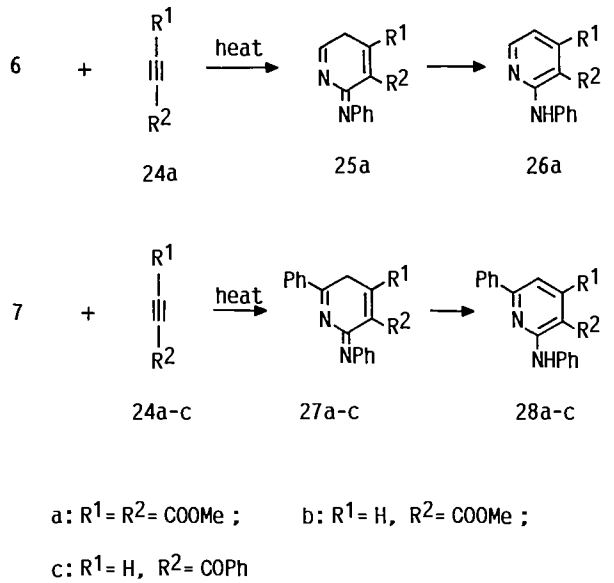

Scheme 6.

tive, and the new compound **23** was easily assigned on the basis of a comparison of the spectral data with those of **15c**.

The cycloaddition reaction of **6** or **7** with activated acetylenes, **24a** or **24a—c**, respectively, in bromobenzene under refluxing also resulted in the formation of a pyridine derivative **26a** or **28a—c** in modest yield (Scheme 6). The results are summarized in Table 4. The spectral data of the new compounds, **26a** and **28a—c**, were consistent with the proposed structures. In the reaction of **7** with **24b,c**, regioselectivity was observed and only one regioisomer was obtained in each case. The regioselectivity was rationalized with the frontier molecular orbital consideration (vide infra).

Molecular Orbital Consideration. A frontier molecular orbital treatment has been successfully applied in order to rationalize both the reactivity and regioselectivity of cycloaddition reactions.[21] We found that this treatment predicts the high regioselectivity for cycloaddition reactions of the vinylcarbodiimide **7**. The frontier orbital energies and coefficients of butadiene (**29**), 2-aza-1,3-butadiene (**30**), vinylcarbodiimide (**31**) (model for **6**, **7**, **8**, and **9**), aminoethylene (**32**) (model for enamines **10a—c**), acetylene (**33**) (model for phenylacetylene), and propynal (**34**) (model for activated acetylenes **24a—c**) were estimated using the MNDO method (Fig. 2). In the [4+2] cycloaddition reaction, both the HOMO(diene)-LUMO(dienophile) and LUMO(diene)-HOMO(dienophile) interactions are important.[21] Since the HOMO of propynal (**34**) is located in a plane including the molecular framework (H-C≡CCH=O), the NHOMO is considered to be the frontier orbital. As shown in Fig. 2, the energy levels of HOMO and LUMO of vinylcarbodiimide **31** are lower than those of butadiene (**29**) and 2-aza-1,3-butadiene (**30**). The lower energy of LUMO (**31**) would increase the interaction with HOMO of dienophiles, such as aminoethylene (**32**). The magnitudes of coefficients of the LUMO (**31**)-HOMO (**32**) interactions were in accord with the observed regioselectivity in the reaction of **7** with unsymmetrical enamine **10c**. Carbodiimide **6**, **7**, **8**, and **9**, all of which have a phenyl group on the nitrogen atom, and **7**, **8**, and **9** are further conjugated with phenyl, C=C and C=O double bond, respectively. Consequently, the energy level of the

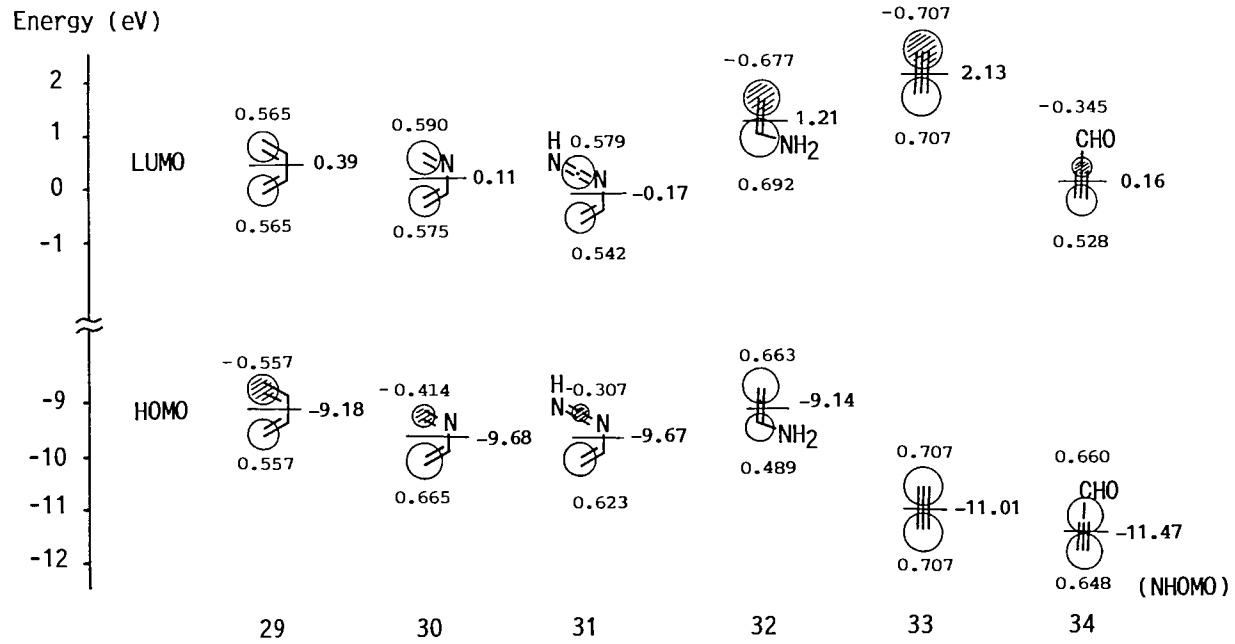

Fig. 2. Energies and coefficients of HOMO and LUMO estimated with MNDO method.

HOMO's of these compounds are expected to be raised and those of the LUMO's are lowered, and the LUMO(**6**—**9**)-HOMO(**10a**—**c**) interaction seems to be operative in the reaction of *N*-vinylcarbodiimides with enamines. Thus, the assignments of the structures of **17c**, **18c**, and **20c** also seems to be reasonable.

On the contrary, the lower energy of the LUMO (**34**) would increase the interaction with HOMO (**31**). The magnitude of the coefficient of the HOMO of **31** was also in accord with the observed regioselectivity in the reaction of **7** with unsymmetrical activated acetylenes, **24b,c**. In the reaction of **7** with phenylacetylene (**22**), the regioselectivity was not observed, and a pair of regioisomers was obtained.

In conclusion, the *N*-phenyl-*N'*-vinylcarbodiimides, which are easily prepared by the reaction of (vinylimino)triphenylphosphoranes with phenyl isocyanate, underwent a regioselective [4+2] cycloaddition reaction with electron-rich enamines as well as activated acetylenes. This type of cycloaddition reaction could also serve as a convenient route for the preparation of pyridines and an annulated pyridine ring system.

Experimental

The IR spectra were recorded on a Shimadzu IR-400 spectrometer. The ^{1}H NMR spectra were recorded on a Hitachi R-24, R-90H, JEOL JNM-PMX60SI, and JNM-GSX400 spectrometers, and the chemical shifts are given in ppm (δ) relative to the internal $SiMe_4$ standard. Mass spectral and high-resolution mass spectral studies were run on a Shimadzu GCMS-QP1000 or a JEOL DX-300 spectrometer. All of the melting points are uncorrected.

Preparation of *N*-Phenyl-*N'*-vinylcarbodiimide (6). A solution of (vinylimino)triphenylphosphorane (**2**)[18] (303 mg, 1 mmol) and phenyl isocyanate (143 mg, 1.2 mmol) in anhydrous benzene (5 ml) was refluxed for 4 h under a nitrogen atmosphere. After the reaction mixture was concentrated in vacuo, the residue was dissolved in hexane and the mixture was filtered to remove insoluble materials. The filtrate was concentrated and chromatographed on silica gel using hexane as an eluent to give **6** (74 mg, 51%): ^{1}H NMR (60 MHz, CCl_4) δ=4.73 (1H, d, J=7.6 Hz, H-*trans*), 5.06 (1H, d, J=15.0 Hz, H-*gem*), 6.43 (1H, dd, J=15.0, 7.6 Hz, H-*cis*), 7.01—7.36 (5H, m, Ph); IR (film) 3056, 2914, 2139, 1623, 1594, 1449, 1487, 1202, 1161, 1070, 755 cm^{-1}. Found: m/z 144.0651. Calcd for $C_9H_8N_2$: 144.0688.

Preparation of *N*-Phenyl-*N'*-(1-phenylvinyl)carbodiimide (7). A solution of [(1-phenylvinyl)imino]triphenylphosphorane (**3**) (3.78 g, 10 mmol) and phenyl isocyanate (1.19 g, 10 mmol) in anhydrous benzene (20 ml) was stirred for 30 min at room temperature under a nitrogen atmosphere. After the reaction mixture was concentrated in vacuo, hexane was added to the residue. The mixture was filtered to remove any insoluble materials, and the filtrate was concentrated. The resulting residue was chromatographed on silica gel using ether-hexane (1/49) as an eluent to give **7** (1.65 g, 75%): ^{1}H NMR (60 MHz, CCl_4) δ=5.08 (1H, s, H-*cis*), 5.25 (1H, s, H-*trans*), 7.00—7.69 (10H, m, Ph); IR (film) 3040, 2258, 2132, 1586, 1480, 1253, 1195, 749 cm^{-1}. Found: m/z 220.0995. Calcd for $C_{15}H_{12}N_2$: M, 220.1002.

Preparation of *N*-(1,3,5-Cycloheptatrienyl)-*N'*-phenylcarbodiimide (8). A solution of [(1,3,5-cycloheptatrienyl)imino]triphenylphosphorane (**4**) (3.67 g, 10 mmol) and phenyl isocyanate (1.19 g, 10 mmol) in anhydrous benzene was stirred for 20 min at room temperature under a nitrogen atmosphere. The reaction mixture was concentrated in vacuo and hexane was added to the residue. After the mixture was filtered to remove any insoluble materials, the filtrate was concentrated and the residue was chromatographed on silica gel using ether-hexane (1/19) as an eluent to give **8** (1.70 g, 82%): ^{1}H NMR (90 MHz, $CDCl_3$) δ=2.61 (2H, d, J=6.9 Hz, H-7), 5.45 (1H, td, J=7.1, 9.0 Hz, H-6), 6.00—6.10 (1H, m, H-2), 6.22 (1H, dm, J=9.0 Hz, H-5), 6.40—6.50 (2H, m, H-3,4), 7.00—7.40 (5H, m, Ph); IR (film) 3016, 2881, 2123, 1611, 1593, 1501, 1239, 1161, 1072, 756, 708, 690 cm^{-1} Found: m/z 208.1001. Calcd for $C_{14}H_{12}N_2$: M, 208.1002.

Reaction of 6 with Enamine 10a. A solution of **6** (74 mg, 0.5 mmol) and enamine **10a** (167 mg, 1 mmol) in anhydrous toluene (3 ml) was refluxed for 15 min under a nitrogen atmosphere. The reaction mixture was separated by TLC on silica gel using AcOEt-hexane (1/2) as a developer to give 5,6,7,8-tetrahydro-1-(phenylamino)isoquinoline **12** (10 mg, 6%): Mp 181—182.5 °C (picrate); ^{1}H NMR (90 MHz, $CDCl_3$) δ=1.65—2.00 (4H, m, H-6, 7), 2.33—2.71 (4H, m, H-5, 8), 6.15 (1H, broad s, NH), 6.40 (1H, d, J=5.0 Hz, H-4), 6.90—7.00 (1H, m, Ph), 7.14—7.51 (4H, m, Ph), 7.85 (1H, d, J=5.0 Hz, H-3); IR ($CHCl_3$) 3422, 2925, 1606, 1578, 1518, 1502, 1443, 1388, 1358 cm^{-1}. Found: m/z 224.1303. Calcd for $C_{15}H_{16}N_2$: M, 224.1315.

General Procedure for the Reaction of 7 with Enamines 10a—c and 13a,b. A solution of **7** (110 mg, 0.5 mmol) and enamines **10a**—**c** and **13a,b** (3 molar equiv) in anhydrous bromobenzene (3 ml) was refluxed for 30 min under a nitrogen atmosphere. The reaction mixture was chromatographed on silica gel using AcOEt-hexane (1/19) as an eluent to give pyridine derivatives **15a**—**c**. The results are summarized in Table 1. The structural proof for the pyridine derivatives **15a**—**c** were based on the following physical data.

5,6,7,8-Tetrahydro-1-phenylamino-3-phenylisoquinoline (**15a**): Mp 159—160 °C (from ethanol); ^{1}H NMR (60 MHz, $CDCl_3$) δ=1.60—2.00 (4H, m, H-6, 7), 2.30—2.90 (4H, m, H-5, 8), 6.19 (1H, broad s, NH), 6.90—7.50 (7H, m, H-4 and Ph), 7.68 (2H, dm, J=7.8 Hz, Ph), 7.90—8.10 (2H, m, Ph); IR ($CHCl_3$) 3456, 3014, 2936, 1603, 1571, 1517, 1495, 1425, 1409, 1389 cm^{-1}. Found: m/z 300.1639. Calcd for $C_{21}H_{20}N_2$: M, 300.1628.

6,7-Dihydro-1-phenylamino-3-phenyl-5*H*-cyclopenta[*c*]pyridine (**15b**): Mp 128.5—129.5 °C (from ethanol); ^{1}H NMR (60 MHz, $CDCl_3$) δ=1.85—2.35 (2H, m, H-6), 2.66 (2H, t, J=7.0 Hz, H-7), 2.85 (2H, t, J=6.2 Hz, H-5), 6.00 (1H, broad s, NH), 6.90—7.50 (7H, m, H-4 and Ph), 7.60 (2H, dm, J=8.0 Hz, Ph), 7.90—8.10 (2H, m, Ph); IR ($CHCl_3$) 3441, 3011, 2961, 1605, 1573, 1521, 1497, 1447, 1413, 1401 cm^{-1}. Found: m/z 286.1480. Calcd for $C_{20}H_{18}N_2$: M, 286.1471.

2-Phenylamino-4,6-diphenylpyridine (**15c**): Mp 220.5—222.0 °C (picrate): ^{1}H NMR (400 MHz, $CDCl_3$) δ=6.79 (1H, broad s, NH), 7.02 (1H, d, J=1.1 Hz, H-3), 7.07 (1H, tt, J=7.3, 1.1 Hz, Ph), 7.36 (2H, t, J=8.1 Hz, Ph), 7.42 (1H, d, J=1.1 Hz, H-5), 7.42—7.50 (8H, m, Ph), 7.62—7.65 (2H, m, Ph), 8.04—8.06 (2H, m, Ph); IR ($CHCl_3$) 3416, 3002, 1594,

1550, 1498, 1450, 1419, 1077, 1010 cm^{-1}. Found: *m/z* 322.1469. Calcd for $C_{23}H_{18}N_2$: M, 322.1471.

General Procedure for the Reaction of 8 with 10a—c. A solution of **8** (104 mg, 0.5 mmol) and enamines **10a—c** (3 molar equiv) in anhydrous bromobenzene (2 ml) was refluxed for 30 min under nitrogen atmosphere. The reaction mixture was chromatographed on silica gel using AcOEt-hexane (1/19) as an eluent to give a mixture of pyridine derivatives **17a—c** and **18a—c**. The results are summarized in Table 2.

2,3,4,7-Tetrahydro-5-phenylamino-1*H*-cyclohepta[*c*]-isoquinoline (**17a**) and 2,3,4,9-tetrahydro-5-phenylamino-1*H*-cyclohepta[*c*]isoquinoline (**18a**): ^1H NMR (90 MHz, $CDCl_3$) δ=1.70—2.00 (4H, m, H-2, 3), 2.30—2.90 (4H, m, H-1, 4), 2.39 (0.7 H, t, *J*=6.3 Hz, **18a**-H-9), 3.13 (1.3 H, d, *J*=6.3 Hz, **17a**-H-7), 5.60—7.70 (10H, m, olefin, Ph, and NH); IR ($CHCl_3$) 3456, 3011, 2941, 2876, 1598, 1581, 1555, 1499, 1441, 1381 cm^{-1}. Found: *m/z* 288.1619. Calcd for $C_{20}H_{20}N_2$: M, 288.1628.

1,2,3,6-Tetrahydro-4-(phenylamino)cyclohepta[*b*]cyclopenta[*d*]pyridine (**17b**) and 1,2,3,8-tetrahydro-4-(phenylamino)cyclohepta[*b*]cyclopenta[*d*]pyridine (**18b**): ^1H NMR (90 MHz, $CDCl_3$) δ=1.95—2.25 (2H, m, H-2), 2.44 (1.5H, t, *J*=6.7 Hz, **18b**-H-8), 2.50—3.00 (4H, m, H-1, 3), 3.18 (0.5H, d, *J*=6.8 Hz, **17b**-H-6), 5.50—7.70 (10H, m, olefin, Ph, and NH); IR ($CHCl_3$) 3440, 2965, 2855, 1587, 1567, 1499, 1437, 1395, 1369, 1303, 910 cm^{-1}. Found: *m/z* 274.1481. Calcd for $C_{19}H_{18}N_2$: M, 274.1471.

4-Phenyl-2-phenylamino-9*H*-cyclohepta[*b*]pyridine (**17c**) and 4-phenyl-2-phenylamino-7*H*-cyclohepta[*b*]pyridine (**18c**): ^1H NMR (60 MHz, CCl_4) δ=2.45 (0.8H, t, *J*=6.6 Hz, **18c**-H-7), 3.09 (1.2H, d, *J*=6.0 Hz, **17c**-H-9), 5.50—7.32 (16H, m, olefin, H-4, Ph, and NH); IR ($CHCl_3$) 3416, 3011, 1593, 1561, 1497, 1417, 1401 cm^{-1}. Found: *m/z* 310.1482. Calcd for $C_{22}H_{18}N_2$: M, 310.1471.

General Procedure for the Reaction of *N*-(3-Oxo-1-cyclohexenyl)-*N'*-phenylcarbodiimide (9) with Enamines 10a—c. A solution of [(3-oxo-1-cyclohexenyl)imino]-triphenylphosphorane (**10**) (186 mg, 0.5 mmol) and phenyl isocyanate (71 mg, 0.6 mmol) in anhydrous bromobenzene (3 ml) was stirred for 1 h under a nitrogen atmosphere. To the solution was added enamines **10a—c** (3 molar equiv) and the mixture was refluxed another 3 h. The reaction mixture was concentrated and the residue was chromatographed on silica gel using AcOEt-hexane (1/4) as an eluent to give quinoline derivatives **20a—c**. The results are summarized in Table 3.

6-Phenylamino-3,4,7,8,9,10-hexahydro-1(2*H*)-phenanthridinone (**20a**): Mp 164—165 °C (from ethanol); ^1H NMR (60 MHz, $CDCl_3$) δ=1.60—2.20 (6H, m, H-3, 8, 9), 2.20—2.75 (4H, m, H-2, 7), 2.85—3.30 (4H, m, H-4, 10), 6.49 (1H, broad s, NH), 6.80—7.40 (3H, m, Ph), 7.62 (2H, dm, *J*=8.0 Hz, Ph); IR ($CHCl_3$) 3451, 3006, 2946, 2876, 1657, 1598, 1563, 1497, 1438, 1375, 1271, 1179 cm^{-1}. Found: *m/z* 292.1573. Calcd for $C_{19}H_{20}N_2O$: M, 292.1577.

4-Phenylamino-1,2,3,6,7,8-hexahydro-9*H*-cyclopenta-[*c*]quinolin-9-one (**20b**): Mp 182.5—183.5 °C (from ethanol); ^1H NMR (60 MHz, $CDCl_3$) δ=1.90—2.40 (4H, m, H-2, 7), 2.40—2.70 (4H, m, H-3, 8), 3.02 (2H, t, *J*=6.0 Hz, H-6), 3.34 (2H, t, *J*=8.0 Hz, H-1), 6.30 (1H, broad s, NH), 6.90—7.40 (3H, m, Ph), 7.62 (2H, dm, *J*=8.0 Hz, Ph); IR ($CHCl_3$) 3436, 2956, 1661, 1605, 1573, 1497, 1443, 1369, 1271 cm^{-1}. Found: *m/z* 278.1405. Calcd for $C_{18}H_{18}N_2O$: M, 278.1420.

4-Phenyl-2-phenylamino-7,8-dihydro-5(6*H*)-quinolinone (**20c**): Mp 182.5—183.5 °C (from ethanol); ^1H NMR (60 MHz, $CDCl_3$) δ=1.90—2.35 (2H, m, H-7), 2.54 (2H, t, *J*=6.0 Hz, H-6), 2.99 (2H, t, *J*=5.9 Hz, H-8), 6.40 (1H, s, NH), 6.90—8.00 (11H, m, H-3 and Ph); IR ($CHCl_3$) 3406, 3011, 2956, 1663, 1581, 1543, 1493, 1411, 1289 cm^{-1}. Found: *m/z* 314.1427. Calcd for $C_{21}H_{18}N_2O$: M, 314.1420.

Reaction of 7 with Phenylacetylene (22). A solution of **7** (1.01 g, 4.59 mmol) and phenylacetylene (1.40 g, 13.7 mmol) in anhydrous bromobenzene (3 ml) was refluxed for 3 h. The reaction mixture was separated by column chromatography on silica gel. The fractions eluted with ether-hexane (1/49) contained 2-phenylamino-3,6-diphenylpyridine (**23**) (81 mg, 5%): Mp 115.5—116 °C (from ethanol); ^1H NMR (400 MHz, $CDCl_3$) δ=6.66 (1H, broad s, NH), 6.99 (1H, tt, *J*=7.3, 1.1 Hz, Ph), 7.30 (2H, tm, *J*=7.3 Hz, Ph), 7.34 (1H, d, *J*=7.7 Hz, H-5), 7.41 (1H, tt, *J*=7.3, 1.1 Hz, Ph), 7.43—7.53 (8H, m, H-4 and Ph), 7.67 (2H, broad d, *J*=7.7 Hz, Ph), 8.08—8.10 (2H, m, Ph); IR (KBr) 3406, 3051, 1603, 1587, 1563, 1519, 1493, 1429, 1409, 1331, 1184, 750, 694 cm^{-1}. Found: *m/z* 322.1447. Calcd for $C_{23}H_{18}N_2$: M, 322.1471.

The fractions eluted with AcOEt-hexane (5/95) contained **15c** (26 mg, 2%).

Reaction of 6 with Dimethyl Acetylenedicarboxylate (24a). A solution of **6** (30 mg, 0.21 mmol) and **24a** (118 mg, 0.84 mmol) in anhydrous toluene (2 ml) was refluxed for 72 h under nitrogen atmosphere. The reaction mixture was concentrated and separated by TLC on silica gel using AcOEt-hexane (5/1) as a developer to give 2-phenylamino-3,4-bis(methoxycarbonyl)pyridine (**26a**) (12 mg, 20%): Mp 145.5—147 °C (picrate); ^1H NMR (90 MHz, $CDCl_3$) δ=3.91 (6H, s, Me), 6.74 (1H, d, *J*=3.2 Hz, H-5), 7.07 (1H, t, *J*=8.1 Hz, Ph), 7.33 (2H, t, *J*=8.1 Hz, Ph), 7.58 (2H, d, *J*=8.1 Hz, Ph), 8.39 (1H, d, *J*=3.2 Hz, H-6), 9.64 (1H, broad s, NH); IR ($CHCl_3$) 3337, 3008, 2960, 1731, 1697, 1600, 1580, 1562, 1525, 1434, 1286, 1158, 1122, 1014 cm^{-1}. Found: *m/z* 286.0941. Calcd for $C_{15}H_{14}N_2O_4$: M, 286.0954.

General Procedure for the Reaction of 7 with 24a—c. A solution of **7** (110 mg, 0.5 mmol) and **24a—c** in anhydrous bromobenzene (3 ml) was refluxed for the period indicated in Table 4 under a nitrogen atmosphere. The reaction mixture was concentrated and the residue was chromatographed on silica gel using CH_2Cl_2. The fractions eluted with CH_2Cl_2 were concentrated and further separated by TLC on silica gel using AcOEt-hexane (3/1) as a developer to give pyridine derivatives **28a—c**. The results are summarized in Table 4.

2-Phenylamino-6-phenyl-3,4-bis(methoxycarbonyl)pyridine (**28a**): Mp 107.0—107.5 °C (from ethanol); ^1H NMR (90 MHz, $CDCl_3$) δ=3.82 (3H, s, Me), 3.87 (3H, s, Me), 7.00—7.50 (7H, m, H-5 and Ph), 7.70 (2H, dm, *J*=8.0 Hz, Ph), 7.90—8.10 (2H, m, Ph), 9.85 (1H, broad s, NH); IR ($CHCl_3$) 3325, 3000, 2945, 1733, 1688, 1599, 1578, 1549, 1241, 1160, 1126 cm^{-1}. Found: *m/z* 362.1247. Calcd for $C_{21}H_{18}N_2O_4$: M, 362.1267.

2-Phenylamino-6-phenyl-3-(methoxycarbonyl)pyridine (**28b**): Mp 66.5—67.0 °C (from ethanol); ^1H NMR (90 MHz, $CDCl_3$) δ=3.88 (3H, s, Me), 6.90—7.50 (6H, m, Ph), 7.14 (1H, d, *J*=8.1 Hz, H-5), 7.73—8.00 (4H, m, Ph), 8.22 (1H, d, *J*=8.1 Hz, H-4), 10.23 (1H, broad s, NH); IR ($CHCl_3$) 3325, 3004, 2857, 1586, 1603, 1590, 1571, 1293, 1251, 1146 cm^{-1}. Found: *m/z* 304.1231. Calcd for $C_{19}H_{16}N_2O_2$: M, 304.1213.

3-Benzoyl-2-phenylamino-6-phenylpyridine (**28c**): Mp 118.0—118.5 °C (from ethanol); ^{1}H NMR (90 MHz, $CDCl_3$) δ=6.90—7.60 (11H, m, Ar), 7.12 (1H, d, J=8.4 Hz, H-3), 7.75—8.10 (4H, m, Ph), 7.88 (1H, d, J=8.4 Hz, H-4), 11.10 (1H, broad s, NH); IR ($CHCl_3$) 3280, 3008, 1601, 1590, 1563, 1519, 1500, 1298, 1245, 909 cm^{-1}. Found: m/z 350.1409. Calcd for $C_{24}H_{18}N_2O$: M, 350.1420.

Financial support by the Science and Engineering Research Laboratory of Waseda University is greatly acknowledged.

References

1) Part 16: M. Nitta, M. Ohnuma, and Y. Iino, *J. Chem. Soc., Perkin Trans. 1,* in press.

2) A part of this paper was presented at the National Meeting of the Chemical Society of Japan, Sendai, October 1988, Abstr., No. 1A302.

3) D. L. Boger, *Chem. Rev.*, **86**, 781 (1986); T. Kametani and S. Hibino, *Adv. Heterocycl. Chem.*, **42**, 246 (1987).

4) A. Demoulin, H. Gorissen, A.-M. H.-Frisque, and L. Ghosez, *J. Am. Chem. Soc.*, **97**, 4409 (1975).

5) R. Gompper and U. Heinemann, *Angew. Chem., Int. Ed. Engl.*, **20**, 296 (1981).

6) Y. Nomura, Y. Takeuchi, S. Tomoda, and M. M. Itoh, *Bull. Chem. Soc. Jpn.*, **54**, 2779 (1981).

7) F. Sainte, B. Serckx-Poncin, A.-M. Hasbain-Frisque, and L. Ghosez, *J. Am. Chem. Soc.*, **104**, 1428 (1982); P. Bayard and L. Ghoses, *Tetrahedron Lett.*, **29**, 6115 (1988); and references cited therein.

8) J. Barluenga, F. J. Gonzalez, V. Gotov, and S. Fustero, *J. Chem. Soc., Perkin Trans. 1,* **1988**, 1739; J. Barluenga, J. Joglar, S. Fustero, V. Gotov, C. Kruger, and M. J. Romao, *Chem. Ber.*, **118**, 3652 (1985).

9) J. Barluenga, F. J. Gonzalez, S. Fustero, and V. Gotov, *J. Chem. Soc., Chem. Commun.*, **1986**, 1179.

10) J. Barluenga, F. J. Gonzalez, S. Fustero, M. de la C. F. Foces, F. H. Cano, and A. S. Faliciano, *J. Chem. Res., Synop.*, **1898**, 66.

11) G. Wulff and H. Bohnke, *Angew. Chem., Int. Ed. Engl.*, **25**, 90 (1986); J. Barluenga, M. Ferrero, and F. Palacios, *Tetrahedron Lett.*, **29**, 4863 (1988).

12) J. Barluenga, M. Tomas, A. Ballesteros, and V. Gotov, *J. Chem. Soc., Chem. Commun.*, **1987**, 1195.

13) T. Saito, M. Nakane, M. Endo, M. Yamashita, Y. Oyamada, and S. Motoki, *Chem. Lett.*, **1986**, 135.

14) P. Molina, P. M. Fresneda, and F. de Ciencias, *Tetrahedron Lett.*, **29**, 379 (1988).

15) J. Barluenga, M. Ferrero, and F. Palacios, *Tetrahedron Lett.*, **29**, 4863 (1988).

16) Y. Iino, T. Kobayashi, and M. Nitta, *Heterocycles,* **24**, 2437 (1986).

17) M. Nitta, H. Soeda, and Y. Iino, *Bull. Chem. Soc. Jpn.*, **63**, 932 (1990); Y. Iino, E. Hara, and M. Nitta, *Bull. Chem. Soc. Jpn.*, **62**, 1913 (1989).

18) Y. Iino and M. Nitta, *Bull. Chem. Soc. Jpn.*, **61**, 2235 (1988); M. Nitta and Y. Iino, *J. Chem. Soc., Perkin Trans. 1,* **1990**, 435.

19) N. Kanomata and M. Nitta, *J. Chem. Soc., Perkin Trans. 1,* **1990**, 1119.

20) M. Nitta, Y. Iino, E. Hara, and T. Kobayashi, *J. Chem. Soc., Perkin Trans. 1,* **1989**, 51; and references cited therein.

21) I. Fleming, "Frontier Orbitals and Organic Reactions," John Wiley and Sons, London (1976).

Cross-Dehydrocycloaddition of 1,3-Butadiene with Isoprene over MgO and ZrO_2

Hiroyasu SUZUKA and Hideshi HATTORI*
Department of Chemistry, Faculty of Science, Hokkaido University, Sapporo 060
(Received October 3, 1990)

A mixture comprising of equal amounts of 1,3-butadiene (BD) and isoprene (IPN) was allowed to react over MgO and ZrO_2 at 473 K in order to examine the relation between the product distribution and the reaction mechanisms. Over ZrO_2 the most abundant product was 4-ethyltoluene, which was produced by a base-catalyzed Diels-Alder reaction between BD and IPN, followed by double-bond migration and dehydrogenation. In the Diels-Alder reaction, IPN acts as a diene and BD acts as a dienophile. Over MgO, *o*-xylene was primarily produced by anionic mechanisms. Among the products formed from BD and IPN, 4-ethyltoluene was produced most, though the production of 3-ethyltoluene was considerable. The active sites on ZrO_2 were strongly poisoned by both CO_2 and NH_3. The active sites on MgO were completely poisoned by CO_2, and were modified by NH_3 in such a way that the reaction mechanisms changed from the anionic mechanisms to those involving the Diels-Alder reaction.

The dehydrocyclodimerization of dienes to aromatics has been reported to proceed over metal-acid bifunctional catalysts and solid acid catalysts at reaction temperatures above 673 K.[1-6] We recently found that the dehydrocyclodimerization of conjugated dienes to form aromatics proceeds over solid base catalysts even below 473 K. Among solid base catalysts, MgO and ZrO_2 exhibit high activity.[7] The product distribution over MgO is different from that over ZrO_2. In the dehydrocyclodimerization of 1,3-butadiene (BD), *o*- and *p*-xylenes were mainly produced over MgO, whereas ethylbenzene was the main product over ZrO_2. We proposed that different mechanisms operate in the reaction for MgO and ZrO_2.[8] Anionic intermediates are involved in the reaction over MgO, while the base-catalyzed Diels-Alder reaction precedes double-bond isomerization, followed by dehydrogenation over ZrO_2.

In the reaction of a mixture containing equal amounts of two different dienes, three different combinations of dienes result. In the case of a mixture containing equal amounts of BD and isoprene (IPN), products arising from combinations of BD-BD, BD-IPN, and IPN-IPN are possible. It is expected that the mechanistic differences are reflected in the product distribution caused by different combinations of the dienes. In the present study, a mixture of BD and IPN was allowed to react over MgO and ZrO_2 in order to examine how the differences in the mechanism reflect the product distribution in the cross-dehydrocycloaddition of BD with IPN.

Experimental

MgO was purchased from Merck. ZrO_2 was prepared from a 10% aqueous solution of $ZrOCl_2$ by hydrolysis with 28% aqueous ammonia to precipitate $Zr(OH)_4$ followed by washing with deionized water, drying at 373 K and calcining at 773 K.

The reactions were carried out in an all-glass H-shaped batch-type reactor. Two branches were separated by a breakable seal. A catalyst sample (200 mg) was placed in one branch, pretreated at 1073 K for MgO or 773 K for ZrO_2, and sealed. Since the product distributions were not significantly changed with the pretreatment temperature for both catalysts in the reaction of BD,[8] the pretreatment temperature was fixed at one temperature for each catalyst in the present study. The reactant, a mixture of 0.19 mmol BD and 0.19 mmol IPN, was stored in the other branch until it was introduced into the branch containing the catalyst thermostated at liquid-nitrogen temperature. The reaction was started by rapid melting of the reactant at the reaction temperature. Most of the reactions were run at 473 K for 17 h. The products were collected in a liquid-nitrogen trap and dissolved into 1 cm^3 of benzene, and then analyzed by gas chromatography. Styrene was used as an internal standard.

Poisoning experiments using carbon dioxide and ammonia as poisons were performed. Following a pretreatment of the catalyst, the poison was adsorbed at room temperature for 10 min, followed by evacuation at the same temperature for 10 min. The amounts of poisons adsorbed on the catalyst were measured as follows. The poisoned catalyst was heated to 1073 K, while the evolved poison was trapped in liquid nitrogen. The trapped poison was evaporated and measured volumetrically.

Results and Discussion

The product distributions in the reaction of a mixture containing equal amounts of BD and IPN, both with and without catalyst, are given in Table 1. Without catalyst, practically no reaction occurred at 393 K. At 473 K, though products resulting from the Diels-Alder reaction were formed, no aromatics were formed. The percentages of the products containing carbon numbers 8, 9, and 10 were 22, 52, and 26%, respectively. The ease to combine two diene molecules for a non-catalytic reaction is in the following order:

$$\text{BD}+\text{IPN} \gg \text{IPN}+\text{IPN} > \text{BD}+\text{BD}$$

Table 1. Cross-Dehydrocycloaddition of 1,3-Butadiene and Isoprene

Catalyst	Reac. temp.	Yield of product[a]/mol%										
	K	C_8	EB	*p*-X	*o*-X	C_9	4ET	3ET	CM	C_{10}	*m*-C	*p*-C
MgO	393	0.3	0	0	0	Trace	0	0	0	0	0	0
	473	0.6	1.6	2.3	4.8	0.4	1.2	0.9	0	0	0.7	0.3
ZrO_2	393	1.0	1.1	0	0	0.6	4.6	Trace	1.1	0	0	2.9
	473	Trace	4.8	0	0	0	6.9	1.8	2.6	0	0	2.4
None	393	Trace	0	0	0	0	0	0	0	0	0	0
	473	3.3	0	0	0	7.8	0	0	0	3.6	0	0

a) Mol of each product to 200 mol of a reactant mixture. C_8: dimer of 1,3-butadiene, EB: ethylbenzene, *o*-X: *o*-xylene, *p*-X: *p*-xylene, CM: isopropylbenzene (cumene), 4ET: 4-ethyltoluene, 3ET: 3-ethyltoluene, C_9: adduct of 1,3-butadiene to isoprene, C_{10}: dimer of isoprene, *p*-C: *p*-cymene, *m*-C: *m*-cymene. Gaseous compounds were produced, but not counted into calculation of composition. Catalyst weight 200 mg, Reactant: 1,3-butadiene 0.19 mmol, isoprene 0.19 mmol, Reaction time 17 h.

In the Diels-Alder reaction, both BD and IPN may act as a dienophile and diene. For the combination of BD with IPN, the possible reactions and the products are as follows:

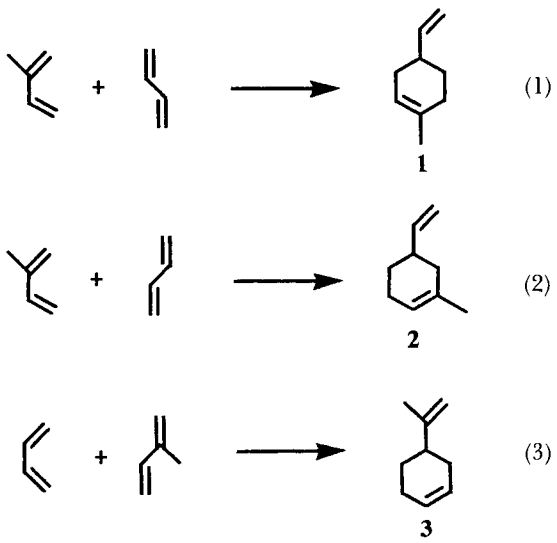

In Eqs. 1 and 2, IPN acts as a diene and BD as a dienophile. In Eqs. 3 and 4, BD acts as a diene and IPN as a dienophile.

The product distributions among compounds containing carbon number 9, excluding aromatics, are given in Table 2. The relative amounts of 1-methyl-4-vinyl-1-cyclohexene (**1**): 1-methyl-5-vinyl-1-cyclohexene (**2**): 4-isopropenyl-1-cyclohexene (**3**): 4-methyl-4-vinyl-1-cyclohexene (**4**) were 8.5 (57.8%): 1.3 (8.8%): 3.6 (24.6%): 1.3 (8.8%), which correspond to the reaction probability of equation (1): (2): (3): (4). A reaction in which BD acts as a dienophile and IPN as a diene is predominant. This is expected because the Diels-Alder reaction is favored due to the presence of electron-releasing groups in the diene.

With a catalyst, the reaction proceeded to some extent, even at 393 K. In particular, the formation of

Table 2. Product Distribution of C_9 Products

Catalyst	Poison	Amount of poison	Reac. temp.	Product distribution/10^{-3} mmol			
		mol g^{-1}	K	1M4VCH[a]	2M4VCH[b]	4IPCH[c]	4V4MCH[d]
MgO	None		393	0	0	0	0
	None		473	0	0	0	0.7
	CO_2	2.3×10^{-4}	473	6.0	0.6	2.1	0.6
	NH_3	8.4×10^{-5}	473	0	0	0	0
ZrO_2	None		393	0	0	0	1.0
	None		473	0	0	0	0
	CO_2	2.7×10^{-4}	473	1.0	0	0	0
	NH_3	2.7×10^{-4}	473	4.2	0	1.9	0.6
None			393	0	0	0	0
			473	8.5	1.3	3.6	1.3

a) 1-Methyl-4-vinyl-1-cyclohexene. b) 1-Methyl-5-vinyl-1-cyclohexene. c) 4-Isopropenyl-1-cyclohexene. d) 4-Methyl-4-vinyl-1-cyclohexene.

aromatics was observed over ZrO_2 at this temperature. At 473 K, the product yields greatly exceeded those observed without a catalyst; the products consisted mostly of aromatics over both MgO and ZrO_2.

The product distributions were different for MgO and ZrO_2. Over ZrO_2, the percentages of the products containing carbon numbers 8, 9, and 10 were 26, 61, and 13, respectively. These percentages are close to those observed in non-catalytic product distribution, 22 : 52 : 26. The ease to combine two diene molecules for a ZrO_2-catalyzed reaction is in the following order:

$$BD + IPN \gg BD + BD > IPN + IPN$$

The combination of BD with IPN is the most favorable. A small difference in the combination between a ZrO_2-catalyzed reaction and a non-catalytic reaction is that the combination of two BD molecules is more favorable than that of two IPN molecules over ZrO_2. In a non-catalytic reaction, the combination of two IPN molecules is slightly favorable.

The relative amounts of C-9 aromatics produced over ZrO_2 were 4-ethyltoluene (6.9%), 3-ethyltoluene (1.8%), isopropylbenzene (2.6%). 4-Ethyltoluene, 3-ethyltoluene, and isopropylbenzene are formed from 1-methyl-4-vinyl-1-cyclohexene (**1**), 1-methyl-5-vinyl-1-cyclohexene (**2**) and 4-isopropenyl-1-cyclohexene (**3**), respectively, by successive double-bond migration and dehydrogenation. 4-Methyl-4-vinyl-1-cyclohexene (**4**) is not able to undergo double-bond migration and dehydrogenation and is difficult to convert to aromatics unless the C-C bond cleaves. The relative amounts of non-catalytic Diels-Alder reaction products are close to the relative amounts of the corresponding C-9 aromatics formed over ZrO_2, though the formation of 3-ethyltoluene over ZrO_2 was twice as great as that of 1-methyl-5-vinyl-1-cyclohexene by a non-catalytic Diels-Alder reaction.

Almost the same percentages of the two main products over ZrO_2 (4-ethyltoluene and isopropylbenzene) to those produced without a catalyst (1-methyl-4-vinyl-1-cyclohexene and 4-isopropenyl-1-cyclohexene) suggest that dehydrocycloaddition results from a ZrO_2 catalyzed Diels-Alder reaction, followed by double-bond migration and dehydrogenation.

The percentages of the products for MgO were 73, 19, and 8% for products containing carbon numbers 8, 9, and 10, respectively, which are different from those for a non-catalytic reaction and a reaction over ZrO_2. The ease to combine two diene molecules over MgO is in the following order:

$$BD + BD \gg BD + IPN > IPN + IPN$$

A reaction involving two BD molecules is the most favorable combination over MgO. By this combination, *o*- and *p*-xylenes were mainly formed. As reported in a previous paper,[8] the formation of *o*- and *p*-xylenes results from anionic intermediates.

In the combination of BD with IPN, if an anionic mechanism is operating, 3-ethyltoluene would predominantly be formed as compared to 4-ethyltoluene, since the formation of 3-ethyltoluene involves a primary anion, while a less stable secondary anion is involved in the formation of 4-ethyltoluene, as illustrated below.

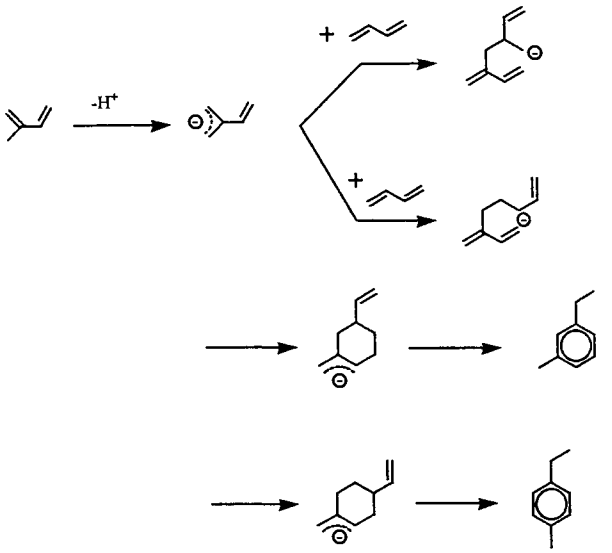

The ratio of 3-ethyltoluene to 4-ethyltoluene formed over MgO was 0.9/1.2, which is much larger than the ratio 1.8/6.8 over ZrO_2. This also supports the idea that the contribution of the anionic mechanism takes place to a considerable extent in a reaction over MgO, though the occurrence of a Diels-Alder reaction can not be neglected.

In the IPN molecule, the allylic hydrogen on the methyl group can be released much more easily as a proton. However, for the formation of isopropylbenzene by the anionic intermediate, an H atom on the carbon atom 4 of IPN should be abstracted, which is not plausible. Therefore, isopropylbenzene is difficult to form by an anionic mechanism. No isopropylbenzene was formed over MgO, in contrast to its formation over ZrO_2, which also suggests that the anionic mechanism is favored, compared with the Diels-Alder reaction over MgO.

As reported in the previous paper,[8] the active sites on ZrO_2 for dehydrocyclodimerization were completely poisoned by both carbon dioxide and ammonia. The poisoning effects on the active sites of MgO are different for carbon dioxide than for ammonia. Although carbon dioxide completely poisoned the active sites, ammonia modified them. The results of poisoning experiments for a mixture containing BD and IPN over MgO and ZrO_2 are given in Table 3. The amounts of the poisons retained on the surfaces were small compared with that of the reactant.

Although no aromatics were produced over the ZrO_2 poisoned by ammonia and carbon dioxide, the Diels-

Table 3. Cross-Dehydrocycloaddition of 1,3-Butadiene and Isoprene over Poisoned MgO and ZrO_2

Catalyst	Poison	Yield of product[a]/mol%										
		C_8	EB	*p*-X	*o*-X	C_9	4ET	3ET	CM	C_{10}	*m*-C	*p*-C
ZrO_2	None	Trace	4.8	0	0	0	6.9	1.8	2.6	0	0	2.4
	CO_2	1.4	0	0	0	0.6	0	0	0	0	0	0
	NH_3	2.2	0	0	0	3.6	0	0	0	1.3	0	0
MgO	None	0.6	1.6	2.3	4.8	0.4	1.2	0.9	0	0	0.7	0.3
	CO_2	2.1	0	0	0	4.9	0	0	0	2.3	0	0
	NH_3	0.4	0.7	0	0	0	1.0	0.4	0.3	0	0	0

a) Mol of each product to 200 mol of a reactant mixture. EB: ethylbenzene, *o*-X: *o*-xylene. C_8: dimer of 1,3-butadiene, *p*-X: *p*-xylene, CM: isopropylbenzene (cumene), 4ET: 4-ethyltoluene, 3ET: 3-ethyltoluene, C_9: adduct of 1,3-butadiene to isoprene, C_{10}: dimer of isoprene, *p*-C: *p*-cymene, *m*-C: *m*-cymene. Gaseous compounds were produced, but not counted into calculation of composition. Catalyst weight 200 mg, Reactant: 1,3-butadiene 0.19 mmol, isoprene 0.19 mmol, Reaction time 17 h, Reaction temperature: 473 K.

Alder reaction proceeded to some extent at the same level as those without a catalyst. The poisoning effect with ammonia on the activity of ZrO_2 was more severe than that with carbon dioxide. The product distribution was essentially the same as that for the non-catalytic type. The ZrO_2 poisoned by NH_3 was inert to the Diels-Alder reaction.

With a MgO catalyst, carbon dioxide completely poisoned all of the active sites. The product distribution was the same as that of the non-catalytic type.

Ammonia preadsorption decreased the activity of MgO to a small extent. However, marked effects by ammonia preadsorption appeared in the product distribution. Upon the adsorption of ammonia, the formations of *o*- and *p*-xylenes and 3-ethyltoluene greatly decreased, and isopropylbenzene, which was not formed on unpoisoned MgO, appeared. By an anionic mechanism, *o*- and *p*-xylenes as well as 3-ethyltoluene were favored; isopropylbenzene was unfavored. The decrease in the *o*- and *p*-xylenes and 3-ethyltoluene, and the formation of isopropylbenzene suggest that ammonia retards the formation of anionic intermediates, but not the Diels-Alder reaction and the following isomerization and dehydrogenation. This is consistent with the result of BD, as reported in a previous paper.[8] The relative ease to combine two diene molecules also changed upon ammonia preadsorption on MgO. The combination of BD with IPN became most favorable. The catalytic behavior of the MgO preadsorbing ammonia was similar to that of ZrO_2. Therefore, ammonia preadsorption modified the active sites on MgO so that the mechanisms for dehydrocycloaddition changed from one involving anionic intermediates to those involving a Diels-Alder reaction followed by isomerization and dehydrogenation.

References

1) T. K. Bhatia and M. J. Phillips, *J. Catal.*, **110**, 150 (1988).
2) S. M. Csicsery, *J. Catal.*, **17**, 207 (1970).
3) S. M. Csicsery, *J. Catal.*, **17**, 216 (1970).
4) S. M. Csicsery, *J. Catal.*, **17**, 315 (1970).
5) S. M. Csicsery, *J. Catal.*, **17**, 323 (1970).
6) S. M. Csicsery, *J. Catal.*, **18**, 30 (1970).
7) H. Suzuka and H. Hattori, *Appl. Catal.*, **47**, L7 (1989).
8) H. Suzuka and H. Hattori, *J. Mol. Catal.*, **63**, 371 (1990).

Synthesis and Properties of High Molecular Weight Polypeptides Containing of Tryptophan[1)]

Yasuko IIZUKA, Toshiya ENDO,† and Masanao OYA*
Department of Biochemistry and Engineering, Faculty of Engineering,
Gunma University, Kiryu-shi, Gunma 376
(Received October 11, 1990)

High purity *N*-carboxy-DL-tryptophan anhydride (DL-4-indoylmethyl-2,5-oxazolidinedione, DL-Trp NCA) was synthesized in good yield. Copolypeptides with a random sequence of DL-Trp with L-alanine (Ala) and DL-alanine (DL-Ala) were synthesized by copolymerization of the corresponding *N*-carboxy-α-amino acid anhydrides (NCA) in solution. Copolypeptides of DL-Trp with L-Ala and DL-Ala were partially soluble in water. The water-soluble copolypeptides of DL-Trp and L-Ala mostly gave disordered conformations, while the water-insoluble copolypeptides were found in a mixture of α- and disordered conformations. The solubility of the copolypeptides was not influence by the tryptophan content in the polypeptides but, rather, by the conformation of the polypeptides.

Tryptophan (Trp, **1**) is widely found in native proteins or several peptide hormones such as snake venom neutrotoxin, ACTH, glucagon, and tyrocidin as a minor component of one to two percent. A very small amount of tryptophan residue influences the emergence of their toxicity or higher-order conformations.[2,3)] Tryptophan has a side chain comprising the indole nucleus, which is characteristic of both a hydrophilic aromatic group and a hydrophobic indol nitrogen capable of hydrogen bonding as a donor. Tryptophan has an interesting structual arrangement in water-soluble proteins, such as cobrotoxin.[2,3)]

High molecular weight synthetic copolypeptides containing the tryptophan residue are therefore both interesting and important in the conformational and biological approach to proteins.

E. Kachalski, et al. first reported the synthesis of poly(DL- or L-tryptophan), which are obtained by the polymerization of *N*-carboxy-DL or L-tryptophan anhydride (Trp NCA) at 150 °C in a high vacuum.[4)] Cosani, et al. have reported on a block copolymer (ethyl DL-glutamate)$_m$(L-Trp)$_n$. High-molecular-weight and synthetic random copolypeptides of tryptophan, however, are very little known.[5)]

In this paper we report on the copolymerization of DL-Trp NCA (**2**) with L-Ala NCA (**3**) to produce high molecular-weight copolypeptides (**4**). In addition, the solubility and conformation of the copolypeptide in solvents and in the solid state were studied.

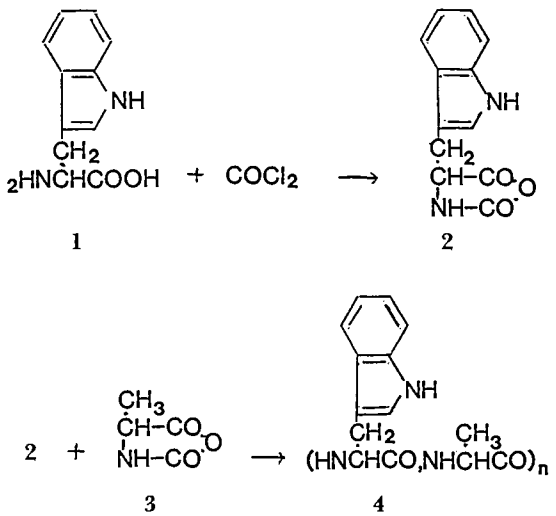

† Present adress: Department of Chemistry, Faculty of Science, Nagoya University, Furou-cho, Tikusa-ku, Nagoya 460-01.

Experimental

Synthesis of NCA (2,3). All NCA were prepared in high purity and good yield by a previously reported method.[6)] DL-Trp NCA was reprecipitated volumetrically by adding hexane to the ethyl acetate solution of NCA, producing high-purity DL-Trp NCA in 46% yield; mp 135—138 °C. Found: C, 61.16; H, 4.56; N, 11.46%. Calcd for $C_{12}H_{10}O_3N_2$: C, 62.60; H, 4.34; N, 12.17%.

Polymerization of NCAs. NCA were copolymerized in 1,2-dichloroethane or ethyl acetate at the concentrations given in Table 1.

Copolypeptides Soluble in Water. The copolypeptide (1g) was placed into water (100 ml) at 20—30 °C, and kept in a refrigerator for 24 h at about 8 °C. An insoluble polymer was separated on a sintered-glass filter and then washed with water and a small amount of ethanol. The residue was dried in vacuo at room temperature. The filtrate was lyophilized under reduced pressure. A water-soluble copolypeptide was obtained.

Viscosity Measurement. The viscosities of the copolypeptides were measured in a solution of 1,1,1,3,3,3-hexafluoro-2-propanol (HFIP) using ubbelohde viscometer at 25 °C.

Gel Filtration. High-performance liquid chromatography was performed on a Shimadzu LC-6A. A column (1.3×30 cm, void volume 1×10^5) TSK Gel G3000SW was calibrated in Tris HCl (Buffer pH 7.5) using carbonic anhydrase (MW 29000), albumine, bovine serum (MW 66000), and Cytochrome C (MW 12400) as standards of the molecular weight.

Spectroscopic Measurements. Tryptophan components in the copolymers were estimated from the UV absorbance at

268 nm for solutions of the copolymers in HFIP. Circular dichroism (CD) spectra were recorded on a JASCO J-20A at wavelengths of 300 to 190 nm at 21—23 °C, using a 0.1 mm path length cell, at a concentration of about 0.03 mol/1000 cm³ (residue basis) in HFIP.

The reduced mean residue ellipticity, $[\theta]'$, was defined as

$$[\theta]' = 3 \cdot \theta / C \cdot L \cdot 10 \cdot (n^2+2),$$

where θ is the observed ellipticity in deg, L the optical path length in cm, C the polymer concentration in mol/1000 cm³ (residue basis) and n the refractive index (n_D^{20} 1.275) of the solvent.[7] The infrared spectra were recorded on a Nippon Densi JIR FX 6160 by KBr disks or nujol mull.

Results

DL-Trp NCA was copolymerized with L-Ala NCA and DL-Ala NCA in solution to produce copolypeptides. The polypeptides were obtained by filtration of the polymerization mixture and then dried in vacuo. The polymerization conditions and properties of copolypeptides are shown in Table 1.

Yields of copolypeptides were remarkably decreased by increasing the fed Trp NCA. The composition of the Trp residue in the copolymer formed was normally less than that of the initial monomer ratio. Katchalski reported the polymerization of Trp NCA in the fusion state because of difficulty in the polymerization of Trp NCA in solution.[4] High-purity DL-Trp NCA polymerized at a slower rate than that of Ala NCA in a solution of 1,2-dichloroethane with butylamine as an initiator. In a previous paper we reported that when the polymerization of DL- or L-Ala NCA is initiated with butylamine, the initiation reaction is completed within 60 min, for a monomer conversion of about 10%. The polymerization reaction after this time takes place for 23 h at a conversion of about 70%; it must be proceeded only through the propagation reaction. This suggests that the initiation rate is faster than that of propagation reaction.[8] Most polymerizations of NCAs in acetonitrile were considered regarding this mechanism. The polymerizaton of NCA in 1,2-dichloroethane may proceed by almost the same mechanism as in acetonitrile. The copolymerization of L-Ala NCA with DL-Trp NCA suggests that the propagation reaction of the Trp residue with DL-Trp NCA is slower than the other propagation i.e., a reaction of the Ala residue with Ala NCA and Trp NCA, and a reaction of the Trp residue with Ala NCA.

The water-soluble parts of the obtained copolypeptides could be increased by increasing the amount of Trp NCA fed. In the copolypeptides of DL-Ala and DL-Trp, the water-soluble parts were not proportional to the contained DL-Trp residue. Although all of the copolypeptides formed were soluble in dichloroacetic acid and trifluoroacetic acid, very soon a blue precipitate separated out. Cosani determined the degree of polymerization of the copolymer by the ratio of the initiator to the amount of NCAs fed.[5] The degree of polymerization, however, did not always depend on the ratio of the monomer with the initiator when the polymerization was propagated by activated NCA.[9] The viscosity of the copolypeptides was thus measured in a solution of HFIP. The results are given in Table 1. No relationship has been studied between the viscosity of the HFIP solution and the molecular weight of the polypeptides. The molecular weights of poly(γ-benzyl L-glutamate) (poly(OBzlGlu)) and poly(DL-Ala) are given by the equations (1)[10] and (2),[8] respectively, and $[\eta]$ is given by the equation (3):

$$[\eta] = 2.78 \times 10^{-5} M^{0.87} \quad (1)$$

$$[\eta] = 5.1 \times 10^{-4} M^{0.74} \quad (2)$$

and

$$[\eta] = (\ln \eta_{rel})/c, \quad \eta_{sp} = \eta_{rel} - 1. \quad (3)$$

Here, $[\eta]$ is the intrinsic viscosity, M the molecular

Table 1. Synthesis and Properties of Copolypeptides of L-[a] and DL-Alanine[b] with DL-Tryptophan

Entry No.	NCA (Ala/Trp) Ratio	NCA Concentration mol dm⁻³	Conversion %	Copolypeptides Water soluble part(A) %	Ala/Trp	η_{sp}/c[c]	Water insoluble part(B) %	Ala/Trp	η_{sp}/c[c]
1[a]	95/5	0.12	94	2	97.6/2.4	0.35	98	97.3/2.7	1.12
2[a]	91/9	0.19	92	14	94.2/5.8	0.26	86	94.4/5.6	0.48
3[a]	84/16	0.17	86	20[f]	89.8/10.2	0.16	75	88.1/11.9	0.28
4[a]	81/19	0.17	86	24	90.4/9.6	0.17	76	88.6/11.4	0.19
5[a]	71/29	0.15	67	31	85.5/14.5	0.13	69	71.6/28.4	0.19
6[a]	61/39	0.14	48	37	84.2/15.8	0.12	63	70.6/29.4	0.19
7	0/100	0.21	36	18	0/100	0.58[d]	82	0/100	
8[b]	97/3	0.47	98	33	97.8/2.2	0.78	67	95.4/4.6	
9[b]	84/16	0.38	98	41	96.2/3.8	0.98	59	88.6/11.4	
10[b]	75/25	0.34	36	17	87.5/12.5	0.43[e]	83	75.8/24.2	

a) Polymerization was initiated with butylamine (BA). at an NCA-to-BA molar ratio of 200 at 30 °C for 15 d in 1,2-dichloroethane. b) Polymerization was initiated with BA at an NCA-to-BA molar ratio 100, at 30 °C for 14 d in ethyl acetate. c) c=0.25 g/100 cm³ in HFIP. d) c=0.1 g/100 cm³. e) c=0.25 g/100 cm³ in mixed solvent HFIP/DCE: 4/1. Insoluble part of 7—10b have low solubility to measure the viscosity of solutions. f) Yield after cutting off a low molecular weight by dialysis tube of 3000 dalton.

weight of the polymer, c the concentration of the polymer (g/100 cm^3), η_{rel} the relative viscosity, and η_{sp}/c the specific viscosity of the dichloroacetic acid solution. The specific viscosity of the poly(OBzl-Glu), with a molecular weight of 20000, is 0.04 in a solution of HFIP at a concentration of 0.5 g/100 cm^3 at 30 °C. The specific viscosity of poly(DL-Ala) with a molecular weight of 6000 (determined by the specific viscosity 0.45 in dichloroacetic acid) was 0.4 in HFIP at 25 °C at a concentration of 0.25 g/100 cm^3. T. Ozaki, et al.[11] reported that in the oligomeric peptides derived from OBzlGlu the formation of α-helix begins in the range from the hexapeptides to the octapeptides derived from γ-benzyl L-glutamate. Most oligomeric peptides are capable of forming a secondary structure, such as an α-helix or β-sheet conformation, in a range which is almost the same as the chain length of poly(OBzlGlu). Gel permitation chromatography was carried out in order to evaluate the relation between the specific viscosity and molecular weight of copoly(Trp, Ala). The result (Fig. 1) shows that the specific viscosity of a copolymer (No. 3,(A)) with a molecular weight of 15000—18000, (plotted as a calibration curve for the elution parameter) is 0.16 in HFIP. This suggests that these copoly(Trp, Ala) have a chain length which is capable of constructing a secondary conformation, such as an α-helix or β-structure. Poly(L-Ala) is insoluble in water, and poly(DL-Trp) partly soluble. Entry 1 in Table 1 is for a copolypeptide formed containing 2.2% of a water-soluble copolypeptide which contains 2.4 mol% of the Trp residue. The indol nucleus of the Trp residue exerts a hydrophilic group in the copolypeptides. The insoluble part of the copolypeptides mentioned in the same entry, however, contained 2.7 mol% of the Trp residues. The tryptophan content in the water-soluble copolypeptide was less than that in the water-insoluble copolypeptide in each entry. The viscosity of the water-soluble parts was lower than that of the water-insoluble parts in each entry. This suggests that the solubility of the copolypeptides in water is essentially independent of the rate of the tryptophan residue in the copolypeptides.

The circular dichroism spectra observed for water-insoluble copolypeptides (Table 1) are shown in Figs. 2-1 and -2. The CD spectra of the polypeptides in the helical, β-sheet, and random forms have been studied extensively.[12-17] The ellipticity bands between 185 and 225 nm are associated with the α-helix, β-sheet, and random-coil peptide. The negative dichroisms near 206 and 220 nm have been used for assigning the helix, and the strong negative band near 190 nm for the random-coil of the polypeptides. The insoluble polymer (No. 1—4 in Fig. 2) exhibited a maximum peak at about 190 nm, a minimum at 204 nm, and a shoulder peak at about 220 nm. For all four poly-

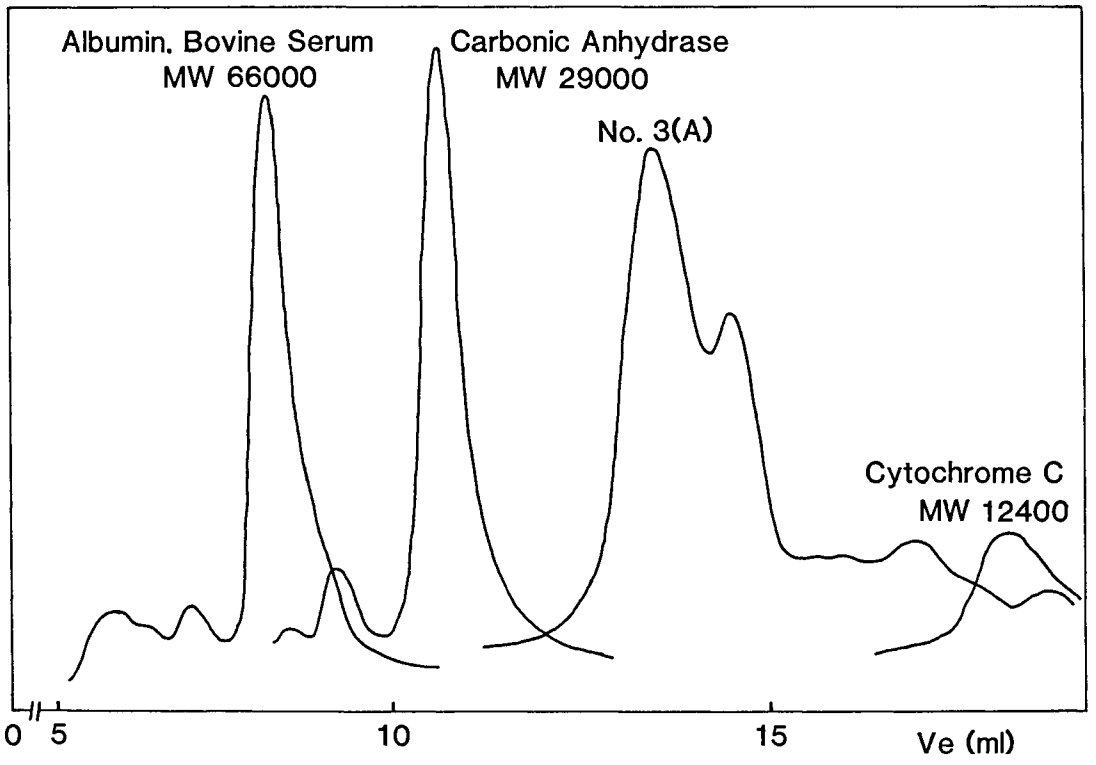

Fig. 1. GPC elution curve of water-soluble copolymer No. 3(A) after dialysis and cutting off MW below 3000) and standard proteins. Column; TSK Gel G3000SW, Developer: 100 mM Tris (pH 7.0), Flow: 0.3 ml min^{-1}, Wave: 280 nm.

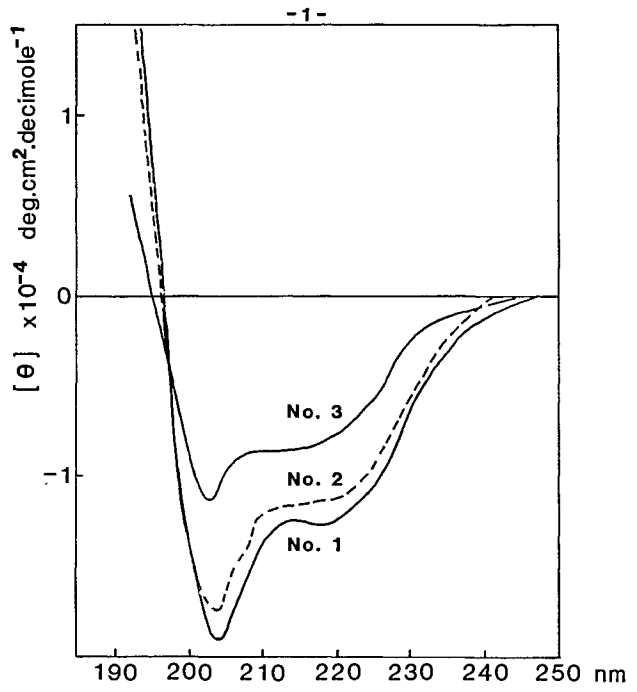

Fig. 2-1. Circular dichroism spectra of water-insoluble copolypeptides(B) shown in Table 1.

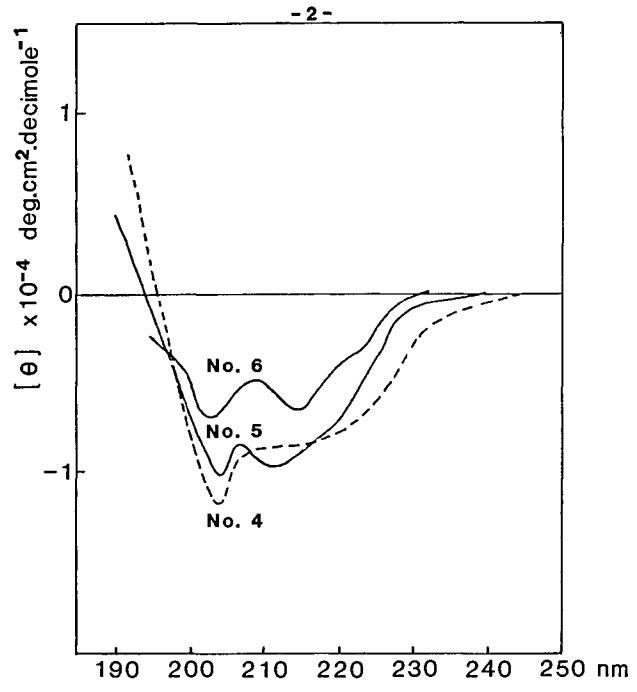

Fig. 2-2. Circular dichroism spectra of water insoluble copolyptides(B) shown in Table 1.

mers given in Fig. 2, the spectra indicate that a right-handed α-helix conformation can be assumed. The intensity of negative peak, which is proportional to the helix content, was decreased by an increase in the tryptophan residue. Polymers No. 5 and 6 given in Fig. 2 have two negative peaks at 212 and 216 nm, respectively, in addition to those of Entries 1—4. These differences in the spectrum patterns could result in an overlapping pattern of the α-helix with β I. The CD spectra of many water-soluble copolypeptides shown in Table 1 (Fig. 3) gave a minimum peak at 197 nm. Furthermore, a minimum peak was observed at

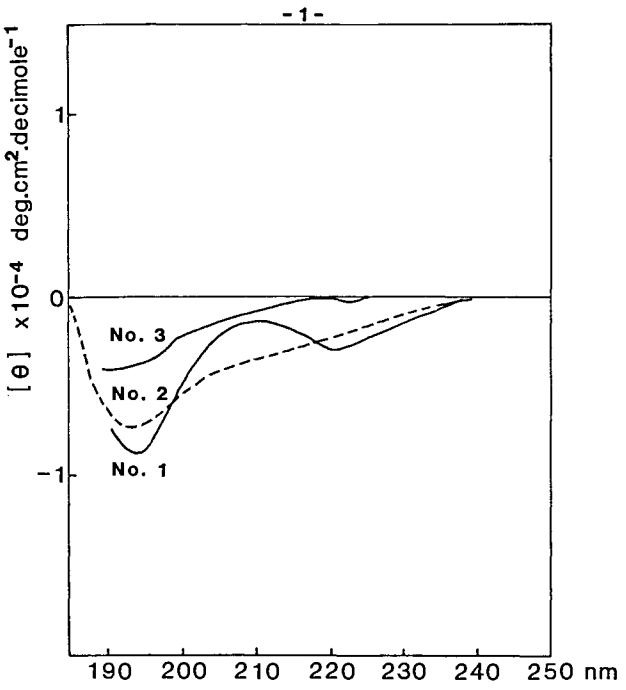

Fig. 3-1. Circular dichroism spectra of water-soluble copolypeptides(A) shown in Table 1.

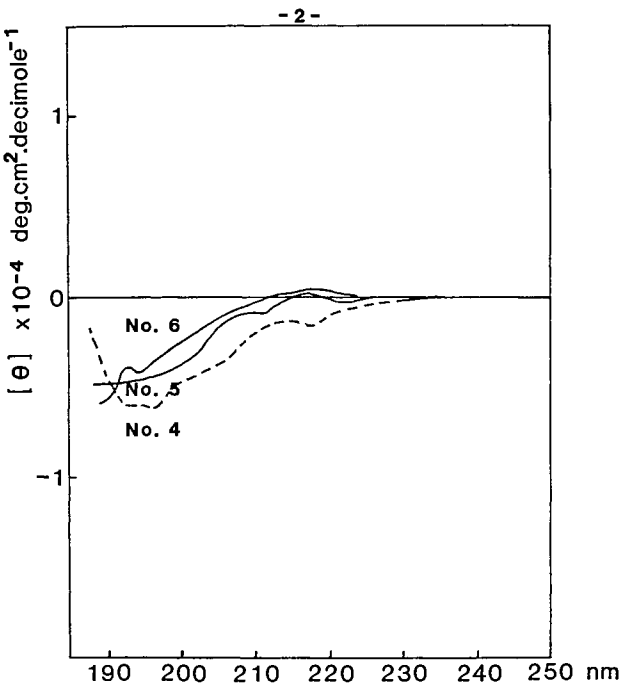

Fig. 3-2. Circular dichroism spectra of water-soluble copolypeptides(A) shown in Table 1.

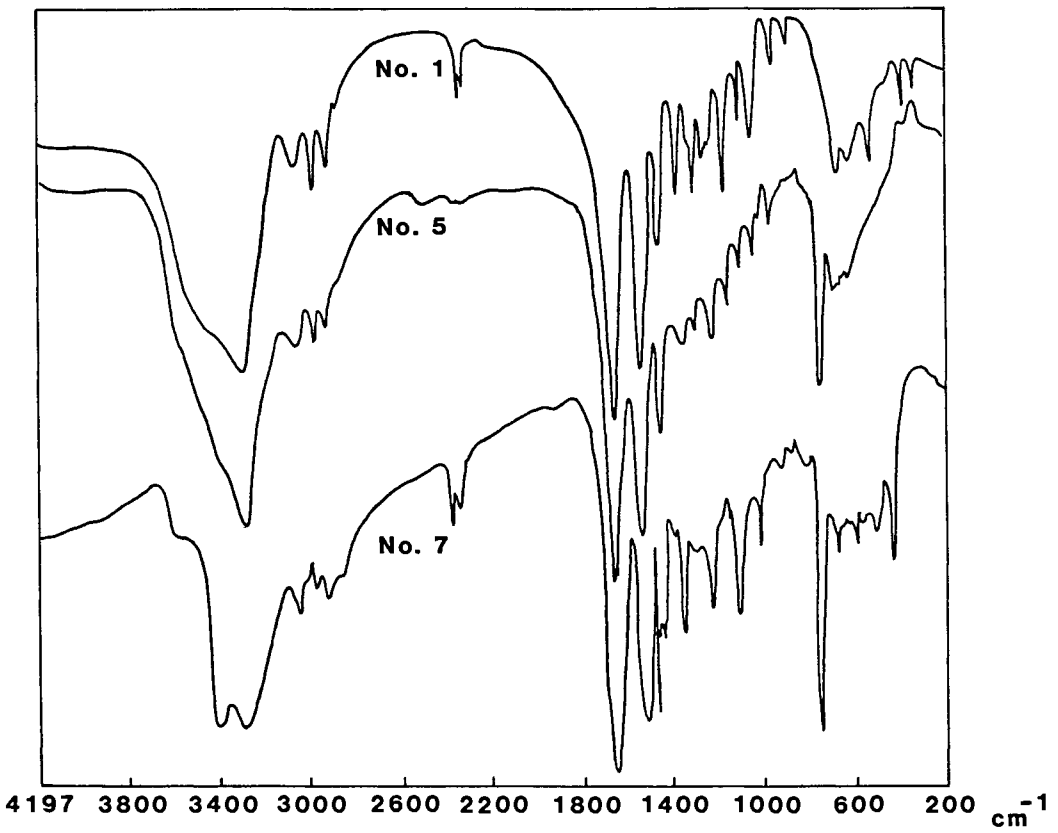

Fig. 4. Infrared spectra of water-insoluble copolypetides(B) shown in Table 1 in KBr disk.

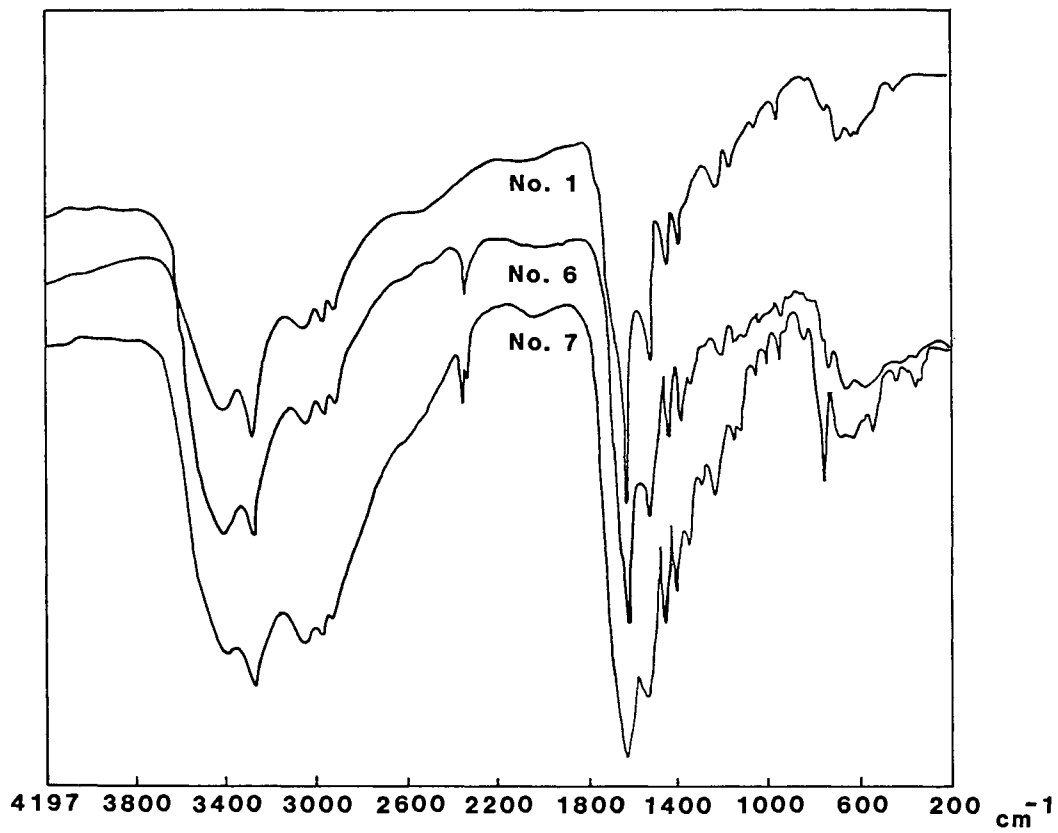

Fig. 5. Infrared spectra of water-soluble copolypeptides(A) shown in Table 1 in KBr disk.

225 nm for Entry 1 and a maximum peak at 222 nm for Entries 5 and 6. Fasman reported a strong negative peak of CD at 197 nm and a weak maximum peak at 217 nm for a poly(L-Lys) aqueous solution to be characteristic of a disordered conformation. Although the shapes were similar, the positive peak of polymer Entries 5 and 6 were higher than that of poly(L-Lys).

The infrared spectra of the copolypeptides listed in Table 1 are shown in Figs. 4 and 5. The insoluble fraction of poly(DL-Trp) gave amide I and II bands at 1654 and 1520 cm^{-1}, respectively. The insoluble fraction of polymer No. 1 gave amide I and II bands at 1656 and 1542 cm^{-1}, respectively, in addition to a band at 1306 cm^{-1}. The frequency value of these bands correspond to those for α-helical poly(L-alanine),[18-20] and the band at 1306 cm^{-1} is considered to be the characteristic of crystalline α-poly(L-Ala).[21] As is evident from the spectra in Entries 2—6 in Table 1, an insoluble polymer with a Trp residue content of 5.6—29.4 mol% gives the amide I band at 1654 and 1634 cm^{-1}, the II band at 1538 and 1305 cm^{-1}, as shown in Entry 5 of Fig. 4. The relative intensity of the 1654 cm^{-1} band was stronger than that of 1634, but almost identity upon increasing the Trp residue. Although the band at 1634 cm^{-1} corresponds to β-polypeptide,[20] the other bands for the β-conformation disappear. This may indicate that only the strongest peak of amide I for the β-conformation was observed, due to the small content of the β-conformational polypeptide. Thus, the infrared spectra coincided with the result of the CD spectra. This would also mean that the conformation of the insoluble polymers in the solid state produces little change in the solution of HFIP. The water-soluble fraction of poly(DL-Trp) No. 7 shows peaks at 1623 and 1540 cm^{-1} due to the β-conformation. The soluble fraction of Entries 1B—6B gave peaks at 1695 and 1628 cm^{-1} (amide I), due to an antiparallel and extended β-conformation, and no peak at about 610 cm^{-1} due to the α-helix conformation. Polymer 1B gave an additional peak at 445 cm^{-1}, which is characteristic of β-polyalanine. As described above, the CD spectra of the soluble polymer indicate a coiled conformation. This may indicate that the conformation of the soluble polymers in the solid state changed from β to a disordered form upon dissolution in HFIP. The infrared spectra of water-soluble copolypeptides No. 8—10 gave an amide I band at 1715—25, 1655 and amide II at 1540 cm^{-1}, characteristic of an α-helix-like conformation of (Ala-Ala-Ala-D-Ala)$_n$.[22] These bands were different from that of the water-soluble parts of Entries 1—6. For water-insoluble parts No. 8—10, bands at 1652 and 1530 cm^{-1} were observed, which are characteristic of a parallel β-conformation. These conformations were different from that of the water-insoluble parts of Entries 1—6.

The authors wish to express their thanks to Professor emeritus Dr. Y. Iwakura of the University of Tokyo, Dr. T. Hayashi of Kyoto University, and Mr. M. Iwatsuki of Ajinomoto Company for useful advice. The present work was partly supported by a Grant-in-Aid for Scientific Research No. 61490008 from the Ministry of Education, Science and Culture.

References

1) A part of this work was presented at the 33rd IUPAC International Symposium on Macromolecules, Montreal, Canada, July 8—13, 1990, Abstr., No. 2.10.5.
2) T. Endo, M. Oya, K. Hayashi, and T. Miyazawa, *J. Protein Chem.*, **8**, 575 (1989).
3) T. Endo, M. Oya, F. J. Joubert, K. Hayashi, and T. Miyazawa, *J. Protein Chem.*, **8**, 583 (1989).
4) A. Pachornik, M. Dela, and E. Katchalski, *J. Am. Chem. Soc.*, **76**, 299 (1954).
5) A. Cosani, E. Peggion, A. S. Verdini, and M. Terbojevich, *Biopolymers*, **6**, 963 (1968).
6) M. Oya and R. Katakai, "Shin Jikken Kagaku Koza No. 19-1; Polypeptides," ed by Nippon Kagaku Kai, Maruzen, Tokyo (1978), p. 244.
7) G. D. Fasman, "Poly-α-Amino Acid," Marcel Dekker, New York (1967), p. 293.
8) Y. Iwakura, K. Uno, and M. Oya, *J. Polym. Sci., Part A*, **6**, 2165 (1968).
9) M. Goodman, *J. Am. Chem. Soc.*, **86**, 3384 (1964); **88**, 3627 (1966).
10) P. Doty, *J. Am. Chem. Soc.*, **78**, 947 (1956).
11) T. Ozaki, A. Shoji, and M. Furukawa, *Macromol. Chem.*, **183**, 771 (1982).
12) G. Holzwarth and P. Doty, *J. Am. Chem. Soc.*, **87**, 218 (1965).
13) J. R. Parrishi and E. R. Blout, *Biopolymers*, **10**, 1491 (1971).
14) Y. A. Zubkov, T. M. Birshtein, and I. S. Milevskaya, *Biopolymers*, **10**, 2051 (1971).
15) S. R. Snell and G. D. Fasman, *Biopolymers*, **11**, 1723 (1972).
16) W. C. Johnson and Ignacio Tinoco, *J. Am. Chem. Soc.*, **94**, 4389 (1972).
17) G. Wouters, R. Katakai, W. J. Becket, and M. Goodman, *Macromolecules*, **15**, 31 (1982).
18) K. Itoh, T. Nakahara, T. Shimanouchi, M. Oya, K. Uno, and Y. Iwakura, *Biopolymers*, **6**, 1759 (1968).
19) K. Itoh, T. Shimanouchi, and M. Oya, *Biopolymers*, **7**, 649 (1969).
20) K. Itoh, M. Oya, and T. Shimanouchi, *Biopolymers*, **11**, 1137 (1972).
21) Y. Iwakura, K. Uno, and M. Oya, *J. Polym. Sci., Part A*, **1**, 2867 (1967).
22) T. Ozaki, M. Oya, and K. Itoh, *Polym. J.*, **13**, 225 (1981).

Formation of Acrylaldehyde by Vapor-Phase Aldol Condensation I. Basic Oxide Catalysts

Mamoru Ai
Research Laboratory of Resources Utilization, Tokyo Institute of Technology,
4259 Nagatsuta, Midori-ku, Yokohama 227
(Received October 30, 1990)

Vapor-phase aldol condensation of formaldehyde with acetaldehyde to form acrylaldehyde was studied with various oxides supported on silica gel using 35% formalin as the source of formaldehyde. The silica gel unsupported catalyst prepared from colloidal silica showed a relatively high activity and selectivity to form acrylaldehyde. The catalytic activity was markedly enhanced by the incorporation of a basic or amphoteric oxide into the silica gel, while it fell with the incorporation of an acidic oxide such as P_2O_5 or B_2O_3. The highest yields of acrylaldehyde were obtained with the Si-Mg, Si-Li, Si-Na, and Si-Zn oxide systems. Effects of reaction variables were also studied using a catalyst with an Si : Mg atomic ratio of 100 : 10.

Acrylaldehyde is currently produced by a partial oxidation of propene, which process has already been well studied. On the other hand, acrylaldehyde is obtained also by an aldol condensation of formaldehyde (HCHO) with acetaldehyde (AcH) in the presence of basic catalyst. This reaction is called "Tollence Reaction":[1,2]

$$CH_3CHO + HCHO \longrightarrow CH_2(OH)CH_2CHO$$
$$\longrightarrow CH_2{=}CHCHO + H_2O.$$

Schulz and Wanger[3] reported a process involving a contact catalytic conversion of an equimolecular amount of AcH and 30% HCHO aqueous solution on silica gel impregnated with 10% sodium silicate [$Na_2Si_2O_5$] at 305 to 310 °C.[4] The yield of acrylaldehyde was 41 mol% with an AcH conversion of 48%; the selectivity was about 85 mol%. The yield (mol%) is defined as 100×(moles of product)/(moles of AcH fed). The selectivity is defined as 100×(moles of product)/(moles of AcH consumed). Malinowski et al.[5] reported 46—62 mol% yields of acrylaldehyde over alkali and alkaline earth hydroxides.

This reaction is attractive in view of the utilization of C_1 chemical resources. However, aside from the above-cited works,[3,5] very little has been reported on this reaction in the literature. In this study, various kinds of metal oxides were examined as catalysts for this reaction, and then, characteristics of this reaction were studied using a silica gel containing MgO in about 10 mol%.

Experimental

Catalysts. The catalysts used in this study were oxides supported on silica gel. For example, the Si-Mg catalyst with an atomic ratio of 100 : 10 was prepared as follows. Magnesium nitrate [$Mg(NO_3)_2 \cdot 6H_2O$] (25.6 g) was dissolved in 100 ml of water and the solution was added to 300 g of colloidal silica "Snowtex O" (Nissan Chem. Ind.) containing SiO_2in 20%. Excess water was evaporated with stirring by means of a hot air current to yield a cake. This cake was dried in an oven for 6 h by gradual heating from 50 to 200 °C. The resulting solid was ground and sieved to get the 8—20 mesh portion. It was finally calcined at 500 °C for 6 h in a stream of air.

Reaction Procedures. The reaction was carried out with a continuous-flow system at atmospheric pressure. The reactor was made of a stainless steel tube, 50 cm long and 1.8 cm in i.d., mounted vertically and immersed in a lead bath. Nitrogen was fed in from the top of the reactor at a fixed rate of 140 $cm^3\,min^{-1}$ as the carrier or diluent, and a mixture of AcH and 35% formalin (containing methanol in about 8%) was introduced into a preheating section of the reactor by means of a syringe pump. Unless otherwise indicated, the feed rates of AcH, HCHO, methanol, water, and nitrogen were 13, 26, 5.6, 71, and 350 $mmol\,h^{-1}$, respectively. The effluent gas from the reactor was led into four chilled scrubbers to recover the water-soluble compounds. After 1 h time-on-stream, the contents of the scrubbers were collected (100 cm^3). The products were analyzed by gas chromatogarphy using a 6 m column of propylene carbonate for CO_2 and a 2 m column of PEG (polyethylene glycol) 20 M at 110 °C for aldehydes and alcohols.

The contact time, defined as (volume of catalyst)/(flow rate of gaseous feed), was changed by changing the amount of catalyst used with the feed rate fixed.

Results and Discussion

Performance of Metal Oxides Supported on Silica Gel. Various kinds of oxides supported on silica gel were tested as catalysts. The main products were acrylaldehyde, CO_2 and methanol. A very small amount of methyl formate was found in the product, but crotonaldehyde was not detected. In some cases, a large deviation was observed between the acrylaldehyde yield and the AcH conversion. It thus seems likely that the deviation is to be ascribed to formation of unidentified polymers. The conversions and yields obtained for each catalyst tested at a fixed temperature of 320 °C are listed in Tables 1 and 2.

The silica gel catalyst, prepared from the colloidal silica "Snowtex O," possesses a certain activity; the yield of acrylaldehyde reached 78 mol% with the selectivity of 98 mol% when the amount of catalyst used was 20 g (the contact time was about 10 s). The

Table 1. Performances of Silica-Supported Alkali and Alkaline Earth Metal Oxide Catalysts[a)]

Catalyst (Atomic ratio)	wt/g	AcH conv. %	Yield/mol% Acryl[b)]	CO_2	Methanol
Si alone	2	13	13	0	0
	5	32	32	0	0
	20	80	78	0.9	4
Si-Cs (100-4)	2	74	65	1.9	4
	4	85	51	4.7	6
Si-K (100-2)	2	50	44	0	2
	10	88	82	2.0	3
(100-6)	2	58	47	0.5	2
	10	95	63	5.2	12
Si-Na (100-4)	2	45	36	0.7	0
	10	89	87	2.8	3
(100-10)	2	31	28	0.5	2
	20	95	90	4.0	6
Si-Li (100-4)	2	57	47	1.4	0
	10	92	91	9.7	4
Si-Ba (100-10)	2	30	30	0.6	2
	10	54	51	5.0	6
	20	85	74	5.0	6
Si-Ca (100-0)	2	60	58	8.0	22
	6	84	75	19.0	50
Si-Mg (100-0)	1	53	51	4.0	10
	2	75	75	5.9	10
	3	80	80	9.3	28
	4	88	88	15.0	66

a) Conditions: temperature=320 °C; AcH/HCHO/methanol/water/nitrogen feed rates=13/26/5.6/71/350 mmol h^{-1}. b) Acryl=acrylaldehyde.

Table 2. Performances of Silica-Supported Oxide Catalysts[a)]

Catalyst (Atomic ratio)	wt/g	AcH conv. %	Yield/mol% Acryl[b)]	CO_2	Methanol
Si alone	2	13	13	0	0
	5	32	32	0	0
	20	80	78	0.9	4
Si-P (100-1)	2	low	6	0	0
Si-B (100-10)	20	33	32	0	0
Si-V (100-2)	2	43	38	2	10
	10	83	46	7.1	10
Si-Al (100-4)	2	41	38	0.5	10
	6	73	46	1.7	6
	8	81	40	2.3	6
(100-15)	1	30	25	0.9	10
	2	42	32	1.2	10
	20	99	0	7.5	6
Si-Zn (100-4)	2	52	52	4.7	8
	10	90	90	22.0	50
Si-Fe (100-4)	2	28	27	5.2	15
	8	60	55	35.0	45
Si-Sn (100-4)	2	30	28	3.3	10
	12	74	58	12.0	10
Si-Pb (100-4)	2	66	40	58.0	62
Si-Cu (100-4)	2	low	1	76.0	38

a) Conditions: temperature=320 °C; AcH/HCHO/methanol/water/nitrogen feed rates=13/26/5.6/71/350 mmol h^{-1}. b) Acryl=acrylaldehyde.

incorporation of a basic oxide, such as alkali or alkaline earth oxide, induces a large increase in the activity. However, it seems hard to get a clear correlation between the electronegativity of metal ions and the activity. The acrylaldehyde yield exceeds 85 mol% with the Si-Li, Si-Na, and Si-Mg systems. However, the yield does not exceed 75 mol% with the Si-Cs, Si-Ba, and Si-Ca systems.

The incorporation of an acidic oxide, such as P_2O_5 or B_2O_3, decreases the activity (Table 2). The effect of the amounts of both P_2O_5 and MgO on the activity is shown in Fig. 1. The activity increases sharply with the incorporation of a small amount of MgO, while it decreases sharply with that of P_2O_5. The results strongly suggest that the reaction is promoted by basic sites, as generally believed. However, it should be noted that the silica-supported MgO catalysts are much more active than the unsupported MgO catalyst. Possibly, the combination of silica-gel with metal oxides induces a large increase in surface area and, moreover, a generation of new acidic sites which may also serve to promote the reaction.

The incorporation of V_2O_5 or Al_2O_3 increases strongly the activity. However, the yield of acrylaldehyde does not exceed 50 mol%, though the formation of CO_2 and methanol is relatively slow. Possibly, the acrylaldehyde formed initially is converted to unidentified polymers under the action of strongly acidic sites present on the Si-V and Si-Al oxides:

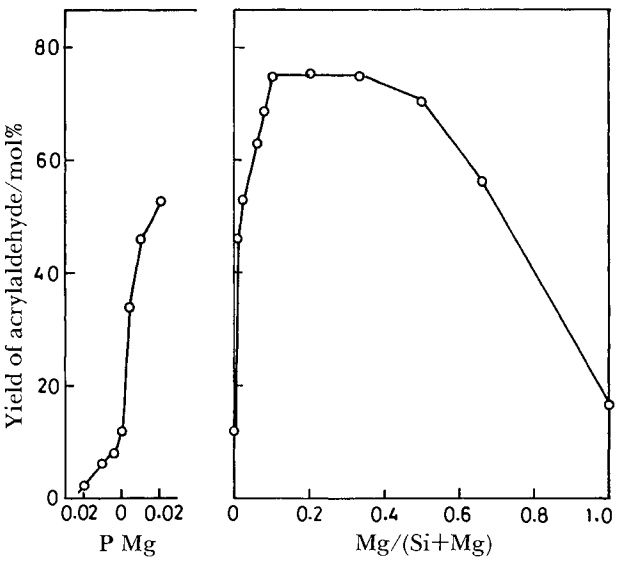

Fig. 1. Effect on activity of the amount of MgO or P_2O_5 incorporated in silica gel. Temperature=320 °C; the amount of catalyst used=20 g.

$$CH_3CHO + HCHO \longrightarrow CH_2{=}CHCHO \longrightarrow \text{polymers.}$$

A relatively good performance in both activity and selectivity was obtained with the Si-Zn oxide catalyst. The yield of acrylaldehyde reached 90 mol% with a

selectivity of almost 100 mol%, though the formation of by-products such as CO_2 and methanol is relatively fast.

The incorporation of an oxide of heavy metal, such as Fe_2O_3, PbO_2, or CuO, promotes strongly the formation of by-products. The amount of obtained methanol is almost in parallel with that of CO_2, which suggests that these two by-products are formed from HCHO via the process,

$$2HCHO \longrightarrow HCOOCH_3 \longrightarrow CH_3OH + HCOOH$$
$$\longrightarrow CH_3OH + CO_2 + H_2.$$

It has been reported that the formation of methyl formate by dimerization of HCHO is promoted by an acid-base dual function,[6] and that the decomposition of formic acid to CO_2 and H_2 is promoted very strongly by basic sites.[7] Possibly, the balance of acidic and basic properties of these catalysts may fit for the dimerization of HCHO.

It should also be noted that the incorporation of V_2O_5, an amphoteric oxide, or an oxide of heavy metal can enhance the catalytic activity to the level of catalysts comprising an alkali or alkaline earth metal oxide. This finding leads us to assume that active sites with a strong base, araising from alkali or alkaline earth metal oxide, are poisoned selectively by acidic reactants such as CO_2 and, further, that the reactions, especially the proton-abstraction from AcH

$$CH_3CHO + OH^- \longrightarrow {}^-CH_2CHO + H_2O,$$

are promoted enough by active sites with a very weak base, araising from V_2O_5 and amphoteric oxides.

Effects of Reaction Variables. The study in the preceding section has revealed that the Si-Li, Si-Na, Si-Mg, and Si-Zn catalysts exhibit a good performance for the acrylaldehyde formation. Thus, the characteristics of this reaction were studied using the catalyst with an Si : Mg atomic ratio of 100 : 10.

Product Distribution. The yields of acrylaldehyde, CO_2, and methanol obtained at 280 °C are shown in Fig. 2 as a function of contact time. The yield of acrylaldehyde on the AcH basis reaches 96 mol%, whereas those of CO_2 and methanol reach 12 and 43 mol%, respectively. The sum of the yields of the three products exceeds far 100 mol%. This also indicates that CO_2 and methanol are not formed from AcH but from HCHO.

Effect of Temperature. The yields of acrylaldehyde btained at four temperatures are shown in Fig. 3 as a function of contact time. From the initial rates at 240 and 280 °C, the apparent activation energy was calculated to be about 15 kcal mol^{-1}. The yield of acrylaldehyde reaches 96 mol% at a temperature between 280 and 340 °C.

Effect of AcH Concentration on Rate. The effect of AcH concentration was studied by changing the initial concentration in the feed gas from 0.78 to 5.6 mol%, while fixing the concentrations of HCHO, methanol, and water at about 6, 1.2, and 16 mol%, respectively. The rate increases steadily with the AcH concentration.

Effect of the HCHO/AcH Molar Ratio on the Yield of Acrylaldehyde. The effect of the HCHO/AcH molar ratio on the yield of acrylaldehyde was studied

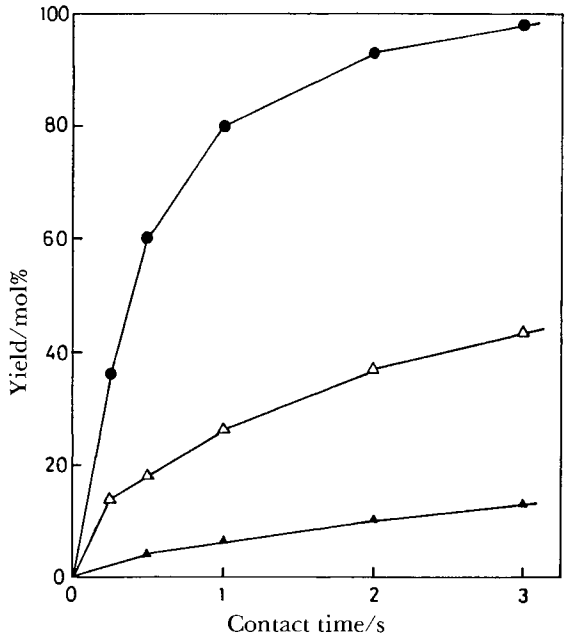

Fig. 2. Reaction of HCHO with AcH with the Si : Mg=100 : 10 catalyst. ● Acrylaldehyde; ▲ CO_2; △ methanol.

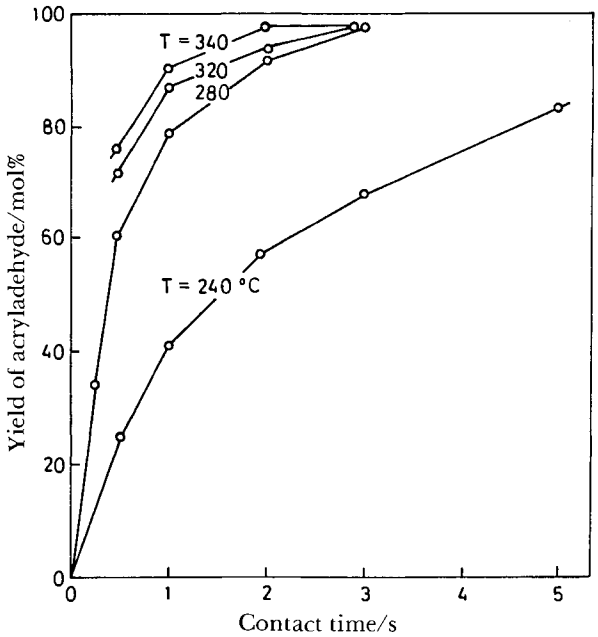

Fig. 3. Effect of temperature on the yield of acrylaldehyde.

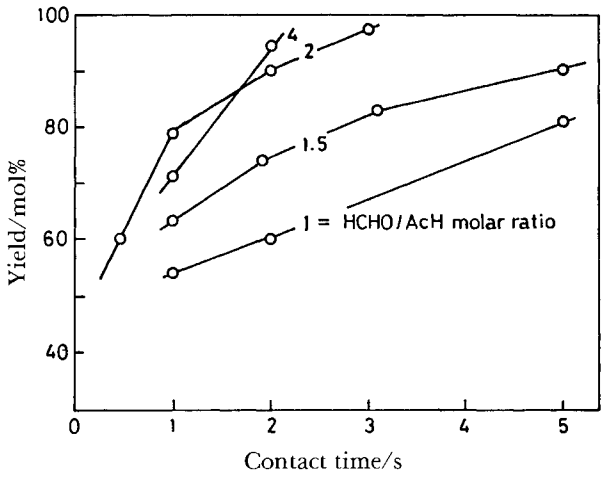

Fig. 4. Effect of the HCHO/AcH molar ratio on the yield of acrylaldehyde. Temperature=280 °C.

at a fixed AcH feed rate of about 13 mmol h^{-1} by changing the feed rate of formalin. Figure 4 shows the yields obtained at 280 °C with four different HCHO/AcH ratios. Longer contact time is required to achieve a certain level of acrylaldehyde yield as the HCHO/AcH ratio decreases, which indicates that the rate increases with the HCHO concentration, too.

Effect of Feed Rate. The reaction was conducted by changing the feed rates of AcH and HCHO, while fixing the HCHO/AcH molar ratio at 2. The initial rate of acrylaldehyde formation at 240 °C increased steadily with the increase in the feed rate, as reasonably expected from the above-mentioned results.

Conclusion. The silica gel prepared from the colloidal silica exhibits a relatively good catalytic performance in both activity and selectivity to form acrylaldehyde by aldol condensation of HCHO with AcH. The incorporation of a small amount of alkali or alkaline earth oxide, V_2O_5, an amphoteric oxide, or an oxide of heavy metal enhances markedly the activity. However, the formation of acrylaldehyde is accompanied by two side-reactions the polymerization of produced acrylaldehyde to unidentified polymers and the dimerization of HCHO to methyl formate which is decomposed readily to methanol and CO_2. The highest acrylaldehyde yields are obtained with the Si-Na, Si-Li, Si-Mg, and Si-Zn oxides.

References

1) B. Tollens and P. Wigand, *Justus Liebigs Ann. Chem.*, **265**, 316 (1891).
2) P. Rave and B. Tollens, *Justus Liebigs Ann. Chem.*, **276**, 58 (1893).
3) H. Schulz and H. Wanger, *Angew. Chem.*, **62**, 105 (1950).
4) Z. G. Hajios, "Carbon-Carbon Bond Formation," Marcel Dekker, New York and Basel (1979), Vol. 1, p. 1.
5) S. Malinowski, H. Jablczynska-Jedrzejewska, S. Basinski, and S. Benbenek, *Chim. Ind. (Paris)*, **85**, 885 (1961); *Chem. Abstr.*, **56**, 2321g (1962).
6) M. Ai, *J. Catal.*, **83**, 141 (1983).
7) M. Ai, *J. Catal.*, **50**, 291 (1977).

Formation of Acrylaldehyde by Vapor-Phase Aldol Condensation II. Phosphate Catalysts

Mamoru Ai
Research Laboratory of Resources Utilization, Tokyo Institute of Technology,
4259 Nagatsuta, Midori-ku, Yokohama 227
(Received October 30, 1990)

Vapor-phase aldol condensation of formaldehyde with acetaldehyde to form acrylaldehyde was studied with various oxide and phosphate catalysts using 35% formalin as the source of formaldehyde. Almost all of the tested oxides exhibited a certain activity as the catalysts. Acidic oxides, such as MoO_3 and WO_3 showed a relatively high selectivity to acrylaldehyde, though the activities were low. V_2O_5 and amphoteric oxides exhibited a much higher activity, but they promoted also the formation of CO_2 and methanol. The catalytic performance was improved, to a certain extent, by combination of an acidic oxide with an amphoteric oxide. Further, the combination of phosphorus with V_2O_5 or an amphoteric oxide induced a large increase in the selectivity to acrylaldehyde. A good performance was obtained with the Ni-P, Mn-P, Fe-P, and V-P systems. The yield of acrylaldehyde reached 86 mol% on the AcH basis with a very slow formation of CO_2 and methanol.

The preceding paper[1] was concerned with performances of silica-supported basic oxides used as catalysts in the vapor-phase aldol condensation of formaldehyde (HCHO) with acetaldehyde (AcH) to form acrylaldehyde:

$$CH_3CHO + HCHO \longrightarrow CH_2{=}CHCHO + H_2O.$$

It was recently found that the aldol condensation of HCHO with a carboxylic acid, such as acetic acid or propionic acid

$$RCH_2COOH + HCHO \longrightarrow CH_2{=}CRCOOH + H_2O \quad (R{=}H, CH_3),$$

is promoted selectively with phosphate catalysts, for example, V-P,[2,3] V-Ti-P,[4] and V-Si-P[5] oxides. On the other hand, basic oxides were found to be unsuitable as catalysts, because they promote the side-reaction

$$2RCH_2COOH \longrightarrow RCH_2COCH_2R + CO_2 + H_2O \quad (R{=}H, CH_3).$$

This led us to infer that certain phosphates would exhibit performance comparable to that of basic oxides as catalysts for the condensation of HCHO with aldehydes, much as for the reaction with carboxylic acids. In this study, we focused our attention on finding out some phosphate catalysts effective for the formation of acrylaldehyde.

Experimental

Catalysts. The catalysts used in this study were various kinds of single, binary, and ternary oxides. Some of them were the same as those used in our previous studies.[2-4] For example, the Ni-P oxide with an atomic ratio of 1 : 0.9 was prepared as follows. Nickel nitrate [$Ni(NO_3)_2 \cdot 6H_2O$] (291 g) was dissolved in 200 ml of water and 104 g of 85% H_3PO_4 was added to the solution. Excess water was evaporated with stirring in a hot air current to yield a viscous paste. This paste was then dried in an oven at 200 °C for 6 h. The obtained solid was ground and sieved to get the 8—20 mesh portion. It was finally calcined at 500 °C for 6 h in a stream of air.

Reaction Procedures. The reaction procedures were almost the same as those described in the preceding paper.[1] As the source of HCHO, 35% formalin, containing methanol in about 8%, was used. Unless otherwise indicated, the feed rates of AcH, HCHO, methanol, water, and nitrogen were 13, 26, 5.6, 71, and 350 mmol h^{-1}, respectively.

Results and Discussion

Performance of Metal Oxide Catalysts. Since little information has been reported on this reaction, it seems necessary to make a character sketch of catalytic function. Therefore, various kinds of oxides were tested as catalysts. Table 1 shows the conversions of AcH and the yields of acrylaldehyde, CO_2, and methanol obtained at 320 °C with 20 g portions of single and binary oxide catalysts.

The results may be summarized as follows.

(1) The acidic oxides, such as MoO_3 and WO_3, show a relatively high selectivity to form acrylaldehyde, though the activity is low.

(2) V_2O_5 shows a high activity, but it promotes also the formation of CO_2 and the selectivity to acrylaldehyde is low.

(3) Amphoteric oxides, such as TiO_2, SnO_2, and Fe_2O_3, show a high activity, but they also promote the formation of CO_2 and methanol and the selectivity to acrylaldehyde is low.

(4) MgO shows a low activity. The Mg-K=9-1 oxide shows a relatively high activity, but the selectivity to acrylaldehyde is low.

(5) The catalytic performance is improved by combination of V_2O_5 or an amphoteric oxide with an acidic oxide, such as MoO_3 or WO_3.

(6) The best performances are obtained with the W-Sn and W-Fe oxide systems. The yield of acrylaldehyde reached 67 mol%.

Table 2 shows the results obtained with various phosphate catalysts. The results may be summarized as follows.

Table 1. Performances of Metal Oxide Catalysts[a]

Catalyst (Atomic ratio)		AcH[b] conv.	Yield/mol%			Catalyst (Atomic ratio)		AcH[b] conv.	Yield/mol%		
		%	Acryl[b]	CO_2	MeOH[b]			%	Acryl[b]	CO_2	MeOH[b]
Mo		15	14	1	1	Ti		89	37	19	19
Mo-V	(8-2)	30	30	0	0	Ti-Mo	(9-1)	43	42	6	16
Mo-Ti	(9-1)	57	15	46	0		(8-2)	52	51	8	22
	(8-2)	54	13	47	0	Ti-W	(9-1)	67	40	8	24
Mo-Sn	(9-1)	54	8	92	0		(7-3)	36	29	1	4
Mo-Fe	(9-1)	32	29	1	0	Ti-V	(9-1)	82	28	34	36
	(7-3)	32	29	2	0	Sn		56	56	27	60
Mo-Bi	(8-2)	15	13	2	0	Sn-Mo	(9-1)	17	16	60	60
	(5-5)	45	21	30	0		(7-3)	61	13	63	36
W		38	35	1	2	Sn-W	(7-3)	57	50	6	8
W-V	(8-2)	22	20	2	0		(5-5)	55	50	7	10
W-Ti	(8-2)	39	28	1	2	Fe		68	42	69	62
	(6-4)	50	28	1	0	Fe-Mo	(7-3)	58	49	29	23
W-Sn	(8-2)	40	40	2	4	Fe-W	(7-3)	79	66	38	65
	(5-5)	55	50	7	10	Sb		Low	2	0	0
W-Fe	(8-2)	48	46	1	4	Sb-V	(8-2)	24	21	14	15
	(7-3)	62	60	3	12	Mg		18	17	2	0
	(5-5)	73	67	14	15	Mg-K	(9-1)	48	24	34	32
V		60	28	34	0						

a) Conditions: temperature=320 °C; amount of catalyst used=20 g; contact time=10 to 15 s; AcH/HCHO/methanol/water/nitrogen feed rates=13/26/5.6/71/350 mmol h^{-1}. b) AcH=acetaldehyde; Acryl=acrylaldehyde; MeOH=methanol.

Table 2. Performances of Phosphate Catalysts[a] (1)

Catalyst (Atomic ratio)		AcH[b] conv.	Yield/mol%			Catalyst (Atomic ratio)		AcH[b] conv.	Yield/mol%		
		%	Acryl[b]	CO_2	MeOH[b]			%	Acryl[b]	CO_2	MeOH[b]
Mo		15	14	1	0	Ni-P	(6-4)	94	48	33	50
Mo-P	(8-2)	Low	3	0	0		(5-5)	79	66	1	0
W		38	35	1	2	Co-P	(6-4)	92	68	21	30
W-P	(9-1)	Low	7	1	0		(5-5)	36	35	1	0
V		60	28	34	0	Mn-P	(6-4)	86	86	11	23
V-P	(1-1.06)	75	70	2	0		(5-5)	Low	4	1	0
Ti		89	37	19	19	Cr-P	(5-5)	32	3	3	0
Ti-P	(9-1)	67	57	3	5		(4-6)	4	3	0	0
	(8-2)	73	66	2	18	Cu-P	(6-4)	50	43	21	0
	(6-4)	43	42	1	0		(5-5)	Low	1	0	0
Sn		56	56	27	60	B-P	(5-5)	20	20	1	0
Sn-P	(9-1)	60	59	7	10	Al-P	(5-5)	Low	0	0	0
	(7-3)	60	60	4	10	Zr-P	(5-5)	25	21	0	0
	(6-4)	15	15	0	0	Zn-P	(6-4)	27	27	4	4
Fe		68	42	69	62	Bi-P	(7-3)	37	35	55	62
Fe-P	(9-1)	83	21	64	60		(5-5)	42	42	7	12
	(8-2)	68	65	33	32		(4-6)	Low	1	0	0
	(6-4)	62	55	3	0	Mg-P	(5-5)	20	10	0	0
	(5-5)	16	15	1	0						
	(4-6)	Low	4	0	0						
$Fe_4(P_2O_7)_3$		45	43	1	0						

a) Conditions: temperature=320 °C; amount of catalyst used=20 g; contact time=10 to 15 s; AcH/HCHO/MeOH/water/nitrogen feed rates=13/26/5.6/71/350 mmol h^{-1}. b) AcH=acetaldehyde; Acryl=acrylaldehyde; MeOH=methanol.

(1) The combination of phosphorus with an acidic oxide, such as MoO_3 or WO_3, decreases the activity markedly.

(2) The V-P oxide consisting of divanadium(IV) dioxide pyrophosphate [$V_2O_2(P_2O_7)$] exhibits a relatively good performance in both activity and selectivity.

(3) The combination of phosphorus with a certain

amphoteric oxide, such as TiO_2, SnO_2, Fe_2O_3, NiO, Co_3O_4, MnO_2, Cr_2O_3, or CuO, induces a large increase in the selectivity to acrylaldehyde, though the activity decreases gradually as the content of phosphorus increases. Therefore, there exists an optimum value in the amount of phosphorus.

(4) The combination of phosphorus with an oxide without oxidizing function, such as B_2O_3, Al_2O_3, ZrO_2, ZnO, Bi_2O_3, or MgO, is less effective.

(5) The best performances are obtained with the Ni-P, Co-P, Mn-P, Fe-P, and V-P oxide systems.

To get more detailed information about the catalytic functions, the effect of contact time on the AcH conversion and yields was examined for several phosphate catalysts which had showed a good performance. The results are listed in Table 3. The results may be summarized as follows.

(1) The best performance in the yield of acrylaldehyde is obtained with the Ni-P oxide with a P/Ni atomic ratio of 0.9/1.

(2) The next best catalyst is the Fe-P oxide with a P/Fe atomic ratio of 0.75/1.

(3) The combination of TiO_2 with the V-P oxide, which improves the performance for the reaction of HCHO with acetic acid,[4] increases the activity markedly, but the maximum yield of acrylaldehyde decreases from 79 to 63 mol%.

Table 3. Performances of Phosphate Catalysts[a] (2)

Catalyst (Atomic ratio)		wt/g	AcH conv. %	Yield/mol% Acryl[b]	CO_2	Methanol
V-P	(1-1.06)	2	17	16	0	0
		20	74	70	2	1
		40	87	79	3	4
V-Ti-P	(1-2-5.5)	2	46	45	0	0
		4	71	63	1	2
		6	78	63	2	4
		8	89	63	3	4
Fe-P	(1-0.75)	2	30	30	1	0
		16	86	80	9	13
Ni-P	(1-0.67)	2	42	41	3	4
		5	77	72	20	40
		20	94	48	33	50
	(1-0.9)	2	37	37	0	0
		15	91	86	1	8
		20	94	80	2	8
	(1-1)	20	79	66	1	0
		40	86	75	1	0
Co-P	(1-0.67)	2	42	41	3	0
		10	77	75	9	15
		20	92	68	21	30
	(1-0.75)	2	20	20	0	0
		12	75	65	2	0
		20	90	63	12	0
Mn-P	(1-0.67)	2	37	37	1	0
		5	53	52	6	8
		20	86	86	11	23

a) Conditions: temperature=320 °C; AcH/HCHO/methanol/water/nitrogen feed rates=13/26/5.6/71/350 mmol h^{-1}. b) Acryl=acrylaldehyde.

The Mo-P and W-P oxides consisting of heteropoly compounds, such as $H_3PMo_{12}O_{40}$ and $H_3PW_{12}O_{40}$, which possess strongly acidic sites, are not active as catalysts for this reaction, which suggests that the reaction is not promoted solely by acidic sites. V_2O_5, amphoteric oxides, and oxides of heavy metals, which are considered to be more basic than MoO_3 and WO_3 because of the lower electronegativity of metal ions, show a higher catalytic activity. Further, the activity of these oxides falls with the incorporation of phosphorus. These findings suggest that the reaction is catalyzed by basic sites. However, the sites required to promote the acrylaldehyde formation seem to consist of very weakly basic sites, present in metal tungstates, molybdates, and phosphates, but not of strongly basic sites, which is in conformity with the results obtained in the preceding study.[1]

The formation of acrylaldehyde is accompanied by the following side-reactions, as has been pointed out in the preceding work:[1] (i) formation of CO_2 and methanol from HCHO via methyl formate, which is promoted mainly by basic sites, and (ii) polymerization of acrylaldehyde to unidentified polymers, which is promoted by strongly acidic sites.

The activity and selectivity may, therefore, be governed by the balance of acidic and basic properties. When the basic property is too strong, the formation of CO_2 and methanol is promoted. On the other hand, when the basic property is suppressed too much by the incorporation of an acidic oxide, the catalyst loses the activity.

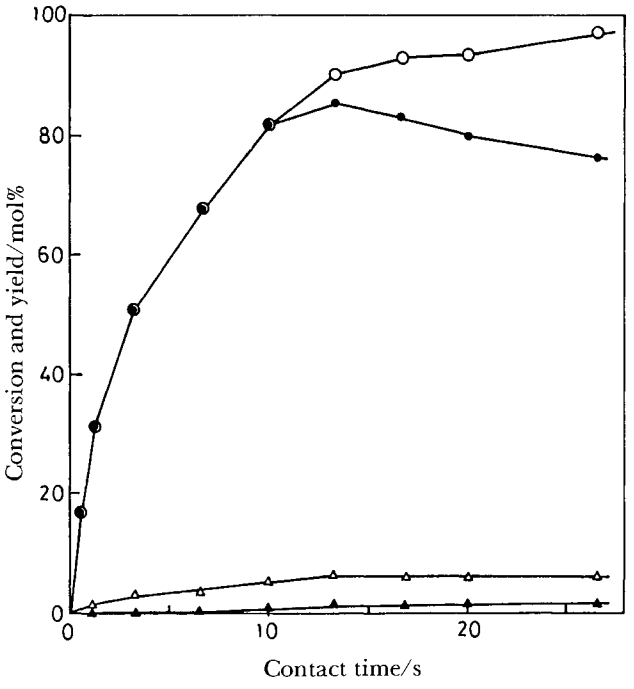

Fig. 1. Performance of the catalyst with an Ni:P atomic ratio=1:0.9. ○ AcH conversion; ● acrylaldehyde; ▲ CO_2; △ methanol.

The control of the acid-base property of catalysts is performed by the combination of an acidic oxide with a more basic oxide. It is, therefore, considered that the acid-base properties of the Ni-P, Mn-P, Co-P, Fe-P, and V-P oxide systems are best fit for promoting solely the formation of acrylaldehyde.

Performance of the Ni-P=1-0.9 Catalyst. The study in the preceding section has revealed that the best results for the formation of acrylaldehyde are obtained with the nickel phosphate with a P/Ni atomic ratio of 0.9/1. Thus, the characteristics of this catalyst were studied.

Product Distribution. The conversion of AcH and the yields of acrylaldehyde, CO_2, and methanol obtained at 280 °C are plotted in Fig. 1 as a function of contact time. The selectivity to acrylaldehyde is almost 100 mol% up to the AcH conversion of 80%, but it falls gradually with a further increase in the conversion. The results indicate that the acrylaldehyde formed initially is converted to polymers. The maximum yield of acrylaldehyde is about 85 mol%. This value is lower than those obtained with silica-supported basic oxides (96 mol%).[1] However, the formation of CO_2 and methanol is clearly slower than that obtained with the silica-supported basic oxides.[1] Possibly, the Ni-P oxide catalyst possesses strongly acidic sites, while the silica-supported basic oxides possess strongly basic sites.

Effect of Temperature. The yield of acrylaldehyde obtained with 2 g portions of catalyst (contact time 1.3 s) are plotted in Fig. 2 as a function of temperature. It was found that the effect of temperature on the rate is very small. The apparent activation energy was calculated to be about 3.5 kcal mol^{-1}. This value is clearly lower than that observed with the Si-Mg catalyst (15 kcal mol^{-1}),[1] which suggests that the active sites of the Ni-P catalyst are different from those of the Si-Mg catalyst. Possibly, the rate determining step is different; for example, it is the protonation of HCHO by acidic sites, $HCHO+H^+ \longrightarrow H_2C^+OH+H_2O$, over the Si-Mg catalyst, whereas over the Ni-P catalyst it is the proton abstraction from AcH by basic sites, $CH_3CHO+OH^- \longrightarrow {}^-CH_2CHO+H_2O$.

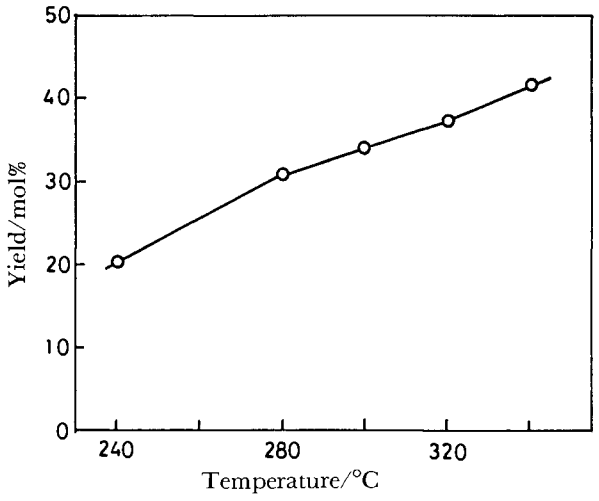

Fig. 2. Effect of temperature on the yield of acrylaldehyde. Contact time=1.3 s.

The effect of temperature on the selectivity to acrylaldehyde was studied. The results obtained at the AcH conversion of around 90% are shown in Table 4. It was found that the selectivity is scarcely affected by temperature up to 320 °C. It is, therefore, concluded that the optimum temperature is 320 °C.

Effect of Feed Rate. The effects of the AcH concentration and AcH-HCHO feed rate on reaction rate were studied at 280 °C. The results were similar to those obtained with the Si-Mg catalyst in the preceding study;[1] the rate increases steadily with the increase in either the AcH concentration or AcH-HCHO feed rate (the HCHO/AcH molar ratio was fixed at 2).

Table 5 shows the effect of the HCHO/AcH molar

Table 4. Effect of Temperature on Acrylaldehyde Formation

Temp.	Contact time	Conversion of AcH	Yield of acryl[a]	Selectivity to acryl[a]
°C	s	%	mol%	mol%
250	27	89	79	88
280	13	91	85	93
300	13	94	85	90
320	10	91	86	94
360	6	84	81	96
	10	92	71	77

a) Acryl=acrylaldehyde.

Table 5. Effect of HCHO/AcH Molar Ratio on Acrylaldehyde Formation[a]

HCHO/AcH Molar ratio	Contact time	Conversion of AcH	Yield of acryl[b]	Selectivity to acryl[b]
	s	%	mol%	mol%
1.5	20	90	85	94
2.0	13	91	85	93
4.0	5	92	90	98

a) Temperature=280 °C. b) Acryl=acrylaldehyde.

Table 6. Effect of AcH-HCHO Feed Rate on Acrylaldehyde Formation[a]

HCHO/AcH Feed rate[a]	Contact time	Conversion of AcH	Yield of acryl[b]	Selectivity to acryl[b]
mmol/h	s	%	mol%	mol%
17/8.5	10	88	85	97
26/13	13	91	85	93
52/26	27	75	73	98
52/26*	27	90	86	95
104/52**	27	89	73	82

a) Temperature=280 °C; *320 °C; **360 °C. b) Acryl=acrylaldehyde.

ratio on the selectivity to acrylaldehyde. It was found that the selectivity is scarcely affected by the change in the HCHO/AcH molar ratio, though the rate decreases as the HCHO/AcH ratio decreases. This is understood from the finding that the Ni-P catalyst is inactive for the formation of CO_2 and methanol, which proceeds in parallel with the formation of acrylaldehyde.

The effect of the AcH-HCHO feed rate on the selectivity to acrylaldehyde was studied with the HCHO/AcH molar ratio fixed at 2. As is seen in Table 6, the effect of the feed rate on the selectivity is small. This is also understood from the finding that the catalyst is inactive for the side-reaction.

References

1) M. Ai, *Bull. Chem. Soc. Jpn.*, **64**, 1342 (1991).
2) M. Ai, *J. Catal.*, **107**, 201 (1987).
3) M. Ai, *Appl. Catal.*, **36**, 221 (1988).
4) M. Ai, *Appl. Catal.*, **48**, 51 (1989).
5) M. Ai, *Bull. Chem. Soc. Jpn.*, **63**, 1217 (1990).

Mixed-Ligand Palladium(II) and Platinum(II) Complexes—Photosensitizers of $^1O_2$ Production and Chemical Quenchers of $^1O_2$

Shobha S. KAMATH, Santwana SHUKLA, and Tapeshwari S. SRIVASTAVA*
Department of Chemistry, Indian Institute of Technology, Powai, Bombay 400076, India
(Received July 9, 1990)

[M(nn)(dhn)] (where M is Pd(II) or Pt(II), nn is 2,2′-bipyridine, 1,10-phenanthroline, 2,2′-biquinoline, or 4,7-diphenyl-1,10-phenanthroline, and dhn is dianion of 2,3-naphthalenediol) photooxidizes the 2,2,6,6-tetramethyl-4-piperidinol in *N,N*-dimethylformamide via $^1O_2$ when irradiated with light of wave-lengths of 420 to 800 nm in presence of molecular oxygen. The presence of $^1O_2$ as an intermediate is confirmed by quenching studies using bis(dibutyldithiocarbamato)nickel(II) and 20% water in DMF. The relative efficiency of $^1O_2$ production sensitized by the above complexes depends on nature of metal, ligand, and geometry of the complexes. However, [Pd(bpy)(dmt)] and [Pd(phen)(dmt)] undergo photooxidation via $^1O_2$ when sensitized by hematoporphyrin IX and its metal derivatives on photolysis under similar conditions. The relative efficiency of $^1O_2$ production depends on the nature of metal in porphyrin.

Photolysis of chloroform solution of [Pt(bpy)(dmt)] (where bpy is 2,2′-bipyridine and dmt is dianion of 3,4-toluenedithiol) at 577 nm in ligand-to-ligand charge-transfer (LLCT) transition region results in an electron transfer from the complex to chloroform. A ligand-centered radical (probably the easily oxidized dmt) $[Pt(bpy)(dmt)]^+$ decomposes into unidentified products.[1] Photolysis of [Ni(phen)(dmde)] (where phen is 1,10-phenanthroline and dmde is dianion of cis-1,2-diphenylethylene-1,2-dithiol) in $CHCl_3$ in LLCT transition region has also promoted analogous photooxidation.[2] Similar mixed-ligand complexes of palladium(II) and platinum(II) complexes of formula [M(nn)(xx)] (where M is Pd(II) or Pt(II), nn is 2,2′-bipyridine or 1,10-phenanthroline, and xx is dianion of catechol, 4-*t*-butylcatechol, 3,4-dimercaptotoluene or thiosalicylic acid (tsa)) in *N,N*-dimethylformamide (DMF) have been used to photosensitize the singlet molecular oxygen ($^1O_2$) production when irradiated in their LLCT transition region between 400 and 700 nm in presence of molecular oxygen.[3,4] However, [Pt(nn)(dmt)] and [Pt(nn)(tsa)] undergo self-sensitized photooxidation via $^1O_2$,[4-6] and [Ni(nn)(dmt)] as physical quenchers of $^1O_2$.[7] In this paper we report the photo-sensitizing ability of [M(nn)(dhn)] (where nn is 2,2′-bipyridine, 1,10-phenanthroline, 2,2′-biquinoline (biq), or 4,7-diphenyl-1,10-phenanthroline (dpp) and dhn is dianion of 2,3-naphthalenediol) in DMF to produce $^1O_2$, and the chemical quenching of $^1O_2$ by [Pd(bpy)(dmt)] and [Pd(phen)(dmt)] using hematoporphyrin IX and its metal derivatives as photosensitizers.

Experimental

Materials: [Pd(nn)(dmt)] and [M(nn)(dhn)] were prepared and characterized as described elsewhere.[4,8] Bis(dibutyldithiocarbamato)nickel(II), [Ni(dbdc)$_2$], was prepared by the reported procedure.[9] Nickel(II), palladium(II), and platinum(II) complexes of hematoporphyrin IX were prepared and purified by the literature methods.[10,11] Chemicals used were of reagent grade and purified before use. The reagent grade solvents were purified before use by the standard procedures.[12]

Physical Measurements: Phosphorescence measurements were made with a SPEX 1934C phosphorimeter with RCA C13034 photomultiplier attachment having facility to give corrected emission spectra. Metal complexes dissolved in ethanol (1×10^{-6} M, 1M=1 mol dm^{-3}) were frozen in liquid nitrogen (77 K) in a 10 mm quartz cuvette and the spectra of the frozen solutions were recorded using different wavelengths of excitation. Other physical methods used were described elsewhere.[3,8]

General Irradiation Procedures: The irradiation of molecular oxygen saturated DMF solutions of metal complexes were carried out in a triple jacket merry-go-round apparatus as described earlier,[3] except 250 W tungsten halogen lamp was used in place of 150 W.

The photochemical measurements were also carried out by following modified method of Diamond and coworkers[13] as described elsewhere.[6]

Results and Discussion

Phosphorescence Spectra of [M(bpy)(dhn)]. The phosphorescence spectra of [M(bpy](dhn)] (where M is Pd(II) or Pt(II)) in ethanol glass at 77 K on excitations at their different absorption maxima show a broad band at about 600 nm. [Pd(bpy)(dhn)] on excitation at 457, 337, and 297 nm gives a phosphorescence band at 607 nm. [Pt(bpy)(dhn)] exhibits a band at 601 nm on excitation at 478, 338, and 296 nm as shown in Fig. 1. The phosphorescence band at about 600 nm in the above complexes is due to the longest wavelength LLCT transition as reported earlier for [Pt(bpy)(dmt)].[1] These data suggest that the triplet state of LLCT transition is expected to be involved in the following photooxidation reactions.

Photooxidation of 2,2,6,6-Tetramethyl-4-piperidinol (XH) and Its Quenching Studies: Molecular oxygen saturated DMF solution of [M(nn)(dhn)] (200 μM) in presence of XH (10 mM) was irradiated with light of wavelengths from 420 to 800 nm for different irradi-

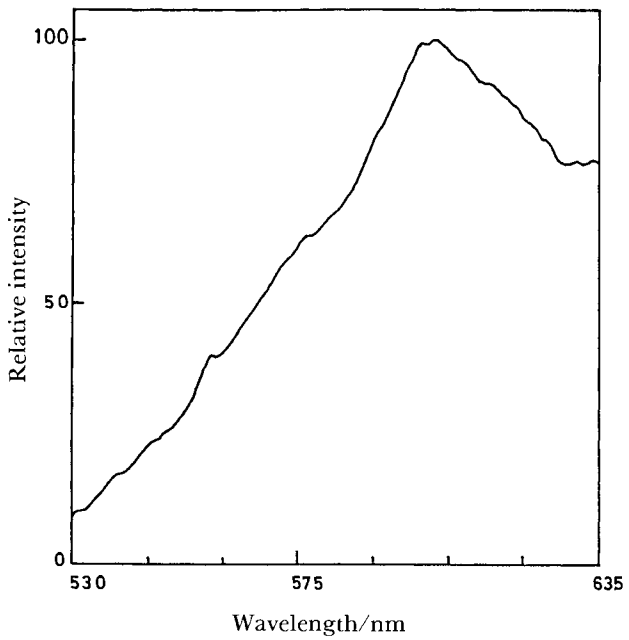

Fig. 1. A phosphorescence spectrum of [Pt(bpy)-(dhn)] in ethanol glass at 77 K.

ation times in a merry-go-round apparatus. The $^1O_2$ molecules formed combine with XH molecules to produce 4-hydroxy-2,2,6,6-tetramethylpiperidinyloxy free radicals (XO) which is measured by EPR method.[3] There is a linear relationship between the amount of XO free radicals formed and the irradiation times for different [M(nn)(dhn)] as shown in Fig. 2. It is supposed that [Pd(dpp)(dhn)] yields the maximum amount of $^1O_2$ as it has the highest slope, whereas [Pd(biq)(dhn)] yields the lowest amount of $^1O_2$ as it exhibits the smallest slope. The relative yields of $^1O_2$ production referred to [Pd(dpp)(dhn)] are given in Table 1. The values of relative efficiency calculated after correcting for the amounts of light absorbed using relative integrated areas under the absorption curves. After correcting the wavelength distribution of the lamp, they are given in Table 1. The relative efficiencies follow the order: [Pd(dpp](dhn)]>[Pt(dpp)(dhn)]>[Pt(bpy)(dhn)]>[Pt(phen)(dhn)]>[Pt(biq)(dhn)]>[Pd(biq)(dhn)]≈[Pd(bpy)(dhn)]≈[Pd(phen)(dhn)].

The formation of nitroxide free radicals was not observed when the solution of [M(nn)(dhn)] or 2,2,6,6-tetramethyl-4-piperidinol was kept in dark or irradiation in presence of molecular nitrogen. There was also no change in the position and intensity of absorption bands between 420 and 800 nm of [M(nn)(dhn)] in molecular oxygen saturated DMF after irradiations for two hours. The photooxidation of XH sensitized by [M(nn)(dhn)] was studied in 20% water-DMF. In these experiments the molecular oxygen saturated solutions of [Pd(dpp)(dhn)] (200 μM) in presence of XH (10 mM) in 20% water-DMF and in 100% DMF respectively were irradiated with light of wavelengths from 420 to 800 nm for different irradiation times. The plots of amount of XO free radicals against irradiation time are given in Fig. 3. The slope decreases in 20% water-DMF. The shortening of lifetime (τ) of $^1O_2$ can be affected by using mixed solvents such as 20% water in DMF (τ of $^1O_2$ in pure water is 2 μs and τ of $^1O_2$ in pure DMF is 7.1 μs).[14] There is an appreciable decrease in slope in 20% water in DMF than in pure DMF as shown in Fig. 3.

The quenching of photooxidation of 2,2,6,6-tetramethyl-4-piperidinol sensitized by [M(nn)(dhn)] was studied using bis(dibutyldithiocarbamato)nickel-(II) as physical quenchers of $^1O_2$. In these quenching experiments the molecular oxygen saturated solutions containing [Pt(phen)(dhn)] (5×10^{-5} M), bis(dibutyldithiocarbamato)nickel(II) (10^{-5} M or 10^{-6} M) and five different concentrations of XH (varying from 1×10^{-2} to 2×10^{-3} M) were irradiated using light of wavelengths from 420 to 800 nm for 1 h. The amount of XO free radicals produced was measured by EPR method.[3] The 1/[XO] was plotted against 1/[XH] for two concentrations of the nickel(II) complex. Two linear plots with their intercepts meeting at a

Table 1. Relative Yields and Efficiencies of [M(nn)(dhn)] for Sensitizing the Generation of $^1O_2$[a]

Complex	Relative yield of $^1O_2$ production referred to [Pd(dpp)(dhn)]	Relative efficiency of $^1O_2$ production referred to [Pd(dpp)(dhn)]
[Pd(dpp)(dhn)]	1.00	1.00
[Pt(dpp)(dhn)]	0.27	0.63
[Pt(bpy)(dhn)]	0.22	0.15
[Pt(phen)(dhn)]	0.30	0.13
[Pt(biq)(dhn)]	0.12	0.07
[Pd(biq)(dhn)]	0.04	0.05
[Pd(bpy)(dhn)]	0.05	0.04
[Pd(phen)(dhn)]	0.08	0.02

a) Relative integrated areas under absorption curves between 420 and 800 nm of [Pd(dpp)(dhn)], [Pt(dpp)(dhn)], [Pt(bpy)(dhn)], [Pt(phen)(dhn)], [Pt(biq)(dhn)], [Pd(biq)(dhn)], [Pd(bpy)(dhn)], and [Pd(phen)(dhn)] for 5×10^{-5} M are in the ratio 1.00 : 0.43 : 1.49 : 2.39 : 1.71 : 0.89 : 1.11 : 3.50, respectively.

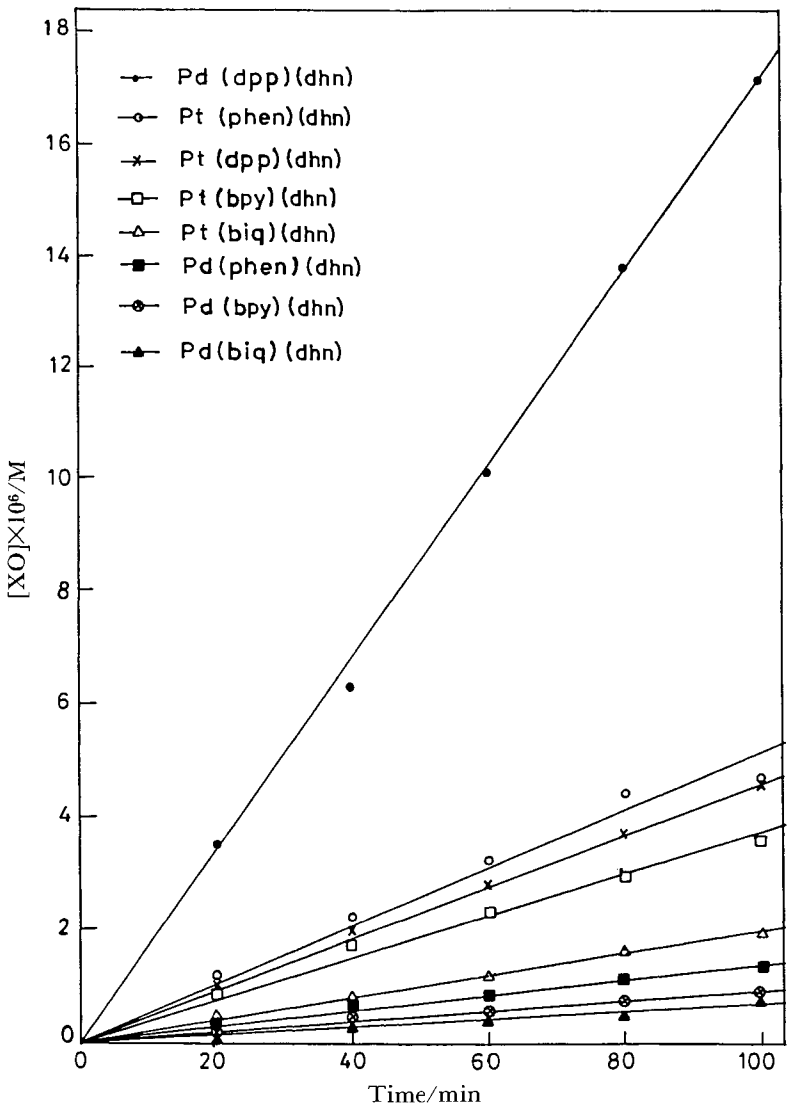

Fig. 2. Plots of XO free radical concentration versus irradiation time of solutions of [M(nn)(dhn)] (2×10^{-4} M) in presence of 2,2,6,6-tetramethyl-4-piperidinol (1×10^{-2} M) in DMF.

same point on the y-axis were obtained and they are given in Fig. 4. The relative amount of light absorbed by the nickel(II) complex in the wavelength range of 420 to 800 nm, at 10^{-5} or 10^{-6} M, is less than 0.1% as compared to [Pt(phen)(dhn)] and, therefore, there is no competition for light absorption between the sensitizer and the quencher.

The above results suggest that the photooxidation of 2,2,6,6-tetramethyl-4-piperidinol sensitized by [M(nn)(dhn)] involves the $^1O_2$ as an intermediate and the triplet state of LLCT transition in [M(nn)(dhn)] is responsible for the production of the $^1O_2$ by energy transfer.[3] The following Scheme 1 suggests the mechanism for the above reaction.[3] (S is one of the [M(nn)(dhn)] as photosensitizer, ^1S and ^3S are its first excited singlet and triplet states respectively, $h\nu$ is the energy of a photon, ISC is the inter system crossing, ET is the energy transfer, k_d is the rate constant of

$$S \xrightarrow{h\nu} {}^1S \quad \text{(i)}$$

$$^1S \xrightarrow{ISC} {}^3S \quad \text{(ii)}$$

$$^3S + {}^3O_2 \xrightarrow{ET} {}^1S + {}^1O_2 \quad \text{(iii)}$$

$$^1O_2 \xrightarrow{k_d} {}^3O_2 \quad \text{(iv)}$$

$$^1O_2 + XH \xrightarrow{k_r} XO \quad \text{(v)}$$

$$^1O_2 + Q \xrightarrow{k_q} {}^3O_2 + Q \quad \text{(vi)}$$

Scheme 1.

quenching of $^1O_2$ by DMF molecules, k_r is the rate constant of chemical quenching of $^1O_2$ by XH to produce XO, and k_q is the physical quenching of $^1O_2$ by the bis(dibutyldithiocarbamate)nickel(II) (Q).

On the assumption of above mechanism (see Scheme

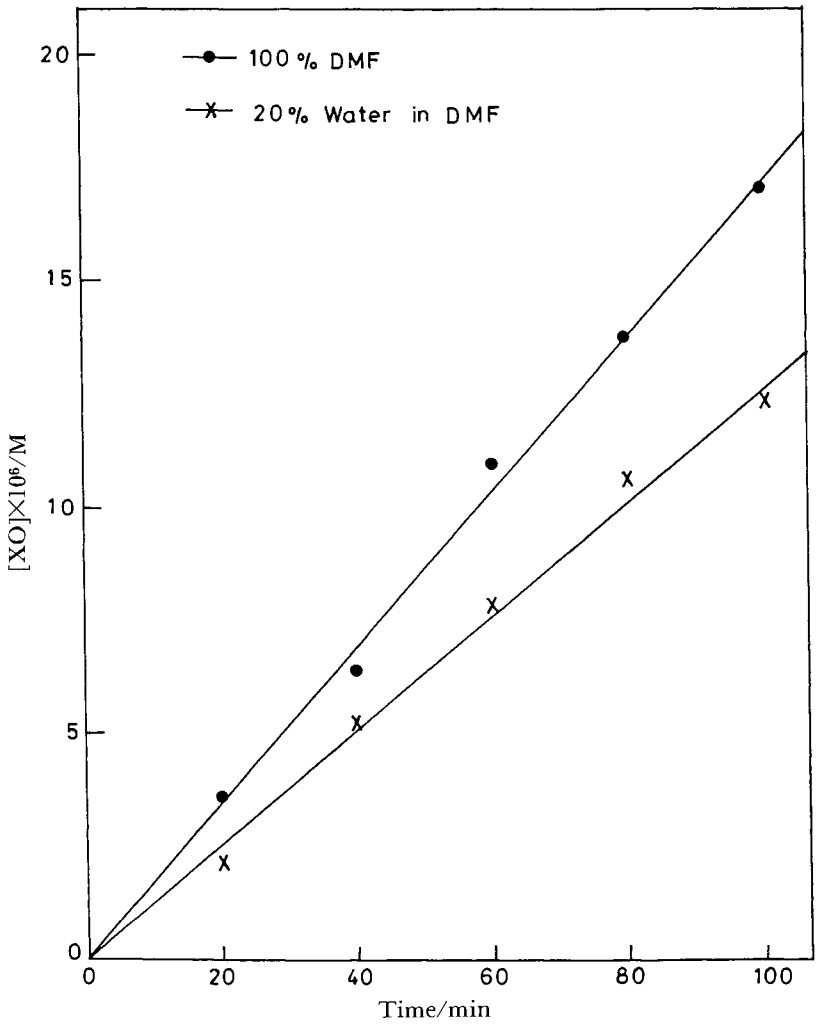

Fig. 3. Plots of XO free radical concentration versus irradiation time of [Pd(dpp)(dhn)] (2×10^{-4} M) and 2,2,6,6-tetramethyl-4-piperidinol (1×10^{-2} M) in DMF and 20% H_2O in DMF.

1) the rate of formation of XO free radicals by oxidation of XH with $^1O_2$ using steady state approximation, can be given by Eq. 1.[3] (I_{abs} is the intensity of

$$\frac{d[XO]}{dt} = I_{abs}\,\phi_{^1O_2}\frac{k_r[XH]}{k_r[XH]+k_d}, \qquad (1)$$

irradiation and $\phi_{^1O_2}$ is the quantum yield of $^1O_2$ production). If I_{abs} is not constant for [M(nn)(dhn)] and k_d, k_r, and [XH] are kept constant, the slope of the plot of the amount of nitroxide radicals produced versus irradiation time is related to $I_{abs}\phi_{^1O_2}$ (called yield of $^1O_2$ production). The slopes of linear plots of amount of nitroxide radicals produced versus irradiation time for [M(nn)(dhn)] are shown in Fig. 2. The relative yields of $^1O_2$ production for [M(nn)(dhn)] referred to [Pd(dpp)(dhn)] were obtained from the slopes of Fig. 2 and they are given in Table 1.

On correcting for the relative amounts of light absorbed by [M(nn)(dhn)] using Eq. 2, the relative

$$\frac{(\phi_{^1O_2})_2}{(\phi_{^1O_2})_1} = \frac{(\text{slope})_2}{(\text{slope})_1}\times\frac{(I_{abs})_1}{(I_{abs})_2}, \qquad (2)$$

efficiencies of $^1O_2$ production for [M(nn)(dhn)] referred to [Pd(dpp)(dhn)] were obtained. These values are also given in the last column of Table 1 and the order follows as given above. The efficiency order seems to depend on nature of metal ion, nature of α-diimine ligand, and the energy of ligand-field A_2 state with respect to the lowest triplet state (π,π^*).[3,15]

If the last step in parentheses of the above mechanism is included, Eq. 3 is obtained as

$$\frac{1}{[XO]} = \frac{1}{[^1O_2]} + \frac{k_q[Q]+k_d}{k_r}\times\frac{1}{[^1O_2]}\times\frac{1}{[XO]}. \qquad (3)$$

On plotting 1/[XO] against 1/[XH] (see Fig. 4) a linear plot is obtained with the slope=$1/[^1O_2]\times(k_q[Q]+k_d)/k_r$ and the intercept=$1/[^1O_2]$. Knowing k_d (1.4×10^5 s^{-1} in DMF),[14] k_r (2.45×10^7 $M^{-1}s^{-1}$)[3,16] and concentrations of Q (1×10^{-5} M or 1×10^{-6} M), slope and inter-

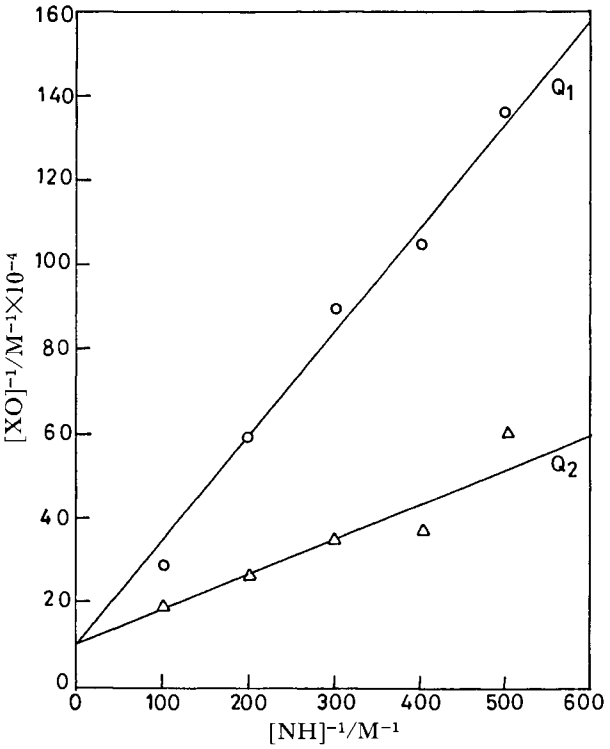

Fig. 4. Plots of reciprocal of XO free radical concentration versus reciprocal of 2,2,6,6-tetramethyl-4-piperidinol in presence of bis(dibutyldithiocarbamato)nickel(II) (10^{-5} M (Q_1) and 10^{-6} M (Q_2)) using [Pt(phen)(dhn)] (5×10^{-5} M) as a photosensitizer.

cept (from above mentioned plot), the k_q can be obtained. The k_q values obtained for bis(dibutyldithiocarbamato)nickel(II) ([Ni(dbdc)$_2$]) at concentrations of 1.0×10^{-5} and 1×10^{-6} M are 4.6×10^{10} and 6.3×10^{10} $M^{-1}s^{-1}$, respectively. Thus, the average value of k_q is 5.5×10^5 $M^{-1}s^{-1}$, which is higher than the reported value.[14] For the two plots as given in Fig. 4, the intercepts meet at a point on the y-axis for 1×10^{-5} M and 1×10^{-6} M [Ni(dbdc)$_2$]. However, the slope increases with increase in concentrations of [Ni(dbdc)$_2$]. This suggests that the physical quenching of $^1O_2$ by the [Ni(dbdc)$_2$] is involved and it rules out any quenching of excited sensitizer [Pt(phen)(dhn)].[14]

Photooxidation of [Pd(nn)(dmt)] Sensitized by Hematoporphyrin IX and Its Metal Derivatives: A solution of [Pd(bpy)(dmt)] or [Pd(phen)(dmt)] (5×10^{-4} M) and porphyrin (5×10^{-5} M) in DMF was bubbled with DMF saturated molecular oxygen for 15 min. This solution was taken in a stoppered quartz cuvette of 1 cm path length and was then irradiated for different intervals of time by the light source directed first through the filter and then through an acrylic cylinder.[13] The course of the photolysis of [Pd(bpy)(dmt)] or [Pd(phen)(dmt)] (5×10^{-4} M) sensitized by a free porphyrin or a metal porphyrin (5×10^{-5} M), after irradiating with light of wavelengths between 455 and 800 at different irradiation time (0 to 10 min), was followed by the difference absorption spectroscopy using same concentration of free porphyrin or metal porphyrin (5×10^{-5} M) in a reference cuvette in the visible region using a Shimadzu UV-260 spectrophotometer. The absorbance (A) of the [Pd(bpy)(dmt)] or [Pd(phen)(dmt)] at different time of photolysis was calculated by substracting the reduction of absorbance at 498 or 500 nm obtained by difference absorption spectroscopy from the initial absorbance of the [Pd(bpy)(dmt)] or [Pd(phen)(dmt)] (5×10^{-4} M). The reduction of absorbance of the palladium(II) complex (5×10^{-4} M) due to photolysis for 10 min irradiation was less than 1% of total absorbance of a free porphyrin or a metal porphyrin (5×10^{-5} M).

The plots of logarithm A of [Pd(bpy)(dmt)] at 498 nm versus different irradiation time of 0 to 10 min for free hematoporphyrin IX and its metal derivatives are shown in Fig. 5. These linear plots have different slopes and the ratio of these slopes is related to relative yields of $^1O_2$ production for different metal hematoporphyrin IX as compared to free hematoporphyrin IX (with its normalized value taken as 1) and these ratios are given in Table 2.

The relative efficiencies of $^1O_2$ production by the

Table 2. Relative Yields and Efficiencies of Hematoporphyrin IX and Its Metal Derivatives to Sensitize the Generation of $^1O_2$

Porphyrin	[Pd(bpy)(dmt)] as chemical quencher		[Pd(phen)(dmt)] as chemical quencher		2,2,6,6-Tetramethytl-4-piperidiol as chemical quencher	
	Relative yield of $^1O_2$ production referred to H_2HP	Relative efficiencies of $^1O_2$ production referred to H_2HP[a)]	Relative yield of $^1O_2$ production referred to H_2HP	Relative efficiencies of $^1O_2$ production referred to H_2HP[a)]	Relative yield of $^1O_2$ production referred to H_2HP	Relative efficiencies of $^1O_2$ production referred to H_2HP[a)]
H_2HP	1.00	1.00	1.00	1.00	1.00	1.00
PdHP	0.76	0.63	0.72	0.60	0.78	0.65
PtHP	0.48	0.40	0.50	0.42	0.51	0.43
NiHP	0.03	0.03	0.03	0.03	0.03	0.03

a) Relative integrated areas under absorption curves between 420 and 800 nm of hematoporphyrin IX (H_2HP), PdHP, PtHP, NiHP for 1×10^{-5} M after correcting for amounts of light absorbed are in ratio of 1.0 : 1.2 : 1.2 : 1.1, respectively.

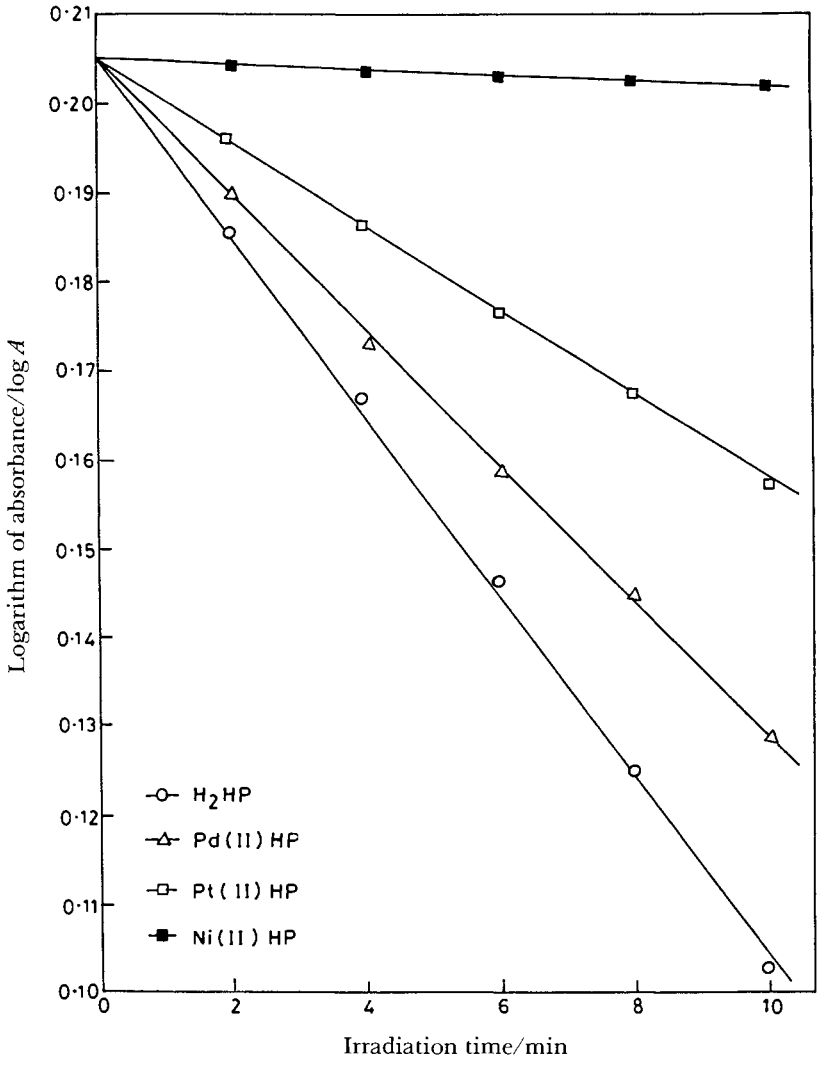

Fig. 5. Plots of log A versus irradiation time (A is absorbance at 498 nm of [Pd(bpy)(dmt)] (5×10^{-4} M) in DMF containing porphyrins (5×10^{-4} M)).

different metal hematoporphyrin IX referred to free hematoporphyrin IX after making corrections for the relative amounts of light absorbed by them have been compared and the values are also given in Table 2. The relative yields or the relative efficiencies of $^1O_2$ production by above porphyrins using [Pd(bpy)(dmt)] as a chemical quencher (see Table 2) follow the order: $H_2HP>PdHP>PtHP\gg NiHP$. Similar plots were obtained using [Pd(phen)(dmt)] as a chemical quencher. In this case the relative yields or relative efficiencies of $^1O_2$ production by porphyrins (see Table 2) follow the same order: $H_2HP>PdHP>PtHP\gg NiHP$.

Hematoporphyrin IX and its metal derivatives are good photosensitizers of $^1O_2$ production[17] and this $^1O_2$ oxidizes the chemical quenchers [Pd(bpy)(dmt)] and [Pd(phen)(dmt)].[18] The mechanism suggested earlier to explain the photooxidation of [Pd(bpy)(dmt)] and [Pd(phen)(dmt)] sensitized by hematoporphyrin IX is also acceptable when Ni(II), Pd(II), and Pt(II) hematoporphyrin IX complexes were used as photosensitizers in place of hematoporphyrin IX in the above photooxidation reactions. The steps involved in these photooxidation reactions are same as given for Scheme 1 (see above) except that S is one of the porphyrins acting as sensitizer, and XH and Q are replaced by Q′ (where Q′ is [Pd(bpy)(dmt)] or [Pd(phen)(dmt)] because the Q′ behaves both as chemical and physical quencher (see steps V and VI in Scheme 1). In the light of this mechanism the log[Q′] can be given by the following relationship.[18,19]

$$\log[Q'] = -kt + c \quad (\text{if } k_d \gg (k_q + k_r)[Q'], \tag{4}$$

and

$$k = I_{abs}\phi_{^1O_2}\frac{k_r}{k_d}, \tag{5}$$

where I_{abs} is the intensity of absorbed light, $\phi_{^1O_2}$ is the quantum yield of $^1O_2$ production, k_d is the rate constant of quenching of $^1O_2$ by DMF, k_q is the rate constant of physical quenching of $^1O_2$ by Q′, k_r is the rate constant of chemical quenching of $^1O_2$ by Q′, Q′ is quencher [Pd(bpy)(dmt)] or [Pd(phen)(dmt)], and t is irradiation time.

If the decay of Q′ is followed by visible spectroscopy, a plot of log[Q′] (or log$A$) against different irradiation time gives a straight line with the slope of k (see Eq. 4) as given in Fig. 5. If I_{abs} is not constant for different porphyrins and the k_d, k_r and the initial concentration of Q′ are kept constant in Eq. 5, the slope of log[Q′] versus irradiation time is related $I_{abs}\phi_{^1O_2}$ (yield of $^1O_2$ production). The relative yields of $^1O_2$ production for different metal hematoporphyrin IX relative to free hematoporphyrin IX were obtained from the slopes (see Fig. 5) and are given in Table 2. If the correction for the relative amounts of light absorbed by different porphyrins is made using Eq. 6, the relative efficiencies of $^1O_2$ production for

$$\frac{(\phi_{^1O_2})_2}{(\phi_{^1O_2})_1}=\frac{k_2\times(I_{abs})_1}{k_1\times(I_{abs})_2}, \quad (6)$$

different metal porphyrins referred to free porphyrin were obtained. The relative efficiencies of $^1O_2$ production follow the order: $H_2HP>PdHP>PtHP \gg NiHP$.

The irradiation of DMF solution of only [Pd(bpy)(dmt)] or [Pd(phen)(dmt)] (5×10^{-4} M) in presence of molecular oxygen or molecular nitrogen for more than 10 min shows no change in absorbance of [Pd(bpy)(dmt)] at 498 nm or [Pd(phen)(dmt)] at 500 nm. Similar irradiation of DMF solution of free hematoporphyrin IX (5×10^{-5} M) in presence of molecular oxygen or molecular nitrogen for more than 10 min shows also no change of absorbance of 498 or 500 nm.

The relative efficiencies of $^1O_2$ generation by the free base hematoporphyrin IX and its metal derivatives were further obtained by the EPR method using 2,2,6,6-tetramethyl-4-piperidinol as a chemical acceptor of $^1O_2$.[16] This method has advantage that 2,2,6,6-tetramethyl-4-piperidinol is a specific quencher of $^1O_2$, which does not react with superoxide ions, hydrogen peroxide and hydroxyl radicals.[16,20] In this method a solution of a free base porphyrin or a metal porphyrin (5×10^{-5} M) and 2,2,6,6-tetramethyl-4-piperidinol (2.5×10^{-3} M) was irradiated on the merry-go-round apparatus[3] for different irradiation time. The photoproduction of $^1O_2$ was measured by recording the EPR spectra of the nitroxide free radicals

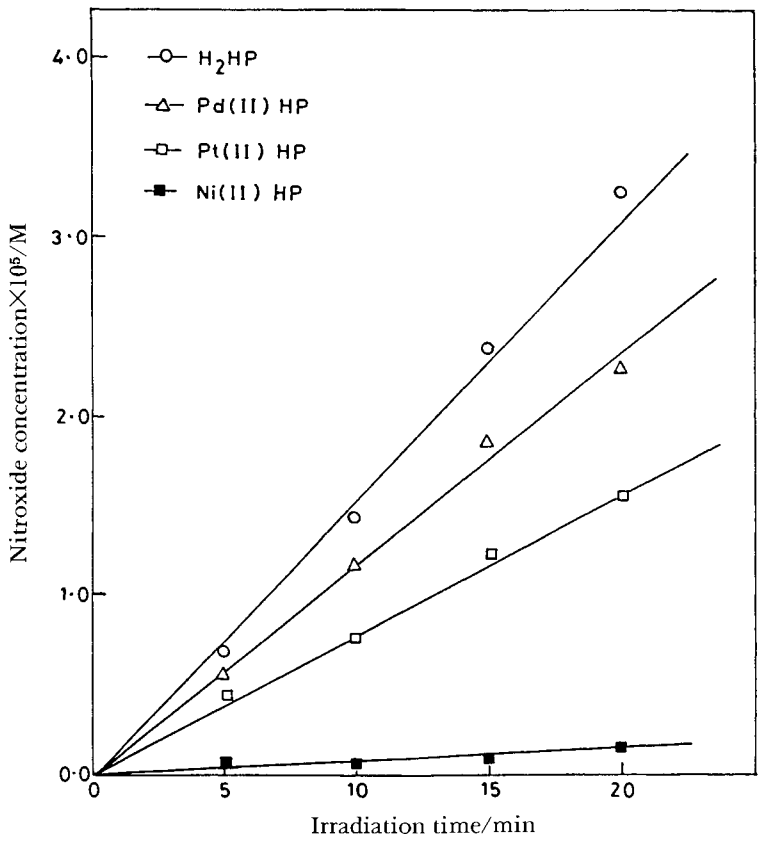

Fig. 6. Plots of XO free radical concentration versus irradiation time of DMF solution of 2,2,6,6-tetramethyl-4-piperidinol (2.5×10^{-3} M) and porphyrins (5×10^{-5} M).

generated by the reaction of 2,2,6,6-tetramethyl-1,4-piperidinol with $^1O_2$.[3,21] The linear plots of amount of nitroxide radicals produced for a free base hematoporphyrin IX and its metal derivatives versus irradiation time are given in Fig. 6. Hematoporphyrin IX gives the largest slope and the NiHP gives the smallest slope. The relative yields and relative efficiencies of $^1O_2$ production for different metal hematoporphyrin IX, as compared to free hematoporphyrin IX are given in Table 2.

The relative yields or relative efficiencies of $^1O_2$ production by the porphyrins follow the order: $H_2HP>PdHP>PtHP\gg NiHP$. This order is same as obtained above using [Pd(bpy)(dmt)] and [Pd(phen)(dmt)] as chemical quenchers.

The above results suggest that PdHP and PtHP are expected to have the energy of their $^3B_{1g}$ state arising from the d-d transition of d^8 configuration of metal ion in a square planar crystal field well above the first triplet state of porphyrin arising from π-π^* transition.[15] On the other hand NiHP shows virtually no photosensitizing ability to produce $^1O_2$ because its ligand-field $^3B_{1g}$ state has energy just lower than that of phosphorescent triplet state of porphyrin. The ligand-field $^3B_{1g}$ state provides the pathway of radiationless decay and thus reduces very considerably the transfer of energy from $^3O_2$ to produce $^1O_2$. The higher efficiency of PdHP as compared to PtHP may be due to longer lifetime of triplet state of former than later.[22]

Conclusion

The above study shows that the Pd(II) and Pt(II) complexes of α-diimine ligands with 3,4-naphthalenediol dianion can sensitize the photooxidation of 2,2,6,6-tetramethyl-4-piperidinol involving $^1O_2$ as intermediate. This intermediate is produced by energy transfer from triplet state of LLCT transition of the complexes to molecular oxygen. In addition [Pd(nn)(dmt)] as chemical quenchers of $^1O_2$ can be used in determining the relative efficiency of $^1O_2$ production sensitized by porphyrins.

We are grateful to DST and DAE (Govt. of India) for financial support and Dr. K. H. Puthraya for his help in earlier research.

References

1) A. Vogler and H. Kunkely, *J. Am. Chem. Soc.*, **103**, 1559 (1981).
2) A. Vogler and H. Kunkely, *Angew. Chem., Int. Ed. Engl.*, **20**, 386 (1981).
3) S. Shukla, S. S. Kamath, and T. S. Srivastava, *J. Photochem. Photobiol., A, Chem.*, **117**, 287 (1989).
4) K. H. Puthraya and T. S. Srivastava, *Polyhedron*, **4**, 1579 (1985).
5) K. H. Puthraya and T. S. Srivastava, *J. Indian Chem. Soc.*, **LXII**, 843 (1985).
6) S. Shukla, S. S. Kamath, and T. S. Srivastava, *J. Photochem. Photobiol., A, Chem.*, **50**, 199 (1989).
7) S. Shukla and T. S. Srivastava, *J. Photochem. Photobiol., A, Chem.*, **48**, 249 (1989).
8) S. S. Kamath, V. Uma, and T. S. Srivastava, *Inorg. Chim. Acta*, **166**, 91 (1989).
9) A. Zweig and W. A. Henderson, *J. Polym. Sci., Polym. Chem. Ed.*, **13**, 717 (1975).
10) J. P. Macquet and T. Theophanides, *Can. J. Chem.*, **51**, 219 (1973).
11) L. Edwards, D. H. Dolphin, M. Gouternan, and A. D. Adler, *J. Mol. Spectrosc.*, **38**, 16 (1971).
12) B. S. Furniss, A. J. Hannafort, V. Rogers, P. W. G. Smith, and A. B. Tuchel, "Vogel's Textbook of Practical Organic Chemistry," Longman, London (1978), pp. 264—279.
13) I. Diamond, S. G. Graneth, and A. F. McDonagh, *Biochem. Med.*, **17**, 121 (1977).
14) B. Ranby and J. F. Rebek, "Singlet Oxygen," Wiley, New York (1978), pp. 60—110.
15) D. Eastwood and M. Gouterman, *J. Mol. Spectrosc.*, **35**, 359 (1970).
16) Y. Lion, S. Gandin, and A. Van de Voorst, *Photochem. Photobiol.*, **31**, 305 (1980).
17) K. M. Smith, "Porphyrins and Metalloporphyrins," Elsevier, Amsterdam (1975), pp. 667—700.
18) T. S. Srivastava and S. Shukla, *Proc. Indian Acad. Sci., (Chem. Sci.)*, **102**, 329 (1990).
19) E. Gandin, Y. Lion, and A. Van de Voorst, *Photochem. Photobiol.*, **37**, 271 (1983).
20) A. Rigo, E. Argese, R. Stenanto, E. F. Orsega, and P. Viglino, *Inorg. Chim. Acta*, **24**, L71 (1977).
21) S. Cannistraro, A. Van de Voorst, and G. Jori, *Photochem. Photobiol.*, **28**, 257 (1978).
22) M. Gouterman, "Excited States of Matter," ed by C. W. Shoppee, Texas Tech. Univ., Lubbock, Texas (1973), Vol. 2, pp. 63—101.

Crystal Structure of 2′-*O*-Succinyladenosine 3′,5′-(Cyclic)phosphate Monohydrate: A Model Compound to Study Protein-Nucleic Acid Interactions

Natarajan PADMAJA, Suryanarayana Rao RAMAKUMAR,* and Mysore A. VISWAMITRA
Department of Physics and Jawaharlal Nehru Centre for Advanced Scientific Research, India Institute of Science, Bangalore 560012, India
(Received June 13, 1990)

The crystal and molecular structure of 2′-*O*-succinyladenosine 3′,5′-(cyclic)phosphate monohydrate has been determined by X-ray diffraction techniques. The compound crystallizes in the orthorhombic space group $P2_12_12_1$; Z=4 with a=5.633(1), b=15.853(2), c=20.607(3) Å. The final R value is 0.029. The adenine base is protonated at N(1). The base is in syn conformation (χ=−95.8°) with respect to the sugar, which has a C(3′)-*endo*-C(4′)-*exo* pucker ($_4T^3$). A six-membered ring formed by phosphate group and ribose shows chair conformation. The succinic acid moiety, which resembles side chains of certain amino acids, is found to have a bent skeleton. The cyclic AMP, which is known to play diverse roles in many metabolic processes, forms the nucleotide portion of the title compound. The succinic acid moiety that is covalently linked to this nucleotide in the present compound, shows direct and water mediated interactions with phosphate and base nitrogens of the nucleotide respectively. Such compounds can therefore serve as models to study the protein-nucleic acid interactions, which play a central role in many of the biological processes.

Adenosine cyclic 3′,5′-phosphate (cAMP) is known to play a central role in various hormonal metabolic control mechanisms.[1,2] It is also known to influence the activity of certain enzymes.[3,4] In light of these observed biological properties a few crystal structure studies of cyclic nucleotides and their analogues have been carried out in the past,[5] to understand the conformational flexibility and interactions of the cyclic nucleotide in the presence of different chemical groups. We report in this context, the crystal structure of 2′-*O*-succinyladenosine 3′,5′-(cyclic)phosphate monohydrate. It has the cyclic nucleotide covalently linked to a succinic acid moiety that resembles the side chains of amino acids like glutamic acid, aspartic acid etc. It is of interest to study the interactions between the nucleotide and the succinic acid moiety in the title compound, as a model for amino acid side chain-nucleic acid interactions, which are important in determining the structures and functions of protein-nucleic acid assemblies. Structural studies on similar model compounds have been reported in literature.[6-10]

Experimental Studies and Structure Determination

Needle-shaped crystals were grown from an aqueous solution of the title compound which was purchased from Sigma Chemicals. Intensity data were collected on a CAD-4 diffractometer with Ni-filtered Cu $K\alpha$(λ=1.5418 Å) radiation using a crystal of dimensions 0.04×0.06×0.64 mm. Cell parameters refined from 18 accurately measured reflections. The crystal data are given in Table 1.

Intensities were measured using ω-2θ scans. Three strong reflections monitored periodically showed that the crystal was stable to X-rays. Absorption correction[11] applied: transmission factors varied from 91.9 to 98.1%. Lorentz and polarization corrections were also applied. 1784 reflections were measured in the range $0<\theta<65°$, of which 1656 reflections were considered to be observed with $|F_o| \geqslant 3\sigma(F)$.

Table 1. Crystal Data

Formula	$C_{14}H_{16}N_5O_9P_1 \cdot H_2O$
F.W.	447.30
Crystal system	Orthorhombic
Space group	$P2_12_12_1$
a/Å	5.633(1)
b/Å	15.853(2)
c/Å	20.607(3)
V/Å^3	1840.2
Z	4
D_x/g cm^{-3}	1.55

The structure was solved by the direct methods using MULTAN11/82[12] and the calculations were performed with the Enraf-Nonius Structure Determination Package[13] on a PDP11-44 computer. An E-map computed with the best set of phases (CFOM=2.979) revealed the atoms of the six-membered ring formed by phosphate group and ribose sugar. A weighted Fourier synthesis at this stage gave rest of the structure. Of the 18 hydrogens, 17 were located from difference Fourier maps computed at various stages of full-matrix least-squares refinement on F's using SHELX 400[14] with the non-H atoms refined anisotropically and the H atoms refined isotropically. One of the water hydrogens which was not located from the difference maps, was fixed in the direction of the hydrogen bond initially, but was varied in the final stages of refinement. Final R=0.029, R_w=0.032; no. of parameters refined were 343. Individual weights $w \propto 1.0/[\sigma^2(F)+0.002\ F^2]$ were used. Maximum shift/error is 0.11; residual density in the final difference electron density map is within ±0.20 e Å^{-3}. The atomic scattering factors are as supplied in SHELX 76.

Results and Discussion

The conformation of the molecule along with atomic numbering scheme is shown in Fig. 1. The

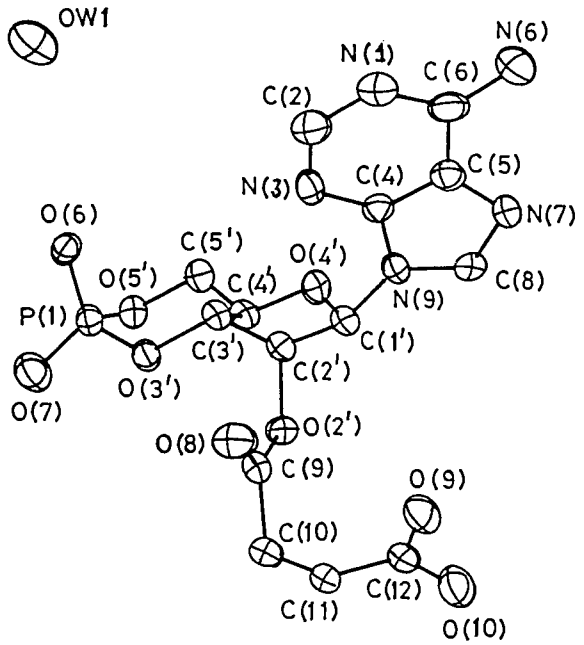

Fig. 1. A perspective view of the molecule with atomic numbering scheme and the thermal ellipsoids at 50% probability level.

Table 2. Final Fractional Coordinates and Equivalent Temperature Factors for Non-Hydrogens along with e.s.d.'s in Parentheses

$$U_{eq}=(1/3)\sum_i\sum_j U_{ij}\mathbf{a}^*_i\mathbf{a}^*_j\mathbf{a}_i\cdot\mathbf{a}_j$$

Atom	x[a)]	y[a)]	z[a)]	U_{eq}[a)]/Å^2
P(1)	4376(1)	2183(0)	7157(0)	283(2)
O(6)	3078(4)	1770(1)	7699(1)	380(7)
O(7)	4185(5)	3104(1)	7083(1)	444(8)
C(1')	5841(6)	−185(2)	5762(1)	259(8)
C(2')	3773(6)	457(2)	5791(1)	241(8)
O(2')	4109(4)	1019(1)	5249(1)	271(6)
C(3')	4291(5)	896(2)	6431(1)	244(8)
O(3')	3548(4)	1758(1)	6480(1)	281(6)
C(4')	6977(6)	833(2)	6474(2)	270(9)
O(4')	7342(4)	−32(1)	6309(1)	327(6)
C(5')	7811(6)	1067(2)	7138(2)	323(9)
O(5')	7129(4)	1945(1)	7206(1)	343(7)
N(1)	114(5)	−2357(2)	6690(1)	377(9)
C(2)	280(7)	−1521(2)	6811(2)	398(11)
N(3)	1848(5)	−1009(2)	6563(1)	359(8)
C(4)	3350(6)	−1418(2)	6162(1)	268(8)
C(5)	3430(6)	−2272(2)	6022(1)	303(9)
C(6)	1665(6)	−2781(2)	6311(1)	334(9)
N(6)	1421(8)	−3604(2)	6225(2)	488(11)
N(7)	5235(5)	−2455(2)	5599(1)	348(8)
C(8)	6198(6)	−1718(2)	5478(1)	305(9)
N(9)	5123(5)	−1065(1)	5797(1)	267(7)
O(8)	157(4)	1170(2)	5153(1)	468(9)
O(9)	3730(5)	225(1)	3894(1)	541(9)
O(10)	6855(6)	620(2)	3345(1)	547(9)
C(9)	2120(6)	1314(2)	4959(1)	270(9)
C(10)	2672(7)	1857(2)	4382(2)	348(10)
C(11)	4945(7)	1663(2)	4022(2)	345(10)
C(12)	5091(7)	780(2)	3750(1)	386(10)
OW1	4632(7)	758(2)	9593(2)	681(12)

a) $\times 10^4$.

Table 3. Bond Lengths (l) and Bond Angles (Φ) Involving Non-Hydrogen Atoms along with the e.s.d.'s in Parentheses

Bond	l/Å	Bond	l/Å
P(1)-O(6)	1.487(2)	C(2)-N(3)	1.304(5)
P(1)-O(7)	1.472(2)	N(3)-C(4)	1.349(4)
P(1)-O(3')	1.618(2)	C(4)-C(5)	1.385(4)
P(1)-O(5')	1.599(2)	C(4)-N(9)	1.370(4)
C(1')-O(4')	1.430(3)	C(5)-C(6)	1.412(4)
C(1')-C(2')	1.548(5)	C(5)-N(7)	1.370(4)
C(1')-N(9)	1.454(4)	C(6)-N(6)	1.324(5)
C(2')-C(3')	1.520(3)	N(7)-C(8)	1.312(4)
C(2')-O(2')	1.441(3)	C(8)-N(9)	1.368(4)
C(3')-C(4')	1.519(4)	C(9)-O(2')	1.353(4)
C(3')-O(3')	1.433(4)	C(9)-O(8)	1.198(4)
C(4')-C(5')	1.494(6)	C(9)-C(10)	1.501(5)
C(4')-O(4')	1.428(4)	C(10)-C(11)	1.511(6)
C(5')-O(5')	1.451(4)	C(11)-C(12)	1.510(5)
N(1)-C(2)	1.352(5)	C(12)-O(9)	1.204(4)
N(1)-C(6)	1.351(4)	C(12)-O(10)	1.322(4)
Angle	**Φ/°**	**Angle**	**Φ/°**
O(6)-P(1)-O(7)	118.6(1)	N(1)-C(2)-N(3)	125.8(3)
O(6)-P(1)-O(5')	109.0(1)	C(2)-N(3)-C(4)	111.5(3)
O(6)-P(1)-O(3')	108.8(1)	N(3)-C(4)-C(5)	128.2(3)
O(7)-P(1)-O(5')	108.1(1)	N(3)-C(4)-N(9)	126.7(3)
O(7)-P(1)-O(3')	107.6(1)	C(5)-C(4)-N(9)	105.1(2)
O(3')-P(1)-O(5')	103.6(1)	C(4)-C(5)-C(6)	116.6(3)
P(1)-O(3')-C(3')	111.9(2)	C(4)-C(5)-N(7)	111.3(3)
C(2')-C(3')-C(4')	102.2(2)	C(6)-C(5)-N(7)	132.0(3)
O(3')-C(3')-C(2')	116.2(2)	C(5)-C(6)-N(1)	114.5(3)
O(3')-C(3')-C(4')	110.5(2)	C(5)-C(6)-N(6)	125.4(3)
C(3')-C(4')-O(4')	101.1(3)	N(1)-C(6)-N(6)	120.0(3)
C(3')-C(4')-C(5')	110.5(3)	C(5)-N(7)-C(8)	103.8(3)
O(4')-C(4')-C(5')	114.3(3)	N(7)-C(8)-N(9)	113.6(3)
C(4')-C(5')-O(5')	104.1(3)	C(8)-N(9)-C(4)	106.1(2)
P(1)-O(5')-C(5')	118.5(2)	C(8)-N(9)-C(1')	125.4(2)
C(4')-O(4')-C(1')	105.4(2)	C(4)-N(9)-C(1')	128.5(2)
O(4')-C(1')-C(2')	107.6(2)	O(2')-C(9)-O(8)	123.4(3)
O(4')-C(1')-N(9)	106.7(2)	O(8)-C(9)-C(10)	124.4(3)
N(9)-C(1')-C(2')	114.8(2)	O(2')-C(9)-C(10)	112.1(3)
C(1')-C(2')-C(3')	101.0(2)	C(9)-C(10)-C(11)	116.6(3)
C(1')-C(2')-O(2')	106.1(2)	C(10)-C(11)-C(12)	114.6(3)
O(2')-C(2')-C(3')	111.4(2)	C(11)-C(12)-O(9)	123.4(3)
C(2')-O(2')-C(9)	116.6(2)	C(11)-C(12)-O(10)	116.9(3)
C(6)-N(1)-C(2)	123.3(3)	O(9)-C(12)-O(10)	119.6(3)

final positional parameters with equivalent isotropic temperature factors for the non-H atoms are given in Table 2.[15] Bond lengths and bond angles are listed in Table 3.

Base: The molecule is found to be in zwitter ionic form with the adenine base protonated at N(1) and a single negative charge on the phosphate group. The bond lengths and bond angles in the base are in good agreement with the average values reported[16] for structures with protonated adenine base. The base shows syn conformation[17] with χ (C(8)-N(9)-C(1')-O(4'))=−95.8°.

Ribose: The ribose in the present structure is covalently linked to succinic acid moiety at 2'-position and is cyclized between 3' and 5' ends by the phosphate group. The ribose ring shows C(3')-

endo-C(4′)-*exo* pucker, a conformation generally found in cyclic 3′,5′-phosphate nucleotide structures.[5,18,19] The pseudorotation parameters[20] of the furanose ring are P=49.9° and τ_m=47.8°.

Phosphate: The six-membered ring formed by phosphate group and ribose is in the chair form with the best mirror bisecting C(4′) and P(1) atoms and with asymmetry parameter[21] ΔC_s[C(4′)-P(1)]=3.3°. The torsion angles ω' (O(5′)-P-O(3′)-C(3′)) and ω (C(5′)-O(5′)-P-O(3′)) fall in the region for 3′,5′-cyclic monophosphate nucleotides on ω' vs. ω map.[22]

Succinic Acid: The succinic acid moiety in the present structure is neutral. It shows a bent skeleton conformation (C(9)-C(10)-C(11)-C(12)=59.5°), which is not uncommon to this moiety.[23,24] In an analysis carried out on the energetically favored side-chain conformations of amino acids,[25] the glutamine and glutamic acid side chains which have a similar carbon backbone structure as that of succinic acid, show this bent conformation in about 50% of these residues in the total sample of oligopeptides considered. Also, this folded or gauche conformation is observed in many of the crystal structures of the compounds containing glutamic acid.[26]

A Comparison with the Biologically Important cAMP: The conformation of the nucleotide part in the present structure (χ=−95.7°, P=49.9°, and τ_m=47.8°) is close to that of one of the molecules in the asymmetric unit (χ=−90°, P=50°, and τ_m=48°) in the crystal structure of cAMP free acid.[5]

The ribose in the cyclic 3′,5′-phosphate nucleotides generally shows a small range of conformations ${}_4T^3 \leftrightarrow {}^3T_4$ and the six-membered ring containing the phosphate group is observed to have chair conformation with a slight flattening at the phosphate end. The flexibility of the cyclic nucleotide seems to lie mostly about the glycosidic bond, C(1′)-N(9), as can be seen from the fact that the cAMP and its analogues have been observed to be in anti or syn conformation and not generally restricted to the anti conformer as in the crystal structures of cyclic monophosphates of pyrimidines.

Hydrogen Bonding Pattern: The crystal structure is stabilized by a number of hydrogen bonds, the details of which are shown in Fig. 2 and Table 4. No base stacking has been observed.

In the present structure, a water molecule forms hydrogen-bonded bridge between the N(6) and N(7) of the same adenine base. This pattern has also been observed in crystal structure of a modified cAMP.[18] In a recent review,[27] on hydration of oligonucleotides in crystals, it is cited that such intra-residue bridges

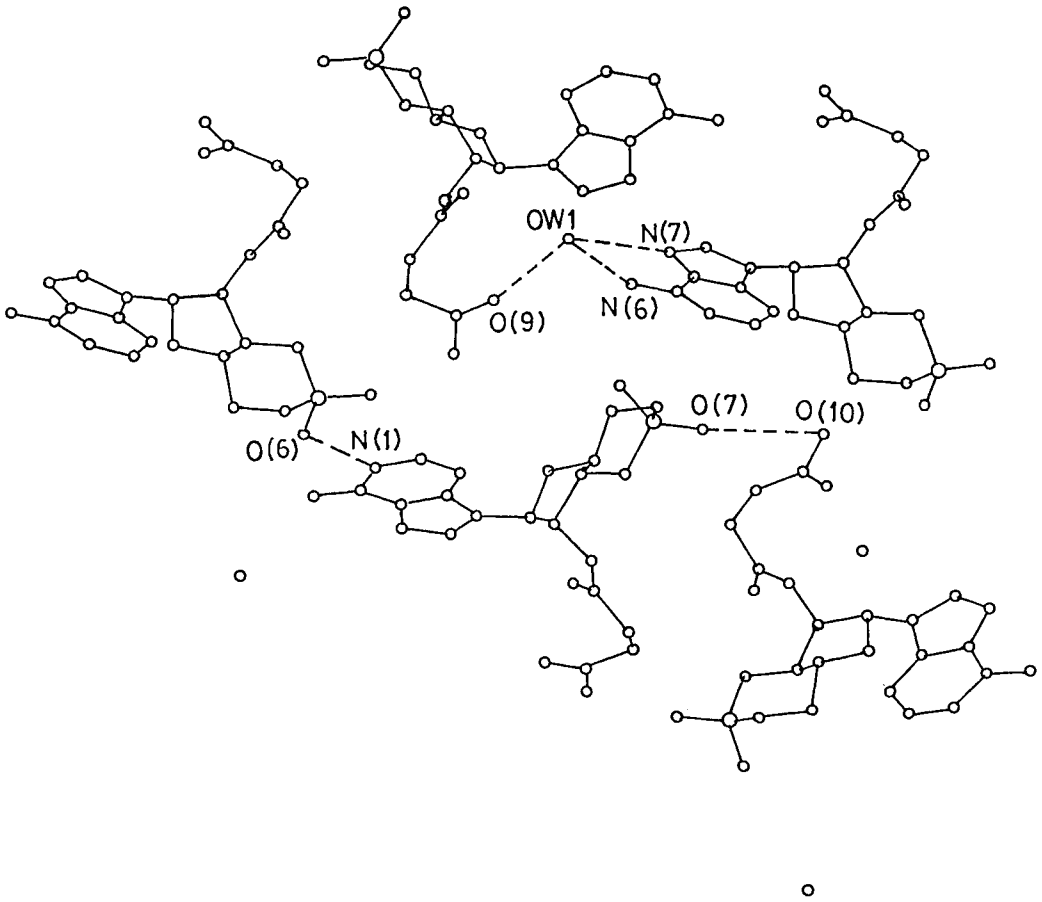

Fig. 2. Hydrogen bonding pattern in the crystal structure of the title compound.

Table 4. Details of Hydrogen Bonding

	D···A(l/Å)	H···A(l/Å)	D-H···A(Φ/°)
Base-phosphate			
N(1)-H···O(6^{i})	2.60	1.58	176.4
Succinic acid-phosphate			
O(10)-H···O(7^{ii})	2.57	1.50	166.7
Water-Succinic acid			
OW1-H···O(9^{iii})	2.84	2.06	171.4
Water-base			
OW1···H-N(6^{iv})	2.97	2.12	166.8
OW1-H···N(7^{iv})	2.86	1.99	154.2

(i) $-x$, 0.5+y, 1.5−z: (ii) 0.5+x, 0.5−y, 1.0−z; (iii) 0.5−x, −y, 0.5+z; (iv) 1.0−x, 0.5+y, 1.5−z.

have been observed for purines in crystals of all the three (A, B, and Z) forms of DNA. In general, bridging water molecules in several nucleic acid structures[28,29] are believed to play a significant role.

The hydroxyl oxygen atom, O(10), of the succinic acid moiety forms a direct hydrogen bond with the phosphate oxygen, O(7), and the carbonyl oxygen atom, O(9), hydrogen bonds to the water molecule (Fig. 2, Table 4) which bridges the N(6) and N(7) atoms of the adenine base. It is interesting to note that a similar mode of interaction, although not involving a water molecule, is observed in the crystal structures of cAMP-Catabolite activator protein (CAP) complex[30] and cAMP and adenosine-CAP mutant complex,[4] where the hydroxyl group of Ser side chain is at hydrogen-bonding distance from the same two nitrogens, N(6) and N(7) of adenine base. This mode of interaction could be a recurring feature, considering the fact that these nitrogens are free to take part in additional hydrogen-bonding interactions even for an adenine base involved in Watson-Crick base pairing. Water mediated interaction between the nucleotide part and the amino acid-like succinic acid moiety observed in the present structure seems to be a biologically important mode of interaction. A similar interaction has been observed in the crystal structure of 1:1 cytosine-*N*-(benzyloxycarbonyl)-glutamic acid dihydrate,[31] where in a water molecule oxygen is at hydrogen-bonding distance from both carboxyl oxygen of glutamic acid and O(2) atom of the cytosine base. In fact, such indirect interactions have also been observed between amino acid side chains and the nucleotides in the crystal stuctures of certain repressor-operator complexes.[32] In the crystal structure of 434 phage repressor-DNA operator complex,[33] four of the six water molecules present are involved in bridging the residues Arg 43, Gln 33, and Ser 30 to base pairs and phosphates of the DNA operator. Also, in the crystal structure of Trp repressor-DNA operator complex,[34] water mediated polar contacts to the bases appear to contribute part of the specificity. The structure shows three water mediated hydrogen bonds, two of which bridging peptide nitrogens of Ile 79 and Ala 80 to adenine and guanine bases, and the third water molecule interacts with hydroxyl of Thr 83 and both the nitrogens N(6) and N(7) of adenine 7 of the DNA operator.

The authors thank the Departments of Science and Technology, Biotechnology, ICMR Centre on Cell Biology and Government of India for financial support.

References

1) E. W. Sutherland and T. W. Rall, *Pharmacol. Rev.*, **12**, 265 (1960).
2) G. A. Robinson, R. W. Butcher, and E. W. Sutherland, "Advances in Biochemical Psychopharmacology," Academic Press, New York (1971).
3) T. A. Langan, *Science*, **162**, 579 (1968).
4) M. C. Vaney, G. L. Gilliland, J. G. Harman, A. Peterkofsky, and I. T. Weber, *Biochemistry*, **28**, 4568 (1989).
5) K. I. Varughese, C. T. Lu, and G. Kartha, *J. Am. Chem. Soc.*, **104**, 3398 (1982) and references cited there of.
6) M. Sundaralingam and S. K. Arora, *J. Mol. Biol.*, **71**, 49 (1972).
7) R. Parthasarathy, J. M. Ohrt, and G. B. Chheda, *Biochemistry*, **16**, 4999 (1977).
8) T. Ishida, A. Tanaka, M. Inoue, T. Fujiwara, and K.-I. Tomita, *J. Am. Chem. Soc.*, **104**, 7239 (1982).
9) M. Takimoto, A. Takenaka, and Y. Sasada, *Acta Crystallogr., Sect. C*, **39**, 73 (1983).
10) I. Saito, H. Sugiyama, T. Matsuura, and K. Fukuyama, *Tetrahedron Lett.*, **26**, 4467 (1985).
11) A.C.T. North, D. C. Phillips, and F. D. Mathews, *Acta Crystallogr., Sect. A*, **24**, 351 (1968).
12) P. Main, S. J. Fiske, S. E. Hull, L. Lessinger, G. Germain, J.-P. Declercq, and M. M. Woolfson, MULTANll 82. A System of Computer Programs for the Automatic Solution of Crystal Structures from X-Ray Diffraction Data. Univs. of York, England and Louvain, Belgium (1982).
13) "Structure Determination Package," Enraf-Nonius, Delft, The Netherlands (1982).
14) G. M. Sheldrick, SHELX 76. Program for Crystal Structure Determination. Univ. of Cambridge, England (1976).
15) The Tables of anisotropic parameters of non-hydrogen atoms, the atomic and thermal parameters of hydrogen atoms, and the F_o−F_c tables are deposited as Document No. 9093 at the Office of the Editor of Bull.

Chem. Soc. Jpn.
16) R. Taylor and O. Kennard, *J. Am. Chem. Soc.*, **104**, 3209 (1982).
17) M. Sundaralingam, *Biopolymers*, **7**, 821 (1969).
18) F. A. Cotton, R. G. Gillen, R. N. Gohil, Jr., E. E. Hazen, C. R. Kirchner, J. Nagyvary, I. P. Rouse, A. G. Stanislowski, J. D. Stevens, and P. W. Tucker, *Proc. Natl. Acad. Sci. U.S.A.*, **72**, 1335 (1975).
19) W. Depmeier, J. Engels, and K. H. Klaska, *Acta Crystallogr., Sect. B*, **33**, 2436 (1977).
20) C. Altona and M. Sundaralingam, *J. Am. Chem. Soc.*, **94**, 8205 (1972).
21) W. L. Duax and D. A. Norton, "Atlas of Steroid Structures," IFI/Plenum, New York (1975), Vol. 1.
22) M. Sundaralingam, T. P. Haromy, and P. Prusiner, *Acta Crystallogr., Sect. B*, **38**, 1536 (1982).
23) J. A. Kanters, H. M. Doesburg, and T. Koops, *Acta Crystallogr., Sect. B*, **33**, 1286 (1977).
24) Y. Schouwstra, *Acta Crystallogr., Sect. B*, **29**, 1 (1973).
25) F. Benedetti, G. Morelli, G. Nemethy, and H. A. Scheraga, *Int. J. Pept. Protein Res.*, **22**, 1 (1983).
26) N. Hirayama, K. Shirahata, Y. Ohashi, and Y. Sasada, *Bull. Chem. Soc. Jpn.*, **53**, 30 (1980).
27) E. Westhof, *Int. J. Biol. Macromol.*, **9**, 186 (1987).
28) A. H.-J. Wang, G. J. Quigley, F. J. Kolpak, J. L. Crawford, J. H. van Boom, G. van der Marel, and A. Rich, *Nature*, **282**, 680 (1979).
29) G. J. Quigley, A. H.-J. Wang, G. Ughetto, G. van der Marel, J. H. van Boom, and A. Rich, *Proc. Natl. Acad. Sci. U.S.A.*, **77**, 7204 (1980).
30) I. T. Weber and T. A. Steitz, *J. Mol. Biol.*, **198**, 311 (1987).
31) T. Hata, M. Yoshikawa, S. Sato, and C. Tamura, *Acta Crystallogr., Sect. B*, **31**, 312 (1975).
32) R. G. Brennan and B. W. Matthews, *Trends Biochem. Sci.*, **14**, 286 (1989).
33) A. K. Aggarwal, D. W. Rodgers, M. Drottar, M. Ptashne, and S. C. Harrison, *Science*, **242**, 899 (1988).
34) Z. Otwinowski, R. W. Schevitz, R.-G. Zhang, C. L. Lawson, A. Joachimiak, R. Q. Marmorstein, B. F. Luisi, and P. B. Sigler, *Nature*, **335**, 321 (1988).

Damage of Egg Phosphatidylcholine Liposomes by DNA-Binding Cytotoxic Agents

Charmian J. O'Connor,* William A. Denny,† Diane P. Emery, Holger Tank,††
Toshinori Sato,†† and Junzo Sunamoto†††
Department of Chemistry, School of Medicine, University of Auckland, Private Bag, Auckland, New Zealand
†Cancer Research Laboratory, School of Medicine, University of Auckland, Private Bag, Auckland, New Zealand
††Department of Industrial Chemistry, Faculty of Engineering, Nagasaki University, Nagasaki 852
†††Laboratories of Materials Sciences of Polymers and Artificial Cell Technology, Department of Polymer Chemistry, Faculty of Engineering, Kyoto University, Sakyo-ku, Yoshida Hommachi, Kyoto 606
(Received July 23, 1990)

The stability of small unilamellar vesicles (SUV) formed by egg phosphatidylcholine has been examined in the presence of four DNA-intercalating drugs—carboxamides of acridine, anthracene, phenylquinoline, and phenylbenzimidazole. The physicochemical stability of the vesicle-membrane changed as the total drug concentration increased and, of the four drugs investigated, the phenylquinolinecarboxamide was the most destructive. The presence of cholesterol in the liposomal bilayer increased resistance to physicochemically induced damage by the drugs except the anthracenecarboxamide. In all cases, coating the liposomes with a polysaccharide made the liposomal surface more hydrophobic and led to the vesicle rupture by the cytotoxic agents. The cytotoxic 9-anilinoacridine derivatives, amsacrine and 9-[2-methoxy-4-(methylsulfonylamino)-anilino]-5-methylacridine-4-*N*-methylcarboxamide (CI-921), were too insoluble to be encapsulated within the aqueous core of liposomes, but the neutral form of CI-921 was intercalated into the liposomal membrane of pullulan-derivative-coated liposomes. In this formulation, CI-921 was more effective against BM 314 carcinoma-cells than the free drug, but an anticarcinoembrionic antigen (anti-CEA) antibody binding liposome provided no additional advantage.

N-[4-(9-Acridinylamino)-3-methoxyphenyl]methanesulfonamide, amsacrine (**1**) was the first synthetic DNA-intercalating agent successfully to enter clinical use,[1] and has been shown to be beneficial in the treatment of leukemia but not for the more common solid tumors.[2] Multi-parameter structure-activity relationships for amsacrine analogues suggested that alterations in the DNA-binding acridine moiety would be beneficial.[3] While high activity was associated with strong binding to DNA, it was also important to develop analogues with better distributive properties which could reach remote tumor sites. The requirement was, therefore, for weakly basic compounds which would have a higher proportion of the diffusable free base, and focussed attention on electron-withdrawing substituents with hydrogen bonding donor/acceptor properties.[4]

In 1982 the analogue 9-[2-methoxy-4-(methylsulfonylamino)anilino]-5-methylacridine-4-*N*-methylcarboxamide (CI-921) (**2**) was selected for clinical evaluation on the basis of its experimental solid tumor activity and its different physicochemical prop-

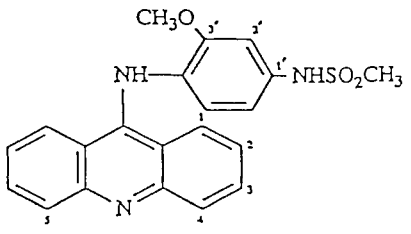

Amsacrine
1

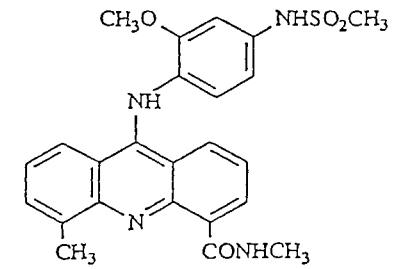

CI-921
2

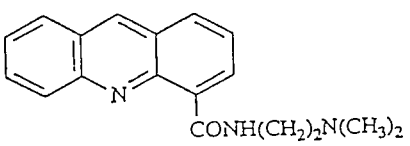

Acridine-4-*N*-(2-dimethylaminoethyl)carboxamide
3

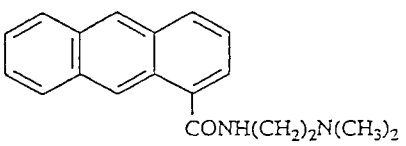

Anthracene-1-*N*-(2-dimethylaminoethyl)carboxamide
4

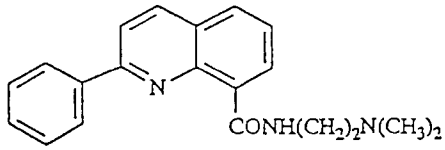

2-Phenylquinoline-8-*N*-(2-dimethylaminoethyl)carboxamide
5

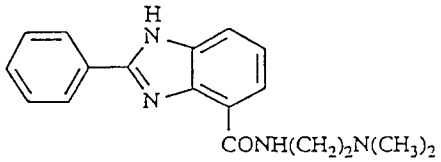

2-Phenylbenzimidazole-4-*N*-(2-dimethylaminoethyl)carboxamide
6

erties compared with amsacrine (stronger DNA-binding, higher water-solubility, and lower pK_a).[5]

Later studies showed that, although high DNA-binding affinity correlates with high in vitro and in vivo drug potency for several series of DNA-intercalating agents, it also limits the distributive properties of the compounds. Emphasis was therefore placed on the development of weakly-binding cationic DNA-intercalating agents.[1,6] One of the first of these was the acridinecarboxamide (**3**), which showed extraordinary activity against the remotely-sited Lewis lung carcinoma in mice.[6] A considerable number of tricyclic carboxamides has now been prepared and evaluated, and these are represented in this study by the linear tricyclic anthracene (**4**)[7] and two '2-1' tricyclic systems, the phenylquinoline (**5**)[8] and the pheylbenzimidazole (**6**).[9] This last cornpound, which possesses the chromophore of lowest aromaticity, displays the lowest DNA-binding constant of all the tricyclic carboxamides which have been investigated.[9]

Liposomes have been of particular interest in cancer chemotherapy, where treatment is required to be systemic to deal with metastatic disease, and is nearly always limited by the toxic side-effects of the drugs. Drug encapsulation within tumour-cell specific liposomes has been chosen to permit smaller quantities to be administered, reducing general side effects. Active targeting of the liposomes to specific tissues such as the lung, or to specific cell types such as alveolar macrophages, may be enhanced by coating them with naturally occurring polysaccharide-derivatives such as mannan and amylopectin[10] anchored by a cholesterol moiety. However, the most deliberate approach to the specific targeting of liposomes has been to attach them to monoclonal antibody fragments capable of recognizing tumor associated antigens. Recent work has shown that such "immunoliposomes" bind selectively to target tumor cells in vitro[11] and in vivo,[12] and that doxorubicin encapsulated into such liposomes is more effective against human lung tumor xenografts in mice than either free drug or drug encapsulated in conventional liposomes.[13]

In this paper we examine first the extent of damage of a variety of egg phosphatidylcholine liposomes caused by the antitumor agents (**3—6**) and how this varies with drug hydrophobicity. Through this experiment, we are able to obtain two different sorts of information. The first is information about the membrane toxicity of these drugs since liposomes are considered to be a simple model of intact cells. The more destructive drug for liposomes should, in general, be more membrane toxic to any kind of cells. The second is information of more technical concern; namely, if one wishes to encapsulate an anti tumor drug into the liposomal drug carrier, the carrier liposome should not be destructed by drugs during the encapsulation procedure. We, therefore, report on the effectiveness of **2**, encapsulated in a carcinoembrionic antigen (CEA)-specific immunoliposome, against a CEA-producing cell line, BM 314, and a CEA-nonproducing cell line, RPMI#4788.

The drugs investigated herein belong to the DNA-intercalating class of antitumor agents. They possess planar aromatic ring systems capable of intercalating reversibly between the basepairs of the double helix and distorting the DNA geometry.

Materials and Methods

Materials. Egg yolk phosphatidylcholine was isolated and purified from egg yolk as described in the literature[14,15] and found to be pure by thin layer chromatography (using a precoated silica gel plate and development with chloroform/methanol/water (65 : 25 : 4, v/v/v). Carboxyfluorescein (CF), the marker entrapped in the liposomes, was from Eastman Kodak. The polysaccharide [CHP-50-1.9 (AECM 2.1)] (i.e. pullulan of average molecular weight 50000, and the primary alcohol moieties are substituted by 2.1 free *N*-(2-aminoethyl)carbamoylmethyl (AECM) residues per 100 glucose units, of which 1.9 residues are bound to cholesterol), was similar to that used in previous work.[11]

Cell Lines. Human colon carcinoma cells (BM 314 and RPMI#4788) were maintained in RPMI 1640 medium (Nissui Pharmaceutical Co. Ltd., Tokyo) supplemented with 10% heat inactivated Fetal Calf Serum (FCS, Protein Institute, Osaka University).

Cytotoxic Assay. 3×10^4 BM 314- or RPMI#4788-cells in 0.5 ml of RPMI 1640 (10% FCS) were added into each of a 24 well culture plate (Corning). Subsequently, an aliquot of CI-921-encapsulated liposome or immunoliposome was added to the cell suspension. The mixture was maintained at 37 °C under 5% CO_2-95% air condition for 3 days. After the cells were stripped from the culture wells by treatment with 0.05% trypsin-0.02% ethylenediaminetetraacetic acid (EDTA), the cell number was counted by trypan blue dye

exclusion.

Preparation of Liposomes. Small unilamellar vesicles, SUV, encapsulating 6-carboxyfluorescein in the interior water phase, were prepared by the method described elsewhere.[16] Polysaccharide-coated liposomes were prepared as follows. After sonication of a suspension of lecithin (30 mg) in a 4 ml solution of carboxyfluorescein (200 mM, 1 M=1 mol dm^{-3}) in tris(hydroxymethyl)methanamine (Tris) buffer (20 mM, pH 8.6) containing 200 mM NaCl, the polysaccharide, CHP-50-1.9 (AECM 2.1) (3 mg), in 0.5 ml of Tris buffer containing 200 mM NaCl, was added. The 1 : 10 (by wt) mixture of polysaccharide: liposome was stirred gently for 30 min and then separated from the multilamellar vesicles (MLV) by gel chromatography. Cholesterol containing liposomes (1 : 10 mol percent) were prepared by adding cholesterol (1.5 mg) to the solution of lecithin (30 mg) in an appropriate amount of chloroform at the beginning of the preparation. For all preparations, the concentration of phosphatidylcholine in the liposomal suspension was determined as inorganic phosphate according to the procedure of Eibl and Lands.[17]

Large unilamellar vesicles (LUV) were prepared by the method of reversed-phase evaporation. Lecithin (60 mg) was dissolved in diethyl ether (8 ml) and an aqueous solution (4 ml) of the material to be encapsulated was added. The mixture was sonicated in an ultrasonicator bath until formation of a homogeneous emulsion was obtained. This step is important, as difficulties in achieving high encapsulation or a primarily unilamellar population of vesicles may arise from failure to obtain a good emulsion. The organic solvent was then removed by rotary evaporation for 60 min at 350 mmHg[a] followed by a further 30 min at 650 mmHg.[a] The jelly-like residue was dissolved in Tris-HCl buffer, 20 mM, in 200 mM NaCl and centrifuged for 30 min at 35,000 G. After each centrifugation the supernatant was decanted and replaced by fresh Tris buffer and the process was repeated three times. The addition of excess buffer to the gel state has been found to decrease the time required to go from the gel state to the final liposomal dispersion, without reducing significantly the percent encapsulation of the initial aqueous material.[18] Sodium chloride is required in the buffer solution to balance the osmolarity between the interior and exterior of the liposome.

Preparation of Immunoliposomes. Dry pyridine (5 ml) was added to 3 ml dry dimethyl sulfoxide containing the CHP-50-1.9 (AECM 2.1) (300 mg) and *N*-[4-maleimidobutyryloxy]succinimide (50 mg) (Dojindo Laboratories, Kumamoto) at room temperature. Substitution of the 4-maleimidobutyryl (GNB) group into the free AECM group in the polysaccharide[11] was completed in 48 h, as confirmed by the fluorescamine test.[19] The reaction mixture was poured into 300 ml ethanol, stored overnight, and then the water soluble portion of the precipitate was lyophilized to yield the polysaccharide derivative coded as GMB-CHP.

Egg phosphatidylcholine liposomes containing CI-921 were prepared in Tris-buffer (200 mM NaCl), pH 8.6. Immediately after sonication, the liposome suspension was mixed with 1 ml Tris buffer (pH 8.6) containing 200 mM NaCl, and containing 3 mg of CMG-CHP. After stirring for 1 h at room temperature, 2 ml of the mixture were adjusted to pH 6.2 with 0.1 M HCl. Phosphate buffer (1.5 ml, pH 6.2) containing 72.5 μg of the anti-carcinoembrionic antigen (CEA) antibody fragment Fab′ (personal donation from S. Nishi, the First Department of Biochemistry, School of Medicine, Hokkaido University) was added and the reaction mixture was incubated with gentle stirring for 20 h at 4 °C. After gel filtration of the immunoliposomal suspension (using phosphate buffer (pH 6.2) as eluant), the MLV fraction (3.6 ml) contained 30.5 μg CI-921 and 4.6 Fab′ as determined by the fluorescamine test[20] (22% of the antibody employed) per ml. The corresponding GMB-CHP-coated multilamellar liposomes, kept at pH 8.6, contained 42.4 μg CI-921 per ml after gel filtration. Thus the loss of CI-921 during the change of pH from 8.6 to 6.2 and the conjugation of the antibody fragment was ca. 30%.

Monitoring the Release of 6-Carboxyfluorescein. A 3 ml sample of 0.1 mM 6-carboxyfluorescein-loaded SUV suspen-

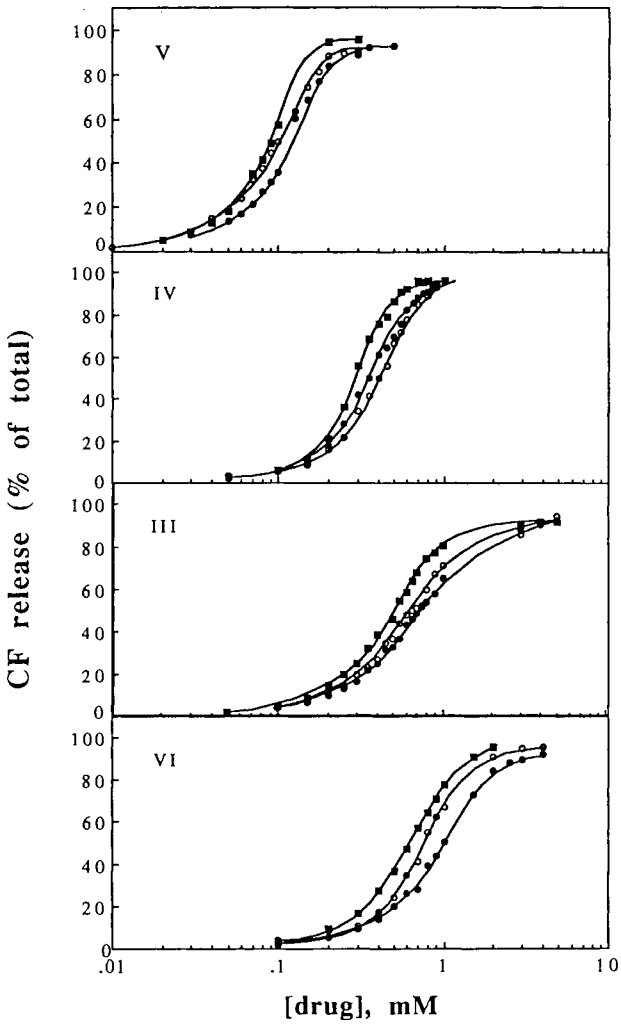

Fig. 1. Cytotoxic agent-induced leakage of 6-carboxyfluorescein (CF) from a 0.1 mM egg phosphatidylcholine small unilamellar vesicle suspension in 200 mM NaCl at 36.5 °C: ○, uncoated liposomes; ●, liposomes containing 10 mol % cholesterol: ■, liposomes coated with pullulan anchored by a cholesterol moiety. The drugs used were the carboxamide derivative of acridine (**3**), anthracene (**4**), the phenylquinoline (**5**), and phenylbenzimidazole (**6**).

[a] 1 mmHg=133.322 Pa.

sion in 20 mM Tris-HCl buffer (pH 8.6) containing 200 mM NaCl was placed in a thermoregulated cuvette cell and preincubated for 10 min at 36.5 °C. During the preincubation, we found no spontaneous release of the marker. The carboxyfluorescein-release (induced by adding 200 μl of an aqueous solution of the drug under investigation) was followed by monitoring an increase in the fluorescence intensity, I, at 520 nm, by excitation at 470 nm on a Shimadzu RF540 fluorescence spectrometer. The intensity of the total amount of the liposome-encapsulated marker, I_∞, was determined after complete destruction of the liposomes with 100 μl of Triton X-100 (10% v/v). The measured percentage of 6-carboxyfluorescein released was obtained by the following equation: % 6-carboxyfluorescein released$=((I_t-I_0)/(I_\infty-I_0))\times 100$, where t and 0 refer to times of sampling and to the instant when the solution of the drug was applied to the liposomal suspension. A standard time of 5 min was used to determine the relative ability of the drugs to effect lysis. Duplicate experiments were performed and the data shown in Fig. 1 represent the mean of two measurements. The experimental error was within ±2%.

Due to interference between the fluorescent properties of the probe and the compounds under investigation (e.g. the acridinecarboxamide, **3**, and the anthracene carboxamide, **4**, possessed fluorescence maxima at excitation wavelengths of 380 and 402 nm, and emission wavelengths of 450 and 472 nm, respectively), it was necessary to apply a correction factor equal to (I_∞(in the absence of drug))/(I_∞(in the presence of drug)) to the measured percent probe released.

Results

Stability of Liposome-Encapsulated Drug Formulations. The amount of amsacrine in the liposomal fraction was below the spectroscopic (λ_{max} 435 nm, ε=12300) detection limit (<80 ng ml^{-1}), but the concentration of neutral CI-921 (λ_{max} 445 nm, ε=10300) dissolved in the lipid membrane increased to 3—8 μg ml^{-1} for the cationic form. Coating the liposomes with cholesterol-substituted pullulan increased the concentration of neutral drug embedded in liposomal bilayer to 70—80 μg ml^{-1} CI-921 and 1.2 μg ml^{-1} amsacrine. The neutral form of CI-921 precipitates rapidly from the uncoated liposomes after sonication and gel filtration, but the polysaccharide-coated liposomes are stabilized and release the drug slowly: at 0, 8, and 11 days the relative concentrations were 90, 66, and 55 μg ml^{-1}, respectively. At the same time the lipid concentration decreased from 2.5 to 2.3 mM.

However, the tricyclic carboxamides (**3**—**6**) were not able to be encapsulated, and in fact degraded liposomal membranes. The rate of this destruction was measured by carboxyfluorescein release. Figure 1 shows comparative data for the percent release of liposome-encapsulated carboxyfluorescein by increasing concentrations of the acridine-(**3**), anthracene-(**4**),

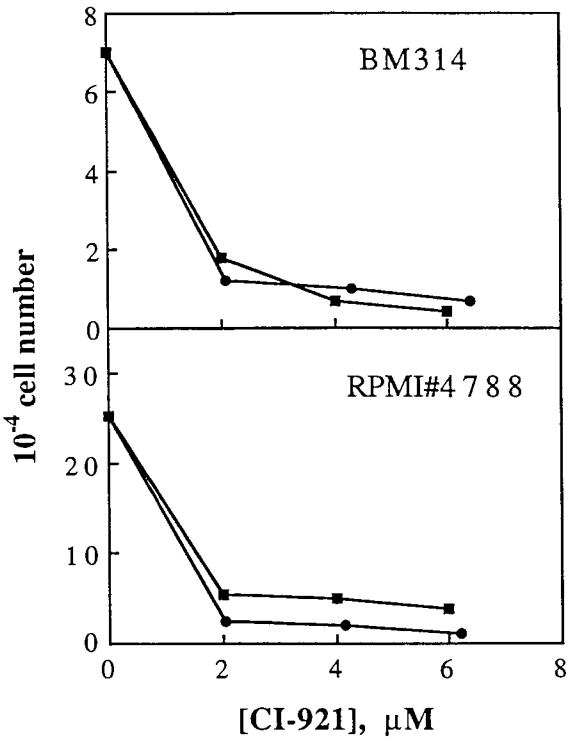

Fig. 2. Antitumor activity of CI-921. The protonated free drug, ●, and the deprotonated form of the drug encapsulated in 60 μM egg phosphatidylcholine MLV, ■, were incubated with CEA-producing BM-314 cells (upper plot) and RPMI#4788 (lower plot) for 3 days at 37 °C. The initial cell number was 3×10^4.

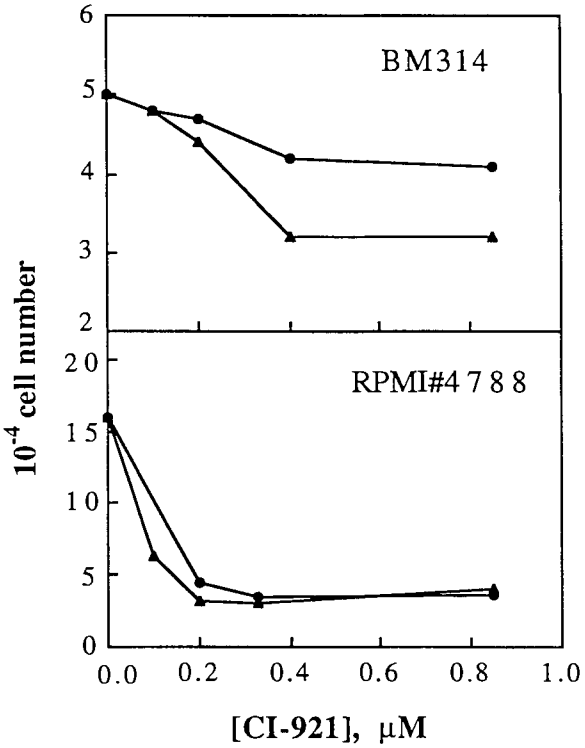

Fig. 3. Antitumor activity of CI-921. The deprotonated drug encapsulated in GMB-CHP coated liposomes, ●, and in immunoliposomes, ▲, were incubated with BM-314 cells (upper plot) and RPMI#4788 cells (lower plot) for 3 days at 37 °C. The initial cell number was 3×10^4.

phenylquinoline-(**5**), and phenylbenzimidazolecarboxamides (**6**) from a variety of liposomes (uncoated, with 10% cholesterol, and coated with pullulan anchored by a cholesterol moiety in the lipid bilayer).

Comparative Antitumor Effect of Liposome Encapsulation of CI-921. The cytotoxicity of CI-921, which was presented to BM-314 and RPMI#4788 tumor cell lines in vitro as either the free drug in its protonated form or the deprotonated drug encapsulated into MLV, is compared in Fig. 2. There was a minor difference in effectiveness in the latter case but no difference in the former.

The deprotonated drug was also encapsulated into GMB-CHP-coated liposomes and into immunoliposomes, and the results for the two cell lines are compared in Fig. 3. In the case of BM-314 cells, the immunoliposome-encapsulated drug was less effective, while for RPMI#4788 there was no significant difference.

Discussion

Our initial interest was to determine whether egg phosphatidylcholine liposomes could be used as a carriers for the cytotoxic drugs amsacrine (**1**), CI-921 (**2**), and acridinecarboxamide (**3**). We had thought that acridinecarboxamide would be the most promising compound for encapsulation because of its high solubility in water (>17 mg ml^{-1}) compared with amsacrine (0.12 mg ml^{-1} in water, 2—3 μg ml^{-1} in saline) and CI-921 (0.72 mg ml^{-1} in water, 23 μg ml^{-1} in saline). Surprisingly, LUV containing the acridinecarboxamide, prepared by the reversed-phase evaporation method, were found to encapsulate only 0.2 to 0.4 percent of the compound. This unexpected result arose from drug induced damage of the liposomal membrane and therefore this compound proved to be unsuitable for encapsulation within egg phosphatidylcholine liposomes. By analogy, therefore, these membrane destructive drugs would be expected to cause some membrane toxic effects even on normal cells in vivo.

Because of their low solubility in water, both amsacrine and CI-921 were unsuitable for encapsulation into the aqueous phase. Furthermore, attempts to encapsulate them into the liposome showed that amsacrine was not detectable in the liposomal fraction and the concentration of CI-921 was less than 0.4 μg ml^{-1}. However, when the pH was raised and the drugs were presented to the liposome in their neutral form, there was a significant increase in the concentration of CI-921 incorporated within the lipid bilayers of MLV. Coating the liposomes with cholesterol substituted pullulan (CHP-50-1.9) increased the drug content of CI-921 more than ten fold.

Of the three compounds investigated, only CI-921 was suitable for encapsulation into liposomes, and then only when applied in its neutral form and when the surface of the liposomes was coated with polysaccharide. When the deprotonated drug was encapsulated in pullulan coated liposomes (results not shown) it appeared to be more effective than the free drug against BM-314 cells, but less effective for RPMI#4788-cells. Anti-CEA bearing immunoliposomes (which encapsulated deprotonated CI-921) were also less effective than the free drug, tested against RPMI#4788 and BM-314 cells, even though Sunamoto et al.[13] have shown that these immunoliposomes are very effectively endocytosed by target (BM-314) cells which are CEA-producing. The cytotoxicity of empty egg-PC liposomes and of anti-CEA monoclonal antibodies, at the concentrations employed herein, was negligible (data not shown).

Since the ability of antitumor agents to lyse a cell membrane may be an important parameter in the design of more effective chemotherapeutic agents, we investigated in more detail the ability of four tricyclic carboxamide DNA-intercalating agents, differing in the aromaticity of their tricyclic chromophore, to interact with egg phosphatidylcholine membranes. In order that these lipid-bilayer structures could act as more effective mimics of a cell membrane they were modified by adding cholesterol therein and by coating them with polysaccharide anchored by a cholesterol moiety.

The results shown in Fig. 1 suggest that cholesterol containing liposomes acquired increased resistance against physicochemically induced damage. High concentrations of both the parent phenylquinoline and phenylbenzimidazole were needed to lyse the cholesterol containing liposomal membrane compared with the concentrations required for the conventional and polysaccharide-coated vesicles.

Unexpectedly, the polysaccharide-uncoated liposomes showed greater resistance to lysis compared with the cholesterol containing vesicles if the lysing drug were the parent anthracene (**4**). However, only ten mol percent cholesterol to phospholipid had been added into the membrane and it is possible that at higher concentrations of cholesterol the liposomal membrane may have shown improved stability. Unfortunately, by increasing the ratio of cholesterol to phospholipid above that of ten percent, one runs the risk of altering the structure of the liposomal membrane to such an extent that the bilayer is damaged. Similar results to these present ones were found by O'Connor et al.[20] who reported that incorporation of cholesterol into the liposomes did not affect the ability of some bile salts to lyse the membrane. In fact, in the case of chenodeoxycholic acid, even the addition of fifty mol percent cholesterol to phospholipid did not significantly alter the magnitude of carboxyfluorescein-release from the liposomal membrane.

Previously, Sunamoto et al. had assembled a cell wall-like coat on the outer surface of liposomes using the modified polysaccharides, *O*-palmitoylpullulan

and *O*-palmitoylamylopectin and showed that such liposomes were more tolerant against permeability of water soluble drugs[21] and changes in ionic strength, pH, osmotic pressure as well as enzymatic lysis by lipases or lipoxygenases.[10] However, unlike these previous experiments the present study dealt with the cytotoxic agents which were injected into the external media rather than being encapsulated within the aqueous interior. Under these conditions, the liposomes coated with pullulan-derivative showed the greater susceptibility to lysis. Interestingly, the present results reported on the cytotoxic agents are similar to those obtained by O'Connor et al.[20] for lysis of polysaccharide-coated liposomes by bile salts. They found that coating the surface of SUV with *O*-palmitoylpullulan led to faster release of carboxyfluorescein for all the bile salts investigated. Coating the liposomes with polysaccharides made the vesicles more hydrophobic and resulted in enhanced lysis by the bile salts.[20]

It seems probable, therefore, that the cytotoxic agents interact more favorably with the polysaccharide-coated vesicles than with the unmodified or cholesterol containing liposomes because of the increased hydrophobicity of the interface. Furthermore, it seems that the increased hydrophobicity of the neutral drugs themselves plays a major role in determining lysis. The relative hydrophobicity values[22] of the carboxamides of the parent phenylbenzimidazole, acridine, anthracene, and phenylquinoline are −0.26, −0.20, −0.02, and 0.01, respectively (determined by liquid-liquid chromatography[22,23] compared with the values of log(1/10% lysis) (i.e. the log of the inverse of the concentration (molar) of drug needed to achieve 10 percent release of carboxyfluorescein from SUV after 5 min at 36.5 °C) equal to 3.54, 3.73, 3.80, and 4.49, respectively.

An investigation of the lysing ability of an extended series of phenylquinolines and phenylbenzimidazoles has been reported separately.[23]

We are indebted to T. Koji and N. Ishii (Health Administration Center, Nagasaki University) for the generous donation of the cell lines and N. Nishi (Hokkaido University) for the gift of the monoclonal antibody. H. Tank acknowledges the award of a New Zealand Universities' Grants Committee postdoctoral fellowship. C. J. O'Connor, W. A. Denny, and J. Sunamoto acknowledge financial support from the Research Committees of the New Zealand Universitie' Grants Committee and the University of Auckland, the Auckland Division of the Cancer Society of New Zealand, and the Ministry of Education, Science and Culture, Japan, respectively.

References

1) W. A. Denny, *Drug Des. Delivery*, **3**, 99 (1988).
2) M. A. Robbie, B. C. Baguley, W. A. Denny, J. B. Gavin, and W. R. Wilson, *Cancer Res.*, **48**, 310 (1988).
3) W. A. Denny, B. F. Cain, G. J. Atwell, C. Hansch, A. Panthananickal, and A. Leo, *J. Med. Chem.*, **25**, 276 (1982).
4) W. A. Denny, G. J. Atwell, and B. C. Baguley, *J. Med. Chem.*, **27**, 363 (1984).
5) B. C. Baguley, W. A. Denny, G. J. Atwell, G. J. Finlay, G. W. Rewcastle, S. J. Twigden, and W. R. Wilson, *Cancer Res.*, **44**, 3245 (1984).
6) G. J. Atwell, G. W. Rewcastle, B. C. Baguley, and W. A. Denny, *J. Med. Chem.*, **30**, 664 (1987).
7) B. D. Palmer, G. W. Rewcastle, G. J. Atwell, B. C. Baguley, and W. A. Denny, *J. Med. Chem.*, **31**, 707 (1988).
8) G. W. Rewcastle, B. C. Baguley, and W. A. Denny, *J. Med. Chem.*, **32**, 396 (1989).
9) W. A. Denny, G. W. Rewcastle, and B. C. Baguley, *J. Med. Chem.*, **33**, 814 (1990).
10) J. Sunamoto, K. Iwamoto, M. Takada, T. Yuzuriha, and K. Katayama, "Polymers in Medicine: Biomedical and Pharmacological Applications," ed by P. Guisti and E. Chiellini, Plenum Press, New York (1983), p. 157.
11) J. Sunamoto, T. Sato, M. Hirota, K. Fukushima, K. Hiratani, and K. Hara, *Biochim. Biophys. Acta*, **898**, 323 (1987).
12) T. Sato, J. Sunamoto, N. Ishii, and T. Koji, *J. Bioact. Compat. Polym.*, **3**, 195 (1988).
13) M. Hirota, K. Fukushima, K. Hiratani, J. Kadota, K. Kawano, M. Oka, A. Tomonaga, K. Hara, T. Sato, and J. Sunamoto, *J. Liposome Res.*, **1**, 15 (1989).
14) A. J. De Konig, *J. Chem. Educ.*, **51**, 48 (1974).
15) B. J. White, C. L. Tripton, and M. Dressel, *J. Chem. Educ.*, **51**, 533 (1974).
16) C. Huang, *Biochemistry*, **8**, 344 (1969).
17) H. Eibl and W. E. M. Lands, *Anal. Biochem.*, **30**, 51 (1969).
18) F. Szoka, Jr. and D. Paphadjopoulos, *Proc. Natl. Acad. Sci. U.S.A.*, **75**, 4194 (1978).
19) S. Udenfriend, S. Stein, P. Bohlen, W. Dairman, W. Leimgraber, and W. Weigele, *Science*, **178**, 871 (1972).
20) C. J. O'Connor, R. G. Wallace, K. Iwamoto, T. Taguchi, and J. Sunamoto, *Biochim. Biophys. Acta*, **817**, 95 (1985).
21) J. Sunamoto, S. Toshinori, and R. M. Ottenbrite, "Current Topics in Polymer Science," ed by R. M. Ottenbrite, L. A. Ultracki, and S. Inove, Hanser Publishers, Munish, Vienna, New York (1987), Vol. 1, p. 101.
22) B. F. Cain., G. J. Atwell, and W. A. Denny, Potential antitumour agents. 17. 9-Anilino-10-methylacridinium salts., *J. Med. Chem.*, **19**, 772 (1976).
23) C. J. O'Connor, D. P. Emery, H. Tank, W. A. Denny, and J. Sunamoto, *Chem.-Biol. Interact.*, **75**, 93 (1990).

Formation of Small Cobalt Clusters from CoNaY by Reduction with H_2 and Consecutive H_2-O_2 Treatments

Jae C. Kim† and Seong I. Woo*
Department of Chemical Engineering, Korea Advanced Institute of Science and Technology, P.O. Box 131, Cheongryang, Seoul 130-650, Korea
(Received May 11, 1990)

In order to raise the degree of reduction and promote the formation of zerovalent cobalt clusters, repetitive treatments of CoNaY with hydrogen and oxygen were carried out. The intensity of FMR (ferromagnetic resonance) band of CoNaY reduced for 36 h at 773 K with intermittent oxygen treatments was twice as much as that of CoNaY reduced only with hydrogen. This fact meant that reduction of CoNaY with H_2-O_2 treatments favored to produce zerovalent cluster due to the increase in the mobility of Co^{2+} ions in CoNaY. The size of clusters is so small that such conventional methods as hydrogen chemisorption, X-ray diffraction, and TEM can not detect the quantity of zerovalent cobalt clusters. FMR spectroscopy, H_2-consumption measurement, and catalytic probe reaction method were used to measure the degree of reduction and were correlated well with one another.

During the last decade, the properties of small metal cluster have become of increasing interest to physics and physical chemistry of catalysts.[1-3] The prospect of catalytic applications has motivated a large body of research about the preparation of well-defined metal clusters and their characterization to find out the electronic and structural properties in the range of size less than 1 nm. However, the physicochemical properties of supported small metal clusters of size less than 1 nm have not been studied extensively. The major obstacles are the preparation of supported small metal clusters showing stability toward agglomerization and reactant accessibility to the supported metal clusters of very small size. Ag, Cu, Ni, Pt, Pd, and Ru ions exchanged with NaY were easily reduced with hydrogen below 773 K.[4-6] However, these metals were found to migrate to the exterior surface of the zeolite to form clusters of size larger than 1 nm in diameter during reduction. In the case of cobalt, although it was very difficult to reduce cobalt ions exchanged in zeolite even at 773 K, reduced cobalt clusters remained inside zeolite pores.[1,9] This material is adequate to study the catalytic properties of small clusters of size less than 1 nm. Hence, our aim is to find out the method to increase the degree of reduction of cobalt ions in CoNaY to produce more cobalt metal clusters in CoNaY.

Many investigators reported that oxidation-reduction treatments of metal surface can change their catalytic properties in various catalytic reactions.[10-19] This phenomenon was explained based on the surface cleaning by O_2 treatment,[10] the possible promoting influence of oxygen remaining in chemisorbed state on the sub-surface region of metals,[11,12] or the increase in the surface area due to the repeated oxidation and reduction.[13] Amariglio et al.[14-16] recently reported that catalytic activities of cobalt ribbon in CO_2 methanation reaction was largely dependent on various oxidation-reduction treatments due to the significant rearrangement of the surface indicated by AES(Auger electron spectroscopy) and electron microscopy. This rearrangement was ascribed to the increase in the mobility of cobalt atom during oxidation cycles. These studies on the effects of H_2-O_2 suggested that repeated oxidation and reduction of CoNaY might increase the degree of reduction of Co^{2+} in CoNaY. The degree of reduction was measured with FMR which can detect the small amounts of zerovalent cobalt clusters of size less than 1 nm as well as paramagnetic cobalt ions in CoNaY. This FMR result was compared with the results of static H_2-consumption measurement and CO hydrogenation probe reaction.

Experimental

Preparation of Cobalt-Exchanged NaY (CoNaY). NaY zeolite (Strem Chem. Inc.) was used for cobalt ion-exchange. It was pretreated with 0.1 M of NaCl aqueous solution (1 M= 1 mol dm^{-3}) to remove sodium deficiency in NaY. Chloride ions were completely removed by washing with deionized water until AgCl was not precipitated when $AgNO_3$ was added to the spent deionized water. The detailed procedures are described elsewhere.[20] The cobalt loadings of CoNaY were found to be 5.4 wt%. This sample will be abbreviated as Co-IE-5.4 in the following text.

Measurement of H_2-Consumption during the Reduction of CoNaY. The amount of hydrogen consumed at 773 K was measured using chemisorption apparatus to estimate the degree of reduction of Co-IE-5.4 with reduction time. One gram of Co-IE-5.4 was dehydrated under 1.2×10^{-5} Torr (1 Torr=133.322 Pa) at 773 K for 2 h to remove physisorbed water and part of hydroxyl groups on the surface of the zeolite. After dehydration, known volume of H_2 purified with oxytrap and molecular sieve column was introduced to the chemisorption cell. The pressure changes inside the cell during the reduction of CoNaY at 773 K were recorded

† Present address: Chemical Engineering Division, Research Institute of Industrial Science and Technology, Pohang 790-600, Korea.

with MKS Baratron Pressure Guage (Model 170 series). After 20 h of reduction of CoNaY at 773 K, the pressure change with time was insignificant. Total amount of hydrogen either consumed in the reduction of CoNaY, adsorbed on zeolite, or adsorbed on the cobalt clusters reduced at 773 K was calculated from the pressure changes in the cell. In order to find out the exact amount of H_2 only consumed for the reduction of CoNaY, the reduced CoNaY was evacuated to 10^{-5} Torr at 773 K to remove H_2 either physisorbed on zeolite or chemisorbed on the reduced cobalt clusters. And then known volume of H_2 was introduced again into the cell. Because the reduction of CoNaY was completed in the first treatment of hydrogen, the pressure changes in this second treatment are due to the hydrogen adsorbed on zeolite and cobalt clusters. The difference between the amount of first hydrogen consumption and that of second hydrogen consumption indicated the amount of hydrogen consumed for the reduction of CoNaY at 773 K.

FMR Study. FMR spectra were recorded with Varian E-4 ESR (electron spin resonance) spectrometer equipped with a temperature controller to record the FMR spectra in the range of temperature from 153 K to 573 K. The spectrometer was operated in the X-band microwave frequency (9.115 GHz) with a modulation frequency of 100 kHz. An in situ FMR cell to pretreat CoNaY without contact of air reported elsewhere was used.[20] 0.3 g of Co-IE-5.4 was dehydrated under 1.2×10^{-5} Torr at 773 K for 1 h to avoid the complication of water vapor during the pretreatment at 773 K. This dehydrated sample was reduced in 60 ml min^{-1} flow of hydrogen then oxidized in 40 ml min^{-1} flow of oxygen at 773 K. This procedure was repeated. After this pretreatment, sample was evacuated to 10^{-5} Torr for 1 h at 773 K to remove chemisorbed H_2 or O_2 and lowered to 298 K under vacuum. Then the sample was transferred to quartz ESR tube attached to the in situ FMR cell. This ESR tube (o.d.: 4 mm) was placed in the cavity of the ESR spectrometer to record FMR spectra.

CO Hydrogenation Reaction. CO hydrogenation reaction was carried out at 1 atm in a differential flow tubular reactor. Carbon monoxide (Research grade, 99.95%, Takachiho, Japan) and hydrogen (99.995% purity) prepared with electrolysis (Teledyne Electro Cell hydrogen gas generator, Model MG 251) were further purified with oxytrap and molecular sieve trap. Oxygen (UHP, 99.99%, Matheson, USA) was used for oxidation of catalyst. Small amount of iron carbonyl was removed by decomposing it above 623 K in the preheating zone. The flow rates of CO and H_2 were controlled with fine metering valve and mass flow meter (Brooks Inc., Model 5841). Reaction temperature was controlled with digital programmable controller with microprocessor (PID type controller, RKC Instrument Inc. Model Rex-100). Reaction products were analyzed with a gas chromatograph (Hewlett-Packard, Model 5840A) equipped with porapak Q column (0.32 cm diameter, 1.83 m long). 0.2 g CoNaY was introduced to the reactor and pretreated with 60 ml min^{-1} of hydrogen flow at 523 K for 30 min. Temperature was raised slowly to the desired reduction or oxidation temperature (10 °C min^{-1}). After reduction-oxidation pretreatments, temperature was set at the reaction temperature under 20 ml min^{-1} of hydrogen flow. CO hydrogenation reaction was initiated by introducing 10 ml min^{-1} of carbon monoxide.

Results

Measurement of the Degree of Reduction. The amount of H_2-consumption during the reduction of Co-IE-5.4 was measured to estimate the degree of reduction of Co-IE-5.4. The amount of cobalt clusters was calculated from the amount of H_2 consumed in reducing Co^{2+} ions to Co metal clusters ($Co^{2+}+H_2\rightarrow Co+2H^+$). Figure 1(A) showed total amount of

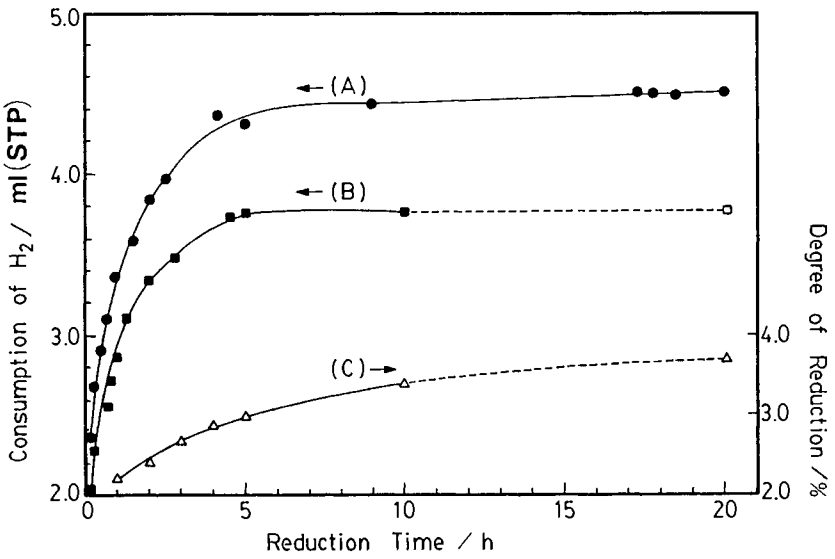

Fig. 1. H_2-consumption and % degree of reduction measured at 773 K as a function of reduction time. (A): total amount of H_2-consumption, (B): amount of H_2 adsorbed either on zeolite or reduced cobalt cluster at 773 K, (C): amount of H_2 consumed only for the reduction.

hydrogen consumed as a function of reduction time at 773 K. Total consumption of H_2 increased rapidly up to 1 h followed with a slow increase. The amount of H_2-consumption was very small after 3 h and negligible after 25 h. This sample was evacuated at 10^{-5} Torr and 773 K for 30 min, then the experiment was repeated to measure the amount of reversible adsorption (Fig. 1(B)). By subtracting the amount of H_2 reversibly adsorbed from total amount of H_2 consumed, the amount of H_2-consumption to reduce Co^{2+} ions to Co metal clusters was calculated. Percent degree of reduction was calculated from this value as shown in Fig. 1(C). The degree of reduction is 3.8% after 20 h of reduction at 773 K. Lee and Ihm[21] measured the degree of reduction with the method developed by Jacobs et al.[22] Their value is almost twice as much as ours, because the amount of H_2 consumption by Jacobs' method included H_2 physisorbed on zeolite or chemisorbed on cobalt clusters formed during reduction.

The general static method of H_2-chemisorption at room temperature with this reduced Co-IE-5.4 did not give any reproducible results either because the amount of zerovalent cobalt clusters (0.2 wt%) is too small or because H_2 chemisorption is suppressed on the cobalt clusters of size less than 1.3 nm in NaY.

FMR Study on the Formation of Cobalt Clusters on CoNaY. FMR spectra of Co-IE-5.4 reduced only with hydrogen at 773 K are shown in Fig. 2. An FMR band of weak intensity appeared overlapped with a weak EPR (electron paramagnetic resonance) band of Co^{2+} (g=2.007) after 1 h of reduction (Fig. 2(A)). A broad and asymmetric band appeared after reduction of Co-IE-5.4 with H_2 for 6 h (see Fig. 2(B)). The temperature dependence of this FMR spectrum is shown in Fig. 3. The FMR band of Fig. 2(B) was deconvoluted based on the assumption that the band is composed of two bands, i.e., broad band (I) of Gaussian type and narrow band (II) of Lorenzian type. Computer simulation with adequate g-values, band widths, and band heights of bands (I) and (II) gives the amount of contribution of bands (I) and (II) to total bands as shown in Table 1. A symmetric and broad band (band (I)) appeared (g=2.278, ΔH_{pp}, peak-to-peak band width=900 G) at the FMR recording temperature of 303 K (Fig. 3). A sharp band (band (II)) started to appear (g=2.132, ΔH_{pp}=330 G) at the FMR recording temperature of 423 K, which was superimposed with band (I). Because of appearance of band (II) the whole FMR band became asymmetric, which was more pronounced at 523 K. FMR spectra of Co-IE-5.4 became symmetric and ΔH_{pp} decreased as the reduction time increased as shown in Figs. 2(C) and 2(D).

It was expected that as the reduction time increased, the size of cobalt clusters must increase, which should be reflected in the increase in ΔH_{pp}. However, the opposite phenomenon was observed. At the initial stage of reduction for 1 h, a broad FMR of weak intensity appeared (Fig. 2(A)). The intensity of this broad band increased rapidly during the reduction for 6 h. Cobalt ions located in the sodalite and the

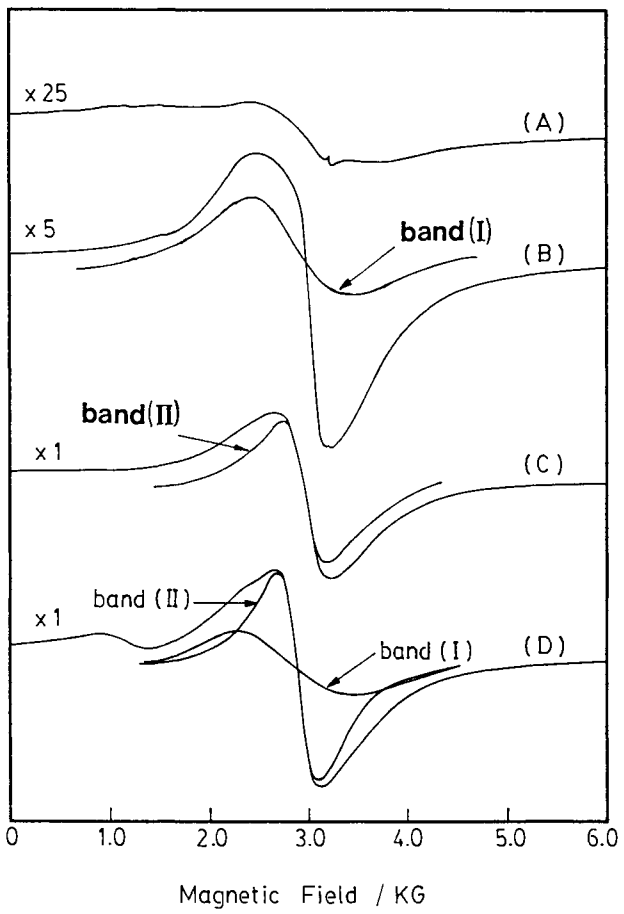

Fig. 2. FMR spectra of Co-IE-5.4 recorded at 523 K reduced with H_2 at 773 K. (A): reduced for 1 h, (B): reduced for 6 h, (C): reduced for 20 h, (D): reduced for 40 h.

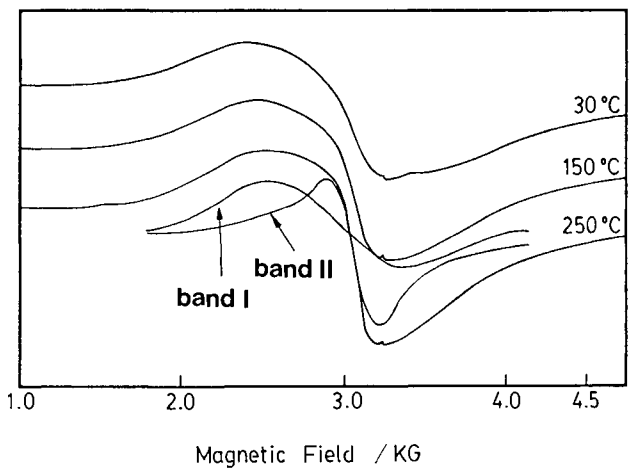

Fig. 3. FMR spectra of Co-IE-5.4 reduced at 773 K for 6 h as a function of recording temperature.

Table 1. Relative Portions of Band(II) in Total FMR Band of CoNaY Reduced with Hydrogen and H_2-O_2 Cycles

Seq. No.	Pret. cond.	Amplitude of total band[a)]	ΔH_{pp} / G	Amplitude of band(II)	Ratio of amplitude of band(II) to that of total band
	R-6	12.4	760	10.6	0.85
	R-20	35.0	600	31.8	0.88
	R-40	45.0	490	43.2	0.96
1	R-3	1.7	825	1.2	0.71
2	O-1-R-5	12.8	840	8.4	0.65
3	O-1-R-12	43.0	900	17.0	0.40
4	O-1-R-15	55.0	880	14.0	0.25

a) Amplitude indicates the height of FMR band (a.u.).

supercage are found to be reduced very slowly.[20] Hence, the band of Fig. 2(A) and the broad band of Fig. 2(B) must be ascribed to unexchanged cobalt hydroxide remained on the exterior surface or the cobalt ions located on the exterior surface of the zeolite because of their fast reduction rate. However, the amount of this cobalt species was smaller than cobalt ions located inside zeolite pores. Further redution of Co-IE-5.4 produced more cobalt clusters inside zeolite pores, resulting in the increase of the intensity of narrow FMR band (Fig. 2(C)) overlapped with broad band (I) whose intensity is much less than that of narrow band (II) (see Table 1). After reduction for 40 h, ΔH_{pp} was 490 G at 523 K while g-value did not vary much (g=2.20). The intensity of band (II) increased more rapidly than that of band (I) as reduction time increased.

The FMR spectra of Co-IE-5.4 reduced with H_2-O_2 cycles are shown in Fig. 4. The FMR spectrum of Co-IE-5.4 after reduction for 3 h showed two peaks similar to the FMR band of Co-IE-5.4 reduced for 6 h (see Fig. 4(A) and Fig. 2(B)). After oxidation for 1 h and further reduction for 5 h, the intensity of band (I) increased, while the contribution of band (II) superimposed with band (I) decreased as compared with that of Co-IE-5.4 reduced with only H_2 for 6 h (see Fig. 2(B) and Table 1). However, band (II) is clearly present in Fig. 4(B) (g=2.122, ΔH_{pp}=300 G). After repeated pretreatments of H_2-O_2 the shape of FMR band became symmetric without much change in ΔH_{pp} and g-value ($800<\Delta H_{pp}<900$ G and g=2.3). However, the intensity of the band increased.

The intensity of FMR band obtained from the double integration of FMR spectrum is proportional to the amount of Co metal clusters reduced from Co-IE-5.4 if the magnetic susceptibility per cobalt atom is constant regardless of size and shape of cobalt clusters. The intensity of FMR band of cobalt clusters reduced from Co-IE-5.4 with H_2 is shown in Fig. 5(A). When Co-IE-5.4 was pretreated with H_2-O_2 repeatedly, the intensity of FMR band increased more rapidly as shown in Fig. 5(B). The intensity of FMR band of Co-IE-5.4 reduced for 36 h at 773 K with intermittent oxygen treatments is twice as much as that of Co-IE-5.4 reduced with H_2 only.

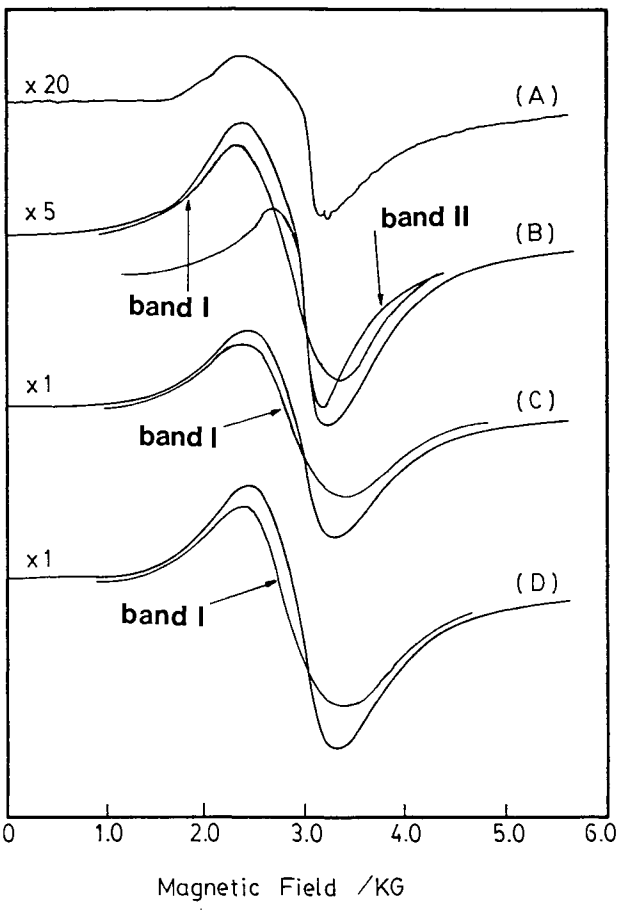

Fig. 4. FMR spectra of Co-IE-5.4 after repetitive pretreatments of H_2-O_2 recorded at 523 K. (A): reduced only for 3 h, (B): oxidized for 1 h and then reduced for 5 h after pretreatment of (A), (C): oxidized for 1 h and then reduced for 12 h after pretreatment of (B), (D): oxidized for 1 h and then reduced for 15 h after pretreatment of (C).

CO Hydrogenation Reaction. Catalytic activities per gram of cobalt of Co-IE-5.4 reduced by either H_2 or cyclic pretreatments of H_2 and O_2 are shown in Figs. 6(A) and (B), respectively. Co-IE-5.4 was pretreated by O_2 at 773 K for 1 h at each point in Fig. 6(B) and purged by helium for 30 min before reduction with

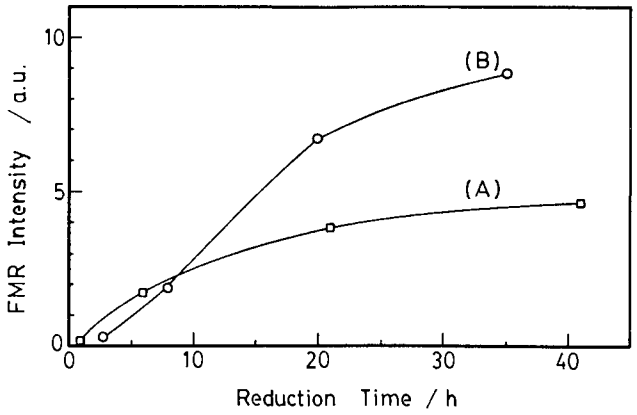

Fig. 5. The intensity of FMR band obtained from double integration of FMR band. (A): as a function of reduction time, (B): as a function of total reduction time. One hour of oxidation was carried out at each point prior to reduction.

H_2. The activities of Co-IE-5.4 reduced by H_2-O_2 treatments were higher by 1.6 times than that of Co-IE-5.4 reduced by only H_2 after 36 h of reduction. In the case of reduction with H_2 only, the pattern of increase in the catalytic activity with reduction time was different from that of increase in the amount of zerovalent cobalt cluster as shown in Figs. 1 and 5. The activity did not increase much up to 25 h of reduction but increased rapidly after 25 h of reduction. In contrast, the catalytic activity of Co-IE-5.4 reduced with H_2-O_2 cycles increased more rapidly than that of Co-IE-5.4 reduced with H_2 only up to 20 h of reduction. After 20 h of reduction, the activity of Co-IE-5.4 reduced with H_2-O_2 cycles increased in the rate similar to that of Co-IE-5.4 reduced with H_2 only.

Selectivities, activities, and TON are shown in Tables 2 and 3. The methane selectivity of Co-IE-5.4 pretreated with only H_2 was lower than that of Co-IE-

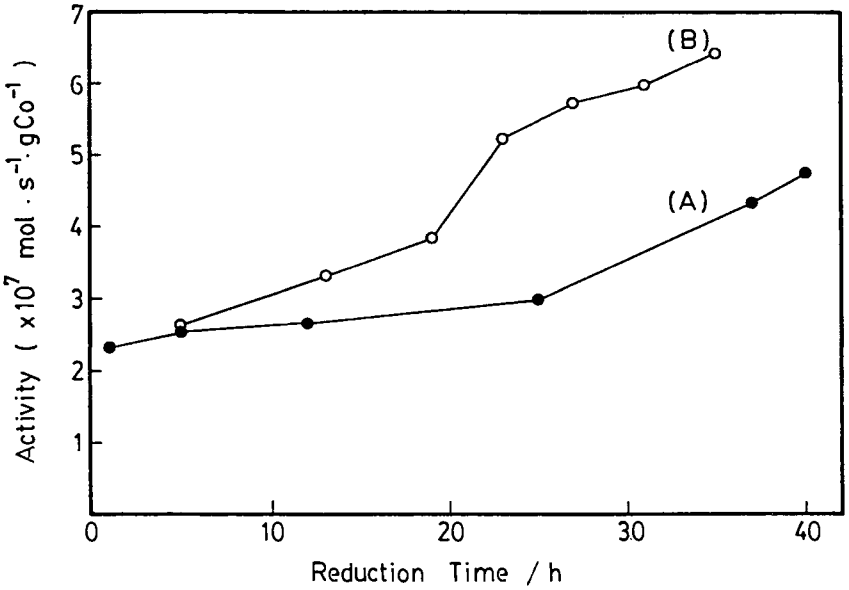

Fig. 6. The catalytic activities of Co-IE-5.4 in CO hydrogenation reaction. (A): as a function of reduction time, (B): as a function of total reduction time. Oxidation was carried out for 1 h at each point prior to reduction.

Table 2. Catalytic Activities and Selectivities of Co-IE-5.4 in CO Hydrogenation Reaction at 723 K as a Function of Reduction Time

Pret. cond.	Activity[b]	Selectivity/mol%			TON[c]
	$\times 10^7$ mol s^{-1} (g-Co)$^{-1}$	C_1	C_2	C_3	$\times 10^3$ s^{-1}
R-1[a]	2.33	71.0	23.9	5.1	0.01
R-5	2.55	74.4	21.1	4.5	0.50
R-12	2.67	75.2	20.5	4.3	0.46
R-25	2.99	75.2	20.5	4.3	0.48
R-37	4.43	77.6	19.1	3.3	—
R-40	4.78	77.2	19.1	3.7	—

a) R-1 means reduction in H_2 flow (60 ml min^{-1}) for 1 h at 773 K. b) Based on the amount of hydrocarbons produced after 30 min of reaction. c) TON based on the amount of zerovalent cobalt cluster of 100% dispersion measured with H_2 consumption method.

Table 3. Catalytic Activities and Selectivities of Co-IE-5.4 in CO Hydrogenation Reaction at 723 K after Cyclic Pretreatments of H_2-O_2

Sequence No.	Pret. cond.	Activity[b]	Selectivity/mol%		
		$\times 10^7$ mol s^{-1} (g-Co)$^{-1}$	C_1	C_2	C_3
1	R-5	2.55	74.4	21.1	4.5
2	O-1-R-8[a]	3.32	78.4	18.0	3.6
3	O-1-R-6	3.84	78.8	17.8	3.4
4	O-1-R-4	5.25	81.8	15.3	2.9
5	O-1-R-4	5.71	84.1	13.2	2.7
6	O-1-R-4	5.99	84.5	12.9	2.6
7	O-1-R-4	6.41	85.5	12.1	2.4

a) O-1-R-8 means that after experiment of seq. no. 1, Co-IE-5.4 was oxidized at 773 K for 1 h, then reduced at 773 K for 8 h. b) Based on the amount of hydrocarbons produced after 30 min of reaction.

5.4 pretreated H_2-O_2 cycles. In both cases, the activities and selectivities of methane increases with increasing reduction time. Ethane and propane were not produced. Only ethylene and propylene were produced. In contrast, the cobalt clusters of size larger than 2 nm at 723 K in CO hydrogenation reaction produced only methane.

Discussion

Reducibility of Co^{2+} Ions in Co-IE-5.4. As shown in Fig. 1(C), 90% of reduction proceeded within 10 h and thereafter reduction proceeded very slowly (H_2-consumption rate=0.06 ml h^{-1}). Co^{2+} ions in CoNaY were reduced rapidly at the initial stage of reduction (H_2-consumption rate=0.46ml h^{-1}). This result suggests that the location of cobalt ions in CoNaY to be reduced determines the rate of reduction. Co^{2+} ions located on the exterior surface of CoNaY or on supercage (site II and site III) are reduced more rapidly than Co^{2+} ions located in sodalite cage (site I′ and site II′), resulting in higher H_2-consumption rate at the initial stage of reduction. Co^{2+} ions located in hexagonal prism (site I) may not be reduced at all. Our sample used in H_2-consumption measurement was dehydrated at 773 K to avoid adverse effect of water vapor on the reduction of Co^{2+} with H_2. During dehydration, Co^{2+} ions were migrated from supercage into either sodalite cage or hexagonal prism.[23-25] Gallezot and Imelik[25] reported through their X-ray diffraction study that 83 and 17% of Co^{2+} ions were located in hexagonal prism and sodalite cage, respectively, when 55% cobalt-changed CoNaY was completely dehydrated. When CoNaY was partially dehydrated, 41, 37, and 22% of Co^{2+} ions were located in hexagonal prism, sodalite cage, and supercage, respectively. The degree of ion-exchange in Co-IE-5.4 is 58%, which is similar to that of the work of Gallezot and Imelik. Our sample has a small amount of Co^{2+} ions located in the supercage which can be reduced rapidly at the initial stage of reduction. Most of Co^{2+} ions located inside sodalite cage and hexagonal prism can not be reduced, resulting in the small degree of reduction (3.8%).

FMR results are also in agreement with H_2-consumption measurement. After 1 h of reduction, band (I) appeared without the appearance of band (II) (Fig. 2(A)). Band (II) was ascribed to the cobalt clusters located in supercage indicated by the narrow ΔH_{pp} and its Lorenzian line shape according to the results of Che et. al.[26] Jacobs et. al.[27] also reported that Lorenzian line shape or Gaussian line shape of FMR band was obtained if the spherical metal particles had a certain particle size distribution and that FMR band of Gaussian line shape was assigned to the population of large particles. The FMR bands of Co-IE-5.4 reduced with H_2 were composed of band (I) of Gaussian line shape and band (II) of Lorenzian line shape estimated by Poole's method.[28] The intensity of band (II) increased with reduction time, suggesting that Co^{2+} ions inside zeolite cage were slowly reduced. The relative portion of band (II) superimposed with band (I) increased with reduction time (see Table I). ΔH_{pp} and g-values of band (II) did not change much with recording temperature (see Fig. 3), which is characteristic of superparamagnetic cobalt particles. Prolonged reduction did not cause ΔH_{pp} of band (II) to be increased indicating that there was no sintering of cobalt clusters. Cobalt clusters are stabilized inside zeolite pores (see Table 1, Figs. 2(B) and 2(D)). Band (I) appeared right after the reduction started. And its contribution to the total FMR band of Co-IE-5.4 reduced for 40 h at 773 K is only 4% (see Table 1). These results indicated that cobalt ions present as a hydroxide form on the exterior surface or in the half sphere of supercage on the exterior surface are reduced to show band (I).

Iton et. al.[3] reported the FMR spectra of cobalt clusters prepared from the reduction of $Co(NH_3)_6^{3+}$-exchanged Y zeolite. High temperature FMR data suggested that a small amount of Co metal particles was produced. ΔH_{pp} of their FMR spectrum of cobalt clusters at FMR recording temperature of 523 K was 600 G, which is larger than that of Co-IE-5.4 reduced

with hydrogen for 40 h at 773 K (ΔH_{pp}=490 G). This indicated that the size of cobalt clusters in Co-IE-5.4 is less than that of cobalt clusters reported by Iton et al.[3] Zerger et al.[29] also reported the FMR spectra of cobalt clusters supported on NaX obtained from the decomposition of $Co_2(CO)_8$ with microwave discharge. The ΔH_{pp} of prepared cobalt clusters (30 Å in diameter) was 1050 G at 523 K, which is larger than that of our sample. From these previous results, it can be concluded that the size of cobalt clusters obtained from the reduction of Co-IE-5.4 with H_2 is the smallest and that the size of cobalt clusters is dependent on the preparation method of cobalt clusters, although we failed to measure the size of cobalt clusters in CoNaY with TEM and hydrogen chemisorption method.

Reduction of Co-IE-5.4 Facilitated with H_2-O_2 Treatments. The FMR spectra of Co-IE-5.4 reduced with H_2 with intermittent oxygen treatments are presented in Fig. 4. The relative portion of Lorenzian band (II) in the FMR band decreased as the number of oxygen treatment increased (see Table 1). In addition to the change in line shape of FMR band, the degree of reduction with H_2-O_2 treatment is twice as much as that of reduction with only hydrogen (see Fig. 5).

It is clear that H_2-O_2 treatment facilitated the reduction of cobalt ions in Co-IE-5.4. It produced cobalt clusters larger than those produced by H_2-reduction. This result can be explained by the fact that O_2 pretreatment increases the mobility of Co^{2+} ions in CoNaY, resulting in the migration of nonreducible Co^{2+} ions located either in hexagonal prism or in sodalite cage to supercage. Co^{2+} ions in supercage were reduced more easily than Co^{2+} ions in hexagonal prism and sodalite cage. The probability that Co^{2+} ions can migrate to the supercage and the exterior surface of zeolite and collide with the cobalt clusters to form a large cobalt cluster was enhanced during the oxygen treatment at 773 K. The contribution of band (I) to the total FMR band increased with the number of oxygen treatment at 773 K indicating that the cobalt clusters inside supercage migrated out to the exterior surface of zeolite to form larger cobalt clusters. However, the size of cobalt clusters on the exterior surface of zeolite is still in the range of superparamagnetic particles evidenced by the fact that the g-value, intensity, ΔH_{pp} and symmetric shape of FMR band of cobalt clusters produced did not change much with the FMR recording temperature.

Catalytic Properties of Small Cobalt Clusters in CoNaY. Many authors showed that TON's in CO hydrogenation reaction increased with decreasing dispersion in the case of Co,[30,31] Ni,[32,33] Ru,[34,35] and Fe.[36] Jung et al.[36] reported that the TON increased more than 20 fold as iron crystallite size increased from about 1 to 10 nm, whereas the activities of gram iron or gram catalyst basis were similar because the low TON's on high dispersion catalysts were compensated by the higher iron surface area. We reported that TON of cobalt clusters (100 nm in diameter) prepared by impregnating aqueous $Co(NO_3)_2 \cdot 6H_2O$ solution to NaY (10 wt% cobalt loading) is 34 s^{-1} and that TON of cobalt clusters prepared by the reduction of Co-IE-5.4 (0.8 nm in diameter by CO chemisorption method) is 0.46×10^{-3} s^{-1} in the CO hydrogenation reaction at 723 K.[20] The TON's of cobalt clusters obtained by the H_2 reduction of Co-IE-5.4 are in the range of order of 10^{-4} s^{-1} in the CO hydrogenation reaction at 723 K (see Tables 2 and 3). We suspected that this small catalytic activity may come from the impurity of metals in NaY produced by H_2 reduction. Hence, we reduced NaY with H_2 in the same manner as the reduction of CoNaY and found out that NaY reduced with H_2 has no catalytic activity in the CO hydrogenation reaction at 723 K. This allows us to conclude that the small catalytic activity of Co-IE-5.4 reduced with H_2 is ascribed to the small cobalt clusters produced. This low catalytic activity must be due to the suppression of hydrogen chemisorption on the small cobalt clusters less than 1.3 nm, which is the approximate size of the supercage in NaY. The appreciable amount of H_2 could not be chemisorbed on cobalt clusters in Co-IE-5.4 at room temperature. However, very small amount of H_2 can be dissociatively chemisorbed at 723 K, because the H_2 chemisorption on cobalt clusters is known to be an activated chemisorption.[37] The appreciable catalytic activity in CO disproportionation reaction at 393 K with small cobalt clusters of Co-IE-5.4[38] indicated that CO is easily dissociatively chemisorbed on the cobalt clusters of sizes less than 1.3 nm at 393 K. These results lead us to conclude that the small catalytic activity of small cobalt clusters in the CO hydrogenation reaction is due to the suppression of H_2 chemisorption. The capability to produce C_2- and C_3-hydrocarbon at the reaction temperature of 723 K also suggests a unique catalytic properties of small cobalt clusters. The suppression of H_2 chemisorption is also evidenced by the formation of C_2- and C_3-olefinic hydrocarbons.

The catalytic activity in CO hydrogenation reaction increased with reduction time as shown in Fig. 6(A). The activity of Co-IE-5.4 increased more rapidly with intermittent O_2 treatments between each reduction steps than with reduction by only H_2. The similar increasing trend of activity with that of FMR intensity means that the increase in the catalytic activity is related to the increase in the amount of cobalt metal clusters reduced from CoNaY whether it is prepared by H_2 only or repetitive H_2-O_2 treatment. This result indicated that the reduction is facilitated by the intermittent O_2 treatment due to the increase in the mobility of Co^{2+}, which is consistent with FMR results.

In summary, small cobalt clusters obtained by the reduction of CoNaY are adequate materials to study the catalytic properties of supported small cobalt clusters of diameters less than 1.3 nm. The reduction was facilitated by the consecutive H_2-O_2 treatment evi-

denced by FMR and CO hydrogenation probe reaction results. The chemisorption of H_2 on the very small size of cobalt clusters in Co-IE-5.4 was suppressed, while the CO chemisorption was not suppressed. The extraordinarily low catalytic TON's and 100% selectivity toward to olefinic hydrocarbons are supporting the suppression of H_2 chemisorption on the small cobalt clusters of Co-IE-5.4.

This work was partially funded by KAIST Basic Research Grant (1985) and KOSEF Basic Fundamental Research Grant (1986—1989).

References

1) Kh. M. Minachev, G. V. Antoshin, E. S. Shpiro, and Yu. A. Yusifov, *Proc. Int. Congr. Catal., 6th*, **2**, 621 (1977).
2) J. R. Pearce, W. J. Mortier, and J. B. Uytterhoeven, *J. Chem. Soc., Faraday Trans. 1*, **77**, 937 (1981).
3) L. E. Iton, R. B. Beal, and P. J. Hamot, *J. Mol. Catal.*, **27**, 95 (1984).
4) H. Beyer, P. A. Jacobs, and J. B. Uytterhoeven, *J. Chem. Soc., Faraday Trans. 1*, **72**, 674 (1976).
5) P. A. Jacobs, J. Ph. Linnart, H. Nijs , J. B. Uytterhoeven, and H. K. Beyer, *J. Chem. Soc., Faraday Trans. 1*, **73**, 1745 (1977).
6) C. Naccache, M. Primet, and M. V. Mathien, *Adv. Chem. Ser.*, **121**, 480 (1973).
7) B. Coughlan, S. Narayan, W. A. McCann, and W. M. Caroll, *J. Catal.*, **49**, 97 (1977).
8) R. Oukasi, A. Sayari, and J. G. Goodwin, Jr., *J. Catal.*, **102**, 127 (1986).
9) J. B. Uytterhoeven, *Acta Phys. Chem.*, **24**, 53 (1978).
10) J. C. Schlatter and M. Boudart, *J. Catal.*, **24**, 482 (1972).
11) D.G. Castner, R. L. Blackadar, and G. A. Somorjai, *J. Catal.*, **66**, 257 (1980).
12) R. L. Palmer and D. A. Vroom, *J. Catal.*, **50**, 244 (1977).
13) H. J. Krebs, H. P. Bonzel, and W. Schwarting, *J. Catal.*, **72**, 199 (1981).
14) A. Jnioui, M. Eddouasse, A. Amariglio, J. J. Ehrhardt, J. Lambert, M. Alnot, and H. Amariglio, *Surf. Sci.*, **162**, 368 (1985).
15) A. Amariglio and H. Amariglio, *J. Catal.*, **68**, 86 (1981).
16) A. Amariglio, M. Lakhdar, and H. Amariglio, *J. Catal.*, **81**, 247 (1983).
17) D. J. Dwyer and G. A. Somorjai, *J. Catal.*, **52**, 291 (1978).
18) S. J. Cochran and F. P. Larkins, *J. Chem. Soc., Faraday Trans. 1*, **81**, 2179 (1985).
19) M. Audier, J. Klinowski, and R. E. Benfield, *J. Chem. Soc., Chem. Commun.*, **1984**, 626.
20) J. C. Kim and S. I. Woo, *Appl. Catal.*, **39**, 107 (1988).
21) D. K. Lee and S. K. Ihm, *J. Catal.*, **106**, 386 (1987).
22) P. A. Jacobs, M. Tielen, J. P. Linart, J. B. Uytterhoeven, and H. Beyer, *J. Chem. Soc., Faraday Trans. 1*, **72**, 2793 (1976).
23) P. J. Hutta and J. H. Lunsford, *J. Chem. Phys.*, **66**, 4716 (1977).
24) T. A. Egerton, A. Hayen, F. S. Stone, and J. C. Vickermann, *J. Chem. Soc., Faraday Trans. 1*, **68**, 723 (1972).
25) P. Gallezot and B. Imelik, *J. Chim. Phys.*, **71**, 155 (1974).
26) M. Che, M. Richard, and D. Olivier, *J. Chem. Soc., Faraday Trans. 1*, **76**, 1526 (1980).
27) P. A. Jacobs, H. Nijs, J. Verdonck, E. G. Derouane, J. P. Gilson, and A. J. Simoens, *J. Chem. Soc., Faraday Trans. 1*, **75**, 1196 (1979).
28) C. P. Poole, Jr., "Electron Spin Resonance," 2nd ed, Wiley, N. Y., Chap. 12.
29) R. P. Zerger, K. C. McMahon, M. D. Seltzer, R. G. Michel, and S. L. Suib, *J. Catal.*, **99**, 498 (1986).
30) L. Fu and C. H. Bartholomew, *J. Catal.*, **92**, 376 (1985).
31) R. C. Reuel and C. H. Bartholomew, *Ind. Eng. Chem. Prod. Res. Dev.*, **24**, 56 (1985).
32) M. A. Vannice, *J. Catal.*, **44**, 152 (1976).
33) C. H. Bartholomew, R. B. Pannell, and J. C. Butler, *J. Catal.*, **65**, 335 (1980).
34) R. A. Dalla Betta, G. A. Pikea, and M. Shelef, *J. Catal.*, **35**, 54 (1974).
35) C. S. Kellner and A. T. Bell, *J. Catal.*, **75**, 251 (1982).
36) H. J. Jung, P. L. Walker, Jr., and M. A. Vannice, *J. Catal.*, **75**, 416 (1982).
37) J. M. Zowtiak and C. H. Bartholomew, *J. Catal.*, **83**, 107 (1983).
38) C. S. Kim and S. I. Woo, paper in preparation (1990).

The Conformational Changes of Poly(L-ornithine) with Organic Counter Ions in Aqueous Sodium 1-Decanesulfonate Solution

Makoto AOYAGI, Tamaki MAEDA, Katumitu HAYAKAWA, and Iwao SATAKE*
Department of Chemistry, Faculty of Science, Kagoshima University, Korimoto, Kagoshima 890
(Received October 3, 1990)

Synopsis. The circular dichroism study was made of the coil-helix transitions of poly(L-ornithine) with 1-alkanesulfonate counter ions of the chain length from 3 to 6 in sodium 1-decanesulfonate solution. The conformational change is insensitive to the counter ion chain length and becomes appreciable even at surfactant concentrations as low as $(1—2)\times10^{-4}$ mol dm^{-3}.

It is well known that additions of the ionic surfactants to the oppositely charged polypeptides in neutral solutions induce conformational transitions from coil to ordered structures.[1-9] For instance, poly(L-ornithine) (PO) undergoes a coil to helix transition in solutions of anionic surfactants such as sodium alkyl sulfate[10-12] and alkanesulfonate[8,9] even at remarkably lower concentrations than critical micelle concentrations. It has been inferred from the binding isotherm measurements that the surfactant ion binds cooperatively onto PO chain to give rise to a micelle like cluster.[8,9,12] The presence of such clusters has been pointed out to be essential for the surfactant-induced coil to helix transition of PO.[8]

So far as we know, however, all of the studies reported so far are concerned only with the ionic polypeptides with inorganic counter ions. It is thus interesting to study the surfactant induced conformational change of polypeptide with organic counter ion of varying hydrophobicity, since the presence of such counter ions is anticipated to affect the binding characteristics of surfactant ion. In this paper we report on the conformational changes of poly(L-ornithine) with 1-alkanesulfonate counter ions of carbon atoms n=3, 4, 5, and 6 (PO·C$_n$) in sodium 1-decanesulfonate (SDeS) solution.

Experimental

SDeS was synthesized from vacuum distilled 1-bromodecane by the sulfonation with sodium sulfite. Sodium 1-alkanesulfonates (Guaranteed grade, Tokyo Kasei Kogyo Co., Ltd.) were used without further purifications. Hydrochloride of PO (PO·Cl) and PO·C$_n$ were prepared by dialyzing hydrobromide of PO (Sigma, MW=41000 for n=5 and 6, and 25000 for the rest) against 0.1 mol dm^{-3} HCl and the corresponding sodium 1-alkanesulfonate respectively, and then against distilled water. The polypeptide concentration (C_p) in molarity of ionic groups was determined by colloid titration with poly(potassium vinyl sulfate) (Wako Pure Chemical Industries Ltd.).

Circular dichroism (CD) spectra of PO·Cl and PO·C$_n$ were measured as a function of SDeS concentration under the condition of constant C_p of 2.5×10^{-4} mol dm^{-3}. The spectra were recorded on JASCO spectropolarimeter J-20A. The potentiometric measurement on PO·C$_5$ - SDeS system was made with a cell based on nitrobenzene membrane electrode. The construction of the cell was described elsewhere.[13] All measurements were conducted in the absence of added salt at 25 °C.

Results and Discussion

Figure 1 shows the typical CD spectra of PO·C$_5$ recorded shortly after mixing with SDeS solutions of varying concentrations (C). Similar results are also obtained for PO·Cl and PO·C$_n$ with n=3, 4, and 6. In all cases, the CD spectrum varies successively from a characteristic spectrum of random coil at C=0 to that of helical conformation with a double minimum located around 207 and 222 nm. The presence of the isoelliptic point at 205 nm suggests the occurrence of a simple conformational transition from coil to helix under our experimental conditions.

According to the theory of polyelectrolyte solutions, the fraction of condensed counter ions is given by

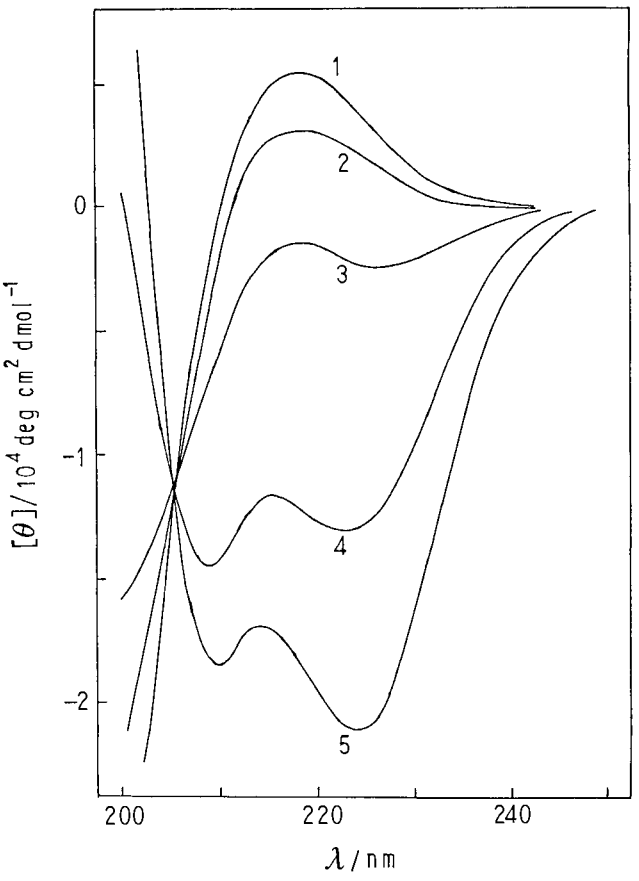

Fig. 1. The change in CD spectrum of PO·C$_5$ with SDeS concentration (C). C_p=2.5×10^{-4} mol dm^{-3}; C/mmol dm^{-3}=0 (1), 0.25 (2), 0.5 (3), 1.25 (4), 3.0 (5).

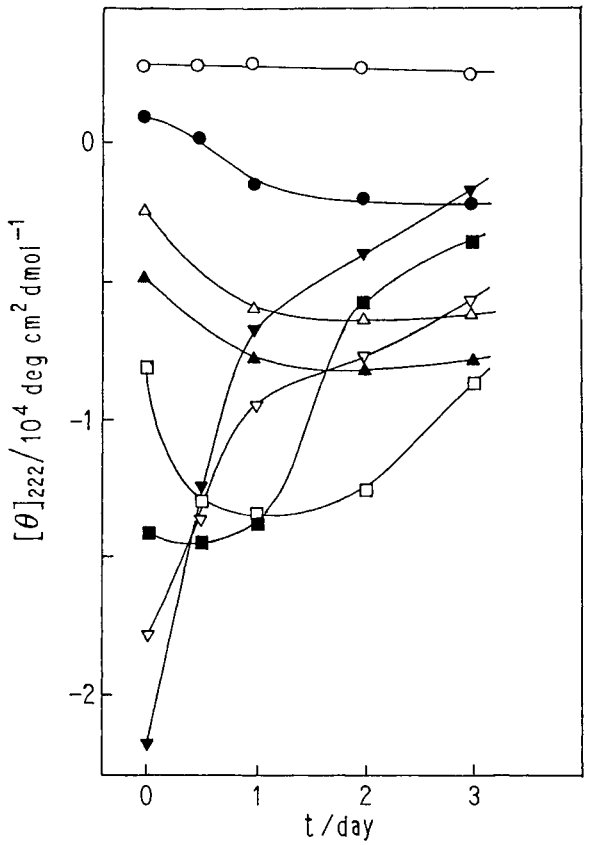

Fig. 2. The time-course of $[\theta]_{222}$ for PO·C_5 in SDeS solutions. C_P=2.5×10^{-4} mol dm^{-3}; C/mmol dm^{-3}=0 (○), 0.50 (●), 0.75 (△), 1.00 (▲), 1.25 (□), 1.50 (■), 2.00 (▽), 3.00 (▼).

$1-1/\xi$, where ξ represents a dimensionless structural parameter defined in terms of the average axial charge spacing (d) in nm as $\xi=0.714/d$ in water at 25 °C.[14,15] For the present systems, the structural consideration suggests that roughly 50% of counter ions are condensed onto PO chain. Therefore, it is highly probable that the average hydrophobicity around PO chain increases monotonically with increasing chain length of the counter ion even in the absence of surfactant ion. Nevertheless, CD spectrum of PO shows the characteristics of a random coil regardless of n. This fact implies that the presence of condensed hydrophobic counter ions with n up to 6 is insufficient to induce a conformational change of PO·C_n alone.

The CD spectrum of PO·C_n in SDeS solution varies gradually over a period of days on standing. A typical example for PO·C_5 is shown in Fig. 2. At lower surfactant concentrations, the mean residue ellipticity at 222 nm, $[\theta]_{222}$, the magnitude of which is proportional to the helical content, decreases monotonically with time and tends eventually to a constant. At higher surfactant concentrations, however, $[\theta]_{222}$ goes through a minimum or increases rapidly with time, because of the progress of aggregation process. Taking these into consideration, we adopted the minimum value of $[\theta]_{222}$ as a measure of helical content at a given surfactant concentration.

In Fig. 3 are plotted the values of $[\theta]_{222}$ thus determined as a function of surfactant concentration. In all cases, the helical content of PO increases monotonically with increasing surfactant concentration and becomes eventually constant at higher concentrations where the visible precipitate of PO—surfactant complex appears.

An interesting feature of Fig. 3 is an unexpected resemblance among $[\theta]_{222}$ vs. C curves for PO with counter ions of varying hydrophobicity. As a result of counter ion condensation phenomenon as noted above, the average hydrophobicity around binding

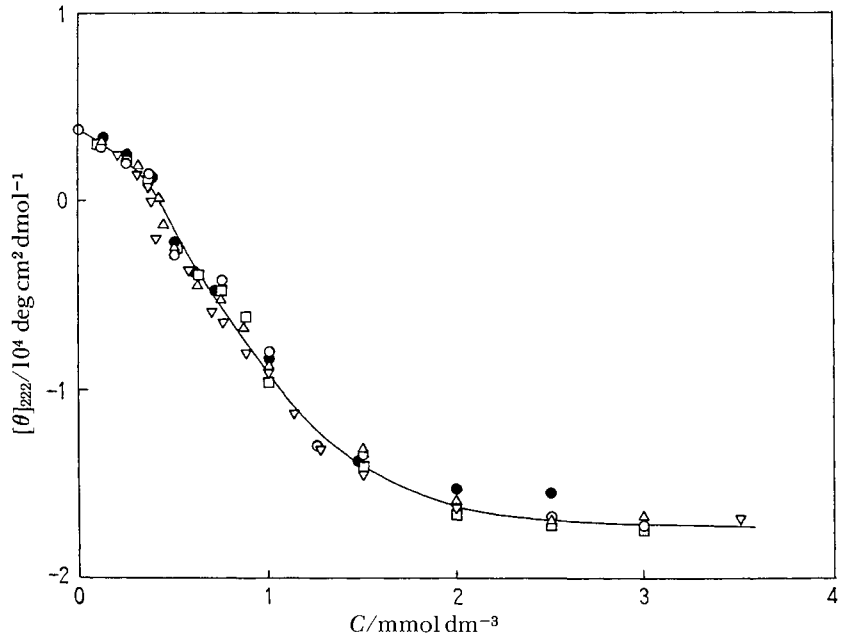

Fig. 3. The change in $[\theta]_{222}$ for PO·Cl and PO·C_n with SDeS concentration. C_P=2.5×10^{-4} mol dm^{-3}: ○, PO·Cl; △, n=3; □, n=4; ▽, n=5; ●, n=6.

site is supposed to increase regularly with increasing chain length of the counter ion. This effect will bring about a change in the intrinsic binding constant of the surfactant ion to PO. In addition, the bound surfactant ions are anticipated to form a mixed cluster with condensed counter ions, especially of a longer chain length. In solutions of PO·C_n, therefore, the binding mechanism on which the conformational change rests is considered to differ somewhat from that in solutions of PO with inorganic counter ions. In the latter case, the average cluster size of the bound surfactant ions is pointed out to be a primary determinant of the surfactant induced coil to helix transition.[8] Although the detailed explanation for the observed resemblance among $[\theta]_{222}$ vs. C curves can not be offered at the present stage, it is probable that the overall hydrophobicity of PO·C_n-surfactant complex at a given surfactant concentration is nearly identical with one another regardless of the counter ion chain length.

Another feature of Fig. 3 is the onset of conformational change at remarkably low concentration range as low as $(1—2)\times10^{-4}$ mol dm^{-3}. This behavior is in marked contrast with that of PO·Cl in SDeS solutions in the presence of added NaCl.[8,9] Under the conditions of $C_p=2.15\times10^{-4}$ mol dm^{-3} and [NaCl]$=2.1\times10^{-2}$ mol dm^{-3}, $[\theta]_{222}$ of PO·Cl was found to decrease abruptly around $C=7\times10^{-4}$ mol dm^{-3}, where the steep rise in binding isotherm occurs.[8,9] Moreover, an addition of the salt has been noted to affect the binding characteristics of the surfactant ion to polyelectrolyte in such a way that the logarithm of the equilibrium surfactant concentration at half binding decreases linearly with the logarithm of the added salt concentration.[16–18] Thus the present result can reasonably be attributed to an onset of surfactant ion binding in the concentration range much lower than that in salt solutions. In order to make this point clear, the potentiometric study was made for PO·C_5 system. Figure 4 shows the plots of electromotive force (E) of the cell vs. log C for SDeS solutions with and without PO·C_5. In the absence of PO·C_5, the electrode responds to the 1-decanesulfonate ion down to 5×10^{-5} mol dm^{-3} with a slope of 58.2 mV. In the presence of PO·C_5, E vs. log C curve is seen to deviate remarkably from that of SDeS solution alone. Under our experimental conditions, the interference of 1-pentanesulfonate ion can safely be neglected since the selectivity coefficient of 1-pentanesulfonate ion with respect to 1-decanesulfonate ion is of the order of 3×10^{-3}.[19] Unfortunately, we can not construct the binding isotherm from Fig. 4 because of the lack of a detailed knowledge of the counter ion activity coefficient in such a complex system as surfactant-polyelectrolyte solution without added salt. With these reservations in mind, an equilibrium surfactant concentration is considered to be small enough even at the lowest concentration studied ($C=2\times10^{-4}$ mol dm^{-3}). This in turn supports the foregoing presumption that the surfactant ion binding starts at remarkably low concentration range around $(1—2)\times10^{-4}$ mol dm^{-3}.

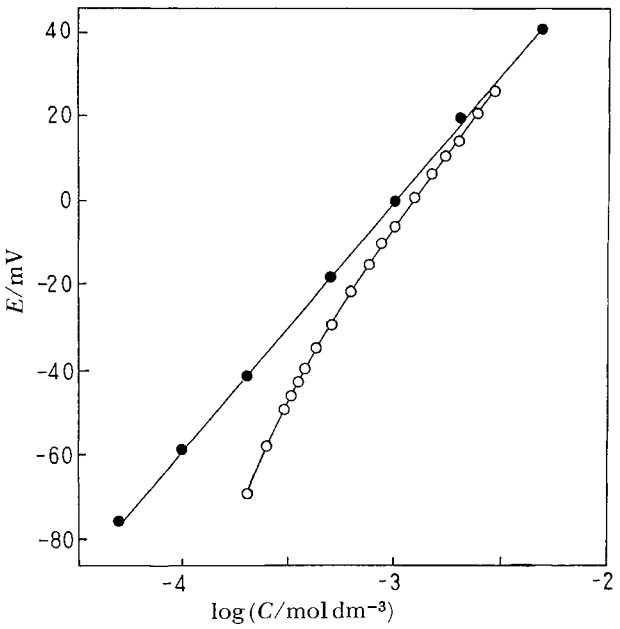

Fig. 4. Plots of the electromotive force (E) of the cell vs. log (C/mol dm^{-3}).
●, SDeS alone; ○, in the presence of PO·C_5 ($C_p=2.5\times10^{-4}$ mol dm^{-3}).

This work was supported in part by a Grant-in-Aid for Scientific Research No. 02640351 (to I. S.) from the Ministry of Education, Science and Culture.

References

1) I. Satake, *Hyomen*, **15**, 511 (1977).
2) K. Takeda, *Hyomen*, **23**, 351 (1985).
3) E. D. Goddard, *Colloids Surf.*, **19**, 301 (1986).
4) H. Maeda, M. Kimura, and S. Ikeda, *Macromolecules*, **18**, 2566 (1985).
5) H. Maeda, Y. Tanaka, and S. Ikeda, *Bull. Chem. Soc. Jpn.*, **59**, 769 (1986).
6) H. Maeda, K. Fujio, and S. Ikeda, *Colloid Polym. Sci.*, **266**, 248 (1988).
7) H. Maeda, T. Nezu, K. Fukuda, and S. Ikeda, *Macromolecules*, **21**, 1154 (1988).
8) I. Satake and K. Hayakawa, *Chem. Lett.*, **1990**, 1051.
9) K. Hayakawa, H. Murata, and I. Satake, *Colloid Polym. Sci.*, **268**, 1044 (1990).
10) M. J. Grourke and J. H. Gibbs, *Biopolymers*, **5**, 586 (1967).
11) I. Satake and J. T. Yang, *Biochem. Biophys. Res. Commun.*, **54**, 930 (1973).
12) I. Satake and J. T. Yang, *Biopolymers*, **15**, 2263 (1976).
13) I. Satake, K. Hayakawa, M. Komaki, and T. Maeda, *Bull. Chem. Soc. Jpn.*, **57**, 2995 (1984).
14) G. S. Manning, *J. Chem. Phys.*, **51**, 924 (1969).
15) G. S. Manning, *Acc. Chem. Res.*, **12**, 443 (1979).
16) K. Hayakawa and J. C. T. Kwak, *J. Phys. Chem.*, **86**, 3866 (1982).
17) K. Hayakawa and J. C. T. Kwak, *J. Phys. Chem.*, **87**, 506 (1983).
18) A. Malovikova, K. Hayakawa, and J. C. T. Kwak, *J. Phys. Chem.*, **88**, 1930 (1984).
19) I. Satake, S. Noda, and T. Maeda, *Bull. Chem. Soc. Jpn.*, **56**, 2581 (1983).

Electrochemical Halogenation of Trisubstituted Germanes and Silanes

Mitsutoshi OKANO* and Kunio MOCHIDA
Department of Chemistry, Faculty of Science, Gakushuin University, 1-5-1 Mejiro, Toshima-ku, Tokyo 171
(Received November 14, 1990)

Synopsis. Electrochemical halogenation of trisubstituted germanes and silanes in acetonitrile occurred in the cathode compartment in contrast to the well-known electrochemical halogenations which always occur in the anode compartment.

Organogermanium compounds and organosilicon compounds are interesting as the objects of electrochemical studies, because (1) they easily undergo electrochemical reactions as a result of their higher HOMO levels and lower LUMO levels compared with the carbon analogues,[1] and (2) electrochemically generated germanium and silicon species, such as anions, radicals, and cations, may have chemical properties, which are different from those of the corresponding carbon species.[2]

It is well-known that electrochemical halogenations occur in the anode compartment and dehalogenations in the cathode compartment.[3] Such electrochemical dehalogenations have also been reported for halogermanes and halosilanes.[4] The authors wish to report here an unusual cathodic halogenations, in which trisubstituted germanes and silanes afford halogenated germanes and silanes.

Experimental

All trisubstituted germanes and silanes were synthesized by the reduction of chloro-germanes and -silanes with $LiAlH_4$. They were identified by comparing their physical properties with those of reported values.[5]

Constant current electrolyses were carried out in a two-compartment cell using platinum plates (electrode surface= 6 cm^2) as the anode and the cathode. Aboout 2.5×10^{-4} mol of trisubstituted germanes or silanes was dissolved in 20 cm^3 of acetonitrile solution containing 0.1 mol dm^{-3} of tetrabutylammonium perchlorate (TBAP) or tetrabutylammonium tetrafluoroborate (TBATFB). Current density passed was about 0.17 mA cm^{-2}.

After the electrolyses, alliquots were sampled from each compartment and analysed directly with GC-MS for qualitative analyses and with HPLC for qualitative and quantitative analyses.

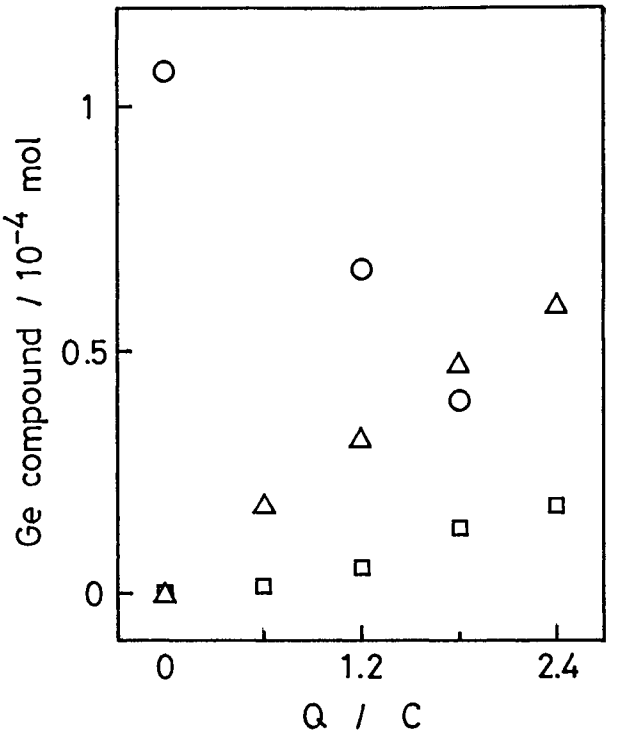

Fig. 1. Generation of Ph_3GeCl (△) and $(Ph_3Ge)_2O$ (□) in the cathode compartment during the electroreduction of Ph_3GeH (○).

Results and Discussion

The results in Fig. 1 were obtained by the constant current (1 mA) electrolysis of Ph_3GeH in the presence of TBAP. In the cathode compartment, Ph_3GeCl and $(Ph_3Ge)_2O$ were generated at constant rates while Ph_3GeH decreased at a constant rate. No such products were found in the anode compartment. After the passage of 0.21 F mol^{-1} of electricity, 63% yield of Ph_3GeCl and 37% yield of $(Ph_3Ge)_2O$ were obtained. A novel reaction pathway must be given for the formation of $(Ph_3Ge)_2O$ in the catholyte because the hydro-

Table 1. Products in the Catholyte Solution Detected by GC-MS. Typical Yields Determined by HPLC are Shown in Parentheses

Compound	Products (yield/%)			
	with TBAP		with TBATFB	
Ph_3GeH	Ph_3GeCl, (60)	$(Ph_3Ge)_2O$ (40)	Ph_3GeF, (a)	$(Ph_3Ge)_2O$ (70)
Ph_3SiH	—,	$(Ph_3Si)_2O$ (80)	Ph_3SiF, (a)	$(Ph_3Si)_2O$ (90)
Ph_2MeGeH[b]	$Ph_2MeGeCl$,	$(Ph_2MeGe)_2O$	Ph_2MeGeF,	$(Ph_2MeGe)_2O$
Ph_2MeSiH[b]	—,	$(Ph_2MeSi)_2O$	—,	$(Ph_2MeSi)_2O$

a) The yield could not be determined by HPLC. b) Yields are not shown because halogenated compounds were readily hydrolyzed.

lysis of Ph_3GeCl did not occur under the experimental conditions. Supposing a one electron reaction for the conversion of Ph_3GeH, the current efficiency is as high as 300—400%. Assuming again a one electron reaction for the following electrochemical generation of Ph_3GeCl, the current efficiency is calculated as 240% (see below Eqs. 1 and 2). The chlorine source for the Ph_3GeCl must be the electrolyte TBAP because there is no other chlorine source. Oxygen may come from TBAP, O_2, and/or residual H_2O in the electrolyte solution.

Table 1 summarises the experimental data. Typical product yields are shown though they varied experiment to experiment. When TBATFB was used as the supporting electrolyte, Ph_3GeF was obtained. The fluorine source must be TBATFB. The generation of $(Ph_3Ge)_2O$ here reveals that the oxygen source was O_2 and/or residual H_2O in the system. In the electrolysis of Ph_3SiH in the presence of TBAP, Ph_3SiCl was not obtained although the experiments were repeated carefully. Using TBATFB as the electrolyte, a trace amount of Ph_3SiF was detected by GC-MS, but it was not detectable by HPLC. These product distributions may be undersood by means of the lower dissociation energy of Si-Cl bond compared with that of Si-O.[6]

Electrolyses were also carried out with other compounds, such as Ph_2MeEH, $PhMe_2EH$, and Et_3EH (E= Ge and Si). However, the expected products, such as Ph_2MeEX, $PhMe_2EX$, and Et_3EX (X=Cl and F) were readily hydrolyzed under the experimental conditions. Among the expected products, only $Ph_2MeGeCl$ and Ph_2MeGeF were detected by GC-MS analyses besides germoxanes and siloxanes.

Germyl (silyl) anions and germyl (silyl) radicals are candidates for the reaction intermediates (see Eqs. 1 and 2).

$$R_3EH + e \longrightarrow R_3E^- + H\cdot \quad (1)$$

$$R_3EH + e \longrightarrow R_3E\cdot + H^- \quad (2)$$

Accordingly, the reactivity of anions was examined as follows. Firstly, Ph_3Ge^- was prepared in tetrahydrofuran (THF) from Ph_3GeBr and Li. An alliquot was added to a THF solution containing 0.1 mol dm^{-3} of TBAP. Another alliouot was added to an acetonitrile solution containing 0.1 mol dm^{-3} of TBAP. However, no halogenated products were obtained in either case. Therefore, it was concluded that anions do not react with TBAP directly. In addition, it was found that the anions are not stable in acetonitrile, because only trace amount of Ph_3GeH was observed after hydrolysis.

Nextly, the reactivity of radicals was examined. Ph_3GeH was heated up to 80 ° in acetonitrile to generate $Ph_3Ge\cdot$. Trace amount of Ph_3GeCl was observed in the presence of TBAP after 6 h. Another experiment without Ar blanket gave $(Ph_3Ge)_2O$ as an additional product.

These results suggest that radical species are more probable as the reaction intermediates. However, it should be noted that by the electrochemical method Ph_3GeCl was obtained with a good yield. It seems that the reaction mechanism is more complicated than the simple reaction scheme: the generation of radicals by electrochemical reduction followed by their attack toward TBAP (or TBATFB).[7]

The authors would like to express their thanks to Miss Tomoko Ueda for her hard work in the very beginning stage of this work.

References

1) M. Okano and K. Mochida, *Chem. Lett.*, **1990**, 701.

2) K. Mochida and T. Kugita, *Main Group Metal Chemistry*, **11**, 215 (1988).

3) A. P. Tomilov, S. G. Mairanovskii, M. Ya. Fioshin, and V. A. Smirnov, "Electrochemistry of Organic Compounds," Halsted Press, Jerusalem (1972).

4) R. E. Dessy, W. Kitching, and T. Chivers, *J. Am. Chem. Soc.*, **88**, 453 (1966); W. G. Boberski and A. L. Allred, *J. Organomet. Chem.*, **88**, 73 (1975); R. J. Boczkowski and R. S. Bottei, *J. Organomet. Chem.*, **49**, 389 (1973); R. J. P. Corriu, G. Dabosi, and M. Martineau, *J. Organomet. Chem.*, **188**, 63 (1980).

5) E. E. Brooks, F. Glockling, and K. A. Hooton, *J. Chem. Soc.*, **1965**, 4283 ; J. Satge and P. Riviere, *Bull. Soc. Chim. Fr.*, **1966**, 1773; J. Satge, *Ann. Chim.*, **6**, 519 (1961); H. H. Reynolds, L. A. Bigelow, and C. A. Kraus, *J. Am. Chem. Soc.*, **51**, 3067 (1929); H. Gilman, G. D. Lichtenwalter, and D. Wittenberg, *J. Am. Chem. Soc.*, **81**, 5320 (1959); R. A. Benkeser and D. J. Foster, *J. Am. Chem. Soc.*, **74**, 5314 (1952); S. Tannenbaum, S. Kaye, and G. P. Lewenz, *J. Am. Chem. Soc.*, **75**, 3753 (1982).

6) D. A. Armitage, "Comprehensive Organometallic Chemistry," ed by G. Wilkinson, E. G. S. Stone, and E. W. Abel, Pergamon Press, Oxford (1982), Vol. 2.

7) Lately, it has been suggested by the authors that germyl and silyl radicals have a strong tendency to lose one electron to give the corresponding cations; M. Okano and K. Mochida, 37th Symposium on Organometallic Chemistry, Japan, 1990, Osaka. These cations are also candidates for the reaction intermediate. However, existence of such cations is not yet generally accepted in chemistry of organogermanium and organosilicon compounds and reactivity of them is still unknown.

Reaction between Nitrogen Monoxide and Carbon Monoxide over Superconducting Bi-Sr-Ca-Cu and Related Mixed Oxides

Noritaka MIZUNO,† Hisashi TOYAMA,†† Mika TANAKA, Mika YAMATO,††† and Makoto MISONO*
Department of Synthetic Chemistry, Faculty of Engineering,
The University of Tokyo, Hongo, Bunkyo-ku, Tokyo 113
(Received November 26, 1990)

Synopsis. Bi-Sr-Ca-Cu-O mixed oxides having a $Bi_2Sr_2CaCu_2O_y$ structure were very active for reactions between nitrogen monoxide and carbon monoxide among the prepared catalysts having perovskite and related structures.

Nitrogen oxides (NO_x) from vehicle engines and industrial boilers cause air pollution and acid rain, and their removal or suppression is an urgent social necessity.[1] The reductions of nitrogen monoxide (NO) by carbon monoxide (CO) and hydrocarbon are the major reaction pathways for the removal of NO_x from automobile exhaust.[2]

It has been reported that superconducting $YBa_2Cu_3O_y$ shows interesting catalytic properties for the ammoxidation of toluene, oxidation of methane, and the dehydrogenation of methanol.[3] Bi-Sr-Ca-Cu mixed oxides are new superconducting materials, and extensive studies of their electronic properties and structures have been reported. However, little is known of their catalytic properties.

Here, we wish to report on the high catalytic activity of a Bi-Sr-Ca-Cu mixed oxide having a $Bi_2Sr_2CaCu_2O_y$ structure for the reaction between nitrogen monoxide and carbon monoxide.

Experimental

All of the perovskite- and K_2NiF_4-type mixed oxides were prepared by calcining the precipitate from the appropriate mixture of aqueous solutions of the metal acetates or nitrates of each components at 1123—1273 K in air in the same manner as has been described previously.[4,5] Although the actual compositions may be nonstoichiometric with respect to oxygen, i.e., $La_{1-x}Sr_xBO_{3\pm\delta}$($x$=0—0.4, B=Co, Mn, Cr, δ; nonstoichiometry) and $La_{2-x}A'_xCuO_{4\pm\delta}$($x$=0—0.5, A'=Ce, Sr), in this paper they are designated as $La_{1-x}Sr_xBO_3$ and $La_{2-x}A'_xCuO_4$, respectively. Y-Ba-Cu-O and Bi-Sr-Ca-Cu-O mixed oxides were prepared by the calcination of appropriate mixtures of metal oxides and/or metal carbonates with nominal compositions of Y : Ba : Cu=1 : 2 : 3 and Bi : Sr : Ca : Cu=4 : 3 : 3 : 4 or 1 : 1 : 1 : 2, respectively, in O_2 at 1123—1193 K according to the methods described in the literature.[6,7] Bi-Sr-Ca-Cu-O mixed oxide was further annealed at 1123 K for 24 h. Bi-Sr-Ca-Cu-O mixed oxides with nominal compositions of Bi : Sr : Ca : Cu=4 : 3 : 3 : 4 and 1 : 1 : 1 : 2 are designated as Bi-Sr-Ca-Cu-O (4 : 3 : 3 : 4) and Bi-Sr-Ca-Cu-O (1 : 1 : 1 : 2), respectively. These structures were confirmed by their X-ray diffraction patterns. A reaction between NO and CO was carried out in a closed circulation system (ca. 190 cm^3), as described previously.[5,6b] The catalysts (25—200 mg) were mixed with inert SiC (250 mg) to prevent any undesirable temperature rise. The standard procedures were as follows: After the catalysts were treated in O_2 at 573 K for 1 h, the system was evacuated for 15 min. Then, the catalysts were exposed to the reaction gas mixture at ca. 8 kPa (NO : CO=1 : 1). Small portions of the reaction gas were intermittently taken from the system using a glass sampler and then analyzed with a gas chromatograph that was directly connected to the reaction system. The N and C balances were confirmed to be good.

Results and Discussion

The crystal structures and surface areas are summarized in Table 1. The X-ray diffraction pattern of Bi-Ca-Sr-Cu-O (4 : 3 : 3 : 4) showed only a $Bi_2Sr_2CaCu_2O_y$' structure, while two extra peaks at 35.5 and 38.7° corresponding to CuO were observed for Bi-Sr-Ca-Cu-O (1 : 1 : 1 : 2), as was reported in Ref. 7. Although the nonstoichiometry of those catalysts was not determined, it is known that Bi-Sr-Ca-Cu-O, thus prepared, exhibits superconductivity. The X-ray diffraction patterns of the other catalysts showed only a perovskite-type, K_2NiF_4-type, or orthorhombic $YBa_2Cu_3O_y$ structure. It has been reported that y in $YBa_2Cu_3O_y$, thus prepared, ranges from 6.5 to 6.9[8] and that y' in $Bi_2Sr_2CaCu_2O_{y'}$ was ca. 8.13.[7]

NO reacted with CO at 573 K over Bi-Sr-Ca-Cu-O (1 : 1 : 1 : 2, Fig. 1) to form N_2 and CO_2 in an approximately stoichiometric ratio in accordance with the reaction $NO+CO \rightarrow 1/2N_2+CO_2$; the amount of NO uptake was comparable with that of CO uptake and the amount of N_2O formed was small. The reaction proceeded over Bi-Sr-Ca-Cu-O (4 : 3 : 3 : 4) at 573 K in a similar way to that of Bi-Sr-Ca-Cu-O (1 : 1 : 1 : 2). A similar time course was observed upon performig a repeated reaction. Absorption of NO was not observed for either Bi-Sr-Ca-Cu-O (1 : 1 : 1 : 2) or Bi-Sr-Ca-Cu-O (4 : 3 : 3 : 4) mixed oxides. No change in the XRD pattern of Bi-Sr-Ca-Cu (1 : 1 : 1 : 2) was observed between fresh and used catalysts.

The selectivities and rates changed little when the reaction was repeated over perovskite-type mixed oxides, while the rates of K_2NiF_4-type mixed oxides and $YBa_2Cu_3O_y$ varied in various ways, depending on the catalysts, as reported previously.[5,6b]

The rate and selectivity of Bi-Sr-Ca-Cu-O (4 : 3 : 3 : 4) were close to those of Bi-Sr-Ca-Cu-O (1 : 1 : 1 : 2), while the former has a CuO phase in addition to the $Bi_2Sr_2CaCu_2O_{y'}$ phase. We previously reported that the catalytic activity of $La_{1.8}Ce_{0.2}CuO_4$ for the reaction of NO and CO was little affected by the small amount of coexisting CuO.[5] These facts indicate that the coexisting Cu or CuO had little influence on the rate and selectivity.

† Present address: Catalysis Research Center, Hokkaido University, Sapporo 060.
†† Present address: Central Research Laboratory, Hitachi Ltd., Kokubunji, Tokyo 185.
††† Present address: Asahi Chemical Industry Co., Ltd., Yako, Kawasaki-ku, Kanagawa 210.

Table 1. Structure, Surface Area, and Catalytic Activity

Catalyst	Structure	Reaction temp./K	Surface area	Rate[a]	Selectivity[b]/%	
			$m^2 g^{-1}$	10^{-6} mol $min^{-1} m^{-2}$	N_2	N_2O
Bi-Sr-Ca-Cu-O (4:3:3:4)	$Bi_2Sr_2CaCu_2O_{y'}$ (T[c])	573	0.7	114	88	12
Bi-Sr-Ca-Cu-O (1:1:1:2)	$Bi_2Sr_2CaCu_2O_{y'}$ (T) +CuO (0.23[d])	573	0.8	128	90	10
Y-Ba-Cu-O	$YBa_2Cu_3O_y$ (O[c])	573	0.7—0.8	68—140	ca. 90	ca. 10
$La_{1.9}Ce_{0.1}CuO_4$[e]	K (O)	673	0.5	60	78	22
La_2CuO_4[e]	K (O)	673	1.2	96	83	17
$La_{1.8}Sr_{0.2}CuO_4$	K (T)	573	2.8	16	78	22
$La_{1.8}Sr_{0.2}CuO_4$[e]	K (T)	673	2.8	159	90	10
$La_{1.5}Sr_{0.5}CuO_4$	K (T)	673	1.2	106	88	12
$LaCoO_3$	P (R[c])	573	2.4	40	11	89
$La_{0.8}Sr_{0.2}CoO_3$	P (C[c])	573	2.8	22	11	89
$LaMnO_3$	P (O)	573	7.0	12	7	93
$LaCrO_3$	P (O)	573	3.2	5	13	87

a) The average rates of the CO consumption for the first 10 min. b) The selectivity of the reaction products of NO after 10 min. The composition was nearly constant for the first 10 min. c) T; tetragonal. O; orthorhombic. R; rhombohedral. C; cubic. d) The intensity ratio of main signal of $Bi_2Sr_2CaCu_2O_{y'}$ phase to that of CuO phase. e) Cited from Ref. 5.

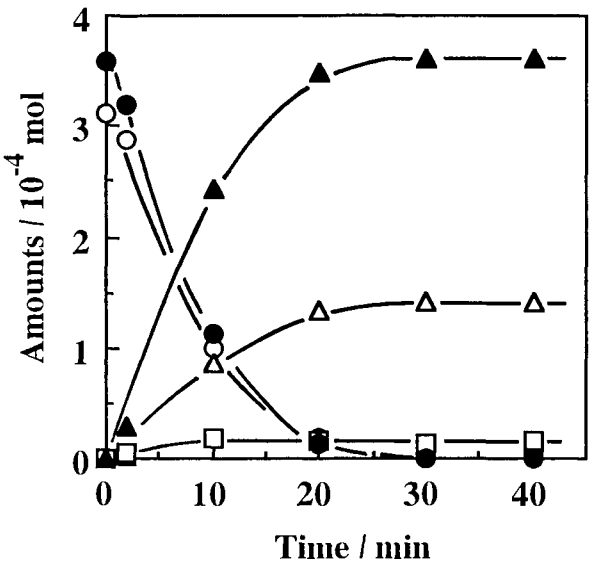

Fig. 1. Reaction between NO and CO at 573 K over Bi-Sr-Ca-Cu-O (1:1:1:2) catalyst.
○, NO; △, N_2; □, N_2O; ●, CO; and ▲, CO_2. Catalyst weight, 0.2 g.

The number of surface copper ions for Bi-Sr-Ca-Cu-O (4:3:3:4), calculated from the crystallographic data of the $Bi_2Sr_2CaCu_2O_y$ structure (assuming that the most frequently exposed plane is CuO_2 plane where the concentration of copper ions is the highest in this structure), is 6.8×10^{18} ions·m^{-2}. The total turnover number of Bi-Sr-Ca-Cu-O (i.e., the number of CO reacted per number of surface copper ions) for Runs 1—4 was greater than five hundred, showing that the reaction is catalytic. It is noteworthy that the catalytic activity of Bi-Sr-Ca-Cu-O mixed oxides for the reaction of NO and CO, as well as the selectivity to N_2, were of the highest level among the catalysts listed in Table 1, which summarizes the stationary rates and selectivities.[9] The formal charge of copper for $Bi_2Sr_2CaCu_2O_{8.13}$ is 2.13. It is remarkable that this value is close to that of $La_{1.8}Sr_{0.2}CuO_4$ (2.10), which was the most active for the reaction of NO and CO among $La_{2-x}A'_xCu_{1-y}B'_yO_4$(A'=Sr, Ce; B'=Al, Zr; x or y=0—0.5) catalysts.[5]

Even using the highest number of surface copper ions (6.8×10^{18} ions·m^{-2}), the calculated turnover frequency was still 1.7×10^{-1} mol s^{-1}(Cu-atom)$^{-1}$, which was 10^2 times higher than the turnover frequency of Rh/Al_2O_3 catalyst (1.7×10^{-3} mol s^{-1}(Rh-atom)$^{-1}$ at 573 K, extrapolated value in Ref. 1b).

As for the other catalysts, the following trends were noted. The rate decreased with Sr^{2+}-substitution for $LaCoO_3$, and $LaMnO_3$ (perovskite-type structure), while the rate increased in the case of La_2CuO_4.[5] Copper-containing catalysts showed the high selectivity to N_2.

The activity of $YBa_2Cu_3O_{y'}$ which changed among the different lots, was comparative to, or a little lower than, that of Bi-Sr-Ca-Cu-O. The difference in the rates between the lots of $YBa_2Cu_3O_y$ may be due to the water which was either absorbed or adsorbed.[10] In fact, the activity of $YBa_2Cu_3O_y$ changed considerably after its exposure to water vapor. The more NO that was absorbed, the higher the activity of Y-Ba-Cu-O for the reaction between NO and CO was. It has been reported for Ba-Cu-O that NO is absorbed into the bulk as in the case of $YBa_2Cu_3O_y$[5b] and that the absorptivity of NO is accelerated by the coexistence of Cu^{3+}.[11] Therefore, the valence of copper may be another influential factor regarding the activity for the reaction between NO and CO.

In contrast, the activity of Bi-Sr-Ca-Cu-O was reproducible. It is noteworthy in the above respect that Bi-Sr-Ca-Cu-O is stable in water vapor and carbon dioxide.[12]

This study was supported by a Grant-in-Aid for Scientific Research No. 02227202 from the Ministry of Education, Science and Culture.

References

1) a) *Chem. Eng. News,* **Dec. 8, 1986**, p. 20. b) G. B. Fisher, S. H. Oh, J. E. Carpenter, C. L. Dimaggio, and S. J. Schmieg, "Catalysis and Automotive Pollution Control," Elsevier, Amsterdam (1987), p. 215.

2) S. H. Oh, *J. Catal.,* **124,** 477 (1990).

3) S. Hansen, J. C. Otamiri, J-O. Bovin, and A. Andersson, *Nature,* **334**, 143 (1988); J. C. Otamiri, S. L. T. Andersson, and A. Andersson, *Appl. Catal.,* **65**, 159 (1990); I. Halasz, *Appl. Catal.,* **47**, L17 (1989); J. G. McCarthy, M. A. Quinlan, and H. Wise, "Proc. 9th Intl. Congr. Catal., Calgary, 1988," The Chemical Institute of Canada, 1988, Vol. 4, p. 1818.

4) T. Nakamura, M. Misono, T. Uchijima, and Y. Yoneda, *Nippon Kagaku Kaishi,* **1980**, 1679.

5) N. Mizuno, M. Yamato, M. Tanaka, and M. Misono, *Chem. Mater.,* **1**, 232 (1989).

6) a) F. Izumi, H. Asano, T. Ishigaki, A. Ono, and F. P. Okamura, *Jpn. J. Appl. Phys.,* **26**, L611 (1987). b) N. Mizuno, M. Yamato, and M. Misono, *J. Chem. Soc., Chem Commun.,* **1988**, 887.

7) J. M. Tarascon, Y. LePage, P. Barboux, B. G. Bagley, L. H. Greene, W. R. McKinnon, G. W. Hull, M. Giroud, and D. M. Hwang, *Phys. Rev. B,* **37**, 9382 (1988); R. S. Liu, Y. T. Huang, J. M. Jiang, P. T. Wu, and C. T. Chang, *Jpn. J. Appl. Phys.,* **28**, L395 (1988).

8) K. Kishio, J. Shimoyama, T. Hasegawa, K. Kitazawa, and K. Fueki, *Jpn. J. Appl. Phys.,* **26**, L611 (1987).

9) The time course of each catalyst in the second run was similar to that in the third run. In this work, the stationary rate and selectivity were defined by those for the first 10 min in the second run.

10) The effect of water vapor on the chemical and catalytic properties of $YBa_2Cu_3O_y$ is significant. For example, the treatment of $YBa_2Cu_3O_y$ with water vapor remarkably accelerated the absorption of NO (H. Toyama, N. Mizuno, and M. Misono, 1989 Intl. Chem. Congr. Pacific. Basin Soc., Honolulu, Dec.1989). Further study is in progress. The reaction of $YBa_2Cu_3O_y$ with water vapor has also been reported (H. S. Horowitz, R. K. Bordia, R. B. Flippen, R. E. Johnson, and U. Chowdhry, *Mat. Res. Bull.,***23**, 821 (1988)).

11) M. Machida, K. Yasuoka, K. Eguchi, and H. Arai, *J. Chem. Soc., Chem. Commun.,* **1990**, 1165.

12) D. W. Johnson, Jr. and W. W. Rhodes, *J. Am. Ceram. Soc.,* **72**, 2346 (1989).

Spinning Effect on Magic-Angle-Spinning NMR Spectra of Silicone Rubber

Shigenobu HAYASHI* and Kikuko HAYAMIZU
National Chemical Laboratory for Industry, Tsukuba, Ibaraki 305
(Received December 11, 1990)

Synopsis. High-resolution solid-state ^{13}C, ^{29}Si, and ^{1}H NMR spectra of silicone rubber have been measured using the magic-angle spinning of the sample. The spectra of the three nuclei split into two or three components in the range of the spinning rate between 1.4 and 2.0 kHz. Below 1.4 kHz and above 2.0 kHz, the spectra consist of only one component. Stress caused by the fast spinning is considered to cause conformational changes in the polydimethylsiloxane chains.

Silicone rubber is a very popular material which is widely used in a daily life as well as in chemical laboratories. It is very flexible, and is usually composed of polydimethylsiloxane. Molecular motions are very rapid in silicone rubber as if they were in liquid state from the standpoint of NMR. The dipolar interactions between the nuclei are weak, and they can be easily averaged out by the magic-angle spinning (MAS) of the sample. Thus, one can get high-resolution spectra of ^{13}C, ^{29}Si, and ^{1}H nuclei in silicone rubber only by MAS. Due to this favorable property, silicone rubber has been used as the shift reference frequently.[1] Cross polarization (CP) is not at all effective in this material.

Recently we have measured the NMR spectra of silicone rubber with very high resolution to determine the chemical shift precisely. In the course of the measurement we have found that the line shape changes in a certain range of the spinning rate.[2] In other words, the spinning induces a change in the NMR spectra. We have recently reported spinning-rate dependent phenomena; one is Cu and halogen NMR signals in copper (I) halides,[3] and the other is ^{31}P MAS NMR spectra of inorganic pyrophosphates.[4] In the former case, the Lorentz force working on the charged particles excites the ion motion, resulting in the frequency shift. In the latter, the homonuclear dipole-dipole interaction is not averaged out by MAS.[5] Bjorholm and Jakobsen[6] have reported a crystalline-to-plastic phase transition induced by MAS in ^{31}P NMR in P_4S_3, although the true origin is the temperature rise induced by the spinning. In the present case, the stress caused by the spinning is considered to influence the conformation of silicone rubber. In this note, we present the spinning-induced changes in the ^{13}C, ^{29}Si, and ^{1}H MAS NMR spectra of silicone rubber. To our knowledge, this is the first observation of the conformational change induced by the stress in MAS NMR.

Experimental

The instrument used for the NMR measurements was a Bruker MSL400 pulsed spectrometer, whose magnetic field strength was 9.4 T. The resonance frequencies were 100.614, 79.496, and 400.136 MHz for ^{13}C, ^{29}Si, and ^{1}H, respectively. The details of the high-resolution measurements were described previously.[2] Chemical shifts were referenced directly to pure tetramethylsilane under MAS, being expressed the higher frequency side as positive. The experimental errors in the shift values was about ±0.004 ppm, and the relative shifts in the same sample had the better accuracies with errors less than ±0.002 ppm. Temperature was 294 K. Two kinds of pulse sequences were used; single pulse, and single pulse with ^{1}H decoupling only during the data aquisition. Simulation of the spectra was carried out using the CLINFIT program supplied by Bruker.

Materials were available commercially. Although there were many kinds of silicone rubber, we have characterized the sample by NMR, as described below.

Results and Discussion

^{1}H and ^{13}C MAS NMR spectra have only one signal,

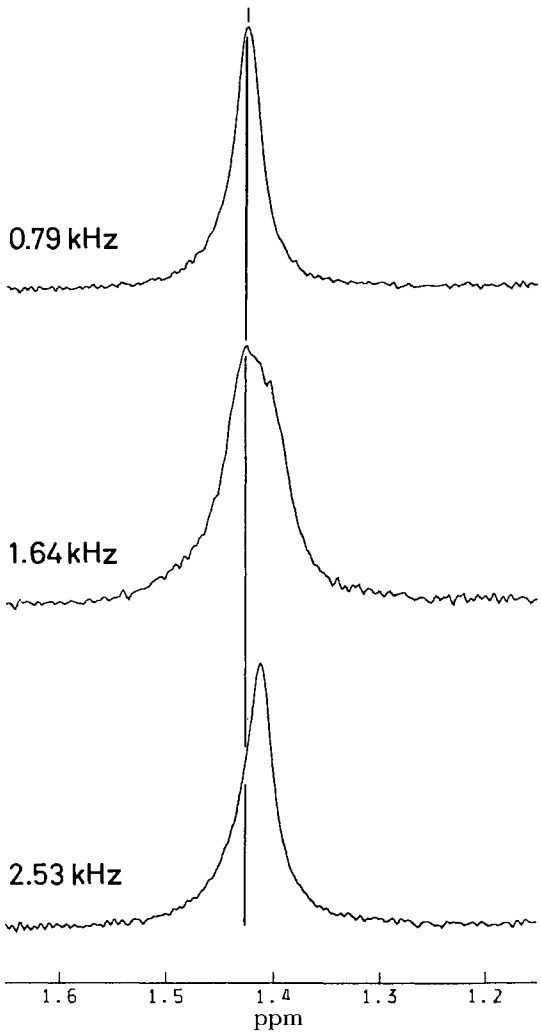

Fig. 1. ^{13}C MAS NMR spectra of silicone rubber with ^{1}H decoupling (ν_0=100.614 MHz). Numbers in the figure are the spinning rates.

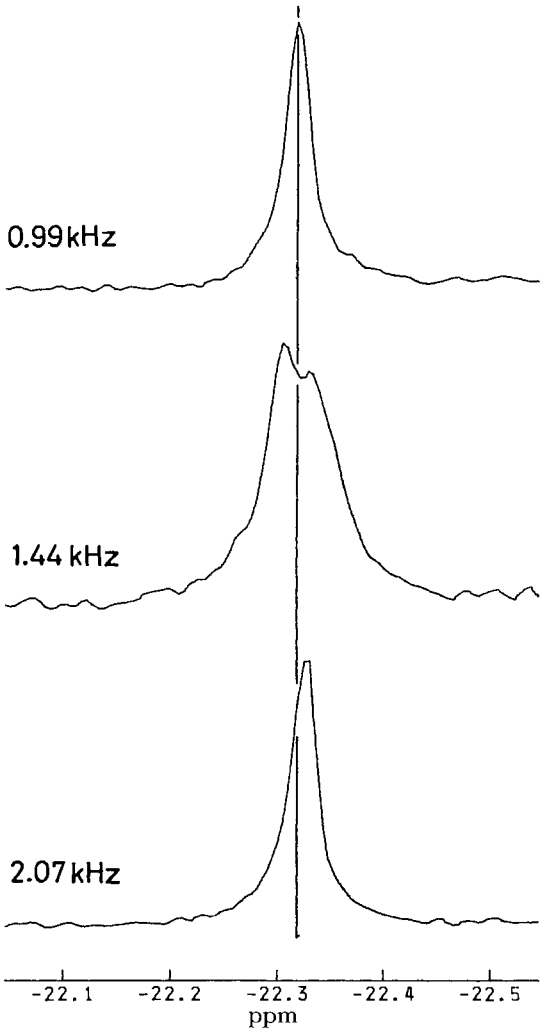

Fig. 2. ^{29}Si MAS NMR spectra of silicone rubber with ^{1}H decoupling (ν_0=79.496 MHz).

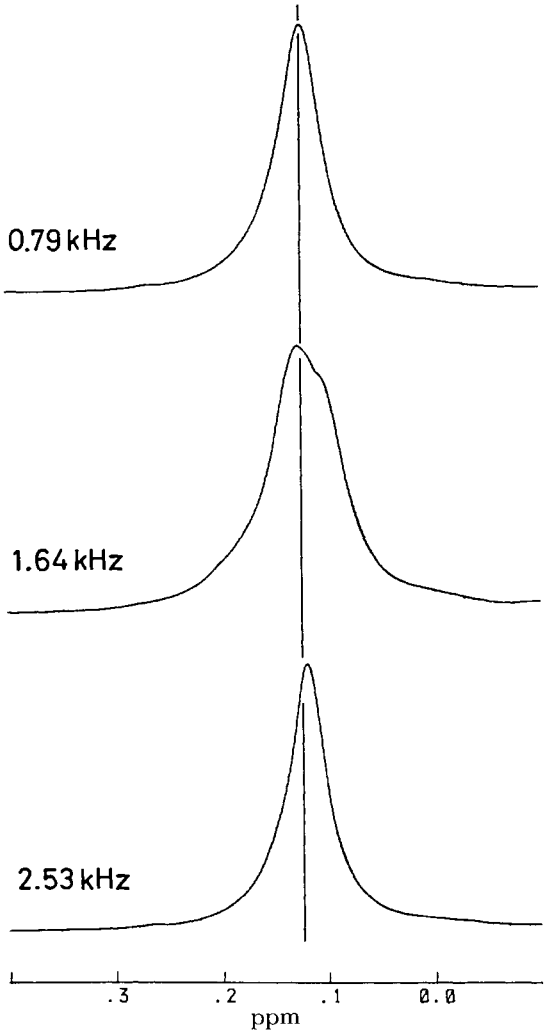

Fig. 3. ^{1}H MAS NMR spectra of silicone rubber (ν_0=400.136 MHz).

which is attributed to methyl groups attached to Si. ^{29}Si MAS NMR spectra have two signals; one is O-Si$(CH_3)_2$-O, and the other is amorphous SiO_2. The amorphous SiO_2 has a broad signal centered at −108 ppm with a full width at half maximum (FWHM) of about 13 ppm, and its mole fraction is 21% of the total Si. The upper limits of the presence of the other species are 2.2, 0.14, and 0.01% for C, Si, and H atoms, respectively, being estimated from the noise levels in the spectra. From these results, it can be concluded that the material is composed of linear polydimethylsiloxane chains and amorphous silica. The density of the sample is 1.17 g cm^{-3}.

Figure 1 shows ^{13}C MAS NMR spectra with ^{1}H decoupling. Note that the spectrum at the spinning rate 1.64 kHz shows line broadening and that the other two spectra have similar narrow linewidths. In the ^{1}H-coupled spectra, the scalar coupling can be observed, whose constant $^{1}J(^{13}C\text{-}^{1}H)$ is 118 Hz. The scalar coupling constant does not change with the spinning rate. Similar spectral changes are observed also in ^{29}Si and ^{1}H MAS NMR spectra, as shown in Figs. 2 and 3. The scalar coupling with ^{1}H is observed also in ^{29}Si spectra without decoupling ($^{2}J(^{29}Si\text{-}^{1}H)$=7.3 Hz). The spectral changes are reversible, and we can observe them repeatedly.

The spectral changes take place in the range of 1.4 to 2.0 kHz, called a "transition region." Below 1.4 (a slow spinning region) and above 2.0 kHz (a fast spinning region) the spectra consist of only one component, whose line shape is Lorentzian. The spectra between 1.4 and 2.0 kHz have fine structures, which can be deconvoluted into two or three Lorentzian lines. We present only the ^{1}H NMR results in Table 1. The ^{13}C and ^{29}Si results show similar behavior to ^{1}H, although there are no correlations among the three nuclei. From the table and the figures, several trends common to the three nuclei can be extracted:

(1) The chemical shifts in the fast spinning region deviate slightly towards lower frequency from those in the low spinning region.

(2) In the transition region, one component has a higher frequency than the signal in the slow spinning region, and the other has a lower frequency than that in the fast spinning region. Consequently, the spectra in the transition region are not the superposition of those in the slow and fast spinning regions. Apparently, the signal splitting takes place, keeping

Table 1. ^{1}H MAS NMR Results

Spinning rate	No. of components	δ	FWHM	Fraction
kHz		ppm	ppm	%
0.79	1	0.122	0.051	
1.01	1	0.123	0.047	
1.20	1	0.124	0.046	
1.64	2	0.128	0.064	88
		0.097	0.029	12
1.68	3	0.132	0.039	62
		0.113	0.018	9
		0.095	0.027	29
2.00	3	0.130	0.061	91
		0.110	0.006	1
		0.097	0.023	8
2.50	1	0.118	0.044	
2.53	1	0.119	0.045	
3.03	1	0.120	0.047	
3.53	1	0.119	0.050	

the weight point almost constant.

As described above, we have recently reported several spinning-induced phenomena. However, in the present case, the stress caused by the spinning is considered to influence the conformation of silicone rubber. Temperature rise induced by the spinning is negligible in the range of the spinning rate used in this work.

Silicone rubber can be regarded as liquid from the standpoint of the NMR measurement. The high flexibility is considered to make the silicone rubber easily influenced by the spinning. The magnitude of the stress, S, can be estimated using the formula presented previously,[5]

$$S=(1/3)\,\rho\, r^2\omega_r^2, \qquad (1)$$

where ρ is the density, r is the distance from the spinning axis, and ω_r is the spinning rate expressed in angular frequency unit. In the present case, ρ=1.17 g cm^{-3} and $0 \leqq r \leqq 0.28$ cm. The maximum stresses just inside the wall of the rotor are 2.4×10^5 and 5.0×10^5 Pa for ν_r=1.4 and 2.0 kHz, respectively.

The characteristics of the present phenomena is that the conformation changes as if there were a phase transition. No monotonic change is observed with the spinning rate. Conformations in the slow and fast spinning regions are homogeneous. In the slow spinning region the conformation is relaxed, while it is deformed in the fast spinning region. The conformation in the transition region is not a mixture of the relaxed and deformed forms, but a kind of "transition form." Several conformations are considered to coexist inhomogeneously in the transition form.

Recently, spinning rates above 20 kHz are possible.[7] In those cases, more rigid solids than silicone rubber might undergo the similar transition. The maximum stress at ν_r=20 kHz amounts to 5.0×10^7 Pa.

Aside from the range between 1.4 and 2.0 kHz, silicone rubber is a good shift standard. Even in the range between 1.4 and 2.0 kHz, it can be used as a shift standard, since the spectral change of the order of 0.04 ppm is usually negligible if compared with the larger linewidth in normal solids.

In summary, we have found that the conformation in silicone rubber is influenced by the fast spinning in MAS NMR. This effect might become more general as the spinning rate as high as 20 kHz is applied.

References

1) S. Hayashi and K. Hayamizu, *Bull. Chem. Soc. Jpn.*, **62**, 2429 (1989).
2) S. Hayashi and K. Hayamizu, *Bull. Chem. Soc. Jpn.*, **64**, 685 (1991).
3) S. Hayashi and K. Hayamizu, *J. Chem. Phys.*, **92**, 2818 (1990).
4) S. Hayashi and K. Hayamizu, *Chem. Phys. Lett.*, **161**, 158 (1989).
5) A. Kubo and C. A. McDowell, *J. Chem. Phys.*, **92**, 7156 (1990).
6) T. Bjorholm and H. J. Jakobsen, *J. Magn. Reson.*, **84**, 204 (1989).
7) S. F. Dec, R. A. Wind, G. E. Maciel, and F. E. Anthonio, *J. Magn. Reson.*, **70**, 355 (1986).

Photolysis of Thietane and Thietane-d_6 in Argon Matrix: Infrared Spectra of Matrix-Isolated Thioformaldehyde and Thioformaldehyde-d_2

Osamu WATANABE, Eiichi SUZUKI, and Fumio WATARI*
Department of Resource Chemistry, Faculty of Engineering, Iwate University, Morioka 020
(Received December 17, 1990)

Synopsis. Argon-matrix isolated thietane at 10 K decomposed by irradiation (λ>290 nm) to form ethylene and thioformaldehyde. The photolysis of thietane under these conditions has been shown to be a clean source of thioformaldehyde. The CH_2S and CD_2S molecules generated this way are indefinitely stable and their infrared spectra could be recorded.

Thioformaldehyde easily polymerizes to a cyclic trimer (trithiane) under normal conditions. It has been generated by pyrolysis or photolysis of various precursors for spectroscopic investigations.[1] Recently infrared spectrum of thioformaldehyde generated by photolysis of matrix isolated methylene trithiocarbonate has been fully analyzed.[2]

Pyrolysis or photolysis in general results in formation of by-products that obscure frequently parts of spectrum of an aimed species in infrared studies. Haines et al.[3] reported that thietane decomposed by the action of light to form only ethylene as a gaseous product and a white solid which was probably a trimer of thioformaldehyde. We expected that photolysis of thietane in the argon matrix would produce thioformaldehyde in a monomeric form and ethylene,

$$H_2C\begin{matrix}H_2\\ C\\ S\end{matrix}CH_2 \xrightarrow{h\nu} H_2CS + CH_2{=}CH_2$$

and the infrared spectrum of thioformaldehyde would be obtained by subtraction of absorptions of ethylene from the spectrum of the photolysis products.

Experimental

Thietane (Tokyo Kasei Kogyo Co.) was distilled under vacuum before use. Thietane-d_6 was prepared from 1,3-dibromopropane-d_6 (MSD ISOTOPES, Montreal) by the method similar to the procedure of Bordwell and Pitt[4] for preparation of thietane, and purified by trap-to-trap distillation. Ethylene-d_4 was prepared by dehydration of ethanol-d_6 (MSD ISOTOPES, Montreal) with sulfuric acid-d_2.

A mixture of thietane or thietane-d_6 with argon gas (Ar : thietane=200 : 1 in a mole ratio) was prepared using standard manometric procedure. The mixture was deposited within 2 h on a CsI plate cooled at 20 K by a CTI Cryogenics Cryodyne Cryocooler Model 21 closed-cycle helium refrigerator. The argon-matrix isolated precursor cooled down to 10 K was exposed to radiation from a high-pressure mercury lamp (Ushio Denki) through a water filter (10 cm) fitted with quartz windows. Since this irradiation experiment resulted in complicated fragmentation, a cut-off filter was used. The irradiation through a UV-29 filter (Toshiba Glass) gave favorably clean infrared spectra, though it took a long exposure time to decompose the precursor completely.

Infrared spectra (4000—250 cm^{-1}) were recorded on a Hitachi Model 260-50 grating spectrometer, which was calibrated with standard gases.[5]

Results and Discussion

Irradiation (λ>290 nm) of argon-matrix isolated thietane and thietane-d_6 for 8 h resulted in the disappearance of the initial infrared spectra, Figs. 1(a) and 2(a), and the appearance of new absorptions, Figs. 1(b) and 2(b). The absorptions due to ethylene and ethylene-d_4 in Figs. 1(b) and 2(b) could be identified by comparing them with the spectra of argon-matrix isolated ethylene and ethylene-d_4 (Figs. 3(a) and 3(b)). By the agreement with the absorptions observed previously,[2] the remaining spectra could be evidently identified as those of CH_2S and CD_2S. The observed frequencies were collected in Table 1 together with the results of Torres et al.[2]

Three absorptions remained at 3019(vw), 2956(m), and 2863(w) cm^{-1} after elimination of the CH_2 stretchings of ethylene in the CH stretching region, in agreement with previous observations, and in the CD stretching region two absorptions were observed at 2277(vw) and 2149(m) cm^{-1} aside from the CD_2 stretch-

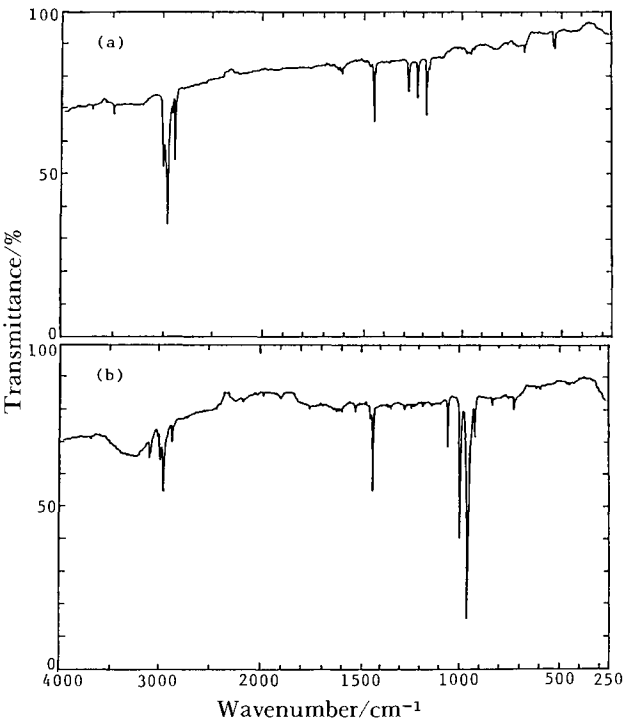

Fig. 1. Infrared spectra of (a) argon-matrix isolated thietane at 10 K and (b) after subsequent 8 h irradiation (λ>290 nm) of (a).

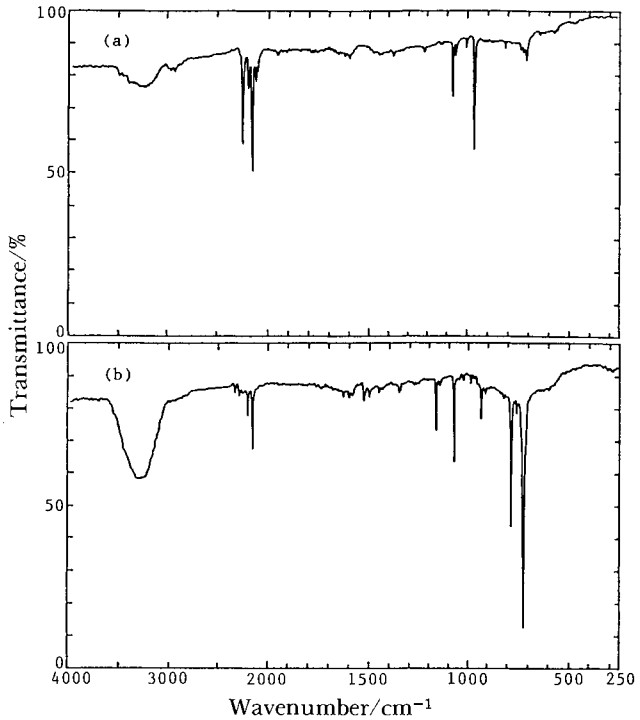

Fig. 2. Infrared spectra of (a) argon-matrix isolated thietane-d_6 at 10 K and (b) after subsequent 8 h irradiation (λ>290 nm) of (a).

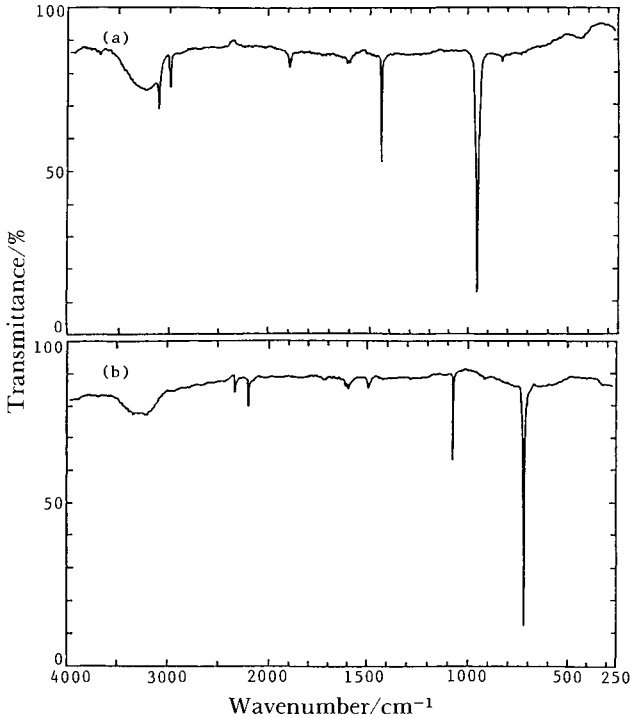

Fig. 3. Infrared spectra of argon-matrix isolated ethylene (a) and ethylene-d_2 (b) at 10 K.

Table 1. Observed Frequencies (cm^{-1}) of CH_2S and CD_2S

CH_2S		CD_2S		Assignment
This work	Torres[a]	This work	Torres[a]	
3019 (vw)	3017	2277 (w)	2280	ν_5 $CH_2(CD_2)$ stretch
2956 (m)	2965	2149 (m)	2155	ν_1 $CH_2(CD_2)$ stretch
2863 (w)	2869			$2\nu_2$
1436[b]	1447	1162 (m)	1167	ν_2 $CH_2(CD_2)$ sym def
1052 (m)	1052	934 (m)	932	ν_3 C=S stretch
994 (s)	988	783 (s)	779	ν_6 $CH_2(CD_2)$ wag
990 (sh)	980	779 (sh)	773	ν_4 $CH_2(CD_2)$ rock

a) Photolysis of matrix isolated methylene trithiocarbonate, Ref. 2. b) Overlaps with the symmetric CH_2 deformation of ethylene.

ings of ethylene-d_4 also in agreement with the previous observations. The 2863 cm^{-1} band has been assigned to $2\nu_2$,[2] whereas $2\nu_2$ of CD_2 must overlap with the 2327 cm^{-1} band of ethylene-d_4, if would appear.

Torres et al. assigned the symmetric CH_2 deformation to the absorption at 1447 cm^{-1} and it was observed to be slightly stronger than the C=S stretch (1052 cm^{-1}).[2] In Fig. 1(b), there is a very weak absorption at 1449 cm^{-1}, but it is too weak as compared with the C=S stretch (1052 cm^{-1}). On the other hand, the symmetric CD_2 deformation of CD_2S is distinguishable from the symmetric CD_2 deformation (1071 cm^{-1}) of ethylene-d_4 (Fig. 2(b)). Thus the symmetric CH_2 deformation of CH_2S must accidentally overlap with the symmetric CH_2 deformation of ethylene.

For the out-of-plane and in-plane CH_2 deformations, there is only a prominent absorption at 994 cm^{-1}, which is accompanied with a shoulder at 990 cm^{-1}. There is often observed a vibrational mode as splitting into various bands in a matrix spectrum. However, on the basis of no splittings for the other bands, these should be interpreted to be due to different modes and we tentatively assinged the strong band at 994 cm^{-1} to the out-of-plane CH_2 deformation and the shoulder at 990 cm^{-1} to the in-plane in accordance with the interpretation of Torres et al.[2] Two bands of CD_2S at 783(s) and 779 (shoulder) cm^{-1} were assigned similarly.

The exclusive photolysis product of ethylene and the good agreement of the remaining spectrum with the CH_2S absorptions previously reported shows that thietane is a clean source compound for the photochemical generation of thioformaldehyde.

References

1) D. R. Johnson, F. X. Powell, and W. H. Kirchhoff, *J.*

Mol. Spectrosc., **39**, 136 (1971); J. W. C. Johns and W. B. Olson, *ibid.*, **39**, 479 (1971); M. E. Jacox and D. E. Milligan, *ibid.*, **58**, 142 (1975); D. J. Bedwell and G. Duxbury, *ibid.*, **84**, 531 (1980); D. J. Clouthier, C. M. L. Kerr, and D. A. Ramsay, *Chem. Phys.*, **56**, 73 (1981); P. H. Turner, L. Halonen, and J. M. Mills, *J. Mol. Spectrosc.*, **88**, 402 (1981).

2) M. Torres, I. Safarik, A. Clement, and O. P. Strausz, *Can. J. Chem.*, **60**, 1187 (1982).

3) W. E. Haines, G. L. Cook, and J. S. Ball, *J. Am. Chem. Soc.*, **78**, 5213 (1956).

4) F. G. Bordwell and B. M. Pitt, *J. Am. Chem. Soc.*, **77**, 572 (1955).

5) IUPAC, "Tables of Wavenumbers for the Calibration of Infrared Spectrometers," 2nd ed, Pergamon Press, New York (1977).

^{1}H NMR Conformational Study of Viologen-Linked Porphyrins (*p*-PC*n*V)

Yasuhiko YAMAMOTO, Sumio NODA,† Norishige NANAI, Ichiro OKURA,† and Yoshio INOUE*
Department of Biomolecular Engineering, Tokyo Institute of Technology,
O-okayama, Meguro-ku, Tokyo 152
†Department of Bioengineering, Tokyo Institute of Technology,
O-okayama, Meguro-ku, Tokyo 152
(Received January 5, 1991)

Synopsis. Conformation of viologen-linked porphyrins (*p*-PC*n*V, *n*=4—7), which are capable of intramolecular electron transfer, was studied by ^{1}H NMR in order to gain insight into the relative geometry of the donor and acceptor during the electron transfer process. The orientation of the viologen with respect to the porphyrin was interpreted in terms of the rate of the intramolecular electron transfer between the two π-systems.

The viologen-linked porphyrins (Fig. 1) exhibit the intramolecular electron transfer process from the porphyrin to the viologen.[1-5] The rate of this process depends crucially on the length of the methylene chain intervening between the two π-systems. The electron transfer rate of *m*-PC*n*V in dimethylsulphoxide (DMSO) decreases monotonously with the methylene chain length and, in the case of *p*-PC*n*V in DMSO, only *p*-PC4V exhibits the intramolecular electron transfer with the rate comparable to that of *m*-PC3V.[5] We have studied the conformation of *p*-PC*n*V in DMSO by ^{1}H NMR. The orientation of the viologen with respect to the porphyrin ring in *p*-PC*n*V was compared with that of *m*-PC*n*V[6] and the difference of the efficiency in the electron transfer process for these compounds was interpreted in terms of the distance between the porphyrin and the bipyridine, based on a proposed relationship, i. e., an exponential dependence of the electron transfer rate on the distance of the donor-acceptor separation.[7]

Experimental

Materials. The viologen-linked porphyrins (*p*-PC*n*V) were synthesized as described previously.[5] Dimethyl-d_6 sulfoxide (DMSO-d_6) was purchased from MSD Isotopes.

NMR Measurements. Solutions of 10 mM *p*-PC*n*V in DMSO-d_6 (1M=1 mol dm^{-3}) were used for ^{1}H NMR measurements. 500 MNz ^{1}H NMR spectra were recorded on a JEOL GSX-500 FT-NMR spectrometer at 27 °C. Typical spectra were recorded with 64 transients, 32 k data points,

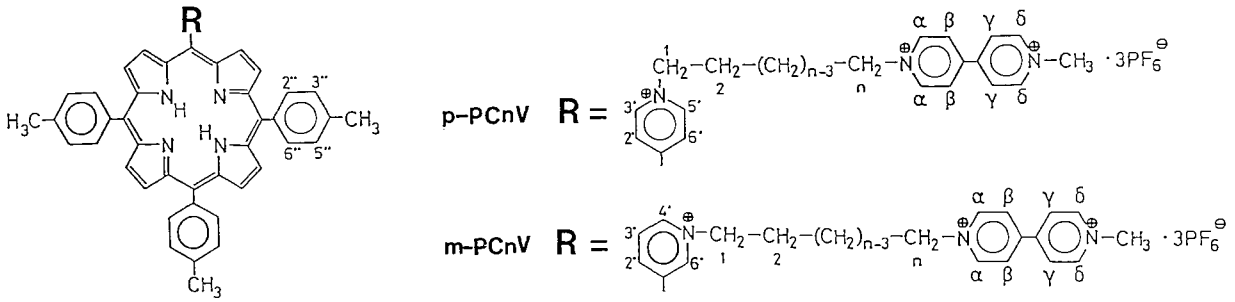

Fig. 1. Molecular structures and numbering systems of viologen-linked porphyrins (*p*-PC*n*V and *m*-PC*n*V).

Table 1. Chemical Shifts[a] on Viologen ^{1}H Resonances of *p*-PC*n*V(*n*=4—7) in DMSO-d_6

Protons	*p*-PC4V	*p*-PC5V	*p*-PC6V	*p*-PC7V
Methylene Chain				
1-CH_2	5.00(+0.34)	4.95(+0.34)	4.93(+0.34)	4.92(+0.34)
2-CH_2	2.35(+0.34)	2.36(+0.34)	2.30(+0.37)	2.26(+0.33)
3-CH_2	2.35(+0.34)	1.64(+0.28)	1.62(+0.28)	1.58(+0.24)
4-CH_2	4.92(+0.31)	2.24(+0.26)	1.62(+0.25)	1.55(+0.13)
5-CH_2		4.84(+0.17)	2.14(+0.21)	1.51(+0.13)
6-CH_2			4.79(+0.13)	2.08(+0.15)
7-CH_2				4.75(+0.08)
Bipyridyl				
α	9.50(+0.17)	9.47(+0.12)	9.45(+0.11)	9.42(+0.09)
β	8.85(+0.07)	8.84(+0.06)	8.83(+0.06)	8.79(+0.02)
γ	8.79(+0.06)	8.70(−0.04)	8.79(+0.04)	8.72(−0.01)
δ	9.31(+0.03)	9.15(−0.13)	9.28(+0.01)	9.24(−0.03)
N-Me	4.46(+0.02)	4.28(−0.16)	4.44(0.00)	4.41(−0.02)

a) Chemical shifts are given in ppm from TMS. The numbers in the parentheses are the porphyrin ring-current induced shift changes and positive value indicates the downfield shift.

7000 Hz spectral width, and 5.9 μs 90° pulse. Chemical shifts were referenced to the solvent peak (2.5 ppm relative to the signal of tetramethylsilane) and are given in parts per million, ppm.

Results and Discussion

^{1}H NMR spectra of *p*-PC*n*V have been unambiguously assigned from the combined analyses of the connectivities in ^{1}H-^{1}H chemical shift correlated and nuclear Overhauser effect correlated spectroscopies. Chemical shifts for the viologen proton resonances of *p*-PC*n*V are given in Table 1. Pyridyl 2′, 6′ and 3′, 5′ protons resonate at 9.09 and 9.52 ppm, respectively, and the shifts of the other proton resonances are essentially identical with those of the corresponding resonances of *m*-PC*n*V previously reported. These shifts are essentially independent of the sample concentration (1—50 mM), indicating the absence of significant intermolecular interaction. The porphyrin ring current induced shifts for the viologen proton resonances of *p*-PC*n*V were calculated using the data obtained for appropriate model compounds as previously described.[6] The ring current shifts (δ_{RC}) of the viologen proton resonances are summarized in Fig. 2 and their plots are individually compared with those of *m*-PC*n*V in Fig. 3. The δ_{RC} value of the 1-CH_2 proton resonance for *p*-PC*n*V is +0.34 ppm and decreases to ca. 0 almost monotonously for protons further away, along chemical bonds, from the porphyrin ring. Similarity in their δ_{RC} plots (Fig. 2) indicates that the orientation of the viologen with respect to the porphyrin is not significantly different among the *p*-PC*n*V. These results suggest that the methylene chain of *p*-PC*n*V is in energetically stable all-*trans* extended conformation as found for *m*-PC*n*V. Anomalously large negative δ_{RC} detected for the δ and N-Me protons of *p*-PC5V may not be explained in terms of its conformational features.

Assuming the extended all-*trans* conformation for the methylene chain, the closest edge-to-edge distances between the two π-systems ($R_{\pi\pi}$) in *p*-PC*n*V with *n*=4, 5, and 6 are 1.03, 1.13, and 1.27 nm, respectively, and are compared with $R_{\pi\pi}$ of 0.85, 0.92, and 1.09 nm for *m*-PC*n*V with the corresponding *n* value, respectively. Therefore, the fact that *p*-PC*n*V (*n*>4) does not exhibit the intramolecular electron transfer leads to conclusions that the electron transfer in DMSO occurs

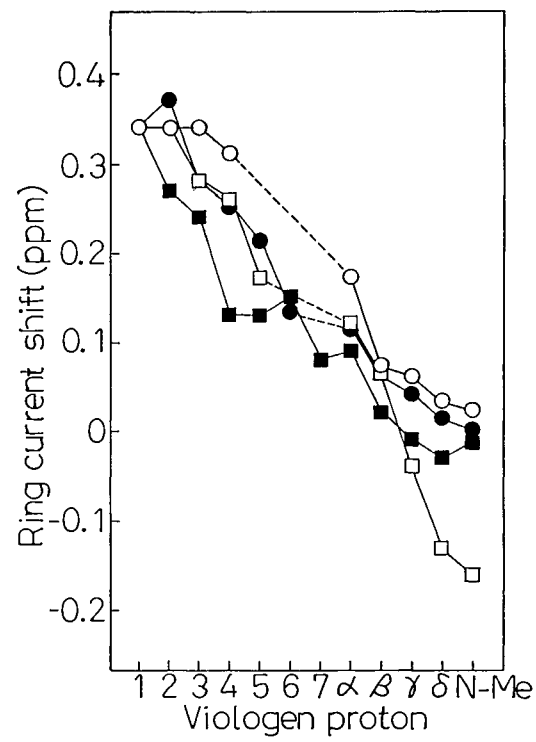

Fig. 2. Plots of the ring current induced chemical shift against viologen protons of *p*-PC*n*V in DMSO-d_6. *p*-PC4V(○), *p*-PC5V (□), *p*-PC6V (●), *p*-PC7V (■).

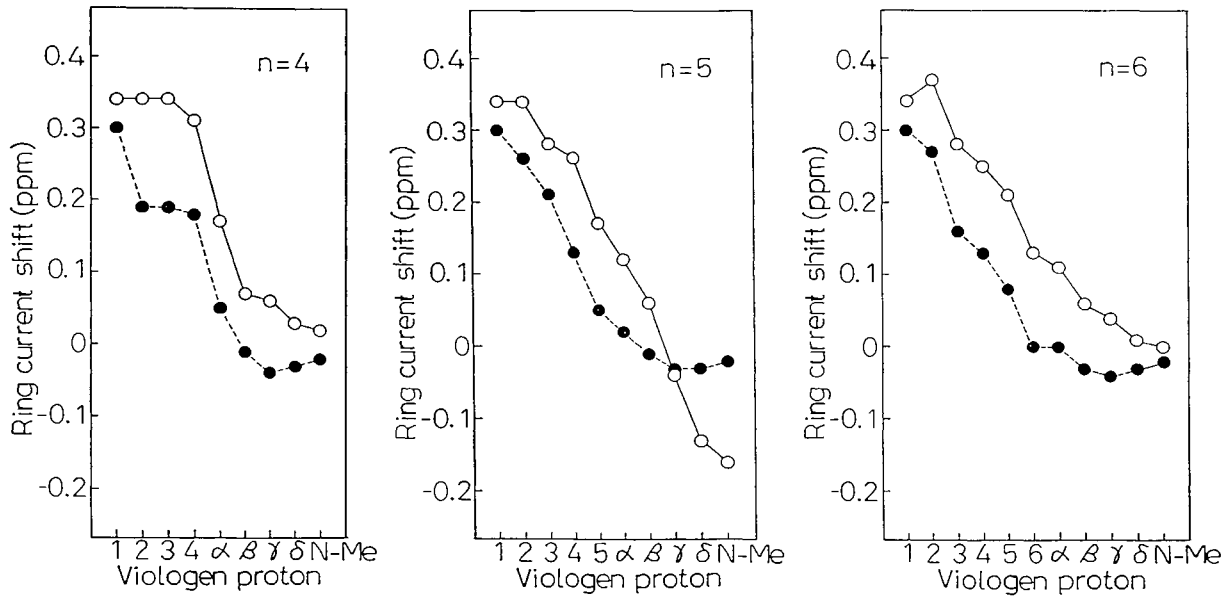

Fig. 3. Plot of the ring current induced chemical shift against viologen proton resonance of *p*-PC*n*V (○) in DMSO-d_6. Similar data for *m*-PC*n*V (●)[6] are also shown for comparison.

when $R_{\pi\pi}<$ ca. 1.1 nm and that the electron is not transfered through the methylene chain. $R_{\pi\pi}$ of 1.1 nm is greater than the theoretical estimate, 0.8 nm, for electron transfer by a short-range tunneling mechanism.[8] Furthermore, $R_{\pi\pi}$ should be considered as a semiquantitative parameter for interpreting the intramolecular electron transfer rate in terms of the molecular structure of these viologen-linked porphyrins, because it does not account for the fact that *m*-PC3V and *p*-PC4V exhibit similar rates.[5] Considering both the conformational flexibility of the methylene chain in solution and the time scale, ns, of the process, $R_{\pi\pi}$ calculated for a molecular structure infered from NMR data may not simply correlate to the electron transfer rate. A conformational change around one of the C-C bonds in themethylene chain, for example, *trans*→*gauche*, alters $R_{\pi\pi}$ as much as ca. 10 and ca. 15% for *p*- and *m*-PC*n*V, respectively.

References

1) S. Aono, N. Kaji, and I. Okura, *J. Chem. Soc., Chem. Commun.*, **1986**, 170.
2) N. Kaji, S. Aono, and I. Okura, *J. Mol. Catal.*, **36**, 201 (1986).
3) I. Okura, N. Kaji, S. Aono, and T. Nishisaka, *Bull. Chem. Soc. Jpn.*, **60**, 1243 (1987).
4) S. Noda, H. Hosono, I. Okura, Y. Yamamoto, and Y. Inoue, *J. Chem. Soc., Faraday Trans. 1*, **86**, 811 (1990).
5) S. Noda, H. Hosono, I. Okura, Y. Yamamoto, and Y. Ionue, *J. Photochem. Photobiol. A: Chem.*, **53**, 423 (1990).
6) Y. Yamamoto, S. Noda, N. Nanai, I. Okura, and Y. Inoue, *Bull. Chem. Soc. Jpn.*, **62**, 2152 (1989).
7) D. Gust, T. A. Moore, P. A. Liddell, G. A. Nemeth, L. R. Makings, A. L. Moore, D. Barrett, P. J. Pessiki, R. V. Bensasson, M. Rougee, C. Chachaty, F. C. De Schryver, M. Van der Auweraer, A. R. Holzwarth, and J. S. Connolly, *J. Am. Chem. Soc.*, **110**, 2670 (1988).
8) J. D. Hopfield, *Proc. Nat. Acad. Sci.*, **71**, 3640 (1974).

Synthesis of Ti-Containing Pillared Montmorillonite Using a Trinuclear Acetatochlorohydroxo Titanium(III) Complex

Tsuyoshi KIJIMA,*,† Hiromoto NAKAZAWA, and Satoshi TAKENOUCHI
National Institute for Research in Inorganic Materials, Namiki 1-1, Tsukuba, Ibaraki 305
(Received August 22, 1990)

Synopsis. Trinuclear acetato-chloro-hydroxo titanium(III) chloride, $[Ti^{III}_3(OCOCH_3)_{6.4}Cl_{1.2}(OH)_{0.4}]Cl \cdot 11H_2O$, was prepared; its aqueous solution was reacted with Ca- and Cu-montmorillonites in air. Titanium(III) complex ions were mostly hydrolyzed, oxidized and condensed into their polynuclear forms, replacing the interlayer metal ions of montmorillonite. The calcined forms of both reaction products maintain large interlayer spacings of 22.2 and 21.3 Å, and have specific surface areas of 105 and 128 m^2g^{-1}, respectively.

Much attention has been paid to the pillaring of layered compounds by bulky inorganic or organic species,[1] including other host molecules, such as cyclodextrins.[2] Similar to zeolites, smectite clays may have micropores, thus affording another family of shape selective catalysts if they are pillared by polynuclear hydroxy metal cations. Titanium oxide is a typical photocatalyst which in combination with, for instance, platinum, is responsible for a variety of organic reactions, such as a one-step preparation of phenol from benzene.[3] These considerations have led to an expectation that smectite clays pillared with titanium oxide may act as a new type of photocatalyst possessing shape-selectivity.

In order to incorporate titanium oxide clusters into the interlayer space of montmorillonite, an attempt was made similar to a method applied to the synthesis of an iron oxide pillared montmorillonite.[4] Ca- and Cu-montmorillonites were reacted with aqueous solutions of a trinuclear acetato-chloro-hydroxotitanium(III) complex, resulting in the formation of titanium-containing pillared montmorillonites. After the present work was underway, Yamanaka, Nishihara, Hattori, and Suzuki[5] reported the synthesis of a titanium oxide pillared clay using montmorillonite and titanium hydoxide soll prepared by the hydrolysis of titanium alkoxide. This was followed by the report of Yoneyama, Haga, and Yamanaka[6] on the photocatalytic activities of the pillared materials.

Experimental

The Na-, Ca-, and Cu-montmorillonite samples used were the same as those used in previous studies.[7] An acetato complex of titanium(III) was prepared by a manner similar to that[8] reported for acetato complexes of iron(III), chrominum(III), and aluminum with a general composition of $[M_3(OCOCH_3)_7(OH)\ (H_2O)_n]NO_3$(M=Fe(III), Cr(III), Al; n=0—4). Fifty cm^3 of anhydrous acetic anhydride were slowly added to a mixed solution of 6.17 g of titanium trichloride, 10 cm^3 of ethyl alcohol, and 5.8 cm^3 of water.

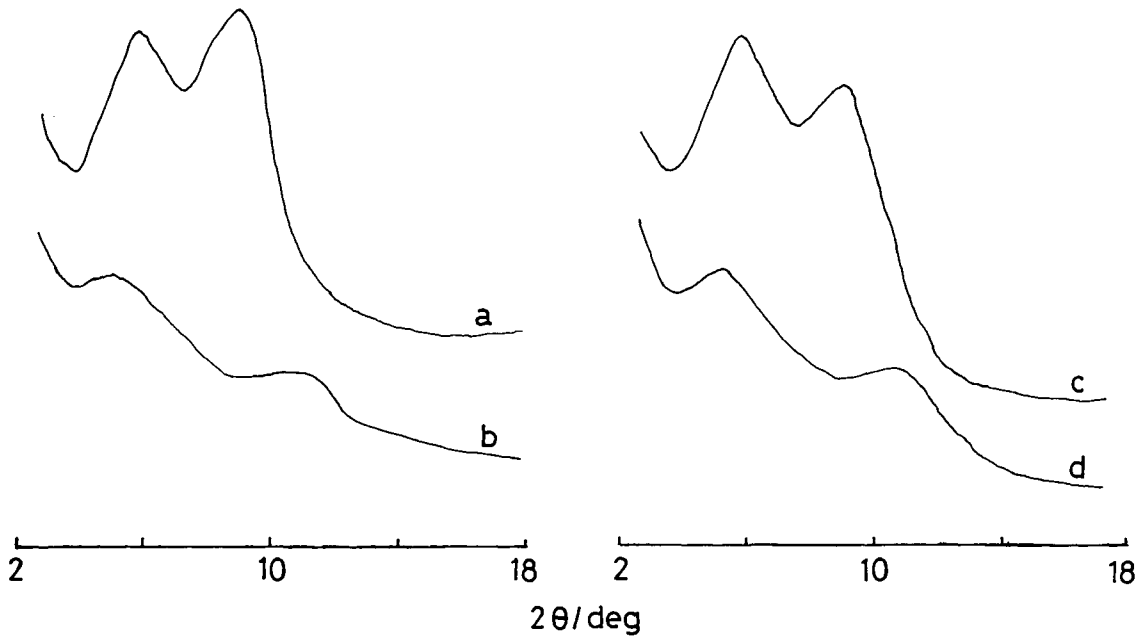

Fig. 1. X-Ray diffraction patterns of the reaction products of (left) Ca- and (right) Cu-montmorillonites heated at 40 °C (a, c) and 400 °C (b, d).

† Present adress: Department of Industrial Chemistry, Faculty of Engineering, Miyasaki University, Miyazaki city, Miyazaki 889-21.

After stirring for 12 h, the resulting solid, black in color and ca. 2.9 g in weight, was separated by filtration. A part of the solid was washed with acetic anhydride and diethylether, allowed to stand in a stream of nitrogen for 2 h, and used for a microanalysis. The other part of the solid was used without washing for a reaction with montmorillonite.

The montmorillonite sample (1 g) was weighed in a flask containing 100 cm^3 of an aqueous solution of the acetato titanium(III) complex (10 g), and kept at 25 °C for 24 h with stirring while the flask was unstoppered in air. The final products were centrifuged, fully washed with water, and dried in air at 40 °C, followed by calcination at 400 °C. When the Ca- and Cu-montmorlllonites were reacted with the acetato titanium complex solution in a stoppered flask, no significant indication of interlayer expansion was observed in the X-ray diffraction patterns of the resulting solids.

X-Ray diffraction measurements were carried out using Fe-$K\alpha$ radiation. The contents of C, H, and metal cations in the resulting materials were determined by a combined use of ICP or atomic absorption, C, H, N elemental and thermogravimetric analyses. A part of the purified acetatotitanium(III) sample was dissolved in water, hydrolyzed with sodium hydroxide, and centrifuged; the chlorine concentration of the supernatant was measured by a Dionex 2000i ion chromatograph. The surface area was measured by a conventional BET method using nitrogen at −196 °C.

Results and Discussion

The composition analysis of the acetatotitanium complex yielded: Ti, 17.7; C, 18.9; H, 3.7; Cl, 9.7 in wt%. This corresponded to a composition of $[Ti^{III}_3(OCOCH_3)_{6.4}(OH)_{0.4}Cl_{1.2}]Cl \cdot 11H_2O$, indicating that the acetatotitanium(III) complex prepared in this work is a trinuclear complex of titanium(III) isotypic with known trivalent metal acetato complexs, but partly including chlorine atoms as a ligand. It was also observed that the complex is gradually oxidized in air accompanying a weight loss and a change in color from black to white.

Table 1. Chemical Analyses of the Ca- and Cu-Montmorillonites Reacted with An Aqueous Solution of Trinuclear Acetato-Chloro-Hydroxo Titanium(III) Complex in Air

	Ca-Product	Cu-Product
	wt%	
Mg	1.9	1.7
Ti	10.8	15.8
Ca	0.1	—
Cu	—	0.04
C	0.36	0.59
Ignit. loss[a)]	16.7	22.0
Molar content based on $O_{10}(OH)_2$ anion		
Silicate layer composition		
Si	3.83	3.83
Al(O)	0.17	0.17
Al(T)	1.60	1.60
Fe	0.10	0.10
Mg	0.32	0.32
Interlayer composition[b)]		
Ti	0.92	1.51
Ca	0.01	—
Cu	—	0.005
OH	3.22	5.51
H_2O	1.46	4.0
Acetoxy	0.061	0.11

a) Total weight loss observed by heating up to 1000 °C in air. b) Tentative values for the OH and H_2O contents were determined by assuming $y=0$ in $Ti_xO_y(OH)_z(Acetoxy)_w$ for the incorporated titanium complex ions.

The X-ray diffraction patterns of the reaction products are shown in Fig. 1. The dried forms of the Ca- and Cu-exchanged products show a strange XRD pattern, in that the d values of the first reflections are 18.2 and 18.8 Å and the second ones are 12.2 and 12.1 Å, respectively. Both apparently show no rational relation. One interpretation is that the first and the second reflection peaks are so broad that they partly overlap each other and, thus, their separation is apparently reduced. In the present case, however, it seems to be difficult to find two such elementary peaks. It is, therefore, much more likely that the dried forms comprise two phases or, more likely, two types of domains with interlayer spacings of 18.2 or 18.8 and 12.2 or 12.1 Å. On the other hand, the calcined forms show two orders of reflections corresponding to interlayer spacings of 22.2 and 21.3 Å, respectively. These observations suggest that during calcination two types of interlayer titanium complexes in the dried form are rearranged to form a single phase of titanium-containing intercalate with larger spacings.

When the acetatotitanium(III) complex had been partly oxidized before dissolving in water, the reaction products showed a distinct peak at $2\theta=31.95°$ ($d=3.52$ Å) attributable to the 101 reflection of titanium dioxide (anatase). However, the above dried and the calcined samples showed no trace of the titanium oxide peak.

Analytical data for products dried at 40 °C are summarized in Table 1. Preliminary analyses of the reaction products indicated that the intralayer composition of the initial montmorillonites remained unexchanged in a reaction with the acetato-hydroxo titanium(III) complex. The chemical formulae of the dried products were, therefore, determined on the basis of the intralayer anion composition, $O_{10}(OH)_2$, as well as the observed content of magnesium ions in the intralayer octahedral sheets.

From the color (white) of the reaction products, the titanium ions incorporated between the silicate layers were assumed to be tetravalent. The amounts of the acetoxy groups were calculated from the carbon content. The total weight loss observed upon heating to 1000 °C in air was attributed to a loss of interlayer water and acetoxy groups, as well as the water produced by condensation of the intra- and inter-layer hydroxide groups. Although the incorporated titanium complex ions would have a composition of $Ti_xO_y(OH)_z(acetoxy)_w$, it is difficult to precisely determine the hydrogen content and the total weight loss for an evaluation of y and z. Tentative values for z and the water content were calculated by assuming $y=0$; the results are listed in Table 1.

Both of the initial Ca- and Cu-momtmorillonites contain 0.203 moles of interlayer Ca^{2+} and Cu^{2+} ions per formula weight.[7] According to the composition data listed in Table 1, the interlayer cations are almost completely replaced by titanium complex ions. This exchange reaction is accompanied by a large decrease in the molar ratio of acetoxy to titanium for the exchanged ions, relative to an expected value of 7/3 for the initial acetatochlorohydroxo titanium(III) complex. The molar exchange ratios of titanium to the initial interlayer Ca^{2+} and Cu^{2+} ions are 4.8 and 7.4, respectively.

When the dried Ca- and Cu-samples were heated at 400 °C, the resulting solids were fully decarbonized, and decreased in weight by 13.5 and 18.7 wt%, respectively, due to a loss of interlayer water and acetoxy groups as well as the water produced by the interlayer condensation. This observations suggest that the interlayer species in calcined samples are formed from titanium(IV) complex ions, during which the molar ratio of intralayer cations to titanium remains unexchanged.

The thicknesses of the titanium complex ion layer for the calcined samples can be estimated by subtracting 9.5 Å for the silicate layer from the observed interlayer spacings of 22.2 and 21.3 Å, yielding 12.7 and 11.8 Å, respectively. The latter two values are in good agreement with a value of 12.1 Å for the van der Waals length of a HO-Ti-O-Ti-OH sequence. These facts suggest that the titanium complex ions taken up by Ca- and Cu-montmorillonites are polynuclear hydroxooxotitanium(IV) ions comprising mainly HO-Ti-O-Ti-OH units directed to the silicate layers. Such polynuclear ions would be formed by an incomplete hydrolysis of the initial acetato titanium complex ions and subsequent condensation. Specific surface areas of 105 and 128 $m^2 g^{-1}$ were obtained for the calcined forms of the Ca- and Cu-montmorillonite based products. These values are much smaller than 300 $m^2 g^{-1}$ for a titanium oxide pillared montmorillonite, obtained by the hydrolysis of titanium alkoxide.[5] This is probably due to the polynuclear forms of titanium resulting from trinuclear acetatochlorohydroxo titanium(III) ions, which are smaller in size than those from titanium alkoxide.

The reaction product obtained from Na-montmorillonite showed a much smaller tendency to intercalate polynuclear titanium complex ions, presumably due to the higher population of interlayer Na^+ ions than that of Ca^{2+} or Cu^{2+} ions.

References

1) T. J. Pinnavia, *Science*, **220**, 365 (1983).
2) T. Kijima, J. Tanaka, M. Goto, and Y Matsui, *Nature*, **310**, 45 (1984); **316**, 280 (1985).
3) I. Izumi, W. W. Dunn, K. O. Wilboun, Furen F. Fan, and A. J. Bard, *J. Phys. Chem.*, **84**, 3207 (1980).
4) S. Yamanaka, T. Doi, S. Sako, and M. Hattori, *Mat. Res. Bull.*, **19**, 161 (1984).
5) S. Yamanaka, T. Nishihara, M. Hattori, and Y. Suzuki, *Mat. Chem. Phys.*, **17**, 87 (1987).
6) H. Yoneyama, S. Haga, and S. Yamanaka, *J. Phys. Chem.*, **93**, 4833 (1989).
7) T. Kijima, H. Nakazawa, and M. Kobayashi, *Bull. Chem. Soc. Jpn.*, **61**, 4277 (1988).
8) K. Starke, *J. Inorg. Nucl. Chem.*, **13**, 254 (1960).

Cobalt(IV) Amine Complexes with Organic Ligands. XI.[1] The Preparation and Properties of Tetraammine(7-chloro-5-nitro- or 5,7-dinitro-8-quinolinolato)cobalt(IV) Complexes and the Corresponding Cobalt(III) Complexes

Yoshihisa YAMAMOTO,* Eiko TOYOTA, and Hidetaka KONNO†
Faculty of Pharmaceutical Sciences, Higashi Nippon Gakuen University, Ishikari-Tobetsu, Hokkaido 061-02
†Faculty of Engineering, Hokkaido University, Sapporo 060
(Received November 13, 1990)

Synopsis. Tetraammine(7-chloro-5-nitro- or 5,7-dinitro-8-quinolinolato)cobalt(IV) complexes and the corresponding cobalt(III) complexes have been isolated, and characterized by analytical, spectroscopic, magnetic, and XPS methods. The effective magnetic moments of cobalt(IV) complexes were ca. 1.6 BM, suggesting an unpaired spin. An unpaired spin on the complex is located over the π-orbitals of the 7-chloro-5-nitro- or 5,7-dinitro-8-quinolinolato ligand (abbreviation: chelated ligand) and on the cobalt atom from the results of the C 1s and Co 2p spectra by XPS. The Cl 2p binding energy of the chloride ion suggests that the valence electrons of the chloride ions may have some interaction with the π-orbitals of the chelated ligand.

In this series, the preparation, properties, and electronic states of cobalt(IV) complexes, $[Co(5\text{-}NO_2sal)L]Cl(NO_3)\cdot nH_2O$ (L: $(NH_3)_4$, $(bpy)_2$, quadridentate amine),[2] radical cobalt(III) complexes, $[Co(5\text{-}NO_2salam)(NH_3)_4]Cl_2(NO_3)$[3] and $[Co(5\text{-}NO_2salam)_2(NH_3)_2]Cl(NO_3)\cdot 2H_2O$,[1] and biradical cobalt(II) complex, $[Co(5\text{-}NO_2salam)_2(NH_3)_2]Cl(NO_3)\cdot 2H_2O$,[1] have been reported. The electronic states of the above mentioned complexes have been solved by physicochemical and XPS methods. Through the above studies, there was an implication that free chloride ions in the complexes may contribute to their stability. So far, the electronic state of the chloride ions has remain unsolved, since no measurement of the chloride ions by XPS was carried out. The present paper deals with the preparation and properties of the title cobalt(IV) complexes, and with the role of the chloride ions in the complexes.

Experimental

Measurements. The XPS measurements were carried out with a VG ESCALAB Mk-II electron spectrometer by irradiating Mg $K\alpha$ X-rays (60—150 W). Sample was placed either on a nickel holder with a copper mesh adhesive or on a indium foil with a gold mesh, and then introduced into the spectrometer. After evacuation to a vacuum of better than 3×10^{-6} Pa, the sample was cooled to ca. 200 K. Sample cooling was initiated within 10 min of the introduction to the spectrometer. Spectra were analysed using a VGS-5000 data system: Peak separation was carried out by a nonlinear least squares method using a mixed Gaussian-Lorentzian curve shape; background level was determined by a method proposed by Shirley,[4] and the contribution from X-ray satellites was subtracted. The electron-binding energies, E_B, were calibrated by assigning either 285.0 eV to the C 1s peak of 8-quinolinol or 407.0 eV to the N 1s peak of the nitrate free anion. The latter value was an average of the values from previous studies;[1,2b,5] the 90% confidence limits of the average are ±0.15 eV. The ^{1}H NMR spectra were recorded with an FX-90Q apparatus (JEOL). The visible absorption spectra were recorded with a Shimadzu UV-210 recording spectrophotometer. The magnetic susceptibilities were measured by the Faraday method using a magnetic balance (Shimadzu) from liquid N_2 to room temperature. The electric conductivities of aqueous solutions were determined by the use of a conductometer, CM-30 (Shimadzu), at room temperature.

Preparation of Complexes. Tetraammine(5,7-dinitro-8-quinolinolato)cobalt(III) Dinitrate (2a) and Tetraammine(5,7-dinitro-8-quinolinolato)cobalt(IV) Trinitrate (3a): Eight cm^3 of 60% HNO_3 were added, drop by drop, to 2.0 g (5.06 mmol) of $[Co(oxin)(NH_3)_4](NO_3)_2$ (**1a**).[6] Soon, a crystalline precipitate (complex **2a**) separates out, and was collected by filtration, and recrystallized from water. The green filtrate was added to acetone (150 cm^3) and stirred at 5 °C. The green cobalt(IV) complex (**3a**), thus precipitated, was filtered, washed with acetone and ether at 5 °C, and dried. Yields: 0.68 g (27.7%) for **2a**, 0.91 g (32.8%) for **3a**. Found **2a**: C, 22.06; H, 3.54; N, 25.77%. Calcd for $CoC_9H_{16}N_9O_{11}$: (MW 485.22) C, 22.28; H, 3.32; N, 25.98%. Found **3a**: C, 19.47; H, 3.09; N, 25.32%. Calcd for $CoC_9H_{16}N_{10}O_{14}$: (MW 547.25) C, 19.75; H, 2.95; N, 25.60%. Absorption spectra **2a** (H_2O): 383 (ε 13800), 398 nm^{sh} (12500); **3a** (60% HNO_3): 384 (5000), 398^{sh} (4600), 670 (1100). Λ=240 S cm^2 mol^{-1} for **2** in water. ^{1}H NMR (DMSO-d_6) **2a**: δ=3.60 (3H, NH_3), 3.75 (6H, NH_3), 4.18 (3H, NH_3); δ=8.25 (q, H_3), 8.74 (d, H_2), 9.15 (s, H_6), 9.40 (d, H_4).

Tetraammine(7-chloro-5-nitro-8-quinolinolato)cobalt(III) Dinitrate (2b), Tetraammine(7-chloro-5-nitro-8-quinolinolato)cobalt(IV) Dichloride Nitrate (3b), and Tetraammine(5,7-dinitro-8-quinolinolato)cobalt(IV) Chloride Dinitrate (3c): Eight cm^3 of 60% HNO_3 were added, drop by drop, to 2.0 g (5.55 mmol) of $[Co(oxin)(NH_3)_4]Cl_2\cdot H_2O$ (**1b**).[7] The precipitated yellowish-brown crystalline complex **2** (mixture of **2a** and **2b**) was collected by filtration and recrystallized from water. The green filtrate was added to acetone (200 cm^3) and stirred. Thus, the precipitated green cobalt(IV) complex **3** (mixture of **3b** and **3c**) was filtered, washed with acetone and ether, and dried. Complex **2b** was isolated from an orange-colored acetone filtrate of **3**. The ratio of **2b** and **2a** in **2** was 7 to 3, according to the results of elemental analyses and ^{1}H NMR spectra, and the ratio of **3b** and **3c** in **3** was 7 to 3 from the results of elemental analyses. Yields **2b**: 0.32 g (12.15%); **2**: 0.91 g (34.3%); **3**: 0.56 g (20.4%). Found **2b**: C, 22.56; H, 3.61; N, 23.52; Cl, 7.19%. Calcd for $CoC_9H_{16}N_8O_9Cl$: (MW 474.66) C, 22.77; H, 3.40; N, 23.61; Cl, 7.47%. Found **2**: C, 22.24; H, 3.62; N, 24.12, Cl, 5.61%. Calcd for $CoC_9H_{16}N_{8.3}O_{9.6}Cl_{0.7}$: (MW 477.85) (**2b**:**2a**=7:3) C, 22.62; H, 3.38; N, 24.33, Cl, 5.19%. Found **3**: C, 22.15; H, 3.55; N, 21.81; Cl, 16.88%. Calcd for $CoC_9H_{16}N_{7.6}O_{7.5}Cl_{2.4}$: (MW 494.70) (**3b**:**3c**=7:3) C, 21.85; H, 3.26; N, 21.52, Cl, 17.20%. Absorption spectra **2b** (H_2O): 412 nm (ε 11800); **2** (H_2O): 407 (12800); **3** (60% HNO_3): 405 (3340), 720 (1500). Λ=240 for **2b** and 410 S cm^2 mol^{-1} for **3**

in water. ^{1}H NMR (DMSO-d_6) **2b**: δ=3.54 (3H, NH_3), 3.65 (6H, NH_3), 4.11 (3H, NH_3); δ=8.10 (q, H_3), 8.64 (d, H_2), 8.69 (s, H_6), 9.40 (d, H_4).

Results and Discussion

Complexes **2a** and **3a** have been obtained from a reaction mixture of **1a** and 60% HNO_3. Complexes **2b**, **2**, and **3** have been obtained from a reaction mixture of **1b** and 60% HNO_3 (Scheme 1). The colors of **2a**, **2b**, and **2** are yellowish-brown, yellowish-orange, and yellowish-orange, respectively and those of **3a** and **3** are green. Complexes **2a**, **2b**, and **2** were soluble in DMSO, and slightly soluble in water and methanol. Complexes **3a** and **3** were soluble in 60% HNO_3 and DMSO.

In the ^{1}H NMR spectra in DMSO-d_6, the signals at δ=3.5—4.2 (12H) and at δ=8.1—9.4 (4H) of **2a**, **2b**, and **2** were assigned to the ammine protons and the coordinated 8-quinolinolato ligand, respectively. The signals at δ=8.25, 8.74, 9.15, and 9.40 of **2a** were very close to those of 5,7-dinitro-8-quinolinol,[8] while those at δ=8.10, 8.64, 8.69, and 9.40 of **2b** were very close to those of 7-chloro-5-nitro-8-quinolinol.[8] This indicates that **2a** and **2b** contain the coordinated 5,7-dinitro-8-quinolinolato and 7-chloro-5-nitro-8-quinolinolato ligands, respectively. A proportion between **2b** and **2a** in **2** was estimated to be 7 to 3 from the intensity ratio of the H_6 proton signals of **2** (Fig. 1). The electric conductivities of **2a**, **2b**, and **2** in the aqueous solutions are ca. 240 S cm^2 mol^{-1}. Complexes **2a**, **2b**, and **2** were diamagnetic by the magnetic susceptibility. Absorption bands at 383—412 nm in water of **2a**, **2b**, and **2** were assigned to the charge-transfer band.[6] In XPS, the Cl $2p_{3/2}$ spectra of **2b** and **2** were observed at 200.4—200.5 eV (Fig. 2). The peak at 200.4—200.5 eV was assigned to the chlorine atom of the coordinated 7-chloro-5-nitro-8-quinolinolato ligand, since the E_B of the peak was close to that (201.0 ev) of chlorobenzene,[9] but was different from that (197.6 ev) of **1b**. The N 1s spectra of **2a**, **2b**, and **2** were observed at ca. 400 and ca. 406 eV. The lower E_B peak was separated to two peaks which were assigned to -NH= and NH_3 nitrogens. The higher E_B peak was also separated into three peaks which were assigned to 5-NO_2, 7-NO_2, and NO_3 nitrogens (Table 1).[1,2b,3]

The magnetic susceptibilities of **3** and **3a** obeyed the Curie-Weiss law, with an effective magnetic moment of 1.58 BM for **3** and 1.50 BM for **3a**, suggesting the presence of an unpaired spin. The absorption spectra in 60% HNO_3 of **3** and **3a** showed two peaks at 405 and 720 nm for **3** and three peaks at 384, 398(sh), and 670 nm for **3a**. The peaks at 720 and 670 nm are due

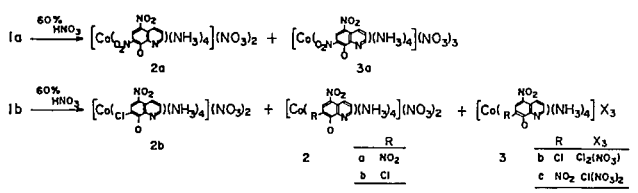

Scheme 1.

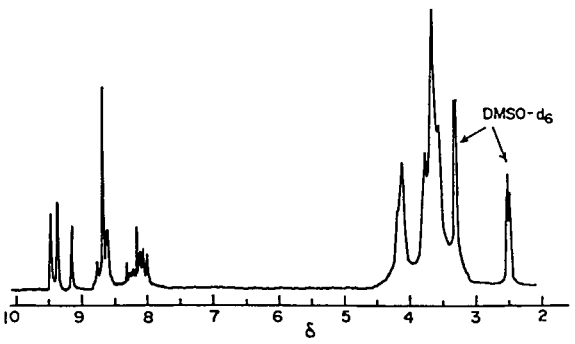

Fig. 1. The ^{1}H NMR spectrum of complex **2**.
2: [Co(5-NO_2-7-R-oxin)(NH_3)$_4$](NO_3)$_2$ (R: Cl, NO_2).

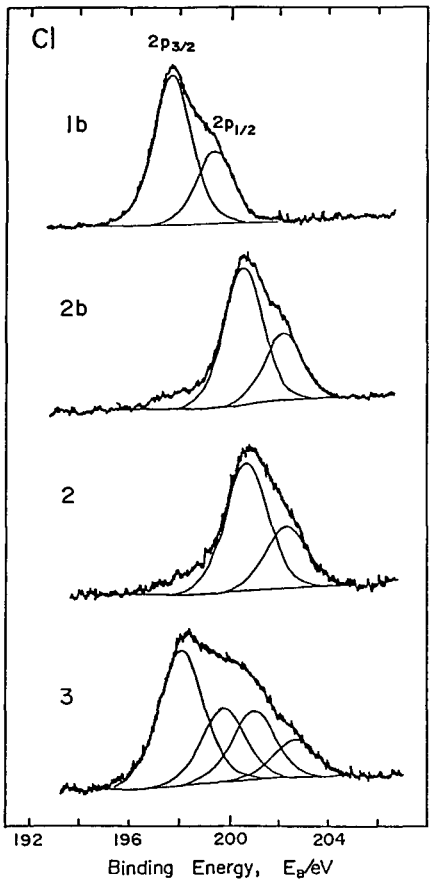

Fig. 2. The XPS in the Cl 2p region of complexes.
1b: [Co(oxin)(NH_3)$_4$]$Cl_2 \cdot H_2O$
2b: [Co(7-Cl-5-NO_2-oxin)(NH_3)$_4$](NO_3)$_2$
2: [Co(5-NO_2-7-R-oxin)(NH_3)$_4$](NO_3)$_2$ (R: Cl, NO_2)
3: [Co(5-NO_2-7-R-oxin)(NH_3)$_4$]X_3 (R: Cl, NO_2; X_3: $Cl_2(NO_3)$, $Cl(NO_3)_2$).

to the unpaired spin.[3] The ^{1}H NMR spectra of **3** and **3a** did not show the expected signals, because of paramagnetism. The electric conductivity in an aqueous solution of **3** was 410 S cm^2 mol^{-1}. In the XPS of **3**, the N 1s spectrum was observed at ca. 400 and ca. 406 eV. Each peak was separated into two (-N= and NH_3) or three peaks (5-NO_2, 7-NO_2, and NO_3) (Table 1). The C 1s peak was separated into two peaks at 285.6 and 288.2 eV. The peak that appeared in the higher E_B region was assigned to the electron-

Table 1. XPS of Complexes

Complex No.	Binding energies of electrons, E_B/eV					
	Co $2p_{3/2}$	Co $2p_{1/2}$	Splitting	C 1s	N 1s	Cl $2p_{3/2}$
2a	782.3(±0.2) FWHM 2.74 (±0.28)	797.3(±0)	15.0	285.6(±0.1) Broad[a] [Weak]	399.5(±0.4) -N= 400.5(±0.2) NH_3 404.9(±0.5) 5-NO_2 406.3(±0.1) 7-NO_2 407.0[b] NO_3^- FWHM 2.13(±0.19)	
2b	782.2(±0.2) FWHM 2.20 (±0.28)	797.2(±0.2)	15.0	285.5(±0.2) Broad[a] [Weak]	399.4(±0.5) -N= 400.3(±0) NH_3 405.5(±0.3) 5-NO_2 407.0[b] NO_3^- FWHM 1.74(±0.03)	200.4(±0.1) -Cl FWHM 1.90(±0.11)
2	782.3(±0.1) FWHM 2.20 (±0.08)	797.3(±0.2)	15.0	285.5(±0.2) Broad[a] [Weak]	399.4(±0) -N= 400.3(±0.2) NH_3 404.6(±0.2) 5-NO_2 406.0(±0.2) 7-NO_2 407.0[b] NO_3^- FWHM 1.86(±0)	200.5(±0.1) -Cl FWHM 2.06(±0.09)
3	782.2(±0.2) FWHM 2.58 (±0.48)	797.3(±0.1)	15.1	285.6(±0.2) 288.2(±0.3)	399.4(±0.3) -N= 400.3(±0.2) NH_3 404.7(±0.4) 5-NO_2 406.0(±0.1) 7-NO_2 407.0[b] NO_3^- FWHM 1.99(±0.16)	198.0(±0.2) Cl^- 200.8(±0.1) -Cl FWHM 2.11 (±0.13)
1b	782.0(±0.3) FWHM 2.13 (±0.35)	797.0(±0)	15.0	285.0[c] Broad[a] [Weak]	399.5(±0.1) -N= 400.2(±0.1) NH_3 FWHM 1.70(±0.01)	197.6(±0.2) Cl^- FWHM 1.86(±0.05)
5				285.0	402.2 $=N^+=$	196.7 Cl^-
6				285.4	402.3	197.1 Cl^-

a): In higher E_B region. b): An average E_B [N 1s] for NO_3^- calculated from the previous data,[1,3,7] 407.00±0.15 eV, was used to the energy calibration. c): An average E_B [C 1s] for carbons in 8-quinolinol was taken to be 285.0 eV. Uncertainties in parentheses are 90% confidence limits.

poor carbons[1,3] relative to the normal ring carbons at 285.5 eV. The proportion of electron-poor carbons in the higher binding energy region was about 2-times larger than that of **2**. The Co $2p_{3/2}$ peak at 782.2 eV showed satellites. These results are in agreement with those of tetraammine(5-nitrosalicylato)cobalt-(IV) complexes,[2b] $[Co(5\text{-}NO_2sal)(NH_3)_4]Cl(NO_3)\cdot H_2O$ (**4**), previously reported. Thus, an unpaired spin is located over the π-orbitals of the chelated ligand and on the cobalt atom. The Cl $2p_{3/2}$ spectrum of **3** was observed at 198.0 and 200.8 eV (Table 1 and Fig. 2). The peak at 198.0 eV was assigned to a free chloride ion (Cl^-), and the peak at 200.8 eV was assigned to the chlorine atom of the coordinated 7-chloro-5-nitro-8-quinolinolato ligand. The intensity ratio between the lower E_B and higher E_B peaks was about 2 to 1. The E_B (198.0 eV) of the chloride ion is higher than those (196.7—197.6 eV) of **1b**, hexadecyltrimethylammonium chloride, $[(C_{16}H_{33})(CH_3)_3N]Cl$ (**5**), and tetramethylammonium chloride,[10] $[(CH_3)_4N]Cl$ (**6**) (Table 1). The higher E_B suggests that the valence electrons of the chloride ions in **3** may have some interaction with the π-orbitals of the chelated ligand and a part of electrons of the chloride ion may flow over the π-orbitals of the chelated ligand, since such a shift to higher E_B is not observed for compounds without a localized spin on the π-orbitals, which is the case in **2**. Further, **3a**, which has an unpaired spin but no chloride ions as a free anion, is unstable under X-ray irradiation and in an aqueous solution. These experimental results indicate that the interaction between the chloride ions and the π-orbitals of the chelated ligand contributes to the stability of **3**.

References

1) Part X. Y. Yamamoto and H. Konno, *Bull. Chem. Soc. Jpn.*, **60**, 1299 (1987).

2) a) Y. Yamamoto, E. Toyota, and N. Mitsudera, *Bull. Chem. Soc. Jpn.*, **53**, 3517 (1980); b) Y. Yamamoto, M. Mori, and H. Konno, *Bull. Chem. Soc. Jpn.*, **54**, 1995 (1981); c) Y. Yamamoto, S. Shimokawa, and E. Yamada, *Bull. Chem. Soc. Jpn.*, **57**, 1153 (1984).

3) Y. Yamamoto and E. Toyota, *Bull. Chem. Soc. Jpn.*, **59**, 617 (1986).

4) D. A. Shirley, *Phys. Rev. B*, **5**, 4709 (1972).

5) Y. Yamamoto, H. Kudo, M. Mori, and H. Konno, *Bull. Chem. Soc. Jpn.*, **55**, 136 (1982).

6) Y. Yamamoto, R. Kataoka, S. Imahara, and T. Amano, *Bull. Chem. Soc. Jpn.*, **54**, 2972 (1981).

7) Y. Yamamoto, *Chem. Lett.*, **1980**, 1555.

8) H. Gershon and M. W. McNeil, *J. Heterocycl. Chem.*, **8**, 821 (1971).

9) D. T. Clark, D. Kilcast, and W. K. R. Musgrave, *J. Chem. Soc., Chem. Comm.*, **1971**, 516.

10) H. Konno and Y. Yamamoto, *Bull. Chem. Soc. Jpn.*, **60**, 2561 (1987).

Difference in Kinetic Behavior on the Photosensitized Decomposition of the Tris(oxalato)cobaltate(III) Ion by Tris(2,2′-bipyridine)ruthenium(II) and Bis(3,3′-biisoquinoline) (2,2′-bipyridine)ruthenium(II)

Masako KATO, Yuki OHONISHI, and Masaru KIMURA*
Department of Chemistry, Faculty of Science, Nara Women's University, Nara 630
(Received November 21, 1990)

Synopsis. The photo-sensitized decomposition of $[Co(ox)_3]^{3-}$ (ox=oxalate) was performed using $[Ru(bpy)_3]^{2+}$ (bpy=2,2′-bipyridine) and $[Ru(i\text{-}biq)_2(bpy)]^{2+}$ (*i*-biq=3,3′-biisoquinoline). The dramatic difference in the decomposition behavior appeared between them. In appearance, the decomposition rate obeys first-order with respect to the $[Co(ox)_3]^{3-}$ concentration for $[Ru(i\text{-}biq)_2(bpy)]^{2+}$ system, whereas zero-order for the $[Ru(bpy)_3]^{2+}$ system. The cause was discussed on the basis of the kinetic analysis.

It is widely known that the tris(2,2′-bipyridine)-ruthenium(11) complex, $[Ru(bpy)_3]^{2+}$, acts as a useful homogeneous photocatalyst for many photochemical systems. The photosensitized reductive decomposition of the tris(oxalato)cobaltate(III) ion, $[Co(ox)_3]^{3-}$, is one of the typical examples.[1] In our previous work, it was found that the rate of the decomposition is of zero-order with respect to the concentration of $[Co(ox)_3]^{3-}$ and is proportional to the incident light-intensity only.[2] For the purpose of comparing the catalytic behavior, we have been used several analogous ruthenium(II) complexes in place of $[Ru(bpy)_3]^{2+}$ as photosensitizers of the reaction. $[Ru(i\text{-}biq)_2(bpy)]^{2+}$ (*i*-biq=3,3′-biisoquinoline) contains only one bpy ligand on which an excited electron can be populated in the lowest MLCT excited state. As *i*-biq ligands in the complex hardly affect the lowest excited state, the photophysical properties such as emission energy and emission lifetime of $[Ru(i\text{-}biq)_2(bpy)]^{2+}$ are very similar to those of $[Ru(bpy)_3]^{2+}$.[3,4] Nevertheless, the dramatic difference between $[Ru(i\text{-}biq)_2(bpy)]^{2+}$ and $[Ru(bpy)_3]^{2+}$ was observed in the decomposition behavior of $[Co(ox)_3]^{3-}$ in appearance. Thus we have carried out the kinetic approach in order to explain the difference between them.

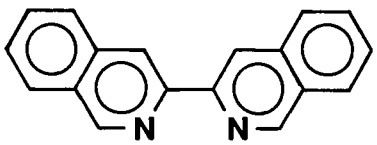

i-biq

Experimental

$[Ru(bpy)_3]Cl_2 \cdot 6H_2O$[5] and $K_3[Co(ox)_3] \cdot 3H_2O$[6] were prepared according to the literatures and recrystallized twice. 3,3′-Biisoquinoline and the $[Ru(i\text{-}biq)_2(bpy)]^{2+}$ complex were available from previous investigation.[3] To obtain higher solubility in water, chloride of the complex was prepared by the anion exchange (Dowex 1-X8). The other chemicals used are of guaranteed reagent grade.

The sample solution for the photo-sensitized decomposition was prepared as follows: 2×10^{-5} mol dm^{-3} of the ruthenium(II) complex, 3×10^{-3} mol dm^{-3} of $[Co(ox)_3]^{3-}$, 0.095 mol dm^{-3} of HCl, and 0.2 mol dm^{-3} of NaCl. For the solution that sodium oxalate was added, the concentration of NaCl was lowered to keep the ionic strength constant. The solution was irradiated continuously with visible light (>400 nm) at 25 °C using the same apparatus as reported previously.[2] The reaction solution was purged of oxygen by bubbling pure nitrogen gas through it. Aliquot samples were withdrawn at appropriate times to measure the absorbance of $[Co(ox)_3]^{3-}$ at 602 nm (ε=148 mol^{-1} dm^3 cm^{-1}). While, the concentration of the ruthenium(II) complexes was checked by the absorption spectra after removal of the $[Co(ox)_3]^{3-}$ ion by the anion-exchange resin (Dowex 1-X8).

Results and Discussion

Figure 1 shows plots of the absorbance of $[Co(ox)_3]^{3-}$ vs. time under three different conditions. In the presence of $[Ru(bpy)_3]^{2+}$, $[Co(ox)_3]^{3-}$ decomposed efficiently in proportion to the time (Fig. 1A). When $[Ru(i\text{-}biq)_2(bpy)]^{2+}$ was used instead of $[Ru(bpy)_3]^{2+}$ as a photosensitizer under the same acid conditions, the decomposition of $[Co(ox)_3]^{3-}$ was as slow as the self-decomposition by the intramolecular electron transfer, showing the very small photosensitizing effect (Fig. 1C). In the system, absorbance at 395 nm of $[Ru(i\text{-}biq)_2(bpy)]^{2+}$ decreased with time and a new

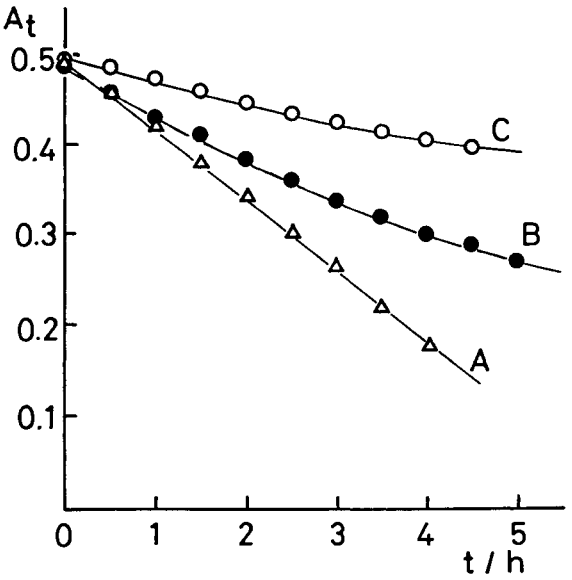

Fig. 1. Plots of the absorbance of $[Co(ox)_3]^{3-}$ vs. time in the presence of: (A) 2×10^{-5} mol dm^{-3} of $[Ru(bpy)_3]^{2+}$, (B) 2×10^{-5} mol dm^{-3} of $[Ru(i\text{-}biq)_2(bpy)]^{2+}$ and 0.05 mol dm^{-3} of $Na_2C_2O_4$, (C) 2×10^{-5} mol dm^{-3} of $[Ru(i\text{-}biq)_2(bpy)]^{2+}$.

absorption band at 370 nm appeared instead. The peak corresponds to the spectrum of a tervalent complex, $[Ru(i\text{-}biq)_2(bpy)]^{3+}$ obtained by the oxidation of $[Ru(i\text{-}biq)_2(bpy)]^{2+}$ using PbO_2 in a 1 mol dm^{-3} sulfuric acid. This indicates that $[Ru(i\text{-}biq)_2(bpy)]^{3+}$, generated due to the oxidative quenching by $[Co(ox)_3]^{3-}$, accumulated during the reaction time. This phenomenon for the mixed ligand complex results from a little higher stability of the tervalent state of the ruthenium ion than that for the tris(bipyridine) complex. The standard redox potentials are 1.26 V and 1.17 V vs. NHE for $[Ru(bpy)_3]^{2+}$ and $[Ru(i\text{-}biq)_2(bpy)]^{2+}$, respectively.[7] In the case of the tris(bipyridine) complex, $[Ru(bpy)_3]^{3+}$ can be reduced rapidly to the bivalent state by the oxalate ion released by the reductive decomposition of $[Co(ox)_3]^{3-}$. Thus when sodium oxalate as a reductant of ruthenium(III) species was beforehand added to the sample solution with $[Ru(i\text{-}biq)_2(bpy)]^{2+}$, the decomposition of $[Co(ox)_3]^{3-}$ proceeded smoothly keeping the constant concentration of $[Ru(i\text{-}biq)_2(bpy)]^{2+}$ (Fig. 1B). However, the apparent kinetic behavior was quite different from that for the $[Ru(bpy)_3]^{2+}$ catalysis. In the case of $[Ru(i\text{-}biq)_2(bpy)]^{2+}$ catalysis, the decomposition rate of $[Co(ox)_3]^{3-}$ seems to be of first-order rather than of zero-order with respect to the $[Co(ox)_3]^{3-}$ concentration.

To explain the difference, we carried out the kinetic approach. The photo-sensitized decomposition takes place as shown in Scheme 1. According to the scheme, the kinetic expression can be described as Eq. 1

$$-d[Co']/dt = (k_{et}+k_{en})[{}^*Ru][Co^{III}] - k_{be}[Ru^{III}\cdots Co^{II}] - k_d[Ru^{II}\cdots {}^*Co] \quad (1)$$

where [Co'] represents the total concentration of $[Co(ox)_3]^{3-}$ involving an encounter complex in the ground state denoted by $[Ru^{II}\cdots Co^{III}]$: [*Ru], $[Co^{III}]$, $[Ru^{III}\cdots Co^{II}]$, and $[Ru^{II}\cdots {}^*Co]$ indicate the concentrations of the excited species of the ruthenium complexes, $[Co(ox)_3]^{3-}$, and encounter complexes generated by electron- and energy-transfer, respectively: The rate constant on each step is defined as shown in Scheme 1. The association constant for $[Ru(bpy)_3]^{2+}$ with $[Co(ox)_3]^{3-}$ on the ground state was reported to be 1900 mol^{-1} dm^3 at zero ionic strength.[7] Using the

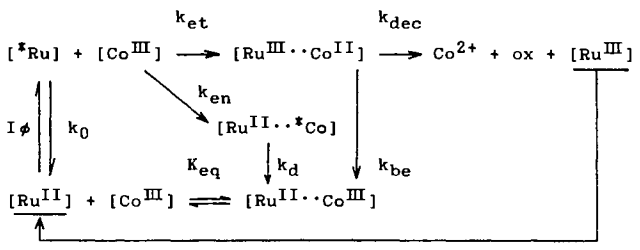

$[Ru^{II}]$ = Ruthenium(II) Complexes

$[Co^{III}] = [Co(ox)_3]^{3-}$

$ox = (COO)_2^{2-}$

Scheme 1.

value and 2×10^{-5} mol dm^{-3} for the $[Ru(bpy)_3]^{2+}$ concentration, it is estimated that only a few percents of $[Co(ox)_3]^{3-}$ are paired with $[Ru(bpy)_3]^{2+}$. Under the experimental conditions of much higher ionic strength, the ion pairing of the ground state species would be negligible. The assumption of the steady state concentration for [*Ru], $[Ru^{III}\cdots Co^{II}]$ and $[Ru^{II}\cdots {}^*Co]$ leads to Eq. 2:

$$[Co'] + k_0/k_q \ln [Co'] = -Bt + C. \quad (2)$$

In this equation, k_q is the bimolecular quenching rate constant:

$$k_q = k_{et} + k_{en}, \quad (3)$$

and B is a constant related to the quantum yield of the reaction:

$$B = I\phi k_{et}k_{dec}/(k_{et}+k_{en})(k_{dec}+k_{be}). \quad (4)$$

Equation 2 indicates that the reaction obeys the zero order rate law under the conditions of $[Co'] \gg |k_0/k_q \ln[Co']|$, while the first-order rate law under the conditions of $[Co'] \ll |k_0/k_q \ln[Co']|$. Thus the data for both $[Ru(bpy)_3]^{2+}$ and $[Ru(i\text{-}biq)_2(bpy)]^{2+}$ were analyzed on the basis of Eq. 2. The decomposition data were corrected for the self-decomposition of $[Co(ox)_3]^{3-}$. The decay rate constant (k_0) of $[Ru(bpy)_3]^{2+}$ was fixed to the value of 1.7×10^6 s^{-1}.[8] On the other hand, a similar value of k_0 is also expected for $[Ru(i\text{-}biq)_2(bpy)]^{2+}$ from the data in acetonitrile (1.0×10^6 s^{-1}).[8] As shown in Fig. 2, both data were well fitted by Eq. 2 with reasonable values of k_0 and k_q. The result indicates that the quenching rate constant of $[Ru(i\text{-}biq)_2(bpy)]^{2+}$ in the system is smaller than that for $[Ru(bpy)_3]^{2+}$. It would be related to the existence of the bulky ligands which do not participate in the lowest excited states for $[Ru(i\text{-}biq)_2(bpy)]^{2+}$. Such a situation particularly makes the intermolecular elec-

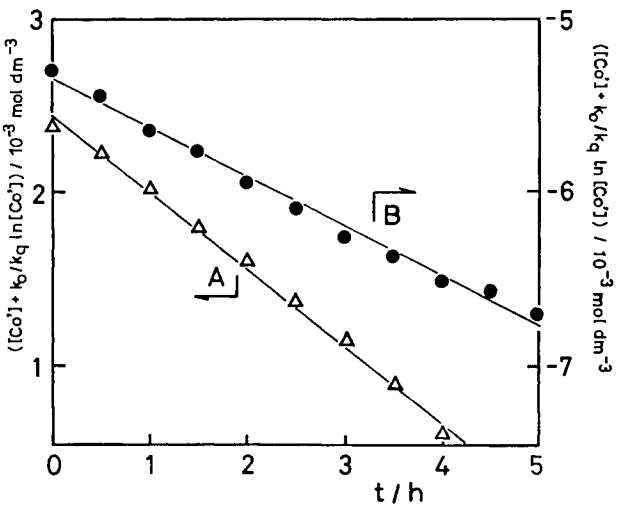

Fig. 2. Plots of $([Co']+k_0/k_q \ln[Co'])$ vs. time in the systems of (A) $[Ru(bpy)_3]^{2+}$ and (B) $[Ru(i\text{-}biq)_2(bpy)]^{2+}$. The straight lines are the least-square-fitting lines on the basis of Eq. 2: (A) $k_0=1.7\times10^6$ s^{-1}, $k_q=1\times10^{10}$ mol^{-1} dm^3 s^{-1}, $B=7.4\times10^{-6}$ mol dm^{-3} s^{-1}, (B) $k_0=1.5\times10^6$ s^{-1}, $k_q=1\times10^9$ mol^{-1} dm^3 s^{-1}, $B=4.7\times10^{-6}$ mol dm^{-3} s^{-1}.

tron transfer (i.e. k_{et}-path) much more difficult.

$[Ru(i\text{-}biq)_2(bpy)]^{2+}$ has several advantages as a photosensitizer compared with $[Ru(bpy)_3]^{2+}$. For example, the lowest excited state of $[Ru(i\text{-}biq)_2(bpy)]^{2+}$ could act as a stronger reductant than that for $[Ru(bpy)_3]^{2+}$, since the oxidation potential of the excited species is estimated to be -0.95 V and -0.79 V vs. NHE for $[Ru(i\text{-}biq)_2(bpy)]^{2+}$ and $[Ru(bpy)_3]^{2+}$, respectively, from the potential of the ground state and the zero-zero excitation energy. The wider and stronger absorption bands in the visible region due to charge transfer to both *i*-biq and bpy ligands for $[Ru(i\text{-}biq)_2(bpy)]^{2+}$ is another merit as a photosensitizer. Nevertheless, $[Ru(i\text{-}biq)_2(bpy)]^{2+}$ is not so effective as $[Ru(bpy)_3]^{2+}$ as indicated by the *B* values (7.4×10^{-6} mol dm^{-3} s^{-1} for $[Ru(bpy)_3]^{2+}$ and 4.7×10^{-6} mol dm^{-3} s^{-1} for $[Ru(i\text{-}biq)_2(bpy)]^{2+}$). The smaller value for the $[Ru(i\text{-}biq)_2(bpy)]^{2+}$ system would come from the yield in the electron transfer step, the part of $k_{et}/(k_{et}+k_{en})$ in the *B* value (Eq. 4). For the $[Ru(bpy)_3]^{2+}$ system, the limiting quantum yield of the photosensitized decomposition of $[Co(ox)_3]^{3-}$ was reported to be 0.85 in 0.05 mol dm^{-3} H_2SO_4.[1] Such a high yield suggests that $k_{et}/(k_{et}+k_{en})$ in Eq. 2 must be a fairly high value near one. This results in a relation of $k_{et}>k_{en}$ for the $[Ru(bpy)_3]^{2+}$ system. On the other hand, k_q (i.e. $k_{et}+k_{en}$) for the $[Ru(i\text{-}biq)_2(bpy)]^{2+}$ system has been estimated to be smaller than that for the $[Ru(bpy)_3]^{2+}$ system by one order as discussed above. Assuming that k_{en} is similar between both systems, there is a possibility that k_{et} is comparable to k_{en} in the $[Ru(i\text{-}biq)_2(bpy)]^{2+}$ system. A sensitive change in $k_{et}/(k_{et}+k_{en})$ and thus the *B* value can occur in the situation. As for the part of $k_{dec}/(k_{dec}+k_{be})$ in Eq. 4, the higher value is expected for the $[Ru(i\text{-}biq)_2(bpy)]^{2+}$ system rather than the $[Ru(bpy)_3]^{2+}$ system because the bulkiness for $[Ru(i\text{-}biq)_2(bpy)]^{2+}$ makes the stability of the encounter complex, $[Ru^{III}\cdots Co^{II}]$, weaker.

In conclusion, the different behavior on the photosensitized decomposition of $[Co(ox)_3]^{3-}$ by $[Ru(bpy)_3]^{2+}$ and $[Ru(i\text{-}biq)_2(bpy)]^{2+}$ can be explained in terms of the difference in the electron transfer step (k_{et}) from the ruthenium complexes to $[Co(ox)_3]^{3-}$.

This research was supported by Grant-in-Aid for Scientific Research from the Ministry of Education, Science and Culture (Nos. 01470051 and 02854071).

References

1) J. N. Demas and A. W. Adamson, *J. Am. Chem. Soc.*, **95**, 5159 (1973).
2) M. Kimura, T. Yamashita, and S. Nishida, *Inorg. Chim. Acta*, **89**, 193 (1984).
3) M. Kato, S. Yamauchi, and N. Hirota, 38th Symposium on Coordination Chemistry of Japan, Tokushima, 1988, Abstr., No. 3B17.
4) A. Juris, F. Barigelletti, V. Balzani, P. Belser, and A. von Zelewsky, *Inorg. Chem.*, **24**, 202 (1985).
5) R. A. Palmer and T. S. Piper, *Inorg. Chem.*, **5**, 864 (1966).
6) J. C. Bailer, Jr. and E. M. Jones, *Inorg. Synth.*, **1**, 37 (1939).
7) J. N. Demas and J. W. Addington, *J. Am. Chem. Soc.*, **98**, 5800 (1976).
8) A. Juris, V. Balzani, F. Barigelletti, S. Campagna, P. Belser, and A. von Zelewsky, *Coord. Chem. Rev.*, **84**, 85 (1988).

Syntheses and Characterization of 2,4-Dioxo-3,3-pentanediselenolato Platinum(II) Complex and Its Dithiolato Analog Prepared by Se–C and S–C Bond Cleavages of 2,3-Diseleno-1,1,4,4-tetraacetylbutane and 2,3-Dithio-1,1,4,4-tetraacetylbutane

Shinsaku YAMAZAKI,* Tamio UENO,† and Masashi HOJO††
Chemistry Laboratory, Kochi Gakuen College, 292 Asahi Tenjin-cho, Kochi 780
†Department of Agriculture, Kyoto University, Oiwake-cho, Kita-Shirakawa, Sakyo-ku, Kyoto 606
††Department of Chemistry, Faculty of Sciences, Kochi University, 2-5-1 Akebono-cho, Kochi 780
(Received November 29, 1990)

Synopsis. 2,4-Dioxo-3,3-Pentanediselenolato(Se_2-ac) platinum(II) complex [Pt(Se_2-ac)(PMe_2Ph)$_2$] and its dithiolato analog [Pt(S_2-ac)(PMe_2Ph)$_2$] have been prepared by treating *cis*-[$PtCl_2$(PMe_2Ph)$_2$] with 2,3-diseleno-1,1,4,4,-tetraacetylbutane and 2,3-dithio-1,1,4,4-tetraacetylbutane in a KOH/acetone-methanol mixed solution. The IR, ^{1}H, ^{13}C, and ^{31}P NMR and mass spectra of these complexes are discussed.

In our previous paper, a 2,4-dioxo-2-pentene-3-thiolato Pt(II) complex was prepared via the S–S bond cleavage of 2,3-dithio-1,1,4,4-tetraacetylbutane under basic conditions.[1] We have newly synthesized a 2,4-dioxo-3,3-pentanediselenolato Pt(II) complex and its dithiolato analog by treating *cis*-[$PtCl_2$(PMe_2Ph)$_2$] with 2,3-diseleno-1,1,4,4-tetraacetylbutane and 2,3-dithio-1,1,4,4-tetraacetylbutane in a KOH/acetone-methanol mixed solution. These novel Pt(II) complexes, which were produced via S–C and Se–C bond cleavages, were rather unstable in solution. Their IR, ^{1}H, ^{13}C, and ^{31}P NMR and mass spectra are discussed in this paper.

Experimental

Bis-(dimethylphenylphosphine)(2,4-dioxo-3,3-pentane diselenolato)platinum(II), [Pt(Se_2-ac)(PMe_2Ph)$_2$]: To *cis*-[$PtCl_2$(PMe_2Ph)$_2$] (0.51 g) in acetone charged with N_2 was added 0.33 g of 2,3-diseleno-1,1,4,4-tetraacetylbutane,[2] followed by KOH (ca. 0.11 g) in methanol. The solution, after stirring overnight, was evaporated to produce a brownish-orange solid. The product was developed with TLC(SiO_2) in acetone–CH_2Cl_2. An eluate of the brownish-orange band was developed again with TLC. The eluate was evaporated to produce a brownish-orange residue, which was crystallized from CH_2Cl_2–hexane to give brownish-orange needles (0.25 g: 37%). Anal. Found: C, 34.68; H, 3.90%. Calcd for $C_{21}H_{28}O_2P_2Se_2Pt$: C, 34.67; H, 3.88%. Electron impact mass spectrum (In-beam direct method at 70 eV). *m/z* 727 M^+, 684 $[M-CH_3CO]^+$, 648 $[M-Se]^+$. [Pt(Se_2-ac)(PMe_2Ph)$_2$] is soluble in $CHCl_3$, CH_2Cl_2, and acetone, but is insoluble in diethylether and hexane. The complex in CH_2Cl_2 or $CHCl_3$, by allowing the solution to stand fo several hours, undergoes a decompositon.

Bis-(dimethylphenylphosphine)(2,4-dioxo-3,3-pentane dithiolato)platinum(II), [Pt(S_2-ac)(PMe_2Ph)$_2$]: To *cis*-[$PtCl_2$(PMe_2Ph)$_2$] (0.6 g) in acetone charged with N_2 was added 0.29 g of 2,3-dithio-1,1,4,4-tetraacetylbutane,[3,4] followed by KOH (ca. 0.13 g) in methanol. After stirring the solution for 2 d, a white precipitate was filtered, and the filtrate was evaporated. A brownish-orange product was developed with TLC(SiO_2) in acetone–CH_2Cl_2. A brownish-orange band was eluted by acetone-methanol. The eluate, after the addition of diethylether and hexane, was allowed to stand in a refrigerator for 3 d to give a brownish-orange solid (0.41 g: 52% yield). Anal. Found: C, 39.82; H, 4.47%. Calcd for $C_{21}H_{28}O_2P_2S_2Pt$: C, 39.81; H, 4.45%. The complex is soluble in CH_2Cl_2, $CHCl_3$, and acetone, but is insoluble in hexane. The complex gradually decomposes in CH_2Cl_2 or $CHCl_3$ and changes into an insoluble white solid whose empirical formula is [Pt(SCO-ac)(PMe_2Ph)$_2$], with its molecular ion at *m/z* 628 (100) by SIMS. This white product has not been characterized. SIMS of [Pt(S_2-ac)(PMe_2Ph)$_2$](3-nitrobenzyl alcohol). *m/z* 633 (5) M^+, 602 (13) $[Pt(S\text{-}ac)(PMe_2Ph)_2]^+$, 471 (12) $[Pt(PMe_2Ph)_2]^+$, 336 (56) $[Pt(PMe_2Ph)]^+$. The other intense peaks at 455 (100) and 488 (56) were assigned to $[Pt(C_6H_4NO_2)(PMe_2Ph)]^+$ and $[PtS(C_6H_4NO_2)(PMe_2Ph)]^+$ which may be formed by a decomposition in the matrix. In addition, a peak was observed at *m/z* 628 (38).

Elemental analyses were performed at the micro Analytical Center, Kyoto University. ^{1}H NMR spectra at 90.04 MHz and ^{13}C NMR spectra at 22.66 MHz were recorded on a Hitachi R-90-H FT NMR spectrometer operating Fourier transform modes in sealed tubes saturated with N_2. The IR spectra were recorded on a Hitachi 260-10 infrared spectrometer. An electron impact mass spectrum was, recorded on a Hitachi M-80 mass spectrometer and secondary ion mass spectra were produced using 3-nitrobenzyl alcohol as a matrix and Xe gas as the first ion source.

Results and Discussion

2,3-Diseleno-1,1,4,4-tetraacetylbutane[2] has been obtained from 2,2,4,4-tetraacetyl-1,3-diselenetane[2,3] by reducing it with aq HI. 2,3-Diseleno-1,1,4,4-tetraacetylbutane has a dienolic from both in solid and solution, which is analogous with 2,3-diseleno-1,1,4,4-tetraacetylbutane.[3,4] These bis(β-dicarbonyls) ligands linked by selenium or sulfur atoms between the two β-diketones under basic conditions readily undergo a cleavage of the M–M or M–C (M=S or Se) bond. We have thus prepared a 2,4-dioxo-2-pentene-3-thiolato Pt(II) complex[1] via an S–S bond cleavage of 2,3-dithio-1,1,4,4-tetraacetylbutane. A treatment of *cis*-[$PtCl_2$(PMe_2Ph)$_2$] with 2,3-diseleno-1,1,4,4-tetraacetylbutane and 2,3-dithio-1,1,4,4-tetraacetylbutane in a KOH/acetone-methanol mixed solution gave 2,4-dioxo-3,3-pentanediselenolato (Se_2-ac) and -dithiolato (S_2-ac) Pt(II) complexes, [Pt(Se_2-ac)-(PMe_2Ph)$_2$] and [Pt(S_2-ac)(PMe_2Ph)$_2$] via a Se–C′ and an S–C′ bond cleavage of the corresponding bis(β-dicarbonyls) respectively.

Table 1. ^{1}H, $^{13}C\{^{1}H\}$, and $^{31}P\{^{1}H\}$ NMR and IR spectral data for $[Pt(M_2\text{-ac})(PMe_2Ph)_2]$ (M=S, Se)

Compound	IR[a]		^{1}H NMR[b]		^{13}C NMR[c]				^{31}P NMR[d]
	(C=O)		δ_{Me}	δ_{Me} (PMe_2Ph)	δ_{CO}	δ_{Me}	δ_{C^3}	δ_{Me} (PMe_2Ph)	
DSTAB[e]			2.43						
TADSN[f]	1687(vs)	1673(vs)	2.63			24.67			
$[Pt(Se_2\text{-ac})(PMe_2Ph)_2]$	1699(vs)	1656(vs)	2.64	1.51 (9.78) [33.98] (0.18) [34.07]	205.59 [18.66]	24.39	59.0 [53.89]	13.32 (19.69) [39.38]	−21.13 [2947.41]
$[Pt(S_2\text{-ac})(PMe_2Ph)_2]$	1700(vs)	1670(vs)	2.52	1.52 (9.00)	206.66 [22.8]	23.69	82.2 [55.97]	13.08 (19.69) [58.72]	

a) In cm^{-1}; Measured in CH_2Cl_2. b) Measured in $CDCl_3$; Chemical shifts are relative to $SiMe_4$. J(P-H) and J(Pt-H) are in parentheses and brackets respectively. c) Measured in $CDCl_3$; Chemical shifts are relative to $SiMe_4$. J(P-C) and J(Pt-C) are in parentheses and brackets respectively. d) Measured in $CDCl_3$; Chemical shift is relative to 85% H_3PO_4. $J(^{195}Pt\text{-}P)$ is in bracket. e) 2,3-Diseleno-1,1,4,4-tetraacetylbutane is abbreviated as DSTAB. f) 2,2,4,4-Tetraacetyl-1,3-diselenetane is abbreviated as TADSN.

The ^{1}H, ^{13}C, and ^{31}P NMR and IR spectral data of $[Pt(M_2\text{-ac})(PMe_2Ph)_2]$ (M=Se, S) are given in Table 1. Carbonyl stretching absorption bands observed for $[Pt(Se_2\text{-ac})(PMe_2Ph)_2]$ are at 1699 and 1656 cm^{-1}, and exhibit two carbonyls of the 2,4-pentanedione group in the keto form. The other absorption pattern very closely resembles those of 2,2,4,4-tetraacetyl-1,3-diselenetane. ^{1}H NMR resonance arising from methyl protons of the 2,4-pentanedione in the complex at 2.64 is appreciably close to 2.63 of 2,2,4,4-tetraacetyl-1,3-diselenetane. These spectral data indicate that two acetyl group of the 2,4-pentanedione is symmetrically arranged in the complex. A ^{13}C NMR resonance arising from its C^3 at 59.0 is in a region which is sufficiently higher field as observed for the central carbon bonded complexes of 2,4-pentanedione[5] and 1,1,2,2-tetraacetylethane.[6] $J(^{195}Pt\text{-}C)$ 53.89 found in $[Pt(Se_2\text{-ac})(PMe_2Ph)_2]$ apparently exhibits no Pt-C bond included, but Se-C^3 bonds maintained.[7] Resonance arising from methyl carbons of the 2,4-pentanedione group in the complex, as is consistent with its ^{1}H NMR, shows a singlet at 24.39, which is also noticeably close to 24.67 of 2,2,4,4-tetraacetyl-1,3-diselenetane. On the other hand, the ^{13}C NMR resonance arising from the methyl carbons of PMe_2Ph unexpectedly exhibits an ABC spin system (Fig. 1), but no AB spin system as predicted for the phosphines arranged at a cis-position mutually. The spectrum is in good agreement with the simulated lines of [ABC(3.5)+ABCM(1)] with $J_{AB}=J_{AC}=19.69$ Hz and $J_{AM}=39.38$ Hz. This ABC spin system which arises from $^{31}P\text{-}^{31}P$ coupling could not be discerned in its ^{1}H NMR spectra as observed in *trans*-$[PtI_2(PMe_2Ph)_2]$ and $[Pd(PMe_2Ph)_3(2,9\text{-}R_2\text{-phen})][BF_4]_2$.[9] The ^{13}C NMR at the present case suggests that two phosphines in the complex are symmetrically arranged with the P-Pt-P bond angle fairly unusually expanded from 90° to give a $^{31}P\text{-}^{31}P$ coupling magnetically. Its ^{31}P NMR with J(Pt-P)=2947 Hz is consistent with the ^{13}C NMR, and the J(Pt-P) is intermediate between 2379 Hz for *trans*-$[PtCl_2(PMe_3)_2]$[10] and 3480 Hz for *cis*-$[PtCl_2(PMe_2Ph)_2]$,[11] in addition to 2311 and 3407 Hz for $[PtCl(PMe_2Ph)_3][PF_6]$.[1] $[Pt(Se_2\text{-ac})(PMe_2Ph)_2]$ is relatively unstable in solution. Its EIMS by In-beam direct method, however, explicitly shows a molecular ion peak at m/z 727. The structure of $[Pt(Se_2\text{-ac})(PMe_2Ph)_2]$ is supposed to have a high symmetry with a diselenetane framework in which the 2,4-dioxo-3,3-pentanediselenolate ligand bonds to Pt(II) as a (η^2-Se_2)-linkage, as is found in a diselenocarbonate Rh(III) complex.[12] Any other conceivable structure

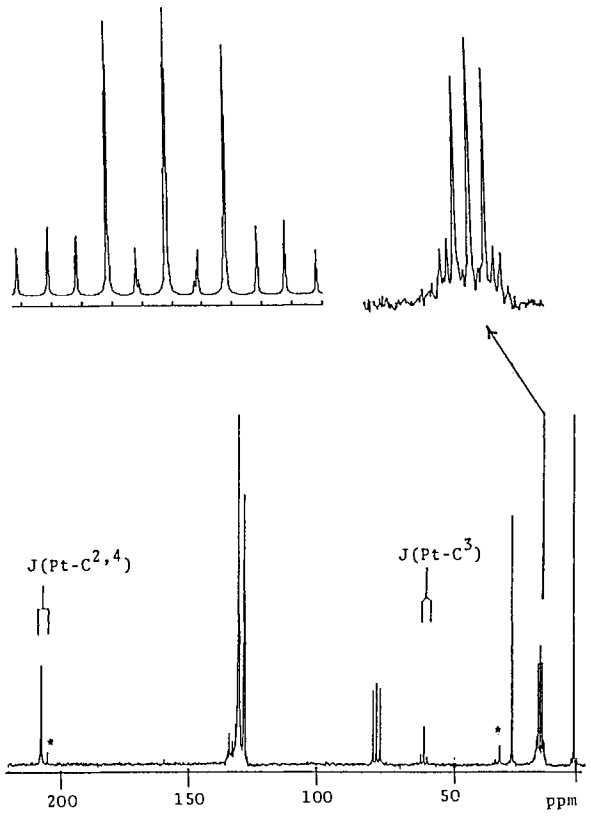

Fig. 1. $^{13}C\{^{1}H\}$ NMR spectrum of $[Pt(\eta^2\text{-}Se_2\text{-ac})(PMe_2Ph)_2]$ in $CDCl_3$ and a simulated line as ABC spin system (expanded) of Me-carbons of PMe_2Ph. *An acetone impurity included.

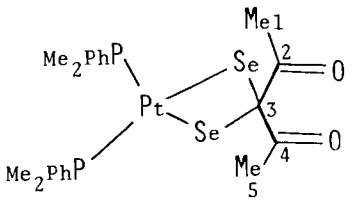

Fig. 2. A supposed structure of [Pt(Se$_2$-ac)-(PMe$_2$Ph)$_2$].

for [Pt(Se$_2$-ac)(PMe$_2$Ph)$_2$], in which a 3-acetyl-4-oxo-1,2-pentanediselenolate ligand may bond to Pt(II) as a (C^3, Se)-chelate, can be excluded since no corresponding J(Pt-C^3) could be obtained and the ^{31}P NMR datum explicitly shows an equivalency of the phosphines. It is also unlikely that the 2,4-dioxo-3,3-pentanediselenolate ligand with a diselenetane framework having a Se-Se bond can coordinate Pt(O) through its oxygen atoms, since J(Pt-$C^{2,4}$)=18.66 Hz observed in [Pt(Se$_2$-ac)(PMe$_2$Ph)$_2$] is quite different from such a presumed configuration.[13]

[Pt(S$_2$-ac)(PMe$_2$Ph)$_2$] is less stable than the corresponding diselenolato Pt(II) complex, and gradually decomposes in $CHCl_3$ producing an insoluble white precipitate(uncharacterized). The ^{1}H and ^{13}C NMR data of [Pt(S$_2$-ac)(PMe$_2$Ph)$_2$] listed in Table 1 involve resonances due to this white species(10—15% included under the condition). The predominant resonances due to [Pt(S$_2$-ac)(PMe$_2$Ph)$_2$] are however sufficiently comparable with those of [Pt(Se$_2$-ac)(PMe$_2$Ph)$_2$]. SIMS datum of [Pt(S$_2$-ac)(PMe$_2$Ph)$_2$] exhibited a molecular ion peak at m/z 633 with a relatively weak intensity(5), although the spectrum was accompanied by an intense peak at m/z 628 due to the white product already formed by a decomposition in the matrix (experimental section).

[Pt(η^2-M$_2$-ac)(PMe$_2$Ph)$_2$] (M=S, Se) produced via a Se′-C′ or S′-C′ bond cleavage of 2,3-diseleno-1,1,4,4-tetraacetylbutane and 2,3-dithio-1,1,4,4-tetraacetylbutane may be given by supposing subsequent reaction steps: a Se′-C′ or S′-C′ bond cleavage of the 3,3′-diseleno or -dithiobis (β-dicarbonyls) and a synchronous Se′-C or S′-C bond formation causes a Se-Se′ or S-S′ bond cleavage resulting in the formation of M$_2$-ac^{2-}, and a following metathesis of the complex. A 2,4-dioxo-2-pentene-3-thiolato Pt(II) complex[1] was previously isolated via an S-S′ bond cleavage of 2,3-dithio-1,1,4,4-tetraacetylbutane under basic conditions. In the present case, no analogous 2,4-dioxo-2-pentene-3-selenolato Pt(II) complex was obtained, which may be formed via a Se-Se′ bond cleavage of 2,3-diseleno-1,1,4,4-tetraacetylbutane. It should also be noticed that 2,2,4,4-tetraacetyl-1,3-diselenetane undergoes a cleavage of the Se-C′ bonds by reducing with aq HI to afford 2,3-diseleno-1,1,4,4-tetraacetylbutane with a Se-Se′ bond. Accordingly, a supposed rearrangement forming (η^2-M$_2$)-bonding to the metal interestingly seems to be a reversed pattern from the reaction cited above (Scheme 1). Yet, J(Pt-P) obtained in [Pt(Se$_2$-ac)(PMe$_2$Ph)$_2$] may be valid only in the configuration of a d-8 electron species.

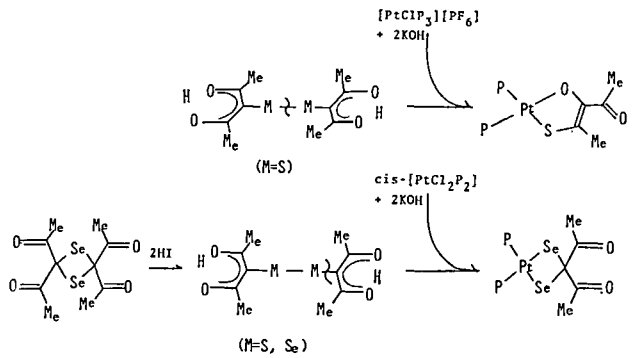

Scheme 1. (Reaction scheme of S-S, S-C, and Se-C bond cleavages of 2,3-dithio-1,1,4,4-tetraacetylbutane and 2,3-diseleno-1,1,4,4-tetraacetylbutane).

An author (Shinsaku Yamazaki) appreciates Dr. Tomoharu Ama (Department of Chemistry, Faculty of Sciences, Kochi University) for obtaining NMR spectra.

References

1) S. Yamazaki, T. Ama, M. Hojo, and T. Ueno, *Bull. Chem. Soc. Jpn.*, **62**, 4036 (1989).
2) G. T. Morgan and H. D. K. Drew, *J. Chem. Soc.*, **117**, 1456 (1920); G. T. Morgan, H. D. K. Drew, and T. V. Barker, *J. Chem. Soc.*, **121**, 2432 (1922).
3) D. H. Dewar, J. E. Fergusson, P. P. Hentschel J. Wilkins, and P. P. Williams, *J. Chem. Soc.*, **1964**, 688.
4) L. F. Power and R. D. Jones, *Acta Crystallogr., Sect. B*, **27**, 181 (1971).
5) T. Ito, T. Kiriyama, Y. Nakamura, and A. Yamamoto, *Bull. Chem. Soc. Jpn.*, **49**, 3257 (1976); T. Yamamoto, Y. Nakamura, and A. Yamamoto, *Bull. Chem. Soc. Jpn.*, **49**, 191 (1976).
6) S. Yamazaki, *Polyhedron*, **5**, 1183 (1986); S. Yamazaki, T. Ama, and Z. Taira, *Polyhedron*, **7**, 353 (1988); S. Yamazaki and T. Ama, *Bull. Chem. Soc. Jpn.*, **62**, 931 (1989).
7) J. G. Verkade and L. D. Quin, "Phosphorous-31 NMR Spectroscopy in Stereochemical Analysis-Organic Compounds and Metal Complexes," VCH Publisher (1987).
8) J. M. Jenkins and B. L. Shaw, *J. Chem. Soc. A*, **1966**, 770.
9) S. Yamazaki, *Polyhedron*, **4**, 1915 (1985); T. Sakai, Z. Taira, S. Yamazaki, and T. Ama, *Polyhedron*, **8**, 1989 (1989).
10) R. Favez, R. Roulet, A. A. A. Pinkerton, and D. Schwarzenbach, *Inorg. Chem.*, **19**, 1356 (1980).
11) P. L. Goggin, R. J. Goodfellow, S. R. Haddock, J. R. Knight, F. J. S. Reed, and B. F. Taylor, *J. Chem. Soc., Dalton Trans.*, **1974**, 523.
12) C. Bianchi, C. Mealli, A. Meli, and M. Sabat, *J. Chem. Soc., Chem. Commun.*, **1984**, 1647; C. Bianchi, D. Masi, C. Mealli, A. Meli, M. Sabat, and F. Bizza, *Inorg. Chem.*, **27**, 3716 (1988); Saul Patai and Zvi Rapport, "The Chemistry of Organic Selenium and Tellurium Compounds," John Wiley & Sons, New York (1986), Vol. 1.
13) B. E. Mann and B. F. Taylor, "^{13}C NMR Data for Organometallic Compounds," Academic Press, New York (1981).

Fluorogenic Substrate of Pepsin

Hiroo YONEZAWA* and Nobuo IZUMIYA†
Department of Chemistry, Faculty of Science, Kagoshima University, 1-Korimoto, Kagoshima 890
†Laboratory of Biochemistry, Faculty of Engineering, Kyushu Sangyo University, Fukuoka 813
(Received August 13, 1990)

Synopsis. Fluorogenic substrates of pepsin; Dns-Ala-Phe-Trp-Val-Leu-OCH_2Py and Dns-Phe-Trp-Val-Leu-OCH_2Py were synthesized by a solution method. Incubation of pepsin with Dns-Ala-Phe-Trp-Val-Leu-OCH_2Py resulted in specific cleavage at the Phe-Trp bond and the time-dependent increase in fluorescence intensity at 345 nm paralleling the extent of substrate hydrolysis. The optimum pH of the substrate was 3.0 and the K_m and k_{cat} values were 8.0×10^{-5} M and 0.10 s^{-1}, respectively. The linearity of the plot of fluorescence intensity vs. enzyme concentration was satisfactory in the range of 50 nM to 500 nM of pepsin at a substrate concentration of 50 μM. Because of its simplicity and rapidity, this method is useful for the measurement of pepsin action. In contrast, Dns-Phe-Trp-Val-Leu-OCH_2Py was not cleaved by pepsin.

Pepsin [EC. 3.4.4.1.] is a gastric proteinase active in acidic solutions (pH 1—5). To determine the pepsin activity, hemoglobin is generally used as a protein substrate.[2] In addition, many synthetic substrates have been used for the measurement of pepsin activity.[3,4] The widely used analytical procedures to estimate the hydrolysis rate are based on the determination of amine products by observing their reaction with ninhydrin. These procedures usually require much intension and are time-consuming. The task of enzymic activity assay is simplified by use of chromogenic substrates. However, a good chromogenic substrate for pepsin has not been obtained. For example, pepsin does not cleave *p*-nitroanilide substrates.

Inouye et al. synthesized chromogenic substrates containing *p*-nitrophenylalanine at the P_1 site such as Z-His-Phe (NO_2)-Phe-OMe and determined the rate of hydrolysis in terms of the increase in absorbance at 310 nm.[5] However, the sensitivity of these substrates for the pepsin action was low.

Fluorometric methods are employed for the detection of peptidase activity as convenient and very sensitive methods. Most of the fluorogenic substrates for peptidases are acyl derivatives of highly fluorescent amines.[6,7] These substrates would not be cleaved by pepsin in analogy with *p*-nitroanilide substrates.[8,9] Latt et al. reported the synthesis of intramolecularly quenching substrates for carboxypeptidase, where the resonance energy transfer phenomenon was utilized with dansylated tryptophan-peptides.[10] Recently, Sato et al. reported applications of 3,4,6,7-tetramethyl-9,10-dioxa-*syn*-bimane to prepare intramolecularly quenching substrates for assay of some peptidases.[11,12]

Since pepsin cleaves the peptide bond between two aromatic amino acids, the peptides containing a dansyl group at the NH_2-terminal, phenylalanine at the P_1 site and tryptophan at the P_1' site must be cleaved between two aromatic amino acid residues by pepsin, with a concomitant increase in the tryptophan fluorescence. However, N-protected peptides are not soluble in acidic buffers. Then, 4-pyridylmethyl ester of N-protected substrates for pepsin was employed, since it confers moderate solubility in acidic buffers.[13] Z-Ala-Ala-Phe(NO_2)-Phe-$O(CH_2)_3Py$ and Phe-Gly-His-Phe(NO_2)-Phe-Val-Leu-OMe are reported by good substrates for pepsin.[9] In view of this, Dns-Phe-Trp-Val-Leu-OCH_2Py (**1**) and Dns-Ala-Phe-Trp-Val-Leu-OCH_2Py (**2**) have been synthesized in the present work as fluorogenic substrates for pepsin.

Results and Discussion

The substrates and the peptides which will arise from cleavage of the substrates were synthesized by a solution method. Each protected amino acid was coupled with amino acid 4-pyridylmethyl ester or peptide 4-pyridylmethyl esters from C-terminus. The obtained Boc-peptide-OCH_2Pys were treated with HCl/AcOH and the resulting deblocked peptide 4-pyridylmethyl esters were dansylated by the usual manner. The dansyl peptides obtained gave one spot by thin layer chromatography and a single peak by HPLC. Compounds **1** and **2** were sufficiently soluble in an acidic buffer containing 10% DMF for use in kinetic studies. The chromatographic patterns for the mixtures of substrates (**2** and **1**) and products (Dns-Ala-Phe, Dns-Phe, and Trp-Val-Leu-OCH_2Py) are shown in Fig. 1-A and 1-C. The elution times of synthetic peptides were as follows: **2**, 27.2 min; **1**, 27.2 min; Dns-Ala-Phe, 20.0 min; Dns-Phe, 18.9 min; Trp-Val-Leu-OCH_2Py, 18.9 min.

The substrates **2** and **1** were incubated, respectively, with pepsin for 3 h and the reaction mixtures were applied on HPLC. Fig. 1-B indicates disappearance of the substrate (**2**) and concomitant appearance of two products (Dns-Ala-Phe and Trp-Val-Leu-OCH_2Py). This result suggests that the substrate was cleaved quantitatively at a single bond between phenylalanine and tryptophan. On the other hand, compound **1** was not cleaved by pepsin (Fig. 1-D).

As seen in Fig. 2, hydrolysis of the substrate (**2**) decreased dansyl emission (500 nm) and increased tryptophan fluorescence (345 nm). When pepsin was added to the substrate solution, the fluorescence at 345 nm increased momentarily, then decreased gradually up to about 2 min. Subsequently, the fluorescence at 345 nm increased linearly in proportion to the concentration of added pepsin. Consequently, measurement of the increase in the fluorescence was started at the incubation time of 2 min. Similarly, addition of pepsin to the substrate produced an increase in the fluorescence intensity at 500 nm. This indicates that the dansyl group of the substrate was bound at a hydrophobic region of the enzyme.[14] Then, the fluo-

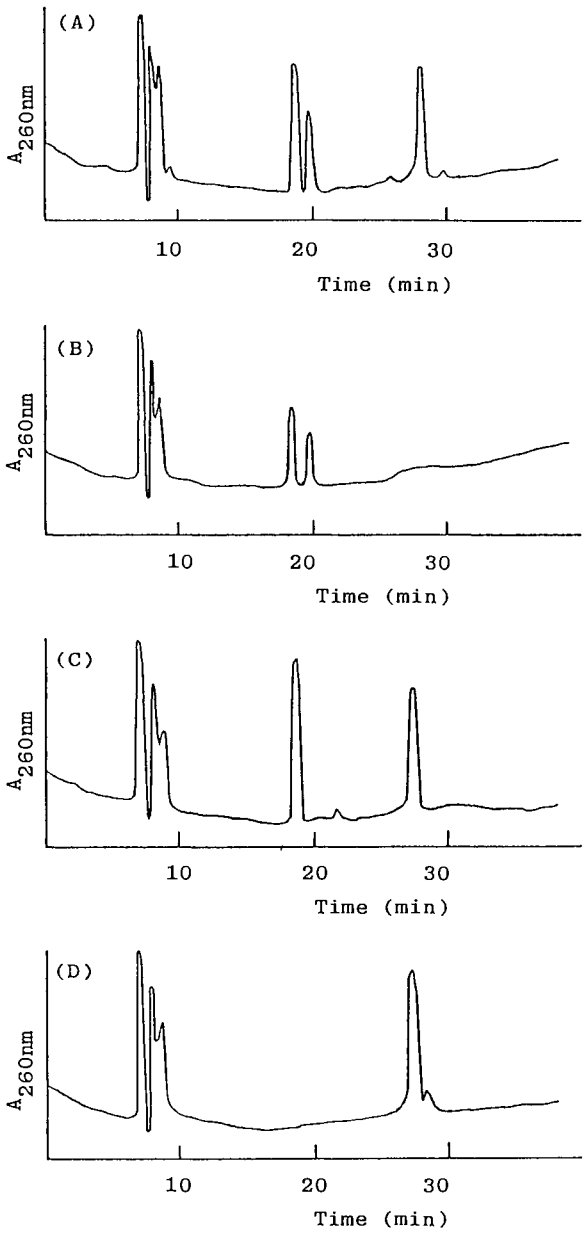

Fig. 1. HPLC traces of fluorogenic substrates and reaction products. (A) Mixture of **2**, Dns-Ala-Phe, and Trp-Val-Leu-OCH_2Py; (B) Reaction mixture of **2** and pepsin; (C) Mixture of **1**, Dns-Phe, and Trp-Val-Leu-OCH_2Py; (D) Reaction mixture of **1** and pepsin.

rescence at 500 nm decreased with the hydrolysis of the substrates. The increase in the fluorescence at 345 nm subsequent to complete hydrolysis of the substrate by pepsin was not influenced by the amount of added pepsin. The molar fluorescence intensity of the complete hydrolysis of compound **2** was 50000.

Comparative measurements of the effect of pH on the pepsin action were made with compound **2**. The optimum pH was 3.0. A pH 3.0 buffer was thus used as solvent for the substrate in the following experiments. K_m and k_{cat} values of 8.0×10^{-5} M and 0.10 s^{-1} were obtained from the Lineweaver-Burk plot of compound **2**. The linearity of the plot of fluorescence

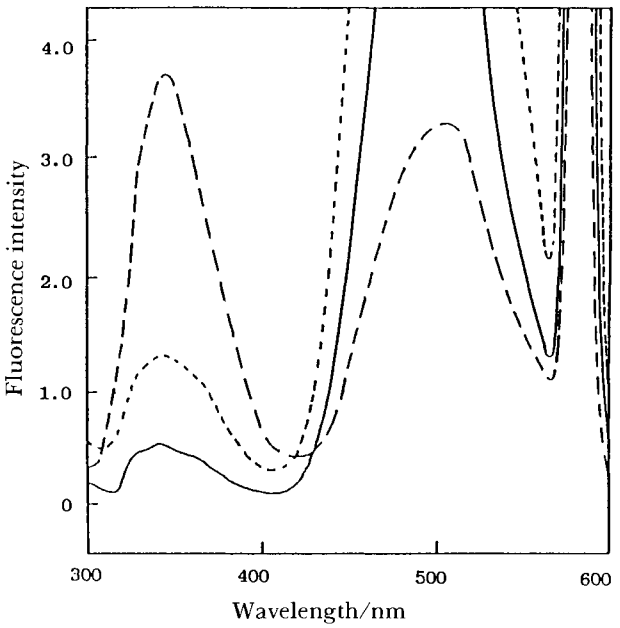

Fig. 2. Fluorescence emission spectra of **2** and the hydrolysate of **2**. (——) **2**; (------) **2** was incubated with pepsin for 10 s; (— —) **2** was incubated with pepsin for 3 h.

intensity vs. enzyme concentration was satisfactory in the range of 50 nM to 500 nM of pepsin.

Compound **2** is the first fluorogenic substrate of pepsin. The resultant assay for pepsin was sensitive and convenient. The product formed can be detected directly as hydrolysis occurs. This contrasts with the case of the nynhydrin methods, where at least several minutes elapse between the formation and detection of the products. The fluorogenic substrate described here may be useful for the assay of pepsin activity.

Experimental

All melting points are uncorrected. Optical rotations were determined with a JASCO spectropolarimeter J-20A. Fluorescence measurements were performed with a Shimadzu spectrofluorophotometer RF-5000.

Synthesis of Substrates. Boc-Leu-OCH_2Py (3). To a solution of Boc-Leu (2.31 g, 10 mmol) and 4-pyridylmethanol (1.09 g, 10 mmol) in CH_2Cl_2 (20 ml) was added DCC (2.06 g, 10 mmol) at 0 °C. The mixture was stirred for 2 h at 0 °C and overnight at room temperature, then evaporated in vacuo, and ethyl acetate was added to the residue. After dicyclohexylurea was filtered off, the filtrate was washed successively with 4% sodium bicarbonate, 10% citric acid and water. The organic layer was dried over anhydrous sodium sulfate and was evaporated in vacuo to yield Boc-Leu-OCH_2Py as an oil (3.07 g). ^1H NMR ($CDCl_3$) δ=0.94 (6H, d, J=5 Hz), 1.40 (9H, s) 1.40—1.92 (3H, m), 4.48 (1H, q, J=6 Hz), 4.90 (1H, d, J= 6 Hz), 5.15 (2H, s), 7.22 (2H, dd, J=1 and 5 Hz), 8.58 (2H, dd, J=1 and 5 Hz).

Boc-Val-Leu-OCH_2Py (4). Compound **3** (3.07 g) was treated with 1M (1 M=1 mol dm^{-3}) HCl/AcOH for 1 h at room temperature and the resulting HCl · Leu-OCH_2Py was converted into free base as described previously.[13] The obtained oily Leu-OCH_2Py was coupled with Boc-Val (2.17 g, 10 mmol) in the same manner using DCC (1.65 g, 8 mmol) in CH_2Cl_2 (30 ml) to yield Boc-Val-Leu-OCH_2Py as an oil (3.16 g). ^1H NMR ($CDCl_3$) δ=0.95 (12H, d, J=6 Hz), 1.40

(9H, s), 1.37—1.87 (2H, m), 2.03 (2H, t, J=6 Hz), 3.88 (1H, dd, J=6 and 8 Hz), 4.73 (1H, q, J=7 Hz), 5.06 (1H, brd, J=7 Hz), 5.13 (2H, s), 6.47 (1H, brd, J=8 Hz), 7.23 (2H, brd, J=4 Hz), 8.62 (2H, dd, J=2 and 4 Hz).

Boc-Trp-Val-Leu-OCH_2Py (5). Boc-Trp (3.0 g, 10 mmol) and Val-Leu-OCH_2Py (derived from 3.16 g of **4** in the manner descrived for Leu-OCH_2Py) were coupled in the same manner using DCC (1.56 g, 7.6 mmol) in CH_2Cl_2 (30 ml). The product was recrystallized from ethyl acetate-petroleum ether; yield, 3.75 g, (81%); mp 89—91 °C; $[\alpha]_D^{25}$ −22.5° (c 1, DMF).

Found: C, 64.59; H, 7.72; N, 11.04%. Calcd for $C_{33}H_{45}O_6N_5 \cdot 1/2H_2O$: C, 64.26; H, 7.35; N, 11.36%.

Boc-Phe-Trp-Val-Leu-OCH_2Py (6). Compound **5** (3.1 g, 5.1 mmol) was treated with 1 M HCl/AcOH for 1 h at room temperature and the solvent evaporated in vacuo. The resulting crystals were collected with the aid of ether; yield, 3.5 g. The product (3.5 g) was dissolved in water (8 ml) and cooled in an ice bath. To this solution was added 50% saturated aqueous K_2CO_3 (13 ml) and the resulting precipitate was collected by filtration, washed with water and dried. The resulting Trp-Val-Leu-OCH_2Py and Boc-Phe (1.33 g, 5 mmol) were coupled in the same manner using DCC (0.9 g, 4.5 mmol) in DMF (10 ml) and CH_2Cl_2 (20 ml). The product was recrystallized from ethyl acetate-petroleum ether; yield, 1.94 g, (57%); mp 121—123 °C; $[\alpha]_D^{25}$ −18.0° (c 1, DMF).

Found: C, 66.15; H, 7.05; N, 11.00%. Calcd for $C_{42}H_{54}O_7N_6 \cdot 1/2H_2O$: C, 66.03; H, 7.26; N, 11.00%.

Boc-Ala-Phe-Trp-Val-Leu-OCH_2Py (7). Boc-Ala (80 mg, 0.42 mmol) and Phe-Trp-Val-Leu-OCH_2Py (derived from 0.3 mmol of **6** in the manner described for Leu-OCH_2Py) were coupled in the same manner using DCC (65 mg, 0.32 mmol) in DMF (1 ml) and CH_2Cl_2 (4 ml). The product was recrystallized from ethyl acetate-petroleum ether; yield, 200 mg, (81%); mp 161—163 °C; $[\alpha]_D^{25}$ −19.5° (c 1, DMF).

Found: C, 64.85; H, 7.23; N, 11.75%. Calcd for $C_{45}H_{59}O_8N_7 \cdot 1/2H_2O$: C, 64.73; H, 7.24; N, 11.74%.

Dns-Phe-Trp-Val-Leu-OCH_2Py (1). Compound **6** (90 mg, 0.12 mmol) was treated with 1 M HCl/AcOH for 1 h at room temperature, and the resulting deblocked peptide ester was dansylated according to the procedure described by Gray.[15] The product was recrystallized from ethyl acetate-petroleum ether; yield, 65 mg, (61%); mp 125—127 °C; $[\alpha]_D^{25}$ −41.0° (c 1, DMF).

Found: C, 65.48; H, 6.34; N, 10.87%. Calcd for $C_{49}H_{57}O_7N_7S_1 \cdot 1/2H_2O$: C, 65.60; H, 6.52; N, 10.93%.

Dns-Ala-Phe-Trp-Val-Leu-OCH_2Py (2). This compound was obtained from **7** (120 mg, 0.15 mmol) by the same procedure as described above, and recrystallized from DMF-ether; yield, 72 mg, (50%); mp 232—234 °C; $[\alpha]_D^{25}$ −31.5° (c 1, DMF).

Found: C, 64.29; H, 6.52; N, 11.68%. Calcd for $C_{52}H_{62}O_8N_8S_1 \cdot 1/2H_2O$: C, 64.51; H, 6.56; N, 11.57%.

Dns-Ala-Phe (8). This compound was obtained from Ala-Phe (200 mg, 0.17 mmol) by the same procedure as described above. The product was recrystallized from ethyl acetate-petroleum ether; yield, 160 mg, (48%); mp 114—116 °C; $[\alpha]_D^{25}$ +7.5° (c 1, DMF).

Enzyme and Methods. Pepsin (salt free crystalline sample from Worthington Biochemical Co. U.S.A.) was dissolved in 0.1 M citrate buffer pH 3.0. The substrates were dissolved in 0.1 M citrate buffer (pH 3.0) containing 10% DMF.

Analysis of Reaction Products. Fifty microliters of the pepsin solution (0.1 mM) was added to 5 ml of the substrate solutions (50 μM) at 37 °C. After incubation for 3 h, the reaction mixtures were subjected HPLC assays. The reaction mixtures (100 μl) were applied to a C_{18} reversed-phase column (DYNAMAX-60A, 4.6×250 mm, Rainin Instrument) and eluted with a linear gradient of 10—70% 2-propanol/acetonitrile (7/3. v/v) in 0.1% trifluoroacetic acid for 30 min at a flow rate of 0.5 ml min^{-1}.

Measurement of Fluorescence Emission Spectrum. The substrate (**2**) was dissolved in a 0.1 M citrate buffer (50 μM). Fifty microliters of the pepsin solution (0.1 mM) was added to the substrate solution (5 ml) at 37 °C. After incubation for 10 s and 3 h, the fluorescence emission spectrum was measured (excitation at 290 nm).

pH-Activity Curve. The substrate (**2**) was dissolved in 0.1 M citrate buffers in the pH range 2.0—4.5 (50 μM). Fifty microliters of the pepsin solution (0.1 mM) was added to the substrate solutions (5 ml) at 37 °C. After incubation for 2 min, the increase in emission at 345 nm was recorded during the following 6 min of the incubation time at 37 °C (excitation at 290 nm).

Linear Relation of the Fluorescence Intensity vs. Enzyme Concentration. Various amounts (5—100 μl) of the pepsin solution (0.1 mM) was added to 5 ml of the substrate solutions (50 μM, pH 3.0) at 37 °C and the increase in emission was measured in the manner described above.

Kinetic Parameter Measurement. Twenty five microliters of the pepsin solution (0.1 mM) was added to various concentrations (5—50 μM) of the substrate solution (5 ml) at 37 °C, and the increase in emission was measured in the manner described above.

References

1) Abbreviations used in this work: Dns, dansyl; Py, 4-pyridyl; DCC, dicyclohexylcarbodiimide; Phe(NO_2), p-nitrophenylalanine.

2) M. L. Anson, *J. Gen. Physiol.*, **22**, 79 (1938).

3) J. S. Fruton, "Acid Proteases," ed by J. Tang, Plenum Press, New York (1977), p. 131.

4) A. J. Barrett and J. K. McDonald, "Mammalian Proteases," Academic Press, New York (1980), Vol. 1, p. 303.

5) K. Inouye and J. S. Fruton, *Biochemistry*, **6**, 1765 (1967).

6) M. Roth, *Clin. Chim. Acta*, **8**, 574 (1963).

7) H. Oya, T. Yamamoto, and T. Nagatsu, *Arch. Oral Biol.*, **13**, 941 (1968).

8) K. Inouye and J. S. Fruton, *Biochemistry*, **7**, 1611 (1968).

9) J. S. Fruton, "Hydrolytic Enzymes," ed by A. Neuberger and K. Brocklehurst, Elsevier, New York (1987), p. 1.

10) S. A. Latt, D. S. Auld, and B. L. Vallee, *Anal. Biochem.*, **50**, 56 (1972).

11) E. Sato, M. Sakashita, Y. Kanaoka, and E. M. Kosower, *Bioorg. Chem.*, **16**, 298 (1988).

12) E. Sato, S. Nishikawa, and Y. Kanaoka, *Chem. Pharm. Bull.*, **37**, 145 (1989).

13) G. P. Sachdev and J. S. Fruton, *Biochemistry*, **8**, 4231 (1969).

14) G. P. Sachdev, M. A. Johnston, and J. S. Fruton, *Biochemistry*, **11**, 1080 (1972).

15) W. R. Gray, "Methods in Enzymology," Academic Press, New York (1967), Vol. 11, p. 139.

Halogenative Allylation and Reduction of Aromatic Acetals by Double Substitution of Alkoxyl Groups in Acetal

Takeshi ORIYAMA,* Katsuyuki IWANAMI, Kazuhisa TSUKAMOTO, Yuichi ICHIMURA, and Gen KOGA
Department of Chemistry, Faculty of Science, Ibaraki University, Bunkyo, Mito 310
(Received September 27, 1990)

Synopsis. In the presence of excessive amount of acetyl halide along with a catalytic amount of tin(II) halide, aromatic acetals react with allyltrimethylsilane or triethylsilane to give α-allylbenzyl halides or benzyl halides, respectively, in good to excellent yields.

In continuation of our studies of the new carbon-carbon bond formation between acetals and silyl nucleophiles effected by the combined use of a catalytic amount of tin(II) halide (SnX_2) and an excessive amount of reactive organic halide such as acetyl chloride (AcCl) and methoxymethyl chloride (MOMCl), we have already demonstrated a convenient synthesis of conjugated enones from acetals and silyl enol ethers.[1]

Now we wish to report novel reaction of aromatic acetals with allyltrimethylsilane[2] or triethylsilane[3] as a silyl nucleophile to give α-allylbenzyl halides or benzyl halides respectively.

In the first place, we have examined the allylation according to the procedure similar to that for the aldol-type reaction reported in the previous paper.[1] Reaction of benzaldehyde dimethyl acetal (**1**) with allylsilane using a combined activator, $SnCl_2$ and AcCl both in a catalytic amount, afforded the known product, 4-methoxy-4-phenyl-1-butene (**3**), in 72% yield (Run 1 in Table 1). In a striking contrast, when 2.5 molar amount of AcCl to the acetal was employed, an allylation with concomitant substitution of methoxyl for chloride[4] occurred to give 4-chloro-4-phenyl-1-butene (**2**, X=Cl) in 83% yield (Run 2 in Table 1). AcCl did not function as an electrophile to acylate allylsilane. Screening of various combined activator system using benzaldehyde dimethyl acetal as a reference substrate revealed that SnX_2/AcX (molar ratio of acetal : SnX_2 : AcX=1.0 : 0.05 : 2.0—2.5) gave the best result as shown in Table 1. When a combination of $SnBr_2$/AcBr was used as an activator, corresponding 4-bromo-1-butene was obtained as a sole product (Run 8 in Table 1). The results of the reaction with various acetals are summarized in Table 2.

The reaction is similarly effective to ketone acetal,

Table 2. Synthesis of 4-Aryl-4-halo-1-butene (**5**) from Acetals (**4**)[a,b]

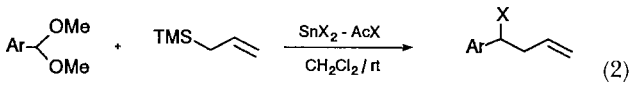

(2)

4 5

Run	Ar	X	Time/h	Yield of 5[c]/%
1	Ph	Cl	2	83
2	Ph	Br	2	87
3	Ph[d]	Cl	2	79
4	*p*-BrC_6H_4	Cl	12	85
5	*p*-BrC_6H_4	Br	24	84
6	*p*-ClC_6H_4	Br	6	65
7	*m*-$MeOC_6H_4$	Br	3	63

a) Molar ratio of acetal : SnX_2 : AcX=1.0 : 0.05 : 2.0—2.5. b) All the products gave satisfactory ^1H NMR and IR spectra. c) Isolated yield. d) Diethyl acetal was used in place of dimethyl acetal.

Table 1. The Effect of Activator System of the Reaction between Benzaldehyde Dimethyl Acetal (**1**) and Allyltrimethylsilane[a]

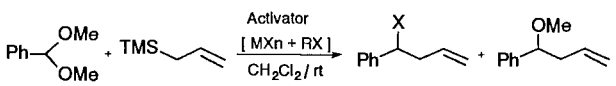

(1)

1 2 3

Run	Activator [MX_n+RX] (molar ratio to the acetal)			Time/h	Yield[b]/%	
					2	3
1	$SnCl_2$	(0.05) + AcCl	(0.05)	2.5	0	72
2	$SnCl_2$	(0.05) + AcCl	(2.5)	2	83	0
3	$ZnCl_2$	(0.05) + AcCl	(2.5)	2	87	Trace
4	$Sn(OTf)_2$	(0.05) + AcCl	(2.5)	2	59	16
5	$SnCl_2$	(0.05) + MOMCl	(2.5)	2	66	0
6	$SnCl_2$	(0.05) + TMSCl	(2.0)	6	Trace	69
7	$SnBr_2$	(0.05) + MOMBr	(2.5)	2	77	0
8	$SnBr_2$	(0.05) + AcBr	(2.0)	2	87	0

a) Molar ratio of acetal : allylsilane=1 : 1.2. b) Isolated yield.

e.g. cyclohexanone dimethyl acetal, to result in 1-allyl-1-bromocyclohexane (Eq. 3).

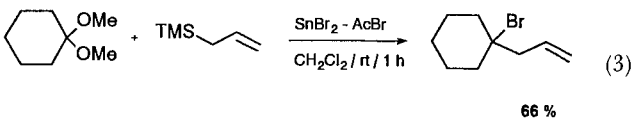

(3)

4-Aryl-4-bromo-1-butenes (**6**), above obtained, were easily converted to 1-aryl-1,3-butadienes (**7**) by a convenient procedure as illustrated in Eq. 4.

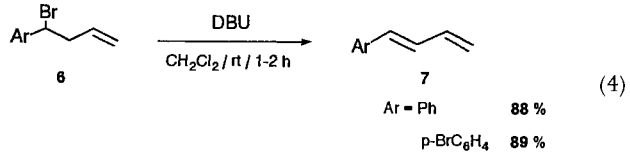

(4)

The above shown double substitution of alkoxyl groups in acetal by a nucleophile from reactive silanes and a halogen from reactive organic halides has led us to examine the hydride reduction of acetals with simultaneous halogen substitution to obtain benzyl halides. Thus, the reduction of aromatic dimethyl acetals by triethylsilane in the presence of a combined AcX/SnX_2 reagent was tried and was proven to be successful as well. The results are summarized in Table 3.

Reaction of alkyl halides with *n*-Bu_3SnH under radical conditions[5] gave the corresponding alkane in good yield as shown in Eqs. 6 and 7. This overall three step reduction from carbonyl to methylene provides a mild and effective alternative to conventional Wolff-Kishner[6] and Clemmensen reductions,[7] both of which necessitate drastic reaction conditions.

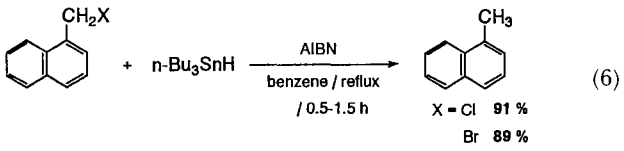

(6)

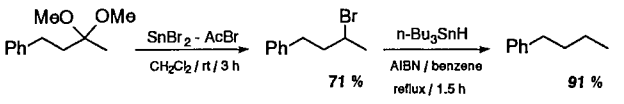

(7)

Table 4. Halogenative Reduction of Various Acetals of Benzaldehyde (**9**)[a,b]

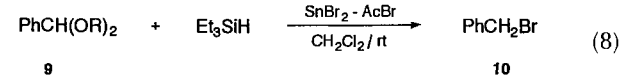

(8)

Run	R, R	Time/h	Yield of **10**[c]/%
1	Me, Me	3	89
2	Et, Et	3	91
3	$-(CH_2)_2-$	3	96
4	$-(CH_2)_3-$	3	82
5	Ac, Ac	3[d]	77

a) Molar ratio of acetal : SnBr : AcBr = 1.0 : 0.05 : 2.5. b) All the products gave satisfactory ^1H NMR and IR spectra. c) Isolated yield. d) The reaction was carried out in refluxing 1,2-dichloroethane.

Benzaldehyde diethyl acetal, ethylene acetal, and acylal were also transformed to benzyl bromide in good yield as shown in Table 4.

Experimental

General Procedure. To a suspension of tin(II) bromide

Table 3. Synthesis of Benzyl Halides (**8**) from Acetals (**4**)[a,b]

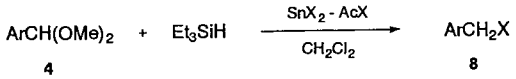

(5)

Run	Ar	X	Temp/°C	Time/h	Yield of **8**[c]/%
1	Ph	Cl	R.T.	3	76
2		Br	R.T.	3	89
3	*m*-$MeOC_6H_4$	Cl	R.T.	3	97
4		Br	R.T.	2	99
5	*p*-MeC_6H_4	Cl	R.T.	3	89
6		Br	R.T.	3	86
7	*p*-ClC_6H_4	Cl	R.T.	12	79
8		Br	R.T.	2	87
9	*p*-BrC_6H_4	Cl	R.T.	5	92
10		Br	R.T.	7	97
11	α-Naph	Cl	0	2	92
12		Br	0	1	96
13	β-Naph	Cl	0	5	91
14		Br	0	3	94

a) Molar ratio of acetal : SnX_2 : AcX = 1.0 : 0.05 : 2.5. b) All the products gave satisfactory ^1H NMR and IR spectra. c) Isolated yield.

(5.1 mg, 0.02 mmol) and benzaldehyde dimethyl acetal (54.8 mg, 0.36 mmol) in dichloromethane (2.5 ml) were added triethylsilane (65.0 mg, 0.56 mmol) in dichloromethane (1.5 ml) and acetyl bromide (96.8 mg, 0.79 mmol) in dichloromethane (1 ml), successively at room temperature under argon atmosphere. The mixture was stirred for 3 h at this temperature, and quenched with a phosphate buffer (pH 7). The organic materials were extracted with dichloromethane and dried over Na_2SO_4. Benzyl bromide (54.7 mg, 89%) was isolated by thin layer chromatography on silica gel.

It should be noted that the present halogenative allylation and reduction of aromatic acetals are extremely mild and exceptionally simple in operation.

The present work was partially supported by a Grant-in-Aid for Scientific Research No. 02854053 from the Ministry of Education, Science and Culture.

References

1) T. Oriyama, K. Iwanami, Y. Miyauchi, and G. Koga, *Bull. Chem. Soc. Jpn.*, **63**, 3716 (1990).
2) For reaction of acetals with allylsilanes, see: A. Hosomi, M. Endo, and H. Sakurai, *Chem. Lett.*, **1976**, 941; T. Tsunoda, M. Suzuki, and R. Noyori, *Tetrahedron Lett.*, **21**, 71 (1980); H. Sakurai, K. Sasaki, and A. Hosomi, *ibid.*, **22**, 745 (1981); T. Mukaiyama, H. Nagaoka, M. Murakami, and M. Ohshima, *Chem. Lett.*, **1985**, 977.
3) For reaction of acetals with triethylsilane, see: G. A. Olah, T. Yamato, P. S. Iyer, and G. K. S. Prakash, *J. Org. Chem.*, **51**, 2826 (1986).
4) F. G. Mann and F. H. C. Stewart, *J. Chem. Soc.*, **1954**, 2819.
5) H. G. Kuivila and L. W. Menapace, *J. Org. Chem.*, **28**, 2165 (1963).
6) D. Todd, *Org. React.*, **4**, 378 (1948), and references cited therein.
7) E. L. Martin, *Org. React.*, **1**, 155 (1942), and references cited therein.

Cyclotriveratrylene Crown Ethers: Metal Ion Extraction and Transport Abilities through Organic Membrane

Sadatoshi AKABORI,* Masakazu TAKEDA, and Hiroshi KAWAKAMI
Department of Chemistry, Faculty of Science, Toho University, Funabashi, Chiba 274
(Received November 19, 1990)

Synopsis. Extraction abilities of cyclotriveratrylene crown ethers (**2**) toward alkali, alkaline earth, and other metal ions were examined. Transport of metal ions by **2** through a liquid membrane was also examined.

Many research groups are recently modifying crown ethers in order to develop a new kind of functionality in the host-guest chemistry.[1] Cyclotriveratrylene attracts considerable attention for the following reasons: i) it exists in a "crown (or cone)" conformation with a high energy barrier for interconversion;[2,3] ii) it forms stoichiometric inclusion compounds with small neutral molecules.[4] Although syntheses of the cyclotriveratrylene crown ethers such as **2b** and **2c** and the isolation of their 1 : 3 complexes with sodium and potassium thiocyanates have already been reported by Frensch and Vögtle,[5] the complexing ability of **2** for metal ions has not been studied in detail. In this paper we report the extraction and transport of metal ions by **2**.

Cyclotriveratrylene crown ethers **2a**, **2b**, and **2c** were prepared by the method of Frensch and Vögtle with minor modification.[5] Thus, compound **2a** was obtained in a 4.8% yield by the reaction of benzo-12-crown-4 (**1a**) with formaldehyde in the presence of hydrochloric acid.

The extraction abilities of the crown ethers **1a—c** and **2a—c** toward alkali, alkaline earth, and other metal ions were determined by the method described in our previous paper.[6] However, the measurement of extraction and transport abilities was carried out using a three-fold concentration of **1a—c** compared with that of **2a—c** in order to clarify the selectivities of **2a—c** and the corresponding monomers **1a—c**. The results are summarized in Table 1. The extraction ability of cyclotriveratrylene crown ether **2a** toward alkali, alkaline earth metals, and other bivalent metal ions is low or zero. Similar results were obtained with the corresponding monomer **1a**. In addition, it was found that **2c** showed a relatively high extraction ability toward alkali metal (excluding lithium) ion, alkaline earth metal ions, silver(I) ion, and thallium(I) ion, while it showed little or no extraction ability toward Li^+, Mg^{2+}, Ca^{2+}, Co^{2+}, Ni^{2+}, and Cu^{2+}. Furthermore, **2c** showed only slightly higher extraction abilities toward Na^+, Rb^+, Cs^+, Sr^{2+}, Ba^{2+}, and Ag^+ than those of the corresponding monomer **1c**. Similar results were obtained in the case of **2b** (except for Sr^{2+} and Ba^{2+}), although the extraction ability of **2b** is relatively low compared with that of **2c**. Consequently, the extraction abilities of cyclotriveratrylene crown ethers **2a**, **2b**, and **2c** are very similar to those of the corresponding monomers **1a**, **1b**, and **1c**, although the complexing manner of the cyclotriveratrylene

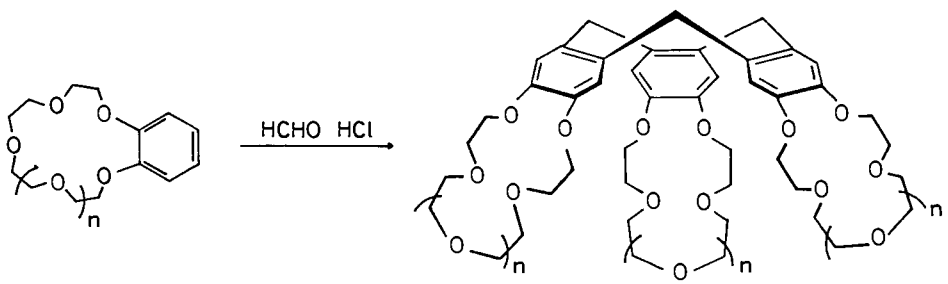

1a : n=0
1b : n=1
1c : n=2

2a : n=0
2b : n=1
2c : n=2

Table 1. Extraction of Metal Picrates from the Aqueous to the Organic Phase (%)

Compd	Li^+	Na^+	K^+	Rb^+	Cs^+	Mg^{2+}	Ca^{2+}	Sr^{2+}	Ba^{2+}	Co^{2+}	Ni^{2+}	Cu^{2+}	Ag^+	Tl^+
2a[a]	0	9	10	11	12	4	0	0	2	0	1	0	12	27
1a[b]	0	8	14	15	17	4	0	0	3	0	1	0	9	31
2b[a]	6	48	87	81	37	2	2	2	4	3	3	1	72	95
1b[b]	3	44	81	60	23	1	1	1	2	2	2	1	57	85
2c[a]	6	53	99	96	98	5	7	55	36	5	10	3	94	100
1c[b]	3	35	98	90	88	1	3	43	25	3	7	2	88	99

a) Solvent: Water and dichloromethane (equal volumes). Picric acid=7.0×10^{-5} M. Metal nitrate=0.1 M. Crown ether=7.0×10^{-4} M. b) Crown ether=2.1×10^{-3} M.

crown ether **2** with metal ions cannot be determined from the present results.

Alkali metal cation transport mediated by **1** and **2** through an organic liquid membrane was investigated using a double cylindrical glass cell in which the inner and outer aqueous phases were bridged by a dichloromethane solution containing crown ether **1** or **2**. Practically no ion transport occurred in the absence of the crown ether. The results and the selectivity of Rb^+ over other alkali metal cations are summarized in Tables 2 and 3, respectively. The rate of ion transport is dependent on the ring size of the cyclotriveratrylene crown ethers and the kind of metal ions. Crown ethers **2a** and **2c** showed a similar tendency of ion transport abilities toward alkali metal cations with the corresponding monomers **1a** and **1c**, although **1a** and **1c** generally showed slightly higher ion transport abilities compared with **2a** and **2c**, respectively. However, **2b** showed much higher ion transport abilities toward alkali metal cations compared with those of the corresponding monomer **1b**. Interestingly, **2b** transported Rb^+ more efficiently than **1b**, while the transport abilities of **2b** and **1b** toward Li^+, Na^+, K^+, and Cs^+ were nearly the same. These observations suggest that the Rb^+ ion is incorporated into the cavity surrounded by the three benzo-crown ether moieties of **2b**, thereby forming a 1 : 1 complex. Furthermore, **2b** showed higher transport abilities toward K^+ and Cs^+ ions compared with the corresponding monomer **1b**, although complexing manner cannot be detailed at present. As shown in Table 3, the difference in the selectivity of Rb^+ over other alkali metal cations between **1** and **2** may be insignificant and the preference of Rb^+ over Na^+ in the transport was in the range from 0.3 to 6.9 except for **2c**. However, it is noticeable that the selectivity (Rb^+/Na^+) of **2c** in the transport was 43.8. This value is very large compared with that (5.5) of the corresponding monomer **1c**, or those of the other crown ethers **1a**, **1b**, **2a**, and **2b**. It is well known that in ion-transport from an IN aq phase to an OUT aq phase across a liquid membrane, there exist two possible rate-determing steps: ion-extraction from the IN aq phase to the membrane phase and ion-releasing from the membrane phase to the OUT aq phase. Therefore, the high selectivity of **2c** for Rb^+/Na^+ may be mainly due to the slow ion-releasing step of Na^+, because the extraction abilities (48 and 53%) of **2b** and **2c** for Na^+ are nearly the same, while the transport abilities (2.18 and 0.66) of **2b** and **2c** for Na^+ are very different.

Table 2. Amounts of Alkali Metal Ions Transported through Liquid Membranes (μmol)[a]

Carrier	Li^+	Na^+	K^+	Rb^+	Cs^+
2a[b]	0.00	0.38	0.08	0.12	0.17
1a[c]	0.00	0.45	0.33	0.13	0.37
2b[b]	0.76	2.18	8.82	15.06	2.27
1b[c]	0.70	3.61	5.97	3.40	0.91
2c[b]	0.30	0.66	6.44	28.90	7.70
1c[c]	0.28	7.31	27.19	39.89	13.43

a) In 24 h. b) 0.33 mM. c) 1.0 mM.

Table 3. Selectivity of Liquid Membrane Transport

Carrier	Rb^+/Na^+	Rb^+/K^+	Rb^+/Cs^+
2a	0.3	1.5	0.7
1a	0.8	1.2	1.1
2b	6.9	1.7	6.6
1b	0.9	0.6	3.7
2c	43.8	4.5	3.8
1c	5.5	1.5	3.0

Experimental

All melting points are uncorrected. ^1H NMR spectra were measured on a Hitachi R-1100 spectrometer (60 MHz) with TMS as the internal standard. Mass spectra were taken on a Hitachi M-80 spectrometer.

Materials. Benzo-12-crown-4 (**1a**), benzo-15-crown-5 (**1b**), and benzo-18-crown-6 (**1c**) were prepared according to a method reported in the literature.[7] Other reagents employed were either commercially available or synthesized by the usual methods. The solvents were purified by distillation.

6,9,12,15,23,26,29,32,40,43,46,49-Dodecaoxaheptacyclo-[$O^{3,18}$.$O^{5,16}$.$O^{20,35}$.$O^{22,33}$.$O^{37,1}$.$O^{39,50}$]heptaconta-3,5(16),17,20,22(33),34,37,39(50),51-nonaene (2a). To a mixture of concentrated hydrochloric acid (135 ml) and 37% formalin (10 ml, 0.13 mol), benzo-12-crown-4 (**1a**) (4.03 g, 18 mmol) was added under stirring at 0 °C. After being stirred for 7 h at 30 °C, the viscous solution was poured onto water. The mixture was then extracted with chloroform and the extracts were washed with water until they became neutral. The combined extract was dried over $MgSO_4$ and concentrated under reduced pressure. Chromatography on silica gel using ethyl acetate as the eluent gave a colorless solid. Recrystallization of the solid from chloroform-hexane gave **2a** (0.2g, 4.8%) as a colorless powder, mp 253-256 °C. ^1H NMR ($CDCl_3$) δ=6.99(s, 6H), 4.75 (d, J=14.0 Hz, 3H), 4.40—3.72 (m, 36H), 3.54 (d, J=14.0 Hz, 3H). MS m/z 708 (M^+). Found: C, 62.09, H, 6.52%. Calcd for $C_{39}H_{48}O_{12}$. 1/2$CHCl_3$: C, 61.74, H, 6.36%.

Compounds **2b** and **2c** were also obtained by a method similar to that previously described.[5]

2b: Yield 3.6%, mp 204.5—206.0 °C (lit,[5] 203.5—205.5 °C).

2c: Yield 12%, mp 166.0—167.0 °C (lit,[5] 169—172 °C).

Solvent Extraction. Equal volumes (5 ml) of dichloromethane containing 7×10^{-4} M of **2** and/or 2.1×10^{-3} M of **1** and an aqueous solution containing 0.1 M of metal nitrate and 7.0×10^{-5} M of picric acid were mixed and agitated (1 M=1 mol dm^{-3}). The solution was then separated by centrifugation. The upper solution was withdrawn and its absorbance was measured at 380 nm. A similar extraction and measurement were performed with pure dichloromethane and an aqueous solution containing 0.1 M metal nitrate and 7.0×10^{-5} M picric acid. Extraction abilities were calculated by the following equation: extraction ability=$(A_0-A)/A_0\times100$. A_0 is the absorbance in the absence of a crown ether and A is the absorbance in its presence.

Cation Transport through Liquid Membranes. Cation transport experiments were conducted using a double cylindrical glass cell (cylinder diameter: inner, 7 mm; outer, 16 mm) in which the inner cylinder had small channels connecting the inner and outer areas at its bottom. A dichloromethane solution (5 ml) containing 0.33 mM of crown ether **2** or 1 mM of crown ether **1** was placed at the bottom. Atop the dichloromethane solution inside the inner cylinder

was placed 1.5 ml of water. Simultaneously, atop the outer ring of the dichloromethane solution was placed an aqueous solution (3 ml) containg metal thiocyanate (1 M). The organic phase was gently stirred at ca. 130 rpm and 24 °C using a stirrer. At specified time intervals, the concentrations of metal ion in the receiving phase were determined by atomic absorption spectroscopy.

References

1) F. Vögtle and F. Weber, "Host Guest Complex Chemistry Macrocycles," Springer-Verlag, Berlin (1985).
2) A. S. Lindsey, *J. Chem. Soc.*, **1965**, 1685.
3) H. Erdtman, F. Haglid, and R. Ryhage, *Acta Chem. Scand.*, **18**, 1249 (1964).
4) V. Caglioti, A. M. Liquori, N. Gallo, E. Giglio, and M. Scrocco, *J. Inorg. Nucl. Chem.*, **8**, 572 (1958).
5) K. Frensch and F. Vögtle, *Liebigs Ann. Chem.*, **1979**, 2121.
6) S. Akabori, T. Kumagai, Y. Habata, and S. Sato, *J. Chem. Soc., Perkin Trans. 1*, **1989**, 1497.
7) J. C. Pedersen, *J. Am. Chem. Soc.*, **89**, 7017 (1967).

A Convenient Synthesis of 4-(Phenylsulfonylthio)-2-azetidinones[1)]

Hideo TANAKA, Masatoshi TANIGUCHI, Seiryu UTO,† Takashi SHIROI,† Michio SASAOKA,† and Sigeru TORII*
Department of Applied Chemistry, Faculty of Engineering, Okayama University, Okayama 700
†Tokushima Research Laboratories, Otsuka Chemical Co., Ltd., Tokushima 771-01
(Received September 12, 1990)

Synopsis. 4-(Phenylsulfonylthio)-2-azetidinones have been prepared conveniently by the reaction of 4-(2-benzothiazolyldithio)-2-azetidinones with 2-benzothiazolyl benzenethiosulfonates. A combination of this reaction with the electrolytic cross-coupling of bis(benzothiazolyl) disulfide and ammonium benzenesulfinate can establish a recycling system, in which *S*-(2-benzothiazolyl) benzenethiosulfonate is regenerated to play a critical role in penicillin-cephalosporin conversions.

4-(Phenylsulfonylthio)-2-azetidinones **2** are versatile intermediates for the synthesis of useful β-lactam antibiotics.[2)] For example the ene-type chlorination and/or C=C bond fission of **2** followed by intramolecular cyclization can provide C(3)-substituted cephems, such as 3-chloromethyl-[3)] and 3-hydroxycephems **3** (Y=CH_2Cl or OH),[4)] wherein the phenylsulfonyl group works not only as a protecting group of the 4-thiol moiety but also as a leaving group in the cephem-ring forming process. (Scheme 1). In spite of a strong interest of **2** in cephem synthesis, only a few reports for the preparation of **2** have appeared so far.[4,5)] Woodward and Gosteli prepared **2** by the replacement of the 2-benzothiazolylthio moiety of Kamiya's disulfides **1** derived from penicillins[6)] with arylsulfonyl groups.[4)] However, the method has disadvantages that it inevitably requires a stoichiometric or excessive amount of heavy metal salts or silver salt of arenesulfinates. Thermolysis of penicillin sulfoxides in the presence of arenesulfinic acids was also attempted by Allan et al.,[5)] but they failed in obtaining **2** owing to a terminal/internal olefin migration of the *N*-alkenyl substituent of **2** (R^2=CH_2CCl_3) under the conditions. Thus, the lack of an acceptable method for the large scale production of **2** enabled us to develop an alternative access to **2**.

Incidentally, the reaction of **1** with arenesulfinates **4** produced **2** together with 2-benzothiazolethiolate **5** but the reaction reached rapidly a state of equilibrium and only 30—45% yields of **1** were obtained. Hence, one can expect that removal of **5** from the equilibrium mixture may shift the equilibrium to the right so as to complete the reaction leading to **2**. Herein, we disclose a new device for this purpose, in which 2-benzothiazolyl benzenethiosulfonate **6** works as an efficient trapping agents of **5** and at the same time liberates benzenesulfinate **4** to complete the transformation of **1** to **2** as illustrated in Scheme 1.

A representative procedure is as follows (Entry 1 in Table 1): A mixture of 4-(2-benzothiazolyldithio)-2-azetidinone **1a** (R^1=$PhOCH_2$; R^2=CH_2Ph) and *S*-(2-benzothiazolyl) benzenethiosulfonate **6** (1 : 1.1) in aqueous acetone containing a catalytic amount of sodium benzenesulfinate **4** was stirred at an ambient temperature for 3.5 h. During the course of the reaction, pale yellow precipitates were formed. The solids were collected by filtration and air-dried to afford disulfide **7** (96%) and the filtrates afforded the 4-(phenylsulfonylthio)-2-azetidinone **2** in 91% yield. The presence of a catalytic amount of **4** is influential to effect the reaction smoothly. Indeed, the reaction hardly started without **4** and did not complete even after the prolonged reaction time (Entry 2).[7)] In place of **4**, sodium 2-benzothiazolethiolate **5** can be used without any disadvantages (Entry 3) presumably because **5** reacts with **6** liberating **4** together with disulfide **7**.

The elimination of the disulfide **7** as precipitates from the equilibrium mixture (vide supra) is also essential to shift the equilibrium to the desired direction. The disulfide **7** is virtually insoluble in various

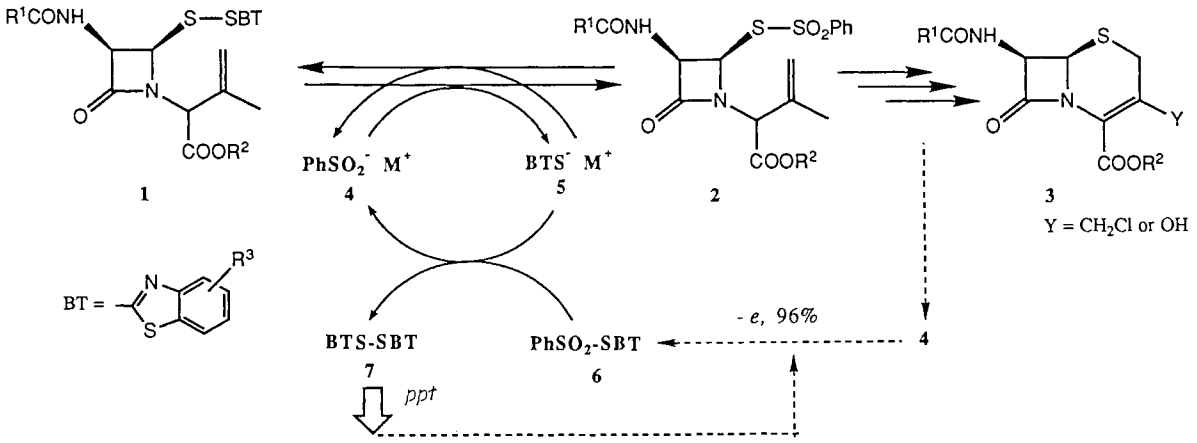

Scheme 1.

Table 1. Reaction of Kamiya's Disulfides with *S*-(2-Benzothiazolyl)benzenethiosulfonates

Entry	1	R^1	R^2	R^3	Additive	Time/h	Yield[a]/%
1	**1a**	$PhOCH_2$	$PhCH_2$	H	$PhSO_2Na$	3.5	91
2	**1a**	$PhOCH_2$	$PhCH_2$	H	—	7	77
3	**1a**	$PhOCH_2$	$PhCH_2$	H	BTSNa	3.5	89
4	**1b**	$PhCH_2$	PMB[b]	H	$PhSO_2Na$	5	91
5	**1b**	$PhCH_2$	PMB[b]	H	BTSNa	1.5	92
6	**1c**	$PhOCH_2$	$PhCH_2$	5-CH_3O	BTSNa	3.5	91
7	**1d**	$PhOCH_2$	$PhCH_2$	4-CH_3	$PhSO_2Na$	3.5	90

a) Isolated yields based on disulfides **1**. b) *p*-Methoxybenzyl.

solvents and, thus, chloroform, acetonitrile, benzene, nitromethane, and isopropyl alcohol were successfully used in place of aqueous acetone without any appreciable change of the products.

The reaction of azetidinones **1b**, **1c**, and **1d** with **6** was performed in a similar manner, affording the corresponding 4-(phenylsulfonylthio)-2-azetidinones **2** in good yields (Entries 4—7 in Table 1).

It has already been described that azetidinones **2** were able to be converted to 3-substituted cephems **3**[3,4] and ammonium benzenesulfinate **4** was liberated in the course of the thiazolidine ring formation. On the other hand, we have recently reported a facile electrolytic cross-coupling of benzenesulfinates **4** and disulfide **7** affording **6** in good yields.[8] These two interesting results provided a clue that **6** could be supplied from **4** given in the course of **2**→**3** transformation for the **1**→**2** conversion as indicated by dotted arrows in Scheme 1.

Experimental

Melting points were determined on a Yamato melting point apparatus Model MP-21 and were uncorrected. IR spectra were obtained on a JASCO IRA-1 grating spectrometer or a JEOL RFX-3002 FTIR spectrophotometer. ^1H NMR spectra were mesured at 60 MHz with a Hitachi R-24 spectrometer or at 300 MHz with a Varian VXR-300S spectrometer. Chemical shifts are expressed in parts per million downfield from Me_4Si as an internal reference. Mass spectra were obtained on a Hitachi M-80 spectrometer. Elemental analyses were performed in our laboratory on a Yanaco CHN corder MT-3. 4-(2-Benzothiazolyldithio)-2-azetidinones **1**[6] and *S*-(2-benzothiazolyl) benzenethiosulfonates **6**[8,9] were prepared by the reported procedures.

4-Phenylsulfonylthio-3-phenoxyacetamido-1-(1-benzyloxycarbonyl-2-methyl-2-propenyl)-2-azetidinone (2a): Procedure A (Table 1, Entry 1). 4-(2-benzothiazolyldithio)-2-azetidinone **1a** (R^1=$PhOCH_2$, R^2=$PhCH_2$, R^3=H, 1.68 g, 2.8 mmol), 2-benzothiazolyl benzenethiosulfonate **6** (0.89 g, 2.9 mmol), and sodium benzenesulfinate hydrate (26 mg, 0.13 mmol) in acetone (35 mL) and water (5 mL) was stirred at room temperature for 3.5 h. The mixture was filtered and the solids were washed with acetone (5 mL) and air-dried to give bis(benzothiazolyl) disulfide (0.88 g, 96%). The filtrate and washings were combined and concentrated in vacuo. The residue was taken up with benzene (30 mL), washed with water (20 mL), and dried (Na_2SO_4). After evaporation of the solvents, the residue was chromatographed (SiO_2, benzene/EtOAc: 5/1) to afford **2a**[10] (1.46 g, 91%) as colorless solids: IR(KBr) 1794, 1756, 1692, 1615, 1537 cm^{-1}; ^1H NMR ($CDCl_3$, 300 MHz) δ=1.79 (s, 3H), 4.38 (d, J=15 Hz, 1H), 4.15 (s, 1H), 4.51 (d, J=15 Hz, 1H), 4.83 (s, 1H), 4.85 (s, 1H), 5.14 (d, 12 Hz, 1H), 5.21 (d, J=12 Hz, 1H), 5.30 (dd, J=5 and 8 Hz, 1H), 5.92 (d, 5 Hz, 1H), 6.90—7.90 (m, 16H); MS (FD) *m/z* 780 (M^+).

Anal. Calcd for $C_{29}H_{28}N_2O_7S_2$: C, 59.98; H, 4.86; N, 4.82%. Found: C, 59.80; H, 4.84; N, 4.76%.

Procedure B (Table 1, Entry 3). A mixture of 4-(2-benzothiazolyldithio)-2-azetidinone **1a** (R^1=$PhOCH_2$, R^2=$PhCH_2$, R^2=H, 200 mg, 0.33 mmol), S-(2-benzothiazolyl) benzenethiosulfonate **6** (112 mg, 0.36 mmol), and sodium 2-benzothiazolethiolate (1 mg, 0.005 mmol) in acetone (5 mL) and water (1.5 mL) was stirred at room temperature for 3.5 h. Workup in the same manner as described above afforded **2a** (171 mg, 89%).

The reactions of 4-(2-benzothiazolyldithio)-2-azetidinone **1b** (R^1=$PhCH_2$, R^2=*p*-$CH_3OC_6H_4CH_2$, R^3=H), **1c** (R^1=$PhOCH_2$, R^2=$PhCH_2$, R^3=5-CH_3O), and **1d** (R^1=$PhOCH_2$, R^2=$PhCH_2$, R^3=4-CH_3O) with *S*-(2-benzothiazolyl) benzenethiosulfonates **6** were carried out according to Procedure A and/or B. Reaction conditions and results are summarized in Table 1.

4-Phenylsulfonylthio-3-phenylacetamido-1-[1-(*p*-methoxybenzyloxycarbonyl)-2-methyl-2-propenyl]-2-azetidinone (2b): Mp 115—116 °C from $CHCl_3/C_2H_5OH$ (1/10); IR (KBr) 1794, 1749, 1653, 1627, 1557, 1531 cm^{-1}; ^1H NMR ($CDCl_3$, 300 MHz) δ=1.73 (s, 3H), 3.56 (d, J=16 Hz, 1H), 3.62 (d, J=16 Hz, 1H), 3.82 (s, 3H), 4.43 (s, 1H), 4.75 (s, 1H), 4.76 (s, 1H), 5.04 (d, J=12 Hz, 1H), 5.10 (d, J=12 Hz, 1H), 5.11 (dd, J=5 and 8 Hz, 1H), 5.78 (d, J=5 Hz, 1H), 5.87 (d, J=8 Hz, 1H), 6.90—7.90 (m, 14H); MS (FD) *m/z* 594 (M^+).

Anal. Calcd for $C_{30}H_{30}N_2O_7S_2$: C, 60.59; H, 5.09; N, 4.71%. Found: C, 60.45; H, 5.07; N, 4.58%.

Refereces

1) Penicillin-Cephalosporin Conversion XV; Part XIV: H. Tanaka, M. Taniguchi, Y. Kameyama, M. Monnin, M. Sasaoka, T. Shiroi, S. Nagao, and S. Torii, *Chem. Lett.*, **1990**, 1867.

2) See for example: "Topics in Antibiotic Chemistry," ed by P. G. Sammes, Ellis Norwood Ltd., Chichester (1980), Vol. 4.

3) S. Torii, H. Tanaka, N. Saitoh, T. Siroi, M. Sasaoka, and J. Nokami, *Tetrahedron Lett.*, **23**, 2187 (1982).

4) H. R. Pfaender, P. A. Rossy, J. Gosteli, and R. B. Woodward, *Heterocycles*, **5**, 293 (1976); J. Gosteli, *Chimia*, **30**, 13 (1976).

5) R. D. Allan, D. H. R. Barton, M. Giriavallabhan, and P. G. Sammes, *J. Chem. Soc., Perkin Trans. 1*, **1974**, 1456.

6) T. Kamiya, T. Teraji, Y. Saito, and M. Hashimoto, *Tetrahedron Lett.*, **1973**, 3001.

7) Some unknown contaminants seemed to act as a nucleophile to react with **1** or **6** to generate **5** or **4**. However, it is likely that the concentration of **5** and **4** is too low to efficiently promote the reaction.

8) H. Tanaka, Y. Kameyama, S. Uto, M. Sasaoka, M. Taniguchi, and S. Torii, *Chem. Express*, **4**, 669 (1989).
9) R. J. Arnold, U.S. Patent, 3732192 (1974); *Chem. Abstr.*, **79**, 54668y (1976); T. Weidner and S. S. Block, *J. Med. Chem.*, **10**, 1167 (1967).
10) S. Torii, H. Tanaka, N. Tada, S. Nagao, and M. Sasaoka, *Chem. Lett.*, **1984**, 877.

Reactions of 1,1-Diphenyl-2-methylpropene Cation Radicals with Methanol. Ketone Formation Involving Carbocation Rearrangement

Ryoichi AKABA,*,† Shin AIHARA, Hirochika SAKURAGI, and Katsumi TOKUMARU*
Department of Chemistry, University of Tsukuba, Tsukuba, Ibaraki 305
(Received November 26, 1990)

Synopsis. Anodic oxidation of 1,1-diphenyl-2-methylpropene (**1**) in an acetonitrile-methanol mixture under argon gave 3,3-diphenyl-2-butanone (**2**) in high yield together with small amounts of 1,2-diphenyl-2-methyl-1-propanone (**3**) and benzophenone (**4**). Similar anodic oxidation of **1** in the presence of oxygen was also carried out, and the mechanisms for the novel ketone forming reactions are discussed.

Photoinduced electron transfer generating cation radicals has gathered sustained interest during the last decade.[1] Among the cation radicals which have so far been studied, olefin cation radicals have attracted continuing interest. Reactions of the olefin cation radicals with nucleophiles such as methanol have been studied by electrochemical generation of the cation radicals as well as by photoinduced electron transfer. For example, it is well-known that the photochemically generated cation radicals of aromatic olefins react with methanol to give anti-Markovnikoff adducts.[2] In contrast, electrochemical oxidation of olefins in methanol usually gives dimethoxylated monomeric or dimeric products.[3-6]

During the course of our investigation of photosensitized oxygenation of 1,1-diphenyl-2-methylpropene (**1**) in acetonitrile,[7] we have found that electrochemical oxidation of **1** in the presence of methanol gives almost exclusively a skeletally rearranged product, 3,3-diphenyl-2-butanone (**2**). This is a novel example demonstrating that the electrochemically generated aromatic olefin cation radical reacts with methanol to give the skeletally rearranged carbonyl compounds instead of the usually observed dimethoxylation products, although similar skeletal rearrangement was observed in photosensitized electron transfer reaction of styrylcyclopropane in methanol.[8] We have also carried out electrochemical oxidation of **1** in the presence of oxygen in acetonitrile/methanol mixed solvents in order to compare the reactivities of the olefin cation radical toward oxygen and methanol.

Results and Discussion

Controlled-potential electrolysis of **1** (45.4 mg, 0.22 mmol) in acetonitrile/methanol (4:1) under argon at 1.6 V/SCE for 3.2 h gave **2** in 79% yield together with small amounts of 1,2-diphenyl-2-methyl-1-propanone (**3**, 4%) and benzophenone (**4**, 4%). The yields of the products were monitored as a function of the electricity passed, and are shown in Fig. 1. The results show that the reaction involves two one-electron oxidation processes as shown in Scheme 2. Thus, electrochemical oxidation of **1** generates the cation radical of **1**, $\mathbf{1}^{+\cdot}$, which is captured by methanol to afford a β-alkoxy radical, **5**. Radical **5** is further oxidized electrochemically to produce a carbocation **6**. Rapid 1,2-migration of a methyl group followed by addition of methanol gives an acetal, **7**, which will be hydrolyzed

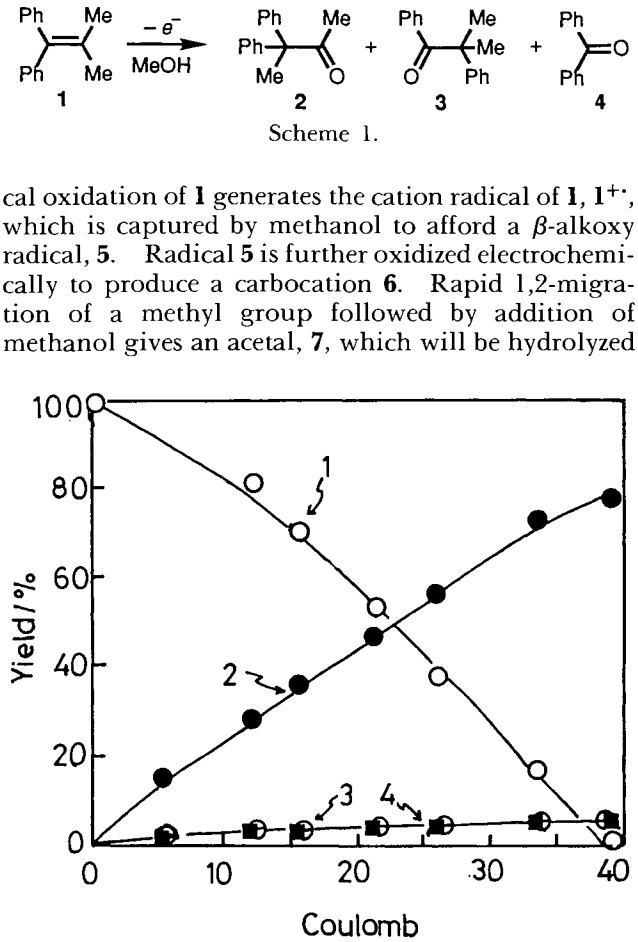

Fig. 1. Correlations of product yields with the electricity passed on electrochemical oxidation of **1** in CH_3CN/CH_3OH under argon.

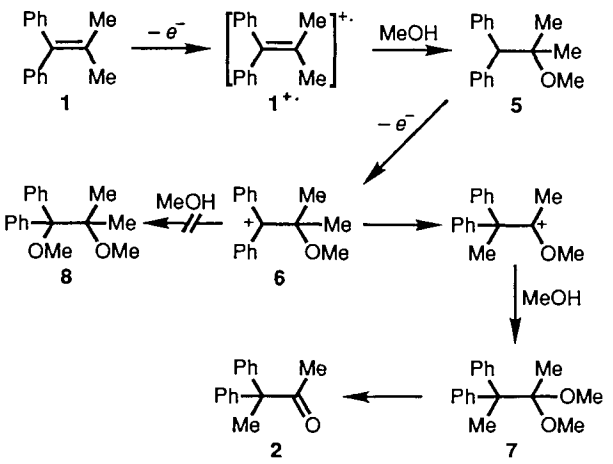

Scheme 2.

† Present address: Gunma College of Technology, Toriba-machi, Maebashi, Gunma 371.

during work-up to afford **2**. Attempts to isolate the acetal were unsuccessful, although similar conversion of an acetal was observed in 9,10-dicyanoanthracene-sensitized electron-transfer reactions of styrylcyclopropane in methanol.[8]

The mechanism shown in Scheme 2 is supported by coulometric studies, which indicated that the electricity of 2 F mol^{-1} was required for 99% consumption of **1**. The formation of **3** can be similarly explained by 1,2-migration of a phenyl group in the carbocation formed by addition of methanol to $\mathbf{1}^{+\cdot}$ at the phenylated carbon. Benzophenone **4** may be afforded by the reaction of $\mathbf{1}^{+\cdot}$ with residual oxygen (vide infra).[9]

In order to get further insight into the reactivity of $\mathbf{1}^{+\cdot}$, we have also carried out electrochemical oxidation of **1** in the presence of oxygen in acetonitrile/methanol. Thus, as in the case under argon, **1** (45.1 mg, 0.22 mmol) was oxidized at 1.6 V/SCE for 3.7 h in acetonitrile/methanol under an oxygen stream to give **2**, **3**, and **4** in 67, 6, and 22% yields, respectively. A plot of the yields of the products as a function of the electricity passed (Fig. 2) indicates that the presence of oxygen significantly decreases the yield of **2** but enhances that of **4**, suggesting that $\mathbf{1}^{+\cdot}$ reacts competitively with methanol and oxygen. The mechanism for formation of **4** was previously explained in terms of the decomposition of a dioxetane afforded by a reaction of $\mathbf{1}^{+\cdot}$ with molecular oxygen followed by the reduction by the electrode and/or **1** (ECbE mechanism).[9] The decrease of the total current (10%) passed in the presence of oxygen is not inconsistent with the ECbE mechanism for the formation of **4**.

The above result that the skeletal rearrangement product **2** is formed in a good yield is in contrast with electrochemical oxidation of olefins usually giving dimethoxylation products.[3-6] The formation of **2** in high yield and the complete absence of dimethoxylated products in **1** indicate that $\mathbf{1}^{+\cdot}$ is reluctant to undergoing self-dimerization or addition to **1**, and

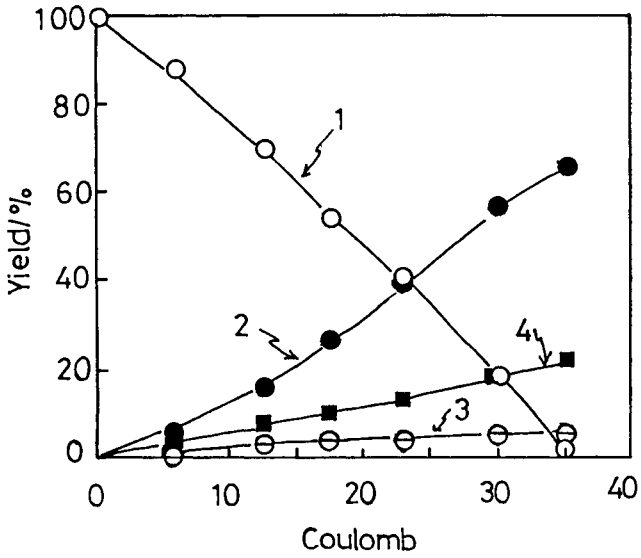

Fig. 2. Correlations of product yields with the electricity passed on electrochemical oxidation of **1** in CH_3CN/CH_3OH in the presence of oxygen.

that the resulting **5** does not dimerize but is rapidly oxidized at the electrode to give carbocation **6**. Rapid rearrangement of **6** followed by the addition of methanol prevents 1,2-addition of methanol.

The dominant formation of **2** over **3** shows that the addition of methanol to $\mathbf{1}^{+\cdot}$ takes place preferentially at the ethenyl carbon with the methyl groups. It is of particular interest to point out that the observed orientation is seemingly contradicting to that expected from the distribution of the spin density and positive charge in $\mathbf{1}^{+\cdot}$; recent ESR[10] and CIDNP[11] studies indicate that the spin density is higher at the methylated carbon than at the phenylated one, and that the latter is more positively charged than the former. Therefore, assuming that steric effects by phenyl and methyl groups are similar at each olefinic carbon, the present findings suggest that the regiochemistry of addition of nucleophiles such as methanol to olefin cation radicals is not governed by the distribution of positive charge on the ethenyl carbons but by the stability of the resulting free radicals; **5** is more stable than the other species $\cdot CMe_2CPh_2OMe$. This trend is parallel to the orientation often observed in the addition of atoms or free radicals and electrophiles to olefins giving free radicals and carbocations, respectively.

Once **6** is produced from **5**, only a methyl group can migrate to give the final product. This situation is consistent with the result of pinacol rearrangement of a glycol of **1**, $Ph_2C(OH)CMe_2OH$,[12] where the dehydration takes place exclusively from the phenylated carbon to give a more stabilized cation, $^{+}CPh_2CMe_2OH$. This carbocation results in the migration of a methyl group affording **2** finally as a sole product though the absolute migratory aptitude is much higher for a phenyl group than for a methyl group in pinacol rearrangement.[13]

In conclusion, we have shown that the electrochemically generated $\mathbf{1}^{+\cdot}$ reacts with methanol to give the skeletally rearranged ketone **2**. This is unusual since the electrochemical oxidations of aromatic olefins in methanol usually give dimethoxylated monomeric or dimeric products. It should be also emphasized that the present study revealed that $\mathbf{1}^{+\cdot}$ reacts competitively with molecular oxygen as a radical and methanol as a cation in solution.

Experimental

General. Nuclear magnetic resonance spectra were taken on a JEOL MH-100 or a JEOL FX-100 FT NMR spectrometer at room temperature in $CDCl_3$. IR spectra were measured with a Hitachi 215 infrared spectrophotometer. Gas chromatographic analyses were performed with a Shimadzu GC-4CM-PF gas chromatograph with an FID. Acetonitrile was distilled over phosphorus pentaoxide and then over potassium carbonate. Commercially available methanol was distilled once and stored over molecular sieve (Waco synthetic zeolite A-3).

Materials. 1,1-Diphenyl-2-methylpropene (**1**),[14] 3,3-diphenyl-2-butanone (**2**)[15] and 1,2-diphenyl-2-methyl-1-propanone (**3**)[16] were prepared by the published procedures, and their IR, ^1H, and ^{13}C NMR spectra were consistent with their structures.

Preparative Electrolysis. Preparative electrolyses were done in a three-compartment cell separated with glass frits (G-3.5). The working and counter electrodes were platinum wire, and the reference electrode was an SCE. Preelectrolysis of the solvent containing a supporting electrolyte under argon was carried out to remove possible electroactive impurities before the substrate was injected into the solvent. A Hokuto HA-201 potentiostat, a Hokuto HB-104 function generator, and a Rika Denki RE-11 X-Y recorder were employed.

Typically, 45.4 mg (0.22 mmol, 4×10^{-3} M, 1 M=1 mol dm^{-3}) of **1** was dissolved in the preelectrolyzed acetonitrile/methanol mixed solvent with tetrabutylammonium perchlorate (TBAP, 0.1 M) as a supporting electrolyte, and the solution was electrolyzed at 1.6 V/SCE for 3.2 h until **1** ,was almost consumed (99%). The progress of the reaction was monitored by taking aliquots periodically from the reaction mixture and examining them by GLC. The GLC analyses of the reaction mixture indicated the formation of 3,3,-diphenyl-2-butanone **2**, 1,2-diphenyl-2-methyl-1-propanone **3**, and benzophenone **4** in 79, 5, and 5% yields, respectively. For isolation of the products, the reaction mixture was poured into water and then extracted with benzene to remove TBAP. The resulting benzene solution was then subjected to TLC separation. The products were identified by comparing their NMR and IR spectra with those of authentic samples.

References

1) O. Hammerich and V. D. Parker, in "Advances in Physical Organic Chemistry," ed by V. Gold and D. Bethell, Academic Press, New York (1984), Vol. 20, p. 55; K. Yoshida, "Electrooxidation in Organic Chemistry. Role of Cation Radicals as Synthetic Intermediates," Wiley-Interscience, New York (1984), p. 194; F. D. Lewis, in "Photoinduced Electron Transfer Part C, Photoinduced Electron Transfer Reactions: Organic Substrates," ed by M. A. Fox and M. Chanon, Elsevier, Amsterdam (1988), p. 1.

2) R. A. Neunteufel and D. R. Arnold, *J. Am. Chem. Soc.*, **95**, 4080 (1973); Y. Shigemitsu and D. R. Arnold, *J. Chem. Soc., Chem. Commun.*, **1975**, 407; D. R. Arnold and A. J. Maroulis, *J. Am. Chem. Soc.*, **98**, 5931 (1976); A. J. Maroulis and D. R. Arnold, *ibid.*, **99**, 7355 (1977); M. Yasuda, C. Pac, and H. Sakurai, *Bull. Chem. Soc. Jpn.*, **53**, 502 (1980); S. L. Mattes and S. Farid, *J. Am. Chem. Soc.*, **104**, 1454 (1982); D. R. Arnold and Xi Du, *ibid.*, **111**, 7666 (1989).

3) T. Inoue, K. Koyama, T. Matsuoka, K. Matsuoka, and S. Tsutsumi, *Tetrahedron Lett.*, **1963**, 1409; T. Inoue, K. Koyama, T. Matsuoka, and S. Tsutsumi, *Bull. Chem. Soc. Jpn.*, **40**, 162 (1967).

4) E. Steckhan, *J. Am. Chem. Soc.*, **100**, 3526 (1978).

5) H. Schaefer and E. Steckhan, *Angew. Chem., Int. Ed. Engl.*, **8**, 518 (1969).

6) M. Kojima, H. Sakuragi, and K. Tokumaru, *Chem. Lett.*, **1981**, 1707.

7) S. Konuma, H. Misawa, H. Sakuragi, and K. Tokumaru, presented at the Annual Meeting of the Chemical Society of Japan, Kyoto, April 1989; S. Konuma, H. Misawa, R. Akaba, H. Sakuragi, and K. Tokumaru, to be published.

8) K. Mizuno, K. Yoshida, and Y. Otsuji, *J. Chem. Soc., Chem. Commun.*, **1984**, 1665.

9) R. Akaba, M. Tsuchiya, S. Aihara, H. Sakuragi, and K. Tokumaru, "Recent Advances in Electroorganic Synthesis," (Studies in Organic Chemistry 30), ed by S. Torii, Kodansha, Tokyo (1987), pp. 75—78; S. F. Nelsen and R. Akaba, *J. Am. Chem. Soc.*, **103**, 2096 (1981).

10) L. Bonazzola, J.-P. Michaut, J. Roncin, H. Misawa, H. Sakuragi, and K. Tokumaru, *Bull. Chem. Soc. Jpn.*, **63**, 347 (1990).

11) T. Miyashi, Y. Takahashi, T. Mukai, H. D. Roth, and M. L. M. Schilling, *J. Am. Chem. Soc.*, **107**, 1079 (1985).

12) W. Parry, *J. Chem. Soc.*, **107**, 108 (1915).

13) E. S. Gould, "Mechanism and Structure in Organic Chemistry," Henry Holt (1960), p. 608; C. K. Ingold, "Structure and Mechanism in Organic Chemistry," 2nd ed, Cornell University Press, New York (1969), p. 723.

14) A. Brodhag and C. R. Hauser, *J. Am. Chem. Soc.*, **77**, 3024 (1955).

15) H.-G. Heine, W. Hartman, D. R. Kory, J. L. Magyar, C. E. Hoyle, J. K. Mcvey, and F. D. Lewis, *J. Org. Chem.*, **39**, 691 (1974).

16) E. M. Schlutz, J. B. Bicking, S. Mickey, and F. S. Crossley, *J. Am. Chem. Soc.*, **75**, 1072 (1953).

Reinvestigation of the Phosphazo Method and Synthesis of *N*-(*t*-Butoxycarbonyl)-L-arginine *p*-Nitroanilide and a Chromogenic Enzyme Substrate for the Factor Xa

Hidekazu OYAMADA, Takashi SAITO, Shinsaku INABA, and Masaaki UEKI*
Department of Applied Chemistry, Faculty of Science, Science University of Tokyo, 1-3 Kagurazaka, Tokyo 162
(Received November 27, 1990)

Synopsis. Reaction conditions for the phosphazo method were reinvestigated in order to apply this method to the synthesis of *p*-nitroanilide(*p*NA)s of *t*-butoxycarbonyl(Boc)- and benzyloxycarbonyl(*Z*)-amino acids.

p-Nitroanilides of amino acids and peptides are among the most popular chromogenic enzyme substrates and their synthesis has been studied intensively. However, since *p*-nitroaniline is a very poor nucleophile, the usual peptide bond forming reactions including the dicyclohexylcarbodiimide-*N*-hydroxybenzotriazole method[1] and the mixed anhydride method[2] could not give sufficient results. As an alternative, the reaction of N^{α}-protected amino acids with *p*-nitrophenyl isocyanate, isolated[3] or obtained in situ by the modified Curtius reaction using diphenyl phosphorazidate,[4] has up until now been the method of choice. The phosphazo method,[5] which had fallen into disuse as a general method for peptide synthesis, was recently utilized for the synthesis of *p*-nitroanilides.[1] However, its applicability to Boc-amino acids had not been examined. In this study we reinvestigated and optimized the conditions for the formation and reaction of the phosphazo compound from *p*-nitroaniline in order to establish a synthetic method for Boc-amino acid *p*-nitroanilides including Boc-arginine *p*-nitroanilide.

Results and Discussion

Optimization of the conditions of the phosphazo method was achieved by focusing on the following points; 1) the reaction time necessary for the complete formation of the phosphazo derivative of *p*-nitroaniline, 2) the lowest necessary temperature for the reaction of the phosphazo compound with acyl components, and 3) molar ratios.

p-Nitroaniline (**1**) was mixed with phosphorus trichloride (**2**) in pyridine at room temperature for 1 h to afford the corresponding phosphazo compound, *N*,*N*′-bis(4-nitrophenyl)phospheneimidous amide (**3**). To this *Z*-L-Phe-OH (**4**) was added (molar ratio of **2**:**4**=1:1) and the mixture stirred for 30 min. Then the temperature was elevated stepwisely to 30, 40, 50, and finally to 60 °C maintaining each temperature for 30 min. At the end of each period the amount of *Z*-L-Phe-*p*NA (**5**) formed was quantitated by HPLC. The yield dramatically increased (24→84%) when the temperature was elevated from 30 °C to 40 °C. Therefore, it was concluded that the lowest necessary temperature for the reaction of **3** with the acyl component was 40 °C. This temperature is much lower than the boiling point of pyridine which had been previously used.[5]

In the above reaction the first step (the reaction of **1** with **2**) was carried out for 1 h. When this step was interrupted after 15 min, as described in the literature,[5] by the addition of **4** and warming the mixture to 40 °C, the reaction was not complete after 4 h. On the other hand, when the first step was continued for 1 h, subsequent reaction with **4** was complete after 1 h. Although this reaction time was not the minimal time required, it was used in the subsequent reactions.

The molar ratio of **2** to **4** appears to be another important factor. In the phosphazo method carboxyl components are usually used in excess, however yields of *p*-nitroanilides under these conditions are low. Better results were obtained when the phosphazo derivative of *p*-nitroaniline was used in excess. When 1.2 and 2.0 equivalents of the phosphazo compound (molar ratios of **2**:**4**=0.6:1 and 1:1, assuming the complete formation of the phosphazo compound) were used yields of the *p*-nitroanilide **5** after 1 h were 81% and quantitative, respectively. Since the former yield could not be significantly improved by increasing the reaction time, it was concluded that an equimolar amount of the phosphazo compound, which corresponds to 2 equivalents of the acyl component, should be used.

In summarizing the above results the optimal conditions for the synthesis of protected amino acid *p*-nitroanilides were decided as follows: 2 mol of *p*-nitroaniline are mixed with 1 mol of PCl_3 in pyridine for 1 h at room temperature. After the addition of 1 mol of a protected amino acid to the mixture the reaction is performed at 40 °C for 1 h or more depending on the structure of the amino acid used.

Under these conditions syntheses of various kinds of N^{α}-protected amino acid *p*-nitroanilides were performed and the results are summarized in Table 1. As the result of the lowering of the reaction temperature, preparation of Boc- and *p*-methoxybenzyloxycarbonyl-amino acid *p*-nitroanilides was possible (Entries 6, 7, 8, 9, and 10). It should also be noted that dicyclohexylamine (DCHA) salts of protected amino acids could be used quite as same as the free acids. Using this technique *p*-nitroanilide of Boc-L-glutamine was obtained, albeit in modest yield because of nitrile formation.[10]

N^{α}-Acylated arginine *p*-nitroanilides are well-known as substrate for trypsin,[11] papain,[12] tissue plasminogen activator, and plasmin.[13] In the synthesis of these compounds the guanidino function of arginine was protected by nitro[11,13] or arenesulfonyl groups.[12] However strong acid treatment in the total deprotection step often gives a complex mixture of

Table 1. Preparation of Protected Amino Acid *p*-Nitroanilides

Entry	Product (Method[a])	Reaction time/h	Yield %	Mp/°C (solvent)[b]	Elemental analysis	$[\alpha]_D$/degree (c 1, CH_3OH)	R_f[c] A	B	C	D
1	Z-L-Phe-*p*NA(A)	1.5	91	158—160(A)[d]		+48.4(25 °C)	0.23	0.91		
2	Z-L-Val-*p*NA(A)	3.0	73	188—191(A)	($C_{19}H_{21}N_3O_5$)C,H,N	−14.8(27 °C)[e]	0.17	0.85		
3	Z-L-Leu-*p*NA(A)	1.5	79	128—129(A)[f]	($C_{20}H_{23}N_3O_5$)C,H,N	−21.1(28 °C)	0.22	0.89		
4	Z-L-Ile-*p*NA(A)	4.0	49	163—164(B)	($C_{20}H_{23}N_3O_5$)C,H,N	−10.6(28 °C)	0.20	0.89		
5	Z-L-Arg-*p*NA·HCl(A)	4.0	94	176—179[g]	($C_{20}H_{25}N_6O_5Cl$)C,H,N	−12.0(28 °C)			0.39	0.52
6	Z(OMe)-L-Leu-*p*NA(B)	1.5	74	107—108(A)	($C_{21}H_{25}N_3O_6$)C,H,N	−11.9(29 °C)	0.19	0.90		
7	Boc-L-Leu-*p*NA(A)	1.5	89	123—125(C)[h]	($C_{17}H_{25}N_3O_5$)C,H,N	−28.5(29 °C)	0.26	0.91		
8	Boc-L-Leu-*p*NA(B)	1.5	87	121—123(C)[h]		−30.0(26 °C)	0.26	0.93		
9	Boc-L-Lys(Z)-*p*NA(A)	2.0	60	Amorphous[i]	($C_{25}H_{32}N_4O_7$)C,H,N	−7.6(30 °C)	0.10	0.83		
10	Boc-L-Gln-*p*NA(B)	2.0	43	166—168(decomp)(A)	($C_{16}H_{22}N_4O_6$)C,H,N	−14.0(28 °C)		0.34		0.84
11	Boc-L-Arg-*p*NA·HCl(A)	4.0	75	195—198(decomp)(D)[j]	($C_{17}H_{27}N_6O_5Cl$)C,H,N	−9.6(29 °C)[e]			0.31	0.51

a) See Experimental. b) A: ethyl acetate–petroleum ether; B: ethyl acetate–ether–petroleum ether; C: ether–petroleum ether; D: ethanol. c) A: chloroform; B: chloroform:methanol=9:1; C: chloroform:methanol:acetic acid=20:5:1. d) Lit,[6] mp 158.5—159.5 °C. e) (c 0.5, CH_3OH). f) Lit,[7] mp 148—151 °C. g) Lit,[8] mp 181—182 °C, $[\alpha]_D^{20}$ −16.0° (c 1, EtOH). h) Lit,[4] mp 91—96 °C, $[\alpha]_D^{20}$ −30.4° (c 1, CH_3OH); Lit,[2] mp 80—81 °C, $[\alpha]_D^{20}$ −27.5° (c 1, CH_3OH). i) Lit,[4] mp 113—114 °C, $[\alpha]_D^{20}$ −8.3° (c 1, CH_3OH). j) Lit,[9] mp 190—192 °C.

products. The most important feature of the modified phosphazo method is the facile availability of Boc-L-Arg-*p*NA, which was obtained as a crystalline hydrochloride (**6**) in 75% yield starting from Boc-L-Arg-OH·HCl·H_2O. To the best of our knowledge, synthesis of Boc-L-Arg-*p*NA by direct coupling of Boc-arginine and *p*-nitroaniline with phosphorus trichloride in pyridine has been recorded only in a patent.[9]

Compound **6** thus obtained was then utilized for the preparation of a peptide *p*-nitroanilide, Bz-L-Ile-L-Glu(OMe)-Gly-L-Arg-*p*NA (**7**), which is known as a substrate for the factor Xa.[14] Protected *N*-terminal tripeptide ester, Boc-L-Ile-L-Glu(OMe)-Gly-OPac, was obtained by stepwise elongation by the mixed anhydride method using dimethylphosphinothioyl chloride.[15] After the Boc group was changed to benzoyl group, the C-terminal phenacyl ester was removed to give protected tripeptide acid, Bz-L-Ile-L-Glu(OMe)-Gly-OH (**8**). Segment condensation of **8** with arginine *p*-nitroanilide dihydrochloride (**9**), which was obtained by deprotection of **6** with HCl in acetic acid, was performed using dimethylphosphinothioyl azide[16] in *N,N*-dimethylformamide. Since the final deprotection step was not necessary in this synthesis, the pure product was readily obtained.

Experimental

Thin-layer chromatography was carried out on silica-gel plates (Merck, Kieselgel 60 F_{254}) in the following solvent systems; A: $CHCl_3$, B: $CHCl_3$:CH_3OH=9:1, C: $CHCl_3$:CH_3OH=4:1, D: $CHCl_3$:CH_3OH:CH_3CO_2H=20:5:1. For amino acid analysis peptides were hydrolyzed with constant boiling hydrochloric acid in evacuated and sealed ampoules for 24 h at 110 °C. The analyses were performed on an Atto Model 203 Amino Acid Analyzer. Optical rotations were determined using a JASCO DIP-360 digital polarimeter. ^1H NMR spectra were observed with a Hitachi R-1100 and JEOL JNM-PMX-60 spectrometers (60 MHz). Analytical reversed-phase HPLC was performed using a Unisil Q C_{18} column (4.6×300 mm) with an isocratic solvent system (0.01 M HCl:CH_3OH=35:65, flow rate 1.0 ml min^{-1}) at 60 °C using Shimadzu LC 6A liquid chromatograph system monitored at 254 nm (1 M= 1 mol dm^{-3}).

General Procedure for the Preparation of Protected Amino Acid *p*-Nitroanilides: To a solution of phosphorus trichloride (0.872 ml, 10 mmol) in pyridine (10 ml) was added *p*-nitroaniline (1.38 g, 20 mmol) at 25 °C, and the mixture stirred for 1 h. To this solution was added a protected amino acid (Method A) or a protected amino acid DCHA salt (Method B) (10 mmol) in pyridine (20 ml) and the mixture stirred at 40 °C for the period given in Table 1. After removal of the solvent under reduced pressure the residue was triturated with ethyl acetate and water and filtered. The organic layer was separated and washed successively with a 5% citric acid solution (3 times), water, a 5% sodium hydrogencarbonate solution (3 times), water and saline, and dried over sodium sulfate. After removal of the solvent, the crystalline residue was rinsed with cold benzene or chloroform and then with ether before recrystallization. When necessary silica-gel column chromatography using dichloromethane for elution was performed prior to recrystallization.

***N*-(*t*-Butoxycarbonyl)-L-arginine *p*-Nitroanilide Hydrochloride (6):** To a solution of the phosphazo compound prepared from PCl_3 (0.436 ml, 5 mmol) and *p*-nitroaniline (1.381 g, 10

mmol) was added Boc-L-Arg-OH·HCl·H_2O (1.644 g, 5 mmol) in pyridine (5 ml). The mixture was stirred at 40 °C for 4 h and the solvent removed under reduced pressure. The residue was dissolved in water (50 ml) and ether (20 ml) and kept at 0 °C overnight. Precipitates were collected by filtration, washed successively with ether, dichloromethane and a small quantity of ethanol and recrystallized from ethanol-ether to give **6** as a colorless granular solid; 1.616 g (75%); ^{1}H NMR ($CDCl_3$+DMSO-d_6) δ=1.4 (s, 9H), 1.5—1.9 (m, 6H), 3.1—3.4 (m, 2H), 4.25 (br, 1H), 6.7—7.3 (m, 4H), 7.6—8.2 (m, 5H), 10.9 (s, 1H).

***N*-(*t*-Butoxycarbonyl)-L-glutamine *p*-Nitroanilide and *N*-(*t*-Butoxycarbonyl)-(2-cyanoethyl)glycine *p*-Nitroanilide:** Boc-L-Gln-OH·DCHA (4.276 g, 10 mmol) was treated with the phosphazo compound as described above. After the usual washing procedures, the products were separated by silica-gel column chromatography using dichloromethane-methanol (50 : 1 v/v) as eluent to give 1.578 g (43%) of Boc-L-Gln-*p*NA as colorless crystals; ^{1}H NMR ($CDCl_3$+DMSO-d_6) δ=1.4 (s, 9H), 1.8—2.6 (m, 4H), 4.1—4.4 (br, 1H), 6.0—6.4 (br, 2H), 6.8—7.0 (br, 2H), 7.7 (d, 2H), 8.1 (d, 2H), 10.5 (br, 1H). Further elution gave 0.802 g (23%) of Boc-(2-cyanoethyl)glycine-*p*-nitroanilide as a fluffy solid; mp 148—149 °C; $[\alpha]_D^{27}$ −21.1° (*c* 1.1, CH_3OH); IR (KBr) 2260 cm^{-1} (C≡N); ^{1}H NMR ($CDCl_3$) δ=1.4 (s, 9H), 1.9—2.7 (m, 4H), 4.3—4.7 (br, 1H), 5.5—6.9 (br, 1H), 7.6 (d, 2H), 8.0 (d, 2H), 9.2—9.5 (br, 1H).

L-Arginine *p*-Nitroanilide Dihydrochloride (9): To a solution of **6** (1.077 g, 2.5 mmol) in acetic acid (2 ml) was added 2.17 M HCl in acetic acid (23 ml) at RT. The mixture was kept standing for 2 h and diluted with ether. Precipitates were collected by filtration, washed with ether and dried to give **9** as a pale yellow powder: 883 mg (96%); mp 262—264 °C (decomp); $[\alpha]_D^{26}$ +73.2° (*c* 1, 0.1 M HCl). Lit,[8] mp 245 °C; $[\alpha]_D^{20}$ +80.6° (*c* 1, water). Found: C, 39.44; H, 5.55; N, 22.65%. Calcd for $C_{12}H_{18}N_6O_3$·2HCl: C, 39.25; H, 5.49; N, 22.88%.

***N*-Benzoyl-L-isoleucyl-L-α-glutamylglycyl-*N*-(4-nitrophenyl)-L-argininamide Methyl Ester [Bz-L-Ile-L-Glu(OMe)-Gly-L-Arg-*p*NA] (7):** To an ice-cooled solution of Bz-L-Ile-L-Glu(OMe)-Gly-OH (0.218 g, 0.5 mmol), **9** (0.184 g, 0.5 mmol) and triethylamine (70 μl, 0.5 mmol) in *N*,*N*-dimethylformamide (1 ml) was added dimethylphosphinothioyl azide (0.081 g, 0.6 mmol) in *N*,*N*-dimethylformamide (0.5 ml) and triethylamine (70 μl, 0.5 mmol). The mixture was stirred for 24 h at 0 °C and concentrated. The residue was solidified by trituration with ether and cold 1 M hydrochloric acid and purified by preparative thin-layer chromatography ($CHCl_3$: CH_3OH : CH_3CO_2H=20 : 5 : 1) and gel chromatography on Sephadex LH-20 (CH_3OH) to give 224 mg (58%) of **7** as an amorphous solid: $[\alpha]_D^{26}$ −31.3° (*c* 0.5, CH_3OH); R_{f_4}=0.51. Amino Acid Ratios: Ile, 0.96; Glu, 1.01; Gly, 1.00; Arg, 1.04. Found: C, 51.76; H, 6.26; 16.65%. Calcd for $C_{33}H_{45}O_9N_9$·HCl·H_2O: C, 51.73; H, 6.31; N, 16.45%.

References

Abbreviations according to IUPAC-IUB Commision, *Eur. J. Biochem.*, **138**, 9 (1984), are used throughout. Additional abbreviations in addition to those shown in the text: Ac, acetyl; Bz, benzoyl; OPac, phenacyl ester; *p*NA, *p*-nitroanilide; TEA, triethylamine; Z(OMe), *p*-methoxybenzyloxycarbonyl.

1) Y. Okada, Y. Tsuda, A. Hirata, Y. Nagamatsu, and U. Okamoto, *Chem. Pharm. Bull.*, **30**, 4060 (1982).

2) K. Noda, M. Oda, M. Sato, and N. Yoshida, *Int. J. Peptide Protein Res.*, **36**, 197 (1990).

3) N. Nishi, S. Tokura, and J. Noguchi, *Bull. Chem. Soc. Jpn.*, **43**, 2900 (1970).

4) T. Shioiri, M. Murata, and Y. Hamada, *Chem. Pharm. Bull.*, **35**, 2698 (1987).

5) S. Goldschmidt and G. Rosculet, *Chem. Ber.*, **93**, 2387 (1960).

6) E. V. Ramenskii, M. M. Botvinik, and R. U. Beisembaeva, *Khim. Prir. Soedin.*, **4**, 23 (1968); *Chem. Abstr.*, **69**, 87424n (1968).

7) H. Tuppy, U. Wiesbauer, and E. Wintersberger, *Hoppe-Seyler's Z. Physiol. Chem.*, **329**, 278 (1962).

8) O. Somorin, N. Nishi, and J. Noguchi, *Bull. Chem. Soc. Jpn.*, **51**, 1255 (1978).

9) S. Bajusz, A. Juhase, E. Barabas, D. Bagdi, and L. Mohai, *Hung. Teljes* HU 40615; *Chem. Abstr.*, **108**, 112956w (1988).

10) D. T. Gish, P. G. Katsoyannis, G. P. Hess, and R. T. Stedman, *J. Am. Chem. Soc.*, **78**, 5954 (1956); C. Ressler, *ibid.*, **78**, 5956 (1956).

11) S. Tokura, N. Nishi, and J. Noguchi, *J. Biochem.*, **69**, 599 (1971).

12) H. Nakata and S. Ishii, *Biochem. Biophys. Res. Commun.*, **41**, 393(1970).

13) S. K. Sharma and F. J. Castellino, *Thromb. Res.*, **57**, 127 (1990).

14) L. Aurell, R. Simonsson, S. Arielly, G. Karlsson, P. Friberger, and G. Claeson, *Haemostasis*, **7**, 92 (1978).

15) M. Ueki and T. Inazu, *Chem. Lett.*, **1962**, 45.

16) M. Ueki, K. Okazaki, and S. Ikeda, "Peptide Chemistry 1984: Proc. of the 22nd Symposium on Peptide Chemistry," ed by N. Izumiya, Protein Research Foundation, Osaka (1984), p. 67.

New Chiral Auxiliary; 4,5-Diphenyl-1-methyl-2-imidazolidinone. Its Utility in Highly Enantioselective Aldol Reaction

Wongsiri SANKHAVASI,† Makoto YAMAMOTO, Shigeo KOHMOTO, and Kazutoshi YAMADA*
Department of Materials Science, Faculty of Engineering, Chiba University,
1-33 Yayoi-cho, Chiba 260
†Graduate School of Science and Technology, Chiba University,
1-33 Yayoi-cho, Chiba 260
(Received November 29, 1990)

Synopsis. The aldol reaction of the boron enolate bearing the titled chiral auxiliary proceeded with high face selectivity.

In the last few years, we have investigated the utility of acyclic urea (**1**) in enantioselective Diels-Alder[1] and aldol reactions.[2] Though the stereoselectivity observed in these reactions was moderate, the urea auxiliary possessed excellent separability[1-3] so that we could obtain both of enantiomerically pure forms of the products. In order to gain absolute asymmetric induction in a modified system, we have designed the new recyclable chiral auxiliary, 4,5-diphenyl-1-methyl-2-imidazolidinone (**2**).[4] Owing to the rigidity and the planarity of five-membered ring of **2**, complete *syn* selectivity ($\geqslant$99% de) was resulted in this aldol addition reaction.

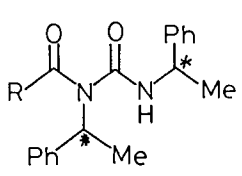

1

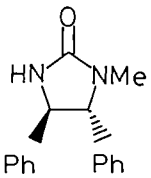

(+)-**2**

N-propionyl derivative (+)-(**7**) was prepared from (+)-(1*R*,2*R*)-1,2-diphenyl-1,2-ethanediamine (**3**) in three steps. Initially, **3** and urea (**4**) were heated with few drops of H_2O at 200 °C for 2 h to give 2-imidazolidinone (**5**) in 87% yield.[5] Monoacylated product (**6**) was obtained by treatment of **5** with 2 equiv of *n*-BuLi (−10 °C, THF) followed by stirring with 1 equiv of propionyl chloride at ambient temperature (84%).[4] The last step was carried out by deprotonation of **6** (*n*-BuLi, 1 equiv, −10 °C, THF) and methylation with excess of methyl iodide (r.t., 79%).

Our first attempt to investigate the utility and the limitations of this chiral auxiliary was made on an aldol reaction. Enolization of **7** with *n*-Bu_2BOTf (1.1 equiv)[6] and *N*,*N*-diisopropylethylamine (*i*-Pr_2NEt, 1.2 equiv) at 0 °C for 30 min, and subsequent addition of aldehydes (1—3 equiv, −73 °C then slowly warmed to room temperature) afforded only optically active syn aldol adduct (**8**). The results are summarized in Table 1. Good yields were obtained with benzaldehyde and 2-naphthaldehyde (Entries 1 and 3). In the case of benzaldehyde, triethylamine also worked well

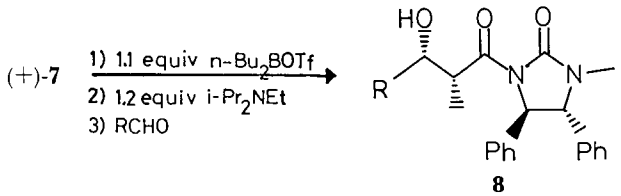

Scheme 2.

Table 1. Aldol Reaction of **7** with Aldehydes

Entry	RCHO	Yield[a]/%	de of **8**[b]/%
1	PhCHO (**8a**)	66	$\geqslant$99
2	PhCHO[c] (**8a**)	72	$\geqslant$99
3	2-NaphCHO (**8b**)	69	$\geqslant$99
4	MeCHO (**8c**)	48	$\geqslant$99
5	EtCHO (**8d**)	38	$\geqslant$99
6	CH_2=CHCHO (**8e**)	23	$\geqslant$99

a) Isolated yield after chromatography. b) Determined by 500 MHz ^{1}H NMR spectroscopy. c) The amine used was Et_3N.

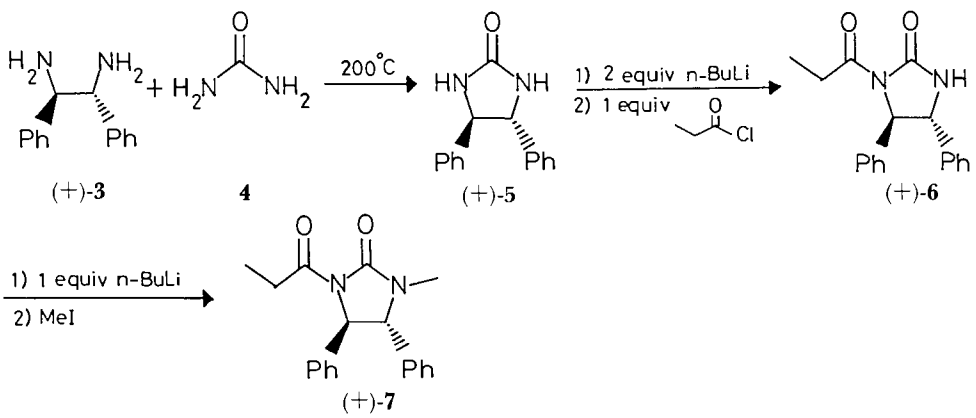

Scheme 1.

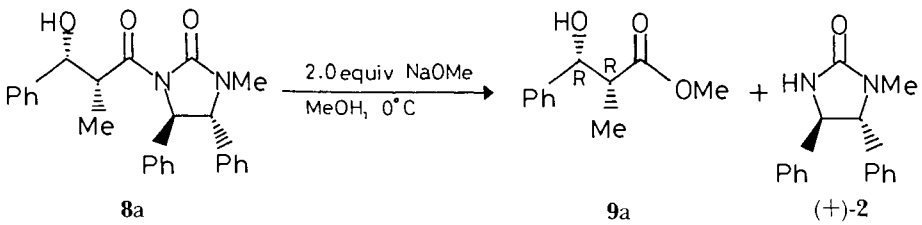

8a 9a (+)-2

Scheme 3.

as a base (Entries 1 and 2). The lower yields with acetaldehyde and propionaldehyde (Entries 4 and 5) may be due to the presence of their active α hydrogens. Because of the long reaction time, acrylaldehyde might polimerize before to react with boron enolate, which resulted in only 23% yield of the aldol adduct (Entry 6). This chiral 2-imidazolidinone boron enolate did not react with hindered 2,2-dimethylpropionaldehyde.

An aldol reaction of **6** was also examined under similar conditions (2.2 equiv n-Bu_2BOTf, 2.3 equiv i-Pr_2NEt) but merely the recovery of the starting material was observed.

The absolute stereochemical assignment of aldol (**8a**) was firmly established by comparison of the optical rotation of methyl ester (**9a**) with the literature value (Scheme 2)[7,8] after methanolysis of it with sodium methoxide (2 equiv, 0 °C then r.t., 17 h, MeOH). In a similar manner all aldol adducts were attested to have syn stereochemistry.

From the results above we propose that the boron enolate formed should have Z-geometry as in the oxazolidinone system and the observed stereoselectivity can be rationalized by the transition state model proposed by Evans.[8]

These results demonstrate that chiral 2-imidazolidinone has the comparable efficacy in asymmetric induction as a 2-oxazolidinone,[8] oxazolidine,[9] 2-oxazolidinethione,[10] or prolinol.[9]

Experimental

Melting points were determined on a Yanaco MP-S3 apparatus and are uncorrected. Infrared spectrum were run on a JASCO A-202 infrared spectrophotometer. ^{1}H NMR spectra were recorded on a Hitachi R-600, JOEL JNM-GX270, JNM-FX270, GSX-400, and GSX-500 spectrometers. ^{13}C NMR spectra were recorded on a JEOL JNM-GX270 and JNM-FX270 spectrometers. Chemical shifts are reported in ppm downfield from trimethylsilane and splitting patterns are designated as s, singlet; d, doublet; t, triplet; q, quartet; m, multiplet; br, broad. Mass spectra were taken with a Hitachi RMU-7M mass spectrometer at 70 eV. Optical rotations were recorded at 21 °C on a JASCO DIP-140 Digital Polarimeter. Tetrahydrofuran (THF) was distilled from lithium aluminium hydride and stored over molecular sieves 5A 1/16. Dichloromethane was distilled from calcium hydride and stored over molecular sieves 5A 1/16. Diisopropylethylamine and triethylamine were used after simple distillation. The purity of all the aldol adducts were shown to be diastereomerically pure by HPLC and ^{1}H NMR spectroscopy.

Preparation of (4*R*,5*R*)-4,5-Diphenyl-2-imidazolidinone (5). (1*R*,2*R*)-1,2-Diphenyl-1,2-ethanediamine **3** (0.606 g, 2.86 mmol), urea **4** (0.172 g, 2.86 mmol), and H_2O (5 drops) were reflux at 200 °C for 2 h. Flash chromatography (ethyl acetate) of the residue gave 0.590 g (87%) of **5**; mp 196.0—197.5 °C; $[\alpha]_D^{21}$ +58.6° (*c* 1.06, $CHCl_3$); IR ($CHCl_3$) 3460, 3250 (broad), 3010, 1710, and 700 cm^{-1}; ^{1}H NMR (60 MHz, $CDCl_3$) δ=4.55 (s, 2H), 5.85 (br s, 2H) 7.33 (s, 10H); ^{13}C NMR (67.8 MHz, $CDCl_3$) δ=66.0, 126.5, 128.3, 128.8, 140.2, 163.0; HRMS Found: *m/z* 238.1098. Calcd for $C_{15}H_{14}N_2O$: 238.1107. Found: C, 75.33; H, 5.93; N, 11.75%. Calcd for $C_{15}H_{14}N_2O$: C, 75.60; H, 5.92; N, 11.76%.

Preparation of (4*R*,5*R*)-4,5-Diphenyl-1-propionyl-2-imidazolidinone (6). To a solution of **5** (0.856 g, 3.60 mmol) in 20 ml of THF, butyllithium (1.55 M in hexane (1 M=1 mol dm^{-3}), 4.60 ml, 7.13 mmol) was added drpowise at −10 °C and stirred for 30 min before propionyl chloride (0.330 g, 3.57 mmol) was added. The reaction temperature was gradually raised to room temperature and stirring was continued overnight. After quenching the reaction mixture with saturated aqueous ammonium chloride, the solution was diluted with dichloromethane and the organic layer was separated. The aqueous layer was extracted with dichloromethane (20 ml×2) and the combined organic layer was dried ($MgSO_4$) and evaporated. Flash chromatography (ethyl acetate-hexane) gave white solid **6** (0.885 g, 84%); mp 120.0—121.0 °C; $[\alpha]_D^{22}$ +98.6° (*c* 0.29, $CHCl_3$); IR ($CHCl_3$) 3475, 3280, 3230, 1740, 1695, 1455, 1374, 1340, 1280, and 700 cm^{-1}; ^{1}H NMR (60 MHz, $CDCl_3$) δ=1.02 (t, *J*=7.6 Hz, 3H), 2.91 (q, *J*=7.6 Hz, 2H), 4.48 (d, *J*=3.4 Hz, 1H), 5.10 (d, *J*=3.4 Hz, 1H), 6.65 (br s, 1H), 7.31 (s, 10H); ^{13}C NMR ($CDCl_3$) δ=8.4, 29.4, 61.0, 66.1, 125.5, 125.6, 128.2, 128.7, 129.1, 129.3, 140.8, 140.9, 156.4, 174.0; HRMS Found: *m/z* 294.1371. Calcd for $C_{18}H_{18}N_2O_3$: 294.1369. Found C, 73.32; H, 6.17; N, 9.55%. Calcd for $C_{18}H_{18}N_2O_3$: C, 73.45; H, 6.16; N, 9.52%.

Preparation of (4*R*,5*R*)-4,5-Diphenyl-1-methyl-3-propionyl-2-imidazolidinone (7). Butyllithium (1.58 M in hexane, 0.75 ml, 1.18 mmol) was added to a solution of **6** (0.317 g, 1.08 mmol) in THF (10 ml) at −10 °C. The mixture was stirred for 30 min and methyl iodide (0.296 g, 2.09 mmol) was added. The temperature was raised to ambient temperature and stirred overnight. Work up with saturated aqueous ammonium chloride and extraction with dichloromethane (10 ml×2) before flash chromatography (ethyl acetate-hexane) afforded **7** (0.262 g, 79%); mp 67.5—69.5 °C; $[\alpha]_D^{21}$ +119.6° (*c* 0.76, $CHCl_3$); IR ($CHCl_3$) 3040, 1733, 1670, 1430, 1390, 1195, 1150, and 700 cm^{-1}; ^{1}H NMR (500 MHz, $CDCl_3$) δ=1.13 (t, *J*=7.3 Hz, 3H), 2.79 (s, 3H), 3.06 (q, *J*=7.3 Hz, 2H), 4.26 (d, *J*=3.6 Hz, 1H), 5.05 (d, *J*=3.6 Hz, 1H), 7.16—7.43 (m, 10H); ^{13}C NMR (67.8 MHz, $CDCl_3$) δ=8.6, 29.1, 29.4, 63.5, 67.4, 125.4, 126.2, 128.1, 129.0, 129.1, 129.4, 138.6, 141.0, 155.0, 174.0; MS *m/z* (rel intensity, %) 308 (M^+, 83), 251 (79), 175 (23), 132 (100), 120 (49), 118 (38), 91 (20), 77 (20), 57 (20), 29 (20). Found; C, 73.86; H, 6.56; N, 9.05%. Calcd for $C_{19}H_{20}N_2O_3$: C, 74.00; H, 6.54; N, 9.09%.

General Procedure for the Aldol Addition of 7. To a solution of **7** (0.2 mmol) in dichloromethane (0.2—0.5 M) at 0 °C were added dibutylboron triflate (1 M in dichloromethane, 1.1 equiv) and diisopropylethylamine (1.2 equiv).

The mixture was stirred at 0 °C for 30 min and cooled to −73 °C, and the solution of the corresponding aldehyde in dichloromethane (1—2 equiv) was added. After stirring at −73 °C for 2 h, the mixture was slowly warmed to ambient temperature and stirred overnight. The mixture was quenched with phosphate buffer (pH 7) and diluted with ether. The layers were separated, the aqueous layer was extracted with ether (4 ml×2), and the solvent was removed on a rotary evaporator. The residue was dissolved in 3 ml of methanol and cooled to 0 °C, and 1 ml of 30% H_2O_2 was added dropwise. After 60 min at 0 °C, 3 ml of water was added and the methanol was removed in vacuo. The aqueous layer was extracted with ether (3 ml×3) and the combined organic layer was washed with saturated aqueous sodium hydrogencarbonate (3 ml), and brine (3 ml), and dried ($MgSO_4$). After evaporation of the solvent, the crude product was purified by flash chromatography (ethyl acetate-hexane) to give the corresponding aldol adducts.

(4*R*,5*R*)-3-[(2*R*,3*R*)-3-Hydroxy-2-methyl-1-oxo-3-phenylpropyl]-4,5-diphenyl-1-methyl-2-imidazolidinone (8a). Yield 66%. Colorless glass; $[\alpha]_D^{22}$ +45.4° (*c* 0.32, $CHCl_3$); IR ($CHCl_3$) 3510, 3070, 3010, 2945, 1720, 1665, 1450, 1430, 1380, 1360, and 700 cm^{-1}; ^1H NMR (500 MHz, $CDCl_3$) δ=1.15 (d, *J*=7.2 Hz, 3H), 2.77 (s, 3H), 3.42 (d, *J*=2.2 Hz, 1H, OH), 4.23 (d, *J*=3.8 Hz, 1H), 4.42 (dq, *J*=3.6, 7.2 Hz, 1H), 5.0 (d, *J*=3.6 Hz, 1H), 5.1 (m, 1H), 7.08—7.44 (m, 15H); ^{13}C NMR (125 MHz, $CDCl_3$) δ=11.0, 29.1, 44.4, 63.4, 67.2, 73.3, 124.9, 126.2, 127.1, 128.1, 128.3, 129.0, 138.2, 140.4, 141.6, 154.3, 177.2. HRMS Found: *m/z* 414.1954. Calcd for $C_{26}H_{26}N_2O_3$: 414.1945.

(4*R*,5*R*)-3-[(2*R*,3*R*)-3-Hydroxy-2-methyl-3-(2-naphthyl)-1-oxopropyl]-4,5-diphenyl-1-methyl-2-imidazolidinone (8b). Yield 69%. White solid; mp 171.0—172.5 °C, $[\alpha]_D^{22}$ +22.9° (*c* 0.19, $CHCl_3$); IR ($CHCl_3$) 3510, 3025, 1725, 1665, 1382, 1360, and 700 cm^{-1}; ^1H NMR (500 MHz, $CDCl_3$) δ=1.19 (d, *J*=7.0 Hz, 3H), 2.75 (s, 3H), 3.57 (br s, 1H, OH), 4.20 (d, *J*=3.8 Hz, 1H), 4.57 (dq, *J*=3.7, 7.0 Hz, 1H), 5.04 (d, *J*=3.8 Hz, 1H), 5.29 (d, *J*=3.7 Hz, 1H), 7.00—7.91 (m, 17H); ^{13}C NMR (125 MHz, $CDCl_3$) δ=11.3, 29.1, 44.2, 63.4, 67.1, 73.5, 124.4, 124.9, 125.0, 125.6, 125.9, 126.1, 127.6, 127.8, 128.1, 128.2, 128.9, 129.2, 129.4, 132.8, 133.2, 138.1, 139.1, 140.3, 154.3, 177.0. HRMS Found: *m/z* 464.2089. Calcd for $C_{30}H_{28}N_2O_3$: 464.2101. Found: C, 77.39; H, 6.15; N, 5.99%. Calcd for $C_{30}H_{28}N_2O_3$: C, 77.56; H, 6.08; N, 6.03%.

(4*R*,5*R*)-3-[(2*R*,3*S*)-3-Hydroxy-2-methyl-1-oxobutyl]-4,5-diphenyl-1-methyl-2-imidazolidinone (8c). Yield 48%. Colorless oil; IR ($CHCl_3$) 3525, 3010, 2950, 2900, 1728, 1665, 1445, 1430, 1390, 1280, 1240, 930, 700 cm^{-1}; ^1H NMR (500 MHz, $CDCl_3$) δ=1.19 (d, *J*=6.6 Hz, 3H), 1.23 (d, *J*=7.1 Hz, 3H), 2.79 (s, 3H), 3.28 (br s, 1H), 4.03 (dq, *J*=2.6, 7.1 Hz, 1H), 4.16 (dq, *J*=2.6, 6.6 Hz, 1H), 4.26 (d, *J*=3.8 Hz, 1H), 5.08 (d, *J*=3.8 Hz, 1H), 7.18—7.44 (m, 10H); ^{13}C NMR (68 MHz, $CDCl_3$) δ=10.7, 19.3, 29.1, 43.1, 63.5, 67.2, 67.6, 124.9, 126.2, 128.2, 129.0, 129.2, 129.4, 138.2, 140.4, 154.6, 177.4. HRMS Found: *m/z* 352.1789. Calcd for $C_{21}H_{24}N_2O_3$: 352.1788.

(4*R*,5*R*)-3-[(2*R*,3*S*)-3-Hydroxy-2-methyl-1-oxopentyl]-4,5-diphenyl-1-methyl-2-imidazolidinone (8d). White solid; IR ($CHCl_3$) 3510, 3020, 2975, 1730, 1663, 1454, 1428, 1389, and 699 cm^{-1}; ^1H NMR (500 MHz, $CDCl_3$) δ=0.99 (t, *J*=7.4 Hz, 3H), 1.22 (d, *J*=7.2 Hz, 3H), 1.45 (m, 1H), 1.58 (m, 1H), 2.79 (s, 3H), 3.23 (br s, 1H, OH), 3.86 (m, 1H), 4.09 (dq, *J*=2.2, 7.2 Hz, 1H), 4.25 (d, *J*=3.8 Hz, 1H), 5.08 (d, *J*=3.8 Hz, 1H), 7.18—7.45 (m, 10H); ^{13}C NMR (68 MHz, $CDCl_3$) δ=10.5, 10.6, 26.5, 29.2, 41.6, 63.5, 67.2, 72.9, 76.5, 124.9, 125.0, 126.0, 126.2, 128.2, 129.1, 129.2, 129.5, 129.6, 138.2, 140.5, 154.5, 177.9. HRMS Found: *m/z* 366.1933. Calcd for $C_{22}H_{26}N_2O_3$: 366.1945.

(4*R*,5*R*)-3-[(2*R*,3*S*)-3-Hydroxy-2-methyl-1-oxo-4-butenyl]-4,5-diphenyl-1-methyl-2-imidazolidinone (8e). Colorless oil. IR ($CHCl_3$) 3500, 3010, 1725, 1660, 1450, 1425, 1390, 923, 698 cm^{-1}; ^1H NMR (500 MHz, $CDCl_3$) δ=1.21 (d, *J*=7.0 Hz, 3H), 2.79 (s, 3H), 3.20, (br s, 1H), 4.17 (dq, *J*=3.1, 7.0 Hz, 1H), 4.26 (d, *J*=3.8 Hz, 1H), 4.52 (br m, 1H), 5.09 (d, *J*=3.8 Hz, 1H), 5.20 (ddd, *J*=1.6, 1.6, 10.4 Hz, 1H), 5.36 (ddd, *J*=1.6, 1.6, 17.0 Hz, 1H), 5.85 (ddd, *J*=5.2, 10.4, 17.0 Hz, 1H), 7.17—7.45 (m, *J*=10 Hz). HRMS Found: *m/z* 364.1779. Calcd for $C_{22}H_{24}N_2O_3$: 366.1788.

References

1) K. Kishikawa, M. Yamamoto, S. Kohmoto, and K. Yamada, *Chem Lett.*, **1988**, 1623; *idem., J. Org. Chem.*, **54**, 2428 (1989).

2) K. Kishikawa, M. Yamamoto, S. Kohmoto, and K. Yamada, *Chem. Lett.*, **1989**, 787.

3) K. Kishikawa, K. Horie, M. Yamamoto, S. Kohmoto, and K. Yamada, *Chem. Lett.*, **1990**, 1009.

4) An only enantioselective reaction using a chiral 2-imidazolidinone was performed in alkylation reaction. G. Cardillo, A. D'Amico, M. Orena, and S. Sandri, *J. Org. Chem.*, **53**, 2354 (1988).

5) A. L. Wilson, U. S. Patent., 2517750 (1950).

6) The addition reaction of lithium and magnesium enolate with benzaldehyde was performed but the remarkable selectivity was not observed. Nevertheless, all of the diastereomers could be purified by high-performance liquid chromatography.

7) The Moshers' ester of **9a** also supported that the aldol adduct produced was enantiomerically homogeneous.

8) D. A. Evans, J. Bartroli, and T. L. Shih, *J. Am. Chem. Soc.*, **103**, 2127 (1981) ; D. A. Evans, J. V. Nelson, and T. R. Taber, *Top. Stereochem.*, **13**, 1 (1982).

9) D. A. Evans and L. R. McGee, *J. Am. Chem. Soc.*, **103**, 2876 (1981).

10) Y. Nagao, S. Yamada, T. Kumagai, M. Ochiai, and E. Fujita, *J. Chem. Soc., Chem. Commun.*, **1985**, 1418.

Preparative Derivatization of *endo*-Dicyclopentadiene via Metallation

Takashi KUMAGAI,† Michihiro AGA, Keiji OKADA, and Masaji ODA*
Department of Chemistry, Faculty of Science, Osaka University, Toyonaka, Osaka 560
†School of Chemistry, Faculty of Education, Ehime University, Matsuyama, Ehime 790
(Received December 5, 1990)

Synopsis. *endo*-Dicyclopentadiene has been selectively metallated with the base complex BuLi·*t*-BuOK in hexane at the olefinic positions in the norbornene moiety and a number of derivatives prepared by reaction of the metallated intermediate with electrophilic reagents. In particular, bromodicyclopentadiene thus obtained is a useful stock precursor for lithiodicyclopentadiene.

endo-Dicyclopentadiene (*endo*-tricyclo [5.2.1.$0^{2,6}$] deca-3,8-diene) (**1**) is an important compound as a direct precursor of synthetically useful cyclopentadiene. In view of ready thermal cycloreversion of dicyclopentadiene to cyclopentadiene, dicyclopentadienes can be regarded as stabilized as well as protected forms of usually labile cyclopentadienes. However, only a small number of substituted dicyclopentadienes have been obtained mostly by thermal dimerization of the corresponding monomers, and no practical way for derivatization of **1** itself has been described.[1] Here we report a metallation and functionalization of **1**.

Norbornene and norbornadiene have been metallated at the olefinic position with the base complex BuLi·*t*-BuOK.[2] There are essentially three possible sites for metallation with a strong base in the molecule of dicyclopentadiene (**1**) from the viewpoint of acidity of C-H bond; namely, the olefinic position of the norbornene part, the olefinc and allylic positions of the cyclopentene part. In fact, **1** was found to be metallated with the base complex selectively at the olefinic positions of the norbornene part (C-8 or -9). The metallated intermediate was assigned to be the potassium compound **2** in analogy with the metallation of norbornene.[2,3] Reactions of **2** with electrophilic reagents gave about 1 : 2.5 mixture of 8- and 9-substituted dicyclopentadienes, **3** and **4**, in moderate yields (Table 1, Method A). Hexane as solvent gave

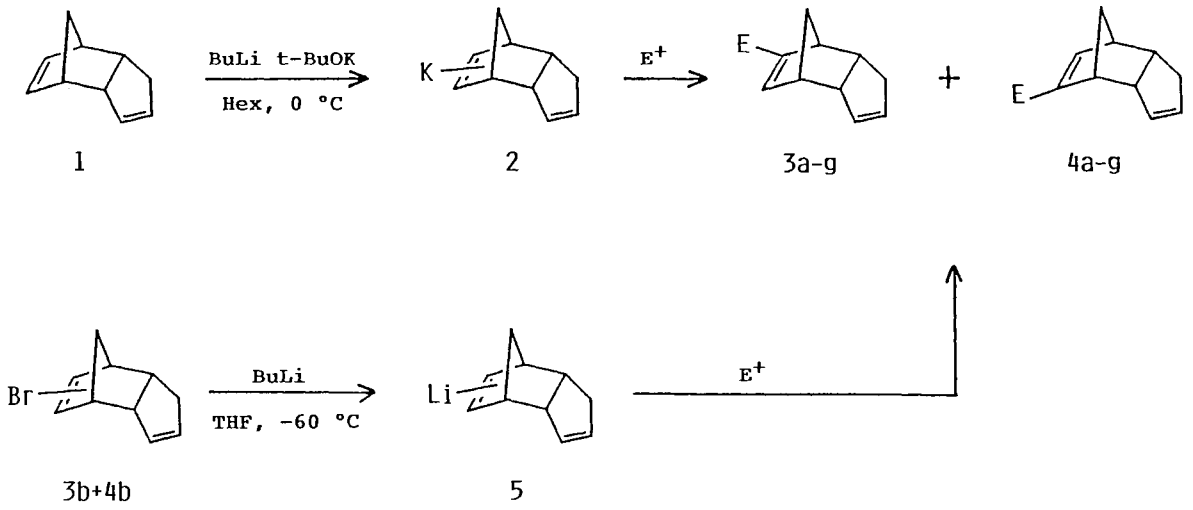

Scheme 1.

Table 1. Yields and Some NMR Data of Derivatives of Dicyclopentadiene

Entry	Electrophile	Product[a] (3+4)	Yield/%		^{1}H NMR[b]	
			Method A	Method B	δ(HC=)	δ(HC=CH)
a	$HCON(CH_3)_2$	E=CHO	42	57	6.9	5.4
b	$BrCH_2CH_2Br$	Br	61		5.95	5.6
c	C_6H_5CHO	$CH(OH)C_6H_5$	46	91	5.7	5.5
d	$(C_6H_5)_2CO$	$C(OH)(C_6H_5)_2$	63	91	5.2—5.7	
e	$(CH_3)_2CO$	$C(OH)(CH_3)_2$	13	45	5.7	5.45
f[c]	$ClCO_2Et$	CO_2Et	41	52	6.7	5.45
g	$(C_6H_5)_2S$	SC_6H_5	55	89	5.7	5.5

a) High-resolution mass spectroscopy gave the expected mol. weights. b) Data of mixture at 90 MHz. c) The anion solution was inversely added to an ethereal solution of excess reagent.

the best results for the metallation. Use of tetrahydrofuran (THF) resulted in very poor yields of products even at low temperatures. In hexane, the metallation was most conveniently and reproducibly conducted by stirring a 2:1 mixture of **1** and the base complex at 0 °C (ice bath) for 4—6 h.

Bromodicyclopentadiene (**3b**+**4b**), which can be prepared in fairly large quantity by Method A, is also a useful precursor for a metallated dicyclopentadiene; thus, treatment of the bromide mixture with BuLi in THF at −60 °C smoothly generated lithiodicyclopentadiene (**5**) which generally afforded quenching products in higher yields (Table 1, Method B).[4)]

The product ratios were little affected by reaction conditions and the mixtures were usually difficult to separate, although **3a** and **4a**, and **3d** and **4d** were partially separated by chromatography on silica gel. The structures of products were mainly elucidated by ^{1}H NMR spectroscopy. The 400 MHz ^{1}H NMR spectrum of the bromide mixture (**3b**+**4b**) in $CDCl_3$ shows a set of two signals particularly for the three olefin protons (H-3,4, and H-8 or 9) and the bridgehead proton at C-1 (H-1) with 1:2.4 ratio. Appearance of two doublets (J=3.3 Hz) at δ=6.00 (0.7H) and 5.94 (0.3H), which are assignable to H-8 or -9, indicates introduction of the bromine atom at the norbornene double bond (C-8 or -9). H-1 is observed at δ=3.38 and 3.29 with the former predominant. Since H-1 of **4b** is expected to resonate at lower field than H-1 of **3b** owing to anisotropic effect of nearby bromine atom, the observation suggests the predominance of **4b** over **3b**. This is also supported from ^{1}H NMR analysis of other quenching products.

Although the present metallation and functionalization of **1** affords mixtures of two regioisomers, they can be used in mixtures for organic syntheses, because both isomers should lead to the same products through thermolytic cycloreversion.

Experimental

^{1}H NMR spectra were recorded on a JEOL FX-90Q or JEOL GSX-400 spectrometer in $CDCl_3$ using tetramethylsilane as an internal standard. IR spectra were obtained from Hitachi EPI-G3 spectrometer, and mass spectra measured on a JEOL JMS-OlSG-2 or JEOL JMS-SX102 spectrometer. The microanalysis was performed at the Elemental Analysis Center, Faculty of Science, Osaka University.

Hexane was distilled from sodium metal and stored on sodium wire. Tetrahydrofuran (THF) was freshly distilled from sodium metal using diphenylketyl as indicator. BuLi and *t*-BuOK were purchased and used as such. Dicyclopentadiene was distilled in vacuo and middle fraction was used. For large scale preparation of bromodicyclopentadiene, commercial dicyclopentadiene was successfully used without further purification.

Metallation and Formylation of Dicyclopentadiene—A Standard Procedure for Method A. To a suspension of *t*-BuOK (1.12 g, 0.01 mol) in hexane (8 ml) was added dropwise hexane solution of BuLi (1.6 M, 6.6 ml) over a few min using a syringe with stirring in an ice bath under nitrogen atmosphere (1 M=1 mol dm^{-3}). After 15 min, dicyclopentadiene (**1**) (2.64 g, 0.02 mol) was added and the mixture stirred for 5 h. A solution of dimethylformamide (1.10 g, 0.015 mol) in dry ether (3 ml) was added in a few minutes. After 20 min, the reaction mixture was poured into ice-dil aq HCl, and extracted with ether (2×25 ml). The ether extract was washed with brine, dried over $MgSO_4$, and concentrated under reduced pressure. The residue was chromatographed on a short silica-gel column (hexane: AcOEt=9:1) to afford a mixture of **3a** and **4a** (0.67 g, 42% yield based on *t*-BuOK used) as a colorless oil. Found: m/z 160.0882. Calcd for $C_{11}H_{12}O$ 160.0888. ^{1}H NMR spectrum of this mixture showed two singlets of formyl proton at δ=9.52 (assigned for **4a**) and 9.63 (**3a**) in 2.5:1 integral ratio. The mixture was partially separated to **3a** and **4a** by careful chromatography.

3a: IR (CCl_4) 1675, 1590 cm^{-1}; ^{1}H NMR (90 MHz) δ=1.3—1.9 (m, 3H), 2.25 (m, 1H), 2.7—3.6 (m, 4H), 5.46 (s-like, 2H), 6.89 (d, J=3.0 Hz, 1H), 9.63 (s, 1H).

4a: IR (CCl_4) 1675, 1590 cm^{-1}; ^{1}H NMR (90 MHz) δ=1.3—1.9 (m, 3H), 2.25 (m, 1H), 2.7—3.6 (m, 4H), 5.52 (s-like, 2H), 6.96 (d, J=3.0 Hz, 1H), 9.52 (s, 1H).

Large Scale Preparation of Bromodicyclopentadiene (3b+4b): In a 1 L three necked flask equipped with a thermometer and two dropping funnels was placed dry hexane (350 ml) and then *t*-BuOK (44.88 g, 0.4 mol) under nitrogen atmosphere. The mixture was cooled below −50 °C in an ethanol-Dry Ice bath and added dropwise with BuLi in hexane (1.5 M, 280 ml, 0.42 mol) over 35 min under efficient magnetic stirring. After 15 min, **1** (100 ml, 98.6 g, 0.75 mol) was added over 10 min. The cold bath was replaced with an ice-bath and stirring continued for 6 h. The mixture was cooled again below −40 °C and 1,2-dibromoethane (42 ml, 91.6 g, 0.49 mol) in THF (60 ml) added at such rate that the inner temperature did not exceed −35 °C (ca. 40 min). The reaction mixture was allowed to warm up to about 0 °C over 1 h, and then added dropwise with water (100 ml). The organic layer was separated, washed with brine, dried over $MgSO_4$, and concentrated under reduced pressure. The residue was fractionally distilled in vacuo using a distilling column (1.5×25 cm) packed with glass helix: fraction 1, bp 40—49 °C/6 Torr (1 Torr=133.322 Pa), unreacted **1**, 54.8 g (0.415 mol); fraction 2, bp 52—83 °C/5 Torr, mixture of **1** and (**3b**+**4b**), 7.5 g; fraction 3, bp 85—87 °C/5 Torr (bp 76 °C/3 Torr), (**3b**+**4b**), 52.1 g (0.247 mol, 61.7%). ^{1}H NMR (400 MHz) δ=1.33 (d, J=8.0 Hz, 1H), 1.74—1.85 (m, 1.7H), 2.22—2.32 (m, 1.3H), 2.75 (m, 0.7H), 2.85—2.95 (m, 2.3H), 3.29 (m, 0.3H), 3.38 (m, 0.7H), 5.47 (m, 0.3H), 5.57 (m, 1H), 5.66 (m, 0.7H), 5.94 (d, J=3.3 Hz, 0.3H), 6.00 (d, J=3.3 Hz, 0.7H). Found: C, 57.15; H, 5.32; Br, 37.33%. Calcd for $C_{10}H_{11}Br$: C, 56.90; H, 5.25; Br, 37.85%.

Lithiation and Formylation of Bromodicyclopentadiene (3b+4b)—A Standard Procedure for Method B. To a solution of (**3b**+**4b**) (3.13 g, 0.015 mol) in THF (8 ml) was added dropwise BuLi (1.6 M in hexane, 8.3 ml, 0.013 mol) over a few minutes at −60 °C. The solution became cloudy in 20 min due to separation of LiBr. Dimethylformamide (1.16 g, 0.016 mol) was added dropwise, and the mixture allowed to warm up to room temperature over 30 min. The reaction mixture was worked up as described for Method A to afford (**3a**+**4a**) (1.21 g, 57%).

This work was supported by the Grant-in-Aid for Scientific Research on Priority Area No. 01648003 from the Ministry of Education, Science and Culture.

References

1) K. Alder, F. H. Flock, A. Houswieler, and R. Reeber, *Chem. Ber.*, **87**, 1752 (1954); K. Alder and F. H. Flock, *ibid.*, **87**, 1916 (1954); M. Rosenblum, *J. Am. Chem. Soc.*, **79**, 3179 (1957); R. B. Woodward and T. J. Katz, *Tetrahedron*, **5**, 70

(1959).
2) M. Stahle, R. Lehman, J. Kramer, and M. Schlosser, *Chimia*, **50**, 229 (1985); H. D. Verkruijsse and L. Brandsma, *Recl. Trav. Chim. Pays-Bas*, **105**, 66 (1986).
3) M. Schlosser and J. Hartmann, *Angew. Chem.*, **85**, 544 (1973).
4) Cyclohexanone gave adducts also in only moderate yield similar to acetone. Abstraction of active hydrogen may have competed with nucleophilic addition for these aliphatic ketones.

Palladium-Catalyzed Synthesis of *N*-Benzoyl-2-arylethenesulfonamides from [2-(Benzoylsulfamoyl)ethyl]pyridinium Chloride and Aryl Halides

Syuzi HIROOKA, Yuzi TANBO, Katsuya TAKEMURA, Hironori NAKAHASHI, Tsuyoshi MATSUOKA, and Shigeyasu KURODA*
Department of Materials Science and Engineering, Faculty of Engineering, Toyama University, Gofuku 3190, Toyama 930
(Received December 20, 1990)

Synopsis. A new, general synthesis of *N*-benzoyl-2-arylethenesulfonamides by the reaction of aryl halides including heteroaryl halides with [2-(benzoylsulfamoyl)ethyl]-pyridinium chloride in the presence of palladium acetate is described.

Although palladium-catalyzed vinylation of aryl halides with olefinic derivatives, known as the Heck reaction,[1] has been widely investigated for its usefulness in organic synthesis, there has been no report concerning a vinylation reaction of aryl halides with saturated ethane derivatives as a versatile vinyl synthon. We have been studying the chemistry of 2-arylethenesulfonamides regarding their biological activity and important precursors of 2-arylethynyl-sulfonamides.[2] Only their benzene derivatives have been known,[3] because heteroaryl derivatives are difficult to prepare by the known method.[4] Then, for the synthesis of these compounds, palladium-catalyzed ethenesulfonamidation of aryl halides by applying the Heck reaction was examined. We found that aryl halides react with [2-(benzoyl-sulfamoyl)ethyl]pyridinium chloride (**1**) as a versatile vinyl synthon in the presence of a catalytic amount of palladium acetate ($Pd(OAc)_2$) and triethylamine (NEt_3) in dry *N*,*N*-dimethylformamide (DMF) to give *N*-benzoyl-2-arylethenesulfonamides. It is the first example, to our knowledge, of such a coupling reaction. Here, we wish to report on general syntheses of the *N*-benzoyl-2-arylethenesulfonamides by two procedures.

A two-step synthesis of *N*-benzoyl-2-arylethene-sulfonamides was successfully achieved as follows. Ethenesulfonamide (**2**)[5] reacted with various aryl halides in the presence of palladium acetate[6] to give the *E*-form of 2-aryl ethenesulfonamides **7**—**14**. The *E*-configuration of these compounds was confirmed by their ^{1}HNMR spectral data, such as the ^{1}H-^{1}H coupling constants (J=14—15.5 Hz) of the protons on the vinyl moiety. In this reaction, a great improvement in the yields of 2-arylethenesulfonamide **7**, **8**, and 4-phenyl-1,3-butadiene-1-sulfonamide **9**[7] was obtained, compared to those of the former method (Table 1). Furthermore, 2-(heteroaryl)ethenesulfonamides **10**—**14** could be prepared only by this method. 2-(2,4-Dimethoxy-5-pyrimidinyl)ethenesulfonamide (**13**) and its 6-methyl derivatives **14** were transformed to the uracil derivative of ethenesulfonamides **15** and its 6-methyl derivative **16**, respectively. They are of interest regarding their antitumor activity because of their structural similarity to the sparsomicine[8] and potential precursor for 5-uracilethynesulfonamides, which is known to have an antitumor activity.[9] Since the generality and superiority of this method were verified, compounds **7**, **10**, and **11**, chosen as typical examples for comparing the yields of the following one-step synthesis, were benzoylated with benzoyl chloride to give **22**—**24** (Table 1). Similarly,3-aryl-2-propene-1-sulfonamides **17**—**21**, homoderivatives of 2-arylethenesulfonamides, were prepared without isomerization of the double bond by the reaction of aryl halides with 2-propene-1-sulfonamide (**4**)[10] in the place of **3**.

Since it was considered that the use of *N*-benzoyl-ethenesulfonamide (**3**) would shorten the preparation steps of *N*-benzoyl-2-arylethenesulfonamides **22**—**24**, benzoylation of ethenesulfonamide **2** in the presence of pyridine used as a base was attempted. However, this benzoylation reaction gave only unexpected pyridinium salt **1** in 56% yield.

It was incidentally found that the reaction of this salt **1** with aryl halides in the presence of a catalytic

Table 1. Synthesis of 2-Arylethenesulfonamides **7**—**14** and 3-Aryl-2-propene-1-sulfonamides **17**—**21**

Aryl Halide	2-Arylethene-sulfonamide	Yield/%	3-Aryl-2-propene-sulfonamide	Yield/%
Iodobenzene	**7**	55 (21)[a]		
Bromobenzene	**7**	61	**17**	42
1-Bromonaphthalene	**8**	72 (19)[b]	**18**	38
2-Bromostyrene	**9**	56 (13)[a]		
2-Bromothiophene	**10**	56	**19**	39
3-Bromopyridine	**11**	54	**20**	30
4-Bromopyridine	**12**	30		
5-Bromo-2,4-dimethoxy-pyrimidine	**13**	10	**21**	10
5-Bromo-2,4-dimethoxy-6-methylpyrimidine	**14**	16		

a) Yield from Ref. 6. b) Our own result obtained by using Culbertson's method.

amount of $Pd(OAc)_2$ and triethylamine in dry DMF gave *N*-benzoyl-2-arylethenesulfonamides **22—24** in better yields than those of the former two-step synthesis (Table 1), and that 20—30% of the unreacted aryl halides were recovered in all cases. The use of **1** is better than that of **2**, not only regarding yields but also in view of the easiness of preparation of **1**, though it was derived from **2**.

A detailed examination of this reaction in order to obtain more information about its mechanism revealed that the salt **1** does not change in the absence of triphenylphosphine and triethylamine at 140 °C. However, the treatment of **1** with triethylamine as a base in DMF at 140 °C gave *N*-benzoylethenesulfonamide (**3**) in 65.8% yield. In consideration of this result, benzoylation of **2** in the presence of NEt_3 (but not pyridine) successfully gave **3** in 13.4% yield. The reaction of **3** with a typical aryl halide of bromobenzene under similar conditions as above gave an expected *N*-benzoyl-2-phenylethenesulfonamide (**22**), but in low yield (16%), which is rather lower yield than that of the case used pyridinium salt **1**. Thus, the above results suggest that the salt **1** was generated *N*-benzoylethenesulfonamide (**3**) in situ under the conditions and that it reacted with aryl halides to give *N*-Benzoyl-2-arylethenesulfonamides **22—24**.

Experimental

All melting points are uncorrected. The IR spectra were taken on a IR-810 spectrometer. The ^1H NMR spectra were taken on Hitachi R-24 (60 MHz) and JEOL-FX 90 (90 MHz) spectrometers in chloroform-*d* (TMS as internal standard), and dimethyl-d_6 sulfoxide (TMS). The ^{13}C NMR spectra were taken on a JEOL-FX 90 (23 MHz) spectrometer in chloroform-*d* (TMS) and dimethyl-d_6 sulfoxide (TMS). The Mass spectra were taken on a JEOL-OISG-2 mass spectrometer.

General Procedures for the Preparation of 2-Arylethenesulfonamides 7—14 and 3-Aryl-2-propene-1-sulfonamides 17—21. A solution of triphenylphosphine (61 mg, 0.23 mmol) and palladium acetate (26 mg, 0.116 mmol) in DMF (16 mL) was stirred at room temperature for a few min under a nitrogen atmosphere. To this solution, a mixture of aryl bromide (5.88 mmol), **2** (or **4** for **17—21**) (7.01 mmol), and triethylamine (1.480 g, 14.7 mmol) was added. The mixture was heated at 140 °C for 24 h under a nitrogen atmosphere with stirring and, after cooling, filtered. The filtrate was concentrated under reduced pressure. The residue was dissolved in 50 mL of 1 M-sodium hydroxide (1M=1 mol dm^{-3}). The resulting solution was heated with 5 g of active carbon and filtered. The filtrate was brought to pH 3 with dil hydrochloric acid and the precipitate was collected by filtration.

7: Colorless needles; mp 140-142 °C (water), (lit,[3] 143 °C).

2-(1-Naphthyl)ethenesulfonamide (8): Colorless needles, mp 162—165 °C (ethanol); IR (KBr) 3345s, 3230s, 3050w, 1625m, 1495m, 1445m, 1319vs, 1308vs, 1172s, 989m, 908s, 748s cm^{-1}; ^1H NMR (DMSO-d_6) δ=8.23 (m, 1H), 8.00—7.20 (m, 10H); MS *m/z* 217 (M^+, 57%). Anal. ($C_{12}H_{11}NO_2S$) C, H.

4-Phenyl-1,3-butadienesulfonamide (9): Colorless needles, mp 193—194 °C, (lit,[7] 198—199 °C).

2-(2-Thienyl)ethenesulfonamide (10): Colorless needles, mp 144—145 °C (by adding ethyl acetate dropwise to a solution of **10** in water); IR (KBr) 3360s, 3260s, 3080w, 1600m, 1520w, 1400w, 1300s, 1270s, 1140s, 960w, 900w, 820m, 780w, 720m cm^{-1}; ^1H NMR (DMSO-d_6) δ=7.69 (d, *J*=5.0 Hz, 1H, H-3), 7.53 (d, *J*=15.5 Hz, 1H, H-b, CH_b=CH_aSO_2), 7.52 (d, *J*=3.2 Hz, 1H, H-5), 7.15 (dd, *J*=5.0 & 3.2 Hz, 1H, H-4), 7.14 (s, 2H, NH_2), 6.90 (d, *J*=15.5 Hz, 1H, H-a); ^{13}C NMR δ=136.9 (s), 131.2 (d), 129.7 (d), 129.2 (d), 128.4 (d), 128.3 (d); MS *m/z* 189 (M^+, 41%), 108 (100%). Anal. ($C_6H_7NO_2S_2$) C, H.

2-(3-Pyridyl)ethenesulfonamide (11): Pale yellow needles, mp 167—169 °C (water); IR (KBr) 3300s, 3050w, 2900m, 2650w, 1615m, 1590m, 1475m, 1421m, 1331vs, 1202m, 1139vs, 1122m, 969s, 900m, 870s, 815s, 778s cm^{-1}; ^1H NMR (DMSO-d_6) δ=8.83 (bs, 1H, H-2), 8.60(bd, *J*=6.5 Hz, 1H, H-6), 8.15 (dt, *J*=1.0 & 7.5 Hz, 1H, H-4), 7.43 (m, 3H, H-5, H-a, b, CH_a=CH_bSO_2), 7.28 (bs, 2H, NH_2); ^{13}C NMR (DMSO-d_6) δ=150.7 (d), 149.4 (d), 134.9 (d), 133.4 (d), 132.2 (d), 128.9 (s), 122.9 (d); MS *m/z* 184 (M^+, 53%), 104 (100%); Anal. ($C_7H_8N_2O_2S$) C, H.

2-(4-Pyridyl)ethenesulfonamide (12): Colorless needles, mp 180 °C (decomp) (water); IR (KBr) 3320s, 3060w, 2980w, 2420w, 1596s, 1410m, 1322vs, 1135vs, 990m, 972vs, 932m, 810m, 795s cm^{-1}; ^1H NMR (DMSO-d_6) δ=8.59 (dd, *J*=1.2 & 6.2 Hz, 2H, H-2, 6), 7.59(dd, *J*=1.2 & 6.2 Hz, 2H, H-5, 3), 7.51(dd, *J*=1.0 & 15.7 Hz, 1H, H-b, CH_b=CH_aSO_2), 7.24 (bs, 2H, NH_2), 7.22 (d, *J*=15.7 Hz, 1H, H-a); MS *m/z* 184 (M^+, 74%), 104 (92%). Anal. ($C_7H_8N_2O_2S$) C, H.

2-(2,4-Dimethoxy-5-pyrimidinyl)ethenesulfonamide (13): Colorless crystals, mp 172—173 °C (ethyl acetate); IR (KBr) 3300m, 3220m, 1590s, 1540s, 1470s, 1400m, 1380m, 1320s, 1300s, 1230m, 1130s, 1060m, 1000m, 850m, 809m, 759m cm^{-1}; ^1H NMR (DMSO-d_6) δ=8.61 (s, 1H, H-6), 7.23 (s, 2H, H-a,b, CH_a=CH_bSO_2), 7.08 (s, 2H, NH_2), 4.01 (s, 3H, OMe), 3.92 (s, 3H, OMe); ^{13}C NMR (DMSO-d_6) δ=168.2 (s), 165.0 (s), 160.1 (d), 130.9 (d), 128.2 (d), 108.4 (s), 54.9 (q), 54.4 (q); MS *m/z* 245 (M^+, 100%), 164 (72%). Anal. ($C_8H_{11}N_3O_4S$) C, H.

2-(2,4-Dimethoxy-6-methyl-5-pyrimidinyl)ethenesulfonamide (14): Colorless needles, mp 195—197 °C (ethyl acetate); IR (KBr) 3300m, 3140w, 3020w, 1610m, 1560s, 1470s, 1450m, 1370s, 1130s, 1060m, 910m, 800m, 785m cm^{-1}; ^1H NMR (DMSO-d_6) δ=7.33 (d, *J*=15.6 Hz, 1H, H-b, CH_b=CH_aSO_2), 7.09 (d, *J*=15.6 Hz, 1H, H-a), 7.06 (s, 2H, NH_2), 4.00 (s, 3H, OMe), 3.90 (s, 3H, OMe), 2.46 (s, 3H, Me); ^{13}C NMR (DMSO-d_6) δ=168.9 (s), 168.7 (s), 163.3 (s), 132.5 (d), 126.9 (d), 105.8 (s), 54.6 (q), 54.4 (q), 22.3 (q); MS *m/z* 259 (M^+, 100%), 178 (93%). Anal. ($C_9H_{13}N_3O_4S$) C, H.

3-Phenyl-2-propene-1-sulfonamide (17): Colorless crystals, mp 110—111 °C (benzene) (lit,[10] 126—127 °C).

3-(1-Naphthyl)-2-propene-1-sulfonamide (18): Pale yellow needles, mp 176—178 °C (EtOH); IR (KBr) 3350s, 3260s, 3050w, 1596w, 1416m, 1310vs, 1145vs, 975s, 890m, 820m, 800s, 772s cm^{-1}; ^1H NMR (DMSO-d_6) δ=8.18 (m, 1H), 7.90—7.50 (m, 7H), 6.69 (s, 2H, NH_2), 6.25 (dt, *J*=15.0 & 6.0 Hz, 1H, H-b, CH_c=$CH_bCH_{a2}SO_2$), 3.50 (d, *J*=6.0 Hz, 2H, CH_2); MS *m/z* 247 (M^+, 8%), 116 (100%). Anal. ($C_{13}H_{13}NO_2S$) C, H.

3-(2-Thienyl)-2-propene-1-sulfonamide (19): Pale yellow crystals, mp 141—142 °C (benzene); IR (KBr) 3390vs, 3280s, 3040w, 1642m, 1550m, 1400m, 1328vs, 1138vs, 1125vs, 965s, 930m, 842m, 810m, 739m, 700s cm^{-1}; ^1H NMR (DMSO-d_6) δ=7.42 (d, *J*=5.0 Hz, 1H, H-5), 7.00 (m, 2H, H-2, 4), 6.92 (bs, 2H, NH_2), 6.82 (d, *J*=14.5 Hz, 1H, H-b, CH_c=$CH_bCH_{a2}SO_2$), 5.98 (dt, *J*=14.5 & 7.2 Hz, 1H, H-c), 3.85 (d, *J*=7.2 Hz, 1H, H-a); MS *m/z* 203 (M^+, 3%), 122 (100%). Anal. ($C_7H_9NO_2S_2$) C, H.

3-(3-Pyridyl)-2-propene-1-sulfonamide (20): Colorless needles, mp 120—121 °C (H_2O); IR (KBr) 3260vs, 3050w, 2900s, 2620s, 1640w, 1580m, 1558m, 1460m, 1318vs, 1285vs, 1232s, 1150s, 1128vs, 962s, 800m, 780s, 718 cm^{-1}; ^1H NMR (DMSO-d_6) δ=8.62 (bs,1H, H-2), 8.43 (bd, *J*=7.0 Hz, 1H, H-6), 7.89 (dt, *J*=9.5 & 1.1 Hz, 1H, H-4), 7.35 (dd, *J*=9.5 & 7.0 Hz, 1H, H-5), 6.93 (bs, 2H, NH_2), 6.72 (d, *J*=14.5 Hz, 1H, H-c, CH_c=CH_b-CH_{a2}), 6.40 (dt, *J*=14.5 & 8.0 Hz, 1H, H-b), 3.92

(d, J=8.0 Hz, 2H, H-a); MS m/z 200 (M^+, 7%), 118 (100%). Anal. ($C_8H_{10}N_2O_2S$) C, H.

3-(2,4-Dimethoxy-5-pyrimidinyl)-2-propene-1-sulfonamide (21): Colorless crystals, mp 273 °C (decomp AcOEt); IR (KBr) 3280m, 3160w, 1590s, 1480s, 1400s, 1380s, 1330s, 1160m, 1000s, 960m, 780m cm^{-1}; ^1H NMR (DMSO-d_6) δ=8.44 (s, 1H, H-6), 6.88 (s, 2H, NH_2), 6.60 (d, J=15.8 Hz, 1H, H-c, CH_c=CH_b-CH_{a2}), 6.30 (dt, J=15.8 & 7.9 Hz, 1H, H-b), 3.98 (s, 3H, OMe), 3.89 (s, 2H, H-a), 3.80 (s, 3H, OMe); MS m/z 259 (M^+, 43%), 179 (-SO_2NH_2, 100%). Anal. ($C_9H_{13}N_3O_4S$) C, H.

2-(1,2,3,4-Tetrahydro-2,4-dioxo-5-pyrimidinyl)ethenesulfonamide (15). A solution of **13** (1.00 g, 4.00 mmol) and sodium iodide (1,84 g, 12 mmol) in acetic acid (9 mL) was heated at 100 °C with stirring for 4 h. After cooling, the solvent was evaporated in vacuo and the residue was dissolved in water (9 mL). To this solution was added dil sodium thiosulfate untill the color of the solution disappeared. The precipitate was collected by filteration to give **15** (83%): colorless crystals, mp 266—268 °C decomp (water); IR (KBr) 3320s, 3220m, 3020w, 1710s, 1690vs, 1670vs, 1620m, 1500w, 1420m, 1320s, 1230s, 1150s, 810m, 769m cm^{-1}; ^1H NMR (DMSO-d_6) δ=11.45 (m, 2H, NH), 8.02 (d, J=7.0 Hz, 1H, H-6), 7.49 (d, J=15.1 Hz, 1H, H-b, CH_b=CH_a-SO_2), 7.01 (d, J=15.1 Hz, 1H, H-a), 6.88 (s, 2H, NH_2); ^{13}C NMR (DMSO-d_6) δ=162.7 (s), 150.2 (s), 145.7 (d), 130.1 (d), 128.3 (d), 105.9 (s); MS m/z 217 (M^+, 3%), 137 (100%). Anal. ($C_6H_7N_3O_4S$) C, H.

2-(1,2,3,4-Tetrahydro-2,4-dioxo-6-methyl-5-pyrimidinyl)-ethenesulfonamide (16). Similarly 6-methyl derivative **16** was obtained from **14** by the above method: Colorless crystals, mp 269—272 °C decomp (water); IR (KBr) 3300s, 3220s, 3080m, 1700vs, 1660vs, 1580m, 1540m, 1412s, 1310s, 1140s, 900m, 760m cm^{-1}; ^1H NMR (DMSO-d_6) δ=11.21 (bs, 2H, NH), 7.56 (d, J=15.1 Hz, 1H, H-b, CH_b=CH_aSO_2), 7.02 (d, J=15.1 Hz, 1H, H-a), 6.89 (s, 2H, NH_2), 2.26 (s, 3H, Me); ^{13}C NMR (DMSO-d_6) δ=162.7 (s), 155.6 (s), 149.9 (s), 129.0 (d), 127.9 (d), 102.3 (s), 16.6 (q); MS m/z 231 (M^+, 7%), 151 (100%). Anal. ($C_7H_9N_3O_4S$) C, H.

[2-(Benzoylsulfamoyl)ethyl]pyridinium Chloride (1). To a solution of **2** (9.29 g, 86.8 mmol) and dry pyridine (14.73 g, 186 mmol) in dry acetone (30 mL) was added benzoyl chloride (25.95 g, 184 mmol) dissolved in dry benzene (10 mL). The mixture was refluxed for 30 min and, after cooling, the precipitate was collected by filteration to give salt **1** (15.38 g, 53%): Pale yellow prisms; mp 186—187 °C (DMF); IR (KBr) 3128m, 1690s, 1343s, 1150s cm^{-1}; ^1H NMR (DMSO-d_6) δ=9.42 (d, J=5.8 Hz, 2H, H-2, 6), 8.63 (t, J=7.7 Hz, 1H, H-4), 8.54—7.45 (m, 4H, H-3,5, and NH_2), 5.26 (t, J=6.4 Hz, 2H, CH_2-C-SO_2), 4.42 (t, J=6.4 Hz, 2H, CH_2SO_2); ^{13}C NMR (DMSO-d_6) δ=166.6, 146.1, 145.8, 133.2, 131.4, 128.9, 128.3, 127.6, 54.7, 52.4. Anal. ($C_{14}H_{15}N_2O_3S$) C, H.

***N*-Benzoylethenesulfonamide (3).** To a solution of **2** (10.8 g, 0.10 mol) and triethylamine (12.7 g, 0.12 mol) in acetone (55 mL) was added benzoyl chloride (17.8 g, 0.13 mol) dropwise with stirring at room temperature. After the addition, the reaction mixture was stirred at room temperature for 30 min. The salt was removed by filteration and the filterate was evaporated in vacuo. The residue was chromatographed on silica gel with dichloromethane as eluent to give **3** (2.7 g, 13%): Colorless needles, mp 87—92 °C (ether); IR (KBr) 3274m, 1710s, 1336s, 1151s, 1060m, 899m, 848m, 733m, 842m cm^{-1}; ^1H NMR ($CDCl_3$) δ=9.50 (bs, 1H, NH), 7.92 (m, 2H, ortho protons on Ph), 7.28 (m, 3H, *m*- & *p*-protons on Ph), 6.99 (dd, J=16.6 & 9.7 Hz, 1H, H-a), 6.49 (d, J=16.6 Hz, 1H, H-b), 6.14 (d, J=9.7 Hz, 1H, H-c); ^{13}C NMR δ=165.5, 135.3, 133.6, 131.0, 130.4, 128.9, 128.1; MS m/z 211 (M^+, 5%), 105 (−$PhCO^+$, 100%). Anal. ($C_9H_9NO_3S$) C, H.

***N*-Benzoyl-2-arylethenesulfonamide (22—24). Method A:** The procedure for the preparation of **22**, **23**, and **24** is similar to that described in general procedure for the arylethenesulfonamines, except for using **1** in place of ethenesulfonamide **2**.

Method B: 2-Arylethenesulfonamides **7**, **10**, and **11** were treated with benzoyl chloride in a manner similar to the case of **3**, giving **22**.

22: (**A**: 23%; **B**: 19%) Colorless needles, mp 232—232.5 °C; IR (KBr) 3290s, 1692s, 1418s, 1335s, 1159s, 1061s, 870m, 839m, 752m, 703m cm^{-1}; ^1H NMR (DMSO-d_6) δ=12.1—12.5 (bm, 1H), 8.01—7.34 (m, 12H); ^{13}C NMR (DMSO-d_6) δ=165.6, 143.2, 133.0, 132.1, 131.6, 131.1, 128.9, 128.8, 128.5, 125.8; MS m/z 223 (M^+ −SO_2, 0.7%). Anal. ($C_{15}H_{13}NO_3S$) C, H.

23: (**A**: 24%; **B**: 9%) Colorless needles, mp 191—192 °C (methanol); IR (KBr) 3290m, 1695s, 1418vs, 1335s, 1159s, 840s, 718s, 702s cm^{-1}; ^1H NMR (DMSO-d_6) δ=12.0—12.5 (bm, 1H, NH), 8.00—7.40 (m, 8H), 7.35—7.05 (m, 2H); ^{13}C NMR (DMSO-d_6) δ=165.7, 136.1, 133.3, 133.1, 131.6, 131.3, 128.6, 128.5, 128.4, 123.2; MS m/z 229 (M^+ −SO_2), 126 (100%), 105 (64%), 77 (88%). Anal. ($C_{13}H_{11}NO_3S_2$) C, H.

24: (**A**: 21%; **B**: 16%) Pale brown crystals, mp 224—225 °C (DMF); IR (KBr) 3060w, 3020w, 2850m, 1696s, 1623m, 1596m, 1509m, 1349s, 1260s, 1157vs, 843m, 791s, 718s cm^{-1}; ^1H NMR (DMSO-d_6) δ=8.97 (d, J=1.8 Hz, 1H, H-2), 8.65 (dd, J=4.8 & 1.8 Hz, 1H, H-5), 8.30 (dt, J=7.4 & 1.8 Hz, 1H, H-4), 7.95 (bd, J=5.1 Hz, 2H, ortho protons on Ph), 7.73 (s, 2H, CH_b=CH_a-SO_2), 7.50 (m, 4H, NH & *m*-, *p*-protons on Ph); ^{13}C NMR (DMSO-d_6) δ=165.8, 151.5, 150.1, 139.9, 135.4, 133.7, 133.1, 128.5, 128.4, 128.3, 128.0, 124.0; MS m/z 289 (M^+ +1, 0.3%), 224 (1.2%), 121 (100%). Anal. ($C_{14}H_{12}N_2O_3S$) C, H.

References

1) R. F. Heck, *Org. React.*, **27**, 345 (1982); R. F. Heck, "Palladium Reagents in Organic Syntheses," Academic Press, New York (1985), pp. 179—319.

2) M.-J. Brienne, D. Varech, M. Leclerg, J. Jacues, N. Randembino, M.-C. Dassalles, G. Mahuzier, C. Gueyouche, C. Bories, P. Loiseau, and P. Gayral, *J. Med. Chem.*, **30**, 2232 (1987).

3) K. Hasegawa and S. Hirooka, *Bull. Chem. Soc. Jpn.*, **45**, 525 (1972); K. Hasegawa, T. Sasaki, and S. Hirooka, *ibid.*, **46**, 2894 (1973); K. Hasegawa, S. Hirooka, and T. Sasaki, *ibid.*, **48**, 1513 (1975).

4) B. M. Culbertson and S. Dietz, *J. Chem. Soc. C*, **1968**, 992.

5) A. S. Matlack, *J. Org. Chem.*, **23**, 729 (1958); D. Ludstech and H. Distler, Belg. Patent 615081 (1962); *Chem. Abstr.*, **58**, 10082e (1963).

6) A. Halberg and C. Westerlund, *Chem. Lett.*, **1982**, 1993.

7) K. Hasegawa, S. Hirooka, T. Sasaki, S. Ikeda, and S. Hashimoto, *Nippon Kagaku Kaishi*, **1975**, 1028.

8) A. D. Argoudelis and R. R. Her, *Antimicrob. Agents Chemorther.*, **1962**, 789; P. F. Wiley and F. A. MacKellar, *J. Am. Chem. Soc.*, **92**, 417 (1970).

9) K. Edo, T. Sakamoto, and H. Yamanaka, *Chem. Pharm. Bull.*, **26**, 3843 (1978); D. E. Derstrom and M. K. Ogawa, *J. Am. Chem. Soc.*, **100**, 8106 (1978); C. F. Bigge, P. K. Kalarities, J. R. Deck, and M. P. Mertes, *J. Am. Chem. Soc.*, **102**, 2033 (1989); M. J. Robins and P. T. Barr, *J. Org. Chem.*, **46**, 1854 (1983).

10) M. A. Belous and I. Ya. Postovskii, *Zh. Obshch. Khim.*, **20**, 1701 (1950); *Chem. Abstr.*, **45**, 2391g (1950).

11) C. M. Suter and E. Truce, *J. Am. Chem. Soc.*, **66**, 1105 (1944).

Oxidation by Cobalt(III) Acetate. Part 13.[1] Oxidation of Substituted Phenols with Cobalt(III) Acetate in Acetic Acid

Masao HIRANO, Tadamichi ISHII, and Takashi MORIMOTO*
Department of Applied Chemistry, Faculty of Technology, Tokyo University of Agriculture and Technology, Koganei, Tokyo 184
(Received December 20, 1990)

Synopsis. The oxidation of 2,6-di- and 2,4,6-tri-substituted phenols with cobalt(III) acetate has been investigated in acetic acid under an inert atmosphere; the former gave the corresponding diphenoquinones in excellent yields, and the latter yielded side-chain or nuclear acetoxylated products in moderate to good yields.

In connection with natural organic products and antioxidants, phenols enjoy important and specific positions in organic chemistry. The oxidation of phenols has also been of considerable significance in the synthesis of a variety of organic chemicals, especially for the biogenetic syntheses of natural products. Thus, fairly extensive methodologies have been demonstrated for the phenol oxidations using ample chemical and biological processes; viz. oxidation with metal oxidants (particularly with iron(III) salts), organic and inorganic peroxides (or peroxy acids), halides, quinones, and Fremy's salt, and electrolytic, enzymatic, auto-, and photo-oxidations and so on.[2]

Although cobalt(III) acetate (**1**) is a potent and versatile one-electron oxidant and has been successfully used for the transformation of various functional groups, especially for the selective oxidation of alkylbenzenes[3] and olefins[1,4] via an electron-transfer mechanism, little attention has been paid to the oxidation of the hydroxyl compounds. We have thus recently examined product and/or kinetic studies concerning the catalytic[5] and stoichiometric oxidations of alcohols[6] and glycols[7] with **1** in acetic acid. Nevertheless, since there have been no data on the oxidation of phenols, the validity of **1** for the hydroxyl compounds has not been fully established. In this article we wish to describe some observations concerning the phenol oxidation with **1**. This is the first case in which **1** has been utilized for this objective.

Results and Discussion

The oxidation of phenols with **1** in acetic acid was carried out under nitrogen in order to exclude any influence of autoxidation. The reaction was stopped at a time in which the dark-green color of the reaction solution disappeared, a clear indication of the complete reduction of the cobalt(III) species into cobalt(II). After the conventional work-up procedures (see the Experimental section), the oxidation products formed were isolated and/or analyzed by GLC.

2,6-Dimethylphenol (**2a**) was readily oxidized at 70 °C, giving 3,3′,5,5′-tetramethyl-4,4′-diphenoquinone (**3a**) as the main product, along with a minor amount of 2,6-dimethyl-*p*-benzoquinone (**4a**). The other 2,6-disubstituted phenols (**2b—e**) exclusively afforded the corresponding diphenoquinones **3b—e** in fairly good yields, while the benzoquinones **4b—e** were absent (Table 1). Thus, *para-para* coupling predominates in the oxidation of the 2,6-disubstituted phenols. On the other hand, the oxidation of 2,4-di-*t*-butylphenol (**5**) at ambient temperature for 15 h ([**1**]/[**5**]=1.2; mole ratio) yielded solely the 2,2′-biphenyldiol (**6**) in 87 mol% GLC yield at 94% conversion, as a result of exclusive *ortho-ortho* coupling.[8]

Table 1. Oxidation of 2,6-Disubstituted Phenols[a]

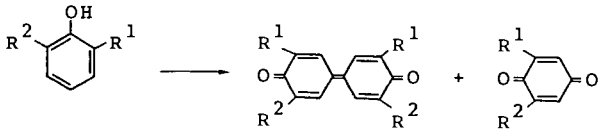

2 **3** **4**

Phenols **2**		Temp	Time	[**1**]/[**2**]	Isolated yields/%	
R^1	R^2	°C	h	Mole ratio	**3**	**4**
(a) Me	Me	70	5.5	2.5	75	23
(b) Me	*t*-Bu	70	15	2.5	97	
(c) *i*-Pr	*i*-Pr	50	15	5.0	91	
(d) *t*-Bu	*t*-Bu	70	72	2.5	95	
(e) MeO	MeO	Ambient	24	2.5	95	

a) Under nitrogen, [$Co(OAc)_3$]=0.420 mol dm^{-3}; 8.4 mmol of phenols were used in every run.

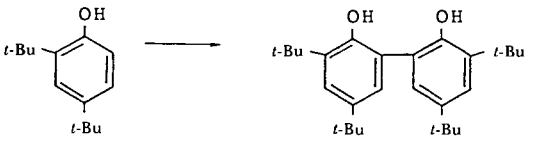

5 **6**

These results are of considerable interest in considering the steric and electronic effects of the substituents on the reactivity of the phenols, as well as product selectivity. As compared with "less" hindered phenols, **2a—c**, a steric hindrance of the *t*-Bu groups of **2d** is prominent; they may severely limit the initial attack of **1** on the "more" hindered hydroxyl group. For example, when oxidations of **2a—d** were conducted at 50 °C ([**1**]/[**2**]=2.5), the reaction times required for complete reduction of **1** were 16, 20, 24, and 72 h, respectively. These results are well consistent with the previous observation that oxidation with **1** is highly sensitive to steric factors.[3c-e,4a-c] The selectivity of the products can also be explained in terms of a steric hindrance of the substituents; thus, carbon-

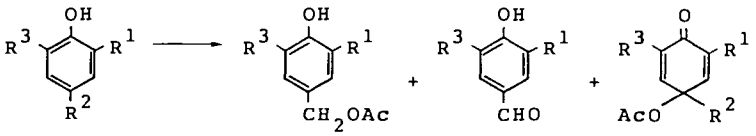

7 8 9 11

Scheme 1. (a); R^1=Me, R^2=Me, R^3=Me: (b); R^1=*t*-Bu, R^2=Me, R^3=*t*-Bu: (c); R^1=*t*-Bu, R^2=*t*-Bu, R^3=*t*-Bu.

carbon couplings occurred at the unhindered *para*- of **2a—e** and *ortho*-position of **5**. Smooth oxidation of **2e**, even at room temperature, evidently indicates that the electron-donating group contributes to promote the reaction. A similar electronic effect has been observed in the oxidations of alkylbenzenes[3a,b] and olefins.[4d,e]

The oxidation of 2,4,6-trisubstituted phenols (**7a—c**) was conducted in a manner analogous to that of **2** in acetic acid (Scheme 1). The oxidation of **7a, b** ([**1**]/[**7**]=2.5) at 50 °C for 1 and 15 h, respectively, afforded 49 and 73 mol% of the benzyl acetates (**8**), and 27 and 7 mol% of the benzaldehydes (**9**) (GLC yields), respectively. In the latter case, a small amount of 3,3′,5,5′-tetra-*t*-butyl-4,4′-stilbenequinone (**10**) was formed (3 mol% by GLC).[9] Control experiments showed that

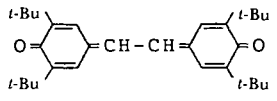

10

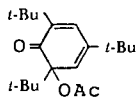

12

upon treatment of **8a, b** with **1** ([**1**]/[**8**]=2.5) at 50 °C for 1 and 15 h, respectively, **9a, b** were formed as the sole products in 67 and 47 mol% yields, respectively, implying that **9** was derived from a consecutive oxidation of **8**, as expected. The difference in the reactivity of **7a** and **7b** can also be explained by the difference in the steric effect of the Me and the *t*-Bu groups, as noted above. The oxidation of **7c**, having no labile hydrogen on the side-chains, with 2.5 equiv of **1** at 50 °C for 15 h, gave 4-acetoxy-2,4,6-tri-*t*-butyl-2,5-cyclohexadien-1-one (**11**) in 83% yield, along with only a trace amount of the 2-acetoxylated derivative (**12**). It has been comparatively rare that such a *p*-acetoxylated product as **11** is selectively formed in high yield. In fact, it has been reported that a mixture of **11** and **12** is obtained from **7c**, where **12** is formed (≈60%) in preference to **11** (<30%) as typically observed in Pb oxidations.[10]

In order to obtain some information on the possible route leading to **8**, close GLC as well as GC-MS analyses of the product mixtures obtained from **7a, b** were carried out, where components (<10%; GLC selectivities) assignable to the 4-methylene-2,5-cyclohexadien-1-ones (**13**) were detected. Although

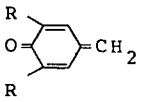

13

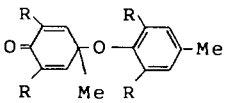

14 [(a); R=Me, (b); R=*t*-Bu]

the isolation of **13a, b** from the product mixtures of **7a, b** failed because of their extreme instability, these facts may be suggestive of a reaction pathway via the 4-aryloxy-2,5-cyclohexadien-1-ones (**14**) as key intermediates, as proposed in the oxidations with Pb, Mn, and DDQ.[11]

The oxidation of phenol and *p*-cresol only afforded amorphous solids, which were infusible upon heating over 350 °C; possibly, polymeric materials were formed.

Experimental

^{1}H NMR spectra were measured with a JEOL JNM-C-HL model spectrometer for solutions in carbon tetrachloride or deuteriochloroform. The IR spectra were recorded for KBr disks or nujol mull on a JASCO DS-403G spectrophotometer. GLC was carried out on a Shimadzu GC-4CM instrument, with a 2 m column packed with 1.5% Silicone OV-17 on Shimalite WAW-DMCS, with temperature programming. The mass spectra were determined on a Shimadzu GC-MS 7000 spectrometer which was coupled via a heated 2 m column packed with 1.5% Silicone OV-17 on Shimalite WAW-DMCS to a GLC apparatus. Melting points were measured on a Yamato capillary mp apparatus and were uncorrected.

Starting Materials. All phenols were commercially available and were purified by recrystallization just before use. Cobalt(III) acetate in acetic acid was prepared by the oxidation of cobalt(II) acetate tetrahydrate with ozone in acetic acid containing acetic anhydride.[12]

Oxidation Procedures. The typical oxidation procedures are as follows: 2,6-Dimethylphenol (**2a**, 1.02 g, 8.4 mmol) was mixed with a solution of cobalt(III) acetate (2.5 mole equiv) in acetic acid in a reaction vessel. The vessel was then flushed with dry nitrogen gas, sealed with a glass stopper, and maintained at a controlled temperature in a thermostat without agitation. After a given period, the reaction mixture was poured into water to precipitate a dark-red solid. Separation of the solid by filtration, followed by recrystallization from acetic acid, afforded dark-purple needles **3a**: 1.51 g, 75%; mp 203—204 °C (lit,[13] 206 °C).

The aqueous filtrate was extracted three times with ether; the combined ether was successively washed with water, 10% aqueous sodium carbonate, and water and then dried (Na_2SO_4). Removing the ether on a rotary evaporator left a red solid, which was chromatographed on silica gel with chloroform as an eluent to give crude **4a**. Upon recrystallization from petroleum ether, the solid yielded yellow needles of pure **4a**: 0.263 g, 23%; mp 71—72 °C(lit,[14] 70—72 °C).

All products thus obtained were known compounds, and were identified by the mps as well as comparisons of the NMR and IR spectra and/or GLC retention times with those of authentic samples prepared independently. For the measurement of the GLC yields of the products, biphenyl or benzophenone was added to the reaction mixture as an internal standard; they were found to be intact

under the reaction conditions employed.

References

1) Part 12; M. Hirano, T. Hamaguchi, X. Zhuang, and T. Morimoto, *J. Chem. Soc., Perkin Trans. 2*, **1989**, 2141.

2) Full outline of phenol oxidations is available by means of a combination of the following reviews; M. Hudlicky, "Oxidations in Organic Chemistry," Am. Chem. Soc., Washington, DC (1990), p. 163; T. Kametani and K. Fukumoto, "Phenol Oxidations," Giho-do, Tokyo (1970); P. D. McDonald and G. A. Hamilton, "Oxidation in Organic Chemistry," ed by W. S. Trahanovsky, Academic Press, New York (1973), Part B, p. 97; J. Cason, "Organic Reactions," (1948), Vol. 4, p. 305; T. Matsuura and A. Nishinaga, "Chemistry of Free Radicals," Nankou-do, Tokyo (1967), p. 161.

3) a) E. I. Heiba, R. M. Dessau, and W. J. Koehl, Jr., *J. Am. Chem. Soc.*, **91**, 6830 (1969); b) T. Morimoto and Y. Ogata, *J. Chem. Soc. B*, **1967**, 1353; c) Y. Kamiya and M. Kashima, *Bull. Chem. Soc. Jpn.*, **46**, 905 (1973); d) K. Sakota, Y. Kamiya, and N. Ohta, *Can. J. Chem.*, **47**, 387 (1969); e) A. Onopchenko, J. G. D. Schulz, and R. Seekircher, *J. Org. Chem.*, **37**, 1414 (1972).

4) a) L. Verstraelen, M. Lalmand, A. J. Hubert, and P. Teyssie, *J. Chem. Soc., Perkin Trans. 2*, **1976**, 1285; b) M. Hirano, K. Nakamura, and T. Morimoto, *ibid.*, **1981**, 817; c) M. Hirano and T. Morimoto, *ibid.*, **1985**, 1105; d) *idem., ibid.*, **1984**, 1033; e) T. Morimoto, M. Hirano, K. Echigoya, and T. Satoh, *ibid.*, **1986**, 1205.

5) T. Morimoto, M. Hirano, M. Wachi, and T. Murakami, *J. Chem. Soc., Perkin Trans. 2*, **1984**, 1949.

6) M. Hirano, T. Morimoto, and K. Itoh, *Bull. Chem. Soc. Jpn.*, **61**, 3749 (1988); M. Hirano and T. Morimoto, *ibid.*, **62**, 4069 (1989).

7) T. Morimoto and M. Hirano, *J. Chem. Soc., Perkin Trans. 2*, **1982**, 1087; *idem., ibid.*, **1983**, 123; T. Gunji, M. Hirano, and T. Morimoto, *ibid.*, **1985**, 1827.

8) W. W. Kaeding, *J. Org. Chem.*, **28**, 1063 (1963).

9) J. Sugita, *Nippon Kagaku Kaishi*, **87**, 1082 (1966).

10) W. A. Bubb and S. Sternhell, *Tetrahedron Lett.*, **1970**, 4499; M. J. Harrison and R. O. C. Norman, *J. Chem. Soc. C*, **1970**, 728.

11) C. M. Orlando, Jr., *J. Org. Chem.*, **35**, 3714 (1970); H.-D. Becker, *ibid.*, **30**, 982 (1965).

12) S. S. Lande, C. D. Folk, and J. K. Kochi, *J. Inorg. Nucl. Chem.*, **33**, 4101 (1971).

13) J. Sugita, *Nippon Kagaku Kaishi*, **87**, 603 (1966).

14) L. I. Smith and B. Irwin, *J. Am. Chem. Soc.*, **63**, 1036 (1941).

The Reaction between Hydrogen Spiro-Borates and Carbinol Form of Crystal Violet in Toluene with Applications to Reagent Selection in Extraction-Spectrophotometry of Boron

Susanta K. SENGUPTA* and O. BALASUBRAMANIAN
Department of Chemistry, Faculty of Science, Banaras Hindu University, Varanasi 221005, India
(Received July 21, 1990)

Synopsis. A study on equilibrium and kinetics of the reactions of boron complexes of a judiciously chosen series of hydroxy and dicarboxy acids (benzilic acid, mandelic acid, 3-chloro- and 4-hydroxy mandelic acid, salicylic acid, and phenylmalonic acid) as well as of the free acids with carbinol form of crystal violet in toluene demonstrated the distinct superiority of mandelic acid over the others, as a reagent for extraction-photometry of boron.

A popular method for the determination of boron is extraction-spectrophotometry of $(dye)^+(spiroborate)^-$ ion pair in a low dielectric constant aprotic solvent. Boron as boric acid is well-known to complex with a diol, hydroxy acid or gem-dicarboxy acid (H_2R) to form hydrogen spiro-borate, HBR_2. A spiroborate anion (BR_2^-), if sufficiently hydrophobic, can be extracted even into a toluene-like solvent in pairing with a triphenylmethae dye cation. Spectrophotometry of the ion pair $(dye^+BR_2^-)_{org}$ is used to determine boron. In fact, combinations of various H_2Rs such as α-hydroxy acids, *o*-hydroxy benzoic acids, catechols or naphthols, dye cations, and solvents were tried to get the best possible reagent system.[1-5] These extraction processes are considered to follow the mechanism.[2]

$$H_2R \rightleftarrows (H_2R)_{org} \quad (1a)$$

$$dye^+ + (H_2R)_{org} \rightleftarrows (dye^+)(HR^-)_{org} + H^+ \quad (1b)$$

$$H_3BO_3 + 2(H_2R)_{org} + dye^+ \rightleftarrows (dye^+)(BR_2^-)_{org} + 3H_2O + H^+ \quad (1c)$$

$$(dye^+HR^-)_{org} + H_2O \longrightarrow (dye\text{-}OH)_{org} + (H_2R)_{org} \quad (1d)$$

$$(dye^+\ BR_2^-)_{org} + H_2O \longrightarrow (dye\text{-}OH)_{org} + (HBR_2)_{org} \quad (1e)$$

In such extraction systems, color fading based on hydrolysis of a cationic dye to the colorless carbinol, dye-OH has been skillfully used to diminish the absorbance of a reagent blank. To develop a sensitive method, the overall rate of Eq. 1d must be sufficiently larger than that of Eq. 1e. Further, the equilibrium of Eq. 1b can be considered as equivalent to the sequences,

$$dye^+ + H_2O \rightleftarrows (dye\text{-}OH)_{org} + H^+ \quad (1b')$$

$$(H_2R)_{org} + (dye\text{-}OH)_{org} \rightleftarrows (dye^+\ HR^-)_{org} + H_2O \quad (1b'')$$

and that of Eq. 1c can be to 1b′ and

$$H_3BO_3 + 2(H_2R)_{org} \rightleftarrows (HBR_2)_{org} + 3H_2O \quad (1c')$$

$$(HBR_2)_{org} + (dye\text{-}OH)_{org} \rightleftarrows (dye^+\ BR_2^-)_{org} + H_2O \quad (1c'')$$

So, determinations of rate constants of Eqs. 1d and 1e and of equilibrium constants of Eqs. 1b″, 1c″ and of 1b′, 1c′ would allow complete evaluation and prediction of such extraction systems. It can be shown that given a dye, solvent and pH for the suitability of a H_2R in boron determination, both the equilibrium constant and the rate constant of the reverse step of Eq. 1b″ must be sufficiently larger than those of Eq. 1c″. The case has been critically examined for a selected set of H_2Rs (salicylic acid, mandelic acid, 3-chloro- and 4-hydroxy mandelic acid, benzilic acid, and phenylmalonic acid) in reference to Crystal Violet dye for toluene as extractant. Herein, are reported the results.

Experimental

Reagents: Reagents used were either of analytical reagent grade or highly purified by standard procedures. Carbinol form of Crystal Violet was prepared by basification of the aqueous dye solution (10^{-5} M) by 2 M NaOH (M=mol dm^{-3}) and subsequent extraction into toluene.[7] HBR_2 was prepared by reacting a definite quantity of a H_2R with aqueous boric acid, followed by extraction into toluene cxcept for 3-chloro- and 4-hydroxy mandelic acid. Its toluene solution was obtained by careful evaporation of chloroform extract and dissolution in toluene.

Choice of Reagents: The medium chosen was toluene due to its relatively low toxicity.[2] The choice of the dye fell on Crystal Violet because its carbinol form is enough basic to undergo slow reaction with acids of widely different strengths in benzene and the like media.[7-9] Any hydroxy carboxy or dicarboxy acid (H_2R) reagent chosen should form a boric acid complex (HBR_2) having sufficient solubility and stability in toluene. Accordingly, the choice fell on H_2Rs having aromatic moiety: phenylmalonic acid, salicylic acid, benzilic acid, mandelic acid, and 3-chloro- and 4-hydroxy mandelic acid.

Procedure: Kinetics as well as equilibrium of the reaction of the carbinol form of Crystal Violet (1.12×10^{-5} M) with both a HBR_2 and the corresponding H_2R (10^{-4} to 10^{-3} M) in toluene were followed by measurements of absorbance at 610 nm in a Shimadzu 160A spectrophotometer as well as in a Systronics 103 spectrocolorimeter at 25±0.5 °C.

Results and Discussion

The carbinol form of Crystal Violet (tris-4-(dimethylamino) phenyl methanol) is an example of an aquo-base.[6] Its reaction with an acid is written in a general form as

$$D + HA \rightleftarrows DH^+A^- \quad (2)$$

Where, D stands for the colorless carbinol form and DH^+A^- is the colored ion pair. The equilibrium constant is defined as:

$$K = \frac{[DH^+A^-]}{[D][HA]^n}. \quad (3)$$

Where, the acid exponent, n, is greater than unity but nonintegral and significantly dependent on the spe-

cific acid (HA), solvent and temperature as well.[7,10,11] The equilibrium 2 should thus be writlen as

$$D + fHA \rightleftarrows DH^+A^- + rHA \quad (4)$$

where, f and r stand for acid exponents of the forward and the reverse steps, respectively. Symbolizing the rate constant for forward and reverse reaction as k_1 and k_{-1} respectively, the following relations follow:

$$n \text{ (overall acid exponent)} = f - r, \quad (5)$$

$$K = k_1/k_{-1}. \quad (6)$$

When [HA]≫[D] the kinetic data[7-9] fitted the formula

$$k = \frac{2.303}{t} \log \frac{x_e}{x_e - x}, \quad (7)$$

where, x_e and x stand for $[DH^+A^-]$ at equilibrium and at the time interval t, respectively, in terms of absorbance. The rate constant, k, can be expressed as

$$k = k_1[HA]^f + k_{-1}[HA]^r. \quad (8)$$

Combining the relations 5, 6, and 8, the following equation can be derived

$$\log\left(\frac{k}{K+[HA]^{-n}}\right) = \log k_{-1} + f \log[HA]. \quad (9)$$

A plot of the left hand side of the Eq. 9 vs. log[HA] was linear for many acids.[7-9] Using the above relations one can obtain K (Eq. 3), k (Eq. 7), k_1 (Eq. 6), k_{-1} (Eq. 9), n (Eq. 3), f (Eq. 9), and r (Eq. 5).

Under the present conditions, where [HA]/[D] is in general 10—500, it was observed that for the reaction of the carbinol form of Crystal Violet with the HBR_2 as well as the H_2R chosen in wet toluene the equilibrium and the kinetic data fitted well the relations 3, 7, and 9. The results and the parameters (obtained by least square analysis) were given in Tables 1, 2, 3, and 4.

Implications of the Results in Boron Determination: On the basis of the mechanism (Eqs. 1a—1e) the extraction-photometry of boron would be more sensitive, larger the overall rate of hydrolysis of a (dye^+HR^-) compared to that of the corresponding ($dye^+BR_2^-$). The relative rate of hydrolysis, for a given dye, extractant and pH, depends on the differences in the intrinsic quantities k_{-1} and K (Eqs. 1b″ and 1c″) as also on the difference between $[H_2R]_{org}$ and $[HBR_2]_{org}$. Use of $[H_2R] \gg [HBR_2]$, a general condition in the boron determination, is thus of advantage to the method's sensitivity. Results on k_{-1} and K (Tables 3 and 4) lead clearly to the prediction that except salicylic acid, all the other acids should be potential reagents and that among these, mandelic acid or phenylmalonic acid should be preferred over benzilic acid and 3-chloro- and 4-hydroxy mandelic acid. However, the last one would be a poor choice owing to very low extractability of its BR_2^- into toluene. Further, between mandelic acid and phenylmalonic acid, the magnitudes of k_{-1} and K cause the rate of hydrolysis of dye^+HR^- very high for both the acids but that of $dye^+BR_2^-$ distinctly less for the former acid.

Thus, evaluation of the physicochemical results distinguishes mandelic acid as the most potential one

Table 1. Results at Fixed [D] (1.12×10^{-5} M)[a] at Different $[HBR_2]$ at 25±0.5 °C

HBR_2	$[HA]\times10^3$ / M	x_e	$\log\frac{[DH^+A^-]}{[D]}$[b]	k / min^{-1}	$\log\frac{k}{K+[HA]^{-n}}$
Hydrogen bis(salicylato)borate	0.10	0.14	−0.30	0.247	−6.95
	0.20	0.20	−0.04	0.790	−6.19
	0.30	0.27	0.26	1.036	−5.97
	0.40	0.32	0.51	1.458	−5.76
	0.50	0.36	0.78	1.612	−5.69
Hydogen bis(benzilato)borate	0.07	0.12	−0.40	0.433	−7.22
	0.14	0.22	0.04	0.766	−6.68
	0.21	0.27	0.26	1.013	−6.56
	0.24	0.31	0.45	1.051	−6.40
	0.28	0.34	0.63	1.471	−6.23
Hydrogen bis(mandelato)borate	3.00	0.17	−0.17	0.029	−7.59
	3.60	0.19	−0.08	0.037	−7.38
	4.20	0.24	0.13	0.042	−7.25
	5.10	0.26	0.21	0.051	−7.09
	6.00	0.33	0.56	0.054	−7.03
Hydrogen bis(3-chloro- and 4-hydroxy mandelato)borate	1.54	0.19	−0.08	0.037	−8.93
	2.16	0.22	0.04	0.043	−8.67
	3.08	0.35	0.70	0.045	−8.54
	4.32	0.38	0.98	0.057	−8.39
Hydrogen bis(phenylmalonato)borate	1.50	0.10	−0.51	1.448	−5.94
	2.50	0.20	−0.04	1.773	−5.54
	3.00	0.24	0.13	1.812	−5.45
	4.00	0.29	0.35	1.858	−5.35
	5.00	0.34	0.63	2.086	−5.25

a) Total concentration of the carbinol form of Crystal Violet in terms of absorbance=b=0.42.
b) $[DH^+A^-]/[D] = x_e/(b - x_e)$.

Table 2. Results at Fixed [D] (1.12×10^{-5} M)[a] at Different [H_2R] at 25±0.5 °C

H_2R	$\frac{[HA]\times10^3}{M}$	x_e	$\log\frac{[DH^+A^-]}{[D]}$[b]	$\frac{k}{min^{-1}}$	$\log\frac{k}{K+[HA]^{-n}}$
Salicylic acid	1.01	0.17	−0.18	0.550	−7.16
	1.51	0.22	0.04	0.691	−6.89
	2.01	0.25	0.18	1.184	−6.58
	3.02	0.32	0.51	1.555	−6.28
	4.02	0.37	0.87	1.935	−6.24
Benzilic acid	0.60	0.17	−0.18	0.230	−9.89
	0.69	0.21	0.00	0.385	−9.69
	0.90	0.27	0.26	0.509	−9.46
	1.00	0.29	0.35	0.710	−9.29
	1.50	0.35	0.70	0.762	−9.17
Mandelic acid	1.05	0.20	−0.04	0.185	−9.12
	1.58	0.26	0.21	0.237	−8.85
	2.10	0.32	0.51	0.402	−8.55
	2.63	0.36	0.78	0.944	−8.14
3-Chloro- and	0.30	0.42	∞	0.064	−∞
4-hydroxy mandelic	0.50	0.42	∞	0.115	−∞
acid	0.60	0.42	∞	0.160	−∞
Phenylmalonic acid	0.20	0.42	∞	—[c]	—

a) Total concentration of the carbinol form of Crystal Violet in terms of absorbance=b=0.42. b) $[DH^+A^-]/[D]=x_e/(b-x_e)$. c) Very large (too fast for ordinary spectrophotometry).

Table 3. Association Constant (K), Individual Rate Constants (k_1, k_{-1}), and Acid Exponents (n, f, r) for Hydrogen Spiro-Borate-Carbinol Form of Crystal Violet Reaction in Toluene at 25±0.5 °C

Hydrogen spiro-borate	$\log K$	$\log k_1$	$\log k_{-1}$	n	f	r
Hydrogen bis(salicylato)borate	5.81	6.35	0.54	1.56	1.86	0.30
Hydrogen bis(benzilato)borate	6.29	5.43	−0.86	1.61	1.52	−0.09
Hydrogen bis(mandelato)borate	5.63	2.80	−2.83	2.32	1.87	−0.45
Hydrogen bis(3-chloro- and 4-hydroxy mandelato)borate	7.10	1.50	−5.60	2.57	1.17	−1.40
Hydrogen bis(phenylmalonato)borate	5.46	3.24	−2.22	2.12	1.30	−0.82

Table 4. Association Constant (K), Individual Rate Constants (k_1, k_{-1}), and Acid Exponents (n, f, r) for H_2R-Carbinol Form of Crystal Violet Reaction in Toluene at 25±0.5 °C

H_2R	$\log K$	$\log k_1$	$\log k_{-1}$	n	f	r
Salicylic acid	6.46	5.54	−0.92	1.67	1.55	−0.12
Benzilic acid	8.96	6.87	−2.09	2.16	1.83	−0.33
Mandelic acid	8.04	8.12	0.08	2.04	2.36	0.32
3-Chloro- and 4-hydroxy mandelic acid	—[a]	—[b]	—[b]	—	—	—
Phenylmalonic acid	—[a]	—[c]	—[c]	—	—	—

a) K, very large (virtually complete reaction, Table 2). b) k_1, large and k_{-1} very small (*vide* k from Table 2 and very large K). c) k_1, very large and k_{-1}, moderate (*vide* very large k from Table 2, and very large K).

among the reagents considered and justifies its wider use in boron determination.[1,2,5,12,13]

The work was supported by grant from the University Grants Commission, New Delhi, India.

References

1) S. Sato, *Anal. Chim. Acta*, **151**, 465 (1983).
2) M. Oshima, S. Motomizu, and K. Toei, *Anal. Chem.*, **56**, 948 (1984).
3) J. R. Garbarino, T. R. Steinheimer, and H. E. Taylor, *Anal. Chem.*, **57**, 46R (1985).
4) M. Oshima, K. Shibata, T. Gyouten, S. Motomizu, and K. Toei, *Talanta*, **35**, 351 (1988).
5) P. MacCarthy and R. W. Klusman, *Anal. Chem.*, **61**, 269R (1989).
6) R. P. Bell, "The Proton in Chemistry," 2nd ed, Chapman and Hall, London (1973), p. 12.
7) S. R. Bhowmik and S. R. Palit, *J. Indian Chem. Soc.*, **44**, 1049 (1967).
8) G. K. Saxena and S. R. Palit, *J. Indian Chem. Soc.*, **49**, 351 (1972).
9) A. Ghosh and S. R. Palit, *Indian J. Chem.*, **14A**, 19 (1976).
10) G. K. Saxena and S. R. Palit, *J. Indian Chem. Soc.*, **49**, 971 (1972).
11) A. Ghosh and S. R. Palit, *Indian J. Chem.*, **12**, 382 (1974).
12) S. Sato and S. Uchikawa, *Mem. Fac. Educ. Kumamoto Univ. Nat. Sci.*, **33**, 17 (1984).
13) S. Sato, *Talanta*, **32**, 447 (1985).

Studies on Some Dithiocarbamato-Bridged Heterobimetallic Complexes: Part II

N. K. SINGH,* Chetna KAW, and Nanhai SINGH
Department of Chemistry, Banaras Hindu University, Varanasi 221005, India
(Received July 30, 1990)

Synopsis. Some dithiocarbamato-bridged heterobimetallic complexes of the type $M^{I}[Zn(dtc)_3]$ and $M^{II}[Zn(dtc)_3]_2$, (M=Co(II), Ni(II), Cu(II), Pd(II), Pb(II), Cd(II), Tl(I), Ag(I), dtc=diethyldithiocarbamate), have been synthesized and characterized by elemental analysis, molar conductance, magnetic susceptibility, (^{1}H, ^{13}C) NMR, UV-visible, and infrared spectral studies. The complexes are nonelectrolytes. The infrared spectral bands and NMR signals indicate the presence of only one type of dithiocarbamate group. The electronic spectra of the complexes recorded in chloroform, pyridine, and dimethyl sulfoxide are similar to their nujol mull spectra indicating no change in the geometry of the central metal. Magnetic moment, electronic spectra, and ESR studies are commensurate with a square-planar geometry around Co(II), Ni(II), Pd(II), and Cu(II).

In the previous paper,[1] the synthesis and spectroscopic studies of some novel xanthato-bridged heterobimetallic complexes of the type M[M'(Etxant)$_3$]$_2$ and M[M'(Etxant)$_3$] have been reported. The ligand dithiocarbamate is closely related to xanthate, nevertheless due to replacement of oxygen with nitrogen some interesting changes in bonding behavior and reactivity of the complexes may be expected. With this viewpoint, we wish to report here the synthesis and structural studies of some analogous dithiocarbamato-bridged heterobimetallic complexes involving some transition and non-transition metal ions.

Experimental

All the chemicals used in the preparative work were BDH (AR) or equivalent grades. The solvents were freshly distilled. Sodium diethyldithiocarbamate trihydrate (Nadtc·3H$_2$O) was prepared according to literature procedure.[2] The experimental details pertaining to analysis of metals, sulfur, carbon, hydrogen, nitrogen, room-temperature magnetic susceptibility measurements, and recording of infrared and NMR spectra are same as described earlier.[1] ESR spectrum of Cu[Zn(dtc)$_3$]$_2$ was recorded in $CHCl_3$ on a Varian E-117 X-band spectrophotometer using DPPH (g=2.00277) as a g marker at room temperature.

Preparation of the Complexes: Na[Zn(dtc)$_3$] required for the synthesis of M[Zn(dtc)$_3$] and M[Zn(dtc)$_3$]$_2$ was prepared[3] in situ by adding 25 cm^3 acetone solution of zinc acetate (1 mmol, 0.220 g) to 40 cm^3 acetone-water mixture 90:10 (v/v) solution of Nadtc·3H$_2$O (3 mmol, 0.675 g). To the above Na[Zn(dtc)$_3$] solution, 25 cm^3 solution (1 mmol or 0.5 mmol) of $AgNO_3$ (0.17 g), Tl_2SO_4 (0.12 g), $CoCl_2·6H_2O$ (0.12 g), $NiCl_2·6H_2O$ (0.12 g), $CuSO_4·5H_2O$ (0.12 g), $Pb(NO_3)_2$ (0.16 g), $CdSO_4$ (0.15 g), or K_2PdCl_4 (0.16 g) dissolved in acetone-water 80:20 (v/v) was added gradually with constant stirring. All the heterobimetallic complexes which precipitated as fine crystalline material were filtered, washed with acetone-water 50:50 (v/v) mixture and dried in vacuum.

Results and Discussion

The analytical results (Table 1) indicate the formation of heterobimetallic complexes of the types M[Zn(dtc)$_3$] and M[Zn(dtc)$_3$]$_2$ by the metathetic reaction of Na[Zn(dtc)$_3$] and the corresponding metal salts in an appropriate molar ratio. The heterobimetallic complexes do not melt but decompose in the temperature range 165—225 °C. They are insoluble in water but soluble in most of the common organic solvents such as methanol, benzene, chloroform, *N*,*N*-dimethylformamide, dimethyl sulfoxide, and pyri-

Table 1. Analytical Data, Magnetic Moment, and Molar Conductance of Heterobimetallic Dithiocarbamates

Complex	Color	Mp/Decomp[b] temp °C	Found (Calcd)/% Zn	M	S	C	H	N	μ_{eff} BM	Molar coductance[a]
Ni[Zn(dtc)$_3$]$_2$	Light green	174(d)	12.30 (12.14)	5.8 (5.5)	36.12 (35.65)	33.80 (33.41)	5.74 (5.56)	7.66 (7.79)	Diamag.	1.58
Co[Zn(dtc)$_3$]$_2$	Green	225(d)	12.43 (12.14)	5.38 (5.47)	35.02 (35.66)	33.90 (33.40)	5.42 (5.56)	7.60 (7.79)	2.03	6.89
Cu[Zn(dtc)$_3$]$_2$	Brown	180(d)	11.93 (12.09)	5.43 (5.87)	30.83 (31.32)	33.08 (33.26)	5.47 (5.54)	7.38 (7.76)	2.23	1.35
Ag[Zn(dtc)$_3$]	Sky blue	165(d)	10.25 (10.59)	18.02 (17.49)	30.96 (31.10)	29.46 (29.15)	4.68 (4.85)	6.56 (6.80)	—	—
Tl[Zn(dtc)$_3$]	Dirty white	176(d)	8.56 (9.16)	29.01 (28.63)	26.03 (26.89)	24.58 (25.21)	4.43 (4.20)	5.98 (5.88)	—	2.14
Pb[Zn(dtc)$_3$]$_2$	Dirty white	166(d)	10.93 (10.67)	17.24 (16.90)	30.09 (31.32)	28.57 (29.36)	5.01 (4.89)	6.57 (6.85)	—	1.01
Cd[Zn(dtc)$_3$]$_2$	Dirty white	205	11.93 (11.56)	10.09 (9.93)	34.26 (33.94)	32.02 (31.82)	5.60 (5.30)	7.69 (7.42)	—	1.58
Pd[Zn(dtc)$_3$]$_2$	Yellow	173(d)	— (11.64)	— (9.29)	— (34.19)	29.43 (32.06)	5.04 (5.34)	6.39 (7.42)	—	2.56

a) In methanol. b) (d) Decomposition temp.

dine. The very low molar conductance values (1.01—6.89 $S cm^2 mol^{-1}$) in methanol are indicative of their nonelectrolytic nature.[4]

The magentic moment value of 2.03 BM and electronic spectral bands at 7000, 11400, 15600, and 20000 cm^{-1} for $Co[Zn(dtc)_3]_2$ suggest square-planar geometry around Co(II). The first and third bands are assigned to $^2A_{1g} \rightarrow {}^2E_{1g}$ and $^2A_{1g} \rightarrow {}^2E_{2g}$ transitions, respectively.[1] The most characteristic band at 11400 cm^{-1} for square-planar Co(II) complex gives the value of B=760 cm^{-1}.

The magnetic moment value of 2.23 BM for $Cu[Zn(dtc)_3]_2$ corresponds to one unpaired electron. Three bands at ca. 13600, ca. 14900, and ca. 21700 cm^{-1} in the visible region spectrum of this complex are assigned to $^2B_{1g} \rightarrow {}^2A_{1g}$, $^2B_{1g} \rightarrow {}^2B_{2g}$ and $^2B_{1g} \rightarrow {}^2E_g$ transitions in a square planar geometry[5,6] around Cu(II). The room-temperature ESR spectrum of $Cu[Zn(dtc)_3]_2$ in chloroform which gives the parameters $g_{\parallel}$=2.02, $g_{\perp}$=2.02, and g_{av}=2.02, together with the electronic spectral bands, indicate a four coordinate square-planar Cu(II) species.

The diamagnetic nature of $Ni[Zn(dtc)_3]_2$ and occurrence of bands at ca. 15900 and ca. 20400 cm^{-1} suggest square planar geometry around Ni(II). The latter absorption bands may be assigned to $^1A_{1g} \rightarrow {}^1B_{1g}$ and $^1A_{1g} \rightarrow {}^1A_{2g}$ transitions,[1] respectively. The value of the ligand field paremeter, Δ_1=18700 cm^{-1}, places the dithiocarbamate after xanthate in the spectrochemical series in a planar NiS_4 environment.

As expected $Pd[Zn(dtc)_3]_2$ complex is diamagnetic and exhibits a band at 22900 cm^{-1} which may be assigned to metal-ligand charge transfer. As compared to Ni(II) complexes, the first spin-allowed d-d transition in the Pd(II) complex is expected to occur at higher energy but it is generally not observed probably because it is masked by the tail of the following charge-transfer band.

In order to study the Lewis acid behavior, the heterobimetallic complexes containing Co(II), Ni(II), Pd(II), or Cu(II) as one of the metal ions have been dissolved in some coordinating as well as non-coordinating solvents like dimethyl sulfoxide, pyridine, chloroform and their UV-visible spectra were studied. The electronic spectral pattern of the complexes is almost similar to their nujol mull spectra, indicating no change in the geometry of the central metal and ruling out the possibility of ligand coordination to cobalt, nickel, palladium, or copper. $M[Zn(dtc)_3]_2$ [M=Ni(II), Co(II), or Cu(II)] complexes are quite insensitive to axial perturbation and their electronic spectra in donor solvents such as pyridine remain unchanged. In general NiS_4 complexes vary substantially in their ability to interact with Lewis bases. This tendency is closely related to the change in the electronic properties of the ligand as a whole rather than to the donor atoms alone. Thus xanthate,[7] dithiophosphate[8] complexes interact strongly, while dithiocarbamate complexes are generally unperturbed similar to the 1,2-dithiolene complexes[9] by dissolution in strong donor solvents such as pyridine. The reluctance of dithiocarbamate complexes to undergo axial interaction has been rationalized[2,10] by considering that sulfur atoms can donate electrons of π-symmetry into a nonbonding MO containing $4p_z$ function of the nickel ion. Any strong π-interaction of this kind should decrease the availability of the $4p_z$ orbital for interaction with bases. Thus the behavior of NiS_4 in this context suggests substantial S→Ni π-bonding and that the π-bonding increases in the order dithiophosphates≈xanthates<dithiocarbamates< dithiolene. This is also because, resonance form (b) is more dominating in dithiocarbamate complexes similar to dithiolene while resonance form (a) is dominating in case of binary metal xanthates. Electronic spectra of these complexes as nujol mull are almost similar to those of the analogous xanthato-bridged heterobimetallic complexes but the solution spectra show the absence of ligand-metal interaction.

The infrared spectra of all the heterobimetallic complexes studied over the region 4000—200 cm^{-1} (Table 2) are very similar and have been assigned on the basis of earlier studies.[2] The thioureide bands occurring at 1445—1460 cm^{-1} are attributed to the CN stretching vibration of the S_2C-NC_2H_5 bond. This band is in the midway of ν(C-N) (1250—1350 cm^{-1}) and ν(C=N) (1640—1690 cm^{-1}) and shows an increase in the double bond character of the C-N bond thereby justifying the major contribution of resonance form (b) for

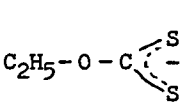

(a)

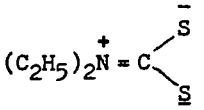

(b)

Table 2. Selected Infrared Spectral Bands (cm^{-1}) and ^1H and ^{13}C Chemical Shifts of the Complexes

Complexes	ν(C=N)	ν(C=S)	^1H		^{13}C	
			$-CH_3$	$-CH_2$	CH_3	CH_2
$Ni[Zn(dtc)_3]_2$	1460	1070, 1095	1.24(t)	3.62(q)	12.40	43.77
$Co[Zn(dtc)_3]_2$	1455	990, 975	1.27(q)	3.77(m)	12.13	42.74
					12.56	49.24
$Cu[Zn(dtc)_3]_2$	1460	1070, 1090	1.20	3.87	—	—
$Ag[Zn(dtc)_3]$	1445	990, 970				
$Tl[Zn(dtc)_3]$	1455	1070, 1090	1.33(t)	3.84(q)	12.14	49.20
$Pd[Zn(dtc)_3]_2$	1450	1070, 1095	1.33(t)	3.84(q)	12.20	48.44
$Cd[Zn(dtc)_3]_2$	1455	1070, 1095	1.34(t)	3.84(q)	12.13	49.89
$Pd[Zn(dtc)_3]_2$	1450	1070, 1090	1.32(5)	3.77(q)	12.40	49.24

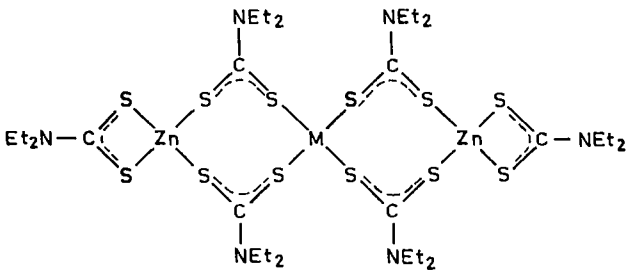

1. $M[Zn(dtc)_3]_2$

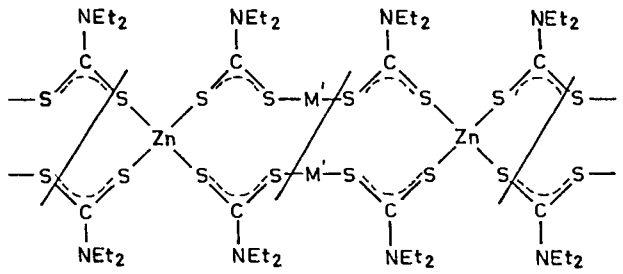

2. $M'[Zn(dtc)_3]$

Fig. 1.

dithiocarbamate complexes. The two bands occurring in the region 990—1070 and 970—1095 cm^{-1} are associated with $\nu(C\cdots S)$ vibrations, indicating unsymmetrical bidentate/bridging behavior of the dithiocarbamate moiety linked to two different metal centers. The bands observed below 400 cm^{-1} are due to metal-sulfur stretching vibrations.

^1H NMR spectra of the complexes (Table 2) exhibit signals due to $-CH_3$ and $-CH_2$ protons[10] around δ=1.24—1.34 and 3.62—3.84 in the intensity ratio of 3 : 2 which are in between monodentate and bidentate dithiocarbamate. This may be probably due to the bridging/unsymmetrical bidentate behavior of dithiocarbamate linked to two different metal centers. The downfield shift observed in $-CH_3$ protons and the upfield shift in $-NCH_2$ protons as compared to sodium dithiocarbamate indicate the deshielding of $-CH_3$ protons and shielding of $-NCH_2$ protons in these complexes. For $Co[Zn(dtc)_3]_2$ the increased number of peaks for $-CH_3$ and $-NCH_2$ protons is due to the presence of paramagnetic Co(II) and diamagnetic Zn(II) centers. However, in the case of $Cu[Zn(dtc)_3]_2$, the $-CH_3$ and $-NCH_2$ protons show broad signals because of the presence of paramagnetic Cu(II) center.

^{13}C NMR spectra of the diamagnetic complexes show two signals at δ=12.13—12.4 and 43.77—49.89 corresponding to $-\underline{C}H_3$ and $-N\underline{C}H_2$ carbons respectively and suggest the intermediate behavior (unidentate and bidentate) of dithiocarbamate attached to two metal centers. Each of these signals shows splitting for $Co[Zn(dtc)_3]_2$ indicating the presence of two types of $-N\underline{C}H_2-\underline{C}H_3$ carbons due to the presence of unpaired electron of Co(II).

On the basis of these studies the complexes are expected to have structures similar to the xanthato-bridged heterobimetallic complexes[1] (Fig. 1).

References

1) N. Singh, N. K. Singh, and C. Kaw, *Bull. Chem. Soc. Jpn.*, **62**, 3328 (1989).
2) D. Coucouvanvanis, *Prog. Inorg. Chem.*, **11**, 233 (1970); **26**, 301 (1979).
3) a) J. A. McCleverty and N. J. Morrison, *J. Chem. Soc., Chem. Commun.*, **1974**, 1048; b) J. A. McCleverty, S. Gill, R. S. Z. Kowalski, N. A. Bailey, H. Adams, K. W. Lumbard, and M. A. Murphy, *J. Chem. Soc., Dalton Trans.*, **1982**, 493.
4) W. J. Geary, *Coord. Chem. Rev.*, **7**, 81 (1971).
5) M. F. Corrigan, K. S. Murray, B. O. West, and J. R. Pilbrow, *Aust. J. Chem.*, **30**, 2455 (1977).
6) M. V. Rajsekharan, C. N. Setholakshmi, P. T. Manoharan, and H. Gudel, *Inorg. Chem.*, **15**, 2657 (1976).
7) D. L. Coffen, P. E. Garrett, and D. R. Williams, *J. Chem. Soc., Chem. Commun.*, **1968**, 652.
8) a) F. A. Cotton and R. H. Soderberg, *Inorg. Chem.*, **3**, 1 (1964); b) F. A. Cotton and R. C. Elder, *Inorg. Chem.*, **4**, 1145 (1965).
9) F. A. Cotton and J. F. Gibson, *J. Chem. Soc. A*, **1971**, 803.
10) R. Eisenberg, *Prog. Inorg. Chem.*, **12**, 295 (1971).
11) J. M. C. Alison and T. A. Stephenson, *J. Chem. Soc., Dalton Trans.*, **1973**, 254.

Synthesis of Tribromoacetic Anhydride and Its Reaction with Dimethyltin(IV) Oxide

Ram PARKASH,* Meena MEENA, and Sukhjinder SINGH
Department of Chemistry, Panjab University, Chandigarh 160014, India
(Received July 12, 1990)

Synopsis. The synthesis of previously unknown tribromoacetic anhydride and its reaction with dimethyltin(IV) oxide is reported. The compounds were characterized by analytical methods, IR, ^{1}H, ^{13}C, ^{119}Sn NMR, and MS (EI) spectral studies.

Conventional method of preparing carboxylic anhydrides by heating the respective carboxylic acid with P_4O_{10} and subsequent distillation of the anhydride formed, even under reduced pressure, lead to partial decomposition of the product in certain cases.[1] Consequently, a few halo carboxylic anhydrides were yet to be synthesized.[2-4] In continuation of the synthesis of dibromoacetic anhydride in these laboratories,[1] preparation of previously unknown tribromoacetic anhydride is reported by a similar method. Its reaction with dimethyltin(IV) oxide and the structural diagnosis of $(CH_3)_2Sn(O_2CCBr_3)_2$ using various techniques especially the multinuclear NMR spectral studies, was also carried out keeping in view the wide application of diorganotin(IV) carboxylates as catalysts and stabilizers.[5]

Experimental

Tribromoacetic acid (Fluka) was used as such. Dimethyltin(IV) oxide was prepared by literature methods.[6,7] The solvents were dried and distilled before use.

The IR spectra were recorded as Nujol/hexachlorobutadiene/CCl_4 smears between AgCl plates on a Perkin-Elmer 1430 IR spectrophotometer. ^{1}H, ^{13}C (proton decoupled), and ^{119}Sn NMR spectra were taken on a JEOL-FX-90Q spectrometer using TMS (Me_4Si), TMS(Me_4Si), and TMT (Me_4Sn), respectively, as external references. Mass spectra (EI) were obtained on a Vg Micromass 7070 F at 70 eV. Melting points are uncorrected. All manipulations were carried out in a dry box filled with nitrogen.

Synthesis of Tribromoacetic Anhydride. Tribromoacetic acid (9.45 g, 31.8 mmol) and phosphorus(V) oxide (14.5 g) were loaded into a 100 cm^3 Pyrex reactor in a dry box, and 60 cm^3 of CCl_4 was added to it. The reactor was then fitted with a reflux condenser and a drying tube. The contents were refluxed at 77 °C for 20 h. The reaction mixture was filtered under positive pressure of dry nitrogen, and the residual portion was repeatedly washed with CCl_4 (5×10 cm^3). Tribromoacetic anhydride (7.35 g, 12.8 mmol) was obtained as a white solid, mp 62—64 °C, yield: 80% after removing the solvent from the filtrate in vacuo. The product was checked for the absence of phosphorus and then recrystallized from CCl_4 as a shining white solid, mp 63—64 °C, yield: 72%. Found: C, 8.31; Br, 82.94%. Calcd for $C_4Br_6O_3$: C, 8.33; Br, 83.33%. IR#: 1855 sh, 1830 vs, 1778 m, 1265 vw, 1125 m, 1085 ms, 935 m, 780 m, 745 sh, 685 vw, 615 ms, 580 sh cm^{-1}.

Preparation of Dimethyltin(IV) Tribromoacetate. Tribromoacetic anhydride (1.18 g, 2 mmol) dissolved in 30 cm^3 of CCl_4 was added to 0.33 g (2 mmol) of dimethyltin(IV) oxide in a 100 cm^3 Pyrex reactor in a dry box. The contents were heated to reflux (80 °C) till a clear solution was obtained. The white solid separated out on cooling the solution to room temperature, was filtered under positive pressure of dry nitrogen and washed twice with CCl_4 (1 cm^3) and finally dried in vacuo. $(CH_3)_2Sn(O_2CCBr_3)_2$ (1.36 g, 1.8 mmol) was obtained as a white solid, mp 145—147 °C, yield: 90%. Found: C, 9.6; H, 0.83; Br, 64.1; Sn, 15.6%. Calcd for $C_6H_6Br_6O_4Sn$: C, 9.72; H, 0.81; Br, 64.8; Sn, 16.02%. IR: 1605 s, 1460 vw, 1360 ms, 1277 vw, 955 mw, 925 w, 805 mw, 760 ms, 720 sh, 515 vw, 460 m cm^{-1}. NMR (CD_2Cl_2) ^{1}H, δ=1.19 ($^{2}J(^{119}Sn, ^{1}H)$ 83.5 Hz); ^{119}Sn, δ=−190.6; ^{13}C (C_6D_6) δ=4.6 ($^{1}J(^{119}Sn, ^{13}C)$ 680 Hz).

Results and Discussion

Reaction between tribromoacetic acid and phosphorus(V) oxide in CCl_4 at 77 °C results in the formation of tribromoacetic anhydride in good yield.

$$2CBr_3COOH \xrightarrow[20\ h,\ 77\ ^{\circ}C]{P_4O_{10},\ CCl_4} (CBr_3CO)_2O$$

The progress of the reaction was monitored by ^{1}H NMR and IR spectroscopy. The reaction was considered to be complete when the test solution did not show any peak relating to OH of the CBr_3COOH in its IR and ^{1}H NMR spectra (tribromoacetic acid has sufficient solubility in warm CCl_4 to check its IR and NMR). Attempts to purify tribromoacetic anhydride by distillation, even under reduced pressure (0.1 Torr, 1 Torr=133.322 Pa), resulted in its significant decomposition. Purification was rather achieved by recrystallizing the product from CCl_4.

Tribromoacetic anhydride is a shining white powder stable at room temperature for more than 20 days in a dry atmosphere. Nearly 5% decomposition of the product was observed in 40 days. The decomposition of $(CBr_3CO)_2O$ was taken into account by the formation of free Br_2 in the storage vessel. Tribromoacetic anhydride is soluble in common organic solvents giving colorless solutions. It is extremely moisture sensitive and reacts readily with water to give tribromoacetic acid. The IR spectrum of $(CBr_3CO)_2O$ free from CBr_3COOH absorptions was obtained as a Nujol smear between AgCl optics. The anhydride is reactive towards KBr plates. Attempts to obtain IR spectra of neat anhydride led to the formation of some CBr_3COOH due to its hydrolysis by atmospheric moisture. A parent or molecular peak was not observed in the EI mass spectra of $(CBr_3CO)_2O$. However, peaks relating to CBr_3COO^+, CBr_3CO^+, CBr_3^+, CBr_2COOH^+, CBr_2CO^+, Br_2CH^+, Br_2C^+, Br_2^+, $BrCO^+$, $BrCH^+$, BrC^+, BrH^+, Br^+ fragment ions were observed. The

s, strong; m, medium; w, weak; v, very; sh, shoulder.

above protonated fragment ions observed in the mass spectra are due to hydrolysis of $(CBr_3CO)_2O$ by traces of moisture either in the probe or during manipulations.

The reaction between dimethyltin(IV) oxide and tribromoacetic anhydride in CCl_4 at 80 °C produces dimethyltin(IV) tribromoacetate in good yield:

$$(CH_3)_2SnO + (CBr_3CO)_2O \xrightarrow[80\,^\circ C]{CCl_4,\ 6\ h} (CH_3)_2Sn(O_2CCBr_3)_2$$

The reaction was complete in nearly 6 h, when a clear solution was obtained (dimethyltin(IV) oxide is completely insoluble in CCl_4 by itself). That the product is soluble in hot CCl_4 but separates out on cooling the solution to room temperature, serves the purpose of recrystallization. So this reaction provides a facile synthesis of $(CH_3)_2Sn(O_2CCBr_3)_2$ in one pot. The yield was not quantitative as some of the product remained in solution even at room temperature.

The preparation of $(CH_3)_2Sn(O_2CCBr_3)_2$ by the above route is not unprecedented. Dialkyltin(IV) acetates have been prepared by reacting dialkyltin(IV) oxide with acetic anhydride.[8]

Dimethyltin(IV) tribromoacetate, a white solid is extremely moisture sensitive and soluble in common organic solvents. It has, however, very low solubility in CCl_4 at ambient temperature.

A comparison of IR frequencies of $(CH_3)_2Sn(O_2CCBr_3)_2$ (see experimental section) with that of sodium tribromoacetate[9] revealed the covalently bonded tribromoacetato ligands in the former. The magnitude of $\Delta\nu$ ($\nu_{as}CO_2-\nu_sCO_2$) in $(CH_3)_2Sn(O_2CCBr_3)_2$ of the order of 245 cm^{-1} ($\nu_{as}CO_2-\nu_sCO_2$=1605−1360=245 cm^{-1}) is less than that in NaO_2CCBr_3 (1664−1355=309 cm^{-1}) and is thus indicative of bidentate tribromoacetato ligand. The magnitude of $\Delta\nu$ has been used in deciding the bonding modes of a carboxylato group. Generally, the magnitude of $\Delta\nu$ in a given carboxylate complex greater or lesser than that of sodium carboxylate reveals the unidentate or bidentate carboxylato ligand.[10,11] The splitting of ν_sCO_2 mode i.e. an additional weak band at 1460 cm^{-1}, may be attributed to the unsymmetrical bidentate tribromoacetato ligand.

The excellent agreement[12] of the NMR prediction and X-ray structure determination for $(CH_3)_2Sn(O_2CCH_3)_2$ has reinforced the power of the NMR structure correlations developed previously[13-15] for the structural analysis of methyltin(IV) compounds in solution and in solid state. It has been shown that the magnitude of tin-hydrogen J coupling, $|^2J(^{119}Sn, ^1H)|$ ($|^2J|$), is related to the H_3C-Sn-CH_3 angle according to the quadratic expression:[14]

$$\theta = (0.0161)\,(|^2J|)^2 - 1.32(|^2J|) + 133.4$$

and the magnitude of tin-carbon J coupling, $^1J(^{119}Sn, ^{13}C)$ ($|^1J|$), is linearly related to the H_3C-Sn-CH_3 angle by the following equation:[14]

$$|^1J| = 11.4(\theta) - 875$$

Where θ is the H_3C-Sn-CH_3 angle in deg and $|^1J|$ and $|^2J|$ are in Hz.

These relationships provide a simple method for estimating H_3C-Sn-CH_3 angles of methyltin(IV) solids from coupling constant values.

The ^1J and ^2J values for $(CH_3)_2Sn(O_2CCBr_3)_2$ are found to be 680 and 83.5 Hz, respectively. H_3C-Sn-CH_3 angle calculated for $(CH_3)_2Sn(O_2CCBr_3)_2$ from ^1J and ^2J values by using the above expressions, comes out to be 136.4° and 135.4°, respectively. These findings are in excellent agreement with that calculated (135°) for $(CH_3)_2Sn(O_2CCH_3)_2$ from $^1J(^{119}Sn, ^{13}C)$ both in solution and solid state and from $^2J(^{119}Sn, ^1H)$ values.[12,14] H_3C-Sn-CH_3 angle in $(CH_3)_2Sn(O_2CCH_3)_2$ has been found to be 135.9° by X-ray structural studies.[12] So distorted octahedral geometry may be anticipated around tin in $(CH_3)_2Sn(O_2CCBr_3)_2$ similar to that in $(CH_3)_2Sn(O_2CCH_3)_2$ on the basis of H_3C-Sn-CH_3 angle. The ^{119}Sn chemical shift of the order of −190.6 ppm relative to TMT also supports the six coordination[12,15-17] around tin in $(CH_3)_2Sn(O_2CCBr_3)_2$.

We wish to thank Ashwani Vij for recording ^1H and ^{119}Sn NMR spectra.

References

1) R. Parkash, S. Singh, and Meena, *Polyhedron*, **8**, 2941 (1989).
2) J. M. Tedder, *J. Chem. Soc.*, **1954**, 2646.
3) D. Martin, A. Wiese, and K. Nadolski, *Chem. Ber.*, **98**, 3286 (1965).
4) R. C. Mehrotra and R. Bohra, "Metal Carboxylates," Academic Press, London (1983).
5) C. J. Evans and S. J. Karpel, *J. Organomet. Chem. Libr.*, **16**, 1 (1985).
6) R. K. Ingham, S. O. Rosenberg, and H. Gilman, *Chem. Rev.*, **60**, 459 (1960).
7) E. G. Rochow and D. Seyferth, *J. Am. Chem. Soc.*, **75**, 2877 (1953).
8) Y. Maeda and R. Okawara, *J. Organomet. Chem.*, **10**, 247 (1967).
9) E. Spinner, *J. Chem. Soc.*, **1964**, 4217.
10) N. W. Alcock and V. M. Tracy, *J. Chem. Soc., Dalton Trans.*, **1976**, 2243.
11) G. B. Deacon and R. J. Phillips, *Coord. Chem. Rev.*, **33**, 227 (1980).
12) T. P. Lockhart, J. C. Calabrese, and F. Davidson, *Organometallics*, **6**, 2479 (1987).
13) T. P. Lockhart, W. F. Manders, and J. Zuckerman, *J. Am. Chem. Soc.*, **107**, 4546 (1985).
14) T. P. Lockhart, W. F. Manders, and E. M. Holt, *J. Am. Chem. Soc.*, **108**, 6611 (1986).
15) T. P. Lockhart and W. F. Manders, *Inorg. Chem.*, **25**, 892 (1986).
16) J. Otera, T. Hinoishi, Y. Kawabe, and R. Okawara, *Chem. Lett.*, **1981**, 273.
17) J. Otera, *J. Organomet. Chem.*, **221**, 57 (1981).

Comments on the "Synthesis and Characterization of Some New Organophosphonates and Their Adducts with Some Metals" by Saad and Ramadan[1]

Eli BREUER* and Amiram GOLDBLUM
Department of Pharmaceutical Chemistry, The Hebrew University School of Pharmacy, Jerusalem, 91120 Israel
(Received December 12, 1990)

Synopsis. This NOTE criticized experimental work, calculations and the conclusions based on them, in a paper recently publishied.[1]

In the above paper the authors claim to have synthesized ethyl hydrogen benzoylphosphonate and ethyl hydrogen butyrylphosphonate by hydrolyzing the corresponding diethyl esters by sodium hydroxide. They claim to have obtained the compounds, although they describe neither their appearance and criteria for their purity nor analytical results, except for ionization constants and selected infrared data.

The authors of the paper cited above are apparently unaware of the long known fact that dialkyl acylphosphonates are sensitive to alkaline conditions,[2-5] and hydrolyze rapidly to the corresponding carboxylic acids and to dialkyl phosphonate. Thus diethyl benzoylphosphonate and diethyl butyrylphosphonate certainly have undergone hydrolysis to benzoic or butyric acid and to diethyl (and/or ethyl hydrogen) phosphonate under the forcing conditions used by Saad and Ramadan (heating at 80 °C with a 6-fold molar excess of sodium hydroxide for 5 h in a sealed flask). This assumption is supported by the fact that the related dimethyl acetylphosphonate has been shown to hydrolyze with a half life of seconds at pH 7 at room temperature.[6] More detailed studies of the kinetics of the hydrolysis have also been reported.[7,8] Acylphosphonates are generally sensitive towards bases. For instance primary amines readily cleave the C-P bond in acylphosphonates and yield carboxamides and dialkyl phosphonates.[9]

Because of this sensitivity to hydrolytic conditions, the preparation of salts of unesterified acylphosphonic acids requires the use of silyl halide dealkylation.[10] Similarly, the preparation of salts of alkyl hydrogen acylphosphonate requires the use of a non-hydrolytic method, namely nucleophilic dealkylation by halides.[11]

We were the first to isolate and to characterize acylphosphonic acids and the corresponding monoesters.[12] Comparison of the infrared carbonyl frequencies reported by Saad and Ramadan for ethyl hydrogen benzoylphosphonate (1718 cm^{-1}) and ethyl hydrogen butyrylphosphonate (1740 cm^{-1}) with those reported by us for methyl hydrogen benzoylphosphonate (1650 cm^{-1}) and alkanoylphosphonates (1690 cm^{-1}) suggests that Saad and Ramadan had indeed benzoic acid and butyric acid, and not the compounds they claim, in their hand.

It is unfortunate that Saad and Ramadan did not make an effort to purify their hydrolysis products and seek proof of purity such as elemental analysis or homogeneity by chromatographic techniques. There is no doubt that the correct structures of the products would have become apparent if such efforts would have been made or if the products would have been examined by ^{31}P nuclear magnetic resonance spectroscopy.

The authors used the HMO method to correlate

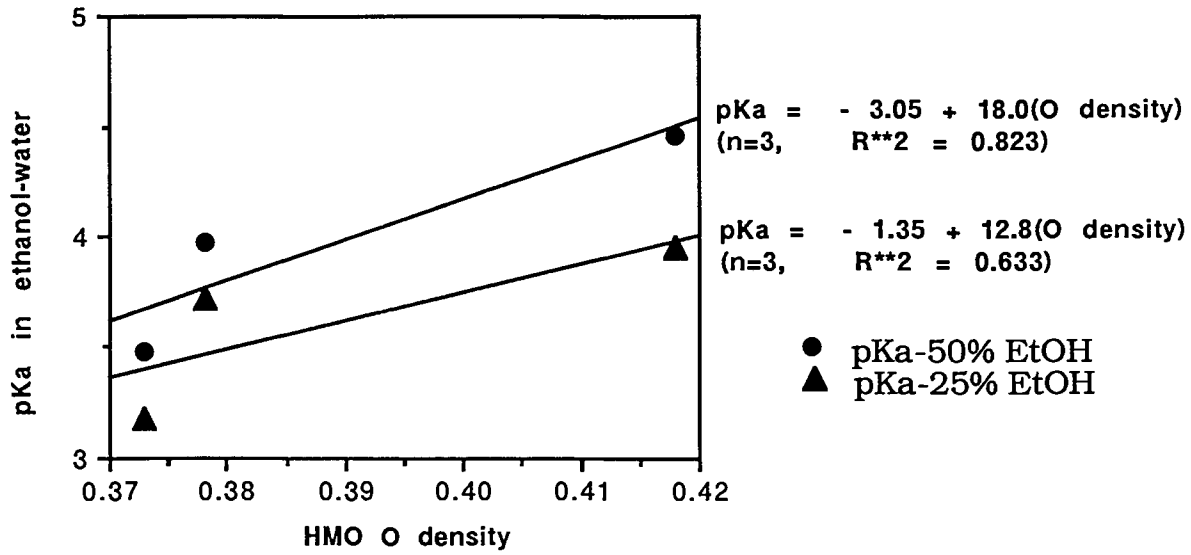

Fig. 1. pK_a dependence on oxygen densities, as reported by Saad and Ramadan.[1] The equations and correlations are marked on the right hand side for each of the two lines, for 50% and 25% ethanol-water.

between measured pK_a values and electron density on the hydroxylic oxygen in these compounds. We would like to comment on the use of Hückel calculations by the authors as well as on their claim of existing correlation.

The reference for HMO cited by the authors[13] does not list any parameters for phosphorus, and the paper does not indicate which parameters were employed for α and for β of this element. In addition, it is clear, and also established by X-ray data (e.g. for sodium hydrogen acetylphosphonate[14]), that the phosphonate group is not planar. In such cases nonplanarity should be taken into account by variation of the value of β for the relevant atoms according to their angular deviation from planarity.[13] This is not mentioned as the procedure which was followed.

pK_a values represent a difference in stability between the neutral and deprotonated molecules in the current environment. Such an environment effect is reflected also in the experimental differences found by the authors between 50% and 25% ethanol-water mixtures. It is possible, in the framework of HMO,[13] to study such differences between neutral molecules and their anions. Unfortunately, the authors do not appear to have tested this option.

The authors further claim that the decrease in electron densities of the hydroxylic oxygen in the three compounds "··· is consistent with the order of increasing acidity and accounts for the closest pK_a values of the butanoyl and benzoyl derivatives, 3.98 and 3.48, respectively". However, the correlation coefficient for the three compounds is very poor with R^2=0.823, for these pK_a values in 50% ethanol-water. The correlation for the 25% ethanol-water is even poorer, with R^2=0.633. Figure 1 clarifies this point.

A final point concerns the values of electron densities obtained by the authors. The overall density on the phenyl ring of the benzyl derivative is 5.272 (out of the original 6 electrons). In the benzoyl derivative, it is 5.610. This indicates that with their calculations, the authors find that a carbonyl adjacent to a phenyl ring is donating electrons to the ring, compared to a methylene at the same position, all other things being equal. This result should have made clear to the authors that something is wrong with the results, with the method or with their scheme of parametrization.

References

1) E. A. Saad and R. M. Ramadan, *Bull. Chem. Soc. Jpn.*, **62**, 3697 (1989).
2) M. I. Kabachnik and P. A. Rossiiskaya, *Izv. Akad. Nauk SSSR, Otd. Khim. Nauk*, **1945**, 364.
3) B. Ackerman, T. A. Jordan, C. P. Eddy, and D. Swern, *J. Am. Chem. Soc.*, **78**, 4444 (1956).
4) K. D. Berlin and H. A. Taylor, *J. Am. Chem. Soc.*, **86**, 3862 (1964).
5) Yu. A. Zhdanov, L. A. Uzlova, and Z. I. Glebova, *Russ. Chem. Rev. (Engl. Transl.)*, **49**, 843 (1980).
6) R. Kluger, D. C. Pike, and J. Chin, *Can. J. Chem.*, **56**, 1792 (1978).
7) W. Jugelt, S. Andreae, and G. Schubert, *J. Prakt. Chem.*, **313**, 83 (1971).
8) S. Andreae and W. Jugelt, *Z. Chem.*, **13**, 136 (1973).
9) M. Sekine, M. Satoh, H. Yamagata, and T. Hata, *J. Org. Chem.*, **45**, 4162 (1980).
10) M. Sekine and T. Hata, *J. Chem. Soc., Chem. Commun.*, **1978**, 285.
11) T. A. O'Brian, R. Kluger, D. C. Pike, and R. B. Gennis, *Biochim. Biophys. Acta*, **613**, 10 (1980).
12) R. Karaman, A. Goldblum, E. Breuer, and H. Leader, *J. Chem. Soc., Perkin Trans. 1*, **1989**, 765.
13) A. Streitwieser, "Molecular Orbital Theory for Organic Chemists," Wiley, New York (1961).
14) P. G. Jones and O. Kennard, *Acta Crystallogr., Sect. B*, **34**, 2309 (1978).

Spin-Trapping Studies on the Reaction of Iron Complexes with Peroxides and the Effects of Water-Soluble Antioxidants

Masahiro KOHNO,* Masako YAMADA, Keiichi MITSUTA, Yokio MIZUTA, and Toshikazu YOSHIKAWA†
ESR Application Laboratory, Analytical Instruments Division, JEOL Ltd.,
1-2 Musashino 3-Chome, Akishima, Tokyo 196
† First Department of Medicine, Kyoto Prefectural University of Medicine, Kamigyo-ku, Kyoto 602
(Received October 29, 1990)

Using ESR spin-trapping techniques we measured the levels of free radical species generated from six different systems (hypoxanthine–xanthine oxidase, iron(II)–hydrogen peroxide, iron(III)–hydrogen peroxide, iron(II)–*t*-butyl hydroperoxide, iron(III)–*t*-butyl hydroperoxide, and catalase (CAT)–*t*-butyl hydroperoxide). Six types of radicals ($O_2^{-\cdot}$, ·OH, ·H, ·CH_3, $(CH_3)_3CO$·, and $(CH_3)_3COO$·) were detected as spin adducts of spin traps 5,5-dimethylpyrroline 1-oxide (DMPO) or 3,5-dibromo-4-nitrosobenzene sulfonate (DBNBS). Quantitative analysis of the levels of generated radicals by means of an ESR instrument also presents important information regarding the reduction of peroxides [hydrogen peroxide (H_2O_2) or *t*-butyl hydroperoxide (ROOH)] by iron(II) or iron(III) as well as catalase. In addition, the scavenging potencies of different water-soluble antioxidants such as L-ascorbic, D-isoascorbic, gallic, sorbic, and protocatechuic acids were evaluated in terms of their ability to reduce the peaks of spin adducts.

Active oxygens such as superoxide anion radical ($O_2^{-\cdot}$, ·OOH), hydroxyl radical (·OH), hydrogen peroxide (H_2O_2), and singlet oxygen ($^1O_2$) have been implicated as being major damaging species in pathology and have been widely investigated.[1] These compounds react with the lipids of membranes and through a series of reactions generate carbon-centered (R·), alkoxyl (RO·), and then peroxyl (ROO·) radicals, all of which are used as markers of lipid peroxidation and the disruption of cellular homeostasis.[2,3] Also widely explored are studies scavenging phenomena of these active oxygens and free radicals by such antioxidants as vitamins C and E, and glutathione, and by scavengers such as superoxide dismutase (SOD) as well as catalase (CAT).[4-7]

The ESR spin-trapping technique is very useful for stabilizing short-lived free radicals. This technique has therefore been a powerful tool for studying generation mechanisms of free radicals and active oxygens[8-10] as of free radicals.[11-23]

The present study was carried out in order to establish a detection method for such free radicals as $O_2^{-\cdot}$, ·OH, ·H, ·CH_3 (R·), $(CH_3)_3CO$· (RO·), and $(CH_3)_3COO$· (ROO·). The six radical-generating systems were: hypoxanthine–xanthine oxidase which generates $O_2^{-\cdot}$ and ·OOH; iron(II)– hydrogen peroxide which gives ·OH; iron(III)–hydrogen peroxide, ·OH; iron(II)–*t*-butyl hydroperoxide and iron(III)-*t*-butyl hydroperoxide, R·, RO·, ROO·, and CAT–*t*-butyl hydroperoxide, RO·. The mechanism in Fenton's or catalase reactions between iron(II), iron(III), or CAT and ROOH or H_2O_2, are also described based on the results obtained from experiments performed under several conditions. Finally, the potencies of water-soluble antioxidants (L-ascorbic acid, D-isoascorbic acid, gallic acid, sorbic acid, and protocatechuic acid) in scavenging $O_2^{-\cdot}$, ·OH, ROO·, and/or RO· are described.

Experimental

Materials. Spin trapping reagents 5,5-dimethylpyrroline I-oxide (DMPO) and 3,5-dibromo-4-nitrosobenzene sulfonate (DBNBS), were supplied by Mitsui Toatu Chemicals and by Sigma Chemical Co., Ltd., respectively. Diethylenetriamine-*N*,*N*,*N*′,*N*″,*N*″-pentaacetic acid (DETAPAC), used to chelate trace metal impurities, was obtained from Wako Pure Chemical. The following were the sources of different radicals and their corresponding suppliers: sources of superoxide radical [hypoxanthine (HPX) from Sigma Chemical, and xanthine oxidase (XOD) from Boehringer Mannheim, cow milk]; source of hydroxyl radical [iron(II) sulfate heptahydrate (ferrous iron) and iron(III) sulfate *n*-hydrate (ferric iron) from Wako Pure Chemical Ins., Ltd., and hydrogen peroxide (H_2O_2)]; source of methyl, *t*-butoxyl, *t*-butylperoxyl radicals [iron(II) or iron(III) and *t*-butyl hydroperoxide (ROOH) from Nakarai Kagaku Co.]. Antioxidant reagents L-ascorbic acid, D-isoascorbic acid (erythorbic acid), and gallic acid were purchased from Daiichi Pure Chemical, while sorbic acid and protocatechuic acids were obtained from Wako Pure Chemical Ins.

Instruments. ESR spectra were recorded on a JEOL JES-RE1X spectrometer using aqueous quartz flat cell (Inner size 60 mm×10 mm×0.31 mm) with an effective sample volume 160 μl.

Preparation of Samples. All measurements were carried out both in 0.1 M (M=mol dm^{-3}) of PBS (sodium phosphate buffer solution) (pH=7.8) and in pure water at room temperature. Both peroxides, H_2O_2 and ROOH, were used as aqueous solutions. The concentration of the antioxidants used in this experiment was 1.0 mM (1 mM=1.0×10^{-3} mol dm^{-3}). Superoxide radicals were generated from a hypoxanthine xanthine oxidase reaction system under the conditions reported previously.[15,17]

Results and Discussion

Detection and Identification of Radicals [$O_2^{-\cdot}$, ·OH, ·H, R·, RO·, and ROO·]. The ESR spectra of the spin

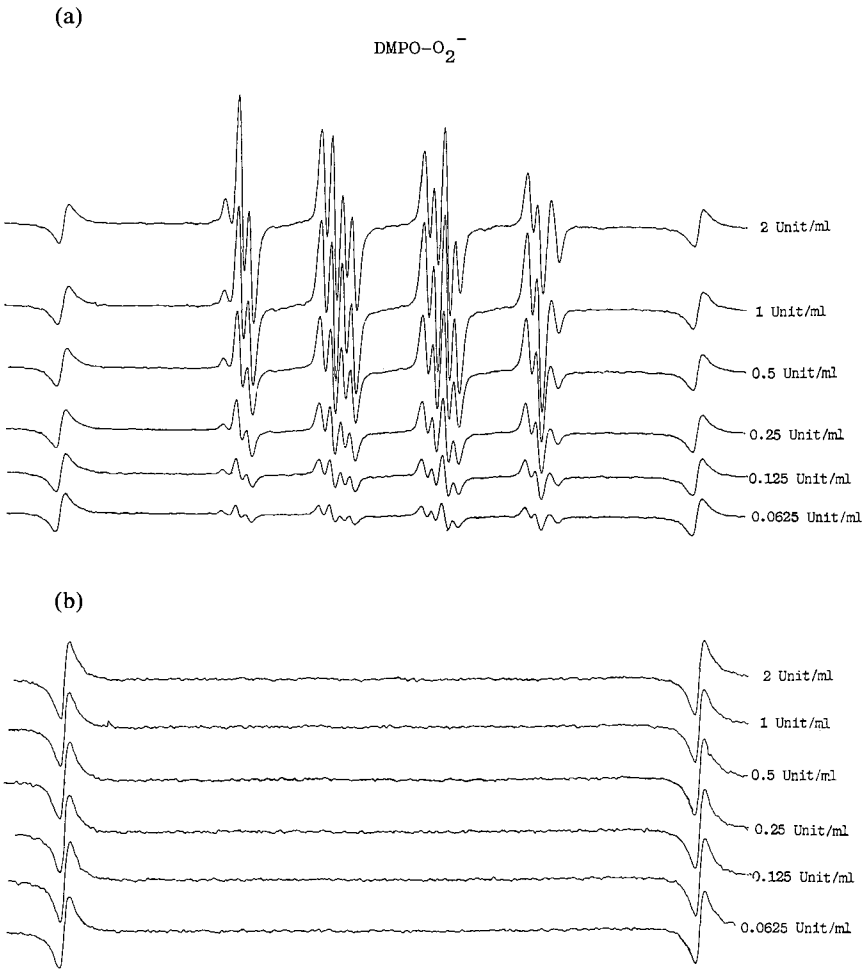

Fig. 1. ESR spectra of spin adducts of $O_2^{-\cdot}$, observed by the use of spin traps DMPO (a) and DBNBS (b). Spectrum (a) recording started 30 s after mixing 50 μl 2 mM HPX, 35 μl 5.5 mM DETAPAC, 15 μl 9.2 M DMPO (a), 50 μl 0.1—0.5 U ml^{-1} XOD, and 50 μl PBS. Spectrum (b) was observed under same conditions but without 15 μl 60 mM DBNBS.

adducts obtained in the hypoxanthine–xanthine oxidase reaction by using two kinds of spin traps, DMPO and DBNBS, are shown in Figs. 1a and 1b. In these figures, the peaks at either ends are of Mn^{2+} in MgO, which is used as an internal standard. The g values of both peaks are 2.0334 and 1.9810 at the resonance frequency of 9450.0 MHz, respectively. The method of measurement and the reaction conditions used in the experiments have been described previously.[10,17] As shown in Fig. 1a, a spin trapped by DMPO increases with the XOD concentration, and the hyperfine coupling constants (hfcc) obtained from the spectra coincide with the values of DMPO–O_2^- reported previously.[8] Using the spin trap DBNBS instead of DMPO, no signals were observed under the same conditions (Fig. 1b). However, the addition of DBNBS (60 mM) reduced the signal intensity of DMPO–O_2^-. From the experimental results for changing the concentration of DBNBS, the value of 50% inhibition(ID_{50}) of DMPO–O_2^- was measured to be 0.3 mM. The reaction rate constant (k_2) of DBNBS with $O_2^{-\cdot}$ in a hypoxanthine–xanthine odixase reaction were determined to be 3.9×10^4 M^{-1} s^{-1} at pH=7.8 from ID_{50} by treating for competitive reaction.[14] This value is 5.9-times larger than the previous reported value, 6.6×10^3 M^{-1} s^{-1} at pH=7.0, obtained by a pulse radiolysis method.[26] The difference may be due to differences in the pH and generation system of $O_2^{-\cdot}$. The results clearly indicate that both DMPO and DBNBS react with $O_2^{-\cdot}$. However, only DMPO gives a spectrum of the $O_2^{-\cdot}$ spin adduct. No $O_2^{-\cdot}$ spin adduct signals can be detected in the case of DBNBS. It is speculated that nitrones are better than nitroso compounds in detecting $O_2^{-\cdot}$ as a spin adduct.

Figures 2a and 2b show the spectra of the spin adducts obtained using DMPO or DBNBS, respectively, in reactions between 0.1 mM iron(II) chelated by DETAPAC (0.1 mM) and H_2O_2 (1 mM) in pure water.

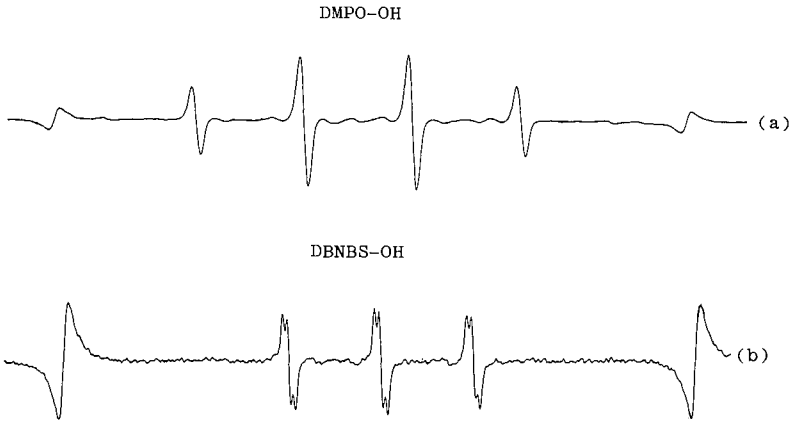

Fig. 2. ESR spectra of spin adducts of ·OH observed by the use of spin traps DMPO (a) and DBNBS (b). Spectra recording started 30 s after mixing 75 μl 0.1 mM iron(II) chelated by 0.1 mM DETAPAC before use [iron(II)-DETAPAC], 75 μl 1 mM H_2O_2, 50 μl 60 mM DMPO and 60 mM DBNBS, in 50 μl pure water.

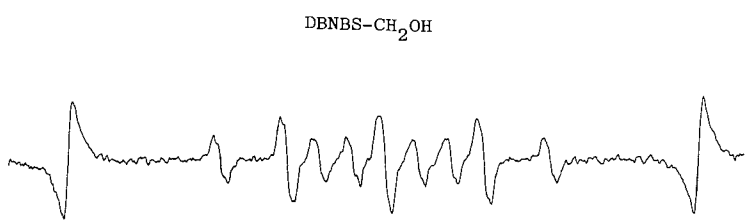

Fig. 3. ESR spectra of spin adducts of ·CH_2OH after mixing 75 μl 0.1 mM iron(II)-DETAPAC, 75 μl 1 mM H_2O_2, 15 μl 60 mM DBNBS and 50 μl 1.6 mM methanol.

In the case of DMPO (Fig. 2a), a typical hfcc was obtained as a_N=1.48 and $a_{H\beta}$=1.48 mT, which is the same as the typical value of DMPO-OH.[12] Using iron(III) (0.1 mM) instead of iron(II), less DMPO-OH is generated (Fig. 2b).

The results of the above-mentioned experiments demonstrate that iron(II) is more active than iron(III) in the reduction reaction of H_2O_2. With DBNBS, the hfcc of the signal is analyzed as a_N=1.24 mT and a_H=0.063 mT (Fig. 2b), which coincide with those reported previously.[26,27] However, the previous studies have many uncertainties,[27] since this adduct was assigned to DBNBS-O_2^-. In order to confirm that this radical species was DBNBS-OH, the methanol, which is a specific scavenger of ·OH, was added to the reaction system. Then, the signal decayed with increasing methanol concentration. When 1.6 mM methanol was added, another spin adduct, which is assigned as methanol radical (DBNBS-CH_2OH; a_N= 1.36 mT, a_H=0.91 mT and a_H=0.06 mT),[20,27] is detected as is shown in Fig. 3. In addition, a concomitant increase in the intensity of the DBNBS-OH signal is observed with increasing amount of added H_2O_2 (Fig. 4). Thus,·OH can be trapped not only by DMPO, but also by DBNBS. The rate constant (k_2) for the reaction of DBNBS with ·OH is determined to be 2.2×10^{10} M^{-1} s^{-1}, as measured from its competitive reaction with DMPO in trapping ·OH radicals. In this treatment, $k_2=3.4\times10^9$ M^{-1} s^{-1} [19] was used as the rate constant for the reaction of DMPO to trap ·OH. From these values, DBNBS is more sensitive than DMPO for detecting ·OH.

In the reaction between iron(II) of 0.1 mM chelated by DETAPAC of 0.1 mM, and H_2O_2 (0.01 mM), two kinds of spin adducts, DMPO-OH and DMPO-H, are observed (Fig. 5). Thus, from these spectra, it is confirmed that at least two types of radicals (·H and ·OH) are generated in the reaction. The concentration of the generated DMPO-OH agrees with that of DMPO-H under this reaction.

Using DMPO, both the reactions between iron(II) or iron(III) and ROOH give three kinds of spin adducts of methyl (R·), *t*-butoxyl (RO·), and *t*-butylperoxyl (ROO·) radicals (Fig. 6). However, when DBNBS was used, only the spin adduct of methyl radical (DBNBS-CH_3: a_N=1.37 mT and a_{CH_3}=1.35 mT and a_H=0.07 mT) was observed (Fig. 7). The reaction between the iron(III) and ROOH give a relatively weak signal of methyl

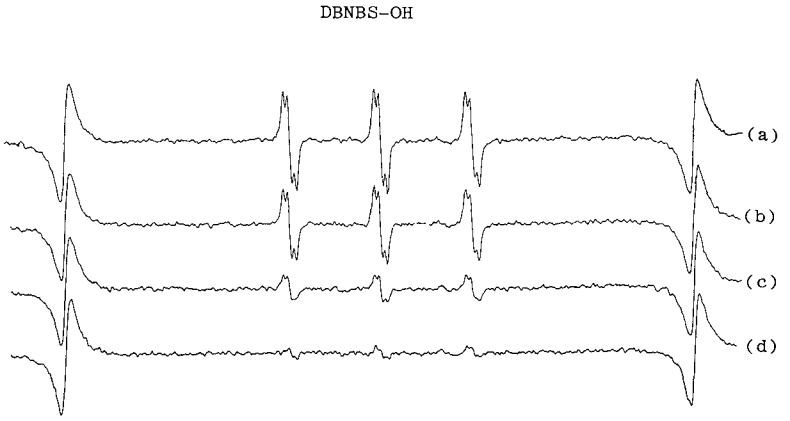

Fig. 4. ESR spectra of spin adducts of ·OH observed by the use of spin trap DBNBS. 75 μl 0.1 mM iron(II)–DETAPAC, 75 μl of (a) 1 mM, (b) 0.5 mM, (c) 0.25 mM and (d) 0.125 mM H_2O_2 concentration, 15 μl 60 mM DBNBS, in 50 μl pure water.

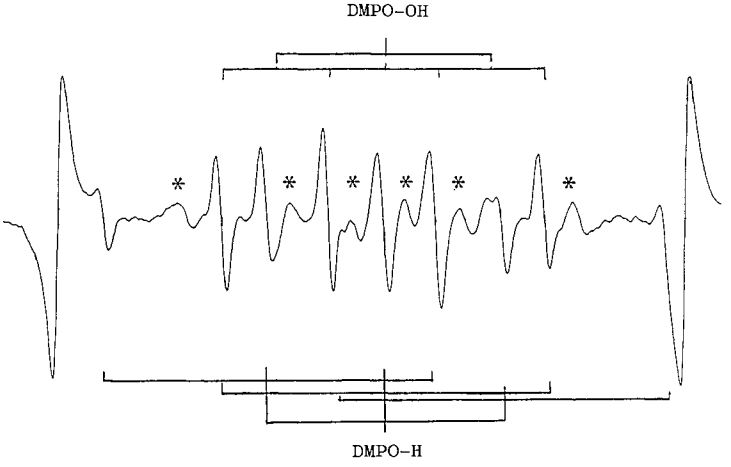

Fig. 5. ESR spectra of spin adducts of ·OH and ·H after mixing 75 μl 0.1 mM iron(II)–DETAPAC, 75 μl 0.01 mM H_2O_2, 15 μl, 0.92 M DMPO, in 50 μl pure water. The signal with "*" is the adduct of carbon center radical.

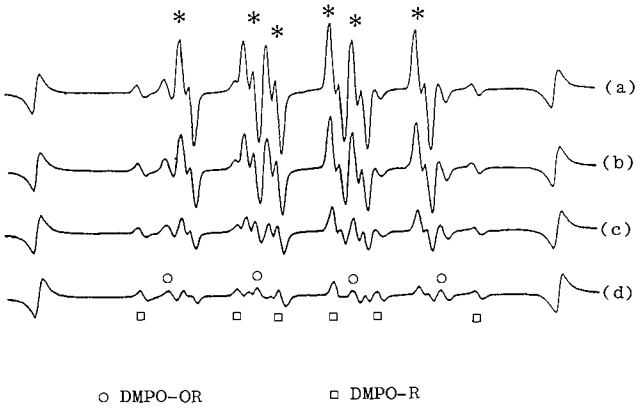

Fig. 6. ESR spectra observed in the reaction between 0.1 mM iron(II)–DETAPAC and ROOH of (a) 10 mM, (b) 5 mM, (c) 2.5 mM, (d) 1.25 mM ROOH concentration. The signal with "*" is the adduct of ROO·.

Table 1. Hyperfine Coupling Constants of Spin Adduct of Radicals, O_2^{-}, ·OH, ·H, R·, RO·, and ROO·[a)]

Spin adduct.	a_N	a_H^β	a_H^γ
DMPO-O_2^-	1.41	1.14	0.13
DMPO-OH	1.48	1.48	
DMPO-H	1.64	2.25	
DMPO-OOR	1.45 (1.45)	1.05 (1.05)	0.14 (0.15)
DMPO-OR	1.49 (1.48)	1.57 (1.60)	
DMPO-R	1.64	2.24	

a) ( ) is reported values.

adducts (Fig. 7). In the case of the reaction with CAT, only RO· is observed (Fig. 8). The spin adducts of R·, RO·, and ROO· were identified using the hfcc values listed in Table 1.[29,30)] As shown in Figs. 7 and 8, the spin adducts of ROO· and RO· changed, depending on each concentration of iron(II), CAT and ROOH.

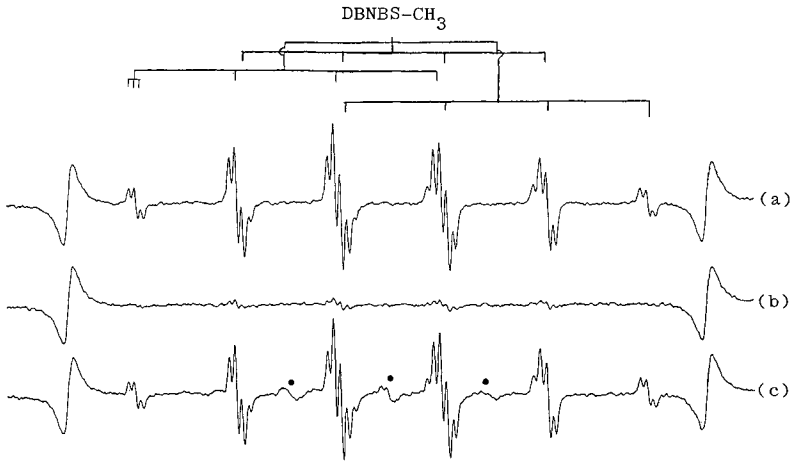

Fig. 7. ESR spectrum of $\cdot CH_3$ was observed by the use of DBNBS in the reaction between 1.0 mM iron(II) (a), iron(III) (b), iron(II)–DETAPAC (c) and 10 mM ROOH. The signal with "*" is the adduct of carbon center radical.

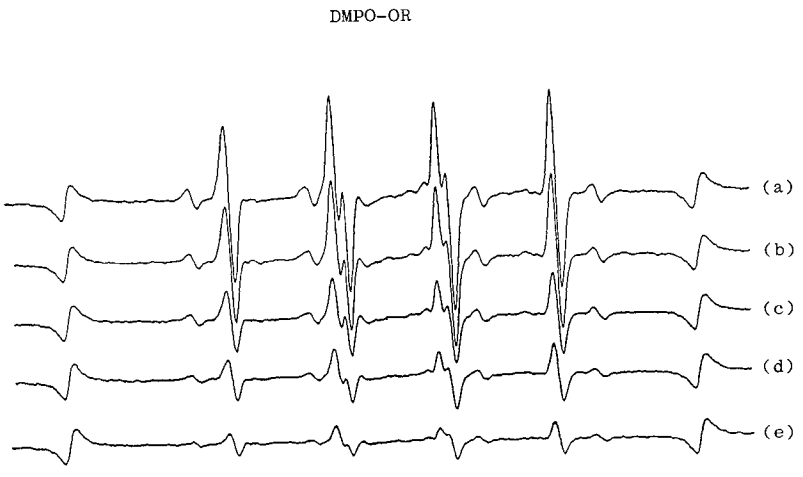

Fig. 8. ESR spectra observed in the reaction between ROOH and catalase of (a) 0.086 mM, (b) 0.043 mM, (c) 0.022 mM, (d) 0.011, (e) 0.006 mM catalase concentration.

In spin-trapping experiments, it can be confirmed that the results are very much affected by the concentration of DMPO used. For instance, if the DMPO concentration changed from 23 mM to 690 mM, the main observed spin adduct changed from RO· to ROO·, as well as the experiments for detecting ·OH and ·H. Thus, varying the DMPO concentration allows one to analyze specific radicals.

Reactivity of Water Soluble Antioxidants with $O_2^{-\cdot}$, ·OH, ROO·, and RO·. When DMPO was added to a solution of a radical-generating system, several spin adducts such as DMPO-O_2^-, DMPO-OH, DMPO-OOR, and DMPO-OR were detected. Various antioxidants such as L-ascorbic acid, D-isoascorbic acid, gallic acid, sorbic acid, and protocatechuic acid were diluted to 1 mM in pure water and added to a solution of the radical-generating system. Then, the amount of each spin adduct was found to decrease. These changes in the intensity of the ESR spectra were evaluated for the scavenging potencies of various antioxidants on $O_2^{-\cdot}$, ·OH, ROO·, and RO·. Table 2 shows the percent intensities of the spin adducts after the addition of antioxidants under the measurement conditions, as shown in the table, all of which were of equal concentration (1 mM). Based on Table 2, the scavenging action on $O_2^{-\cdot}$ of various antioxidants investigated decrease in the order D-isoascorbic acid > gallic acid > L-ascorbic acid > protocatechuic acid ≫ sorbic acid. As for ·OH, the potencies of antioxidants decrease in the order D-isoascorbic acid > L-ascorbic acid ≫ gallic acid = protocatechuic acid = sorbic acid=0%. For RO·, that order is gallic acid > protocatechuic acid ≫ sorbic

Table 2. Scavenging Activities(%) of Water Soluble Antioxidants L-Ascorbic Acid, D-Isoascorbic Acid, Sorbic Acid Protocatechuic Acid, and Gallic Acid against $O_2^{-\cdot}$, ·OH, ROO·, and RO·

Compound	$O_2^{-\cdot}$ [a]	·OH [b]	ROO· [c]	RO· [d]
L-Ascorbic acid	93.3	70.3	0	0
D-Isoascorbic acid	100.0	100.0	0	0
Sorbic acid	0	0	0	5.8
Protocatechuic acid	63.6	0	10.3	3.0
Gallic acid	96.5	0	0	28.5

Measurement conditions for generating $O_2^{-\cdot}$, ·OH, RO·, ROO· are shown as follows. a) $O_2^{-\cdot}$, 2 mM HPX+5.5 mM DETAPAC+0.4 U ml^{-1}+0.7 M DMPO. b) ·OH, 0.1 mM iron(II)-DETAPAC+1 mM H_2O_2+0.92 M DMPO. c) ROO·, 1.0 mM iron(II)-DETAPAC+5 mM ROOH+0.07 M DMPO. d) RO·, 1.0 mM iron(II)-DETAPAC+5 mM ROOH+0.07 M DMPO.

acid $\gg$ L-ascorbic acid = D-isoascorbic acid= 0%. In the case of ROO·, only protocatechuic acid show the function.

Reaction Mechanisms

The Fenton's Reaction. It has been reported that the formation of ·OH in a Fenton's reaction was directly confirmed using the spin trapping technique.[31,32] However, the reaction mechanism between iron(II) and H_2O_2 was assumed[33] to be

$$H_2O_2 + Fe^{2+} + H^+ \longrightarrow \cdot OH + Fe^{3+} + H_2O. \quad (1)$$

In our experiment two radical species (·OH and ·H) were observed in a Fenton's reaction used the H_2O_2 of low concentration for the concentration of iron(II). We thus propose the following reaction scheme, whereby both ·OH and ·H are generated:

$$H_2O_2 + Fe^{2+} \longrightarrow Fe^{3+}\text{-}OOH^- + \cdot H \quad (2)$$
$$Fe^{3+}\text{-}OOH^- \longrightarrow Fe^{4+}{=}O^{2-} + \cdot OH \quad (3)$$
$$H_2O_2 + Fe^{2+} \longrightarrow \cdot H + \cdot OH + Fe^{4+}{=}O^{2-} \quad (4)$$

In addition, it can be speculated that the existence of ·OOH generates a reaction between O_2 and ·H. In the case of a high H_2O_2 concentration,[13] ·OH is mainly observed. We therefore propose the follow reaction:

$$H_2O_2 + Fe^{2+} \longrightarrow \cdot OH + Fe^{3+}\text{-}OH. \quad (5)$$

Catalase Reaction. As in the case of a Fenton's reaction, this catalase reaction mechanism with regard to the radical reaction has not been proven experimentally. The proposed catalase reaction mechanism is according to

$$\text{Catalase} + 2H_2O_2 \longrightarrow 2H_2O + O_2. \quad (6)$$

To clarify the mechanism for the oxidation of H_2O_2, the reaction of iron(II), iron(III), or ROOH with CAT and H_2O_2 were assayed under different conditions. Mixtures of just catalase and H_2O_2 gave no signals. However, the ESR spectrum of alkoxyl radical[$(CH_3)_3CO\cdot$] was detected in a reaction between the catalase and ROOH. We therefore propose the existence of the following reaction mechanism:

$$\text{Catalase} + (CH_3)_3COOH \longrightarrow (CH_3)_3CO\cdot + \text{catalase-OH} \quad (7)$$

$$2\ \text{Catalase} + H_2O_2 \longrightarrow 2\ \text{catalase-OH (Compound-II)}^{7} \quad (8)$$

However, the generation of molecular O_2 in the reaction (Eq. 6) has been confirmed. Unknown factors in the mechanisms in the catalase reaction are as follows:

$$H_2O_2 \longrightarrow 2\cdot OH \quad (9)$$
$$H_2O_2 \longrightarrow \cdot H + \cdot OOH \quad (10)$$
$$\cdot OOH \longrightarrow \cdot H + O_2 \quad (11)$$
$$2\cdot H + 2\cdot OH \longrightarrow 2H_2O \quad (12)$$
$$2H_2O_2 \longrightarrow 2H_2O + O_2 \quad (13)$$

The net equation (Eq. 13) is the same as that of Eq. 6.

Peroxides Reaction.[34] The reaction between iron(II) and ROOH generates three kinds of radicals (RO·, R·, and ROO·). Catalase reacts with ROOH, and generates RO·. Both results show that radical generation is modulated by the redox state and the conformation of the iron sites. The reaction of catalase is expressed as a function of the peroxidase.

These studies confirmed the previous results obtained from indirect assays, which indicated that $O_2^{-\cdot}$, ·OH, ·H, R·, RO·, and ROO· are generated by bio-relative reaction systems. Whether these compounds are the natural microbiological products of the oxidation process or simply intermediates in a complex series of reactions has yet to be determined. The methods employed here allow us to measure the antioxidant potencies of L-ascorbic, D-isoascorbic, sorbic, protocatechuic, and gallic acids on radical species such as $O_2^{-\cdot}$, ·OH, ROO·, and RO·.

References

1) R. J. Korthuis and D. N. Granger, in "Physiology of Oxygen Radicals," ed by A. E. Tayler, S. Matalon, and P. A. Warld, Williams & Wilkins, Baltimore MD (1986), p. 217—249.

2) M. G. Simic, D. S. Bergtold, and L. R. Karam, *Mutat. Res.*, **214**, 3 (1989).

3) M. G. Simic, *Mutat. Res.*, **202**, 377 (1988).

4) I. Fridovich, *Adv. Enzymol.*, **41**, 35 (1974).

5) J. M. McCord and I. Fridovich, *J. Biol. Chem.*, **244**, 6049 (1969).

6) N. Shimizu, K. Kobayashi, and K. Hayashi, *J. Biol. Chem.*, **259**, 4414 (1984).

7) I. Yamazaki, *Protein, Nucleic Acid Enzyme*, **33**, 2934 (1988).

8) E. Finkelstain, G. M. Rosen, E. J. Raukckman, and J. Paxton, *Mol. Pharmacol.*, **16**, 676 (1979).
9) E. Finkelstain, G. M. Rosen, E. J. Raukckman, and J. Paxton, *Arch. Biochem. Biophys.*, **200**, 1 (1980).
10) I. Ueno, M. Kohno, K. Mitsuta, Y. Mizuta, and S. Kanegasaki, *J. Biochem.*, **105**, 905 (1989).
11) M. Makino, M. M. Mossoba, and P. Riese, *J. Am. Chem. Soc.*, **102**, 4994 (1980).
12) M. Makino, M. M. Mossoba, and P. Riese, *J. Phys. Chem.*, **87**, 1369 (1983).
13) M. Makino, M. M. Mossoba, and P. Riese, *FEBS Lett.*, **100**, 23 (1979).
14) K. Mitsuta, Y. Mizuta, M. Kohno, H. Hiramatsu, and A. Mori, *Bull. Chem. Soc. Jpn.*, **63**, 187 (1990).
15) I. Ueno, M. Kohno, K. Yoshihira, and I. Hirano, *J. Pharm. Dyn.*, **7**, 563 (1984).
16) I. Ueno, M. Kohno, K. Yoshihira, and I. Hirano, *J. Pharm. Dyn.*, **7**, 798 (1984).
17) H. Hiramatsu and M. Kohno, *JEOL News*, **23A**, 7 (1987).
18) H. Miyagawa, T. Yoshikawa, T. Tanigawa, N. Yoshida, S. Sugino, M. Kondo, H. Nishikawa, and M. Kohno, *J. Clin. Biochem. Nutr.*, **5**, 1 (1988).
19) T. Tanigawa, *J. Kyoto Pref. Univ. Med.*, **99**, 133 (1990).
20) Y. Mizuta, K. Mitsuta, and M. Kohno, Proceeding of the 4th Biennial General Meeting of the Society for Free Radical Research, Kyoto, 1988, Abstr., pp. 9—13.
21) A. Mori, R. Edamatsu, M. Kohno, and S. Ohmori, *Neuroscience*, **15**, 371 (1989).
22) S. Uchida, M. Hiramatsu, A. Mori, G. Monaka, I. Nishioka, M. Niwa, and M. Ozaki, *Med. Sci. Res.*, **15**, 831 (1987).
23) F. Hayase, S. Hirashima, G. Okamoto, and H. Kato, *Agric Biol. Chem.*, **53**, 3383 (1989).
24) T. Hatano, R. Edamatsu, M. Hiramatsu, A. Mori, Y. Fuzita, T. Yasuhara, T. Yoshida, and T. Okuda, *Chem. Pharm. Bull.*, **37**, 2016 (1989).
25) E. G. Janzen, D. E. Nutter, and E. D. Davis, *Can. J. Chem.*, **56**, 2237 (1978).
26) N. B. Nazhat, G. Yang, R. E. Allen, D. R. Blake, and P. Jones, *Biochem. Biophys. Res. Commun.*, **166**, 807 (1990).
27) T. Ozawa and A. Hanaki, *Biochem. Biophys. Res. Commun.*, **136**, 657 (1986).
28) A. Samuni, A. Samuni, and H. M. Swartz, *Free Radicals Med. Biol.*, **7**, 37 (1989).
29) G. R. Buettner, *Free Radicals Med. Biol.*, **3**, 259 (1987).
30) B. Kalyanaraman, C. Mottley, and R. P. Mason, *J. Biol. Chem.*, **258**, 3855 (1983).
31) I. Yamazaki and L. H. Piette, *J. Biol. Chem.*, **265**, 13589 (1990).
32) J. M. C. Gutteridge, L. Maidt, and L. Poyer, *Biochem. J.*, **269**, 169 (1990).
33) C. C. Winterbourn, *Free Radicals Med. Biol.*, **3**, 33 (1987).
34) R. A. Floyd, *Biochim. Biophys. Acta*, **756**, 204 (1983).

Preferential Incorporation of a Cyclopropyl σ Bond Over an Ethylenic π Bond in the TCNE Cycloaddition of 1,2-Dicyclopropylethylene. Occurrence of the Type-II Reaction in Some Disubstituted Substrates

Shinya NISHIDA,* Masakazu MASUI, Masashi MURAKAMI, Toshiro IMAI, and Takashi TSUJI†
Department of Chemistry, Faculty of Science, Hokkaido University, Sapporo, Hokkaido 060
(Received November 29, 1990)

Among the two types of cycloadditions known to take place in the reactions of cyclopropyl-substituted ethylenes (**1**) with tetracyanoethylene (TCNE) (type-I gives a cyclobutane derivative (**2**) and type-II yields a vinylcyclopentane derivative (**3**)), the type-II reaction has been practically limited to occur in reactions of tetrasubstituted substrates. However, some disubstituted substrates, namely *cis*- and *trans*-1,2-dicyclopropylethylene (**4** and **5**), were found to produce a mixture of **2** (R^1=R^2 or R^3=H, R^2 or R^3=*cyclo*-Pr) and **3** (R^1=R^2 or R^3=H, R^2 or R^3=*cyclo*-Pr). In acetonitrile at 80 °C, **2** predominated in the reactions of both **4** and **5**, but **3** became the major adduct in 1,2-dichloroethane or benzene. The other 1,2-disubstituted ethylenes, such as 1-cyclopropylpropene, 1-cyclopropyl-3-methyl-1-butene and 1-cyclopropyl-3,3-dimethyl-1-butene, produced a small amount of **3** in solvents of low polarity; the type-II, however, has never become a major process. Parent vinylcyclopropane failed to give the type-II adduct in all of the solvents examined. Participation of the cyclopropyl σ bond in the reaction with TCNE is thus shown to have a scope wider than that presumed previously; hence, both the type-I and the type-II processes may be the two principal modes of the reaction of **1** with TCNE.

It may be natural to expect that an ethylenic π bond is more reactive than a cyclopropyl σ bond towards an electrophilic reagent.[1] Thus, it was not surprising when we observed that mono- and disubstituted cyclopropylethylenes **1** (R^1, R^2, and/or R^3=H) reacted with electrophilic tetracyanoethylene (TCNE) at their π bond to give a cyclobutane derivative **2** (type I reaction).[2] However, we found successively that TCNE preferentially reacted with the cyclopropyl σ bond of certain trisubstituted **1** (R^1, R^2, and R^3≠H) to give a vinylcyclopentane derivative **3** (type II reaction).[3] Although it has recently been demonstrated that the spiro-activation of a cyclopropane ring brought about a change of the reaction course from type-I to type-II in the reaction of 1,1,2-tricyclopropylethylene,[4] the type-II reaction has actually been limited to occur only in the reaction of tetrasubstituted olefins.[3]

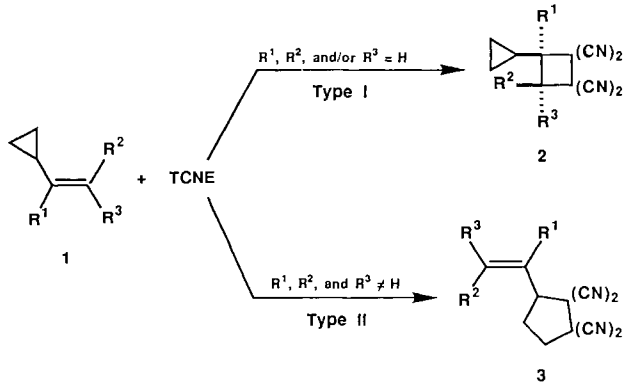

1 2 3

In a previous paper[2] we reported that *cis*- and *trans*-1,2-dicyclopropylethylenes (**4** and **5**) were not exceptions for the disubstituted substrates. Namely, they gave crystalline **2**, albeit in relatively low yields, in a reaction with TCNE at elevated temperature in a polar solvent.[5] Recently, however, we noticed a second oily product, which was assignable to **3**. This finding occurred to us when we examined the mutual isomerization of **4** and **5** in the presence of some acceptor molecules. The observation suggests that the type-II reaction could have a scope wider than what we had presumed.[3,4] Accordingly, we carried out minute investigations on the reactions of some rather simple cyclopropylethylenes. In the present paper we report that the type-II reaction, indeed, gains significance to a certain extent in the reaction of some 1,2-disubstituted substrates.

4 5

Results and Discussion

Substrates. The ethylenes examined in the present study include, in addition to **4** and **5**,[6,7] *cis*- and *trans*-1-cyclopropylpropene (**6** and **7**),[8] vinylcyclopropane (**8**),[9] *cis*-1-cyclopropyl-3-methyl-1-butene (**9**), and *cis*-1-cyclo-

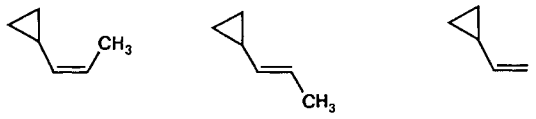

6 7 8

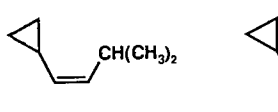

9

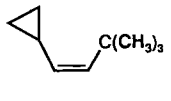

10

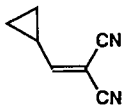

11

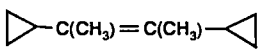

12

propyl-3,3-dimethyl-1-butene (**10**). The relative reactivities of these substrates toward TCNE were **5**>**4**>**6**=**7**=**8**>**9**>**10**.

Reactions of 4 and 5 with TCNE. In the previous study we examined the reactions of **4** and **5** as a part of an investigation aimed to show the generality of the type-I reaction.[2] Thus, the reaction of **4** was previously observed to occur at 100 °C in nitromethane[5] and crystalline *cis*-3,4-dicyclopropylcyclobutane-1,1,2,2-tetracarbonitrile (**2**: R^1=R^3=H, R^2=cyclo-Pr) was obtained in 25% isolated yield; **5** yielded *trans*-**2** (R^1=R^2=H, R^3=*cyclo*-Pr) in 11% yield. Since **2** was usually obtained in crystalline forms and was known to undergo fragmentation readily upon heating,[10] no effort, such as GC analysis, was made for the remaining oily portion of the reaction mixture.

In the present study we reexamined the same reaction in various solvents and found that 3-(2-cyclopropylvinyl)-cyclopentane-1,1,2,2-tetracarbonitrile (**3**: R^2 or R^3=*cyclo*-Pr) is produced as an oily product in addition to crystalline **2** (R^2 or R^3=*cyclo*-Pr). We realized that **3** is stable under GC conditions; it was therefore purified by preparative GC. As expected, **2** (R^2 or R^3=*cyclo*-Pr) underwent fragmentation under GC conditions to give two molecules of cyclopropylmethylenemalononitrile (**11**). Although the GC peak of **2** (R^2 or R^3=*cyclo*-Pr) was not symmetric (a steep maximum with a relatively long tailing), the shape was reproducibly recorded during each analysis. It was therefore possible to analyze the reactions of **4** and **5** with GC.[11]

As summarized in Table 1, heating **4** and TCNE in acetonitrile for 30 h resulted in a 76% consumption of **4**; **2** and **3** were produced in 74 and 18% GC yields, respectively.[12] The recovered olefin was found to be a mixture of **4** and **5** in a 53:47 ratio. In a separate experiment, **2** was isolated in 62% yield as an 84:16 mixture of geometrical isomers,[13,14] whereas **3** was collected by preparative GC in 11% yield; it was found to be a 52:48 mix-

Table 1. Reactions of Cyclopropylethylenes with TCNE at 80 °C

Substrate	Solvent (Time[a]/h)	Conversion %	Recov. olefin *c* : *t*	Yield of product[b]/% **2** (*c* : *t*)[c]	**3** (*c* : *t*)[c]
4[d]	A (30)	76	53 : 47	74 (4 : 1)[e,f]	18 (2 : 1)[g,f]
	D (48)	74	99 : 1	16 (9 : 1)[e]	82 (24 : 1)[g]
	B(168)	55	99 : 1	4 (s)[e]	62 (s)[g]
	C(960)	73	98 : 2	4 (s)[e]	43 (16 : 1)[g]
5[d]	A (48)	81	12 : 88	45 (1 : 9)[e,f]	44 (1 : 32)[g,f]
	D (48)	82	5 : 95	—[h]	99 (s)[g]
	B(168)	71	2 : 98	—[h]	66 (s)[g]
	C(960)	76	2 : 98	3 (s)[e]	45 (s)[g]
6[d]	A (27)	77	27 : 73	65 (6 : 4)[i]	—[h]
	D(144)	78	—[j]	63 (4 : 1)[i]	2 (s)[g]
	B(912)	48	—[j]	31 (s)[i]	5 (s)[g]
7[d]	A (48)	86	20 : 80	67 (3 : 7)[i]	<1 (s)[g]
	D(132)	82	—[j]	47 (s)[i]	3 (s)[g]
	B(864)	62	—[j]	25 (s)[i]	10 (s)[g]
8	A (8)	83		65	—[h]
	D (90)	81		69	—[h]
	B(912)	57		—[k]	—[h]
9[d]	A(648)	55	99 : 1	—[l]	4 (s)[g]
	D(600)	66	—[j]	—[l]	10 (s)[g]
10[d]	D(648)	58	—[j]	—[l]	7 (s)[g]
12[m]	A (2)	87		76[n]	6
	D (2)	81		17	65
	B (18)	85		—[h]	68

a) A=acetonitrile, D=1,2-dichloroethane, B=benzene, and C=carbon tetrachloride. Reaction time is given in h. b) In the reactions of **4** and **5**, yields of **2** and **3** were determined by GC analysis, whereas yields in the reactions of **6**—**10** were based on the amount of the adduct isolated. c) An abbreviation "s" refers to stereochemically practically single (>99 : <1) on either HPLC or GC analysis. d) More than 99% isomerically pure. e) Based on the HPLC analysis. f) In the text, the ratio of isomers (500 MHz ^{1}H NMR) observed in isolation experiments is given.[13] g) Analyzed by GC. h) Undetectable either by HPLC or by GC. i) By 100 MHz ^{1}H NMR. j) On the GC analysis with an $AgNO_3$-glycerol column, the peak of the olefin overlapped badly with the solvent peak so that no reliable figure could be obtained. k) See the text. l) No characterizable material corresponding to **2** was isolated although the yield of **3** was relatively low. m) A mixture of stereoisomers in a 6 : 4 ratio. n) See the experimental section.

ture of isomeric **3** possessing a *cis*- and a *trans*-2-cyclopropylvinyl side chain.

In 1,2-dichloroethane (48 h at 80 °C), **3** was found to be the major product (82%) accompanied by **2** (16%). Both **2** and **3** obtained in this solvent were more rich in the cis isomer (9 : 1 and 24 : 1, respectively) than those obtained in acetonitrile. In benzene, the reaction was found to proceed slowly to give 4% of **2** and 62% of **3**,[15] which were practically free from contamination of the corresponding trans isomer. The recovered **4** was also not contaminated by **5**. Since TCNE was hardly soluble in carbon tetrachloride, even at 80 °C, the reaction in this solvent was heterogeneous throughout; stereochemically, though, nearly single **2** and **3** were produced in 4 and 43% yields, respectively, after 40 d at 80 °C (73% conversion).[15]

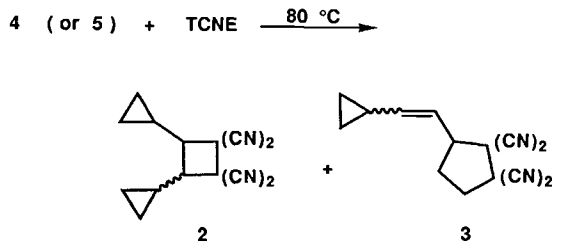

The trans isomer **5** behaved similarly to **4**, except for the fact that the production of **3** was more prominent than that observed in the reaction of **4**. Thus, after 48 h at 80 °C in acetonitrile (81% conversion), **2** and **3** were produced in 45 and 44% yields, respectively. In a separate experiment, a 38% yield of **2** (*cis* : *trans*=20 : 80)[13,16] and 30% of **3** (*cis* : *trans*=4 : 96) was isolated; the recovered olefin was found to be a mixture of **4** and **5** (see Table 1). GC analysis of the product mixture obtained in the reaction of **5** in 1,2-dichloroethane indicated that **2** was practically absent, and quantitatively produced **3** was free from the corresponding geometrical isomer. Similarly, *trans*-**3** (66%) was the sole detectable adduct produced in benzene. In a reaction in carbon tetrachloride, although a small amount of **2** (ca. 3% yield) was detected, the major product was pure *trans*-**3** (45% yield).[15]

Reactions of Other Cyclopropylethylenes. Since the type-II process is observed to occur even in reactions of disubstituted **4** and **5**, we were interested in examining the reactions of **6**, **7**, **9**, and **10**, as well as **8**. In acetonitrile, although both **6** and **7** produced practically no **3**, a small amount (2—10%) of **3** (R^2 or R^3=Me) was found in the product mixtures obtained in 1,2-dichloroethane or in benzene. In contrast to the reactions of **4** and **5**, however, **2** (R^2 or R^3=Me) remained the major product (25—31%), even in benzene.[15] The stereochemical results (Table 1) were similar to those observed in the reactions of **4** and **5**.

The reaction of parent **8** proceeded nicely in acetonitrile to give **2** (R^1=R^2=R^3=H) in 65% yield after 8 h at 80 °C (83% conversion). In 1,2-dichloroethane, the reaction proceeded much more slowly to give **2** (69% yield), which was not contaminated by **3** (GC). In a reaction in benzene (38 d at 80 °C; 57% conversion), no **2** could be isolated, although its production was suggested by observing the signals of fragments on the ^{1}H NMR analysis of the product mixture.[15] It should be noted, however, that no peak corresponding to **3** was observed in the GC analysis. Apparently, the type-II process is totally unimportant in the reaction of **8**.

The reactivities of **9** and **10** were much lower than those of **4**—**8** and, hence, a prolonged reaction time was required. We failed to isolate **2** in these reactions, probably because of the thermal instability of **2**; however, a small amount of **3** (R^2 or R^3=*i*-Pr or *t*-Bu; 4—10% yield) was unambiguously produced, as indicated by a GC analysis.[15]

Reaction of 2,3-Dicyclopropyl-2-butene. Since it appears that **4** and **5** are somewhat exceptional among the substrates examined for undergoing a preferential type-II reaction, it is of interest to investigate the reaction of a tetrasubstituted ethylene which maintains a substitution pattern similar to that of **4** or **5**. Accordingly, we studied the reaction of 2,3-dicylopropyl-2-butene (**12**). Although this olefin was readily prepared by a McMurry coupling[17] of cyclopropyl methyl ketone, the separation of stereoisomers was unsuccessful in all attempts. Thus, a 6 : 4 mixture of the stereoisomers was unavoidably used in the present study. The olefin **12** reacted smoothly with TCNE in acetonitrile to give a 76% yield of **2** and 6% yield of **3** after 2 h at 80 °C (87% conversion). In 1,2-dichloroethane, **12** gave **2** in 17% yield and **3** in 65% yield. We anticipated that tetrasubstituted **12** would give **3** in an amount larger than that produced in the reaction of **4** or **5**; actually, though, **12** produced a somewhat smaller amount of **3**. The calculated yields of **2** and **3** to be produced in the reaction of a 4 : 6 mixture of **4** and **5** are 57 and 32% in acetonitrile and 6 and 91% in 1,2-dichloroethane, respectively.

The aforementioned results indicate that **4** and **5** are two particular substrates prone to undergo a type-II reaction. In the reactions of 1-cyclopropyl-1-alkenes only a limited amount of **3** is produced, even in a solvent of low polarity. From steric grounds, **4** and **5** should be intermediate between **6**—**7** and **9**—**10**. Therefore, it can be concluded that the steric hindrance around the π bond is not the major factor for the relative importance of the type-II process. The present results might perhaps be rationalized in a way similar to that proposed in previous cases,[2-4,18] since **4** and **5** (IP^V=8.4 eV, E_p^{ox} vs. SCE=1.5 V[19]) can be oxidized more readily than **6**, **7** (IP^V=8.9 eV, E_p^{ox} vs. SCE=1.7 V) or **8** (IP^V=9.3 eV,[20] E_p^{ox} vs. SCE=2.1 V). However, the thermal SET, even in the case of **4** or **5**, is expected to be highly endothermic.[21] If we grant that the previous scheme for the formation of **3** can be applied in the present cases, we must therefore assume that the cation radical, which is produced only in

a very minute amount, is extremely prone to be attacked by a nearly TCNE anion radical. Since it is known that the cyclopropane to be cleaved in a nucleophilic attack should be substituted by appropriate activating groups, preferably by two electron-withdrawing groups in a geminal manner,[22] the cyclopropyl group in the present type-II reaction should be activated by some means. Although activation of the cyclopropyl group in the transformation of **1** to $\mathbf{1}^{\ddagger}$ and the anticipated nucleophilicity of the TCNE anion radical may make the ring cleavage probable, the highly endothermic nature of the SET process requires further consideration. A mechanistic justification must, therefore, await additional investigations.

It was unfortunate that considerable isomerization of the starting olefin took place, particularly in acetonitrile. However, the isomerization was less significant in 1,2-dichloroethane and practically absent in benzene; the **2** and **3** produced in benzene were nearly, or totally, free from contamination of the stereoisomer. From these results it may be concluded that both the type-I and type-II cycloadditions are stereospecific, at least in a solvent of low polarity. The extensive isomerization of the starting olefin observed in acetonitrile may be due to the reversibility of the type-I cycloaddition.[23]

In conclusion, it is demonstrated that both the type-I and type-II reactions may be the two principal modes of the reaction of **1** with TCNE. In the reaction of 1,1-disubstituted substrates, the type-I process is so facile[2,3] that the type-II process can hardly compete with it. However, when the type-I reactivity of the substrate is relatively low, as in **4**—**7** and **9** and **10**, the type-II process gains significance to a certain extent. The fact that the type-II process is somewhat less prominent in the reaction of **12** than those of **4**/**5** might be rationalized on the basis that the intermediate for the type-I process produced in the reaction of **12** holds the tertiary carbocationic center, whereas that yielded in the reaction of **4**/**5** merely has a secondary carbocationic portion. The type-I process is therefore somewhat more facilitated in the reaction of **12**.

Experimental

General Methods. IR spectra were recorded on a Hitachi 270-30 spectrophotometer. ^{1}H NMR spectra were recorded on either a JEOL FX-100, JEOL GX-270, JEOL FX-500, or Hitachi R-600 NMR spectrometer and are reported in parts per million downfield of internal tetramethylsilane. Mass spectra were taken on a JEOL LMS-D300 mass spectrometer. GC analyses were carried out with Hitachi 063 and 163 gas chromatographs with a column packed by APL 15% on Celite 545, 2m, and with temperature programing from 80 to 220 °C, unless otherwise specified. In analyses of stereoisomeric olefins, an $AgNO_3$–glycerol column was used. HPLC analyses were performed with Hitachi 635 and 655 liquid chromatographs with a μ-Polasil column. A mixture of hexane–ether (2:1) was used as an eluant and a UV detector was set at 215 nm. E^{ox} were obtained in the same manner as reported previously.[4b] IP^{V} were obtained from the UPS spectra, which were recorded on a VG ADES400 photoelectron spectrometer with a He(I) resonance lamp. The resolution was 34 meV for the Ar(^{3}P) signal. Elemental analyses were performed at the Center for Instrumental Analysis of Hokkaido University. The melting and boiling points are uncorrected.

Substrates. Olefins rich in the cis isomer were prepared by the Wittig reaction.[6] The cis/trans ratios observed in the preparation of **4**,[6] **6**,[7] **9**, and **10** were 86/14, 73/27, 90/10, and >99/<1, respectively. Stereochemically pure substrates (> 99%) were obtained with preparative GC. Trans olefins **5**[6] and **7**[7] were alternatively prepared by the addition of dibromocarbene to 1-cyclopropyl-1,3-butadiene[10b,24] or 1,3-pentadiene, both rich in the trans isomer, followed by reduction with sodium in ethanol.[9] As in the reactions with the Seyferth's reagent, however, an addition of dibromocarbene to the 1-substituted-1,3-butadiene under the phase-transfer reaction conditions was not as regioselective as that observed in the addition of fluorenylidene to 1-cyclopropyl-1,3-butadiene.[7] Accordingly, the overall yields of **5** and **7** were relatively low. Vinylcyclopropane (**8**) was prepared by following procedures reported previously.[9]

***cis*-1-Cyclopropyl-3,3-dimethyl-1-butene (10).** In a 500 ml three-necked flask fitted with a mechanical stirrer and a reflux condenser, 20.2 g (110 mmol) of sodium bis(trimethylsilyl)amide in 200 ml of THF was placed. Under a nitrogen atmosphere, 43.7 g (110 mmol) of (cyclopropylmethyl)triphenylphosphonium bromide[6] was added; the mixture was refluxed for 1 h. A resulting orange suspension was cooled to −78 °C, and then 9.5 g (110 mmol) of 2,2-dimethylpropanal was slowly added with a syringe. The mixture was stirred at −78 °C for 1 h, and then at room temperature for 12 h. To the resultant mixture, 200 ml of water was added and organic material was extracted with 5 portions of pentane (100 ml). The combined pentane solution was washed with dilute hydrochloric acid, aqueous sodium hydrogencarbonate, and water, and dried over anhydrous sodium sulfate. An oily residue obtained by evaporation of the solvent was distilled to give a fraction boiled at 55—85 °C at 150 Torr (15.1 g; 1 Torr=101, 325/760 Pa), which was found to contain 10.0 g (74%) of *cis*-**10** (GC); *trans*-**10** was not detected. Rectification of the fraction gave pure *cis*-**10** (7.1 g, 53% yield); Bp 130—134 °C; IR (liquid film) 3088, 3008, 2960, 1660 cm^{-1}; ^{1}H NMR (100 MHz, $CDCl_3$) δ=5.27 (d, 1H, J=12 Hz), 4.53 (dd, 1H, J=12, 10 Hz), 1.90—1.57 (m, 1H), 1.17 (s, 9H), 0.83—0.54 (m, 2H), 0.50—0.03 (m, 2H); MS (70 eV) m/z (rel intensity) 124 (M^+, 33), 67 (100). Anal. (C_9H_{16}) C, H.

***cis*-1-Cyclopropyl-3-methyl-1-butene (9).** In a similar manner, **9**, which was contaminated by 10% of the trans isomer, was obtained in 62% yield. Pure **9** was obtained by preparative GC followed by distillation: Bp 116—117 °C; IR (liquid film) 3088, 3008, 2960, 2872, 1655 cm^{-1}; ^{1}H NMR (100 MHz, $CDCl_3$) δ= 5.14 (dd, 1H, J=9, 11 Hz), 4.61 (dd, 1H, J=9, 11 Hz), 2.93—2.57 (m, 1H), 1.72—1.37 (m, 1H), 1.00 (d, 6H, J=6.5 Hz), 0.80—0.21 (m, 4H); MS (70 eV) m/z (rel intensity) 110 (M^+, 33), 43 (100). Anal. (C_8H_{14}) C, H.

2,3-Dicyclopropyl-2-butene (12). A McMurry coupling of cyclopropyl methyl ketone with a low valent titanium reagent prepared from titanium trichloride and metallic magnesium[25] gave **12** in 17% yield. Separation of geometrical isomers by means of GC was unsuccessful in all attempts. Accordingly, the mixture was used in the following investigations: Bp 75—

80 °C at 17 Torr; IR (liquid film) 3084, 3004, 2920, 1650, 1600 cm^{-1}; ^1H NMR (60 MHz, $CDCl_3$) δ=2.2—1.5 (m, 2H), 1.52 (s, 3.6H), 1.39 (s, 2.4H), 0.9—0.3 (m, 8H). Anal. ($C_{10}H_{16}$) C, H.

GC Analyses of the Reactions. The relative reactivities of **4**—**10** with TCNE under given conditions were determined by following the consumption of the starting olefin at appropriate time intervals. The time required for the half-consumption of the olefin in 1,2-dichloroethane at 80 °C was: **4**: 18 h, **5**: 10 h, **6**: 32 h, 7: 32 h, **8**: 32 h, **9**: 168 h, and **10**: 312 h. The reactions of **4** and **5**, but not those of others, with TCNE were analyzed directly by GC (see Table 1).[11]

Reaction of 4 with TCNE in Acetonitrile. A reddish violet solution obtained on mixing of **4** (108 mg, 1.0 mmol) with TCNE (135 mg, 1.06 mmol) in acetonitrile (10 ml, containing 56 mg of octane as an internal standard) was degassed and sealed in a tube. After being heated at 80 °C for 48 h, the tube was opened (the consumption of **4** being 83% and recovered olefin being a mixture of **4** and **5** in a 41 : 59 ratio). The solution was then concentrated and a residue (230 mg) was subjected to column chromatography with silica gel (40 g). Elution of the column with chloroform gave a white solid (159 mg), which was recrystallized from cyclohexane to give colorless needles (121 mg, 62%) as a mixture of *cis*-**2** and *trans*-**2** in a ratio of 84 : 16. Repeated recrystallizations from cyclohexane gave an analytically pure *cis*-**2** (R^2=*cyclo*-Pr, R^1=R^3=H), mp 156—158 °C (lit,[2] mp 165—167 °C). Since the mp of the adduct differed significantly from that reported previously, the product was subjected to a precise analysis. IR (KBr disc) 3092, 3016, 2250 cm^{-1}; ^1H NMR (100 MHz, $CDCl_3$) δ=2.66—2.42 (AA'XX', 2H, J_{AA}=9, J_{AX}=11, J_{AX}=0.3 Hz), 1.49—1.20 (m, 2H), 1.10—0.70 (m, 4H), 0.56—0.28 (m, 4H); MS (70 eV) *m*/*z* (rel intensity) 236 (M^+, 0.2), 91 (100). Anal. ($C_{14}H_{12}N_4$) C, H, N.

A yellow oil obtained in the concentration of mother liquors of the recrystallizations (42 mg) was analyzed by GC and found to be a mixture of two components. These were collected by preparative GC to give 21 mg (11%) of a 52 : 48 mixture of *cis*-**3** and *trans*-**3**. Each isomer was purified by repeated GC collections. *cis*-**3** (R^2=*cyclo*-Pr, R^1=R^3=H): Oil; IR (liquid film) 3012, 2250, 1656 cm^{-1}; ^1H NMR (270 MHz, $CDCl_3$) δ=5.36—5.26 (AA'XX', 2H, $J_{AA'}$=11, J_{AX}=9, J_{AX}=0.7), 4.06 (ddd, 1H, *J*=9, 7, 4 Hz), 2.92 (ddd, 1H, *J*=14.5, 9, 6 Hz), 2.83 (ddd, *J*=14.5, 10.5, 6 Hz), 2.54 (dddd, 1H, *J*=17, 9, 6, 7 Hz), 2.12 (dddd, 1H, *J*=17, 10.5, 6, 9 Hz), 1.65—1.53 (m, 1H), 1.02—0.86 (m, 2H), 0.63—0.46 (m, 2H); MS (70 eV) *m*/*z* (rel intensity) 236 (M^+, 39), 93 (100). Anal. ($C_{14}H_{12}N_4$) C, H, N. *trans*-**3** (R^3=*cyclo*-Pr, R^1=R^2=H): Oil; IR (liquid film) 3012, 2250, 1664, 968 cm^{-1}; ^1H NMR (270 MHz, $CDCl_3$) δ=5.57—5.42 (AA'XX', 2H, $J_{AA'}$=16, J_{AX}=7, J_{AX}=0.7), 3.45 (ddd, 1H, *J*=9, 7, 4.5 Hz), 2.89 (ddd, 1H, *J*=14.5, 9, 6 Hz), 2.78 (ddd, 1H, *J*=14.5, 10.5, 6 Hz), 2.44 (dddd, 1H, *J*=18, 9, 6, 4.5 Hz), 2.15 (dddd, 1H, *J*=18, 10.5, 6, 9 Hz), 1.56—1.44 (m, 1H), 0.92—0.80 (m, 2H), 0.55—0.44 (m, 2H); MS (70 eV) *m*/*z* (rel intensity) 236 (M^+, 29), 93 (100). Anal. ($C_{14}H_{12}N_4$) C, H, N.

Reaction of 5 with TCNE in Acetonitrile. A reddish purple solution of **5** (109 mg, 1.01 mmol), TCNE (132 mg, 1.03 mmol), and octane (54 mg, as an internal standard) in acetonitrile (10 mL) was degassed in a tube and heated at 80 °C for 48 h. The consumption of **5** was 86%; recovered olefin was a mixture of **4** and **5** in a 12 : 88 ratio. After concentrating the resultant brown solution, a residue (254 mg) was subjected to column chromatography with silica gel (40 g). Elution of the column with chloroform gave adduct fractions comprising a white solid and a liquid (178 mg). Recrystallization of the solid from cyclohexane gave colorless needles (77 mg, 38% yield), mp 143—153 °C, which were a mixture of *cis*-**2** and *trans*-**2** in a 20 : 80 ratio. Repeated recrystallizations of the needles from cyclohexane gave analytically pure *trans*-**2** (R^3=*cyclo*-Pr, R^1=R^2=H): Mp 153—155 °C (lit,[2] mp 159—160.5 °C); IR (KBr disc) 3100, 3012, 2250 cm^{-1}; ^1H NMR (100 MHz, $CDCl_3$) δ=2.53—2.27 (AA'XX', 2H, J_{AA}=11, J_{AX}=9, J_{AX}=0.4 Hz), 1.25—0.74 (m, 6H), 0.66—0.43 (m, 4H); MS (70 eV) *m*/*z* (rel intensity) 236 (M^+, 0.1), 91 (100). Anal. ($C_{14}H_{12}N_4$) C, H, N. From the oily portion of the product, 61 mg (30%) of **3** (cis : trans=4 : 96) was obtained.

Reaction of 5 in 1,2-Dichloroethane. The reaction produced *trans*-**3** quantitatively (Table 1). When the reaction (108 mg, 1.00 mmol, of **5**, 132 mg, 1.03 mmol of TCNE, and 57 mg of octane in 10 ml of the solvent) was carried out in the presence of methanol (325 mg, 10 equivalent), **3** (cis : trans=4 : 96) was produced in 64% GC yield (46% by isolation). In no fraction on the silica-gel column chromatography was the MeO signal observed by ^1H NMR spectroscopy.

Reaction of 6. In acetonitrile (15 ml, containing 102 mg of heptane as an internal standard), the reaction of **6** (123 mg, 1.50 mmol) with TCNE (198 mg, 1.55 mmol) at 80 °C for 27 h (77% conversion; recovered olefin being a mixture of **6** and 7 in a 27 : 73 ratio) gave a geometrical mixture of **2** (cis : trans=6 : 4, 158 mg, 65%). In 1,2-dichloroethane at 80 °C for 144 h (78% conversion), the same reaction produced **2** (cis : trans=4 : 1, 155 mg, 63%) and **3** (5 mg, 2%). From this product mixture, *cis*-**2** (R^2=Me, R^1=R^3=H) was isolated by repeated recrystallization: Mp 156—157 °C; IR (KBr disc) 3008, 2250 cm^{-1}; ^1H NMR (100 MHz, $CDCl_3$) δ=3.40 (dq, 1H, *J*=9.1, 7.2 Hz), 2.54 (dd, 1H, *J*=10.6, 9.1 Hz), 1.63 (d, 3H, *J*=7.2 Hz), 1.87—1.10 (m, 1H), 0.97—0.33 (m, 4H); MS (70 eV) *m*/*z* (rel intensity) 210 (M^+, 0.15), 67 (100). Anal. ($C_{12}H_{10}N_4$) C, H, N.

In the reaction in benzene at 80 °C for 912 h (48% conversion), 47 mg (31%) of *cis*-**2**, mp 155.0—156.5 °C, and 7 mg (5%) of **3** were isolated. The type-I adduct was not contaminated by *trans*-**2** (100 MHz ^1H NMR) in this case. From the combined oily products, *cis*-**3** (R^2=Me, R^1=R^3=H) was isolated by preparative GC: Oil; IR (liquid film) 3028, 2952, 2250, 1662 cm^{-1}; ^1H NMR (100 MHz, $CDCl_3$) δ=6.09 (dq, 1H, *J*=10.7, 7.1 Hz), 5.57 (ddq, 1H, *J*=9.3, 10.7, 1.8 Hz), 3.94 (q, 1H, *J*=9.3 Hz), 2.97—2.78 (m, 2H), 2.70—1.95 (m, 2H), 1.85 (dd, 3H, *J*=7.1, 1.8 Hz); MS (70 eV) *m*/*z* (rel intensity) 210 (M^+, 5.4), 67 (100). Anal. ($C_{12}H_{10}N_4$) C, H, N.

Reaction of 7. In a similar manner (see Table 1 for the reaction conditions), the reaction of **7** (124 mg, 1.51 mmol) with TCNE (200 mg, 1.56 mmol) in acetonitrile (15 ml) gave colorless needles (181 mg, 67%), which were a 3 : 7 mixture of *cis*-**2** and *trans*-**2**, and oily **3** (3 mg, 1%). In 1,2-dichloroethane, practically pure *trans*-**2** (120 mg, 47%) was obtained in addition to oily **3** (8 mg, 3%). *trans*-**2** (R^3=Me, R^1=R^2=H): Mp 113—115 °C; IR (KBr disc) 3012, 2980, 2250 cm^{-1}; ^1H NMR (100 MHz, $CDCl_3$) δ=3.24 (dq, 1H, *J*=11, 6.4 Hz), 2.17 (dd, 1H, *J*=11, 9.3 Hz), 1.51 (d, 3H, *J*=6.4 Hz), 1.38—1.15 (m, 1H), 1.11—0.38 (m, 4H); MS (70 eV) *m*/*z* (rel intensity) 210 (M^+, 0.14), 67 (100). Anal. ($C_{12}H_{10}N_4$) C, H, N.

The reaction in benzene gave 49 mg (25%) of *trans*-**2** and 20 mg (10%) of **3**, from the latter, pure *trans*-**3** (R^3=Me, R^1=R^2=H) was obtained: Oil; IR (liquid film) 2968, 2250, 1672, 968 cm^{-1}; ^1H NMR (100 MHz, $CDCl_3$) δ=6.05 (dq, 1H, *J*=15,

6.4 Hz), 5.50 (dd, 1H, J=15, 7.9 Hz), 3.47 (dt, 1H, J=10, 8.6 Hz), 3.01—2.76 (m, 2H), 2.67—2.00 (m, 2H), 1.85 (d, 3H, J=6.4 Hz); MS (70 eV) m/z (rel intensity) 210 (M^+, 4.3), 67 (100). Anal. ($C_{12}H_{10}N_4$) C, H, N.

Reaction of 8. In degassed acetonitrile (20 ml), a mixture of **8** (136 mg, 2.00 mmol), TCNE (264 mg, 2.06 mmol), and octane (130 mg) was heated at 80 °C for 8 h (83% conversion) in an ampoule. From the reaction mixture, **2** (R^1=R^2=R^3=H; 211 mg, 65%), mp 123.5—124.5 °C (lit,[2] mp 124—125 °C), was obtained as colorless plates. Similarly, **2** was obtained in 69% yield in 1,2-dichloroethane (80 °C for 90 h; 81% conversion). In a reaction in benzene (912 h at 80 °C; 57% conversion), **2** did not crystallize out after a work-up as mentioned above. ^{1}H NMR analyses of fractions obtained on silica-gel column chromatography indicated the occurrence of fragmentation. In no case was the formation of **3** indicated by GC analyses.

Reaction of 9. A mixture of **9** (110 mg, 1.00 mmol), TCNE (134 mg, 1.05 mmol), and octane (103 mg) in degassed acetonitrile (10 ml) was heated in an ampoule for 648 h (45% conversion). Work-up of the reaction mixture (as mentioned above) gave an oily product (30 mg), from which oily **3** (4 mg, 4%) was obtained by preparative GC. The same reaction in 1,2-dichloroethane (66% conversion) gave 16 mg (10%) of *cis*-**3** (R^2=*i*-Pr, R^1=R^3=H): Oil; IR (liquid film) 3012, 2964, 2872, 2252, 1660 cm^{-1}; ^{1}H NMR (500 MHz, $CDCl_3$) δ=5.79 (t, 1H, J=11 Hz), 5.29 (t, 1H, J=11 Hz), 3.86 (q, 1H, J=10 Hz), 2.90 (ddd, 1H, J=15, 9, 5 Hz), 2.82 (ddd, 1H, J=15, 11, 6 Hz), 2.63 (dq, 1H, J=17, 6 Hz), 2.45 (ddt, 1H, J=14, 6, 9 Hz), 2.14—2.06 (m, 1H), 1.11 (d, 3H, J=7 Hz), 1.02 (d, 3H, J=7 Hz); MS (70 eV) m/z (rel intensity) 238 (M^+, 4.9), 69 (100). Anal. ($C_{14}H_{14}N_4$) C, H, N. Most of the material in the reaction mixture did not elute out of the silica-gel column.

Reaction of 10. In acetonitrile, the reaction of **10** with TCNE did not proceed to a reasonable extent, even after 14 days at 80 °C. In 1,2-dichloroethane, 58% consumption of **10** was noted after 648 h at 80 °C. From the reaction mixture (124 mg, 1.00 mmol, of **10** and 132 mg, 1.03 mmol, of TCNE in 10 ml of the solvent), 35 mg of an oil was isolated after the work-up mentioned above. The oil comprised 4 products (GC), from which *cis*-**3** (R^2=*t*-Bu, R^1=R^3=H; 10 mg, 7% yield) was isolated: Oil; IR (liquid film) 2964, 2872, 2252, 1660 cm^{-1}; ^{1}H NMR (100 MHz, $CDCl_3$) δ=5.91, (d, 1H, J=12 Hz,)5.23 (dd, 1H, J=12, 10 Hz), 4.22 (dt, 1H, J=9, 10 Hz), 2.94—2.76 (m, 2H), 2.67—1.98 (m, 2H), 1.20 (s, 9H); MS (70 eV) m/z (rel intensity) 252 (M^+, 1.7), 41 (100). HRMS Calcd for $C_{15}H_{16}N_4$: M, 252.1375. Found: m/z 252.1356.

Reaction of 12. A mixture of **12** (136 mg, 1.00 mmol), TCNE (132 mg, 1.03 mmol), and dodecane (60 mg) in acetonitrile (10 ml) was heated at 80 °C under a nitrogen atmosphere. After 2 h, 87% consumption of **12** was noted by GC analysis. Concentration of the reaction mixture gave a brown oil (270 mg), which was subjected to silica-gel colume chromatography (20 g). Elution of the column with benzene gave a white solid and a pale yellow oil (total of 188 mg). The solid was recrystallized from 99% ethanol to give colorless needles (158 mg, 69%), mp 130—135 °C, which was assigned to be **2** (R^1 and R^2 or R^3=Me, R^2 or R^3=*cyclo*-Pr): IR (KBr disc) 3012, 2250 cm^{-1}; ^{1}H NMR (60 MHz, $CDCl_3$) δ=1.9—1.35 (m, 2H), 1.26 (s, 3.4H), 1.09 (s, 2.6H), 0.9—0.3 (m, 8H); MS (70 eV) m/z (rel intensity) 264 (M^+, 0.4), 105 (100). Anal. ($C_{16}H_{16}N_4$) C, H, N. The oily portion obtained in the column chromatography comprised mostly **2** (60 MHz ^{1}H NMR; **2**:**3**=93:7), and hence the total yield of **2** was calculated to be 76%. Concentrated mother liquors of the recrystallization gave an oil, from which **3** (R^1 and R^2 or R^3=Me, R^2 or R^3=*cyclo*-Pr; 13 mg, 6% yield) was isolated.

The reaction in 1,2-dichloroethane (2 h at 80 °C, 81% conversion) gave **2** in 17% and **3** in 65% yield, respectively. In the reaction in benzene (18 h at 80 °C; 85% conversion), 60 MHz ^{1}H NMR spectral analysis of the adduct fraction revealed no formation of **2**. An oily product obtained in silica-gel column chromatography was found to be **3** (68% yield). Repeated preparative GC of the products allowed isomeric **3** to be separated, although stereochemical assignments were not accomplished:

3-I: Oil; IR (liquid film) 3088, 3008, 2260, 1630 cm^{-1}; ^{1}H NMR (100 MHz, $CDCl_3$) δ=4.77 (t, 1H, J=9 Hz), 2.95—2.78 (m, 2H), 2.48—2.23 (m, 2H), 2.0—1.4 (m, 1H), 1.85 (s, 3H), 1.60 (s, 3H), 0.90—0.50 (m, 4H); MS (70 eV) m/z (rel intensity) 264 (M^+, 39), 121 (100). Anal. ($C_{16}H_{16}N_4$) C, H, N.

3-II: Oil; IR (liquid film) 3088, 3004, 2260, 1632 cm^{-1}; ^{1}H NMR (100 MHz, $CDCl_3$) δ=4.28 (t, 1H, J=9 Hz), 2.94—2.78 (m, 2H), 2.49—2.17 (m, 2H), 2.1—1.5 (m, 1H), 2.00 (s, 3H), 1.58 (s, 3H), 0.90—0.50 (m, 4H); MS (70 eV) m/z (rel intensity) 264 (M^+, 49), 121 (100). Anal. ($C_{16}H_{16}N_4$) C, H, N.

Fragmentation of 2. Since **2** is known to decompose during a GC analysis,[10] the decomposed material of **2** (R^1=R^3=H, R^2=*cyclo*-Pr and R^1=R^2=H, R^3=*cyclo*-Pr) was collected. From 25.0 mg (0.11 mmol) of *cis*-**2**, 20.4 mg (82%) of colorless liquid was obtained, which was found to be **11**: Oil; IR (liquid film) 3032, 2232, 1600 cm^{-1}; ^{1}H NMR (100 MHz, $CDCl_3$) δ=6.63 (d, 1H, J=11 Hz), 2.35—1.99 (m, 1H), 1.57—0.96 (m, 4H); MS (70 eV) m/z (rel intensity) 118 (M^+, 27), 91 (100). Anal. ($C_7H_6N_2$) C, H, N. Similarly, *trans*-**2** gave **11** in 71% yield.

The present research was supported by a Grant-in-Aid for Scientific Research No. 01430005 from the Ministry of Education, Science and Culture to which we are very grateful. We thank Professor Masahiro Kawasaki of Hokkaido University, Research Institute of Applied Electricity, for generous loan of the ADES400 spectrometer.

References

1) M. Charton, "The Chemistry of Alkenes," ed by J. Zabicky, Interscience, London (1970), Vol. 2, Chap. 10. M. A. Battiste and J. M. Coxon, "The Chemistry of the Cyclopropyl Group," ed by Z. Rappoport, John Wiley, New York (1987), Part 1, Chap. 6. T. T. Tidwell, *ibid.*, Part 1, Chap. 10.

2) S. Nishida, I. Moritani, and T. Teraji, *J. Chem. Soc., Chem. Commun.*, **1970**, 501. S. Nishida, I. Moritani, and T. Teraji, *J. Org. Chem.*, **38**, 1878 (1973).

3) S. Nishida, I. Moritani, and T. Teraji, *J. Chem. Soc., Chem. Commun.*, **1971**, 36. F. Kataoka and S. Nishida, *Chem. Lett.*, **1980**, 1115. T. Tsuji and S. Nishida, *Acc. Chem. Res.*, **17**, 56 (1984).

4) a) S. Nishida, M. Murakami, T. Mizuno, and T. Tsuji, *J. Org. Chem.*, **54**, 3868 (1989). Cf. also b) S. Nishida, M. Murakami, H. Oda, T. Tsuji, T. Mizuno, M. Matsubara, and N. Kikai, *ibid.*, **54**, 3859 (1989).

5) Since we were primarily concerned with generality of the type-I process in our previous study,[2] and the type-I reaction was known to proceed readily in a polar solvent, the reactions

of **4** and **5** were examined only in nitromethane at 100 °C.

6) T. Teraji, I. Moritani, E. Tsuda, and S. Nishida, *J. Chem. Soc. C*, **1971**, 3252.

7) Attempted preparation of **5** by an addition of dihalocarbene followed by reduction was unsatisfactory because of poor regioselectivity in the carbene addition stage (see Experimental Section): S. Nishida, Z. Komiya, T. Mizuno, A. Mikuni, T. Fukui, T. Tsuji, M. Murakami, and N. Shimizu, *J. Org. Chem.*, **49**, 495 (1984).

8) W. E. Farneth and M. W. Thomson, *J. Am. Chem. Soc.*, **105**, 843 (1983).

9) S. Nishida, I. Moritani, K. Ito, and K. Sakai, *J. Org. Chem.*, **32**, 939 (1967).

10) Cyclobutane-1,1,2,2-tetracarbonitrile derivatives are known to undergo fragmentation at ca. 150 °C: N. Shimizu and S. Nishida, *J. Chem. Soc., Chem. Commun.*, **1978**, 931. F. Kataoka, N. Shimizu and S. Nishida, *J. Am. Chem. Soc.*, **102**, 711 (1980). S. Nishida, T. Imai, K. Hamatsu, T. Tsuji, and M. Murakami, *J. Chem. Soc., Chem. Commun.*, **1983**, 1191.

11) GC analyses were successful only in the reactions of **4** and **5**, which produced symmetric **2**. Unsymmetrically substituted **2** exhibited a somewhat complex GC diagram and hence the GC analysis was not reliable for the quantitative study.

12) The yield given hereafter is based on the consumed amount of the starting olefin.

13) Based on the ^{1}H NMR analysis of a fraction containing **2** obtained in the column chromatography. The figure determined by HPLC was somewhat low in accuracy, because **2** lacked a chromophore suitable for the HPLC analysis. In some cases, the ratio of the stereoisomers in **3** was also determined by ^{1}H NMR.

14) Previously, *cis*-**2** was obtained in 25% yield after repeated recrystallizations.[2)]

15) Whereas **3** was thermally stable, **2** decomposed gradually on prolonged heating.

16) Previously, *trans*-**2** was obtained in 11% yield.[2)]

17) J. E. McMurry, *Acc. Chem. Res.*, **16**, 405 (1983). The cyclopropyl group is known to be stable under McMurry coupling conditions: S. Nishida and F. Kataoka, *J. Org. Chem.*, **43**, 1612 (1978).

18) Although trapping of the intermediate with methanol was examined in the reaction of **5** in 1,2-dichloroethane, in which **3** is expected to be the exclusive product, the attempt was unsuccessful (see Experimental Section).

19) The Oxidation was irreversible in all case, and E_p^{ox} values varied with the sweep rate. Accordingly, merely round numbers are given.

20) Reported IP^v=9.2 eV: Y. Harada, K. Seki, A. Suzuki, and H. Inokuchi, *Chem. Lett.*, **1973**, 893. P. Bruckmann and M. Klessinger, *Chem. Ber.*, **107**, 1108 (1974). R. Gleiter, *Top. Curr. Chem.*, **86**, (1977).

21) D. Rehm and A. Weller, *Ber. Bunsenges. Phys. Chem.*, **73**, 834 (1969); *Isr. J. Chem.*, **8**, 259 (1970). Cf. also Ref. 4b.

22) S. Danishefsky, *Acc. Chem. Res.*, **12**, 66 (1979); and references cited therein. R. Verhé and N. De Kimpe, "The Chemistry of the Cyclopropyl Group," ed by Z. Rappoport, John Wiley, New York (1987), Part 1, Chap. 9. See also H.-U. Reissig, *ibid.*, Chap. 8.

23) R. Huisgen, *Acc. Chem. Res.*, **10**, 117, 119 (1977).

24) H. M. Frey and A. Krants, *J. Chem. Soc. A*, **1969**, 1159. M. Hanack and H. Eggensperger, *Justus Liebigs Ann. Chem.*, **663**, 31 (1963).

25) R. Dams, M. Malinowski, I. Westdrop, and H. Y. Geise, *J. Org. Chem.*, **47**, 248 (1982). J.-M. Pons and M. Santelli, *Tetrahedron*, **44**, 4295 (1988).

Palladium Catalyzed Reaction of Silacyclobutanes with Acetylenes

Yoshihiro TAKEYAMA, Kyoko NOZAKI, Kozo MATSUMOTO, Koichiro OSHIMA,* and Kiitiro UTIMOTO*
Department of Industrial Chemistry, Faculty of Engineering, Kyoto University, Sakyo-ku, Kyoto 606
(Received December 6, 1990)

Whereas the reaction of 1,1-dimethyl-1-silacyclobutane (**1a**) with dimethyl acetylenedicarboxylate in the presence of Pd catalyst provides dimethyl 1,1-dimethyl-1-sila-2-cyclohexene-2,3-dicarboxylate almost exclusively, the reaction of **1a** with phenylacetylene affords allyldimethylstyrylsilane as a major product. The reaction of silacyclobutane with phenylallene provided three isomeric products.

Strained small ring molecules are versatile building blocks and often provide short and elegant routes in organic synthesis. From the interest in the development of synthetic use of silacyclobutane, we have studied stereoselective formation of silacyclopentanes by the reaction of silacyclobutane with lithium carbenoids[1] and the base induced reaction of silacyclobutane with aldehyde to give oxasilacyclohexanes.[2] During the course of these studies, accidentally, it was found that the palladium catalyzed reaction of silacyclobutane with acetylenes provided a mixture of silacyclohexene derivatives and allylvinylsilane derivatives.

Sakurai and Imai have reported[3] that 1,1-dimethyl-1-silacyclobutane (**1a**) reacted smoothly with dimethyl acetylenedicarboxylate, methyl propiolate, or phenylacetylene to give dimethyl 1,1-dimethyl-1-sila-2-cyclohexene-2,3-dicarboxylate (**3a**), methyl 1,1-dimethyl-1-sila-2-cyclohexene-3-carboxylate (**3b**), or 1,1-dimethyl-3-phenyl-1-sila-2-cyclohexene (**3c**), respectively (Scheme 1).

Meanwhile, we have found that allylvinylsilane derivative **4** was formed in addition to the silacyclohexene derivative **3** in the reaction of **1** with acetylenic compounds. For instance, $PdCl_2(PPh_3)_2$ catalyzed reaction of 1,1-dimethyl-1-silacyclobutane (**1a**) with methyl propiolate in benzene under an argon atmosphere gave a mixture of methyl 1,1-dimethyl-1-sila-2-cyclohexene-3-carboxylate (**3b**) and methyl (*E*)-4,4-dimethyl-4-sila-2,6-heptadienoate (**4b**, **3b**/**4b**=4/6, Scheme 2). The representative results are summarized in Table 1.

As shown in Table 1, the ratios of two types of the products, silacyclohexene **3** and allylvinylsilane derivative **4** heavily depend on the nature of acetylenic compounds. The reaction of silacyclobutane with dimethyl acetylenedicarboxylate provided the former product, silacyclohexene **3**, as a major product. In contrast, the reaction with phenylacetylene afforded the latter allylvinylsilane derivative **4** mainly. Whereas palladium complexes such as $Pd(PPh_3)_4$ and $PdCl_2(P(o\text{-tolyl})_3)_2$ were as effective as $PdCl_2(PPh_3)_2$, $PdCl_2(Ph_2PCH_2CH_2PPh_2)$ was not effective as a catalyst and phenylacetylene was recovered unchanged in the reaction with **1a**. The catalysts prepared in situ from $PdCl_2$ and PPh_3 or $PdCl_2(PPh_3)_2$ and pyridine were also ineffective. The ratios of two products were not affected by the ligand on palladium complex. Thus, the ratio of **3c** and **4c** was always 1/9—2/8 in the reaction of 1,1-dimethyl-1-silacyclobutane with phenylacetylene ($PdCl_2(PPh_3)_2$, 1/9; $PdCl_2(P(o\text{-tolyl})_3)_2$, 2/8; $PdCl_2$–$2P(OEt)_3$, 1/9). Tetrahydrofuran and dimethylformamide as well as benzene were suitable solvent for the reaction. Regioselective formation of single isomers **3** and **4** was observed for the reaction of methyl propiolate or phenylacetylene.

Prosaic acetylenic compound such as 1-dodecyne reacted very sluggishly to give the corresponding products in poor yield (17%, 3-decyl-1,1-dimethyl-1-sila-2-cyclohexene/(*E*)-allyl(1-dodecenyl)dimethylsilane=4/6).

Treatment of 3-deuterio-3-methyl-1,1-diphenyl-1-silacyclobutane **5**[4] with acetylenic compounds in the presence of $PdCl_2(PPh_3)_2$ gave the corresponding products

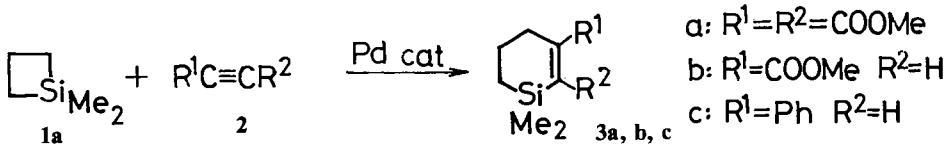

Scheme 1.

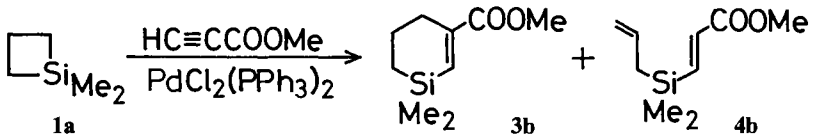

Scheme 2.

Table 1. Palladium Catalyzed Reaction of Silacyclobutanes with Acetylenes[a)]

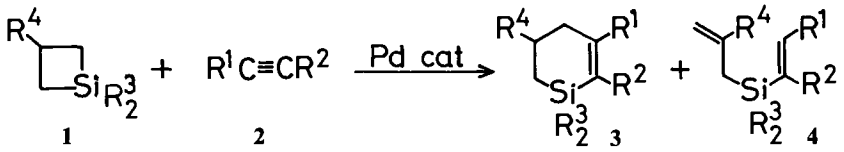

Entry	Silacyclobutane 1		Acetylene 2		Yield/%	
	R^3	R^4	R^1	R^2	3	4
1	Me	H (1a)	COOMe	COOMe	50 (3a)	18 (4a)
2	Me	H (1a)	COOMe	H	27 (3b)	41 (4b)
3	Me	H (1a)	Ph	H	6 (3c)	51 (4c)
4	Ph	H (1b)	COOMe	COOMe	86 (3d)	7 (4d)
5	Ph	H (1b)	COOMe	H	50 (3e)	26 (4e)
6	Ph	H (1b)	Ph	H	16 (3f)	60 (4f)
7	Me	Me (1c)	COOMe	COOMe	61 (3g)	13 (4g)
8	Me	Me (1c)	COOMe	H	43 (3h)	32 (4h)
9	Me	Me (1c)	Ph	H	12 (3i)	29 (4i)
10	Ph	Me (1d)	COOMe	COOMe	82 (3j)	4 (4j)
11	Ph	Me (1d)	COOMe	H	71 (3k)	26 (4k)
12	Ph	Me (1d)	Ph	H	50 (3l)	36 (4l)

a) One mmol of silacyclobutane, 1 mmol of acetylene, and a catalytic amount of $PdCl_2(PPh_3)_2$ were employed. The reaction mixture was refluxed for 2 h.

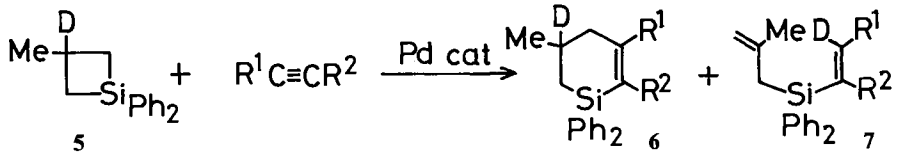

Scheme 3.

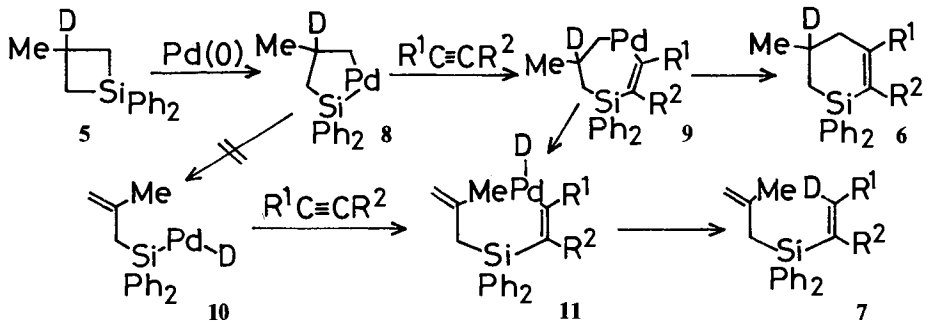

Scheme 4.

6 and **7**. In the case of the reaction with methyl propiolate, methyl (*E*)-2-deuterio-6-methyl-4,4-diphenyl-4-sila-2,6-heptadienoate **7b** (R^1=COOMe, R^2=H) was obtained (12% yield) along with methyl 5-deuterio-5-methyl-1-sila-2-cyclohexene-3-carboxylate **6b** (R^1=COOMe, R^2=H, 76% yield). Deuterium occupied 2-position of 4-sila-2,6-heptadienoate **7b**. The ^{1}H NMR signal of δ=6.30 for the corresponding compound **4k** (methyl 6-methyl-4,4-diphenyl-4-sila-2,6-heptadienoate) completely disappeared in the product **7b**. The reaction with phenylacetylene or dimethyl acetylenedicarboxylate also provided the corresponding deuterated compounds **6** and **7** (Scheme 3)

Based on these results, we are tempted to assume the following reaction mechanism: (1) Insertion of Pd(0) into silacyclobutane leading to ring-expanded compound **8**,[5)] (2) regioselective silylpalladation of acetylenic compounds to provide seven-membered ring intermediate **9**, and (3) reductive elimination of Pd(0) to afford silacyclohexene **6** or β-elimination of Pd–D followed by reductive elimination of Pd(0) to give allylvinylsilane derivative **7** (Scheme 4).[10)]

Alternatively, the formation of allylvinylsilane derivatives **7** might be explained by the addition of CH_2=$CMeCH_2SiPh_2$–Pd–D (**10**), which is derived by β-elimination of Pd–D from **8**, to acetylenic compounds providing **11** and successive reductive elimination of Pd(0) from **11**. However, this route was ruled out by

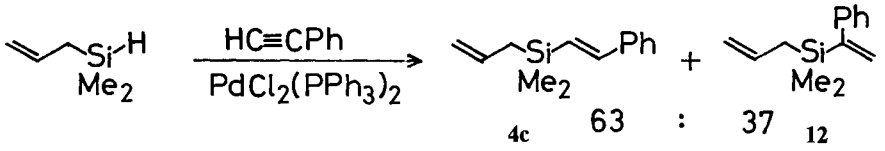

Scheme 5.

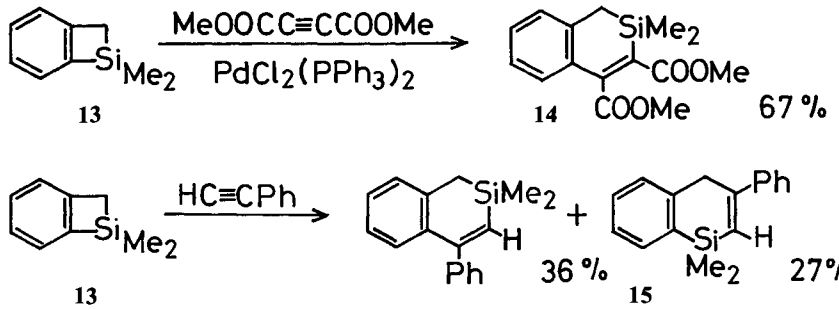

Scheme 6.

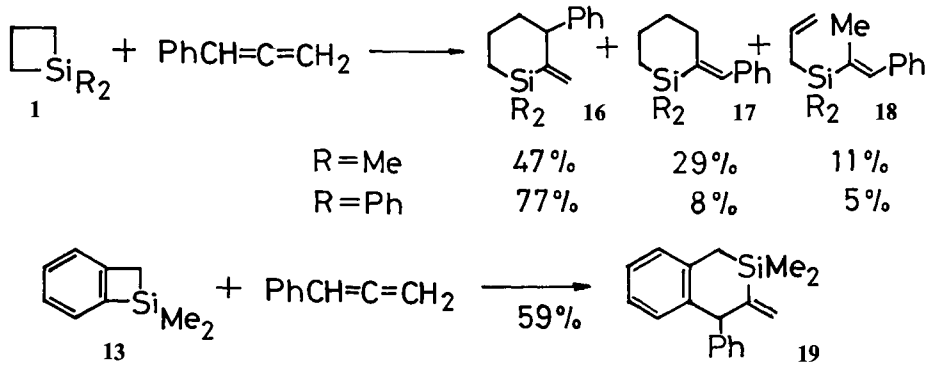

Scheme 7.

the following fact. Treatment of phenylacetylene with allyldimethylsilane in the presence of $PdCl_2(PPh_3)_2$ gave a regioisomeric mixture of allyldimethylstyrylsilane **4c** and allyldimethyl(1-phenylvinyl)silane **12** in low yield (<15% combined yield, **4c**/**12**=63/37) as depicted in Scheme 5.

The reaction of 1,2-dihydro-1,1-dimethyl-1-silabenzocyclobutene (**13**), which has no β-hydrogen, with dimethyl acetylenedicarboxylate or phenylacetylene under similar conditions gave the corresponding dihydrosilanaphthalenes, **14** or **15**, respectively (Scheme 6).

Phenylallene also easily reacted with silacyclobutanes in the presence of $PdCl_2(PPh_3)_2$ catalyst to give a mixture of three components, **16**, **17**, and **18**. On the other hand, 1,2-dihydro-1-silabenzocyclobutene **13** provided 1,2,3,4-tetrahydro-2-silanaphthalene **19** in 59% yield as a single product (Scheme 7).

Experimental

Distillations of the products were performed by use of Kugelrohr (Büchi), and boiling points are indicated by air-bath temperature without correction. ^1H NMR and ^{13}C NMR spectra were taken on a Varian XL-200 spectrometer, $CDCl_3$ was used as solvent, and chemical shifts being given in δ with tetramethylsilane as an internal standard. IR spectra were determined on a JASCO IR-810 spectrometer. The elemental analyses were carried out at the Elemental Analyses Center of Kyoto University.

Preparation of Silacyclobutane Derivatives. 1,1-Dimethyl-1-silacyclobutane (**1a**) was purchased from Shinetsu Silicone Chemicals and used as delivered. 1,1-Diphenyl-1-silacyclobutane (**1b**) was prepared in 86% yield by treatment of 1,1-dichloro-1-silacyclobutane (obtained from Petrarch Systems) with phenylmagnesium bromide in ether. 1,1,3-Trimethyl-1-silacyclobutane (**1c**) and 3-methyl-1,1-diphenyl-1-silacyclobutane (**1d**) were obtained from 2-methylallyl chloride. Hexachloroplatinic(IV) acid catalyzed hydrosilylation with $HSiClMe_2$ or $HSiClPh_2$ followed by treatment of the resulting $ClSiMe_2CH_2CH(Me)CH_2Cl$ or $ClSiPh_2CH_2CH(Me)CH_2Cl$ with Mg provided **1c** or **1d** in 26% or 35% overall yield, respectively.[4] 1,2-Dihydro-1-silabenzocyclobutene (**13**) was prepared following the reported procedure.[11]

General Procedure for the Reaction of Silacyclobutane with Acetylenic Compounds or Phenylallene in the Presence of Pd Catalyst. The reaction of 1,1-dimethyl-1-silacyclobutane with methyl propiolate is representative. A catalytic amount of $PdCl_2(PPh_3)_2$ (115 mg, 0.02 mmol) was added to a solution of 1,1-dimethyl-1-silacyclobutane (**1a**, 0.20 g, 2.0 mmol) and methyl propiolate (0.17 g, 2.0 mmol) in benzene (5 ml) under an argon atmosphere. The pale yellow mixture

was heated at reflux for 2 h. The resulting dark brown mixture was concentrated in vacuo and the residual oil was submitted to silica-gel column chromatography to give a mixture of methyl 1,1-dimethyl-1-sila-2-cyclohexene-3-carboxylate (**3b**[3], 0.10 g, 27% yield) and methyl (*E*)-4,4-dimethyl-4-sila-2,6-heptadienoate (**4b**, 0.15 g, 41% yield). **4b**: Bp 65 °C (1.0 Torr, 1 Torr=133.322 Pa, bath temp); IR(neat) 2948, 1730, 1308, 1271, 1250, 1227, 1168, 995, 846 cm^{-1}; ^1H NMR ($CDCl_3$) δ=0.13 (s, 6H), 1.62 (d, J=8.0 Hz, 2H), 3.75 (s, 3H), 4.86 (bd, J=9.5 Hz, 1H), 4.87 (bd, J=17.6 Hz, 1H), 5.74 (ddt, J=9.5, 17.6, 8.0 Hz, 1H), 6.25 (d, J=18.9 Hz, 1H), 7.23 (d, J=18.9 Hz, 1H); ^{13}C NMR ($CDCl_3$) δ=−4.03, 22.69, 51.17, 114.0, 133.7, 134.4, 148.1, 166.2. Found: C, 58.38; H, 9.05%. Calcd for $C_9H_{16}O_2Si$: C, 58.65; H, 8.75%.

Methyl (*E*)-3-Methoxycarbonyl-4,4-dimethyl-4-sila-2,6-heptadienoate (4a): Bp 95 °C (1.0 Torr, bath temp); IR(neat) 2952, 1728, 1436, 1341, 1238, 1198, 1174, 1039, 890 cm^{-1}; ^1H NMR ($CDCl_3$) δ=0.19 (s, 6H), 1.69 (d, J=8.0 Hz, 2H), 3.73 (s, 3H), 3.81 (s, 3H), 4.90 (d, J=17.5 Hz, 1H), 4.91 (d, J=8.0 Hz, 1H), 5.73 (ddt, J=17.5, 8.0, 8.0 Hz, 1H), 6.08 (s, 1H); ^{13}C NMR ($CDCl_3$) δ=−4.45, 21.98, 52.02, 114.8, 129.5, 132.8, 154.0, 164.4, 170.8. Found: C, 54.37; H, 7.43%. Calcd for $C_{11}H_{18}O_4Si$: C, 54.52; H, 7.49%.

(*E*)-Allyldimethylstyrylsilane (4c): Bp 90 °C (1.0 Torr, bath temp); IR(neat) 3074, 2954, 1629, 1604, 1572, 1493, 1248, 1154, 988, 851, 687, 645 cm^{-1}; ^1H NMR ($CDCl_3$) δ=0.16 (s, 6H), 1.66 (d, J=8.0 Hz, 2H), 4.87 (d, J=10.2 Hz, 1H), 4.89 (d, J=16.9 Hz, 1H), 5.83 (ddt, J=10.2 Hz, 1H), 6.50 (d, J=19.3 Hz, 1H), 6.91 (d, J=19.3 Hz, 1H), 7.15—7.45 (m, 5H); ^{13}C NMR ($CDCl_3$) δ=−3.46, 23.66, 113.2, 126.4, 127.4, 128.1, 128.5, 134.8, 138.2, 144.5. Found: C, 76.95; H, 9.09%. Calcd for $C_{13}H_{18}Si$: C, 77.16; H, 8.96%.

Dimethyl 1,1-Diphenyl-1-sila-2-cyclohexene-2,3-dicarboxylate (3d): Bp 200 °C (1.0 Torr, bath temp); IR(neat) 2946, 1719, 1600, 1430, 1280, 1236, 1191, 1145, 1114, 1050, 1029, 776, 730, 698, 661 cm^{-1}; ^1H NMR ($CDCl_3$) δ=1.18—1.33 (m, 2H), 1.88—2.08 (m, 2H), 2.62 (t, J=5.8 Hz, 2H), 3.48 (s, 3H), 3.79 (s, 3H), 7.33—7.70 (m, 10H); ^{13}C NMR ($CDCl_3$) δ=9.62, 19.83, 31.64, 51.52, 52.30, 127.8, 129.8, 132.6, 133.3, 135.4, 155.3, 169.4. Found: C, 68.56; H, 6.00%. Calcd for $C_{21}H_{22}O_4Si$: C, 68.82; H, 6.05%.

Methyl (*E*)-3-Methoxycarbonyl-4,4-diphenyl-4-sila-2,6-heptadienoate (4d): Bp 200 °C (1.0 Torr, bath temp); IR(neat) 2948, 1726, 1430, 1339, 1239, 1197, 1173, 1112, 1036, 897, 770, 736, 699 cm^{-1}; ^1H NMR ($CDCl_3$) δ=2.32 (d, J=7.8 Hz, 2H), 3.66 (s, 3H), 3.72 (s, 3H), 4.93—5.10 (m, 2H), 5.84 (ddt, J=17.6, 9.8, 7.8 Hz, 1H), 6.10 (s, 1H), 7.35—7.68 (m, 10H); ^{13}C NMR ($CDCl_3$) δ=19.97, 51.97, 52.06, 116.2, 128.1, 130.3, 131.2, 132.2, 133.5, 135.6, 150.6, 164.4, 170.3. Found: C, 68.59; H, 6.25%. Calcd for $C_{21}H_{22}O_4Si$: C, 68.82; H, 6.05%.

Methyl 1,1-Diphenyl-1-sila-2-cyclohexene-3-carboxylate (3e): Bp 150 °C (0.3 Torr, bath temp); IR(neat) 3066, 3000, 2922, 1715, 1590, 1428, 1293, 1221, 1112, 776, 734, 698 cm^{-1}; ^1H NMR ($CDCl_3$) δ=1.18—1.33 (m, 2H), 1.88—2.08 (m, 2H), 2.56 (t, J=5.8 Hz, 2H), 3.76 (s, 3H), 7.30—7.70 (m, 11H); ^{13}C NMR ($CDCl_3$) δ=9.07, 20.96, 29.32, 52.02, 128.0, 129.7, 133.7, 134.9, 135.3, 150.1, 167.3. Found: m/z 308.1227. Calcd for $C_{19}H_{20}O_2Si$: M, 308.1233.

Methyl (*E*)-3-(Allyldiphenylsilyl)acrylate (4e): Bp 150 °C (0.3 Torr, bath temp); ^1H NMR ($CDCl_3$) δ=2.25 (d, J=1.1 Hz, 2H), 3.75 (s, 3H), 4.90—5.08 (m, 2H), 5.82 (ddt, J=17.0, 10.1, 7.9 Hz, 1H), 6.31 (d, J=18.9 Hz, 1H), 7.30—7.70 (m, 11H); ^{13}C NMR ($CDCl_3$) δ=20.43, 51.68, 115.5, 128.0, 129.9, 132.7, 132.8, 135.8, 137.6, 143.8, 165.8.

1,1,3-Triphenyl-1-sila-2-cyclohexene (3f): Bp 145 °C (0.2 Torr, bath temp); IR(neat) 3064, 2918, 1589, 1565, 1493, 1427, 1110, 794, 729, 697 cm^{-1}; ^1H NMR ($CDCl_3$) δ=1.28 (m, 2H), 2.10 (m, 2H), 2.74 (t, J=5.5 Hz, 2H), 6.42 (s, 1H), 7.25—7.75 (m, 15H); ^{13}C NMR ($CDCl_3$) δ=20.00, 21.29, 33.10, 119.7, 125.6, 127.6, 128.2, 129.3, 129.9, 134.9, 136.7, 138.8, 144.9. Found: C, 84.56; H, 6.73%. Calcd for $C_{23}H_{22}Si$: C, 84.61; H, 6.79%.

(*E*)-1,1,3-Triphenyl-3-sila-1,5-hexadiene (4f): Bp 145 °C (0.2 Torr, bath temp); IR(neat) 3064, 2918, 1428, 1110, 794, 731, 697 cm^{-1}; ^1H NMR ($CDCl_3$) δ=2.26 (d, J=7.9 Hz, 2H), 4.91 (d, J=9.9 Hz, 1H), 4.98 (d, J=17.2 Hz, 1H), 5.89 (ddt, J=17.2, 9.9, 7.9 Hz, 1H), 6.75 (d, J=19.4 Hz, 1H), 6.98 (d, J=19.4 Hz, 1H), 7.25—7.88 (m, 15H); ^{13}C NMR ($CDCl_3$) δ=21.30, 114.8, 122.9, 126.7, 127.7, 127.9, 128.45, 128.54, 129.5, 133.8, 134.8, 135.4, 148.3. Found: C, 84.83; H, 6.79%. Calcd for $C_{23}H_{22}Si$: C, 84.61; H, 6.79%.

Dimethyl 1,1,5-Trimethyl-1-sila-2-cyclohexene-2,3-dicarboxylate (3g): Bp 90 °C (1.0 Torr, bath temp); IR(neat) 2950, 1719, 1604, 1432, 1229, 1144, 830, 801 cm^{-1}; ^1H NMR ($CDCl_3$) δ=0.19 (s, 3H), 0.21 (s, 3H), 0.45 (dd, J=14.3, 12.8 Hz, 1H), 0.87 (d, J=14.3 Hz, 1H), 1.08 (d, J=6.2 Hz, 3H), 1.80—2.03 (m, 1H), 2.04 (dd, J=18.1, 10.8 Hz, 1H), 2.53 (d, J=18.1 Hz, 1H), 3.75 (s, 3H), 3.77 (s, 3H); ^{13}C NMR ($CDCl_3$) δ=−2.75, −2.54, 20.25, 25.91, 27.53, 38.96, 51.57, 52.02, 136.4, 151.0, 169.0, 170.1. Found: C, 56.36; H, 8.12%. Calcd for $C_{12}H_{20}O_4Si$: C, 56.22; H, 7.86%.

Methyl (*E*)-3-Methoxycarbonyl-4,4,6-trimethyl-4-sila-2,6-heptadienoate (4g): Bp 90 °C (1.0 Torr, bath temp); IR(neat) 2950, 1725, 1637, 1434, 1338, 1235, 1195, 1172, 1037, 843 cm^{-1}; ^1H NMR ($CDCl_3$) δ=0.23 (s, 6H), 1.719 (s, 3H), 1.723 (s, 2H), 3.75 (s, 3H), 3.83 (s, 3H), 4.54—4.60 (m, 1H), 4.68—4.73 (m, 1H), 6.11 (s, 1H); ^{13}C NMR ($CDCl_3$) δ=−3.88, 25.12, 25.75, 51.95, 110.1, 129.3, 141.5, 154.4, 164.4, 170.8. Found: C, 56.27; H, 8.01%. Calcd for $C_{12}H_{20}O_4Si$: C, 56.22; H, 7.86%.

Methyl 1,1,5-Trimethyl-1-sila-2-cyclohexene-3-carboxylate (3h): Bp 70 °C (1.0 Torr, bath temp); IR(neat) 2950, 1717, 1434, 1272, 1249, 1219, 1059, 1048, 850, 801 cm^{-1}; ^1H NMR ($CDCl_3$) δ=0.110 (s, 3H), 0.114 (s, 3H), 0.37 (dd, J=14.3, 12.8 Hz, 1H), 0.81 (d, J=14.3 Hz, 1H), 1.08 (d, J=6.2 Hz, 3H), 1.60—1.93 (m, 2H), 2.50—2.73 (m, 1H), 3.75 (s, 3H), 7.00 (s, 1H); ^{13}C NMR ($CDCl_3$) δ=−2.27 −2.20, 20.38, 26.42, 28.56, 37.27, 51.78, 138.0, 147.2, 167.5. Found: C, 60.46; H, 9.33%. Calcd for $C_{10}H_{18}O_2Si$: C, 60.56; H, 9.15%.

Methyl (*E*)-4,4,6-Trimethyl-4-sila-2,6-heptadienoate (4h): Bp 70 °C (1.0 Torr, bath temp); IR(neat) 2952, 1732, 1436, 1306, 1271, 1251, 1227, 1195, 1168, 997, 843, 803 cm^{-1}; ^1H NMR ($CDCl_3$) δ=0.17 (s, 6H), 1.65 (s, 2H), 1.70 (s, 3H), 3.76 (s, 3H), 4.49—4.53 (m, 1H), 4.62—4.65 (m, 1H), 6.27 (d, J=18.9 Hz, 1H), 7.27 (d, J=18.9 Hz, 1H); ^{13}C NMR ($CDCl_3$) δ=−3.49, 25.18, 26.71, 51.63, 109.3, 134.1, 142.3, 148.5, 166.1. Found: C, 60.49; H, 9.30%. Calcd for $C_{10}H_{18}O_2Si$: C, 60.56; H, 9.15%.

1,1,5-Trimethyl-3-phenyl-1-sila-2-cyclohexene (3i): Bp 100 °C (1.0 Torr, bath temp); IR(neat) 2950, 2902, 2876, 1589, 1568, 1492, 1453, 1442, 1206, 847, 787, 693 cm^{-1}; ^1H NMR ($CDCl_3$) δ=0.10 (s, 3H), 0.12 (s, 3H), 0.42 (dd, J=14.0, 12.8 Hz, 1H), 0.84 (d, J=14.0 Hz, 1H), 1.11 (d, J=6.4 Hz, 3H), 1.83—2.10 (m, 1H), 2.18 (ddd, J=16.9, 10.5, 2.4 Hz, 1H), 2.57 (ddd, J=16.9, 3.1, 1.6 Hz, 1H), 6.01 (s, 1H), 7.20—7.53 (m, 5H); ^{13}C NMR ($CDCl_3$) δ=−1.47, −1.37, 20.75, 26.79, 29.23, 41.47, 124.2, 125.5, 127.1, 128.1, 145.2, 156.6. Found:

C, 77.50; H, 9.54%. Calcd for $C_{14}H_{20}Si$: C, 77.71; H, 9.32%.

(*E*)-3,3,5-Trimethyl-1-phenyl-3-sila-1,5-hexadiene (4i): Bp 95 °C (1.0 Torr, bath temp); IR(neat) 2956, 1636, 1604, 1493, 1447, 1247, 987, 852 cm^{-1}; ^1H NMR ($CDCl_3$) δ=0.19 (s, 6H), 1.67 (s, 2H), 1.73 (s, 3H), 4.53—4.58 (m, 1H), 4.60—4.68 (m, 1H), 6.47 (d, J=19.2 Hz, 1H), 6.90 (d, J=19.2 Hz, 1H), 7.25—7.53 (m, 5H); ^{13}C NMR ($CDCl_3$) δ=−2.87, 25.29, 27.73, 108.6, 126.4, 128.0, 128.5, 138.3, 143.4, 144.3. Found: C, 77.97; H, 9.58%. Calcd for $C_{14}H_{20}Si$: C, 77.71; H, 9.32%.

Dimethyl 5-Methyl-1,1-diphenyl-1-sila-2-cyclohexene-2,3-dicarboxylate (3j): Bp 180 °C (0.3 Torr, bath temp); IR(neat) 2948, 2918, 1719, 1601, 1429, 1236, 1191, 1144, 1111, 1039, 779, 730, 697 cm^{-1}; ^1H NMR ($CDCl_3$) δ=1.00 (dd, J=14.5, 13.0 Hz, 1H), 1.11 (d, J=6.3 Hz, 3H), 1.30 (d, J=14.5 Hz, 1H), 1.95—2.20 (m, 1H), 2.27 (dd, J=18.5, 10.9 Hz, 1H), 2.66 (d, J=18.5 Hz, 1H), 3.49 (s, 3H), 3.79 (s, 3H), 7.30—7.78 (m, 10H); ^{13}C NMR ($CDCl_3$) δ=18.99, 26.11, 27.40, 39.72, 51.51, 52.28, 127.8, 127.9, 129.77, 129.85, 132.3, 133.2, 135.3, 135.4, 155.1, 169.3. Found: C, 69.18; H, 6.43%. Calcd for $C_{22}H_{24}O_4Si$: C, 69.44; H, 6.36%.

Methyl (*E*)-3-Methoxycarbonyl-6-methyl-4,4-diphenyl-4-sila-2,6-heptadienoate (4j): ^1H NMR ($CDCl_3$) δ=1.60 (s, 3H), 2.30 (s, 2H), 3.65 (s, 3H), 3.72 (s, 3H), 4.62 (s, 1H), 4.70 (s, 1H), 6.15 (s, 1H), 7.30—7.80 (m, 10H). Analytically pure sample could not be obtained because of its small yield.

Methyl 5-Methyl-1,1-diphenyl-1-sila-2-cyclohexene-3-carboxylate (3k): Bp 155 °C (0.3 Torr, bath temp); IR(neat) 2948, 2918, 1715, 1597, 1454, 1429, 1271, 1219, 1113, 1057, 790, 776, 732, 712, 698 cm^{-1}; ^1H NMR ($CDCl_3$) δ=0.92 (dd, J=14.0, 12.0 Hz, 1H), 1.14 (d, J=5.8 Hz, 3H), 1.37 (d, J=12.0 Hz, 1H), 1.80—2.20 (m, 2H), 2.67—2.92 (m, 1H), 3.77 (s, 3H), 7.25—7.70 (m, 11H); ^{13}C NMR ($CDCl_3$) δ=18.34, 26.52, 28.51, 37.50, 52.04, 128.0, 129.7, 133.6, 134.8, 134.9, 135.1, 149.6, 167.2. Found: C, 74.20; H, 6.91%. Calcd for $C_{20}H_{22}O_2Si$: C, 74.49; H, 6.88%.

Methyl (*E*)-6-Methyl-4,4-diphenyl-4-sila-2,6-heptadienoate (4k): Bp 155 °C (0.3 Torr, bath temp); IR(neat) 2948, 1720, 1429, 1271, 1224, 1190, 1169, 1112, 789, 777, 732, 712, 698 cm^{-1}; ^1H NMR ($CDCl_3$) δ=1.58 (s, 3H), 2.25 (s, 2H), 3.76 (s, 3H), 4.60 (bs, 1H), 4.70 (bs, 1H), 6.30 (d, J=19.0 Hz, 1H), 7.25—7.75 (m, 11H); ^{13}C NMR ($CDCl_3$) δ=24.66, 25.50, 51.78, 111.2, 129.9, 133.3, 135.3, 137.5, 141.5, 144.4, 165.9. Found: C, 74.63; H, 6.90%. Calcd for $C_{20}H_{22}O_2Si$: C, 74.49; H, 6.88%.

5-Methyl-1,1,3-triphenyl-1-sila-2-cyclohexene (3l): Bp 175 °C (0.3 Torr, bath temp); IR(neat) 3064, 3016, 2948, 2916, 2864, 1591, 1565, 1492, 1444, 1428, 1264, 1207, 1187, 1111, 843, 793, 758, 730, 696 cm^{-1}; ^1H NMR ($CDCl_3$) δ=0.93 (dd, J=13.3, 14.1 Hz, 1H), 1.16 (d, J=6.4 Hz, 3H), 1.39 (d, J=14.1 Hz, 1H), 2.00—2.26 (m, 1H), 2.35 (ddd, J=17.1, 10.7, 2.4 Hz, 1H), 2.73 (d, J=17.1 Hz, 1H), 6.38 (s, 1H), 7.24—7.75 (m, 15H); ^{13}C NMR ($CDCl_3$) δ=18.75, 26.80, 29.10, 41.65, 119.6, 125.7, 127.6, 127.8, 128.2, 129.3, 134.8, 135.0, 145.0, 159.7. Found: C, 84.53; H, 7.04%. Calcd for $C_{24}H_{24}Si$: C, 84.65; H, 7.10%.

(*E*)-5-Methyl-1,3,3-triphenyl-3-sila-1,5-hexadiene (4l): Bp 170 °C (0.3 Torr, bath temp); IR(neat) 3064, 3018, 2960, 2914, 1638, 1599, 1570, 1493, 1446, 1428, 1277, 1263, 1110, 1028, 997, 873, 795, 733, 697 cm^{-1}; ^1H NMR ($CDCl_3$) δ=1.62 (s, 3H), 2.26 (s, 2H), 4.61 (s, 1H), 4.67 (s, 1H), 6.79 (d, J=19.1 Hz, 1H), 6.96 (d, J=19.1 Hz, 1H), 7.24—7.75 (m, 15H); ^{13}C NMR ($CDCl_3$) δ=25.30,25.60, 110.5, 123.4, 126.7, 127.8, 128.4, 128.5, 129.5, 135.1, 135.5, 138.1, 142.4, 148.2. Found: C, 84.48; H, 7.04%. Calcd for $C_{24}H_{24}Si$: C, 84.65; H, 7.10%.

Preparation of 3-Deuterio-3-methyl-1,1-diphenyl-1-silacyclobutane (5). The title compound was obtained following the procedure described for the preparation of **1d**. Hydrosilylation of 2-methylallyl chloride with diphenyldeuteriochlorosilane ($Ph_2Si(D)Cl$) in the presence of platinum catalyst gave 3-chloro-2-deuterio-2-methylpropyldiphenylchlorosilane in 36% yield: Bp 130—150 °C (0.2 Torr); IR(neat) 3068, 3048, 2998, 2962, 2870, 1457, 1429, 1378, 1283, 1246, 1115, 815, 766, 727, 697, 652 cm^{-1}; ^1H NMR ($CDCl_3$) δ=1.00 (s, 3H), 1.31 (d, J=15.1 Hz, 1H), 1.68 (d, J=15.1 Hz, 1H), 3.40 (d, J=10.7 Hz, 1H), 3.44 (d, J=10.7 Hz, 1H); ^{13}C NMR ($CDCl_3$) δ=20.27, 21.27, 31.18, (t, J=20.1 Hz), 53.11, 128.1, 130.5, 130.6, 134.1, 134.2. Treatment of 3-chloro-2-deuterio-3-methylpropyldiphenylchlorosilane with Mg gave **5** in 79% yield: Bp 100 °C (0.3 Torr, bath temp); IR(neat) 3064, 3046, 3010, 2946, 2912, 2854, 1450, 1428, 1196, 1151, 1114, 842, 789, 736, 717, 696 cm^{-1}; ^1H NMR ($CDCl_3$) δ=1.13 (d, J=15.6 Hz, 2H), 1.23 (s, 3H), 1.69 (d, J=15.6 Hz, 2H), 7.38—7.78 (m, 10H); ^{13}C NMR ($CDCl_3$) δ=22.25, 27.49, 129.6, 134.5, 134.7, 135.9, 137.1. The signal for the carbon bearing deuterium could not be observed even with high concentrated sample. Found: C, 80.48; H, 7.85%. Calcd for $C_{16}H_{17}DSi$: C, 80.27; H, 8.00%.

The Reaction of 5 with Dimethyl Acetylenedicarboxylate. Heating a benzene solution of **5** (0.23 g, 0.97 mmol), dimethyl acetylenedicarboxylate (0.14 g, 1.0 mmol), and $PdCl_2(PPh_3)_2$ (7 mg, 0.01 mmol) at 80 °C for 3 h under argon atmosphere. The resulting mixture was concentrated in vacuo and the residual oil was submitted to silica-gel column chromatography to give **6a** (0.31 g, 84%) and **7a** (12 mg, 3%). Methyl 5-deuterio-5-methyl-1,1-diphenyl-1-sila-2-cyclohexene-2,3-dicarboxylate (**6a**): Bp 180 °C (0.3 Torr, bath temp); IR(neat) 2948, 2916, 1719, 1602, 1450, 1429, 1238, 1205, 1192, 1145, 1113, 1040, 898, 779, 759, 733, 698 cm^{-1}; ^1H NMR ($CDCl_3$) δ=0.99 (d, J=14.6 Hz, 1H), 1.10 (s, 3H), 1.29 (d, J=14.6 Hz, 1H), 2.26 (d, J=19.0 Hz, 1H), 2.65 (d, J=19.0 Hz, 1H), 3.49 (s, 3H), 3.79 (s, 3H), 7.36—7.75 (m, 10H); ^{13}C NMR ($CDCl_3$) δ=18.86, 26.02, 39.65, 51.54, 52.31, 127.8, 127.9, 129.8, 129.9, 135.3, 135.4, 155.2, 169.4. The signal for the carbon bearing deuterium could not be observed. Found: C, 68.98; H, 6.40%. Calcd for $C_{22}H_{23}DO_4Si$: C, 69.26; H, 6.60%.

Reaction of Allyldimethylsilane with Phenylacetylene in the Presence of $PdCl_2(PPh_3)_2$ or H_2PtCl_6. A benzene solution of allyldimethylsilane (0.15 g, 1.5 mmol) and phenylacetylene (0.10 g, 1.0 mmol) was heated in the presence of catalytic amount of $PdCl_2(PPh_3)_2$ (10 mg, 0.014 mmol) at reflux for 2 h. The resulting dark brown solution was concentrated and the residual oil was submitted to silica-gel column chromatography to give a mixture of allyldimethylstyrylsilane (**4c**) and allyldimethyl(1-phenylvinyl)silane (**12**, 30 mg, **4c**/**12**=63/37) in <15% combined yield. **12**: ^1H NMR ($CDCl_3$) δ=5.65 (d, J=2.9 Hz, 1H), 5.90 (d, J=2.9 Hz, 1H). Meanwhile, stirring a mixture of allyldimethylsilane (0.30 g, 3.0 mmol) and phenylacetylene (0.30 g, 3.0 mmol) in the presence of $H_2PtCl_6 \cdot 6H_2O$ (5 mg) at room temperature for 15 h gave a mixture of **4c** and **12** (0.31 g, **4c**/**12**=2.4/1) in 52% yield.[12]

Dimethyl 1,2-Dihydro-2,2-dimethyl-2-silanaphthalene-3,4-dicarboxylate (14): Bp 119 °C (1.0 Torr, bath temp); IR(neat) 2950, 1734, 1715, 1584, 1554, 1435, 1302, 1231, 1208, 1070, 810 cm^{-1}; ^1H NMR ($CDCl_3$) δ=0.20 (s, 6H); 2.19 (s, 2H), 3.77 (s, 3H), 3.91 (s, 3H), 7.10—7.24 (m, 4H); ^{13}C NMR ($CDCl_3$) δ=−3.96, 20.77, 51.82, 52.40, 126.0, 129.1, 129.9, 131.4, 131.9,

137.5, 145.4, 153.3, 169.6, 169.9. Found: C, 61.89; H, 6.32%. Calcd for $C_{15}H_{18}O_4Si$: C, 62.04; H, 6.25%.

1,2-Dihydro-2,2-dimethyl-4-phenyl-2-silanaphthalene (15a): Mp 76.5—77.0 °C (hexane); IR(neat before crystallization) 3040, 2945, 2840, 1570, 1540, 1475, 1435, 1242, 1203, 822, 797, 761, 698 cm^{-1}; ^1H NMR ($CDCl_3$) δ=0.13 (s, 6H), 2.22 (s, 2H), 6.14 (s, 1H), 6.98—7.30 (m, 4H), 7.37 (bs, 5H); ^{13}C NMR ($CDCl_3$) δ=−3.63, 21.41, 125.0, 127.1, 127.3, 128.0, 128.2, 129.4. Found: C, 81.52; H, 7.11%. Calcd for $C_{17}H_{18}Si$: C, 81.54; H, 7.24%.

1,4-Dihydro-1,1-dimethyl-3-phenyl-1-silanaphthalene (15b): Bp 120 °C (0.3 Torr, bath temp); IR(neat) 3052, 2952, 1595, 1492, 1436, 1247, 1136, 844, 772, 741, 693 cm^{-1}; ^1H NMR ($CDCl_3$) δ=0.32 (s, 6H), 4.07 (s, 2H), 6.33 (s, 1H), 7.25—7.68 (m, 9H); ^{13}C NMR ($CDCl_3$) δ=−1.21, 38.78, 123.9, 125.7, 125.8, 127.5, 128.3, 128.6, 128.8, 133.1, 134.0, 144.7, 144.8, 155.1. Found: C, 81.38; H, 7.26%. Calcd for $C_{17}H_{18}Si$: C, 81.54; H, 7.24%.

2-Methylene-1,1-dimethyl-3-phenyl-1-silacyclohexane (16a): Bp 100 °C (1.0 Torr, bath temp); IR(neat) 2954, 2920, 2852, 1729, 1630, 1599, 1491, 1447, 1250, 1154, 1121, 1073, 1032, 961, 892, 835, 758, 695 cm^{-1}; ^1H NMR ($CDCl_3$) δ=0.12 (s, 3H), 0.17 (s, 3H), 0.50—0.80 (m, 1H), 0.80—1.00 (m, 1H), 1.60—1.90 (m, 2H), 1.90—2.03 (m, 1H), 2.03—2.13 (m, 1H), 3.40—3.60 (m, 1H), 4.84 (t, J=2.5 Hz, 1H), 5.24 (t, J=2.5 Hz, 1H), 7.10—7.45 (m, 5H); ^{13}C NMR ($CDCl_3$) δ=−3.05, 15.19, 23.61, 36.77, 52.50, 122.0, 125.9, 128.1, 128.5, 143.8, 155.7. Found: C, 77.82; H, 9.50%. Calcd for $C_{14}H_{20}Si$: C, 77.71; H, 9.32%.

2-Benzylidene-1,1-dimethyl-1-silacyclohexane (17a): Bp 100 °C (1.0 Torr, bath temp); IR(neat) 2950, 2916, 2848, 1729, 1598, 1492, 1445, 1429, 1249, 1139, 1111, 900, 871, 828, 776, 751, 732, 712, 698 cm^{-1}; ^1H NMR ($CDCl_3$) δ=0.17 (s, 6H), 0.65—0.80 (m, 2H), 1.40—1.70 (m, 2H), 1.75—1.95 (m, 2H), 2.55—2.70 (m, 2H), 6.68 (s, 1H), 7.10—7.50 (m, 5H); ^{13}C NMR ($CDCl_3$) δ=−3.49, 15.36, 24.37, 30.70, 31.60, 126.3, 128.0, 128.9, 134.1, 138.1, 145.5. Found: C, 77.75; H, 9.47%. Calcd for $C_{14}H_{20}Si$: C, 77.71; H, 9.32%.

Allyldimethyl(α-methylstyryl)silane (18a): Bp 90 °C (1.0 Torr, bath temp); IR(neat) 2954, 2922, 2852, 1630, 1598, 1490, 1447, 1250, 1153, 1120, 1072, 1031, 961, 930, 892, 835, 758, 694 cm^{-1}; ^1H NMR ($CDCl_3$) δ=0.15 (s, 6H), 1.66 (d, J=8.0 Hz, 2H), 1.94 (d, J=1.8 Hz, 3H), 4.80—5.00 (m, 2H), 5.83 (ddt, J=17.0, 10.0, 8.0 Hz, 1H), 6.77 (s, 1H), 7.10—7.50 (m, 5H); ^{13}C NMR ($CDCl_3$) δ=−4.26, 16.57, 22.74, 113.1, 122.0, 126.5, 128.0, 128.5, 129.0, 135.0, 137.8, 138.2, 138.6. Found: C, 77.77; H, 9.56%. Calcd for $C_{14}H_{20}Si$: C, 77.71; H, 9.32%.

2-Methylene-1,1,3-triphenyl-1-silacyclohexane (16b): Bp 175 °C (0.25 Torr, bath temp); IR(neat) 3062, 3048, 3020, 2916, 2850, 1491, 1451, 1429, 1111, 938, 814, 732, 711, 698 cm^{-1}; ^1H NMR ($CDCl_3$) δ=1.15—1.45 (m, 1H), 1.45—2.12 (m, 4H), 2.18—2.35 (m, 1H), 3.52 (d, J=10.0 Hz, 1H), 5.06 (s, 1H), 5.20 (s, 1H), 7.10—7.80 (m, 15H); ^{13}C NMR ($CDCl_3$) δ=12.45, 23.88, 36.87, 52.81, 126.0, 127.0, 127.7, 128.2, 128.5, 129.47, 129.52, 134.0, 134.7, 135.2, 135.5, 143.7, 151.2. Found: C, 84.56; H, 7.20%. Calcd for $C_{24}H_{24}Si$: C, 84.65; H, 7.10%.

2-Benzylidene-1,1-diphenyl-1-silacyclohexane (17b): Bp 175 °C (0.4 Torr, bath temp); ^1H NMR ($CDCl_3$) δ=1.25—2.20 (m, 6H), 2.65—2.80 (m, 2H), 6.67 (s, 1H), 7.20—7.80 (m, 15H); ^{13}C NMR ($CDCl_3$) δ=12.64, 24.14, 30.42, 32.15, 126.6, 127.9, 128.0, 129.0, 135.5, 139.3, 141.2. Found: C, 84.36; H, 6.98%. Calcd for $C_{24}H_{24}Si$: C, 84.65; H, 7.10%.

Allyldiphenyl(α-methylstyryl)silane (18b): Bp 175 °C (0.3 Torr, bath temp); ^1H NMR ($CDCl_3$) δ=2.07 (s, 3H), 2.35 (d, J=8.0 Hz, 2H), 4.85—5.03 (m, 2H), 5.80—6.15 (m, 1H), 6.90 (s, 1H), 7.20—7.80 (m, 15H); ^{13}C NMR ($CDCl_3$) δ=17.65, 20.53, 114.8, 126.9, 127.8, 128.1, 129.1, 134.1, 134.4, 135.6, 142.4. Found: C, 84.57; H, 6.96%. Calcd for $C_{24}H_{24}Si$: C, 84.65; H, 7.10%.

1,2,3,4-Tetrahydro-2,2-dimethyl-3-methylene-4-phenyl-2-silanaphthalene (19): Mp 85—86 °C (hexane); IR(neat before crystallization) 3058, 3026, 2944, 1491, 1481, 1447, 1246, 922, 834, 805, 776, 754, 736, 697, 649 cm^{-1}; ^1H NMR ($CDCl_3$) δ=−0.04 (s, 3H), 0.06 (s, 3H), 1.65 (d, J=14.8 Hz, 1H), 1.84 (d, J=14.8 Hz, 1H), 4.72 (s, 1H), 5.59 (d, J=2.6 Hz, 1H), 5.91 (d, J=2.6 Hz, 1H), 7.05—7.38 (m, 9H); ^{13}C NMR ($CDCl_3$) δ=−2.42, −0.80, 20.87, 60.58, 125.5, 125.9, 126.5, 127.1, 127.5, 128.1, 130.0, 130.9, 138.0, 140.8, 141.7, 151.3. Found: C, 81.72; H, 7.57%. Calcd for $C_{18}H_{20}Si$: C, 81.76; H, 7.62%.

Financial support by the Ministry of Education, Science and Culture (Grant-in-Aid for Scientific Research No. 02650624) is acknowledged.

References

1) K. Matsumoto, K. Oshima, and K. Utimoto, *Tetrahedron Lett.*, **31**, 6055 (1990).

2) Y. Takeyama, K. Oshima, and K. Utimoto, *Tetrahedron Lett.*, **31**, 6059 (1990).

3) H. Sakurai and T. Imai, *Chem. Lett.*, **1975**, 891.

4) J. Laane, *J. Am. Chem. Soc.*, **89**, 1144 (1967).

5) 1,1-Dimethyl-1-silacyclobutane is known to undergo various insertion reactions with SO_2,[6] SO_3,[7] carbene,[8] $Fe(CO)_4$.[9]

6) J. Dubac and P. Mazerolles, *Bull. Soc. Chim. Fr.*, **1969**, 3608.

7) J. Dubac, P. Mazerolles, M. Lesbre, and M. Joly, *J. Organomet. Chem.*, **25**, 367 (1970).

8) D. Seyferth, R. Damrauer, and S. S. Washbune, *J. Am. Chem. Soc.*, **89**, 1538 (1967); D. Seyferth, R. Damrauer, S. B. Andrews, and S. S. Washburne, *ibid.*, **93**, 3709 (1971); D. Seyferth, Houng-Min Shin, J. Dubac, P. Mazerolles, and B. Serres, *J. Organomet. Chem.*, **50**, 39 (1971); H. M. Frey, R. Walsh, and I. M. Watts, *J. Chem. Soc., Chem. Commun.*, **1989**, 284.

9) C. S. Cundy and M. F. Lappert, *J. Chem. Soc., Chem. Commun.*, **1972**, 445.

10) The rate of reductive elimination is enhanced by electron abstraction from palladium metal. For instance, Schwartz et al. have reported that reductive elimination proceeded smoothly in the presence of maleic anhydride (J. S. Temple, M. Riediker, and J. Schwartz, *J. Am. Chem. Soc.*, **104**, 1310 (1982)). Thus, the difference in the product ratio (**3**:**4**) between dimethyl acetylenedicarboxylate and phenylacetylene might be ascribed to the electron density on palladium in the intermediate **9**. The electron density on palladium in the compound **9** (R^1=R^2=COOMe) might be lower than that in the intermediate **9** (R^1=Ph, R^2=H) and facile reductive elimination would take place in the compound **9** (R^1=R^2=COOMe) to give silacyclohexene derivative mainly.

11) C. Eaborn, D. R. M. Walton, and M. Chan, *J. Organomet. Chem.*, **9**, 251 (1967).

12) R. A. Benkeser, *Pure Appl. Chem.*, **13**, 133 (1966).

Stereochemical Control in Microbial Reduction. 18. Mechanism of Stereochemical Control in the Diastereoselective Reduction with Bakers' Yeast

Kaoru NAKAMURA,* Yasushi KAWAI, Takehiko MIYAI,†† Sohichi HONDA, Nobuyoshi NAKAJIMA,† and Atsuyoshi OHNO
Institute for Chemical Research, Kyoto University, Uji, Kyoto 611
† Department of Food and Nutrition, Okayama Prefectural Junior College, Okayama 700
(Received December 25, 1990)

Reduction of a variety of 2-alkyl-3-oxobutanoates with bakers' yeast yields the corresponding L-(3*S*)-hydroxy esters with exclusive enantioselectivity, while the diastereoselectivity, syn/anti ratio, varies depending on the structure of the alkoxyl moiety. In order to elucidate the mechanism for this stereochemical control, oxidoreductases that reduce 2-alkyl-3-oxobutanoate have been isolated from the cells of bakers' yeast and purified. Two dominant competing 2-alkyl-3-hydroxybutanoate oxidoreductases have been obtained: one of them reduces 2-alkyl-3-oxobutanoates stereoselectively yielding the corresponding L-*syn*-hydroxy esters, whereas the other affords a mixture of L-*syn*- and L-*anti*-hydroxy esters. The experimental results on stereoselectivity have nicely been simulated using kinetic parameters elucidated.

Optically active 2-alkyl-3-hydroxyalkanoates are versatile chiral building blocks in organic synthesis[1] because they have two chiral centers necessary for asymmetric synthesis as well as two functional groups that are readily convertible into many other functions. A number of researchers have made efforts to obtain the compounds of this class.[2-4] Recently, we developed the methods to synthesize optically active 2-alkyl-3-hydroxy esters under the catalysis of biological systems:[5-10] bakers' yeast reduces various 2-alkyl-3-oxobutanoates affording the corresponding L-(3*S*)-hydroxy esters with exclusive enantioselectivity, while the diastereoselectivity varies depending on the structure of the alkoxyl group. The presence or absence of a substituent at the carbon adjacent to the alkoxyl oxygen is crucial to control the reduction course leading to the *syn*- or *anti*- product.[11] For example, the reduction of neopentyl 2-methyl-3-oxobutanoate (**1c**) affords the corresponding (2*R*,3*S*)-*syn*-hydroxy ester with 92% diastereomer excess (d.e.), whereas the reduction of *t*-butyl 2-allyl-3-oxobutanoate (**2b**) yields the corresponding (2*S*,3*S*)-*anti*-hydroxy ester with 88% d.e. (Scheme 1).

In order to clarify the mechanism for stereochemical control in microbial reduction, we isolated certain β-hydroxy ester oxidoreductases effective to the reduction of 2-alkyl-3-oxobutanoates from the cells of bakers' yeast and studied the kinetics as well as stereochemical properties of the enzymes. In the previous paper of this series, we reported that the studies at the enzyme level is successful to explain stereochemical behavior of their host microbe under various reaction conditions at least qualitatively.[12]

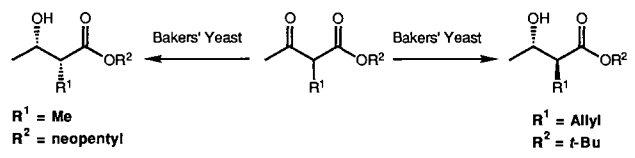

Scheme 1.

Experimental

Instruments. ^{1}H NMR spectra were recorded on a Varian VXR-200 spectrometer in $CDCl_3$ with Me_4Si as an internal standard. Gas chromatograms were recorded on a Yanaco G-2800 (PEG-20M, 1.5 m) and a Shimadzu GC-14A (PEG-20M Bonded, 25 m) gas chromatographs. Preparative gas chromatography was done on a Varian Aerograph Model 920 gas chromatograph (PEG-20M, 1.5 m, 150 °C). UV spectra were obtained on a Hitachi U-3210 spectrophotometer. Optical rotation was measured with a Perkin-Elmer 241 polarimeter.

Materials. Organic reagents and solvents were purchased from Nacalai Tesque Co., Tokyo Kasei Co., and Aldrich Chemical Co. unless otherwise indicated. Bakers' yeast was purchased from Oriental Yeast Co. and stored in a refrigerator. The substrates (**1a—c**) and (**2a—c**) were prepared according to the method described in our previous paper.[7] The detailed procedure for purification of the enzymes was described in the previous paper.[12]

Enzyme Assay. A 50 μl aliquot of a fraction of chromatography was added to a 3.10 ml solution (0.10 M potassium phosphate buffer at pH 7.0, 1M=1 mol dm^{-3}) containing ethyl 2-allyl-3-oxobutanoate (**2a**) (9.32×10^{-4} M) and NADPH (9.00×10^{-5} M). The kinetics was followed spectrophotometrically at 30 °C following the decreases in absorbance of NADPH at 340 nm. One unit of the enzyme activity was defined as the amount of an enzyme which catalyzes the oxidation of 1 μmol NADPH per minute at 30 °C under the assay conditions.

Reduction of Alkyl 2-Alkyl-3-oxobutanoate with Enzymes. In a 10 ml round-bottomed flask equipped with magnetic stirrer and silicone stopper, were placed a concentrated solution of an enzyme (1 unit), NADPH (8 mg), a substrate (5 mg), and 0.1 M phosphate buffer (pH 7.0, 4 ml). The flask

†† Present address: Nissei Kagaku Kogyo Co., Ltd., 1-8-7 Fukumachi, Nishiyodogawa-ku, Osaka 555.

was protected from light and the mixture was stirred for 24 h at 30 °C. The mixture was extracted with ether, washed with water and brine, and dried over anhydrous sodium sulfate. The diastereomer excess (% d.e.) in the hydroxy ester was determined by gas chromatographic analyses (PEG-20M Bonded, 25 m, 90 °C for 2-methyl-3-hydroxy esters and 150 °C for 2-allyl-3-hydroxy esters).[13]

Results

Purification of 2-Alkyl-3-hydroxybutanoate Oxidoreductases. 2-Alkyl-3-hydroxy ester oxidoreductases were separated from the cell-free solution of bakers' yeast by column chromatography on DEAE-Toyopearl anion exchange resin, and two enzymes were found to exert the desired activity. One of them (E1) was not adsorbed on the anion exchange resin, whereas the other (E2) was adsorbed on it at pH 7.0 (10 mM phosphate buffer). Both enzymes were further purified with chromatographic techniques including ion-exchange, hydrophobic, and gel filtration chromatographies. The activity was determined based on the velocity of the reduction of ethyl 2-allyl-3-oxobutanoate (**2a**). Both enzymes utilize NADPH preferentially as the coenzyme. Total activities of these enzymes measured under the assay and preparative conditions are summarized in Table 1.

In the previous paper, we reported that bakers' yeast has four β-hydroxy ester oxidoreductases. Two of them (L-enzymes) afford the corresponding L-hydroxy esters, whereas the other two (D-enzymes) give the D-hydroxy esters.[12] Since the yeast reduction of 2-alkyl-3-oxobutanoates affords the corresponding L-(3*S*)-hydroxy esters exclusively, it is probable that these two 2-alkyl-3-hydroxy ester oxidoreductases are identical with the two L-enzymes reported previously. In order to confirm the identity, the substrate specificities of E1 and E2 were kinetically studied for the reductions of ethyl 4-chloro-3-oxobutanoate and found, together with the chromatographic evidence, that non-adsorbed enzyme (E1) and adsorbed enzyme (E2) are identical with the previously reported L-enzyme-1 and L-enzyme-2, respectively. Detailed descriptions of the purification methods and enzyme properties are given in the previous paper.[12]

The diastereoselectivity in the reduction of various esters of 2-methyl-3-oxobutanoates (**1**) or 2-allyl-3-oxobutanoates (**2**) with these two enzymes were determined (Scheme 2) and the results are summarized in Table 2.

In order to characterize the enzymes, the kinetic parameters, K_M and V_{max}, for the present particular substrates were elucidated from the Lineweaver–Burk plot[14] and the results are listed in Table 3.

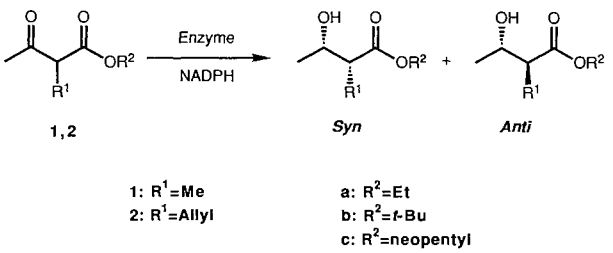

Scheme 2.

Table 1. Total Activities of Enzymes for Ethyl 2-allyl-3-oxobutanoate (**2a**) as Substrate

Enzyme	Total activity (unit)	
	[S]=1 mM[a]	[S]=40 mM[b]
E1	8.8[c]	102
E2	93	273

a) Substrate concentration under the assay conditions. b) Substrate concentration under the preparative reaction conditions. c) Note that [S]≪K_M under the assay conditions.

Table 2. Reduction of Alkyl 2-Methyl- and 2-Allyl-3-oxobutanoates (**1**) and (**2**) with Isolated Enzymes

Substrate	*syn*:*anti* Ratio in the product	
	E1	E2
1a	>99:1	82:18
1b	97:3	51:49
1c	>99:1	96:4
2a	>99:1	6:94
2b	>99:1	3:97
2c	>99:1	19:81

Table 3. Kinetic Parameters for the Enzymes[a]

Substrate	K_M/mM		k_{cat}/s^{-1}		$10^6 V_{max}$/M s^{-1} mg^{-1} protein		$10\,k_{cat}/K_M$/s^{-1} mM^{-1}	
	E1	E2	E1	E2	E1	E2	E1	E2
1a	6.4	3.1	4.06	0.179	41.0	1.80	6.35	0.577
1b	15	2.3	2.87	0.070	28.9	0.701	1.91	0.302
1c	0.72	2.0	8.55	0.128	86.1	1.29	119	0.642
2a	15	2.1	3.48	0.452	35.1	4.56	2.32	2.15
2b	30[b]	2.1	8.32	1.22	83.8	12.3	2.77	5.80
2c	1.1	1.0	1.90	0.403	19.1	4.06	17.3	4.03

a) Errors in K_M and k_{cat} are estimated to be less than ±10%. b) The error in this value is about ±20% because the solubility of this substrate is only 3 mM.

Discussion

Several hydroxy ester oxidoreductases have been isolated from bakers' yeast. Shieh et al. isolated three kinds of β-hydroxy ester oxidoreductases, which reduced ethyl 4-chloro-3-oxobutanoate.[15] One of them possesses similar properties to fatty acid synthetase (FAS) and reduces β-keto esters to afford D-hydroxy ester. One of the other enzymes also gives D-hydroxy ester (D-enzyme), whereas the last one yields L-hydroxy ester (L-enzyme). Their L-enzyme is distinct from our both L-enzymes since there have different molecular weight and kinetic constants. Furuich et al. isolated a β-hydroxy ester oxidoreductase from bakers' yeast.[16] It reduces benzyl 2-methyl-3-oxobutanoate affording the corresponding L-hydroxy ester (L-enzyme). This enzyme differs from our enzymes, because the latter enzymes are able to reduce ethyl 2-methyl-3-oxobutanoate (**1a**), whereas the former inactive toward this substrate. Although they reported the isolation of another oxidoreductase from *Saccharomyces fermentati*, this enzyme also differs from our enzymes both in molecular weight and substrate specificity.[17]

As listed in Table 2, E1 is distinct from E2 in diastereoselectivity of the reduction. The former affords the L-*syn*-hydroxy ester with exclusive stereoselectivity for all the substrates. On the other hand, the diastereoselectivity of the latter enzyme depends on the structure of the substrate; not only on the structure of the alkoxyl group but also on the structure of the substituent at the C_2-position. The substrates (**1**) that have a methyl group at the C_2-position tend to afford the corresponding *syn*-hydroxy esters under the catalysis of E2, whereas the substrates (**2**) having an allyl group at the same position prefer to afford the corresponding *anti*-hydroxy esters under the same reaction conditions.

In the reaction with E2, the values of K_M remains almost constant regardless of the structure through all of the substrates employed. However, this tendency is not held in the reaction with E1: the K_M for the neopentyl ester is small but that for the *t*-butyl ester is large in both of 2-methyl and 2-allyl derivatives. That is, it has been elucidated that the active site of E1 is adopted to the neopentyl derivative more effectively than to the ethyl derivative. The *t*-butyl derivative is the least effective substrate.

In addition, it is interesting to compare the substrate selectivity of E1 with that of E2 from the viewpoint of the stereochemistry at the C_2-position. Only the (2*R*)-isomer can be recognized by E1 as the substrate affording the (2*R*)-*syn*-product exclusively. The (2*S*)-isomer is not reduced until it is converted into the (2*R*)-isomer by isomerization equilibrium. This characteristics of the reaction is independent of the structure of the substituent at the C_2-position. On the contrary, E2 has a rather wide selectivity on stereochemistry at the C_2-position: although a substrate which has the 2-methyl substituent exerts a tendency to react as the (2*R*)-isomer, the selectivity at the C_2-position depends largely on the structure of the alkoxyl moiety. Namely, the neopentyl ester (**1c**) is reduced almost exclusively through the (2*R*)-isomer (2*R*:2*S*=96:4), whereas there is no enantiomeric discrimination between the (2*S*)- and (2*R*)-configurations in the *t*-butyl ester (**1b**) (2*R*:2*S*= 51:49).

In the reduction with E2, the substrate with the 2-allyl substituent reacts mainly through the (2*S*)-isomer. Among three substrates studied, the *t*-butyl ester (**2b**) exerts the largest (2*S*)-selectivity, which is a distinct contrary to the selectivity on the 2-methyl derivative mentioned above. In other words, it may be concluded that the *t*-butoxyl group prefers to afford the (2*S*)-*anti*-product, but the neopentyloxyl group suits to yield the (2*R*)-*syn*-product.

Knowing relative activities of the enzymes in bakers' yeast and the concentration of the substrate, we can simulate the stereoselectivity of the microbial reduction theoretically. The substrate concentration employed for the present preparative reactions is 40 mM.[7] Although **1a** and **2a** have enough solubility to maintain this stoichiometric concentration during the reaction, **1b**, **1c**, **2b**, and **2c** are less soluble to water and their concentrations in saturated aqueous solutions are about 12, 3, 3, and 1 mM, respectively. That is, the effective concentrations of the substrates in the latter group are much smaller than 40 mM in the preparative reactions. Therefore, the diastereoselectivities of the reduction can be evaluated based on the effective concentrations of the substrates, the relative activities: velocity (listed in Table 3) × total unit (listed in Table 1), and the syn/anti selectivities of these two competing enzymes. The results are summarized in Table 4. The diastereoselectivities experimentally observed for the reduction with bakers' yeast[7] are also listed in Table 4 for comparison. It is apparent that the calculated selectivities are in good agreement with the experimental values.

The mechanism for stereochemical control in the reduction with bakers' yeast by modification of the alkoxyl group is thus explicated by kinetic parameters

Table 4. Calculated Diastereoselectivity of the Reduction Based on Kinetic Parameters

Substrate	*syn*:*anti* Ratio in the product	
	Bakers' yeast[a]	Calcd
1a	87:13	92:8
1b	72:28	78:22
1c	96:4	99:1
2a	35:65	31:69
2b	6:94	9:91
2c	56:44	37:63

a) Ref. 8.

for the combinations of various substrates and enzymes. The K_M values for E2 do not change appreciably upon the modification in structure of the alkoxyl group, whereas those for E1 change so that they increase when the alkoxyl oxygen is bound directly to a tertiary carbon such as in the *t*-butyl group, and decrease when a methylene group is inserted between the alkoxyl oxygen and a bulky alkyl group such as in the neopentyl group.

It is conceivable that the binding site of E1 has a shape such that there is no enough room to set a bulky tertiary carbon in the vicinity of the alkoxyl oxygen. The steric tension in the pocket can be released, however, by the insertion of a methylene group between the alkoxyl oxygen and a bulky alkyl group because the molecule now procures an ability to fracture the bulky substituent to assume the least volume.[7] Consequently, the presence or absence of a methylene group adjacent to the alkoxyl oxygen is crucial to control the diastereoselectivity of the reduction.

The pocket of E2, on the other hand, is so vague that not only the structure of the alkoxyl group but also the stereochemistry at the C_2-position are not discriminated strictly by this enzyme. It is assumed that a substrate can be contained in the pocket of E2 setting either of its 2*S*- and 2*R*-isomer against the reacting function of the enzyme without causing serious steric strain. The dominant effect to choose the isomer is the force to set the substrate in the stable form in the pocket of the enzyme. The *syn*- and *anti*-products are, therefore, afforded in various ratios under the catalysis of E2 depending on the structure of substituent at the C_2-position.

The enzymatic studies of bakers' yeast for other substrates are now in progress in our laboratory and will be reported elsewhere.

We thank financial support for this research by the Ministry of Education, Science and Culture, under the Grant-in-Aid Nos. 01470022, 01303007, and 02303004.

References

1) S. Masamune and W. Choy, *Aldrichimica Acta,* **15**, 47 (1982).
2) J. D. Morrison, "Asymmetric Synthesis," Academic Press, New York (1985), Vol. 3.
3) G. Fráter, U. Müller, and W. Günter, *Tetrahedron,* **40**, 1269 (1984).
4) R. Noyori, T. Ikeda, T. Ohkuma, M. Widhalm, M. Kitamura, H. Takaya, S. Akutagawa, N. Sayo, T. Saito, T. Taketomi, and H. Kumobayashi, *J. Am. Chem. Soc.,* **111**, 9134 (1989).
5) K. Nakamura, T. Miyai, K. Nozaki, K. Ushio, S. Oka, and A. Ohno, *Tetrahedron Lett.,* **27**, 3155 (1986).
6) K. Nakamura, T. Miyai, K. Ushio, S. Oka, and A. Ohno, *Bull. Chem. Soc. Jpn.,* **61**, 2089 (1988).
7) K. Nakamura, T. Miyai, A. Nagar, S. Oka, and A. Ohno, *Bull. Chem. Soc. Jpn.,* **62**, 1179 (1989).
8) K. Nakamura, T. Miyai, Y. Kawai, N. Nakajima, and A. Ohno, *Tetrahedron Lett.,* **31**, 1159 (1990).
9) K. Nakamura, T. Miyai, K. Fukushima, Y. Kawai, B. B. Ramesh, and A. Ohno, *Bull. Chem. Soc. Jpn.,* **63**, 1713 (1990).
10) K. Nakamura, Y. Kawai, T. Miyai, and A. Ohno, *Tetrahedron Lett.,* **31**, 3631 (1990).
11) For simplicity of expression, we use the terms *syn* and *anti* for *erythro* and *threo*, respectively. The terms *syn* and *anti* denote the configuration of (2*R*,3*S*) and (2*S*,3*S*), respectively.
12) K. Nakamura, Y. Kawai, N. Nakajima, and A. Ohno, *J. Org. Chem.,* in press.
13) K. Nakamura, T. Miyai, A. Nagar, B. B. Ramesh, T. Ando, and A. Ohno, *Bull. Chem. Soc. Jpn.,* **63**, 298 (1990).
14) I. H. Segel, "Enzyme Kinetics," John Wiley & Sons, New York (1975).
15) W. -R. Shieh, A. S. Gopalan, and C. J. Sih, *J. Am. Chem. Soc.,* **107**, 2993 (1985).
16) A. Furuichi, H. Akita, H. Matsukura, T. Oish, and K. Horikoshi, *Agric. Biol. Chem.,* **49**, 2563 (1985).
17) A. Furuichi, H. Akita, H. Matsukura, T. Oish, and K. Horikoshi, *Agric. Biol. Chem.,* **51**, 293 (1987).

Enantio- and Diastereo-Selective Synthesis of (+)-Grandisol

Koichi NARASAKA,* Hiroyuki KUSAMA, and Yujiro HAYASHI
Department of Chemistry, Faculty of Science, The University of Tokyo,
Hongo, Bunkyo-ku, Tokyo 113
(Received December 27, 1990)

(+)-Grandisol, an insect pheromone having cyclobutane skeleton, is synthesized enantio- and diastereoselectively. The key steps in the synthesis are the asymmetric [2+2] cycloaddition reaction catalyzed by a chiral titanium reagent and the diastereoselective conjugate addition reaction by the combined use of Me_2CuLi and trimethylsilyl trifluoromethanesulfonate.

(+)-Grandisol, which was first isolated by Tumlinson et al. in 1967,[1] is one of the components of the male-produced pheromone of the cotton boll weevil (*Anthonomus Grandis*). This compound attracted much attention of many synthetic organic chemists not only due to its biological activity but also to its unique cyclobutane structure, and many synthetic studies have been reported[2,3] including several asymmetric syntheses.[4-6] The crucial step in these asymmetric syntheses is the preparation of optically active cyclobutanes, which includes optical resolutions of cyclobutane derivatives,[4] syntheses from chiral building blocks of natural compounds,[5] and diastereoselective [2+2] photocycloaddition reactions using substrates having chiral auxiliaries.[6]

We have recently reported the asymmetric [2+2] cycloaddition reaction between 3-acryloyl-1,3-oxazolidin-2-one derivatives and ketene dithioacetal promoted by a catalytic amount of the chiral titanium reagent prepared from dichlorodiisopropoxytitanium and a tartrate-derived chiral diol.[7] This reaction gives chiral cyclobutane derivatives in high enantioselectivity and, furthermore, both enantiomers of the chiral cyclobutanes are easily obtained by choosing the appropriate enantiomer of the chiral 1,4-diol. These chiral products are expected to be synthetically useful chiral building blocks. In fact, the total synthesis of carbocyclic oxetanocin analogues was performed starting from the optically active [2+2] adduct.[8] For a further application, the asymmetric synthesis of (+)-grandisol **1** has been attempted and, in this report, the detail of the synthesis is summarized.

In the following retrosynthetic scheme, the key steps are: (1) the construction of the chiral cyclobutane **5** with high enantioselectivity, (2) the diastereoselective introduction of α-methyl group to the methyl cyclobutylideneacetate **10** or **12**.

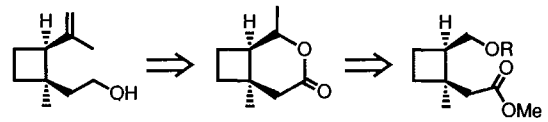

(+)-Grandisol **1**

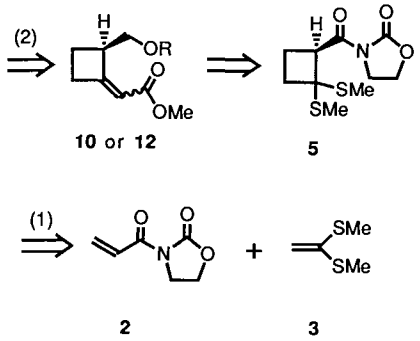

Results and Discussion

The asymmetric [2+2] cycloaddition reaction between 3-acryloyl-1,3-oxazolidin-2-one (**2**) and 1,1-bis(methylthio)ethylene (**3**) was examined. The chiral titanium reagent was prepared *in situ* by mixing dichlorodiisopropoxytitanium and (−)-(2*S*,3*S*)-1,1,4,4,-tetraphenyl-2,3-*O*-(1-phenylethylidene)-1,2,3,4-butanetetrol (**4**) derived from (−)-tartaric acid.[9] The reaction of **2** and **3** in the presence of 10% mol of the above chiral titanium catalyst and Molecular Sieves 4A in a toluene–petroleum ether mixture at 0 °C for 1 h afforded the corresponding cyclobutanecarboxylic acid derivative **5** in 80% yield with 88% ee.

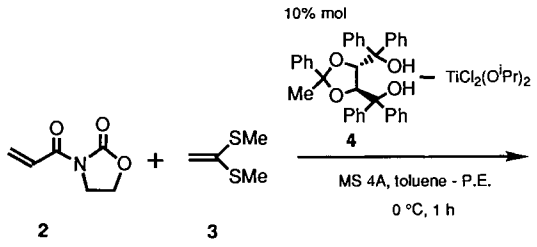

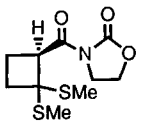

80% yield, 88% ee
recryst. from benzene - hexane >98% ee

The optically pure material **5** (>98% ee) was obtained by the recrystallization from benzene–hexane. The optical purity was checked by the 500 MHz ^{1}H NMR analysis of the Mosher's (+)-methoxy trifluoromethyl phenyl acetate ((+)-MTPA ester)[10] derived from **7**. The X-ray crystallographic analysis of the single crystal of **5** was shown in the following figure. Although the absolute configuration of **5** could not be determined by this X-ray analysis, it is considered to be *S* based on the previously reported [2+2] cycloaddition reaction of 3-[3-(methoxycarbonyl)acryloyl]-1,3-oxazolidin-2-one and ketene dithioacetal **3**.[7]

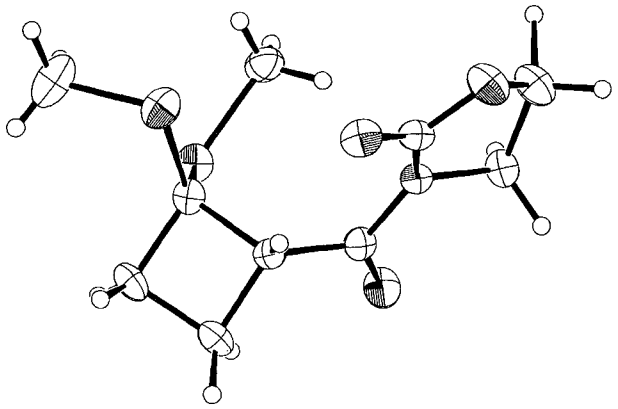

Fig. 1. The ORTEP drawing of **5**.

The transformation of the optically pure cyclobutane **5** to the α,β-unsaturated ester **10a** was performed as shown in Scheme 1. Treatment of **5** with magnesium methoxide gave the methyl ester **6**. Reduction of **6** with $LiAlH_4$ afforded the alcohol **7**, whose hydroxyl group was protected as *t*-butyldiphenylsilyl (TBDPS) ether **8** in 94% overall yield from **5** in 3 steps. Subsequently, hydrolysis of dithioacetal group of **8** with *N*-chlorosuccinimide and silver nitrate[11] gave the cyclobutanone **9** in 95% yield. The Peterson olefination of **9** [$LiN(c\text{-}C_6H_{11})_2$, $TMSCH_2CO_2Me$ (TMS=trimethylsilyl)][12] gave the (*Z*)-α,β-unsaturated ester **10a** quantitatively as a single stereoisomer.

Then, the introduction of methyl group to the (*Z*)-ester **10a** was investigated. The (*Z*)-**10a**, a β,β-disubstituted unsaturated ester, was considered to be a poor Michael acceptor toward organocopper(I) reagents.[13] In fact, as shown in Table 1, the reactions of **10a** with lithium dimethylcuprate(I) and methylcopper-(I) did not proceed (Entries 1 and 2). The mixed reagents, MeCu–BF_3·OEt_2 or Me_2CuLi–BF_3·OEt_2,[13,14] also did not give the methylated product (Entries 3 and 4). By the use of Me_2CuLi–TMSCl,[15,16] however, the addition product **11a** was obtained, but the yield was not sufficiently high (60%) (Entry 5). Since more effective activation reagent was thought to be required, the reaction was examined by using trimethylsilyl trifluoromethanesulfonate (TMSOTf), a much stronger Lewis acid (Entry 6). Treatment of **10a** with Me_2CuLi in the presence of TMSOTf in Et_2O at −78 °C afforded the addition product **11a** almost quantitatively as an inseparable mixture of *cis* and *trans* isomers (*cis*:*trans*= 2.5:1). Relative stereochemistry of these two isomers were determined by NOESY spectrum (see Experimental Section).

In order to realize much higher stereoselectivity, the reaction was further examined in detail. And it was found that the stereoselectivity was not influenced on

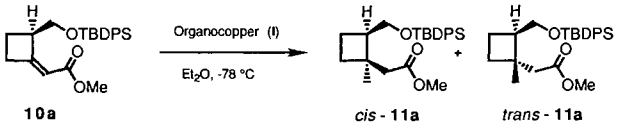

Table 1. The Conjugate Addition Reaction of Organocopper (I) Reagents with **10a**

Entry	Organocopper (I)	Lewis acid	Yield (*x*/%)	**11a** *cis*:*trans*[a]
1	MeCu		0	
2	Me_2CuLi		0	
3	MeCu	BF_3·OEt_2	0	
4	Me_2CuLi	BF_3·OEt_2	0	
5	Me_2CuLi	TMSCl	60	2:1
6	Me_2CuLi	TMSOTf	quant.	2.5:1

a) The ratio of *cis*:*trans* was determined by the integration ratio of the singlet peak of the quaternary methyl groups (500 MHz ^{1}H NMR).

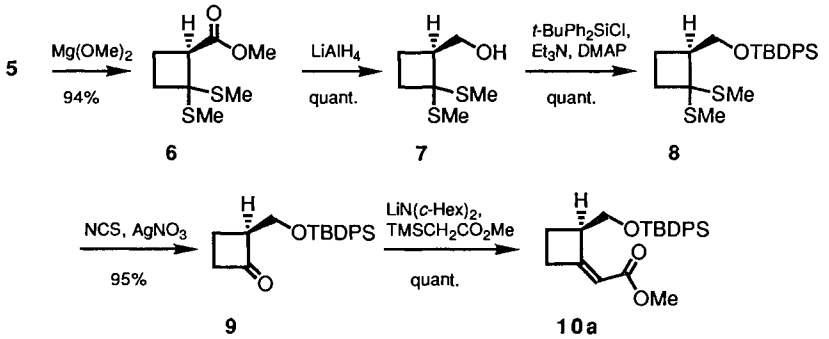

Scheme 1.

the solvent and the reaction temperature. The use of higher order organocuprates(I) was also ineffective. On the other hand, the diastereoselectivity was found to be largely dependent on the protective group of the hydroxyl group and the geometry of the α,β-unsaturated ester moiety.

The (*E*)-α,β-unsaturated esters having various hydroxyl protective groups were prepared from the (*Z*)-ester **10a** as shown in Scheme 2. The desilylation of the (*Z*)-ester **10a** with $Bu_4N^+F^-$ in THF at room temperature was accompanied with the isomerization to the (*E*)-ester **13**, though the complete racemization occurred at the same time with the fluoride anion. The isomerization was, therefore, tried with PhSLi in THF and the (*E*)-ester **12a** was obtained in 73% yield (the (*Z*)-ester **10a** was recovered in 26% yield). Deprotection of **12a** with hydrochloric acid in MeOH and the introduction of various protective groups gave the corresponding (*E*)-esters **12b,c**. By the ^1H NMR analysis of the (+)-MTPA ester[10] of the alcohol **13**, no sign of racemization could be detected. The (*Z*)-esters **10b,c** were prepared by desilylation of **10a** with hydrochloric acid followed by the protection of the resulting alcohol.

The addition reaction to various (*Z*)- and (*E*)-esters **10** and **12** were examined with Me_2CuLi and TMSOTf at −78 °C in Et_2O. When the (*Z*)- or (*E*)-esters protected as *t*-butyldiphenylsilyl ether or methyl ether **10a,b** and **12a,b** were employed, the stereoselectivity was not improved (Table 2, Entries 1—4). In the case of the reaction of the (*Z*)-ester having TMS ether **10c**, the selectivity was also low (Entry 5). On the contrary,

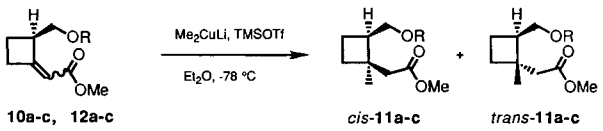

Table 2. The Conjugate Addition Reaction to (*Z*) and (*E*)-Esters **10** and **12**[a]

Entry	R		**11a—c** ratio of *cis*:*trans*[b]
1	*t*-$BuPh_2Si$	**10a**	2.5:1
2	*t*-$BuPh_2Si$	**12a**	2.5:1
3	Me	**10b**	1.5:1
4	Me	**12b**	2:1
5	Me_3Si	**10c**	2:1
6	Me_3Si	**12c**	15:1

a) The yields of the addition products **11a—c** were almost quantitative. b) The ratio of *cis*:*trans* was determined by the integration ratio of the quaternary methyl peaks (500 MHz ^1H NMR).

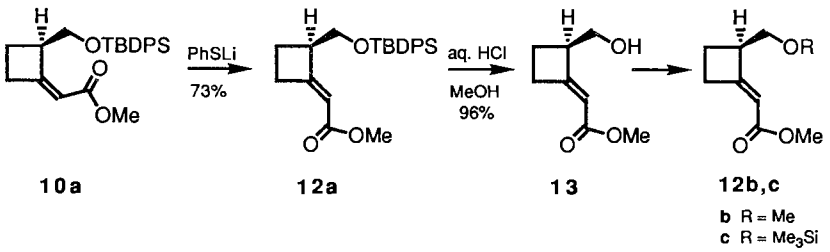

Scheme 2.

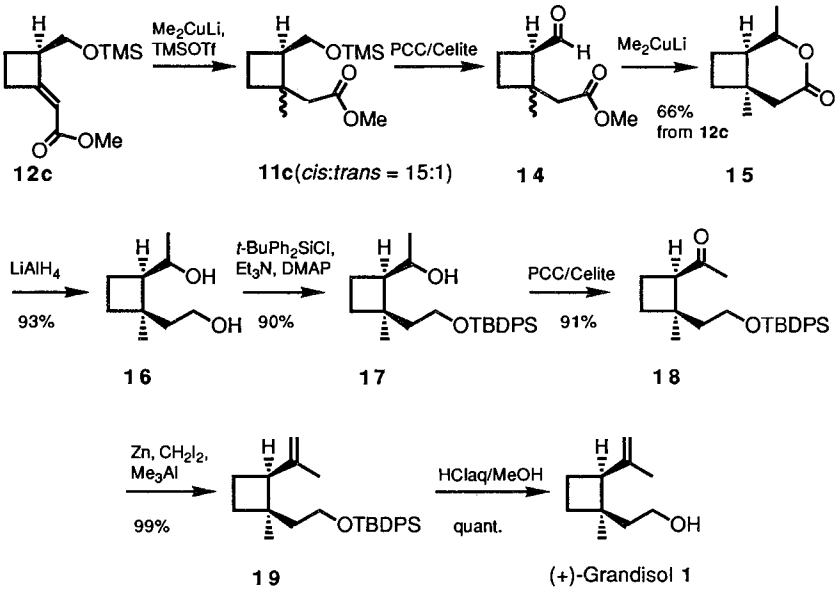

Scheme 3.

it was noted that the reaction of the TMS ether of the (*E*)-ester **12c** gave the addition product **11c** in high stereoselectivity (the ratio of *cis*:*trans*=15:1) (Entry 6). These results indicate that the introduction of a small silyl group and the (*E*)-geometry of the double bond are indispensable to achieve high stereoselectivity.

Then the transformation of the stereoselectively prepared **11c** to (+)-grandisol **1** was executed as shown in Scheme 3. Oxidation of the crude Michael product **11c** (*cis*:*trans*=15:1) with pyridinium chlorochromate (PCC)/Celite in CH_2Cl_2 followed by the treatment with Me_2CuLi in Et_2O gave the *cis* bicyclic lactone **15** as a single stereoisomer (stereochemistry not determined) in 66% yield from **12c** in 3 steps. Reduction of the lactone **15** with $LiAlH_4$ afforded the diol **16** (93% yield), whose primary hydroxyl group was protected as *t*-butyldiphenylsilyl ether **17** in 90% yield. Oxidation of **17** with PCC/Celite (91% yield) and the treatment of the resulting ketone **18** with Zn, CH_2I_2 and Me_3Al[17] gave the methylenation product **19** in 99% yield. Finally, deprotection of **19** with hydrochloric acid in MeOH afforded (+)-grandisol **1** quantitatively.

The overall yield of **1** from **2** was ca. 25% in 17 steps. The spectral data were in good agreement with those of the literature.[4b,c,5b] The optical rotation of the synthesized (+)-grandisol was $[\alpha]_D^{27}$ +18.6° (*c*=1.00, hexane). The dextrorotatory of **1** confirmed the absolute stereochemistry of **5** to be *S* as expected.

To avoid the risk of determining the optical purity from the $[\alpha]_D$ value, the present sample **1** was converted to the corresponding Mosher's (+)-MTPA ester.[10] By the 500 MHz ^{1}H NMR analysis of this (+)-MTPA ester, the optical purity of our (+)-grandisol was confirmed to be >98% ee.

Experimental

General. NMR spectra were recorded on Hitachi R24B and Bruker AM500 spectrometers using tetramethylsilane as the internal standard. $CDCl_3$ was used as solvent. IR spectra were measured with Horiba FT-300S spectrometer. High-mass spectra were obtained with JEOL JMS-D300 mass spectrometer operating at 70 ev. The optical rotations were measured with JASCO DIP-370 digital polarimeter.

Column chromatography was conducted on silica gel (E. Merck, 7734, 70—230 mesh) and Florisil (Wako, 100—200 mesh) and medium pressure column chromatography was performed with the YFLC-254 system of Yamazen Corp. Preparative thin-layer chromatography (TLC) was carried out on a silica gel (Wakogel B-5F).

Dichloromethane was distilled from P_2O_5, then from CaH_2, and dried over MS 4A. Toluene and petroleum ether were distilled and dried over MS 4A. Tetrahydrofuran (THF) and diethyl ether (Et_2O) were freshly distilled from sodium diphenylketyl. Dichlorodiisopropoxytitanium was prepared from titanium(IV) chloride and titanium(IV) isopropoxide according to the literature method.[18] 1,1-Bis(methylthio)-ethylene (**3**)[19] and (2*S*,3*S*)-1,1,4,4-tetraphenyl-2,3-*O*-(1-phenylethylidene)-1,2,3,4-butanetetrol (**4**)[9] were prepared according to the literature procedures. All the operations were performed under an argon atmosphere.

3-Acryloyl-1,3-oxazolidin-2-one (2). To a THF suspension (200 ml) of NaH (60% oil dispersion, 12.2 g, 0.30 mol) was added 1,3-oxazolidin-2-one (26.5 g, 0.30 mol) and the mixture was heated to reflux for 1 h and then cooled to 0 °C. A THF solution (100 ml) of acryloyl chloride (25.0 g, 0.28 mol) was added dropwise, and the mixture was stirred for 4 h. The pH 7 phosphate buffer was slowly poured into the mixture and the organic materials were extracted with ethyl acetate. The organic layers were washed with brine and dried over Na_2SO_4 with a catalytic amount of hydroquinone to prevent polymerization at 0 °C. Solvent was evaporated in vacuo below 10 °C. When the solvent was removed, the crude product was immediately purified by column chromatography (silica gel, dichloromethane) to give the title compound **2** (12.6 g, 42% yield). The pure material should be kept in a refrigerator. ^{1}H NMR (60 MHz) δ=3.83—4.13 (2H, m), 4.28—4.57 (2H, m), 5.82 (1H, dd, *J*=2.0, 10.0 Hz), 6.47 (1H, dd, *J*=2.0, 16.8 Hz), 7.43 (1H, dd, *J*=10.0, 16.8 Hz).

(*S*)-3-[2,2-Bis(methylthio)-1-cyclobutylcarbonyl]-1,3-oxazolidin-2-one (5). Toluene (300 ml) was added to dichlorodiisopropoxytitanium (1.40 g, 5.9 mmol), the chiral diol **4** (3.12 g, 5.9 mmol), and Molecular Sieves 4A (powder, 3.0 g) at 0 °C and the mixture was stirred for 30 min. Then **2** (10.0 g, 71 mmol) and petroleum ether (200 ml) were added. And a petroleum ether solution (100 ml) of **3** (10.0 g, 83 mmol) was added to the mixture, which was stirred at 0 °C for 1 h. The reaction was quenched by pH 7 phosphate buffer and inorganic materials were removed by filtration. The organic materials were extracted with ethyl acetate and the extracts were washed with brine and dried over Na_2SO_4. After evaporation of the solvent, the crude product was purified by column chromatography (silica gel, hexane:ethyl acetate=5:1) to afford the title compound **5** (14.8 g, 80% yield, 88% ee). The optically pure **5** was obtained by two recrystallizations from benzen–hexane (80% recovery). The optically pure **5** was used in the following experiments. Mp 90.5—92.0 °C; IR (KBr) 1780, 1690 cm^{-1}; ^{1}H NMR (500 MHz) δ=2.00 (3H, s), 2.12 (3H, s), 2.25—2.31 (1H, m), 2.32—2.38 (1H, m), 2.42—2.47 (1H, m), 2.53—2.60 (1H, m), 4.07 (2H, dt, *J*=5.5, 8.1 Hz), 4.41 (2H, t, *J*=8.1 Hz), 4.61—4.65 (1H, m); ^{13}C NMR (125 MHz) δ=12.36, 12.66, 18.81, 33.61, 42.62, 49.47, 61.55, 61.96, 153.03, 170.51; $[\alpha]_D^{26}$ −59.4° (*c* 1.17, CH_2Cl_2), >98% ee; Anal. Calcd for $C_{10}H_{15}NO_3S_2$: C, 46.00; H, 5.78; N, 5.36; S, 24.53%. Found: C, 45.88; H, 5.69; N, 5.36; S, 24.92%.

Crystallographic data: M. F.=$C_{10}H_{15}NO_3S_2$, M. W.=261.35, orthorhombic, *a*=8.285 (3), *b*=22.304 (7), *c*=6.726 (2) (Å), *V*=1242.8 (7) (Å^3), space group $P2_12_12_1$, *Z*=4, D_c=1.40 g cm^{-3}, μ(Mo*K*α)=4.11 cm^{-1}. Data collection: crystal size=0.10×0.25×1.00 mm, T_c=25 °C, Mo*K*α radiation (graphite monochrometer), 1704 reflections (2θ<55.0°). The structure was finally refined anisotropically for S, C, O, and N, and isotropically for H to give an *R* factor of 0.052 for 1192 independent reflections with $I>3.0\sigma(I)$.

Methyl (*S*)-2,2-Bis(methylthio)cyclobutane-1-carboxylate (6). Dry methanol (40 ml) and a few drops of carbon tetrachloride was added to metal magnesium (1.9 g, 78 mmol) at 0 °C to generate magnesium methoxide. When all the magnesium dissolved, a THF (30 ml) solution of the [2+2] adduct **5** (6.7 g, 26 mmol) was added. The reaction was

immediately quenched with saturated aqueous ammonium chloride solution and the methyl ester was extracted with ethyl acetate. The organic layers were washed with brine and dried over Na_2SO_4. After evaporation of the solvent, the crude product was purified by column chromatography (silica gel, hexane:ethyl acetate=14:1) to afford the methyl ester **6** (5.0 g, 94% yield). IR (KBr) 1736 cm^{-1}; ^1H NMR (500 MHz) δ=2.01 (3H, s), 2.10 (3H, s), 2.21—2.34 (3H, m), 2.51—2.56 (1H, m), 3.38—3.42 (1H, m), 3.73 (3H, s); ^{13}C NMR (125 MHz) δ=12.27, 12.69, 16.80, 33.43, 51.53, 51.71, 60.70, 171.12; $[\alpha]_D^{24}$ −119.3° (*c* 1.12, CH_2Cl_2); HRMS Found: *m/z* 206.0431. Calcd for $C_8H_{14}O_2S_2$: M, 206.0436.

(*S*)-[2,2-Bis(methylthio)-1-cyclobutyl]methanol (7). A THF solution (20 ml) of **6** (2.66 g, 12.9 mmol) was added to a THF suspension (30 ml) of lithium aluminum hydride (1.0 g, 26 mmol) at 0 °C and the mixture was stirred for 5 min. Then saturated aqueous sodium sulfate solution was added dropwise until hydrogen evolution ceased. Inorganic materials were removed by filtration and washed with portions of hot isopropyl alcohol. The filtrate was concentrated in vacuo. The crude product was purified by column chromatography (silica gel, hexane:ethyl acetate=9:1) to give the title compound **7** (2.30 g, quant.). IR (KBr) 3394 cm^{-1}; ^1H NMR (500 MHz) δ=1.89—1.94 (1H, m), 2.05 (3H, s), 2.07 (3H, s), 2.20—2.29 (4H, m), 2.65—2.69 (1H, m), 3.73 (1H, dd, *J*=4.8, 11.7 Hz), 3.83 (1H, dd, *J*=7.8, 11.7 Hz); ^{13}C NMR (125 MHz) δ=12.39, 12.50, 19.08, 33.59, 49.33, 61.04, 63.46; $[\alpha]_D^{25}$ −34.1° (*c* 1.02, CH_2Cl_2); HRMS Found: *m/z* 178.0485. Calcd for $C_7H_{14}OS_2$: M, 178.0487.

Optical Purity of 7. The optical purity was checked by the ^1H NMR (500 MHz) analysis of the corresponding (+)-MTPA ester[10] of the alcohol **7**. The two sets of two singlet signals due to the methylthio groups of the racemate appeared at 1.89, 1.92 and 1.92, 1.95 ppm. In the present sample, only one set of two singlet peaks was observed at 1.92, 1.95 ppm and the other set could not be detected. So this sample was determined to be >98% ee.

***t*-Butyldiphenylsilyl Ether of 7.** To a dichloromethane (CH_2Cl_2) solution (20 ml) of **7** (1.47 g, 8.2 mmol) was added a CH_2Cl_2 solution (5 ml) of triethylamine (1.68 g, 16.6 mmol) at 0 °C. Then a CH_2Cl_2 solution (5 ml) of *t*-butylchlorodiphenylsilane (2.73 g, 9.9 mmol) and a catalytic amount of 4-dimethylaminopyridine were added. After being stirred overnight, the reaction was quenched by pH 7 phosphate buffer and the organic materials were extracted with CH_2Cl_2. The extracts were washed with brine and dried over Na_2SO_4. After evaporation of the solvent, the crude product was purified by column chromatography (silica gel, hexane:ethyl acetate=14:1) to afford the TBDPS ether **8** (3.49 g, quant). ^1H NMR (500 MHz) δ=1.04 (9H, s), 1.70—1.77 (1H, m), 2.02 (3H, s), 2.06 (3H, s), 2.07—2.24 (3H, m), 2.77—2.81 (1H, m), 3.58 (1H, dd, *J*=5.8, 10.8 Hz), 3.95 (1H, dd, *J*=8.6, 10.8 Hz), 7.36—7.44 (6H, m), 7.66—7.71 (4H, m); $[\alpha]_D^{25}$ −15.6° (*c* 1.00, CH_2Cl_2).

(*S*)-2-*t*-Butyldiphenylsiloxymethyl-1-cyclobutanone (9). A solution of **8** (2.20 g, 5.3 mmol) in acetonitrile (20 ml) was added quickly to a well-stirred solution of *N*-chlorosuccinimide (2.11 g, 15.8 mmol) and silver nitrate (3.14 g, 18.5 mmol) in aqueous 90% acetonitrile (20 ml) at 0 °C. The mixture was stirred for 5 min and treated successively at 1-min intervals with saturated aqueous sodium sulfite, saturated aqueous sodium carbonate, and brine (10 ml each). And then inorganic materials were removed by filtration. The organic material was extracted with ethyl acetate and the organic layers were washed with brine and dried over Na_2SO_4. After evaporation of the solvent, the crude product was purified by column chromatography (silica gel, hexane:ethyl acetate=14:1) to give the title compound **9** (1.69 g, 95% yield). IR (KBr) 1784 cm^{-1}; ^1H NMR (500 MHz) δ=1.04 (9H, s), 2.08—2.23 (2H, m), 3.02 (2H, t, *J*=8.5 Hz), 3.40—3.44 (1H, m), 3.70 (1H, dd, *J*=3.8, 10.6 Hz), 3.98 (1H, dd, *J*=4.1, 10.6 Hz), 7.37—7.44 (6H, m), 7.59—7.69 (4H, m); ^{13}C NMR (125 MHz) δ=13.54, 19.28, 26.74, 45.96, 61.23, 62.43, 127.70, 129.71, 133.00, 135.51, 210.85; $[\alpha]_D^{27}$ −16.0° (*c* 1.02, CH_2Cl_2).

Methyl [(*R*),(*Z*)-2-(*t*-Butyldiphenylsiloxy)methyl-1-cyclobutylidene]acetate (10a). A solution of dicyclohexylamine (2.65 g, 14.6 mmol) in THF (20 ml) was treated with BuLi (8.8 ml, 1.66 M (1 M=1 mol dm^{-3}) in hexane) at −78 °C. After the mixture was stirred for 30 min at −78 °C, a solution of methyl trimethylsilylacetate (2.14 g, 14.6 mmol) in THF (10 ml) was added dropwise, and the resulting solution was stirred for 30 min at −78 °C. Then to this solution was added dropwise a THF (10 ml) solution of **9** (2.42 g, 7.2 mmol) at −78 °C. The reaction mixture was stirred for 1 h and then treated with pH 7 phosphate buffer. The organic materials were extracted with ethyl acetate and the extracts were washed with brine and dried over Na_2SO_4. After the solvent was removed in vacuo, the crude material was purified by column chromatography (silica gel, hexane:ethyl acetate=14:1) to afford the title compound **10a** (2.82 g, quant.). IR (KBr) 1718, 1676 cm^{-1}; ^1H NMR (500 MHz) δ=1.05 (9H, s), 2.19—2.24 (2H, m), 2.62—2.69 (1H, m), 2.88—2.96 (1H, m), 3.54 (3H, s), 3.52—3.58 (1H, m), 3.88 (1H, dd, *J*=3.8, 9.9 Hz), 4.03 (1H, dd, *J*=5.5, 9.9 Hz), 5.64 (1H, dd, *J*=2.2, 4.3 Hz), 7.32—7.40 (6H, m), 7.62—7.68 (4H, m); ^{13}C NMR (125 MHz) δ=19.34, 20.70, 26.81, 30.73, 47.78, 50.71, 63.89, 113.55, 127.51, 129.52, 133.70, 135.59, 166.23, 168.09; $[\alpha]_D^{25}$ −124.4° (*c* 0.95, CH_2Cl_2).

Methyl [(*R*),(*E*)-2-(*t*-Butyldiphenylsiloxy)methyl-1-cyclobutylidene]acetate (12a). To a solution of thiophenol (31.7 mg, 0.29 mmol) in THF (2 ml) was added a hexane solution (0.18 ml) of BuLi (1.57 M in hexane) at 0 °C and the resulting solution was stirred for 10 min. Then a THF (2 ml) solution of **10a** (115.4 mg, 0.29 mmol) was added. After the mixture was stirred overnight, the reaction was quenched by pH 7 phosphate buffer and the organic materials were extracted with ethyl acetate. The organic layers were washed with brine and dried over Na_2SO_4. After the solvent was evaporated, the crude product was purified by column chromatography (silica gel, hexane:ethyl acetate=9:1) to afford the (*E*)-form ester **12a** (83.8 mg, 73% yield) and the recovered starting material **10a** (30.2 mg, 26% yield). Then the same operations with the recovered **10a** were carried out once again. The (*E*)-form compound **12a** was totally obtained in 91% yield. IR (KBr) 1718, 1676 cm^{-1}; ^1H NMR (500 MHz) δ=1.06 (9H,s), 1.85—1.91 (1H, m), 2.15 (1H, ddt, *J*=6.1, 9.3, 11.2 Hz), 2.96—3.10 (2H, m), 3.23—3.28 (1H, m), 3.69 (3H, s), 3.73 (2H, d, *J*=6.4 Hz), 5.74 (1H, dd, *J*=2.4, 4.6 Hz), 7.34—7.45 (6H, m), 7.65—7.68 (4H, m); ^{13}C NMR (125 MHz) δ=19.22, 20.67, 26.80, 31.05, 46.52, 50.84, 65.28, 112.32, 127.65, 129.65, 133.50, 135.59, 166.94, 168.54; $[\alpha]_D^{27}$ +1.5° (*c* 1.61, CH_2Cl_2).

Assignment of the Stereochemistry of 10a and 12a. The stereochemistry (*E* or *Z*) of the α,β-unsaturated ester **10a** and **12a** was determined by NOESY spectra. The NOEs were

observed between the olefinic proton and Ha in **10a** and between the olefinic proton and $H_{b'}$ in **12a** as shown in the figure.

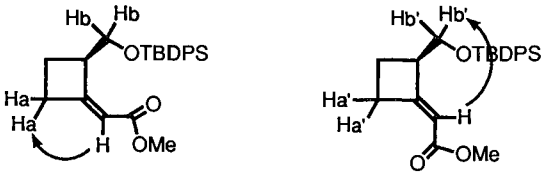

10a (*Z*)-form **12a** (*E*)-form

Methyl [(*R*),(*E*)-2-Hydroxymethyl-1-cyclobutylidene]acetate (13). To a methanol solution (10 ml) of **12a** (245 mg, 0.62 mmol) was added a few drops of concd hydrochloric acid at room temperature. After being stirred for 3.5 h, the mixture was treated with pH 7 phosphate buffer and the organic materials were extracted with ethyl acetate. The extracts were washed with brine and dried over Na_2SO_4. After evaporation of the solvent, the crude product was purified by column chromatography (silica gel, hexane:ethyl acetate=9:1) to give the alcohol **13** (92.8 mg, 96% yield). IR (KBr) 3450, 1711, 1676 cm^{-1}; ^1H NMR (500 MHz) δ=1.61—1.64 (1H, bs), 1.89—1.96 (1H, m), 2.22 (1H, ddt, J=6.1, 9.2, 11.3 Hz), 3.00—3.14 (2H, m), 3.25—3.31 (1H, m), 3.69 (3H, s), 3.68—3.72 (1H, m), 3.78 (1H, dd, J=6.3, 10.9 Hz), 5.74 (1H, dd, J=2.5, 4.8 Hz); $[\alpha]_D^{25}$ +20.7° (*c* 1.45, CH_2Cl_2); HRMS Found: *m/z* 156.0763. Calcd for $C_8H_{12}O_3$: M, 156.0786.

Methyl [(*R*),(*E*)-2-(Trimethylsiloxy)methyl-1-cyclobutylidene]-acetate (12c). A CH_2Cl_2 solution (3 ml) of triethylamine (313 mg, 3.1 mmol) was added to a CH_2Cl_2 solution (5 ml) of **13** (152 mg, 0.97 mmol) at 0 °C. Then a CH_2Cl_2 solution (2 ml) of chlorotrimethylsilane (218 mg, 2.0 mmol) and a catalytic amount of 4-dimethylaminopyridine were added to the mixture. After being stirred overnight at room temperature, the resulting solution was quenched by pH 7 phosphate buffer and the organic materials were extracted with CH_2Cl_2. The organic layers were washed with brine and dried over Na_2SO_4. After the solvent was removed, the crude product was purified by column chromatography (florisil, hexane:ethyl acetate=9:1) to give the TMS ether **12c** (212 mg, 95% yield). IR (KBr) 1716, 1676 cm^{-1}; ^1H NMR (500 MHz) δ=0.09 (9H, s), 1.76—1.83 (1H, m), 2.12—2.20 (1H, m), 2.94—3.08 (2H, m), 3.17—3.23 (1H, m), 3.63 (2H, d, J=7.0 Hz), 3.66 (3H, s), 5.69—5.71 (1H, m); $[\alpha]_D^{23}$ +5.9° (*c* 1.43, CH_2Cl_2).

(*Z*)-form **10c**: ^1H NMR (500 MHz) δ=0.08 (9H, s), 1.97—2.03 (1H, m), 2.16 (1H, ddd, J=8.6, 11.1, 17.3 Hz), 2.58—2.65 (1H, m), 2.77—2.86 (1H, m), 3.38—3.53 (1H, m), 3.65 (3H, s), 3.78 (1H, dd, J=8.1, 10.5 Hz), 3.90 (1H, dd, J=4.0, 10.5 Hz), 5.60—5.62 (1H, m).

Methyl [(*R*)-1-Methyl-2-(trimethylsiloxy)methyl-1-cyclobutyl]-acetate (11c). To an Et_2O suspension (5 ml) of CuI (324 mg, 1.7 mmol) was added dropwise MeLi (3.0 ml, 1.15 M in Et_2O) at −23 °C to generate lithium dimethylcuprate(I). The resulting solution was stirred for 30 min and then cooled to −78 °C. An Et_2O solution (3 ml) of **12c** (77.2 mg, 0.34 mmol) and TMSOTf (375 mg, 1.7 mmol) was added dropwise at −78 °C. After being stirred overnight at that temperature, the mixture was treated with saturated aqueous sodium hydrogencarbonate and inorganic materials were filtered off. The organic materials were extracted with ether and the extracts were washed with brine and dried over Na_2SO_4. After evaporation of the solvent, the crude product **11c** was directly used for further transformation. IR (KBr) 1739 cm^{-1}; ^1H NMR (500 MHz) *cis*-**11c** δ=0.07 (9H, s), 1.20 (3H, s), 1.50—1.67 (2H, m), 1.88—2.02 (2H, m), 2.14—2.17 (1H, m), 2.37 (1H, d, J=14.5 Hz), 2.53 (1H, d, J=14.5 Hz), 3.53 (1H, dd, J=6.3, 10.6 Hz), 3.61 (3H, s), 3.59—3.63 (1H, s); *trans*-**11c** δ=1.10 (3H, s), 3.65 (3H, s); ^{13}C NMR (125 MHz) δ=−0.52, 18.64, 27.59, 30.57, 38.73, 40.00, 46.29, 51.09, 63.00, 173.27; HRMS Found: *m/z* 244.1502. Calcd for $C_{12}H_{24}O_3Si$: M, 244.1495.

Assignment of the Stereochemistry of the Conjugate Addition Product. The relative stereochemistry of the conjugate addition products was determined by the NOESY spectrum of **11a**. In the major isomer, the NOEs were observed between the quaternary methyl group and H_a proton, H_b and H_c respectively, as shown in the following figure. The stereochemistry of the major isomer was assigned as *cis* and the minor was *trans*. The singlet signal of the methyl group of the *cis* isomer appeared at 1.26 ppm and that of *trans* isomer appeared at 1.16 ppm.

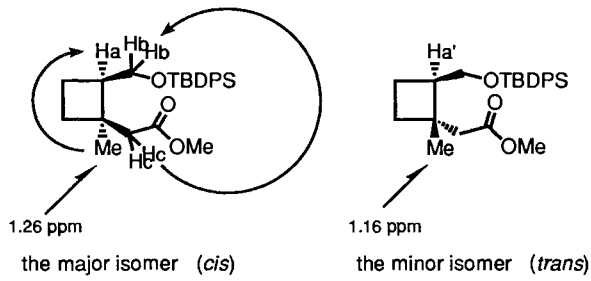

the major isomer (*cis*) the minor isomer (*trans*)

In the case of the compound **11c**, the stereochemistry was assigned from the chemical shift of the quaternary methyl group. The major isomer of **11c**, whose methyl singlet signal appeared at lower field (1.20 ppm), was determined to be *cis* isomer and the minor isomer (the methyl signal was observed at 1.10 ppm) was assigned as *trans*. These assignments of the stereochemistry were confirmed by the formation of the lactone **15** from the major isomer. The minor isomer (*trans*) could not form a lactone.

Methyl [(*R*)-1-Methyl-2-formyl-1-cyclobutyl]acetate (14). To a well-stirred suspension of pyridinium chlorochromate (PCC) (150 mg, 0.7 mmol) and celite (300 mg) in CH_2Cl_2 (3 ml) was added a CH_2Cl_2 solution (2 ml) of the crude product **11c** at 0 °C. After being stirred for 3 h, the mixture was filtered through silica gel. Then the filtrate was concentrated and the crude product **14** was directly used for further transformation. IR (KBr) 1736, 1714 cm^{-1}; ^1H NMR (500 MHz) the *cis*-isomer δ=1.31 (3H, s), 1.72—1.78 (1H, m), 1.81—1.96 (2H, m), 2.20—2.27 (1H, m), 2.35 (1H, d, J=15.7 Hz), 2.52 (1H, d, J=15.7 Hz), 2.95—2.98 (1H, m), 3.57 (3H, s), 9.81 (1H, d, J=1.8 Hz); the *trans*-isomer δ=1.12 (3H, s), 1.58—1.64 (1H, m), 1.81—1.96 (2H, m), 2.35—2.39 (1H, m), 2.44 (1H, d, J=15.0 Hz), 2.56 (1H, d, J=15.0 Hz), 3.11—3.14 (1H, m), 3.62 (3H, s), 9.76 (1H, s).

(1*R*,6*R*)-2,6-Dimethyl-3-oxabicyclo[4.2.0]octan-4-one (15). To an Et_2O suspension (5 ml) of CuI (325 mg, 1.7 mmol) was added dropwise MeLi (3.0 ml, 1.15 M in Et_2O) at −23 °C to generate lithium dimethylcuprate(I). The resulting solution was stirred for 30 min and then cooled to −78 °C, to which an Et_2O solution (2 ml) of the crude **14** was added dropwise at

−78 °C. After being stirred for 15 min, the mixture was treated with saturated aqueous sodium hydrogencarbonate and inorganic materials were filtered off. The organic materials were extracted with ether and the extracts were washed with brine and dried over Na_2SO_4. After distillation of the solvent, the crude product was purified by thin-layer chromatography (hexane:ethyl acetate=3:1) to give the *cis* bicyclic lactone **15** (34.4 mg) in 66% overall yield from **12c** in 3 steps. IR (KBr) 1739 cm^{-1}; ^1H NMR (500 MHz) δ=1.19 (3H, s), 1.29 (3H, d, J=6.4 Hz), 1.62—1.68 (1H, m), 1.88—1.92 (1H, m), 1.94 (2H, t, J=8.5 Hz), 2.21 (1H, ddd, J=8.7, 12.6, 17.5 Hz), 2.36 (1H, d, J=15.0 Hz), 2.58 (1H, d, J=15.0 Hz), 4.34 (1H, dq, J=6.4, 8.7 Hz); ^{13}C NMR (125 MHz) δ=17.93, 19.06, 28.22, 32.21, 35.71, 42.24, 44.34, 78.93, 173.14; $[\alpha]_D^{24}$ −102.9° (*c* 1.13, CH_2Cl_2); HRMS Found: *m/z* 154.0947. Calcd for $C_9H_{14}O_2$: M, 154.0994.

2-[(1*R*,2*R*)-1-Methyl-2-(1-hydroxyethyl)-1-cyclobutyl]ethanol (16). A THF solution (2 ml) of **15** (43.3 mg, 0.28 mmol) was added to a THF suspension (3 ml) of lithium aluminum hydride (37.0 mg, 0.97 mmol) at 0 °C and the mixture was stirred for 5 min. Then saturated sodium sulfate solution was added dropwise until hydrogen evolution ceased. Inorganic materials were removed by filtration and washed with portions of hot isopropyl alcohol. After the filtrate was concentrated in vacuo, the crude product was purified by thin-layer chromatography (hexane:ethyl acetate=2:1) to give the title compound **16** (41.3 mg, 93% yield). IR (KBr) 3323 cm^{-1}; ^1H NMR (500 MHz) δ=0.99 (3H, d, J=6.1 Hz), 1.11 (3H, s), 1.37—1.44 (1H, m), 1.49—1.60 (3H, m), 1.79—1.85 (2H, m), 2.02 (1H, ddd, J=7.5, 8.7, 14.2 Hz), 3.00—3.10 (2H, bs), 3.60 (1H, ddd, J=4.2, 7.4, 10.5 Hz), 3.71 (1H, ddd, J=6.5, 8.9, 10.5 Hz), 3.81 (1H, dq, J=6.1, 9.7 Hz); $[\alpha]_D^{24}$ +27.3° (*c* 1.59, CH_2Cl_2).

***t*-Butyldiphenylsilyl Ether of 16.** To a CH_2Cl_2–dimethylformamide 1:1 solution (6 ml) of **16** (36.7 mg, 0.23 mmol) was added a CH_2Cl_2 solution (1.5 ml) of triethylamine (79.5 mg, 0.79 mmol) at 0 °C. Then a CH_2Cl_2 solution (1.5 ml) of *t*-butylchlorodiphenylsilane (114 mg, 0.42 mmol) and a catalytic amount of 4-dimethylaminopyridine were added. After being stirred overnight, the mixture was treated with pH 7 phosphate buffer and the organic materials were extracted with CH_2Cl_2. The extracts were washed with brine and dried over Na_2SO_4. After evaporation of the solvent, the crude product was purified by thin-layer chromatography (hexane:ethyl acetate=5:1) to afford the silyl ether **17** (82.8 mg, 90% yield). IR (KBr) 3392 cm^{-1}; ^1H NMR (500 MHz) δ=1.01 (3H, d, J=6.3 Hz), 1.03 (3H, s), 1.05 (9H, s), 1.38—1.48 (2H, m), 1.50—1.60 (2H, m), 1.74—1.82 (2H, m), 1.84 (2H, t, J=7.2 Hz), 3.66—3.71 (1H, m), 3.74—3.81 (2H, m), 7.35—7.43 (6H, m), 7.68—7.72 (4H, m); $[\alpha]_D^{25}$ +15.5° (*c* 0.81, CH_2Cl_2).

(1*R*,2*R*)-2-[2-(*t*-Butyldiphenylsiloxy)ethyl]-2-methyl-1-cyclobutyl Methyl Ketone (18). To a well-stirred suspension of pyridinium chlorochromate (PCC) (42.5 mg, 0.17 mmol) and celite (85 mg) in CH_2Cl_2 (2 ml) was added a solution of the alcohol **17** (34.2 mg, 0.09 mmol) in CH_2Cl_2 (2 ml) at 0 °C. After being stirred for 4 h, the mixture was filtered through silica gel. Then the filtrate was concentrated in vacuo and the crude product was purified by thin-layer chromatography (hexane:ethyl acetate=5:1) to afford the title compound **18** (31.1 mg, 91% yield). IR (KBr) 1705 cm^{-1}; ^1H NMR (500 MHz) δ=1.02 (9H, s), 1.23 (3H, s), 1.54—1.61 (1H, m), 1.68—1.74 (2H, m), 1.79 (1H, ddd, J=6.0, 8.0, 13.4 Hz), 1.99 (3H, s), 2.23 (1H, ddd, J=8.8, 11.2, 18.3 Hz), 2.91 (1H, t, J=8.2 Hz), 3.60 (1H, ddd, J=6.0, 8.0, 10.4 Hz), 3.66 (1H, ddd, J=6.0, 8.0, 10.4 Hz), 7.35—7.43 (6H, m), 7.63—7.65 (4H, m); ^{13}C NMR (125 MHz) δ=16.19, 19.02, 26.80, 28.00, 29.52, 30.42, 37.31, 42.86, 57.28, 60.44, 127.60, 129.55, 133.71, 135.53, 208.34; $[\alpha]_D^{24}$ −29.5° (*c* 1.32, CH_2Cl_2).

***t*-Butyldiphenylsilyl Ether of (+)-Grandisol 19.** The operations were carried out according to the literature procedure.[17] A solution of diiodomethane (220 mg, 0.82 mmol) in THF (3 ml) was added to activated zinc powder (135 mg, 2.1 mmol) and then a hexane solution (1.6 ml) of trimethylaluminum (1.0 M in hexane) was added. The resulting suspension was stirred for 10 min. A THF solution (2 ml) of the ketone **18** (66.2 mg, 0.17 mmol) was added dropwise to the mixture. After being stirred for 1 h, the mixture was cooled to 0 °C and diluted with ether and 1 M hydrochloric acid was added dropwise until all the zinc dissolved. The organic materials were extracted with ether and the extracts were washed with brine and dried over Na_2SO_4. After evaporation of the solvent, the crude product was purified by thin-layer chromatography (hexane:ethyl acetate=5:1) to give the title compound **19** (65.4 mg, 99% yield). ^1H NMR (500 MHz) δ=1.05 (9H, s), 1.08 (3H, s), 1.40 (1H, dddd, J=1.2, 6.1, 8.9, 13.7 Hz), 1.46—1.59 (2H, m), 1.62 (3H, d, J=0.7 Hz), 1.70—1.79 (2H, m), 1.83—1.92 (1H, m), 2.47 (1H, t, J=9.1 Hz), 3.66 (1H, ddd, J=5.8, 8.9, 10.0 Hz), 3.72 (1H, ddd, J=6.0, 8.9, 10.2 Hz), 4.60 (1H, bs), 4.80 (1H, bs), 7.36—7.43 (6H, m), 7.67—7.69 (4H, m); ^{13}C NMR (125 MHz) δ=19.10, 19.15, 23.17, 26.88, 28.41, 29.22, 36.17, 41.29, 52.69, 61.17, 109.55, 127.56, 129.49, 134.08, 135.61, 145.25; $[\alpha]_D^{23}$ +2.6° (*c* 1.28, CH_2Cl_2).

(+)-Grandisol (1). To a methanol solution (5 ml) of **19** (64.0 mg, 0.16 mmol) was added as few drops of concd hydrochloric acid at room temperature. After being stirred for 2 h, the mixture was diluted with pH 7 phosphate buffer and the organic materials were extracted with ether. The extracts were washed with brine and dried over Na_2SO_4. After distillation of the solvent, the crude product was purified by thin-layer chromatography (hexane:ethyl acetate=2:1) to give the (+)-grandisol **1** (25.3 mg, quant.). IR (KBr) 3342, 3080, 2949, 2868, 1645, 1450, 1375, 1240, 1053, 1012, 887 cm^{-1}; ^1H NMR (500 MHz) δ=1.15 (3H, s), 1.42 (1H, dddd, J=1.2, 6.2, 9.4, 13.4 Hz), 1.35—1.45 (1H, m), 1.55—1.67 (2H, m), 1.65 (3H, s), 1.70—1.81 (2H, m), 1.91—1.99 (1H, m), 2.52 (1H, bt, J=9.0 Hz), 3.63 (1H, ddd, J=5.6, 9.4, 10.2 Hz), 3.66 (1H, ddd, J=6.2, 9.4, 10.2 Hz), 4.62 (1H, bs), 4.81 (1H, bs); ^{13}C NMR (125 MHz) δ=19.14, 23.20, 28.34, 29.30, 36.91, 41.28, 52.48, 59.94, 109.73, 145.19; $[\alpha]_D^{27}$ +18.6° (*c* 1.00, hexane), >98% ee.

Optical Purity of 1.[5b] The optical purity of **1** was determined by the ^1H NMR (500 MHz) analysis of the (+)-MTPA ester[10] of **1**. A set of the singlet signals of the methyl group adjacent to the quaternary carbon of the racemate appeared at 1.141 and 1.151 ppm. The corresponding (+)-MTPA ester of the optically active sample **1** showed only one singlet signal of the methyl group at 1.151 ppm. Therefore, the enantiomeric excess of **1** was determined absolutely to be >98% ee.

We thank Toray Industries, Inc. for the kind gift of (−)-tartaric acid.

References

1) J. H. Tumlinson, R. C. Gueldner, D. D. Hardee, A. C. Thompson, P. A. Hedin, and J. P. Minyard, *J. Org. Chem.*, **36**, 2616 (1971).

2) For reviews, see: J. A. Katzenellenbogen, *Science*, **194**, 139 (1976); C. A. Henrick, *Tetrahedron*, **33**, 1845 (1977); K. Mori, "The Synthesis of Insect Pheromones," in "The Total Synthesis of Natural Products," ed by J. Apsimon, John Wiley & Sons, New York (1981), Vol. 4, pp. 80—85.

3) The syntheses of (±)-grandisol not cited in Ref. 2, see: E, Negishi, L. D. Boardman, J. M. Tour, H. Sawada, and C. L. Rand, *J. Am. Chem. Soc.*, **105**, 6344 (1983); H. R. Sonawane, B. S. Nanjundiah, and M. U. Kumar, *Tetrahedron Lett.*, **25**, 2245 (1984); G. Rosini, E. Marotta, M. Petrini, and R. Ballini, *Tetrahedron*, **41**, 4633 (1985); G. Rosini, M. Geier, E. Marotta, M. Petrini, and R. Ballini, *ibid.*, **42**, 6027 (1986); I. A.-Solaja, M. Rey, and A. S. Dreiding, *Helv. Chim. Acta*, **70**, 1302 (1987); E. Negishi, L. D. Boardman, H. Sawada, V. Bagheri, A. T. Stoll, J. M. Tour, and C. L. Rand, *J. Am. Chem. Soc.*, **110**, 5383 (1988); T. Kametani, T. Toya, K. Ueda, M. Tsubuki, and T. Honda, *J. Chem. Soc., Perkin Trans. 1*, **1988**, 2433; A. Ghosh, U. K. Banerjee, and R. V. Venkateswaran, *Tetrahedron*, **46**, 3077 (1990).

4) a) K. Mori, *Tetrahedron*, **34**, 915 (1978); b) J. B. Jones, M. A. W. Finch, and I. J. Jakovac, *Can. J. Chem.*, **60**, 2007 (1982); c) F. X. Webster and R. M. Silverstein, *J. Org. Chem.*, **51**, 5226 (1986).

5) a) P. D. Hobbs and P. D. Magnus, *J. Am. Chem. Soc.*, **98**, 4594 (1976); b) K. Mori and M. Miyake, *Tetrahedron*, **43**, 2229 (1987).

6) A. I. Meyers and S. A. Fleming, *J. Am. Chem. Soc.*, **108**, 306 (1986); M. Demuth, A. Palomer, H.-D. Sluma, A. K. Dey, C. Krüger, and Y.-H. Tsay, *Angew. Chem., Int. Ed. Engl.*, **25**, 1117 (1986).

7) Y. Hayashi and K. Narasaka, *Chem. Lett.*, **1989**, 793; **1990**, 1295; Y. Hayashi, S. Niihata, and K. Narasaka, *ibid.*, **1990**, 2091.

8) Y. Ichikawa, A. Narita, A. Shiozawa, Y. Hayashi, and K. Narasaka, *J. Chem. Soc., Chem. Commun.*, **1989**, 1919.

9) H. Minamikawa, S. Hayakawa, T. Yamada, N. Iwasawa, and K. Narasaka, *Bull. Chem. Soc. Jpn.*, **61**, 4379 (1988); K. Narasaka, N. Iwasawa, M. Inoue, T. Yamada, M. Nakashima, and J. Sugimori, *J. Am. Chem. Soc.*, **111**, 5340 (1989); N. Iwasawa, Y. Hayashi, H. Sakurai, and K. Narasaka, *Chem. Lett.*, **1989**, 1581; K. Narasaka, Y. Hayashi, S. Shimada, and J. Yamada, *Isr. J. Chem.*, accepted for publication.

10) J. A. Dale, D. L. Dull, and H. S. Mosher, *J. Org. Chem.*, **34**, 2543 (1969).

11) E. J. Corey and B. W. Erickson, *J. Org. Chem.*, **36**, 3553 (1971).

12) H. Taguchi, K. Shimoji, H. Yamamoto, and H. Nozaki, *Bull. Chem. Soc. Jpn.*, **47**, 2529 (1974).

13) Y. Yamamoto, *Angew. Chem., Int. Ed. Engl.*, **25**, 947 (1986).

14) K. Maruyama and Y. Yamamoto, *J. Am. Chem. Soc.*, **99**, 8068 (1977); Y. Yamamoto and K. Maruyama, *ibid.*, **100**, 3240 (1978).

15) E. J. Corey and N. W. Boaz, *Tetrahedron Lett.*, **26**, 6019 (1985).

16) E. Nakamura, S. Matsuzawa, Y. Horiguchi, and I. Kuwajima, *Tetrahedron Lett.*, **27**, 4029 (1986); S. Matsuzawa, Y. Horiguchi, E. Nakamura, and I. Kuwajima, *Tetrahedron*, **45**, 349 (1989).

17) K. Takai, Y. Hotta, K. Oshima, and H. Nozaki, *Bull. Chem. Soc. Jpn.*, **53**, 1698 (1980).

18) C. Dijkgraaf and J. P. G. Rousseau, *Spectrochim. Acta, Part A*, **24**, 1213 (1968).

19) R. Kaya and N. R. Beller, *J. Org. Chem.*, **46**, 196 (1981).

An Useful Synthetic Method for 3-Substituted δ-Lactones. Synthesis of (±)-Secocrispiolide

Michiharu KATO,* Akihiko OUCHI, and Akira YOSHIKOSHI
Chemical Research Institute of Non-Aqueous Solutions, Tohoku University, Katahira, Aoba-ku, Sendai 980
(Received January 23, 1991)

2-Phenylthio-2-penten-5-olide (**1**) acted as a reactive Michael acceptor toward some typical carbon neucleophiles to give 3-substituted 2-phenylthio-5-pentanolides (**2**) which were convertible both to 3-substituted 5-pentanolides by reductive desulfurization and to 3-substituted 2-penten-5-olides by sulfenic acid *syn* elimination of the sulfoxides **4** derived from **2**. The Pummerer rearrangement of **4** provided 3-substituted 2-phenylthio-2-penten-5-olides and/or 2-hydroxy-2-penten-5-olides. (±)-Secocrispiolide was synthesized via the adduct obtained by the Michael reaction of **1** with the Grignard reagent prepared from 2,6-dimethylbenzyl bromide and magnesium.

Lactone function is found as a structural subunit in many classes of natural product.[1] Up to date, considerable attention for the syntheses of natural products having this group has been attracted especially in connection with investigation of their biological activities.[2] Although a variety of efficient methods for construction of γ-lactones have been developed,[3] comparatively a few are general methods for the syntheses of δ-lactones. In the course of our synthetic study on a natural product, we required an efficient preparation of 3-substituted 2-penten-5-olides. However, methodologies for the syntheses of these useful compounds were, to our knowledge, not well defined. We wish to report here a versatile synthetic method for 3-substituted 5-pentanolides and 2-penten-5-olides, starting with 2-phenylthio-2-penten-5-olide (**1**) which acts as a common building block upon this purpose.[4]

Our contributions to this objective are illustrated in Scheme 1. In contrast to 2-penten-5-olide (**8**), 2-phenylthio-2-penten-5-olide (**1**) was deemed most favorable as a starting material in that the phenylthio group would not only serve as an activator for the Michael reaction,[5] but also subsequently act as a key substituent for introduction of a double bond in the adduct. A series of reactions used in this study is as follows; (i) reactions of **1** with some carbon nucleophiles would proceed exclusively in 1,4 addition fashion to give the required 3-substituted 2-phenylthio-5-pentanolides (**2**) which are convertible to 3-substituted 5-pentanolides (**3**) in reductive cleavage of the phenylthio group, (ii) thermolysis of the sulfoxides **4** derived from **2** provides 3-substituted 2-penten-5-olides (**5**), and (iii) exposure of **4** to the conditions of the Pummerer rearrangement leads to 3-substituted 2-phenylthio-2-penten-5-olides (**6**), which would keep the capacity to act as a reactive Michael acceptor toward 3,3-disubstituted 5-pentanolide synthesis. This strategy has mostly proven to be successful as described below.

Results and Discussion

We started our synthesis with preparation of 2-phenylthio-5-pentanolide (**10**) (Scheme 2). Treatment of freshly distilled δ-valerolactone (**9**) with lithium diisopropylamide (LDA) followed by addition of diphenyl disulfide provided **10** in moderate yield. On this occasion, an attempt to improve the yield of **10** by sulfenylation with *S*-phenyl benzenethiosulfonate[6] was fruitless. Furthermore, sulfenylation of the silyl enol ether **11**, prepared

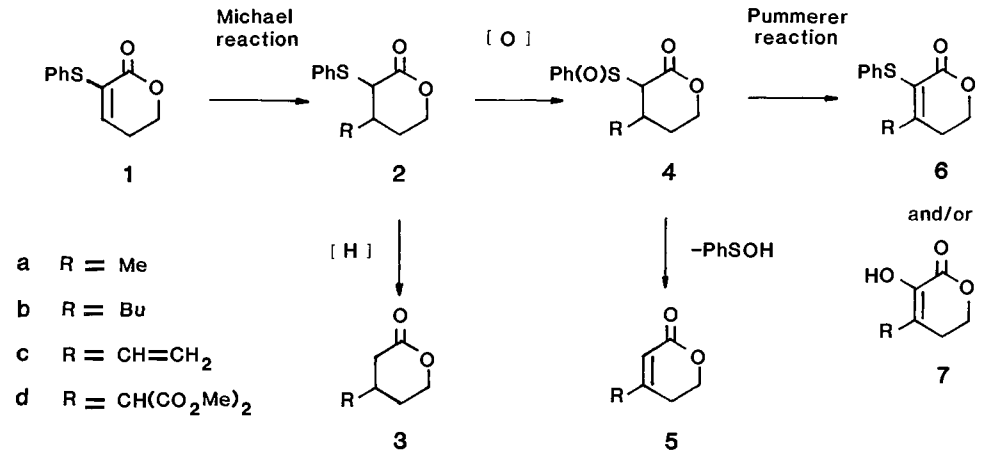

Scheme 1.

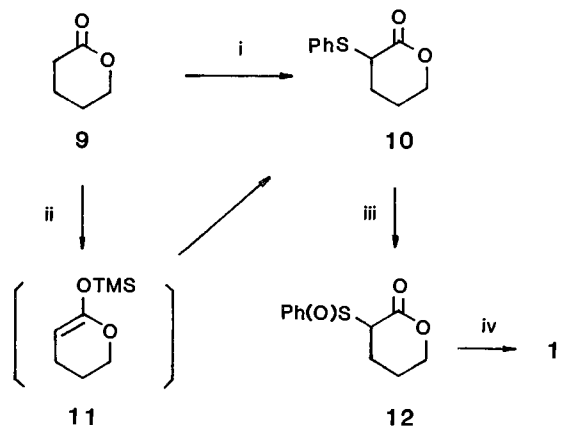

Scheme 2. (i) LDA, THF, HMPA, then Ph_2S_2, −78°C—r.t. (53%): (ii) LDA, Me_3SiCl, THF, then PhSCl, −78°C—r.t. (44%): (iii) *m*CPBA (1.0 equiv), CH_2Cl_2, −15°C: (iv) $(CF_3CO)_2O$, CH_2Cl_2, r.t. (98% from **10**).

Table 1. Yields (%)[a] of 3-Substituted 5-Pentanolides **2**—**4** and 2-Penten-5-olides **5**

Compound	2	3	4	5
a R=Me	91	74	100	72
b R=Bu	80	76	100	79
c R=CH=CH_2	82	42	100	73
d R=$CH(CO_2Me)_2$	73	56	100	80

a) Isolated yield.

from **9** by treatment with LDA (1 equiv) followed by chlorotrimethylsilane, with benzenesulfenyl chloride provided disappointing 44% yield of **10**. The substrate **10** was converted by oxidation with equimolar *m*-chloroperbenzoic acid (*m*CPBA) to the sulfoxide **12** which on exposure to trifluoroacetic anhydride led to **1** in 52% overall yield from **9**.

We turned our attention to conjugate addition of **1** with representative carbon nucleophiles. The nucleophiles used in this study were lithium dimethylcuprate (**i**), lithium dibutylcuprate (**ii**), vinylmagnesium bromide–copper(I) iodide 1:1-complex (**iii**), and dimethyl sodiomalonate (**iv**). Reactions of **1** with eqimolar cuprates, **i** and **ii**, proceeded smoothly, to our expectations, to give the 1,4-addition products, 3-substituted 2-phenylthio-5-pentanolides, **2a** and **2b**, in excellent yields (Scheme 1 and Table 1). On the other hand, on reaction with the reagents, **iii** and **iv**, 2.0 equivalent amount of the reagents was required to maximize yields of the adducts, **2c** and **2d**. While the pentanolides obtained were inseparable diastereomeric mixtures, it would be reasonable to estimate that the thermodynamically stable *trans*-isomers are in large quantities, although relatively small vicinal coupling constants (6.4—6.5 Hz, PhS–CH–CH) were observed in their ^1H NMR spectra. In order to verify the effect of the phenylthio group used as an activator, the Michael reactions of 2-penten-5-olide (**8**) with the nucleophiles, **ii** and **iii**, were examined for comparison, giving 3-butyl-[7] and 3-vinyl-5-pentanolides, (**3b**) and (**3c**), in such poor yields as 45 and 13%, respectively. After all, it was demonstrated that 2-phenylthio-2-penten-5-olide (**1**) has highly electrophilic reactivity enough to act as a common Michael acceptor.

Table 2. The Pummerer Rearrangement of Sulfoxides **4**

Run	4	Conditions	Product, yield (%)[a]		
			6	7	5c
1	**a** R=Me	3d[b]	52	18	—
2	**a** R=Me	1h[c]	14	59	—
3	**b** R=Bu	2d[b]	49	Trace	—
4	**c** R=CH=CH_2	3d[b]	10	—	74
5	**d** R=$CH(CO_2Me)_2$	1d[b]	—	34	—

a) Isolated yield. b) Room temperature. d; day. c) 0°C, then quenched with aqueous sodium hydrogencarbonate. h; hour.

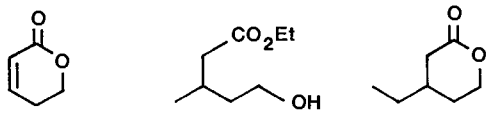

8 13 14

Desulfurization of **2** was next examined (Scheme 1 and Table 1). Reaction of **2b** with W-4 Raney nickel in ethanol proceeded smoothly to give 3-butyl-5-pentanolide (**3b**)[7] in good yield, whereas desulfurization of **2a** and **2c** under the similar reaction conditions produced hydroxy ester **13** and 3-ethyl-5-pentanolide (**14**),[8] respectively, as the result of concomitant ethanolysis for the former and hydrogenation of the vinyl group for the latter. These unexpected results were suppressed as follows. Replacement of ethanol into acetone resulted in good formation of **3a** from **2a**. On the other hand, **3c** was obtained on reduction of **2c** with Raney nickel deactivated with acetone. Finally, **2d** was desulfurized in acetone to afford **3d** in good yield.

Synthesis of 3-substituted 2-penten-5-olides **5a**—**d**[9] was accomplished readily by oxidation of **2a**—**d** with equimolar *m*CPBA followed by refluxing the resulting sulfoxides **4a**—**d** in benzene containing catalytic amount of pyridine, wherein the oxidation and thermal elimination of sulfenic acid proceeded in quantitative and in good yield, respectively, (Scheme 1 and Table 1).

Table 2 details the result obtained by the Pummerer reaction of sulfoxides **4a**—**d**. Contrary to our expectations, the reactions of **4a**—**c** with trifluoroacetic anhydride proceeded considerably slowly to produce unexpected 2-hydroxy-2-penten-5-olides (**7**) as well as the desired 2-phenylthio-2-penten-5-olides (**6**) (Scheme 1), so that this type of reactions showed marked dependence on reaction conditions employed and/or on type of the substituent at C(3) of **4**. Treatment of **4a** with trifluoroacetic anhydride at room temperature afforded a mixture of **6a**[10] and 2-hydroxy-2-penten-5-olide (**7a**),

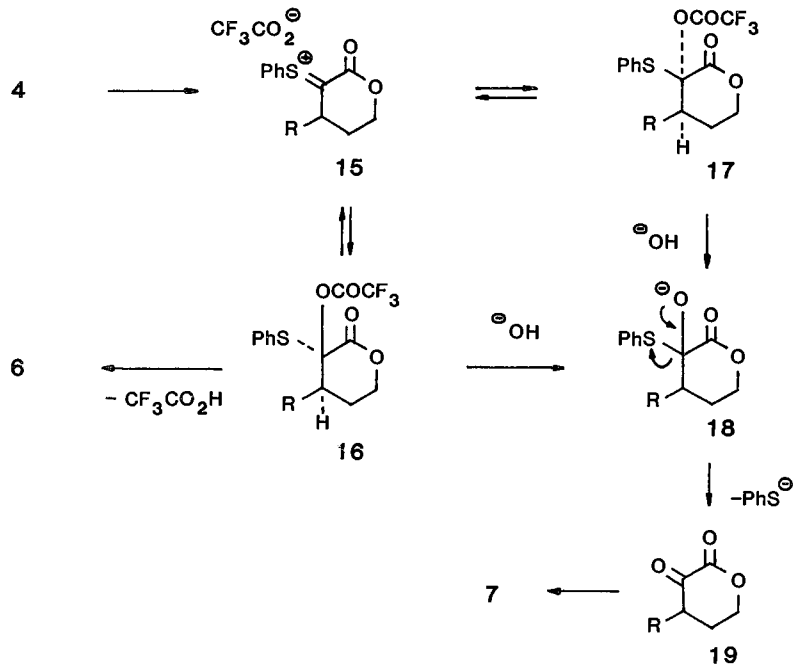

Scheme 3.

in which the former predominated (Run 1). On the contrary, **7a** was obtained predominantly when the reaction was carried out at low temperature, followed by quenching with aqueous sodium hydrogencarbonate (Run 2). Compound **6b** was derived in fair yield from **4b** along with a trace of 2-hydroxy-2-penten-5-olide (**7b**) which was detectable by the TLC analysis (Run 3). On the other hand, the pummerer reaction of **4c** provided low yield of **6c**, and in this case, the major product isolated in 74% yield was unexpected **5c** (Run 4). In the case of **4d**, the only product obtained in low yield was **7d** (Run 5).

The following mechanism would be surmised to account for the formation of **6** and **7** (Scheme 3). Exposure of the sulfoxide **4** to trifluoroacetic anhydride leads to the Pummerer intermediate **15**. On reacting with a trifluoroacetate anion, **15** provides two kinds of trifluoroacetates, **16** with cis relationship between the trifluoroacetoxy group and the substituent (R), and **17** with trans relationship between the two. These trifluroacetates would exist as comparatively stable intermediates in equilibrium. 2-Penten-5-olide **6** is derived only from **16** in trans elimination fashion of trifluoroacetic acid. On the other hand, hydrolysis of **16** and **17** on hydrolytic workup using aqueous sodium hydrogencarbonate leads to the alkoxide **18**, which spontaneously eliminates the phenylthio group to give α-keto lactone **19**. Subsequent tautomerization of **19** affords 2-hydroxy-2-penten-5-olide (**7**). In the case of **4d** which has a bulky bis(methoxycarbonyl)methyl group as a substituent (R), **17d** whose R and trifluoroacetoxy groups are in a trans relationship is formed exclusively to provide **7d** on hydrolytic workup. Formation of **5c** (Table 2, Run 4) would be rationalized by surmising that, because of high acidity of the allylic β-hydrogen in **4c**, *syn* elimination of sulfenic acid readily occurs, before the Pummerer rearrangement initiates.

A parallel study on the conjugate addition to 3-substituted 2-phenylthio-2-penten-5-olides obtained reproduced the important role of the phenylthio group as the activator: Reactions of **6a** and **6b** with lithium dimethylcuprate provided 3,3-disubstituted δ-lactones, **20**, and **21**, respectively, albeit in low yields, whereas 3-methyl- and 3-butyl-2-penten-5-olides, (**5a**) and (**5b**), were recovered unchanged on treatment with this cuprate reagent. It is noteworthy that reaction of 3-vinyl-2-penten-5-olide (**5c**) with lithium dimethylcuprate underwent regioselective conjugate addition to give a mixture of 1,6-addition products, **22** and **23**.

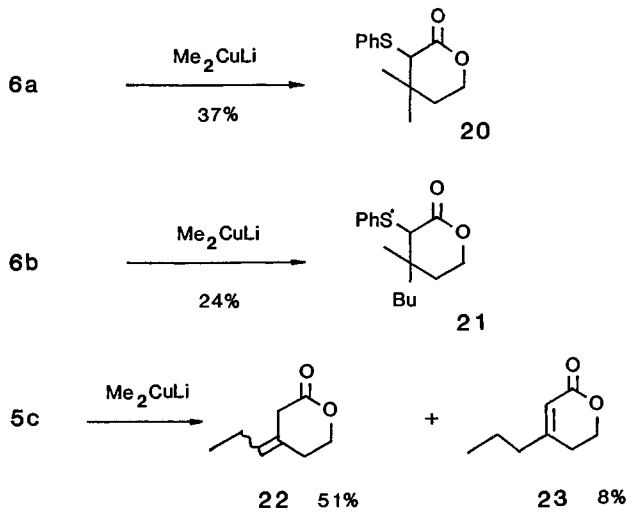

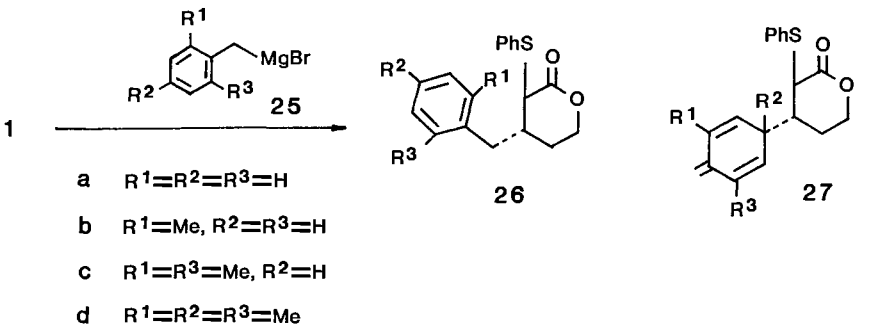

Scheme 4.

Table 3. Conjugate Addition of **1** with Benzylic Grignard Reagents **25**

Run		25			Product		Recoverd **1**, (%)[a]
		R^1	R^2	R^3	**26**, yield (%)[a]	**27**, yield (%)[a]	
1	**a**	H	H	H	82	—	16
2	**b**	Me	H	H	62	—	16
3	**c**	Me	H	Me	34	65	—
4	**d**	Me	Me	Me	6[b]	10[b]	75

a) Isolated yield. b) Calculated from the integral ratio in the ^{1}H NMR of the mixture.

In an effort to extend the scope of this methodology, conjugate addition of **1** with a few benzylic Grignard reagents was examined for the purpose of the synthesis of secocrispiolide **24**,[11] a seco-sesquiterpene lactone isolated from *Plicaria crispa* Sch. Bip. The Grignard reagents **25** used in this study and the results thereby obtained are shown in Scheme 4 and Table 3, respectively.

It is known that condensation of the benzylic Grignard reagent with carbon dioxide or some aldehydes occasionally provides an abnormal product resulting from the so-called allylic rearragement of the reagent.[12] While exposure of **1** to benzyl- and 2-methylbenzylmagnesium bromides, (**25a**) and (**25b**), gave diastereomeric mixtures of the normal adducts, **26a** and **26b**, respectively, (Table 3, Run 1, 2), the abnormal adduct **27c** was produced together with the normal **26c** in a ratio of ca. 2:1, when **1** was treated with 2,6-dimethylbenzylmagnesium bromide (**25c**) (Run 3). These results indicated that the steric bulk at the benzyl face would impose the allylic rearrangement on the ortho-disubstituted benzylic Grignard reagents to give the para addition products. **27c** was an unstable oil and, to our surprise, the structure possessing a cross-conjugate methylenecyclohexadiene skeleton was clarified as follows. Two resonances [δ=5.59 (2H, br s) and 2.28 (6H, d, J= 1 Hz)] in the ^{1}H NMR and those [δ=125.1 (d) and 19.9 (q)] in the ^{13}C NMR showed the presence of two trisubstituted double bonds possessing a methyl group. In addition, resonances due to an *exo*-methylene group appeared at δ=5.04 (2H, br s) in the ^{1}H NMR and δ= 107.7 (t) and 128.2 (s) in the ^{13}C NMR. In fact, aromatization of **27c** with catalytic *p*-toluenesulfonic acid readily occured to give a stable compound **28**. An analogous trend was observed on reaction of **1** with 2,4,6-trimethylbenzylmagnesium bromide (**25d**) (Run 4).

The procurement of the synthetic intermediate **26c** prompted us to complete the synthesis of secocrispiolide (**24**). The lithium enolate obtained from treatment of **26c** with LDA was submitted to methylation with methyl iodide in the presence of hexamethylphosphoric triamide (HMPA), providing 2-methyl-δ-lactone (**29**) as an inseparable 3:1 mixture of diastereomers. Oxidation of **29** with equimolar *m*CPBA followed by elimination of sulfenic acid from the resulting sulfoxide **30** afforded (±)-secocrispiolide (**24**) and an *endo*-olefin regioisomer **31** in 23 and 69% yields, respectively. The spectra (IR, ^{1}H NMR and MS) of the synthetic **24** were identical with those of the natural product.[13]

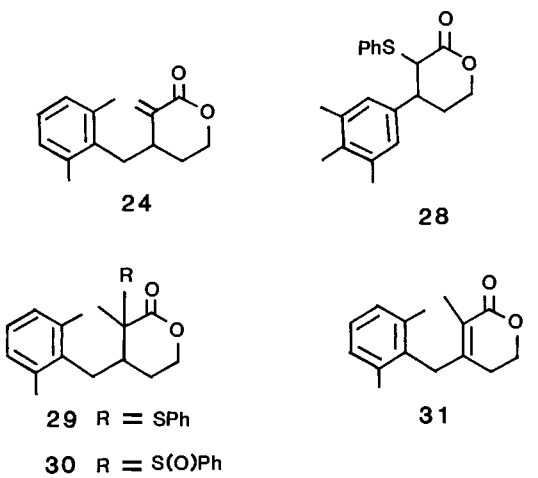

In conclusion, we have developed an useful method for the synthesis of a variety of 3-substituted δ-lactones starting with 2-phenylthio-2-penten-5-olide (**1**), and (±)-secocrispiolide (**24**) was synthesized via the Michael adduct **26c**.

Experimental

Melting points are uncorrected. IR spectra were obtained with a JASCO A-3 infrared spectrophtometer. ^{1}H NMR spectra were recorded on a JEOL FX90Q spectrometer in deuterochloroform with tetramethylsilane as internal standard. High resolution mass spectra were obtained by a JEOL JMS-DX 300 spectrometer. δ-Valerolactone was purchased from Aldrich Chemical Co. Dry tetrahydrofuran (THF) and diethyl ether were obtained by distillation over sodium benzophenone ketyl. Other organic solvents were purified and dried by using standard procedures. All reactions were carried out under N_2 or Ar atmosphere with use of standard procedures for the exclusion of moisture. Column chromatography was performed by using silica gel (Merck, Kieselgel 60, 70—230 mesh). Kieselgel GF_{254} was employed for preparative thin-layer chromatography (TLC) and a mixed solvent (hexane–ether, 1:2) was used for elution, unless otherwise stated. Na_2SO_4 was employed for the drying of extracts.

2-Phenylthio-5-pentanolide (10). (a) To a stirred solution of diisopropylamine (5.133 g, 50.8 mmol) in THF (50 ml) at −78 °C was added dropwise a 1.5 M solution (1 M=1 mol dm^{-3}) of butyllithium in hexane (30.0 ml, 46.91 mmol). The bath was replaced by an ice bath and the mixture was stirred for 10 min, then recooled at −78 °C. A solution of freshly distilled δ-valerolactone (**9**) (1.959 g, 19.5 mmol) in THF (15 ml) was added dropwise and stirring was continued for 30 min. To the reaction mixture, a solution of diphenyl disulfide (8.535 g, 39.1 mmol) in HMPA (40 ml) and THF (50 ml) was added and the temperature was gradually raised to room temperature over 10 h. The reaction was quenched by addition of saturated aqueous ammonium chloride (30 ml) and the phases were separated. The aqueous phase was extracted with ether. The combined organic solutions were washed with 0.1 M HCl and brine, and dried. Evaporation of the solvent left an oil, which was chromatographed on 50 g of silica gel with ether–hexane (1:3) as the eluant to give **10** (2.139 g, 53%) as a colorless oil: IR (film) 1730 cm^{-1} (C=O); ^{1}H NMR ($CDCl_3$) δ= 1.6—2.6 [4H, m, $(CH_2)_2$], 3.92 (1H, t, J=6.5 Hz, SCH), 4.4 (2H, m, CH_2O), and 7.2—7.7 (5H, m, Ph).

Found: C, 63.50; H, 5.85%. Calcd for $C_{11}H_{12}O_2S$: C, 63.45; H, 5.81%.

(b) A solution of lithium diisopropylamide in THF was prepared from a 1.5 M solution of buthyllithium in hexane (35.1 ml, 54.9 mmol) and diisopropylamine (6.05 g, 59.9 mmol) in THF (30 ml), and a solution of **9** (5.00 g, 59.9 mmol) in THF (15 ml) was added dropwise with stirring at −78 °C. After being stirred for 40 min, chlorotrimethylsilane (6.51 g, 59.9 mmol) was added. Two hours later, a solution of benzenesulfenyl chloride (10.83 g, 74.9 mmol) in THF (15 ml) was added and the reaction was warmed to room temperature and stirred for 20 h, then quenched with aqueous ammonium chloride. The mixture was extracted with ether and the combined extracts were washed with brine and dried. Evaporation followed by purification of a residue with column chromatography on silica gel using ether–hexane (1:1) as the eluant gave **10** (4.57 g, 44%) and recovered **9** (1.29 g, 26%).

2-Phenylthio-2-penten-5-olide (1). To a stirred solution of **10** (1.614 g, 7.76 mmol) in CH_2Cl_2 (50 ml) at −16 °C, was added dropwise over 30 min a solution of *m*CPBA (80% purity 1.673 g, 7.76 mmol) in CH_2Cl_2 (20 ml). After stirring for 30 min, the reaction mixture was washed with aqueous sodium thiosulfate, aqueous sodium hydrogencarbonate, and brine, and dried. Evaporation of the solvent afforded practically pure sulfoxide **12** (1.617 g) as an oil: IR (film) 1720 cm^{-1} (C=O); ^{1}H NMR ($CDCl_3$) δ=1.5—2.6 [4H, m, $(CH_2)_2$], 3.6 (1H, t, J=7.5 Hz, SCH), 4.4 (2H, m, CH_2O), and 7.55 (5H, m, Ph). To a solution of **12** in CH_2Cl_2 (10 ml) precooled at −15 °C, trifluoroacetic anhydride (10 ml) was added. The mixture was stirred for 12 h and allowed to warm gradually to room temperature. The mixture was diluted with CH_2Cl_2 and washed with aqueous sodium hydrogencarbonate and brine, and dried. Filtration followed by evaporation left an oil, which was passed through a short silica-gel column with ether to provide **1** (1.644 g, 98%) as an oli: IR (film) 1710 cm^{-1} (C=O); ^{1}H NMR ($CDCl_3$) δ=2.48 (2H, m, CH_2C=C), 4.41 (2H, t, J=5.4 Hz, CH_2O), 6.25 (1H, t, J=5.5 Hz, C=CH), and 7.40 (5H, m, Ph).

Found: m/z 206.0398. Calcd for $C_{11}H_{10}O_2S$: M, 206.0401.

3-Methyl-2-phenylthio-5-pentanolide (2a). To a stirred mixture of copper(I) iodide (51 mg, 0.27 mmol), dimethyl sulfide (0.5 ml), and ether (3 ml) at −35 °C was added dropwise 1.6 M methyllithium in ether (0.33 ml, 0.53 mmol). After stirring for 50 min at −35 °C, a solution of **1** (50.2 mg, 0.24 mmol) in THF (2 ml) was added, and stirring was continued for an additional 30 min at the range of −35 to −18 °C. The reaction was quenched by addition of aqueous ammonium chloride followed by 25% aqueous ammonia, and the product was extracted with CH_2Cl_2. The combined extracts were washed with brine, and dried. Evaporation of the solvent left an oil which was purified by TLC to give **2a** (49.3 mg, 91%) as a colorless oil: IR (film) 1730 cm^{-1} (C=O); ^{1}H NMR ($CDCl_3$) δ=1.25 (3H, d, J=7.2 Hz, Me), 1.4—2.3 (3H, m), 3.41 and 3.85 (1H in total, d, J=6.5 and 6.3 Hz, each, 9:1 ratio by integration, SCH), 4.2—4.5 (2H, m, CH_2O), 7.2—7.6 (5H, m, Ph).

Found: m/z 222.0702. Calcd for $C_{12}H_{14}O_2S$: M, 222.0714.

3-Butyl-2-phenylthio-5-pentanolide (2b). According to the procedure described for the preparation of **2a**, treatment of copper(I) iodide (48.6 mg, 0.26 mmol) with 1.5 M butyllithium in hexane (0.32 ml, 0.51 mmol), followed by addition of **1** (49.8 mg, 0.24 mmol) provided **2b** (51.0 mg, 80%) as a colorless oil: IR (film) 1730 cm^{-1} (C=O); ^{1}H NMR ($CDCl_3$) δ=0.90 (3H, br t, Me), 1.1—2.3 (9H, m), 3.51 and 3.92 (1H, in total, d, J=6.4 and 5.4 Hz each, 9:1 ratio by integration, SCH), 4.2—4.6 (2H, m, CH_2O), and 7.2—7.6 (5H, m, Ph).

Found: m/z 264.1182. Calcd for $C_{15}H_{20}O_2S$: M, 264.1183.

2-Phenylthio-3-vinyl-5-pentanolide (2c). According to the procedure described for the preparation of **2a**, treatment of copper(I) iodide (388 mg, 2.04 mmol) with 1.09 M vinylmagnesium bromide (1.79 ml, 1.94 mmol) at −55 °C, followed by addition of **1** (200 mg, 0.97 mmol) gave **2c** (185 mg, 82%) as a colorless oil: IR (film) 1730 cm^{-1} (C=O); ^{1}H NMR ($CDCl_3$) δ=1.5—2.8 (3H, m), 3.61 and 3.85 (1H in total, d, J=6.4 and 5.0 Hz, 7:1 ratio by integration, SCH), 4.3—4.7 (2H, m, CH_2O), 5.1—5.38 (2H, m, $C\underline{H}_2$=CH), 5.7—6.1 (1H, m, CH_2=$C\underline{H}$), and 7.2—7.6 (5H, m, Ph).

Found: m/z 234.0722. Calcd for $C_{13}H_{14}O_2S$: M, 234.0714.

3-[Bis(methoxycarbonyl)methyl]-2-phenylthio-5-pentanolide (2d). To a stirred suspension of 60% sodium hydride in min-

eral oil (20 mg, 0.49 mmol) in ether (4 ml) was added dimethyl malonate (64.2 μl, 0.53 mmol). After stirring for 25 min, a solution of **1** (50 mg, 0.24 mmol) in THF (2 ml) was added at 0 °C and stirring was continued for an additional 1.5 h at 0 °C. The mixture was poured into aqueous ammonium chloride and extracted with CH_2Cl_2. The combined extracts were washed with brine, and dried. Evaporation of the solvent followed by purification of a residue by TLC afforded **2d** (60 mg, 73%) as a colorless oil: IR (film) 1730 cm^{-1} (C=O); ^1H NMR ($CDCl_3$) δ=1.6—2.2 (3H, m), 2.7 (1H, m), 3.76 and 3.78 (3H, s each, Me), 3.8 (1H, s, SCH), 4.2—4.5 (2H, m, CH_2O), and 7.3—7.6 (5H, m, Ph).

Found: *m/z* 338.0848. Calcd for $C_{16}H_{18}O_6S$: M, 338.0823.

3-Methyl-5-pentanolide (3a). A mixture of **2a** (36 mg), W-4 Raney nickel (500 mg) and acetone (3 ml) was stirred at room temperature for 3.5 h, and filtered through a short celite column. The filtrate was evaporated to leave an oil, whose purification by TLC afforded **3a** (14 mg, 74%) as an oil: IR (film) 1730 cm^{-1} (C=O); ^1H NMR ($CDCl_3$) δ=1.02 (3H, d, *J*=6.0 Hz, Me), 1.1—2.8 (5H, m), and 4.1—4.5 (2H, m, CH_2O).

3-Butyl-5-pentanolide (3b). (a) According to the procedure described for the preparation of **3a**, treatment of **2b** (60 mg) with W-4 Raney nickel (1 g) in ethanol (10 ml) afforded **3b** (26 mg, 76%) as an oil: IR (film) 1740 cm^{-1} (C=O); ^1H NMR ($CDCl_3$) δ=0.90 (3H, br t, Me), 1.1—2.8 (11H, m), 4.1—4.6 (2H, m, CH_2O).

(b) According to the procedure described for the preparation of **2a**, treatment of copper(I) iodide (94 mg, 0.49 mmol) with 1.5 M butyllithium in hexane (0.62 ml, 0.98 mmol) at −40 °C, followed by addition of **8** (40 mg, 0.41 mmol) afforded **3b** (29 mg, 45%).

3-Vinyl-5-pentanolide (3c). (a) According to the procedure described for the preparation of **3a**, desulfurization of **2c** (47 mg) in acetone (3 ml) with W-4 Raney nickel (500 mg) deactivated with refluxing acetone provided **3c** (11 mg, 42%) as a colorless oil: ^1H NMR ($CDCl_3$) δ=1.2—2.9 (5H, m), 4.1—4.6 (2H, m, CH_2O), 4.9—5.2 (2H, m, $C\underline{H}_2$=CH), and 5.6—6.0 (1H, m, CH_2=C$\underline{H}$).

Found: *m/z* 126.0679. Calcd for $C_7H_{16}O_2$: M, 126.0680.

(b) According to the procedure described for the preparation of **2a**, treatment of copper(I) iodide (117 mg, 0.61 mmol) with 1.09 M vinylmagnesium bromide (0.52 ml, 0.56 mmol) at −50 °C, followed by addition of **8** (51 mg, 0.52 mmol) gave **3c** (9 mg, 17%).

3-[Bis(methoxycarbonyl)methyl]-5-pentanolide (3d). According to the procedure described for the preparation of **3a**, reaction of **2d** (31 mg) with W-4 Raney nickel (500 mg) in acetone (3 ml) gave **3d** (12 mg, 56%) as an oil: ^1H NMR ($CDCl_3$) δ=1.3—2.8 (5H, m), 3.3 (1H, br d, COCHCO), 3.75 and 3.81 (6H in total, s each, Me_2), and 4.2—4.5 (2H, m, CH_2O).

Found: *m/z* 230.0793. Calcd for $C_{10}H_{14}O_6$: M, 230.0790.

Ethyl 5-Hydroxy-3-methylpentanoate (13) and 3-Ethyl-5-pentanolide (14). A mixture of **2a** (42 mg), W-4 Raney nickel (500 mg) and ethanol (5 ml) was stirred for 4 h. Workup according to the procedure described for the preparation of **3a** followed by purification of a residue by TLC gave **13** (23 mg, 75%) as a colorless oil: IR (film) 3300 (OH) and 1730 cm^{-1} (C=O); ^1H NMR ($CDCl_3$) δ=0.98 (3H, d, *J*=6.0 Hz, CH$\underline{Me}$), 1.28 (3H, t, *J*=7.0 Hz, $CH_2\underline{Me}$), 1.6 (2H, m), 2.0 (1H, m, C$\underline{H}$Me), 2.25 (2H, m, CH_2CO), 3.65 (2H, t, *J*=6.0 Hz, $C\underline{H}_2OH$), and 4.17 (2H, q, *J*=6.0 Hz, $MeC\underline{H}_2$).

By the similar procedure, reaction of **2c** (31 mg) with W-4 Raney nickel (500 mg) in ethanol (5 ml) afforded **14** (14 mg, 86%) as an oil: IR (film) 1730 cm^{-1} (C=O); ^1H NMR ($CDCl_3$) δ=1.1—2.8 (10H, m), 4.1—4.6 (2H, m, CH_2O).

Found: *m/z* 128.0830. Calcd for $C_7H_{12}O_2$: M, 128.0837.

General Procedure for the Preparation of 3-Substituted 2-penten-5-olide (5). To a stirred solution of **2** (0.3 mmol) in CH_2Cl_2 (15 ml) at −10 °C for **2a**, **b**, **d** and at −50 °C for **2c**, was added dropwise over 30 min a solution of *m*CPBA (0.3 mmol) in CH_2Cl_2 (10 ml). After addition was complete, stirring was continued for an additional 10 min at −10 °C for **2a**, **b**, **d** and at −20 °C for **2c**, and the mixture was washed with aqueous sodium thiosulfate, aqueous sodium hydrogencarbonate, and brine, and dried. Evaporation gave practically pure and oily sulfoxide **4** in quantitative yield. To a solution of **4** in benzene (10 ml) was added pyridine (100 μl) and the mixture was gently refluxed for 1.5 h. After cooling, the mixture was diluted with benzene and washed with aqueous sodium hydrogencarbonate, aqueous copper(II) sulfate and brine, and dried. Evaporation of the solvent followed by purification of a residue by TLC afforded **5** as a colorless oil.

3-Methyl-2-phenylsulfinyl-5-pentanolide (4a). ^1H NMR ($CDCl_3$) δ=0.75 and 1.30 (3H in total, both d, *J*=6.8 Hz, 1:9 ratio by integration, Me), 1.2—2.4 (3H, m), 3.38 and 3.85 (1H in total, d, *J*=5.4 and 5.7 Hz each, 9:1 ratio by integration, SOCH), 4.1—4.5 (2H, m, CH_2O), and 7.4—8.0 (5H, m, Ph).

3-Butyl-2-phenylsulfinyl-5-pentanolide (4b). ^1H NMR ($CDCl_3$) δ=0.8—2.6 (12H, m), 3.38 and 3.82 (1H in total, d, *J*=4.3 and 5.4 Hz each, 9:1 ratio by integration, SOCH) 4.2—4.7 (2H, m, CH_2O), and 7.4—8.0 (5H, m, Ph).

2-Phenylsulfinyl-3-vinyl-5-pentanolide (4c). ^1H NMR ($CDCl_3$) δ=1.5—2.8 (3H, m), 3.82 and 4.02 (1H in total, both d, *J*=5.4 Hz, 7:1 ratio by integration, SOCH), 4.4 (2H, m, CH_2O), 5.1—5.3 (2H, m, $C\underline{H}_2$=CH), 5.7—6.2 (1H, m, CH_2=C$\underline{H}$), and 7.3—8.0 (5H, m, Ph).

3-[Bis(methoxycarbonyl)methyl]-2-phenylsulfinyl-5-pentanolide (4d). ^1H NMR ($CDCl_3$) δ=1.6—2.4 (2H, m), 2.84—3.5 (2H, m), 3.6—4.0 (7H, m), 4.3—4.7 (2H, m, CH_2O), and 7.3—8.0 (5H, m, Ph).

3-Methyl-2-penten-5-olide (5a). 72% yield from **2a**; IR (film) 1720 (C=O) and 1645 cm^{-1} (C=C); ^1H NMR ($CDCl_3$) δ=2.0 (3H, d, *J*=1.6 Hz, Me), 2.40 (2H, t, *J*=5.8 Hz, $C{=}CCH_2$), 4.38 (2H, t, *J*=6.1 Hz, CH_2O), and 5.80 (1H, q, *J*=1.6 Hz, C=CH).

Found: *m/z* 112.0519. Calcd for $C_6H_8O_2$: M, 112.0524.

3-Butyl-2-penten-5-olide (5b). 79% yield from **2b**; ^1H NMR ($CDCl_3$) δ=0.95 (3H, br t, Me), 1.1—1.8 (4H, m), 2.1—2.5 (4H, m, $C{=}CCH_2$), 4.38 (2H, t, *J*=6.1 Hz, CH_2O), and 5.80 (1H, s with fine splittings, C=CH).

Found: *m/z* 154.1009. Calcd for $C_9H_{14}O_2$: M, 154.0994.

3-Vinyl-2-penten-5-olide (5c). 73% yield from **2c**; IR (film) 1720 (C=O), 1630 (C=C), and 1590 cm^{-1} (C=C); ^1H NMR ($CDCl_3$) δ=2.58 (2H, t, *J*=6.4 Hz, $C{=}CCH_2$), 4.44 (2H, t, *J*=6.4 Hz, CH_2O), 5.58 (1H, d, *J*=10.5 Hz, $C\underline{H}_aH_b$=CH), 5.65 (1H, d, *J*=17.3 Hz, $CH_a\underline{H}_b$=CH), 5.92 (1H, s, C=CHCO), and 6.56 (1H, dd, *J*=17.3, 10.5 Hz, CH_2=C$\underline{H}$).

3-[Bis(methoxycarbonyl)methyl]-2-penten-5-olide (5d). 80% yield from **2d**; IR (film) 1730 (C=O) and 1640 cm^{-1} (C=C); ^1H NMR ($CDCl_3$) δ=2.63 (2H, t with fine splittings, *J*=5.8 Hz, $C{=}CCH_2$), 3.80 (6H, s, Me_2), 4.3—4.5 (3H, m, CH_2O, COCHCO), and 6.0 (1H, s with fine splittings, C=CHCO).

Found: *m/z* 228.0669. Calcd for $C_{10}H_{12}O_6$: M, 228.0633.

General Procedure for the Pummerer Reaction of 4. The sulfoxide **4** was prepared by oxidation of **2** with equimolar *m*CPBA according to the aforementioned procedure. Trifluoroacetic anhydride was added to **4** at −60 °C and the

resulting mixture was stirred, and allowed to warm gradually to room temperature. The reaction mixture was diluted with CH_2Cl_2 and washed with aqueous sodium hydrogencarbonate and brine, and dried. Filtration followed by removal of the solvent left an oil, which was purified by TLC to give **6** and/or **7**.

3-Methyl-2-(phenylthio)-2-penten-5-olide (6a) and 2-Hydroxy-3-methyl-2-penten-5-olide (7a). (a) A solution of **4a** (190 mg) prepared from **2a** (183 mg, 0.82 mmol) and trifluoroacetic anhydride (4 ml) was stirred for 3d to give **6a** (94 mg, 52% from **2a**) and **7a** (19 mg, 18% from **2a**).

6a: an oil; IR (film) 1720 (C=O) and 1605 cm^{-1} (C=C); ^1H NMR ($CDCl_3$) δ=2.28 (3H, s, Me), 2.65 (2H, t, *J*=5.7 Hz, C=CCH_2), 4.40 (2H, t, *J*=5.7 Hz, CH_2O), and 7.18 (5H, br s, Ph).

Found: *m/z* 220.0548. Calcd for $C_{12}H_{12}O_2S$: M, 220.0557.

7a: an oil; IR (film) 3350 (OH), 1700 (C=O), and 1580 cm^{-1}; ^1H NMR ($CDCl_3$) δ=1.91 (3H, t, *J*=1.3 Hz, Me), 2.47 (2H, tt, *J*=5.3, 1.3 Hz, C=CCH_2), 4.39 (2H, t, *J*=6.3 Hz, CH_2O), and 5.59 (1H, s, OH).

Found: *m/z* 128.0470. Calcd for $C_6H_8O_3$: M, 128.0473.

(b) **4a** (47 mg) prepared from **2a** (42 mg, 0.19 mmol) was treated with trifluoroacetic anhydride (3 ml) and the temperature was gradually raised to 0 °C over 3 h. The reaction mixture was diluted with CH_2Cl_2 and poured into ice-cooled aqueous sodium hydrogencarbonate. Workup gave **6a** (5 mg, 14% from **2a**) and **7a** (14 mg, 59% from **2a**).

3-Butyl-2-phenylthio-2-penten-5-olide (6b). A solution of **4b** (71 mg) prepared from **2b** (63 mg, 0.24 mmol) and trifluoroacetic anhydride (2 ml) was stirred for 2d to give **6b** (31 mg, 49% from **2b**) as an oil: IR (film) 1720 (C=O) and 1600 cm^{-1}; ^1H NMR ($CDCl_3$) δ=0.95 (3H, t, Me), 1.1—1.8 (4H, m), 2.5—2.8 (4H, m, C=CCH_2×2), 4.40 (2H, t, *J*=6.7 Hz, CH_2O), and 7.22 (5H, m, Ph).

Found: *m/z* 262.1026. Calcd for $C_{15}H_{18}O_2S$: M, 262.1027.

2-Phenylthio-3-vinyl-2-penten-5-olide (6c). A solution of **4c** (39 mg) prepared from **2c** (33 mg, 0.14 mmol) and trifluoroacetic anhydride (2 ml) was stirred for 3d to give **6c** (4 mg, 10% from **2c**) and **5c** (13 mg, 74% from **2c**).

6c: a colorless oil; ^1H NMR ($CDCl_3$) δ=2.64 (2H, t, *J*=6.1 Hz, C=CCH_2), 4.48 (2H, t, *J*=6.1 Hz, CH_2O), 5.45 (1H, d, *J*=10.4 Hz, CH_aH_b=CH), 5.52 (1H, d, *J*=18.0 Hz, CH_aH_b=CH), and 6.95 (1H, dd, *J*=10.4, 18.0 Hz, CH_2=CH).

2-Hydroxy-3-[bis(methoxycarbonyl)methyl]-2-penten-5-olide (7d). A solution of **4d** (54 mg) prepared from **2d** (50 mg, 0.15 mmol) and trifluoroacetic anhydride (2 ml) was stirred for 2d to give **7d** (12 mg, 34% from **2d**): IR (film) 3350 (OH) and 1730 cm^{-1} (C=O); ^1H NMR ($CDCl_3$) δ=2.70 (2H, t, *J*=6.4 Hz, C=CCH_2), 3.81 (6H, s, Me), 4.47 (2H, t, *J*=6.4 Hz, CH_2O), 4.92 (1H, s, COCHCO), and 6.0 (1H, br, OH).

3,3-Dimethyl-2-phenylthio-5-pentanolide (20). Acoording to the procedure described for the preparation of **2a**, treatment of copper(I) iodide (19 mg, 0.10 mmol) with 1.25 M methyllithium in ether (160 μl, 0.18 mmol) at −13 °C, followed by addition of **6a** (18 mg, 0.08 mmol) gave **20** (6 mg, 32%): ^1H NMR ($CDCl_3$) δ=1.24 (6H, s, Me_2), 1.4—2.1 (4H, m), 3.43 (1H, br s, SCH), 4.4 (2H, m, CH_2O), and 7.2—7.7 (5H, m, Ph).

Found: *m/z* 236.0867. Calcd for $C_{13}H_{16}O_2S$: M, 236.0870.

3-Butyl-3-methyl-2-phenylthio-5-pentanolide (21). Acoording to the procedure for the preparation of **2a**, treatment of copper(I) iodide (16 mg, 0.08 mmol) with 1.22 M methyllithium in ether (0.13 ml, 0.16 mmol) at −25 °C, followed by addition of **6b** (18 mg, 0.07 mmol) gave **21** (5 mg, 24%). ^1H NMR ($CDCl_3$) δ=0.9 (3H, br t, Me), 1.1—2.23 (11H, m), 3.52 (1H, br s, SCH), 4.1—4.6 (2H, m, CH_2O), and 7.2—7.7 (5H, m, Ph).

Found: *m/z* 278.1347. Calcd for $C_{16}H_{22}O_2S$: M, 278.1340.

Reaction of 5c with Lithium Dimethylcuprate. Acoording to the procedure described for the preparation of **2a**, treatment of copper(I) iodide (102 mg, 0.54 mmol) with 1.6 M methyllithium in ether (0.67 ml, 1.07 mmol) at −30 °C, followed by addition of **5c** (61 mg, 0.49 mmol) gave **22** (35 mg, 51%) and **23** (6 mg, 8%).

22: IR (film) 1750 cm^{-1} (C=O); ^1H NMR ($CDCl_3$) δ=0.95 (3H, t, *J*=7.1 Hz, Me), 2.0 and 2.5 (2H, m each, CH_2CH_2O and C=CCH_2Me), 3.3 (2H, m, CH_2CO), 4.2—4.42 (2H, m, CH_2O), and 5.35 (1H, br t, C=CH).

Found: *m/z* 140.0841. Calcd for $C_8H_{12}O_2$: M, 140.0837.

23: IR (film) 1710 (C=O) and 1640 cm^{-1} (C=C); ^1H NMR ($CDCl_3$) δ=0.98 (3H, t, *J*=7.0 Hz, Me), 1.1—2.1 (4H, m), 2.42 (2H, m, CH_2CH_2O), 4.2—4.5 (2H, m, CH_2O), and 6.0 (1H, s, with fine splittings, C=CH).

Found: *m/z* 140.0829. Calcd for $C_8H_{12}O_2$: M, 140.0837.

General Procedure for the Reaction of 1 with Benzylic Grignard Reagents 25. Benzyl or substituted benzyl bromide (3 equiv) was added to a mixture of finely powdered magnesium (30 equiv) and a catalytic amount of 1,2-dibromoethane in ether. The resulting suspension was stirred at room temperature for 30 min, and then with refluxing for an additional 10 min, and cooled at −12 °C. A solution of **1** (1.0 equiv) in THF (1—2 ml) was added with stirring and stirring was continued for an additional 20—30 min. The reaction was quenched by addition of aqueous ammonium chloride, and the product was extracted with CH_2Cl_2, washed with brine, and dried. Removal of the solvent left an oil which was purified by TLC to give **26** and/or **27**, along with recovered **1** on the reactions with the Grignard reagents **25a**, **b**, **d**.

3-Benzyl-2-phenylthio-5-pentanolide (26a). Reaction of **1** (49 mg, 0.24 mmol) with the Grignard reagent **25a**, prepared from magnesium (175 mg, 7.29 mmol) and benzyl bromide (125 mg, 0.23 mmol) in ether (3 ml), gave **26a** (58 mg, 82%) and **1** (8 mg, 16%). **26a**: a colorless oil; IR (film) 1730 cm^{-1} (C=O); ^1H NMR ($CDCl_3$) δ=1.2—2.8 (3H, m), 3.2 (2H, m, CH_2Ph), 3.58 and 3.75 (1H in total, d, *J*=5.7 and 3.6 Hz each, 9:1 ratio by integration, SCH), 4.2—4.4 (2H, m, CH_2O), and 7.1—7.6 (10H, m, Ph).

Found: *m/z* 298.1026. Calcd for $C_{18}H_{18}O_2S$: M, 298.1027.

3-(2-Methylbenzyl)-2-phenylthio-5-pentanolide (26b). Reaction of **1** (50 mg, 0.24 mmol) with the Grignard reagent **25b** prepared from magnesium (176 mg, 7.33 mmol) and 2-methylbenzyl bromide (139 mg, 0.73 mmol) in ether (4 ml), provided **26b** (47 mg, 62%) and **1** (8 mg, 16%). **26b**: a colorless oil; IR (film) 1730 cm^{-1} (C=O); ^1H NMR ($CDCl_3$) δ=1.3—2.8 (5H, m), 2.26 (3H, s, Me), 3.57 and 3.80 (1H in total, d, *J*=6.1 and 4.7 Hz each, 9:1 ratio by integration, SCH), 4.1—4.5 (2H, m, CH_2O), and 7.0—7.6 (9H, m, Ph, ArH).

Found: *m/z* 312.1193. Calcd for $C_{19}H_{20}O_2S$: M 312.1183.

3-(2,6-Dimethylbenzyl)-2-phenylthio-5-pentanolide (26c) and 3-(3,5-Dimethyl-4-methylene-2,5-cyclohexadienyl)-2-phenylthio-5-pentanolide (27c).[4b] Reaction of **1** (105 mg, 0.51 mmol) with the Grignard reagent **25c**, prepared from magnesium (350 mg, 14.59 mmol) and 2,6-dimethylbenzyl bromide (195 mg, 1.48 mmol) in ether (4 ml), afforded **26c** (58 mg, 34%) and **27c** (108 mg, 65%).

26: Found: *m/z* 326.1339. Calcd for $C_{20}H_{22}O_2S$: M 326.1340.

27: Found: *m/z* 326.1340. Calcd for $C_{20}H_{22}O_2S$: M 326.1340.

3-(2,4,6-Trimethylbenzyl)-2-phenylthio-5-pentanolide (26d) and 3-(1,3,5-Trimethyl-4-methylene-2,5-cyclohexadienyl)-2-phenylthio-5-pentanolide (27d).[4b] Reaction of **1** (50 mg, 0.4 mmol) with the Grignard reagent **25d**, prepared from magnesium (175 mg, 7.29 mmol) and 2,4,6-trimethylbenzyl bromide (155 mg, 0.72 mmol) in ether (3 ml), gave a mixture of **26d** and **27d** (14 mg in total, 6 and 10%, respectively) and recoverd **1** (37 mg, 75%). The yields of **26d** and **27d** were calculated from the integral ratio of the aromatic and aliphatic methyls in **26d** and **27d**, respectively, in the ^{1}H NMR spectrum of the mixture.

2-Phenylthio-3-(2,4,6-trimethylphenyl)-5-pentanolide (28).[4b] A mixture of **27** (40 mg) and a catalytic amount of *p*-toluenesulfonic acid in anhydrous benzene (1 ml) was allowed to stir at room temperature for 10 h. After removal of the solvent, an oily residue was purified by TLC (CH_2Cl_2) to give **28** (39 mg, 98%) as colorless crystals, mp 107—108 °C.

Found: C, 73.58; H, 6.70%. Calcd for $C_{20}H_{22}O_2S$: C, 73.60; H, 6.79%.

3-(2,6-Dimethylbenzyl)-2-methyl-2-phenylthio-5-pentanolide (29). According to the procedure described for the preparation of **10**, lithium diisopropylamide was prepared from diisopropylamine (62 mg, 0.61 mmol) and 1.5 M butyllithium in hexane (0.37 ml, 0.58 mmol) in THF (5 ml). A solution of **26c** (181 mg, 0.54 mmol) in THF (5 ml) was added to the above solution at −70 °C with rapid stirring, and stirring was continued for an additional 30 min. To this mixture, HMPA (1 ml) followed by methyl iodide (91 mg, 0.64 mmol) was added and the temperature was gradually raised to −10 °C over 3.5 h. The reaction was quenched by addition of aqueous ammonium chloride, and the product was extracted with CH_2Cl_2. The combined extracts were washed with brine and dried. Evaporation followed by purification of a residue by TLC gave a mixture of diastereomers **29** (135 mg, 72%) as an oil; IR (film) 1720 cm^{-1} (C=O); ^{1}H NMR ($CDCl_3$) δ=1.59 (3H, s, Me), 1.7 (2H, m, $C\underline{H}_2CH_2O$), 2.35 (6H, s, Ar$\underline{Me}$), 2.2—3.3 (3H, m, $PhC\underline{H}_2C\underline{H}$), 4.2—4.5 (2H, m, CH_2O), 7.0 (3H, br s, Ar$\underline{H}$), and 7.2—7.7 (5H, m, Ph).

Found: *m/z* 340.1498. Calcd for $C_{21}H_{24}O_2S$: M 340.1496.

(±)-Secocrispiolide (24) and 3-(2,6-Dimethylbenzyl)-2-methyl-2-penten-5-olide (31). To a stirred solution of **29** (91 mg, 0.27 mmol) in CH_2Cl_2 (10 ml) at −20 °C was added a solution of 80% *m*CPBA (58 mg, 0.27 mmol) in CH_2Cl_2 (8 ml) over 30 min. The mixture was stirred for 30 min, diluted with CH_2Cl_2, and washed with aqueous sodium thiosulfate, aqueous sodium hydrogencarbonate and brine, and dried. Evaporation of the solvent gave the sulfoxide **30** (94 mg, quantitative), which was dissolved in benzene (5 ml). The resulting solution was gently refluxed for 30 min and cooled to room temperature. Removal of the solvent followed by purification of a residue with TLC gave a mixture of (±)-secocrispiolide (**24**) and **31** in 1:3 ratio (57 mg in total). Separation of the mixture by HPLC (Waters Associates, column 25 cm/0.46 (i.d.), silica gel, 9:2 hexane–chloroform) provided pure **24** and **31**. The spectra (IR, ^{1}H NMR and MS) of the synthetic **24** were identical with those of the natural material.[12]

24: a colorless oil; IR ($CHCl_3$) 1730 (C=O) and 1625 cm^{-1} (C=C); ^{1}H NMR ($CDCl_3$) δ=1.9—2.1 (2H, m, $C\underline{H}_2CH_2O$), 2.30 (6H, br s, Me_2), 2.7—3.1 (3H, m, $ArC\underline{H}_2C\underline{H}$), 4.1—4.3 (2H, m, CH_2O), 5.38 (1H, br s, $C\underline{H}_aH_b$=C), 6.42 (1H, br s, $CH_a\underline{H}_b$=C), and 7.04 (3H, s, ArH).

Found: *m/z* 230.1304. Calcd for $C_{15}H_{18}O_2$: M 230.1306.

31: a colorless oil; IR (film) 1710 cm^{-1} (C=O); ^{1}H NMR ($CDCl_3$) δ=1.8—2.1 (2H, m, $C\underline{H}_2CH_2O$), 2.08 (3H, s, C=CMe), 2.25 (6H, s, Ar$\underline{Me}$), 3.50 (2H, br s, $PhC\underline{H}_2$), 4.18 (2H, br t, *J*=5 Hz, CH_2O), and 7.05 (3H, br s, Ph).

Found: *m/z* 230.1296. Calcd for $C_{15}H_{18}O_2$: M 230.1306.

This work was supported by a Grant-in-Aid for Scientific Research No. 56470024 from the Ministry of Education, Science and Culture.

References

1) For example, T. K. Devon, and A. I. Scott, "Handbook of Naturally Occuring Compounds, Vol. II, Terpens," Academic Press, New York & London (1972).

2) For example, J. ApSimon, "The Total Synthesis of Natural Products," A Wiley-Interscience Publication, John Wiley & Sons, 1983, Vol. 5; Nair and A. K. Sinhababu, *J. Org. Chem.*, **45**, 1893 (1980); and references cited therein.

3) (Review) Y. S. Rao, *Chem. Rev.*, **76**, 625 (1976); N. Petragnani, H. M. C. Ferraz, and G. V. J. Silva, *Synthesis*, **1986**, 157; P. Brownbrigde, E. Egert, P. G. Hunt, O. Kennard, and S. Warren, *J. Chem. Soc., Perkin Trans. 1*, **1981**, 2751, and references cited therein.

4) Reported in part in preliminary communications: a) M. Kato, A. Ouchi, and A. Yoshikoshi, *Chem. Lett.*, **1983**, 1511; b) M. Kato, A. Ouchi, and A. Yoshikoshi, *Chem. Lett.*, **1984**, 1697.

5) For analogous reactions: see K. Iwai, H. Kosugi, and H. Uda, *Chem. Lett.*, **1974**, 1237; H. J. Monterio, *J. Org. Chem.*, **42**, 2324 (1977); F. Kido, Y. Noda, and A. Yoshikoshi, *J. Am. Chem. Soc.*, **104**, 5509 (1982); M. Kato, B. Vogler, Y. Tooyama, and A. Yoshikoshi, *Chem. Lett.*, **1990**, 151.

6) B. M. Trost and G. S. Massiot, *J. Am. Chem. Soc.*, **99**, 4405 (1977).

7) A. I. Meyers, R. K. Smith, and C. E. Whitten, *J. Org. Chem.*, **44**, 2250 (1979); F. E. Ziegler and P. J. Gilligan *J. Org. Chem.*, **46**, 3874 (1981).

8) J. B. Jones and K. P. Lok, *Can. J. Chem.*, **57**, 1025 (1979); B. M. Trost and T. R. Verhoven, *J. Am. Chem. Soc.*, **102**, 4743 (1980).

9) For 3-methyl-2-penten-5-olide (**5a**): See references cited in Ref. 4a.

10) W. A. Skinner, F. Fuhrmann, L. C. Rutledge, M. A. Moussa, and C. E. Schreck, *J. Pharm. Sci.*, **69**, 196 (1980).

11) F. Bohlmann, K.-H. Knoll, and N. A. El-Emary, *Phytochemistry*, **18**, 1231 (1972).

12) M. S. Kharasch and O. Reinmuth, "Grignard Reactions of Non-Metallic Substances," Prentice-Hall, Inc., New York (1954), p. 1133. The terminology "abnormal" indicates the reaction at ortho or para position of a benzyl group.

Light-Induced Electron-Transfer Reaction into *Rs. rubrum* Chromatophores from a Pt Electrode

Tatsuo ERABI,* Kiyoharu MATSUMOTO, Noritaka TAKAHASHI, Kumiko HIRATA, and Masanori WADA
Department of Materials Science, Faculty of Engineering, Tottori University, Koyama, Tottori 680
(Received August 10, 1990)

A platinum electrode immersed in a chromatophore suspension brought about, upon illumination, a cathodic photocurrent under potentiostatic conditions. The photocurrent action spectrum coincided fairly well with the absorption one of a chromatophore suspension, showing maxima at 600, 800, and 875 nm. The photocurrent increased with an increasing cathodic shift of the applied potential up to about −500 mV; two successive waves were observed on the photocurrent. The mechanism for the generation of the photocurrent is discussed.

Serious environmental problems, including air pollution with NO_x and SO_x and the release of vast amounts of CO_2 into atmosphere, limit the utility of fossil fuels. The development of solar energy technology has therefore been desired, while promising a substantial future contribution to growing energy demands. The primary processes of photosynthesis are the most efficient to convert solar energy to chemical energy and, consequently, could possibly be used as the basis for modified photosynthetic processes applicable in solar energy conversion.[1] Supporting this viewpoint, many studies[2] have demonstrated the possibility of employing photoactive biological components in photoelectrochemical cells, in connection with studies on the mechanism of photosynthetic primary processes as well as solar energy conversion projects. We have been studying photoelectrochemical behavior using a photosynthetic apparatus, chromatophores, of photosynthetic bacterium, *Rhodospirillum rubrum,* at a platinum electrode.[3,4] Still, questions regarding the electron-transfer mechanism between chromatophores and the electrode remain unanswered. The present paper deals with a further detailed photoresponse of chromatophores at a platinum electrode and with a plausible mechanism to account for the photoresponse.

Experimental

A carotenoid-less blue-green mutant strain (G-9) of *Rs. rubrum* was used throughout the present study. The cells were grown anaerobically at 30 °C for 3 days under continuous illumination from tungsten lamps, as described previously.[5] Chromatophores were prepared from light-grown cells by sonication, followed by centrifugation.[6] Chromatophores, thus prepared, were suspended in a 0.12 M (M=mol dm^{-3}) GTA buffer comprising an equimolar mixture of 3,3-dimethylglutaric acid, tris(hydroxymethyl)methanamine, and 2-amino-2-methyl-1,3-propanediol, which was adjusted to various pH values by adding HCl or NaOH. The concentration of chromatophores is expressed in terms of the absorbance of bound bacteriochlorophyll at 873 nm (A_{873}; corresponding to 7.1 μM of bound bacteriochlorophyll[7]). An experimental cell[4] with a light path length of 0.4 mm comprised a platinum plate working electrode (2×3 cm^2 of surface area), a platinum wire counter electrode and a saturated calomel reference electrode. All of the potentials listed in this paper were corrected against a normal hydrogen electrode. For a potentiostatic measurement, the potential of the electrode was controlled with a Hokuto Model potentiostat (HA-104 or HA-501), and the resulting current was recorded. The photocurrent was measured after electrolyzing for 30 min in the dark at a certain potential, while approaching a steady state of electrolysis. The light source was a 300 W projector lamp, usually used in combination with a 12 cm thick water filter in order to eliminate any thermal effects (a 500 W xenon arc lamp (Wacom Model MX-500) was used in combination with a JASCO Model CT-25N grating monochromator equipped with a cut-off filter (UV-39 or VR-69) for measuring the photocurrent action spectrum). The intensity of monochromatic light was measured with a calibrated thermopile (Model 404 of Spectra-Physics). Ten units·ml^{-1} of glucose oxidase, 2 mM of glucose and 13 units·ml^{-1} of catalase were added to the suspension to remove any dissolved oxygen; oxygen-free nitrogen was passed through the suspension for 30 min before electrolysis. The suspension was kept at 25 °C using a thermostat. The electrochemical cell, thus prepared, was placed in a dark box under a nitrogen atmosphere; it was shielded with a common ground against any electromagnetic perturbations.

Results and Discussion

A platinum electrode immersed in a chromatophore suspension brought about, upon illumination, a cathodic photocurrent (I_p) under potentiostatic conditions, as reported previously.[3,4] Although the magnitude of the cathodic photocurrent depended on the concentration of chromatophores, incident light intensity, and applied potential,[3] no anodic photocurrents could be observed, even under anodic polarization. This may be due to a structural anisotropy in the chromatophore membrane at which the functional positions of such electron-transport components as cytochromes, ubiquinone 10 and the reaction center complex are important in consideration of the transfer of electrons and protons within and across the membrane.

If electrons injected into the electron-transport components bound to the chromatophore membrane equilibrate with the electrode during the primary photoact, the action spectrum of the photocurrent should correspond to the absorption one of the chromatophore suspension. The photocurrent action spectra were mea-

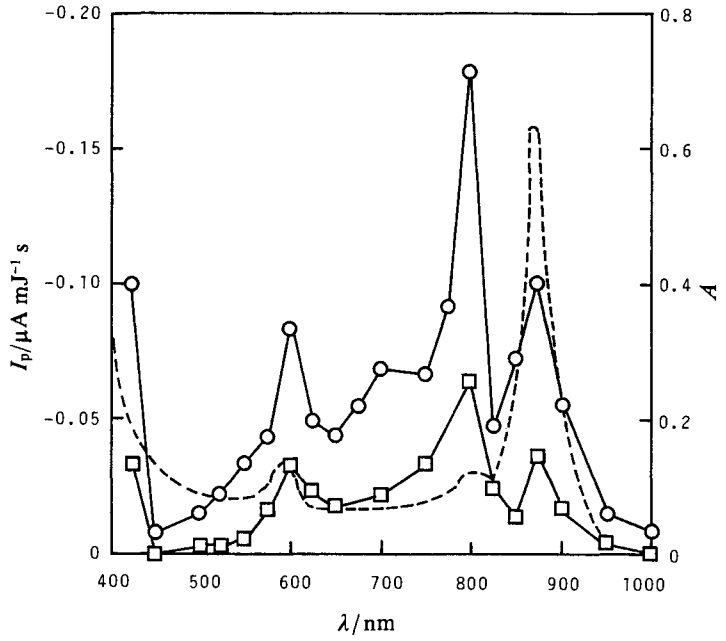

Fig. 1. Photocurrent action spectra (solid lines) and absorption spectrum of chromatophore suspension (dotted line). ○ and □ represent the values of photocurrent obtained at −500 mV and −100 mV of applied potentials, respectively. The concentration of chromatophores was kept constant at A_{873}=75.

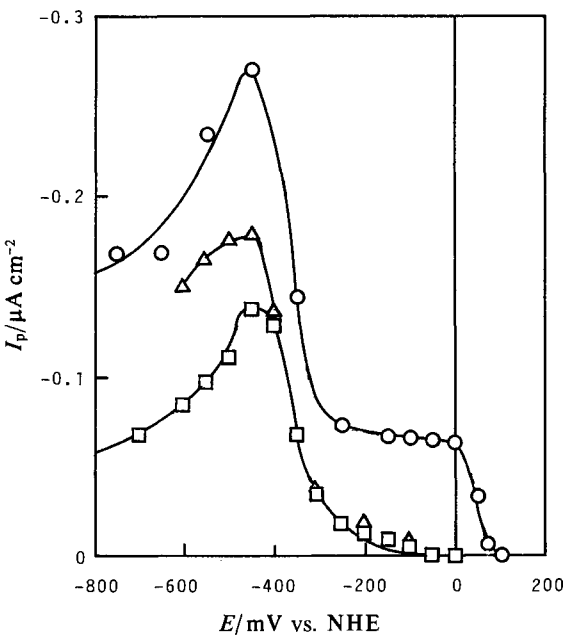

Fig. 2. Dependence of photocurrent on applied potential. ○, □, and △ represent the values obtained by native chromatophores, quinone-extracted ones, and reaction center complexes, respectively. The concentration of chromatophores and reaction centers were at A_{873}=75, and A_{802}=5, respectively. The light intensity was kept at 6000 lx of illuminance.

sured at low light intensity (1—10 J $m^{-2}s^{-1}$) and at different electrode potentials. The results are shown in Fig. 1, together with the absorption spectrum of the chromatophore suspension. It is evident that both the photocurrent action spectra and that for absorption coincide fairly well, showing maxima at 600, 800, and 875 nm assigned to chromatophore-bound bacteriochlorophyll absorption (588, 804, and 873 nm).[8] This result suggests that the bound bacteriochlorophyll, especially the reaction center bacteriochlorophyll called P870, assumes some roles in the generation of the cathodic photocurrent.

In order to specify the electrochemically active species bound to chromatophores the behavior of the photocurrent was examined in some detail against the applied potential under potentiostatic conditions at various pH values. A typical result at pH 8.0 is shown in Fig. 2. In this figure the cathodic photocurrent increases with the more cathodic shift of the applied potential up to about −500 mV, and then decreases. The decrease in the photocurrent in a more cathodic region than about −500 mV may be due to competitive hydrogen evolution resulting from the electrolysis of water, as well as an irreversible reduction of the chromatophore membrane.[9] In addition, two successive waves were observed on the cathodic photocurrent and two potential onsets of the waves were +100 and −275 mV, respectively.

Earlier, Higuti et al.[10] found that 90—95% of ubiquinone 10 and rhodoquinone are easily extractable from lyophilized chromatophores with 2,2,4-trimethylpentane; the various activities, thus depressed, are restored by adding extracts or ubiquinone 10 to the extracted chromatophores. The photocurrent generated by quinone-extracted chromatophores was lowered to about 45% or less than the original level, as also shown in Fig. 2. The effect of extracting ubiquinone 10 was especially larger in the more positive potential region, and the photocurrent became hardly observable. In addition, the voltammetric behavior of ubiquinone 10 bound to chromatophores has been reported,[9] and the redox potential at pH 8.0 was estimated to be +20 mV. These facts indicate a possibility that the first photocurrent-generating component is ubiquinone 10 bound to the chromatophores.

The chromatophore membrane can be easily disintegrated with *N*,*N*-dimethyldodecylamine *N*-oxide; a reaction center complex was purified by repeating molecular-sieve and ion-exchange chromatographies for the disintegrated membrane.[11] When the photocurrent was measured for the reaction center complex, thus prepared, the potential dependence of the cathodic photocurrent was similar to the more negative wave of the photocurrent generated by chromatophores. This result is also shown in Fig. 2. It therefore seems reasonable that the second photocurrent-generating component is one of the photooxidized constituents localized on the outside of the reaction center complex. It is generally accepted that in chromatophores the majority of bacte-

riochlorophyll molecules are harvesters of light quanta and the remainder are functional in driving the electron-transport system (reaction center bacteriochlorophyll, P870). Earlier, Okayama et al.[12] distinguished the reaction center bacteriochlorophyll into two different kinds regarding functions, Liac-860 (E_{m7}=450 mV) and Liac-890 (E_{m7}<−100 mV). In addition, we[9] have reported that chromatophores bound two reactable components on a voltammetric electrode; one is ubiquinone 10 and the other was a component named POC_{-170}, corresponding to Liac-890. It therefore seems presumable that the photooxidized constituent may correspond to a reaction center bacteriochlorophyll, Liac-890. However, it has been indicated by immunological experiments[13] that the reaction center bacteriochlorophyll should be situated at or near the periplasmic aspect of the chromatophore membrane (inside of chromatophore vesicle). It may thus be difficult for the P870 to be directly reduced on the electrode, due to the insulation of the redox center from the electrode by the structure protein. It is now being attempted to specify which of the extrinsic constituents takes role in the generation of a second cathodic photocurrent; more details regarding the photoelectrochemical behavior of reaction center complexes will be reported elsewhere.

References

1) P. Weaver, S. Lien, and M. Seibert, "Photobiological Production of Hydrogen—A Solar Energy Conversion Option," SERI/TR-33-122 (1979).

2) For example: on use of chloroplasts, H. Ochiai, H. Shibata, Y. Sawa, and T. Katoh, *Photochem. Photobiol.*, **35**, 149 (1982); S. Lemieux and R. Carpentier, *ibid.*, **48**, 115 (1988): On use of reaction center complexes, M. Seibert, A. F. Janzen, and M. Kendall-Tobias, *ibid.*, **35**, 193 (1982): On use of algae, K. Kobayashi, T. Sagara, M. Okada, and K. Niki, *Chem. Lett.*, **1983**, 373.

3) T. Erabi, H. Hiura, M. Hayashi, M. Yamada, T. Endo, J. Yamashita, M. Tanaka, and T. Horio, *Chem. Lett.*, **1978**, 341.

4) T. Erabi, K. Matsumoto, H. Itoh, N. Takahashi, K. Nishimura, and M. Wada, *Bull. Chem. Soc. Jpn.*, **60**, 3805 (1987).

5) T. Horio, K. Nishikawa, M. Katsumata, and J. Yamashita, *Biochim. Biophys. Acta*, **94**, 371 (1965).

6) N. Nishi, M. Kataoka, G. Soe, T. Kakuno, T. Ueki, J. Yamashita, and T. Horio, *J. Biochem.*, **86**, 1211 (1979).

7) T. Kakuno, R. G. Bartsch, K. Nishikawa, and T. Horio, *J. Biochem.*, **70**, 79 (1971).

8) K. Hosoi, G. Soe, and T. Horio, "Seitaimaku Jikkenho," Kyoritsu Shuppan, Tokyo (1974), p. 321.

9) T. Erabi, T. Higuti, T. Kakuno, J. Yamashita, M. Tanaka, and T. Horio, *J. Biochem.*, **78**, 795 (1975).

10) T. Higuti, T. Erabi, T. Kakuno, and T. Horio, *J. Biochem.*, **78**, 51 (1975).

11) C. Vadeboncoeur, H. Noel, L. Poirier, Y. Cloutier, and G. Gingras, *Biochemistry*, **18**, 4301 (1979).

12) S. Okayama, T. Kakuno, and T. Horio, *J. Biochem.*, **68**, 19 (1970).

13) S. Kaplan and C. J. Arntzen, "Photosynthesis," ed by Govindjee, Academic Press, New York (1982), Vol. 1, p. 100.

Selective Potential Response of a Poly(*N*,*N*-dimethylaniline)/ Poly(*o*-chloroaniline) Dual-Layer Coated Electrode to Dissolved Iodide Ions

Jun YANO
Department of Chemistry, Faculty of Education, Yamanashi University, Kofu, Yamanashi 400
(Received Octover 29, 1990)

Poly(*N*,*N*-dimethylaniline) (PDA) was easily obtained by an anodic oxidation of *N*,*N*-dimethylaniline in acidic media. PDA is a semiconductor having positively charged sites as quaternary ammonium groups in its polymeric backbone. It was possible for a PDA-film coated electrode to incorporate I^- electrostatically; I^- in the film was then oxidized electrochemically. Further, the oxidized products of I^- still remained in the film. Although the electrode responded to dissolved I^- potentiometrically, the response was disturbed by the presence of other redox species. On the other hand, poly(*o*-chloroaniline) (PCA) was also easily prepared by the electro-oxidation of *o*-chloroaniline in acidic solutions. On a PCA-film coated electrode, only the redox wave of I_2/I^- was observed, though PCA, itself, was electroinactive. In other words, the PCA film responded to I^- selectively. The dual-layer (a PDA film incorporated oxidized products of I^- and PCA film) showed a selective Nernstian response to dissolved I^-.

Polyaniline, which is now a familiar conducting polymer, is easily obtained by anodic oxidation of aniline in acidic media. If the anodic oxidation of aniline derivatives, instead of aniline, also gave electroactive conducting polymers, they would have unique properties other than polyaniline. We have already examined the possibility of forming functional polymer films onto Pt electrodes by anodic oxidation.[1] The products of electro-oxidation were classified as follows: (1) deposition of an electroactive polymer film which shows a redox wave of polymer, itself; (2) deposition of an electroactive polymer film which does not show any redox wave of the polymer, itself; (3) formation of soluble products not adhering to an electrode surface; and (4) deposition of an electroinactive polymer film.

The only polymer that belongs to group (2) is poly(*N*,*N*-dimethylaniline) (PDA). PDA can incorporate anionic redox species electrostatically due to its structure, having positively charged sites as quaternary ammonium groups in the polymeric backbone.[2] This means that the PDA-film coated electrodes which incorporate certain oxidized (reduced) products have a potentiometric response to the corresponding dissolved reduced (oxidized) species. For example, a PDA film which incorporates oxidized products of I^- is sure to respond to dissolved I^- potentiometrically. Unfortunately, the response must be disturbed by the presence of other redox species, because PDA is itself conducting.

Only the redox wave of I_2/I^- was obviously observed on some of the polymer films of group (4) described above, although the films were not expected to have any useful functions.[3-5] In other words, those polymer films responded to only I^-, though they were electroinactive. The author would like to employ poly(*o*-chloroaniline) (PCA) here as a representative of group (4).

If a polymer-coated electrode responds to a certain dissolved ion selectively, it would be useful in various fields as a new type of ion sensor. Such a sensor would also have some advantage compared with conventional ion-selective electrodes, particularly regarding miniaturization. There have, however, not been many studies on polymer-coated electrodes used for such sensors. Ohnuki et al. reported that selective film permeation of H^+, Br^-, and Fe^{2+} has been observed in a few polymer-coated electrodes.[6] The electrodes probably act as amperometric sensors for them. On the other hand, a poly(*o*-phenylenediamine)-coated electrode may be applicable to voltammetric pH measurements.[7,8] In studies up to now, the kinds of dissolved ions to be measured (coating polymer materials and so on) have been limited. In this paper the author describes the unique potentiometric sensor of dissolved I^- using the PDA/PCA dual-layer coated electrode.

Experimental

For an electrochemical cell a standard three-electrode system was used for all electrolyses. In measurements of cyclic voltammograms, a platinum wire having a geometry of 1 mm in diameter and 10 mm in length (area=ca. 0.3 cm^2) was employed as the working electrode. In preparing PDA samples for elemental analysis, the electrode substrate used was a platinum plate having a surface area of ca. 8 cm^2. The counter electrode was either a platinum wire or a platinum plate. The reference electrode was a saturated calomel electrode (SCE). The platinum electrodes were treated with 6 M (1 M=1 mol dm^{-3}) HNO_3 and polarized by repeated potential cycling between −0.2 and 1.2 V vs. SCE in 0.1 M H_2SO_4. The electrodes showed the well-known redox waves of platinum. Measurements were carried out with a potentiostat/galvanostat (Model HA-301, Hokuto Denko Co., Ltd.) with a function generator (Model HB-104, Hokuto Denko Co., Ltd.) and an X-Y recorder (Model RW-21, Rikadenki Co., Ltd.).

N,*N*-dimethylaniline and *o*-chloroaniline (Tokyo Kasei Co., Ltd.) were used after distilling under reduced pressure. Other chemicals were of reagent grade and used as received. All of the aqueous solutions were prepared with doubly distilled deionized water.

In order to examine whether dissolved I^- permeates through a PDA film, a technique using a rotating disk electrode (RDE) was employed. Measurements were carried out using an RDE-measuring system (Model HR-103A, Hokuto Denko Co., Ltd.). A platinum disk of 5.0 mm diameter (area=ca. 0.196 cm^2) was used as the working electrode. Prior to use, it was polished and then polarized by repeated potential cycling between −0.2 and 1.2 V vs. SCE in 0.1 M H_2SO_4. A platinum plate (area=ca. 8 cm^2) was used as the counter electrode and an SCE was also used as the reference electrode.

Elemental analyses of carbon, hydrogen, and nitrogen were carried out with a Perkin-Elmer 240-C. Those of chlorine and iodine were carried out by the following method. The PDA samples were subjected to perfect combustion; the gases produced were absorbed in water and the amounts of chlorine and iodine in the aqueous solution determined by ion chromatography (Dionex 2000-I). Procedures for the preparation of the polymer-film coated electrodes are described in more detail in the Results and Discussion sections. All experiments were carried out at room temperature.

Results and Discussion

Preparation of PDA-Film and PCA-Film Coated Electrodes. PDA and PCA films were formed onto platinum electrodes using the same type electrolysis methods as were described in a previous paper,[1] except that the electrolytic solutions were 1.0 M HCl containing 0.5 M respective monomers. Cyclic voltammograms of the film-forming process of PDA onto a platinum electrode are shown in Fig. 1 (a). During the first positive sweep monomeric *N,N*-dimethylaniline was oxidized, exhibiting a distinct irreversible current peak at about 0.85 V. As soon as this peak current flowed, red powdery products were observed near the electrode surface. The products continued to diffuse from the surface to the bulk, while potential cycling was repeated. After about 100 cycles, however, deposition of a brown film on the electrode surface was clearly seen. The potential cycling was further continued for up to 300 cycles in preparation of the PDA-film coated electrode.

Redox peaks at ca. 0.55 V were observed until about the fiftieth cycle. The peaks corresponded to the *N,N,N',N'*-tetramethylbenzidine/the quinone diimine redox pair.[9-11] In Fig. 1 (a), the two anodic peak potentials shift more positively, and cathodic one more negatively, as the number of cycles increases. This is probably due to an *iR* drop of the growing PDA film. In fact, the conductivity of PDA in the dry state was determined to be 6.2×10^{-6} S cm^{-1} by the four-point probe method.[3]

Figure 1 (b) shows cyclic voltammograms for a coating process of the PCA film onto a platinum electrode. The anodic peak current for the oxidation of *o*-chloroaniline diminishes immediately during the first five cycles. This means that the resulting PCA film is electroinactive and quite an insulator.

The morphologies of the PCA films and the PDA films on platinum electrodes were observed using a scanning electron microscope (SEM). The PCA film

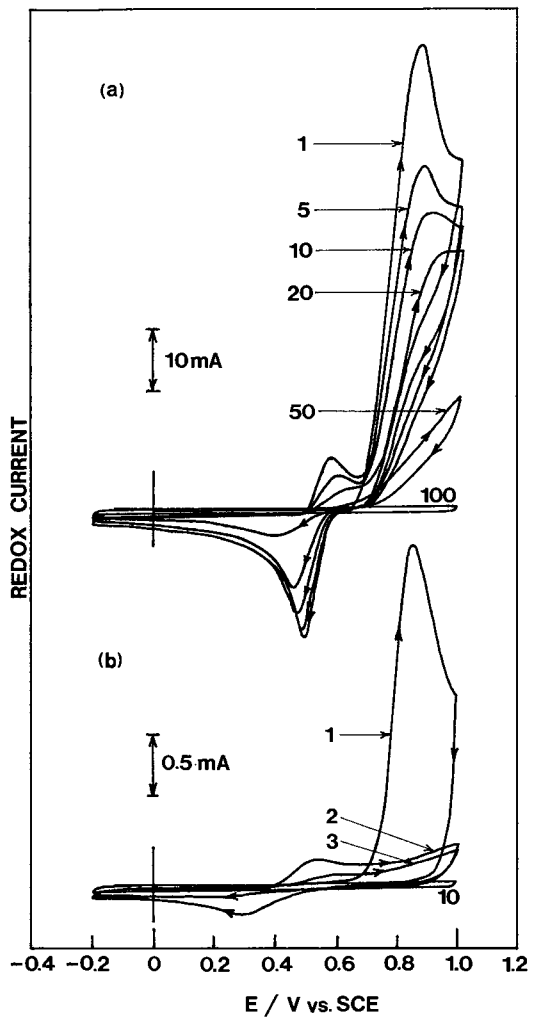

Fig. 1. (a) Cyclic voltammograms in the film forming process of poly(*N,N*-dimethylaniline) (PDA). Sweep rate: 50 mV s^{-1}, Solution: 0.5 M *N,N*-dimethylaniline+1.0 M HCl, Electrode area: 0.307 cm^2. (b) Cyclic voltammograms in the film forming process of poly(*o*-chloroaniline) (PCA). Sweep rate: 50 mV s^{-1}, Solution: 0.5 M *o*-chloroaniline+1.0 M HCl, Electrode area: 0.311 cm^2. Numbers in the figure indicate the number of potential cycles.

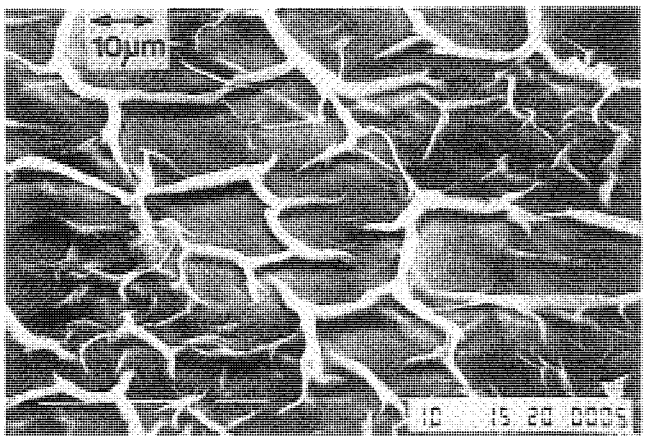

Fig. 2. Scanning electron microphotograph of the surface of the PDA film.

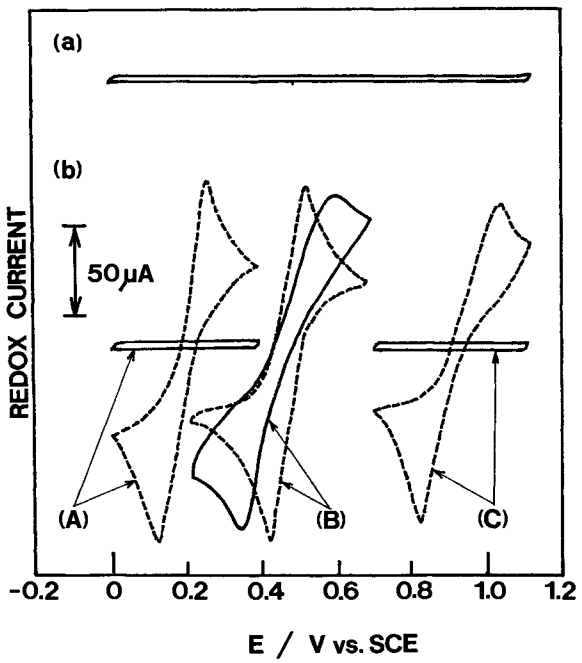

Fig. 3. (a) Voltammogram showing the electroactivity of the PCA film itself in an acetate buffer solution (pH 3.5). Sweep rate: 20 mV s^{-1}. (b) Voltammograms for the redox reactions of $[Fe(CN)_6]^{3-}/[Fe(CN)_6]^{4-}$ (A), I_2/I^- (B), and Br_2/Br^- (C) at both a bare platinum electrode (broken line) and the PCA-film coated electrode (solid line). Concentration of the species: $[Fe(CN)_6^{4-}]$=4 mM, $[I^-]=[Br^-]$=2 mM, Supporting electrolyte: acetate buffer solution (pH 3.5), Sweep rate: 20 mV s^{-1}.

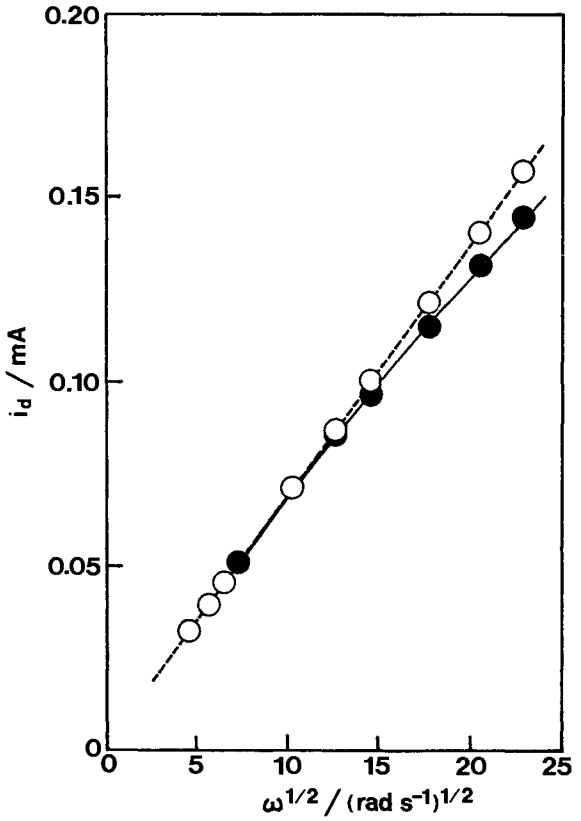

Fig. 4. Plots of the limiting anodic current (i_d) versus the square root of the rotation rate ($\omega^{1/2}$) for the electro-oxidation of dissolved I^- on the PCA-film coated platinum disk electrode (solid line) and a bare platinum disk electrode (broken line). Solution: 0.1 M H_2SO_4 containing 10 mM KI.

had a featureless smooth surface. Figure 2 shows a typical morphology of the PDA films. In contrast to the PCA film, it is interesting to clearly observe defined fibrils on a compact microspheroid underlayer of the polymer. The fibril diameter (ca. 3 μm) is greater than that found in polyaniline (ca. 1 μm).[12] In addition, the dry film thickness of PCA and PDA was determined to be ca. 6 μm and 15 μm, respectively, from observations of the cross-sectional morphologies of the films.

Redox Reactions of Dissolved Species on the PCA-Film Coated Electrode. Figure 3 (b) shows voltammograms for the redox reactions of Br_2/Br^-, I_2/I^-, and $[Fe(CN)_6]^{3-}/[Fe(CN)_6]^{4-}$ at both a naked platinum electrode and the PCA-film coated electrode. Although the PCA film is itself electroinactive (see Fig. 3 (a)), the redox wave of only the I_2/I^- is evident. In addition, the PCA-film coated electrode gave no redox waves for Fe^{3+}/Fe^{2+}, *o*-quinone/catechol, *p*-quinone/hydroquinone, MnO_2/Mn^{2+}, and Tl^{3+}/Tl^+.

Insulator-film coated electrodes do not respond to dissolved species unless the films are permeable. The PCA film is probably permeable to dissolved I^- since it is an insulator.[3] In order to confirm this, the RDE voltammograms for the oxidation of dissolved I^- were measured with both the PCA-film coated disk electrode and a naked platinum disk electrode. The PCA-film coated electrode was prepared by the same type electrolysis described in Fig. 1 (b). The limiting anodic current (i_d) vs. the square root of the rotation rate ($\omega^{1/2}$) plots obtained are shown in Fig. 4. Deviations of i_d for a PCA-film coated electrode from a linear Levich line obtained with a naked platinum electrode gradually increase with the rotation rate, in particular when $\omega^{1/2}>44.7$ $(rpm)^{1/2}$. This is evidence that the PCA film is permeable to dissolved I^-.[13] Therefore, in the selective response of the PCA-film coated electrode, the charge transfer is caused by the following mechanism. Dissolved I^- permeates through the film selectively and is then electro-oxidized on the platinum substrate.

Redox Reactions of Dissolved Species on the PDA-Film Coated Electrode. Most organic conduting polymers, such as polyaniline, have a redox activity; nonconducting polymers do not show such activity. Practically, a PCA film which has no redox activity is nonconducting and electroinative to dissolved species, except for I^- which can permeate the film. The PDA film also produces no redox waves originating from redox reactions of the film, itself (Fig. 5 (a)).[1] However, a marked difference of PDA film is that the film, itself, is

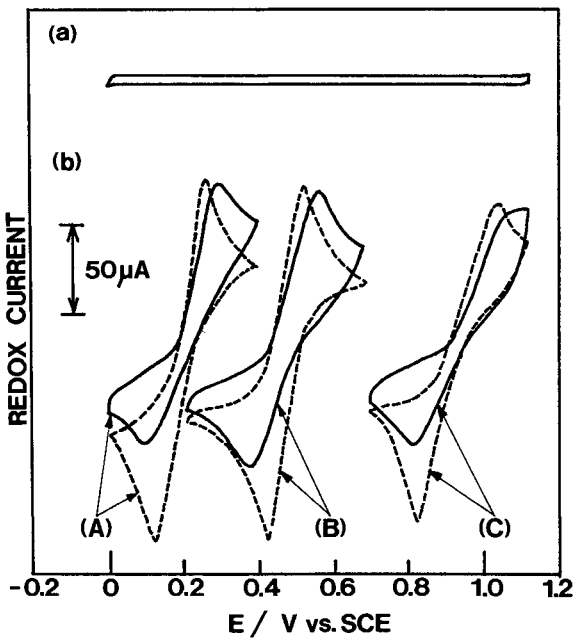

Fig. 5. (a) Voltammogram showing the electroactivity of the PDA film itself in the acetate buffer solution (pH 3.5). Sweep rate: 20 mV s^{-1}. (b) Voltammograms for the redox reactions of $[Fe(CN)_6]^{3-}/[Fe(CN)_6]^{4-}$ (A), I_2/I^- (B), and Br_2/Br^- (C) at both a bare platinum electrode (broken line) and the PDA-film coated electrode (solid line). Concentration of the species: $[Fe(CN)_6^{4-}]$=4 mM, $[I^-]=[Br^-]$=2 mM, Supporting electrolyte: acetate buffer solution (pH 3.5), Sweep rate: 20 mV s^{-1}.

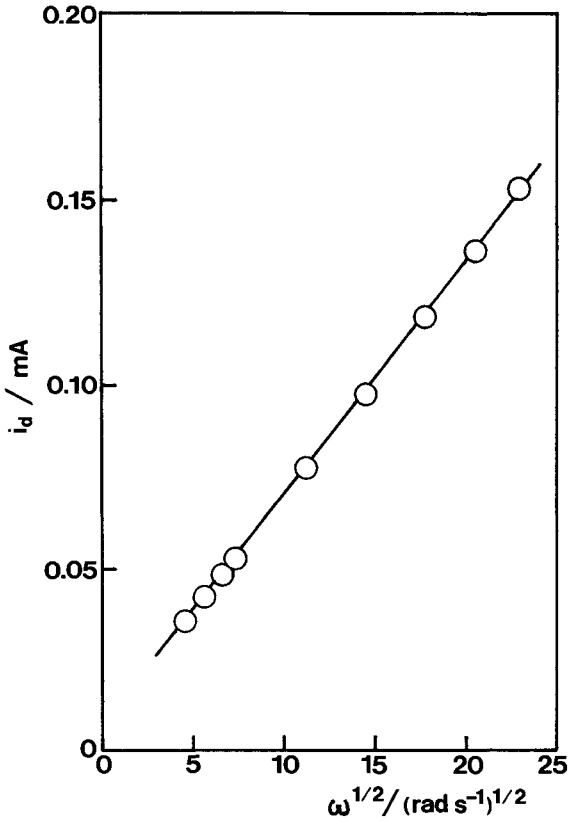

Fig. 6. Levich plots ($\omega^{1/2}$—i_d plots) for the electro-oxidation of dissolved I^- on the PDA-film coated platinum disk electrode. Solution: 0.1 M H_2SO_4 containing 10 mM KI.

electrically conducting.[3] Therefore, a PDA-film coated electrodes is expected to be active towards the electrode reactions of dissolved species. Figure 5 (b) shows voltammograms for the redox reactions of Br_2/Br^-, I_2/I^-, and $[Fe(CN)_6]^{3-}/[Fe(CN)_6]^{4-}$ at both a naked platinum electrode and the PDA-film coated electrode. Although the reversibility of the redox reactions is somewhat poor, compared with that of naked platinum, the PDA film does respond to redox couples. Another characteristics of the PDA film is that the cathodic current of the redox couples is always suppressed with this electrode. A similar behavior was also observed with MnO_2/Mn^{2+}, Tl^{3}/Tl^{+}, Fe^{3+}/Fe^{2+}, *p*-quinone/hydroquinone, and *o*-quinone/catechol. Judging from the conductivity, the PDA film is a typical semiconductor. Suppression of the cathodic current may be correlated, at least in part, to a rectification effect of a *p*-type semiconductor. A polyaniline-film coated electrode is active to dissolved redox species only in the limited potential range where polyaniline, itself, is electroactive.[14] The PDA-film coated electrode has no such limitation. The oxidation peaks of Br^-, Mn^{2+}, and Tl^+ were clearly observed with the PDA-film coated electrode, while the polyaniline-film coated electrode was found to be inactive to these species. A nonconducting polyaniline film, which exhibits no redox wave of polymer, itself, shows a limited response towards the redox reactions of dissolved species.[6] The electrochemical response for such a case was observed only for relatively small ions which can permeate through the film. On the other hand, the PDA-film coated electrode was found to be electroactive to all dissolved species studied, regardless of their size and redox potentials.

In order to examine whether the PDA film is permeable to dissolved species in the redox reactions or not, the RDE technique was employed. An iodide ion was used here as being representative of dissolved species. A PDA-film coated disk electrode was prepared by the same type electrolysis process as shown in Fig. 1 (a). By using this electrode, voltammograms for the oxidation of dissolved I^- were measured at different rotation rates from 200 to 5000 rpm. A Levich plot obtained from the voltammograms is shown in Fig. 6. The limiting anodic current is proportional to the square root of the rotation rate, as can readily be seen in Fig. 6. If dissolved species permeate through polymer films and then electro-oxidized on the electrode substrate, Levich plots do not give a straight line.[13] The proportionality shown in Fig. 6 means that such a permeation does not occur; in other words, it is not on the electrode substrate, but on the PDA film that the electro-oxidation

of I^- takes place.

A polyaniline-film coated electrode is useful only within a limited pH range.[15] For example, the redox wave of $[Fe(CN)_6]^{3-}/[Fe(CN)_6]^{4-}$ is not observed in neutral or alkaline solutions (pH>4). As long as the redox reaction of the $[Fe(CN)_6]^{3-}/[Fe(CN)_6]^{4-}$ couple is concerned, the PDA-film coated electrode gave a constant electrochemical response over the entire pH range studied (pH 1—13).

Incorporation of Anionic Redox Species into the PDA Films on Platinum Electrodes. The mechanism of electropolymerization of *N,N*-dimethylanilne has yet not been clarified. Various coupling patterns, such as para–para coupling[9] and ortho–para coupling,[11] have been reported. In any case, the resulting PDA films have structures with positively charged sites as quaternary ammonium groups in their polymeric backbones (Fig. 7).

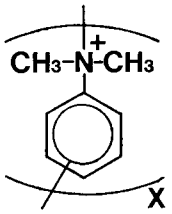

Fig. 7. Possible molecular structure of PDA.

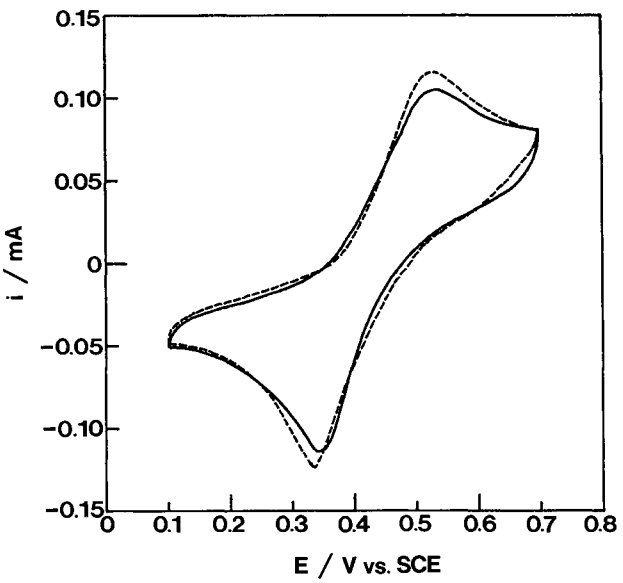

Fig. 8. Redox wave of the I^- incorporated into the PDA film. The broken line indicates the redox wave before the water immersion of one day (see text).

PDA film can incorporate $[Fe(CN)_6]^{4-}$ due to its structure (Fig. 7).[2] Several other multiply-charged anionic redox species can also be incorporated into the PDA film.[16] In order to confirm that the PDA film can incorporate dissolved I^-, the following was carried out. A PDA-film coated electrode was prepared by the same electrolysis method as shown in Fig. 1 (a). After rinsing the deposited PDA layer with water the electrode was immersed in 0.1 M KI aqueous solution for ten minutes.[17] The electrode was rinsed again and then transferred into water for one day. A cyclic voltammogram of the electrode measured in 0.1 M H_2SO_4 is shown in Fig. 8. The redox wave of the I^- incorporated in the film is evident, though the redox charge decreases slightly with water immersion. In this case, the amount of the I^- incorporated in the film was roughly evaluated to be 2.5×10^{-8} mol cm^{-2} by a graphical integration of the voltammogram.

The amounts of Cl^- and I^- ions incorporated into the PDA films were determined by elemental analysis of PDA. Three PDA samples were prepared for this purpose. The first sample (Sample 1) was an original PDA film which was prepared by the electro-oxidation of 1.0 M HCl containing 0.5 M *N,N*-dimethylaniline under continuous potential cycling in the range from −0.2 to 1.0 V on the SCE scale. The second sample (Sample 2) was basically the same as Sample 1, but was immersed in a 1 mM KI aqueous solution for one day. The third sample (Sample 3) was also the same as Sample 1, but was immersed in a 1 mM I_2 aqueous solution for one day. All of the samples were scratched off from the electrode substrate and washed with water sufficiently. They were dried in vacuo at 50 °C for 12 h and subjected to elemental analysis. The obtained results are summarized in Table 1. Although the data lack precise consistency, it is undoubted that the PDA film has anion exchangeability. The original PDA film (Sample 1), which was analysed just after preparation in a 1.0 M HCl solution, contained Cl^- ions with an atomic ratio of roughly 0.6 with respect to the nitrogen content. Hand and Nelson have reported that the electro-oxidation of *N,N*-dimethylaniline gives such secondary amines as *N*-(*p*-dimethylaminobenzyl)-*N*-methylaniline, as well as *N,N*-dimethylanilines.[18] The atomic ratio

Table 1. Elemental Composition of PDA

Sample	Treatment	Elemental composition				
		C	H	N	Cl	I
1	As prepared in HCl[a]	8	10.79	1.07	0.61	
2	1 was immersed in a KI solution[a]	8	10.34	1.06	0.02	0.58
3	1 was immersed in an I_2 solution[a]	8	12.62	1.04	0.43	0.20

a) For details, see text.

being less than unity is probably due to the presence of tertiary amino groups in the polymeric backbone. The data from Sample 2 is evidence regarding the anion exchangeability of the PDA film. The Cl^- ions in the PDA film are almost replaced by I^- ions after immersing the film in a KI aqueous solution, although only a few Cl^- ions still remain. It is noteworthy that not only I^-, but also I_2, which is electroneutral, is incorporated into the PDA film (see the data of Sample 3).

Selective Potential Response of a PDA/PCA Dual-Layer Coated Electrode to Dissolved Iodide Ions. As described previously, dissolved I^- can be incorporated in a PDA-film coated electrode and then electro-oxidized to generate oxidized products of I^-. If these products still remain in the electrode, the electrode will show a potentiometric response to dissolved I^-. Further, if the electrode responds to only I^- by coating the PDA layer with a PCA layer, it is applicable to potentiometric sensing of dissolved I^-.

The PDA/PCA dual-layer coated electrode for potentiometric sensing of I^- was prepared by means of the following. Initially, a PDA-film coated electrode was prepared under the same electrolytic condition as shown in Fig. 1 (a). After adequate rinsing of the electrode with water, the electrode was immersed in an aqueous 0.1 M KI solution for ten minutes. Coating of the PCA film on the electrode was next performed under the same conditions as shown in Fig. 1 (b). The PDA/PCA dual-layer coated electrode obtained was finally held at 0.7 V vs. SCE for five minutes in 0.1 M H_2SO_4 to change the incorporated I^- into its oxidized products. Figure 9 (a) shows the potential response of a bare platinum electrode, a PDA-film coated, and a PDA/PCA dual-layer coated electrode to dissolved I^-. Both the PDA-film coated electrode and the PDA/PCA dual-layer coated electrode have a Nernstian response to I^-, with the slope of -56 mV/log[I^-]. This potential response is evidence that the oxidized products of I^- still remain in the PDA layer. The products seem to be I_2 and a little I_3^-, judging from the slope.

Figure 9 (b) shows the effect of interfering substances on the potential response. The interfering substance in this case is the redox pair of $[Fe(CN)_6]^{3-}/[Fe(CN)_6]^{4-}$. The PDA/PCA dual-layer coated electrode obviously has the potential response, while the PDA-film coated electrode itself without the PCA-layer coating has no such response. The response of the PDA/PCA dual-layer

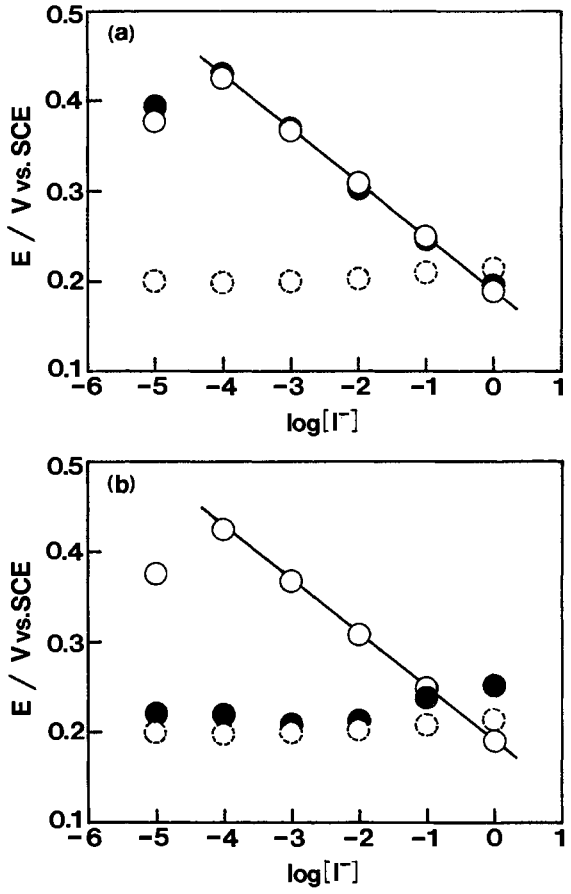

Fig. 9. (a) Potential response of a bare platinum electrode (○), the PDA-film coated electrode (●), and the PDA/PCA dual-layer coated electrode (○) with changes in log[I^-] from -5 to 0. Solution: acetate buffer solutions containing KI (pH 3.5). The response time of the PDA-film coated electrode and the PDA/PCA dual-layer coated electrode were less than ten seconds. (b) Effect of interfering substance on the potential response of (a). The interfering substance was the redox pair of $[Fe(CN)_6]^{4-}/[Fe(CN)_6]^{3-}$. Solution: acetate buffer solutions containing not only KI but also 10 mM $K_4[Fe(CN)_6]$ and $K_3[Fe(CN)_6]$.

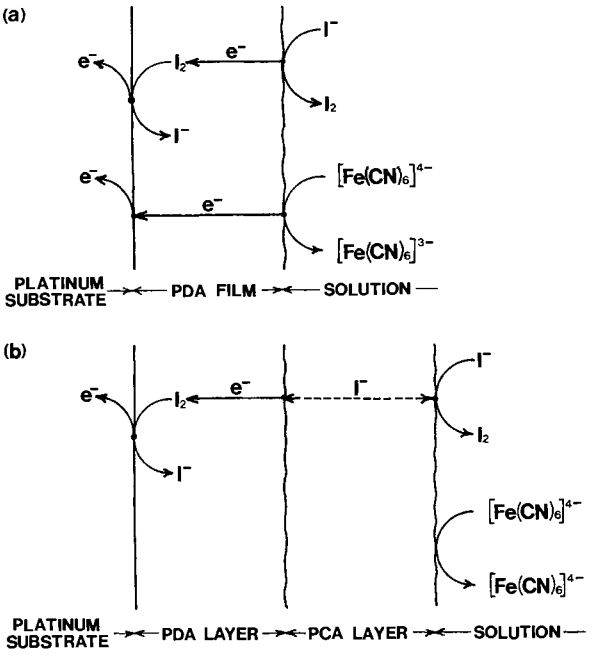

Fig. 10. Schematic depiction of the response mechanisms of dissolved I^- on the PDA-film coated electrode (a) and the PDA/PCA dual-layer coated electrode (b).

coated electrode was not disturbed by the presence of Fe^{3+}/Fe^{2+}, *p*-quinone/hydroquinone, and $Fe(edta)^-/Fe(edta)^{2-}$ and by a change of the solution pH, although they are not illustrated in Fig. 9 (b).

Figure 10 is a schematic depiction explaining how a PDA-film coated electrode and a PDA/PCA dual-layer coated electrode respond to dissolved I^-. In the case of the PDA-film coated electrode, the charge transfer between the oxidized products of I^- in the film and dissolved I^- can occur spontaneously. The oxidized product is regarded as being I_2 in this case. Consequently, the electrode has a Nernstian response to dissolved I^-. The reason why the electrode, itself, does not have a selective potential response is that the PDA film is electrically conducting, as is the electrode substrate. Charge transfer between other redox couples, such as $[Fe(CN)_6]^{3-}/[Fe(CN)_6]^{4-}$, takes place on the electrode as well, and the response of I^- is disturbed (Fig. 10 (a)). This disturbance can be repressed by a coating with a PCA layer. The PCA layer blocks the permeation of other dissolved species than I^-. As a result, the PDA/PCA dual-layer coated electrode shows a selective potential response to dissolved I^- (Fig. 10 (b)). For $[I^-]<10^{-5}$ M, it does not give a response anymore. However, this limitation might be improved by changing the amount of oxidized products of I^- in the PDA layer, the thickness of the respective layers, and so on.

The author thanks Dr. Akira Kitani and Dr. Kazuo Sasaki, Hiroshima University, for letting him use an RDE-measuring system. This work was partly supported by a grant from the Casio Science Promotion Foundation.

References

1) J. Yano, A. Kitani, R. E. Vasquez, and K. Sasaki, *Nippon Kagaku Kaishi*, **1985**, 1124.
2) A. Kitani, J. Yano, and K. Sasaki, *Chem. Lett.*, **1984**, 1565.
3) J. Yano and T. Tanaka, *Chem. Lett.*, **1988**, 1943.
4) J. Yano and T. Tanaka, *Denki Kagaku*, **57**, 744 (1989).
5) J. Yano, *J. Electrochem. Soc.*, **138**, 455 (1991).
6) Y. Ohnuki, H. Matsuda, T. Ohsaka, and N. Oyama, *J. Electroanal. Chem.*, **158**, 55 (1983).
7) W. R. Heineman, H. J. Wieck, and A. M. Yacynych, *Anal. Chem.*, **52**, 345 (1980).
8) I. Rubinstein, *Anal. Chem.*, **56**, 1135 (1984).
9) T. Mizoguchi and R. N. Adams, *J. Am. Chem. Soc.*, **84**, 2058 (1962).
10) Z. Galus and R. N. Adams, *J. Am. Chem. Soc.*, **84**, 2061 (1962).
11) Z. Galus, R. M. White, F. S. Rowland, and R. N. Adams, *J. Am. Chem. Soc.*, **84**, 2065 (1962).
12) A. Kitani, M. Kaya, S. Tsujioka, and K. Sasaki, *J. Polym. Sci., Part A*, **26**, 1531 (1988).
13) D. A. Gough and J. K. Leypoldt, *Anal. Chem.*, **51**, 439 (1979).
14) N. Oyama, Y. Ohnuki, K. Chiba, and T. Ohsaka, *Chem. Lett.*, **1983**, 1759.
15) A. Kitani, J. Izumi, J. Yano, Y. Hiromoto, and K. Sasaki, *Bull. Chem. Soc. Jpn.*, **57**, 2254 (1984).
16) T. Ohsaka, T. Okajima, and N. Oyama, *J. Electroanal. Chem.*, **200**, 159 (1986).
17) The author tested the relationship between the amount of I^- in the film and the immersion time, so that the I^- ions were incorporated sufficiently as long as the immersion time was more than five minutes.
18) R. Hand and R. F. Nelson, *J. Electrochem. Soc.*, **117**, 1353 (1970).

 © 1991 The Chemical Society of Japan Bull. Chem. Soc. Jpn., 64, 1497—1508 (1991)

On the Facilitation Effect of Neutral Macrocyclic Ligands on the Ion Transfer across the Interface between Aqueous and Organic Solutions. I. Theoretical Equation of Ion-Transfer-Polarographic Current-Potential Curves and Its Experimental Verification

Hiroaki MATSUDA,* Yutaka YAMADA, Kazuo KANAMORI, Yoshihiro KUDO, and Yasuyuki TAKEDA
Department of Chemistry, Faculty of Science, Chiba University, Yayoi-cho 1-33, Chiba 260
(Received November 29, 1990)

A theoretical equation of the reversible polarographic current-potential curves for the ion transfer across the aqueous/organic interface facilitated by the neutral macrocyclic ligand present in the o-phase is derived without any limitation on the magnitude of distribution constant of the ligand. In two limiting cases, which have been employed in common experimental practice, i.e., (A) the bulk concentration of cation, c^*_M, in the aqueous phase $\gg$ that of ligand, c^*_L, in the organic phase and (B) the reverse condition, $c^*_M \ll c^*_L$, the equation of current-potential curves becomes the same in form as that of reversible D. C. polarographic waves. It is shown that the limiting current is controlled by diffusion of ligand in the organic phase for (A) and of cation in the aqueous phase for (B) and, on the other hand, the half-wave potential depends on c^*_M for (A) and on c^*_L for (B). Furthermore, an analysis method to determine the complex formation constants in the organic phase (and in the aqueous phase for favorable cases) from the concentration dependence of the half-wave potential is presented. The theoretical predictions are verified experimentally using dibenzo-18-crown-6 and 18-crown-6 as macrocyclic ligands and sodium, cesium, barium, and oxonium ions as transferred cations.

Natural and synthetic macrocyclic compounds, such as valinomysin, nonactin, and various crown ethers, are known to form selectively stable complexes with a variety of cations, especially alkali and alkaline-earth metal ions, by holding a cation in their central cavity, and then to allow the cation to be transferred from the aqueous phase (w-phase) into the organic phase (o-phase), because of the hydrophobic outer envelope of the complexes thus produced. This function of macrocyclic ligands has stimulated a great deal of interest in various branches of chemistry and biology. Potential applications have been made in liquid membrane ion-selective electrode and in making specific separations by solvent extraction and membrane transport methods. Liquid membrane containing macrocyclic compounds have also been recognized as a good model of the selective and up-hill ion transport through biological membranes.

In recent years, electrochemical methods have been employed for studies on the ion transfer across the water/nitrobenzene or water/1,2-dichloroethane interface facilitated by various natural and synthetic macrocyclic ligands. The studies done with electrochemical methods have been thoroughly reviewed by Koryta.[1-3] However, all the macrocyclic ligands hitherto employed have had large values of the distribution constant. Hence, it has been assumed that the ligands added to the o-phase cannot penetrate the w/o-interface and thus does not exist in the w-phase. Highly lipophilic crown ethers such as dibenzo-18-crown-6 (DB18C6) and its substituted derivatives have been used very frequently as the neutral carriers in ion-selective electrodes and in membrane transport experiments. On the other hand, unsubstituted crown ethers such as 15-crown-5 and 18-crown-6 (18C6), of which the distribution constants are relatively small, have been used for elucidating the behavior of crown ether complexes in the w-phase.

In the present paper, taking into account the above circumstances, we shall derive a theoretical equation of current–potential curves for the ion transfer across the w/o-interface facilitated by neutral macrocyclic ligands, without any limitation on the magnitude of distribution constant of the ligands. Then, the theoretical predictions obtained will be verified experimentally, using the ion-transfer-polarographic method with the electrolyte dropping electrode.[1]

Theory

In deriving a general equation of current-potential curves expressing the facilitation effect of neutral macrocyclic ligands on the ion transfer across the interface of the water drop growing into the organic solution, we shall make the following assumptions:

(i) The expanding plane model, which has been used as a good mathematical model for the dropping mercury electrode in polarography, is employed here for the moving interface between the water drop (w-phase) and the organic solution (o-phase). Then, the w/o-interface is taken as the origin of coordinates (x=0) and the w- and o-phases are placed in the regions: $-\infty \leqslant x \leqslant 0$ and $0 \leqslant x \leqslant +\infty$, respectively.

(ii) The complete dissociation of electrolytes present both in the w- and the o-phase is assumed for the sake of simplicity. Any effect of ion pair formation can be neglected.

(iii) At the beginning of the drop growth, the w-phase contains only the relevant metal ion M^{z+} at the uniform concentration $c_M{}^*$, except for indifferent electrolytes to be added if necessary, while the o-phase con-

tains the neutral macrocyclic ligand L at the uniform concentration c_L^* and an indifferent electrolyte.

(iv) Only the 1:1 complex ML^{z+} is formed in both phases. The rates of the complex formation and dissociation processes are sufficiently large in comparison with the corresponding diffusion rates, so that it may be assumed that the complex formation and dissociation are at equilibrium even when current is flowing. Then we have

$$\beta_1^\alpha = c_{ML}^\alpha / c_M^\alpha c_L^\alpha \quad (\alpha = w, o) \tag{1}$$

where c_j^α and β_1^α denote the concentration of the species j (j=M, L, ML) and the over-all formation constant of ML^{z+} in the α-phase, respectively.

An extention to the more general case, in which a series of complexes, such as 1:1, 1:2,···, 1:n complexes, are formed under the presence of a large excess of the ligand in the o-phase, will be treated in a later section.

(v) The rates of transfer of all relevant species across the w/o-interface are sufficiently large in comparison with the corresponding diffusion rates,[4] so that the interfacial concentrations of all species in question satisfy the equilibrium relations, even when current is flowing. For the electrostatically neutral species L, we have

$$K_D = (c_L^o)_{x=0} / (c_L^w)_{x=0} \tag{2}$$

K_D denotes the distribution constant of L, which is assumed to be independent of the potential difference $\Delta\phi = \phi^w - \phi^o$ at the w/o-interface, where ϕ^α is the inner potential of the α-phase. On the other hand, the distribution constants of the charged species M^{z+} and ML^{z+} may depend on the potential difference and their potential dependence is assumed to be governed by the Nernst equation. Thus we have

$$\exp(\zeta'_M) = (c_M^o)_{x=0} / (c_M^w)_{x=0} \tag{3}$$

$$\exp(\zeta'_{ML}) = (c_{ML}^o)_{x=0} / (c_{ML}^w)_{x=0} \tag{4}$$

with

$$\zeta'_M = (zF/RT)(\Delta\phi - \Delta\phi^{o\prime}_M) \tag{5}$$

$$\zeta'_{ML} = (zF/RT)(\Delta\phi - \Delta\phi^{o\prime}_{ML}) \tag{6}$$

where $\Delta\phi_j^{o\prime}$ is termed the formal potential of the species j for the ion transfer across the w/o-interface. Frequently, the following stoichiometric equation is employed for the facilitated ion trasfer across the w/o-interface:

$$M^{z+}(\text{w-phase}) + L(\text{o-phase}) \rightleftharpoons ML^{z+}(\text{o-phase}) \tag{7}$$

For this process the Nernst equation may be written as

$$\exp(\zeta'_{M/ML}) = (c_{ML}^o)_{x=0} / (c_M^w)_{x=0} (c_L^o)_{x=0} \tag{8}$$

with

$$\zeta'_{M/ML} = (zF/RT)(\Delta\phi - \Delta\phi^{o\prime}_{M/ML}), \tag{9}$$

where $\Delta\phi^{o\prime}_{M/ML}$ denotes the formal potential of the process expressed by Eq. 7. Taking into consideration the relations expressed by Eqs. 1—6, we can readily verify that the following relations hold among $\Delta\phi^{o\prime}_M$, $\Delta\phi^{o\prime}_{ML}$ and $\Delta\phi^{o\prime}_{M/ML}$:

$$\Delta\phi^{o\prime}_{ML} = \Delta\phi^{o\prime}_M - (RT/zF)\ln(K_D\beta_1^o/\beta_1^w) \tag{10}$$

$$\begin{aligned}\Delta\phi^{o\prime}_{M/ML} &= \Delta\phi^{o\prime}_M - (RT/zF)\ln\beta_1^o \\ &= \Delta\phi^{o\prime}_{ML} - (RT/zF)\ln(K_D/\beta_1^w)\end{aligned} \tag{11}$$

(vi) For simplicity we assume that the diffusion coefficients of relevant species in the α-phase (α=w, o) have the common value D^α.

(vii) Any interfacial excess of the relevant species, due to adsorption etc., is assumed to be absent at the w/o-interface.

Under the assumptions (i)—(vii) described above, the boundary value problem for the diffusion processes of the species M^{z+}, L and ML^{z+} can be formulated, as follows:

$$\mathscr{D}^\alpha c_M^\alpha = R_1^\alpha \tag{12}$$

$$\mathscr{D}^\alpha c_L^\alpha = R_1^\alpha \tag{13}$$

$$\mathscr{D}^\alpha c_{ML}^\alpha = -R_1^\alpha \quad (\alpha = w, o) \tag{14}$$

with

$$R_1^\alpha = k_1^\alpha (c_{ML}^\alpha - \beta_1^\alpha c_M^\alpha c_L^\alpha) \tag{15}$$

where the diffusion operator for the expanding plane model, $\mathscr{D}^\alpha$, defined by

$$\mathscr{D}^\alpha = \partial/\partial t - D^\alpha \partial^2/\partial x^2 - (2x/3t)\partial/\partial x, \tag{16}$$

is employed for simplicity of description and k_1 denotes the rate constant of the dissociation process of ML^{z+}. The initial and boundary conditions are derived from the assumptions (iii), (vi), and (vii), as follows:

$$t = 0 : \left\{ \begin{array}{llll} c_M^w = c_M^*, & c_L^w = 0, & c_{ML}^w = 0 \\ c_M^o = 0, & c_L^o = c_L^*, & c_{ML}^o = 0 \end{array} \right\} \tag{17}$$

$$\left. \begin{array}{llll} x \to -\infty : & c_M^w = c_M^*, & c_L^w = 0, & c_{ML}^w = 0 \\ x \to +\infty : & c_M^o = 0, & c_L^o = c_L^*, & c_{ML}^o = 0 \end{array} \right\} \tag{18}$$

$$x=0:\begin{cases}(f_M)_t=-\{D^w(\partial c_M{}^w/\partial x)+D^w(\partial c_{ML}{}^w/\partial x)\}\\ \quad=D^o(\partial c_M{}^o/\partial x)+D^o(\partial c_{ML}{}^o/\partial x) & (19)\\ (f_L)_t=-\{D^w(\partial c_L{}^w/\partial x)+D^w(\partial c_{ML}{}^w/\partial x)\}\\ \quad=D^o(\partial c_L{}^o/\partial x)+D^o(\partial c_{ML}{}^o/\partial x) & (20)\end{cases}$$

where $(f_j)_t$ denotes the total flux of the species j (j=M, L) at the w/o-interface. Here, it is noticed that in spite of the assumption (iv) the reaction term R_l must be added to the diffusion equations of individual species. The reasoning is: since the equilibrium condition given by Eq. 1 is approached only when k_l^α approaches infinity, the term R_l^α becomes indeterminate. This difficulty can be avoided by introducing the total concentrations of the metal ion and the ligand, defined by

$$(c_M^\alpha)_t=c_M^\alpha+c_{ML}^\alpha \tag{21}$$

$$(c_L^\alpha)_t=c_L^\alpha+c_{ML}^\alpha \quad(\alpha=\mathrm{w},\ \mathrm{o}) \tag{22}$$

Then, our diffusion problem can be reduced to

$$\mathscr{D}^\alpha(c_M^\alpha)_t=0 \tag{23}$$

$$\mathscr{D}^\alpha(c_L^\alpha)_t=0 \tag{24}$$

with the initial and boundary conditions:

$$\left.\begin{matrix}t=0\\ x\to\pm\infty\end{matrix}\right\}:\left\{\begin{matrix}(c_M{}^w)_t=c_M{}^*,\ (c_L{}^w)_t=0\\ (c_M{}^o)_t=0,\quad (c_L{}^o)_t=c_L{}^*\end{matrix}\right\} \tag{25}$$

$$x=0:\begin{cases}(f_M)_t=-D^w\{\partial(c_M{}^w)_t/\partial x\}=D^o\{\partial(c_M{}^o)_t/\partial x\} & (26)\\ (f_L)_t=-D^w\{\partial(c_L)_t/\partial x\}=D^o\{\partial(c_L{}^o)_t/\partial x\} & (27)\end{cases}$$

The boundary value problem expressed by Eqs. 23—27 has already been solved in a previous paper,[5] in which it has been shown that the following relations hold between the total interfacial concentration $\{(c_j^\alpha)_t\}_{x=0}$ and the corresponding flux $(f_j)_t$:

$$\{(c_M{}^w)_t\}_{x=0}=c_M{}^*-(D^w)^{-1/2}I_M \tag{28}$$

$$\{(c_M{}^o)_t\}_{x=0}=(D^o)^{-1/2}I_M \tag{29}$$

$$\{(c_L{}^w)_t\}_{x=0}=-(D^w)^{-1/2}I_L \tag{30}$$

$$\{(c_L{}^w)_t\}_{x=0}=c_L{}^*+(D^o)^{-1/2}I_L \tag{31}$$

with

$$I_j=\left(\frac{7}{3\pi}\right)^{1/2}\int_0^t\frac{(f_j)_t u^{2/3}\mathrm{d}u}{(t^{7/3}-u^{7/3})^{1/2}}\quad(\mathrm{j}=\mathrm{M},\ \mathrm{L}) \tag{32}$$

Hence we obtain immediately from Eqs. 28—31

$$\{(c_M{}^w)_t\}_{x=0}+\xi\{(c_M{}^o)_t\}_{x=0}=c_M{}^* \tag{33}$$

$$\{(c_L{}^w)_t\}_{x=0}+\xi\{(c_L{}^o)_t\}_{x=0}=\xi c_L{}^* \tag{34}$$

where

$$\xi=(D^o/D^w)^{1/2} \tag{35}$$

Substituting the relations expressed by Eqs. 1—4 and 10 into Eqs. 33 and 34 and performing some calculations yields

$$(c_M{}^w)_{x=0}\{(1+\exp\zeta_M)+\beta_1{}^w(1+\exp\zeta_{ML})(c_M{}^w)_{x=0}\}=c_M{}^* \tag{36}$$

$$(c_L{}^w)_{x=0}\{(1+\xi K_D)+\beta_1{}^w(1+\exp\zeta_{ML})(c_M{}^w)_{x=0}\}=\xi c_L{}^* \tag{37}$$

with

$$\zeta_M=\zeta_M'+\ln\xi=(zF/RT)(\Delta\phi-\Delta\phi_M^{o\prime})+\ln(D^o/D^w)^{1/2} \tag{38}$$

$$\zeta_{ML}=\zeta_{ML}'+\ln\xi=(zF/RT)(\Delta\phi-\Delta\phi_{ML}^{o\prime})+\ln(D^o/D^w)^{1/2} \tag{39}$$

Eliminating $(c_M{}^w)_{x=0}$ from Eqs. 36 and 37, we obtain the algebraic equation of the second order with respect to $(c_L{}^w)_{x=0}$, the solution of which is

$$(c_L{}^w)_{x=0}=\xi c_L{}^*(1-\Psi)/(1+\xi K_D) \tag{40}$$

with

$$\Psi=\frac{2\gamma_M}{\left[\left(1+\dfrac{1+\xi K_D}{\beta_1^w c^*}\,\dfrac{1+\exp\zeta_M}{1+\exp\zeta_{ML}}\right)+\left\{\left(1+\dfrac{1+\xi K_D}{\beta_1^w c^*}\,\dfrac{1+\exp\zeta_M}{1+\exp\zeta_{ML}}\right)^2-4\gamma_M\gamma_L\right\}^{1/2}\right]} \tag{41}$$

$$c^*=c_M{}^*+\xi c_L{}^* \tag{42}$$

$$\gamma_M=c_M{}^*/c^*,\quad \gamma_L=\xi c_L{}^*/c^*\quad(\gamma_M+\gamma_L=1) \tag{43}$$

Substituting Eq. 40 into Eq. 36 and performing some rearrengements yields

$$(c_M{}^w)_{x=0}=(c_M{}^*-\xi c_L{}^*\Psi)/(1+\exp\zeta_M) \tag{44}$$

Introducing Eqs. 40 and 44 into Eq. 1 with α=w, we obtain

$$(c_{ML}{}^w)_{x=0}=\xi c_M{}^*\Psi/(1+\exp\zeta_{ML}) \tag{45}$$

The current flowing, i, is defined as the total amount

of the net positive charges transferred from the w- to the o-phase per unit time. Hence, the current can be related to the total flux of metal ion at the interface, $(f_M)_t$, as follows:

$$i = zFA(t)(f_M)_t \tag{46}$$

where $A(t)$ denotes the surface area of the water drop. If the water drop is assumed to be a complete sphere as for the dropping mercury electrode in polarography, we obtain

$$A(t) = 4\pi(3vt/4\pi)^{2/3} \tag{47}$$

where v is the constant volume flow rate of aqueous solution.

Therefore, substituting Eqs. 44—46 into Eq. 28 yields

$$\left(\frac{7}{3\pi}\right)^{1/2}\int_0^t \frac{(i/zFA)u^{2/3}\mathrm{d}u}{(t^{7/3}-u^{7/3})^{1/2}} = \frac{\sqrt{D^w}\,c_M^*}{1+\exp(-\zeta_M)} + \left\{1-\frac{1+\exp(-\zeta_{ML})}{1+\exp(-\zeta_M)}\right\}\frac{\sqrt{D^o}\,c_L^*\Psi}{1+\exp(-\zeta_{ML})} \tag{48}$$

This is the Abel integral equation with respect to (i/zFA), which can readily be solved by using the standard method.[6] Thus we obtain

$$i = i_M + \left\{1-\frac{1+\exp(-\zeta_{ML})}{1+\exp(-\zeta_M)}\right\} i_{fw} \tag{49}$$

where

$$i_M = (i_d)_M/[1+\exp(-\zeta_M)] \tag{50}$$

$$i_{fw} = (i_d)_L\Psi/[1+\exp(-\zeta_{ML})] \tag{51}$$

with

$$(i_d)_M = \sqrt{7/3\pi}\; zFA(t)\sqrt{D^w}\,c_M^*/\sqrt{t} \tag{52}$$

$$(i_d)_L = \sqrt{7/3\pi}\; zFA(t)\sqrt{D^o}\,c_L^*/\sqrt{t} \tag{53}$$

Here, $(i_d)_M$ and $(i_d)_L$ denote the limiting diffusion currents, expressed by the Ilkovic equation, which are obtained when the currents would be controlled completely by the diffusion processes of M in the w-phase and of L in the o-phase, respectively. Equation 49 with Eqs. 50 and 51 is the general expression for the reversible current–potential curves. The first term on rhs of Eq. 49 denotes the current due to the transfer of M^{z+}, which would be obtained without adding L to the o-phase, while the second term expresses the current facilitated by the presence of L in the o-phase.

Now, our consideration will be resticted to the case, in which well-defined facilitated waves are observed at sufficiently more negative potentials than $\Delta\phi_M^{o\prime}$. Then, within the potential region where the facilitated wave appears, we have

$$\exp(-\zeta_M) \longrightarrow \infty$$

Hence the facilitated current is given by i_{fw}, the expression of which can be given, after introducing the explicit expression for Ψ, as follows:

$$i_{fw} = \frac{(i_d)_M + (i_d)_L}{1+\exp(-\zeta)} \times \frac{2\gamma_M\gamma_L}{1+\left\{1-4\gamma_M\gamma_L\left(\frac{1+\exp(-\zeta_{ML})}{1+\exp(-\zeta)}\right)^2\right\}^{1/2}} \tag{54}$$

where

$$\left.\begin{aligned}\gamma_M &= \frac{c_M^*}{c^*} = \frac{(i_d)_M}{(i_d)_M+(i_d)_L},\\ \gamma_L &= \frac{c_L^*}{c^*} = \frac{(i_d)_L}{(i_d)_M+(i_d)_L}\end{aligned}\right\} \tag{43'}$$

$$\begin{aligned}\zeta &= \zeta_{ML} - \ln\{(1+\xi K_D+\beta_1^w c^*)/\beta_1^w c^*\}\\ &= \zeta_M - \ln\{(1+\xi K_D+\beta_1^w c^*)/K_D\beta_1^o c^*\}\end{aligned} \tag{55}$$

Under the limiting current conditions we have

$$\exp(-\zeta) \longrightarrow 0 \text{ and } \exp(-\zeta_{ML}) \longrightarrow 0$$

Hence, the limiting current, $(i_{fw})_{lim}$, can be given as

$$(i_{fw})_{lim} = \begin{cases}(i_d)_L \text{ for } c_M^* > \xi c_L^* \;(\gamma_L/\gamma_M < 1) & (56)\\ (i_d)_M \text{ for } \xi c_L^* > c_M^* \;(\gamma_M/\gamma_L < 1) & (56')\end{cases}$$

This equation indicates that the limiting current is controlled only by the diffusion process of the species with smaller bulk concentration.

If we solve Eq. 54 with respect to $\Delta\phi$, the formula of current-potential curves can be rewritten as

$$\begin{aligned}\Delta\phi = \Delta\phi_M^{o\prime} &- \frac{RT}{zF}\ln\xi\\ &+ \frac{RT}{zF}\ln\left\{\frac{1+\xi K_D+\beta_1^w c^*[1-2\gamma_M\gamma_L(x_M+x_L)]}{K_D\beta_1^o c^*(1-x_M)(1-x_L)/(x_M+x_L)}\right\}\\ &+ \frac{RT}{zF}\ln\frac{1}{2}\left\{1+\left[1-4\gamma_M\gamma_L(1-x_M)(1-x_L)\right.\right.\\ &\left.\left.\times\left(\frac{\beta_1^w c^*}{1+\xi K_D+\beta_1^w c^*[1-2\gamma_M\gamma_L(x_M+x_L)]}\right)^2\right]^{1/2}\right\}\end{aligned} \tag{57}$$

with

$$x_M = i_{fw}/(i_d)_M, \quad x_L = i_{fw}/(i_d)_L \tag{58}$$

The half-wave potential can be obtained by introducing into Eq. 57 $i_{fw}=\frac{1}{2}(i_d)_L$ for $c_M^* \geqslant \xi c_L^*$ and $i_{fw}=\frac{1}{2}(i_d)_M$ for $\xi c_L^* \geqslant c_M^*$, respectively, as follows:

$$\Delta\phi_{1/2} = \begin{cases} \Delta\phi_M^{\circ\prime} - \dfrac{RT}{zF}\ln\xi + \dfrac{RT}{zF}\left[\ln\left(\dfrac{1+\xi K_D+\beta_1^w c_M^*}{K_D\beta_1^\circ c_M^*}\right)\right. \\ \quad - \ln\left(1-\dfrac{1}{2}\dfrac{\gamma_L}{\gamma_M}\right) \\ \quad + \ln\dfrac{1}{2}\left\{1+\left[1-\left(\dfrac{\gamma_L}{\gamma_M}\right)\left(2-\dfrac{\gamma_L}{\gamma_M}\right)\right.\right. \\ \quad \left.\left.\times\left(\dfrac{\beta_1^w c_M^*}{1+\xi K_D+\beta_1^w c_M^*}\right)^2\right]^{1/2}\right\}\Bigg] \\ \qquad \text{for } c_M^* \geqslant \xi c_L^* \ (\gamma_L/\gamma_M \leqslant 1) \end{cases} \tag{59}$$

$$\begin{cases} \Delta\phi_M^{\circ\prime} - \dfrac{RT}{zF}\ln\xi + \dfrac{RT}{zF} \\ \quad [\text{terms obtained by exchanging } c_M^* \text{ and } \xi c_L^*] \\ \qquad \text{for } \xi c_L^* > c_M^* \ (\gamma_M/\gamma_L < 1) \end{cases} \tag{59'}$$

In most experimental practice, the two limiting conditions, i.e., (A) $c_M^* \gg \xi c_L^*$ and and (B) $\xi c_L^* \gg c_M^*$, have been employed, in order to simplify analysis of current-potential curves. In the following we shall examine these two cases in some detail.

(A) $c_M^* \gg c_L^*$

When the condition:

$$\gamma_L/\gamma_M = \xi c_L^*/c_M^* \leqslant \frac{z}{25}\left(1+\frac{\beta_1^w c_M^*}{1+\xi K_D}\right) \tag{60}$$

is satisfied, the general formula of facilitated waves can be simplified very much within errors of ca. 1 mV and Eq. 57 can be reduced to

$$\Delta\phi = \Delta\phi_{1/2}^A + (RT/zF)\ln[i_{fw}/\{(i_d)_L - i_{fw}\}] \tag{61}$$

with

$$\Delta\phi_{1/2}^A = \Delta\phi_M^{\circ\prime} - \frac{RT}{zF}\ln\xi + \frac{RT}{zF}\ln\left(\frac{1+\xi K_D+\beta_1^w c_M^*}{K_D\beta_1^\circ c_M^*}\right) \tag{62}$$

Hence the log-plots of the current-potential curve, i.e., $\log[i_{fw}/\{(i_d)_L - i_{fw}\}]$ vs. $\Delta\phi$ plots, yield a straight line with a reciprocal slope of 2.3 (RT/zF), as in D. C. polarography. Equation 62 indicates that the half-wave potential depends only on the bulk concentration of metal ion, which is present in the w-phase in a large excess in comparison with the bulk concentration of ligand in the o-phase. Figure 1 is a schematic diagram showing the concentration dependence of the half-wave potential. As can readily be seen from the figure, the behavior of the concentration dependence can be divided into three types, as follows:

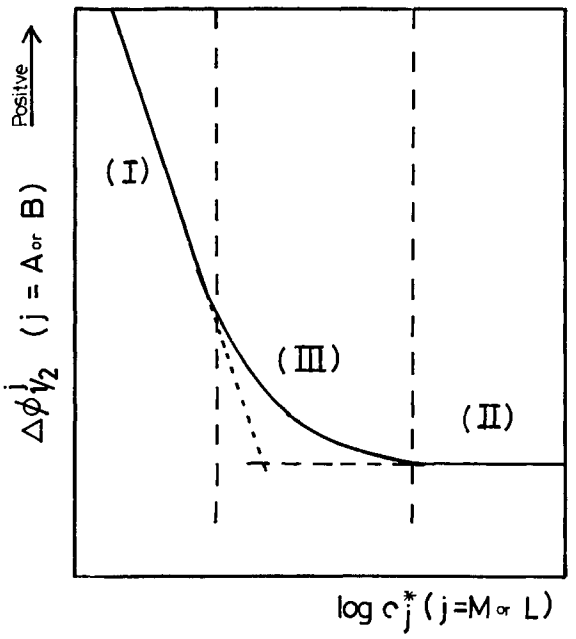

Fig. 1. Schematic diagram showing the concentration dependence of the half-wave potential. $\Delta\phi^A_{1/2}$ vs. $\log c^*_M$ plot for the cell (A). $\Delta\phi^B_{1/2}$ vs. $\log c^*_L$ plot for the cell (B).

Type (I): The plots of $\Delta\phi_{1/2}^A$ vs. $\log c_M^*$ yields a straight line with the slope of -2.3 (RT/zF). This type can be obtained when the following condition is satisfied:

$$(1+\xi K_D) \geqslant 20\,\beta_1^w c_M^* \tag{63}$$

Type (II): The half-wave potential becomes independent of $\log c_M^*$ and the plot of $\Delta\phi_{1/2}^A$ vs $\log c_M^*$ gives a horizontal line. For this type the following inequality holds:

$$\beta_1^w c_M^* \geqslant 20(1+\xi K_D) \tag{64}$$

Type (III): This is the intermediate type between the types (I) and (II). In this case we have

$$(1+\xi K_D) \sim \beta_1^w c_M^* \tag{65}$$

In order to analyze the concentration dependence of the half-wave potentials precisely, we introduce the following function F_A:

$$F_A \equiv \exp(zF/RT)(\Delta\phi_{1/2}^A - \Delta\phi_M^{\circ\prime})$$
$$= (\beta_1^w/\xi K_D\beta_1^\circ) + \{(1+\xi K_D)/\xi K_D\beta_1^\circ\}(1/c_M^*) \tag{66}$$

Then the plots of the function F_A vs. $(1/c_M^*)$ yields a straight line, of which the slope and the intercept are $\{(1+\xi K_D)/\xi K_D\beta^o{}_1\}$ and $(\beta^w{}_1/\xi K_D\beta^o{}_1)$, respectively. Hence, if the value of ξK_D is known, we can determine the values of the complex formation constants both in the w- and the o-phase from the slope and the intercept, respectively. In practice, however, it frequently happens that the $\Delta\phi^{\wedge}_{1/2}$ vs. $\log c_M^*$ curve belongs to the type (I) and the F_A vs. $(1/c_M^*)$ plot passes through the origin within experimental errors. In such a case we can obtain only the value of the complex formation constant in the o-phase from the slope. For the complex formation constant in the w-phase we obtain only the following inequality condition from Eq. 63:

$$\beta_1^w \leqslant (1 + \xi K_D)/\{20(c_M^*)_{max}\} \tag{67}$$

where $(c_M^*)_{max}$ denotes the maximum concentration of metal ion employed in the experiment. On the other hand, in some case the concentration dependence of the half-wave potential belongs to the type (II) and the F_A vs. $(1/c_M^*)$ plot becomes a horizontal line within experimental errors. In this case only the ratio $(\beta^w{}_1/\beta^o{}_1)$ is determinable from the intercept, and from Eq. 64 we have the following inequality condition:

$$\beta_1^w \geqslant 20(1 + \xi K_D)/(c_M^*)_{min} \tag{68}$$

where $(c_M^*)_{min}$ is the minimum concentration of metal ion used in the experiment.

(B) $c_L^* \gg c_M^*$

For the case:

$$\gamma_M/\gamma_L = c_M^*/\xi c_L^* \leqslant \frac{z}{25}\left(1 + \frac{\xi\beta_1^w c_L^*}{1 + \xi K_D}\right) \tag{69}$$

the general equation 57 can be simplified to

$$\Delta\phi = \Delta\phi^B_{1/2} + (RT/zF)\ln[i_{fw}/\{(i_d)_M - i_{fw}\}] \tag{70}$$

with

$$\Delta\phi^B_{1/2} = \Delta\phi^{o\prime}_M - \frac{RT}{zF}\ln\xi + \frac{RT}{zF}\ln\left(\frac{1 + \xi K_D + \xi\beta_1^w c_L^*}{\xi K_D\beta_1^o c_L^*}\right) \tag{71}$$

within errors of ca. 1 mV. Further we introduce the following function F_B:

$$F_B \equiv \exp(zF/RT)(\Delta\phi^B_{1/2} - \Delta\phi^{o\prime}_M) = (\beta_1^w/\xi K_D\beta_1^o) + \{(1 + \xi K_D)/\xi K_D\beta_1^o\}(1/\xi c^*{}_L) \tag{72}$$

Equations 70—72 can also be obtained by exchanging c_M^* by ξc_L^* in Eqs. 61, 62, and 66, respectively. Hence, all arguments described above in (A) may be applicable to the present case.

Extention to More General Case. It has been known in solvent extraction and membrane transport experiments that when the ionic crystal diameter of metal ion is somewhat larger than the cavity size of macrocyclic ligands, the 1:2 complex, i.e., the so-called sandwich type complex, as well as the ordinary 1:1 complex are formed under the presence of a large excess of the macrocyclic ligands in the o-phase. Hence, we shall extend the above theory to the more general case, in which a series of complex species ML_p^{z+} (p=1, 2,···, n) are formed under the condition (B).

In this case, the total concentrations of the metal ion and the ligand are defined as

$$(c_M^\alpha)_t = c_M^\alpha + \sum_{p=1}^{n} c_{ML_p}^\alpha \tag{73}$$

$$(c_L^\alpha)_t = c_L^\alpha + \sum_{p=1}^{n} p c_{ML_p}^\alpha \quad (\alpha = w,\ o) \tag{74}$$

Then these two total concentrations satisfy the diffusion boundary value problem defined by Eqs. 23—27 and thus the solutions are given by Eqs. 28—31. The successive complex formation in the α-phase may be characterized by the following over-all formation constant:

$$\beta_p^\alpha = c_{ML_p}^\alpha/c_M^\alpha(c_L^\alpha)^p \quad (\alpha = w,\ o;\quad p = 1,\ 2,\cdots,\ n) \tag{75}$$

On the other hand, the transfer of complex species ML_p^{z+} (p=0, 1, 2, ···, n) across the w/o-interface may be governed by the Nernst equation:

$$\exp(\zeta'_{ML_p}) = (c_{ML_p}{}^o)_{x=0}/(c_{ML_p}{}^w)_{x=0} \tag{76}$$

with

$$\zeta'_{ML_p} = (zF/RT)(\Delta\phi - \Delta\phi^{o\prime}_{ML_p}) \tag{77}$$

where $\Delta\phi^{o\prime}_{ML_p}$ is the formal potential of the complex species ML_p^{z+} for the ion transfer across the w/o-interface and may be related to $\Delta\phi^{o\prime}_M$ as follows:

$$\Delta\phi^{o\prime}_{ML_p} = \Delta\phi^{o\prime}_M - (RT/zF)\ln(K_D^p\beta_p^o/\beta_p^w) \tag{78}$$

Hence, introducing Eqs. 75 and 76 into Eqs. 33 and 34 yields

$$(c_M{}^w)_{x=0}\{(1 + \exp\zeta_M) + \sum_{p=1}^{n}\beta_p{}^w(1 + \exp\zeta_{ML_p})[(c_L{}^w)_{x=0}]^p\} = c_M^* \tag{79}$$

$$(c_L{}^w)_{x=0}\{(1 + \xi K_D) + (c_M{}^w)_{x=0}\sum_{p=1}^{n} p\beta_p{}^w(1 + \exp\zeta_{ML_p})[(c_L{}^w)_{x=0}]^p\} = \xi c_L^* \tag{80}$$

Elimination of $(c_M{}^w)_{x=0}$ from the above two equations

results in an algebraic equation of $(n+1)$-th order with respect to $(c_L^w)_{x=0}$. Under the condition (B), in which $c_L^* \gg c_M^*$ holds, this $(n+1)$-th order algebraic equation can be factorized and the solution becomes

$$(c_L^w)_{x=0} = \xi c_L^*/(1 + \xi K_D) \tag{81}$$

Hence, we can obtain the expression for $(c_M^w)_{x=0}$ by substituting Eq. 81 into Eq. 79 and then the expression of $(c_{ML_p}^w)_{x=0}$ can be derived from introducing $(c_M^w)_{x=0}$ thus obtained and Eq. 81 into Eq. 75. Substituting the interfacial concentrations of a series of complex species obtained in this way into Eq. 73 and performing some calculation by using the Eq. 78, we have

$$\{(c_M^w)_i\}_{x=0} = c_M^*/\{1 + \exp(zF/RT)(\Delta\phi - \Delta\phi_{1/2}^B)\} \tag{82}$$

with

$$\Delta\phi_{1/2}^B = \Delta\phi_M^{\circ\prime} - \frac{RT}{zF}\ln\xi + \frac{RT}{zF}\ln\left\{\frac{1 + \sum_{p=1}^{n}\beta_p^w[\xi c_L^*/(1 + \xi K_D)]^p}{1 + \sum_{p=1}^{n}\beta_p^\circ[\xi K_D c_L^*/(1 + \xi K_D)]^p}\right\} \tag{83}$$

Hence, introducing Eqs. 46 and 82 into Eq. 28 yields the Abel integral equation similar to Eq. 48, the solution of which gives for current–potential curves

$$i = (i_d)_M/\{1 + \exp(zF/RT)(\Delta\phi - \Delta\phi_{1/2}^B)\} \tag{84}$$

where $\Delta\phi_{1/2}^B$ is the half-wave potential given by Eq. 83. Of course, for $n=1$ Eq. 83 can be reduced to Eq. 71.

Very frequently, especially for hydrophobic macrocyclic ligands, the following conditions are satisfied:

$$K_D \gg 1, \quad K_D \gg (\beta_p^w)^{1/p} c_L^*$$

In such a case Eq. 83 may be reduced to

$$\Delta\phi_{1/2}^B = \Delta\phi_M^{\circ\prime} - (RT/zF)\ln\xi - (RT/zF)\ln\{1 + \sum_{p=1}^{n}\beta_p^\circ(c_L^*)^p\} \tag{85}$$

This equation is the same in form as that of the reversible half-wave potential for the polarographic reduction of complex metal ions. Therefore, by using the DeFord–Hume method[7] in polarography, we can determined the values of β_p° ($p=1, 2, \cdots, n$) succesively from the concentration dependence of the half-wave potential.

Experimental

Chemicals. Nitrobenzene, employed as the o-phase, was purified by the method described by Kakutani et al.[4] Four-times distilled water was used to prepare the aqueous electrolyte solutions. Tetrabutylammonium tetraphenylborate (TBATPB), which was used as the supporting electrolyte in the o-phase, was prepared by the equimolar addition of an aqueous solution of sodium tetraphenylborate (Kanto Chemical Co.) to an aqueous solution of tetrabutylammonium chloride (Kanto Chemical Co.). The resulting precipitate was solved into 1,2-dichloroethane (DCE), washed repeatedly with distilled water, and then recrystallized by pouring the DCE solution into distilled ethanol. Commercial DB18C6 (Merck, Schuchardt) and 18C6 (Nippon Soda Co.) were recrystallized from benzene and acetonitrile, and dried under reduced pressure. All other chemicals were of analytical grade and used without further purification. The nitrobenzene solution of TBATPB and the aqueous solution were equilibrated with each other by shaking overnight before use.

Electrochemical Measurements. The electrolysis cell employed here is essentially the same as that described by Kihara and Yoshida,[8] except for wearing the water jacket around the cell. The cell temperature was controlled at 25±0.3 °C by circulating thermostated water through the jacket. The aqueous solution was dropped upword into the nitrobenzene solution from a teflon capillary (diameter 0.8 mm) with the volume flow rate $\nu=(5—15)\times10^{-3}$ cm^3 s^{-1} and the drop time $t_d=2—5$ s. The potential difference at the test electrode was controlled by means of a four-electrode potentiostat (Huso-seisakusho, defferential potentiostat HECS 310B) with a positive feedback circuit for iR compensation.

The galvanic cells employed for the control or the measurement of the potential difference at the w/o-interface were the following two cells, corresponding to the conditions (A) $(c^*_M \gg c^*_L)$ and (B) $(c^*_L \gg c^*_M)$, respectively:

Cell (A):

(RE1) Ag	AgCl	0.05 mol dm^{-3} TBACl	0.05 mol dm^{-3} TBATPB + y mmol dm^{-3} L
		I (w)	II (o)

*	z mol dm^{-3} $M^{I}Cl$ or $M^{II}Cl_2$	sat. KCl salt bridge	0.05 mol dm^{-3} NaCl	
	III (w)		IV (w)	

AgCl | Ag (RE2)

Cell (B):

(RE1) Ag	AgCl	0.05 mol dm^{-3} TBACl	0.05 mol dm^{-3} TBATPB + y' mol dm^{-3} L
		I (w)	II (o)

$$\left|\begin{array}{l|l|l} z' \text{ mmol dm}^{-3}\ \mathrm{M^{I}Cl} & \text{sat. KCl} & 0.05\ \text{mol dm}^{-3} \\ +\,0.1\ \text{mol dm}^{-3}\ \mathrm{MgSO_4} & \text{salt bridge} & \mathrm{NaCl} \end{array}\right|^{*}$$

III (w) IV (w)

$$\mathrm{AgCl}\ |\ \mathrm{Ag\,(RE2)}$$

Here the test interface is marked by asterisk and L and M denote the macrocyclic ligand and the cation in question, respectively. The reference electrode for the nitrobenzene phase, RE1, was a Ag|AgCl|0.05 mol dm^{-3} TBACl(W) electrode, which was connected to nitrobenzene phase II through sintered glass. On the other hand, the reference electrode for the aqueous phase, RE2, was a Ag|AgCl|0.05 mol dm^{-3} NaCl(W) electrode and connected to aqueous phase III through a salt-bridge containing saturated KCl solution. For the cell (B), 0.1 mol dm^{-3} $MgSO_4$ was added to the aqueous phase III as a supporting electrolyte. Two counter electrodes were platinum wires immersed in two aqueous MCl solutions, which, in turn, were connected to the aqueous phase I and III through sintered glass, respectively. The linear sweep voltage was applied at the rate of 2 mV s^{-1} by means of a potential scanner (Huso seisakusho, potential sweep unit HECS 321B) and polarograms were recorded using a X-Y recorder (Graphtec Co., WX 1200).

The voltage, V_{app}, applied to the cells was defined as the potential of the terminal of RE2, E_{RE2}, against to that of RE1, E_{RE1}, i.e., $V_{app}=E_{RE2}-E_{RE1}$. Therefore, if we neglect the potential difference through the salt bridge, we obtain $V_{app}=\Delta\phi$ +const. The constant term was evaluated under the well-known extrathermodynamic assumption that the standard transfer free energies of tetraphenylarsonium cation ($TPhAs^+$) and tetraphenylborate anion ($TPhB^-$) are equal,[9] as follows: using the cells (A) and (B) in the absence of any ligand in the o-phase, we measured the half-wave potential of tetramethylammonium ion (TMA^+), from which we determined the formal potential, $(\Delta\phi^{o'}_{TMA})_{meas}$, after correcting the diffusion coefficient term $(RT/F)\ln\sqrt{D^o/D^w}=-0.009$ V.[10] Since the literature value of $\Delta\phi^{o'}_{TMA}$ under the TPhAs-TPhB assumption is 0.035 V,[2] we have $\Delta\phi=V_{app}-[(\Delta\phi^{o'}_{TMA})_{meas}-0.035\ \mathrm{V}]$. The values of potential $\Delta\phi$ given in the present paper are those calculated in this way and designated as V vs. TPh(As/B)E.

The flow of the positive charge from the w- to the o-phase was taken as the positive current. The current values used for the wave-form analysis were corrected appropriately for the residual currents which were obtained using the cells in the absence of ligands in the o-phase.

Results and Discussion

In the following we shall verify experimentally the theoretical predictions obtained above, especially for the two limiting conditions (A) and (B). As typical macrocyclic ligands we employ DB18C6 and 18C6, of which the distribution constants are very large ($K_D=2.3\times10^4$)[11] and relatively small ($K_D=0.10$),[11] respectively. On the other hand, sodium, cesium, barium, and oxonium ions are chosen as the cations yielding facilitated waves. The wave-form analysis is performed in the same mannar as in the polarographic practice.

DB18C6.

(1) DB18C6-Na^+ System. First, we examine the behavior of DB18C6-Na^+ complex, using both the cells (A) and (B). The well-defined facilitated waves were always observed at the potentials 150—200 mV more negative than the final rise. The limiting currents were diffusion-controlled with respect to the ligand in the o-phase for the cell (A) and to the metal ions in the w-phase for the cell (B), as proved from the fact that the diffusion current constant, defined by

$$(I_d)_j = (i_d)_j/m^{2/3}t_d^{1/6}c^*_j \quad (j = \mathrm{L\ or\ M}),$$

was constant within experimental errors, when values of c^*_j (0.2—1 mmol dm^{-3}), ν (5—15×10^{-3} cm^3 s^{-1}) and t_d (2—6 s) were changed. The ratio, $(I_d)_L/(I_d)_M$, of the diffusion current constants obtained for the cells (A) and (B), respectively, was 0.50. The log-plots of current-potential curves yielded straight lines with the reciprocal slopes of 61±2 mV/decade for the cell (A) and of 63±1 mV/decade for the cell (B). These facts indicate that the facilitated waves of DB18C6-Na^+ system are reversible and diffusion-controlled.

In Fig. 2, the half-wave potentials obtained both for the cells (A) and (B), $\Delta\phi^A_{1/2}$ and $\Delta\phi^B_{1/2}$, are given in

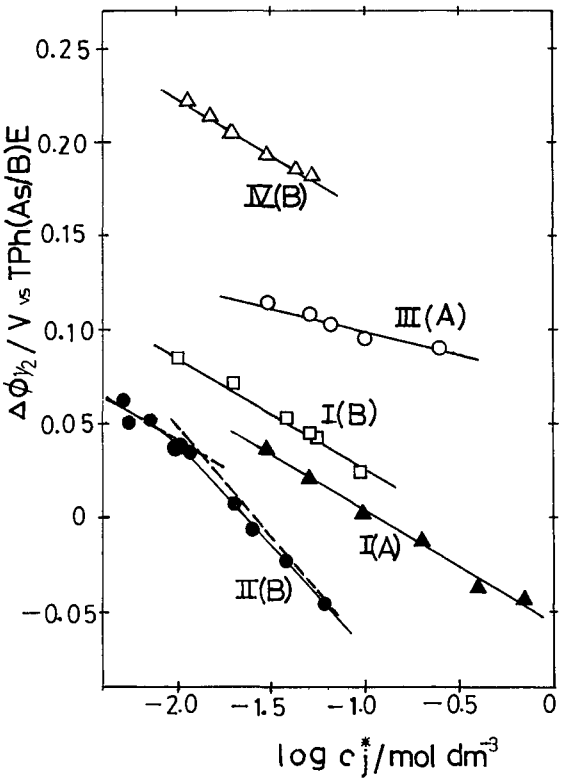

Fig. 2. Half-wave potentials of the DB18C6 complexes in dependence of log c^*_j (j=M for the cell (A) and L for the cell (B)). I: Na^+, II: Cs^+, III: Ba^{2+}, and IV: H_3O^+. (A) and (B) denote the kind of cell employed.

dependence of $\log c^*_M$ and $\log c^*_L$ by the curves I(A) and I(B), respectively. For both cases, we have straight lines with the slope of −60 mV/decade, indicating that the DB18C6–Na^+ system corresponds to the type (I) described in Fig. 1. As can readily be seen from Fig. 2, the straight line I(A) is located at ca. 20 mV more negative potential than that of I(B). Comparing Eq. 62 with Eq. 71 yields for $c^*_M=c^*_L$

$$\Delta\phi^A_{1/2} - \Delta\phi^B_{1/2} = (RT/zF)\ln\xi \quad (86)$$

Therefore, this value of −20 mV may be comparable to the theoretical prediction of −18 mV, which can be calculated from the above equation with $\xi=(I_d)_L/(I_d)_M=0.50$.

In Fig. 3, the values of functions F_A and F_B calculated from Eqs. 66 and 72 with $\Delta\phi^\circ_{Na}=0.355$ V vs. TPh(As/B)E[12] are plotted against $(1/c^*_j)$ (j=M for I(A) and L for I(B)). These plots fall on straight lines with the slope of 1.3×10^{-7} mol^{-1} dm^3 for I(A) and 2.8×10^{-7} mol^{-1} dm^3 for I(B) and with the intercept of zero for both I(A) and I(B) within experimental errors. The fact that the slope of I(B) is ca. 2.1 times larger than that of I(A) may be explained from the following relation: [slope of F_B vs. $(c^*_L)^{-1}$ plot]/[slope of F_A vs. $(c^*_M)^{-1}$ plot]$=\xi^{-1}$, which can be derived from Eqs. 66 and 72.

As described in the theoretical part, we can evaluate the complex formation constant in the o-phase from the value of slope to be $\log\beta^\circ_1=6.8$. On the other hand, the formation constant in the w-phase cannot be determined, sicne the value of intercept becomes zero. From Eq. 67 we obtain only the following inequality condition: $\log\beta^w_1<2.9$. In this connection the literature value of $\log\beta^w_1$ is 1.16.[13]

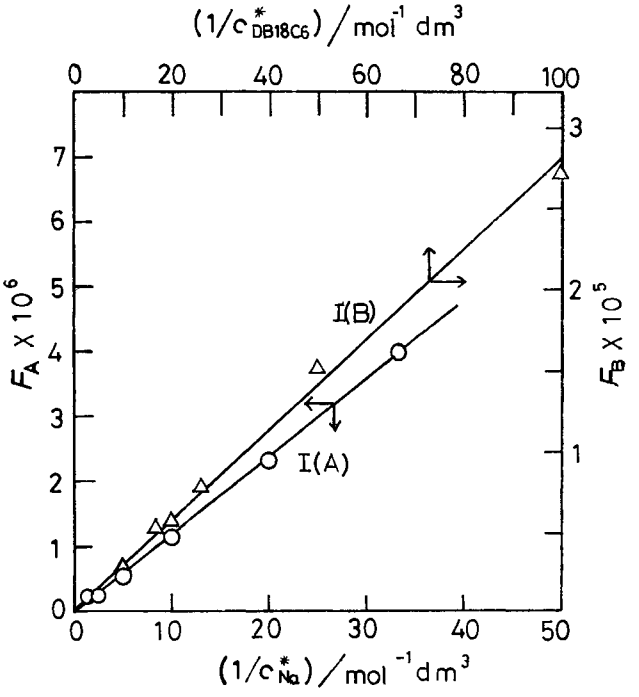

Fig. 3. F_A vs. $(1/c^*_{Na})$ and F_B vs. $(1/c^*_{DB18C6})$ plots for DB18C6–Na^+ system. I(A): F_A vs. $(1/c^*_{Na})$, I(B): F_B vs. $(1/c^*_{DB18C6})$.

(2) DB18C6–Cs^+ System. As is well-known, cesium ion is bulky compared with the other alkali metal ions, so that the standard ion-transfer potential becomes relatively negative. Hence, if we employ the cell (A), the corresponding potential window becomes very narrow, and we cannot observe any well-defined facilitated wave. On this ground, the behavior of facilitated waves of cesium ion was examined only for the cell (B).

In the absence of ligand in the o-phase, we observed a well-defined wave at the potential ca. 100 mV more negative than the final rise, which was regarded as being due to the transfer of cesium simple ion across the w/o-interface. This wave was reversible and diffusion-controlled, as verified from the constancy of diffusion current constant and the log-plot analysis of current–potential curves. The half-wave potential obtained is 0.131 V vs. TPh(As/B)E.

Addition of DB18C6 in the o-phase in a large excess (c_L^*=5—40 mmol dm^{-3}) shifted the wave of cesium ion to the potential region +0.06—−0.05 V vs. TPh(As/B)E. The limiting currents of these facilitated waves are diffusion-controlled with respect to Cs^+, as verified from the constancy of diffusion-current constant. The log-plots of current-potential curves yield straight lines with the reciprocal slope of 63±3 mV/decade. The half-wave potentials determined from log-plots are given in dependence of $\log c_L^*$ by curve II(B) in Fig. 2. As can readily be seen from figure, curve II(B) is asymptotic to a straight line with the slope of −120 mV/decade at high ligand concentration, while it approaches a straight line with the slope of −60 mV/decade with a decrease in ligand concentration. In accord with the fact that the ionic radius of Cs^+ (1.67 Å)[14] larger than the cavity radius of DB18C6 (1.34—1.43 Å),[15] this result suggests that the cesium ion forms the so-called sandwich type 1:2 (metal to ligand) complex with DB18C6 at higher ligand concentration. Since K_D-value of DB18C6 is very large (2.3×10^4) and the literature value of $\log\beta_1^w$ is 0.83,[13] the concentration dependence of the half-wave potential may be expressed by Eq. 85. Hence, we can evaluate the values of β°_p (p=1, 2, ···) by means of the DeFord–Hume method[7] in polarography. We define the DeFord–Hume F_o-function as

$$F_o \equiv \exp(zF/RT)\{(\Delta\phi^B_{1/2})_M - \Delta\phi^B_{1/2}\} = 1 + \sum_{p=1}^{n}\beta_p^\circ(c^*_L)^p \quad (87)$$

where $(\Delta\phi^B_{1/2})_M$ denotes the half-wave potential of simple cesium ion. Then, we define, in general, the DeFord–Hume F_p-function (p=1, 2, ···) as

$$F_p = \{F_{p-1} - \lim(c_L^* \longrightarrow 0)F_{p-1}\}/c_L^* \quad (88)$$

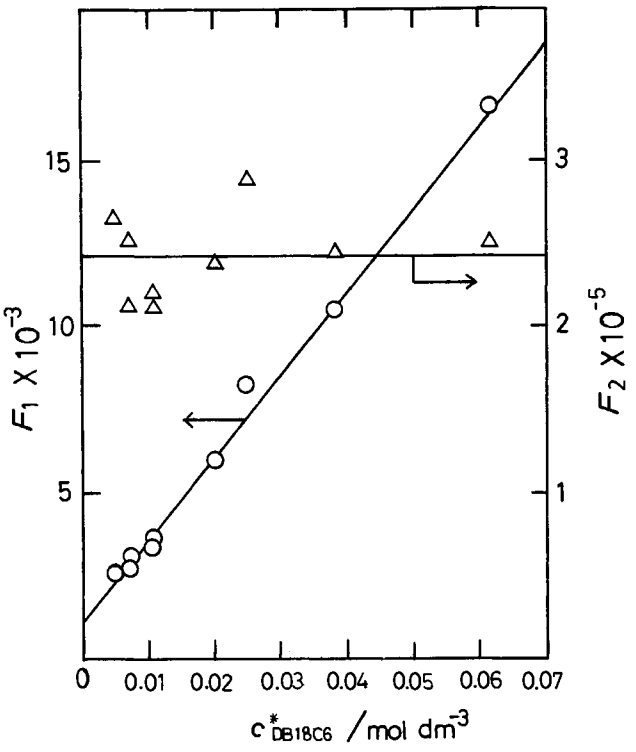

Fig. 4. DeFord-Hume functions F_1 and F_2 in dependence of c^*_L for the DB18C6-Cs^+ system.

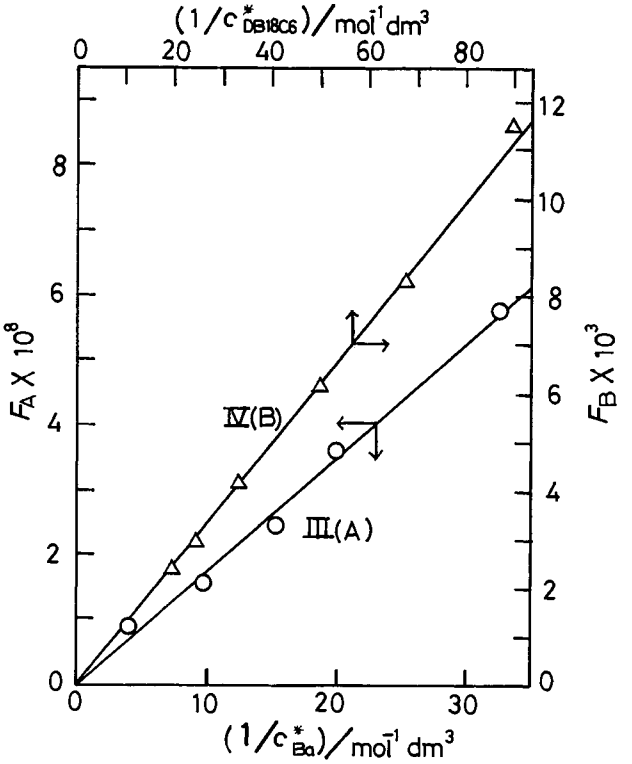

Fig. 5. F_A vs. $(1/c^*_{Ba})$ plot for the DB18C6-Ba^{2+} system and F_B vs. $(1/c^*_{DB18C6})$ plot for the DB18C6-H_3O^+ system. III(A): DB18C6-Ba^{2+}, IV(B): DB18C6-H_3O^+.

where $\lim(c_L^* \to 0)F_p$ denotes the value of F_p extrapolated to $c_L^*=0$, which is equal to β^o_p, as can be seen from Eqs. 87 and 88. In this way, from the extrapolated values of F_p (p=1, 2, ···) vs. c_L^* plots, we can evaluate succesively the values of β^o_1, β^o_2, ···.

In Fig. 4, the DeFord-Hume functions F_1 and F_2 are plotted against c_L^*, where the experimentally determined value of 0.131 V vs. TPh(As/B)E is employed for $(\Delta\phi^B_{1/2})_{Cs}$. As can be seen from the figure, the extrapolated values of these functions yield $\log \beta^o_1=3.1$ and $\log \beta^o_2=5.4$.

(3) DB18C6-Ba^{2+} System. As an example of alkaline earth metal ions, we examined the behavior of barium ion, using the cell (A). The well-defined facilitated waves were always observed at the potential ca. 100 mV more negative than the final rise. The limiting currents were verified to be diffusion-controlled with respect to the ligand and the value of diffusion current constant was ca. 1.8 times larger than that of DB18C6-Na^+ complex obtained for the cell (A). The log-plot analysis of current-potential curves yielded straight lines with the reciprocal slope of 32±2 mV/decade. These results indicate that these facilitated waves correspond to the reversible transfer of divalent cation across the w/o-interface as can readly be expected. The half-wave potentials determined from the log-plot analysis are plotted against the logarithm of Ba^{2+} bulk concentration in Fig. 2 (see curve III(A)). This plot yields a straight line with the slope of −28 mV/decade, indicating that the DB18C6-Ba^{2+} system corresponds to the type (I). The F_A vs. $(1/c^*_{Ba})$ plot is given by curve III(A) in Fig. 5, where the values of F_A have been calculated using the literature value $\Delta\phi^o_{Ba}$=0.328 V vs. TPh(As/B)E.[2] We can see that this plot yields a straight line passing through the origin within experimental errors. Since $K_D \gg 1$, we can obtain directly from the slope the value of $\log \beta^o_1$ as 8.8. For the value of β^w_1, from Eq. 64 we have only the inequality equation, $\log \beta^w_1 < 3.0$, while the literature value of $\log \beta^w_1$ is 1.95.[13]

(4) DB18C6-H_3O^+ System. The facilitation effects of DB18C6 on oxonium ion were small, so that we employed here only the cell (B), because we could not separate the facilitated waves from the final rise for the cell (A) containing a large excess of oxonium ion in the w-phase. The facilitated waves were observed at the potenitals only 40—60 mV more negative than the final rise. Hence the data obtained were rather inaccurate comparing with those of other cases, although corrections for residual currents were carried out as carefully as possible. The limiting currents were proved to be diffusion-controlled from the constancy of diffusion current constant. The log-plot analysis yielded straight lines with a reciprocal slope of 56±4 mV/decade, though the data were fairly scattered. The plot of half-wave potentials vs. $\log c_L^*$ yields a straight line with the

slope of −61 mV/decade, as shown by curve IV(B) in Fig. 2. The plot of F_B vs. $(1/c^*_L)$ is shown by curve IV(B) in Fig. 5, where F_B values have been calculated with $\Delta\phi^\circ_H$=0.337 V vs. TPh(As/B)E.[12] As can be seen from the figure, this plot yields a straight line passing through the origin. For the cell (B), we can obtain from the slope the value of log $(\xi\beta^\circ_1)$ as 3.7. The value of ξ for this complex was estimated as follows: the diffusion current constant $(I_d)_H$ is 1.5 times larger than that of Na^+ obtained for the cell (B). Further, the value of ξ for the DB18C6–Na^+ system is 0.5, as given above. Hence the value of ξ for DB18C6–H_3O^+ system may be estimated to be 0.5/1.5=0.33. Using this value of ξ yields log β°_1=4.2.

18C6.

Since the K_D-value of 18C6 is 0.10, the interfacial concentration of L in the w-phase may become 10 times larger than that of the o-phase. Hence, the diffusion layer formed in the vicinity of the w/o-interface in the w-phase may be presumed to become unstable, especially for the cell (B) for which the ligand is present in a large excess. On this ground, we examined the behavior of current–potential curves only for the cell (A). Even when the cell (A) was employed, a gradual decrease in the limiting current was observed during repeating measurements for a long time, due to loss of ligand from the o- to the w-phase. Hence, in order to obtain reproducible results, it was required to start measurements as soon as possible after constructing the cell.

(1) 18C6-Na^+ System. The well-defined facilitated waves were obtained at the potentials about 160 mV more negative than the final rise, with the diffusion-controlled limiting currents with respect to the ligand concentration. The log-plot analysis of current–potential curves yielded straight lines with the reciprocal slope of 63±4 mV/decade. The half-wave potentials in dependence of log c^*_{Na} are shown by curve I(A) in Fig. 6. As can be seen from the behavior of the curve, the concentration dependence of the half-wave potential belongs to the intermediate type(III). The F_A vs. $(1/c^*_M)$ plot is given in Fig. 7, from which we can see that the plot points fall on a straight line with non-zero values of both the slope and the intercept. Hence, we can fortunately, in this case, determine the formation constants both in the w- and the o-phase. Using K_D=0.10 and assuming ξ=0.5 yields log β^w_1=0.7 and log β°_1=8.5. The former value may compare with the literature value of log β^w_1=0.8 obtained by calorimetry.[16]

(2) 18C6-Ba^{2+} System. The 18C6–Ba^{2+} complex yields well-defined facilitated waves at the potentials 100 mV more negative than the final rise, with limiting currents controlled by diffusion of the ligand. The log-plot analysis of current–potential curves gives straight lines with the reciprocal slope of 32±3 mV/decade, indicating that the transfered ion is divalent. The concentration dependence of the half-wave potential is given by curve III(A) in Fig. 6, from which we can see that the

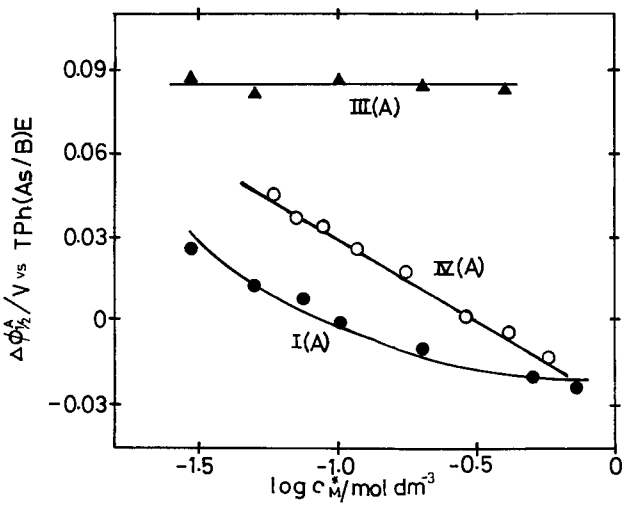

Fig. 6. Half-wave potentials of the 18C6 complexes in dependence of log c^*_M. I(A): Na^+, III(A): Ba^{2+}, and IV(A): H_3O^+.

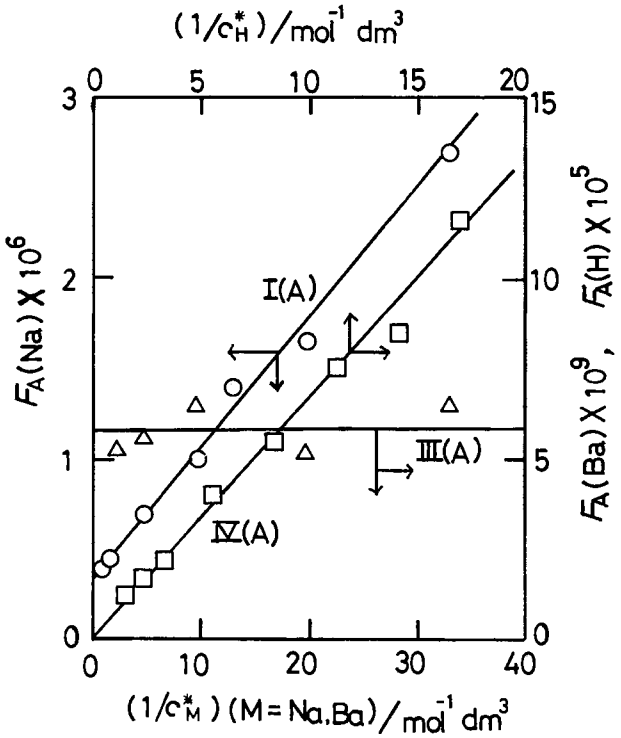

Fig. 7. F_A vs. $(1/c^*_M)$ plots for the 18C6–Na^+, –Ba^{2+}, and –H_3O^+ systems. I(A): 18C6-Na^+, III(A): 18C6–Ba^{2+}, IV(A): 18C6–H_3O^+.

half-wave potential is independent of the Ba^{2+}-concentration and this system belongs to the type (II). The F_A vs. $(1/c^*_{Ba})$ plot yields a straight line with zero slope within experimental errors, as seen from Fig. 7. Hence, we can obtain only the ratio β°_1/β^w_1 from the value of intercept. Using K_D=0.10 and ξ=0.5 yields log $(\beta^\circ_1/\beta^w_1)$= 9.5. If we use the literature value of 3.87 for log β^w_1,

which has been obtained by Izatt et al.[16] using calorimetry, we obtain $\log \beta^{o}{}_{1}=13.4$. On the other hand, from Eq. 68 we obtain the following inequality equation: $\log \beta^{w}{}_{1}>3$, which is consistent with the literature value.

(3) 18C6-H_3O^+ System. Finally we examined the behavior of oxonium ion. In contrast to the DB18C6-H_3O^+ system, the 18C6-H_3O^+ system exhibited well-defined facilitated waves at the potential ca. 120 mV more negative than the final rise, with diffusion-controlled limiting currents with respect to the ligand concentration. The log-plot analysis of current-potenial curves yielded straight lines with the reciprocal slope of 59±3 mV/decade. The half-wave potentials obained are plotted against $\log c^{*}{}_{H}$ in Fig. 6 (curve IV(A)). As can be seen from the figure, this plot gives a straight line with the slope of −57 mV/decade, indicating that the 18C6-H_3O^+ system belongs to the type (I). In Fig. 7, the values of F_A are plotted against $(1/c_L^*)$, from which we can see that this plot yields a straight line passing through the origin, in spite of small K_D-value of 18C6. From the value of slope we obtain $\log \beta^{o}{}_{1}=7.5$, where ξ is assumd to be 0.5, since for the cell (A) the diffusing species in both the w- and o-phases may be regarded as the ligand. On the other hand, for $\beta^{w}{}_{1}$, we have only the inequality equation: $\log \beta^{w}{}_{1}\leqslant -1$, from Eq. 67. Hence it can be seen that the formation constant of oxonium ion in the w-phase is very small.

In conclcusion, it can be stated that the theoretical equation derived without any limitation on the magnitude of distribution constants of macrocyclic ligands explaines extensively the behavior of facilitated ion transfer across the water/introbenzene interface and allows to evaluate the complex formation constants in the nitrobenzene phase and for favorable cases those of both the nitrobenzene and water phase.

In the present paper we have selected the polarographic method with the electrolyte dropping electrode from various electrochemical methods available at present. However, the theoretical equations obtained here can easily be transformed to those of other various polarographic and voltammetric techniques in the same manner as done in usual polarography and voltammetry.

References

1) J. Koryta, *Electrochim. Acta,* **24**, 293 (1979).
2) J. Koryta, *Electrochim. Acta,* **29**, 445 (1984).
3) J. Koryta, *Electrochim. Acta,* **33**, 189 (1988).
4) T. Kakutani, Y. Nishiwaki, T. Osakai, and M. Senda, *Bull. Chem. Soc. Jpn.,* **59**, 781 (1986).
5) H. Matsuda and Y. Ayabe, *Bull. Chem. Soc. Jpn.,* **28**, 422 (1955); H. Matsuda, *Z. Elektrochem.,* **61**, 489 (1957).
6) K. Hidaka, "Oyo-sekibunhoteishiki-ron," (Applied theory of integral equations), Kawade-shobo, Tokyo (1943), pp. 130—134.
7) D. D. DeFord and D. N. Hume, *J. Am. Chem. Soc.,* **73**, 5321 (1951).
8) S. Kihara, M. Suzuki, K. Maeda, K. Ogura, S. Umetani, M. Matsui, and Z. Yoshida, *Anal. Chem.,* **58**, 2954 (1986).
9) A. J. Parker, *Electrochim. Acta,* **21**, 671 (1976).
10) T. Osakai, T. Kakutani, and M. Senda, *Bull. Chem. Soc. Jpn.,* **57**, 370 (1984).
11) T. Iwachido, M. Minami, A. Sadakane, and K. Toei, *Chem. Lett.,* **1977**, 1511.
12) J. Rais, *Collect. Czeck. Chem. Commun.,* **36**, 3253 (1971).
13) E. Shchori, N. Nae, and J. Jagur-Grodzinski, *J. Chem. Soc., Dalton Trans.,* **1975**, 2381.
14) R. D. Shannon and C. T. Prewitt, *Acta Crystallogr., Sect. B,* **25**, 925 (1969).
15) J. D. Lamb, R. M. Izatt, and J. J. Christensen, "Progress in Macrocyclic Chemistry," ed by R. M. Izatt and J. J. Christensen, J. Wiley & Sons, New York, N. Y. (1981), Vol. 2, Chap. 2, pp. 41—90.
16) R. M. Izatt, R. E. Terry, B. L. Haymore, L. D. Hansen, N. K. Dalley, A. G. Avondet, and J. J. Christensen, *J. Am. Chem. Soc.,* **98**, 7620 (1976).

 © 1991 The Chemical Society of Japan Bull. Chem. Soc. Jpn., 64, 1509—1513 (1991)

Electron Spin Resonance Study of Intrinsic Paramagnetism of Soluble Polyaniline Perchlorates

Masaki IIDA, Tetsuo ASAJI,* Motomichi INOUE,*,† Heriberto GRIJALVA,†
Michiko B. INOUE,† and Daiyu NAKAMURA
Department of Chemistry, Faculty of Science, Nagoya University,
Nagoya 464-01
†Centro de Investigación en Polímeros y Materiales, Universidad de Sonora,
Apdo. Postal 130, Hermosillo, Sonora, Mexico
(Received December 10, 1990)

An ESR study was carried out on two polyaniline perchlorates prepared by different chemical methods: Soluble perchlorate I prepared by the use of copper(II) perchlorate as an oxidative coupling agent, and perchlorate II (corresponding to polyemeraldine perchlorate) obtained by treating a polymer base with perchloric acid. The ESR signal intensity of perchlorate I shows a thermally activated temperature dependence at temperatures between 95 and 300 K. The ESR signal intensity of perchlorate II was temperature-independent. When this polymer adsorbed oxygen, the ESR signal showed a thermally activated paramagnetism resembling that of perchlorate I. These paramagnetic properties can be explained by polaron spins that are antiferromagnetically coupled with each other, and are different from the Pauli-type paramagnetism. This suggests that the charge-transport cannot be explained by the migration of paramagnetic polarons along a polymer chain alone.

The charge transport of polyaniline is sensitively dependent on the protonation of the polymer chains,[1,2] and the protonation results in a significant enhancement of paramagnetism.[1-3] The relation between the charge transport and the magnetic properties is the important subject of the conducting polyaniline. Usually electroconducting polymers contain a significant number of unpaired electrons due to defects of polymer chains. The susceptibility of these defect spins is strongly temperature-dependent. This makes it difficult to study the intrinsic paramagnetism, which is expected to be weakly temperature-dependent. Recently, we have reported that a polymerization of aniline by the use of copper(II) perchlorate as an oxidative coupling agent yields a polyaniline perchlorate that has a doping level of ca. 0.4 per polymer unit and is soluble in dimethyl sulfoxide (DMSO).[4] The solubility is expected to be due to a low degree of chain defect and/or cross linking of polymer chains. Therefore, the new polyaniline perchlorate is a good material for studying the intrinsic magnetism of conducting polyaniline. Preliminarily we have reported that the electron spin resonance (ESR) signal intensity of this perchlorate shows a thermally activated temperature dependence differing from the Pauli-type paramagnetism.[5] The present paper is the full report of the ESR study.

Experimental

Perchlorate I in Table 1 was prepared by the method reported in our previous paper:[4] Freshly distilled aniline was polymerized by the use of copper(II) perchlorate as an oxidative coupling agent in acetonitrile. The resulting powder material was washed with acetonitrile in a Soxhlet extractor to eliminate possible oligomer components and copper perchlorate. The obtained polymer did not show an ESR signal attributable to Cu(II) species. A polymer base was obtained by treating the perchlorate with 4.5 M NH_3 solution for 20 h. By treating this polymer base with 3 M perchloric acid for 3 h, perchlorate II was obtained. The compositions determined by elemental analyses for the three polymers are shown in Table 1 together with the room-temperature conductivity. The elemental analyses were performed by Huffman Laboratories, Golden, CO., U.S.A.

Table 1. ESR Data Observed for Polyanilines at Room Temperature: g Value and Molar Magnetic Susceptibility χ (in emu mol^{-1}) per $-C_6H_4NH_y-$ Unit and Peak-to-Peak Width W in Oxygen-Free and Oxygen-Adsorbing States

Polyaniline	σ/S cm^{-1}	g	$10^6\chi$	W/G	
				O_2-free	O_2-ads
Perchlorate I[a]	1.3	2.0027	40	0.28	2.0
Polymer base[b]	10^{-10}	2.0036	0.3	8.5	8.5
Perchlorate II[c]	1.8	2.0027	45	0.42	1.5

a) As-prepared perchlorate: $[(-C_6H_4NH-)(ClO_4)_{0.4}\cdot 0.4H_2O]_n$. b) Base: $[(-C_6H_4NH-C_6H_4NH-)_{1-x}(-C_6H_4N=C_6H_4=N-)_x\cdot 0.4H_2O]_n$ ($x\approx 0.6$). c) Perchlorate prepared from the base: $[(-C_6H_4NH-)(ClO_4)_{0.4}\cdot 0.6H_2O]_n$.

The ESR spectra were obtained with the aid of a JEOL SCXA ESR spectrometer. The sample temperature was controlled by flowing a cold nitrogen gas between 95—300 K. Mn^{2+}/MgO and DPPH were used as references. The ESR spectra were recorded on the two conditions for each material: 1) The oxygen-free samples were sealed with He gas in a quartz tube after kept in dynamic vacuum for 3—4 h, and 2) the oxygen-adsorbing samples were sealed in a cell with He gas after equilibrated with atmospheric oxygen. Each observed derivative curve was digitized and doubly integrated: The error of the integration was ca. 20%. The magnetic susceptibility was calculated by referring to the signal intensity of Mn^{2+}/MgO powder used as a marker, the susceptibility of which was calibrated with DPPH. The molar susceptibility was calculated for each $-C_6H_4NH_y-$ unit. The electrical conductivity was determined on the compressed pellets of the powder materials by van der Pauw's four-probe method.

Results

Electrical Conductivities. The room-temperature conductivities are shown in Table 1. The two perchlorates show a semiconductive property with an activation energy of 0.04 eV at high temperatures, and the temperature dependence throughout the temperature range investigated (80—300 K) is explained by the variable-range hopping model (Figs. 1 and 2):[6]

$$\sigma = (T_0/T)^{1/2}\exp[-(A/kT)^{1/4}] \quad (1)$$

The parameters obtained were: T_0=4.2×10^{11} K and A/k=3.2×10^6 K for perchlorate I, and T_0=5.5×10^{12} K and A/k=4.5×10^6 K for perchlorate II. No significant difference is appreciable for the charge-transport properties of the two perchlorates.

ESR of Perchlorate I (As-Prepared Perchlorate). The ESR spectrum of perchlorate I showed a symmetric signal with a g value of 2.0027 and a peak-to-peak width W of 0.28 G (G=10^{-4} T). The g value was temperature-independent. In contrast, the W was temperature-dependent as shown in Fig. 3: It showed a maximum at 185 K. The magnetic susceptibility calculated from the signal intensity at 297 K was 0.3×10^{-6} emu g^{-1}, which gave a molar magnetic susceptibility of 40×10^{-6} emu mol^{-1} for each aniline unit. Figure 4 shows the temperature dependence of the relative signal intensity I_r= $I(T\,\mathrm{K})/I(297\,\mathrm{K})$, which is proportional to the magnetic susceptibility. The I_r gradually decreased with decreasing temperature, differing from that reported for polyemeraldine salts[3] prepared by the use of ammonium peroxodisulfate, $(NH_4)_2S_2O_8$, as an oxidative coupling agent.

When the perchlorate was exposed to air, the peak-to-peak width increased (W=2.0 G at 297 K), and showed a strong temperature-dependence (Fig. 3). The ESR relaxation is markedly influenced by the adsorption of oxygen molecules. On the other hand, the integrated signal intensity was unchanged by oxygen adsorption.

ESR of Polymer Base. The treatment of perchlorate I with an alkaline solution yielded an insulating polymer base $[(-C_6H_4-NH-C_6H_4-NH-)_{1-x}(-C_6H_4-N=C_6H_4=N-)_x]_n$

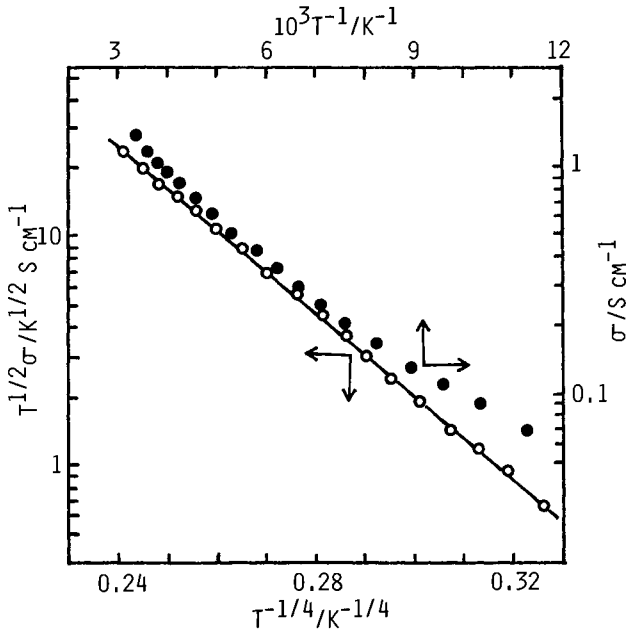

Fig. 1. Electrical conductivity σ of the as-prepared polyaniline (perchlorate I). The solid line shows the hopping model.

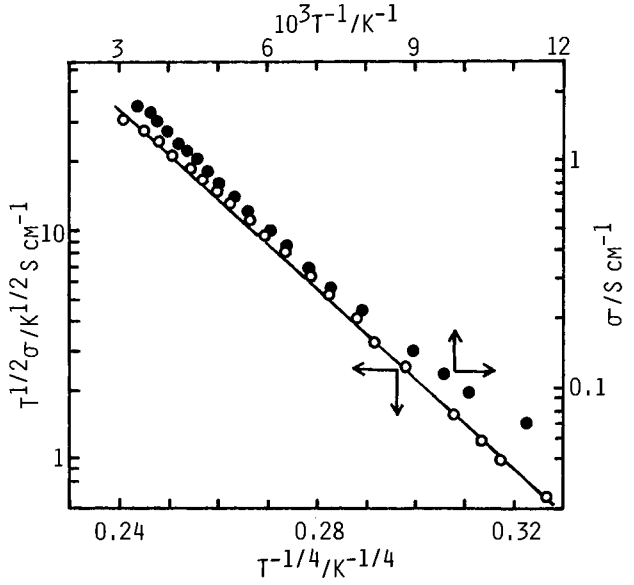

Fig. 2. Electrical conductivity σ of perchlorate II obtained by the protonation of polyemeraldine base. The solid line shows the hopping model.

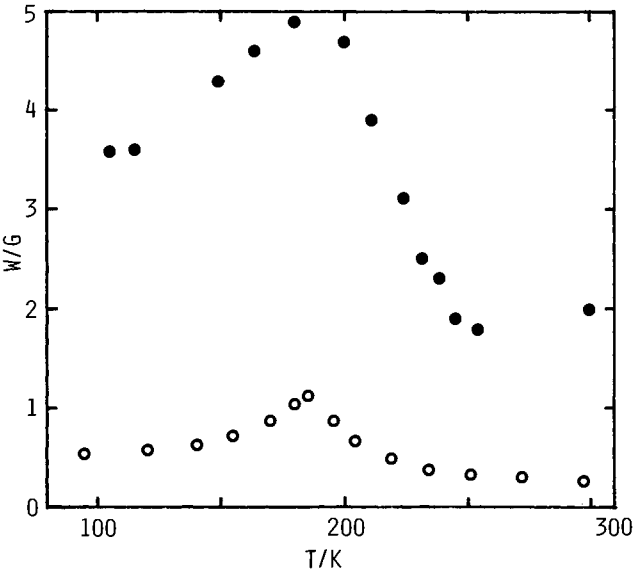

Fig. 3. Temperature dependence of the peak-to-peak width W/G (G=10^{-4} T) of perchlorate I in oxygen-free (○) and oxygen-adsorbing (●) states.

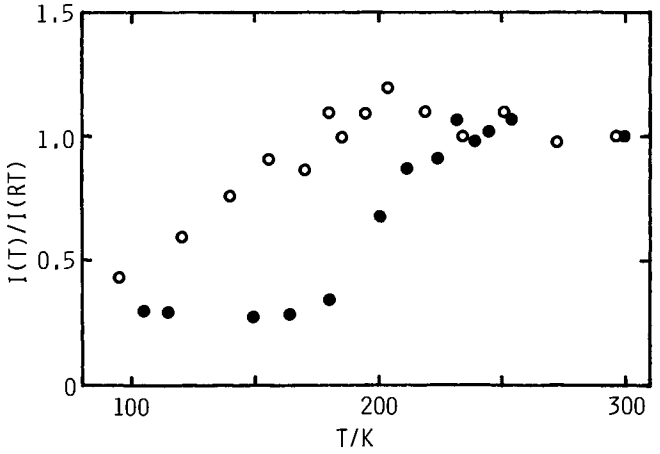

Fig. 4. Temperature dependence of the relative signal intensity $I(T\ \mathrm{K})/I(\mathrm{Room\ Temp})$ of perchlorate I in oxygen-free (○) and oxygen-adsorbing (●) states.

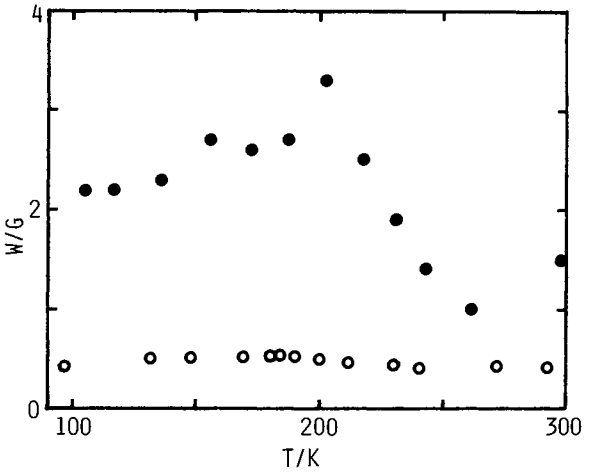

Fig. 5. Temperature dependence of the peak-to-peak width W/G (G=10^{-4} T) of perchlorate II in oxygen-free (○) and oxygen-adsorbing (●) states.

with $x\approx0.6$; the composition is practically identical with that of polyemeraldine base. The polymer base showed a broad ESR signal with a g value of 2.0036 and a peak-to-peak width W of 8.5 G at 297 K. These ESR parameters were temperature-independent throughout the temperature range investigated. The magnetic susceptibility was 3×10^{-9} emu g^{-1}: This gave a molar susceptibility of 3×10^{-7} emu mol^{-1} for each $-C_6H_4NH_y-$ unit. The signal intensity $I_r=I(T\ \mathrm{K})/I(297\ \mathrm{K})$ obeyed the Curie–Weiss law $I_r=C/(T-\theta)$ with $\theta=-21$ K throughout the temperature range investigated (95—300 K). These magnetic properties were not substantially influenced by adsorption of oxygen: g=2.0036, W=8.5 G at 297 K, and $\theta=-14$ K for the oxygen-adsorbing polymer. The Curie constant C was calculated to be 9×10^{-5} emu K mol^{-1} for each ring by referring to the room temperature susceptibility. A spin system containing one unpaired electron on each site has the Curie constant 0.375 emu K mol^{-1}. The ratio C/0.375 gave a spin density of 2×10^{-4} per $-C_6H_4NH_y-$ unit. This spin density is much smaller than that reported for polyemeraldine base prepared by the conventional method.[3] The polymer obtained by the use of the new oxidant contains a very small number of chain defects.

ESR of Perchlorate II (Perchlorate Obtained from Polymer Base). When the polymer base was treated with perchloric acid, the ESR signal narrowed (W= 0.42 G and g=2.0027 at 293 K), and the signal intensity increased by a factor of 100. The susceptibility of this perchlorate was equal to that of the as-prepared polymer (perchlorate I) within the experimental error (Table 1). Figures 5 and 6 show the peak-to-peak width W and the signal intensity I_r, respectively, as functions of temperature. The I_r showed a very weak temperature-dependence. Upon adsorbing oxygen, the signal broadened markedly (Fig. 5), whereas the integrated signal intensity at room temperature was unchanged. The I_r of the oxygen-adsorbing sample showed a thermally

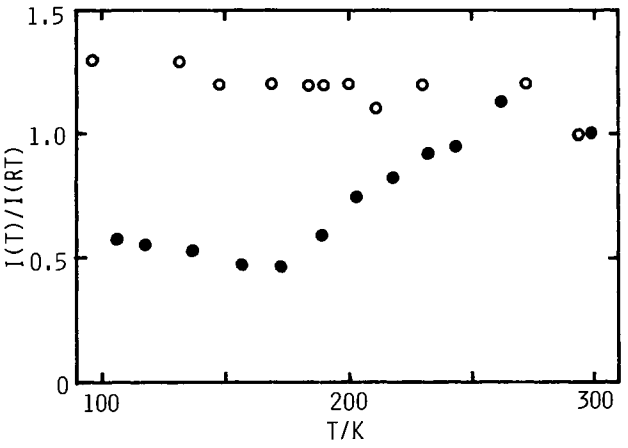

Fig. 6. Temperature dependence of the relative signal intensity $I(T\ \mathrm{K})/I(\mathrm{Room\ Temp})$ of perchlorate II in oxygen-free (○) and oxygen-adsorbing (●) states.

activated temperature dependence (Fig. 6), in contrast to the oxygen-free sample.

Discussion

The solution electronic spectrum of the as-prepared polymer (perchlorate I) shows that the charge carriers are paramagnetic polarons rather than diamagnetic bipolarons.[4] The intrinsic magnetism of the polarons is expected to be observed for the polymer. The nature of the ESR spectra is markedly influenced by oxygen adsorption. The similar oxygen-adsorption effect has been extensively studied for polyacetylene, and it has been interpreted by the coexistence of mobile spins and trapped spins, although the ESR signals of the two different spin species have not been observed individually.[7] The ESR peak-to-peak width W of perchlorate I markedly increases upon oxygen adsorption. The oxygen-adsorbing polymer shows a clear maximum of

W at ca. 185 K. Around this temperature, the differential scanning calorimetry showed no appreciable thermal anomaly; usually, a sudden change of ESR relaxation accompanies a phase transition. Therefore, it is probable that additional spin sites are formed by oxygen adsorption, as proposed for polyacetylene: The temperature dependence of W can be explained by the presence of two spin species, line-widths of which exhibit different temperature dependence. The more important experimental result is that the temperature dependence of the signal intensity observed for the polymer is different from that reported for polyemeraldine salts. The signal intensity of the latter polymer increases with decreasing temperature, but it deviates from the Curie–Weiss law. This magnetic behavior has been explained by the superposition of a strong Curie-type paramagnetism and a weak temperature-independent paramagnetism.[1-3,8] In contrast, the signal intensity of polyaniline perchlorate I decreases with decreasing temperature. Obviously, at least one of the two possible spin species in perchlorate I shows a thermally activated temperature dependence, although their ESR signals cannot be distinguished from each other. This magnetic property is not explained by the Pauli-type paramagnetism. In polyaniline, the molecular planes of the neighboring $-C_6H_4NH-$ groups are twisted with one another due to a steric effect,[2,9] and hence the electronic band formed by the π-electron overlap is not expected to be wide enough to show the Pauli paramagnetism. A thermally activated paramagnetism similar to that of the perchlorate has been reported for a variety of paramagnetic compounds that have a strong antiferromagnetic interaction via superexchange interaction mechanism.[10] This type of magnetic interaction is operative between unpaired electrons that reside on the conjugated system of a polymer chain.[11] A conceivable interaction mechanism for polyaniline is schematically shown in Fig. 7: A polaron spin that resides on a positively charged nitrogen atom induces a spin polarization of a π electron on the adjacent carbon atom, and this spin polarization is induced in succession until another unpaired electron is encountered on a nitrogen atom. Consequently, the two unpaired electrons are antiferromagnetically coupled with each other. This antiferromagnetic interaction may occur among a number of polaron spins existing on a polymer chain. The ground level of this spin system is singlet and the paramagnetism is induced by a thermal activation.

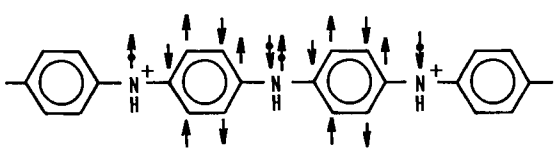

Fig. 7. Superexchange interaction operative between two polaron spins in a polyaniline chain. An unpaired electron on a positively charged nitrogen atom causes the spin polarization of a π electron on the adjacent carbon atom. The spin polarization is induced in succession until another unpaired electron is encountered. Consequently, the two unpaired electrons are coupled antiferromagnetically.

In the course of the treatment of a polymer base with acid, protonation is expected to occur in preference at the quinone-imine nitrogen and to yield bipolarons that have no unpaired electron. The magnetic susceptibility of the resulting polymer salt, however, is a factor of 100 larger than that of the parent polymer base. On the basis of this observation, Ginder et al.[8] have proposed that a bipolaron produced by protonation is converted to two polarons by an internal redox reaction and the resulting polarons migrate successively so as to reduce the Coulomb repulsion. This mechanism well explains the origin of the paramagnetism induced by protonation. On the other hand, the X-ray photoelectron spectra (XPS) of polyemeraldine salts exhibit a weak nitrogen Is peak attributable to bipolarons in addition to a strong polaron peak.[12-14] The solution electronic spectrum and the XPS of polyaniline perchlorate II have evidenced that a small number of bipolarons coexist with polarons in the polymer chains, whereas perchlorate I contains no significant number of bipolarons.[4,14] This is an important structural difference between perchlorates I and II. A bipolaron that is diamagnetic may be thermally excited to two neighboring paramagnetic polarons. When these two states are in a thermal equilibrium, a thermally activated magnetism is expected to be observed. The interconversion between a bipolaron state and a two-polaron state is, however, accompanied by a polymer conformation rearrangement,[4] which requires a large activation energy. In a normal temperature range, therefore, the thermal activation of a bipolaron to two polarons in solid state is hardly observed in the susceptibility vs. temperature curve. On the other hand, the superexchange interaction is readily influenced by the electronic state of intervenient atoms between interacting polarons. In this manner, bipolarons that coexist with polarons in perchlorate II may result in the difference between the magnetic properties of the two perchlorates in oxygen-free states. In oxygen-adsorbing states, the two perchlorates show an identical temperature dependence of signal intensity. Since the oxygen-adsorbing materials show a stronger temperature dependence than that of the corresponding oxygen-free materials, the oxygen-adsorption enhances the magnetic interaction between polarons, so that the effect of the structural difference is smeared out.

The charge-transport of polyaniline has been explained by the hopping of paramagnetic polarons along the polymer chains. The present study has shown that the polyaniline chains do not show the Pauli-type paramagnetism. Two explanations are conceivable: 1) Hopping polarons responsible for charge-transport do

not show the Pauli-type paramagnetism, and 2) there is no direct relation between the two physical properties. The second case is consistent with a recent theoretical calculation of doped polyaniline, which has indicated that large spin densities are distributed on nitrogen atoms whereas large net-charge densities exist on phenyl rings.[9] These results suggest that the charge transport in polyaniline cannot be explained by paramagnetic polaron migration along a polymer chain alone. An additional effect contributes to the charge transport. For example, a charge transfer between phenyl rings that face to each other in proximity may be one of the important contributing factors.

The work at the Universidad de Sonora was supported by the Consejo Nacional de Ciencia y Tecnología, Mexico (Grant No. P228CCOX891769).

References

1) Proceedings of International Conference of Science and Technology of Synthetic Metals, Santa Fe, NM, U.S.A., 1988, *Synth. Met.*, **29**, (1989).

2) E. M. Geniès, A. Boyle, M. Lapkowski, and C. Tsintavis, *Synth. Met.*, **36**, 139 (1990).

3) H. H. S. Javadi, R. Laversanne, A. J. Epstein, R. K. Kohli, E. M. Scherr, and A. G. MacDiarmid, *Synth. Met.*, **29**, E439 (1989), and references cited therein.

4) M. Inoue, R. E. Navarro, and M. B. Inoue, *Synth. Met.*, **30**, 199 (1989).

5) M. Inoue, H. Grijalva, M. B. Inoue, M. Iida, T. Asaji, R. Ikeda, and D. Nakamura, Proceedings of International Conference of Science and Technology of Synthetic Metals, Tübingen, Germany, 1990, *Synth. Met.*, **41**, 679 (1991).

6) F. Zuo, M. Angelopoulos, A. G. MacDiarmid, and A. J. Epstein, *Phys. Rev. B: Condens. Matter*, **39**, 3570 (1989).

7) M. Nechtschein, F. Devreux, F. Genoud, M. Guglielmi, and K. Holczer, *Phys. Rev. B: Condens. Matter*, **27**, 61 (1983).

8) J. M. Ginder, A. F. Richter, A. G. MacDiarmid, and A. J. Epstein, *Solid State Commun.*, **63**, 97 (1987).

9) K. Tanaka, S. Wang, and T. Yamabe, *Synth. Met.*, **36**, 129 (1990).

10) J. B. Goodenough, "Magnetism and the Chemical Bond," Interscience, New York (1963).

11) M. Inoue, M. B. Inoue, M. M. Castillo-Ortega, M. Mizuno, T. Asaji, and D. Nakamura, *Synth. Met.*, **33**, 355 (1989).

12) E. T. Kang, K. G. Neoh, T. C. Tang, S. H. Khor, and K. L. Tan, *Macromol.*, **23**, 2918 (1990).

13) S. N. Kumar, F. Gaillard, G. Bouyssoux, and A. Sartre, *Synth. Met.*, **36**, 111 (1990).

14) M. B. Inoue, K. W. Nebesny, Q. Fernando, and M. Inoue, *J. Mat. Chem.*, **1**, 213 (1991).

Reproduction of Bifurcation Structure of Belousov–Zhabotinskii Reaction in Flow System by Oscillatory Flow Term Oregonator

Shinji SAKANOUE, Chiaki MURASE,† and Mitsuo ENDO*
Department of Chemistry, Faculty of General Education, Tokyo University of Agriculture and Technology, Saiwaicho, Fuchu, Tokyo 183
† Department of Physics, Faculty of General Education, Tokyo University of Agriculture and Technology, Saiwaicho, Fuchu, Tokyo 183
(Received December 28, 1990)

Simulation has been made on the oscillatory flow term Oregonator model (OFO) proposed in our previous paper for the Belousov–Zhabotinskii reaction (BZ reaction) accompanying constant feed. When the amplitude of the forced oscillation term in OFO is taken extremely small, the computational simulation with this model finely reproduces the oscillatory mode, many types of wave patterns including nonperiodic chaotic behaviors and the bifurcation structure, which appear in the experimental results of the BZ reaction in flow system.

There have been numbers of experimental and theoretical studies[1-5] on the Belousov–Zhabotinskii reaction (BZ reaction) in a continuous-flow stirred tank reactor. Hudson et al.[1] have investigated experimentally BZ reaction in the flow system and found complex phenomena such as several types of periodic multipeak oscillations and chaotic(nonperiodic) behavior. In our previous paper[6,7] for the purpose of reproducing these phenomena by computational simulation, we proposed a model in which a flow term was added to the original Oregonator's equation[8] proposed by Tyson[9], i.e. Oregonator+flow term. Mathematically the model can be expressed by the following differential equations:

$$\mathrm{d}\boldsymbol{X}/\mathrm{d}t = \boldsymbol{O}(\boldsymbol{X}) + R(\boldsymbol{X}^{\mathrm{I}} - \boldsymbol{X}), \tag{1A}$$

where the first term $\boldsymbol{O}(\boldsymbol{X})$ denotes the original Oregonator and the second term $R(\boldsymbol{X}^{\mathrm{I}}-\boldsymbol{X})$ the flow term; or more explicitly,

$$\begin{aligned} \mathrm{d}X/\mathrm{d}t &= (1/\varepsilon)(X + Y - qX^2 - XY) + R(X^{\mathrm{I}} - X), \\ \mathrm{d}Y/\mathrm{d}t &= -Y + fZ - XY + R(Y^{\mathrm{I}} - Y), \\ \mathrm{d}Z/\mathrm{d}t &= (1/p)(X - Z) + R(Z^{\mathrm{I}} - Z), \end{aligned} \tag{1B}$$

where all variables are set dimensionless; and X, Y, and Z are the component of the concentration $\boldsymbol{X}$ corresponding to the concentrations of the three chemical species $HBrO_2$, Br^-, and Ce^{4+}, respectively; and ε, p, and q are the parameters with regard to the rate constants of elementary reactions and f is the paprameter with reference to a stoichiometric coefficient, R corresponds to the flow rate, and t is the time variable. The terms containing R in Eq. 1 are the flow terms to be added to the original Oregonator $\boldsymbol{O}(\boldsymbol{X})$. The X^{I}, Y^{I}, and Z^{I} in them are the components of inflow term $\boldsymbol{X}^{\mathrm{I}}$, and they consist of both the time-independent term $\boldsymbol{X}^0(X^0, Y^0, Z^0)$ and the time-dependent one $\boldsymbol{X}^{\mathrm{I}}(X^{\mathrm{I}}, Y^{\mathrm{I}}, Z^{\mathrm{I}})$:

$$\boldsymbol{X}^{\mathrm{I}} = \boldsymbol{X}^0 + \boldsymbol{X}^{\mathrm{I}}(t), \tag{2A}$$

and the components of $\boldsymbol{X}^{\mathrm{I}}$ are taken as follows

$$\begin{aligned} X^{\mathrm{I}} &= X^0 + Q_x \sin(-\Omega t), \\ Y^{\mathrm{I}} &= Y^0 + Q_y \cos \Omega t, \\ Z^{\mathrm{I}} &= Z^0 + Q_z \sin(-\Omega t), \end{aligned} \tag{2B}$$

where Ω is the angular frequency of the oscillation of the time-dependent term $\boldsymbol{X}^{\mathrm{I}}(t)$, and Q_x, Q_y, and Q_z are the amplitudes of the oscillation of $\boldsymbol{X}^{\mathrm{I}}(t)$. We called the above model the "oscillatory flow term Oregonator" ("OFO"). When $\boldsymbol{X}^{\mathrm{I}}=\boldsymbol{X}^0$, that is the OFO without the time-dependent term $\boldsymbol{X}^{\mathrm{I}}$, we called it the "constant flow term Oregonator" ("CFO"). Here we took the time-independent term $\boldsymbol{X}^0(X^0, Y^0, Z^0)$ to be the steady state of the original Oregonator. Figure 1 shows the three types of global behaviors of the trajectories of CFO projected onto Y–Z plane, which we call the extended state, the intermediate state and the localized state as shown in Fig. 2. In the intermediate state an orbit falls into $\boldsymbol{X}^0$, but a large part of a limit cycle, which we call the semi-global limit cycle, remains around $\boldsymbol{X}^{\mathrm{S}}$. One of the steady state $\boldsymbol{X}^0$ of CFO is common with the steady state of the original oregonator $\boldsymbol{O}(\boldsymbol{X})$ in Eq. 1 and exist for all values of flow rate R. The additional

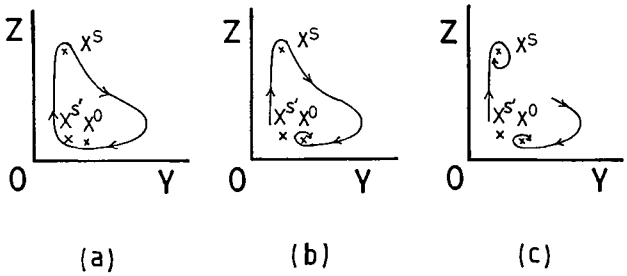

Fig. 1. Schematic representation of three types of behaviors of trajectories of the constant flow term Oregonator (CFO model) in Y–Z plane. $\boldsymbol{X}^0$, $\boldsymbol{X}^{\mathrm{S}}$, $\boldsymbol{X}^{\mathrm{S}'}$; steady states. (a) extended state, (b) intermediate state, and (c) local state.

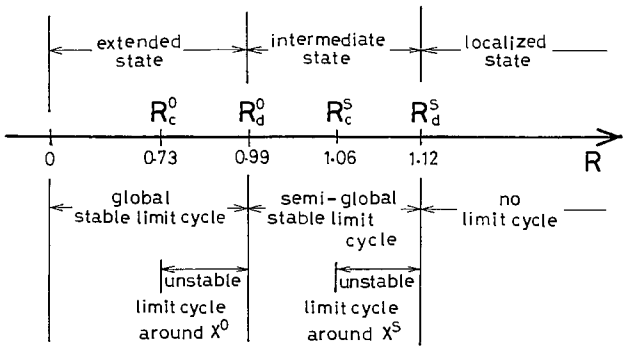

Fig. 2. Relation between three types of global behaviors of CFO and the existence of limit cycles for the ranges of flow rate R.

two steady states X^S and $X^{S'}$ of CFO exist in the flow rate range $0.54<R<5.99$. For the range of the flow rate 0.95—1.10 to be considered later three steady states exist; and consequently, CFO is in a multisteady state. The cross signs in Fig. 1 denote the positions of these three steady states. The CFO can also have a stable and an unstable limit cycle in a certain range of R as shown in Fig. 2.

In the previous paper[6] we showed the behavior of OFO in which the parameters ε, q, f, p, and Ω in Eq. 1 were chosen as follows;

$$\varepsilon = 0.05, \quad q = 0.01, \quad f = 1.8, \quad p = 3 \quad \Omega = 0.75, \quad (3)$$

and the components of the amplitude $\boldsymbol{Q}$ of the forced oscillation in Eq. 2 were set to

$$Q_x = 2, \quad Q_y = 0.5, \quad Q_z = 1. \quad (4)$$

These values of the amplitude $\boldsymbol{Q}$ were chosen about 1/15—1/40 of the amplitude of the stable limit cycle of the original Oregonator. This implies that the forced oscillation very weakly acts in OFO. In order to distinguish the combined parameter set of (3) and (4) from the parameter set in this paper, we call it the "OFO-I". In the previous paper[6] we indicated that the OFO-I could qualitatively exhibit the characteristic features of the experimental results by Hudson et al., but we could not succeed in reproducing the fine details of the oscillatory modes, the wave patterns and the nonperiodic chaotic behaviors which appear in the experiment on the BZ reaction of flow system.

In this study we take the values of the amplitude $\boldsymbol{Q}$ as

$$Q_x = 0.07, \quad Q_y = 0.0175, \quad Q_z = 0.035, \quad (5)$$

which is extremely smaller than the values of (4) of OFO-I. These magnitudes of the amplitude of forced oscillation are about 1/1000—3/1000 of the amplitude of the limit cycle of the original Oregonator, and is about 1/29 of the amplitude of forced oscillation of OFO-I. The other parameters ε, q, p, f, and Ω are set fixed again to the same values of the set (3). We call the OFO with the combined parameter set of (3) and (5) the "OFO-II". The following would show that the simulational results on the OFO-II can exhibit not only the elementary features of the experiment qualitatively, but also a fine agreement with the experimental results on the oscillatory modes, the wave patterns and the nonperiodic chaotic behaviors. Simply speaking the OFO-II can reproduce the detailed bifurcation structure of the flow rate R.

Results

We carry out the computational simulation on the OFO model of the Eq. 1 with the parameter set of the OFO-II, where the magnitudes of the amplitude $\boldsymbol{Q}$ in the time-dependent term X^1 in Eq. 2B are set extremely small values of Eq. 5. The time variation of the OFO-II is determined by the Runge–Kutta Gill's method. The value of the flow rate R is varied by the increase of 0.002 throughout the range of 0.950—1.100, which include both the upper end of the extended state and all the range of the intermediate state of CFO shown in Fig. 2. Figure 3 shows the projections of the typical trajectories of both the OFO-I and the OFO-II onto Y–Z plane, where the three steady states X^0, X^S, and $X^{S'}$ of CFO are marked with the crosses. In the range of R mentioned above, X^0 is a stable focus while X^S changes from an unstable focus to a stable focus, and $X^{S'}$ is a saddle point as shown in Fig. 4. As can be seen from Fig. 3, the orbit of OFO-I turns around X^S while that of OFO-II passes through X^S and turns around X^0. For $0.73<R<0.99$, CFO has an unstable limit cycle around X^0 as shown in Fig. 2. The typical oscillatory wave patterns from the OFO-II are shown in Figs. 5—7 for the series of values of the flow rate R. In these figures the patterns from the experiment by Hudson et al.[1] are also shown for comparison. Here we adopted the abbreviated notations of the mode for oscillatory patterns introduced by Tomita et al.[10] like as; (1) $\Pi(n)$ denotes an n-peaked periodic mode, (2) $\Pi_{l_n,l_m}(n, m)$ a periodic switching between l_n times $\Pi(n)$-like and l_m times $\Pi(m)$-like mode, (3) $\chi(n, m)$ a chaotic switching between $\Pi(n)$-like and $\Pi(m)$-like modes. We introduce the notation $\Pi(S)$ for the periodic oscillation with a small amplitude only.

We have ever summarized the qualitative features of oscillation behaviors of the results of the experiment by Hudson et al.[1] into the following three points; (a) two types of the peaked oscillations, one with a large amplitude and the other with a small amplitude, (b) multi-peaked oscillations with a large amplitude and some small amplitudes, and (c) the mixing of two types of oscillations and the sandwiched structure in the bifurcation structure for the flow rate R. We could express these three features more explicity using the notation of oscillation mode mentioned above; (a) the 2-peaked

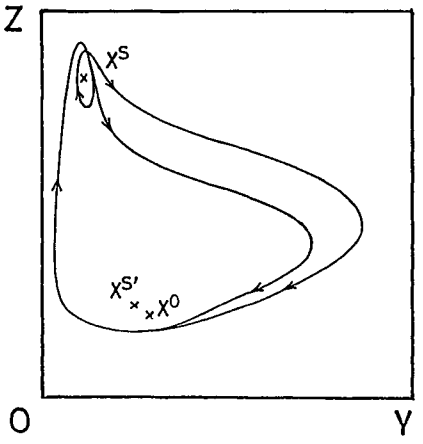

(a) OFO-I Q_x=2.0, Q_y=0.5, Q_z=1.0, R=1.06.

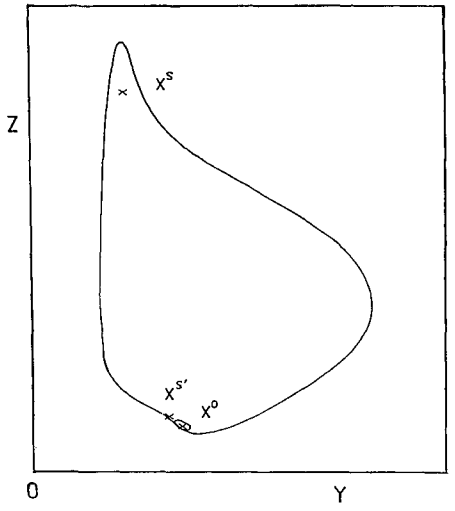

(b) OFO-II Q_x=0.07, Q_y=0.0175, Q_z=0.035, R=1.00.

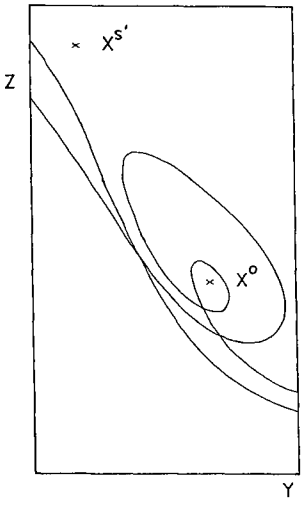

(c) Magnification of orbit around X^0 in (b).

Fig. 3. Typical behaviors of the two types of trajectories in Y–Z plane corresponding to the different two amplitudes in OFO model. $\boldsymbol{X}^0$, $\boldsymbol{X}^S$, $\boldsymbol{X}^{S'}$; steady states.

Stationary state	R				
	0	0.54	0.73	0.74	1.06
$\boldsymbol{X}^0$	UF		SF		
$\boldsymbol{X}^S$	—	UN		UF	SF
$\boldsymbol{X}^{S'}$	—	S			

Fig. 4. Change of local behaviors of orbits around steady states with varitaion of flow rate R. UF: unstable focus, SF: stable focus, UN: unstable node, S: saddle, —: nonexistence of the stationary state.

oscillation $\Pi(2)$, for example, is composed of one large amplitude oscillation and one small amplitude oscillation, (b) $\Pi(5)$, for example, expresses the 5-peaked oscillation with one of the large amplitude and four of the small amplitude, (c) $\Pi_{1,1}(1,3)$, for example, implies the mixing oscillation of $\Pi(1)$ and $\Pi(3)$, and the sandwiched structure of those two types of modes means that the range of the flow rate R at which $\Pi_{1,1}(1,3)$ appears is sandwiched by the range of $\Pi(1)$ and that of $\Pi(3)$. In the previous paper we have showed that OFO-I can properly exhibit three qualitative features of experimental results. While, as we can see in Figs. 5—7, the OFO-II not only can exhibit the qualitative features (a)—(c) above mentioned, but also can reproduce all kinds of periodic oscillatory modes and wave patterns to be found in the Hudson's experimental results. Only the exception on this correspondence is that the mode $\Pi(4)$ from the experiment could not be found stably in the simulational results, but appear temporarily. For example the mode $\Pi(4)$ sometimes appears near the flow rate R=1.066 and continue to exist for some time, but as time goes on some other modes always mix with $\Pi(4)$ mode. This seems to mean that the mode $\Pi(4)$ cannot exist stably in OFO-II model, and we have judged that $\Pi(4)$ cannot be found in our simulation.

Figure 8 shows the bifurcation structures of oscillatory modes both from the simulation with OFO-II and from the Hudson's experiment. In the figure of the bifurcation structure we put the mark "○" on the value of R at which a periodic oscillation appears, and no mark on the other values of R at which nonperiodic oscillations, i.e. chaotic behaviors, are realized. The simulational results of the bifurcation structure agree very well qualitatively with the experimental one. On this correspondence there are two exceptions that the mode of $\Pi(4)$ can not be found in the simulational results as mentioned above, and the modes $\Pi_{1,1}(1,3)$ and $\Pi(2)$ are situated in reverse order one another on the increase of R value between (a) and (b) in Fig. 8.

From the analysis of the Hudson's experimental data Tomita et al.[10] found that the period T_p of a p-peaked periodic mode obeys a simple rule, namely

$$T_p = T + (p-1)\tau, \tag{6}$$

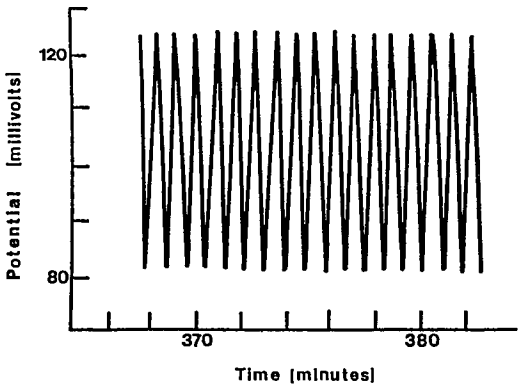

(a-1) Flow rate=2.91 ml min^{-1}

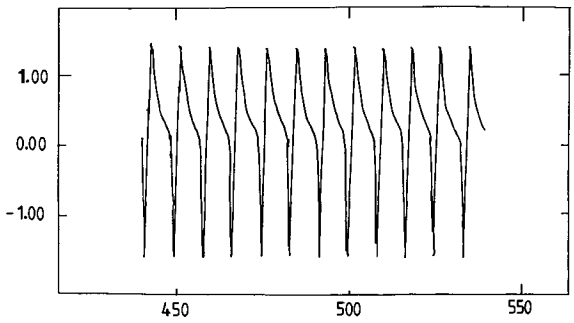

(a-2) $\Pi(1)$, R=0.9520

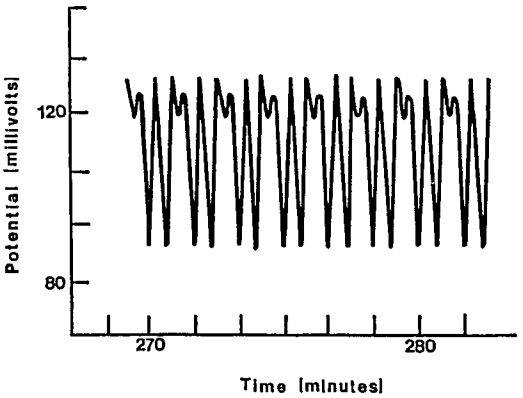

(b-1) Flow rate=3.76 ml min^{-1}

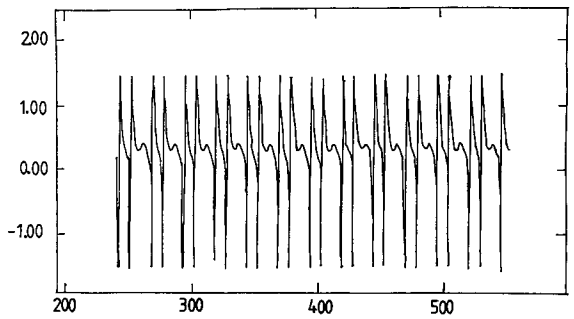

(b-2) $\Pi_{1,1}(1,2)$, R=0.9660

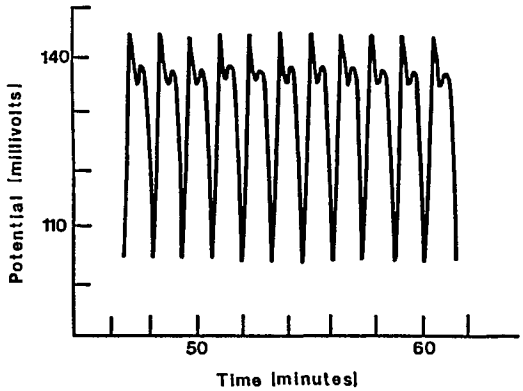

(c-1) Flow rate=4.06 ml min^{-1}

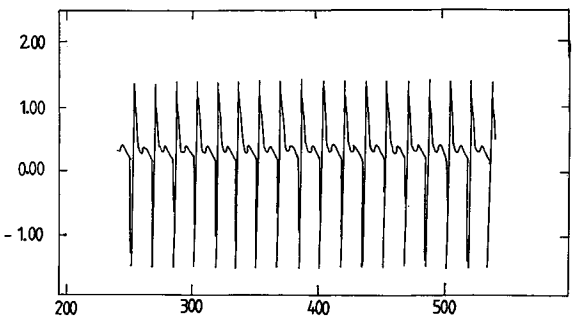

(c-2) $\Pi(2)$, R=1.0240

Fig. 5. Comparison of the wave patterns from OFO-II model (right hand side figures 2) with those from Hudson's experiment of Ref. 1 (left hand side figures 1) for the flow rate. (a-1), (b-1), and (c-1) are recordings from bromide ion electrode; T=25°C; Ce^{3+}catalyst. (a-2), (b-2), and (c-2) are our simulations for Q_x=0.07, Q_y=0.0175, Q_z=0.035.

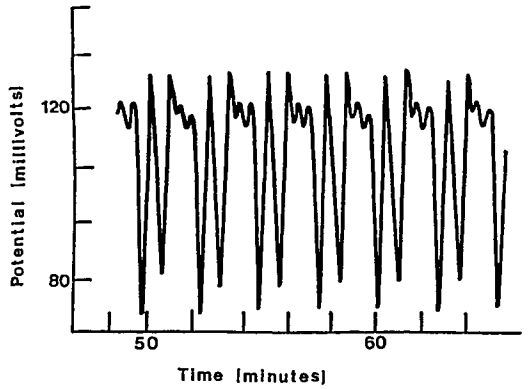

(d-1) Flow rate=3.99 ml min^{-1}

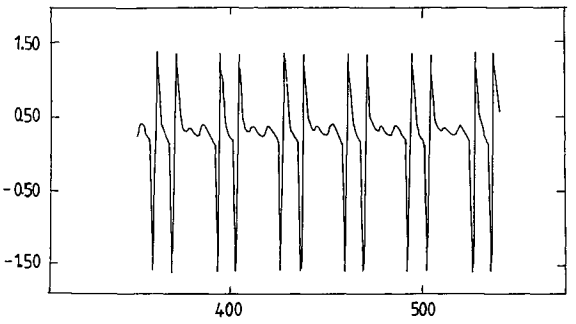

(d-2) $\Pi_{1,1}(1,3)$, R=1.0440

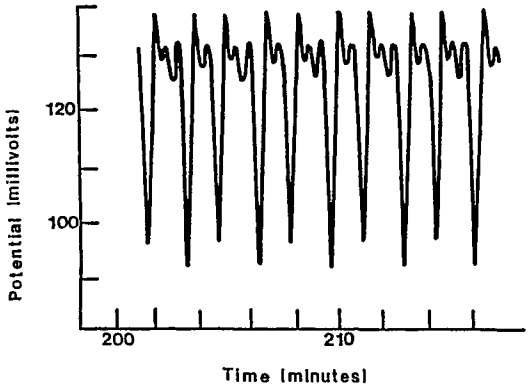

(e-1) Flow rate=4.11 ml min^{-1}

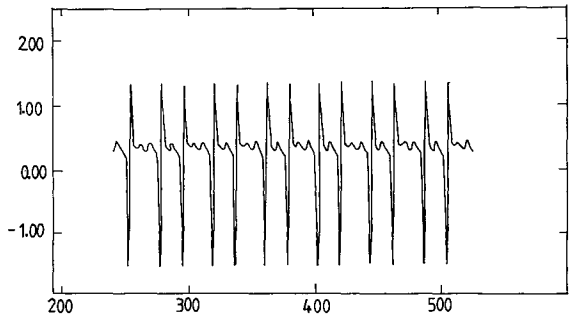

(e-2) $\Pi_{1,1}(2,3)$, R=1.0600

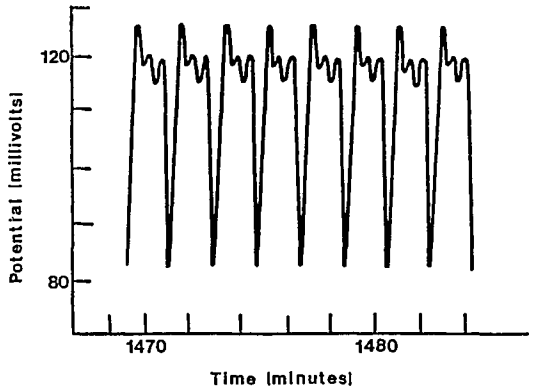

(f-1) Flow rate=4.34 ml min^{-1}

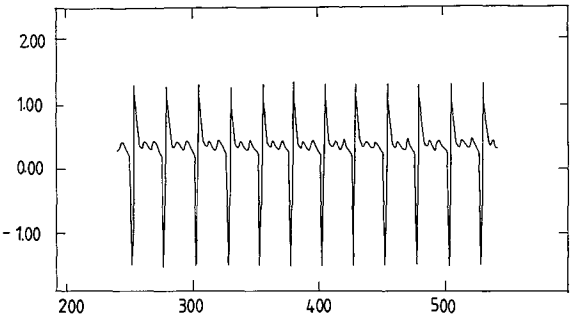

(f-2) $\Pi(3)$, R=1.0800

Fig. 6. Comparison of the wave patterns from OFO-II model (right hand side figures 2) with those from Hudson's experiment of Ref. 1 (left hand side figures 1) for the flow rate. (d-1), (e-1), and (f-1) are recordings from bromide ion electrode; T=25°C; Ce^{3+}catalyst. (d-2), (e-2), and (f-2) are our simulations for Q_x=0.07, Q_y=0.0175, Q_z=0.035.

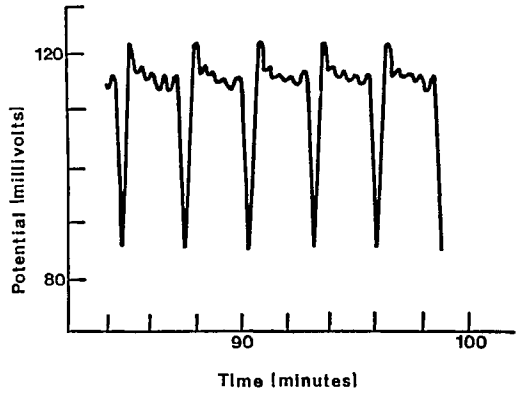

(g-1) Flow rate=4.81 ml min^{-1}

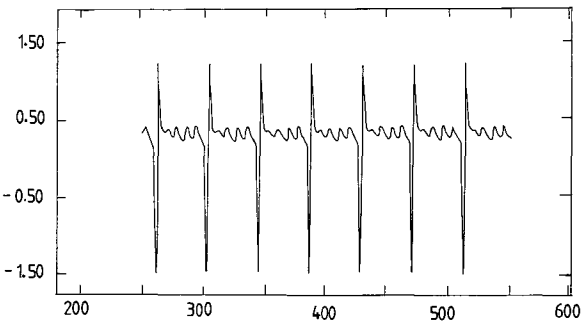

(g-2) $\Pi(5)$, R=1.0902

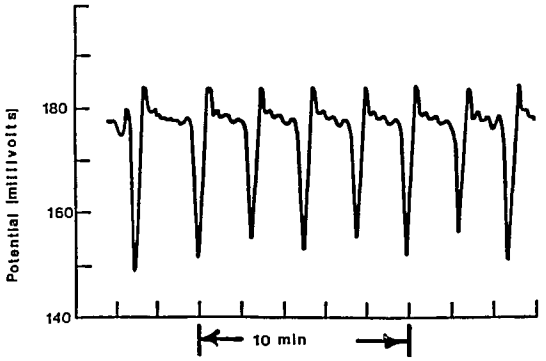

(h-1) Flow rate=4.76 ml min^{-1}

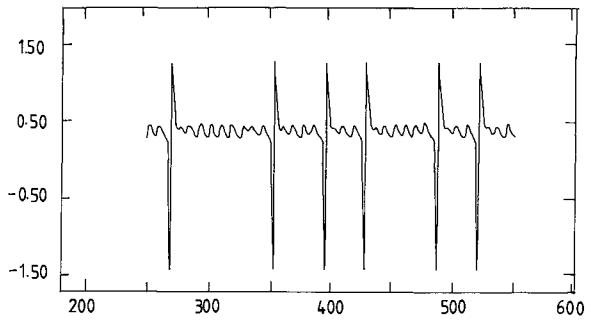

(h-2) χ, R=1.0912

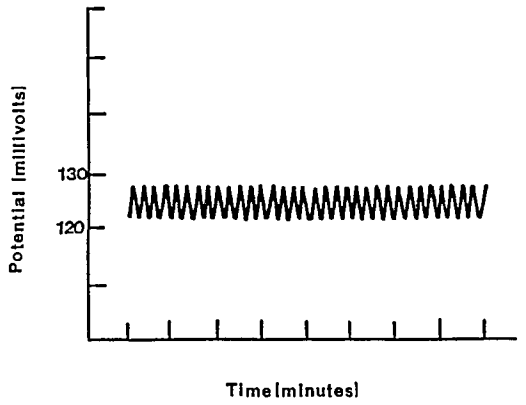

(i-1) Flow rate=5.42 ml min^{-1}

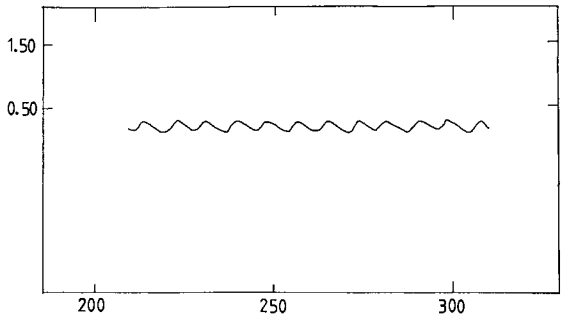

(i-2) $\Pi(S)$, R=1.0980

Fig. 7. Comparison of the wave patterns from OFO-II model (right hand side figures 2) with those from Hudson's experiment of Ref. 1 (left hand side figures 1) for the flow rate. (g-1), (h-1), and (i-1) are recordings from bromide ion electrode; T=25°C; Ce^{3+}catalyst. (g-2), (h-2), and (i-2) are our simulations for Q_x=0.07, Q_y=0.0175, Q_z=0.035.

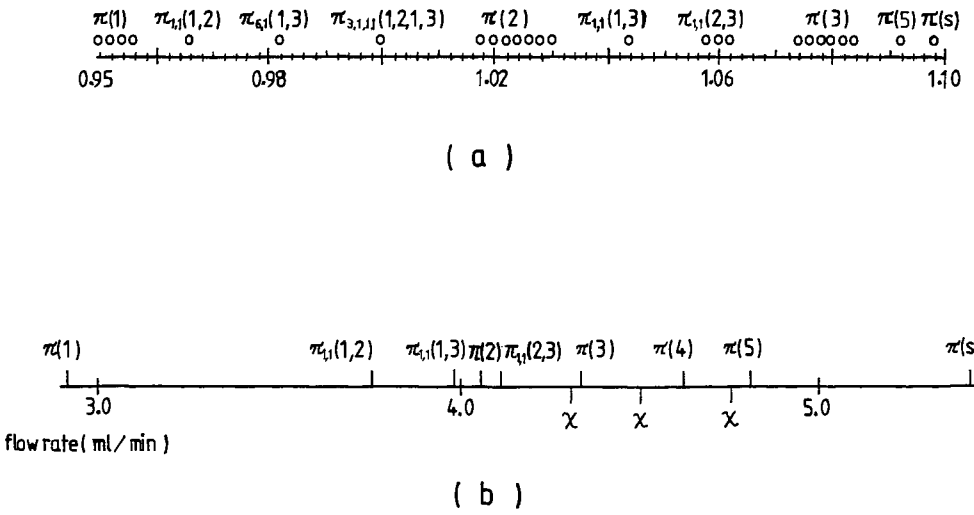

Fig. 8. Bifurcation structure of OFO-II model for flow rate R and its comparison with the Hudson's experimental results of Ref. 1. (a) Bifurcation structure from OFO-II. (b) Bifurcation structure from Hudson's experiment.

Table 1. Periods from Simulations and from Theoretical Formula (6)

Flow rate	Multiplicity	Periods	
R	p in π (P)	T_p(obs)[a]	T_p(theor)[b]
0.952	1	10.41	10.41
1.024	2	16.78	17.81
1.080	3	25.13	25.21
1.090	5	41.93	40.01

a) T_p(obs): period obtained from simulations. b) T_p(theor)$=T+(p-1)\tau$, $T=10.41$, $\tau=7.40$ (6).

where $p=1,2,3,4$, and 5, and both of T and τ are constants. Tomita gave $\tau=0.48$ and $T=0.96\approx 2\tau$. Here, we tried to apply this rule to our simulational data based on OFO-II. When $\tau=7.40$ and $T=10.41$, we confirmed very good agreement between the period predicted from Eq. 6 and the period obtained by the simulation data. The result is indicated in Table 1, where T_p(theor) is the period predicted from Eq. 6 and T(obs) is that of the simulational data. Here the value of $T(=10.41)$ is smaller than $2\tau=2\times 7.40=14.80$ and $\tau(=7.40)$ is also slightly smaller than the value of the period $2\pi/\Omega=8.38$ to be expected from the angular frequency Ω of the oscillation. It is interesting, however, that the every difference is not so large.

Discussion

We studied the behaviors of the oscillatory flow term Oregonator (OFO model) to compare our results with the experimental results of Hudson et al.[1] The simulation of OFO has been made under the values of parameters of OFO-II which is same as OFO-I except the extremely small amplitude of the forced oscillation. It can be concluded that the OFO-II model is very suitable for reproducing the experimental results by Hudson et al.

In the previous paper[6,7] we have shown that the trajectory of CFO changes both globally and locally according to the value of the flow rate R as shown in Fig. 1. And the behavior of CFO is primarily determined by the competitions among some attractors like as steady states and a stable or an unstable limit cycle. We think that these behaviors of CFO still perform a part of the background of the behaviors of OFO because the only difference of OFO from CFO is the existence of the forced oscillation term of which amplitude is set extremely small of order 1/500 compared with the amplitude of the limit cycle of CFO. Therefore, the steady states, $\boldsymbol{X}^0$, $\boldsymbol{X}^S$, $\boldsymbol{X}^{S'}$, and the limit cycles in CFO may also be at work as the latent attractors in OFO. In the previous paper we summarized the following conditions for the exhibition of the characteristic features of the Hudson's experimental results by OFO: (1) The CFO, which could be the background of the OFO, should have two steady states $\boldsymbol{X}^0$ and $\boldsymbol{X}^S$ at least. (2) The stability of steady states $\boldsymbol{X}^0$ and $\boldsymbol{X}^S$ should become larger with the increase of the flow rate R. (3) The value of R should be taken near the value at which the CFO could realize the intermediate state as shown in Fig. 2. (4) The curved surface formed by the orbits near $\boldsymbol{X}^S$ should be enough flat to be able to form the turning orbit around it.

Here, it is newly confirmed that in order to reproduce more finely the Hudson's experimental results by OFO the following conditions should be added. (5) The amplitude of the oscillation in the time-dependent term

of OFO should be extremely smaller than that of OFO-I. Thus the forced oscillation should be so weak that the trajectory is attracted not to the steady state X^S, but to the steady state X^0 and turns around it. (6) The stability of X^0 should be moderate; or more definitely, the stability of X^0 should be as high as a running orbit can be attracted to X^0 and turns around X^0 while it should be as low as the trajectory finally falls not to the steady state X^0, but comes out to the global stable limit cycle which may surpass X^0 in stability. If an unstable limit cycle exists around X^0, the curved surface formed by the orbit inside this unstable limit cycle should be also flat enough, which is same as the condition (4) around X^S. This circumstance corresponds to the condition that the stability of the focus X^0 should be as low as that mentioned in (6). If the stability of X^0 is comparatively low and at the same time the magnitude of the amplitude Q is larger than a certain threshold, the trajectory passes through near X^0 without turning around it. In this case the oscillatory modes, the wave patterns and the bifurcation structure would differ in fine details from those of Hudson's experimental results.

Here, we must pay attention to the fact that no forced oscillation was set in the Hudson's experimental system[1] while the OFO has the time-dependent flow term implying a forced oscillation. This is a discrepancy between the Hudson's experimental system and the OFO model. From the microscopic point of view, however, local fluctuation in concentrations of chemical species necessarily comes always into the experimental system. The time-dependent term in OFO could be regarded as a correspondence on this fluctuation. Now, there are two discrepancies between the experimental results and the simulational results based on OFO-II. Namely, one of them is the lack of the mode $\Pi(4)$ in the simulational results and the other is an inversion in the order of the appearance of the mode $\Pi_{1,1}(1,3)$ and $\Pi(2)$ with the increase of R. These discrepancies would be due to the difference between the random fluctuation in the expeprimental system and the trigonometric functional oscillation in the OFO model system. But we think that the discrepancies between two results are not so significant and not so essential because qualitatively the OFO-II shows totally a very good reproduction of the bifurcation structure of the experimental results. If these considerations are appropriate, the simulational results mean that the smaller amplitude of forced oscillation in the OFO model guarantees the better correspondence between the OFO model and the real experimental system. From this point of view it can be said that the OFO-II model may have better correspondence to the experimental system than the OFO-I model.

We would like to thank Dr. A. Kouda for valuable discussion. The authors are much indebted to Dr. J. L. Hudson, Dr. M. Hart, and Dr. D. Marinko for kindly permitting us to quote many figures in their paper of Ref. 1.

References

1) J. L. Hudson, M. Hart, and D. Marinko, *J. Chem. Phys.*, **71**, 1601 (1979).
2) C. Vidal, S. Bachelart, and A. Rossi, *J. Phys.*, **43**, 7 (1982).
3) J. C. Roux, *Physica*, **7D**, 57 (1983).
4) T. Yamaguchi, Y. Yamamoto, and K. Imaeda, *J. Phys. Soc. Jpn.*, **58**, 1550 (1989).
5) T. Yamaguchi, Y. Yamamoto, and K. Imaeda, *J. Phys. Soc. Jpn.*, **59**, 857 (1990).
6) C. Murase, S. Sakanoue, and M. Endo, *Prog. Theor. Phys.*, **77**, 1307 (1987).
7) C. Murase, S. Sakanoue, and M. Endo, *Prog. Theor. Phys.*, **77**, 1319 (1987).
8) R. J. Field and R. M. Noyes, *J. Chem. Phys.*, **60**, 1877 (1974).
9) J. J. Tyson, *J. Chem. Phys.*, **66**, 905 (1977).
10) K. Tomita and I. Tsuda, *Prog. Theor. Phys.*, **64**, 1138 (1980).

Physical Characteristic and Molecular Structure of Spin-Crossover Iron(III) Complexes of Monoclinic Form with Hexadentate Ligands Derived from Triethylenetetramine and Salicylaldehyde [Fe(sal$_2$trien)]BPh$_4$·acetone

Yonezo MAEDA,* Hiroki OSHIO,† Yuichi TANIGAWA, Takayuki ONIKI,†† and Yoshimasa TAKASHIMA
Department of Chemistry, Faculty of Science, Kyushu University, Hakozaki, Higashiku, Fukuoka 812
† The Institute for Molecular Science, Okazaki, Aichi 444
†† Kyushu Dental College, Tokuyoshi, Kokuraminamiku, Kitakyushu 803-02
(Received October 18, 1990)

Iron(III) complexes of [FeL]BPh$_4$·acetone containing the hexadentate ligand derived from triethylenetetramine and salicylaldehyde have been synthesized. These complexes were grown in two crystalline forms, monoclinic and the twin crystals. The crystal structure of the monoclinic form was determined at 290 K, at which temperature the complex is in a transition spin-state between high- and low-spin states; the spin-state interconversion rate of the monoclinic form is as fast as the inverse of the Mössbauer lifetime (1×10^{-7} s) above 200 K. The monoclinic crystal of [FeL]BPh$_4$·acetone is of space group $P2_1/a$, with a=27.418(4), b=10.097(2), c=14.726(3) Å, β=98.00(1)°, and Z=4. The average bond distances of Fe–O (1.875 Å), Fe–N_{imine} (1.988 Å), and Fe–N_{amine} (2.069 Å) are in good agreement with the expected values for the transition spin-state between high- and low-spin states. Twin crystals are in a high-spin state over the temperature range 78—320 K.

The dynamics of spin-state interconversion in a solution and a solid at ambient temperature have been the subject of a number of papers.[1-3] The measured ^{2}T(LS)$\rightleftharpoons$ ^{6}A(HS) relaxation rates are of the order of 10^7 s^{-1} in the solution state at high temperature; there are few solids for which both the solution and solid-state spin-state interconversion rates have been determined.[4,5] The solid-state rates are supposed to be consistently slower than the corresponding solution rates.

The spin-state interconversion rates in [FeL]Y (H_2L; Schiff base derived from triethylenetetramine and salicylaldehyde) with Y=PF_6^-, NO_3^-, BPh_4^-, I^-, and Cl^- in solution were measured by Tweedle and Wilson, and are about 10^7 s^{-1}.[5] The magnetic properties and the crystal structures for some of their solid complexes have been reported and the interconversion rate for the PF_6 salt has been estimated to be slower than 10^7 s^{-1}.[6]

Some examples in which the electronic spin-state is dependent on the crystal form are known. For example, Fe(phen)$_2$(NCS)$_2$ and Fe(bpy)$_2$(NCS)$_2$ have polymorph,[7-9] and the magnetic behaviors are different from each other. [Fe(oep)(3-Clpy)$_2$]ClO$_4$[10,11] (oep: octaethylporphyrin, 3-Clpy: 3-chloropyridine) of monoclinic form is a quantum-admixed intermediate-spin state; the triclinic one shows a thermal spin equilibrium, although the solution susceptibilities of both crystalline forms are identical.

We are interested in the differences in the spin-state interconversion rates between the solution- and solid-state, and in the effect of the difference of the crystal forms on the spin-crossover.

Experimental

Sample Preparation. The ligand was prepared by slowler adding 0.73 g (5 mmol) of triethylenetetramine in 20 ml of methanol to 1.22 g (10 mmol) of salicylaldehyde in 100 ml of methanol; the mixture was kept for 1 h at room temperature.[12] Then, 1.12 g (20 mmol) of KOH in 50 ml of methanol was added to the mixture. This mixture was used without separating the ligand as a solid. Iron complexes were prepared by the addition of 2.0 g (5 mmol) of iron nitrate in 50 ml of methanol to the ligand solution. The precipitation was separated with a glassfilter and 1.36 g (4 mmol) of sodium tetraphenylborate in 50 ml of methanol was slowly poured into the filtrate. The crude product was collected by filtration, washed with methanol and recrystallized from acetone. Two crystal forms were produced, filtrated, washed with acetone and separated mechanically. The crystals of each form were collected and recrystallized from acetone. The analytical data for [FeL]BPh$_4$·acetone are as follows: Found for monoclinic crystals: C, 72.01; H, 6.40; N, 7.15%. Found for twin crystals: C, 71.93; H, 6.51; N, 7.23%. Calcd for $BC_{47}H_{50}FeN_4O_3$: C, 71.85; H, 6.42; N, 7.13%.

Physical Measurements. The magnetic susceptibilities of the polycrystalline samples were measured by the Faraday method using a type-2002 (Cahn Instruments) electrobalance with an electromagnet (8000 G, 0.8 T). The temperature was controlled over the range 78—320 K by using a digital temperature controller (model 3700; Scientific Instruments). Compound HgCo(NCS)$_4$ was used as a calibration standard. Effective magnetic moments were calculated by using the formula $\mu_{eff}=2.84\,(\chi_M T)^{1/2}$, where χ_M is the molar susceptibilities after applying a diamagnetic correction.

The Mössbauer spectra were measured with a constant-acceleration spectrometer (Austin Science Associates). Data were stored in a 1024-channel pulse-height analyzer (type 5200; Inotech Inc.). The temperature was monitored with a calibrated copper–constantan thermocouple within a variable-temperature cryostat (type ASAD-4V). A cobalt 57 source of 10 mCi diffused into a palladium foil was used for the absorption measurement. All spectra were fitted by Lorentzian line shapes using a least-squares fitting procedure at the Computer Center, Kyushu university. The velocity scale was normalized with respect to the centre of the spectrum of metallic iron at 296 K.

The relaxation fits were based on the method reported in Ref. 13 for relaxation between two quadrupole split doublets representing the low- and high-spin electronic states. The quadrupole splittings of the low- and high-spin doublets in these fits were kept constant at 2.85 and 0.28 mm s^{-1}, respectively. The high- and low-spin population fractions determined from the magnetic data were used. We used values of 2.58 BM for the low-spin electronic state and 5.60 BM for high-spin electronic state, of which value is popularly observed for high-spin iron(III) complexes. The line widths for the doublets were assumed to be 3.03 mm s^{-1} for the low-energy line 0.86 mm s^{-1} for the high-energy line of the high-spin species; those for low-spin species were 0.44 and 0.31 mm s^{-1}, respectively. The values were varied according to the fraction of the high-spin/low-spin population in fitting as inevitable management, since the high-spin species shows very broad line widths due to spin-spin relaxation. (The values used in practice for fitting were less than 2.199 mm s^{-1}, although 3.03 mm s^{-1} appeared to be too large.)

The IR spectra for both samples were measured using a JASCO FT/IR-5000; the peak positions of N–H or C=N stretching vibration for monoclinic crystals (complex **a**) were similar to those for the twin crystals. No existence of strong hydrogen bonding in N(2)–H(23)–OS(1) is supposed for both complexes.

Electron paramagnetic resonance data at the X-band frequency were collected on a FEX (JEOL, Ltd) spectrometer.

Crystal Structure Determination of Monoclinic [Fe(sal$_2$trien)]BPh$_4$·acetone. Suitable single crystals of monoclinic [FeL]BPh$_4$·acetone were obtained by slow evaporation of acetone at room temperature.

Crystal Data. $BC_{47}H_{50}FeN_4O_3$, M=785.5. Monoclinic, a=27.418(4), b=10.097(2), c=14.726(3)A, β=98.00(1)°, V=4037(0)Å^3 (by least squares refinement on diffractomer angles 25°<2θ<30° for 50 automatically centered reflections, λ=0.71073 Å), space group $P2_1/a$ (No. 14), Z=4, D_c=1.29 g cm^{-3}, D_o=1.30 g cm^{-3}, blue black, crystal dimensions: 0.2×0.2×0.3 mm, μ(Mo $K\alpha$)=16.46 cm^{-1}.

Data Collection and Processing. Diffraction data were collected at 290 K on a Rigaku AFC5 four-circle diffractometer using the $\omega-2\theta$ scan technique; graphite monochromated Mo $K\alpha$ radiation; 10333 reflections measured(−35<h<35, 0<k<13, 0<l<19), 5287 independent data with $|F_o|>3\sigma(F_o)$. The crystal was covered with glue in order to avoid any release of acetone molecules from the crystal during measurements. The intensities of the three standard reflection were monitored every 100 reflections, and showed no greater fluctuations during the data collection than that expected from Poisson statistics. Intensity data were corrected for both Lorentz and polarization factors, but not for adsorption and extinction.

Structure Analysis and Refinement. The structure was solved by the conventional heavy-atom method and refined by a block-diagonal least-squares method with anisotropic thermal parameters for non-hydrogen atoms and isotropic for Hydrogen atoms. The weighting scheme $w=[\sigma_c^2+(0.025|F_o|)^2]^{-1}$ was employed, where σ_c was estimated from the counting statistics. The final indices, R and R', were 7.2 and 9.3%, respectively, which are defined as $R=\Sigma(|F_o|-|F_c|)/\Sigma|F_o|$ and $R'=[\Sigma w(|F_o|-|F_c|)^2/\Sigma w|F_o|^2]^{1/2}$. The atomic scattering factors for non-hydrogen atoms were taken from Ref. 14, and those for hydrogen atoms from Stewart et al.[15] The effects of anomalous scattering for non-hydrogen atoms were corrected for in structure factor calculations. A determination of the structural parameters was carried out with the universal Crystallographic Computation Program System UNICS III,[16] using a HITAC M-680 Computer at the Computer Center of The Institute for Molecular Science. The final atomic coordinates are given in Table 1.

Table 1. Positional Parameters of the Cation and Acetone Molecule for Monoclinic [Fe(sal$_2$trien)]BPh$_4$·acetone with Estimated Standard Deviations in Parentheses (×10^5 for Fe and ×10^4 for the Other Atoms)

Atom	x	y	z
Fe	12683 (3)	8787 (7)	20157 (5)
O(1)	1167 (1)	−904 (4)	1687 (2)
O(2)	650 (1)	1292 (4)	2348 (2)
N(1)	1034 (2)	1450 (4)	734 (3)
N(2)	1469 (2)	2847 (4)	2156 (3)
N(3)	2003 (2)	682 (5)	1847 (4)
N(4)	1526 (2)	375 (5)	3293 (3)
C(1)	881 (2)	−1422 (5)	975 (4)
C(2)	778 (2)	−2765 (5)	964 (4)
C(3)	492 (2)	−3353 (6)	247 (5)
C(4)	290 (2)	−2613 (7)	−505 (4)
C(5)	387 (2)	−1296 (7)	−536 (4)
C(6)	685 (2)	−655 (5)	202 (3)
C(7)	782 (2)	720 (5)	112 (3)
C(8)	1110 (3)	2861 (6)	538 (4)
C(9)	1154 (2)	3595 (6)	1422 (4)
C(10)	2015 (2)	3037 (6)	2183 (4)
C(11)	2221 (2)	1956 (7)	1645 (5)
C(12)	2253 (3)	62 (10)	2663 (9)
C(13)	2021 (3)	−163 (12)	3415 (5)
C(14)	1302 (2)	500 (5)	4005 (4)
C(15)	811 (2)	1014 (5)	3983 (3)
C(16)	628 (2)	1121 (6)	4822 (4)
C(17)	167 (2)	1555 (7)	4875 (4)
C(18)	−131 (2)	1895 (6)	4079 (4)
C(19)	36 (2)	1815 (6)	3240 (4)
C(20)	515 (2)	1355 (5)	3169 (3)
OS(1)	1202 (2)	4969 (6)	3376 (4)
CS(1)	937 (3)	5665 (6)	3747 (4)
CS(2)	981 (3)	7114 (7)	3755 (5)
CS(3)	572 (4)	5088 (9)	4299 (8)

Results and Discussion

We isolated solids of two crystalline forms with a solvent. The temperature-dependent magnetic susceptibilities for the two crystalline forms were different from each other. The crystal structure of the monoclinic form, which shows thermal spin-crossover, was determined. Twin crystals give a different powder X-ray diffraction pattern from the monoclinic one and are in a high-spin state over the temperature range 78–320 K.

Magnetic Susceptibilities and ESR. Figure 1 shows variable temperature magnetic data for both complexes. The data for the monoclinic form indicate an anomalous magnetic behavior characteristic of an LS⇌HS spin-crossover behavior; the magnetic susceptibility is of an intermediate value at 296 K, and the electronic

state of 40% high-spin and 60% low-spin states. The twin crystals remain fully in the high-spin state, even at 78 K.

ESR spectra were measured for both samples. As the temperature of complex **a** was decreased, the low-spin signals (g_1=2.20, g_2=2.194, g_3=1.944) increased in intensity at the expense of the high-spin signals(g=4 and 2). These high- and low-spin ESR signals are typical for ferric centers of this type. In the twin crystals broad signals at g=2.1, 3.7, and 5.3 were observed at 296 K.

Mössbauer Spectra. The Mössbauer spectra of the monoclinic form were measured at various temperatures (Fig. 2). The spectrum at 78 K is typical of low-spin iron(III); the residual paramagnetic species was not observed, although the magnetic moment (2.58 BM at 80 K) is more than the spin-only value (1.98 BM). The full widths at half maximum(FWHM) at high temperature became broad due to a spin-spin interaction. The spectral data reported in Table 2 characterize anomalous magnetic properties arising from a spin-state interconversion; the spectra are not a superimposition of

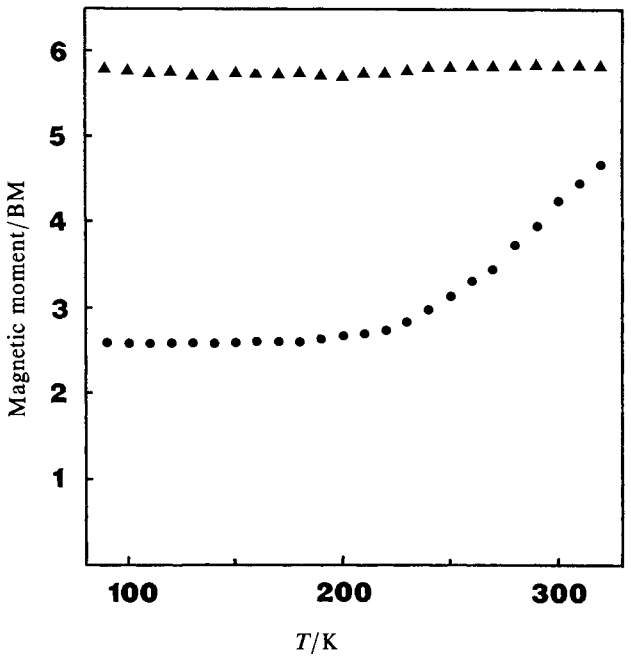

Fig. 1. Temperature dependences of magnetic moments for monoclinic [FeL]BPh_4·acetone (●) and twin crystals (▲).

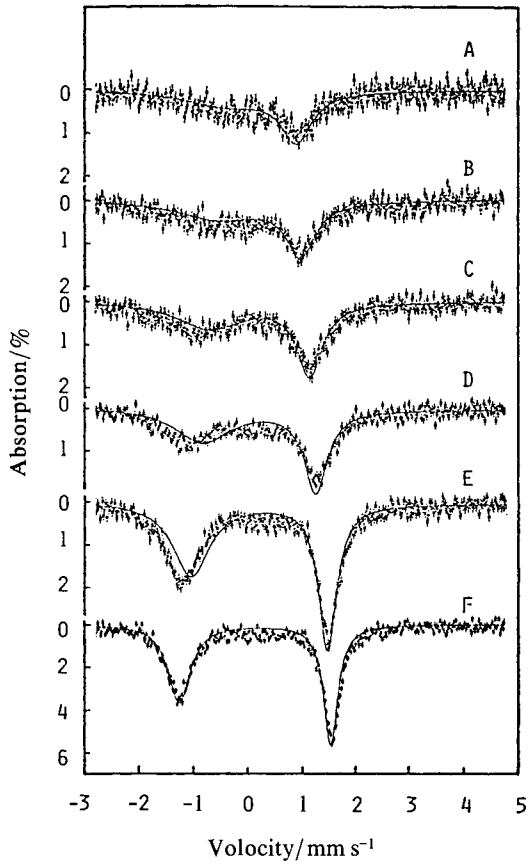

Fig. 2. Temperautre dependence of representative Mössbauer spectra for monoclinic [FeL]BPh_4·acetone and fits. (A) 320 K, $\tau=0.39\times10^{-8}$, f=0.60; (B) 310 K, $\tau=0.47\times10^{-8}$, f=0.53; (C) 296 K, $\tau=0.60\times10^{-8}$, f=0.40; (D) 280 K, $\tau=0.70\times10^{-8}$, f=0.30; (E) 250 K, $\tau=0.87\times10^{-8}$, f=0.13; (F) 200 K, $\tau=0.98\times10^{-8}$, f=0.02.

Table 2. Mössbauer Parameters with Two Lorentzian Lines, High-Spin Fraction and Average Interconversion Rate for Monoclinic [Fe(sal_2trien)]BPh_4·acetone

T	ΔE[a]	δ[b]	Γ_l[c]	Γ_h[d]	χ[e]	f[f]	k'[g]
K	mm s^{-1}	mm s^{-1}	mm s^{-1}	mm s^{-1}		%	s^{-1}
320	1.165	0.364	2.199	0.659	469	60	1.3×10^8
310	1.453	0.286	2.155	0.688	511	53	1.1×10^8
296	1.986	0.168	1.708	0.732	464	40	8.2×10^7
280	2.226	0.170	1.709	0.705	617	30	6.6×10^7
250	2.658	0.153	0.791	0.457	566	13	3.9×10^7
200	2.799	0.164	0.543	0.357	584	2	1.4×10^7
78	2.852	0.223	0.438	0.310	535	0	—

a) Quadrupole splitting. b) Isomer shift relative to metallic iron. c) Full width at half maximum for low energy line. d) Full width at half maximum for high energy line. e) Total of residual sum, free degree is 493. f) High-spin population fraction estimated from the data of magnetic susceptibilities. g) Average interconversion rate tentatively estimated from the Mössbauer fitting.

both high- and low-spin absorptions, but comprise the time-averaged state in both electronic spin-states. The quadrupole splitting values are decreased with increasing population of the high-spin state. These facts indicate that the lifetimes of the low- and high-spin states are as short as or less than the Mössbauer lifetime of ^{57}Fe (1×10^{-7} s).

If we assume that the magnetic moments for low- and high- spin states of the monoclinic crystals are 2.58 and 5.60 BM, respectively, and temperature-independent values are assumed for the low- and high-spin effective magnetic moments, the high-spin population fraction (x) at ambient temperature can be calculated using the $\mu_{obs}^2=x\mu_{hs}^2+(1-x)\mu_{ls}^2$ relation (collected in Table 2).

The relaxation time, τ, is represented by $\tau=\tau_l\tau_h/(\tau_l+\tau_h)$, where τ_l and τ_h are the lifetimes of the low- and high-spin species, respectively. The observed spectra show a rapid relaxation between the high- and low-spin states with the rate of the Mössbauer time scale of 10^{-7} s. Although a fitting is one of many attempts, such a treatment should involve computing the distribution of the relaxation spectra, a correction for the line broadening resulting from the thick absorber and the temperature dependence of the quadrupole splitting for the low-spin species. Such a complex treatment was not attempted herewith and, consequently, the absolute values of the relaxation rate should be taken with caution. Our best fits are illustrated in Fig. 2. The rates for the forward k_1 and reverse k_{-1} rate constants for the spin interconversion LS$\rightleftharpoons$HS are defined as $1/\tau_{ls}$ and $1/\tau_{hs}$, respectively. The low-spin population fraction, f_{ls}, times k_1 is equal to the high-spin fraction, f_{hs}, times k_{-1}, *i.e.*,

$$f_{hs}+f_{ls}=1 \text{ and } k_1f_{ls}=k_{-1}f_{hs}$$

are fulfilled. An equilibrium constant, $K=k_{-1}/k_1$, plot of the temperature-dependent LS$\rightleftharpoons$HS relaxation rates described above deviates from a straight line (Fig. 3); the enthalpy for this process could therefore not be determined accurately. Nonetheless, the fitting of the Mössbauer spectra shown in Fig. 2 can serve as a qualitative of a rapid interexchange system. Sinn et al.[6] have reported that the average rate, $k'=\sqrt{k_1k_{-1}}$, for [FeL]$^+$ in solution is 1.4×10^7 s^{-1} at room temperature. The $\tau=0.6\times10^{-8}$ s in the spectrum (c) of Fig. 2 corre-

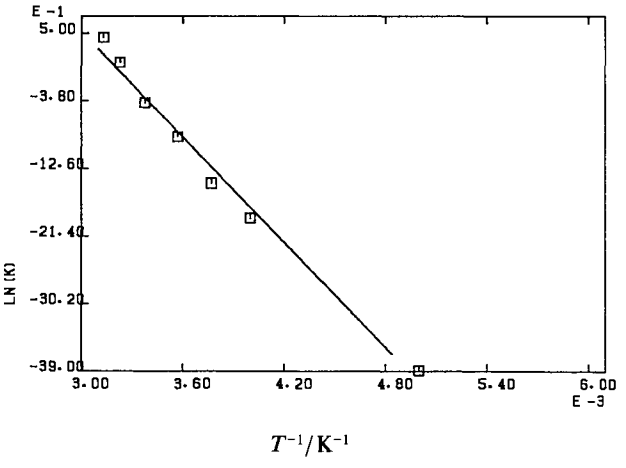

Fig. 3. Plots of natural logarithm of equilibrium constant $K=k_1/k_{-1}$ vs. $1/T$ for monoclinic [FeL]BPh$_4$·acetone (inclination of a straight line is -0.23×10^4 K).

Table 3. Interatomic Distances (Å) for the Cation and Acetone Molecule of Monoclinic [Fe(sal$_2$trien)]BPh$_4$·acetone with Estimated Standard Deviations in Parentheses

Fe-O(1)	1.875(4)	Fe-O(2)	1.875(4)
Fe-N(1)	1.993(4)	Fe-N(2)	2.065(4)
Fe-N(3)	2.073(5)	Fe-N(4)	1.982(5)
O(1)-C(1)	1.326(6)	C(1)-C(2)	1.385(8)
C(2)-C(3)	1.361(8)	C(3)-C(4)	1.385(9)
C(4)-C(5)	1.359(9)	C(5)-C(6)	1.421(7)
C(6)-C(1)	1.420(7)	C(6)-C(7)	1.423(8)
C(7)-N(1)	1.297(6)	N(1)-C(8)	1.474(8)
C(8)-C(9)	1.488(9)	C(9)-N(2)	1.491(7)
N(2)-C(10)	1.506(7)	C(10)-C(11)	1.504(9)
C(11)-N(3)	1.466(8)	N(3)-C(12)	1.441(13)
C(12)-C(13)	1.371(15)	C(13)-N(4)	1.450(10)
N(4)-C(14)	1.293(8)	C(14)-C(15)	1.438(8)
C(15)-C(16)	1.402(8)	C(16)-C(17)	1.349(9)
C(17)-C(18)	1.376(9)	C(18)-C(19)	1.377(9)
C(19)-C(20)	1.410(8)	C(20)-O(2)	1.315(6)
C(20)-C(15)	1.395(7)		

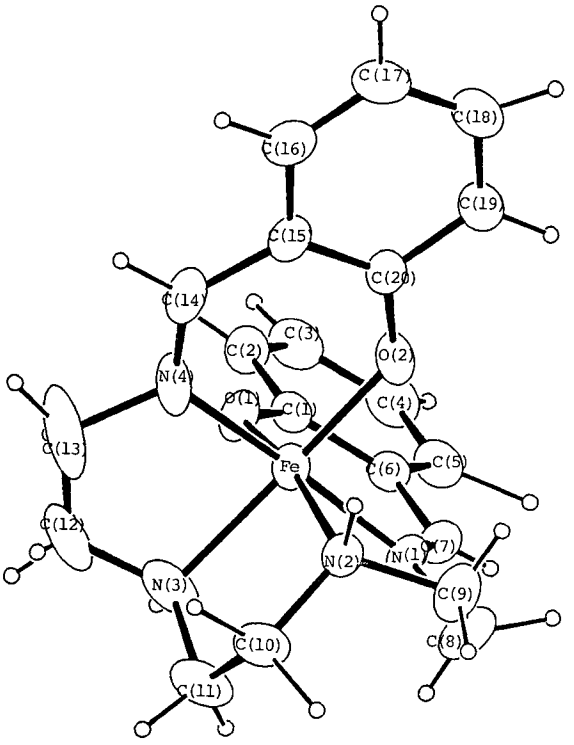

Fig. 4. Ortep figure for the cation of monoclinic [FeL]BPh$_4$·acetone.

sponds to the rate $k'=\sqrt{k_1 k_{-1}}=8.2\times10^7$ s^{-1} and is compared with solution rate. This result is consistent with a report that the spin-state interconversion rates are dependent on the crystal packing and that intermolecular interaction can induce a faster rate than that in an isolated system.[17]

Crystal Structure. The crystal structure of the monoclinic form was determined at 290 K; interatomic distances for the cation and acetone molecule, and bond angles for the cation are listed in Tables 3 and 4, respectively. Steric structure and numbering system for the cation are drawn in Fig. 4 using ORTEP.[18] The structure of the complex contains cation and anion layers in an ac plane, as shown in Fig. 5. The $[FeL]^+$ ion is hydroden bonded via an amine nitrogen (H(23) attached to the nitrogen atom N(2)) to oxygen atom of the

Table 4. Bond Angles (°) for the Cation of Monoclinic [Fe(sal$_2$trien)]BPh$_4$·acetone with Estimated Standard Deviations in Parentheses

O(1)-Fe-O(2)	100.0(2)	O(1)-Fe-N(1)	91.0(2)
O(1)-Fe-N(2)	168.0(2)	O(1)-Fe-N(3)	89.4(2)
O(1)-Fe-N(4)	91.1(2)	O(2)-Fe-N(1)	89.9(2)
O(2)-Fe-N(2)	89.8(2)	O(2)-Fe-N(3)	168.8(2)
O(2)-Fe-N(4)	91.5(2)	N(1)-Fe-N(2)	82.1(2)
N(1)-Fe-N(3)	96.0(2)	N(1)-Fe-N(4)	177.3(2)
N(2)-Fe-N(3)	81.7(2)	N(2)-Fe-N(4)	95.6(2)
N(3)-Fe-N(4)	82.2(2)	Fe-O(1)-C(1)	129.2(3)
O(1)-C(1)-C(2)	119.5(5)	C(1)-C(2)-C(3)	122.1(5)
C(2)-C(3)-C(4)	120.5(6)	C(3)-C(4)-C(5)	119.8(6)
C(4)-C(5)-C(6)	121.0(5)	C(5)-C(6)-C(1)	118.6(5)
C(1)-C(6)-C(7)	123.4(4)	C(6)-C(1)-O(1)	122.4(5)
C(6)-C(1)-C(2)	118.1(5)	C(5)-C(6)-C(7)	118.0(5)
C(6)-C(7)-N(1)	125.3(4)	C(7)-N(1)-C(8)	119.0(4)
C(7)-N(1)-Fe	125.0(4)	Fe-N(1)-C(8)	115.4(3)
N(1)-C(8)-C(9)	107.9(5)	C(8)-C(9)-N(2)	110.9(5)
C(9)-N(2)-C(10)	115.4(4)	C(9)-N(2)-Fe	107.2(3)
Fe-N(2)-C(10)	112.0(3)	N(2)-C(10)-C(11)	109.7(5)
C(10)-C(11)-N(3)	109.7(5)	C(11)-N(3)-C(12)	113.0(5)
C(11)-N(3)-Fe	111.7(4)	Fe-N(3)-C(12)	107.5(5)
N(3)-C(12)-C(13)	121.6(7)	C(12)-C(13)-N(4)	111.7(7)
C(13)-N(4)-C(14)	118.7(5)	C(13)-N(4)-Fe	114.7(4)
Fe-N(4)-C(14)	126.7(4)	N(4)-C(14)-C(15)	124.5(5)
C(14)-C(15)-C(16)	117.3(5)	C(15)-C(16)-C(17)	121.9(5)
C(16)-C(17)-C(18)	118.9(6)	C(17)-C(18)-C(19)	121.1(6)
C(18)-C(19)-C(20)	121.0(5)	C(19)-C(20)-C(15)	117.0(5)
C(20)-C(15)-C(16)	120.1(5)	C(20)-C(15)-C(14)	122.6(5)
C(19)-C(20)-O(2)	118.1(4)	C(15)-C(20)-O(2)	125.0(5)
C(20)-O(2)-Fe	129.2(3)		

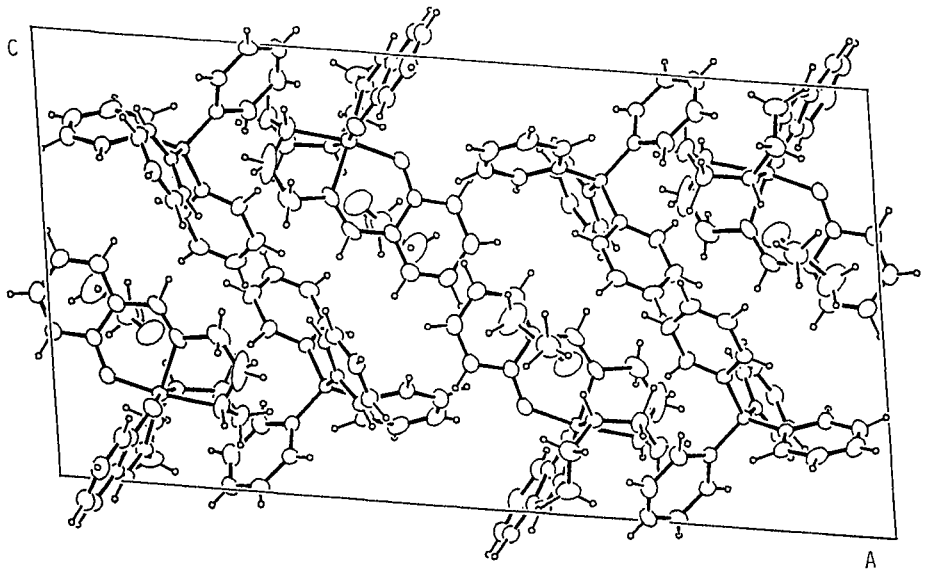

Fig. 5. Packing diagram in ac plane for monoclinic [FeL]BPh$_4$·acetone.

acetone molecule; bond lengths OS(1)–H(23)=2.073 Å, H(23)–N(2)=0.999 Å, OS(1)–N(2)=2.953 Å. The coordination sphere around the iron atom in the cation is approximately octahedral with the two terminal oxygen atom *cis* to each other. The configuration of the hexadentate ligand about the metal atom is analogous to that of low-spin [FeL]NO_3·H_2O (complex **b**) and [FeL]Cl·2H_2O (complex **c**), of which the structures were determined by Sinn et al.[6]; the deviation from octahedral geometry in the FeN_4O_2 unit is larger than those of complexes **b** and **c**. The angles O(1)–Fe–N(2), O(2)–Fe–N(3), and N(1)–Fe–N(4) are 168.0°, 168.8°, and 177.3°, respectively. The iron-ligand bond lengths are Fe–O^{av} 1.875, Fe–N_{imine}^{av} 1.988, and Fe–N_{amine}^{av} 2.069 Å. The Fe–O^{av} bond length for **a** is a little less than those for **b** and **c** 1.885 Å. The Fe–N bond length for **a** is larger than those for **b** and **c**. The bonds to the oxygen atoms are shortest, followed by those to the imine and the amine nitrogen atoms. These bond lengths are less than those for typical high-spin complexes with a Schiff base, in accordance with the electronic spin-state of this complex; i.e. the high-spin population fraction is 40% at 296 K.

With respect to the difference in the bond angles, Fe–O–C, between low-spin [FeL]X(X=NO_3, Cl) and complex **a**, the bond angles of Fe–O(1)–C(1) (129.2°) and Fe–O(2)–C(20) (129.2°) for **a** are about 4° larger than those for **b** or **c** respectively. The difference is larger than those for any other angles; four Fe–N–C angles for **a** are analogous to those corresponding to **b** or **c**. We have pointed out that the ease to transform the Fe–O–C bond angle between both spin-states is important regarding the spin-crossover behavior of FeN_4O_2 Schiff base complexes.[19,20]

The octahedral coordination around an iron atom is stable in the coordination structure represented by Fig. 4; other coordination structures have great strain.[21] Therefore, the coordination structure of twin crystals would be analogous to that shown in Fig. 4, and there would be a faint difference in the molecular structures between the monoclinic- and twin-type crystals.

It is reasonable that the hydrogen bonding interaction produces an increase in the low-spin populations. Complexes **b** and **c** with a strong hydrogen-bonding network are in a low-spin state and, therefore, the electronic states of complex **a** with weak hydrogen bonding and of the desolvated [FeL]BPh_4 may be on the spin-crossover point. It would be very interesting to clarify which difference in the molecular structure in these complexes brings about the spin-state difference. We are now trying to obtain single crystals of the other form (twin crystals).

Desolvated complexes [FeL]BPh_4 are also spin-crossover complexes, and the spin-state interconversion rate is slower than the inverse of the Mössbauer lifetime.[6] It is therefore not necessary to have acetone molecules in the crystal to cause a spin-crossover behavior. Rapid spin-state interconversion may result from the incorporation of acetone molecules, by which any soft modes are devoted to lattice vibration.

Supplementary Materials are Available: Tables of (1) positional parameters except hydrogen atoms, (2) positional parameters for hydrogen atoms, (3) anisotropic temperature factors, (4) mean square displacement tensor for atoms, and (5) observed and calculated structure factors for monoclinic [Fe(sal$_2$trien)]BPh_4·acetone are deposited as Document No. 9110 at the Office of the Editor of Bull. Chem. Soc. Jpn.

References

1) P. Gütlich, *Struct. Bonding (Berlin)*, **44**, 83 (1981).
2) W. R. Scheidt and C. A. Reed, *Chem. Rev.*, **81**, 543 (1981).
3) Y. Maeda and Y. Takashima, *Comm. Inorg. Chem.*, **7**, 41 (1988).
4) E. V. Dose, K. M. Murphy, and L. J. Wilson, *Inorg. Chem.*, **15**, 2622 (1976).
5) M. F. Tweedle and L. J. Wilson, *J. Am. Chem. Soc.*, **98**, 4824 (1976).
6) E. Sinn, G. Sim, E. V. Dose, M. F. Tweedle, and L. J. Wilson, *J. Am. Chem. Soc.*, **78**, 3375 (1978).
7) E. König and K. Medeja, *Inorg. Chem.*, **6**, 48 (1967). P. Ganguli, P. Gütlich, E. W. Müller, and W. Irler, *J. Chem. Soc., Dalton Trans.*, **1981**, 441.
8) B. Gallois, J. A. Real, C. Hauw, and J. Zarembowitch, *Inorg Chem.*, **29**, 1152 (1990).
9) E. König, K. Madeja, and K. J. Watson, *J. Am. Chem. Soc.*, **90**, 1146 (1968).
10) W. R. Scheidt, D. K. Geiger, and K. J. Haller, *J. Am. Chem. Soc.*, **104**, 495 (1982).
11) W. R. Scheidt, D. K. Geiger, R. G. Hayes, and G. Lang, *J. Am. Chem. Soc.*, **105**, 2625 (1983).
12) B. D. Sarma and J. C. Bailar, *J. Am. Chem. Soc.*, **77**, 5476 (1955).
13) J. A. Pople, W. G. Schneider, and H. J. Bernstein, "High Resolution Nuclear Magnetic Resonance," McGraw-Hill, New York (1959); Y. Maeda, Y. Takashima, N. Matsumoto, and A. Ohyoshi, *J. Chem. Soc., Dalton Trans.*, **1986**, 1115.
14) J. A. Ibers and W. C. Hamilton, "International Tables for X-Ray Crystallography," Kynoch Press, Birmingham, England (1974), Vol. IV.
15) R. F. Stewart, E. R. Davidson, and W. T. Simpson, *J. Chem. Phys.*, **42**, 3175 (1965).
16) T. Sakurai and K. Kobayashi, *Sci. Rep. Inst. Chem. Phys. Res. Jpn.*, **55**, 69 (1979).
17) Y. Maeda, M. Tomokiyo, K. Kitazaki, and Y. Takashima, *Bull. Chem. Soc. Jpn.*, **61**, 1953 (1988).
18) C. K. Johnson, ORTEP, Report ORNL-3794, Oak Ridge National Laboratory, Oak Ridge, Tennessee (1965).
19) Y. Maeda, H. Oshio, K. Toriumi, and Y. Takashima, to be published.
20) B. J. Kenedy, A. C. McGrath, K. S. Murray, B. W. Skelton, and A. H. White, *Inorg. Chem.*, **26**, 483 (1987).
21) B. das Sarma and J. C. Bailar, Jr., *J. Am. Chem. Soc.*, 77, 5476 (1955).

Structure of Cobalt(II) Ion and Tri- and Tetrachlorocobaltate(II) Complexes in *N,N*-Dimethylformamide Determined by the Fluorescent EXAFS Method

Kazuhiko OZUTSUMI,* Kazuyuki TOHJI,† Yasuo UDAGAWA,† and Shin-ichi ISHIGURO††
Department of Chemistry, University of Tsukuba, Tsukuba 305
† Department of Molecular Structure, Institute for Molecular Science, Myodaiji, Okazaki 444
†† Department of Electronic Chemistry, Tokyo Institute of Technology at Nagatsuta, Midori-ku, Yokohama 227
(Received November 30, 1990)

EXAFS (extended X-ray absorption fine structure) spectra were measured for *N,N*-dimethylformamide (DMF) solutions containing cobalt(II) ion and its chloro complexes of low concentration (20—40 mmol dm^{-3}) by a laboratory EXAFS spectrometer modified for the fluorescence detection. The analysis of the EXAFS data for a cobalt(II) perchlorate DMF solution showed that cobalt(II) ion in DMF has an octahedral structure with six DMF molecules. The Co–O (DMF) bond length within $[Co(dmf)_6]^{2+}$ in DMF is 206(1) pm and is practically the same as that within $[Co(H_2O)_6]^{2+}$ (208 pm) in water within experimental uncertainties. It was also shown that the tri- and tetrachlorocobaltate(II) complexes in DMF have a tetrahedral structure. The Co–O and Co–Cl lengths within $[CoCl_3(dmf)]^-$ in DMF are 202(1) and 227(1) pm, respectively. The Co–Cl distances within $[CoCl_4]^{2-}$ in DMF and in water are the same and 229(1) pm.

Extended X-ray absorption fine structure (EXAFS) spectroscopy has been widely applied to the structure determination of metal complexes in solution. Most of EXAFS measurements of solution samples were performed by the transmission mode. However, this mode can not be used for dilute solutions. It turned out that the fluorescence detection is effective for very dilute systems.[1,2] In fact, EXAFS spectroscopy by the fluorescence detection is indispensable for the structural determination of metal complexes in nonaqueous media, where solubility of metal complexes is usually very low compared with aqueous media.

Complex formation reactions of divalent transition metal with halide ions have been studied in *N,N*-dimethylformamide (DMF).[3-7] Since metal ions are solvated in solution, solvation structure of metal(II) ions is essential to understand the thermodynamics of complexation. Direct structural information on the solvation structure of copper(II) and cadmium(II) ions in DMF has so far been provided by solution X-ray diffraction.[8,9]

With cobalt(II), a series of mononuclear $[CoCl]^+$, $[CoCl_2]$, $[CoCl_3]^-$, and $[CoCl_4]^{2-}$ complexes are formed in DMF. In particular, the tri- and tetrachloro complexes are extensively formed as the main species at suitable mole ratios of chloride to cobalt(II) ions.[3] However, since the solubility of $((CH_3CH_2)_4N)_2[CoCl_4]$ in DMF is low (less than 20 mmol dm^{-3}), it is difficult to apply the transmission EXAFS method for the structural study. Therefore, in the present study we employed the fluorescent EXAFS method to determine the structure of the solvated cobalt(II) ion and the tri- and tetrachlorocobaltate(II) complexes in DMF. The structure of mono- and dichlorocobalt(II) complexes was not determinable because of their suppressed formation in DMF.

Experimental

Reagents. All chemicals used were of reagent grade. Cobalt(II) perchlorate and cobalt(II) chloride were recrystallized once from water. Cobalt(II) perchlorate DMF solvate was prepared by the same method as described elsewhere.[3] Lithium chloride and tetraethylammonium chloride were used without further purification and dried at 100 °C. *N,N*-Dimethylformamide was purified as described elsewhere.[5]

Preparation of Solutions. Five sample solutions were prepared for EXAFS measurements. Solution AQ0 is an aqueous cobalt(II) perchlorate solution. Solution AQ4 was prepared by dissolving cobalt(II) chloride in an aqueous 13 mol dm^{-3} lithium chloride solution. The former and latter solutions contain $[Co(H_2O)_6]^{2+}$ and $[CoCl_4]^{2-}$ complexes, respectively, of known structure.[10,11] Solution DMF0 is a cobalt(II) perchlorate DMF solution. Solutions DMF3 and DMF4 were prepared by dissolving cobalt(II) perchlorate DMF solvate and tetraethylammonium chloride in DMF at suitable C_{Cl}/C_{Co} mole ratios. The tri- and tetrachlorocobaltate(II) complexes are the main species in solutions DMF3 and DMF4, respectively, according to the stability constants of cobalt(II) chloro complexes in DMF.[3] The compositions of the solutions are given in Table 1.

EXAFS Measurements. EXAFS spectra were measured on a laboratory EXAFS spectrometer[12] modified for the fluorescence detection[13] at the Institute for Molecular Science.

A rotating anode X-ray generator (Rigaku RU-200) was

Table 1. The Composition of Sample Solutions

Solution	C_{Co}/mol dm^{-3}	C_{Cl}/mol dm^{-3}	C_{Cl}/C_{Co}
AQ0	0.0203	0	0
DMF0	0.0405	0	0
DMF3	0.0413	0.123	2.98
DMF4	0.0192	0.171	8.91
AQ4	0.100	13	130

operated at the voltage of 12 kV and the current of 200 mA. Monochromatized X-rays were obtained by a Johansson cut bent crystal (Ge(220)). Helium bags were placed along the beam path to prevent absorption by air. Sample solutions were held in a 5 mm thick glass cell with a Mylar window.

The incident X-ray intensity I_0 and the fluorescence intensity I were simultaneously measured by an ion chamber and an NaI scintillation counter with 2 inches in diameter combined with a filter (iron foil with thickness of 10 μm), respectively, and more than 1×10^6 counts of I were obtained at each data point above the edge. The observed spectra $\mu\,(=I/I_0)$ are shown in Fig. 1.

Analysis of EXAFS Data. Background other than that for the K edge of cobalt atom was estimated by least-squares fitting first-order polynomial function to the pre-edge and was subtracted from the raw spectrum by extrapolation. The smooth background μ_0 due to an isolated atom was evaluated by fitting a smooth curve to the observed spectrum using an eighth-order polynomial function.

The EXAFS pattern was then extracted and normalized by the following equation;

$$\chi(k) = \{\mu(k) - \mu_0(k)\}/\mu_0(k), \tag{1}$$

where $k(=\{2m(E-E_0)\}^{1/2}/\hbar)$ is the photoelectron wave vector. E represents the energy of the incident X-rays and E_0 is the threshold energy of a K-shell electron. The E_0 value was selected as the position of the half-height of the edge jump in each sample and was set to be 7.722 keV in the present study. The extracted EXAFS spectra weighted by k^3 are depicted in Fig. 2. The $k^3\cdot\chi(k)$ values are converted to the radial structure function $F(r)$ as

$$F(r) = (1/2\pi)^{1/2}\int_{k_{min}}^{k_{max}} k^3\cdot\chi(k)\cdot W(k)\cdot\exp(-2ikr)dk. \tag{2}$$

$W(k)$ is the window function of the Hanning type.[14] The $F(r)$ values are shown in Fig. 3.

A curve fitting procedure in the k-space for the refinements of structure parameters was applied to the Fourier filtered $k^3\cdot\chi(k)_{obsd}$ values to minimize the error-square sum U:

$$U = \Sigma k^6(\chi(k)_{obsd} - \chi(k)_{calcd})^2. \tag{3}$$

The model function $\chi(k)_{calcd}$ is given by the single scattering theory as[15-18]

$$\chi(k)_{calcd} = \Sigma\{n_j/(k\cdot r_j^2)\}\exp(-2\sigma_j^2k^2 - 2r_j/\lambda)F_j(\pi,k) \times\sin(2kr_j + \alpha_j(k)), \tag{4}$$

where $F_j(\pi, k)$ is the backscattering amplitudes from each of n_j scatterers j at distances r_j from the X-ray absorbing atom.

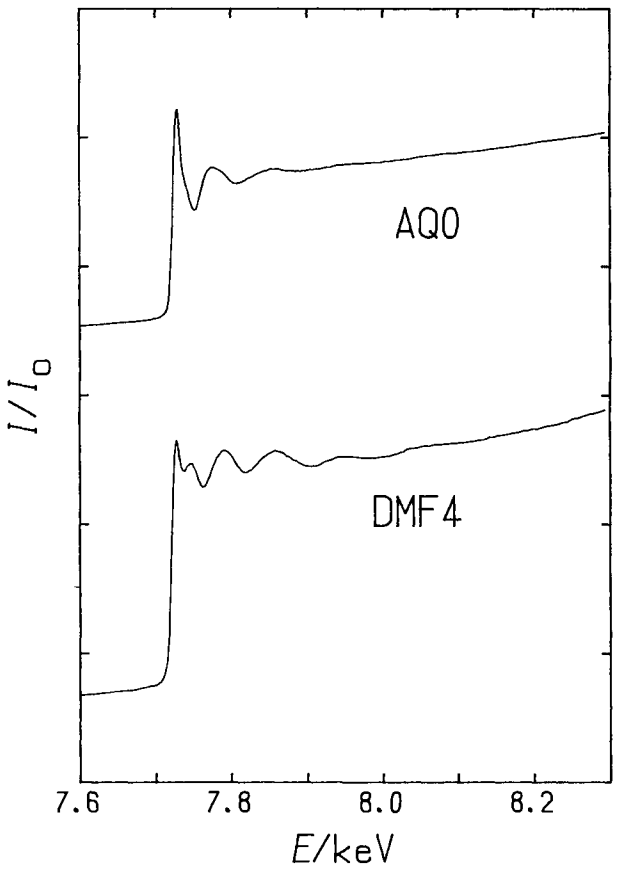

Fig. 1. The raw EXAFS spectra for sample solutions AQ0 and DMF4 of low concentration (ca. 20 mmol dm^{-3}) by the fluorescence detection.

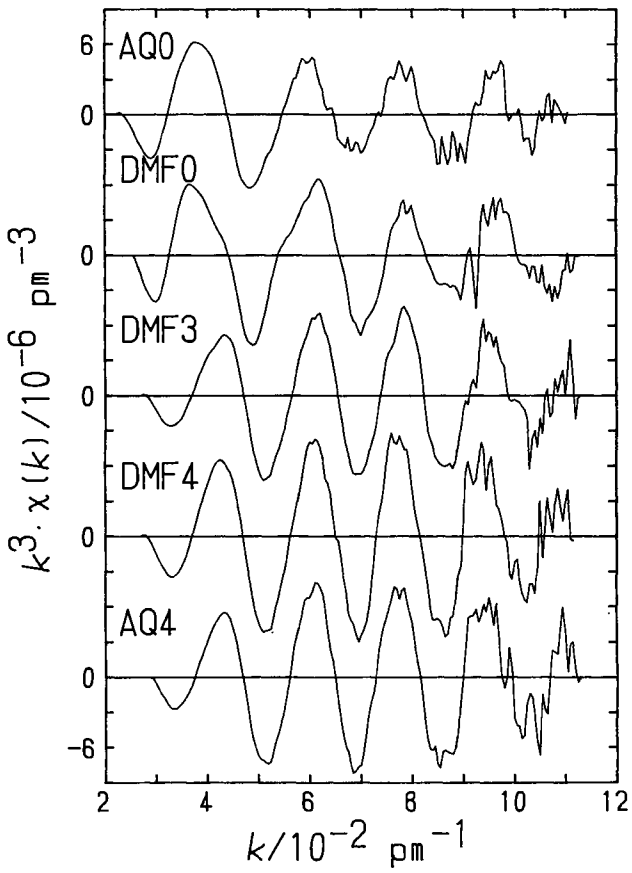

Fig. 2. The extracted EXAFS oscillations multiplied by k^3 for sample solutions. AQ0: $Co(ClO_4)_2$ in water, DMF0: $Co(ClO_4)_2$ in DMF, DMF3: $[CoCl_3]^-$ in DMF, DMF4: $[CoCl_4]^{2-}$ in DMF, and AQ4: $[CoCl_4]^{2-}$ in water.

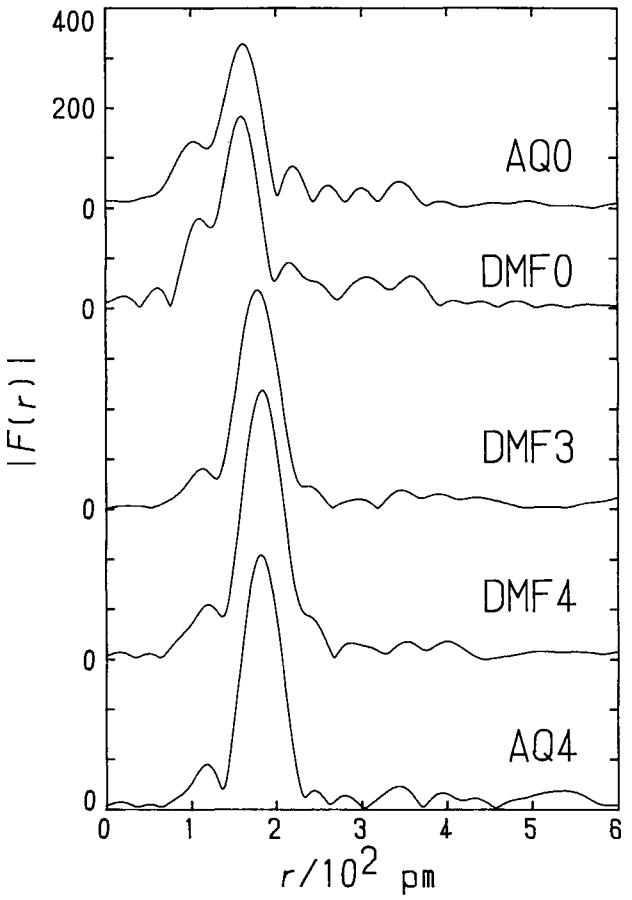

Fig. 3. The Fourier transforms $F(r)$ of the $k^3 \cdot \chi(k)$ curves shown in Fig. 2, phase shift uncorrected.

σ_j^2 is the mean square displacement of the equilibrium distance r_j and λ is the mean free path of the photoelectron. $\alpha_j(k)$ is the total scattering phase shift experienced by the photoelectron. The values of $F_j(\pi, k)$ in Eq. 4 were taken from the tables reported by Teo and Lee.[19] The phase shift $\alpha_j(k)$ was approximated by the function $a_0+a_1k+a_2k^2+a_3/k^3$,[20] where the a_0, a_1, a_2, and a_3 values were obtained by fitting the function to the phase shift values by Teo and Lee.[19] In the least-squares calculations, the parameters a_0, a_1, and λ were first determined from the standard samples of known structure. The a_2 and a_3 values were fixed at the above values during the refinement. An aqueous cobalt(II) perchlorate solution containing $[Co(H_2O)_6]^{2+}$ (AQ0) and a cobalt(II) chloride in a 13 mol dm^{-3} LiCl solution containing $[CoCl_4]^{2-}$ (AQ4) were used as the standard for the Co–O and Co–Cl atom pairs, respectively.[10,11] The parameters were then used as constants in the course of the structural analysis of unknown samples, while r, σ, and n values were optimized.

Results and Discussion

Figure 2 shows the extracted EXAFS oscillations in the form of $k^3 \cdot \chi$ (k) for solutions AQ0, DMF0, DMF3, DMF4, and AQ4. In Fig. 3, the Fourier transforms of the $k^3 \cdot \chi(k)$ values of the test solutions are depicted. The first intense peaks at 150—180 pm are ascribable to the bonds between cobalt(II) ion and oxygen atom and/or chloride ion in the first coordination sphere.

Solutions AQ0 and DMF0 contain the solvated cobalt(II) ion in water and DMF, respectively. Both solutions show a similar pattern in intensity and phase over the k-range of the measurements (Fig. 2). A slightly different feature in the $k^3 \cdot \chi(k)$ curves between solutions AQ0 and DMF0 at 4.5 and 5.5×10^{-2} pm^{-1}, i.e. two shoulders in the curve of solution DMF0, may be due to the nonbonding Co···C (DMF) interactions. Indeed, similar shoulders due to M···C interactions were observed for the aqueous solutions involving copper(II) bidentate chelate complexes.[21] The first intense peaks around 150 pm in the Fourier transform for both solutions are also practically unchanged in intensity and positions as in Fig. 3. Therefore, the structure of solvated cobalt(II) ion in DMF may be octahedral like the hexaaquacobalt(II) ion in water[10]

According to the species distribution of the cobalt(II) chloro complexes in DMF,[3] the tri- and tetrachlorocobaltate(II) complexes are the predominant species in solutions DMF3 and DMF4, respectively. The relative amounts of the predominant complex in the solutions exceed 90%, on the basis of the molar absorption coefficients of individual cobalt(II) chloro complexes in DMF.[3] Hence, we treated solution DMF3 or DMF4 to contain only tri- or tetrachlorocobaltate(II) complex, respectively.

It has been revealed that a structure change from octahedral to tetrahedral around cobalt(II) ion occurs upon the formation of the dichlorocobalt(II) complex on the basis of the thermodynamic quantities of complexation and the electronic spectra of individual cobalt(II) chloro complexes in DMF.[3]

Very similar $k^3 \cdot \chi(k)$ and $F(r)$ curves were in fact obtained for solutions AQ4 and DMF4 as shown in Figs. 2 and 3. This is expected because the two solutions contain the four-coordinate $[CoCl_4]^{2-}$ complex.

The structure parameters of these complexes were finally determined by a least-squares calculation applied to the Fourier filtered $k^3 \cdot \chi(k)$ values over the range $4.0 < k/10^{-2}\,\text{pm}^{-1} < 10.0$. The Fourier filtering was performed over the r-range including the main peak in the $F(r)$ curve for each sample. The phase function and the λ values were first evaluated for the Co–O and Co–Cl atom pairs from respective solutions AQ0 involving the hexaaquacobalt(II) ion[10] and AQ4 involving the tetrachlorocobaltate(II) complex of known structure.[11] In the fitting procedures, the Co–O and Co–Cl bond distances and the numbers of the relevant interactions were fixed at the interature values,[10,11] while the parameters σ, λ, a_0, and a_1 were optimized as independent variables.

The interatomic distances and Debye–Waller factors for the cobalt(II) complexes in DMF were then refined by adopting the phase function and the λ values in water evaluated above. The coordination numbers were fixed during the calculations at the given values in Table 2

Table 2. Results of the Least-Squares Refinements of Structure Parameters for Cobalt(II) Ion and Its Chloro Complexes in *N,N*-Dimethylformamide[a)]

Complex	Solution	Interaction	r/pm	σ/pm	n
$[Co(H_2O)_6]^{2+}$ (in water)	AQ0	Co–O	208[b,c)]	7.3(2)	6[b,c)]
$[Co(dmf)_6]^{2+}$ (in DMF)	DMF0	Co–O	206(1)	6.2(1)	6[b)]
$[CoCl_3(dmf)]^-$ (in DMF)	DMF3	Co–O	202(1)	6.7(6)	1[b)]
		Co–Cl	227(1)	5.1(1)	3[b)]
$[CoCl_4]^{2-}$ (in DMF)	DMF4	Co–Cl	229(1)	5.0(1)	4[b)]
$[CoCl_4]^{2-}$ (in water)	AQ4	Co–Cl	229[b,d)]	5.4(1)	4[b,d)]

Standard deviations are given in parentheses. a) λ_O=630(20) and λ_{Cl}=853(38) pm. b) The values were kept constant during the calculations. c) Ref. 10. d) Ref. 11.

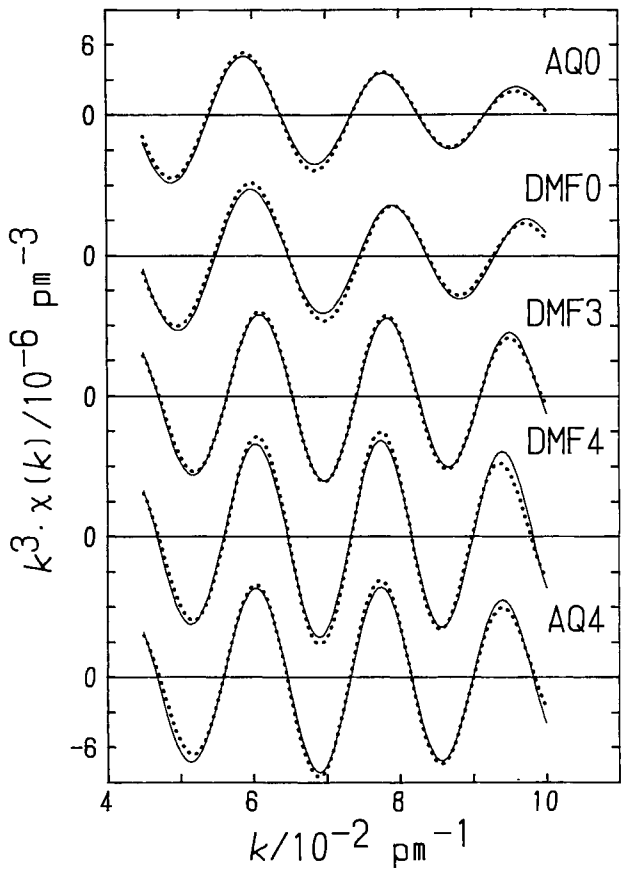

Fig. 4. The Fourier filtered $k^3 \cdot \chi(k)$ curves of the main peak depicted in Fig. 3. The observed values are shown by dots and ones calculated using parameter values in Table 2 by solid lines.

which are suggested by the spectrophotometric and calorimetric studies.[3)] This is reasonable because, when the coordination numbers were also optimized, the numbers converged to 6.2(2) for the Co–O (DMF) bonds of the solvated cobalt(II) ion (solution DMF0) and 4.4(2) for the Co–Cl bonds of the tetrachlorocobaltate(II) complex (solution DMF4), suggesting the six- and four-coordination structures, respectively. The final results are given in Table 2. The solid curves calculated by using the parameter values in the table well reproduce the experimental points, as shown in Fig. 4.

The solvated cobalt(II) ion in DMF has a six-coordinate octahedral structure and described as $[Co(dmf)_6]^{2+}$ similar to $[Co(H_2O)_6]^{2+}$ in water.[10)] The Co–O bond distance within $[Co(dmf)_6]^{2+}$ in DMF is 206(1) pm and is practically the same as that (208 pm) within $[Co(H_2O)_6]^{2+}$ in water[10)] within experimental uncertainties.

Both tri- and tetrachlorocobaltate(II) complexes in DMF have a four-coordinate tetrahedral structure. The Co–Cl bond distances within $[CoCl_4]^{2-}$ in DMF and in water[11)] are the same and 229(1) pm. The Co–Cl bond length within $[CoCl_3(dmf)]^-$ in DMF is 227(1) pm and is practically the same as that within $[CoCl_4]^{2-}$ in DMF within experimental uncertainties. On the other hand, the Co–O bond length within $[CoCl_3(dmf)]^-$ is 202(1) pm and shorter than that within six-coordinate $[Co(dmf)_6]^{2+}$. However, the distance is much longer than that (194 pm) within four-coordinate $[Co(hmpa)_4]^{2+}$ in hexamethylphosphoric triamide (HMPA).[22)].

References

1) J. Jaklevic, J. A. Kirby, M. P. Klein, A. S. Robertson, G. S. Brown, and P. Eisenberger, *Solid State Commun.*, **23**, 679 (1977).

2) S. S. Hasnain, P. D. Quinn, G. P. Diakun, E. M. Wardell, and C. D. Garner, *J. Phys. E*, **17**, 40 (1984).

3) S. Ishiguro, K. Ozutsumi, and H. Ohtaki, *J. Chem. Soc., Faraday Trans. 1*, **84**, 2409 (1988).

4) S. Ishiguro, K. Ozutsumi, and H. Ohtaki, *Bull. Chem. Soc. Jpn.*, **60**, 531 (1987).

5) S. Ishiguro, B. G. Jeliazkova, and H. Ohtaki, *Bull. Chem. Soc. Jpn.*, **58**, 1143 (1985).

6) K. Ozutsumi and S. Ishiguro, *J. Chem. Soc., Faraday Trans.*, **86**, 271 (1990).

7) S. Ishiguro, K. Ozutsumi, M. Miyauchi, and H. Ohtaki, *Inorg. Chem.*, **28**, 3258 (1989).

8) K. Ozutsumi, S. Ishiguro, and H. Ohtaki, *Bull. Chem. Soc. Jpn.*, **61**, 945 (1988).

9) K. Ozutsumi, T. Takamuku, S. Ishiguro, and H. Ohtaki, *Bull. Chem. Soc. Jpn.*, **62**, 1875 (1989).

10) H. Ohtaki, T. Yamaguchi, and M. Maeda, *Bull. Chem. Soc. Jpn.*, **49**, 701 (1976).

11) H. -G. Lee, Y. Matsumoto, T. Yamaguchi, and H. Ohtaki, *Bull. Chem. Soc. Jpn.*, **56**, 443 (1983).

12) K. Tohji, Y. Udagawa, T. Kawasaki, and K. Masuda,

Rev. Sci. Instrum., **54**, 1482 (1983).
13) K. Tohji, T. Mizushima, and Y. Udagawa, *Jpn. J. Appl. Phys.*, **29**, 2171 (1990).
14) F. J. Harris, *Proc. IEEE*, **66**, 51 (1978).
15) D. E. Sayers, E. A. Stern, and F. W. Lytle, *Phys. Rev. Lett.*, **27**, 1204 (1971).
16) E. A. Stern, *Phys. Rev. B*, **10**, 3027 (1974).
17) E. A. Stern, D. E. Sayers, and F. W. Lytle, *Phys. Rev. B*, **11**, 4836 (1975).
18) B. Lengeler and P. Eisenberger, *Phys. Rev. B*, **21**, 4507 (1980).
19) B. -K. Teo and P. A. Lee, *J. Am. Chem. Soc.*, **101**, 2815 (1979).
20) P. A. Lee, B. -K. Teo, and A. L. Simons, *J. Am. Chem. Soc.*, **99**, 3856 (1977).
21) K. Ozutsumi and T. Kawashima, *Inorg. Chim. Acta*, **180**, 231 (1991).
22) K. Ozutsumi, K. Tohji, Y. Udagawa, Y. Abe, and S. Ishiguro, to be published.

Studies on the Secondary Structure of Bradykinin in Aqueous Solution. Syntheses, Circular Dichroism Spectra, and Biological Activities of Bradykinin Analogs Containing 5-Aminovaleric Acid Residue

Chikao HASHIMOTO,*,† Makoto TAMAKI,†† Shosuke SOFUKU, and Ichiro MURAMATSU
Department of Chemistry, College of Science, Rikkyo University,
Toshima-ku, Nishi-Ikebukuro, Tokyo 171
(Received November 14, 1990)

Eight bradykinin analogs containing 5-aminovaleric acid residue were synthesized by a solution method. Based on the consideration concerning their CD spectra, the presence of an intramolecular 3→1 hydrogen bond between the carbonyl oxygen of Ser^6 and the amide proton of Phe^8, an intramolecular 4→1 hydrogen bond between the carbonyl oxygen of Pro^2 and the amide proton of Phe^5, and a salt bridge between the guanidino group of Arg^1 and the carboxyl group of Arg^9, was proposed for the secondary structure of bradykinin in aqueous solution. The biological activities of these analogs depend on the presence of both Phe residues at positions 5 and 8, and Arg residues at positions 1 and 9. No correlation between the biological activities and the secondary structure could be found.

Bradykinin (BK) was discovered by Rocha e Silva et al.,[1] isolated by Elliott et al.,[2] and synthesized by Boissonnas et al.[3] This peptide shows mainly activities on uterus and smooth muscle contraction, pain, and blood pressure etc. To date, a large number of BK analogs have been prepared in order to examine the relationship between structure and activity. The secondary structure of BK in solution has been studied by several research groups. Initial studies on the secondary structure of BK were made by Bodanszky et al.[4] and Brady et al.[5] They suggested that BK existed in an extended conformation, namely a random coil, from the results of the ORD and CD spectra. From a study on the CD spectra of BK, its fragments, and model compounds, a secondary structure model of BK was proposed by Cann et al.[6] It has an intramolecular 3→1 hydrogen bond between the carbonyl oxygen of Ser^6 and the amide proton of Phe^8, which was considered to cause the CD band at 234 nm of the peptide. On the basis of studies by electron spin resonance and fluorescence energy transfer, Ivanov et al.[7] suggested ionic bond formation between the guanidino group of Arg^1 and the carboxyl group of Arg^9. A ^{13}C NMR study by London et al.[8] provided evidence for the existence of the 3→1 hydrogen bond, but not for the formation of a salt bridge. Chipens et al.[9] implied a certain similarity in the secondary structure between the BK and *cyclo*-BK analogs from studies of their CD spectra. In the past, we reported on preliminary results of a study of BK analogs containing a 5-aminovaleric acid (5-Ava) residue.[10-12]

In this paper we wish to report on the syntheses, the CD spectra, and the biological activities of eight BK analogs containing the 5-Ava residue shown in Table 1. When each sequence of two adjacent amino acid residues is replaced by one residue of 5-Ava, each amide group is substituted by an ethylene group, and each side chain by a hydrogen atom, respectively. The contributions of each amide bond and each side chain to the secondary structure and the biological activity of BK is discussed here on the basis of the results of the CD spectra and biological activities.

Table 1. Primary Sequences of Bradykinin and Eight Bradykinin Analogs Containing 5-Ava Residue

	1	2	3	4	5	6	7	8	9	
Bradykinin (BK)	H–Arg–	Pro–	Pro–	Gly–	Phe–	Ser–	Pro–	Phe–	Arg–	OH
[5-Ava$^{1-2}$]-BK (**9**)	H–	5-Ava	–							–OH
[5-Ava$^{2-3}$]-BK (**16**)	H–	–	5-Ava	–						–OH
[5-Ava$^{3-4}$]-BK (**26**)	H–		–	5-Ava	–					–OH
[5-Ava$^{4-5}$]-BK (**32**)	H–			–	5-Ava	–				–OH
[5-Ava$^{5-6}$]-BK (**37**)	H–				–	5-Ava	–			–OH
[5-Ava$^{6-7}$]-BK (**46**)	H–					–	5-Ava	–		–OH
[5-Ava$^{7-8}$]-BK (**50**)	H–						–	5-Ava	–	–OH
[5-Ava$^{8-9}$]-BK (**56**)	H–							–	5-Ava	–OH

† Present address: Department of Chemistry, The Jikei University School of Medicine, 8-3-1, Kokuryo-cho, Chofu-shi, Tokyo 182.

†† Present address: Department of Chemistry, Faculty of Science, Toho University, Miyama, Funabashi-shi, Chiba 274.

Results and Discussion

Synthesis of BK Analogs Containing 5-Ava Residue. The synthetic methods for BK analogs containing the 5-Ava residue are shown in Figs. 1—8. All of them were synthesized by a solution method. Following protecting groups were used for synthesizing those compounds: Z[13] or Boc group for the α-amino groups; methyl, ethyl, or benzyl ester group for the carboxyl groups; and nitro group for the guanidino group of arginine. The hydroxyl group of serine was not protected. The above-mentioned protecting groups were deprotected by the following methods: HCl/THF, HCl/dioxane, or TFA for Boc group, HBr/AcOH or H_2/Pd for Z group, saponification for methyl and ethyl ester groups, and H_2/Pd for benzyl ester and nitro groups. For peptide bond formation, DCC,[14] DCC/HOBt,[15]

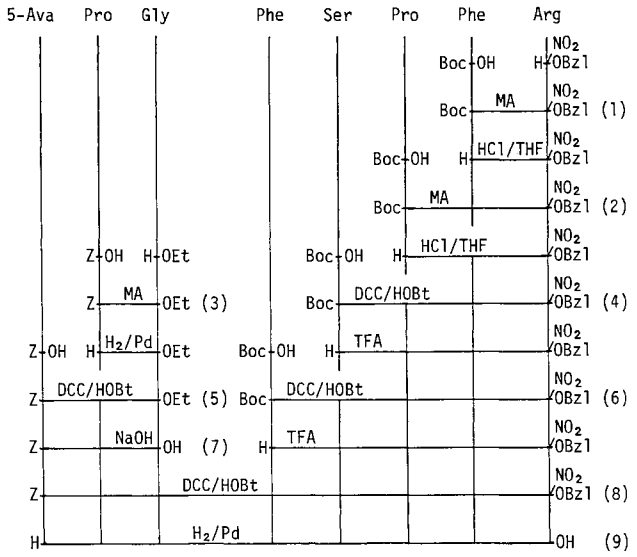

Fig. 1. Synthetic scheme of [5-Ava[1-2]]-BK.

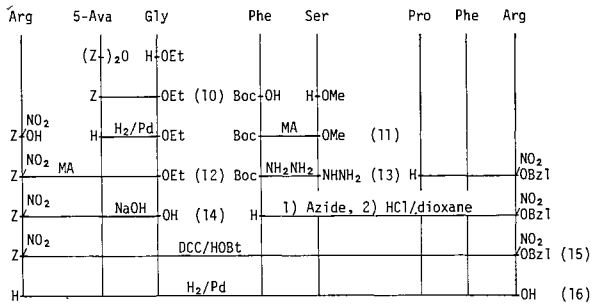

Fig. 2. Synthetic scheme of [5-Ava[2-3]]-BK.

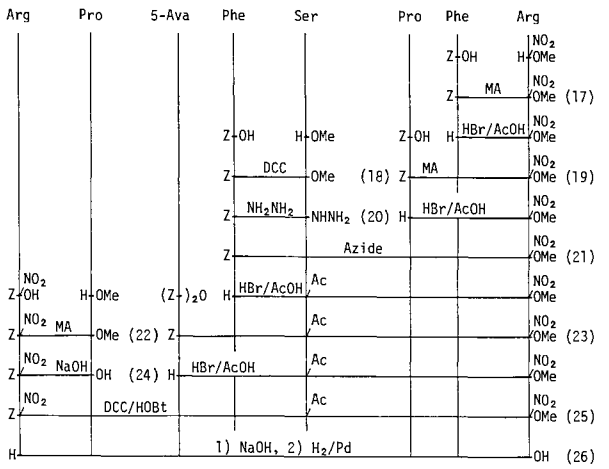

Fig. 3. Synthetic scheme of [5-Ava[3-4]]-BK.

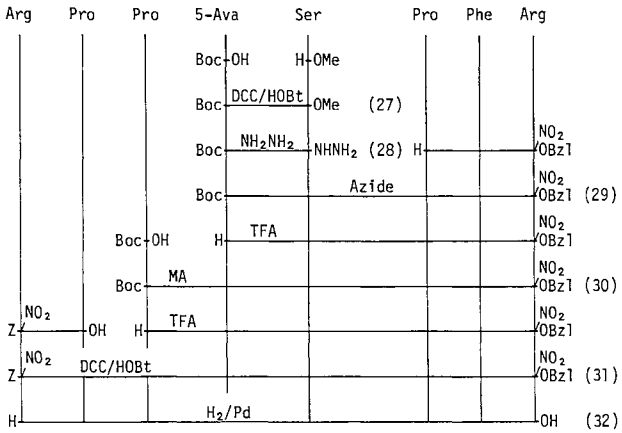

Fig. 4. Synthetic scheme of [5-Ava[4-5]]-BK.

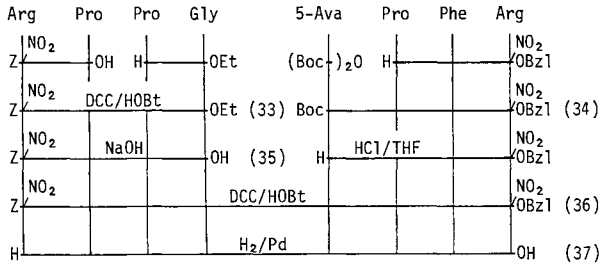

Fig. 5. Synthetic scheme of [5-Ava[5-6]]-BK.

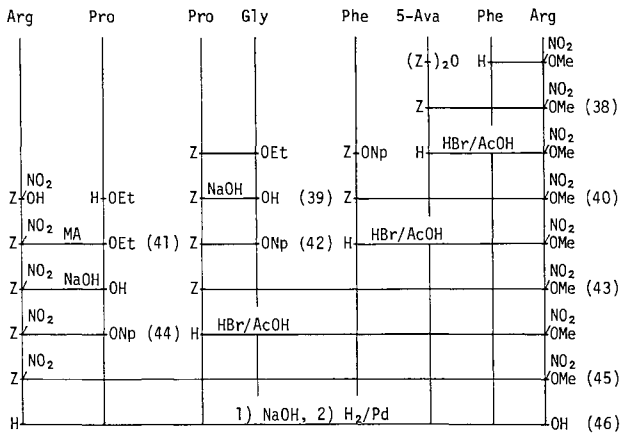

Fig. 6. Synthetic scheme of [5-Ava[6-7]]-BK.

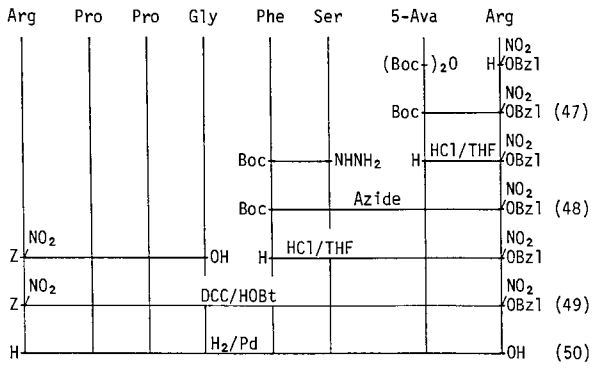

Fig. 7. Synthetic scheme of [5-Ava$^{7-8}$]-BK.

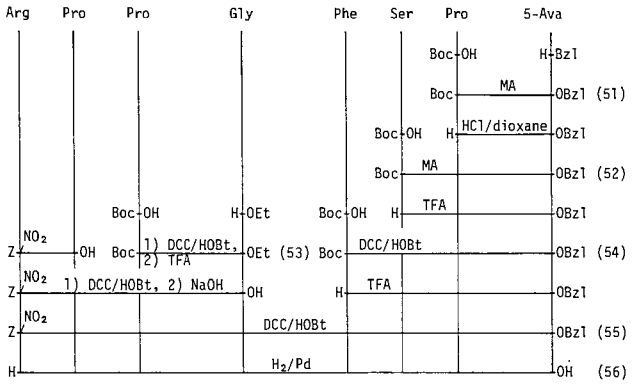

Fig. 8. Synthetic scheme of [5-Ava$^{8-9}$]-BK.

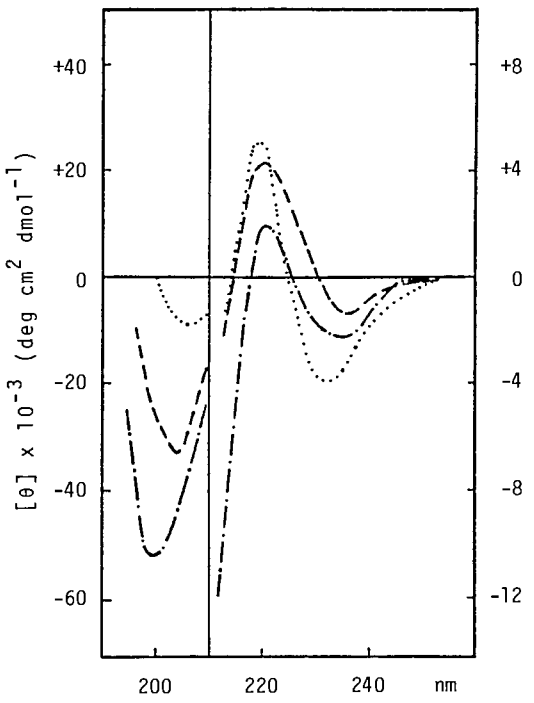

Fig. 9. CD spectra of [5-Ava$^{3-4}$]-BK (**26**) (·····), [5-Ava$^{5-6}$]-BK (**37**) (————), and [5-Ava$^{8-9}$]-BK (**56**) (—·—·—) in water.

MA,[16] azide,[17] active ester,[18] and symmetrical anhydride methods were employed. The final deprotection of protected [5-Ava$^{1-2}$]-BK (**8**), [5-Ava$^{2-3}$]-BK (**15**), [5-Ava$^{4-5}$]-BK (**31**), [5-Ava$^{5-6}$]-BK (**36**), [5-Ava$^{7-8}$]-BK (**49**), and [5-Ava$^{8-9}$]-BK (**55**) was carried out by catalytic hydrogenation. On the other hand, deprotection of protected [5-Ava$^{3-4}$]-BK (**25**) and [5-Ava$^{6-7}$]-BK (**45**) was performed by saponification followed by catalytic hydrogenation.

In coupling of the carboxyl group of 5-Ava, a mixed anhydride method gave some by-products; a DCC method did not afford the expected product. A symmetrical anhydride and DCC/HOBt methods gave satisfactory results. Purification of protected octapeptides was performed by gel filtration on a Sephadex LH-20 column using DMF as the eluent. Free peptides were purified by ion-exchange chromatography on a carboxymethyl cellulose column, gel filtration on a Sephadex G-10 column, and partition chromatography on a Sephadex G-25 column.[19] The purity of all products was confirmed by TLC, elemental analysis, and amino acid analysis. Table 2 shows physical data concerning other compounds, except for those described in the experimental section.

CD Spectra of BK Analogs Containing 5-Ava Residue. The CD spectra were measured in the region of about 190 to 270 nm in aqueous solution. The data are reported as molar ellipticity, [θ], which is expressed in degree square centimeter per decimole.

The CD spectrum of BK shows a negative band at 234 nm, a positive band at 221 nm, and a deep negative band at about 200 nm (Fig. 11). The CD spectra of the BK analogs containing the 5-Ava residue are classified into three types in the region 210—260 nm. The CD spectra of [5-Ava$^{3-4}$]-BK (**26**), [5-Ava$^{5-6}$]-BK (**37**), and [5-Ava$^{8-9}$]-BK (**56**) (Fig. 9) show a negative band near 234 nm and a positive band near 221 nm, resembling that of BK. In the region near 200 nm, [5-Ava$^{3-4}$]-BK shows a considerably shallower trough, as compared with that of BK. The CD spectra of [5-Ava$^{1-2}$]-BK (**9**), [5-Ava$^{2-3}$]-BK (**16**), and [5-Ava$^{4-5}$]-BK (**32**) (Fig. 10) near 234 nm are similar to that of BK, although their peak near 221 nm is lower. Concerning the negative band near 200 nm, [5-Ava$^{1-2}$]-BK and [5-Ava$^{2-3}$]-BK show a much shallower trough. The CD spectra of [5-Ava$^{6-7}$]-BK (**46**) and [5-Ava$^{7-8}$]-BK (**50**) (Fig. 11) do not show a negative band at 234 nm and exhibit a simple peak near 221 nm. The ellipticity of [5-Ava$^{6-7}$]-BK is very large. Regarding the negative band near 200 nm, the ellipticity of [5-Ava$^{7-8}$]-BK is similar to that of BK, although that of [5-Ava$^{6-7}$]-BK is small.

In [5-Ava$^{6-7}$]-BK and [5-Ava$^{7-8}$]-BK, the absence of the negative band at 234 nm suggests that both the amide bonds of Ser^6–Pro^7 and Pro^7–Phe^8 of BK relate to this negative band. That is, these two analogs can

Table 2. Yields, Physical Properties, and Analytical Data of Intermediate and Final Peptides[a)]

Compound	Yield/%	Mp θ_m/°C	$[\alpha]_D^{24}$/° (*c* 1.0, DMF)	Molecular formula	Elemental analysis/% Found (F:), Calcd (C:)	C	H	N	R_f[b)]
3	95	Oil	—	—			—		R^1 0.77, R^2 0.52
5	68	Oil	—	—			—		R^1 0.69, R^4 0.74, R^5 0.71
7	88	Oil	—	—			—		R^4 0.48, R^5 0.58
9	52	—	−64.7[f)] (*c* 0.1, H_2O)	$C_{44}H_{63}O_{10}N_{11}\cdot CH_3COOH\cdot 2.5H_2O$	F:	54.64	6.75	15.07	R^9 0.61 (Cellulose)
					C:	54.64	7.18	15.24	
12	66	97—102	+1.7 (*c* 1.24)	$C_{23}H_{35}O_8N_7\cdot H_2O$	F:	49.60	6.39	18.09	R^1 0.40, R^4 0.53, R^8 0.71
					C:	49.72	6.71	17.65	
13	54	165	−3.6 (*c* 0.84)	$C_{17}H_{26}O_5N_4\cdot 1/2H_2O$	F:	54.22	7.73	15.70	R^4 0.36
					C:	54.38	7.24	14.92	
14	63	139—142	−3.5 (*c* 0.90, MeOH)	$C_{21}H_{31}O_8N_7\cdot 1/2H_2O$	F:	48.84	6.24	18.88	R^5 0.49
					C:	48.64	6.22	18.91	
15	41	135—140	−35.4 (*c* 0.88)	$C_{60}H_{78}O_{16}N_{16}\cdot 6H_2O$	F:	52.69	5.77	15.68	R^1 0.11, R^4 0.24, R^8 0.79
					C:	51.94	6.53	16.15	
16	15	—	−36.7 (*c* 0.1, H_2O)	$C_{45}H_{68}O_{10}N_{14}\cdot 2CH_3COOH\cdot 3H_2O$	F:	51.78	6.98	17.85	R^6 0.87, R^7 0.28, R^8 0.64
					C:	51.65	7.25	17.21	(Cellulose)
23	81	204—208	−45.2[g)]	$C_{48}H_{62}O_{13}N_{10}$	F:	57.74	6.28	13.93	R^1 0.53, R^2 0.50
					C:	58.40	6.33	14.19	
25	37	168—171	−53[d)] (*c* 0.5)	$C_{59}H_{80}O_{17}N_{16}$	F:	56.02	6.21	17.73	R^2 0.23, R^5 0.73
					C:	55.13	6.27	17.43	
26	63	—	−77.2[e)] (*c* 0.1, H_2O)	$C_{48}H_{72}O_{10}N_{14}\cdot 2CH_3COOH\cdot 5H_2O$	F:	51.71	7.04	16.09	R^8 0.43, R^{10} 0.66
					C:	51.39	7.46	16.13	
27	66	Oil	—	—			—		R^1 0.44
31	71	123—125.5 (Decomp)	−53.1 (*c* 0.167)	$C_{59}H_{80}O_{16}N_{16}\cdot 2H_2O$	F:	54.45	6.32	17.49	R^1 0.29, R^4 0.36, R^5 0.63
					C:	54.29	6.49	17.17	
32	44	—	−93.7[f)] (*c* 0.1, H_2O)	$C_{44}H_{70}O_{10}N_{14}\cdot 2CH_3COOH\cdot 3H_2O$	F:	51.09	7.01	17.54	R^8 0.29, R^5 0.45, R^6 0.65,
					C:	51.05	7.50	17.36	R^8 0.56 (Cellulose)
34	80	Oil	—	—			—		R^2 0.47
36	80	Oil	—	—			—		R^1 0.41
37	5	—	−64.1[e)] (*c* 0.1, H_2O)	$C_{43}H_{68}O_9N_{14}\cdot 2CH_3COOH\cdot 7H_2O$	F:	47.98	6.67	16.58	R^8 0.35
					C:	48.19	7.74	16.74	
38	60	110—111	−9.6	$C_{29}H_{39}O_8N_7$	F:	56.01	6.73	15.33	R^2 0.40
					C:	56.76	6.41	15.98	
40	70	127—129	−11.7[e)]	$C_{38}H_{48}O_9N_8$	F:	60.12	6.31	14.60	R^2 0.55
					C:	59.99	6.36	14.73	
41	49	146—147	−39.4	$C_{21}H_{30}O_7N_6$	F:	52.90	6.47	17.25	R^2 0.63
					C:	52.71	6.32	17.56	
44	33	78—94	−61.5[d)]	$C_{25}H_{29}O_9N_7$	F:	53.57	5.66	17.01	R^2 0.60
					C:	52.53	5.11	17.15	
45	35	124—126	−31.5[d)] (*c* 0.1)	$C_{56}H_{76}O_{15}N_{16}$	F:	55.34	6.21	18.26	R^3 0.65
					C:	55.44	6.31	18.47	
46	56	—	−27.0[e)] (*c* 0.1, H_2O)	$C_{47}H_{70}O_9N_{14}\cdot 2CH_3COOH\cdot 6H_2O$	F:	50.42	7.06	16.19	R^{10} 0.41, R^{10} 0.78
					C:	50.90	7.54	16.30	(Cellulose)

Table 2. (Continued)

Compound	Yield/%	Mp θ_m/°C	$[\alpha]_D^{24}$/°	Molecular formula	Elemental analysis/% Found (F:), Calcd (C:) C	H	N	R_f[b]
50	9	—	−40.5[e] (*c* 1.0, DMF)	$C_{41}H_{66}O_{10}N_{14}\cdot 2CH_3COOH\cdot 4H_2O$	F: 48.81	7.47	17.71	R^9 0.44 (Cellulose)
			(*c* 0.12, H_2O)		C: 48.82	7.46	17.71	
51	73	Oil	—	—		—		R^1 0.83, R^4 0.90
52	52	134—135.5	−29.6	$C_{25}H_{37}O_7N_3$	F: 61.42	7.75	8.51	R^1 0.65, R^4 0.80, R^5 0.86
					C: 61.08	7.59	8.55	
53	100	Oil	—	—		—		R^1 0.79, R^4 0.81
54	97	Oil	—	—		—		R^1 0.60, R^4 0.76, R^5 0.87
55	97	108—113	−53.8	$C_{55}H_{72}O_{14}N_{12}\cdot H_2O$	F: 57.89	6.56	14.68	R^1 0.33, R^4 0.37, R^5 0.61
					C: 57.78	6.52	14.70	

a) Compound **1**[24] has mp 155—157 °C; **2**[24] mp 85—92 °C; **4**[24] mp 155.5—159 °C; **6**[24] mp 110—113 °C; **11**[25] mp 67—69 °C; **17**[26] mp 152—155 °C; **18**[3] mp 126—129 °C; **19**[26] mp 135—138 °C; **20**[3] mp 189 °C; **22**[27] mp 162—164 °C; **24**[28] mp 114—117 °C; **33**[29] mp 87—90 °C; **39**[26] oil; **42**[26] mp 143.5—144 °C. Compound **21** produced in 62% yield; **47** 40% yield; **48** 66% yield; **49** 45% yield: other data of these compounds are unlisted. b) The solvent systems were described in experimental section. Silica-gel plate was used for TLC except when noted herein. c) At 19 °C. d) At 20 °C. e) At 21 °C. f) At 22 °C. g) At 25.5 °C.

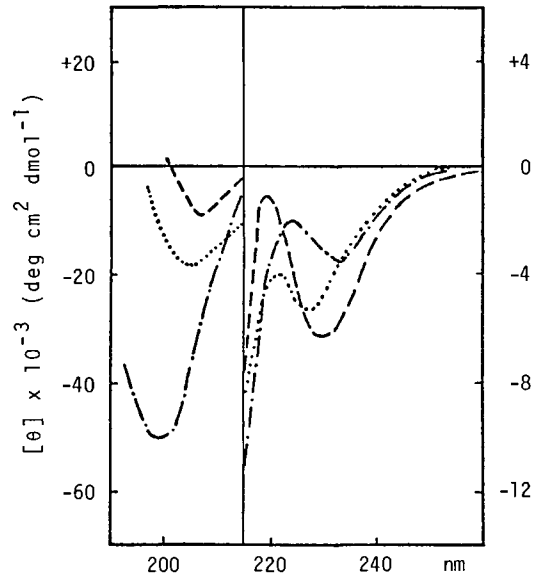

Fig. 10. CD spectra of [5-Ava[1-2]]-BK (**9**) (·····), [5-Ava[2-3]]-BK (**16**) (————), and [5-Ava[4-5]]-BK (**32**) (—·—·—) in water.

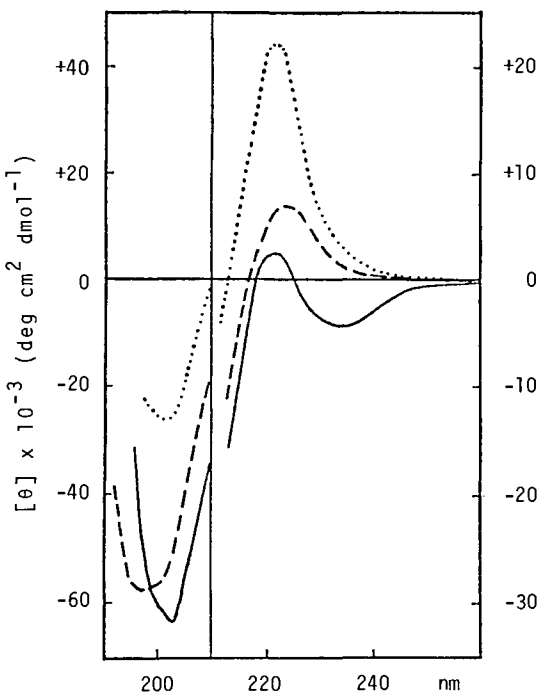

Fig. 11. CD spectra of BK (————), [5-Ava[6-7]]-BK (**46**) (·····), and [5-Ava[7-8]]-BK (**50**) (————) in water.

not form an intramolecular 3→1 hydrogen bond between the carbonyl oxygen of Ser[6] and the amide proton of Phe[8] as the result of replacement with the 5-Ava residue. The existence of the hydrogen bond in the BK molecule was pointed out by Cann et al.[6] Our result provides additional evidence for the formation of the intramolecular 3→1 hydrogen bond.

Cann et al. indicated the importance of an N-terminal sequence and Phe residues as a contribution for the positive band at 221 nm, suggesting an intramolecular 3→1 hydrogen bond between the carbonyl oxygen of Pro^2 and the amide proton of Gly^4.[6] Ivanov et al. proposed four energetically preferable BK-conformers which contain the salt bridge.[7] One of them forms an intramolecular 4→1 hydrogen bond between the carbonyl oxygen of Pro^2 and the amide proton of Phe^5 in the molecule. Although the positive band near 221 nm is generally referred to as arising from a Phe residue, the present result suggests that both amide bonds of Pro^2–Pro^3 and Gly^4–Phe^5 also contribute to this band. This result may be explained by supposing the formation of a partial structure stabilized with the intramolecular 4→1 hydrogen bond. Also, the similarity of the positive bands of [5-Ava^{3-4}]-BK and BK appears to make the 3→1 hydrogen bond in N-terminal sequence unlikely. In addition, the peak of [5-Ava^{1-2}]-BK, which lacks the strongly basic group on the side chain of Arg^1, is lower than those of [5-Ava^{2-3}]-BK and [5-Ava^{4-5}]-BK. This may be due to a change of secondary structure, owing to an impossibility to form the salt bridge between the guanidino group of Arg^1 and the C-terminal carboxyl group, proposed by Ivanov et al.[7] The similarity of the positive bands near 220 nm of BK-amide and [5-Ava^{1-2}]-BK implies the presence of the salt bridge in BK.[12] That is, the stability of the intramolecular 4→1 hydrogen bond is lowered by the incapability of salt-bridge formation because of a blocking of the C-terminal carboxyl group. This impossibility may bring about a decrease of ellipticity near 221 nm. The similarity between the peaks of BK and [5-Ava^{8-9}]-BK, in which the formation of salt bridge is possible, supports this supposition.

The analogs, (in which each sequence of Arg^1–Pro^2, Pro^2–Pro^3, Pro^3–Gly^4, Phe^5–Ser^6, and Ser^6–Pro^7 was replaced with a 5-Ava residue), show a shallower trough near 200 nm, as compared with that of BK; that is, this band probably arises mainly from the both sequences of Arg^1–Pro^2–Pro^3–Gly^4 and Phe^5–Ser^6–Pro^7 in BK.

The contributions for each CD band of BK are suggested as follows: the intramolecular 3→1 hydrogen bond for 234 nm band, Phe residues and the intramolecular 4→1 hydrogen bond for 221 nm band, and the both sequences of Arg^1–Pro^2–Pro^3–Gly^4 and Phe^5–Ser^6–Pro^7 for about the 200 nm band. Much smaller ellipticities of BK, compared with other peptides carrying a rigid conformation, such as gramicidin S, may reflect a higher flexibility in the backbone structure of BK.

Biological Activities of BK Analogs Containing 5-Ava Residue. The biological activities of these analogs were examined for uterus contraction of rat and blood flow of dog. The results shown in Table 3 are expressed as relative activity compared with the threshold dose of BK. [5-Ava^{1-2}]-BK, [5-Ava^{4-5}]-BK, [5-Ava^{5-6}]-BK, [5-Ava^{7-8}]-BK, and [5-Ava^{8-9}]-BK have no activity, while [5-Ava^{2-3}]-BK, [5-Ava^{3-4}]-BK, and [5-Ava^{6-7}]-BK indicate some of the activity, although very weak compared with that of BK. It has been known that the biological activity of BK analogs are drastically reduced by substitution of both or one of the Arg residue at positions 1 and 9 with a neutral amino acid or acidic amino acid residue, whereas the substitution of the Arg residue with other basic amino acids preserves considerable biological activities. [5-Ava^{1-2}]-BK and [5-Ava^{8-9}]-BK lack in Arg residue at positions 1 and 9, respectively. The present results also emphasize the importance of these two basic amino acid residues regarding biological activity. One or two of the Phe residues at positions 5 and 8 in BK can be substituted with an amino acid containing a restricted side chain, such as tyrosine methyl ether and 3-cyclohexylalanine, without any striking change regarding the biological activities.[20,21] However, replacement of the Phe residue by an aliphatic amino acid residue, such as the Ala, Leu, or Ile residue, results in a loss of activity.[21-23] [5-Ava^{4-5}]-BK, [5-Ava^{5-6}]-BK, [5-Ava^{7-8}]-BK, and [5-Ava^{8-9}]-BK did not show any biological activity. These results indicate similarly the importance for biological activity of the Phe residues at positions 5 and 8.

It is an interesting problem to elucidate the relationship between the structure in an aqueous solution and the activities of BK. [5-Ava^{3-4}]-BK, in which the peptide bond substituted with 5-Ava residue does not take part in the intramolecular 4→1 hydrogen bond, showed biological activity. Also, [5-Ava^{2-3}]-BK and [5-Ava^{6-7}]-

Table 3. Biological Activities of Eight Bradykinin Analogs Containing 5-Ava Residue

Compound	Blood flow[a] (dog, femoral artery)	Uterus contraction[b] (rat, isolated)
Bradykinin (BK)	1	1
[5-Ava^{1-2}]-BK (**9**)	Inactive	Inactive
[5-Ava^{2-3}]-BK (**16**)	4×10^{-5}	1×10^{-2}
[5-Ava^{3-4}]-BK (**26**)	1×10^{-3} [c]	1×10^{-3}
[5-Ava^{4-5}]-BK (**32**)	Inactive	Inactive
[5-Ava^{5-6}]-BK (**37**)	Inactive	Inactive
[5-Ava^{6-7}]-BK (**46**)	1×10^{-2}	1×10^{-3}
[5-Ava^{7-8}]-BK (**50**)	Inactive	Inactive
[5-Ava^{8-9}]-BK (**56**)	Inactive	Inactive

a) The threshold dose of BK: 1×10^{-9} g (=1). b) The threshold dose of BK: 1×10^{-9} g ml^{-1} (=1). c) Rat.

BK have biological activity, although not so strong as that of BK, in spite of an absence of the carbonyl oxygen of Pro^2 or Ser^6, which participates in the intramolecular 4→1 hydrogen bond or the intramolecular 3→1 hydrogen bond, respectively. These results imply that the biological activities of BK are affected by the absence of Arg and Phe residues, rather than the one of the intramolecular hydrogen bonds. On account of the structural flexibility of these linear peptides, a number of conformers may exist in equilibrium in solution. Therefore, the contribution of secondary structure for biological activity is ambiguous. We could not find any appreciable relationship between the CD spectra and the biological activities.

Experimental

Melting points were measured by a micro melting-point apparatus (Yanagimoto MFG Co.) and are given as uncorrected values. Optical rotations were determined with a polarimeter 111 (Shimadzu Co.). Amino acid analyses were performed on a JLC-6AS automatic analyzer (JEOL) after acid hydrolysis with 6 M (1 M=1 mol dm^{-3}) HCl in a sealed tube at 110 °C for 16—24 h. The theoretical values of the amino acid ratios are shown in parentheses after each result.

Thin-layer chromatography was performed on a TLC plate of silica gel 60 F_{254} (Merck and Co.) or cellulose (Avicel), using the following solvent systems (volume ratios): R_f^1, chloroform–methanol (9:1); R_f^2, chloroform–methanol–acetic acid (95:5:3); R_f^3, chloroform–methanol–acetic acid (95:15:3); R_f^4, chloroform–methanol–acetic acid (9:1:1); R_f^5, 1-butanol–acetic acid–water (4:1:1); R_f^6, 1-butanol–pyridine–acetic acid–water (15:10:3:12); R_f^7, 1-butanol–pyridine–acetic acid–water (16:3:1:4); R_f^8, 1-butanol–pyridine–acetic acid–water (4:1:1:2); R_f^9, 1-butanol–pyridine–acetic acid–water (16:10:3:12); R_f^{10}, 1-butanol–pyridine–water–ethanol (4:1:5:4). Silica-gel plate was used for TLC if not mentioned otherwise.

CD measurements were performed using a JASCO J-20 CD, ORD spectropolarimeter at 21—23 °C. A 0.50-mm thick cell was used. The measurements were carried out at concentrations of $(3.2—4.2)\times10^{-4}$ M and at pH 5.49—7.30.

Female rats weighing 180—250 g were used in order to assay the ability for the contraction of isolated rat uterus. A uterus horn applied to the load-tension of 0.5 g was suspended in an organ-bath of de Jalon's solution (10 ml) at 26 °C. The uterus contractions caused by the addition of BK analogs were recorded as isometric data using a JD-111S physiological displacement transducer (Nihonkoden Kogyo Co.). A dose-response curve was obtained in the concentration range of 3×10^{-6}—1×10^{-5} g ml^{-1} by using a cumulative method.

After a dog was anesthetized with sodium pentobarbital (30 mg kg^{-1}), hepaline was injected into a vein. The blood flow in the femoral artery of the dog was measured by using an electromagnetic blood flowmeter. The injection-volume into the artery of the BK analogs was $(1—3)\times10^{-5}$ l, and the administration range of these was $2\times(10^{-6}—10^{-4})$ g.

N^{α}-Boc groups were removed by TFA, HCl/THF, or HCl/dioxane with or without anisole, respectively. The reaction was run in an ice-bath or at room temperature according to the requisite. The concentration of HCl in the solution was kept above 2.5 M and at 10—30 equivalents for each peptide. N^{α}-Z groups were removed by H_2/Pd in an acidic solution at room temperature or the treatment with 25% HBr/AcOH for 1.0—2.5 h at room temperature. The symmetrical anhydrides described in the schemes were prepared by DCC. The protected products were purified by the usual methods. Only the typical procedures are herein described.

Z-5-Ava-Pro-Gly-Phe-Ser-Pro-Phe-Arg(NO_2)-OBzl (8) by a DCC/HOBt Method. The deprotection of **6** (0.719 g) with TFA (7.0 ml) and anisole (0.50 ml) in the usual manner gave an oily residue. DCC (0.239 g) in DMF (2.0 ml), and an ice-chilled solution of the above residue and NMM (0.349 ml) in DMF (8.0 ml) were added to an ice-cooled solution of **7** (0.427 g) and HOBt (0.285 g) in DMF (7.0 ml). The mixture was stirred for 1 h in an ice-bath and then for 41 h at room temperature. After the precipitates were removed, the solvent was evaporated. The residue was dissolved in ethyl acetate. The ethyl acetate solution was washed by the routine method. After removing the solvent, the residue was crystallized from diethyl ether. The crude product was further recrystallized from ethyl acetate–diethyl ether: Yield 0.640 g (67%); mp 103—106.5 °C; $[\alpha]_D^{24}$ −31.5° (*c* 0.5, DMF); R_f^1 0.71, R_f^4 0.70, R_f^5 0.80, R_f^8 0.77. Amino acid ratios in acid hydrolyzate: Ser 0.83 (1), Pro 2.21 (2), Gly 1.03 (1), Phe 1.81 (2), 5-Ava 1.19 (1), Arg+Orn 0.93 (1). Found: C, 59.85; H, 6.75; N, 14.01%. Calcd for $C_{59}H_{74}O_{14}N_{12}$: C, 60.29; H, 6.35; N, 14.30%.

Z-5-Ava-Gly-OEt (10) by a Symmetrical Anhydride Method. $(Z\text{-}5\text{-}Ava)_2O$ (3.03 g) was added to a solution of HCl·H-Gly-OEt (1.12 g) and Et_3N (2.50 ml) in chloroform (30 ml). After stirring for 2 d, the solvent was evaporated. The residue was dissolved in ethyl acetate. The organic layer was washed using the usual method. After evaporation of the solvent, the residue was recrystallized from ethyl acetate: Yield 0.81 g (35%); mp 62—64.2 °C; $[\alpha]_D^{24}$ −12.8° (*c* 0.265, DMF); R_f^1 0.59. Found: C, 60.22; H, 7.28; N, 8.86%. Calcd for $C_{17}H_{24}O_5N_7$: C, 60.70; H, 7.19; N, 8.33%.

Boc-5-Ava-Ser-$NHNH_2$ (28). Compound **27** (4.210 g) was dissolved in methanol (12.0 ml), and to this solution was added 80% $NH_2NH_2\cdot H_2O$ (8.05 ml). The mixture was stirred for 45 h at room temperature. The resulting crystals were collected, then washed onto a filter funnel with methanol–diethyl ether (1:1), and further triturated with ethanol: Yield 3.483 g (83%); mp 171—173.5 °C; $[\alpha]_D^{24}$ −1.0° (*c* 1.0, DMF); R_f^8 0.65. Amino acid ratios in acid hydrolyzate: Ser 0.92 (1), 5-Ava 1.08 (1). Found: C, 49.01; H, 8.81; N, 17.65%. Calcd for $C_{13}H_{26}O_5N_4$: C, 49.04; H, 8.23; N, 17.60%.

Boc-5-Ava-Ser-Pro-Phe-Arg(NO_2)-OBzl (29) by an Azide Method. The treatment of **2** (1.961 g) in dioxane (11.1 ml) with 5.04 M HCl/dioxane (11.90 ml) in the presence of anisole (1.0 ml) for 1 h in an ice-bath gave a solid. A solution of **28** (0.952 g) in DMF (12 ml) was cooled below −30 °C. To the solution were added 5.04 M HCl/dioxane (1.79 ml) and isopentyl nitrite (0.402 ml) with stirring. The mixture was stirred for 15 min at −22 °C and then chilled below −30 °C. To the mixture were added Et_3N (1.25 ml) and an ice-chilled solution of the above solid and Et_3N (0.42 ml) in DMF (11 ml). After stirring for ca. 3 d, the solvent was evaporated. The residue was dissolved in ethyl acetate. The organic layer was washed using the usual procedure. After concentration of the solution, the residue was crystallized from diethyl ether. The product was further recrystallized from ethanol–diethyl ether:

Yield 2.156 g (86%); mp 110.5—114.5°C; $[\alpha]_D^{24}$ −36.7° (*c* 0.5, DMF); R_f^1 0.38, R_f^5 0.90. Amino acid ratios in acid hydrolyzate: Ser 0.93 (1), Pro 1.05 (1), Phe 0.99 (1), 5-Ava 1.12 (1), Arg+Orn 0.91 (1). Found: C, 56.60; H, 6.84; N, 15.19%. Calcd for $C_{40}H_{57}O_{11}N_9 \cdot 1/2H_2O$: C, 56.59; H, 6.89; N, 14.85%.

Boc-Pro-5-Ava-Ser-Pro-Phe-Arg(NO_2)-OBzl (30) by an MA Method. Compound **29** (0.400 g) was treated with TFA (4.0 ml) for 50 min to yield a solid in the usual manner. Boc-Pro-OH (0.103 g) was dissolved in THF (2.0 ml) and the solution was chilled below −40 °C. NMM (0.053 ml) and ethyl chloroformate (0.046 ml) were added to this solution. The mixture was stirred for 5 min at −13—−15 °C, and then chilled below −40°C. To the mixture was added an ice-chilled solution of the above solid and NMM (0.083 ml) in DMF (3.5 ml). The mixture was stirred in an ice-bath and then at room temperature for 22 h. After evaporation of the solvent, the residue was dissolved in ethyl acetate. The organic layer was washed in the usual method. After the solution was concentrated, the residue was recrystallized from ethyl acetate–diethyl ether: Yield 0.309 g (69%); mp 103.5—107.5 °C; $[\alpha]_D^{24}$ −45.5° (*c* 0.5, DMF); R_f^1 0.49, R_f^5 0.80. Amino acid ratios in acid hydrolyzate: Ser 0.86 (1), Pro 1.97 (2), Phe 1.04 (1), 5-Ava 1.15 (1), Arg+Orn 0.98 (1). Found: C, 56.13; H, 6.87; N, 14.39%. Calcd for $C_{45}H_{64}O_{12}N_{10} \cdot H_2O$: C, 56.59; H, 6.97; N, 14.67%.

Z-Arg(NO_2)-Pro-Pro-Gly-OH (35). To an ice-chilled solution of **33** (0.506 g) in ethanol (3.0 ml) was added 1.90 M NaOH (0.85 ml). The mixture was stirred for 30 min at room temperature and then 1 M HCl (1.70 ml) was added to this solution in an ice-bath. After evaporation of ethanol, to the residual solution were added ethyl acetate and 5% Na_2CO_3. The aqueous layer was acidified with concd HCl in an ice-bath, and then saturated with NaCl. It was extracted with ethyl acetate and the organic layer was washed with water saturated with NaCl. The aqueous layer was further extracted with ethyl acetate in the same manner. The organic layers were combined and the solvent was evaporated. The residue was crystallized from diethyl ether: Yield 0.463 g (96%); mp 112.5—118 °C; $[\alpha]_D^{24}$ −54.8° (*c* 0.5, DMF); R_f^4 0.17, R_f^5 0.47. Amino acid ratios in acid hydrolyzate: Pro 2.21 (2), Gly 0.79 (1), Arg+Orn 0.60 (1). Found: C, 47.96; H, 5.69; N, 16.69%. Calcd for $C_{26}H_{36}O_9N_8 \cdot 3H_2O$: C, 47.41; H, 6.42; N, 17.01%.

Z-Pro-Gly-Phe-5-Ava-Phe-Arg(NO_2)-OMe (43) by an Active Ester Method. Compound **40** (1.52 g) was treated with 25% HBr/AcOH (3.0 ml) for 1 h at room temperature to afford a solid in the usual way. Compound **42** (0.890 g) was added to a solution of the above solid, Et_3N (0.30 ml), and NMM (0.60 ml) in DMF (5.0 ml). After stirring for 7 d at room temperature, water (200 ml) was added to this mixture. The resulting precipitates were washed onto a filter funnel as usual. The crude product was washed with ethyl acetate, and then recrystallized from ethanol. The product was washed with diethyl ether: Yield 0.960 g (53%); mp 140—143 °C; $[\alpha]_D^{19.5}$ −25.0° (*c* 1.0, DMF); R_f^2 0.32. Found: C, 58.90; H, 6.67; N, 15.35%. Calcd for $C_{45}H_{58}O_{11}N_{10}$: C, 59.07; H, 6.39; N, 15.31%.

H-Arg-Pro-Pro-Gly-Phe-Ser-Pro-5-Ava-OH (56). Compound **55** (201 mg) in a solution of DMF–water–acetic acid (10 – 5 – 1 ml) was hydrogenated over palladium black for 7 d. Water (14 ml) was added to the mixture during the hydrogenation. After the catalyst was removed, the solution was concentrated. The residue was dissolved in ammonium acetate buffer (0.04 M, pH 6.0) (3.0 ml) and subjected to a carboxymethyl cellulose column (1.7×22.3 cm; Whatman CM-52). It was eluted with ammonium acetate buffers (0.04—0.40 M, pH 6.0) by a linear gradient method. Fractions of 3.0 g each were collected and checked by UV absorption at 254 nm, TLC, and amino acid analysis. Fractions 37—42 were combined and concentrated. The residue was dissolved in 4% acetic acid (2.0 ml) and applied to a Sephadex G-10 column (1.7×41 cm) using the same solvent. Fractions 11—17 (2.5 g each) were combined and concentrated. For further purification, the residue was dissolved in 1-butanol–pyridine–acetic acid–water (16 : 10 : 3 : 12) (1.0 ml) and applied to a column (1.7×26.0 cm) of Sephadex G-25. Fractions 12—25 (3.0 g each), including a pure peptide, were combined and concentrated. The residue was lyophilized from water: Yield 72.7 mg (42%); $[\alpha]_D^{22}$ −97.7° (*c* 0.1, H_2O); R_f^9 0.62 (cellulose). Amino acid ratios in acid hydrolyzate: Ser 0.89 (1), Pro 3.07 (3), Gly 0.98 (1), Phe 1.00 (1), 5-Ava 1.14 (1), Arg 0.92 (1). Found: C, 52.60; H, 6.76; N, 16.10%. Calcd for $C_{40}H_{61}O_{10}N_{11} \cdot CH_3COOH \cdot 2H_2O$: C, 52.98; H, 7.30; N, 16.18%.

The authors are grateful to the Research Laboratory of Toyo Jozo Co., Ltd. for the elemental and amino acid analyses. We would also like to thank Toyo Jozo Co., Ltd. for the biological assays of uterus contraction of compounds **9** and **56**, and the Research Laboratory of Nihon Kayaku Co., Ltd. for obtaining the other biological-activity data.

References

1) M. Rocha e Silva, W. T. Beraldo, and G. Rosenfeld, *Am. J. Physiol.*, **156**, 261 (1949).

2) D. F. Elliott, G. P. Lewis, and E. W. Horton, *Biochem. Biophys. Res. Commun.*, **3**, 87 (1960).

3) R. A. Boissonnas, St. Guttmann, P.-A. Jaquenoud, *Helv. Chim. Acta*, **43**, 1349 (1960).

4) A. Bodanszky, M. Bodanszky, E. J. Jorpes, V. Mutt, and M. A. Ondetti, *Experientia*, **26**, 948 (1970).

5) A. H. Brady, J. W. Ryan, and J. M. Stewart, *Biochem. J.*, **121**, 179 (1971).

6) J. R. Cann, J. M. Stewart, and G. R. Matsueda, *Biochemistry*, **12**, 3780 (1973).

7) V. T. Ivanov, M. P. Filatova, Z. Reissman, T. O. Reutova, E. S. Efremov, V. S. Pashkov, S. G. Galaktionov, G. L. Grigoryan, and Yu. A. Ovchinnikov, "Peptides," ed by R. Walter and J. Meienhofer, Ann Arbor Publishers, Michigan (1975), p. 151.

8) R. E. London, J. M. Stewart, J. R. Cann, and N. A. Matwiyoff, *Biochemistry*, **17**, 2270 (1978).

9) G. I. Chipens, F. K. Mutulis, N. V. Myshlyakova, I. P. Misina, R. O. Vitolina, V. J. Klusha, and B. S. Katayev, *Int. J. Pept. Protein Res.*, **26**, 460 (1985).

10) S. Sofuku, K. Shiino, I. Muramatsu, H. Naganawa, and T. Takita, "Peptide Chemistry 1973," ed by H. Kotake, Protein Research Foundation, Osaka (1974), p. 62.

11) M. Tamaki, S. Sofuku, I. Muramatsu, and A. Hagitani, "Peptide Chemistry 1975," ed by S. Yamada, Protein Research Foundation, Osaka (1976), p. 117.

12) C. Hashimoto, M. Tamaki, H. Uchida, S. Nozaki, S. Sofuku, and I. Muramatsu, "Peptide Chemistry 1978," ed by

N. Izumiya, Protein Research Foundation, Osaka (1979), p. 115.

13) The amino acids except glycine used are of L-configuration. The abbreviations used are those recommended by IUPAC-IUB Joint Commission on Biochemical Nomenclature (JCBN): *Eur. J. Biochem.*, **138**, 9 (1984). The following additional abbreviations are used: 5-Ava, 5-aminovaleric acid; Z, benzyloxycarbonyl; Boc, *t*-butoxycarbonyl; THF, tetrahydrofuran; AcOH, acetic acid; DCC, dicyclohexylcarbodiimide; HOBt, 1-benzotriazolol; MA, mixed anhydride; TFA, trifluoroacetic acid; DMF, *N*,*N*-dimethylformamide; NMM, *N*-methylmorpholine; Et_3N, triethylamine; Ac, acetyl.

14) J. C. Sheehan and G. P. Hess, *J. Am. Chem. Soc.*, **77**, 1067 (1955).

15) W. König and R. Geiger, *Chem. Ber.*, **103**, 788 (1970).

16) G. W. Anderson, J. E. Zimmerman, and F. M. Callahan, *J. Am. Chem. Soc.*, **88**, 1338 (1966).

17) J. Honzl and J. Rudinger, *Collect. Czech. Chem. Commun.*, **26**, 2333 (1961).

18) M. Bodanszky and V. du Vigneaud, *J. Am. Chem. Soc.*, **81**, 5688 (1959).

19) D. Yamashiro, *Nature*, **201**, 76 (1964).

20) J. M. Stewart, *Fed. Proc., Fed. Am. Soc. Exp. Biol.*, **27**, 63 (1968).

21) A. T. Chi, A. R. Day, J. A. Radding, and R. J. Freer, *J. Med. Chem.*, **22**, 334 (1979).

22) E. Schröder and R. Hempel, *Experientia*, **20**, 529 (1964).

23) W. K. Park, S. A. St-Pierre, J. Barabé, and D. Regoli, *Can. J. Biochem.*, **56**, 92 (1978).

24) R. Tomatis, R. Ferroni, M. Guarneri, and C. A. Benassi, *J. Med. Chem.*, **16**, 1053 (1973).

25) R. Schwyzer and G. Karlaganis, *Justus Liebigs Ann. Chem.*, **1973**, 1298.

26) M. A. Ondetti, *J. Med. Chem.*, **6**, 10 (1963).

27) E. Schröder and H. Gibian, *Justus Liebigs Ann. Chem.*, **649**, 168 (1961).

28) H. Yajima, K. Kitagawa, and T. Segawa, *Chem. Pharm. Bull.*, **21**, 2500 (1973).

29) G. C. Barrett, P. M. Hardy, T. A. Harrow, and H. N. Rydon, *J. Chem. Soc., Perkin Trans. 1*, **1972**, 2634.

Triethylborane Induced Perfluoroalkylation of Silyl Enol Ethers and Ketene Silyl Acetals with Perfluoroalkyl Iodides

Katsukiyo MIURA, Yoshihiro TAKEYAMA, Koichiro OSHIMA,* and Kiitiro UTIMOTO*
Department of Industrial Chemistry, Faculty of Engineering, Kyoto University, Sakyo-ku, Kyoto 606
(Received December 6, 1990)

Reaction of perfluoroalkyl iodides with silyl enol ethers mediated by Et_3B in the presence of base such as 2,6-dimethylpyridine provides mixtures of perfluoroalkylated trialkylsilyl enol ethers and α-perfluoroalkylated ketones. The yield and distribution of the products heavily depend on the nature of base employed. Treatment of a reaction mixture consisting of perfluoroalkylated silyl enol ether and α-perfluoroalkylated ketone with concd HCl in THF gives α-perfluoroalkylated ketone as a single product. Reaction of ketene silyl acetals with perfluoroalkyl iodides in the absence of base affords α-perfluoroalkylated esters in excellent yields.

Recently, much attention has been paid to a method of introducing a perfluoroalkyl chain to a carbonyl compound and several reports have appeared in the literature.[1] The methods, however, have some drawbacks and there is still a need for a new method preparing perfluoroalkylated compounds from carbonyl compounds such as aldehydes, ketones, and esters. Previously we have reported that Et_3B induced the successful addition of perfluoroalkyl iodides to acetylenes and olefins (Scheme 1).[2] Here we report further exploitation of this method to (1) the reaction of perfluoroalkyl iodides with trialkylsilyl enol ethers providing perfluoroalkylated silyl enol ethers[3] and (2) the reaction of perfluoroalkyl iodides with ketene silyl acetals affording perfluoroalkylated esters.

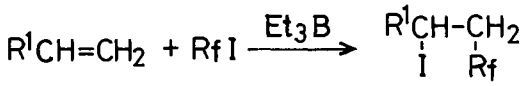

Scheme 1.

(1) The Reaction of Perfluoroalkyl Iodides with Trialkylsilyl Enol Ethers. Treatment of a hexane solution of 1-trimethylsiloxy-1-cyclohexene (**1**) and perfluorohexyl iodide with a catalytic amount of triethylborane[4] in the presence of base such as 2,6-dimethylpyridine gave a mixture of perfluoroalkylated silyl enol ether (**2** and **3**) and 2-(perfluorohexyl)cyclohexanone (**4**)[1d] in 76% combined yield (**2**+**3**/**4**=86/14, Scheme 2).

The distribution of the products heavily depends on the nature of base employed. The base and the yields of **2**+**3** (ratio of **2**/**3**) and **4** in the reaction between 1-trimethylsiloxy-1-cyclohexene (**1**) and perfluorohexyl iodide are given below: Et_3N, 47 (59/41), 26; 2,2,6,6-tetramethylpiperidine, 63 (68/32), 11; hexamethyldisilazane, 24 (0/100), 44; pyridine, 0, 20; diisopropylethylamine, 12 (65/35), 29. The amount of base also affected the distribution of the products (Scheme 3). The presence of excess base (2,6-dimethylpyridine, 3.0 mmol per 1.0 mmol of silyl enol ether) caused the formation of 2-(perfluorohexylidene)cyclohexanone **5** in 6% yield along with **2**+**3** (49%) and **4** (23%). The use of slightly deficient amount of 2,6-dimethylpyridine suppressed the formation of **5**. The representative results using 2,6-dimethylpyridine (0.95 mmol per 1.0 mmol of silyl enol ether) as a base are summarized in Table 1.

The use of triisopropylsilyl enol ether **6** instead of trimethylsilyl enol ether **1** gave better yields of perfluoroalkylated silyl enol ethers **7** and **8** with less contamination by 2-(perfluoroalkyl)cyclohexanones **4** (Runs 3 and

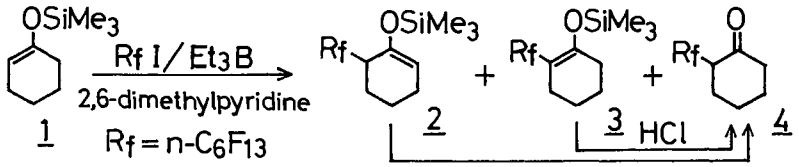

Scheme 2.

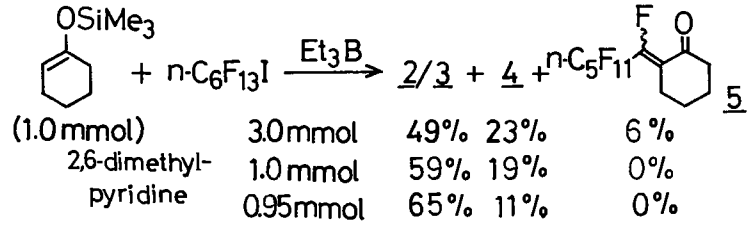

Scheme 3.

Table 1. Reaction of Silyl Enol Ether with Perfluoroalkyl Iodide[a)]

Run	Silyl enol ether		R_fI	Product (%)		
	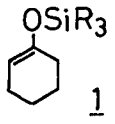			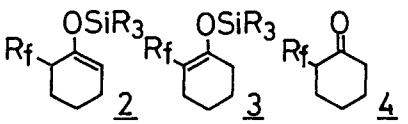		
1		R=Me	n-$C_6F_{13}I$	44	21	11
2		R=Me	i-C_3F_7I	41	11	9
3		**6**: R=*i*-Pr	n-$C_6F_{13}I$	57 (**7**)	14 (**8**)	<5
4		R=*i*-Pr	i-C_3F_7I	47	25	<2
	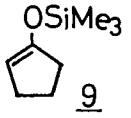			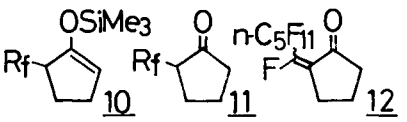		
5			n-$C_6F_{13}I$	35	26	3
	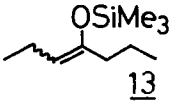			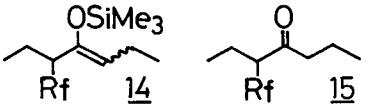		
6			n-$C_6F_{13}I$	71 (E/Z=60/40)		16
7			i-C_3F_7I	66 (E/Z=70/30)		<2
	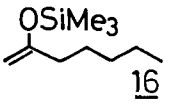			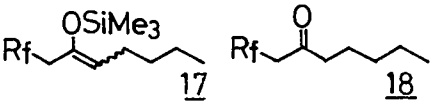		
8			n-$C_6F_{13}I$	54 (E/Z=28/72)		24
9			i-C_3F_7I	56 (E/Z=33/67)		15
	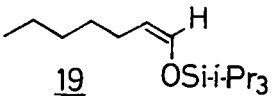			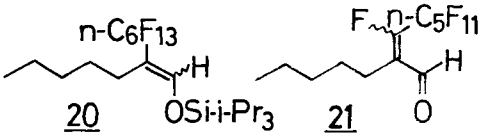		
10			n-$C_6F_{13}I$	38 (88/12)[b)]		46 (71/29)[b)]

a) Silyl enol ether (2.0 mmol), perfluoroalkyl iodide (2.6 mmol), 2,6-dimethylpyridine (1.90 mmol), and triethylborane (0.4 mmol) were employed. b) Stereochemistry could not be determined.

4). Treatment of 1-trimethylsiloxy-1-cyclopentene **9** with perfluorohexyl iodide gave a mixture of 5-(perfluorohexyl)-1-trimethylsiloxy-1-cyclopentene **10**, 2-(perfluorohexyl)cyclopentanone **11**, and 2-(perfluorohexylidene)cyclopentanone **12** in 35, 26, and 3% yields, respectively. 2-(Perfluorohexyl)-1-trimethylsiloxy-1-cyclopentene was not detected in the reaction mixture. The reaction proceeded with acyclic silyl enol ether as well as cyclic silyl enol ether. In the case of silyl enol ether **13** or **16**, derived from acyclic ketone such as 4-heptanone or 2-heptanone, 5-(perfluoroalkyl)-4-trimethylsiloxy-3-heptenes **14** or 1-(perfluoroalkyl)-2-trimethylsiloxy-2-heptenes **17** was obtained as a single regioisomer as the reaction of 1-trimethylsiloxy-1-cyclopentene **9**. The other isomeric silyl enol ether (3-(perfluoroalkyl)-4-trimethylsiloxy-3-heptene or 1-(perfluoroalkyl)-2-trimethylsiloxy-1-heptene) was not observed in the reaction mixture. Reaction of silyl enol ether **19** derived from heptanal afforded a mixture of 2-(perfluoroalkyl)-1-triisopropylsiloxy-1-heptene **20** and 2-(perfluorohexylidene)heptanal **21**.

Treatment of the reaction mixture consisting of **2**, **3**, and **4** with concd hydrochloric acid in THF at 25 °C for 10 min afforded 2-(perfluoroalkyl)cyclohexanone **4** as a single product in 74% overall yield. The yields of perfluoroalkylated carbonyl compounds after acidic workup were 78, 73, and 56% for the reaction described in Runs 6, 8, and 9.

Trifluoromethylated organic compounds are of importance from the biological point of view.[5)] Thus, we focussed our attention on trifluoromethylation of carbonyl compounds and examined the reactions of silyl

Table 2. Reaction of Silyl Enol Ether with CF_3I or CF_3CH_2I

Silyl enol ether (1.0 mmol)	R–X (mmol)	Reaction time/h	Product	Y/%
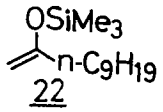 22	CF_3I (10)	40	CF_3CH_2CO-*n*-C_9H_{19} **23a**	64
	CF_3CH_2I (2)	15	$CF_3(CH_2)_2CO$-*n*-C_9H_{19} **23b**	79
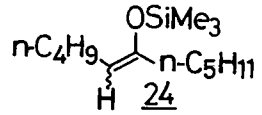 24	CF_3I (10)	48	*n*-$C_4H_9CH(CF_3)CO$-*n*-C_5H_{11} **25a**	32
	CF_3CH_2I (2)	20	*n*-$C_4H_9CH(CH_2CF_3)CO$-*n*-C_5H_{11} **25b**	4

enol ether with trifluoromethyl iodide or 2,2,2-trifluoroethyl iodide (Table 2). Treatment of terminal silyl enol ether **22** with excess trifluoromethyl iodide or 2,2,2-trifluoroethyl iodide gave 1,1,1-trifluoro-3-dodecanone **23a** or 1,1,1-trifluoro-4-tridecanone **23b** in 64 or 79% yield, respectively after quenching the reaction mixture by concd HCl. Meanwhile, the reaction of internal silyl enol ether such as **24** with CF_3I or CF_3CH_2I gave the corresponding trifluoro ketone **25a** or **25b** in poor yield.

Reaction of **26** prepared from cyclopropyl methyl ketone with perfluoroalkyl iodides followed by treatment with concd HCl provided the corresponding 5-iodo-1-(perfluoroalkyl)-2-pentanones under cleavage of cyclopropane ring.[6] The reaction proceeded without base such as 2,6-dimethylpyridine. The intermediary silyl enol ether **27b** was isolated in the reaction of **26** with *i*-C_3F_7I in 85% yield (Scheme 4).

Thus, a new method provided us with a synthetic tool

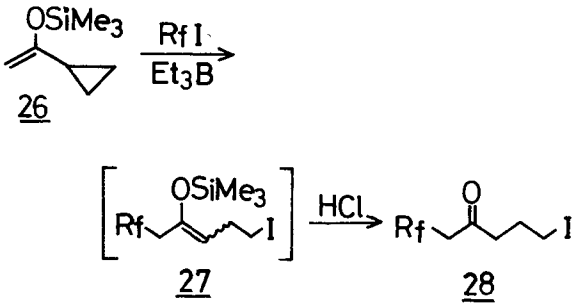

R_f a: *n*-C_6F_{13} 25°C 20 min 88%
b: *i*-C_3F_7 25°C 20 min 83%
c: CF_3 −78°C—5°C 3 h 67%

Scheme 4.

for the preparation of newly functionalized trimethyl silyl enol ethers as well as α-perfluoroalkyl ketones.[7]

We are tempted to assume following reaction mechanism for the formation of perfluoroalkylated silyl enol ethers (Scheme 5): (1) Perfluoroalkyl radical, generated by the action of ethyl radical on perfluoroalkyl iodide, adds to silyl enol ether to give a radical **A**, (2) the radical **A** abstracts iodine from R_fI to give the adduct **B** and regenerates perfluoroalkyl radical, and (3) the coexisting base causes the elimination of HI to give a mixture of two perfluoroalkylated silyl enol ethers (**2** and **3**). The regioselective formation of **B** would be attributed to the electrophilic attack of reactive R_f radical on the electron-rich carbon of silyl enol ether.

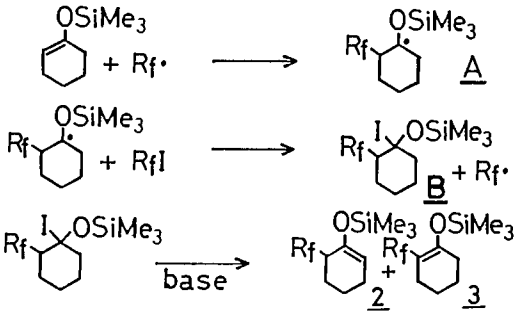

Scheme 5.

(2) The Reaction of Perfluoroalkyl Iodides with Ketene Silyl Acetals. Reaction of ketene silyl acetals with perfluoroalkyl iodides also proceeded easily in the presence of triethylborane catalyst to give α-perfluoroalkylated esters in excellent yields. Exposure of ketene silyl acetal **29** (1.0 mmol) to *n*-$C_6F_{13}I$ (1.3 mmol) in the presence of 2,6-dimethylpyridine (0.95 mmol) provided

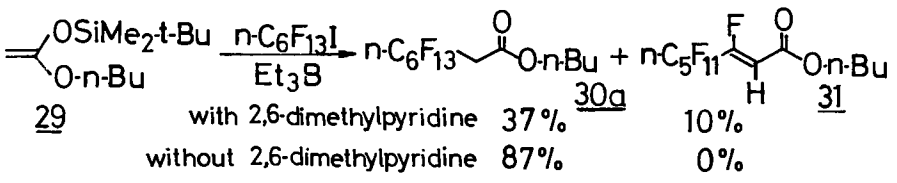

Scheme 6.

Table 3. Reaction of Ketene Silyl Acetal with Perfluoroalkyl Iodide

Ketene silyl acetal	R_fI	Reaction time/min		Product %
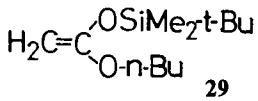 **29**	*n*-$C_6F_{13}I$	10	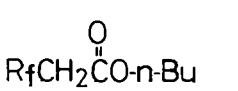 **30**	87 (**30a**)
	i-C_3F_7I	30		61 (**30b**)
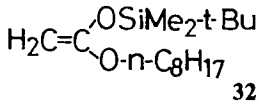 **32**	CF_3I	120	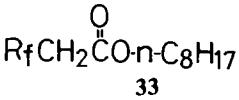 **33**	81 (**33b**)
	CF_3CH_2I	30		62 (**33c**)
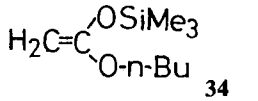 **34**	*n*-$C_6F_{13}I$	20[a]	**30**	96 (**30a**)
	i-C_3F_7I	20		49 (**30b**)
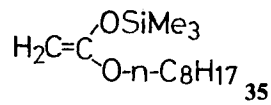 **35**	*i*-C_3F_7I	20	**33**	96 (**33a**)
	CF_3I	120[a]		90 (**33b**)
	CF_3CH_2I	60[a]		77 (**33c**)
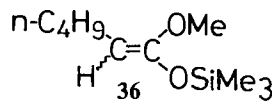 **36**	*n*-$C_6F_{13}I$	20	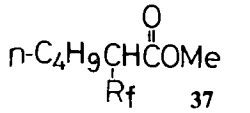 **37**	83 (**37a**)
	i-C_3F_7I	20		40 (**37b**)
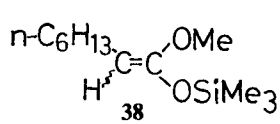 **38**	*i*-C_3F_7I	20[a]	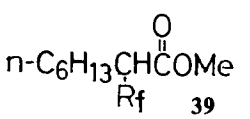 **39**	88 (**39a**)
	CF_3I	120[a]		66 (**39b**)
	CF_3CH_2I	120[a]		32 (**39c**)
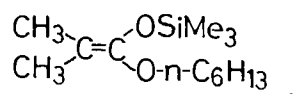 **40**	*n*-$C_6F_{13}I$	4 h	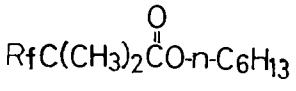 **41**	63 (**41a**)
	i-C_3F_7I	16 h		27 (**41b**)
	CF_3I	12 h		22 (**41c**)

a) TBAF was added prior to work-up. See experimental part.

butyl 2-(perfluorohexyl)acetate (**30a**, 37%) along with butyl 2-(perfluorohexylidene)acetate (**31**, 10%). In contrast, treatment of **29** (2.0 mmol) with *n*-$C_6F_{13}I$ (1.0 mmol) in the absence of 2,6-dimethylpyridine in hexane provided **30a** (87% based on *n*-$C_6F_{13}I$) as a single product (Scheme 6). The yields of **30a** depend on the molar ratio of ketene silyl acetal and perfluoroalkyl iodide employed. The yields of **30a** in the reaction of **34** (x mmol) with *n*-$C_6F_{13}I$ (1.0 mmol) in the presence of catalytic amount of Et_3B (0.2 mmol) are as follows: **34** (2.0 mmol), 96%; **34** (1.5 mmol), 93%; **34** (1.2 mmol), 89%. Slight excess (1.2 equiv) of ketene silyl acetal was enough for the successful reaction. However, the reactions were performed using 2.0 equiv of ketene silyl acetals to obtain better yields and the results are summarized in Table 3.

Not only *n*-$C_6F_{13}I$, *i*-C_3F_7I but also CF_3I[7] or CF_3CH_2I reacted easily to give the corresponding perfluoroalkylated esters in good yields. Perfluoroalkylated ketene silyl acetal could not be detected. Trimethylsilyl acetal (**34** or **35**) reacted equally as dimethyl-*t*-butylsilyl acetal (**29** or **32**) to give the same perfluoroalkylated ester upon treatment with perfluoroalkyl iodides.

Alkyl group substituted ketene silyl acetals (**36**, **38**, and **40**) were prepared and their behavior toward perfluoroalkyl iodides were examined. Whereas the acetals **36** and **38** easily reacted with R_fI to provide the corresponding perfluoroalkylated esters in good yields, the acetal **40** reacted slowly because of its steric hindrance to give ester **41** in poor yields.

Treatment of ketene silyl acetal **42** with *n*-$C_6F_{13}I$ afforded a cyclized product **43** (10%) along with perfluoroalkylated ester **44** (50%) (Scheme 7). The formation of **43** suggests an intermediacy of carbon radical bearing OR and $OSiMe_3$ groups. The result also shows that C–C double bond of ketene silyl acetal is much more reactive than that of simple olefin.

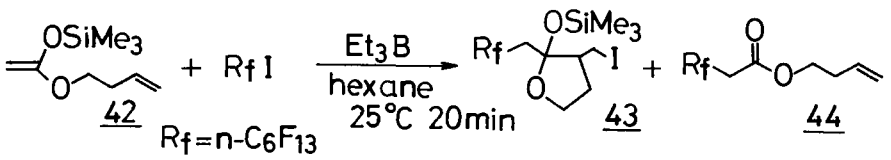

Scheme 7.

Experimental

Distillations of the products were performed by use of Kugelrohr (Büchi), and boiling points are indicated by air-bath temperature without correction. Melting point was obtained on a Yanako MP-50929 melting point apparatus and are uncorrected, too. ^{1}H NMR and ^{13}C NMR spectra were taken on a Varian XL-200 spectrometer, $CDCl_3$ was used as solvent, and chemical shifts being given in δ with tetramethylsilane as an internal standard. ^{19}F NMR spectra were recorded on JEOL JNM-FX 90Q spectrometer and the chemical shifts are given in δ with $CFCl_3$ as an internal standard. IR spectra were determined on a JASCO IR-810 spectrometer and the mass spectra on a Hitachi M-80 machine. The analyses were carried out at the Elemental Analyses Center of Kyoto University. Tetrahydrofuran (THF) was freshly distilled from sodium diphenylketyl.

Preparation of Silyl Enol Ethers. Trimethylsilyl enol ethers **1**, **9**, **13**, **16**, **22**, and **24** were prepared by the reported procedure.[8-11] Triisopropylsilyl enol ether **6** and **19** were prepared according to the Corey's method.[12] 1-Trimethylsiloxy-1-cyclopropylethylene was obtained following the reported procedure.[13] The physical data are shown below for the silyl enol ethers whose physical data have not been described in the literature.

1-Triisopropylsiloxy-1-cyclohexene (6): Bp 91—96 °C (1 Torr, 1 Torr=133.322 Pa, bath temp); IR(neat) 2936, 2892, 2864, 1670, 1465, 1367, 1195, 885, 826, 680 cm^{-1}; ^{1}H NMR ($CDCl_3$) δ=1.02—1.23 (m, 21H), 1.45—1.57 (m, 2H), 1.60—1.72 (m, 2H), 1.95—2.10 (m, 4H), 4.89 (t, J=3.7 Hz, 1H); ^{13}C NMR ($CDCl_3$) δ=12.66, 17.98, 22.38, 23.27, 23.87, 29.92, 103.6, 150.6; MS (70 eV) m/z (rel intensity) 254 (11), 211 (100), 183 (26), 141 (18), 81 (20), 75 (48), 61 (36), 59 (28), 41 (20). Found: C, 70.54; H, 12.02%. Calcd for $C_{15}H_{30}OSi$: C, 70.80; H, 11.88%.

(Z)-1-Triisopropylsiloxy-1-heptene (19): Bp 81—86 °C (1 Torr, bath temp); IR(neat) 2926, 2864, 1655, 1465, 1256, 1135, 1092, 1069, 882, 683, 662 cm^{-1}; ^{1}H NMR ($CDCl_3$) δ=0.88 (t, J=6.5 Hz, 3H), 1.03—1.20 (m, 21H), 1.22—1.42 (m, 6H), 2.04—2.15 (m, 2H), 4.39 (td, J=7.2, 5.8 Hz, 1H), 6.27 (dt, J=5.8, 1.5 Hz, 1H); ^{13}C NMR ($CDCl_3$) δ=11.98, 14.10, 17.74, 22.57, 23.54, 29.39, 31.63, 110.0, 138.9; MS (70 eV) m/z (rel intensity) 270 (2), 228 (20), 227 (100), 103 (21), 75 (24), 61 (15), 59 (29). Found: C, 70.94; H, 12.85%. Calcd for $C_{16}H_{34}OSi$: C, 71.04; H, 12.67%.

2-Trimethylsiloxy-1-undecene (22). This compound was prepared from 2-undecanone in 79% yield along with 2-trimethylsiloxy-2-undecene (93/7): Bp 85—86 °C (1 Torr); IR (neat) 2954, 2924, 2852, 1654, 1637, 1252, 1013, 845 cm^{-1}; ^{1}H NMR ($CDCl_3$) δ=0.20 (s, 9H), 0.88 (t, J=6.4 Hz, 3H), 1.20—1.53 (m, 14H), 2.01 (t, J=7.3 Hz, 2H), 4.04 (s, 2H); ^{13}C NMR ($CDCl_3$) δ=0.15, 14.11, 22.70, 26.89, 29.15, 29.35, 29.52, 29.60, 31.93, 36.53, 89.75, 159.7; MS (70 eV) m/z (rel intensity) 242 (4), 144 (14), 143 (100), 130 (70), 115 (40), 75 (52), 73 (97), 43 (18), 41 (21). Found: C, 69.57; H, 12.72%. Calcd for $C_{14}H_{30}OSi$: C, 69.35; H, 12.47%.

(E) and (Z)-6-Trimethylsiloxy-5-undecene (24, (E):(Z)=69:31). The title compound was prepared from 6-undecanone in 82% yield: Bp 75—78 °C (1 Torr); IR(neat) 2956, 2926, 2858, 1664, 1251, 1177, 1100, 888, 842 cm^{-1}; ^{1}H NMR ($CDCl_3$) δ=0.17 (s, 9H), 0.89 (t, J=6.5 Hz, 6H), 1.23—1.52 (m, 10H), 1.87—2.07 (m, 4H), 4.44 (t, J=6.8 Hz, 0.31H), 4.60 (t, J=7.6 Hz, 0.69H); ^{13}C NMR ($CDCl_3$) δ=0.37, 0.62, 14.03, 22.25, 22.58, 25.07, 26.57, 26.78, 31.13, 31.47, 31.56, 32.18, 32.96, 36.63, 107.8 (*E*), 108.4 (*Z*), 150.2 (*Z*), 151.4 (*E*); MS (70 eV) m/z (rel intensity) 242 (14), 227 (9), 200 (18), 199 (100), 171 (9), 143 (14), 130 (23), 73 (15), 69 (10). Found: C, 69.09; H, 12.66%. Calcd for $C_{14}H_{30}OSi$: C, 69.35; H, 12.47%.

The Reaction of Silyl Enol Ether with Perfluorohexyl or Perfluoroisopropyl Iodide in the Presence of Base (Procedure A). Perfluoroalkylation of cyclohexanone trimethylsilyl enol ether is representative. Et_3B[4] (1.0 M hexane solution, 0.4 ml, 0.4 mmol, M=mol dm^{-3}) was added to a solution of 1-trimethylsiloxy-1-cyclohexene **1** (0.34 g, 2.0 mmol), perfluorohexyl iodide (1.19 g, 2.6 mmol), and 2,6-dimethylpyridine (0.20 g, 1.9 mmol) in hexane (5 ml) at room temperature. After stirring for 8 h at 25 °C, resulting precipitate was filtered through Celite 545. The filtrate was concentrated in vacuo. The residual oil was submitted to silica-gel column chromatography to give perfluoroalkylated silyl enol ether (**2a** and **3a**, 0.64 g, 65% yield, **2a**/**3a**=68/32) and 2-(perfluorohexyl)cyclohexanone (**4a**,[14] 92 mg, 11% yield). (Procedure A') Treatment of the reaction mixture consisting of **2a**, **3a**, and **4a** with acid afforded 2-(perfluoroalkyl)cyclohexanone (**4a**) as a single product. Thus, the residual oil after concentration of the filtrate was treated with concd aq HCl (35 wt%, 1 ml) in THF (5 ml) for 10 min. Reaction mixture was slowly poured into sat. aq $NaHCO_3$ (40 ml) and extracted with AcOEt (30 ml×2).[15] The combined organic layer was dried over anhydrous Na_2SO_4 and concentrated in vacuo. Purification by silica-gel column chromatography gave only **4a** in 74% yield.

6-Perfluorohexyl-1-trimethylsiloxy-1-cyclohexene (2a): Bp 68—71 °C (1 Torr, bath temp); IR(neat) 2958, 1669, 1324, 1239, 1203, 1146, 1120, 913, 846, 694, 660 cm^{-1}; ^{1}H NMR ($CDCl_3$) δ=0.20 (s, 9H), 1.48—1.88 (m, 3H), 1.96—2.16 (m, 3H), 2.95 (tm, J=15.6 Hz, 1H), 5.11 (t, J=4.1 Hz, 1H); ^{13}C NMR ($CDCl_3$) δ=—0.10, 18.82, 23.18 (two peaks), 41.77 (t, J=20.4 Hz), 108.6, 141.1. ^{13}C-Signals of perfluorohexyl group could not be observed for all perfluorohexyl compounds; ^{19}F NMR ($CDCl_3$) δ=—81.39 (t, J=9.8 Hz, 3F), —108.1 (dm, J=284 Hz, 1F), —113.8 (dm, J=284 Hz, 1F), —121.2 (bs, 2F), —122.2 (bs, 2F), —123.2 (bs, 2F), —126.4——126.8 (m, 2F); MS (70 eV) m/z (rel intensity) 488 (10), 169 (14), 133 (12), 77 (61), 75 (6), 74 (8), 73 (100), 69 (27), 55 (19), 45 (11), 41 (17). Found: C, 37.17; H, 3.49%. Calcd for $C_{15}H_{17}F_{13}OSi$: C, 36.89; H, 3.51%.

2-Perfluorohexyl-1-trimethylsiloxy-1-cyclohexene (3a): Bp 68—72 °C (1 Torr, bath temp); IR(neat) 2944, 1661, 1375,

1292, 1238, 1204, 1145, 1119, 1074, 1065, 933, 861, 848, 704 cm^{-1}; ^{1}H NMR ($CDCl_3$) δ=0.20 (s, 9H), 1.55—1.75 (m, 4H), 2.14—2.19 (m, 4H); ^{13}C NMR ($CDCl_3$) δ=0.50, 22.10, 22.45, 23.51 (t, J=5.0 Hz), 31.38, 117.1 (t, J=32.7 Hz), 155.8 (t, J=5.5 Hz); ^{19}F NMR ($CDCl_3$) δ=−81.39 (tt, J=9.7, 3.6 Hz, 3F), −108.5 (t, J=14.0 Hz, 2F), −122.1—−123.2 (m, 6F), −126.4—−126.8 (m, 2F); MS (70 eV) m/z (rel intensity) 488 (7), 220 (15), 219 (92), 169 (7), 77 (46), 74 (9), 73 (100), 69 (9), 45 (11), 41 (19). Found: C, 37.15; H, 3.56%. Calcd for $C_{15}H_{17}F_{13}OSi$: C, 36.89; H, 3.51%.

2-(Perfluorohexylidene)cyclohexanone (5): Bp 78—83 °C (7 Torr, bath temp); IR(neat) 1722, 1228, 1204, 1164, 1144, 724 cm^{-1}; ^{1}H NMR ($CDCl_3$) δ=1.81—2.05 (m, 4H), 2.54—2.73 (m, 4H); ^{13}C NMR ($CDCl_3$) δ=25.01, 25.44, 27.45, 43.35, 129.2 (d, J=6.0 Hz), 198.5; ^{19}F NMR ($CDCl_3$) δ=−81.28 (tt, J=9.8, 3.0 Hz, 3F), −114.1—−114.6 (m, 2F), −121.1 (bs, 1F), −123.3 (bs, 2F), −124.1 (bs, 2F), −126.4—−126.7 (m, 2F); MS (12 eV) m/z (rel intensity) 396 (7), 369 (10), 368 (77), 150 (8), 149 (100), 127 (21), 99 (99), 67 (36), 41 (18). Found: C, 36.51; H, 2.09%. Calcd for $C_{12}H_8F_{12}O$: C, 36.38; H, 2.04%.

6-Perfluoroisopropyl-1-trimethylsiloxy-1-cyclohexene (2b): Bp 50—53 °C (1 Torr, bath temp); IR(neat) 2960, 1664, 1287, 1255, 1219, 1159, 1118, 1099, 985, 964, 936, 902, 846 cm^{-1}; ^{1}H NMR ($CDCl_3$) δ=0.18 (s, 9H), 1.33—1.55 (m, 1H), 1.65—2.10 (m, 5H), 3.03—3.22 (m, 1H), 5.03 (t, J=4.4 Hz, 1H); ^{13}C NMR ($CDCl_3$) δ=−0.15. 20.92, 23.34, 23.56 (d, J=10.6 Hz), 41.08 (d, J=18.9 Hz), 93.92 (dm, J=205 Hz), 107.3, 121.2 (qd, J=289, 29.3 Hz), 145.2; ^{19}F NMR ($CDCl_3$) δ=−72.99 (d, J=4.9 Hz, 6F), −173.4—−173.9 (m, 1F); MS (70 eV) m/z (rel intensity) 338 (19), 169 (27), 77 (64), 73 (100), 55 (11), 45 (14), 41 (14). Found: C, 42.76; H, 5.23%. Calcd for $C_{12}H_{17}F_7OSi$: C, 42.60; H, 5.06%.

2-Perfluoroisopropyl-1-trimethylsiloxy-1-cyclohexene (3b): Bp 50—55 °C (1 Torr, bath temp); IR(neat) 2942, 1669, 1369, 1299, 1272, 1259, 1217, 1172, 1144, 1065, 967, 956, 899, 848 cm^{-1}; ^{1}H NMR ($CDCl_3$) δ=0.19 (s, 9H), 1.55—1.76 (m, 4H), 2.10—2.21 (m, 4H); ^{13}C NMR ($CDCl_3$) δ=0.89, 22.30 (d, J=3.7 Hz), 22.39, 23.67 (d, J=10.7 Hz), 31.35, 93.21 (dm, J=197 Hz), 101.5 (d, J=22.8 Hz), 121.3 (qd, J=288, 28.7 Hz), 153.1 (d, J=6.0 Hz); ^{19}F NMR ($CDCl_3$) δ=−74.68 (d, J=6.1 Hz, 6F), −177.1 (sep, sep=septet, J=6.1 Hz, 1F); MS (70 eV) m/z (rel intensity) 338 (17), 269 (11), 177 (10), 169 (27), 149 (13), 77 (50), 73 (100), 65 (10), 45 (16), 41 (24). Found: C, 42.49; H, 5.14%. Calcd for $C_{12}H_{17}F_7OSi$: C, 42.60; H, 5.06%.

2-(Perfluoroisopropyl)cyclohexanone (4b): Bp 82—87 °C (36 Torr, bath temp); IR(neat) 1733, 1292, 1274, 1224, 1161, 1134, 1109, 1098, 972 cm^{-1}; ^{1}H NMR ($CDCl_3$) δ=1.60—2.15 (m, 5H), 2.30—2.60 (m, 3H), 3.16—3.30 (m, 1H); ^{13}C NMR ($CDCl_3$) δ=24.61, 27.41, 28.45, 42.74, 51.95 (d, J=20.1 Hz), 92.61 (dm, J=207 Hz), 120.9 (qd, J=288, 27.4 Hz), 202.9 (d, J=4.8 Hz); ^{19}F NMR ($CDCl_3$) δ=−72.85—−73.54 (m, 6F), −178.3—−178.9 (m, 1F); MS (70 eV) m/z (rel intensity) 266 (71), 238 (11), 237 (16), 141 (15), 127 (13), 77 (10), 69 (18), 55 (100), 42 (20), 41 (14). Found: C, 40.90; H, 3.33%. Calcd for $C_9H_9F_7O$: C, 40.61; H, 3.41%.

6-Perfluorohexyl-1-triisopropylsiloxy-1-cyclohexene (7a): Bp 100—105 °C (1 Torr, bath temp); IR(neat) 2946, 2894, 2868, 1668, 1466, 1239, 1200, 1145, 1119, 883, 688, 660 cm^{-1}; ^{1}H NMR ($CDCl_3$) δ=1.01—1.26 (m, 21H), 1.55—1.83 (m, 2H), 2.00—2.18 (m 4H), 2.85—3.10 (m, 1H), 5.08 (t, J=4.0 Hz, 1H); ^{13}C NMR ($CDCl_3$) δ=12.75, 17.90 (d, J=3.9 Hz), 18.46, 23.08, 23.31, 41.54 (dd, J=21.0, 18.9 Hz), 107.2, 144.3 (t, J=2.7 Hz); ^{19}F NMR ($CDCl_3$) δ=−81.29 (t, J=9.8 Hz, 3F), −107.6 (d, J=271 Hz, 1F), −113.5 (d, J=271 Hz, 1F), −121.4 (bs, 2F), −122.3 (bs, 2F), −123.2 (bs, 2F), −126.6 (bs, 2F); MS (70 eV) m/z (rel intensity) 572 (2), 529 (30), 349 (17), 105 (50), 77 (100), 63 (13), 59 (13), 43 (34), 41 (17). Found: C, 44.22; H, 5.02%. Calcd for $C_{21}H_{29}F_{13}OSi$: C, 44.06; H, 5.11%.

2-Perfluorohexyl-1-triisopropylsiloxy-1-cyclohexene (8a): Bp 98—103 °C (1 Torr, bath temp); IR(neat) 2950, 2868, 1653, 1375, 1240, 1205, 1145, 1073 cm^{-1}; ^{1}H NMR ($CDCl_3$) δ=1.03—1.30 (m, 21H), 1.58—1.80 (m, 4H), 2.10—2.32 (m, 4H); ^{13}C NMR ($CDCl_3$) δ=13.69, 17.83, 22.14, 22.74, 23.82, 31.67, 102.5 (t, J=21.1 Hz), 156.3 (t, J=4.9 Hz); ^{19}F NMR ($CDCl_3$) δ=−81.32 (t, J=9.8 Hz, 3F), −108.6 (bs, 2F), −122.4 (bs, 4F), −123.3 (bs, 2F), −126.4—−126.8 (m, 2F); MS (70 eV) m/z (rel intensity) 530 (M^+−i-Pr+1, 20), 529 (M^+−i-Pr, 79), 105 (50), 77 (100), 63 (15), 59 (12), 43 (24), 41 (19). Found: C, 43.81; H, 5.21%. Calcd for $C_{21}H_{29}F_{13}OSi$: C, 44.06; H, 5.11%.

6-Perfluoroisopropyl-1-triisopropylsiloxy-1-cyclohexene (7b): Bp 78—83 °C (1 Torr, bath temp); IR(neat) 2944, 2892, 2868, 1664, 1466, 1288, 1268, 1218, 1196, 1159, 1120, 1099, 1064, 965, 897, 882, 832, 677 cm^{-1}; ^{1}H NMR ($CDCl_3$) δ=0.95—1.30 (m, 21H), 1.34—1.55 (m, 1H), 1.64—2.08 (m, 5H), 2.99—3.14 (m, 1H), 5.08 (t, J=4.0 Hz, 1H); ^{13}C NMR ($CDCl_3$) J=12.90, 17.90 (d, J=6.3 Hz), 20.85, 23.30, 23.72 (d, J=7.8 Hz), 40.94 (d, J=17.1 Hz), 93.86 (dm, J=208 Hz), 107.3, 121.2 (qd, J=288, 28.1 Hz), 146.0; ^{19}F NMR ($CDCl_3$) δ=−72.73 (qd, J=8.6, 6.1 Hz, 3F), −73.65 (qd, J=8.6, 6.1 Hz, 3F), −172.1—−172.7 (m, 1F); MS (70 eV) m/z (rel intensity) 422 (3), 379 (15), 199 (24), 179 (18), 159 (15), 105 (49), 79 (17), 77 (100), 63 (23), 59 (23), 43 (45), 41 (32). Found: C, 51.18; H, 6.99%. Calcd for $C_{18}H_{29}F_7OSi$: C, 51.17; H, 6.92%.

2-Perfluoroisopropyl-1-triisopropylsiloxy-1-cyclohexene (8b): Bp 76—81 °C (1 Torr, bath temp); IR(neat) 2946, 2896, 2870, 1645, 1467, 1371, 1293, 1216, 1180, 1160, 1146, 1067, 984, 968, 959, 898, 884, 844, 771, 723, 686 cm^{-1}; ^{1}H NMR ($CDCl_3$) δ=0.99—1.26 (m, 21H), 1.52—1.74 (m, 4H), 2.07—2.26 (m, 4H); ^{13}C NMR ($CDCl_3$) δ=13.83, 17.90, 22.38, 22.55, 24.03 (d, J=2.2 Hz), 32.26, 93.12 (dm, J=207 Hz), 99.00 (d, J=15.1 Hz), 121.5 (qd, J=289, 28.8 Hz), 155.2; ^{19}F NMR ($CDCl_3$) δ=−74.74 (d, J=6.1 Hz, 6F), −177.2 (sep, J=6.1 Hz, 1F); MS (70 eV) m/z (rel intensity) 422 (0.2), 379 (42), 227 (32), 207 (42), 179 (18), 105 (31), 77 (100), 63 (19), 43 (25), 41 (22). Found: C, 51.03; H, 6.98%. Calcd for $C_{18}H_{29}F_7OSi$: C, 51.17; H, 6.92%.

5-Perfluorohexyl-1-trimethylsiloxy-1-cyclopentene (10): Bp 65—70 °C (1 Torr, bath temp); IR(neat) 1666, 1654, 1381, 1240, 1205, 1146, 1120, 867, 848 cm^{-1}; ^{1}H NMR ($CDCl_3$) δ=0.21 (s, 9H), 2.05—2.46 (m, 4H), 3.10—3.36 (m, 1H), 4.89 (bs, 1H); ^{13}C NMR ($CDCl_3$) δ=−0.43, 22.82, 27.07, 47.52 (dd, J=22.8, 20.3 Hz), 106.9, 148.9; ^{19}F NMR ($CDCl_3$) δ=−81.33 (t, J=9.4 Hz, 3F), −109.5 (t, J=12.8 Hz, 1F), −116.0—−117.1 (m, 1F), −121.6 (bs, 1F), −122.1—−123.5 (m, 5F), −126.3—−126.8 (m, 2F); MS (70 eV) m/z (rel intensity) 475 (M^++1, 11), 474 (M^+, 52), 459 (25), 205 (39), 155 (15), 77 (54), 73 (100), 55 (59). Found: C, 35.50; H, 3.13%. Calcd for $C_{14}H_{15}F_{13}OSi$: C, 35.45; H, 3.19%.

2-(Perfluorohexyl)cyclopentanone (11): Bp 89—94 °C (5 Torr, bath temp); IR(neat) 2890, 2882, 1768, 1350, 1238, 1206, 1147, 733 cm^{-1}; ^{1}H NMR ($CDCl_3$) δ=1.76—2.51 (m, 6H), 2.77—3.03 (m, 1H); ^{13}C NMR ($CDCl_3$) δ=20.16, 24.51, 38.67, 49.29 (dd, J=24.1, 20.0 Hz), 208.9 (d, J=2.4 Hz); ^{19}F NMR

($CDCl_3$) δ=−81.38 (tt, *J*=10.9, 2.4 Hz, 3F), −115.1—−116.0 (m, 2F), −121.3 (bs, 2F), −122.4 (bs, 2F), −123.2 (bs, 2F), −126.3—−126.8 (m, 2F); MS (70 eV) *m/z* (rel intensity) 403 (M^++1, 17), 402 (M^+, 100), 383 (11), 382 (46), 354 (12), 343 (8), 340 (10). Found: C, 32.77; H, 1.76%. Calcd for $C_{11}H_7F_{13}O$: C, 32.58; H, 1.75%.

2-(Perfluorohexylidene)cyclopentanone (12): Stereochemistry of alkene could not be determined. Bp 110—115 °C (37 Torr, bath temp); IR(neat) 1747, 1669, 1238, 1194, 1143, 1111, 724 cm^{-1}; ^1H NMR ($CDCl_3$) δ=1.95—2.10 (m, 2H), 2.38—2.46 (m, 2H), 2.82—2.95 (m, 2H); ^{13}C NMR ($CDCl_3$) δ=19.89, 25.83, 38.79, 141.9, (d, *J*=30.3 Hz), 202.6; ^{19}F NMR ($CDCl_3$) δ=−81.34 (t, *J*=8.5 Hz, 3F), −116.6—−117.2 (m, 3F), −123.5 (bs, 4F), −126.6 (bs, 2F); MS (70 eV) *m/z* (rel intensity) 382 (9), 135 (11), 121 (20), 113 (100), 107 (95), 69 (23), 57 (17), 55 (21). Found: C, 34.38; H, 1.51%. Calcd for $C_{11}H_6F_{12}O$: C, 34.57; H, 1.58%.

(*Z*)-5-Ethyl-6,6,7,7,8,8,9,9,10,10,11,11,11-tridecafluoro-4-trimethylsiloxy-3-undecene ((*Z*)-14a): Bp 95—100 °C (35 Torr, bath temp); IR(neat) 2966, 1671, 1362, 1299, 1240, 1195, 1147, 1121, 1087, 847, 733, 706 cm^{-1}; ^1H NMR ($CDCl_3$) δ=0.20 (s, 9H), 0.95 (t, *J*=7.4 Hz, 3H), 0.96 (t, *J*=7.5 Hz, 3H), 1.58—1.85 (m, 2H), 1.92—2.15 (m, 2H), 2.60 (tdd, *J*=14.8, 10.3, 4.3 Hz, 1H), 4.59 (t, *J*=7.1 Hz, 1H); ^{13}C NMR ($CDCl_3$) δ=0.83, 11.55, 14.01, 18.07, 19.33, 50.47 (t, *J*=20.5 Hz), 115.5, 141.9; ^{19}F NMR ($CDCl_3$) δ=−81.30 (tt, *J*=9.8, 2.4 Hz, 3F), −113.8—−114.7 (m, 2F), −121.2 (bs, 2F), −122.3 (bs, 2F), −123.3 (bs, 2F), −126.3—−126.7 (m, 2F); MS (70 eV) *m/z* (rel intensity) 504 (23), 489 (10), 448 (9), 207 (14), 143 (14), 77 (34), 73 (100), 70 (14), 69 (9), 55 (30). Found: C, 37.82; H, 4.03%. Calcd for $C_{16}H_{21}F_{13}OSi$: C, 38.10; H, 4.20%.

(*E*)-5-Ethyl-6,6,7,7,8,8,9,9,10,10,11,11,11-tridecafluoro-4-trimethylsiloxy-3-undecene ((*E*)-14a): Bp 50—55 °C (1 Torr, bath temp); IR(neat) 2966, 1664, 1241, 1146, 962, 886, 848, 659 cm^{-1}; ^1H NMR ($CDCl_3$) δ=0.19 (s, 9H), 0.90 (t, *J*=7.4 Hz, 3H), 0.96 (t, *J*=7.4 Hz, 3H), 1.60—2.08 (m, 4H), 3.07 (tdd, *J*=15.1, 10.5, 4.1 Hz, 1H), 4.77 (t, *J*=7.5 Hz, 1H); ^{13}C NMR ($CDCl_3$) δ=0.00, 11.15, 14.83, 17.24, 20.16, 43.85 (t, *J*=20.7 Hz), 112.9, 143.0; ^{19}F NMR ($CDCl_3$) δ=−81.35 (t, *J*=9.8 Hz, 3F), −113.6 (bs, 2F), −121.8—−122.4 (m, 4F), −123.2 (bs, 2F), −126.4—−126.9 (m, 2F); MS (70 eV) *m/z* (rel intensity) 505 (M^++1, 12), 504 (M^+, 53), 489 (22), 448 (20), 207 (24), 143 (17), 77 (36), 73 (100), 55 (27). Found: C, 38.33; H, 4.04%. Calcd for $C_{16}H_{21}F_{13}OSi$: C, 38.10; H, 4.20%.

5-Ethyl-6,6,7,7,8,8,9,9,10,10,11,11,11-tridecafluoro-4-undecanone (15a): Bp 97—102 °C (35 Torr, bath temp); IR(neat) 2970, 1731, 1363, 1239, 1207, 1146, 694, 651 cm^{-1}; ^1H NMR ($CDCl_3$) δ=0.94 (t, *J*=7.3 Hz, 6H), 1.55—1.73 (m, 2H), 1.78—2.09 (m, 2H), 2.46 (dt, *J*=18.4, 7.2 Hz, 1H), 2.60 (dt, *J*=18.4, 7.3 Hz, 1H), 3.21 (tdd, *J*=15.0, 10.2, 4.5 Hz, 1H); ^{13}C NMR ($CDCl_3$) δ=11.39, 13.31, 16.37, 18.81 (t, *J*=5.1 Hz), 46.19, 54.85 (t, *J*=19.8 Hz), 204.1; ^{19}F NMR ($CDCl_3$) δ=−81.32 (tt, *J*=9.8, 2.4 Hz, 3F), −113.6—−114.1 (m, 2F), −121.1 (bs, 2F), −122.3 (bs, 2F), −123.3 (bs, 2F), −126.3—−126.8 (m, 2F); MS (70 eV) *m/z* (rel intensity) 432 (0.5), 388 (5), 72 (5), 71 (100), 69 (6), 47 (14), 43 (55), 41 (11). Found: C, 35.88; H, 2.98%. Calcd for $C_{13}H_{13}F_{13}O$: C, 36.13; H, 3.03%.

(*Z*)-5-Ethyl-6,7,7,7-tetrafluoro-6-trifluoromethyl-4-trimethylsiloxy-3-heptene ((*Z*)-14b): Bp 82—87 °C (35 Torr, bath temp); IR(neat) 2966, 1670, 1384, 1298, 1256, 1224, 1186, 1160, 1127, 1101, 1088, 1069, 952, 847 cm^{-1}; ^1H NMR ($CDCl_3$) δ=0.20 (s, 9H), 0.95 (t, *J*=7.4 Hz, 6H), 1.58—1.85 (m, 2H), 1.97—2.12 (m, 2H), 2.56—2.70 (m, 1H), 4.63 (t, *J*=7.2 Hz, 1H); ^{13}C NMR ($CDCl_3$) 0.92, 12.50, 13.89, 18.56, 19.54, 50.43 (d, *J*=20.1 Hz), 92.76 (dm, *J*=204 Hz), 115.5, 121.1 (qd, *J*=288, 28.8 Hz), 121.3 (qd, *J*=289, 26.6 Hz), 141.5 (d, *J*=6.5 Hz); ^{19}F NMR ($CDCl_3$) δ=−73.10 (d, *J*=7.3 Hz, 6F), −174.7—−175.7 (m, 1F); MS (70 eV) *m/z* (rel intensity) 355 (M^++1, 12), 354 (M^+, 62), 339 (47), 298 (49), 247 (14), 185 (22), 143 (16), 77 (31), 73 (100). Found: C, 44.14; H, 6.08%. Calcd for $C_{13}H_{21}F_7OSi$: C, 44.06; H, 5.97%.

(*E*)-5-Ethyl-6,7,7,7-tetrafluoro-6-trifluoromethyl-4-trimethylsiloxy-3-heptene ((*E*)-14b): Bp 77—82 °C (35 Torr, bath temp); IR(neat) 2966, 1661, 1297, 1255, 1224, 1159, 1135, 1123, 892, 848 cm^{-1}; ^1H NMR ($CDCl_3$) δ=0.19 (s, 9H), 0.87 (t, *J*=7.3 Hz, 3H), 0.96 (t, *J*=7.5 Hz, 3H), 1.57—2.06 (m, 4H), 3.04—3.18 (m, 1H), 4.75 (t, *J*=7.6 Hz, 1H); ^{13}C NMR ($CDCl_3$) δ=−0.26, 11.91, 14.82, 17.93, 20.31, 43.79 (d, *J*=20.5 Hz), 92.51 (dm, *J*=203 Hz), 113.3, 121.1 (qd, *J*=290, 27.3 Hz); 121.4 (qd, *J*=290, 27.6 Hz), 142.3 (d, *J*=6.0 Hz); ^{19}F NMR ($CDCl_3$) δ=−72.98—−73.91 (m, 6F), −174.7—−176.1 (m, 1F); MS (70 eV) *m/z* (rel intensity) 354 (11), 339 (9), 298 (12), 185 (9), 143 (9), 77 (33), 73 (100), 55 (10). Found: C, 44.18; H, 6.22%. Calcd for $C_{13}H_{21}F_7OSi$: C, 44.06; H, 5.97%.

5-Ethyl-6,7,7,7-tetrafluoro-6-trifluoromethyl-4-heptanone (15b): Bp 71—76 °C (49 Torr, bath temp); IR(neat) 2968, 2938, 1733, 1299, 1260, 1226, 1163, 1145, 1131, 971 cm^{-1}; ^1H NMR ($CDCl_3$) δ=0.89 (t, *J*=7.9 Hz, 3H), 0.93 (t, *J*=7.4 Hz, 3H), 1.55—1.89 (m, 3H), 1.93—2.17 (m, 1H), 2.43 (dtd, *J*=18.3, 7.0, 1.2 Hz, 1H), 2.64 (dtd, *J*=18.3, 7.3, 1.6 Hz, 1H), 3.10—3.25 (m, 1H); ^{13}C NMR ($CDCl_3$) δ=12.31, 13.25, 16.57, 19.00, 48.06, 53.00 (d, *J*=8.6 Hz), 92.19 (dm, *J*=205 Hz), 120.6 (qd, *J*=287, 27.7 Hz), 120.8 (qd, *J*=287, 28.0 Hz), 204.1; ^{19}F NMR ($CDCl_3$) δ=−73.05 (dq, *J*=8.6, 8.5 Hz, 3F), −74.43 (dq, *J*=9.8, 8.5 Hz, 3F), −176.4—−176.9 (m, 1F); MS (70 eV) *m/z* (rel intensity) 239 ($M^+-C_3H_7$, 2), 171 (2), 127 (3), 72 (5), 71 (100), 43 (88), 41 (24). Found: C, 42.30; H, 4.46%. Calcd for $C_{10}H_{13}F_7O$: C, 42.56; H, 4.64%.

(*Z*)-8,8,9,9,10,10,11,11,12,12,13,13,13-Tridecafluoro-6-trimethylsiloxy-5-tridecene ((*Z*)-17a): Bp 94—99 °C (5 Torr, bath temp); IR(neat) 2958, 2930, 1675, 1350, 1240, 1195, 1145, 1121, 1097, 990, 846, 707 cm^{-1}; ^1H NMR ($CDCl_3$) δ=0.20 (s, 9H), 0.90 (t, *J*=6.8 Hz, 3H), 1.25—1.37 (m, 4H), 1.99—2.10 (m, 2H), 2.75 (t, *J*=18.4 Hz, 2H), 4.72 (t, *J*=7.1 Hz, 1H); ^{13}C NMR ($CDCl_3$) δ=0.37, 13.82, 22.41, 25.55, 31.61, 38.32 (t, *J*=22.1 Hz), 116.5, 139.1; ^{19}F NMR ($CDCl_3$) δ=−81.32 (t, *J*=9.8 Hz, 3F), −113.0—−113.5 (m, 2F), −122.1—−122.6 (m,2F), −123.4 (bs, 2F), −123.8 (bs, 2F), −126.3—−126.9 (m, 2F); MS (70 eV) *m/z* (rel intensity) 505 (M^++1, 7), 504 (M^+, 27), 462 (14), 461 (89), 175 (10), 77 (17), 73 (100), 55 (38). Found: C, 37.90; H, 4.15%. Calcd for $C_{16}H_{21}F_{13}OSi$: C, 38.10; H, 4.20%.

(*E*)-8,8,9,9,10,10,11,11,12,12,13,13,13-Tridecafluoro-6-trimethylsiloxy-5-tridecene ((*E*)-17a): Bp 71—76 °C (1 Torr, bath temp); IR(neat) 2960, 2930, 1670, 1360, 1240, 1195, 1145, 1122, 847, 733, 707 cm^{-1}; ^1H NMR ($CDCl_3$) δ=0.20 (s, 9H), 0.90 (t, *J*=7.0 Hz, 3H), 1.27—1.37 (m, 4H), 1.89—2.00 (m, 2H), 2.86 (t, *J*=18.4 Hz, 2H), 4.91 (t, *J*=7.6 Hz, 1H); ^{13}C NMR ($CDCl_3$) δ=0.09, 13.87, 22.19, 26.91, 32.31, 33.26 (t, *J*=22.2 Hz), 113.5, 140.6; ^{19}F NMR ($CDCl_3$) δ=−81.32 (t, *J*=9.8 Hz, 3F), −112.3—−112.7 (m, 2F), −122.3 (bs, 2F), −123.4 (bs, 2F), −123.8 (bs, 2F), −126.4—−126.9 (m, 2F); MS (70 eV) *m/z* (rel intensity) 504 (6), 461 (23), 175 (8), 77

(22), 74 (9), 73 (100), 55 (46). Found: C, 38.25; H, 4.17%. Calcd for $C_{16}H_{21}F_{13}OSi$: C, 38.10; H, 4.20%.

8,8,9,9,10,10,11,11,12,12,13,13,13-Tridecafluoro-6-tridecanone (18a): Bp 100—105 °C (43 Torr, bath temp); IR(neat) 2960, 2934, 1732, 1363, 1240, 1204, 1145, 1124, 706 cm^{-1}; ^1H NMR ($CDCl_3$) δ=0.90 (t, J=6.7 Hz, 3H), 1.23—1.40 (m, 4H), 1.55—1.70 (m, 2H), 2.58 (t, J=7.3 Hz, 2H), 3.16 (t, J=18.7 Hz, 2H); ^{13}C NMR ($CDCl_3$) δ=13.84, 22.37, 22.88, 31.03, 43.10 (t, J=22.1 Hz), 44.48, 200.0; ^{19}F NMR ($CDCl_3$) δ=−81.29 (bs, 3F), −111.2—−112.0 (m, 2F), −122.2 (bs, 2F), −123.4 (bs, 4F), −126.3—−126.8 (m, 2F); MS (70 eV) m/z (rel intensity) 432 (5), 376 (100), 361 (45), 356 (95), 341 (47), 99 (45), 56 (36), 43 (61). Found: C, 36.06; H, 2.94%. Calcd for $C_{13}H_{13}F_{13}O$: C, 36.13; H, 3.03%.

***(Z)*-1,1,1,2-Tetrafluoro-2-trifluoromethyl-4-trimethylsiloxy-4-nonene (*(Z)*-17b):** Bp 50—55 °C (1 Torr, bath temp); IR(neat) 2958, 2930, 1675, 1378, 1332, 1286, 1221, 1187, 1163, 1151, 1117, 1069, 999, 978, 846 cm^{-1}; ^1H NMR ($CDCl_3$) δ=0.19 (s, 9H), 0.89 (t, J=6.5 Hz, 3H), 1.26—1.36 (m, 4H), 1.94—2.06 (m, 2H), 2.73 (d, J=21.5 Hz, 2H), 4.71 (t, J=7.3 Hz, 1H); ^{13}C NMR ($CDCl_3$) δ=0.46, 13.88, 22.29, 25.39, 31.39, 36.08 (d, J=19.7 Hz), 91.39 (dm, J=206 Hz), 116.3, 120.8 (qd, J=288, 27.9 Hz), 139.9 (d, J=2.8 Hz); ^{19}F NMR ($CDCl_3$) δ=−76.60 (d, J=7.3 Hz, 6F), −183.0 (tsep, tsep=triplet, septet, J=22.0, 7.3 Hz, 1F); MS (70 eV) m/z (rel intensity) 354 (4), 311 (22), 219 (10), 77 (15), 74 (9), 73 (100). Found: C, 43.95; H, 6.02%. Calcd for $C_{13}H_{21}F_7OSi$: C, 44.06; H, 5.97%.

***(E)*-1,1,1,2-Tetrafluoro-2-trifluoromethyl-4-trimethylsiloxy-4-nonene (*(E)*-17b):** Bp 49—54 °C (1 Torr, bath temp); IR(neat) 2958, 2932, 1671, 1332, 1286, 1224, 1187, 1163, 1118, 998, 918, 846 cm^{-1}; ^1H NMR ($CDCl_3$) δ=0.18 (s, 9H), 0.90 (t, J=7.0 Hz, 3H), 1.25—1.37 (m, 4H), 1.89—2.02 (m, 2H), 2.86 (d, J=20.8 Hz, 2H), 4.80 (t, J=7.6 Hz, 1H); ^{13}C NMR ($CDCl_3$) δ=−0.08, 13.90, 22.25, 26.87, 30.89 (d, J=20.9 Hz), 32.28, 91.21 (dm, J=206 Hz), 112.5, 120.8 (qd, J=286, 24.5 Hz), 141.0; ^{19}F NMR ($CDCl_3$) δ=−76.82 (d, J=6.1 Hz, 6F), −182.3 (tsep, J=20.8, 6.1 Hz, 1F); MS (70 eV) m/z (rel intensity) 354 (22), 312 (18), 311 (100), 298 (15), 219 (32), 77 (16), 73 (68), 57 (24), 56 (11), 43 (22), 41 (22). Found: C, 44.14; H, 6.07%. Calcd for $C_{13}H_{21}F_7OSi$: C, 44.06; H, 5.97%.

1,1,1,2-Tetrafluoro-2-trifluoromethyl-4-nonanone (18b): Bp 82—87 °C (45 Torr, bath temp); IR(neat) 2958, 2934, 1729, 1340, 1288, 1227, 1164, 1131, 1108, 996 cm^{-1}; ^1H NMR ($CDCl_3$) δ=0.90 (t, J=6.7 Hz, 3H), 1.20—1.40 (m, 4H), 1.53—1.68 (m, 2H), 2.56 (t, J=7.1 Hz, 2H), 3.07 (d, J=21.9 Hz, 2H); ^{13}C NMR ($CDCl_3$) δ=13.66, 22.35, 22.94, 30.97, 40.33 (d, J=19.1 Hz), 44.44, 90.69 (dm, J=208 Hz), 120.4 (qd, J=287, 27.8 Hz), 200.6; ^{19}F NMR ($CDCl_3$) δ=−77.01 (d, J=7.3 Hz, 6F), −183.0 (tsep, J=22.0, 7.3 Hz, 1F); MS (70 eV) m/z (rel intensity) 282 (7), 253 (5), 239 (15), 227 (21), 226 (100), 211 (36), 206 (6), 186 (3), 99 (5). Found: C, 42.83; H, 4.65%. Calcd for $C_{10}H_{13}F_7O$: C, 42.56; H, 4.64%.

3,3,4,4,5,5,6,6,7,7,8,8,8-Tridecafluoro-2-pentyl-1-triisopropylsiloxy-1-octene (20, Major, Stereochemistry (*E* or *Z*) could not be determined): Bp 92—97 °C (1 Torr, bath temp); IR(neat) 2948, 2868, 1659, 1466, 1240, 1145, 1112, 882, 708, 686, 653 cm^{-1}; ^1H NMR ($CDCl_3$) δ=0.88 (t, J=6.7 Hz, 3H), 1.03—1.56 (m, 27H), 2.12—2.20 (m, 2H), 6.83 (t, J=2.0 Hz, 1H); ^{13}C NMR ($CDCl_3$) δ=11.79, 13.97, 17.44, 22.49, 23.99, 28.53, 32.04, 111.1 (t, J=20.4 Hz), 146.4 (t, J=12.5 Hz); ^{19}F NMR ($CDCl_3$) δ=−81.35 (t, J=9.8 Hz, 3F), −109.2—−109.6 (m, 2F), −122.1—−122.5 (m, 4F), −123.2 (bs, 2F), −126.4—−126.7 (m, 2F); MS (12 eV) m/z (rel intensity) 546 (M^+−^{t}Pr+1, 26), 545 (M^+−^{t}Pr, 100), 489 (4), 395 (3), 139 (2), 133 (3), 121 (2), 105 (2). Found: C, 45.18; H, 5.89%. Calcd for $C_{22}H_{33}F_{13}OSi$: C, 44.90; H, 5.65%.

3,3,4,4,5,5,6,6,7,7,8,8,8-Tridecafluoro-2-pentyl-1-triisopropylsiloxy-1-octene (20, Minor): Bp 105—110 °C (4 Torr, bath temp); IR(neat) 2950, 2868, 1656, 1466, 1281, 1240, 1202, 1146, 1130, 882, 808, 710, 685 cm^{-1}; ^1H NMR ($CDCl_3$) δ=0.89 (t, J=6.7 Hz, 3H), 1.00—1.50 (m, 27H), 1.98—2.05 (m, 2H), 6.59 (s, 1H); ^{13}C NMR ($CDCl_3$) δ=11.67, 14.01, 17.37, 22.39, 27.78, 30.01, 31.27, 107.3 (t, J=20.3 Hz), 146.8 (t, J=5.7 Hz); ^{19}F NMR ($CDCl_3$) δ=−81.32 (t, J=9.8 Hz, 3F), −108.9—−109.3 (m, 2F); −122.2—−122.7 (m, 4F), −123.3 (bs, 2F), −126.3—−126.8 (m, 2F); MS (12 eV) m/z (rel intensity) 546 (M^+−i-Pr+1, 26), 545 (M^+−i-Pr, 100), 489 (10), 395 (15), 157 (14), 133 (12), 121 (11), 105 (43), 77 (67), 43 (12). Found: C, 44.83; H, 5.54%. Calcd for $C_{22}H_{33}F_{13}OSi$: C, 44.90; H, 5.65%.

3,4,4,5,5,6,6,7,7,8,8,8-Dodecafluoro-2-pentyl-2-octenal (21, Major, Stereochemistry (*E* or *Z*) could not be determined): Bp 91—96 °C (27 Torr, bath temp); IR(neat) 2960, 2932, 2866, 1697, 1658, 1361, 1301, 1237, 1201, 1166, 1145, 1113, 724 cm^{-1}; ^1H NMR ($CDCl_3$) δ=0.89 (t, J=6.7 Hz, 3H), 1.24—1.50 (m, 6H), 2.41—2.51 (m, 2H), 10.00 (s, 1H); ^{13}C NMR ($CDCl_3$) δ=13.75, 22.23, 23.32 (d, J=3.8 Hz), 27.73, 31.46, 132.3 (d, J=9.1 Hz), 187.5 (d, J=8.3 Hz); ^{19}F NMR ($CDCl_3$) δ=−81.25 (t, J=9.8 Hz, 3F), −107.1 (bs, 1F), −111.6 (bs, 2F), −123.3 (bs, 4F), −126.5 (bs, 2F); MS (12 eV) m/z (rel intensity) 412 (7), 384 (23), 364 (19), 357 (34), 356 (53), 335 (50), 143 (100). Found: C, 38.03; H, 2.90%. Calcd for $C_{13}H_{12}F_{12}O$: C, 37.88; H, 2.93%.

3,4,4,5,5,6,6,7,7,8,8,8-Dodecafluoro-2-pentyl-2-octenal (21, Minor): Bp 88—93 °C (24 Torr, bath temp); IR(neat) 2960, 2934, 2874, 1700, 1660, 1362, 1237, 1205, 1144, 1113, 724 cm^{-1}; ^1H NMR ($CDCl_3$) δ=0.89 (t, J=6.5 Hz, 3H), 1.23—1.46 (m, 6H), 2.26—2.34 (m, 2H), 10.23 (s, 1H); ^{13}C NMR ($CDCl_3$) δ=13.77, 22.17 (two peaks), 29.21, 31.72, 129.3, 187.6 (d, J=18.8 Hz); ^{19}F NMR ($CDCl_3$) δ=−81.26 (t, J=9.8 Hz, 3F), −115.6 (bs, 2F), −123.1 (bs, 4F), −126.2—−126.6 (m, 3F); MS (12 eV) m/z (rel intensity) 412 (0.6), 335 (5), 145 (11), 143 (100), 95 (7), 85 (24), 68 (8), 56 (24). Found: C, 37.58; H, 2.86%. Calcd for $C_{13}H_{12}F_{12}O$: C, 37.88; H, 2.93%.

The Reaction of Silyl Enol Ether with Trifluoromethyl Iodide in the Presence of Base. Typical procedure is as follows. CF_3I (2.88 g, 14.7 mmol) was introduced into the flask pre-cooled to −78 °C, then hexane (7.4 ml), silyl enol ether (**22** (purity: 93%), 354 mg, 1.36 mmol), 2,6-dimethylpyridine (159 mg, 1.47 mmol) and Et_3B (0.96 M hexane solution, 0.30 ml, 0.29 mmol) were slowly added to the flask. After addition of these reagents, the reaction mixture was warmed to room temperature and stirred for 40 h. The resulting precipitate was filtered through Celite 545 and the filtrate was concentrated in vacuo. Treatment of the crude product with concd aq HCl in THF and purification by silica-gel column chromatography gave **23a** in 64% yield. 1,1,1-Trifluoro-3-dodecanone (**23a**): Mp 44.5—45.5 °C; IR($CDCl_3$) 2926, 2854, 1731, 1367, 1341, 1274, 1255, 1160, 1139 cm^{-1}; ^1H NMR ($CDCl_3$) δ=0.88 (t, J=6.4 Hz, 3H), 1.27 (bs, 12H), 1.53—1.70 (m, 2H), 2.53 (t, J=7.3 Hz, 2H), 3.21 (q, J=10.5 Hz, 2H); ^{13}C NMR ($CDCl_3$) δ=14.04, 22.63, 23.16, 28.90, 29.21, 29.31, 29.36, 31.83, 43.50, 46.18 (q, J=28.2 Hz), 123.7 (q, J=277 Hz), 200.2; ^{19}F NMR ($CDCl_3$) δ=−62.91 (t,

J=10.3 Hz); MS (12 eV) m/z (rel intensity) 238 (12), 220 (23), 164 (26), 153 (26), 150 (34), 139 (32), 127 (30), 126 (88), 112 (100), 110 (46), 71 (25). Found: C, 60.72; H, 9.10%. Calcd for $C_{12}H_{21}F_3O$: C, 60.49; H, 8.88%.

5-Trifluoromethyl-6-undecanone (25a): Bp 79—84 °C (1 Torr, bath temp); IR(neat) 2958, 2932, 2870, 1729, 1261, 1163, 1123, 1091 cm^{-1}; ^{1}H NMR ($CDCl_3$) δ=0.90 (t, J=6.8 Hz, 6H), 1.17—1.47 (m, 8H), 1.53—1.99 (m, 4H), 2.47 (dt, J=17.9, 7.1 Hz, 1H), 2.61 (dt, J=17.9, 7.3 Hz, 1H), 3.19 (dqd, J=9.2, 8.9, 4.7 Hz, 1H); ^{13}C NMR ($CDCl_3$) δ=13.59, 13.80, 22.39 (two peaks), 22.70, 25.61, 29.02, 31.07, 43.64, 55.56 (q, J=25.0 Hz), 124.9 (q, J=280 Hz), 204.4; ^{19}F NMR ($CDCl_3$) δ=−67.33 (d, J=8.9 Hz); MS (12 eV) m/z (rel intensity) 238 (3), 167 (4), 126 (5), 100 (7), 99 (100), 85 (4), 72 (4), 71 (19), 56 (6), 43 (7). Found: C, 60.20; H, 9.10%. Calcd for $C_{12}H_{21}F_3O$: C, 60.49; H, 8.88%.

The Reaction of Silyl Enol Ether with 2,2,2-Trifluoroethyl Iodide in the Presence of Base. The reactions were performed according to Procedure A′ described for the reaction of silyl enol ether with R_fI with some variation of the quantity of reagents and reaction time, which are shown below.

1,1,1-Trifluoro-4-tridecanone (23b). Et_3B (0.96 M hexane solution, 0.42 ml, 0.40 mmol) was added to a solution of silyl enol ether (**22** (purity: 93%), 486 mg, 1.86 mmol), CF_3CH_2I (840 mg, 4.00 mmol) and 2,6-dimethylpyridine (205 mg, 1.91 mmol) in hexane (5 ml) at room temperature. The resulting mixture was stirred for 15 h. Acidic work-up followed by purification gave **23b** in 79% yield: Bp 90—95 °C (1 Torr, bath temp); IR(neat) 2926, 2854, 1723, 1442, 1364, 1315, 1256, 1231, 1143, 1091, 612 cm^{-1}; ^{1}H NMR ($CDCl_3$) δ=0.88 (t, J=6.5 Hz, 3H), 1.27 (bs, 12H), 1.52—1.70 (m, 2H), 2.28—2.53 (m, 4H), 2.64—2.72 (m, 2H); ^{13}C NMR ($CDCl_3$) δ=13.99, 22.61, 23.73, 27.86 (q, J=29.8 Hz), 29.11, 29.21, 29.32, 29.36, 31.82, 34.76 (q, J=2.7 Hz), 42.76, 127.0 (q, J=277 Hz), 207.1; ^{19}F NMR ($CDCl_3$) δ=−67.17 (t, J=10.3 Hz); MS (12 eV) m/z (rel intensity) 252 (9), 155 (66), 153 (16), 141 (29), 140 (100), 112 (37), 110 (21), 85 (15), 71 (28), 57 (20). Found: C, 62.04; H, 9.48%. Calcd for $C_{13}H_{23}F_3O$: C, 61.88; H, 9.19%.

5-(2,2,2-Trifluoroethyl)-6-undecanone (25b): Bp 65—70 °C (1 Torr, bath temp); IR(neat) 2956, 2930, 2862, 1719, 1467, 1459, 1378, 1257, 1131, 1102, 1075 cm^{-1}; ^{1}H NMR ($CDCl_3$) δ=0.90 (t, J=6.8 Hz, 6H), 1.15—1.75 (m, 12H), 1.88—2.21 (m, 1H), 2.48 (t, J=7.5 Hz, 2H), 2.57—2.90 (m, 2H); ^{13}C NMR ($CDCl_3$) δ=13.77, 13.88, 22.44, 22.54, 23.00, 28.79, 31.25, 31.82, 34.53 (q, J=28.4 Hz), 42.80, 44.93 (q, J=2.7 Hz), 126.6 (q, J=277 Hz), 211.5; ^{19}F NMR ($CDCl_3$) δ=−65.50 (t, J=10.8 Hz); MS (12 eV) m/z (rel intensity) 252 (3), 196 (8), 140 (7), 100 (6), 99 (100), 71 (15), 43 (4). Found: C, 62.04; H, 9.46%. Calcd for $C_{13}H_{23}F_3O$: C, 61.88; H, 9.19%.

The Reaction of 1-Trimethylsiloxy-1-cyclopropylethylene (26) with Perfluorohexyl or Perfluoroisopropyl Iodides. Perfluoroisopropylation of **26** is representative. Et_3B (1.0 M hexane solution, 0.20 ml, 0.20 mmol) was added to a solution of silyl enol ether (0.16 g, 1.0 mmol) and i-C_3F_7I (0.50 g, 1.7 mmol) in hexane (2 ml). After stirring for 20 min, the reaction mixture was concentrated in vacuo. Purification by silica-gel column chromatography gave **27b** in 85% yield. Treatment of crude product with concd aq HCl in THF according to Procedure A′ and purification by distillation gave **28b** in 83% yield.

(*Z*), (*E*)-6,7,7,7,-Tetrafluoro-1-iodo-6-trifluoromethyl-4-trimethylsiloxy-3-heptene (27b, (*Z*):(*E*)=81:19): Bp 92—97 °C (1 Torr, bath temp); IR(neat) 2960, 1671, 1374, 1333, 1286, 1222, 1164, 1149, 1121, 1003, 845 cm^{-1}; ^{1}H NMR ($CDCl_3$) δ=0.22 (s, 9H), 2.53 (dt, J=7.6, 7.0 Hz, 0.38H), 2.60 (td, J=7.4, 7.0 Hz, 1.62H), 2.75 (d, J=21.6 Hz, 1.62H), 2.86 (d, J=21.0 Hz, 0.38H), 3.10 (t, J=7.4 Hz, 1.62H), 3.14 (t, J=7.0 Hz, 0.38H), 4.75 (t, J=7.0 Hz, 0.81H), 4.80 (t, J=7.6 Hz, 0.19H); ^{13}C NMR for (*Z*)-isomer ($CDCl_3$) δ=0.43, 4.00, 30.12, 35.99 (d, J=19.5 Hz), 91.41 (dm, J=207 Hz), 114.5, 120.9 (qd, J=288, 28.8 Hz), 142.4 (d, J=2.6 Hz); ^{13}C NMR for (*E*)-isomer ($CDCl_3$) δ=−0.15, 5.92, 31.21, 31.49 (d, J=19.0 Hz), 111.0, 143.6 (d, J=3.4 Hz), (^{13}C of $^iC_3F_7$ could not be detected); ^{19}F NMR ($CDCl_3$) δ=−76.56 (d, J=6.1 Hz, 4.86F), −76.79 (d, J=7.3 Hz, 1.14F), −182.1 (tsep, J=20.8, 7.3 Hz, 0.19F), −183.0 (tsep, J=22.0, 6.1 Hz, 0.81F); MS (70 eV) m/z (rel intensity) 452 (2), 326 (18), 325 (100), 233 (8), 73 (18). Found: C, 29.16; H, 3.58%. Calcd for $C_{11}H_{16}F_7IOSi$: C, 29.22; H, 3.57%.

6,7,7,7-Tetrafluoro-1-iodo-6-trifluoromethyl-4-heptanone (28b): Bp 73—78 °C (1 Torr, bath temp); IR(neat) 1728, 1338, 1289, 1223, 1165, 1117, 1045, 1002 cm^{-1}; ^{1}H NMR ($CDCl_3$) δ=2.04—2.18 (m, 2H), 2.75 (t, J=7.0 Hz, 2H), 3.11 (d, J=21.9 Hz, 2H), 3.23 (t, J=6.6 Hz, 2H); ^{13}C NMR ($CDCl_3$) δ=5.31, 26.60, 40.55 (d, J=19.0 Hz), 44.69, 90.52 (dm, J=209 Hz), 120.3 (qd, J=288, 27.0 Hz), 199.1; ^{19}F NMR ($CDCl_3$) δ=−76.98 (d, J=4.9 Hz, 6F), −182.8 (bs, 1F); MS (70 eV) m/z (rel intensity) 253 (M^+−I, 61), 211 (100), 155 (14), 95 (14), 69 (36), 42 (19), 41 (27). Found: C, 25.51; H, 2.29%. Calcd for $C_8H_8F_7IO$: C, 25.28; H, 2.12%.

6,6,7,7,8,8,9,9,10,10,11,11,11-Tridecafluoro-1-iodo-4-undecanone (28a): Bp 100—105 °C (1 Torr, bath temp); IR(neat) 1729, 1345, 1241, 1209, 1146 cm^{-1} δ=^{1}H NMR ($CDCl_3$) δ=2.07—2.20 (m, 2H), 2.78 (t, J=6.9 Hz, 2H), 3.22 (t, J=18.6 Hz, 2H), 3.25 (t, J=6.7 Hz, 2H); ^{13}C NMR ($CDCl_3$) δ=5.26, 26.52, 43.20 (t, J=22.1 Hz), 44.66, 198.4; ^{19}F NMR ($CDCl_3$) δ=−81.45 (bs, 3F), −111.5 (bs, 2F), −122.2 (bs, 2F), −123.4 (bs, 4F), −126.7 (bs, 2F); MS (70 eV) m/z (rel intensity) 403 (M^+−I, 67), 362 (9), 361 (100), 341 (9), 197 (11), 169 (8), 155 (7), 69 (13), 41 (8). Found: C, 24.85; H, 1.52%. Calcd for $C_{11}H_8F_{13}IO$: C, 24.93; H, 1.52%.

The Reaction of 1-Trimethylsiloxy-1-cyclopropylethylene with Trifluoromethyl Iodide. CF_3I (0.40 ml, 5.0 mmol) was collected in the flask pre-cooled to −78 °C. Hexane (2 ml), silyl enol ether (0.16 g, 1.0 mmol) and Et_3B (0.20 mmol) were added to CF_3I and the mixture was warmed to 5 °C over 3 h. After evaporation of solvent, the crude product was treated with concd aq HCl in THF. Purification by distillation gave **28c** in 67% yield: Bp 65—70 °C (1 Torr, bath temp); IR(neat) 1733, 1419, 1380, 1270, 1223, 1159, 1142, 1091, 626 cm^{-1}; ^{1}H NMR ($CDCl_3$) δ=2.05—2.18 (m, 2H), 2.72 (t, J=6.9 Hz, 2H), 3.24 (t, J=6.6 Hz, 2H), 3.26 (q, J=10.4 Hz, 2H); ^{13}C NMR ($CDCl_3$) δ=5.55, 26.30, 43.59, 46.18 (q, J=28.3 Hz), 123.4 (q, J=277 Hz), 198.6; ^{19}F NMR ($CDCl_3$) δ=−62.85 (t, J=9.8 Hz); MS (70 eV) m/z (rel intensity) 153 (M^+−I, 58), 127 (7), 111 (100), 91 (6), 83 (12), 42 (9), 41 (11), 39 (8). Found: C, 25.57; H, 2.79%. Calcd for $C_6H_8F_3IO$: C, 25.74; H, 2.88%.

Preparation of Ketene Silyl Acetals. The following ketene silyl acetals were prepared by the reported procedure.[9,16] The physical data for 1-hexyloxy-2-methyl-1-trimethylsiloxy-1-propene (**40**) is described in the literature.[17] The physical data for other compounds are shown below.

1-Butoxy-1-(*t*-butyldimethylsiloxy)ethylene (29): Bp 66—68 °C (2 Torr); IR(neat) 2958, 2930, 1653, 1277, 1254, 837,

784 cm^{-1}; ^{1}H NMR ($CDCl_3$) δ=0.17 (s, 6H), 0.93 (s, 9H), 0.94 (t, J=7.3 Hz, 3H), 1.33—1.52 (m, 2H), 1.59—1.72 (m, 2H), 3.06 (d, J=2.3 Hz, 1H), 3.22 (d, J=2.3 Hz, 1H), 3.68 (t, J=6.4 Hz, 2H); ^{13}C NMR ($CDCl_3$) δ=−4.56, 13.73, 18.09, 19.31, 25.62, 30.95, 60.32, 67.48, 161.5; MS (70 eV) m/z (rel intensity) 230 (9), 174 (14), 159 (13), 131 (78), 117 (91), 75 (100), 73 (67), 57 (15), 43 (14), 41 (23). Found: C, 62.27; H, 11.62%. Calcd for $C_{12}H_{26}O_2Si$: C, 62.55; H, 11.37%.

1-(t-Butyldimethylsiloxy)-1-octyloxyethylene (32): Bp 114—117 °C (2 Torr); IR(neat) 2954, 2928, 2856, 1651, 1276, 1254, 829, 785 cm^{-1}; ^{1}H NMR ($CDCl_3$) δ=0.17 (s, 6H), 0.89 (t, J=6.6 Hz, 3H), 0.93 (s, 9H), 1.28 (bs, 10H), 1.60—1.73 (m, 2H), 3.05 (d, J=2.3 Hz, 1H), 3.22 (d, J=2.3 Hz, 1H), 3.67 (t, J=6.5 Hz, 2H); ^{13}C NMR ($CDCl_3$) δ=−4.54, 14.07, 18.13, 22.65, 25.63, 26.11, 28.89, 29.22 (two peaks), 31.80, 60.32, 67.78, 161.5; MS (70 eV) m/z (rel intensity) 286 (2), 187 (28), 175 (18), 119 (17), 117 (100), 75 (67), 73 (44), 43 (23). Found: C, 67.23; H, 12.23%. Calcd for $C_{16}H_{34}O_2Si$: C, 67.07; H, 11.96%.

1-Butoxy-1-(trimethylsiloxy)ethylene (34): Bp 95—101 °C (39 Torr); IR(neat) 2960, 1657, 1278, 1252, 1088, 1023, 849, 757 cm^{-1}; ^{1}H NMR ($CDCl_3$) δ=0.22 (s, 9H), 0.94 (t, J=7.2 Hz, 3H), 1.34—1.52 (m, 2H), 1.60—1.73 (m, 2H), 3.06 (d, J=2.5 Hz, 1H), 3.21 (d, J=2.5 Hz, 1H), 3.70 (t, J=6.4 Hz, 2H); ^{13}C NMR ($CDCl_3$) δ=0.05, 13.69, 19.26, 30.91, 60.03, 67.54, 161.2; MS (70 eV) m/z (rel intensity) 188 (3), 131 (26), 117 (94), 75 (100), 73 (97), 72 (23), 57 (22), 56 (41), 45 (26), 43 (80), 41 (43). Found: C, 57.20; H, 10.91%. Calcd for $C_9H_{20}O_2Si$: C, 57.40; H, 10.70%.

1-(Trimethylsiloxy)-1-octyloxyethylene (35): Bp 91—96 °C (1 Torr); IR(neat) 2956, 2926, 2854, 1656, 1277, 1252, 1019, 848 cm^{-1}; ^{1}H NMR ($CDCl_3$) δ=0.22 (s, 9H), 0.88 (t, J=6.5 Hz, 3H), 1.28 (bs, 10H), 1.60—1.73 (m, 2H), 3.05 (d, J=2.5 Hz, 1H), 3.20 (d, J=2.5 Hz, 1H), 3.68 (t, J=6.5 Hz, 2H); ^{13}C NMR ($CDCl_3$) δ=0.08, 14.03, 22.62, 26.09, 28.87, 29.22 (two peaks), 31.78, 60.03, 67.85, 161.2; MS (70 eV) m/z (rel intensity) 244 (2), 187 (20), 133 (42), 117 (100), 75 (43), 73 (48), 56 (21), 43 (51), 41 (23). Found: C, 63.62; H, 11.51%. Calcd for $C_{13}H_{28}O_2Si$: C, 63.88; H, 11.55%.

1-Methoxy-1-(trimethylsiloxy)-1-hexene (36, (*E*):(*Z*)=83:17): Bp 102—105 °C (36 Torr); IR(neat) 2956, 1682, 1254, 1227, 1174, 1089, 906, 845 cm^{-1}; ^{1}H NMR ($CDCl_3$) δ=0.19 (s, 1.53H), 0.23 (s, 7.47H), 0.89 (t, J=6.8 Hz, 3H), 1.25—1.40 (m, 4H), 1.90—2.01 (m, 2H), 3.47 (t, J=6.8 Hz, 0.17H), 3.48 (s, 0.51H), 3.52 (s, 2.49H), 3.67 (t, J=7.1 Hz, 0.83H); ^{13}C NMR for (*E*)-isomer ($CDCl_3$) δ=−0.32, 13.92, 22.20, 24.10, 32.91, 54.76, 85.33, 153.5; MS (70 eV) m/z (rel intensity) 202 (8), 159 (47), 89 (19), 73 (58), 59 (11), 55 (100), 45 (11). Found: C, 59.47; H, 11.22%. Calcd for $C_{10}H_{22}O_2Si$: C, 59.35; H, 10.96%.

1-Methoxy-1-(trimethylsiloxy)-1-octene (38, (*E*):(*Z*)=88:12): Bp 68—70 °C (1 Torr); IR(neat) 2956, 2922, 2852, 1682, 1253, 1227, 1170, 1091, 902, 845 cm^{-1}; ^{1}H NMR ($CDCl_3$) δ=0.19 (s, 1.08H), 0.23 (s, 7.92H), 0.88 (t, J=6.5 Hz, 3H), 1.28 (bs, 8H), 1.89—2.03 (m, 2H), 3.47 (t, J=6.8 Hz, 0.12H), 3.48 (s, 0.36H), 3.51 (s, 2.64H), 3.67 (t, J=7.3 Hz, 0.88H); ^{13}C NMR for (*E*)-isomer ($CDCl_3$) δ=−0.30, 14.07, 22.68, 24.43, 28.85, 30.67, 31.78, 54.78, 85.42, 153.5; MS (70 eV) m/z (rel intensity) 230 (10), 160 (11), 159 (75), 89 (16), 73 (52), 59 (11), 55 (100), 41 (11). Found: C, 62.68; H, 11.63%. Calcd for $C_{12}H_{26}O_2Si$: C, 62.55; H, 11.37%.

1-(3-Butenyloxy)-1-(trimethylsiloxy)ethylene (42): Bp 90—91 °C (39 Torr); IR(neat) 2958, 1653, 1277, 1253, 1088, 1018, 990, 911, 847, 758 cm^{-1}; ^{1}H NMR ($CDCl_3$) δ=0.22 (s, 9H), 2.43 (qt, J=6.7, 1.3 Hz, 2H), 3.07 (d, J=2.6 Hz, 1H), 3.23 (d, J=2.6 Hz, 1H), 3.75 (t, J=6.7 Hz, 2H), 5.08 (ddt, J=10.2, 1.8, 1.3 Hz, 1H), 5.13 (ddt, J=17.0, 1.8, 1.3 Hz, 1H), 5.84 (ddd, J=17.0, 10.2, 6.7 Hz, 1H); ^{13}C NMR ($CDCl_3$) δ=0.09, 33.28, 60.26, 67.00, 117.0, 134.4, 161.0; MS (70 eV) m/z (rel intensity) 186 (3), 101 (21), 75 (61), 73 (100), 55 (73), 54 (85), 43 (45). Found: C, 57.74; H, 9.82%. Calcd for $C_9H_{18}O_2Si$: C, 58.02; H, 9.74%.

The Reaction of 1-Butoxy-1-(*t*-butyldimethylsiloxy)ethylene with Perfluorohexyl Iodide in the Presence of 2,6-Dimethylpyridine (Procedure A). This reaction gave a mixture of **30a** and **31** in 37 and 10% yields respectively. Butyl 3,3,4,4,5,5,6,6,7,7,8,8,8-tridecafluorooctanoate (**30a**): Bp 76—81 °C (7 Torr, bath temp); IR(neat) 2964, 1754, 1396, 1353, 1241, 1208, 1146, 1122, 1064, 709, 628 cm^{-1}; ^{1}H NMR ($CDCl_3$) δ=0.94 (t, J=7.2 Hz, 3H), 1.31—1.49 (m, 2H), 1.57—1.73 (m, 2H), 3.14 (t, J=17.7 Hz, 2H), 4.20 (t, J=6.6 Hz, 2H); ^{13}C NMR ($CDCl_3$) δ=13.53, 18.94, 30.37, 37.02 (t, J=22.5 Hz), 65.91, 163.9; ^{19}F NMR ($CDCl_3$) δ=−81.34 (tt, J=7.4, 3.0 Hz, 3F), −111.6—−112.6 (m, 2F), −112.1 (bs, 2F), −123.4 (bs, 4F), −126.3—−126.8 (m, 2F); MS (70 eV) m/z (rel intensity) 434 (0.2), 361 (26), 69 (18), 57 (42), 56 (100), 55 (12), 41 (35). Found: C, 33.45; H, 2.46%. Calcd for $C_{12}H_{11}F_{13}O_2$: C, 33.20; H, 2.55%. (*E*)-Butyl 3,4,4,5,5,6,6,7,7,8,8,8-dodecafluoro-2-octenoate (**31**): Bp 83—88 °C (13 Torr, bath temp); IR(neat) 2964, 1736, 1702, 1350, 1275, 1239, 1206, 1143, 1114, 723, 644 cm^{-1}; ^{1}H NMR ($CDCl_3$) δ=0.96 (t, J=7.3 Hz, 3H), 1.33—1.51 (m, 2H), 1.60—1.76 (m, 2H), 4.24 (t, J=6.6 Hz, 2H), 6.00 (d, J=29.8 Hz, 1H); ^{13}C NMR ($CDCl_3$) δ=13.45, 19.02, 30.44, 65.64, 107.2 (t, J=4.0 Hz), 161.6 (d, J=2.7 Hz); ^{19}F NMR ($CDCl_3$) δ=−81.14—−81.43 (m, 3F), −107.7—−108.7 (m, 1F), −118.9—−119.4 (m, 2F), −123.2 (bs, 4F), −126.6 (bs, 2F); MS (12 eV) m/z (rel intensity) 359 ($M^+-C_4H_7$, 6), 341 (5), 57 (5), 56 (100), 55 (2). Found: C, 35.02; H, 2.49%. Calcd for $C_{12}H_{10}F_{12}O_2$: C, 34.80; H, 2.43%.

The Reactions of Ketene Silyl Acetals with Perfluorohexyl Iodide without Base (Procedure B). Following procedure for the reaction of ketene *t*-butyldimethylsilyl acetal derived from butyl acetate with perfluorohexyl iodide is typical. Under argon atmosphere, Et_3B was added to a solution of ketene silyl acetal (**29**, 456 mg, 1.98 mmol) and perfluorohexyl iodide (440 mg, 0.99 mmol) in hexane (4.9 ml). After stirring for 10 min, sat. aq $NaHCO_3$ (5 ml) was added to the reaction mixture. The mixture was vigorously stirred for 40 min, then poured into water (30 ml) and extracted with hexane (30 m×2). The combined organic layer was dried over anhydrous Na_2SO_4 and concentrated in vacuo. The residual oil was purified by silica-gel column chromatography to give **30a** in 87% yield.

Methyl 2-Butyl-3,3,4,4,5,5,6,6,7,7,8,8,8-tridecafluorooctanoate (37a): Bp 98—103 °C (20 Torr, bath temp); IR(neat) 2964, 2936, 2870, 1757, 1458, 1437, 1350, 1239, 1194, 1145, 1116, 712, 695, 652 cm^{-1}; ^{1}H NMR ($CDCl_3$) δ=0.91 (t, J=6.8 Hz, 3H), 1.21—1.47 (m, 4H), 1.74—2.07 (m, 2H), 3.06—3.29 (m, 1H), 3.78 (s, 3H); ^{13}C NMR ($CDCl_3$) δ=13.42, 22.19, 24.87, 28.98, 48.15 (dd, J=22.6, 20.6 Hz), 52.28, 168.1 (d, J=7.8 Hz); ^{19}F NMR ($CDCl_3$) δ=−81.32 (t, J=9.8 Hz, 3F), −113.7 (dm, J=266 Hz, 1F), −116.4 (dm, J=266 Hz, 1F), −121.8—−122.4 (m, 4F), −123.3 (bs, 2F), −126.3—−126.9 (m, 2F); MS (70 eV) m/z (rel intensity) 448 (0.1), 392 (11), 129 (16), 123 (100), 91 (13), 88 (14), 87 (12), 69 (14), 59 (68), 57 (11), 55

(24), 43 (13), 42 (14), 41 (21). Found: C, 34.82; H, 2.84%. Calcd for $C_{13}H_{13}F_{13}O_2$: C, 34.84; H, 2.92%.

Hexyl 3,3,4,4,5,5,6,6,7,7,8,8,8-Tridecafluoro-2,2-dimethyloctanoate (41a): Bp 69—74 °C (2 Torr, bath temp); IR(neat) 2960, 2932, 2862, 1746, 1477, 1277, 1241, 1195, 1177, 1147, 1112, 1063, 697, 658 cm^{-1}; ^{1}H NMR ($CDCl_3$) δ=0.89 (t, J=6.5 Hz, 3H), 1.23—1.42 (m, 6H), 1.46 (s, 6H), 1.57—1.71 (m, 2H), 4.14 (t, J=6.5 Hz, 2H); ^{13}C NMR ($CDCl_3$) δ=13.74, 19.99, 22.48, 25.46, 28.29, 31.34, 48.48 (t, J=20.8 Hz), 66.02, 170.6 (t, J=3.1 Hz); ^{19}F NMR ($CDCl_3$) δ=−81.33, (tt, J=9.9, 2.5 Hz, 3F), −112.4 (bs, 2F), −114.7 (bs, 2F), −118.1 (bs, 2F), −123.1 (bs, 2F), −126.3—−126.8 (m, 2F); MS (12 eV) m/z (rel intensity) 407 ($M^+-C_6H_{11}$, 15), 85 (49), 84 (100), 69 (9), 57 (11), 56 (37), 43 (51). Found: C, 39.22; H, 3.89%. Calcd for $C_{16}H_{19}F_{13}O_2$: C, 39.20; H, 3.91%.

The Reaction of Ketene Silyl Acetals with Perfluoroisopropyl Iodide. Et_3B (0.2 mmol) was added to a solution of ketene silyl acetal (2.0 mmol) and perfluoroisopropyl iodide (1.0 mmol) in hexane (5 ml) at 0 °C. After an addition of Et_3B, the reaction mixture was immediately warmed up to room temperature and stirred for appropriate time given in Table 3. Work-up and purification were performed according to Procedure B. In the case of ketene trimethylsilyl acetals **34** or **35**, butyl or octyl 2-(trimethylsilyl)acetate was obtained as by-product. These trimethylsilyacetates could be produced by isomerization of starting ketene acetals **34** and **35** under the reaction conditions. Tetrabutylammonium fluoride (TBAF, 1.0 mmol per 1.0 mmol of ketene silyl acetal) was added to the reaction mixture prior to work-up to remove these by-products from perfluoroalkylated esters **30** and **33**. Thus, TBAF was added and the resulting mixture was stirred for 10 min at room temperature. The resulting mixture was poured into dil aq NH_4Cl (sat. aq NH_4Cl:water=1:10). Extraction and purification by silica-gel column chromatography provided the desired perfluoroalkylated esters.

Butyl 3,4,4,4-Tetrafluoro-3-trifluoromethylbutanoate (30b): Bp 68—73 °C (36 Torr, bath temp); IR(neat) 2962, 1753, 1346, 1296, 1229, 1202, 1168, 1129, 1060, 1004, 703 cm^{-1}; ^{1}H NMR ($CDCl_3$) δ=0.94 (t, J=7.1 Hz, 3H), 1.30—1.48 (m, 2H), 1.57—1.71 (m, 2H), 3.07 (d, J=20.4 Hz, 2H), 4.17 (t, J=6.6 Hz, 2H); ^{13}C NMR ($CDCl_3$) δ=13.46, 18.91, 30.26, 34.21 (d, J=19.8 Hz), 65.96, 89.98 (dm, J=211 Hz), 120.4 (qd, J=288, 27.9 Hz), 164.4 (d, J=2.5 Hz); ^{19}F NMR ($CDCl_3$) δ=−77.25 (d, J=7.3 Hz, 6F), −182.9 (tsep, J=20.1, 7.3 Hz, 1F); MS (70 eV) m/z (rel intensity) 284 (0.6), 255 (3), 229 (5), 212 (6), 211 (100), 191 (2), 163 (2), 56 (3). Found: C, 38.26; H, 3.94%. Calcd for $C_9H_{11}F_7O_2$: C, 38.04; H, 3.90%.

Octyl 3,4,4,4-Tetrafluoro-3-trifluoromethylbutanoate (33a): Bp 69—74 °C (1 Torr, bath temp); IR(neat) 2958, 2930, 2860, 1754, 1347, 1296, 1230, 1202, 1169, 1061, 1006, 703 cm^{-1}; ^{1}H NMR ($CDCl_3$) δ=0.89 (t, J=6.5 Hz, 3H), 1.28 (bs, 10H), 1.59—1.73 (m, 2H), 3.06 (d, J=20.4 Hz, 2H), 4.16 (t, J=6.7 Hz, 2H); ^{13}C NMR ($CDCl_3$) δ=13.94, 22.60, 25.69, 28.26, 29.11 (two peaks), 31.75, 34.22 (d, J=19.9 Hz), 66.24, 89.99 (dm, J=211 Hz), 120.4 (qd, J=288, 28.2 Hz), 164.4; ^{19}F NMR ($CDCl_3$) δ=−77.23 (d, J=6.9 Hz, 6F), −182.9 (tsep, J=20.2, 6.9 Hz, 1F); MS (12 eV) m/z (rel intensity) 229 ($M^+-C_8H_{15}$, 12), 112 (55), 84 (100), 83 (81), 82 (30), 70 (84), 69 (34), 68 (29), 56 (52). Found: C, 46.06; H, 5.81%. Calcd for $C_{13}H_{19}F_7O_2$: C, 45.89; H, 5.63%.

Methyl 2-(Perfluoroisopropyl)hexanoate (37b): Bp 78—83 °C (50 Torr, bath temp); IR(neat) 2962, 2934, 2878, 1757, 1460, 1439, 1282, 1222, 1169, 1135, 1111, 1092, 984, 720 cm^{-1}; ^{1}H NMR ($CDCl_3$) δ=0.91 (t, J=7.0 Hz, 3H), 1.15—1.50 (m, 4H), 1.69—1.86 (m, 1H), 1.91—2.12 (m, 1H), 3.10—3.24 (m, 1H), 3.77 (s, 3H); ^{13}C NMR ($CDCl_3$) δ=13.56, 22.12, 25.44, 29.84, 46.90 (d, J=20.1 Hz), 52.51, 91.53 (dm, J=208 Hz), 120.7 (qd, J=289, 29.9 Hz), 168.3 (d, J=6.0 Hz); ^{19}F NMR ($CDCl_3$) δ=−74.04 (d, J=7.3 Hz, 6F), −178.6 (dsep, J=12.2, 6.1 Hz, 1F); MS (70 eV) m/z (rel intensity) 298 (0.2), 267 (23), 255 (21), 242 (80), 173 (100), 141 (11), 129 (18), 59 (13). Found: C, 40.25; H, 4.54%. Calcd for $C_{10}H_{13}F_7O_2$: C, 40.28; H, 4.39%.

Methyl 2-(Perfluoroisopropyl)octanoate (39a): Bp 85—90 °C (24 Torr, bath temp); IR(neat) 2958, 2930, 2860, 1757, 1459, 1439, 1302, 1229, 1168, 1134, 1114, 1093, 976, 718 cm^{-1}; ^{1}H NMR ($CDCl_3$) δ=0.89 (t, J=6.5 Hz, 3H), 1.28 (bs, 8H), 1.67—1.89 (m, 1H), 1.92—2.13 (m, 1H), 3.09—3.23 (m, 1H), 3.77 (s, 3H); ^{13}C NMR ($CDCl_3$) δ=13.77, 22.41, 25.69, 27.67, 28.64, 31.38, 46.90 (d, J=20.2 Hz), 52.39, 91.48 (dm, J=209 Hz), 120.6 (qd, J=287, 27.0 Hz), 168.0—168.2 (m); ^{19}F NMR ($CDCl_3$) δ=−74.03 (d, J=6.1 Hz, 6F), −178.7 (dsep, J=13.4, 6.1 Hz, 1F); MS (70 eV) m/z (rel intensity) 326 (2), 297 (25), 295 (13), 255 (58), 242 (100), 173 (91), 59 (17), 55 (14), 43 (17), 41 (16). Found: C, 43.96; H, 5.27%. Calcd for $C_{12}H_{17}F_7O_2$: C, 44.18; H, 5.25%.

Hexyl 3,4,4,4-Tetrafluoro-3-trifluoromethylbutanoate (41b): Bp 72—77 °C (3 Torr, bath temp); IR(neat) 2958, 2932, 2860, 1743, 1472, 1287, 1228, 1190, 1166, 1149, 1116, 1033, 995, 726 cm^{-1}; ^{1}H NMR ($CDCl_3$) δ=0.90 (t, J=6.6 Hz, 3H), 1.26—1.45 (m, 6H), 1.50 (s, 6H), 1.58—1.74 (m, 2H), 4.12 (t, J=6.6 Hz, 2H); ^{13}C NMR ($CDCl_3$) δ=13.84, 21.23, 22.46, 25.44, 28.15, 31.29, 46.54 (d, J=19.0 Hz), 66.23, 93.87 (dm, J=216 Hz), 121.2 (qd, J=289, 28.7 Hz), 171.4; ^{19}F NMR ($CDCl_3$) δ=−70.76 (d, J=4.9 Hz, 6F), −178.0 (bs, 1F); MS (12 eV) m/z (rel intensity) 257 ($M^+-C_6H_{11}$, 27), 85 (65), 84 (62), 69 (11), 57 (24), 56 (32), 43 (100). Found: C, 45.93; H, 5.81%. Calcd for $C_{13}H_{19}F_7O_2$: C, 45.89; H, 5.63%.

The Reaction of Ketene Silyl Acetals with Trifluoromethyl Iodide. CF_3I (1.0 mmol) was introduced into the flask precooled to −78 °C, then hexane (5.0 ml) and ketene silyl acetal (2.0 mmol) were added to the flask. Et_3B (0.2 mmol) was added and the reaction mixture was immediately warmed up to room temperature. After stirring for several hours (Table 3), extractive work-up followed by purification gave the corresponding trifluoromethylated ester.

Octyl 3,3,3-Trifluoropropanoate (33b): Bp 56—61 °C (1 Torr, bath temp); IR(neat) 2956, 2926, 2856, 1754, 1418, 1399, 1364, 1269, 1221, 1119 cm^{-1}; ^{1}H NMR ($CDCl_3$) δ=0.89 (t, J=6.5 Hz, 3H), 1.28 (bs, 10H), 1.59—1.74 (m, 2H), 3.17 (q, J=10.1 Hz, 2H), 4.18 (t, J=6.7 Hz, 2H); ^{13}C NMR ($CDCl_3$) δ=14.01, 22.60, 25.69, 28.34, 29.09 (two peaks), 31.72, 39.66 (q, J=30.9 Hz), 65.95, 123.4 (q, J=277 Hz), 164.1 (q, J=4.2 Hz); ^{19}F NMR ($CDCl_3$) δ=−64.02 (t, J=10.4 Hz); MS (70 eV) m/z (rel intensity) 129 ($M^+-C_8H_{15}$, 6), 112 (23), 84 (94), 83 (73), 70 (100), 69 (45), 68 (30), 56 (73). Found: C, 55.21; H, 8.13%. Calcd for $C_{11}H_{19}F_3O_2$: C, 54.99; H, 7.97%.

Methyl 2-Trifluoromethyloctanoate (39b): Bp 78—83 °C (24 Torr, bath temp); IR(neat) 2956, 2928, 2860, 1755, 1459, 1439, 1354, 1272, 1209, 1165, 1107 cm^{-1}; ^{1}H NMR ($CDCl_3$) δ=0.89 (t, J=6.4 Hz, 3H), 1.21—1.41 (m, 8H), 1.67—2.01 (m, 2H), 3.11 (dqd, J=9.9, 8.4, 4.8 Hz, 1H), 3.78 (s, 3H); ^{13}C NMR ($CDCl_3$) δ=13.87, 22.44, 26.11, 26.70, 28.74, 31.37, 50.28 (q, J=27.4 Hz), 52.44, 124.7 (q, J=280 Hz), 168.2 (q,

J=2.7 Hz); ^{19}F NMR ($CDCl_3$) δ=−68.86 (d, J=8.5 Hz); MS (12 eV) m/z (rel intensity) 226 (0.3), 155 (23), 143 (13), 142 (100), 116 (27), 115 (18), 85 (27), 84 (16). Found: C, 53.05; H, 7.82%. Calcd for $C_{10}H_{17}F_3O_2$: C, 53.09; H, 7.57%.

Hexyl 3,3,3-Trifluoro-2,2-dimethylpropanoate (41c): Bp 58—63 °C (5 Torr, bath temp); IR(neat) 2956, 2932, 2860, 1745, 1476, 1401, 1282, 1206, 1152, 1119 cm^{-1}; ^{1}H NMR ($CDCl_3$) δ=0.89 (t, J=6.6 Hz, 3H), 1.24—1.39 (m, 6H), 1.42 (s, 6H), 1.58—1.73 (m, 2H), 4.16 (t, J=6.6 Hz, 2H); ^{13}C NMR ($CDCl_3$) δ=13.87, 19.67, 22.46, 25.36, 28.32, 31.28, 48.45 (q, J=25.5 Hz), 65.84, 126.4 (q, J=282 Hz), 170.5; ^{19}F NMR ($CDCl_3$) δ=−75.42 (s); MS (12 eV) m/z (rel intensity) 157 ($M^+-C_6H_{11}$, 31), 139 (8), 85 (32), 84 (100), 69 (24), 57 (13), 56 (68), 43 (50), 42 (9). Found: C, 55.09; H, 8.18%. Calcd for $C_{11}H_{19}F_3O_2$: C, 54.99; H, 7.97%.

The Reaction of Ketene Silyl Acetals with 2,2,2-Trifluoroethyl Iodide. The reactions were performed according to Procedure B.

Octyl 4,4,4-Trifluorobutanoate (33c): Bp 72—77 °C (1 Torr, bath temp); IR(neat) 2958, 2928, 2858, 1744, 1332, 1265, 1230, 1192, 1145, 1112, 985 cm^{-1}; ^{1}H NMR ($CDCl_3$) δ=0.89 (t, J=6.5 Hz, 3H), 1.30 (bs, 10H), 1.57—1.71 (m, 2H), 2.33—2.63 (m, 4H), 4.11 (t, J=6.7 Hz, 2H); ^{13}C NMR ($CDCl_3$) δ=13.99, 22.60, 25.83, 27.09 (q, J=3.3 Hz), 28.50, 29.14 (two peaks), 29.35 (q, J=29.6 Hz), 31.74, 65.26, 126.5 (q, J=277 Hz), 170.9; ^{19}F NMR ($CDCl_3$) δ=−67.56 (t, J=10.4 Hz); MS (12 eV) m/z (rel intensity) 143 ($M^+-C_8H_{15}$, 27), 112 (44), 84 (96), 83 (83), 82 (24), 70 (100), 69 (36), 68 (23), 56 (59). Found: C, 56.84; H, 8.61%. Calcd for $C_{12}H_{21}F_3O_2$: C, 56.68; H, 8.32%.

Methyl 2-(2,2,2-Trifluoroethyl)octanoate (39c): Bp 88—93 °C (24 Torr, bath temp); IR(neat) 2954, 2928, 2858, 1744, 1438, 1381, 1260, 1203, 1153, 1126, 1096 cm^{-1}; ^{1}H NMR ($CDCl_3$) δ=0.88 (t, J=6.5 Hz, 3H), 1.27 (bs, 8H), 1.45—1.77 (m, 2H), 2.05—2.33 (m, 1H), 2.47—2.77 (m, 2H), 3.72 (s, 3H); ^{13}C NMR ($CDCl_3$) δ=13.97, 22.49, 26.68, 28.86, 31.51, 32.52, 35.87 (q, J=29.1 Hz), 39.34, 51.96, 126.2 (q, J=277 Hz), 174.6; ^{19}F NMR ($CDCl_3$) δ=−65.93 (t, J=10.4 Hz); MS (70 eV) m/z (rel intensity) 240 (0.9), 169 (18), 156 (100), 87 (42), 59 (22), 57 (11), 55 (18), 43 (18), 41 (21). Found: C, 54.70; H, 8.18%. Calcd for $C_{11}H_{19}F_3O_2$: C, 54.99; 7.97%.

The Reaction of 42 with Perfluorohexyl Iodide. Following the procedure B, treatment of ketene silyl acetal **42** with perfluorohexyl iodide provided a cyclized product **43** (10%) and perfluoroalkylated ester **44** (50%). 3-Iodomethyl-2-(2,2,3,3,4,4,5,5,6,6,7,7,7-tridecafluoroheptyl)-2-(trimethylsiloxy)-oxolane (**43**): Bp 93—98 °C (1 Torr, bath temp); IR(neat) 2956, 2894, 1363, 1234, 1146, 1123, 1018, 908, 845, 719, 709, 634 cm^{-1}; ^{1}H NMR ($CDCl_3$) δ=0.14 (s, 9H), 1.73—1.94 (m, 1H), 2.28—2.76 (m, 4H), 3.04 (dd, J=10.2, 9.9 Hz, 1H), 3.38 (dd, J=9.9, 4.2 Hz, 1H), 3.81 (ddd, J=10.6, 8.6, 6.2 Hz, 1H), 4.01 (ddd, J=8.6, 8.3, 2.0 Hz, 1H); ^{13}C NMR ($CDCl_3$) δ=1.06, 3.54, 32.86, 39.10 (t, J=20.0 Hz), 51.10, 65.81, 103.7; ^{19}F NMR ($CDCl_3$) δ=−81.31 (tt, J=9.8, 3.0 Hz, 3F), −112.7—−114.1 (m, 2F), −122.1 (bs, 2F), −123.4 (bs, 2F), −124.0 (bs, 2F), −126.3—−126.8 (m, 2F); MS (12 eV) m/z (rel intensity) 632 (0.1), 618 (12), 506 (21), 505 (100), 489 (8), 304 (6), 303 (49), 299 (15), 55 (54). Found: C, 28.72; H, 2.96%. Calcd for $C_{15}H_{18}F_{13}IO_2Si$: C, 28.49; H, 2.87%.

3-Butenyl 3,3,4,4,5,5,6,6,7,7,8,8,8-Tridecafluorooctanoate (44): Bp 91—96 °C (27 Torr, bath temp); IR(neat) 1755, 1352, 1241, 1207, 1145, 1122, 709, 628 cm^{-1}; ^{1}H NMR ($CDCl_3$) δ=2.43 (qt, J=6.7, 1.3 Hz, 2H), 3.14 (t, J=17.5 Hz, 2H), 4.26 (t, J=6.7 Hz, 2H), 5.11 (ddt, J=10.2, 1.7, 1.3 Hz, 1H), 5.13 (ddt, J=17.1, 1.7, 1.3 Hz, 1H), 5.78 (ddt, J=17.1, 10.2, 6.7 Hz, 1H); ^{13}C NMR ($CDCl_3$) δ=32.81, 36.92 (t, J=22.5 Hz), 64.99, 117.5, 133.3, 163.8; ^{19}F NMR ($CDCl_3$) δ=−81.31 (tt, J=6.9, 3.0 Hz, 3F), −111.6—−112.5 (m, 2F), −122.2 (bs, 2F), −123.3 (bs, 4F), −126.3—−126.8 (m, 2F); MS (12 eV) m/z (rel intensity) 432 (2), 362 (9), 361 (100), 341 (16), 55 (5), 54 (93). Found: C, 33.49; H, 2.23%. Calcd for $C_{12}H_9F_{13}O_2$; C, 33.35; H, 2.10%.

Financial support by the Ministry of Education, Science and Culture (Grant-in-Aid for Scientific Research No. 63470074) is acknowledged.

References

1) a) T. Umemoto, *Yuki Gosei Kagaku Kyokai Shi*, **41**, 251 (1983). b) T. Umemoto and Y. Gotoh, *Bull. Chem. Soc. Jpn.*, **60**, 3823 (1987). c) T. Umemoto and S. Ishihara, *Tetrahedron Lett.*, **31**, 3579 (1990). d) D. Cantacuzene, C. Wakselman, and R. Dorme, *J. Chem. Soc., Perkin Trans. 1*, **1977**, 1365; T. Umemoto, Y. Kuriu, S. Nakayama, and O. Miyano, *Tetrahedron Lett.*, **23**, 1471 (1982). e) K. Uneyama and K. Ueda, *Chem. Lett.*, **1988**, 853. f) T. Okano, T. Uekawa, and S. Eguchi, *Bull. Chem. Soc. Jpn.*, **62**, 2575 (1989). g) T. Okano, T. Uekawa, H. Sawaki, and S. Eguchi, *Synlett.*, **1990**, 403.

2) Y. Takeyama, Y. Ichinose, K. Oshima, and K. Utimoto, *Tetrahedron Lett.*, **30**, 3159 (1989).

3) A part of this work was published in communications: K. Miura, M. Taniguchi, K. Nozaki, K. Oshima, and K. Utimoto, *Tetrahedron Lett.*, **31**, 6391 (1990).

4) We thank Tosoh Akzo Co. for a gift of Et_3B.

5) "Biomedicinal Aspects of Fluorine Chemistry," ed by R. Filler and Y. Kobayashi, Kodansha Ltd., Tokyo (1982).

6) The reaction of vinylcyclopropane with R_f has been reported. K. Miura, K. Oshima, and K. Utimoto, *Bull. Chem. Soc. Jpn.*, **63**, 1665 (1990).

7) Recently Magnus et al. have reported sequential electrophilic addition of trialkylsilyl enol ether. P. Magnus and B. Mugrage, *J. Am. Chem. Soc.*, **112**, 462 (1990). Double hydroxylation of enol silyl ether have been reported. Y. Horiguchi, E. Nakamura, and I. Kuwajima, *Tetrahedron Lett.*, **30**, 3323 (1989).

8) H. O. House, L. J. Czuba, M. Gall, and H. D. Olmstead, *J. Org. Chem.*, **34**, 2324 (1969).

9) E. W. Colvin, "Silicon Reagents in Organic Synthesis," Academic Press Inc., London (1988), Chap. 15, pp. 99—118.

10) S. Locioro, L. Pellacani, and P. A. Tardella, *Tetrahedron Lett.*, **24**, 593 (1983).

11) E. J. Corey and A. W. Gross, *Tetrahedron Lett.*, **25**, 495 (1984).

12) E. J. Corey, H. Cho, C. Rücker, and D. H. Hua, *Tetrahedron Lett.*, **22**, 3455 (1981).

13) P. A. Grieco and Y. Ohfune, *J. Org. Chem.*, **43**, 2720 (1978).

14) D. Cantacuzene and R. Dorme, *Tetrahedron Lett.*, **1975**, 2031.

15) 4-Chloro-1-butanol, ring-opening product derived from THF, was not detected in the reaction mixture after treatment with concd HCl for 10 min.

16) C. Ainsworth, F. Chen, and Y-N. Kuo, *J. Organomet. Chem.*, **46**, 59 (1972).

17) N. Slougui and G. Rousseau, *Tetrahedron*, **41**, 2643 (1985).

Dynamic NMR as a Nondestructive Method for the Determination of Rates of Dissociation. XVIII. Factors Affecting the Rates of Dissociation of N–B Bond in the Coordinated Form of 9-[2-(Dialkylaminomethyl)-phenyl]-9-borabicyclo[3.3.1]nonanes[1)]

Shinji Toyota and Michinori Ōki*
Department of Chemistry, Faculty of Science, Okayama University of Science, Ridaicho, Okayama 700
(Received January 7, 1991)

NMR spectra of the title compounds reveal that they exist in the intramolecularly N–B coordinated form. The NMR signals exhibited dynamic behaviors accompanied with the dissociation of the N–B bond and total line shape analyses of the exchanging nuclei afforded kinetic parameters for the topomerization. Entropies of activation are large and positive, typical for the dissociation of coordination bonds. Examination with the multiple probes shows that the nitrogen inversion requires additional energy after the N–B bond dissociation. The barrier for the topomerization is affected by *N*-alkyl groups due to their F-strain. The barrier height is reduced in nonpolar solvents and not influenced by nucleophilicity of solvents. These solvent effects are discussed in connection with polarity of the N–B bond and steric hindrance of the boron atom.

The dynamic NMR method is a convenient technique for observation of dynamic processes of ligands in various coordination compounds,[2-4)] of which uniqueness is that rates of bond dissociation can be determined in the absence of foreign materials in organic solvents. An amine ligand is one of the well investigated examples. The dissociative processes of lignads were observed by NMR for tin–amine,[5)] silicon–amine,[6)] boron–amine,[7,8)] and other complexes.[9)] From the ease of dissociation, the kinetic basicity of an amine ligand or the kinetic Lewis acidity of a metal center can be estimated.

Recently, the kinetic parameters for the N–B bond dissociation in an intramolecular boronate–amine complexes (**1**) were determined by the total line shape analysis.[1)] The low barrier of the dissociation (**1a** $\Delta G^{\neq}_{233}$ 11.5 kcal mol^{-1}) was ascribed to the weak Lewis acidity of the boron atom which accepts electron from two attached oxgen atoms by p_π–p_π interactions. Trialkylborane–amine complexes should exhibit higher barriers to the N–B bond dissociation, since in these compounds the carbon atoms attached to the boron do not bear lone-pair electrons that suppress the acidity of the boron, and indeed trialkylboranes are known to be better electron acceptors than boronates.[10)]

In 1984, Kalbarczyk and Pasynkiewicz reported the synthesis of this type of compound, 9-[2-(dimethylaminomethyl)phenyl]-9-borabicyclo[3.3.1]nonane (**2**), which was stable in the air.[11)] They proposed the intramolecularly coordinated form with a four-coordinated center of boron from the chemical shift data in ^{1}H NMR spectrum. It seemed convincing on one hand, but on the other their ^{13}C NMR data were not in conformity with the expected structure. They reported that the *N*-methyl groups were diastereotopic and the carbon atoms in the positions 2(4) and 6(8) in the borabicyclononane skeleton (2(4)-C and 6(8)-C) and those in the positions 3 and 7 (3-C and 7-C) were isochronous. Since the molecule has a σ plane, passing N, B, 3-C, and 7-C, the *N*-methyl groups should be enantiotopic in the coordinated form. On the other hand, the 2-C/8-C pair as well as the pairs of 4-C/6-C and 3-C/7-C should not be equivalent in the coordinated form. From our experience, however, we were convinced that compounds **2** should exist as a coordinated form in solution and were prompted to reexamine this compound as a model for the trialkylborane-amine complexes. Evidence for the structure, the coordinated form, will be presented in this paper.

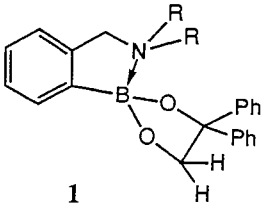

1

a : R= Me
b : R= Et

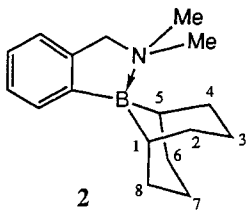

2

The strength of the N–B bond is affected by steric hindrance and solvents in addition to the basicity of the nitrogen atom and the acidity of the boron atom.[1)] Since the barrier to the dissociation in **1b** was lower than that in **1a** due to the steric effect (F-strain), the steric effect is expected to become more important, when the electron acceptor is bulky, as is the case of the 9-borabicyclo[3.3.1]-9-nonyl (9-BBN) group. Polarity and nucleophilicity of the solvent affected the rates of the N–B bond dissociation in **1** by affecting the ground state stability and by assisting the leaving of the amino moiety, respecively. These effects are expected to be affected by the bulkiness of the borane as well. It should be of interest to compare the strength of coordination in the 9-BBN system bearing various *N*-alkyl groups in various solvents because the data can assist us to get further insight into the acid-base properties of the amine-borane complexes in solution.

Results and Discussion

Since compound **2** possesses no convenient diastereotopic proton pairs for the NMR line shape analysis, the topomerization process in this compound must be observed by ^{13}C NMR spectra. To make this system amenable to ^{1}H NMR dynamic study, we designed **3** and **4**; instead of two methyl groups in **2**, **3** carries two ethyl groups and **4** a methyl group and an alkyl group.

These compounds were synthesized according to a known method shown in Scheme 1. The treatment of *o*-lithio-*N*,*N*-dialkylbenzylamines (**7**) with 9-BBN afforded the desired compounds. The point which deserves mention here is the steric effect in the preparation of the lithio compounds. The *o*-lithiation of *N*,*N*-diethylbenzylamine with butyllithium requires several days[12] although that of *N*,*N*-dialkylbenzylamine (**5**) proceeds smoothly during a day or so,[13] when one of the alkyl groups is a methyl and another in an alkyl group which has no branch at α- or β-position. For the syntheses of **3**, **4e**, **4f**, and **4h**, the corresponding lithio compounds

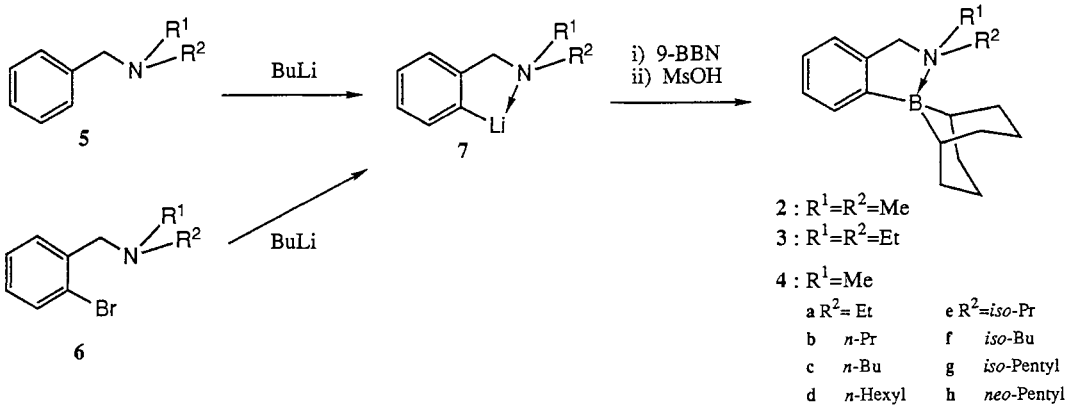

Scheme 1.

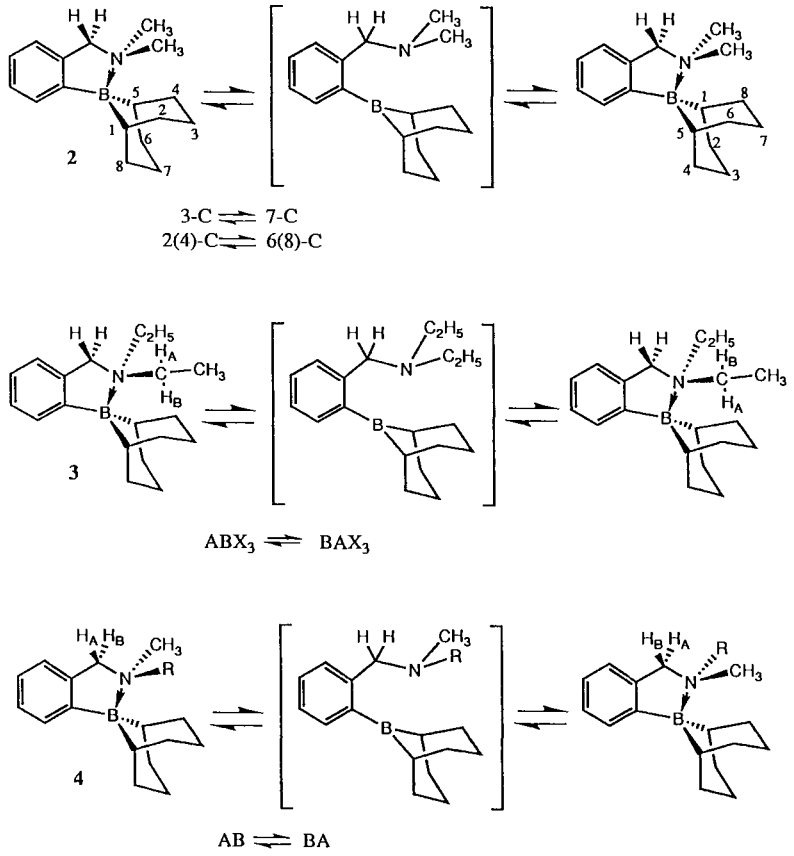

Scheme 2. Idealized topomerization processes in **2**, **3**, and **4**.

were prepared from *o*-bromo-*N*,*N*-dialkylbenzylamines (**6**) and butyllithium by the halogen–lithium exchange method,[14] because the corresponding benzylamines were too slowly lithiated under ordinary conditions.

Both ^{1}H NMR and ^{13}C NMR spectra were in conformity with the expected structure of compounds **2**, **3**, and **4**. The two methyl groups were equivalent, whereas 2(4)-C and 6(8)-C were not equivalent in **2**. Nonequivalent signals of ring carbons were reported in intermolecular 9-BBN complexes with pyridine.[15] The methylene protons in the ethyl groups were nonequivalent in **3**. Compound **4** showed nonequivalent benzylic methylene protons and other similar characteristics with those mentioned for **2**. These are in accord with the coordinated forms of these compounds.

The methylene protons in the ethyl groups in **3**, which are diastereotopic unless the dissociation of the N–B bond is too rapid on the NMR time scale, exchange their sites after the dissociation of the N–B bond followed by the nitrogen inversion and recoordination. Similarly, the benzylic methylene protons in compound **4** satisfy the requirement as a probe. Idealized topomerization processes in these compounds are shown in Scheme 2.

^{11}B NMR signals of these compounds were observed at 9.5 ppm (**2**), 10.5 ppm (**3**), and 9.3 ppm (**4a**) with reference to BF_3:OEt_2, these shifts being in accord with those in other trialkylborane–amine complexes[15,16] and being at higher fields by ca. 70 ppm relative to the nitrogen-free borane (cf. 9-phenyl-9-BBN; 80.35 ppm).[17] Such a high field shift of a coordinated tetrahedral boron compared with a trivalent one was reported in similar compounds.[8,17]

Kinetic Parameters for Topomerization in 2 and 3. The methylene protons of the ethyl group in compound **3** showed broad signals at room temperature and they became sharp (AB part of the ABX_3 system) at −20 °C. ^{13}C NMR signals due to the carbons at 2(4)-C/6(8)-C exhibited line broadening at room temperature as well. The total line shape analyses of these spectra afforded kinetic parameters for the topomerization shown in Table 1. We could also obtain the kinetic parameters for **2** by taking advantage of the diastereotopic carbon pairs, carbons at 3-C/7-C and 2(4)-C/6(8)-C. The data are also compiled in Table 1.

Several points of interest can be mentioned here. Firstly, both compounds **2** and **3** give much higher barriers to the topomerization than **1**. As expected, the N–B coordination in borane–amine complexes is stronger than that in boronate–amine complexes, although the steric effects could reverse the situation. The result can be well explained by the enhanced Lewis acidity of the boron atom. Secondly, the entropy of activation is large, positive in every case. This value is typical, when the ground state possesses the ionic character which is reduced at the transition state, and is often observed in the dissociation of coordination bonds. The dissociation in borane–amine complexes is no exceptions. Thirdly, there is no concentration effect on the kinetic parameters for the topometrization. Therefore we can compare the parameters obtained in different concentrations directly.

Mechanism of Topometization in 3. The free energies of activation for the topomerization obtained from the proton and the carbon probes in **3** are significantly different, the proton probe giving a 1.2 kcal mol^{-1} higher barrier than the carbon probe (Table 1). We wish to explain the result in the following way.

The site exchange of the methylene protons takes place after dissociation of the N–B bond followed by inversion of the nitrogen atom (and then rotation about an N–C bond) and recombination to form the N–B bond. Thus the difference in barriers obtained by the two probes suggests that the nitrogen inversion requires additional energy after the N–B bond dissociation and that the rate-limiting step is the nitrogen inverstion rather than the N–B bond dissociation.

Nitrogen inversion in *N*,*N*-dialkylbenzylamine complexes was reported to be much faster than the N–M bond scission in boronate–amine complex (**1**)[1] and tertiary amine hydrogen chlorides.[18] Barriers to nitrogen inversion in *N*,*N*-dialkylamines are relatively high (ca. 11 kcal mol^{-1}), although inversion in open-chain amines generally requires lower activation energy than this value.[19] Therefore, unless otherwise affected, nitrogen inversion in general should exhibit lower barriers than the N–B bond dissociation.

However, the nitrogen inversion in compound **3** is specifically affected by the steric effects. The nitrogen inversion is effected by either displacing one of the ethyl groups to the position where the lone pair electrons has occupied before inversion, or by true inverstion of the nitrogen. The latter seems too much energy-requiring because the two ethyl groups which change their posi-

Table 1. Kinetic Parameters for the Topomerization in **2** and **3** in Toluene-d_8[a]

Compound	Probe	$\Delta H^{\neq}$/kcal mol^{-1}	$\Delta S^{\neq}$/cal mol^{-1} K^{-1}	$\Delta G^{\neq}_{323}$/kcal mol^{-1}	r[b]
2	^{13}C	23.7±0.5	16.6±1.4	18.3	0.9996
3	^{13}C	18.9±0.5	14.9±1.6	14.1	0.9997
3	^{1}H	22.8±1.7	23.1±5.6	15.3	0.9991
3	^{1}H[c]	23.0±1.1	24.0±3.4	15.3	0.9992

a) 1 cal=4.184 J. Concentration ca. 200 mmol dm^{-3} unless otherwise mentioned. b) Correlation coefficient. c) Concentration 31 mmol dm^{-3}.

tions will strongly interact with the 9-BBN moiety. Even the former, however, suffers from the steric hindrance of the 9-BBN group because one of the ethyl groups must come very close to the 9-BBN during the site exchange. It may be argued that the nitrogen inversion can take palce after rotation about the benzyl carbon-to-nitrogen bond. This process, however, also requires much energy because the two ethyl groups interfere strongly with the 9-BBN group during the rotation, if nitrogen inversion does not take place.

On the other hand, the site-exchange of the ring carbons is caused by rotation of the C_{Ph}–B bond after the N–B bond dissociation. If the rotation about the bond in question is much faster than the dissociation, the rate-limiting step should be the latter process and the rates of topomerization should be equal to half of the rates of the N–B bond dissociation. Although it is difficult to conclude which is faster by the data presented in this paper, the following paper[20] provides a clue for the diagnosis.

In the paper, dissociation of an S–B bond and sulfur-inversion in a similar complex are discussed. The sulfur-inversion is a faster process than the rotation about the C_{Ph}–B bond. The free energy of activation for the rotation is ca. 12.5 kcal mol^{-1}. Because of the similar steric situations in both compound **3** and the sulfur compoud, in which a lone-pair electron lobe directs toward the 9-BBN group, we may take the activation energy for the sulfur compound as an approximate value for the rotation of the 9-BBN group in **3**. Since this value is well below the activation energy for the topomerization obtained with the carbon probe, we may now conclude that the activation energy obtained with the carbon probe is indeed that of the N–B bond scission.

It is tempting to consider that the entropy of activation observed by the carbon probes are larger, positive than that observed by the proton probe because freedom increases in the transition state for the nitrogen inversion. Although it is difficult to justify or to exclude the possibility that the transition state structure for the nitrogen inversion is such that rotation about the benzylic carbon-to-nitrogen bond takes place to some extent with simultaneous partial exchange of the positions of the ethyl group and the N-lone pair electrons, the results clearly show that nitrogen inversion is a slower process than the N–B bond dissociation.

We conclude that the proton probes and the carbon ones give information on different processes in this molecule: the carbon probes give information on the N–B bond dissociation and the proton probe that on nitrogen inversion. Unfortunately, the information on the nitrogen inversion cannot be quantitative becaues the process is influenced by the N–B bond dissocaiton. This is clear from the entropy of activation for the nitrogen inversion which is large positive. Independent nitrogen inversion is known to show near-zero entropy of activation.[19]

Steric Effects on Rates of Topomerization. The free energy of activation in the dimethyl compound (**2**) was ca. 4 kcal mol^{-1} higher than that in the diethyl compound (**3**), as is revealed by comparison of kinetic parameters obtained by the carbon probes (Table 1). The reduction of the barrier height in **3** is attributed to the steric effect (F-strain).[21] This phenomenon was also observed in the boronate–amine system **1** and the difference in the free energies of activation between the dimethyl and the diethyl compounds was 1.5 kcal mol^{-1}.[1] The more bulky the borane in borane–amine complexes, the more important the F-strain. The result presented here is in accord with this generalization because 9-BBN is a very bulky group.[22]

To get further insight into the steric effects of *N*-alkyl groups on the topomerization, the kinetic parameters for compound **4** were similarly determined. The bezylic methylene protons were used as a probe in unsymmetrical compounds **4**, the carbon probe (3-C/7-C) being also used for **4a** for comparison. The kinetic data thus obtained are listed in Table 2.

Compounds **4a–d**, which possess a methyl group and a straight chain alkyl group, give almost the same barriers to the topomerization. This is reasonable becasue the steric effects on the stability of the ground state is given by the first methylene group which is attached to the nitrogen and those methylene groups in β- and farther positions will direct away from the boron to minimize the steric effects. In addition, the basicity of

Table 2. Kinetic Parameters for the Topomerization of Benzylic Methylene Protons in **4** in Toluene-d_8

Compound	$\Delta H^{\neq}$/kcal mol^{-1}	$\Delta S^{\neq}$/cal mol^{-1} K^{-1}	$\Delta G^{\neq}_{323}$/kcal mol^{-1}	k_{323}/s^{-1}	r
4a	24.5±0.5	18.9±1.2	18.4	2.4	0.9997
4a[a]	20.1±1.1	10.8±3.2	16.6	38	0.9993
4b	25.1±0.4	21.8±1.1	18.0	4.3	0.9998
4c	24.7±0.3	21.0±0.9	18.2	3.4	0.9999
4d	25.0±0.4	21.0±1.0	18.2	3.3	0.9998
4e	20.4±0.3	19.3±1.1	14.1	1900	0.9998
4f	23.4±0.4	22.7±1.2	16.1	86	0.9998
4g	24.8±0.6	20.3±1.7	18.2	3.1	0.9996
4h	19.8±0.5	20.4±1.8	13.2	8000	0.9995

a) Obtained from carbon probes in the 9-BBN group.

the amines is not affected appreciably by the chain-length of the alkyl group. Although this situation should affect the entropy of the ground state and consequently the entropy of activation in principle, it does not increase the entropy of activation to a significant extent as is seen in Table 2.

Comparison of free energies of activation for compounds **2**, **3**, and **4a**, obtained with the proton and carbon probes provides other points of interest. On one hand, compound **4a** shows medium barrier height among the compunds, when they are determined with carbon probes. This means the steric effects of the alkyl groups on the amino-nitrogen is significant. On the other hand, if the barrier is determined with proton probes, **4a** gives a higher barrier than that obtained with the carbon probes. This will mean that the steric effects given by a methyl group on inversion of the amine after the N–B bond dissociation is strong enough to make the barrier significantly higher than that for the N–B bond dissociation.

In **4e–g** bearing an isoalkyl group, the free energy of activation decreases in the order **4g**>**4f**>**4e**. Apparently branching at the α-position of the alkyl group which is attached to the nitrogen has a very large effect which lowers the barrier hight. Branching at the β-position has a small effect but that at farther positions inserts little effect on the N–B bond scission. In order to see the effect of further branching at the β-position of the alkyl group, we introduced a neopentyl group. As is seen in Table 2, compound **4h** shows the lowest barrier to the N–B bond dissociation among the compounds examined. This type of steric effects are known as γ-effect in ^{13}C NMR spectroscopy[23] and this is the manifestation of the similar effect in kinetics. The series of compounds **4e**—**4h** together with **4a**—**4d** constitute clear examples which show that destabilization of the ground state without affecting the transition state significantly indeed lowers the barrier to dissociation.

Solvent Effects on Topomerization in 3 and 4a. Kinetic parametrs for the topomeization in **3** and **4a**, determined for solutions of various solvents, are listed in Tables 3 and 4, respectively. Solvents are arranged in the order of their dielectric constants in these tables.

There are unambiguous solvent effects on the rates of topomerization; the more polar the solvent, the larger the free energy of activation at 323 K. The free energy of activation obtained in cyclohexanes, typical nonpolar solvents, are ca. 2 kcal mol^{-1} smaller than those obtained

Table 3. Solvent Effect on Kinetic Parameters for the Topomerization of the Methylene Protons in the Ethyl Groups in **3**

Solvent	$\Delta H^{\neq}$/kcal mol^{-1}	$\Delta S^{\neq}$/cal mol^{-1}K^{-1}	$\Delta G^{\neq}_{323}$/kcal mol^{-1}	k_{323}/s^{-1}	r
$C_6D_{11}CD_3$[a]	22.4±0.7	24.7±2.3	14.4	1280	0.9995
$C_6D_5CD_3$	23.0±1.1	24.0±3.4	15.3	320	0.9992
$(C_2D_5)_2O$	23.9±0.6	28.3±1.9	14.8	680	0.9997
$CDCl_3$	24.1±0.4	27.6±1.2	15.2	360	0.9998
C_6D_5Cl	25.7±0.8	31.8±2.5	15.5	230	0.9996
THF-d_8	22.9±0.3	22.1±0.7	15.7	155	0.9999
$C_2D_2Cl_4$[b]	21.7±0.6	18.2±1.7	15.8	145	0.9997
CD_2Cl_2	22.5±0.7	21.4±2.1	15.6	185	0.9997
$(CD_3)_2CO$	22.0±0.4	18.6±1.3	16.0	105	0.9998
CD_3NO_2	24.4±0.8	24.6±2.4	16.5	47	0.9995
CD_3CN	27.1±0.8	33.5±2.4	16.3	67	0.9997
DMF-d_7	22.1±0.6	17.9±1.9	16.3	59	0.9997

a) Methylcyclohexane-d_{14}. b) 1,1,2,2-Tetrachloroethane-d_2.

Table 4. Solvent Effect on Kinetic Parameters for the Topomerization of the Benzylic Methylene Protons in **4a**

Solvent	$\Delta H^{\neq}$/kcal mol^{-1}	$\Delta S^{\neq}$/cal mol^{-1} K^{-1}	$\Delta G^{\neq}_{323}$/kcal mol^{-1}	k_{323}/s^{-1}	r
C_6D_{12}[a]	23.0±0.3	16.9±0.8	17.6	8.5	0.9999
$C_6D_{11}CD_3$[b]	22.7±0.4	15.8±1.0	17.6	8.5	0.9998
C_6D_6	24.7±0.7	19.3±2.0	18.5	2.1	0.9997
$C_6D_5CD_3$	24.5±0.4	18.9±1.2	18.4	2.4	0.9997
$CDBr_3$	24.9±0.5	19.0±1.2	18.7	1.5	0.9998
C_6D_5Cl	25.0±0.3	19.8±0.8	18.6	1.7	0.9999
$C_2D_2Cl_4$[c]	25.5±0.2	20.9±0.6	18.8	1.3	0.9999
Pyridine-d_5	23.4±0.4	14.3±1.2	18.7	1.5	0.9998
$C_6D_5NO_2$	26.6±0.3	22.1±0.8	19.4	0.48	0.9999
CD_3NO_2	26.7±0.9	21.9±2.3	19.6	0.38	0.9996
CD_3CN	28.0±0.6	26.2±1.6	19.5	0.42	0.9998
DMF-d_7	24.2±0.8	15.3±1.4	19.2	0.65	0.9997
DMSO-d_6	25.5±0.5	18.0±1.2	19.7	0.35	0.9998

a) Cyclohexane-d_{12}. b) Methylcyclohexane-d_{14}. c) 1,1,2,2-Tetrachloroethane-d_2.

in polar solvents. Though the proton probes afford the barrier to nitrogen inverstion, it is not separated from the barrier to the bond dissociation and thus the solvent affects the activation parameters. We attribute the results to the stabilization of the ground state in polar solvents. Since the N–B coordination bond is polar, the ground state is more polar than the transition state in the topomerization process. A polar solvent stabilizes the ground state better than the transition state by solvation: Consequently, the barrier to the topomerization is enhanced in the polar solvent.

Similar solvent effects were observed in the boronate–amine complexes (**1a**).[1] Some irregularities, however, existed in rates of dissociation in **1a**. Oxygen-contatining solvents, especially ethers, gave larger rate constants than that expected from their polarity. We postulated that the dissociation of the N–B bond was assisted by solvent molecules in these solvents (S_N2 type dissociation). Such irregularities are insignficant in **3** and **4a**. This difference can be ascribed to the steric environments of the boron atoms. Back-side approach of the solvent molecules to the boron atom is unfavorable in **3** and **4a** because of the bulkiness of the substituents on the boron atom in the 9-BBN group: They resemble the *t*-alkyl case in S_N2 reactions.

The kinetic parameters in **4a** could be obtained even in pyridine-d_5, which is well known to be a good donor, and the rates are normal on the stand point of expectation from its polarity. This result also suggests that solvent polarity rather than nucleophilicity of solvent molecules plays important role in the dissociation processes. Although methanol-d_4 and acetic acid-d_4 were used for a solvent, these solvent were unsuitable for a solvent because of reaction with the complexes.

Experimental

Melting points are uncorrected. Elemental analyses were performed on a Perkin–Elmer 240C analyzer. High resolution mass spectra were measured with a JEOL JMS-DX303 spectrometer. Silica gel used for column chromatography was Wako-gel C-200. *N,N*-Dimethylbenzylamine (Tokyo Kasei Co.) and a THF solution of 9-BBN (Aldrich Chemical Co.) were commercially available. *N*-Alkyl-*N*-methylbenzylamines[24] and *o*-bromo-*N*-alkyl-*N*-methylbenzylamines[14] were prepared according to known methods and these amines were distilled before use. Deuterated solvents for NMR measurements were purchased from Aldrich Chemical Co., E. Merck, or MSD ISOTOPES.

General Procedure for the Syntheses of Compound 2,3, and 4. For the preparation of an *o*-lithio-*N,N*-dialkylbenzylamine solution in ether, *N,N*-dialkylbenzylamines were used for the case of **2**, **4a**—**d**, and **4g** (Method A) and *o*-bromo-*N,N*-dialkylbenzylamines were used for others (Method B).

Method A. To a solution of an *N,N*-dialkylbenzylamine (20 mmol) in 30 ml of dry ether was added 13 ml (20 mmol) of a 1.5 mol dm^{-3} hexane solution of butyllithium at −78 °C under a nitrogen atmosphere. The mixture was allowed to stand until the temperature became ambient and stirred for another 12 h at the temperature. The mixture was slowly transferred to 40 ml of a 0.50 mol dm^{-3} THF solution of 9-BBN and stirred for 10 min at room temperature. To the reaction mixture cooled to 0 °C, 1.3 ml (20 mmol) of methanesulfonic acid was added. Then white precipitate was formed with evolution of hydrogen gas. After the gas evolution ceased, the reaction mixture was stirred for 1 h at room temperature and filtered with a glass filter. The filtrate was evaporated under reduced pressure and the residue was extracted with 30 ml of ether for three times. The combined extracts were evaporated and the crude material was purified by recrystallization from hexane–ether and/or chromatography on silica gel (eluent: hexane).

Method B. To a solution of an *o*-bromo-*N,N*-dialkylbenzylamine (20 mmol) in 40 ml of dry ether was added 13 ml (20 mmol) of 1.5 mol dm^{-3} hexane solution of butyllithium at −78 °C under a nitrogen atmosphere. The mixture was allowed to stand until the temperature became ambient and stirred for another hour at the temperature. The solution was slowly transferred to 40 ml of a 0.50 mol dm^{-3} THF solution of 9-BBN. The following procedures are the same as in Method A.

9-[2-(Dimethylaminomethyl)phenyl]-9-borabicyclo[3.3.1]nonane (2). **2** was obtained in 45% yield. Mp 124.5—126.0 °C. Found: C, 80.10; H, 10.41; N, 5.45%. Calcd for $C_{17}H_{26}NB$: C, 80.01; H, 10.27; N, 5.49%. ^{1}H NMR ($CDCl_3$) δ=0.90 (2H, m), 1.60—1.76 (6H, m,) 1.89—2.30 (6H, m), 2.70 (6H, s), 3.96 (2H, s), 7.02 (1H, m), 7.09 (1H, dt, *J*=1.3 and 7.4 Hz), 7.18 (1H, m), 7.68 (1H, d, *J*=7.4 Hz). ^{13}C NMR ($CDCl_3$)[25] δ=21.9 (br), 23.7 and 23.9 (3-C/7-C), 30.4 and 33.6(2(4)-C/6(8)-C), 49.1, 69.7, 121.2, 124.6, 126.2, 133.3, 138.0. ^{11}B NMR ($CDCl_3$) δ=9.5.

9-[2-(Diethylaminomethyl)phenyl]-9-borabicyclo[3.3.1]nonane (3). **3** was obtained in 17% yield. Mp 122.0—125.0 °C (with decomp). Found: C, 80.34; H, 10.84; N, 4.95%. Calcd for $C_{19}H_{30}NB$: C, 80.56; H, 10.68; N, 4.95%. ^{1}H NMR ($CDCl_3$) δ=0.93 (2H, br s), 1.12 (6H, t, *J*=7.2 Hz), 1.5—2.4 (12H, br m), 3.08—3.27 (4H, br m), 4.01 (2H, s), 7.01 (1H, d, *J*=7.5 Hz), 7.07 (1H, dt, *J*=1.0 and 7.4 Hz), 7.16 (1H, dt, *J*=1.0 and 7.4 Hz), 7.66 (1H, d, *J*=7.5 Hz). ^{13}C NMR ($CDCl_3$)[25] δ=10.9, 22.7 (br), 23.7, 31.1 and 34.0 (br, 2(4)-C/6(8)-C), 51.6, 61.5, 120.6, 124.5, 125.9, 132.7, 138.8. ^{11}B NMR ($CDCl_3$) δ=10.5.

9-[2-(Ethylmethylaminomethyl)phenyl]-9-borabicyclo[3.3.1]-nonane (4a). **4a** was obtained in 17% yield. Mp 144.5—147.0 °C (with decomp). Found: C, 80.27; H, 10.61; N, 5.18%. Calcd for $C_{18}H_{28}NB$: C, 80.30; H, 10.48; N, 5.20%. ^{1}H NMR ($CDCl_3$) δ=0.90 (1H, br s), 0.96 (1H, br s), 1.19 (3H, t, *J*=7.3 Hz), 1.57—1.73 (6H, m), 1.89—2.37 (6H, m), 2.60 (3H, s), 3.20 (2H, q, *J*=7.3 Hz), 3.87 and 4.04 (2H, ABq, *J*=13.3 Hz), 7.03 (1H, d, *J*=7.5 Hz), 7.09 (1H, dt, *J*=1.0 and 7.2 Hz), 7.18 (1H, t, *J*=7.2 Hz), 7.69 (1H, d, *J*=7.2Hz). ^{13}C NMR ($CDCl_3$)[25] δ=8.0, 22(br), 23.6 and 23.9 (3-C/7-C), 30.4, 30.7, 33.6, 34.1, 42.9, 52.5, 63.4, 121.3, 124.6, 126.2, 133.4, 138.0. ^{11}B NMR ($CDCl_3$) δ=9.3.

9-[2-(Methylpropylaminomethyl)phenyl]-9-borabicyclo[3.3.1]-nonane (4b). **4b** was obtained in 23% yield. Mp 111.0—113.0 °C (with decomp). Found: C, 80.79; H, 10.97; N, 4.94%. Calcd for $C_{19}H_{30}NB$: C, 80.56; H, 10.68; N, 4.95%. ^{1}H NMR ($CDCl_3$) δ=0.93 (3H, t, *J*=7.2 Hz), 0.95 (2H, br m), 1.50—1.77 (8H, m), 1.89—2.38 (6H, m), 2.63 (3H, s), 3.03 (2H, m), 3.90 and 4.07 (2H, ABq, *J*=13.4 Hz), 7.01 (1H, d,

Table 5. Temperature Dependence of the Chemical Shift Difference, Coupling Constant, and T_2 of Methylene Protons in Ethyl Groups in Compound **3**

Solvent	Correlation[a]		Coupling constant/Hz			T_2/s
	$\Delta\nu_{AB}$/Hz	$\Delta\nu_{AX}$/Hz	J_{AX}	J_{BX}	J_{AB}	
$C_6D_{11}CD_3$[b]	$-0.148t+25.9$	$-0.145t+846.2$	7.2	7.5	−13.3	0.15
$C_6D_5CD_3$	$-0.145t+21.0$	$+0.167t+845.0$	7.2	7.4	−13.4	0.20
$C_6D_5CD_3$[c]	$-0.123t+21.4$	$+0.155t+844.8$	7.2	7.4	−13.4	0.18
$(C_2D_5)_2O$	$-0.210t+32.2$	$-0.146t+844.0$	7.2	7.3	−13.3	0.19
$CDCl_3$	$-0.162t+32.6$	$-0.135t+834.9$	7.2	7.4	−13.4	0.21
C_6D_5Cl	$-0.142t+24.8$	$-0.090t+838.3$	7.2	7.4	−13.3	0.16
THF-d_8	$-0.203t+39.1$	$-0.214t+854.7$	7.2	7.4	−13.2	0.23
$C_2D_2Cl_4$[d]	$-0.184t+35.9$	$-0.145t+832.2$	7.1	7.3	−13.5	0.16
CD_2Cl_2	$-0.155t+33.2$	$-0.180t+842.8$	7.3	7.3	−13.3	0.21
$(CD_3)_2CO$	$-0.155t+41.5$	$-0.244t+857.2$	7.2	7.4	−13.2	0.25
CD_3NO_2	$-0.151t+40.8$	$-0.228t+862.5$	7.2	7.3	−13.3	0.19
CD_3CN	$-0.139t+38.1$	$-0.235t+859.6$	7.2	7.4	−13.3	0.16
DMF-d_7	$-0.124t+41.5$	$-0.201t+853.3$	7.2	7.4	−13.3	0.20

a) $\Delta\nu$/Hz$=xt/°C+y$. Spin A in the ABX_3 system represents the methylene signals in lower magnetic field. b) Methylcyclohexane-d_{14}. c) Concentration 200 mmol dm^{-3}. d) 1,1,2,2-Tetrachloroethane-d_2.

J=7.2 Hz), 7.08 (1H, dt, J=1.1 and 7.4 Hz), 7.18 (1H, t, J=7.0 Hz), 7.69 (1H, d, J=7.5 Hz).

9-[2-(Butylmethylaminomethyl)phenyl]-9-borabicyclo[3.3.1]-nonane (4c). **4c** was obtained in 15% yield. Mp 113.5—117.0 °C (with decomp). Found: C, 80.63; H, 11.04; N, 4.70%. Calcd for $C_{20}H_{32}NB$: C, 80.80; H, 10.85; N, 4.71%. ^{1}H NMR ($CDCl_3$) δ=0.90 (1H, br s), 0.96 (3H, t, J=7.4 Hz), 1.0 (1H, br s), 1.32 (2H, sextet, J=7.4 Hz), 1.48—1.73 (8H, m), 1.90—2.38 (6H, m), 2.62 (3H, s), 3.08 (2H, m), 3.89 and 4.07 (2H, ABq, J=13.7 Hz), 7.02 (1H, d, J=7.5 Hz), 7.08 (1H, dt, J=1.0 and 7.5 Hz), 7.18 (1H, t, J=7.5 Hz), 7.69 (1H, d, J=7.5 Hz).

9-[2-(Hexylmethylaminomethyl)phenyl]-9-borabicyclo[3.3.1]-nonane (4d). **4d** was obtained in 14% yield. Mp 78.0—79.5 °C. Found: C, 81.40; H, 11.42; N, 4.35%. Calcd for $C_{22}H_{36}NB$: C, 81.22; H, 11.15; N, 4.31%. ^{1}H NMR ($CDCl_3$) δ=0.83—0.98 (5H, m), 1.22—1.38 (6H, m), 1.46—1.75 (8H, m), 1.89—2.38 (4H, m), 2.61 (3H, s), 3.07 (2H, m), 3.88 and 4.07 (2H, ABq, J=13.4 Hz), 7.02 (1H, d, J=7.2 Hz), 7.08 (1H, dt, J=1.0 and 7.4 Hz), 7.18 (1H, dt, J=1.0 and 7.4 Hz), 7.69 (1H, d, J=7.2 Hz).

9-[2-(Isopropylmethylaminomethyl)phenyl]-9-borabicyclo-[3.3.1]nonane (4e). **4e** was obtained in 13% yield. Mp 114.0—119.0 °C (with decomp). Found: C, 80.40; H, 10.94; N, 5.17%. Calcd for $C_{19}H_{30}NB$: C, 80.56; H, 10.68; N, 4.95%. ^{1}H NMR ($CDCl_3$, r.t.) δ=0.7—2.6 (20H, br m), 2.76 (3H, s), 3.58 (1H, septet, J=6.5 Hz), 3.8—4.2 (2H, br), 6.96 (1H, d, J=7.5 Hz), 7.05 (1H, dt, J=1.4 and 7.4 Hz), 7.14 (1H, t, J=7.4 Hz), 7.59 (1H, d, J=7.4 Hz). ($CDCl_3$, −20 °C) δ=0.78 (1H, br s), 0.86 (3H, d, J=6.5 Hz), 1.09 (1H, br s), 1.24 (3H, d, J=6.5 Hz), 1.50—2.18 (10H, m), 2.48—2.62 (2H, m), 2.78 (3H, s), 3.59 (1H, septet, J=6.5 Hz), 3.91 and 4.12 (2H, ABq, J=14.5 Hz), 7.00 (1H, d, J=7.5 Hz), 7.08 (1H, dt, J=1.0 and 7.5 Hz), 7.17 (1H, t, J=7.5 Hz), 7.60 (1H, d, J=7.5 Hz).

9-[2-(Isobutylmethylaminomethyl)phenyl]-9-borabicyclo[3.3.1]-nonane (4f). **4f** was obtained in 8% yield. Mp 118.0—121.0 °C (with decomp). Found: C, 80.99; H, 11.10; N, 4.70%. Calcd for $C_{20}H_{32}NB$: C, 80.80; H, 10.85; N, 4.71%. ^{1}H NMR ($CDCl_3$) δ=0.92 (2H, br s), 0.99 (3H, d, J=6.8 Hz), 1.07 (3H, d, J=6.8 Hz), 1.45—2.40 (13H, br m), 2.67 (3H, s), 2.94 and 3.01 (2H, AB part of ABX system, J_{AB}=14.1 Hz, J_{AX}=J_{BX}=4.8 Hz), 3.96 and 4.08 (2H, ABq, J=13.3 Hz), 7.01 (1H, d, J=7.5 Hz), 7.08 (1H, dt, J=1.0 and 7.2 Hz), 7.18 (1H, dt, J=0.7 and 7.4 Hz), 7.68 (1H, d, J=7.2 Hz).

Table 6. Temperature Dependence of the Chemical Shift Difference, Coupling Constant, and T_2 of Benzylic Methylene Protons in Compound **4**

Compound	Solvent	$\Delta\nu_{AB}$/Hz[a]	J_{AB}/Hz	T_2/s
4a	C_6D_{12}[b]	$-0.243t+71.7$	−13.0	0.19
4a	$C_6D_{11}CD_3$[c]	$-0.252t+72.3$	−13.0	0.20
4a	C_6D_6	$-0.337t+82.9$	−13.5	0.19
4a	$C_6D_5CD_3$	$-0.272t+73.8$	−13.3	0.21
4a	$CDBr_3$	$-0.153t+67.3$	−13.4	0.18
4a	C_6D_5Cl	$-0.233t+72.2$	−13.4	0.19
4a	$C_2D_2Cl_4$[d]	$-0.165t+73.1$	−13.6	0.18
4a	Pyridine-d_5	$-0.179t+68.7$	−13.7	0.22
4a	$C_6D_5NO_2$	$-0.129t+65.1$	−13.8	0.17
4a	CD_3NO_2	$-0.118t+68.6$	−13.9	0.20
4a	CD_3CN	$-0.129t+66.1$	−13.9	0.18
4a	DMF-d_7	$-0.121t+63.0$	−13.9	0.20
4a	DMSO-d_6	$-0.132t+62.4$	−13.9	0.18
4b	$C_6D_5CD_3$	$-0.203t+74.4$	−13.4	0.19
4c	$C_6D_5CD_3$	$-0.272t+91.4$	−13.3	0.20
4d	$C_6D_5CD_3$	$-0.239t+84.4$	−13.5	0.18
4e	$C_6D_5CD_3$	$-0.041t+39.5$	−14.5	0.18
4f	$C_6D_5CD_3$	$+0.142t+39.0$	−13.5	0.18
4g	$C_6D_5CD_3$	$-0.333t+105.4$	−13.4	0.18
4h	$C_6D_5CD_3$	$+0.175t+107.3$	−13.4	0.14

a) Chemical shift differences between AB signals: $\Delta\nu_{AB}$/Hz$=xt/°C+y$. b) Cyclohexane-d_{12}. c) Methylcyclohexane-d_{14}. d) 1,1,2,2-Tetrachloroethane-d_2.

9-[2-(Isopentylmethylaminomethyl)phenyl]-9-borabicyclo-[3.3.1]nonane (4g). **4g** was obtained in 35% yield. Mp 103.0—105.0 °C. Found: C, 81.09; H, 11.12; N, 4.71%. Calcd for $C_{21}H_{34}NB$: C, 81.02; H, 11.01; N, 4.50%. ^{1}H NMR ($CDCl_3$) δ=0.90 (1H, br s), 0.93 (3H, d, J=6.2 Hz), 0.94 (3H, d, J=6.2 Hz), 0.97 (1H, br s), 1.40—1.78 (9H, m), 1.90—2.23 (5H, m), 2.30—2.42 (1H, m), 2.59 (3H, s), 3.13 (2H, m), 3.86 and 4.07 (2H, ABq, J=13.5 Hz), 7.02 (1H, d, J=7.2 Hz), 7.08

(1H, dt, J=1.0 and 7.2 Hz), 7.18 (1H, t, J=7.2 Hz), 7.69 (1H, d, J=7.2 Hz).

9-[2-(Methylneopentylaminomethyl)phenyl]-9-borabicyclo-[3.3.1]nonane (4h). **4h** was obtained in 2% yield. Mp 106.0—111.0 °C (with decomp). Found: M^+ 311.2820. Calcd for $C_{21}H_{34}N^{11}B$: M^+ 311.2785. ^1H NMR ($CDCl_3$, r.t.) δ=0.94 (2H, br s), 1.18 (9H, s), 1.35—2.40 (12H, br m), 2.71 (3H, s), 2.8—3.5 (2H, br), 3.9—4.5 (2H, br), 7.01 (1H, d, J=7.2 Hz), 7.09 (1H, dt, J=0.7 and 7.2 Hz), 7.18 (1H, t, J=7.2 Hz), 7.68 (1H, d, J=7.2 Hz). ($CDCl_3$, −20 °C) δ=0.85 (1H, br s), 1.04 (1H, br s), 1.19 (9H, s), 1.50—2.22 (10H, m), 2.35—2.52 (2H, m), 2.70 (3H, s), 2.96 and 3.36 (2H, ABq, J=14.4 Hz), 4.11 and 4.33 (2H, ABq, J=13.7 Hz), 7.06 (1H, d, J=7.2 Hz), 7.13 (1H, dt, J=1.0 and 7.2 Hz), 7.21 (1H, t, J=7.2 Hz), 7.70 (1H, d, J=7.2 Hz).

NMR Measurement and Line Shape Analysis. ^1H and proton-decoupled ^{13}C NMR spectra were measured on a JEOL GSX-400 spectrometer operating at 399.8 MHz and 100.5 MHz, respectively. Temperature were calibrated using the chemical shift differences of methanol and ethylene glycol. Unless otherwise mentioned the concentration of the solution was ca. 30 and 200 mmol dm^{-3} for ^1H and ^{13}C NMR measurement, respectively. The FID data were accumulated more than 8 times for ^1H and more the 100 times for ^{13}C. The line

Table 7. Rate Constants of Topomerization Obtained from Proton Probes in Compounds **3** and **4**

Compound	Solvent	k/s^{-1} (temperature/°C)
3	$C_6D_{11}CD_3$[a]	6.0(8.0), 11.2(12.0), 19.8(16.0), 33.5(20.0), 54(24.0), 88(28.0), 155(32.0), 265(36.0)
3	$C_6D_5CD_3$	7.4(19.9), 12.5(23.8), 20.5(27.8), 34(32.0), 58(36.0), 78(38.0), 102(40.0)
3	$C_6D_5CD_3$[b]	7.7(20.0), 14.2(26.5), 26.5(30.0), 51(35.0), 98(40.0)
3	$(C_2D_5)_2O$	6.7(15.0), 9.5(17.6), 13.5(20.0), 18.8(22.5), 27.5(25.0), 39(27.5), 56(30.0), 80(33.0)
3	$CDCl_3$	3.9(16.1), 7.2(20.0), 13.0(24.1), 22.0(28.0), 38(32.0), 63(36.0), 100(40.0), 172(44.0), 290(48.0), 410(50.8)
3	C_6D_5Cl	6.5(24.0), 11.6(28.0), 20.0(32.0), 34.5(36.0), 60(40.0), 102(43.5), 160(47.0)
3	THF-d_8	3.6(19.9), 6.3(23.9), 10.8(28.1), 18.0(32.0), 29.2(36.0), 47(39.9), 76(44.0), 125(48.0), 195(52.0)
3	$C_2D_2Cl_4$[c]	7.2(24.0), 11.5(28.0), 17.8(32.0), 29.5(36.0), 47(39.9), 74(44.0), 115(47.9), 160(50.7)
3	CD_2Cl_2	4.7(19.9), 7.8(24.0), 12.8(28.0), 21.6(32.0), 31.5(35.0), 47(38.1), 66(40.9)
3	$(CD_3)_2CO$	4.7(24.0), 8.0(28.0), 12.8(32.0), 21.0(36.0), 34.5(40.0), 53(44.0), 82(48.0)
3	CD_3NO_2	4.7(32.0), 8.5(36.0), 12.6(40.0), 22.5(43.9), 37.0(48.1), 60(52.0), 98(56.0), 150(59.9)
3	CD_3CN	5.2(31.9), 9.8(36.1), 16.2(40.0), 31.0(44.1), 54(48.1), 88(52.0), 145(56.0)
3	DMF-d_7	4.4(28.0), 7.3(32.0), 12.4(36.0), 18.8(40.0), 29.5(43.9), 46(47.9), 75(52.0)
4a	C_6D_{12}[d]	8.5(50.1), 13.5(54.0), 20.8(58.0), 31(62.0), 48(66.0), 74(70.0), 110(74.0), 160(78.0), 235(82.0)
4a	$C_6D_{11}CD_3$[a]	8.8(50.0), 13.2(54.0), 20.2(58.0), 31(62.0), 46.5(66.0), 70(70.0), 106(74.0), 155(78.0), 230(82.0)
4a	C_6D_6	4.0(55.1), 6.7(60.0), 10.6(64.0), 17.2(68.0), 26.5(72.0), 39.5(76.0), 58(79.5)
4a	$C_6D_5CD_3$	7.8(60.3), 11.9(64.1), 19.2(68.1), 29.8(72.2), 47(76.2), 68(80.2), 102(84.0), 148(88.1), 220(92.1), 310(96.2)
4a	$CDBr_3$	8.8(65.0), 14.4(69.5), 23.6(74.0), 34.5(78.0), 54(81.9), 82(85.9), 120(90.0), 175(94.0)
4a	C_6D_5Cl	8.8(64.0), 13.6(68.0), 21.2(72.0), 33.5(76.0), 50(80.0), 75(83.9), 115(88.0), 168(92.0), 240(96.0)
4a	$C_2D_2Cl_4$[c]	8.0(65.0), 13.8(69.5), 22.4(74.0), 34.5(78.0), 53(82.0), 80(86.0), 118(90.0), 175(93.9), 260(97.9)
4a	Pyridine-d_5	7.1(64.0), 10.4(68.0), 15.6(72.0), 23.4(76.0), 31.5(78.9), 42.0(82.0), 63(85.9), 170(97.0)
4a	$C_6D_5NO_2$	5.6(70.0), 9.8(74.9), 16.6(79.5), 27.6(84.0), 41.5(88.0), 64(91.9), 95(96.0), 140(100.0), 205(104.0)
4a	CD_3NO_2	4.7(69.9), 7.7(74.9), 13.8(80.0), 23.8(85.0), 42.0(90.0), 62(93.9), 94(97.9)
4a	CD_3CN	5.0(69.0), 7.4(72.0), 10.2(74.9), 14.6(77.9), 18.4(79.9), 24.2(82.3), 31(84.3)
4a	DMF-d_7	6.4(70.0), 9.5(74.0), 14.0(78.0), 21.2(82.0), 30.2(86.0), 45.5(90.0), 69(94.0), 98(97.9), 140(101.9)
4a	DMSO-d_6	6.3(75.0), 10.4(79.5), 16.8(84.0), 25.6(88.0), 37.5(91.9), 55(95.9), 82(100.0), 115(104.0)
4b	$C_6D_5CD_3$	7.7(55.0), 14.6(60.0), 22.4(63.9), 35(67.9), 54(71.9), 86(75.9), 128(80.0), 190(84.0), 295(88.0)
4c	$C_6D_5CD_3$	5.9(55.0), 11.0(60.0), 17.5(63.9), 27.2(67.9), 41(71.9), 64(75.9), 95(79.9), 150(84.5), 235(89.0), 370(93.8)
4d	$C_6D_5CD_3$	6.0(55.1), 11.2(60.0), 17.8(64.0), 28.0(68.0), 42.5(72.0), 66(76.0), 102(80.0), 145(84.0), 220(88.0), 330(91.9)
4e	$C_6D_5CD_3$	6.1(1.8), 11.0(6.0), 19.5(10.0), 32(14.0), 52.5(18.1), 83(22.0), 135(26.0), 215(29.9), 350(33.9)
4f	$C_6D_5CD_3$	7.4(30.0), 12.1(33.9), 19.5(38.0), 33.0(42.0), 55(46.0), 86(50.0), 135(53.9), 210(57.9)
4g	$C_6D_5CD_3$	8.8(59.0), 14.3(63.0), 23.4(67.0), 36.5(71.0), 56(75.0), 83(79.0), 124(82.9), 180(87.0), 290(91.9)
4h	$C_6D_5CD_3$	5.6(−10.1), 9.6(−6.0), 18.5(−2.0), 32(1.9), 57(6.0), 95(10.0), 155(14.0), 230(17.9), 380(22.0), 610(26.0)

a) Methylcyclohexane-d_{14}. b) Concentration 200 mmol dm^{-3}. c) 1,1,2,2-Tetrachloroethane-d_2. d) Cyclohexane-d_{12}.

shape analysis was performed using DNMR3K program.[36] The coupling constants and chemical shift differences of exchanging nuclei were checked at several points where the exchange was negligibly slow. The coupling constants were constant throughout the temperature ranges. The chemical shift differences were linearly correlated with temperature. T_2 values were estimated from the line width of exchanging signals at the slow exchange limit. For the simulation of methylene protons of ethyl groups in **3**, the calculations were performed only for the AB part in the $ABX_3 \rightleftarrows BAX_3$ system. The benzylic methylene protons in **4** were simulated as the $AB \rightleftarrows BA$ system. These parameters are listed in Tables 5 and 6. The rate contants are compiled in Table 7.

The line shape analyses for compound **2** were performed by using ^{13}C NMR signals due to 3-C/7-C and 2(4)-C/6(8)-C as the $A \rightleftarrows X$ exchange. Input parameters and rate constants follow: 3-C/7-C: $\Delta\nu$=0.037 t+24.5 Hz, T_2 0.30, 030 s. 2(4)-C/6(8)-C: $\Delta\nu$=−0.071 t+329.1 Hz, T_2 0.36, 0.38 s. Rate constant k/s^{-1} (temperature/°C): 5.0(55.0), 8.5(60.0), 15.6 (65.0), 25(69.9), 40(75.0), 64(79.9), 110(84.9), 190(89.9), 300(95.0), 450(99.9), 1000(109.8) in toluene-d_8.

The carbon signals in **3** and **4a** observed in toluene-d_8 were similarly analyzed. **3** 2(4)-C/6(8)-C: $\Delta\nu$=0.135 t+285.5 Hz; T_2 0.19, 0.20 s; k/s^{-1} (temperature/°C): 49(14.9), 90(20.0), 165(25.0), 280(30.0), 470(35.0), 740(40.0), 1950(49.6). **4a** 3-C/7-C: $\Delta\nu$=29.2 Hz (constant); T_2 0.20, 0.21 s; k/s^{-1} (temperature/°C): 13.5(39.8), 22.5(45.0), 37(50.1), 50(52.9), 65(55.1), 100(60.0).

^{11}B NMR spectra were measured on the same spectrometer operating at 128.2 MHz at room temperature. The chemical shifts were recorded relative to BF_3:OEt_2 used as an external reference.

This work was supported by Grants-in-Aid for Fundamental Scientific Research Nos. 02230108 and 01740320 from the Ministry of Education, Science and Culture. The 400 MHz NMR and mass spectra were measured at the Analytical Center in Okayama University of Science.

References

1) For part XVII of the series, see S. Toyota and M. Ōki, *Bull. Chem. Soc. Jpn.*, **63**, 1168 (1990).
2) M. Ōki, *Pure Appl. Chem.*, **61**, 699 (1989).
3) M. Ōki, "Applications of Dynamic NMR Spectroscopy to Organic Chemistry," VCH Publishers, Deerfield Beach (1985).
4) "Dynamic Nuclear Magnetic Reasonance Spectroscopy," ed by L. M. Jackman and F. A. Cotton, Academic Press, New York (1975).
5) G. van Koten and J. G. Noltes, *J. Am. Chem. Soc.*, **98**, 5393 (1976).
6) R. J. P. Corriu, G. Royo, and A. de Saxcè, *J. Chem. Soc., Chem., Commun.*, **1980**, 892; R. J. P. Corriu, A. Kpoton, M. Poirier, G. Royo, and J. Y. Corey, *J. Organomet, Chem.*, 277, C25 (1984).
7) A. H. Cowley and J. L. Mills, *J. Am. Chem. Soc.*, **91**, 2911 (1969); H. Kessler, G. Zimmermann, H. Fietza, and H Möhrle, *Chem. Ber.*, **111**, 2605 (1978).
8) T. Burgemeister, R. Grobe-Einsler, R. Grotstollen, A. Mannschreck, and G. Wulff, *Chem. Ber.*, **114**, 3403 (1981).
9) For example see, J. T. B. H. Jastrzebski, G. van Koten, D. G. Tuck, H. A. Meinema, and J. G. Noltes, *Organometallics*, **1**, 1492 (1982).
10) J. D. Odom, "Comprehensive Organometallic Chemistry," ed by G. Willkinson, F. G. A. Stone, and E. W. Abel, Pergamom, Oxford (1982), Vol. 1, pp. 298—301.
11) E. Kalbarczyk and S. Pasynkiewicz, *J. Organomet. Chem.*, **262**, 11 (1984).
12) M. Ōki and M. Ohira, *Bull. Chem. Soc. Jpn.*, **57**, 3117 (1984).
13) F. N. Jones, M. F. Zinn, and C. R. Hauser, *J. Org. Chem.*, **28**, 663 (1963); F. N. Jones, R. L. Vaulx, and C. R. Hauser, *J. Org. Chem.*, **28**, 3461 (1963).
14) F. N. Jones and C. R. Hauser, *J. Org. Chem.*, **27**, 4389 (1962).
15) H. C. Brown and J. A. Soderquist, *J. Org. Chem.*, **45**, 846 (1980).
16) R. G. Kidd, "NMR of Newly Accessible Nuclei," ed by P. Laszlo, Academic Press, New York (1983), Vol. 2, pp. 49—60; H. Nöth and B. Wrackmeyer, *Chem. Ber.*, **107**, 3070 (1974).
17) E. Kalbarczyk and S. Pasynkiewicz, *J. Organomet. Chem.*, **292**, 119 (1985).
18) T. Morita and M. Ōki, *Bull, Chem. Soc. Jpn.*, **61**, 1185, (1988).
19) J. B. Lambert, *Top, Stereochem.*, **6**, 19 (1971); Ref. 3, Chap. 5.
20) S. Toyota and M. Ōki, *Bull. Chem. Soc. Jpn.*, **64**, 1563 (1991).
21) H. C. Brown, *J. Am. Chem. Soc.*, **67**, 378, 1452 (1945).
22) H. C. Brown, E. F. Knights, and C. G. Scouten, *J. Am. Chem. Soc.*, **96**, 7765 (1974).
23) For example see, E. Breitmaier and W. Voelter, "Carbon-13 NMR Spectroscopy," VCH Publishers, New York (1987), p. 115.
24) E. Wedekind and F. Ney. *Chem. Ber.*, **45**, 1298 (1912).
25) The signal due to *ipso* carbon attached to the boron atom was not observed.
26) A Modified version of the DNMR3 program[27] by Dr. H. Kihara of Hyogo University of Teacher Education.
27) G. Binsh, *Top. Stereochem.*, **3**, 97 (1968).

Dynamic NMR as a Nondestructive Method for the Determination of Rates of Dissociation. XIX. Sulfur Inversion in 9-[2-(Ethylthiomethyl)phenyl]-9-borabicyclo[3.3.1]nonane Proceeds via Dissociative Mechanism[1)]

Shinji TOYOTA and Michinori ŌKI*
Department of Chemistry, Faculty of Science, Okayama University of Science, Ridaicho, Okayama 700
(Received January 7, 1991)

Kinetic parameters for sulfur inversion in the title compound were determined by the dynamic NMR method in CD_2Cl_2 as follows: $\Delta H^{\neq}$ 14.2±0.1 kcal mol^{-1}, $\Delta S^{\neq}$ 11.3±0.3 cal mol^{-1} K^{-1}, $\Delta G^{\neq}_{233}$ 11.6 kcal mol^{-1}. The large and positive entropy of activation suggests that the inversion takes place through dissociative mechanisms. Comparison of the rate constants obtained with multiple probes shows that the rotation about the C_{Ph}–B bond requires further energy after the dissociation of the S–B bond. The solvent effect on the sulfur inversion is small but distinct; the more polar a solvent, the higher the barrier to the inversion. Dynamic behaviors of a related compound are also discussed.

Although inversion at a trivalent sulfur atom is one of the interesting phenomena in stereochemistry, there have been few general methods to investigate mechanisms of the inversion. Dynamic NMR spectroscopy was found to be a useful technique in studying sulfur inversion, especially in coordination compounds.[2,3)] Recently, we reported sulfur inversion in sulfonium salts,[4)] thioether–Lewis acid complexes,[5)] and platinum(II) complexes[6)] by the use of this method. These results are generalized that entropy of activation ($\Delta S^{\neq}$) is a convenient guide for diagnosing the mechanisms of sulfur inversion: Entropy of activation is large positive if the bond dissociation is the rate-limiting step (dissociative mechanism), whereas it is nearly zero if sulfur inversion takes place without bond scission (pyramidal inversion).

An organostannane compound **1** was one of the examples in the former case, but analogous boron compound **2** failed to show dynamic processes even at −90 °C due to low barrier to the S–B bond dissociation.[5)] Many of organoboron–thioether adducts were known to be unstable because of the weak basicity of the sulfur atom toward the boron atom.[7)] We expected that introduction of a boron atom bearing two alkyl groups should enhance S–B bond energy with respect to the boronate S–B bond. Our recent work revealed that the boron atom in 9-borabicyclo[3.3.1]-9-nonyl (9-BBN) group, which has unusual stability as a diakylboryl group,[8)] was a stronger Lewis acid toward amine ligands than that in boronates.[1,9)] We decided to use this boron atom as an acceptor and chose 9-[2-(ethylthiomethyl)phenyl]-9-BBN (**3**) for our study on the dissociation of the S–B bond.

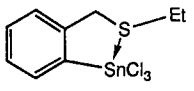

1

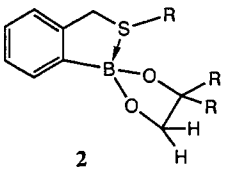

2
R=H or Me

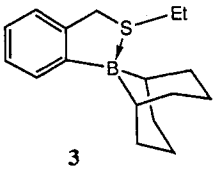

3

We have been interested in solvent effects on the rates of sulfur inversion as well. The barriers for the inversion in platinum(II)–thioether complexes are independent of solvents, in which the sulfur inverts without bond dissociation.[6)] On the other hand, there is no available information about solvent effects in dissociative mechanisms. Polar solvents decelerate the dissociation of coordination bonds involving a boron atom from our experiences[1,9)] and the same effects are expected in the dissociation of the S–B bond. In order to make the relationship between the inversion mechanism and solvent effects clear, we observed inversion processes of compound **3** in various solvents.

Results and Discussion

Synthesis and NMR Spectra of 3. Compound **3** was prepared in a modified procedure of the known method for the syntheses of 9-aryl-9-BBN's[10)] shown in Scheme 1. A solution of ethyl *o*-lithiobenzyl sulfide (**5**), prepared from 1-bromo-2-(ethylthiomethyl)benzene (**4**) and butyllithium, was treated with 9-BBN followed by methanesulfonic acid to give an oily mixture containing the desired compound. The reaction products were separated by HPLC and subsequent recrystallization afforded **3** in 19% yield as white crystals, which were air stable and soluble in ordinary organic solvents.

Other three products were identified as **6** (39%), **7** (7%), and **8** (4%) from their NMR and mass spectra: Compound **6** is a hydrolysis product of **5** and compounds **7** and **8** are butylated products of **3** and **6**, respectively. We believe that compounds **7** and **8** are formed in the following way. The benzylic protons in **3** and **6** are firstly lithiated by lithium hydride that results

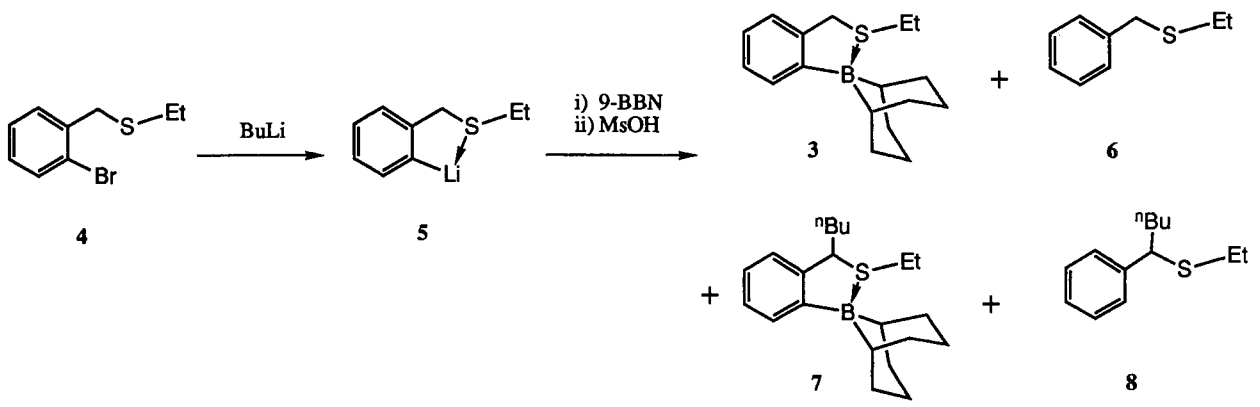

Scheme 1.

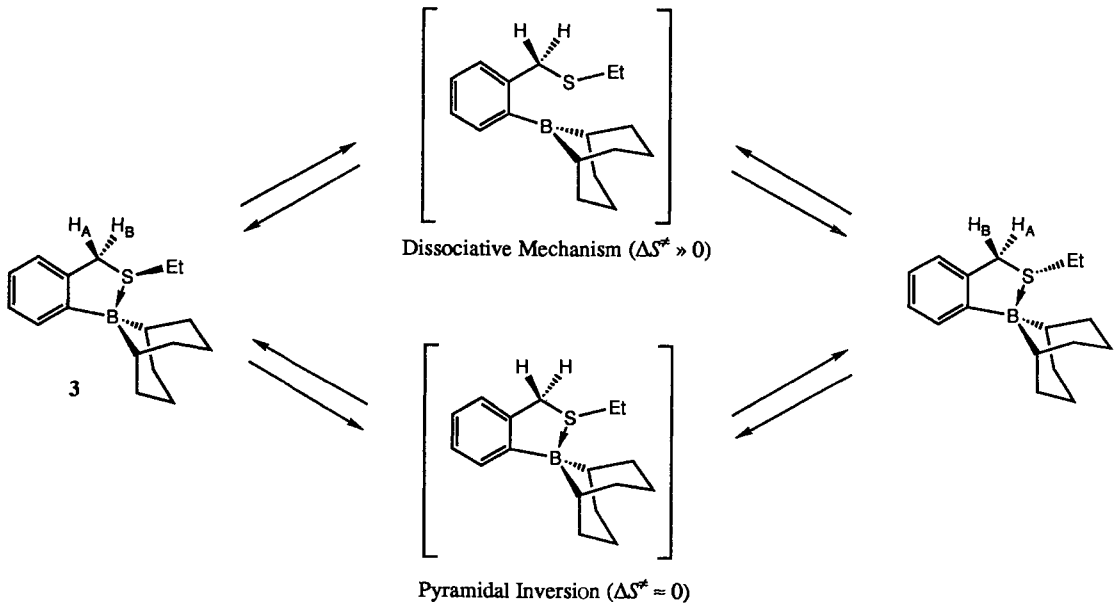

Scheme 2. Possible mechanisms for the sulfur inversion in compound **3**.

from treatment of **5** with 9-BBN, although it is difficult to rule out that other lithium species react with them because various lithium sources may exist in the reaction mixture. Then butyl bromide derived from butyllithium attacks the benzylic positions to form compounds **7** and **8**. Prolonged stirring before the addition of methanesulfonic acid increased yields of the butylated compounds; this fact supports the mechanisms mentioned above.

Compound **3** possesses some diastereotopic pairs of protons and carbons which exchange their sites on the topomerization shown in Scheme 2. The benzylic methylene protons exhibited a sharp singlet at room temperature. With lowering the temperature, the signal began to broaden and became an AB quartet signal at −70 °C in CD_2Cl_2. Other proton signals except for the aromatic and the methyl ones also exhibited line shape changes in the temperature range. Carbon signals due to the 9-BBN group were broad even at room temperature and separated into eight signals at −70 °C. These observations suggests that the sulfur atom coordinates to the boron atom in **3** at low temperatures. The sulfur inversion takes place faster than the NMR time scale at room temperature and this process is frozen at −70 °C.

The chemical shift of ^{11}B NMR (**3**: 14.4 ppm) supports a coordinated structure as well. This value is typical for a tetrahedral boron and at a higher field than those in trialkylboranes.[11] The high field shifts caused by sulfur coordinations were observed in 9-halo-9-BBN complexes with dimethyl sulfide relative to free 9-halo-9-BBN's.[12]

Kinetic Parameters and Mechanism of Sulfur Inversion. We firstly selected benzylic methylene protons as a probe for the observation of dynamic processes at the

sulfur atom. Altough the methylene protons in the ethyl group also seemed to satisfy the requirement as a probe, we excluded them because of overlapping of the signals with those of the ring protons. The total line shape analyses were carried out with the use of DNMR3K program[13] and observed and simulated NMR signals for the benzylic methylene protons are shown in Fig. 1. Eyring plot of rate constants thus obtained affords kinetic parameters for the topomerization (Table 1).

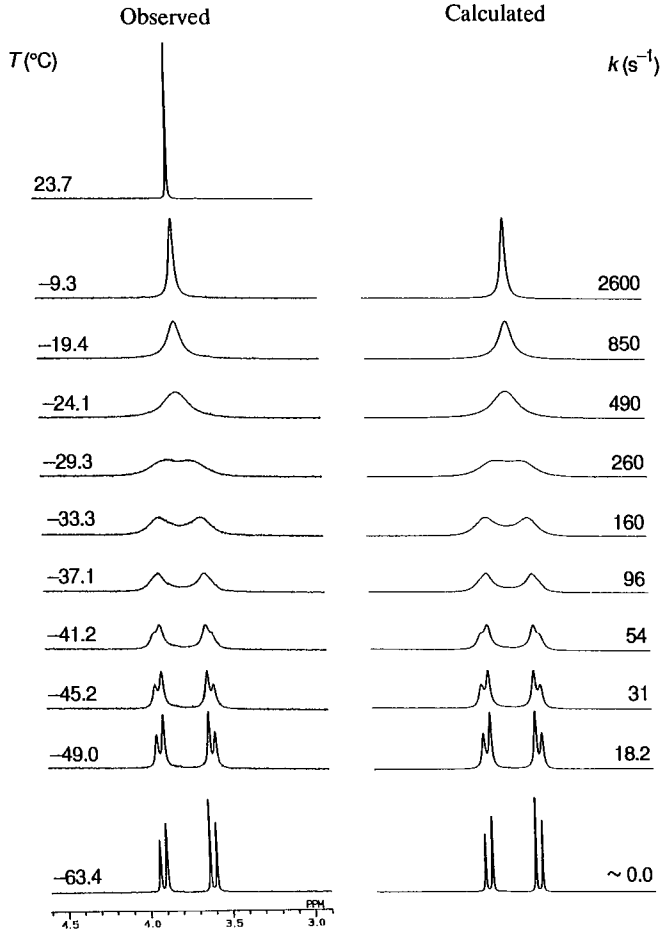

Fig. 1. Observed (solvent CD_2Cl_2) and calculated (DNMR3K program) line shapes for the benzylic methylene protons in compound **3**.

Entropy of activation is large positive as is expected for the dissociative mechanism, in which the ground state is ionic and the transition state is less ionic. Consequently, the dissociation of the S–B bond is the rate-limiting step for the topomerization of the benzylic methylene protons and the topomerization completes after the recombination from another side to form an S–B bond (Scheme 2). Strictly speaking, the rate constants of the topomerization should be doubled when we take account of the dissociation of the S–B bond. The dissociated sulfur atom recoordinates to the boron atom at the same site or at the other site with the same probabilities.

The S–B bond in **3** is more than 3 kcal mol^{-1} stronger than those in boronates (**2**)[15] and ca. 4 kcal mol^{-1} weaker than that in 3,3,4,4-tetramethylthiolane-boron tribromide complex.[5] These results are consistent with the general order of Lewis acidity of the boron atom: trihaloborane>trialkylborane>boronate.[7]

We have reported that, in platinum(II)-thioether complexes, the sulfur inversion takes place without scission of the Pt–S bond.[6] The results reported here contrast in the mechanisms of inversion. In the case of platinum, the pπ–dπ interaction is possible to stabilize the planar transition state for inversion. In the case of boron, the d-orbitals are of so high energy that such an interaction to stabilize the planar transition state for inversion is not effective. These differences must be responsible to the difference in the mechanisms of the sulfur inversion.

Comparison of Kinetic Parameters Obtained from Multiple Probes. We could also obtain kinetic parameters for the topomerization from diastereotopic proton and carbon pairs in the 9-BBN moiety in dichloromethane-d_2, these data being compiled in Table 1. Three probes that follow were used other than the benzylic methylene proton probe: The protons and carbons at 1,5-positions (1,5-H and 1,5-C) and the carbons at 3,7-positions (3,7-C) in the 9-BBN group.

The rate constants obtained from 3,7-C are ca. 7 times smaller than that obtained from the benzylic methylene proton probe. Namely, the topomerization observed by 3,7-C probe requires additional energy, 0.9 kcal mol^{-1}, compared with the latter probe. The site

Table 1. Kinetic Parameters for the Topomerization Obtained with Multiple Probes in Compound **3**[a]

Probe	$\Delta H^{\neq}$	$\Delta S^{\neq}$	$\Delta G^{\neq}_{233}$	k_{233}	r[b]
	kcal mol^{-1}	cal mol^{-1} K^{-1}	kcal mol^{-1}	s^{-1}	
^{1}H CH_2[c]	14.2±0.1	11.3±0.4	11.6	65	0.9999
^{1}H CH_2[c,d]	14.3±0.3	11.9±1.3	11.6	64	0.9998
^{1}H 1,5-*H*			11.5 (245 K)[e]		
^{13}C 3,7-*C*	15.3±0.8	11.9±3.2	12.5	8.7	0.9993
^{13}C 1,5-*C*			11.5 (249 K)[e]		

a) 1 cal=4.184 J. Concentration ca. 40 and ca. 400 mmol dm^{-3} for ^{1}H and ^{13}C probes, respectively, unless otherwise mentioned. b) Correlation coefficient. c) Benzylic methylene protons. d) Concentration 400 mmol dm^{-3}. e) $\Delta G^{\neq}$ at coalescence temperature (T_c) obtained by the coalescence method.

Table 2. Solvent Effects on the Kinetic Parameters for the Topomerization of Benzylic Methylene Protons in Compound **3**

Solvent	ε[a)]	$\Delta H^{\neq}$	$\Delta S^{\neq}$	$\Delta G^{\neq}_{233}$	k_{233}	r
		kcal mol^{-1}	cal mol^{-1} K^{-1}	kcal mol^{-1}	s^{-1}	
$C_6D_{11}CD_3$[b)]	2.02	13.5±0.3	9.4±1.2	11.3	129	0.9997
Toluene-d_8	2.38	14.3±0.3	11.4±0.9	11.7	54	0.9998
$(C_2D_5)_2O$	4.20	15.1±0.4	15.1±1.0	11.6	61	0.9998
THF-d_8	7.58	14.7±0.2	11.9±0.7	11.9	31	0.9999
CD_2Cl_2	8.93	14.2±0.1	11.3±0.4	11.6	65	0.9999
Acetone-d_6	20.56	14.5±0.3	11.4±0.9	11.8	42	0.9998
DMF-d_7	36.71	14.6±0.2	10.6±0.8	12.2	20	0.9999

a) Dielectric constants for non-deuterated solvents from Ref. 20. b) Methylcyclohexane-d_{14}.

exchange of 3,7-C requires bond rotaion about the C_{Ph}–B as well as the dissociation of the S–B bond. Although the sulfur inversion without the S–B bond breakage might explain the discrepancy of the rates, this process is eliminated from being the course for the observed topomerization because the inversion took place in dissociative mechanisms as judged from the value of entropy of activation mentioned above. On a steric point of view, pyramidal inversion seems to be an unfavorable process; steric hindrance between the 9-BBN group and the ethyl group must be serious at the transition state for the pyramidal inversion.

The differences in the rates are due to hindered rotation about the C_{Ph}–B bond after the dissociation of the S–B bond. Thus the rate-limiting step for the exchange of 3,7-C is the C–B bond rotation rather than the S–B bond dissociation. A 9-BBN group, in which wing protons overhang outside, is known to be bulky and its bulkiness is superior to that of a *t*-butyl group. It is probable that the rotation about the C_{Ph}–B bond is slow though there is no report on restricted rotation in an *o*-substituted 9-aryl-9-BBN.

The kinetic parameters for the exchanges of 1,5-H and 1,5-C were only determined by the coalescence method because their signals were very broad owing to spin-spin couplings with ^{10}B and ^{11}B. Both of the free energies of activation at the coalescence temperature are almost the same as that obtained from the benzylic methylene probe. This result is natural if one considers the topomerization mechanism; the site exchange of 1,5-positions completes by the sulfur inversion regardless of the C–B bond rotation.

Solvent Effects on the Dissociation of S–B Bond. The rates of dissociation in various solvents are listed in Table 2. As expected, an increase in solvent polarity tends to decelerate the dissociation of the S–B bond. The same effect in N–B bond dissociation has been explained on the basis of better stabilization of the polar ground state in polar solvents than the less polar transition state.[1,9] It is reasonable to assume that this explanation is also the case for the S–B bond dissociation.

A careful comparison of the rate constants shows that the solvent effect on the S–B bond dissociation in **3** is smaller than that on the N–B bonds: a relative rate constant in methylcyclohexane-d_{14} and DMF-d_7, k(methylcyclohexane-d_{14})/k(DMF-d_7), is 6.5 in **3**, whereas it is 22 in 9-[2-(diethylaminomethyl)phenyl]-9-BBN (**9**).[1] The small solvent effect can be interpreted in terms of polarity of a coordination bond. Since an S–B bond is less ionic than an N–B bond, the solvation which stabilizes the ground state in the dissociation process is less important in the S–B bond case than that in the N–B. Anyway, there are unambiguous solvent effects on the dissociation of the S–B bond.

In contrast, there are little solvent effects on the sulfur inversion in platinum(II)–thioether complexes, in which the inversion took place without bond dissociation.[6] Therefore, solvent effects can be a clue to distinguish the two mechanisms of sulfur inversion; presence of solvent effects described above in the dissociative mechanism and absence of solvent effect in the pyramidal inversion. It is necessary to evaluate the solvent effects carefully because the difference in rate constants tend to be small in the dissociative mechanism.

Solvent assisted dissociation (S_N2 type dissociation) is observed for the N–B bond dissociation in an amine–boronate complex.[9] This assistance seems to be improbable in the 9-BBN system, compound **3** as well as **9**, due to steric hindrance of the bicyclic frame work. The rate constants of the dissociation obtained in donor solvents, diethyl-d_{10} ether, THF-d_8, and DMF-d_7, are not apart from those expected from their polarities. This finding supports the non-assisted dissociation mechanism.

Dynamic Behaviors in 7. The structural feature and some dynamic behaviors of the by-product **7** are also interesting. The structure was determined from its NMR and mass spectra (M^+ 328), these data suggesting existence of an extra butyl group compared with the structure of **3**. Since this compound has a chiral center at the benzylic carbon, two diastereomers should exist if the dissociation of S–B bond is negligibly slow.

The NMR spectra observed at various temperature exhibited line shape changes. This compound gave broad proton and carbon signals in the aliphatic region

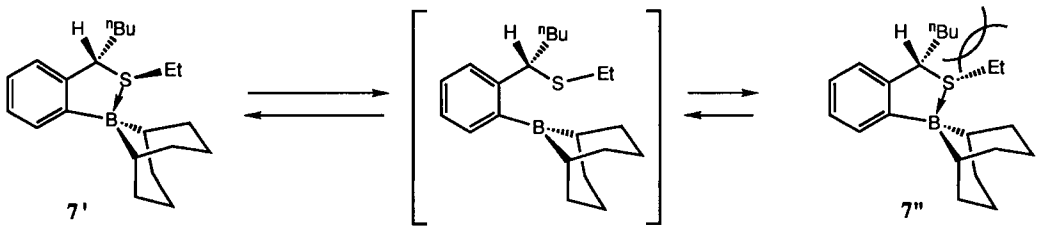

Scheme 3. Topomerization process between diastereomers in compound 7.

at room temperature and these signals became sharp at −40 °C. These dynamic processes are also caused by the S–B bond dissociation shown in Scheme 3.

The NMR spectrum observed at −40 °C where the dynamic process is virtually frozen suggests that this compound exist in two forms, the major isomer being in 97% and the minor in 3% from integrated intensities of signals due to the benzylic methine proton. We assume that 7′ should be the major isomer because another isomer 7″, in which the butyl group and the ethyl are eclipsing, is sterically unfavorable. The population of the isomers shows that the major form is more stable by 1.6 kcal mol^{-1} than the minor one. The carbon signals observed at −40 °C are in accord with the structure of 7′.

The signals due to the benzylic methine proton showed line broadening at 0 °C and this change is interpreted in terms of the interconversion between the two isomers. Roughly estimated free energy of activation for the isomerization is 12 kcal mol^{-1} from the major isomer to the minor. This barrier is comparable to that for the S–B bond dissociation in **3**. This is in accord with the idea that the S–B bond scission is the rate-limiting step for the diastereomerization.

Experimental

Melting points are uncorrected. Silica gel 60 (Merck, 70—230 mesh) and Silica gel 60 F_{254} (Merck, 0.25 mm) were used for column and thin-layer chromatography, respectively. Preparative HPLC was carried out with a Hitachi L-6250 intelligent pump using a Chemcosolb Si column (5 μ, 25 mmϕ×500 mm). Elemental analyses were performed by a Perkin-Elmer 240C analyser. Mass spectra were measured with a JEOL JMS-DX303 spectrometer.

NMR Measurement and Line Shape Analysis. ^{1}H and ^{13}C NMR spectra were measured on a JEOL GSX-400 spectrometer operating at 399.8 MHz and 100.5 MHz, respectively. Temperatures were calibrated with a methanol sample. The concentration of the solution was ca. 40 mmol dm^{-3} and ca. 400 mmol dm^{-3} for ^{1}H and ^{13}C NMR measurement, respectively. The line shape analysis was performed by DNMR3K program.[13] Coupling constants and chemical shift differences were measured at several points where rates were almost zero. The chemical shift differences were linearly correlated with temperature, but the coupling constants were constant at every temperature. Spin–spin relaxation times (T_2) were estimated from the line width of exchanging signals at the slow exchange limit and line shapes of non-exchanging signals at the temperature where the exchange takes place. Input parameters for the simulation for the benzylic methylene protons (AB⇄BA) are listed in Table 3. The analyses for the carbon probe (3,7-C) were performed similarly under the A⇄X exchanging system with the use of the following parameters: $\Delta\nu$=54.5 Hz, T_2=0.17 s. The rate constants obtained are shown in Table 4. The barrier for the topomerization of 1,5-H and 1,5-C were determined by the coalescence method. The coalescence temperatures (T_c) and chemical shift differences ($\Delta\nu$) are −28±1 °C and 129.6 Hz for the 1,5-H and −24±1 °C and 201.0 Hz for the 1,5-C probe, respectively.

Table 3. Temperature Dependence of the Chemical Shift Difference, Coupling Constant, and T_2 of Benzylic Methylene Protons in Compound **3**

Solvent	$\Delta\nu_{AB}$/Hz[a]	J_{AB}/Hz[b]	T_2/s[c]
$C_6D_{11}CD_3$	0.609t+187.2	−15.9	0.14—0.16
Toluene-d_8	205.9[e]	−16.3	0.14—0.15
$(C_2D_5)_2O$	0.626t+156.3	−16.3	0.11—0.13
THF-d_8	0.594t+100.1	−16.2	0.13—0.16
CD_2Cl_2	0.323t+140.3	−16.4	0.18—0.19
CD_2Cl_2[d]	0.365t+142.6	−16.4	0.14—0.16
Acetone-d_6	0.486t+76.5	−16.4	0.17—0.18
DMF-d_7	0.246t+59.3	−16.5	0.13—0.16

a) Chemical shift differences between benzylic methylene protons (AB signal): $\Delta\nu_{AB}$/Hz=xt/°C+y. b) Coupling constants between A and B protons. These were constant throughout the temperature range. c) Spin-spin relaxation times for the signals. d) Concentration ca. 400 mmol dm^{-3}. e) Constant throughout the temperature range.

^{11}B NMR spectra were measured on the JEOL GSX-400 spectrometer with a multinuclear tunable probe operating at 128.2 MHz. The chemical shifts are given to an external BF_3:OEt_2 (δ=0) reference.

9-[2-(Ethylthiomethyl)phenyl]-9-borabicyclo[3.3.1]nonane (3). To a solution of 3.34 g (14.4 mmol) of 1-bromo-2-(ethylthiomethyl)benzene[17] in ether (20 ml) was added 9.25 ml (14.4 mmol) of a 1.5 mol dm^{-3} hexane solution of butyllithium at −30 °C under a nitrogen atmosphere. The mixture was allowed to warm up to 0 °C and added to 28.8 ml (14.4 mmol) of a 0.5 mol dm^{-3} THF solution of 9-borabicyclo[3.3.1]nonane (Aldrich Co. Inc.) at 0 °C during the course of 1 min. Immediately after the addition, methanesulfonic acid (1.39 g, 14.4 mmol) was added at 0 °C and the mixture was stirred for 1 h at room temperature. The precipitate was filtered off by a glass filter and the filtrate was evaporated under reduced pressure. The residue was chromatographed on silica gel with hexane to give 2.34 g of a nonpolar mixture (colorless oil),

Table 4. Rate Constants of Topomerization Obtained with the Proton Probe (Benzylic Methylene Protons) in Compound **3**

Solvent	k/s^{-1} (temperature/°C)
$C_6D_{11}CD_3$	20.5 (−53.7), 39 (−49.1), 70 (−44.2), 135 (−39.6), 215 (−35.7), 350 (−31.8), 610 (−27.4), 1000 (−23.0), 1800 (−18.0)
Toluene-d_8	16.8 (−48.2), 34.0 (−43.3), 67 (−38.3), 135 (−33.4), 240 (−28.3), 440 (−23.4), 830 (−18.5), 1450 (−13.5), 2400 (−8.4)
$(C_2D_5)_2O$	13.2 (−50.3), 22.5 (−46.3), 44 (−42.3), 87 (−37.8), 162 (−33.3), 300 (−28.3), 580 (−23.4), 1050 (−18.5), 1850 (−13.4), 3500 (−8.5)
THF-d_8	9.8 (−48.0), 19.0 (−43.4), 41.0 (−38.2), 78 (−33.4), 145 (−28.4), 270 (−23.4), 560 (−17.4), 1600 (−8.4)
CD_2Cl_2	18.2 (−49.0), 31.0 (−45.2), 54 (−41.2), 96 (−37.1), 160 (−33.3), 260 (−29.3), 490 (−24.1), 850 (−19.4), 2600 (−9.3)
CD_2Cl_2[a]	10.6 (−52.2), 28.0 (−45.9), 58.5 (−40.8), 118 (−35.7), 225 (−30.6), 425 (−25.4), 750 (−20.3)
CD_2Cl_2[b]	8.0 (−40.8), 18 (−35.7), 37 (−30.6), 70 (−25.4), 125 (−20.3), 400 (−10.2)
Acetone-d_6	6.8 (−52.7), 12.8 (−48.2), 22.1 (−44.3), 39.0 (−40.3), 68 (−36.3), 122 (−32.0), 220 (−27.5), 440 (−21.4), 920 (−15.5)
DMF-d_7	11.8 (−43.4), 23.5 (−38.9), 42.5 (−34.5), 78 (−29.8), 135 (−25.4), 230 (−21.0), 390 (−16.5), 650 (−11.9)

a) Concentration ca. 400 mmol dm^{-3}. b) Obtained with the carbon probe (3,7-C).

which consisted of four major products (R_f=0.42, 0.38, 0.36, and 0.31. eluent: hexane) and other minor products. The fractions containing the desired compound (R_f=0.36) were purified by HPLC (hexane as an eluent). Recrystallization from hexane-ether afforded 0.74 g (19%) of the desired compound as white crystals. Mp 116.0—118.0 °C. Found: C, 75.13; H, 9.41%; M^+, 272. Calcd for $C_{17}H_{25}BS$: C, 75.00; H, 9.26%; M^+, 272. ^1H NMR ($CDCl_3$) δ=1.00 (2H, br s), 1.28 (3H, t, J=7.4 Hz), 1.63—1.72 (2H, br m), 1.76—2.10 (10H, br m), 2.34 (2H, q, J=7.5 Hz), 3.89 (2H, s), 7.08—7.14 (2H, m), 7.19 (1H, dt, J=2.1 and 6.8 Hz), 7.69 (1H, d, J=7.5 Hz). ^{13}C NMR ($CDCl_3$)[18] δ=12.1, 23 (very broad, coupled with ^{10}B and ^{11}B), 24.1, 24.5, 32.8 (br), 37.2, 125.0, 125.1, 126.3, 132.3, 138.5. ^{11}B NMR ($CDCl_3$) δ=14.4.

Following three products were also identified.

9-[2-(1-Ethylthiopentyl)phenyl]-9-borabicyclo[3.3.1]nonane (7). **7** (R_f=0.42) was isolated by recrystallization from hexane. Yield 0.38 g (7%), mp 78.5—80.0 °C. Found: C, 76.80; H, 10.24%; M^+, 328. Calcd for $C_{21}H_{33}BS$: C, 76.81; H, 10.13%; M^+, 328. ^1H NMR ($CDCl_3$, r.t.) δ=0.94 (3H, t, J=7.4 Hz), 0.96 (2H, br), 1.32 (3H, t, J=7.5 Hz), 1.34—2.48 (19H, m), 2.53 (1H, m), 3.95 (1H, m), 7.08 (1H, d, J=7.2 Hz), 7.12 (1H, dt, J=1.0 and 7.2 Hz), 7.19 (1H, dt, J=1.4 and 7.2 Hz), 7.69 (1H, d, J=7.2 Hz). (CD_2Cl_2, −40 °C) δ=0.72 (1H, br s), 0.84 (3H, t, J=7.4 Hz), 0.93 (1H, br s), 1.24 (3H, t, J=7.4 Hz), 1.16—2.10 (18H, m), 2.33 (1H, m), 2.48 (1H, m), 3.89 (1H, dd, J=1.4 and 7.4 Hz, benzylic methine proton for the major isomer), 4.36 (br m, benzylic methine proton for the minor isomer), 6.98—7.17 (3H, m), 7.58 (1H, d, J=7.2 Hz). ^{13}C NMR ($CDCl_3$, r. t.)[18] δ=12.7, 13.9, 22.3, 24.5 (br), 25.5, 30.9, 21—38 (very broad), 56.5, 124.9, 125.0, 126.2, 132.5, 144.1. (CD_2Cl_2, −40 °C) δ=12.4, 13.9, 21.7 (br), 22.3, 24.0, 24.7, 25.4, 27.2 (br), 30.0, 30.9, 31.1, 32.9, 35.0, 37.4, 56.2, 125.0, 124.3, 126.0, 132.4, 144.3, 154.1. ^{11}B NMR ($CDCl_3$) δ=12.9. The free energy of activation for the topomerization between the two diastereomers was determined by the coalescence method with the signals due to benzylic methine protons (δ=3.89 and 4.36) in dichloromethane-d_2. The coalescence temperature was −17± 3 °C and the chemical shift difference was 184.8 Hz. The population of the minor isomer was 3.1% at −40 °C determined from the integration of the signals and the difference in free energies was 1.6 kcal mol^{-1} at the temperature. Other signals due to the minor isomer were not assigned because of various ambiguity.

Ethyl 1-Phenylpentyl Sulfide (8). **8** (R_f=0.38) was not isolated and its yield (0.13 g or 4%) was determined from the signal intensity of ^1H NMR. This compound was synthesized by another method as follows. A solution of α-lithiobenzyl ethyl sulfide (13.1 mmol) in ether (20 ml) prepared from benzyl ethyl sulfide and butyllithium in an ordinary manner was treated with 1-bromobutane (15.7 mmol) at 0 °C. Addition of 1 mol dm^{-3} HCl (20 ml) gave the desired sulfide (2.39 g, 87%) together with recovered benzyl ethyl sulfide (0.17 g, 9%). Bp 92—94 °C/0.4 mmHg (1 mmHg=133.322 Pa). Found: M^+, 208.1274. Calcd for $C_{13}H_{20}S$: M^+, 208.1285. ^1H NMR ($CDCl_3$) δ=0.84 (3H, t, J=7.0 Hz), 1.14 (3H, t, J=7.5 Hz), 1.17—1.37 (4H, m), 1.77—1.92 (2H, m), 2.25 and 2.29 (2H, AB part of the ABX_3 system, J_{AX}=J_{BX}=7,5 Hz, J_{AB}=12.3 Hz), 3.77 (1H, dd, J=6.5 and 8.6 Hz), 7.19—7.34 (5H, m). ^{13}C NMR ($CDCl_3$) δ=13.8, 14.4, 22.4, 24.8, 29.8, 36.2, 49.4, 126.8, 127.7, 128.3, 143.1.

Benzyl Ethyl Sulfide (6). **6** (R_f=0.31), which was obtained in 39% yield, was identified by comparison of ^1H NMR data with an authentic sample prepared by a standard method.[19] ^1H NMR ($CDCl_3$) δ=1.23 (3H, t, J=7.4 Hz), 2.44 (2H, q, J=7.4 Hz), 3.72 (2H, s), 7.21—7.33 (5H, m). ^{13}C NMR ($CDCl_3$) δ=14.3, 25.1, 35.8, 126.8, 128.4, 128.8, 138.5.

When the reaction mixture was stirred for 1 h at room temperature before the addition of methanesulfonic acid in the procedure of synthesis of **3**, yields of the products were 20, 30, 11, and 23% for **3**, **6**, **7**, and **8**, respectively. Separation of the products was tedious.

This work was supported by Grants-in-Aid for Fundamental Scientific Research Nos. 02230108 and 01740320 from the Ministry of Education, Science and Culture. The 400 MHz NMR and mass spectra were measured at the Analytical Center in Okayama University of Science.

References

1) For part XVIII of the series, see S. Toyota and M.

Ōki, *Bull. Chem. Soc. Jpn.*, **64**, 1554 (1991).
2) E. W. Abel, S. K. Bhargava, and K. G. Orrell, *Prog. Inorg. Chem.*, **32**, 1 (1981); K. G. Orrell, *Coord. Chem. Rev.*, **96**, 1 (1989).
3) M. Ōki, *Pure Appl. Chem.*, **61**, 699 (1989).
4) M. Ōki and Y. Yamada, *Bull. Chem. Soc. Jpn.*, **61**, 1181 (1988).
5) M. Ōki and Y. Yamada, *Bull. Chem. Soc. Jpn.*, **61**, 1191 (1988).
6) S. Toyota, Y. Yamada, K. Kaneyoshi, and M. Ōki, *Bull. Chem. Soc. Jpn.*, **62**, 1509 (1989).
7) J. D. Odom, "Comprehensive Organometallic Chemistry," ed by G. Willkinson, F. G. A. Stone, and E. W. Abel, Pergamon, Oxford (1982), Vol. 1, p. 298.
8) H. C. Brown, E. F. Knights, and C. G. Scouten, *J. Am. Chem. Soc.*, **96**, 7765 (1974).
9) S. Toyota and M. Ōki, *Bull. Chem. Soc.*, **63**, 1168 (1990).
10) H. C. Brown and M. M. Rogić, *J. Am. Chem. Soc.*, **91**, 4304 (1969).
11) R. G. Kidd, "NMR of Newly Accessible Nuclei," ed by P. Laszlo, Academic Press, New York (1983), Vol. 2, pp. 49—60.
12) H. C. Brown and S. U. Kulkarni, *J. Org. Chem.*, **44**, 2422 (1979).
13) A modified version of the DNMR3 program[14] by Dr. H. Kihara of Hyogo University of Teacher Education.
14) G. Binsh, *Top. Stereochem.*, **3**, 97 (1968).
15) Estimated from Ref. 5. Rate constant of the dissociation of S–B bond is more than 10^3 s^{-1} at −90 °C.
16) M. Ōki, "Applications of Dynamic NMR Spectroscopy to Organic Chemistry," VCH Publishers, Deerfield Beach (1985), Chap. 5.
17) G. Bähr and K-H. Thiele, *Chem. Ber.*, **90**, 1578 (1957).
18) The signals due to *ipso* aromatic carbon attached to the boron atom could not be observed.
19) H. Gilman and N. J. Beaber, *J. Am. Chem. Soc.*, **47**, 1449 (1925).
20) C. Reichardt, "Solvent and Solvent Effects in Organic Chemistry," VCH Publishers, Cambridge (1988), pp. 407—411.

Unusual EPR Profile Obtained by Laser Photoreaction of Cardiovascular Tissue

Kouichi NAKAGAWA†
Department of Chemistry, Boston University, Boston, Massachusetts 02215, USA
(Received September 11, 1990)

Using spin trap methods, laser generated free radicals from cardiovascular tissue in high viscosity blood solution have been studied by EPR. The EPR spectra obtained are compared with spectra of free radicals produced by both cw and pulsed excimer laser irradiation. Nitroxide spin adducts produced by excimer laser irradiation show an unusual EPR hyperfine structure. In addition, the EPR spectra obtained by continuous wave (cw) laser irradiation are different from those obtained by excimer laser irradiation. The observed β-hydrogen hyperfine coupling for pulsed laser is approximately 1 Gauss smaller than those for cw laser irradiation. The present EPR results provide firm evidence that different free radical reaction intermediates are produced for each laser mode.

The detection and characterization of transient free radical intermediates generated by laser photoablation of biological tissue are essential to the understanding of the mechanism of laser–tissue interaction. Recently, there has been a great interest in studying the formation and determination of laser ablated molecular intermediates in the area of laser medicine.[1-5] Electron paramagnetic resonance (EPR) techniques using spin trap methods have been employed to determine the nature of free radical fragments which are formed by laser photoablation processes.[3-4] By examining the ablated fragments, it may also be possible to trace back the molecular details of the initial photoproduced events of laser ablation on the tissue surface.

Several experimental attempts have been made to elucidate the mechanism of laser interaction with tissue samples. For example, photoacoustic spectra of normal artery wall and of atherosclerotic plaque are reported by Singleton et al.[1] Threshold fluences (in units of [J cm^{-2}]) for excimer laser ablated gaseous products were calculated from the photoacoustic spectrum. Acoustic measurements of vascular tissue by pulsed laser has been performed by Cross et al.[6] They succeeded in measuring pulsed laser generated thermoelastic stress-waves on a 10 nanosecond time scale using acoustic transducers. Clarke et al.[4] suggested that by comparing two different energy sources, pulsed laser and ultrasound, it could be determined if free radicals are produced by the photoacoustic shock wave following the laser pulse. Gaseous products accompanying cw and pulsed laser ablation of cardiovascular tissue[2] and arterial wall[1] have been determined by gas chromatography. The pulsed laser ablation at high fluence of tissue results in plasma emission. Some of the emitted species have been identified, such as atomic calcium, C_2, and CN.[5] The results imply that radical fragments are common products of secondary reactions occurring in the plasma and should not be used to support mechanistic models for laser ablation. Hence, the formation and characterization of the fragments has not been well established.

† Present address: Department of Chemistry, University of Denver, Denver, Colorado 80208, USA.

Nitroxide spin traps have great potential for application to biological systems. A number of biological systems have recently been investigated to probe the structure of biological free radicals.[7-10] As an extension, the free radicals produced by laser irradiation of tissue samples in high viscosity blood media are investigated. We hope to extend our findings to achieve better understandings of how free radicals are produced and what types of free radicals are produced by laser irradiation of cardiovascular tissue. The results are discussed in terms of the various laser wavelengths and a correlation between the laser generated free radicals produced by the action of continuous wave (cw) vs. pulsed laser irradiation.

Materials and Methods

Tissue sample preparation has been described in elsewhere.[1] A spin trap reagent: *N*-(4-pyridylmethylene)-*t*-butylamine *N,N'*-dioxide (4-POBN) was purchased from Aldrich Chemical Co. and used as is. The water soluble spin trap reagent 4-POBN was chosen because of its stability, solubility in water, and insensitivity to light. 4-POBN was dissolved in canine blood to a concentration of 50 mM (M=mol dm^{-3}). The canine blood containing heparin was used without deoxygenation and centrifuging or filtration in this in vitro experiment. The size of myocardium sample was approximately the diameter of an EPR tube (5 mm) and the tissue sample was mounted in the bottom of the EPR tube. The sample was in contact with a fused silica optical fiber connected to the laser and was directly irradiated through the optical fiber by the output of a focused laser beam.[3] The blood solution without tissue sample was also irradiated through the optical fiber coupled with the laser beam. The laser output power from the optical fiber was kept at ca. 0.3 W. Right after laser irradiation of the tissue sample, the spin trap-blood solution was immediately transferred to an EPR aqueous quartz cell and mounted in the EPR cavity.

EPR measurements were made with a Varian E 104 X-band spectrometer. EPR spectra were recorded at room temperature. The recording conditions were the following: microwave power, 20 mW; microwave frequency, 9.42 GHz; modulation amplitude, 1.0 G; modulation frequency, 100 kHz; time constant, 1.0 s; scan rate, 20 Gauss per minute (1 Gauss=10^{-4} T). The resonance fields were measured relative to the standard free radical, 2,2-diphenyl-1-picrylhydrazyl (DPPH).

Results

The background signals of the spin trap reagent (4-POBN) and the 4-POBN dissolved in blood solution are shown in Fig. 1(A) and (B), respectively. As evidenced by Fig. 1(A) and (B), there is no EPR detectable background signal from the spin trap reagent as well as spin trap-blood solution. The EPR signal of spin trapped free radicals generated by cw 514 nm irradiation of cardiovascular tissue is a doublet of triplet as shown in Fig. 1(C). The laser irradiation of spin trap-blood solution, without tissue sample, irradiated by cw 514 nm argon ion laser is shown in Fig. 1(D). Figure 1(D) shows a nitrogen dominated triplet overlapping with a weak doublet of triplet. This spectrum is indicative of the decomposition of 4-POBN such as di-*t*-butylnitroxide ($a^N \approx 17$ Gauss). These experimental procedures were repeated for cw 351 nm and pulsed 308 nm irradiation. The obtained results are shown in Figs. 2 and 3, respectively. The EPR spectra observed for both cw 514 nm and 351 nm irradiation of tissue sample are very similar as shown in Figs. 1(C) and 2(C), respectively. Both EPR spectra are dominated by a nitrogen triplet hyperfine pattern and further split by β-hydrogen.

Figure 3 shows that the trapped free radicals produced by pulsed UV laser ablation of the tissue sample are not the same as those by the irradiation of spin trap-blood solution. The EPR spectrum obtained on pulsed excimer laser irradiation of tissue under high viscosity blood solution is not a simple nitrogen triplet signal, as shown in Fig. 3(C). This EPR signal is a weak boublet. In addition, the previously obtained EPR spectra for pulsed 308 nm and 351 nm irradiation of tissue sample under low viscosity cyclohexane show a simple three line pattern.[3] In contrast, the EPR spec-

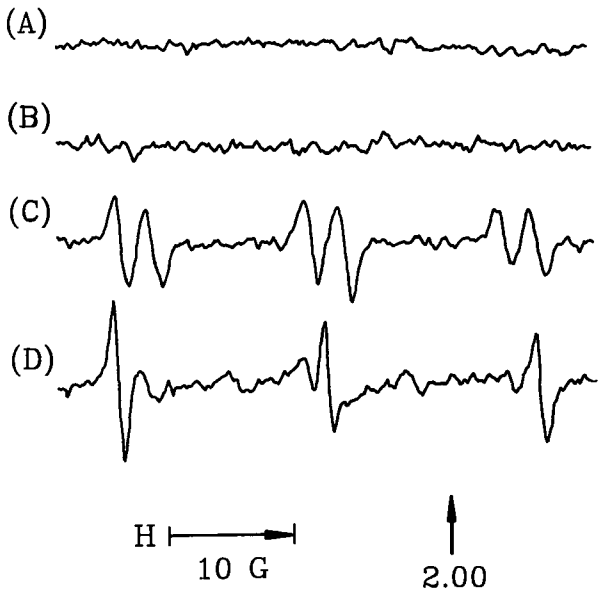

Fig. 1. Observed EPR spectra for cw 514 nm: (A) 4-POBN reagent before laser irradiation; (B) 4-POBN dissolved in blood before irradiation; (C) laser irradiation of myocardium in 4-POBN blood solution; and (D) irradiation of 4-POBN blood solution without myocardium. The calibrated g-value, 2.00_0, is marked. (Not DPPH, g=2.0036) EPR conditions are in the experimental section.

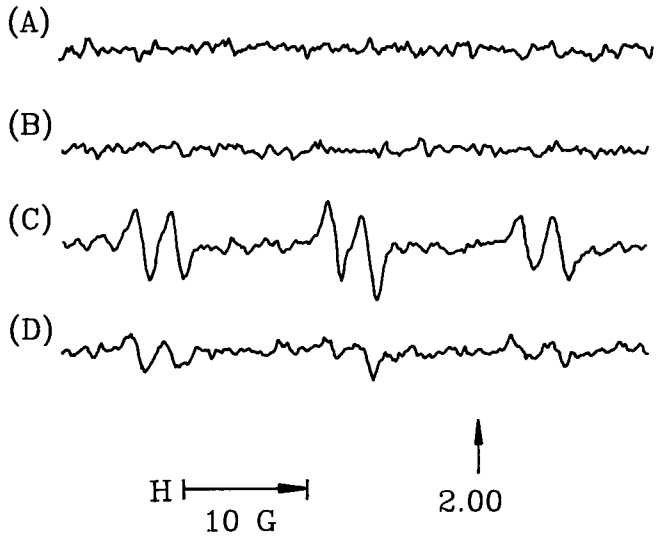

Fig. 2. Observed EPR spectra for cw 351 nm irradiation: (A) 4-POBN reagent before laser irradiation; (B) 4-POBN dissolved in blood before irradiation; (C) laser irradiation of myocardium in 4-POBN blood solution; and (D) irradiation of 4-POBN blood solution without myocardium.

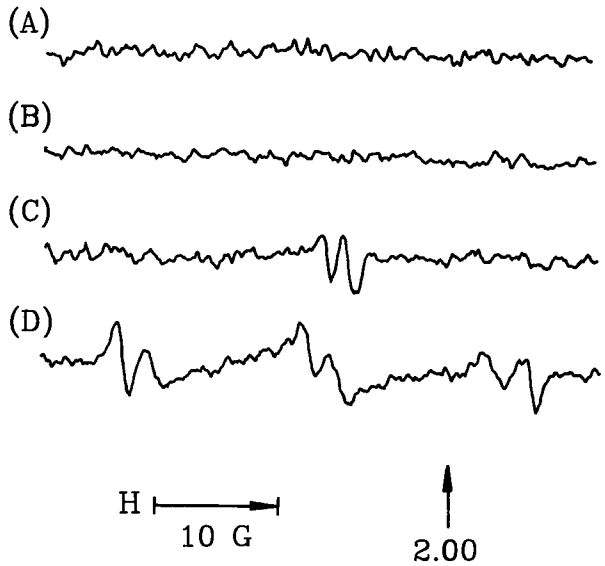

Fig. 3. Observed EPR spectra for pulsed 308 nm: (A) 4-POBN reagent before laser irradiation; (B) 4-POBN dissolved in blood before irradiation; (C) laser irradiation of myocardium in 4-POBN blood solution; and (D) irradiation of 4-POBN blood solution without myocardium.

trum obtained from excimer laser irradiation of blood solution shows a broad nitrogen dominated hyperfine structure (Fig. 3(D)). This EPR pattern presumably consists of di-*t*-butylnitroxide which is formed by photodecomposition 4-POBN and blood cell.

Comparison of the EPR spectra for trapped free radicals generated by laser irradiation of tissue sample is shown in Fig. 4. We immediately recognize three major EPR spectral differences between cw and pulsed laser irradiation. First of all, the hyperfine structure obtained for pulsed laser irradiation is obviously distinct from those obtained for cw laser irradiation. Second, the center line for pulsed laser irradiation is shifted towards high magnetic field. Thus, the *g*-value associated with the photogenerated free radicals is smaller than those for cw laser irradiation. Third, the hyperfine splitting for pulsed excimer laser photolysis is smaller (ca. 1 Gauss) than those for cw laser irradiation, as listed in Table 1. In addition, the pulsed 308 nm ablation of tissue sample did not produce thermal damage to the target site or the surrounding blood solution. However, cw 514 and 351 nm irradiation of the tissue sample resulted in thermal damage to the tissue target site and formed a thermally damaged cloud in the surrounding blood solution.

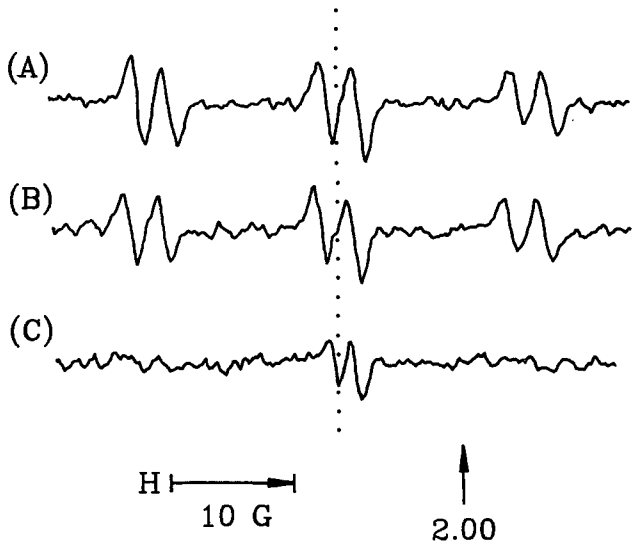

Fig. 4. Comparison of the EPR spectra for (A) cw 514 nm, (B) cw 351 nm, and (C) pulsed 308 nm laser irradiation of myocardium in the presence of 4-POBN in blood. The vertical dotted line represents a reference line. The calibrated *g*-value, 2.00$_0$, is marked. (Not DPPH, g=2.0036).

Table 1. EPR Parameters of Trapped Free Radicals by 4-POBN

R·	a^{N}_{NO} [b)]	a^{H}_{β} [b)]	Comments
Unidentified	15.77±0.07	2.66±0.06	cw 514 nm irrad.
Unidentified	15.63±0.09	2.86±0.06	cw 351 nm irrad.
Unidentified	—	1.78±0.08	pulsed 308 nm irrad.
H	16.2	10.2	Ref. 16
LOO	15.8	2.56	Ref. 17[a)]

a) Lipid peroxy radical. b) Units in Gauss.

Addition comparison of the EPR spectra for cw 514 nm, 351 nm, and pulsed 308 nm irradiation of blood solution in the presence of 4-POBN is shown in Fig. 5. Figure 5(A) shows that the decomposition of spin trap results in a sharp three line pattern building on a weak doublet of triplet signal. Changing the laser wavelength to 351 nm a weak doublet of triplet signal is observed. The main spectral differences between (A) and (B) in Fig. 5 are due to the light absorption property of canine blood. The absorption spectrum of canine blood is shown in Fig. 6. A peak at 412 nm is

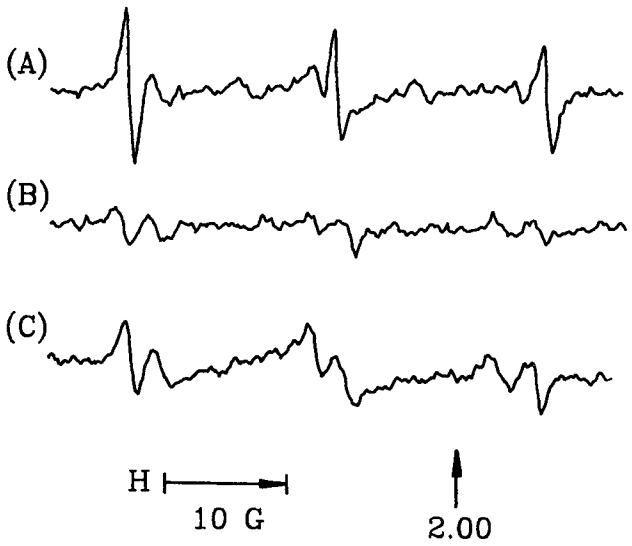

Fig. 5. Comparison of EPR spectra for (A) cw 514 nm, (B) cw 351 nm, and (C) pulsed 308 nm laser irradiation of blood solution in the presence of 4-POBN.

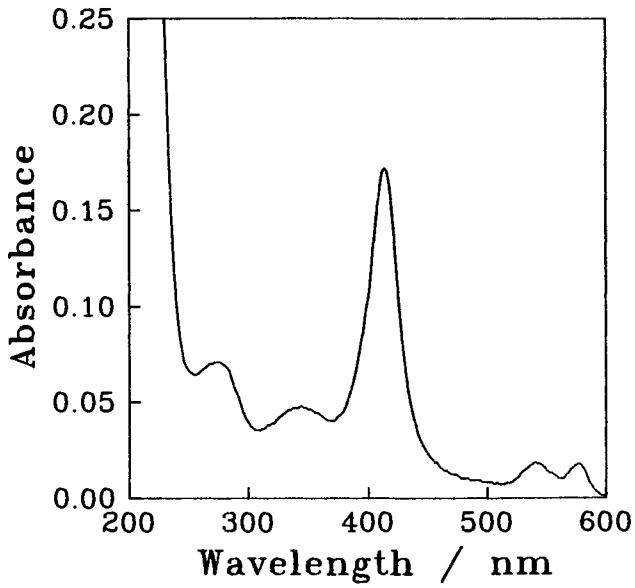

Fig. 6. The canine blood absorption spectrum.

characteristic hemoglobin absorption. The relative intensity of absorption at 351 nm is six times stronger than that at 514 nm. Switching to pulsed 308 nm irradiation of canine blood, a broad doublet of triplet signal is observed without thermal damage to the site. The signal might be due to decomposition of blood cell as well as spin trap. This broad EPR signal might result from slow tumbling motion of the trapped free radicals. Slow molecular motion generally results in the broadness of EPR signals.[11] However, there is no similarity on the EPR signal between laser irradiation of the blood solution and laser ablation of the tissue sample.

Discussion

The mechanism of laser-tissue interaction has been the subject of great concern. The light delivery of cw or pulsed energy has quite different consequences in its effect on the tissue target site. A schematic illustration of laser-tissue interaction is presented in Fig. 7. In the case of light delivered in a cw mode, several groups have reported the extensive thermal damaged to the tissue target site.[2,3,12] In contrast, high energy excimer laser ablates the tissue with no evidence for thermal damage.[1-3,6,12] However, both laser modes cw and pulse involve the production of free radicals accompanying laser interaction with tissue. The species of free radicals are weakly dependent depending on laser wavelengths and strongly dependent on laser operational mode: cw and pulse.

A. CW Laser Irradiation. A photon 514 nm wavelength is equivalent to 2.4 eV. This energy is not enough to break the average C–C bond which is ca. 3.6 eV. The excited molecules at the target site undergo internal coversion to a vibrational excited states, and any subsequent decomposition can be considered as a thermal process in which the photons merely act as a source of thermal energy.[13] This heat accumulation of the tissue may play an important role of the free radical generation and propagation. As a matter of fact, sever thermal damage to the tissue target site was observed for 514 nm laser irradiation of the cardiovascular tissue.

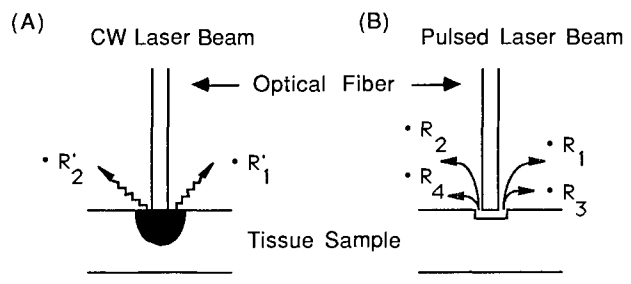

Fig. 7. A schematic illustration of short-lived free radicals produced by laser irradiation of the tissue sample. $\cdot R'_1$ and $\cdot R'_2$ represent cw laser generated free radicals, and $\cdot R'_1$, $\cdot R'_2$, $\cdot R'_3$, and $\cdot R'_4$ represent pulsed laser generted free radicals where pulsed laser produces free radicals more efficient compared to cw laser (Ref. 3). (A) CW laser irradiation shows severe thermal damage to the target site. (B) Excimer laser irradiation shows clean tissue removal without thermal damage.

A photon energy of cw 351 nm wavelength is 3.9 eV. This laser also produces thermal damage to the tissue target site.[3] Thus, the fundamental radical generation scheme might be similar to that for cw 514 nm radiation. However, the tissue sample absorbs more cw 351 nm laser light than cw 514 nm.[14] Thus, the UV laser light excites the tissue sample more effectively and may break weak bonds of the protein sample. The slight differences (ca. 0.2 Gauss) in β-hydrogen splitting in the observed EPR spectra between cw 514 nm and 351 nm, as listed in Table 1, could explain the differences. Both EPR spectra obtained by two different cw laser wavelength irradiations of myocardium may not be distinguished clearly without additional characteristic EPR structure.

Therefore, the trapped radicals for cw visible and ultraviolet laser photolysis should have some similarities, and the free radicals are photothermally produced. Thermally excited water in the tissue and oxygen in blood is involved for their generation and propagation. Oxygen centered free radicals are the most likely produced. Hydrogen radicals may not be trapped because the typical hyperfine values for the trapped hydrogen radical ($a^N \approx 16.3$, $a_\beta^H \approx 10.2$ Gauss[15]) do not match the hyperfine values obtained by laser irradiation of tissue as listed in Table 1.

B. Excimer Laser Irradiation. A photon energy at 351 nm for pulsed laser is the same as that of the cw UV 351 nm. However, the pulsed laser beam is very is very intense, that is, a large number of photons are produced within a 20 nanosecond laser pulse. Such a direct impact of photons from the laser causes nonthermal ablation of the tissue samples and the expulsion of the fragments at supersonic velocities.[13] This pulsed laser excitation could have enough energy to fragment the tissue protein chains without thermal damage at the target site.

The present results show that there are clear differences in observed EPR spectra between cw and pulsed laser irradiation of the tissue sample under blood solution as well as laser irradiation of the spin trap-blood solution without the tissue sample, as shown in Figs. 4 and 5, respectively. The EPR spectra obtained by cw laser photolysis of the tissue sample show a doublet of triplets. On the other hand, the EPR spectrum obtained by excimer laser ablation has a unique profile (Fig. 4(C)). The unusual EPR profile for excimer laser excitation can be accounted for by the followings: First, recent laser photoablation studies have indicated that various molecules are produced by pulsed UV laser irradiation of biological material and organic polymer.[1-3,5,18,19] If the tissue sample is exposed to a pulsed UV laser beam, it will break down into various molecular fragments of the protein sample. These free radical fragments can subsequently react with 4-POBN and

become stable free radicals. Second, the various size of free radicals might be a key to the unusual EPR spectrum. The tumbling motion of a nitroxide spin adduct affects changes in EPR lines due to loss of spectral symmetry. If the size of the spin adduct is large, the rotational correlation time for the spin adducts increases considerably. Third, viscosity of the blood solution might contribute to the unusual hyperfine structure for excimer laser irradiation of tissue. The viscosity of blood is about 4.8 relative to water.[20] If a nitroxide spin adduct is immobilized due to the higher viscosity, the EPR spectrum loses the spectral symmetry of nitrogen hyperfine structure.[10, 21]

As conformation of the interpretation, Collagen as the model compound was irradiated by excimer laser in the same manner as the irradiation of the tissue samples. The EPR signal obtained by excimer laser ablation of collagen is identical to that of the tissue sample.[22] Therefore, carbon centered various free radicals from the tissue sample can be trapped by excimer laser.

Summary

Considering the above discussed, the possible free radicals for pulsed UV laser ablation are C-terminal with various chain molecules. Various free radicals are produced by pulsed and cw laser operational modes. The contingent reaction scheme is

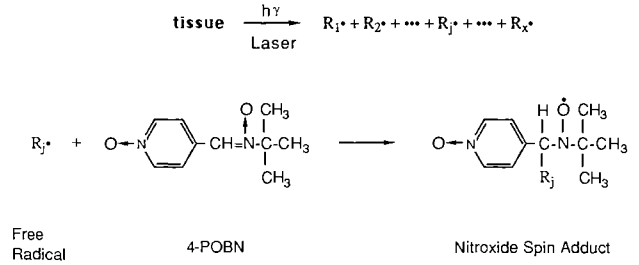

where R_1·, R_2·, R_j·, and R_x·, represents unidentified free radical fragments formed on either cw or pulse laser irradiation of the tissue. Those free radicals react with 4-POBN and become stable nitroxide spin adducts. For cw laser irradiation, R· can be oxygen centered radicals. C-terminal R· are most likely produced by pulsed laser. The present EPR results suggest that the backbone of amino acids, lipids, or other biological building blocks are cleaved during the ablation. Moreover, the carbon centered long chain free radicals derived from peptide main chain scission were produced by Hg–Xe lamp photolyses[23] and C-terminal radicals are observed by high output power cw laser irradiation of the tissue samples.[24]

Finally, it is interesting to note that those different types of laser generated short-lived free radicals should be converted to stable free radicals by biochemical manner based on the species for practical applications. The present results do not provide full details regarding laser generated free radicals. In the presence of multiple free radicals such as in our system, the identification of unknown radicals becomes more difficult using conventional cw EPR techniques. It is important to see substantial hyperfine structures in the EPR spectrum of the spin adduct. In most cases the hyperfine structure is a key to identification of the trapped radicals. Therefore, it might be useful to employ other techniques to regain some missing details of the hyperfine other techniques to regain some missing details of the hyperfine structure of the spin adducts in order to provide full information regarding the laser generated free radicals.

The author grately acknowleges Dr. J. M. Isner of New England Medical Center for the gift of canine blood sample. He thanks Drs. K. Kuwata, M. Kuwabara, T. Kumagai, and T. Tajima, R. H. Clarke for useful discussion during his visit. He also thanks referees for excellent suggestions on the manuscript.

References

1) D. L. Singleton, G. Paraskevopoulos, G. S. Jolly, R. S. Irwin, D. J. Mckenney, W. S. Nip, E. M. Farrel, and L. A. J. Higginson, *Appl. Phys. Lett.*, **48**, 878 (1986).
2) J. M. Isner, P. G. Steg, and R. H. Clarke, *IEEE J. Quantum Electron.*, **QE-23**, 17561 (1987).
3) R. H. Clarke, K. Nakagawa, and J. M. Isner, *Free Radical Biol. Med.*, 4, 209 (1988).
4) R. H. Clarke, K. Nakagawa, and J. M. Isner, *Photochem. Photobiol.*, **48**, 205 (1988).
5) T. D. Gauthier, R. H. Clarke, and J. M. Isner, *J. Appl. Phys.*, **64**, 2736 (1988).
6) F. W. Cross, R. K. Al-Dhahir, P. E. Dyer, and A. J. MacRobert, *Appl. Phys. Lett.*, **50**, 1019 (1987).
7) J. L. Poyer, P. B. McCay, E. K. Lai, E. G. Janzen, and E. R. Davis, *Biochem. Biophys. Res. Commun.*, **91**, 1154 (1980).
8) E. Albano, K. A. Lott, T. F. Slater, A. Stier, M. C. R. Symons, and A. Tomasi, *Biochem. J.*, **204**, 593 (1982).
9) S. Kubow, C. M. DuBose, E. G. Janzen, J. R. Carlson, and T. M. Bray, *Biochem. Biophys. Res. Commun.*, **114**, 168 (1983).
10) S. Kubow, E. G. Janzen, and T. M. Bray, *J. Biol. Chem.*, **259**, 4447 (1984).
11) J. E. Wertz and J. B. Bolton, "Electron Spin Resonance Elementary Theory and Practical Applications," McGraw-Hill Inc., New York (1972).
12) L. I. Deckelbaum, J. M. Isner, R. F. Donaldson, R. H. Calrke, S. Laliberte, A. S. Aharon, and J. S. Berstein, *Am. J. Cardiol.*, **56**, 662 (1985).
13) R. Srinivasan, *Science*, **234**, 559 (1986).
14) G. Yoon, A. J. Welch, M. Montamedi, and M. C. J. Van Gemert, *IEEE J. Quantum Electron.*, **QE-23**, 1721 (1987).
15) G. R. Buetner, *Free Radical Biol. Med.*, **3**, 259 (1987).
16) A. J. Carmichael, K. Makino, and P. Riesz, *Radiat. Res.*, **100**, 222 (1984).
17) H. D. Connor, V. Fisher, and R. P. Mason, *Biochem. Biopys. Res. Commun.*, **141**, 614 (1986).
18) G. Koren and J. T. C. Yeh, *J. Appl. Phys.*, **56**, 2120

(1984).
19) W. R. Creasy and J. T. Brenna, *Chem. Phys.*, **126**, 453 (1988).
20) R. Fahraeus and T. Lindqvist, *Am. J. Physiol.*, **96**, 562 (1931).
21) E. G. Janzen and G. A. Coulter, *J. Am. Chem. Soc.*, **106**, 1962 (1984).
22) K. Nakagawa, Ph. D. Thesis, Boston University (1989).
23) P. Riesz and I. Rosenthal, *Can. J. Chem.*, **60**, 1474 (1982).
24) S. Jain, X. Shi, M. Billie, A. C. Jain, and N. S. Dalal, *Lasers Surg. Med.*, **9**, 616 (1989).

Biosynthesis of Mutant β-D-Galactosidases Containing Nonnatural Aromatic Amino Acids by *Escherichia coli*

Takehiko UEDA,* Mitsuyoshi UEDA,† Atsuo TANAKA,† Masahiko SISIDO,††
and Yukio IMANISHI
Department of Polymer Chemistry, Kyoto University, Kyoto 606
† Department of Industrial Chemistry, Kyoto University, Kyoto 606
†† Research Laboratory of Resources Utilization, Tokyo Institute of Technology, Kanagawa 227
(Received November 20, 1990)

Mutant β-D-galactosidases containing nonnatural aromatic amino acids were produced by misincorporation during protein overproduction by *Escherichia coli*. The incorporation of 3-(1-pyrenyl)-L-alanine (pyrAla) was confirmed by fluorescence measurement of the produced enzyme, although the replacement frequency was low. Some of mutant enzymes showed improved thermostability.

Chemical treatment and protein engineering have produced many modified or mutant proteins, which are more effective in enzymatic activity than the original ones. In the meantime, the introduction of functional residues by means of chemical modification is limited only to functional groups on the protein surface, where modifying reagents are sterically reachable. On the other hand, site-directed mutagenesis provides a means of substitution at precise position of the sequence with natural amino acids. If protein engineering also enables utilization of nonnatural amino acids, we can design novelly functionalized enzymes easier.

Proofreading system prevents protein biosynthesis from mistranslation in every step of biosynthetic process.[1] However, the system could not function properly against nonnatural amino acids because it works most strictly against naturally occurring amino acids. So far, many kinds of nonnatural amino acids, whose structure is very similar to a natural one, have been introduced into proteins by using *Escherichia coli*. The substitution rate of a target amino acid with a nonnatural amino acid was found to be about 10% to 90% in the cases of alkaline phosphatase,[2-8] aspartate transcarbamylase,[9] β-D-galactosidase[10] human epidermal growth factor (hEGF).[11] Schlesinger and co-workers have succeeded in incorporation of various amino acid analogs into bacterial alkaline phosphatase.[2-7] Alkaline phosphatase gene is expressed under the control of *phoA* promoter that is induced by lowering the phosphate concentration of the culture medium. The biosynthesis of the other probably toxic abnormal proteins is not active under these conditions except the production of abnormal alkaline phosphatase. In this method, Miyazawa and co-workers succeeded in preparing hEGF substituted with one norleucine for methionine by biosynthesis of alkaline phosphatase signal peptide-hEGF fusion protein.[11] On the other hand, incorporation of nonnatural amino acids, whose structure is very different from a natural one, is a difficult task. One of approaches to realize this purpose is that the protein-biosynthesis system is accelerated to obtain the mutant enzymes containing nonnatural amino acids as much as possible.

In this paper, incorporation of fluorescent nonnatural amino acids into β-D-galactosidases was studied by using *E.coli* in the overproduced state on the protein synthesis. 3-(1-Pyrenyl)-L-alanine (pyrAla) was incorporated into β-D-galactosidases and relatively high thermostability was found in some of the mutant enzyme.

Experimental

o-Nitrophenyl β-D-galactopyranoside (ONPG), bovine serum albumin (BSA), and *E.coli* β-D-galactosidase (M.W. 130 kDa) were purchased from Sigma, USA. Bacterial endonucleases BamHI and EcoRV, bacterial alkaline phosphatase (BAP), and T4 DNA ligase were purchased from Toyobo Co., Ltd., Japan. Bacto-Trypton and Bacto-Yeast-Extract were purchased from DIFCO Laboratory, USA. *E.coli* B357 (wild type) and *E.coli* DH5α (F⁻, *endA*1, *hsdR*17 (rk⁻, mk⁺), *supE*44, *thi*⁻¹, *recA*1, *gyrA*96, *relA*1, Δ (*argF*-laczya) U169, φ 80d*lacZ* λ M15, λ⁻) were used for expression of β-D-galactosidase.

Ultraviolet absorption spectra were recorded by a Hitachi Model 200-10 spectrometer. Fluorescence emission and excitation spectra were recorded by a Hitachi MPF-4 autocorrected fluorescence spectrometer. Fluorescence excitation spectra were monitored at wavelength 397 nm for pyrAla and at wavelength 415 nm for 3-(9-anthryl)-L-alanine (antAla).

The recombinant plasmid pUC19Z was synthesized from the plasmid pUC19 and pMC1871 (Pharmacia, Sweden). A 3.0 kbp fragment containing the lacZ gene was excised from the pMC1871 plasmid with BamHI, and ligated into the pUC19, digested with BamHI and dephosphorylated with BAP. The resultant plasmid pUC19Z was transformed into DH5α strain and the transformants exhibiting β-D-galactosidase activity were picked on 2% agar plates of LB-medium (1% (w/w) bacto-trypton/0.5% (w/w) bacto-yeast-extract) in the presence of ampicillin, 5-bromo-4-chloro-3-indolyl β-D-galactopyranoside and isopropyl β-D-galactopyranoside. The plasmid DNA was isolated with the method of alkaline treatment.[15]

The *E.coli* strain DH5α harboring plasmid pUC19Z was precultured in a 500 ml flask containing 100 ml of LB-medium at 37 °C, with shaking for 16 h. The cells were collected by centrifugation at 3,000 rpm for 5 min and suspended in 30 ml of deionized water. An aliquot (1 ml) of the precultured cell

suspension was inoculated into 100 ml of LB-medium in a 500 ml flask and cultivated to the exponential growth phase. Then 10 mg of chloramphenicol was added and the flask was shaken for further 1 h. The cells were harvested by centrifugation and suspended in 30 ml of deionized water again. A portion of cell suspension (20 ml) was inoculated into 2.0 liter of LB-medium in the presence of 50 μg ml^{-1} of nonnatural fluorescent amino acid and 0.1% lactose instead of glucose and cultured to the exponential growth phase at 37 °C. After cultivation, the cells washed with deionized water were suspended in 400 ml of 0.3 M (1 M=1 mol dm^{-3}) potassium phosphate buffer (pH 7.2) in the presence of 3 mM $MgCl_2$. Cell growth was monitored at absorbance of 600 nm. 1 OD corresponds to 10^8 cells ml^{-1}.

Cell-free extracts were prepared by disintegrating the cells with a Braun cell homogenizer (Type 853023, B. Brown, Germany). The cell homogenate was centrifuged at 12,000 rpm for 5 min, the supernatant obtained being further centrifuged at 45,000 rpm for 60 min at 4 °C. The cell-free extract obtained finally was concentrated through a DIAFLOW membrane filter (Ultrafiltration Cell Model 12, AMICON Corp., USA). The total amount of protein was estimated by the Lowry's method.[16] The β-D-galactosidase protein was analyzed with sodium dodecyl sulfate-polyacrylamide gel electrophoresis (SDS-PAGE).

The proteins were recovered from the cell-free extracts with saturated ammonium sulfate. It was solubilized again with 100 mM potassium phosphate buffer (pH 7.2) and dialyzed for 24 h at 4 °C against 500-fold volume of the potassium phosphate buffer to remove ammonium sulfate. Thereafter, the fluorescence excitation spectra of the protein solution and the dialyzing buffer were measured at every 2.5 h of dialysis against 500-fold volume of the buffer at 4 °C. After the dialysis for ten times (25 h), the protein solution was added to the same volume of dimethyl sulfoxide (DMSO) and stirred overnight at 4 °C to wash out the nonnatural amino acid followed by further 20 times of the dialysis. The content of the nonnatural amino acid was monitored by following the fluorescence spectrum during the dialysis treatment.

β-D-Galactosidase was purified with a gel-filtration chromatography followed by nondenaturing polyacrylamide gel electrophoresis. The proteins were applied to a Sephacryl S-300 column (2.5×85 cm) equilibrated with 100 mM potassium phosphate buffer (pH 7.2) containing 10 mM $MgCl_2$. A single peak of the β-D-galactosidase activity was found and the fractions were collected and concentrated. The concentrated solution was applied to a nondenaturing polyacrylamide gel electrophoresis (7%) and the gel band corresponding to β-D-galactosidase was excised and eluted out with an Extraphore electrophoretic concentrator (Pharmacia). The preparation finally obtained was used as a purified β-D-galactosidase.

The nonnatural amino acid contents in the β-D-galactosidases were estimated by the fluorescence measurement. The fluorescence from the enzyme is attributed to both the original tryptophan residues and the incorporated nonnatural amino acid residues. Assuming that the fluorescence intensity of the tryptophan residues ($F_{trp}(\lambda)$) gives a maximum at wavelength λ_{trp} and the intensity of the nonnatural amino acid residues ($F_{aa}(\lambda)$) gives a maximum at wavelength λ_{aa}, we have a ratio (R) of the fluorescence intensity from the nonnatural amino acid residues to that from the tryptophan residues as follows.

$$F_{obs}(\lambda) = XF_{trp}(\lambda) + YF_{aa}(\lambda)$$

$$R_{obs} = F_{obs}(\lambda_{aa}) \,/\, F_{obs}(\lambda_{trp})$$

$$R_{trp} = F_{trp}(\lambda_{aa}) \,/\, F_{trp}(\lambda_{trp})$$

$$R_{aa} = F_{aa}(\lambda_{aa}) \,/\, F_{aa}(\lambda_{trp})$$

$$R = YF_{aa}(\lambda_{aa}) \,/\, XF_{trp}(\lambda_{trp})$$
$$= R_{obs}(1 - R_{trp}/R_{obs}) \,/\, (1 - R_{obs}/R_{aa})$$

where $F_{obs}(\lambda)$ represents the observed fluorescence intensity at wavelength λ and X and Y represent the contributions of each fluorescent residue. The nonnatural amino acid content C (mol/mol tryptophan residue) was estimated from a calibration curve for 1 mg ml^{-1} bovine serum albumin solution.

The β-D-galactosidase activity was measured at 30 °C by following the increase in absorbance of *o*-nitrophenol produced through the hydrolysis of ONPG at 405 nm.

Results

The construction of plasmid pUC19Z to express β-D-galactosidase is illustrated in Fig. 1. *E.coli* DH5α was transformed with the pUC19Z. Several transformants exhibiting β-D-galactosidase activity (blue-colored col-

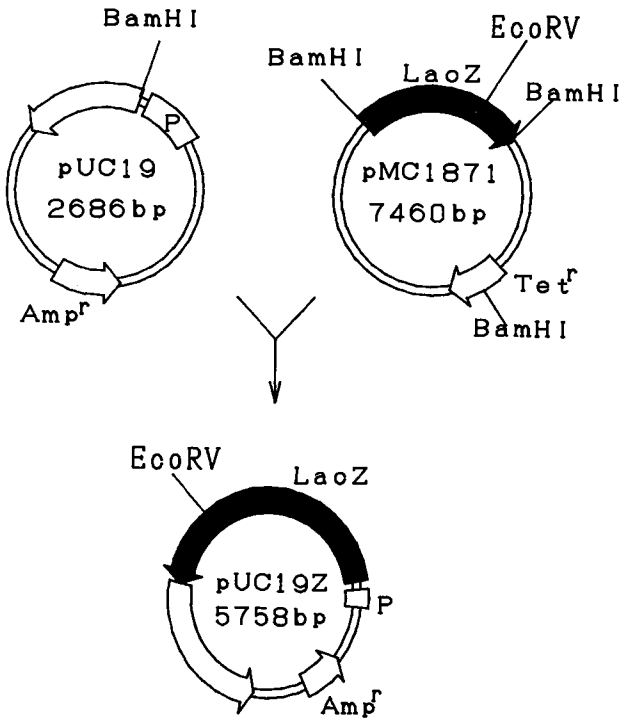

Fig. 1. Construction of β-D-galactosidase expressing plasmid pUC19Z. BamHI and EcoRV represent the restriction sites on the plasmid. P is the promoter, and lacZ is the structural gene of β-D-galactosidase. Some of the colonies were screened for the presence of lacZ gene by agalose electrophoresis. A positive colony had a band corresponding to the open-circular plasmid DNA band digested at the site of EcoRV in lacZ gene.

onies) and having 5.7 kbp fragment of plasmid pUC19Z were obtained. The enzymatic activities of β-D-galactosidase in various *E.coli* strains, grown in the absence of nonnatural amino acids, were measured and are summarized in Table 1. The activity of the wild strain B357 was 73-fold higher in lactose-grown cells than in glucose-grown cells. The protein produced in the presence of lactose from the DH5α strain, transformed with pUC19Z and treated with chloramphenicol, showed two thousands-fold activity of that in the presence of glucose. The content of β-D-galactosidase in the total protein was estimated over 65% judging from the calculation of specific activity (126 μmol min^{-1} mg^{-1} in the cell free extract; 171 μmol min^{-1} mg^{-1} in the purified preparation).

The reduction in growth of strain B357 was within 20% when the concentration of each nonnatural amino acid added in medium was lower than 50 μg ml^{-1}. The amount of proteins produced and β-D-galactosidase activity are shown in Table 2. In the presence of 3-(1-naphthyl)-L-alanine (napAla), both the protein production and the activity per cell increased slightly. In this case, the effect of incorporation of napAla was not observed. In comparison, in the presence of antAla, the protein production per cell increased, while the activity per cell did not increase significantly, and in the presence of pyrAla, the protein production per cell did not decrease, while the activity per cell was reduced considerably. These results might be due to the incorporation of the nonnatural amino acid into β-D-galactosidase.

The amount of a nonnatural amino acid in a protein was estimated by the fluorescence intensity of the nonnatural amino acid taking that of tryptophan in the protein as standard. For the calibration of fluorescence intensity, fluorescence of nonnatural amino acids was measured in the presence of BSA.

The fluorescence intensity ratio R and the residual content C were plotted on log-log graph paper and a calibration curve was obtained by the least-squares method. The curve was expressed by $C=9.28R^{0.615}$ (mmol/mol tryptophan residue) for antAla in the range of $R<15$ and by $C=0.795R^{1.55}$ (mmol/mol tryptophan residue) for pyrAla in the range of $R<10$.

The protein solution from the wild strain B357 grown in the presence of the nonnatural amino acid was added to the same volume of DMSO and the nonnatural amino acid that nonspecifically bound to the protein was removed by dialysis. The fluorescence intensity ratio during the dialysis was followed and is shown in Fig. 2. The ratio was decreased exponentially, but a certain intensity was remained after the sufficient dialysis for 75 h. The minimum R was 0.30 for antAla and

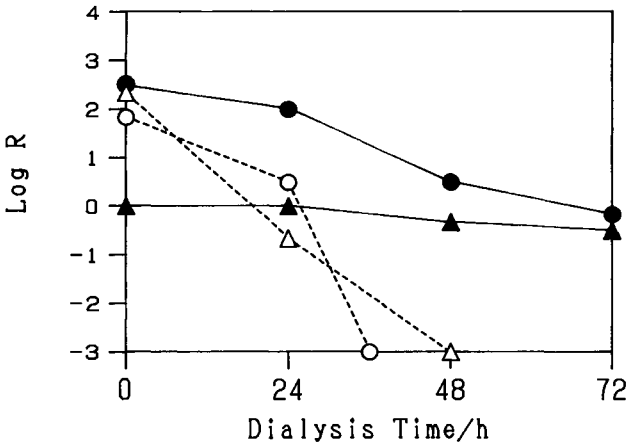

Fig. 2. Change in fluorescence intensity ratio during dialysis treatment. The fluorescence intensity ratio of the protein solutions obtained from the cells of strain B357 were followed during the dialysis. ●, Sample from the cells grown in the presence of pyrAla; ○, mixture of sample from the cells grown without nonnatural amino acid and 40 μg ml^{-1} of pyrAla; ▲, sample from the cells grown in the presence of antAla; △, mixture of sample from the cells grown without nonnatural amino acid and 40 μg ml^{-1} of antAla.

Table 1. β-D-Galactosidase Activity of Various *E. coli* Strains

Strain	Plasmid[b]	Induction[c]	CP[a,d]	Specific activity[e]
B357	None	None	None	0.0645
B357	None	+	None	4.73
DH5α	pUC19Z	+	+	126
DH5α	None	+	+	0.00

a) CP represents chloramphenicol treatment b) Transformation with the plasmid. c) Induction with lactose. d) CP treatment for 1 h. e) Specific activity was expressed in units per milligram of the β-D-galactosidase (μmol min^{-1} mg^{-1}).

Table 2. The Relative Amount of Proteins Obtained from the Cells of Strain B357 and the Relative β-D-Galactosidase Activity

Nonnatural amino acid[a]	Growth[b]	Amount of protein[c]	Specific activity[d]	Change[e]
None	1	1	1	—
Nap	1.04	1.06	1.09	+9%
Ant	0.91	1.38	0.95	−5%
Pyr	0.80	1.35	0.75	−25%

a) Nap, Ant, and Pyr represent 3-(1-naphthyl)-L-alanine, 3-(9-anthryl)-L-alanine, 3-(1-pyrenyl)-L-alanine, respectively. b) The relative growth of the cells. c) The relative amount of proteins per cell. d) The relative specific activity of β-D-galactosidases. e) The change in the specific activity.

was 0.65 for pyrAla. The residual content C was obtained using the calibration curve as 4.5 mmol mol^{-1} for antAla and 0.42 mmol mol^{-1} for pyrAla. In comparison, the protein solution of the B357 grown without nonnatural amino acids was mixed with a solution of 40 μg ml^{-1} nonnatural amino acids and stirred at 4 °C for 24 h. The fluorescence intensity ratio during the dialysis was followed after washing with DMSO. As shown in Fig. 2, the fluorescence of the nonnatural amino acids disappeared in 48 h, indicating that the nonspecifically bound nonnatural amino acids were completely removed by the dialysis.

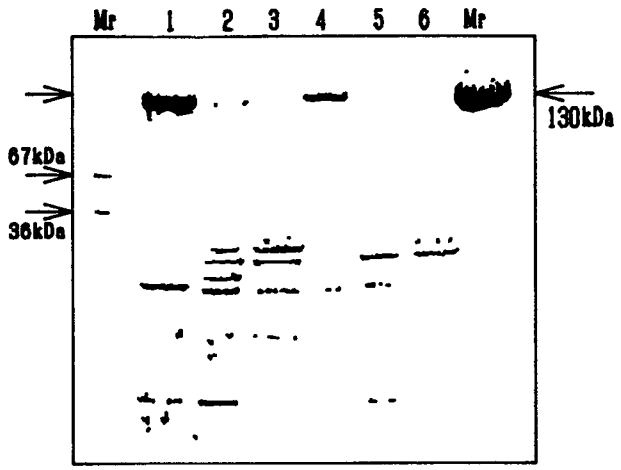

Fig. 3. The SDS-PAGE profile of produced β-D-galactosidases. β-D-Galactosidase was obtained from various strains without nonnatural amino acid. Mr, Marker; lanes 1 and 4, DH5α strain harboring pUC19Z; lanes 2 and 5, DH5α strain harboring pUC19; lanes 3 and 6, DH5α without transformation. Lanes 1, 2, and 3, 20 μg protein each; lanes 4, 5, and 6, 10 μg protein each.

β-D-Galactosidase was purified from the protein solution obtained from the DH5α cells harboring pUC19Z without nonnatural amino acid (Fig. 3). Similarly, β-D-galactosidase was purified from the protein solution obtained from the DH5α cells harboring pUC19Z grown in the presence of 50 μg ml^{-1} nonnatural amino acids. Each 200 μg of purified β-D-galactosidase was obtained from 1 mg of the crude preparation through the nondenaturing polyacrylamide gel electrophoresis.

A significant fluorescence of pyrenyl moiety was observed in the purified β-D-galactosidase obtained from the cells grown in the presence of pyrAla (Fig. 4). It was found that the fluorescence intensity ratio R_{obs} was 0.796 from the fluorescence excitation spectrum of the purified β-D-galactosidase monitored at wavelength 397 nm. The residual content C was determined as 0.556 mmol mol^{-1} from the calibration curve.

β-D-Galactosidases were incubated in a water bath at 60 °C. Aliquots were removed at various times over 180 s period, placed on ice and then measured for the residual activity (Fig. 5). The activity of the purified β-D-galactosidases obtained from the cells grown in the presence of pyrAla or antAla remained after the incubation of 120 s at 60 °C, while that obtained from the cells grown without nonnatural amino acids was lost completely in 120 s. This indicates that the thermostability of β-D-galactosidase was improved by the incorporation of nonnatural amino acids.

It can be derived from the Michaelis-Menten's reaction kinetics that a specific activity of an enzyme is proportional to the rate constant k_{cat} in the case of sufficiently high substrate concentration. The activation energy of the catalytic reaction was calculated from the

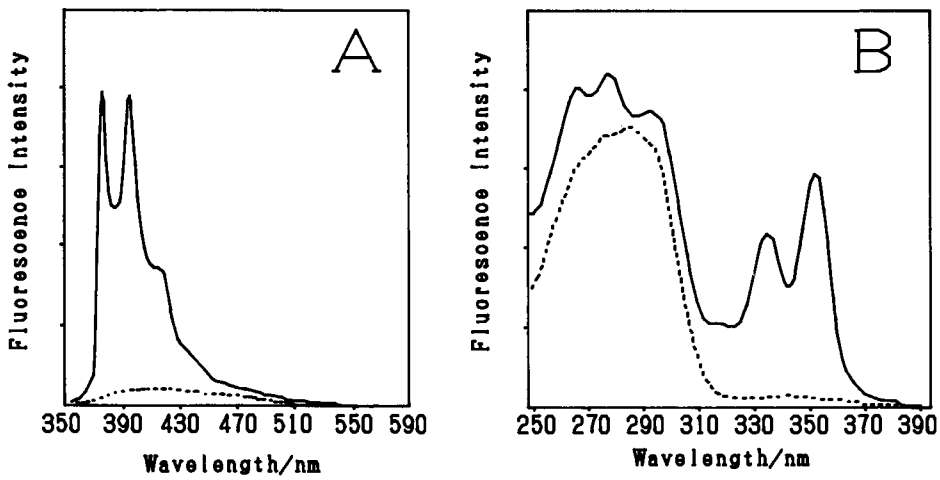

Fig. 4. Fluorescence emission and excitation spectra of the purified β-D-galactosidase obtained from the cells of strain DH5α grown with or without pyrAla. A, fluorescence emission spectra excited at 345 nm; B, fluorescence excitation spectra monitored at 395 nm. —, spectra of the purified β-D-galactosidase obtained from the cells grown in the presence of pyrAla; ···, spectra of that obtained from the cells without nonnatural amino acid.

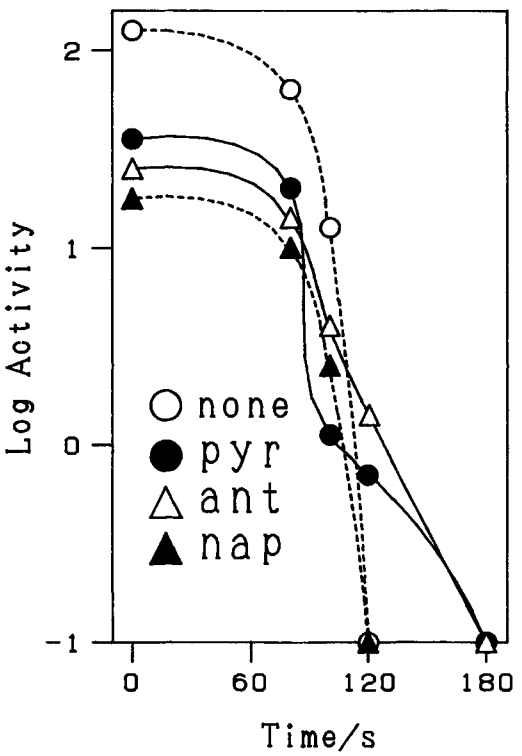

Fig. 5. Thermostability of purified β-D-galactosidases. Log specific activity is plotted against incubation times of 80 s, 100 s, 120 s, and 180 s. ○, Sample obtained from the cells of strain DH5α grown without nonnatural amino acid; ●, △, and ▲, samples obtained from the cells of strain DH5α grown in the presence of pyrAla, antAla, and napAla, respectively.

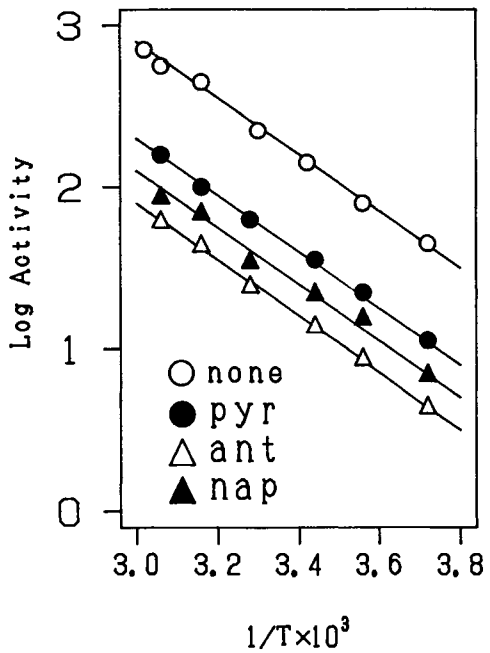

Fig. 6. The log specific activity vs. $1/T$ plot of purified β-D-galactosidases. ○, Sample obtained from the cells of strain DH5α grown without nonnatural amino acid; ●, △, and ▲, samples obtained from the cells of strain DH5α grown in the presence of pyrAla, antAla, and napAla, respectively.

plot of log specific activity against $1/T$ as shown in Fig. 6. The activation energy of β-D-galactosidase obtained from the cells grown in the presence of various nonnatural amino acids was identical with that for β-D-galactosidase obtained from the cells grown without the nonnatural amino acids.

Discussion

In general, a tRNA is not mischarged with nonnatural amino acids, because aminoacyl-tRNA synthetase precisely discriminates the corresponding amino acid from the others. Nonnatural amino acids found in natural polypeptides is usually formed in the process of the posttranslational modification. In some cases, the nonnatural amino acid-containing proteins show resistance to the digestion by proteases. The natural amino acid analogs, such as canavanine, 2-azetidinecarboxylic acid, and 4-fluorophenylalanine, were shown to be incorporated during the accelerated biosynthesis of protein after viral infection of bacteria.[12] The mutant proteins inhibited the self-assembly of the viral proteins. On the other hand, it has been reported that cleavage of the signal sequence of pre-prolactin synthesized in the presence of hydroxynorvaline is inhibited by incorporation of the analog.[12] In most cases, incorporation of analogs resulted in reduction of protein functions. Abnormal (mutant) proteins accumulated in a cell are known to be digested by intracellular proteases. The accumulation of abnormal proteins leads to an expression of protease La, which digests the abnormal proteins.[13] In addition, cell growth will be inhibited because high frequency of production of abnormal proteins may cause reduction of normal protein production. For these reasons, it was difficult to prepare abnormal proteins incorporated with nonnatural amino acids.

Parker reported that the amino acid substitutions did not lead to proteins recognized as grossly abnormal by the proteolysis systems in cells. Abnormal proteins in which substitution frequency was under 10% were not eliminated in a cell, and abnormal subunits of ribosome were found in cells grown normally.[14] Taking these results into consideration abnormal proteins may be prepared by lowering substitution frequency. Abnormal β-D-galactosidase was prepared in the presence of various fluorescent nonnatural amino acids with low frequency of incorporation. In order for the protein not to be recognized as a foreign abnormal protein, β-D-galactosidase was synthesized in *E.coli*. The nonnatural amino acids used in this study were not analogous to any natural amino acids, so that the nonatural amino acids were mischarged to tRNAs to be incorporated into proteins in sufficiently low frequency. Fluorescent amino acids can be detected in abnormal proteins even in low frequency of incorporation.

We have succeeded in overproduction of β-D-galactosidase using the DH5α strain with plasmid

pUC19Z in the level of two thousands times higher than the wild strain (Table 1). AntAla and pyrAla were found in the proteins of the wild strain synthesized in the presence of these nonnatural amino acids (Fig. 2), indicating that *E.coli* utilized these nonnatural amino acids to some extent in protein biosynthesis. Fluorescence emission of pyrenyl moiety was observed in the purified β-D-galactosidase synthesized in the presence of pyrAla, and the residual content was estimated to be 0.556 mmol mol^{-1} tryptophan residue. Thus, one pyrAla residue per 46 molecules of β-D-galactosidase was found because there are 39 tryptophan residues in a β-D-galactosidase molecule. However, pyrAla may be attached to the hydrophobic surface of BSA used in the calibration experiment, so that this value is the minimum in the case of the absence of pyrenyl moiety quenching by surrounding charges or dipoles.

The specific activity of the proteins obtained in the presence of antAla or pyrAla was reduced (Table 2), while the amount of proteins per cell was not affected. This indicates that protein biosynthesis was not lowered by the addition of the nonnatural amino acids. The β-D-galactosidase content of the total proteins was found to increase continuously throughout the cultivation, indicating that the reduction of the specific activity was not the result of proteolytic digestion of abnormal β-D-galactosidase but the result of the production of β-D-galactosidase with low activity. On the other hand, the activation energy of the purified β-D-galactosidase did not decrease (Fig. 6). Thus, it is considered that the nonnatural amino acids were incorporated into the active site of β-D-galactosidase and the activity of some β-D-galactosidase was lost. In this case, incorporated amino acids are thought to be on the protein surface and easily quenched. In addition, incorporation of a highly hydrophobic amino acid into the hydrophilic surface may cause instabilization of β-D-galactosidase.

At least 2.2% of β-D-galactosidase was estimated to have one pyrAla residue. As shown in Fig. 5, several per cent of the mutant β-D-galactosidases resulted in the improved thermostability of the enzyme, indicating that the nonnatural amino acids were incorporated into the hydrophobic region of β-D-galactosidase and a higher-order structure of the enzyme was stabilized. In this case, the incorporated nonnatural amino acids should be located apart from the protein surface and are hardly quenched.

In conclusion, we have succeeded in preparing mutant β-D-galactosidases substituted by the nonnatural amino acids. By lowering substitution frequency, cell growth and protein biosynthesis rate were not reduced.

The authors are grateful to Dr. Yoshihito Inai for his kind gift of napAla and pyrAla and to Dr. Hiroki Sasaki for his generous supply of antAla.

References

1) G. L. Igloi, F. Haar, and F. Cramer, *Biochemistry,* **17**, 3459 (1978).
2) S. Schlesinger and M. J. Schlesinger, *J. Biol. Chem.,* **242**, 3369 (1967).
3) S. Schlesinger, *J. Biol. Chem.,* **243**, 3877 (1968).
4) S. Schlesinger and M. J. Schlesinger, *J. Biol. Chem.,* **244**, 3803 (1969).
5) J. Attias, S. Schlesinger, and M. J. Schlesinger, *J. Biol. Chem.,* **244**, 3810 (1969).
6) H. Morris and M. J. Schlesinger, *J. Bacteriol.,* **111**, 203 (1972).
7) B. D. Sykes, H. I. Weingarten, and M. J. Schlesinger, *Proc. Natl. Acad. Sci. U.S.A.,* **471**, 469 (1974).
8) D. T. Browne and J. D. Otvos, *Biochem. Biophys. Res. Commun.,* **468**, 907 (1976).
9) P. Gueguen, M. Padron, B. Perbal, and G. Herve, *Biochim. Biophys. Acta,* **615**, 59 (1980).
10) F. Naider, Z. Bohak, and J. Yariv, *Biochemistry,* **411**, 3202 (1972).
11) H. Koide, S. Yokoyama, G. Kawai, J. Ha, T. Oka, S. Kawai, T. Miyake, T. Fuwa, and T. Miyazawa, *Proc. Natl. Acad. Sci. U.S.A.,* **485**, 6237 (1988).
12) M. J. Wilson and D. L. Hatfield, *Biochim. Biophys. Acta,* **781**, 205 (1984).
13) S. A. Goff and A. L. Goldberg, *Cell,* **441**, 587 (1985).
14) J. Parker, *J. Biol. Chem.,* **256**, 9770 (1981).
15) T. Maniatis, E. F. Fritsch, and J. Sambrook, "Molecular Cloning: A Laboratory Manual," Cold Spring Harbor, New York (1982), pp. 90—91.
16) D. H. Lowry, N. J. Rosebrough, A. L. Farr, and R. J. Randall, *J. Biol. Chem.,* **193**, 265 (1951).

Nucleophilic Ring-Opening of Chlorooxiranes: A New Synthesis of α-Hydroxy α′-Substituted Ketones from Carbonyl Compounds and 1-Chloroalkyl *p*-Tolyl Sulfoxides

Tsuyoshi SATOH, Asako OGURA, Youko IKEDA, and Koji YAMAKAWA*
Faculty of Pharmaceutical Sciences, Science University of Tokyo,
Ichigaya-funagawara-machi, Shinjuku-ku, Tokyo 162
(Received December 19, 1990)

The addition of 1-chloroalkyl *p*-tolyl sulfoxides to carbonyl compounds gave adducts which were then converted to chlorooxiranes in two steps with good overall yields. The treatment of the chlorooxiranes with various nucleophiles gave α-hygroxy α′-substituted ketones or α-hydroxy ketones in good yields.

The homologation method of carbonyl compounds from lower carbonyl compounds by carbon–carbon coupling reactions is now one of the most important and extensively used methods for obtaining desired carbonyl compounds.[1] Recently, we reported a method to synthesize α-substituted carbonyl compounds **4** from carbonyl compounds **1** and 1-chloroalkyl phenyl sulfoxides **2** through α,β-epoxy sulfoxides **3** (Scheme 1).[2] In this method the carbonyl carbon of **1** was acylated and

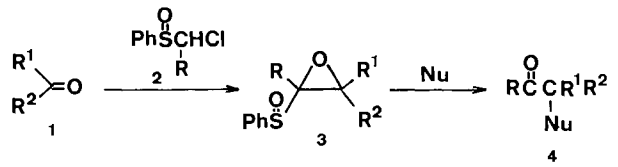

Scheme 1.

the carbonyl oxygen was replaced by nucleophiles.

In a continuation of our study on the use of 1-chloroalkyl aryl sulfoxides in organic synthesis, we describe here a novel method for the synthesis of α-hydroxy α′-substituted ketones **9** from carbonyl compounds **1** and 1-chloroalkyl *p*-tolyl sulfoxides **5** through chlorooxiranes **8** (Scheme 2).[3] It is worth noticing that in this method **5** acted as an α-substituted acyl anion equivalent.

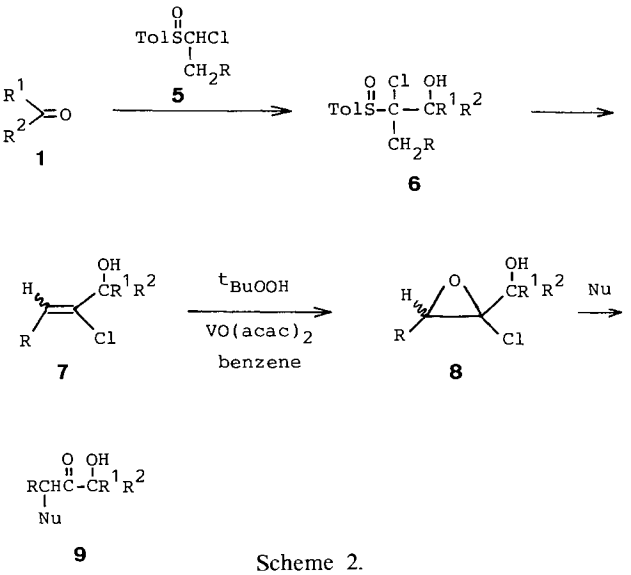

Scheme 2.

Results and Discussion

The representative example of this procedure using 1-chlorobutyl *p*-tolyl sulfoxide **10**[4] and cycloheptanone as a carbonyl compound is as follows. The treatment of **10** with lithium diisopropylamide (LDA) in THF at −60°C and then with cycloheptanone gave chloro alcohol **11** in 92% yield. The sulfinyl group of **11** was found to be prone to eliminate under heating; refluxing **11** in toluene for 5 min cleanly gave the desired vinyl chloride **12** in 88% yield. Among the procedures reported for epoxidation of allylic alcohols[5] we selected a *t*-butyl hydroperoxide (ᵗBuOOH)-vanadyl acetylacetonate ($VO(acac)_2$) system for the epoxidation of vinyl chloride **12**, since the product chlorooxirane **13** was presumed to be unstable under acidic conditions.

The epoxidation of **12** was carried out by adding a solution of ᵗBuOOH (1.2 equivalents) to a dry benzene solution of **12** and $VO(acac)_2$ (0.12 equivalents) at room

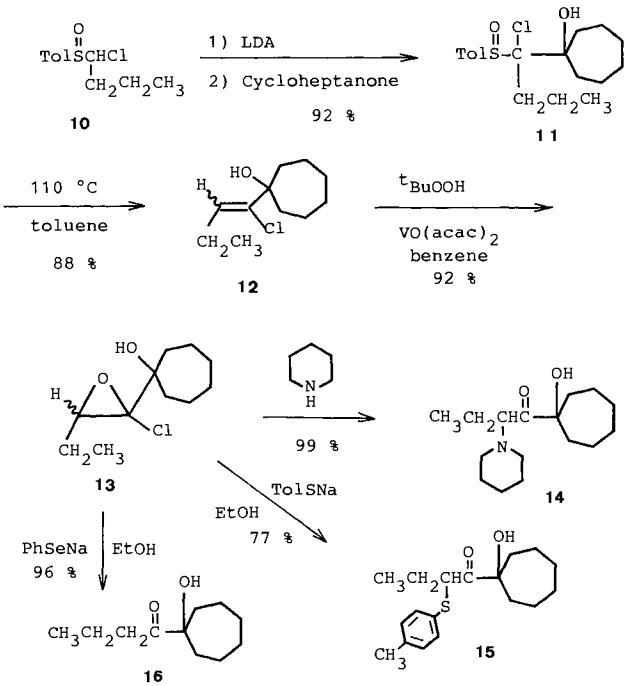

Scheme 3.

temperature (**Method A**). A slightly exothermic reaction took place to afford the desired chlorooxirane **13** in 92% yield. Chlorooxirane **13** was found to be stable under these reaction conditions and the usual workup system; it is storable for a few months in a refrigerator without any detectable decomposition.

We next investigated the reactivity of **13** with some nucleophiles. The treatment of **13** with piperidine[2c] without a solvent at room temperature gave the desired α-hydroxy α'-piperidino ketone **14** in quantitative yield within 10 min. The treatment of **13** with sodium *p*-toluenethiolate[2b] in ethanol at room temperature gave α-*p*-tolylthio ketone **15** in 77% yield within 10 min. The treatment of **13** with sodim benzeneselenolate[2a,6] in ethanol at room temperature gave α-hydroxy ketone **16** in 96% yield. From these results it became apparent that the reactivity of chlorooxirane **13** with the nucleophiles was quite similar to that of α,β-epoxy sulfoxides **3**.[2]

Encouraged by these results, we synthesized vinyl chlorides **17**—**20** from **10** or 1-chloroethyl *p*-tolyl sulfoxide (**5**; R=H) with cyclohexanone, cycloheptanone, 3-phenylpropanal, and decanal in a similar way to that described above.

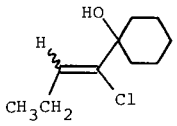

17

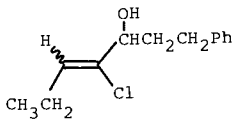

18

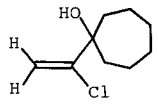

19

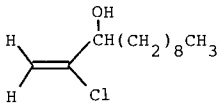

20

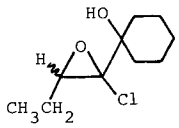

21

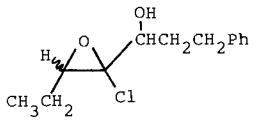

22

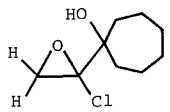

23

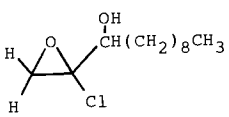

24

The epoxidation of **17** using **Method A** took place smoothly to give chlorooxirane **21** in 86% yield. The reaction of **21** with several nucleophiles gave α-hydroxy α'-substituted ketones **25**—**28** in high yields (see Table 1; Entry 1—4). Even sodium methoxide reacted with **21** at room temperature for 3 h to give α-hydroxy α'-methoxy ketone **27** in good yield (Entry 3).

We came across a problem in the epoxidation of vinyl chloride **18**—**20**. The epoxidation of **18**—**20** using **Method A** gave either no or an incomplete reaction; unfortunately, those vinyl chlorides (**18**—**20**) and chlorooxiranes (**22**—**24**) have the same (or quite close) R_f-value on silica-gel TLC, respectively. The other procedures reported for the epoxidation of allylic alcohols were unsuccessful. For instance, the epoxidation of **19** with ^{t}BuOOH–titanium(IV) isopropoxide or *m*-chloroperbenzoic acid (MCPBA) both gave mainly cycloheptanone and some unknown products.

After several investigations we found that the treatment of vinyl chlorides with ^{t}BuOOH and a very low concentration of $VO(acac)_2$ gave the desired chlorooxiranes in good yields. Thus, for example, to a solution of **18** and ^{t}BuOOH in benzene at 50 °C was added a dilute solution of $VO(acac)_2$ in benzene over a period of 1 h (**Method B**) to give **22** in quantitative yield as a low melting point solid. Monosubstituted chlorooxiranes **23** and **24** were synthesized by **Method B**; however, the yields were rather low compared with the disubstituted ones (**13**, **21**, and **22**). Chlorooxirane **23** was found to be unstable; it decomposed slowly, even on storage in a refrigerator. However, if it was used immediately after being prepared, the desired α-hydroxy α'-substituted ketones (**32** and **33**) were obtained in high yields without any problem. Representative examples for the synthesis of α-hydroxy α'-substituted ketones from carbonyl compounds are summarized in Table 1.

Nucleophilic ring-opening was investigated using some alkylmetals as carbon nucleophiles. The treatment of chlorooxirane **21** with *n*-butyllithium (3 equiv; −55 °C, 1 h), methylmagnesium bromide (3 equiv; −40 °C, 2 h), or lithium dimethylcuprate (3 equiv; 0 °C, 1.5 h) gave almost no reaction.

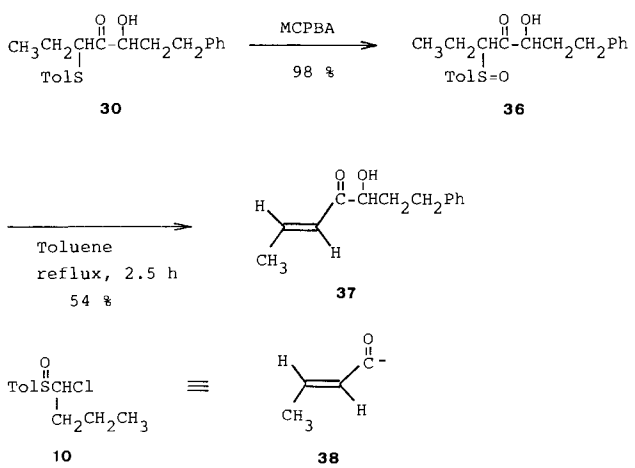

30 **36** **37** **10** **38**

Scheme 4.

Table 1. Synthesis of α-Hydroxy α′-Substituted Ketones **9** from Carbonyl Compounds through Chlorooxiranes **8**

Entry	Vinyl chloride (Yield/%)[a]	Epoxidation method[b]	Chlorooxirane (Yield/%)	Nucleophile	Product (Yield/%)	
1	**17** (93)	A	**21** (86)	Piperidine	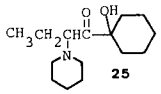 **25**	(95)
2				TolSNa	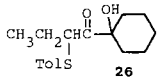 **26**	(92)
3				CH_3ONa	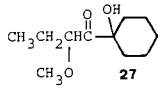 **27**	(83)
4				PhSeNa	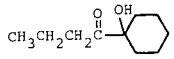 **28**	(98)
5	**18** (82)	B	**22** (98)	Piperidine	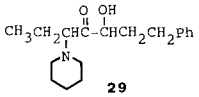 **29**	(52)
6				TolSNa	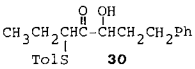 **30**	(99)
7				PhSeNa	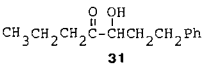 **31**	(60)
8	**19** (90)	B	**23** (74)	Piperidine	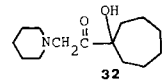 **32**	(92)
9				TolSNa	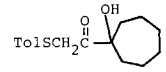 **33**	(99)
10	**20** (91)	B	**24** (62)	Piperidine	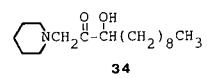 **34**	(95)
11				TolSNa	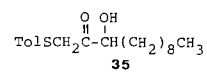 **35**	(92)

a) Two-step overall yield from 1-chloroalkyl *p*-tolyl sulfoxide and carbonyl compound. b) See text.

The application of this procedure to a synthesis of α-hydroxy α′,β′-unsaturated ketone was made with **30** (Scheme 4). The α-tolylthio ketone **30** was oxidized with MCPBA to sulfoxide **36** in quantitative yield as a diastereomeric mixture. Heating **36** in refluxing toluene for 2.5 h afforded (*E*)-5-hydroxy-7-phenyl-2-hepten-4-one **37** in 54% yield. In this entire sequence **10** acted as an α,β-unsaturated acyl anion equivalent **38**.

In conclusion a new and versatile procedure for the synthesis of α-hydroxy α′-substituted ketones has been developed from 1-chloroalkyl *p*-tolyl sulfoxides and carbonyl compounds through the reaction of chlorooxiranes with nucleophiles. Because of its simplicity and the good overall yields obtained, we believe that the presented method will prove to be valuable in the synthesis of α-hydroxy ketones, α-hydroxy α′-substituted ketones, and α-hydroxy α′,β′-unsaturated ketones.

Experimental

All of the melting points are uncorrected. The ^1H NMR spectra were measured in a $CDCl_3$ solution with a JEOL FX-100 spectrometer. Electron-impact mass spectra (MS) were obtained at 70 eV by direct insertion. Silica gel BW-127 ZH (Fuji-Devison) containing 2% of fluorescence reagent 254 and

a quartz column were used for column chromatography; products having UV absorption were detected by UV irradiation. In experiments requiring dry solvents, THF was distilled from diphenylketyl; benzene, toluene, and diisopropylamine were dried over CaH_2 and distilled. $VO(acac)_2$ was recrystallized from acetone.

1-(1-Chloro-1-butenyl)-1-cycloheptanol (12). A solution of **10** (1.15 g; 5 mmol) in 3 ml of dry THF was added dropwise to a stirred solution of LDA (6 mmol) in 6 ml of THF at −60 °C. The mixture was then stirred at −60 °C for 10 min; cycloheptanone (0.71 ml; 6 mmol) was then added to the reaction mixture. After 10 min the reaction was quenched with sat. aq NH_4Cl. The entire mixture was extracted with ether–benzene. The usual workup followed by silica-gel column chromatography gave chloro alcohol **11** (1.58 g; 92%) as a colorless oil, IR (neat) 3400 (OH), 1070, 1040 (SO) cm^{-1}.

A solution of **11** (1.3 g) in 15 ml of toluene was refluxed under N_2 for 5 min. The solvent was evaporated under vacuum and residue was separated by flash chromatography (hexane–AcOEt=20 : 1) to give 680 mg (88%) of **12** as a colorless oil. IR (neat) 3410 (OH), 1655 (C=C) cm^{-1}; ^1H NMR δ=1.01 (3H, t, J=7 Hz), 1.2—2.1 (13H, m), 2.21 (2H, quintet, J=7 Hz), 5.78 (1H, t, J=7 Hz); MS m/z (%) 202 (M^+, 22), 173 (73), 145 (96), 41 (100). Found: m/z 202.1127. Calcd for $C_{11}H_{19}ClO$: M, 202.1124.

1-(1-Chloro-1,2-epoxybutyl)-1-cycloheptanol (13). ^{t}BuOOH (anhydrous, 3 M solution in 2,2,4-trimethylpentane, 1 M= 1 mol dm^{-3}; 3.3 mmol) was added dropwise to a solution of **12** (527 mg; 2.6 mmol) and $VO(acac)_2$ (93 mg; 0.35 mmol) in 12 ml of dry benzene. A slightly exothermic reaction took place; the reaction mixture was stirred at room temperature for 1 h. The reaction mixture was passed through a short pad of Florisil. The solvent was evaporated and the residue was purified by silica-gel column chromatography to give **13** as a low melting point solid. IR (neat) 3480 (OH) cm^{-1}; ^1H NMR δ=1.06 (3H, t, J=7 Hz), 1.4—2.3 (15H, m), 3.32 (1H, t, J=7 Hz); MS m/z (%) 219 ([M+H]$^+$, trace), 189 ([M−C_2H_5]$^+$, 0.8), 113 (100).

1-(1-Hydroxycycloheptyl)-2-piperidino-1-butanone (14). A mixture of **13** (113 mg) in 2 ml of piperidine was stirred at room temperature for 10 min. The piperidine was evaporated and the residue was dissolved in benzene. The solution was washed once with water, and then dried over $MgSO_4$. The usual workup followed by silica-gel column chromatography gave **14** (137 mg; 99%) as an oil. IR (neat) 3250 (OH), 1710 (CO) cm^{-1}; ^1H NMR δ=0.78 (3H, t, J=7 Hz), 1.2—2.2 (21H, m), 2.50 (4H, m), 3.58 (1H, dd, J=10, 3 Hz); MS m/z (%) 266 (M^+, 0.2), 238 (0.1), 210 (0.1), 154 (0.3), 126 (100). Found: m/z 266.2118. Calcd for $C_{16}H_{28}NO_2$: M, 266.2118.

1-(1-Hydroxycycloheptyl)-2-(*p*-tolylthio)-1-butanone (15). To 3 ml of EtOH at room temperature was added NaH (0.78 mmol) and then *p*-toluenethiol (105 mg; 0.85 mmol). A solution of **13** (85 mg; 0.39 mmol) in 0.5 ml of EtOH was added to a solution of the thiolate; the reaction mixture was stirred at room temperature for 10 min. Powdered NH_4Cl was added to this mixture, and the EtOH was evaporated under vacuum. The residue was extracted with benzene and the usual workup was followed by silica-gel column chromatography, giving 92 mg (77%) of **15** as colorless crystals. Mp 70—72 °C (AcOEt–hexane); IR (KBr) 3525 (OH), 1690 (CO) cm^{-1}; ^1H NMR δ=0.92 (3H, t, J=7 Hz), 1.3—2.2 (15H, m), 2.33 (3H, s), 4.03 (1H, t, J=7 Hz), 7.0—7.3 (4H, m). Anal. Calcd for $C_{18}H_{26}O_2S$: C, 70.55; H, 8.55; S, 10.46%. Found: C, 70.57; H, 8.60; S, 10.40%.

1-(1-Hydroxycycloheptyl)-1-butanone (16). $NaBH_4$ (153 mg; 4.05 mmol) was added to a solution of diphenyl diselenide (630 mg; 2.03 mmol) in 9 ml of EtOH at room temperature. After all of the $NaBH_4$ reacted, a solution of **13** (147 mg; 0.67 mmol) in 1 ml of EtOH was added to the benzeneselenolate solution. The reaction mixture was stirred at room temperature for 10 min; powdered NH_4Cl was then added. The EtOH was evaporated under vacuum and the residue extracted with benzene–ether. The organic layer was washed once with sat. aq NH_4Cl and the usual workup followed by silica-gel column chromatography gave 119 mg (96%) of **16** as a colorless oil. IR (neat) 3480 (OH), 1700 (CO) cm^{-1}; ^1H NMR δ=0.92 (3H, t, J=7 Hz), 1.3—2.0 (14H, m), 2.52 (2H, t, J=7 Hz); MS m/z (%) 184 (M^+, 0.25), 167 (0.15), 113 (100). Found: m/z 184.1468. Calcd for $C_{11}H_{20}O_2$: M, 184.1462.

1-(1-Chloro-1-butenyl)-1-cyclohexanol (17). This vinyl chloride was synthesized from **10** and cyclohexanone in a similar manner as that described for **12** in 93% overall yield. Colorless oil; IR (neat) 3410 (OH), 1655 (C=C) cm^{-1}; ^1H NMR δ=1.01 (3H, t, J=7 Hz), 1.2—1.9 (10H, m), 2.22 (2H, quintet, J=7 Hz), 5.80 (1H, t, J=7 Hz); MS m/z (%) 188 (M^+, 50), 159 ([M−C_2H_5]$^+$, 100). Found: m/z 188.0965. Calcd for $C_{10}H_{17}ClO$: M, 188.0966.

Vinyl Chloride (18—20). These vinyl chlorides were reported in the previous paper: see Ref. 7.

1-(1-Chloro-1,2-epoxybutyl)-1-cyclohexanol (21). This chlorooxirane was synthesized from **17** in a similar manner (**Method A**) as that described for **13** in 86% yield. Colorless low melting solid. IR (KBr) 3525 (OH) cm^{-1}; ^1H NMR δ=1.06 (3H, t, J=7 Hz), 1.4—2.0 (13H, m), 3.30 (1H, t, J=7 Hz); MS m/z (%) 175 ([M−C_2H_5], 0.3), 146 (3), 99 (100).

4-Chloro-4,5-epoxy-1-phenyl-3-heptanol (22). A solution of $VO(acac)_2$ (106 mg; 0.4 mmol) in 50 ml of dry benzene was added dropwise to a stirred solution of **18** (440 mg; 1.95 mmol) and ^{t}BuOOH (4.5 mmol) in 10 ml of dry benzene at 50 °C over a period of 1 h (**Method B**). The reaction mixture was passed through a short pad of Florisil and the solvent evaporated. The residue was purified by silica-gel column chromatography to afford 457 mg (98%) of **22** as a low melting point solid. IR (KBr) 3400 (OH) cm^{-1}; ^1H NMR δ=1.07 (3H, t, J=7 Hz), 1.4—2.4 (5H, m), 2.6—3.0 (2H, m), 3.14 (1H, t, J=6 Hz), 3.86 (1H, dd, J=8, 4 Hz), 7.22 (5H, m); MS m/z (%) 240 (M^+, 0.5), 205 (2.5), 193 (2), 104 (100). Found: m/z 240.0918. Calcd for $C_{13}H_{17}ClO_2$: M, 240.0916.

Chlorooxirane (23, 24). These chlorooxiranes were synthesized from **19** and **20** in a similar manner as that described for **22** (**Method B**).

1-(1-Chloro-1,2-epoxyethyl)-1-cycloheptanol **23**: Colorless oil; 74% yield; IR (neat) 3475 (OH) cm^{-1}; ^1H NMR δ=1.4—2.3 (13H, m), 3.01 (1H, d, J=5 Hz), 3.24 (1H, d, J=5 Hz); MS m/z (%) 149 (0.5), 113 ([M−C_2H_2ClO]$^+$, 100).

2-Chloro-1,2-epoxy-3-dodecanol **24**: Colorless oil; 62% yield; IR (neat) 3425 (OH) cm^{-1}; ^1H NMR δ=0.87 (3H, t, J=6 Hz), 1.0—2.2 (16H, m), 3.07 (2H, s), 3.82 (1H, m); MS m/z (%) 235 ([M+H]$^+$, 0.3), 234 (M^+, 0.1), 198 (2), 155 (40), 83 (100).

1-(1-Hydroxycyclohexyl)-2-piperidino-1-butanone (25). Colorless oil; IR (neat) 3280 (OH), 1720 (CO) cm^{-1}; ^1H NMR δ=0.87 (3H, t, J=7 Hz), 1.0—2.0 (18H, m), 2.50 (4H, m), 3.54

(1H, dd, J=10, 4 Hz); MS m/z (%) 253 (M^+, trace), 252 (0.2), 126 (100). Found: m/z 253.2026. Calcd for $C_{15}H_{27}NO_2$: M, 253.2039.

1-(1-Hydroxycyclohexyl)-2-(*p*-tolylthio)-1-butanone (26). Colorless crystals; mp 63—64 °C (AcOEt–hexane); IR (KBr) 3510 (OH), 1700 (CO) cm^{-1}; ^1H NMR δ=0.90 (3H, t, J=7 Hz), 1.4—2.0 (12H, m), 2.32 (3H, s), 4.04 (1H, dd, J=8, 7 Hz), 7.0—7.3 (4H, m); MS m/z (%) 292 (M^+, 14), 222 (3), 194 (16), 166 (58), 124 (100). Anal. Calcd for $C_{17}H_{24}O_2S$: C, 69.82; H, 8.27; S, 10.96%. Found: C, 69.58; H, 8.21; S, 10.85%.

1-(1-Hydroxycyclohexyl)-2-methoxy-1-butanone (27). NaH (1 mmol) was added to dry methanol (2.5 ml); a solution of **21** (62 mg; 0.3 mmol) in 0.5 ml of methanol was then added to the methoxide solution. The reaction mixture was stirred at room temperature for 3 h. Powdered NH_4Cl was added to the reaction mixture, and the methanol was evaporated under vacuum. The residue was extracted with benzene–ether. The solution was washed once with water. The usual workup followed by silica-gel column chromatography gave **27** (50 mg; 83%) as a colorless oil. IR (neat) 3510 (OH), 1720 (CO) cm^{-1}; ^1H NMR δ=0.95 (3H, t, J=7 Hz), 1.4—2.0 (12H, m), 3.33 (3H, s), 4.10 (1H, dd, J=6, 5 Hz); MS m/z (%) 200 (M^+, trace), 173 (0.3), 172 (3), 99 (100). Found: m/z 200.1430. Calcd for $C_{11}H_{20}O_3$: M, 200.1411.

1-(1-Hydroxycyclohexyl)-1-butanone (28). Colorless oil; IR (neat) 3510 (OH), 1710 (CO) cm^{-1}; ^1H NMR δ=0.92 (3H, t, J=7 Hz), 1.0—1.9 (12H, m), 2.53 (2H, t, J=7 Hz); MS m/z (%) 170 (M^+, 0.4), 159 (0.5), 99 (100). Found: m/z 170.1303. Calcd for $C_{10}H_{18}O_2$: M, 170.1305.

3-Hydroxy-1-phenyl-5-piperidino-4-heptanone (29). Diastereomeric mixture with respect to the two chiral carbon (ratio about 1:1). Colorless oil; IR (neat) 3450 (OH), 1715 (CO) cm^{-1}; ^1H NMR δ=0.81, 0.85 (each triplet, J=7 Hz), 4.0—4.3 (1H, m), 7.21 (5H, m); MS m/z (%) 288 ($[M-H]^+$, trace), 261 (0.2), 204 (4), 126 (100).

3-Hydroxy-1-phenyl-5-(*p*-tolylthio)-4-heptanone (30). Diastereomeric mixture (ratio about 2:1). Colorless oil; IR (neat) 3510 (OH), 1710 (CO) cm^{-1}; ^1H NMR δ=0.97 (3H, t, J=7 Hz), 1.5—2.2 (4H, m), 2.31 (3H, s), 2.72 (2H, m), 3.50 (2/3H, t, J=7 Hz), 3.76 (1/3H, t, J=7 Hz), 4.22 (1/3H, m), 4.56 (2/3H, m), 7.0—7.4 (9H, m); MS m/z (%) 328 (M^+, 20), 205 (5), 165 (100). Found: m/z 328.1495. Calcd for $C_{20}H_{24}O_2S$: M, 328.1495.

3-Hydroxy-1-phenyl-4-heptanone (31). Colorless oil; IR (neat) 3500 (OH), 1715 (CO) cm^{-1}; ^1H NMR δ=0.91 (3H, t, J=7 Hz), 1.4—2.3 (4H, m), 2.39 (2H, t, J=7 Hz), 2.76 (2H, m), 4.12 (1H, dd, J=8, 3 Hz), 7.21 (5H, m); MS m/z (%) 206 (M^+, 2), 134 (12), 117 (20), 102 (46), 91 (100). Found: m/z 206.1302. Calcd for $C_{13}H_{18}O_2$: M, 206.1305.

1-(1-Hydroxycycloheptyl)-2-piperidino-1-ethanone (32). Colorless crystals; mp 87—89 °C (AcOEt–hexane); IR (KBr) 3225 (OH), 1720 (CO) cm^{-1}; ^1H NMR δ=1.2—2.0 (18H, m), 2.45 (4H, m), 3.29 (2H, s); MS m/z (%) 239 (M^+, trace), 211 (0.7), 149 (0.3), 98 (100). Anal. Calcd for $C_{14}H_{25}NO_2$: C, 70.25; H, 10.53; N, 5.85%. Found: C, 70.42; H, 10.58; N, 5.94%.

1-(1-Hydroxycycloheptyl)-2-(*p*-tolylthio)-1-ethanone (33). Colorless oil; IR (neat) 3510, 3410 (OH), 1705 (CO) cm^{-1}; ^1H NMR δ=1.4—2.0 (12H, m), 2.31 (3H, s), 3.89 (2H, s), 7.0—7.4 (4H, m); MS m/z (%) 278 (M^+, 10), 166 (31), 138 (73), 124 (100). Found: m/z 278.1335. Calcd for $C_{16}H_{22}O_2S$: M, 278.1338.

3-Hydroxy-1-piperidino-2-dodecanone (34). Colorless oil; IR (neat) 3370 (OH), 1720 (CO) cm^{-1}; ^1H NMR δ=0.87 (3H, t, J=7 Hz), 1.0—1.9 (22H, m), 2.42 (4H, m), 3.24 (2H, s), 4.22 (1H, m); MS m/z (%) 283 (M^+, 0.1), 282 (0.3), 196 (1), 155 (10), 98 (100). Found: m/z 283.2490. Calcd for $C_{17}H_{33}NO_2$: M, 283.2509.

3-Hydroxy-1-(*p*-tolylthio)-2-dodecanone (35). Colorless crystals; mp 69—71 °C (AcOEt–hexane); IR (KBr) 3550, 3380 (OH), 1720 (CO) cm^{-1}; ^1H NMR δ=0.88 (3H, t, J=6 Hz), 1.0—1.9 (16H, m), 2.31 (3H, s), 3.72 (2H, s), 4.40 (1H, m), 7.0—7.4 (4H, m); MS m/z (%) 322 (M^+, 32), 137 (48), 124 (100). Anal. Calcd for $C_{19}H_{30}O_2S$: C, 70.76; H, 9.38; S, 9.94%. Found: C, 70.69; H, 9.44; S, 9.70%.

(*E*)-5-Hydroxy-7-phenyl-2-hepten-4-one (37). MCPBA (2.75 mmol) was added to a stirred solution of the sulfide **30** (820 mg; 2.5 mmol) in 30 ml of CH_2Cl_2. The reaction mixture was stirred at −50 °C for 30 min; the mixture was then diluted with CH_2Cl_2 and the solution washed successively with 5% NaOH and sat. aq NH_4Cl. The usual workup followed by silica-gel column chromatography afforded a diastereomeric mixture of sulfoxide **36** (840 mg; 98%).

A solution of **36** (830 mg) in 20 ml of toluene was refluxed under N_2 for 2.5 h. The solvent was evaporated under vacuum and the residue purified by silica-gel column chromatography (hexane:AcOEt=20:1) to afford 265 mg (54%) of enone **37** as a colorless oil. IR (neat) 3470 (OH), 1690 (CO), 1630 (C=C) cm^{-1}; ^1H NMR δ=1.6—2.3 (2H, m), 1.90 (3H, dd, J=7, 1 Hz), 2.76 (2H, m), 4.32 (1H, dd, J=9, 4 Hz), 6.17 (1H, dq, J=16, 1 Hz), 6.96 (1H, dq, J=16, 7 Hz), 7.20 (5H, m); MS m/z (%) 204 (M^+, 0.6), 117 (12), 100 (90), 91 (100). Found: m/z 204.1147. Calcd for $C_{13}H_{16}O_2$: M, 204.1149.

We are grateful to Dr. Mikio Takeda, Tanabe Seiyaku Co., Ltd., for the elemental analysis, and to Noriko Sawabe and Fukiko Hasegawa of this laboratory for the NMR and MS measurements. This work was supported by a Grant-in-Aid for Scientific Research No. 01571168 from the Ministry of Education, Science and Culture, which is gratefully acknowledged.

References

1) For reviews: O. William Lever, Jr., *Tetrahedron,* **32**, 1943 (1976); S. F. Martin, *Synthesis,* **1979**, 633; J. C. Stowell, *Chem. Rev.,* **84**, 409 (1984).

2) a) T. Satoh, Y. Kaneko, T. Izawa, K. Sakata, and K. Yamakawa, *Bull. Chem. Soc. Jpn.,* **58**, 1983 (1985); b) T. Satoh, T. Kumagawa, and K. Yamakawa, *ibid.,* **58**, 2849 (1985); c) T. Satoh, Y. Kaneko, K. Sakata, and K. Yamakawa, *ibid.,* **59**, 457 (1986); d) T. Satoh, M. Itoh, T. Ohara, and K. Yamakawa, *ibid.,* **60**, 1839 (1987); e) T. Satoh and K. Yamakawa, *Yuki Gosei Kagaku Kyokai Shi,* **47**, 734 (1989).

3) A few studies with halogenated epoxides were reported: J. Gasteiger and C. Herzig, *Angew. Chem., Int. Ed. Engl.,* **20**, 868 (1981); M. Spraul and K. Griesbaum, *Chem. Ber.,* **116**, 2641 (1983); H. Keul, B. Pfeffer, and K. Griesbaum, *ibid.,* **117**, 2193 (1984); K. Griesbaum, G. O. Lie, and H. Keul, *J. Org. Chem.,* **49**, 679 (1984).

4) T. Satoh, K. Onda, and K. Yamakawa, *Tetrahedron Lett.,* **31**, 3567 (1990).

5) a) K. B. Sharpless and T. R. Verhoeven, *Aldrichimica Acta,* **12**, 63 (1979); b) T. Itoh, K. Jitsukawa, K. Kaneda, and S. Teranishi, *J. Am. Chem. Soc.,* **101**, 159 (1979); c) A. S. Rao, S. K. Paknikar, and J. G. Kirtane, *Tetrahedron,* **39**, 2323 (1983).

6) M. Miyashita, T. Suzuki, and A. Yoshikoshi, *Tetrahedron Lett.,* **28**, 4293 (1987); M. Miyashita, M. Hoshino, and A. Yoshikoshi, *ibid.,* **29**, 347 (1988).

7) T. Satoh, K. Onda, and K. Yamakawa, *J. Org. Chem.,* in press.

Characteristics of the Membrane Permeability of Temperature-Sensitive Liposome

Masaharu UENO,* Shoshin YOSHIDA, and Isamu HORIKOSHI†
Faculty of Pharmaceutical Sciences, Toyama Medical & Pharmaceutical University,
2630 Sugitani, Toyama 930-01
† Department of Hospital Pharmacy, Toyama Medical & Pharmaceutical University,
2630 Sugitani, Toyama 930-01
(Received December 20, 1990)

The relationship between the temperature-sensitivity of the release of an entrapped drug from liposome as well as the type of drug or liposome is discussed. The drug release from DPPC liposome (dipalmitoylphosphatidylcholine liposome) has been confirmed to increase abruptly near its phase-transition temperature for both low-molecular-weight compouds (such as calcein) and high-molecular-weight compounds (such as dextran). The amount of temperature-sensitive calcein released from the liposomes was dependent on the method of liposome preparation: that is, the release from REV (reverse phase evaporated vesicle) was the highest; next was that from LUV (large unilamellar vesicle prepered by detergent removal method), and lowest was from SUV (small unilamellar vesicle prepared by an ultrasonication method). In order to examine the size effect of liposomes on temperature-sensitive drug release, REV was fractionated into three groups according to their average sizes and calcein release for each group was investigated. The temperature at which calcein release showed a maximum was almost the same in each of three groups; while as the average liposome size of a group was larger, the initial rate of calcein release became higher and the temperature at which calcein release began became lower. The amount of release of a entrapped drug was primarily dependent on the molecular weight of the drug, in spite of the variety of drugs investigated.

Liposomes have been regarded as having promise for use as a new type of drug carrier. They can encapsulate either hydrophilic or hydrophobic drugs in their inner core or membrane matrix. They can be expected to have different forms of interactions with bioorgan than do other types of drug carriers, such as emulsions or microspheres, judged from a similarity with biological cell membranes regarding both structure and nature. They can also be considered as being biodegradable and to have little toxity.[1,2] One obstacle in putting liposomes to practical use as drug carriers has been a difficulty in controlling the release of encapsulated drugs. Yatbin et al.[3] and Weinstein et al.[4] showed the possibility of medical applications of the so-called "temperature-sensitive liposome", which enables the control of drug release from a liposome using the nature of the phospholipid membrane; the barrier efficiency of the membrane abruptly decreases near the phase transition temperature of a gel-to-liquid crystalline of the phospholipid membrane.[5] This report concerns an extension of their idea. In order to extend the application of a temperature-sensitive liposome, it is especially important to clarify the characteristics of the temperature-sensitive membrane permeability. In this report the effects of various entrapped drugs and the forms of liposomes on the temperature-sensitive drug release were studied. Especially, results concerning the possibility of controlling the release of macromolecule drugs would stimulate the use of temperature-sensitive liposomes for medical applications, since many macromolecular drugs, such as urokinase, are easily inactivated by a variety of inhibitors in the blood;[6] also, their clearance from blood is very rapid.

Experimental

Materials. L-α-phosphatidylcholine from egg yolk (egg PC) was purchased from Green Cross Co. (no less than 99% purity). L-α-dipalmitoylphosphatidylcholine (DPPC) was obtained from Sigma Co. (no less than 99% purity determined by thin-layer chromatography). *N*-octyl β-D-glucoside and calcein (3,3′-bis[*N*,*N*-(dicalboxymethyl)aminomethyl]fluorescein) were obtained from Dojindo Laboratories. Dextran ($\overline{M_W}$; 70000) and inulin were purchased from Wako Chemicals. Urokinase was obtained from Kyorin Co, (the trade name is caltokinase). Sinthesized fluorescenced urokinase substrate, Glutaryl-Gly-Arg-MCA (4-methylcoumarinamide), was obtained from Protein Research Foundation. ^{3}H-dextran (specific activity; 336 μCi mg^{-1}) and ^{14}C-inulin (specific activity; 2.6 μCi mg^{-1}) were obtained from Amercham. Hydrophobic beads used for detergent removal were Amberlite XAD-2 obtained from Tokyo Organic Chemicals. All other reagents were of reagent grade from Wako Chemicals or Nakarai Chemicals.

Methods. Liposome Preparation. DPPC-SUV (small unilamellar vesicle) was prepared according to a method of Weinstein et al.[4] or Watt et al.[7] as follows: a dried, thin film of dipalmitoylphosphatidylcholine was swollen with buffer solution, (if necessary, containing an appropriate drug,) for 2 min at 50°C followed by shaking for 20 s; this process was repeated 3 times. The resulting suspension was sonicated using a probe-type sonicator (Taiyo Seiki Co., model UR-200P) at 50 °C for 60 min, followed by standing for 15 min at 50 °C. The suspension was then ultracentrifuged at 100000×*g* for 15 min using a centrifuge (Hitachi automatic preparative ultracentrifuge, 55p-72). SUV was obtained from the supernatant.

DPPC-LUV (large unilamellar vesicle) was prepared according to a method described in previous papers[8-10] as follows: a dried thin film of phospholipid was solubilized by octyl glucoside (molar ratio of pospholipid to octyl glucoside was 1/10);

the solubilized micellar solution was rapidly passed through a XAD-2-loaded column at 50 °C. The liposomes prepared by this method have been known to be mostly unilamellar vesicle. LUV was obtained after 15 passages through the column.

DPPC- or EggPC-REV (reverse-phase evaporated vesicle) was prepared according to a method of Szoka et al.[11] The preparation of an emulsion during this procedure was accomplished using diisopropyl ether / chloroform (1/1) at 47 °C for DPPC-REV preparation, and diethyl ether at 4 °C for EggPC-REV.

Any untrapped drug was removed by centrifugation for REV or gel chromatography using Sephadex G-50 for LUV or SUV. The drug-loaded liposomes were resuspended in Tris-HCl buffer (150 mM NaCl / 10 mM Tris-HCl / pH 7.4, 1 M=1 mol dm^{-3}) and, if necessary, concentrated or diluted to make an appropriate concentration for succeeding release experiments.

Size Fractionation of REV. Since REV contained various sizes of liposomes, it was fractionated by centrifugation as follows: First, REV suspension was centrifuged at 30000×*g* at 4 °C for 20 min. Small REV (S-REV) was obtained from the supernatant. The precipitate was resuspended in Tris-buffer after being washed by a cold buffer 3 times, and centrifuged at 1000×*g* at 4 °C for 20 min. Medium REV (M-REV) was obtained from the supernatant and large REV (L-REV) from the precipitate. These suspensions were either diluted or concentrated to make an appropriate concentration for the succeeding release experiment.

Entrapping Efficiency and Captured Volume. The entrapping efficiency and captured volume were evaluated by adding a fluorescence quencher in a calcein-containing liposome suspension[12] as follows: liposome was prepared in 10 μM of a calcein solution; the remaining fluorescence intensities were measured after the fluorescence of untrapped calcein was quenched by the addition of an appropriate amount of 100 mM $CoCl_2$. The entrapping efficiency was calculated by using the following equation:

$$\text{entrapping efficiency (\%)} = \frac{f_{in}\, r_1 - f_{total,q}\, r_2}{f_{total} - f_{total,q}\, r_2} \times 100,$$

where f_{in} is the fluorescence intensity of the internal calcein; f_{total} and $f_{total,q}$ are the total fluorescence intensity of the calcein before and after liposome destruction, respectively; r_1 and r_2 are correction factors for the volume increase upon adding a $CoCl_2$ solution and the Triton X-100 solution, respectively. They were 2620/2600 and 2625/2600 in our experiments. The fluorescence intensity of calcein was measured by a fluorophotometer (Shimadzu, difference spectrofluorophotometer, RF-503A) at 490 nm for exitation and 520 nm for emission. The captured volume was defined as being the total internal volume per mole of phospholipid, calculated from the amount of drug captured.

Release Measurement of Entrapped Drug. Calcein release was evaluated by a fluorescence self-quenching method according to Yatvin et al.[3] or Senior et al.[13]; 20 μl of a liposome suspension containing 100 mM of calcein was added to 2.5 ml of a buffer solution which had been kept at the desired temperature in advance. With this method the temperature was rapidly controlled. ^{14}C-inulin and ^{3}H-dextran release was monitored by measuring their radioactivity (using an Aloka scintilation system, LSC-900) in the supernatant by centrifugation at 40000×*g* for 20 min at 4 °C after an appropriate incubation time of the liposome suspensions at the desired temperature.

Urokinase release was monitored enzymatically using a fluorescenced urokinase substrate according to the method of Morita et al.[14]

Other Methods. The liposome size was evaluated by quasielastic light scattering (QELS) using a laser particle analyzing system (Otsuka Electronics Co. LPA 3000/3100). The phase-transition temperature was monitored by calorimetry using a differential scanning calorimeter (2nd Seiko Co. SSC-560). Phospholipid concentrations were determined by the micro method of Bartlet.[15]

Results

Characterization of Liposomes. The size and entrapping efficiency of liposomes prepared by several methods are summarized in Table 1. REV was the largest regarding both size and entrapping efficiency. The stability or barrier efficiency of DPPC-REV in a buffer solution at 4 °C are shown in Table 2. About 90% of the low-molecular-weight compound (calcein) and about 100% of the high-molecular-weight compound (dextran) were retained in the liposomes after 4 weeks of incubation. Judged from these observations, the liposomes could be regarded as having a high barrier efficiency against both low- or high-molecular-weight compounds at a temperature below their phase-transition temperature.

Calcein Release and Phase Transition. In order to examine the characteristics of the temperature-sensitive membrane permeability, the release of calcein from the liposome was investigated under several conditions. In Fig. 1, DSC curve of DPPC-REV and calcein release (%) from the liposome after 2 min incubation at several temperatures are shown. An endthermal peak due to the phase transition of DPPC hydrocarbon chains was observed at 42 °C. At the corresponding temperature

Table 1. Characterization of Various DPPC-Liposomes Used in This Study

	SUV	LUV	REV
Diameter/nm	40	345	1800
Entrapping efficiency[a]/%	1.9±0.4	8.7±2.7	17.7±2.9
Captured volume[b] (l/mole of lipid)	2.8±0.7	8.4±2.6	13.6±1.8

a) mean±S.D. (n=6). b) mean±S.D. (n=3).

Table 2. Barrier Efficiency of DPPC-REV in Buffer at 4 °C

	Remaining/% (mean±S.D., n=3)		
	1 day	1 week	4 weeks
Calcein	99.2±0.2	93.9±2.7	90.7±3.5
Dextran	98.3±7.5	97.0±5.5	98.2±8.3

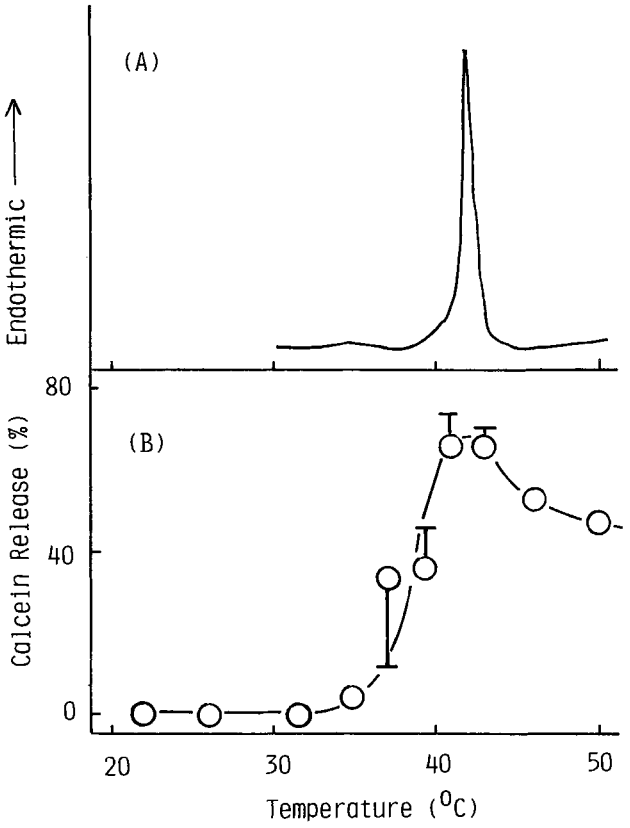

Fig. 1. Relationship between phase-transition temperature of DPPC-REV and calcein release (%) for 2 min incubation. (A): differential scanning calorimetry thermogram. (B): calcein release (%). Each point represents mean±S.D. (n=4—5).

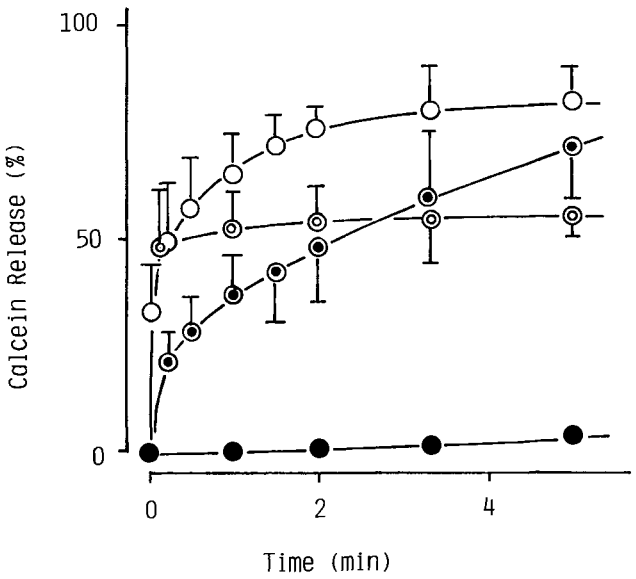

Fig. 2. Time course of calcein release from DPPC-REV. ●, 34.5°C; ◉, 39.3°C; ○, 41.0°C; ◎, 46.0°C. Each point represents the mean±S.D. (n=4—5).

the liposome showed maximum release. The time course of calcein release from DPPC-REV is shown in Fig. 2. The initial rate of calcein release seemed to become faster as the incubation temperature become higher; the rate at 46 °C was the highest measured, while the total amount of calcein released during 2 min of incubation became largest at 41 °C, near the phase-transition temperature, instead of 46 °C. At 46 °C, calcein release plateaued at a levels (ca. 50% of entrapped calcein) after 1 min of incubation. The drastic release observed during the initial stage at 46 °C would be due to the temporary experience of the optimum temperature of calcein release, (that is, the phase-transition temperature of the membrane phospholipid), during a temperature rise from room temperature to 46 °C. The saturation phenomenon regarding release % after 1 min of incubation at 46 °C suggests that the liposome again came to have a high barrier efficiency at a higher temperature than the transition temperature.

The Temperature-Sensitivity of Calcein Release Depending on the Preparation Method of the Liposomes. The calcein release % from liposomes prepared by several methods is shown in Fig. 3. EggPC-REV, whose phase-transition temperature is below 0 °C, did not practically make calcein release within experimental temperature range (24—47 °C), while DPPC liposomes prepared by any method showed (more or less) a temperature-sensitivity in calcein release near 40 °C. The release % of

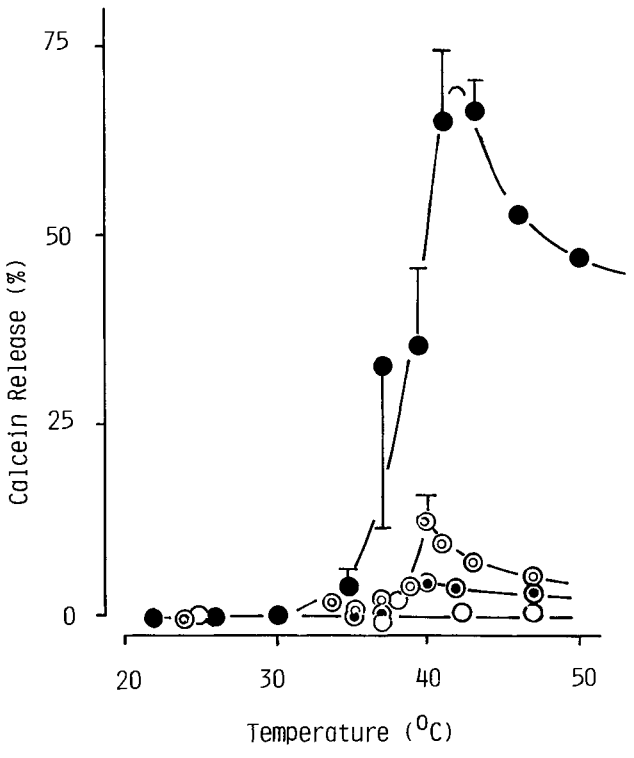

Fig. 3. Temperature dependence of calcein release from various types of liposomes. ○, eggPC-REV; ●, DPPC-REV; ◎, DPPC-LUV; ◉, DPPC-SUV. Each point represents mean±S.D. (n=4—5).

calcein was dependent on the method of liposome preparation; calcein release % from REV was the highest of all, followed by LUV, and then SUV.

Dextran Release from REV. Concerning DPPC-REV, which had showed the highest temperature-sensitivity for the release of calcein adopted as a model compound for low-molecular-weight drugs, the behavior of dextran release as a model compound for high-molecular-weight drugs was studied. The results are given in Figs. 4 and 5. As shown in Fig. 4, REV showed the maximum release (%) of dextran near 40 °C, similar to the case of a low-molecular-weight compound: that is, REV was found to possess the characteristics of temperature-sensitivity, even for the release of a high-molecular-weight compound. As shown in Fig. 5, the time course of dextran release from REV was also similar to that of calcein; that is, an initial high release followed by a dull release was observed. On the whole, the release % of dextran was smaller than that of calcein. For a high-molecular-weight compound, a saturation phenomenon was observed during its release, even at optimum temperature. The maximum amount of dextran released at the transition temperature was only 20% of encapsulated amount, while that of calcein was 70—90%. These observations suggest the inhomogeneity of the liposome in size and/or property; that is, the coexistance of both vesicles (permeable and inpermeable) for macro molecules, even at the transition temperature.

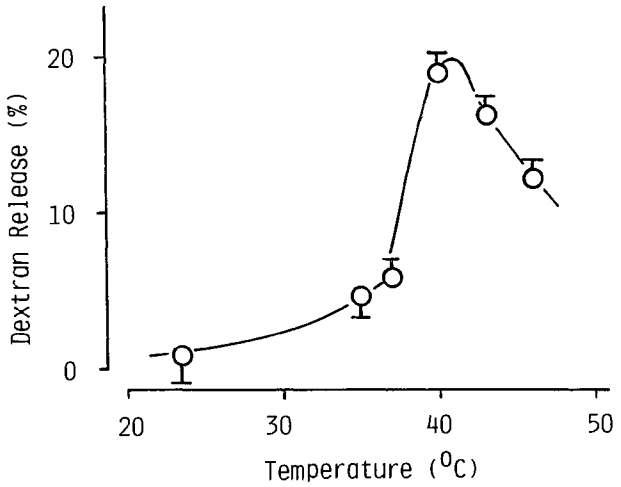

Fig. 4. Temperature dependence of dextran release from DPPC-REV. Each point represents mean±S.D. (n=4—5).

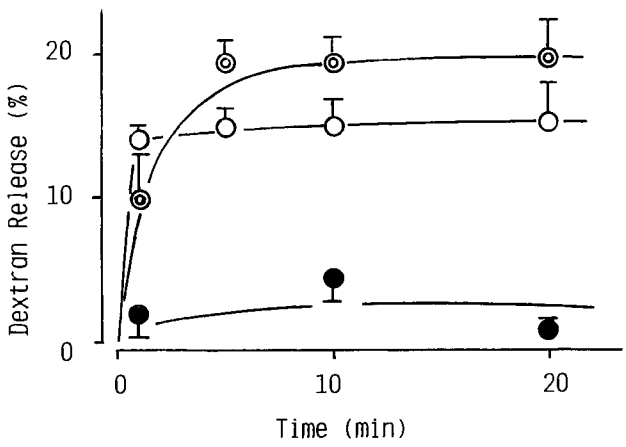

Fig. 5. Time course of dextran release from DPPC-REV at several temperatures. ●, 37 °C; ◎, 40 °C; ○, 42 °C. Each point represents the mean±S.D. (n=4).

Caracteristics of the Temperature-Sensitive Membrane Permeability. A pattern analysis of the time course of calcein release from DPPC-REV was carried out. In Fig. 6, the time course of the remaining percent of calcein in REV at 34.5 °C is shown on a logarithmic scale. At 34.5 °C the rate of calcein release was extremely slow and obeyed the first-order efflux. At 39.7 or 41.0 °C (near phase transition temperature) the efflux pattern seemed to have two or more phases; that is, an initial high efflux followed by a slow efflux was observed. These observations suggest that these liposomes must be inhomogenous in the size and/or property. In order to confirm the above suggestion, these liposomes were tentatively fractionated into 3 groups by centrifugation as S-REV with 100 nm of average diameter, M-REV with 2000 nm and L-REV with 3000 nm; the calcein efflux from each fractionated liposome was tested (data not shown). The calcein release rate was of the order of L-REV, M-REV, and S-REV. The polyphase of the efflux pattern for calcein release from the liposomes would be mainly due to the polydispersity of

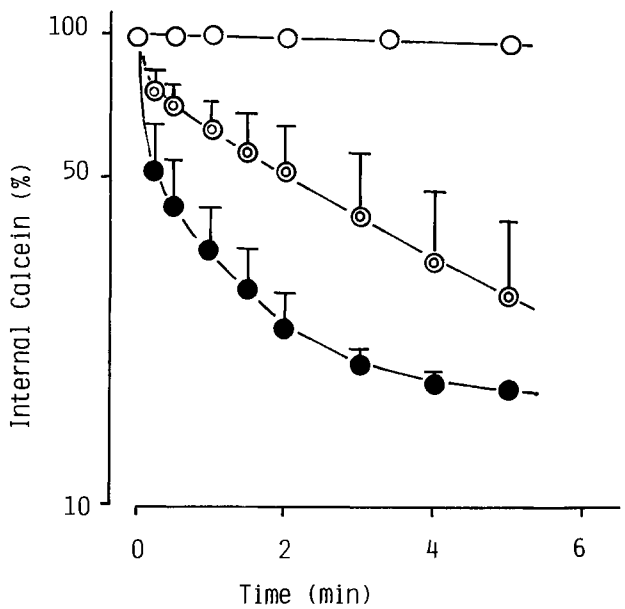

Fig. 6. Time course of remaining calcein (%) in DPPC-REV in logarithmic scale at several incubation temperatures. ○, 34.5 °C; ◎, 39.3 °C; ●, 41.0 °C. Each point represents the mean±S.D. (n=4).

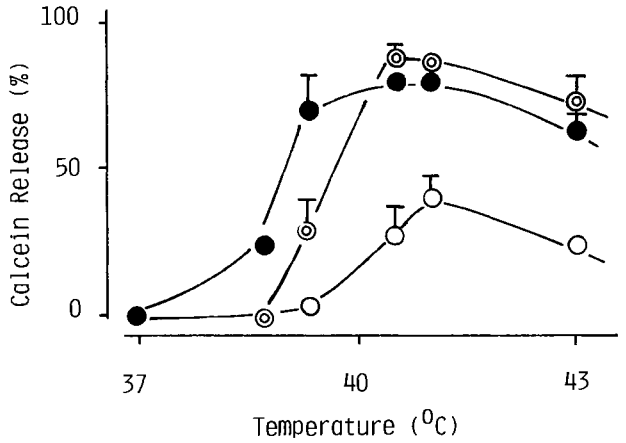

Fig. 7. Effect of liposome size on temperature-dependent calcein release. ●, L-REV; ◎, M-REV; ○, S-REV. Each point represents the mean±S.D. (n=3-4).

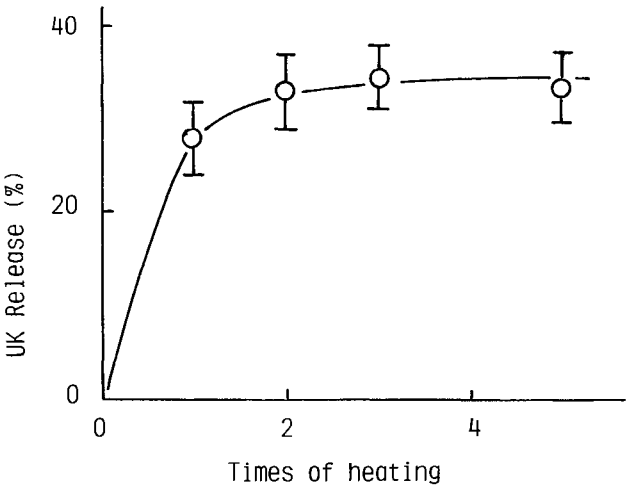

Fig. 8. Influence of the repeated heating on the release of urokinase from DPPC-REV. Each point represents mean±S.D. (n=3).

the liposomes in relation to size. In Fig. 7, the temperature dependence of calcein release for each fraction of the liposomes is shown. The temperature at which calcein release starts was found to shift to a lower temperature as the liposome size became larger. The maximum release % of L-REV and M-REV was almost the same as each other. The release % of S-REV was about half that of M-REV and L-REV. This observation also shows that the liposomes, which are registant for calcein release even at their transition temperature, somewhat exist in the liposome preparations, especially in S-REV.

Urokinase Release by Repeated Heating. One-minute heating of REV contaning urokinase was repeated several times at 5 min intervals. In Fig. 8, the urokinase release % is plotted against the number of repeating times. About 28% of the urokinase release was observed after the first 1 min of heating. Urokinase release upon a second heating was only 5%. After a third heating, no further urokinase release was observed. These results show that drug release from the temperature-sensitive liposome came to completion within two or so minutes heating, as is predicted by Fig. 2 for low-molecular-weight compound, or Fig. 5 for high-molecular-weight compound. Furthermore, these results suggest that there exist about 60% liposomes which are inpermeable for urokinase, even at the transition temperature.

Effect of the Molecular Weight of Encapsulated Compounds on Liposomal Permeation. The releases of several compounds with different molecular weights after 1 min incubation at 43 °C were plotted against the molecular weight in logarithmic scale, as shown in Fig. 9. The plotts fell into one curve according to their molecular weights, independent of the types of compounds: that is, low-molecular-weight organic compounds, proteins, polysaccarides. These results show that the releases of entrapped compounds from temperature-sensitive liposomes near their transition temperatures could be primarily governed by their molecular weight, in spite of the variety of drugs.

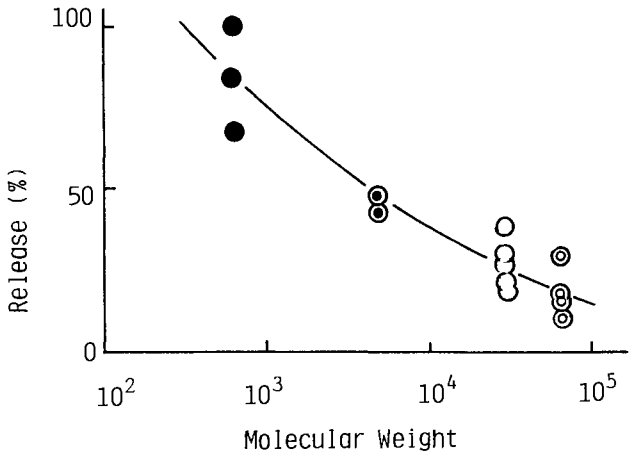

Fig. 9. Molecular weight dependence on the release of model drugs from DPPC-REV. ●, calcein; ◉, inulin; ○, urokinase; ◎, dextran.

Discussion

The initial release rate of both a low-molecular-weight compound (calcein) and a high-molecular-weight compound (dextran) from liposomes became larger as the incubation temperature was elevated within the experimental temperature limit (34.5—46 °C). At temperatures higher than the phase-transition temperature, the release amount attained saturation within a few minutes of incubation. Regarding calcein release at 46 °C, saturation was achieved within 1 min of incubation, and the released calcein upon saturation was about 50% of the calcein entrapped in the

liposome. No further release was added, even after long-time incubation. These observations suggest that the high initial rate at a temperature above the phase-transition temperature might be brought about when the liposome experiences the phase-transition temperature while increasing the temperature from low temperature to a fixed temperature; the liposome might again have a high barrier efficiency after the temperature exeeds the phase transition temperature.

Even at the transition temperature, a saturation phenomenon was also observed in the case of the release of a macromolecule. Saturation was achieved within a few minutes. The amount of release at saturation was dependent on the molecular weight of the compounds entrapped, and was 20—40% of the total macromolecules entrapped. No release exeeding 20—40% was observed, even after long-time incubation. These phenomena might be due to the polydispersity of the liposome size and properties: that is, 2 or more species of liposomes (one liposome could be perturbed enough large to bring about membrane release of macromolecules and the others not,) coexisted. Strictly speaking, even for a low-molecular-weight compound, no 100% release occured at all; thus, about 10% of the liposome was impermeable, even at the transition temperature. Judged from the results that the extent of temperature-sensitivity of drug release from a vesicle was dependent on the method of liposome preparation as well as on fractionation by centrifugation of the liposomes, larger liposomes seemed to generate a higher-temperature-sensitive drug release, suggesting that the extent of structural deformation of the membrane at the phase-transition temperature would vary among liposomes, especially depending on the liposome size.

Regarding the structural deformation of the membrane at the phase-transition temperature, which brings about an abrupt lowering of the membrane barrier efficiency, several hypotheses have been reported: (1) the apearance of a boundary between the gel phase and the liquid crystalline phase accompanying lateral phase separation,[16,17] (2) a change in the lateral compresibility between adjacent phospholipid molecules with an increase in membrane fluidity,[18] and (3) the formation of statistical pores by the rotation of phospholipid molecules with isomerization.[19] Since these hypotheses are based on the behavior of low-molecular-weight compound or ions, it is difficult to restrict the mechanism for such a rapid permeation of a high-molecular-weight compound as observed in our present experiments. In any case, it should at least be concluded that a large perturbation, which enables even a rapid permeation of macromolecules, must arise in a membrane on the occasion of a phase transition; also, the degree of perturbation must vary with the properties of the liposomes, especially regarding their size.

This work was supported by a Grant-in Aid for Scientific Research No. 60460218 (M.U.) and No. 6187009 (I.H.) from the Ministry of Education, Science and Culture.

References

1) G. Gregoriadis, "Liposomes as Drug Carriers," Wiley, New York (1988).
2) M. Ueno, *Med. Drug J.*, **22**, 2045 (1986).
3) M. B. Yatvin, J. N. Weinstein, W. H. Dennis, and R. Blumenthal, *Science*, **202**, 1290 (1978).
4) J. N. Weinstein, R. L. Magin, R. L. Cysyk, and D. S. Zaharko, *Cancer Res.*, **40**, 1388 (1980).
5) D. Papahadjopoulos, K. Jacobson, S. Nir, and T. Isac, *Biochim. Biophys. Acta*, **311**, 330 (1973).
6) E. K. Waller, W. D. Schlennig, and E. Reich, *Biochem. J.*, **215**, 123 (1983).
7) A. Watts, D. Marsh, and P. F. Knowles, *Biochemistry*, **17**, 1792 (1978).
8) M. Ueno, C. Tanford, and J. A. Reynolds, *Biochemistry*, **23**, 3070 (1984).
9) M. Ueno, *Biochim. Biophys. Acta*, **904**, 140 (1987).
10) M. Ueno, N. Tanaka, and I. Horikoshi, *J. Membr. Sci.*, **40**, 269 (1989).
11) F. Szoka and D. Papahadjopoulos, *Proc. Natl. Acad. Sci. U.S.A.*, **75**, 4194 (1978).
12) N. Oku, D. A. Knedall, and R. C. Macdonald, *Biochim. Biophys. Acta*, **691**, 332 (1982).
13) J. Senior and G. Gregoriadis, *Life Sci.*, **30**, 2123 (1982).
14) T. Morita, H. Kato, S. Iwanaga, K. Takada, T. Kimura, and S. Sakakibara, *J. Biochem.*, **82**, 1495 (1977).
15) G. R. Bartlett, *J. Biol. Chem.*, **234**, 466 (1959).
16) D. Marsh, A. Watts, and P. F. Knowles, *Biochemistry*, **15**, 3570 (1976).
17) M. I. Kanehisa and T. Y. Tsong, *J. Am. Chem. Soc.*, **100**, 424 (1978).
18) J. F. Nagle and H. L. Scott, Jr, *Biochim. Biophys. Acta*, **513**, 236 (1978).
19) A. Seeling and J. Seeling, *Biochemistry*, **13**, 4839 (1974).

Difference of the Final Products of the Photochemical Reactions of Azanaphthalenes and Naphthalene in Mixed Crystals of Durene

Nagahiro HOSHI,*,† Seigo YAMAUCHI,†† and Noboru HIROTA*
Department of Chemistry, Faculty of Science, Kyoto University, Kyoto 606
† Department of Applied Chemistry, Faculty of Engineering, Chiba University, Yayoicho, Chiba 260
†† Chemical Research Institute of Non-Aqueous Solutions, Tohoku University, Katahira, Sendai 980
(Received September 25, 1990)

Final products of the photochemical reactions of quinazoline, quinoline, and naphthalene in 1,2,4,5-tetramethylbenzene (durene) mixed crystals are investigated on the basis of the phosphorescence and fluorescence spectra of the products. Quinazoline in durene is considered to transform into a benzene derivative, whereas naphthalene and quinoline tranform into anthracene derivatives. These products are different from a pyrazine derivative found in the case of quinoxaline, which is specific to the reaction in a durene mixed crystal. The cause of this difference is discussed in terms of the configurations of guests in the mixed crystals and the difference of the molecular structures.

One of the interesting features of the chemical reactions in single crystals is the generation of reaction products specific to single crystals.[1,2] Yamauchi, Terazima, and Hirota reported a unique product of the photochemical reaction of quinoxaline (Qx) in a single crystal of 1,2,4,5-tetramethylbenzene (durene (D)).[3] The final product of this reaction was found to be a pyrazine derivative with two hydrogen atoms attached to the benzene ring of Qx. In the hydrogen abstraction reactions of Qx in solution, the reaction product is the 1,4-dihydro-1-quinoxalinyl radical (QxH) with a hydrogen attached to the nitrogen of Qx.[4-8] Pyrazine derivatives have never been found in the reactions in solution.

In a series of papers, we have recently discussed the photochemical reactions of naphthalene (N) and azanaphthalenes (Qx, quinazoline (Qz), and quinoline (Q)) in durene mixed crystals schematically shown by the scheme in Fig. 1. In all cases, the initial steps (1) of the reactions are the hydrogen abstraction reactions of the triplet states of these molecules and quantum mechanical tunneling plays an essential role in these steps.[9-12] We have discussed the observed temperature, pressure and deuterium isotope effects on the reaction rates in terms of the Siebrand model of hydrogen tunneling.[13] As for the final products, we have hitherto discussed only the case of Qx mentioned above. In the present work, we have made a spectroscopic investigation on the reaction products of Qz, Q, and N in mixed crystals of durene (hereafter these systems are abridged as Qz/D, Q/D, and N/D). The final products of these reactions are found to be quite different depending on the system. The reaction product of Qz/D gives a phosphorescence spectrum characteristic of a benzene derivative, whereas the products of Q/D and N/D give fluorescence spectra characteristic of anthracene derivatives, indicating that dimerization of Q (N) and durene occurs. The difference in the products is rationalized on the basis of the configurations of the guest molecules in the mixed crystals and the difference in the molecular structures.

Experimental

Q was purified by vacuum distillation. Qz was purified by vacuum sublimation. N was recrystallized from ethanol and

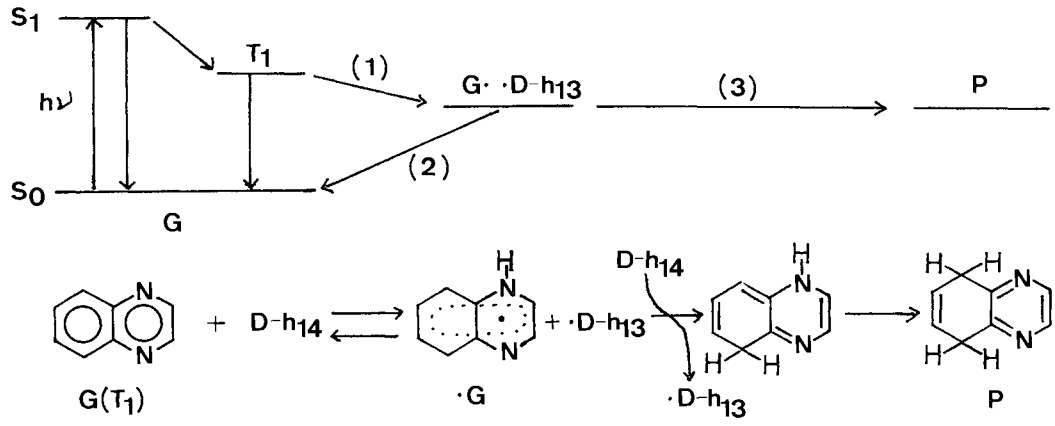

Fig. 1. General reaction scheme of the photochemical reaction of azanaphthalene/durene and naphthalene/durene. Reaction (3) may consist of several steps. G, D-h_{14}, D-h_{13}, and P represent a guest molecule, durene, 2,4,5-trimethylbenzyl radical, and product, respectively. The reaction process of quinoxaline/durene is also shown below the scheme.

zone refined. Indan was purified by vacuum distillation. Durene was recrystallized from ethanol followed by column chromatography and zone refined. Mixed single crystals were grown from melts containing about 0.1 mol% of guest molecules by the standard Bridgman method.

The UV irradiation was provided by a 900 W Xe lamp whose output was passed through a saturated $NiSO_4$ solution and a Toshiba UV-D33S glass filter. Samples were irradiated at room temperature for about 30 min to induce photochemical reactions. Phosphorescence spectra of the reaction products were obtained at 4.2 K with a Spex Model 1704 1-m monochromator equipped with an EMI 9502B photomultiplier. Phosphorescence lifetimes were measured using a mechanical shutter. Fluorescence spectra were observed at room temperature with a Shimadzu fluorometer (RF-502A).

Results and Discussion

Quinazoline/Durene. When Qz/D is irradiated at room temperature, the green fluorescence of a 2,4,5-trimethylbenzyl radical with a maximum peak at 495 nm appears as the phosphorescence of Qz decreases. The phosphorescence of Qz disappears completely after prolonged (30 min.) irradiation. After irradiation, the ESR signal of a pentamethylcyclopentadienyl radical produced via the 2,4,5-trimethylbenzyl radical was obtained.[14] These experimental results are similar to those found for Qx/D,[3] indicating that the 2,4,5-trimethylbenzyl radical is produced by the photoinduced hydrogen abstraction of Qz from durene.

Figure 2(a) shows the phosphorescence spectrum of "Qz/D" at 4.2 K after irradiation at room temperature. The phosphorescence of Qz (0–0 band: 454.4 nm) is absent, but instead a new spectrum with an 0–0 band at 359.7 nm is obtained. The phosphorescence lifetime is 3.2 s. On the analogy of the result of Qx/D, it may be expected that the final product of the photochemical reaction of Qz/D is a pyrimidine derivative. The observed phosphorescence spectrum, however, cannot be due to a pyrimidine derivative, because the phosphorescence lifetime of pyrimidine is about 12 ms.[15] The long lifetime (3.2 s) and the location of the 0–0 band of the phosphorescence indicate that the phosphorescence is likely to arise from a benzene derivative.[16] The energy of the 0–0 band of the observed phosphorescence (27798 cm^{-1}) is very close to that of durene (28000 cm^{-1})[17] and there are two possibilities for the assignment of the observed spectrum.

(1) The energy of the triplet state of the reaction product is lower than that of durene and the observed phosphorescence is genuinely due to the reaction product.

(2) The energy of the triplet state of the reaction product is higher than that of durene and the observed phosphorescence is due to a durene X-trap.

The second possibility cannot be excluded, if the reaction

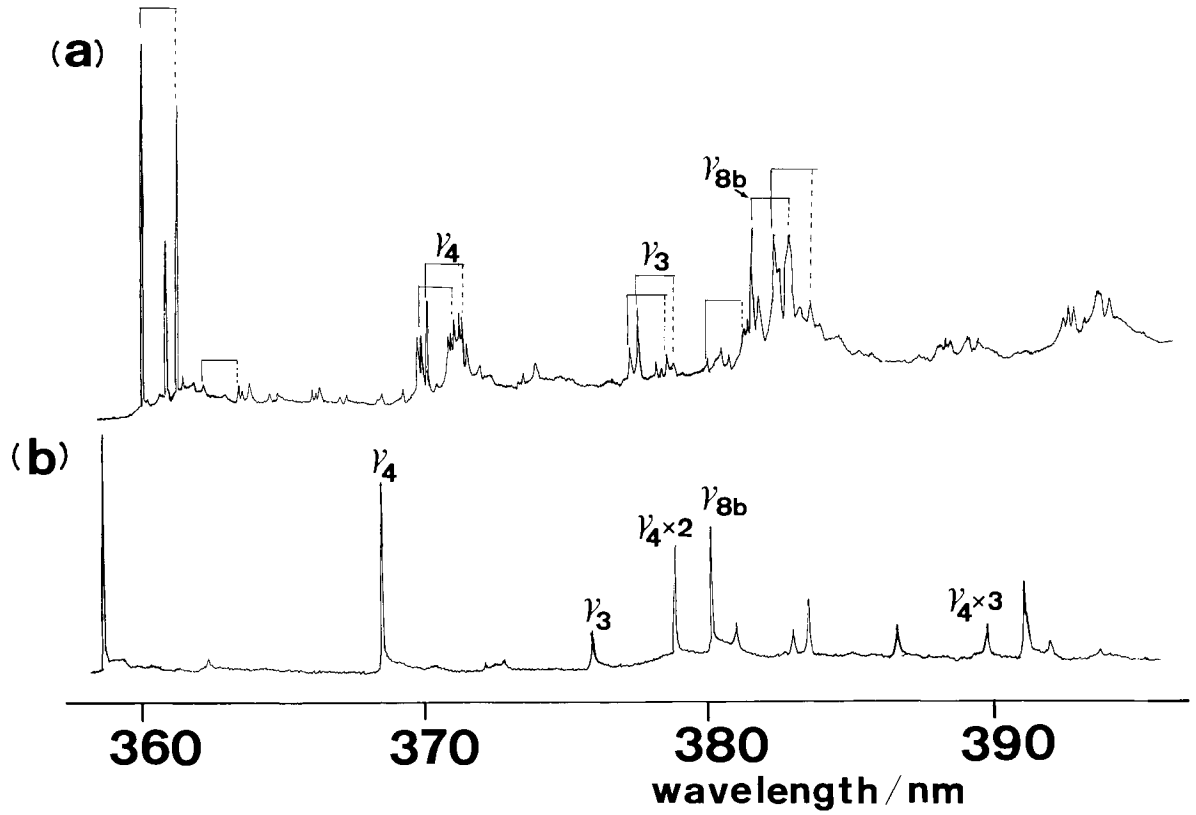

Fig. 2. (a) Phosphorescence spectrum of quinazoline/durene at 4.2 K after irradiation at room temperature. (b) Phosphorescence spectrum of durene X-trap obtained by doping indan in a durene single crystal at 4.2 K.

product is a pyrimidine derivative. This is because the 0–0 energy of $^3(n, \pi^*)$ pyrimidine (28112 cm^{-1} in *p*-xylene and 28240 cm^{-1} in methylcyclohexane[18]) is slightly higher than that of the lowest triplet state of durene.

In order to assign the observed phosphorescence, we have studied the phosphorescence spectrum of a durene X-trap obtained by doping indan in a durene single crystal (Fig. 2(b)). The vibrational analysis and the assignment of the vibronic bands of the phosphorescence are shown in Table 1(a) and (b). The assignment was made on the basis of the Raman data of durene.[19] The energy of the 0–0 band of the durene X-trap is 90 cm^{-1} higher than that of Qz/D after irradiation. Vibronic bands characteristic of the benzene ring can be found in the durene X-trap phosphorescence. The vibronic bands at 760, 1290, and 1582 cm^{-1} are assigned as ν_4, ν_3, and ν_{8b} modes of the benzene ring,[19,20] respectively. These vibrations are the C–C–C out-of-plane bending, the C–H in-plane bending, and the C–C stretching modes, respectively. As for Qz/D after irradiation, vibronic bands from two different sites are clearly observed with a splitting of 91 cm^{-1}. The vibronic bands characteristic of the benzene ring (ν_4, ν_3, and ν_{8b}) are also observed, indicating that the phosphorescence comes from a benzene derivative. There are, however, significant differences between the Qz/D spectrum and the X-trap spectrum. First, in the Qz/D spectrum, there are some bands that are not observed in the durene X-trap, for example, the vibronic bands at 741, 839, 1269 cm^{-1} etc. The band at 741 cm^{-1} may be assigned to the C–H bending mode of an aliphatic skeleton as observed in 1,4-dihydronaphthalene.[21] Second, some overtone (754×2, 754×3) and combination bands in the durene X-trap are not observed in Qz/D. These differences seem to indicate that the phosphorescence of Qz/D after irradiation comes from the reaction product, and not a durene X-trap.

Table 1(a). Vibrational Analysis of the Phosphorescence Spectrum of Quinazoline/Durene at 4.2 K after Irradiation
(As for the vibronic bands from different sites, only those with the lower energy are shown. Weak bands are not shown in the table.)

λ/Å	ν/cm^{-1}	Δν/cm^{-1}	Intensity	Assignment
3597.3	27798	0	v.s.	0–0
3605.6	27735	63	s.	
3634.9	27511	287	m.	b_{3g}
3659.5	27326	472	m.	
3694.8	27085	733	m.	
3695.9	27057	741	s.	C–H bend. (aliphatic)
3698.5	27038	760	s.	ν_4
3706.1	26983	815	m.	
3706.6	26979	819	m.	
3709.4	26959	839	s.	
3712.6	26935	863	m.	
3769.5	26529	1269	m.	
3772.5	26508	1290	s.	ν_3
3814.4	26216	1582	s.	ν_{8b}
3815.5	26209	1589	m.	
3821.5	26168	1630	s.	b_{2g}
3823.0	26157	1641	s.	

Table 1(b). Vibrational Analysis of the Phosphorescence Spectrum of Durene X-Trap at 4.2 K

λ/Å	ν/cm^{-1}	Δν/cm^{-1}	Intensity	Assignment
3586.3	27884	0	v.s.	0–0
3602.9	27755	128	w.	
3604.8	27741	143	w.	
3623.3	27599	285	w.	b_{3g}
3685.9	27130	754	v.s.	ν_4
3701.8	27014	870	w.	
3703.6	27001	883	w.	
3721.0	26874	1010	w.	
3724.0	26853	1031	w.	ν_{18a}
3725.1	26845	1039	w.	
3727.4	26828	1056	w.	
3759.3	26601	1283	m.	ν_3
3789.3	26390	1494	s.	754×2
3801.5	26305	1579	s.	ν_{8b}
3809.8	26248	1636	m.	b_{2g}
3826.5	26134	1750	w.	
3830.0	26110	1774	m.	754+1031
3833.4	26087	1797	w.	
3835.3	26074	1810	s.	754+1056
3867.2	25859	2025	m.	754+1283
3898.5	25651	2233	m.	754×3
3911.9	25563	2321	s.	754+1579

This product comes most likely from Qz for the following reason. The reaction products originating from durene are considered to be 2,4,5-trimethylbenzyl and pentamethylcyclopentadienyl radicals. These radicals give, however, no phosphorescence. Furthermore, in the case of Qx/D and Q/D, no phosphorescence similar to that found for the reaction product of Qz/D is observed, though durene is used as the host in all cases. Moreover, durene neat crystal does not give such phosphorescence after irradiation for about 1 h. Intermediate 1,3-dihydro-1-quinazolinyl and 2,4,5-trimethylbenzyl radicals may combine to produce a 3,4-dihydro-3-(2,4,5-trimethylbenzyl)quinazoline like product. The 0–0 band of the phosphorescence spectrum of such a product, however, should be much lower than that of the observed one because of the conjugation of a double bond with the benzene ring as discussed in Reaction Mechanism.

Quinoline/Durene. Different from the cases of Qx and Qz, no new phosphorescence appears after irradiation at room temperature when observed at 4.2 K. However, very intense blue fluorescence starts to grow gradually as the green phosphorescence of Q diminishes upon irradiation. Figure 3 shows the fluorescence spectrum of the reaction product of Q/D after irradiation for about 30 min at room temperature. The emission spectrum (obtained by irradiation at 285 nm) starts to rise at 361 nm accompanied by two vibronic bands at 418 and 442 nm and a shoulder at 397 nm. The wavelength range of the emission and the interval of the vibronic

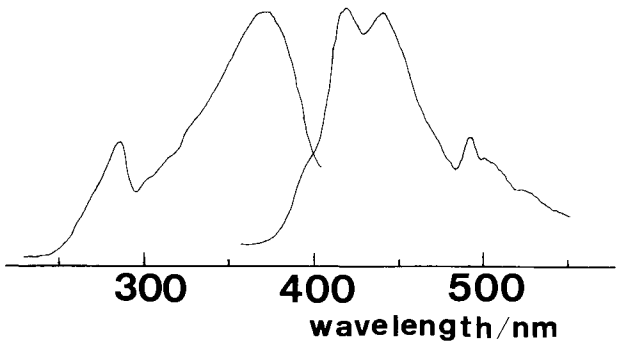

Fig. 3. Fluorescence emission (irradiated at 285 nm) and excitation (monitored at 418 nm) spectra of quinoline/durene at room temperature after irradiation.

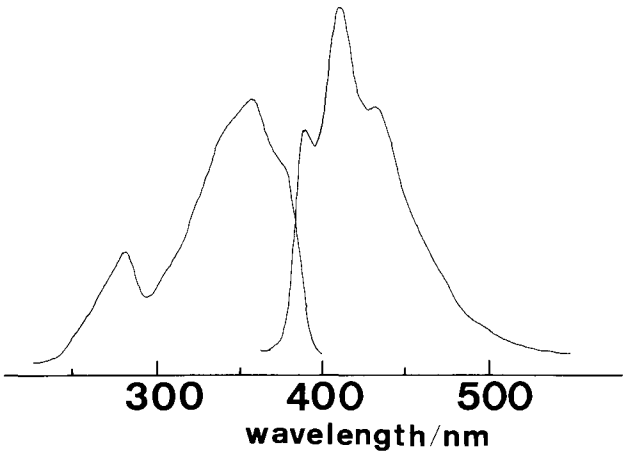

Fig. 4. Fluorescence emission (irradiated at 285 nm) and excitation (monitored at 410 nm) spectra of naphthalene/durene at room temperature after irradiation.

bands (1300 cm^{-1}) are similar to those of anthracene,[22] and the excitation spectrum monitored at 418 nm is also similar to the absorption spectrum of anthracene.[23] Because of the broad nature of the spectrum, we cannot ascertain that this fluorescence arises from only one product. But the above mentioned features of the spectrum seems to indicate that the main fluorescent product is an anthracene derivative.

The fluorescence peaks observed lower than 490 nm are due to the 2,4,5-trimethylbenzyl radical which is produced by the hydrogen abstraction reaction.

Naphthalene/Durene. Intense blue fluorescence increases during the UV irradiation at room temperature as Q/D. Figure 4 shows the fluorescence emission and excitation spectra of the reaction product after irradiation. The emission (irradiated at 285 nm) starts at about 370 nm with three vibronic bands at 389, 410, and 433 nm. The wavelength range of the fluorescence and the interval of the vibronic bands (1300 cm^{-1}) are similar to those of anthracene.[22] The excitation spectrum with a peak at 361 nm (emission at 410 nm) is also similar to the absorption spectrum of anthracene.[23] Therefore, the reaction product of N/D is also considered to be one of the anthracene derivatives as in the case of Q/D.

Neither the fluorescence spectrum of the 2,4,5-trimethylbenzyl radical nor the ESR spectrum of the pentamethylcyclopentadienyl radical was observed. This is probably because the back reaction in the initial hydrogen abstraction process ((2) in Fig. 1) is so efficient that the steady state concentrations of the intermediate 2,4,5-trimethylbenzyl and 1,4-dihydro-1-naphthyl radicals become too low to be detected by ESR.[10] The fluorescence of 2,4,5-trimethylbenzyl radical seems to be much weaker than that of anthracene derivative because of its low steady state concentration and quantum yield.

Reaction Mechanisms. There are three questions about the experimental results given above.

(1) What are the exact structures of the reaction products ?

(2) Why is Qz transformed into a benzene derivative, not a pyrimidine derivative ?

(3) Why are Q and N transformed into anthracene derivatives, but not Qx and Qz ?

We discuss these questions on the basis of the configurations of the guest molecules in the mixed crystals and the molecular structures of the guest molecules.

Figure 5 shows the proposed reaction mechanism of Qz/D. In the case of Qz/D, according to the potential energy calculation by McCool et al., there are two sites for Qz in durene, one rotated by 18° and the other by −25° in the molecular plane with respect to the molecular axis of durene.[24] Figure 6 shows the configuration of Qz at the −25° site in durene as a representative. The following discussion can also be applied to Qz at the +18° site. The hydrogen atom from durene is expected to attack the nitrogen of Qz via tunneling in the initial process of the reaction as reported before.[11] The molecular center of Qz deviates by 0.9 Å from that of durene.[24] The durene nearest to the nitrogen at position 1 of Qz is located along the *c* axis of the lattice (2 in Fig. 6). On the other hand, the durene nearest to the nitrogen at position 3 of Qz is located in the *ab* plane of the lattice (3 in Fig. 6). When a reaction proceeds via tunneling, a reaction rate constant depends sensitively on the tunneling distance (the distance between the nitrogen of Qz and the abstracted hydrogen of durene).[13] For example, a decrease of the tunneling distance by 0.1 Å is known to enhance the reaction rate constant by one or two order of magnitude. Because the tunneling distance for the nitrogen at position 3 of Qz is smaller (0.2 Å for the +18° site and 1.5 Å for the −25° site) than that at position 1, the hydrogen atom from durene is predicted to attack position 3 of Qz preferentially to produce a 1,3-dihydro-1-quinazolinyl radical (QzH). Therefore the hydrogen abstraction at position 1 of Qz is negligible to that at position 3 in the initial process of the reaction.

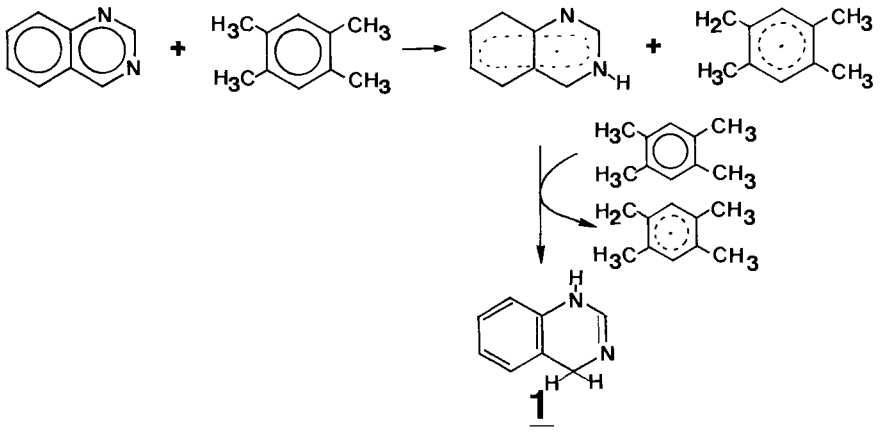

Fig. 5. Proposed reaction mechanism of quinazoline/durene.

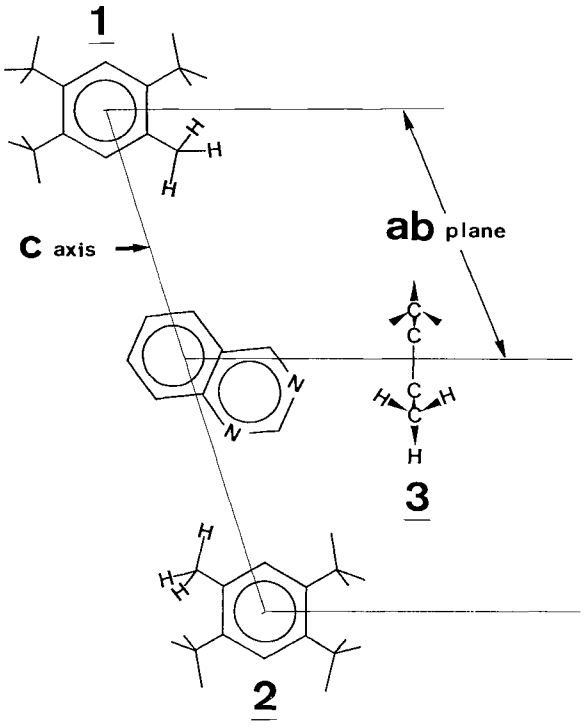

Fig. 6. Configuration of −25° site of quinazoline in durene mixed crystal. Molecules along the *c* axis are not in the same plane in reality.

Hydrogen abstraction via tunneling at the benzene ring of Qz is also negligible to that at the pyrimidine ring because the tunneling distance to the benzene ring is much larger than that to the pyrimidine ring because of the deviation of the molecular center of Qz from that of durene. In order to produce a stable benzene derivative, one more hydrogen must attack the pyrimidine ring of Qz. There are three possible benzene derivatives shown in Fig. 7, but neither product **2** and **3** can be the final product. Because of the conjugation of the double bond with the benzene ring, the triplet energies of products **2**

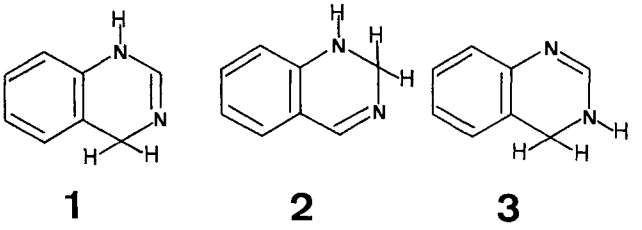

Fig. 7. Possible benzene derivatives produced from quinazoline.

and **3** are expected to be as low as that of 1H-indazole (23590 cm^{-1})[25]. On the other hand, product **1** does not have the conjugaton of the double bond with the benzene ring, producing a triplet energy as high as that of aniline (27659 cm^{-1}).[26] Therefore, we consider product **1** as the final product. Though the vibronic bands corresponding to the N–H bond are not found, the existence of the C–H bending mode of an aliphatic skeleton in the phosphorescence spectrum supports this assignment.

A possible way to explain how the final benzene derivative is produced is the following. The hydrogen of durene along the *c* axis attacks the nitrogen atom at position 1 of QzH, accompanying the transfer of the hydrogen from position 3 to position 4 simultaneously.

Though there is no direct experimental evidence that a pyrimidine derivative is not produced, we consider that the attack of the hydrogen on position 3 of Qz and the deviation of the molecular center of Qz from that of durene inhibit the formation of a pyrimidine derivative. In the case of Qx/D, the molecular axes of Qx is the same as those of durene and the deviation of the molecular center is considered to be small compared to that of Qz. In this system, first, the hydrogen of durene along the *c* axis attacks position 1 of Qx whose tunneling distance is the smallest, producing a 1,4-dihydro-4-quinoxalinyl radical (QxH). Then, the hydrogen attacks position 5 (benzene ring of QxH) which is equivalent to position 1. Finally, the hydrogen attached to position 1 is transferred

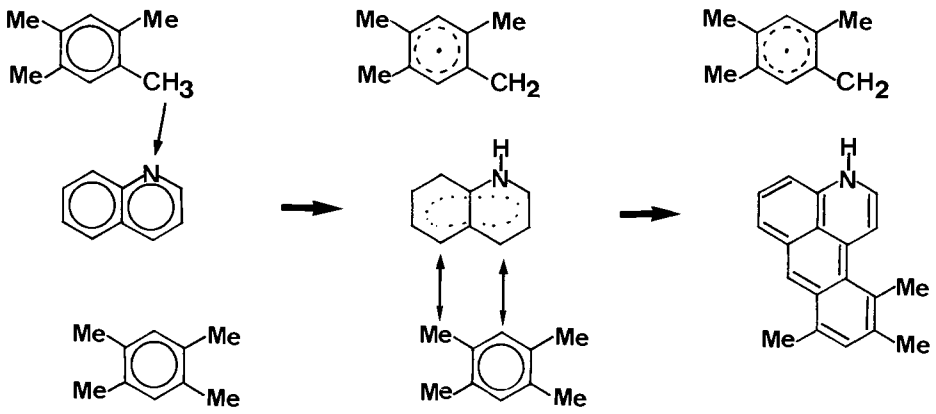

Fig. 8. Probable reaction mechanism of quinoline/durene. The orientation of quinoline and durene in the figure is almost the same as that in durene mixed crystal.

to the neighboring position 8 to produce the pyrazine derivative. The crucial process in proceeding the pyrazine derivative is the attack of the hydrogen of durene on the benzene ring of Qx (position 5). In the case of Qz/D where the hydrogen is attached at position 3, the second hydrogen cannot attack position 5 or 8 because the attachment to these positions destroys the conjugation of the system. The positions in the benzene ring of QzH on which the hydrogen can attack are 6 and 7. The distances from durene to these positions are, however, larger than that of position 5 or 8 on which the hydrogen attacks in Qx/D. Moreover, because the molecular center of Qz deviates by 0.9 Å from that of the replaced durene, the distance between the benzene ring of Qz and durene becomes larger than that for Qx. Therefore, the second hydrogen is expected to attack on the second nearest nitrogen at position 1 of Qz to produce the benzene derivative.

Figure 8 shows a possible reaction mechanism of Q/D. On the analogy of the reaction in solutions[27] and on the basis of the crystal structure,[28] the hydrogen from durene attacks position 1 of Q to produce a 1,4-dihydro-4-quinolinyl radical. After the hydrogen transfers from durene to Q, the 1,4-dihydro-4-quinolinyl radical and durene located at the other position along the *c* axis may dimerize to produce a benzo[*de*]anthracene like derivative. We cannot discuss this dimerization process in detail because the orientation of the intermediate radical is not known. When the orientation of the radical is the same as that of Q, the location of Q and durene along the *c* axis becomes favorable for the dimerization, because Q and durene need not change their orientation greatly to dimerize. However, five hydrogen atoms are released after dimerization. These hydrogen atoms may attach to the neighboring durene molecules to produce pentamethylcyclopentadienyl radicals. On the basis of the fact that the orientation of N is almost the same as that of Q,[29] the photochemical reaction of N/D is also expected to proceed in the same way.

The reason why Qx and Qz do not produce anthracene derivatives may be found in the fact that these molecules have two nitrogen atoms. If such a reaction should occur, durene would attack the nitrogen at position 4 of QxH to form a dimerized product. QxH and durene, however, cannot dimerize because a conjugated system including the nitrogen cannot be formed. In the case of Qz/D, there can be two ways to produce a dimerized product in view of the configuration in the mixed crystal (Fig. 6.) and the attachment of the hydrogen at position 3 of QzH.

(a) Durene 2 attacks the nitrogen at position 1 of QzH.

(b) Durene 1 attacks the carbon at position 4 of QzH.

In the case of (a), the dimerization of QzH and durene 2 does not occur for the same reason as given for Qx. In the case of (b), because of the deviation of the molecular center and the rotation in the molecular plane, the distance between durene 1 and position 4 of QzH becomes much larger than that between durene 2 and position 1 of QzH. Therefore the hydrogen abstraction from durene 2 to QzH is considered to occur more efficiently than the dimerization of QzH with durene 1.

In summary, it is found that the final products of the photochemical reactions of Qx/D, Qz/D, Q/D, and N/D are quite different depending on the system despite the fact that the initial steps of the reactions are similar. This difference can be rationalized on the basis of the difference in the molecular structures and the configuration of the guest molecules in the mixed crystals.

References

1) A. Savezzoti and M. Simonetta, *Chem. Rev.*, **82**, 1 (1982).

2) V. Ramamurthy and K. Venkatesan, *Chem. Rev.*, **87**, 433 (1987).

3) S. Yamauchi, M. Terazima, and N. Hirota, *J. Phys.*

Chem., **89**, 4804 (1985).
4) G. Allan, A. Castellano, J. P. Catteau, and A. Lablache-Combier, *Tetrahedron*, **27**, 4704 (1971).
5) D. V. Bent, E. Hayon, and P. N. Moorthy, *J. Am. Chem. Soc.*, **97**, 5065 (1975).
6) S. Basu, K. A. McLauchlan, and G. R. Sealy, *Chem. Phys. Lett.*, **88**, 84 (1982).
7) S. Basu, K. A. McLauchlan, and A. J. D. Ritchie, *Chem. Phys.*, **79**, 95 (1983).
8) S. Yamauchi and N. Hirota, *J. Phys. Chem.*, **88**, 4631 (1984).
9) N. Hoshi, S. Yamauchi, and N. Hirota, *J. Phys. Chem.*, **92**, 6615 (1988).
10) N. Hoshi, S. Yamauchi, and N. Hirota, *Chem. Phys. Lett.*, **169**, 326 (1990).
11) N. Hoshi, S. Yamauchi, and N. Hirota, *J. Phys. Chem.*, **94**, 7523 (1990).
12) N. Hoshi, K. Hara, S. Yamauchi, and N. Hirota, *J. Phys. Chem.*, in press.
13) W. Siebrand, T. A. Wildman, and M. Z. Zgierski, *J. Am. Chem. Soc.*, **106**, 4083 (1984); *ibid.*, **106**, 4089 (1984).
14) J. L. Monge and M. Scotto, *J. Chem. Phys.*, **70**, 1555 (1973).
15) a) S. W. Mao, T. C. Wang, and N. Hirota, *Chem. Phys. Lett.*, **13**, 199 (1972); b) D. M. Burland and J. Schmidt, *Mol. Phys.*, **22**, 19 (1971).
16) E. R. Bernstein, S. D. Colson, D. S. Tinti, and G. W. Robinson, *J. Chem. Phys.*, **48**, 4632 (1968).
17) S. P. McGlynn, T. Azumi, and K. Kinoshita, "Molecular Spectroscopy of the Triplet State," Prentice-Hall Inc., Englewood Criffs, New Jersey (1969).
18) C. J. Nonhof and J. H. van der Waals, *Chem. Phys. Lett.*, **92**, 588 (1982).
19) A. Chosson, M. Martin-Bouyer, and P. Faure, *J. Chim. Phys.*, **72**, 1139 (1975).
20) V. I. Berezin and M. D. Elkin, *Opt. Spectrosc.*, **36**, 528 (1974).
21) von W. Huckel, C-M. Jennewein, M. Wartini, and J. Wolfering, *Ann. Chem.*, **686**, 51 (1965).
22) J. B. Birks and A. J. Cameron, *Proc. R. Soc. London, Ser. A*, **249**, 297 (1959).
23) W. V. Mayneord and E. M. F. Roe, *Proc. R. Soc. London, Ser. A*, **152**, 299 (1935).
24) B. J. McCool, B. R. Markey, and R. Bramlay, *Mol. Phys.*, **51**, 935 (1984).
25) M. Noda and N. Hirota, *J. Am. Chem. Soc.*, **105**, 6790 (1983).
26) H. M. van Noort, Ph. J. Vergragt, J. Herbich, and J. H. van der Waals, *Chem. Phys. Lett.*, **71**, 5 (1980).
27) J. A. Leone and W. S. Koski, *J. Am. Chem. Soc.*, **88**, (1966).
28) H. Blok, J. Kooter, and J. Schmidt, *Chem. Phys. Lett.*, **30**, 160 (1975).
29) A. Hutchison, Jr. and B. W. Mangum, *J. Chem. Phys.*, **34**, 308 (1961).

Mechanism of Cis-Trans Isomerization of Fluoranthenylethylenes on Direct Irradiation

Hideo FURUUCHI, Yasunao KURIYAMA, Tatsuo ARAI,* Hirochika SAKURAGI, and Katsumi TOKUMARU*
Department of Chemistry, University of Tsukuba, Tsukuba, Ibaraki 305
(Received November 19, 1990)

On direct irradiation 8-styrylfluoranthene (SF) and 8-(3,3-dimethyl-1-butenyl)fluoranthene (BF) underwent two-way and one-way isomerizations, respectively, in the triplet manifold after intersystem crossing of the initially produced singlet excited state.

Recently, we have shown that in the triplet sensitized isomerization of olefins the introduction of an anthracene nucleus results in the cis→trans one-way isomerization, no matter which of an alkyl or an aryl group may be substituted on the other ethylenic carbon.[1-3] This is very much contrasted with the mutual two-way isomerization between the cis and trans isomers,[4,5] as well investigated for stilbenes.

Furthermore, we have reported that the olefins substituted by a pyrene[6] or a fluoranthene nucleus[7] whose triplet excitation energy, 48 or 54 kcal mol^{-1},[8] is slightly higher than that of anthracene, 42 kcal mol^{-1},[8] exhibit intermediate behavior between the two-way and one-way isomerizations on triplet sensitization. When a *t*-butyl group is substituted on the other ethylenic carbon, the one-way isomerization occurs with a quantum chain process. On the contrary, when a phenyl group is attached, the two-way isomerization involving a similar quantum chain process takes place.

The direct excitation of olefins also results in their isomerization; however, the mechanism, particularly the spin multiplicity in which the isomerization actually proceeds, depends on the olefins. Stilbene isomerizes in the singlet excited state before intersystem crossing on direct excitation,[9,10] whereas the anthrylethylenes undergo cis→trans one-way isomerization with a quantum chain process on the triplet manifold after intersystem crossing.[1-3] For the olefins exhibiting the intermediate behavior between the two-way and one-way isomerizations, we have recently shown that the direct excitation of the pyrenylethylene with a *t*-butyl group or a phenyl group on the other ethylenic carbon led to the isomerization in the triplet manifold in the same way as the triplet sensitization.[11]

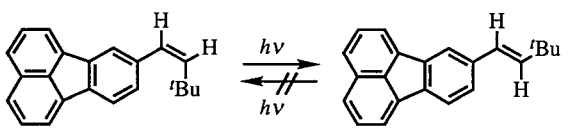

cis-BF *trans*-BF

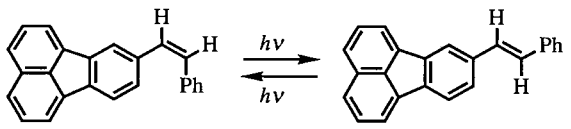

cis-SF *trans*-SF

These results prompted us to examine whether direct excitation of the fluoranthenylethylenes, whose excitation energies are higher than those of the pyrenylethylenes, brings about the isomerization in the singlet manifold as observed in stilbenes or in the triplet manifold as demonstrated in the anthryl- and pyrenylethylenes.

Experimental

Proton (^{1}H) NMR spectra were recorded on a JEOL JMN-MH-100 spectrometer. Ultraviolet absorption spectra (UV) were taken on a Hitachi 200-20 and a JASCO 660 spectrophotometer. Fluorescence spectra were measured on a Hitachi F-4000 and a Hitachi MPF-4 fluorescence spectrofluorometer. Fluorescence lifetimes were measured using a single photon counting apparatus, Horiba NAES 1100.

Materials. Solvent benzene for photochemical measurements was distilled over calcium hydride. Biacetyl was purified by distillation.

8-Styrylfluoranthene (SF). 8-(Hydroxymethyl)fluoranthene prepared by reducing methyl 8-fluoranthenecarboxylate[12] with lithium aluminum hydride in boiling ether[13] was converted to 8-(bromomethyl)fluoranthene by treating with phosphorus tribromide in the presence of pyridine in chloroform at 0°C.[13]

8-(Bromomethyl)fluoranthene was refluxed with triphenylphosphine in xylene to give (8-fluoranthenylmethyl) triphenylphosphonium bromide.

The Wittig reaction of benzaldehyde with the ylide prepared from (8-fluoranthenylmethyl)triphenylphosphonium bromide with sodium ethoxide in ethanol gave a mixture of *cis*- and *trans*-8-styrylfluoranthene (SF). Column chromatography on silica gel eluting with hexane and benzene (4 : 1) followed by crystallization from hexane afforded *cis*- and *trans*-SF.

cis-SF: Mp 100—101°C; UV (benzene) 304 nm (log ε 4.56), 372 (4.09); ^{1}H NMR ($CDCl_3$, 100 MHz) δ=6.63 (d, 1H, *J*=12.2 Hz, C=CH), 6.69 (d, 1H, *J*=12.2 Hz, C=CH), 7.2—7.9 (m, 14H, ArH). Calcd for $C_{24}H_{16}$: C, 94.70; H, 5.30%. Found: C, 94.64; H, 5.29%.

trans-SF: Mp 131—133°C; UV (benzene) 322 nm (log ε 4.59), 372 (4.10); ^{1}H NMR ($CDCl_3$, 100 MHz) δ=7.2—7.9 (m, 16H). Calcd for $C_{24}H_{16}$: C, 94.70; H, 5.30%. Found: C, 94.58; H, 5.25%.

8-(3,3-Dimethyl-1-butenyl)fluoranthene (BF). A mixture

of *cis*- and *trans*-BF was prepared by the Wittig reaction of 2,2-dimethylpropanal with the ylide prepared from (8-fluoranthenylmethyl)triphenylphosphonium bromide with butyllithium in ether. The pure cis and trans isomers were separated by column chromatography on silica gel eluting with petroleum ether.

cis-BF: UV (benzene) 302 nm (log ε 4.65), 330 (3.91).

trans-BF: UV (benzene) 294 nm (log ε 4.56), 327 (3.82), 349 (3.90), 365 (4.95). ^{1}H NMR ($CDCl_3$, 100 MHz) δ=1.06 (s, 9H, $C(CH_3)_3$), 5.77 (d, 1H, J=15 Hz, C=CH), 6.65 (d, 1H, J=15 Hz, C=CH), 7.62—8.08 (m, 14H, ArH). Calcd for $C_{22}H_{20}$: C, 92.91; H, 7.09%. Found: C, 92.61; H, 7.15%.

Steady State Irradiation. Irradiation of benzene solutions containing *cis*- or *trans*-SF was performed with 436-nm light from a 400-W high-pressure mercury lamp through a filter solution ($CuSO_4 \cdot 5H_2O + NaNO_2$). Similarly, benzene solutions of *cis*- and *trans*-BF were irradiated with 313-nm light isolated from a 400-W high-pressure mercury lamp through an aqueous potassium chromate solution filter and a Toshiba UV-D36B glass filter. For measurements of isomerization quantum yields the sample solutions containing the cis or trans isomer (≥98%, checked by HPLC) were deaerated by bubbling with argon, and irradiated so that the conversions of the isomer were within 20%. The concentrations of the cis and trans isomers in the irradiated samples were determined by HPLC (Waters 600 Multisolvent Delivery System) equipped with an LC spectrophotometer (Waters 490 Programmable Multiwavelength Detector).

The light intensity was measured by a potassium tris(oxalato)ferrate(III) chemical actinometer.

Laser Flash Photolysis. Direct excitation of SF with 351-nm light was performed with a XeF excimer laser (Lambda Physik EMG-101, 10-ns fwhm). Direct excitation at 308 and 337 nm, and biacetyl sensitization with 425-nm light of BF were performed with a XeCl excimer laser (Lambda Physik EMG-101, 10-ns fwhm), a nitrogen laser (National Research Group Inc., 5-ns fwhm), and an excimer laser-pumped dye laser (Lambda Physik FL-3002, Stilbene 3), respectively.

The monitoring beam obtained from a xenon lamp was oriented perpendicularly to the exciting laser beam, passed through a sample cell and a grating monochromator (JASCO CT-25C), and detected with a photomultiplier (Hamamatsu Photonix R928, R446, or R212). The amplified signal was recorded as the time profile of a transmittance change on a storage oscilloscope (Iwatsu TS-8123) and transferred to a personal computer where it was analyzed.

Results

Absorption and Fluorescence Spectra. Figure 1 depicts the absorption and fluorescence spectra of cis and trans isomers of BF and SF. The cis and trans isomers exhibit different fluorescence spectra with different lifetimes from each other. The singlet excitation energies corresponding to the maximum wavelengths of fluorescence spectra (λ_{max}^{fl}) are estimated as 60 kcal mol^{-1} for both *cis*- and *trans*-SF, and 63 and 62 kcal mol^{-1} for *cis*- and *trans*-BF, respectively (Table 1). Because of the broad fluorescence band for every fluoranthenylethylene the energy of the 0–0 transition cannot be determined precisely. When the 0–0 band is assumed to correspond

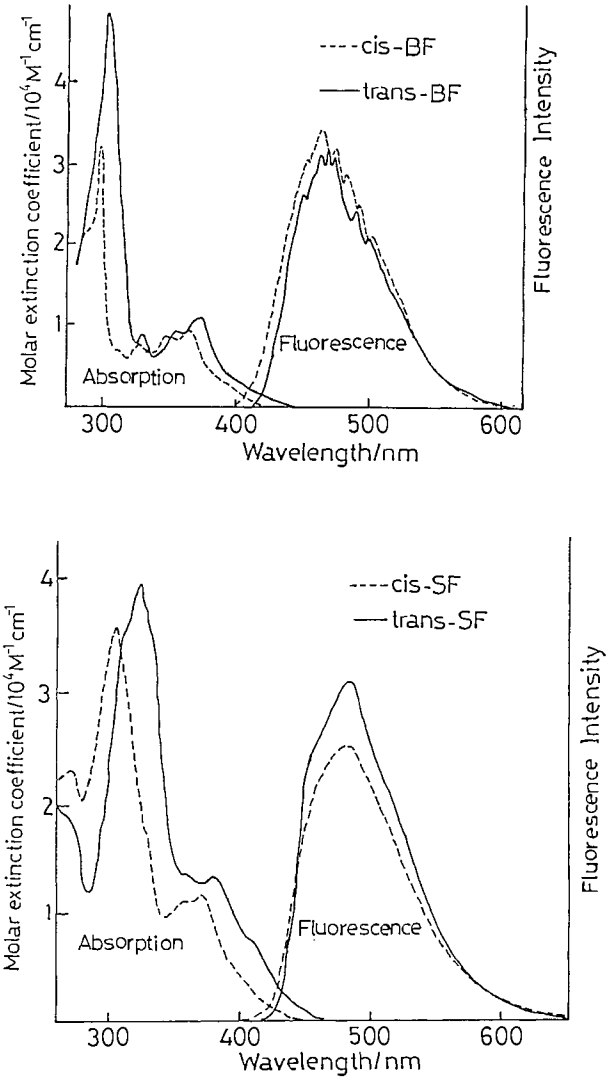

Fig. 1. Absorption and fluorescence spectra of BF and SF in benzene.

to the crossing point of the absorption and fluorescence spectra, the energies of the 0–0 transition are estimated as 67 and 65 kcal mol^{-1} for *cis*- and *trans*-SF, respectively, and 70 and 69 kcal mol^{-1} for *cis*- and *trans*-BF, respectively (Table 1).

In Fig. 1, the differences in energy between the absorption and fluorescence spectra (the Stokes shifts, here defined as the difference in wavelength between the longest absorption maximum and the emission maximum) are calculated as 6000 and 5600 cm^{-1} for *cis*- and *trans*-SF, respectively, and as 5600 and 5200 cm^{-1} for *cis*- and *trans*-BF, respectively. These results indicate that the photoexcitation causes a pronounced change in their structure from the ground states, as reported for the parent hydrocarbon, fluoranthene.[14]

The fluorescence quantum yields (Φ_f) were determined in benzene as 0.40 and 0.48 for *cis*- and *trans*-SF, respectively, and 0.16 and 0.19 for *cis*- and *trans*-BF, respectively, by using anthracene (Φ_f=0.27)[8] (for SF) or

Table 1. Physical Data for the Singlet Excited State of Fluoranthene, BF, and SF

Compound	λ^{fl}_{max}/nm (E/kcal mol^{-1})	$\lambda_{0\text{-}0}$[a]/nm (E_S/kcal mol^{-1})	E_T/kcal mol^{-1}	τ_S/ns	Φ_f
Fluoranthene	463 (62)	405 (71)	54	43.7	0.30[b]
cis-BF	457 (63)	410 (70)	52	28.3	0.16
trans-BF	465 (62)	415 (69)	49	19.4	0.19
cis-SF	480 (60)	430 (67)	46	12.4	0.40
trans-SF	480 (60)	440 (65)	44	9.7	0.48

a) See text. b) In hexane; Ref. 8.

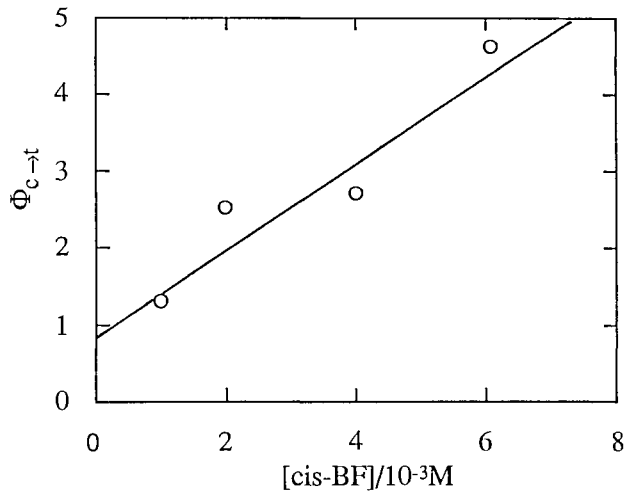

Fig. 2. Plot of the quantum yields for cis→trans isomerization of BF on direct irradiation in benzene.

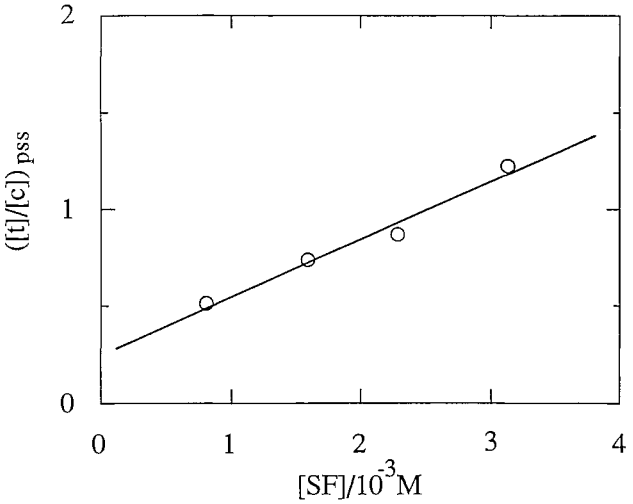

Fig. 3. Plot of the photostationary state isomer ratios against the total SF concentration on direct irradiation in benzene.

fluoranthene (Φ_f=0.30 in hexane)[14] (for BF) as a standard. The singlet lifetimes measured in benzene by the single photon counting method (SPC) are 12.4, 9.7, 28.3, and 19.4 ns for *cis*-SF, *trans*-SF, *cis*-BF, and *trans*-BF, respectively. The fluorescence quantum yields and lifetimes of the BF and SF isomers are summarized in Table 1.

Isomerization Quantum Yields and Photostationary State Isomer Ratio. On direct excitation as well as on triplet sensitized irradiation,[7b] BF underwent cis→trans one-way isomerization. Figure 2 illustrates a concentration dependence of the quantum yield ($\Phi_{c\to t}$) for cis→trans isomerization on direct irradiation. This figure indicates that $\Phi_{c\to t}$ increases with increasing *cis*-BF concentration, attaining nearly 5 at [*cis*-BF]=6×10^{-3} M (1M=1 mol dm^{-3}). On biacetyl sensitization, $\Phi_{c\to t}$ also increased with increasing [*cis*-BF] up to nearly 20 at [*cis*-BF]= 3×10^{-3} M.

The photostationary state isomer composition, ([t]/[c])$_{pss}$, for SF was determined on irradiation with a 436-nm line to be 0.51 at the total olefin concentration of 9×10^{-4}M. The ([t]/[c])$_{pss}$ value increased with increasing olefin concentration to attain 0.94 at [SF]=2.3×10^{-3} M (Fig. 3). The quantum yields of cis-trans isomerization, $\Phi_{c\to t}$ and $\Phi_{t\to c}$ were determined on 436-nm excitation as 0.22 and 0.029, respectively, on starting with pure *cis*- and *trans*-SF at [SF]= 2.3×10^{-3}M.

The ([t]/[c])$_{pss}$ value is expressed by the product of the ratios of isomerization quantum yields and of the extinction coefficients ($\varepsilon_c/\varepsilon_t$) at the irradiation wavelength as described by Eq. 1.

$$([t]/[c])_{pss}=(\varepsilon_c/\varepsilon_t)(\Phi_{c\to t}/\Phi_{t\to c}) \quad (1)$$

The extinction coefficients at 436 nm were determined as 310 and 2500 for *cis*- and *trans*-SF. Thus, at an olefin concentration of 2.3×10^{-3}M the ([t]/[c])$_{pss}$ value is calculated from Eq. 1 as 0.94 [=(310/2500)×(0.22/0.029)], which is in good agreement with the observed value.

Laser Flash Photolysis Studies. The transient absorption spectra were observed on 308- or 337-nm laser excitation of *cis*- and *trans*-BF (4×10^{-4} M) in benzene. Both isomers exhibited the same spectra having two bands at 400—480 and 550—650 nm with the same lifetime (τ_T=25 μs) as measured at the peak wavelengths.

The spectra and lifetimes were essestially identical with those observed on triplet sensitized excitation.[7a] Under similar conditions fluoranthene exhibited its T-T absorption at 400—440 nm (τ_T=30 μs). The transient absorption spectra of SF were effectively quenched by azulene (E_T=39.8 kcal mol^{-1});[15] the quenching rate constant was determined as 3.6×10^{-9} M^{-1} s^{-1} on excitation of *cis*-BF.

On excitation of *cis*- and *trans*-SF (6×10^{-5}M) with 351-nm laser pulses in benzene, both isomers exhibited the same transient absorption spectra with a sharp intense and a broad weak band around 490 and 600 nm, respectively. The spectra decayed with a lifetime of 500 ns under deaerated conditions. The spectral properties are identical with those observed on camphorquinone-sensitized laser excitation.[7b] From these results the observed transient spectra can be reasonably assigned to the trans triplets in both cases.

Discussion

Isomerization Mechanism of BF and SF on Direct Excitation. The results of stationary irradiation and flash photolysis indicate that the triplet mechanism describes the cis→trans one-way isomerization of BF on direct irradiation. Thus, the cis triplet (^{3}c*) produced by intersystem crossing of the cis excited singlet (^{1}c*) undergoes twisting around the double bond to give the trans triplet (^{3}t*), which subsequently undergoes unimolecular deactivation to the trans isomer or energy transfer to the cis isomer to regenerate ^{3}c* leading to a quantum chain process (Scheme 1). According to this mechanism, the quantum yield ($\Phi^{dir}_{c\to t}$) for cis→trans isomerization is expressed by Eq. 2.

$$\Phi^{dir}_{c\to t} = \Phi_{isc}(1 + k_{tc}\tau_T[cis\text{-BF}]) \quad (2)$$

where Φ_{isc}, k_{tc}, and τ_T denote the quantum yield for intersystem crossing of *cis*-BF, the rate constant for energy transfer from ^{3}t* to *cis*-BF, and the lifetime of the trans triplet of BF.

Figure 2 gives a slope, $\Phi_{isc}k_{tc}\tau_T$, of 600 M^{-1}, an intercept, Φ_{isc}, of 0.83, and therefore, $k_{tc}\tau_T$ of 720 M^{-1}. The obtained value for Φ_{isc}, 0.83, is very close to $1-\Phi_f=1-0.16=0.84$, showing that the singlet excited state of *cis*-BF decays through either fluorescence emission or intersystem crossing to ^{3}c*. Dividing the obtained $k_{tc}\tau_T$ values by τ_T (=25 μs, determined by laser flash photolysis) affords k_{tc} of 2.9×10^7 M^{-1} s^{-1}.

In the excited singlet state, the energy transfer from ^{1}t* to ^{1}c leading to the quantum chain process could not compete with the deactivation of ^{1}t* with $k_{td}(=1/\tau_S)=5\times10^7$ s^{-1}; the energy transfer via the resonance mechanism could not operate because of an insufficient overlap of the *trans*-SF emission and *cis*-SF absorption (Fig. 1), and the energy transfer via the exchange mechanism might be much slower ($\ll10^{10}$ M^{-1} s^{-1}) than diffusion-controlled since this process is nearly 1 kcal mol^{-1} endothermic on the basis of the fluorescence data. Thus, the pseudo-first-order energy transfer rate may be $\ll10^7$ s^{-1} in the concentration range of ca. 10^{-3} M. A mechanism involving a ground state complex can be also ruled out since there was no evidence for the formation of such a complex in either absorption or fluorescence spectra for various concentrations of *trans*-BF.

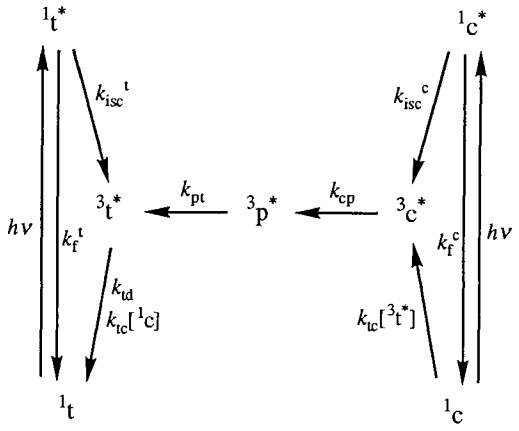

Scheme 1.

As mentioned above, k_{tc} is determined to be 2.9×10^7 M^{-1} s^{-1}. The following equation is established for endothermic energy transfer:[16]

$$k_{tc} = A\exp(-E_a/RT), \quad (3)$$

where

$$-E_a = \Delta E_T = E_T(trans\text{-BF}) - E_T(cis\text{-BF}) \quad (4)$$

On substituting $k_{tc}=2.9\times10^7$ M^{-1} s^{-1} into this equation and assuming $k_{tc}=5\times10^9$ M^{-1} s^{-1} at $\Delta E_T=0$,[16] the energy transfer from ^{3}t* to *cis*-BF is estimated to be endothermic by 3 kcal mol^{-1}. Therefore, the triplet energy of *cis*-BF is nearly 3 kcal mol^{-1} higher than that of *trans*-BF.

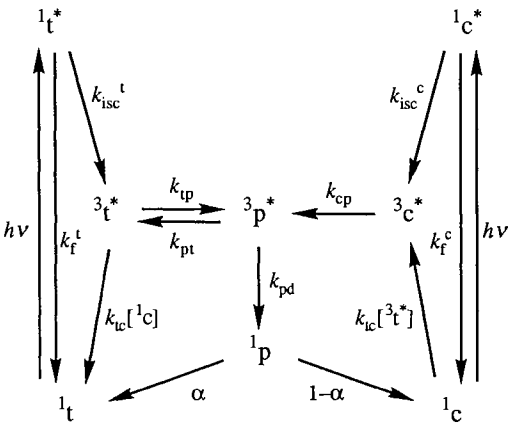

Scheme 2.

Contrary to BF, SF undergoes two-way isomerization on direct irradiation similarly to the previously reported triplet sensitization.[7b] *cis*-SF exhibited the fluorescence spectrum with a different lifetime and different spectral properties from those of *trans*-SF. Moreover, the T–T absorption spectrum was also observed on direct excitation of *cis*-SF. The photostationary state isomer composition $([t]/[c])_{pss}$ increased with increasing total olefin concentration. These results clearly indicate that the isomerization on direct excitation proceeds through the triplet manifold as shown in Scheme 2.

Potential Energy Surface of Fluoranthenylethylenes. The excited singlet states of fluoranthenylethylenes emit fluorescence or undergo intersystem crossing with decay rate constants of $1/\tau_S=8.1\times10^7\ s^{-1}$ for *cis*-SF and $3.5\times10^7\ s^{-1}$ for BF, but the isomerization cannot be detected in the singlet manifold. Therefore, the latter process might be slower than 1/100 of $1/\tau_S$, $10^6\ s^{-1}$. If we assume a frequency factor A of 10^{11}—$10^{12}\ s^{-1}$ for twisting around the double bond as reported for some triplet olefins,[2b,17] the activation barrier for isomerization might be higher than 7 kcal mol^{-1} in the singlet manifold. Thus, the potential energy surfaces of SF are depicted in Fig. 4a taking into account the previously reported triplet energy surface.[7b]

In Fig. 4a, the direct excitation of *cis*- and *trans*-SF produces the respective singlet excited states which emit fluorescence or undergo intersystem crossing to produce the triplet states, which are deactivated to the ground state from either the perpendicular or trans triplet state, resulting in the photostationary mixture of cis and trans isomers.

On direct irradiation, BF undergoes one-way isomerization in the triplet manifold after intersystem crossing, and its potential energy surfaces is similarly drawn in Fig. 4b.

As mentioned above, on direct irradiation the two-way isomerizing olefins such as stilbene usually undergo isomerization in the singlet manifold, while the one-way isomerizing olefins undergo isomerization in the triplet manifold. The fluoranthenylethylenes employed also isomerize in the triplet manifold irrespective of the substituent on the other ethylenic carbon, *t*-butyl or phenyl, therefore behaving similarly to the anthryl- and pyrenylethylenes.

On the triplet energy surface of olefins, the introduction of an aromatic group with a low triplet energy lowers the energy of $^3t^*$ and $^3c^*$ to put them, instead of $^3p^*$, at the energy minima. A similar situation may happen on the singlet energy surface. On substitution of an aryl group on the terminal carbon of styrene, those with low singlet excitation energies like 8-fluoranthenyl (80 kcal mol^{-1})[8] make both $^1c^*$ and $^1t^*$ fluorescent and apt to intersystem cross to the triplet state with considerable efficiencies (Table 1), whereas those with high singlet energies like phenyl (110 kcal mol^{-1})[8] and 2-naphthyl (92 kcal mol^{-1})[8] do not make $^1c^*$ fluorescent but lead it to isomerize in the singlet manifold before intersystem crossing.[8] These results indicate that the substitution of the aromatic group with a low singlet energy sufficiently stabilizes $^1c^*$

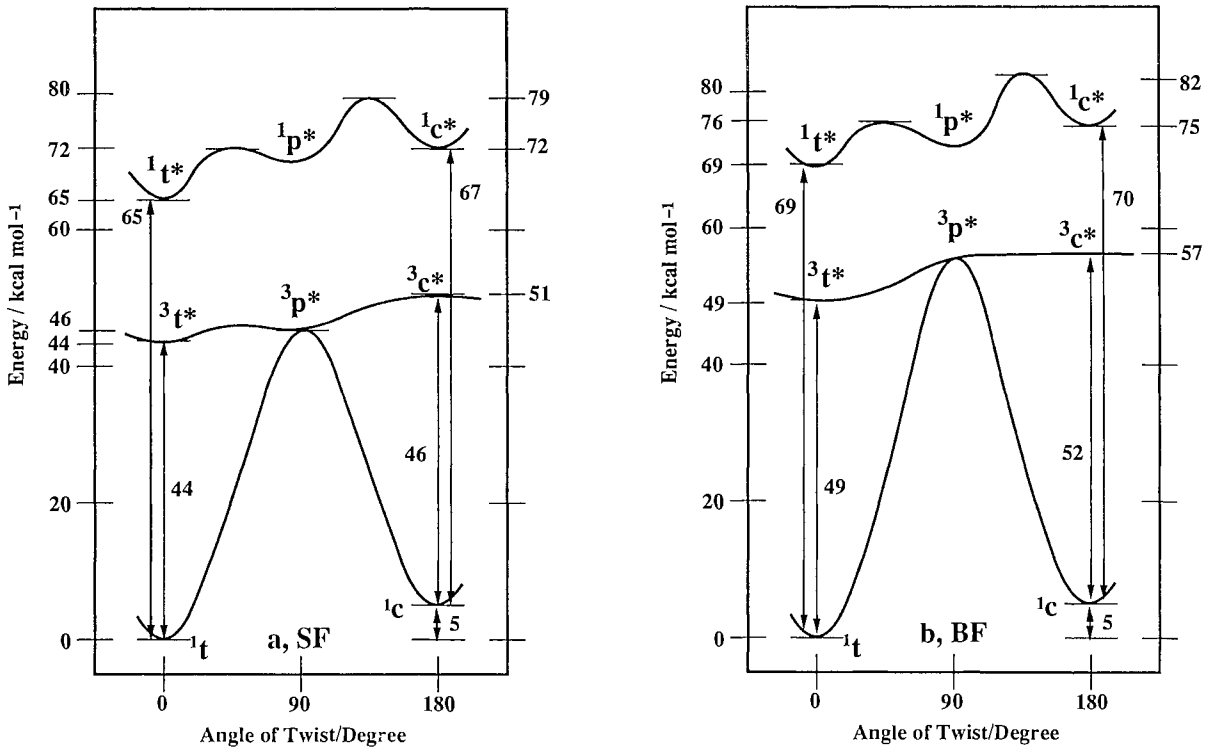

Fig. 4. Potential energy surfaces of cis-trans isomerization of SF (a) and BF (b).

to reside at an energy minimum and to have a sufficient lifetime to emit fluorescence. This situation may reflect the presence of a considerable energy barrier for isomerization in the singlet manifold. Therefore, the isomerization takes place in the triplet state after intersystem crossing. This is contrasted to the effect of substitution of the aromatic group with higher energies as observed in stilbene, where $^1c^*$ is not so stabilized as to fluoresce practically and isomerizes facilely on the singlet energy surface. Therefore, the singlet and triplet excitation energies of the aromatic group on the double bond control the course of isomerization, (1) the spin multiplicity in which the isomerization takes place on direct excitation, and (2) the mode of isomerization, two-way or one-way, in the triplet state.

The authors thank to the Ministry of Education, Science and Culture for partial support of this work by Grant-in-Aid for Special Project Research Nos. 61123001, 62113001, and 63104001 (K. T.) and by Grant-in-Aid for Scientific Research Nos. 61740242, 01740255 (T. A.), and 02453019 (K. T.). Thanks are also due to University of Tsukuba for partial support by the President's Special Grant for Education and Research, 1990 (K. T.).

References

1) a) T. Arai, T. Karatsu, H. Sakuragi, and K. Tokumaru, *Tetrahedron Lett.*, **24**, 2873 (1983); b) T. Karatsu, T. Arai, H. Sakuragi, and K. Tokumaru, *Chem. Phys. Lett.*, **115**, 9 (1985); c) H. Hamaguchi, M. Tasumi, T. Karatsu, T Arai, and K. Tokumaru, *J. Am. Chem. Soc.*, **108**, 1698 (1986).

2) a) T. Arai, T. Karatsu, M. Tsuchiya, H. Sakuragi, and K. Tokumaru, *Chem. Phys. Lett.*, **149**, 161 (1988); b) T. Karatsu, M. Tsuchiya, T. Arai, H. Sakuragi, and K. Tokumaru, *Chem. Phys. Lett.*, **169**, 36 (1990).

3) T. Arai, T. Karatsu, H. Misawa, Y. Kuriyama, H. Okamoto, T. Hiresaki, H. Furuuchi, H. Zeng, H. Sakuragi, and K. Tokumaru, *Pure Appl. Chem.*, **60**, 989 (1988), and references cited therein.

4) a) J. Saltiel, J. D'Agostino, E. D. Megarity, L. Metts, K. R. Neuberger, M. Wrighton, and O. C. Zafiriou, in "Organic Photochemistry," ed by O. L. Chapman, Marcel Dekker, New York (1973), Vol. 3, p. 1; b) J. Saltiel and J. L. Charlton, in "Rearrangement in Ground and Excited States," ed by P. de Mayo, Academic Press, New York (1980), Vol. 3, p. 25.

5) G. S. Hammond, J. Saltiel, A. A. Lamola, N. J. Turro, J. B. Bradshaw, D. O. Cowan, R. Counsell, V. Vogt, and C. Dalton, *J. Am. Chem. Soc.*, **86**, 3197 (1964).

6) a)T. Arai, H. Okamoto, H. Sakuragi, and K. Tokumaru, *Chem. Phys. Lett.*, **157**, 46 (1989); b) H. Okamoto, T. Arai, H. Sakuragi, and K. Tokumaru, *Bull. Chem. Soc. Jpn.*, **63**, 2881 (1990).

7) a) T. Arai, Y. Kuriyama, T. Karatsu, H. Sakuragi, K. Tokumaru, and S. Oishi, *J. Photochem.*, **36**, 125 (1987); b) H. Furuuchi, T. Arai, Y. Kuriyama, H. Sakuragi, and K. Tokumaru, *Chem. Phys. Lett.*, **162**, 211 (1989).

8) S. L. Murov, "Handbook of Photochemistry," Marcel Dekker, New York (1973), p. 5.

9) J. Saltiel, A. Marinari, D. W.-L. Chang, J. C. Mitchener, and E. D. Megarity, *J. Am. Chem. Soc.*, **101**, 2983 (1979).

10) M. Sumitani and K. Yoshihara, *J. Chem. Phys.*, **76**, 738 (1982).

11) H. Okamoto, T. Arai, H. Sakuragi, and K. Tokumaru, *Bull. Chem. Soc. Jpn.*, **64**, 216 (1991).

12) a) J. v. Braun and G. Manz, *Justus Liebigs Ann. Chem.*, **496**, 170 (1932); b) N. Campbell and W. W. Easton, *J. Chem. Soc.*, **1949**, 340; c) T. Sasaki, K. Kanematsu, and T. Hiramatsu, *J. Chem. Soc., Perkin Trans. 1*, **1974**, 1213.

13) S. Akiyama, S. Misumi, and M. Nakagawa, *Bull. Chem. Soc. Jpn.*, **35**, 1826 (1962).

14) I. B. Berlman, "Handbook of Fluorescence Spectra of Aromatic Molecules," Academic Press, New York (1971), p. 390.

15) A. A. Gorman, I. Hamblett, M. Irvine, P. Raby, M. C. Standen, and S. Yeates, *J. Am. Chem. Soc.*, **107**, 4404 (1985).

16) W. G. Herkstroeter and G. S. Hammond, *J. Am. Chem. Soc.*, **88**, 4769 (1966).

17) H. Misawa, T. Karatsu, T. Arai, H. Sakuragi, and K. Tokumaru, *Chem. Phys. Lett.*, **146**, 405 (1988).

Insulator-to-Metal-to-Semiconductor Transitions of One-Dimensional Bis(1,2-dione dioximato)Pt(II) Complexes at High Pressures

Ichimin SHIROTANI,* Akira KAWAMURA, Kazunaga SUZUKI, Wataru UTSUMI,† and Takehiko YAGI†
Muroran Institute of Technology, 27-1, Mizumoto, Muroran 050
† The Institute for Solid State Physics, The University of Tokyo, Roppongi, Minato-ku, Tokyo 106
(Received December 12, 1990)

The electrical resistivities and absorption spectra of one-dimensional bis(1,2-dione dioximato)Pt(II) have been studied at high pressures. The resistivities of needle crystals of $Pt(dmg)_2$ and $Pt(bqd)_2$ were measured in detail under a quasi-hydrostatic pressure of up to 7 GPa. $Pt(dmg)_2$ is an insulator with a resistivity of 10^{15} Ω cm, and $Pt(bqd)_2$ is a semiconductor with 10^3 Ω cm at atmospheric pressure. A pressure-induced insulator (semiconductor)-to-metal transition was observed for both complexes. This transition arises from a crossing of the $5d_{z^2}$ valence and $6p_z$ conduction bands. When the pressure was further increased, a metal-to-semiconductor transition took place at around the pressure that showed a resistivity minimum. A new pressure-induced absorption band was found in the visible region for the Pt complexes. The new band did not shift with pressure; the intensity of the band, however, increased with pressure over a narrow pressure region. The pressure-induced band may be due to intramolecular d–d transitions. The metal-to-semiconductor transition may arise from a change in the electronic states at high pressure, since no anomaly in the strucutre was observed.

Square planar d^8 metal complexes with various kinds of 1,2-dinoe dioximes (Fig. 1) crystallize in columnar structures. These columns are formed by complex molecules with metal–metal distances varying from 3.2 to 3.6 Å in the direction of the stacks.[1] These poorly conducting one-dimensional complexes show an interst-ing behavior at high pressure. The electrical resistivity,[2-5] electronic and infrared spectra,[4-8] and crystal structure[9] of the complexes have already been studied at high pressures. Their resistivities rapidly decrease and an absorption band ascribed to the d–p transition shifts remarkably to a longer wavelength with pressure. The electrical and optical properties of the complexes are very sensitive to the metal–metal distance in a linear chain.

Pressure-induced electrical and optical anomalies in bis(dimethylglyoximato)Pt(II), $Pt(dmg)_2$, were observed at around 6.5 GPa; the electrical resistivity drastically decreases, by a factor 10^{-16}, with increasing pressure up to the pressure that indicates a resistivity minimum.[2,3] A new pressure-induced absorption band at around 540 nm was found above 6 GPa.[4,5] Bis(1,2-benzoquinone dioximato)Pt(II), $Pt(bqd)_2$, has the shortest Pt–Pt dis-tance (3.17 Å) in the known bis(1,2-dione dioximato)Pt(II)

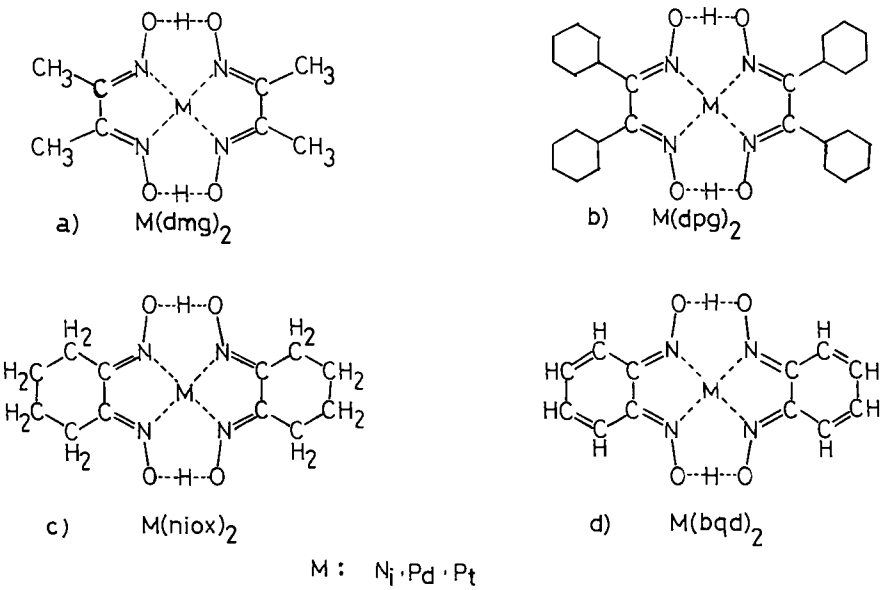

Fig. 1. Molecular structure of bis(1,2-dione dioximato)M(II) (M: Ni, Pd, Pt); a) bis(dimethylglyoximato)M(II), $M(dmg)_2$, b) bis(diphenylglyoximato)M(II), $M(dpg)_2$, c) bis(1,2-cyclohexanedione dioximato)M(II), $M(niox)_2$ (1,2-cyclo-hexanedione dioxime is usually called nioxime), d) bis(1,2-benzoquinone di-oximato)M(II), $M(bqd)_2$.

compounds; it is a semiconductor with a thermal energy gap of 0.25 eV at atmospheric pressure.[10] The resistivity along the needle axis is about $10^3\,\Omega$ cm at room temperature. An absorption band polarized parallel to the linear chain, which is assigned to the electronic transition between $5d_{z^2}$ and $6p_z$, is located at around 1300 nm. The interesting properties are mainly interpreted in terms of a short Pt–Pt distance of 3.17 Å.

We recently reported preliminary results concerning insulator-to-metal-to-semiconductor transitions of $Pt(dmg)_2$ at high pressure; this complex behaves as an insulator(semiconductor) in the pressure range 0—4.5 GPa, as a metal around 5 GPa, and again as a semiconductor above 6 GPa.[5] Similar phenomena have also been observed for $Pt(bqd)_2$ at high presessures.

In this paper we present some findings concerning electrical and optical anomalies in the four platinum complexes shown in Fig. 1 and discuss the mechanism of the phase transitions at high pressure.

Experimental

Platinum complexes were prepared by mixing a hot alcohol solution of 1,2-dione dioximes and an aqueous solution of K_2PtCl_4. The products were purified by repeated recrystallization from *o*-dichlorobenzene or dimethylformamid. The needle crystals were grown from these solutions of the complexes. The compositions of all of the materials used were confirmed by elemental analysis.

Measurements of the electrical resistance were carried out up to 7 GPa in a cubic-anvil press; cemented tungusten carbide anvils had square faces of 6 mm edge length. Each sample was placed in the center hole of a pyrophyllite cube that had an 8 mm edge length. The sample assembly has already been reported in a previous paper.[12] The crystal was covered by an epoxy resin, which was used as a pressure-transmitting medium. The resistance was measured over a temperature range of 25 to 100 °C at various pressures under quasi-hydrostatic conditions.

A diamond-anvil pressure cell was used for the measurement of the absorption spectra at high pressures.[4] The optical system comprised a standard microscope and a monochrometer with an associated photodetection system. The pressure was determined from the pressure shift in the sharp R-line fluorescence spectrum of ruby.[13] Water was used as the pressure-transmitting medium.

Results and Discussion

$Pt(dmg)_2$ is a square planar complex in which each Pt^{2+} ion is surrounded by four nitrogen atoms of two dimethylglyoxime anions. The d orbitals of the Pt^{2+} ion are split by a crystal field of D_{4h} symmetry. The 8 electrons of the Pt^{2+} ion core fill the d_{z^2}, d_{xy}, d_{yz}, and d_{zx} states. The complex crystallizes in columnar structures. The columns are formed by square planar complex molecules with a relatively short Pt–Pt distance of 3.26 Å in a direction of the stacks. The overlap of the d_{z^2} orbitals can, thus, produced a band that is completely filled and separated from the next empty band

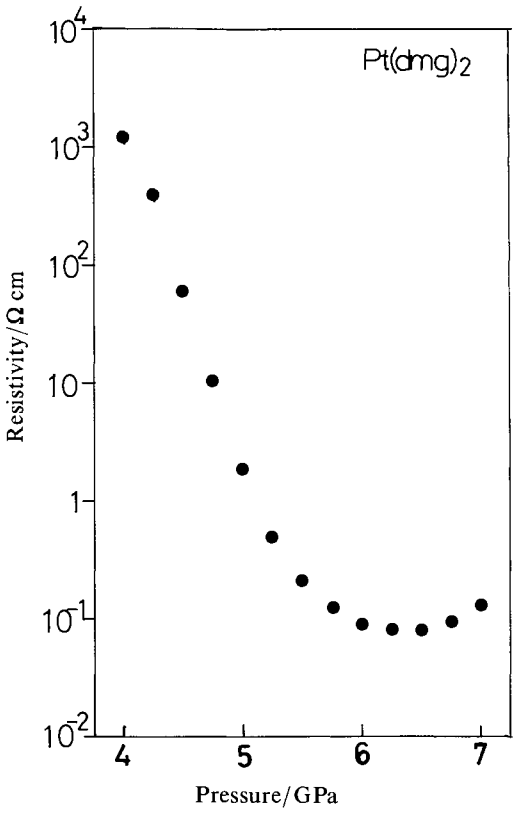

Fig. 2. Electrical resistivity of the single crystal of $Pt(dmg)_2$ at high pressure.

formed by p_z orbitals by a large gap. The complex is an insulator with a resistivity of $10^{15}\,\Omega$ cm at atmospheric pressure.[14]

Figure 2 shows the electrical resistivity along the stacking axis of a single crystal of $Pt(dmg)_2$ at high pressures. The resistivity drastically decreases with pressure up to the pressure that shows the resistivity minimum. The lowest resistivity along the stacking axis of the single crystal is about $10^{-2}\,\Omega$ cm at room temperature and high pressure. Figure 3 shows the temperature dependence of the resistivity at various pressures. The resistivity linearly increases with increasing temperature at around 5 Gpa. A pressure-induced insulator-to-metal transition was observed. The thermal energy gap rapidly decreases with decreasing Pt–Pt distance, reaching zero at around 5 GPa.

The absorption spectrum of $Pt(dmg)_2$ comprises two bands at 320 and 660 nm in the visible region; the former band is ascribed to a metal-to-ligand charge-transfer transition (M–L transition); the latter band is assigned to the $5d_{z^2}$–$6p_z$ transition.[15] This latter band indicates a large red shift with pressure, at a rate of $-2700\,cm^{-1}/GPa$. Since the absorption edge is located at about $12.8\times10^3\,cm^{-1}$, the optical energy gap between the $5d_{z^2}$ and $6p_z$ bands becomes zero at around 5 GPa. Thus, the insulator-to-metal transition at around 5 GPa arises from a crossing of the $5d_{z^2}$ valence and the $6p_z$ conduction bands.

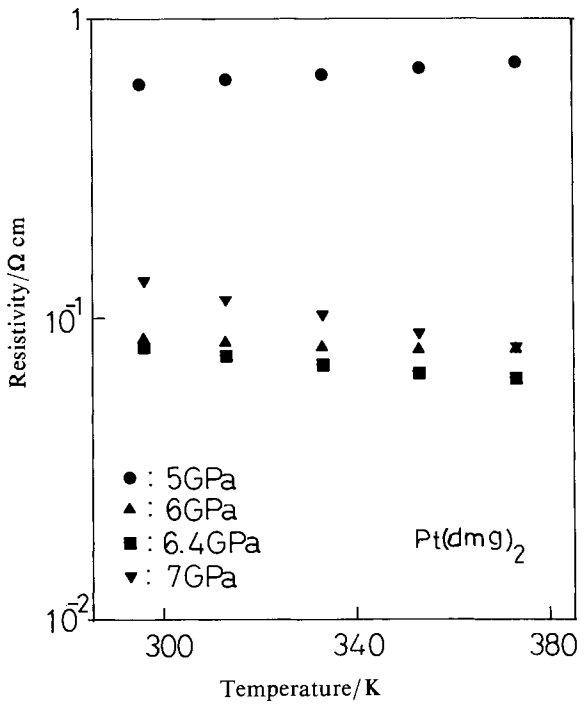

Fig. 3. Temperature dependence of the resistivity of $Pt(dmg)_2$ at high pressures.

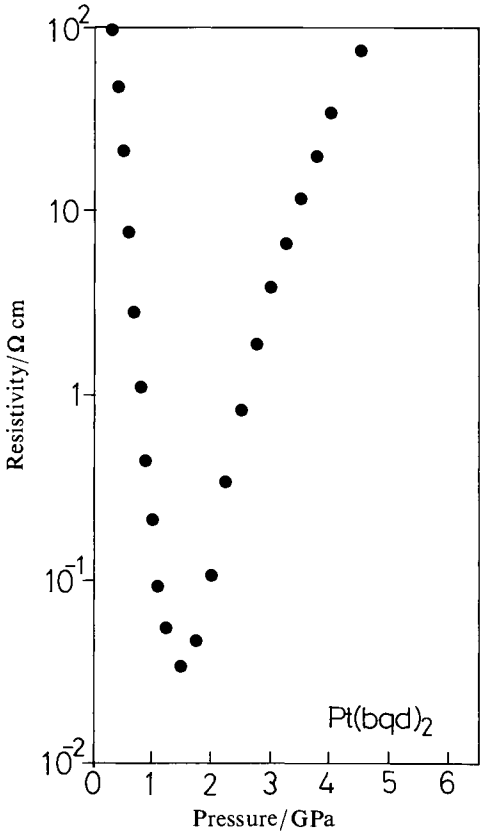

Fig. 4. Electrical resistivity of the needle crystal of $Pt(bqd)_2$ at high pressure.

The effect of pressure on the Pt–Pt distance has already been studied by powder X-ray diffraction.[4] The distance within a linear chain decreases from 3.26 Å at atmospheric pressure to 2.77 Å at 13 GPa. The Pt–Pt distance of metallic $Pt(dmg)_2$ is about 2.90 Å, slightly longer than that of a one-dimensional metal, such as $K_2Pt(CN)_4Br_{0.3}\cdot 3H_2O$ (KCP).

The temperature dependence of resistivity again changed at around 6 GPa; the resistivity slightly decreased with increasing temperature. Semiconductive-like behavior was again observed above 6 GPa. The one-dimensional metal was only stable within a narrow pressure region. This result seems to suggest a Peierls transition, due to the strong one-dimensional character in $Pt(dmg)_2$. Recently, an X-ray study of a single crystal of $Pt(dmg)_2$ was carried out up to 4 GPa.[9] The *a* and *b* lattice constants decrease monotonically with pressure. The Pt–Pt distance within the linear chains, $c/2$, decreases continuously from 3.26 Å at atmospheric pressure to 2.97 Å at 3.84 GPa. This agrees with the result concerning powder X-ray diffraction. The *b*-axis rapidly shrinks with pressure up to 1.5 GPa, but slowly decreases above this pressure. The intermolecular interaction of CH···O type grow stronger by a shrinking of the *b*-axis at high pressure. The intermolecular distance between O and C of the adjacent chains decreases from 3.28 Å at atmospheric pressure to 2.97 Å at 2.38 GPa. The intermolecular interaction between adjacent chains increases with pressure. The anomaly in the crystal structure along the *c*-axis, as anticipated for a Peierls distortion, was not found in the X-ray diffraction of the single crystal at around 7 GPa.[16]

A new pressure-induced absorption band appears at around 540 nm above 6 GPa.[3,4] The absorption intensity of the new band abruptly increases with increasing pressure over a narrow pressure range of 6 to 9 GPa. The absorption peak of the band does not shift with pressure at least up to 15 GPa. On the other hand, Tkacz and Drickamer have found that the intensity of the d–p band exhibits a sharp drop over the same pressure range.[7] The new band grows with a disappearance of the d–p transition. These results suggest that the metal-to-semiconductor transition at around 6 GPa is not due to a Peierls transition but, rather, to a change in the electronic states with pressure.

The resistivity of a needle crystal of $Pt(bqd)_2$ is about $10^3\ \Omega$ cm at room temperature.[10] The complex is a semiconductor with a thermal energy gap of 0.25 eV at atmospheric pressure. Figure 4 depicts the resistivity of a needle crystal at high pressure. The crystals were obtained by recrystallization from an *o*-dichlorobenzene solution. The resistivity rapidly decreases with pressure up to 1.7 GPa; above that pressure it abruptly increases with an increase in the pressure. The resistivity at the resistance minimum is about $10^{-2}\ \Omega$ cm at room temperature and high pressure. Figure 5 shows the temperature dependence of the resistivity at various pressures. The resistivity rises with increasing temperature

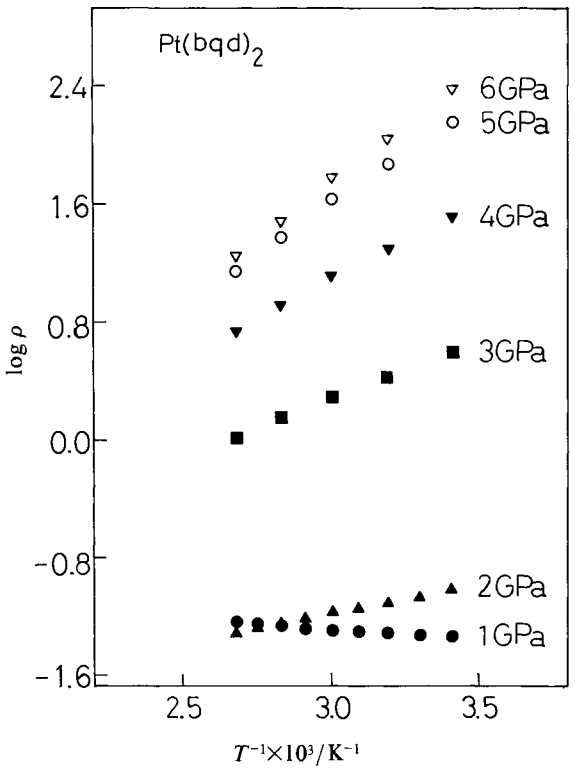

Fig. 5. Temperature dependence of the resistivity of $Pt(bqd)_2$ at high pressures.

at around 1 GPa. The thermal energy gap of 0.25 eV at atmospheric pressure became zero at around 1 GPa. A semiconductor-to-metal transition was found for $Pt(bqd)_2$.

An oriented film of $Pt(bqd)_2$ is prepared by evaporation onto a quartz or a glass substrate held at room temperature in a vacuum of 1.33×10^{-4} Pa (10^{-6} Torr, 1 Torr=133.322 Pa).[17] The absorption bands of the oriented film are located at around 360, 420, and 1300 nm. The latter band is assigned to the $5d_{z^2}$–$6p_z$ transtition. The pressure effect of the bands has not yet been studied. When the Pt–Pt distance of $Pt(dmg)_2$ skrinks from 3.26 Å to the Pt–Pt distance of $Pt(bqd)_2$ (3.17 Å), the peak of the d–p band shifts from 15200 to 13000 cm^{-1}. This value of $Pt(dmg)_2$ is much larger than the energy of the d–p band of $Pt(bqd)_2$, 7700 cm^{-1}. It is therefore expected that the d–p band of $Pt(bqd)_2$ has a very large red shift with pressure. The $6p_z$ conduction band must cross the $5d_{z^2}$ valence band at around 1 GPa.

The temperature dependence of the resistivity again changed at around 1.4 GPa; the resistivity of $Pt(bqd)_2$ decreased slightly with increasing temperature. The metal-to-insulator transition took place at around 1.4 GPa. The complex again behaved as a semiconductor above that pressure. The one-dimensional metal was stable within only a narrow pressure region. Figure 6 shows the absorption spectra of $Pt(bqd)_2$ at high pressures. A new pressure-induced absorption band

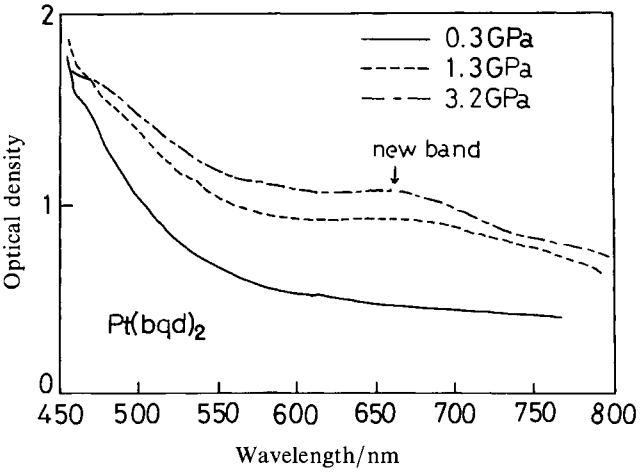

Fig. 6. Pressure effect of absorption spectra of $Pt(bqd)_2$.

appeared at around 660 nm above 1.3 GPa; the absorption intensity of the new band increased with pressure. The metal-to-semiconductor transition was found at around the pressure in which the optical anomaly was observed. Anomalous electronic and infrared spectra have been observed in a evaporated film of $Pt(bqd)_2$ on a NaCl substrate;[17] the 1300 nm band ascribed to the d–p transition disappears an asymmetric O···H–O bridge is formed, and the C=N stretching band splits into 1600 and 1610 cm^{-1}. The optical behavior of $Pt(bqd)_2$ is similar to that of $Pt(dmg)_2$ at high pressure.

The metal-to-semiconductor transition took place at around 6 GPa for $Pt(dmg)_2$, and 1.4 GPa for $Pt(bqd)_2$. The one-dimensional metal of both Pt complexes was stable over a very narrow pressure region. The pressure-induced absorption band and the resistivity minimum were observed near to the transition pressures. The absorption peaks of the new bands did not shift with pressure. An intramolecular d–d transition of metal complexes generally indicates a small blue shift with pressure.[6] The spin-allowed d–d transitions (d_{xy}–$d_{x^2-y^2}$, d_{z^2}–$d_{x^2-y^2}$, d_{yz} and d_{zx}–$d_{x^2-y^2}$) in square planar d^8 complexes can be observed, even though the absorption intensity is weak.[18] However, the transitions did not appear in the Pt complexes at atmospheric pressure. If vibronic modes of the complexes (especially the e_u mode) strongly couple to the d states with pressure, the intensity of the d–d transitions will increase at high pressure. The d–d transitions coupled by an e_u mode may borrow intensity from the M–L and d–p transitions. The absorption intensity of the d–p transition rapidly decreased over the narrow pressure region where the new band appeared. The pressure effect of the intensity of the M–L band has not been studied for Pt complexes. The a and b lattice constants (a=16.774 Å, b=10.579 Å) are so long that the $d_{x^2-y^2}$ orbitals between adjacent complex molecules in the ab plane hardly overlap. It is expected that the d–d bands hardly shift with pressure, since the $d_{x^2-y^2}$ orbital in the

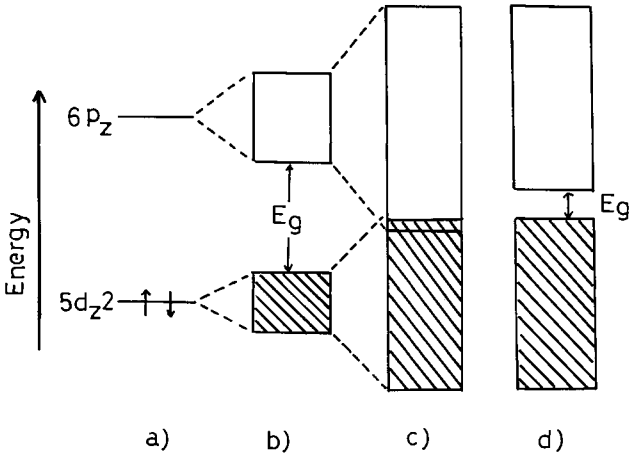

Fig. 7. Schematic energy diagram in $Pt(dmg)_2$ and $Pt(bqd)_2$ complexes; a) the energy separation between the filled $5d_{z^2}$ and the empty $6p_z$ orbitals of the complex molecules, b) the filled $5d_{z^2}$ valence and the empty $6p_z$ conduction bands are produced at atmospheric pressure, c) the $6p_z$ conduction band crosses the $5d_{z^2}$ valence band at high pressure. Pressure-induced insulator-to-metal transition takes place at room temperature, d) the energy gap between the $6p_z$ conduction and the $6p_{z^2}$ valence band is again observed at higher pressures. Pressure-induced metal-to-semiconductor transition takes place at room temperature.

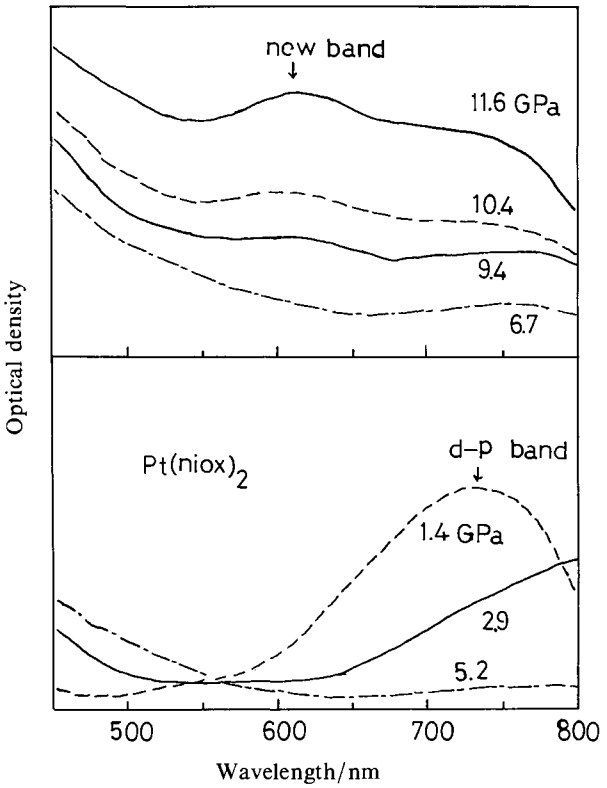

Fig. 8. Pressure effect of absorption spectra of $Pt(niox)_2$.

Pt complexes is not sensitive to pressure. We thus suggest that the new band of the Pt complexes is due to an intramolecular d–d transition as the intensity of the new band becomes stronger with pressure and the absorption peak does not shift with pressure. Therefore, the metal-to-semiconductor transition mainly arises from a change in the electronic states at high pressure.

We have found a pressure-induced insulator (semiconductor)-to-metal-to-semiconductor transitions for $Pt(dmg)_2$ and $Pt(bqd)_2$ over a narrow pressure region. A schematic energy diagram of the Pt complexes is given in Fig. 7.

A thin film of bis(1,2-cyclohexanedione dioximato)Pt(II), $Pt(niox)_2$, was prepared by evaporation in a high vacuum. The absorption spectrum of the thin film is similar to that of $Pt(dmg)_2$. The absorption bands of $Pt(niox)_2$ are located at 320 and 670 nm at atmospheric pressure; the former band is ascribed to the M–L transition, and the latter band is assigned to the d–p transition. Figure 8 exhibits the absorption spectra of $Pt(niox)_2$ at high pressures. The d–p band shifted remarkably toward longer wavelengths; the intensity of the band decreased with pressure. A new pressure-induced band at around 625 nm was observed above 9.5 GPa; the absorption intensity of the band increased with increasing pressure. The resistance of polycrystals of $Pt(niox)_2$ decreases rapidly with pressure, reaching a resistance minimum at 9.4 GPa.[3] The lowest resistivity of the powder sample is about 2 Ω cm at high pressure. A pressure-induced band of $Pt(niox)_2$ was observed around the pressure showing the resistivity minimum. This behavior is smimilar to that of $Pt(dmg)_2$ and $Pt(bqd)_2$. A single crystal of $Pt(niox)_2$ has not yet been prepared. If the resistivity of the single crystal is measured in detail at high pressure, the phase transitions may be found.

The resistivity of bis(diphenylglyoximato)Pt(II), $Pt(dpg)_2$, decreased at least up to 22 GPa; no minimum was found. The lowest resistivity was 3×10^2 Ω cm at room temperature, much higher than that of the other Pt complexes. The band at 550 nm under atomospheric pressure is due to the $5d_{z^2}$–$6p_z$ transition, and the 394 nm band is assigned as the M–L transition. Both bands indicate large red shifts with pressure. No pressure-indued absorption band was found. No electrical or optical anomalies were found at high pressure.

References

1) E. Frasson, C. Panattoni, and R. Zannetti, *Acta Crystallogr.*, **12**, 1027 (1959); L. E. Godycki and R. E. Rundle, *Acta Crystallogr.*, **6**, 487 (1953).

2) Y. Hara, I. Shirotani, and A. Onodera, *Solid State Commun.*, **19**, 171 (1976).

3) I. Shirotani, A. Onodera, and Y. Hara, *J. Solid State Chem.*, **40**, 180 (1981).

4) I. Shirotani and T. Suzuki, *Solid State Commun.*, **59**, 533 (1986).

5) I. Shirotani, M. Konno, and Y. Taniguchi, *Synth. Met.*, **29**, F123 (1989).

6) H. G. Drickarmer and J. C. Zhanar, *Adv. Chem. Phys.*, **4**, 161 (1962).
7) M. Tkacz and H. G. Drickamer, *J. Chem. Phys.*, **85**, 1184 (1986).
8) Y. Hara and M. Nicol, *Bull. Chem. Soc. Jpn.*, **51**, 1982 (1978).
9) M. Konno, T. Okamoto, and I. Shirotani, *Acta Crystallogh., Sect. B*, **45**, 142 (1989).
10) M. M. Bélombé, *J. Solid State Chem.*, **22**, 151 (1977).
11) J. W. Brill, M. M. Bélombé, and M. Novotny, *J. Chem. Phys.*, **68**, 585 (1978).
12) I. Shirotani, A. Fukizawa, H. Kawamura, T. Yagi, and S. Akimoto, "Solid State Physics under High Pressure," ed by S. Minomura, KTK Scientific Publisher, Tokyo (1985), p. 207.
13) J. D. Barnett, S. Block, and G. J. Piermarini, *Rev. Sci. Instrum.*, **44**, 1 (1973).
14) L. Atkinson, P. Day, and R. J. P. Williams, *Nature*, **218**, 668 (1968).
15) Y. Ohashi, I. Hanazaki, and S. Nagakura, *Inorg. Chem.*, **9**, 2551 (1970).
16) N. Hamaya, private communication.
17) I. Shirotani, N. Minobe, Y. Ohotsuki, H. Yamochi, and G. Saito, *Chem. Phys. Lett.*, **147**, 231 (1988).
18) H. B. Gray, "Transition Metal Chemistry," ed by R. L. Garlin, Marcel Dekker (1996).

 © 1991 The Chemical Society of Japan Bull. Chem. Soc. Jpn., 64, 1613—1617 (1991)

NMR Studies on Reorientational Motion of Hydrated D_2O Molecules of Halaide Ions (F^-, Cl^-, Br^-, and I^-) in Dilute Aqueous Solutions

Akio SHIMIZU and Yoshihiro TANIGUCHI*
Department of Chemistry, Faculty of Science and Engineering, Ritsumeikan University, Kita-ku, Kyoto 603
(Received December 25, 1990)

The spin-lattice relaxation rates of the D and ^{17}O nuclei of D_2O molecules have been measured for dilute aqueous solutions of potassium halides (KF, KBr, KCl, KI) in the concentration range below 1.0 mol kg^{-1} at 25 °C. The agreement between the B_X' coefficients of the spin-lattice relaxation rate (reorientational motion) and the B coefficients of the solution viscosity of the anions is somewhat better than that of the cations. The reorientational motion of hydration for D_2O molecules of Cl^-, Br^-, and I^- ions was anisotropic; this anisotropic motion is enhanced with increasing ion radius. On the other hand, the hydration D_2O molecule of the F^- ion was approximately isotropic.

The concentration effect on the reorientational correlation times of hydrated water molecules in electrolyte solutions is both important and necessary in understanding the dynamic features of ionic hydration. Measurements of the spin-lattice relaxation rate (R_1) have mainly been carried out in the high concentration range above 1.0 mol kg^{-1}.[1-9] These data are expressed by a quadrutic polynominal equation as a function of the concentration in order to provide reorientational correlation times of hydrated water molecules for each ion at infinite dilution. We have recently carried out systematic NMR studies concerning the reorientational correlation times of hydrated water molecules in low the concentration range below 1.0 mol kg^{-1} [10-14] in order to elucidate the ion-water interactions. Since R_1 varies linearly with concentration below 1.0 mol kg^{-1}, each hydration sphere of the ions can be isolated from each other.

It is well known that the dynamic properties of aqueous electrolyte solutions are influenced by the ionic radius as well as the charge of ions. The structure-breaking effect of halide ions on the viscosity of solutions is greater than that of alkali metal ions, since the ionic radius of halide ions is larger than that of alkali metal ions. Studies concerning the dynamic properties of hydrated water molecules of ions have attracted both physical and biochemical attention, since the behavior of water in aqueous electrolyte solutions plays an essential role in biological reactions and protein stability.[15]

A D_2O molecule has a D and an ^{17}O nuclei which relax by a quadrupole interaction. Their spin-lattiice relaxation rates have been measured by NMR. The main component of the quadrupole interaction tensor at the D nuclei lies along the O-D bond axis, and the main component at the ^{17}O nucleus is the perpendicular axis to the molecular plane of a D_2O molecule.[16,17] The reorientational correlation times of the D and ^{17}O nuclei furnish information on the reorientational motion of the O-D axis and the axis perpendicular to the D_2O molecular plain.

In the present study we focused attention on the dynamic properties of the hydration D_2O molecule of halide ions (F^-, Cl^-, Br^-, and I^-) and measured the concentration dependence of the D and ^{17}O spin-lattice relaxation rates of D_2O molecules below 1.0 mol kg^{-1}. Comparing the D relaxation rate with that of the ^{17}O nucleus on the basis of the two-state model, we can discuss the dynamic behavior of a hydrated D_2O molecule.

Experimental

Samples. Potassium halide (KF, KCl, KBr, KI) salts from Nakarai Tesque Inc. (extra pure grade) were recrystallized from water. D_2O obtained from CEA contained over 99.8% of D.

NMR Measurement. The D and ^{17}O relaxation times (T_1) were obtained on a JEOL GX-270 spectrometer operating at 41.5 and 36.6 MHz, respectively. T_1 was measured by using the inversion-recovery method (180°-t-90° pulse sequence). The T_1 values were determined for each sample at 16 different time intervals (t); the pulse delay time was more than $10T_1$. The reproducibility of the T_1 measurements was within 2%. The temperature was controlled to 25±0.1° by a GVT 1 temperature-control unit (JEOL).

Results and Discussion

B_X and B_X' Coefficients. The relation between the R_1/R_1^0 values of the D and ^{17}O nuclei of D_2O molecules in potassium halaide aqueous solutions and their concentrations at 25 °C is shown in Figs. 1 and 2. The slopes of the D and ^{17}O nuclei shown in Figs. 1 and 2 are in the following order:

$$KI < KBr < KCl < 1 < KF.$$

This tendency corresponds to the B-coefficient of the solution viscosity. The R_1/R_1^0 values of the D and ^{17}O nuclei vary linearly with increasing concentration up to 1.0 mol kg^{-1}, in a manner similar to other salts;[10-12] the concentration dependences of R_1/R_1^0 are given by the following equations:

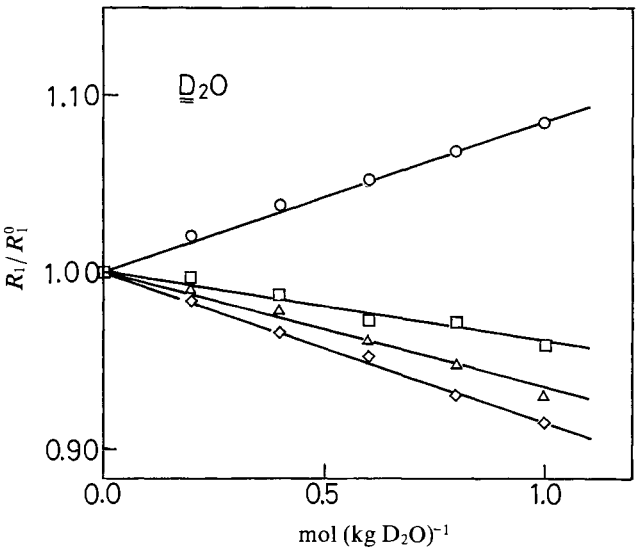

Fig. 1. Plots of D relaxation rates (R_1/R_1^0) of D_2O molecules in potassium halide solutions at 25°C. ○: KF, □: KCl, △: KBr, ◇: KI.

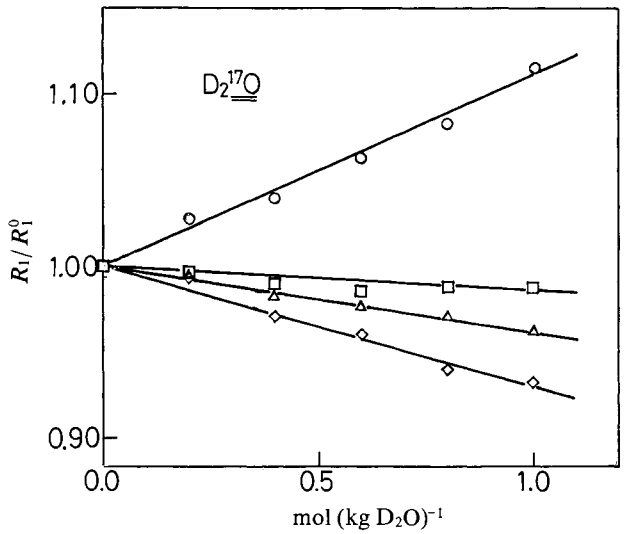

Fig. 2. Plots of ^{17}O relaxation rates (R_1/R_1^0) of D_2O molecules in potassium halide solutions at 25°C. ○: KF, □: KCl, △: KBr, ◇: KI.

$$R_1/R_1^0 = 1 + B_x \cdot m \tag{1}$$

and

$$R_1/R_1^0 = 1 + B_x' \cdot c \quad (x = D \text{ or } {}^{17}O), \tag{2}$$

where R_1 and R_1^0 are the spin-lattice relaxation rates of D_2O molecules at a certain concentration, m (mol kg^{-1}) or c (mol dm^{-3}), and pure D_2O, respectively. The B_X values are separated into contributions from individual ions on the basis of the following conventional assumptions:[18,19]

$$B(KCl) = B^+(K^+) + B^-(Cl^-), \text{ and } B^+(K^+) = B^-(Cl^-). \tag{3}$$

From Eqs. 1 and 3, the following relation is obtained:

$$R_1/R_1^0 = 1 + (B_x^+ + B_x^-)m, \tag{4}$$

where B_X^+ and B_X^- are the contributions from a cation and an anion, respectively. Similarly, $B_X^{+\prime}$ and $B_X^{-\prime}$ were determined by the same method as mentioned above.

The D and ^{17}O nuclei are quadrupole nuclei with spin quantum numbers of $I=1$ and 5/2, respectively. Under an extreme motional narrowing condition, the relation between R_1 and the reorientational correlation time (τ) is given by

$$R_1 = \frac{3}{40}\frac{2I+3}{I^2(2I-1)}\left(\frac{e^2qQ}{\hbar}\right)^2\left(1+\frac{\eta^2}{3}\right)\tau, \tag{5}$$

where, η is an asymmetric parameter, and $e^2qQ/\hbar$ is a quadrupole coupling constant.

The observed R_1 values represent a fractional ($x^{\pm}$) average of the spin-lattice relaxation rate of bulk D_2O (R_1^0), the cation hydrated D_2O (R_1^+), and the anion hydrated D_2O (R_1^-) molecules. When the exchange of D_2O molecules between a hydrated D_2O bulk D_2O is much faster than nucleus relaxation, the follow equation holds:

$$R_1 = (1 - x^+ - x^-)R_1^0 + x^+R_1^+ + x^-R_1^- \tag{6}$$

Further,

$$x^{\pm} = n^{\pm} \cdot m/50.0, \tag{7}$$

where n^+ and n^- are the coordination numbers of the cation and the anion, respectively. From Eqs. 4, 5, 6, and 7 the following relations are obtained:

$$\frac{R_1}{R_1^0} = 1 + \left\{n^+\left(k^+ \cdot \frac{\tau_x^+}{\tau^0} - 1\right) + n^-\left(k^- \cdot \frac{\tau_x^-}{\tau^0} - 1\right)\right\}\frac{m}{50.0} \tag{8}$$

and

$$k^{\pm} = \{(e^2qQ/\hbar)^{\pm}\}^2/\{(e^2qQ/\hbar)^0\}^2. \tag{9}$$

Here, the k^- value of the D and ^{17}O nuclei is 0.69 for the F^- ion, within experimental error.[8] The k^- values for the Cl^-, Br^-, I^- ions are determined by the following method. Ab initio calculations give the D quadrupole coupling constant as a function of the intramolecular O–D bond length of a D_2O molecule. The relation between the O–H distance and the D coupling constant is given by the following equation:[8]

$$(e^2qQ/\hbar)_D^{\pm} = (e^2qQ/\hbar)_D^0 - p(r_{OH}^{\pm} - r_{OH}^0), \tag{10}$$

Table 1. The B_X, $B_{\bar{X}}$, B'_X, and $B_{\bar{X}}'$ of NMR and B^-[a] of Solution Viscosity at 25°C

Salt	B_X (kg mol^{-1})		B'_X (l mol^{-1})		$B_{\bar{X}}$ (kg mol^{-1})		$B_{\bar{X}}'$ (l mol^{-1})		B^- (l mol^{-1})
	D	^{17}O	D	^{17}O	D	^{17}O	D	^{17}O	
KF	0.088	0.105	0.097	0.116	0.109	0.114	0.120	0.126	0.096[b]
KCl	−0.042	−0.017	−0.046	−0.019	−0.021	−0.009	−0.021	−0.008	−0.02
KBr	−0.067	−0.035	−0.074	−0.039	−0.046	−0.027	−0.051	−0.030	−0.05
KI	−0.087	−0.071	−0.096	−0.078	−0.066	−0.063	−0.073	−0.069	−0.10

a) Ref. 19. b) This is the H_2O value, deteils see text.

where p is 18058 KHz/nm, $r^{\pm}_{OH}$ the intramolecular O–H bond length of a hydrated water, and r^0_{OH}=0.098 nm the intramolecular O–H bond length of pure water. The deuterium isotope effect on the O–H bond length has been neglected. The k^+ value of the D nucleus for the K^+ ion, calculated by using Eq. 10 (r^+_{OH}=0.097 nm), is 1.14. Under an extrem narrowing condition, there is no different $k^{\pm}$ value for the D and ^{17}O nuclei of a hydrated water molecule.[8] Since Cl^-, Br^-, and I^- ions are structure-breaking ions similar to K^+ ion, we may use 1.14 as the k^-, value of the D and ^{17}O nuclei for the Cl^-, Br^-, I^- ions. In this case, different orientations of water molecules around the anions and cations may be neglected. Finally, from Eqs. 4 adn 8 we can obtain

$$B^{\pm}_X = \left(k^{\pm}\cdot\frac{\tau^{\pm}_x}{\tau^0_x} - 1\right)\frac{n^{\pm}_x}{50.0}. \tag{11}$$

Table 1 shows the B_X, $B_{\bar{X}}$, B'_X, and $B_{\bar{X}}'$values of the NMR and B^- values[19] of the solution viscosities in potassium halides–D_2O systems. In these cases we assumed that B^- of the F^- ion of the D_2O system is equal to that of the H_2O system, since the solvent isotrope effect on the $B^{\pm}$ values for positive hydration ions is small.[19] The mol kg^{-1} unit of B_X and $B^{\pm}_X$ and the mol dm^{-3} unit of B'_X and $B^{\pm\prime}_X$ have a linear relation to the $B^{\pm}$ (mol l^{-1} unit) of the solution viscosity. The effect of the structure-making F^- ion on the $B^-_{^{17}O}$ value for ^{17}O relaxation is larger than that on B^-_D, and the effect of the structure-breaking Cl^-, Br^-, and I^- ions on the $B_{\bar{X}}$ values is reversed. On the other hand, the effects of the structure-making Li^+ and Na^+ cations and the structure-breaking K^+ and Cs^+ cations on B^+_D are larger than those of $B^+_{^{17}O}$.[10] The relation between $B_{\bar{X}}'$ and B^- in the D_2O system is of the order of $B_{\bar{X}}' \geqq B^-$. These results regarding the D_2O system are in contrast with the relation $B_{\bar{H}} < B^-$ in the H_2O system reported by Hertz et al.[1] The reason is due to a different relaxation mechanism between the ^1H nucleus and the D and ^{17}O nuclei. Although the ^1H nucleus is relaxed by dipole–dipole (intra and intermolecular) interactions, the D and ^{17}O nuclei are relaxed by the quadrupole (intramolecular) interaction. Our experimental condition below 1.0 mol kg^{-1} was different from that for the concentration above 1.0 mol kg^{-1} studied by Hertz et al. The relation

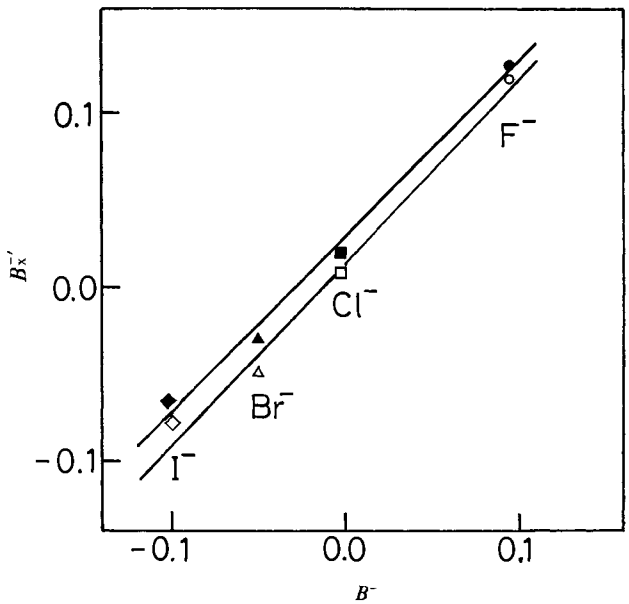

Fig. 3. The relation between $B_{\bar{X}}'$ of NMR method and B^- of solution viscosity at 25°C. The open and closed symboles are X=D and ^{17}O, respectively. The open symbols for different anions are ○: F^-, □: Cl^-, △: Br^-, ◇: I^-.

between $B_{\bar{X}}'$ from the NMR method and B^- from the solution viscosity of halide anions is shown in Fig. 3. The observed linear correlations between $B^{\pm\prime}_X$ and $B^{\pm}$ (mol l^{-1} unit) are given by the following equations:

$$B_{\bar{D}}' = 1.0B^- + 0.012 \tag{12a}$$

and

$$B^-_{^{17}O} = 1.0B^- + 0.024 \tag{12b}$$

for anions; for cations[10] it is given by

$$B_{\bar{D}}' = 0.75B^- + 0.0022 \tag{12a}$$

and

$$B^-_{^{17}O} = 0.61B^- + 0.0046 \tag{12b}$$

The agreement between the $B^{\pm\prime}_X$ values of NMR (reori-

Table 2. The Limiting Values of a Hydrated D_2O Molecules in Halides Ions at 25°C

Ion	$(R_1)^-_D/(R_1)^0_D$	$(R_1)^-_{^{17}O}/(R_1)^0_{^{17}O}$	$(R_1)^-_D$ s^{-1}	$(R_1)^-_{^{17}O}$ s^{-1}	τ^-_D ps	$\tau^-_{^{17}O}$ ps	$\tau^-_D/\tau^-_{^{17}O}$
F^-	1.91	1.96	4.34	344	6.47	6.64	0.97
Cl^-	0.819	0.908	1.86	160	1.70	1.89	0.90
Br^-	0.638	0.733	1.45	129	1.33	1.51	0.88
I^-	0.433	0.534	0.983	94.0	0.900	1.10	0.82
Pure water			2.27	176	2.38	2.37	1.00

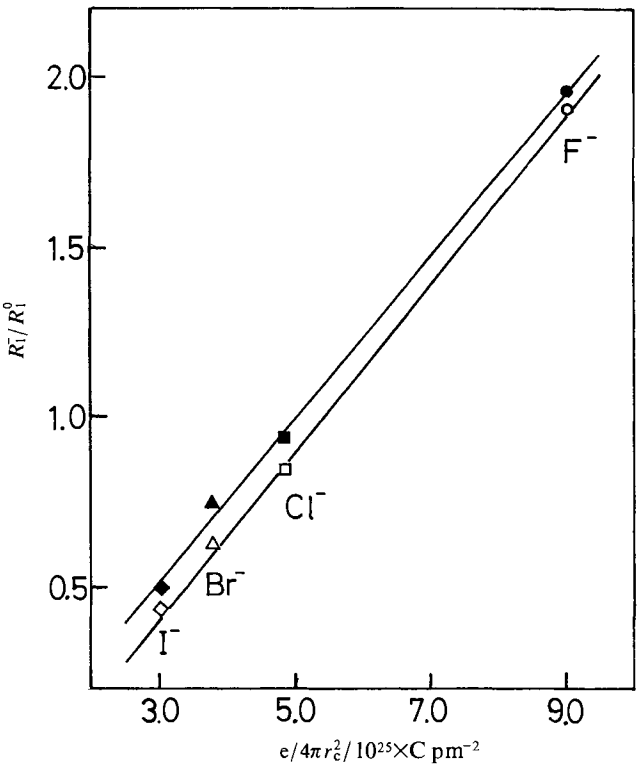

Fig. 4. The relation between the relative relaxation rates (R_1^-/R_1^0) and the surface charge density of ions. The open and closed symboles are X=D and ^{17}O, respectively. The open symbols employed for different anions are O: F^-, □: Cl^-, △: Br^-, ◇: I^-.

entational motion) and the B^- values for the solution viscosity of anions is somewhat better than those for the cations.

Reorientational Motion of a Hydrated D_2O Molecule. Van der Maarel et al. estimated the relaxation of both the D and ^{17}O nuclei of the hydrated water molecules of cations in the limit of infinite dilution by using a polynominal relation between R_1/R_1^0 and the salt concentration. Both reorientational correlation times of the D and ^{17}O nuclei of hydrated water molecules of an hydration sphere are equal within the experimental error, as in the case of pure D_2O molecules, i.e., isotropic reorientational motion. On the other hand, the relaxation rate of the D nucleus of hydrated water molecules is smaller than that of the ^{17}O nucleus in the high-concentration range above 1.0 mol kg^{-1}, i.e., anisotropic reorientational motion. From this result at high concentration, they expected anisotropic reorientational motion of hydrated water molecules at infinite dilution. Especially for the F^- ion, being the largest surface-charge density among univalent anions, a significant ion-water interaction was suggested from several experimental results.

Table 2 shows the corrected $(R_1)^-_X/(R_1)^0_X$, $(R_1)^-_X$, τ^-_X, and $\tau^-_D/\tau^-_{^{17}O}$ values at infinite dilution. They were determined from the linear relation between $(R_1)^-_X/(R_1)^0$ given by Eqs 8—11 and the surface charge density of ions, as shown in Fig. 4. As shown in Table 2, although the reorientational motion of a hydrated D_2O molecule in Cl^-, Br^-, and I^- ions (negative hydration anions) is anisotropic, the reorientational motion of a hydrated D_2O molecule in F^- ions is approximetly isotropic. From these results, it is clear that the anisotropy of reorientational motion of an anionic hydrated D_2O molecule is enhanced with increasing anionic radius.

We are indebted to Professor J. C. Leyte of Lyeden University for his helpful discussion.

References

1) L. Endom, H. G. Hertz, B. Thull, and M. D. Zeidler, *Ber. Bunsen-Ges. Phys. Chem.*, **71**, 1008 (1967).
2) F. Fister and H. G. Hertz, *Ber. Bunsen-Ges. Phys. Chem.*, **71**, 1032 (1967).
3) G. Engel and H. G. Hertz, *Ber. Bunsen-Ges. Phys. Chem.*, **72**, 808 (1968).
4) H. G. Hertz, R. Tutsch, and H. Versmid, *Ber. Bunsen-Ges. Phys. Chem.*, **75**, 1177 (1971).
5) D. Lankhorst, J. Schriever, and J. C. Leyte, *Ber. Bunsen-Ges. Phys. Chem.*, **86**, 215 (1982).
6) C. W. R. Muulder, J. Schriever, W. J. Jesse, and J. C. Leyte, *J. Phys. Chem.*, **87**, 2336 (1983).
7) C. W. R. Muulder, J. Schriever, W. J. Jesse, and J. C. Leyte. *J. Phys. Chem.*, **87**, 2342 (1983).
8) J. R. C. van der Maarel, D. Lankhorst, J. de Bleijster, and J. C. Leyte, *J. Phys. Chem.*, **90**, 1470 (1986).
9) R. P. W. J. Struis, J. de Bleijser, and J. C. Leyte, *J. Phys. Chem.*, **91**, 1639 (1987).
10) A. Shimizu and Y. Taniguchi, *Bull. Chem. Soc. Jpn.*, **63**, 1572 (1990).
11) A. Shimizu and Y. Taniguchi, *Bull. Chem. Soc. Jpn.*, **63**, 3255 (1990).
12) A. Shimizu and Y. Taniguchi, *Bull. Chem. Soc. Jpn.*, **64**, 221 (1991).

13) H. Uedaira, M. Ikura, and H. Uedaira, *Bull. Chem. Soc. Jpn.*, **62**, 1 (1989).
14) H. Uedaira and H. Uedaira, *Nippon Kagaku Kaishi*, **1986**, 1265.
15) A. Kibanov, *Adv. Appl. Microbiol.*, **29**, 1 (1983).
16) H. W. Spiess, B. B. Garrett, and R. K. Sheline, *J. Chem. Phys.*, **51**, 1201 (1969).
17) D. E. Wossner, *J. Chem. Phys.*, **40**, 2341 (1964).
18) M. Kaminsky, *Discuss. Faraday Soc.*, **24**, 171 (1957).
19) K. Ibuki and M. Nakahara, "The Review of Physical Chemistry Japan., Special Issue," (1990), p. 145.

Phase Separation Coupled with Gelation in Polyethylene Glycol–Gelatin–Aqueous Buffer System

Takashi NEZU and Hiroshi MAEDA*,†
Department of Chemistry, Faculty of Science, Nagoya University, Nagoya 464-01
† Department of Chemistry, Faculty of Science, Kyushu University, Fukuoka 812
(Received January 5, 1991)

Phase behavior of a pseudoternary system, gelatin–polyethylene glycol–acetate buffer, was examined. Phase diagram was constructed by determining the compositions of separated phases. One phase contained mostly gelatin but a trace amount of polyethylene glycol. When temperature was lower than the gelation temperature corresponding to the composition of the separated phase, diverse outlooks of the whole system were found. Observation of solutions under an optical microscope revealed microgels or network structure when gelatin was labeled with sirius red. Two different types of microgel formation were noted: nucleation-growth and spinodal decomposition. Size of the microgels formed by spinodal decomposition decreased with quench temperature.

Multicomponent polymer solutions often undergo phase separation either due to mutual incompatibility[1,2] or due to difference between their interactions with solvent ($\Delta\chi$-effect).[3] When one of separated phases gels, it is anticipated that phase separation process becomes involved and diverse outlooks are observed. Furthermore, if gelation takes place before the completion of the phase separation, we can expect to fix intermediate stages of phase separation by gelation. In the present study, we examine phase behavior of aqueous mixtures of gelatin and polyethylene glycol (PEG). Gelatin–water two component system undergoes gelation rather than phase separation when temperature is lowered in contrast to another popular aqueous two component system agarose–water where microgels are produced as a result of phase separation.[4] Microgels of gelatin has been prepared through simple coacervation induced by the addition of a poor solvent such as alcohol.[5] Later, microgels of gelatin was obtained in aqueous media by the addition of polyethylene glycol.[6] This type of phase separation will be examined in the present study.

Experimental

Gelatin (Sigma type B from bovine skin) was dialyzed against distilled water and freeze-dried subsequently. Weight-average molecular weights of polyethylene glycol (PEG) (Wako Pure Chemical Industries, Ltd.) and purified gelatin were $(2.6\pm0.1)\times10^4$ and $(9\pm1)\times10^4$, respectively as determined from light scattering. Both PEG and gelatin samples showed single peaks on GPC. Acetate buffer (pH 5.0; 5×10^{-2} M, 1 M= 1 mol dm^{-3}) was used as solvent unless otherwise stated.

Concentrations of gelatin (C_g) and PEG (C_{PEG}) of separated phases were determined with HPLC (TSK G4000PW gel). Gelatin concentration was determined from absorption at 260 nm where absorption of PEG was negligible (molar extinction of PEG was about 1/20 of that of gelatin). Refractive index increment consisted of contributions from both polymers and their additivity was confirmed from preliminary measurements. PEG concentration was then obtained by subtracting gelatin contribution from the total refractive index increment. Polymer concentrations were expressed in weight percent; grams of one polymer component in 100 g solution. For microscopic observation an Olympus model BHA microscope equipped with a photographing unit PM-10A was used. Stage was thermostatted within ±0.5 °C.

Result

Phase Separation and Gelation. Two examples of various states accompanying the phase separation are shown in Fig. 1(A) and (B) for polyethylene glycol concentration C_{PEG} of 1.5% and 2% respectively. Gelling process taking place in a gelatin-rich phase gives rise to diverse appearance of the whole system. A solid curve in Fig. 1(A) or (B) represents critical solution temperatures, a kind of binodal line. At temperatures higher than this line a single solution phase is stable, while two phases are expected to appear at temperatures below this line. Actually, two solution phases (⊖) appeared at temperatures not far from the line. Sometimes one of the two phases was dispersed in another phase and the whole system looked like a single turbid solution (□). When temperatures were low, sol–gel (◒) or rarely gel–gel (▲) type phase separation took place. When temperature was lowered further, gelation occurred rapidly before separated microdomains merged into a macroscopic phase. In this case, single turbid gel resulted (●). Under certain conditions, flocculates accumulated at the interface between upper sol and lower gel and hence exhibited three phase behavior (sol–flocculates–gel). All these results were reproducible and irrespective of the direction to reach the final temperature either from higher or lower temperature side. Essentially similar results were obtained at other PEG concentrations.

These results are schematically summarized in Fig. 2. A solid curve represents critical solution temperatures (binodal). At temperatures just below the line, liquid–liquid phase separation usually takes place (region II). Region IV, which is below the gelation curve of gelatin, is always associated with gelation. Complex behaviors appear in region III.

In Fig. 3, critical solution temperatures (c—g) or gelation temperatures (a,b) are shown for different PEG concentrations. At C_{PEG}=0.55%, gelation instead of

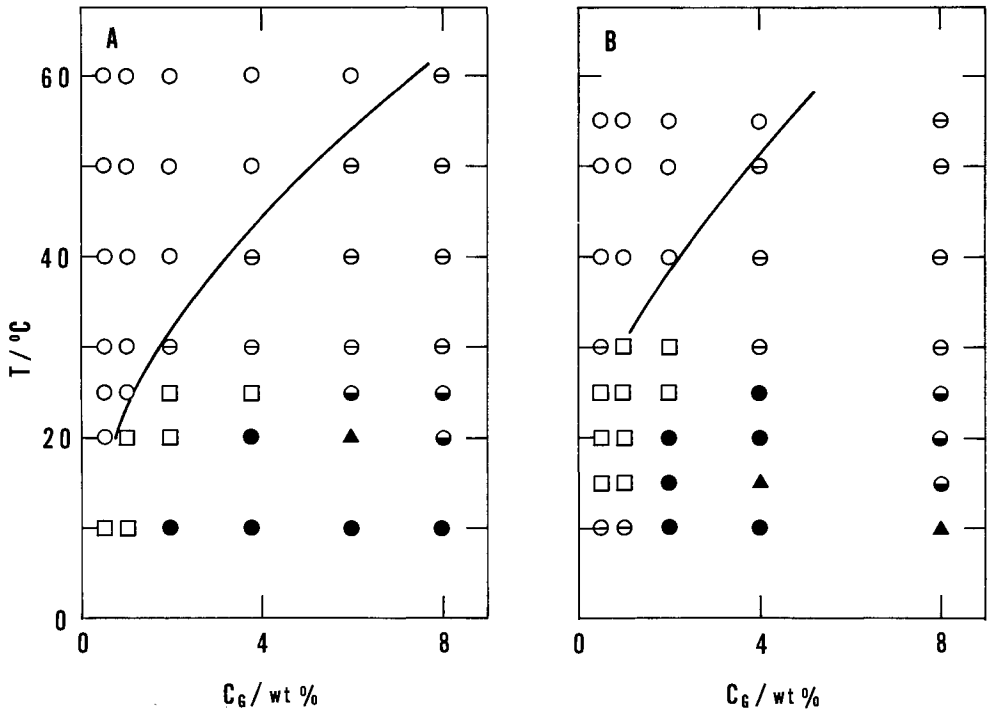

Fig. 1. Phase diagram of gelatin-PEG-aqueous buffer. (A) C_{PEG}=1.5%, (B) C_{PEG}=2.0%. Various symbols representing various apparently different states: (○) single solution, (⊖) two solutions, (◒) solution-gel, (●) gel(turbid), (▲) gel-gel, and (□) emulsion (turbid).

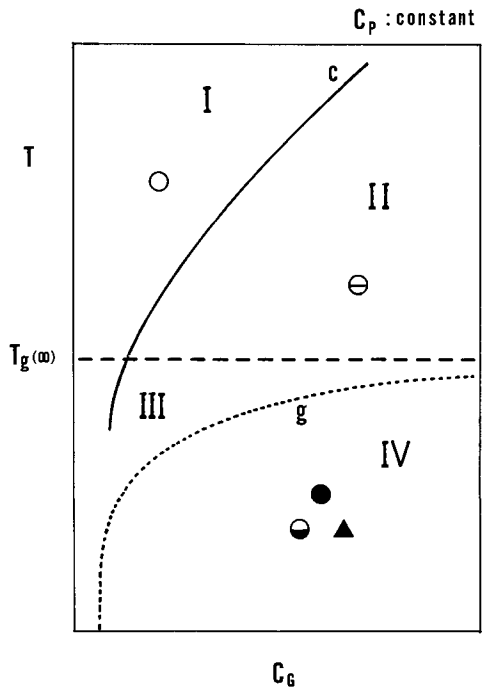

Fig. 2. Schematic presentation of four regions encountered in gelatin-PEG-aqueous buffer. A solid curve c represents critical solution temperatures. Dotted curve g represents gelation temperatures T_g of gelatin solution. $T_g(\infty)$ is the gelation temperature at infinite gelatin concentration.

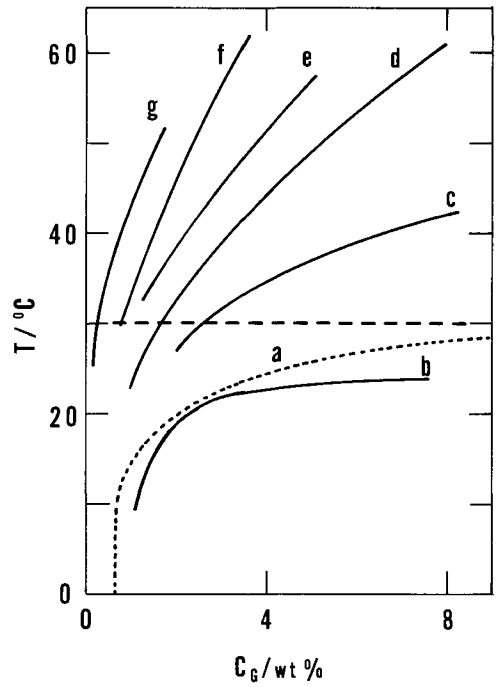

Fig. 3. Effect of PEG concentration on phase behavior. Solid curves represent critical solution temperatures (c—g) or gelation temperatures (b). Dotted curve (a) and dashed curve represent gelation temperatures of gelatin solution and $T_g(\infty)$, respectively. C_{PEG}(%): (a) 0, (b) 0.55, (c) 1.0, (d) 1.5, (e) 2.0, (f) 3.0, and (g) 4.0.

phase separation occurred. Gelation curve (b) at C_{PEG}=0.55% lies at lower temperatures than that of gelatin (a). This indicates that PEG molecules are excluded from gelatin gel and remain in solution phase; 'gel point depression' is expepcted to occur.

Effect of pH was examined at an ionic strength of 0.05 M for pH 5.0, 6.0, and 7.0. Little difference was observed with respect to phase behavior among these pHs. Effect of ionic strength was examined at a pH of 5.1 (10 mM acetate buffer). The solution was turbid in the absence of 0.2 M NaCl but it was clear in the presence of 0.2 M NaCl.

Compositions of Separated Phases. Concentrations of gelatin and PEG in two separated phases were determined with HPLC as described in Experimental section. Results obtained at 40 °C and 25 °C are shown in Fig. 4(A) and (B), respectively. In constructing phase diagrams shown in Fig. 4, we approximated aqueous acetate buffer as a single component. We found that two separated phases showed identical pH which coincided with that of original solution before phase separation. Preferential binding of one of two buffer components to either of the polymer components was thus ruled out. We assumed that buffer concentrations did not differ much on phase separation. As shown in Fig. 4(B), two solutions characterized with different initial compositions give approximately identical compositions of two separated phases, in so far as initial compositions lie on a common tie line. This supports that phase equilibrium was attained in the present study. Binodal lines are close to both axes indicating that separated phases were rich in either of the two components. In particular, PEG concentrations in gel phase were zero within experimental error in all cases examined. This suggests that repulsive interaction between the two polymer components plays an important role to induce the phase separation. Compositions of flocculates in two apparently three-phase systems were examined at 25 °C: C_g=4.0%–C_{PEG}=3.0% and C_g=3.0%–C_{PEG}=2.0%. The compositions were found to be identical to those of gel phase. This has provided a good example indicating that in the present study we dealt with two phase system in thermodynamic sence in spite of three-phase appearance.

All these diverse phase behaviors were expected to originate from inhibited growth or merge of microscopic domains (enriched with gelatin) formed at the initial stage of the phase separation. If gelation had not occurred, these microdomains could have grown and could have merged into three dimensional network (modulated structure in spinodal decomposition) which eventually could have changed into another bulk liquid phase. It is expepcted, therefore, that translational movement of gelatin molecules becomes inhibited by gelation and that the whole process of phase separation is kinetically frozen. If this is to be the case, intermediate stages of phase separation can be visuallized, for example, by staining gelatin with sirius red as was done in the present study.

Observation of Phase Separation under a Microscope. We observed under a microscope solutions containing labeled gelatin. With dilute solutions, a large number of red spherical microgels were observed after phase separation. However, time intervals prior to their emergence differed greatly depending on the compositions of initial solutions. For a solution (C_g=1.25% and C_{PEG}=1.0%) microdroplets first appeared about 8 h after it was brought to the final temperature (25 °C) and sizes of these microbeads did not change appreciably for 24 h. These beads were considered to be produced through nucleation-growth process (NG regime). For another solution (C_g=2.0% and C_{PEG}=1.3%) under the same conditions, on the other hand, microgels appeared immediately after quenching. Phase separation in this case is considered to occur through spinodal decomposition (SD regime). Microdroplets appeared immediately after quenching were not gel-like but of liquid nature. They grew up and merged

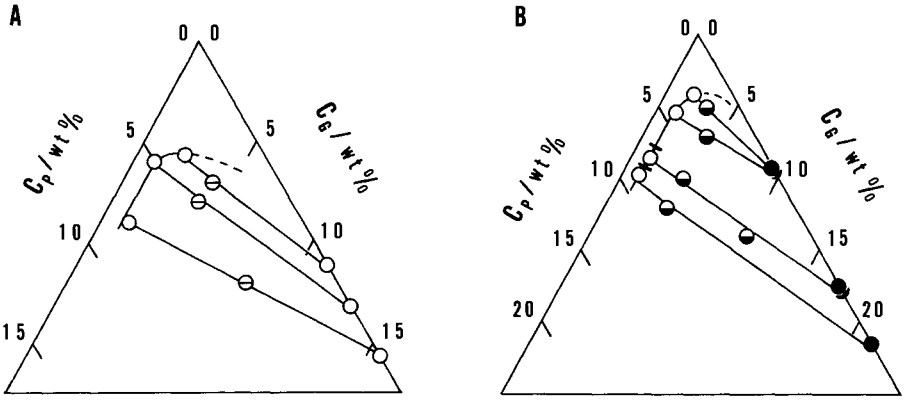

Fig. 4. Phase diagram of gelatin–PEG–aqueous buffer (A) 40°C and (B) 25°C. Symbols are used in the same sense as in Fig. 1 and correspond to the final state.

with each other and their size became bigger with time but reached eventually a constant level at 50—60 min after quenching, probably as a result of loss of fluidity due to advancement of gelation. Their average diameters (d) measured at 55 min. (or later) after quenching were 1.70, 2.01, and 2.76 μm at quench temperatures of 11.7, 16.2, and 20.5 °C, respectively. Calibration of dimension was carried out with polystyrene latex (d=5.854 μm; SD=0.21). Distributions of d about the average value were rather narrow at three temperatures examined. Spinodal temperature (T_S) of the system was determined to be 23.8±1.0 °C from the maximum light scattering intensity. In Fig. 5, values of $\log d$ are plotted against $\log \Delta T$, where $\Delta T(=T_s-T)$ represents a quench depth. The result can be expressed as $d \propto (\Delta T)^{-n}$ with n=0.4±0.1. That is, we get smaller beads as quench depth increases.

When solutions were more concentrated and quenched to low temperatures, we observed network structure (as shown in Fig. 6) rather than dispersed microbeads. This

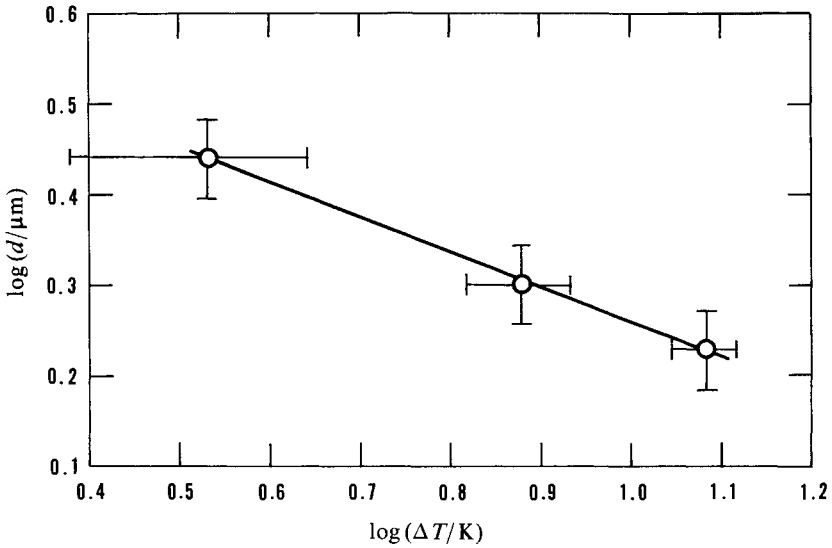

Fig. 5. Dependence of particle diameters d on quench depth ΔT. C_g= 2.0%, C_{PEG}=1.3%, T_s=296.9 K (23.8 °C). Three points correspond to quench temperatures of 11.7, 16.2, and 20.5 °C. Slope of the straight line is −0.4±0.1.

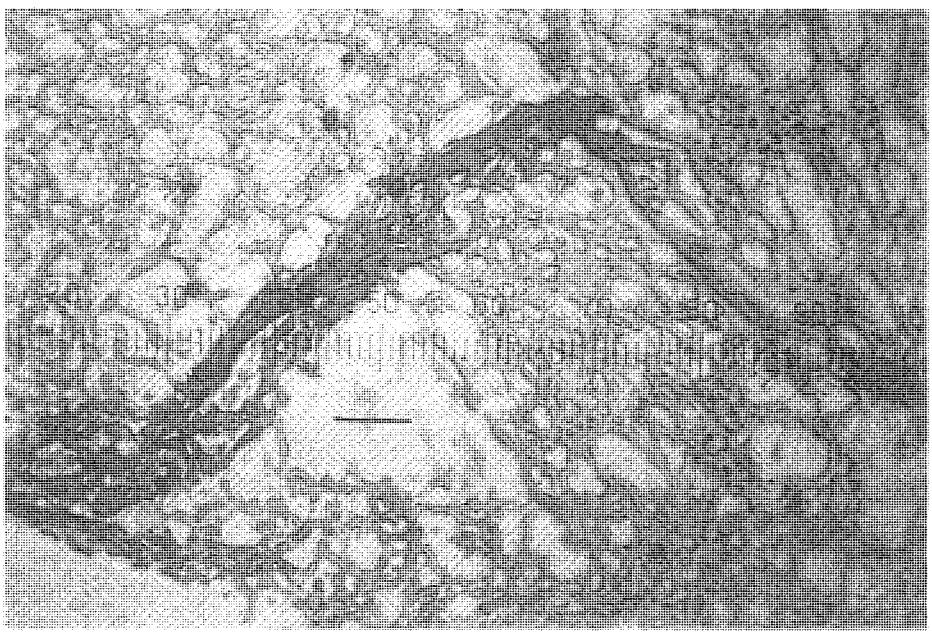

Fig. 6. Network structure consisting of gel (observed at 25 °C) formed at intermediate stage of phase separation at −10 °C. Solution (C_g=2.5% and C_{PEG}= 2.0%) was incubated at −10 °C for 3 h. A horizontal bar corresponds to 100 μm.

picture (Fig. 6) was obtained when a solution (C_g=2.5% and C_{PEG}=2.0%) at 60 °C was quenched at −10 °C for 3 h and then brought to 25 °C for observation. The network structure was stable at 25 °C for more than 30 min indicating it was gel. When the same solution was quenched at −10 °C for 30 min, thin branches melted and only thick branches remained during observation. When quenching duration was further reduced to 10 min, no network structure was seen any more when brought to 25 °C for observation. The dependence of strength of network structure on quenching duration suggests that gelation became predominant over phase separation with decreasing temperature, although both processes became slow at low temperatures. Generally, we can expect this situation from the following consideration. Aggregation of gelatin chains occurs prior to gelation. These aggregates make the phase separation process slower and hence enhance the aggregation further. It is reasonable, therefore, that gelation predominates over phase separation due to this autocatalytic effect.

In Fig. 6, both thin and thick branches consist of gelatin gel. Gelatin concentration in these gels is consistent with phase equilibrium at 25 °C rather than at −10 °C where they were formed. This is because gel composition changed to the equilibrium value at 25 °C during observation primarily through solvent movement. However, observed structural pattern itself reflects the intermediate stages of phase separation at the quench temperature of −10 °C.

Modulated structure has been observed under a microscope for other multicomponent polymer systems.[9-11]

Discussion

In the present study, microgels or network structures were observed in SD regime. It is pertinent to examine whether or not these observations are consistent with, at least qualitatively, the prediction of general theory of SD.

According to Cahn's theory,[7] concentration fluctuation taking place at initial stages of SD is characterized with a particular wavelength λ_m, which is given as follows.[8]

$$\lambda_m = 2\pi\, l\, [3\Delta T/T_s]^{-1/2} \quad (1)$$

Here l is related to some characteristic dimension of poymer coils. It is to be noted that Eq. 1 has been derived for two component systems,[7,8] either polymer–polymer or polymer–solvent. Dependence of λ_m on ΔT originates from a term related to the mixing free energy, which is a function of single concentration variable in the theory.[7,8] On the other hand, mixing free energy depends on two concentration variables in the present pseudoternary system. However, essential step of the phase separation undoubtedly involves translational movement of two kinds of polymers toward opposite directions. Consequently, phase separation in the present study is expected to be approximated with that occurs in a polymer–polymer two component system. If microgels are formed through spinodal decomposition, then their size d should be closely related to the characteristic wavelength λ_m. According to Eq. 1, $\log \lambda_m$ decreases with $\log \Delta T$ with a slope of −0.5. Experimentally, a slope of about −0.4 was observed (Fig. 5). We are not in a position, however, to compare the experimental and the theoretical values of the slope, since there are many uncertain factors to be clarified in both theoretical and experimental aspects.

The authors wish to thank Professors Akira Takahashi (Mie University) and Takashi Inoue (Tokyo Institute of Technology) and Dr. Minoru Ueda (Kuraray Central Research Institute) for their enlightening comments. The present work was partially supported by a Grant-in-Aid for Scientific Research No. 02403004 from the Ministry of Education, Science and Culture.

References

1) R. L. Scott, *J. Chem. Phys.*, **17**, 279 (1949).
2) H. Tompa, *Trans. Faraday Soc.*, **45**, 1142 (1949).
3) L. Zerman and D. Patterson, *Macromolecules,* **5**, 513 (1972).
4) G. T. Feke and W. Prins, *Macromolecules,* 7, 527 (1974).
5) R. E. Phares, Jr. and G. J. Sperandio, *J. Pharm. Sci.*, **53**, 515 (1964).
6) H. Jizomoto, *J. Pharm. Sci.*, **73**, 879 (1984).
7) J. W. Cahn, *J. Chem. Phys.*, **42**, 93 (1965).
8) J. J. van Aartsen, *Eur. Polym. J.*, **6**, 919 (1970).
9) T. Ougizawa, T. Inoue, and H. W. Kammer, *Macromolecules,* **18**, 2089 (1985).
10) T. Ougizawa and T. Inoue, *Polym. J.*, **18**, 521 (1986).
11) T. Okada, H. Saito, M. Yamazaki, and T. Inoue, *Polymer,* **31**, 469 (1990).

Combustion Reactions in Methane–Air Premixed Flames

Seishiro FUKUTANI,* Keizo SAKAGUCHI, Nílson KUNIOSHI, and Hiroshi JINNO†
Department of Industrial Chemistry, Faculty of Engineering, Kyoto University, Yoshida-honmachi, Sakyo-ku, Kyoto 606
† Department of Chemistry, Faculty of Science and Engineering, Sophia University, Kioicho 7-1, Chiyoda-ku, Tokyo 102
(Received February 5, 1991)

A reaction scheme reproducing methane combustion by computer simulation under a wide range of stoichiometric ratio has been proposed and applied to flat methane–air premixed flames to elucidate factors determining their propagation mechanisms and the role of C_2 reaction pathways. Main methane combustion reactions, which progress sequentially from the fuel to carbon dioxide, are inhibited at low temperatures due to retarded production of oxygen atoms which are necessary for the oxidation of methyl radicals. The role of C_2 routes have been investigated by comparison of the results obtained by use of the C_2 scheme and a simplified C_1 scheme. Some of the methyl radicals are once recombined to ethane but most of the produced ethane is dissociated again to methyl via ethyl radicals. Then the C_2 routes work as a temporary storage of species and hinder the main combustion reactions which go through C_1 species.

There are two alternative approaches to study in detail the mechanism of a chemical reaction consisting of many elementary reactions; one of them is an analytical approach where the chemical change is divided into the contribution of each elementary reaction based on the measurements of the temperature, the species concentrations and so on, and the other one is a synthetic approach where the chemical change is constructed step by step with possible elementary reactions. The former is usually used in experimental studies and the latter in computer simulations.

This study has simulated methane–air premixed flames using a detailed reaction scheme to investigate the following two points of methane combustion: Why methane flames propagate according to the thermal theory; and how important is the C_2 routes for methane combustion under various conditions. A simplified reaction scheme has also been proposed and used to estimate the second point.

Simulation Model

We used the same assumptions as those described in a previous work[1] in constructing the simulation model, and obtained the following governing equations for flat flames:

$$\frac{\partial \rho}{\partial t} + \frac{\partial}{\partial x}(\rho v) = 0 \tag{1}$$

$$\frac{\partial}{\partial t}(c_p \rho T) + \frac{\partial}{\partial x}(c_p \rho T v) = \frac{\partial}{\partial x}\left(\lambda \frac{\partial T}{\partial x}\right) + \sum_i D_i \rho \frac{\partial h_i}{\partial x}\frac{\partial \omega_i}{\partial x} - \sum_i h_i \phi_i \tag{2}$$

$$\frac{\partial}{\partial t}(\rho \omega_i) + \frac{\partial}{\partial x}(\rho \omega_i v) = \frac{\partial}{\partial x}\left(D_i \rho \frac{\partial \omega_i}{\partial x}\right) + \phi_i \tag{3}$$

$$p = \rho R T \sum_i \frac{\omega_i}{m_i} \tag{4}$$

where ω_i and ϕ_i are, respectively, the mass fraction and the chemical production rate of the i-th species. The other symbols have their usual meanings.

The partial differential terms in the governing equations were transformed into the corresponding finite difference terms according to the control-volume method.[2] The obtained finite-difference equations were solved numerically under the following boundary conditions; at the unburned side the temperature is 298K and the combustible gas mixture is composed of the fuel and air, and at the burned side the gas is heated up to the adiabatic flame temperature, which is evaluated beforehand based on the combustion condition, and has the equilibrium composition at that temperature. The solutions individually converge to certain values independent of the initial condition only when the flow velocity given as one of the boundary conditions just agrees with the burning velocity which is the eigenvalue for the combustion condition.

Reaction Scheme for Methane Combustion

Methane combustion actually consists of a wide variety of elementary reactions including those occurring among C_2 and higher hydrocarbons, particularly when air is supplied insufficiently, because soot is produced under such conditions. Reaction schemes including higher hydrocarbons have been proposed[3-5] and used for combustion of fuels containing eight or more carbon atoms in their molecules. Those schemes are, however, too complicated to be applied to methane combustion, though they should be employed when soot-formation processes, for example, are discussed.

In this investigation, we composed a reaction scheme comprising only C_1 and C_2 hydrocarbons (Table 1), and applied it to methane combustion under various conditions. Nitrogen works as the source of thermal NO_x in actual flames but in this investigation it is assumed to be inert due to the consideration of the production rate of NO_x.[1] Most of the rate coefficients except those of

Table 1. CH_4-O_2 Reaction Scheme
$k=AT^n\exp(-E/T)$

No.	Reaction	A	n	E	Ref.
R1	$CH_4+M\rightarrow CH_3+H+M$	1.41E10	0.0	44500.0	6
R2	$CH_4+OH\rightarrow CH_3+H_2O$	3.47E-3	3.08	1010.0	6
R3	$CH_4+H\rightarrow CH_3+H_2$	2.20E-2	3.0	4400.0	7
R4	$CH_4+O\rightarrow CH_3+OH$	1.20E01	2.1	3840.0	7
R5	$CH_3+HO_2\rightarrow CH_3O+OH$	3.24E07	0.0	0.0	6
R6	$CH_3+O_2\rightarrow CH_3O+O$	2.51E07	0.0	14600.0	6
R7	$CH_3+OH\rightarrow HCHO+H_2$	3.98E06	0.0	0.0	6
R8	$CH_3+O\rightarrow HCHO+H$	7.00E07	0.0	0.0	7
R9	$CH_3+CH_3\rightarrow C_2H_6$	4.00E06	0.0	0.0	6
R10	$CH_3+CH_3\rightarrow C_2H_5+H$	8.00E07	0.0	13400.0	7
R11	$CH_3+CH_3\rightarrow C_2H_4+H_2$	1.00E10	0.0	16100.0	7
R12	$CH_3O+O_2\rightarrow HCHO+HO_2$	1.00E06	0.0	3020.0	6
R13	$CH_3O+M\rightarrow HCHO+H+M$	5.01E07	0.0	10600.0	6
R14	$HCHO+OH\rightarrow CHO+H_2O$	7.59E06	0.0	85.5	6
R15	$HCHO+H\rightarrow CHO+H_2$	3.31E08	0.0	5280.0	6
R16	$HCHO+O\rightarrow CHO+OH$	5.01E07	0.0	2310.0	6
R17	$HCHO+M\rightarrow CHO+H+M$	3.31E10	0.0	40800.0	6
R18	$CHO+OH\rightarrow CO+H_2O$	1.00E08	0.0	0.0	6
R19	$CHO+H\rightarrow CO+H_2$	2.00E08	0.0	0.0	6
R20	$CHO+O\rightarrow CO+OH$	1.00E08	0.0	0.0	6
R21	$CHO+O_2\rightarrow CO+HO_2$	3.98E06	0.0	3520.0	6
R22	$CHO+M\rightarrow CO+H+M$	5.00E09	0.0	8460.0	7
R23	$CO+OH\rightarrow CO_2+H$	4.40E00	1.5	−373.0	7
R24	$CO+O+M\rightarrow CO_2+M$	5.89E03	0.0	2060.0	6
R25	$CO+HO_2\rightarrow CO_2+OH$	1.51E08	0.0	11900.0	6
R26	$CO+O_2\rightarrow CO_2+O$	3.16E05	0.0	18900.0	6
R27	$C_2H_6+OH\rightarrow C_2H_5+H_2O$	1.12E07	0.0	1230.0	6
R28	$C_2H_6+H\rightarrow C_2H_5+H_2$	5.37E-4	3.5	2620.0	6
R29	$C_2H_6+O\rightarrow C_2H_5+OH$	2.51E07	0.0	3200.0	6
R30	$C_2H_6+CH_3\rightarrow C_2H_5+CH_4$	5.50E-7	4.0	4170.0	6
R31	$C_2H_5+O_2\rightarrow C_2H_4+HO_2$	1.00E06	0.0	2520.0	6
R32	$C_2H_5+M\rightarrow C_2H_4+H+M$	2.00E09	0.0	15100.0	6
R33	$C_2H_4+OH\rightarrow C_2H_3+H_2O$	4.79E06	0.0	619.0	6
R34	$C_2H_4+H\rightarrow C_2H_3+H_2$	1.51E01	2.0	3020.0	6
R35	$C_2H_4+M\rightarrow C_2H_3+H+M$	6.31E12	0.0	54700.0	6
R36	$C_2H_4+M\rightarrow C_2H_2+H_2+M$	9.33E10	0.0	38800.0	6
R37	$C_2H_4+OH\rightarrow CH_3+HCHO$	2.00E06	0.0	483.0	6
R38	$C_2H_4+O\rightarrow CH_3+CHO$	3.31E06	0.0	569.0	6
R39	$C_2H_4+O\rightarrow HCHO+CH_2$	2.51E07	0.0	2520.0	6
R40	$C_2H_3+H\rightarrow C_2H_2+H_2$	2.00E07	0.0	1260.0	6
R41	$C_2H_3+O_2\rightarrow C_2H_2+HO_2$	1.00E06	0.0	5030.0	6
R42	$C_2H_3+M\rightarrow C_2H_2+H+M$	7.94E08	0.0	15900.0	6
R43	$C_2H_2+OH\rightarrow C_2H+H_2O$	6.03E06	0.0	3520.0	6
R44	$C_2H_2+H\rightarrow C_2H+H_2$	2.00E08	0.0	9560.0	6
R45	$C_2H_2+O\rightarrow C_2H+OH$	3.24E09	−0.6	8550.0	6
R46	$C_2H_2+M\rightarrow C_2H+H+M$	1.00E08	0.0	57400.0	6
R47	$C_2H_2+OH\rightarrow CH_2CO+H$	3.24E05	0.0	101.0	6
R48	$C_2H_2+O\rightarrow HCCO+H$	3.55E-2	2.7	699.0	6
R49	$C_2H_2+O\rightarrow CH_2+CO$	6.76E07	0.0	2010.0	6
R50	$C_2H_2+O_2\rightarrow CHO+CHO$	3.98E06	0.0	14100.0	6
R51	$C_2H+O_2\rightarrow CHO+CO$	1.00E07	0.0	3520.0	6
R52	$C_2H+O\rightarrow CH+CO$	5.01E07	0.0	0.0	6
R53	$CH_2CO+OH\rightarrow HCCO+H_2O$	1.00E07	0.0	0.0	6
R54	$CH_2CO+H\rightarrow HCCO+H_2$	1.00E07	0.0	0.0	6
R55	$CH_2CO+O\rightarrow HCCO+OH$	1.00E07	0.0	0.0	6
R56	$CH_2CO+OH\rightarrow HCHO+CHO$	2.82E07	0.0	0.0	6
R57	$CH_2CO+H\rightarrow CH_3+CO$	1.10E07	0.0	1710.0	6
R58	$CH_2CO+O\rightarrow CHO+CHO$	1.00E07	0.0	1210.0	6
R59	$CH_2CO+M\rightarrow CH_2+CO+M$	2.00E10	0.0	30200.0	6
R60	$HCCO+OH\rightarrow CHO+CHO$	1.00E07	0.0	0.0	6
R61	$HCCO+H\rightarrow CH_2+CO$	5.01E07	0.0	0.0	6
R62	$HCCO+O\rightarrow CO+CHO$	3.39E07	0.0	1010.0	6
R63	$CH_2+OH\rightarrow CH+H_2O$	2.69E05	0.67	12900.0	6
R64	$CH_2+H\rightarrow CH+H_2$	2.69E05	0.67	12900.0	6

Table 1. (Continued)

No.	Reaction	A	n	E	Ref.
R65	$CH_2+O \rightarrow CH+OH$	1.91E05	0.68	12600.0	6
R66	$CH_2+O_2 \rightarrow CHO+OH$	1.00E08	0.0	1860.0	6
R67	$CH+O_2 \rightarrow CHO+O$	1.00E07	0.0	0.0	6
R68	$CH+O_2 \rightarrow CO+OH$	1.35E05	0.67	12900.0	6
R69	$H+O_2 \rightarrow OH+O$	2.20E08	0.0	8450.0	8
R70	$O+H_2 \rightarrow OH+H$	1.80E04	1.0	4480.0	8
R71	$OH+OH \rightarrow O+H_2O$	6.30E06	0.0	550.0	8
R72	$OH+H_2 \rightarrow H+H_2O$	2.20E07	0.0	2590.0	8
R73	$H+H+M \rightarrow H_2+M$	2.60E06	−1.0	0.0	8
R74	$O+O+M \rightarrow O_2+M$	1.90E01	0.0	−900.0	8
R75	$H+O+M \rightarrow OH+M$	3.60E06	−1.0	0.0	9
R76	$OH+H+M \rightarrow H_2O+M$	4.06E10	−2.0	0.0	8
R77	$H+O_2+M \rightarrow HO_2+M$	5.00E03	0.0	−500.0	8
R78	$H+HO_2 \rightarrow H_2+O_2$	2.50E07	0.0	350.0	8
R79	$H+HO_2 \rightarrow OH+OH$	2.50E08	0.0	950.0	8
R80	$H+HO_2 \rightarrow O+H_2O$	9.00E05	0.5	2000.0	8
R81	$OH+HO_2 \rightarrow H_2O+O_2$	5.00E07	0.0	500.0	9
R82	$O+HO_2 \rightarrow OH+O_2$	6.30E07	0.0	350.0	10

The rate constants are expressed in m, mol, s units.

hydrogen–oxygen reactions were selected from the values proposed by Westbrook[6] and Warnatz.[7] Some of the frequency factors, however, were modified to make the scheme applicable for combustion of methane under wide conditions and, in addition, for that of ethane, ethylene and acetylene under stoichiometric and lean conditions.

The thermal conductivities and diffusion coefficients of the component gases were evaluated as functions of temperature according to Eucken's and Hirschfelder's approximations,[12] respectively. The values of these properties for the gas mixtures were estimated by summation of the corresponding values of the individual components with multiplication by factors depending on the gas compositions.

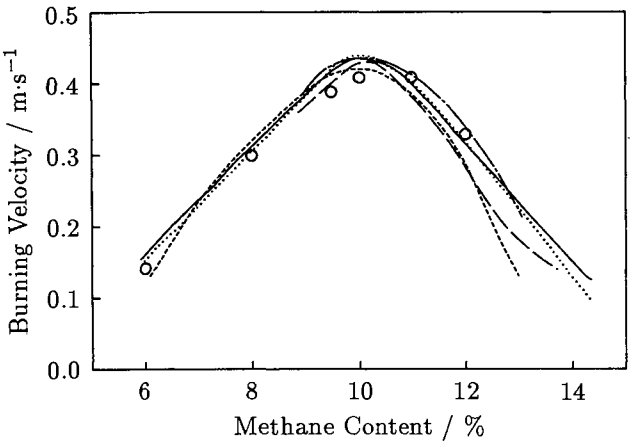

Fig. 1. Comparison of the predicted burning velocities (circles) with the experimental ones which were summarized by Andrews et al.[13]

Table 2. Stoichiometric Hydrocarbon-Air premixed Flames

Hydrocarbons	C_2H_2	C_2H_4	C_2H_6	CH_4
Buring velocity/m s^{-1}	1.56	0.76	0.49	0.39
Initial mole fraction of fuel/%	7.73	6.53	5.65	9.48
Adiabatic flame temperature/K	2550	2380	2260	2230
Experimental burning velocity[14]/m s^{-1}	1.56	0.78	0.48	0.42

Results and Discussion

Validity of Proposed Reaction Scheme. The calculated burning velocities of methane–air premixed flames with various equivalence ratios were compared with those obtained experimentally[13] (Fig. 1). The predicted burning velocities for stoichiometric ethane–, ethylene–, and acetylene–air flames were also checked with the experimental values (Table 2).

The burning velocity predicted by use of computer simulation is given as an overall result of interactions among chemical and physical processes constituting the model. Good agreement between the predicted and the experimental burning velocities leads to the conclusion that the model including the reaction scheme proposed in this investigation are valid for simulation of actual methane flames.

Combustion Reaction in Stoichiometric Methane Flame. Figure 2 shows the profiles of the temperature and the mole fractions of stable species in a stoichiometric methane–air premixed flame. Water vapor, one of the final combustion products, is already present even at a very early stage; carbon dioxide, on the contrary, is not produced in a large amount until most methane has been consumed. These changes suggest that carbon and hydrogen contained in the fuel molecule are oxidized through different routes in methane combustion.

The mole-fraction profiles of active or intermediate

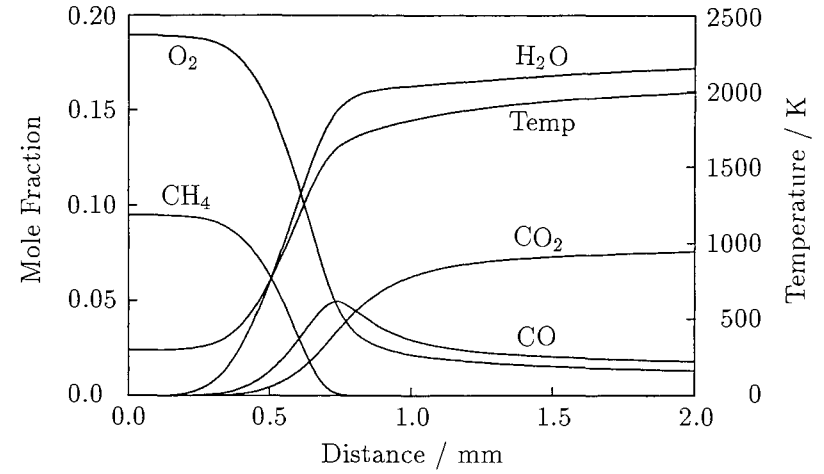

Fig. 2. Profiles of the temperature and the concentrations of stable species in a stoichiometric methane-air premixed flame.

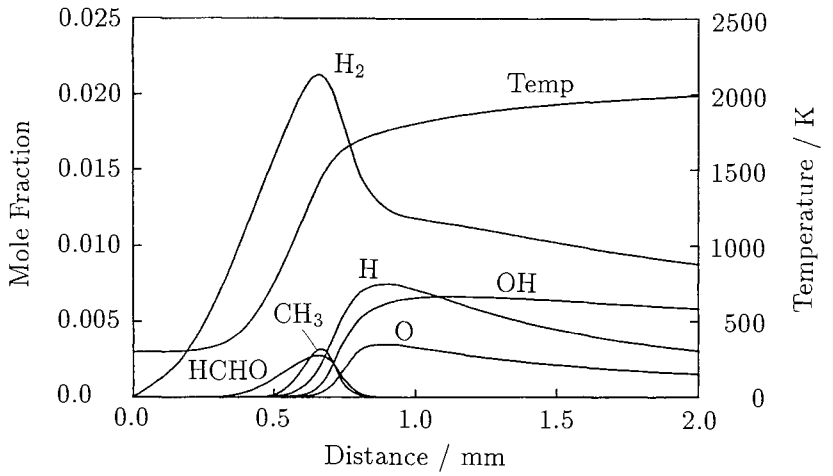

Fig. 3. Profiles of the temperature and the concentrations of active species in the stoichiometric methane-air premixed flame.

species are given in Fig. 3. The three active species, hydroxyl radicals and hydrogen and oxygen atoms, generally holding a decisive role in combustion, do not increase until the temperature becomes higher than 1000 K. These profiles are quite different from those in hydrogen premixed flames,[1] where hydrogen atoms diffusing from the flame front to the low-temperature region carry enthalpy as chemical energy, release it as thermal energy through reactions toward less active species, and raise temperature there.

Figure 4 shows the heat increase rates due to the four possible terms which appear in the conservation equation of thermal energy, Eq. 2, that is, convection, conduction, heat transfer accompanying species diffusion and heat release by chemical reactions. The condition that the summation of the above four contributions must be zero at any position in a steady flame is satisfied. Thermal energy is practically accumulated both by conduction and heat release at low temperatures but increases only by heat release at high temperatures. Species diffusion does not contribute to the transfer of thermal energy as also observed in hydrogen flames.

Temperature must be raised at any part of a flame for its steady propagation. It is easy to raise temperature in the high-temperature region because of the intense heat release through reactions, but is difficult in the low-temperature region; therefore the mode how the temperature is raised there governs the propagation mechanism of the whole flame. Two theories have been proposed for the propagation mechanism of a premixed flame depending on which of the two factors, conduction and heat release, is considered to be responsible for the thermal energy increase in its low-temperature region;[15] the thermal propagation theory, which assumes that the former is predominant, and the active-species diffusion theory, which is constructed on the mechanism that active species diffuse to the low-temperature region from the flame front and are degraded to stable species through exothermic reactions. In the latter theory the active species can be considered to be hydrogen atoms

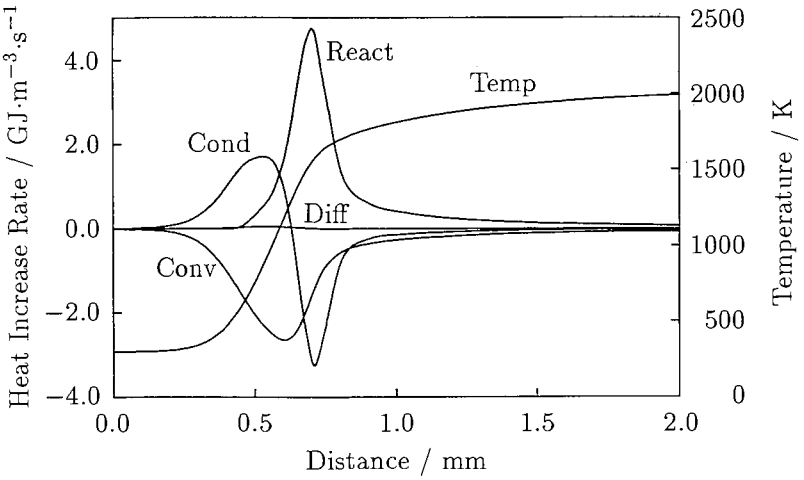

Fig. 4. Rates of the heat increase due to convection (Conv), conduction (Cond), heat transfer accompanying species diffusion (Diff), and heat release through reactions (React) in the stoichiometric methane–air premixed flame.

without substantial error because of their large diffusion coefficient. In the stoichiometric methane–air premixed flame, chemical reactions do not release yet thermal energy in a large amount at low temperatures as shown in Fig. 4, suggesting that this flame is a typical example of thermally-propagating flames.

We now discuss the reasons why the methane flame propagates thermally.

One of the characteristics of the distribution of heat-release rate in the methane flame is that heat is evolved at fairly high temperatures comparing with that in a stoichiometric hydrogen-air flame;[1] the contribution of heat release in the methane flame increases at about 1000K, equals that of conduction at 1120K, and decreases steeply after reaching its maximum at 1550K, while in the hydrogen flame it becomes significant already at about 400K and exceeds the thermal conduction at 450K. This comparison between these changes in the heat-release profiles suggests that initiation of the combustion reaction is retarded in the methane flame.

According to simulation of methane premixed flames, the main combustion reactions proceed sequentially as $CH_4 \rightarrow CH_3 \rightarrow HCHO \rightarrow CHO \rightarrow CO \rightarrow CO_2$ under stoichiometric or lean conditions.[7] At 1550 K in the stoichiometric flame, the reaction pathways are shown in Fig. 5 and the predominant reactions for each step are:

$$CH_4 + OH \rightarrow CH_3 + H_2O, \quad (R2)$$

$$CH_4 + H \rightarrow CH_3 + H_2; \quad (R3)$$

$$CH_3 + O \rightarrow HCHO + H; \quad (R8)$$

$$HCHO + H \rightarrow CHO + H_2, \quad (R15)$$

$$HCHO + OH \rightarrow CHO + H_2O; \quad (R14)$$

$$CHO + M \rightarrow CO + H + M. \quad (R22)$$

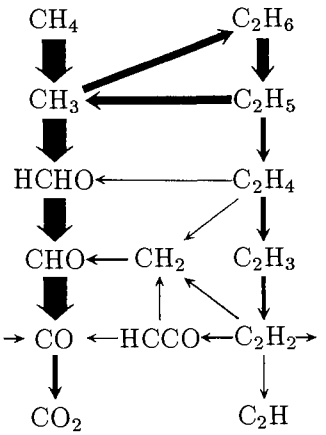

Fig. 5. Reaction pathways at 1550 K in the stoichiometric methane flame. The widths of the arrows are proportional to the rates of the corresponding reactions.

The contributions of reactions (R2) and (R3) are, respectively, 55% and 37% for the total methane dehydrogenation; 88% of the methyl oxidation is ascribed to reaction (R8); 63% and 22% of formyl radicals are produced by reactions (R15) and (R14), respectively; almost all formyl radicals are decomposed to carbon monoxide by reaction (R22).

About 85% of the carbon monoxide cannot be oxidized yet into carbon dioxide even at this temperature. Its oxidation is activated only after the fuel has been exhausted. Almost all carbon monoxide reacts with hydroxyl radicals via reaction

$$CO + OH \rightarrow CO_2 + H. \quad (R23)$$

The slow oxidation of carbon monoxide is explained as follows. There are several reactions consuming hydroxyl radicals such as reactions (R2), (R72), (R14), and

(R23) at high temperatures. The oxidation step of carbon monoxide, however, has the smallest rate constant among them, though it has a negative activation temperature (see Table 1). It can be activated for the first time after all the other consumption reactions of hydroxyl radicals have actually been completed.

Methoxyl radicals are present at low temperatures. At 1120 K, where the rates of heat increase due to conduction and heat release are equal, for instance, about 40% of the methyl radicals are once oxidized to methoxyl radicals via reaction

$$CH_3 + HO_2 \rightarrow CH_3O + OH. \quad (R5)$$

These radicals are further decomposed through reactions

$$CH_3O + M \rightarrow HCHO + H + M \quad (R13)$$

and

$$CH_3O + O_2 \rightarrow HCHO + HO_2, \quad (R12)$$

in the stoichiometric flame. The rest of the methyl radicals are oxidized through reaction (R8). The direct oxidation of methyl to formaldehyde increases with increasing temperature.

A chemical process composed of a sequence of elementary reactions cannot proceed as a whole when any step is delayed. The oxidation step of methyl radicals is mostly due to reaction (R8); therefore oxygen atoms must be present for smooth progression of methane combustion. That species, however, cannot be supplied by diffusion because of its small diffusion coefficient. Hence they must be inevitably supplied by reactions.

Oxygen atoms are produced mostly through a chain-branching reaction

$$H + O_2 \rightarrow OH + O \quad (R69)$$

over a wide range of temperature. As shown in Table 1, this reaction is competing with reaction

$$H + O_2 + M \rightarrow HO_2 + M. \quad (R77)$$

Reaction (R77) is activated in a low-temperature region because of its negative activation energy, so that reaction (R69) becomes faster than reaction (R77) at temperatures as high as 1100K; in other words, oxygen atoms cannot be produced in a sufficient amount and, hence, the whole combustion reaction of methane cannot be accelerated at low temperatures. This is the main reason why methane flames propagate thermally, and has been also confirmed by experiments.[16]

The propagation mechanism of a premixed flame is also controlled by the possibility of efficient formation of free hydrogen atoms; when they are sufficiently produced in a flame its propagation can be explained according to the active-species diffusion theory. Hydrogen atoms initially contained in methane molecules are finally oxidized into water molecules via several kinds of species. The number of hydrogen atoms shared in the fuel decreases almost linearly with rising temperature and instead that shared in water vapor increases, and the number of hydrogen atoms contained in hydrogen molecules is kept around 10% throughout the whole temperature range. The stable final product is directly produced from the fuel at the first step of the combustion, that is, reaction (R2), and holds about half of the hydrogen atoms at temperature as low as 1000 K; thus free hydrogen atoms cannot be appreciably liberated until complete consumption of the fuel.

Heat release due to chemical reactions is caused predominantly by the following reactions: reaction (R1) at low temperatures, reaction (R9) at 950—1300 K, reaction (R8) at 1400—1650 K, reaction (R23) at 1700—1800 K, and reactions (R76) and (R77) at higher temperatures. The contribution of reaction (R8) is the most important; the fairly steep decrease in the heat-release rate after passing its maximum as shown in Fig. 4 is ascribable to the decrease in the rate of this reaction. It is noteworthy that reaction

$$CH_4 + M \rightarrow CH_3 + H + M \quad (R1)$$

proceeds in the reverse direction and release a remarkable amount of thermal energy in a low-temperature region, though this reaction is generally considered to be one of the initiation reactions. The rate constant of its reverse reaction must be exactly evaluated from the viewpoint of the heat release at low temperatures.

Combustion Reactions under Various Conditions and Role of C_2 Routes. The combustion reactions in methane–air premixed flames proceed in various mechanisms depending on their initial fuel concentrations. The reaction paths via C_2 hydrocarbons are not important under the stoichiometric condition as described above though its contribution is not negligible. They are, however, of importance as a combustion route and also a starting step of soot formation under rich conditions. We simulated five other methane flames with various equivalence ratios and carried out a comparative study of their reaction mechanisms.

The equivalence ratios of the additional flames are 1.30, 1.18, 1.06, 0.83, and 0.61, and the calculated burning velocities are 0.33, 0.41, 0.41, 0.30, and 0.14 m s^{-1}, respectively. These velocities are in good agreement with the corresponding experimental values as shown in Fig. 1.

As the equivalence ratio increases, the oxidation of carbon monoxide is naturally suppressed and a larger amount of carbon monoxide is left unburned even at the adiabatic flame temperature. More than 5% of the carbon atoms are, however, contained temporarily in the C_2 hydrocarbons even in the flame with the equivalence ratio of 0.61, and the maximum ratio of the carbon atoms shared in the C_2 hydrocarbons monotonically increases with the increasing equivalence ratio reaching about 14%

in the richest flame among those investigated here; the temperature where the maximum ratio is achieved ranges from 1100K (at the leanest condition) to 1360K (at the richest one).

We estimated the roles of the C_2 routes from chemical viewpoints.

Some of methyl radicals are recombined to ethane through reaction

$$CH_3 + CH_3 \rightarrow C_2H_6, \quad \text{(R9)}$$

and the ethane is predominantly dehydrogenated through

$$C_2H_6 + H \rightarrow C_2H_5 + H_2 \quad \text{(R28)}$$

and

$$C_2H_6 + OH \rightarrow C_2H_5 + H_2O \quad \text{(R27)}$$

in all the flames throughout wide ranges of temperature. It should be noted that more than half of the ethyl radicals dissociate again into methyl radicals by the reaction with hydrogen atoms:

$$C_2H_5 + H \rightarrow CH_3 + CH_3 \quad \text{(R10)}$$

In other words, the C_2 routes partly work just as a temporary storage of the carbon-containing species and, in addition, as radical-consuming steps for methane combustion. Therefore, we evaluated the net roles of the C_2 routes by use of the ratio between the amounts of methyl radicals reacting to methoxyl or formaldehyde and that of ethyl radicals reacting to ethylene. Figure 6 shows those ratios in the stoichiometric and rich flames as functions of temperature. According to this figure, the ratios become minimum at around 1200 K in both flames indicating that the relative importance of the C_2 routes are almost similar as a whole independently of the equivalence ratio and also are remarkable at low temperatures.

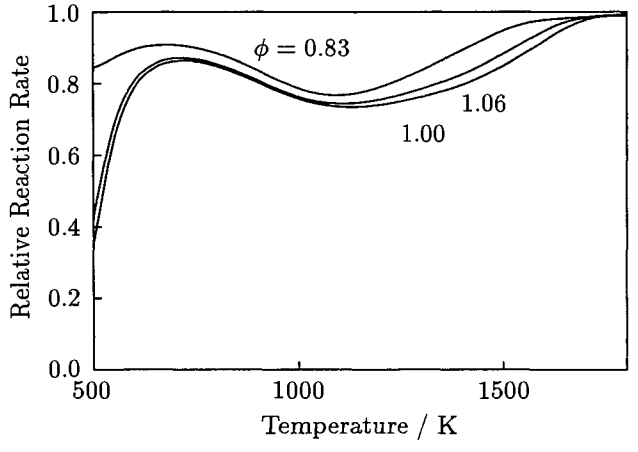

Fig. 6. Relative reaction rates of the C_1 and the C_2 routes in the three methane flames depicted with the equivalence ratio.

About 40% of the ethyl radicals further react as C_2 species. In all the flames simulated in this investigation, the C_2 routes starting from ethyl radicals progress predominantly as $C_2H_5 \rightarrow C_2H_4 \rightarrow C_2H_3 \rightarrow C_2H_2$ though there are some side pathways (see Fig. 5); acetylene is consequently produced through the sequence of reactions

$$C_2H_5 + M \rightarrow C_2H_4 + H + M; \quad \text{(R32)}$$

$$C_2H_4 + H \rightarrow C_2H_3 + H_2, \quad \text{(R34)}$$

$$C_2H_4 + OH \rightarrow C_2H_3 + H_2O; \quad \text{(R33)}$$

$$C_2H_3 + H \rightarrow C_2H_2 + H_2, \quad \text{(R40)}$$

$$C_2H_3 + M \rightarrow C_2H_2 + H + M. \quad \text{(R42)}$$

The contribution of reaction (R32) for the first step is more than 90% at 1550 K in the stoichiometric flame, for instance; those of reactions (R34) and (R33) for the dehydrogenation of ethylene are 73% and 27%, respectively; about 52% and 44% of acetylene is produced through reactions (R40) and (R42), respectively.

More than 80% of the acetylene is oxidized with oxygen atoms by either of the following two reactions, which have almost the same contributions in the above-mentioned flame:

$$C_2H_2 + O \rightarrow HCCO + H \quad \text{(R48)}$$

$$C_2H_2 + O \rightarrow CH_2 + CO. \quad \text{(R49)}$$

The rest of the acetylene is further dehydrogenated through reactions

$$C_2H_2 + H \rightarrow C_2H + H_2 \quad \text{(R44)}$$

and

$$C_2H_2 + OH \rightarrow C_2H + H_2O. \quad \text{(R43)}$$

Application of Simple Reaction Scheme. The reaction paths through C_2 hydrocarbons are not major routes of methane combustion at least under the stoichiometric and lean conditions. Therefore, some combustion phenomena particularly in real flames have been investigated applying simplified reaction schemes to avoid complexities; reaction schemes which are composed of only three or four reactions have been proposed,[17,18] for instance.

Those schemes are useful for confined purposed such as general surveys of combustion reactions in flames having complicated flow fields and discussion in considering chemical reactions only as heat-releasing processes. But they are too simple and, furthermore, are not necessarily composed of so-called elementary reactions; they are not satisfactory at least for the analyses of reaction mechanisms of combustion. Here we made a simple reaction scheme which is composed of C_1 hydrocarbon elementary reactions and, at the same

time, is exact enough to reproduce methane combustion reactions, though they can only be applied for combustion under stoichiometric and lean conditions. The simple reaction scheme is also expected to elucidate the importance of the C_2 routes in comparison with the results obtained by use of the full and the simple reaction schemes.

The proposed simple reaction scheme consists in thirtyseven pairs of elementary reactions (Table 3). At first, we assumed the same rate coefficients, that is, A, n, and E, as those in Table 1 for each reaction of the simple scheme. However, the predicted burning velocity of the stoichiometric methane flame, for example, was as large as $0.49 ms^{-1}$, while both burning velocities obtained by experiments and predicted with the full reaction scheme are around $0.4 ms^{-1}$.

An elementary reaction should universally have the same rate coefficients independently of what reaction scheme it belongs to. This principle, however, is strictly followed only when the reaction is a constituent of a complete scheme. On the contrary, when it belongs to an abbreviated scheme, its rate coefficients may be modified to compensate the influences coming from the omission of reactions, though the omitted reactions individually have only negligible effects on the whole combustion process. A trial and error method led to the

Table 3. Simple CH_4-O_2 Reaction Scheme
$k=AT^n\exp(-E/T)$

No.	Reaction	A	n	E
R1	$CH_4+M\rightarrow CH_3+H+M$	1.41E10	0.0	44500
R2	$CH_4+OH\rightarrow CH_3+H_2O$	3.47E-3	3.08	1010
R3	$CH_4+H\rightarrow CH_3+H_2$	2.20E-2	3.0	4400
R4	$CH_4+O\rightarrow CH_3+OH$	1.20E01	2.1	3840
R5	$CH_3+HO_2\rightarrow CH_3O+OH$	3.24E07	0.0	0
R6	$CH_3+O_2\rightarrow CH_3O+O$	2.51E07	0.0	14600
R7	$CH_3+OH\rightarrow HCHO+H_2$	3.98E06	0.0	0
R8	$CH_3+O\rightarrow HCHO+H$	7.00E07	0.0	0
R9	$CH_3O+O_2\rightarrow HCHO+HO_2$	1.00E06	0.0	3020
R10	$CH_3O+M\rightarrow HCHO+H+M$	5.01E07	0.0	10600
R11	$HCHO+OH\rightarrow CHO+H_2O$	7.59E06	0.0	85.5
R12	$HCHO+H\rightarrow CHO+H_2$	3.31E08	0.0	5280
R13	$HCHO+O\rightarrow CHO+OH$	5.01E07	0.0	2310
R14	$HCHO+M\rightarrow CHO+H+M$	3.31E10	0.0	40800
R15	$CHO+OH\rightarrow CO+H_2O$	1.00E08	0.0	0
R16	$CHO+H\rightarrow CO+H_2$	2.00E08	0.0	0
R17	$CHO+O\rightarrow CO+OH$	1.00E08	0.0	0
R18	$CHO+O_2\rightarrow CO+HO_2$	3.98E06	0.0	3520
R19	$CHO+M\rightarrow CO+H+M$	1.42E09	0.0	8460
R20	$CO+OH\rightarrow CO_2+H$	4.40E00	1.5	−373
R21	$CO+O+M\rightarrow CO_2+M$	5.89E03	0.0	2060
R22	$CO+HO_2\rightarrow CO_2+OH$	1.51E08	0.0	11900
R23	$CO+O_2\rightarrow CO_2+O$	3.16E05	0.0	18900
R24	$H+O_2\rightarrow OH+O$	1.20E11	−0.91	8310
R25	$O+H_2\rightarrow OH+H$	1.80E04	0.0	4480
R26	$OH+OH\rightarrow O+H_2O$	6.30E06	0.0	550
R27	$OH+H_2\rightarrow H+H_2O$	2.20E07	0.0	2590
R28	$H+H+M\rightarrow H_2+M$	2.60E06	−1.0	0
R29	$O+O+M\rightarrow O_2+M$	1.90E01	0.0	−900
R30	$H+O+M\rightarrow OH+M$	3.60E06	−1.0	0
R31	$OH+H+M\rightarrow H_2O+M$	4.06E10	−2.0	0
R32	$H+O_2+M\rightarrow HO_2+M$	5.00E03	0.0	−500
R33	$H+HO_2\rightarrow H_2+O_2$	2.50E07	0.0	350
R34	$H+HO_2\rightarrow OH+OH$	2.50E08	0.0	950
R35	$H+HO_2\rightarrow O+H_2O$	9.00E05	0.5	2000
R36	$OH+HO_2\rightarrow H_2O+O_2$	5.00E07	0.0	500
R37	$O+HO_2\rightarrow OH+O_2$	6.30E07	0.0	350

The rate constants are expressed in m, mol, s units.

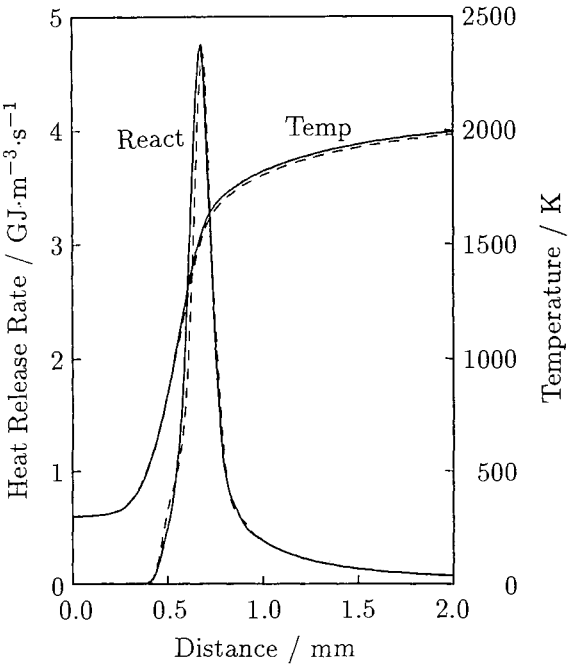

Fig. 7. Comparison of the temperature and the heat-release rate predicted by use of the C_2 scheme (solid lines) and the C_1 scheme (dashed lines).

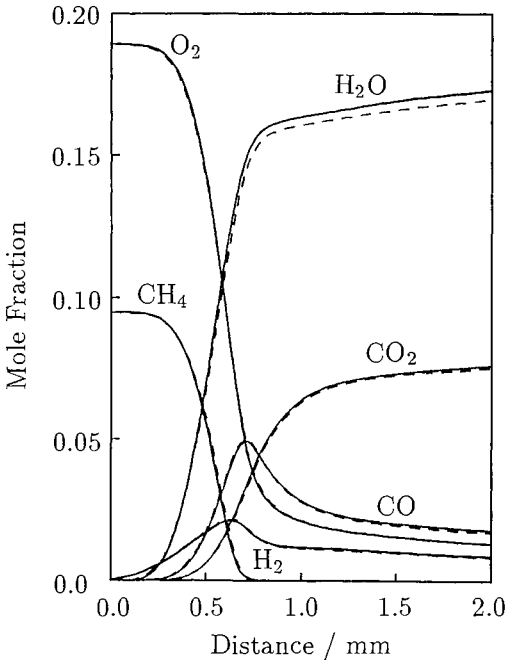

Fig. 8. Comparison of the concentrations of the stable species predicted by use of the C_2 scheme (solid lines) and the C_1 scheme (dashed lines).

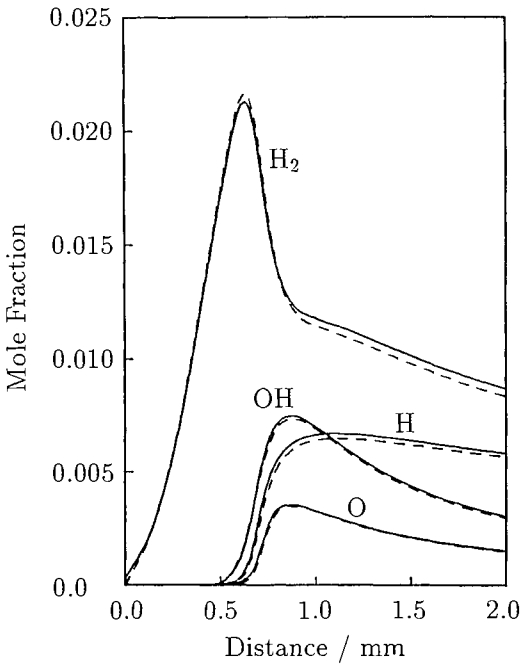

Fig. 9. Comparison of the concentrations of the intermediate species predicted by use of the C_2 scheme (solid lines) and the C_1 scheme (dashed lines).

result that multiplication of the frequency factor of reaction (R22) in Table 1 by a factor of 0.284 is the most suitable modification. The routes via the C_2 hydrocarbons are, therefore, approximately equivalent to the suppression of the rate of the sequential oxidation of methane via the C_1 hydrocarbons. In other words, those routes have inhibiting effects on methane combustion.

Then, the burning velocity was improved to be 0.38 m s^{-1} for the stoichiometric methane flame. Figure 7 shows the profiles of the temperature and the heat-release rate of the stoichiometric methane flame calculated by using both reaction schemes. Figures 8 and 9 designate the mole-fraction profiles of the stable and active or intermediate species, respectively. These profiles are in good agreement except those of water and hydrogen. The number of the carbon atoms shared in the other species except methane, carbon monoxide and carbon dioxide obtained by means of the C_2-hydrocarbon scheme is about 1.5 times as large as that calculated by using the C_1-hydrocarbon reaction scheme.

Conclusions

Two reaction schemes for combustion reactions of C_1 and C_2 hydrocarbons were proposed and applied to flat premixed methane flames. The following conclusions were obtained:

1. Methane combustion proceeds predominantly via the C_1 routes under stoichiometric and lean conditions; the C_2 routes hold only a subordinate role. However the omission of the C_2 routes from the reaction scheme causes increase in the burning velocity because they work as a temporary storage of the species. The rate constant of reaction (R22) should be reduced to compensate the unreasonable raise of the burning velocity in a simplified reaction scheme which comprises only the C_1 routes.

2. A methane premixed flame propagates mainly according to the thermal theory, which is applicable to the propagation of flames where reactions do not occur in the low-temperature regions, because methane combustion reactions have not been activated until the temperature is raised up to about 1100 K; the oxidation of methyl radicals inevitably requires oxygen atoms but these cannot be supplied at lower temperatures due to a competition reaction for their formation.

References

1) S. Fukutani, N. Kunioshi, and H. Jinno, *Bull. Chem. Soc. Jpn.*, **63**, 2191 (1990).
2) S. V. Patankar, "Numerical Heat Transfer and Fluid Flow," Hemisphere Publishing Co., New York (1980), Chap. 3.
3) J. Warnatz, "Combustion Chemistry," ed by W. C. Gardiner, Jr., Springer-Verlag, New York (1984), pp. 197—360.
4) C. K. Westbrook, J. Creighton, C. Lund, and F. L. Dryer, *J. Phys. Chem.*, **81**, 2542 (1977).
5) P. Dagaut, M. Cathonnet, J. C. Boettner, and F. Gaillard, *Combust. Flame*, **71**, 295 (1988).
6) C. K. Westbrook, F. L. Dryer, and K. P. Schug, *Combust. Flame*, **52**, 299 (1983).
7) J. Warnatz, H. Bockhorn, A. Möser, and H. W. Wenz, "Nineteenth Symposium (International) on Combustion," The Combustion Institute, Pittsburgh (1982), pp. 197—209.
8) D. L. Baulch, D. D. Drysdale, D. G. Horne, and A. C. Lloyd, "Evaluated Kinetic Data for High Temperature Reactions," Butterworths, London (1972), Vol. 1.
9) D. E. Jensen and G. A. Jones, *Combust. Flame*, **32**, 1 (1978).
10) M. P. Heap, T. J. Tyson, J. E. Cichanowicz, R. Gershman, C. J. Kau, G. B. Martin, and W. S. Lanier, "Sixteenth Symposium (International) on Combustion," The Combustion Institute, Pittsburgh (1977), pp. 535—545.
11) D. L. Baulch, D. D. Drysdale, J. Duxbury, and S. Grant, "Evaluated Kinetic Data for High Temperature Reactions," Butterworths, London (1976), Vol. 3.
12) R. H. Perry and C. H. Chilton, "Chemical Engineer's Handbook," 5th ed, McGraw-Hill, New York (1973).
13) G. E. Andrews and D. Bradley, *Combust. Flame*, **20**, 77 (1973).
14) R. Günther and G. Janische, *Chemi.-Ing.-Tech.*, **43**, 975 (1971).
15) A. G. Gaydon and H. G. Wolfhard, "Flames," 4th ed, Chapman and Hall, London (1979), Chap. 5.
16) S. Fukutani, T. Sasaki, and H. Jinno, *Nenryo Kyokai Shi*, **69**, 946 (1990).
17) G. Paczko, P. M. Lefdal, and N. Peters, "Twenty-first Symposium (International) on Combustion," The Combustion Institute, Pittsburgh (1986), pp. 739—748.
18) N. Peters and F. A. Williams, *Combust. Flame*, **68**, 185 (1987).

 © 1991 The Chemical Society of Japan Bull. Chem. Soc. Jpn., 64, 1632—1640 (1991)

Intramolecular Energy Transfer in Covalently Linked Polypyridine Ruthenium(II)/Osmium(II) Binuclear Complexes. $Ru(II)(bpy)_2Mebpy-(CH_2)_n-MebpyOs(II)(bpy)_2$ (n=2, 3, 5, and 7)

Masaoki FURUE,* Toshiyuki YOSHIDZUMI, Shuichi KINOSHITA,†,†† Takashi KUSHIDA,† Shun-ichi NOZAKURA, and Mikiharu KAMACHI

Department of Macromolecular Science, Faculty of Science, Osaka University, Toyonaka, Osaka 560

† Department of Physics, Faculty of Science, Osaka University, Toyonaka, Osaka 560

(Received November 19, 1990)

A novel series of polymethylene-linked heterobinuclear complexes of polypyridine ruthenium(II)/osmium(II) complex $Ru(II)(bpy)_2Mebpy-(CH_2)_n-MebpyOs(II)(bpy)_2$(bpy=2,2′-bipyridine and n=2, 3, 5, and 7), **1**, was prepared. The photophysical behavior was examined in various solvents. The emission spectra of **1** (excitation wavelength: 455nm) showed a nearly complete quenching of $Ru^{II}\rightarrow\pi^*$(bpy) metal-to-ligand charge transfer (MLCT) emission and the enhancement of $Os^{II}\rightarrow\pi^*$(bpy) MLCT emission. The luminescence lifetime measurements by a time-correlated single photon-counting method provided evidence that intramolecular energy transfer is a significant pathway for the observed emission quenching. The rate constants of the intramolecular energy transfer in ethanol are 5.3×10^8, 3.3×10^8, 1.3×10^8, and $1.0\times10^8 s^{-1}$ for **1**(n=2, 3, 5, and 7), respectively. They were found to be proportional to the inverse sixth power on the center-to-center distance of the two complexes. The mechanism is discussed in terms of the Förster (a dipole–dipole interaction) mechanism.

There has been considerable interest in photochemical and photophysical processes of molecular assemblies consisting of polypyridine and porphyrin complexes of the transition metals.[1-5] A possible use of these materials is to control photochemical processes in which optical excitation is followed by spatially directed energy or electron transfer.[6-10] We have studied the photochemical and photophysical properties of $Ru(bpy)_3^{2+}$-containing polymers in which $Ru(bpy)_3^{2+}$ complexes are covalently incorporated into poly(4-methyl-4′-vinyl-2,2′-bipyridine).[11] In our recent study, covalently linked dimers of $Ru(bpy)_3^{2+}$ (complex **2**) as a dimer model for $Ru(bpy)_3^{2+}$-containing polymers exhibited rather different photophysical behaviors in comparison with those of aromatic hydrocarbon and porphyrin dimers.[12-15] In excited **2**, no intramolecular interaction leading to the enhanced quenching between the excited and ground states was found. However, an efficient intramolecular triplet–triplet annihilation process was found under the high intensity irradiation of laser light.[16] These results aroused our interest in the heterobinuclear system.

The intramolecular energy-transfer processes in a variety of weakly coupled dimers of transition metal complexes have been the subjects of both theoretical and mechanistic studies.[17-20] Two major mechanisms for energy transfer in organic systems have been recognized.[21,22] Energy transfer can take place via a dipole–dipole interaction between an electronically excited donor and an acceptor in the ground state (i.e., the Förster mechanism).[23] The other mechanism involved in energy transfer is an electron-exchange mechanism in which a spatial overlap of the donor and acceptor is required (i.e., the Dexter mechanism).[24] Since electronic transition in transition metal complexes are frequently symmetry and spin forbidden, the Förster-type energy transfer based on a dipole–dipole interaction is usually unimportant in these systems. However, it cannot be dismissed for some transition metal complexes. An appreciable amount of singlet character in luminescent excited states of $Ru(bpy)_3^{2+}$ and $Os(bpy)_3^{2+}$ has been recognized.[25,26] There are a few examples of binuclear complexes for which the Förster mechanism is conceivable in the excited state. Schmehl has discussed the intramolecular energy transfer of covalently linked ruthenium(II) dimers in terms of a dipolar coupling mechanism, namely the Förster mechanism.[18] We have also discussed the intramolecular energy transfer of a heterobinuclear complex of polypyridine–ruthenium(II) and –osmium(II), (complex **3**) using the Förster mechanism.[27]

The Förster and Dexter mechanisms are typically distinguished by evaluating the dependence of the rate of energy transfer on the distance of donor–acceptor separation. The dependence of the inverse sixth power of the distance is expected for a dipole–dipole coupling process, while an exponential dependence of distance is observed for the Dexter mechanism. There has been no systematic examination of the distance dependency of energy transfer for covalently linked complexes of this type.

We have recently established a synthetic method regarding polymethylene linked dimers of 4-methyl-2,2′-bipyridine. This work presents 1) the preparation of the ligand dimers and a novel series of polymethylene-linked heterobinuclear complexes comprising the polypyridine ruthenium(II)/osmium(II) complex $Ru(II)(bpy)_2Mebpy-(CH_2)_n-MebpyOs(II)(bpy)_2$ (bpy=2,2′-bipyridine, n=2,3,5 and 7), **1**,

2) their spectroscopic and electrochemical properties,

†† Present Address: Research Institute of Applied Electricity, Hokkaido University, Sapporo 060.

and

3) a kinetic study of intramolecular energy transfer in excited **1** by a time-correlated single-photon counting method. For these complexes, the rate constant of the intramolecular energy transfer (k_{en}) decreases with increasing number of methylene chains. The results are elucidated by the Förster mechanism. Electron localization in the excited MLCT state of the ruthenium part is also discussed in conjunction with the results for Ru(II)(bpy)$_2$Mebpy-[CH$_2$CH(OH)CH$_2$]-MebpyOs(II)-(bpy)$_2$, **3** and Ru(II)(Me$_2$bpy)$_2$Mebpy-[CH$_2$CH(OH)CH$_2$]-MebpyOs(II)(bpy)$_2$, **4**.

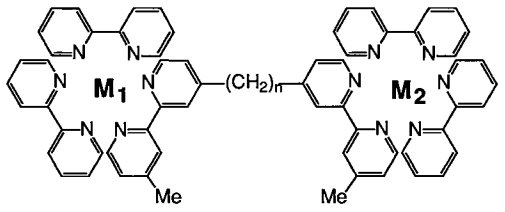

1: M_1 = Ru(II), M_2 = Os(II), n=2,3,5,7

2: M_1 = M_2 = Ru(II), n=2,3,5

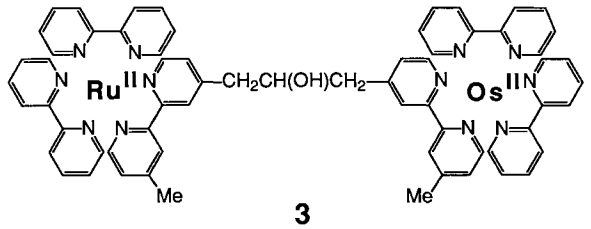

3

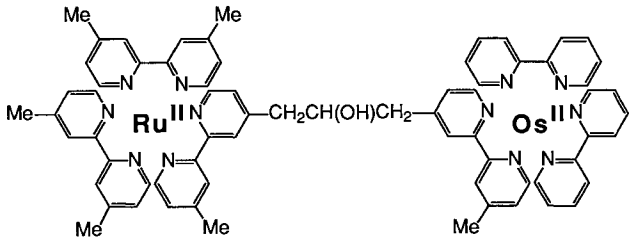

4

Experimental

Materials. The synthesis of **1** is outlined in Scheme 1. The starting material, 4,4′-dimethyl-2,2′-bipyridine, was purchased from Tokyo Kasei and recrystallized from ethanol.

4-Methyl-2,2′-bipyridine-4′-carbaldehyde (7). A mixture of 4,4′-dimethyl-2,2′-bipyridine (12.5 g, 68 mmol) and selenium dioxide (7.52 g, 68 mmol) in diglyme (120 ml) was stirred at 130—135 °C for 6 h. The reaction mixture was dissolved in 1 l of hot water and filtered to remove selenium metals. The filtrate was adjusted to pH 9—10 with an aqueous NaOH solution (10%) and extracted four times with 300 ml of the $CHCl_3$ portions. The extract was dried ($MgSO_4$) and evaporated to give a pale-yellow solid. Column chromatography on silica gel (ethyl acetate) afforded a white solid **7** (5.3 g, 40%), mp 135—136 °C: ^{1}H NMR ($CDCl_3$) δ=2.5(s, 3H), 7.0—9.0(m, 6H), 10.3 (s, 1H); IR (Nujol) 1710 cm^{-1}. Anal. Calcd for $C_{12}H_{10}N_2O$: C, 72.71; H, 5.08; N, 14.13. Found: C, 72.74; H, 5.11; N, 14.03%.

4-Hydroxymethyl-4′-methyl-2,2′-bipyridine (8a). A solution of **7** (5.3 g, 27 mmol) and sodium borohydride (3 g, 79 mmol) in anhydrous ethanol (350 ml) was stirred at room temperature for 1.5 h. Water (300 ml) was then added dropwise, and the mixture stirred at room temperature overnight. The solution was then extracted with $CHCl_3$ (4×300 ml). The extract was dried ($MgSO_4$) and evaporated to give a white solid. Recrystallization from ethanol provided 4.5 g (84%) of **8a**, mp 124—125 °C: ^{1}H NMR ($CDCl_3$) δ=2.4 (s, 3H), 3.9—4.6 (s, 1H), 4.7 (s, 2H), 7.0—8.6 (m. 6H); IR (Nujol) 3200 cm^{-1}. Anal. Calcd for $C_{12}H_{12}N_2O$: C, 71.98; H, 6.04; N, 13.99%. Found: C, 72.27; H, 6.08; N, 13.98%.

4-Bromomethyl-4′-methyl-2,2′-bipyridine (9a). A mixture of **8a** (2.0 g, 10 mmol) and thionyl bromide (5 ml, 63 mmol) in 25 ml of CH_2Cl_2 was stirred at room temperature for 3 h under the flow of nitrogen gas. Water (200 ml) was added. The reaction mixture was neutralized (pH 8—9) with a saturated Na_2CO_3 solution and extracted with 500 ml of CH_2Cl_2.

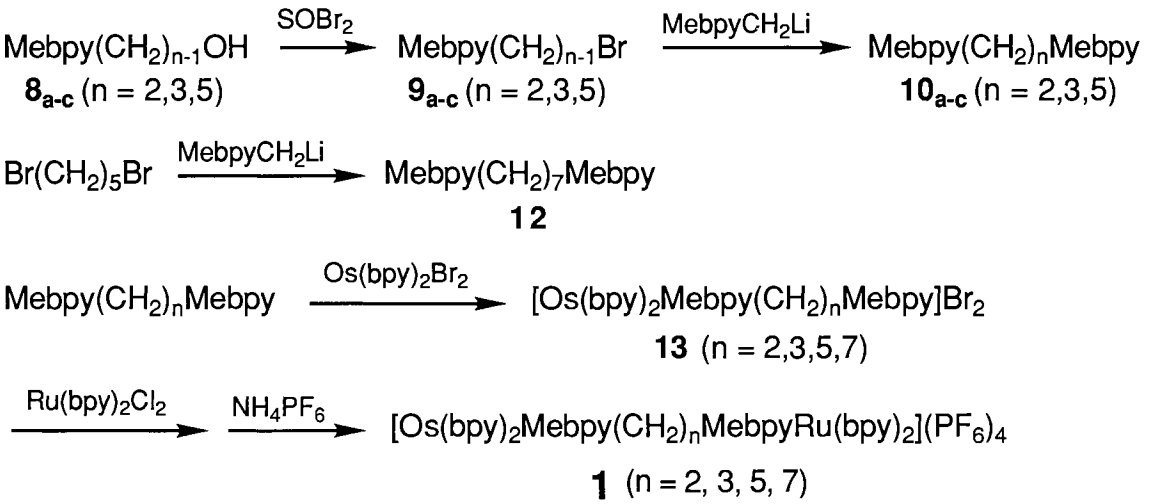

Scheme 1.

After the extract was dried ($MgSO_4$) and evaporated below room temperature, the crude product was chromatographed on a silica-gel column by eluting with ethyl acetate–CH_2Cl_2 (3:2) to give 0.78 g (30%) of white crystals of **9a**, mp 76—77 °C: ^1H NMR ($CDCl_3$) δ=2.4 (s, 3H), 4.5 (s, 2H), 7.0—8.8 (m, 6H). Anal. Calcd for $C_{12}H_{11}N_2Br$: C, 54.77; H, 4.21; N, 10.65%. Found; C, 54.48; H, 4.21; N, 10.56%.

Lithiation of 4,4′-Dimethyl-2,2′-bipyridine. To a solution of 4,4′-dimethyl-2,2′-bipyridine (3.4 g, 18 mmol) in 200-ml of THF, lithium diisopropylamide (12 mmol) in THF (10 ml) was added at 0 °C under an argon atmosphere. After the solution was stirred for 1.5 h it was ready for subsequent steps.

1,2-Bis(4′-methyl-2,2′-bipyridyl-4-yl)ethane (10a). To a stirred solution of lithiated 4,4′-dimethyl-2,2′-bipyridine, **9a** (2.0 g, 7.6 mmol) in 70 ml of THF was added dropwise at room temperature. The mixture was stirred for 1 h. Methanol (10 ml) and then water (100 ml) were added. The resulting solution was extracted with 1 l of ether. The extract was dried ($MgSO_4$) and evaporated. The residue was placed on a silica gel column, eluted with a gradient mixture of ethyl acetate–CH_2Cl_2 from 1:9 to 3:1 to remove any 4,4′-dimethyl-2,2′-bipyridine and unidentified by-products, and with methanol to provide a white solid of **10a**. Recrystallization from ethanol yielded 1.4 g (50%) of **10a**, mp 198—199 °C: ^1H NMR ($CDCl_3$) δ=2.5 (s, 6H), 3.2 (s, 4H), 7.0—9.0 (m, 6H). Anal. Calcd for $C_{24}H_{22}N_4$: C, 78.66; H, 6.05; N, 15.29%. Found: C, 78.66; H, 6.05; H, 15.23%.

4-(2-Bromoethyl)-4′-methyl-2,2′-bipyridine (9b). Using 4-(2-hydroxyethyl)-4′-methyl-2,2′-bipyridine, **8b**[28] (3.0 g, 14 mmol) and thionyl bromide (7.5 ml, 95 mmol) as the starting materials, the reaction was worked up using the procedure described regarding the preparation of **9a**. It provided 1.8 g (46%) of **9b** as a clear oil: ^1H NMR ($CDCl_3$) δ=2.4 (s, 3H), 3.2 (t, 2H), 3.6 (t, 2H), 7.0—8.7 (m, 6H). Anal. Calcd for $C_{13}H_{13}N_2Br$: C, 56.52; H, 4.71; N, 10.07%. Found; C, 56.52; H, 4.82; N. 10.15%.

1,3-Bis(4′-methyl-2,2′-bipyridyl-4-yl)propane (10b). 10b was prepared from **9b** (1.3 g, 5 mmol) by the same procedure described regarding the preparation of **10a**. 4-Methyl-4′-vinyl-2,2′-bipyridine (0.3 g) as a by-product was obtained from the early eluates. Yield of **10b** was 1.2 g (63 %), mp 128 °C: ^1H NMR ($CDCl_3$) δ=2.1 (q, 2H), 2.4 (s, 6H), 2.8 (t, 4H), 7.0—8.7 (m, 12H). Anal. Calcd for $C_{25}H_{24}N_4$; C, 79.04; H, 6.32; N, 14.64%. Found: C, 78.71; H, 6.41; N, 14.61%.

1,3-Bis(4′-methyl-2,2′-bipyridyl-4-yl)-2-propanol (11). Ethyl formate (0.88 ml, 12 mmol) was added dropwise to a solution of monolithiated 4,4′-dimethyl-2,2-bipyridine (30 mmol) in 150 ml of THF at room temperature. The mixture was stirred overnight at room temperature, quenched with 150 ml of water, neutralized (pH 8—9) with 10% (v/v) methanolic HCl, and extracted four times with 100 ml $CHCl_3$ portions. The extracts were dried ($MgSO_4$) and evaporated to give a brownish-yellow solid. Purification of the crude product was achieved through several recrystallizations from methanol to provide a white solid **11** in a yield of 20%, mp 159—160 °C. ^1H NMR ($CDCl_3$) δ=2.45 (s, 6H), 2.93 (dd, 4H), 4.33 (m, 1H), 7.12—8.54 (m, 12H), MS *m/z* 396. Anal. Calcd for $C_{25}H_{24}NO$: C, 75.73; H, 6.10; N, 14.13%. Found: C, 75.93; H, 6.12; N, 13.97%.

4-(4-Hydroxybutyl)-4′-methyl-2,2′-bipyridine (8c). To a solution of lithiated 4,4′-dimethyl-2,2′-bipyridine (48 mmol), 1-bromo-3-(tetrahydro-2-pyranyloxy)propane[29] (10 g, 45 mmol) in 70-ml of THF was added dropwise. The resulting mixture was stirred overnight at room temperature. Methanol (10 ml) and then water (100 ml) were added. The solution was extracted with 1 l of chloroform. The extract was dried ($MgSO_4$) and evaporated. The residue was placed on an alumina column and eluted with benzene to provide 11.7 g of 4-methyl-4′-[4-(tetrahydro-2-pyranyloxy)butyl]-2,2′-bipyridine. ^1H NMR ($CDCl_3$) δ=1.4—1.8 (m, 10H), 2.4 (s, 3H), 2.7 (t, 2H), 3.3—4.0 (m, 4H), 4.6 (t, 2H), 7.0—8.6 (m, 6H). 4-Methyl-4′-(4-tetrahydropyran-2-yloxybutyl)-2,2′-bipyridine (11.7 g) in 300 ml of ethanol was treated with *p*-toluenesulfonic acid to give 3.3 g (30%) of **8c**. ^1H NMR ($CDCl_3$) δ=1.7 (m, 4H), 2.4 (s, 3H), 2.7 (t, 2H), 3.6 (t, 2H), 7.1—8.6 (m, 6H).

4-(4-Bromobutyl)-4′-methyl-2,2′-bipyridine (9c). A mixture of **8c** (3.5 g, 14 mmol) and thionyl bromide (25 g, 120 mmol) in 30 ml of CH_2Cl_2 was stirred at room temperature for 3 h under the flow of nitrogen gas. Water (200 ml) was added. The reaction mixture was neutralized (pH 8—9) with an aqueous solution saturated with Na_2CO_3 and extracted with 500 ml of CH_2Cl_2. After the extract was dried ($MgSO_4$) and evaporated below room temperature, the crude product was chromatographed on a silica-gel column by eluting with ethyl acetate–CH_2Cl_2 (3:2) to give 3.7 g (84%) of **9c**. ^1H NMR ($CDCl_3$): δ=1.8 (m, 4H), 2.4 (s, 3H), 2.7 (t, 2H), 3.4 (t, 2H), 7.1—8.6 (m, 6H).

1,5-Bis(4′-methyl-2,2′-bipyridyl-4-yl)pentane (10c).[30] To a solution of lithiated 4,4′-dimethyl-2,2′-bipyridine (24 mmol), **9c** (3.7 g, 12 mmol) in 30 ml of THF was added dropwise at room temperature. Methanol(10 ml) and then water (100 ml) were added. The resulting solution was extracted with 1 l of chloroform. The extract was dried ($MgSO_4$) and evaporated. The residue was placed on a silica gel column and eluted with a mixture of acetone–CH_2Cl_2 (1:9 v/v) to provide a white solid of **10c**. Recrystallization from methanol yielded 2.4 g (48 %) of **10c**, mp 115—116 °C; ^1H NMR ($CDCl_3$) δ=1.3—1.9 (m, 6H), 2.4 (s, 6H), 2.7 (t, 4H), 7.1—8.6 (m, 12H), MS *m/z* 408. Anal Calcd for $C_{27}H_{28}N_4$: C, 79.38; H, 6.91; N, 13.71%. Found: C, 79.40; H, 6.84; N, 13.70%.

1,7-Bis(4′-methyl-2,2′-bipyridyl-4-yl)heptane (12). To a solution of lithiated 4,4′-dimethyl-2,2′-bipyridine (27 mmol), 1,5-dibromopentane (1.85 ml, 14 mmol) was added dropwise at room temperature. The mixture was stirred for 20 h. The solution was quenched with methanol and neutralized with methanol–HCl. The reaction mixture was diluted with 100 ml of water and extracted with dichloromethane. The extract was dried ($MgSO_4$) and evaporated. The residue was placed on a silica-gel column and eluted with a mixture of CH_2Cl_2–acetone (9:1, v/v) to give a white solid. Recrystallization from ethanol yielded 2.2 g (37%) of **12**, mp 86—87 °C: ^1H NMR ($CDCl_3$) δ=1.36 (m, 6H), 1.69 (q, 4H), 2.43 (s, 6H), 2.67 (t, 4H), 7.11 (d, 4H), 8.21 (s, 4H), 8.53 (dd, 4H). Anal. Calcd for $C_{29}H_{32}N_4$: C, 79.78; H, 7.39; N, 12.83%. Found: C, 79.62, H, 7.36; N, 12.66%.

Os(II)(bpy)$_2$Mebpy-(CH$_2$)$_n$-Mebpy (13) and Ru(II)(bpy)$_2$-Mebpy-(CH$_2$)$_n$-MebpyOs(II)(bpy)$_2$(PF$_6$)$_4$ (1). Compound **13** was obtained by refluxing a mixture (10:1) of α,ω-bis(4′-methyl-2,2′-bipyridyl-4-yl)alkane and $Os(bpy)_2Br_2$ in methanol for 24 h. After the isolation of **13** by chromatography on a Sephadex LH-20 with a methanol eluent, treatment of **13** with $Ru(bpy)_2Cl_2$ in methanol under reflux, and then with ammonium hexafluorophosphate in water, afforded **1**. Compound **1** was purified by the same procedure with **13** and was recrys-

tallized from water as a PF_6^- salt.

Ru(II)(bpy)$_2$Mebpy-[CH$_2$CH(OH)CH$_2$]-MebpyOs(II)(bpy)$_2$ (3) and **Ru(II)(Me$_2$bpy)$_2$Mebpy-[CH$_2$CH(OH)CH$_2$]-MebpyOs(II)(bpy)$_2$, (4).** Compounds **3** and **4** were prepared from **11**, Os(bpy)$_2$Br$_2$, and Ru(bpy)$_2$Cl$_2$ (or Ru(Me$_2$bpy)$_2$Cl$_2$), according to the procedure described for **1**.

Measurements. Samples for luminescence measurements were deoxygenated by purging with argon gas. Solvents for spectroscopic measurements were purchased from Nakarai Chemicals as in spectrograde. Static absorption and luminescence measurements were performed using a Shimadzu UV-2100 spectrometer and an RF-502A spectrofluorimeter, respectively. The luminescence lifetime was measured by the time-correlated single photon counting method, as described elsewhere.[31] The luminescence lifetimes for the complexes at room temperature are listed in Table 1; the reported lifetimes represent the average of several independent determinations. Electrochemical measurements were performed in a conventional single-compartment cell equipped with a glassy carbon or platinum working electrode and a saturated calomel electrode as a reference electrode (SCE). All measurements were carried out using a NF function generator (FG-12113) and a Hokuto Potentiostat (HA-301) at a scan rate 0.2V s^{-1}. Tetrabutylammonium perchlorate (TBAP) was used as the supporting electrolyte and acetonitrile as the solvent. The sample solution (1 mM, 1 M=1 mol dm^{-3}) was deaerated by bubbling with argon gas.

Results and Discussion

The bridging ligand was first coupled with 1/10 equimolar Os(bpy)$_2$Br$_2$ and purified by repeated Sephadex LH-20 chromatography to remove any unreacted bridging ligand and Os(II)(bpy)$_2$Mebpy-(CH$_2$)$_n$-MebpyOs(II)-(bpy)$_2$. Treatment of Os(II)(bpy)$_2$Mebpy-(CH$_2$)$_n$-Mebpy with Ru(bpy)$_2$Cl$_2$ and ammonium hexafluorophosphate afforded **1** as a PF_6 salt. Purification of **1** was achieved by repreated chromatography using Sephadex LH-20 methanol as an eluent. On the basis of lifetime measurements, the possible existence of Ru(II)(bpy)$_2$Mebpy-(CH$_2$)$_n$-MebpyRu(II)(bpy)$_2$ or Ru(II)(bpy)$_2$Mebpy-(CH$_2$)$_n$-Mebpy as impurities was found to be less than 0.5%. (vide infra).

The redox and electronic properties of **1** in the ground state was compared with those of its component complexes, (4,4′-dimethyl-2,2′-bipyridine)bis(2,2′-bipyridine)osmium(II), **5**, and -ruthenium(II), **6**, and a 1:1 mixture of **5** and **6**. Redox potentials in acetonitrile (MeCN) were measured by cyclic voltammetry using a glassy carbon or a platinum electrode. As an illustration, a cyclic voltammogram of **1** (n=3) is shown in Fig. 1. Irrespective of the number of methylene chains, **1** shows two reversible oxidation waves at 0.78 and 1.22 V vs. SCE for the Os(III)/Os(II) and Ru(III)/Ru(II) couples, which correspond to those of **5** and **6**, respectively. The peak-to-peak splitting for these waves is 60—70 mV, indicating that in **1**, two successive one-electron oxidation processes take place. A typical absorption spectrum for **1** (n=3) in methanol is shown in Fig. 2. As showm in Fig. 2, the electronic absorption spectrum of **1** (n=3) is identical with the superimposed spectrum of equimolar **5** and **6**. This was also observed in **1** (n=2,5, and 7). Thus, a comparison for the redox and electronic properties of **1** with its component complexes gave no evidence of an interaction between the ruthenium and osmium moieties of **1** in the ground state. This represents a marked difference from the covalently linked porphyrin dimers, in which the interaction between the porphyrin rings has been reported.[14,15]

The luminescence spectra of **1** (excitation wavelength: 455 nm) was recorded with an argon-gas bubbled methanol solution at room temperature and compared with that of a 1:1 mixture of **5** and **6** at the same substrate concentration. The efficient quenching of emission at 615 nm from a ruthenium complex and the enhancement of emission intensity at 730 nm from osmium complex were observed in **1** (n=3). In a mixture of **5** and **6**, no such quenching process could be observed because of the low substrate concentration (Fig. 3). For all **1** systems, a comparison of the spectra given in Fig. 4 shows that the degrees of quenching at 615 nm and sensitization at 730 nm increase in shorter

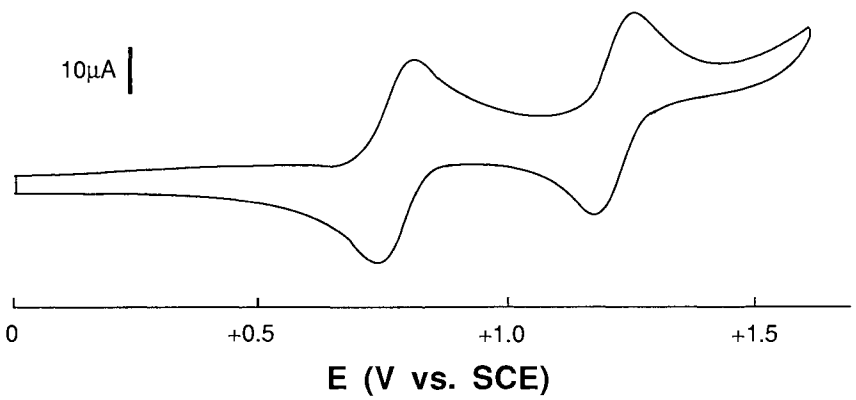

Fig. 1. Cyclic voltammogram of **1** (n=3) (1 mM) in MeCN solution with n-Bu$_4$NClO$_4$ as supporting electrolyte at a Pt disc electrode. Sweep rate was 200 mV s^{-1}.

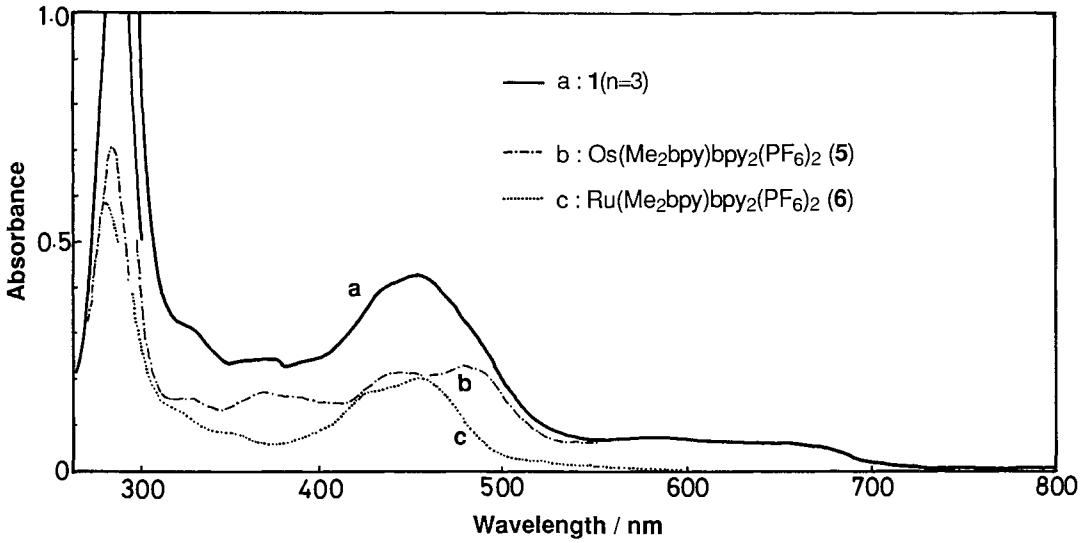

Fig. 2. Absorption spectra in water for **1** (n=3) (a), **5** (b), and **6** (c). [substrate]=1.5×10^{-5} M.

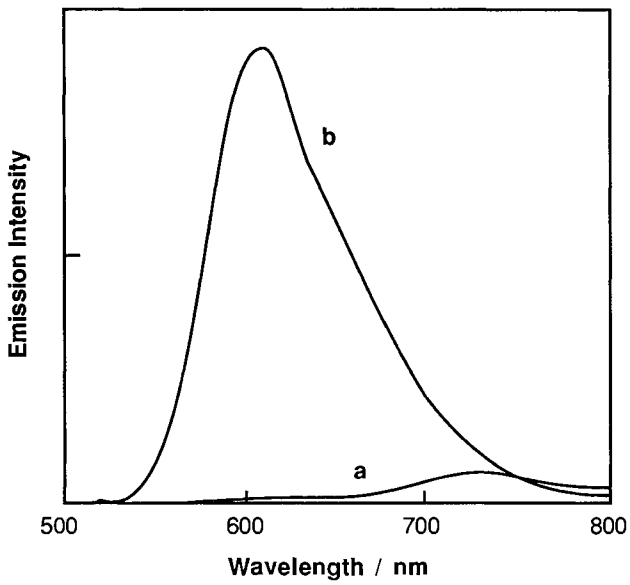

Fig. 3. Emission spectra of **1** (n=3) (a) and [**5**+**6**] (b) in MeOH. [substrate]=1.5×10^{-5} M. Excitation at 455 nm.

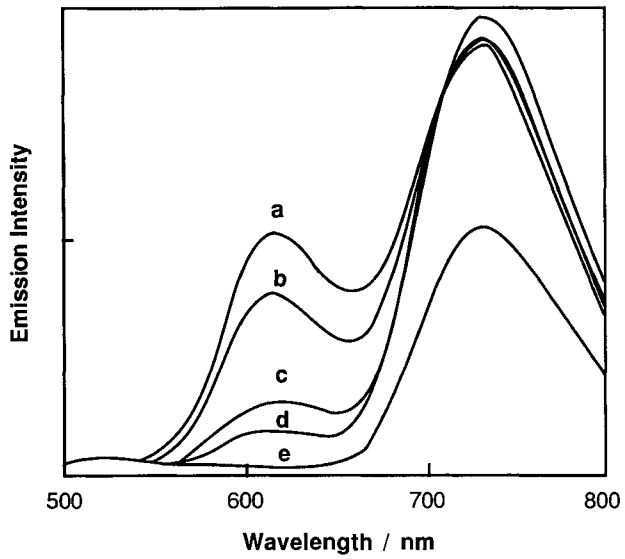

Fig. 4. Emission spectra of **1** in MeCN. [substrate]= 1.5×10^{-5} M. Excitation at 455 nm. **1** (n=7) (a), **1** (n=5) (b), **1** (n=3) (c), and **1** (n=2) (d). (e): The estimated contribution due to the direct excitation of osmium complex.

methylene chains. The molar absorption coefficients of **5** and **6** at 455 nm are equal. This overlap of absorption endows the equal probability of excitation of the Ru and Os moieties in **1**. In Fig. 4, spectrum e reveals the contribution due to a direct excitation of an osmium complex of **1** at 455 nm. The enhancement of emission at 730 nm indicates that the sensitization of the osmium complex by an excited ruthenium complex occurs through an intramolecular process in **1**.

As for the quenching mechanism, energy transfer from *Ru(II) to Os(II) and reductive electron transfer from Os(II) to *Ru(II) are conceivable. In acetonitrile, the first reduction potential of the $Ru^{2+/+}$ couple is -1.39 V, and the first oxidation potential of the $Os^{3+/2+}$ couple is 0.78 V vs.SCE (by cyclic voltammetry). Since substitution of one bpy-ligand of $Ru(bpy)_3^{2+}$ and $Os(bpy)_3^{2+}$ with 4,4′-dimethyl-2,2′-bipyridine does not show a marked difference in the absorption and emission maxima, the excited energies of the Ru-complex and the Os-complex of **1** can be assumed to be almost the same as those of $Ru(bpy)_3^{2+}$ and $Os(bpy)_3^{2+}$, respectively. The excited-state energy of the Ru-complex and the Os-complex of **1** were estimated to be 2.10[32] and 1.78 eV,[33] respectively. The photophysical behavior of **1** can be described in terms of an energy level diagram that is simply made by superimposing the low-lying excited states of the $Ru(bpy)_3^{2+}$ and $Os(bpy)_3^{2+}$ units on

the redox potentials in the ground state. The reductive quenching of the excited Ru-complex is slightly endergonic (ΔG=0.07 eV) based on a comparison of the reduction potential (0.71 V) for the $Ru^{2+*/+}$ couple with the oxidation potential (0.78 V) for the $Os^{3+/2+}$ couple. On the other hand, energy transfer can be more favorable by 0.32 eV, which corresponds to the observed difference in the emission maxima of the Ru-complex (E_{em}=1.63×10⁴cm⁻¹) and the Os-complex (E_{em}=1.37×10⁴ cm⁻¹) of **1**. The thermodynamical aspect allows us to conclude that energy transfer instead of electron transfer constitutes the quenching mechanism.

The occurrence of energy transfer can be detected by observing the enhancement of the emission intensity of the osmium chromophore along with a decrease in the emission intensity of the ruthenium chromophore. The decay of $Ru^{II}\rightarrow\pi^*$(bpy) MLCT emission at 610 nm and the rise and decay of $Os^{II}\rightarrow\pi^*$(bpy) MLCT emission at 800 nm were measured in various solvents by using a time-correlated single photon counting method[31] (excitation wavelength at 457.9 nm and instrumental width of 300 ps). Deconvolution of the luminescence profiles at 610 nm afforded the best fit by single exponential decay. In some cases, a minor, long-lived component was present (<0.5%). The amplitude of this component was sensitive to the degree of sample purification, it therefore most probably represents an impurity. Figure 5 shows the emission decay profile of an excited Ru-complex of **1** (n=7) in MeCN, with which a computer-calculated fit is superimposed. The fast exponential decay (12.1 ns: 8.3×10⁷ s⁻¹) is attributed to a deactivation of the ruthenium-excited state by an intramolecular energy transfer to the osmium complex. The double exponential analysis for the rise and decay of the excited-osmium complex at 800 nm gave 12 ns (8.3×10⁷ s⁻¹) for a rise corresponding to a decay of the excited ruthenium complex and 56 ns (1.8×10⁷ s⁻¹) for the decay, respectively. Table 1 contains the parameter

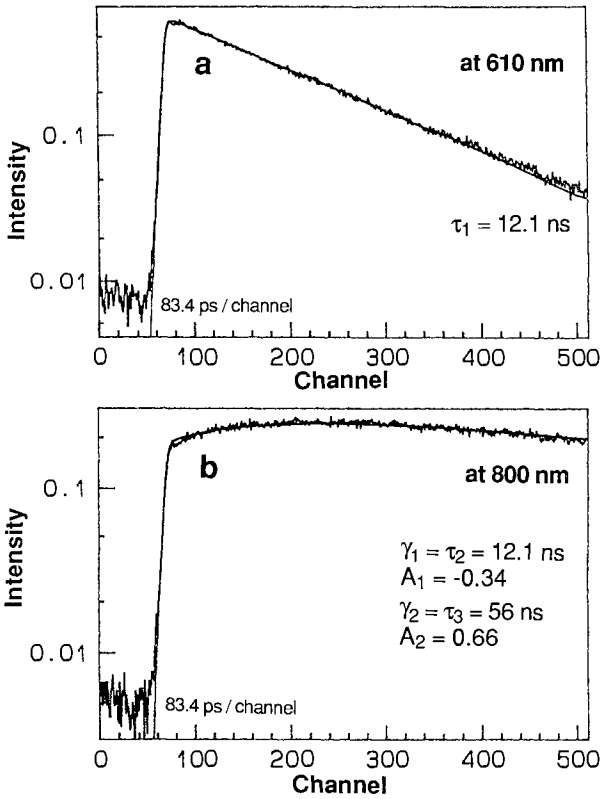

Fig. 5. Emission rise and decay for **1** (n=7) monitored at 610 nm (a) and 800 nm (b). 83.4 ps/channel, [**1**]=1×10⁻⁴M, solvent: MeCN.

Table 1. Emission Lifetimes and Energy-Transfer Rates[a]

Complex	Solvent	τ_1/ns[b]	τ_2/ns[c]	τ_3/ns[c]	k_{en}/s⁻¹[d]
1 (n=2)	H_2O	0.86[e]	0.93 (−0.25)	23 (0.75)	1.1×10⁹
	EtOH	1.9	1.9 (−0.33)	52 (0.67)	5.3×10⁸
	MeCN	1.2	1.2 (−0.38)	55 (0.62)	8.3×10⁸
1 (n=3)	H_2O	2.2	2.2 (−0.32)	18 (0.68)	4.5×10⁸
	EtOH	3.0	3.0 (−0.35)	37 (0.65)	3.3×10⁸
	MeCN	2.5	2.5 (−0.35)	44 (0.65)	4.0×10⁸
1 (n=5)	H_2O	5.8	5.8 (−0.35)	19 (0.65)	1.7×10⁸
	EtOH	8.0	8.0 (−0.36)	42 (0.64)	1.3×10⁸
	MeCN	7.9	7.9 (−0.33)	48 (0.67)	1.3×10⁸
1 (n=7)	H_2O	8.1	8.1 (−0.32)	20 (0.68)	1.2×10⁸
	EtOH	9.6[e]	10 (−0.36)	42 (0.64)	1.0×10⁸
	MeCN	12.1	12 (−0.34)	56 (0.66)	8.1×10⁷
3	H_2O	2.2	2.2 (−0.33)	19 (0.67)	4.5×10⁸
	EtOH	3.0	3.0 (−0.34)	41 (0.66)	3.3×10⁸
	MeCN	2.5	2.5 (−0.31)	41 (0.69)	4.0×10⁸
4	H_2O	1.1	1.1 (−0.32)	22 (0.68)	9.1×10⁸
	EtOH	1.9	1.9 (−0.34)	53 (0.66)	5.3×10⁸
	MeCN	1.4	1.4 (−0.32)	63 (0.68)	7.1×10⁸

a) All data represent averages and were measured at room temperature. The errors are less than 10%. b) Emission at 610 nm. c) Emission at 800 nm; the number in parenthesis indicates preexponential factors A_1 and A_2 for double exponential fit. d) Calcd from $1/\tau_1-1/\tau_0$; τ_0 is a lifetime of **6**. Values are 518, 729, and 859 ns in H_2O, EtOH, and MeCN, respectively. e) Average value of double exponential decay.

for the fit.

The excitation of **1**, denoted by Ru-C_n-Os at 457.9 nm, affords two excited states, namely *Ru-C_n-Os and Ru-C_n-Os* (Eq. 1a and 1b). In addition to the normal deactivation process (Eq. 1c and 1f), the reductive quenching of *Ru-C_n-Os by an intramolecular electron transfer process (Eq. 1d) and the buildup of Ru-C_n-Os* by the intramolecular energy transfer process (Eq. 1e) are taken into account:

$$\text{Ru-C}_n\text{-Os} \xrightarrow{h\nu} \text{*Ru-C}_n\text{-Os}, \quad (1a)$$

$$\text{Ru-C}_n\text{-Os} \xrightarrow{h\nu} \text{Ru-C}_n\text{-Os*}, \quad (1b)$$

$$\text{*Ru-C}_n\text{-Os} \xrightarrow{k_1} \text{Ru-C}_n\text{-Os} + (h\nu + \Delta), \quad (1c)$$

$$\text{*Ru-C}_n\text{-Os} \xrightarrow{k_{el}} \text{Ru-C}_n\text{-Os}, \quad (1d)$$

$$\text{*Ru-C}_n\text{-Os} \xrightarrow{k_{en}} \text{Ru-C}_n\text{-Os*}, \quad (1e)$$

and

$$\text{Ru-C}_n\text{-Os*} \xrightarrow{k_2} \text{Ru-C}_n\text{-Os} + (h\nu + \Delta). \quad (1f)$$

The relevant rate equations are

$$d[\text{*Ru-C}_n\text{-Os}]/dt = -(k_1 + k_{el} + k_{en})[\text{*Ru-C}_n\text{-Os}] \quad (2a)$$

and

$$d[\text{Ru-C}_n\text{-Os*}]/dt = k_{en}[\text{*Ru-C}_n\text{-Os}] - k_2[\text{Ru-C}_n\text{-Os*}] \quad (2b)$$

Equation (2b) yields

$$[\text{Ru-C}_n\text{-Os*}] = A_1\exp(-\gamma_1 t) + A_2\exp(-\gamma_2 t), \quad (3)$$

where $A_1=k_{en}[\text{*Ru-C}_n\text{-Os}]_0/(\gamma_2-\gamma_1)$, $A_2=[\text{Ru-C}_n\text{-Os*}]_0-A_1$, $\gamma_1=k_1+k_{el}+k_{en}$, $\gamma_2=k_2$, and $[\text{*Ru-C}_n\text{-Os}]_0$ and $[\text{Ru-C}_n\text{-Os*}]_0$ denote the initial concentration. γ_1 can be obtained from the decay time at 600 nm and the rise time at 800 nm. γ_2 can be also obtained from the decay time at 800 nm. The values of k_2 calculated from τ_3 ($=1/\tau_2$) in Table 1 are of the order of $2-5\times10^7$ s^{-1}. The value of k_1 is 2×10^6 s^{-1} based on the lifetime of **6**.

Since the molar absorption coefficients of **5** and **6** at 457.9 nm are quite similar, we can deduce $[\text{*Ru-C}_n\text{-Os}]_0=[\text{Ru-C}_n\text{-Os*}]_0$. The ratio of the preexponential factors is given by

$$A_2/A_1 = (k_2 - k_1 - k_{el})/k_{en} - 2. \quad (4)$$

As indicated in Table 1, the A_2/A_1 values from the parameter for the computer fits of the experimental rise, and the decay profiles at 800 nm are close to -2. Equation 4 yields $(k_2-k_1-k_{el})/k_{en}\approx0$. Since k_2 is of the order of $2-5\times10^7$ s^{-1} and k_1 is 2×10^6 s^{-1}, k_{el} can be estimated to be of the order of 10^7 s^{-1} or less. The values of γ_1 ($=k_1+k_{el}+k_{en}$) calculated from τ_1 in Table 1 are $8-1\times10^8$ s^{-1}. By combining the estimated values of k_1 and k_{el}, k_{en} is found to be of the order of 10^8 s^{-1}; thus, $k_{en}\gg k_{el}$. This implies that the quantum efficiency of the energy transfer is almost 1, irrespective of the length of the methylene chain examined in the present study. Accordingly the electron transfer process by reductive quenching can be ruled out regarding **1**.

The rate constant, k_{en}, of energy-transfer can then be calculated via

$$k_{en} = k_{obs} - k_1, \quad (5)$$

where k_{obs} and k_1 can be calculated from the observed lifetime (τ_1) at 610 nm and the emission lifetime of **6**, $Ru(bpy)_2(dmb)^{2+}$(dmb=4,4′-dimethyl-2,2′-bipyridine), respectively. As presented in Table 1, k_{en} depend strongly on the length of the methylene chain, and increase in shorter methylene chains. Two mechanisms are possible for the present energy-transfer. The Förster mechanism operates via a dipole-dipole interaction between the transition moment and, therefore, requires no direct contact between the energy donor and acceptor. The Dexter mechanism depends upon the electron exchange and, thus, requires a spatial overlap. Discrimination between the Förster and the Dexter mechanisms can be achieved by studying the effect of varying the donor-acceptor separation (R). The rate constant for the Förster dipole-dipole transfer is expected to fall off with the inverse sixth power of R. The rate constant of the Dexter transfer, however, is predicted to parallel any decrease in the electronic overlap with increasing R, which may approximated by an exponential function. Although it is admittedly difficult to estimate the distance of **1** (n=2), space-filling molecular models indicate that, by using the molecular radius 4.7 Å of $Ru(bpy)_3^{2+}$ and assuming a fully extended trans-conformation for alkane bridges of the bridging

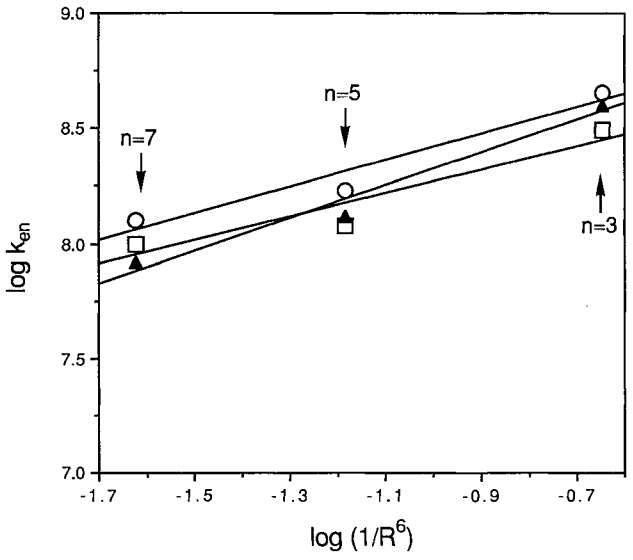

Fig. 6. Dependence of the rate of energy transfer on distance in various solvents. ○: in H_2O, ▲: in EtOH, and □: in MeCN.

ligands, the center-to-center separation distances in **1** are 12.8, 15.8, and 18.6 Å for n=3,5, and 7, respectively. It is adequate to evaluate R for a dipole–dipole interaction with a center-to-center rather than an edge-to-edge distance of both metal complexes. As shown in Fig. 6, the distance dependence of k_{en} in series **1** in water, ethanol, and acetonitrile can be fitted to an inverse sixth power law of the Förster mechanism. Instead, a steep drop of the rate is predicted by the Dexter mechanism in which k_{en} is expressed via an exponential dependence on the distance. Plots of the rate (k_{en}) vs. exp ($-R$) could not give a linear ralationship. These observations led us to conclude that a Förster-type interaction mechanism is operating in the intramolecular energy transfer in **1**.

A quantitative treatment of the Förster mechanism leads to the following expression for k_{en};[23]

$$k_{en} = \frac{9000 \ln 10 \kappa^2 \phi_D}{128\pi^5 n^4 N \tau_D R^6} \int_0^\infty F_D(\nu)\varepsilon_A(\nu)\frac{d\nu}{\nu^4} \qquad (6)$$

Here, ν is the wave number, $F_D(\nu)$ is the spectral distribution of the donor emission in quanta normalized to unity, $\varepsilon_A(\nu)$ is the molar extinction coefficient for the acceptor absorption, n is the refractive index of the solvent, κ is an orientation factor which equals $(2/3)^{1/2}$ for a random distribution of donor and acceptor molecules, ϕ_D is the quantum yield of donor emission, τ_D is the actual donor emission lifetime, N is Avogadro's number, and R is the distance between the donor and acceptor molecules. The overlap integral was calculated from numerical integration over the emission of **6** and the absorption of **5** in water and the value was 5.57×10^{-11} mol^{-1} cm^6. Based on the observed values of ϕ_D=0.028 and τ_D=4.77×10^{-7} s and assuming κ^2=2/3 and R=12.8 Å for **1** (n=3), the calculated k_{en} value was 1.4×10^8 s^{-1}, which was reasonably close to the observed value (4.5×10^8 s^{-1}).

Creutz and Sutin reported that the bimolecular quenching rate constant between excited $Ru(bpy)_3^{2+}$ and $Os(bpy)_3^{2+}$ was 1.5×10^9 M^{-1} s^{-1}, and that the reaction is almost diffusion-controlled.[34] The observed first-order rate constant for **1** seemed unexpectedly small. This fact might result from an electrostatic repulsion between two chromophores of **1**, which prevents any collisional quenching process based on an electron exchange (Dexter mechanism). It has been known that the intramolecular electron transfer via collisional processes in a trimethylene-linked donor-acceptor is influenced the solvent viscosity.[35] The dependence of solvent viscosity on the energy transfer rate (k_{en}) was examined for **1** (n=5) in three different solvents [ethanol(0.012), ethylene glycol (0.17), and glycerol (10.7) (in parentheses: viscosity in poise)]. In spite of the large difference in the viscosity, the observed k_{en} were in good agreement, that is, $(1.1—1.2)\times10^8$ s^{-1} irrespective of the solvent used. This finding also supports the Förster mechanism.

As shown in Table 1, a remarkable difference of k_{en} between **3** and **4** exists. According to the Förster formulation (Eq. 6), the rate constant is proportional to the spectral overlap and the reciprocal value of the radiative lifetime. The emission maxima (E_{em}), quantum yields (ϕ_{em}) and emission lifetime in water are 1.63×10^4 cm^{-1}, 0.028, and 477 ns for $Ru(bpy)_2(dmb)^{2+}$ and 1.61×10^4 cm^{-1}, 0.023, and 333 ns for $Ru(dmb)_3^{2+}$, respectively, which correspond to the ruthenium complex of **3** and **4**. Hence, the true radiative lifetimes are 17.0 μs for $Ru(bpy)_2(dmb)^{2+}$ and 14.5 μs for $Ru(dmb)_3^{2+}$. These values can not explain the observed differences. It is known that the excited electron in MLCT excited state of $Ru(bpy)_3^{2+}$ is fully localized on one of three equivalent ligands, at least for a time long enough for this ligand and its neighboring solvent to adjust to the geometry of fully charged bpy^-. Vibrational relaxation and localization have been suggested to come to completion within a few picoseconds.[36] In **3**, optical electron may preferentially reside on a bridging ligand rather than on a bpy ligand. On the contrary, the MLCT transition involves the π* orbital of dmb ligands, rather than a bridging ligand in **4**. The orientation of the MLCT transition in **4** is possibly more favorable for the dipole–dipole interaction.

In the Förster mechanism, the mutual orientation of donor and acceptor complexes is important for determining the energy transfer rate. The polypyridine complex has two configurational isomers, namely *Δ* and *Λ*-isomers. It has been recognized that the dimer of polypyridine ruthenium complex, **2** (n=3), consists of a 1:1 diastereomeric mixture of (*Δ*–*Δ*) and (*Δ*–*Δ*+*Λ*–*Λ*).[12] **1** is also assumed to have the same composition of configurational isomers. A careful examination of the decay profiles indicates that there is no marked difference in the rate of the intramolecular energy transfer between these configurational isomers. Solvation may also cause a conformational change. The binuclear complex, **3** has an OH group on the bridging ligand. Protic solvents may interact with the OH group of **3**. Since the photophysical behavior of **1** (n=3) and **3** is quite the same, such an interaction is not important for intramolecular energy transfer.

It can be concluded that electrostatic repulsion prevents any collisional interaction between two chromophores of **1**, and that the dipole–dipole interaction is the main pathway for intramolecular energy transfer. The structural difference due to the configuration (*Δ* and *Λ*) of each chromophores is not important in the intramolecular energy transfer in the present case.

References

1) T. J. Meyer, *Acc. Chem. Res.*, **22**, 163 (1989).
2) D. Gust and T. A. Moore, *Science*, **244**, 35 (1989).
3) J. R. Norris, Jr. and D. Meisel, "Photochemical Energy Conversion," Elsevier, New York (1989), pp. 366.

4) M. A. Fox and M. Chanon, "Photoinduced Electron Transfer," Elsevier, Amsterdam (1988).
5) V. Balzani, "Supramolecular Photochemistry," D. Reidel Publishing Co., Doedrecht (1987).
6) R. Duesing, G. Tapolsky, and T. J. Meyer, *J. Am. Chem. Soc.*, **112**, 5378 (1990).
7) K. S. Schanze and L. Cabana, *J. Phys. Chem.*, **94**, 2740 (1990).
8) A. Osuka, K. Maruyama, N. Mataga, T. Asahi, I. Yamasaki, and N. Tamai, *J. Am. Chem. Soc.*, **112**, 4958 (1990).
9) D. Gust, T. A. Moore, A. L. Moore, S. Lee, E. Bittersmann, D. K. Luttrull, A. A. Rehms, J. M. DeGraziano, X. C. Ma, F. Gao, R. E. Belford, and T. T. Trier, *Science*, **248**, 199 (1990).
10) G. Tapolsky, R. Duesing, and T. J. Meyer, *Inorg. Chem.*, **29**, 2285 (1990).
11) K. Sumi, M. Furue, and S. Nozakura, *J. Polym. Sci., Polym. Chem. Ed.*, **23**, 3059 (1985).
12) M. Furue, N. Kuroda, and S. Nozakura, *Chem. Lett.*, **1986**, 1209.
13) J. B. Birks, "Photophysics of Aromatic Molecules," Wiley-Interscience, New York (1970).
14) Y. Kaizu, H. Maekawa, and H. Kobayashi, *J. Phys. Chem.*, **90**, 4234 (1986).
15) O. Ohno, Y. Ogasawara, M. Asano, Y. Kajii, Y. Kaizu, K. Obi, and H. Kobayashi, *J. Phys. Chem.*, **91**, 4269 (1987).
16) M. Furue, N. Kuroda, T. Yoshidzumi, S. Shun-ichi Nozakura, M. Kamachi, T. Ohno, W. E. Jones, Jr., and T. J. Meyer, *Polym. Prepr. Jpn.*, **38**, 1814 (1989).
17) C. A. Bignozzi, M. T. Indelli, and F. Scandola, *J. Am. Chem. Soc.*, **111**, 5192 (1989).
18) R. H. Schmehl, R. A. Auerbach, and W. F. Wacholtz, *J. Phys. Chem.*, **92**, 6202 (1988).
19) C. K. Ryu and R. H. Schmehl, *J. Phys. Chem.*, **93**, 7961 (1989).
20) R. Sahai, D. A. Baucom, and D. P. Rillema, *Inorg. Chem.*, **25**, 3843 (1986).
21) A. A. Lamola, "Energy Transfer and Organic Photochemistry," Interscience, New York (1969), pp. 17.
22) N. J. Turro, "Modern Molecular Photochemistry," The Benjamin/Cummings, Menlo Park, California (1978).
23) Th. Förster, *Discuss. Faraday Soc.*, **27**, 7 (1959).
24) D. L. Dexter, *J. Chem. Phys.*, **21**, 836 (1953).
25) F. Felix, J. Ferguson, H. U. Guedel, and A. Ludi, *J. Am. Chem. Soc.*, **102**, 4096 (1980).
26) E. M. Kober and T. J. Meyer, *Inorg. Chem.*, **23**, 3877 (1984).
27) M. Furue, S. Kinoshita, and T. Kushida, *Chem. Lett.*, **1987**, 2355.
28) K. Sumi, M. Furue, and S. Nozakura, *J. Polym. Sci., Polym. Chem. Ed.*, **22**, 3779 (1984).
29) F. B. Bohlmann, H. Bornowski, and P. Herbst, *Chem. Ber.*, **93**, 1931 (1960).
30) R. H. Schmehl, R. A. Auerbach, W. F. Wacholtz, C. M. Elliott, R. A. Freitag, and J. W. Merkert, *Inorg. Chem.*, **25**, 2440 (1986).
31) S. Kinoshita and T. Kushida, *Anal. Instrum.*, **14**, 503 (1985).
32) R. J. Watts, *J. Chem. Educ.*, **60**, 834 (1983).
33) C.-T. Lin and N. Sutin, *J. Phys. Chem.*, **80**, 97 (1976).
34) C. Creutz, M. Chou, T. L. Netzel, M. Okumura, and N. Sutin, *J. Am. Chem. Soc.*, **102**, 1309 (1980).
35) S. Russo and P. J. Thistlethwaite, *Chem. Phys. Lett.*, **106**, 91 (1984).
36) P. J. Carroll and L. E. Brus, *J. Am. Chem. Soc.*, **109**, 7613 (1987).

Synthesis and Absorption Spectral Properties of New Merocyanine Dyes Derived from 1,1-Diaryl-2-propyn-1-ols[1)]

Shin'ichi NAKATSUJI,*† Tomio YAHIRO, Kenichiro NAKASHIMA, Shuzo AKIYAMA,* and Hiroyuki NAKAZUMI††
School of Pharmaceutical Sciences, Nagasaki University, 1-14 Bunkyo-machi, Nagasaki 852
†† Department of Applied Chemistry, College of Engineering, University of Osaka Prefecture, Sakai 592
(Received December 25, 1990)

A series of push-pull butadiene dyes (new merocyanine dyes) containing 3,6-bis(dimethylamino)fluorenylidene, thioxanthenylidene, or 10-(9-xanthenylidene)-9(10*H*)-anthrylidene chromophore was easily synthesized from the corresponding 1,1-diaryl-2-propyn-1-ol systems. Their absorption spectral properties were examined and the relationship between their light absorption properties and chemical structures is discussed in comparison with the results from PPP-SCF-CI-MO calculations. The influence of the solvent polarity on the $1/\lambda_{max}$(=wave number)-values of the dyes was investigated, and the solvatochromic nature compared with the known solvent polarity parameters such as E_T30, Z, χ_R, π^*_{azo} on 2-[2-[3,6-bis(dimethylamino)fluorenylidene]ethylidene]-1,3-indandione.

Merocyanine dyes are a well-known class of dyes, which have such practical applications as photoconductive or imaging materials (photographic films or electrographic systems);[2)] they have also been proposed as dyes for organic solar cells.[3)] Moreover, these dyes are used as important materials for photophysical[4)] or biochemical investigations.[5)] More recently, special interest has been focused on these dyes as possible candidates for nonlinear optics, owing to the development of optical and laser storage technologies.[6)]

During the course of our studies on the acetylenic analogs of triphenylmethane dyes (triphenylmethane dye ethynologs),[7)] we have developed a simple and convenient method for the preparation of aryl-substituted push–pull butadienes, a family of merocyanine dyes.[8)]

In this paper we report on the syntheses of novel push–pull-type merocyanine dyes containing bis[4-(dimethylamino)]phenylmethylene (**A**), 3,6-bis(dimethylamino)-fluorenylidene (**B**), thioxanthenylidene (**C**), and 10-(9-xanthylenylidene)-9(10*H*)-anthrylidene (**D**) chromophores from the corresponding 1,1-diaryl-2-propyn-1-ols. Successively, a mutual relation between their light-

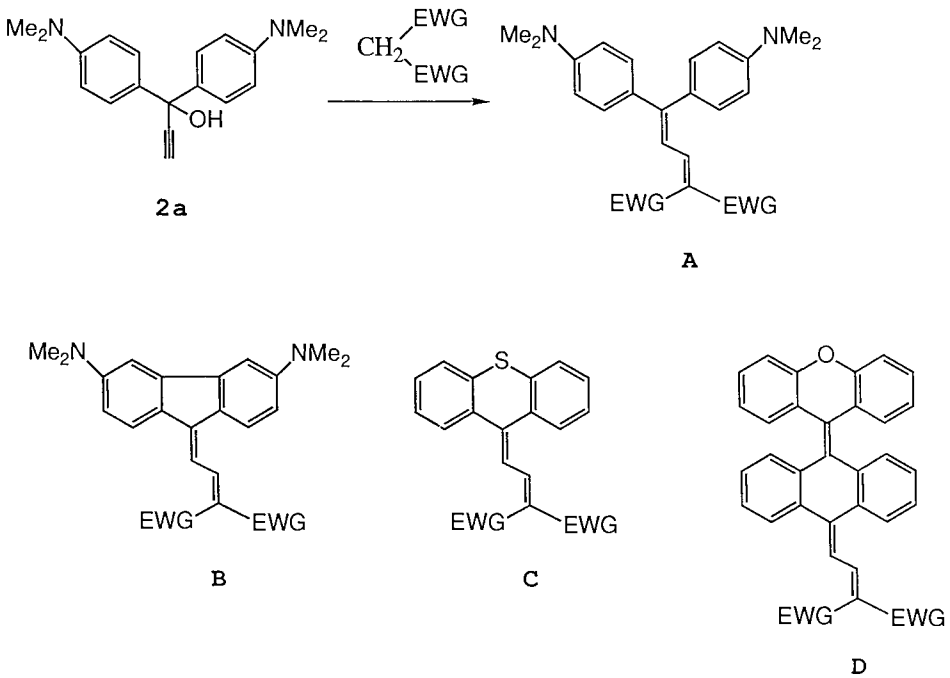

EWG=Electron-Withdrawing Group

Chart 1.

† Present address: Department of Materials Science, Faculty of Science, Himeji Institute of Technology, Shosha 2167, Himeji, Hyogo 671-22.

absorption properties and chemical structures was investigated and compared with Pariser–Paar–Pople MO (PPP-MO) calculations. Moreover, the solvatochromic properties were examined on 2-[2-[3,6-(dimethylamino)fluorenylidene]ethylidene]-1,3-indandione (**3b**) as a representative of the prepared dyes.

Results and Discussion

Synthesis of Dyes. Each of the precursors, i.e., the 1,1-diaryl-2-propyn-1-ol systems (**2a—d**), were prepared by ethynylation of the corresponding ketones.[9] Several nucleophiles, i.e., active methylene compounds, were allowed to react with **2a—d**, yielding a variety of new merocyanine dyes [(**3a—d**—**5a—d**), (**6a—c**), (**7a, b**), (**8a, b**), and (**9b**)], as shown in Scheme 1. In some cases the reactions proceeded easily at ambient temperature by mixing the substrates and each reagent without either heating or adding a catalyst, e.g., reactions with barbituric acid or thiobarbituric acid. Although isolated yields were good for the above-mentioned cases; in some cases appropriate heating was necessary to complete the reaction; there were also cases in which no reaction proceeded (see Experimental). It seems apparent that these reactivities depend on both the acidity of the nucleophiles employed and the electrophilicity of the substrates. A sort of acid-catalyzed propargylic rearrangement would participate in the reaction;[10] a plausible reaction process is shown in Scheme 2.

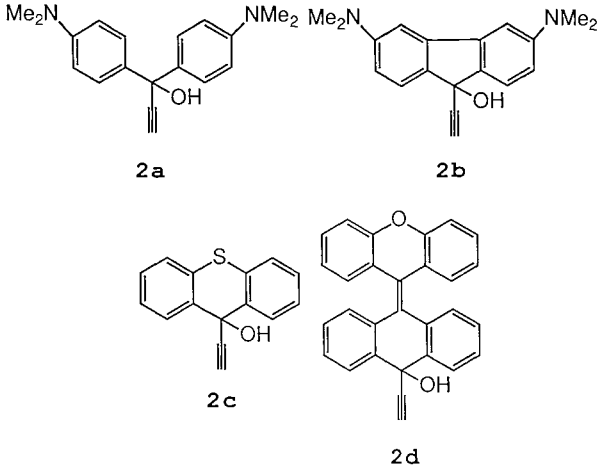

Absorption Spectral Properties. Absorption spectral data for the longest wavelength region of the prepared dyes are listed in Table 1. The bathochromic shift of the absorption band of the push–pull butadiene dyes (**A—D**) (Chart 1) depended on the electron-donating residue according to the sequence: **D>B>A>C**. The influence of the electron acceptor residue similarly followed the

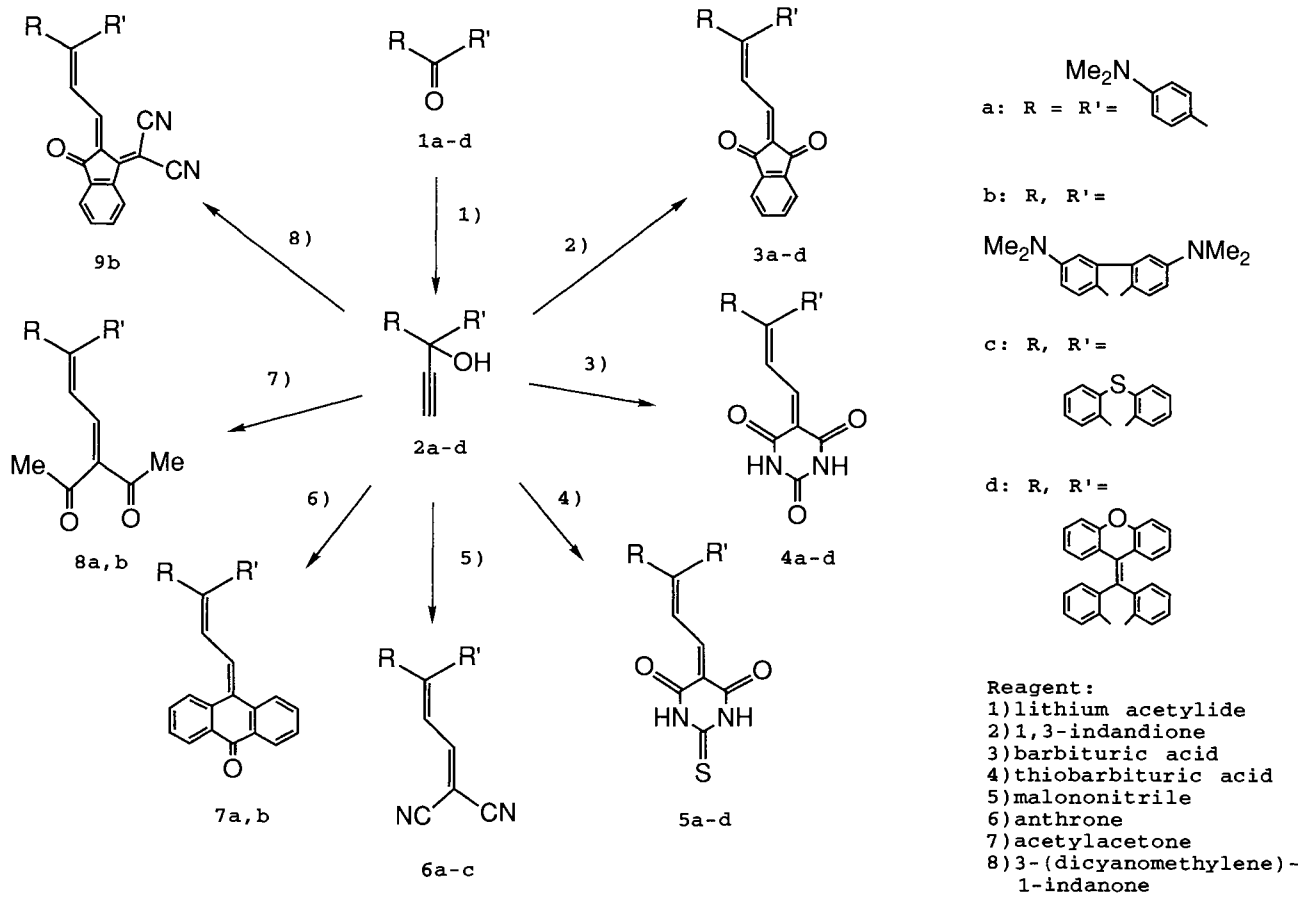

Scheme 1.

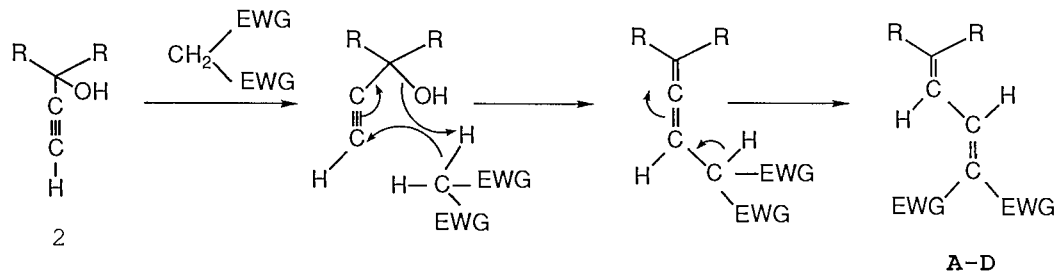

Scheme 2.

Table 1. Light Absorption Properties of Merocyanine Dyes **A**, **B**, **C**, **D**

Compound	λ_{max}/nm ($\varepsilon\times10^{-4}$)			Compound	λ_{max}/nm ($\varepsilon\times10^{-4}$)			Compound	λ_{max}/nm ($\varepsilon\times10^{-4}$)	
	CH_2Cl_2	EtOH	Calcd[a]		CH_2Cl_2	EtOH	Calcd[a]		CH_2Cl_2	EtOH
3a	565 (4.98)	578 (4.33)	459	**3b**	588 (5.89)	610 (5.62)	492	**3c**	473 (2.38)	472 (2.40)
4a	566 (5.60)	558 (3.86)	489	**4b**	598 (3.41)	597 (1.22)	523	**4c**	486 (1.62)	464 (1.25)
5a	595 (8.06)[b]	592 (5.67)	548	**5b**	634 (1.85)	637 (1.07)	579	**5c**	514 (0.94)	486 (0.68)
6a	498 (3.32)[b]	497 (4.19)	493	**6b**	531 (4.91)	529 (2.83)	532	**6c**	454 (1.69)	447 (1.38)
7a	503 (2.28)	504 (2.98)	507	**7b**	526 (3.50)	525 (2.38)	525	**3d**	672 (3.43)	667 (1.48)
8a	442 (3.04)	445 (1.83)	454	**8b**	473 (1.34)	481 (1.30)	488	**4d**	652 (3.13)	650 (2.05)
				9b	707 (6.40)	707 (—)[c]		**5d**	664 (4.01)	665 (1.14)

a) Calcd by PPP-SCF-CI-MO. b) Reported in Ref. 8. c) Insoluble.

Table 2. Calculated Results for the First and Second Absorption Bands of **4b** with Various Tautomers

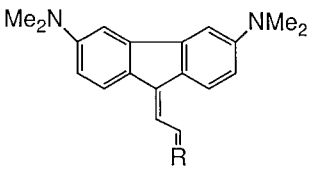

B

	4b$_1$	**4b**$_2$	**4b**$_3$	**4b**$_4$	**4b**$_5$
R=	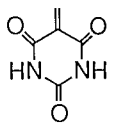	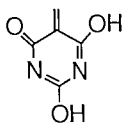	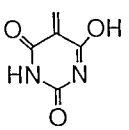	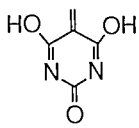	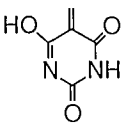
λ_{max_1}	523	530	527	510	513
λ_{max_2}	498	485	496	486	478

order: 3-(dicyanomethylene)-1-indanone>thiobarbituric acid>barbituric acid>1,3-indandione>malononitrile>anthrone>acetylacetone. The dicyanovinylindanone derivative of 3,6-bis(dimethylamino)fluorenylidene dye (**9b**) absorbs in the longest region among the dyes investigated (707 nm). The calculated results by the PPP-SCF-CI-MO method are also shown in Table 1.[11] The calculations were carried out on some of the **A** and **B** systems with the normal parameter sets proposed by Griffiths.[12] Although reasonable results were obtained in some of the compounds studied, there is some disagreement regarding **3a**, **b** and for the barbiturate series (or thiobarbiturate series), which in some cases showed deviations of 50—70 nm between the observed and calculated results with diketo forms. In barbituric or thiobarbituric acid derivatives, tautomeric effects might be considered to explain the experimental results. From the calculated results of **4b**, considering not only diketo forms but also keto/enol or dienol forms (see Table 2), however, no significant difference was observed between them, giving slightly better results in the keto/enol forms (**4b**$_2$ and **4b**$_3$). The bathochromic behavior of the thiobarbituric acid derivatives, compared with that of barbituric derivatives, agreed well with the calculated results. Also, the bathochromic tendency by ring closure of the *o*- and *o'*-positions of the diphenylmethane

component of **A** to the fluorenylidene component, **B**, was well reproduced by a MO calculation, i.e., a lowering tendency of the LUMO level of the diphenylmethane component by ring closure was elucidated by a comparison of each of the MO energy levels.[13] This shift was calculated to be 18—39 nm, showing reasonable agreement to the experimental shift (21—45 nm in EtOH).

Since one of the most remarkable shifts was observed for **3b**, we further investigated the solvatochromic effect by using 17 kinds of solvents. As shown in Table 3, the linear bathochromicity of the absorption of the longest wavelength was observed according to an increase in the solvent polarity. The correlation was investigated between the solvatochromism of the dye and the commonly used solvent polarity parameters: Dimroth and Reicharts' E_T30;[14] Kosower's Z;[15] Brooker's χ_R;[16] as well as recently proposed Buncel's π^*_{azo}.[17] As shown in Fig. 1, a good correlation was observed for the latter two, which are both based on merocyanine dyes. On the contrary, a weaker correlation was found for the former two (Correlation coefficient: r=0.92 and 0.87), both based on ionic betaine dyes. Because of the case of preparation and clear solvatochromic behavior, **3b** would be a possible candidate for a solvent polarity parameter.

In conclusion, four series of push–pull butadiene-type merocyanine dyes **A**—**D** were prepared by reactions of the corresponding diarylpropynols with various nucleophiles. The absorption spectral properties of **A**—**D** were investigated along with the calculated results by PPP-MO method, showing the characteristic spectral behavior derived from the electron-donating nature of the donor part and electron-withdrawing nature of the acceptor part. The solvatochromic nature of **3b** was estimated by using 17 solvent sets to make comparisons with the commonly used E_T30, Z, χ_R, or π^*_{azo} giving good correlations with the latter two.

Tale 3. Longest Absorption Maxima of **3b** in Various Solvents

Solvent	λ_{max}/nm	Solvent	λ_{max}/nm
Hexane	528	Ethylmethylketone	587
Cyclohexane	532	CH_2Cl_2	588
CCl_4	546	$CHCl_3$	596
Dioxane	552	DMF	600
Toluene	554	*i*-PrOH	608
Benzene	560	EtOH	610
THF	568	BuOH	612
Acetone	576	MeOH	612
Acetonitrile	578		

Experimental

All of the melting points are uncorrected. UV-visible spectra were recorded on Shimadzu UV-265F and Hitachi 210 spectrometers. IR spectra were obtained on a JASCO IRA 810 spectrophotometer. ^{1}H NMR spectra were measured on a JNM-GX 400 spectrometer; the chemical shifts are given in δ-values with respect to TMS used as an internal standard. MS spectra were taken using a JEOL JMS-DX 303 mass spectrometer.

Preparation of Alcohols (2b—d):[9] **General Method.** The reaction of an excess amount (ca. 5—15 equiv) of lithium acetylide (prepared by Midland's method[18]) with the ketones[19] in THF at −60 °C for several h gave the corresponding alcohols

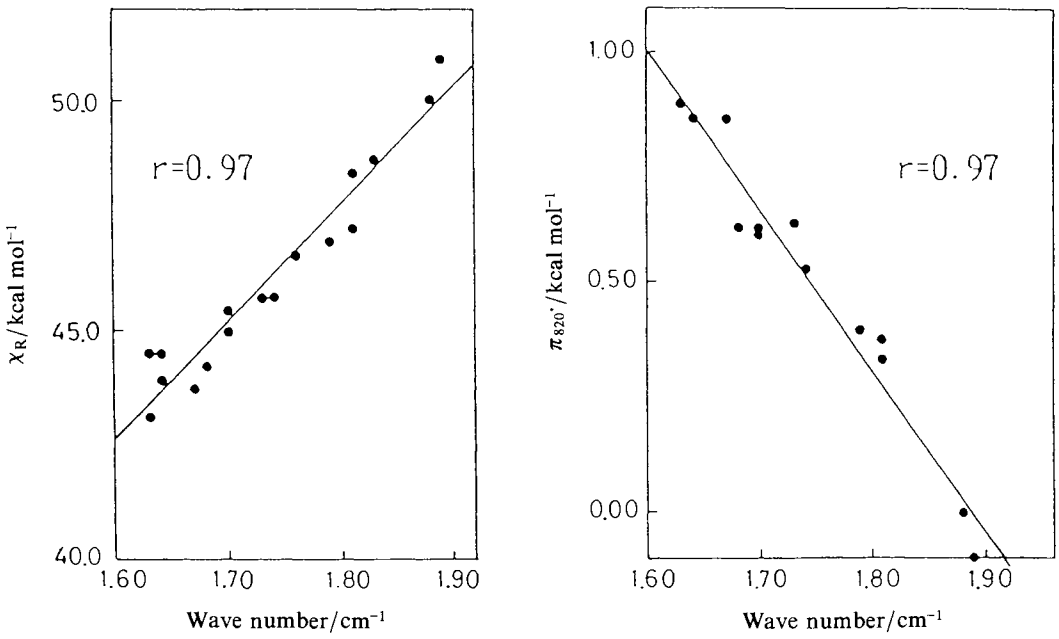

Fig. 1. Correlation diagram of the wave number of **3b** with χ_R and π_{azo}* (r: Correlation coefficienct).

after the usual work-up.

2b: Colorless crystals, 77%. Mp 230 °C. Found: C, 77.54; H, 6.95; N, 9.50%. Calcd for $C_{19}H_{20}N_2O$: C, 78.05; H, 6.90; N, 9.58%. IR (Nujol) 3260 (C≡CH), 2100 (C≡C), and 1610 cm^{-1} (C=C); FAB-MS (*m/z*) 293 (M+1); ^{1}H NMR (DMSO-d_6) δ=2.97 (6H, s, Me), 3.06 (1H, s, C≡CH), 3.19 (6H, s, Me), 5.85 (1H, s, OH), 6.57 (2H, dd, *J*=2 and 8 Hz, ArH), 7.09 (2H, d, *J*=2 Hz, ArH), and 7.33 (2H, d, *J*=8 Hz, ArH).

2c: Pale yellow crystals, 75%. Mp 98—100 °C (lit, 98—99 °C).[20] IR (Nujol) 3400 (OH), 3300 (C≡CH), 2120 (C≡C), and 1580 cm^{-1} (C=C); EI-MS (*m/z*) 238 (M$^+$); ^{1}H NMR ($CDCl_3$) δ=2.91 (1H, s, C≡CH), 2.94 (1H, s, OH), 7.23—7.55 (6H, m, ArH), and 8.00—8.17 (2H, m, ArH).

2d: Colorless crystals, 89%. Mp 211—214 °C. IR (KBr) 3400 (OH), 3280 (C≡CH), and 1600 cm^{-1} (C=C); EI-MS (*m/z*) 398 (M$^+$); ^{1}H NMR ($CDCl_3$) δ=2.45 (1H, s, C≡CH), 3.20 (1H, s, OH), and 6.72—7.33 (14H, m, ArH).

Synthesis of Merocyanine Dyes: Bis[4-(dimethylamino)-phenyl]methylene System; General Method [Indandione Derivative (3a)]. 1,3-Indandione (50 mg, 0.17 mmol) was mixed with acetylenic alcohol (**2a**) (25 mg, 0.17 mmol) in EtOH (20 ml) at ambient temperature. The resulting violet solution was then heated under reflux for 1 h. After concentrating the reaction mixture under reduced pressure, green needles, thus obtained, were filtered and dried in vacuo while affording an analytically pure sample (55 mg, 76%). Mp 182—183 °C (decomp). Found: C, 79.67; H, 6.31; N, 6.31%. Calcd for $C_{28}H_{26}N_2O_2$: C, 79.59; H, 6.20; N, 6.63%. EI-MS (*m/z*) 422 (M$^+$); ^{1}H NMR ($CDCl_3$) δ=3.06 (6H, s, Me), 3.07 (6H, s, Me), 6.65 (2H, d, *J*=9 Hz, ArH), 6.74 (2H, *J*=9 Hz, ArH), 7.15—7.89 (9H, m, ArH and olefinic H), and 8.28 (1H, d, *J*=13 Hz, olefinic H). In the same method, **4a**, **7a**, and **8a** were prepared. The preparations of **5a** and **6a** were already reported.[8]

4a: Deep red crystals, 79%. Mp 269—271 °C (decomp). Found: C, 66.51; H, 6.28; N, 13.35%. Calcd for $C_{23}H_{24}O_3N_4 \cdot 1/2H_2O$: C, 66.81; H, 6.09; N, 13.35%. IR (KBr) 3170 (NH), 1715 (C=O), 1655 (C=O), and 1595 cm^{-1} (C=C); FAB-MS (*m/z*) 405 (M+1); ^{1}H NMR (DMSO-d_6) δ=3.02 (12H, s, NMe_2), 6.76 (2H, d, *J*=10 Hz, ArH), 6.81 (2H, d, *J*=10 Hz, ArH), 7.09 (2H, d, *J*=10, ArH), 7.28 (2H, d, *J*=10 Hz, ArH), 7.83 (1H, d, *J*=14 Hz, olefinic H), 8.20 (1H, d, *J*=14 Hz, olefinic H), and 10.88 (2H, s, NH).

7a: Reddish brown crystals, 45%. Mp 277—278 °C (decomp). Found: C, 82.64; H, 6.62; N, 5.87%. Calcd for $C_{33}H_{30}N_2O \cdot 1/2H_2O$: C, 82.64; H, 6.51; N, 5.84%. IR (KBr) 1650 (C=O) and 1605 cm^{-1} (C=C); EI-MS (*m/z*) 470 (M$^+$); ^{1}H NMR ($CDCl_3$) δ=2.99 (6H, s, Me), 3.09 (6H, s, Me), 6.65 (2H, d, *J*=9 Hz, ArH), 6.81 (2H, d, *J*=9 Hz, ArH), and 6.68—8.42 (14H, m, ArH and olefinic H).

8a: Reddish-orange crystals, 80%. Mp 159—160 °C (decomp). Found: C, 76.49; H, 7.56; N, 7.40%. Calcd for $C_{24}H_{28}N_2O_2$: C, 76.56; H, 7.50; N, 7.44%. IR (KBr) 1650 (C=O) and 1605 cm^{-1} (C=C); EI-MS (*m/z*) 376 (M$^+$). ^{1}H NMR ($CDCl_3$) δ=2.19 (3H, s, Me), 2.43 (3H, s, Me), 3.00 (6H, s, Me) 3.04 (6H, s, Me), 6.61 (2H, d, *J*=9 Hz, ArH), 6.73 (2H, d, *J*=9 Hz, ArH), 6.89 (1H, d, *J*=11 Hz, olefinic H), 7.15 (2H, d, *J*=9 Hz, ArH), 7.30 (2H, d, *J*=9 Hz, ArH), and 7.37 (1H, d, *J*=11 Hz, olefinic H).

3,6-Bis(dimethylamino)fluorenylidene System: General Method [Indandione Derivative (3b)]. To a stirred solution of acetylenic alcohol (**2b**) (0.20 g, 0.68 mmol) in EtOH (40 ml) was added 1,3-indandione (0.11 g, 0.68 mmol) at ambient temperature. After stirring for 3 h, the reaction mixture was concentrated in vacuo to give crystals, which were recrystallized from dichloromethane. Compound **3b** was obtained as deep green crystals (0.24 g, 84%). Mp 240 °C. Found: C, 79.59; H, 5.89; N, 6.58%. Calcd for $C_{28}H_{24}N_2O_2$: C, 79.98; H, 5.75; N, 6.66%. IR (Nujol) 1710, 1660 (C–O), and 1600 cm^{-1} (C=C); EI-MS (*m/z*) 420 (M$^+$); ^{1}H NMR ($CDCl_3$) δ=3.10 (6H, s, Me), 3.11 (6H, s, Me), 6.40—6.60 (2H, m, ArH), 6.80—6.90 (2H, m, ArH), 7.60—8.00 (6H, m, ArH), 8.24 (1H, d, *J*=14 Hz, olefinic H), and 8.55 (1H, d, *J*=14 Hz, olefinic H). In the similar method, barbituric and thiobarbituric acid derivatives (**4b** and **5b**) were prepared.

4b: Deep bluish-violet crystals, 88%. Mp 305 °C. Found: C, 65.70; H, 5.43; N, 13.39%. Calcd for $C_{23}H_{22}N_4O_3 \cdot H_2O$: C, 65.70; H, 5.75; N, 13.33%. IR (Nujol) 1730, 1625 (C=O), and 1603 cm^{-1} (C=C); FAB-MS (*m/z*) 403 (M+1); ^{1}H NMR (DMSO-d_6) δ=3.11 (12H, s, Me), 6.59 (1H, d, *J*=9 Hz, ArH), 6.63 (1H, d, *J*=9 Hz, ArH), 7.25 (2H, d, *J*=9 Hz, ArH), 7.46 (1H, d, *J*=9 Hz, ArH), 7.73 (1H, d, *J*=9 Hz, ArH), 8.19 (1H, d, *J*=14 Hz, olefinic H), 8.84 (1H, d, *J*=14 Hz, olefinic H), 11.00 (1H, s, NH), and 11.06 (1H, s, NH).

5b: Deep blue crystals, 74%. Mp >330 °C. Found: 63.33; H, 5.35; N, 12.85%. Calcd for $C_{23}H_{22}N_4O_2 \cdot H_2O$: C, 63.28; H, 5.35; N, 12.85%. IR (Nujol) 1680, 1640 (C=O), and 1605 cm^{-1} (C=C); FAB-MS (*m/z*) 419 (M+1); ^{1}H NMR (DMSO-d_6) δ=3.14 (12H, s, Me), 6.58 (1H, d, *J*=9 Hz, ArH), 8.20 (1H, d, *J*=14 Hz, olefinic H), 8.81 (1H, d, *J*=14 Hz, olefinic H), 12.10 (1H, s, NH), and 12.17 (1H, s, NH). In the cases of malononitrile, anthrone, acetylacetone, and 3-(dicyanomethylene)-1-indanone derivatives (**6b—9b**), appropriate heating for several hours was necessary due to the low reactivities of the reactants.

6b: Deep green crystals, 78%. Mp 300—305 °C. Found: C, 77.53; H, 5.97; N, 16.38%. Calcd for $C_{22}H_{20}N_4$: C, 77.62; H, 5.92; N, 16.46%. IR (Nujol) 2210 (C≡N) and 1605 cm^{-1} (C=C); EI-MS (*m/z*) 340 (M$^+$); ^{1}H NMR ($CDCl_3$) δ=3.14 (12H, s, Me), 6.40—6.60 (2H, m, ArH), 6.83 (2H, d, *J*=2 Hz, ArH), 6.90 (1H, d, *J*=13 Hz, olefinic H), 7.49 (2H, d, *J*=8 Hz, ArH), and 8.34 (1H, d, *J*=13 Hz, olefinic H).

7b: Deep reddish-violet crystals, 35%. Mp 289—292 °C. IR (Nujol) 1660 (C=O) and 1600 cm^{-1} (C=C); FAB-MS (*m/z*) 469 (M+1); ^{1}H NMR ($CDCl_3$) δ=3.09 (6H, s, Me), 3.15 (6H, s, Me), 6.50—7.10 (4H, m, ArH and olefinic H), 7.35—7.70 (6H, m, ArH and olefinic H), and 7.90—8.45 (6H, m, ArH and olefinic H).

8b: Brown crystals, 28%. Mp 210 °C. Found: C, 76.72; H, 6.68; N, 8.01%. Calcd for $C_{24}H_{26}N_2O_2$: C, 76.98; H, 7.00; N, 7.48%. EI-MS (*m/z*) 374 (M$^+$); IR (Nujol) 1640 (C=O) and 1610 cm^{-1} (C=C); ^{1}H NMR ($CDCl_3$) δ=2.48 (6H, s, Me), 3.10 (6H, s, Me), 3.12 (6H, s, Me), 6.50—6.65 (2H, m, ArH), 6.85—7.10 (3H, m, ArH and olefinic H), 7.40—7.80 (2H, m, ArH), and 8.29 (1H, d, *J*=13 Hz, olefinic H).

9b: Deep green crystals, 84%. Mp 274—278 °C. IR (Nujol) 2230 (C=N), 1700 (C=O), and 1600 cm^{-1} (C=C); EI-MS (*m/z*) 468 (M$^+$); ^{1}H NMR (DMSO-d_6) δ=3.46 (12H, s, NMe_2), 6.49 (2H, dd, *J*=2, 9 Hz, ArH), 7.16 (2H, d, *J*=9 Hz, ArH), 7.68—7.82 (5H, m, ArH), 8.45—8.55 (2H, m, ArH and olefinic H), and 8.97 (1H, d, *J*=14 Hz, olefinic H).

Thioxanthenylidene System: General Method [Indandione Derivative (3c)]. 1,3-Indandione (0.12 g, 0.84 mmol) was added to a stirred solution of acetylenic alcohol (**2c**) (0.20 g, 0.84 mmol) in EtOH. After stirring for 30 min, the reaction

mixture was heated under reflux for 3 h and then evaporated under reduced pressure to give deep reddish-violet crystals, which after recrystallization from dichloromethane yielded 0.13 g (43%). Mp 232 °C. IR (Nujol) 1720, 1690 (C=O), and 1600 cm^{-1} (C=C); EI-MS (*m/z*) 366 (M^+); ^1H NMR ($CDCl_3$) δ=7.37—8.00 (13H, m, ArH and olefinic H) and 8.33 (1H, d, *J*=12 Hz, olefinic H).

4c: Reddish-violet crystals, 38%. Mp 328—329 °C. Found: C, 64.72; H, 3.59; N, 7.85%. Calcd for $C_{19}H_{12}N_2O_3 \cdot 0.3H_2O$: C, 64.51; H, 3.59; N, 7.92%. IR (Nujol) 1640 (C=O) and 1560 cm^{-1} (C=C); FAB-MS (*m/z*) 349 (M+1); ^1H NMR (DMSO-d_6) δ=7.45—7.88 (8H, m, ArH), 8.02 (1H, d, *J*=12 Hz, olefinic H), 8.30 (1H, d, *J*=12 Hz, olefinic H), and 11.15 (2H, s, NH).

5c: Brown crystals, 85%. Mp >300 °C. Found: C, 61.95; H, 3.34; N, 7.20%. Calcd for $C_{19}H_{12}N_2O_2S_2 \cdot 0.2H_2O$: C, 62.01; H, 3.40; N, 7.61%. IR (Nujol) 1640 (C=O) and 1560 cm^{-1} (C=C); FAB-MS (*m/z*) 365 (M+1); ^1H NMR (DMSO-d_6) δ=6.98—7.63 (8H, m, ArH), 8.03 (1H, d, *J*=12 Hz, olefinic H), 8.33 (1H, d, *J*=12 Hz, olefinic H), and 12.25 (2H, m, NH).

6c: Brown crystals, 92%. Mp 290 °C. Found: C, 75.01; H, 3.83; N, 9.34%. Calcd for $C_{18}H_{10}N_2S$: C, 75.49; H, 3.52; N, 9.79%. IR (Nujol) 2240 (C≡N) and 1580 cm^{-1} (C=C); EI-MS (*m/z*) 286 (M^+); ^1H NMR ($CDCl_3$) δ=6.70 (1H, d, *J*=14 Hz, olefinic H), 7.26—7.57 (8H, m, ArH), and 7.81 (1H, d, *J*=14 Hz, olefinic H). Other derivatives, such as anthrone or acetylacetone, could not be prepared, even upon changing the reaction conditions: i.e., raising the reaction temperature by using alcohols with higher boiling points or prolonging the reaction time.

10-(9-Xanthenylidene)-9(10*H*)-anthrylidene System; General Method [Indandione Derivative (3d)]: 1,3-Indandione (37 mg, 0.25 mmol) was added to acetylenic alcohol (**2d**) (0.10 g, 0.25 mmol) in EtOH and the reaction mixture was heated under reflux for 24 h. Reddish-violet crystals were obtained after evaporating the solvent, adding ether, and recrystallizing the resulting crystals (42 mg, 32%). Mp >340 °C. IR (Nujol) 1630 (C=O) and 1590 cm^{-1} (C=C); FAB-MS (*m/z*) 526 (M+1); ^1H NMR ($CDCl_3$) δ=6.64 (2H, d, *J*=9 Hz, ArH), 7.26—7.79 (15H, m, ArH and olefinic H), and 8.70—8.92 (6H, m, ArH and olefinic H).

4d: Violet crystals, 35%. Mp >340 °C. Found: C, 74.40; H, 4.13; N, 5.00%. Calcd for $C_{33}H_{20}N_2O_4 \cdot 1.3H_2O$: C, 74.51; H, 4.28; N, 5.27%. IR (KBr) 1710, 1620 (C=O), and 1595 cm^{-1} (C=C); FAB-MS (*m/z*) 509 (M+1); ^1H NMR (DMSO-d_6) δ=6.69 (2H, d, *J*=9 Hz, ArH), 7.35—7.94 (12H, m, ArH and olefinic H), 8.66 (2H, d, *J*=9 Hz, ArH), 8.75 (1H, dd, *J*=2 and 9 Hz, ArH), 9.16 (1H, d, *J*=2 Hz, ArH), 10.44 (1H, s, NH), and 11.00 (1H, s, NH).

5d: Reddish-violet crystals, 57%. Mp >340 °C. Found: C, 72.49; H, 3.86; N, 4.97%. Calcd for $C_{33}H_{20}N_2O_3S \cdot 1.3H_2O$: C, 72.49; H, 4.16; N, 5.11%. IR (KBr) 1630 (C=O) and 1595 cm^{-1} (C=C); FAB-MS (*m/z*) 524 (M+1); ^1H NMR (DMSO-d_6) δ=6.77—7.00 (2H, m, ArH), 7.29—8.04 (12H, m, ArH and olefinic H), 8.66 (2H, d, *J*=9 Hz, ArH), 8.84 (1H, dd, *J*=2 and 9 Hz, ArH), 9.25 (1H, s, ArH), and 11.54 (2H, s, NH). Other derivatives such as malononitrile, anthrone, or acetylacetone derivatives could not be isolated.

We thank Professors (Emeritus) Masazumi Nakagawa of Osaka University, Masahiko Iyoda of Tokyo Metropolitan University, and Teijiro Kitao of University of Osaka Prefecture for helpful discussions. Financial support by Grants-in-Aid for Scientific Research Nos. 62470035 and 63540406 from the Ministry of Education, Culture and Science is gratefully acknowledged.

References

1) A portion of this work has been published as a preliminary communication: S. Nakatsuji, T. Yashiro, K. Nakashima, S. Akiyama, and H. Nakazumi, *Chem. Express,* **4**, 601 (1989). For part 9 in the series Ethynologues of Triphenylmethane Dyes, see S. Nakatsuji, H. Nakazumi, H. Fukuma, T. Yahiro, M. Iyoda, and S. Akiyama, *J. Chem. Soc., Chem. Commun.,* **1990**, 489.

2) Cf. H. Meier, "Spectral Sensitization," Focal, London (1968); T. H. James, "The Theory of Photographic Process," 4th ed, Macmillan, New York (1977); J. Simon and J. -J. Andre, "Molecular Semiconductors," Springer-Verlag, Berlin (1985).

3) D. L. Morel, *Appl. Phys. Lett.,* **32**, 495 (1978); *idem., Mol. Cryst. Liq. Cryst.,* **50**, 127 (1978); G. A. Chamberlain, P. J. Cooney, and S. Dennison, *Nature,* **289**, 45 (1981); K. Iriyama, M. Yoshiura, Y. Ozaki, T. Ishii, and S. Yasui, *Thin Solid Films,* **132**, 229 (1985), and references cited therein.

4) T. B. Tang, K. Seki, H. Inokuchi, Y. Kohno, and T. Tani, *J. Appl. Phys.,* **59**, 5 (1986); K. Tamagake, Y. Kohno, Y. Shiota, and Y. Fujita, *Nippon Kagaku Kaishi,* **1984**, 82; H. Funakoshi, K. Tamagaki, and Y. Fujita, *ibid.,* **1989**, 56, 706.

5) L. B. Cohen, B. M. Salzberg, H. V. Davila, W. N. Ross, D. Landowne, A. S. Waggoner, and C. H. Wong, *J. Membr. Biol.,* **19**, 1 (1974); P. R. Dragsten and W. W. Webb, *Biochemistry,* **17**, 5228 (1978); J. T. Russell, T. Beeler, and A. Martonosi, *J. Biol. Chem.,* **254**, 2047 (1979); L. M. Loew, *J. Biochem. Biophys. Methods,* **6**, 243 (1982); K. S. Schanze, D. M. Schin, and D. G. Whitten, *J. Am. Chem. Soc.,* **107**, 507 (1985).

6) Cf., D. J. Williams, *Angew. Chem.,* **96**, 637 (1984); *Angew. Chem., Int. Ed. Engl.,* **23**, 690 (1984); D. S. Chamla and J. Zyss, "Nonlinear Optical Properties of Organic Molecules and Crystals," Academic Press, New York (1987); M. Blanchard-Desce, I. Ledoux, J. M. Lehn, J. Malthete, and J. Zyss, *J. Chem. Soc., Chem. Commun.,* **1988**, 736; A. Samala-Schwok, M. Blanchard-Desce, and J. M. Lehn, *J. Phys. Chem.,* **94**, 3894 (1990).

7) S. Akiyama, S. Nakatsuji, K. Nakashima, M. Watanabe, and H. Nakazumi, *J. Chem. Soc., Perkin Trans. 1,* **1988**, 3155, and references cited therein.

8) S. Nakatsuji, K. Nakashima, M. Iyoda, and S. Akiyama, *Bull. Chem. Soc. Jpn.,* **61**, 2253; (1988); S. Nakatsuji, T. Yahiro, K. Nakashima, and S. Akiyama, in "Chemistry of Functional Dyes," ed by Z. Yoshida and T. Kitao, Mita Press, Tokyo (1989), p. 63.

9) The synthesis of **2a** was already reported in Ref. 8.

10) Cf. F. Theron, M. Verny, and R. Vessiere, "Chemistry of Carbon-Carbon Triple Bond," ed by S. Patai, John Wiley & Sons, New York (1978), Part 1, Chap. 10.

11) The details of the procedure of PPP-MO calculations are described in Ref. 7.

12) J. Griffiths, *Dyes Pigm.,* **3**, 211 (1982).

13) Cf. J. Fabian and H. Hartmann, "Light Absorption of Organic Colorants," Springer-Verlag, Berlin (1980), p. 157.

14) K. Dimroth, C. Reichardt, T. Siepmann, and F. Bohlmann, *Ann. Chem.,* **661**, 1 (1963).

15) E. M. Kosower, *J. Am. Chem. Soc.*, **80**, 3253 (1958).
16) L. G. S. Brooker, A. C. Craig, D. W. Heseltine, P. W. Jenkins, and L. L. Lincoln, *J. Am. Chem. Soc.*, **87**, 2443 (1965).
17) E. Buncel and S. Rajagopal, *J. Org. Chem.*, **54**, 798 (1989).
18) M. M. Midland, *J. Org. Chem.*, **40**, 2250 (1975).
19) 3,6-Bis(dimethylamino)fluorenone was prepared by Barkers' method (A. Barker and C. C. Barker, *J. Chem. Soc.*, **1954**, 870). We are grateful to Profs. Y. Abe and T. Misono, Department of Industrial Chemistry, Faculty of Science and Technology, Tokyo University of Science, for informing us experimental details on the modified Barkers' method. 10-(9-Xanthenylidene)anthrone was prepared by Schönberg's method, A. Schönberg, A. F. A. Ismil, and W. Asker, *J. Chem. Soc.*, **1946**, 442.
20) K. Nakasuji, K. Takatoh, M. Nakatsuka, and I. Murata, *J. Chem. Soc., Chem. Commun.*, **1981**, 717.

Syntheses of Titanium Butoxide Tris(polyfluoroalkanoate) and Surface Modification of Calcium Carbonate

Norio YOSHINO,* Yukihide SHIRAISHI, and Hidefumi HIRAI
Department of Industrial Chemistry, Faculty of Engineering, Science University of Tokyo, Kagurazaka, Shinjuku-ku, Tokyo 162
(Received January 29, 1991)

Titanium butoxide tris(5*H*-octafluoropentanoate), $Ti(O^nC_4H_9)[OCO(CF_2)_4H]_3$, titanium butoxide tris(7*H*-undecafluoroheptanoate), $Ti(O^nC_4H_9)[OCO(CF_2)_6H]_3$, titanium butoxide tris(9*H*-hexadecafluorononanoate), $Ti(O^nC_4H_9)[OCO(CF_2)_8H]_3$, and titanium butoxide tris(perfluorooctanoate), $Ti(O^nC_4H_9)[OCO(CF_2)_6CF_3]_3$, were prepared by the reaction of titanium butoxide trichloride with sodium fluoro-substituted acylates in 1,1,2-trichloro-1,2,2-trifluoroethane. These compounds were characterized on the basis of elemental analysis as well as their IR, ^1H NMR, ^{13}C NMR, and ^{19}F NMR spectra. In the compounds produced, a Ti–OCO bond was stable in water, although a Ti–OR bond was only moderately stable in water. A surface modification against calcium carbonate was attempted by using these products. From measurements of the contact angles $\theta(°)$ of water and toluene against a modified calcium carbonate surface, titanium butoxide tris(perfluorooctanoate) was found to be an effective substance for a new-type coupling agent, which increases the affinity between organofluoro polymers and some inorganic substances.

Metal alkoxides have been the subject of extensive research owing to their potential as precursor materials for several applications, such as new-ceramics, adhesives, and coupling agents, which are molecular bridges between the interface of an inorganic filler and an organic polymer. Many alkyl or aryl titanates and their halogenated derivatives were prepared[1] and the reactivities of these titanates towards various types of electron donors (such as amides, amines, ethers, and amino acids) have been reported.[2] The number of worldwide commercial applications for coupling agents established using monoalkoxyl-type titanates, such as titanium isopropoxide tris(2-heptylundecanoate), are now very substantial, as indicated by over one hundred patents.[3-6]

In recent years, dramatic developments have been made in the utilization of organofluoro compounds, resulting in materials with high performance. However, only a few research reports concerning fluoro-substituted alkoxides of metals have appeared in the literature.[7-11] In a previous paper we reported on the syntheses of fluoroalkyl and fluoroaryl titanates[12] as well as the syntheses of fluoroalkyl silicates.[13] Although these alkoxides were expected to be stable against moisture, since many of the compounds having the fluorinated carbon structure possess water repellency, all of the products were very sensitive to water and easy to decompose.

In this paper, the results of the syntheses and characterizations of new titanium compounds having both three fluoro-substituted alkanoyloxyl groups and one butoxyl group are reported. The application for the surface modification against calcium carbonate will be also reported.

Experimental

Special precautions were adopted in order to avoid any hydrolysis of the starting materials and products; all experiments were carried out under an atmosphere of purified nitrogen to preclude oxygen and moisture.

Materials. Titanium tetrachloride (bp 136 °C) and titanium tetrabutoxide (bp 184—185 °C/665 Pa) were commercially available and purified by distillation. Titanium butoxide trichloride (bp 94—96 °C/80 Pa) was synthesized by the method of Jennings;[16] Found: Ti, 20.1; Cl, 46.9%. Calcd for $C_4H_9Cl_3OTi$: Ti, 20.1; Cl, 46.8%. ^1H NMR (in THF-d_8, TMS standard) δ=0.92 (CH_3, t(triplet), J=6.0 Hz), 1.10—1.90 (CH_2–CH_2, m(multiplet)), 4.96 (OCH_2, t, J=6.0 Hz). 5*H*-octafluoropentanoic acid (bp 40—42 °C/120 Pa), 7*H*-undecafluoroheptanoic acid (bp 60—61 °C/100 Pa), 9*H*-hexadecafluorononanoic acid (bp 92—93 °C/53 Pa), and perfluorooctanoic acid (bp 89—90 °C/4000 Pa) were obtained from PCR Inc and purified by distillation. Sodium acylate derivatives were synthesized by the reaction of fluoro-substituted acids with excess sodium hydrogencarbonate in THF. The solvents used were purified by the usual methods. Calcium carbonate powder (specific gravity; 2.60, average particle size; 3.0×10^{-6} m, specific surface area (BET); 5.5 $m^2 g^{-1}$) was obtained from Shiraishi Industries, Ltd.

Measurements. FT-IR spectra were measured in a liquid film or by a KBr method with a JEOL JIR 5300 spectrophotometer. Pulsed Fourier Transform 100-MHz, ^1H and 25-MHz ^{13}C NMR were run in THF-d_8 with TMS as an internal standard using a JEOL JNR-PX-100 spectrometer at room temperature: ^1H NMR spectra (pulse repetition time, 5s; number of accumulations, 20) and ^{13}C NMR spectra (pulse repetition time, 2.0s; number of accumulations, 40000). The FT mode 90-MHz ^{19}F NMR was recorded at 27 °C on a JEOL JNM-FX-90Q in THF with fluorobenzene (−113.6 ppm[14] from $CFCl_3$ in $CDCl_3$) as an external standard: pulse repetition time, 0.5s; number of accumulations, 20. The assignments of the ^{19}F NMR spectra were referred to in the data book.[14] Gas chromatograms were performed with a Hitachi 063 (PEG-6000 supported Chromosorb A NAW 30/60 mesh 5 m packed column, TCD) or Hitachi G-3000 gas chromatograph (OV-1 25 m Fused capillary column, FID) and these intensities were measured with a Hitachi 834 chromato processor or a Hitachi D-2500 chromato integrator. The contact angles $\theta(°)$ were measured at 23 °C with a ELMA-Kougaku Co. Gonio-type apparatus. Ultrasonic operations were carried out using a Branson Ultrasonics Corporation Model 250 Sonifier Cell

Disruptor System (200 W, 20 kHz).

Analytical Methods. Titanium was determined gravimetrically as titanium oxide after the hydrolysis of titanium compounds by adding aqueous ammonia and burned in a quartz crucible. Chlorine was quantified by the Mohr method. Butoxyl group was measured quantitatively as 1-butanol by GLC after hydrolysis of the products by adding a sodium hydroxide solution. The contents of the fluorinated alkanoyloxyl group having hydrogen at the end of the chain were estimated indirectly from the intensities against oxymethylene protons in the butoxyl group by ^{1}H NMR spectra.

Synthesis of Titanium Butoxide Tris(polyfluoroalkanoate). Synthesis of Titanium Butoxide Tris(5*H*-octafluoropentanoate), Ti(O^{n}C$_4$H$_9$)[OCO(CF$_2$)$_4$H]$_3$: To a stirred solution of titanium butoxide trichloride, 2.00 g (8.75 mmol) in 110 ml 1,1,2-trichloro-1,2,2-trifluoroethane, sodium 5*H*-octafluoropentanoate 8.48 g (31.6 mmol) was added at room temperature into a two-necked 200-ml flask connected to a reflux condenser and a three-way stop cock. The heterogeneous mixture was refluxed with stirring for 10 h. Completion of the reaction was checked by adding a silver nitrate solution to a portion of the clear upper solution. Sodium chloride produced and excess sodium 5*H*-octafluoropentanoate were removed by filtration. A transparent slightly brown liquid was obtained after removing the solvent under reduced pressure (yield 5.25 g, 69.8%): IR 2970, 2943, 2883, 1772, 1716, 1684, 1653, 1443, 1400, 1362, 1333, 1275, 1227, 1170, 1130, 1080, 1051, 955, 926, 906, 802, 750, 708, 660, 582, 538, 536, 459 cm^{-1}; ^{1}H NMR δ=0.90(CH$_3$, t, J=8.1 Hz), 1.18—1.84 (CH$_2$, m), 4.30 (OCH$_2$, t, J=6.9 Hz), 6.39 (HCF$_2$, t(t) (triplet(triplet)), J=51.4(5.7) Hz); ^{13}C NMR δ=11.7 (f, s(singlet)), 17.7(g, s), 29.2(h, s), 67.2(i, s), 107.3(a, t(t), J=252.8(30.8) Hz), 107.4(b, t(m), J=255.1 Hz), 108.6(c, t(m)(triplet(multiplet)), J=260.8 Hz), 109.6(d, t(t), J=266.7(31.5) Hz), 157.3(e, t, J=24.9 Hz) for (HC^{a}F$_2$C^{b}F$_2$C^{c}F$_2$C^{d}F$_2$C^{e}OO)$_3$Ti(OC^{f}H$_2$C^{g}H$_2$C^{h}H$_2$C^{i}H$_3$); ^{19}F NMR δ=−25.9(a, d(doublet), J=51.3 Hz), −17.9(b, s), −12.4(c, m), −6.7(d, m, J=11.0 Hz) for (HCF$_2^a$CF$_2^b$CF$_2^c$CF$_2^d$COO)$_3$Ti(O^{n}C$_4$H$_9$). Found: Ti, 5.71; C$_4$H$_9$O, 8.48; H(CF$_2$)$_4$COO, 85.7%. Calcd for C$_{19}$H$_{12}$F$_{24}$O$_7$Ti: Ti, 5.59; C$_4$H$_9$O, 8.54; H(CF$_2$)$_4$COO, 85.9%.

Synthesis of Titanium Butoxide Tris(7*H*-dodecafluoroheptanoate), Ti(O^{n}C$_4$H$_9$)[OCO(CF$_2$)$_6$H]$_3$: The synthesis was carried out in a similar manner to that of titanium butoxide tris(5*H*-octafluoropentanoate). It took about 80 h for the reaction to come to completion. From a reaction of titanium butoxide trichloride 1.20 g (5.28 mmol) and sodium 7*H*-dodecafluoroheptanoate 6.80 g (18.5 mmol) as starting materials, slightly brown liquid product was obtained (4.51 g, yield 74.0%): IR 2972, 2945, 2883, 1772, 1718, 1669, 1558, 1506, 1446, 1402, 1363, 1323, 1203, 1142, 1082, 1061, 970, 926, 862, 837, 795, 766, 725, 671, 602, 565, 538, 509 cm^{-1}; ^{1}H NMR δ=0.95(CH$_3$, t, J=8.6 Hz), 1.20—1.88(CH$_2$, m), 4.38(OCH$_2$, t, J=6.7 Hz), 6.56(HCF$_2$, t(t), J=51.4(5.7) Hz); ^{13}C NMR δ=13.8(h, s), 19.7(i, s), 31.2(j, s), 69.4(k, s), 109.3(a, t(t), J=253.5(30.8) Hz), 111.5(b, t(m), J=249.1 Hz), 112.0(c, t(m), J=252.0 Hz), 112.6(d, t(m), J=255.0 Hz), 113.3(e, t(m), J=249.8 Hz), 113.6(f, t(m), J=260.8 Hz), 159.1(g, t, J=28.4 Hz) for (HC^{a}F$_2$C^{b}F$_2$C^{c}F$_2$C^{d}F$_2$C^{e}F$_2$C^{f}F$_2$C^{g}OO)$_3$Ti(OC^{h}H$_2$C^{i}H$_2$C^{j}H$_2$C^{k}H$_3$); ^{19}F NMR δ=−26.3(a, d, J=51.3 Hz), −17.4 (b, s), −11.1 (c and d, m), −9.6 (e, m), −6.3(f, m) for (HCF$_2^a$CF$_2^b$CF$_2^c$CF$_2^d$CF$_2^e$CF$_2^f$COO)$_3$Ti(O^{n}C$_4$H$_9$). Found: Ti, 4.08; C$_4$H$_9$O, 6.45; H(CF$_2$)$_6$COO, 89.6%. Calcd for C$_{25}$H$_{12}$F$_{36}$O$_7$Ti: Ti, 4.14; C$_4$H$_9$O, 6.32; H(CF$_2$)$_6$COO, 89.5%.

Synthesis of Titanium Butoxide Tris(9*H*-hexadecafluorononanoate), Ti(O^{n}C$_4$H$_9$)[OCO(CF$_2$)$_8$H]$_3$: The solution of titanium butoxide trichloride (8.93 g, 29.5 mmol) in 170 ml 1,1,2-trichloro-1,2,2-trifluoroethane was added to a stirred dispersion of sodium 9*H*-hexadecafluorononanoate (64.6 g, 138 mmol) in 80 ml of 1,1,2-trichloro-1,2,2-trifluoroethane. After refluxing the dispersion with stirring for 200 h, the upper clear solution was checked with silver nitrate as well as the synthesis of titanium butoxide tris(5*H*-octafluoropentanoate), and the precipitate was then removed by filtration and the solvent was removed by evaporation under vacuum. Slightly brown liquid product was obtained (4.51 g, yield 74.0%): IR 2972, 2945, 2883, 1772, 1734, 1668, 1653, 1616, 1558, 1506, 1450, 1446, 1402, 1363, 1338, 1211, 1147, 1084, 999, 860, 804, 768, 731, 698, 661, 538, 507 cm^{-1}; ^{1}H NMR δ=0.87 (CH$_3$, t, J=7.2 Hz), 1.05—1.88 (CH$_2$, m), 4.03 (OCH$_2$, t, J=6.6 Hz), 6.44 (HCF$_2$, t(t), J=51.2(5.3) Hz); ^{13}C NMR δ=12.9(j, s), 19.0(k, s), 30.4(l, s), 69.0(m, s), 108.6(a, t(t), J=253.5(30.8)Hz), 97.2—125.0(b—h, No detectable), 158.0(i, t, J=29.3 Hz) for (HC^{a}F$_2$-C^{b}F$_2$C^{c}F$_2$C^{d}F$_2$C^{e}F$_2$C^{f}F$_2$C^{g}F$_2$C^{h}F$_2$C^{i}OO)$_3$Ti(OC^{j}H$_2$C^{k}H$_2$C^{l}H$_2$C^{m}H$_3$); ^{19}F NMR δ=−25.7 (a, d(m), J=51.3 Hz), −17.0(b, m), −10.7(c, m), −10.0(d, m), −9.2(e, f and g, m), −5.5(h, m) for (HCF$_2^a$CF$_2^b$-CF$_2^c$CF$_2^d$CF$_2^e$CF$_2^f$CF$_2^g$CF$_2^h$COO)$_3$Ti(O^{n}C$_4$H$_9$). Found: Ti, 3.24; C$_4$H$_9$O, 5.13; H(CF$_2$)$_8$COO, 91.5%. Calcd for C$_{31}$H$_{12}$F$_{48}$O$_7$Ti: Ti, 3.29; C$_4$H$_9$O, 5.02; H(CF$_2$)$_8$COO, 91.7%.

Synthesis of Titanium Butoxide Tris(perfluorooctanoate), Ti(O^{n}C$_4$H$_9$)[OCO(CF$_2$)$_6$CF$_3$]$_3$: This procedure and purification technique were almost the same as those for the preparation of titanium butoxide tris(5*H*-octafluoropentanoate). From the reaction (100 h) of titanium butoxide trichloride 2.15 g (9.45 mmol) and sodium perfluorooctanoate 14.90 g (34.2 mmol) as starting materials, slightly brown liquid product was obtained (7.65 g, yield 59.7%): IR 2972, 2945, 2883, 1784, 1716, 1653, 1558, 1506, 1446, 1394, 1363, 1240, 1209, 1149, 1088, 1018, 985, 922, 889, 804, 802, 800, 746, 737, 721, 700, 665, 642, 561, 530 cm^{-1}; ^{1}H NMR δ=0.88 (CH$_3$, t, J=7.9 Hz), 1.10—1.82 (CH$_2$, m), 4.32 (OCH$_2$, t, J=7.0 Hz); ^{13}C NMR δ=13.6 (i, s), 19.7(j, s), 31.1(k, s), 69.4(l, s), 110.7(b, t(m), J=266.1 Hz), 112.0(c, t(m), J=253.9 Hz), 112.1(d, t(m), J=252.7 Hz), 113.4(e, t(m), J=260.0 Hz), 113.6(f, t(m), J=256.9 Hz), 114.9(g, t(m), J=255.7 Hz), 118.4(a, q(t), J=288.0(32.9) Hz), 158.9(h, t, J=28.7 Hz) for (C^{a}F$_3$C^{b}F$_2$C^{c}F$_2$C^{d}F$_2$C^{e}F$_2$C^{f}F$_2$C^{g}F$_2$C^{h}OO)$_3$-Ti(OC^{i}H$_2$C^{j}H$_2$C^{k}H$_2$C^{l}H$_3$); ^{19}F NMR δ=−14.1(b, s), −10.4(c and d, m), −9.7(e and f, m), −6.4(g, m), 30.8(a, m) for (CF$_3^a$CF$_2^b$CF$_2^c$CF$_2^d$CF$_2^e$CF$_2^f$CF$_2^g$COO)$_3$Ti(O^{n}C$_4$H$_9$). Found: Ti, 3.65; C$_4$H$_9$O, 5.33%. Calcd for C$_{28}$H$_9$F$_{45}$O$_7$Ti: Ti, 3.52; C$_4$H$_9$O, 5.38%.

Surface Modification of Calcium Carbonate. In a 50 ml vial, 0.10—0.35 g titanium butoxide tris(7*H*-dodecafluoroheptanoate) was added to the dispersion of calcium carbonate (1.00 g) in 30 ml THF; the heterogeneous mixture was irradiated by ultrasonic waves (200 W, 20 kHz) for 30 min. A surface-modified calcium carbonate powder was obtained after filtration of the mixture through a sintered glass disk; it was then thoroughly washed with THF and dried under reduced pressure. The surface wettabilities of modified calcium carbonate were evaluated by contact angles θ(°) against water and toluene, which were measured by the tablet method. The tablet used to measure the contact angles θ(°) was prepared as follows. Pressed cellulose disks were preliminary made by pressing 40 mg cellulose powder in a die for IR tablets at 200 kg cm^{-2} for 10 min; 0.15 g of surface modified calcium

carbonate was then placed on it. Surface-flattened tablets of the calcium carbonate were obtained by again pressing at 200 kg cm^{-2} for 15 min in the die. The contact angles $\theta(°)$ were measured using 1.0×10^{-6} dm^{-3} of water or toluene drops. The contact angles $\theta(°)$ were evaluated by extrapolating to time zero from a plot of the advancing contact angle $\theta(°)$ vs. time.[15]

Results and Discussion

The reaction of the synthesis of titanium butoxide tris(polyfluoroalkanoate) was heterogeneous in every case; it took long time to complete the reaction, especially in the case where the sodium fluoro-substituted acylate had a longer chain. Although the fluoro-substituted alkoxides of titanium were sensitive to moisture,[12] the prepared titanium butoxide tris(polyfluoroalkanoate)s were insensitive to water, except for the Ti–OC_4H_9 bond. These obtained titanium compounds were seemingly unchanged in excess water upon standing for one month at room temperature and held in an oily state at the bottom of a flask. The ^1H NMR spectrum of the oily state product showed that the intensity ratio of the alkanoyloxyl groups to the alkoxyl group were 3.0:0.8. This result shows that the Ti–OCO bond is stable and that the Ti–OC_4H_9 bond is moderately stable under these conditions. These stabilities against hydrolysis is caused by a steric hindrance of the three fluoro-substituted alkanoyloxyl groups, which exhibit the nature of water repellency.

Figure 1 shows a variation of the contact angles $\theta(°)$ of water against the wt% of titanium butoxide tris(7*H*-dodecafluoroheptanoate) vs. calcium carbonate used for the surface modification of calcium carbonate. From the results given in Fig. 1, the concentration used in the modification was found to be sufficient at 35 wt% titanium compounds against calcium carbonate; the authors thus used this concentration in all of the other runs. The results of the measurements of the contact angles $\theta(°)$ of water and toluene for the modified calcium carbonate by using the synthesized titanium butoxide tris(polyfluoroalkanoate)s are given in Table 1. These results show that the abilities of water and oil repellency of the surface-modified calcium carbonate were affected by the length of the fluorocarbon chains forming the titanium compounds. Also, the ability was more effective for fluorocarbon chains having a CF_3 group at the end of the chain in titanium compounds.

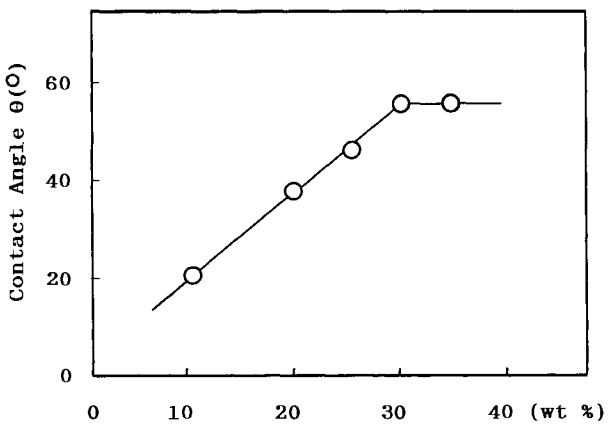

Fig. 1. Relation between contact angles $\theta(°)$ of water against the surface modified calcium carbonate and amount (wt%) of titanium butoxide tris(7*H*-dodecafluoroheptanoate) vs. $CaCO_3$.

Table 1. Extrapolated Contact Angles $\theta(°)$ of the Surface Modified Calcium Carbonate against Water and Toluene

Titanium butoxide tris(polyfluoroalkanoate)	Contact angle $\theta(°)$	
	Water	Toluene
Untreated	0[a]	0[a]
$Ti(O^nC_4H_9)[OCO(CF_2)_4H]_3$	44	14
$Ti(O^nC_4H_9)[OCO(CF_2)_6H]_3$	56	23
$Ti(O^nC_4H_9)[OCO(CF_2)_8H]_3$	65	32
$Ti(O^nC_4H_9)[OCO(CF_2)_6CF_3]_3$	88	74

a) Untreated calcium carbonate absorbed water and toluene drops too rapidly to measure the contact angles, then both of the contact angles were described 0°.

The authors are grateful to Mr. Noboru Komine and Mr. Shin-ichi Tominaga for their assistance in carrying out part of the present experiment.

The present work was partially supported by a Grant-in-Aid for Scientific Research No. 62550618 from the Ministry of Education, Science and Culture, to which the authors are also grateful.

References

1) a) D. C. Bradley, D. C. Hancock, and W. Wardlaw, *J. Chem. Soc.*, **1952**, 2773: b) D. C. Bradley, F. M. El-Halim, R. C. Mehrotra, and W. Wardlaw, *J. Chem. Soc.*, **1952**, 4609: c) J. S. Jennings, W. Wardlaw, and W. J. Way, *J. Chem. Soc.*, **1936**, 637.

2) a) N. Yoshino and T. Yoshino, *Kogyo Kagaku Zasshi*, **71**, 1025 (1968); **73**, 1161 (1970); **74**, 1673 (1971): b) N. Yoshino, K. Dohya, and T. Yoshino, *Kogyo Kagaku Zasshi*, **74**, 2138 (1971): c) N. Yoshino and T. Yoshino, *Bull. Chem. Soc. Jpn.*, **45**, 3172 (1972); **46**, 2899 (1973).

3) Jpn. Kokai Tokkyo Koho JP 59-99616 [84-99616].

4) Jpn. Kokai Tokkyo Koho JP 59-93741 [84-93741].

5) S. J. Monte and G. Surgerman, *Mod. Plast.*, **61(5)**, 74 (1984).

6) S. J. Monte and G. Surgerman, *Rubber World*, **190(1)**, 20 (1984); **190 (1)**, 24 (1984).

7) D. C. Bradley, M. E. Redwood, and C. J. Willis, *Proc. Chem. Soc.*, **1964**, 416.

8) M. E. Redwood and C. J. Willis, *Can. J. Chem.*, **43**, 1893 (1965).

9) P. N. Kapoor and R. C. Mehrotra, *Chem. Ind.*, **1966**, 1034.

10) P. N. Kapoor, R. N. Kapoor, and R. C. Mehrotra, *Chem. Ind.*, **1968**, 1314.

11) K. S. Mazdiyasni, B. J. Schaper, and L. M. Brown, *Inorg. Chem.*, **10**, 889 (1971).

12) N. Yoshino, J. Tomita, and H. Hirai, *Bull. Chem. Soc. Jpn.*, **62**, 2208 (1989).
13) N. Yoshino, H. Terajima, and H. Hirai, *Synth. React. Inorg. Met. -Org. Chem.*, **20(6)**, 729 (1990).
14) K. Kushida and A. Watanabe, "Proton and Fluorine Nuclear Magnetic Resonance Spectral Data 1988 Edition," ed by Varian Instruments Ltd., Tokyo, Japan and Japan Halon Co., Ltd., Tokyo, Japan.
15) J. Kimura, T. Itoh, and M. Koishi, *Shikizai*, **50**, 431 (1977).

Thermal and Electrooptical Properties of Ferroelectric Liquid Crystals Having OH Groups

Kazuo SUGIYAMA,* Koichi KATO, and Kohei SHIRAISHI
Department of Industrial Chemistry, Faculty of Engineering, Kinki University, Hirokoshinkai, Kure, Hiroshima 737-01
(Received November 13, 1990)

Four kinds of ferroelectric liquid crystals (FLCs) possessing OH groups, ((*S*)-2-methylbutyl 4-[4-(11-hydroxyundecyloxy)benzylideneamino]cinnamate **4a**, (*S*)-2-methylbutyl 4-[4-(11-hydroxyundecyloxy)-2-hydroxybenzylideneamino]cinnamate **4b**, (*S*)-2-hydroxypropyl 4-[4-(11-hydroxyundecyloxy)benzylideneamino]cinnamate **4c**, and (*S*)-2-hydroxypropyl 4-[4-(11-hydroxyundecyloxy)-2-hydroxybenzylideneamino]cinnamate **4d**) were prepared in order to understand how the introduction of OH groups in FLCs affect the phase behavior and electrooptical effects. α,ω-Diols **4c** and **4d** show a higher transition temperature of the smectic A (S_A) phase than do ω-hydroxyl compounds **4a** and **4b**. Comparing **4b** and **4d** both of which have an OH group at the *o*-position of the benzylidene group with **4a** and **4c**, the former samples show a higher S_A-isotropization (I) transition temperature than do the latter ones. It is suggested from IR spectroscopic results that inter- and intramolecular hydrogen bonding contribute to the stabilization of the S_A phase. The order of the helical pitch in the chiral smectic C (S_c*) phase was found to be **4b**>**4a**>**4d**>**4c** within 1.8—6.6 μm. From an electrooptical effect due to a deformation of the helical structure in the S_c phase, the rise time of the surface director (τ_{sr}) and the rise time of the bulk director (τ_{br}) were measured to be as follows: τ_{sr} are 850, 1500, 30, and 70 μs, and τ_{br} are 12, 100, 0.17, and 0.35 ms for **4a**, **4b**, **4c**, and **4d**, respectively. It was found that the intramolecular hydrogen bonding results in a slower optical response time, whereas intermolecular hydrogen bonding results in a faster one.

Since the discovery of a ferroelectric property in the S_c* phase by Meyer et al.,[1] (*S*)-2-methylbutyl-4-[4-(decyloxy)benzylideneamino]cinnamate (DOBAMBC) has attracted much attention regarding both fundamental physical science[2-5] and practical view points concerning various types of electrooptical materials with small switching times and memory effects.[6-10] Many scientific and practical efforts have also been concentrated on families of FLCs, such as chiral compounds with benzylideneaniline,[11-13] biphenyl,[14,15] phenylbenzoate[16-18] used as mesogenic units. On the other hand, ferroelectric liquid crystalline polymers (FLCPs) that combine the mechanical properties of polymeric material and the physical properties of FLCs have also been an active, growing area of research interest for many years. FLCPs have been achieved in various polymers having chiral mesogens as a pendant group on the main chain such as polysiloxane,[19,20] polyvinyl[21-23] and polyester backbones.[24-26] Few FLCPs having chiral mesogenic groups as blocks within the main chain are presently known.[27] In previous papers[28-30] we have reported on the properties of terminal-terminal-type FLCs as twin models for the main-chain-type of FLCs which contain mesogenic units interconnected through spacer groups. As a part of an ongoing study of FLCPs, we have prepared novel DOBAMBC analogous with the structures designated **4a**—**4d** in scheme 1. α,ω-FLC diols **4c**, **4d** can be used as mesogenic units in FLCPs with various structures such as polyurethane, polyester, and polycarbonate. In the present study differential scanning calorimetry (DSC) and polarized optical microscopy (POM) were applied to an investigation of the thermal behavior of FLCs, also two types of electrooptical effects, such as a surface-stabilized FLC (SSFLC) cell and a transient scattering mode (TMS) device, were measured for possible applications.

Experimental

Syntheses: Novel types of FLCs **4a**—**4d** were prepared using the following route, as shown in Scheme 1.

4-(11-Hydroxyundecyloxy)benzaldehydes **1**; Aldehyde **1a** and **1b** were obtained from a reaction of 4-hydroxybenzaldehyde or 2,4-dihydroxybenzaldehyde and 11-bromoundecanol in the presence of K_2CO_3 and KI, according to the method of Ringsdorf et al.[31]

4-(11-Hydroxyundecyloxy)benzaldehyde **1a**: 80.5% yield; mp 61—62 °C; ^{1}H NMR ($CDCl_3$) δ=1.12—2.28 (m, 18H), 3.72—3.92 (t, 2H), 4.20—4.44 (t, 2H), 8.32—8.48 (q, 4H), and 10.05 (s, 1H). Found: C, 73.82; H, 9.48%. Calcd for $C_{18}H_{28}O_3$ (M, 292.422): C, 73.93; H, 9.65%.

2-Hydroxy-4-(11-hydroxyundecyloxy)benzaldehyde **1b**: 57.3% yield; mp 56—58 °C; ^{1}H NMR ($CDCl_3$) δ=1.06—2.09 (m, 18H), 3.33—3.69 (t, 2H), 3.81—4.03 (t, 2H), 6.22—7.37 (q, 3H), and 9.18 (s, 1H). Found: C, 70.05; H, 9.02%. Calcd for $C_{18}H_{28}O_4$ (M, 308.421): C, 70.10; H, 9.15%.

(*S*)-2-Hydroxypropyl 4-nitrocinnamate **2a**: To 0.2 mol (*S*)-1,2-propanediol and 50 mL pyridine in 300 mL freshly distilled THF, 0.16 mol 4-nitrocinnamoyl chloride in 100 mL THF was added with stirring at 0 °C for 2 h. After stirring for an additional 10 h at room temperature, the reaction mixture was evaporated to dryness, and ca. 300 mL of chloroform was added to the residue. The chloroform layer was washed with water and evaporated to dryness. The obtained product was recrystallized from methanol to give yellow crystals: 73.3% yield; mp 72—74 °C; ^{1}H NMR ($CDCl_3$) δ=1.12—1.52 (m, 3H), 3.28—3.64 (m, 1H), 4.04—4.60 (m, 2H), 6.60—6.80 (d, J=16 Hz, 1H), and 7.60—8.48 (q, 5H). Found: C, 57.41; H, 5.25; N, 5.34%. Calcd for $C_{12}H_{13}NO_5$ (M, 251.241): C, 57.37; H, 5.22; N, 5.58%.

(*S*)-2-Hydroxypropyl 4-aminocinnamate **3a**: To 0.04 mol **2a** and 0.84 mol $FeCl_2$ in 300 mL methanol, gaseous NH_3 was gently introduced with stirring at room temperature for 1.5 h.

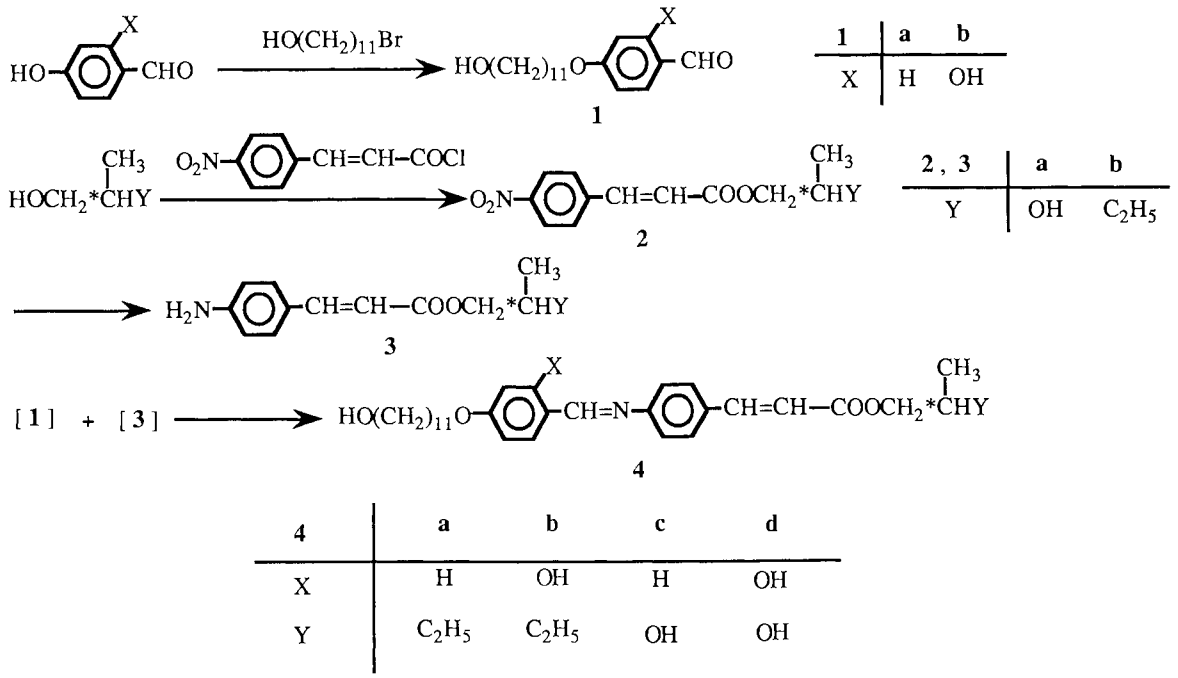

4	a	b	c	d
X	H	OH	H	OH
Y	C_2H_5	C_2H_5	OH	OH

Scheme 1. Preparation of ferroelectric liquid crystalline α,ω-diols.

Table 1. NMR Spectra and Elemental Analysis of **4**

4	^{1}H NMR ($CDCl_3$)	Elemental analysis/%			Phase transition temperature	$\Delta T_{S_C^*}$	ΔT_{S_A}
	δ/ppm	C	H	N	°C	°C	°C
4a	0.80—1.08 (m, 6H), 1.14—2.00 (m, 21H), 3.50—3.72 (t, 2H), 3.84—4.24 (m, 4H), 6.18—6.48 (d, J=16 Hz, 1H), 6.80—7.88 (m, 9H), 8.30 (s, 1H)	$C_{32}H_{45}O_4N$=507.720			K 68 S_C* 91 S_A 109 I	23	18
		Found 75.46	9.06	2.61			
		Calc. 75.70	8.93	2.76			
4b	0.74—1.07 (m, 6H), 1.12—1.96 (m, 21H), 3.43—3.71 (t, 2H), 3.78—4.18 (m, 4H) 6.26—6.36 (d, J=16 Hz, 1H), 7.34—7.64 (m, 8H), 8.43 (s, 1H)	$C_{32}H_{45}O_5N$=523.719			K 62 S_C* 86 S_A 120 I	24	34
		Found 73.84	8.55	2.58			
		Calc. 73.99	8.66	2.67			
4c	0.80—1.56 (m, 18H), 1.60—1.90 (m, 3H), 3.28—3.56 (t, 3H), 3.68—4.08 (m, 4H) 6.16—6.44 (d, J=16 Hz, 1H), 6.68—7.76 (m, 9H), 8.22 (s, 1H)	$C_{30}H_{41}O_4N$=496.665			K 57 S_H* 112 S_C* 132 S_A 147 I	20	15
		Found 72.60	8.32	2.60			
		Calc. 72.70	8.34	2.83			
4d	0.90—1.56 (m, 18H), 1.62—1.92 (m, 3H), 3.34—3.58 (t, 3H), 3.68—4.12 (m, 4H), 6.20—6.48 (d, J=16 Hz, 1H), 7.00—7.66 (m, 9H), 8.46 (s, 1H)	$C_{30}H_{41}O_5N$=511.664			K 67 S_C* 107 S_A 155 I	40	48
		Found 70.38	8.15	2.61			
		Calc. 70.42	8.08	2.74			

After reduction was completed, the reaction mixture was evaporated to dryness. The residue was extracted three times with 100 mL of dichloromethane. The dichloromethane layer was washed with water and evaporated to dryness. The obtained product was chromatographed on silica gel (Wakogel C-200) with diethyl ether to give yellow crystals; 74.8% yield; mp 83—84 °C; ^{1}H NMR ($CDCl_3$) δ=1.04—1.44 (m, 3H), 3.26—3.84 (m, 1H), 4.04—4.40 (m, 2H), 6.28—6.44 (d, J=16 Hz, 1H), 6.60—7.82 (m, 5H). Found: C, 64.93; H, 6.71; N, 6.10%. Calcd for $C_{12}H_{15}NO_3$ (M, 221.258): C, 65.14; H, 6.83; N, 6.33%.

Shiff Bases 4: An equimolar mixture of aldehyde **1** and 4-aminocinnamate **3** in 10 mL of absolute ethanol was allowed to stand for 24 h. The precipitate was filtered and recrystallized twice from the absolute ethanol; the yield was ca. 90%. The thermal behaviors and characterization of (*S*)-2-methylbutyl 4-[4-(11-hydroxyundecyloxy)benzylideneamino]-cinnamate **4a**, (*S*)-2-methylbutyl 4-[4-(11-hydroxyundecyloxy)-2-hydroxybenzylideneamino]cinnamate **4b**, (*S*)-2-hydroxypropyl 4-[4-(11-hydroxyundecyloxy)benzylideneamino]cinnamate **4c**, and (*S*)-2-hydroxypropyl 4-[4-(11-hydroxyundecyloxy) 2-hydroxybenzylideneamino]cinnamate **4d** are tabulated in Table 1.

Measurements: ^{1}H NMR measurements were carried out with a 100 MHz JEOL JNM-MH 100 spectrometer. The

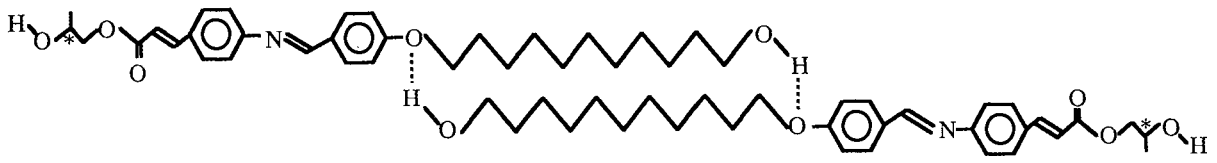

Fig. 1. Structure of intermolecular hydrogen bonds of **4c**.

phase-transition temperature was determined by DSC using a Rigaku Thermoflex apparatus (DSC-8230B). Sample quantities varied from 5 to 10 mg. POM was performed using an Olympus nicroscope (BH-2), with a heating stage attached to a temperature controller. Thin samples were sandwiched between two glass slides, the surfaces of which had been unidirectionally rubbed with cotton wool to obtain a homogeneous alignment. The spacing between the top and bottom glass plates was 25 μm, with a stretched polyester film used as the spacer material. Electrooptical measurements were carried out as follows. The surfaces of glass plates were coated with a transparent conductive material (In_2O_3); the surface resistance was about 100 Ω m^{-2}. The sample cell (thickness: 25 μm) was set without a polarizer in the optical path of a He-Ne laser (NEC-GLG, 5313, wavelength 632.8 nm, and output power 1 mW). The incident light was damped with an attenuator and arranged with a slit. Changes in the transmission upon the application of an electric field were monitored with a photodiode, and processed with a personalcomputer (NEC 9801).

Results and Discussion

Thermal Properties. According to DSC and POM, samples **4a**—**4d** show two or more mesophases upon cooling; at the transition from the I to the S_A phase, a fan-shaped texture with the focal conic texture first appears. Upon further cooling, the S_A phase and the following S_c* phase result, showing a focal conic texture with stripes due to a helical structure.

The phase-transition temperature of a samples determined using DSC is compatible with that obtained by means of POM and the electro-optical measurements mentioned below. The results are summarized in Table 1. From the obtained results it was found that although these samples resemble typical FLC, DOBAMBC (S_H 63 S_c* 95 S_A 118 I) very closely in mesomorphic behavior, their phase-transition temperature is somewhat higher than that of DOBAMBC, itself. The OH stretch vibrations of **4c** and **4d** are broad bands centered at 3425 and 3340 cm^{-1} due to intermolecular hydrogen bonds in the crystalline phase (K), respectively.

It is, thus, suggested that in FLC α,ω-diols **4c** and **4d** hydrogen bonds exist between the hydroxyl hydrogen and the phenyl ether oxygens, as described regarding 4,4′-bis(6-hydroxyhexyloxy)biphenyl.[32] The structure of hydrogen bonding in **4c** is speculated to be as shown in Figure 1. Comparing the thermal behavior of **4b** and **4d** with that of the corresponding liquid crystals, **4a** and **4c**, the former samples show a wider temperature range of both the S_A phase (ΔT_{S_A}) and the S_c* phase (ΔT_{S_c*}) than do that of latter ones. In addition, the phase-

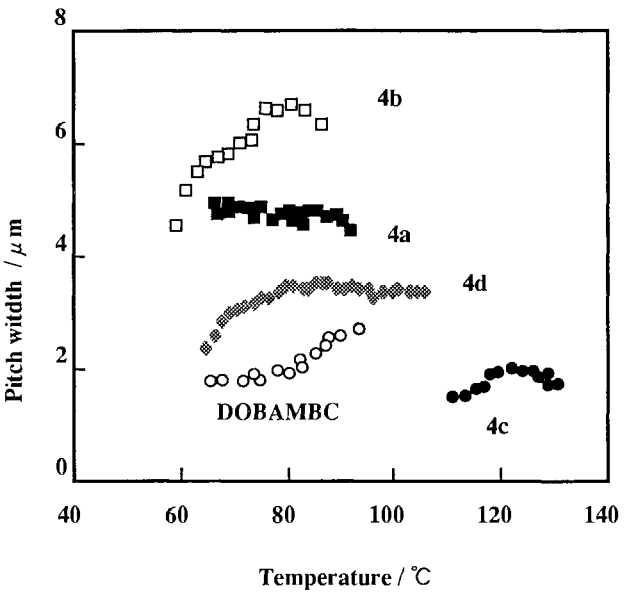

Fig. 2. Temperature dependence of pitch width of helical structure in the S_c* phase of α,ω-diols **4** and DOBAMBC.

transition temperatures of the S_A-I transition of **4b** and **4d** was higher than those of **4a** and **4c**. These results can be explained as follows: the thermal stability of the smectic state in liquid crystals having an OH group at the *o*-position of the benzylidene group, such as in **4b** and **4d**, is increased by an interaction between adjacent molecules in the smectic layers when the hydroxyl hydrogen is intramolecular hydrogen-bonded to give a cis conformation with a narrow molecular breadth and a coplanarity of the two benzene rings.[12,33]

The pitches of the helical structure of the S_c* phase, which are important factors concerning the electrooptical effect in FLCs, were measured by averaging the spacing of the stripes at ten different places in a micrograph of their textures. Figure 2 shows the temperature dependence of the pitch of the helical structure in the S_c* phase. The order of the average pitch of the samples was found to be as follows:

4b>4a>4d>4c.

FLC α,ω-diols (**4d** and **4c**) show a narrower pitch than do the others (**4b** and **4a**), while intramolecular hydrogen bonded **4b** and **4d** show a wider pitch than do **4a** and **4c**. This result may be explained in terms of the

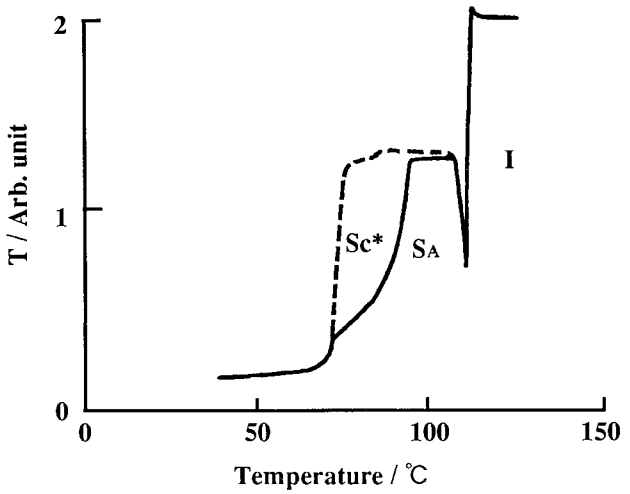

Fig. 3. Transmission intensity (T) of **4a** on cooling cycles: (——); E=0, (-----); E=16 kV cm^{-1}.

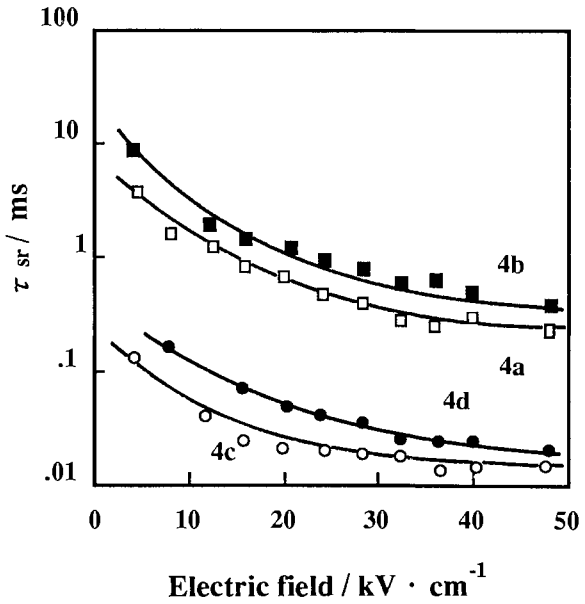

Fig. 4. Electric field dependence of the rise time of surface director (τ_{sr}) in the ferroelectric S_c* phase α,ω-diols **4**.

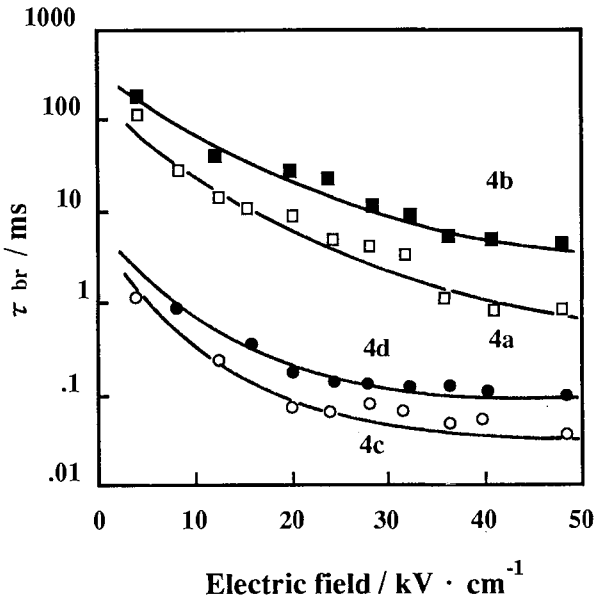

Fig. 5. Electric field dependence of the rise time of bulk director (τ_{br}) in the ferroelectric S_c* phase α,ω-diols **4**.

layer spacing in a smectic phase, depending on the hydrogen bonds between the molecular layers.

Electrooptical Properties. FLC α,ω-diols were measured regarding electrooptical effects in order to obtain basic data for practical uses of FLCs. Figure 3 shows the transmission intensity (T) of the He–Ne laser through the **4a** cell upon cooling. When no voltage was applied, T below 91 °C gradually decreased due to light scattering in the wound phase of the helical structure of the S_c* phase. On the other hand, upon application of a d.c. electric field, T never decreased within the temperature range of the S_c* phase. In this measurement, it was found that T decreases slightly just after a d.c. field application, and then increases remarkably. The applied field induces a fluctuation of the boundary due to a reorientation of the molecular alignment in the layer near to the electrode surface resulting in a decrease of T within a short time (τ_{sr}). This electrooptical effect can be regarded as being a response time of a surface-stabilized ferroelectric liquid crystal (SSFLC) cell.[10] On the other hand, the main response (τ_{br}) corresponding to an increase in T is relatively slow. The slow response, called the transient scattering mode (TSM) effect,[34] is believed to be due to a transformation of a wound phase (S_c*) to unwound phase (S_c): that is, a transition from a helical structure to a uniform monodomain structure. The electrooptical response time corresponding to the change in T caused by a d.c. field application was measured over an electric field from 0.4 to 48 kV cm^{-1} at T_{Sc^*} −10 °C (cell thickness; 25 μm). τ_{sr} and τ_{br} are the times taken to reach the stage of a T decrease and increase of up to 90%, respectively. In order to determine the effect of the applied field on the response times, τ_{sr} and τ_{br} were used to measure the S_c* phase by changing the applied voltage. Figures 4 and 5 show the field dependence of the response time in the **4** cell. These figures show that an increase in the applied voltage results in a faster optical response time; an increase in the pitch of helical structure results in a slower response. It was also found by comparing the **4b** and **4d** existing intramolecular hydrogen bonding with **4a** and **4c**, the former samples show a slower optical response time than do the latter ones. In addition, the optical response times of α,ω-FLC diols **4c** and **4d** are faster than that of ω-hydroxyl FLCs **4a** and **4b**. For development of the S_c* phase, it is well known that intermolecular interactions are limited to

Table 2. Thermal and Electrooptical Properties of 4[a)]

4	$T_{S_A\text{-}S_c^*}$ / °C	$T_{S_c^*\text{-}K}$ / °C	Pitch / μm	τ_{sr}[b)] / μs	τ_{br}[b)] / ms
4a	91	23	4.7 (76°C)	850 (76°C)	12 (76°C)
4b	86	24	6.6 (75°C)	1500 (75°C)	100 (75°C)
4c	132	20	1.8 (114°C)	30 (114°C)	0.17 (114°C)
4d	107	40	3.5 (89°C)	70 (89°C)	0.35 (89°C)
DOBAMBC	95	33	1.7 (90°C)	200 (90°C)	120 (75°C)

a) Cell thickness; 25 μm. b) Electric field=16 kV cm^{-1}.

excluded volume effects and dispersive forces. In our case, in addition to the interaction due to these two factors, hydrogen bonding plays an important role in the formation of the S_c^* phase and in the optical response time corresponding to a change in the helical structure in the S_c^* phase. So far, the relationship between the pitch and the response time in our samples is not explicable, since it is not at all clear how large their spontaneous polarization (P_s) and viscosity (η) are. An explanation for this observed interesting relationship will be provided when the P_s and η are measured. The optical response times at 16 kV cm^{-1} are summarized in Table 2. Since the samples obtained as new types of FLCs show a relatively high-speed electrooptical effect with a low-threshold field of less than 5 kV cm^{-1}, these samples can be practically applied as display devices.

From the results concerning the thermal and electrooptical characterization of DOBAMBC analogous FLCs **4a**—**4d**, the following conclusions can be drawn:

1. α,ω-Diols **4c** and **4d** show a higher transition temperature of S_A phase than do ω-hydroxyl compounds **4a** and **4b**. Since α,ω-diols **4c** and **4d** also exhibit a higher S_A transition temperature than does DOBAMBC, the introduction of OH as terminal groups was found to stabilize the S_A phase, based on intermolecular hydrogen bonding.

2. Comparing **4b** and **4d** having an OH group at the *o*-position of the benzylidene group with **4a** and **4c**, the former samples show a higher transition temperature of S_A–I than do the latter ones. It is suggested that intramolecular hydrogen bonding contributes to a stabilization of the S_A phase.

3. Intramolecular hydrogen bonding results in a wider helical pitch, while the intermolecular hydrogen bonding results in a narrower one.

4. From the electrooptical measurements, it was found that a wider helical pitch results in a slower optical response time.

5. The τ_{sr} for SSFLC of **4a**—**d** is slower than that of DOBAMBC, whereas the τ_{br} for TSM is faster than that of DOBAMBC.

References

1) R. B. Meyer, L. Liebert, L. Strzelecki, and P. Keller, *J. Phys. Lett.*, **36**, L-69 (1975).
2) N. Maruyama, *Ferroelectrics*, **63**, 49 (1985).
3) S. Kai, T. Hashimoto, M. Nomiyama, and M. Imasaki, *Jpn. J. Appl. Phys., Suppl.*, **24**, 890 (1985).
4) H. Takezoe, Y. Ouchi, K. Ishikawa, and A. Fukuda, *Mol. Cryst. Liq. Cryst.*, **139**, 27 (1986).
5) K. Kondo, S. Era, M. Isogai, and A. Mukoh, *Jpn. J. Appl. Phys.*, **24**, 1389 (1985).
6) J. S. Patel, *Appl. Phys. Lett.*, **47**, 1277 (1985).
7) M. Ozaki, S. Kishio, Y. Shigeno, and K. Yoshino, *Jpn. J. Appl. Phys., Suppl.*, **24**, 63 (1985).
8) K. Yoshino, M. Ozaki, T. Sakurai, and M. Honma, *Jpn. J. Appl. Phys., Suppl.*, **24**, 59(1985).
9) K. Yoshino, S. Kishio, M. Ozaki, T. Sakurai, N. Mikami, and R. Higuchi, *Jpn. J. Appl. Phys.*, **25**, L976 (1986).
10) S. Kishio, M. Ozaki, K. Yoshino, and A. Sakamoto, *Mol. Cryst. Liq. Cryst.*, **144**, 43 (1987).
11) T. Kitamura, A. Mukoh, M. Isogai, T. Inukai, K. Furukawa, and K. Terashima, *Mol. Cryst. Liq. Cryst.*, **136**, 167 (1986).
12) B. Otterholm, M. Nilsson, S. T. Lagerwall, and K. Skarp, *Liq. Cryst.*, **2**, 757 (1987).
13) A. Ezcurra, M. A. P. Jubindo, M. R. De La Fuente, J. Etxebarria, A. Remon, and M. J. Tello, *Liq. Cryst.*, **4**, 125 (1989).
14) T. Sakurai, N. Mikami, R. Higuchi, M. Honma, M. Ozaki, and K. Yoshino, *J. Chem. Soc., Chem. Commun.*, **1986**, 978.
15) J. W. Goodby, E. Chin, T. M. Leslie, J. M. Greary, and J. S. Patel, *J. Am. Chem. Soc.*, **108**, 4729 (1986).
16) K. Skarp and G. Andersson, *Ferroelectr., Lett. Sect.*, **6**, 67 (1986).
17) D. M. Walba, R. T. Vohra, N. A. Clark, M. A. Handschy, J. Xue, D. S. Parmar, S. T. Lagerwall, and K. Skarp, *J. Am. Chem. Soc.*, **108**, 7424 (1986).
18) Y. Haramoto and H. Kamogawa, *Chem. Lett.*, **1987**, 755.
19) T. Suzuki, T. Okawa, T. Ohnuma, and Y. Sakon, *Makromol. Chem., Rapid Commun.*, **9**, 755 (1988).
20) M. Dumon, H. T. Nguyen, M. Mauzac, C. Destrade, M. F. Achard, and H. Gasparoux, *Macromolecules*, **23**, 355 (1990).

21) S. Uchida, K. Morita, K. Miyoshi, K. Hashimoto, and K. Kawasaki, *Mol. Cryst. Liq. Cryst.*, **155**, 93 (1988).
22) V. P. Shibaev, M. V. Kozlovsky, N. A. Platé, L. A. Beresnev, and L. M. Blinov, *Liq. Cryst.*, **8**, 545 (1990).
23) K. Sugiyama and K. Shiraishi, *Makromol. Chem.*, **190**, 2381 (1989).
24) S. Bualek and R. Zentel, *Makromol. Chem.*, **189**, 797 (1988).
25) R. Zentel, G. Reckert, S. Bualek, and H. Kapitza, *Makromol. Chem.*, **190**, 2869 (1989).
26) S. Ujiie and K. Iimura, *Chem. Lett.*, **1990**, 1031.
27) J. Watanabe, A. Morita, M. Hayashi, and S. Kinoshita, *Polym. Prep. Jpn.*, **38**, 2371 (1989).
28) K. Shiraishi, K. Kato, and K. Sugiyama, *Chem. Lett.*, **1990**, 971.
29) K. Shiraishi, K. Kato, and K. Sugiyama, *Bull. Chem. Soc. Jpn.*, **63**, 1848 (1990).
30) K. Sugiyama, K. Kato, and K. Shiraishi, in contribution to *Chem. Lett.*
31) M. Portugall, H. Ringsdorf, and R. Zentel, *Makromol. Chem.*, **183**, 2311 (1982).
32) G. Smyth, S. K. Pollack, W. J. Macknight, and S. L. Hsu, *Liq. Cryst.*, **7**, 839 (1990).
33) A. Hallsby, M. Nilsson, and B. Otterholm, *Mol. Cryst. Liq. Cryst. Lett.*, **82**, 61 (1982).
34) K. Yoshino and M. Ozaki, *Jpn. J. Appl. Phys.*, **23**, L385 (1984).

Methanol Synthesis from CO_2 and H_2 over CuO–ZnO Catalysts Combined with Metal Oxides under 13 atm Pressure

Zheng Xu, Zaihu Qian, Liqun Mao, Kozo Tanabe,† and Hideshi Hattori*,†
Department of Chemistry, Jilin University, Changchun, China
† Department of Chemistry, Faculty of Science, Hokkaido University, Sapporo 060
(Received November 28, 1990)

The synthesis of methanol from CO_2 and H_2 in a flow reactor was studied over CuO–ZnO catalysts combined with ZrO_2, MgO, Al_2O_3, or Cr_2O_3 under a presssure of 13 atm. CuO–ZnO–Al_2O_3, CuO–ZnO–ZrO_2, and CuO–ZnO–MgO showed higher activity and higher selectivity for methanol than did CuO–ZnO. The selectivity for methanol formation became higher as the reaction temperature was lower, or any of the H_2/CO_2 ratio, the pressure and the space velocity were higher. On the basis of analyses by XRD, XPS, and ultraviolet diffused reflectance spectroscopy, the active centers of CuO–ZnO–ZrO_2 seem to be a Cu^+–ZnO species stabilized by ZrO_2.

Methanol synthesis from CO_2 and H_2 has recently been studied over various mixed oxide catalysts. The binary mixed oxides used were CuO–Al_2O_3,[1,2] CuO–ZnO,[2,3] CuO supported on MgO, La_2O_3, Sm_2O_3, ThO_2–K, and ZrO_2[2] and ZnO supported on MgO, Al_2O_3, SiO_2, TiO_2, ZrO_2, and Nb_2O_5.[4] The ternary mixed oxides used were CuO–ZnO–Al_2O_3,[2,3,5,6] CuO–ZnO–Cr_2O_3,[3] and CuO–ZnO supported on MgO, Y_2O_3, In_2O_3, La_2O_3, Nd_2O_3, ThO_2, and SiO_2.[6] Among these catalysts, CuO–ZnO–MgO, CuO–ZnO–Al_2O_3, CuO–ZnO–La_2O_3, and CuO–ZnO–ThO_2 showed high catalytic activity and selectivity for methanol formation. In the present work, CuO–ZnO–ZrO_2 was examined and the activity and selectivity of CuO–ZnO–ZrO_2 compared with those of CuO–ZnO–MgO, CuO–ZnO–Al_2O_3, and CuO–ZnO–Cr_2O_3; further, the active sites on CuO–ZnO–ZrO_2 were studied by means of XRD, XPS, and ultraviolet diffused reflectance spectroscopy.

Experimental

Catalyst. CuO-ZnO catalysts with different compositions were prepared by the hydrolysis of a mixed solution of $Cu(NO_3)_2$ and $Zn(NO_3)_2$ with an aqueous solution of Na_2CO_3, followed by thoroughly washing the co-precipitates with distilled water and drying overnight. The dried catalysts were calcined in air at 350 °C for 3 h and then at 500 °C for 1 h.

CuO–ZnO–ZrO_2, CuO–ZnO–MgO, CuO–ZnO–Al_2O_3, and CuO–ZnO–Cr_2O_3 catalysts with different compositions were prepared by directly adding $Zr(OH)_4$, $Mg(OH)_2$, $Al(OH)_3$, and $Cr(OH)_3$, respectively, to the $Cu(OH)_2$–$Zn(OH)_2$ co-precipitates obtained above, followed by drying and calcining, as described above. Zirconium tetrahydroxide was obtained by the hydrolysis of $ZrOCl_2$ with aqueous ammonia and $Mg(OH)_2$, $Al(OH)_3$, and $Cr(OH)_3$ were prepared by hydrolysis of the respective nitrates with an aqueous solution of Na_2CO_3.

Catalysts after being sieved to 20—40 mesh size were reduced with H_2 at 300 °C for 6 h in a reactor and subjected to evaluation.

Preparation of Standard Samples. A standard sample of Cu^0 was obtained by etching a pure Cu metal plate with Ar^+ ions at an electric current of 20 μA for 10 min until the O_{1s} lines in the XPS spectra disappeared. Pure CuO sample was prepared by calcining a pure Cu metal plate at 500 °C for 3 h in air. Pure $Cu_2O(Cu^+)$ was obtained by etching the pure CuO with Ar^+ ions in an ultra high vacuum at a lower electronic current (15 μA) for 10 min.[7]

Reaction Procedures. A reaction of CO_2 with H_2 was carried out in a flow reactor. A mixture containing H_2 and CO_2 at a mole ratio 3:1 was fed through a constant volume of catalyst (1.8 cm^3) at a total pressure of 13 atm. The products were analyzed by gas chromatography with a Porapak Q column.

XPS Measurement. XPS spectra were measured by the use of an ESCALAB MK spectrometer (V. G. Scientific Ltd., UK) equipped with an in-situ reaction cell and a pretreatment chamber, using Mg $K\alpha$ radiation ($h\nu$=1253.6 eV). Catalyst specimens were prepared by pressing powder samples to a small plate, followed by evacuation at room temperature of about 10^{-9} Torr in the pretreatment chamber. After being transferred to a small reactor equipped inside the pretreatment chamber, each specimen was reduced with H_2 (1 atm) at 300 °C for 2 h (a mixture of 25% CO_2+75% H_2 (1 atm) was adsorbed on it at room temperature) and then evacuated to 10^{-3} Torr at 250 °C. The specimen was cooled down, and transferred back to the pretreatment chamber, evacuated to about 5×10^{-8} Torr, and then transferred to the analyzing chamber for an XPS measurement. The charging effects of various specimens were minimized by taking the binding energy of the $Zn(2p_{2/3})$ level at 1021.7 eV as the internal standard.

XRD Measurement. The X-ray powder diffraction patterns were recorded by using a Rigaku D/MAX III-A X-ray diffractometer with Cu $K\alpha$ (0.15418 nm) radiation. Samples were mounted on a glass slide by using double-seal tape and inserted into the sample holder.

UDRS Measurements. Ultraviolet diffused reflectance spectra were measured by utilizing a UV-240 spectrometer in the range of 250—800 nm; $BaSO_4$ was used as a standard. Samples were reduced for 6 h and then placed in infrasil front-window cells without exposure to air, either by transfer under nitrogen or by direct reduction in a closed system.

Results and Discussion

Catalytic Activity and Selectivity. Table 1 shows both the activity and selectivity of CuO–ZnO catalysts with different compositions. Only CuO showed a very low activity (CO_2 conversion), no methanol being formed; only ZnO showed low activity and formed

Table 1. Activity and Selectivity of CuO-ZnO Catalysts in CO_2+H_2 Reaction[a]

Catalyst	SV	Reac. temp	X_{CO_2}[b]	Selectivity/%			Y_{CO_2}[c]
	h^{-1}	°C	%	CH_3OH	CO	CH_4	%
ZnO	3500	240	6.0	16.9	74.7	8.5	1.0
CuO/ZnO	3600	220	7.2	13.5	79.1	7.3	1.0
(10/90)		240	15.1	12.1	82.3	5.6	1.8
CuO/ZnO	3600	220	20.0	42.6	53.8	3.7	8.5
(30/70)		240	32.4	20.6	76.5	2.9	6.7
CuO/ZnO	3600	220	21.2	56.7	40.3	3.1	12.0
(47/53)		240	31.6	38.9	56.5	4.0	12.3
CuO/ZnO	3600	220	19.1	41.0	56.2	2.8	7.8
(90/10)		240	33.5	28.3	67.7	4.0	9.5
CuO	3600	240	1.7	0	81.0	19.0	0

a) Reaction conditions: mole ratio of $H_2/CO_2=3/1$, total pressure 13 atm. The catalyst of 1.8 cm^3 was used after reduction with H_2 at 300 °C for 6 h. b) X_{CO_2}=Conversion of CO_2. c) Y=yield.

Table 2. Activity and Selectivity of CuO-ZnO-ZrO_2 Catalysts in CO_2+H_2 Reaction[a]

Catalyst	SV	Reac. temp	X_{CO_2}[b]	Selectivity/%			Rate of reaction[d]			Y_{CH_3OH}[c]
	h^{-1}	°C	%	CH_3OH	CO	CH_4	CO	CH_3OH	CO_2	%
CuO/ZnO/ZrO_2	3600	220	21.2	56.7	40.3	3.1	3.3	4.7	8.2	12.0
(47/53/0) A_1		240	31.6	38.9	56.5	4.6	6.9	4.8	12.2	12.3
CuO/ZnO/ZrO_2	3600	220	12.5	68.9	27.4	3.8	1.5	3.7	5.4	8.6
(45/50/5) A_2		240	19.8	60.7	34.9	4.4	3.0	5.2	8.55	12.0
CuO/ZnO/ZrO_2	3600	160	5.4	94.8	4.4	0.8	0.1	2.3	2.4	5.1
(42/47/11) A_3		180	9.4	88.8	10.3	0.9	0.4	3.8	4.3	8.4
		200	17.9	73.0	26.0	1.0	2.1	6.0	8.2	13.1
		220	29.1	59.9	38.4	1.6	5.1	8.0	13.3	17.4
		240	37.1	39.6	56.5	3.9	8.7	6.8	17.2	14.9
		260	39.3	22.8	69.5	7.7	12.5	4.1	17.9	9.0
		280	42.8	18.6	72.4	8.9	14.2	3.6	19.5	8.0
CuO/ZnO/ZrO_2	3600	220	21.6	72.4	25.7	1.9	3.0	8.6	11.8	15.6
(32/35/33) A_4		240	27.5	51.4	46.6	2.0	7.0	7.8	15.1	14.1
CuO/ZnO/ZrO_2	3600	220	20.5	68.3	29.3	2.3	4.3	9.9	14.6	14.0
(21/24/55) A_5		240	29.7	46.4	50.3	3.2	10.6	9.8	21.1	13.8
CuO/ZnO/ZrO_2	3600	240	6.9	78.7	17.0	4.3	0.8	3.6	4.6	5.4
(11/12/77) A_6										

a) Reaction conditions: mole ratio of $H_2/CO_2=3/1$, total pressure 13 atm. The catalyst of 1.8 cm^3 was used after reduction with H_2 at 300 °C for 6 h. b) X_{CO_2}=Conversion of CO_2. c) Y=yield. d) mmol g^{-1} h^{-1}.

methanol, its selectivity being 17%. However, the mixed oxides, CuO-ZnO, showed much higher activity for CO_2 conversion and much higher selectivity for the formation of methanol than did CuO or ZnO alone. A CuO-ZnO catalyst with a molar ratio=47/53 showed the higher yield (12.3%) of methanol at 240 °C, the CO_2 conversion and methanol selectivity being 31 and 39% at 240 °C, respectively.

The results for the reaction of CO_2 with H_2 over CuO-ZnO-ZrO_2 catalysts of different compositions are given in Table 2. The selectivities for methanol were high for all of the CuO-ZnO-ZrO_2 catalysts, compared with that for CuO-ZnO. A CuO-ZnO-ZrO_2 catalyst with a molar ratio of 42/47/11 exhibited the highest yield (17.4%) of methanol at 220 °C, and the highest selectivity (94.8%) for methanol at 160 °C. The lower was the reaction temperature, the higher was the methanol selectivity. On the other hand, the conversion of CO_2 and the selectivity for CO or CH_4 increased with increasing the reaction temperature.

The effects of the H_2/CO_2 ratio, pressure, and space velocity on the activity and selectivity of CuO-ZnO-

ZrO_2 (42/47/11) are shown in Figs. 1, 2, and 3, respectively. With an increase in the H_2/CO_2 ratio, the CO_2 conversion and methanol selectivity increased linearly, and the CO selectivity decreased. With an increase in the pressure, the CO_2 conversion and methanol selectivity increased, and the CO selectivity decreased. With an increase in the space velocity, and methanol selectivity increased over an SV range smaller than 3600 h^{-1}, while a small increase was observed above 3600 h^{-1}; CO selectivity decreased considerably.

Since the addition of ZrO_2 to CuO–ZnO caused a high yield of methanol, we attempted to examine the additive effect of MgO, Al_2O_3, or Cr_2O_3 on the activity and selectivity of CuO–ZnO. As shown in Table 3, the methanol yield was found to be highest over CuO–ZnO–Al_2O_3. The addition of Cr_2O_3 resulted in a marked decrease in the activity. No reaction was appreciable over CuO–ZnO–Cr_2O_3 below 300 °C. Although the amount of Cr_2O_3 was higher than those of the other catalyst supports, the decrease in the activity was so great that it cannot be explained by the amount of support. Thus, the order of methanol yield over verious catalysts is CuO–ZnO–Al_2O_3>CuO–ZnO–ZrO_2>CuO–ZnO–MgO>CuO–ZnO≫CuO–ZnO–Cr_2O_3.

Structure and Surface Area. The XRD powder pattern of a calcined CuO–ZnO sample showed that it comprises of tetragonal CuO and hexagonal ZnO. When a small amount (11 mol%) of ZrO_2 was added, the pattern of CuO–ZnO was not changed, as is shown in Fig. 4, indicating that ZrO_2 forms an amorphous

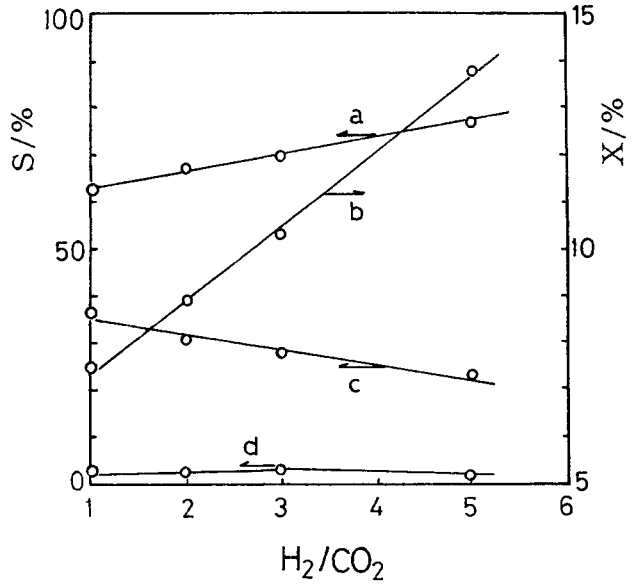

Fig. 1. Effect of H_2/CO_2 ratio on activity and selectivity of CuO–ZnO–ZrO_2 (42/47/11) catalyst. (a: S_{CH_3OH}, b: X_{CO_2}, c: S_{CO}, d: S_{CH_4}).

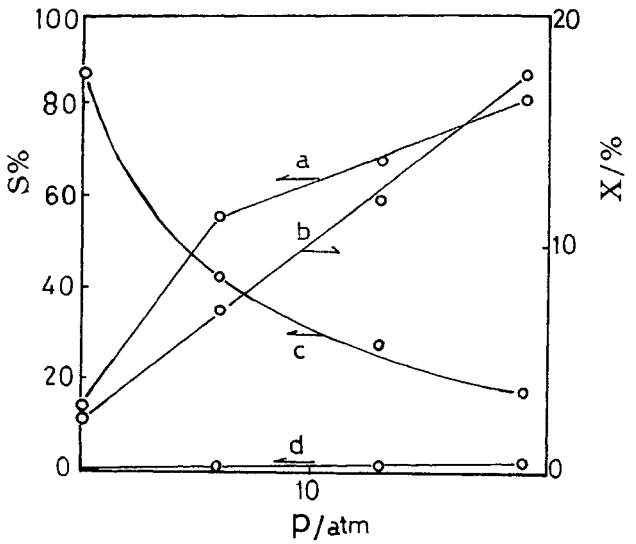

Fig. 2. Effect of pressure on activity and selectivity of CuO–ZnO–ZrO_2 (42/47/11) catalyst. (a: S_{CH_3OH}, b: X_{CO_2}, c: S_{CO}, d: S_{CH_4}).

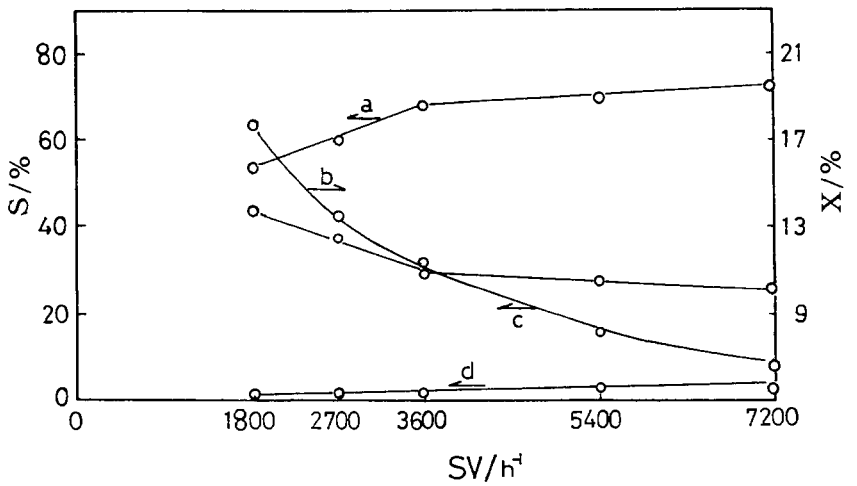

Fig. 3. Effect of space velocity on activity and selectivity of CuO–ZnO–ZrO_2 (42/47/11) catalyst. (a: S_{CH_3OH}, b: X_{CO_2}, c: S_{CO}, d: S_{CH_4}).

Table 3. Activity and Selectivity of CuO-ZnO-(MgO, Al_2O_3, or Cr_2O_3) Catalysts in CO_2+H_2 Reaction[a)]

Catalyst	SV	Reac. temp	X_{CO_2}[b)]	Selectivity/%			Rate of reaction[d)]			Y_{CH_3OH}[c)]
	h^{-1}	°C	%	CH_3OH	CO	CH_4	CO	CH_3OH	CO_2	%
CuO-ZnO	3600	160	4.4	78.4	21.5	0	0.2	0.7	0.9	3.4
(50/50) B_1		180	8.2	57.2	42.8	0	0.7	0.9	1.7	4.7
		200	14.6	40.6	59.4	0	1.6	1.2	3.0	6.0
		220	27.3	31.9	68.1	0	3.8	1.8	5.5	8.7
		240	35.9	22.2	77.8	0	5.7	1.6	7.3	8.0
		260	39.7	21.1	78.9	0	6.3	1.7	8.0	8.4
		280	39.9	15.4	84.6	0	6.8	1.2	8.1	6.2
CuO/ZnO/MgO	3600	160	9.6	96.8	3.0	0	0.6	1.9	2.0	9.3
(47/47/6) B_2		180	12.3	91.8	8.3	0	0.2	2.3	2.6	11.3
		200	11.2	72.1	27.9	0	6.5	1.7	2.3	8.1
		220	19.1	57.0	53.0	0	2.1	1.9	4.0	9.0
		240	30.7	41.2	58.9	0	3.8	2.6	6.4	12.6
		260	39.0	26.7	73.3	0	5.9	2.2	8.1	10.4
		280	41.2	26.1	74.0	0	6.3	2.3	8.6	10.7
CuO/ZnO/Al_2O_3	3600	160	20.6	97.9	2.1	0	0.1	6.0	6.2	20.2
(47/47/6) B_3		180	27.2	95.3	4.7	0	0.4	7.6	8.1	25.9
		200	23.9	82.4	17.6	0	1.3	5.9	7.2	19.7
		220	35.3	64.7	35.3	0	3.7	6.8	10.6	22.8
		240	48.3	57.9	42.0	0	6.1	8.4	14.5	28.0
		260	43.3	61.7	38.3	0	4.8	7.8	12.7	26.7
		280	45.7	37.8	62.2	0	8.5	5.2	13.7	17.3
CuO/ZnO/Cr_2O_3	3600	300	2.4	31.1	51.1	0				0.7
(34.5/34.5/31) B_4		320	5.8	25.5	49.9	0				1.6
		340	11.0	14.8	73.2	0				1.6
		360	17.8	8.1	56.0	31.7				1.4
		380	27.0	4.0	0	95.5				1.0

a) Reaction conditions: mole ratio of $H_2/CO_2=3/1$, total pressure 13 atm. The catalyst of 1.8 cm^3 was used after reduction with H_2 at 300°C for 6 h. b) X_{CO_2}=Conversion of CO_2. c) Y=yield. d) mmol g^{-1} h^{-1}.

phase. With the addition of a larger amount (77 mol%) of ZrO_2, almost all of the patterns of CuO and ZnO disappeared. This disappearance of the patterns is considered to be due to a high dispersion of CuO and ZnO over ZrO_2. The surface area (29 cm^2 g^{-1}) of CuO-ZnO (47/53) increased to 37 cm^2 g^{-1} for CuO-ZnO-ZrO_2 (42/47/11) and 42 cm^2 g^{-1} for CuO-ZnO-ZrO_2 (21/24/55). The activation energy for CO_2 conversion decreased from 71.2 kJ mol^{-1} over CuO-ZnO (47/53) to 61.1 kJ mol^{-1} over CuO-ZnO-ZrO_2 (42/47/11) and 47.2 kJ mol^{-1} over CuO-ZnO-ZrO_2 (21/24/55). These changes seem to be due to the high dispersion of CuO-ZnO over ZrO_2.

Active Centers. Figure 5 shows the ultraviolet diffused reflectance spectra of reduced CuO, ZnO, CuO-ZnO, and CuO-ZnO-ZrO_2. The absorption edges of ZrO_2, ZnO, and Cu^0 were confirmed to be 330, 360, and 560 nm, respectively. The spectral feature of ZnO was observed for CuO-ZnO and CuO-ZnO-ZrO_2, but that of ZrO_2 was not found for those samples. The spectra characteristic of Cu^0 were shifted toward lower frequencies in CuO-ZnO and CuO-ZnO-ZrO_2. The shape of the spectra also changed. The characteristic edge (600—800 nm) of Cu^0 in CuO increased its intensity in CuO-ZnO and CuO-ZnO-ZrO_2 up to 55% of the ZrO_2 content. With increasing the ZrO_2 content to 77%, the characteristic edge of Cu^0 became close to that in CuO. This trend corresponds to a difference in the catalytic activity for methanol formation over CuO and CuO-ZnO-ZrO_2 catalysts with the different ZrO_2 contents shown in Tables 1 and 2. The visible absorption edge of the reduced catalysts was different from those of Cu_2O(610 nm),[8)] Cu(560 nm), CuO(850 nm),[9)] and Cu^{2+} existing in a Cu^{2+}-ZnO solid solution. This characteristic absorption edge was reported to be caused by Cu^+ which existed in Cu^+-ZnO solid solution.[10)] Since Cu^+ and Zn^{2+} are isoelectric ions, the replacement of Zn^{2+} by Cu^+, and resulting dissolution of Cu^+ in ZnO, may be possible. The addition of high valent Zr^{4+} may supply positive charge to Cu^+, thus making dissolution easy. As a result, the intensity of the absorption edges for Cu' is considered to increase.

According to an XPS measurement, the $Cu2p_{3/2}$ peak in CuO has two strong shoulders toward its high-energy side called a "satellite shake up peak".[11)] Although the $Zn2p_{3/2}$ and $Zr3d_{5/2}$ peaks in CuO-ZnO-ZrO_2 were very similar to those of ZnO and ZrO_2, respectively, the two $Cu2p_{3/2}$ shoulder peaks were slightly wider and weaker in intensity than those in CuO. It can be said that Cu ions are located in a center of more distorted symmetry as the intensity ratio of the satellite-to-main peak

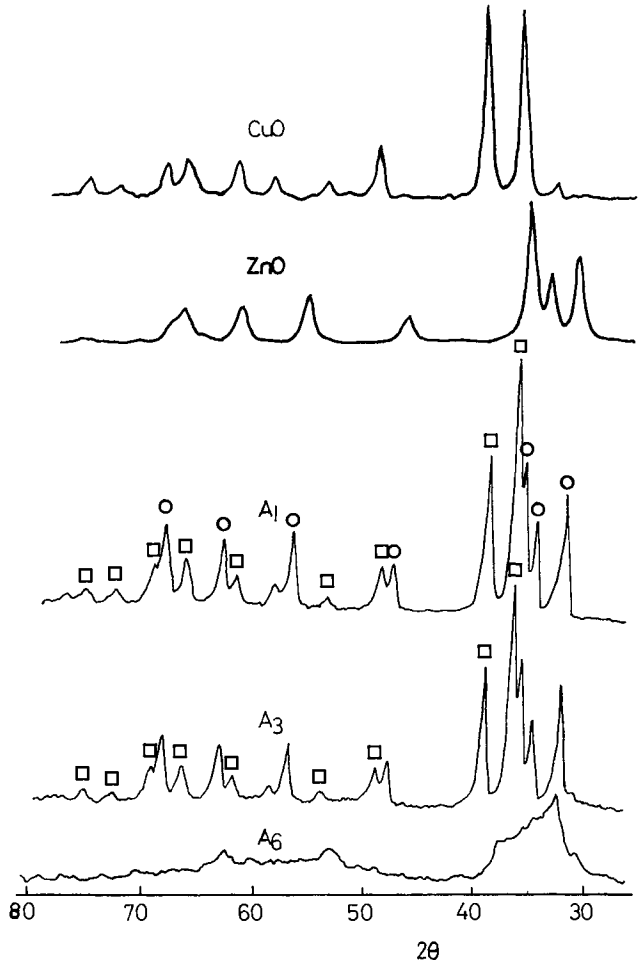

Fig. 4. XRD spectra of pure CuO and calcined samples ($CuO-ZnO-ZrO_2$) A_1, A_3, A_6. O; ZnO, □; CuO.

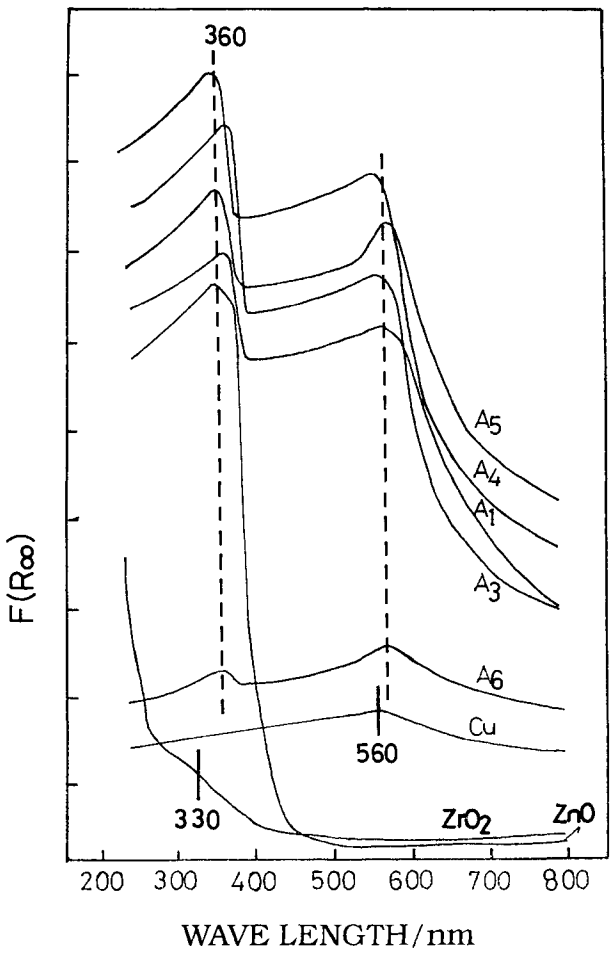

Fig. 5. Ultraviolet diffused reflectance spectra of the $CuO-ZnO-ZrO_2$ catalyst.

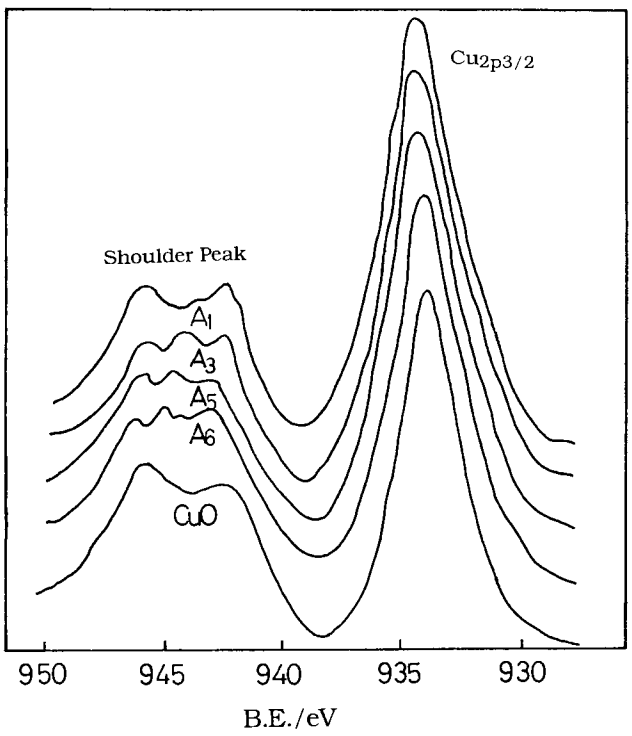

Fig. 6. XPS spectra of $Cu2p_{3/2}$ region for calcined samples. ($CuO-ZnO-ZrO_2$).

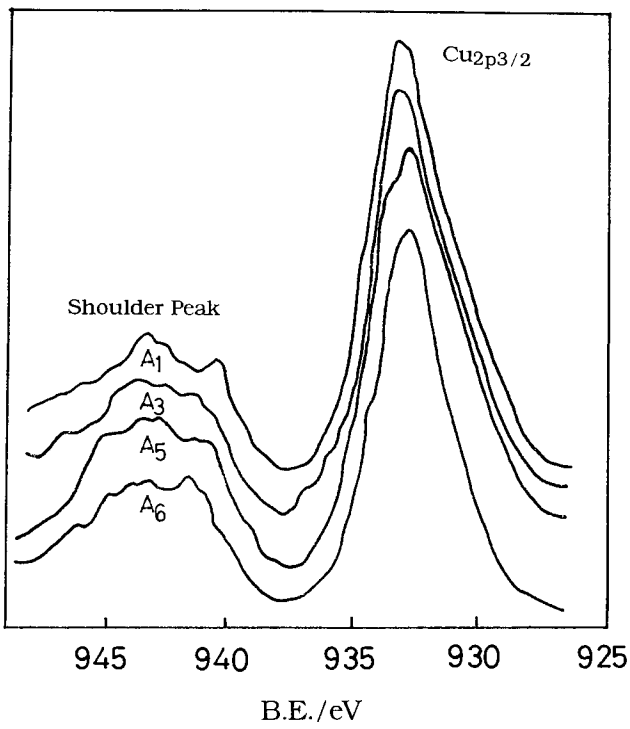

Fig. 7. XPS spectra of $Cu2p_{3/2}$ region for the samples ($CuO-ZnO-ZrO_2$) after reaction.

(S/M) becomes large.[11]

The $Zn2p_{3/2}$ and $Zr3d_{5/2}$ peaks of the used catalysts were the same as those of unused ones, and the $Cu2p_{3/2}$ peak shifted by approximately lev, similar to that of Cu. In contrast, Cu(LMM) Auger electron energy was different from that of Cu and similar to that of Cu_2O. The XPS spectra in the region of $Cu2p_{3/2}$ for the catalysts after calcination and after use for the reaction are shown in Figs. 6 and 7, respectively. Compared with the calcined catalysts, and used catalysts exhibited lower S/M values for the calcined catalysts (A_1, A_3, A_5, and A_6): 0.46, 0.46, 0.41, and 0.42, respectively; they changed to 0.25, 0.20, 0.34, and 0.31, respectively.

The decrease in the S/M value of $Cu2p_{3/2}$ is considered to be due to the formation of a solid solution comprising of Cu^{2+} and ZnO.[12] In used catalysts, although two shoulder peaks of $Cu2p_{3/2}$ also existed, their binding energy shifted toward lower energy, indicating that Cu^{2+} was reduced to lower valencies. However, the similarity of Cu(LMM) of the used catalysts to that of Cu_2O seems to suggest that the reduced Cu is partially oxidized and that the surface is partly converted with oxygen to prevent any further oxidation of Cu.[13] The shoulder peaks are usually observed for CuO, but not for Cu_2O and Cu. However, Cu^{2+} was not detected for the used catalysts in the present work. Therefore, the shoulder peaks of $Cu2p_{3/2}$ are considered to be due to the formation of Cu^+ in a Cu_2O–ZnO solid solution. During the prereduction condition, Cu^{2+} is easily reduced to Cu^+ and dissolved into ZnO, resulting in the formation of a Cu_2O and ZnO solid solution, making it difficult for any further reduction to take place since Cu^+ and Zn^{2+} are isoelectric ions. This result is in agreement with that obtained by UDRS. Thus, Cu^+ and ZnO in Cu_2O–ZnO solid solutions are suggested to be active centers under the reaction conditions.

References

1) V. N. Ipatieff and G. C. Monroe, *J. Am. Chem. Soc.*, **67**, 2168 (1945).
2) B. Denise and R. P. A. Sneeden, *Appl. Catal.*, **28**, 235 (1986).
3) T. Tagawa, G. Pleizier, and Y. Amenomiya, *Appl. Catal.*, **18**, 285 (1985).
4) T. Inoue, T. Iizuka, and K. Tanabe, *Bull. Chem. Soc. Jpn.*, **60**, 2663 (1987).
5) Y. Amenomiya and T. Tagawa, "Proc. 8th Intern. Congr. Catalysis," Verlag Chemie, Weinheim (1984), Vol. II, p. 557.
6) E. Ramaroson, R. Kieffer, and A. Kiennemann, *Appl. Catal.*, **4**, 281 (1983).
7) G. Panzner, B. Egert, and H. P. Schmidt, *Surf. Sci.*, **151**, 400 (1985).
8) J. Bloem, *Phillips Res. Rep.*, **13**, 167 (1958).
9) F. S. Stone, *Bull. Soc. Chim. Fr.*, **1966**, 819.
10) R. G. Herman, K. Klier, G. W. Simmons, B. P. Finn, and J. B. Bulko, *J. Catal.*, **56**, 407 (1979).
11) D. Brigge, "Handbook of X-Ray and Ultraviolet Photoelectron Spectroscopy," ed by D. Briggs, Heyden & Son Ltd., London (1977), p. 190.
12) F. Garbassi and G. Petrini, *J. Catal.*, **90**, 106 (1984).
13) O. Ruggeri, F. Trifieo, and A. Vaccari, *J. Solid State Chem.*, **42**, 120 (1982).

Support Effect of Re Catalyst on Methanol Synthesis from CO_2 and H_2 under a Pressure of 5 atm

Zheng Xu, Zaihu Qian, Kozo Tanabe,† and Hideshi Hattori*,†
Department of Chemistry, Jilin University, Changchun, China
† Department of Chemistry, Faculty of Science, Hokkaido University, Sapporo 060
(Received November 29, 1990)

Methanol synthesis by the reaction of CO_2 with H_2 over Re supported on ZrO_2, CeO_2, La_2O_3, and Al_2O_3 was studied under a pressure of 5atm by the use of a flow reactor. Methanol was formed over Re/CeO_2, Re/ZrO_2, and Re/La_2O_3, but not over Re/Al_2O_3 and ZrO_2 alone. On the basis of XPS analysis, the active state of Re was suggested to be Re^0 for Re/ZrO_2 and Re/CeO_2. For Re/Al_2O_3, Re was incompletely reduced, resulting in no formation of methanol. Methanol synthesis was inferred to proceed via CO in the case of Re/ZrO_2, and via the reaction of CO_2 with surface OH in the case of Re/CeO_2 by FT-IR analysis.

The support effect of rhenium catalyst on methanol synthesis from CO_2 and H_2 under 10 atm was reported to be remarkable, the selectivity for methanol formation being of the order Re/ZrO_2(73%)>Re/Nb_2O_5(52%)>Re/SiO_2(23%)>Re/Zeolon(18%)=Re/MgO (17.5%).[1,2] In the present work, we attempted to examine the effects of CeO_2, La_2O_3, and Al_2O_3, together with ZrO_2, as supports of a rhenium catalyst in the reaction of CO_2 with H_2 under 5 atm; we also studied the active sites and the reaction mechanisms by XPS and FT-IR analysis.

Experimental

Preparation of Catalysts. Supported Re catalysts were prepared by impregnating La_2O_3, CeO_2, ZrO_2, and Al_2O_3 (20—40 mesh) with an NH_4ReO_4 aqueous solution. This was followed by drying in a vacumm at 100 °C and reducing with hydrogen at 200 °C for 2 h, and then at 400 °C for 4 h; they were then cooled down to the reaction temperature under hydrogen and kept at the reaction temperature for 2 h. The amount of Re was adjusted to be 1.5 wt% for all catalysts. La_2O_3 and CeO_2 were obtained by thermal decomposition of $La(NO_3)_3$ and $(NH_4)_2Ce(NO_3)_4$ at 500 °C in air for 24 h. ZrO_2 was prepared by hydrolysis of $ZrOCl_2$ with aqueous ammonia, followed by drying at 110 °C for 12 h and calcining at 500 °C for 12 h. Al_2O_3 was a commercially available γ-Al_2O_3, which was used after calcination at 500 °C for 12 h.

Reaction Procedures. The reaction of CO_2 with H_2 was carried out in a flow reactor within the temperature range: 160—340 °C. A mixture containing H_2 and CO_2 at a mole ratio of 3:1 was fed through a constant volume of catalyst (1.8 ml) at a total pressure of 5 atm. The products were analyzed by gas chromatography using a column Porapak Q.

XPS and IR Measurements. Auger and X-ray photoelectron spectroscopic analyses were carried out by the use of an ESCA LABMK II electronic Auger spectrometer with an Al $K\alpha$ (1486.6 eV) excitation source. The infrared spectra of CO_2 and H_2 adsorbed on a catalyst placed in an in situ vacuum cell with CaF_2 windows were recorded with a NICOLET 5DX FT-IR spectrometer.

Results and Discussion

Catalytic Activity. Methanol was formed over Re/CeO_2, Re/ZrO_2, and Re/La_2O_3, but not over Re/Al_2O_3 and ZrO_2, or CeO_2 alone, although C_1 compounds (CH_3OH, CO, or CH_4) were the main products over all catalysts (Table 1). The product distribution changed, depending on the reaction temperature and space velocity. With an increase in the reaction temperature, the conversion of CO_2 increased and methanol selectivity decreased. With an increase in the space velocity, the conversion of CO_2 decreased, while methanol selectivity increased over the range 3000—12000 h^{-1}. Under the best reaction conditions, the highest selectivity for methanol formation was observed to be 76.7% over Re/CeO_2 at a reaction temperature of 160 °C.

Active Centers. The XPS spectra of Re/ZrO_2, Re/CeO_2, and Re/Al_2O_3 are shown in Figs. 1, 2, and 3, respectively. In both cases of Re/ZrO_2 and Re/CeO_2, the Re_{4f} peaks of those samples which were reduced with hydrogen at 400 °C were similar to the peak of Re metal, Re^0. The spectra of untreated NH_4ReO_4/ZrO_2 and NH_4ReO_4/CeO_2 were also similar to that of NH_4ReO_4, whose oxidation state of Re is 7+. This indicates that Re^{7+} on the surfaces was almost reduced to Re^0 by reduction

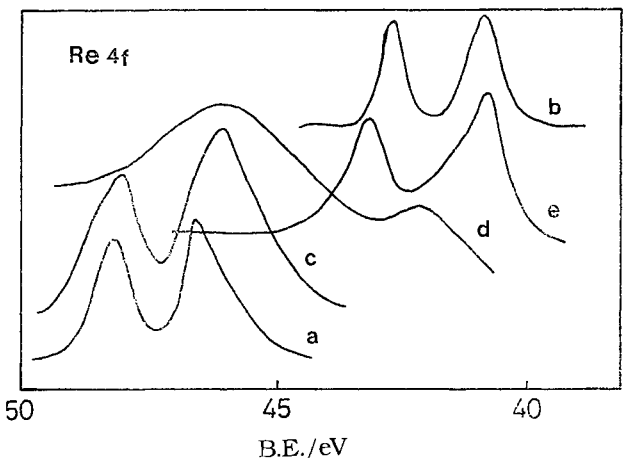

Fig. 1. XPS spectra of NH_4ReO_4/ZrO_2. a: NH_4ReO_4 powder, b: Re^0 powder, c: NH_4ReO_4/ZrO_2, d: NH_4ReO_4/ZrO_2 reduced with H_2 at 200 °C, e: NH_4ReO_4/ZrO_2 reduced with H_2 400 °C.

Table 1. Activity and Selectivity of Supported Re Catalyst[a)]

Catalyst	SV h^{-1}	Reac. temp °C	X_{CO_2}[b)]	Selectivity/%				Rate of reaction[d)]			Y[f)]
				$CO+CH_4$	CH_3OH	C_2–C_5[c)]	Me_2O	CO	C_2–C_5[c)]	CH_3OH	%
Re/CeO_2	6000	160	1.4	17.9	76.7	5.4	0	0.2	0.2	0.2	0.6
		200	4.0	41.9	56.3	1.8	0	0.6	0.6	0.4	1.5
		240	13.9	62.8	26.6	10.6	0	3.1	1.5	0.4	1.2
		260	20.8	77.6	7.9	16.2	0	4.4	2.4	0.2	0.6
		300	39.7	72.6	11.1	16.0	0.3	7.2	5.7	0.6	1.9
		340	49.8	73.0	0.3	26.4	0.3	7.4	8.8	0.0	0.1
	3000	200	5.3	44.8	16.0	39.2	0				
	12000	200	2.1	35.1	64.9	Trace	0	0.5	0.3	0.5	0.6
	24000	200	0.8	100.0	Trace	0	0	0.2	0.1	Trace	0
Re/ZrO_2	3750	260	15.5	60.0	26.3	12.0	1.7	3.6	2.2	0.8	1.9
Re/Al_2O_3	3330	260	19.3	83.0	0	16.9	0.2	6.0	2.1	0	0
Re/La_2O_3	5000	200	0.3	85.7	0	0	14.3	0.1	0.8[e)]	0	0
		260	3.4	46.1	52.1	0	1.8	0.9	0.2	10.5[e)]	0.4
ZrO_2		200	0.0	79.1	0	20.9	0				0
		240	0.2	87.1	0	12.9	0				0
CeO_2		200	1.0	100.0	0	0	0				0
		260	0.0	100.0	0	0	0				0

a) Reaction conditions: molar ratio of $H_2/CO_2=3/1$, total pressure 5 atm. Catalyst of 1.8 cm^3 was used after reduction with H_2 at 200°C for 2 h and then at 400°C for 4 h. b) X_{CO_2}=Conversion of CO_2 in 30 min when reaction became steady state. c) Hydrocarbons containing carbon number 2—5. d) mmol g^{-1} h^{-1}. f) Y=yield.

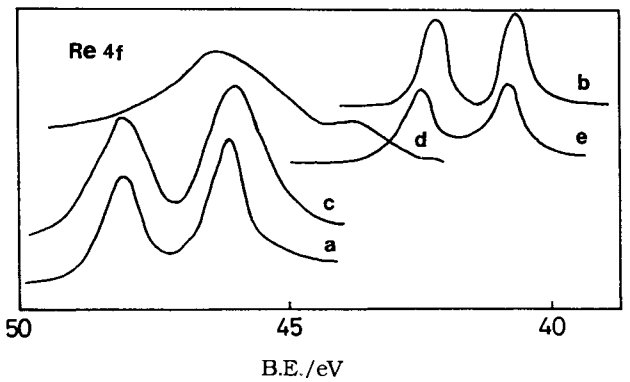

Fig. 2. XPS spectra of NH_4ReO_4/CeO_2. a: NH_4ReO_4 powder, b: Re^0 powder, c: NH_4ReO_4/CeO_2, d: NH_4ReO_4/CeO_2 reduced with H_2 at 200°C, e: NH_4ReO_4/CeO_2 reduced with H_2 at 400°C.

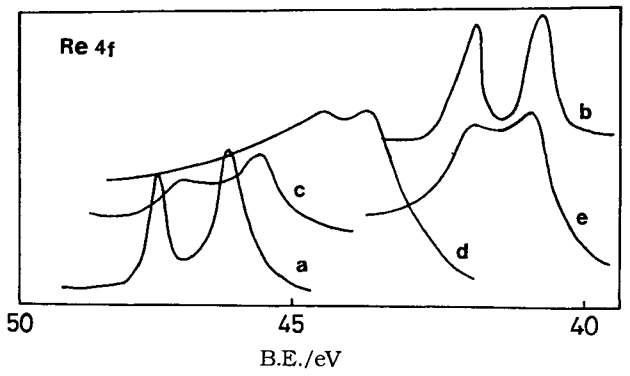

Fig. 3. XPS spectra of NH_4ReO_4/Al_2O_3. a: NH_4ReO_4 powder, b: Re^0 powder, c: NH_4ReO_4/Al_2O_3, d: NH_4ReO_4/Al_2O_3 reduced with H_2 at 400°C, e: NH_4ReO_4/Al_2O_3 reduced with H_2 at 600°C.

with hydrogen at 400 °C.

On the other hand, the spectra of Re/Al_2O_3 were different from that of Re metal, even when reduced with hydrogen at 600 °C; untreated NH_4ReO_4/Al_2O_3 also showed spectra different from NH_4ReO_4 alone. This is considered to be due to a strong interaction between the Re and Al_2O_3 support. This interaction makes the reduction of Re^{7+} to Re^0 difficult. This is in agreement with the conclusion by Yao and Shelef[3)] made on the bases of chemisorption, ESR, and temperature-programmed reduction. They reported that the dispersed phase of Re interacts strongly with the α-Al_2O_3 and, as a result, it can be reduced to a zero-valent state by H_2 only at a high temperature above 500 °C.

The methanol selectivity is considered to be affected by the adsorbed state of CO_2 on Re catalysts and, in particular, the the C–O bond strength. To determine the state of adsorbed CO_2, CO_2 was adsorbed and evacuated at room temperature and the XPS was measured. XPS in the region of O_{1s} are shown in Fig. 4. With the Re/γ-Al_2O_3 catalyst, C_{1s} peaks appeared at 290.3 and 284.6 eV. The former peak was assigned to the CO_3^{2-} species.

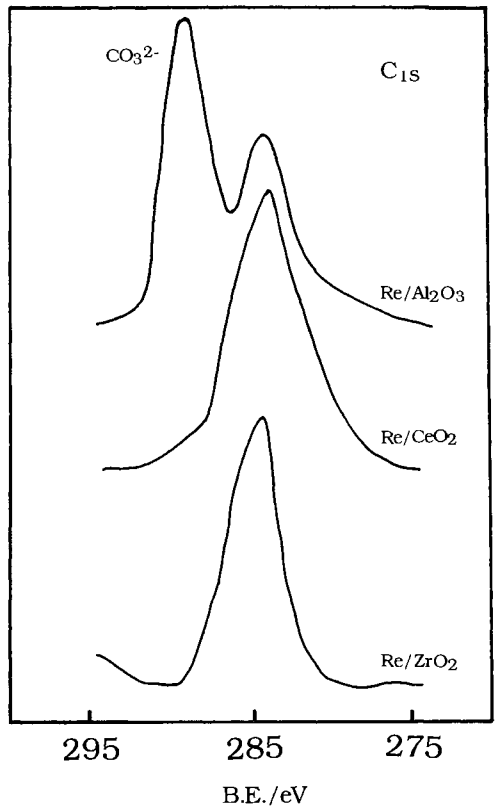

Fig. 4. XPS spectra of Re/CeO_2, Re/ZrO_2, and Re/Al_2O_3 after adsorption of CO_2 followed by evacuation at room temperature.

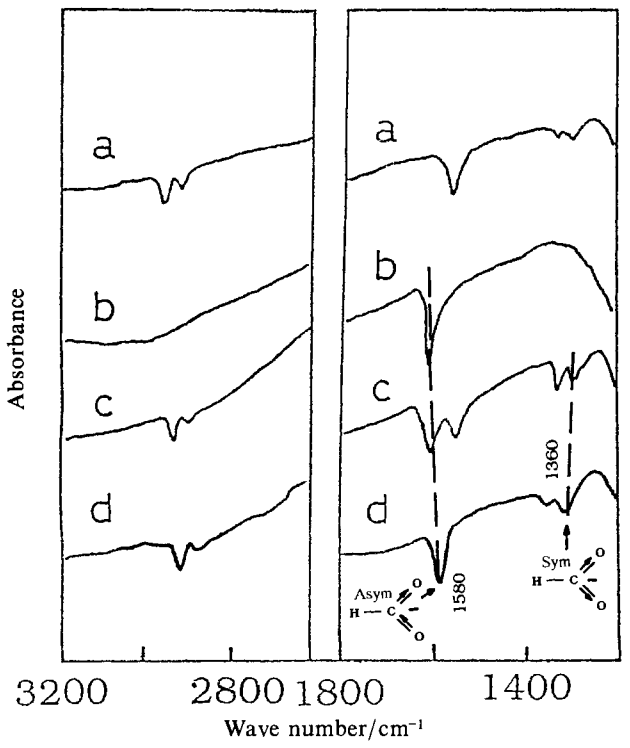

Fig. 5. IR spectra for CO_2/H_2 adsorbed on ZrO_2. a: CO_2/H_2, b: CO_2, c: CO_2/H_2 at 130°C, d: CO_2/H_2 at 230°C.

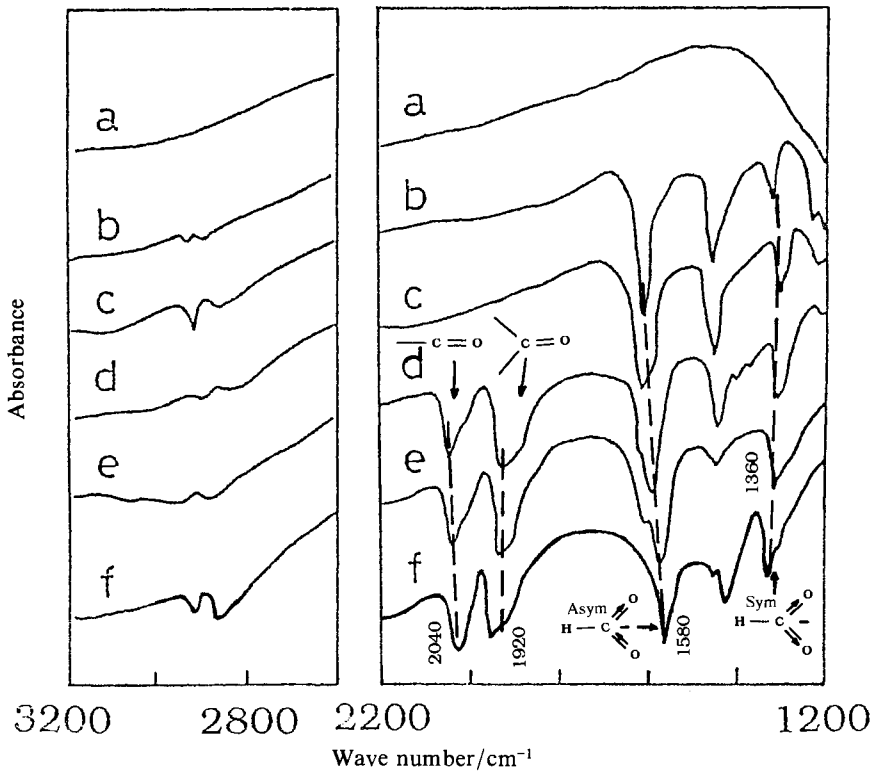

Fig. 6. IR spectra for CO_2/H_2 adsorbed on Re/ZrO_2. a: background, b: at 25°C, c: at 25°C in 8 h, d: at 100°C, e: at 200°C, f: at 300°C.

With Re/CeO_2 and Re/ZrO_2 catalysts, only one peak appeared at 284.6 eV, which was assigned to carbon atom. The C–O bond should be very strong in the state of CO_3^{2-}. No formation of methanol on Re/Al_2O_3 can be interpreted by the strong interaction between Re and γ-Al_2O_3, which causes a strong C–O bond.

Mechanism of Reaction. Figures 5, 6, and 7 show the FT-IR spectra of CO_2 and H_2 adsorbed on ZrO_2, Re/ZrO_2, and Re/CeO_2, respectively. The absorption bands at 1360, 1390, 1580, and 2880 cm^{-1}, which are assigned to $HCOO^-$(ad), appeared on the surfaces of both ZrO_2 and Re/ZrO_2 (Figs. 5 and 6). However, the bands at 2040 and 1920 cm^{-1}, which are assigned to CO(ad), appeared on Re/ZrO_2 (Fig. 6), but not on ZrO_2 (Fig. 5). The bonds at 2040 and 1920 cm^{-1} were assigned to linear and bridging carbonyls, respectively. Since the catalytic activity of Re/ZrO_2 for the reaction of CO_2 with H_2 was found to be much higher than that of ZrO_2, the $HCOO^-$(ad) species is not considered to be the active intermediate in the reaction. It seems likely that the CO(ad) species which was observed over Re/ZrO_2, but not over ZrO_2, is the active intermediate, although it is not certain which carbonyl is the intermediate. Since the CO species appeared at the adsorption temperature of 100 °C, at which no reaction took place, it is considered that the CO species did not result in the product, but from the adsorption of CO_2 and H_2. Thus, the reaction is considered to proceed by the conversion of CO_2 to CO(ad) followed by a reaction of CO(ad) with H(ad) formed on Re. This is in agreement with Iizuka's conclusion drawn from a comparative study between CO_2+H_2 and $CO+H_2$, for a Re/ZrO_2 catalyst.[2)]

The spectra for Re/CeO_2 were different from those for Re/ZrO_2. The band at 1220, 1300, 1410, 1460, and 1570 cm^{-1} were observed at the room temperature. The 1570 cm^{-1} band, which has a shoulder band at 1610 cm^{-1}, decreased its intensity and shifted to 1580 cm^{-1} with an increase in the temperature up to 130 °C, two new weak bands being formed at 1397 and 1550 cm^{-1}. The bands

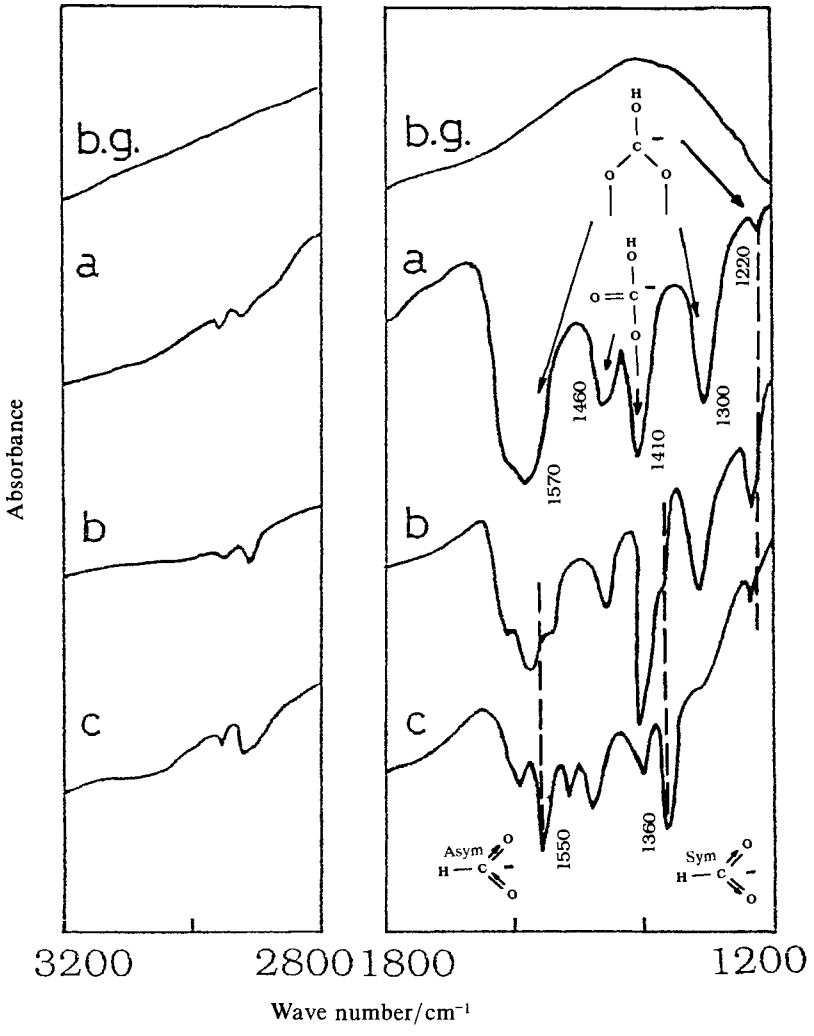

Fig. 7. IR spectra for CO_2/H_2 adsorbed on Re/CeO_2. b.g.: background, a: at room temp, b: at 130 °C, c: at 230 °C.

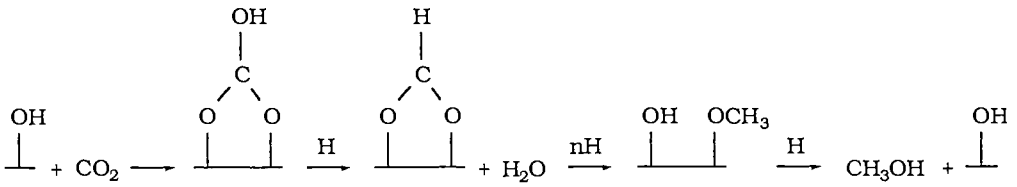

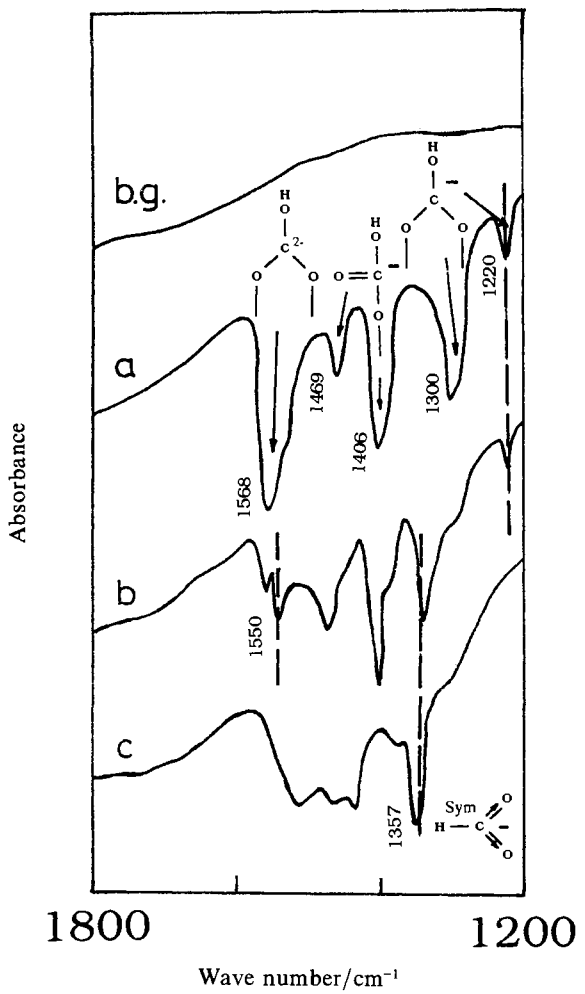

Fig. 8. IR spectra for CO_2 adsorbed on CeO_2. b.g.: background, a: at room temp, b: at 130 °C, c: at 230 °C.

at 1200 and 1610 cm^{-1} disappeared and the intensity of the bands at 1360, 1397, and 1550 cm^{-1} increased when temperature was raised to 230 °C. Since the $HCOO^-$(ad) species, which is evidenced by the bands at 1360 and 1550 cm^{-1}, exists on the surface of Re/CeO_2 at 230 °C under which a high yield of methanol was observed, it is suggested that the $HCOO^-$(ad) species is an active intermediate in the reaction over Re/CeO_2.

As shown in Fig. 8, the bands at 1220, 1300, 1406, 1469, and 1568 cm^{-1} were observed in the IR spectra of CO_2 adsorbed on CeO_2 at room temperature, but that the $HOCO_2^-$(ad) species, which is evidenced by 1220 cm^{-1}, disappeared when the temperature was increased to 230 °C; the 1357 cm^{-1} band was also observed at a higher temperature. This indicates that the $HOCO_2^-$(ad) and $HCOO^-$(ad) species could be formed on the surface of CeO_2 without Re. The XPS spectrum of the reduced Re/CeO_2 showed that an intense peak appeared at 530 eV, which was assigned to O_{1s} of the OH group. This indicates that a large amount of the OH group exists on the surface of Re/CeO_2. Therefore, CO_2 is considered to react with the surface OH (inserted to Ce–OH) to form $HOCO_2^-$(ad), as shown by the shoulder band at 1610 cm^{-1} in Fig. 6, in the first step. Then, $HOCO_2^-$(ad) reacts with H dissociated on Re (H–Re) to form $HCOO^-$(ad) over the surface Ce site on CeO_2 oxide, followed by the formation on CH_3O^- and CH_3OH by successive hydrogenation with hydrogen atoms which was dissociated on Re (H–Re). This can be illustrated by the scheme shown at the top of this page.

References

1) T. Iizuka, M. Kajima, and K. Tanabe, *J. Chem. Soc., Chem. Commun.*, **1983**, 638.

2) T. Iizuka, "Proc. 8th Intern. Congr. Catalysis," Verlag Chemie, Weinheim (1984), Vol. II, p. 221.

3) H. I. Yao and M. Shelef, *J. Catal.*, **44**, 392 (1976).

Increase of Solvent-Soluble Products of Coal by Repeated Butylation with Zinc and Butyl Iodide under Mild Conditions

Yoshiharu YONEYAMA,* Yutaka YAMAMURA, Kiyoshi HASEGAWA, and Tsutomu KATO
Department of Industrial Chemistry, Faculty of Engineering, Toyama University, Gofuku, Toyama 930
(Received November 29, 1990)

Yubari and Taiheiyo coals were repeatedly butylated with zinc metal powder and butyl iodide under mild conditions. After the benzene-soluble products (BS) from each reaction were combined the mixture was further butylated. The BS and its butylation products (Bu.BS) were fractionated by gel permeation chromatography. At each reaction step, BS with a similar structural character but different degrees of polymerization were solubilized for Taiheiyo coal; for Yubari coal BS with similar characteristics were solubilized. A large portion of these Bu.BS from both coals were solubilized in hexane. The molecular weight of BS decreased after butylation. These results suggest that this procedure brings about depolymerization as well as the introduction of butyl groups, while enhancing solubilization.

We previously developed a new alkylation procedure for coal solubilization,[1] which can effectively convert coal to benzene-soluble products under mild conditions (at 130 °C for 3—5 h under atmospheric pressure). The solvent-solubility of products is very high. Also, because of the ease of treating by the use of zinc metal powder and butyl iodide, this is a simple and safe method for coal solubilization; it is also suitable for examining coal structures.

In a previous paper we showed that the solubilization of low-rank coal in benzene is not increased by this method to a large extent,[1] and that the cleavage of the aliphatic linkage in coal structures increased with increasing number of alkyl groups attached to the aromatic rings.[2] In studies of coal solubilization under mild conditions, repeated reactions usually promoted bond cleavages.[3,4] It is thus expected that repeated butylation causes a high degree of coal solubilization; it is therefore of interest to examine changes in the degree of polymerization and that in the structural characteristics of coal products upon butylation.

The purpose of this study was to determine the solubility of reaction products obtained by repeated butylation, and to examine changes in their structural

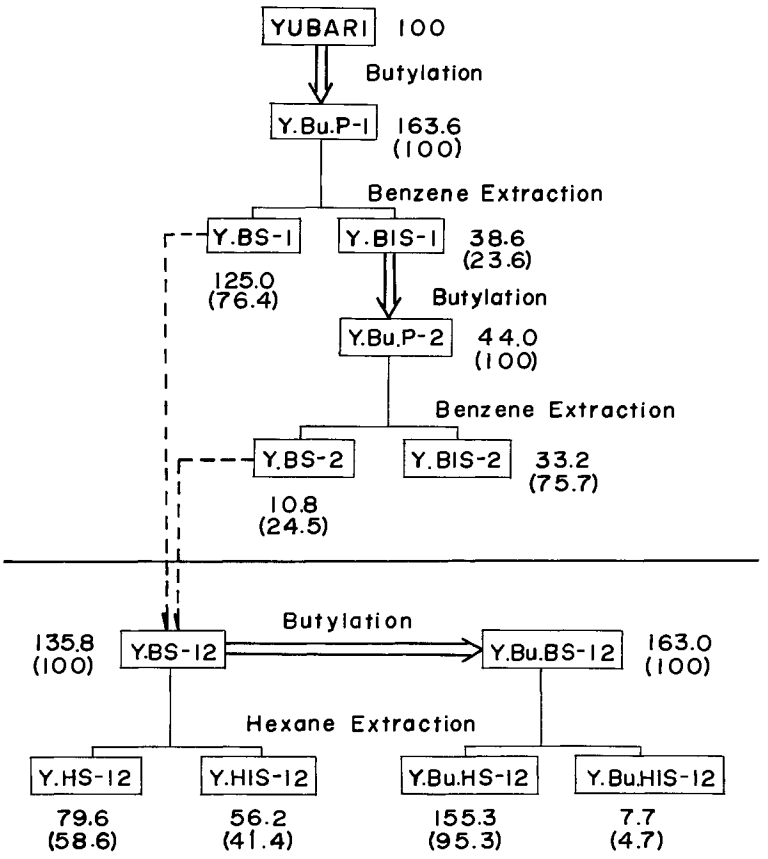

Scheme 1.

features.

Experimental

Yubari (C, 83.4%; H, 6.1%; N, 2.0%; Odiff, 8.5%; Ash, 5.1%) and Taiheiyo coals (C, 75.4%; H, 6.1%; N, 1.4%; Odiff, 17.1%; Ash, 8.3%) were used. The reaction was carried out in a similar way to that of a previous study:[1] 10 g of a coal sample, 40 g of zinc metal powder, and 100 ml of butyl iodide were placed in a 300 ml three-neck flask, while being agitated, the mixture was heated at 130 °C for 3.5—5 h under nitrogen in an oil bath. Then, unreacted butyl iodide was removed by evaporation and the mixture was washed with dilute hydrochloric acid to remove any unreacted zinc metal. The products were exhaustively extracted with hot benzene. The benzene-insoluble products (BIS) were successively butylated, twice for Yubari coal, and three times for Taiheiyo coal. The butylated products (Bu.P) were extracted with benzene, as described above. The benzene-soluble products (BS) from each reaction were combined, and the combined products further butylated. The BS and butylated BS (Bu.BS) were fractionated into hexane-soluble (HS) and hexane-insoluble products (HIS) by extraction with hexane. Details are given in Schemes 1 and 2. The BS and Bu.BS were separated into 8 and 7 fractions, respectively, by gel permeation chromatography (GPC), using packed columns of Bio-Beads S-X4 and S-X8 (25.4 mm i.d.×100 cm long); benzene was used as the eluent (cut volume, 6 ml). The number-average molecular weight (M_w) of each fraction was determined by VPO at 4—10 g kg^{-1} with a CORONA 114, using benzene as the solvent, and extrapolated to infinite dilution. Since most of the samples contained a small amount of iodine, the content was determined by the Schoeniger's method[5] to correct for analytical data. The FT-IR spectra were measured by a diffuse reflectance procedure using a JASCO FT/IR-3 spectrometer. The samples were ground with KBr prior to measurement. The structural parameters were estimated according to equations proposed by Brown and Ladner[6] and modified by Yokoyama et al.[7] The concerned structural parameters are as follows: The ratio of the number of aromatic carbons to the total number of carbons, f_a; the ratio of the number of peripheral aromatic carbons to total number of aromatic carbons (degree of aromatic ring condensation), H_{au}/C_a; the degree of aromatic ring substitution of the aliphatic chain, σ_{al}; the degree of aromatic

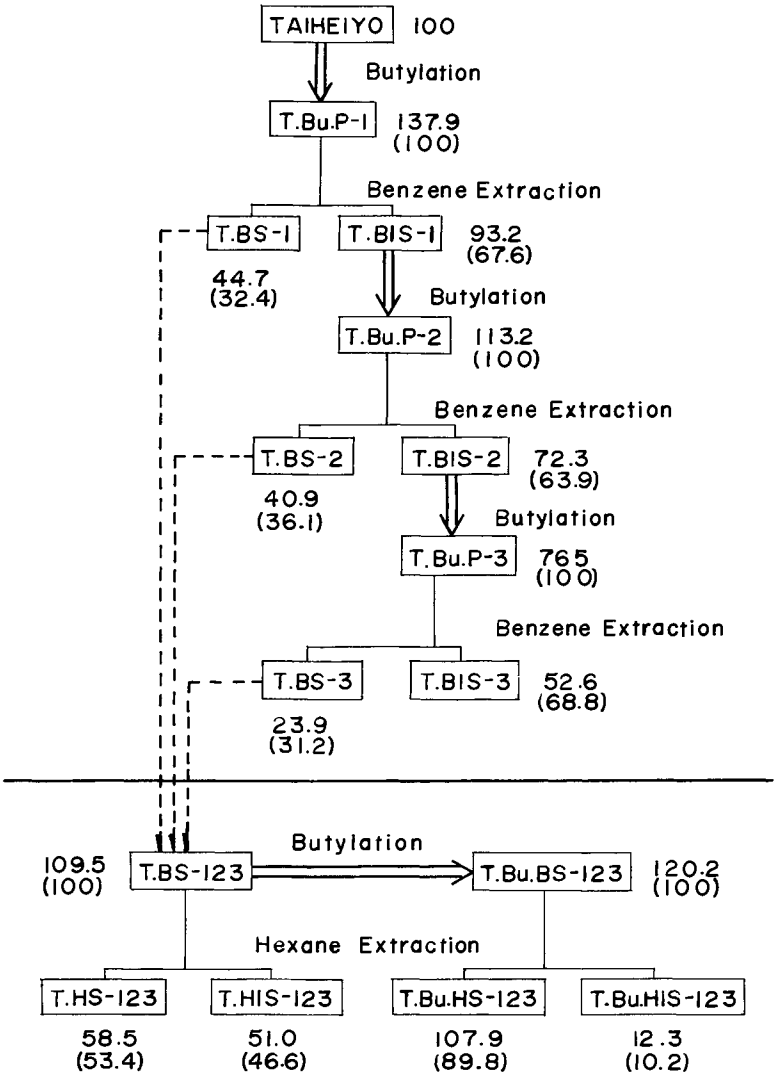

Scheme 2.

ring substitution of groups other than the aliphatic chain, σ_0; and the length of the aliphatic chain, n ($H_0/H_\alpha+1$). ^1H and ^{13} NMR spectra were taken on a JEOL JNM-FX 90Q spectrometer. Samples for measurements of the ^{13}C NMR spectra were prepared by dissolving approximately 100 mg of the coal products in 0.2—0.3 ml of $CDCl_3$; the spectra were measured with proton decoupling at a frequency of 22.49 MHz. The required pulse numbers were approximately 10000.

Results and Discussion

The yields of each fraction are shown in Schemes 1 and 2. The yields (daf) are based on the weights of the original coals and reactants, and are shown out of and within parentheses, respectively. Although the first Bu.P of Yubari coal could be dissolved in benzene to a high extent, the second one was less successful. In contrast, the benzene-solubility of Taiheiyo-Bu.P was almost constant at 30%, irrespective of the number of butylations. Table 1 shows the number of butyl groups introduced per 100 carbon atoms and the values of BS/Butyl calculated by the following equation:

$$\text{BS/Butyl (wt/wt)} = \frac{\text{Bu.P Yield (wt\%)} \times \text{BS Yield (wt\%)}/100}{\text{Bu.P Yield (wt\%)} - 100}.$$

These values, which are hereafter termed "solubilization efficiency (Es)", provide diagnostic criteria for judging coal solubilization. The butyl groups were much more easily introduced into coal during the first reaction than during later reactions; further, the introduction of butyl groups did not increase additional butylations. As can be seen from Figs. 1 and 2, the IR

Table 1. Number of Butyl Groups Introduced per 100 Original Carbon Atoms of the Reactant

Product	No. of butyl groups/100C				BS/Butyl (wt/wt)
	A.R.[a]	C.B.[b]	M.B.[c]	Mean	
Yubari					
Y.Bu.P-1	13.8	17.9	16.1	15.9	1.97
Y.Bu.P-2	4.1	3.5	3.5	3.7	2.00
Taiheiyo					
T.Bu.P-1	9.3	11.6	10.6	10.5	1.18
T.Bu.P-2	4.1	6.7	5.8	5.5	2.04
T.Bu.P-3	(4.2)	1.5	1.5	1.5	5.69

a) From change of H/C atomic ratio. b) From carbon balance. c) From material balance.

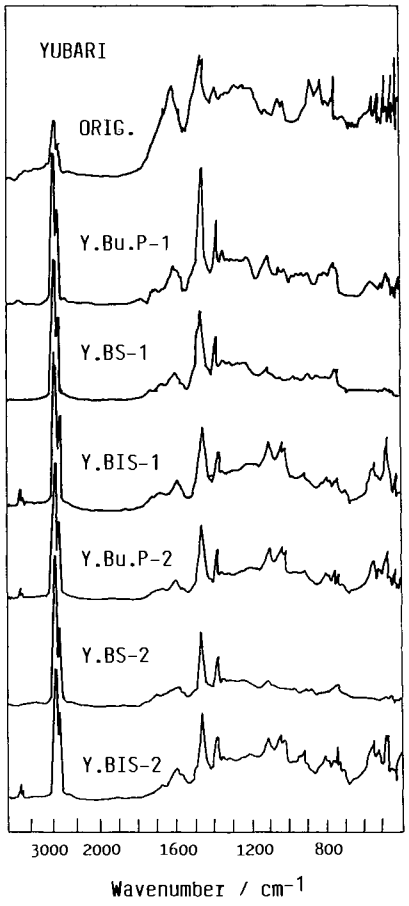

Fig. 1. FT-IR spectra of the products of Yubari coal.

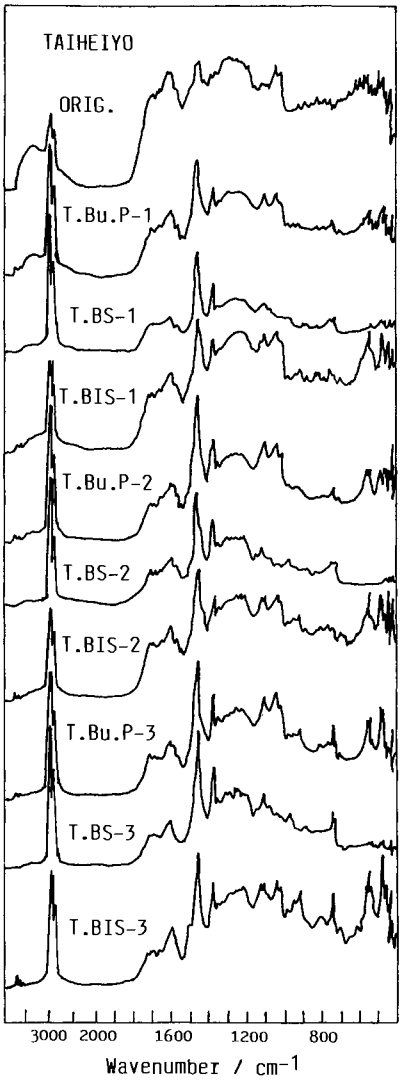

Fig. 2. FT-IR spectra of the products of Taiheiyo coal.

spectra of the BIS from both coals showed a moderately intense band of apliphatic CH stretching at 2958—2871 cm^{-1}, and an aliphatic CH deformation at 1465 and 1379 cm^{-1}, upon gradually increasing Es; this was opposite to the decrease of the number of butyl groups introduced. From these facts, it is concluded that many butyl groups remained in BIS support of further dissolution of Bu.P during additional reactions. As described above, since the cleavage of aliphatic linkages of coal structures increases with increasing number of alkyl groups attached to aromatic rings, it seems that the linkage-cleavage reactions significantly occur during later butylation.

In the solubilization of coal by alkylation methods it is difficult to determine whether the solvent-soluble products are derived from the coal or the by-products.[8] In this study the values of Es were larger than 1, and no significant absorption peaks due to by-products, which may arise from the reaction with only butyl iodide and zinc, were present in the ^{13}C NMR spectra of all the solvent-soluble products. This allows us to confirm that the solvent-soluble products are derived from coal and that butylation really occurs.

Tables 2 and 3 summarize the ultimate analyses, M_w and the results of structural analyses. For Taiheiyo coal, the M_w of the BS gradually increased upon the repetition of the reaction, while for Yubari coal their M_w were almost the same at each step. For both coals, the results of the structural analyses of BS at each step were similar each other. These results indicate that for Taiheiyo coal products with similar structures and different degrees of polymerization solubilized.

It has been reported that repeated reactions usually promote the reaction on coal solubilization under mild conditions.[3,4] A similar result was obtained in this study; even Taiheiyo coal, a low-lank coal, solubilized in benzene to a high extent.

It has also been reported that the ease of cleavage of the aliphatic linkage in the coal structure increases with increasing the number of alkyl groups on the aromatic rings.[2] In this study, all of the BS obtained during each step was combined, and then further butylated,

Table 2. Elemental Analyses, Structural Parameters, and M_w of the Products of Butylated Yubari Coal

Product	Elemental analysis/wt%[a]					Structural parameters					M_w
	C[b]	H[b]	N[b]	O[c]	I	f_a	σ_{al}	σ_o	H_{au}/C_a	n[d]	
Y.Bu.P-1	87.4	10.0	1.0	1.6	4.5	—	—	—	—	—	—
Y.BS-1	86.6	9.9	0	3.5	3.1	0.43	0.62	0.11	0.65	3.4	2540
Y.BIS-1	84.9	9.5	1.2	4.4	2.8	—	—	—	—	—	—
Y.Bu.P-2	84.8	10.4	1.0	3.8	4.1	—	—	—	—	—	—
Y.BS-2	85.0	10.1	0	4.9	3.6	0.39	0.66	0.17	0.64	3.7	2420
Y.BIS-2	83.6	10.0	1.0	5.4	3.2	—	—	—	—	—	—
Y.BS-12	85.9	9.7	0	4.5	3.0	0.44	0.61	0.15	0.60	3.5	2500
Y.Bu.BS-12	87.4	11.0	0	1.6	4.0	0.36	0.73	0.06	0.65	3.7	2670
Y.HS-12	85.9	10.5	0	3.6	2.5	0.38	0.62	0.11	0.71	3.6	1820
Y.HIS-12	80.5	8.8	0	10.7	3.2	0.45	0.52	0.29	0.77	3.1	22600
Y.Bu.HS-12	87.8	11.2	0	1.0	4.4	0.35	0.76	0.03	0.66	3.8	2360
Y.Bu.HIS-12	85.0	9.9	0	5.1	4.3	0.40	0.60	0.20	0.84	3.0	10000

a) Dry ash free basis. b) Iodine corrected values. c) By difference. d) $n=H_o/H_\alpha+1$.

Table 3. Elemental Analyses, Structural Parameters, and M_w of the Products of Butylated Taiheiyo Coal

Product	Elemental analysis/wt%[a]					Structural parameters					M_w
	C[b]	H[b]	N[b]	O[c]	I	f_a	σ_{al}	σ_o	H_{au}/C_a	n[d]	
T.Bu.P-1	80.0	8.8	1.0	10.2	3.4	—	—	—	—	—	—
T.BS-1	84.6	10.4	0	5.0	2.7	0.38	0.62	0.18	0.65	4.1	1590
T.BIS-1	78.1	8.2	1.2	12.5	2.4	—	—	—	—	—	—
T.Bu.P-2	81.5	9.5	0.9	8.1	5.1	—	—	—	—	—	—
T.BS-2	83.3	9.8	0	6.9	4.3	0.40	0.60	0.21	0.71	3.5	2530
T.BIS-2	81.7	9.2	1.0	8.1	4.7	—	—	—	—	—	—
T.Bu.P-3	81.9	10.1	0.9	7.1	6.1	—	—	—	—	—	—
T.BS-3	84.4	10.4	0	5.2	3.5	0.36	0.65	0.17	0.74	3.6	3140
T.BIS-3	80.9	9.6	0.8	8.7	3.2	—	—	—	—	—	—
T.BS-123	83.2	10.5	0	6.3	3.6	0.35	0.59	0.25	0.65	4.8	1880
T.Bu.BS-123	84.7	10.9	0	4.4	4.1	0.34	0.66	0.17	0.66	4.5	2310
T.HS-123	84.2	10.9	0	4.9	2.9	0.34	0.61	0.18	0.69	4.6	1050
T.HIS-123	82.5	9.6	0	7.9	5.2	0.40	0.61	0.26	0.70	3.5	12900
T.Bu.HS-123	83.7	10.9	0	5.4	2.8	0.33	0.63	0.19	0.76	4.2	1780
T.Bu.HIS-123	80.7	9.7	0	9.6	5.6	0.39	0.55	0.23	0.99	2.9	15000

a) Dry ash free basis. b) Iodine corrected values. c) By difference. d) $n=H_o/H_\alpha+1$.

structural parameters of these mixture and their butylation products, which were separated by GPC, are given in Tables 2 and 3. The changes of M_w and hexane-solubility are in Scheme 3. Repeated butylation increases the weight of the reactants. Butyl-free M_w of the butylated BS of Yubari (Y.Bu.BS-12) and Taiheiyo coals (T.Bu.BS-123) were 2140 and 2120, respectively. For Yubari coal, M_w of BS decreases after butylation. For Taiheiyo coal, M_w of the butylated BS (T.Bu.BS-123) was slightly higher than that of BS (T.Bu.BS-123). However, because the yields of the hexane-soluble products (HS) increased from 46.6% to 89.8%, it seems that M_w of the BS decreases due to this reaction. These results suggest that some linkages present in coal structures may cleave, as is expected from the results obtained from a study using model compounds.[2]

The GPC elution curves are shown in Figs. 3 and 4, and the M_w and structural parameters of these GPC fractions are listed in Tables 4 and 5. In each GPC separation, the samples which do not contain benzene-insoluble products were well fractionated in order of decreasing M_w; all of them were almost recovered after elution. Larsen et al.[9] have been reported that a larger-

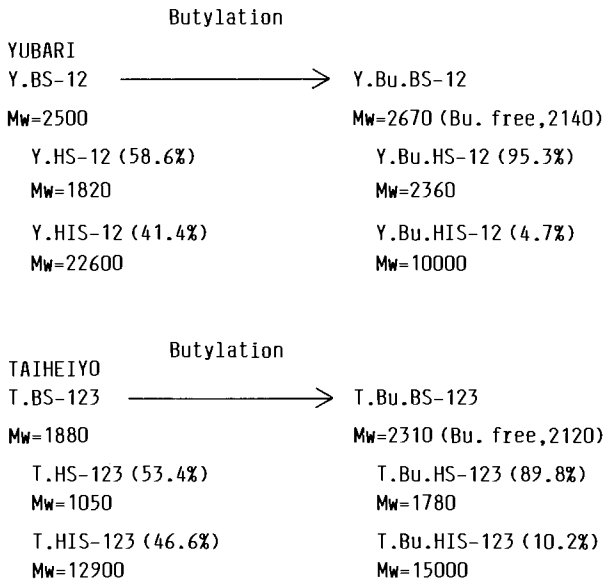

Scheme 3.

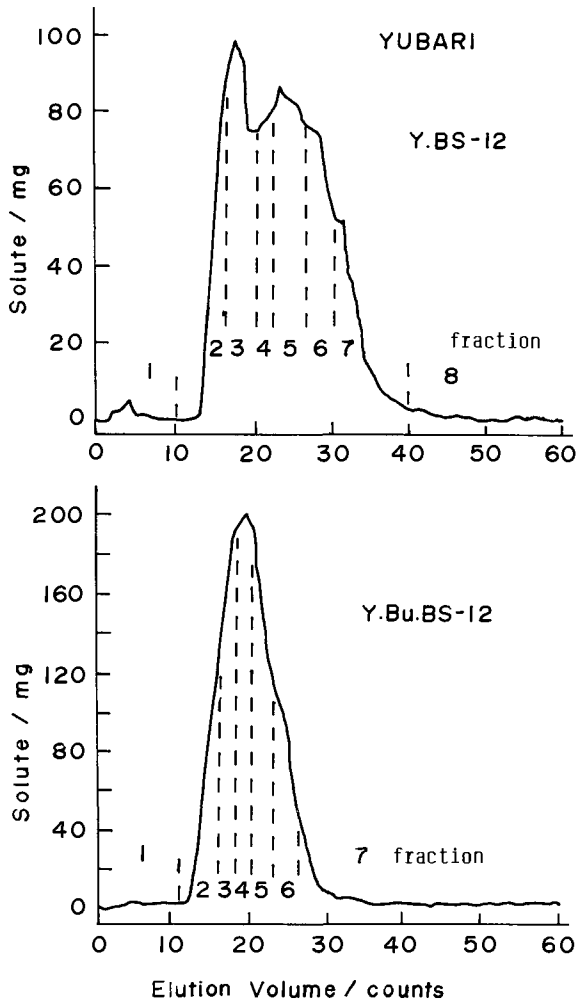

Fig. 3. GPC elution curves of benzene soluble products of Yubari coal.

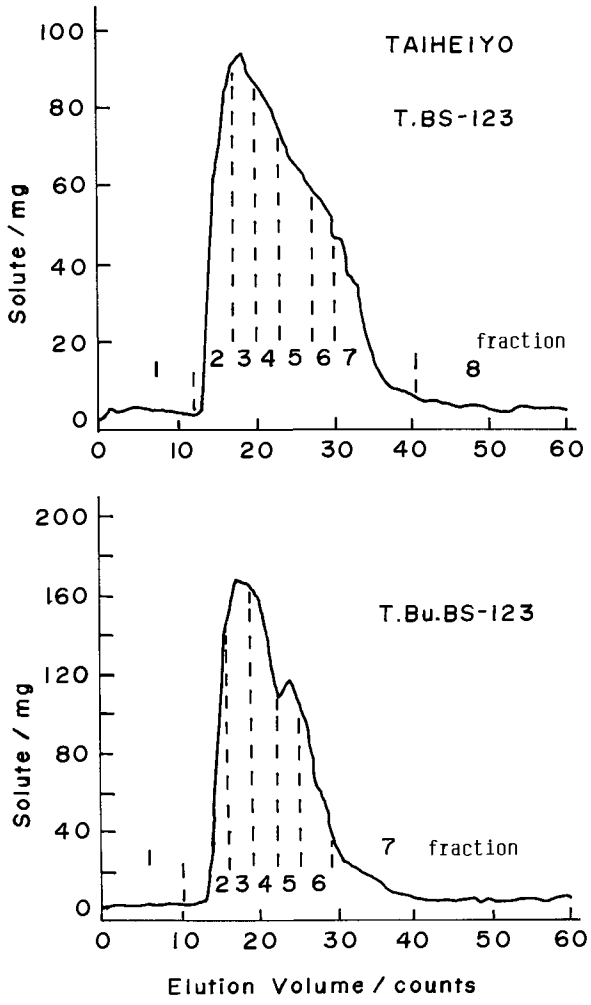

Fig. 4. GPC elution curves of benzene soluble products of Taiheiyo coal.

Table 4. Yields, M_w, and Structural Parameters of Yubari GPC Fractions

Sample	GPC Fr. No.	Yield %	M_w	Atomic ratio[a] H/C	O/C	Structural parameters f_a	σ_{al}	σ_o	n[b]	H_{au}/C_a
Y.BS-12	1	0.4	—	—	—	—	—	—	—	—
	2	11.6	4100	1.31	0.06	0.44	0.59	0.19	3.3	0.65
	3	22.6	4090	1.36	0.04	0.42	0.64	0.15	3.7	0.58
	4	12.3	3300	1.34	0.04	0.43	0.64	0.15	3.4	0.61
	5	21.6	3010	1.34	0.05	0.42	0.64	0.17	3.4	0.62
	6	16.4	2380	1.39	0.03	0.41	0.66	0.13	3.5	0.62
	7	10.5	1170	1.46	0.03	0.38	0.63	0.13	3.9	0.66
	8	1.0	—	1.50	0.08	0.35	0.42	0.28	5.3	0.82
Bu.Y.BS-12	1	0.6	—	—	—	—	—	—	—	—
	2	17.7	5390	1.44	0.03	0.38	0.71	0.11	3.7	0.60
	3	20.2	4600	1.48	0.02	0.37	0.75	0.09	3.6	0.64
	4	21.4	4060	1.48	0.02	0.37	0.74	0.06	3.8	0.62
	5	22.7	1830	1.48	0.02	0.37	0.73	0.10	3.9	0.61
	6	12.3	1320	1.49	0.02	0.36	0.76	0.08	3.9	0.60
	7	6.3	—	1.62	0.05	0.29	0.65	0.23	5.4	0.68

a) These values are corrected by the iodine weight (except Y.BS-12 Fr. 8 and Bu.Y.BS-12 Fr. 7). b) $n=H_o/H_a+1$.

Table 5. Yields, M_w, and Structural Parameters of Taiheiyo GPC Fractions

Sample	GPC Fr. No.	Yield %	M_w	Atomic ratio[a] H/C	O/C	Structural parameters f_a	σ_{al}	σ_o	n[b]	H_{au}/C_a
T.BS-123	1	1.2	—	—	—	—	—	—	—	—
	2	19.1	4710	1.42	0.06	0.38	0.64	0.21	3.6	0.69
	3	17.6	4000	1.43	0.06	0.38	0.62	0.23	3.7	0.71
	4	19.5	2740	1.45	0.05	0.38	0.63	0.21	3.9	0.68
	5	18.0	2280	1.48	0.05	0.36	0.64	0.20	3.9	0.71
	6	12.2	1750	1.50	0.06	0.35	0.63	0.23	4.2	0.70
	7	12.0	910	1.54	0.04	0.33	0.66	0.19	4.8	0.65
	8	1.6	—	1.55	0.11	0.32	0.47	0.37	4.9	0.91
Bu.T.BS-123	1	0.5	—	—	—	—	—	—	—	—
	2	14.9	7480	1.45	0.06	0.37	0.63	0.21	3.7	0.71
	3	26.1	4620	1.41	0.03	0.39	0.70	0.15	3.8	0.60
	4	21.1	3180	1.47	0.03	0.36	0.73	0.12	4.1	0.60
	5	17.3	2560	1.53	0.05	0.34	0.65	0.20	4.3	0.69
	6	12.7	1350	1.57	0.07	0.32	0.60	0.28	4.7	0.76
	7	8.4	—	1.74	0.04	0.24	0.62	0.26	7.8	0.66

a) These values are corrected by the iodine weight (except T.BS-123 Fr. 8 and Bu.T.BS-123 Fr. 7). b) $n=H_o/H_a+1$.

molecular-weight material is strongly associated with one another and significant amounts of low-molecular-weight materials were incorporated into them, consisting of a cross-linked structure found by the GPC separation. It seems that such incorporation can also occur during this reaction.

As can be seen from Tables 4 and 5, there was a downward tendency for f_a, and an upward one for σ_{al} with increasing number of butyl groups introduced. The decrease in the values of σ_o is attributed to a cleavage of the functional oxygen-containing groups, as reported in the results regarding model compound studies.[2]

To obtain a large amount of solvent-soluble products under this mild condition, the resulting sample is suitable for estimating the coal structure. However, the solvent-soluble products are so heavy that high-molecular-weight materials incorporated a significant amount of low-molecular-weight ones. Therefore, to obtain detailed information concerning the coal structure, the pretreatment of coal products (such as hydrogenation under mild conditions and/or chemical-type separation) would be required.

Some portions of the cross-linkage of the coal structure were cleaved into solvent-soluble products, as described above. However, M_w of the HS obtained by this method corresponds to that of a preasphaltene by other methods.[10] Sternberg and Delle Donne[11] have reported that because petroleum asphaltene, in contrast to coal, contained a considerable number of alkyl groups attached to the aromatic clusters, they are largely soluble in benzene, in spite of the fact that they comprise a large number of aromatic rings per cluster, in compari-

son with coal. These facts indicate that the high extractability of butylated BS with hexane can be attained by introducing many butyl groups; the occurrence of some cleavage of the aliphatic linkages was suggested by the model compound study.

References

1) H. Tsukashima, T. Kato, Y. Yoneyama, and Y. Sakai, *Fuel. Process. Technol.*, **14**, 193 (1986).
2) Y. Yoneyama, Y. Akaki, and T. Kato, *Bull. Chem. Soc. Jpn.*, **62**, 3959 (1989).
3) K. Niemann and H. -P. Hombach, *Fuel*, **58**, 853 (1979).
4) K. Ouchi, Y. Yokoyama, T. Katoh, and H. Itoh, *Fuel*, **60**, 1115 (1987).
5) A. Nara, "Yuuki-Biryo-Teiryobunseki," ed by K. Hozumi, Nankodo, Tokyo (1969), p. 383.
6) J. K. Brown and W. R. Ladner, *Fuel*, **39**, 87 (1960).
7) S. Yokoyama, H. Uchino, T. Katoh, and Y. Sanada, *Nenryokyokaishi*, **58**, 771 (1979).
8) R. H. Schlosberg, M. L. Gorbaty, and T. Aczel, *J. Am. Chem. Soc.*, **100**, 4188 (1976).
9) J. W. Larsen, L. Urban, G. Lawson, and D. Lee, *Fuel*, **60**, 267 (1981).
10) J. W. Larsen and P. Choudhury, *J. Org. Chem.*, **44**, 2856 (1979).
11) H. W. Sternberg and C. L. Delle Donne, *Am. Chem. Soc., Div. Fuel Chem., Prepr. Pap.*, **12**, 13 (1965).

UV and DSC Analyses of Suspensions of Mixtures of Phosphatidylcholine and a Fatty Acid Having a Diene Group

Etsuo HASEGAWA, Masanori HATASHITA, Noboru KIMURA, and Eishun TSUCHIDA*
Department of Applied Chemistry, Waseda University, Tokyo 169
(Received December 9, 1990)

Synopsis. The aqueous suspensions of the mixtures of a phosphatidylcholine (1,2-Bis[(2*E*,4*E*)-2,4-octadecadienoyl]-sn-glycero-3-phosphocholine (**1b**) and 1,2-dioctadecanoyl-sn-glycero-3-phosphocholine (**1a**)) with a fatty acid ((2*E*,4*E*)-2,4-octadecadienoic acid and octadecanoic acid), having a diene chromophore were analyzed by DSC and UV measurements. The phase transition was dependent on the composition of the lipid mixtures. The UV spectral change of the diene chromophore of a fatty acid for the **1a** mixtures corresponded well with the phase transition determined by DSC analyses, but not for the **1b** mixtures.

Liposomes composed of phosphatidylcholine and other lipids have been studied as biological membrane models.[1] However, liposomes are often unstable and tend to aggregate and precipitate during storage. To overcome these problems, charged compounds such as fatty acid, phosphatidic acid, dihexadecyl hydrogenphosphate, and octadecylamine, which can control the surface potential of liposomes, are incorporated in phosphatidylcholine bilayers. Among them, fatty acids are interesting because they are one of the components of biological membranes and are present at high concentrations in certain membranes: for example, 8% in rat liver plasma.[2] They control various membrane-mediated cellar functions,[3-6] such as the enzyme activity, membrane fluidity, permeability, and fusion. A mixture of fatty acid and phosphatidylcholine is a simple model membrane used for understanding the roles of fatty acids in biological membranes.

Studies on the mixtures of a fatty acid and a phosphatidylcholine having saturated acyl chains have revealed:[7-10] (1) fatty acids eliminate the pretransition; (2) mixing is good at the 1:2 molar ratio of saturated phosphatidylcholine and fatty acids having the same carbon numbers (1:2 complex formation); (3) the thermal phase transition is a lamellar-to-nonlamellar phase, and (4) the apparent pKa of fatty acid in the lipid bilayer is surprisingly large.

A phase-transition analysis of lipid bilayer membranes is normally carried out by DSC, NMR, and ESR methods. In addition to these types of measurements, a simple method using UV measurements has been reported: for example, on lamellar aggregates of single-chain amphiphiles containing a chromophore, such as an azobenzene residue.[11] The shift of λ_{max} of the chromophore is useful for a phase-transition analysis. A phosphatidylcholine having polymerizable groups (dienes) in acyl chains is also used as a UV probe of bilayer transitions.[12]

We describe here an application of a diene-containing fatty acid to bilayer transition analysis of fatty acid–phosphatidylcholine mixtures by a UV measurement, and compare the results with those of a DSC measurement.

Experimental

Materials. 1,2-Bis[(2*E*,4*E*)-2,4-octadecadienoyl]-sn-glycero-3-phosphocholine (**1b**), (2*E*,4*E*)-2,4-octadecadienoic acid (**2b**), and 1,2-dioctadecanoyl-sn-glycero-3-phosphocholine (**1a**) were purchased from Nippon Oil & Fats Co., Ltd. 1-Hexadecanoyl-(2*E*,4*E*)-2,4-octadecadienoyl-sn-glycero-3-phosphocholine (**1c**) was prepared.[13] The purity was confirmed by thin-layer chromatography on silica gel. Octadecanoic acid was purchased from Kishida Chem. Co., Ltd. **2b** was recrystallized once from hexane. Benzene was distilled from calcium hydride. Phosphatidylcholine and fatty acid mixtures were prepared by freeze-drying from dry benzene.

Lipid suspensions were prepared by adding a prescribed amount of distilled water to the freeze-dried powder. They were suspended with glass beads (diameter: 2—3 mm) on a Vortex mixer at a temperature above the transition temperature under a nitrogen atmosphere for 15 min.

DSC was performed by using DSC 10 (Seiko I&E). Samples were placed into silver microtubes, and measurements were run with temperature scanning at 2 °C min^{-1} under a nitrogen atmosphere.

The temperature-dependence of the absorption maximum corresponding to the diene groups of lipid suspension was analyzed in a quartz cell (path-length: 10 mm) with UV spectrometry (Shimadzu MPS-2000) with a heating rate of 1 °C min^{-1}.

Results and Discussion

A saturated phospholipid (1,2-dioctadecanoyl-sn-glycero-3-phosphocholine (**1a**)) and an unsaturated one (1,2-bis-[(2*E*,4*E*)-2,4-octadecadienoyl]-sn-glycero-3-phosphocholine (**1b**)) were used and mixed with a saturated fatty

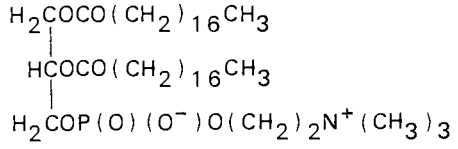

1a

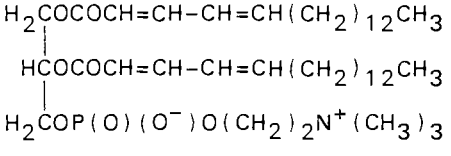

1b

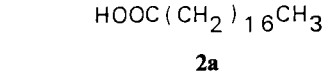

2a

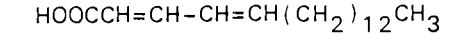

2b

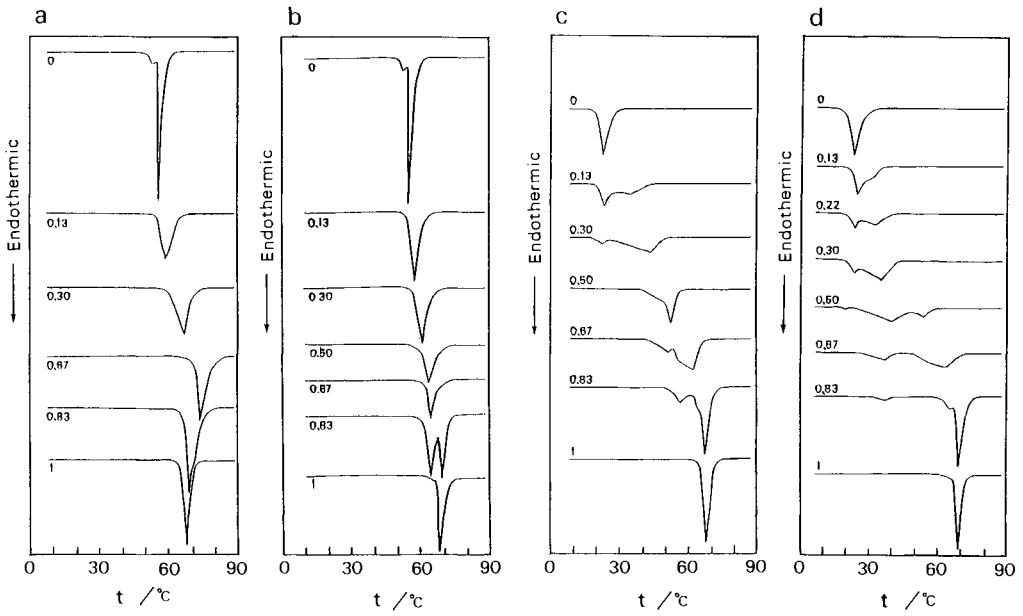

Fig. 1. DSC thermograms for the various mixtures of the phospholipids and the fatty acids with different molar ratios. (a): **1a**/**2a**, (b): **1a**/**2b**, (c): **1b**/**2a**, (d): **1b**/**2b**. Mole fraction of fatty acid is indicated beside each thermogram.

acid (octadecanoic acid (**2a**)) or an unsaturated one ((2*E*,4*E*)-2,4-octadecadienoic acid (**2b**)). All of the compounds have acyl chains of the same carbon numbers (18), since it has been reported that mixing strongly depends on a combination of the chain length of a phospholipid acyl chain and the fatty acid.[8] The phase-transition behaviors were analyzed by DSC measurements and by observing the UV spectral change of the diene chromophores upon increasing the temperature at a constant rate.

The DSC analyses were performed on lipid suspensions packed in silver microtubes, but not on aluminum ones, due to the presence of an acid compound. Figure 1 shows DSC curves for various mixtures of the phospholipids and the fatty acids with different molar ratios. As shown in Fig. 1b, the mixture of **1a** and **2b** showed a single peak upon increasing the fraction of the fatty acid component up to 0.67 and the transition temperature increased, as in the case of mixtures of **1a** and **2a** (Fig. 1a). This means that two components mix well under mole fractions of the fatty acid up to 0.67. An increase of the fatty acid component to more than 0.67 causes the formation of a domain of excess fatty acid, in addition to a homogeneously mixed domain of **1a** and **2b** with a molar ratio of 1:2. This can be seen by the appearance of two peaks.

Apart from these two mixtures, those related to unsaturated phospholipid **1b** showed complexed behaviors, as indicated in Figs. 1c and 1d. The mixtures showed three transitions in the DSC curves with increasing the mole fraction of the fatty acid component. This indicates that the good mixing found in mixtures of the saturated phospholipid **1a** with fatty acids did not occur in those of the unsaturated phospholipid **1b** mixtures. Figures 1c and 1d indicate that the phase transitions at lower temperatures change to transitions at higher temperatures with an increase in the fatty acid fraction.

At mole fractions of a fatty acid less than 0.3 the mixture showed two peaks, corresponding to the presence of two blocks: one comprising pure **1b**, and the other comprising **1b** and a fatty acid with a molar ratio of 1.6—2.0:1.0. The molar ratio could be calculated from a decrease in the endothermic heat change, compared to that of a pure **1b** suspension. Upon further increases in the mole fraction of a fatty acid component up to 0.67, the first intermediate mixture changed to the second and third mixtures along with a concomitant decrease of **1b**, itself, and the first intermediate mixture. At a much higher content of a fatty acid, the **1b** mixtures form a block of excess fatty acid; this was confirmed by the appearance of an endothermic peak of pure fatty acid **2a** or **2b**, as in the cases of mixtures of **1a** and a fatty acid. Therefore, the third peak may be responsible for the 1:2 homogeneous mixtures that are normally found in the saturated lipid systems described above.

It has been reported that the UV chromophores of phospholipids and synthetic surfactants can be used to determine the phase-transition temperatures of their molecular assemblies.[11,12] The absorption maxima change sharply at the transition temperature. Here, we tried to use the diene chromophore of fatty acid **2b** to analyze mixtures with phospholipids **1a** or **1b**.

Mixtures of **1a**/**2b** gave a spectral change in the UV region with the temperature. Figure 2 summarizes the changes in the absorption maxima of various mixtures of **1a** and **2b** with increased temperature. The changes were sharp in the mixtures (the mole fraction of **2b** up to 0.67) and the phase-transition temperatures could be calculated. Mixtures of **1b** with a fatty acid had only one transition.

Table 1. Comparison of Transiton Temperatures Determined by DSC and UV Measurements[a)]

Lipid mixture	Transition temperature (T_c)/°C							
	Mole fraction of fatty acid							
	0.0	0.13	0.22	0.30	0.50	0.67	0.83	1.00
1a/2a	55	55	—	61	—	72	66	65
1a/2a (2b)	(54)	(57)	—	(62)	(68)	(69)	—	—
1a/2b	55	54	—	58	61	62	62, 69	68
	(54)	(54)	—	(58)	(63)	(63)	—	—
1b/2a	19	17, 26	—	17, 24	49	43, 52	52, 65	65
	(18)	(19)	(22)	(27)	(36)	(35)	—	—
1b/2b	19	21	20, 25	18, 24	16, 26, 47	27, 49	25, 62, 68	68
	(18)	(21)	(21)	(23)	(31)	(27)	—	—

a) The values in the parentheses mean transition temperatures determined by UV measurements.

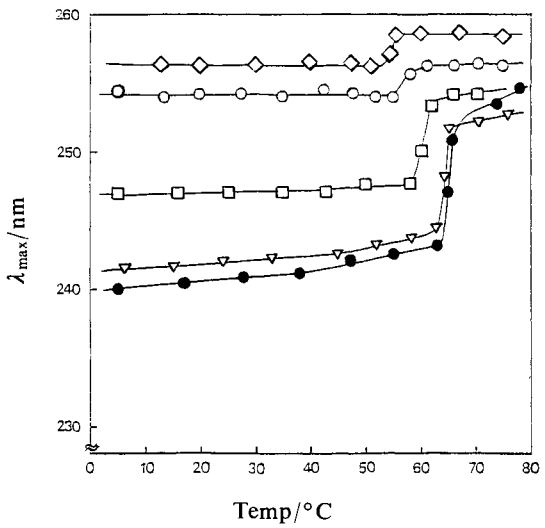

Fig. 2. Temperature dependence of the absorption maxima for diene groups in various mixtures of **1a** and **2b**. Mole fraction of **2b**: 0 (◇), 0.13 (○), 0.30 (□), 0.50 (▽), 0.67 (●).

Table 1 summarizes the transition temperatures (T_c) of various lipid mixtures determined by DSC and UV measurements. For **1a**/**2b** and **1a**/**2a** mixtures, both measurements gave the same transition temperatures, respectively, but not for the mixtures of **1b** with a fatty acid. The results show that care must be taken when using a UV probe for the determination of phase-transition temperatures.

These results indicate for the miscibility of phosphatidyl choline with fatty acid that: (1) the (2*E*,4*E*)-diene group containing a fatty acid is capable of mixing well with saturated phosphatidylcholine as does a saturated fatty acid; (2) the presence of the (2*E*,4*E*)-diene moiety in diacyl chains of phosphatidylcholine interferes with the homogeneous mixing with a fatty acid. In addition to these results, a diene-containing phospholipid, 1-hexadecanoyl-2-[(2*E*,4*E*)-2,4-octadecadienoyl]-sn-glycero-3-phosphocholine (**1c**, T_c: 24 °C),[12)] gave a single transition peak (T_c: 57 °C) when it was mixed with **2a** with a molar ratio of 1:2. This indicates that the (2*E*,4*E*)-2,4-octadecadienoyl group at the 2-position of the glycerol backbone is not responsible for non-homogeneous mixing of **1b** with a fatty acid.

References

1) G. Gregoriadis, "Liposome Technology," CRC Press, Flo., U. S. A. (1983), Vol. II; J. H. Fendler, "Membrane Mimetic Chemistry," John Wiley and Sons, New York, U. S. A. (1984).

2) T. K. Ray, V. P. Skipski, M. Barclay, E. Essner, and F. M. Archibald, *J. Biol. Chem.*, **244**, 5528 (1969).

3) J. Orly and M. Schramm, *Proc. Natl. Acad. Sci. U. S. A.*, **72**, 3433 (1975).

4) D. Papahadjopoulos, D. Hui, and G. Poste, *Biochim. Biophys. Acta*, **448**, 245 (1976).

5) N. Schramm, B. Eisenkraft, and E. Barkai, *Biochim. Biophys. Acta*, **135**, 44 (1967); L. Wojtczak, *J. Bioenerg. Biomembr.*, **8**, 293 (1976); T. J. Andreasen and M. G. McNamee, *Biochemistry*, **19**, 4719 (1980); N, Muranishi, N. Takagi, S. Muranishi, and H. Sezaki, *Chem. Phys. Lipids*, **28**, 269 (1981); K. D. Philipson and P. R. Ward, *J. Biol. Chem.*, **260**, 9666 (1985).

6) Q. F. Ankong, D. Fisher, W. Tampion, and J. A. Lucy, *Biochem. J.*, **136**, 147 (1973); H. L. Kator and J. H. Prestegard, *Biochemistry*, **17**, 3592 (1978); C. E. Creutz, *J. Cell. Biol.*, **91**, 247 (1981); L. G. Herbette, C. Fevreau, K. Segalman, C. A. Napolitano, and J. Watras, *J. Biol. Chem.*, **259**, 1325 (1984).

7) S. P. Verma, D. F. H. Wallach, and J. D. Sakura, *Biochemistry*, **19**, 574 (1980).

8) S. Mabrey and J. M. Sturtevant, *Biochim. Biophys. Acta*, **486**, 444 (1977); *idem.*, *Methods Membr. Biol.*, **9**, 237 (1978).

9) D. Marsh and J. M. Seddon, *Biochim. Biophys. Acta*, **690**, 117 (1982); T. Heimberg, N. J. P. Ryba, U. Wuerz, and D. Marsh, *ibid.*, **1025**, 77 (1990).

10) H. L. Kantor and J. H. Prestegard, *Biochemistry*, **17**, 3592 (1978); M. Ptak, M. Egret-Charlier, A. Sanson, and O. Bouloussa, *Biochim. Biophys. Acta*, **600**, 387 (1980); S. E. Schullery, T. A. Seder, D. A. Weinstein, and D. A. Bryant, *Biochemistry*, **20**, 6818 (1981).

11) M. Shimomura, R. Ando, and T. Kunitake, *Ber. Bunsenges. Phys. Chem.*, **87**, 1134 (1983).

12) S. Takeoka, H. Iwai, H. Ohno, and E. Tsuchida, *Bull. Chem. Soc. Jpn.*, **62**, 102 (1989), and references cited therein.

13) E. Hasegawa, N. Kimura, M. Hatashita, C. Makino, and E. Tsuchida, *Macromolecules*, (1990), to be submitted.

Terminal Polar Substituent Effect on the Liquid Crystalline Properties of a Series of 4-Octyloxy-*N*-(4-substituted benzylidene)anilines

Seiichi MIYAJIMA,* Takehiko ENOMOTO, Tomohiro KUSANAGI, and Takehiko CHIBA
Department of Chemistry, College of Humanities and Sciences, Nihon University,
Sakurajosui, Setagaya-ku, Tokyo 156
(Received January 5, 1991)

Synopsis. Mesomorphic properties are studied on the title compounds where substituents are F, Cl, Br, I, NO_2, and CN. Besides the known mesophases, nematic and smectic Ad, in CN and NO_2 homologues, stable smectic A and B phases were observed in either of the Cl and Br derivatives. Metastable nematic and smectic A phases were found in F derivative. The effects of terminal polar substituents, stabilization of the smectic A phase by moderately polar substituents, and of the nematic phase by strongly polar substituents, were confirmed.

The liquid crystalline compound, 4-octyloxy-*N*-(4-cyanobenzylidene)aniline (CBOOA) has been studied extensively as one of the typical compounds having smectic A (S_A) and nematic (N) phases. CBOOA is very popular not only because it exhibits stable S_A and N phases at relatively low temperatures but also because of its interesting physical properties. McMillan's early study[1] which suggested the existence of a second order S_A–N phase transition in this compound stimulated a good number of experiments on the nature of this phase transition.[2-7] It is also of particular interest that CBOOA was shown to exhibit a thermotropic reentrant nematic (RN) phase transition at high pressures.[8,9] It has been conceived until now that this peculiar property is attributable to the strong antiferroelectric intermolecular interaction caused by the cyano end group.[10,11] Noting that strong polarity of the terminal substituent is essential, Prasad et al.[12] studied whether RN phase also appeared at high pressures when the cyano group is replaced by nitro group. In this homologue (NBOOA), however, the S_{Ad}/N phase boundary was quite straight in the p–T phase diagram, and the reentrant nematic phase transition did not take place until up to 2 kbar. In this way the kind of terminal substituent delicately affects the liquid crystalline properties. In a recent paper[13] we showed that terminal polar substituents counteracts on the thermodynamical stability of the S_A state, namely, moderately polar substituents stabilize the S_A state whereas strongly polar substituents relatively stabilize the N state. It was also shown that all of the parameters of the Kobayashi–McMillan's pair and mean field potentials were determined experimentally. In order to further study the terminal polar substituent effect, we prepared a series of compounds, 4-octyloxy-*N*-(4-substituted benzylidene)anilines, where X are H,

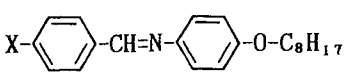

F, Cl, Br, and I. The liquid crystalline properties are studied and compared among the seven compounds including the known cyano and nitro derivatives, and the substituent effect is compared with the results obtained in the three-ring systems.[13] Although the conventional namings XBOOA may also be used, the symbols [X] are used for short in this paper.

Experimental

The materials were synthesized through dehydration condensation of 4-X-substituted benzaldehyde with 4-octyloxy aniline, the latter of which was prepared from potassium 4-acetamidophenoxide by Williamson's method.[14] Chemical analyses gave good agreement with the formulae.

Dipole moment of the molecule was determined with heterodyne beat method in dilute benzene solutions at 25 °C. The temperatures and the entropies of phase transitions were measured with a Seiko Electronics DSC 20 calorimeter. The temperature was calibrated by the melting of zone-refined biphenyl, and the transition enthalpy was calibrated by the solid–solid phase transition of potassium nitrate and the melting transitions of gallium, indium, tin, and biphenyl. Smectic layer spacings were determined from the first order quasi-Bragg reflection of copper $K\alpha$ radiation. The scattering angle was calibrated by the (001) peak of the monoclinic c-polytype powder of stearic acid. Proton NMR lineshape was recorded in [Cl] and [Br] to assess the molecular alignments in the smectic phases with a laboratory-made Fourier-transform NMR spectrometer. The liquid crystalline phases were identified with the aids of texture observation, X-ray diffraction, proton NMR spectrum, and the DSC experiments.

Results and Discussion

Dipole Moment of the Molecule. Values of the dipole moments, μ, of the molecules are given in Table 1. Since the value of μ in [H], 1.77 D (1 D=1 Debye=3.3356×10^{-30} C m), measures contributions from the linkage groups, –CH=N– and –O–, the larger values for the other six compounds show that a permanent dipole parallel to the long molecular axis is formed by the polar substituent. The halogeno compounds exhibit values in the range of 2.60 ± 0.08 D, and [NO_2] and [CN] have values greater than 5 D.

Identification of the Liquid Crystalline Phases. In the known compound, [CN] and [NO_2],[12,15,16] the reported mesophases, S_A and N, were confirmed from the microscopic texture observations. Differential scanning calorimetry and the texture observation revealed that no liquid crystalline phases appear in [H] and [I]. [F] showed metastable N and S_A phases of only narrow temperature ranges on cooling from the isotropic (I) phase. In either of [Cl] and [Br], two liquid crystalline phases were found, both of which were of smectic type in microscopic appearances. DSC study revealed that the smectic-to-smectic and the smectic-to-isotropic phase transitions were strongly of first order, and the entropy of the former transition was about half in mag-

Table 1. Dipole Moment μ of the Molecule, and the Smectic Layer Spacings, d, in the S_B and S_A Phases

Compound	μ/Debye	d/Å (S_B)	d/Å (S_A)
[H]	1.77	—	—
[F]	2.52	—	—
[Cl]	2.56	25.1	24.7
[Br]	2.68	25.8	25.4
[I]	2.65	—	—
[NO_2]	5.14	—	31.9
[CN]	5.21	—	35.7

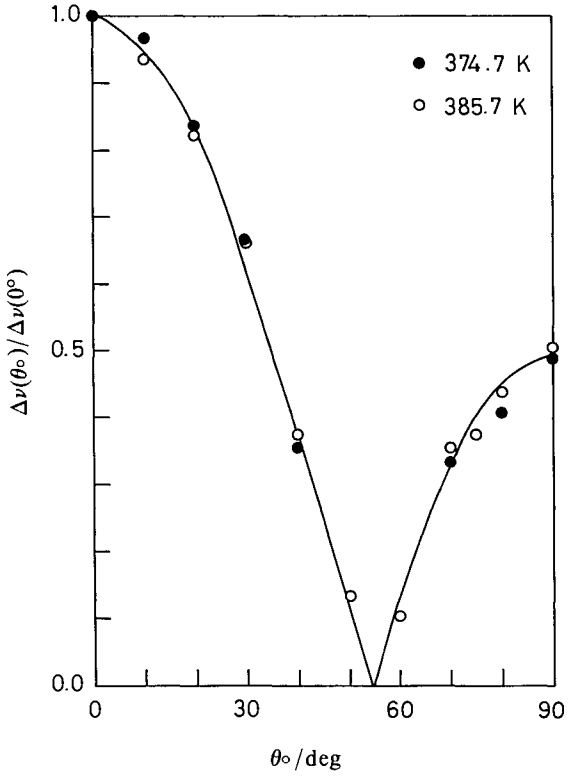

Fig. 1. The angular dependence of the proton NMR splitting frequency normalized to that taken at $\theta_o=0°$ in the high (○) and low (●) temperature smectic phases of [Br]. Each phase is assigned to S_A and S_B in the text. θ_o is the angle between the external magnetic field and the averaged direction of the director. The solid line represents $p_2(\cos\theta_o)$ where p_2 is the Legendre polynomial of rank two.

nitude that of the latter transition. More decisive results in identifying these phases were obtained from the angular dependence studies of the proton NMR lines. Figure 1 shows the angular dependence of the dipolar splitting of the phenyl protons in [Br]. The open and the filled circles show the data taken in the high and low temperature smectic phases, respectively. If the smectic states are of the orthogonal type (in which the averaged direction of the molecular long axis is not tilted from the layer normal), the dipolar splitting frequency is given by the equation,[17]

$$\Delta\nu(\theta_o)/\Delta\nu(0°) = |p_2(\cos\theta_o)|, \quad (1)$$

irrespective of the magnitude of orientational order parameter. Here θ_o is the angle between director and the external magnetic field, and p_2 (x) is the Legendre polynomial of rank two. Figure 1 clearly show that the experimental results follow Eq. 1, and the dipolar splitting vanishes as θ_o approaches the magic angle (54.7°). Both of the smectic phases are thus revealed to be of orthogonal type. The result in [Cl] was quite similar to that of [Br]. Judging also from the textures, DSC, and X-ray results, the high and low temperature mesophases were concluded to be S_A and S_B, respectively. The phase transition behaviors of all the compounds studied are summarized in Table 2.

Layer Spacings in the Smectic Phases. The smectic layer spacings were measured in S_A and S_B phases, and are summarized in Table 1. Judging from the stereochemical molecular model, the molecular length along the long axis is 23—24 Å in this series of compounds. The observed values of d in the S_A phases of [Cl] and [Br] shows that these mesophases are of the monolayer type, whereas those in [NO_2] and [CN] belong to S_{Ad} modification, as has been already reported. The observed d in the low temperature smectic (S_B) phase in [Cl] and [Br] is consistent with the monolayer model, and is also consistent with the NMR result.

Entropies of Phase Transitions. The temperatures and the entropies of phase transitions are summarized in Table 2. The entropies of N–I phase transitions, ΔS_{NI}, observed in [NO_2] and [CN] were 0.249 R and 0.273 R, respectively, where R is the gas constant. These are considerably smaller than the universal value of 0.42 R predicted by the statistical theories of Maier and Saupe[18] and McMillan.[19] On the other hand, the entropies of S_B–S_A transition, ΔS_{BA}, observed in [Cl] and [Br] were 0.908 R and 1.034 R, respectively, both of which are larger than 0.559 R predicted by Meyer and McMillan.[20] The S_{Ad}–N transition entropy was too small to be detected in [CN], while it amounted to 0.165 R in [NO_2]. Details on the difference in nature of the two S_{Ad}–N phase transitions will be described elsewhere.[21] Table 2 also summarizes the total amount of the entropies of phase transitions in each of the compounds. It is of some interest to point out that the accumulated entropies of phase transitions in each of the compounds amount to like values, 116±8 J K^{-1} mol^{-1}, proving that the entropy of the condensed state in such a rod-like compound is acquired mainly at the phase transitions in a stepwise manner until the isotropic symmetry is finally obtained. This fact was first pointed out by Tsuji et al.[22] in the 4-substituted *N*-(4-hexyloxybenzylidene)anilines, analogues to our series having reversed linkage group and shorter alkyl chain, where the accumulated entropy was 93.6±2.5 J K^{-1} mol^{-1}. The latter value is comparable to but a little smaller than our result. The difference (22 J K^{-1} mol^{-1}) is attributable to the difference in chain length because of the following assessment. If three conformations are allowed for each of the methylene group, the conformational entropy shared by the two methylene units is $2R \ln 3$=18.3 J K^{-1} mol^{-1}, which explains the above dif-

Table 2. Temperatures and Entropies of Phase Transitions

Observed stable phases are designated by *. The plain figures represent the temperatures of phase transition in Kelvin, and the parenthesized figures stand for the discontinuities of entropy at the phase transitions in the unit of J K^{-1} mol^{-1}. Accumulated entropy of phase transitions for each compound is shown in the last column.

Compound	CII		CI		S_B		S_A		N		I	$(\Sigma\Delta S_{tr})$
[H]	*	—		—		—		—		342.7	*	
										(121)		(121)
[F][a)]	*	—		—		—		—		360.5	*	
										(124)		(124)
[Cl]	*	—		363.3	*	370.4	*	—		381.4	*	
				(84.7)		(7.55)				(16.3)		(108.6)
[Br]	*	—		365.5	*	384.8	*	—		388.2	*	
				(80.3)		(8.60)				(19.8)		(108.7)
[I]	*	378.53	*	—		—		—		392.83	*	
		(21.4)								(92.2)		(113.6)
[NO_2]	*	—		—		336.5	*	349.3	*	358.5	*	
						(107)		(0.360)		(2.07)		(109.4)
[CN]	*	339.9	*	—		347.0	*	356.2	*	382.1	*	
		(33.19)				(85.6)		(ca. 0)		(2.27)		(121.1)

a) Metastable N and S_A phases were found on cooling from I.

ference fairly well.

Effect of Terminal Polar Substituents on the Liquid Crystalline Properties. It was shown by the present authors[13] that terminal polar substituents bring about increase in the intermolecular attractive force, and also bring about counteracting contributions to the stability of the S_A phase in the homologous series of 4-substituted *N*-[4-(4-octyloxybenzoyloxy) benzylidene]anilines (OBBX series). In that case, the tendency of liquid crystal formation was strongly enhanced in the homologous compounds with polar end groups compared with the unsubstituted one. It was also shown that moderately polar substituents like halogens significantly stabilized the S_A phase, but extremely polar substituents such as cyano group relatively stabilized the N phase. The general conclusions still hold in the present series: namely, the liquid crystalline nature is enhanced in [Cl], [Br], [NO_2], and [CN] compared with the non-mesogen [H]. It is also recognized that N phase is relatively stabilized in [NO_2] and [CN], whereas destabilized and lost in [Cl] and [Br]. It is the expected tendency that the halogeno compounds favor the S_A state. It should be noted, however, that two-ring compounds generally have less tendency of forming the liquid crystalline phase than three-ring compounds, and it is the major difference in the phase transition behaviors of the present and the OBBX series. The survival of the high temperature crystalline phase up to above 390 K in [I] and the existence of only metastable N and S_A phases in [F] will be attributable to this general tendency.

We thank Dr. Hatsumi Mori for her kind advice and collaboration in DSC measurements.

References

1) W. L. McMillan, *Phys. Rev. A*, **7**, 1419 (1973).
2) P. E. Cladis, *Phys. Rev. Lett.*, **31**, 1200 (1973).
3) S. Torza and P. E. Cladis, *Phys. Rev. Lett.*, **32**, 1406 (1974).
4) K. C. Chu and W. L. McMillan, *Phys. Rev. A*, **11**, 1059 (1975).
5) R. A. Wise, A. Olah, and J. W. Doane, *J. Phys. [Paris], Colloq.*, **36**, C1-117 (1975).
6) M. F. Achard, F. Hardouin, G. Sigaud, and H. Gasparoux, *J. Chem. Phys.*, **65**, 1387 (1976).
7) D. Armitage and F. P. Price, *Mol. Cryst. Liq. Cryst.*, **38**, 229 (1977).
8) P. E. Cladis, R. K. Bogardus, and D. Aadsen, *Phys. Rev. A*, **18**, 2292 (1978).
9) D. Guillon, P. Cladis, D. Aadsen, and W. B. Daniels, *Phys. Rev. A*, **21**, 658 (1980).
10) L. Longa and W. H. de Jeu, *Phys. Rev. A*, **26**, 1632 (1982).
11) J. Prost and P. Barois, *J. Chim. Phys. (Paris)*, **80**, 65 (1983).
12) S. Krishna Prasad, S. Pfeiffer, G. Heppke, and R. Shashidhar, *Z. Naturforsch., A*, **40**, 632 (1985).
13) S. Miyajima, K. Nakazawa, K. Niikura, Y. Ujiiye, M. Yashiro, and T. Chiba, *Liq. Cryst.*, **8**, 707 (1990).
14) P. Keller and L. Liebert, "Solid State Physics," ed by F. Seitz and D. Turnbull, Academic Press, New York (1978), Supplement Vol. 14, pp. 19—76.
15) R. A. Vora and N. Dixit, "Liquid Crystals," ed by S. Chandrasekhar, Heydon, London (1980), pp. 585—588.
16) P. C. Jain, S. R. S. Kafle, R. A. Vora, and N. Dixit, *Mol. Cryst. Liq. Cryst.*, **103**, 287 (1983).
17) C. A. Veracini, "Nuclear Magnetic Resonance of Liquid Crystals," ed by J. W. Emsley, D. Reidel Publ. Co., Dordrecht (1985), Chap. 5, pp. 99—121.
18) W. Maier and A. Saupe, *Z. Naturforsch., A*, **13**, 564 (1958); *ibid.*, **14**, 882 (1959); *ibid.*, **15**, 287 (1960).
19) W. L. McMillan, *Phys. Rev. A*, **4**, 1238 (1971); *ibid.*, **6**, 936 (1972).
20) R. J. Meyer and W. L. McMillan, *Phys. Rev. A*, **9**, 899 (1974).
21) S. Miyajima and T. Chiba, unpublished result.
22) K. Tsuji, M. Sorai, H. Suga, and S. Seki, *Mol. Cryst. Liq. Cryst.*, **90**, 85 (1982).

A Method for Preparing New Elongated-Shaped Silica Sols

Akitoshi YOSHIDA,* Yoshitane WATANABE, Mikio ANDOO, and Kenji TANIMOTO
Central Research Institute, Nissan Chemical Industries, Ltd., 722 Tuboi-cho, Funabashi, Chiba 274
(Received February 6, 1991)

Synopsis. An active silicic acid sol was added to a mixture of a $Ca(NO_3)_2$ aqueous solution and a NaOH aqueous solution, then the mixture was heated for several hours under stirring at 100—150 °C to obtain a silica sol. The silica sol consisted of elongated-shaped colloidal particles desirable for film formation.

Most of the commercially available silica sols have spherical particles[1,2] of 4—150 nm in diameter or cocoon-like nonspherical particles.[3] Iler[4] prepared an amorphous silica sol by heating a wet silica gel in an autoclave.

However, he did not succeed in establishing the conditions to prepare sols with other shapes, such as an elongated shape which is desirable for filmformation.

In this note, we first report the preparation of elongated-shaped silica sols. The method is based on the addition of Ca^{2+} ions to an active silicic acid sol, and is represented by the following scheme:

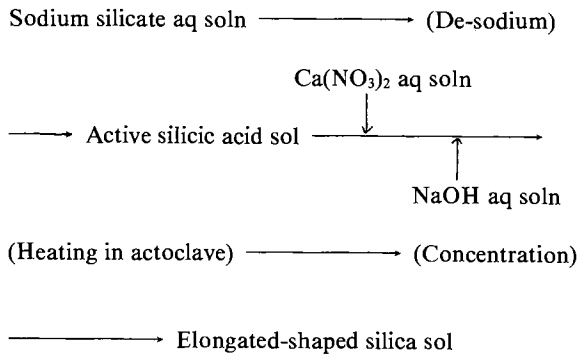

In this process, several factors such as (1) the amount of Ca^{2+} and Na^+ ions contained in silica sols, (2) the reaction temperature, and (3) silica concentration, significantly influenced on shape of the final silica sol particles.

The experimental findings are qualitatively summarized as follows:

1) The Ca^{2+} ion is strongly adsorbed to the surface of the active silicic acid sol. In the course of heating the sol in an autoclave, the Ca^{2+} ion plays a crucial role in the formation of elongated-shaped particles, namely, the ion controls the directionality of particle growth. Too high a Ca^{2+} ion content leads to rapid gelation of the sol, while too low a Ca^{2+} ion content makes the particle shape spherical.

2) A base such as NaOH is necessary for the particle growth of colloidal silica where the Na^+ ion is strongly adsorbed to the surface of the active silicic acid sol. When the Na^+ ion content is too high, the particle-shape becomes spherical, while the sol is liable to gelate if it is too low.

3) When the silica content is too high, the sol readily gelates during the reaction.

4) A moderately high reaction temperature gives silica sols with a large specific surface area and the elongatedshape. Too high a temperature leads to rapid gelation of the silica sols, and too low a temperature gives spherical particles with a small specific surface area. To obtain the elongated-shaped silica sols it is essential to control these factors strictly. For instance, when a silica sol composed of SiO_2 3.2%, CaO 208 ppm, and Na_2O 550 ppm (SiO_2/Na_2O molar ratio=60) was allowed to react at 130 °C for 6 h and then concentrated up to 20% in silica content, the sol is elongated. A transmission electromicroscope (TEM) photograph of the elongated-shaped silica sol thus obtained is shown in Fig. 1. It is seen that the elongated-shaped sol growing in one direction has an almost uniform size of 10—15 nm in diameter. The average particleslength measured by the dynamic light scattering method (N4,

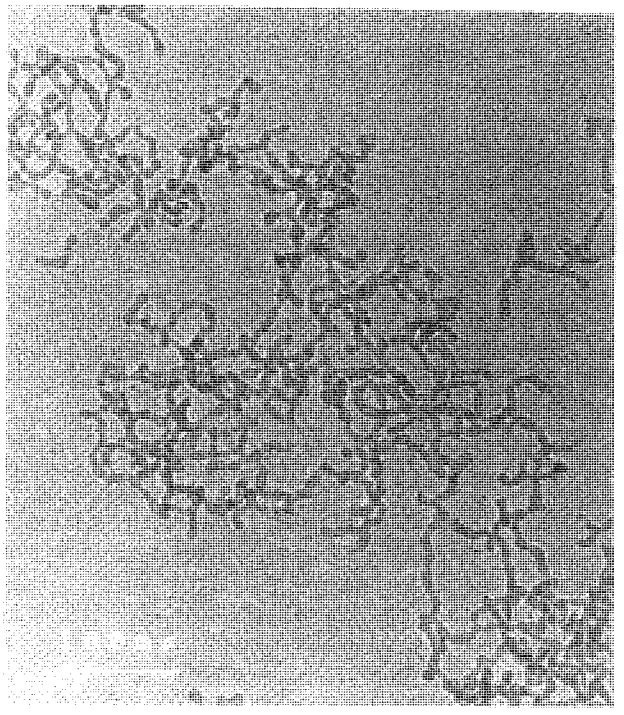

Fig. 1. TEM image of the elongated silica sol.

Table 1. Characteristics of the Elongated Silica Sol

Specific gravity (at 20 °C)	1.130
pH (at 25 °C)	9.65
Viscosity/cP[a] (at 25 °C)	46.3

a) 1 P=10^{-1} Pa s.

D1nm) was 65.8 nm, and the ratio of the particle size measured by this method and by the BET method (D2nm) was 5.4. The characteristics of the sol are given in Table 1.

Under the above-mentioned preparation conditions, the amounts of Ca^{2+} and Na^{+} ions correspond to 0.65 wt% and 1.7 wt% of SiO_2, respectively. Hence, on assumption that the silanol sites on the surface of the elongated-shaped silica particles are exchanged with these ions during the reaction, the fractions of these ions in the total surface silanol sites (i.e., the surface coverages of the ions) are 3.9% for Ca^{2+} and 18.7% for Na^{+}.

References

1) R. K. Iler, "Colloid Chemistry of Silica and Silicate," Cornell Univ. Press (1956), p. 200.
2) T. Graham, *J. Chem. Soc. London,* **15**, 216 (1862).
3) W. Cummings, B. P. 1244334 (1971).
4) E. Matijevic, "Surface and Colloid Science," John Wiley & Sons, New York (1973), Vol. 6, p. 13.

XANES Spectra of $Co(ala)_3$ and $Co(acac)_3$ in Solid and Solution

Mitsuru SANO
Department of Chemistry, College of General Education, Nagoya University, Nagoya 464-01
(Received May 28, 1990)

Synopsis. XANES spectra of $[Co(ala)_3]$ and $[Co(acac)_3]$ have been measured in solid and solution. Comparisons of spectra of the species in solid and solution give a basis for the spectral change being attributable to intermolecular interactions.

X-Ray absorption spectra near K-edge have been measured for many years. The relations between XANES features and electronic structures of the absorbing atom have been extensively studied. In spite of some successful studies,[1] full understanding still remains for further systematic studies.

In recent papers,[2,3] the author reported that systematic measurements of Co K-edge XANES for Co(III) complexes showed counter-ion effect for $[Co(NH_3)_6]X_3$ (X=Cl, Br, and I), and that the Co XANES spectra of $[Co(H_2O)_6](ClO_4)_2$, $[Co(H_2O)_6]SO_4$, and $[Co(NH_3)_6]Br_3$ in solid are different from those in solution. These findings suggest that "the counter ion effect" in solid does not originate from a long-range effect as ejected electrons directly interact with counter ions but from a short range effect where XANES is influenced by slight distortion of a local electronic and geometrical structure induced by counter ions. Then, if this suggestion is correct, it is expected that XANES spectra of non-charged compounds without counter ions in solution will differ from those in the crystal in which a strong intermolecular interaction such as hydrogen-bonding exists. In order to make sure this, I measured XANES spectra of (+)mer-$[Co(ala)_3]$ (ala^-=alaninate) which has hydrogen bonds in the crystal and those of $[Co(acac)_3]$ ($acac^-$=4-pentanedionate) which has no strong intermolecular interaction in the solid, and compared them with those in solution.

The cobalt(III) complexes were prepared and recrystalized according to standard methods.[4] Organic solvents were purified by distillation. A solid sample was ground and diluted with boron nitride and contained in a plastic cell. A small volume of each sample solution (0.1 M, 1 M=1 mol dm^{-3}) was contained in a teflon cell with teflon windows. X-Ray absorption measurements were carried out at the BL-10B on the storage ring of Photon Factory (KEK). Synchrotorn radiation (2.5 GeV, 120—280 mA) was monochromatized with a chnnel-cut Si(311) monochromater. Other instrumental details are given in Ref. 5. The absorption spectra were measured in the transmission mode at room temperature. All spectra have been normalized to give an edge jump of 1.0.

Figure 1 shows the XANES spectra and their first

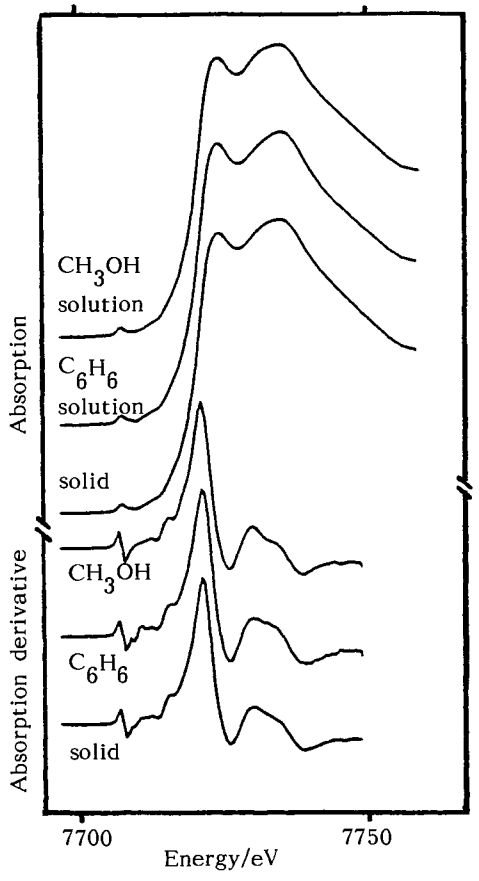

Fig. 1. Co K edge spectra and their derivatives of $[Co(acac)_3]$ in solid and solutions.

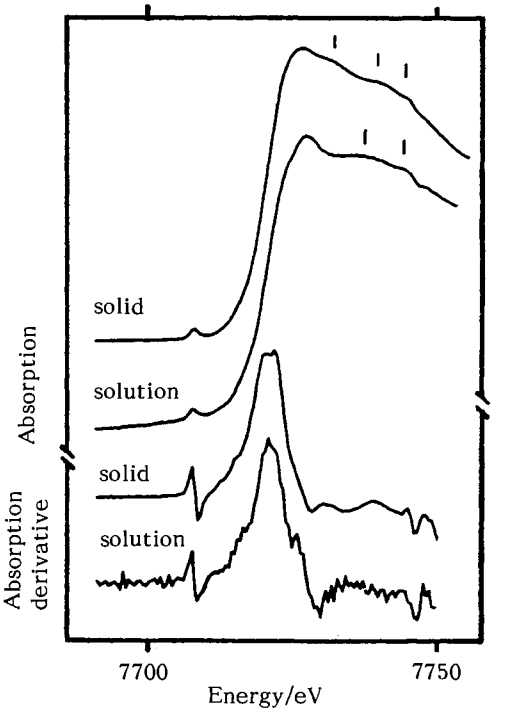

Fig. 2. Co K edge spectra and derivatives of mer-$[Co(ala)_3]$ in solid and aqueous solutions.

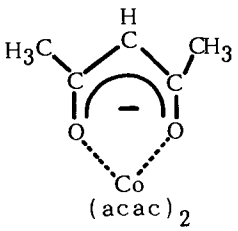

Scheme 1.

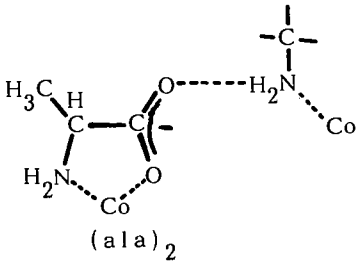

Scheme 2.

derivatives of $[Co(acac)_3]$ in crystal and solution, and Fig. 2 the corresponding spectra of $[Co(ala)_3]$. The spectra of $[Co(acac)_3]$ are similar to each other and also similar to those of its acetonitrile and dimethylformamide solutions. Although the XANES spectrum of $[Co(ala)_3]$ in crystal generally resembles that in aqueous solution, some small differences are found in 7725—7750 eV; two absorptions can be observed in solution and three absorptions in solid.

The crystal structures of both complexes have been well studied.[6-7] The coordination form for $[Co(acac)_3]$ is schematically shown by Scheme 1 and six Co–O bond lengths are practically the same (Co–O=1.883—1.892 Å).[5] This suggests the absence of strong intermolecular interactions in solid $[Co(acac)_3]$. This is also supported by the fact that the compound easily sublimes. Since there is no strong intermolecular interaction in solid $[Co(acac)_3]$, it is expected that the conditions of geometrical and electronic structures are the same in solid and in solution. This can be the reason for the XANES spectra being similar to each other. In $[Co(ala)_3]$,[7] the alaninate ions coordinate to a cobalt ion as shown in Scheme 2. Strong hydrogen bonds exist between the complexes in the crystal in Scheme 2. This strong interaction between the molecules causes a change in the geometrical arrangement and charge distribution within the molecule, which will result in a change in the electronic state. The interaction between the complex and water in aqueous solution is much weaker than that between the complexes in solid. The intermolecular interaction in crystal different from that in solution results in a change in a different geometrical and electronic structure and thus a change in the spectra of $[Co(ala)_3]$.

The present result exemplifies that the XANES spectral change is attributable to the intermolecular interaction associated with a geometrical and electronic local change rather than direct interactions of the electron wave with surrounding atoms. It also discloses what is "the counter-ion effect". Yamashita et al.[8] reported a correlation between XANES patterns and crystal packing structures. These findings demonstrate how much change of XANES in solid by intermolecular interaction. It is useful to compare with XANES of solid compounds and theoretical consideration.

The author thank professor Hideo Yamatera at Daido Institute of Technology for his useful discussion and his encouragement. This work has been performed under the approval of the Photon Factory Program Advisory Committee (Proposal No. 86015).

References

1) N. Kosugi, *Kotai Butsuri*, **25**, 329 (1990), and the references cited therein; A. Bianconi, J. Garcia, and M. Benfatto, *Top. Curr. Chem.*, **145**, 30 (1988); T. Miyanaga, I. Watanabe, S. Ikeda, K. Tashiro, and T. Fujikawa, *Bull. Chem. Soc. Jpn.*, **61**, 3199 (1988), and the references cited therein.

2) M. Sano, *Inorg. Chem.*, **27**, 4249 (1988).

3) M. Sano, *Chem. Phys. Lett.*, **148**, 331 (1988).

4) B. E. Douglas and S. Yamada, *Inorg. Chem.*, **4**, 1561 (1965); H. F. Bauer and W. C. Drinkard, *J. Am. Chem. Soc.*, **82**, 5031 (1960).

5) H. Oyanagi, T. Matsushita, M. Ito, and H. Kuroda, *KEK Report*, **1983**, 83—100.

6) G. J. Krunger and E. C. Reynhardt, *Acta Crystallogr., Sect. B*, **30**, 822 (1974).

7) R. Herak, B. Prelesnik, and I. Krstanovic, *Acta Crystallogr., Sect. B*, **34**, 91 (1978).

8) S. Yamashita, Y. Yanase, T. Yamaguchi, and H. Wakita, *Bull. Chem. Soc. Jpn.*, **62**, 2902 (1989).

Intercalation of a Triethylenetetramine-Substituted Cyclodextrin by Co(II)- and Ni(II)-Montmorillonites

Tsuyoshi KIJIMA,* Hiromoto NAKAZAWA,† and Satoshi TAKENOUCHI†
Department of Industrial Chemistry, Faculty of Engineering, Miyazaki University, Miyazaki 889-21
† National Institute for Research in Inorganic Materials, Tukuba, Ibaraki 305
(Received September 26, 1990)

Synopsis. The intercalation of mono[6-[(8-amino-3,6-diazaoctyl)amino]-6-deoxy]-β-cyclodextrin (CDtrien) by Co(II)- and Ni(II)-montmorillonites was examined at 25 °C. At low uptakes, the CDtrien molecules in both minerals form a monolayer, 13—14 Å thick, with their cavity axes perpendicular to the silicate layers. At higher loadings, guest molecules with the same orientation form a bilayer in Co- (21.8 Å thick) and Ni-montmorillonites (17.6 Å). Their thicknesses are larger than those for the Cu-and Zn-analogues, 16.1 Å, i.e. twice the molecular thickness.

New porous solids have been required for the platforms of immobilized enzymes, for improved columns in adsorption and ion-exchange chromatography, and for effecting gas separations.[1] Our attention has been focused on developing microporous inclusion compounds having novel characteristics. An organic and inorganic double host material is an example which can be obtained by the intercalation of host molecules such as cyclodextrins in inorganic hosts.[2-4] We recently studied the intercalation of mono[6-[(8-amino-3,6-diazoctyl)amino]-6-deoxy]-β-cyclodextrin(CDtrien) by Na-, Ca-, Cu-, and Zn-montmorillonites, and revealed the mechanism of the CDtrien intercalation and the arrangement of the guest molecules in the host cavities.[5] This paper reports on the intercalation of CDtrien by Co(II) and Ni(II)-montmorillonites.

In a previous paper,[5] the mode of intercalation by Ca-montmorillonite was explained by the formation of CDtrien$(H_2O)_2$–Ca complexes. However, after this paper was published, it was found by analytical scanning electron microscopy that the uptake of CDtrien by Ca-montmorillonite is accompanied by a remarkable release of Ca, which forms a second phase. A reexamination by X-ray diffraction suggested that the second phase is calcium carbonate. Thus, the previous explanation must be modified as follows: the intercalation by Ca-montmorillonite proceeds by an ion exchange of interlayer Ca^{2+} ions with the divalent cationic forms of CDtrien, as in the case of Na-montmorillonite.

Experimental

The CDtrien and the Na-montmorillonite used as starting minerals were the same as those used in a preceding study.[5] The Co(II)- and Ni(II)- exchanged minerals were prepared by placing the Na-montmorillonite in a 1.25 mol dm^{-3} solution of $CoCl_2$ and $NiCl_2$ at 25°C for 10d, respectively. The exchanged products were fully washed with water, centrifuged, and lyophilized. The Co(II)- and Ni(II)-clays were soaked in an aqueous solution containing 0.25, 1, 1.5, and 3.0 mmol of CDtrien per gram of clay at 25 °C for 10 d, centrifuged, fully washed with water, and air-dried at 40 °C. The CDtrien and water contents in the resulting solids were determined by thermogravimetric analysis. An X-ray diffraction measurement was made using Fe-$K\alpha$ radiation, and 1-tetradecanol having a long d-spacing (39.90 Å) was used as an external standard.

Results and Discussion

The uptakes of CDtrien for Co(II)- and Ni(II)-montmorillonites are plotted against the amount of CDtrien added (Fig. 1). The interlayer spacings of the resulting solids were determined from 001 reflections in the X-ray diffraction patterns. Figure 2 shows the variation of Δ, the thickness of the intercalated layer obtained by subtracting 9.5 Å, the thickness of the silicate layer, from the observed d-spacings. When 0.25 mmol of CDtrien was added per gram of each clay, a phase with a Δ value of 12.9—14.1 Å appeared and coexisted with its parent host phase. With a further addition of CDtrien the solids were converted into a single phase with a Δ value of 21.8 (Co-intercalate) or 17.6 Å (Ni-intercalate). The uptake curves of both intercalates showed saturation. The CDtrien uptakes were accompanied by the release of interlayer metal ions, as shown in Fig. 1.

Table 1 summarizes the Δ values and compositions of intercalates of Co- and Ni-montmorillonites with

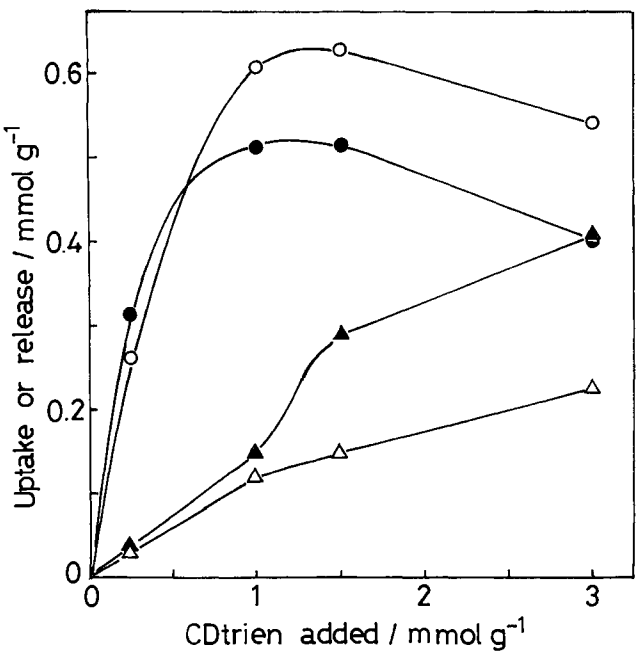

Fig. 1. CDtrien uptake by (○) Co- and (●) Ni-montmorillonites and release of (△) Co^{2+} and (▲) Ni^{2+} ions as a function of CDtrien added.

Table 1. Characterization of Intercalates of Co(II)- and Ni(II)-Monmorillonites with CDtrien at Its Full Loadings

Interlayer metal ion	Δ/Å	Amount of releasable metal ions/mmol g^{-1} clay[a]						Amount of CDtrien/mmol g^{-1} clay[a,d]		
		Initial			Desorbed		Remaining	Total	Neutral form	Divalent cationic form
		Total	Int[b]	Ext[c]	Int[b]	Ext[c]				
Co	21.8	0.63	0.54	0.09	0.06	0.09	0.48	0.63	0.57 (90.5)	0.06 (9.5)
Ni	17.6	0.61	0.54	0.07	0.22	0.07	0.32	0.51	0.29 (56.9)	0.22 (43.1)

a) Anhydrous form of clay. b) The amount of exchangeable cation held as interlayer counter ions for the negatively charged silicate layers. c) The amount of adsorbed cations as any neutralized species on the external surface of crystals. d) Contents in mol% are given in parentheses.

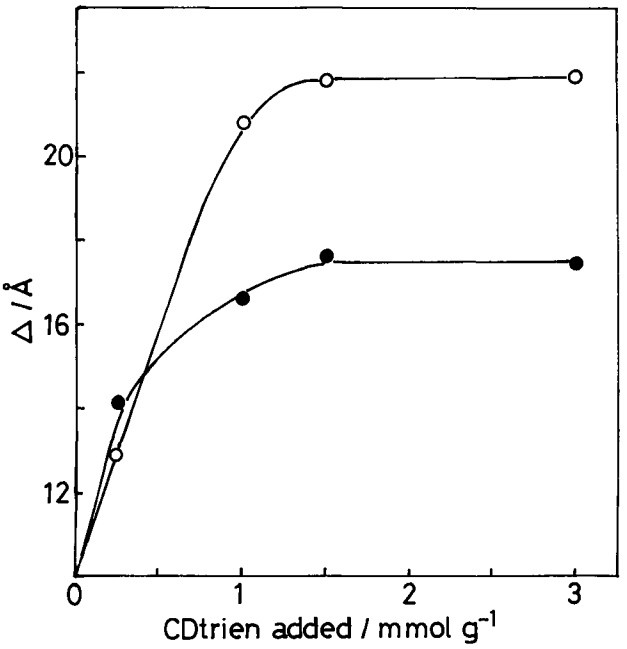

Fig. 2. The thickness of the intercalated layer, Δ (see text), as a function of CDtrien added. Key as in Fig. 1.

CDtrien obtained at an addition level of 1.5 mmol g^{-1}. The initial amounts of the cationic and the neutral forms of interlayer metal ions in Co(II)- and Ni(II)-montmorillonites were evaluated as described previously.[5]

The uptake reaction for Co-and Ni-montmorillonites took place in the pH range of as narrow as 8.3—8.9. Similarly to the previous discussion,[5] the above-mentioned data indicate that the intercalation of CDtrien by Co-and Ni-montmorillonites proceeds by the formation of CDtrien–Co^{2+} or CDtrien–Ni^{2+} complexes at low uptakes and by the combined modes of complexation and an ion exchange of Co^{2+} or Ni^{2+}/CDtrien2H^+ at higher loadings, where CDtrien2H^+ is the divalent form of CDtrien. We can, thus, evaluate the amounts of interlayer metal ions desorbed and those of both neutral and ionized forms of intercalated CDtrien (Table 1). At addition levels of more than 1.5 mmol g^{-1}, the uptake of CDtrien shows a tendency to decrease, in contrast to an increase in the release of interlayer metal ions. This can be explained by assuming that the CDtrien uptake due to ion exchange increases, whereas that due to complexation decreases appreciably, resulting in a decrease in the total uptake of CDtrien.

According to the literature,[6] the stability constants for trien–Cu^{2+}, trien–Ni^{2+}, trien–Zn^{2+}, and trien–Co^{2+} complexes in solution are $10^{20.4}$, $10^{14.0}$, $10^{12.1}$, and $10^{11.0}$, respectively. If stability constants of CDtrien–metal ion complexes in the solid state are assumed to be comparable to those in solution, the complexation tendency would be of the order of $Cu^{2+} \gg Ni^{2+} > Zn^{2+} > Co^{2+}$. In contrast, the experimental result is the order Co^{2}(90.5)$\gg Cu^{2+}$(65.9)$> Ni^{2+}$(56.9)$\gg Zn^{2+}$(23.8), where the amounts of the neutral form of intercalated CDtrien in mol% are given in parentheses. The high degree of complexation for Co^{2+} ion could be explained in terms of the extremely high stability of the structure of interlayer CDtrien complexes, as is discussed later. The relatively high degree of complexation for the Ni^{2+} ion can also probably be attributed to a similar structural effect.

The previous observations[5] showed that Cu(II)- and Zn-montmorillonites intercalate CDtrien to form a bilayer at high uptakes: the bilayered molecules are in a close contact with each other at a van der Waals distance of 16.1 Å, with their cavity axes perpendicular to the silicate layers and with the trien groups pointing both upward and downward in the intramolecular-complexing or divalent cationic forms. On the other hand, the Δ values for the Co(II)- and Ni(II)-intercalates are greater by 5.7 and 1.5 Å than those for the Cu- and Zn-analogues, respectively. This fact suggests that the CDtrien molecules in the former two intercalates are also arranged as a bilayer with the same orientation, but with a looser contact of 5.7 or 1.5 Å between the layers.

Upon heating up to 150 °C, the CDtrien layers of the Co(II)-intercalate contracted in thickness from 21.8 to 19.7 Å, due to the release of interlayer water. No interlayer contraction, on the other hand, was observed for the Cu- and Zn-intercalates. These observations suggest that at least a part of the interlayer water molecules participates as a ligand in the formation of the expanded bilayer in the Co-intercalate. It is thus suggested that the CDtrien molecules in Co(II)-montmorillonite form a 1:1 octahedral aqua complex, CDtrien$(H_2O)_2$–Co^{2+}, and that they are dimerized with a tail-to-tail arrangement, as illustrated in Fig. 3. The intercalated CDtrien$(H_2O)_2$–Co^{2+} complex would be highly stabilized by such a dimerization. A similar dimerized structure was observed for the CDen intercalate of Cu-montmorillonite.[2]

The intercalated layers of the Ni(II)-intercalate is also contracted in thickness from 17.6 to 16.2 Å upon heating up to 150 °C. This fact suggests that a slight expansion

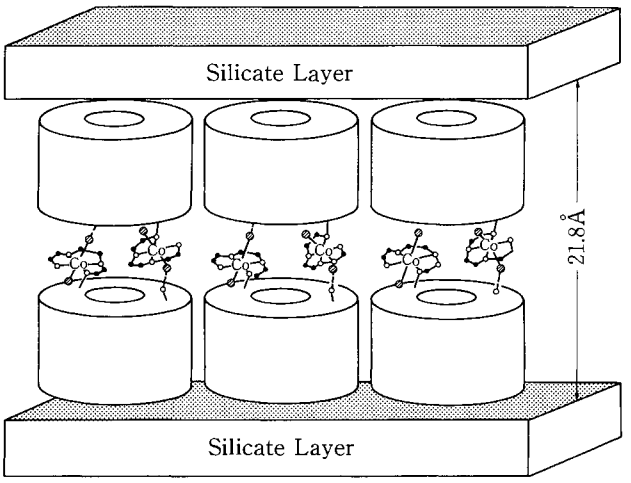

Fig. 3. A tentative model of the arrangement of CDtrien molecules in the interlayer space of Co-montmorillonite. ●, C; ○, N; ◍, water molecule.

of the CDtrien bilayer in the Ni(II)-intercalate also results from the interlayer water molecules and that the anhydrous form of the intercalate may have a structure similar to that of the Cu(II)- and Zn-intercalates. Thus, the CDtrien molecules in Ni(II)-montmorillonite are likely to make an isolated octahedral aqua complex, CDtrien$(H_2O)_2$–Ni^{2+}. The slight increase in the thickness of CDtrien$(H_2O)_2$–Ni^{2+} complex bilayer can be understood by assuming that they are more rigid and more bulky than the square plannar CDtrien–Cu^{2+} or tetrahedral CDtrien–Zn^{2+} complex.

The authors wish to thank Dr. Haruo Ohashi for his helpful discussions.

References

1) T. J. Pinnavia, *Science,* **220**, 365 (1983).
2) T. Kijima, J. Tanaka, M. Goto, and Y. Matsui, *Nature,* **310**, 45 (1984); **316**, 280 (1985).
3) T. Kijima and Y. Matsui, *Nature,* **322**, 533 (1986).
4) T. Kijima, *J. Inclusion Phenom.,* **4**, 333 (1986).
5) T. Kijima, H. Nakazawa, and M. Kobayashi, *Bull. Chem. Soc. Jpn.,* **61**, 4277 (1988).
6) N. Nakasuga and K. Doi, "Complexation Reaction," ed by The Japan Society of Analytical Chemistry, Maruzen, Tokyo (1974), p. 42.

Determination of Rhodium by Third-Derivative Spectrophotometry with *o*-Hydroxyhydroquinonephthalein in the Presence of *N*-Hexadecylpyridinium Chloride†

Itsuo MORI,* Yoshikazu FUJITA, Minako TOYODA, and Sachi MAEKUBO
Osaka University of Pharmaceutical Sciences, Matsubara-shi, Osaka 580
(Received November 29, 1990)

Synopsis. A third-derivative spectrophotometric determination ($d^3A/d\lambda^3$) of rhodium with *o*-hydroxyhydroquinonephthalein (Qnph) in the presence of *N*-hexadecylyridinium chloride (HPC) was proposed by measuring the distance of $d^3A/d\lambda^3$ on the peak at 530 nm (λ_3) and the troughs at 500 nm (λ_2) and 560 nm (λ_4). Beer's law was valid for the range 0—10 μg rhodium 10^{-1} cm^3; the apparent molar $d^3A/d\lambda^3$ was 7.37×10^5 dm^3 mol^{-1} cm^{-1}.

The most popular spectrophotometric method for the determination of rhodium, one of the platinum metals, is based on reaction between rhodium(III) and tin(II) chloride in hydrochloric acid medium.[1-3] However, this method is not sensitive and lacks reproducibility. On the other hand, the derivative spectrophotometric method has recently been found to be more sensitive, selective, and reversible than classical zero-order derivative spectrophotometries.[4-6] In addition, we have recognized that *o*-hydroxyhydroquinonephthalein (Qnph) used as a xanthene dye is a most useful organic agent.[7-9] Also, the coexisting effect of such surfactants as *N*-hexadecylpyridinium chlorid (HPC) has been reported in various spectro- or fluoro-photometries.[10-12] Accordingly, for the purpose of establishing a sensitive and simple spectrophotometric determination of rhodium, a third-derivative spectrophotometric determination with Qnph was investigated in the surfactant micellar media.

Experimental

Apparatus and Reagents. Absorption and high-derivative spectra were recorded on a Shimadzu UV 160 spectrophotometer with a 1.0-cm matched cell. The third-derivative spectrum was recorded by a fixed third-order differentiation circuit of $\Delta\lambda$=31.5 nm with a scan speed of 1500 nm per min. A Hitachi-Horiba F-7AD glass electrode pH meter was used for pH measurements.

A Qnph solution, 1.0×10^{-3} mol dm^{-3} was prepared by dissolving Qnph in methanol. A 5.0×10^{-4} mol dm^{-3} rhodium(III) solution was diluted by using a standard atomic absorption spectroscopy solution (Wako chemical Co., Ltd.). A 1.0×10^{-2} mol dm^{-3} HPC solution was prepared by dissolving HPC in water; a Sörensen phosphate buffer solution (pH 6.4—7.2) was used for the pH adjustments. Deionized water was used throughout.

Standard Procedure. To a solution containing 0—10 μg rhodium(III) in a 10-cm^3 volumetric flask, 3.0 cm^3 of a 2.0×10^{-2} mol dm^{-3} buffer solution (pH 6.5), 1.0 cm^3 of a 1.0×10^{-2} mol dm^{-3} HPC solution and 0.8 cm^3 of 5.0×10^{-4} mol dm^{-3} Qnph solution were added; the mixture was diluted to volume with water (Solution A), kept at 75 °C for 30 min, then cooled to room temperature (10—25 °C) for 5 min. The $d^3A/d\lambda^3$ distances at 500 nm (trough λ_2), 530 nm (peak λ_3) and 560 nm (trough λ_4) were measured against a reagent blank (Solution B).

Results and Discussion

Absorption Spectra. Figure 1 shows the absorption spectra of the Qnph–rhodium(III) solution (Solution A) and the Qnph solution (Solution B) in the presence of HPC as a cationic surfactant (or absence). The color formation reaction in the presence of HPC was stable and exhibited a large absorbance in comparison with that in the absence of HPC. In addition, the derivative spectrum (third-derivative, $d^3A/d\lambda^3$) of Solution A against Solution B was most sharp and apparent. Figure 2 shows two peaks (λ_1 480 nm, λ_3 530 nm) and three valleys (λ_2 500 nm, λ_4 560 nm, λ_5 610 nm). The analytical response was obtained by measuring the absorbance distance between the peak at 530 nm (λ_3) and the valleys at 500 nm (λ_2) and 560 nm (λ_4); its value was large compared with the zero-order derivative absorption spectrum.

Effect of pH. The maximum and constant $d^3A/d\lambda^3$ was obtained within limited ranges of pH 6.4—7.2,

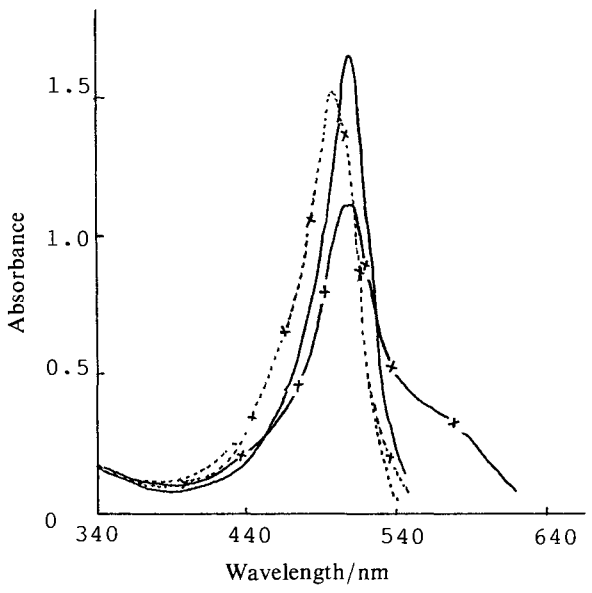

Fig. 1. Absorption spectra of Qnph–rhodium(III) solution (Solution A) and Qnph solution (Solution B) in the presence or absence of HPC at pH 7.0. Rhodium(III), 2.5 ppm, Qnph, 2.5×10^{-5} mol dm^{-3}; HPC, 1.0×10^{-3} mol dm^{-3}; Reference, water -------, Qnph; ----×----, Qnph–rhodium(III); ———, Qnph–HPC (Solution B); ——×——, Qnph–HPC–rhodium(III) (Solution A).

† Application of Xanthene Derivatives for Analytical Chemistry, Part LXXXVI. Part LXXXV: I. Mori, Y. Fujita, M. Toyoda, A. Obana, M. Nakamura, and S. Oka, *Anal. Lett.*, **23**, 2303 (1990).

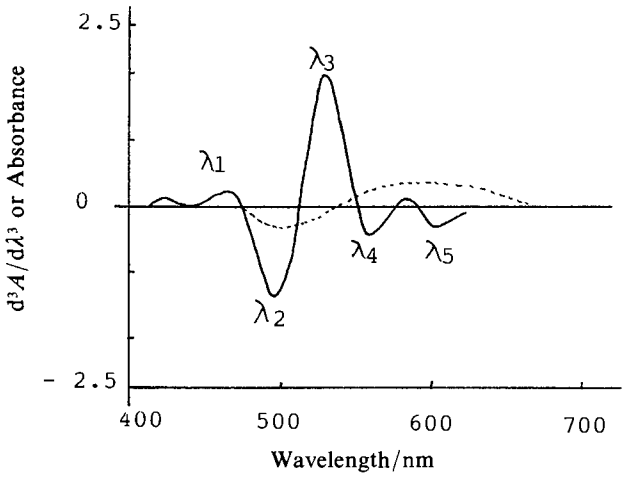

Fig. 2. Zero-order and third-derivative spectra of Qnph–rhodium(III) solution (Solution B) in the presence of HPC. Rhodium(III), 5.0×10^{-6} mol dm^{-3}; Qnph, 4.0×10^{-5} mol dm^{-3}; HPC, 1.0×10^{-3} mol dm^{-3}; pH 6.5; Reference, reagent blank (Solution B). -------, Zero-order spectrum; ———, Third-derivative spectrum.

Table 1. Effect of Various Surfactants on Zero-Order and Third-Derivative Spectrophotometries

Surfactant	Zero-order		$d^3A/d\lambda^3$
	max	Absorbance	
—	535	0.105	b) 0.50
HPC	572	0.540	3.70
SLS	532	0.115	b) 0.80
LS	532	0.117	b) 0.80
Brij 35	532	0.135	b) 0.85
HPC+Brij 35	570	0.390	2.90
HPC[a)]+Brij 35	530	0.132	b) 0.85
SLS+Brij 35	504	0.09	b) 0.65

Rhodium(III) 5.0 μg 10 cm^{-3}; Qnph, 5.0×10^{-4} mol dm^{-3}; pH, 6.5; HPC, 1.0×10^{-3} mol dm^{-3}; other surfactants, 0.01%. a) HPC, 1.0×10^{-4} mol dm^{-3}. b) Insufficiency.

using 2.0—3.0 cm^3 of a 2.0×10^{-1} mol dm^{-3} phosphate buffer solution. Accordingly, 3.0 cm^3 of a buffer solution (pH 6.5) was used for pH adjustments in all further work.

Effect of Surfactants. The complex formation reactions between Qnph and rhodium(III) were systematically investigated by using the $d^3A/d\lambda^3$-method in the absence or presence of only a surfactant, or its combination; cationic-, anionic, nonionic-, and amphoteric-surfactants—HPC, sodium dodecylsulfate (SDS), Tween 20, sodium *N*-lauroylsarcosine (LS). The coexistence of only the cationic surfactant was most effective, and its color was stable and abundant regarding reproducibility. In tested cationic surfactants such as hexadecyltrimethylammonium chloride (HTAC), benzyldimethyltetradecylammonium chloride (Zephiramine, Zp), benzyltriethylammonium chloride (TBBAC), and HPC, the presence of 5.0×10^{-3} mol dm^{-3} HPC was most effective.

Table 2. Effect of Foreign Ions

Foreign ions	Added		$d^3A/d\lambda^3$	Error
	as	μg/10 cm^3		%
—	—	—	3.80	—
Co(II)	Nitrate	0.30	3.81	+0.3
Ni(II)	Nitrate	4.40	3.83	+0.8
Zn(II)	Nitrate	3.27	3.82	+0.6
Bi(III)	Nitrate	0.52	3.88	+2.1
Th(IV)	Nitrate	1.16	3.81	+0.3
S^{2-}	Sodium	0.80	3.79	−0.3
$S_2O_3^{2-}$	Sodium	0.28	3.80	+0
$C_2O_4^{2-}$	Sodium	6.6	3.79	−0.3
Citrate	Sodium	14.10	3.78	−0.6
F^-	Potassium	144.50	3.80	±0

Rhodium(III) taken, 5.0 μg 10 cm^{-3}; Qnph, 5.0×10^{-4} mol dm^{-3}; HPC, 1.0×10^{-3} mol dm^{-3}; pH, 6.5; Reference, reagent blank (Solution B).

Accordingly, final 1.0×10^{-3} mol dm^{-3} HPC was used for a further investigation.

Effect of Concentration of Qnph. The recommended concentration of Qnph was final 0.4—1.0×10^{-4} mol dm^{-3}, and final 5.0×10^{-5} mol dm^{-3} Qnph was used for subsequent procedures.

Effect of Stability. The effects of the temperature and heating time were examined at 10—80 °C for 2—60 min. The optimum heating condition was at 70 °C for 5—20 min; further work was carried out at 70 °C for 5 min.

Calibration Graph and Reproducibility. Beer's law held at lower than 10 μg of rhodium(III) per 10 cm^3, and apparent molar $d^3A/d\lambda^3$ was 7.37×10^5 dm^3 mol^{-1} cm^{-1}. The reproducibility for 5 μg/10 cm^3 rhodium(III) (5 experiments) was 1.5%.

Interferences. Although nickel(II), zinc(II), bismuth(III), thorium(IV), and other platinum metals, such as palladium, gave a positive error, and citrate, oxalate, thiocyanate ions gave negative errors, the infuluence of foreign ions on the proposed $d^3A/d\lambda^3$-method was reduced to about half, compared with zero-order spectrophotometry. For a mixture of rhodium and other platinum metals, pre-separation by other techniques, such as ion exchange chromatography,[13,14] was necessary.

Composition of Complex. The molar ratio of rhodium(III) to Qnph in a color formation reaction in the presence of HPC was determined by continuous variation (Job's) and molar-ratio methods to be 2:3; the molar ratio of rhodium(III) to HPC, however, was not investigated.

Conclusion. The complex formation reaction between Qnph and rhodium(III) in the presence of a cationic surfactant alone, such as HPC at pH 6.5, was very stable and abundant regarding reproducibility. Accordingly, this Qnph-rhodium(III) complex was newly used for a sensitive and simple third-derivative spectrophotometry of rhodium(III). The $d^3A/d\lambda^3$-method was compared with zero-order spectrophotometry; the calibration graph was linear over the range 0—10 μg rhodium(III) per 10 cm^3. The proposed method was 5-times more sensitive, and the influence of foreign ions

was reduced by half compared with the zero-order method. Also, the method was 10-fold more sensitive than Chromazurol S, and 30-fold more sensitive than the Eriochrome Cyanine R and 4-(2-pyridylazo)resorcinol methods.[15,16]

References

1) G. H. Ayres, B. L. Triffly, and J. S. Forrester, *Anal. Chem.*, **27**, 1742 (1955).
2) S. Iwasaki, T. Nagai, E. Miki, M. Mizumachi, and T. Ishimori, *Bull. Chem. Soc. Jpn.*, **57**, 386 (1984).
3) F. E. Beamish, C. L. Lewis, and J. C. Van Loon, *Talanta*, **16**, 1 (1969).
4) A. Melegarjo Gallardo, A. Céspedes Gallordo, and J. M Cano Parón, *Analyst*, **114**, 109 (1989).
5) R. L. Sharma and H. B. Shingh, *Analyst*, **111**, 551 (1986).
6) J. A. Murillo, J. M. Lemus, A. M. Pena, and F. Salinas, *Analyst*, **113**, 1439 (1982).
7) I. Mori, Y. Fujita, and S. Kitano, *Bunseki Kagaku*, **32**, E1 (1983).
8) I. Mori, Y. Fujita, and T. Enoki, *Bunseki Kagaku*, **26**, 480 (1977).
9) I. Mori, Y. Fujita, and K. Fujita, *Bull. Chem. Soc. Jpn.*, **55**, 3649 (1982).
10) Qi Wen-Bin and Zhun L-Zhung, *Talanta*, **32**, 1013 (1985).
11) S. Hur and X. Kau, *Fenxi Shiyanski*, **5**, 23 (1986); *Anal. Abst.*, **49**, 6B197 (1987).
12) D. Nanov' and K. Stoyanov, *Anal. Chim. Acta*, **183**, 321 (1982).
13) S. S. Berman, *Can. J. Chem.*, **36**, 835, 845 (1958).
14) F. Cocufalik and M. Svach, *Fresenius Z. Anal. Chem.*, **173**, 113 (1960).
15) H. Duchková, L. Ćemáková, and M. Malát, *Anal. Lett.*, **8**, 115 (1975).
16) J. R. Stokeley and W. D. Jacobs, *Anal. Chem.*, **35**, 149 (1963).

Syntheses and Properties of Binuclear Manganese(III) and Manganese(IV) Complexes with 1,2,3,4-Tetrakis(salicylideneamino)-2,3-diphenylbutane

Masaaki NAKAMURA,* Sayuri SHIMOKAWA, Yuri MIYANAKA, Hu HUANG,† and Fumiaki KAI†
Department of Chemistry, Faculty of Science, Kumamoto University, Kumamoto 860
† Department of Environmental Science, Graduate School of Natural Science and Technology, Kumamoto University, Kumamoto 860
(Received December 1, 1990)

Synopsis. A new dichlorodimanganese(III) and novel tetrachlorodimanganese(IV) complexes with 1,2,3,4-tetrakis-(salicylideneamino)-2,3-diphenylbutane were prepared and characterized. The obtained dimanganese(IV) complex was rather stable to moisture in the solid state, but readily reduced to the corresponding dimanganese(III) complex in a methanol solution. The complexes can not be electrochemically formed as mixed valence states.

Binuclear manganese(III) and (IV) complexes have been receiving considerable attention as model systems for the photosynthetic oxygen-evolving complex.[1-4] From the viewpoint of these interests, many of the oxygen-bridged (μ-oxo, μ-hydroxo, and/or μ-phenyloxo) type binuclear manganese(III) and some μ-oxo type binuclear manganese(IV) complexes have been prepared and characterized.[5-9] In these complexes, the bridging oxo ligands are considered to play a role in connecting two or more high-valent manganese ions in the molecules. Actually, the binuclear manganese(IV) complexes reported hitherto regarding the above-mentioned interests are almost limited to the μ-oxo type complexes.[6-9]

In this paper we report on the syntheses and properties of a new type of binuclear manganese(III) and (IV) complexes with an octadentate Schiff base ligand, 1,2,3,4-tetrakis(salicylideneamino)-2,3-diphenylbutane (H_4sabzta), which do not contain a bridging oxo ligand. For the sake of a comparative study, the corresponding mononuclear manganese(III) and (IV) complexes with 1,2-bis(salicylideneamino)-1-phenylethane (H_2sabzen) were also prepared.

Experimental

Syntheses. The ligands, H_4sabzta and H_2sabzen, were prepared by a method described in our previous paper.[10]

[Mn_2(sabzta)Cl_2]: Manganese(II) chloride tetrahydrate (3.64 mmol) and tetrabutylammonium permanganate, (TBA)MnO_4, (0.78 mmol) were added to a dry ethanol solution (20 cm^3) containing H_4sabzta (2.21 mmol). This solution was refluxed for 2 h and then cooled to ambient temperature. The dark-brown crystalline powder obtained was collected. The crude product was recrystallized from methanol. The yield was ca. 42%. Found: C, 60.01; H, 4.24; N, 6.14%. Calcd for $C_{44}H_{34}N_4O_4Mn_2Cl_2 \cdot H_2O$: C, 59.95; H, 4.12; N, 6.36%.

[Mn(sabzen)Cl]: This complex was obtained as a dark-brown crystalline powder by reacting manganese(II) chloride tetrahydrate (1.79 mmol), (TBA)MnO_4 (0.60 mmol) and H_2sabzen (2.39 mmol) in dry ethanol (20 cm^3) in a way similar to the method for Mn_2(sabzta)Cl_2. The crude product was recrystallized from methanol. The yield was ca. 45%. Found: C, 59.42; H, 4.34; N, 6.02%. Calcd for $C_{22}H_{18}N_2O_2MnCl \cdot 3/4H_2O$: C, 59.21; H, 4.40; N, 6.28%.

[Mn_2(sabzta)Cl_4]: Mn_2(sabzta)Cl_2 (0.11 mmol) was suspended in dry acetone (20 cm^3); a methanol solution (2 cm^3) containing hydrochloric acid (0.21 mmol) was then added dropwise to the suspension. The obtained deep-green clear solution was filtered and the filtrate was concentrated under reduced pressure. The deep-green crystals obtained were collected and washed with dry acetone. The yield was ca. 23%. Found: C, 57.06; H, 4.22; N, 5.50%. Calcd for $C_{44}H_{34}N_4O_4Mn_2Cl_4 \cdot C_3H_6O$: C, 56.87; H, 4.06; N, 5.64%.

[Mn(sabzen)Cl_2]: This complex was obtained as deep-green crystals by treating Mn(sabzen)Cl (0.11 mmol) with hydrochloric acid in a way similar to that for Mn_2(sabzta)Cl_4. The yield was ca. 30%. Found: C, 56.25; H, 4.00; N, 5.77%. Calcd for $C_{22}H_{18}N_2O_2MnCl_2$: C, 56.43; H, 3.87; N, 5.98%.

Measurements. The IR spectra were recorded on a JASCO A-102 grating spectrometer on a KBr disk. Electronic spectra were recorded on a Hitachi 220A recording spectrophotometer. The electric conductivities were determined by a Horiba Conductivity Meter (Model DS-14). Polarograms were recorded on a Yanagimoto Polarographic Analyzer (Model P-1100) in dichloromethane containing 0.1 mol dm^{-3} tetrabutylammonium perchlorate as the supporting electrolyte, by the use of a three-electrode cell equipped with glassy carbon as a working electrode, a platinum coil as an auxiliary electrode, and a saturated calomel electrode (SCE) as a reference electrode. In practice, all of the potentials were normalized by the use of ferrocene as an internal standard. The magnetic susceptibilities were measured by the Faraday method over the temperature range 85—300 K.

Results and Discussion

[Manganese(III) Complexes]. Since the binucleating ligand H_4sabzta has two "salen-like" donating sites, where H_2salen denotes 1,2-bis(salicylideneamino)ethane, the two manganese(III) ions in Mn_2(sabzta)Cl_2 are expected to hold in each of the above-mentioned donating sites. The IR spectrum of Mn_2(sabzta)Cl_2 is almost similar to that of the corresponding mononuclear complex Mn(sabzen)Cl and Mn(salen)Cl.[11] Further, it does not show any characteristic bands at 700—600 cm^{-1}, due to the presence of the μ-oxo or μ-peroxo structure.[6] The magnetic moments of Mn_2(sabzta)Cl_2 and Mn(sabzen)Cl per one manganese atom at room temperature are 5.08 and 4.90 BM, respectively. These obtained values are consistent with the spin-only value expected for a d^4 high-spin manganese(III) complex. The magnetic moment of the binuclear complex was almost independent of the temperature over the range 85—300 K, indicating the absence of a spin-exchange interaction between the metal ions. This is in contrast with the magnetic properties of the μ-oxo type dimanganese(III) complexes, in which a rather strong antiferromagnetic spin-exchange interaction between the manganese ions via oxo group(s) has been observed.[5-8]

Table 1. Electronic Spectral Data for Manganese(III) and (IV) Complexes

Complex	Solvent	$\tilde{\nu}/10^3$ cm^{-1} (log ε)			
Mn_2(sabzta)Cl_2	CH_2Cl_2	20.3 (3.24)	23.8 (3.67)	31.3 (4.21)	35.7 (4.33)
	CH_3OH		25.0 (3.79)		35.0 (4.33)
Mn(sabzen)Cl	CH_2Cl_2	20.8 (3.24)	23.8 (3.86)	31.7 (4.37)	35.7 (4.50)
	CH_3OH		25.3 (3.37)		35.5 (4.29)
Mn_2(sabzta)Cl_4	CH_2Cl_2	15.9 (3.61)	23.8 (3.83)	32.9 (4.32)	37.0 (4.56)
	CH_3OH		25.4 (3.67)		35.7 (4.19)
Mn(sabzen)Cl_2	CH_2Cl_2	15.9 (3.56)	23.8 (3.80)	33.0 (4.29)	37.2 (4.53)
	CH_3OH		24.9 (3.69)		35.6 (4.22)
Mn(salen)Cl_2[a]	CH_2Cl_2	15.4 (3.60)	23.0 (3.78)		

a) Ref. 15.

The obtained complexes are soluble in both nondonor and donor solvents such as dichloromethane, chloroform, methanol, ethanol, and dimethylformamide. However, the electronic spectra of the complexes are sensitive to a kind of solvent; namely, different spectral features are observed in dichloromethane and in methanol (Table 1). These spectral properties resemble those of the pentacoordinated manganese(III) complexes with a "salen"-type ligand.[11-13] The molar conductivities of Mn_2(sabzta)Cl_2 and Mn(sabzen)Cl in methanol are 163 and 78 S cm^2 mol^{-1} at 25 °C, respectively, which are consistent with the expected values for 1:2 and 1:1 electrolytes, respectively.[14] These results strongly suggest that the chloride ions in the complexes are extensively dissociated and that solvated di- and monocationic complex ions, $[Mn_2(sabzta)]^{2+}$ and $[Mn(sabzen)]^+$, are formed in a methanol solution, respectively. It is concluded that the two manganese(III) sites do not interact intramolecularly, but act independently as the corresponding mononuclear complex.

[Manganese(IV) complexes]. In this study, a synthetic method for the mononuclear manganese(IV) complexes Mn(salen)Cl_2 and its homologues[15] was applied for the preparation of Mn_2(sabzta)Cl_4 and Mn(sabzen)Cl_2. The magnetic moments of these complexes are 3.90 and 3.80 BM per one manganese at room temperature, respectively; their values coincided well with the spin-only moment expected for the d^3 manganese(IV) ion. Matsushita et al. have reported that in manganese complexes with "salen"-type ligands a lower-frequency shift of ν(C–O) at the phenolate moiety was observed upon going from manganese(III) to (IV).[15] An analogous relationship exists in the present complexes; bands are observed at 1290 and 1300 cm^{-1} for the manganese-(IV) and (III) complexes, respectively.

The manganese(IV) complexes obtained are soluble in dichloromethane, chloroform, and dry acetone; a deep-green solution is formed. The electronic spectra of these complexes in dichloromethane exhibit a new intense absorption band around 15900 cm^{-1} (Table 1), which is assignable to the CT transition from the Cl^- to the Mn(IV) ion on the basis of a resemblance to the reported spectra of Mn(salen)Cl_2 and its homologues.[15] From the magnetic and spectral properties of the binuclear manganese(IV) complex, it is concluded that the two manganese(IV) ions in this complex are also held in each of the two "salen-like" donating sites and have an octahedral geometry by coordinating two chloride ions at axial positions as well as the mononuclear complex, Mn(sabzen)Cl_2 and Mn(salen)Cl_2. As described above, it should be emphasized that this complex is the first example of a binuclear manganese(IV) complex lacking a bridging oxo ligand.

Table 2. Electrochemical Data for Manganese(III) and (IV) Complexes

Complex	E_{pc}	E_{pa}	ΔE_p	$E'_{1/2}$[a]	$E_{1/2}$
	V	V	mV	V	V
Mn_2(sabzta)Cl_2	−0.690	−0.590	100	−0.640	−0.650
					0.650
Mn(sabzen)Cl	−0.695	−0.595	100	−0.645	−0.655
					0.615
Mn_2(sabzta)Cl_4	−0.710	−0.600	110	−0.655	−0.655
					0.350
Mn(sabzen)Cl_2	−0.700	−0.590	110	−0.645	−0.645
					0.360

a) $E'_{1/2}=(E_{pc}+E_{pa})/2$.

The methanolic solutions of manganese(IV) complexes do not show a deep-green color, but brown. Their electronic spectra are quite similar to those of the corresponding manganese(III) complexes in methanol (Table 1). The spectral difference of the manganese(IV) complex for dichloromethane and methanol solutions strongly indicates that the manganese(IV) complexes are reduced to the corresponding manganese(III) complexes. Unfortunately, it is ambiguous at present that the manganese(IV) complexes are reduced by either methanol or trace water contained in this solvent. Whereas Mn_2(sabzta)Cl_4 and Mn(sabzen)Cl_2 are rather stable to moisture in the solid state and show no appreciable changes in appearance, their IR spectra are observed when they are exposed to air for several months.

Both the present mononuclear and binuclear complexes exhibit redox waves at nearly the same potentials in dichloromethane (Table 2). Each of these four complexes exhibits only one reduction wave at around −0.65 V, which can be assigned to a quasi-reversible or irreversible one-electron reduction process for Mn(III) to Mn(II) on the basis of the peak separations (ΔE_p=100—110 mV) and their wave shapes in cyclic voltammograms.

However, their peak currents observed for the binuclear complexes are about twice, compared with the current of the corresponding redox waves for the mononuclear complexes, respectively. This electrochemical property is almost similar to that of the dicopper(II) complex with the same ligand, Cu_2(sabzta),[10] and can be interpreted in terms of the fact that binuclear complexes are electrochemically reduced by two simultaneous monoelectronic steps at nearly the same potential as that for the corresponding mononuclear complexes. In other words, the present binuclear manganese complexes can not be electrochemically formed as mixed valence states, such as Mn(III)–Mn(II).

The redox waves observed at the anodic region are also assigned to the irreversible one-electron redox process of Mn(III/IV), since the oxidation waves of the coordinated Schiff base ligands and chloride ion in these four complexes appeared at a more positive potential region. The reduction of Mn(IV) to Mn(III) for the manganese(IV) complexes occurs at about a 300 mV more cathodic region, compared with the corresponding oxidation potentials for the manganese(III) complexes. This shift of the redox potentials should indicate a stabilization of the manganese(IV) state by coordinating two chloride ions to metal centers.

We wish to express our thanks to Professor Sigeo Kida and Associate Professor Hisashi Ōkawa of Kyushu University for help in obtaining the magnetic data.

References

1) G. D. Lawrence and D. T. Sawyer, *Coord. Chem. Rev.*, **27**, 173 (1978).
2) G. Renger, *Angew. Chem., Int. Ed. Engl.*, **26**, 643 (1987).
3) J. E. Penner-Hahn, R. M. Fronko, V. L. Pecoraro, C. F. Yocum, S. D. Betts, and N. R. Bowlby, *J. Am. Chem. Soc.*, **112**, 2549 (1990).
4) J. A. Kirby, A. S. Robertson, J. P. Smith, A. C. Thompson, S. R. Cooper, and M. P. Klein, *J. Am. Chem. Soc.*, **103**, 5529 (1981).
5) K. Wieghardt, *Angew. Chem., Int. Ed. Engl.*, **28**, 1153 (1989).
6) T. Matsushita, T. Yarino, I. Masuda, T. Shono, and K. Shinra, *Bull. Chem. Soc. Jpn.*, **46**, 1712 (1973).
7) K. Wieghardt, U. Bossek, B. Nuber, J. Weiss, J. Bonvoisin, M. Corbella, S. E. Vitols, and J. J. Griered, *J. Am. Chem. Soc.*, **110**, 7398 (1988).
8) P. A. Goodson, J. Glerup, D. J. Hodgson, K. Michelsen, and E. Pedersen, *Inorg. Chem.*, **29**, 503 (1990).
9) T. Matsushita, L. Spencer, and D. T. Sawyer, *Inorg. Chem.*, **27**, 1167 (1988).
10) M. Nakamura, T. Masumoto, and F. Kai, *Polyhedron*, **6**, 513 (1987).
11) L. J. Boucher and M. O. Farrel, *J. Inorg. Nucl. Chem.*, **35**, 3731 (1973).
12) L. J. Boucher and D. R. Herrington, *Inorg. Chem.*, **13**, 1105 (1974).
13) L. J. Boucher, *J. Inorg. Nucl. Chem.*, **36**, 531 (1974).
14) W. J. Geary, *Coord. Chem. Rev.*, **7**, 81 (1971).
15) T. Matsushita, H. Kono, and T. Shono, *Bull. Chem. Soc. Jpn.*, **54**, 2646 (1981).

Synthesis and Characterization of Six-Membered Cyclometallated Complexes of 2-Bezylpyridine with Rhodium(III)

Katsuma HIRAKI,* Masayoshi ONISHI, and Hiroko KISHINO
Department of Industrial Chemistry, Faculty of Engineering, Nagasaki University, Bunkyo-machi, Nagasaki 852
(Received December 25, 1990)

Synopsis. 2-Benzylpyridine (Hpiph) is metallated with $RhCl_3 \cdot 3H_2O$ to give $[\{Rh(piph)Cl_2(Hpiph)\}_2] \cdot H_2O$ [piph=2-(2-picolyl)phenyl] in which piph is coordinated at phenyl-1-C and picolyl-N atoms. This complex reacts with tertiary phosphines (PR_3) such as PEt_3, PEt_2Ph, and PPh_3 to yield $[Rh(piph)Cl_2(PR_3)_2]$.

Considerable interest has developed concerning cyclometallated complexes owing to not only the direct activation of the carbon–hydrogen bonds with transition metal complexes,[1-3] but also the wide range of the utilization for organic synthesis,[4] optical resolution of organic compounds,[5] catalyst precursors,[6] and so on. Several articles have already been published concerning five-members-chelated organorhodium(III) complexes derived from nitrogen-containing ligands, such as 2-phenylpyridine,[7] benzo[*h*]quinoline,[7] azobenzenes,[8] aromatic oximes,[9] 1-phenylpyrazole,[10] and 8-methylquinoline.[11] However, six-membered cyclometallated complexes with rhodium(III) are very scarce.

We have studied six-membered cyclopalladated complexes of 2-benzylpyridine,[12] 2-benzoylpyridine,[13] and 2-neopentylpyridine.[14] Here, we will report the synthesis and characterization of new six-membered cyclometallated complexes of 2-benzylpyridine with rhodium(III).

Results and Discussion

When 2-benzylpyridine was heated with $RhCl_3 \cdot 3H_2O$ in 2-methoxyethanol at 80 °C, a yellow-brown complex, $[\{Rh(piph)Cl_2(Hpiph)\}_2] \cdot H_2O$ [piph=2-(2-picolyl)phenyl] (**1**) was formed in 45% yield. Complex **1** was so poorly soluble in organic solvents that NMR spectra of **1** could not be obtained. However, **1** was tentatively ascribed to a chloro-bridged dimeric structure on the basis of the elemental analysis and the poor solubility. Treatment of **1** with excess amounts of tertiary phosphines in refluxing dichloromethane afforded mononuclear complexes, $[Rh(piph)Cl_2(PR_3)_2]$ (**2a**, R=Et; **2b**, PR_3=PEt_2Ph; **2c**, R=Ph). The elemental analyses of **2a**—**c** were satisfactory. Their IR spectra showed a weak absorption near 1600 cm^{-1} and fairly strong bands near 1430 and 1485 cm^{-1}, ascribable to ν(C=N) of the pyridyl group and phosphine moieties, respectively, supporting the above formulations.

The $^{13}C\{^1H\}$ NMR spectrum of **2a** showed a double triplet at δ=145.4 ($^1J_{CRh}$=29.3 Hz, $^2J_{CP}$=17.6 Hz, RhC), disclosing clearly that direct metallation took place at one aromatic carbon of 2-benzylpyridine and that the metallated carbon was situated cis to the two phosphine ligands (Fig. 1). In general, a pyridyl nitrogen is coordinated easily to a trivalent rhodium atom.[7] Indeed, in the ^1H NMR spectrum of **2a**, pyridyl 6-H of the piph moiety resonates at a considerably lower field (at δ=10.33) than that (δ=8.56) of free 2-benzylpyridine, indicating the coordination of the pyridyl group. Accordingly, it is certain that the rhodium-bonded carbon (1-C), located ortho to the picolyl group, and the pyridyl nitrogen are coordinated together to the rhodium atom, forming a new six-membered chelate structure, piph-C^1, N-Rh, similarly to the cases of $\{Pd(piph)(CH_3CO_2)\}_2$] and its related complexes.[12]

2-Benzylpyridine, in which the phenyl and the 2-pyridyl groups are separated by the methylene group, reacted with $RhCl_3 \cdot 3H_2O$ in the alcohlic solvent at ca. 80 °C to afford the dimeric complex, **1** containing one metallated piph unit per Rh atom. This bears analogy with the cyclometallated rhodium(III) complexes of 8-methyl-quinoline,[11] in which the methyl group was not involved apparently in the conjugate system of the quinoline moiety. It is noted that these are in sharp contrast with the other N-containing ligands, such as 2-phenylpyridine,[7] benzo[*h*]quinoline,[7] azobenzenes,[8] aromatic oximes,[9] and 1-phenylpyrazole,[10] each of which consists of a continuous conjugate system and reacted with $RhCl_3 \cdot 3H_2O$ in refluxing ethanol to give a dimeric complex containing two metallated C,N-chelate units per Rh atom.

In the $^{13}C\{^1H\}$ NMR spectrum of **2a**, the methylene carbons of ethyl groups resonated as a triplet at δ=14.8 owing to virtual coupling with the two phosphorus atoms. Furthermore, the ^1H NMR spectrum of **2a** exhibited a quintet at δ=0.73 ascribable to the methyl protons, and its signal splitting was due to coupling with two vicinal methylene protons and virtual coupling with the two phosphorus atoms ($^3J_{HH}$=$^{3+5}J_{HP}$=7.3 Hz). These data imply unambiguously that the two phosphine

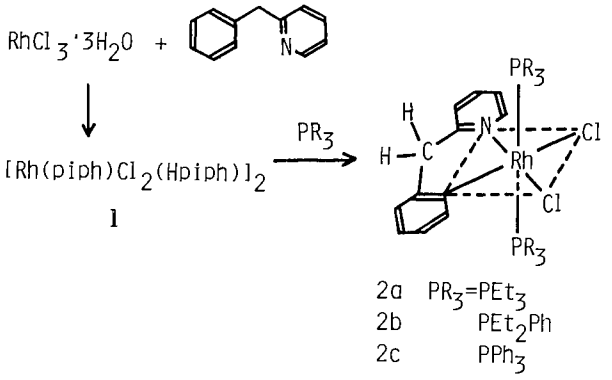

Fig. 1. The 2-(2-picolyl)phenyl-C^1,N-rhodium(III) complexes.

ligands in **2a** are equivalent and located trans to each other, similarly to the case of $[Rh(CH_2\text{–}C_9H_6N)X_2(PBu^n_3)_2]$ (C_9H_6N=8-quinolyl).[11]

In the ^1H NMR spectrum of **2a**, the picolyl methylene protons appeared as a singlet at δ=4.22, which showed no change in the range of +30—−60°C. These facts indicate that the two methylene protons are equivalent and that the piph moiety is plain and situated in the same plane as the $RhCl_2$ moiety forms. In addition, the piph moiety is rigid and shows no inversion motion, in sharp contrast with the piph moiety in $[Pd(piph)Cl\{C_5H_3N(Me)_2\text{-}3.5\}]$.[12] The rigid plain structure of the piph moiety in **2a** is due to steric effect of the two tertiary phosphine ligands, located above and below the central rhodium atom.

In the $^{13}C\{^1H\}$ NMR spectrum of **2b**, the signal patterns of the rhodium-bonded carbon and the methylene carbons of the ethyl groups are quite similar to those of the corresponding carbons in **2a**, indicating that **2b** has an analogous structure to **2a**. This is also supported by the facts that the ipso-carbons of the phosphine phenyl groups exhibited a triplet owing to virtual coupling ($^{1+3}J_{CP}$=7.3 Hz), and that the phosphine ortho-protons showed a quartet due to combination of virtual coupling and H–H coupling ($^{3+5}J_{HP}=^3J_{HH}$=7 Hz). Its ^1H NMR spectrum exhibited two quintets at δ=0.81 and 1.02 (each 6H, $^3J_{HH}=^{3+5}J_{HP}$=7.3 Hz, CH_3), one broad quartet at δ=2.06 (4H, $^3J_{HH}$=ca. 7 Hz, CH_2CH_3), and two multiplets at δ=2.50 and 2.77 (each 2H, $CH_AH_BCH_3$). Irradiation at the quintet at δ=0.81 converted the broad quartet into a broad singlet, whereas that at the quintet at δ=1.02 changed the two multiplets into two broad doublets [each, $^2J(H_AH_B)$=15.6 Hz]. These data imply that two ethyl groups in the PEt_2Ph ligand are unequivalent owing to the restriction of rotation of the PEt_2Ph ligands and that two methylene protons in one of the two ethyl groups are also nonequivalent. Furthermore, it is notable that $^{2+4}J_{HP}$ of the methylene protons in the PEt_2Ph ligands was too small to be detected. In fact, the corresponding $^2J_{HP}$ of methylene prontons in uncoordinated PEt_3 is very small (0.5 Hz).[15] However, the coupling constant of PEt_3 varies depending on the coordination. For example, $[PdBr_2(PEt_3)_2]$ and $[PdBrPh(PEt_3)_2]$ exhibited 4 Hz of $^{2+4}J_{HP}$ of the methylene protons.[16]

Complex **2c** is scarcely soluble in organic solvents and the NMR data could not be obtained.

Experimental

2-Benzylpyridine was available from Tokyo Kasei Kogyo Co., Ltd. General procedures were described previously.[17]

Reaction of 2-Benzylpyridine with $RhCl_3\cdot3H_2O$. A 2-methoxyethanol solution (20 cm^3) containing $RhCl_3\cdot3H_2O$ (300 mg, 1.20 mmol) and 2-benzylpyridine (1.00 g, 6.0 mmol) was heated at 80°C for 0.5 h. After cooling, the resulting products were filtered and the precipitates were washed with diethyl ether to give a pale yellow solid, $[Rh(piph)Cl_2(Hpiph)]_2\cdot H_2O$ (**1**). Yield 280 mg (45%). Mp 242—250°C. IR (KBr) 760 (o-C_6H_4), 1020 (Py ring), 1480 (CH_2), 1560, 1605 (Py), and 3030 cm^{-1} (aromatic CH). Found: C, 55.49; H, 4.11; N, 5.26%. Calcd for $C_{24}H_{23}N_2Cl_2ORh$: C, 55.41; H, 4.26; N, 5.38%.

$[Rh(piph)Cl_2(PEt_3)_2]$ (2a). A dichoromethane suspension (10 cm^3) containing **1** (100 mg, 0.10 mmol) and triethylphosphine (0.08 cm^3, 0.55 mmol) was refluxed for 1 h to afford a yellow solution. The yellow solution was evaporated to dryness under reduced pressure. The resulting solid was recrystallized from dichloromethane and hexane to yield lemon yellow powders, **2a**. Yield 41 mg (86%). Mp 207—212°C, IR (KBr) 755 (o-C_6H_4), 1030 (Py ring), 1420 (PCH_2), 1450 (CH_2), 1570, 1600 (Py), 2890, 2940, 2970 (CH), and 3025 cm^{-1} (aromatic CH); ^1H NMR (CD_2Cl_2) **PEt_3**: δ=0.73 (18H, quintet, $^3J_{HH}=^{3+5}J_{HP}$=7.3 Hz, CH_3), 1.71 (12H, m, PCH_2); **piph:** δ=4.22 (2H, s, $PyCH_2$), 6.92 (1H, t, ^3J=7.3 Hz, CH), 6.95 (1H, d, ^3J=ca. 6.5 Hz, CH), 6.97 (1H, t, ^3J=7.0 Hz, CH), 7.20 (1H, dt, ^3J=7.3 Hz, ^4J=1.5 Hz, CH), 7.39 (1H, d, ^3J=7.0 Hz, CH), 7.75 (1H, dt, ^3J=7.3 Hz, ^4J=1.5 Hz, CH), 8.20 [1H, d, ^3J=7.3 Hz, 3-H(Py)], and 10.33 [1H, d, ^3J=6.0 Hz, 6-H(Py)]; $^{13}C\{^1H\}$ NMR (CD_2Cl_2) **PEt_3**: δ=7.53 (s, CH_3), 14.79 (t, $^{1+3}J_{CP}$=12.7 Hz, PCH_2); **piph:** 49.45 (s, $PyCH_2$), 122.3 (s), 123.7 (s), 125.2 (s), 125.8 (s), 127.2 (s), 135.9 (s), 138.8 (s), 140.5 (s), 145.4 (dt, $^1J_{CRh}$=29.3 Hz, $^2J_{CP}$=17.6 Hz, Rh-C), 157.7 (s, quarternary C), and 161.0 (s, quarternary C). Found: C, 49.58; H, 6.81; N, 2.34%. Calcd for $C_{24}H_{30}NCl_2P_2Rh$: C, 49.84; H, 6.97; N, 2.42%.

$[Rh(piph)Cl_2(PEt_2Ph)_2]CH_2Cl_2$ (2b). A dichloromethane suspension (10 cm^3) containing **1** (100 mg, 0.10 mmol) and diethylphenylphosphine (0.09 cm^3 0.50 mmol) was refluxed for 1.5 h to afford a reddish yellow solution. The solvent was removed under reduced pressure. The resulting solids were recrystallized from dichloromethane and diethyl ether to give a yellow solid, **2b**. Mp 207—214°C; IR (KBr) 735 (o-C_6H_4), 1030 (Py ring), 1435 (PCH_2), 1455 (CH_2), 1490 (PC_6H_5), 1575, 1610 (Py), 2880, 2940, 2970 (CH), and 3050 cm^{-1} (aromatic CH). ^1H NMR (CD_2Cl_2) **PEt_2Ph**: δ=0.81 (6H, quintet, $^3J_{HH}=^{3+5}J_{HP}$=7.3 Hz, CH_3), 1.02 (6H, quintet, $^3J_{HH}=^{3+5}J_{HP}$=7.3 Hz, CH_3), 2.06 (4H, broad quartet, $^3J_{HH}$=ca. 7 Hz, CH_2), 2.50 (2H, m, CH_2), 2.77 (2H, m, CH_2), 6.81 (4H, t, ^3J=7.3 Hz, m-CH), 6.93 (4H, quartet, $^3J_{HH}=^{3+5}J_{HP}$=7 Hz, o-CH), ca. 6.9 (2H, overlapping, p-CH); **piph:** δ=3.55 (2H, s, CH_2), 6.36 (1H, d, ^3J=7.3 Hz, CH), 6.71 (1H, t, ^3J=7.3 Hz, CH), 6.9—7.05 (3H, overlapping, CH), 7.07 (1H, t, ^3J=6.9 Hz, CH), 8.42 [1H, d, ^3J=8.0 Hz, 3-H(Py)], and 9.93 [1H, d, ^3J=6.3 Hz, 6-H(Py)]; $^{13}C\{1H\}$ NMR (CD_2Cl_2) **PEt_2Ph**: δ=7.51 (2C, s, CH_3), 7.7 (2C, s, CH_3), 13.5 (2C, t, $^{1+3}J_{CP}$=13.7 Hz, CH_2), 14.5 (2C, t, $^{1+3}J_{CP}$=13.7 Hz, CH_2), 127.6 (4C, s, m-C), 128.9 (2C, s, p-C), 131.3 (4C, s, o-C), 132.7 (2C, t, $^{1+3}J_{CP}$=7 Hz, ipso-C); **piph:** δ=48.6 (s, CH_2), 122.3 (s), 123.9 (s), 124.8 (s), 127.2 (s), 136.1 (s), 137.3 (s), 140.7 (s), 145.3 (1C, dt, $^1J_{CRh}$=27 Hz, $^2J_{CP}$=15 Hz, RhC), 156.3 (s, quarternary C), and 159.0 (s, quarternary C). Found: C, 54.84; H, 6.03; N, 2.08%. Calcd for $C_{32}H_{40}NCl_2P_2Rh+CH_2Cl_2$: C, 54.75; H, 5.85; N, 1.98%.

$[Rh(piph)Cl_2(PPh_3)_2]$ (2c). A dichloromethane suspension (15 cm^3) involving **1** (100 mg, 0.10 mmol) and triphenylphosphine (130 mg, 0.50 mmol) was refluxed for 2.5 h to yield an orange solution. The solution was evaporated to dryness under reduced pressure and the residue was washed with dichloromethane to give yellow powders, **2c**. Yield 35 mg, 20%. Mp 189—194°C. IR (KBr) 745 (o-C_6H_4), 1090 (Py ring), 1435, 1485 (PC_6H_5), 1450 (CH_2), 1575, 1610 (Py), and 3050 cm^{-1} (aromatic CH). Found: C, 66.34; H, 4.82; N, 1.67%. Calcd for $C_{48}H_{40}NCl_2P_2Rh$: C, 65.91; H, 5.53; N, 1.60%.

The authors wish to express their thanks to Shoei Chemical Industry Inc. for its financial support to the present work.

References

1) D. E. Webster, *Adv. Organomet. Chem.*, **15**, 147 (1977).

2) I. Omae, "Organometallic Intramolecular Coordination Compounds," Elsevier, Amsterdam (1986).
3) G. R. Newkome, W. E. Puckett, V. K. Gupta, and G. E. Kiefer, *Chem. Rev.*, **86**, 451 (1986).
4) A. D. Ryabov, *Int. J. Methods Synthetic Org. Chem.*, **1985**, 233.
5) K. Tani, L. D. Brown, J. Ahmed, J. A. Ibers, M. Yokota, A. Nakamura, and S. Otsuka, *J. Am. Chem. Soc.*, **99**, 7876 (1977).
6) P. K. Santra and C. R. Saha, *J. Mol. Catal.*, **39**, 279 (1987).
7) M. Nonoyama and K. Yamasaki, *Inorg. Nucl. Chem. Lett.*, **7**, 943 (1971).
8) M. I. Bruce, M. Z. Iqbal, and F. G. A. Stone, *J. Organomet. Chem.*, **40**, 393 (1972).
9) H. Onoue and I. Moritani, *J. Organomet. Chem.*, **44**, 189 (1972).
10) M. Nonoyama, *J. Organomet. Chem.*, **86**, 263 (1975).
11) M. Nonoyama, *J. Organomet. Chem.*, **74**, 115 (1974).
12) K. Hiraki, Y. Fuchita, and K. Takechi, Inorg. Chem., **20**, 4316 (1981).
13) Y. Fuchita, K. Hiraki, and Y. Kage, *Bull. Chem. Soc. Jpn.*, **55**, 955 (1982).
14) Y. Fuchita, K. Hiraki, and T. Uchiyama, *J. Chem. Soc., Dalton Trans.*, **1983**, 897.
15) J. B. Hendrickson, M. L. Maddox, J. J. Sims, and H. D. Kaesz, *Tetrahedron*, **20**, 449 (1964).
16) Y. Fuchita, K. Hiraki, Y. Kamogawa, M. Suenaga, K. Tohgoh, and Y. Fujiwara, *Bull. Chem. Soc. Jpn.*, **62**, 1081 (1989).
17) Y. Fuchita, K. I. Hardcastle, K. Hiraki, and M. Kawatani, *Bull. Chem. Soc. Jpn.*, **63**, 1961 (1990).

Structural and Compositional Changes of Hydrated Sodium Molybdenum Bronze by Heat Treatments in Air

Noriyuki SOTANI,* Kazuo EDA, Kouichi FURUSAWA,† Fumikazu HATAYAMA,†† and Sadao TAKAGI†
College of Liberal Arts, Kobe University, Tsurukabuto, Nada, Kobe 657
† Department of Chemistry, Faculty of Science and Technology, Kinki University, Kowakae, Higashi-Osaka 577
†† School of Allied Medical Science, Kobe University, Tomogaoka, Suma, Kobe 654-01
(Received December 25, 1990)

Synopsis. When hydrated sodium molybdenum bronze, VD, was heated in air, dehydration as well as both irreversible and reversible phase changes took place as follows:

$$Na_{0.22}(H_2O)_{0.43}H_{0.03}MoO_{3.11} \xrightarrow{442\ K} Na_{0.21}H_{0.03}MoO_{3.14} \xrightarrow{555\ K} Na_2Mo_4O_{13} + MoO_3 \xrightarrow{801\ K} \text{melt.}$$

Interest has been focused on studies of alkali molybdenum bronzes which show low-dimensional electronic properties,[1] such as semiconductor-metal transitions[2,3] and superconductivity.[4] Wold et al.[2] first prepared sodium molybdenum bronze, $Na_{0.9}Mo_6O_{17}$, by fusing the desired molar proportion of a mixture of MoO_3 and Na_2MoO_4 at 823 K for 1 h. However, the authors[5] obtained $Na_{0.9}Mo_6O_{17}$ from the hydrated sodium molybdenum bronze by heating in nitrogen at about 600 K. This is a useful and effective preparation method for the following reasons: (1) The treating temperature is lower by about 200 K than that for the usual fused method. (2) Although the usual preparation method of $Na_{0.9}Mo_6O_{17}$ proceeds in the liquid phase, in our method there is a solid phase without any intermediate products.[5] (3) The hydrated sodium molybdenum bronze already contains Na before any treatment. It is, therefore, important to have detailed information concerning the hydrated sodium molybdenum bronze as a starting material for the preparation of $Na_{0.9}Mo_6O_{17}$. However, no detailed characterization has yet been performed.[6-9] The authors have recently reported[10] on the characterization of hydrated sodium molybdenum bronzes by the use of TG-DTA and NMR. In a series of investigations concerning the hydrated alkali metal molybdenum bronze, we studied both the structural and compositional changes of the hydrated sodium molybdenum bronze by a heat treatment in air; they are described in this paper.

Experimental

The sample was obtained by the method of Thomas and MacCarron.[9] The air-dried sample (named "AD") was unstable. A sample called "VD" was stable and was used for the experiment; it was obtained from AD by vacuum drying at room temperature overnight or by standing in air for more than 30 d. TG-DTA curves were obtained using a MAC SCIENCE TG-DTA 2000 with a heating rate of 10 K min^{-1}. Samples heated at various temperatures were studied using a RIGAKUDENKI GEIGER D-1 FLEX X-ray diffractometer and a JASCO 701G IR spectrophotometer. Changes in surface area were measured using a QUANTACHROME QUNTASORB Jr. The contents of Na and Mo in the samples were measured using a HITACHI 180-80 atomic absorption spectrometer with the 330.23-nm line for Na and the 313.26-nm line for Mo. Mo^{5+} was determined by using the method of Choain and Marion.[11]

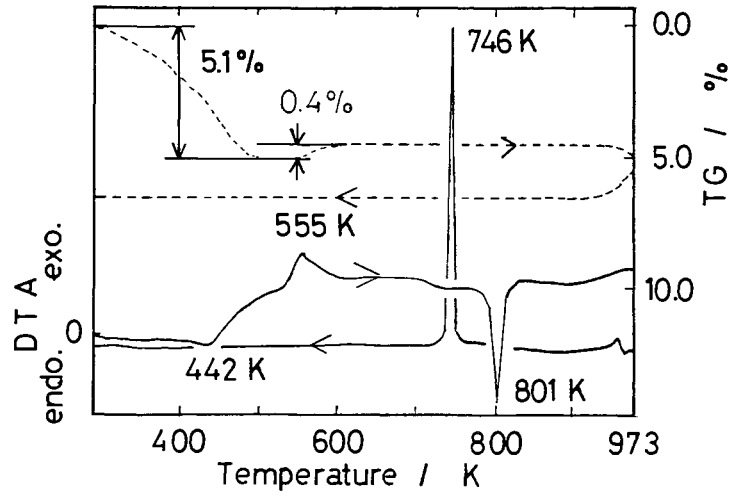

Fig. 1. TG-DTA curves of VD in air. The curves were obtained by heating (—>—) with a heating rate of 10 K min^{-1} and then by cooling (—<—) naturally to room temperature.

Results

Figure 1 shows the TG-DTA curves of hydrated sodium molybdenum bronze, VD, which were obtained by heating to 973 K and then cooling naturally to room temperature. Upon heating, two endothermic peaks at 442 and 801 K and an exothermic peak at 555 K appeared. The endothermic peak at 442 K was accompanied by a weight loss (5.1%) and the exothermic peak at 555 K, by a weight gain (0.4%); the endothermic peak at 801 K showed no weight change. Upon cooling, two exothermic peaks with no weight change appeared at 746 and 937 K. The endothermic peak at 442 K and the exothermic peak at 555 K upon heating gave no corresponding peak upon cooling. It is, therefore, suggested that an irreversible phase transition takes place. On the other hand, the endothermic peak at 801 K upon heating corresponds to the exothermic peak at 746 K upon cooling, and is attributed to a reversible phase transition.

Figure 2 shows the X-ray diffraction patterns of samples heated at various temperatures. The pattern of the sample heated at 498 K is identical with that of VD, although the X-ray peaks are broad. The samples heated at 593 and 828 K show patterns attributed to $Na_2Mo_4O_{13}$ and MoO_3.

The IR spectra of the samples heated at the same temperatures as in the case of X-ray studies were obtained. Although the spectra of samples heated at 423 and 498 K were identical with that of VD, those of the samples heated at 593 and 828 K were very complicated.

The surface areas of the samples heated at the same temperatures as in the case of the X-ray studies are shown in Table 1. Although the surface areas of samples with the VD structure were nearly constant, they decreased steeply when samples with the VD structure were completely transformed to $Na_2Mo_4O_{13}$ and MoO_3. It is clear that the change in the surface area depends on the crystal structure.

The TG results and the results obtained by chemical analyses are given in Table 1. According to these results, samples having the VD structure necessarily contain Mo^{5+}, which is produced by reduction of Mo^{6+}, resulting from an insertion of cations. On the contrary, samples without the VD structure did not contain Mo^{5+}, even though they contained Na.

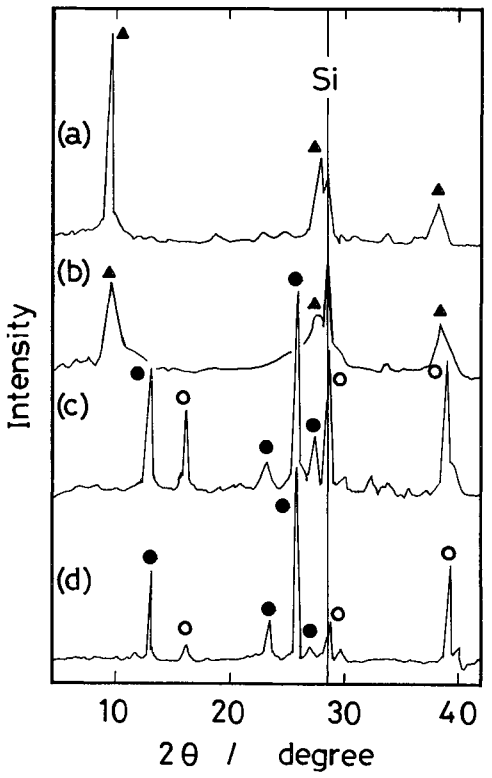

Fig. 2. X-Ray diffraction patterns of the samples heated in air at (a): 423, (b): 498, (c): 593, and (d): 828 K. ▲ represents VD, ●, MoO_3 and ○, $Na_2Mo_4O_{13}$, respectively.

Discussion

According to chemical analyses, VD contains 0.25 mol of Mo^{5+} and 0.22 mol of Na^+, as shown in Table 1. The NMR results[10] have proved that VD contains protons. Considering these results, it is suggested that the concentration of protons is 0.03 (=0.25−0.22) mol. VD is therefore, formulated as $Na_{0.22}(H_2O)_{0.43}H_{0.03}MoO_{3.11}$. The weight gain (0.4%) at around 555 K should be due to a recombination of oxygens in air to make up for the lattice oxygens consumed by the protons. This value corresponds to 0.02 mol of oxygens and to 0.04 mol of protons, which agrees rather well with that of 0.03 mol evaluated from the results of the chemical analysis.

The results obtained by chemical analyses of the samples heated at 498 and 593 K are the same, except that a sample heated at 498 K contains 0.04 mol of Mo^{5+}. This sample has the VD structure. The NMR result also shows the presence of a small number of protons. Protons in a Type-I hydrogen bronze can be kept at a temperature of more than 550 K.[12] Considering these results, 0.03 mol of protons should be maintained in the

Table 1. Composition of Hydrated Sodium Molybdenum Bronze Heated at Various Temperatures in Air

	H_2O	Mo	Na	O	x	SA
	%	%	%	%	(Mo^{5+})	$m^2\ g^{-1}$
V D	5.10	60.36	3.33	31.21		10.1
a)	(0.43)	(1.00)	(0.22)	(3.11)	0.25	
423 K	3.29	61.90	3.11	31.69		9.1
a)	(0.28)	(1.00)	(0.21)	(3.07)	0.19	
498 K		64.50	3.30	32.20		8.8
a)		(1.00)	(0.21)	(3.14)	0.04	
593 K		63.48	3.22	33.30		3.5
a)		(1.00)	(0.21)	(3.14)	0.00	
733 K		64.20	3.40	32.40		1.6
a)		(1.00)	(0.22)	(3.03)	0.00	
828 K		63.56	3.28	33.16		0.3
a)		(1.00)	(0.22)	(3.13)	0.00	

a) Molar ratio to Mo.

sample. Therefore, the composition is $Na_{0.21}H_{0.03}MoO_{3.14}$; the sample heated at 593 K has a different structure, and the composition is $Na_{0.21}MoO_{3.14}$. This X-ray result proves that the sample heated at 593 K and then cooled to the room temperature comprises a mixture of $Na_2Mo_4O_{13}$ and MoO_3. The Na_2MoO_4/MoO_3 ratio of the sample is about 1/9, agreeing well with the range of coexistence with $Na_2Mo_4O_{13}$ and MoO_3 according to a Na_2MoO_4–MoO_3 phase diagram.[13-15] The exothermic peak at 555 K is due to an irreversible phase transition from VD to $Na_2Mo_4O_{13}$ and MoO_3.

The sample heated at 828 K and then cooled to room temperature apparently shows a glassy state. The X-ray results prove that it comprises $Na_2Mo_4O_{13}$ and MoO_3. According to the phase diagram, an eutectic temperature of 810 K appears when the $Na_2Mo_4O_{13}/MoO_3$ ratio is between 23/77 and 6/94. In this range, the samples can produce solid solutions at an eutectic temperature such as for $Na_2Mo_4O_{13}\cdot MoO_3$ and $Na_2Mo_4O_{13}\cdot 2MoO_3$.[13] Since the Na_2MoO_4/MoO_3 ratio of 1/9 found in this study just falls within this range and the X-ray results show the presence of $Na_2Mo_4O_{13}$ and MoO_3 (as mentioned above), it can be concluded that the endothermic peak at 801 K upon heating is due to the eutectic point, (which corresponds to the melting point of the solid solution), and the exothermic peak at 746 K upon cooling, to solidification. According to above consideration, we conclude that the hydrated sodium molybdenum bronze, VD, is changed by a heat treatment in air as follows:

$$Na_{0.22}(H_2O)_{0.43}H_{0.03}MoO_{3.11} \xrightarrow{442\ K} Na_{0.21}H_{0.03}MoO_{3.14}$$
$$\xrightarrow{555\ K} Na_2Mo_4O_{13} + MoO_3 \xrightarrow{801\ K} \text{melt.}$$

References

1) M. Greenblatt, *Chem. Rev.*, **88**, 31 (1988).
2) A. Wold, W. Kunnmann, R. J. Arnott, and A. Ferretti, *Inorg. Chem.*, **3**, 545 (1964).
3) P. Strobel and M. Greenblatt, *J. Solid State Chem.*, **36**, 331 (1981).
4) M. Greenblatt, W. H. McCaroll, R. Niefeld, M. Groft, and J. V. Waszczak, *Solid State Commun.*, **51**, 671 (1984).
5) K. Eda, K. Furusawa, F. Hatayama, S. Takagi, and N. Sotani, *Bull. Chem. Soc. Jpn.*, **64**, 161 (1991).
6) R. Schöllorn, R. Kuhlmann, and J. O. Besenhard, *Mater. Res. Bull.*, **11**, 83 (1976).
7) S. Son, F. Kanamaru, and M. Koizumi, *Inorg. Chem.*, **18**, 400 (1979).
8) T. Iwamoto, Y. Itoh, K. Ohkura, and M. Takahashi, *Nippon Kagaku Kaishi*, **1983**, 273.
9) D. Thomas and E. MacCarron, III, *Mater. Res. Bull.*, **21**, 945 (1986).
10) N. Sotani, K. Eda, and M. Kunitomo, *J. Solid State Chem.*, **89**, 123 (1990).
11) C. Choain and F. Marion, *Bull. Chim. Fr.*, **1963**, 212.
12) N. Sotani, K. Eda, M. Sadamatu, and S. Takagi, *Bull. Chem. Soc. Jpn.*, **62**, 903 (1989).
13) P. Caillet, *Bull. Chim. Fr.*, **1967**, 4750.
14) J.-M. Réau and C. Fouassier, *Bull. Chim. Fr.*, **1971**, 398.
15) "Gmelin Handbuch: Molybdän," Springer-Verlag, Berlin (1975), Vol. 53, Teil Bl, s. 211.

Catalytic Behavior of Rhodium(I) Complexes in Hydrogermylation and Hydrosilylation of Phenylacetylene

Fumio WADA,* Seiji ABE, Norio YONEMARU, Kiyoshi KIKUKAWA,† and Tsutomu MATSUDA
Department of Organic Synthesis, Faculty of Engineering, Kyushu University, Hakozaki, Higashi-ku, Fukuoka 812
† Department of Industrial Chemistry, Faculty of Engineering, Kinki University in Kyushu, Kayanomori, Iizuka 820
(Received December 17, 1990)

Synopsis. Rhodium complexes, $Rh(L)(C_2H_4)_2$ {L=$(CH_3C{=}O)_2CH$ (acac), and $(CF_3C{=}O)_2CH$ (hfa)}, catalyze hydrogermylation and hydrosilylation of phenylacetylene with Bu_3GeH and R_3SiH (R=Bu, Et), respectively, to produce $Ph(R_3M)C{=}CH_2$ (M=Ge, Si) selectively. Other rhodium complexes, that is, $[RhCl(C_2H_4)_2]_2$, $Rh_2Cl_2(cod)_2$, $Rh(tmhd)(C_2H_4)_2$ {tmhd=$(t\text{-BuC}{=}O)_2CH$}, and $Rh(dbm)(C_2H_4)_2$ {dbm=$(PhC{=}O)_2CH$}, also catalyze these reactions, but with less regioselectivity.

Hydrosilylation, hydrostannylation, and hydrogermylation of terminal acetylenes under transition metal catalysis have been widely studied[1] because of their potential utility in the synthetic organic chemistry of vinylic organometals with 14(IV B) series elements (Eq. 1).

$$R_3MH + R'\text{-}C{\equiv}CH \xrightarrow{cat.} \underset{\text{1 (}\alpha\text{-adduct)}}{\overset{R'}{\underset{R_3M}{\diagdown\!\!\diagup}}C{=}CH_2} + \underset{\text{2 (}\beta\text{-adducts, }E\text{ and }Z\text{)}}{\overset{R}{\underset{H}{\diagdown\!\!\diagup}}C{=}CH{\sim}MR_3} \quad (1)$$

M=Si, Sn, Ge
R,R'=alkyl, phenyl

The selective formation of β-adducts (**2**) has been thoroughly investigated under transition metal catalysis or radical conditions.[1b-e] However, catalysts yielding α-adduct (**1**) selectively have not been well-studied, except for rhodium catalysts used for the hydrostannylation of terminal acetylenes. We report here on a new rhodium catalyst which is effective for the selective formation of an α-adduct in the hydrogermylation and hydrosilylation of phenylacetylene.

Experimental

Materials. The rhodium complexes used in the present study were prepared by using ordinary methods,[2] and were stored at −25 °C. The solvents and other reagents were purified by distillation before use.

General Procedure. All operation were carried out under a nitrogen atmosphere. The typical procedure was as follows. To a mixture of $Rh(hfa)(C_2H_4)_2$ {1.46 mg (4.0×10^{-3} mmol)} and CH_2Cl_2 (10 ml) was added phenylacetylene {0.41 g (4.0 mmol)}, and the mixture was stirred at 40 °C for 10 min. Then, (n-Bu)$_3$GeH {0.098 g (0.4 mmol)} was added rapidly and the reaction was monitored by GLC. The reaction products were isolated by short-pass distillation. The characterization and the product distribution of products were determined by ^{1}H NMR and GLC.

Table 1. Rhodium-Catalyzed Hydrogermylation and Hydrosilylation of PhC≡CH[a]

Run	Catalyst[b]	Temp	Time	PhC≡CH/R_3MH	Yield[c]	Products (% ratio)[d]	
		°C	h	(Molar ratio)	%	**1**	**2** (E/Z)
M=Ge				R=Bu			
1	$RhCl(CO)(PPh_3)_2$	0	6	10	65	7	93 (70/23)
2	$RhCl(CO)(PPh_3)_2$-galvinoxyl	0	2	10	73	1	99 (91/8)
3	$[RhCl(C_2H_4)_2]_2$	0	0.5	1	84	15	85 (36/49)
4	$[RhCl(C_2H_4)_2]_2$	0	1	10	89	61	39 (20/19)
5	$[RhCl(cod)]_2$	40	9	10	88	23	76 (49/27)
6	$Rh(acac)(C_2H_4)_2$	40	0.5	1	89	81	19 (16/1)
7	$Rh(acac)(C_2H_4)_2$	40	0.5	10	91	86	14 (13/1)
8	$Rh(acac)(C_2H_4)_2$-galvinoxyl	40	1	10	96	81	19 (18/1)
9	$Rh(tmhd)(C_2H_4)_2$	40	1	10	96	56	44 (40/4)
10	$Rh(dbm)(C_2H_4)_2$	40	0.5	10	97[d]	54	46 (43/3)
11	$Rh(hfa)(C_2H_4)_2$	40	1	10	100[d]	95	5 (4/1)
M=Si				R=Bu			
12	$Rh(acac)(C_2H_4)_2$	40	22	10	77	75	25 (25/0)
13	$Rh(acac)(C_2H_4)_2$	40	33	1	83[d]	71	29 (25/4)
14	$Rh(tmhd)(C_2H_4)_2$	40	7	10	97	60	40 (39/1)
M=Si				R=Et			
15	$Rh(acac)(C_2H_4)_2$	40	1	10	99[d]	86	14 (14/0)
16	$Rh(hfa)(C_2H_4)_2$	40	1	10	100[d]	96	4 (4/0)

a) The reaction was monitored by GLC for it's completion. Isomerization among the isomers did not observed under the conditions. b) One mol% of a catalyst was used. cod=1,5-cyclooctadiene; acac=$(CH_3C{=}O)_2CH$; tmhd=$(t\text{-BuC}{=}O)_2CH$; dbm=$(PhC{=}O)_2CH$; hfa=$(CF_3C{=}O)_2CH$. c) Isolated yields by short pass distillation based on R_3MH. d) Determined by GLC.

Table 2. Solvent Effects on the Hydrogermylation and the Hydrosilylation

Catalyst[a]	Solvent	Temp °C	Time h	PhC≡CH/R_3MH (Molar ratio)	Yield[b] %	Products (% ratio)[c] 1	2 (*E*/*Z*)
M=Ge				R=Bu			
$Rh(acac)(C_2H_4)_2$	CH_2Cl_2	40	0.5	1	89	81	19 (16/3)
	THF	40	6	1	98	43	57 (38/19)
	C_6H_6	40	9	1	95	41	59 (44/15)
M=Si				R=Et			
$Rh(acac)(C_2H_4)_2$	CH_2Cl_2	40	1	10	99	86	14 (14/0)
	CH_2ClCH_2Cl	65	3	10	94	79	21 (19/2)
	THF	40	1	1	89	48	52 (37/15)
	C_6H_6	65	1	1	86	46	54 (45/9)
	C_6H_6	40	3	1	80	50	50 (40/10)

a) One mol% of the catalyst was used. b) Isolated yields by short pass distilation based on R_3MH. c) Determined by GLC.

Hydrosilylation was also carried out by the same method mentioned above.

Results and Discussion

Rhodium complexes {$RhClL_3$, $RhCl(CO)L_2$, $[RhCl(cod)]_2$; L=PPh_3} were previously found to catalyze the hydrostannylation of acetylene with Bu_3SnH to produce an α-adduct, $Ph(Bu_3Sn)C=CH_2$ selectively, and a combination of galvinoxyl (radical inhibitor) and $RhCl(CO)(PPh_3)_2$ in the hydrostannylation of phenylacetylene proved to give an α-adduct exclusively in excellent yield.[3] In the hydrogermylation of phenylacetylene, however, these catalysts gave β-adducts (**2**) as the main products, and the presence of the radical inhibitor suppressed the formation of the α-adduct and (*Z*)-β-adduct, as shown in Table 1 (Run 2). When we used a large excess of PhC≡CH to Bu_3GeH (>10), only $[RhCl(C_2H_4)_2]_2$ produced the α-adduct with moderate selectivity (61%), probably because of an effective exchange of the ethylene with PhC≡CH.

Interestingly, $Rh(acac)(C_2H_4)_2$, in which chloride in $[RhCl(C_2H_4)]_2$ is replaced by acetylacetonate, gave the α-adduct in good yields, irrespective of the molar ratio of PhC≡CH/R_3GeH, although the catalytic activity was somewhat less than that of $[RhCl(C_2H_4)_2]_2$. The catalyst also acted as an effective catalyst for the hydrosilylation of PhC≡CH with R_3SiH (R=Bu, Et) under the same conditions as those in hydrogermylation, but not for hydrostannylation. When we used $(CF_3C=O)_2CH$ instead of acac as a β-diketonate ligand, the regioselectivity toward the α-adduct in both reaction systems was greatly improved (select.=ca. 95%). On the other hand, the other complexes with a bulky β-diketonate ligand, that is $Rh(tmhd)(C_2H_4)_2$ and $Rh(dbm)(C_2H_4)_2$, also catalyzed both reactions, but with less selectivity. These results indicate that the regioselectivity in both reaction systems is influenced by both electronic and steric effects of the ligands around the rhodium metal. In this catalyst system, the reaction temperature and solvent also affected the regioselectivity toward the α-adduct. For example, in the $Rh(acac)(C_2H_4)_2$ catalyst system, as shown in Table 2, dichloromethane having a small coordination ability was found to be appropriate as a reaction medium.

Compared with Bu_3GeH, Bu_3SiH required a longer reaction time because of the less reactivity of Bu_3SiH, and the regioselectivity toward the α-adduct was somewhat less than that of Bu_3GeH (Runs 7 and 12). However, with less crowded triethylsilane, Et_3SiH, regioselectivity toward the α-adducct increased, giving almost the same selectivity to that of Bu_3GeH. The solvent effect was almost the same with that in the hydrogermylation as shown in Table 2.

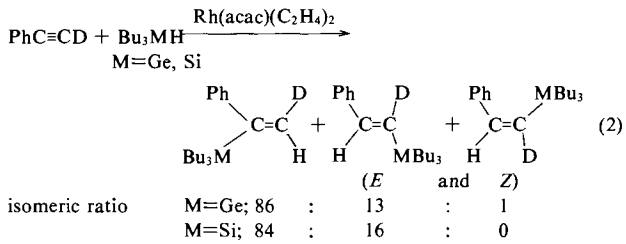

(2)

The $Rh(acac)(C_2H_4)_2$ system proved to give $Ph(Bu_3M)C=CHD$ (M=Ge, Si) stereoselectively in the reaction of PhC≡CD with Bu_3GeH and Bu_3SiH, respectively (Eq. 2).

This result supports the *syn*-addition process in the present α-directive hydrogermylation and hydrosilylation which is generally observed in the transition metal-catalyzed hydrostannylation[4] and hydrosilylation.[5]

The catalytic behaviors of $Rh(acac)(C_2H_4)_2$ and $Rh(hfa)(C_2H_4)_2$ for α-adduct selectivity have not get been clarified. Consequently, $Rh(hfa)(C_2H_4)_2$ is a useful catalyst which provides a simple method for the preparation of $Ph(R_3M)C=CH_2$ (M= Ge, Si; R=Bu, Et) with regard to the starting materials and procedures.

References

1) a) R. J. P. Corriu and J. E. Morean, *J. Organomet. Chem.*, **40**, 73 (1972); b) Y. Ichinose, H. Oda, K. Oshima, and K. Uchimoto, *Bull. Chem. Soc. Jpn.*, **60**, 3468 (1987); c) A. J. Leusink and H. A. Budding, *J. Organomet. Chem.*, **11**, 533 (1968); d) T. K. Gar, A. A. Buyakov, A. V. Kisin, and V. F. Mironov, *Zh. Obsch. Khim.*, **41**, 1589 (1971); e) R. A. Benkeser, M. L. Burrous, L. E. Nelson, and J. V. Swisfer, *J. Am. Chem. Soc.*, **83**, 4385 (1961); f) R. A. Benkeser and R. A. Hickner, *J. Am. Chem. Soc.*, **80**, 5298 (1958); g) J. E. Hill and T. A. Nile, *J. Organomet. Chem.*, **137**, 293 (1977); h) M. Green, J. L. Spences, and F. G. A. Stone, *J. Chem. Soc., Dalton Trans.*, **1977**, 1525; and i) "Comprehensive Organometallic Chemistry," ed by G.

Wilkinson, F. G. A. Stone, and E. W. Abel, Pergamon Press, Oxford (1982), Vol. 2.

2) a) Rh(hfa)(C_2H_4)$_2$; B. T. Golding and C. Pierpoint, *J. Chem. Soc., Dalton Trans.*, **1984**, 219. b) Rh(acac)(C_2H_4)$_2$; R. Cramer, *J. Am. Chem. Soc.*, **86**, 217 (1964). c) RhCl(CO)(PPh_3)$_2$; D. Evans, J. A. Osborn, and G. Wilkinson, *Inorg. Synth.*, **11**, 99 (1968).

3) K. Kikukawa, H. Umekawa, F. Wada, and T. Matsuda, *Chem. Lett.*, **1988**, 881.

4) R. A. Benkeser, *Pure Appl. Chem.*, **13**, 133 (1966).

5) K. Tamao, J. Yoshida, M. Yamamoto, T. Kakui, H. Matsumoto, M. Takahashi, A. Kurita, M. Murata, and M. Kumada, *Organometallics*, **1**, 355 (1982).

Reactions of 2-Hydrazino- and 8-Hydrazinocyclohepta[*b*]pyrroles with Dimethyl Acetylenedicarboxylate

Noritaka ABE* and Kumiko YATABE
Department of Chemistry, Faculty of Science, Yamaguchi University, Yamaguchi 753
(Received January 16, 1991)

Synopsis. 2-Hydrazinocyclohepta[*b*]pyrrole reacted with dimethyl acetylenedicarboxylate (DMAD) to give the hydrazones (**2a**), the pyrimidinone-fused cyclohepta[*b*]pyrrole (**3**), 1,2,4-triazinone-fused cyclohepta[*b*]pyrroles, and the 1,2-dihydro-3*H*-pyrazol-3-one derivative. Thermolysis of **2a** gave **3** and tetramethyl pyrrole-2,3,4,5-tetracarboxylate. The reaction of ethyl cyclohepta[*b*]pyrrole-3-carboxylate with DMAD at room temperature gave the hydrazone and the spiro-pyrazoline derivative.

It is known that hydrazino-substituted heterocycles react with dimethyl acetylenedicarboxylate (DMAD) to give the hydrazones, and that subsequent cyclization gives either 1,2,4-triazin-5-ones or 5-pyrazolones.[1] Although cyloadditions of azaazulenes are of interest and some studies have been carried out,[2-7] cycloadditions of hydrazinoazaazulenes have not yet been studied. In this paper we report on the reactions of 2-hydrazino- and 8-hydrazinocyclohepta[*b*]pyrroles with DMAD.

The treatment of 2-hydrazinocyclohepta[*b*]pyrrole (**1a**) with two molar amount of DMAD in benzene at room temperature for 3 h gave dimethyl 2-[1-[(*E*)-1,2-bis(methoxycarbonyl)vinyl]cyclohepta[*b*]pyrrol-2(1*H*)-ylidenehydrazono]succinate (**2a**) (22%), methyl 2-oxo-2*H*-cyclohepta[4,5]pyrrolo[1,2-*a*]pyrimidime-4-carboxylate (**3**)[3] (1%), dimethyl 2-[(cyclohepta[*b*]pyrrol-2-yl)hydrazono]succinate (**4a**) (4%), methyl 3,4-dihydro-4-oxo-2*H*-cyclohepta[4,5]pyrrolo[2,1-*c*][1,2,4]triazin-4-ylideneacetate (**5**) (4.5%), methyl 3,4-dihydro-4-oxo-2*H*-cyclohepta[4,5]pyrrolo[2,1-*c*][1,2,4]triazin-3-ylideneacetate (**6**) (3%), and methyl 1-(cyclohepta[*b*]pyrrol-2-yl)-2,5-dihydro-5-oxo-1*H*-pyrazole-3-carboxylate (**7**) (12%). When **1a** was treated with one molar amount of DMAD in acetonitrile at room temperature, **7** (46%) was obtained as a major product, and **2a** and **3** were not obtained. The treatment of **1a** with three molar amounts of DMAD in acetonitrile at room temperature gave **2a** (43%) as the major product; the yield of **7** was low (2%). For an improvement of the yield of cycloadducts (**5** and **6**), although the reaction was tried under reflux or in the presence of Pd-C, no particular change was observed.

These structures were deduced on the basis of spectral data, especially ^{1}H NMR spectra, as well as elemental analyses.

Compound **3** was considered to be a thermolyzed product of **2a**. Thus, **2a** was heated in *t*-butylbenzene under reflux for 6 h and gave **3** (19%) and **8**[8] (30%).

The reactions of ethyl 2-hydrazinocyclohepta[*b*]pyrrole-3-carboxylate (**1b**) with DMAD somewhat differed from those of **1a**. Thus, a treatment of **1b** with DMAD in acetonitrile at room temperature gave the ethoxycarbonyl **4b** (65%) and 3-ethyl 4',5'-dimethyl 1-[(*Z*)-1,2-bis(methoxycarbonyl)vinyl]-1',2'-dihydrospiro[cyclohepta[*b*]pyrrole-2(1*H*),3'-[3*H*]pyrazole]-3,4'5'-tricarboxylate (**9**) (3%), and a treatment in refluxing xylene gave 1-ethyl 4,5-dimethyl 2-[(*Z*)-1,2-bis(methoxycarbonyl)vinylhydrazono]-2*H*-cyclohepta[*gh*]pyrrolizine-1,4,5-tricarboxylate (**10**) (4%), **4b** (7%), **8** (16%), and 10-ethyl 2,3-dimethyl cyclohepta[4,5]pyrrolo[1,2-*a*]imidazole-2,3,10,-tricarboxylate (**11**)[9] (10%). Compounds **10**, **8**, and **11** would be secondary reaction products. Thus, **4b** was treated with DMAD in refluxing xylene and compounds **10**, **8**, and **11** were obtained.

The formation of the spiro-pyrazoline derivative resembles the reaction of benzophenone phenylhydrazone with DMAD.[10]

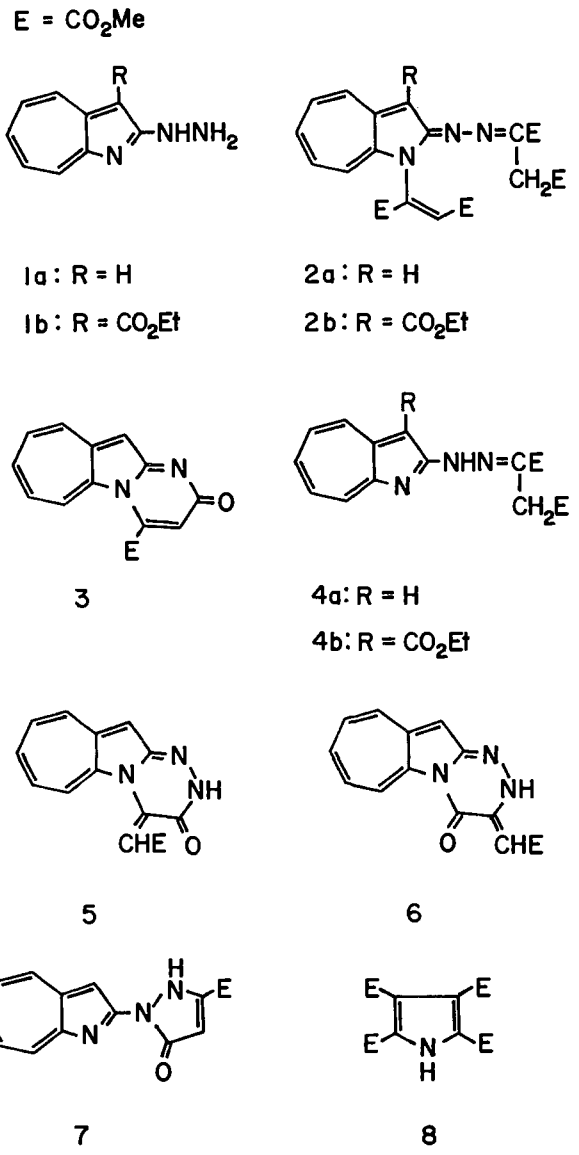

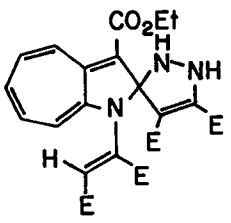

9

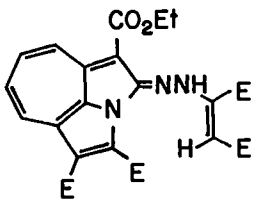

10

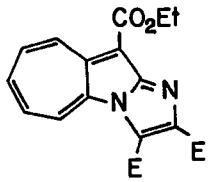

11

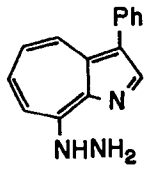

12

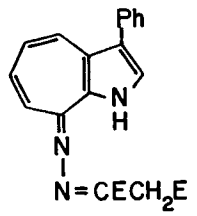

13

The reaction of 8-hydrazino-3-phenylcyclohepta[*b*]-pyrrole (**12**) with DMAD gave dimethyl 2-[3-phenylcyclohepta[*b*]pyrrol-8(1*H*)-ylidenehydrazono]succinate (**13**) in 56% yield. From the expectation of cyclization, compound **13** was treated with acetic anhydride or triethylamine, as previously used;[1] no distinct product was obtained.

Experimental

The melting points are uncorrected. ^{1}H NMR spectra (250 MHz) and ^{13}C NMR spectra (62.87 MHz) were taken on a Hitachi R-250H spectrometer using $CDCl_3$ as a solvent (TMS as an internal standard). IR spectra were recorded for Nujol mulls with a Hitachi 270-50 infrared spectrophotometer. High-resolution mass spectra were determined with a JEOL-01SG-2 spectrometer at 70 eV of ionization energy. Column chromatography was performed on Kieselgel 60.

Reaction of 1a with DMAD. a) A mixture of **1a** (0.500 g) and DMAD (0.893 g) in dry benzene (100 ml) was stirred for 3 h at room temperature and evaporated. The residue was chromatographed with chloroform to give **2a** (0.305 g, 22%), **3**[3] (0.005 g, 1%), **4a** (0.040 g, 4%), **5** (0.038 g, 4.5%), **6** (0.028 g, 3%), and 7 (0.102 g, 12%), successively.

2a: Red prisms; mp 186—187 °C (from hexane); ^{1}H NMR δ=3.65 (3H, s), 3.75 (3H, s), 3.82 (2H, s), 3.87 (3H, s), 3.88 (3H, s), 6.40 (1H, s), 6.65—6.95 (6H, m), and 7.26 (1H, d, J=11.0 Hz); ^{13}C NMR δ=32.55 (t), 51.74 (q), 52.31 (q), 52.50 (q), 52.85 (q), 102.23 (d), 112.62 (d), 128.74 (d), 129.44 (d), 129.66 (d), 131.98 (d), 133.00 (d), 133.97 (s), 145.25 (s), 147.09 (s), 147.24 (s), 147.28 (s), 162.18 (s), 164.05 (s), 165.44 (s), 165.70 (s), and 169.64 (s); IR 1752, 1740, 1726, 1706 (C=O), and 1660 cm^{-1} (C=N). Found: C, 57.19; H, 4.79; N, 9.15%. Calcd for $C_{21}H_{21}N_3O_8$: C, 56.88; H, 4.78; N, 9.48%.

4a: Orange prisms; mp 165—167 °C (from hexane); ^{1}H NMR δ=3.73 (3H, s), 4.01 (3H, s), 4.77 (2H, s), 6.17 (1H, s), 7.06 (1H, s), 7.45—7.70 (3H, m), 8.21 (1H, d, J=10.4 Hz) and 8.23—8.29 (1H, m); IR 3348 (NH), 1738, 1704 (C=O), and 1640 cm^{-1} (C=N). Found: C, 59.68; H, 4.95; N, 13.98%. Calcd for $C_{15}H_{15}N_3O_4$; C, 59.80; H, 5.02; N, 13.95%.

5: Brown needles; mp 242—244 °C (from hexane–dichloromethane); ^{1}H NMR δ=3.74 (3H, s), 5.98 (1H, brd, J=7.9 Hz), 6.14 (1H, s), 6.40—6.60 (3H, m), 6.69 (1H, s), 6.93 (1H, d, J=11.6 Hz), and 9.05 (1H, brs); IR 3160 (NH), 1696, 1652 (C=O), and 1622 cm-1 (C=C). Found: C, 62.59; H, 4.24; N, 15.65%. Calcd for $C_{14}H_{11}N_3O_3$: C, 62.45; H, 4.12; N, 15.61%.

6: Red brown needles; mp 201—202 °C (from hexane–dichloromethane); ^{1}H NMR δ=3.86 (3H, s), 6.08 (1H, s), 6.34 (1H, s), 6.35—6.55 (3H, m), 6.86 (1H, d, J=10.4 Hz), 6.90 (1H, brd, J=6.7 Hz), and 8.79 (1H, brs); IR 3160 (NH), 1710, 1660 (C=O), and 1610 cm^{-1} (C=C). Found: C, 62.43; H, 4.55; N, 15.25%. Calcd for $C_{14}H_{11}N_3O_3$: C, 62.45; H, 4.12; N, 15.61%.

7: Yellow brown needles; mp 190—191 °C (from hexane–dichloromethane); ^{1}H NMR δ=3.98 (3H, s), 6.14 (1H, s), 7.65 (1H, s), 7.70—7.95 (3H, m), 8.53 (1H, d, J=9.2 Hz), and 8.55 (1H, d, J=9.8 Hz); IR 3100 (NH), 1720, 1715, 1652 (C=O), and 1622 cm-1 (C=C). Found: C, 62.68; H, 4.29; N, 15.20%. Calcd for $C_{14}H_{11}N_3O_3$: C, 62.45; H, 4.12; N, 15.61%.

b) A mixture of **1a** (0.318 g) and DMAD (0.290 g) in dry acetonitrile (100 ml) was stirred for 3 h at room temperature and evaporated. The residue was chromatographed with chloroform to give **4a** (0.006 g, 1%), **5** (0.015 g, 2.5%), **6** (0.014 g, 2%), and 7 (0.274 g, 46%), successively.

Thermolysis of 2a. A solution of **2a** (0.180 g) in *t*-butylbenzene (15 ml) was refluxed for 6 h and evaporated. The residue was chromatographed with benzene–chloroform (1:1) to give **3** (0.020 g, 19%) and **8**[8] (0.037 g, 30%).

Reaction of 1b with DMAD. a) A mixture of **1b** (1.000 g) and DMAD (1.230 g) in dry acetonitrile (100 ml) was stirred for 3 h at room temperature and evaporated. The residue was chromatographed with chloroform to give **4b** (1.050 g, 65%) and **9** (0.074 g, 3%), successively.

4b: Yellow prisms; mp 150—151 °C (from hexane–dichloromethane); ^{1}H NMR δ=1.53 (3H, t, J=7.3 Hz), 3.71 (3H, s), 3.81 (2H, s), 3.92 (3H, s), 4.58 (2H, q, J=7.3 Hz), 7.50—7.90 (3H, m), 8.54 (1H, d, J=9.8 Hz), 9.17 (1H, d, J=9.8 Hz), and 14.01 (1H, s); IR 3248 (NH), 1734, 1710, and 1668 cm^{-1} (C=O). Found: C, 58.15; H, 5.18; N, 11.14%. Calcd for $C_{18}H_{19}N_3O_6$: C, 57.91; H, 5.13; N, 11.25%.

9: Red brown prisms, mp 197—198 °C (from hexane–dichloromethane); ^{1}H NMR δ=1.43 (3H, t, J=7.3 Hz), 3.50 (1H, brs), 3.68 (3H, s), 3.76 (3H, s), 3.80 (3H, s), 3.95 (3H, s), 4.35 (2H, dq, J=11.6 and 7.3 Hz), 5.08 (1H, brs), 5.56 (1H, s), 6.31 (1H, d, J=9.2 Hz), 6.69 (1H, dd, J=11.0 and 9.2 Hz), 6.94 (1H, dd, J=11.0 and 9.2 Hz), 6.97 (1H, d, J=11.6 and 9.2 Hz), and 8.41 (1H, d, J=11.6 Hz); IR 1760, 1744, 1694, and 1678 cm^{-1} (C=O). Found: m/z 515.1538. Calcd for $C_{24}H_{25}N_3O_{10}$: M, 515.1538.

b) A mixture of **1b** (0.500 g) and DMAD (0.920 g) in dry xylene (50 ml) was refluxed for 5 h and evaporated. The residue was chromatographed with benzene–chloroform (1:1) to give **10** (0.040 g, 4%), **4b** (0.054 g, 7%), **8** (0.101 g, 16%), and **11**[9] (0.079 g, 10%), successively.

10: Red prisms, mp 210—212 °C (from hexane–dichloromethane); ^{1}H NMR δ=1.42 (3H, t, J=7.3 Hz), 3.43

(3H, s), 3.61 (3H, s), 3.83 (3H, s), 3.97 (3H, s), 4.41 (2H, q, J=7.3 Hz), 6.08 (1H, s), 6.56 (1H, dd, J=11.6 and 9.2 Hz), 6.89 (1H, dd, J=11.6 and 9.2 Hz), 7.69 (2H, d, J=11.6 Hz), and 10.62 (1H, brs, exch.); IR 3356 (NH), 1746, 1734, 1712, and 1690 cm^{-1} (C=O). Found: m/z 513.1376. Calcd for $C_{24}H_{23}N_3O_{10}$: M, 513.1382.

11: Dark violet needles, mp 162—163 °C (from hexane–dichloromethane) (lit,[9] mp 161 °C).

Reaction of 4b with DMAD. A mixture of **4b** (0.250 g) and DMAD (0.190 g) in dry xylene (50 ml) was refluxed for 3 h and evaporated. The residue was chromatographed with benzene–chloroform (1:1) to give **10** (0.015 g, 4%), **4b** (0.164 g, 47.5%), **8** (0.072 g, 30%), and **11** (0.010 g, 4%), successively.

Reaction of 12 with DMAD. a) A mixture of **12**[11] (0.235 g) and DMAD (0.285 g) in dry acetonitrile (100 ml) was stirred for 1 h and evaporated. The residue was chromatographed with chloroform to give **13** (0.210 g, 56%), which was recrystallized from cyclohexane to give yellow needles, mp 120—121 °C; ^{1}H NMR δ=3.61 (3H, s), 3.85 (2H, s), 3.96 (2H, s), 6.72 (1H, dd, J=10.4 and 8.9 Hz), 7.17 (1H, dd, J=12.2 and 8.9 Hz), 7.41 (1H, s), 7.38—7.55 (5H, m), 7.61 (1H, d, J=10.4 Hz), 8.11 (1H, d, J=12.2 Hz), and 10.30 (1H, brs); ^{13}C NMR δ=35.01 (t), 51.93 (q), 52.57 (q), 122.81 (d), 123.52 (d), 123.90 (d), 126.78 (s), 127.00 (d), 127.60 (s), 128.52 (d×2), 129.27 (d×2), 131.37 (d), 133.33 (s), 134.20 (s), 135.15 (d), 147.01 (s), 156.34 (s), 165.35 (s), and 171.92 (s); IR 3288 (NH), 1706 (C=O), 1622 (C=N), and 696 cm^{-1} (phenyl). Found: C, 67.03; H, 5.05; N, 10.96%. Calcd for $C_{21}H_{19}N_3O_4$: C, 66.83; H, 5.07; N, 11.03%.

We thank Dr. Akira Mori, Kyushu University, for the measurements of the mass spectra and elemental analyses.

References

1) D. J. LeCount and A. T. Greer, *J. Chem. Soc., Perkin Trans. 1,* **1974**, 297.
2) T. Nishiwaki and N. Abe, *Heterocycles,* **15**, 547 (1981).
3) N. Abe and T. Takehiro, *Bull. Chem. Soc. Jpn.,* **61**, 1225 (1988), and references cited therein.
4) N. Abe and T. Ueno, *Bull. Chem. Soc. Jpn.,* **63**, 2121 (1990), and references cited therein.
5) O. Meth-Cohn, C. Moore, and P. H. van Rooyen, *J. Chem. Soc., Perkin Trans. 1,* **1985**, 1793.
6) K. Hafner, *Lect. Heterocycl. Chem.,* **3**, 33 (1976), and references cited therein.
7) G. R. Tian, A. Mori, and H. Takeshita, *Bull. Chem. Soc. Jpn.,* **62**, 3727 (1989).
8) T. Zaima, Y. Matsunaga, and K. Mitsuhashi, *J. Heterocycl. Chem.,* **20**, 1 (1983).
9) N. Abe, *Heterocycles,* **26**, 51 (1987).
10) M. K. Saxena, M. N. Gudi, and M. V. George, *Tetrahedron,* **29**, 101 (1973).
11) K. Yamane, K. Fujimori, J.-K. Sin, and T. Nozoe, *Bull. Chem. Soc. Jpn.,* **50**, 1184 (1977).

Hydroformylation–Amidocarbonylation of Methylvinylphosphinate. Application to Synthesis of Glufosinate

Toshiyasu SAKAKURA, Xin-Yan HUANG, and Masato TANAKA*
National Chemical Laboratory for Industry, Tsukuba, Ibaraki 305
(Received January 17, 1991)

Synopsis. Glufosinate, 2-amino-4-[(hydroxy)methylphosphinyl]butanoic acid, (**2a**) was synthesized from 2-chloroethyl methylvinylphosphinate (**1a**) via successive hydroformylation–amidocarbonylation. Hydroformylation of **1a** catalyzed by $Co_2(CO)_8$ in methanol gave 2-chloroethyl (3,3-dimethoxypropyl)methylphosphinate (**5**). Crude **5** was subjected to cobalt-catalyzed amidocarbonylation to afford *N*-acylglufosinic acid methyl ester (**2b**). Hydrolysis of **2b** under acidic conditions gave **2a** quantitatively.

Transition metal-catalyzed carbonylations with carbon monoxide are useful methods to synthesize carbonyl compounds from easily accessible starting materials like olefins, halides, etc. Applications of these reactions to functionalized substrates are expected to provide new and facile synthetic routes to multifunctional compounds.[1] Now, we wish to report a convenient synthesis of glufosinate (**2a**) from a methylvinylphosphinate (**1a**) via successive carbonylations catalyzed by transition metal complexes (Eq. 1).

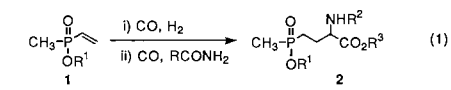

1 2

1a: $R^1 = CH_2CH_2Cl$ 2a: $R^1 = R^2 = R^3 = H$
2b: $R^1 = CH_2CH_2Cl$, $R^2 = PhCO$, $R^3 = Me$
2c: $R^1 = CH_2CH_2Cl$, $R^2 = PhCO$, $R^3 = H$

Glufosinate (phosphinothricin) is the first naturally occurring amino acid with a phosphinic acid moiety and shows strong herbicidal and antibiotic activities. There have been a considerable number of precedents about the synthesis of glufosinate.[2,3] The synthetic routes are mainly divided into two categories. One is Strecker reaction of phosphinyl aldehydes.[2b-d] The other is the Michael addition of an amino acid derivative to the methylvinylphosphinate (**1**).[2e-j] The process via carbonylation (Eq. 1) is superior to these reactions in the following aspects. i) Highly toxic cyanide which requires troublesome treatment of aqueous waste is not involved. ii) The amino acid moiety is introduced inexpensively with carbon monoxide and an amide. The starting compound **1a** is easily obtained by the dehydrochlorination of 2-chloroethyl 2-chloroethylmethylphosphinate which is synthesized by the reaction of dichloromethylphosphine and ethylene oxide in a high yield.[4]

Hydroformylation of **1a** (Eq. 2) with cobalt carbonyl took place with high linear-selectivities over 85% irrespective of solvents (Table 1). However, the yield of the aldehyde was low due to the formation of high-boiling by-products. Optimization of various reaction conditions finally resulted in the finding that the reaction in methanol afforded the desired linear aldehyde in a very high yield as a form of dimethyl acetal (Eq. 3). A similar observation was reported by Wakamatsu et al. in the hydroformylation of acrylonitrile with $Co_2(CO)_8$.[5]

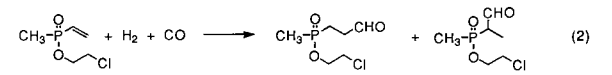

1a 3 4

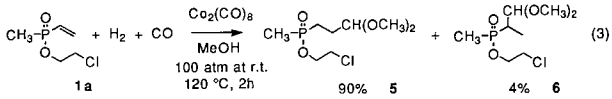

1a 90% 5 4% 6

On the other hand, the problem in rhodium-catalyzed hydroformylation of **1a** using $Rh_4(CO)_{12}$, $Rh_2Cl_2(CO)_4$, or $HRh(CO)(PPh_3)_3$ was low linear selectivity rather than low aldehyde yield (Table 2). It is noteworthy that the high linear- or the branched-selectivities observed in

Table 1. Hydroformylation of **1a** with $Co_2(CO)_8$[a]

Solvent	Conv./%	Yield of aldehyde/%	Linear-sel./%
Benzene	84	42	94
t-BuOH	85	32	89
Et_2O[b]	45	15	86
Acetone[c]	21	15	92
DMF	0	0	—

a) $Co_2(CO)_8$ 0.1 mmol, **1a** 10 mmol, solvent 9 ml, 120°C, $CO/H_2=1/1$, 100 atm at room temperature, 2 h, linear-sel.=100×**3**/(**3**+**4**). b) 150°C. c) 4.5 h.

Table 2. Hydroformylation of **1a** with Rhodium Catalysts[a]

Catalyst	Conv./%	Yield/%		Linear-sel./%
		Aldehydes	Hydrogenation	
$Rh_4(CO)_{12}$	100	61	13	11
$Rh_2Cl_2(CO)_4$	100	70	19	22
$HRh(CO)(PPh_3)_3$	100	80	9	9
$Rh(acac)\{P(OPh)_3\}_2$[b]	56	53	1	97

a) Rh 0.01 mg-atom, **1a** 10 mmol, solvent 9 ml, 100°C, $CO/H_2=1/1$, 100 atm at room temperature, 5—19 h, linear-sel.=100×**3**/(**3**+**4**). b) Rh complex 0.05 mmol, **1a** 5.7 mmol, $P(OPh)_3$ 0.13 mmol, benzene 1.4 ml, $CO/H_2=1/1$, 1 atm, 45°C, 2 h. acac: acetylacetonate.

the hydroformylation of **1a** with cobalt or rhodium catalysts, respectively, are similar to those reported for the hydroformylation of an α,β-unsaturated carboxylate with $Co_2(CO)_8$ or $Rh_4(CO)_{12}$.[6] On the other hand, Trzeciak et al. have reported an unusually high linear selectivity in the rhodium-catalyzed hydroformylation of ethyl acrylate with the Rh–$P(OPh)_3$ system.[7] The catalytic system was successfully applied to the hydroformylation of **1a** to achieve a high linear selectivity under mild conditions (Table 2).[8]

Since a high linear selectivity and a high yield have been achieved in the hydroformylation of **1a** with $Co_2(CO)_8$ in MeOH (Eq. 3), we next investigated the amidocarbonylation[9] of the resulting acetal (**5**) (Eq. 4). Although examples of amidocarbonylation of acetals have been rare,[10] the reaction of **5** proceeded smoothly to give a mixture of the methyl ester (**2b**) and presumably the free carboxylic acid (**2c**);[11] the latter could be quantitatively converted to the former via the treatment with trimethylsilyldiazomethane.[12] The amidocarbonylation proceeded in various solvents such as benzene, ethyl acetate, dioxane, and tetrahydrofuran; the last one gave the highest reaction rate. Since the amidocarbonylation is slow in methanol, the solvent should be exchanged after the hydroformylation.

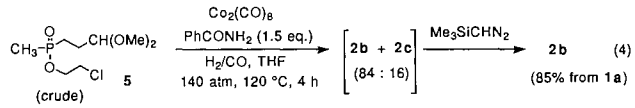

The hydrolysis of **2b** was easily carried out under acidic conditions to give glufosinate quantitatively. Thus, glufosinate can be efficiently synthesized via successive hydroformylation–amidocarbonylation of the methylvinylphosphinate. The resolution of racemic glufosinate and the conversion of the optical isomer to its racemate have already been established.[13]

Experimental

^1H and ^{13}C NMR signals were referred to tetramethylsilane as an internal standard. Chemical shift in ^{31}P NMR was referred to H_3PO_4.

$Co_2(CO)_8$ was recrystallized from toluene at a low temperature. Rh(acac)$[P(OPh)_3]_2$ was synthesized according to the literature.[14] The methylvinylphosphinate (**1a**) was obtained from Nissan Chemical Industries Ltd.

Hydroformylation of 1a. Octacarbonyldicobalt (0.1 mmol), the methylvinylphosphinate (10 mmol), and methanol (9 ml) were added to a 27 ml Hastelloy-C autoclave under nitrogen. Synthesis gas ($H_2/CO=1/1$) was charged up to 100 atm at room temperature. The autoclave was heated in an oil bath at 120°C for 2 h. The reaction mixture was analyzed by capillary GC (OV-1701 and PEG-20M, 25 m) using tridecane as an internal standard. Rhodium catalyzed reactions were conducted similarly; see Table 2 for reaction conditions.

Amidocarbonylation of 5. Hydroformylation of **1a** was carried out in methanol as stated above. The reaction mixture was concentrated. The resulting oil, octacarbonyldicobalt (0.2 mmol), benzamide (15 mmol) and tetrahydrofuran (10 ml) were added to a 27 ml Hastelloy-C autoclave under nitrogen. Synthesis gas ($H_2/CO=1/1$) was charged up to 140 atm. The autoclave was heated in an oil bath at 120°C for 3.8 h. The reaction mixture was analyzed by HPLC (ODS, methanol: $H_2O=1/1$) using benzene as an internal standard after the esterification of the free amino acid with trimethylsilyldiazomethane.[10]

The products were isolated by distillation (Kugelrohr) or preparative thin-layer chromatography (silica gel, $CHCl_3$: MeOH=15:1). Spectral data were listed below.

2-Chloroethyl Methylvinylphosphinate (1a). ^1H NMR[2d] ($CDCl_3$) δ=1.57 (d, J=14 Hz, 3H, CH_3P), 3.70 (t, J=6 Hz, 2H, CH_2Cl), 4.0–4.4 (m, 2H, OCH_2), 6.0–6.5 (m, 3H, $CH=CH_2$); ^{13}C NMR ($CDCl_3$) δ=14.9 (d, J=102 Hz, CH_3P), 43.1 (d, J=7 Hz, CH_2Cl), 63.8 (d, J=6 Hz, OCH_2), 129.6 (d, J=121 Hz, $C\underline{H}=CH_2$), 135.8 (s, $CH=C\underline{H}_2$); MS m/z (%) 171 ($M^+(^{37}Cl)+H$, 0.3), 169 ($M^+(^{35}Cl)+H$, 1.0), 153 ($M^+(^{35}Cl)-Me$, 4), 133 (M^+-Cl, 100), 119 (15), 107 (24), 91 (20). Found: m/z 133.0407 (M^+-Cl). Calcd for $C_5H_{10}O_2P$: M, 133.0418.

2-Chloroethyl Ethylmethylphosphinate. Bp 80–90°C/0.5 mmHg (1 mmHg≈133.3 Pa); ^1H NMR ($CDCl_3$) δ=1.19 (dt, J=19 and 8 Hz, 3H, $C\underline{H}_3CH_2$), 1.50 (d, J=14 Hz, 3H, CH_3P), 1.80 (dq, J=15 and 8 Hz, 2H, $C\underline{H}_2CH_3$), 3.70 (t, J=6 Hz, 2H, CH_2Cl), 4.1–4.3 (m, 2H, OCH_2); ^{13}C NMR ($CDCl_3$) δ=6.1 (d, J=5 Hz, $CH_2\underline{C}H_3$), 13.2 (d, J=90 Hz, CH_3P), 22.8 (d, J=95 Hz, CH_2P), 43.4 (d, J=7 Hz, CH_2Cl), 63.7 (d, J=6 Hz, OCH_2); MS m/z (%) 173 ($M^+(^{37}Cl)+H$, 0.1), 171 ($M^+(^{35}Cl)+H$, 0.3), 155 ($M^+(^{35}Cl)-Me$, 2), 141 ($M^+(^{35}Cl)-Et$, 9), 135 (100), 121 (16), 115 (14), 107 (17), 91 (54). Found: m/z 171.0336 (M^++H). Calcd for $C_5H_{13}ClO_2P$: M, 171.0341.

2-Chloroethyl Methyl(3-oxopropyl)phosphinate (3). Bp 150–180°C/0.4 mmHg; IR (neat) 1730 cm^{-1} (CO); ^1H NMR ($CDCl_3$) δ=1.56 (d, J=14 Hz, 3H, CH3P), 2.10 (dt, J=14 and 8 Hz, 2H, CH_2P), 2.7–3.0 (m, 2H, $C\underline{H}_2CHO$), 3.71 (t, J=5 Hz, 2H, CH_2Cl), 4.1–4.3 (m, 2H, OCH_2), 9.83 (s, 1H, CHO); ^{13}C NMR ($CDCl_3$) δ=14.5 (d, J=92 Hz, CH_3P), 21.8 (d, J=96 Hz, CH_2P), 36.1 (d, J=3 Hz, $\underline{C}H_2CHO$), 43.3 (d, J=7 Hz, CH_2Cl), 64.0 (d, J=6 Hz, OCH_2), 199.1 (d, J=13 Hz, CHO); MS m/z (%) 201 ($M^+(^{37}Cl)+H$, 0.3), 199 ($M^+(^{35}Cl)+H$, 1.0), 163 (M^+-Cl, 21), 144 (17), 142 (48), 135 (100), 127 (24), 119 (86), 107 (100). Found: m/z 199.0279 (M^++H). Calcd for $C_6H_{13}ClO_3P$: M, 199.0289.

2-Chloroethyl Methyl(1-methyl-2-oxoethyl)phosphinate (4). Bp 140–160°C/0.35 mmHg; IR (neat) 1720 cm^{-1} (CO); ^1H NMR ($CDCl_3$) (diastereomer) δ=1.407 and 1.423 (dd, J=16 and 7 Hz, 3H, $PCHC\underline{H}_3$), 1.547 and 1.569 (d, J=14 Hz, 3H, CH_3P), 3.0–3.5 (m, 1H, $C\underline{H}CHO$), 3.73 (t, J=5 Hz, 2H, CH_2Cl), 4.2–4.4 (m, 2H, OCH_2), 9.80 and 9.87 (d, J=2 Hz, 1H, CHO); ^{13}C NMR ($CDCl_3$) (diastereomer) δ=7.61 (s, $CH\underline{C}H_3$), 7.67 (d, J=1.5 Hz, $CH\underline{C}H_3$), 12.77 and 12.94 (d, J=93 Hz, $\underline{C}H_3P$), 43.06 and 43.10 (d, J=7 Hz, CH_2Cl), 50.33 and 50.39 (d, J=79 Hz, $\underline{C}HCH_3$), 64.51 and 64.63 (d, J=6 Hz, OCH_2), 197.77 (d, J=3 Hz, CHO), 197.89 (s, CHO); MS m/z (%) 200 ($M^+(^{37}Cl)$, 3), 198 ($M^+(^{35}Cl)$, 11), 163 (M^+-Cl, 55), 149 (M^+-CH_2Cl, 15), 137 (15), 136 (26), 135 (100), 119 (59), 117 (13), 115 (17), 109 (42), 107 (61), 97 (24), 91 (44). Found: m/z 198.0222 (M^+). Calcd for $C_6H_{12}ClO_3P$: M, 198.0212.

2-Chloroethyl (3,3-Dimethoxypropyl)methylphosphinate (5). Bp 100°C/5.6×10^{-4} mmHg; ^1H NMR ($CDCl_3$) δ=1.52 (d, J=14 Hz, 3H, CH_3P), 1.7–2.0 (m, 4H, PCH_2CH_2), 3.34 (s, 6H, OCH_3), 3.70 (t, J=6 Hz, 2H, CH_2Cl), 4.1–4.3 (m, 2H, OCH_2), 4.3–4.5 (m, 1H, $CH_2C\underline{H}$); ^{13}C NMR ($CDCl_3$) δ=14.0 (d, J=92 Hz, CH_3P), 24.4 (d, J=70 Hz, CH_2P), 25.4 (d, J=21 Hz, $PCH_2\underline{C}H_2$), 43.3 (d, J=6 Hz, CH_2Cl), 53.4 (d, J=3 Hz, CH_3O), 63.8 (d, J=6 Hz, OCH_2), 104.0 (d, J=17 Hz, CH); MS m/z (%) 245 ($M^+(^{37}Cl)-H$, 0.3), 243 ($M^+(^{37}Cl)-H$, 1.0), 231 ($M^+(^{37}Cl)-CH_3$, 6), 229 ($M^+(^{35}Cl)-CH_3$, 18), 215 ($M^+(^{37}Cl)-OCH_3$, 52), 214 (17), 213 ($M^+(^{35}Cl)-OCH_3$, 100), 199 (16), 197 (38), 193 (11), 177 (28), 165 (35), 161 (10), 151 (11), 149 (39), 141 (12), 135 (44), 133 (39), 131 (20), 121 (36), 119 (59), 107 (17), 101 (15), 93 (17). Found: m/z 243.0566 (M^+-H). Calcd for $C_8H_{17}ClO_4P$: M, 243.0553; Found: m/z 229.0398 (M^+-CH_3). Calcd

for $C_7H_{15}ClO_4P$: M, 229.0396.

2-Chloroethyl (2,2-Dimethoxy-1-methylethyl)methylphosphinate (6). This minor product formed in hydroformylation in methanol was identified only by GCMS. MS *m/z* (%) 245 ($M^+(^{37}Cl)-H$, 0.6), 243 ($M^+(^{35}Cl)-H$, 1.5), 231 ($M^+(^{37}Cl)-CH_3$, 8), 229 ($M^+(^{35}Cl)-CH_3$, 24), 215 ($M^+(^{37}Cl)-OCH_3$, 24), 213 ($M^+(^{35}Cl)-OCH_3$, 67), 199 (14), 197 (31), 177 (11), 173 (17), 165 (27), 149 (64), 143 (29), 141 (82), 135 (30), 133 (13), 125 (17), 123 (11), 117 (19), 115 (35), 111 (16), 107 (15), 102 (69), 93 (55), 79 (67), 76 (18), 75 (100). Found: *m/z* 243.0560 (M^+-H). Calcd for $C_8H_{17}ClO_4P$: M, 243.0553. Found: *m/z* 229.0413 (M^+-CH_3). Calcd for $C_7H_{15}ClO_4P$: M, 229.0396.

2-Chloroethyl [3-Benzoylamino-3-(methoxycarbonyl)propyl]methylphosphinate (2b). IR (neat) 3450 cm^{-1} (NH), 1740 cm^{-1} (CO_2Me), 1660 cm^{-1} (PhCO); ^1H NMR ($CDCl_3$) (diastereomer) δ=1.525 and 1.546 (d, *J*=14 Hz, 3H, CH_3P), 1.75–2.05 (m, 2H, PCH_2), 2.05–2.4 (m, 2H, CH_2CH), 3.6–3.75 (m, 2H, CH_2Cl), 3.79 (s, 3H, CO_2CH_3), 4.1–4.3 (m, 2H, OCH_2), 4.75–5.0 (m, 1H, NCH), 7.35–8.0 (m, 6H, Ph and NH); ^{13}C NMR ($CDCl_3$) (diastereomer) δ=14.2 (d, *J*=94 Hz, CH_3P), 24.5 (s, CH_2CH), 26.01 and 26.11 (d, *J*=93 Hz, PCH_2), 43.27 and 43.32 (d, *J*=7 Hz, CH_2Cl), 52.8 (s, $CO_2\underline{C}H_3$), 52.8 (d, *J*=21 Hz, CH), 64.1 (d, *J*=7 Hz, OCH_2), 127.4 (s, Ph, meta), 128.6 (s, Ph, ortho), 129.9 (s, Ph, para), 133.4 (s, Ph, C_1), 167.4 (d, *J*=2.5 Hz, CO_2), 172.3 (s, PhCO); ^{31}P NMR ($CDCl_3$) δ=55 (s); MS *m/z* (%) 363 ($M^+(^{37}Cl)$, 0.5), 361 ($M^+(^{35}Cl)$, 1.4), 304 ($M^+(^{37}Cl)-CO_2CH_3$, 19), 302 ($M^+(^{35}Cl)-CO_2CH_3$, 48), 284 (8), 256 (12), 105 (100),. Found: *m/z* 361.0865 (M^+). Calcd for $C_{15}H_{21}ClNO_5P$: M, 361.0845. Anal. ($C_{15}H_{21}ClNO_5P$) C, H, N, Cl.

Hydrolysis of 2b. The methyl ester **2b** (182 mg) was dissolved in 6 mol dm^{-3} hydrochloric acid (4 ml) and refluxed overnight. The resulting mixture was washed with benzene to remove benzoic acid. The water layer was concentrated to dryness in vacuo to give pure glufosinate (**2a**) (96 mg, 100%). ^1H NMR[2j] (D_2O) δ=1.42 (d, *J*=14 Hz, 3H, CH_3P), 1.7–2.2 (m, 4H, PCH_2CH_2), 4.06 (t, *J*=6 Hz, 1H, $CHCO_2$); ^{13}C NMR[2d,j] (D_2O) δ=14.4 (d, *J*=92 Hz, CH_3P), 23.5 (d, *J*=2 Hz, $PCH_2\underline{C}H_2$), 26.0 (d, *J*=93 Hz, PCH_2), 53.6 (d, *J*=17 Hz, CH), 172.0 (s, CO_2H).

The authors thank Messrs. Shinichiro Takigawa and Shuzo Shinke (Nissan Chemical Industries, Ltd.) for the generous gift of the phosphinate (**1a**) and for useful discussions.

References

1) "New Syntheses with Carbon Monoxide," ed by J. Falbe, Springer-Verlag, Berlin (1980); C. Botteghi, R. Gauzerla, M. Lenarda, and G. Moretti, *J. Mol. Catal.*, **40**, 129 (1987).

2) a) E. Bayer, K. H. Gugel, K. Hägele, H. Hagenmaier, S. Jessipow, W. A. König, and H. Zähner, *Helv. Chim. Acta*, **55**, 224 (1972). b) E. Gruszecka, P. Mastalerz, and M. Soroka, *Rocz. Chem.*, **49**, 2127 (1975). c) E. Gruszecka, M. Soroka, and P. Mastalerz, *Pol. J. Chem.*, **53**, 937 (1979). d) A. Suzuki, T. Tsuruoka, K. Mizutani, and S. Inouye, *Meiji Seika Kenkyu Nempo*, **No. 20**, 33 (1981). e) H. Gross and T. Gnauk, *J. Prakt. Chem.*, **318**, 157 (1976). f) L. Maier and P. J. Lea, *Phosphorus Sulfur*, **17**, 1 (1983). g) L. Maier, G. Rist, and P. J. Lea, *ibid.*, **18**, 349 (1983). h) N. Minowa, S. Fukatu, T. Niida, M. Takada, and K. Sato, *Tetrahedron Lett.*, **24**, 2391 (1983). i) N. Minowa, M. Hirayama, and S. Fukatsu, *ibid.*, **25**, 1147 (1984). j) N. Minowa, M. Hirayama, and S. Fukatsu, *Bull. Chem. Soc. Jpn.*, **60**, 1761 (1987). k) C. Wasielewski and K. Antczak, *Synthesis*, **1981**, 540. l) E. W. Logusch, *Tetrahedron Lett.*, **27**, 5935 (1986). m) H.-J. Zeiss, *ibid.*, **28**, 1255 (1987). n) I. A. Natchev, *Bull. Chem. Soc. Jpn.*, **61**, 3699 (1988).

3) The synthesis of glufosinate via one-pot hydroformylation–amidocarbonylation of the methylvinylphosphinate has been preliminary published by one of the authors and others; S. Takigawa, S. Shinke, and M. Tanaka, *Chem. Lett.*, **1990**, 1415.

4) I. A. Rogacheva and E. L. Gefter, *Zh. Obshch. Khim.*, **41**, 2634 (1971).

5) J. Kato, H. Wakamatsu, R. Iwanaga, and T. Yoshida, *Kogyo Kagaku Zasshi*, **64**, 2139 (1931).

6) Y. Takegami, C. Yokokawa, and Y. Watanabe, *Bull. Chem. Soc. Jpn.*, **39**, 2430 (1966); Y. Takegami, Y. Watanabe, and H. Masada, *ibid.*, **40**, 1459 (1967).

7) A. M. Trzeciak and J. J. Ziolkowski, *J. Mol. Catal.*, **43**, 15 (1987).

8) Factors to control regioselectivity and reaction rate in the hydroformylation by the $Rh-P(OR)_3$ system were investigated by the authors using ethyl acrylate as a substrate. The results will be published separately.

9) For recent developments in amidocarbonylation, see I. Ojima, M. Okabe, K. Kato, H. B. Kwon, and I. T. Horvath, *J. Am. Chem. Soc.*, **110**, 150 (1988); I. Ojima, K. Hirai, M. Fujita, and T. Fuchikami, *J. Organomet. Chem.*, **279**, 203 (1985); J.-J. Parnaud, G. Campari, and P. Pino, *J. Mol. Catal.*, **6**, 341 (1979); K. Izawa, *Yuki Gosei Kagaku Kyokaishi*, **46**, 218 (1988).

10) K. Izawa and S. Nishi, Jpn. Patent Kokai. 60-142948 (1985).

11) Formation of a free carboxylic acid as a byproduct has been found in amidocarbonylation of an acetal.[10] Although convincing evidence to support the structure of **2c** is not available in the present experiment, the following observations are in agreement with the proposed structure. (1) The compound appeared sooner than the ester in the reversed phase HPLC. This indicates the compound is more polar than the ester. (2) Upon methylation with trimethylsilyldiazomethane, the compound disappeared and the yield of the ester consistently increased.

12) S. Mori, I. Sakai, T. Aoyama, and T. Shioiri, *Chem. Pharm. Bull.*, **30**, 3380 (1982); N. Hashimoto, T. Aoyama, and T. Shioiri, *ibid.*, **29**, 1475 (1981).

13) a) Hoechst A.-G., Ger. Offen. DE 3048612 (1982); *Chem. Abstr.*, **97**, 125725z (1982). **b)** Hoechst A.-G., Ger. Offen. DE 3334849 (1985); *Chem. Abstr.*, **104**, P19809h (1986).

14) A. M. Trzeciak and J. J. Ziolkowski, *Inorg. Chem. Acta*, **64**, L267 (1982).

Cycloadditions of 2,8,11-Triphenyl-7,9,10,11b-tetraazanaphth[1,2,3-*cd*]azulene and 2,8,10-Triphenyl-9-oxa-7,10b-diazaindeno[4,5,6-*cd*]azulene with Dimethyl Acetylenedicarboxylate

Noritaka ABE,* Yoshimasa HIRAI,† and Yoshimasa FUKAZAWA†
Department of Chemistry, Faculty of Science, Yamaguchi University, Yamaguchi 753
† Department of Chemistry, Faculty of Science, Hiroshima University, Higashisenda-machi, Hiroshima 730
(Received January 21, 1991)

Synopsis. Cycloadditions of the title compounds with dimethyl acetylenedicarboxylate gave 1:2-cycloadducts. The structural assignments of the products were deduced by spectral inspections; the structure for one compound was established by X-ray crystallography.

Many investigations have been carried out concerning the reactions of heterocycles with dimethyl acetylenedicarboxylate (DMAD) due to interesting surprises regarding their reactions and usefulness for building heterocyclic rings.[1-3] The reaction of poly-fuzed heterocyclies having multi reaction sites with DMAD is very interesting. One of the authors (NA) has been investigating the syntheses and cycloadditions of azaazulenes, and recently reported the syntheses of pyridazine-, furan-, and thiophene-fused 2a,5-diazabenz[*cd*]azulenes (**1**, **2a**, and **2b**).[4] The cycloaddition of these compounds is attractive, since they comprise different aromatic heterocyclic moieties. The authors have therefore advanced the reaction.

The treatment of **1** with DMAD in refluxing acetonitrile for 70 h gave a 1:2-adduct (**3**) in 78.7% yield. Its structure was elucidated using spectroscopic data as well as elemental analysis. Its ^{1}H NMR spectrum displays four ester-methyl singlets at δ=3.38, 3.64, 3.80, and 3.95; four seven-membered protons at δ=5.47, 5.95, 6.07, and 6.38; 15H phenyl protons at δ=7.0-8.0; and one singlet at δ=6.69. Information concerning chemical shifts of the seven-membered ring protons have suggested that compound **3** retains the 2a,5-diazabenz[*cd*]azulene nuclei.[4] Since the chemical shift of the singlet is comparable to that of **1**, the environments of both singlet protons would be similar. It is therefore considered that the reaction occured at both the N-9 and C-8 positions. In the ^{13}C NMR spectrum of **2**, one sp^3 carbon (s) was observed at δ=63.51; the other signals are in accord with the structure. This reaction is comparable to that of 4-methylphthalazine with DMAD.[5]

Treatment of **2a** with DMAD in refluxing acetonitrile for 50 h gave the 1:2-adduct (**4**) in 45.8% yield. The structure was assumed by spectroscopic data and established by an X-ray analysis. In its ^{1}H NMR spectrum, four ester-methyl singlets at δ=3.21, 3.48, 3.49, and 3.63; four seven-menbered protons at δ=6.67, 7.11, 7.64, and 7.73; 15H phenyl protons at δ=7.2—7.9; and one singlet at δ=6.41 were observed. The chemical shifts and signal patterns of seven-membered ring protons resemble those of **5**.[6] In the ^{13}C NMR spectrum of **4**, two sp^3 carbons were observed at δ=58.05 (d) and 94.52 (s); these are comparable to dihydrofuran derivatives. The mass spectrum of **4** displays intense peaks at *m*/*z* 384 and 336, which would be attributed to ions of the cyclazine and furan moieties, respectively, produced by fragmentation of the molecular ion; this strongly suggests the structure (the structure of **4** is shown in Fig. 1).

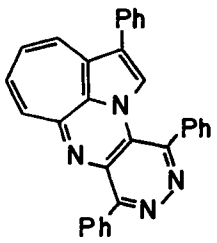

1

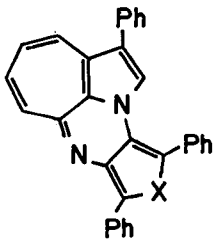

2a: X = O
2b: X = S

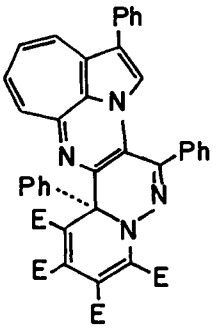

3: E = CO_2Me

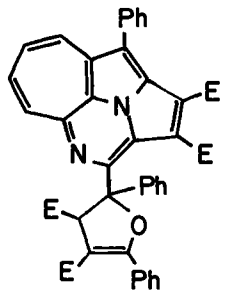

4: E = CO_2Me

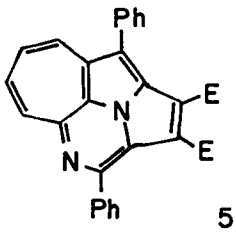

5: E = CO_2Me

A plausible mechanism for the formation of **4** is shown in Scheme 1. DMAD initially attacks the furan moiety of **2a** to give intermidiate **A**; a successive attack of a second molar of DMAD on **A** gives **B**. Bond scission attended by aromatization of **B** leads to **4**. The second step followed by aromatization is similar to a reaction in which 1,4-diphenyl-2a,5-diazabenz[*cd*]azulene reacts

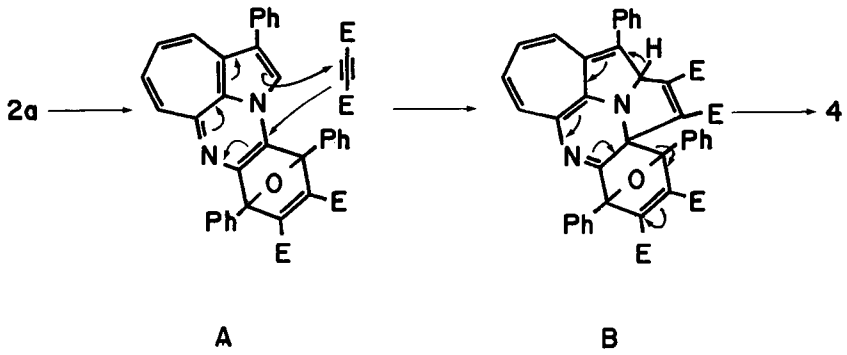

Scheme 1.

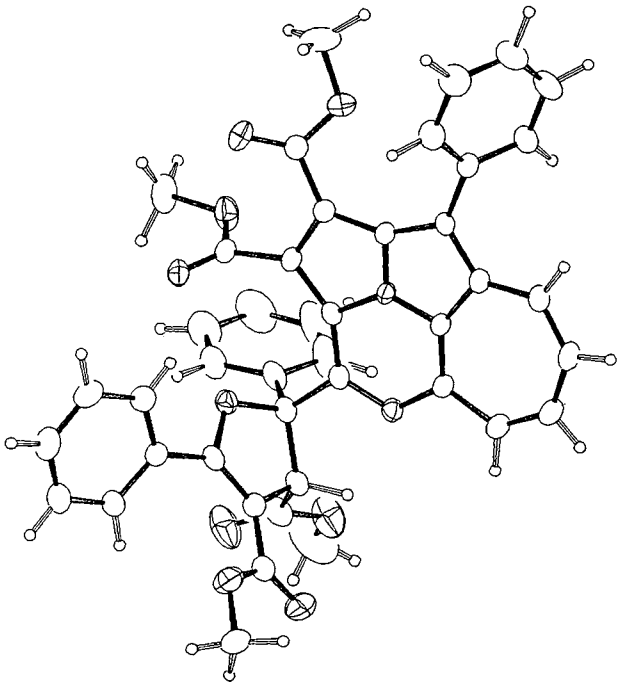

Fig. 1. Molecular structure of **4**.

with DMAD to give **5**.[6]

Compound **2b** did not react with DMAD under the conditions used.

Experimental

All melting points are uncorrected. ^{1}H NMR spectra (250 MHz) and ^{13}C NMR spectra (62.87 MHz) were taken on a Hitachi R-250H spectrometer using $CDCl_3$ as a solvent (TMS as an internal standard). IR spectra were recorded for Nujol mulls with a Hitachi 270-50 infrared spectrophotometer. Mass spectra were determined with a JEOL-01SG-2 spectrometer an ionization energy of 70 eV. Column chromatography was performed on a Kieselgel 60.

Reaction of 1 with DMAD. A mixture of **1** (0.070 g) and DMAD (0.150 g) in dry acetonitrile (50 ml) was refluxed for 70 h and evaporated. Elution with benzene–chloroform (1:1) gave **3** (0.090 g, 78.7%), which was recrystallized from cyclohexane to give reddish-brown needles; mp 283—284 °C; ^{1}H NMR δ=3.38, 3.64, 3.80, 3.95 (each 3H, s, OMe), 5.47 (1H, dd, J=11.6 and 7.9 Hz, H-5), 5.95 (1H, dd, J=12.2 and 7.9 Hz, H-4), 6.07 (1H, d, J=12.2 Hz, H-3), 6.38 (1H, d, J=11.6 Hz, H-6), 6.69 (1H, s, H-2), 7.05 (2H, dd, J=7.9 and 1.8 Hz, H-*o*-phenyl), 7.27—7.45 (9H, m, H-*m*,*p*-phenyl), 7.61 (2H, dd, J=7.9 and 1.8 Hz, H-*o*-phenyl), and 7.90 (2H, dd, J=7.9 and 1.8 Hz, H-*o*-phenyl); ^{13}C NMR δ=52.01 (q), 52.24 (q), 52.83 (q×2), 63.51 (s), 103.23 (s), 103.74 (s), 114.61 (d), 119.10 (s), 123.89 (s+d), 125.44 (s), 127.29 (d×2), 127.34 (d×2), 127.49 (s), 127.52 (d×2), 128.57 (d×2), 128.62 (d×3), 129.33 (d), 129.63 (d), 130.11 (d×2), 130.83 (d), 132.11 (s), 133.28 (s), 135.10 (d), 135.29 (d), 136.06 (s), 136.19 (s), 137.29 (s), 142.73 (s), 147.64 (s), 157.01 (s), 162.40 (s), 163.23 (s), 164.84 (s), and 166.79 (s); IR 1746, 1740, and 1710 (C=O), 780, 764, 736, 707, and 696 cm^{-1} (phenyl). Found: C, 70.44; H, 4.65; N, 7.48%. Calcd for $C_{43}H_{32}N_4O_8$: C, 70.48; H, 4.36; N, 7.64%.

Reaction of 2a with DMAD. A mixture of **2a** (0.140 g) and DMAD (0.30 g) in dry acetonitrile (80 ml) was refluxed for 50 h and then evaporated. The residue was chromatographed. Elution with benzene gave recoverded **2a** (0.038 g, 27.1%). Elution with benzene–chloroform (1:1) gave **4** (0.106 g, 45.8%), which was recrystallized from cyclohexane to give red needles; mp 274—275 °C; ^{1}H NMR δ=3.21, 3.48, 3.49, 3.63 (each 3H, s, OMe), 6.41 (1H, s, H-3'), 6.67 (1H, dd, J=11.0 and 8.6 Hz, H-7), 7.11 (1H, dd, J=11.6 and 8.6 Hz, H-8), 7.25—7.60 (13H, m, H-phenyl), 7.64 (1H, d, J=11.0 Hz, H-6), 7.73 (1H, d, J=11.6 Hz, H-9), and 7.77 (2H, dd, J=7.9 and 1.8 Hz, H-*o*-phenyl); ^{13}C NMR δ=51.15 (q), 51.34 (q), 51.54 (q), 52.46 (q), 58.05 (d), 94.52 (s), 104.05 (s), 115.21 (s), 115.64 (s), 122.43 (s), 124.80 (d), 126.46 (d×2), 126.78 (s), 127.30 (d×4), 127.70 (d), 127.73 (d×2), 127.96 (s), 128.06 (d), 128.79 (s), 129.34 (s), 129.68 (d×2), 130.35 (d), 130.48 (d×2), 131.72 (d), 131.93 (d), 132.72 (s), 132.91 (d), 137.75 (s), 141.71 (s), 151.02 (s), 163.31 (s), 164.28 (s), 166.34 (s), and 171.06 (s); IR 1742, 1724, and 1705 (C=O), 774, 754, and 696 cm^{-1} (phenyl). MS m/z (rel intensity) 721 (0.8, M$^+$+1), 720 (0.6, M$^+$), 719 (6), 384 (6), 336 (14), 105 (30), 81 (42), 69 (70), 32 (100). Found: C, 71.82; H, 4.73; N, 3.78%. Calcd for $C_{43}H_{32}N_2O_9$: C, 71.66; H, 4.48; N, 3.89%.

Single Crystal X-Ray Structure Determination of 4. The crystals of **4** belong to a monoclinic system with cell dimensions of a= 16.513 (3) Å, b= 21.153 (7) Å, c= 10.714 (4) Å, β=107.14 (2)°, and V= 3621.8 (17) Å^3. The space group is $P2_1/n$, and Z= 4. The empirical formula is $C_{43}H_{32}N_2O_9$, the molecular weight is 720.47, and the caluculated density is 1.29 g cm^{-3}. Three-dimensional X-ray data were collected by the use of graphite-monochromated Mo $K\alpha$ radiation (λ=0.71073 Å) on a Syntex R3 automatic four-circle diffractometer up to a maximum 2θ of 50°. The intensity data from 5762 independent reflections were collected and 3513 with $|F_o|>3\sigma|F_o|$ were used in the present X-ray analysis. The structure was solved by a direct method (MULTAN78). All non-hydrogen atoms were located by an initial E synthesis. The remaining hydrogens were located by a difference Fourier map, and were included in additional calculations. Block-diagonal least

squares refinements with anisotropic 54 non-hydrogen atoms and 32 isotropic hydrogens converged to a conventional R factor of 0.066. All of the calculations were carried out on a HITAC M-680H computer of Hiroshima University using a structure analysis program system (UNICS3).[7,8]

We thank Dr. Akira Mori (Kyushu University) for performing mass spectra and elemental analyses.

References

1) R. M. Acheson and N. F. Elmore, *Adv. Heterocycl. Chem.*, **23**, 263 (1978).
2) R. M. Acheson, *Lect. Heterocycl. Chem.*, **6**, 59 (1982).
3) M. V. George, S. K. Khetan, and R. K. Gupta, *Adv. Heterocycl. Chem.*, **19**, 279 (1976).
4) N. Abe and T. Ueno, *Bull. Chem. Soc. Jpn.*, **63**, 2121 (1990).
5) R. M. Acheson and M. W. Foxton, *J. Chem. Soc. C*, **1966**, 2218.
6) N. Abe, *Heterocycles*, **26**, 59 (1987).
7) T. Sakurai and K. Kobayashi, *Rep. Inst. Phys. Chem. Res. (Jpn.)*, **55**, 69 (1979).
8) Tables of the bond lengths, bond angles, fractional atomic coordinates, and anisotropic thermal parameters are deposited as Document No. 9111 at the Office of the Editor of Bull. Chem. Soc. Jpn.

Molybdenum Pentachloride-Induced Reaction of Cyclopropyl-Substituted Carbonyl Compounds

Toshikazu HIRAO,* Shinichiro NAGATA, Makoto YAMAGUCHI, and Yoshiki OHSHIRO*
Department of Applied Chemistry, Faculty of Engineering, Osaka University,
Yamadaoka, Suita, Osaka 565
(Received February 12, 1991)

Synopsis. Molybdenum pentachloride induced the ring-opening reactions of cyclopropyl phenyl ketone or propyl 2-(trimethylsilylmethyl)cyclopropanecarboxylate to give 1-phenyl-1,2,4-trichloro-1-butene or *cis*-2-chloro-4-pentanolide, respectively.

Molybdenum pentachloride is an excellent reagent for *cis*-chlorination of olefins.[1] In our previous papers, molybdenum pentachoride has been disclosed to work well as a Lewis acid to cleave a carbon–oxygen bond of acetals in the reaction with vinylsilanes.[2] This characteristic is expected to be useful in the transformations of carbonyl compounds via molybdenum enolates. Ring-opening reactions of small-ring compounds provide a versatile synthetic method.[3] We herein report the molybdenum pentachloride-induced reactions of cyclopropyl-substituted carbonyl compounds.

Cyclopropyl phenyl ketone (**1**) was treated with molybdenum pentachloride in dichloromethane to give 1-phenyl-1,2,4-trichloro-1-butene (**2**). Ring cleavage[4] and chlorination are achieved by this procedure. An increase in the amount of molybdenum pentachloride raised the yield of **2** as shown in Table 1 (Eq. 1).

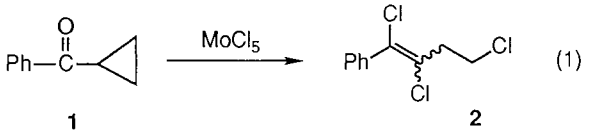

1 2 (1)

Table 1. Synthesis of **2**

$MoCl_5$/equiv	Time/h[a)]	Yield/% **2**
2	45	10
3	45	22
4	24	34

a) Reaction temperature, room temperature.

Propyl *cis*-2-phenylcyclopropanecarboxylate (**3**), however, did not undergo the ring-opening reaction under similar conditions, and was isomerized to the *trans* isomer **4** in 70% yield (Eq. 2). This result indicates that the reactivity of the ester function is lower towards molybdenum pentachloride.

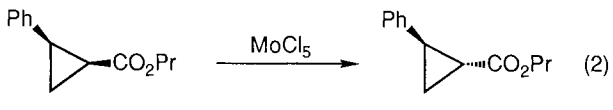

3 4 (2)

On the contrary, it should be noted that the reaction of propyl 2-(trimethylsilylmethyl)cyclopropanecarboxylate (**5**) with molybdenum pentachloride led to desilylation and ring-opening lactonization giving *cis*-2-chloro-4-pentanolide (**6**) stereoselectively in 45% yield (Eq. 3).

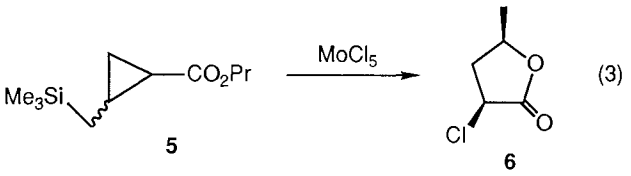

5 6 (3)

Such a ring-opening reaction was not observed in the case of propyl 2-butyl-3-(trimethylsilyl)cyclopropanecarboxylate (**7**) even on treatment at 80 °C in DMF. The ester **7** was recovered quantitatively, suggesting that the presence of trimethylsilylmethyl group appears to facilitate ring opening as is the case with 1-[2-(trimethylsilylmethyl)cyclopropylcarbonyl]imidazole.[5]

The reaction scheme is explained by the intervention of an enolate intermediate based on the operation of molybdenum pentachloride as a Lewis acid, which is considered to be supported by the isomerization of **3** to **4**. Desilylative ring cleavage of **5** gives the enolate, which undergoes recyclization and *cis*-chlorination possibly with molybdenum pentachloride.[1] Chlorination seems to take place at the α- and γ-positions of the ketone **1**, being accompanied by the transformation of the ketone function to the corresponding olefinic chloride.

Molybdenum pentachloride is demonstrated to be a versatile Lewis acid with the capability of chlorination.

Experimental

IR and ^{1}H NMR spectra were recorded with Hitachi 270-30 and JEOL JNM-FX90Q spectrometers, respectively. Electron impact mass spectra were recorded with JEOL JMS-DX303 at the Faculty of Engineering, Osaka University.

The cyclopropanecarboxylates **3** and **5** were prepared according to the reported method.[6]

Synthesis of 1,2,4-Trichloro-1-phenyl-1-butene (2). To a solution of molybdenum pentachloride (1.37 g, 5.0 mmol) in dichloromethane (5.0 mL) was dropwise added cyclopropyl phenyl ketone (**1**, 0.183 g, 1.25 mmol) over 30 min at 0 °C. The mixture was warmed to room temperature and was stirred for 24 h. Ether (20 mL) and conc. HCl (2 mL) were added to the resulting mixture, which was extracted with ether (3×20 mL). The combined ethereal solution was washed with 10% aqueous $Na_2S_2O_3$ (10 mL), saturated aqueous NH_4Cl (10 mL), and brine (10 mL), dried ($MgSO_4$), and concentrated. GLC analysis (1.2 m PEG 20M 10% column, 180 °C) of the residue showed the formation of **2** (34%). **2** (*E* and *Z* mixture): IR (neat) 1660 cm^{-1}; ^{1}H NMR ($CDCl_3$ with TMS, 90 MHz) δ=2.82 (t, 1.04H, J=6.9 Hz), 3.21 (t, 0.96H, J=6.9 Hz), 3.71 (t, 1.04H, J=6.9 Hz), 3.81 (t, 0.96H, J=6.9 Hz), 7.3—8.3 (m, 5H); MS m/z 238 (M^++4), 236 (M^++2), 234 (M^+). Anal. ($C_{10}H_9Cl_3$) C, H, Cl.

Synthesis of *cis*-2-Chloro-4-pentanolide (6). To a solution of molybdenum pentachloride (0.137 g, 0.50 mmol) was dropwise added propyl 2-(trimethylsilylmethyl)cyclopropanecarboxylate (**5**, 0.107 g, 0.50 mmol) over 5 min at 0 °C. The mixture was stirred at 0 °C for 5 min and then at room temperature for 20 h. Methanol aqueous solution (50%, 2 mL) was added to the reaction mixture, which was stirred at room temperature for 1 h and was extracted with ether (3×20 mL). The combined ethereal solution was washed with brine, dried (Na_2SO_4), and concentrated. GLC analysis (1.2 m PEG 20M 10% column, 150 °C) of the residue showed the formation of **6** (45% yield). **6:** IR (neat) 1780 cm^{-1}; ^1H NMR ($CDCl_3$ with TMS, 90 MHz) δ=1.46 (d, 3H, J=6.6 Hz), 2.33 (dd, 1H, J=8.5, 6.7 Hz), 2.48 (dd, 1H, J=5.6, 2.9 Hz), 4.43 (dd, 1H, J=6.7, 2.9 Hz), 4.89 (ddq, 1H, J=8.5, 6.6, 5.6 Hz); MS m/z 136 (M^++2), 134 (M^+). Anal. ($C_5H_7O_2Cl$) C, H, Cl.

Isomerization of Propyl *cis*-2-Phenylcyclopropanecarboxylate (3) to the *trans*-Ester 4. The reaction of **3** was carried out in a similar manner as mentioned above. The ester **4** was produced in 70% yield with the recovery (30%) of the starting ester **3**.

References

1) J. S. Filippo, A. F. Sowinski, and L. J. Romano, *J. Am. Chem. Soc.*, **97**, 1599 (1975).

2) T. Hirao, S. Kohno, J. Enda, Y. Ohshiro, and T. Agawa, *Tetrahedron Lett.*, **22**, 3633 (1981); T. Hirao, S. Kohno, Y. Ohshiro, and T. Agawa, *Bull. Chem. Soc. Jpn.*, **56**, 1569 (1983).

3) A. de Meijere, "Topics in Current Chemistry, Small Ring Compounds in Organic Synthesis I-IV," Springer-Verlag, Berlin (1986, 1987, 1988, 1990); D. Tunemoto and K. Kondo, *J. Synth. Org. Chem. Jpn.*, **35**, 1070 (1977).

4) L. Bagnell, A. Meisters, and T. Mole, *Aust. J. Chem.*, **28**, 821 (1975).

5) T. Hirao, D. Misu, and T. Agawa, *J. Chem. Soc., Chem. Commun.*, **1986**, 26.

6) T. Hirao, Y. Harano, Y. Yamada, Y. Hamada, S. Nagata, and T. Agawa, *Bull. Chem. Soc. Jpn.*, **59**, 1341 (1986).

Thermal Properties of Liquid-Crystalline Polyitaconates with Paired Mesogens.

Kazuo SUGIYAMA* and Kohei SHIRAISHI
Department of Industrial Chemistry, Faculty of Engineering, Kinki University,
Hirokoshinkai, Kure, Hiroshima 737-01
(Received December 20, 1990)

Synopsis. 2-Methylenesuccinates (Itaconates) (**2**) having two 4-methoxyazobenzene moieties as paired mesogenic groups were prepared. The monomer **2** was radically homopolymerized and copolymerized with non-mesogenic monomer, dioctadecyl itaconate (DOI). Paired mesogenic homopolyitaconate exhibits a nematic phase and the copolymers of the monomer **2** with DOI also show a mesomorphic phase up to 25 mol% of DOI content. The enhancement of mesophase formation by paired mesogens is discussed.

In order to obtain comprehensive knowledge concerning the structure–property relation of thermotropic liquid crystalline side-group polymers (TLCPs), numerous polymers have been prepared and their mesomorphic properties investigated with a variation of the type of mesogen and the spacer in polyacrylates,[1,2] polymethacrylates,[3] polyesters[4,5] and polysiloxanes.[6] The properties of TLCPs are varied by the mesogenic structure and how mesogens are incorporated into the backbones. TLCPs with accentuated liquid-crystalline properties were prepared with paired mesogenic units fixed to a polysiloxane main chain.[7,8]

The concentration of mesogens along the polymer chain could also be achieved by making use of polymethylenesuccinates (polyitaconates).[9] The polymerization reactivity of itaconate monomers with paired mesogens and the mesomorphic properties of the polymers are, however, not obvious concerning detail. In recent papers, the syntheses and thermal behaviors of non-vinyl TLCPs were reported. The polymers considered were polyfumarate[10] or polyitaconate[11] backbones, a methylene spacer and 4-(4-methoxyphenylazo)-phenoxy and 4-(4-cyanophenoxycarbonyl)phenoxy mesogenic groups. In this brief note, we described the enhancement of mesophase formation by pairing the mesogens in polyitaconates, poly[bis[6-[4-(4-methoxyphenylazo)phenoxy]hexyl]itaconate].

Experimental

Preparation of Monomers: Bis[6-[4-(4-methoxyphenylazo)phenoxy]hexyl] itaconate **2** was prepared as follows: a benzene solution of 0.05 mol of itaconic anhydride and a 0.11 mol of 6-[4-(4-methoxyphenylazo)phenoxy]-1-hexanol was refluxed in the presence of a catalytic amount of *p*-toluenesulfonic acid for 3 d. After removing the solvent, the crude product was recrystallized twice from benzene. 83.9% yield; mp 121—122.4 °C; ^{1}H NMR ($CDCl_3$) δ=1.12—1.86 (m, 16H, $-CH_2(CH_2)_4CH_2-$), 3.36 (s, 2H, $-CH_2-$), 3.84—4.33 (m, 8H, $-CH_2(CH_2)_4CH_2-$), 3.91 (s, 6H, $-OCH_3$), 5.72—5.80 (m, 1H, H–CH=), 6.30—6.45 (m, 1H, H–CH=), 6.89—7.93 (m, 16H, Aromatic). Found: C, 68.78; H, 7.01; N, 7.44%. Calcd for $C_{43}H_{50}O_8N_4$ (M, 750.900): C, 68.78; H, 6.71; N, 7.46%.

Dioctadecyl itaconate (DOI) was prepared from the reaction of 0.18 mol of itaconic anhydride and 0.40 mol of 1-octadecanol according to the preparation method of **2**. 83.6% yield; mp 59.4—59.8 °C; ^{1}H NMR ($CDCl_3$) δ=0.77—1.74 (m, 70H, $-CH_2(CH_2)_{16}CH_3$), 3.26 (s, 2H, $-CH_2-$), 3.88—4.18 (m, 4H, $-CH_2(CH_2)_{16}CH_3$), 5.48—5.62 (m, 1H, H–CH=), 6.12—6.24 (s, 1H, H–CH=). Found: C, 77.66; H, 12.25%. Calcd for $C_{41}H_{78}O_4$ (M, 635.076): C, 77.54; H, 12.38%.

6-[4-(4-methoxyphenylazo)phenoxy]hexyl methacrylate was prepared by adding dropwise a slight excess of methacryloyl chloride to 6-[4-(4-methoxyphenylazo)phenoxy]-1-hexanol dissolved in anhydrous THF at 0 °C and in the presence of triethylamine. 66.3% yield; mp 81.2—82 °C; ^{1}H NMR ($CDCl_3$) δ=1.43—2.00 (m, 8H, $-CH_2(CH_2)_4CH_2-$), 2.08 (s, 3H, $-CH_3$), 4.14 (s, 3H, $-OCH_3$), 3.56—4.52 (m, 4H, $-CH_2-(CH_2)_4CH_2-$), 5.76—5.93 (m, 1H, H–CH=), 6.32—6.49 (s, 1H, H–CH=), 7.20—8.41 (m, 8H, Aromatic). Found: C, 69.68; H, 7.12; N, 16.14%, Calcd for $C_{23}H_{28}O_4N_2$ (M, 396.491): C, 69.66; H, 7.08; N, 16.33%.

Polymerization: The polymerization procedure was the same as that described by Sugiyama.[12] Polymers were reprecipitated twice from benzene and methanol. The intrinsic viscosities [η] of the polymer were determined in benzene at 30 °C with an Ubbelohde viscometer. The composition ratios of the copolymers were calculated from the nitrogen content as obtained by elemental analysis.

Results and Discussion

Itaconates with mono- and paired mesogenic units, the monomers **1** and **2**, are shown in Scheme 1. The polymerization of the monomer **2** was carried out using a free-radical initiator. The results given in Table 1 show that monomer **2** polymerizes to give mesomorphic polyitaconates with moderate conversion. As far as the viscosity behavior in benzene is concerned, their intrinsic viscosities are relatively small. The weight-averaged molecular weight was estimated to be 3430 for the polymer of [η]=0.027 dL g^{-1} by means of GPC measure-

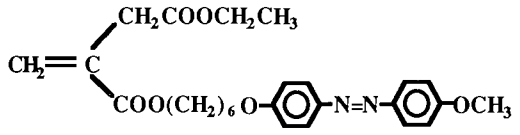

Monomer 1

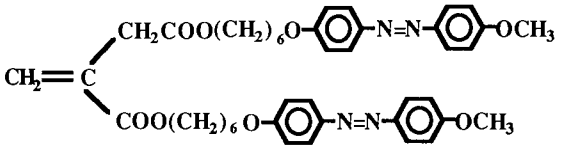

Monomer 2

Scheme 1. Structure of monomers **1** and **2**.

Table 1. Radical Polymerization and Phase Transition Temperature of **2**[a]

2	[ACN]×10²	Yield	$[\eta]$[b]	Phase transition temp/°C	
mmol	mmol	%	dL g^{-1}	T_m	T_i
0.67	1.34	8.3	0.059	101	136
0.67	2.68	10.4	0.052	100	130
0.67	4.02	18.2	0.044	98	137
0.67	5.36	25.0	0.042	97	131
0.67	6.70	58.0	0.027	97	122

a) Polymerized with 1,1′-Azobis(cyclohexanecarbonitrile) (ACN) in benzene (2 mL) at 100°C for 7 d. b) Measured in benzene at 30°C. c) Measured by DSC on heating cycle.

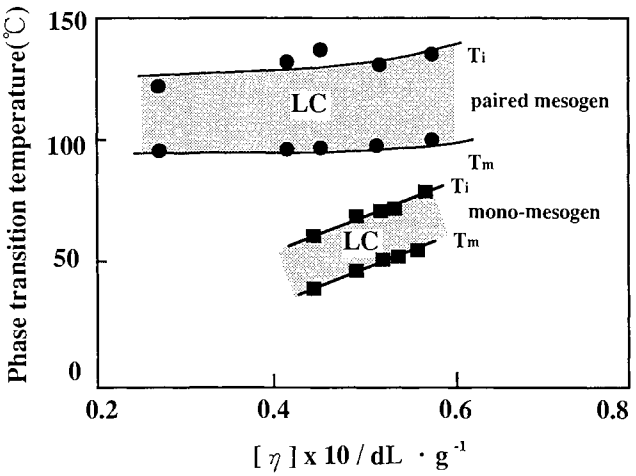

Fig. 1. Relationship between phase transition temperature and $[\eta]$ for the mono-mesogenic (■) and the paired mesogenic (●) polyitaconates.

ment.[13]

The molecular weight of polyitaconates seems to high sufficient to discuss the liquid crystalline properties. A DSC study showed that all of the paired mesogenic polyitaconates as well as mono-mesogenic polymers[11] turned into mesophase, since they showed two endothermic peaks and an exothermic peak upon heating and cooling cycles, respecctively. The mono-mesogenic polyitaconates showed rather broad melting and clearing peaks,[11] while the paired mesogenic polyitaconates showed sharp transition peaks at higher temperatures than the mono- would be favorable for liquid crystalline alignment and give sharp peaks in thermal analysis. According to polarized optical microscopy (POM), the mesophase of polyitaconates showed a schlieren texture and was confirmed to be nematic phase. The schlieren texture of polyitaconates was retained unchanged up to room temperature. It is suggested from a DSC trace on cooling cycles and POM that the polyitaconates are frozen in the mesophase at room temperature. The phase-transition temperatures determined by means of DSC measurements are tabulated in Table 1. Figure 1

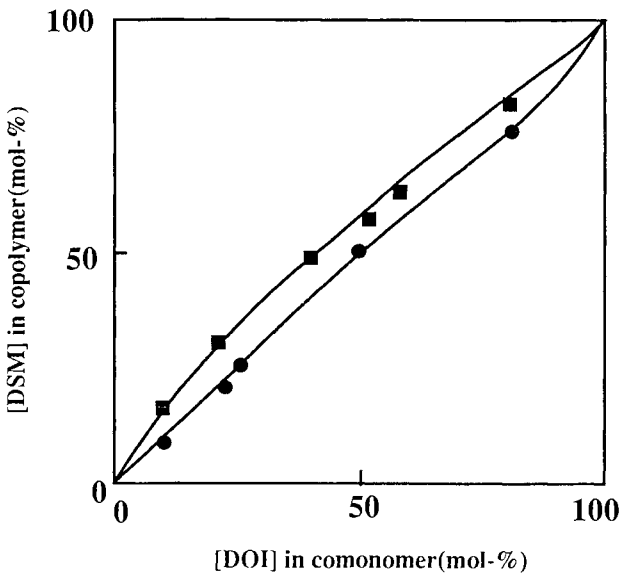

Fig. 2. Composition curve for the polymerization of monomers **1** (■) and **2** (●) with DOI (M_1) initiated with 1,1′-azobis(cyclohexanecarbonitrile) in benzene at 100°C.

shows the relationships between the phase-transition temperature and the intrinsic viscosity for the polyitaconates. The clearing temperature (T_i) of polyitaconates gradually increases with an increase in the intrinsic viscosity values, as observed in liquid crystalline polyacryrates with $[\eta]$ below 0.1 dL g^{-1}.[14] Comparing the two kind of polymers, paired mesogenic polyitaconates show a higher T_i and a wider range of nematic states than do the mono-mesogenic ones. This is explained by concentrating the mesogenic groups along the main chain: paired mesogenic groups favor a lateral interaction between successive pendant groups. It is known that the distance between successive pendent mesogenic groups along the polymer backbone plays an important role for mesophase formation in alternating mesogenic copolymers.[15]

In order to reinforce the enhancement of mesophase formation by paired mesogens, the copolymerization of itaconates (M_2) with non-mesogenic DOI monomer (M_1) was carried out radically with 1 mol% for monomer amounts of ACN in bulk at 100°C. The obtained copolymers were 30—50% in yield with 0.041—0.045 dL g^{-1} intrinsic viscosities. Figure 2 shows the composition curves for copolymerization. Applying the data in Fig. 2 to a curve-fitting method, the monomer reactivity ratios were calculated to be r_1=0.45 and r_2=0.95 for monomer **1** and r_1=1.02 and r_2=0.81 for monomer **2**, respectively. It is suggested that two kinds of polyitaconates radicals are nearly equal in reactivity for the DOI monomer, while the DOI radical decreases reactivity for itaconate with a paired mesogenic group, as is known from the steric effect of the bulky nature of the pendant groups. Thermal analyses of these random copolymers provided information concerning the

Table 2. Comparison of Phase Transition Temperature of Various Mesomorphic Side Chain Polymers[a)]

R	$[\eta]$/dL g^{-1}	T_m/°C	T_i/°C
-H[18)]	0.060	97	130
$-CH_3$[b)]	0.072	85	121
$-CH_2COOC_2H_5$[11)]	0.056	45	78
$-CH_2COO-(CH_2)_6-O-\langle\bigcirc\rangle-N=N-\langle\bigcirc\rangle-OCH_3$	0.059	101	136

a) $-[-CH_2-C(R)-]_n-$ with $R = COO-(CH_2)_6-O-\langle\bigcirc\rangle-N=N-\langle\bigcirc\rangle-OCH_3$.

b) Polymethacrylate was obtained from the polymerization of 6-[4-(4-methoxyphenylazo)phenoxy]hexyl methacrylate initiated by 1 mol% of 1,1'-azobisisobutyronitrile in the presence of 3.5 mol% of mercaptoacetic acid in benzene at 60°C for 24 h.

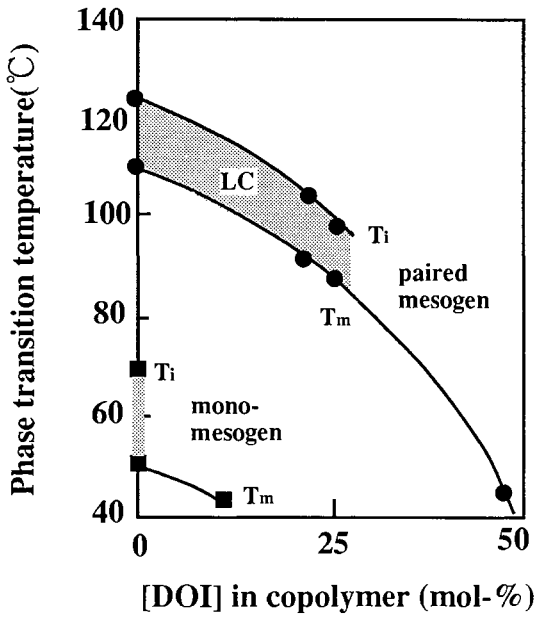

Fig. 3. Relationship between phase transition temperature and DOI content in copolymer of monomers **1** (■) and **2** (●) with DOI.

enhancement of the mesophase by introducing a pairing of the mesogens. Figure 3 exhibits the effect of nonmesogenic component on mesophase formation in a random copolymer. Paired mesogenic polyitaconates showed a nematic phase up to 25 mol% of DOI content, although the dilution lowered the phase-transition temperatures. On the other hand, copolymers of monomesogenic itaconates with nonmesogenic DOI showed no mesophase, even when the polyitaconates were diluted with 10 mol% of DOI content; it showed only the melting point. It is concluded that paired mesogens enhance the interaction of successive pendants in the liquid crystalline state and that the mesophase of copolymers with nonmesogenic DOI can be retained.

It is well known that the variation of substituents at the α-position of mesomorphic vinyl polymers causes a change in the kind of mesophase and transition temperature.[16,17)] Table 2 shows the transition temperature of various polymers bearing methoxyazobenzene moieties as a mesogenic group. In the case of monomesogenic liquid-crystalline polymers, large substituents at the α-position lower the transition temperature, since it accounts for the prevention of the mesogenic units from a liquid crystalline aligning due to their bulky nature. On the other hand, a paired mesogenic polymer shows a higher transition temperature based on a close packing of the mesogenic groups.

References

1) F. Hessel, R-P. Herr, and H. Finkelmann, *Makromol. Chem.*, **188**, 1597 (1987).
2) J. J. Mallon and S. W. Kantor, *Macromolecules*, **23**, 1249 (1990).
3) M. L. Tsai and S. H. Chen, *Macromolecules*, **23**, 1908 (1990).
4) S. Bualek and R. Zentel, *Makroml. Chem.*, **189**, 797 (1988).
5) I. G. Voigt-Martin, H. Durst, B. Reck, and H. Ringsdorf, *Macromolecules*, **21**, 1620 (1988).
6) C. H. Hsu, J. M. Rodriguez-Parada, and V. Percec, *J. Polym. Sci., Part A, Polym. Chem.*, **25**, 2425 (1987).
7) S. Diele, B. Hisgen, B. Reck, and H. Ringsdorf, *Makromol. Chem., Rapid Commun.*, **7**, 267 (1986).
8) S. Diele, S. Oelsner, F. Kuschel, B. Hisgen, H. Ringsdrof, and R. Zentel, *Makromol. Chem.*, **188**, 1993 (1987).
9) P. Keller, *Macromolecules*, **18**, 2337 (1985).
10) K. Shiraishi and K. Sugiyama, *Chem. Lett.*, **1990**, 1697.
11) K. Shiraishi, K. Sugiyama, and T. Otsu, *Bull. Chem. Soc. Jpn.*, **62**, 4083 (1989).
12) K. Sugiyama, *J. Macromol. Sci., -Chem.*, **A23**, 1155 (1986).
13) GPC measurements was carried out in THF with TSKgel G1000H, TSKgel G2000H, and TSKgel G3000H columns based on polystyrene as standard with an HLC-8020.
14) S. G. Kostromin, R. V. Talrose, V. P. Shibaev, and N. A. Platé, *Macromol. Chem., Rapid Commun.*, **3**, 803 (1982).
15) Y. Frere, F. Yang, P. Gramain, D. Guillon, and A. Skoulios, *Makromol. Chem.*, **189**, 419 (1988).
16) M. Portugall, H. Ringsdorf, and R. Zentel, *Makromol. Chem.*, **183**, 2311 (1982).
17) R. Zentel and H. Ringsdorf, *Makromol. Chem., Rapid Commun.*, **5**, 393 (1984).
18) A. S. Angeloni, D. Caretti, C. Carlini, E. Chiellini, G. Galli, A. Altomare, R. Salaro, and M. Laus, *Liq. Cryst.*, **4**, 513 (1989).

Aggregates in Langmuir-Blodgett Films of Spiropyrans Having Hydroxyl or Hydroxymethyl Group

Akio MIYATA,* Yutaka UNUMA, and Yoshiyuki HIGASHIGAKI
Tokyo Research Laboratories, Sharp Corporation, Kashiwa, Chiba 277
(Received November 29, 1990)

The optical properties of monomolecular layers at an air–water interface and also of Langmuir–Blodgett (LB) films of several photochromic spiropyrans with a single hydrophobic long chain and either a hydroxyl or a hydroxymethyl group have been investigated. Changes in the optical spectra of these films were induced by either UV irradiation or heating. UV-visible, and IR absorption spectra showed that spiropyran SP145 formed J-aggregates and SP147 formed H-aggregates. The half-decay period of the J-aggregate to the spiropyran (SP) form was longer than that of the colored monomeric photomerocyanine (PMC) to the SP form. It was concluded that hydrogen bonding between neighboring colored PMC molecules via hydroxyl, hydroxymethyl, and nitro groups stabilizes the aggregate state.

Spiropyran (SP) molecules are converted into the photomerocyanine (PMC) form on UV irradiation, and a reverse change takes place when the colored product is irradiated with visible light of a specific wavelength. This photochromic reaction can be applied to developing high density optical recording information storage media. In view of this, several workers[1–4] have studied the photochromic reactions of spiropyran monomolecular layers and multilayers prepared by the Langmuir–Blodgett (LB) technique.

The LB technique is useful to prepare a well-ordered molecular aggregation state of spiropyran molecules. Under such conditions these molecules often exhibit spectroscopic changes due to aggregate formation, i.e., red-shifted J-aggregates and blue-shifted H-aggregates. Ando et al.[5] reported that SP1822 (Fig. 1) LB films mixed with hexadecane formed J-aggregates after successive UV irradiation and heat treatment procedures at 35—50 °C. The J-aggregate state is featured by its sharper, more intensely colored band at a longer wavelength (λ_{max}=618 nm) than in the PMC state (λ_{max}=583 nm). A small Stokes shift in the fluorescence peak is another characteristic of the J-aggregate. The SP1801 (Fig. 1) LB films, however, formed a J-like aggregate (λ_{max}=600 nm) when either stearic acid or octadecyl alcohol was used as matrix molecules.[6] These films do not form an aggregate without admixing. This J-like aggregate formation was also noted in alternating LB films of SP1801 and stearic acid.

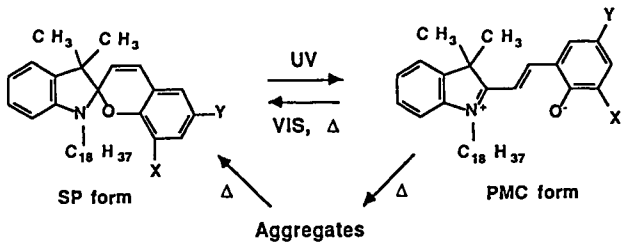

	X	Y
SP144	H	OH
SP145	CH_2OH	NO_2
SP147	OH	NO_2
SP18	H	NO_2
SP1801	OCH_3	NO_2
SP1822	$CH_2OCOC_{21}H_{43}$	NO_2

Fig. 1. Chemical structures of spiropyran derivatives used.

Only a few studies have been done on the aggregate formation of amphiliphilic spiropyrans, though the characterization of dye aggregate states in general has been performed by many researchers. Their formation of well-ordered J- and H-aggregate states, and examination of a correlation between the structure and aggregate forming ability of spiropyrans are therefore of interest. Molecules in an aggregate interact through various cohesive forces, i.e., hydrogen, ionic, and covalent bonding. In this paper the importance of hydrogen bonding in aggregation is emphasized.

The present work deals with the photochromic behavior of spiropyran derivatives prepared as monolayers at the air–water interface or as LB films. The spiropyrans used here contain a long alkyl chain and a hydroxyl group. These formed an LB film without matrix molecules such as stearic acid or octadecyl alcohol. The colored PMC form and the J- and H-aggregate forms are highly stable, and the results suggest that these aggregates are formed through hydrogen bonding.

Experimental

Materials. The spiropyrans (Fig. 1) were purchased from the Nippon Kankoh-Shikiso Kenkyusho Co., and were used without further purification. The spreading solvent was spectroscopic grade chloroform.

Procedures. Measurements of surface pressure–area (π–A) isotherms and the deposition of monolayers onto quartz slides were performed by means of a conventional Langmuir trough (Joyce Loebl, Langmuir Trough IV, UK) equipped with a Whilhelmy balance. The substrates for visible spectroscopic measurements were rendered hydrophobic by immersion in a 10% chloroform solution of trimethylchlorosilane. The LB films were deposited at a surface pressure of 20 mN m^{-1} and a dipping speed of 15 mm min^{-1}. The subphase

was maintained at 20 °C, pH 5.8.

The visible absorption spectra of monolayers were measured with a multichannel spectrophotometer (Otsuka Electronics Co., model MCPD-200), whereas a double-beam UV-visible spectrophotometer (Japan Spectroscopic Co., model UVIDEC-610C) was used for multilayers. Infrared spectra of the LB films were measured with an IR spectrophotometer (Japan Spectroscopic Co., model IR-810), and fluorescence spectra were detected by means of a monochromator (Japan Spectroscopic Co., model CT-25C) combined with photomultiplier (Hamamatsu Corp., model R943-02) by excitation at 550 nm. The monochromator had a spectral band width of ca. 0.1 nm. To make proceed photochromic reactions from the SP to the PMC form on the subphase, the monolayer was irradiated with a UV lamp (366 nm, UVP Inc., model UVL-56, USA).

Results

Surface Pressure-Area (π-A) Isotherms. When monolayers of the spiropyran derivatives were compressed after conversion from the SP to the PMC form by UV irradiation, it was possible to deposit them as an LB film onto the substrate. Figure 2 shows the π-A isotherms for the monolayers of SP144, SP145, and SP147 after UV irradiation. The monolayers were stable up to a surface pressure of 40 mN m^{-1}, and the limiting areas are 0.53 nm^2 (SP144), 0.57 nm^2 (SP147), and 0.58 nm^2 (SP145).

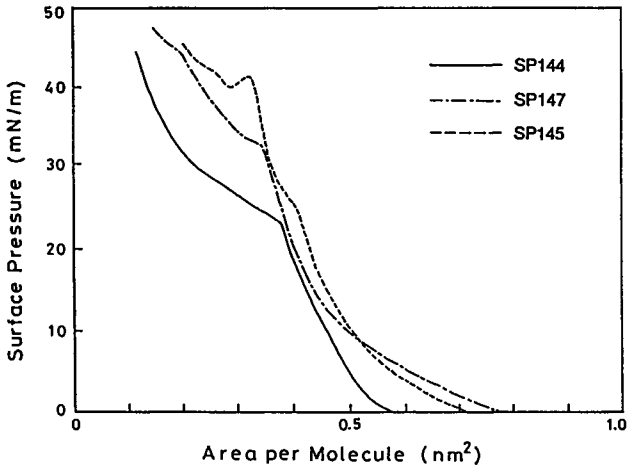

Fig. 2. Surface pressure-area isotherms for monolayers of spiropyran derivatives after UV irradiation.

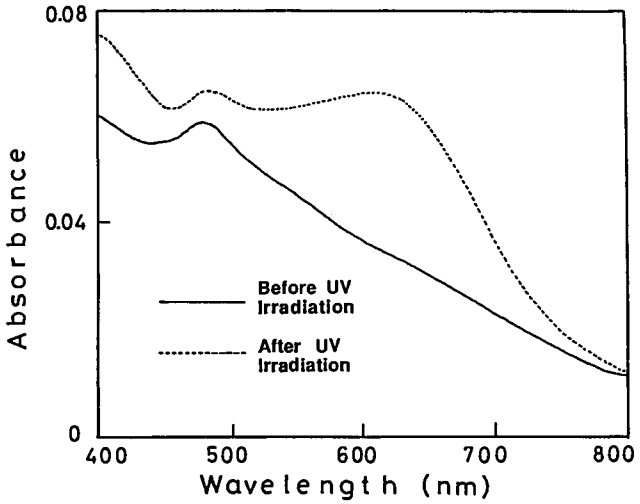

Fig. 3. SP144 LB film absorption spectra.

Photochromic Behavior of SP144. The absorbance of the SP144 monolayer at the air-water interface was negligible because its colored PMC without NO_2 group had a small extinction coefficient. Spectral measurements became possible with ten double multilayers formed on both sides of the substrate. Figure 3 shows the absorption spectra before UV irradiation, where the dye was in the SP form, and after UV irradiation. In the latter case a broad band is seen around 610 nm arising from the PMC form. On visible irradiation, the absorption spectrum returned to the original one, which was obtained also by heating in darkness. This reversible transformation was repeated using UV light and heating, and the change from the PMC to the SP form took place with a half-decay time of 2 min at 25 °C. A small absorption band at 480 nm is probably due to H-aggregates. No further changes were noted in the visible spectrum when the SP144 LB film was irradiated with UV light (366 nm, 1.0 mW cm^{-2}) for more than 10 min. This indicates that new aggregates are not formed after photoisomerization from the SP to the PMC form.

Infrared spectral analysis of the SP144 LB films was performed on a calcium fluoride support. The results

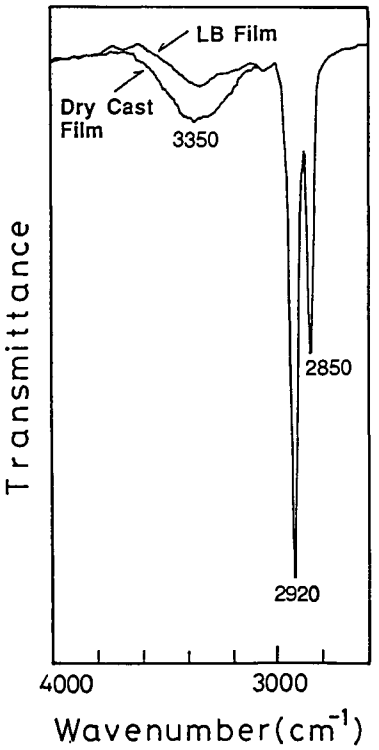

Fig. 4. SP144 IR spectra in the region 4000—2600 cm^{-1}.

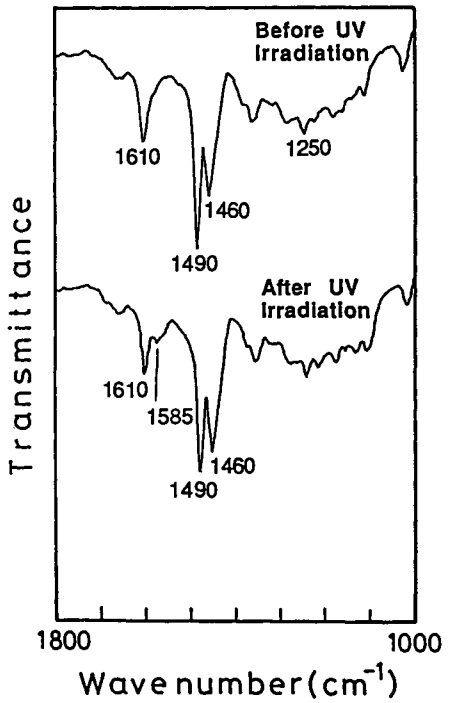

Fig. 5. SP144 LB film IR spectra in the region 1800—1000 cm^{-1}.

are shown in Figs. 4 and 5. In CCl_4 the SP form molecules exhibit a peak at 3620 cm^{-1} reflecting the free O–H stretching. However, in the LB films this free OH-band is absent and instead a broad band peaking at 3350 cm^{-1}, which appeared also in a dry SP144 film cast from a dichloromethane solution, is observed due to the stretching of the hydrogen bonded OH groups (Fig. 4). In the LB films deposited at pH 9.0, the broad band did not exist due possibly to deprotonation of the hydroxyl groups. As seen in Fig. 5, no substantial change took place in the spectral shape over a wavenumber range 1800 to 1000 cm^{-1} in going from the SP to the PMC form in the LB film. The intensity of the 1610 cm^{-1} peak, assignable to the C=C stretching of *trans*-photomerocyanine,[3] did not increase by UV irradiation. Therefore, we conclude that no significant change took place in the molecular skeleton, and the PMC form is an alternatively open form (cisoid) and not a completely open (almost planar) form, or the so called transoid. An IR study by Morinaka et al.[7] demonstrated the occurrence of similar phenomena, namely hydrogen-bond formation and no cisoid-transoid isomerization in vacuum-deposited films of a spiropyran having a hydroxy group but no long alkyl chain. Reportedly they observed a stabilization of the PMC form via intermolecular hydrogen bonding in the vacuum-deposited films, but we were unable to prepare a stable PMC form in the LB films. Presumally the strengths of the hydrogen bonding are different between the two experiments because of a difference in the molecular orientation in the films.

Photochromic Behavior of SP145. A larger extinction coefficient of spiropyrans having nitro groups enabled measurement of their monolayers at the air–water interface. Monolayer absorption spectra after UV irradiation are displayed in Fig. 6. A broad band (555 nm) assigned to the PMC form appeared at a surface pressure of 5 mN m^{-1}, whereas a relatively sharp band (638 nm) reflecting the J-aggregate form appeared at surface pressures of 15—25 mN m^{-1}.

The J-aggregated state was maintained by the transfer of surface monolayers onto the substrate. Figure 7 shows the absorption spectra of the transferred LB films. The J-aggregate (λ_{max}=638 nm) was converted into the colorless SP form with a half-life of 560 min at 25 °C in darkness. Subsequent UV irradiation of the SP form regenerated the PMC form (λ_{max}=585 nm) without J-aggregate formation. The half-decay period for the PMC-to-SP conversion of SP145 is 135 min, being longer than those of the colored PMC forms of SP18 (15 min) and SP1801 (30 min)[6] for which no intermolecular hydrogen bonding was observed by IR

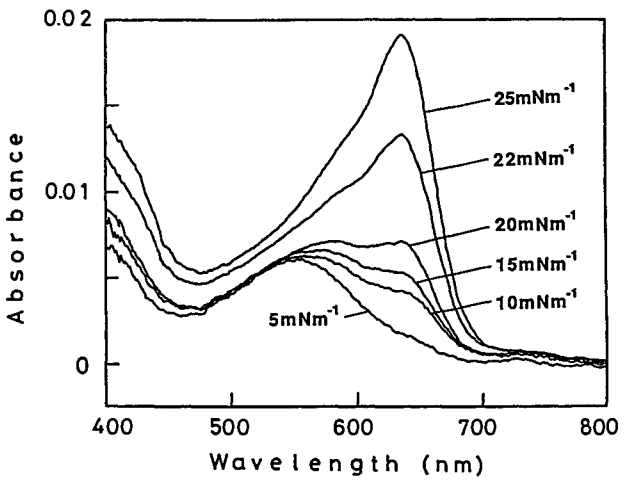

Fig. 6. Absorption spectra of the SP145 monolayer at the air–water interface.

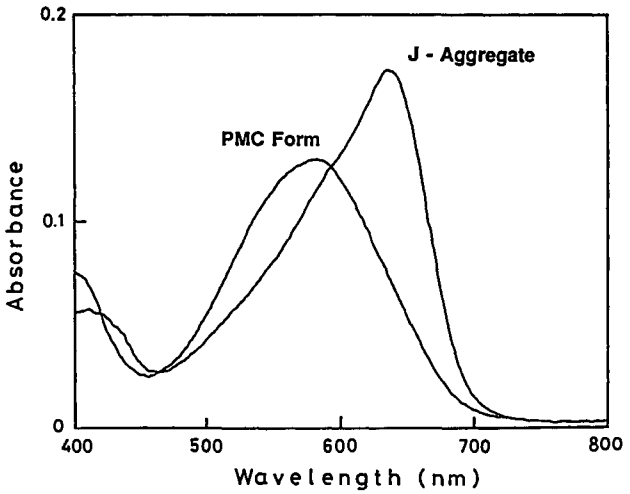

Fig. 7. SP145 LB film absorption spectra.

spectroscopy. A possible reason for the non-reformation of J-aggregates may be that their two-dimensional arrangements were sterically hindered by a molecular structural change during the conversion from the initial J-aggregated state to the SP form. Once such a change has occurred, recovery on the substrate is apparently impossible because an arrangement favorable for the J-aggregate formation may take place only at the air–water interface.

In order to examine whether the absorption band at 638 nm was due to J-aggregates, the fluorescence spectrum of the SP145 LB film was measured. A relatively small Stokes shift (65 nm) suggests that the dye is in a J-aggregated state as shown in Fig. 8. The Stokes shift, however, is larger than that (16 nm) of SP1822 having two long alkyl chains. This may reflect an inhomogeneous arrangement of the SP145 J-aggregate, or suggest that SP1822 J-aggregate is more tightly packed and well-ordered. Figure 9 shows the IR spectra for the J-aggregate, SP, and PMC form of the SP145 LB film. The NO_2 asymmetrical stretching at 1520 cm^{-1} in the SP form is shifted to 1518 cm^{-1} in both the J-aggregate and the PMC form. In contrast, the symmetrical NO_2 stretching mode at 1340 cm^{-1} in the SP form is shifted to 1295 cm^{-1} in the PMC form, and to split peaks at 1280 and 1250 cm^{-1} in the J-aggregate form. Since the colored PMC form has a zwitterion structure, the wavenumber lowering of the symmetrical NO_2 stretching peak may be a result of a resonance effect between the phenoxide ion and *p*-nitro group. The significantly lower frequency and larger intensity of the symmetrical NO_2 stretching bands in J-aggregate may reflect a stronger resonance effect, which promotes an intermolecular charge transfer from the negative oxygen atom of phenoxide ion in the pyran ring to the positive nitrogen atom in the indoline ring of an adjacent PMC molecule. Similarly, in the SP1822 LB film the sysmetrical NO_2 stretching peak was shifted from

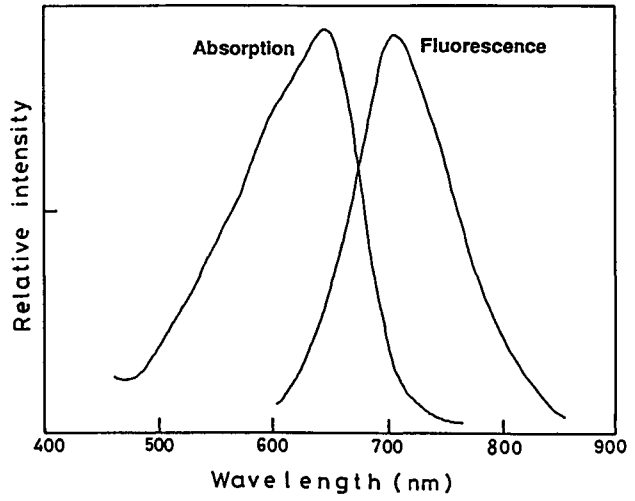

Fig. 8. Absorption and fluorescence spectra of J-aggregates in SP145 LB film.

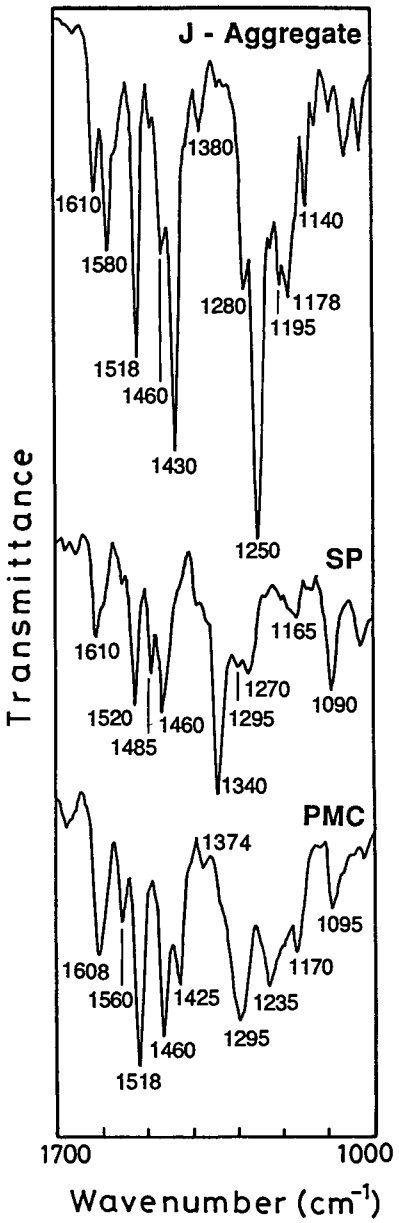

Fig. 9. IR spectra in the region 1700—1000 cm^{-1} for SP145 LB film.

1340 cm^{-1} in the SP form to 1290 cm^{-1} in the PMC and J-aggregate form.[8] To examine the state of the OH group, IR spectra were measured in the region 4000—2400 cm^{-1}. The SP form in CCl_4 showed a free OH-band at 3600 cm^{-1}. In the LB films, a weak band at 3220 cm^{-1} reflecting the O–H stretching in a hydrodgen bonded state was observed in both the PMC and the J-aggregate form, but not in the SP form. This demonstrates the formation of intermolecular hydrogen bonding in the PMC and J-aggregate form. The IR spectra for a SP145 cast film onto a CaF_2 substrate is shown in Fig. 10. By the SP-to-PMC conversion, the intensity of a broad peak at 3350 cm^{-1} increased while that of sharp peak at 3550 cm^{-1} decreased to a shoulder of the former peak. The 3550 cm^{-1} band is assigned to free

O–H streching. Accompanying the ring closure by 580-nm irradiation and by heating, the intensity of the free OH-band (3550 cm^{-1}) was recovered and that of the hydrogen-bonded OH-band decreased. These spectral changes were well reproducible. The intensity of the hydrogen-bonded OH-band in the dry cast films, however, was much larger than that in the LB films.

Photochromic Behavior of SP147. After spiropyan SP147 was spread on water, the colored PMC form (λ_{max}=590 nm) was observed without UV irradiation. The absorption spectra for the monolayer after UV irradiation are shown in Fig. 11. In the LB film a broad band at 590 nm is transformed into a new absorption band at 560 nm due to aggregate formation by heat treating at 35 °C for 120 min (Fig. 12). This peak shift seems the higher dipole interaction energy increased due to formation of either H-dimer or H-aggregate containing three or four molecules. This H-aggregate was stable and did not decay for more than a month.

The IR spectra of the PMC and the H-aggregate form are depicted in Fig. 13. On heating the LB films, the intensities of the hydrogen-bonded O–H stretching (3220 cm^{-1}) and of the symmetric NO_2 stretching (1290 cm^{-1}) increased. This suggests that hydrogen-bond formation among the NO_2 group, phenoxide ion, and OH group is responsible for the formation of the H-aggregate. By heat treatment, the SP147 dry cast film behaved in essentially the same manner as the LB film with regard to these features. Hydrogen bonding is

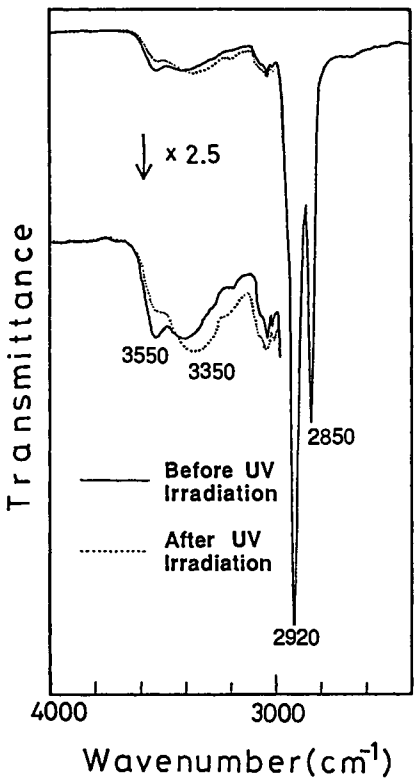

Fig. 10. IR spectra in the region 4000—2400 cm^{-1} for SP145 dry cast film.

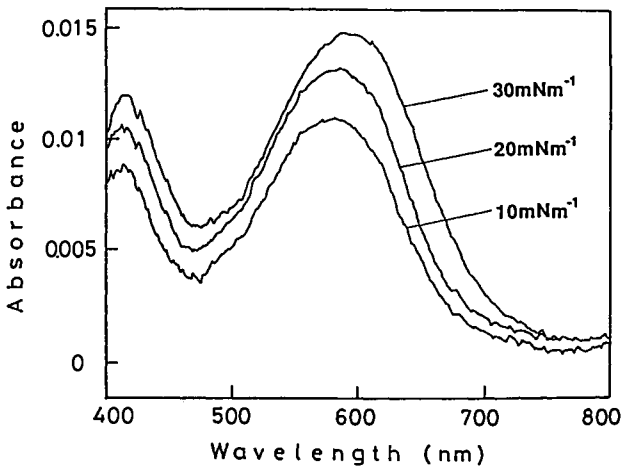

Fig. 11. Absorption spectra for the SP147 monolayer at the air–water interface.

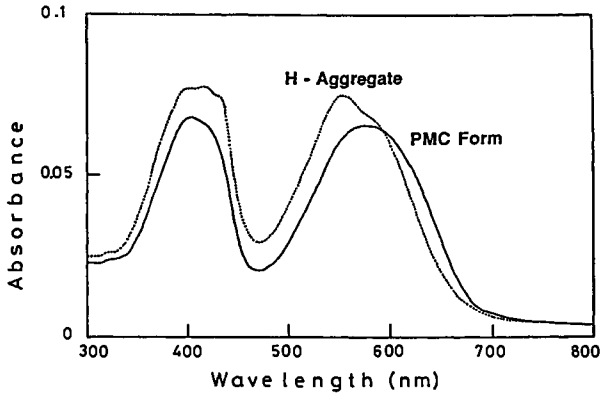

Fig. 12. SP147 LB film absorption spectra.

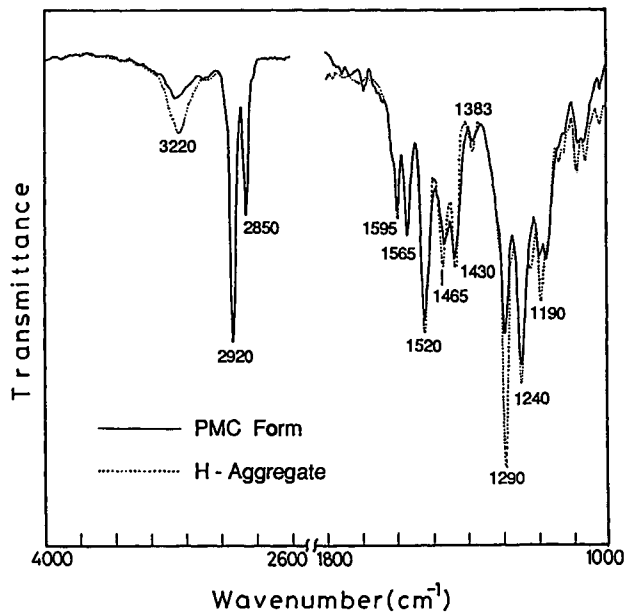

Fig. 13. IR spectra in the region 4000—2600 cm^{-1}, and 1800—1000 cm^{-1} for SP147 LB film.

one of the key driving forces for aggregate formation. An intramolecular hydrogen bonding may also occur in the PMC molecules, but the IR band reflecting this may have been hidden by the asymmetrical and symmetrical $-CH_2-$ stretching peaks (2910 and 2850 cm^{-1}) of the long alkyl chain.

Discussion

The photochromic behaviors of the spiropyran derivatives studied here are summarized in Table 1. UV-generated PMCs of SP18 (X=H),[9,10] SP145 (X=CH_2OH), and SP1822 (X=$CH_2OCOC_{21}H_{43}$)[11] have a head-to-tail configuration due to dipole–dipole interaction, and form J-aggregates in the monolayer at the air–water interface. Since the PMC form is more polar than the SP form, an electrostatic interaction may occur between neighoring PMCs in the J-aggregate. Previous studies have shown that the SP18 J-aggregate is unstable and readily converted into the PMC form in the LB films.[9,10] As verified in the presented work, the PMC of SP145 formed a J-aggregates which is more stable than the SP18 J-aggregate in the LB films. The stability of J-aggregates is a result of stronger dye–dye interaction and prevents the PMC-to-SP isomerization via formation of microcrystals. In contrast, the UV-generated PMCs of SP1801 (X=OCH_3)[11] and SP147 (X=OH) having the electron donating groups did not form J-aggregate in the monolayer on water. The SP147 PMC form, however, changed to an H-aggregate or an H-dimeric state by heat treatment in the LB film and dry cast film.

Table 1. Aggregate Formation in the Monolayer and LB Film

	Monolayer	LB film
SP144	No Data[a]	PMC (H-aggregate)
SP145	J-aggregate	J-aggregate
SP147	PMC	H-aggregate
SP18	J-aggregate	J-aggregate
SP1801	PMC	PMC
SP1822	J-aggregate	J-aggregate

a) Signal not measurable.

Based on the blue-shifted visible absorption band and intensity increase of IR OH-band, we propose four types of molecular configuration for a hydrogen-bonded SP147 dimer in Fig. 14. It is generally known that H-dimer and H-aggregate assume a side-by-side arrangement.[12] In the type a and b the hydrogen bonding occurs among the OH group, phenoxide ion, and the NO_2 group. The transition dipole moments of the two molecules are in parallel, and this molecular configuration should exhibit a bule-shifted absorption from the monomer band. In type c the hydrogen bond forms between the OH group and the phenoxide ion, and here

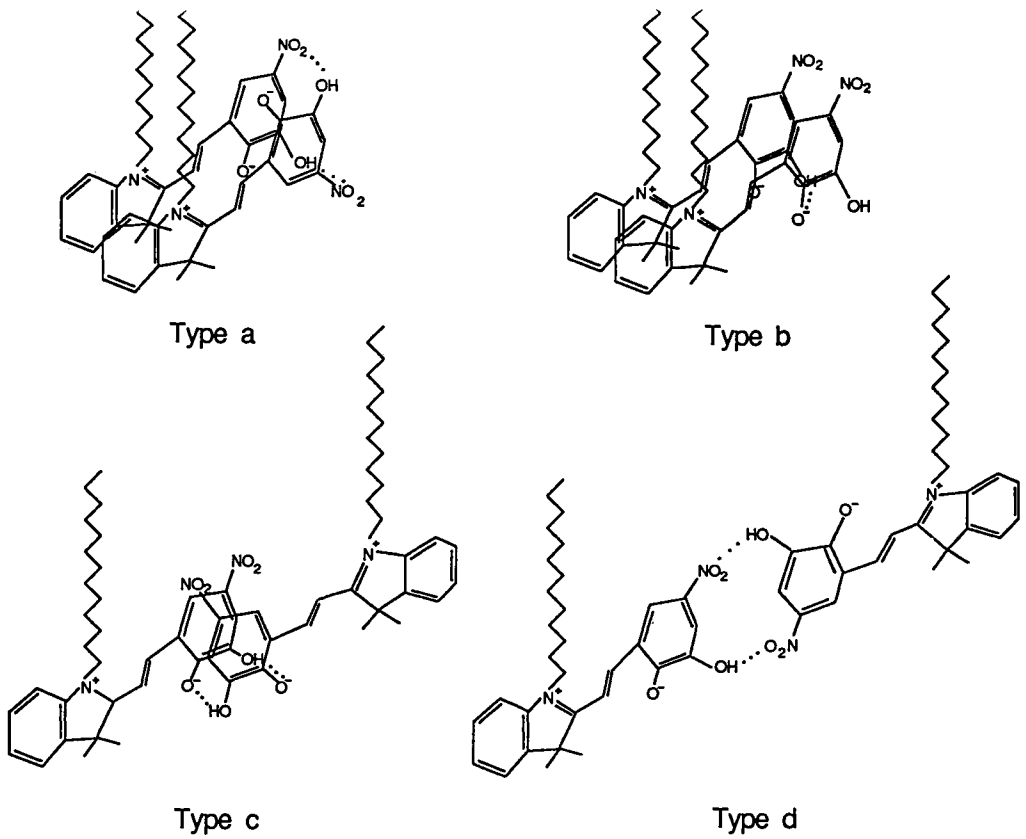

Fig. 14. Molecular configuration models of SP147 dimer.

the two transition moments are oriented anti-parallel. The slip angle between the molecular long axis and the center-to-center line, is small. Thus PMC molecules are essentially in a head-to-head arrangement. In type d, the hydrogen bond forms between the OH group and the NO_2 group. Again, PMC molecules are in a head-to-head arrangement. Both type c and d should hence exhibit a red-shifted absorption. In view of these, type a or b is the most plausible configuration for the reported H-dimer or H-aggregate.

In conclusion, intermolecular hydrogen bonding acts in stabilizing the colored PMC form and in promoting aggregation of spiropyrans having hydrophilic OH and CH_2OH groups, in systems where hydrophilic matrix molecules are absent. Spiropyrans with an NO_2 group and either OH or CH_2OH groups form diffrent types of aggregates depending on the mode of configurations of open-ring PMC molecules in the LB films and the dry cast films.

The authors are grateful to Drs. Mistuyuki Soma and Yuko Soma of the National Institute of Environmental Studies for IR assignments, and to Dr. David Heard of Sharp Corporation and Professsor Akihiko Yamagishi of the University of Tokyo for valuable discussions.

This work was performed under the management of the FED (the R&D Association for Future Electron Devices) as a part of the R&D of Basic Technology for Future Industries supported by NEDO (New Energy and Industrial Technology Development Organization).

References

1) E. E. Polymeropoulos and D. Möbius, *Ber. Bunsen-Ges. Phys. Chem.*, **83**, 1215 (1979).
2) M. Morin, R. M. Leblanc, and I. Gruda, *Can. J. Chem.*, **58**, 2038 (1980).
3) C. B. McArdle, H. Blair, A. Barraud, and A. Ruaudel-Teixeier, *Thin Solid Films*, **99**, 181 (1983).
4) D. A. Holden, H. Ringsdorf, V. Deblauwe, and G. Smets, *J. Phys. Chem.*, **88**, 716 (1984).
5) E. Ando, J. Miyazaki, K. Morimoto, H. Nakahara, and K. Fukuda, *Thin Solid Films*, **133**, 21 (1985).
6) E. Ando, J. Hibino, T. Hashida, and K. Morimoto, *Thin Solid Films*, **160**, 279 (1988).
7) A. Morimoto, T. Yoshida, and N. Funakoshi, Proc. Int. Symp. on Optical Memory, 1987; *Jpn. J. Appl. Phys.*, **26**, Supplement 26-4 (1987).
8) J. Hibino, E. Ando, K. Morimoto, J. Umemura, and T. Takenaka, 56th Annual Meeting of the Chemical Society of Japan, Tokyo, April 1988, Abstr., No. 3II-H03.
9) E. Ando, K. Arita, and K. Morimoto, 56th Annual Meeting of the Chemical Society of Japan, Tokyo, April 1988, Abstr., No. 3II-H01.
10) E. Ando, K. Moriyama, K. Arita, and K. Morimoto, *Langmuir*, **6**, 1451 (1990).
11) E. Ando, M. Suzuki, K. Moriyama, and K. Morimoto, *Thin Solid Films*, **178**, 103 (1989).
12) V. Czikkely, H. D. Föresterling, and H. Kuhn, *Chem. Phys. Lett.*, **6**, 207 (1970).

Shock Tube Studies of the H_2-O_2-CO Reaction by Atomic Resonance Absorption Spectroscopy

Tohru KOIKE
Department of Chemistry, National Defense Academy, Hashirimizu, Yokosuka 239
(Received December 20, 1990)

The atomic resonance absorptions of O- and H-atoms in the reaction of shock-heated $H_2/O_2/CO/Ar$(1/1/1/97 and 0.2/1/1/97.8) mixtures were observed over a relatively low temperature range from 1000 to 1400 K. The induction times, determined from the absorptions, were investigated by means of computer modeling which included a sensitivity test. The rate constant for the important initiation reaction, $CO+O_2=CO_2+O$, was evaluated to be $k_{13}=10^{13.1\pm0.6}$ exp $(-196.9\pm14.9$ kJ/$RT)$ cm^3 mol^{-1} s^{-1}, which may supplement the lack of reported rate constants in the low-temperature region.

The reaction

$$CO+O_2=CO_2+O \quad (13)$$

is a radical-producing step which initiates CO oxidation and has drawn the attention of many researchers, where the reaction number is in accordance with that given in Table 1. Recently, Thielen and Roth[1] studied CO oxidation in a shock-heated CO/O_2 system employing atomic resonance absorption spectroscopies (ARAS) of O-atoms. In a CO–O_2 mixture, the overall oxidation reaction is not so fast that it requires a high-temperature environment to observe the progress of the reaction within the restricted observation time of the shock-tube system. They determined the k_{13} value in the high-temperature region of 1700—3500 K.

Gardiner et al.[2] studied the reaction in both H_2/O_2 and $H_2/O_2/CO$ systems by means of UV absorption spectroscopy of the ground-state OH-radicals at temperatures of 1400—2500 K. They compared the induction times of OH absorption in the $H_2/O_2/CO$ system with those in the H_2/O_2 system and obtained k_{13} in the lower temperature region by computer modeling.

Reviews concerning elementary reactions in $H_2/O_2/CO$ system were given in detail by a group at the University of Leeds,[3] and more recently by Warnatz.[4] These two groups proposed the same k_{13} value in the temperature range 1500—3000 K.[3,4]

We have also adopted the $H_2/O_2/CO$ system and have observed the growth rates of O- and H-atoms directly by ARAS and have determined the k_{13} value in a low-temperature region in order to supplement the lack of reported rate constants.

Experimental

Since details concerning the incident shock-tube and the ARAS optical system were given in a previous paper,[5] we discuss them here only briefly.

The ARAS system comprises a light source and a detector. Gas mixtures of H_2 or O_2 diluted in He (by 1% flowing at 2 Torr through a quartz tube, 1 Torr=133.322 Pa) were excited by a microwave generator (Raytheon, PGM10X1); the accompanied emissions were used for the light source. A combination of a vacuum-UV-monochromator (Minuteman, 302-VM dispersion=40 nm/mm), of which wavelength was centered at 121.6 nm of the Lyman-α line by H-atoms or at 130.5 nm of the O-triplet line by O-atoms, and a solar blind photomultiplier (Hamamatsu, R-1459) was used as the detector. The signals of the absorption time profiles were recorded on a digital oscilloscope (Iwatsu, DS-6121) combined with an XY-recorder.

The test section of the shock tube was evacuated to less than 10^{-5} Torr before each run. The leak rate was ca. 10^{-5} Torr min^{-1}, and the shock waves were actuated within 3 min after closing all valves of the shock-tube.

Gases for the test gases ($H_2/O_2/CO/Ar$=1/1/1/97 and 0.2/1/1/97.8) were 99.99999% pure H_2, 99.999% pure O_2, 99.6% pure CO and 99.999% pure Ar and were used without further purification.

Results and Discussion

Figure 1 is a sample oscillogram of the absorption history at 121.6 nm for the 1/1/1 ($H_2/O_2/CO$) mixture; it shows the slight rise at the shock front, a low plateau,

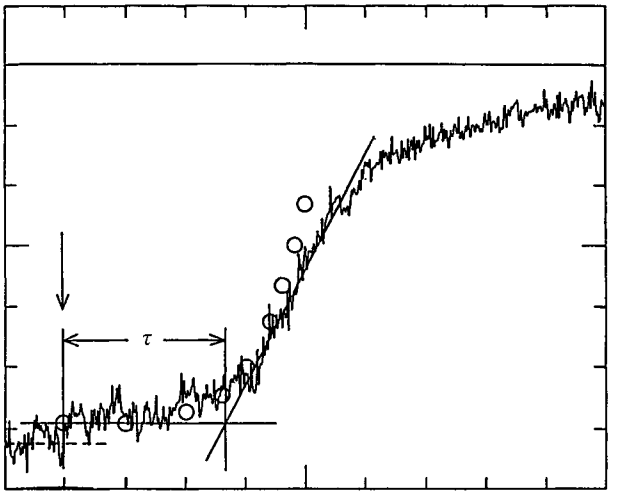

Fig. 1. A sample oscillogram of the absorption profile at 121.6 nm.
Test gas: $H_2/O_2/CO/Ar$=1/1/1/97,
P_1=20 Torr, T_2=1173 K.
The time-scale is 50 μs/div. The upper line shows the zero-level of the incident light intensity. The arrow shows the shock front. The induction time, τ, was evaluated as in the figure. The circles show the results by computer modeling with the reaction mechanism in Table 1.

and an exponential increase. Such a time profile was also obtained for absorption at 130.5 nm. Since the absorption by H_2 for the two light sources are smaller than those by O_2 and CO,[1,5,6] the absorption time profiles are not so different between the two mixtures. From the oscillograms, the induction times, τ, defined as the time interval between the shock arrival at the observation window and the foot of the exponential absorption rise, were evaluated on the laboratory base. As is shown in Fig. 1, the foot is the intersection of the low plateau and the extrapolated line of the absorption increase. The low plateau of the absorption after the shock front can be attributed to absorption by O_2 and CO.[1,5,6] Since the total absorption is the summation of each absorption of the contributing species, this revised

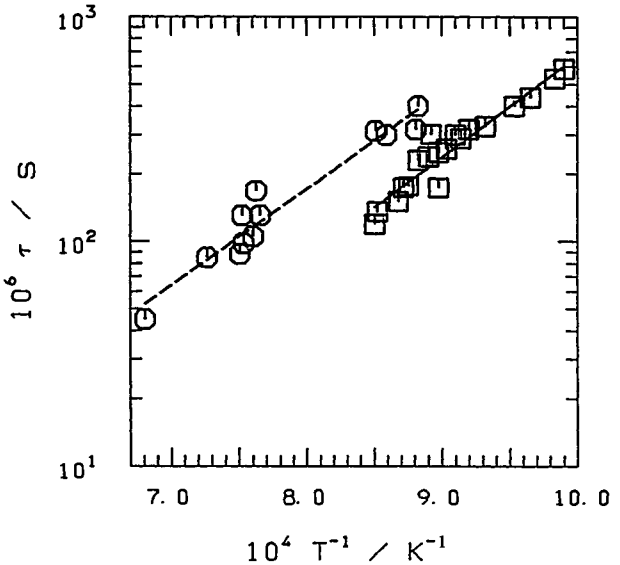

Fig. 2. Induction times, τ, at 121.6 nm vs. $10^4/T$.
Squares: for the 1/1/1 (H_2/O_2/CO) mixture,
Octagonals: for the 0.2/1/1 mixture.
The lines show the least-squares fits for the data points.

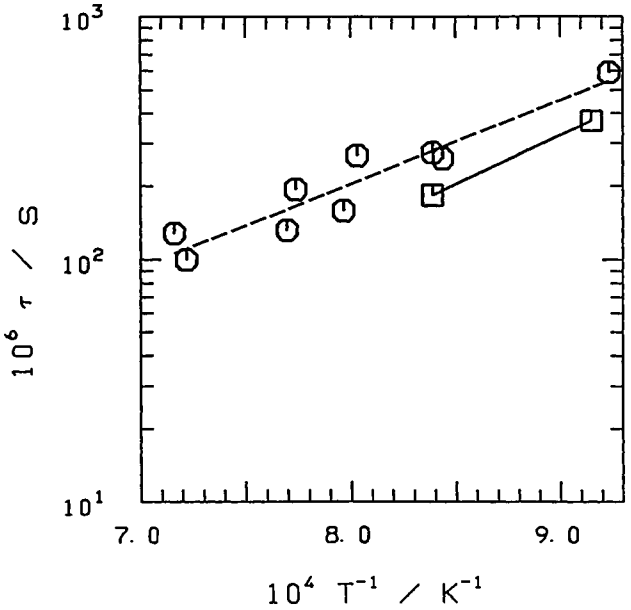

Fig. 3. Induction times, τ, at 130.5 nm vs. $10^4/T$.
Squares: for the 1/1/1 mixture,
Octagonals: for the 0.2/1/1 mixture.
The lines show the least-squares fits for the data points.

definition of τ must be more reasonable than those adopted in a previous study.[5]

The data points of the experimental τ values obtained from the 121.6 and 130.5 nm absorption profiles are shown in Figs. 2 and 3, respectively. Each line exhibits a least-squares result for the data points. The temperature dependences of both lines are almost equal and the τ values in the 1/1/1 mixture are smaller than those in the 0.2/1/1 mixture.

These results were subjected to interpretation by computer modeling. The induction time for the modeling is defined as being the time interval between shock arrival and the attainment of certain values of the

Table 1. Reaction Mechanism and Rate Constant
$k=AT^n \exp(-E/RT)$ (mol, cm, s, and J units)

	Reaction	A	n	E	Ref.
1)	$H_2+O_2=H+HO_2$	2.8+15[a]	0.	2.60+5	See Text
2)	$H_2+AR=H+H+Ar$	2.2+14	0.	3.77+5	4
3)	$O_2+AR=O+O+Ar$	1.2+14	0.	4.51+5	4
4)	$H+O_2=OH+O$	1.22+17	−0.91	6.91+4	4
5)	$O+H_2=OH+H$	1.5+7	2.0	3.16+4	4
6)	$OH+H_2=H_2O+H$	1. +8	1.6	1.38+4	4
7)	$H+O_2+AR=HO_2+Ar$	7. +17	−0.8	0.	4
8)	$OH+OH=H_2O+O$	1.5+9	1.14	0.	4
9)	$H+HO_2=OH+OH$	1.5+14	0.	4.18+3	4
10)	$OH+HO_2=H_2O+O_2$	2. +13	0.	0.	4
11)	$O+HO_2=OH+O_2$	2. +13	0.	0.	4
12)	$CO+OH=CO_2+H$	4.4+6	1.5	−3.1+3	4
13)	$CO+O_2=CO_2+O$	1.3+13	0.	1.97+5	This Work
14)	$CO+O+AR=CO_2+AR$	5.3+13	0.	−1.9+4	4

a) The number after + exhibits an index for 10.

radical concentrations. These concentrations for H- and O-atoms were assumed to be 8.3×10^{-13} and 1.66×10^{-12} mol cm^{-3}, respectively.[5,6] These are almost in accord with the detection limit of the present ARAS system; the induction times, thus defined, in computer modeling are considered to be compatible with the induction times obtained from an oscillogram of the absorption profile.[5]

The reaction mechanism used in the computer modeling of the present study is shown in Table 1. This mechanism comprises H_2–O_2 reaction steps of Reactions (1)—(11),[4] derived in a former study,[5] and CO steps to form CO_2, Reactions (12)—(14). Excepting the k_1 and k_{13} values, the k values are those recently recommended by Warnatz.[4] He re-evaluated the values by Baulch et al.[3] as well as those by other groups that have appeared after Baulch's review.

In order to comprehend the roles of each reaction in the progress of the H_2–O_2–CO reaction, we carried out a sensitivity test for the reaction mechanism shown in Table 1 by changing each rate constant by factors of five and one-fifth. Figure 4 shows the results of the sensitivity test. The variations of the τ values are dominant for the sensitivity tests for Reactions (1), (4), (5), (6), and (13). A similar tendency of the variations was obtained for the two 1/1/1 and 0.2/1/1 mixtures.

Reaction (1) was found to be an important initiation in the H_2–O_2 reaction; we[5] thus had derived the k_1 value by means of ARAS and computer modeling which included a sensitivity test. The k_1 value in Table 1 is, however, that re-evaluated from the revised τ, as obtained above for the H_2/O_2 mixture. In the present system of the $H_2/O_2/CO$ mixture, Reaction (1) has a smaller effect on the variation of the τ values. Reactions (4)—(6) are bi-molecular reactions which include one radical; they are representative reaction steps in the H_2/O_2 reaction system. The rate constants for those steps had been well established in studies of the H_2/O_2 system. Reaction (13) is a radical-producing step to initiate CO oxidation, as is emphasized in the introduction; it is the most influential reaction on the τ values

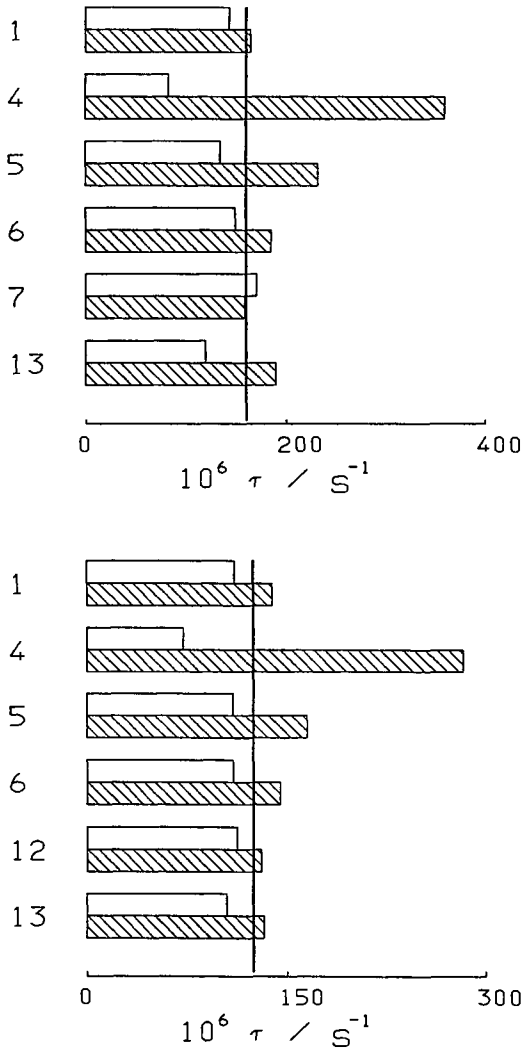

Fig. 4. Sensitivity calculation for τ.
Upper: for the result of Fig. 1 by H-atoms.
The numbers at the left hand side show the elementary reactions in Table 1. The above bar for each number shows the τ value obtained by computer modeling when each rate constant was multiplied by a factor of 5. The lower hatched bar was obtained by using the rate constant divided by the same factor. The elementary reactions giving small variations of τ are not shown in the figure. The vertical line through the bars shows the standard value of τ given by using the reaction parameters in Table 1.
Lower: for the 0.2/1/1 mixture at 1385 K by O-atoms. The numbers, the bars and the vertial line have the same meaning as those above.

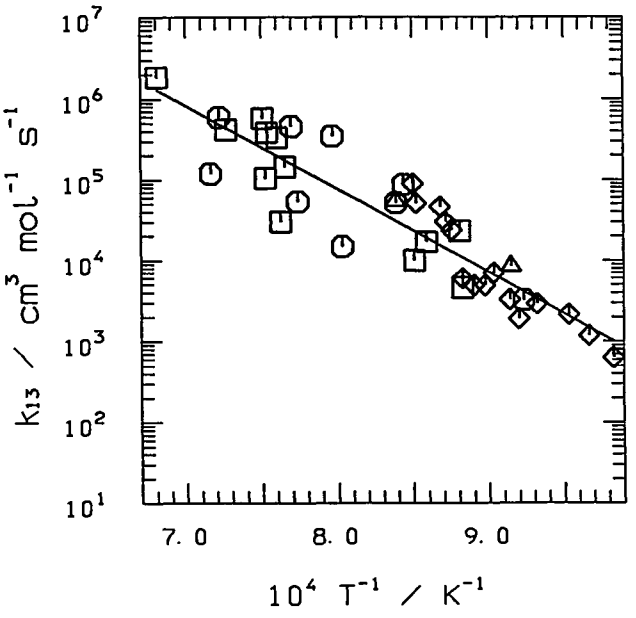

Fig. 5. Arrhenius plots of derived k_{13}.
Squares: for the 0.2/1/1 mixture at 121.6 nm,
Octagonals: for the 0.2/1/1 mixture at 130.5 nm,
Diamonds: for the 1/1/1 mixture at 121.6 nm,
Triangles: for the 1/1/1 mixture at 130.5 nm.
The line shows the least-squares fit for the data points.

among the CO participating reaction steps.

In the present study, we fit the τ values by computer modeling to the experimental τ values given in Figs. 2 and 3 by adjusting the k_{13} value. The k_{13} values, thus determined, are shown vs. $10^4/T$ in Fig. 5. We see no distinctive dependences of the k_{13} values on the test gas mixtures, as well as the species, H- or O-atoms, observed. The line shows the result of least-squares fitting for the k_{13} values and following Arrhenius expression could be derived:

$$k_{13} = 10^{13.1\pm0.6} \exp(-196.9\pm14.9 \text{ kJ}/RT) \text{ cm}^3 \text{ mol}^{-1} \text{ s}^{-1},$$

where the values with $\pm$ exhibit one standard deviation.

Computer modeling with the reaction mechanism given in Table 1 was also carried out for the absorption time profile given in Fig. 1. The absorptivity of H-atoms used in the computer modeling was 5×10^{10} $\text{cm}^2 \text{ mol}^{-1}$, which was determined in a study of the H_2O pyrolysis at temperatures above 2000 K (described later). The agreement of the absorption profile between the experiment and computer modeling is good for the early period of the reaction. At later stages, however, the absorption determined by modeling is larger than that found by experiment. These modeling results are due to the fact that the absorptivity of H-atoms becomes smaller at higher concentrations;[1,6] such effects were not taken into account in the computer modeling.

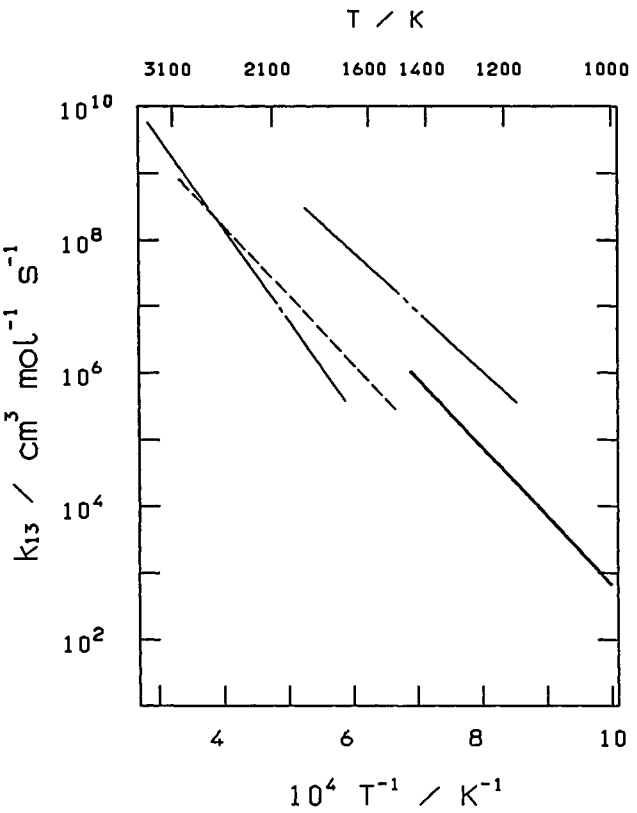

Fig. 6. Arrhenius expression of k_{13}.
Solid line: This work.
Chain line: by Thielen and Roth.[1]
Broken line: by Baulch et al.[3]
Chain-broken line: by Brabbs et al.[7]

Figure 6 shows an Arrhenius expressions for k_{13} from different sources by Thielen and Roth,[1] Baulch et al. (the same one by Warnatz)[3,4] and Brabbs et al.,[7] along with our value. Baulch et al.[3] took into account the expression by Gardiner et al.[2] in recommending their k_{13} value. Thus, the value given by Gardiner et al.[2] can be considered to be the data reviewed by Baulch et al.[3] and is not shown in the figure.

As shown in Fig. 6, most of these reported k_{13} values were obtained at higher temperatures than ours. The value by Brabbs et al.[7] was obtained in a temperature region close to the present study, but is larger than ours. Their value is also larger than the extrapolated values of Thielen and Roth[1] as well as Baulch et al.[3] by almost one order of magnitude. The discrepancies were so large that Gardiner et al.[2] examined the results by Brabbs et al.[7] by taking into account such view points as 1) the purities of the test gas mixtures used, 2) the difference of the vibrational relaxation times of CO depending on the compositions of the test gas mixtures used, and 3) a few uncertainties concerning the emission spectroscopy adopted.

Although Gardiner et al.[2] were not successful in explaining the larger value of k_{13} by Brabbs et al.,[7] their points[2] seem to cover most of the important criterions necessarily to consider the discrepancies.

Our k_{13} value determined in the present study is smaller than the value by Brabbs et al.,[7] but larger than the extrapolated values by Thielen and Roth[1] as well as Baulch et al.;[3] examinations of the present results through any appropriate criterions are thus required. We adopted Gardiner's view points for the examination. His view point concerned with the emission spectroscopy could be excluded in the present case. Gardiner's second view point is based on the vibrational relaxation of CO, which depends on the compositions of test gas mixtures; it could be ignored in the present case, since the present experimental conditions, including the composition of the test gas mixtures, are almost the same as those adopted by Gardiner et al.[2]

The first view point of the Gardiner et al.[2] concerns impurities of the test gas mixtures used; we examined our experiments in terms of this view point. The purities of H_2, O_2 and Ar used for the experiments were above 99.999%; we discarded them for the present from considerations of the impurities. Although the purity of CO was given as 99.6%, we mainly focused our attention on the impurity problem origining from the CO gas used.

A trial experiment for CO/Ar mixtures both with and without O_2 was carried out under the same experimental conditions as the present by using the ARAS. It was observed that only a small absorption, starting at the shock front and continuing with a constant value, appeared. Since no growing absorption was observed during the reaction period, the influence of the impuri-

ties, if any, on the progress of reaction is considered to be negligible within the present temperature range.

With regard to the influence of impurities,[3] a question always arises whether or not a trace amount of H_2O derived from the CO container might accelerate the reaction to be measured. We, therefore, studied the reactivity of H_2O both by computer modeling and experiment. Computer modeling was carried out according to the reaction mechanism given in Table 1 for a test gas mixture of $H_2/O_2/CO/H_2O=1/1/1/0.01$ in Ar. No acceleration of the reaction (estimated from the growth rates of O-atoms and H-atoms) with the presence of H_2O was observed to occur in the modeling. Furthermore, the experimental verifications were done for test gas mixtures of H_2O/Ar and H_2O/O_2/Ar. No absorption under the present experimental conditions was observed for the growth of O- and H-atoms, which could be produced directly or indirectly by the decomposition of H_2O. It has been confirmed that H_2O is very stable within the present temperature range. The influence of H_2O on the reaction progress is thus also negligible. Detailed reports on the reaction of H_2O measured using the present technique may appear elsewhere.

In conclusion, we could establish a reliable k_{13} in the lower temperature region, though we could not elucidate the discrepancies between the present k_{13} value and extrapolations of the reported k_{13} values[1,3,4] to the lower temperature region.

The present author wishes to thank Professor Kihei Morinaga, National Defense Academy, for providing him with many helpful suggestions.

References

1) K. Thielen and P. Roth, *Ber. Bunsen-Ges. Phys. Chem.*, **87**, 920 (1983).
2) W. C. Gardiner, Jr., M. McFarland, K. Morinaga, T. Takeyama, and B. F. Walker, *J. Phys. Chem.*, **75**, 1504 (1971).
3) D. L. Baulch, D. D. Drysdale, J. Duxbury, and S. Grant, "Evaluated Kinetic Data for High Temperature Reactions," Butterworths (1976), Vol. 3.
4) J. Warnatz, "Combustion Chemistry," ed by W. C. Gardiner, Jr., Springer-Verlag (1984).
5) T. Koike, *Bull. Chem. Soc. Jpn.*, **62**, 2480 (1989).
6) P. Frank and Th. Just, *Ber. Bunsen-Ges. Phys. Chem.*, **89**, 181 (1985).
7) T. A. Brabbs, F. E. Belles, and R. S. Browkaw, 13th Int. Symp. Combust., 1971, p. 129.

Mechanism of the Reaction of NH($^1\Delta$) with NO in Argon Matrix

Keiichi YOKOYAMA, Hiroshi KITAIKE, and Takayuki FUENO*
Department of Chemistry, Faculty of Engineering Science, Osaka University, Toyonaka, Osaka 560
(Received January 28, 1991)

Matrix-isolated hydrazoic acid HN_3 admixed with NO was photolyzed by a low-pressure mercury discharge lamp. Product analysis based on the FTIR spectroscopy has revealed the formations of NH, N_2O, OH, HNO, and HONO as photoproducts. From the comparisons of the amount of HN_3 consumed with that of N_2O produced, we conclude that the reaction of NH($^1\Delta$) with NO proceeds mainly through the process NH($^1\Delta$)+NO→N_2O+H. The quantum yield of N_2O is found to be $\phi_1=0.7\pm0.1$. The conclusion is in line with our previous results of the gas phase experiments at room temperature.

We have previously investigated the gas-phase reaction of NH($^1\Delta$) with NO both theoretically and experimentally.[1] The theoretical studies have shown that the reaction should proceed through an intermediacy of the HNNO adduct and that two channels are open for the unimolecular decomposition of the HNNO adduct:

$$NH(^1\Delta)+NO \longrightarrow [HNNO] \begin{cases} \longrightarrow N_2O+H & (1a) \\ \longrightarrow N_2+OH & (1b) \end{cases}$$

The entire reaction is expected to be essentially collision-controlled, and the HNNO decompositions as the product-determining step have energy barrier heights lower than the heat of the adduct formation, with a marginal advantage of reaction (1a) over reaction (1b). The expectation that the primary product of the reaction should be N_2O was borne out by the experimental determination of the quantum yield of N_2O being ca. 0.7, under the assumption that the quantum yield of NH($^1\Delta$) in the photodissociation is 1.0.

$$HN_3 \xrightarrow{h\nu} NH(^1\Delta)+N_2 \qquad \phi=1 \text{ at } 2537\,\text{Å} \qquad (2)$$

It is feared, however, that in the gas phase N_2O might well be formed by some routes other than the direct process (1a). Hack et al. carried out laser photolysis of HN_3 in the presence of NO in the gas phase at room temperature.[2] On the basis of the laser-induced fluorescence signal intensity of OH, they concluded that the primary product is OH($X^2\Pi$) to be formed by reaction (1b). They suggested the possibility that the formation of N_2O was rather a consequence of subsidiary reactions as follows:

$$NH(^1\Delta)+HN_3 \longrightarrow NH_2+N_3 \qquad (3)$$

$$N_3+NO \longrightarrow N_2O+N_2 \qquad (4)$$

In the present work, we have undertaken studies of the photo-induced reaction of HN_3 with NO in argon matrix. Our principal purpose here is to examine whether our previous gas-phase product determination study has indeed reflected the kinetics of reaction (1a). In a matrix there are not only isolated monomers but also dimers, polymers, and complexes with other molecular species, but generally there are little mobilities for isolated molecules except for the H atom. Thus, photoinduced reactions are thought to be completed within single cages of argon matrix. Contributions of subsidiary processes to the overall reaction could be examined more closely in this study.

Experimental

The cryogenic apparatus used in the matrix experiments is schematically shown in Fig. 1. A Cryomini D310 closed-cycle helium system (Iwatani Cryo-Techno Inc.) was used to refrigerate the deposition target made of CsI of 20 mm in diameter and 2 mm in thickness. An indium gasket was inserted between the CsI disk and the copper sample holder mounted on the cold head. Two Pylex nozzles of 0.5 mm in internal diameter were placed at a distance of 3 cm from the target in the direction orthogonal to each other to spray sample gases onto the target. Only one of these nozzles was used in the present experiments. A thermocouple of Chromel vs. Au–0.07% Fe was embedded on the sample holder. The ordinary operating temperature was measured to be 12 K. A liquid nitrogen trap and an oil diffusion pump were used to evacuate all of these devices placed within a stainless steel envelope.

IR spectra were measured through two KRS-5 windows located on both sides of the target on the envelope. In the direction perpendicular to the IR beam, there were two quartz

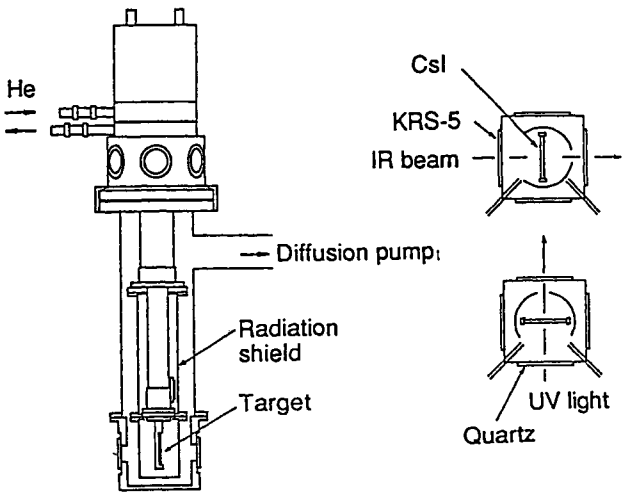

Fig. 1. Schematic drawing of the cryogenic apparatus. Top right, target alignment for IR measurement. Bottom right, that for deposition of the sample gases and UV photolyses.

windows for UV irradiation. The target was rotatable on a horizontal plane for IR measurement and UV irradiation. The UV light source used was a 22W low-pressure mercury discharge lamp (Ultra Violet Prod. Inc.) placed just in front of the quartz window of 2 mm in thickness without lens nor filter. This alignment provided homogeneous exposure of the target to the 2537 Å UV light. It is thought that another mercury line 1849 Å will little influence the measurements because of the absorption by the quartz window (not suprasil) at this wavelength. A Fourier-transform infrared spectrometer FT/IR-5000 (Japan Spectroscopic Co., Ltd.) was operated with a resolution of 4 cm^{-1} and the spectra were calculated from the coaddition of 100 interferograms. The deposition rates of sample gases were controlled with a teflon needle valve and a capacitance manometer CMLB-1000 (Vacuum General Inc.).

HN_3/NO/Ar(=0.1—1/0.08—1/100) gas mixtures were sprayed out through the nozzle at a rate of 2 mmol h^{-1} for ca. 3.5 h. After measurements of IR spectra for deposited samples, UV irradiation was started. Photolyzed matrix spectra were measured at the irradiation times of 0.5, 1, 2, 4, 6, 10, 20, 30, 60, and 120 min. A single measurement took about 4 min. The matrix temperature was monitored to be maintained at 12 K during irradiation. A relative intensity of the N_2O ν_3 (2224 cm^{-1}) to the HN_3 ν_2 (2138 cm^{-1}) band was evaluated on the basis of the matrix spectra of N_2O/HN_3/Ar of known compositions.

HN_3 was synthesized by the reaction of NaN_3 with excess stearic acid at 80—90 °C in a vacuum glass line. After the purification by means of trap-to-trap distillations at −80 °C, HN_3 gas was stored in a 6-l Pyrex bulb. NO (99.99%), Ar (99.9999%), and N_2O (99.999%) (Takachiho Kagaku Inc.) were used without further purification. Gas mixtures diluted in argon were kept in a 6-l Pyrex bulb overnight for mixing.

Results

(A) Assignment of Complexes. The HN_3/NO/Ar matrix spectra have exhibited, in the vicinity of the HN_3 ν_2 band (2138 cm^{-1}), a perturbed ν_2 band at 2150 cm^{-1} due to the hydrogen-bonded HN_3 dimer.[3] More highly aggregated molecules may also contribute to this peak since annealing experiments broadened the ν_2 band. By contrast, the ν_2 band was not resolved by possible complexation of HN_3 with NO, which might reflect a weaker hydrogen bonding between the two components.

A new peak was observed at 1882 cm^{-1} near the isolated NO stretching (1874 cm^{-1}). It is assigned essentially to the HN_3–NO complex on the basis of the following observations. First, this peak is observed in the HN_3/NO/Ar spectra but is absent in either of the HN_3/Ar and NO/Ar matrix spectra. Second, as can be seen in Fig. 2, the relative peak heights of the complexes vs. NO remain constant, irrespective of the molar fraction of NO in the sample gas used. It is possible, however, that the assigned peak is actually overlaped with that of the $(HN_3)_2$–NO complex, as will be considered later.

(B) Photoproducts. Figure 3 shows a difference spectrum of an HN_3/NO/Ar matrix after photolysis for 1 h. The irradiation diminishes HN_3 and the complexes and gives rise to $NH(X^3\Sigma^-)$, N_2O, OH, HNO, HONO, and NO_2. Little change was observed in absorbance of the peak due to the isolated NO monomer

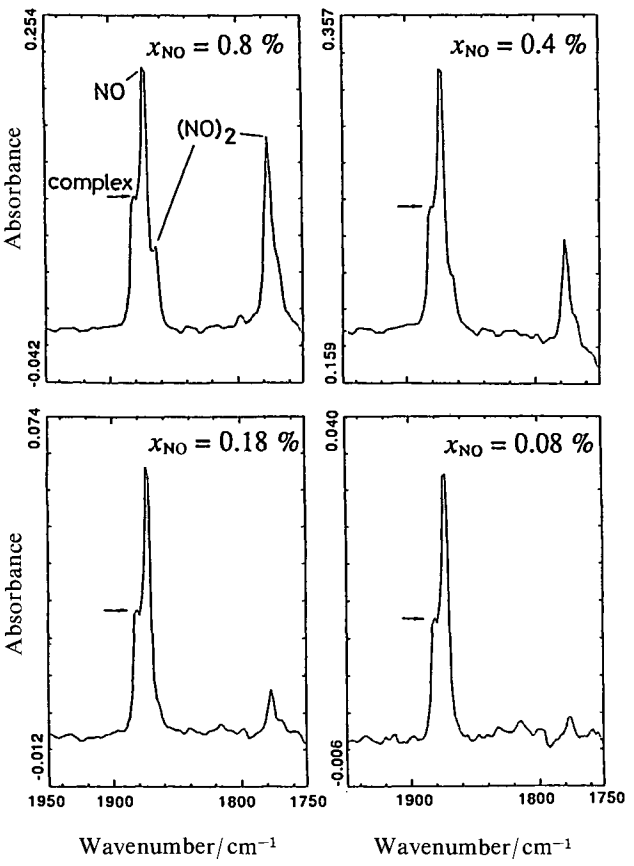

Fig. 2. Absorbance changes for the NO stretching bands of the NO monomer and dimer and for the complexes in the spectra of the HN_3/NO/Ar=1/0.08—0.8/100 matrices.

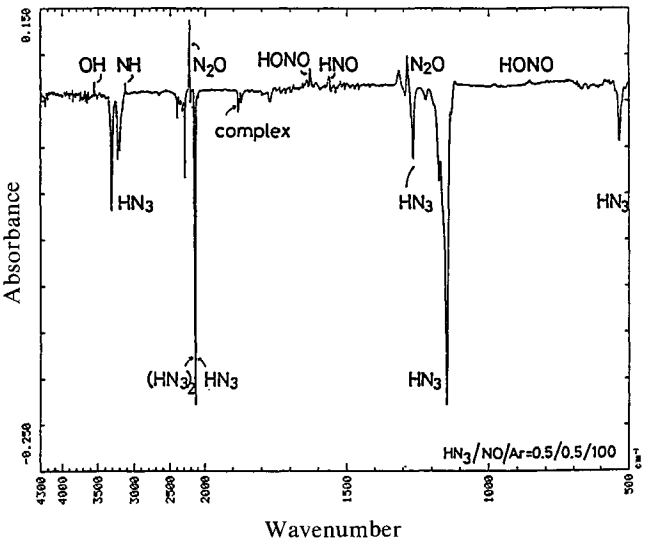

Fig. 3. FTIR difference spectrum of the HN_3/NO/Ar=0.5/0.5/100 matrix at 12 K after 1 h photolysis.

Table 1. Infrared Absorption Frequencies for the Products Formed in the Photolyses of the HN_3/NO/Ar Matrices

Frequency / cm^{-1}	Assignment	Lit. value / cm^{-1}	Ref.
3554	OH	3548.2	10
3136	NH	3133	12
2744			
2718	HNO	2717	13
2224	N_2O	2221	14
1758			
1686	*trans*-HONO	1690	15
1644			
1630	*cis*-HONO	1633	15
1609	NO_2	1610	15
1566	HNO	1563	13
1510			
1503			
1499[a)]	NH_2	1499	6
1317			
1286	N_2O	1284.9	14
1215			
856	*cis*-HONO	850	15
800	*trans*-HONO	800	15
719			
661			
588	N_2O	588	14

a) Observed in the photolysis of the HN_3/Ar matrix.

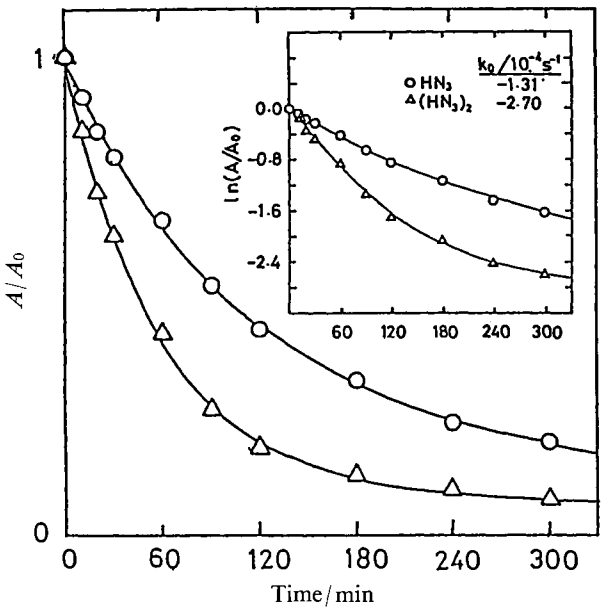

Fig. 4. Differernce between relative decay curves for the HN_3 monomer (2138 cm^{-1}) and dimer (2150 cm^{-1}) in the spectrum of HN_3/NO/Ar=0.5/0.5/100. Solid curve is obtained from biexponential fitting. Insert is log plots of the decays. Note that initial slope ratio is about 1 : 2 (monomer : dimer).

(1874 cm^{-1}). Assignments of the product peaks are listed in Table. 1, together with the literature values. In the vicinity of the NH_2 ν_2 band (1499 cm^{-1}), no significant peak was observed.

Evidently, N_2O is the primary product of the present matrix experiments also. As we believe, it has arisen from reaction (1a) directly, even though the mechanism proposed by Hack et al.,[2] i.e., the succession of reactions (3) and (4), cannot wholly be negated at this stage. Importantly, the concurrent formation of HNO lends strong support to our belief. Namely, the H atom which should have been formed together with N_2O by reaction (1a) could migrate in argon matrix cages to undergo recombination with NO:

$$NO + H + M \longrightarrow HNO + M \quad (5)$$

Reaction (1a) followed by reaction (5) seems to be the only route for the formation of HNO under our experimental conditions.

(C) Time Evolution. The HN_3 ν_2 band absorbances for monomer (2138 cm^{-1}) and dimer (2150 cm^{-1}) are plotted in Fig. 4 as the functions of irradiation time. Two curves have apparently different time constants. Log plots of these decay curves manifest that the dimer is photodecomposed nearly twice as rapidly as is the monomer; the initial slope ratio for dimer to monomer is about 2. The results indicate that the dimerization does not perturb the IR intensity of the ν_2 band nor the UV dissociation cross section of HN_3. In addition, it seems that highly aggregated HN_3 molecules, if any, hardly contribute to the absorption at 2150 cm^{-1}

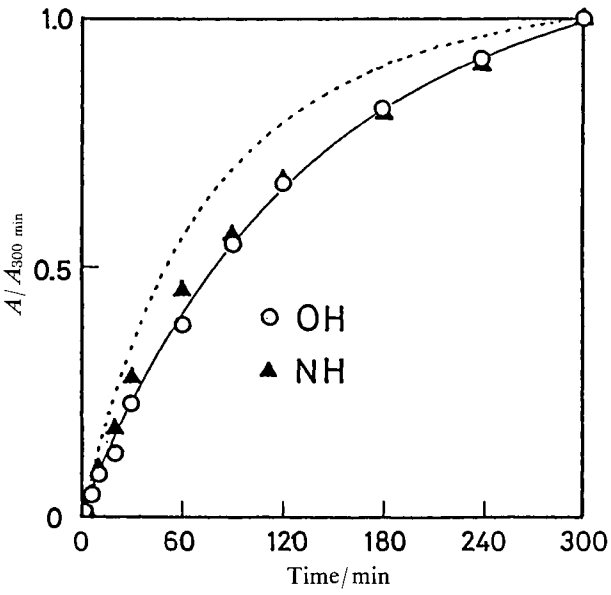

Fig. 5. Comparisons of the OH (3554 cm^{-1}) or the NH (3136 cm^{-1}) production profile with the HN_3 monomer and dimer decay profiles. The solid and dashed curves provide decrements in absorbance at the HN_3 (2138 cm^{-1}) and $(HN_3)_2$ (2150 cm^{-1}) ν_2 bands, respectively. HN_3/NO/Ar=1/1/100.

because they should be photodecomposed further more rapidly.

Figure 5 shows the increases in the OH (3554 cm^{-1}) and NH (3136 cm^{-1}) absorbances with the elapsing irradiation time. For the purpose of comparisons in

shape, measured absorbances have been arbitrarily normalized to a constant value at 300 min. Shown by the solid and dotted curves are the *decrements* in absorbance of HN_3 (2138 cm^{-1}) and $(HN_3)_2$ (2150 cm^{-1}), respectively, as the functions of time (Fig. 4). It can be seen that both the OH and NH increment curves fit the HN_3 monomer decrement curve. The results suggest that NH arises from the photolysis of the HN_3 monomer and that the precursor for OH is the 1 : 1 HN_3–NO complex.

The absorbance of N_2O ν_2 band (2224 cm^{-1}) was also found to increase with time but to be fitted with neither of the HN_3 and $(HN_3)_2$ decay curves. The time profile showed a somewhat faster saturation curve. This is presumably due to a photodecomposition process of N_2O itself.[4]

$$N_2O \xrightarrow{h\nu} N_2 + O(^1\Delta) \qquad \lambda < 2300\ \text{Å} \qquad (6)$$

Under such circumstances, we have decided to examine the initial rate of the formation of N_2O relative to that of the consumption of HN_3 monomer as the function of the molar fraction χ_{HN_3} of HN_3 present in the sample gas deposited. Note that the word "initial" used here means such an early time region that the secondary photodecomposition does not affect $[N_2O]$, normally less than 4 min.

Figure 6 shows the initial production rate of N_2O (2224 cm^{-1}), $d[N_2O]/dt$ (t=0), relative to the initial decay rate of HN_3 monomer (2138 cm^{-1}), i.e., $-d[HN_3]/dt$ (t=0), at the varying initial molar fraction χ_{HN_3}. It can be seen in Fig. 6 that the relative initial rate $-d[N_2O]/d[HN_3]$ (t=0), is constant at 0.52, irrespective of χ_{HN_3}. The results indicate that N_2O is produced from the HN_3 monomer complexes; i.e. HN_3–$(NO)_{1,2}$.

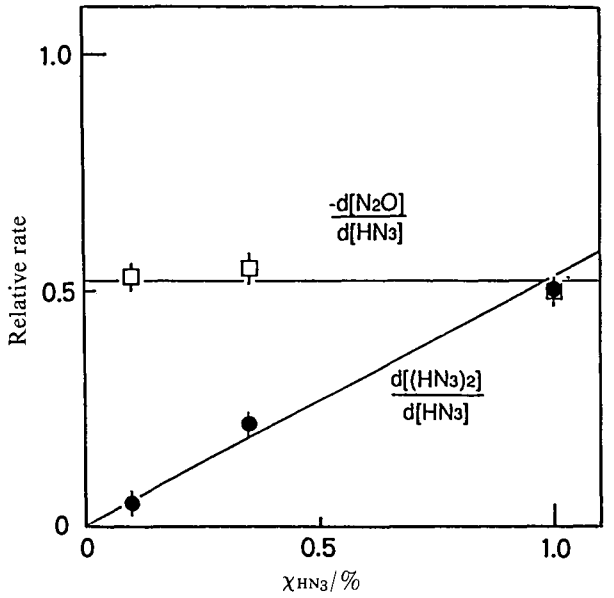

Fig. 6. Dependence of the production of N_2O on the fraction of HN_3. Dependence of the monomer: dimer ratio of HN_3 is also shown.

In addition, the initial rate of the consumption of $(HN_3)_2$ (2150 cm^{-1}) was measured relative to $-d[HN_3]/dt$ (t=0). The relative rate $d[(HN_3)_2]/d[HN_3]$ (t=0) was confirmed to be proportional to χ_{HN_3}. Therefore, if the photolysis of $(HN_3)_2$–$(NO)_{1,2}$ had given rise to N_2O, the plots of $-d[N_2O]/d[HN_3]$ against χ_{HN_3} would have shown a significant positive slope. Constancy of $-d[N_2O]/d[HN_3]$ indicates that the photolysis of the 2 : 1 or 2 : 2 complex $(HN_3)_2$–$(NO)_{1,2}$ has hardly contributed to the N_2O production. The results entirely negate the contribution of the succession of reactions (3) and (4) in the N_2O production under the present conditions.

(D) Yield of N_2O. We have evaluated the yield of N_2O formed by the photolysis of the 1 : 1 complex. In the measurements of the yield, there are two complexities. One is that N_2O may be formed by the photolysis of the 1 : 2 complex as well. The other is that the absorption at 1882 cm^{-1}, which was used to measure the amount of the 1 : 1 complex, may have overlaped with that of the 2 : 1 complex. Therefore, appropriate corrections are needed in evaluating the yield from the rates of the N_2O production and the complex consumption.

Let the yields of N_2O arising from the photolyses of the 1 : 1 and 1 : 2 complexes be denoted as ϕ_1 and ϕ_2, respectively. Since N_2O is assumed to be formed from both complexes, we may write

$$d[N_2O] = -\phi_1\, d[HN_3\text{–}NO] - \phi_2\, d[HN_3\text{–}(NO)_2]. \qquad (I)$$

The apparent overall yield of N_2O, defined as $\Phi \equiv -d[N_2O]/d[HN_3\text{–}NO]$ is then expressed as

$$\Phi = \phi_1 + \phi_2\, d[HN_3\text{–}(NO)_2]/d[HN_3\text{–}NO]. \qquad (II)$$

The second term $d[HN_3\text{–}(NO)_2]/d[HN_3\text{–}NO]$ is expected to be proportional to χ_{NO}, which will be confirmed later. Thus, plots of Φ vs. χ_{NO} should provide the ϕ_1 value as the intercept at $\chi_{NO} \to 0$.

In order to evaluate the Φ value, the initial rate of the consumption of the 1 : 1 complex is needed. The complex peak at 1882 cm^{-1} which is the only peak distinguishable at the present resolution contains both the 1 : 1 and 2 : 1 complexes:

$$-dC/dt = -d[HN_3\text{–}NO]/dt - d[(HN_3)_2\text{–}NO]/dt, \qquad (III)$$

where C is the amount of the complexes absorbing at 1882 cm^{-1}. Dividing both sides by $d[N_2O]/dt$, we can write

$$-dC/d[N_2O] = \Phi^{-1} - d[(HN_3)_2\text{–}NO]/d[N_2O], \qquad (IV)$$

where the second term $d[(HN_3)_2\text{–}NO]/d[N_2O]$ should be proportional to χ_{HN_3} in view of the results illustrated in Fig. 6. Hence, by plotting $-dC/d[N_2O]$ against χ_{HN_3}, we obtain the reciprocal Φ from the intercept.

In practice, the values of dC/dt have been evaluated from the absorbance changes at 1882 cm^{-1} in the initial 4 min period. The initial decreasing rates of C have been divided by the initial production rates of N_2O (2224 cm^{-1}). Plots of the quotients against χ_{HN_3} at a fixed χ_{NO} value of 1.0%, for instance, have indeed proved to

be linear, as is shown in Fig. 7. The intercept 0.48 leads to Φ=2.08 at χ_{NO}=1.0%.

The values of Φ at various χ_{NO} values have been measured in a similar way. Figure 8 shows the plots of Φ vs. χ_{NO}. As has been anticipated in the form of Eq. II, the plots are linear. The intercept gives ϕ_1=0.7± 0.1.

For the absorption peaks of HN_3, N_2O, and $(HN_3)_{1,2}$-NO, proportionalities between the concentrations and the absorbances have been assumed. Relative absorption coefficients are measured to be 1 : 1.15 : 0.225 for HN_3 (2136 cm^{-1}): N_2O (2224 cm^{-1}): $(HN_3)_{1,2}$-NO (1882 cm^{-1}). These values have been obtained from the IR spectra of the matrices made of the sample gases of known compositions. The absorption coefficient of the complex peak (1882 cm^{-1}) has been assumed to be equal to that of isolated NO monomer, because the IR absorption intensity of the N-O stretching would not be perturbed largely by the complexation.

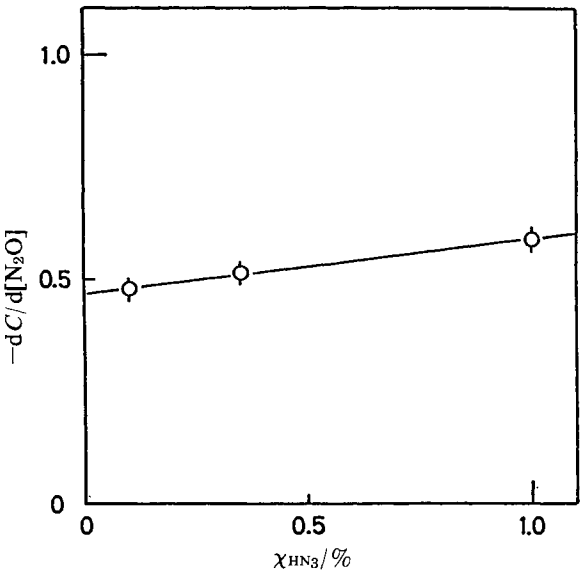

Fig. 7. χ_{HN_3} dependence of reciprocal yield, $-dC/d[N_2O]$, at a fixed χ_{NO} value of 1.0%. The intercept corresponds to the value of Φ^{-1}.

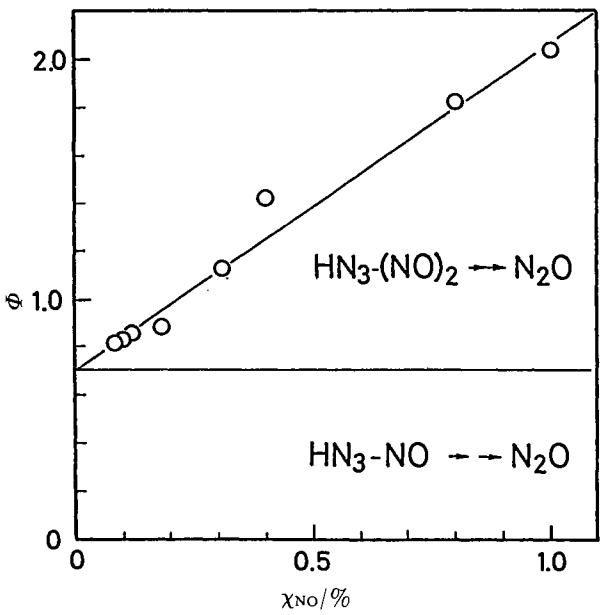

Fig. 8. [NO] dependence of the yield of N_2O from the photolysis of the 1 : 1 and 1 : 2 complexes HN_3-NO and HN_3-$(NO)_2$. The intercept corresponds to the absolute yield ϕ_1 of N_2O in reaction (1).

Discussion

Since NH($a^1\Delta$) formed by the photolysis of HN_3 is metastable, there may exist a physical quenching to NH($X^3\Sigma^-$):

$$NH(^1\Delta) + Ar \longrightarrow NH(^3\Sigma^-) + Ar. \quad (7)$$

Ramsthaler-Sommer et al. measured the lifetime of NH($a^1\Delta$) in argon matrix.[5] Their reported value of ca. 0.7 s at 12 K is long enough to allow the barrierless reaction (1) to complete without an influence of the quenching process (7).

The photoinduced reaction of the 1 : 1 complex can be regarded as reaction (1) in argon matrix cages. The value 0.7±0.1 obtained for ϕ_1 indicates that N_2O arises dominantly from reaction (1a) via the HNNO intermediacy. The result is perfectly compatible with the observation of HNO, whose production is a quite likely event as a fate of the H atom formed in reaction (1).

We have already noted the failure in detecting NH_2. For the purpose of more quantitative discussion, the infrared intensity of the NH_2 ν_2 band 1499 cm^{-1} is needed. Thus, we conducted separate photolysis experiments of NH_3/Ar and NH_3/CO in order to isolate the radical.

$$NH_3 \xrightarrow{h\nu} NH_2 + H. \quad (8)$$

A low-pressure mercury discharge lamp with suprasil window provides 1849 Å UV light which should efficiently photodecompose NH_3. In the case of NH_3/Ar, the NH_2 ν_2 band at 1499 cm^{-1} showed only a slight absorption after an irradiation over a period of five hours, probably because of the recombination between the dissociated NH_2 and the H atom. In the NH_3/CO photolysis, on the other hand, effective productions of NH_2, HCO, and $HCONH_2$ have been observed.[6] Assuming that the amount of NH_2 produced is equal to that of NH_3 consumed, we have estimated a lower limit of the relative intensity of the NH_2 ν_2 band to the N_2O ν_3 band to be $I_{NH_2}/I_{N_2O}>0.1$. Obviously, this value is underestimated owing to the production of a significant amount of $HCONH_2$. By appling this value to a spectrum for HN_3/NO/Ar, in which an absorbance ratio A_{NH_2}/A_{N_2O} is found to be less than 0.01, we estimate an upper limit of the production ratio $d[NH_2]/d[N_2O]$ to be less than 0.1. Therefore, only less than 10% of N_2O might be formed via the succession of reaction (3) and

(4), if any.

We have also been cautious of the possibility that N_2O may be formed directly from NO. Although isolated NO monomer cannot be decomposed by irradiation with a low-pressure mercury discharge lamp, the dimer is susceptible to the photodissociation:[7]

$$ONNO \xrightarrow{h\nu} N_2O + O \qquad \lambda < 2400\,\text{Å} \qquad (9)$$

However, in the present experiments, reaction (9) will not participate significantly, since the intense Hg resonance line at 1849 Å has been attenuated to a large extent through the window used in this study. In fact, the initial production rate $d[N_2O]/dt$ ($t=0$) in the photolysis of NO/Ar (1/100) was found to be less than 2% that in the photolysis of HN_3/NO/Ar (1/1/100). Thus, N_2O formed in the photolysis of HN_3/NO/Ar has no doubt originated nearly exclusively from the photodecomposition of HN_3.

Our original aim of the present work was to detect the HNNO intermediate. This was unsuccessful, however. It is supposed that the nascent vibrationally excited HNNO has an extremely short lifetime compared to a period of time required for stabilization by collisions with Ar. Thus, fragmentation will take place prior to stabilization. Also, the photodecomposition might be so fast that the amount of HNNO could not reach the detection limit.

We have assigned a peak at 3554 cm^{-1} to the OH radical in the spectrum of an HN_3/NO/Ar matrix photolyzed. The infrared absorption of OH in argon matrix has not been established yet. There are some discrepancies among the reported values.[8-10] Acquista et al.[8] and Suzar et al.[9] conducted the photolysis of H_2O at 1218 Å and decomposition of H_2O by means of electron impact in argon matrix, respectively. Both of them assigned two absorptions near 3452 and 3428 cm^{-1} to the OH vibration. On the other hand, Cheng et al.[10] found a new peak at 3548.2 cm^{-1}, which was concluded to be due to the OH radical prepared in solid argon by means of the reactions of atomic H with NO_2, O_3, and atomic O. The shift of 21.4 cm^{-1} from 3569.6 cm^{-1} as the gas-phase fundamental band is within the common range of matrix shifts.[11] They pointed out the possibility that the absorptions at 3452 and 3428 cm^{-1} previously assigned to OH may be due to the hydroxyl radical in complex with either H_2O or one Ar atom. Our observation 3554 cm^{-1} supports the conclusion by Cheng et al. The difference of 6 cm^{-1} between their wavenumber and ours may have been caused by an interaction of OH with N_2, which has been formed simultaneously with OH via reaction (1b). N_2 matrix experiments to isolate OH will be interesting.

The formation of HONO observed in a considerable amount probably stems from the 1:2 complex HN_3–$(NO)_2$. By virtue of weakness of the N–N bonding in $(NO)_2$, its photolysis will be apt to form the same intermediate HNNO as does reaction (1).

$$NH(^1\Delta) + ONNO \longrightarrow [HNNO]^* + NO \qquad (11)$$

If HNNO formed in this reaction has still enough excess energy, reaction (1b) will follow to give OH, which may in turn recombine with the other NO molecule to form HONO.

$$OH + NO + Ar \longrightarrow HONO + Ar \qquad (12)$$

Finally, in addition to the chemical channels (1a) and (1b), a quenching process must be considered.

$$NH(^1\Delta) + NO \longrightarrow NH(^3\Sigma^-) + NO \qquad (1c)$$

Hack et al. measured the rate constant of reaction (1c) in the gas phase, to claim that its branching ratio was as large as 0.4.[2] If so, the reaction of $NH(^1\Delta)$ with NO will inevitably be accompanied by the reaction of $NH(^3\Sigma^-)$ with NO under the present conditions as well. Since N_2O may arise from $NH(^3\Sigma^-)$ as well as $NH(^1\Delta)$, our value of ϕ_1 (=0.7) may not directly correspond to the branching ratio of the singlet reaction (1a) alone. This final point is still open to inquiry. Nevertheless, the conclusion that reaction (1a) is the most dominant channel of the reacion between $NH(^1\Delta)$ and NO will be basically correct.

Conclusions

Product analyses of the photochemical reactions in HN_3/NO/Ar matrices at 12 K were conducted to investigate the microscopic mechanism of the reaction of $NH(^1\Delta)$ with NO. NH, N_2O, OH, HONO, and HNO were identified by the IR spectra. The absolute yield of N_2O from the phtolysis of the 1:1 complex HN_3–NO was found to be $\phi_1=0.7\pm0.1$. Also, a considerable amount of N_2O was confirmed to arise from the 1:2 complex HN_3–$(NO)_2$. The photolysis of the 2:1 or 2:2 complex $(HN_3)_2$–$(NO)_{1,2}$ was found not to contribute to the production of N_2O, indicating that $NH(^1\Delta)$ fragmented from one of two HN_3 would react with the other HN_3 preferentially.

This work was supported by the Grant-in-Aid No. 62303002 from the Ministry of Education, Science and Culture.

References

1) T. Fueno, M. Fukuda, and K. Yokoyama, *Chem. Phys.*, **124**, 265 (1988).

2) W. Hack and K. Rathmann, private communication.

3) G. C. Pimentel, S. W. Charles, and K. Rosengren, *J. Chem. Phys.*, **44**, 3029 (1966).

4) G. P. Kevopoulos and R. J. Cvetanovic, *J. Am. Chem. Soc.*, **91**, 7572 (1969).

5) A. Ramsthaler-Sommer, K. E. Eberhardt, and U. Schurath, *J. Chem. Phys.*, **85**, 3760 (1986).

6) D. E. Milligan and M. E. Jacox, *J. Chem. Phys.*, **43**, 4487 (1965).

7) J. R. Sodeau and R. Withnall, *J. Phys. Chem.*, **89**, 4484 (1985).

8) N. Acquista, L. J. Schoen, and D. R. Lide, Jr., *J. Chem.*

Phys., **48**, 1534 (1968).
9) S. Suzer and L. Andrews, *J. Chem. Phys.*, **88**, 916 (1987).
10) B. M. Cheng, Y. P. Lee, and J. F. Ogilvie, *Chem. Phys. Lett.*, **151**, 109 (1988).
11) M. E. Jacox, *J. Mol. Spectrosc.*, **113**, 286 (1985).
12) D. E. Milligan and M. E. Jacox, *J. Chem. Phys.*, **41**, 2838 (1964).
13) M. E. Jacox and D. E. Milligan, *J. Mol. Spectrosc.*, **48**, 536 (1973).
14) L. Andrews and G. L. Johnson, *J. Chem. Phys.*, **76**, 2875 (1982).
15) W. A. Guillory and C. E. Hunter, *J. Chem. Phys.*, **54**, 598 (1971).

Formations of OH($X^2\Pi$, $A^2\Sigma^+$) in the Reaction of NH($^3\Sigma^-$) with NO in Incident Shock Waves

Keiichi YOKOYAMA, Yasuo SAKANE, and Takayuki FUENO*
Department of Chemistry, Faculty of Engineering Science, Osaka University, Toyonaka, Osaka 560
(Received January 28, 1991)

Gaseous mixtures of HNCO and NO diluted in Ar were heated by incident shock waves to about 3500 K to investigate the bimolecular reaction of NH($^3\Sigma^-$) with NO. Ultraviolet emissions from the excited NH($A^3\Pi$) and OH($A^2\Sigma^+$) were monitored to determine the rate constants for the ground-state reaction NH($^3\Sigma^-$) $+NO\rightarrow N_2+OH(X^2\Pi)$. The branching ratio defined as the rate constant for the formation of OH relative to that for the NH($^3\Sigma^-$) decay was found to be 0.32±0.07 at the shock-wave temperature adopted. An intense spike of chemiluminescence due to $OH(A^2\Sigma^+\rightarrow X^2\Pi)$ was observed, a finding which indicates a possible participation of the channel $NH(^3\Sigma^-)+NO\rightarrow N_2+OH(A^2\Sigma^+)$ at high temperatures.

We have previously studied the reaction of NH($^1\Delta$) with NO in the gas phase at room temperature.[1] The results have been in essence (1) that the reaction should proceed through an intermediacy of an adduct radical HNNO and (2) that the subsequent decomposition of HNNO gives rise to N_2O+H in prevalence over the channel leading to N_2+OH. Ab initio configuration-interaction (CI) calculations of the potential energy profiles[1] rationalized the experimental results.

Gas-phase reaction of NH($^3\Sigma^-$) with NO is intriguing in connection with the above-mentioned chemistry of NH($^1\Delta$) on one hand and with the issue of the process control for fuel combustions on the other. The reaction has already received interest by several groups of workers,[2–7] who unanimously claim that NH($^3\Sigma^-$) decays essentially at the collision-controlled rate, the rate constant being on the order of 10^{13} cm^3 mol^{-1} s^{-1}. However, product identification as the most important phase of chemical kinetics has remained unsettled.

In the present study, we intend to elucidate the kinetic feature of the NH($^3\Sigma^-$)–NO system, paying due attention to the time-dependent behavior of products. For this purpose, we have shock-heated the HNCO/NO/Ar mixtures of varying composition to ca. 3500 K, to let the NH($^3\Sigma^-$) entity generated by the thermal decomposition[8]

$$HNCO + Ar \longrightarrow NH(^3\Sigma^-) + CO + Ar \qquad (1)$$

react with the coexisting NO. In analogy to the case of NH($^1\Delta$), the reaction is expected to proceed in the following manner:

$$NH(^3\Sigma^-) + NO \longrightarrow [HNNO]^* \begin{cases} \longrightarrow N_2O + H & (2a) \\ \longrightarrow N_2 + OH & (2b) \end{cases}$$

Unfortunately, however, N_2O if formed by reaction (2a) is liable to be readily decomposed into N_2+O under the experimental conditions adopted. Thus, monitoring the OH radical to be formed by reaction (2b) will be a central issue of this study.

Experimental

The conventional incident shock tube described in a previous study[8] was used. Only the optical arrangement was altered. Time-resolved emission spectra were observed in the spectral region of 337.0±3.0 nm for NH($A^3\Pi$–$X^3\Sigma^-$) and 309.1±3.0 nm for OH($A^2\Sigma^+$–$X^2\Pi$). A Nikon-P250 grating monochromator with 1200 lines/mm and F=4.5 and a Hamamatsu 1P28 photomultiplier were used without lens or concave mirror. Time resolution arising from the observation volume was about 2 μs. The signals were amplified with an electronic rise time 2.2RC less than 1 μs and stored in a digital storage scope (Kawasaki Electronica KDS-103). Sample gases were shock-heated to about 3500 K in the pressure range of 210—870 Torr (1 Torr=133.322 Pa). The compositions HNCO/NO/Ar of the samples used were 0.021/0.595/99.4 for the NH measurements and 0.048/1.10/98.9 and 0.053/0.616/99.3 for the OH measurements. The OH emission sensitivity was calibrated on the basis of the H_2/O_2/Ar experiments under the same conditions.

HNCO was synthesized by the reaction of potassium cyanate KCNO with excess stearic acid at 90—110 °C in a vacuum glass line. After removal of water using P_2O_5 and purification by means of trap-to-trap distillations at −80 °C, HNCO was stored at −196 °C and vaporized prior to use. NO (99.99%), H_2 (99.999%), O_2 (99.8%), N_2O (99.9%) (Takachiho Kagaku Inc.), and Ar (99.999%) (Seitetsu Kagaku Inc.) were used without further purification. Gas mixtures diluted in argon were stored in a 6-l Pyrex bulb for more than one day.

Results

(A) Decay of NH. The NH emission-time profiles recorded have exhibited a rapid rise within 10 to 20 μs after the arrival of shock and subsequent decay during 40 to 100 μs. From these decay curves we have evaluated the rate constants k_2 of the overall reaction (2), assuming a pseudo first-order decay law in excess of NO. The rate constant was determined to be k_2=(7.1±0.5)×10^{12} cm^3 mol^{-1} s^{-1} at ca. 3500K.

Figure 1 shows the Arrhenius plots of the reported experimental k_2 values at various temperatures including the value obtained in the present study. A negative temperature dependence is evident. The plotted points are best fitted by the Arrhenius equation, $k_2=A\exp(-E_a/RT)$, with A=(7.8±0.6)×10^{12} cm^3 mol^{-1} s^{-1} and E_a=−(3.5±0.3) kJ mol^{-1}. The results indicate that the association step (HNNO formation) involving no

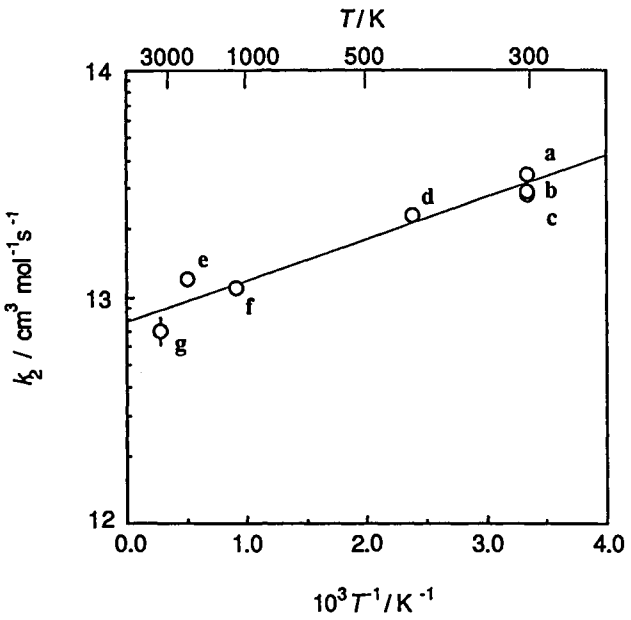

Fig. 1. Arrhenius plots of k_2. **a**, Harrison et al.[2]; **b**, Hansen et al.[3]; **c**, Cox et al.[5]; **d**, Gordon et al.[4]; **e**, Dean et al.[6]; **f**, Kondo[7]; **g**, the present work.

potential energy barrier should be rate-controlling.

(B) Formation of OH. In the OH emission-time profiles, an intense emission was observed during a period of initial 30 μs, as is shown in Fig. 2. We attribute this emission to the OH($A^2\Sigma^+ \rightarrow X^2\Pi$) chemiluminescence, as will be discussed later. After the intense spike, almost steady or slowly increasing emission profiles were observed. These latter emissions are due to OH($A^2\Sigma^+$) which is in thermal equilibration with OH($X^2\Pi$). Thus, the emission intensity of this steady part directly corresponds to the concentration of OH($X^2\Pi$).

In order to determine the rate constant k_{2b} and hence the branching ratio $\beta \equiv k_{2b}/k_2$, we have decided to recourse to the computer simulation technique. Thus, we intend to search for the value of k_{2b} that will best reproduce the time-concentration profiles of OH observed under the varying experimental condition. To this end, we have invoked several elementary reactions to be considered concurrently at high temperatures. The elementary steps chosen for the simulation are listed in Table 1, together with pertinent Arrhenius parameters. For reaction (1), we have chosen the most recent kinetic data obtained by Hanson et al.[9] For

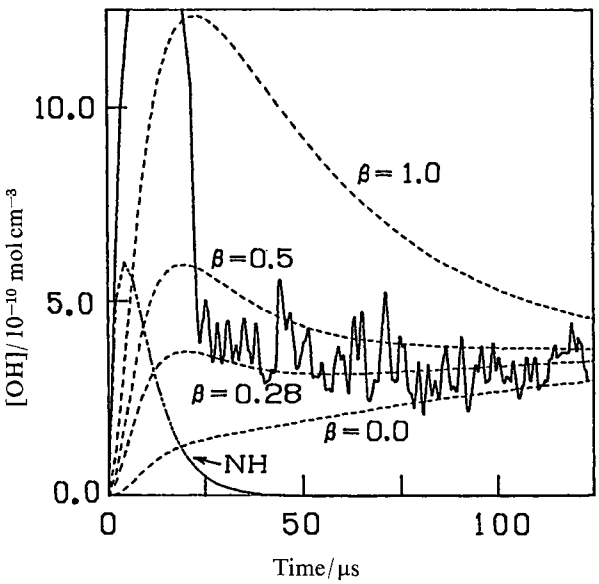

Fig. 2. Comparisons of the computed OH concentration profiles (------) with the observed (——). T_2= 3637 K, P_2=846 Torr, HNCO/NO/Ar=0.053/0.613/99.33.

Table 1. Elementary Reactions Used for the Simulations of the Time-Concentration Profiles of the OH Radical

No.	Reaction[a]	log A / cm^3 mol^{-1} s^{-1}	n	E_a / kJ mol^{-1}	Ref.
1	HNCO+Ar→NH+CO+Ar	35.51	−5.11	460	9
2a	NH+NO →N_2O+H	$(1-\beta)k_2$	0	0	This study
2b	→OH+N_2	βk_2	0	0	This study
3	NH+NH →N_2+2H	13.65	0	0	8
4	NH+Ar →N+H+Ar	14.42	0	316	8
5	H+HNCO→NH_2+CO	14.04	0	223	8
6	NH_2+Ar →NH+H+Ar	23.50	−2.0	382	9
7	NH+CO →CN+OH	13.00	0	0	10
8	OH+H →H_2+O	9.90	1	29	11
		10.26[b]	1[b]	37[b]	11
9	OH+O →O_2+H	13.40	0	0	11
		14.34[b]	0[b]	70.3[b]	11
10	OH+H_2 →H_2O+H	13.34	0	21.7	11
11	OH+Ar →O+H+Ar	18.90	−1	439	11
12	NO+H →OH+N	12.40	0.5	201	11
13	N_2O+Ar →N_2+O+Ar	14.70	0	243	11

a) The rate constant $k=AT^n \exp(-E_a/RT)$ cm^3 mol^{-1} s^{-1}. b) For the reverse processes.

reactions (2a) and (2b) of our present interest, we use the rate constants $(1-\beta)k_2$ and βk_2 respectively, where k_2 is the above-mentioned rate constant for the net decay of NH. Reactions 3 through 6 are those elementary processes which are known to be important in simulating the time-concentration profile of $NH(^3\Sigma^-)$ after its generation by reaction (1).[8] The remaining reactions are all those that are related somehow with the OH radical. Reaction (7) in particular is the key reaction which has turned up to be of importance in the high temperature region above 2300 K.[10] The rate constants for reactions (8) through (13) were all taken from the literature.[11]

An example of the curve-fittings by simulation is shown in Fig. 2. As can be seen in Fig. 2, the calculated OH concentration first tends to increase with the decaying NH concentration. The OH concentration observed in this sample run stays at a nearly constant level of 3×10^{-10} mol cm^{-3} over the time period of 25—125 μs. The curve simulated under the assumption that $\beta=1.0$ definitely overestimates the OH concentration. It appears that the best fit of the calculated curve to the observed is attainable when β is assigned a value of 0.28. Note that the OH concentration approaches the experimentally observed steady level even when reaction (2b) has been assumed to make no contribution at all, i.e., $\beta=0$. This is simply because of the situation that reactions (7) and (12) can make significant contributions in the prolonged time region considered.

Computer simulations as delineated above have been conducted for a total of 9 runs. Results for typical runs are summarized in Table 2, together with the relevant experimental data. The values of β appear to be nearly constant at 0.32 ± 0.07 on the average, the allowance limit attached being the probable error. Taking this branching ratio as granted, the branching ratio for reaction (2a) is estimated to be 0.68 ± 0.07 which is in good agreement with the ratio 0.7 deduced previously for the case of the reaction of $NH(^1\Delta)$ at room temperature.[1]

Discussion

(A) Branching Ratio. The branching ratio depends on the excess energy and temperature. We have calculated the branching ratios at 300 K and 3500 K on the basis of the RRKM theory. Since the reactions to be taken into account are only (2a) and (2b), calculations of only the ratio k_{2a}/k_{2b} suffice.

According to the basic RRKM theory, the ratio of the specific rate constants is given by

$$\frac{k_{2a}(E)}{k_{2b}(E)}=\frac{N_a(E-E_a)}{N_b(E-E_b)} \quad \text{(I)}$$

Here, $k_{2i}(E)$, i being a or b, is the rate constant at a specific energy E, which is measured from the potential energy minimum for HNNO; E_i is the barrier height for reaction (2i); and $N_i(E-E_i)$ is the number of available states for the respective transition states with an energy in excess over E_i. In order to obtain the ratio k_{2a}/k_{2b} Eq. I need be integrated over the energy distribution. We assume that chemically activated HNNO upon its formation by the association of NH with NO would undergo fragmentation before collisional stabilization affects the internal energy distribution. Thus, we may write approximately[12]

$$\frac{k_{2a}}{k_{2b}}=\int_{E_0}^{\infty}\left(\frac{N_a(E-E_a)}{N_b(E-E_b)}\right)F(E)\mathrm{d}E \quad \text{(II)}$$

where E_0 is the reactant potential energy level and where $F(E)$ is the energy distribution function:

$$F(E)=\frac{N(E-E_0)\exp(-E/kT)}{\int_{E_0}^{\infty}N(E-E_0)\exp(-E/kT)\mathrm{d}E} \quad \text{(III)}$$

with $N(E-E_0)$ as the number of available states for HNNO having energy in excess over E_0.

In calculating the ratio k_{2a}/k_{2b} by Eq. II, the energy humps, E_0, E_a and E_b were all taken from the results of our previous CI calculations (Fig. 3).[1] With the vibration zero-point energy corrections, they are 234, 180, and 197 kJ mol^{-1}, respectively. The values of N, N_a, and N_b were all evaluated by the Whitten-Rabinovitch approximation,[13] using the fundamental vibrational frequencies obtained from the ab initio SCF calculations. At 3500 K, k_{2a}/k_{2b} has come out to be 3.2. It follows that $\beta=0.24$, in reasonable agreement with the experimental value of 0.32. The small discrepancy between the calculated and observed values may be due to the uncertainty attached to the calculated potential energies of the transition states as well as the dynamically preferential formation of $OH(X^2\Pi)+N_2$, i.e. the non-statistical behavior of HNNO. Either way, it is confirmed that a sizable amount of OH can arise from reaction (2), although it may not innately be the main product.

Table 2. Run Conditions and the Branching Ratio β for the Reaction $NH(^3\Sigma^-)+NO\rightarrow N_2+OH$

No.	[Ar]	$[HNCO]_0$	$[NO]_0$	P_2	T_2	ρ_{21}	β
	10^{-6} mol cm^{-3}	10^{-9} mol cm^{-3}		Torr	K		
1	1.26	0.61	13.9	279	3539	3.69	0.29
2	1.12	0.59	6.9	233	3355	3.67	0.25
3	1.79	0.95	11.0	380	3404	3.68	0.29
4	1.80	0.95	11.1	359	3207	3.66	0.38
5	3.73	1.98	23.0	846	3637	3.70	0.28
6	4.05	2.15	25.0	871	3444	3.68	0.44

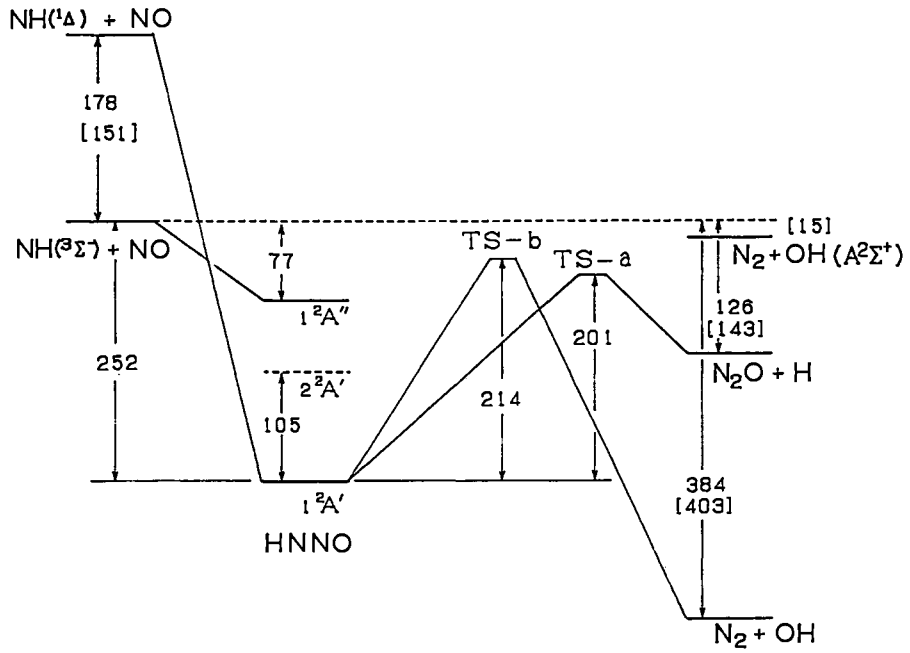

Fig. 3. Potential energy profiles calculated by the MRD-CI(4-31G**//4-31G**) procedure.[1] The energy gaps shown are in units of kJ mol^{-1}. The values given in brackets are those obtained from the relevant thermochemical data.[16] TS-a and TS-b denote the transition states located for the unimolecular steps of reactions (2a) and (2b), respectively.

Further, we have obtained β=0.31 and 0.19 for NH($^1\Delta$)+NO and NH($^3\Sigma^-$)+NO, respectively, both at 300 K. The former value is in good accord with our previous results of the N_2O quantum yield measurements [$\phi_{N_2O}\equiv 1-\beta=0.7$].[1]

Incidentally, the above discussions presume that the HNNO adduct to be formed from NH($^3\Sigma^-$)+NO be in its ground electronic atate (X^2A'), just as in the case of the NH($^1\Delta$)+NO system. The presumption will be acceptable in view of the possibility of an effective "conical" crossing between the two doublet surfaces of the interacting HN ··· NO system.

(B) OH Chemiluminescence. The initial spike in the OH emission profiles is attributed to the OH($A^2\Sigma^+ \rightarrow X^2\Pi$) chemiluminescence on the basis of the following observations. First, the emission was observed in the absorption experiments as well. That is, in order to monitor the OH concentration, we applied also the absorption technique using a He-H_2O microwave-discharge lamp as a light source of the OH absorption. Obtained profiles were of course quite different from the emission profiles, but the initial spike was still an intense emission in contrast to the pattern of the subsequent steady part due to absorption. Second, we confirmed that the peak height of the spike attained a maximum at the wavelength 308 nm, which was consistent with the OH(A-X) emission band. Third, when temperature was raised from 3500 K to 4100 K, the peak height did not increase correspondingly as did the subsequent steady part. Fourth, when $N_2O/H_2/Ar$ gas mixtures were shock-heated, a similar intense spike was observed. In this connection, when O_2 or H_2O, instead of NO, was added to the HNCO/Ar gas mixtures, no emission spike was observed.

A few words will be in order regarding the initial spike which was observed in the reaction system N_2O+H_2. The OH chemiluminescence will be possible in the manner as follows:

$$N_2O + Ar \longrightarrow N_2 + O + Ar \quad (13)$$

$$H_2 + O \longrightarrow OH + H \quad (14)$$

$$N_2O + H \longrightarrow [HNNO]^* \longrightarrow N_2 + OH(A^2\Sigma^+) \quad (15)$$

It should be noted that the initial step of reaction (15) is nothing but the reverse process of the unimolecular step of reaction (2a).

The formation of $OH(A^2\Sigma^+)$ is formally represented as

$$NH(^3\Sigma^-) + NO \longrightarrow [HNNO]^* \longrightarrow N_2 + OH(A^2\Sigma^+) \quad (2c)$$

The branching ratio of reaction (2c) has been estimated from the comparison of the chemiluminescence intensity with the thermal emission intensity. We assume that the relative intensity is equal to the rate of the $OH(A^2\Sigma^+)$ formation through reaction (2c) relative to that through the excitation of $OH(X^2\Pi)$ on collisions with Ar:

$$\frac{I_{chem}}{I_{therm}} = \frac{k_{2c}[NH(^3\Sigma^-)][NO]}{k_{ex}[OH(X^2\Pi)][Ar]} \quad (IV)$$

Here, k_{ex} denotes the rate constant for the collisional

excitation, which may be assumed to be to $k_{quench}K_{ex}$, where k_{quench} is the quenching rate constant[14] and where K_{ex} is the equilibrium constant between $OH(X^2\Pi)$ and $OH(A^2\Sigma^+)$. As a result, we have estimated $k_{2c} \leq 7 \times 10^{10}$ $cm^3\,mol^{-1}\,s^{-1}$. The branching ratio for reaction (2c) is thus less than 0.01. Considering that reaction (2c) is only slightly exothermic, the reaction is expected to have a significantly high barrier.

Hoffmann et al. have already reported on the same chemiluminescence arising from the reaction of N_2O with the H atom having a kinetic energy of ca. 2.5 eV under bulk conditions (single-collision and arrested-relaxation).[15] At lower H-atom kinetic energies (ca. 1.8 eV), however, there was no chemiluminescence. Since the N_2O+H system lies about 1.5 eV below the $NH(^3\Sigma^-)+NO$ system, the threshold energy for the production of $OH(A^2\Sigma^+)+N_2$ from $NH(^3\Sigma^-)+NO$ should lie 0.3 to 1.0 eV above the energy level for $NH(^3\Sigma^-)+NO$.

Previous ab initio MO calculations[1] have revealed that the ground state $HNNO(1^2A')$ surface is correlated to $OH(X^2\Pi)+N_2$ adiabatically. Therefore, it is most likely that for the first excited state $HNNO(2^2A')$ an adiabatic potential energy surface correlates to $OH(A^2\Sigma^+)+N_2$. The virtual excitation energy of the $HNNO(2^2A')$ at the equilibrium geometry of *cis*-$HNNO(1^2A')$ has been calculated by the MRD-CI method to be 105 $kJ\,mol^{-1}$, as is shown in Fig. 3. The excitation energy seems to be low enough for the internal conversion from $1^2A'$ to $2^2A'$ to take place thermally. For clear discussion of the dynamical mechanism of the formation of $OH(A^2\Sigma^+)$, MCSCF calculations on the excited state surface are required.

Conclusions

From the time-concentration profiles of the OH radicals formed in the shock-heated HNCO/NO/Ar mixtures, the branching ratio of the reaction, $NH(^3\Sigma^-)+NO \rightarrow N_2+OH(X^2\Pi)$, was determined to be 0.32 ± 0.07. The experimental result was rationalized by the RRKM treatments of the product-determining step. A new chemiluminescent reaction $NH(^3\Sigma^-)+NO \rightarrow OH(A^2\Sigma^+)+N_2$, was found, although it is a minor channel.

This work was supported by the Grant-in-Aid No. 61470007 from the Ministry of Education, Science and Culture.

References

1) T. Fueno, M. Fukuda, and K. Yokoyama, *Chem. Phys.*, **124**, 265 (1988).
2) J. A. Harrison, A. R. Whyte, and L. F. Phillips, *Chem. Phys. Lett.*, **129**, 346 (1985).
3) I. Hansen, K. Hoinghaus, C. Zetzsch, and F. Stuhl, *Chem. Phys. Lett.*, **42**, 370 (1976).
4) S. Gordon, W. Mulac, and P. Nangia, *J. Phys. Chem.*, **75**, 2087 (1971).
5) J. W. Cox, H. H. Nelson, and J. R. McDonald, *Chem. Phys.*, **96**, 175 (1985).
6) A. M. Dean, M. S. Chou, and D. Stern, *Int. J. Chem. Kinet.*, **16**, 633 (1984).
7) O. Kondo, Doctoral Dissertation, Osaka University (1982).
8) O. Kajimoto, O. Kondo, K. Okada, J. Fujikane, and T. Fueno, *Bull. Chem. Soc. Jpn.*, **58**, 3469 (1985).
9) J. D. Mertens, A. Y. Chang, R. K. Hanson, and C. T. Bowman, *Int. J. Chem. Kinet.*, **21**, 1049 (1989).
10) K. Yokoyama and T. Fueno, *Bull. Chem. Soc. Jpn.*, to be published.
11) F. Westley, "Table of Recommended Rate Constants for Chemical Reactions Occurring in Combustion," National Bureau of Standards, Washington, D. C. (1980).
12) W. N. Olmstead and J. I. Brauman, *J. Am. Chem. Soc.*, **99**, 4219 (1977).
13) G. Z. Whitten and B. S. Rabinovitch, *J. Chem. Phys.*, **38**, 2466 (1963).
14) K. H. Becker, D. Haaks, and Tatarczyk, *Chem. Phys. Lett.*, **25**, 564 (1974).
15) G. Hoffmann, D. Oh, and C. Wittig, *J. Chem. Soc., Faraday Trans. 2*, **85**, 1141 (1989).
16) M. W. Chase, Jr., C. A. Davies, J. R. Downey, Jr., D. J. Frurip, R. A. McDonald, and A. N. Syverud, "JANAF Thermochemical Tables," 3rd ed, National Bureau of Standards, Washington, D. C. (1985).

Structure and Polarized Spectra of *cis*-difluorotetraamminecobalt(III) Perchlorate, *cis*-$[CoF_2(NH_3)_4]ClO_4$

Yoshihiro MITSUTSUKA,* Tomonori AOYAMA,† Shigeru OHBA,† Yoshihiko SAITO,†
Fumiko KANEUCHI,†† and Masamichi TSUBOI†††
Department of Chemistry, Faculty of Science & Engineering, Meisei University, Hodokubo, Hino 191
†Department of Chemistry, Faculty of Science & Technology, Keio University,
3-14-1, Hiyoshi, Kohoku-ku, Yokohama 223
††Japan Spectroscopy Co., Ltd., Hachioji, Tokyo 192
†††Faculty of Science & Engineering, Iwaki-Meisei University, Iwaki, Fukushima 970
(Received September 10, 1990)

The structure of *cis*-$[CoF_2(NH_3)_4]ClO_4$ has been determined by a single-crystal X-ray diffraction method. Crystals are tetragonal, space group $P4_1$ (or $P4_3$), a=7.2645(6), c=16.260(2) Å, V=858.1(2) Å^3, Z=4, T=297(1) K, final R=0.052 for 970 observed unique reflections. The coordinated F and N atoms could be distinguished unambiguously from each other based on the thermal parameters. The bond distances Co–F and Co–N are 1.828(6)—1.870(5) and 1.924(7)—1.944(7) Å, respectively. The absorption spectra of the single crystals have been examined in the visible and infrared regions with polarized radiation by the use of microspectrophotometers. The 584 nm band (B_1) was considered to borrow intensity from some A_1 bands through vibronic coupling with some B_1 vibrations, and the 504 nm band (A_2 & B_2) through some A_2 and B_2 vibrations. Two of the four ammine groups of this cobalt complex were found to give an NH_3 rocking frequency (860 cm^{-1}) higher by 50 cm^{-1} than the other two (at 810 cm^{-1}). This fact has been attributed to two inter-molecular hydrogen bonds (NH···F=2.85—2.68 Å) in which the former two ammine groups are involved.

In structural chemistry, the idea of combining an optical microscope and spectrophotometer emerged a long time ago, and its actual practice started some forty years ago. An extensive use of this combination, however, has become possible only recently, after a number of technological developments were made regarding both microscopes and spectrophotometers. We are now attempting to adopt this combination as a tool for elucidating the detailed electronic structures of some complex molecules in their single crystals, whose sizes cannot readily be greater than 50 μm (order of magnitude). The present paper deals with one part of our work along this line.

cis-Difluorotetraamminecobalt(III) perchlorate, *cis*-$[CoF_2(NH_3)_4]ClO_4$, is one of the new complexes which have recently been prepared.[1] It gives violet needle crystals. The crystal structure has now been determined, as detailed below. It has been found that all of the complex molecules are oriented with their C_2-axes approximately along the crystalline elongation direction, which is now established to be its tetragonal c-axis. Therefore, this crystal is extremely favorable for spectroscopic analyses of the complex molecule presently in question. By the use of polarized radiation, well characterized bands are expected to be newly resolved, and their transition moment directions determined. Some results of such analyses are reported below.

Experimental

Sample Preparation. Single crystals of *cis*-$[CoF_2(NH_3)_4]ClO_4$ were obtained by evaporating the solvent from an aqueous mixture of *cis*-$[Co(NH_3)_4(H_2O)_2](ClO_4)_3$ and NH_4F, as detailed in a previous paper.[1]

Structure Determination. Crystal data are as follows: $[CoF_2(NH_3)_4]ClO_4$, Formula weight 264.5, tetragonal $P4_1$ (or $P4_3$), a=7.2645 (6), c=16.260 (2) Å, V=858.1 (2) Å^3, Z=4, D_m (CCl_4/CH_3I)=2.04 (1), D_x=2.05 Mg m^{-3}, λ (Mo $K\alpha$)=0.71073 Å, μ=2.33 mm^{-1}, $F(000)$=536, T=297 (1) K. Crystals are purple needles elongated along c. A crystal of dimensions 0.08×0.08×0.5 mm was mounted on a Rigaku AFC-5 four-circle diffractometer with graphite-monochromatized Mo $K\alpha$ radiation. The cell parameters were refined by least squares for 25 2θ values ($20<2\theta<30°$). The intensity measurements were performed using a 2θ=55° (h −9→9, k −9→9, l 0→21) by θ–2θ scan technique. Systematic absences were 0 0 l with $l\neq4n$. The variation of five standard reflections was $0.98<\Sigma(|F_o|/|F_o|_{initial})/5\leq1.00$. 4015 reflections were measured and 2482 reflections were observed with $|F_o|<3\sigma(|F_o|)$. The number of unique reflections was 970, with R_{int}=0.022 after an absorption correction ($0.81<A<0.85$). The Laue group and systematic absences showed that the space group is $P4_1$ (or $P4_3$). The positions of the Co and Cl atoms were deduced from the Patterson function. All of the six coordinating atoms around the Co could be located by Fourier synthesis and tentatively refined using the nitrogen scattering factor. The isotropic thermal parameters of two atoms became smaller (1.2 Å^2) than those of the other four atoms, which ranged from 2.3 to 5.2 Å^2. Thus, these two atoms were assigned to be more electron-rich atoms, F. Then, all of the nonhydrogen atoms were refined anisotropically. Five out of twelve H atoms were located by a difference synthesis; the others were calculated. The coordinates of the H atoms were fixed according to the isotopic thermal parameter, B=4 Å^2. The function $\Sigma w||F_o|-|F_c||^2$ was minimized with $w^{-1}=\sigma^2(|F_o|)+(0.015|F_o|)^2$ by a block-diagonal least-squares method. Final R=0.052, wR=0.053, S=2.04 for 970 unique reflections. The space group of the crystal specimen used for data collection appeared to be $P4_3$. The enantiomeric space group, $P4_1$, was rejected because of larger R factors, R=0.059, wR=0.064. The reflection/parameter ratio was 6.1 ($\Delta/\sigma<0.2$, $-0.8<\Delta\rho<1.2$ e Å^{-3}). Complex neutral-atom scattering factors were used.[2] The calculations were carried out on a FACOM M-380R computer at Keio university using the

UNICS-III computation program system.[3]

Visible Absorption Spectrum. The absorption spectra of a single crystal of the cis cobalt complex now in question were examined in the visible spectral region at two different orientations of the electric vector of the polarized radiation. The procedures for the microscopic spectral measurement and a curve-analysis method were both essentially the same as that described in a previous paper.[4]

Infrared Absorption Spectrum. A Jasco Micro FTIR-100 was used. A single crystal with the dimensions of 15×30 μm was placed under a microscope. Its transmittance spectra were recorded at two different polarizations of the radiation: one with $E//c$ and the other $E\perp c$, where E is the electric vector of the infrared radiation. For producing an infrared interferogram, 100 scans were accumulated with a resolution 4 cm^{-1} and with a cosine apodization function. A liquid-nitrogen-cooled mercury cadmium telluride detector was used.

Results and Discussion

Structure of $[CoF_2(NH_3)_4]ClO_4$. The final atomic parameters of non-hydrogen atoms and interatomic distances and bond angles are presented in Tables 1 and 2.[5] The Co atom is coordinated octahedrally by two F atoms and four NH_3 molecules, the former being in the cis positions. The average bond distance of the Co–F, 1.849 (6) Å, is 0.083 Å shorter than that of the Co–N, 1.932 (8) Å. This fact supports the distinction of F from NH_3 based on their thermal parameters in the refinement. The crystal structure is shown in Fig. 1. The bisector of the F–Co–F bond angle is approximately parallel to c. There exist intermolecular hydrogen bonds, N–H···F (or O), as shown in Table 3.

Group Theoretical Predictions. On the basis of the crystal structure just described, the number of optically active vibrations, in which the vibrations in all the

Table 1. Positional Parameters (×10⁴) and Equivalent Isotropic Temperature Factors

Atom	x	y	z	×10 B_{eq}/Å²
Co	2393(1)	2531(2)	0[a]	16
Cl	7448(3)	7402(3)	223(1)	29
F(1)	553(7)	2513(7)	−767(4)	38
F(2)	4216(7)	2516(7)	−812(3)	42
N(1)	532(10)	2575(11)	844(5)	33
N(2)	4296(9)	2555(9)	823(5)	31
N(3)	2383(9)	5205(9)	−47(5)	31
N(4)	2391(8)	−127(8)	−17(5)	24
O(1)	8798(13)	7491(14)	−441(7)	89
O(2)	7539(25)	5924(22)	693(12)	181
O(3)	7576(32)	9133(25)	511(13)	225
O(4)	5874(14)	7542(22)	−137(17)	233

a) This parameter was used to define the origin of the unit cell along z and is listed without e.s.d.

Table 2. Interatomic Distances (Å) and Angles (°)

Co–F(1)	1.828(6)	Co–N(4)	1.931(6)
Co–F(2)	1.870(5)	Cl–O(1)	1.460(11)
Co–N(1)	1.927(8)	Cl–O(2)	1.320(17)
Co–N(2)	1.924(7)	Cl–O(3)	1.345(19)
Co–N(3)	1.944(7)	Cl–O(4)	1.289(16)
F(1)–Co–F(2)	92.1(2)	N(1)–Co–N(4)	91.5(3)
F(1)–Co–N(1)	88.5(3)	N(2)–Co–N(3)	91.2(3)
F(1)–Co–N(2)	178.9(3)	N(2)–Co–N(4)	91.1(3)
F(1)–Co–N(3)	88.7(3)	N(3)–Co–N(4)	176.9(3)
F(1)–Co–N(4)	89.0(3)	O(1)–Cl–O(2)	115.5(9)
F(2)–Co–N(1)	179.2(3)	O(1)–Cl–O(3)	99.8(9)
F(2)–Co–N(2)	89.0(3)	O(1)–Cl–O(4)	104.9(8)
F(2)–Co–N(3)	88.9(3)	O(2)–Cl–O(3)	123.8(11)
F(2)–Co–N(4)	89.1(2)	O(2)–Cl–O(4)	111.8(10)
N(1)–Co–N(2)	90.5(3)	O(3)–Cl–O(4)	98.4(11)
N(1)–Co–N(3)	90.5(3)		

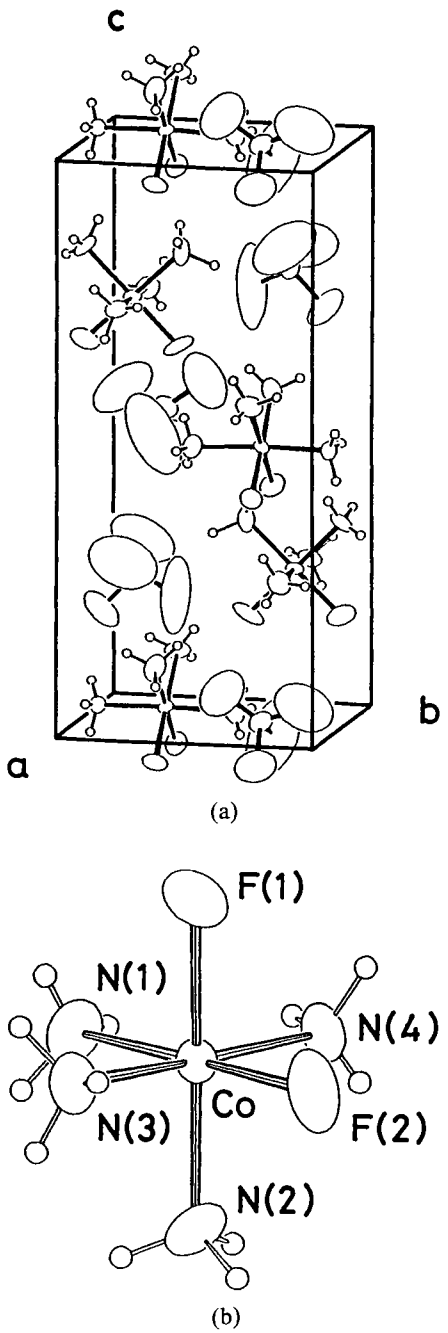

Fig. 1. (a) Crystal structure of *cis*-$[CoF_2(NH_3)_4]ClO_4$ and (b) molecular structure of the complex cation.

Bravais unit cells in the crystal take place in-phase, has been calculated for each type of vibration (Table 4). The $CoF_2(NH_3)_4^+$ ion has $3\times19-6=51$ intramolecular normal vibrations and the ClO_4^- ion has $3\times5-6=9$. Because four $CoF_2(NH_3)_4^+$ ions and four ClO_4^- ions are involved in the Bravais unit cell, $60\times4=240$ optically active intramolecular vibrations are expected for the crystal. Among them, 60 give their transition moments along the *c*-axis, 60 are infrared-inactive, and the remaining 120 are polarized along the perpendicular directions to the *c*-axis.

As long as the strict crystallographic symmetry is concerned, no further characterization is possible for these intramolecular vibrations. In a good approximation, however, every $CoF_2(NH_3)_4^+$ ion here has a pseudo-C_{2v} symmetry. As shown in Fig. 2, the C_2 symmetry axis is oriented along the crystallographic *c*-axis; We designate this the molecular *z*-axis. Two of the four Co–N bonds are in the plane which is formed by the two Co–F bonds; this plane is designated the molecular *xz*-plane, and the two NH_3 groups on the ends of these Co–N bonds are denoted by "NH_3-pair I." The two other Co–N bonds are both along the molecular *y*-axis, and are called "NH_3-pair II." The normal vibrations of the $CoF_2(NH_3)_4^+$ ion are now classified as given in Table 5.

The environment of the *d*-electrons of the Co atom is also considered to have nearly C_{2v} symmetry. The electron configuration of the ground state thus belongs to the A_1 species, and those corresponding to the T_{1g} species for the O_h symmetry turn out into three configu-

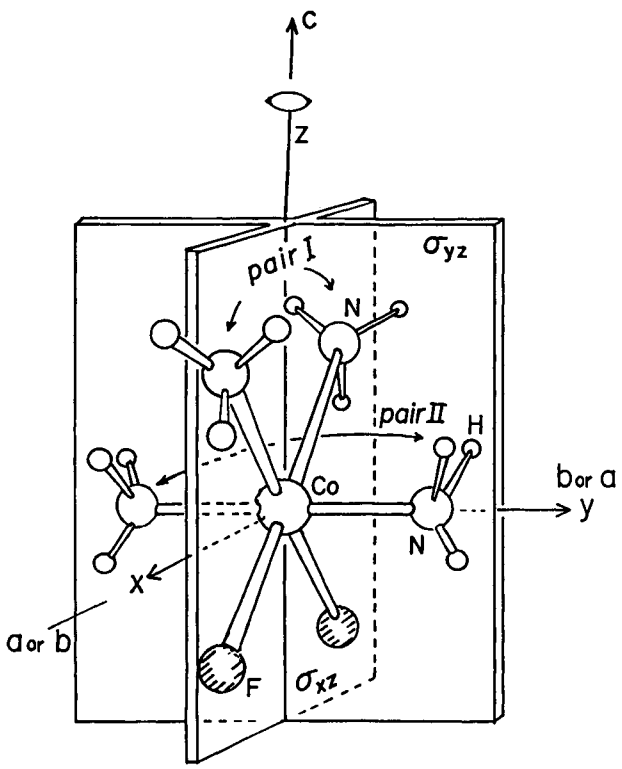

Fig. 2. An approximate symmetry (C_{2v}) of the $CoF_2(NH_3)_4$ ion in its crystal now in question. (*x*, *y*, *z*) are the molecular axes, (*abc*) are the crystallographic axes, and (*XYZ*) are the axes to express the molecular orbitals of the *d* electrons of the Co atom ($d_{X^2-Y^2}$, d_{YZ-ZX}, etc.) when its environment had the O_h symmetry.

Table 3. Intermolecular Hydrogen Bonds (Distances in Å)

A ··· H–B	(Symmetry code)[a]	A ··· B	A ··· H	H–B
F(1) ··· H(13)–N(1)	(i)	3.054(10)	2.424(5)	0.880(8)
F(1) ··· H(22)–N(2)	(i)	2.994(9)	2.276(5)	0.887(7)
F(1) ··· H(43)–N(4)	(i)	2.864(10)	2.358(6)	0.868(7)
F(2) ··· H(12)–N(1)	(ii)	3.065(9)	2.281(5)	0.877(8)
F(2) ··· H(23)–N(2)	(ii)	3.025(9)	2.211(5)	0.891(7)
F(2) ··· H(32)–N(3)	(ii)	2.854(9)	2.117(5)	0.886(8)
O(1) ··· H(33)–N(3)	(iii)	3.154(12)	2.347(10)	0.862(7)
O(4) ··· H(41)–N(4)	(iv)	3.051(14)	2.416(13)	0.689(6)

a) Symmetry code: (i) $-y, -x, -1/4+z$, (ii) $1-y, -x, -1/4+z$, (iii) $1+x, y, z$, (iv) $x, 1+y, z$.

Table 4. Number of In-Phase Normal Vibrations of Each Type in the *cis*-$[CoF_2(NH_3)_4]ClO_4$ Crystal

Space group					$P4_1$(or $P4_3$)	
Isomorphous point group					C_4(Factor group)	
Total number of molecules in the Bravais unit cell					8	
(Number of $CoF_2(NH_3)_4^+$ ions .....4) (Number of ClO_4^- ions .....4)						
Number of atoms in the Bravais unit cell					96	
	T	R	n	IR	Raman	
A	5	6	60	M_c	$\alpha_{a^2+b^2}$	α_{c^2}
B	6	6	60		$\alpha_{a^2-b^2}$	α_{ab}
E	10	12	120	M_a & M_b	α_{bc}	α_{ac}

T=Translational lattice vibrations. R=Rotatory lattice vibrations. n=Intramolecular vibrations.

Table 5. Number of Normal Vibrations of Each Type in the $CoF_2(NH_3)_4^+$ Ion

C_{2v}	IR	Raman	NH_3 sym. str.		NH_3 deg. str.		NH_3 sym. def.		NH_3 deg. def.		NH_3 rock.		NH_3 tors.		Co–N str.		Co–F str.	Skeletal def.	Total
			I	II	I	II	I	II	I	II	I	II	I	II	I	II			
A_1	M_z	α_{xx}, α_{yy}, α_{zz}	1	1	1	1	1	1	1	1	1	1			1	1	1	3	16
A_2		α_{xy}			1	1			1	1	1	1	1	1				2	10
B_1	M_x	α_{zx}	1		1	1	1		1	1	1	1	1		1		1	2	13
B_2	M_y	α_{yz}		1	1	1		1	1	1	1	1		1		1		2	12

sym.=symmetric, deg.=degenerate, str.=stretching, def.=deformation, rock.=rocking, tors.=torsional, I=$NH_3(1)$–$NH_3(2)$ pair, II=$NH_3(3)$–$NH_3(4)$ pair.

rations belonging to the B_1, A_2, and B_2 species. The electronic excited state T_{2g} in the O_h environment, however, splits into three states (A_1, B_2, and A_2) in the C_{2v} environment.

Visible Region Absorption Spectrum. The experimental results are shown in Fig. 3. As can be seen, two bands appear at about 20000 and 27000 cm^{-1}. The first band comprises two components. As was once pointed out by Yamatera,[6] two electronic transitions ($A_2 \leftarrow A_1$ and $B_2 \leftarrow A_1$) in the lower frequency region ($T_{1g} \leftarrow A_{1g}$ for O_h) are expected to have nearly equal frequencies, whereas $B_1 \leftarrow A_1$ should have an appreciably lower frequency than do the other two. Therefore, the lower-frequency component of the lower frequency group of bands is assignable to the $B_1 \leftarrow A_1$ transition ($d_{X^2-Y^2} \leftarrow d_{XY}$ for O_h, see Fig. 2 and its legend) and the other two to $A_2 \leftarrow A_1$ ($d_{X^2-Y^2} \leftarrow d_{YZ+ZX}$ for O_h) and $B_2 \leftarrow A_1$ ($d_{X^2-Y^2} \leftarrow d_{YZ-ZX}$ for O_h). The second group of bands ($T_{2g} \leftarrow A_{1g}$ for O_h) shows no explicit splitting, and is assigned to an overlapping of the following three transitions: $A_1 \leftarrow A_1$ ($d_{Z^2} \leftarrow d_{XY}$ for O_h), $B_2 \leftarrow A_1$ ($d_{Z^2} \leftarrow d_{YZ+ZX}$ for O_h), and $A_2 \leftarrow A_1$ ($d_{Z^2} \leftarrow d_{YZ-ZX}$ for O_h). (Note that the axis system XYZ for O_h is different from the system xyz for C_{2v}, see Fig. 2).

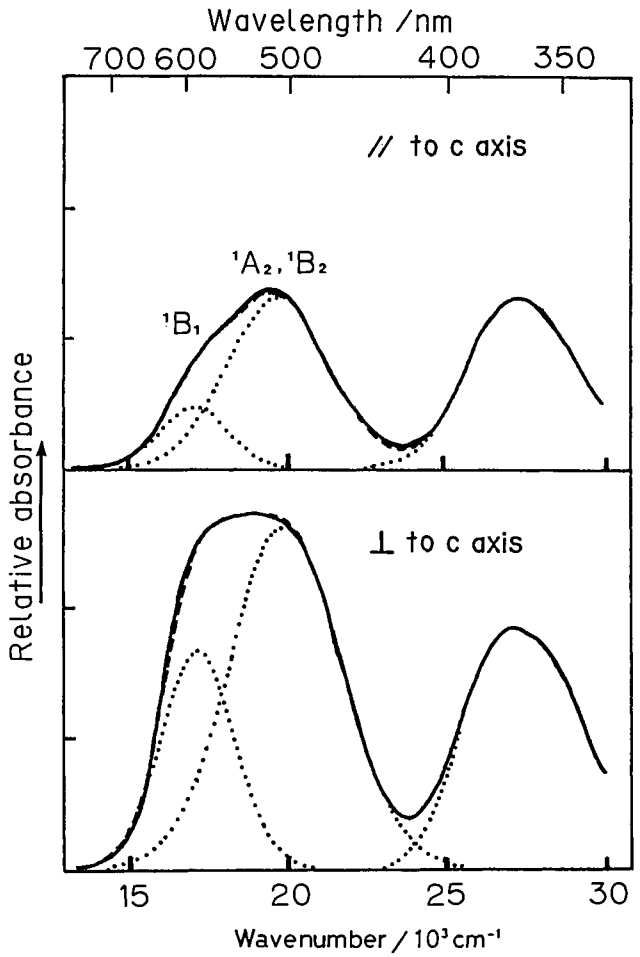

Fig. 3. Dichroic spectrum of a single crystal of *cis*-$[CoF_2(NH_3)_4]ClO_4$. Solid line, observed spectrum; dotted line, calculated Gaussian components; dashed line, sum of the Gaussian components.

We now examine the observed dichroism. Because all of the $CoF_2(NH_3)_4^+$ ions in the crystal are oriented with their C_2-axis along the crystallographic c-axis, only the A_1-type transition is expected to appear in the $E//c$ spectrum, as long as the selection rules of purely electronic transitions are taken into account. Actually, however, appreciable $E//c$ absorption intensities have been found (see Fig. 3) in the spectral regions assigned to the B_1 and A_2 & B_2 transitions. It is therefore quite certain that these intensities should be interpreted while taking vibronic coupling into consideration. The lowest-frequency (at 584 nm) electronic band, B_1, is considered to borrow some intensity from the A_1 band at 366 nm, or, more probably, from stronger A_1 bands somewhere in a higher frequency region through coupling with some of the B_1 vibrations. The higher-frequency components (at 504 nm) of the first band (A_2 and B_2) are considered to borrow some intensities from the A_1 bands through A_2 and B_2 vibrations. As can be seen in Fig. 3, the vibronic couplings are definitely greater for the latter (through A_2 and B_2 vibrations) than for the former (through B_1 vibrations). The number of B_1 normal vibrations is 13; this number is much smaller than the sum (22) of the numbers of the A_2 and B_2 normal vibrations (see the last column of Table 5). Therefore, one might assume that the number of the

vibrations active for intensity borrowing determines the transition intensity. To persue the consequence of this simple assumption, numbers were estimated for every electronic transition (Table 6). As can be seen in the last line of this table, the number of the possible cases of the vibronic couplings turns out to be nearly equal for the $//c$ component to that for the $\perp c$ component in every band now in question. It is therefore rather tempting to attribute the prominent perpendicular dichroisms actually observed for the 584 and 504 nm bands largely to their own electronic properties. It is probable, however, that the vibronic couplings do contribute not only to the $//c$ intensities, but also to the $\perp c$ intensities in these bands. It is also probable that, in every case, some of the possible vibrations and much greater contributions than do some of the other vibrations belonging to the same symmetry species; we must therefore study the nature of such vibronic couplings in more detail in the future.

Infrared Absorption Spectrum. The results of the measurements are given in Fig. 4. Six bands were observed at about 3250, 3180, 1620, 1265, 1090, and 850 cm^{-1}. On the basis of a previous study by Shimanouchi and Nakagawa[7] on $Co(NH_3)_6^{3+}$ and some other ammine complexes, these have been assigned, respectively, to NH_3 degenerate stretching, NH_3 symmetric stretching, NH_3 degenerate deformation, NH_3 symmetric deformation, ClO_4 T_2-type stretching, and NH_3 rocking vibrations (Table 7). Each band is found comprise approximately two components. Although each $CoF_2(NH_3)_4^+$ ion has four NH_3 groups, they are not equivalent to one another regarding the crystallographic symmetry. Practically, however, the two NH_3 groups of pair-I are similar to each other, and two of pair-II are similar (see Table 1 and 2). The two NH_3 groups of pair-I are equivalent if the molecular pseudo-C_{2v} symmetry is taken into account; likewise, the NH_3 groups of pair-II are equivalent. In addition, "inter-pair" vibrational interactions should be very small, based on their geometrical arrangements. For every NH_3 band, therefore, one of the two components is assigned to pair-I and the other to pair-II. These can be distinguished on the basis of the dichroic characters of the components.

An NH_3 symmetric deformation vibration, for example, has its transition moment (p) along the pseudo-C_3 axis. For each of the $NH_3(1)$ and $NH_3(2)$, the transition moment is directed at an angle of 45° to the c-axis. Therefore, the pair-I A_1 vibration causes an absorbance which is proportional to $(2p\cos 45°)^2=2p^2$. The B_1 absorbance should also be $(2p\cos 45°)^2=2p^2$, and no B_2

Table 6. Visible-Region Absorption Bands of *cis*-$[CoF_2(NH_3)_4]ClO_4$ Single Crystal

Frequency	17130 cm^{-1} (584 nm)	19840 cm^{-1} (504 nm)		27310 cm^{-1} (366 nm)		
Observed intensities[a] //|⊥	12/48	37/76		36/53		
Assignment	B_1	A_2	B_2	A_1	B_2	A_2
Intensities expected for purely electronic transitions[b] //|⊥	$0/b_1$	0/0	$0/b_2$	$a_1/0$	$0/b_2'$	0/0
Vibrations to reach A_1(//) Number	B_1 13	A_2 10	B_2 12	A_1 16	B_2 12	A_2 10
Vibrations to reach B_1(⊥) Number	A_1 16	B_2 12	A_2 10	B_1 13	A_2 10	B_2 12
Vibrations to reach B_2(⊥) Number	A_2 10	B_1 13	A_1 16	B_2 12	A_1 16	B_1 13
Average, ⊥	13	12.5	13	12.5	13	12.5
Relative numbers of possible cases of vibronic interaction //|⊥	13/13	22/25.5		38/38		

a) // refers to $E//c$, where E is the electric vector of the incident radiation, and ⊥ refers to $E\perp c$.
b) b_1=a proper intensity for the lowest electronic B_1 transition, b_2=a proper intensity for the lowest electronic B_2 transitions, b_2'=a proper intensity for the second lowest electronic B_2 transition.

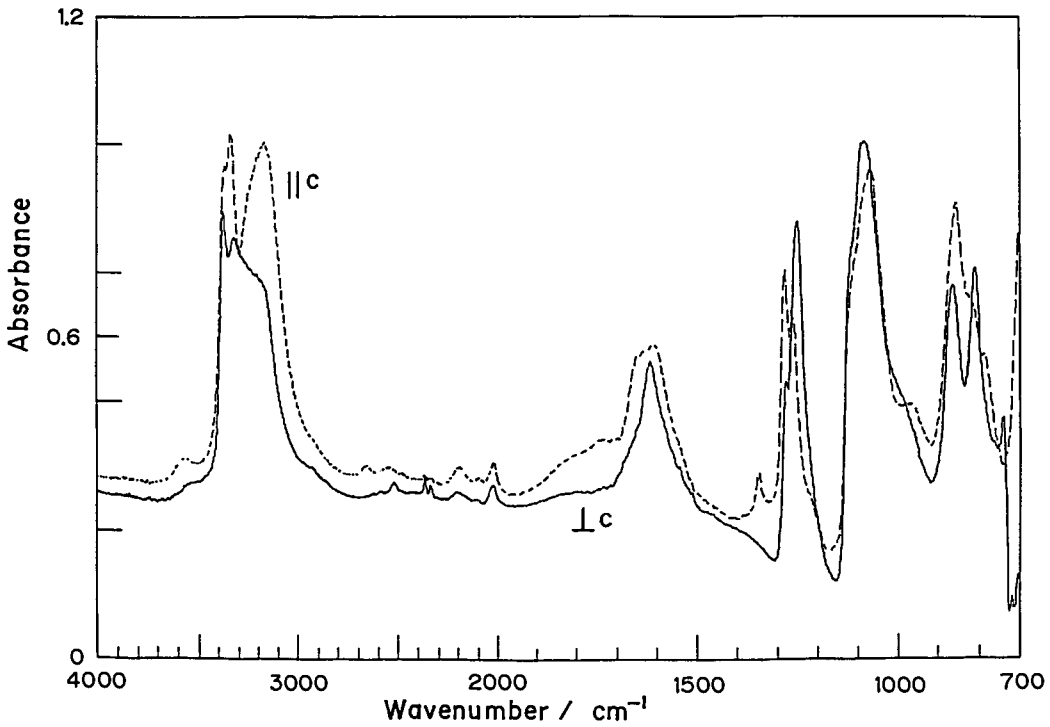

Fig. 4. Infrared dichroism spectrum of a single crystal of *cis*-$[CoF_2(NH_3)_4]ClO_4$. Solid line: the electric vector of the incident radiation is perpendicular to the *c*-axis. Dashed line: the electric vector is parallel to the *c*-axis.

Table 7. Infrared Absorption Bands and Their Dichroisms

Observed			Assignment[a]	Expected relative intensities
Frequency/cm	Dichroism			///⊥
3285	⊥	I	NH_3 deg. str.	2/3
3250	//	II		4/2
3180	//	I	NH_3 sym. str.	2/1
3170	⊥	II		0/2
1660	//	II	NH_3 deg. def.	4/2
1620	⊥	I		2/3
1280	//	I	NH_3 sym. def.	2/1
1250	⊥	II		0/2
1085	⊥		ClO_4 str. (T_2)	1/1
1070	//			
860	//	II	NH_3 rock.	4/2
810	⊥	I		2/3

a) str.=stretching, def.=deformation, rock.=rocking, sym.=symmetric, deg.=degenerate, I=NH_3-pair I (see Fig. 2), II=NH_3-pair II.

absorbance should result. From the average of the contributions of the four $CoF_2(NH_3)_4^+$ ions in the Bravais unit cell, the intensity ratio ///⊥ of the pair-I NH_3 symmetric deformation band should be $2p^2/1p^2=2/1$. For each of the $NH_3(3)$ and $NH_3(4)$, on the other hand, the transition moment (p) now in question is directed perpendicularly to the *c*-axis. The pair-II A_1 vibration, therefore, causes no absorbance, whereas the pair-II B_2 vibration causes absorbance that is proportional to $(2p)^2$. Thus, the ///⊥ intensities average out to $0/2p^2=0/2$. As can be seen in Fig. 4, the NH_3 symmetric deformation band comprises two components at 1280 and 1250 cm^{-1}. At 1280 cm^{-1} the dichroic ratio, ///⊥, is found to be nearly 2/1. whereas at 1250 cm^{-1} it is almost 0/2. Therefore, the 1280 cm^{-1} component is assignable to pair-I and the 1250 cm^{-1} component to pair-II.

An NH_3 degenerate deformation vibration is considered to have two transition moments, which are directed perpendicularly to each other in the plane normal to the NH_3 pseudo-C_3 axis. By taking this into account, a similar analysis has revealed that the pair-I NH_3 degenerate deformation vibration causes the relative intensities $///\perp=2p^2/3p^2$ and that of pair-II $///\perp=4p^2/2p^2$.

Thus, the observed peak at 1660 cm^{-1}, which shows a strong parallel dichroism, is assignable to the pair-II NH_3 degenerate deformation vibration, and that at 1620 cm^{-1} to the pair-I NH_3 degenerate deformation vibration.

In a similar manner, assignments of the components of every band have been made, as shown in Table 7. As can be seen, the greatest frequency difference between the components was for the NH_3 rocking band. Here, the pair-II frequency is higher than that of pair-I by 50 cm^{-1}. This is explained by taking intermolecular hydrogen bonds into account. As shown in Table 3, two strong hydrogen bonds (N···F=2.85—2.86 Å) are found at F(1)···H(43)–N(4) and F(2)···H(32)–N(3). Therefore, some of the effective ∠H–N–Co and ∠H–N–H angle bending force constants should be appreciably greater for the pair-II NH_3 groups than the corresponding ones for the pair-I NH_3 groups. As can be seen in Fig. 4 and Table 7, the pair-II NH_3 degenerate deformation frequency (1660 cm^{-1}) is also higher than that of pair-I (1620 cm^{-1}). This fact may also be explained by the two strong intermolecular hydrogen bonds. A hydrogen bond generally causes a lowering of the stretching force constant of the N–H bond in question. The fact that the pair-II NH_3 degenerate stretching frequency (3250 cm^{-1}) is lower than that (3285 cm^{-1}) of pair-I may be interpreted as indicating such an effect of the hydrogen bonds. The fact, however, that the pair-I NH_3 symmetric deformation frequency (1280 cm^{-1}) is higher than that of pair-II (1250 cm^{-1}) is yet to be explained.

We express appreciation to Dr. Masahiro Morita of the Science University of Tokyo for computer programming for the curve analysis. One (Y.M.) of us is indebted to Professor Tetsuroh yoshida in Meisei University for his helpful discussions. The work in Iwaki Meisei University was partly supported by a Grant-in-Aid No. 02670985, from the Ministry of Education, Science and Culture.

References

1) Y. Mitsutsuka, E. Tursun, and M. Nakahara, *Bull. Chem. Soc. Jpn.*, **63**, 260 (1990).

2) "International Tables for X-ray Crystallography," Kynoch Press Birmingham, (1974), Vol. IV. (Present distributor Kluwer Academic Publishers, Dordrecht.)

3) T. Sakurai and K. Kobayashi, *Rikagaku Kenkyusho Hokoku,* **55**, 69 (1979).

4) Y. Mitsutsuka, I. Kondo, and M. Nakahara, *Bull. Chem. Soc. Jpn.*, **59**, 2767 (1986).

5) Tables of the coordinates of hydrogen atoms, the anisotropic thermal parameters of the nonhydrogen atoms, and the observed and calculated structure factors are deposited as Document No. 9112 at the Office of the Editor of Bull. Chem. Soc. Jpn.

6) H. Yamatera, *Bull. Chem. Soc. Jpn.*, **31**, 95 (1958).

7) T. Shimanouchi and I. Nakagawa, *Inorg. Chem.*, **3**, 1805 (1964).

Synthesis of [6-(1,4,7,10-Tetraaza-12-cyclotridecyl)-1,4,8,11-tetraazacyclotetradecane]dinickel(II) Perchlorate and Its Electrocatalytic Property for Water Reduction

Katsura MOCHIZUKI,* Hajime GOTOH, Masaaki SUWABE, and Tohru SAKAKIBARA
Department of Chemistry, Yokohama City University, Yokohama 236
(Received January 23, 1991)

A new bimacrocyclic ligand, in which 13- and 14-membered rings are linked together by a C–C bond, 6-(1,4,7,10-tetraaza-12-cyclotridecyl)-1,4,8,11-tetraazacyclotetradecane (L^{13-14}), and its dinickel(II) complex, $[Ni^{II}_2L^{13-14}]^{4+}$, were synthesized. The absorption spectra and cyclic voltammograms of $[Ni^{II}_2L^{13-14}]^{4+}$ showed that it has properties of both the 13- and 14-membered rings. Cyclic voltammetry and controlled-potential electrolysis showed that $[Ni^{II}_2L^{13-14}]^{4+}$ can serve as an electrocatalyst for water reduction to produce H_2. The electrocatalytic efficiency for H_2 produclion at −1.5 V was found to be as follows: $[Ni^{II}_2L^{14-14}]^{4+}$ (L^{14-14}: 6,6′-bi(1,4,8,11-tetraazacyclotetradecane)) > $[Ni^{II}_2L^{13-14}]^{4+} \approx [Ni^{II}L^{14}]^{2+}$ (L^{14}: 1,4,8,11-tetraazacyclotetradecane) ≫ $[Ni^{II}_2L^{13-13}]^{4+}$ (L^{13-13}: 12,12′-bi(1,4,7,10-tetraazacyclotridecane)).

The production of hydrogen from water is extremely important, especially for the chemical storage of light or electrical energy. For this purpose, a highly efficient catalytic system generating H_2 (and O_2) from water should be developed. Although the problem of overvoltage must be solved, some Ni(II) complexes with monomacrocyclic ligands are known to have a capability like that of an electrocatalyst.[1] Recently, Sauvage et al. investigated the electrocatalytic properties of a binuclear Ni(II) complex with biscyclam, $[Ni^{II}_2L^{14-14}]^{4+}$, in which two cyclams, L^{14}, are linked together by a C–C bond; they found that the bimacrocyclic complex, $[Ni^{II}_2L^{14-14}]^{4+}$, is a better catalyst than is the corresponding monomacrocyclic, $[Ni^{II}L^{14}]^{2+}$.[2] These findings prompted us to systematically study the electrocatalytic capabilities of this type of bimacrocyclic complexes.

We attempted to clarify how the electrocatalytic property of $[Ni^{II}_2L^{14-14}]^{4+}$ changes upon replacing the 14-membered macrocycles of $[Ni^{II}_2L^{14-14}]^{4+}$ with 13-membered ones. Thus, the dinickel(II) complexes with a bimacrocyclic ligand having two 13-membered rings, L^{13-13}, and with one having 13- and 14-membered rings, L^{13-14}, were required. However, the synthesis of the latter "nonsymmetric" ligand, L^{13-14}, has been unprecedented, to the best of our knowledge.

In this paper we describe the preparation of "nonsymmetric" ligand, L^{13-14}, and its dinickel(II) complex, as well as the electrocatalytic efficiencies of dinickel(II) complexes with L^{13-13}, L^{13-14}, and L^{14-14} for H_2 generation from water.

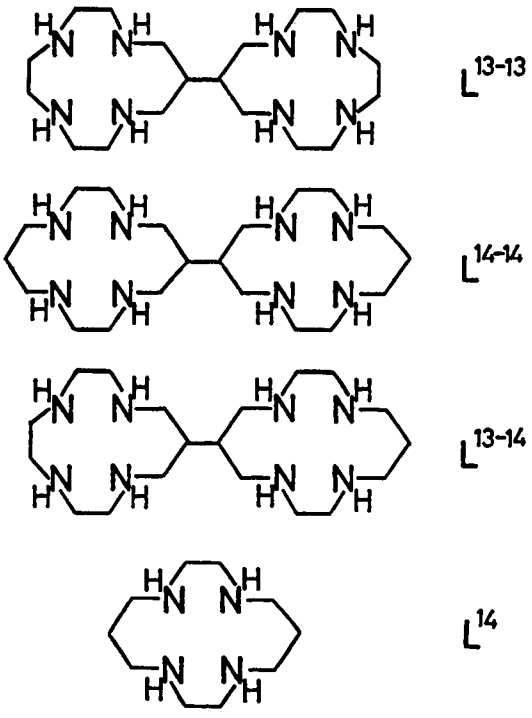

Results and Discussion

Synthesis of L^{13-14} and Its Dinickel(II) Complex. The synthetic route of the intending bimacrocyclic Ni(II) complex is shown in Scheme 1.

Statistic predominance was applied to the preparation of the bimacrocyclic ligand, L^{13-14}. Since the separation of L^{13-14} from the reaction mixture failed, its isolation was performed after conversion of the ligands into dinickel(II) complexes. This idea came from the following speculation based on experimental results.

It is known that in water both $[Ni^{II}L^{14}]^{2+}$ and $[Ni^{II}L^{13}]^{2+}$ (L^{13}: 1,5,8,11-tetraazacyclotridecane) are in equilibrium between square planar and octahedral forms; in the latter two water molecules coordinate to the Ni(II) ion; that the ratio of octahedral forms is slightly higher in $[Ni^{II}L^{14}]^{2+}$ (29%, 25 °C) than in $[Ni^{II}L^{13}]^{2+}$ (13%, 25 °C).[10] This means that the coordination of water to the 14-membered macrocyclic Ni(II) complex predominates slightly over that of the 13-membered one. If a similar relationship holds between the bimacrocyclic Ni(II) complexes and anionic ligands instead of water, $[Ni^{II}_2L^{14-14}]^{4+}$ favors octahedral form than does $[Ni^{II}_2L^{13-13}]^{4+}$. The cationic character of the

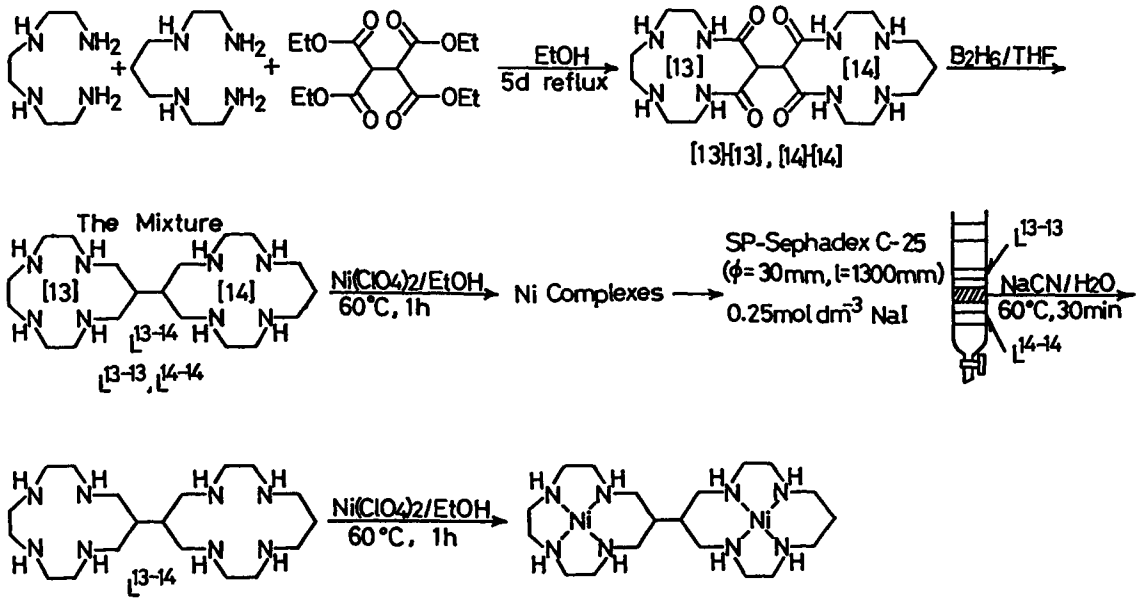

Scheme 1.

complex is thus least in $[Ni^{II}_2L^{14-14}]^{4+}$, and most in $[Ni^{II}_2L^{13-13}]^{4+}$. As a result, separation of the mixture by cation exchange chromatography may be possible.

Condensation between tetraethyl 1,1,2,2-ethanetetracarboxylate and a 1 : 1 mixture of 3,6-diazaoctane-1,8-diamine and 3,7-diazanonane-1,9-diamine, followed by reduction with B_2H_6, afforded a mixture of three ligands: L^{13-13}, L^{13-14}, and L^{14-14} (see Experimental). The gas chromatogram of the mixture showed three peaks: the first was assigned to L^{13-13} (28%) and the third to L^{14-14} (16%) respectively, compared with the respective authentic samples (Fig. 1). We assigned the second peak to L^{13-14} (50%). Indeed, a FAB mass spectrum of the mixture showed three peaks at m/z 371, 385, and 399, which corresponded to $[M+H]^+$ for L^{13-13}, L^{13-14}, and L^{14-14}, respectively.

Separation of these three ligands was accomplished, when the ligands were converted into the dinickel(II) complexes and then chromatographed with SP-Sephadex C-25 cation-exchange resin using 0.25 mol dm^{-3} NaI as the eluent. As expected, $[Ni^{II}_2L^{14-14}]^{4+}$ was eluted first, $[Ni^{II}_2L^{13-14}]^{4+}$ second, and $[Ni^{II}_2L^{13-13}]^{4+}$ last. This clear separation of the three bands indicates that the second band is not a mixture of $[Ni^{II}_2L^{14-14}]^{4+}$ and $[Ni^{II}_2L^{13-13}]^{4+}$, but $[Ni^{II}_2L^{13-14}]^{4+}$, itself; this view is supported by the FAB mass spectrum of the free ligand obtained by treatment of the Ni(II) complex with NaCN (m/z 385, $[M+H]^+$ for L^{13-14}). Since a complete exchange of iodide into the perchlorate ion was tedious, an analytical sample of $[Ni^{II}_2L^{13-14}](ClO_4)_4 \cdot H_2O$ was prepared by treatment of L^{13-14} with $Ni(ClO_4)_2 \cdot 6H_2O$.

The ligand, L^{13-14}, and the $[Ni^{II}_2L^{13-14}]^{4+}$ complex, thus isolated, were characterized as follows.

Although the ^{13}C NMR spectrum of L^{13-14} in $CDCl_3$ was very similar to the sum of the spectrum of L^{14-14} and

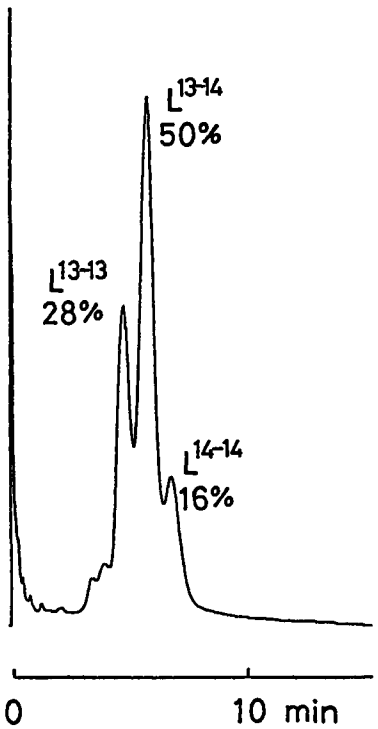

Fig. 1. Gas chromatogram of the mixture of ligands produced by reduction of the condensation product with tetramines (column: 1% OV-1, 0.25 m×2.6 mm; carrier gas: He; column temperature: 220 °C).

that of L^{13-13}, small differences in the chemical shifts around the C–C bridge were observed between, L^{13-14}, L^{13-13}, and L^{14-14}. The 100.614 MHz ^{13}C NMR spectrum of L^{13-14} in D_2O expectedly showed 11 signals (9 triplets and 2 doublets).

Figure 2 shows the absorption spectrum of $[Ni^{II}_2L^{13-14}]^{4+}$ in an aqueous solution; it is almost equal to the

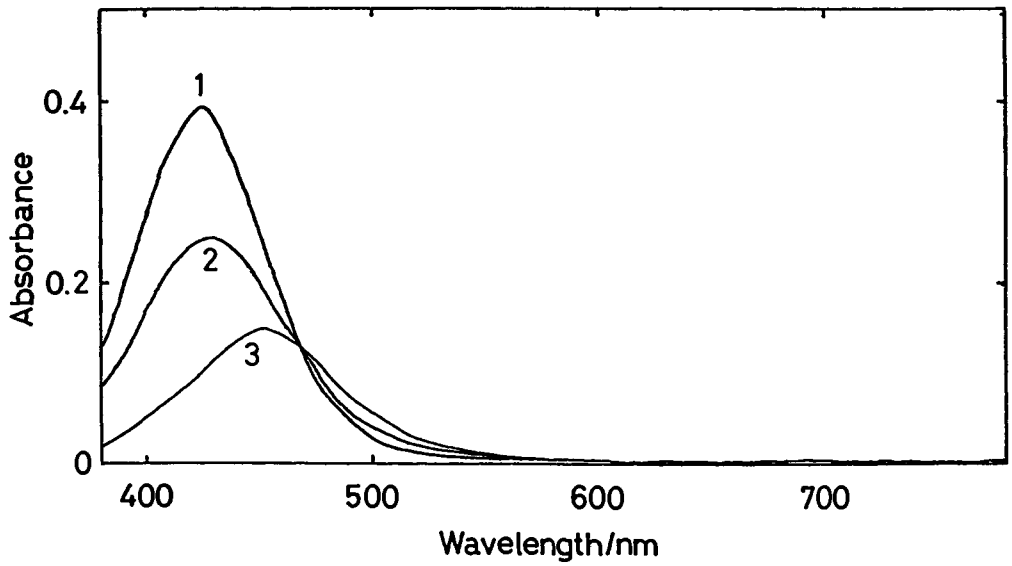

Fig. 2. Absorption spectra of 2×10^{-3} mol dm^{-3} $[Ni_2L^n]^{4+}$ (n=13—13 (1), 13—14 (2), 14—14 (3)) in water at 25 °C.

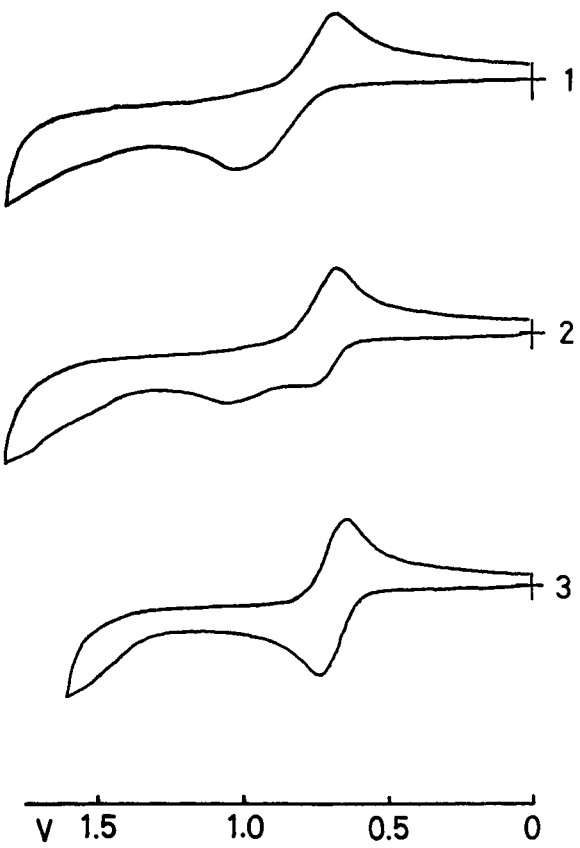

Fig. 3. Cyclic voltammograms of 2×10^{-3} mol dm^{-3} $[Ni_2L^n]^{4+}$ (n=13—13 (1), 13—14 (2), 14—14 (3)) in acetonitrile at 25 °C. Glassy carbon electrode. V vs. Ag-Ag$^+$ (0.01 mol dm^{-3} $AgNO_3$).

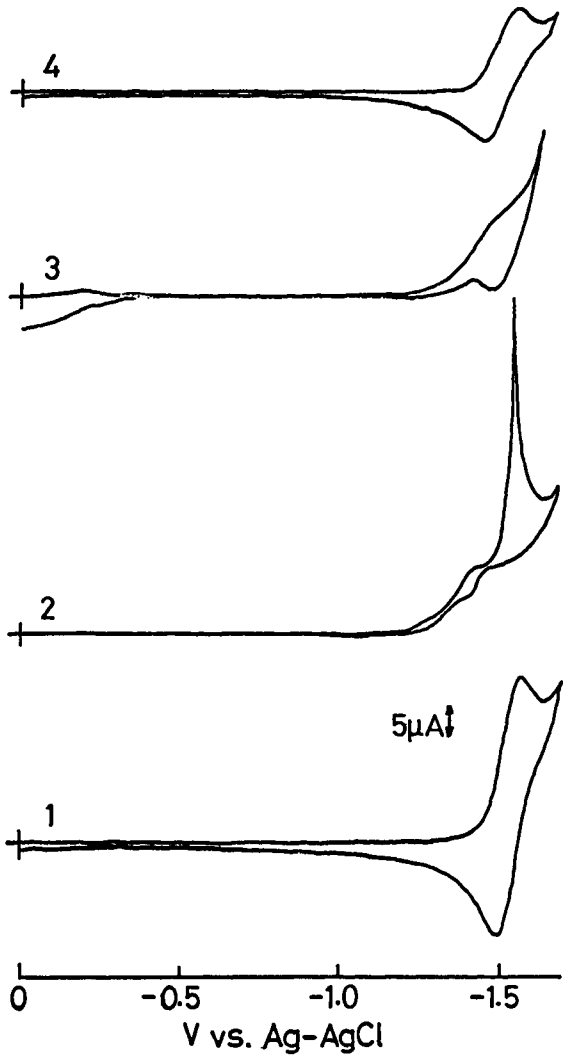

Fig. 4. Cyclic voltammograms of 5×10^{-3} mol dm^{-3} $[NiL^{14}]^{2+}$ (1) and 2×10^{-3} mol dm^{-3} $[Ni_2L^n]^{4+}$ (n= 13—13 (2), 13—14 (3), 14—14 (4)) in 0.1 mol dm^{-3} KCl aqueous solutions at 25 °C. HMDE.

average of the spectrum of $[Ni^{II}_2L^{14-14}]^{4+}$ and that of $[Ni^{II}_2L^{13-13}]^{4+}$. The same conclusion was also obtained by cyclic voltammetry. Figure 3 shows the cyclic voltammograms (CV) observed in the oxidation of $[Ni^{II}_2L^{13-14}]^{4+}$, $[Ni^{II}_2L^{14-14}]^{4+}$, and $[Ni^{II}_2L^{13-13}]^{4+}$,

respectively, in acetonitrile. The CV of $[Ni^{II}_2L^{13-14}]^{4+}$ (E_{pa} 0.80_0; 1.04_5; E_{pc} 0.67_5 V) is again almost equal to the average of the spectrum of $[Ni^{II}_2L^{14-14}]^{4+}$ (E_{pa} 0.74_5; E_{pc} 0.64_5 V) and that of $[Ni^{II}_2L^{13-13}]^{4+}$ (E_{pa} 1.02_5; E_{pc} 0.68_0 V). $[Ni^{II}_2L^{13-14}]^{4+}$ was found to have properties of both the 13- and 14-membered rings.

Thus, a new bimacrocyclic ligand having 13- and 14-membered rings linked bythe C–C bond and its dinickel(II) complex were unequivocally obtained.

Electrocatalytic Properties. Figure 4 shows the CV's for the reduction of Ni(II) complexes in an aqueous solutions containing 0.1 mol dm^{-3} KCl as a supporting electrolyte. Our observations for $[Ni^{II}_2L^{14-14}]^{4+}$ were different from the results previously reported by Sauvage et al.;[2] they did not describe a quasi-reversible wave, but an irreversible wave for Ni^{II}/Ni^{I} couples in a neutral aqueous solution. We observed, here, a quasi-reversible wave at -1.50 V, accompanied by a small adsorption wave at -1.3 V, in a neutral aqueous solution of $[Ni^{II}_2L^{14-14}]^{4+}$ (E_{pc}=-1.55_1 V, E_{pa}=-1.44_9 V, HMDE, scan rate: 100 mV s^{-1}, 0.1 mol dm^{-3} KCl, 25 °C). A couple of cathodic and anodic peaks were observed; they were assignable to the couples of $[Ni^{II}Ni^{II}]/[Ni^{II}Ni^{I}]$ and $[Ni^{II}Ni^{I}]/[Ni^{I}Ni^{I}]$[11] by comparison with the Ni^{II}/Ni^{I} couple of $[Ni^{II}L^{14}]^{2+}$ (E_{pc}=-1.56 V, E_{pa}=-1.48 V), since two Ni(II) in the complex should be reduced at the very close potentials.[12] A similar quasi-reversible wave was observed when 0.1 mol dm^{-3} $NaClO_4$ was used as the supporting electrolyte. On the other hand, the 13-membered ring complex, $[Ni^{II}_2L^{13-13}]^{4+}$, does not show reversible waves, but a cathodic peak at -1.43 and a sharp irreversible peak at -1.54 V; the latter may be caused by strong adsorption of the complex to the Hg electrode. The mixed-ring complex, $[Ni^{II}_2L^{13-14}]^{4+}$, shows a broad wave comprising a broad cathodic peak around -1.47 V assignable to the reduction of two Ni(II) ions in the 13- and 14-membered rings, and an anodic peak around -1.47 V to the oxidation of Ni(I) formed in the 14-membered ring.

Figure 5 shows CV's measured under various conditions. When the solution contained only a supporting electrolyte (0.1 mol dm^{-3} KCl), a supporting electrolyte+phosphate buffer (pH 6.8), or a supporting electrolyte+$[Ni^{II}_2L^{14-14}]^{4+}$ (2×10^{-5} mol dm^{-3}), neither cathodic nor anodic peaks were observed in 0—-1.7 V. Only when both phosphate buffer and $[Ni^{II}_2L^{14-14}]^{4+}$ (2×10^{-5} mol dm^{-3}) was added to 0.1 mol dm^{-3} KCl solution, did a new wave appear at ca. -1.66 V. This was assigned

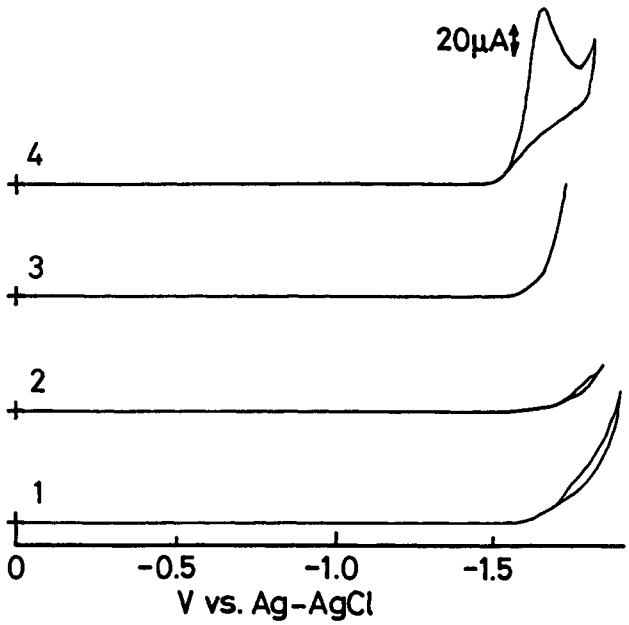

Fig. 5. Cyclic voltammograms of 0.1 mol dm^{-3} KCl aqueous solutions containing no buffers + no catalysts (1), phosphate buffer ($[HPO_4^{2-}]_T$=4×10^{-2} mol dm^{-3}, pH=6.8) (2), 2×10^{-5} mol dm^{-3} $[Ni_2L^{14-14}]^{4+}$ (3), and phosphate buffer ($[HPO_4^{2-}]_T$=4×10^{-2} mol dm^{-3}, pH=6.8)+2×10^{-5} mol dm^{-3} $[Ni_2L^{14-14}]^{4+}$ (4). T= 25 °C. HMDE.

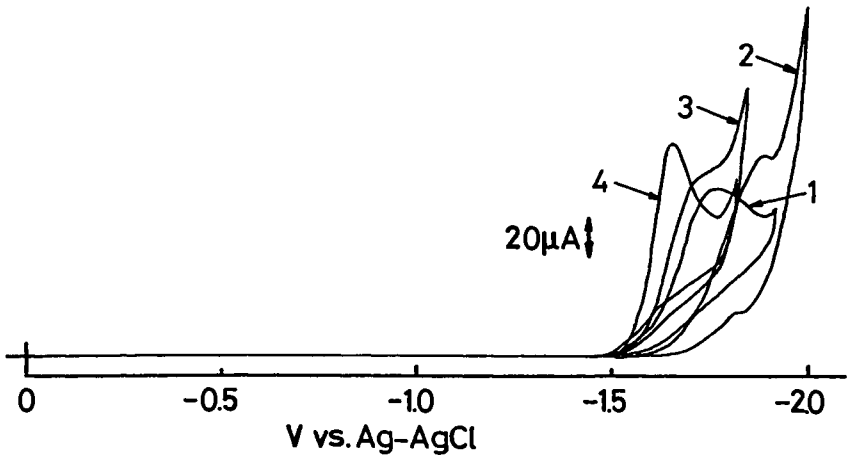

Fig. 6. Cyclic voltammograms of 0,1 mol dm^{-3} KCl aqueous solutions containing phosphate buffer ($[HPO_4^{2-}]_T$=4×10^{-2} mol dm^{-3}, pH=6.8) and 2×10^{-5} mol dm^{-3} Ni(II) complexes: $[NiL^{14}]^{2+}$ (1); $[Ni_2L^n]^{4+}$ (n= 13—13 (2), 13—14 (3), 14—14 (4)). T=25 °C. HMDE.

to the catalytic wave for water reduction, as reported previously.[2] Indeed, the controlled-potential electrolysis at the peak potential produced reasonable amounts of H_2, which was identical with a standard H_2 sample by gas chromatography. Similar catalytic waves were also observed upon the addition of $[Ni^{II}L^{14}]^{2+}$, $[Ni^{II}_2L^{13-14}]^{4+}$, or $[Ni^{II}_2L^{13-13}]^{4+}$.

Figure 6 shows the catalytic waves observed for solutions containing each Ni(II) complex (2×10^{-5} mol dm^{-3}), phosphate buffer, and 0.1 mol dm^{-3} KCl. The peak potentials, $(E_p)_{cata}$, of the catalytic waves are different among these Ni(II) complexes and their peak currents, $(i_p)_{cata}$, lie in 87—110 μA (see Table 1). According to the following order; $[Ni^{II}_2L^{13-13}]^{4+}<[Ni^{II}_2L^{13-14}]^{4+}\approx[Ni^{II}L^{14}]^{2+}<[Ni^{II}_2L^{14-14}]^{4+}$, $(E_p)_{cata}$ shifts toward the positive. As $(E_p)_{cata}$ becomes more positive, the wave begins to rise at a more positive potential; the overvoltage for the water reduction therefore becomes smaller. These results suggest that $[Ni^{II}_2L^{14-14}]^{4+}$ is the most favorable catalyst for H_2 production and that the electrocatalytic capability of $[Ni^{II}_2L^{13-14}]^{4+}$ should lie between those of $[Ni^{II}_2L^{14-14}]^{4+}$ and $[Ni^{II}_2L^{13-13}]^{4+}$, being close to that of mononuclear $[Ni^{II}L^{14}]^{2+}$.

The practical capabilities of the electrocatalysts could be evaluated by measurements of the amount of H_2 evolved by controlled-potential electrolysis: the greater was the amount of H_2, the more effective was the Ni(II) complex. The gas in the flask was analyzed by gas chromatography at an appropriate interval. In all cases, the amount of H_2 that evolved increased linearly with the electrolysis time.

We used a 1×10^{-4} mol dm^{-3} Ni(II) complex, where the concentration of the electrocatalyst has only a minor effect on the efficiency of H_2 production.[2] In the electrolysis at −1.5 V, only a small amount of H_2 is detected on a blank experiment in the absence of the Ni(II) complexes (Fig. 7). The addition of $[Ni^{II}_2L^{13-13}]^{4+}$ to a blank solution does not improve H_2 production, indicating that a Ni(II) complex with only 13-membered rings has a negligible electrocatalytic capability at −1.5 V. On the other hand, when the other Ni(II) complex with a 14-membered ring, $[Ni^{II}L^{14}]^{2+}$, $[Ni^{II}_2L^{13-14}]^{4+}$, or $[Ni^{II}_2L^{14-14}]^{4+}$, is added, a significantly larger amount of H_2 evolves compared with the case of a blank. The efficiency of binuclear $[Ni^{II}_2L^{14-14}]^{4+}$ is higher than that of mononuclear $[Ni^{II}L^{14}]^{2+}$ by about two times; this result, though the efficiency is somewhat lower in our experiments, is similar to that reported by Sauvage et al.[2] The capability of $[Ni^{II}_2L^{13-14}]^{4+}$ is almost equal to that of mononuclear $[Ni^{II}L^{14}]^{2+}$ and lies between those of $[Ni^{II}_2L^{14-14}]^{4+}$ and $[Ni^{II}_2L^{13-13}]^{4+}$. Thus, the order of the electrocatalytic capability derived from the controlled-potential electrolysis well corresponds to that predicted from $(E_p)_{cata}$ in CV experiments.

These data obtained herein undoubtedly show that the electrocatalytic capability strongly depends on the ring sizes of bimacrocyclic Ni(II) complexes, where the capability falls as 14-membered rings are replaced by 13-membered rings, i.e., the "symmetric" bimacrocycle, $[Ni^{II}_2L^{14-14}]^{4+}$, is the most favorable for H_2 generation.

Table 1. Electrochemical Data of Catalytic Waves[a]

Complex	$(E_p)_{cata}$/V	$(i_p)_{cata}$/μA
$[Ni^{II}L^{14}]^{2+}$	−1.77	87
$[Ni^{II}_2L^{14-14}]^{4+}$	−1.66	110
$[Ni^{II}_2L^{13-14}]^{4+}$	−1.75	95
$[Ni^{II}_2L^{13-13}]^{4+}$	−1.89	104

a) Solutions contained 0.1 mol dm^{-3} KCl, phosphate buffer ($[HPO_4^{2-}]_T=4\times10^{-2}$ mol dm^{-3}, pH 6.8), and 2×10^{-5} mol dm^{-3} Ni(II) complex.

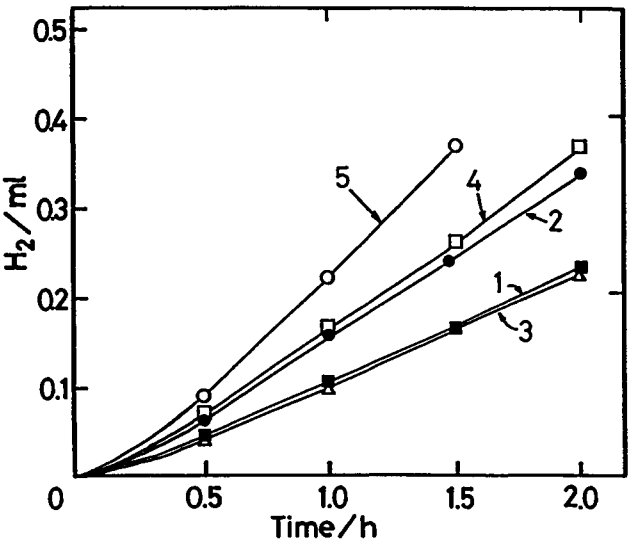

Fig. 7. Amount of H_2 evolved by the electrolysis at −1.5 V vs. Ag–AgCl. Electrolytic solutions contain only phosphate buffer ($[HPO_4^{2-}]_T=0.2$ mol dm^{-3}, pH=6.8) (1) and phosphate buffer+1×10^{-4} mol dm^{-3} Ni(II) complexes: $[NiL^{14}]^{2+}$ (2); $[Ni_2L^n]^{4+}$ (n=13—13 (3), 13—14 (4), 14—14 (5)). Mercury-pool electrode (8 cm^2). T=ca. 23 °C.

Experimental

Materials. The procedures for preparations of the ligand L^{13-14} and of its dinickel(II) complex are as follows.

Tetraoxo Derivatives: Tetraethyl 1,1,2,2-ethanetetracarboxylate (25.5 g, 0.08 mol) was dissolved in dry ethanol (1.6 dm^3) under an N_2 atmosphere, to which was added dropwise in 30 min a mixture of 3,6-diazaoctane-1,8-diamine (11.7 g, 0.08 mol) and 3,7-diazanonane-1,9-diamine (12.8 g, 0.08 mol). The solution was heated under reflux for 5 d. White precipitates which formed were filtered, washed with cold ethanol, and dried over P_2O_5 in a vacuum to give a mixture consisting of three tetraoxo derivatives, 6-(11,13-dioxo-1,4,7,10-tetraaza-12-cyclotridecyl)-1,4,8,11-tetraazacyclotetradecane-5,7-dione), 12,12′-bi[1,4,7,10-tetraazacyclotridecane-11,13-dione], and 6,6′-bi[1,4,8,11-tetraazacyclotetradecane-5,7-dione] in 18% yield. Since several attempts to separate the mixture failed, a crude mixture was subjected to the following procedures.

Reduction of the Mixture of Tetraoxo Derivatives: The mixture (4.0 g) of tetraoxo derivatives was suspended in tetrahydrofuran (300 cm^3) under an N_2 atmosphere, to which

was added B_2H_6 (240 cm^3, 1 mol dm^{-3} in tetrahydrofuran). After the solution was heated under reflux for 6 h, B_2H_6 (160 cm^3) was again added; refluxing was continued for additional 12 h. After the solution was cooled to room temperature, methanol (200 cm^3) was carefully added dropwise (*CAUTION*: this reaction can be explosive) to quench any excess B_2H_6. The resulting solution was evaporated to dryness. To the residue, conc. HCl (30 cm^3), water (60 cm^3), and methanol (160 cm^3) were added; the solution was then evaporated to dryness, this treatment being repeated five times in order to remove boric acid as trimethyl borate. To the residue, thus obtained, was added NaOH (50 cm^3, 1 mol dm^{-3}, pH>13). The reduction products were extracted five times with $CHCl_3$) (100 cm^3). The combined extracts were dried over anhydrous Na_2SO_4 over night and evaporated to dryness to give a white residue, a mixture of three bimacrocyclic ligands: L^{13-13}, L^{13-14}, and L^{14-14}. Yield: 92%.

Separation of the Mixture of Ligands: A mixture (1.5 g) of L^{13-13}, L^{13-14}, and L^{14-14} was dissolved in ethanol (80 cm^3), to which was added nickel(II) perchlorate hexahydrates (2.85 g, 7.8 mmol) in ethanol (160 cm^3). The mixture was stirred at 60 °C for 1 h to give yellow precipitates. The precipitates were suspended in a small amount of water and passed through a column of Cl-form anion-exchange resin (Amberlite IRA-410, ϕ=30 mm, l=300 mm) to exchange the counter ions from perchlorates to chlorides. The resulting clear solution was chromatographed with a cation-exchange column (SP-Sephadex C-25, ϕ=30 mm, l=1300 mm), with a 0.25 mol dm^{-3} sodium iodide solution as the eluent, to give three orange bands. The first and third bands were assigned to $[Ni^{II}_2L^{14-14}]^{4+}$ and $[Ni^{II}_2L^{13-13}]^{4+}$ respectively by comparison with respective authentic samples (see below). The second eluate was concentrated to ca. 200 cm^3, adjusted to pH>13 by adding NaOH, and heated at 60 °C. To the solution was added NaCN (2.4 g, 0.049 mol); the solution was stirred at 60 °C for 30 min. After being cooled to room temperature, the solution was extracted with $CHCl_3$ (100 cm^3) four times. The combined extracts were dried over anhydrous Na_2SO_4 and evaporated to dryness to give a pale-yellow residue of the free ligand, L^{13-14}, in 13 % yield. An analytical sample of hydrochloride was prepared by the following treatment. The residue was dissolved in a small amount of ethanol, to which was added conc. HCl (1 cm^3) to give a white precipitate. The precipitate was washed with dry ethanol and dried over P_2O_5 in a vacuum.

$L^{13-14}\cdot 8HCl\cdot 1.5H_2O$: Found: C, 32.58; H, 8.01; N, 15.77%. Calcd for $C_{19}H_{44}N_8\cdot 8HCl\cdot 1.5H_2O$: C, 32.45; H, 7.88; N, 15.93%.

L^{13-14}: ^{13}C NMR ($CDCl_3$, TMS) δ=29.4 (t), 42.1 (d), 42.3 (d), 47.6 (2t), 49.1 (t), 49.6 (2t), 51.0 (t), 54.5 (t), and 54.9 (t). FAB MS m/z 385 $[M+H]^+$.

$[Ni^{II}_2L^{13-14}](ClO_4)_4\cdot H_2O$: The free ligand L^{13-14} (0.1 g, 0.26 mmol) was dissolved in ethanol (5 cm^3), to which was added nickel(II) perchlorate hexahydrates (0.19 g, 0.52 mmol) in ethanol (10 cm^3). The mixture was stirred at 60 °C for 1 h, cooled at room temperature, and filtered to give yellow precipitates. The precipitates were recrystallized from a small amount of water to give plate crystals, which were washed with cold water and dried at 80 °C over P_2O_5 in a vacuum. Yield: 42%. Found: C, 24.89; H, 4.91; N, 12.34%. Calcd for $C_{19}H_{44}N_8Ni_2Cl_4O_{16}\cdot H_2O$: C, 24.86; H, 5.05; N, 12.21%. VIS (H_2O) 428 (ε 130), (CH_3NO_2) 431 nm (167 mol dm^3 cm^{-1}).

$[Ni^{II}_2L^{14-14}](ClO_4)_4\cdot H_2O$: L^{14-14} was prepared according to a method described in the literature.[6] The dinickel(II) complex of L^{14-14} was prepared by the analogous method described above. Found: C, 25.66; H, 5.02; N, 11.85%. Calcd for $C_{20}H_{46}N_8Ni_2Cl_4O_{16}\cdot H_2O$: C, 25.78; H, 5.19; N, 12.03%. VIS (H_2O) 450 (ε 77), (CH_3NO_2) 456nm (113 mol^{-1} cm^3 cm^{-1}).

L^{14-14}: ^{13}C NMR ($CDCl_3$, TMS) δ=29.1 (t), 42.7 (d), 49.2 (t), 50.7 (t), and 54.8 (t).

$[Ni^{II}_2L^{13-13}](ClO_4)_4\cdot H_2O$: L^{13-13} and its dinickel(II) complex were prepared by the analogous method as described in the preparation of $[Ni^{II}_2L^{14-14}](ClO_4)_4\cdot H_2O$. Found: C, 24.13; H, 4.72; N, 12.48%. Calcd for $C_{18}H_{42}N_8Ni_2Cl_4O_{16}\cdot H_2O$: C, 23.92; H, 4.91; N, 12.40%. VIS (H_2O) 424 (ε 185), (CH_3NO_2) 427 nm (203 mol dm^3 cm^{-1}).

L^{13-13}: ^{13}C NMR ($CDCl_3$, TMS) δ=42.0 (d), 47.3 (t), 49.0 (t), and 54.1 (t).

Measurements. The visible absorption spectra were measured with a Hitachi 340 spectrophotometer. ^{13}C NMR spectra were recorded with JEOL FX90Q or Brucker AM400 spectrometers. FAB mass spectra were measured with a JEOL DX303 spectrometer.

Cyclic voltammograms for the oxidation of dinickel(II) complexes were measured according to a method described in our previous paper.[9] Cyclic voltammograms for the reduction were carried out by using a Yanagimoto Polarographic Analyzer P-1100. A hanging mercury electrode (Metrohm EA-290 equipped with glass capillary EA-1053) and Pt spiral electrode were used as working electrode and counter electrode respectively.

Controlled-potential electrolyses were performed at room temperature (ca. 23 °C), in a gas-tight electrolysis cell under one atmosphere of N_2 with a Fuso potentiostat 315A. The gas-tight cell was a 100 cm^3, three-necked, round-bottomed flask equipped with two side arms. The working electrode used in all the experiments was mercury (8 cm^2) which had been distilled twice. The counter electrode (Pt) and the reference electrode (Ag/AgCl) were separated from the working electrode compartment by a glass frit. The gases occupied 95 cm^3 of the cell volume. Before electrolysis, the aqueous solution (50 cm^3) was degassed by bubbling N_2 for 30 min, after which the admission tap was turned off, the internal pressure within the electrolysis cell being kept equal to 1 atm by means of an oil valve.

Gas samples (0.5 cm^3), taken at various intervals with a gas-tight syringe through a septum, were analyzed on a Shimadzu GC-14A gas chromatograph with a thermal conductivity detector by using a 2.1 m×3 mm column packed with molecular sieve 5A at 60 °C using argon as carrier gas.

References

1) B. Fisher and R. Eisenberg, *J. Am. Chem. Soc.*, **102**, 7361 (1980).

2) J. P. Collin, A. Jouaiti, and J. P. Sauvage, *Inorg. Chem.*, **27**, 1986 (1988).

3) A. M. Tait, M. Z. Hoffman, and E. Hayon, *Inorg. Chem.*, **15**, 934 (1976); D. Meyerstein, *Acc. Chem. Res.*, **11**, 43 (1978), and references therein; J. L. Grant, K. Goswami, L. O. Spreer, J. W. Otvos, and M. Calvin, *J. Chem. Soc., Dalton Trans.*, **1987**, 2105.

4) I. Murase, K. Hamada, and S. Kida, *Inorg. Chim. Acta*, **54**, L171 (1981); I. Murase, K. Hamada, S. Ueno, and S. Kida, *Synth. React. Inorg. Met.-Org. Chem.*, **13**, 191 (1983); I.

Murase, S. Ueno, and S. Kida, *Inorg. Chim. Acta,* **111**, 57 (1986).

5) M. Ciampolini, M. Micheloni, N. Nardi, F. Vizza, A. Buttafava, L. Fabbrizzi, and A. Perotti, *J. Chem. Soc., Chem. Commun.*, **1984**, 998; L. Fabbrizzi, F. Forlini, A. Perotti, and B. Seghi, *Inorg. Chem.*, **23**, 807 (1984); A. Buttafava, L. Fabbrizzi, A. Perotti, A. Poggi, and B. Seghi, *Inorg. Chem.*, **23**, 3917 (1984); R. Schneider, A. Riesen, and T. A. Kaden, *Helv. Chim. Acta,* **68**, 53 (1985).

6) L. Fabbrizzi, L. Montagna, A. Poggi, T. A. Kaden, and L. Siegfried, *Inorg. Chem.*, **25**, 2671 (1986); L. Fabbrizzi, L. Montagna, A. Poggi, T. A. Kaden, and L. C. Siegfried, *J. Chem. Soc., Dalton Trans.*, **1987**, 2631.

7) E. K. Barefield, D. Chueng, D. G. Van Derveer, and F. J. Wagner, *J. Chem. Soc., Chem. Commun.*, **1981**, 302.

8) K. Mochizuki, K. Toriumi, and T. Ito, *Bull. Chem. Soc. Jpn.*, **57**, 881 (1984); K. Mochizuki, *Bull. Chem. Soc. Jpn.*, **61**, 1023 (1988); K. Mochizuki and Y. Endoh, *Bull. Chem. Soc. Jpn.*, **62**, 936 (1989).

9) K. Mochizuki and M. Fujimoto, *Bull. Chem. Soc. Jpn.*, **58**, 1520 (1985).

10) L. Fabbrizzi, *J. Chem. Soc., Dalton Trans.*, **1979**, 1857.

11) Assuming the theoretical separation (36 mV) of the two couples, $E^1_{1/2}$ for $[Ni^{II}Ni^{II}]/[Ni^{II}Ni^{I}]$ and $E^2_{1/2}$ for $[Ni^{II}Ni^{I}]/[Ni^{I}Ni^{I}]$ can be calculated to be -1.48 and -1.52 V respectively. $E^1_{1/2}$ seems to shift to rather positive side compared with $E_{1/2}$ (-1.52 V) of Ni^{II}/Ni^{I} of $[Ni^{II}L^{14}]^{2+}$. One Ni(II) in $[Ni^{II}{}_2L^{14-14}]^{4+}$ might be reduced easier than $[Ni^{II}L^{14}]^{2+}$.

12) It is reported that two Ni(II) in $[Ni^{II}{}_2L^{14-14}]^{4+}$ are oxidized at very close potentials (see Ref. 6).

Monolayer Level Depth Profiling by Laser Induced Fluorescence Spectroscopy

Xing-Zheng Wu, Takehiko Kitamori, Norio Teramae,† and Tsuguo Sawada*
Department of Industrial Chemistry, Faculty of Engineering, The University of Tokyo,
7-3-1 Hongo, Bunkyo, Tokyo 113
†Department of Applied Chemistry, Faculty of Engineering, Nagoya University,
Hurouchou 1, Chigusaku, Nagoya 464
(Received January 28, 1991)

Application limits of the proposed concentration depth profile using laser induced fluorescence spectroscopy based on the reciprocal principle (*Bull. Chem. Soc. Jpn.*, **64**, 755 (1991)) were investigated. Although this method has no limitations regarding film thickness and spatial resolution in the depth direction theoretically, for practical applications, they are limited by the instrumental factors. Effects of uncertainty in the observation angle measurement, which depends on the size of the detector, the mechanical precision of the rotating stage, and experimental errors in the fluorescence intensity measurement on the accuracy of the reconstructed concentration depth profile were discussed in detail. The theoretical results predicted nanometer level depth profiling with our laboratory-constructed instruments. A 29 nm thick model film sample, consisting of long chain molecular bilayers, was used to verify the theoretical analysis results. The concentration depth profile for bilayer level steps of about 5 nm was obtained under our experimental conditions. Possible improvements in this method and monolayer level depth profiling were also considered.

Many problems in thin film chemistry and materials science are concerned with the distribution of chemical species in the depth direction.[1,2] In many situations, vacuum spectroscopic depth profiling methods are undesirable, because they are destructive methods and they need high vacuum conditions which are unsuitable for in situ and in vivo analysis. Optical spectroscopical concentration depth profiling methods such as photoacoustic spectroscopy (PAS) depth profiling,[3] attenuated total reflection (ATR) spectroscopy depth profiling[4] are non-destructive and non-contact methods not requiring high vacuum system.[5,6] Recently, we have reported on the concentration depth profiling technique using laser induced fluorescence spectroscopy under normal incidence conditions based on the reciprocal principle.[7] Using this method, the quantitative concentration depth profile of a 187 nm thick Langmuir–Blodgett (LB) model film sample was obtained by the least square method. This spectroscopic technique is attractive since it has a high spatial resolution in the depth direction and can be used on a film sample thinner than the wavelength of the excitation light. In addition, by using the normal incidence conditions, it is possible to obtain a three dimensional concentration profile by scanning the excitation beam.

However, to function as a basic methodology for practical applications, answers must be got for the following questions: How accurate is the reconstructed concentration depth profile? Is there any limitation to film thickness for this method? What is the spatial resolution in the depth direction? Then it is necessary to investigate the application limits.

In this paper, we investigate application limits, such as film thickness, and accuracy of the reconstructed concentration depth profile by this method. The main instrumental error sources such as the uncertainty in determining observation angle, the mechanical precision of the rotating stage, and the uncertainty in the fluorescence intensity measurement, and their effects on the accuracy of the reconstructed concentration depth profile are discussed. In the experiments, a 29 nm thick LB model film sample where fluorophore is distributed in the form of a nearly linear function is used to verify the theoretical conclusions, and a bilayer level concentration depth profile is obtained.

Theory and Simulation

The basic theory of depth profiling using laser induced fluorescence spectroscopy under normal incidence conditions based on the reciprocal principle has been discussed in our previous paper.[7] Here we summarize it briefly. Figure 1 illustrates the basic optical arrangement. The fluorescence intensity $F(\theta)$ obtained

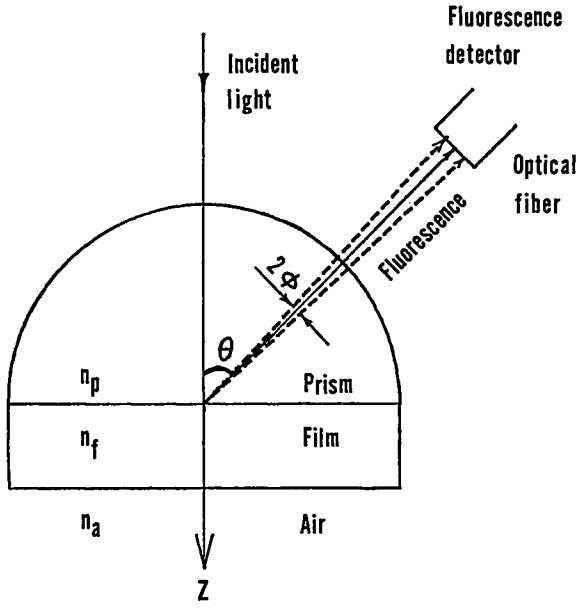

Fig. 1. Measurement principle of the depth profiling method.

at an observation angle θ under normal incidence conditions can be expressed as Eq. 1,

$$F(\theta)=k\int_0^t C(z)T(\theta, z)\mathrm{d}z, \quad (1)$$

where $C(z)$ is the concentration distribution in the depth direction z, t is the thickness of the sample, and k is a constant given by material constants and instrumental factors. The transmission function $T(\theta, z)$ can be obtained by theoretical analysis of multiple reflection of the fluorescence electromagnetic wave between prism/film and film/air interfaces.[8] When θ, z, and t are given, $T(\theta, z)$ can be calculated exactly from the optical parameters such as the fluorescence wavelength and the refractive indices of the prism, film, and air. Thus $C(z)$ can be obtained by resolving the inverse integral of Eq. 1 from a set of fluorescence intensity data. It is well known that resolution of the inverse integral problem is difficult due to the ill-posed problem.[9–11] However, for the present method, if a process leading to the formation of $C(z)$ is estimated beforehand, then $C(z)$ can be easily obtained by the least square method.[7] As shown in the previous experimental reports of this depth profiling method,[7] the experimental errors seriously affect results of the reconstructed concentration profiles. We can discuss the effects of the instrumental error factors on the accuracy and the limitation of the present depth profiling method by a numerical simulation method. Since $C(z)$ is obtained from a set of fluorescence intensities determined at a series of observation angles by the least square method, the following three error sources are considered. First, uncertainty ϕ in observation angle, as shown in Fig. 1, is determined by the size of the detector and the distance between the detector and the illuminated point. Second, the angular error $\Delta\theta$ is determined by the mechanical precision of the rotating stage. Third, the measurement error ΔF in the fluorescence intensity is caused by noise such as electric noise. An influence of base-line drift on ΔF cannot be disregarded, when measurement period is relatively longer than the instrument stability.

Here, three typical concentration distribution cases are discussed. In the first case, $C(z)$ is a linear function form

$$C(z)=Az+B \quad (2)$$

as shown in Fig. 2-A), which was used as a trial function in our previous paper.[7] In the second case, $C(z)$ is an exponential function form

$$C(z)=C_0\exp(-z/l) \quad (3)$$

as shown in Fig. 2-B), which often emerges in chemical kinetics systems. In the third case, $C(z)$ is an error function form

$$C(z)=C_0[1-\mathrm{erf}(-z/l)] \quad (4)$$

as shown in Fig. 2-C), which is usually met in a diffusion limiting process. The parameters A, B, C_0, l can be obtained by the least square method, i. e., by

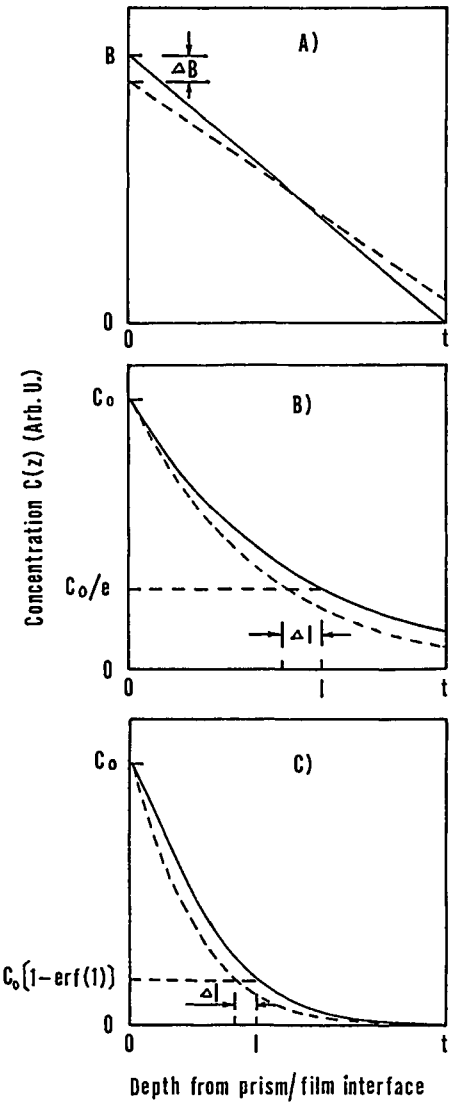

Fig. 2. Model function used in the simulation. The solid and dashed lines represent the original $C(z)$ and reconstructed $C(z)$. A: $C(z)$ is a linear function form. B: $C(z)$ is an exponential function form. C: $C(z)$ is an error function form.

minimizing the following value s,

$$s=\sum_i[F_m(\theta_i)-F_c(\theta_i)]^2/g_{\theta_i}, \quad (5)$$

where i means the i-th measurement data, $F_m(\theta_i)$ and $F_c(\theta_i)$ are the measured and calculated fluorescence intensities, respectively, and g_{θ_i} is a weight factor.

The differences between actual and calculated values of parameters A, B, and l are represented by ΔA, ΔB, and Δl, respectively (Fig. 2). The accuracy of the reconstructed $C(z)$ is evaluated by the relative errors of the parameters in Eqs. 2—4, i. e., $\Delta A/A$ or $\Delta B/B$ for the linear distribution case, and $\Delta l/l$ for the exponential and error function cases.

In this simulation, θ_i is assumed to be varied from 20° to 80° with 1° steps. The calculated fluorescence intensities $F_c(\theta_i)$ in Eq. 5 are obtained according to Eq. 1 for

the above three cases expressed as Eqs. 2—4. The constants in Eqs. 2—4 are normalized as follows: A (% nm^{-1}) and B (%) are $-1(\%)/t(\mathrm{nm})$ and 1(%), respectively, and C_0 (%) and l (nm) are 1(%) and t (nm), respectively. In order to calculate $\Delta A/A$, $\Delta B/B$, and $\Delta l/l$ caused by ϕ, the measured fluorescence intensity $F_m(\theta_i)$ in Eq. 5 is simulated by substituting θ_i with $\theta_i+\phi$. When the effect of $\Delta\theta$ is considered, the observation angle θ_i takes a certain value within the range of $\theta_i\pm\Delta\theta$. In the worst case, θ_i is randomly given by either $\theta_i+\Delta\theta$ or $\theta_i-\Delta\theta$, leading to $F_m(\theta_i+\Delta\theta)$ or $F_m(\theta_i-\Delta\theta)$. Considering ΔF, $F_m(\theta_i)$ in Eq. 5 is within the range of $F_m(\theta_i)\pm\Delta F$, and the value of $F_m(\theta_i)$ in Eq. 5 is also substituted randomly by $F_m(\theta_i)+\Delta F$ or $F_m(\theta_i)-\Delta F$. With these simulated values of $F_m(\theta_i)$, the relative errors of $\Delta A/A$, $\Delta B/B$, and $\Delta l/l$ caused by ϕ, $\Delta\theta$, and ΔF are obtained from Eq. 5. The results are shown in Figs. 5, 6, and 7, respectively.

Experimental

The experimental set up used is the same as reported in our previous paper.[7] An Ar^+ laser (output, 30 mW) provides the excitation light (wavelength, 488 nm). The laser beam was modulated with a chopper. The chopped beam was focused on the focal plane of the hemicylindrical prism (refractive index n, 1.88) which was mounted on two rotating stages. A step index type optical fiber bundle was used to collect the fluorescence transmitted through the prism. The area collecting fluorescence was 0.2 mm×1 mm, and the numerical aperture was 0.57. One end of the optical fiber was fixed at the focal plane of the prism and the other end of the optical fiber was coupled with a monochromator. A film polarizer was placed in front of the optical fiber to restrict the fluorescence collected only to the perpendicularly polarized component. A photomultiplier (Hamamatsu 1P21) was used as a detector. The signal from the photomultiplier was fed into and amplified with a lock-in amplifier. Fluorescence intensity data were obtained at the fluorescence wavelength of 580 nm.

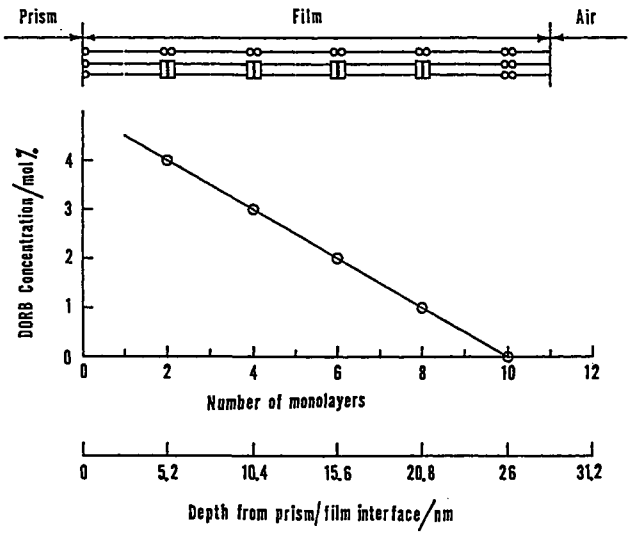

Fig. 3. Concentration depth profile of the model film sample. The upper part is a schematic representation of the model film sample construction. Rectangles represent the head groups of DORB, which are the fluorophores. Circles represent CdC_{20} head groups (nonfluorescent). Long hydrocarbon chains are represented as lines. The lower part is the concentration depth profile represented graphically. The circles and the straight line represent the true and approximate linear function form concentration depth profiles, respectively.

The LB multilayer deposition method was used to prepare a model film sample where $C(z)$ is a nearly linear function form. A model film sample having an exact linear function form or an exponential function form $C(z)$ is difficult to prepare. Details of the preparation procedure were reported previously.[7] The LB multilayers were deposited onto the prism directly. In order to ensure the prism surface was uniform and hydrophobic, a monolayer of CdC_{20} was first deposited. Then a mixture of CdC_{20} and N,N'-dioctadecylrhodamine B (DORB), in which the concentration of DORB varied from 4% to 0%, was deposited in 2 layer steps. The concentration depth profile of the model film sample is shown in Fig. 3, and its $C(z)$ can be precisely expressed as a discrete function with the spacing of a bilayer thickness (5.2 nm) between the values. This concentration depth profile of the model film sample is approximately described as a linear function form in the same manner as the previous report,[7]

$$C(z)(\%) = -0.19(\%\ \mathrm{nm}^{-1})\, z(\mathrm{nm}) + 5(\%). \quad (6)$$

Results and Discussion

In order to obtain $C(z)$ from Eq. 1, the necessary condition is that the partial derivative of $T(\theta, z)$ with respect to z, $\partial T(\theta, Z)/\partial Z$, must not be equal to zero. Otherwise $T(\theta, z)$ is independent of z, that is, $T(\theta, z)$ becomes a constant $T(\theta)$, and Eq. 1 becomes as follows,

$$F(\theta) = kT(\theta)\int_0^t C(z)\mathrm{d}z. \quad (7)$$

It is clear that information on $C(z)$ disappears from the observed $F(\theta)$ expressed in Eq. 7.

Figure 4 shows a calculation example of the relations between $\partial T(\theta, Z)/\partial Z$ and the film thickness at the observation angle of 20°. The calculation results show

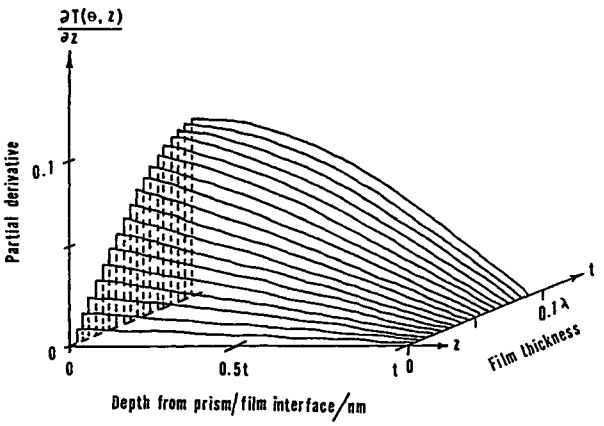

Fig. 4. Calculation results of partial derivative $\partial T(\theta, z)/\partial z$ for different film thicknesses at observation angle 20°. t: film thickness. λ: wavelength of fluorescence.

the partial derivative is not zero, and moreover, $\partial T(\theta, Z)/\partial Z$ has different values at different θ. This means that at different θ_i, $T(\theta_i, z)$ has different function forms. Hence, $C(z)$ can be obtained mathematically from Eq. 1 regardless of t. In other words, theoretically, this method is not limited by the film thickness. It is obvious from Eq. 1 that the measured fluorescence $F(\theta)$ does not involve informations related to concentration distribution $C(z)$ when $\partial T(\theta, Z)/\partial Z$ is zero, even though $T(\theta, z)$ has certain value.

Considering the above theoretical results and the previous experiments,[7] the application limit is considered to depend on instrumental factors and experimental errors. Then, their effects on the accuracy of the reconstructed $C(z)$ were investigated. After that, the application limits of film thickness under our experimental conditions were discussed on the basis of the simulation results.

For the first case in which $C(z)$ is a linear function form, Fig. 5 shows the simulation results of the effects of ϕ, $\Delta\theta$, and ΔF on the accuracy of the reconstructed $C(z)$. The circles and the vertical error bars in Figs. 5-B) and 5-C) represent the average values and variation for ten simulation results taking the values $\theta_i+\Delta\theta$ or $\theta_i-\Delta\theta$, and $F_m(\theta_i)+\Delta F$ or $F_m(\theta_i)-\Delta F$ randomly for Figs. 5-B) and 5-C), respectively. The relative value $\Delta F/F$ in Fig. 5-C) is considered to be the same as the signal to noise ratio (S/N). Since $F_m(\theta)$ takes a value within the range of $F_m(\theta)\pm\Delta F$, the noise is considered as $2\Delta F$. Thus the relation between $\Delta F/F$ and S/N is as follows,

$$\Delta F/F = 1/2(S/N). \tag{8}$$

The vertical axes of Fig. 5 represent the relative error $\Delta B/B$ of the parameter B obtained from Eq. 5 and $\Delta B/B$ decreases with decreasing ϕ. The variation range of

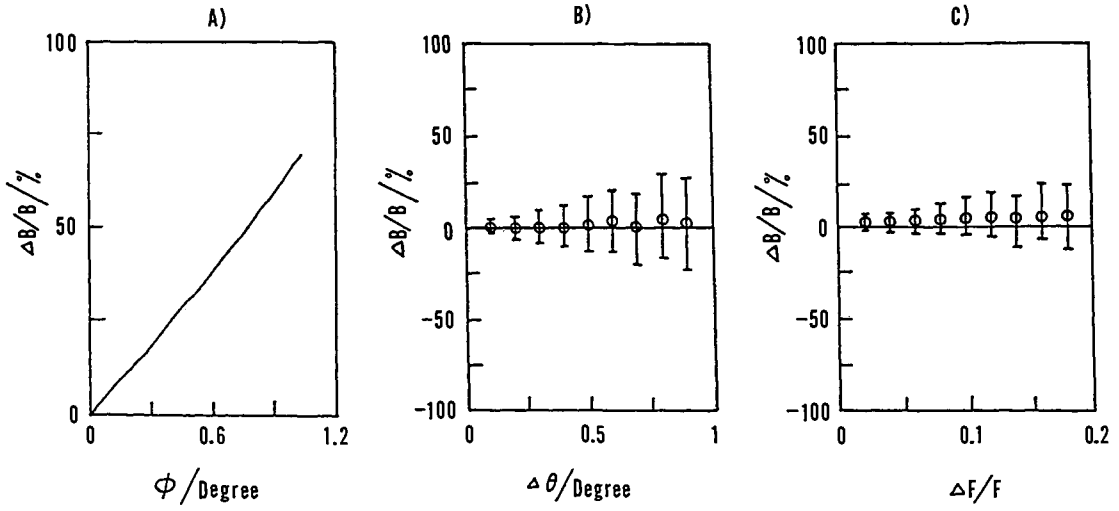

Fig. 5. Effects of instrumental factors on the accuracy of the reconstructed concentration depth profile for the first case. A: effect of ϕ on $\Delta B/B$. B: effect of $\Delta\theta$ on $\Delta B/B$. C: effect of ΔF on $\Delta B/B$.

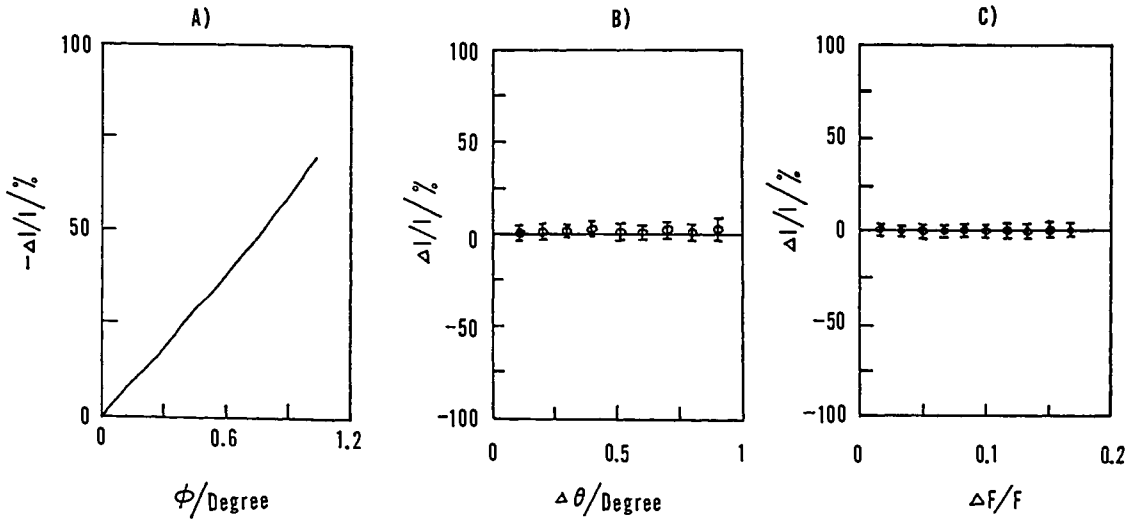

Fig. 6. Effects of instrumental factors on the accuracy of the reconstructed concentration depth profile for the second case. A: effect of ϕ on $\Delta l/l$. B: effect of $\Delta\theta$ on $\Delta l/l$. C: effect of ΔF on $\Delta l/l$.

$\Delta B/B$ also decreases with the decrease of both $\Delta\theta$ and $\Delta F/F$ although the average values of $\Delta B/B$ are nearly equal to zero as shown in Figs 5-B) and 5-C). These results indicate that the accuracy of the reconstructed $C(z)$ depends on the experimental errors. The effects of ϕ, $\Delta\theta$, and ΔF on $\Delta A/A$, which is the relative error of the parameter A of the linear equation function form expressed as Eq. 2, were also simulated and the results are simular to those shown in Fig. 5.

It has been stated that ϕ is determined by the size of the detector, and the distance between the detector and the illuminated point. When using a small sized fiber bundle, ϕ can be decreased, so that accuracy of the reconstructed $C(z)$ can be improved. However, at the same time, S/N decreases which results in a decreased accuracy of the reconstructed $C(z)$. Therefore there is an optimum condition between ϕ and ΔF, which is determined experimentally.

For the second case in which $C(z)$ is an exponential function form, Fig. 6 shows the effects of ϕ, $\Delta\theta$, and ΔF on the accuracy of the reconstructed $C(z)$. It is clear that the relative error $\Delta l/l$ of parameter l in Eq. 3 decreases with decreasing ϕ, but varies hardly at all with $\Delta\theta$ and $\Delta F/F$ in comparison with the first case shown in Fig. 5. For the first and the second cases, Eq. 1 takes the following forms:

$$F(\theta)=k[A\int_0^t zT(\theta, z)\mathrm{d}z+B\int_0^t T(\theta, z)\mathrm{d}z], \quad (9)$$

$$F(\theta)=k\int_0^t c_0 \exp(-z/l)T(\theta, z)\mathrm{d}z. \quad (10)$$

Therefore, the relations between ΔF and ΔA, ΔB and Δl are expressed as Eqs. 11 and 12, respectively.

$$\Delta F=[\Delta A\int_0^t zT(\theta, z)\mathrm{d}z+\Delta B\int_0^t T(\theta, z)\mathrm{d}z], \quad (11)$$

$$\Delta F=k\int_0^t [\exp(-z/(1+\Delta l))-\exp(-z/l)]T(\theta, z)\mathrm{d}z. \quad (12)$$

It can be seen that ΔF has a linear relation with ΔA and ΔB for the first case, but it has an exponential relation with Δl for the second. Thus ΔF has a smaller effect on the exponential distribution than the linear one. When $\Delta\theta$ and $\Delta F/F$ are within the range of 0—1° and 0—0.2, the average values of $\Delta l/l$ in Figs. 6-B) and 6-C) are nearly equal to zero, and the variation range of $\Delta l/l$ is about ±5%. Therefore, in this case, the effects of $\Delta\theta$ and ΔF are small, and ϕ is the main factor affecting the accuracy of reconstructed $C(z)$.

For the third case in which $C(z)$ is an error function form, the effects of ϕ, $\Delta\theta$, and ΔF on the accuracy of reconstructed $C(z)$ were also investigated, and the results are similar with those shown in Fig. 6.

In conclusion, when $C(z)$ is an exponential function form or an error function form, the accuracy of the reconstructed $C(z)$ is mainly determined by the instrumental factor ϕ. When $C(z)$ is a linear function form, the accuracy of the reconstructed $C(z)$ depends on both the instrumental factors ϕ and $\Delta\theta$, and the experimental ΔF. However, if $\Delta\theta$ is smaller than 0.05° and S/N is above 10, $\Delta B/B$ caused by $\Delta\theta$ and ΔF are estimated to be about ±1% and ±4% respectively from Figs. 5-B) and 5-C). Under this situation, ϕ is also the main factor for affecting the linear distribution.

Figure 7 shows the simulation results of the relations between $\Delta B/B$ and film thickness t. The relations between $\Delta l/l$ and the film thickness t for the exponential and error function cases are similar to those shown in Fig. 7. The plotted data indicate that $\Delta B/B$ increases with thinner films. In other words, the accuracy of the reconstructed $C(z)$ becomes worse when the film thickness decreases. For an experimental system, ϕ has a fixed value, thus the applicable limit of film thickness can be obtained according to the required accuracy of the reconstructed $C(z)$, although there is no limitation theoretically. For example, to keep $\Delta B/B$ smaller than ±10%, when ϕ is 0.3°, the limit of film thickness is about 50 nm from Fig. 7.

In our experiment, the accuracy of the rotating stage was 0.05°, and signal to noise ratio was kept above 10. The fiber bundle width was about 0.2 mm, and the distance between the fiber bundle and the illumination point was about 21.4 mm. Thus ϕ is calculated to be 0.13°. The errors of the reconstructed $C(z)$ caused by $\Delta\theta$ and ΔF are estimated to be ±1% and ±4% from Figs. 5-B) and 5-C), respectively. The errors of reconstructed $C(z)$ caused by ϕ, $\Delta\theta$, and ΔF are a cumulative error. Therefore, in order to maintain an accuracy of the reconstructed $C(z)$ of better than 10%, the error of the reconstructed $C(z)$ caused by ϕ must be smaller than ±5%. For this accuracy level and the value of ϕ, the limitation of film thickness is estimated to be about 30 nm from Fig. 7. This theoretical analysis result is verified by the experiments using the 29 nm thick LB model film sample.

Figure 8 shows the experimental and theoretical fluorescence intensity dependence on the observation angle under normal incidence conditions for the model film sample. The theoretical and experimental results are represented by a solid line and circles, respectively. The theoretical values were obtained by substituting

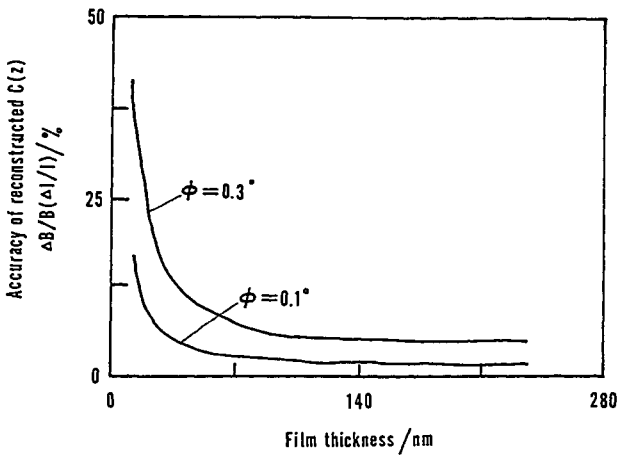

Fig. 7. Dependence of the accuracy of the reconstructed concentration depth profile on film thickness for the case that $C(z)$ is a linear function form.

$C(z)$ expressed as Eq. 6 into Eq. 1. The theoretical values agree well with the experimental ones.

With the fluorescence intensity data presented in Fig. 8, the constants A and B of the linear function form used as the test function were calculated from Eq. 5. Figure 9 shows the results of the reconstructed $C(z)$ with the actual $C(z)$ described in circles. The solid and dotted lines represent the average reconstructed $C(z)$ and its variation range for four times determinations, respectively. The average values calculated for the parameters A and B are -0.21% nm $^{-1}$ and 5.48%, respectively. As shown in Eq. 6, the values of A_0 and B_0 of the model film sample are approximately -0.19 (% nm^{-1}) and 5 (%), respectively (Fig. 3). Hence $\Delta A/A$ and $\Delta B/B$ are got as 10.5% and 9.5%, respectively. Therefore the accuracy of reconstructed $C(z)$ is about 10% which agrees well with the theoretical estimation. The model film sample consists of long chain molecular bilayers, and the concentration changes in each bilayer have been recognized with a reasonable accuracy as shown in Fig. 9. Hence the spatial resolution in the depth direction is estimated to be at least on the order of the bilayer thickness, 5.2 nm.

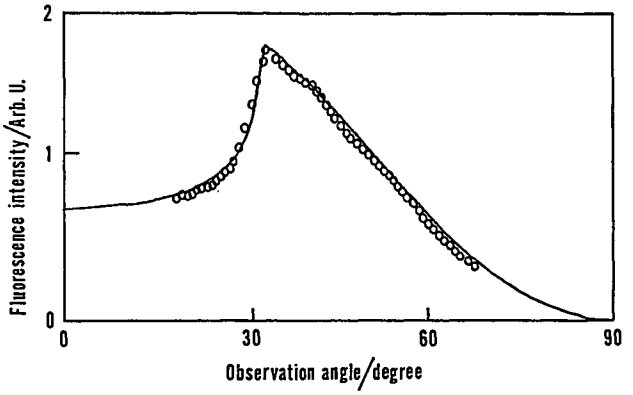

Fig. 8. Theoretical and experimental results of the angular dependency of the fluorescence intensity measured for the model sample. The theoretical values are described by the solid line, and the experimental results are plotted with circles.

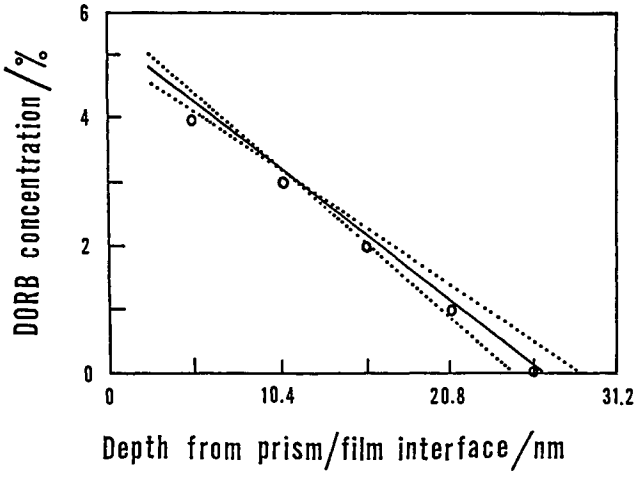

Fig. 9. Reconstructed concentration depth profile for the model film sample. The solid and dotted lines represent the average reconstructed $C(z)$ and the variation range of reconstructed $C(z)$. The circles represent the actual $C(z)$ of the model sample.

The signal to noise ratio can be improved using a more sensitive photomultiplier. For example, a photomultiplier such as Hamamatsu R923 is more sensitive by a factor of 5 than the used one in our experiments (Hamamatsu 1P21). Moreover, it can be improved further by using a photon counting technique. Therefore, the signal to noise ratio can be improved at least by a factor of 10 compared with our present experiments. This means ϕ can be decreased by a factor of 10, then the limitation of the film thickness is estimated to be 5 nm from Fig. 7, and concentration depth profiles on the nm level or molecular level are expected. In fact, Fig. 9 suggests, where the molecule is a long chain molecule, that the concentration depth profile is on the molecular level.

The authors wish to express their thanks to Professor Y. Goshi and Dr. K. Miyamura of the University of Tokyo, for their useful advice in preparation of the model LB film sample.

References

1) D. L. Taylor and Y-L. Wang, "Fluorescence Microscopy of Living Cells in Culture, Pt. B: Quantitative Fluorescence Microscopy-Imaging and Spectroscopy," "Methods in Cell Biology," Academic Press, Inc., London (1989), Vol. 30.

2) E. Kaneko, H. Tanno, and T. Yotsuyanagi, *Mikrochim. Acta*, **III**, 333 (1988).

3) A. Harata and T. Sawada, *J. Appl. Phys.*, **65**, 959 (1989).

4) T. Hirschfeld, *Appl. Spectrosc.*, **31**, 289 (1977).

5) P. W. Bohn, *Anal. Chem.*, **57**, 1203 (1985).

6) D. R. Miller, O. H. Han, and P. W. Bohn, *Appl. Spectrosc.*, **41**, 245 (1987).

7) X-Z. Wu, T. Kitamori, N. Teramae, and T. Sawada, *Bull. Chem. Soc. Jpn.*, **64**, 755 (1991).

8) P. A. Suci and W. M. Reichert, *Appl. Spectrosc.*, **42**, 120 (1988).

9) P. A. Suci and W.M. Reichert, *Lanqmuir*, **4**, 1131 (1988).

10) D. R. Miller and P. W. Bohn, *Anal. Chem.*, **60**, 407 (1988).

11) T. Albert, "Inverse Problem Theory," Elsevier, New York (1987).

The Structure of Notoryne, a Halogenated C_{15} Nonterpenoid with a Novel Carbon Skeleton from the Red Alga *Laurencia nipponica* Yamada[1)]

Hajime KIKUCHI,† Teruaki SUZUKI,* Etsuro KUROSAWA, and Minoru SUZUKI*
Department of Chemistry, Faculty of Science, Hokkaido University, Sapporo 060
(Received November 26, 1990)

A new halogenated C_{15} nonterpenoid with a novel carbon framework, named notoryne, has been isolated from the title alga and its structure was established on the basis of spectroscopic and chemical evidence. In addition, the structure of a rearranged product, whose structure has long remained unsettled, of laurefucin derivative was also determined by spectral and chemical methods. Furthermore, the biogenesis of the halogenated C_{15} nonterpenoids from *L. nipponica* collected at warm current region in Hokkaido is also discussed.

Red algae of the genus *Laurencia* are known to produce halogenated C_{15} nonterpenoid ethers containing different ring systems, which usually have a conjugated enyne or a bromoallene moiety at one end of the molecule.[2,3)] Among the Japanese species of the genus *Laurencia, L. nipponica* displayed a marked variation in the major metabolites, which seems to be mainly dependent upon the growth locality. The major metabolites from this species, collected in the warm current region in Hokkaido, are, with some exception,[4,5)]

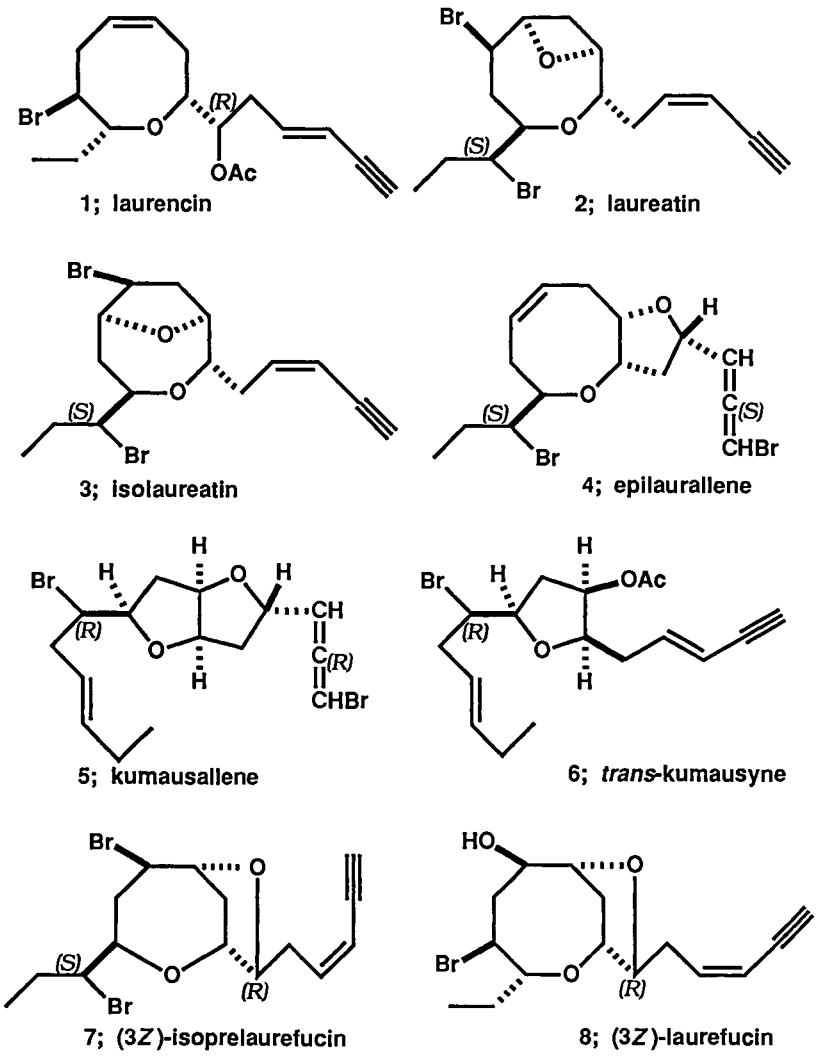

Fig. 1. The main C_{15} nonterpenoids from *Laurencia nipponica* collected in the warm current region in Hokkaido.

† Present address: Tobishi Pharmaceutical Co., Ltd., Ome 198.

composed of C_{15} nonterpenoids, e.g. laurencin (**1**),[6,15] laureatin (**2**),[7,9,15] isolaureatin (**3**),[8,9,15] epilaurallene (**4**),[10,15] kumausallene (**5**),[11,13] *trans*-kumausyne (**6**),[12,13] and (3*Z*)-isoprelaurefucin (**7**)[14] (Fig. 1).

In connection with our studies on this species growing in the warm current region in Hokkaido, we have newly made collection at Notoro Point, near Abashiri, and examined its constituents. This specimen contained (3*Z*)-laurefucin (**8**)[16] as the major metabolite and a new C_{15} nonterpenoid, which we have named notoryne, as a minor one. In this paper we report the isolation and the structure elucidation of notoryne (**9**) as well as the structure of a rearranged product **22**, which has previously been obtained from laurefucin derivative.[17] Furthermore, the biogenesis of C_{15} nonterpenoids from *Laurencia nipponica* collected at warm current region in Hokkaido is also discussed.

Notoryne (**9**), colorless oil, $[\alpha]_D$ +40.3° ($CHCl_3$), had a molecular formula of $C_{15}H_{20}BrClO_2$. The presence of a (*Z*)-2-penten-4-ynyl side chain in **9** was evident from the UV [λ_{max} 223 nm (ε 12500)], IR [ν_{max} 3300 and 2100 cm^{-1}], ^1H NMR [δ=3.13 (1H, dd, *J*=2.4 and 0.8 Hz), 5.60 (1H, dddd, *J*=10.3, 2.4, 1.3, and 1.3 Hz), and 6.08 (1H, dddd, *J*=10.8, 7.3, 7.3, and 0.8 Hz)], and mass [*m/z* 285, 283, and 281 ($M^+-C_5H_5$)] spectra. Furthermore, the ^1H NMR spectrum revealed the presence of a methyl group at δ=1.00 (3H, dd, *J*=7.3 and 7.3 Hz) and six methine groups at δ=3.88 (1H, ddd, *J*=8.3, 7.3, and 6.8 Hz), 3.91 (1H, ddd, *J*=7.3, 7.2, and 3.9 Hz), 3.98 (1H, ddd, *J*=8.3, 6.8, and 5.5 Hz), ca. 4.1 (2H, m), and 4.26 (1H, ddd, *J*=7.3, 7.3, and 5.5 Hz) which are flanked by a bromine, a chlorine, or an oxygen atom. Since the IR spectrum of **9** showed no hydroxyl and carbonyl absorptions, both oxygen atoms in **9** were assumed to be involved in ether links. Moreover, the ^{13}C NMR spectrum of **9** showed no other double bonds other than those of the conjugated enyne moiety, and hence **9** must be composed of two oxide rings.

Extensive spin decoupling experiments in the ^1H NMR spectrum of **9** indicated the presence of the following partial structure (Fig. 2) for **9**. Hydrogenation of **9** with platinum oxide in ethanol gave a hexahydro derivative **10**, $C_{15}H_{26}BrClO_2$. The ^1H NMR spectrum of **10** displayed no signals at δ=3.5—2.9 due to epoxide protons[18] and at near δ=2.7 due to methylene protons on a 1,3-disubstituted oxetane ring.[9,19] Furthermore, the mass spectrum of **10** showed no fragment ions due to a 1-halopropyl or a 1-halohexyl moiety, thus suggesting that the substituents at C-6 and C-13 must not be halogen atoms but oxygen atoms.

The FI mass spectrum of **9** showed significant fragment ions at *m/z* 285, 283, 281 (32:100:80), 179, 177 (45:45), and 171, 169 (3:10). On the other hand, the EI mass spectrum of **9** showed a base peak at *m/z* 133 and significant peaks at *m/z* 97 and 69 along with those at *m/z* 285, 283, 281, 179, and 177. The main fragmentation in both spectra would be explicable as shown in Scheme 1, leading to formula **9** as the most favor-

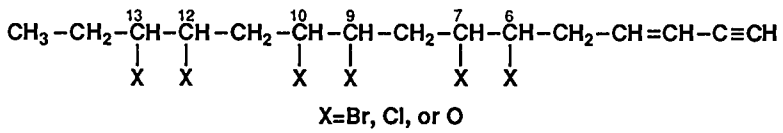

Fig. 2. Partial structure for notoryne (**9**).

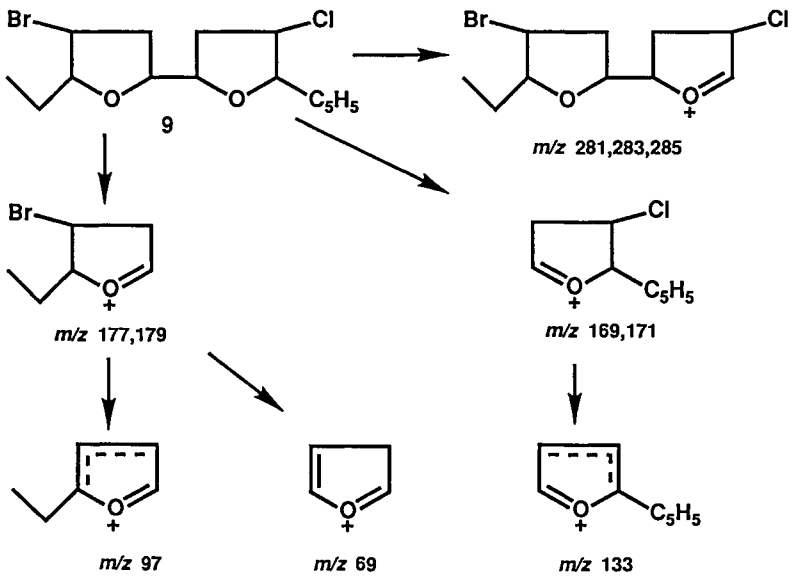

Scheme 1. The main fragmentation in the mass spectra of **9**.

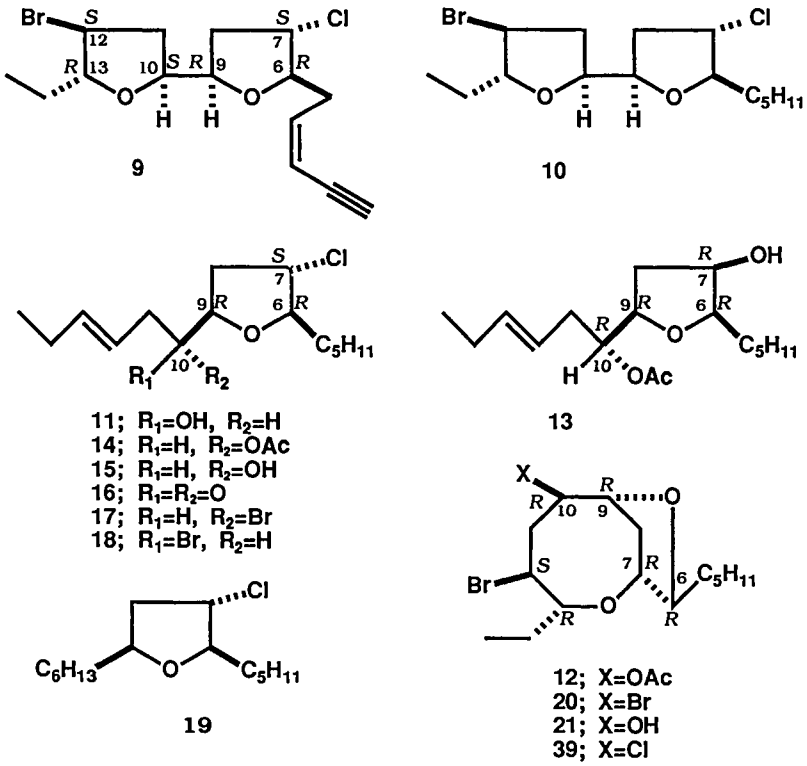

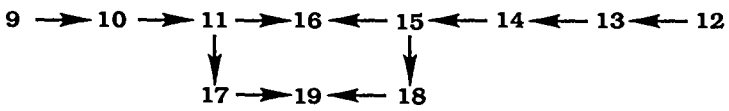

Scheme 2. Chemical correlation of **9**.

able planar structure for notoryne. Confirmation of the structure was obtained by the following chemical correlation with known compound (Scheme 2).

Treatment of **10** with zinc and acetic acid in methanol gave a chloro alcohol **11**, $C_{15}H_{27}ClO_2$, ν_{max} 3550, 3430, 3030, and 970 cm^{-1}. The ^1H NMR spectrum of **11** revealed signals due to a *trans* double bond at δ=5.34 and 5.62 (each 1H, dt, J=15 and 6 Hz). The mass spectrum of **11** showed fragment ions at m/z 207, 205 (3:9; $M^+-C_5H_{11}$) and 177, 175 (4:14; $M^+-C_6H_{11}O$), suggesting **11** possesses an oxolane ring containing a chlorine atom, a C_5-side chain, and a C_6-side chain with a hydroxyl group.

On the other hand, the acetoxy alcohol **13**,[17,20] which was obtained by treatment of hexahydroacetyllaurefucin (**12**)[17,20] with zinc and acetic acid in methanol, was treated with carbon tetrachloride and triphenylphosphine in benzene to give a chloro acetate **14**, $C_{17}H_{29}ClO_3$, whose IR spectrum showed no hydroxyl absorption. This halogenation reaction with carbon tetrahalide and triphenylphosphine usually proceeds in the S_N2 manner with inversion of configuration.[21] Therefore, the configuration at C-7 in **13** must have been inverted from *R* to *S*. Saponification of **14** with potassium carbonate in methanol yielded the corresponding chloro alcohol **15**, $C_{15}H_{27}ClO_2$, whose spectral data showed a close resemblance to those of the chloro alcohol **11** derived from **9**. Collins oxidation of both the chloro alcohols, **11** and **15**, gave the same ketone **16**, $C_{15}H_{25}ClO_2$, thus indicating that the both chloro alcohols are an epimer of the hydroxyl group at C-10. This was confirmed by the following reactions.

On treatment with carbon tetrabromide and triphenylphosphine in benzene, a chloro alcohol **11** gave a bromochloro ether **17**, $C_{15}H_{26}BrClO$. On the other hand, another chloro alcohol **15** also gave a bromochloro ether **18** on bromination with carbon tetrabromide and triphenylphosphine. Both the halo ethers **17** and **18** afforded the same tetrahydrofuran derivative **19**, $C_{15}H_{29}ClO$, by Raney nickel reduction in ethanol, thus proving that the chiral centers at C-6, C-7, C-9, and C-10 of the chloro alcohol **11** should be represented by *R*-, *S*-, *R*-, and *S*-configuration, respectively. Thus the structure of notoryne can be assigned as formula **9** except for the configurations at C-12 and C-13, which are discussed later.

Previously Fukuzawa et al.[17] have observed that a dibromo compound **20**, which was obtained by the bromination of hexahydrolaurefucin (**21**) with thionyl bromide in ether, is converted into a rearranged product

22, which has the same molecular formula of $C_{15}H_{26}Br_2O_2$ as that of **20**, on silica-gel column chromatography. The structure of this rearranged product **22** has long remained unresolved.

The spectral properties of **22** were very similar to those of hexahydronotoryne (**10**), suggesting that **22** possesses the same carbon skeleton, including an ethyl group, a pentyl group, and two bromine atoms, as that of **10**. This was confirmed by the following chemical derivation (Scheme 3).

Treatment of **10** with Raney nickel in refluxing ethanol gave a dehalogenated compound **23**, $C_{15}H_{28}O_2$. On the other hand, the rearranged product **22** was also treated with Raney nickel in ethanol at room temperature to afford a debrominated compound which was found to be identical with **23** in all respects. Above results indicated that the rearranged product **22** possesses the same stereochemistry at C-6, C-9, C-10, and C-13 as that of **10**. The locations of two bromine atoms and their stereochemistry as well as that at C-12 and C-13 were determined as follows.

Treatment of **22** with zinc and acetic acid in methanol gave two unsaturated bromo alcohols, **24** and **25**, which have the same molecular formula of $C_{15}H_{27}BrO_2$, and a glycol **26**[17,20] in 25, 49, and 16% yields, respectively. One of the bromo alcohols, compound **24** showed in its ^1H NMR spectrum the presence of two methyl groups, four methine groups, and a *trans* double bond. The mass spectrum of **24** exhibited significant fragment ions at 221, 219 ($M^+-C_6H_{11}O$) and 99 ($M^+-C_9H_{16}BrO$), arising from the C_9–C_{10} single bond cleavage. As shown in Scheme 3, the assigned structure **24** was confirmed by the correlation with the acetoxy alcohol **13** as in the case of compound **11** derived from hexahydronotoryne (**10**). Collins oxidation of **24** gave a bromo ketone **29**, which was identical with the ketone derived from **13** via a bromo acetate **27** and a bromo alcohol **28**.

Another bromo alcohol **25** also showed in its

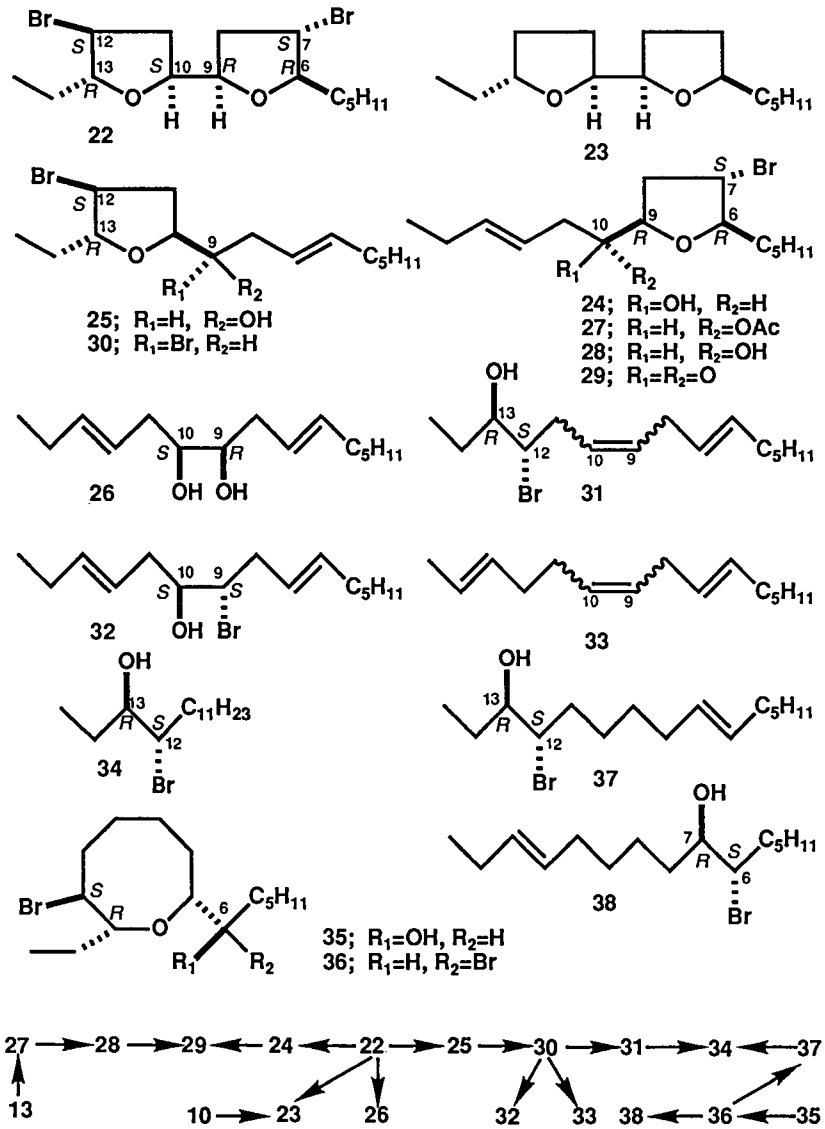

Scheme 3. Chemical correlation of the rearranged product **22**.

^{1}H NMR spectrum the presence of two methyl groups, four methine groups, and a *trans* double bond. The mass spectrum of **25** showed significant fragment ions at 179, 177 ($M^+-C_9H_{17}O$) and 141 ($M^+-C_6H_{10}BrO$), which should also be generated by C_9–C_{10} bond cleavage. These data are consistent with the assigned structure **25**, except for the configurations at C-12 and C-13. The absolute configurations at C-12 and C-13 in **25** were established by the chemical correlation to laurencin (**1**).

Treatment of **25** with carbon tetrabromide and triphenylphosphine in benzene afforded a dibromo compound **30**, $C_{15}H_{26}Br_2O$, which was then treated with zinc and acetic acid in methanol to give three products, two of which were unsaturated bromohydrins **31** and **32**, $C_{15}H_{27}BrO$. Another reduction product was an unsaturated hydrocarbon **33**, $C_{15}H_{26}$. One of the unsaturated bromohydrins, compound **31**, which was found to be a mixture of (9*Z*)- and (9*E*)-isomer (ca. 2:3) by the ^{1}H NMR (400 MHz) spectrum, was hydrogenated with PtO_2 in ethanol to yield a saturated bromohydrin **34**, $C_{15}H_{31}BrO$.

On the other hand, octahydrodeacetyllaurencin (**35**)[6] was treated with carbon tetrabromide and triphenylphosphine in benzene to give a dibromide **36**, $C_{15}H_{28}Br_2O$,[22] which was then subjected to the reduction with zinc and acetic acid in methanol to afford two unsaturated bromohydrins **37** and **38**, $C_{15}H_{29}BrO$. One of the bromohydrins, compound **37** was subsequently hydrogenated with PtO_2 in ethanol to yield a saturated bromohydrin which was identical with the bromohydrin **34** in all respects, thus indicating that the absolute configurations at C-12 and C-13 in compound **25** are assigned as *S* and *R*, respectively. Therefore, it is concluded that the structure of the rearranged product must be represented by formula **22**, including the absolute configuration.

As already mentioned above, the configuration at C-13 of hexahydronotoryne (**10**) is the same as that of the rearranged product **22**, and hence the absolute configuration at C-13 of **10** is also assigned as *R*. The configuration at C-12 of **10** was deduced from the following evidence. In the 400 MHz ^{1}H NMR spectra, the signals due to the methine protons at C-12 in compounds **10** and **22** revealed the same chemical shift and splitting pattern at δ=3.86 (ddd, J=8.3, 7.3, and 6.8 Hz). Furthermore, compound **22**, on treatment with zinc and acetic acid in methanol, gave (12*E*)-olefin **24** as a sole product. Similarly, hexahydronotoryne (**10**) also afforded only (12*E*)-olefin **11** under the same reduction conditions as in the case of **22**. Since the degradation proceeds through E2 mechanism under *trans*-periplanar arrangement of the bromine atom at C-12 and the ethereal oxygen atom at C-13, the (12*E*)-double bond in **11** and **24** should arise from *erythro* configuration between C-12 and C-13. These findings strongly indicated that the absolute configuration at C-12 of hexahydronotoryne (**10**) is *S*, the same as that of **22**.

Accordingly, the structure of notoryne, including the absolute configuration, must be shown as formula **9**.

The structural similarity between hexahydronotoryne (**10**) and the rearranged product **22** suggested that a chloro compound **39**, when treated with silica gel, would give hexahydronotoryne (**10**). As anticipated, the chloro compound **39**, prepared from hexahydrolaurefucin (**21**) by chlorination with thionyl chloride in ether, afforded hexahydronotoryne (**10**) in quantitative yield when it was treated with activated silica gel[23] in hexane at room temperature for 24 h. Furthermore, on treatment with aluminum oxide (Merck, activity II-III) or silica gel (Merck, Kieselgel 60), the chloro compound **39** gave hexahydronotoryne (**10**) and hexahydrolaurefucin (**21**) in about 20 and 80% yields, respectively. On the other hand, on treatment with activated silica gel, the dibromo compound **20** gave the rearranged product **22** in almost quantitative yield. Moreover, compound **20** afforded hexahydrolaurefucin (**21**) in quantitative yield on treatment of aluminum oxide and also afforded **22** and **21** in 40 and 60% yields on treatment with silica gel.

The mechanism of the rearrangement reactions of compounds **20** and **39** would be explained by assuming that an oxonium ion may serve as an intermediate as shown in Scheme 4.

The stereochemistry of the bromine atom at C-10 of the dibromo compound **20** was unambiguously established as a β-oriented configuration by X-ray crystallographic analysis.[24] Since the close resemblance of the chemical shifts and multiplicities in the 400 MHz ^{1}H NMR spectra of **20** and **39** indicated that the configurations at C-10 and the ring conformations in **20** and **39** are nearly identical, the configuration at C-10 in **39** must be *R*. In **20** and **39**, the 2p orbital of the lone pair on the oxygen atom of the oxocane ring is situated close to the C–X (X=Br or Cl) bond at C-10 (about 2.81 Å in the crystalline state), the formation of an oxonium ion **40** can be rationalized by transannular participation of the ether oxygen. Reactions of the resulting oxonium ion **40** with bromide ion or chloride ion at C-7 position would lead to the rearranged product **22** or hexahydronotoryne (**10**), respectively. Furthermore, reaction of cation **40** with water at C-10 position would lead to hexahydrolaurefucin (**21**).

The isomerization reactions described above suggested that notoryne (**9**) could be an artifact generated during the course of the isolation procedure, in which aluminum oxide and silica gel have been used as the absorbent for chromatography. Thus the separation was carried out with high performance liquid chromatography (Finepak SIL-C_{18} with CH_3CN–H_2O (70:30)), under whose condition the synthetic **41**, prepared from (3*Z*)-laurefucin (**8**) by chlorination with thionyl chloride in ether, was unchanged. The HPLC of the neutral oil gave notoryne (**9**) and (3*Z*)-laurefucin (**8**) in ca. 5 and 18% yields, respectively. However, compound **41** could not be detected. Furthermore, the possibility that **9** was produced during the extraction procedure can be ruled out on the basis of the following evidence. Both

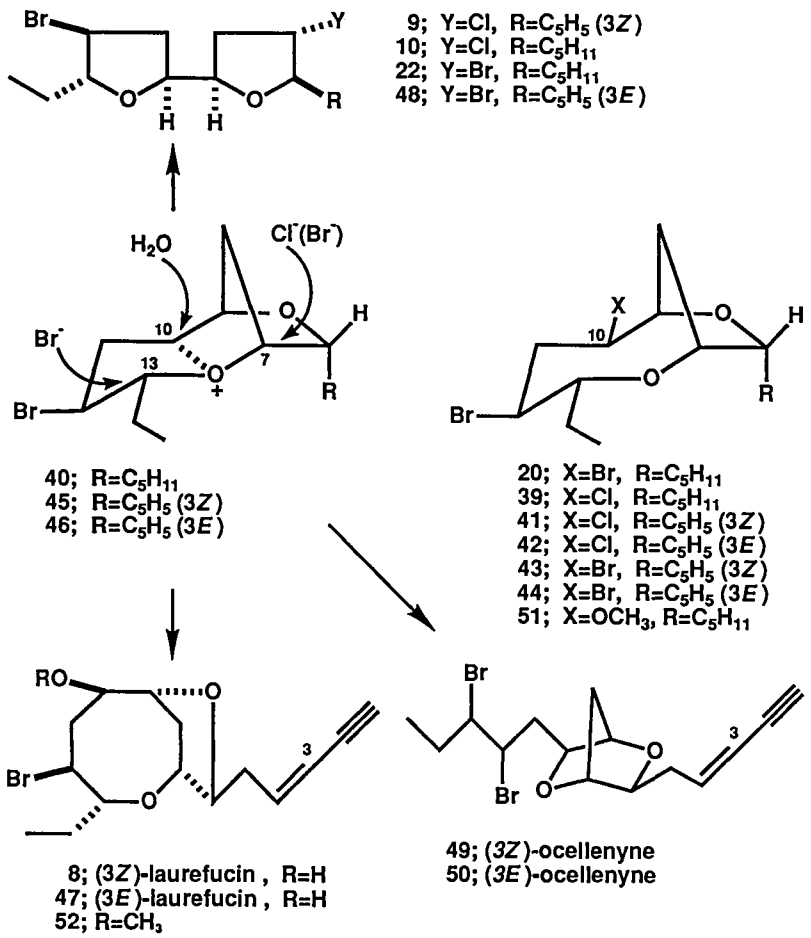

Scheme 4. Mechanism of the rearrangement reaction.

the compounds **20** and **39**, when treated with aqueous methanol, gave an *O*-methyl derivative which was identical with *O*-methylhexahydrolaurefucin (**51**) derived by hydrogenation from *O*-methyllaurefucin (**52**),[25] which has been isolated from the methanol extracts of *Laurencia nipponica* collected at several locations and must be an artifact formed during the extraction procedure. However, the neutral methanol extract of Notoro's specimen displayed the absence of *O*-methyllaurefucin (**52**). These results strongly indicate that notoryne (**9**) is a natural product.

As shown in Scheme 4, notoryne (**9**) would be enzymatically synthesized from compound **41**, designated as (3*Z*)-neoprelaurefucin, via the oxonium ion **45** by attack of chloride ion at C-7. (3*Z*)-Neoprelaurefucin (**41**) and (3*E*)-neoprelaurefucin (**42**) may serve as the precursors of (3*Z*)-laurefucin (**8**) and (3*E*)-laurefucin (**47**), formed via cations **45** and **46** by attack of water at C-10, respectively. Furthermore, compounds **43** and **44**, designated as (3*Z*)-prelaurefucin and (3*E*)-prelaurefucin, could serve also as the precursors of **8** and **47**. *O*-Methyllaurefucin (**52**) (3*E*) would be formed via the oxonium ion **46** by attack of methanol at C-10. Both neoprelaurefucins, **41** and **42**, and prelaurefucins, **43** and **44**, phantasmal metabolites, have not been isolated from natural sources. On the other hand, (3*E*)-prelaurefucin (**44**) would give a dibromide **48**, which has not yet been isolated so far, via the cation **46** by attack of bromide ion at C-7 as in the case of notoryne (**9**). More recently, lauroxolane, which has the same molecular formula and the same carbon skeleton as those of **48**, has been isolated from *Laurencia majuscula* collected off the North Shore of Oahu, Hawaii.[26] A comparison of the spectral data of lauroxolane and those of the rearranged product **22** indicates that the relative stereochemistry of lauroxolane must be different from that of **22**. Furthermore, (3*Z*)-prelaurefucin (**43**) and (3*E*)-prelaurefucin (**44**) also seem to serve as the precursors of (3*Z*)- and (3*E*)-ocellenyne, **49** and **50**, which have previously been isolated from the sea hare *Aplysia oculifera*.[27] Ocellenynes would be formed via the oxonium ion **45** and **46** by attack of bromide ion at C-13.

The C_{15} nonterpenoids isolated from *L. nipponica*, whose major representatives are shown in Fig. 1, may be derived from laurencenyne (**53**)[28,30] or *trans*-laurencenyne (**54**)[29,30,5] via (6*R*,7*R*)- or (6*S*,7*S*)-laurediols, **55** (3*E* or 3*Z*) and **56** (3*E* or 3*Z*),[31] which have also been isolated from the same alga. As illustrated in Schemes 5 and 6, the formation of cyclic ethers with various ring size can be rationalized by the cyclization of the

(9*S*,10*R*)-bromonium ions, **57** and **59**, or (12*S*,13*S*)-bromonium ions, **58** and **60**, derived from laurediols. These bromonium ions may arise from laurediols by the addition of Br^+ generated from Br^- by bromoperoxidase[32,33] to the double bonds at C-9 or C-12. Reaction of the bromonium ion **57** (3*E*) (Scheme 5) with the hydroxyl group at C-6 would lead to the bromo ethers **61** and **62**. The former bromo ether **61** is *trans*-deacetylkumausyne.[12] The latter bromo ether **62**, which has not yet been found so far, may give laureoxanyne (**63**)[34] via (12*S*,13*S*)-bromonium ion. *trans*-Deacetylkumausyne (**61**) may further afford (3*E*)-prelaurefucin (**44**) and (3*E*)-isoprelaurefucin (**64**)[35,14] also via (12*S*,13*S*)-bromonium ion. Kumausallene (**5**) may also arise from *trans*-deacetylkumausyne (**61**) by bromonium ion-catalyzed cyclization. Furthermore, reaction of the bromonium ion **57** with the hydroxyl group at C-7 would give the bromo ether **65**, which must afford laureoxolane (**66**),[36] isolated from this alga as a minor component. Reaction of the bromonium ion **58** (3*E*) with the hydroxyl group at C-7 would lead to the formation of deacetyllaurencin (**67**)[6] and deacetyliso-

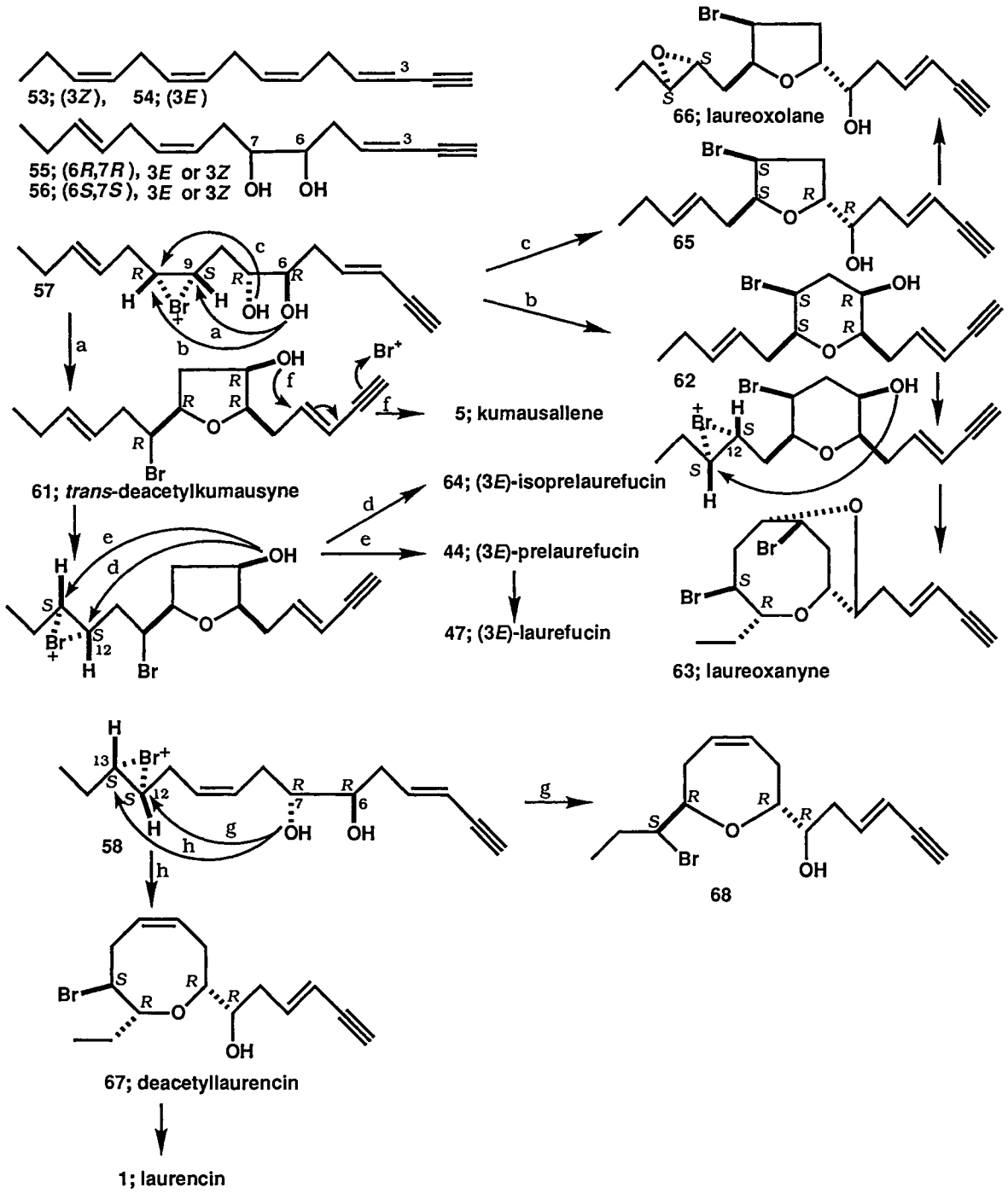

Scheme 5. Biogenesis from (6*R*,7*R*)-laurediols.

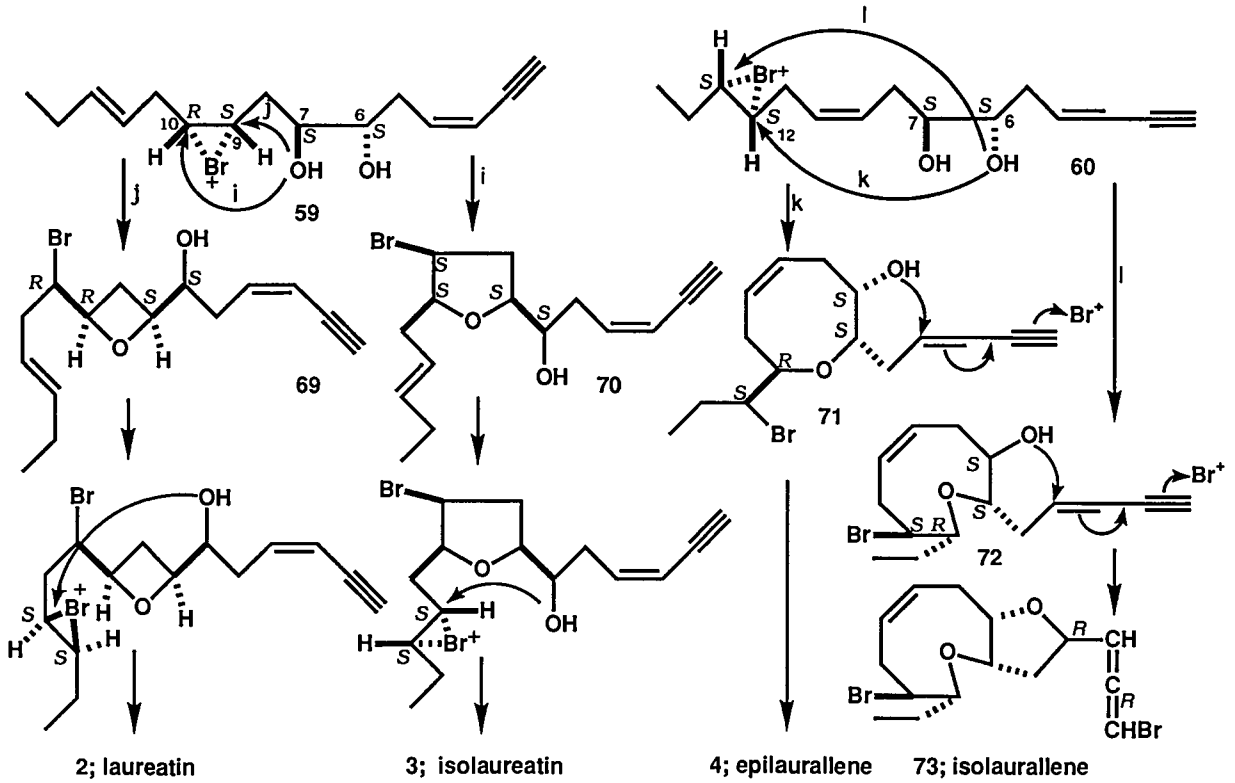

Scheme 6. Biogenesis from (6*S*,7*S*)-laurediols.

laurencin (**68**).[37]

On the other hand, on reaction with the hydroxyl group at C-7, the bromonium ion **59** (3*Z*) (Scheme 6) would give the bromo ethers **69** and **70**, from which laureatin (**2**)[7,9] and isolaureatin (**3**)[8,9] may be derived also via (12*S*,13*S*)-bromonium ions, respectively. Furthermore, reaction of the bromonium ion **60** with the hydroxyl group at C-6 would give two bromo ethers **71** and **72**. Epilaurallene (**4**)[10] or laurallene[38] may arise from the bromo ether **71** by bromonium ion-catalyzed cyclization. Similarly, the bromo ether **72** may give isolaurallene (**73**),[39] which has been isolated from this alga as a minor component.

Experimental

All the melting points were uncorrected. The IR spectra were measured on a JASCO A-102 spectrophotometer and the UV spectra on a Hitachi 124 or a Shimadzu UV-240 spectrophotometer. The ^{1}H NMR spectra were obtained in $CDCl_3$ as the solvent with TMS as the internal standard by using a JEOL JNM-FX-100, JNM-FX-400, or JNM-PS-100 spectrometer. The ^{13}C NMR spectra were recorded on a JEOL JNM-FX-100 spectrometer in $CDCl_3$ solution. The low and high resolution EI-MS spectra were measured on a JEOL JMS-D300 spectrometer, and the low FI-MS spectrum was taken with a JEOL JMS-OISG-2 spectrometer. Optical rotations were measured on a JASCO DIP-140 polarimeter in $CHCl_3$ solution. Aluminum oxide (Merck, activity II-III) and silica gel (Merck, Kieselgel 60, 70—230 mesh) were used for column chromatography. The high performance liquid chromatography (HPLC) was performed on a JASCO TRI-ROTAR using Finepak SIL-C_{18} column (JASCO).

Isolation. Half-dried alga (8 kg), which was collected at Notoro Point, near Abashiri, Hokkaido, in July 31, 1981, was extracted with MeOH and the neutral MeOH exrtract (59 g) obtained by the conventional methods was fractionated by column chromatography over standard alumina. The fraction eluted with hexane gave a mixture of hydrocarbons, which was repeatedly chromatographed on silica-gel column with hexane to yield isodihydrolaurene (2.5% of the neutral oil),[4] laurene (2.1%),[40] and *trans*-laurencenyne (0.7%).[29] The fraction eluted with benzene were further subjected to repeated column chromatography over silica gel with benzene to give nidificene,[13,41] (3*Z*)-laurediol acetate,[31] and crude notoryne which was purified by silica-gel column chromatography with hexane/benzene (1 : 3) to give pure notoryne (**9**) (5.0%). The fraction eluted with benzene/EtOAc (10 : 1) afforded debromoallolaurinterol (1.0%),[16,42] (3*Z*)-acetyllaurefucin (1.3%),[16] and (3*Z*)-7-acetyllaurediol (2.6%). The fraction eluted with EtOAc was further chromatographed on silica-gel column with benzene–EtOAc (1 : 1) to yield (3*Z*)-laurefucin (18%).[16]

Notoryne (9): Colorless oil; $[\alpha]_D$ +40.3° (*c* 1.03); UV (ethanol), λ_{max} 223 nm (ε 12500) and λ_{inf} 220 (ε 10300) and 231 nm (ε 9400); IR (neat), ν_{max} 3300, 3030, 2100, 1615, 1110, 1070, 1025, 970, 920, and 735 cm^{-1}, ^{1}H NMR (400 MHz) δ=1.00 (3H, t, *J*=7.3 Hz, H_3-15), 1.49 (1H, dqd, *J*=14.3, 7.3, 7.2 Hz, H-14), 1.76 (dqd, *J*=14.3, 7.3, 3.9 Hz, H-14), 2.17 (1H, ddd, *J*=13.2, 8.3, 8.3 Hz, H-11), 2.3 (2H, m, H_2-8), 2.59 (1H, dddd, *J*=14.8, 7.3, 7.0, 1.3 Hz, H-5), 2.66 (1H, ddd, *J*=13.2, 6.8, 6.8 Hz, H-11), 2.67 (1H, m, H-5), 3.13 (1H, dd, *J*=2.4, 0.8 Hz, H-1), 3.88 (1H, ddd, *J*=8.3, 7.3, 6.8 Hz, H-12), 3.91 (1H, ddd,

J=7.3, 7.2, 3.9 Hz, H-13), 3.98 (1H, ddd, J=8.3, 6.8, 5.5 Hz, H-10), 4.1 (2H, m, H-6 and H-7), 4.26 (1H, ddd, J=7.3, 7.3, 5.5 Hz, H-9), 5.60 (1H, dddd, J=10.8, 2.4, 1.3, 1.3 Hz, H-3), and 6.08 (1H, dddd, J=10.8, 7.3, 7.3, 0.8 Hz, H-4); ^{13}C NMR (25.0 MHz) δ=10.0 (q, C-15), 25.4 (t, C-14), 34.3 (t, C-5), 38.0 (t, C-11 or C-8), 39.3 (t, C-8 or C-11), 47.2 (d, C-12), 59.1 (d, C-7), 78.8 (d, C-13 or C-6), 79.8 (s, C-2), 79.9 (d, C-6 or C-13), 82.1 (d, C-1), 85.9 (d, C-9 or C-10), 87.0 (d, C-10 or C-9), 110.8 (d, C-3), and 139.5 (d, C-4); EI-MS (70 eV) m/z (rel intensity) 313, 311 (0.3:0.3; M^+−Cl), 285, 283, 281 (5:21:16; M^+−C_5H_5), 284, 282 (1:1; M^+−Cl−C_2H_5), 201 (3; M^+−HBr−HCl−C_2H_5), 179, 177 (3:3; M^+−$C_9H_{10}ClO$), 135 (16), 133 (100; M^+−$C_6H_{10}BrO$−HCl), 105 (14), 97 (47; M^+−$C_9H_{10}ClO$−HBr), 69 (36; M^+−$C_9H_{10}ClO$−Br−C_2H_5), 55 (8), and 41 (17); FI-MS (70 eV), m/z 350, 348, 346 (27:63:43; M^+), 285, 283, 281 (32:100:84; M^+−C_5H_5), 284, 282 (16:16; M^+−Cl−C_2H_5), 269, 267 (6:13; M^+−Br), 179, 177 (45:45; M^+−$C_9H_{10}ClO$), and 171, 169 (3:10; M^+−$C_6H_{10}BrO$). Found: m/z 282.9923. Calcd for $C_{10}H_{15}{}^{81}Br^{35}ClO_2$: M−$C_5H_5$, 282.9923.

Hydrogenation of Notoryne (9). The hydrogenation of **9** (12 mg) was performed in EtOH over PtO_2-catalyst to give an oily product which was chromatographed on silica-gel column with hexane–benzene (2:1) to afford hexahydronotoryne (**10**) (12 mg); colorless oil; $[\alpha]_D$ +52.6° (c 0.980); IR (neat), ν_{max} 1290, 1120, 1100, 1070, 1030, 970, 925, 790, and 740 cm^{-1}; ^{1}H NMR (400 MHz) δ=0.89 (3H, br t, J=6.8 Hz), 1.00 (3H, t, J=7.3 Hz), 1.2—1.6 (9H, m), 1.75 (1H, dqd, J=15.0, 7.3, 4.4 Hz), 2.13 (1H, ddd, J=13.2, 8.3, 8.3 Hz), 2.23 (2H, dd, J=7.3, 5.9 Hz), 2.65 (1H, ddd, J=13.2, 6.8, 6.8 Hz), 3.86 (1H, ddd, J=8.3, 7.3, 6.8 Hz), 3.8—4.0 (4H, m), and 4.22 (1H, ddd, J=7.3, 7.3, 5.4 Hz); EI-MS (70 eV), m/z 318, 316 (0.2:0.2; M^+−HCl), 274, 272 (0.1:0.3; M^+−HBr), 179, 177 (9:9; M^+−$C_9H_{16}ClO$), 177, 175 (8:25; M^+−$C_6H_{10}BrO$), 139 (37; M^+−HCl−$C_6H_{10}BrO$), 121 (12), 97 (100; M^+−$C_9H_{10}ClO$−HBr), 95 (15), 69 (40; M^+−$C_9H_{16}OCl$−Br−C_2H_5), 55 (14), and 41 (23).

Conversion of Hexahydronotoryne (10) into 11. To a solution of **10** (20 mg) and AcOH (80 μl) in MeOH (1 ml) was added activated Zn-dust (150 mg), and the mixture was stirred for 21 h at room temperature under N_2 atmosphere. After being filtered off and evaporated, the mixture was extracted with ether. The ethereal solution was washed successively with water, 5% aqueous $NaHCO_3$, and water. After drying over Na_2SO_4, the solvent was evaporated to give a residual oil which was purified by column chromatography over silica gel with hexane–benzene (1:3) to yield **11** (15 mg); oil; $[\alpha]_D$ +31.6° (c 0.530); IR (neat), ν_{max} 3550, 3430, 3030, 1280, 1120, 1065, 1045, 1020, and 970 cm^{-1}; ^{1}H NMR (100 MHz) δ=0.89 (3H, br t, J=6 Hz), 0.98 (3H, t, J=7 Hz), 1.1—1.8 (8H, m), 1.99 (1H, d, J=2 Hz, OH), 1.8—2.6 (6H, m), 3.79 (1H, dddd, J=7, 7, 4, 2 Hz), ca. 4.0 (2H, m), 4.11 (1H, ddd, J=8, 6, 4 Hz), 5.34 (1H, dt, J=15, 6 Hz), and 5.62 (1H, dt, J=15, 6 Hz); EI-MS (70 eV), m/z 276, 274 (1:3; M^+), 239 (21; M^+−Cl), 221 (11), 207, 205 (3:9; M^+−C_5H_9), 177, 175 (4:14; M^+−$C_6H_{11}O$), 153 (17), 139 (20; M^+−$C_6H_{11}O$−HCl), 121 (38), 99 (8: M^+−$C_9H_{16}ClO$), 95 (74), 83 (31), 81 (41), 70 (21), 69 (M^+−$C_6H_{11}O$−Cl−C_5H_{11}), 67 (28), 57 (20), 55 (95), 43 (32), and 41 (100).

Chlorination of 13 into 14. A solution of **13**[17,20] (73 mg) in dry carbon tetrachloride (1 ml) was refluxed with triphenylphosphine (81 mg) for 23 h in N_2 atmosphere and then cooled. The subsequent removal of the solvent gave an oily substance which was chromatographed over silica gel with hexane–benzene (1:1) to afford **14** (46 mg); oil; $[\alpha]_D$ +23.2° (c 0.860); IR (neat), ν_{max} 3030, 1740, 1240, 1095, 1065, 1035, 970, 945, and 710 cm^{-1}; ^{1}H NMR (100 MHz) δ=0.89 (3H, br t, J=7 Hz), 0.95 (3H, t, J=7 Hz), 1.1—1.7 (8H, m), 1.7—2.7 (6H, m), 2.07 (3H, s), 3.95 (2H, m, W_H=13 Hz), 4.24 (1H, ddd, J=8, 8, 5 Hz), 4.86 (1H, ddd, J=7, 6, 5 Hz), 5.32 (1H, dt, J=16, 7 Hz), and 5.57 (1H, dt, J=16, 6 Hz); EI-MS (70 eV), m/z 318, 316 (0.1:0.3; M^+), 281 (0.7; M^+−Cl), 258, 256 (1:3; M^+−CH_3COOH), 229 (3), 221 (50; M^+−Cl−CH_3COOH), 177, 175 (1:3; M^+−$C_8H_{13}O_2$), 153 (66), 139 (4; M^+−HCl−$C_8H_{13}O_2$), 121 (14), 95 (19), 83 (7), 82 (9), 81 (17), 69 (15; M^+−$C_8H_{13}O_2$−Cl−C_5H_{11}), 67 (8), 55 (17), 43 (100), and 41 (19).

Saponification of 14 into 15. A solution of **14** (18 mg) and K_2CO_3 (50 mg) in MeOH (0.5 ml) was stirred for 1.5 h at room temperature under N_2 atmosphere, then water was added, and most of MeOH was evaporated in vacuo. The mixture was then extracted with ether and the ethereal solution was washed with saturated brine and dried over Na_2SO_4. After removal of the solvent, the residual oil was chromatographed over silica gel with hexane–benzene (1:3) to yield **15** (15 mg); oil; $[\alpha]_D$ +28.9° (c 0.830); IR (neat), ν_{max} 3550, 3430, 3030, 1280, 1120, 1090, 1060, 1040, 970, and 720 cm^{-1}; ^{1}H NMR (100 MHz) δ=0.89 (3H, br t, J=6 Hz), 0.98 (3H, t, J=7Hz), 1.1—1.8 (8H, m), 2.10 (1H, d, J=6 Hz, OH), 1.8—2.5 (6H, m), 3.47 (1H, dddd, J=6, 6, 6, 6 Hz), 3.98 (2H, m), 4.09 (1H, ddd, J=9, 7, 5 Hz), 5.40 (1H, dt, J=16, 6 Hz), and 5.45 (1H, dt, J=16, 6 Hz); EI-MS (70 eV), m/z 276, 274 (1:3; M^+), 239 (5; M^+−Cl), 221 (4; M^+−H_2O−Cl), 207, 205 (12:37; M^+−C_5H_9), 177, 175 (2:6; M^+−$C_6H_{11}O$), 169 (4; M^+−C_5H_9−HCl), 139 (8; M^+−HCl−$C_6H_{11}O$), 121 (28), 95 (68), 93 (14), 82 (24), 80 (46), 70 (31), 69 (67; M^+−$C_6H_{11}O$−Cl−C_5H_{11}), 67 (26), 57 (16), 55 (100), 42 (26), and 41 (68).

Collins Oxidation of 11 into the Chloro Ketone 16. Collins oxidation of **11** (12 mg) was carried out with dry chromium trioxide (30 mg) in dry pyridine (46 μl) and dry CH_2Cl_2 (1 ml) by the usual method to give an oily substance which was chromatographed over silica gel with hexane–benzene (1:3) to give **16** (9 mg); oil; $[\alpha]_D$ +85.0° (c 0.367); IR (neat), ν_{max} 3030, 1715, 1305, 1300, 1115, 1075, 1045, and 970 cm^{-1}; ^{1}H NMR (100 MHz) δ=0.90 (3H, br t, J=6 Hz), 0.99 (3H, t, J=7 Hz), 1.1—1.8 (8H, m), 2.1 (2H, m), 2.40 (2H, m), 3.30 (2H, br d, J=5 Hz), 3.8—4.2 (2H, m), 4.58 (1H, t, J=8 Hz), and 5.3—5.8 (2H, m); EI-MS (70 eV), m/z 274, 272 (0.7:2; M^+), 237 (1; M^+−Cl), 210 (7), 177, 175 (20:91; M^+−C_6H_9O), 139 (36; M^+−C_6H_9O−HCl), 121 (90), 95 (100), 93 (26), 80 (13), 78 (18), 69 (70; M^+−C_6H_9O−Cl−C_5H_{11}), 67 (20), 55 (74), 43 (22), and 41 (74).

Collins Oxidation of 15 into the Chloro Ketone 16. Collins oxidation of **15** (15 mg) was carried out in the same conditions as that in the case of the oxidation of **11** to afford, after the purification by means of silica-gel chromatography, a ketone (12 mg) which was identical with the chloro ketone **16** in all respects (IR, ^{1}H NMR, MS, and specific rotation).

Bromination of 11 into 17. A solution of **11** (20 mg) in dry benzene (2 ml) was refluxed with triphenylphosphine (40 mg) and carbon tetrabromide (50 mg) for 30 min in N_2 atmosphere. The subsequent removal of the solvent gave a residual substance which was subjected to column chromatography over silica gel with hexane to yield **17** (11 mg); mp 122—123 °C (diisopropyl ether); $[\alpha]_D$ +27.6° (c 0.808); IR ($CHCl_3$), ν_{max} 3030, 1665, 1120, 1095, 1070, 1040, 1020, 970, and 925 cm^{-1}; ^{1}H NMR (100 MHz) δ=0.89 (3H, br t, J=6 Hz), 0.98 (3H, t, J=7 Hz), 1.1—1.8 (8H, m), 2.0—2.8 (6H, m), 3.8—4.1 (3H, m), 4.27 (1H, ddd, J=7, 7, 4 Hz), 5.42 (1H, dt, J=15, 6 Hz),

and 5.63 (1H, dt, J=15, 5 Hz); EI-MS (70 eV), m/z 340, 338, 336 (1:3:3; M^+), 303, 301 (12:12; M^+-Cl), 270, 268, 266 (1:3:3; $M^+-C_5H_9-H$), 259, 257 (3:9; M^+-Br), 221 (9: $M^+-Cl-Br-H$), 177, 175 (3:10; $M^+-C_6H_{10}Br$), 139 (7; $M^+-C_6H_{10}Br-HCl$), 121 (23), 111 (18), 107 (22), 95 (74), 83 (39), 81 (21), 79 (22), 69 (78; $M^+-C_6H_{10}Br-Cl-C_5H_{11}$), 67 (39), 55 (100), and 41 (97).

Bromination of 15 into 18. A solution of **15** (16 mg) in dry benzene (3 ml) was refluxed with triphenylphosphine (32 mg) and carbon tetrabromide (40 mg) for 30 min in N_2 atmosphere. After removal of the solvent, a residual oil was subjected to a column chromatography over silica gel with hexane to afford **18** (18 mg); oil; $[\alpha]_D$ +26.9° (c 1.77); IR (neat), ν_{max} 3030, 1660, 1120, 1080, 1065, 1030, 970, 920, 720, and 705 cm^{-1}; ^1H NMR (100 MHz) δ=0.89 (3H, br t, J=6 Hz), 0.99 (3H, t, J=7 Hz), 1.1—2.8 (14H, m), 3.7—4.1 (3H, m), 4.22 (1H, ddd, J=7, 7, 7 Hz), 5.41 (1H, dt, J=15, 6 Hz), and 5.62 (1H, dt, J=15, 5 Hz); EI-MS (70 eV), m/z 340, 338, 336 (1:3:3; M^+), 303, 301 (15:15; M^+-Cl), 259, 257 (3:9; M^+-Br), 258, 256 (1:3; M^+-HBr), 221 (11; $M^+-Cl-Br-H$), 177, 175 (3:10; $M^+-C_6H_{10}Br$), 151 (25), 139 (7; $M^+-C_6H_{10}Br-HCl$), 121 (22), 107 (23), 95 (59), 83 (26), 81 (23), 79 (22), 69 (55; $M^+-C_6H_{10}Br-Cl-C_5H_{11}$), 55 (100), and 41 (94).

Conversion of 17 into 19. To a solution of **17** (10 mg) in EtOH (1 ml) was added W-7 Raney nickel freshly prepared from Al-Ni alloy (2 g), and the mixture was stirred for 17 h at room temperature. After removal of the Ni, the solvent was evaporated to leave a residual oil which was chromatographed on column chromatography over silica gel with hexane-benzene (4:1) to give a chrolo ether **19** (5 mg); oil; $[\alpha]_D$ +21.6° (c 0.190); IR (neat), ν_{max} 1280, 1245, 1120, 1090, 1070, 925, and 720 cm^{-1}; ^1H NMR (100 MHz) δ=0.88 (3H, br t, J=6 Hz), 0.89 (3H, br t, J=6 Hz), 1.1—1.8 (18H, m), 1.7—2.3 (2H, m), and 3.7—4.2 (3H, m); EI-MS (70 eV), m/z 262, 260 (0.1:0.3; M^+), 191, 189 (3:9; $M^+-C_5H_{11}$), 177, 175 (30:100; $M^+-C_6H_{13}$), 139 (14; $M^+-C_6H_{13}-HCl$), 135 (23), 121 (24), 95 (36), 83 (30), 69 (54; $M^+-C_5H_{11}-C_6H_{13}-Cl$), 55 (75), 43 (42), and 41 (38).

Conversion of 18 into 19. To a solution of **18** (21 mg) in EtOH (1 ml) was added W-7 Raney nickel freshly prepared from Al-Ni alloy (2 g), and the mixture was stirred for 17 h at room temperature. After worked up as usual, the resulting oil was purified by silica-gel column chromatography with hexane-benzene (4:1) to yield an ether (10 mg) which was identical with the chloro ether **19** in all respects.

Rearranged Product 22: Oil; $[\alpha]_D$ +49.6° (c 1.02); IR (neat), ν_{max} 1290, 1205, 1200, 1115, 1095, 1065, 1030, 1000, 970, 920, 780, and 740 cm^{-1}; ^1H NMR (400 MHz) δ=0.89 (3H, br t, J=6.8 Hz), 1.00 (3H, t, J=7.3 Hz), 1.2—1.7 (9H, m), 1.75 (1H, dqd, J=15.1, 7.3, 3.9 Hz), 2.18 (1H, ddd, J=13.2, 8.3, 8.3 Hz), 2.33 (2H, dd, J=6.8, 6.8 Hz), 2.65 (1H, ddd, δ=13.2, 6.8, 6.8 Hz), 3.86 (1H, ddd, J=8.3, 7.3, 6.8 Hz), 3.8—4.0 (3H, m), 4.06 (1H, ddd, J=7.3, 4.9, 4.9 Hz), and 4.21 (1H, ddd, J=6.8, 6.8, 5.7 Hz); EI-MS (70 eV), m/z 371, 369, 367 (0.3:0.6:0.3; $M^+-C_2H_5$), 329, 327, 325 (0.7:1.4:0.7; $M^+-C_5H_{11}$), 319, 317 (1:1; M^+-Br), 318, 316 (1:1; M^+-HBr), 247, 245 (1:1; $M^+-C_5H_{11}-HBr$), 221, 219 (10:10; $M^+-C_6H_{10}BrO$), 179, 177 (14:14; $M^+-C_9H_{16}BrO$), 139 (95; $M^+-C_6H_{10}BrO-HBr$), 121 (25), 97 (100; $M^+-C_9H_{16}BrO-HBr$), 95 (26), 69 (60; $M^+-C_9H_{16}BrO-Br-C_5H_{11}$), 55 (20), and 41 (31). Found: m/z 370.9845. Calcd for $C_{13}H_{21}{}^{81}Br_2O_2$: $M-C_2H_5$, 370.9867.

Conversion of 10 into 23. To a solution of **10** (18 mg) in EtOH (3 ml) was added W-7 Raney nickel freshly prepared from Al-Ni alloy (2 g), and the mixture was refluxed for 3.5 h. After worked up as usual, the resulting oil was purified by silica-gel column chromatography with hexane-benzene (1:3) to yield a dehalogenated ether **23** (10 mg); oil; $[\alpha]_D$ −14.5° (c 0.518); IR (neat), ν_{max} 1090, 1070, 1040, and 930 cm^{-1}; ^1H NMR (100 MHz) δ=0.88 (3H, br t, J=7 Hz), 0.90 (3H, t, J=7 Hz), 1.1—2.0 (16H, m), 1.9—2.1 (2H, m), and 3.7—4.0 (4H, m); EI-MS (70 eV), m/z 240 (0.2; M^+), 211 (1; $M^+-C_2H_5$), 169 (1; $M^+-C_5H_{11}$), 141 (43; $M^+-C_6H_{11}O$), 140 (11; $M^+-C_2H_5-C_5H_{11}$), 123 (46), 99 (79; $M^+-C_9H_{17}O$), 98 (23), 81 (100), 67 (14), and 55 (37).

Conversion of 22 into 23. To a solution of **22** (18 mg) in EtOH (2 ml) was added W-7 Raney nickel freshly prepared from Al-Ni alloy (2 g), and the mixture was stirred for 1.5 h at room temperature. After worked up as usual, the residual oil was purified by silica-gel column chromatography with hexane-benzene (1:3) to give a debrominated ether (11 mg) which was identical with the ether **23** in all respects.

Partial Degradation of 22. To a solution of **22** (257 mg) and AcOH (400 μl) in MeOH (5 ml) was gradually added activated zinc dust (800 mg) with stirring for 2.5 h at room temperature under N_2 atmosphere. After the usual work-up, the resulting oil was subjected to column chromatography over silica gel with hexane-benzene (2:1) to afford three products, **24** (52 mg), **25** (101 mg), and **26** (24 mg).

24: Oil; $[\alpha]_D$ +28.5° (c 1.12); IR (neat), ν_{max} 3560, 3430, 3030, 1280, 1120, 1080, 1065, 1045, 1025, 970, and 925 cm^{-1}; ^1H NMR (100 MHz) δ=0.89 (3H, br t, J=6 Hz), 0.98 (3H, t, J=7 Hz), 1.1—1.8 (8H, m), 2.01 (1H, d, J=3 Hz; OH), 2.0—2.3 (5H, m), 2.50 (1H, ddd, J=14, 8, 8 Hz), 3.80 (1H, dddd, J=7, 7, 4, 3 Hz), 3.8—4.2 (3H, m), 5.38 (1H, dt, J=15, 6 Hz), and 5.62 (1H, dt, J=15, 5 Hz); EI-MS (70 eV), m/z 320, 318 (1:1; M^+), 302, 300 (0.5:0.5; M^+-H_2O), 251, 249 (2:2; $M^+-C_5H_9$), 250, 248 (2:2; $M^+-C_5H_9-H$), 239 (12; M^+-Br), 221 (12; M^+-H_2O-Br), 221, 219 (3:3; $M^+-C_6H_{11}O$), 169 (5; $M^+-C_5H_9-HBr$), 151 (25), 139 (37; $M^+-C_6H_{11}O-HBr$), 121 (32), 99 (9; $M^+-C_9H_{16}BrO$), 95 (52), 83 (21), 81 (44; $M^+-C_9H_{16}BrO-H_2O$), 69 (66; $M^+-C_6H_{11}O-Br-C_5H_{11}$), 67 (23), 57 (14), 55 (100), 43 (23), and 41 (70).

25: Mp 36—37 °C (hexane); $[\alpha]_D$ +6.50° (c 1.00); IR (Nujol), ν_{max} 3560, 3440, 3030, 1320, 1300, 1290, 1110, 1080, 1070, 1020, 980, 970, 935, and 920 cm^{-1}; ^1H NMR (100 MHz) δ=0.88 (3H, br t, J=7 Hz), 1.00 (3H, t, J=7 Hz), 1.1—1.9 (8H, m), 2.04 (1H, d, J=2 Hz; OH), 1.9—2.7 (6H, m), 3.7—4.1 (4H, m), 5.36 (1H, dt, J=15, 6 Hz), and 5.57 (1H, dt, J=15, 6 Hz); EI-MS (70 eV), m/z 320, 318 (1:1; M^+), 302, 300 (1:1; M^+-H_2O), 263, 261 (0.3:0.3; $M^+-C_4H_9$), 245, 243 (0.3:0.3; $M^+-H_2O-C_4H_9$), 239 (3; M^+-Br), 221 (8; M^+-Br-H_2O), 209, 207 (3:3; $M^+-C_8H_{15}$), 181 (2; $M^+-HBr-C_4H_9$), 179, 177 (4:4; $M^+-C_9H_{17}O$), 149, 147 (2:2; $M^+-C_9H_{17}O-C_2H_5-H$), 141 (2; $M^+-C_6H_{10}BrO$), 97 (65; $M^+-C_9H_{17}O-HBr$), 81 (17), 69 (100; $M^+-C_9H_{17}O-Br-C_2H_5$), 55 (16), and 41 (27).

26: Mp 95—96 °C (diisopropyl ether); $[\alpha]_D$ −3.90° (c 1.04); IR (Nujol), ν_{max} 3300, 3200, 3030, 1045, 970, and 965 cm^{-1}; ^1H NMR (100 MHz) δ=0.89 (3H, br t, J=7 Hz), 0.99 (3H, t, J=7 Hz), 1.1—1.6 (6H, m), 2.2 (2H, br d, J=3 Hz; OH×2), 1.7—2.4 (8H, m), 3.63 (2H, m), 5.40 (2H, dt, J=15, 6 Hz), 5.61 (1H, dt, J=15, 6 Hz), and 5.65 (1H, dt, J=15, 5 Hz); EI-MS (70 eV), m/z 240 (1; M^+), 222 (2; M^+-H_2O), 204 (1; $M^+-H_2O\times2$), 171 (4; $M^+-C_5H_9$), 165 (1; $M^+-C_4H_9-H_2O$), 153 (8; $M^+-C_5H_9-H_2O$), 129 (5; $M^+-C_8H_{15}$), 111 (16; $M^+-C_7H_{13}O_2$), 93 (12), 81 (23), 79 (29), 70 (19; $M^+-C_6H_{11}O-C_5H_{11}$), 69 (96; $M^+-C_{10}H_{19}O_2$), 67 (19), 57 (19), 55 (100), 43 (19), and 41 (39).

Bromination of 13 into 27. A solution of **13** (88 mg) in dry

benzene (5 ml) was refluxed with triphenylphosphine (155 mg) and carbon tetrabromide (196 mg) for 1 h in N_2 atmosphere. After removal of the solvent, the residual oily substance was subjected to column chromatography on silica gel with hexane–benzene (1 : 1) to afford **27** (106 mg); oil; $[\alpha]_D$ +26.1° (*c* 1.21); IR (neat), ν_{max} 3030, 1740, 1235, 1120, 1090, 1035, 970, and 945 cm^{-1}; ^1H NMR (100 MHz) δ=0.89 (3H, br t, *J*=6 Hz), 0.95 (3H, t, *J*=7 Hz), 1.1—2.5 (14H, m), 2.06 (3H, s), 3.96 (2H, m), 4.24 (1H, ddd, *J*=8, 8, 5 Hz), 4.87 (1H, ddd, *J*=7, 6, 5 Hz), 5.32 (1H, dt, *J*=15, 6 Hz), and 5.58 (1H, dt, *J*=15, 5 Hz); EI-MS (70 eV), *m/z* 362, 360 (0.2 : 0.2; M^+), 302, 300 (2 : 2; M^+-CH_3COOH), 221 (64; $M^+-CH_3COOH-Br$), 153 (29), 139 (14; $M^+-C_8H_{13}O_2-HBr$), 121 (13), 111 (22), 95 (16), 81 (13), 80 (13), 69 (28; $M^+-C_8H_{13}O_2-Br-C_5H_{11}$), 55 (22), 43 (100), and 41 (17).

Saponification of 27 into 28. A solution of **27** (31 mg) and K_2CO_3 (100 mg) in MeOH (1 ml) was stirred for 1.5 h at room temperature under N_2 atmosphere. After the usual work-up, the resulting oily substance was chromatographed on silica-gel column with hexane–benzene (1 : 3) to yield **28** (25 mg); oil; $[\alpha]_D$ +32.4° (*c* 1.14); IR (neat), ν_{max} 3540, 3430, 3030, 1120, 1090, 1055, 1035, and 970 cm^{-1}; ^1H NMR (100 MHz) δ=0.90 (3H, br t, *J*=6 Hz), 0.98 (3H, t, *J*=7 Hz), 1.1—2.6 (14H, m), 2.12 (1H, d, *J*=6 Hz; OH), 3.48 (1H, dddd, *J*=6, 6, 6, 6 Hz), 3.7—4.2 (3H, m), 5.42 (1H, dt, *J*=15, 6 Hz), and 5.62 (1H, dt, *J*=15, 5 Hz); EI-MS (70 eV), *m/z* 320, 318 (1 : 1; M^+), 251, 249 (26 : 26; $M^+-C_5H_9$), 239 (13; M^+-Br), 221 (15; M^+-H_2O-Br), 169 (27; $M^+-C_5H_9-HBr$), 151 (16), 139 (31; $M^+-C_6H_{11}O-HBr$), 133 (10), 123 (13), 121 (31), 95 (71), 83 (27), 81 (58; $M^+-C_9H_{16}BrO$), 70 (34), 69 (87; $M^+-C_6H_{11}O-Br-C_5H_{11}$), 67 (32), 57 (27), 55 (100), 43 (37), and 41 (85).

Collins Oxidation of 24 into the Bromo Ketone 29. Collins oxidation of **24** (12 mg) was carried out with dry chromium trioxide (31 mg) and dry pyridine (50 μl) in dry CH_2Cl_2 (1.2 ml) under the same conditions as that in the case of the oxidation of **11** to give an oily substance which was purified by silica-gel column chromatography with hexane–benzene (3 : 1) to yield **29** (10 mg); oil; $[\alpha]_D$ +66.3° (*c* 0.563); IR (neat), ν_{max} 3030, 1720, 1300, 1115, 1070, and 970 cm^{-1}; ^1H NMR (100 MHz) δ=0.90 (3H, br t, *J*=6 Hz), 0.99 (3H, t, *J*=7 Hz), 1.2—1.7 (8H, m), 2.2 (2H, m), 2.49 (2H, m), 3.30 (2H, br d, *J*=5 Hz), 3.92 (1H, ddd, *J*=6, 5, 5 Hz), 4.15 (1H, m), 4.58 (1H, dd, *J*=8, 8 Hz), and 5.3—5.8 (2H, m); EI-MS (70 eV), *m/z* 318, 316 (2 : 2; M^+), 221, 219 (16 : 16; $M^+-C_6H_9O$), 203, 201 (5 : 5), 139 (68; $M^+-C_6H_9O-HBr$), 121 (94), 95 (97), 69 (91; $M^+-C_6H_9O-Br-C_5H_{11}$), 67 (16), 55 (70), 43 (19), and 41 (100).

Collins Oxidation of 28 into the Bromo Ketone 29. Collins oxidation of **28** (12 mg) was carried out under the same conditions as that in the case of the oxidation of **24** to afford a ketone (10 mg) which was identical with the bromo ketone **29** in all respects.

Bromination of 25 into 30. Bromination of **25** (130 mg) was performed with triphenylphosphine (210 mg) and carbon tetrabromide (270 mg) in dry benzene (20 ml) to give an oily substance, which was chromatographed over silica gel with hexane to yield a dibromide **30** (80 mg); oil; $[\alpha]_D$ +26.5° (*c* 1.23); IR (neat), ν_{max} 3020, 1295, 1110, 1070, 1060, 1010, 970, and 930 cm^{-1}; ^1H NMR (100 MHz) δ=0.88 (3H, br t, *J*=6 Hz), 1.00 (3H, t, *J*=7 Hz), 1.1—2.8 (14H, m), 3.86 (1H, ddd, *J*=8, 8, 7 Hz), 3.8—4.3 (3H, m), 5.41 (1H, dt, *J*=15, 6 Hz), and 5.60 (1H, dt, *J*=15, 6 Hz); EI-MS (70 eV), *m/z* 384, 382, 380 (0.2 : 0.4 : 0.2; M^+), 327, 325, 323 (0.3 : 0.6 : 0.3; $M^+-C_4H_9$), 303, 301 (5 : 5; M^+-Br), 221 (5; $M^+-HBr-Br$), 205, 203 (1 : 1; $M^+-C_6H_{10}BrO$), 179, 177 (5 : 5; $M^+-C_9H_{16}Br$), 97 (79; $M^+-C_9H_{16}Br-HBr$), 81 (11), 79 (11), 69 (100; $M^+-C_9H_{16}Br-Br-C_2H_5$), 67 (23), 57 (20), 55 (31), 43 (10), and 41 (64).

Partial Degradation of 30. To a solution of **30** (82 mg) and AcOH (400 μl) in MeOH (5 ml) was gradually added activated zinc dust (1.5 g) with stirring for 2 h at room temperature under N_2 atmosphere. After the usual work-up, the resulting oil was chromatographed on silica gel with hexane–benzene (3 : 1) to afford three products **31** (22 mg), **32** (21 mg), and **33** (12 mg).

31: Oil; $[\alpha]_D$ −18.0° (*c* 1.68); IR (neat), ν_{max} 3530, 3380, 3020, 1100, 1055, and 970 cm^{-1}. ^1H NMR (100 MHz) δ=0.88 (3H, br t, *J*=7 Hz), 1.01 (3H, t, *J*=7 Hz), 1.1—2.2 (10H, m), 1.94 (1H, d, *J*=3 Hz; OH), 2.4—2.9 (4H, m), 3.64 (1H, m), 4.14 (1H, ddd, *J*=7, 7, 4 Hz), and 5.1—5.8 (4H, m); EI-MS (70 eV), *m/z* 304, 302 (0.1 : 0.1; M^+), 286, 284 (0.1 : 0.1; M^+-H_2O), 275, 273 (0.1 : 0.1; $M^+-C_2H_5$), 223 (3; M^+-Br), 205 (4; M^+-H_2O-Br), 165 (1; $M^+-C_4H_9-HBr$), 153, 151 (1 : 1; $M^+-C_{11}H_{19}$), 95 (15), 93 (14), 85 (15), 81 (20), 79 (29), 69 (40), 67 (38), 59 (16; $M^+-C_{12}H_{20}Br$), 57 (100; $M^+-C_{11}H_{18}BrO$), 55 (42), 43 (26), and 41 (58).

32: Oil; $[\alpha]_D$ −10.8° (*c* 1.68); IR (neat), ν_{max} 3530, 3400, 3020, 1665, 1080, 1060, 1035, and 970 cm^{-1}; ^1H NMR (100 MHz) δ=0.88 (3H, br t, *J*=7 Hz), 0.98 (3H, t, *J*=7 Hz), 1.1—1.5 (6H, m), 1.91 (1H, d, *J*=8 Hz; OH), 1.7—2.2 (4H, m), 2.31 (2H, dd, *J*=6, 6 Hz), 2.66 (2H, dd, *J*=6, 6 Hz), 3.53 (1H, dtd, *J*=8, 7, 3 Hz), 4.06 (1H, ddd, *J*=8, 7, 3 Hz), 5.36 (1H, dt, *J*=15, 7 Hz), 5.39 (1H, dt, *J*=15, 5 Hz), 5.52 (1H, dt, *J*=15, 6 Hz), and 5.65 (1H, dt, *J*=15, 6 Hz); EI-MS (70 eV) *m/z* 304, 302 (0.4 : 0.4; M^+), 286, 284 (0.2 : 0.2; M^+-H_2O), 235, 233 (2 : 2; $M^+-C_5H_9$), 223 (2; M^+-Br), 222 (1; M^+-HBr), 206 (2; $M^+-Br-OH$), 205 (8; M^+-Br-H_2O), 153 (13; $M^+-C_5H_9-HBr$), 135 (14), 83 (12), 81 (14), 70 (61; $M^+-C_9H_{16}Br-C_2H_5$), 69 (100; $M^+-C_{10}H_{18}BrO$), 67 (26), 57 (14), 55 (85), and 41 (81).

33: Oil; IR (neat), ν_{max} 3020, 1075, and 970 cm^{-1}; ^1H NMR (100 MHz) δ=0.88 (3H, t, *J*=7 Hz), 0.97 (3H, br t, *J*=7 Hz), 1.1—1.5 (6H, m), 1.7—2.2 (4H, m), 2.5—2.9 (4H, m), and 5.44 (6H, m); EI-MS (70 eV), *m/z* 206 (1; M^+), 177 (1; $M^+-C_2H_5$), 150 (2), 149 (1; $M^+-C_4H_9$), 121 (3), 108 (14), 95 (64), 93 (29), 81 (33), 80 (32), 79 (82), 69 (17), 67 (100), 57 (13), 55 (42), 43 (32), and 41 (86).

Hydrogenation of 31. Hydrogenation of **31** (14 mg) was performed in EtOH over PtO_2-catalyst. After removal of the catalyst and the solvent, the residual oil was chromatographed over silica gel with hexane–benzene (3 : 1) to give a saturated bromohydrin **34** (11 mg); oil; $[\alpha]_D$ −26.7° (*c* 0.890); IR (neat), ν_{max} 3530, 3400, 1295, 1220, 1105, 1095, 1050, and 970 cm^{-1}; ^1H NMR (100 MHz) δ=0.88 (3H, br t, *J*=6 Hz), 1.02 (3H, t, *J*=7 Hz), 1.1—2.0 (22H, m), 1.97 (1H, d, *J*=6 Hz; OH), 3.61 (1H, dddd, *J*=7, 6, 5, 3 Hz), and 4.18 (1H, ddd, *J*=9, 5, 3 Hz); EI-MS (70 eV), *m/z* 279, 277 (0.2 : 0.2; $M^+-C_2H_5$), 227 (0.2; M^+-Br), 226 (0.1; M^+-Br), 197 (1; $M^+-C_2H_5-HBr$), 149 (2), 71 (6), 59 (100; $M^+-C_{12}H_{24}Br$), 58 (5), 57 (24), 55 (5), 43 (21), and 41 (7).

Bromination of Octahydrodeacetyllaurencin (35)[6] into 36. Bromination of **35** (400 mg) was performed with triphenylphosphine (655 mg) and carbon tetrabromide (830 mg) in dry benzene (15 ml) to give an oily substance which was chromatographed over silica gel with hexane to yield a dibromide **36** (406 mg); oil; $[\alpha]_D$ −2.50° (*c* 1.08); IR (neat), ν_{max} 1185, 1115, 1090, 1070, and 1050 cm^{-1}; ^1H NMR (100 MHz) δ=0.90 (3H, br t, *J*=6 Hz), 0.99 (3H, t, *J*=7 Hz), 1.1—2.2 (18H, m), 3.4—3.8 (2H, m), and 3.8—4.2 (2H, m); EI-MS (70 eV), *m/z* 386, 384, 382 (0.1 : 0.2 : 0.1; M^+), 305, 303 (0.6 : 0.6; M^+-Br), 304,

302 (0.3 : 0.3; M^+-HBr), 247, 245 (9 : 9; $M^+-HBr-C_4H_9$), 221, 219 (4 : 4; $M^+-C_6H_{12}Br$), 165 (38), 139 (34; $M^+-C_6H_{12}Br-HBr$), 111 (12; $M^+-C_6H_{12}Br-Br-C_2H_5$), 109 (50), 97 (32), 95 (86), 81 (60), 79 (50), 69 (100), 67 (65), 55 (83), and 41 (66).

Partial Degradation of 36. To a solution of **36** (264 mg) and AcOH (800 μl) in MeOH (10 ml) was gradually added activated zinc dust (1.5 g) with stirring for 4 h at room temperature under N_2 atmosphere. After the usual work-up, the resulting oily substance was subjected to repeated silica-gel column chromatography with hexane–benzene (3 : 1) to yield **37** (40 mg) and **38** (125 mg).

37: Oil; $[\alpha]_D$ −28.9° (*c* 1.50); IR (neat), ν_{max} 3400, 3020, 1655, 1295, 1230, 1100, 1070, 1050, and 970 cm^{-1}; ^1H NMR (100 MHz) δ=0.89 (3H, br t, *J*=6 Hz), 1.02 (3H, t, *J*=7 Hz), 1.1—2.2 (19H, m), 3.60 (1H, m), 4.17 (1H, ddd, *J*=8, 6, 4 Hz), and 5.37 (2H, m); EI-MS (70 eV), *m/z* 306, 304 (1 : 1; M^+), 288, 286 (2 : 2; M^+-H_2O), 277, 275 (0.3 : 0.3; $M^+-C_2H_5$), 249, 247 (0.3 : 0.3; $M^+-C_4H_9$), 225 (1; M^+-Br), 207 (19; M^+-H_2O-Br), 151 (5; $M^+-OH-Br-C_4H_9$), 123 (35), 111 (10; $M^+-C_7H_{14}BrO$), 109 (60), 97 (16), 95 (100), 83 (19), 81 (65), 69 (83), 67 (55), 59 (79; $M^+-C_{12}H_{22}Br$), 57 (19), 55 (82), and 41 (60).

38: Oil; $[\alpha]_D$ −23.8° (*c* 0.608); IR (neat), ν_{max} 3400, 3020, 1650, 1305, 1280, 1260, 1115, 1070, 1040, 1010, and 965 cm^{-1}; ^1H NMR (100 MHz) δ=0.90 (3H, br t, *J*=6 Hz), 0.96 (3H, t, *J*=7 Hz), 1.1—2.2 (18H, m), 3.69 (1H, m), 4.18 (1H, ddd, *J*=8, 5, 3 Hz), and 5.4 (2H, m); EI-MS (70 eV), *m/z* 306, 304 (0.6 : 0.6; M^+), 288, 286 (0.3 : 0.3; M^+-H_2O), 225 (3; M^+-Br), 207 (6; M^+-Br-H_2O), 141 (7; $M^+-C_6H_{12}Br$), 123 (57), 109 (12), 95 (56), 82 (15), 81 (100), 69 (41; $M^+-C_{10}H_{20}BrO$), 67 (62), 57 (11), 55 (71), 43 (13), and 41 (61).

Hydrogenation of 37. Hydrogenation of **37** (18 mg) was performed in EtOH over PtO_2-catalyst. After removal of the catalyst and the solvent, the resulting oily substance was purified by silica-gel column chromatography with hexane–benzene (3 : 1) to give a saturated bromohydrin (18 mg) which was identical with the bromohydrin **34** in all respects.

Treatment of 39 with Activated Silica Gel. A mixture of **39** (31 mg) and silica gel (Merck, Kieselgel 60, 70—230 mesh) (1.5 g), which was activated at 140 °C for 3 h, in hexane was stirred at room temperature for 24 h. After the silica gel was filtered off and washed with ethyl acetate, the combined solvents were evaporated to leave an oily substance which was chromatographed on silica-gel column with hexane–benzene (1 : 1) to yield hexahydronotoryne (**10**) (31 mg).

Treatment of 39 with Silica Gel. A solution of **39** (20 mg) and silica gel (Merck, Kieselgel 60, 70—230 mesh) (1 g) in hexane (10 ml) was stirred at room temperature for 24 h. After being worked up as described above, the residual oily substance was chromatographed on silica-gel column with hexane–benzene (1 : 1) to give hexahydronotoryne (**10**) (4 mg) and hexahydrolaurefucin (**21**) (16 mg).

Treatment of 39 with Aluminum Oxide. A solution of **39** (19 mg) and aluminum oxide (Merck, activity II-III) (1 g) in hexane (10 ml) was stirred at room temperature for 20 h. After the aluminum oxide was filtered off and then washed with ethyl acetate, the combined solvents were evaporated to give an oily substance which was chromatographed on silica-gel column with hexane–benzene (1 : 1) to yield hexahydronotoryne (**10**) (4 mg) and hexahydrolaurefucin (**21**) (15 mg).

References

1) Part 78 of "Constituents of Marine Plants". Part 77; S. Takeda, E. Kurosawa, K. Komiyama, and T. Suzuki, *Bull. Chem. Soc. Jpn.*, **63**, 3066 (1990).

2) R. E. Moore, "Marine Natural Products," ed by P. J. Scheuer, Academic Press, New York (1978), Vol. 1, pp. 44—58.

3) K. L. Erickson, "Marine Natural Products," ed by P. J. Scheuer, Academic Press, New York (1983), Vol. 5, pp. 201—237 and 249—251.

4) T. Suzuki, H. Kikuchi, and E. Kurosawa, *Bull. Chem. Soc. Jpn.*, **55**, 1561 (1982).

5) M. Suzuki, M. Segawa, H. Kikuchi, T. Suzuki, and E. Kurosawa, *Phytochemistry*, **24**, 2011 (1985).

6) T. Irie, M. Suzuki, and T. Masamune, *Tetrahedron Lett.*, **1965**, 1091; T. Irie, M. Suzuki, and T. Masamune, *Tetrahedron*, **24**, 4193 (1968); A. F. Cameron, K. K. Cheung, G. Ferguson, and J. M. Robertson, *Chem. Commun.*, **1965**, 638; A. F. Cameron, K. K. Cheung, G. Ferguson, and J. M. Robertson, *J. Chem. Soc. B*, **1969**, 559.

7) T. Irie, M. Izawa, and E. Kurosawa, *Tetrahedron Lett.*, **1968**, 2091.

8) T. Irie, M. Izawa, and E. Kurosawa, *Tetrahedron Lett.*, **1968**, 2735.

9) T. Irie, M. Izawa, and E. Kurosawa, *Tetrahedron*, **26**, 851 (1970); E. Kurosawa, A. Furusaki, M. Izawa, A. Fukuzawa, and T. Irie, *Tetrahedron Lett.*, **1973**, 3857.

10) M. Suzuki, K. Koizumi, H. Kikuchi, T. Suzuki, and E. Kurosawa, *Bull. Chem. Soc. Jpn.*, **56**, 715 (1983).

11) T. Suzuki, K. Koizumi, M. Suzuki, and E. Kurosawa, *Chem. Lett.*, **1983**, 1639.

12) T. Suzuki, K. Koizumi, M. Suzuki, and E. Kurosawa, *Chem. Lett.*, **1983**, 1643.

13) M. Suzuki, M. Segawa, T. Suzuki, and E. Kurosawa, *Bull. Chem. Soc. Jpn.*, **56**, 3824 (1983).

14) M. Suzuki, K. Kurata, T. Suzuki, and E. Kurosawa, *Bull. Chem. Soc. Jpn.*, **59**, 2953 (1986).

15) M. Suzuki and E. Kurosawa, *Bull. Chem. Soc. Jpn.*, **60**, 3791 (1987).

16) S. J. Wratten and D. J. Faulkner, *J. Org. Chem.*, **42**, 3343 (1977).

17) A. Furusaki, E. Kurosawa, A. Fukuzawa, and T. Irie, *Tetrahedron Lett.*, **1973**, 4579.

18) K. Tori, T. Komeno, and T. Nakagawa, *J. Org. Chem.*, **29**, 1136 (1964).

19) E. Peretsch, T. Clerc, J. Seible, and W. Simon, in "Tabellen zur Strukturaufklärung organischer Verbindungen," Springer, Berlin (1981), p. H65.

20) A. Fukuzawa, E. Kurosawa, and T. Irie, *Tetrahedron Lett.*, **1972**, 3.

21) J. Hooz and S. S. H. Gilani, *Can. J. Chem.*, **46**, 86 (1968); R. G. Weiss and E. I. Snyder, *J. Chem. Soc., Chem. Commun.*, **1968**, 1358; R. G. Weiss and E. I. Snyder, *J. Org. Chem.*, **36**, 403 (1971).

22) A. Fukuzawa and E. Kurosawa, *Tetrahedron Lett.*, **21**, 1471 (1980).

23) Silica gel (Merck, Kieselgel 60, 70—230 mesh) was activated by heating at 140 °C for 3 h.

24) A. Furusaki, T. Matsumoto, H. Kikuchi, T. Suzuki, M. Suzuki, and E. Kurosawa, *Bull. Chem. Soc. Jpn.*, **56**, 2523 (1983).

25) Unpublished data.

26) I. K. Kim, M. R. Brennan, and K. L. Erickson, *Tetrahedron Lett.*, **30**, 1757 (1989).

27) G. R. Schulte, M. C. H. Chung, and P. J. Scheuer, *J. Org. Chem.*, **46**, 3870 (1981).

28) H. Kigoshi, Y. Shizuri, H. Niwa, and K. Yamada, *Tetrahedron Lett.*, **22**, 4729 (1981).
29) H. Kigoshi, Y. Shizuri, H. Niwa, and K. Yamada, *Tetrahedron Lett.*, **23**, 1475 (1982).
30) H. Kigoshi, Y. Shizuri, H. Niwa, and K. Yamada, *Tetrahedron*, **42**, 3781 (1986).
31) E. Kurosawa, A. Fukuzawa, and T. Irie, *Tetrahedron Lett.*, **1972**, 2121.
32) S. L. Neidleman and J. Geigert, in "Biohalogenation: Principles, Basic Roles and Applications," Ellis Horwood Ltd., Chichester (1986), pp. 46—84.
33) More recently Fukuzawa et al. reported the cyclization of laurediol and its derivatives with lactoperoxidase in the presence of hydrogen peroxide and sodium bromide. A. Fukuzawa, Mya Aye, M. Nakamura, M. Tamura, and A. Murai, *Chem. Lett.*, **1990**, 1287; A. Fukuzawa, Mya Aye, and A. Murai, *Chem. Lett.*, **1990**, 1579.
34) A. Fukuzawa, Mya Aye, M. Nakamura, M. Tamura, and A. Murai, *Tetrahedron Lett.*, **31**, 4895 (1990).
35) E. Kurosawa, A. Fukuzawa, and T. Irie, *Tetrahedron Lett.*, **1973**, 4135.
36) A. Fukuzawa, Mya Aye, Y. Takaya, H. Fukui, T. Masamune, and A. Murai, *Tetrahedron Lett.*, **30**, 3665 (1989).
37) Although isolaurencin has not yet been isolated so far, the related metabolite **74** has been isolated from *L. nipponica* collected at Moheji and Rumoi. Compound **74** may be formed by cyclization between the hydroxyl group at C-7 and C-12 of the (12*S*,13*S*)-bromonium ion **60** (Scheme 6) derived from (6*S*,7*S*)-laurediol (**56**) (3*Z*). The detail of the structure of **74**, which was established by the chemical correlation with laureatin (**2**), will be reported elsewhere.

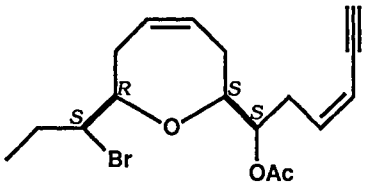

74

Fig. 3.

74: $C_{17}H_{23}BrO_3$, $[\alpha]_D$ −25.7° (*c* 0.737; $CHCl_3$), ^1H NMR (270 MHz, $CDCl_3$) δ=1.06 (3H, t, *J*=7.3 Hz), 2.09 (3H, s), 3.12 (1H, d, *J*=2.2 Hz), 3.48—3.58 (2H, m), 3.90—3.97 (1H, m), 5.04 (1H, ddd, *J*=7.7, 4.9, 4.9 Hz), 5.56 (1H, br d, *J*=10.6 Hz), 5.78 (2H, m), and 6.00 (1H, ddd, *J*=10.6, 7.0, 7.0 Hz); ^{13}C NMR (67.9 MHz, $CDCl_3$) δ=12.15 (q), 21.19 (q), 27.39(t), 31.69 (t), 32.67 (t), 34.50 (t), 61.52 (d), 74.51 (d), 77.23 (d), 80.05 (d), 82.26 (s), 82.88 (d), 110.88 (d), 128.85 (d), 128.89 (d), 140.38 (d), and 170.68 (s).

38) A. Fukuzawa and E. Kurosawa, *Tetrahedron Lett.*, **1979**, 2797.
39) K. Kurata, A. Furusaki, K. Suehiro, C. Katayama, and T. Suzuki, *Chem. Lett.*, **1982**, 1031.
40) T. Irie, T. Suzuki, Y. Yasunari, E. Kurosawa, and T. Masamune, *Tetrahedron*, **25**, 459 (1969).
41) S. W. Waraszkiewicz and K. L. Erickson, *Tetrahedron Lett.*, **1974**, 2003.
42) M. Suzuki and E. Kurosawa, *Bull. Chem. Soc. Jpn.*, **52**, 3349 (1979).

Amination of Carboxylic Acids by Reductive Fixation of Molecular Nitrogen by Glow Discharge Against Aqueous Solution

Kaoru HARADA,* Shun-ichiro IGARI, Toratane MUNEGUMI,†
Michiaki TAKASAKI, and Akira SHIMOYAMA
Department of Chemistry, University of Tsukuba, Tsukuba, Ibaraki 305
(Received November 29, 1990)

Amination of several carboxylic acids by reductive fixation of molecular nitrogen was achieved by glow discharge against aqueous solution of these carboxylic acids. The yield of the aminated product is the highest in the case of maleic acid among carboxylic acids used. The addition of hydrochloric acid to the reaction mixture enhances the yields of aminated products. This may be caused by the fact that chloride anion is oxidized by hydroxyl radicals to chlorate ion, and the fixation of molecular nitrogen proceeds under relatively reducing conditions.

Numerous experimental studies on the formation of bioorganic compounds under possible prebiotic conditions have been reported in the past three decades.[1] Most of the studies were carried out under reducing conditions, using hydrocarbon, ammonia, hydrogen, and carbon monoxide etc. However, if the temperature on the primitive earth was high (1000 °C), the chemical equilibrium of the atmosphere would have shifted to the non-reducing side as shown in Eq. 1. The resulting hydrogen gas would have escaped from the gravitational field of the earth, and the primitive atmosphere would be a mixture of nitrogen, carbon dioxide and water. This is an extreme case of the non-reducing atmosphere of the primitive earth.

$$\begin{aligned} &H_2 + 1/2O_2 \longrightarrow H_2O \\ &CO + 1/2O_2 \longrightarrow CO_2 \\ &CH_4 + 2H_2O \longrightarrow CO_2 + 4H_2 \\ &2NH_3 \longrightarrow N_2 + 3H_2 \end{aligned} \quad (1)$$

Ammonia is one of the important starting materials for the formation of nitrogen-containing bioorganic compounds under prebiotic conditions. If ammonia did not exist on the primitive earth, abiotic formation of nitrogen-containing bioorganic compounds would strongly restricted. The formation of ammonia from molecular nitrogen is thermodynamically favored when hydrogen is present at relatively low temperature (Harber–Bosch methods). However ammonia is difficult to be produced without hydrogen. And ammonia is unstable both thermally and photochemically.

Molecular nitrogen is one of the most inert diatomic molecules, and the reductive fixation of molecular nitrogen with water is thermodynamically difficult because of the large positive ΔG° value as shown in Eq. 2.

$$\begin{aligned} &4/5N_2 + 9/5H_2O \longrightarrow NH_3 + 3/5HNO_3 \\ &\Delta G^\circ = +86.2 \text{ kcal mol}^{-1} \end{aligned} \quad (2)$$

Photochemical conversion of molecular nitrogen in the presence of catalyst[2,3] and hydrolysis of nitrogen–metal complexes[4] are known as reductive fixation of molecular nitrogen, while little study has been carried out on the molecular fixation of notrogen in the absence of a catalyst.[5,6]

In our previous investigation, we reported that direct amination of carboxylic acids in aqueous ammoniacal solution by using glow discharge.[5] It was found that the reductive fixation of molecular nitrogen with water by using glow discharge yields ammonia and nitrate ion.[6] When aqueous acetic acid was added to this system, it was found that aminated product (glycine) was identified.[7]

In this paper, details of the experimental results of the amination reactions of various carboxylic acids using molecular nitrogen and water induced by glow discharge are described. And some of the additive effects on the reductive fixation of nitrogen gas was studied. Under these reactions it was found that a) ammonia and nitrate

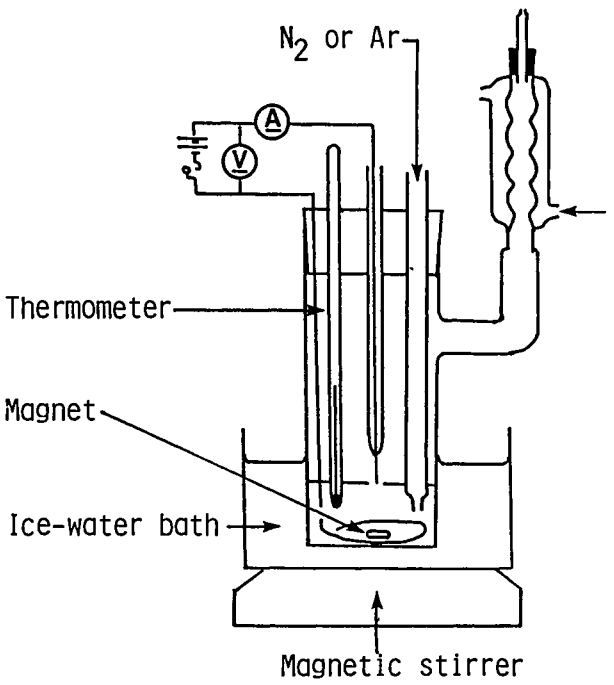

Fig. 1. Apparatus for nitrogen fixation by CGDE.

† Present address: Oyama National College of Technology, Oyama, Tochigi 323.

ions were simultaneously formed in the aqueous solution, and that b) various amino acids and aminated degradation products were formed. Formation of amino acid was chosen because of the ease of identification and also as a model for the formation of the bioorganic compounds under non-reducing conditions.

Experimental

Glow discharge was applied on the surface of water (20 ml) containing a small amount of sulfuric acid (0.025 mmol) under nitrogen atmosphere. The applied electric current was 20—50 mA at 500—600 V. The reaction temperature was kept at 25—40 °C by cooling the reaction mixture in an ice-water bath. The reaction tube for the glow discharge reaction is shown in Fig. 1. A small amount of reaction mixture was withdrawn at intervals and each sample was analyzed with an amino acid analyzer for amino acid and ammonia, and also by ion chromatography for nitrate and nitrite ions.

Results and Discussion

The experimental results of reductive fixation of molecular nitrogen are summarized in Figs. 2 and 3. As shown in Fig. 2, the amount of ammonia and nitrate ion found in the reaction mixture increased as the reaction proceeded and the concentrations of ammonia and nitrate ion were 0.45 mmol/20 ml and 0.38 mmol/20 ml, respectively, after 24 h. As a control reaction, the glow discharge was carried out in a similar way under argon atmosphere. Neither ammonia nor nitrate ion was found in the reaction mixture (Fig. 3). This whole process was also carried out without glow discharge, and ammonia or nitrate ion was not detected. Nitrite ion was not found in the reaction mixture,

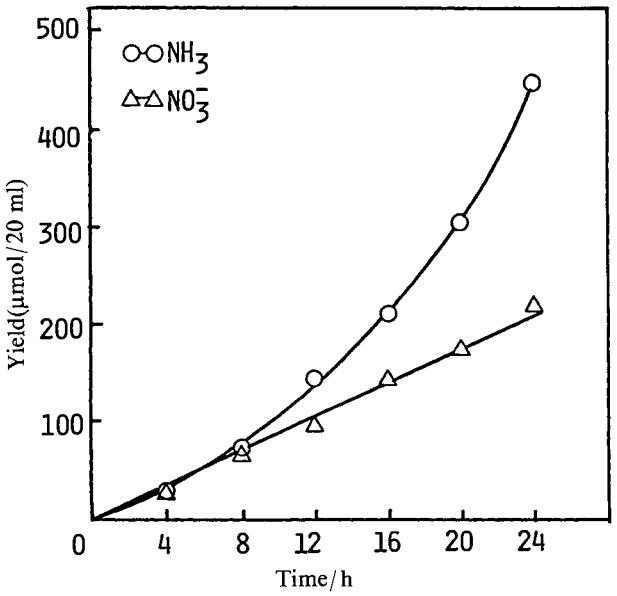

Fig. 2. Formation of NH_3 and NO_3^- from N_2 and H_2O by CGDE.
Reaction conditions: 520—600 V, 50 mA, 35—45 °C.
Substrate: H_2SO_4 0.025 mmol/20 ml H_2O–N_2.

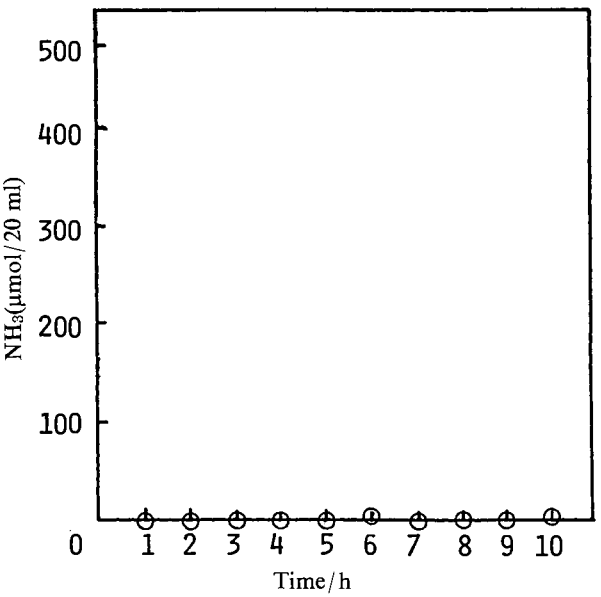

Fig. 3. Ammonia found in the reaction mixture of H_2O–Ar system by CGDE.
Reaction conditions: 720—800 V, 50—60 mA, 40—50 °C.
Substrate: H_2SO_4 0.1 mmol/20 ml H_2O–Ar.

probably because of the rapid oxidation to nitrate ion. A possible pathway for the formation of ammonia and nitrate ion could be shown as follows:

$$N_2 \longrightarrow 2N$$
$$H_2O \longrightarrow OH + H$$
$$N + H_2O \longrightarrow N + H + OH$$
$$N + nH \longrightarrow NH \longrightarrow NH_2 \longrightarrow NH_3$$
$$N + OH \longrightarrow NO_2^- \longrightarrow NO_3^-$$
$$N_2 + H_2O \longrightarrow NH_3 + NO_3^- \quad (3)$$

The nitrogen atom generated under high energy conditions is reduced with hydrogen to form NH and NH_2 radicals, and finally NH_3. Therefore, if some suitable organic amino acceptor is present in the reaction mixture, the glow discharge reaction could result in the formation of several amino compounds. In this study, several aliphatic carboxylic acids were used and the time course of the resulting amino compounds was shown in Figs. 4—9. Carboxylic acids used were acetic acid, propionic acid, succinic acid, acrylic acid and maleic acid in the glow discharge reaction using molecular nitrogen and water. The effect of added sodium chloride and hydrochloric acid on the reductive amination of molecular nitrogen was also studied (Figs. 10—12).

Figure 4 shows the time course of the amination reaction of aqueous acetic acid (10%, 20 ml) by glow discharge under nitrogen atmosphere. The aminated product, glycine, and the aminated degradation product, methylamine, were confirmed. The yields of these aminated products are smaller than those from the reaction of other carboxylic acids.

Figure 5 shows the time course of the amination

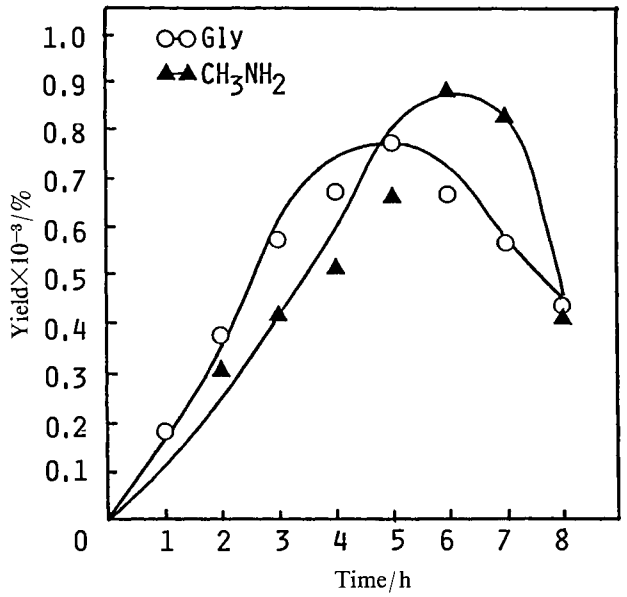

Fig. 4. The amination of acetic acid by CGDE.
Reaction conditions: 540—640 V, 40—50 mA, 30—40 °C.
Substrate: acetic acid 33 mmol/H_2O(total 20 ml) -N_2.

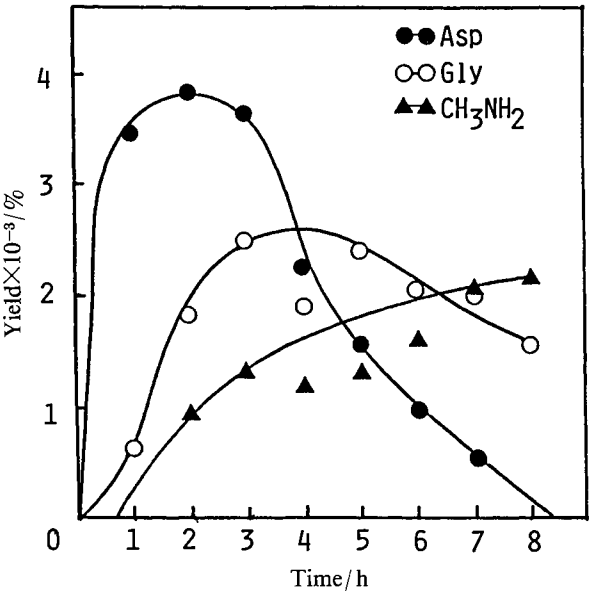

Fig. 6. The amination of succinic acid by CGDE.
Reaction conditions: 560—620 V, 50 mA, 35—45 °C.
Substrate: succinic acid 10 mmol/H_2O(total 20 ml) -N_2.

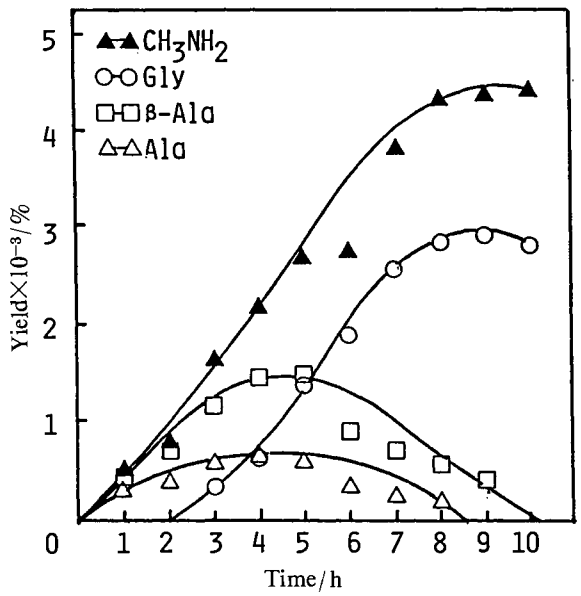

Fig. 5. The amination of propionic acid by CGDE.
Reaction conditions: 560—680 V, 40—60 mA, 35—45 °C.
Substrate: propionic acid 27 mmol/H_2O(total 20 ml) -N_2.

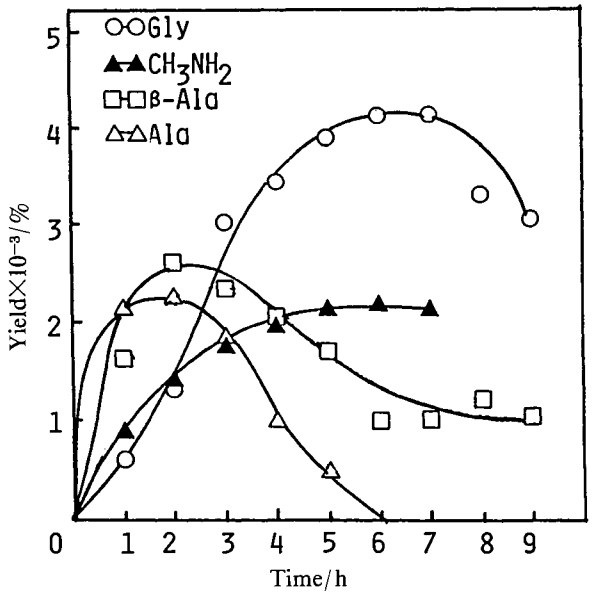

Fig. 7. The amination of acrylic acid by CGDE.
Reaction conditions: 560—600 V, 40—60 mA, 35—45 °C.
Substrate: acrylic acid 8.3 mmol, H_2O(total 20 ml) -N_2.

reaction of propionic acid (10%, 20 ml). β-Alanine and alanine were confirmed as aminated products. The ratio of β-ala : ala after 1 h was roughly 1.5 : 1. Methylamine and glycine, which are the aminated degradation products, were also confirmed. This indicates that the C–C bond could easily be cleaved under the conditions used.

Figure 6 shows the amination of succinic acid (10 mmol/20 ml). The directly aminated product, aspartic acid, formed first, and the aminated degradation products, glycine and methylamine, increased with time. The yields were similar to the case of propionic acid.

Figure 7 shows the time course of amination of acrylic acid (3%, 20 ml) with nitrogen. In this case the concen-

tration of acrylic acid was reduced in order to avoid radical polymerization of the unsaturated carboxylic acid. The direct amination product, β-alanine and alanine, were formed first and the yields of aminated degradation products, glycine and methylamine, increased with the reaction time. The yield of alanine reached almost zero after 6 h in the reaction, while the yield of β-alanine remained at the higher level at that time. This suggests that β-alanine might be formed from the degradation products, for example, by the coupling of methylamine and acetic acid.

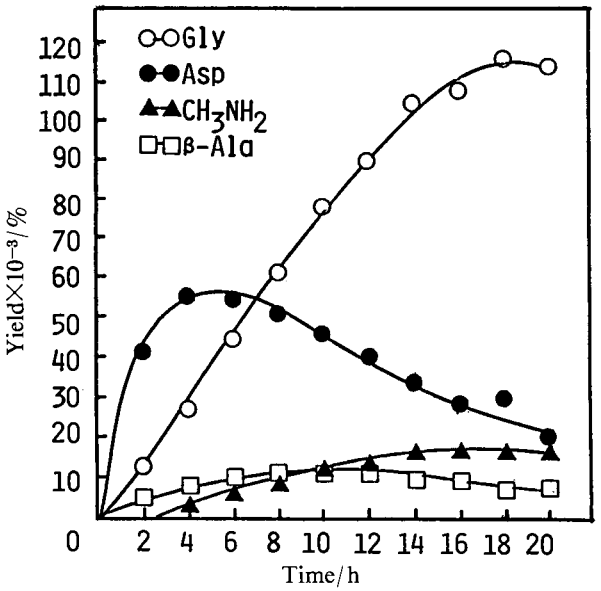

Fig. 8. The amination of maleic acid by CGDE.
Reaction conditions: 460—500 V, 20 mA, 10—20 °C.
Substrate: maleic acid 10 mmol/H_2O(total 20 ml) -N_2.

Figure 8 shows the amination of maleic acid by glow discharge under nitrogen atmosphere. Direct amination product, aspartic acid, was synthesized first, and the aminated degradation products, glycine, methylamine, and β-alanine, were formed with the reaction proceeded. The yields of aminated products in this reaction were much higher (>50×) than those of the other carboxylic acids.

As was described earlier, the direct amination of aliphatic carboxylic acids by using electric discharge was possible in relatively high concentration of aqueous ammonia.[5] In this reductive fixation of nitrogen by using electric discharge, a small amount of ammonia was formed in aqueous solution. Therefore, it is worthwhile to investigate whether the direct amination of carboxylic acid in such a low ammonia concentration proceeds or not under the high energy conditions. When glow discharge was applied to the N_2–H_2O system for 24 h, 450 mol/20 ml of ammonia was produced. The concentration of ammonia is equivalent to about 0.03% aqueous ammonia. Therefore, glow discharge was applied to 10% acetic acid (20 ml) containing 0.03% ammonia. The time course of the reaction is shown in Fig. 9. The highest yield of glycine and methylamine reach 3×10^{-3} and 2×10^{-3}%, and the formation of β-alanine and aspartic acid was confirmed. The yields are higher than those obtained by using molecular nitrogen.

In the following investigation, the effect of additives

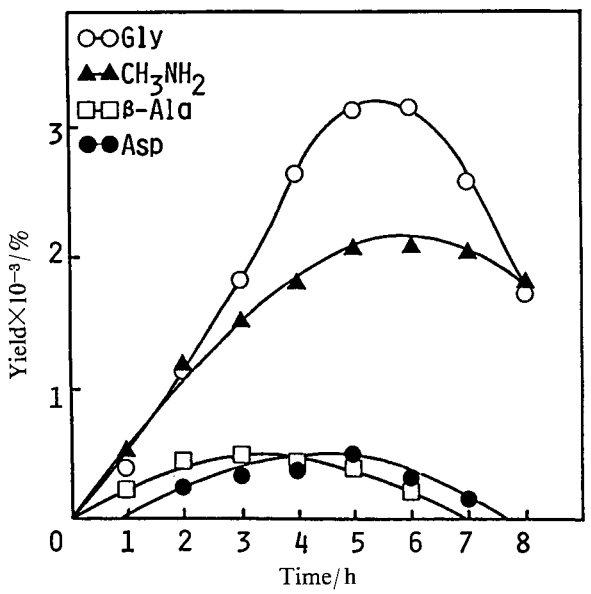

Fig. 9. The amination of acetic acid by CGDE.
Reaction conditions: 540—640 V, 40—60 mA, 35—45 °C.
Substrate: ammonia 17 mmol+acetic acid 33 mmol/H_2O(total 20 ml) -N_2.

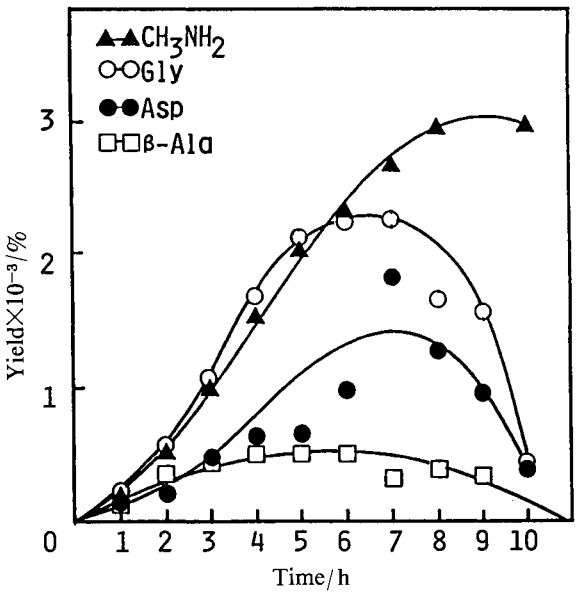

Fig. 10. The amination of acetic acid by CGDE in the presence of NaCl.
Reaction conditions: 520—560 V, 20—40 mA, 20—30 °C.
Substrate: acetic acid 33 mmol, 0.09M-NaCl/H_2O(total 20 ml) -N_2.

(NaCl and HCl) in the reductive amination of carboxylic acids is described. Because chloride anion could be oxidized under the reaction conditions, this might enhance the yields in the reductive amination of nitrogen molecule. The effect of sodium chloride in the amination reaction of acetic acid is shown in Fig. 10. The yield of glycine increased about three times compared with that of reactions without sodium chloride. The yields of other aminated secondary products, methylamine, glycine, β-alanine, and aspartic acid, were also higher than the case without sodium chloride.

The effect of hydrogen chloride addition was investigated in the reaction with acetic acid. The time course of the formation of aminated products using 0.1 M HCl (1 M=1 mol dm^{-3}) is shown in Fig. 11. In addition to the direct amination product, glycine, aminated secondary products, methylamine, β-alanine, and aspartic acid, were synthesized in higher yields. The yield of glycine is much higher (×30) compared with the yields without hydrogen chloride. When the concentration of hydrogen chloride was reduced to 0.01 M, the yield of glycine decreased, but, the yield was still four times higher than that without hydrogen chloride (Fig. 12). Therefore, the effect of hydrogen chloride in the reductive amination by glow discharge in aqueous solution is significant. Similarly, the effect of hydrogen chloride in the reductive amination of maleic acid is shown in Fig. 13. When the concentration of hydrochloric acid was 0.01 M, the yield of aspartic acid is similar to that obtained without hydrochloric acid. However, when the concentration of HCl was increased to 0.1 M, the yields of aspartic acid and glycine increased roughly twice. The formation of chlorate ion (ClO_3^-) was confirmed in the reaction mixture by ion chromatography. This indicates that chloride ion (Cl^-) was oxidized to chlorate ion by hydroxyl radicals ($Cl^- \rightarrow [ClO^-]$

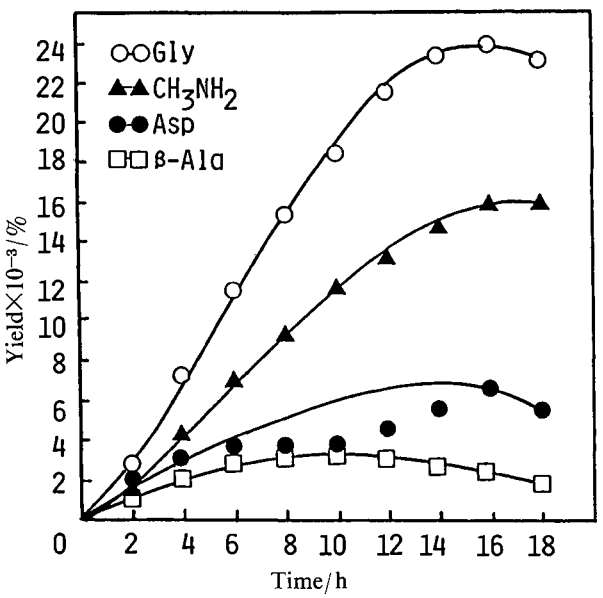

Fig. 11. The amination of acetic acid by CGDE in the presence of HCl.
Reaction conditions: 480—500 V, 20 mA, 10—20 °C.
Substrate: acetic acid 33 mmol, 0.09M-HCl/H_2O(total 20 ml) -N_2.

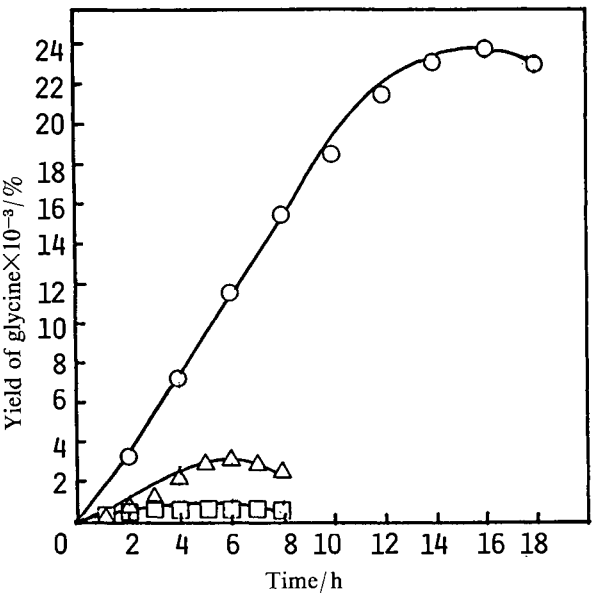

Fig. 12. The amination of acetic acid by CGDE in the presence of HCl.
Reaction conditions: ○—○ 480—500 V, 20 mA, 10—20 °C. △—△ 520—600 V, 40 mA, 30—40 °C. □—□ 540—640 V, 40—50 mA, 35—45 °C.
Substrate: ○—○ acetic acid 33 mmol, 0.09 M-HCl(total 20 ml)-N_2; △—△ acetic acid 33 mmol, 0.009 M-HCl(total 20 ml)-N_2; □—□ acetic acid, H_2O(total 20 ml)-N_2.

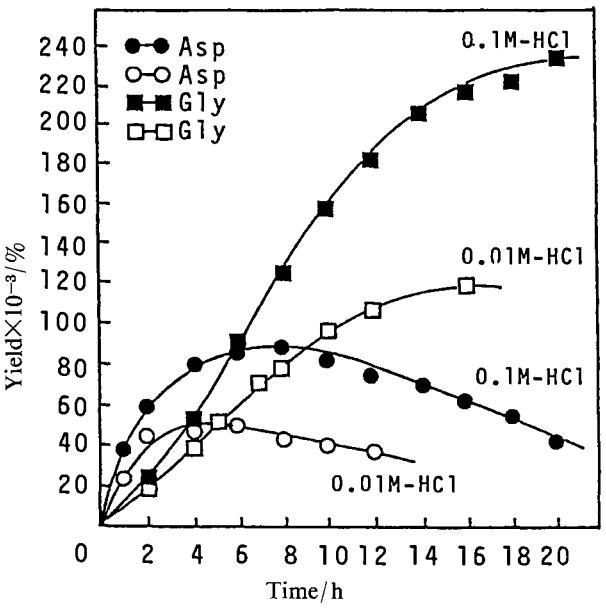

Fig. 13. The amination of maleic acid by CGDE in the presence of HCl.
Reaction conditions: 440—460 V, 20 mA, 10—20 °C.
Substrate: △—△, ○—○ maleic acid 10 mmol/0.01M-HCl(total 20 ml)-N_2; ■—■, ●—● maleic acid 10 mmol/0.1M-HCl(total 20 ml)-N_2.

$\rightarrow ClO_3^-$). When the Cl^- concentration decreased to 55% of the initial concentration of hydrogen chloride (0.1 M), the yield of ClO_3^- reached 45% after glow discharge for 12 h. This suggests that Cl^- serves as a scavenger for hydroxyl radicals, therefore forming relatively reducing reaction conditions, and increasing the yields of reductive amination products.

The formation of ammonia and nitrate ion from molecular nitrogen and water is a new type of chemical reaction that could be regarded as a disproportionation reaction under high energy conditions. The reaction is not controlled thermodynamically. The simultaneous formation of reduced (ammonia) and oxidized (nitrate ion) compounds could be explained by the decomposition of nitrogen and water molecules under high energy conditions and the recombination of the resulting radicals. The active species in the ammination reaction could be NH or NH_2 radicals formed by the coupling reaction of nitrogen and hydrogen atoms generated by glow discharge. The ratio of ala : β-ala produced from propionic acid (1 : 1.5) was similar to that obtained in NH radical reaction to propionic acid (1 : 1.6).[7,8] This indicates that the amination of carboxylic acid by reductive fixation of molecular nitrogen under high energy conditions may proceed via a radical mechanism.

The reductive fixation reaction of molecular nitrogen with water is not only interesting chemically, but also interesting from the point of view of chemical evolution. This type of reaction could be regarded as a model experiment to examine the effect of lightning struck on the hydrosphere in a non-reducing atmosphere (composed mainly of H_2O, N_2, and CO_2) on the primitive earth. The lightning may induce various chemical reactions under aqueous conditions, which could produce various bioorganic compounds that cannot arise thermodynamically.

References

1) S. L. Miller and L. E. Orgel, "The Origins of Life on the Earth," Prentice Hall Inc., Englewood Cliffs, New Jersey, U.S.A. (1974); S. Fox and K. Dose, "Molecular Evolution and the Origins of Life," 2nd ed, Marcel Dekker, New york (1977); A. G. Cairns-Smith, "Genetic Takeover and the Mineral Origins of Life," Cambridge University Press, New York (1982).

2) G. N. Schrauzer and T. D. Guth, *J. Am. Chem. Soc.*, **99**, 7189 (1977).

3) R. I. Bickley and V. Vishwanathan, *Nature*, **280**, 306 (1979).

4) J. Chat, J. R. Dilworth, and R. L. Richards, *Chem. Rev.*, **78**, 589 (1978).

5) K. Harada and T. Iwasaki, *Nature*, **250**, 426 (1974).

6) K. Harada, S. Igari, M. Takasaki, and A. Shimoyama, *J. Chem. Soc., Chem. Commun.*, **1986**, 1384.

7) S. Sano, T. Kitamura, and S. Tsunashima, *Chem. Lett.*, **1980**, 687.

8) S. Tsunashima, T. Kitamura, and S. Sano, *Bull. Chem. Soc. Jpn.*, **54**, 2869 (1981).

Some Unusual Properties of Tris(2,6-dimethoxyphenyl)phosphine Sulfide and the Related Compounds

Masanori WADA,* Mitsuyuki KANZAKI, Masanobu FUJIWARA, Kazuhisa KAJIHARA, and Tatsuo ERABI
Department of Materials Science, Faculty of Engineering, Tottori University, Koyama, Tottori 680
(Received December 11, 1990)

The title sulfide {2,6-$(MeO)_2C_6H_3$}$_3$P=S [abbr. $(2,6)_3$P=S] reacted with acids to form a novel mercaptophosphonium salt [$(2,6)_3$P–SH]X, solution thermolysis of which in the absence or presence of triphenylphosphine resulted in the unusual desulfurization to give the tertiary phosphonium salts [$(2,6)_3$P–OH]X. $(2,6)_3$P=S also reacted with alkyl iodides or bromides under mild conditions to give stable (alkylthio)phosphonium salts [$(2,6)_3$P–SR]X (R=Me, Et, n-Bu), which reacted with thiols at room temperature in the presence of a catalytic amount of the tertiary phosphine $(2,6)_3$P to give [$(2,6)_3$P–H]X and unsymmetrical disulfides.

Triphenylphosphines bearing methoxyl substituents at 2,6-positions of the phenyl groups, such as {2,6-$(MeO)_2C_6H_3$}$_3$P [abbr. $(2,6)_3$P, see Fig. 1], exhibit high basicities and nucleophilicities.[1–3] In our previous paper, we reported some unusual physical and chemical properties of the oxide $(2,6)_3$P=O.[4] In the present paper, we report the details of some unusual properties of its sulfide $(2,6)_3$P=S towards acids and alkyl halides. The preliminary results have been reported elsewhere.[5,6]

Results and Discussion

Preparation and Desulfurization of Mercaptophosphonium Salts. The tertiary phosphine $(2,6)_3$P reacted easily with elemental sulfur in toluene at room temperature to give its sulfide $(2,6)_3$P=S [step (1) of Scheme 1].

In contrast to triphenylphosphine sulfide Ph_3P=S, an addition of 60% $HClO_4$ to a solution of $(2,6)_3$P=S in acetone resulted in immediate precipitation of a novel mercaptophosphonium salt [$(2,6)_3$P–SH]ClO_4 [step (2)]. To our further surprise, when [$(2,6)_3$P–SH]ClO_4 was heated in 2-propanol, it was partly desulfurized to give an equilibrated mixture of [$(2,6)_3$P–H]ClO_4 and [$(2,6)_3$P–SH]ClO_4 in a ratio of 71 : 29 [step (3)]. Heating a solution of $(2,6)_3$P=S in ethyl methyl ketone (MEK) containing aqueous HCl also gave [$(2,6)_3$P–H]$^+$ salt (55% yield). Analogous results were obtained using methanol or 2-propanol as the solvent. The reversibility [step (3')] was confirmed by treating [$(2,6)_3$P–H]Cl·2.5H_2O with sulfur in acetone.

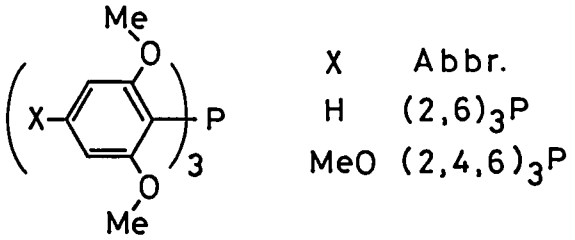

Fig. 1.

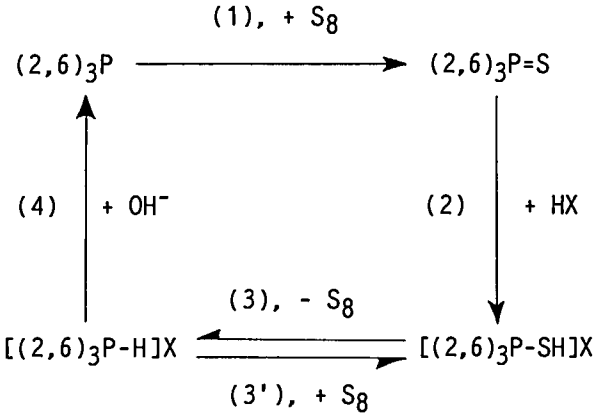

Scheme 1.

Since [$(2,6)_3$P–H]$^+$ salts are easily deprotonated by aqueous sodium hydroxide to give $(2,6)_3$P in quantitative yields [step (4)], the combination of these reactions [steps (2)–(4)] may be used to reduce $(2,6)_3$P=S to $(2,6)_3$P *without using any reducing reagent.*

Although other sulfides $(2,6)_2$PhP=S, $(2,6)Ph_2$P=S, and $(2\text{-}MeOC_6H_4)_3$P=S were prepared from the corresponding tertiary phosphine and elemental sulfur, we had no evidence for the formation of their mercaptophosphonium salts. These sulfides, as well as Ph_3P=S, were stable against the desulfurization in solutions containing HCl or $HClO_4$ even at 70 °C for 8 h. Tris(2,4,6-trimethoxyphenyl)phosphine sulfide $(2,4,6)_3$P=S [(2,4,6)= 2,4,6-$(MeO)_3C_6H_2$], on the other hand, gave a complex mixture containing 1,3,5-trimethoxybenzene, the protonation product at C(–P).

When $(2,6)_3$P=S was treated with Ph_3P in acetone containing HCl at 50 °C for 3 h, a mixture of [$(2,6)_3$P–H]Cl·2.5H_2O and Ph_3P=S was obtained both in quantitative yields. $(2,6)_2$PhP=S also reacted with Ph_3P in the presence of acid to give [$(2,6)_2$PhP–H]$^+$ salt[1] and Ph_3P=S, but $(2,6)Ph_2$P=S and $(2\text{-}MeOC_6H_4)_3$P=S were recovered almost unreacted.

Reactions of Triarylphosphine Sulfides with Alkyl Halides. Although an (alkylthio)phosphonium salt is a key intermediate in the reactions or formation of organodisulfides,[7] its isolation from these reaction mixtures is generally very difficult.[8] We found that $(2,6)_3$P=S reacted very easily with alkyl iodide (RI=MeI, EtI, *n*-BuI) in benzene at room temperature to give imme-

diately precipitates of $[(2,6)_3P–SR]I$ [step (2) of Scheme 2]. The reactions with alkyl bromides were slower under analogous conditions, but $(2,6)_3P=S$ reacted both with EtBr and BuBr in ethanol on heating at 60 °C for 2 h. $(2,6)_2PhP=S$ also reacted with methyl iodide at room temperature to give $[(2,6)_2PhP–SMe]I$, but neither $(2,6)Ph_2P=S$ nor $Ph_3P=S$ reacted with these alkyl halides under these conditions.

The bromides $[(2,6)_3P–SR]Br$ are soluble and stable in water, and an addition of 60% aqueous perchloric acid to the aqueous solution gave the precipitates of $[(2,6)_3P–SR]ClO_4$. These (alkylthio)phosphonium salts are thermally stable even in the presense of base. Thus, they were recovered almost unchanged after heating at 80 °C for 24 h in ethanol containing triethylamine.

The inertness of the P–SR bond to hydrolysis or to alcoholysis can readily be explained by both the steric and electronic effects of the 2,6-dimethoxyl substituents. However, the most attractive explanation involves the interaction between the phosphorus atom and one or more of the oxygen atoms on 2,6-positions in the phosphonium species. The presence of such interactions may interfere both sterically and electronically with additional coordination by oxide anions, a key step for P–SR bond cleavage. An analogous explanation has been cited for the unusual thermal reactions of (2-hydroxyalkyl)phosphonium salts $[(2,6)_3P–CH_2CRR'OH]X$.[2]

Reactions of (Alkylthio)phosphonium Salts with Thiols. Omelańczuk and Mikołajczyk prepared some (methylthio)phosphonium salts by treating the phosphine sulfides with methyl triflate.[9] They also found that reaction of $[Ph_3P–SMe]^+$ salt with NaSEt gave exclusively triphenylphosphine and a mixture of dimethyl, diethyl, and methyl ethyl disulfides. Masui et al. reported that a variety of phosphonium salts $[Ph_3P–SR]ClO_4$ could be prepared electrochemically from Ph_3P and dialkyl (or diaryl) disulfide and that their reaction with thiols in the presence of triethylamine gave Ph_3P and unsymmetrical diorganodisulfides.[10] We also found that $[(2,6)_3P–SR]I$ (R=Me, Et, Bu) reacted with thiols R'SH (R'=Ph, 4-MeC_6H_4, n-C_8H_{17}), in methanol containing a catalytic amount of $(2,6)_3P$ [step (3)]. The mixture was stirred at room temperature for 24 h under argon, and it was worked up to give the tertiary phosphonium salt $[(2,6)_3P–H]I$ and the unsymmetrical disulfides selectively. 2,6-Dimethoxybenzenethiol[11] reacted with $[(2,6)_3P–SR]I$ much slower than the other thiols, due probably to the bulkiness. We expected that in these reactions the catalyst $(2,6)_3P$ (pK_a 9.33)[1,12] worked as a base toward R'SH to form $[(2,6)_3P–H]SR'$, and that the anion $R'S^-$ thus formed reacted with the cation $[(2,6)_3P–SR]^+$ to form RSSR' and to reproduce $(2,6)_3P$. In fact, triethylamine (pK_a 10.75) could be used in place of $(2,6)_3P$ to give triethylammonium iodide and $(2,6)_3P$, as well as RSSR'. The lack of formation of symmetrical disulfides at lower temperatures is astonishing, and it can be best explained as that the exchange of alkylthio group at phosphorus by $R'S^-$ anion[9] is sterically precluded in our compounds. However, the formation of symmetrical disulfides was observed when the reactions were performed at elevated temperatures or when the base was used in larger amounts. We observed no formation of monosulfide RSR' even under these conditions. In the absence of base, the reaction was very slow even at elevated temperatures, and it gave equilibrium mixtures of $[(2,6)_3P–SR]I$, $[(2,6)_3P–H]I$, R'SH, and RSSR'. The reversibility of the reaction could be used for the preparation of (phenylthio)phosphonium salt $[(2,6)_3P–SPh]ClO_4$ by the reaction of $[(2,6)_3P–H]Cl$ and PhSSPh, although the yield was poor.

Since $[(2,6)_3P–H]I$ can easily be deprotonated by aqueous alkali hydroxide, we now obtained a reaction cycle as shown in Scheme 2. This indicates that unsymmetrical disulfides can be prepared under mild conditions from elemental sulfur, alkyl halide, thiol, and aqueous alkali hydroxide using $(2,6)_3P$ as a reproducible reagent.

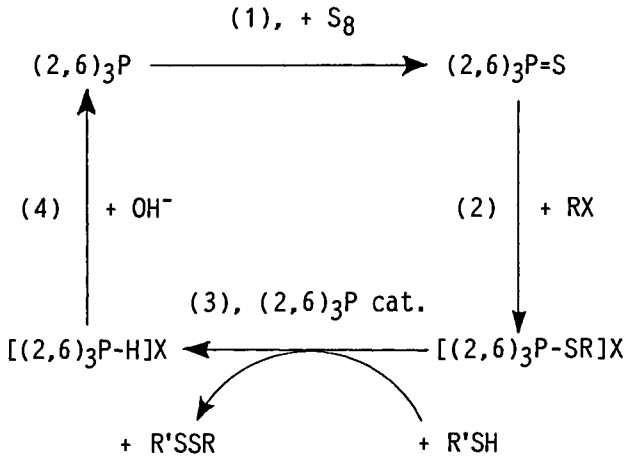

Scheme 2.

Experimental

Physical Measurements. ^1H and ^{13}C NMR spectra were recorded for solutions in $CDCl_3$ using a JEOL model JNM-GX-270 spectrometer operating at 270 and 67 MHz, respectively. IR spectra were recorded for Nujol mull using a Simadzu FTIR-4200 spectrophotometer. Gas–liquid chromatography was recorded on a Hitachi 263-30 gas chromatograph by means of a one m. Silicone gum rubber SE 30 column at 60—250 °C.

The ^1H NMR and ^{13}C NMR spectral data of new compounds are shown in Tables 1 and 2, respectively.

Triarylphosphines. Tris(2,6-dimethoxyphenyl)phosphine, $(2,6)_3P$, was obtained from the K. I. Kasei Co., Ltd. It was purified by washing with water followed by recrystallization from 2-propanol. Other tertiary phosphines, tris(2,4,6-trimethoxyphenyl)phosphine, $(2,4,6)_3P$, bis(2,6-dimethoxyphenyl)phenylphosphine, $(2,6)_2PhP$, (2,6-dimethoxyphenyl)diphenylphosphine, $(2,6)Ph_2P$, and tris(2-methoxyphenyl)phosphine, $(2\text{-}MeOC_6H_4)_3P$, were prepared as described previously.[1,12]

Table 1. ^{1}H NMR Spectral Data[a] for Organophosphorus Compounds

Compounds	4-H[b]	3,5-H[c]	2,6-MeO[d]	Other protons[e]
$(2,4,6)_3P{=}S$	—	6.03[f]	3.53	3.77s(4-MeO)
$(2,6)_3P{=}S$	7.22	6.49	3.53	
$(2,6)_2PhP{=}S$	7.27	6.47	3.47	8.06ddd[15]$_P$[6]$_H$[3]$_H$(2′,6′-H), 7.4—7.2m(3′,4′,5′-H)
$(2,6)Ph_2P{=}S$	—[g]	6.51	3.27	8.0—7.8m(4H) and 7.5—7.3m(7H) (Ph)
$[(2,6)_3P{-}SH]ClO_4$	7.56	6.65	3.66	
$[(2,6)_3P{-}SMe]I$	7.59	6.68	3.60	2.09d[19]$_P$(CH_3)
$[(2,6)_3P{-}SEt]I$	7.58	6.66	3.61	2.51dq[10]$_P$[8]$_H$(CH_2), 1.25dt[2]$_P$[7]$_H$(CH_3)
$[(2,6)_3P{-}SBu]I$	7.58	6.66	3.61	2.48dt[10]$_P$[7]$_H$(P-CH_2), 1.58—1.28m (CH_2CH_2), 0.84t[7]$_H$(CH_3)
$[(2,6)_3P{-}SPh]ClO_4$	7.44	6.52	3.63	7.27—7.13m(Ph)
$[(2,6)_2PhP{-}SMe]I$	7.67	6.73	3.61	2.12d[18]$_P$(CH_3), 7.84—7.58m(Ph)
$[(2,6)_3P{-}H]Cl\cdot 2.5H_2O$	7.61	6.69	3.71	8.48d[546]$_P$(P-H)
$[(2,6)_3P{-}H]I$	7.62	6.68	3.72	8.48d[546]$_P$(P-H)
$(2\text{-}MeOC_6H_4)_3P{=}S$	7.70ddd[16]$_P$[8]$_H$[2]$_H$(6-H), 7.44tdd[8]$_H$[2]$_H$[2]$_P$(5-H), 6.99tdd[8]$_H$[2]$_H$[1]$_P$(4-H), 6.89dd[8]$_H$[6]$_F$(3-H), 3.55s(OMe)			

a) In $CDCl_3$ (δ, s=singlet, d=doublet, t=triplet, m=multiplet, and q=quartet. b) Triplet with J_H 8—9 Hz. c) Double doublets with J_H 8—9 Hz and J_P 4—6 Hz. d) Singlet. e) The coupling constants J_P or J_H (in Hz) given in square brackets. f) Doublet with J_P 4 Hz. g) Overlapped with Ph proton resonances.

Table 2. ^{13}C NMR Spectral Data[a] for Organophosphorus Compounds

Compounds	δ (ppm) in $CDCl_3$
$(2,4,6)_3P{=}S$	—,[b] 162.4d[2], 91.9d[7], 162.7s, 56.0s, 55.2s
$(2,6)_3P{=}S$	—,[b] 161.6s, 105.1d[6], 130.9s, 55.9s
$(2,6)_2PhP{=}S$	114.7d[92], 161.1s, 105.0d[7], 129.5d[3], 55.7s
$(2,6)Ph_2P{=}S$	—,[b] 162.2s, 105.2d[6], 129.9d[4], 55.4s, 136.4d[90], 130.5d[10], 127.7d[12], 134.1s
$[(2,6)_3P{-}SH]ClO_4$	—,[b] 162.0s, 104.9d[8], 136.2s, 56.3s
$[(2,6)_3P{-}SMe]I$	101.0d[99], 162.5s, 104.8d[7], 136.2s, 56.4s, 15.1d[6]
$[(2,6)_3P{-}SEt]I$	101.0d[99], 162.5s, 104.8d[7], 136.2s, 56.4s, 27.4d[6], 14.3d[12]
$[(2,6)_3P{-}SBu]I$	101.0d[99], 162.5s, 104.8d[7], 136.2s, 56.4s, 32.7d[6], 31.3d[12], 22.1s, 13.6s
$[(2,6)_3P{-}SPh]ClO_4$	101.3s[100], 162.2s, 104.5d[4], 136.0s, 56.1s, 134.9d[6], 129.8d[4], 128.6s
$[(2,6)_2PhP{-}SMe]I$	98.3d[96], 162.3s, 105.5d[7], 133.4d[3], 56.7s, 15.05d[5], 124.9d[90], 131.9d[13], 129.3d[15], 137.8s
$[(2,6)_3P{-}H]Cl\cdot 2.5H_2O$	94.7d[105], 162.9s, 104.6d[7], 137.0s, 56.7s
$[(2,6)_3P{-}H]I$	94.8d[105], 162.9s, 104.8d[7], 137.0s, 56.9s
$(2\text{-}MeOC_6H_4)_3P{=}S$	121.7d[91], 160.9d[3], 134.4d[10], 132.8d[3], 120.4d[14], 111.9d[7], 55.6s

a) In the order of C-1, C-2,6, C-3,5, C-4, MeO-2,6, C-1′, C-2′, and others; s=singlet, d=doublet; J_P (in Hz) given in square brackets. b) The C-1 resonance could not be observed.

Preparation of Triarylphosphine Sulfides. $(2,6)_3P{=}S$. To a solution of $(2,6)_3P$ (4.425 g, 10 mmol) in toluene (100 ml) was added elemental sulfur (0.353 g, 11 mmol). The mixture was stirred at room temperature for 4 h. Unreacted sulfur was filtered off, and the filtrate was cooled to −30 °C to give crystals, which were dried at 120 °C for 2 h to give $(2,6)_3P{=}S$ in 88% yield. It can be purified by recrystallization from toluene, ethanol or acetone, followed by drying at 120 °C. Mp 206—208 °C. Anal. ($C_{24}H_{27}O_6PS$) C, H, S.

$(2,4,6)_3P{=}S$. To a solution of $(2,4,6)_3P$ (0.533 g, 1 mmol) in toluene (20 ml) was added elemental sulfur (0.032 g, 1 mmol) to give a clear solution in a few minutes. The mixture was stirred at room temperature for 1 h and was cooled to −30 °C to aid precipitation of the crystals of $(2,4,6)_3P{=}S$ in 70% yield. Mp 221 °C. Anal. ($C_{27}H_{33}O_9PS$) C, H, S.

$(2\text{-}MeOC_6H_4)_3P{=}S$. To a suspension of $(2\text{-}MeOC_6H_4)_3P$ (0.352 g, 1 mmol) in acetone (10 ml) was added elemental sulfur (0.032 g, 1mmol), and the mixture was stirred at room temperature for 3 h to afford the crystals of $(2\text{-}MeOC_6H_4)_3P{=}S$ in 87% yield, which were recrystallized from tetrahydrofuran to give the analytical sample. The melting point was not observed below 230 °C. Anal. ($C_{21}H_{21}O_3PS$) C, H.

$(2,6)_2PhP{=}S$ and $(2,6)Ph_2P{=}S$. Analogous treatments of $(2,6)_2PhP$ or $(2,6)Ph_2P$ as described above resulted in the formation of $(2,6)_2PhP{=}S$ (mp 170 °C) or $(2,6)Ph_2P{=}S$ (mp 159—160 °C) in 80—90% yields. Anal. ($C_{22}H_{23}O_4PS$) C, H, S and ($C_{20}H_{19}O_2PS$) C, H.

Preparation of Mercaptophosphonium Salt. To a solution of $(2,6)_3P{=}S$ (0.485 g, 1 mmol) in acetone (10 ml) was added with stirring 60% aqueous perchloric acid (0.4 ml). The resultant precipitates were filtered, washed with cold acetone, and dried in air to give $[(2,6)_3P{-}SH]ClO_4$ in 95% yield. Mp

181—182 °C. Anal. ($C_{24}H_{28}O_{10}ClPS$) C, H.

Desulfurization of $[(2.6)_3P\text{-}SH]^+$ Salts A suspension of $[(2,6)_3P\text{-}SH]ClO_4$ (0.338 g, 0.6 mmol) in 2-propanol (30 ml) was heated at 70 °C. Aliquots were taken at 1, 4, and 8 h of heating. The solvent was removed under reduced pressure, and the ^1H NMR spectra of the residue showed the presence of $[(2,6)_3P\text{-}SH]ClO_4$ and $[(2,6)_3P\text{-}H]ClO_4$[1] in 32 : 68, 29 : 71, and 29 : 71 ratios, respectively.

To a solution of $(2,6)_3P$=S (0. 2 mmol) in MEK (15 ml) was added 6M HCl (2 ml) (1 M=1 mol dm^{-3}). The resultant suspension was heated at 70 °C for 4 h to give new crystals, which were found to be identical with those of $[(2,6)_3P\text{-}H]Cl \cdot 2.5H_2O$ (55% yield, see below).

Preparation of $[(2.6)_3P\text{-}H]Cl \cdot 2.5H_2O$. To a solution of $(2,6)_3P$ (2.212 g, 5 mmol) in MEK (50 ml) was added 12M HCl (1 ml) dissolved in MEK (4 ml). The resultant precipitates were recrystallized from acetone (120 ml) to give $[(2,6)_3P\text{-}H]Cl \cdot 2.5H_2O$ in 95% yield. Mp 170—187 °C, decomposed. Anal. ($C_{24}H_{33}O_{8.5}ClP$) C, H, Cl.

Reactions of Triarylphosphine Sulfides with Triphenylphosphine in the Presence of Acid. A mixture of $(2,6)_3P$=S (3 mmol) and Ph_3P (0.800 g, 3.05 mmol) in acetone (30 ml) containing 6M HCl (1 ml) was heated at 50 °C for 3 h. The solvent was removed under reduced pressure, and the residual solid was treated with water (100 ml) to leave the crystals of Ph_3P=S (92% yield). To the aqueous filtrate was added 60% aqueous perchloric acid (1 ml) to precipitate the crystals of $[(2,6)_3P\text{-}H]ClO_4$[1] in 99% yield.

$(2,6)_2PhP$=S reacted with Ph_3P in analogous manner to give $[(2,6)_2PhP\text{-}H]ClO_4$[1] in 77% yield.

Preparations of (Alkylthio)phosphonium Salts. $[(2,6)_3P\text{-}SR]I$ (R=Me, Et, *n*-Bu) and $[(2,6)_2PhP\text{-}SMe]I$. To a solution of $(2,6)_3P$=S (1 mmol) in benzene (10 ml) was added MeI (0.2 ml) to give immediately the precipitates of $[(2,6)_3P\text{-}SMe]I$ in quantitative yield. Mp 220 °C, decomposed. Anal. ($C_{25}H_{30}O_6IPS$) C, H.

Analogous treatments of $(2,6)_3P$=S with RI (R=Et, Bu) resulted in the formations of $[(2,6)_3P\text{-}SEt]I$ (mp 206 °C) and $[(2,6)_3P\text{-}SBu]I$ (mp 175 °C) in 80 and 88% yields, respectively. Anal. ($C_{26}H_{32}O_6IPS$) C, H and ($C_{28}H_{36}O_6IPS$) C, H.

An analogous treatment of $(2,6)_2PhP$ with MeI resulted in the formation of $[(2,6)_2PhP\text{-}SMe]I$ in 84% yield. Mp 168—170 °C, decomposed. Anal. ($C_{23}H_{26}O_4IPS$) C, H.

$[(2,6)_3P\text{-}SR]Br$ and $[(2,6)_3P\text{-}SR]ClO_4$ (R=Et, Bu). To a solution of $(2,6)_3P$=S (1 mmol) in ethanol (20 ml) was added EtBr (0.5 ml). The mixture was heated at 55 °C for 2 h. The volatile materials were removed under reduced pressure, and the residual solid was washed with benzene to give $[(2,6)_3P\text{-}SEt]Br$ in 91% yield; mp 194 °C. It was dissolved in water (0.100 g 10 ml) by heating, and 60% aqueous perchloric acid (0.1 ml) was added at room temperature to give the precipitates of $[(2,6)_3P\text{-}SEt]ClO_4$ in 82% yield. The perchlorate salt was served for the elemental analysis. The melting point was not observed below 230 °C. Anal. ($C_{26}H_{32}O_{10}ClPS$) C, H

An analogous treatment of $(2,6)_3P$=S with BuBr resulted in the formation of $[(2,6)_3P\text{-}SBu]Br$ (74% yield, mp 174 °C) and $[(2,6)_3P\text{-}SBu]ClO_4$ (86%, the melting point was not observed below 230 °C. Anal. ($C_{28}H_{36}O_{10}ClPS$) C, H.

Reactions of $[(2,6)_3P\text{-}SR]I$ (R=Me, Et, *n*-Bu) with Thiols. A mixture of $[(2,6)_3P\text{-}SMe]I$ (0.308 g, 0.5 mmol), PhSH (0.1 ml, 0.55 mmol), and $(2,6)_3P$ (0.022 g, 0.05 mmol) in methanol (10 ml) was stirred under argon at room temperature for 24 h. An aliquot was analyzed by GLC to confirm the selective formation of MeSSPh. The mixture was acidified by addition of 1 M HCl (0.1 ml), the volatile materials were removed under reduced pressure, and the residue was treated with benzene (10 ml) to separate the excess PhSH and MeSSPh. The ^1H NMR and the IR spectra of the residue were identical with those for $[(2,6)_3P\text{-}H]I$ (94% yield). The GLC retention time of MeSSPh was measured separately with the sample obtained by exchange reaction[13] of two symmetrical disulfides catalyzed by Ph_3P or $(2,6)_3P$. When $[(2,6)_3P\text{-}SMe]I$ was reacted with 4-MeC_6H_4SH or *n*-$C_8H_{17}SH$ in analogous manners, the ^1H NMR spectrum showed that the residues contained mainly $[(2,6)_3P\text{-}H]I$ (95% yield) and small amounts (<2%) of unreacted $[(2,6)_3P\text{-}SMe]I$. The yields (>90%) of MeSSR were estimated by ^1H NMR or GLC.

Analogous results were obtained for $[(2,6)_3P\text{-}SEt]I$ and $[(2,6)_3P\text{-}SBu]I$, and they reacted with PhSH, 4-MeC_6H_4SH, and $C_8H_{17}SH$ under the same conditions to give $[(2,6)_3P\text{-}H]I$ (>85% yields) and unsymmetrical disulfides (^1H NMR or GLC, >85% yields).

Preparation of $[(2,6)_3P\text{-}H]I$. $(2,6)_3P$ (3 mmol) was dissolved in water (150 ml) containing HCl (7 mmol). Addition of KI (0.548 g, 3.3 mmol) solution in water (3 ml) resulted in the precipitation of crystals, which were recrystallized from water to give $[(2,6)_3P\text{-}H]I$ in 80% yield. Mp 215—217 °C. Anal. ($C_{24}H_{28}O_6PI$) C, H, I.

Preparation of (Phenylthio)phosphonium Salt. A mixture of $[(2,6)_3P\text{-}H]Cl \cdot 2.5H_2O$ (1.572 g, 3 mmol) and PhSSPh (0.218 g, 1 mmol) in methanol (10 ml) was heated in a sealed glass tube at 80 °C for 24 h. The solvent was removed under reduced pressure, and the residue was extracted with benzene (10 ml)-water (45 ml). Addition of 1 M sodium hydroxide (3.5 ml) to the water layer resulted in the precipitation of $(2,6)_3P$ (2.36 mmol). To the filtrate was added 60% percloric acid to result in the precipitation of $[(2,6)_3P\text{-}SPh]ClO_4$ (0.3 mmol). The melting point was not observed below 230 °C. Anal. ($C_{30}H_{32}O_{10}ClPS$) C, H.

Reaction of $[(2,6)_3P\text{-}H]I$ with Base. To a methanol (4 ml) solution of $[(2,6)_3P\text{-}H]I$ (0.570 g, 1 mmol) was added 1 M sodium hydroxide (1.1 ml) to give light yellow precipitates, which were washed well with water and filtered to give $(2,6)_3P$ in 95% yield.

This work was partially supported by the Grant-in-Aid for Scientific Research on Priority Area of Organic Unusual Valency No. 02247215 from the Ministry of Education, Science and Culture, and partly by the Asahi Glass Foundation for Industrial Technology.

References

1) M. Wada and S. Higashizaki, *J. Chem. Soc., Chem. Commun.*, **1984**, 482; M. Wada, S. Higashizaki, and A. Tsuboi, *J. Chem. Res. Synop.*, **1985**, 38; *Miniprint*, 467—490.

2) M. Wada and A. Tsuboi, *J. Chem. Soc., Perkin Trans. 1*, **1987**, 151.

3) M. Wada, A. Tsuboi, K. Nishimura, and T. Erabi, *Nippon Kagaku Kaishi*, **1987**, 1284; H. Kurosawa, A. Tsuboi, Y. Kawasaki, and M. Wada, *Bull. Chem. Soc. Jpn.*, **60**, 3563 (1987).

4) M. Wada, H. Ohta, N. Hashizume, M. Kanzaki, K. Hirata, and T. Erabi, *Chem. Express*, **3**, 471 (1988).

5) M. Wada, M. Kanzaki, H. Ohta, K. Tenma, N. Hashizume, K. Hirata, and T. Erabi, *Chem. Express*, **4**, 257 (1989).

6) M. Wada, M. Kanzaki, M. Fujiwara, K. Kajihara, and T. Erabi, *Chem. Lett.*, **1990**, 867.

7) A. Schönberg and M. Z. Barakat, *J. Chem. Soc.*, **1949**, 892; R. S. Davidson, *J. Chem. Soc. C*, **1967**, 2131; R. Matsueda, H. Maruyama, M. Ueki, and T. Mukaiyama, *Bull. Chem. Soc. Jpn.*, **44**, 1373 (1971).

8) H. Ohmori, S. Nakai, M. Sekiguchi, and M. Masui, *Chem. Pharm. Bull.*, **28**, 910 (1980); and references cited therein.

9) J. Omelańczuk and M. Mikolajczyk, *J. Am. Chem. Soc.*, **101**, 7292 (1979).

10) M. Masui, Y. Mizuki, K. Sakai, C. Ueda, and H. Ohmori, *J. Chem. Soc., Chem. Commun.*, **1984**, 843.

11) M. Wada, K. Tenma, K. Kajihara, K. Hirata, and T. Erabi, *Chem. Express*, **4**, 109 (1989).

12) Y. Yamashoji, T. Matsushita, M. Wada, and T. Shono, *Chem. Lett.*, **1988**, 43; Y. Yamashoji, T. Matsushita, M. Tanaka, and T. Shono, *Polyhedron*, **8**, 1053 (1989).

13) D. N. Harpp and R. A. Smith, *J. Am. Chem. Soc.*, **104**, 6045 (1982).

Titanium(III) Chloride Mediated Reduction of 1-Nitro-2-phenylethenes

Akira SERA,* Shoji FUKUMOTO, Masako TAMURA, Kiyoshi TAKABATAKE, Hiroaki YAMADA, and Kuniaki ITOH
Department of Chemistry, Faculty of Science, Kobe University, Kobe 657
(Received December 14, 1990)

The reaction of 1-nitro-2-phenylethenes (β-nitrostyrenes) with aqueous titanium(III) chloride afforded substituted pyrroles in addition to the expected reduction products, oximes and carbonyl compounds. 2-Substituted 1-nitro-2-phenylethenes yielded divinylamine derivatives instead of pyrroles. The reaction mechanism has been rationalized by taking account of the electron transfer from titanium(III) species to the nitro olefins, followed by protonation, dimerization, cyclization, and/or hydrolysis.

Much attention has been paid to the role of conjugated nitroalkenes as versatile intermediates in organic synthesis, since they may be transformed into legions with diverse functionalities.[1,2] The conversion of nitroalkenes to alkylamines has been accomplished through the use of catalytic hydrogenation, lithium aluminum hydride, or sodium borohydride–boron trifluoride.[3] Carbonyl compounds and their oximes have been prepared from nitroalkenes by means of titanium(III) chloride,[4] Raney nickel/sodium phosphinate,[5] chromium(II) chloride,[6] lithium trialkylhydroborate,[7] zinc/acetic acid,[8] lead/acetic acid,[9] sodium stannite,[10] tin(II) chloride,[11,12] and electrochemical means.[13,14] In addition, nitriles are synthesized by reactions of nitroalkenes with iodotrimethylsilane[15] or by a cathodic reduction in the presence of titanium(IV) chloride.[16]

We previously reported that the reaction of 1-nitro-2-phenylethenes **1** with titanium(III) chloride yields divinylamine derivatives **4** and pyrroles **5**, in addition to the expected oximes **2** and carbonyl compounds **3**.[17] This paper is concerned with the synthetic utility and the mechanistic features of the titanium(III) chloride-mediated reduction of several 1-nitro-2-phenylethenes (**1**, substituted β-nitrostyrenes).

Results and Discussion

A report by McMurry and Melton[4] indicates that 1-nitrocyclooctene is readily reduced with aqueous titanium(III) chloride in tetrahydrofuran at pH <1 to give cyclooctanone in 55% yield. However, we found that the reaction of **1a—d** with titanium(III) chloride under almost neutral conditions (pH=6.5, an ammonium acetate buffer) results in dimerized and/or cyclized products in addition to the expected carbonyl compounds or oximes. The product distribution was dependent on the structural features of the starting 1-nitro-2-phenylethenes (Table 1). The reaction of **1a** with titanium(III) chloride (6 mole equiv) afforded a small amount of 3,4-diphenylpyrrole (**5a**) along with 1,4-dinitro-2,3-diphenylbutane (**6a**). The formation of **5** and **6** is the first example of the reductive dimerization of nitro olefins by chemical means. Since **6a** was thought to be a possible intermediate for pyrrole forma-

Table 1. Reaction of 1-Nitro-2-phenylethenes with Titanium(III) Chloride[a,b]

Nitroethene	Conditions	Products and yields/%[c]				
		2	**3**	**4**	**5**	Others
1a	0 °C/0.5 h	—	—	—	3	**6a**: 7
	35 °C/24 h[d]	—	—	—	32	
1b	0 °C/0.5 h	—	35	—	6	**7b**: 7
	35 °C/24 h[d]	—	60	—	32	
1c	35 °C/24 h[d]	—	61	—	31	
1d	0 °C/1.5 h	62	6	—	—	
	35 °C/24 h[d]	—	38	—	20	
1e	0 °C/5 h	55	10	—	—	
1f	0 °C/4 h	46	15	32	—	
	30 °C/0.5 h[d]	19	22	50	—	
1g	0 °C/20 h	56	27	—	—	
	35 °C/24 h[d]	—	84	14	—	
1h	0 °C/6 h[d]					**8**: 33; **9**: 15
	35 °C/14 h[e]					**8**: 43; **9**: 13
1i	0 °C/0.2 h[f] (pH 7)					Benzil dioxime: 54
1j	0 °C/1.5 h (pH 7)					Benzophenone: 56

a) Taken in part from Ref. 17. b) In aqueous tetrahydrofuran at pH 6.5. Molar $TiCl_3$/**1** ratio was 6. c) Isolated yields. d) Molar $TiCl_3$/**1** ratio was 12. e) Molar $TiCl_3$/**1** ratio was 18. f) In acetonitrile.

tion, the reaction was conducted with 12-fold molar titanium(III) chloride at an elevated temperature. Expectedly, **5a** was obtained in an improved yield (32%). The reaction conditions were then examined to improve the yields of **5a**. As shown in Table 2, the reaction with 12 molar titanium(III) chloride in neutral aqueous 1,4-dioxane at 35 °C gave **5a** in a satisfactory yield (50%). Phenylacetaldehyde (**3a**) could not be isolated because of its instability under the reaction conditions employed.[18] Similar results were obtained for a series of substituted 1-nitro-2-phenylethenes (**1b—d**) possessing a hydrogen atom at the β-position to the nitro group (R^2=H). In all cases, pyrroles **5b—d** as well as carbonyl compounds **3b—d** were obtained. Although many procedures have been documented for pyrrole synthesis,[19] the present reaction may be taken as a new entry into symmetrically substituted pyrroles. The major advantages of the present method are that the operation is simple and the starting compounds are easily prepared from the corresponding aldehydes and nitroalkanes.

Table 2. Reduction of **1a** with Aqueous Titanium(III) Chloride under Various Conditions[a]

Solvent	$TiCl_3$ (molar equivalent)	Yield of **5a**/%[b]
Tetrahydrofuran	6	18
	12	32
Methanol	6	25
	12	43
Acetonitrile	6	22
	12	35
1,4-Dioxane	6	32
	12	50
	12[c]	28
	12 (pH=4.4)	23
	12 (pH<1)	0

a) At 35 °C for 24 h, pH=6.5. b) Isolated yields. c) At 65 °C.

The reaction of **1a** with an insufficient amount (3 mole equiv) of titanium(III) chloride yielded **6a** (15%), **7a** (3%), and 2,3-diphenyl-4-nitrobutanal oxime (**11**, 23%). These partially reduced products were supposed to be the intermediates leading to pyrrole **5a**. Accordingly, **6a** was synthesized by the Michael reaction of **1a** with 1-nitro-2-phenylethane, and the product was separated to the *meso*- and *dl*-**6a**. Titanium(III) chloride reduction of these two isomers did not afford **5a** at all; however, the disodium salt of **6a** could be reduced under the present reduction conditions to produce **5a**. Thus, the dinitronate anion (**B**) of **6a** should be the actual intermediate, and the formation of pyrroles is rationalized by taking account of the stepwise electron transfer-protonation process (Scheme 2).[4] Electron transfer from the titanium(III) species to **1** gives rise to an anion radical (**A**) stabilized by the 2-phenyl substituent. This anion radical is further reduced to give an oxime **2**, which is readily reduced by aqueous titanium(III) chloride to give an imine (overall six-electron transfer).[20,21] Upon hydrolysis this imine gives rise to a carbonyl compound **3**. The formation of a carbonyl compound by direct hydrolysis of oxime is unlikely under the present conditions. The anion radical (**A**) would dimerize to give an intermediate (**B**) which is further reduced by titanium(III) chloride to a diimine through the dioxime **7**. Elimination of ammonia from the imine–enamine tautomeric form (**C**) of the diimine intermediate finally affords the pyrrole derivative **5**. In the reductions of 1-nitro-1-alkenes by known methods,[4–14] no dimeric products were reported. The formation of the dimeric products is therefore characteristic of the reaction with titanium(III) chloride. Chelation of two anion radical intermediates with titanium(III or IV) species would hold both radical centers sufficiently close

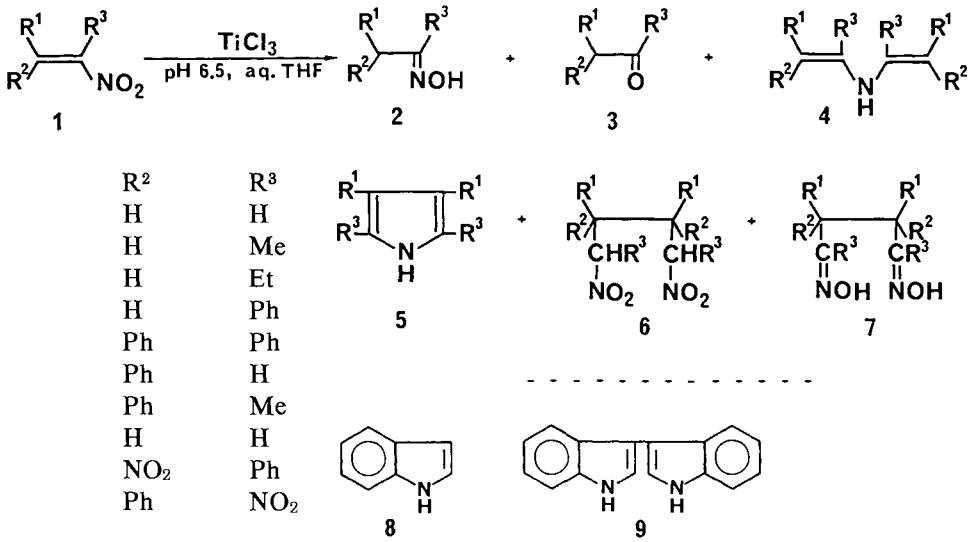

	R^1	R^2	R^3
1a:	Ph	H	H
b:	Ph	H	Me
c:	Ph	H	Et
d:	Ph	H	Ph
e:	H	Ph	Ph
f:	Ph	Ph	H
g:	Ph	Ph	Me
h:	*o*-$NO_2C_6H_4$	H	H
i:	Ph	NO_2	Ph
j:	Ph	Ph	NO_2

Scheme 1.

to achieve radical coupling, just as was proposed for the electrochemical hydrodimerization of cinnamate esters.[22]

On the other hand, the reaction of nitroolefins possessing no β-hydrogen atom **1f,g** with titanium(III) chloride yielded divinylamine derivatives **4f,g**. In these cases carbonyl compounds **3f,g** and oximes **2f,g** were produced, but no pyrrole was detected. The yield of **4f** increased at the expense of that of **2f** with excess titanium(III) chloride at higher temperature. The divinylamines **4f,g** may be regarded as forms of cross-conjugated dienamines (an open chain version of pyrrole). Many cross-conjugated dienamines have been described in the literature.[23] However, those dienamines which possess a structural feature of C=C–N–C=C, like **4f,g**, have been only little documented,[24,25] although many of those possessing the C=C–C=C–N and C=C(N)–C=C functionalities have been synthesized and their characteristics are thoroughly elucidated.[23] The mechanism of divinylamine formation can be considered to be as follows. The intermediate radical anions (**A**) from **1f,g** are highly stabilized and have no tendency to dimerize to (**B**), due to the presence of two bulky phenyl groups on the radical center. The electron transfer-protonation process thus gives rise to oximes **2f,g**, which are reduced further to give imine intermediates. These imines yield carbonyl compounds by hydrolysis or tautomerize to enamines. Spectroscopic studies[24,26] have shown that the equilibrium is usually almost completely in favor of the imine form for simple nonconjugated aldimines and ketimines. Nevertheless, imine–enamine tautomerism has been clearly demonstrated for reactions in which the enamine tautomer reacts with a variety of electrophiles.[27] In the present case the primary enamines are stabilized by conjugation with the two phenyl groups. Intervention of the imine–enamine tautomerism was further confirmed by trapping these species. In the presence of aniline, the titanium(III) chloride reduction of **1f** yielded *N*-(2,2-diphenylethylidene)aniline, produced by the addition of aniline to an imine (2,2-diphenylethanimine) followed by elimination of ammonia. On the other hand, addition of *N*-benzylidene butylamine afforded *N*-benzylidene-2,2-diphenylvinylamine, produced by the addition of an enamine (2,2-diphenylvinylamine) to the Schiff base followed by the elimination of butylamine. From these observations, it is clear that the nucleophilic addition of the enamine to the imine followed by the elimination of ammonia afforded divinylamine **4f**[28] as the final product. The product selectivity is thus governed by both the nature and number of substituents at C_2 of the starting 1-

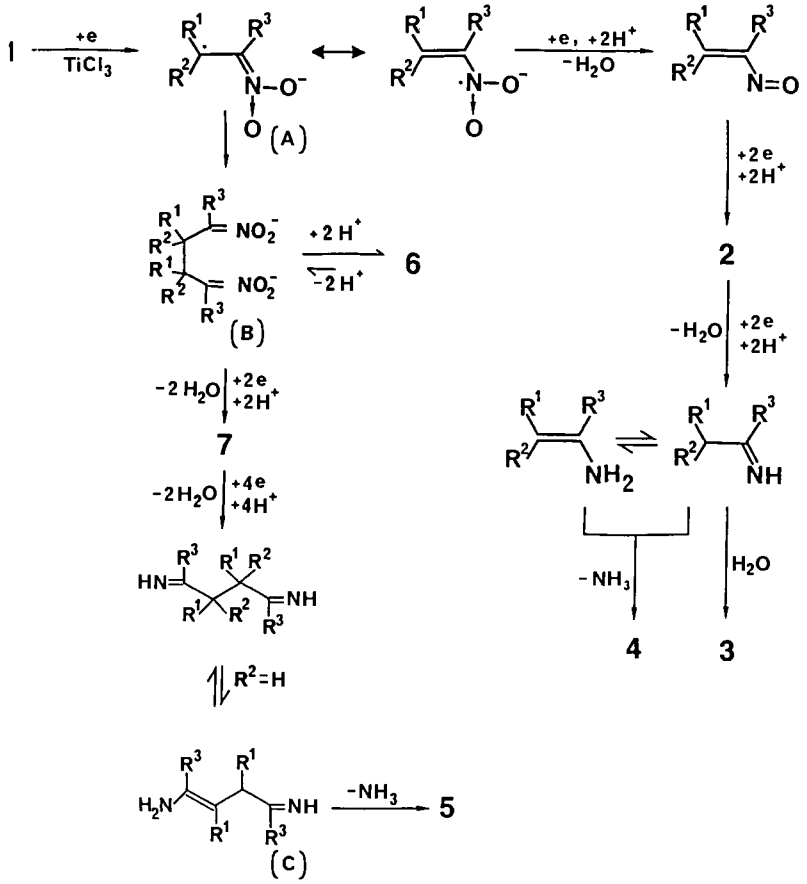

Scheme 2.

nitroethenes.

As expected, 1-nitro-2-(2-nitrophenyl)ethene (**1h**) yielded indole (**8**). 3,3′-Bi-1*H*-indole (**9**) was also produced by dimerization of the intermediate radical anion (**A**) followed by cyclization. The absence of 3,4-bis-(2-aminophenyl)pyrrole, another possible cyclization product from the dimerized intermediate, indicates a predominance of the imine tautomer in the imine–enamine tautomerism of the dimerized intermediate. The titanium(III) chloride reduction of 1,2-dinitro-1,2-diphenylethene (**1i**) and 1,1-dinitro-2,2-diphenylethene (**1j**) resulted only in the formation of benzil dioxime and benzophenone (hydrolysis product), respectively.

Experimental

All melting points were determined on a micro hot-plate melting-point apparatus and are not corrected. IR spectra were measured on a JASCO IRA-3 spectrophotometer. ^{1}H and ^{13}C NMR spectra were recorded on JEOL FX-90Q and PS-100 spectrometers. Chemical shifts are given in ppm downfield from internal tetramethylsilane. Mass spectra were recorded on an ESCO EMD-05A spectrometer.

Substituted nitroethenes were prepared according to methods described in the literatures.[29] Solvents were purified as usual. Aqueous titanium(III) chloride solution was purchased from Wako Chemical Ind., and titrated before use.

General Procedure of Titanium(III) Chloride Reduction. A buffered titanium(III) chloride solution was prepared by adding ammonium acetate (5.5 g, 71 mmol) in 25 ml of water to a 1.76 M aqueous titanium(III) chloride solution (11 ml) under nitrogen (1 M=1 mol dm^{-3}). Adjustment of the pH was achieved by adding 10% (w/v) aqueous ammonia to the solution. A solution of 1-nitro-2-phenylethene (**1**, 3 mmol) in 14 ml of tetrahydrofuran was rapidly added to the buffered titanium (III) chloride solution; the solution was stirred at 0 °C under nitrogen. The reaction was monitored by TLC. After the substrate was completely consumed, the reaction mixture was extracted several times with diethyl ether. The combined extracts were washed successively with aqueous sodium hydrogencarbonate and sodium chloride solutions, and dried over magnesium sulfate. The solvent was removed under reduced pressure and the residue was subjected to silica gel chromatography. The results are given in the Tables.

Representative Products of the Titanium(III) Chloride Reduction. 3,4-Diphenylpyrrole (5a):[30] Oil, IR (neat) 3400, 1720, 1600, and 1560 cm^{-1}; ^{1}H NMR (CCl_4) δ=6.7 (2H, d, J=2.6 Hz), 7.1 (10H, m), and 8.0 (1H, br); MS m/z 219 (M^+), 218, 190, 188, and 164.

1,4-Dinitro-2,3-diphenylbutane (6a): A *meso*–*dl* mixture; mp 178—180 °C; IR (KBr) 1550 and 1380 cm^{-1}; ^{1}H NMR (DMSO-d_6) δ=3.5—5.2 (6H, m) and 7.3 (10H, m); MS m/z 300 (M^+), 254, 223, 208, and 194. Found: C, 63.79; H, 5.50%. Calcd for $C_{16}H_{16}N_2O_4$: C, 63.99; K, 5.37%.

meso and *dl*-**6a**[31] were prepared.

meso-**6a:** Mp 101—102 °C; IR (KBr) 1554, 1380, 790, and 696 cm^{-1}; ^{1}H NMR (DMSO-d_6) δ=3.7—4.1 (2H, br. t), 4.8—5.3 (4H, br), and 6.8—7.4 (10H, s); ^{13}C NMR ($CDCl_3$) δ=45.7, 77.3, 128.6, 128.7, 129.1, and 134.3; MS m/z 300 (M^+), 254, 223, 208, and 194. Found: C, 63.85; H, 5.30; N, 9.25%. Calcd for $C_{16}H_{16}N_2O_4$: C, 63.99; H, 5.37; N, 9.33%.

dl-**6a:** Mp 240—243 °C; IR (KBr) 1554, 1382, 790, and 700 cm^{-1}; ^{1}H NMR (DMSO-d_6) δ=3.7—3.9 (2H, br. t), 4.1—4.3 (2H, br. dd), 4.7—5.1 (2H, br. t), and 7.2—7.7 (10H, m); ^{13}C NMR (DMSO-d_6) δ=46.8, 78.7, 127.9, 128.0, 128.8, and 137.5; MS m/z 300 (M^+), 254, 223, 208, and 194.

2,5-Dimethyl-3,4-diphenylpyrrole (5b):[32] Mp 145—148 °C; IR (KBr) 3350, 1600, 1500, 1450, and 770 cm^{-1}; ^{1}H NMR ($CDCl_3$) δ=2.2 (6H, s), 7.0 (10H, m), and 7.3 (1H, br); MS m/z 247 (M^+), 246, 202, 179, and 77.

3,4-Diphenyl-2,5-hexanedione Dioxime (7b):[32] Mp 370 °C (decomp); IR (KBr) 3240 and 1500 cm^{-1}; ^{1}H NMR (DMSO-d_6) δ=1.5 (6H, s), 4.2 (2H, s), 7.2 (10H, m), and 9.7 (2H, s); MS m/z 296 (M^+), 279, 262, 247, and 188.

2,5-Diethyl-3,4-diphenylpyrrole (5c):[33] Mp 149—150 °C; ^{1}H NMR ($CDCl_3$) δ=1.2 (6H, t), 2.6 (4H, q), 7.1 (10H, m), and 7.5 (1H, br); MS m/z 275 (M^+), 274, 260, 246, 231, and 230.

Benzyl Phenyl Ketone Oxime (2d):[34] Mp 86—89 °C; IR (KBr) 3200, 1605, 1495, and 1450 cm^{-1}; ^{1}H NMR ($CDCl_3$) δ=4.1 (2H, s), 6.5—7.7 (10H, m), and 9.3 (1H, br); MS m/z 211 (M^+), 193, 164, 119, 103, and 91.

2,3,4,5-Tetraphenylpyrrole (5d):[35] Mp 213.5—214 °C; ^{1}H NMR ($CDCl_3$) δ=6.8—7.4 (20H, m) and 8.2 (1H, br); MS m/z 371 (M^+), 370, 293, 265, and 216.

Diphenylacetaldehyde Oxime (2f):[36] Mp 117—118.5 °C; IR (KBr) 3260, 1600, 1450, 1250, 960, and 700 cm^{-1}; ^{1}H NMR ($CDCl_3$) δ=4.9 (1H, d, J=7 Hz), 7.1—7.5 (10 H, s), 7.8 (1H, d, J=7 Hz), and 8.0 (1H, s); ^{13}C NMR ($CDCl_3$) δ=51.3, 127.2, 128.6, 128.8, 140.3, and 153.1; MS m/z 211 (M^+), 194, 180, 167, and 115.

Bis(2,2-diphenylvinyl)amine (4f):[24] Pale yellow needles (benzen–hexane), mp 143.5—144.5 °C; IR (KBr) 3360 and 3200 cm^{-1}; UV (MeCN) λ_{max} 360 nm (ε_{max}=25600); ^{1}H NMR ($CDCl_3$) δ=6.6 (2H, s) and 7.0 (20H, m, Ph and NH); ^{13}C NMR ($CDCl_3$), geminal two phenyl rings are not equivalent, δ=117.5 ($Ph_2\underline{C}$=), 126.7, 127.3, 128.2, 129.4 (C=$\underline{C}$HN–), 129.7, 130.3, 131.2, 139.4, and 142.6; MS m/z 373 (M^+), 372, 296, 206, and 179. Found: C, 89.86, H, 6.28, N, 3.77%. Calcd for $C_{28}H_{23}N$: C, 90.04, H, 6.21, N, 3.75%.

1,1-Diphenyl-2-propanone Oxime (2g):[37] Mp 160—162 °C; IR (KBr) 3420, 1605, 1495, and 1455 cm^{-1}; ^{1}H NMR ($CDCl_3$) δ=1.8 (3H, s), 4.9 (1H, s), 7.1 (10H, m), and 8.5 (1H, s); MS m/z 225 (M^+), 208, 193, 167, 165, and 152. Found: C, 80.03, H, 6.83%. Calcd for $C_{15}H_{15}NO$: C, 79.97, H, 6.71%.

Bis(1-methyl-2,2-diphenylvinyl)amine (4g): Oil, IR ($CHCl_3$) 3400 and 1610 cm^{-1}; ^{1}H NMR ($CDCl_3$) δ=2.2 (6H, s), and 6.8—7.7 (21H, m, Ph and NH); MS m/z 207 (M^+-Ph_2C=CHMe), 206, 178, 165, and 130.

3,3′-Bi-1*H*-indole (9):[38] Mp 280 °C (decomp); IR (KBr) 3380 cm^{-1}; ^{1}H NMR (DMSO-d_6) δ=6.7—7.8 (10H, m) and 10.9 (2H, br); MS m/z 232 (M^+), 231, and 203.

Reduction of 1a with 3 Molar Equivalents of Titanium(III) Chloride. Reaction of **1a** (4.47 g, 30 mmol) with 90 mmol of titanium(III) chloride under the standard conditions for 45 h yielded, after usual work-up, **6a** (15%), **7a** (3%), and 2,3-diphenyl-4-nitrobutanal oxime (**11**, 23%).

2,3-Diphenyl-4-nitrobutanal Oxime (11): An isomer mixture; mp 205—210 °C; IR (KBr) 3400, 1555, 1460, 1385, and 705 cm^{-1}; ^{1}H NMR (DMSO-d_6) δ=3.5—5.0 (8H, m), 6.8 (1H, d, J=8 Hz), 7.2 (1H, d, J=8 Hz), 7,1—7.7 (20H, m), 10.3 (1H, s), and 10.7 (1H, s); ^{13}C NMR (acetone-d_6) δ=44.5 and 49.2, 49.5 and 50.8, 80.3, 128.6 and 129.6, 129.0 and 128.0, 129.8 and 129.7, 129.8 and 129.9, 130.2 and 130.4, 130.2 and 130.5, 139.5, 140.5, 151.1 and 151.4; MS m/z 284 (M^+), 283, 253, 207, and 205. Found: C, 67.34; H, 5.95; N, 9.78%. Calcd for

$C_{16}H_{16}N_2O_3$: C, 67.51; H, 5.67; N, 9.85%.

Reduction of Disodium Salt of 6a with Titanium(III) Chloride. A solution of disodium salt (173 mg, 0.5 mmol) of **6a** in methanol (8 ml) was added to a buffered solution (pH=6.5) of titanium(III) chloride; the mixture was stirred for 24 h at room temperature. After the usual work-up, 20 mg (18%) of **5a** was obtained.

Titanium(III) Chloride Reduction of 1f in the Presence of Aniline or *N*-Benzylidenebutylamine. 1,1-Diphenyl-2-nitroethene (**1f**, 3 mmol) was reduced in a buffered aqueous tetrahydrofuran solution (pH 6.5) containing titanium(III) chloride (18 mmol) and aniline (3 mmol) at 30 °C for 2 h. After the usual work-up, the product was chromatographed on silica gel to give *N*-(2,2-diphenylethylidene)aniline (62%). This compound was easily oxidized by air to give benzophenone (57%) and *N*-formylaniline (47%). A similar reaction carried out in the presence of *N*-benzylidenebutylamine (15 mmol) yielded *N*-benzylidene-2,2-diphenylvinylamine (40%) as yellow crystals: Mp 131.5—133.5 °C; IR (KBr) 1620, 1590, 1550, 1480, and 1440 cm^{-1}; ^1H NMR ($CDCl_3$) δ=7.0—7.7 (16H, m, PhX3 and C=C<u>H</u>–N) and 8.3 (1H, s, –N=C<u>H</u>Ph); MS *m/z* 283 (M^+), 206, 178, and 165. Found: C, 89.20; H, 6.21; N, 4.89%. Calcd for $C_{21}H_{17}N$: C, 89.05, H, 6.01; N, 4.95%.

This work was supported by a Grant-in-Aid for Scientific Research No. 60430008 from the Ministry of Education, Science and Culture. We are indebted to Miss M. Nishinaka for MS determination and microanalysis.

References

1) E. J. Corey and H. Estreicher, *J. Am. Chem. Soc.*, **100**, 6294 (1978).
2) H. H. Bauer and L. Urbas, "The Chemistry of the Nitro and Nitroso Group," ed by H. Feuer, Wiley-Interscience, New York (1970), Part 2, p. 75.
3) R. S. Varma and G. W. Kabalka, *Synth. Commun.*, **15**, 843 (1985).
4) J. E. McMurry and J. Melton, *J. Org. Chem.*, **38**, 4367 (1973).
5) D. Monti, P. Gramatica, G. Speranza, and P. Manitto, *Tetrahedron Lett.*, **24**, 417 (1983).
6) R. S. Varma, M. Varma, and G. W. Kabalka, *Tetrahedron Lett.*, **26**, 3777 (1985); *Synth. Commun.*, **15**, 1325 (1985).
7) M. S. Mourad, R. S. Varma, and G. W. Kabalka, *Synthesis*, **1985**, 654.
8) D. Nightingale and J. R. Janes, *J. Am. Chem. Soc.*, **66**, 352 (1944).
9) S. Sera, H. Yamauchi, H. Yamada, and K. Itoh, *Synlett.*, **1990**, 477.
10) R. S. Varma, M. Varma, and G. W. Kabalka, *Tetrahedron Lett.*, **26**, 6013 (1985).
11) A. Dornow, H. D. Jordan, and G. Muller, *Chem. Ber.*, **15**, 67 (1961).
12) R. S. Varma and G. W. Kabalka, *Chem. Lett.*, **1985**, 243.
13) T. Shono, H. Hamaguchi, H. Mikami, H. Nogusa, and S. Kashimura, *J. Org. Chem.*, **48**, 2103 (1983).
14) S. Torii, H. Tanaka, and T. Katoh, *Chem. Lett.*, **1983**, 607.
15) G. A. Olah, S. C. Narang, L. D. Field, and A. P. Fung, *J. Org. Chem.*, **48**, 2766 (1983).
16) A. Sera, H. Tani, I. Nishiguchi, and T. Hirashima, *Synthesis*, **1987**, 631.
17) A. Sera, S. Fukumoto, T. Yoneda, and H. Yamada, *Heterocycles*, **24**, 697 (1986). *Correction:* the yields of products given in the table are partly incorrect. The correct values are: 62 (0 °C) and 0% (35 °C) for **3**, and 6 (0 °C) and 38% (35 °C) for **4** based on **1c**, respectively.
18) A control experiment showed that **3a** could not survive under the reaction conditions.
19) R. J. Sundberg, "Comprehensive Heterocyclic Chemistry," ed by A. R. Katritzky and C. W. Rees, Pergamon Press, Oxford (1984), Vol. 4, p. 313.
20) Masui and Sayo examined the polarographic behavior and constant potential electrolysis of **1a**, and found that **1a** was reduced to hydroxylamine (and also to imine) by the six-electron transfer process; M. Masui and H. Sayo, *Pharm. Bull. (Tokyo)*, **4**, 332, 337 (1956).
21) G. H. Timms and E. Wildsmith, *Tetrahedron Lett.*, **1971**, 195.
22) L. H. Klemm and D. R. Olson, *J. Org. Chem.*, **38**, 3390 (1973).
23) A. G. Cook, "Enamines: Synthesis, Structure, Reactions," Marcel Dekker, New York (1969).
24) B. Witkop, *J. Am. Chem. Soc.*, **78**, 2873 (1956).
25) T. Zaima, K. Mitsuhashi, and K. Takahashi, *J. Chem. Soc. Jpn., Chem. Ind. Chem.*, **1974**, 2118.
26) G. Bianchetti, P. Della Croce, and D. Pocar, *Tetrahedron Lett.*, **1965**, 2043.
27) P. W. Hickmott, *Tetrahedron*, **38**, 3363 (1982).
28) Divinylamine **4f** was oxidized in solutions by molecular oxygen to give benzophenone and *N*-formyl-2,2-diphenylvinylamine.[24] However, in the absence of molecular oxygen, **4f** was found to be stable even at 110 °C or toward irradiation by a low pressure mercury arc lamp.
29) For **1a,h**, D. E. Warrall, *Org. Synth.*, Coll. Vol. I, 413 (1951); **1b,c**, H. B. Hass, A. G. Susie, and R. L. Heider, *J. Org. Chem.*, **15**, 8 (1950); **1d,e,g**, J. P. Freeman and T. E. Stevens, *J. Org. Chem.*, **23** 136 (1958); F. G. Bordwell and E. W. Garbisch, Jr., *J. Org. Chem.*, **27**, 2322, 3049 (1962); **1f**, K. Yamamura and S. Watarai, *Bull. Chem. Soc. Jpn.*, **48**, 3757 (1975); **1i**, K. N. Campbell, J. Shavel, Jr., and B. K. Campbell, *J. Am. Chem. Soc.*, **75**, 2400 (1953); **1j**, E. Bergmann, L. Engel, and H. Meyer, *Ber.*, **65**, 446 (1932).
30) M. Friedman, *J. Org. Chem.*, **30**, 859 (1965).
31) K. Tatsumi, H. Yamada, H. Yoshimura, and Y. Kawazoe, *Arch. Biochem. Biophys.*, **213**, 689 (1982).
32) J. Hambrecht, *Synthesis*, **1977**, 280.
33) I. I. Grandberg, L. B. Dmitriev, V. I. Sorokin, and Yu. A. Larshin, *Khim. Geterotsikl. Soedin.*, **1979**, 620; *Chem. Abstr.*, **91**, 90908h (1979).
34) M. Shiono, Y. Echigo, and T. Mukaiyama, *Chem. Lett.*, **1976**, 1397.
35) D. Davidson, *J. Org. Chem.*, **3**, 361 (1938).
36) S. N. Danilow, *Zh. Obshch. Khim. (J. Gen. Chem.)*, **18**, 2000 (1948).
37) Z. Y. Kyi and W. Wilson, *J. Chem. Soc.*, **1953**, 789.
38) B. Odd and L. Raffa, *Gazz. Chim. Ital.*, **9**, 562 (1939).

Regiospecific Ring Opening of Epoxides with Cyanotrimethylsilane on Solid Bases: Reaction Features, and Role of Metal Cations of Solid Bases

Keisuke SUGITA, Akihisa OHTA, Makoto ONAKA,* and Yusuke IZUMI*
Department of Synthetic Chemistry, School of Engineering, Nagoya University,
Furo-cho, Chikusa-ku, Nagoya 464
(Received January 14, 1991)

A new attempt of utilizing solid acids and bases for ring opening of epoxides with Me_3SiCN was investigated. Solid strong bases such as calcium oxide and magnesium oxide catalyzed the regio- and chemoselective ring opening of epoxides with Me_3SiCN much more effectively than homogeneous catalysts. On CaO and MgO, the reactions of unsymmetrical epoxides with Me_3SiCN afforded 3-trimethylsiloxyalkanenitriles in high yields through regio- and stereoselective attack of cyanide ion on the less substituted epoxycarbon. Additionally, on CaO, 2,3-epoxy-1-alkanol derivatives were selectively converted to the corresponding C-3 opened products by the attack of cyanide ion. In these cases no isocyanides were formed. It was suggested that CaO acted as a bifunctional catalyst; the lattice oxide anions of CaO activated Me_3SiCN, and simultaneously calcium ions promoted the ring opening of epoxyalkanol as Lewis acid sites.

Cyanotrimethylsilane (Me_3SiCN), which is considered as stabilized hydrogen cyanide, has been widely applied to organic synthesis.[1] Recently Me_3SiCN has been reported to react with epoxyalkanes in the presence of various Lewis acids to give 3-trimethylsiloxyalkanenitriles or 2-trimethylsiloxyalkyl isocyanides.[2] "Hard" acids such as $AlCl_3$,[3,4] Et_2AlCl,[3,5] $Al(O^iPr)_3$,[5] $LuCl_3$,[6] and $Ti(O^iPr)_4$[7] promote the reaction of epoxides with Me_3SiCN to afford 3-trimethylsiloxyalkanenitriles. In contrast, 2-trimethylsiloxyalkyl isocyanides are predominantly produced in the presence of "Soft" acids such as $ZnCl_2$,[8] ZnI_2,[8] $Pd(CN)_2$,[5] and $SnCl_2$.[5] In acid-promoted nitrile formation via ring openings of unsymmetrical epoxides, however, the problems of low regioselectivity and contamination of isocyanides are often encountered.[5]

We have attempted to utilize inorganic solid acids and bases such as zeolites[9] and clay montmorillonite[10] for several types of liquid-phase organic reactions. These heterogeneous organic reactions on inorganic solids are becoming very useful for the following reasons:[11] (1) They are operationally simple, with product isolation involving only filtration and solvent evaporation, (2) they are often more selective and milder than the corresponding homogeneous reactions, (3) a synergistic reaction-promoting effect by acid and base sites is expected because both acid and base sites can exist independently on the surface of solid.

Recently we found that inorganic solid bases could efficiently activate Me_3SiCN to react with carbonyl compounds to afford 3-trimethylsiloxyalkanenitriles.[12] On the basis of this finding, we applied several types of solid bases as promoters to ring openings of unsymmetrical epoxides and 2,3-epoxy-1-alkanol derivatives with Me_3SiCN, and reported in a rapid communication that certain solid bases such as CaO and MgO greatly activated the ring opening of epoxides to produce exclusively 3-trimethylsiloxyalkanenitriles in a highly regioselective manner.[13] Regioselective ring opening of 2,3-epoxy-1-alkanol derivatives with nucleophiles is an intriguing synthetic subject since easily available, optically pure 2,3-epoxy-1-alkanols are important building blocks for synthesis of natural products.[14] In this context, we have previously demonstrated a highly regioselective ring opening of 2,3-epoxy-1-alkanols with several inorganic nucleophiles supported on a solid acid of calcium ion-exchanged Y-typed zeolite, in which the calcium ions bound in zeolite regulated the ring opening by forming a five-membered chelate complex with 2,3-epoxy-1-alkanol.[9b,9c]

In this paper, we describe the details of ring opening of epoxides promoted by inorganic solid bases such as CaO and MgO, comparing with the effects by other soluble promoters of $Al(O^iPr)_3$ and $^nBu_4NF$. In addition, we discuss the role of the metal cations of solid bases in regioselective ring opening of 2,3-epoxy-1-alkanol, based on a spectroscopic evidence for the formation of a five-membered chelate complex of Eu^{3+} with 2,3-epoxy-1-alkanol.

Results and Discussion

1) Reactions of Unsymmetrical Epoxides with Me_3SiCN. The reaction of 1,2-epoxyoctane (**1**) with Me_3SiCN was examined in the presence of various solid catalysts in heptane, and the results are listed in Table 1 (Eq. 1). On solid bases such as CaO, MgO, hydroxy-

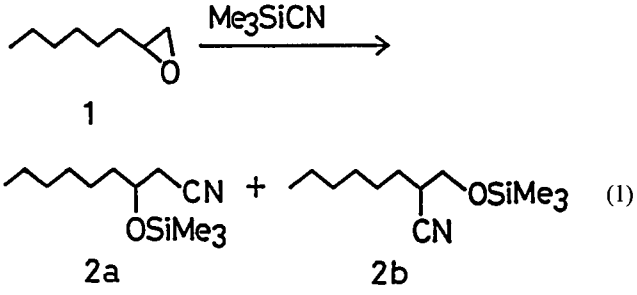

(1)

apatite (HAp, $Ca_{10}(PO_4)_6(OH)_2$),[15] and CaF_2, the ring opening of the epoxide was accelerated to produce 3-(trimethylsiloxy)nonanenitrile (**2a**) in over 97% regiose-

Table 1. Ring Opening of 1,2-Epoxyoctane (**1**) with Me_3SiCN

Run	Solid catalyst	Solvent	Condition Temp/°C (Time/h)	Yield %	**2a : 2b**
1	CaO[a]	Heptane	R.T. (0.5)	98	97 : 3
2	MgO[a]	Heptane	R.T. (0.5)	97	98 : 2
3	HAp[a,b]	Heptane	R.T. (1.5)	97	98 : 2
4	CaF_2[a]	Heptane	R.T. (72)	96	99 : 1
5	SiO_2[a]	Heptane	R.T. (5)	0	
6	Fe-Mont[a,e]	Heptane	R.T. (5)	0	
7	$Al(O^iPr)_3$[b]	Hexane	R.T. (72)	91	97 : 3
8	$^nBu_4NF$[c]	THF	Reflux (4)	96	>99 : 1

a) **1** (1 mmol), Me_3SiCN (2 mmol), and solid catalyst (0.2 g) were used. b) **1** (1 mmol), Me_3SiCN (1.5 mmol), and $Al(O^iPr)_3$ (1.5 mmol) were used. c) **1** (1 mmol), Me_3SiCN (3 mmol), and $^nBu_4NF$ (3 mmol) were used. d) Hydroxyapatite. e) Iron (III) ion-exchanged montmorillonite.

Table 2. Chemical Properties of Solid Acids and Bases

Solid	S.A./$m^2 g^{-1}$[a]	Acid or base strength[b]
CaO	65	$H_- \geqslant +18.4$
MgO	316	$H_- \geqslant +18.4$
HAp	55	$+15.0 > H \geqslant +9.3$
CaF_2	6	c)
SiO_2	585	$+3.3 \geqslant H_o \geq +1.5$
Fe-Mont	37	$-8.2 \geqslant H_o$

a) Specific surface area. b) Maximum acid or base strength were measured by use of Hammett indicators in benzene. c) H_- of CaF_2 could not be determined.

lectivity (Run 1—4). The catalytic activity of solid base decreased in the order of $CaO \fallingdotseq MgO > HAp \gg CaF_2$, correlating to their intrinsic base strengths (Table 2). In contrast to the solid bases, strongly acidic montmorillonite (Fe-Mont), as well as weakly acidic silica (SiO_2), showed no catalytic activity for the ring opening (Run 5, 6). When Me_3SiCN and a soluble Lewis acid such as $Al(O^iPr)_3$ or $^nBu_4NF$ were treated with **1**, reaction rates were largely reduced compared with the cases of CaO and MgO (Run 7, 8).

Since silicon has strong affinities for fluoride ion and oxide ion, when combined with fluoride ion or oxide ion, silicon can expand its coordination number from the normal value of four to five or six to form penta- or hexacoordinated compounds.[16] These penta- and hexacoordinate silicon compounds have higher reactivities than the ordinary tetracoordinate silicon compounds. On the other hand, the basic sites on CaO and MgO were reported to be the surface lattice oxygen (O^{2-}) species.[17] It can be, therefore, presumed that a strongly basic site of O^{2-} on the surface of CaO or MgO coordinates to Me_3SiCN to release a cyanide ion, resulting in nucleophilic ring opening of epoxides (Chart 1).[18]

Next, the reaction of **1** with Me_3SiCN on MgO was examined with respect to the influence of the reaction solvent (Table 3). The reaction rate was remarkably decreased when dimethoxyethane (DME) was used. A polar solvent such as DME may strongly adsorb on the surface of MgO to weaken the interaction between Me_3SiCN and MgO.

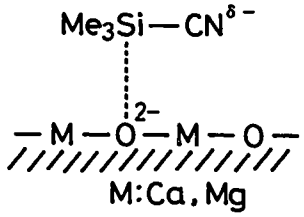

Chart 1.

Table 3. Effects of Solvent in the Reaction of **1** with Me_3SiCN on MgO[a]

Run	Solvent	Time/h[b]	Yield/%	**2a : 2b**
1	Heptane	0.5	97	98 : 2
2	Benzene	0.5	97	98 : 2
3	CH_2Cl_2	0.5	97	99 : 1
4	DME	3	95	96 : 4

a) Ring-opening reaction was carried out at room temperature. b) Reaction was monitored by TLC and GC: Reaction was carried out until **1** was consumed.

Table 4. Ring Opening of Unsymmetrical Epoxides with Me_3SiCN

Run	Solid catalyst	R^1	R^2	R^3	Time h	Yield %	**4a : 4b**
1	CaO[a]	CH_3	CH_3	H	0.5	98	>99 : 1
2	MgO[a]	CH_3	CH_3	H	0.5	78	>99 : 1
3	CaO[a]	CH_3	$-(CH_2)_4-$		4.5	95	99 : 1
4	MgO[a]	CH_3	$-(CH_2)_4-$		3	96	98 : 2
5	$Al(O^iPr)_3$[b]	CH_3	$-(CH_2)_4-$		96	91	76 : 24
6	CaO[a]	CH_3	CH_3	CH_3	24	84	94 : 6
7	MgO[a]	CH_3	CH_3	CH_3	24	84	96 : 4
8	$Al(O^iPr)_3$[b]	CH_3	CH_3	CH_3	48	82	51 : 49

a) Epoxide (1 mmol), Me_3SiCN (2 mmol), and solid catalyst (0.2 g) in heptane, at room temperature. b) Epoxide (1 mmol), Me_3SiCN (1.5 mmol), and $Al(O^iPr)_3$ (1.5 mmol), in heptane, at room temperature.

The synthetic potential of the present method was demonstrated by the successful employment of other epoxides (Eq. 2). Table 4 shows the ring openings of

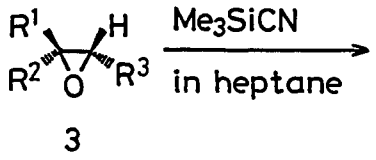

3

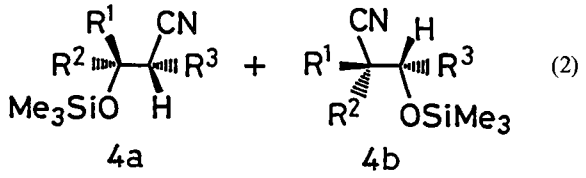

4a 4b (2)

various unsymmetrical epoxides (**3**) with Me_3SiCN on CaO and MgO. All the epoxides investigated quantitatively afforded 3-trimethylsiloxyalkanenitriles by highly regioselective ($\geqslant$94%) attack of cyanide on the less substituted epoxycarbon without the formation of isocyanides. The ring opening in Run 3—5 occurred completely in an S_N2 fashion. Previously it was reported that a soluble strong base such as lithium diethylamide induced the rearrangement of epoxides to the corresponding allylic alcohols.[19] However, CaO and MgO never induced this type of rearrangement.

When Me_3SiCN and a soluble Lewis acid $Al(O^iPr)_3$ were treated with epoxides (**3**), regioselectivity was reduced (Run 5, 8). Consequently, solid bases of CaO and MgO were ascertained to be very effective in the regioselective ring-opening of epoxides with Me_3SiCN.

2) Base Induced Regioselective Ring Openings of 2,3-Epoxy-1-alkanol Derivatives with Me_3SiCN. On CaO, the ring opening of trans-2,3-epoxy-1-hexanol (**5**)[20] with Me_3SiCN (Eq. 3) smoothly took place at

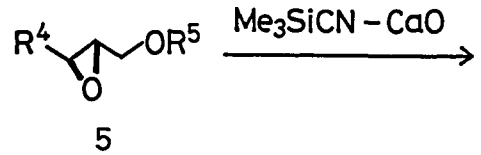

5

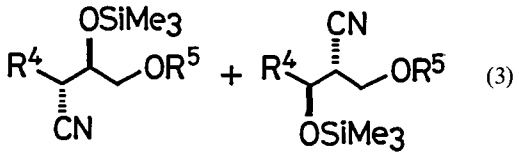

6a 6b (3)

room temperature to afford **6a** and **6b** in good total yield (86%) and good regioselectivity (89 : 11). We assume that such high regioselection is attributed to the formation of a five-membered chelate complex between two oxygen atoms of the epoxyalkanol and a calcium ion of CaO. This chelate formation directs the ring-opening site of epoxide.[9b,9c] When 2,3-epoxy-1-alkanol was acetylated beforehand and then treated with

Table 5. CaO-Directed Reactions of *trans*-2,3-epoxy-1-alkanol and Its Derivative with Me_3SiCN[a]

Run	R^4	R^5	Condition Temp/°C (Time/h)	Yield %	**6a : 6b**
1	^{n}Pr	H	R.T. (4)	86	89 : 11
2	^{n}Pr	Ac	R.T. (4)	91	96 : 4
3	^{i}Pr	Ac	60 °C (1)	75	96 : 4
4	Cyclohexyl	Ac	60 °C (2)	84	97 : 3

a) CaO (0.5 g), epoxides (0.5 mmol), Me_3SiCN (1 mmol), in heptane.

Me_3SiCN on CaO, more regioselective ring opening at the C-3 carbon ($\geqslant$90) was realized as shown in Table 5. This higher regioselectivity would be caused by the inductive effect of the acetyl group in addition to the above-mentioned chelate formation between Ca^{2+} and 2,3-epoxy-1-acetate. In Runs 1—4 the ring openings proceeded with inversion of configuration, and no isocyanides were formed. MgO, HAp, and CaF_2 showed lower activities than CaO.

Compared with heptane, benzene and CH_2Cl_2 induced not only lower rates but lower regioselectivities. Benzene and CH_2Cl_2 may restrain the chelate formation between an epoxyalkanol molecule and a calcium ion. Furthermore, no ring-opening reaction occurred in DME. This strongly negative effect of DME is probably due to chelation of a calcium ion on CaO, so that DME may prevent a calcium ion from electrophilic activation of oxirane ring toward nucleophilic attack. Thus a less polar solvent is preferable in order to increase reaction rate and regioselectivity.

Reportedly, $Ti(O^iPr)_4$ promotes the reaction of *trans*-2,3-epoxy-1-hexanol with Me_3SiCN under DME reflux conditions to give C-3 and C-2 opening products in 83 : 17 regioselectivity and 32% yield.[21] In another control experiment, no reaction occurred when the *trans*-2,3-epoxy-1-hexanol was refluxed in THF with Me_3SiCN (3 equiv) in the presence of $^nBu_4NF$ (3 equiv). CaO thus catalyzed the ring opening of epoxyalkanols much more efficiently and selectively than $Ti(O^iPr)_3$ and $^nBu_4NF$.

3) Investigation on Chelate Complex Formation between 2,3-Epoxy-1-alkanol and Ca^{2+}. In order to clarify the role of Ca^{2+} ions of CaO in the nucleophilic ring opening of 2,3-epoxy-1-alkanol, we tried to confirm a putative intermediate complex formed from Ca^{2+} and 2,3-epoxy-1-alkanol in solution by means of ^1H NMR spectroscopy.[22] Unfortunately, most of calcium salts were sparingly soluble in nonpolar organic solvents suitable for ^1H NMR spectroscopy (e.g. $CDCl_3$). Here we chose $Eu(fod)_3$ instead of Ca^{2+} salts based on the following three reasons. First, Eu^{3+} (0.98 Å) is almost the same as Ca^{2+} (0.99 Å) with respect to ionic radius. Second, the coordination properties of Eu^{3+} have been recognized to be very similar to those of Ca^{2+}: Eu^{3+}, as well as Ca^{2+}, has a strong affinity for oxygen ion.[23]

Third, $Eu(fod)_3$ is freely soluble in organic solvents such as $CDCl_3$.

$Eu(fod)_3$ has been used as a typical NMR shift reagent.[24] Paramagnetic ions such as Lu^{3+} exert stronger magnetic fields on NMR spectra and afford greater spectral spreading properties, when coordinated by organic compounds which possess Lewis base sites. Therefore, the influence of magnetic fields by Lu^{3+} falls away sharply with the distance from Lu^{3+}, and the induced shifts will be significant only if a nucleus is in close average proximity to Lu^{3+}.

Figure 1 demonstrates the changes of chemical shifts in the ^1H NMR spectra (200 MHz) of 1-hexanol and *trans*-2,3-epoxy-1-hexanol with the amount of $Eu(fod)_3$ in $CDCl_3$. As expected, the shift of each proton of 1-hexanol induced by $Eu(fod)_3$ attenuated along the following series: $H_1>H_2>H_3>H_4>H_5>H_6$. However, the shifts observed in the case of *trans*-2,3-epoxy-1-hexanol decreased in the order of $H_3>H_1>H_2>H_4>H_5>H_6$. An anormalous larger shift of H_3 suggests that H_3 of *trans*-2,3-epoxy-1-hexanol is located closer to Eu^{3+}. By the molecular model examination of a bidentate complex of $Eu(fod)_3$ with *trans*-2,3-epoxy-1-hexanol, we could ascertain that the proton at C-3 and Eu^{3+} became so closely spaced each other as to interact strongly (Chart 2). Consequently it is obvious that the epoxyalkanol forms a bidentate complex with Eu^{3+}.

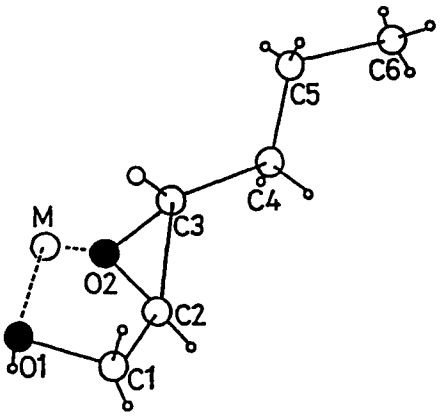

Chart 2.

The reaction of *trans*-2,3-epoxy-1-hexanol with Me_3SiCN in the presence of $Eu(fod)_3$[25] was rather slower and took about 20 h at 98 °C for completion. However, a good regioselectivity (88 : 12) and a good total yield of 80% were obtained as expected from the above mentioned complex formation. This regioselectivity was almost the same as that of the reaction on CaO.

$Ca(OTf)_2$ is easily prepared by adding triflic acid to a suspension of calcium carbonate in dry methanol.[26] $Ca(OTf)_2$ though not soluble in $CHCl_3$ is freely soluble in methanol and DMSO. By using $Ca(OTf)_2$ dissolved

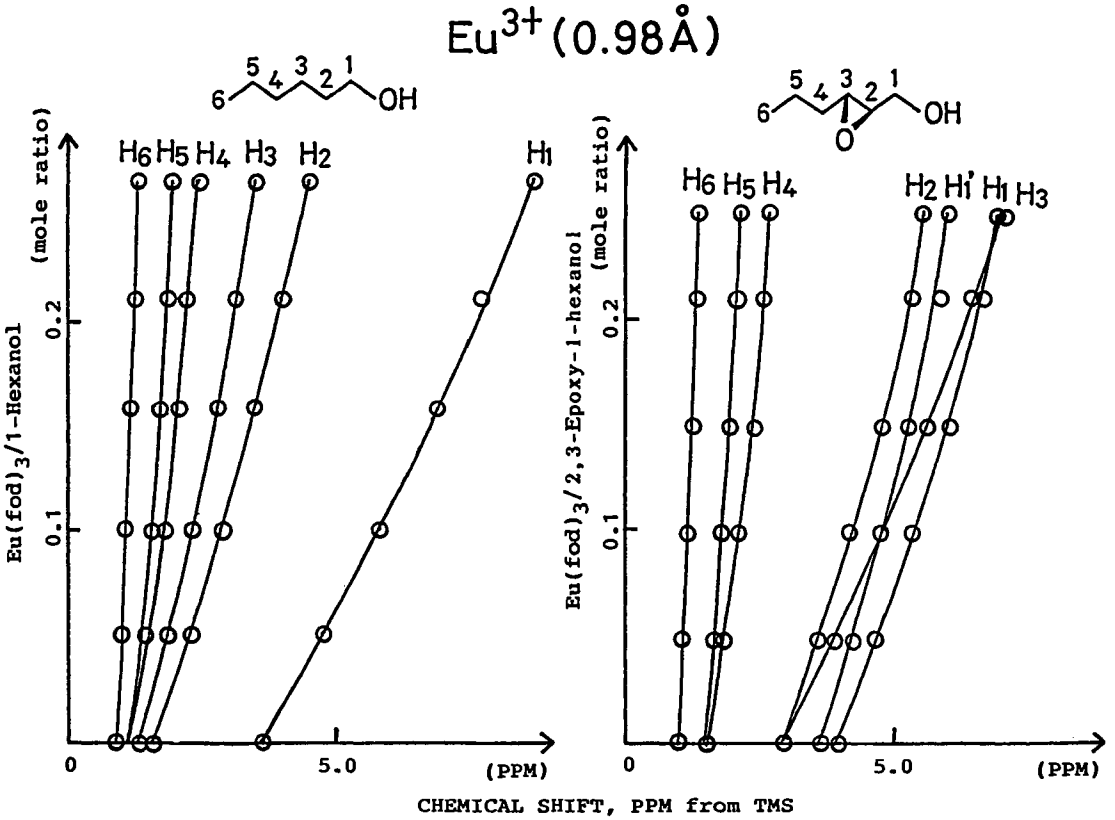

Fig. 1. Chemical shifts as a function of added $Eu(fod)_3$ to 1-Hexanol or 2,3-Epoxy-1-hexanol in 0.55 ml $CDCl_3$. 200 MHz spectra of 1-Hexanol or 2,3-Epoxy-1-hexanol with $Eu(fod)_3$ was measured at room temperature.

Table 6. Reactions of *trans*-2,3-Epoxy-1-hexanol (7) with MeO^-

Run	Promoter	Nucleophile	Condition	Yield %	8a : 8b
1	$Ca(OTf)_2$	MeOH[a]	$CHCl_3$, 50 °C, 3 h	82	79 : 21
2		MeONa[b]	THF, 50 °C, 18 h	36	64 : 36

a) 7 (1 mmol), MeOH (5 mmol), and $Ca(OTf)_2$ (1 mmol), in $CHCl_3$. b) 7 (1 mmol), and MeONa (3 mmol), in THF.

in MeOH–$CHCl_3$ (1 : 30), we could examine homogeneous ring opening of epoxyalkanol (Eq. 4). When

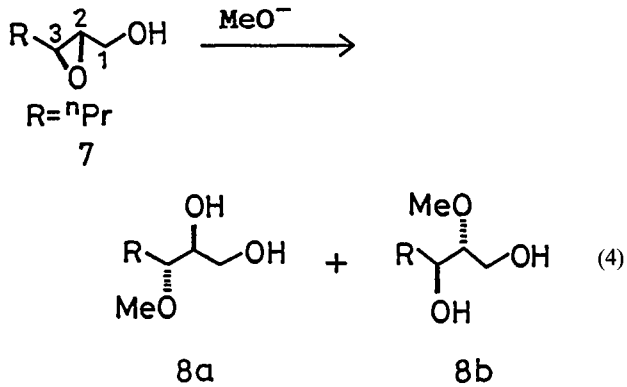

(4)

MeOH and $Ca(OTf)_2$ were treated with *trans*-2,3-epoxy-1-hexanol (7) in $CHCl_3$, a C-3 : C-2 ratio was as high as 79 : 21 (Table 6). On the other hand, when 7 and MeONa were vigorously mixed in THF in the absence of any calcium salt, a lower C-3 : C-2 ratio of 64 : 36 (**8a : 8b**) was obtained (Table 6). Evidently calcium ions could enhance the regioselectivity at C-3 acting as homogeneous Lewis acids.

On the basis of the spectroscopic study using $Eu(fod)_3$ and a comparative experiment using $Ca(OTf)_2$, it is concluded that the calcium ions on the surface of CaO regulate the ring-opening site, probably by forming bidentate chelate complexes with 2,3-epoxy-1-alkanol molecules.

Additionally, compared with the homogeneous Lewis acid-promoted reactions (e.g. $Al(O^iPr)_3$, $Ti(O^iPr)_4$ and $Eu(fod)_3$), CaO-promoted ring openings proceeded more efficiently and regioselectively because CaO served as a bifunctional catalyst; the oxide anions on CaO activated Me_3SiCN, and simultaneously the calcium ions on CaO activated epoxyalkanol as Lewis acids regulating the ring-opening site.

Conclusion

The present synthetic method using inorganic solid base catalysts provides a convenient and simple procedure for the regioselective ring opening of epoxides with Me_3SiCN. Especially the strong base solids such as CaO and MgO enable milder reaction conditions (room temperature, neutral reaction medium), higher regiospecific transformation, and easier product isolation than Lewis acids ever used in the corresponding homogeneous reactions. Further studies are underway to utilize base solids in various types of liquid-phase organic reactions which involve organosilicon reagents.

Experimental

Measurement. Infrared (IR) spectra were measured in $CDCl_3$ or CCl_4 with a JASCO IR-810 spectrometer. The ^1H NMR spectra were measured in $CDCl_3$ with Hitachi R-600 (60 MHz) and Varian GEMINI 200 (200 MHz) spectrometers. Tetramethylsilane (TMS) was used as an internal standard. The chemical shifts are given in δ (ppm) downfield from TMS, and the coupling constants are in hertz. Gas chromatographic analyses were carried out with a Shimadzu GC-8A instrument with a flame ionization detector and a capillary column (OV-1 bonded, 25 m and PEG-HT bonded, 25m).

Materials. MgO and CaO were prepared by calcining their hydroxide (Kishida Chemical Co.) at 500 °C/0.5 Torr (1 Torr=133.322 Pa), for 2 h. Hydroxyapatite[15] (HAp, $Ca_{10}(PO_4)_6(OH)_2$, Nacalai Tesque, Inc.) was dried at 500 °C/0.5 Torr for 2 h. CaF_2 (Kishida Chemical Co.) and Silica (Fuji-Davison B-Type) were dried at 200 °C/0.5 Torr for 2 h. Iron (III) ion-exchanged montmorillonite (Fe-Mont) was prepared from sodium ion exchanged montmorillonite (Kunipia-F, Kunimine Co.) by ion exchange.[10b] Fe-Mont was dried at 120 °C/0.5 Torr for 3 h.

Organic solvents were dried over molecular sieves 3A.

(2*S*,3*S*)-2,3-Epoxy-1-alkanols were prepared from trans allylic alcohols by Sharpless asymmetric epoxidation process.[27]

$Ca(CF_3SO_3)_2$. Trifluoromethanesulfonic acid (5 ml, 0.06 mol) was slowly added to a suspension of calcium carbonate (2 g, 0.02 mol) in dry methanol (20 ml) at room temperature. The reaction mixture was stirred at room temperature for 20 min, then at reflux for 2 h. It was concentrated under reduced pressure, and then the resulting white cake was dried at 130 °C/1 Torr for 3 h to give 6.6 g of calcium triflate (98% yield).

Acid and Base Strength Measurements of Solids. The method of measurement corresponded to Walling's method.[28] The following Hammett indicators (pK_a value) were employed; 4-nitroaniline (+18.4), 2,4-dinitroaniline (+15.0), phenolphthalein (+9.3), bromothymol blue (+7.2), 4-(dimethylamino)azobenzene (butter yellow) (+3.3), 4′-amino-2,3′-dimethylazobenzene (+2.0), 4-(phenylazo)-*N*-phenylaniline (+1.5), crystal violet (+0.8), and anthraquinone (− 8.2).

The color of the indicator adsorbed on the solid was visually observed after the addition of about 5 ml of dry benzene and one drop of a 0.1% solution of the indicator in benzene to 0.1 g of a solid.

Reactions of Unsymmetrical Epoxides with Me_3SiCN and Inorganic Solids. To a suspended mixture of the solid catalyst (0.2 g) and heptane (2 ml) were added a heptane solution

(3 ml) of epoxide (1 mmol), and Me_3SiCN (2 mmol), successively. The mixture was stirred under the conditions listed in Tables 1, 3, and 4. As work-up, ether (5 ml) was added, the solid catalyst was filtered off through a Celite pad and washed with ether. The filtrate was distilled on a Kugelrohr apparatus to yield the products. The regioisomeric ratios of the products were determined by ^1H NMR (200 MHz) and capillary GC (OV-1, 25 m).

Reaction of 1,2-Epoxyoctane with Me_3SiCN and $^nBu_4NF$. A solution of $^nBu_4NF$ in THF (1.1 M, 1 M=1mol dm^{-3}) was stored over activated 3A molecular sieves powders. (Activation of powdered 3A molecular sieves involved heating at 200 °C and 0.5 Torr pressure for at least 3 h.) Under a nitrogen atmosphere, the solution of $^nBu_4NF$ (3 mmol) was added to a solution of a 1,2-epoxyoctane (1 mmol) and Me_3SiCN (3 mmol) in THF (5 ml) at room temperature. The mixture was stirred at 60 °C for 4 h. The THF was removed by evaporation, and the residue was diluted with Et_2O. The reaction mixture was washed with water and the organic layer was dried over anhydrous Na_2SO_4. The organic layer was evaporated and distilled by a Kugelrohr apparatus to yield the products.

Reactions of Unsymmetrical Epoxides with Me_3SiCN and $Al(O^iPr)_3$. Under a nitrogen atmosphere, a mixture of $Al(O^iPr)_3$ (1.5 mmol) and Me_3SiCN (1.5 mmol) in hexane (5 ml) was stirred for 2 h at room temperature. An epoxide (1 mmol) was added and the mixture was stirred at room temperature. Then Me_3SiCN (8 mmol) was added and the mixture was stirred at room temperature for 20 h. As work-up, a mixture of ice and 3M NaOH was added, and the mixture was extracted with ether. The ethereal solution was washed with brine and dried over anhydrous Na_2SO_4. The organic layer was evaporated and distilled by a Kugelrohr apparatus to yield the products.

3-(Trimethylsiloxy)nonanenitrile. Bp 110 °C (bath temperature)/0.5 Torr; IR (CCl_4) 1253, 2251 cm^{-1}; ^1H NMR ($CDCl_3$) δ=0.15 (s, 9H, CH_3Si), 0.88 (t, 3H, J=7.7 Hz, CH_3), 1.10—1.44 (br, 8H, $(CH_2)_4$), 1.44—1.64 (m, 2H, CH_2COSi), 2.44 (d, 2H, J=7.7 Hz, CH_2CN), 3.9 (dddd, 1H, J=5.1, 5.1, 5.1 Hz, CHOSi); ^{13}C NMR δ=—0.1, 13.8, 22.4, 25.0, 26.1, 28.9, 31.5, 37.0, 68.4, 118.0. Found: C, 63.54; H, 11.33; N, 6.15%. Calcd for $C_{12}H_{25}NOSi$: C, 63.38; H, 11.08; N, 6.16%.

***c*-2-Methyl-2-(trimethylsiloxy)-*r*-1-cyclohexanecarbonitrile:** Bp 135 °C (bath temperature)/20 Torr; IR (CCl_4) 1253, 2249 cm^{-1}; ^1H NMR ($CDCl_3$) δ=0.14 (s, 9H, CH_3Si), 1.42 (s, 3H, CH_3), 1.35—1.80 (m, 7H, -(CH_2)-), 1.88—2.06 (m, 1H), 2.60 (dd, 1H, J=7.0, 4.0 Hz, CHCN); ^{13}C NMR ($CDCL_3$) δ=2.1, 21.5, 22.4, 25.8, 26.2, 37.7, 41.0, 73.0, 121.3. Found: C, 62.77; H, 10.21; N, 6.62%. Calcd for $C_{11}H_{12}NOSi$: C, 62.50; H, 10.01; N, 663%.

2,3-Dimethyl-3-(trimethylsiloxy)butanenitrile. Bp 130 °C (bath temperature)/30 Torr; IR (CCl_4) 1253, 2251 cm^{-1}; ^1H NMR ($CDCl_3$) δ=0.12 (s, 9H, CH_3Si), 1.28 (d, 3H, J=7.1 Hz, CH_3CCN), 1.38 (s, 6H, CH_3COSi), 2.69 (q, 1H, J=7.1 Hz, CHCN); ^{13}C NMR ($CDCl_3$) δ=2.0, 12.8, 26.7, 27.6, 39.1, 73.7, 122.0. Found: C, 58.17; H, 10.31; N, 7.64%. Calcd for $C_9H_{19}NOSi$: C, 58.32; H, 10.33; N, 7.56%.

3-Methyl-3-(trimethylsiloxy)butanenitrile. Bp 120 °C (bath temperature)/30 Torr; IR (CCl_4) 1253, 2251 cm^{-1}; ^1H NMR ($CDCl_3$) δ=0.14 (s, 9H, CH_3Si), 1.38 (s, 6H, CH_3COSi), 2.45 (s, 2H, CH_2CN); ^{13}C NMR ($CDCl_3$) δ=2.0, 29.3, 33.8, 71.7, 118.0. Found: C, 56.08; H, 10.10; N, 8.11%. Calcd for $C_8H_{17}NOSi$: C, 56.09; H, 10.00; N, 8.18%

Reactions of (2*S*,3*S*)-2,3-Epoxy-1-alkanol Derivatives with Me_3SiCN and Inorganic Solids. To a suspended mixture of an inorganic solid (0.5 g) and heptane (2 ml) was added a heptane (3 ml) solution of (2*S*,3*S*)-2,3-epoxy-1-alkanol (0.5 mmol) and the mixture was stirred under the conditions listed in Table 5. As work-up, ether (3 ml) was added, the inorganic solid was filtered off through a Celite pad and washed with ether. After organic solvents were evaporated, the reaction mixture was diluted with methanol (3 ml), and 5 equivalents of potassium fluoride was added. The mixture was stirred at 25 °C for 14 h in order to desilylate the organic products. The regioselectivity of the reaction was based on GC (OV-1; 25 m) and ^1H NMR (200 MHz) analysis of the unpurified reaction mixture after acetylation. The hydroxy carbonitriles were treated with Ac_2O (0.5 ml) and pyridine (0.5 ml) in CH_2Cl_2 (1 ml) in the presence of catalytic 4-(*N*,*N*-dimethylamino)pyridine. After the reaction was complete, the reaction mixture was washed with 1 M HCl solution (3 ml) and brine (3 ml), dried over anhydrous Na_2SO_4, and distilled with a Kugelrohr apparatus to yield dihydroxy carbonitriles.

The two regioisomers of dihydroxy carbonitriles were identical with those obtained from the reactions of epoxyalkanols with Me_3SiCN-$Ti(O^iPr)_4$ by GC (OV-1; 25 m) and ^1H NMR (200 MHz) analyses.

Reaction of (2*S*,3*S*)-2,3-Epoxy-1-alkanol with Me_3SiCN and $Ti(O^iPr)_4$. Under a nitrogen atmosphere, $Ti(O^iPr)_4$ (1.5 mmol) was added to solution of an epoxyalkanol (1 mmol) and Me_3SiCN (3 mmol) in DME (5 ml) at room temperature. The mixture was stirred at 80 °C until the epoxyalkanol was consumed. After 5% H_2SO_4 (5 ml) was added, the two phase mixture was stirred vigorously until two clear layers formed. The dihydroxy carbonitriles were extracted with AcOEt and dried over anhydrous Na_2SO_4. The regioselectivity of the reaction was based on GC (OV-1; 25 m) and ^1H NMR (200 MHz) analysis of the unpurified reaction mixture after acetylation.

Reaction of (2*S*,3*S*)-2,3-Epoxy-1-hexanol with Me_3SiCN and $Eu(fod)_3$. Under a nitrogen atmosphere, $Eu(fod)_3$ (1 mmol) was added to solution of a 2,3-epoxy-1-hexanol (1 mmol) and Me_3SiCN (3 mmol) in heptane (4 ml) at room temperature. The reaction mixture was stirred at 98 °C for 20 h. After 5% H_2SO_4 (5 ml) was added, the two phase mixture was stirred vigorously for 1 h at room temperature. The dihydroxy carbonitriles were extracted with AcOEt, and then dried over anhydrous Na_2SO_4. The regioselectivity was determined as described above.

(2*R*,3*R*)-3-Cyano-1,2-hexanediol. Bp 170 °C (bath temperature)/1 Torr; IR (CCl_4) 2250, 3400 cm^{-1}; ^1H NMR ($CDCl_3$) δ=0.98 (br t, 3H, CH_3), 1.10—2.00 (br, 4H, $(CH_2)_2$), 2.50—3.05 (m, 1H, CHCN), 3.30—4.20 (br m, 5H, CH_2OH, CHOH); ^{13}C NMR ($CDCl_3$) δ=13.3, 20.3, 29.7, 35.0, 63.8, 71.1, 120.5. Found: C, 58.52; H, 9.05; N, 9.73%. Calcd for $C_7H_{13}O_2N$: C, 58.72; H, 9.15; N, 9.78%.

(2*R*,3*R*)-3-Cyano-1,2-hexanediol Diacetate. This product was obtained from (2*R*,3*R*)-3-cyano-1,2-hexanediol by acetylation. Bp 150 °C (bath temperature)/1 Torr; IR (CCl_4) 1760, 2250 cm^{-1}; ^1H NMR ($CDCl_3$) δ=0.94 (t, 3H, J=6.8 Hz, CH_3), 1.25—1.80 (br, 4H, $(CH_2)_2$), 2.06 (s, 3H, Ac), 2.08 (s, 3H, Ac), 2.85—3.00 (m, 1H, CHCN), 4.17 (dd, 1H, J=12.5, 5.2 Hz, C(H)HOAc), 4.44 (dd, 1H, J=12.5, Hz, 3.3 Hz, C(H)HOAc), 5.05 (ddd, 1H, J=5.2, 5.2, 3.3 Hz, CHOAc); ^{13}C NMR ($CDCl_3$), δ=13.1, 20.1, 20.4, 20.5, 30.1, 33.2, 62.2, 69.7, 118.6, 170.0, 170.6.

(2*R*,3*R*)-3-Cyano-3-cyclohexyl-1,2-propanediol Diacetate. Bp 190 °C (bath temperature)/0.5 Torr; IR (CCl_4) 1758, 2249 cm^{-1}; ^1H NMR ($CDCl_3$) δ=1.00—2.00 (br, 11H, cyclohexyl), 2.10 (s, 3H, Ac), 2.12 (s, 3H, Ac), 2.84 (dd, 1H, *J*=7.9, 6.0 Hz, CHCN), 4.18 (dd, 1H, *J*=12.4, 5.6 Hz, C(H)HOAc), 4.55 (dd, 1H, *J*=12.4, 2.6 Hz, C(H)HOAc), 5.23 (ddd, 1H, *J*=7.9, 5.6, 2.6 Hz, CHOAc); ^{13}C NMR ($CDCl_3$) δ=20.4, 20.5, 25.4, 25.5, 25.6, 29.2, 31.1, 35.8, 39.8, 62.8, 67.7, 117.7, 170.0, 170.6. Found: C, 63.13; H, 8.14; N, 5.51%. Calcd for $C_{14}H_{21}O_4N$: C, 62.90; H, 7.92; N, 5.24%.

(2*R*,3*R*)-3-Cyano-4-methyl-1,2-pentanediol Diacetate. Bp 130 °C (bath temperature)/0.5 Torr; IR (CCl_4) 1760, 2250 cm^{-1}; ^1H NMR ($CDCl_3$) δ=1.09 (d, 3H, *J*=7.2 Hz CH_3), 1.13 (d, 3H, *J*=7.2 Hz, CH_3), 2.12 (s, 6H, Ac), 2.86 (dd, 1H, *J*=8.4, 5.5 Hz, CHCN), 4.18 (dd, 1H, *J*=12.2, 4.8 Hz, C(H)HOAc), 4.57 (dd, 1H, *J*=12.2, 3.0 Hz, C(H)HOAc), 5.21 (ddd, 1H, *J*=8.4, 4.8, 3.0 Hz, CHOAc); ^{13}C NMR ($CDCl_3$) δ=18.3, 20.4, 20.5, 20.8, 26.6, 40.5, 62.9, 68.2, 117.4, 170.0, 170.6. Found: C, 57.96; H, 7.69; N, 6.25%. Calcd for $C_{11}H_{17}O_4N$: C, 58.14; H, 7.54; N, 6.16%.

Reaction of (2*S*,3*S*)-2,3-Epoxy-1-hexanol with MeOH and $Ca(OTf)_2$. Under a nitrogen atmosphere, $Ca(OTf)_2$ (1 mmol) was added to solution of a 2,3-epoxy-1-hexanol (1 mmol) and CH_3OH (5 mmol) in $CHCl_3$. The reaction mixture was stirred at 50 °C for 3 h. It was diluted with Et_2O (5 ml), washed with H_2O (3 ml), and the organic phase was dried over anhydrous Na_2SO_4. The regioselectivity was based on GC (PEG-HT, 25 m) and ^1H NMR (200 Hz) analysis of the unpurified reaction mixture after acetylation.

Reaction of (2*S*,3*S*)-2,3-Epoxy-1-hexanol with MeONa. Under a nitrogen atmosphere, sodium hydride (3 mmol) was slowly added to solution of MeOH (3 mmol) in THF (2 ml). The solution was stirred for 0.5 h and solution of an epoxyalkanol (1 mmol) in THF was added to it. The reaction mixture was stirred at 60 °C for 18 h. It was then diluted with AcOEt (3 ml) and washed with water (3 ml), and the organic phase was dried over anhydrous Na_2SO_4. The regioselectivity was determined as described above.

(2*R*,3*R*)-3-Methoxy-1,2-hexanediol. 140 °C (bath temperature)/0.6 Torr; IR (CCl_4) 2830, 3450 (br), 3630 cm^{-1}; ^1H NMR ($CDCl_3$) δ=0.70—1.16 (br t, 3H, CH_3), 1.16—1.80 (br m, 4H, $(CH_2)_2$), 2.57 (s, 2H, OH), 3.42 (s, 3H, OCH_3), 3.60—4.10 (m, 4H, CHOMe, CH_2OH, CHOH); ^{13}C NMR ($CDCl_3$) δ=14.0, 18.5, 32.1 , 58.4, 63.2, 72.3, 83.4. Found: C, 56.52; H, 10.80%. Calcd for $C_7H_{16}O_3$: C, 56.73; H, 10.88%.

(2*R*,3*R*)-3-Methoxy-1,2-hexanediol Diacetate. This product was obtained from (2*R*,3*R*)-3-methoxy-1,2-hexanediol by acetylation. 140 °C (bath temperature)/1 Torr; IR (CCl_4) 1750, 2830 cm^{-1}; ^1H NMR ($CDCl_3$) δ=0.90 (tr, 3H, *J*=6.6 Hz, CH_3), 1.20—1.65 (br m, 4H, $(CH_2)_2$), 2.03 (s, 3H, Ac), 2.07 (s, 3H, Ac), 3.25—3.45 (m, 1H, CHOMe), 3.38 (s, 3H, OCH_3), 4.11 (dd, 1H, *J*=12.1, 7.6 Hz, C(H)HOAc), 4.34 (dd, 1H, *J*=12.1, 3.0 Hz, C(H)HOAc), 5.12 (ddd, 1H, *J*=7.6, 4.2, 3.0 Hz, CHOAc); ^{13}C NMR ($CDCl_3$) δ=13.8 18.4, 20.6, 20.8, 32.7, 58.4, 62.6, 72.7, 80.2, 170.6, 171.0.

References

1) a) W. C. Groutas and D. Felker, *Synthesis,* **1980**, 861; b) W. P. Weber, "Silicon Reagents for Organic Synthesis," Springer-Verlag, Berlin (1983), p. 6.

2) a) M. T. Reetz and I. Chatziiosifidis, *Angew. Chem., Int. Ed. Engl.,* **20**, 1017 (1981); b) T. Sasaki, A. Nakanishi, and M. Ohno, *J. Org. Chem.,* **46**, 5445 (1981); c) M. T. Reetz, I. Chatziiosifidis, H. Künzer, and H. Müller-Starke, *Tetrahedron,* **39**, 961 (1983).

3) J. C. Mullis and W. P. Weber, *J. Org. Chem.,* **47**, 2873 (1982).

4) W. Lidy and W. Sundermeyer, *Tetrahedron Lett.,* **1973**, 1449.

5) K. Imi, N. Yanagihara, and K. Utimoto, *J. Org. Chem.,* **52**, 1013 (1987).

6) A. E. Vougioukas and H. B. Kagan, *Tetrahedron Lett.,* **28**, 5513 (1987).

7) a) M. Caron and K. B. Sharpless, *J. Org. Chem.,* **50**, 1557 (1985); b) M. Emziane, P. Lhoste, and D. Sinou, *J. Mol. Catal.,* **49**, L23 (1988).

8) a) P. G. Gassman and T. L. Guggenheim, *J. Am. Chem. Soc.,* **104**, 5849 (1982); b) P. G. Gassman and R. S. Gremban, *Tetrahedron Lett.,* **25**, 3259 (1984); c) P. G. Gassman and L. M. Haberman, *ibid.,* **26**, 4971 (1985); d) P. G. Gassman, K. Okuma, A. Lindbeck, and R. Allen, *ibid.,* **27**, 6307 (1986); e) P. G. Gassman and L. M. Haberman, *J. Org. Chem.,* **51**, 5010 (1986).

9) a) M. Onaka, M. Kawai, and Y. Izumi, *Bull. Chem. Soc. Jpn.,* **59**, 1761 (1986); b) M. Onaka, K. Sugita, and Y. Izumi, *J. Org. Chem.,* **54**, 1116 (1989); c) M. Onaka, K. Sugita, H. Takeuchi, and Y. Izumi, *J. Chem. Soc., Chem. Commun.,* **1988**, 1173.

10) a) M. Onaka, R. Ohno, M. Kawai, and Y. Izumi, *Bull. Chem. Soc. Jpn.,* **60**, 2689 (1987); b) M. Kawai, M. Onaka, and Y. Izumi, *ibid.,* **61**, 1237 (1988); c) M. Kawai, M. Onaka, and Y. Izumi, *ibid.,* **61**, 2157 (1988); d) M. Onaka, R. Ohno, and Y. Izumi, *Tetrahedron Lett.,* **30**, 747 (1989); e) M. Onaka, T. Mimura, R. Ohno, and Y. Izumi, *ibid.,* **30**, 6341 (1989).

11) Recently various porous inorganic solids such as zeolite, silica, and alumina are widely utilized to organic reactions. a) Review: G. H. Posner, *Angew. Chem., Int. Ed. Engl.,* **17**, 487 (1978); b) Review: A. Mckillop and D. W. Young, *Synthesis,* **1979**, 401, 481; c) Review: A. Cornelis and P. Laszlo, *ibid.,* **1985**, 909.

12) M. Onaka, K. Higuchi, K. Sugita, and Y. Izumi, *Chem. Lett.,* **1989**, 1393.

13) To the best our knowledge, this base-catalyzed method is the first example in the reaction of epoxides with Me_3SiCN: K. Sugita, A. Ohta, M. Onaka, and Y. Izumi, *Chem. Lett.,* **1990**, 481.

14) a) K. B. Sharpless, C. H. Behrens, T. Katsuki, A. W. Lee, V. S. Martin, M. Takatani, S. M. Viti, J. Walker, and S. S. Woodard, *Pure Appl. Chem.,* **55**, 589 (1983); b) C. H. Behrens and K. B. Sharpless, *Aldrichimica Acta,* **16**, 67 (1983); c) C. H. Behrens, S. Y. Ko, K. B. Sharpless, and F. J. Walker, *J. Org. Chem.,* **50**, 5687 (1985); d) C. H. Behrens and K. B. Sharpless, *J. Org. Chem.,* **50**, 5696 (1985); e) A. Pfenninger, *Synthesis,* **1986**, 89.

15) J. A. S. Bett, L. G. Christner, and W. K. Hall, *J. Am. Chem. Soc.,* **89**, 5535 (1967).

16) The reactions involving pentacoordinate silicate intermediates have been reported in regio- and stereocontrolled organic synthesis: a) M. Kumada, K. Tamao, and J. Yoshida, *J. Organomet. Chem.,* **239**, 115 (1982); b) M. Kira, K. Sato, and H. Sakurai, *J. Org. Chem.,* **52**, 948 (1987); c) G. Cerveau, C. Chuit, R. J. P. Corriu, and C. Reye, *J. Organomet. Chem.,* **328**, C17 (1987); d) A. Hosomi, S. Kohra, and Y. Tominaga, *J. Chem. Soc., Chem. Commun.,* **1987**, 1517; e) Review: H. Sakurai, *Synlett,* **1**, 1 (1989); f) M. Kira, K. Sato, and H.

Sakurai, *J. Am. Chem. Soc.*, **112**, 257 (1990).

17) The basic site on CaO or MgO was reported to be a surface lattice oxygen (O^{2-}): K. Tanabe and K. Saito, *J. Catal.*, **35**, 247 (1974).

18) Recently we identified the interaction between silicon of Me_3SiCN and O^{2-} on the CaO, by infrared spectrum on the CaO in the course of the above reaction: to be submitted for publication.

19) a) A. C. Cope and J. K. Heeren, *J. Am. Chem. Soc.*, **87**, 3125 (1965); b) B. Rickborn and R. P. Thummel, *ibid.*, **34**, 3583 (1969); c) R. P. Thummel and B. Rickborn, *ibid.*, **92**, 2064 (1970).

20) When Me_3SiCN and CaO were treated with *cis*-2,3-epoxy-1-hexanol, the ring opening was completed within 1 h at room temperature, and a mixture of dihydroxy carbonitriles was isolated in 88% yield. A ^1H NMR analysis of the acetylated crude product revealed a C-3 : C-2 ratio of 97 : 3.

21) The reaction of *trans*-2,3-epoxy-1-hexanol with Nagata's reagent(Et_2AlCN) was reported to give high regioselectivity (94 : 6). See Ref. 7a.

22) In recent years, the solution structures of the complexes formed between 3-alkoxyalkanal and Lewis acid have been confirmed via NMR spectroscopy: a) G. E. Keck and S. Castellino, *J. Am. Chem. Soc.*, **108**, 3847 (1986); b) G. E. Keck, S. Castellino, and M. R. Wiley, *J. Org. Chem.*, **51**, 5478 (1986); c) G. E. Keck and S. Castellino, *Tetrahedron Lett.*, **28**, 281 (1987); d) M. T. Reetz, M. Hüllmann, and T. Seitz, *Anegw. Chem., Int. Ed. Engl.*, **26**, 477 (1987).

23) Review: F. S. Richardson, *Chem. Rev.*, **82**, 541 (1982).

24) a) Review: A. F. Cockerill, G. L. O. Davies, R. C. Harden, and D. M. Rackham, *Chem. Rev.*, **73**, 553 (1973); b) M. D. McCreary, D. W. Lewis, D. L. Wernick, and G. M. Whitesides, *J. Am. Chem. Soc.*, **96**, 1038 (1974).

25) Lanthanide complexes have been utilized as Lewis-acid catalysts to various organic reactions. For a review: a) H. B. Kagan and J. L. Namy, *Tetrahedron*, **42**, 6573 (1986); For a Diels-Alder reaction: b) M. Bednarski and S. Danishefsky, *J. Am. Chem. Soc.*, **105**, 3716 (1983); c) J. Jurczak, A. Golebiowski, and T. Bauer, *Synthesis*, **1985**, 928; d) M. Quimpere and K. Jankowski, *J. Chem. Soc., Chem. Commun.*, **1987**, 676; e) M. M. Midland and M. M. Afonso, *J. Am. Chem. Soc.*, **111**, 4368 (1989); For a ring opening of epoxides: f) A. E. Vougioukas and H. B. Kagan, *Tetrahedron Lett.*, **28**, 6065 (1987); See, also Ref. 9.

26) E. J. Corey and K. Shimoji, *Tetrahedron Lett.*, **24**, 169 (1983).

27) Y. Gao, R. M. Hanson, J. M. Klunder, S. Y. Ko, H. Masamune, and K. B. Sharpless, *J. Am. Chem. Soc.*, **109**, 5765 (1987).

28) a) C. Walling, *J. Am. Chem. Soc.*, **72**, 1164 (1950); b) J. Take, N. Kikuchi, and Y. Yoneda, *J. Catal.*, **21**, 164 (1971).

Formation of 1,2-Dioxanes by the Use of Tris(2,4-pentanedionato)-manganese(III) or Manganese(III) Acetate

Hiroshi NISHINO,* Shin-ichi TATEGAMI, Takashi YAMADA, James D. KORP,† and Kazu KUROSAWA*
Department of Chemistry, Faculty of Science, Kumamoto University, Kurokami 2-39-1, Kumamoto 860
†Department of Chemistry, University of Houston, University Park, Houston, Texas 77204-5641, U.S.A.
(Received January 25, 1991)

The reactions of 1,1-diphenylethene, 1,1-bis(4-chlorophenyl)ethene, 1,1-bis(4-methoxyphenyl)ethene, 1,1-bis(4-methylphenyl)ethene, 1,1-bis(4-fluorophenyl)ethene, styrene, 1-octene, cyclohexene, and cyclooctene with tris(2,4-pentanedionato)manganese(III) ([Mn(acac)$_3$]) in acetic acid at room temperature give 4-acetyl-3-methyl-1,2-dioxan-3-ol in 8—92% yields, together with 3-acetyl-4-hydroxy-3-hexene-2,5-dione. The similar reactions of 1,1-diphenylethene with 2,4-pentanedione, 3-methyl-2,4-pentanedione, 3-ethyl-2,4-pentanedione, 1-phenyl-1,3-butanedione, acetoacetanilide, and 1,3-cyclohexanedione in the presence of manganese(III) acetate also give the corresponding cyclic peroxide in good to moderate yields. The mechanisms of manganese(III)-induced 1,2-dioxane ring formation and concomitant radical side reaction are discussed.

A unique synthetic methodology utilizing manganese(III)-mediated radical inter- or intra-molecular cyclization reactions has been recently and extensively investigated and modified.[1-3] Particularly, manganese(III) acetate and tris(2,4-pentanedionato)manganese(III) ([Mn(acac)$_3$]) are well-known reagents, which perform a very interesting role in acetic acid. That is, two types of reaction occur simultaneously: (1) a one-electron-transfer from an electron-rich organic substrate (donor) to a manganese(III) complex (acceptor) and (2) a radical reaction for ligands which are formed from the thermolysis of a manganese(III) complex or ligand-exchange reaction.[4] These reactions are also influenced by reaction temperature or additives such as acetate ions and water. In the course of a study on the reactions of [Mn(acac)$_3$] with various organic substrates, one of the present authors found that the reaction product from alkenes using this reagent at room temperature differed dramatically from that at the elevated temperature.[5] When 1,1-diphenylethene (**1a**) was treated with [Mn(acac)$_3$] in acetic acid under air *at the reflux temperature*, it gave 3-acetyl-2-methyl-5,5-diphenyl-4,5-dihydrofuran (**2a**), together with a small amount of benzophenone (**4a**). When the reaction was carried out under air *at room temperature* for 12 h, it gave 4-acetyl-3-methyl-6,6-diphenyl-1,2-dioxan-3-ol (**3a**) (the structure was erroneously assigned as 3-acetyl-2-hydroperoxy-2-methyl-5,5-diphenyltetrahydrofuran in the previous paper[5]) along with small amounts of **4a**, 4,4-diphenyl-4-butanolide (**5a**), and 3-acetyl-4-hydroxy-3-hexene-2,5-dione (**8**). Although a lot of cyclic peroxides were synthesized using photosensitized oxygenation[6] and electrochemical cycloaddition,[7] the present reaction is the first example that molecular oxygen is trapped during the manganese(III)-induced radical intermolecular cyclization.[8] We also found that the reaction of **1a** with a 1,3-dicarbonyl compound in the presence of manganese(III) acetate in acetic acid at room temperature gave a similar cyclic peroxide.[8] Therefore, we have been intrigued by these reaction mechanisms and in the possibility of their application to organic synthesis. Herein we report the results of our study.

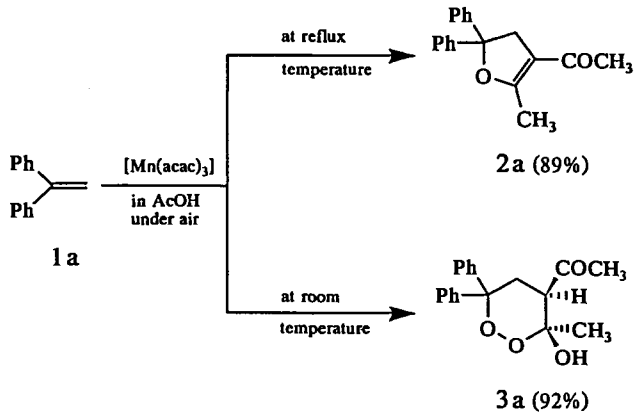

Scheme 1.

Results

Reaction of Alkenes with [Mn(acac)$_3$]. We scrutinized the reaction products from **1a** and found that 4,4-diphenyl-4-butanolide (**5a**), 2,2-diphenyl-2-hydroxyethyl acetate (**6a**), 1-phenyl-1,4-pentanedione (**7a**), and 3-acetyl-4-hydroxy-3-hexene-2,5-dione (**8**) were obtained together with **2a** and **3a** after separation by TLC (Table 1). The structures of these products were determined by analyzing their ^{1}H NMR, IR, and mass spectra as well as by comparing their spectra and melting points with the authentic specimen. The reaction of **3a** with triphenylphosphine gave **2a** (32%), 3-acetyl-2-methyl-5,5-diphenyltetrahydrofuran-2-ol (**9**) (49%), 4-oxo-1,1-diphenylpentyl acetate (**10**) (13%), and triphenylphosphine oxide (83%).[6b,e,9] The structure of **3a** was finally confirmed by an X-ray crystallography. A single crystal of **3a** was successfully grown from ethanol in the orthorhombic space group $P2_12_12_1$ with cell constants a=7.856, b=12.823, and c=15.820 Å. The X-ray structure was solved using the SHELXTL direct

Table 1. Reaction of 1,1-Diphenylethene (**1a**) with Tris(2,4-pentanedionato)manganese(III) in AcOH at 23 °C

Entry	Molar ratio[a]	Time	Recovery	Product (yield/%)[b]						
		h	%	**2a**	**3a**	**4a**	**5a**	**6a**	**7a**	**8**[c]
1	1:0.5	4	25		43	9	7	11		5
2	1:1	11			92	3	2			7
3[d]	1:1	5	57		21	4	2	7		26
4	1:2	19		8	83	5		3		13
5	1:3	24		9	78	5			10	17

a) **1a**: $[Mn(acac)_3]$. b) Isolated yield based on the amount of **1a** used. c) Isolated yield based on the amount of $[Mn(acac)_3]$ used. d) Reaction under an oxygen atmosphere.

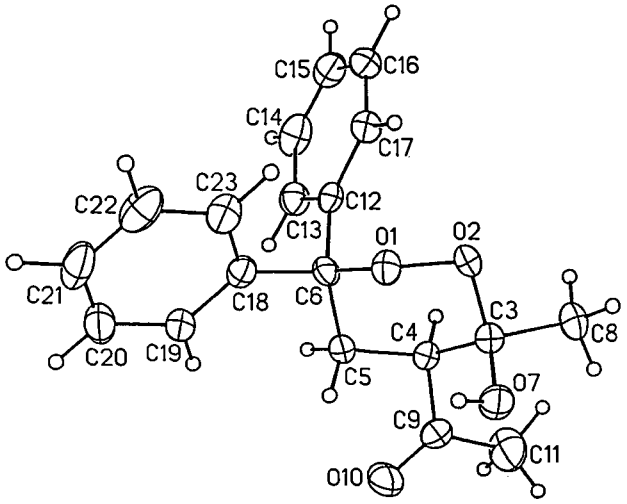

Fig. 1. ORTEP diagram of **3a**. The thermal ellipsoids are 40% equiprobability envelopes, with hydrogens as spheres of arbitrary diameter.

methods program, TREF, which revealed the positions of all of the nonhydrogen atoms. The ORTEP diagram of **3a** is presented in Fig. 1. The O(1)–O(2) bond length is 1.470 Å, the bond angles at O(1) and O(2) are 108.1° and 109.6°, respectively, and the peroxide torsional angle (C(6)–O(1)–O(2)–C(3)) is −74.0°.[10] Unfortunately, we could not determine the absolute configuration because of the lack of a significant anomalous scatterer in the crystal, although **3a** crystallized in a chiral space group (see Experimental Section). However, it should be noted that the cyclic peroxide (**3a**) in the solid state was obtained as the *c*-4-acetyl-3-methyl-1,2-dioxan-*r*-3-ol based on the X-ray analysis. The structure of **7a** was also confirmed by synthesis: the condensation of 2-bromoacetophenone with ethyl 3-oxobutanoate, followed by hydrolysis and acidification, gave **7a** (Scheme 2).

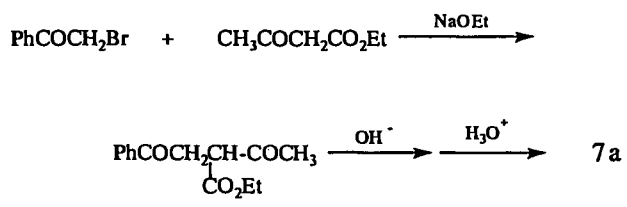

Scheme 2.

The reaction of **1a** with $[Mn(acac)_3]$ in AcOH at 23 °C under air was then carried out at various molar ratios. The best yield of **3a** was attained when the molar ratio was 1 : 1 (Table 1, Entry 2). The reaction under an oxygen atmosphere gave a decreased yield of **3a** with an increase in the yield of **8** (Entry 3). The yield of **3a** decreased at higher molar ratios (Entries 4 and 5).

The reactions were examined for 1,1-bis(4-chlorophenyl)ethene (**1b**), 1,1-bis(4-methoxyphenyl)ethene (**1c**), 1,1-bis(4-methylphenyl)ethene (**1d**), 1,1-bis(4-fluorophenyl)ethene (**1e**), styrene (**1f**), 1-octene (**1g**), cyclohexene (**1h**), and cyclooctene (**1i**) in AcOH to yield the corresponding 1,2-dioxane derivatives (**3b**—**i**) (Scheme 3). It was observed that the molar ratio at which the maximum yield was attained depended on the substrate as shown in Table 2. The alkenes having no aromatic substituents are poor substrates for the 1,2-dioxane formation (Entries 12—14).

Similar reactions of **1a** with (2,4-pentanedionato)-metals such as $[Cr(acac)_3]$, $[Co(acac)_3]$, $[Fe(acac)_3]$, and $[Cu(acac)_2]$ were also carried out, but either **1a** was recovered unchanged or a complex mixture resulted.

Reaction of 1a with 1,3-Diketones in the Presence of Manganese(III) Acetate. When the reaction of **1a** with 2,4-pentanedione in the presence of manganese(III) acetate was carried out at a molar ratio of 1 : 3 : 1, the major product was again **3a**, along with small amounts of **5a**, **7a**, and **8** (Table 3). When 3-methyl-2,4-pentanedione in place of 2,4-pentanedione was added during the oxidation of **1a** with manganese(III) acetate, the products were 4-acetyl-3,4-dimethyl-6,6-diphenyl-1,2-dioxan-3-ol (**11a**), 3-acetyl-2-ethoxy-2,3-dimethyl-5,5-diphenyltetrahydrofuran (**12a**), and **4a**. The reaction of 3-ethyl-2,4-pentanedione also yielded the corresponding 1,2-dioxan-3-ol derivative (**11b**) and 2-ethoxytetrahydrofuran (**12b**). The similar reactions of **1a** using 1-phenyl-1,3-butanedione, acetoacetanilide, and 1,3-cyclohexanedione gave the corresponding cyclic peroxides (**11c**—**e**) (Fig. 2).

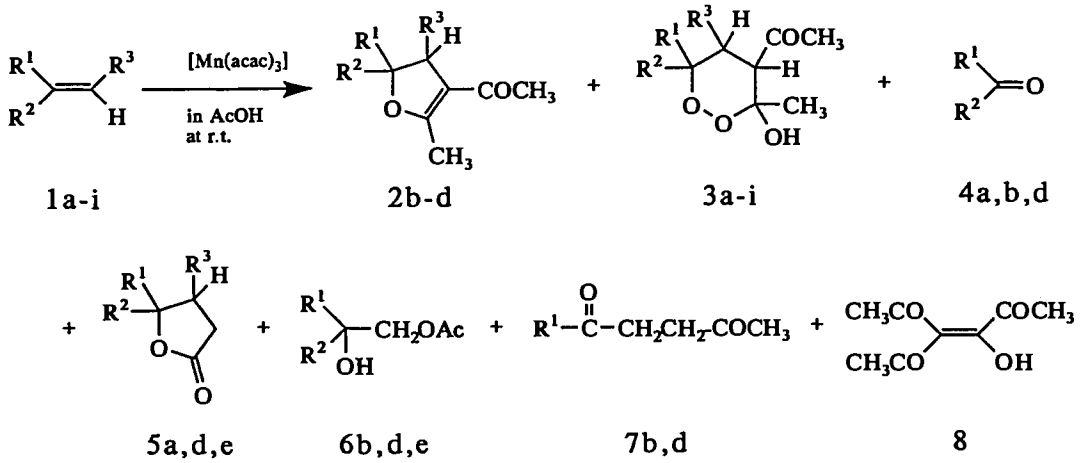

a : R^1=R^2=Ph, R^3=H
b : R^1=R^2=4-ClC_6H_4, R^3=H
c : R^1=R^2=4-$MeOC_6H_4$, R^3=H
d : R^1=R^2=4-MeC_6H_4, R^3=H,
e : R^1=R^2=4-FC_6H_4, R^3=H
f : R^1=Ph, R^2=R^3=H
g : R^1=C_6H_{13}, R^2=R^3=H
h : R^1,R^3=-$(CH_2)_4$-, R^2=H
i : R^1,R^3=-$(CH_2)_6$-, R^2=H

Scheme 3.

Table 2. Reaction of Alkenes (**1a**—**i**) with Tris(2,4-pentanedionato)manganese(III) in AcOH at 23 °C

Entry	Alkene	Molar ratio[a]	Time / h	Product (yield/%)[b,c]						
6	**1a**	1 : 1	11		**3a** (92)	**4a** (3)	**5a** (2)			**8** (7)
7	**1b**	1 : 2	12	**2b** (2)	**3b** (88)	**4b** (3)		**6b** (1)	**7b** (3)	**8** (13)
8	**1c**	1 : 2	12	**2c** (10)	**3c** (87)					**8** (<1)
9	**1d**	1 : 1	13	**2d** (3)	**3d** (77)	**4d** (1)	**5d** (1)	**6d** (4)	**7d** (10)	**8** (11)
10	**1e**	1 : 1	12		**3e** (72)	**4e** (2)	**5e** (2)	**6e** (4)		**8** (14)
11	**1f**	1 : 1	12		**3f** (34)					**8** (10)
12	**1g**	5 : 1	15		**3g** (8)					**8** (<1)
13	**1h**	4 : 1	12		**3h** (11)					**8** (5)
14	**1i**	5 : 1	14		**3i** (43)					

a) Alkene: [Mn(acac)3]. b) Isolated yield based on the amount of the alkene used except for **8**.
c) The yield of **8** was based on the amount of the [Mn(acac)3] used.

Table 3. Reaction of 1,1-Diphenylethene (**1a**) with 1,3-Dicarbonyl Compounds in the Presence of Manganese(III) Acetate in AcOH at 23 °C

Entry	1,3-Dicarbonyl compound	Molar ratio[a]	Time / h	Product (yield/%)[b]						
15	2,4-Pentanedione	1 : 3 : 1	9	**3a** (81)		**4a** (<1)	**5a** (1)	**6a** (1)	**7a** (1)	**8** (3)[c]
16	3-Methyl-2,4-pentanedione	1 : 4 : 1	3	**11a** (49)	**12a** (22)	**4a** (5)				
17	3-Ethyl-2,4-pentanedione	1 : 4 : 1	3	**11b** (62)	**12b** (26)					
18	1-Phenyl-1,3-butanedione	1 : 3 : 1	24	**11c** (43)						
19	Acetoacetanilide	1 : 3 : 1	2	**11d** (91)						
20	1,3-Cyclohexanedione	1 : 3 : 1	12	**11e** (49)		**4a** (12)				

a) **1a**: 1,3-Dicarbonyl compound: Manganese(III) acetate. b) Isolated yield based on the amount of **1a** used.
c) Isolated yield based on the amount of 2,4-pentanedione used.

Discussion

The mechanism for the formation of 1,2-dioxanes in the [Mn(acac)3] system can be depicted as the following. The decomposition of [Mn(acac)3] would produce diacetylmethyl radicals (**I**) which attack the double bond in alkenes, resulting in tertiary radicals (**II**).[4d,5] The radicals (**II**) then react with oxygen to give radicals (**III**),[7a,b] which are cyclized to alkoxyl radicals (**IV**) and could give 1,2-dioxanes (**3**) after abstraction of hydro-

gen from the solvent and/or 2,4-pentanedione which results from the ligand-exchange reaction of $[Mn(acac)_2]$. The radicals (**II**), on the other hand, can be oxidized to carbocations (**V**) with Mn(III) at elevated temperatures since concentration of dissolved oxygen in AcOH is probably small at high temperatures, which eventually give rise to dihydrofuran derivatives (**2**) (Scheme 4). When the reaction of **1b** with $[Mn(acac)_3]$ (1 : 2 molar ratio) was carried out at 23 °C for 12 h under an argon atmosphere, **1b** (38%) was recovered and **2b** (57%) was obtained (see Experimental Section). Any existence of **3b** was not detected. This indicates that the oxygens in the 1,2-dioxane ring did come from molecular oxygen in the air. Unexpectedly, the reac-

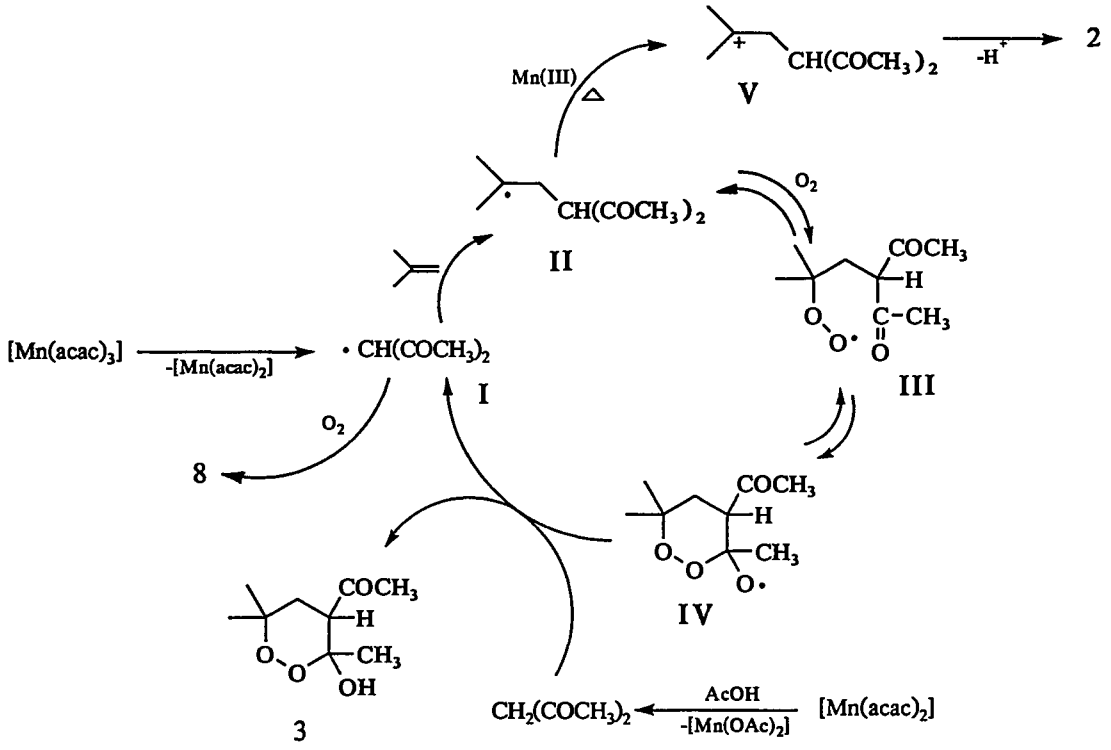

Scheme 4.

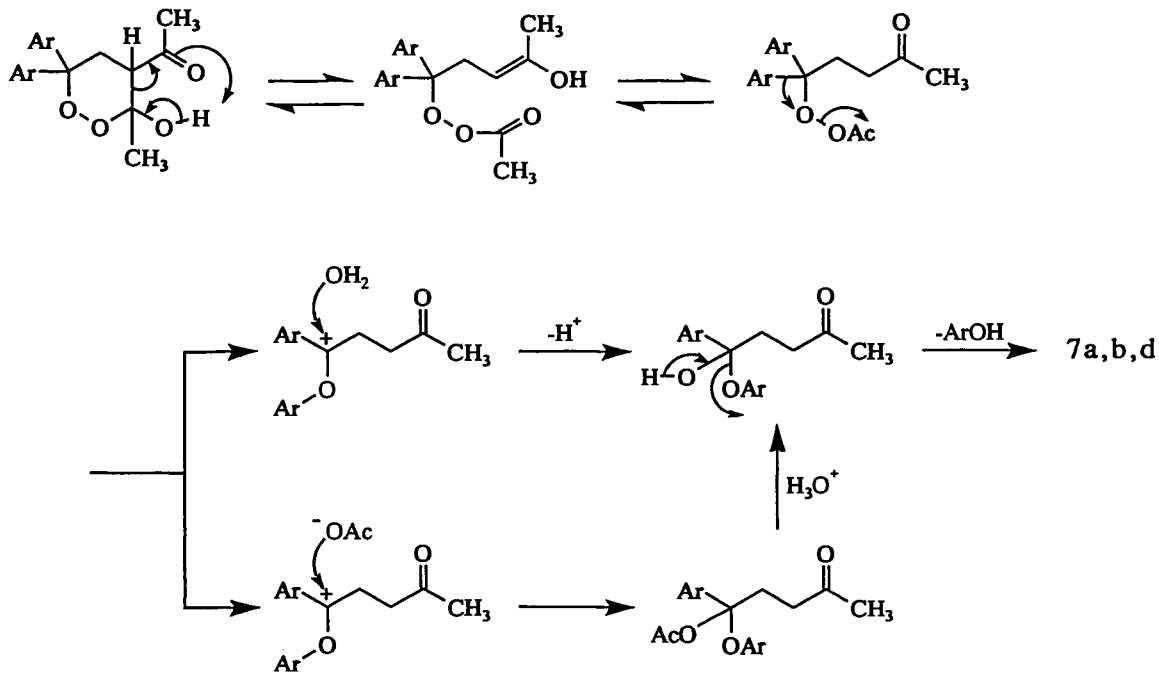

Scheme 5.

tion under an atmosphere of pure oxygen decreased the yield of **3a** and increased the yield of **8**. This may suggest that diacetylmethyl radicals (**I**) formed by the decomposition of [Mn(acac)$_3$] are consumed during dimerization followed by the oxidation with oxygen and the rearrangement, eventually giving **8**. It is worth noting that **3a** was obtained as the *c*-4-acetyl-3-methyl-1,2-dioxan-*r*-3-ol based on the X-ray analysis. This means that the cyclization of peroxyl radical (**III**) is reversible and leads to a thermodynamically stable configuration, that is to say, the *c*-4-acetyl-1,2-dioxan-*r*-3-ol form.[7b]

The formations of 2,2-diaryl-2-hydroxyethyl acetates (**6b**, **d**, **e**) and benzophenones (**4a**, **b**, **d**, **e**) have been well accounted for by the electron-transfer mechanism in the oxidation of **1a** and subsequent cleavage of the resulting diol monoacetate by Mn(III).[11] 4,4-Diaryl-4-butanolides (**5a**, **d**, **e**) are the products of the reaction of alkenes with carboxymethyl radicals, $\cdot CH_2COOH$.[4a–c,12] The formation of 1-aryl-1,4-pentanediones (**7a**, **b**, **d**) showed another feature of the reaction. Probably, they might be formed by retro-Claisen type reaction, followed by Criegee type peroxy ester rearrangement of the corresponding 1,2-dioxanes,[6e] although its mechanism is not yet clarified at present (Scheme 5).

In the case of the manganese(III) acetate system, the ligand-exchange reaction of acetate ligands on manganese(III) acetate and 1,3-dicarbonyl compounds must occur first, because manganese(III) acetate, which is insoluble in AcOH at ambient temperature, does dissolve in the solution of 1,3-diketone–AcOH at room temperature. Although no isolated manganese(III) acetate–1,3-diketone complexes have been reported, it is known that bis(2,4-pentanedionato)manganese(III) carboxylate complexes can be prepared by the ligand-exchange reaction from [Mn(acac)$_3$] and the corresponding carboxylic acids.[13] Slow decomposition of the diketone–Mn(III) complex then yields the corresponding 1,3-diketo radicals(**VI**). This is consistent

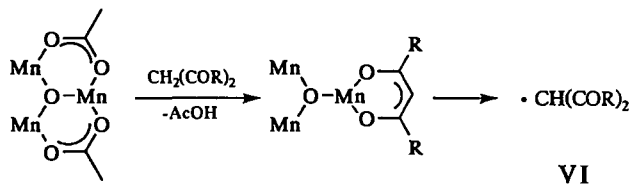

VI

Scheme 6.

with previously proposed mechanism by us[2f,4d,h,14] and others.[2c,4g,15] The radicals **VI** attack the alkene in a similar manner as shown in Scheme 4 to give the cyclic peroxides (**3a**, and **11a**—**e**). The ethoxyl groups in **12a** and **12b** probably come from ethanol which was used as the recrystallizing solvent.

Electrochemical oxidation of 2-alkyl-1,3-diketones in the presence of alkenes under an oxygen atmosphere has been reported and this also gave the substituted 1,2-dioxane ring system.[7] The structure of the cyclic

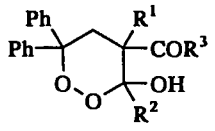

11a : $R^1=R^2=R^3=CH_3$
11b : $R^1=Et$, $R^2=R^3=CH_3$
11c : $R^1=H$, $R^2=CH_3$, $R^3=Ph$
11d : $R^1=H$, $R^2=CH_3$, $R^3=NHPh$
11e : $R^1=H$, $R^2,R^3=-CH_2CH_2CH_2-$

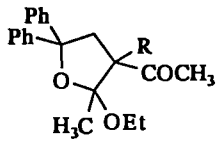

12a : R=CH_3
12b : R=Et

Fig. 2.

peroxide derivative was determined by X-ray analysis. The reaction is also affected by adding azobis(isobutyronitrile) (AIBN) as a radical initiator.[7b] However, the reactions seem to be limited to the 1,3-diketones which produce tertiary radicals during electrochemical oxidation.

The reduction of **3a** with triphenylphosphine deserves comments. The cyclic peroxide (**3a**) can be coordinated to triphenylphosphine with using one of the oxygens in the 1,2-dioxane ring and subsequent rearrangement would give **9** and then **2a**. The formation of **10** would be explained as the result of retro-Claisen reaction of **9** such as the formation of **7** from **3**. These reactions are shown in Scheme 7.

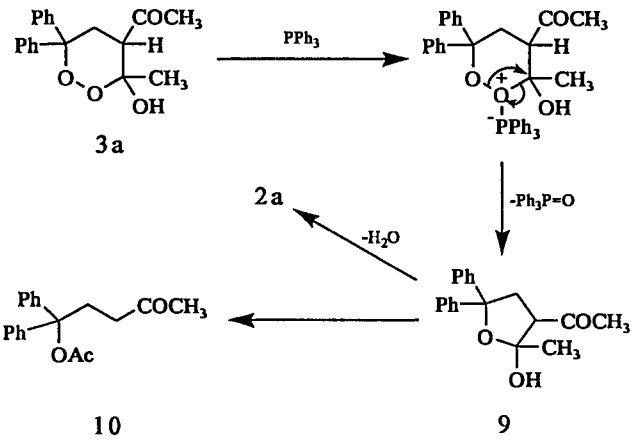

Scheme 7.

We also looked into the mechanisms in which **8** was formed. The hexanedione **8** was formed irrespective of the substrate used. When oxygen was passed through the reaction mixture, the reaction time was decreased by half and the maximum yield of **8** was attained. During the anhydrous work-up of the reaction of [Mn(acac)$_3$] it afforded 3-acetoxy-4-acetyl-3-hexene-2,5-dione (**13**). Therefore, the mechanism can be visualized as shown in Scheme 8. The diacetylmethyl radicals (**I**) dimerize and are then oxidized to a hydroperoxide (**VII**). The hydroperoxide (**VII**) rearranges to **13** and is finally hydrolyzed to give **8** that was formed during the work-up. The acyl migration of this type is probably the first example that occurs in a polyketonic

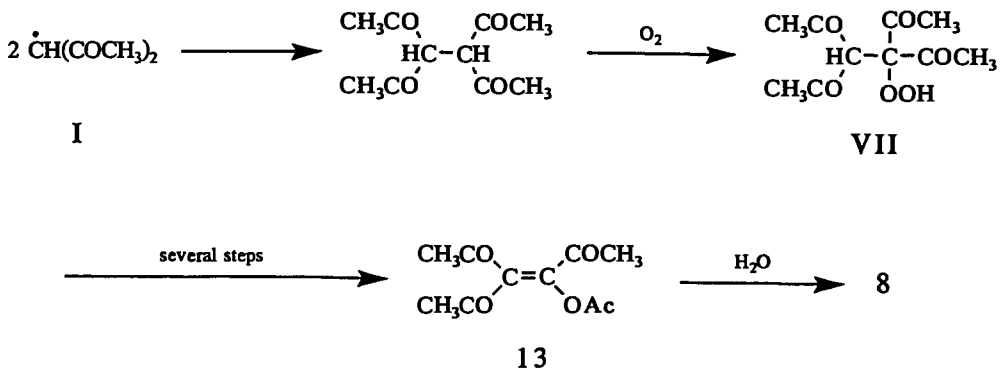

I VII 13

Scheme 8.

compound.

This 1,2-dioxane framework reminds us of bioactive natural occurring cyclic peroxides such as root-growth inhibitor.[16a,b] Therefore, we examined the biological activities for insecticide, bactericide, and herbicide of the 1,2-dioxanes (**3a—e**). Contrary to our expectation, no activity was observed for these compounds.[17] However, we believe that this synthetic method can be used as one of the preparative techniques for natural occurring cyclic peroxides.

Conclusions

The reactions of 1,1-diarylethenes, arylethenes, and alkenes, though to limited extent, with tris(2,4-pentanedionato)manganese(III) or with 1,3-diketones in the presence of manganese(III) acetate at room temperature gave 1,2-dioxane derivatives in moderate to good yields. They may provide a useful tool for the synthesis of a new type peroxide, i.e. 1,2-dioxane derivatives.

Experimental

Instrumentation. Infrared spectra were recorded in chloroform except for **12a** on either a JASCO A-102 or a JASCO FT/IR-7000 infrared spectrometer. The IR spectral data are expressed in cm^{-1}. ^1H NMR spectra were measured in chloroform-*d*, DMSO-d_6, or carbon tetrachloride on either a JEOL JNM-PMX60SI or a Nicolet 300MHz NMR spectrometer at room temperature. Chemical shifts are reported in ppm downfield from an internal TMS standard. Mass spectra were measured on either a JEOL JMS-DX303HF or a Finnigan 6000 GC/MS mass spectrometer at an ionizing voltage of 70 eV. All melting points were determined with a Yanaco MP-J3 micromelting point apparatus (Yanagimoto) and were uncorrected. Elemental analyses were performed by Elemental Analysis Center, Faculty of Science, Kyushu University.

Materials. Tris(2,4-pentanedionato)manganese(III)[18] and manganese(III) acetate[4a] were prepared according to the method previously described. 1,1-Diarylethenes (**1a—e**) were prepared by dehydration of the corresponding alcohols which were synthesized from substituted acetophenones and arylmagnesium bromides.[5] Styrene (Wako), 1-octene (Wako), cyclohexene (Wako), cyclooctene (Wako), and acetic acid (Kanto) were used as received.

Oxidation of Alkenes with Tris(2,4-pentanedionato)-manganese(III) ([Mn(acac)$_3$]). A typical procedure for the oxidation of alkenes with [Mn(acac)$_3$] was as follows. An alkene (1 mmol) was dissolved in acetic acid (25 mL) in a 100 mL round-bottomed flask equipped with a calcium chloride drying tube followed by addition of [Mn(acac)$_3$] (1 mmol) to the mixture. The mixture was stirred at 23 °C under air until the brown color of the Mn(III) species turned a transparent pale yellow. The reaction time is shown in Tables 1 and 2. The solvent was removed in vacuo, and the residue was triturated with 2 M (1 M=1 mol dm^{-3}) hydrochloric acid and then extracted with chloroform. The products were separated on TLC (Wakogel B-10) with chloroform as the developing solvent.

Oxidation Products. 3-Acetyl-2-methyl-5,5-diphenyl-4,5-dihydrofuran (2a): Yellow liquid; (lit,[5] bp 180—185 °C/133 Pa).

4-Acetyl-3-methyl-6,6-diphenyl-1,2-dioxan-3-ol (3a): Colorless prisms (EtOH); mp 165—166 °C (lit,[5] mp 161—162 °C).

Benzophenone (4a): Colorless needles (EtOH); mp 48 °C.[19]

4,4-Diphenyl-4-butanolide (5a): Colorless prisms (EtOH); mp 90—91 °C (lit,[20] mp 87—90 °C).

2,2-Diphenyl-2-hydroxyethyl Acetate (6a): Colorless prisms (EtOH); mp 92.0—92.5 °C (lit,[21] mp 93—93.5 °C).

1-Phenyl-1,4-pentanedione (7a): Pale yellow liquid; bp 116 °C/66.7 Pa (lit,[22] bp 93—94 °C/13.3 Pa).

3-Acetyl-4-hydroxy-3-hexene-2,5-dione (8): Colorless prisms (benzene); mp 116.0—116.3 °C (lit,[4d] mp 115—116 °C).

3-Acetyl-5,5-bis(4-chlorophenyl)-2-methyl-4,5-dihydrofuran (2b): Colorless cubes; mp 95—96 °C (petroleum ether). IR ($CHCl_3$) ν=1670 (COMe). ^1H NMR ($CDCl_3$) δ=2.20 (3H, s, COMe), 2.33 (3H, t, J=1.6 Hz, Me), 3.56 (2H, q, J=1.6 Hz, $-CH_2-$), 7.28 (8H, s, arom.H). MS m/z (rel intensity) 346 (M^+) (91), 303 (67), 275 (26), 225 (26). Found: m/z 346.0526. Calcd for $C_{19}H_{16}O_2{}^{35}Cl_2$: M, 346.0527.

4-Acetyl-6,6-bis(4-chlorophenyl)-3-methyl-1,2-dioxan-3-ol (3b): Colorless needles (EtOH); mp 164—165 °C. IR ($CHCl_3$) ν=3592—3600 (OH), 1699 (COMe). ^1H NMR ($CDCl_3$) δ=1.28 (3H, s, Me), 2.29 (3H, s, COMe), 2.27 (3H, m, $-CH_2-CH<$), 4.12 (1H, br, OH), 7.00—7.50 (8H, m, arom.H). MS m/z (rel intensity) 380 (M^+) (1), 347 (23), 305 (60), 250 (47), 139 (100). Found: C, 59.81; H, 4.79%. Calcd for $C_{19}H_{18}O_4Cl_2$: C, 59.86; H, 4.76%.

4,4′-Dichlorobenzophenone (4b): Colorless needles (benzene–hexane); mp 144.3—145.3 °C (lit,[23] mp 146.5 °C).

2,2-Bis(4-chlorophenyl)-2-hydroxyethyl Acetate (6b):

Colorless prisms (EtOH); mp 95.5—96.2 °C. IR ($CHCl_3$) ν=3604—3200 (OH), 1743 (OAc). ^1H NMR ($CDCl_3$) δ=2.00 (3H, s, OAc), 3.30 (1H, br, OH), 4.62 (2H, s, $-CH_2-$), 7.32 (8H, s, arom.H). Found: C, 59.11; H, 4.30%. Calcd for $C_{16}H_{14}O_3Cl_2$: C, 59.08; H, 4.33%.

1-(4-Chlorophenyl)-1,4-penanedione (7b): Colorless needles (EtOH); mp 74.5—75.0 °C (lit,[22] mp 76 °C).

3-Acetyl-5,5-bis(4-methoxyphenyl)-2-methyl-4,5-dihydrofuran (2c): Colorless needles (benzene–petroleum ether); mp 96—97 °C (lit,[5] mp 96.0—96.5 °C).

4-Acetyl-6,6-bis(4-methoxyphenyl)-3-methyl-1,2-dioxan-3-ol (3c): Pale yellow liquid. IR ($CHCl_3$) ν=3584—3200 (OH), 1700 (COMe). ^1H NMR ($CDCl_3$) δ=1.27 (3H, s, Me), 2.25 (3H, s, COMe), 2.75 (3H, m, $-CH_2-CH\langle$), 3.75 (6H, s, 2×OMe), 4.43 (1H, br, OH), 6.50—7.50 (8H, m, arom.H). MS m/z (rel intensity) 372 (M^+) (1), 312 (9), 242 (52), 211 (21), 188 (33). Found: m/z 372.1570. Calcd for $C_{21}H_{24}O_6$: M, 372.1571.

3-Acetyl-2-methyl-5,5-bis(4-methylphenyl)-4,5-dihydrofuran (2d): Pale yellow liquid. IR ($CHCl_3$) ν=1664 (COMe). ^1H NMR (CCl_4) δ=2.11 (3H, s, COMe), 2.22 (6H, s, 2×Me), 2.27 (3H, t, J=1.6 Hz, Me), 3.35 (2H, q, J=1.6 Hz, $-CH_2-$), 6.90—7.33 (8H, m, arom.H). MS m/z (rel intensity) 306 (M^+) (1), 211 (10), 175 (9), 119 (100). Found: m/z 306.1604. Calcd for $C_{21}H_{22}O_2$: M, 306.1620.

4-Acetyl-3-methyl-6,6-bis(4-methylphenyl)-1,2-dioxan-3-ol (3d): Colorless needles (EtOH); mp 138—139 °C. IR ($CHCl_3$) ν=3580—3200 (OH), 1669 (COMe). ^1H NMR ($CDCl_3$) δ=1.27 (3H, s, Me), 2.25 (6H, s, 2×Me), 2.34 (3H, s, COMe), 2.76 (3H, s, $-CH_2-CH\langle$), 4.40 (1H, br, OH), 7.06—7.50 (8H, m, arom.H). MS m/z (rel intensity), 340 (M^+) (1), 307 (23), 265 (7), 210 (47), 119 (100). Found: C, 73.87; H, 7.14%. Calcd for $C_{21}H_{24}O_4$: C, 74.09; H, 7.11%.

4,4'-Dimethylbenzophenone (4d): Colorless needles; mp 92—94 °C.[24]

4,4-Bis(4-methylphenyl)-4-butanolide (5d): Colorless liquid; (lit,[25] bp 183 °C/67 Pa).

2,2-Bis(4-methylphenyl)-2-hydroxyethyl Acetate (6d): Colorless prisms (benzene–hexane); mp 71.0 °C. IR ($CHCl_3$) ν=3610 (OH), 1742 (OAc). ^1H NMR ($CDCl_3$) δ=1.97 (3H, s, OAc), 2.28 (6H, s, 2×Me), 3.57 (1H, br, OH), 4.60 (2H, s, $-CH_2-$), 7.00—7.33 (8H, m, arom.H). MS m/z (rel intensity) 284 (M^+) (1), 224 (2), 211 (100), 119 (50), 91 (18). Found: C, 76.09; H, 7.08%. Calcd for $C_{18}H_{20}O_3$: C, 76.03; H, 7.09%.

1-(4-Methylphenyl)-1,4-pentanedione (7d): Colorless liquid; (lit,[26] mp 53 °C).

4-Acetyl-6,6-bis(4-fluorophenyl)-3-methyl-1,2-dioxan-3-ol (3e): Colorless prisms (EtOH); mp 142—144 °C. IR ($CHCl_3$) ν=3550—3200 (OH), 1702 (COMe). ^1H NMR ($CDCl_3$) δ=1.30 (3H, s, Me), 2.28 (3H, s, COMe), 2.75 (3H, m, $-CH_2-CH\langle$), 4.23 (1H, br, OH), 7.10—8.00 (8H, m, arom.H). Found: C, 65.53; H, 5.23%. Calcd for $C_{19}H_{18}O_4F_2$: C, 65.51; H, 5.21%.

4,4'-Difluorobenzophenone (4e): Colorless needles; mp 103—105 °C.[27]

4,4-Bis(4-fluorophenyl)-4-butanolide (5e): Yellow liquid. IR ($CHCl_3$) ν=1778 (–O–CO–). ^1H NMR (CCl_4) δ=2.25—3.02 (4H, m, $-CH_2-CH_2-$), 6.83—7.87 (8H, m, arom.H). MS m/z (rel intensity) 274 (M^+) (45), 219 (100), 123 (58). Found: m/z 274.0813. Calcd for $C_{16}H_{12}O_2F_2$: M, 274.0805.

2,2-Bis(4-fluorophenyl)-2-hydroxyethyl Acetate (6e): Colorless needles (petroleum ether); mp 71—72 °C. IR ($CHCl_3$) ν=3596—3200 (OH), 1741 (OAc). ^1H NMR ($CDCl_3$) δ=2.01 (3H, s, OAc), 4.00 (1H, br, OH), 4.63 (2H, s, $-CH_2-$), 7.10—7.60 (8H, m, arom.H). Found: C, 65.86; H, 4.92%. Calcd for $C_{16}H_{14}O_3F_2$: C, 65.75; H, 4.83%.

4-Acetyl-3-methyl-6-phenyl-1,2-dioxan-3-ol (3f): Colorless prisms (EtOH); mp 110—111 °C. IR ($CHCl_3$) ν=3592—3200 (OH), 1698 (COMe). ^1H NMR ($CDCl_3$) δ=1.45 (3H, s, Me), 2.28 (3H, s, COMe), 1.77—3.27 (3H, m, $-CH_2-CH\langle$), 4.10 (1H, s, OH), 5.06 (1H, m, H-5), 7.32 (5H, m, Ph). MS m/z (rel intensity) 237 (M+1) (6), 219 (49), 203 (74), 161 (47). Found: C, 66.00; H, 6.76%. Calcd for $C_{13}H_{16}O_4$: C, 66.08; H, 6.83%.

4-Acetyl-6-hexyl-3-methyl-1,2-dioxan-3-ol (3g). Pale yellow liquid. IR ($CHCl_3$) ν=3580—3200 (OH), 1691 (COMe). ^1H NMR (CCl_4) δ=1.06—2.00 (13H, m, C_6H_{13}), 1.39 (3H, s, Me), 2.24 (3H, s, COMe), 2.33—3.20 (3H, m, $-CH_2-CH\langle$), 4.00 (1H, br, H-5), 4.33 (1H, br, OH). MS m/z (rel intensity), 244 (M^+) (1), 185 (9), 113 (100), 71 (100), 43 (96). Found: m/z 244.1671. Calcd for $C_{13}H_{24}O_4$: M, 244.1674.

5-Acetyl-4-methyl-2,3-dioxabicyclo[4.4.0]decan-4-ol (3h): Pale yellow liquid. IR ($CHCl_3$) ν=3576—3150 (OH), 1692 (COMe). ^1H NMR (CCl_4) δ=0.66—4.00 (11H, m, C_6H_{10}, H-5), 1.26 (3H, s, Me), 2.19 (3H, s, COMe), 5.57 (1H, br, OH). MS m/z (rel intensity) 214 (M^+) (1), 197 (7), 155 (22), 111 (33), 97 (100). Found: m/z 214.1138. Calcd for $C_{11}H_{18}O_4$: M, 214.1204.

12-Acetyl-11-methyl-9,10-dioxabicyclo[6.4.0]dodecan-11-ol (3i): Pale yellow liquid. IR ($CHCl_3$) ν=3600—3200 (OH), 1699 (COMe). ^1H NMR ($CDCl_3$) δ=1.07—3.33 (15H, m, C_8H_{14}, H-12), 1.27 (3H, s, Me), 2.22 (3H, s, COMe), 3.83 (1H, br, OH). MS m/z (rel intensity), 225 (M^+ −17) (20), 183 (8), 167 (13), 121 (17), 97 (50), 71 (55), 43 (100).

Reaction of 1,1-Diphenylethene (1a) with 1,3-Diketones in the Presence of Manganese(III) Acetate.[28] To a mixture of **1a** (1 mmol) and 1,3-diketone (3 or 4 mmol) in acetic acid (25 mL), manganese(III) acetate (1 equivalent) was added. The solution was stirred at 23 °C under air until the brown color of manganese(III) acetate turned colorless. The reaction mixture was then worked-up by the procedure previously described.

Oxidation Products. 4-Acetyl-3,4-dimethyl-6,6-diphenyl-1,2-dioxan-3-ol (11a): Colorless prisms (EtOH); mp 147.8 °C. IR ($CHCl_3$) ν=3596—3200 (OH), 1696 (COMe). ^1H NMR ($CDCl_3$) δ=0.93 (3H, s, Me), 1.40 (3H, s, Me), 2.18 (3H, s, COMe), 2.73 (1H, d, J=14.2 Hz, H-4), 3.22 (1H, d, J=14.2 Hz, H-4), 4.33 (1H, br, OH), 7.06—7.66 (10H, m, 2×Ph). MS m/z (rel intensity) 326 (M^+) (1), 293 (74), 251 (18), 105 (100). Found: C, 73.73; H, 6.84%. Calcd for $C_{20}H_{22}O_4$: C, 73.60; H, 6.79%.

3-Acetyl-2-ethoxy-2,3-dimethyl-5,5-diphenyltetrahydrofuran (12a): Colorless prisms (EtOH); mp 123.5—124.5 °C. IR (KBr) ν=1711 (COMe). ^1H NMR ($CDCl_3$) δ=0.55 (3H, t, J=7.2 Hz, $-OCH_2\underline{CH_3}$), 0.97 (3H, s, Me), 1.62 (3H, s, Me), 2.17 (3H, s, COMe), 2.62 (1H, d, J=13.0 Hz, H-4), 3.34 (2H, q, J=7.2 Hz, $-O\underline{CH_2}CH_3$), 3.82 (1H, d, J=13.0 Hz, H-4), 7.00—7.67 (10H, m, 2×Ph). MS m/z (rel intensity) 338 (M^+) (1), 293 (100), 250 (32). Found: C, 78.13; H, 7.74%. Calcd for $C_{22}H_{26}O_3$: C, 78.07; H, 7.74%.

4-Acetyl-4-ethyl-3-methyl-6,6-diphenyl-1,2-dioxan-3-ol (11b): Colorless prisms (EtOH); mp 144.2 °C. IR ($CHCl_3$) ν=3632—3200 (OH), 1693 (COMe). ^1H NMR ($CDCl_3$) δ=0.33—1.91 (5H, m, Et), 1.51 (3H, s, Me), 1.98 (3H, s, COMe), 2.83 (1H, d, J=14.2 Hz, H-4), 3.20 (1H, d, J=14.2 Hz, H-4), 5.20 (1H, br, OH), 7.13—7.67 (10H, m, 2×Ph). MS

m/z (rel intensity) 340 (M^+) (2), 265 (15), 180 (78), 105 (100). Found: C, 74.19; H, 7.05%. Calcd for $C_{21}H_{24}O_4$: C, 74.09; H, 7.11%.

3-Acetyl-2-ethoxy-3-ethyl-2-methyl-5,5-diphenyltetrahydrofuran (12b): Colorless liquid. IR ($CHCl_3$) ν=1706 (COMe). ^{1}H NMR (CCl_4) δ=0.28—2.00 (5H, m, Et), 0.37 (3H, t, J=7.0 Hz, $-OCH_2\underline{CH_3}$), 1.55 (3H, s, Me), 2.05 (3H, s, COMe), 2.27 (1H, d, J=12.0 Hz, H-4), 3.31 (2H, q, J=7.0 Hz, $-O\underline{CH_2}CH_3$), 3.58 (1H, d, J=12.0 Hz, H-4), 6.97—7.54 (10H, m, 2×Ph). MS *m/z* (rel intensity) 352 (M^+) (2), 307 (30), 264 (100). Found: *m/z* 352.2055. Calcd for $C_{23}H_{28}O_3$: M, 352.2037.

4-Benzoyl-3-methyl-6,6-diphenyl-1,2-dioxan-3-ol (11c): Colorless needles (EtOH); mp 139—141 °C. IR (KBr) ν=3420 (OH), 1659 (C=O). ^{1}H NMR ($CDCl_3$) δ=1.33 (3H, s, Me), 2.70—4.17 (3H, m, $-CH_2CH\langle$), 7.12 (1H, s, OH), 7.17—8.13 (15H, m, 3×Ph). Found: C, 76.80; H, 5.99%. Calcd for $C_{24}H_{22}O_4$: C, 76.98; H, 5.92%.

4-*N*-Phenylcarbamoyl-3-methyl-6,6-diphenyl-1,2-dioxan-3-ol (11d): Colorless microcrystals (EtOH); mp 191 °C. IR ($CHCl_3$) ν=3600—3100 (NH and OH), 1670 (C=O). ^{1}H NMR ($CDCl_3$) δ=1.33 (3H, s, Me), 2.53—3.50 (3H, m, $-CH_2-CH\langle$), 4.90 (1H, br, OH), 6.93—7.63 (15H, m, 3×Ph), 8.87 (1H, s, NH). Found: C, 73.71; H, 5.97; N, 3.55%. Calcd for $C_{24}H_{23}O_4N$: C, 74.02; H, 5.95; N, 3.60%.

1-Hydroxy-4,4-diphenyl-2,3-dioxabicyclo[4.4.0]decan-7-one (11e): Colorless microcrystals (EtOH); mp 184—186 °C. IR (KBr) ν=3600—3200 (OH), 1705 (C=O). ^{1}H NMR (DMSO-d_6) δ=1.36—2.97 (9H, m, C_5H_9), 6.67 (1H, s, OH), 7.06—7.70 (10H, m, 2×Ph). Found: C, 73.92; H, 6.26%. Calcd for $C_{20}H_{20}O_4$: C, 74.05; H, 6.22%.

In the reaction of **1a** with 3-methyl-2,4-pentanedione or 1,3-cyclohexanedione in the presence of manganese(III) acetate, a small amount of benzophenone (**4a**) was also obtained.

Reaction of 1,1-Bis(4-chlorophenyl)ethene (1b) with [Mn(acac)$_3$] under Argon Atmosphere. [Mn(acac)$_3$] was recrystallized from benzene/petroleum ether[29] and stored under argon. The [Mn(acac)$_3$] (454.2 mg) and **1b** (167.5 mg) were put in a 100 mL Schlenk flask under argon. Acetic acid (25 mL), which was purified by distillation from acetic anhydride–chromium trioxide and stored under argon, was added to the flask by a syringe. The mixture was stirred at 23 °C under argon for 12 h. The solvent was removed under high vacuum and the residue was triturated with 2M HCl (25 mL). The aqueous solution was extracted with chloroform. The crude products were separated on TLC using chloroform as the developing solvent to give **1b** (63.6 mg; 38% recovered) and **2b** (132.9 mg; 57%).

Reduction of 3a with Triphenylphosphine. A mixture of **3a** (0.5 mmol) and Ph_3P (0.5 mmol) in anhydrous diethyl ether (30 mL) was stirred at room temperature overnight. The solvent was removed and the residue was triturated with 2 M hydrochloric acid. The mixture was then extracted with chloroform. The following products were obtained after the separation on a silica-gel column.

3-Acetyl-2-methyl-5,5-diphenyltetrahydrofuran-2-ol (9): Colorless liquid. IR ($CHCl_3$) ν=3610—3200 (OH), 1706 (COMe). ^{1}H NMR (CCl_4) δ=1.73 (3H,s, Me), 2.18 (3H, s, COMe), 2.63—3.18 (3H, m, $-CH_2CH\langle$), 3.27 (1H, br, OH), 7.07—7.73 (10H, m, 2×Ph). MS *m/z* (rel intensity) 296 (M^+) (7), 254 (4), 196 (60), 183 (100), 105 (65). Found: *m/z* 296.1385. Calcd for $C_{19}H_{20}O_3$: M, 296.1411.

4-Oxo-1,1-diphenylpentyl Acetate (10): Liquid. IR ($CHCl_3$) ν=1737 (O-$\underline{CO}$Me), 1716 (COMe), 1243 ($\underline{O-CO}$Me). ^{1}H NMR ($CDCl_3$) δ=2.01 (3H, s, Me), 2.12 (3H, s, COMe), 2.17—3.33 (4H, m, $-CH_2-CH_2-$), 7.00—7.56 (10H, m, 2×Ph). FAB MS (solvent: $CHCl_3$; matrix: G+T, G+0.5M-NaI), *m/z* (rel intensity) 319 (M+Na) (21), 279 (26), 259 (56), 237 (100). Found: *m/z* 296.1412. Calcd for $C_{19}H_{20}O_3$: M 296.1394.

Triphenylphosphine Oxide: Colorless prisms (EtOH); mp 152—153 °C (lit,[30] mp 154—155 °C).

Synthesis of 1-Phenyl-1,4-pentanedione (7a). The pentanedione (**7a**) was prepared as follows. To a heated solution of ethyl 3-oxobutanoate (0.06 mol) and metallic sodium (0.05 mol) in anhydrous ethanol, 2-bromoacetophenone (0.05 mol) in anhydrous ethanol was added dropwise. After a few hours reflux, the solvent was removed. The residue was triturated with 2 M sulfuric acid and extracted with benzene. After the removal of the solvent, the reaction mixture was added to a 2 M aqueous sodium hydroxide and stirred at room temperature overnight. The reaction mixture was extracted with benzene, the aqueous solution was acidified with 2 M sulfuric acid and then extracted with diethyl ether. The ethereal solution was dried over anhydrous sodium sulfate. 1-Phenyl-1,4-pentanedione (**7a**, 39%), 3-phenyl-2-cyclopentenone (2%), and 4-oxo-4-phenylbutanoic acid (2%) were obtained after the separation on a silica-gel column.

3-Phenyl-2-cyclopentenone: Colorless prisms (diethyl ether); mp 77.5—78.0 °C (lit,[31] mp 83—84 °C).

4-Oxo-4-phenylbutanoic Acid: Colorless prisms (EtOH); mp 112—113 °C (lit,[32] mp 116.5 °C).

Formation of 13 by Anhydrous Work-up. [Mn(acac)$_3$] (8 mmol) in acetic acid (100 mL) was stirred at 23 °C under air until the brown color of Mn(III) turned yellow. The solvent was removed in vacuo and benzene (150 mL) was added to the residue. After separation of [Mn(OAc)$_2$] by filtration, the solvent was removed under reduced pressure. The residue obtained was purified on TLC to afford a trace amount of **13** and **8**. The product, **13**, was prepared by acetylation of **8** with acetyl chloride: A mixture of **8** and acetyl chloride was heated under reflux for 3 h and then concentrated to dryness. It gave **13**.

3-Acetoxy-4-acetyl-3-hexene-2,5-dione (13): Pale yellow liquid. IR ($CHCl_3$) ν=1687, 1723 (COMe), 1768 (OAc). ^{1}H NMR ($CDCl_3$) δ=1.54 (3H, s, COMe), 2.12 (3H, s, OAc), 2.43 (3H, s, COMe), 2.57 (3H, s, COMe). MS *m/z* (rel intensity) 212 (M^+) (2), 170 (12), 127 (63), 43 (100). Found: *m/z* 212.0685. Calcd for $C_{10}H_{12}O_5$: M, 212.0688.

X-Ray Crystallography of 3a.[33] A clear colorless thin plate of **3a** having the approximate dimensions 0.56×0.44×0.13 mm was mounted in a random orientation on a Nicolet R3m/v automatic diffractometer. The radiation used was Mo $K\alpha$ monochromatized by a highly ordered graphite crystal. Final cell constants, as well as other information pertinent to data collection and refinement, are listed in Table 4. The Laue symmetry was determined to be *mmm*, and from the systematic absences noted, the space group was shown unambiguously to be $P2_12_12_1$. Intensities were measured using the omega scan technique with the scan rate depending on the count obtained in rapid pre-scans of each reflection. Two standard reflections were monitored after every two hours or after every 100 data points collected. These showed no significant variation. In reducing the data, Lorentz and polarization corrections were applied, however, no correction for absorption was made due to the small absorption coefficient.

Table 4. Data Collection and Processing Parameters

Space group	$P2_12_12_1$, orthorhombic
Cell constants	a=7.856(3) Å
	b=12.823(6) Å
	c=15.820(8) Å
	V=1594 Å^3
Molecular formula	$C_{19}H_{20}O_4$
Formula weight	312.39
Formula units per cell	Z=4
Density	ρ=1.30 g cm^{-3}
Absorption coefficient	μ=0.85 cm^{-1}
Radiation (Mo $K\alpha$)	λ=0.71073 Å
Collection range	$4°<2\theta<55°$
Scan width	$\Delta\theta=1.30+(K\alpha_2-K\alpha_1)_o$
Scan speed range	1.5 to 15.0° min^{-1}
Total data collected	2092
Independent data, $I>3\sigma(I)$	1392
Total variables	215
$R=\sum\|\|F_o\|-\|F_c\|\|/\sum\|F_o\|$	0.043
$R_w=[\sum w(\|F_o\|-\|F_c\|)^2/\sum w\|F_o\|^2]^{1/2}$	0.031
Weights	$w=\sigma(F)^{-2}$

The structure was solved by use of the SHELXTL direct methods program TREF, which revealed the positions of all of the nonhydrogen atoms. The usual sequence of isotropic and anisotropic refinement was followed, after which all hydrogens were entered in ideal calculated positions and constrained to riding motion with a single variable isotropic temperature factor. In the final cycles of the least squares the hydroxyl hydrogen H7 was freely refined in order to get accurate hydrogen bonding parameters. The C11 methyl group was treated as a separate rigid body and allowed to rotate freely. Although **3a** crystallizes in a chiral space group, the lack of a significant anomalous scatterer makes determination of the absolute configuration impossible. Therefore, a random choice was made to refine the model having an R configuration at C3. After all nonhydrogen shift/esd ratios were less than 0.3, convergence was reached at the agreement factors listed in Table 4. No unusually high correlations were noted between any of the variables in the last cycle of the full-matrix least squares refinement, and the final difference density map showed a maximum peak of about 0.2 e Å^{-3}. All calculations were made using Nicolet's SHELXTL PLUS (1987) series of crystallographic programs.

We are grateful for financial suport of this work by a Grant-in-Aid for Encouragement of Young Scientists No. 62740301 from the Ministry of Education, Science and Culture. We wish to thank Dr. Teruyoshi Marunaka of the Taiho Pharmaceutical Co., Inc., Tokushima, Japan, for his arrangement of the measurements of the mass spectra. H. N. acknowledges Dr. Abdallah Cherif, Department of Medicinal Chemistry, University of Houston, Houston, Texas, U.S.A. for obtaining the H,C COSY spectrum of **3a** and also thanks Dr. Jean-Luc Lim and Mr. Serge Perrier, Department of Chemistry, University of Houston, for their helpful discussion.

References

1) For reviews, see: a) W. J. De Klein, "Reactions with Manganese(III) Acetate," in "Organic Syntheses by Oxidation with Metal Compounds," ed by W. J. Mijs and C. R. H. I. De Jonge, Plenum, New York (1986), pp. 261—314. b) D. Arndt, "Manganese Compounds as Oxidizing Agents in Organic Chemistry," Open Court, La Salle (1981), pp. 1—25.

2) For intermolecular cyclization, see: a) N. Ito, H. Nishino, and K. Kurosawa, *Bull. Chem. Soc. Jpn.*, **56**, 3527 (1983). b) H. Nishino, *ibid.*, **58**, 217 (1985). c) W. E. Fristad and S. S. Hershberger, *J. Org. Chem.*, **50**, 1026 (1985). d) W. E. Fristad, J. R. Peterson, and A. B. Ernst, *ibid.*, **50**, 3143 (1985). e) E. J. Corey and A. W. Gross, *Tetrahedron Lett.*, **26**, 4291 (1985). f) N. Fujimoto, H. Nishino, and K. Kurosawa, *Bull. Chem. Soc. Jpn.*, **59**, 3161 (1986). g) H. Sato, H. Nishino, and K. Kurosawa, *ibid.*, **60**, 1753 (1987). h) E. J. Corey and A. K. Ghosh, *Tetrahedron Lett.*, **28**, 175 (1987); *Chem. Lett.*, **1987**, 223. i) F. Z. Yang, M. K. Trost, and W. E. Fristad, *Tetrahedron Lett.*, **28**, 1493 (1987). j) P. Breuilles and D. Uguen, *ibid.*, **31**, 357 (1990).

3) For intramolecular cyclization, see: a) E. J. Corey and M. Kang, *J. Am. Chem. Soc.*, **106**, 5384 (1984). b) B. B. Snider, R. Mohan, and S. A. Kates, *J. Org. Chem.*, **50**, 3661 (1985). c) A. B. Ernst and W. E. Fristad, *Tetrahedron Lett.*, **26**, 3761 (1985). d) B. B. Snider, R. Mohan, and S. A. Kates, *ibid.*, **28**, 841 (1987). e) R. Mohan, S. A. Kates, M. A. Dombroski, and B. B. Snider, *ibid.*, **28**, 845 (1987). f) B. B. Snider and M. A. Dombroski, *J. Org. Chem.*, **52**, 5487 (1987). g) J. R. Peterson, R. S. Egler, D. B. Horsley, and T. J. Winter, *Tetrahedron Lett.*, **28**, 6109 (1987). h) B. B. Snider, J. J. Patricia, and S. A. Kates, *J. Org. Chem.*, **53**, 2137 (1988). i) B. B. Snider and J. J. Patricia, *ibid.*, **54**, 38 (1989). j) A. Citterio, D. Fancelli, C. Finzi, and L. Pesce, *ibid.*, **54**, 2713 (1989). k) H. Oumar-Mahamat, C. Moustrou, J.-M. Surzur, and M. P. Bertrand, *ibid.*, **54**, 5684 (1989). l) J. D. White, T. C. Somers, and K. M. Yager, *Tetrahedron Lett.*, **31**, 59 (1990). m) S. A. Kates, M. A. Dombroski, and B. B. Snider, *J. Org. Chem.*, **55**, 2427 (1990).

4) a) E. I. Heiba, R. M. Desau, and W. J. Koehl, Jr., *J. Am. Chem. Soc.*, **91**, 138 (1969). b) H. Nishino and K. Kurosawa, *Bull. Chem. Soc. Jpn.*, **56**, 474 (1983). c) W. E. Fristad and J. R. Peterson, *J. Org. Chem.*, **50**, 10 (1985). d) H. Nishino, *Bull. Chem. Soc. Jpn.*, **59**, 1733 (1986). e) W. E. Fristad, J. R. Peterson, A. B. Ernst, and G. B. Urbi, *Tetrahedron*, **42**, 3429 (1986). f) A. Citterio and D. Fancelli, *Gazz. Chim. Ital.*, **118**, 405 (1988). g) A. Citterio, R. Santi, T. Fiorani, and S. Strologo, *J. Org. Chem.*, **54**, 2703 (1989). h) H. Nishino, K. Tsunoda, and K. Kurosawa, *Bull. Chem. Soc. Jpn.*, **62**, 545 (1989).

5) H. Nishino, *Bull. Chem. Soc. Jpn.*, **58**, 1922 (1985).

6) a) K. Kondo and M. Matsumoto, *J. Chem. Soc., Chem. Commun.*, **1972**, 1332. b) R. W. Denny and A. Nickon, *Org. React.*, **20**, 133. c) R. M. Wilson, E. J. Gardner, R. C. Eider, R. H. Squire, and L. R. Florian, *J. Am. Chem. Soc.*, **96**, 2955 (1974). d) M. Suzuki, H. Ohtake, Y. Kameya, M. Hamanaka, and R. Noyori, *J. Org. Chem.*, **54**, 5292 (1989), and references cited therein. e) S. Patai, "The Chemistry of Peroxides," John Wiley & Sons, New York (1983).

7) a) J. Yoshida, K. Sakaguchi, and S. Isoe, *Tetrahedron Lett.*, **28**, 667 (1987). b) J. Yoshida, S. Nakatani, K. Sakaguchi, and S. Isoe, *J. Org. Chem.*, **54**, 3383 (1989). c) J. Yoshida, S. Nakatani, and S. Isoe, *Tetrahedron Lett.*, **31**, 2425 (1990).

8) For preliminary report, see: S. Tategami, T. Yamada, H. Nishino, J. D. Korp, and K. Kurosawa, *Tetrahedron Lett.*,

31, 6371 (1990).

9) J. I. G. Cadogan and R. K. Mackie, *Chem. Soc. Rev.*, **3**, 87 (1974).

10) Crystallographic data of cyclic peroxides are available in Ref. 6d, and also: M. Sterns *J. Cryst. Mol. Struct.*, **1**, 373 (1971); A. Takenaka, Y. Sasada, and H. Yamamoto, *Acta Crystallogr., Sect. B*, **33**, 3566 (1977).

11) M. G. Vinogradov, Z. V. Todres, G. P. Il'ina, A. Rutavicius, D. N. Kursanov, and G. I. Nikishin, *Izv. Akad. Nauk SSSR, Ser. Khim.*, **1976**, 1331.

12) J. B. Bush, Jr. and H. Finkbeiner, *J. Am. Chem. Soc.*, **90**, 5903 (1968); E. I. Heiba, R. M. Dessau, and W. J. Koehl, Jr., *ibid.*, **90**, 5905 (1968).

13) a) A. F. Nikolaev, K. V. Belogorodskaya, V. G. Shibalovich, E. D. Andreeva, L. V. Bogdanova, and M. V. Vinogradov, *Zh. Prikl. Khim. (Leningrad)*, **46**, 2718 (1973). b) A. F. Nikolaev, K. V. Belogorodskaya, V. G. Shibalovich, E. D. Andreeva, and G. I. Ivanova, *ibid.*, **48**, 2028 (1975). c) A. F. Nikolaev, K. V. Belogorodskaya, L. I. Pushkareeva, and E. D. Andreeva, *ibid.*, **49**, 937 (1976). d) K. V. Belogorodskaya, A. F. Nikolaev, V. G. Shibalovich, and L. I. Pushkareeva, *Vysokomol. Soedin., Ser. B*, **22**, 449 (1980); *Chem. Abstr.*, **93**, 221131r (1980).

14) a) T. Tsuruta, T. Harada, H. Nishino, and K. Kurosawa, *Bull. Chem. Soc. Jpn.*, **58**, 142 (1985). b) H. Yonemura, H. Nishino, and K. Kurosawa, *ibid.*, **59**, 3153 (1986).

15) a) M. Okano, T. Kinoshita, Y. Muramoto, and T. Aratani, *Nippon Kagaku Kaishi*, **1978**, 578. b) K. D. Donnelly, W. E. Fristad, B. J. Gellerman, R. J. Peterson, and B. J. Selle, *Tetrahedron Lett.*, **25**, 607 (1984).

16) a) W. D. Crow, W. Nicholls, and M. Sterns, *Tetrahedron Lett.*, **12**, 1353 (1971). b) M. L. Bolte, W. D. Crow, and S. Yoshida, *Aust. J. Chem.*, **35**, 1411, 1421, 1431 (1982).

17) Biological activity tests were performed by Sumitomo Chemical Co., Inc., Takarazuka, Hyogo, Japan.

18) M. N. Bhattacharjee, M. K. Chaudhuri, and D. T. Khathing, *J. Chem. Soc., Dalton Trans.*, **1982**, 669.

19) C. S. Marvel and W. M. Sperry, *Org. Synth.*, Coll. Vol. 1, 95 (1967).

20) W. S. Jonson, J. W. Petersen, and W. P. Schneider, *J. Am. Chem. Soc.*, **69**, 74 (1947).

21) W. A. Bonner and F. D. Mango, *J. Org. Chem.*, **29**, 430 (1964).

22) H. Stetter and M. Schreckenberg, *Chem. Ber.*, **107**, 2453 (1974).

23) O. G. Backeberg and J. L. Marais, *J. Chem. Soc.*, **1945**, 803.

24) W. T. Nauta, M. J. Ernsting, and A. C. Faber, *Recl. Trav. Chim. Pays-Bas*, **60**, 915 (1941).

25) G. E. Moussa, M. N. Basyouni, and M. E. Shaben, *Indian J. Chem., Sect. B*, **19**, 800 (1980).

26) J. H. Helberger, *Liebigs Ann. Chem.*, **522**, 269 (1936).

27) D. Seyferth and R. J. Spohn, *J. Am. Chem. Soc.*, **90**, 540 (1968).

28) E. I. Heiba and R. M. Dessau, *J. Org. Chem.*, **23**, 3456 (1974).

29) Benzene (Wako) was treated with concd. H_2SO_4, washed with water, aqueous Na_2CO_3 and then with water, dried over anhydrous $CaCl_2$, and distilled from sodium diphenylketyl. Petroleum ether (Nacalai) was extracted with concd H_2SO_4 three times and then with $KMnO_4$–10% H_2SO_4 aqueous solution, washed with water, aqueous Na_2CO_3 and then with water, dried over anhydrous $CaCl_2$, and distilled. The distilled benzene and petroleum ether were stored under argon.

30) N. Staudinger and E. Hauser, *Helv. Chim. Acta*, **4**, 861 (1921).

31) W. Borsche and W. Menz, *Ber.*, **41**, 190 (1908).

32) E. P. Kohler and H. Engelbrecht, *J. Am. Chem. Soc.*, **41**, 764 (1919).

33) Tables 2—8 containing X-ray crystallographic data consisting of atomic coordinates and equivalent isotropic displacement parameters, bond lengths and angles, anisotropic displacement parameters, H-atom coordinates and isotropic displacement parameters, hydrogen bonding parameters, and torsion angles for **3a** (7 pages); and Table 9 containing observed and calculated structure factors (8 pages) are deposited as Document No. 9115 at the Office of the Editor of Bull. Chem. Soc. Jpn.

Alkynylations of Oxiranes with Lithium Acetylides by the Catalysis of Trimethylgallium

Yukitoshi FUKUDA,† Seijiro MATSUBARA,* Claude LAMBERT, Hiroshi SHIRAGAMI, Toshiki NANKO, Kiitiro UTIMOTO,* and Hitosi NOZAKI
Department of Industrial Chemistry, Faculty of Engineering, Kyoto University, Yoshida, Kyoto 606
(Received February 5, 1991)

The reaction of 1-lithio-1-alkynes with oxiranes under the catalytic action of trimethylgallium afforded the corresponding β-hydroxy acetylenic compounds in good yields with excellent regioselectivities. No isomerization of oxiranes was observed during the reactions because of low Lewis acidity of trimethylgallium. The mechanism including activation of an oxirane by the coordination to trimethylgallium was proposed.

The ring-opening reactions of oxiranes with metal acetylides have been used as the most important tool for preparation of β-hydroxy acetylenic compounds,[1-5] which are versatile intermediates in organic syntheses.[6-8] Although several methods have appeared for the reaction, they usually require severe reaction conditions and/or resulted in low yields of the expected products. Recently Yamaguchi et al. reported alkynylation of oxiranes with lithium acetylides by the action of $BF_3 \cdot OEt_2$, and prepared varieties of β-hydroxy acetylenic compounds in good yields.[9] Although the utilities of the BF_3-catalyzed reaction has been proved by several successful applications,[10,11] this reaction requires stoichiometric amount of $BF_3 \cdot OEt_2$. On the other hand, lithium acetylides attack oxiranes under the action of catalytic amount of trimethylgallium to give β-hydroxy acetylenic compounds in good to excellent yields.[12] This paper describes in detail the regioselective reaction of lithium acetylides and oxiranes under trimethylgallium catalysis.

Ring-Opening Reaction of Oxirane with Lithium Acetylides. The reaction of lithium acetylides with oxiranes was tried in the presence of catalytic amount of trimethylgallium; treatment of a THF (tetrahydrofuran) solution of a 1-lithio-1-alkyne with catalytic amount of Me_3Ga and an oxirane was examined. The expected β-hydroxy acetylenic product was obtained in good yield by regioselective attack of acetylide to the less substituted carbon (Scheme 1). In the absence of trimethyl-

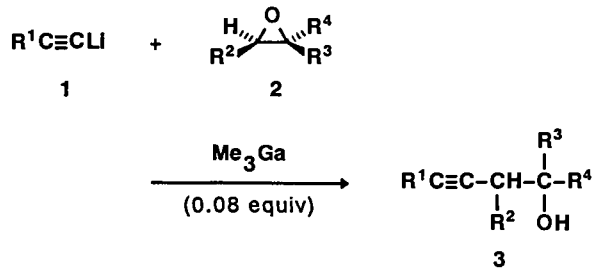

Scheme 1.

Table 1. The Reaction of Oxiranes with Lithium Acetylides in the Presence of Trimethylgallium

R^1	R^2	R^3	R^4	Conditions		Product	Yield[a]/%
C_6H_{13}	H	H	H	R.T.	1 h	**3a**[e]	92 (10)
	H	CH_3	H	R.T.	1.5 h	**3b**	87 (3)
	H	C_2H_5	H	R.T.	5 h	**3c**	74
	H	CH_3	CH_3	R.T.	5 h	**3d**	70
	$-(CH_2)_4-$		H	Reflux	6 h	**3e**	71
	$-(CH_2)_3-$		H	Reflux	6 h[b]	**3f**	82
	H	CH_2Cl	H	0 °C	6 h[b]	**3g**	64
	H	CH_2Cl	H	R.T.	6 h[b]	**3h**	85[c]
C_5H_{11}	H	CH_3	H	R.T.	5 h	**3i**	77
	H	CH_3	CH_3	R.T.	5 h	**3j**	79
	H	Ph	H	50 °C	4 h	**3k**, **3l**[f]	78[d]
C_2H_5	$-(CH_2)_4-$		H	Reflux	5 h	**3m**	80
Ph	H	H	H	R.T.	2 h	**3n**[g]	99 (4)
	H	CH_3	H	R.T.	2 h	**3o**[h]	88 (3)
Me_3Si	H	C_4H_9	H	Reflux	40 min	**3p**	79 (18)

a) Yields in parentheses indicate those obtained by the reaction without Me_3Ga. b) 0.16 equiv of Me_3Ga was used. c) The product was 1,2-epoxy-4-undecyne. d) The product was a mixture of 1-phenyl-3-nonyn-1-ol (**3k**) and 2-phenyl-3-nonyn-1-ol (**3l**) in the ratio of 7:3. e) Ref. 14. f) Ref. 9. g) Ref. 15. h) Ref. 16.

† On leave from Kyowa Yuka Co., Ltd., Yokkaichi, Mie.

gallium, the reaction proceeded sluggishly. Reaction conditions and results are summarized in Table 1.

As shown in Table 1, alkynylation of cyclohexene oxide or cyclopentene oxide gave *trans*-2-alkynylcyclohexanol or -cyclopentanol in good yield under THF reflux. This result is in contrast to that of the reaction with alkynylmagnesium bromide; the reaction of cyclohexene oxide with 1-octynylmagnesium bromide did not gave 2-(1-octynyl)cyclohexanol but afforded a mixture of 2-bromocyclohexanol (58%) and 1-cyclopentyl-2-nonyn-1-ol (31%), indicating the isomerization of cyclohexene oxide into cyclopentanecarbaldehyde under the reaction conditions. It should be noted that no isomerization of oxiranes was observed in the case of trimethylgallium-catalyzed alkynylation of oxiranes. The reaction of epichlorohydrin at 0 °C gave corresponding chlorohydrin **3g**; The reaction at room temperature afforded 1,2-epoxy-4-undecyne **3h**, which was derived from initially produced lithium alkoxide by intramolecular reaction. Among various oxiranes shown in Table 1, reaction with styrene oxide showed relatively good regioselectivity by predominant attack of lithium acetylides on less substituted carbons, whereas BF_3-catalyzed reaction of styrene oxide with 1-lithio-1-heptyne showed non-regioselectivity to give a 1 : 1 mixture of possible two products. These results are shown in Table 1.

In the case of butadiene monoepoxide, Me_3Ga-catalyzed reaction with lithium acetylides showed considerable regioselectivity; the reaction of 1-lithio-1-octyne (**4a**) with butadiene monoepoxide (**5**) gave 1-dodecen-5-yn-3-ol (**6a**) and 2-vinyl-3-decyn-1-ol (**7a**) in the ratio of 71 : 29 without other by-products. The reaction with 1-lithio-2-trimethylsilylethyne (**4b**) gave 6-trimethylsilyl-1-hexen-5-yn-3-ol (**6b**) with high regioselectivity. Above two examples show that alkynyl group was introduced mainly from less substituted carbon of oxirane in the case of trimethylgallium catalyzed alkynylation. On the contrary, in the case of $BF_3 \cdot OEt_2$ mediated alkynylation of butadiene monoepoxide (**5**), the regioselectivity to give **6** is low and several by-products were formed besides regioisomer **7**. Results are summarized in

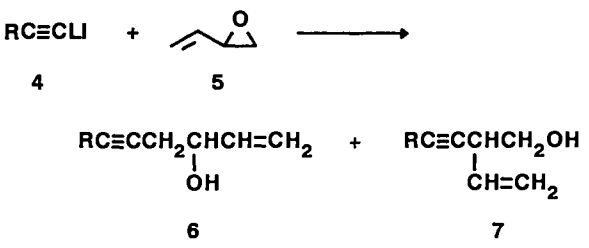

Scheme 2.

Table 2. Alkynylation of Butadiene Monoepoxide

Entry	R	Method[a]	Yield/%	Ratio (6 : 7)
1	C_6H_{13}	A	76	71 : 29
2		B	44[b]	43 : 57
3	Me_3Si	A	78	92 : 8
4		B	35[b]	54 : 46

a) A: in th presence of Me_3Ga (0.2 equiv), 50 °C, 4 h. B: in the presence of $BF_3 \cdot OEt_2$ (1.0 equiv), −78 °C, 30 min. b) Isolated yield after column chromatography.

Table 2.

These results as well as relatively regioselective reaction of styrene oxide indicated that Lewis acidity of trimethylgallium is not so strong to induce the isomerization of oxirane or to produce allylic or benzylic cation species but sufficient to catalyze regioselective reaction of oxirane with lithium acetylides.

Mechanistic Considerations

NMR analyses of the mixtures of oxirane, lithium acetylides, and Me_3Ga were informative to the mechanistic considerations. The peak of oxirane protons of cyclohexene oxide was observed at δ=3.12 in $CDCl_3$–hexane. When slightly excess Me_3Ga (hexane solution) was added to a $CDCl_3$ solution of cyclohexene oxide, that of oxirane protons moved to δ=3.33 with broadening. This result indicates that Me_3Ga affected as a Lewis acid by coordinating to the oxygen of cyclohexene oxide and thus activated for the alkynylation. Lewis acidic activation of oxiranes by trimethylgallium

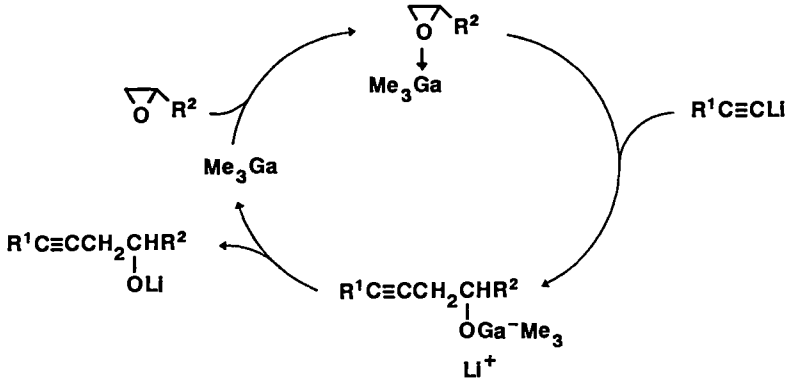

Scheme 3. Catalytic cycle for trimethylgallium-catalyzed alkynylation of oxirane with 1-lithio-1-alkyne.

was also reported in the isonitrile formation by the reaction with cyanotrimethylsilane.[13]

Although exothermic interaction was observed when hexane solution of trimethylgallium was added to THF solution of 1-lithio-1-octyne (1 : 1), any positive evidence could not be obtained for the formation of an ate complex from trimethylgallium and 1-lithio-1-alkyne at this moment.

On the basis of the above discussion, the trimethylgallium catalyzed alkynylation of oxiranes is explained as shown in Scheme 3.

Conclusion

The above described trimethylgallium catalyzed reaction of oxiranes with lithium acetylides to give β-hydroxy acetylenic compounds possesses the following respects: (1) acetylides attacked regioselectively on less substituted carbon with respect to the applied oxiranes, even with styrene oxide and butadiene monoepoxide, (2) relative low Lewis acidity of Me_3Ga did not induce any isomerization of oxiranes before the coupling reaction, (3) catalytic amount of Me_3Ga was sufficient in contrast to the stoichiometric use of $BF_3 \cdot OEt_2$ in reported case, and (4) the expected β-hydroxy acetylenic compounds were obtained in high yields under mild reaction conditions.

Experimental

IR spectra were obtained on a JASCO IR-810 spectrometer. ^1H NMR (200 MHz) were measured on a Varian XL-200. Elemental analyses were performed at Elemental Analysis Center of Kyoto University.

Alkynylation of Oxirane (2) with Lithium Acetylide (1) under the Catalysis of Trimethylgallium (General Procedure): To a THF solution of 1-lithio-1-alkyne (**1**) prepared from 1-alkyne (10 mmol) and butyllithium (1.86 M in hexane, 5.6 ml, 10 mmol, 1 M=1 mol dm^{-3}) 10 ml of THF, trimethylgallium (0.8 M in hexane, 1.0 ml, 0.8 mmol) was added at 0 °C. To the reaction mixture, an oxirane (**2**, 12 mmol, 1.2 eguiv) was added and the whole was stirred for 40 min to 6 h at 0—50 °C or at reflux. The reaction mixture was worked up with brine and extracted with ether. The ethereal solution was washed with brine, dried over anhydrous Na_2SO_4 and concentrated. Chromatographical purification (Silica gel) of the residue gave the product.

4-Undecyn-2-ol (3b): ^1H NMR ($CDCl_3$) δ=0.89 (3H, t, *J*=6.7 Hz), 1.24 (3H, d, *J*=6.2 Hz), 1.20—1.60 (8H, m), 2.15 (2H, dt, *J*=6.7, 2.4 Hz), 2.20 (1H, br-s), 2.32 (2H, tt, *J*=2.4, 6.6 Hz), 3.90 (1H, tq, *J*=5.8, 6.2 Hz); IR (neat) 3600—3000, 1150, 1080, 940 cm^{-1}. Found: C, 78.41; H, 12.22%. Calcd for $C_{11}H_{20}O$: C, 78.51; H, 11.98%.

5-Dodecyn-3-ol (3c): ^1H NMR ($CDCl_3$) δ=0.90 (3H, t, *J*=6.8 Hz), 0.98 (3H, t, *J*=7.8 Hz), 1.19—1.70 (10H, m), 1.96 (1H, d, *J*=5.0 Hz), 2.17 (2H, tt, *J*=2.4, 7.0 Hz), 2.28 (1H, ddt, *J*=7.0, 16.4, 2.4 Hz), 2.42 (1H, ddt, *J*=5.2, 16.4, 2.4 Hz), 3.63 (1H, m); IR (neat) 3600—3050, 1265, 1115, 1070, 1012, 976 cm^{-1}. Found: C, 78.92; H, 12.22%. Calcd for $C_{12}H_{22}O$: C, 79.06; H, 12.16%.

2-Methyl-4-undecyn-2-ol (3d): ^1H NMR ($CDCl_3$) δ=0.90 (3H, t, *J*=6.8 Hz), 1.21—1.56 (8H, m), 1.28 (6H, s), 1.99 (1H, s), 2.20 (2H, tt, *J*=2.2, 7.0 Hz), 2.34 (2H, t, *J*=2.2 Hz); IR (neat) 3700—3100, 1264, 1249, 1210, 1145, 981, 906 cm^{-1}. Found: C, 78.91; H, 12.07%. Calcd for $C_{12}H_{22}O$: C, 79.06; H, 12.16%.

2-(1-Octynyl)cyclohexanol (3e): ^1H NMR ($CDCl_3$) δ=0.91 (3H, t, *J*=6.5 Hz), 1.08—1.85 (15H, m), 1.99 (2H, m), 2.17 (2H, br-t, *J*=6.2 Hz), 2.36 (1H, d, *J*=2.0 Hz), 3.37 (1H, ddt, *J*=2.0, 3.0, 9.5 Hz); IR (neat) 3600—3100, 1285, 1085 cm^{-1}. Found: C, 80.54; H, 11.84%. Calcd for $C_{14}H_{24}O$: C, 80.71; H, 11.61%.

2-(1-Octynyl)cyclopentanol (3f): ^1H NMR ($CDCl_3$) δ=0.88 (3H, t, *J*=6.5 Hz), 1.12—2.03 (14H, m), 1.92 (1H, s), 2.13 (2H, dt, *J*=2.0, 7.0 Hz), 2.50 (1H, ddt, *J*=2.0, 6.0, 6.0 Hz), 4.09 (1H, dt, *J*=6.0, 6.0 Hz); IR (neat) 3600—3100, 1292, 1122, 1073, 1029, 992, 721 cm^{-1}. Found: C, 80.43; H, 11.68%. Calcd for $C_{13}H_{22}O$: C, 80.35; H, 11.41%.

1-Chloro-4-undecyn-2-ol (3g): ^1H NMR ($CDCl_3$) δ=0.90 (3H, t, *J*=6.0 Hz), 1.20—1.65 (8H, m), 2.27 (2H, tt, *J*=2.1, 6.9 Hz), 2.35 (1H, d, *J*=6.0 Hz), 2.48 (1H, tt, *J*=2.1, 7.0 Hz), 2.60 (1H, dq, *J*=7.0, 2.1 Hz), 3.62 (1H, dd, *J*=6.1, 11.0 Hz), 3.74 (1H, dd, *J*=4.6, 11.0 Hz), 3.95 (1H, m); IR (neat) 3600—3050, 1090, 1050, 710, 700 cm^{-1}. Found: C, 65.26; H, 9.72%. Calcd for $C_{11}H_{19}OCl$: C, 65.17; H, 9.45%.

1,2-Epoxy-4-undecyne (3h): ^1H NMR ($CDCl_3$) δ=0.89 (3H, t, *J*=6.0 Hz), 1.15—1.62 (9H, m), 2.15 (2H, tt, *J*=2.3, 7.2 Hz), 2.43 (1H, ddt, *J*=5.0, 17.7, 2.3 Hz), 2.60 (1H, ddt, *J*=4.6, 17.7, 2.3 Hz), 2.65 (1H, dd, *J*=2.5, 4.8 Hz), 2.79 (1H, dd, *J*=3.6, 4.8 Hz), 3.08 (1H, ddd, *J*=2.5, 3.6, 5.0 Hz); IR (neat) 960, 930, 840, 830 cm^{-1}. Found: C, 79.36; H, 11.02%. Calcd for $C_{11}H_{18}O$: C, 79.46; H, 10.92%.

4-Decyn-2-ol (3i): ^1H NMR ($CDCl_3$) δ=0.91 (3H, t, *J*=6.9 Hz), 1.25 (3H, d, *J*=6.4 Hz), 1.20—4.58 (6H, m), 2.06 (1H, d, *J*=4.9 Hz), 2.19 (2H, tt, *J*= 2.3, 7.0 Hz), 2.28 (1H, ddt, *J*=6.8, 16.0, 2.3 Hz), 2.40 (1H, ddt, *J*=5.0, 16.0, 2.3 Hz), 3.90 (1H, dddq, *J*=4.9, 5.0, 6.8, 6.9 Hz); IR (neat) 3650—3100, 1116, 1085, 940 cm^{-1}. Found: C, 77.56; H, 11.95%. Calcd for $C_{10}H_{18}O$: C, 77.86; H, 11.76%.

2-Methyl-4-decyn-2-ol (3j): ^1H NMR ($CDCl_3$) δ=0.92 (3H, t, *J*=6.9 Hz), 1.21—1.59 (6H, m), 1.30 (6H, s), 2.01 (1H, s), 2.19 (2H, tt, *J*=2.5, 7.0 Hz), 2.34 (2H, t, *J*=2.5 Hz); IR (neat) 3600—3100, 1266, 1210, 1146, 975, 906, 762 cm^{-1}. Found: C, 78.49; H, 12.12%. Calcd for $C_{11}H_{20}O$: C, 78.51; H, 11.98%.

2-(1-Butynyl)cyclohexanol (3m): ^1H NMR ($CDCl_3$) δ=1.16 (3H, t, *J*=7.5 Hz), 1.20—2.10 (9H, m), 2.20 (1H, m), 2.21 (2H, dq, *J*=2.0, 7.5 Hz), 3.41 (1H, ddd, *J*=2.5, 9.5, 9.5 Hz); IR (neat) 3650—3100, 1310, 1275, 1075 cm^{-1}. Found: C, 78.60; H, 10.85%. Calcd for $C_{10}H_{16}O$: C, 78.90; H, 10.59%.

1-Trimethylsilyl-1-octyn-4-ol (3p): ^1H NMR ($CDCl_3$) δ=0.16 (9H, s), 0.88 (3H, t, *J*=6.9 Hz), 1.17—1.57 (6H, m), 1.95 (1H, d, *J*=5.0 Hz), 2.29 (1H, dd, *J*=7.0, 16.7 Hz), 2.45 (1H, dd, *J*=5.0, 16.7 Hz), 3.67 (1H, m); IR (neat) 3600—3100, 2174, 1250, 1125, 1082, 1045, 1017, 841, 758, 697 cm^{-1}. Found: C, 66.55; H, 11.36%. Calcd for $C_{11}H_{22}OSi$: C, 66.60; H, 11.18%.

1-Dodecen-5-yn-3-ol (6a): ^1H NMR ($CDCl_3$) δ=0.90 (3H, t, *J*=6.5 Hz), 1.19—1.69 (8H, m), 2.07 (1H, d, *J*=6.0 Hz), 2.18 (2H, tt, *J*=2.5, 6.0 Hz), 2.40 (1H, ddt, *J*=6.5, 16.1, 2.3 Hz), 2.50 (1H, ddt, *J*=6.5, 16.1, 2.7 Hz), 4.17 (1H, m), 5.18 (1H, ddd, *J*=1.1, 1.1, 10.5 Hz), 5.31 (1H, ddd, *J*=1.1, 1.1, 17.0 Hz), 5.91 (1H, ddd, *J*=6.0, 10.5, 17.0 Hz); IR (neat) 3630—3100, 3080, 1379, 1330, 1122, 1034, 992, 923 cm^{-1}. Found: C, 79.69; H, 11.31%. Calcd for $C_{11}H_{20}O$: C, 79.94; H, 11.18%.

2-Vinyl-3-decyn-1-ol (7a): ^{1}H NMR ($CDCl_3$) δ=0.91 (3H, t, J=6.3 Hz), 1.20—1.64 (8H, m), 1.83 (1H, dd, J=6.1, 6.5 Hz), 2.23 (2H, dt, J=2.1, 7.1 Hz), 3.29 (1H, m), 3.55 (1H, ddd, J=6.1, 6.9, 16.0 Hz), 3.69 (1H, ddd, J=6.5, 6.9, 16.0 Hz), 5.21 (1H, ddd, J=1.6, 1.6, 10.0 Hz), 5.40 (1H, ddd, J=1.6, 1.6, 17.0 Hz), 5.75 (1H, ddd, J=6.9, 10.0, 17.0 Hz); IR (neat) 3650—3100, 3082, 1632, 1379, 1331, 1053, 991, 920, 721 cm^{-1}. Found: C, 79.98; H, 11.31%. Calcd for $C_{12}H_{20}O$: C, 79.94; H, 11.18%.

6-Trimethylsilyl-1-hexen-5-yn-3-ol (6b): ^{1}H NMR ($CDCl_3$) δ=0.18 (9H, s), 2.07 (1H, d, J=5.7 Hz), 2.46 (1H, dd, J=6.7, 17.0 Hz), 2.56 (1H, dd, J=5.9, 17.0 Hz), 4.27 (1H, ddddt, J=5.7, 5.9, 6.0, 6.7, 1.5 Hz), 5.17 (1H, ddd, J=1.5, 1.5, 10.0 Hz), 5.29 (1H, ddd, J=1.5, 1.5, 17.5 Hz), 5.89 (1H, ddd, J=6.0, 10.0, 17.5 Hz); IR (neat) 3700—3100, 3082, 3005, 2176, 1250, 1123, 1044, 1001, 926, 842, 759, 697 cm^{-1}. Found: C, 64.21; H, 9.70%. Calcd for $C_9H_{16}OSi$: C, 64.23; H, 9.58%.

4-Trimethylsilyl-2-vinyl-3-butyn-1-ol (7b): ^{1}H NMR ($CDCl_3$) δ=0.15 (9H, s), 1.81 (1H, t, J=6.6 Hz), 3.34 (1H, dtt, J=6.6, 1.2, 6.6 Hz), 3.61 (1H, ddd, J=3.4, 6.6, 6.6 Hz), 3.65 (1H, ddd, J=3.4, 6.6, 6.6 Hz), 5.25 (1H, ddd, J=1.2, 1.2, 10.5 Hz), 5.42 (1H, ddd, J=1.2, 1.2, 17.0 Hz), 5.81 (1H, ddd, J=6.6, 10.5, 17.0 Hz); IR (neat) 3700—3100, 3084, 3010, 2170, 1642, 1299, 1250, 1049, 991, 925, 883, 842, 759, 697, 635 cm^{-1}. Found: 64.23; H, 9.76%. Calcd for $C_9H_{16}OSi$: C, 64.23; H, 9.58%.

Alkynylation of Butadiene Monoepoxide: The alkynylations of butadiene monoepoxide catalyzed by trimethylgallium were carried out along the procedure described above using 0.2 equiv of trimethylgallium. The $BF_3 \cdot OEt_2$ mediated alkynylations were accomplished by the procedure reported in the literature. Thus, $BF_3 \cdot OEt_2$ (2 mmol) was added at −78 °C to THF-hexane solution of 1-lithio-1-alkyne (2 mmol), which was prepared from the reaction of 1-alkyne (2 mmol) with hexane solution of butyllithium (2 mmol). After the whole was stirred at −78 °C for 10 min, butadiene monoepoxide (2 mmol) was added to the solution and the whole was stirred at −78 °C for additional 30 min. The reaction mixture was worked up with sat NH_4Cl and extracted with ether. The ethereal solution was dried (Na_2SO_4) and concentrated to give the crude product, which was purified by column chromatography (silica gel).

This work was financially supported by the Japan Society for the Promotion of Science by a Grant-in-Aid for an International Joint Research Project. The authors are indebted to Tosoh Akzo Co. Ltd. by the kind supply of trimethylgallium.

References

1) V. Jager and H. G. Viehe, "Methoden der Organischen Chemie," 4th ed, ed by E. Muller, Houben-Weyl (1977), Vol. V/2a.
2) J. Fried, C.-H. Lin, and S. H. Ford, *Tetrahedron Lett.*, **1969**, 1379.
3) S. Danishefsky, T. Kitahara, M. Tsai, and J. Dynak, *J. Org. Chem.*, **41**, 1669 (1976).
4) M. Hanack, E. L. Kunzmann, and W. Schumacher, *Synthesis*, **1978**, 26.
5) W. Schumacher and M. Hanack, *Synthesis*, **1981**, 490.
6) S. Watanabe, T. Fujita, K. Suga, and M. Haibara, *Aust. J. Chem.*, **35**, 1739 (1982).
7) K. Utimoto, *Pure Appl. Chem.*, **55**, 1845 (1983).
8) N. R. Jackson, P. Perlmutter, and A. J. Swallridge, *J. Chem. Soc., Perkin Trans. 2*, **1985**, 1509.
9) M. Yamaguchi and I. Hirao, *Tetrahedron Lett.*, **24**, 391 (1983).
10) M. Yamaguchi, Y. Nobayashi, and I. Hirao, *Tetrahedron*, **40**, 4261 (1984).
11) M. J. Eis, J. E. Wrobel, and B. Ganem, *J. Am. Chem. Soc.*, **106**, 3693 (1984).
12) K. Utimoto, C. Lambert, Y. Fukuda, H. Shiragami, and H. Nozaki, *Tetrahedron Lett.*, **25**, 5423 (1984).
13) K. Imi, N. Yanagihara, and K. Utimoto, *J. Org. Chem.*, **52**, 1013 (1987).
14) L. Faucounau, *C. R. Acad. Sci.*, **199**, 605 (1934).
15) G. D. Prestwish, E. Deaton, and D. Wichern, *J. Chem. Ecol.*, **10**, 1201 (1984).
16) H. Normant and T. Cuvigny, *Bull. Soc. Chim. Fr.*, **1957**, 1447.

Complex Formation of Gelatin and Chondroitin Sulfate and the Effects on H^+ Ion Binding

Masakatsu YONESE,* Mikio YANO, and Hiroshi KISHIMOTO
Faculty of Pharmaceutical Sciences, Nagoya City University, Tanabe-dori, Mizuho-ku, Nagoya 467
(Received November 14, 1990)

Soluble and insoluble complex formations of gelatin and chondroitin 6-sulfate (Chs-C) were studied by measuring their viscosities and transmittances; the effects of complex formations on H^+ ion binding were studied by pH titrations. Soluble complexes were formed electrostatically with low ionic strengths; the compositions of the complexes varied with pH from those of solutions. The weight fraction of Chs-C of the saturated soluble complex was found to be 0.294 at pH=5.1. The composition of the insoluble complexes increased in the fraction of Chs-C with decreasing pH. The compositions were found to agree with the theoretical predictions obtained from the condition of electroneutrality. Furthermore, from pH titrations of mixed solutions comprising gelatin and Chs-C, the apparent dissociation constants, pK_a of the carboxylic groups of both polymers were obtained. They were found to increase due to soluble complex formation; soluble complex formation depresses the dissociation of H^+ ions due to a shielding of the positively charged amino groups of gelatin.

Chondroitin sulfates (Chs) are important components of mammalian connective tissues found in vivo as proteoglycans that bind with proteins, such as a collagen. They contribute to tissue elasticity and to the control of bone formation, due to their binding properties with Ca^{2+} and other ions.[1,2] Several kinds of Chs are found in vivo. Chondroitin 4-sulfate (Chs-A) and 6-sulfate (Chs-C), which are typical Chs, are *N*-acetyl-D-galactosamine 4- and 6-sulfate, together with D-glucuronic acids. Their thermodynamic properties, such as counterion binding properties,[3] osmotic coefficients,[4] partial molar volumes,[5] and dilution enthalpies,[6–8] could be explained by the Manning theory based on a line-charge model.[9] One of the characteristics resulting from the alternate arrangement of carboxylic and sulfuric groups in Chs contributes to maintaining the activity of Ca^{2+} ions constant when any pH changes.[3] Furthermore, no differences in these properties were found between Chs-C and -A.[4]

Chs interacts electrostatically with proteins to form complexes. These properties have been studied by light scattering,[10] electrophoresis,[11] and chromatograph methods.[12] In the regions of more acidic pH than the isoionic points of a protein, insoluble complexes were reported to be formed.[13] In gel membranes comprising gelatin and Chs, complex formation affects the membrane characteristics: the membranes shrink, and their water contents and permeabilities decrease due to complex formation.[14–18]

We studied the complex formation of gelatin and Chs-C in solutions and its effects on H^+ ion binding.

Experimental

Materials. Gelatin (Lot. No. P-1710) was offered by Nitta Gelatin Co., Ltd. By passing the gelatin solution through a mixed ion exchange column comprising cation exchange resins (Amberlite IR-120-B) and anion exchange resins (Amberlite IRA-410) an isoionic gelatin was obtained according to Jenus;[19] the isoionic pH was 4.8 (concentration: C_{ge}=1 w/v%). The isoionic gelatin solution was stored under refrigeration. The amino acid composition is shown in Table 1. Sodium salt of chondroitin sulfate C Chs-C was of commercial origin (Seikagaku Kougyou Co., Ltd., Tokyo, Japan) and was used without any purification. All other reagents were special grade from Katayama Co., Ltd. (Nagoya, Japan). Distilled and deionized water was used for the preparation of all solutions.

Viscosity Measurements. The viscosities of the mixed solutions comprising gelatin and Chs-C were measured at 25.0 °C by an Ostwald-type viscometer in which the falling time of water was 92 s.

pH Titration. The pH values of the solutions were measured by using a digital ion meter (Orion, Type 701A) connected to glass and reference electrodes (Orion, Type 91-01 and 90-02). pH titrations of the mixed solutions comprising isoionic gelatin and Chs-C were carried out at 25.0 °C by adding HCl (1.0 mol dm^{-3}) and NaOH (1.0 mol dm^{-3}) under an atmosphere of nitrogen.

From pH titration curves of the mixed solutions, the binding amounts ν of H^+ and OH^- ions were obtained as follows. Equal volumes of the polymer solution and solvent (V dm^3) were titrated by HCl and NaOH solutions (C mol dm^{-3}). When the titrants are added to the polymer and the solvent by ν and ν_0 dm^3, respectively, to attain the same pH, the value ν (mol g^{-1}) is obtained by the following equation[20]

$$\nu=(\nu-\nu_0)\,C/n_p, \tag{1}$$

where n_p (g) is the polymer weight in the sample solution. Since the binding amounts of the OH^- ion are equivalent to

Table 1. Amino Acid Composition of Gelatin

	mmol g^{-1}		mmol g^{-1}
Glycine	3.28	Tyrosine	0.0085
Alanine	1.09	Serine	0.296
Valine	0.195	Threonine	0.155
Leucine	0.226	Methionine	0.025
Isoleucine	0.115	Tryptophan	0
Proline	1.04	Cysteine	0
Hydroxyproline	1.21	Arginine	0.459
Phenylalanine	0.115	Histidine	0.046
Aspartic Acid	0.403	Lysine	0.279
Glutamic Acid	0.671	Hydroxylysine	0.050

the dissociated amounts of H^+ ions, they were defined as negative values.[21]

Composition of Insoluble Complex. The compositions of the insoluble complexes formed under various acidic pH conditions were studied by following two methods: (1) In the transmittance method, mixed solutions comprising gelatin and Chs-C were adjusted at 25 °C to an acidic pH in the region pH=5.6—2.5; after 15 min their transmittances were measured at λ=420 nm. According to A. Nakajima,[22] from compositions showing the transmittance maximum, those of the complexes were determined. (2) In the nitrogen analysis method, from the nitrogen contents of the insoluble complex $(W_N)_{ic}$, gelatin $(W_N)_{ge}$ and Chs-C $(W_N)_{chs}$, the weight fraction of Chs-C of the insoluble complex $(W_{chs})_{ic}$ was obtained by the following relation:

$$(W_{chs})_{ic}=((W_N)_{ge}-(W_N)_{ic})/((W_N)_{ge}-(W_N)_{chs}). \quad (2)$$

After adjusting the pH of the mixed solutions to the acidic region, they were allowed to stand for 15 min. Precipitated bulky insoluble complexes were dried in vacuo (at 80 °C), and their nitrogen contents $(W_N)_{ic}$ were analyzed. The nitrogen contents of gelatin, $(W_N)_{ge}$, and Chs-C, $(W_N)_{chs}$, were 0.178 and 0.267, respectively.

Results

Viscosities of Mixed Solutions Composed of Gelatin and Chondroitin Sulfate. The relative viscosities, η_{rel}, of mixed solutions comprising isoionic gelatin and Chs-C are shown in Fig. 1 as a function of the weight fraction of Chs-C W_{chs}. The total polymer concentrations of the mixed solutions were 0.3 g/100 cm^3, and the added ionic strengths of NaCl J were 0.0, 0.01, and 0.4 mol dm^{-3}. The results of the gelatin solutions did not significantly depend on J, but those of Chs-C solutions did. For J=0.4, the results of the mixed solutions increased linearly with increasing W_{chs}. However, in the cases of J=0.01 and 0, the results deviated from a linear relation; especially in the case of J=0 the deviation became significant. The deviations result from the formation of soluble complexes due to an electrostatic interaction between the gelatin and Chs-C. The ionic strengths resulting from the Na^+ counterion of Chs-C increased from 0 to 0.012 mol dm^{-3} with increasing W_{chs}. Therefore, the total ionic strengths of the mixed solutions varied with W_{chs} and in the region of total ionic strengths smaller than 0.022 mol dm^{-3} soluble complexes were found to be formed.

Chs-C was added to the isoionic gelatin solutions (the concentration C_{ge}=0.3 g/100 cm^3) under various conditions. The specific viscosities of mixed solutions, η_{sp}, defined by Eq. 3 are shown in Fig. 2 as a function of the concentration of Chs-C, C_{chs}:

$$\eta_{sp}=(\eta_{rel}/(\eta_{rel})_0-1), \quad (3)$$

where $(\eta_{rel})_0$ is the relative viscosity of the gelatin solution. In the case of J=0.005 mol dm^{-3} and pH=8.0, the results of η_{sp} increased linearly with increasing C_{chs} and were equal to those of Chs-C solutions (C_{ge}=0). In cases satisfying linearity, no complexes were formed. However, in the case of C_{ge}=0.3 g/100 cm^3 and J=0.005 mol dm^{-3}, the results of η_{sp} showed a steeper increase with C_{chs} and deviated at C_{chs}=0.125 g/100 cm^3 (=$(C_{chs})_c$)

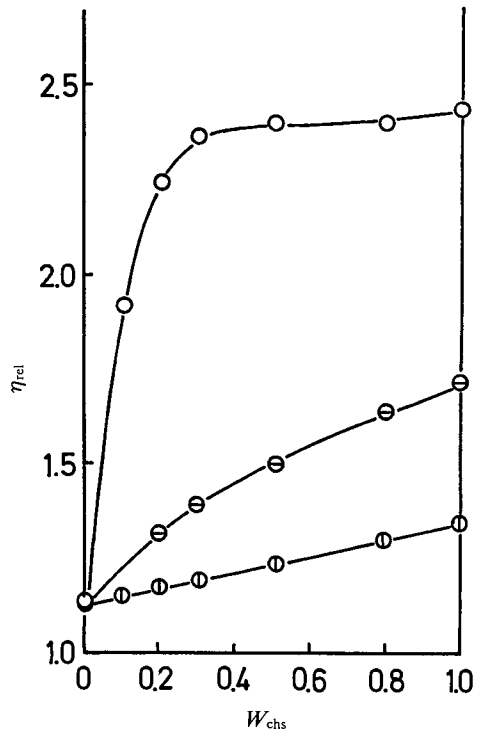

Fig. 1. Relative viscosity of mixed solution composed of gelatin and chondroitin sulfate C in various ionic strengths.
Ionic strength J: ○; 0.0, ⊖; 0.01, ⊙; 0.40 mol dm^{-3}
Total polymer concentrations of the mixed solutions were 0.3 g/100 cm^3, and the ionic strengths were adjusted by adding NaCl.

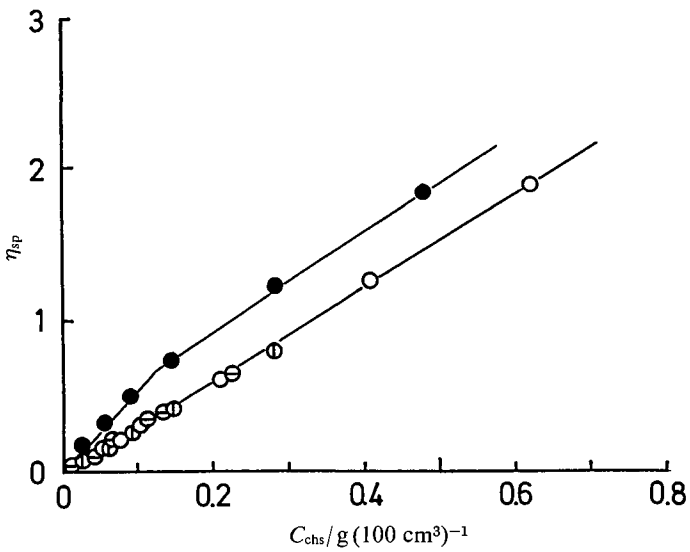

Fig. 2. Effects of adding chondroitin sulfate C to gelatin solutions on specific viscosities.
○: C_{ge}=0 g/100 cm^3, J=0.005 mol dm^{-3}, pH=4.8—5.6, ●: C_{ge}=0.3, J=0.005, pH=4.8—5.4, ⊖; C_{ge}=0.15, J=0.1, pH=4.8—5.4, ⊙; C_{ge}=0.3, J=0.005, pH=8.0.

from linearity. This results from the formation of the soluble complexes. In the region $C_{chs}>(C_{chs})_c$ complexes were formed, and their compositions seemed to vary with C_{chs}, i.e. the fraction of Chs-C in the complexes increased with increasing C_{chs}. At $C_{chs}=(C_{chs})_c$, saturated complexes were formed. In the region $C_{chs}>(C_{chs})_c$, the saturated complex and the free Chs-C present in the solution and the latter increased with increasing C_{chs}. Nakagaki et al. have reported that for soluble complexes formed by a bovine serum albumin (BSA) and Chs-C, BSA molecules bind strongly with Chs-C in a manner like the Langmuir type.[10] By assuming that all of the gelatin and Chs-C contribute to form complexes at $(C_{chs})_c$, the weight fraction of Chs-C in the saturated soluble complex $(W_{chs})_{ssc}$ was estimated to be 0.294.

pH Titrations of Mixed Solutions. The pH values of mixed solutions comprising isoionic gelatin and Chs-C solutions are shown in Fig. 3 as a function of W_{chs} for J=0 and 0.1 mol dm^{-3}. Their total concentrations were 1 g/100 cm^3 and the added ionic strengths J were adjusted by NaCl. The solid curves indicate the pH values calculated by assuming an ideal mixture. In the case of J=0.1 mol dm^{-3}, the results agreed with the calculated values. However, in the case of J=0, the experimental results were more alkaline than the calculated ones in the region $W_{chs}<0.3$; upon increasing W_{chs}, both of the results approached each other. The increments of pH in the region $W_{chs}<0.3$ are considered to result from the formation of soluble complexes.

The binding amounts of H^+ ion on isoionic gelatin and Chs-C, ν mol g^{-1}, were obtained from their pH titration curves by using Eq. 1. The values of ν are shown in Fig. 4 as a function of pH. The saturated binding amount of the isoionic gelatin, ν_{ge}^{∞}, was 0.85×10^{-3}, mol g^{-1}. This is equivalent to the total amount of the basic amino acids of the gelatin,[21] which was 0.83×10^{-3} mol g^{-1} (Table 1). The saturated binding amount of Chs-C, ν_{chs}^{∞}, was 1.60×10^{-3} mol g^{-1}, equal to the concentration of glucuronic acid in Chs-C (1.67×10^{-3} mol g^{-1}), as determined by the carbazole-sulfuric acid method.[23] Figure 4 also shows the results for ν using mixed solutions (W_{chs}=0.177, 0.334, and

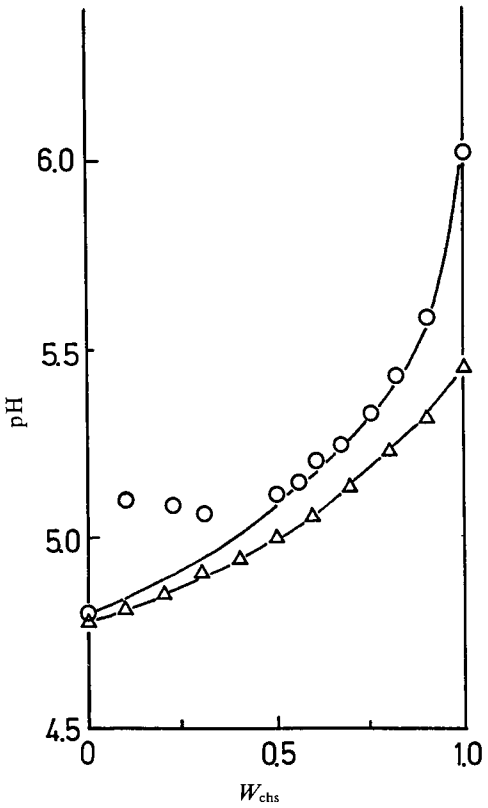

Fig. 3. pH of mixed solutions vs. weight fraction of chondroitin sulfate C.
J: ○; 0.0, △; 0.10 mol dm^{-3}. Solid curves are the calculated values obtained by assuming an ideal mixtures.

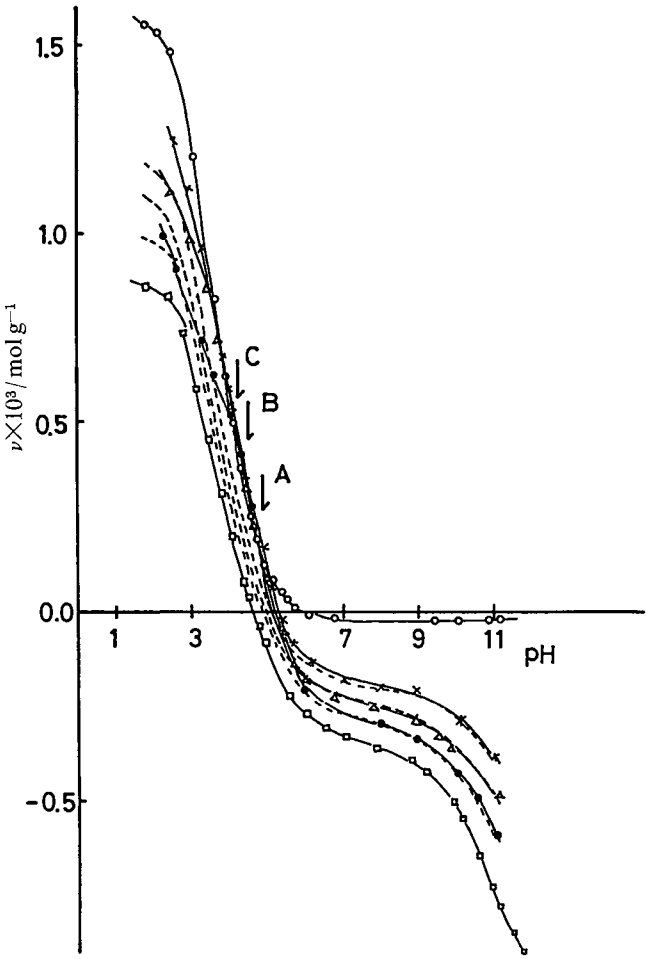

Fig. 4. H^+ and OH^- ion binding amounts of mixed solutions.
W_{chs}: ○; 1.0, ×; 0.461, △; 0.334, ●; 0.177, □; 0.
Arrows show the value of pH at which the insoluble complexes start to be formed, $(pH)_{ic}$, and capital letters by the arrows show W_{chs}, A; 0.177, B; 0.334, C: 0.461. Broken lines are calculated values from Eq. 4 by assuming no effects of interactions between gelatin and Chs-C.

0461); these are the binding amounts of H^+ ions per 1 g of polymers. The results were found to be close to that for a Chs-C solution in the pH region 4.5—6. Upon decreasing the pH of mixed solutions, they became opaque due to the formation of insoluble complexes. The arrows in Fig .4 indicate the pH values at which insoluble complexes start to be formed (=$(pH)_{ic}$). Since the insoluble complexes were deposited onto the glass electrode in the region pH<$(pH)_{ic}$, the experimental results might not be very exact in these regions.

When there was no interaction between the gelatin and Chs-C, the ideal binding amounts of H^+ ions, ν^{ideal}, could be expressed by summing up the binding amounts of the gelatin and Chs-C, ν_{ge} and ν_{chs},

$$\nu^{ideal} = (1-W_{chs})\,\nu_{ge} + W_{chs}\,\nu_{chs}. \quad (4)$$

The calculated values are shown in Fig. 4 with broken lines. In the region of pH greater than about 6, the experimental and calculated results were almost equal. However, in the region of smaller pH, the former were more than the latter. An enhancement of H^+ ion binding is expected from the results shown in Fig. 3, and is considered to result from the formation of complexes.

Compositions of Insoluble Complexes. Upon decreasing the pH of mixed solutions comprising gelatin and Chs-C, a phase separation occurred. The transmittances of the mixed solutions of various compositions were measured at various times after adjusting to acidic pH in the range pH=2.5—5.0. During the initial stage a milky turbidity appeared, but with an elapse of time the bulky insoluble complexes precipitated, even under stirring conditions. The results mesured 15 min after adjusting the pH showed the clearest peaks as a function of W_{chs} (Fig. 5). The values of W_{chs} showing the transmittance maximum at arbitrary acidic pHs, $(W_{chs})_{ic}$, are considered to represent the compositions of insoluble complexes.[22] The $(W_{chs})_{ic}$ results are shown in Fig. 6 as a function of the pH of the solutions. $(W_{chs})_{ic}$ decreased with increasing pH of the solutions.

From the nitrogen contents, $(W_N)_{ic}$, of the insoluble complexes at pH=3, 3.5, and 4.4, the results of $(W_{chs})_{ic}$ were obtained using Eq. 2. They did not depend on the compositions of the mixed solutions, but on the pHs. The mean values of the results are shown in Fig. 6. Taking the errors of the nitrogen analysis into consideration, the results were found to agree fairly well with those from the transmittance method.

The compositions of saturated soluble complexes can vary with the pH of mixed solutions. However, the composition of saturated soluble complexes at only pH=5.1 was estimated to be $(W_{chs})_{ssc}$=0.294 from viscosity measurements. As shown in Fig. 6, $(W_{chs})_{ic}$ and pH.

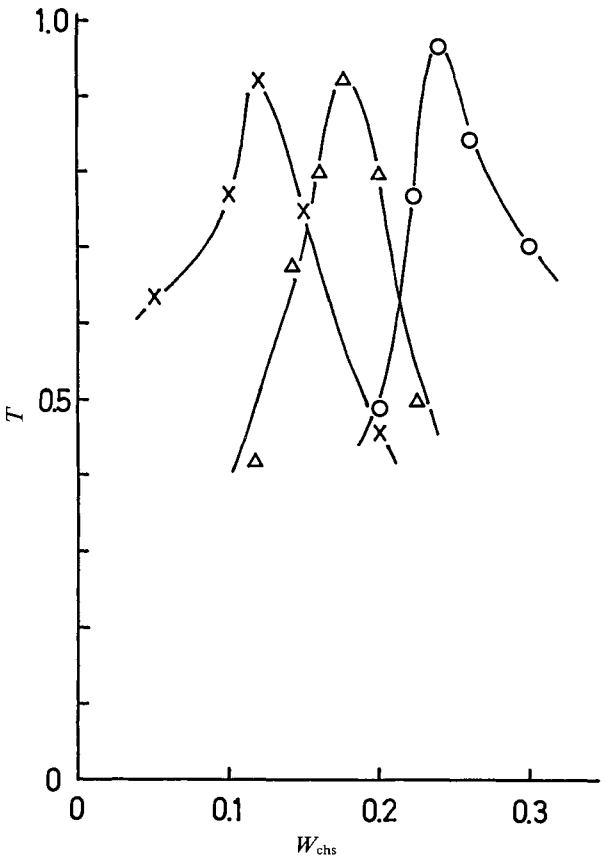

Fig. 5. Transmittance T of mixed solutions at various pH.
pH of the mixed solution: ○; 3.0, △; 3.5, ×; 4.0.

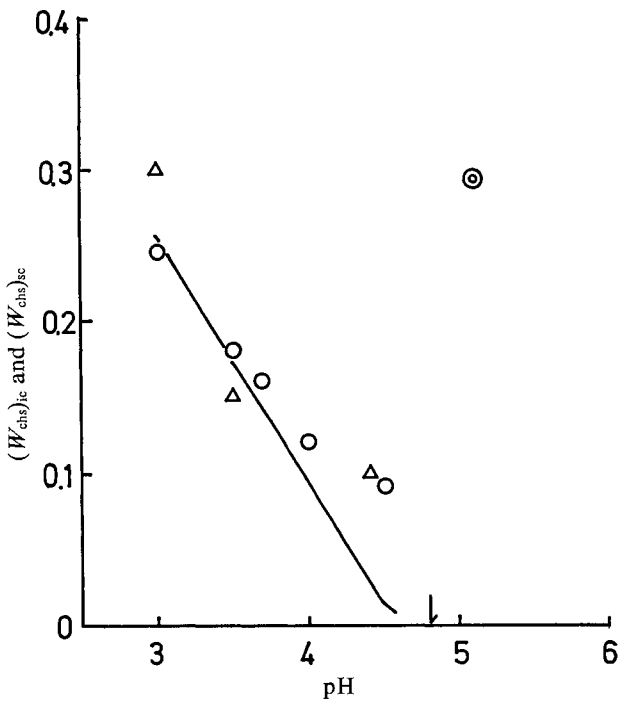

Fig. 6. Fraction of Chs-C of insoluble complexes formed in acidic pH region and saturated soluble complex.
$(W_{chs})_{ic}$: ○; Transmittance method, △; Nitrogen analysis method, $(W_{chs})_{ssc}$: ◎; exprimental result obtained from viscosity measurement. Solid curve shows the calculated values $(W_{chs})_{co}$ from Eq. 10 under the condition of electroneutrality between Z_{chs} and Z_{ge}. An arrow shows the isoionic point of the gelatin.

Discussion

Apparent Dissociation Constant of Carboxylic Groups in Mixed Solutions. The degree of dissociation, α, of the carboxylic group of weak acidic polymers is related to the pH of the solutions by Eq. 5 in the range where α is not close to 0 or 1:[24]

$$pH = pK_a + n \log(\alpha/(1-\alpha)), \quad (5)$$

where pK_a is an apparent dissociation constant and n is a constant. Since the sulfuric groups of Chs-C can be approximated to be fully dissociated in mixed solutions of gelatin and Chs-C,[25,26] their carboxylic groups are responsible for the binding of H^+ ions. Eq. 5 can, thus, be applied to mixed solutions. In mixed solutions the mean value of the degree of dissociation of their carboxylic groups is obtained by

$$\alpha = \frac{(1-W_{chs})\nu_{ge}^{\infty} + W_{chs}\,\nu_{chs}^{\infty} - \nu}{(1-W_{chs})(n_{car})_{ge} + W_{chs}(n_{car})_{chs}}, \quad (6)$$

where $(n_{car})_{ge}$ and $(n_{car})_{chs}$ mol g^{-1} are the contents of the carboxylic groups of the gelatin and Chs-C. $(n_{car})_{ge}$ is 1.074×10^{-3} mol g^{-1}, which is the total content of the acidic amino groups obtained from Table 1; $(n_{car})_{chs}$ is 1.67×10^{-3} mol g^{-1}, which is the content of the glucuronic acid of Chs-C. The relations between pH and $\log(\alpha/(1-\alpha))$ were found to be linear, even for mixed solutions (Fig. 7). The values of pK_a and n obtained from these linearities are the mean values of the carboxylic groups of both polymers. Although the n values were almost constant (the mean value=1.24), the values of pK_a were found to have a maximum at about W_{chs}=0.25 (Fig. 8).

By using the mean value of n, the values of pK_a of the mixed solutions over the full range of W_{chs} can be obtained from the pH results for the mixed solutions shown in Fig. 3. The pK_a values, thus obtained, are

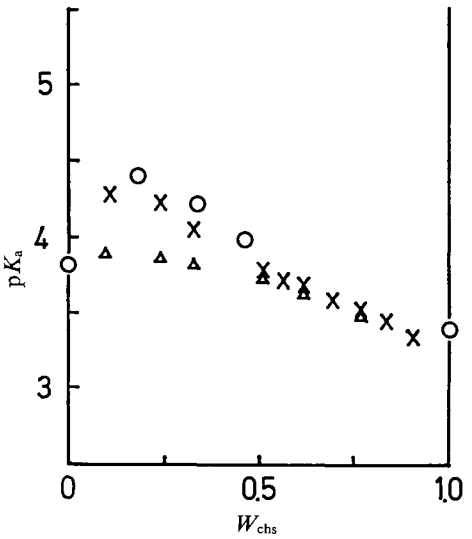

Fig. 8. pK_a values of carboxylic groups in mixed solutions.
○: Results obtained from the linear relations in Fig. 7. ×: Results obtained from Eq. 5 using the mean values of n and α obtained from pH titration curves. △: Calculated values assuming the ideal mixtures.

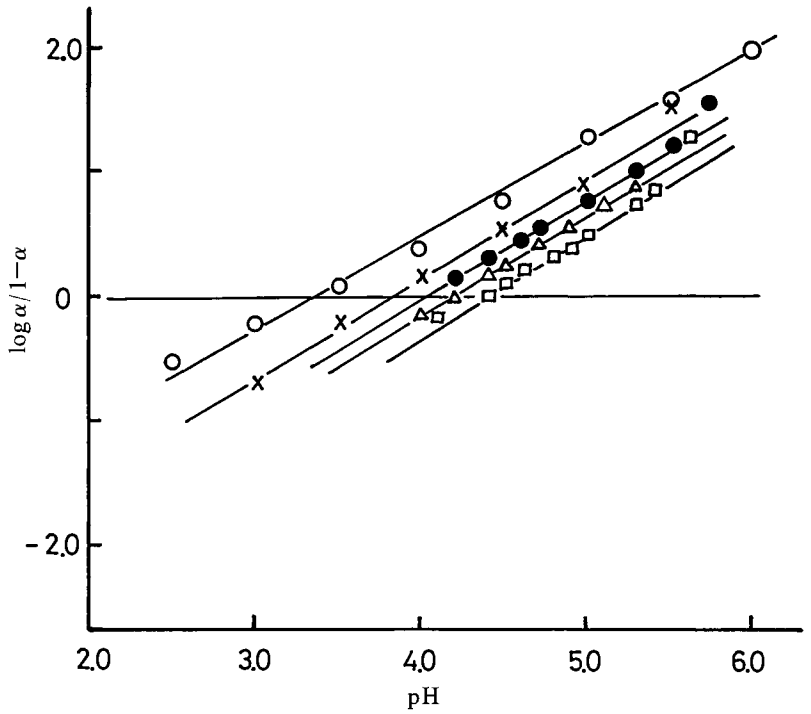

Fig. 7. $\log(\alpha/(1-\alpha))$ vs. pH.
W_{chs}: ×; 0, □; 0.177, △; 0.334, ●; 0.461 , ○; 1.0.

also shown in Fig. 8, and are found to be in good agreements with the results mentioned above. The theoretical values of pK_a obtained by assuming ideal mixtures of Chs-C and gelatin are also shown in Fig. 8. The experimental results of pK_a were found to be greater than the theoretical values in the region $0<W_{chs}<0.4$, and the maximum to be around $W_{chs}=0.25$, which is very near to $(W_{chs})_{ssc}$ (=0.29). The carboxylic groups of the gelatin and Chs-C are responsible for the association of H^+ ions. The latter can be considered to be depressed in the association of H^+ ions for the following reasons: (1) competitive binding with H^+ ions and the amino groups of the gelatin, and (2) electrostatic shielding of the neighboring sulfuric groups due to interaction with the gelatin. The latter reason is expected from the fact that pK_a of chondroitin is less than that of Chs-C.[27] Chondroitin is the same structure as Chs-C except for the lack of sulfuric groups. Therefore, the enhancement of the H^+ ion association due to soluble complex formation is ascribed to that of the carboxylic groups of the gelatin due to a shielding of neighboring positively charged amino groups.

Complex Formations and Charge Densities of Gelatin and Chs-C. The saturated binding amounts of H^+ ions on isoionic gelatin molecules ν_{ge}^{∞} was 0.85×10^{-3} mol g^{-1}, as shown in Fig. 4. The charge amounts of the gelatin at the isoionic pH, $(Z_{ge})_{iip}$, is obtained by

$$(Z_{ge})_{iip}=(C_{OH}-C_H)/C_{ge}, \tag{7}$$

where C_{ge} is the concentration of gelatin (g dm^{-3}); C_{OH} and C_H are those of OH^- and H^+ ions (mol dm^{-3}) at the isoionic pH. From the isoionic pH of the gelatin (=4.8), $(Z_{ge})_{iip}$ was determined to be -1.585×10^{-6} mol g^{-1}, which can be negligible. The isoionic pH can thus be approximated to be equal to the isoelectric point, and the maximum charge amount of the gelatin Z_{ge}^{∞} to be ν_{ge}^{∞}. The charge amounts, Z_{ge}, vary with pH, due to a dissociation of H^+ ions, and can be obtained by subtracting the dissociated amounts of H^+ ions, r_{ge}, from Z_{ge}^{∞},

$$Z_{ge}=Z_{ge}^{\infty}-r_{ge}. \tag{8}$$

Cl^- or Na^+ ions come from the HCl or NaOH present in the solutions. However, the concentrations of these ions were so small that their binding amounts might be negligible. The charge of Chs-C Z_{chs} is the summation of the contributions of the sulfuric and the carboxylic groups ($(Z_{sul})_{chs}$ and $(Z_{car})_{chs}$),

$$Z_{chs}=(Z_{sul})_{chs}+(Z_{car})_{chs}=(Z_{sul})_{chs}-r_{chs}, \tag{9}$$

where r_{chs} is the dissociated amounts of H^+ ions from chondroitin sulfuric acid. The values of Z_{ge} and Z_{chs} in the solutions can be related to the formation of both soluble and insoluble complexes. The pHs which start to form the soluble complexes were almost pH=6, at which Z_{ge} was negative (=−0.026 mol dm^{-3}). Soluble complex formation was, thus, found to occur even between both the negatively charged gelatin and Chs-C, being considered to result from an electrostatic interaction between the positively charged amino groups of the gelatin and the charged groups of Chs-C. As the pH decreases, Z_{ge} increases and the insoluble complexes come to be formed; a phase separation thus occurs.

Composition of Complexes. When the complexes formed by electrostatic interactions satisfy electroneutrality, the weight fraction of the Chs-C of the complex $(W_{chs})_{co}$ are related to Z_{chs} and Z_{ge} by the following equation:

$$(W_{chs})_{co}=-Z_{ge}/(Z_{chs}-Z_{ge}). \tag{10}$$

Using Z_{ge} and Z_{chs}, the values of $(W_{chs})_{co}$ were calculated. They are shown in Fig. 6 together with the experimental results for insoluble complexes $(W_{chs})_{ic}$, and a saturated soluble complex at pH=5.1 $(W_{chs})_{ssc}$. The results for the insoluble complexes $(W_{chs})_{ic}$ agreed with the calculated values. Therefore, the formation of insoluble complexes is found to be due to electrostatic interactions between the negative charge of Chs-C and the effective positive charge of the gelatin. However, when the pH value approaches the isoionic point of the gelatin, the experimental results, $(W_{chs})_{ic}$, became greater than the calculated values.

The weight fraction of Chs-C of the saturated soluble complex $(W_{chs})_{ssc}$ was 0.294 at pH=5.1. However, it can not be estimated from Eq. 10 since Z_{ge} (=−0.05 mol dm^{-3})<0. The soluble complexes are thus considered to be formed by an interaction between Chs-C and the positively charged amino groups of the gelatin. Although the theoretical value of $(W_{chs})_{ssc}$ is difficult to estimate from our results, as an extreame estimation, $(W_{chs})_{ssc}$ was calculated from the electroneutrality between Chs-C and all of the positively charged amino groups at pH=5.1: 0.217, and less than the experimental result. This difference might be explained as follows. Near the isoionic point of gelatin, since it is in a shrinking random coil state, parts of the positively charged amino groups are considered to take part in complex formation. Furthermore, parts of the negatively charged groups of Chs-C are also considered to take part in it, and the residual parts are free states in solutions.

Conclusion

(1) The apparent dissociation constants of carboxylic groups of Chs-C and gelatin decrease due to complex formation; thus, the dissociation of H^+ ions of the carboxylic groups of gelatin was depressed by a shielding of the positively charged amino groups due to an interaction with Chs-C.

(2) Along with decreasing pH of the solutions, insoluble complexes were formed due to the electrostatical interactions between Chs-C and the effective positive charges of gelatin; the composition agrees with the values calculated according to electroneutrality.

References

1) J. H. Fessler, *Biochem. J.*, **76**, 124 (1960).
2) A. Courts and B. G. Giles, "Struc. Function Connective Skeletal Tissue," Proc. St. Andrews, Scotland (1965), p. 235.
3) M. Yonese, H. Tsuge, and H. Kishimoto, *J. Phys. Chem.*, **91**, 1971 (1987).
4) M. Yonese, H. Tsuge, and H. Kishimoto, *Nippon Kagaku Kaishi,* **1978**, 108.
5) H. Tsuge, M. Yonese, and H. Kishimoto, *Nippon Kagaku Kaishi,* **1978**, 609.
6) H. Tsuge, M. Yonese, and H. Kishimoto, *Bull. Chem. Soc. Jpn.*, **52**, 2846 (1979).
7) M. Yonese and H. Kishimoto, *Bull. Chem. Soc. Jpn.*, **54**, 20 (1981).
8) H. Tsuge and M. Yonese, *Nippon Kagaku Kaishi,* **1982**, 1583.
9) G. S. Manning, *Annu. Rev. Phys. Chem.*, **23**, 117 (1972).
10) M. Nakagaki and Y. Sano, *Bull. Chem. Soc. Jpn.*, **45**, 1011 (1972).
11) M. B. Mathews, *Biochem. J.*, **96**, 710 (1965).
12) B. Obrink and A. Wasteson, *Biochem. J.*, **121**, 227 (1971).
13) E. A. MacMullan and F. R. Eirich, *J. Colloid Sci.*, **18**, 526 (1963).
14) M. Yonese and M. Nakagaki, *Yakugaku Zasshi,* **95**, 75 (1975).
15) M. Yonese and M. Nakagaki, *Yakugaku Zasshi,* **95**, 641 (1975).
16) M. Yonese and M. Nakagaki, *Yakugaku Zasshi,* **95**, 665 (1975).
17) M. Yonese and M. Nakagaki, *Yakugaku Zasshi,* **96**, 299 (1976).
18) M. Yonese and M. Nakagaki, *Yakugaku Zasshi,* **101**, 493 (1981).
19) J. W. Janus, A. W. Kenchington, and A. G. Ward, *Research,* **4**, 247 (1951).
20) M. Nakagaki, N. Koga, and H. Terada, *Yakugaku Zasshi,* **86**, 849 (1966).
21) C. Tanford, "Physical Chemistry of Macromolecules," University of Tokyo Press, Tokyo (1969), p. 548.
22) A. Nakajima and K. Shinoda, *J. Colloid Interface Sci.*, **55**, 126 (1976).
23) T. Bitter and H. M. Muir, *Anal. Biochem.*, **4**, 330 (1962).
24) A. Katchalski, N. Shavit, and H. Eisenberg, *Polym. Sci.*, **13**, 69 (1954).
25) M. B. Mathews, *Biochim. Biophys. Acta,* **35**, 9 (1959).
26) I. G. F. Gilbert and N. A. Myers, *Biochim. Biophys. Acta,* **42**, 469 (1960).
27) M. Yonese, unpublished data.

Electronic Spectra of Phenanthrolinediones, Phenanthrolinones, Bipyridinediones, and Amino-Substituted Phenanthrolines

Masaki YAMADA,* Miki KIMURA, Mineyasu NISHIZAWA, Shigeyasu KURODA, and Ichiro SHIMAO
Department of Materials Science and Engineering, Faculty of Engineering,
Toyama University, 3190 Gofuku, Toyama 930
(Received January 16, 1991)

The electronic spectra of three types of 1,10-phenanthroline derivatives having different π-conjugated systems, phenanthrolinedione, phenanthrolinone, and the parent phenanthroline, showed characteristic patterns easily distinguished from each other. Analogous spectral patterns were noted in amino-substituted 1,10-phenanthrolines, and the protonated structures of these compounds were characterized on the basis of such spectral features.

Recently we reported on the preparation of *N,N'*-annelated phenanthrolinedione **1a** and **1b**, and bipyridinedione **2a** and **2b**, as potential precursors of the corresponding dichloro derivatives of 1,10-phenanthroline (phen) and 2,2'-bipyridine (bpy), respectively.[1] These diones seem to be also attractive compounds as "extended" α-pyridinones. From these viewpoints, we investigated in detail the electronic spectra of **1a**, **1b**, **2a**, **2b**, well-known phenanthrolinone **3a**,[2] **3b**,[3] and nonannelated bipyridinedione **2c**.[4] The electronic spectra of **1a,b** and **3a,b** were largely different from that of the parent phen and from each other, whereas there were small differences in spectral patterns between **2a**—**c** and the parent bpy. It was suggested that the characteristic of spectral patterns should be a good means in identifying the formal π-conjugated systems in phen derivatives regardless of the shifts in absorption maxima.[5] Further, spectral patterns analogous to those of **1** and **3** were observed in the spectra of protonated forms of amino-substituted phens, 1,10-phenanthroline-2,9-diamine (**4**)[3] and 1,10-phenanthrolin-2-amine (**5**).[6] The protonated structures of **4** and **5** were characterized by examining the spectral patterns.

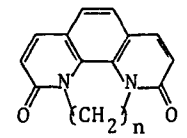

1: **a**; n=2
b; n=3

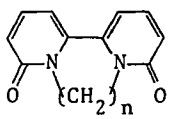

2: **a**; n=2
b; n=3

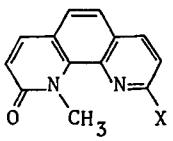

3: **a**; R=H
b; R=Cl

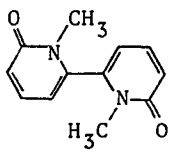

2c

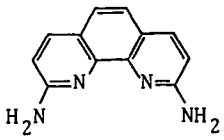

4

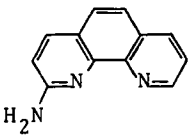

5

Results and Discussion

Electronic Spectra of Phenanthrolinones and Bipyridinones. The electronic spectra of phen, a phenanthrotinone **3a**, and a phenanthrolinedione **1a** in 250—450 nm region are shown in Fig. 1. A strong π-π^* transition band (β'-band) and two additional bands of

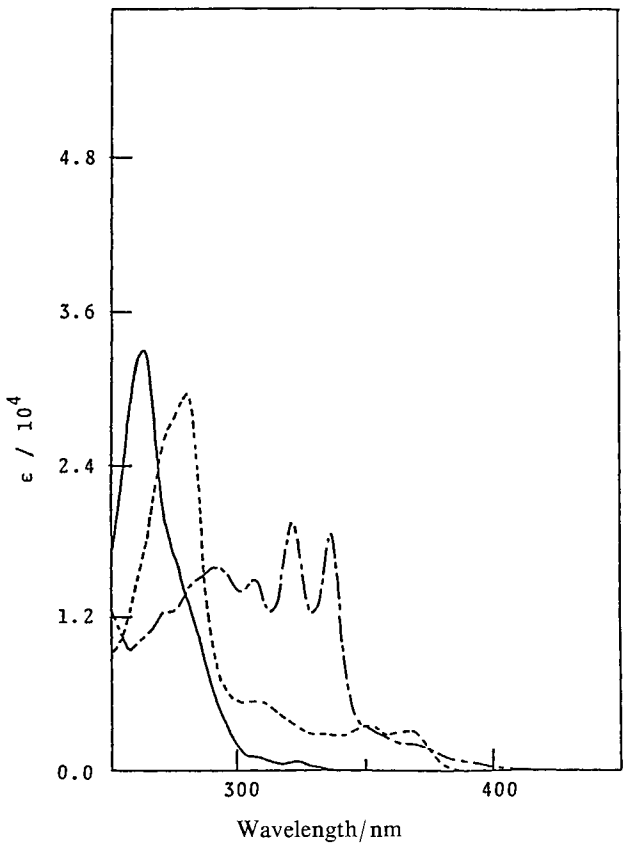

Fig. 1. Electronic spectra of (——): phen, (------): **3a**, and (— - —): **1a** in methanol.

much lower intensity at longer wavelengths (p-band and α-band) appeared in the spectrum of phen.[7] Noticeable differences are observed between the spectrum of **3a** and that of phen, i.e., three clear peaks of much higher intensity than that of p- and α-bands (λ_{max}=308, 352, and 369 nm, with $\log\varepsilon_{max}$=3.74, 3.55, and 3.50, respectively) appeared in the spectrum of **3a**. The spectrum of **1a** is quite different from those of both phen and **3a**, i.e., four peaks of similar intensities (λ_{max}=271, 291, 307, 322, and 337 nm, with $\log\varepsilon_{max}$=4.10, 4.21, 4.18, 4.29, and 4.27, respectively) are observed instead of the β'-band.

The spectral patterns of the parent phen are not affected by simple substituents such as amino,[3,6] chloro,[2,3] and methoxy groups[8,9] at 2- and 9-positions. The only noticeable influences caused by substituents were the red shifts according to the nature and number of substituents and appearances of sub-peaks in β'-bands of disubstituted derivatives, **7** and **9** (Table 1).

The electronic spectra of another phenanthrolinone **3b**[3] and another phenanthrolinedione **1b** along with **3a** and **1a** are depicted in Fig. 2. The chloro substituent in **3b** caused a small red shift compared with **3a**, in a similar manner to the chloro substituent in **6**. Exchange of the ethano-bridge in **1a** by a propano-bridge in **1b** also resulted in a small red shlft.[1,10] Nevertheless, the spectral patterns of **3b** and **1b** are quite similar to those of the corresponding compounds having the same formal π-conjugated systems, **3a** and **1a**, respectively. These results indicate that the characteristic spectral patterns of phen, **3a**, and **1a** reflect the individual π-conjugated systems rather than the substituent effects.

This speculation was supported further by spectral measurement of **1a** in strong acidic media. In concentrated sulfuric acid, the absorbances at wavelengths shorter than 300 nm were increased to a level of the β'-bands (Fig. 3). Since two different sets of isosbestic points appeared successively during spectrometric titration with sulfuric acid (Fig. 3-A and -B), stepwise protonation to the two oxygen atoms in **1a** should take place in strong acidic media, forming **1'a** and **1''a** (Scheme 1). The diprotonated form **1''a** may exist in resonance with **1'''a**, whose π-conjugated system is the same as that of phen.

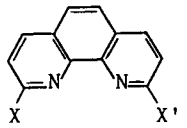

6; X=Cl, X'=H
7; X=X'=Cl
8; X=OMe, X'=H
9; X=X'=OMe

Table 1. Absorption Maxima of β'-Bands of phen Derivatives in Methanol

Compound	λ_{max}/nm ($\log\varepsilon_{max}$)
5	287 (4.45)
4	309 (4.43)
6	268 (4.63)
7	273 (4.54), 293 (4.26)
8	274 (4.53)
9	281 (4.47), 294 (4.34)

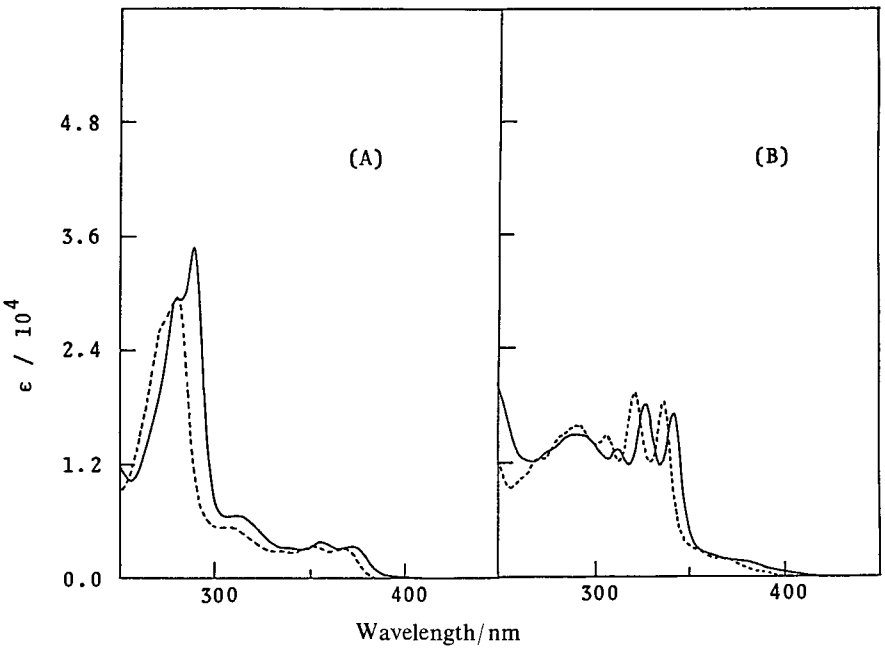

Fig. 2. Electronic spectra of (A) (——): **3b** and (------): **3a**, and (B) (——): **1b** and (----): **1a** in methanol.

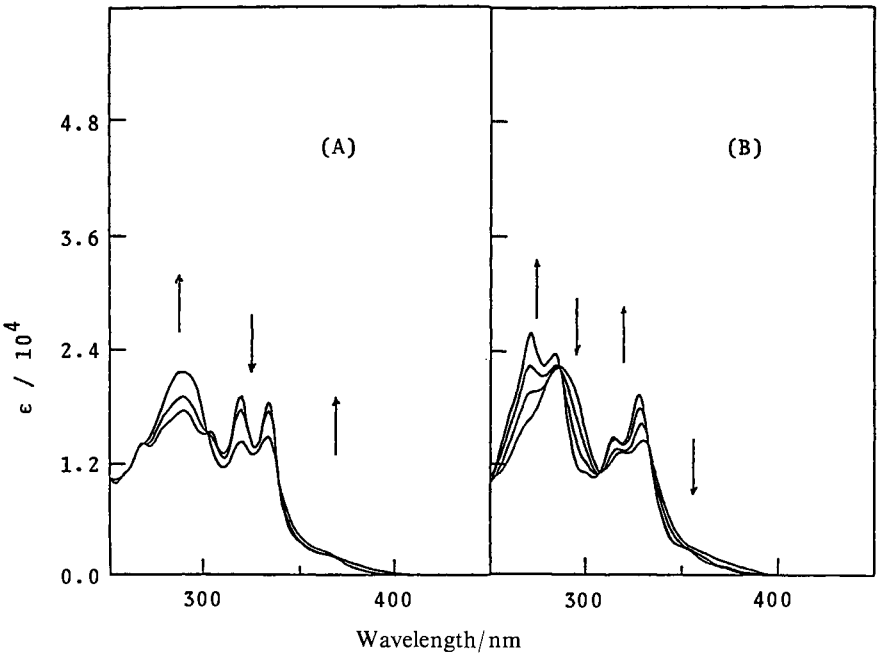

Fig. 3. Spectral change of **1a** by increasing concentration of sulfuric acid. Concentrations of sulfuric acid; (A): 0, 10, and 20%, (B): 30, 40, 50, and 90%.

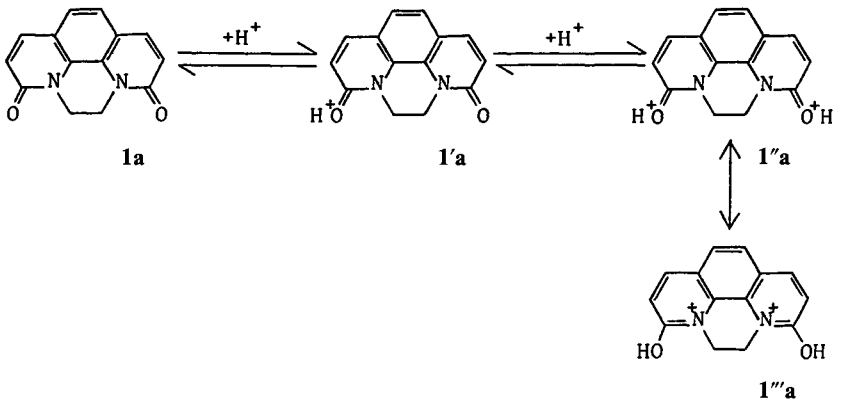

Scheme 1.

The electronic spectra of bipyridinediones **2a**—**c** in 250—450 nm region are displayed in Fig. 4. It is well-known that a strong π–π^* transition band of the parent bpy (β'-band,[11] λ_{max}=280 nm[12]) appears in this region. Analogous bands indeed appear in the spectra of **2a**—**c**. The large red shifts of absorption maxima from that of the parent bpy (93, 63, and 36 nm for **2a**, **2b**, and **2c**, respectively) are noted, which should be attributed to changes in the π-conjugated systems.[5] Large shifts of absorption maxima can take place also by rotation of the interannular bond,[1,13,14] i.e., large blue shifts occur in the spectra of twisted bipyridinediones, **2b** and **2c** (30 and 57 nm, respectively), compared with the planar one, **2a**. Thus we should be careful in identifying the π-conjugated systems of bpy derivatives in terms of the shifts of absorption bands.[5,13]

Amino-Substituted Phen's and Their Protonated Structures. Though the amino substituents at 2- and 9-positions in **4** and **5** do not affect the spectral pattern of phen (see above), protonation to these compounds effected large changes in the spectral pattern. The electronic spectra of amino-substituted phen's, **5** and **4**, and their protonated forms are shown in Fig. 5. A one-step protonation was detected by spectrometric titration of **5** within a pH range of 10 to 0 (pK_a=6.9[15]). A large change in the spectral pattern took place by the protonation, i.e., several prominent peaks appeared at longer wavelengths (Fig. 5-A). In the case of **4**, two-step protonations were observed within a pH range of 10 to 0 (pK_a=7.9 and 2.1[16]). Though the change in the spectral pattern was marginal by the first protonation, it was fairly drastic by the second protonation (Fig. 5-B). In

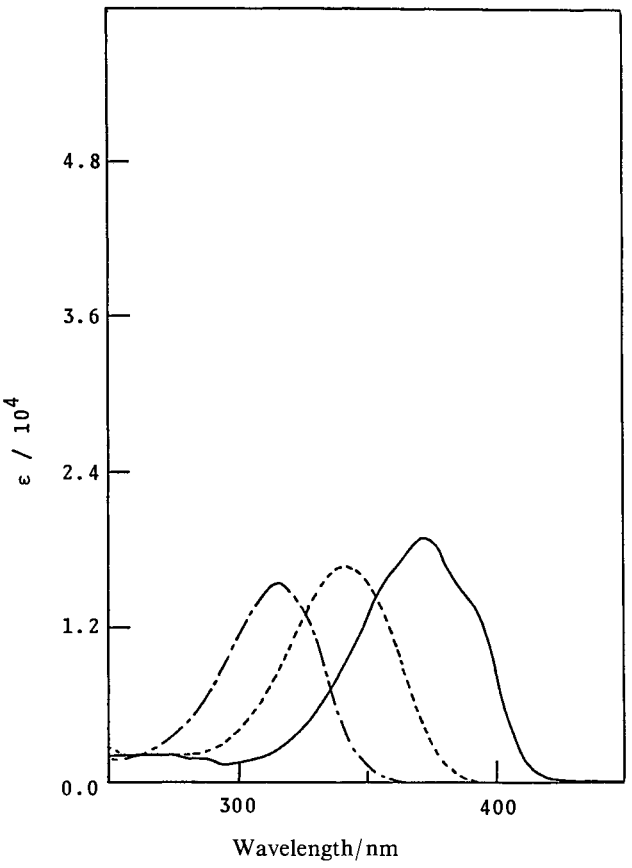

Fig. 4. Electronic spectra of (——): **2a**, (– – –): **2b**, and (— - —): **2c** in methanol.

contrast, only the shifts of the β'-band were noted by the protonation to phen.[17] Since the spectral changes of **4** and **5** are reversible, these changes do not reflect degradation reactions. A comparison between these spectra and some spectra discussed above (Fig. 6) shows that the spectral pattern of the monoprotonated **5** is quite similar to that of **3a** (Fig. 6-A), and that the spectral patterns of diprotonated form of **4** resemble that of phenanthrolinedione **1a**, though the sharpness of each peak is reduced to some extent (Fig. 6-B).

Analogous spectral similarity was observed between simpler heteroaromatic compounds, 2-quinolinamine **10** and 1-methyl-2(1*H*)-quinolinone **11**. A one-step protonation took place in **10** within a pH range of 10 to 0 (pK_a=7.3).[18] The electronic spectra of **10** in free and monoprotonated forms and **11** in a 250—450 nm region are illustrated in Fig. 7. The single peak appearing in

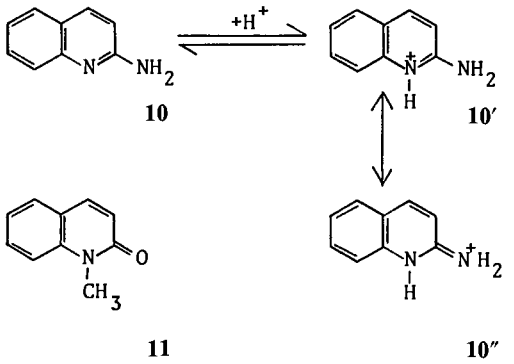

Scheme 2.

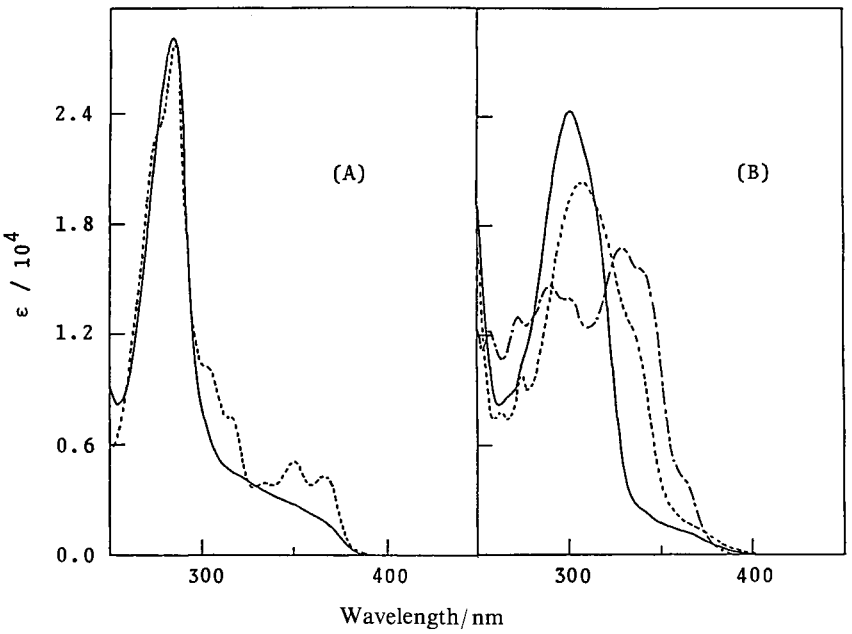

Fig. 5. Electronic spectra of (A) **5** and (B) **4** in aqueous buffer solution; (——): free form, (– – –): monoprotonated form, and (— - —): diprotonated form.

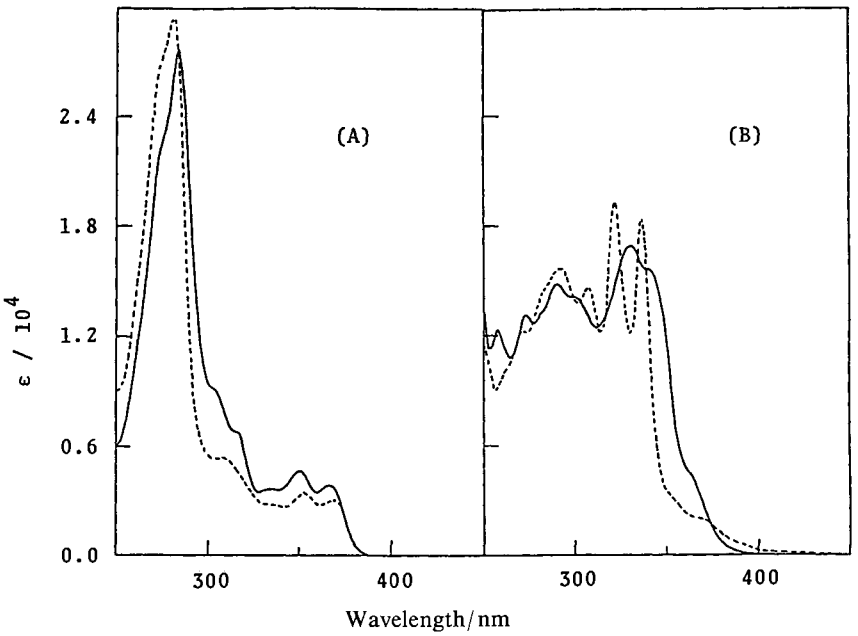

Fig. 6. Spectral comparison of amino-substituted 1,10-phenanthrolines in protonated forms and the corresponding phenanthrolinones; (A) (——): monoprotonated form of **5** in aqueous buffer solution and (- - - -): **3a** in methanol, (B) (——): diprotonated form of **4** in aqueous buffer solution and (- - - -): **1a** in methanol.

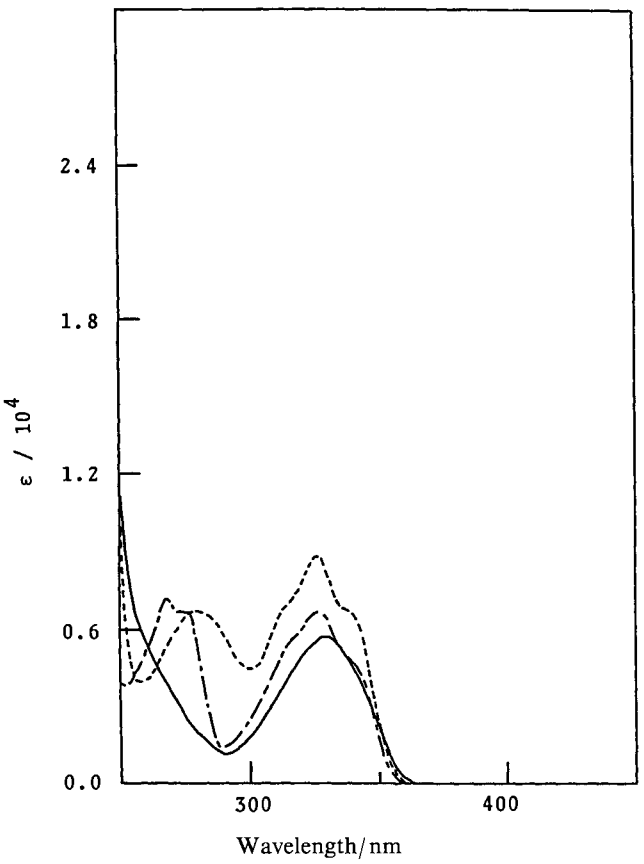

Fig. 7. Electronic spectra of (——): free form of **10** in aqueous buffer solution, (- - - -): monoprotonated form of **10** in aqueous buffer solution, and (— - —): **11** in methanol.

the spectrum of the free form of **10** splitted into two major peaks by protonation. The spectral pattern of monoprotonated **10** was similar to that of **11**. Protonation to **10** took place on the ring nitrogen to form **10′**, because the ring nitrogen of amino-substituted pyridines has much higher basicity than the amino nitrogen.[12,19] There is a large contribution of the resonance structure **10″** in **10′**.[18,20] The spectral similarity of monoprotonated **10** and **11** should be attributed to the similarity of the π-conjugated systems between **10″** and **11** (Scheme 2).

The spectral similarity between monoprotonated **5** and **3a**, and between diprotonated **4** and **1a**, can be rationalized by the same argument. The initial proton-

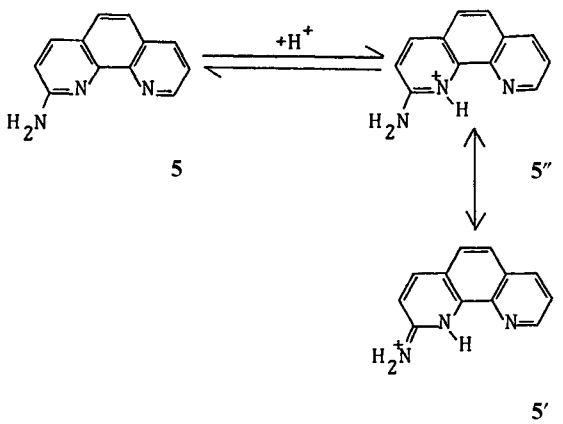

Scheme 3.

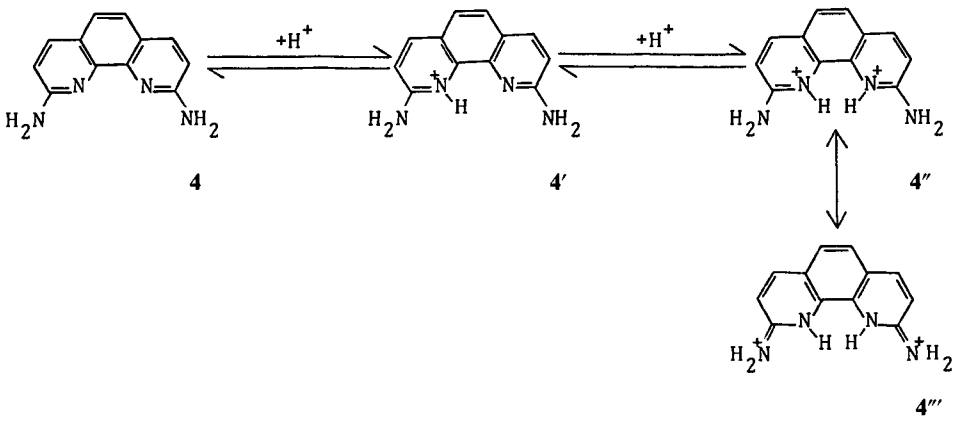

Scheme 4.

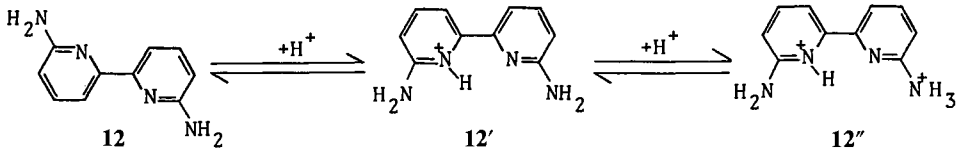

Scheme 5.

ation to **5** takes place on the nitrogen in 1-position rather than in 10-position[6] forming **5'**, because the amino substituent at α-position of the pyridine ring significantly increases the basicity of the neighboring ring nitrogen.[12,18–20] There would be a large contribution of the resonance structure **5''**, which is a conjugated system quite similar to that of **3a** (Scheme 3). For the same reason, the initial protonation to **4** should take place at one of the ring nitrogens, forming **4'**. The second protonation should take place at the other ring nitrogen to form **4''**, which has a resonance structure **4'''**. The formal π-conjugated system of **4'''** is quite similar to that of **1a** (Scheme 4). If the second protonation should take place on one of the amino nitrogens, one cannot draw a π-conjugated system similar to that of **1a**. On the other hand, the spectral pattern of monoprotonated form **4'** resembles that of phen rather than that of **3a**. This suggests that the positive charge in **4'** is delocalized not only over the neighboring amino nitrogen but also over the other pyridine ring and its amino substituent, thereby lowering the contribution of the π-conjugated system similar to that of **5''**.

As discussed above, at least judging from the spectral features of phenanthroline derivatives, both the first and second protonation to **4** appear to take place on the ring nitrogens. It is well-known that the second protonation to the ring nitrogens of phen and bpy occurs only in such strong acidic media as concentrated sulfuric acid because of a repulsion between the neighboring protons in diprotonated forms.[17,21] In the present case, however, the second protonation to the ring nitrogen of **4** is apparantly completed at pH 1. Incidentally, the acid-base properties of 2,2'-bipyridine-6,6'-diamine **12**, a bpy analogue of **4**, have been studied by electronic and ^{1}H NMR spectroscopies,[22] and it has been concluded that the second protonation to **12** takes place at the amino nitrogen rather than the ring nitrogen (Scheme 5). Since there were only minor changes in the spectral patterns by protonation to **12**, there should be some uncertainty as to the actual forms for reasons given above with respect to **2a—c**.

The absorption maxima and the ^{1}H NMR chemical

Table 2. Spectral Comparison of **4** and **12** with the Parent phen and bpy

Compound	λ_{max}/nm[a]	^{1}H NMR/δ[b] (position)			
4 (A)	309	—	6.81 (3,8)	7.88 (4,7)	7.29 (5,6)
phen (B)	264	9.12 (2,9)	7.77 (3,8)	8.50 (4,7)	7.99 (5,6)
(A)—(B)	45	—	−0.96 (3,8)	−0.62 (4,7)	−0.70 (5,6)
12 (C)	334[c]	—	6.38 (5,5')	7.36 (4,4')	7.36 (3,3')[d]
bpy (D)	280[c]	8.43 (6,6')	7.24 (5,5')	7.72 (4,4')	8.15 (3,3')[d]
(C)—(D)	54	—	−0.86 (5,5')	−0.36 (4,4')	−0.79 (3,3')

a) In methanol. b) In dimethyl-d_6 sulfoxide. c) Ref. 12. d) Ref. 22.

shifts for **4** and **12** are summarized in Table 2 together with those of the parent phen and bpy. At least in acid-free forms, the electron donating effects of amino substituents seem to be very similar in the two compounds, as judged from the red shifts in the electronic spectra and the ^{1}H NMR high field shifts.[23] The second protonation to **12** (pK_a=2.2[22]) might also take place at the ring nitrogen in a similar manner to that of **4** (pK_a=2.1). Systematic investigations are needed, however, to settle this problem.

In conclusion, we demonstrated that the electronic spectra of the three types of phen derivatives, **1a,b**, **3a,b**, and the parent phen, show neatly different spectral pattern distinguished from each other by visual inspection. This may reflect the differences in the individual π-conjugated systems. Such a feature could be a good means to elucidate the electronic structure and related properties of phen and the corresponding bpy derivatives.

Experimental

Materials. Preparation of 5,6-dihydropyrazino[1,2,3,4-*lmn*][1,10]phenanthroline-3,8-dione (**1a**), 6,7-dihydro-5*H*-[1,4]diazepino[1,2,3,4-*lmn*][1,10]phenanthroline-3,9-dione (**1b**), 6,7-dihydrodipyrido[1,2-*a*:2′,1′-c]pyrazine-4,9-dione (**2a**), 7,8-dihydrodipyrido[1,2-*a*:2′,1′-c][1,4]diazepine-4,10-dione (**2b**), and 2,9-dichloro-1,10-phenanthroline (**7**) was reported elsewhere.[1] The following materials were prepared by literature procedures: 1-Methyl-1,10-phenanthrolin-2(1*H*)-one (**3a**), mp 123—124 °C (lit,[2] 123—124 °C), 9-chloro-1-methyl-1,10-phenanthrolin-2(1*H*)-one (**3b**), mp 153—154 °C (lit,[3] 154—155 °C), 1,10-phenanthroline-2,9-diamine (**4**), mp 296—298 °C (lit, 1[3] 273—275 °C, lit, 2[9] 296—298 °C), 1,10-phenanthrolin-2-amine (**5**), mp 188—192 °C (lit,[6] 187—190 °C), 2-chloro-1,10-phenanthroline (**6**), mp 129—130 °C (lit,[2] 129—130 °C), 2-methoxy-1,10-phenanthroline (**8**), mp 78—80 °C (lit,[8] 74—76 °C), 2,9-dimethoxy-1,10-phenanthroline (**9**), mp 111—113 °C (lit,[9] 110—111 °C), 1,1′-dimethyl-2,2′-bipyridine-6,6′-(1*H*,1′*H*)-dione (**2c**), mp 224—225 °C (lit,[4] 210—211 °C). 1,10-Phenanthroline (phen) and 2-quinolinamine (**10**) were commercially obtained. 1-Methyl-2(1*H*)-quinolinone (**11**) was prepared by a procedure analogous to that for 3a:[2] recrystallyzed from petroleum ether (bp 30—70 °C), mp 71—72 °C (lit, 1[24] 68—69 °C, lit, 2[25] 73—74 °C).

Spectral Measurements. Electronic spectra were recorded on a Shimadzu UV-265FS Spectrophotometer at 20 °C. ^{1}H NMR spectra were measured with a JEOL JNM-FX90Q Spectrometer at room temperature. The buffer solutions used for spectrometric titrations were as follows:[26] weakly basic area, potassium borate buffer; weakly acidic area, acetic acid-sodium acetate buffer; acidic area, HCl–KCl buffer.

References

1) M. Yamada, Y. Nakamura, S. Kuroda, and I. Shimao, *Bull. Chem. Soc. Jpn.*, **63**, 2710 (1990).

2) B. E. Halcrow and W. O. Kermack, *J. Chem. Soc.*, **1946**, 155.

3) S. Ogawa, T. Yamaguchi, and N. Gotoh *J. Chem. Soc., Perkin Trans. 1*, **1974**, 976.

4) S. Ogawa and S. Shiraishi, *J. Chem. Soc., Perkin Trans. 1*, **1980**, 2527.

5) P. Beak, F. S. Fry, Jr., J. Lee, and F. Steele, *J. Am. Chem. Soc.*, **98**, 171 (1976).

6) S. Ogawa and N. Gotoh, *Kogyo Kagaku Zasshi*, **74**, 83 (1971).

7) R. G. Bray, J. Ferguson, and C. J. Hawkins, *Aust. J. Chem.*, **22**, 2091 (1969).

8) K. G. Claus and J. V. Rund, *Inorg. Chem.*, **8**, 59 (1969).

9) P. J. Pijper, H. van der Goot, H. Timmerman, and W. Th. Nauta, *Eur. J. Med. Chem.-Chim. Ther.*, **19**, 399 (1984).

10) A. L. Black and L. A. Summers, *Tetrahedron*, **24**, 6453 (1968).

11) M. S. Henry and M. Z. Hoffman, *J. Phys. Chem.*, **83**, 618 (1979).

12) M. Yamada, K. Araki, and S. Shiraishi, *Bull. Chem. Soc. Jpn.*, **61**, 2208 (1988).

13) I. C. Calder, T. McL. Spotswood, and C. I. Tanzer, *Aust. J. Chem.*, **20**, 1195 (1967); R. F. Homer and T. E. Tomlinson, *J. Chem. Soc.*, **1960**, 2498.

14) H. Suzuki, *Bull. Chem. Soc.*, **27**, 597 (1954); H. Suzuki, *ibid.*, **32**, 1340 (1959); H. Suzuki, *ibid.*, **32**, 1350 (1959); H. Suzuki, *ibid.*, **32**, 1357 (1959).

15) The value was determined by plot of absorbances at 340 nm vs. pH.

16) The values were determined by plot of absorbances at 302 and 332 nm vs. pH, respectively.

17) R. H. Linnell and A. Kaczmarczyk, *J. Phys. Chem.*, **65**, 1196 (1961); B. N. Bandyopadhyay and A. Harriman, *J. Chem. Soc., Faraday Trans. 1*, **73**, 663 (1977).

18) E. A. Steck and G. W. Ewing, *J. Am. Chem. Soc.*, **70**, 3397 (1948).

19) J. Catalán, O. Mó, P. Pérez, and M. Yáñez, *J. Am. Chem. Soc.*, **101**, 6520 (1979); J. Catalán and M. Yáñaz, *J. Chem. Soc., Perkin Trans. 2*, **1979**, 1627.

20) P. H. Gore and J. N. Phillips, *Nature*, **163**, 690 (1949); A. R. Osborn, K. Schofield, and L. N. Short, *J. Chem. Soc.*, **1956**, 4191.

21) J. H. Baxendale and P. George, *Nature*, **162**, 777 (1948); F. H. Westheimer and O. T. Benefey, *J. Am. Chem. Soc.*, **78**, 5309 (1956); W. A. E. McBryde, *Can. J. Chem.*, **43**, 3472 (1965).

22) N. Kishii, K. Araki, and S. Shiraishi, *Bull. Chem. Soc. Jpn.*, **57**, 2121 (1984).

23) The poor solubility of protonated **4** both in aqueous and organic solvents renders impossible the direct characterization of **4′** and **4″** by ^{1}H NMR spectra under controlled conditions.

24) M. Wózniak, D. J. Buurman, and H. C. van der Plas, *J. Heterocycl. Chem.*, **22**, 765 (1985).

25) E. Späth and F. Galinovsky, *Ber.*, **69**, 2059 (1936).

26) D. D. Perrin and B. Dempsey, "Buffers for pH and Metal Ion Control," Chapman and Hall, London (1974).

Temperature Distribution in Tubular Solid Oxide Fuel Cell

Kiyoshi KANAMURA,* Shoji YOSHIOKA, and Zen-ichiro TAKEHARA
Department of Industrial Chemistry, Faculty of Engineering, Kyoto University,
Yoshida-Honmachi, Sakyo-ku, Kyoto 606
(Received February 7, 1991)

The temperature distribution in the tubular solid oxide fuel cell (SOFC) was calculated by using a finite element method. In this study, specially, the heat generation and consumption caused by the entropy changes at anode and cathode were taken into account for the calculation of temperature distribution in SOFC. In order to estimate the tendency of temperature distribution, the current distribution and the partial pressure distributions of hydrogen, steam, and oxygen were obtained from the calculation by using the simple mathematical model. From the temperature distribution in the tubular SOFC, it can be seen that the temperature difference is largest in the region of porous cathode material. This indicates that the heat generation from the entropy change of cathode reaction has the significant effect for the temperature distribution in tubular solid oxide fuel cell.

Solid oxide fuel cell (SOFC) has been investigated and developed, because of the high energy conversion efficiency. These researches have been concentrated on the development of the electrode materials, the electrolyte materials, and the construction of the cell.[1] Recently the excellent design of SOFC has been achieved by using Electrochemical Vapor Deposition (EVD).[2] The thin electrolyte was deposited on the conductive oxide cathode which was deposited on the porous calcia stabilized zirconia. The tubular SOFC is suitable for EVD process. In this study, the temperature distribution in the tubular SOFC was calculated by a finite element method in order to offer the fundamental knowledge for the development of the high energy conversion SOFC.

The maximum electric energy generated in SOFC corresponds to ΔG of the hydrogen combustion which is the total reaction in SOFC when oxygen and hydrogen are used. ΔH of this reaction, however, is the total energy which can be utilized in SOFC. The energy of $T\Delta S$ cannot be utilized as an electric energy. Since SOFC is operated at high temperature (around 1273 K), the energy of $T\Delta S$ is lost as a heat which amount is much larger than those from other fuel cells operated at low temperature (around 450 K). Moreover, the energy loss is also caused by both overpotentials of hydrogen and oxygen electrodes and the ohmic loss of the electrolyte. These irreversible factors generate the heat in SOFC. In order to minimize the energy loss caused by the overpotential and ohmic resistance, the thickness of electrolyte has to be decreased and the excellent oxygen and hydrogen electrodes have to be developed. The energy loss caused by the entropy change, however, can not be improved, because of the thermodynamic limiting. From this fact, it can be concluded that the temperature distribution caused by the heat generated or consumed by the entropy change of electrode reactions is more important.

The heat management of SOFC is the most important problem for the construction of the SOFC and the determination of the practical operating conditions. Therefore, the calculation of the temperature distribution was conducted by using a finite element method.

Experimental

Yttria stabilized zirconia was prepared by the sintering of the mixture of Y_2O_3 8 mol% and ZrO_2 92 mol% (Toyo Soda Corp.). Its oxygen ion conductance was measured by using AC impedance method at 1273 K. The entropy changes at oxygen and hydrogen electrodes were determined by the measurement of Seebeck coefficients according to the reference.[3]

The temperature distribution in the tubular SOFC was calculated by using the program for a finite element method.[4] From our calculation, the tendency of the temperature distribution can be obtained. The electrochemical parameters of oxygen and hydrogen electrodes reported in reference[5] were used for the estimation of heat generated from oxygen and hydrogen overpotentials. For the simple calculation, some assumptions were adopted.

Results and Discussion

Heat Generation Factors. The heat is generated by the irreversible processes taking place in SOFC and thermodynamic factors in an electrochemical system. In SOFC, the heat is generated or absorbed by the following factors;

(1) Overpotentials of hydrogen and oxygen electrodes.

(2) Ohmic resistance of yttria stabilized zirconia.

(3) Entropy changes at hydrogen and oxygen electrodes.

The overpotentials of hydrogen and oxygen electrodes are dependent on the current. The relationships between the overpotentials and the current for oxygen and hydrogen electrodes have been examined and suggested by many researchers.[5–7] The electrochemical parameters depend on the kind of electrode. In this study, the model cell is constructed by $LaCoO_3$ as a cathode, Ni cermet as an anode, yttria stabilized zirconia as an electrolyte and porous yttria stabilized zirconia as a support. The following equations were adopted in the calculation of the heat generation caused by the

Table 1. Electrochemical Parameters Used in the Calculation of the Current Distribution

Electrochemical parameters	
I_0	9.8 A m^{-2}
K	0.0609 V[a)]
σ[b)]	0.1 S cm^{-1}

a) $K=RT/4\alpha F$ from Ref. 5, α: transfer coefficient, R: gas constant, F: Faraday constant. b) $R=(1/\sigma)(L/S)$; L: thickness of YSZ of element, S: surface area of YSZ of element.

overpotentials in order to simplify the calculation. Table 1 shows the electrochemical parameters which have been suggested in the reference.[5)]

For hydrogen electrode

$$\eta_a = K \ln\left(\frac{I}{I_0}\right) \tag{1}$$

For oxygen electrode

$$\eta_c = 0 \tag{2}$$

where η_a and η_c are overpotentials of anode and cathode, respectively, I_0 is exchange current, I is current, and K is the constant listed in Table 1. The heat generation from the ohmic resistance of yttria stabilized zirconia is also dependent on the current. The relationship between the voltage loss in the electrolyte (ΔV) and the current (I) obeys Ohm's law.

$$\Delta V = IR \tag{3}$$

where R is the resistance of the electrolyte in the tubular SOFC, which is estimated from the conductivity of yttria stabilized zirconia (YSZ). The conductivity of YSZ can be measured by using the impedance method.[8)]

The heat generation caused by the entropy change becomes larger with increasing temperature. The heat caused by the entropy changes at hydrogen and oxygen electrodes has to be taken into account for the calculation of the temperature distribution. The total reaction in SOFC is the hydrogen combustion. The total entropy change (ΔS) is easily estimated from the thermodynamic consideration. The total reaction, however, is separated to cathode and anode reactions in an electrochemical cell. The entropy change is also separated to cathode and anode reactions. In other words, an entropy change of single electrode ($\Delta S_{cathode}$ for the entropy change of cathode reaction, ΔS_{anode} for the entropy change of anode reaction) have to be estimated.

$$\Delta S = \Delta S_{cathode} + \Delta S_{anode} \tag{4}$$

The entropy changes of cathode and anode can be estimated from Seebeck coefficients of oxygen and hydrogen electrodes, as reported in reference.[3)] The entropy change of oxygen electrode reaction was estimated to be -81.6 J K^{-1} mol^{-1} per two electrons under 0.21×10^5 Pa oxygen partial pressure at 1273 K. From Eq. 4, the entropy change of hydrogen electrode can be calculated. These values are dependent on the partial pressure. The dependence can be represented by the following equations.

Total reaction

$$H_2 + \frac{1}{2} O_2 \rightarrow H_2O \tag{5}$$

For hydrogen electrode,

$$\Delta S_{anode} = (S_{H_2O} - R\int_1^{P_{H_2O}} d\ln P) - (S_{H_2} - R\int_1^{P_{H_2}} d\ln P) - S_{O^{2-}}{}^* \tag{6}$$

For oxygen electrode,

$$\Delta S_{cathode} = S_{O^{2-}}{}^* - \frac{1}{2}(S_{O_2} - R\int_1^{P_{H_2O}} d\ln P) \tag{7}$$

where $S_{O^{2-}}{}^*$ is the transported entropy of O^{2-} ion in yttria stabilized zirconia. The entropy changes of hydrogen and oxygen electrodes under various partial pressures can be calculated from Eqs. 6 and 7. $\Delta S_{cathode}$ changes with the partial pressure of oxygen and ΔS_{anode} changes with the partial pressures of hydrogen and steam in SOFC. Therefore, the partial pressure distribution has to be estimated in order to calculate the temperature distribution in the tubular SOFC. The entropy change of single electrode reaction is represented by the function of temperature. In this study, however, it was assumed that the dependence of entropy change on temperature in narrow temperature region was too small to influence the temperature distribution.

Calculation of Current and Partial Pressure Distributions. The current and partial pressure distribution in solid oxide fuel cell have been reported in some references.[9,10)] In this study, the current distribution was calculated by using the model, as shown in Fig. 1. This is the typical tubular SOFC which has metal oxide

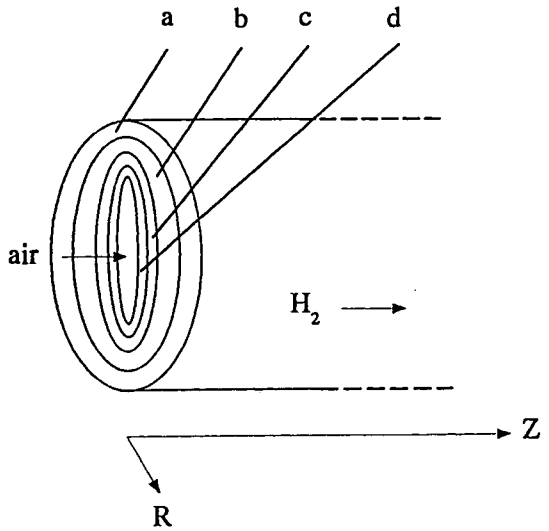

Fig. 1. Schematic illustration of tubular SOFC constructed by electrolyte (yttria stabilized zirconia), anode (Ni zirconia cermet electrode), cathode ($LaCoO_3$), and porous zirconia substrate.

cathode, Ni–ZrO_2 cermet anode, yttria stabilized zirconia electrolyte, and porous yttria stabilized zirconia support. Hydrogen is flown through the outside of cell and oxygen through the inside of cell. The dimension of the cell is summarized in Table 2. In order to calculate the current distribution in this SOFC, the cell is divided to n elements, as shown in Fig. 2. The simple mathematical procedure was used for the calculation of the current and partial pressure distributions in the tubular SOFC. The equivalent circuit for this model is shown in Fig. 3. The current passed through each element is represented by I_i. R_i indicates the resistance of yttria stabilized zirconia electrolyte in i th element. Z_i is the sum of both impedances of oxygen and hydrogen electrodes. The total current (I) is given by the sum of each elementary current (I_i).

$$I = I_1 + I_2 + \cdots + I_i + \cdots + I_n \tag{8}$$

If both electrodes have high electric conductivity, the cell voltage of each element is equal to the cell voltage (V).

$$V = V_1 = V_2 = \cdots = V_i = \cdots = V_n \tag{9}$$

Table 2. Dimension of the Tubular SOFC

Length (L)	20 cm
Diameter inside	10 mm
outside (D)	17 mm
Thickness of cathode	0.5 mm
Thickness of anode	0.5 mm
Thickness of electrolyte	0.5 mm
Thickness of porous substrate	2 mm

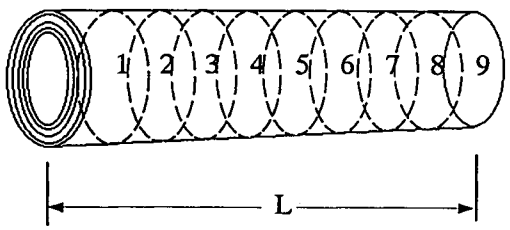

Fig. 2. Model for calculation of current and partial pressure distribution.

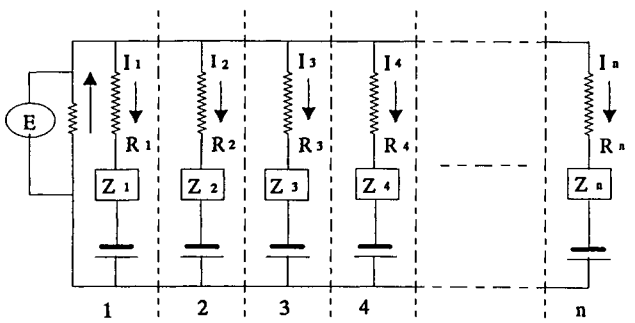

Fig. 3. Equivalent circuit for the model in Fig.2.

For element 1, the relationship between V_1 and I_1 is represented by the following equation,

$$V_1 = E_e - \eta_1 - R_1 I_1 \tag{10}$$

where η_1 is the total overpotential of element 1 and is given by the Eqs. 1, 2, and 11. η_i is given by the sum of both overpotentials of hydrogen and oxygen electrodes.

$$\eta_i = \eta_{ia} + \eta_{ic} \tag{11}$$

where η_{ia} and η_{ic} are the overpotential of hydrogen electrode of element i and that of oxygen electrode of element i, respectively. E_e is the equilibrium voltage of solid oxide fuel cell and is determined from the partial pressures of hydrogen, steam, and oxygen according to Nernst equation.

$$E_e = E_0 - (RT/2F)\ln(P_{H_2O}/P_{O_2}^{1/2} P_{H_2}) \tag{12}$$

For the other elements, the same relationship can be established. The hydrogen and oxygen flow horizontally through the chambers in the cell at constant rate. The partial pressures of oxygen and hydrogen at the entrance of chamber are higher than those at the exit, because oxygen and hydrogen are consumed by the electrode reactions at each element. The partial pressure of steam at the entrance of fuel chamber is lower than that at the exit. The hydrogen partial pressure in element 2 is given by the following equation,

$$P_{H_2,2} = \frac{U_{H_2,1} - \dfrac{I_1}{2F}}{\left(U_{H_2,1} - \dfrac{I_1}{2F}\right) + \left(U_{H_2O,1} + \dfrac{I_1}{2F}\right)} \tag{13}$$

The air and steam partial pressures are given by the similar equations.

$$P_{air,2} = \frac{0.21\,U_{air,1} - \dfrac{I_1}{4F}}{U_{air,1} - \dfrac{I_1}{4F}} \tag{14}$$

$$P_{H_2O,2} = \frac{U_{H_2O,1} + \dfrac{I_1}{2F}}{\left(U_{H_2O,1} + \dfrac{I_1}{2F}\right) + \left(U_{H_2,1} - \dfrac{I_1}{2F}\right)} \tag{15}$$

where $U_{i,1}$ is the flow rate of gas i at the entrance of SOFC (mol s^{-1}). In this way, the partial pressure in element 2 can be obtained. As a result, E_e can be also determined. The elementary current in element 2, I_2, can be calculated from E_e and V by using Eq. 10. Such a procedure is repeated n times. Finally, the current distribution and the partial pressure distribution can be calculated.

Figure 4 shows the equilibrium voltage and the total overpotential distributions along Z-axis in the tubular SOFC calculated from above simple mathematical model, where the total current and gas flow rate are

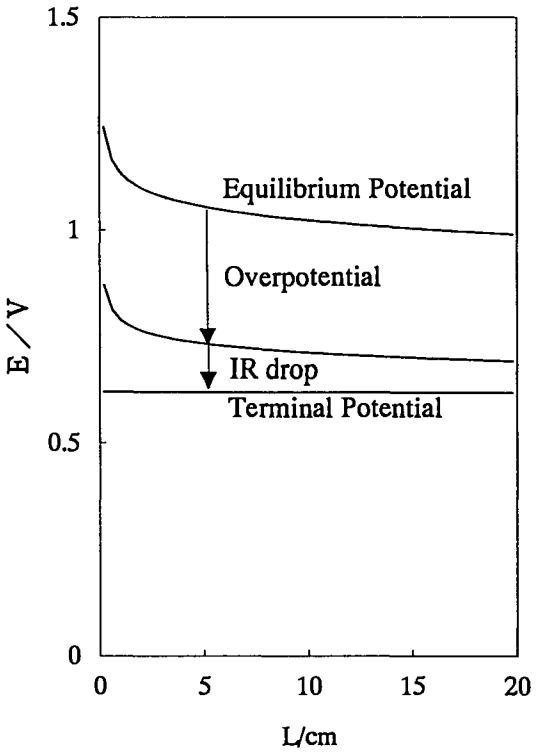

Fig. 4. Distributions of the equilibrium potential and IR drop in the tubular SOFC, discharge current: 200 mA cm^{-2}, flow rate: 5 cm s^{-1}.

assumed to be 200 mA cm^{-2} and 5 cm s^{-1}, respectively. The utilization of hydrogen depends on the flow rate. The flow rate was assumed to be 5 cm s^{-1}, in order to obtain the fuel utilization to be about 10%. These distributions result in the current distribution in the tubular SOFC.

Figure 5 shows the current distribution in SOFC at two flow rates of hydrogen. The average current density is 200 mA cm^{-2}. The partial current near the entrance of SOFC is larger than that near the exit according to the potential distribution in Fig. 4. The current distribution depends on the flow rate and become larger with decreasing of the flow rate. The heat generation caused by the ohmic resistance of electrolyte is seemed to be much larger at the entrance of cell compared with the heat generation at the exit, as expected from the relationship between the heat generation at the electrolyte and the current.

Figure 6 shows the partial pressure distributions of oxygen, hydrogen, and steam in SOFC at 5 cm s^{-1} (0.0376 mol s^{-1}) flow rate. The hydrogen partial pressure gradually decreases along the Z axis from the entrance to the exit. Under these conditions, 10% of hydrogen induced in SOFC is consumed by the electrode reaction. The oxygen partial pressure also decreases. The partial pressure distribution of hydrogen is larger than that of oxygen, because 4 electron per 1 mole oxygen is consumed at the oxygen electrode and 2 electron per 1 mole hydrogen is consumed at the

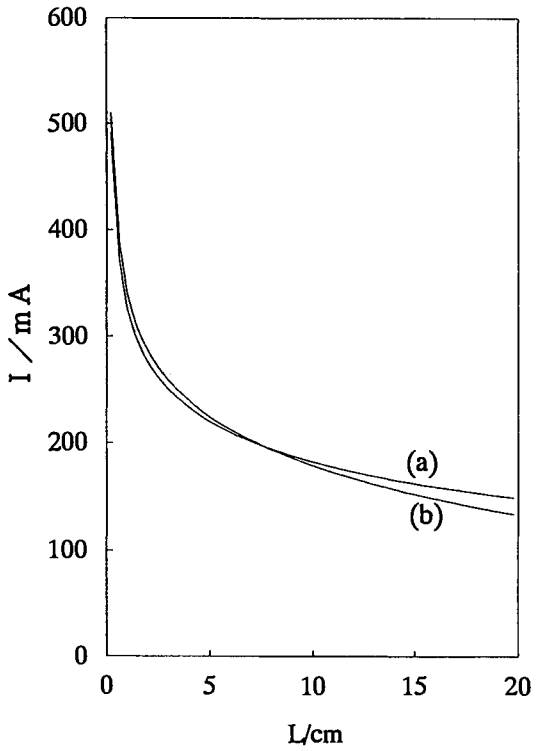

Fig. 5. Current distribution in the tubular SOFC, discharge current: 200 mA cm^{-2}, flow rate: 5 cm s^{-1} (a) and 20 cm s^{-1} (b).

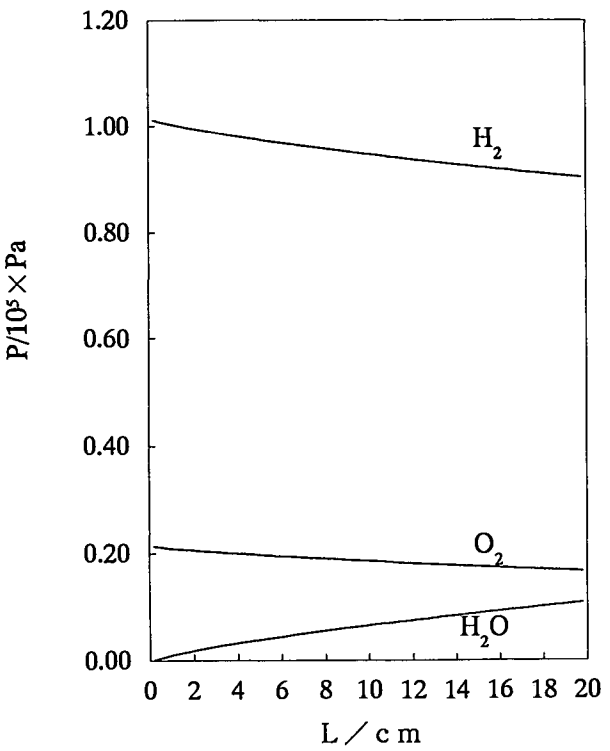

Fig. 6. Partial pressure distributions in the tubular SOFC, discharge current; 200 mA cm^{-2}, flow rate; 5 cm s^{-1}.

hydrogen electrode. The partial pressure distributions of hydrogen and steam are larger than that of oxygen. The heat caused by the entropy change of oxygen and hydrogen electrodes can be estimated from the partial pressure distributions of gasses according to Eqs. 13, 14, and 15.

In this way, the partial pressure distributions of hydrogen, oxygen, and steam and the current distribution in SOFC were obtained. From these results, the heat generation at each element can be estimated. The temperature distribution in SOFC can be calculated by using a finite element method.

Temperature Distribution in Tubular SOFC. Figure 7 shows the model of the tubular SOFC and the initial and boundary conditions for the calculation of a finite element method. The gas temperature was assumed to be 1273 K to simplify the calculation. The temperature distribution at steady state was estimated in this study. The heat conductivities of yttria stabilized zirconia, porous yttria stabilized zirconia support, $LaCoO_3$, and Ni cermet are summarized in Table 3. At the interface between the oxygen chamber and the porous yttria stabilized zirconia, the thermal boundary is assumed. The heat transfer coefficients of the thermal boundary between air and yttria stabilized zirconia support (h_{in}) can be written by

$$h_{in} = Nu\ \kappa / D \tag{16}$$

where Nu (Nusselt constant) is calculated from physicochemical properties of air by using the following equations.

$$Nu = 2.43\ (Re\ Pr\ D/L)^{1/3} \tag{17}$$

$$Pr = C_p\ \mu / \kappa \tag{18}$$

$$Re = Du\ \rho / \mu \tag{19}$$

ρ is the density of gas, μ the viscosity of gas, C_p the heat capacity of gas, κ the heat conductivity, u the flow rate of gas, D the diameter of the cell, L the length of the cell, Pr Prandtl constant, and Re Reynolds number. These parameters are summarized in Table 2 and 4. On the other hand, the heat transfer coefficient of thermal boundary between hydrogen chamber and anode (h_{out}) can be given by the following equation

$$h_{out} = 0.664\ (\kappa / L)\ Re^{1/2}\ Pr^{1/3} \tag{20}$$

In this way, the heat transfer coefficients at the interfaces are easily calculated from these equations. The heat generation at oxygen electrode can be estimated by

$$\frac{dQ}{dt} = IT\Delta S_c + I\eta_c \tag{21}$$

and at hydrogen electrode

$$\frac{dQ}{dt} = IT\Delta S_a + I\eta_a \tag{22}$$

The heat generation from electrolyte is given by

$$\frac{dQ}{dt} = I^2R \tag{23}$$

The hydrogen and oxygen flows along Z-axis from the entrance to the exit. The hydrogen electrode is made from nickel cermet and its thickness is 500 μm. The oxygen electrode is made from $LaCoO_3$ and its thickness is 500 μm. The electrolyte is the yttria stabilized zirconia and its thickness is 500 μm. The thickness of each element is related to the mechanical strength of the cell. The thick element gives the high reliability of the cell. In this study, the thickness of each element was assumed from the point of view of the stability of the cell.

Thus, all parameters used in the calculation of the temperature distribution in the tubular SOFC can be estimated. The calculation by using a finite element method was carried out. Figure 8 shows the temperature distribution in the electrolyte along Z-axis. The temperature at the entrance is lower than that at the exit. From the current distribution, it is expected that the heat energy generated at the entrance is larger than

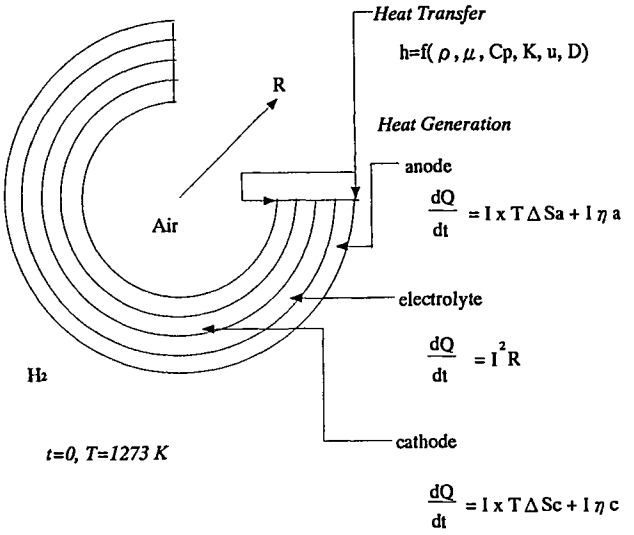

Fig. 7. Model for calculation of temperature distribution and initial and boundary conditions.

Table 3. Heat Conductivities of the Materials in SOFC

Material	κ/J cm^{-1} s^{-1} K^{-1}
YSZ	0.027
Porous YSZ	0.011
$LaCoO_3$	0.022
Ni cermet	0.11

Table 4. Physical Parameters of Hydrogen and Air at 1273 K

	ρ/g cm^{-3}	μ/g cm^{-1} s^{-1}	C_p/J g^{-1} K^{-1}	κ/J cm^{-1} s^{-1} K^{-1}
Air	0.276	6×10^{-5}	1.1×10^{3}	0.2
H_2	0.019	3×10^{-5}	1.4×10^{4}	0.1

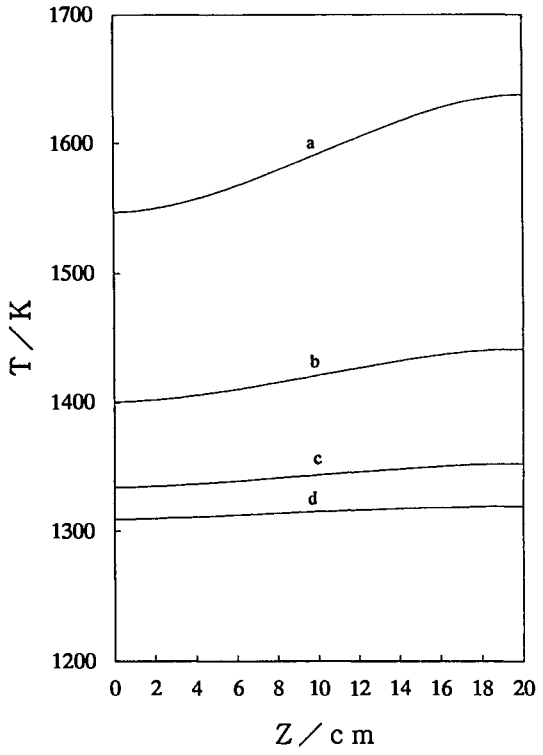

Fig. 8. Temperature distribution in YSZ along Z-axis at a: 5 cm s^{-1}, b: 10 cm s^{-1}, c: 20 cm s^{-1}, and d: 30 cm s^{-1}.

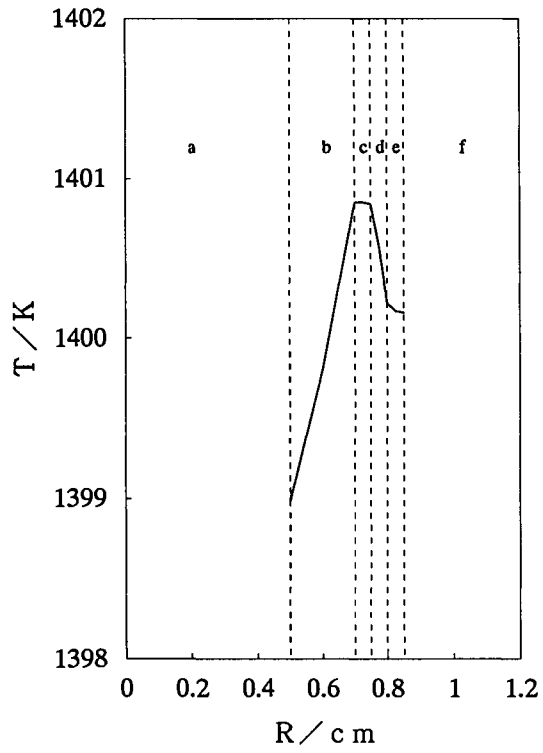

Fig. 9. Temperature distribution along R-axis near the entrance of the tubular SOFC at 10 cm s^{-1}, a: air chamber, b: porous substrate, c: cathode, d: electrolyte, e: anode, f: fuel chamber.

that at the exit. The temperature distribution in Fig. 8, however, is inconsistent with such an expectation. This fact indicates that the heat generated near the entrance of SOFC is transported to hydrogen gas and oxygen gas. At the exit of the tubular SOFC, the heat is transported form hydrogen gas and oxygen gas to the electrolyte during the initial period of the discharge. Therefore the temperature in electrolyte near the exit is higher than that at the entrance. The temperature distribution in SOFC strongly depends on the flow rate. The uniform temperature distribution can be obtained at 30 cm s^{-1} flow rate. The utilization of fuel, however, decreased with increasing of flow rate.

Figure 9 shows the temperature distribution along R-axis near the entrance of SOFC. The highest temperature is observed at the electrolyte region. The temperatures at porous yttria stabilized zirconia and the nickel cermet electrode are lower than that at the electrolyte. The heat is transported from the electrolyte to hydrogen and oxygen gasses. The temperature gradient is largest at the electrolyte region. This result indicates that the thermal stress at the electrolyte region is the most important factor for the decomposition of SOFC. The heat absorbed by hydrogen gas is comparable to that by oxygen gas. The half of heat energy generated in SOFC is transported to the hydrogen gas chamber near the entrance region of the tubular SOFC.

Conclusion

The simulation of the temperature distribution in solid oxide fuel cell was demonstrated. The heat energy produced by the entropy change of electrode reactions was taken into account for the calculation. The calculation under various conditions will give the guideline for the design of solid oxide fuel cell. For the calculation of the temperature distribution in solid oxide fuel cell, the heat produced from the entropy change of electrode reaction will become larger than those by overpotentials and ohmic resistances with the development of the excellent materials and processes.

In this study, the dependencies of thermal and electrochemical parameters on temperature were not taken into account for the calculation of the temperature distribution. However, the deviation from the true temperature distribution in the model cell, which cannot be measured, may not be significant, because the dependencies of parameters on temperature may be negligible small for the temperature distribution in SOFC. The tendency of the temperature distribution calculated in this study might be similar to that of true temperature distribution in the model cell. The calculation under various conditions will provide the useful information for the selection of materials and the construction of SOFC.

This work was supported by the Grant-in-Aid for Scientific Research No. 62603016 from the Ministry of

Education, Science and Culture.

Kyoto University assisted in meeting the publication costs of this article.

References

1) H. S. Isaacs and L. J. Olmer, *J. Electrochem. Soc.*, **129**, 436 (1982).

2) W. Feduska and A. D. Isenberg, *J. Power Sources*, **10**, 89 (1983).

3) Z. Takehara, K. Kanamura, and S. Yoshioka, *J. Electrochem. Soc.*, **136**, 2506 (1989).

4) M. Simoseki and H. Fujinuma, "PC-9801 Finite Element Method/Thermal Stress under Non-Steady State Programing," Nikkan Kogyo Sinbunsha, Tokyo (1989).

5) N. J. Maskalick and D. K. Mclain, *J. Electrochem. Soc.*, **135**, 6 (1988).

6) N. Nakagawa and M. Ishida, *Ind. Eng. Chem. Res.*, **127**, 1181 (1988).

7) E. J. L. Schouler and H. S. Isaacs, *Solid State Ionics*, **5**, 555 (1981).

8) A. E. McHale and H. L. Tuller, *Solid State Ionics*, **5**, 515 (1981).

9) G. Wilemski, *J. Electrochem. Soc.*, **130**, 117 (1983).

10) A. Hirano, S. Nakamura, M. Ippommatsu, and K. Ishimaru, *Denki Kagaku*, **58**, 842 (1990).

Syntheses, Crystal Structures, and Antitumor Activities of Dinuclear Platinum(II) Complexes, Di-μ-sulfoacetato-bis[(diamine)platinum(II)] Trihydrate

T. Ken MIYAMOTO* and Hikaru ICHIDA
Department of Chemistry, Faculty of Science, The University of Tokyo, Hongo, Bunkyo-ku, Tokyo 113
(Received December 15, 1990)

A series of new dinuclear platinum(II) complexes have been prepared from the reaction of $[PtL_2(OH)_2]$ with sulfoacetic acid: $[PtL_2(slac)]_2 \cdot 3H_2O$, where slac=sulfoacetate dianion; L_2=1,2-diaminocyclohexane (**1a**—**1c**) or 1,2-diaminoethane (**2**) and L=isopropylamine (**3**) or ammine (**4**). They have di-μ-carboxylato bridged dinuclear zwitterionic structures in crystals. Among them, complexes (**1a**—**1c**) show significant antitumor activities against mice ieukemia L1210.

Since the discovery of broad-spectrum activities of *cis*-dichlorodiammineplatinum(II) (trade name *cis-platin*), a large number of platinum complexes have been synthesized as antitumor agents. Among them there are promising compounds such as (1,2-diaminocyclohexane)platinum(II) derivatives.[1] Many of these compounds are, however, mononuclear complexes; few oligonuclear platinum complexes have shown antitumor activity.[2]

In recent years, the formation of hydroxo-bridged di-,[3] or tri-nuclear[4] complexes has been reported in the hydrolysis reaction of *cis-platin*. Other platinum oligomers, such as "platinum blue",[5] have also received much attention. These studies emphasized a structural diversity of oligonuclear species in the platinum chemistry; antitumor activities have not been reported concerning these oligomers, except a few examples.

We describe here the syntheses, crystal structures, and antitumor activities of a series of new dinuclear platinum complexes, di-μ-sulfoacetato-bis[(diamine)-platinum(II)] trihydrate, $[Pt(diamine)(slac)]_2 \cdot 3H_2O$. Preliminary accounts of the synthesis and structural work have appeared.[6,7]

Experimental

The Three Isomers of Di-μ-sulfoacetato-bis[(1,2-diamino-cyclohexane)platinum(II)], Compounds 1a—c. The compounds were synthesized by modified methods from those described in a previous publication.[8] Dinitrato[(1*R*,2*R*)-1,2-diaminocyclohexane]platinum(II), [Pt(*RR*-dach)$(NO_3)_2$] (4.30 g, 10 mmol), was dissolved in water (100 cm^3) with heating. The solution was passed through a column packed with an anion-exchange resin (Diaion SA10AOH); and additional amount of water was then passed through the column. To the combined eluate, 1.40 g of sulfoacetic acid (10 mmol) was dissolved. The reaction mixture was evaporated to ca. 30 ml

Table 1. Crystallographic Data for $[Pt(diamine)(slac)]_2 \cdot 3H_2O$

Compound	[Pt(*RR*-dach)(slac)]$_2 \cdot 3H_2O$(**1a**)	[Pt(en)(slac)]$_2 \cdot 3H_2O$(**2**)	[Pt(ipr)$_2$(slac)]$_2 \cdot 3H_2O$(**3**)
T/K	298	298	298
Formula	$Pt_2S_2O_{13}N_4C_{16}H_{38}$	$Pt_2S_2O_{13}N_4C_8H_{18}$	$Pt_2S_2O_{12}N_4C_{16}H_{22}$
Fw	948.80	832.55	916.67
Crystal system	Orthorhombic	Triclinic	Orthorhombic
Space group	$P2_12_12_1$	$P\bar{1}$	$Pbcn$
Lattice parameters/Å	a=19.186(4)	a=10.392(2)	a=18.21(3)
	b=14.577(2)	b=12.363(2)	b=17.790(4)
	c=9.876(1)	c=9.521(2)	c=19.281(2)
		α=105.56(1)°	
		β=113.08(1)°	
		γ=92.351(1)°	
V/Å^3	2762(1)	1069.1(3)	6246(1)
Z	4	2	8
D_x/g cm^{-3}	2.28	2.589	1.95
D_m/g cm^{-3}	2.25	2.59	1.96
Range of transmittance (for Absorption correction)		0.75—1.00	0.50—2.24
F(000)	1816	772	3440
μ/cm^{-1}(Mo $K\alpha$)	108.59	134.59	92.23
$(\Delta\sigma)_{max}$	0.63	0.00	0.69
$(\Delta\rho)_{max}$/eÅ^{-3}	0.88	5.47	2.92
No. Ref. Measured	3261	6590	7800
No. Ref. Observation	2455	3161	1905
R	0.033	0.042	0.078
R_w	0.031	0.045	0.081

Table 2. Positional Parameters and B(eq) for **2**

Atom	x	y	z	B(eq)	Atom	x	y	z	B(eq)
Pt(1)	0.06213(07)	0.13347(06)	0.02400(08)	1.81(2)	C(1)	−0.1765(16)	0.1927(13)	−0.2252(18)	1.7(5)
Pt(2)	0.05529(07)	0.37809(05)	0.01573(08)	1.72(2)	C(2)	−0.3101(19)	0.1476(14)	−0.3774(21)	2.5(6)
S(1)	−0.2802(05)	0.0350(04)	−0.5207(05)	2.4(1)	C(3)	−0.0453(17)	0.2953(13)	0.2273(18)	1.8(5)
S(2)	−0.2474(05)	0.3870(05)	0.3274(06)	3.1(2)	C(4)	−0.0959(19)	0.3203(14)	0.3585(24)	2.8(6)
O(1)	−0.1371(12)	0.1237(10)	−0.1467(14)	2.9(5)	C(5)	0.2612(24)	0.0133(20)	−0.0638(27)	5(1)
O(2)	−0.1195(11)	0.2918(09)	−0.1923(13)	2.2(4)	C(6)	0.3460(22)	0.0922(22)	0.0931(30)	5(1)
O(3)	−0.0005(13)	0.2053(10)	0.2011(14)	2.8(5)	C(7)	0.3163(19)	0.4330(15)	−0.0013(23)	3.1(7)
O(4)	−0.0468(12)	0.3712(10)	0.1630(13)	2.5(4)	C(8)	0.3276(20)	0.5177(17)	0.1472(24)	3.8(7)
O(5)	−0.4151(13)	−0.0022(11)	−0.6598(14)	3.9(5)	H(1)	−0.3389	0.2078	−0.4222	3.1
O(6)	−0.2353(14)	−0.0526(10)	−0.4465(15)	3.7(5)	H(2)	−0.3833	0.1193	−0.3539	3.1
O(7)	−0.1689(13)	0.0836(11)	−0.5520(15)	3.8(5)	H(3)	−0.0197	0.3691	0.4542	4.3
O(8)	−0.2863(13)	0.3843(11)	0.4583(15)	3.5(5)	H(4)	−0.1155	0.2506	0.3761	4.3
O(9)	−0.1969(16)	0.5042(13)	0.3411(19)	5.3(7)	H(5)	0.2432	−0.0591	−0.0532	6.8
O(10)	−0.3524(14)	0.3190(16)	0.1735(17)	6.8(7)	H(6)	0.3126	0.0090	−0.1278	6.8
O(11)	−0.1042(13)	0.8157(10)	0.3597(15)	3.2(5)	H(7)	0.3868	0.1575	0.0822	7.4
O(12)	0.4239(14)	0.3471(12)	0.3847(16)	4.3(6)	H(8)	0.4188	0.0562	0.1508	7.4
O(13)	0.3450(15)	0.3220(12)	0.6042(19)	5.2(6)	H(9)	0.3541	0.3680	0.0221	4.3
N(1)	0.1258(15)	0.0477(12)	−0.1442(17)	2.7(5)	H(10)	0.3669	0.4653	−0.0485	4.3
N(2)	0.2567(14)	0.1273(12)	0.1848(15)	2.4(5)	H(11)	0.2995	0.5855	0.1255	4.7
N(3)	0.1620(15)	0.3980(12)	−0.1172(17)	2.6(5)	H(12)	0.4232	0.5337	0.2256	4.7
N(4)	0.2318(14)	0.4693(12)	0.2101(16)	2.5(5)					

Table 3. Positional Parameters and B(eq) for **3**

Atom	x	y	z	B(eq)	Atom	x	y	z	B(eq)
Pt(1)	0.1827(1)	0.15906(7)	0.54245(6)	2.92(7)	N(3)	0.379(2)	0.174(2)	0.445(1)	4(2)
Pt(2)	0.3382(1)	0.21216(8)	0.53382(6)	3.45(7)	N(4)	0.388(2)	0.133(2)	0.588(1)	5(2)
S(1)	0.177(1)	0.4423(6)	0.4920(6)	5.5(7)	C(1)	0.212(2)	0.295(2)	0.467(2)	2.2(6)
S(2)	0.257(1)	0.282(1)	0.7873(6)	7.2(9)	C(2)	0.195(2)	0.368(2)	0.429(1)	2.6(7)
O(1)	0.171(2)	0.251(1)	0.482(1)	4(1)	C(3)	0.240(3)	0.262(2)	0.648(2)	2.4(7)
O(2)	0.188(2)	0.225(2)	0.627(1)	6(2)	C(4)	0.220(2)	0.316(2)	0.709(1)	2.9(7)
O(3)	0.283(2)	0.296(1)	0.479(1)	4(1)	C(5)	0.115(5)	0.059(4)	0.441(3)	10(2)
O(4)	0.304(2)	0.257(2)	0.624(1)	5(1)	C(6)	0.120(4)	0.008(3)	0.365(3)	10(2)
O(5)	0.118(3)	0.420(2)	0.532(2)	10(3)	C(7)	0.054(5)	0.099(4)	0.438(4)	13(2)
O(6)	0.245(3)	0.454(2)	0.526(2)	12(3)	C(8)	0.117(3)	0.040(2)	0.638(2)	4.0(9)
O(7)	0.161(2)	0.507(2)	0.448(2)	9(2)	C(9)	0.131(3)	−0.035(3)	0.669(2)	6(1)
O(8)	0.240(2)	0.333(2)	0.838(1)	7(2)	C(10)	0.094(3)	0.092(2)	0.691(2)	6(1)
O(9)	0.227(4)	0.212(2)	0.800(2)	14(4)	C(11)	0.460(4)	0.193(4)	0.426(3)	11(2)
O(10)	0.326(4)	0.264(4)	0.781(2)	20(6)	C(12)	0.459(4)	0.276(4)	0.417(3)	12(2)
O(11)	0.678(2)	0.020(1)	0.196(2)	9(2)	C(13)	0.479(3)	0.162(3)	0.353(3)	8(1)
O(12)	0.301(2)	0.095(2)	0.713(1)	5(1)	C(14)	0.468(4)	0.145(4)	0.608(3)	10(2)
N(1)	0.182(2)	0.100(2)	0.455(1)	5(2)	C(15)	0.478(4)	0.211(4)	0.646(3)	12(2)
N(2)	0.188(2)	0.068(2)	0.605(1)	3(1)	C(16)	0.483(4)	0.071(3)	0.653(3)	11(2)

at ca. 60 °C under reduced pressures to give the precipitate of the product, [Pt(*RR*-dach)(slac)]$_2\cdot 3H_2O$ (**1a**). Yield: 3.2 g (3.4 mmol, 67%). A crystal suitable for X-ray crystal analysis was obtained by recrystallization from water as a pale-yellow plate. In a similar manner, two other isomers of di-μ-sulfoacetato-bis[(1,2-diaminocyclohexane)platinum(II)] were synthesized. Found: **1a**: C, 20.05; H, 3.93; N, 5.99; S, 6.76%; **1b**: C, 20.04; H, 4.02; N, 5.97; S, 6.57%; **1c**: C, 20.42; H, 3.94; N, 5.84; S, 6.76%. Calcd for $C_{16}H_{38}N_4O_{13}S_2Pt_2$: C, 20.25, H, 4.04; N, 5.91; S, 6.76%.

Di-μ-sulfoacetato-bis[(1,2-diaminoethane)platinum(II)][Pt(en)(slac)]$_2\cdot 3H_2O$, Compound 2: In a similar way, the title complex was prepared from a 12.0 g (31.6 mmol) portion of dinitrato(1,2-diaminoethane)platinum(II) and 4.5 g (32.1 mmol) of sulfoacetic acid. Yield: 9.0 g (10.7 mmol, 68%). Found: C, 11.13; H, 2.95; N, 6.52; S, 7.28%. Calcd for $C_8H_{26}N_4O_{13}S_2Pt_2$: C, 11.43; H, 3.12; N, 6.67; S, 7.63%. The sample for X-ray crystallography was recrystallized from water as a yellow needle.

Di-μ-sulfoacetato-bis[bis(isopropylamine)platinum(II)][Pt(ipr)$_2$(slac)]$_2\cdot 3H_2O$, Compounds 3: This complex was similarly prepared as a pale yellow powder. Found: C, 19.89; H, 4.72; N, 5.83; S, 6.53%. Calcd for $C_{16}H_{46}N_4O_{13}S_2Pt_2$; C, 20.08; H, 4.85; N, 5.86; S, 6.70%. A crystal for X-ray crystallographic analysis was obtained as a orange-yellow plate by leaving the aqueous solution in a desiccator (desiccant: $CaCl_2$) for 2 months.

Di-μ-sulfoacetato-bis[diammineplatinum(II)][Pt(NH$_3$)$_2$(slac)]$_2\cdot 3H_2O$, Compound 4: A white crystalline solid containing a small amount of green material was obtained. A green impurity could not be removed by recrystallization. Found: C, 5.87; H, 2.77; N, 7.10; S, 7.56%. Calcd for $C_4H_{22}N_4O_{13}S_2Pt_2$: C, 6.09; H, 2.81; N, 7.11; S, 8.13%.

Solubility Test. Solubility (mg cm^{-3}) in H_2O at 26 °C: **1a**:

5; **1b**: 5; **1c**: 50; **2**: 18.

X-Ray Diffraction Measurements and Structure Determination. Among a series of new complexes, three compounds, $[Pt(RR\text{-dach})(slac)]_2 \cdot 3H_2O$ (**1a**), $[Pt(en)(slac)]_2 \cdot 3H_2O$ (**2**), and $[Pt(ipr)_2(slac)]_2 \cdot 3H_2O$ (**3**), were applied to X-ray crystal structure analysis.

The X-ray diffraction intensities were collected on a Rigaku AFC-5R goniometer with graphite-monochromatized Mo $K\alpha$ (λ=0.71069 Å) radiation (40 kV, 120 mA). Details of the X-ray structure analysis on $[Pt(RR\text{-dach})(slac)]_2 \cdot 3H_2O$ were described in a previous report.[7] Crystallographic data are summarized in Table 1 and positional parameters and B(eq) for **2** or **3** are given in Table 2 or 3, respectively. The complete F_o-F_c data are deposited as document No. 9114 at the Office of the Editor of Bull. Chem. Soc. Jpn.

Antitumor Assay in vivo. A preliminary animal test against mice leukemia L1210 was carried out at The Cancer Chemotherapy Center, J. C. R., through the courtesy of Dr. Tazuko TASHIRO. There, 10^5 cells/mouse were transplanted i.p. into CDF_1 mice (6 mice/group), and the samples administered i.p. on days 1,5, and 9. From the mean survival times of treated (T) and control (C) mice, the T/C values were calculated as indicators of activity. Compounds **3** and **4** were not suitable for the animal test because of their instability in saline solution. Thus, comounds **1a**—**c** and **2** were subjected to the primary screening.

Results and Discussion

Syntheses. A series of complexes were synthesized by a neutralization reaction of dihydroxoplatinum(II) complexes with the equivalent mole of sulfoacetic acid (Scheme 1). Compounds **1a**—**c** and **2** were recrystallized from hot water. However, an attempt to recrystallize **3** from a hot aqueous solution led to an immediate decomposition, precipitating a black solid. The

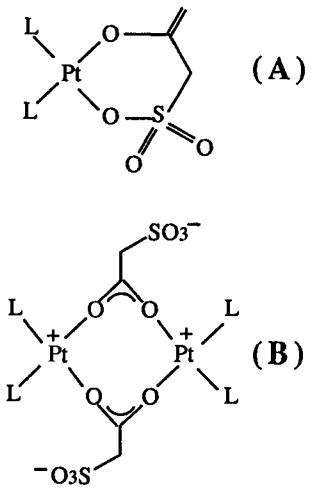

Fig. 1. Possible species of Pt(diamine)(slac); (A) Monomer, (B): Dimer.

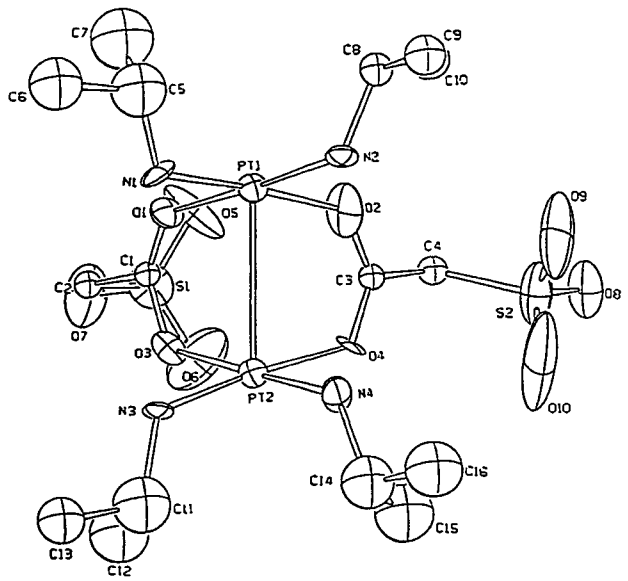

Fig. 3. Molecular structure of **3**.

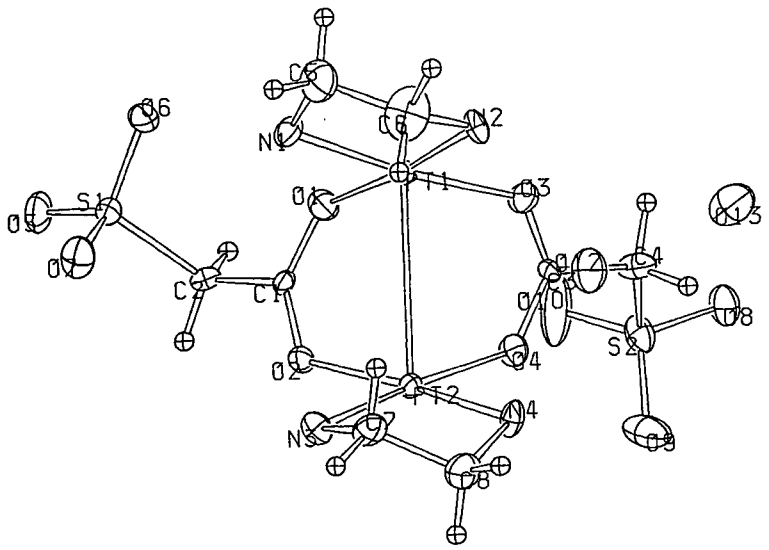

Fig. 2. Molecular structure of **2**.

$$cis\text{-}[PtL_2(NO_3)_2] \xrightarrow[\text{exchange}]{\text{anion}} \{cis\text{-}[PtL_2(OH)_2]\} \xrightarrow[\text{acid}]{\text{sulfoacetic}} [PtL_2(slac)_2]_2 \cdot 3H_2O$$

Scheme 1. Synthetic procedure to dinuclear sulfoacetatoplatinum(II).

crystalline product **3** was, therefore, prepared by long standing of a dilute solution at room temperature in a desiccator (see Experimental). An attempt to recrystallize **4** was also unsuccessful: the colorless solution soon turned to green, presumably forming an oligomeric species.

At the beginning we planned to make mononuclear chelate compounds (Fig. 1(A)). Subsequent X-ray crystal analyses, on the contrary, revealed their dinuclear structures (Fig. 1(B)).

Molecular Structures of 1a, 2, and 3. The molecular structure of **1a** was reported in a previous paper.[7]

The molecular structures of **2** and **3** are shown in Figs. 2 and 3, respectively. The bond lengths and angles are listed in Tables 4 and 5.

As a whole, the molecular structures of **1a**, and **3** resemble each other. They are dinuclear complexes having di-μ-bridged carboxylate ligands. Because of a weak coordination of the sulfonate ligand, a mononuclear structure with six-membered chelation of the sulfoacetate ligand (Fig. 1(A)) might be less stable than the dinuclear structur (Fig. 1(B)).

The local positive charge on Pt atoms(+1) and the negative charge of SO_3 groups(−1), in a formal sense, give a zwitterionic character to the dinuclear complexes. Although the geometric requirement imposed by the bridging carboxyl group causes a relatively short Pt–Pt distances (ca. 3.0 Å), they are slightly too long to be regarded as being metal–metal bonds. The two coordination planes around Pt in a dimeric structure are not parallel to each other. The steric repulsion between the amine ligands may cause such a tilt. The Pt–Pt distances and the dihedral angles(°) between the coordination planes are summarized in Table 6 together with other dinuclear platinum(II) which have been reported so far.[9,10] As a general trend, the steric bulk of amine

Table 4. Selected Bond Lengths (Å) and Angles (°) of **2** with esd's in Parentheses

Bond length (Å)					
Pt1–Pt2	3.049(1)	Pt1–O1	2.04(1)	Pt1–O3	2.04(1)
Pt2–O2	2.06(1)	Pt2–O4	2.08(1)	S1–O5	1.45(1)
S1–O6	1.44(1)	S1–O7	1.45(1)	S1–C2	1.80(2)
S2–O8	1.46(1)	S2–O9	1.47(2)	S2–O10	1.43(1)
S2–C4	1.77(2)	O1–C1	1.26(2)	O2–C1	1.24(2)
O3–C3	1.22(2)	O4–C3	1.25(2)	C1–C2	1.50(2)
C3–C4	1.50(2)				

Bond angle (°)			
Pt2–Pt1–O1	77.3(3)	Pt2–Pt1–O3	77.4(3)
Pt2–Pt1–N1	108.5(4)	Pt2–Pt1–N2	107.8(4)
O1–Pt1–O3	90.5(5)	O1–Pt1–N1	91.6(5)
O1–Pt1–N2	174.7(5)	O3–Pt1–N1	174.1(5)
O3–Pt1–N2	92.2(5)	Pt1–Pt2–O2	78.6(3)
Pt1–Pt2–O4	78.2(3)	Pt1–Pt2–N3	105.5(4)
Pt1–Pt2–N4	104.4(4)	O2–Pt2–O4	93.8(4)
O2–Pt2–N3	89.7(5)	O2–Pt2–N4	175.4(5)
O4–Pt2–N3	175.4(5)	O4–Pt2–N4	90.2(5)
O5–S1–O6	112.9(8)	O5–S1–O7	113.4(8)
O6–S1–O7	111.0(8)	O5–S1–C2	105.2(8)
O6–S1–C2	107.0(7)	O7–S1–C2	106.7(8)
O8–S2–O9	111.6(8)	O8–S2–O10	112.6(9)
O9–S2–O10	117(1)	O8–S2–C4	105.6(8)
O9–S2–C4	104.1(8)	O10–S2–C4	105(1)
Pt1–O1–C1	126(1)	Pt2–O2–C1	125(1)
Pt1–O3–C3	129(1)	Pt2–O4–C3	125(1)
O1–C1–O2	128(1)	O1–C1–C2	115(1)
O2–C1–C2	117(1)	S1–C2–C1	110(1)
O3–C3–O4	127(1)	O3–C3–C4	116(1)
O4–C3–C4	116(1)	S2–C4–C3	117(1)

Table 5. Bond Lengths (Å) and Angles (°) of **3** with esd's in Parentheses

Bond length (Å)					
Pt1–Pt2	2.990(5)	Pt1–O1	2.01(2)	Pt1–O2	2.00(2)
Pt1–N1	1.99(3)	Pt1–N2	2.03(3)	Pt2–O3	2.09(3)
Pt2–O4	2.01(2)	Pt2–N3	1.99(2)	Pt2–N4	1.98(3)
S1–O5	1.37(4)	S1–O6	1.41(4)	S1–O7	1.46(3)
S1–C2	1.82(3)	S2–O8	1.36(3)	S2–O9	1.39(5)
S2–O10	1.29(6)	S2–C4	1.77(3)	O1–C1	1.13(4)
O2–C3	1.23(5)	O3–C1	1.30(4)	O4–C3	1.26(5)
N1–C5	1.44(7)	N2–C8	1.51(5)	N3–C11	1.55(8)
N4–C14	1.52(7)	C1–C2	1.53(4)	C3–C4	1.56(4)
C5–C6	1.71(8)	C5–C7	1.33(9)	C8–C9	1.48(5)
C8–C10	1.45(5)	C11–C12	1.49(7)	C11–C13	1.55(7)
C14–C15	1.39(7)	C14–C16	1.59(7)		

Bond angle (°)			
Pt2–Pt1–O1	79.2(9)	Pt2–Pt1–O2	79(1)
Pt2–Pt1–N1	97(1)	Pt2–Pt1–N2	104.2(9)
O1–Pt1–O2	90(1)	O1–Pt1–N1	87(1)
O1–Pt1–N2	176(1)	O2–Pt1–N1	176(1)
O2–Pt1–N2	89(1)	N1–Pt1–N2	94(1)
Pt1–Pt2–O3	78.1(8)	Pt1–Pt2–O4	77.5(8)
Pt1–Pt2–N3	107.2(9)	Pt1–Pt2–N4	100(1)
O3–Pt2–O4	90(1)	O3–Pt2–N3	89(1)
O3–Pt2–N4	178(1)	O4–Pt2–N3	175(1)
O4–Pt2–N4	88(1)	N3–Pt2–N4	92(1)
O5–S1–O6	118(3)	O5–S1–O7	114(3)
O5–S1–C2	107(2)	O6–S1–C2	105(2)
O7–S1–C2	103(2)	O8–S2–O9	113(3)
O8–S2–O10	117(4)	O8–S2–C4	107(2)
O9–S2–O10	101(4)	O9–S2–C4	108(3)
O10–S2–C4	112(3)	Pt1–O1–C1	130(3)
Pt1–O2–C3	129(3)	Pt2–O3–C1	124(3)
Pt2–O4–C3	129(2)	Pt1–N1–C5	116(3)
Pt1–N2–C8	118(2)	Pt2–N3–C11	119(3)
Pt2–N4–C14	118(4)	O1–C1–O3	128(4)
O1–C1–C2	126(4)	O3–C1–C2	106(4)
S1–C2–C1	109(2)	O2–C3–O4	123(3)
O2–C3–C4	114(4)	O4–C3–C4	123(4)
S2–C4–C3	109(2)	N1–C5–C6	113(6)
N1–C5–C7	116(6)	C6–C5–C7	107(6)
N2–C8–C9	109(4)	N2–C8–C10	110(4)
C9–C8–C10	110(3)	N3–C11–C12	104(6)
N3–C11–C13	111(5)	C12–C11–C13	104(6)
N4–C14–C15	111(7)	N4–C14–C16	101(5)
C15–C14–C16	113(5)		

Table 6. Comparison of Geometric Properties of Oligonuclear Platinum Diammine Complexes

Compound	**1a**	**2**	**3**	**5***	**6***	**7***
Oxid. state[a]	2.0	2.0	2.0	2.25	2.0	2.0
Distance[b]	3.044(1)	3.049(1)	2.990(5)	2.775(1)	2.877(1)	2.992(1)
γ[c]	42.9	43.2	34.1	27.4	30.0	39.6
ω[d]	1.1	13.1	3.0	22.8	20.3	24.9

a) Formal oxidation state of platinum. b) Pt–Pt distance (Å), the shortest one is listed. c) Dihedral angle (°) between the coordination planes. d) Average torsion angle (°) along Pt–Pt vector.
***5**: $[Pt_2(NH_3)_4(C_5H_4NO)_2]_2(NO_3)_5 \cdot H_2O$, Ref. 5. **6**: $[Pt_2(NH_3)_4(C_5H_4NO)_2]_2(NO_3)_4$, Ref. 9. **7**: $[Pt_2(en)_2(C_5H_4NO)_2]_2(NO_3)_4$, Ref. 10.

Table 7. Antitumor Activities against Mice Leukemia L1210

Compound		T/C(%)[a-c]			
		Dose (mg kg^{-1})			
		50	25	12.5	6.25
[Pt(*RR*-dach)(slac)]$_2 \cdot 3H_2O$	**1a**	Toxic	128P	269P(3)	230P(1)
[Pt(*SS*-dach)(slac)]$_2 \cdot 3H_2O$	**1b**	287P(2)	301P(3)	141P	
[Pt(*cis*-dach)(slac)]$_2 \cdot 3H_2O$	**1c**	^{T}191P(1)	335P(3)	383P(5)	
[Pt(en)(slac)]$_2 \cdot 3H_2O$	**2**	^{T}119	113	113	

a) T/C value over 125 was evaluated as anticancer active and indicated with P. b) The number in parentheses indicate 30 days survivors out of 6 mice. c) The weight decrease over 4 g on day 5 was judged as toxic and indicated with a superscript^T.

ligands has a good correlation with the Pt–Pt distances and dihedral angles.

Antitumor Activities. The results of animal tests against mice leukemia L1210 are listed in Table 7. Complex **2** had no detectable antitumor activity. The dach complexes **1a**—**c**, however, have shown the significant antitumor activity in this primary screening. It should thus be emphasized that the dinuclear complex has potential in the drug design of an antineoplastic platinum(II) agent.

References

1) C. F. Bernard, *Platinum Met. Rev.*, **33**, 162 (1989).
2) Y. Okuno, K. Tonosaki, T. Inoue, O. Yonemitsu, and T. Sasaki, *Chem. Lett.*, **1986**, 1947.
3) R. Faggiani, B. Lippert, C. J. L. Lock, and B. Rosenberg, *J. Am. Chem. Soc.*, **99**, 777 (1977).
4) R. Faggiani, B. Lippert, C. J. L. Lock, and B. Rosenberg, *Inorg. Chem.*, **16**, 1192 (1977).
5) J. K. Barton, H. A. Rabinowitz, D. J. Szalda, and S. J. Lippard, *J. Am. Chem. Soc.*, **99**, 2827 (1977).
6) K. Okude, H. Ichida, T. K. Miyamoto, Y. Sasaki, and T. Tashiro, *Chem. Lett.*, **1989**, 119.
7) K. Okude, H. Ichida, T. K. Miyamoto, and Y. Sasaki, *Acta Crystallogr., Sect. C*, **45**, 949 (1989).
8) T. K. Miyamoto, K. Okude, K. Maeda, H. Ichida, Y. Sasaki, and T. Tashiro, *Bull. Chem. Soc. Jpn.*, **62**, 3239 (1989).
9) L. S. Hollis and S. J. Lippard, *J. Am. Chem. Soc.*, **105**, 3494 (1983).
10) L. S. Hollis and S. J. Lippard, *Inorg. Chem.*, **22**, 2600 (1983).

Kinetic Studies of Electron-Transfer Reactions Induced by the Reductive Quenching of Tris(2,2′-bipyrazine)ruthenium(II)

Suzuko YAMAZAKI-NISHIDA and Masaru KIMURA*
Department of Chemistry, Faculty of Science, Nara Women's University, Nara 630
(Received January 14, 1991)

The oxidation reaction of the oxalate ion ($C_2O_4^{2-}$) by the peroxodisulfate ion ($S_2O_8^{2-}$) is greatly accelerated by irradiation with visible light in an aqueous solution containing tris(2,2′-bipyrazine)ruthenium(II) ($[Ru(bpz)_3]^{2+}$). The mechanism constitutes a chain reaction initiated by a reductive quenching of photoexcited $[Ru(bpz)_3]^{2+}$ with $C_2O_4^{2-}$. The rate of reaction increases with an increase of the $[Ru(bpz)_3]^{2+}$ concentration or incident light intensity. On the other hand, the reaction rate hardly depends not only on the concentrations of $C_2O_4^{2-}$ and $S_2O_8^{2-}$, but also on the ionic strength and temperature. The $[Ru(bpz)_3]^{2+}$ acts as a photo-catalyst, although the absorption spectra of the reaction solution are slightly changed during the photoreaction. An analysis of the absorption spectra by a graphic method indicates that another absorbing species than $[Ru(bpz)_3]^{2+}$ is formed in the reaction solution. Such a complex has no photocatalytic effect for the redox reaction between $S_2O_8^{2-}$ and $C_2O_4^{2-}$. The concentration of the produced complex is always coincident with ca. 0.7% of that of the $S_2O_8^{2-}$ reacted. The reaction mechanism and rate law are clarified to account for the results obtained.

Tris(2,2′-bipyridine)ruthenium(II)($[Ru(bpy)_3]^{2+}$) and its derivatives have been extensively investigated from the viewpoint of the solar energy conversion.[1–9] Recently, the analogous tris(2,2′-bipyrazine)ruthenium(II) ion ($[Ru(bpz)_3]^{2+}$) has attracted the attention of many researchers.[10–15] The photochemical properties of $[Ru(bpz)_3]^{2+}$ are similar to those of the $[Ru(bpy)_3]^{2+}$. A salient feature of the former is that the excited state lifetime is longer than that of the latter and that the standard redox potentials are more positive by ca. 0.5 V than those of the corresponding couples for ($[Ru(bpy)_3]^{2+}$), respectively.[16–19] As a result, the photo-excited ruthenium(II) complex ($[Ru(bpz)_3]^{2+*}$) is a stronger oxidant, but poorer reductant, than $[Ru(bpy)_3]^{2+*}$. The $[Ru(bpz)_3]^{2+*}$ has been reported to be reductively quenched with an oxalate ion and ethylenediaminetetraacetic acid (EDTA) in an aqueous solution; the anodic photocurrent obtained in the photoelectrochemical system was attributable to the oxidation of $[Ru(bpz)_3]^{+}$ produced by the quenching reaction.[20–22] As far as the $[Ru(bpy)_3]^{2+}$ is concerned, only a few reductive quenchers, such as Eu^{2+} and ascorbate ion, are known in aqueous solutions.

Various photo-induced electron-transfer reactions with $[Ru(bpy)_3]^{2+}$ as a photocatalyst have been studied kinetically in order to clarify the reaction mechanisms. On the other hand, there have been few kinetic studies on photoreactions with $[Ru(bpz)_3]^{2+}$, except for a reaction system consisting of methylviologen (MV^{2+}), a sacrificial donor (such as EDTA and triethanolamine (TEOA)) and colloidal metal redox catalysts.[12,16,17] In such a system, the $[Ru(bpz)_3]^{2+*}$ is quenched reductively by EDTA or TEOA; the resulting $[Ru(bpz)_3]^{+}$ reacts with MV^{2+} to produce MV^{+} and, subsequently, MV^{+} reduces water in the presence of a catalyst. The quantum yield of the MV^{+} formation by $[Ru(bpz)_3]^{2+}$ is reported to be nearly 100%, while that by $[Ru(bpy)_3]^{2+}$ is only 20% under similar photochemical conditions.

We previously studied the electron-transfer reaction between oxalate and peroxodisulfate induced by photo-excited $[Ru(bpy)_3]^{2+}$.[23] This reaction was initiated by the oxidative quenching of $[Ru(bpy)_3]^{2+*}$ by $S_2O_8^{2-}$.

In this paper we present a kinetic study of the photo-induced electron-transfer reaction between $S_2O_8^{2-}$ and $C_2O_4^{2-}$ by using $[Ru(bpz)_3]^{2+}$ as a photocatalyst. Several remarkable differences between the $[Ru(bpy)_3]^{2+}$ and $[Ru(bpz)_3]^{2+}$ systems are: (1) the photo-induced reaction is initiated by the oxidative quenching reaction of $[Ru(bpy)_3]^{2+*}$ by the $S_2O_8^{2-}$, while by the reductive quenching of $[Ru(bpz)_3]^{2+*}$ by the $C_2O_4^{2-}$; (2) the ligand-substitution reaction for $[Ru(bpy)_3]^{2+}$ does not occur at all, but that for $[Ru(bpz)_3]^{2+}$ occurs to produce the bis(2,2′-bipyrazine)ruthenium(II) complex. The photochemical stability of the ruthenium(II) complex is an important problem concerning utilization as a photosensitizer and -catalyst. This paper also proposes that the ligand-substitution product of $[Ru(bpz)_3]^{2+}$ is inactive for a photo-catalyzed reaction between $C_2O_4^{2-}$ and $S_2O_8^{2-}$.

Experimental

$[Ru(bpz)_3]Cl_3 \cdot 3.5H_2O$ was prepared and purified as described in the literature.[24,25] Ruthenium trichloride and 2,2′-bipyrazine were purchased from Wako Pure Chemical Co. and Aldrich, respectively. The other chemicals used were of guaranteed reagent grade and were used without further purification. Unless otherwise stated, each sample solution was irradiated with visible light from two 100-W tungsten lamps placed 3 dm to the right- and left-hand sides from the center of the reaction vessel. Oxygen dissolved in the solutions was removed by bubbling through pure nitrogen gas. The concentration of $S_2O_8^{2-}$ remaining in the solution was determined as reported previously,[23] except that the amount of cation exchange resin (Dowex 50W-X8, 200—400 mesh, hydrogen form, washed well with distilled water) to remove the $[Ru(bpz)_3]^{2+}$ was twice as much as that for $[Ru(bpy)_3]^{2+}$. The measurement of the spectral changes in a deaerated solution was carried out by using a Shimadzu digital double beam spectrophotometer (UV-200S).

Results

Dependence of the Reaction Rate on the Concentrations of $S_2O_8^{2-}$, $C_2O_4^{2-}$, and $[Ru(bpz)_3]^{2+}$, Light Intensity, Ionic Strength, and Temperature. Plots of the $S_2O_8^{2-}$ concentration against the reaction time are shown in Fig. 1 under the conditions of 5×10^{-5} mol dm^{-3} $[Ru(bpz)_3]Cl_2$, 0.04 mol dm^{-3} $Na_2C_2O_4$, 30 °C, and an ionic strength of 0.4 mol dm^{-3}. The decomposition rate of $S_2O_8^{2-}$ is almost independent of the $S_2O_8^{2-}$ concentration, and decreases gradually with an increase of the reaction time. Such a time-profile is attributable to the concentration change of $[Ru(bpz)_3]^{2+}$ as a photocatalyst (mentioned later). The plots of $[S_2O_8^{2-}]$ vs. t are also independent of the $C_2O_4^{2-}$ concentrations over the range 0.04—0.055 mol dm^{-3}. On the other hand, the decomposition rate of $S_2O_8^{2-}$ increases with an increase of $[Ru(bpz)_3]^{2+}$ concentration or intensity of the incident light as shown in Figs. 2 and 3. The electron-transfer reaction between $S_2O_8^{2-}$ and $C_2O_4^{2-}$ hardly proceeds without either of $[Ru(bpz)_3]^{2+}$ or visible light. The dependences of the reaction rate on the ionic strength and temperature were also examined over the range 0.2—0.5 mol dm^{-3} and 20—40 °C, respectively. It is found that the ionic strength as well as temperature of the reaction solution have little effect on the reaction rate. The kinetic studies were carried out in a neutral solution, although the pH of the solution increases after $S_2O_8^{2-}$ is completely exhausted by the photoreaction. This fact is attributed to water reduction with $[Ru(bpz)_3]^{+}$ (see Eq. 10).

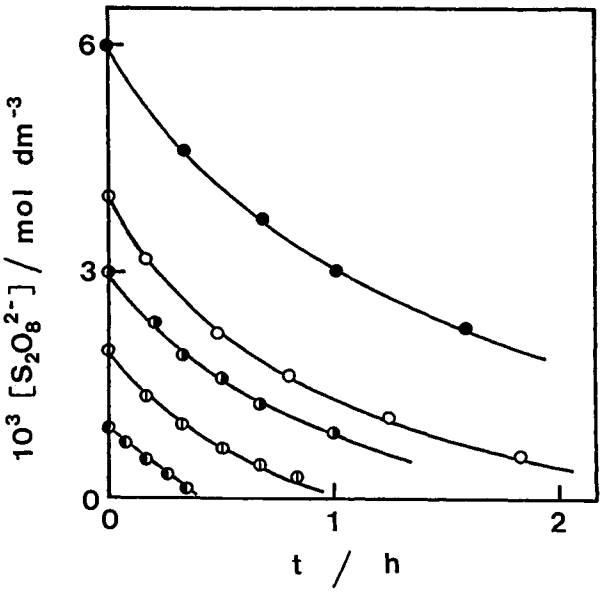

Fig. 1. Plots of $[S_2O_8^{2-}]$ vs. t obtained in the deaerated solution containing 4×10^{-2} mol dm^{-3} $Na_2C_2O_4$ and 5×10^{-5} mol dm^{-3} $[Ru(bpz)_3]Cl_2$ at an ionic strength of 0.4 mol dm^{-3} and 30 °C. Irradiation was done with two lamps. Initial concentrations of $S_2O_8^{2-}$ are (●) 6×10^{-3}, (○) 4×10^{-3}, (◑) 3×10^{-3}, (◔) 2×10^{-3}, and (◐) 1×10^{-3} mol dm^{-3}.

Spectral Change of the Reaction. The typical spectral changes obtained by the irradiation of the reaction solution are presented in Fig. 4. The absorption spectrum at t=0 coincides with that of $[Ru(bpz)_3]^{2+}$. The absorption band of $[Ru(bpz)_3]^{2+}$ at 442 nm decreased with the irradiation time, while new bands appeared at around 380 and 480 nm. Two isosbestic points were

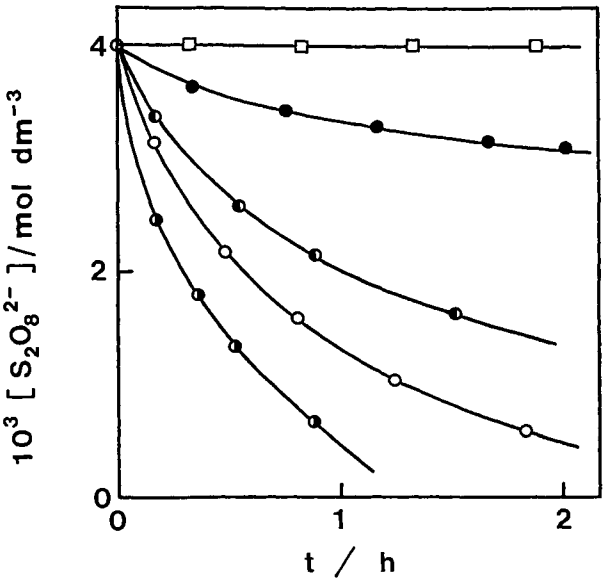

Fig. 2. Effect of the $[Ru(bpz)_3]^{2+}$ ion concentration. Initial concentrations of $[Ru(bpz)_3]Cl_2$ are (□) 0, (●) 1.1×10^{-5}, (◐) 3.1×10^{-5}, (○) 5×10^{-5}, and (◑) 7.7×10^{-5} mol dm^{-3}. Other conditions are the same as in the plots ○ in Fig. 1.

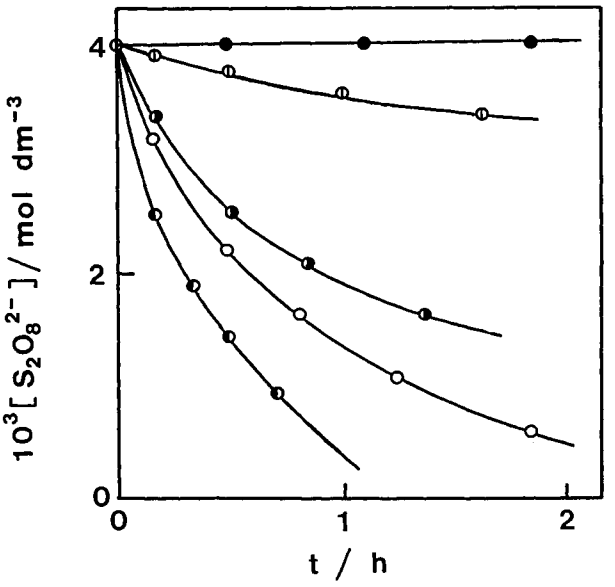

Fig. 3. Effect of the incident light intensity. Conditions:(●) dark, (◔) room light, (◑) 1 lamp, (○) 2 lamps, and (◐) 4 lamps. Other conditions are the same as in the plots ○ in Fig. 1.

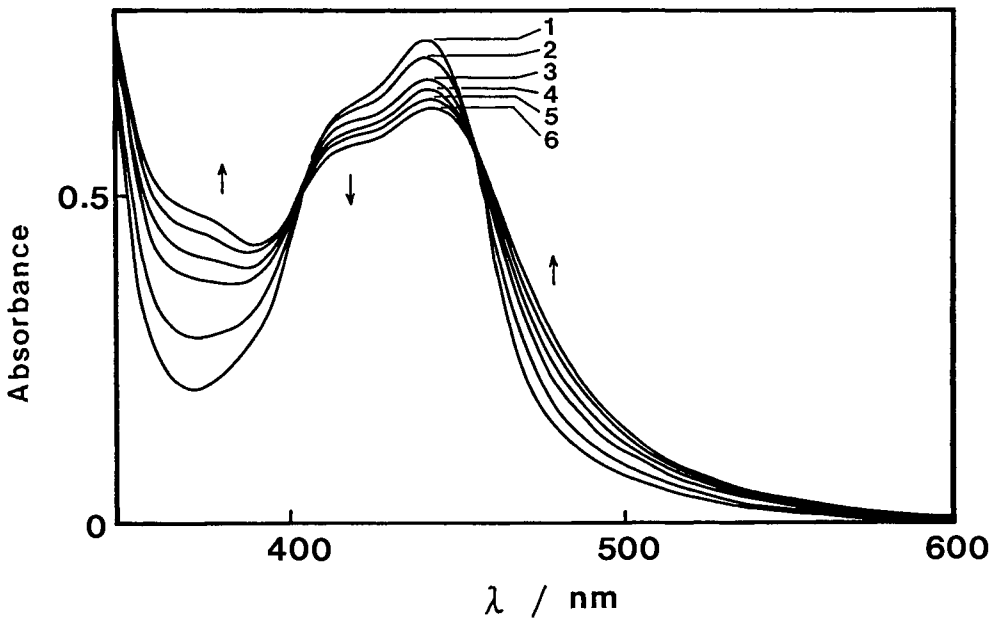

Fig. 4. Spectral change of the solution. Conditions are the same as in the plots O in Fig. 1. Reaction time: (1) 0, (2) 10 min, (3) 28 min, (4) 48 min, (5) 72 min, and (6) 108 min.

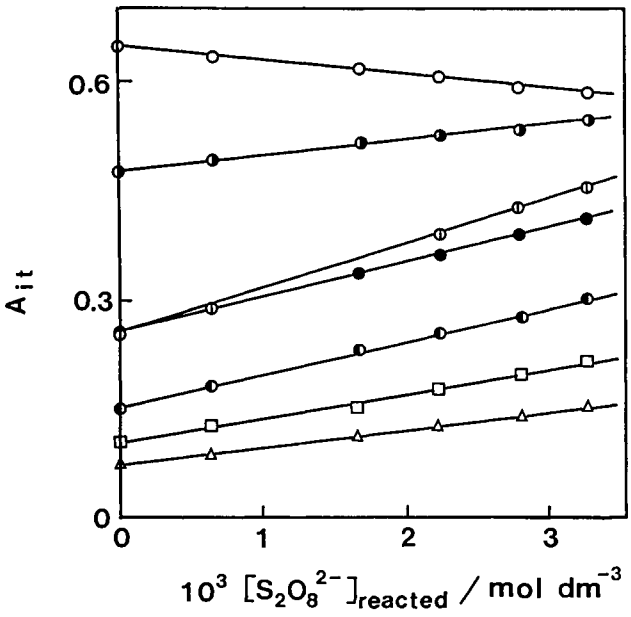

Fig. 5. Plots of A_{it} vs. $[S_2O_8^{2-}]_{reacted}$. Conditions are the same as in Fig. 4. The data are taken at wavelength of (⊙) 380 nm, (○) 420 nm, (◑) 460 nm, (●) 470 nm, (◐) 480 nm, (□) 490 nm, and (△) 500 nm.

observed at 407 and 456 nm. The absorption spectra of $[Ru(bpz)_3]^{2+}$ were not recovered, even if the solution was saturated with air. Figure 5 indicates that plots of A_{it} vs. $[S_2O_8^{2-}]_{reacted}$ are rectilinear; an intercept where A_{it} indicates absorbance at a given wavelength, i, and reaction time, t; $[S_2O_8^{2-}]_{reacted}$ represents the concentration of $S_2O_8^{2-}$ consumed up to $t=t$.

$$A_{it} = a_i + b_i[S_2O_8^{2-}]_{reacted} \quad (1)$$

The intercept, a_i, is the absorbance at a wavelength i and $t=0$. The b_i value varies with the wavelength, whereas it is independent of other experimental factors, such as the initial concentrations of $S_2O_8^{2-}$, $C_2O_4^{2-}$,, and $[Ru(bpz)_3]^{2+}$, light intensity, ionic strength, and temperature. The b_i values are estimated to be 67.9±6.3, −21.8±2.2, 19.9±3.3, 46.3±3.2, 44.7±2.4, 33.8±2.0, and 24.4±1.9, at 380 nm, 420 nm, 460 nm, 470 nm, 480 nm, 490 nm, and 500 nm, respectively.

Quenching Reaction of $[Ru(bpz)_3]^{2+*}$ with $C_2O_4^{2-}$ and $S_2O_8^{2-}$. The quenching rate constants (k_q) of $[Ru(bpz)_3]^{2+*}$ with $C_2O_4^{2-}$ or $S_2O_8^{2-}$ were evaluated from quenching experiments using an unbuffered neutral solution. The Stern–Volmer plots are linear and the k_q values, respectively, 7.2×10^6 and 3.3×10^6 dm^3 mol^{-1} s^{-1} for $C_2O_4^{2-}$ and $S_2O_8^{2-}$ at an ionic strength of 0.4 mol dm^{-3}. Figure 6 depicts the spectral change of a deaerated $[Ru(bpz)_3]^{2+}$ solution containing $C_2O_4^{2-}$ under continuous irradiation. An absorbance at 442 nm decreases the new bands at 420 and 470 nm. The observed absorption spectra did not change along with air saturation in the solution. A similar absorption spectrum has been reported from a flash photolysis of a deaerated solution containing $[Ru(bpz)_3]^{2+}$ and EDTA.[26]

Discussion

The photoexcited $[Ru(bpz)_3]^{2+}$ is quenched reductively by $C_2O_4^{2-}$ and oxidatively by $S_2O_8^{2-}$ with quenching-rate constants of 7.2×10^6 and 3.3×10^6 dm^3 mol^{-1} s^{-1}, respectively. Under the experimental conditions investigated, the concentrations of $C_2O_4^{2-}$ are always ten-

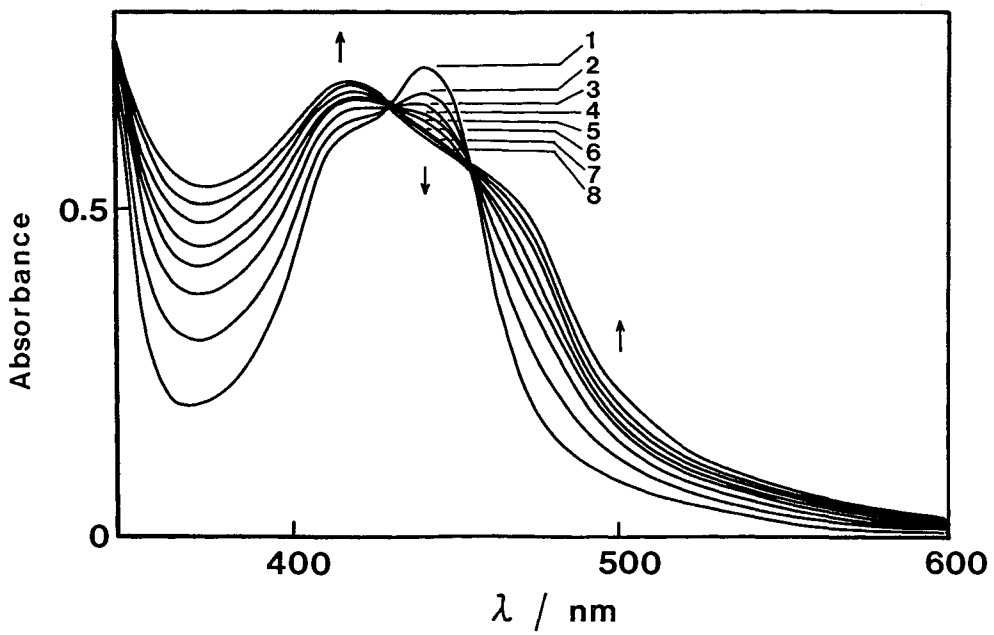

Fig. 6. Spectral change in the reductive quenching reaction of $[Ru(bpz)_3]^{2+*}$ with $C_2O_4^{2-}$. Conditions are the same as in Fig. 1 without an addition of $S_2O_8^{2-}$. Reaction time: (1) 0, (2) 5 min, (3) 10 min, (4) 15 min, (5) 21 min, (6) 30 min, (7) 40 min, and (8) 60 min.

times as much as those of $S_2O_8^{2-}$. Thus, it is most likely that reductive quenching proceeds predominantly in the present system.

The following reaction mechanism is assumed to account for the results obtained:

$$[Ru(bpz)_3]^{2+} + h\nu \longrightarrow [Ru(bpz)_3]^{2+*}, \quad (2)$$

$$[Ru(bpz)_3]^{2+*} \xrightarrow{k_0} [Ru(bpz)_3]^{2+} + h\nu' \text{ or } \Delta \text{ (thermal energy)}, \quad (3)$$

$$[Ru(bpz)_3]^{2+*} + C_2O_4^{2-} \xrightarrow{k_q} [Ru(bpz)_3]^{+} + CO_2^{-} + CO_2, \quad (4)$$

$$[Ru(bpz)_3]^{2+*} + CO_2^{-} \longrightarrow [Ru(bpz)_3]^{+} + CO_2, \quad (5)$$

$$S_2O_8^{2-} + [Ru(bpz)_3]^{+} \longrightarrow SO_4^{-} + SO_4^{2-} + [Ru(bpz)_3]^{2+}, \quad (6)$$

and

$$SO_4^{-} + [Ru(bpz)_3]^{+} \longrightarrow SO_4^{2-} + [Ru(bpz)_3]^{2+}. \quad (7)$$

Assuming a steady state concentration for $[Ru(bpz)_3]^{+}$, SO_4^{-}, and CO_4^{-} radicals, the following reaction rate is obtained:

$$-d[S_2O_8^{2-}]/dt = \frac{k_q I_a \Phi [C_2O_4^{2-}]}{k_0 + k_q [C_2O_4^{2-}]}, \quad (8)$$

Here, I_a is the amount of light absorbed, Φ the quantum yield for the formation of $[Ru(bpz)_3]^{2+*}$ and $I_a\Phi$ corresponds to the formation rate of $[Ru(bpz)_3]^{2+*}$. The I_a can be rewritten as Eq. 9 with an incident light intensity of I_0, and an empirical constant, γ, comprising the molar absorption coefficient of $[Ru(bpz)_3]^{2+}$ and the length of the light path:

$$I_a = I_0(1-\exp(-\gamma[[Ru(bpz)_3]^{2+}])). \quad (9)$$

The rate law (Eq. 8) suggests that the reaction rate is independent of the $S_2O_8^{2-}$ concentration and is dependent on the incident light intensity and the $[Ru(bpz)_3]^{2+}$ concentration. This is coincident with all of the experimental results. Equation 8 also indicates that the reaction rate should depend on the $C_2O_4^{2-}$ concentration. However, the reaction rate observed was almost independent of the $C_2O_4^{2-}$ concentration within the range 0.04—0.055 mol dm^{-3}. The value of $k_q[C_2O_4^{2-}]$ is comparable within such a concentration range to that of k_0 which is estimated to be 9.6×10^5 s^{-1} from the lifetime of $[Ru(bpz)_3]^{2+*}$. The right-hand side of Eq. 8 is rewritten as $I_a\Phi\{1-k_0/(k_0+k_q[C_2O_4^{2-}])\}$; the value of $k_0/(k_0+k_q[C_2O_4^{2-}])$ changes little when the concentration varies by at most 1.5 times as much. Thus, if we were to examine the dependence of the reaction rate on the $C_2O_4^{2-}$ concentration over a wider concentration range, a dependence like that shown in Eq. 8 might be obtained. In fact, however, in the lower concentrations of $C_2O_4^{2-}$, the oxidative quenching of $S_2O_8^{2-}$ for $[Ru(bpz)_3]^{2+*}$ should be considered in the reaction mechanism, while at higher concentrations of $C_2O_4^{2-}$, the dark redox reaction between $S_2O_8^{2-}$ and $C_2O_4^{2-}$ proceeds considerably. According to Eq. 8, the $S_2O_8^{2-}$ decreases linearly with the reaction time under excess concentrations of $C_2O_4^{2-}$. However, as described later, some $[Ru(bpz)_3]^{2+}$ are transformed to an inert complex for the photoreaction, causing a decrease in the reaction rate with the reaction time. The reaction rate was independent of both the ionic strength and temperature of the solution. This finding is attributed to the fact

that the k_q- and k_0-paths have a similar dependence on the ionic strength and temperature. The latter means that the activation energies for both reaction paths are almost the same. The $[Ru(bpz)_3]^+$ is capable of reducing water when all the $S_2O_8^{2-}$ ions are exhausted by the reaction, which is responsible for an increase in the solution pH.

$$[Ru(bpz)_3]^+ + H_2O \longrightarrow [Ru(bpz)_3]^{2+} + 1/2\,H_2O + OH^- \quad (10)$$

Since the $SO_4^{\cdot-}$ radical is a strong oxidant, the following reactions can be considered:

$$SO_4^{\cdot-} + C_2O_4^{2-} \longrightarrow SO_4^{2-} + CO_4^{\cdot-} + CO_2, \quad (11)$$

$$SO_4^{\cdot-} + [Ru(bpz)_3]^{2+} \longrightarrow SO_4^{2-} + [Ru(bpz)_3]^{3+}, \quad (12)$$

and

$$[Ru(bpz)_3]^{3+} + C_2O_4^{2-} \longrightarrow [Ru(bpz)_3]^{2+} + CO^{\cdot-} + CO_2, \quad (13)$$

The $CO_2^{\cdot-}$ radicals produced by reactions 11 and 13 react with $[Ru(bpz)_3]^{2+}$ to form $[Ru(bpz)_3]^+$, which is subsequently oxidized by $S_2O_8^{2-}$ (see Eqs. 5 and 6). When reactions 11—13 could occur, the reaction rate should be dependent on the $S_2O_8^{2-}$ concentration; but being quite different from the obtained results, these reactions have been ruled out.

A graphical analysis has been developed regarding the change in the absorption spectra (Fig. 4) in order to determine the number of species in the solution. A plot of $A_{it}-A_{it'}$ vs. $A_{i't}-A_{i't'}$ gives a straight line through the origin only when two absorbing species exist in the solution.[27,28] From the results given in Fig. 7, we can conclude that another absorbing species (RuL) as well as $[Ru(bpz)_3]^{2+}$ is present in the solution. The following relationship is derived from Eq. 1:

$$\frac{[[Ru(bpz)_3]^{2+}]_{decreased}}{[S_2O_8^{2-}]_{reacted}} = \frac{[RuL]_{produced}}{[S_2O_8^{2-}]_{reacted}} = \frac{b_i}{\varepsilon_i' - \varepsilon_i}, \quad (14)$$

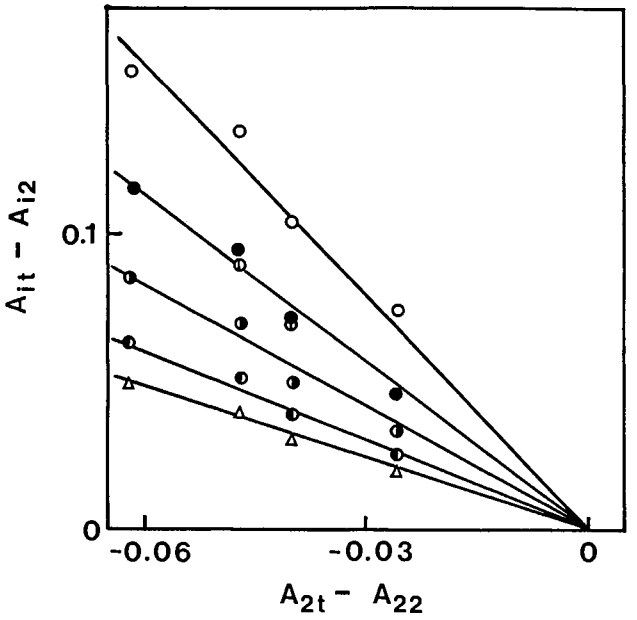

Fig. 7. A graphic method for two absorbing species. The data are taken from Fig. 4. The values of i and t correspond to the wavelength and reaction time, respectively. i=2:420 nm, t=2:10 min. (○) 380 nm, (△) 460 nm, (●) 470 nm, (①) 480 nm, (◑) 490 nm, (◐) 500 nm.

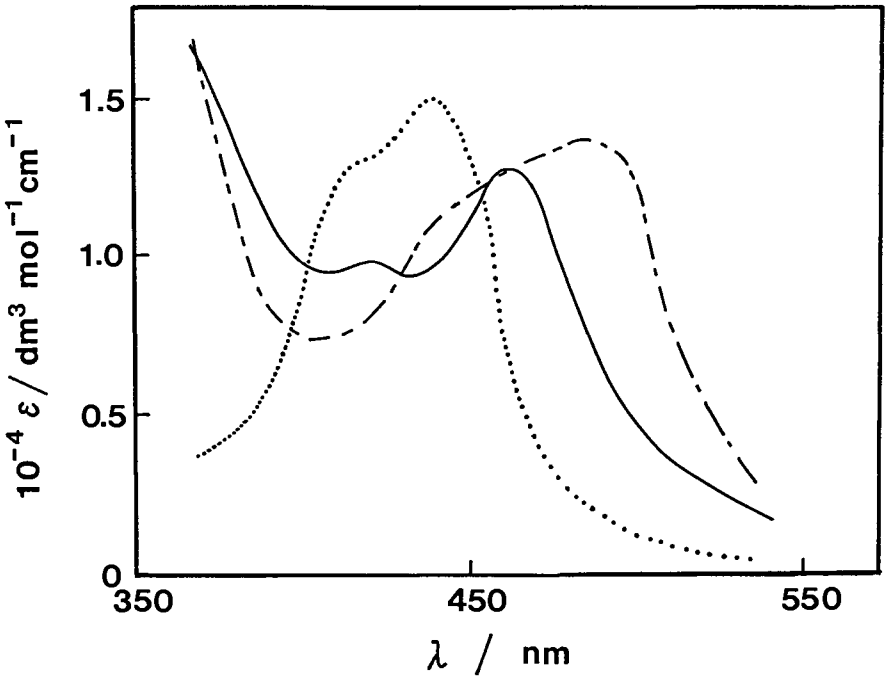

Fig. 8. Absorption spectra of $[Ru(bpz)_3]^{2+}$ (·····), $[Ru(bpz)_3]^+$ (—·—),[17] and RuL (——). The absorption spectra of RuL are calculated from the spectral data in Fig. 4.

where ε_i' indicates the molar absorption coefficient for RuL at wavelength i. Since the value of $b_i/(\varepsilon_i'-\varepsilon_i)$ must be constant for all observed wavelengths, the absorption spectra for RuL is represented in Fig. 8 from the spectral data in Fig. 4 and the b_i values obtained from the plots A_{it} vs. $[S_2O_8^{2-}]_{reacted}$ (Fig. 5). The b_i value was independent of any experimental conditions investigated and the $b_i/(\varepsilon_i'-\varepsilon_i)$ value was estimated to be 7×10^{-3}. Therefore, in the present reaction system, the amount of RuL formed always corresponds to ca. 0.7% of the $S_2O_8^{2-}$ reacted, suggesting that RuL has little photocatalytic effect on the photo-induced redox reaction between $S_2O_8^{2-}$ and $C_2O_4^{2-}$. This causes a decrease in the reaction rate with an increase in the reaction time (as described in Fig. 1). The RuL might be a bis(bipyrazine)ruthenium(II) complex, such as $[Ru(bpz)_2(C_2O_4)]$, $[Ru(bpz)_2(CO_2)(H_2O)]^+$, or $[Ru(bpz)_2(SO_4)(H_2O)]^+$. The former two species are not likely to be formed, since the absorption spectra observed in the reaction solution are different from those obtained in the quenching reaction of $[Ru(bpz)_3]^{2+*}$ with $C_2O_4^{2-}$ (Fig. 6).

In conclusion, $[Ru(bpz)_3]^{2+}$ acts as a photocatalyst in a way similar to $[Ru(bpy)_3]^{2+}$ for a redox reaction between $S_2O_8^{2-}$ and $C_2O_4^{2-}$. The reaction rate law is apparently similar with respect to the concentration of the quencher. However, the reaction mechanism is quite different, i.e., the initial step is the reductive quenching of $[Ru(bpz)_3]^{2+*}$ by $C_2O_4^{2-}$ for $[Ru(bpz)_3]^{2+}$ as a photocatalyst. Some $[Ru(bpz)_3]^{2+}$ is transformed to an inactive species for the photo-induced electron-transfer reactions. The stability of the ruthenium(II) complex during the photoreaction is a serious problem for the utilization of $[Ru(bpz)_3]^{2+}$, although $[Ru(bpz)_3]^{2+}$ has been described as a new photo-catalyst.

This research was supported by Grant-in-Aid for Scientific Research No. 01470051 from the Ministry of Education, Science and Culture.

References

1) K. Kalyanasundaram, *Coord. Chem. Rev.*, **46**. 159 (1982).
2) K. Kalyanasundaram, M. Grätzel, and E. Pelizzetti, *Coord. Chem. Rev.*, **69**, 57 (1986).
3) D. P. Rillema, G. Allen, T. J. Meyer, and D. Conrad, *Inorg. Chem.*, **22**, 1617 (1983).
4) Y. Ohsawa, K. W. Hanck, and M. K. DeArmond, *J. Electroanal. Chem.*, **175**, 229 (1984).
5) C. D. Tait, R. J. Donohoe, M. K. DeArmond, and D. W. Wertz, *Inorg. Chem.*, **26**, 2754 (1987).
6) K. Shinozaki, O. Ohno, Y. Kaizu, H. Kobayashi, M. Sumitani, and K. Yoshihara, *Inorg. Chem.*, **28**, 3680 (1989).
7) Y. Kawanishi, N. Kitamura, and S. Tazuke, *Inorg. Chem.*, **28**, 2968 (1989).
8) T. Ohno, A. Yoshimura, N. Mataga, S. Tazuke, Y. Kawanishi, and N. Kitamura, *J. Phys. Chem.*, **93**, 3546 (1989).
9) C. J. Timpson, C. C. Carter, and J. Olmsted III, *J. Phys. Chem.*, **93**, 4116 (1989).
10) H. Dürr, G. Dörr, K. Zengerle, E. Mayer, J.-M. Curchod, and A. M. Braun, *Nouv. J. Chim.*, **9**. 717 (1985).
11) Y. Kawanishi, N. Kitamura, Y. Kim, and S. Tazuke, *Sci. Pap. Inst. Phys. Chem. Res. (Jpn.)*, **78**, 212 (1984).
12) D. R. Prasad, D. Hessler, and M. Z. Hoffman, *Chem. Phys. Lett.*, **121**, 61 (1985).
13) S. Tazuke, N. Kitamura, and Y. Kawanishi, *J. Photochem.*, **29**, 123 (1985).
14) R. Maidan and I. Willner, *J. Am. Chem. Soc.*, **108**, 8100 (1986).
15) I. Willner, R. Maidan, D. Mandler, H. Dürr, G. Dörr, and K. Zengerle, *J. Am. Chem. Soc.*, **109**, 6080 (1987).
16) N. Kitamura, Y. Kawanishi, and S. Tazuke, *Chem. Lett.*, **1983**, 1185.
17) R. J. Crutchley and A. B. P. Lever, *J. Am. Chem. Soc.*, **102**, 7128 (1980).
18) R. J. Crutchley, N. Kress, and A. B. P. Lever, *J. Am. Chem. Soc.*, **105**, 1170 (1983).
19) J. Gonzales-Velasco, I. Rubinstein, R. J. Crutchley, A. B. P. Lever, and A. J. Bard, *Inorg. Chem.*, **22**, 822 (1983).
20) S. Nishida, Y. Harima, and K. Yamashita, *Inorg. Chem.*, **28**, 4073 (1989).
21) G. Neshvad and M.Z. Hoffman, *J. Phys. Chem.*, **93**, 2445 (1989).
22) S. Y.-Nishida, Y. Harima., and K. Yamashita, to be published.
23) M. Kimura and S. Nishida, *J. Chem. Soc., Dalton Trans.*, **1985**, 355.
24) R. J. Crutchley and A. B. P. Lever, *Inorg. Chem.*, **21**, 2276 (1982).
25) I. P. Evans, A. Spencer, and G. Wilkinson, *J. Chem. Soc., Dalton Trans.*, **1973**, 204.
26) D. R. Prasad and M. Z. Hoffman, *J. Am. Chem. Soc.*, **108**, 2568 (1986).
27) J. S. Coleman, L. P. Varga, and S. H. Mastin, *Inorg. Chem.*, **9**, 1015 (1970).
28) R. J. Crutchley, N. Kress, and A. B. P. Lever, *J. Am. Chem. Soc.*, **105**, 1170 (1983).

The Intercalation of *n*-Alkylamines into Layered Transition Metal Phosphates-Solvent Effect

Yasushi KANZAKI*,† and Mitsuo ABE
Department of Chemistry, Faculty of Science, Tokyo Institute of Technology, 2-12-1 Ohokayama, Meguro-ku, Tokyo 152
†Showa College of Pharmaceutical Sciences, 3-Chome, Higashi-Tamagawagakuen, Machida, Tokyo 194
(Received January 14, 1991)

The intercalation of *n*-alkylamines (carbon number 1—18) into γ-titanium phosphate and γ-zirconium phosphate was examined in aqueous, methanol, and benzene solutions. The interlayer spacings increased with an increase in the carbon number of alkylamines, showing the formation of bilayers of alkylamines in a similar manner to that in previous reports. The intercalation reaction depended on the solvents used to dissolve the alkylamines. For example, an anomaly was observed regarding intercalation in ethanol solutions. The interlayer spacings decreased when the carbon number exceeded 14—16, indicating a distortion or the monolayer formation of alkylamines. The rate of intercalation was also seriously affected by the kind of solvents. Intercalation occurred almost instantaneously in aqueous solutions. The rate of the intercalation reaction was generally faster in benzene solutions than that in ethanol solutions. The formation of bilayers was also more perfect in benzene solutions, and resulting interlayer spacings were slightly larger than those prepared in ethanol solutions. The anomaly in ethanol was attributed to a disturbance due to the cointercalation of methanol molecules. The solvent effect was also accountable due to the dielectric constant, or dipole moment, of solvents.

γ-Titanium phosphate ($Ti(HPO_4)_2 \cdot 2H_2O$: γ-TiP) and γ-zirconium phosphate ($Zr(HPO_4)_2 \cdot 2H_2O$: γ-ZrP) are known to have a layered structure with interlayer spacings of around 1.2 nm.[1,2] They can be compared with the corresponding α-phosphates, the interlayer spacings of which are about 0.76 nm.[3] These layerd compounds are insoluble acid salts and are known to be typical inorganic ion exchangers.[4] They can also intercalate various alkylamines or organic bases as host materials; their interlayer spacing increases corresponding to the geometric size of the guest intercalants. Among them, the intercalation of *n*-alkylamines has been examined extensively for intercalated alkylamine molecules forming well-established bilayers within the layered compond[5] similar to those of biological cell membranes.[6]

The procedure for the intercalation of alkylamines seems to have been definitely established according to previous studies.[5,7] However, such studies reported so far have treated the intercalation reaction too much ideally, and structural considerations of the final products have been of major interest. The detailed mechanisms for the intercalation reaction of alkylamines have not yet been clarified. For example, the roles of the acid-base reaction, ion exchange, and van der Waals forces acting on the Langmuir-type monolayer, etc. have not been treated properly. This paper mainly deals with the solvent effect on the intercalation reaction of *n*-alkylamines into γ-type transition metal phosphates, while discussing the mechanisms of the intercalation reaction in detail.

Experimental

Layered Materials. γ-TiP was prepared according to a procedure reported by Kobayashi et al.[1] Amorphous titanium phosphate prepared from phosphoric acid and titanium(IV) chloride was heated hydrothermally in 10 M phosphoric acid (1 M=1 mol dm^{-3}) for 24 h at 280 °C; a well crystallized H^+ form of γ-TiP was thus obtained (Fig. 1a). The crystal was carefully washed with de-ionized water and stored in a saturated NaCl desiccator. Two types of γ-ZrP (sodium ion form) were used in this study. One was obtained from Dai-ichi Kigenso Kogyo Co. Ltd., which was prepared under atmospheric pressure. The other was prepared hydrothermally at about 190 °C for 1 week according to a procedure by Yamanaka et al.[2] The H^+ form γ-ZrP was prepared by treating the Na^+ form of γ-ZrP with 1 M HCl untill free of sodium ions. After drying, the H^+ form of γ-ZrP was stored in a saturated NaCl desiccator. The empirical formula of the H^+ form of γ-TiP could be represented by $Ti(HPO_4)_2 \cdot 1.7—1.8H_2O$. γ-ZrP also had a similar content of the water of crystallization.

Intercalation of Alkylamines. *n*-Alkylamines with carbon numbers (C_n) from 1 to 18 were dissolved in water, methanol, benzene, etc. and were used for intercalation. The concentrations of *n*-alkylamines were 0.1 M (M=mol dm^{-3}) for C_n=1 to 10 and 0.05 M for C_n=14 to 18. Intercalation was carried out by immersing 3.6×10^{-4} moles of phosphates (0.1 g for γ-TiP and 0.117 g for γ-ZrP) in 20 ml of each *n*-alkylamine solution. The reaction time was varied from 0.5 h to 4 d (96 h) and the temperature was kept at 30±0.1 °C unless otherwise stated. The amount of intercalated amines was determined by acid-base titration with 0.1 M HCl methanol solution. The indicator used was a (bromocresol green+methyl red) mixture.

X-Ray Diffraction. The intercalation compounds were characterized using X-ray diffractometer with Mn filtered Fe-*Kα* radiation. *d*-Values of up to 7 nm (λ=0.193736 nm, 2-$\theta \geqq 1.5°$) were successfully measured with sufficient accuracy. The interlayer spacings (*d*-spacings) were determined by averaging the *d*-values of the integral sequence of hexagonally approximated (00*n*) planes.

Results

Table 1 shows crystallographic data of γ-type phosphates. Figure 1 (a—d) shows SEM photographs of

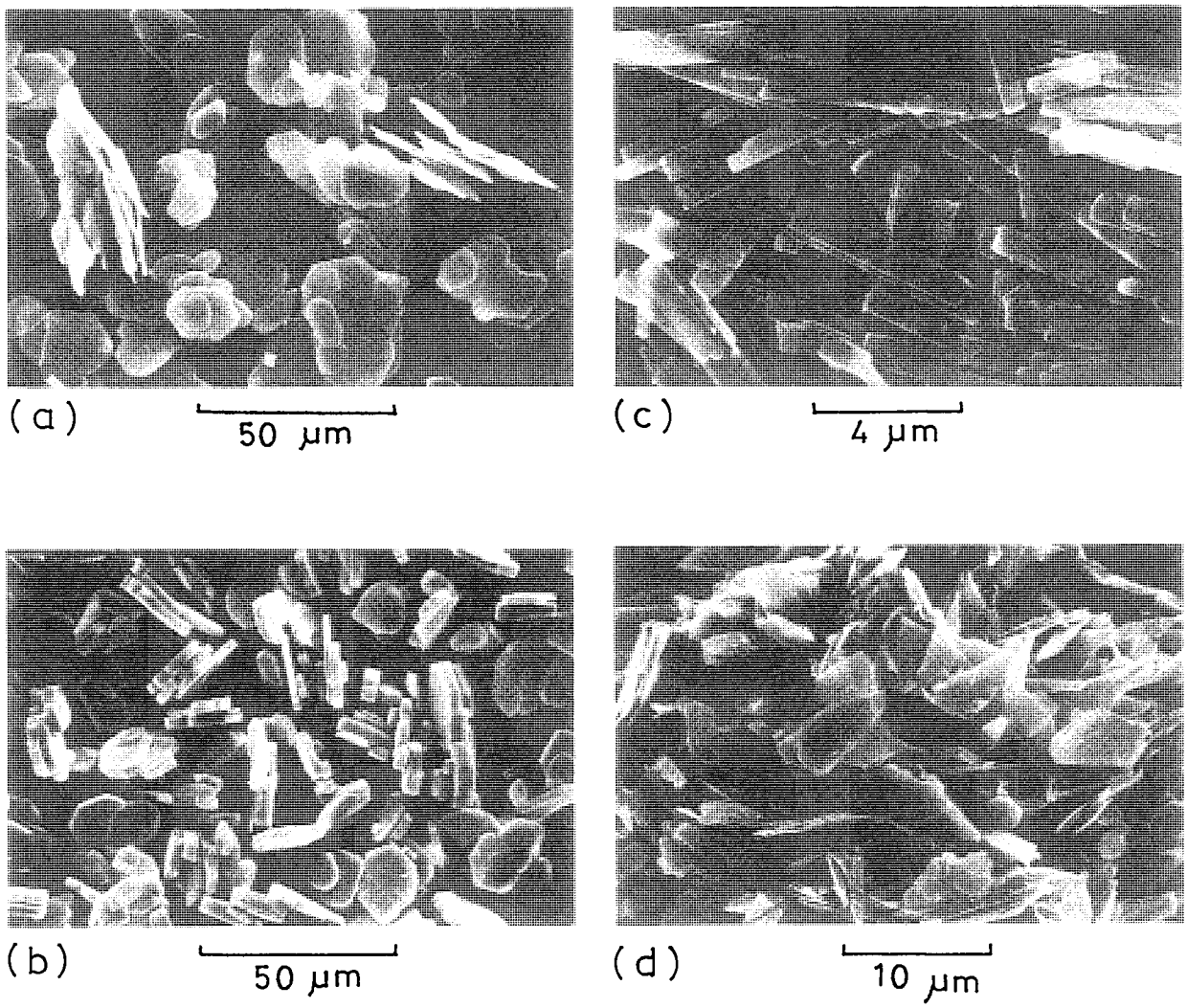

Fig. 1. SEM photographs of γ-TiP (a), octadecylamine intercalated (bilayer) γ-TiP (b), hydrothermal γ-ZrP (c), γ-ZrP supplied from Dai-ichi Kigenso Kogyo Co., Ltd. (d).

Table 1. Crystallographic Data of γ-Phosphates

	γ-TiP	γ-ZrP
System	Monoclinic[a)]	Monoclinic[b)]
a/nm	0.527	0.5376
b/nm	0.642	0.6636
c/nm	2.429	2.456
β/deg	102.5	93.94
Basal spacing/nm	1.16	1.225
Free area/nm^2	0.166	0.178

a) Ref. 1. b) Ref. 2.

the phosphates used. The appearances of the crystals are quite different from each other, even though they are classified as a monoclinic lattice with similar geometric dimensions. The X-ray diffraction pattern of hydrothermal γ-ZrP was quite similar to that of γ-ZrP prepared under atmospheric pressure, though they look quite different from each other. The γ-ZrP prepared under atmospheric pressure was mainly used for the hydrothermal γ-ZrP sometimes gave X-ray diffraction patterns which indicated the presence of mixed phases.

Solvent Effect on Butylamine Intercalation. Figures 2a and 2b show the time dependence of the uptake of butylamine in three different solvents. Intercalation into γ-TiP occurred almost instantaneously in aqueous and benzene solutions. On the other hand, it took three to four days to reach equilibrium in a methanol solution. The maximum uptake was in the order aqueous>benzene>methanol (Molality of protons in solid γ-TiP: 7.25 mmol g^{-1} and γ-ZrP: 6.27 mmol g^{-1}). The reaction was relatively slow in γ-ZrP, though the apparent solvent effect was similar to that in γ-TiP. The speed of the reaction rate in aqueous solution may be attributed to the (strong) basic property of butylamine in the solvent, which results in a neutralization reaction with strong solid acid γ-TiP.

A similar experiment was carried out for the alkylamines with C_n=1 to 18 in methanol solutions. The

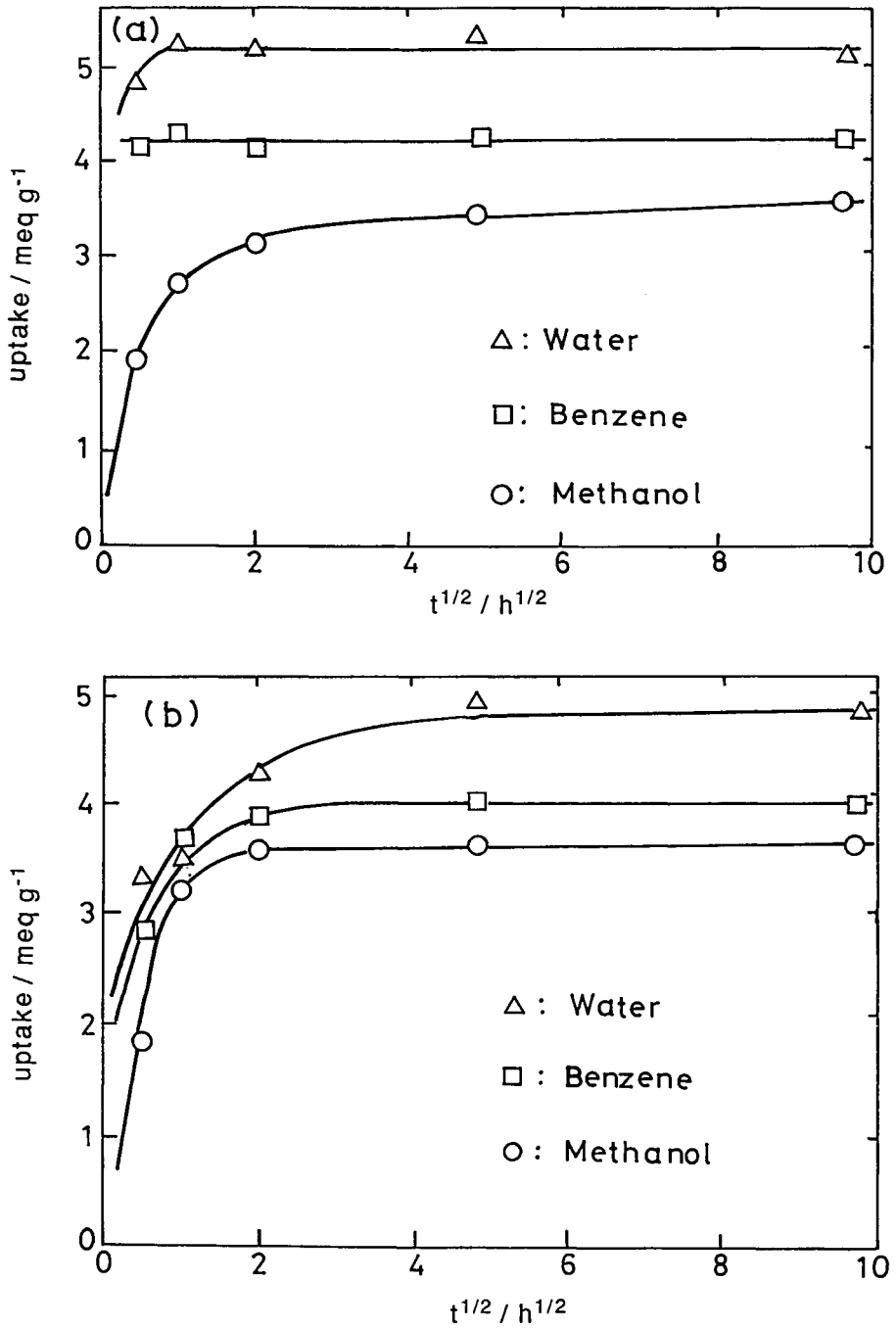

Fig. 2. Uptake of butylamine vs. reaction time in various solvents. (a) γ-TiP, (b) γ-ZrP. Absissa $t^{1/2}$ was taken for convenience and has no chemical significance (same as below).

results are shown in Figs. 3a and 3b. Generally speaking the rate of intercalation became slower as the alkyl-chain of the amines become longer. The intercalation of octadecylamine did not reach the equilibrium point, even after 4 d. The maximum uptake depends considerably on the length of the alkylamines and no easy finding regularity was observed. This fact may suggest a disturbance due to cointercalated methanol molecules. Figure 4 shows the uptake of butylamine into γ-TiP, which was pretreated (immersed) by pure methanol. It was found that the uptake decreased with increasing pretreatment time with methanol. This result suggested the co-intercalation of methanol[5] and, therefore, a disturbance due to the co-intercalated methanol. Figures 5a and 5b shows the results obtained in each benzene solution. The intercalation reached equilibrium points within two days, even in octadecylamine for either γ-TiP or γ-ZrP. The maximum uptakes were almost independent of alkylamines, suggesting a smaller disturbance due to the solvent molecules, unlike

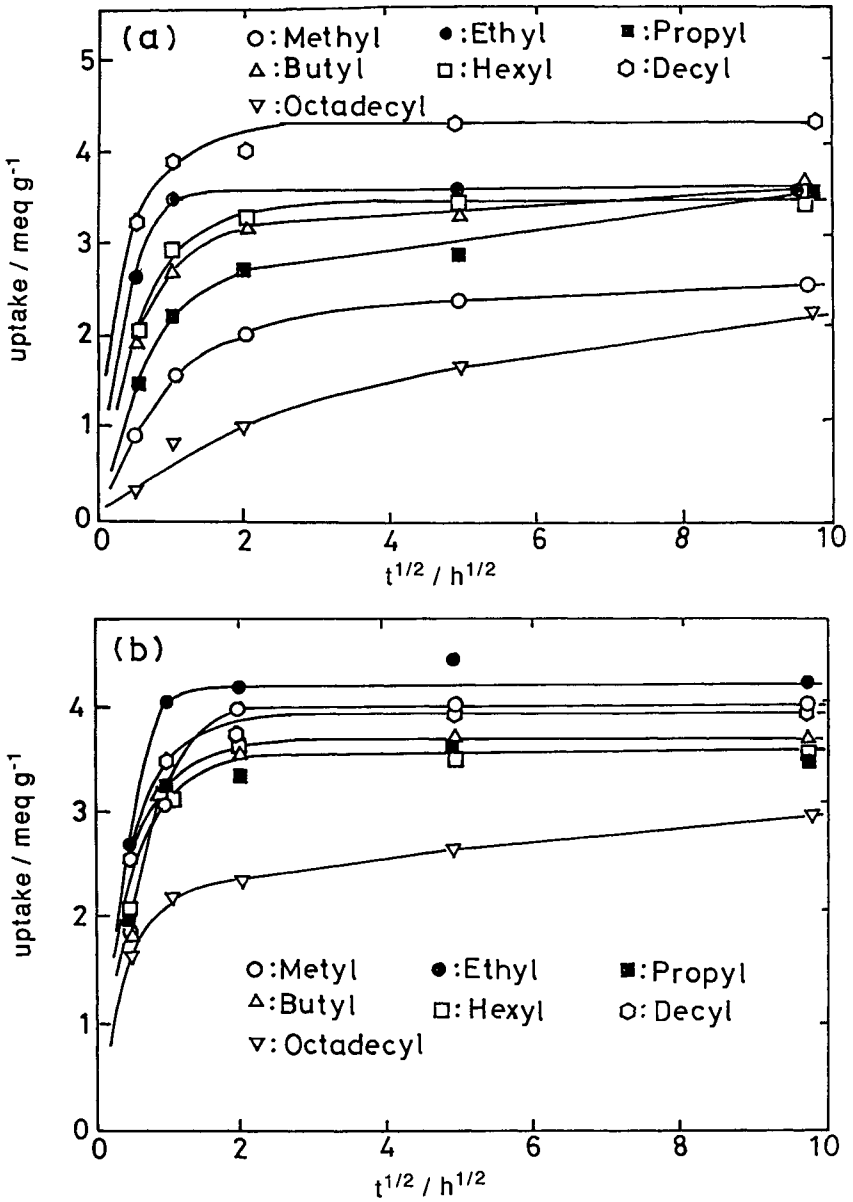

Fig. 3. Uptake of various amines vs. reaction time measured in methanol solutions. (a) γ-TiP, (b) γ-ZrP.

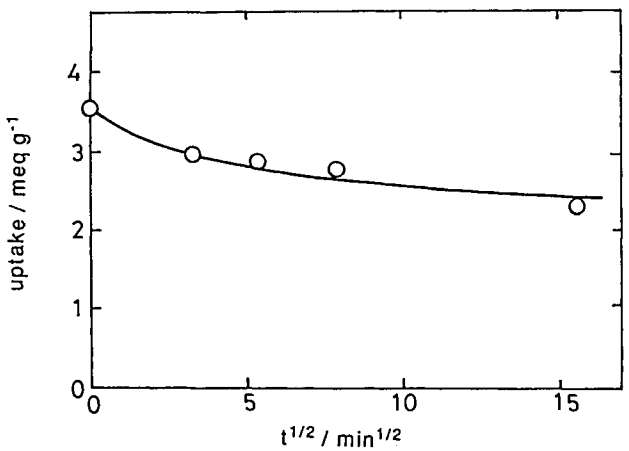

Fig. 4. Uptake of butylamine vs. suspension time in methanol.

those in methanol solutions.

Table 2 shows the amount of intercalated alkylamines [(mole of amine)/(mole of phosphate)] in the products for a reaction time of 4 d. Roughly speaking, the alkylamines intercalated in these phosphates amounted to about 1/2 of the active (or exchangable) protons in the host phosphates. The data obtained by Costantino[5] are listed in the same table for comparison. Our data are in good agreement with those reported by Costantino, except for some combinations (underlined). Small differences between the two data may be attributable to the difference in the preparation procedures of the γ-phosphates. The maximum uptakes were larger in the intercalates prepared in benzene solution than those in methanol solution, corresponding to the reaction rates in both solvents (Figs. 3a, 3b, 5a, 5b).

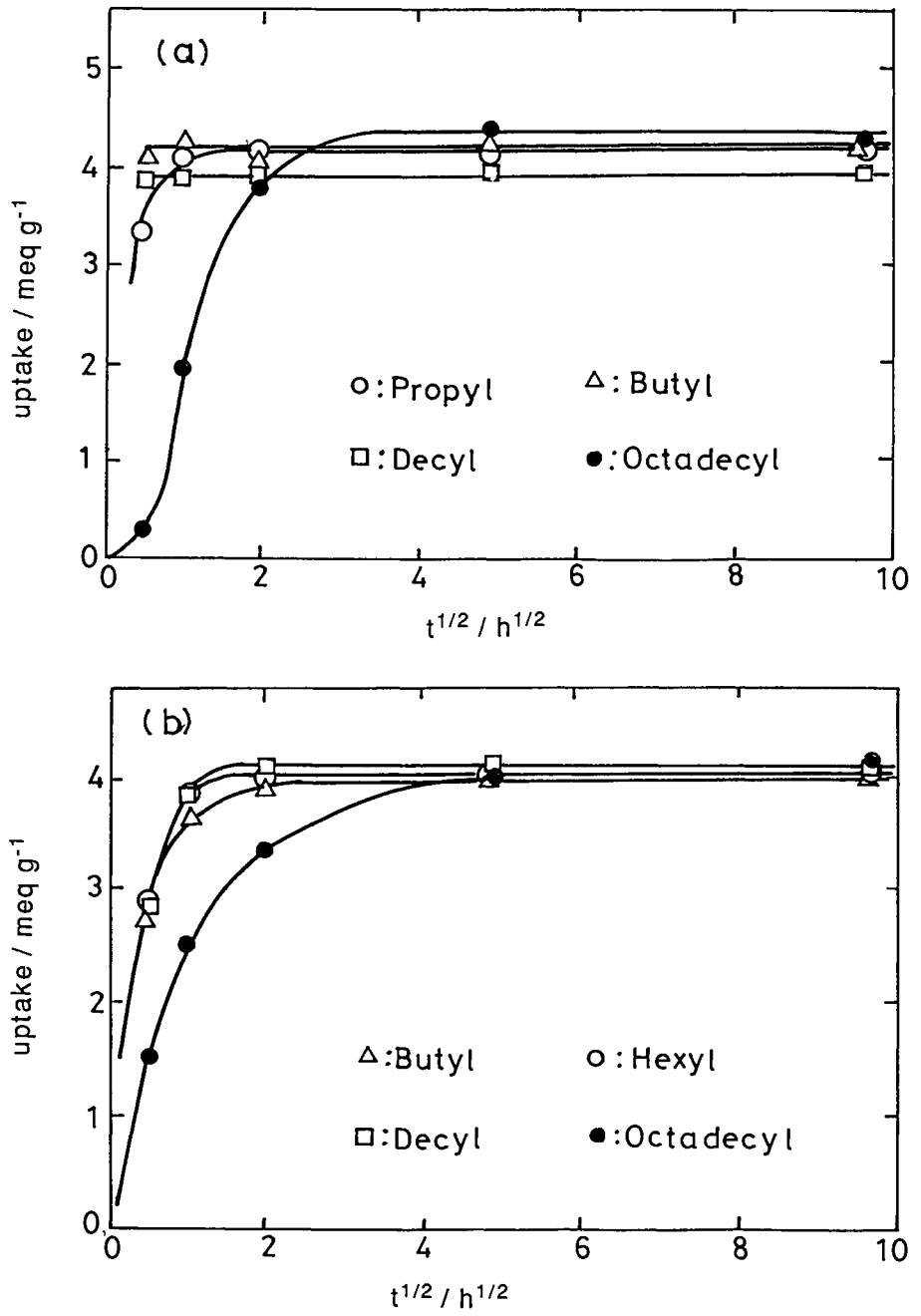

Fig. 5. Uptake of various amines vs. reaction time measured in benzene solutions. (a) γ-TiP, (b) γ-ZrP.

Table 2. Content of *n*-Alkylamine Intercalated in γ-Phosphates (moles/mole of γ-phosphate)

Amines	γ-TiP (Methanol)	γ-TiP (Methanol)[a]	γ-TiP (Benzene)	γ-ZrP (Methanol)	γ-ZrP (Methanol)[a]	γ-ZrP (Benzene)
Methylamine	0.71	—[b]	—	1.26	—	—
Ethylamine	1.08	1.00	—	1.37	1.05	—
Propylamine	0.99	1.08	1.24	1.14	0.95	1.35
Butylamine	0.99	1.02	1.24	1.15	1.00	1.29
Hexylamine	0.95	—	1.15	1.16	—	1.31
Decylamine	1.14	0.93	1.17	1.28	1.05	1.34
Tetradecylamine	1.30	0.67	1.27	1.28	1.33	1.40
Hexadecylamine	1.25	0.58	1.25	1.04	1.33	1.31
Octadecylamine	0.60	0.64	1.24	0.96	1.33	1.33

a) U. Costantino, *J. Inorg. Nucl. Chem.*, **43**, 1895 (1981). b) Not measured.

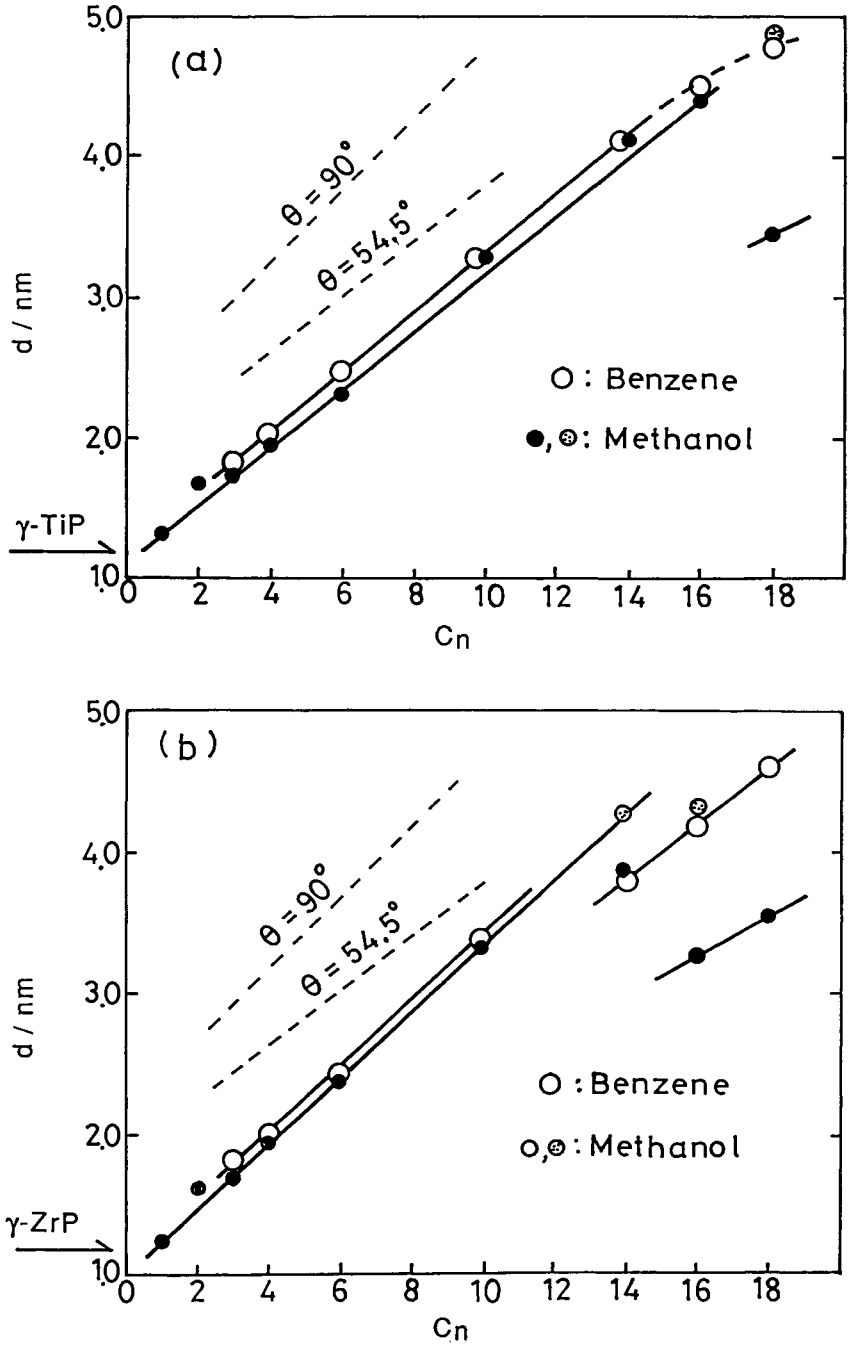

Fig. 6. *d*-Spacing (*d*) vs. number of carbon atom in *n*-alkyl chain (C_n).
(a) γ-TiP, (b) γ-ZrP.

Figures 6a and 6b show the *d*-spacings of the alkylamine intercalates corresponding to those in Table 2. The slope vs. number of carbon atoms (C_n) seems to be almost parallel to the theoretical slope (2×0.127 nm per carbon atom[5]) which was estimated by assuming that the alkyl-chains were intercalated in a bilayer just perpendicular to the basal planes, for C_n lower than 10 (γ-ZrP in both solutions) and lower than 16 (γ-TiP, methanol) or 18 (γ-TiP, benzene). Above these carbon numbers, some distortion might have occurred, such as irregular bilayer formation, inclination, and kink-block distortions.[7] The *d*-spacings for the intercalates of γ-ZrP for C_n=16 and 18 prepared in methanol solution may indicate the formation of monolayer of these amines.

The temperature effect of the intercalation of alkylamines with carbon numbers 14, 16, and 18 was examined in order to clarify the cause of the above mentioned distortion. The combinations of γ-TiP with benzene and γ-ZrP with methanol were selected as to be ideal (no distortion) and non-ideal (much distorted) (Fig. 7), respectively. The bilayer products of γ-TiP were obtained in benzene solutions for temperatures ranging

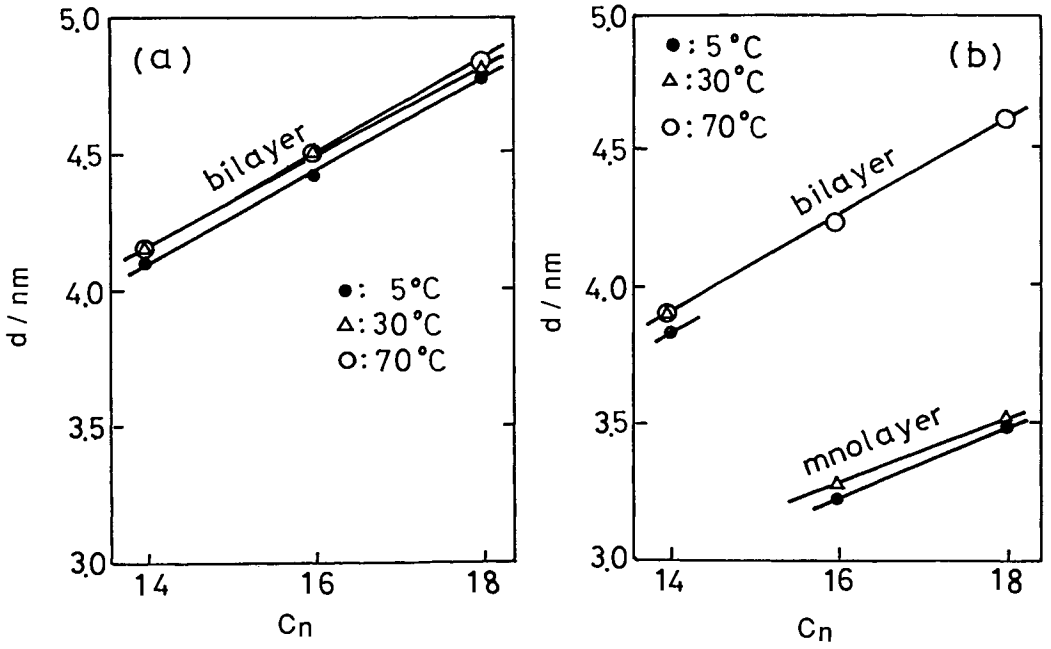

Fig. 7. Temperature dependence of *d*-spacing vs. number of carbon atom in alkyl-chain (C_n). (a) in benzene, (b) in methanol.

between 5 and 70 °C. On the other hand, bilayer products of γ-ZrP for carbon numbers 16 and 18 were obtained in methanol only for a sample prepared at 70 °C. Monolayer products were obtained at lower temperatures. It has been reported that the temperature rise up to this range caused an increase in kink-block distortion, resulting in a decrease in the *d*-spacings.[7] In the present study, however, it was found that the rise in temperature assisted in the formation of more perfect bilayers, presumably due to vibrational motion.

Comparison with Other Solvents. The facility of bilayer formation in the intercalation corresponding to the study illustrated in Fig. 7 (the rate and *d*-spacings) was examined in other solvents, xylene and propanol. Xylene and propanol showed intermediate properties between Figs. 7a and 7b. Thus, the order of facility for the intercalation of *n*-alkylamines was estimated to be as follows:

Benzene > Xylene > Propanol > Methanol

These results may suggest an effect of the dielectric constant of the solvent or the dipole moment of the solvent molecule in addition to the cointercalation of solvent molecules. The slow, imperfect intercalation reaction observed in methanol solutions suggests a strong solvation of the alkyl chain with polar methanol molecules, which may cause a slow desolvation on the occasion of the intercalation process, in addition to the co-intercalation effect stated above.

Ion Exchange and Acid-Base Reactions. The intercalation reaction of *n*-alkylamines into γ-phosphates is fundamentally an acid-base reaction. The ion-exchange reaction of decylammonium cations was examined in both methanol and aqueous solutions (Table 3). No ion-exchange reaction of decylammonium cations occurred in ethanol solution. This result suggests a poor dissociation of decylammonium chloride in the solvent. The *d*-values for the product by ion-exchange reactions of γ-TiP in aqueous solution were similar to that of decylamine intercalates in methanol, and showed the formation of a bilayer compound. On the other hand, the combination of γ-ZrP with decylammonium cations gave a monolayer inter-

Table 3. Interlayer Spacings of *n*-Decylamine and *n*-Decylammonium Ion Intercalates

Solvent	γ-TiP/nm		γ-ZrP/nm	
	Decylamine	Decylammonium	Decylamine	Decylammonium
Methanol	3.58 (Bilayer)	n.i.[a]	3.53 (Bilayer)	n.i.
Water	—[b] (Insoluble)	3.67 (Bilayer)	— (Insoluble)	2.80 (Monolayer)

a) Not intercalated. b) Intercalant was insoluble.

calate. These results indicate that the intercalation of *n*-alkylamines occurred more easily than did that of *n*-alkylammonium ions with a similar alkyl-chain; the intercalation of alkyl-chain was more accelerated by the acid-base reaction than that in an ordinary ion-exchange reaction.

Discussion

This study was designed to reveal that the intercalation of *n*-alkylamines should not be interpreted as being due solely to crystallographic, or visible, considerations regarding intercalated alkylamines, such as packing sequence, inclination of alkyl chain, and kink-block property. It was found from the present study that the crystallographic properties of *n*-alkylamines intercalated in layered compounds depend strongly on the conditions under which the intercalation reaction is carried out. This means that the crystallographic properties of intercalated alkylamines should not be interpreted only in terms of the final products. The crystallographic considerations reported so far should be reexamined by taking into account how they were prepared.

Packing Sequence. It has been proposed that alkyl chains in γ-phosphates are intercalated with an angle of 54.5°.[5] This study suggests, however, that alkyl-chains are intercalated almost perpendicular to the basal plane in γ-ZrP from carbon number 1 to 10 if the length of the carbon chain is assumed to be 0.127 nm/carbon and alkyl chains are closely packed without any distortion. Above that number, alkyl chains do undergo some distortion and, in some cases, intercalation occurs by forming monolayers. Alkylamines are to some extent inclinated in γ-TiP, though the angle is larger than 54.5°. However, it seems insignificant to determine the angle in detail only from the C_n vs. *d*-spacing curve, since the reproducibility of the *d*-value is rather poor and the error in determining the inclination would be large at high angles (near 90°).

Packing Density. It has been estimated that the free areas of the active site (exchangeable proton) are 0.166 and 0.178 nm² for γ-TiP and γ-ZrP, respectively (Table 1). The maximum uptake of alkylamines can not be estimated from the data obtained in ethanol solutions, but can be reasonably be estimated from the data obtained in benzene solutions. The number of alkyl-chains, thus estimated, are 1.22 and 1.33 chains per two active protons for γ-TiP and γ-ZrP, respectively (Table 2). This means that the packing density of the alkyl chains is 0.27 nm² (3.7 alkyl-chains per 1 nm²) in both γ-TiP and γ-ZrP, which approaches the corresponding value 4.17 observed in α-ZrP.[7] It can be concluded, therefore, that the packing density is determined mainly by the cross section of the alkyl chain. The length of the alkyl chain and the free area of the active protons are less important. The kink-block distortion would also be less important if intercalation procedures were settled properly.

The authors wish to thank Mr. K. Ito in Dai-ichi Kigenso Kogyo Co. Ltd., who kindly supplied us γ-ZrP and α-ZrP.

References

1) E. Kobayashi and S. Yamazaki, *Bull. Chem. Soc. Jpn.*, **56**, 1632 (1983).
2) S. Yamanaka and M. Tanaka, *J. Inorg. Nucl. Chem.*, **41**, 45 (1979).
3) A. Clearfield and J. A. Stynes, *J. Inorg. Nucl. Chem.*, **26**, 117 (1964).
4) G. Alberti, "Inorganic Ion Exchange Materials," ed by A. Clearfield, CRC Press, Boca Raton and Florida (1982), Chap. 2.
5) U. Costantino, *J. Inorg. Nucl. Chem.*, **43**, 1895 (1981).
6) S. J. Singer and G. L. Nicolson, *Science*, **175**, 720 (1973).
7) G. Lagaly, *Angew. Chem., Int. Ed. Engl.*, **15**, 575 (1976).

Spectrophotometric Determination of Tetrathionate by Its Oxidation with Iodate

Tomozo KOH* and Masako YAJIMA
Department of Chemistry, Faculty of Science, Tokai University, Hiratsuka, Kanagawa 259-12
(Received January 25, 1991)

The conditions under which tetrathionate is oxidized stoichiometrically to sulfate by iodate have been established by investigating the reaction rate of tetrathionate with iodate in a medium containing varying amounts of sulfuric acid at room temperature and 40 °C. Tetrathionate reacted with iodate with a tetrathionate : iodate mole ratio of 3 : 7 under the conditions of the usual procedure. After a complete reaction, the iodine, formed from excess iodate by the addition of iodide, was spectrophotometrically measured as triiodide. A 14-fold chemical amplification was achieved for the determination of tetrathionate by using the proposed method, compared with the conventional methods via the sulfitolysis and cyanolysis of tetrathionate. A linear calibration graph with a negative slope was obtained over the concentration range 2.5×10^{-7}—2.5×10^{-5} mol dm^{-3} tetrathionate (0.56—56 μg of $S_4O_6^{2-}$ in 10 cm^3); the relative standard deviation was 0.42% at the 1.5×10^{-5} mol dm^{-3} tetrathionate level.

The identification and determination of polythionates in their mixtures are difficult owing to similarities in their chemical and physical properties.[1] Hence, various reactions of individual polythionates, such as cyanolysis,[2–7] sulfitolysis[8–10] and sulfidolysis,[11,12] have been investigated in detail in order to determine a specific polythionate in the presence of other polythionates. These reactions have played an important role in the development of methods for the analysis of mixtures of polythionates.[13–17] All of these methods have been based on the formation of thiosulfate and/or thiocyanate equivalent to the polythionates, and on the spectrophotometric measurements of the reaction products.

It has been stated that iodate can be used as an excellent analytical reagent for standard iodine,[1] because a mixture solution of iodate and the excess amount of iodide is extremely stable and produces quantitatively iodine equivalent to the iodate, by the addition of acid, according to the following equation:

$$IO_3^- + 8I^- + 6H^+ \longrightarrow 3I_3^- + 3H_2O. \quad (1)$$

Further, the molar absorptivity of triiodide at 350 nm is much higher than that of iodine in carbon tetrachloride at 515 nm.[18] With regard to reactions involving oxoacid ions, such as the iodate ion, the potential for its reduction to the iodide ion is expected to increase with an increase in the hydrogen-ion concentration. In a previous paper[19] it was mentioned that thiosulfate can be oxidized by iodate to sulfate in a strong acidic medium, and that a simple, precise method has been developed for the determination of thiosulfate. In this study we attempted to oxidize tetrathionate with iodate in a strong acid medium, and established the conditions under which tetrathionate can be stoichiometrically oxidized to sulfate according to the following equation:

$$3S_4O_6^{2-} + 7IO_3^- + 9H_2O \longrightarrow 12SO_4^{2-} + 7I^- + 18H^+. \quad (2)$$

The proposed method for the determination of tetrathionate, in which the formed iodine equivalent to the excess iodate is measured spectrophotometrically, is very simple and is 14-fold more sensitive than previous methods for tetrathionate by its cyanolysis[15] and sulfitolysis.[8]

Experimental

Apparatus and Reagents. A Shimadzu Model UV-240 recording spectrophotometer with 10-mm quartz cells was used for all of the absorbance measurements. The desired temperatures were controlled by a Taiyo Model M-1 incubator.

All of the chemicals used, except for tetrathionate, were of analytical-reagent grade and were used without further purification. The water used in these experiments was redistilled.

Standard Tetrathionate Solution: Potassium tetrathionate was prepared according to a procedure described by Stamm and Goehring.[20] The obtained tetrathionate was recrystallized with water at temperatures below 60 °C and then dried at room temperature before storage at -10 ± 2 °C. A standard tetrathionate solution (1×10^{-3} mol dm^{-3}) was prepared by dissolving 151.3 mg of the potassium tetrathionate (water content: 0.07%) in water and diluting it to 500 cm^3; it was then stored at 5 ± 2 °C. Working standards were prepared by suitable dilultion.

Standard Iodate Solution: A 0.100/6 mol dm^{-3} iodate solution was prepared by dissolving 3.567 g of potassium iodate (99.98%) in water and diluting to 1000 cm^3. Working standard iodate solutions were prepared by appropriate dilution.

Standard Thiosulfate Solution: An approximately 0.1 mol dm^{-3} solution was prepared by dissolving a known amount of sodium thiosulfate pentahydrate in oxygen-free water containing a small amount of sodium carbonate (0.01% w/v) as a stabilizer. This solution was standardized by iodimetry 1 week after preparation. Working standard thiosulfate solutions (0.01% w/v Na_2CO_3) were prepared by suitable dilution of the standard with oxygen-free water.

Procedure. Pipette 10 cm^3 of a sample solution of up to 2.86×10^{-5}mol dm^{-3} tetrathionate into a 50-cm^3 calibrated flask, and add 3 cm^3 of 5 mol dm^{-3} sulfuric acid and 4.2 cm^3 of $1\times10^{-3}/6$ mol dm^{-3} standard iodate solution. Allow the flask to stand in a thermostat at 40 °C for 30 min in order to oxidize the tetrathionate completely to sulfate according to Eq. 2. Then add 5 cm^3 of 5 mol dm^{-3} acetic acid, 5 cm^3 of 6 mol dm^{-3} sodium hydroxide and 5 cm^3 of 1 mol dm^{-3} potassium iodide, whereupon the iodine equivalent to the excess iodate is quantitatively formed. After diluting to the mark

with water, mix the contents well and measure the absorbance of a solution of the triiodide against water at 350 nm.

Prepare an iodate-free reagent blank by adding 4.2 cm^3 of water in place of 4.2 cm^3 of $1\times10^{-3}/6$ mol dm^{-3} standard iodate solution and treating it exactly the same, and correct it for all the absorbances measured in this study.

Results and Discussion

Calibration Graphs. A series of standard solutions (10 cm^3) of tetrathionate were treated as described in the Procedure section. After the complete reaction of tetrathionate with iodate, the iodine which formed from the excess iodate was spectrophotometrically measured as triiodide. Hence, the proposed method gave a linear calibration graph with a negative slope for an increase in the concentration of tetrathionate. In previous methods, the thiosulfate formed by the sulfitolysis[8] and cyanolysis[15] of tetrathionate was measured by the consumption of iodine according to the following equation:

$$2S_2O_3^{2-} + I_2 \longrightarrow S_4O_6^{2-} + 2I^-, \quad (3)$$

in which 1 mol of thiosulfate furnishes 1 mol of electrons. On the other hand, according to Eq. 2, tetrathionate is oxidized to sulfate by iodate; 1 mol of tetrathionate furnishes 14 mol of electrons. Therefore, when the amount of liberated iodine equivalent to the excess iodate for tetrathionate is measured, a 14-fold chemical amplification can be achieved for the determination of tetrathionate. The calibration graph for tetrathionate obtained by the proposed method is shown, together with the calibration graph obtained for thiosulfate using iodine,[21] in Fig. 1, in which the molar concentration scale for tetrathionate was drawn to 14-times the scale for the thiosulfate concentration. The calibration graph for tetrathionate and that for thiosulfate were parallel to each other; the lower reagent blank obtained by the proposed method can be probably attributed to the oxidation of trace amounts of impurities in the reagents by the iodate and to the higher temperatures caused by the heat of neutralization of a strong acid; at higher temperatures the absorbance of triiodide decreases owing to its dissociation. When the reagent blank obtained for thiosulfate was normalized to that for tetrathionate, both the calibration graphs coincided completely with each other. This confirms that tetrathionate is quantitatively oxidized to sulfate by iodate according to Eq. 2 under the conditions described in the Procedure section.

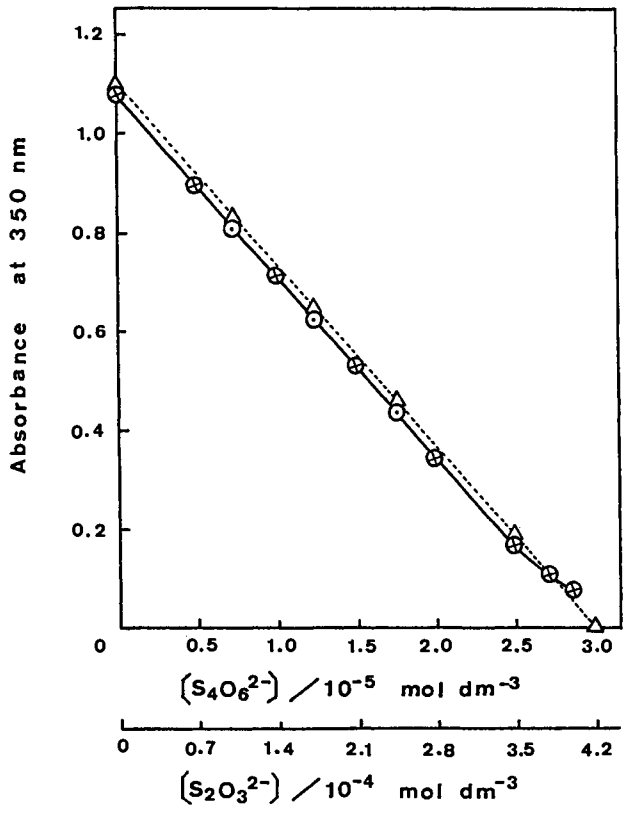

Fig. 1. Calibration graphs for tetrathionate and thiosulfate. ⊗, Tetrathionate by the proposed method; △, thiosulfate by iodine method;[21] ⊙, expected graph (the reagent blank obtained by the iodine method was normalized to that by the proposed method).

The proposed method can be applied to the determination of tetrathionate in the concentration range 2.5×10^{-7}—2.5×10^{-5} mol dm^{-3} (0.056—5.6 ppm). The precision of the method was based on 11 replicate analyses of a 10-cm^3 aliquot of a 1.5×10^{-5} mol dm^{-3} standard tetrathionate solution (33.6 μg of $S_4O_6^{2-}$ in 10 cm^3); the mean value of tetrathionate was found to be 33.5 μg, with a standard deviation of 0.14 μg of $S_4O_6^{2-}$ and a relative standard deviation of 0.42%.

Reaction Rate of Tetrathionate with Iodate. It is normally known that the potential for the redox couples, which involve a large number of hydrogen ions, is strongly dependent on the hydrogen-ion concentration. We therefore made an attempt to oxidize tetrathionate with iodate in an acidic medium of various strong acids: hydrochloric, nitric, perchloric, and sulfuric. Among these acids, only sulfuric acid proved suitable as a medium for the reaction of tetrathionate with iodate.[19] Therefore, the reaction rate was investigated in a medium containing varying amounts of sulfuric acid at 21 °C (i.e., room temparature); tetrathionate was allowed to react with iodate for various periods of time; the amount of iodine liberated from the excess of the iodate by the addition of iodide was then measured. The resulting graphs are shown in Fig. 2. Here, all of the absorbances obtained were normalized to those obtained using 3 cm^3 of 5 mol dm^{-3} sulfuric acid (i.e., all the reagent blanks were normalized to that obtained under the Procedure section). The reaction did not go to completion, even within 2 h in a 0.52 mol dm^{-3} sulfuric acid medium (3-cm^3 addition of 3 mol dm^{-3} H_2SO_4). Still, the reaction rate was accelerated by an increase in the amount of sulfuric acid; the reaction proceeded to stoichiometric completion according to Eq. 2 within 80 min in a 0.70 mol dm^{-3} sulfuric acid

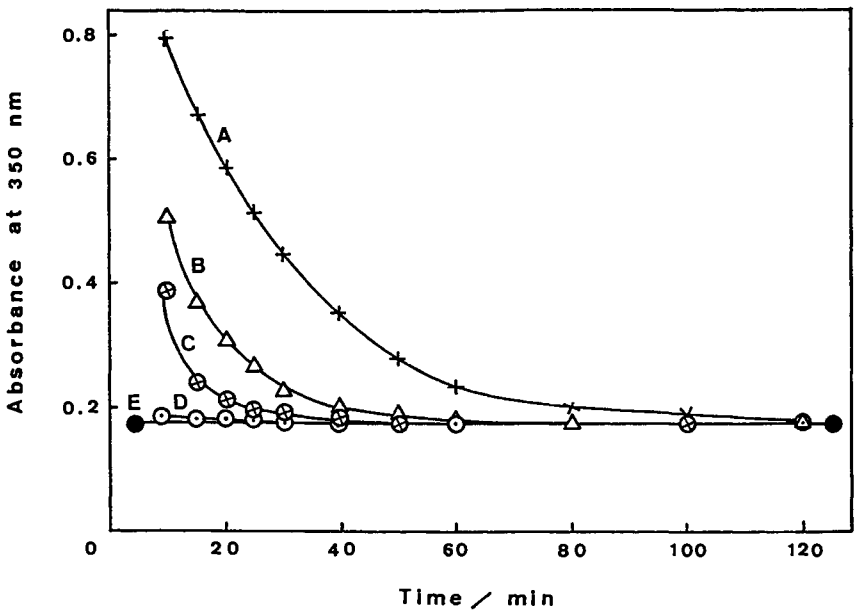

Fig. 2. Reaction rate of tetrathionate with iodate in a medium containing varying amounts of sulfuric acid at 21 °C (i. e., room temperature). A 10-cm^3 solution of 2.5×10^{-5} mol dm^{-3} tetrathionate was used. A, 3-cm^3 addition of 3 mol dm^{-3} H_2SO_4; B, 3-cm^3 addition of 4 mol dm^{-3} H_2SO_4; C, 3-cm^3 addition of 5 mol dm^{-3} H_2SO_4; D, 3-cm^3 addition of 8 mol dm^{-3} H_2SO_4; E, expected value obtained for 3.5×10^{-4} mol dm^{-3} $S_2O_3^{2-}$ using iodine method.[21]

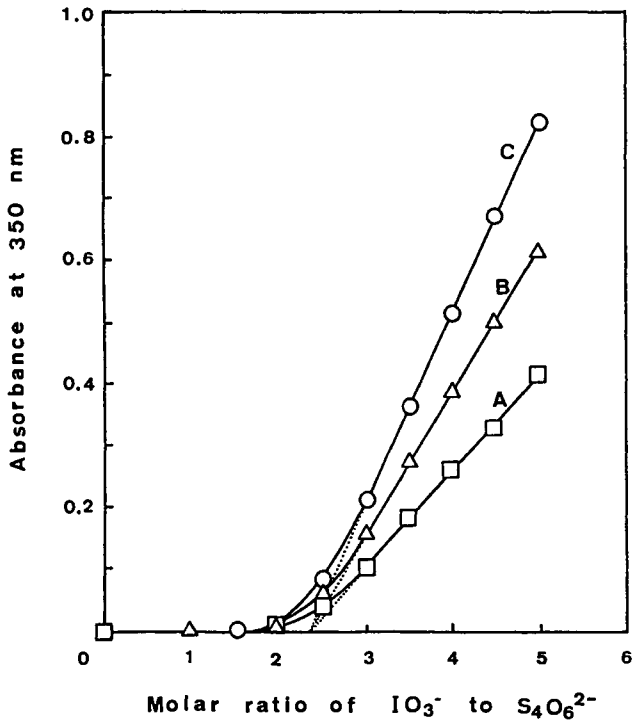

Fig. 3. Molar ratio graphs for the reaction of tetrathionate with iodate. A 10-cm^3 tetrathionate solution with various concentrations was used. A, 1×10^{-5} mol dm^{-3} $S_4O_6^{2-}$; B, 1.5×10^{-5} mol dm^{-3} $S_4O_6^{2-}$; C, 2×10^{-5} mol dm^{-3} $S_4O_6^{2-}$.

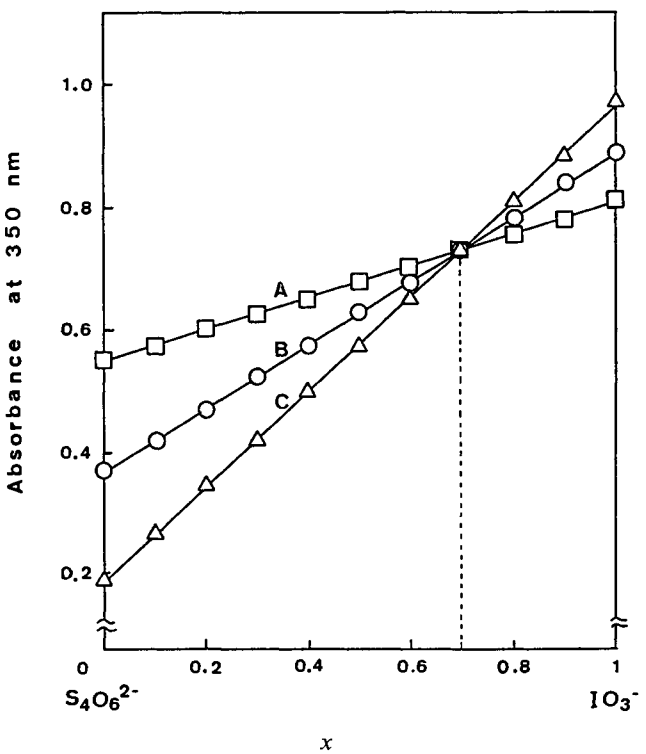

Fig. 4. Continuous variation graphs for the reaction of tetrathionate with iodate. A, $[IO_3^-]+[S_4O_6^{2-}]=5\times10^{-6}$ mol dm^{-3}; B, $[IO_3^-]+[S_4O_6^{2-}]=1\times10^{-5}$ mol dm^{-3}; C, $[IO_3^-]+[S_4O_6^{2-}]=1.5\times10^{-5}$ mol dm^{-3}. A 2.8-cm^3 solution of $1\times10^{-3}/6$ mol dm^{-3} iodate was additionally used.

Table 1. Effect of Foreign Ions on the Determination of 33.6 μg of Tetrathionate in 10 cm^3 of Sample Solution

Ion	Added as[a]	Amount	Amount of $S_4O_6^{2-}$ found	Error
		μg	μg	%
None			33.6	
Na^+	Na_2SO_4	10000	33.6	0
K^+	K_2SO_4	10000	33.6	0
NH_4^+	$(NH_4)_2SO_4$	10000	33.6	0
Mg^{2+}	$MgSO_4$	10000	33.6	0
Zn^{2+}	$ZnSO_4$	10000	33.8	0.6
Ca^{2+}	$Ca(NO_3)_2$	10000	33.2	−1.2
Cd^{2+}	$CdSO_4$	10000	33.6	0
Al^{3+}	$K_2Al_2(SO_4)_4$	10000	33.8	0.6
Pb^{2+}	$Pb(NO_3)_2$	1000	31.6	−6.0
		100	33.6	0
Mn^{2+}	$MnSO_4$	100	22.4	−33.3
		10	33.8	0.6
Cu^{2+}	$CuSO_4$	100	26.9	−19.9
		10	33.8	0.6
Fe^{2+}	$FeSO_4$	1000	22.2	−33.9
		100	34.0	1.8
Fe^{3+}	$Fe(NH_4)(SO_4)_2$	100	25.6	−24.1
		100	33.2[b]	−1.2
F^-	NaF	10000	33.8	0.6
Cl^-	KCl	10000	34.0	1.8
Br^-	KBr	10000	34.7	3.3
I^-	KI	1000	14.1	−58.0
		100	34.5	2.7
SO_4^{2-}	Na_2SO_4	10000	33.6	0
NO_3^-	KNO_3	10000	33.4	−0.6
HPO_4^{2-}	Na_2HPO_4	10000	33.6	0
HCO_3^-	$NaHCO_3$	10000	33.6	0
$HAsO_4^{2-}$	Na_2HAsO_4	10000	33.8	0.6
NO_2^-	$NaNO_2$	10	29.4	−12.5
		10000	33.8[c]	−0.6
HSO_3^-	$NaHSO_3$	10	37.4	11.3
		100	34.0[d]	1.8
S^{2-}	Na_2S	1	35.6	6.0
		10	34.5[d]	2.7

a) Water of crystallization is omitted for brevity. b) Iron(III) was masked by adding 1 cm^3 of 0.2 mol dm^{-3} sodium fluoride. c) Nitrite was decomposed by adding 1 cm^3 of 0.5 mol dm^{-3} amidosulfuric acid. d) The nitrogen gas at a flow-rate of 400 cm^3 min^{-1} was bubbled for 30 min.

medium (3-cm^3 addition of 4 mol dm^{-3} H_2SO_4), within 50 min in a 0.87 mol dm^{-3} sulfuric acid medium (3-cm^3 addition of 5 mol dm^{-3} H_2SO_4) and within 30 min in a 1.4 mol dm^{-3} sulfuric acid medium (3-cm^3 addition of 8 mol dm^{-3} H_2SO_4); the absorbances remained constant. At 40 °C, the reaction rate was accelerated much more and the reaction went to completion within 40 min in a 0.52 mol dm^{-3} sulfuric acid medium, within 30 min in a 0.70 mol dm^{-3} sulfuric acid medium and within 20 min in both 0.87 and 1.4 mol dm^{-3} sulfuric acid media. Hence, for the usual procedure, 3 cm^3 of 5 mol dm^{-3} sulfuric acid was employed and tetrathionate was allowed to react with iodate in the 0.87 mol dm^{-3} sulfuric acid medium for 30 min at 40 °C.

The sulfuric acid used had to be neutralized with a strong base; otherwise, the absorbance of triiodide increased greatly and rapidly with time owing to the formation of iodine in a strong acid medium, as the result of air-oxidation of the iodide added for the liberation of iodine from the excess iodate. Accordingly, each amount of the sulfuric acid used was neutralized with a strong base equivalent to the amount of the sulfuric acid. Further, 5 cm^3 of 5 mol dm^{-3} acetic acid was added to make the solution weakly acidic. However, it was desirable to measure the absorbance of the triiodide as soon as possible after its formation. A 4—8 cm^3 volume of 1 mol dm^{-3} potassium iodide solution proved to be sufficient for the complete liberation of iodine; in the Procedure section, a 5-cm^3 volume of 1 mol dm^{-3} potassium iodide solution was employed.

Stoichiometric Relationship for the Reaction of Tetrathionate with Iodate. An attempt was made to determine the stoichiometric relationship for the reaction of tetrathionate with iodate in a medium of sulfuric acid using both the molar ratio method and the continuous variation method. For applying the molar ratio

method, 10 cm^3 each of 1×10^{-5}, 1.5×10^{-5}, and 2×10^{-5} mol dm^{-3} tetrathionate solutions, and 4.2 cm^3 of each of iodate solutions (with varying concentrations) were used with a varying mole ratios of iodate to tetrathionate. After the addition of 3 cm^3 of 5 mol dm^{-3} sulfuric acid to each mixture, the mixture was allowed to stand for 30 min at 40 °C. The absorbance of the series of the solutions obtained was then measured according to the Procedure section. The resulting graphs are shown in Fig. 3. In order to determine the stoichiometric relationship of iodate to tetrathionate involved in the determination of tetrathionate, straight portions of each graph were extrapolated to the abscissa, since the proposed method gave a straight calibration graph over the concentration range of up to 2.5×10^{-5} mol dm^{-3} tetrathionate. Each dotted line intersected the abscissa at the point 2.3 (7/3). This proves that 3 mol of tetrathionate reacted with 7 mol of iodate under the conditions of the usual procedure.

For the method of continuous variations, each $10x$ (x=mole fraction of iodate) cm^3 of 5×10^{-6}, 1×10^{-5}, and 1.5×10^{-5} mol dm^{-3} iodate solutions, and each $10(1-x)$ cm^3 of 5×10^{-6}, 1×10^{-5}, and 1.5×10^{-5} mol dm^{-3} tetrathionate solutions were used to prepare a series of 10-cm^3 solutions with a varying iodate–tetrathionate mole ratio. To each mixture, 2.8 cm^3 of $1\times10^{-3}/6$ mol dm^{-3} iodate solution was added in order to obtain the absorbance of iodine (as triiodide), even in the region of the excess of tetrathionate ($x<0.7$). Then, 3 cm^3 of 5 mol dm^{-3} sulfuric acid and 1.4 cm^3 of water were added; the resulting volume of the solution was 17.2 cm^3 (as described in the Procedure section). The mixture was allowed to stand for 30 min at 40 °C; then, the absorbance of a series of the solutions was measured at 350 nm against water. Figure 4 shows the resulting plots of absorbance vs. mole fraction of iodate; all three graphs intersected at the point indicating a 0.7 [7/(7+3)] mole fraction of iodate. Further, this point appeared just on the absorbance obtained for the amount of the iodate used additionally. These results signify that tetrathionate reacted with iodate stoichiometrically with a tetrathionate : iodate mole ratio of 3 : 7 under the conditions described in the Procedure section, according with the results obtained by the method of molar ratios.

Effect of Foreign Ions. A 10-cm^3 solution containing 33.6 μg of tetrathionate (1.5×10^{-5} mol dm^{-3} tetrathionate) and various amounts of foreign ions was treated as described in the Procedure Section. The results are given in Table 1. The proposed method is based on the oxidation of tetrathionate with iodate in a strong acid medium, followed by spectrophotometric measurements of the iodine (as triiodide) formed (by the addition of iodide) from the excess iodate. Hence, the ions which oxidize iodide or reduce iodate are thought to interfere with the determination of tetrathionate. Copper(II), iron(III), and nitrite (which oxidize iodide), and sulfite and sulfide (which reduce iodate) gave serious errors when present in small amounts. Still, the nitrite was tolerated in amounts of up to 10000 μg by decomposing it by the addition of 1 cm^3 of 0.5 mol dm^{-3} amidosulfuric acid solution.

References

1) T. Koh, *Anal. Sci.*, **6**, 3 (1990).
2) P. J. Urban, *Fresenius' Z. Anal. Chem.*, **179**, 422 (1961).
3) T. Koh, A. Wagai, and Y. Miura, *Anal. Chim. Acta*, **71**, 367 (1974).
4) O. A. Nietzel and M. A. DeSesa, *Anal. Chem.*, **27**, 1839 (1955).
5) T. Koh and I. Iwasaki, *Bull. Chem. Soc. Jpn.*, **39**, 352 (1966).
6) T. Koh, *Bull. Chem. Soc. Jpn.*, **38**, 1510 (1965).
7) T. Koh and I. Iwasaki, *Bull. Chem. Soc. Jpn.*, **38**, 2135 (1965).
8) T. Koh, K. Taniguchi, Y. Miura, and I. Iwasaki, *Nippon Kagaku Kaishi*, **1979**, 348.
9) T. Koh, K. Taniguchi, and I. Iwasaki, *Bull. Chem. Soc. Jpn.*, **51**, 164 (1978).
10) T. Koh and K. Taniguchi, *Anal. Chem.*, **46**, 1679 (1974).
11) T. Koh, Y. Miura, and M. Suzuki, *Anal. Sci.*, **4**, 267 (1988).
12) T. Koh, Y. Miura, and M. Suzuki, *Analyst (London)*, **113**, 949 (1988).
13) T. Koh and I. Iwasaki, *Bull. Chem. Soc. Jpn.*, **39**, 703 (1966).
14) D. P. Kelly, L. A. Chambers, and P. A. Trudinger, *Anal. Chem.*, **41**, 898 (1969).
15) T. Koh and K. Taniguchi, *Anal. Chem.*, **45**, 2018 (1973).
16) T. Koh, Y. Aoki, and I. Iwasaki, *Analyst (London)*, **104**, 41 (1979).
17) T. Koh, Y. Miura, M. Ishimori, and N. Yamamuro, *Anal. Sci.*, **5**, 79 (1989).
18) T. Ozawa, *Nippon Kagaku Zasshi*, **87**, 573 (1966).
19) T. Koh, K. Kitami, and Y. Yonemura, *Anal. Sci.*, **7**, 81 (1991).
20) H. Stamm and M. Goehring, *Z. Anorg. Allg. Chem.*, **250**, 226 (1942).
21) T. Ozawa, *Nippon Kagaku Zasshi*, **87**, 576 (1966).

Structural Study of Optical Resolution. XVI. The Crystal Structures of a Pair of Diastereomeric Salts of the *lel*$_3$-Tris(*trans*-1,2-cyclohexanediamine)nickel(II) Complex with *d*-Tartrate Dianion

Tsutomu MIZUTA and Katsuhiko MIYOSHI*
Department of Chemistry, Faculty of Science, Hiroshima University,
1-1-89 Higashi-senda-machi, Naka-ku, Hiroshima 730
(Received November 30, 1990)

The crystal structures of the diastereomeric salt pair, *Λ-lel*$_3$-[Ni(*S,S*-chxn)$_3$](*d*-tart)·3H$_2$O (**1**) and *Δ-lel*$_3$-[Ni(*R,R*-chxn)$_3$](*d*-tart)·5H$_2$O (**2**) (chxn=*trans*-1,2-cyclohexanediamine and *d*-tart=(+)-(*R,R*)-tartrate dianion), have been determined by single-crystal X-ray diffraction techniques. Crystal **1** is orthorhombic with the space group $P2_12_12_1$, a=10.093(2), b=13.589(4), c=22.011(4) Å, and Z=4. Crystal **2** is also orthorhombic with the same space group, a=11.197(2), b=13.102(2), c=22.402(2) Å, and Z=4. In **1**, the *d*-tart ion makes a familiar face-to-face contact with the *Λ* complex, in which the two alcoholic and one carboxylic O atoms of the *d*-tart ion are involved in the multiple hydrogen bonds to the three H–N groups on the triangular face of the complex. This contact mode resembles the one found earlier in the chloride *d*-tart salt of the corresponding *Λ* Co(III) complex, *Λ-lel*$_3$-[Co(*S,S*-chxn)$_3$]Cl(*d*-tart)·2H$_2$O (**3**). On the other hand, no such face-to-face contact is present in **2**, though it has been found in the corresponding *Δ* Co(III) complex salt, *Δ-lel*$_3$-[Co(*R,R*-chxn)$_3$]Cl(*d*-tart)·2H$_2$O (**4**) in which the *d*-tart ion is obliged to rotate the distal carboxylato group so as to avoid the steric repulsion otherwise imposed on it by one of the bulky chxn ligands. Detailed comparison of the above four crystal structures revealed that the packing modes of the respective complex cations and counterions are surprisingly similar to one another, indicating that the absence of such a face-to-face contact in **2** is attributed to the weaker affinity of the *d*-tart ion for the divalent *Δ* Ni(II) complex, rather than to the steric demands of the crystal packing in **2**. In **2** are found two deformed contact modes similar to each other, in which the *d*-tart ion directs its three O atoms to the triangular face, but only one of them is hydrogen-bonded to one or two of the three H–N groups on the triangular face. The *d*-tart ion thereby avoids the steric repulsion that would be imposed on it if it should make a usual face-to-face contact with the *Δ* complex.

(+)-(*R,R*)-Tartrate dianion (abbreviated as *d*-tart ion hereafter) is known as an effective resolving agent not only for chiral amines but also for metal–amine complexes.[1,2] To elucidate how this simple chiral anion recognizes the chirality of these complexes, we and other groups have analyzed several crystal structures of *d*-tart salts with some tris(diamine)cobalt(III) complex cations.[3–10] They found a common face-to-face contact mode in which the two alcoholic and one carboxylic O atoms of the *d*-tart ion are hydrogen-bonded to the three H–N groups on the triangular face of the complex along the C_3 axis. When the complex has a *Λ* configuration, the above-mentioned multiple hydrogen bonds are favorably formed without any steric repulsion. On the other hand, the *Δ* complex imposes a steric repulsion on the distal carboxylato group of the *d*-tart ion if it should make a similar face-to-face contact with the triangular face. As a result, either the *d*-tart ion rotates its distal carboxylato group to maintain the face-to-face contact,[9] or the multiple hydrogen bonds to the triangular face are more or less damaged in number and/or in strength.[10] In this way, chiral discrimination with *d*-tart ion is effectively attained, particularly for those metal–amine complexes which have bulky substituents on their chelate rings, such as *lel*$_3$-[Co(*trans*-chxn)$_3$]$^{3+}$ or *fac*- and *mer*-[Co(*cis*-chxn)$_3$]$^{3+}$ (chxn=1,2-cyclohexanediamine), because the bulkier the substituents, the more severe the steric repulsion that *Δ* enantiomers of these complexes impose on the distal carboxylato group.[9,10] However, most of the diastereomeric salts investigated are those of trivalent Co(III) complex cations, and only two divalent Ni(II) complex salts, i.e., *Λ,Λ*-[Ni(en)$_3$](*dl*-tart)·H$_2$O[11] and *Δ*-[Ni(en)$_3$]$_3$(*d*-tart)$_3$·4H$_2$O[11] (en=1,2-ethanediamine) having no substituent on each chelate, have been so far examined. In the present study, the crystal structures have been determined for a pair of diastereomeric salts of the divalent *lel*$_3$-[Ni(*trans*-chxn)$_3$]$^{2+}$ complex with *d*-tart ion, with the aim of elucidating how the valency of the complex cation affects the contact modes with the *d*-tart ion when the complex carries bulky substituents on the diamine chelates.

Experimental

Preparation of *Λ*-[Ni(*S,S*-chxn)$_3$](*d*-tart)·3H$_2$O (1). To an aqueous solution of (1*S*,2*S*)-cyclohexanediamine[9] (2.9 g) in 20 ml of water, was added 1.5 g of nickel *d*-tartrate prepared by mixing sodium *d*-tartrate with an equivalent amount of NiCl$_2$·6H$_2$O in water. The violet solution thus obtained was left standing at room temperature for several days. Violet crystals were deposited and a crystal of suitable size was selected for the structure analysis. Anal. Found: C, 44.07; H, 8.98; N, 13.80%. Calcd for *Λ*-[Ni(*S,S*-chxn)$_3$](*d*-tart)·3H$_2$O (**1**): C, 43.79; H, 8.69; N, 13.93%.

Preparation of *Δ*-[Ni(*R,R*-chxn)$_3$](*d*-tart)·5H$_2$O (2). **2** was prepared in a similar manner using (1*R*,2*R*)-cyclohexanediamine.[9] Anal. Found: C, 41.27; H, 8.72; N, 13.01%. Calcd for *Δ*-[Ni(*R,R*-chxn)$_3$](*d*-tart)·5H$_2$O (**2**): C, 41.33; H,

Table 1. Crystallographic Data

Crystal	1	2
Formula	$C_{18}H_{42}N_6Ni$, $C_4H_4O_6$, $3H_2O$	$C_{18}H_{42}N_6Ni$, $C_4H_4O_6$, $5H_2O$
a/Å	10.093(2)	11.197(2)
b/Å	13.589(4)	13.102(2)
c/Å	22.011(4)	22.402(2)
V/Å^3	3018.8(11)	3286.4(10)
Z	4	4
Fw	603.4	639.4
Space group	$P2_12_12_1$	$P2_12_12_1$
T/°C	20	20
λ/Å	0.71069	0.71069
ρ_{calcd}/g cm^{-3}	1.328	1.292
ρ_{obsd}/g cm^{-3}	1.34	1.30
μ (Mo $K\alpha$)/cm^{-1}	6.96	6.47
R[a]	0.044	0.047
R_w[b]	0.047	0.056

a) $R=\sum(||F_o|-|F_c||)/\sum|F_o|$. b) $R_w=[\sum w(|F_o|-|F_c|)^2/\sum w(F_o)^2]^{1/2}$ and $w=1/(\sigma(F_o))^2$.

Table 2. Atomic Coordinates and Equivalent Temperature Factors for Non-Hydrogen Atoms in Λ-[Ni(S,S-chxn)$_3$](d-tart)·3H$_2$O (**1**)

Atom	x	y	z	B_{eq}/Å^2
Ni	0.28897(6)	0.85323(4)	0.14173(3)	2.3
N1	0.1567(4)	0.9765(3)	0.1391(2)	3.0
N2	0.4037(4)	0.9478(3)	0.0849(2)	2.6
N3	0.1885(4)	0.7826(3)	0.0681(2)	2.7
N4	0.4174(4)	0.7306(3)	0.1317(2)	2.8
N5	0.1652(4)	0.7823(3)	0.2061(2)	2.8
N6	0.3840(4)	0.9029(3)	0.2221(2)	3.0
C1	0.2036(5)	1.0492(3)	0.0932(2)	2.7
C2	0.1467(6)	1.1514(4)	0.1043(2)	4.1
C3	0.2047(8)	1.2281(4)	0.0603(3)	5.2
C4	0.3564(7)	1.2277(4)	0.0633(3)	5.3
C5	0.4115(6)	1.1254(4)	0.0503(2)	4.1
C6	0.3556(5)	1.0497(4)	0.0949(2)	2.7
C7	0.2356(5)	0.6793(3)	0.0653(2)	2.7
C8	0.1978(6)	0.6266(4)	0.0065(2)	4.2
C9	0.2539(7)	0.5209(4)	0.0043(3)	5.0
C10	0.4034(7)	0.5241(4)	0.0103(3)	4.5
C11	0.4426(6)	0.5759(4)	0.0696(3)	4.0
C12	0.3876(5)	0.6801(3)	0.0730(2)	2.6
C13	0.1861(5)	0.8288(3)	0.2659(2)	2.9
C14	0.1271(6)	0.7705(4)	0.3193(2)	4.2
C15	0.1545(7)	0.8216(5)	0.3802(3)	5.7
C16	0.3038(7)	0.8372(5)	0.3882(2)	5.9
C17	0.3650(6)	0.8947(5)	0.3351(2)	4.4
C18	0.3346(5)	0.8441(4)	0.2743(2)	3.0
C19	0.7368(7)	1.0437(4)	0.2549(3)	4.8
C20	0.7639(5)	0.9794(4)	0.1983(2)	3.3
C21	0.7811(5)	0.8711(4)	0.2162(2)	3.2
C22	0.8154(5)	0.8071(4)	0.1598(2)	3.4
O1	0.8254(5)	1.0480(3)	0.2948(2)	7.2
O2	0.6298(5)	1.0888(3)	0.2549(2)	6.7
O3	0.6575(4)	0.9915(3)	0.1572(2)	4.4
O4	0.6656(4)	0.8400(3)	0.2472(2)	4.5
O5	0.7394(4)	0.7362(3)	0.1480(2)	6.0
O6	0.9180(3)	0.8286(3)	0.1322(2)	4.4
OW1	0.8267(5)	0.6148(3)	0.0534(2)	6.8
OW2	0.6308(5)	0.6321(4)	0.2483(2)	7.3
OW3	0.9117(7)	0.5780(5)	0.2225(4)	14.8

8.83; N, 13.14%.

X-Ray Structure Analysis. Cell dimensions were determined and refined on a Syntex R3 single-crystal diffractometer. The results are given in Table 1. The intensity data were collected by the ω-scan technique with graphite-monochromated Mo $K\alpha$ radiation (λ=0.71069 Å). Three check reflections monitored after every 197 reflections showed no decrease in intensity during the data collection. Corrections for Lorentz and polarization effects were applied to the intensities, but no absorption and extinction corrections were made.

Each structure was solved by the well-established heavy-atom methods described in the previous work.[9,12,13] The anomalous dispersion coefficient was used for the Ni atom only,[14] and the absolute configuration of the complex cation was confirmed to be Λ for **1** and Δ for **2**.[15] The final R and R_w values are given in Table 1 together with the crystallographic data on **1** and **2**. Final positional parameters for non-hydrogen atoms are given in Tables 2 and 3 for **1** and **2**,

Table 3. Atomic Coordinates and Equivalent Temperature Factors for Non-Hydrogen Atoms in Λ-[Ni(R,R-chxn)$_3$](d-tart)·5H$_2$O (**2**)

Atom	x	y	z	B_{eq}/Å^2
Ni	0.32019(6)	0.80530(6)	0.35908(3)	2.6
N1	0.2361(4)	0.7502(4)	0.4382(2)	2.9
N2	0.4326(4)	0.6771(4)	0.3754(2)	3.3
N3	0.1967(4)	0.7218(3)	0.3044(2)	3.4
N4	0.3985(4)	0.8327(3)	0.2738(2)	3.1
N5	0.2117(4)	0.9398(4)	0.3527(2)	3.5
N6	0.4337(4)	0.9084(4)	0.4061(2)	3.3
C1	0.2712(5)	0.6411(4)	0.4457(2)	2.9
C2	0.2366(6)	0.5977(5)	0.5065(3)	4.1
C3	0.2821(7)	0.4865(5)	0.5142(3)	5.3
C4	0.4141(7)	0.4821(5)	0.5047(3)	4.7
C5	0.4483(6)	0.5229(5)	0.4427(3)	4.2
C6	0.4066(5)	0.6325(4)	0.4352(2)	3.1
C7	0.2044(5)	0.7649(4)	0.2426(2)	3.1
C8	0.1360(6)	0.7022(6)	0.1969(3)	5.0
C9	0.1548(7)	0.7441(6)	0.1349(3)	6.5
C10	0.2854(8)	0.7491(7)	0.1192(3)	6.7
C11	0.3545(6)	0.8143(6)	0.1646(2)	4.5
C12	0.3366(6)	0.7721(4)	0.2268(2)	3.2
C13	0.2482(6)	1.0094(5)	0.4017(2)	3.3
C14	0.1943(7)	1.1160(5)	0.3953(3)	4.9
C15	0.2370(9)	1.1863(6)	0.4457(3)	7.5
C16	0.3721(9)	1.1902(6)	0.4481(3)	7.5
C17	0.4293(7)	1.0855(6)	0.4523(3)	5.3
C18	0.3839(6)	1.0144(4)	0.4023(2)	3.6
C19	0.9136(6)	0.6921(5)	0.4132(2)	4.1
C20	0.7971(5)	0.6837(5)	0.3771(2)	3.5
C21	0.8195(6)	0.6469(4)	0.3133(2)	3.4
C22	0.7013(5)	0.6458(4)	0.2784(2)	3.4
O1	0.9894(4)	0.7544(4)	0.3929(2)	4.9
O2	0.9177(5)	0.6420(4)	0.4597(2)	6.3
O3	0.7178(5)	0.6168(4)	0.4066(2)	7.0
O4	0.8721(4)	0.5484(4)	0.3130(2)	5.8
O5	0.6652(4)	0.5604(3)	0.2600(2)	5.0
O6	0.6477(4)	0.7290(3)	0.2730(2)	4.7
OW1	0.5832(5)	1.0293(3)	0.2323(2)	5.2
OW2	0.3308(4)	1.4220(4)	0.1691(2)	5.0
OW3	0.3017(6)	1.3675(4)	0.3229(2)	7.3
OW4	−0.0756(5)	0.9262(4)	0.3347(2)	7.6
OW5	0.0864(7)	1.4520(6)	0.2888(3)	12.4

respectively. Tables of the full listing of the crystallographic data, hydrogen atom coordinates, anisotropic thermal parameters for non-hydrogen atoms, bond distances and angles, hydrogen bond distances and angles, and a list of observed and calculated structure factors are deposited as Document No. 9119 at the Office of the Editor of Bull. Chem. Soc. Jpn.

Results and Discussion

Contact Modes in 1 and 2. There has been found a familiar face-to-face contact in the *Λ*-[Ni(*S,S*-chxn)$_3$](*d*-tart)·3H$_2$O (**1**), which is depicted in Fig. 1 with the numbering schemes adopted for the respective atoms. The geometries of the complex cation in **1** are in complete agreement with those reported previously.[16] The *d*-tart ion takes a normal conformation and directs its four O atoms (O2, O3, O4, and O5) to the triangular face of the complex along the C_3 axis. Of the four, two alcoholic and one carboxylic O atoms (O3, O4, and O5) are triply hydrogen-bonded to the three H–N groups (H2–N2, H2–N6, and H2–N4) on the triangular face without any steric repulsion. The two O atoms (O1 and O2) of the distal carboxylato group are far from any of the bulky chxn ligands, but they are hydrogen-bonded to the H1–N5 and H1–N4 groups of another neighboring complex, which are directed along the C_2 axis. Thus, the above contact mode resembles those so far found in some diastereomeric salts of trivalent *Λ* Co(III) complexes such as *Λ*-*lel*$_3$-[Co(en)$_3$]X(*d*-tart)·5H$_2$O[3,5,6] (X=Cl or Br), *Λ*-[Co(sen)]Cl(*d*-tart)·6H$_2$O[4,6] (sen=*N,N'*-bis(2-aminoethyl)-2-[[(2-aminoethyl)-amino]methyl]-2-methyl-1,3-propanediamine), and *Λ*-*lel*$_3$-[Co(*S,S*-chxn)$_3$]Cl(*d*-tart)·2H$_2$O (**3**).[9] It is then confirmed that a familiar face-to-face contact is maintained even in the divalent Ni(II) complex salt with bulky diamine chelates, provided that the complex has a *Λ* configuration. Actually, a similar face-to-face contact mode has been found in the *Λ,Λ*-[Ni(en)$_3$](*dl*-tart)·H$_2$O[11] as well, where the *d*-tart ion makes such a contact with the *Λ* enantiomer only and the *l*-tart ion does with the *Δ* enantiomer only, as expected. The hydrogen bonds pertinent to these face-to-face contact modes are numerically compared in Table 4.

In contrast, no such face-to-face contact mode is present in the *Λ*-[Ni(*R,R*-chxn)$_3$](*d*-tart)·5H$_2$O (**2**). Instead, each *d*-tart ion is sandwiched between the two triangular faces and connects them through the two "deformed" contact modes in **2**, as seen in Fig. 2. One of them is depicted down to the C_3 axis in Fig. 3 together with the atom numbering schemes, where the *d*-tart ion with a usual conformation directs the three O atoms (O1, O2, and O4) to the triangular face, but only the O1 atom is disposed close enough to form a bifurcated hydrogen bond to the H1–N1 and H1–N3 groups on the triangular face. The O2 atom is hydrogen-bonded to the two H–N groups (H2–N1 and H2–N6) directed along the C_2 axis of another neighboring complex and the O4 atom is to a water molecule.

The other "deformed" contact mode is the one in which the remaining three O atoms (O3, O5, and O6) of the *d*-tart ion are directed to the triangular face of another complex cation in the above layer and similar hydrogen bonds are formed without any steric repulsion; O6 to H1–N4 on the triangular face and to H–OW3 (water molecule), O5 to H2–N4 and H2–N5 directed along the C_2 axis of the neighboring complex in the same layer, and O5 to H–OW1 (water molecule). Consequently, it is evident that the overall hydrogen-bonding interaction of the *d*-tart ion with the triangular face of the complex is by far weaker in **2** than in **1** or **3**,

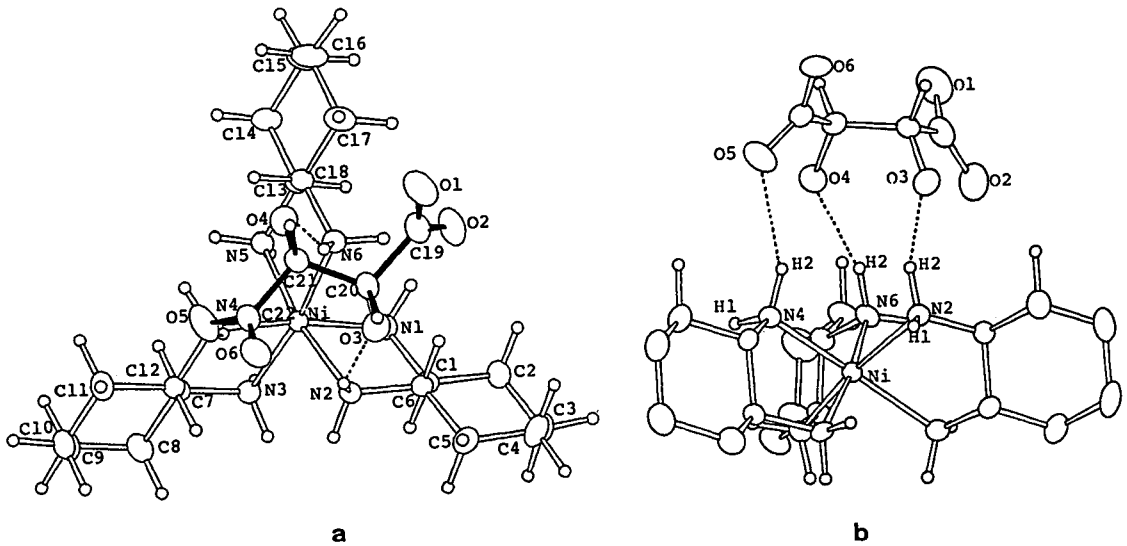

Fig. 1. Drawing of the face-to-face contact mode found in *Λ*-[Ni(*S,S*-chxn)$_3$](*d*-tart)·3H$_2$O (**1**), as viewed down (a) and normal to (b) the C_3 axis of the complex. Possible hydrogen bonds are shown by broken lines and most of the CH protons are omitted for clarity in (b).

Table 4. Comparison of Hydrogen-Bond Distances and Angles in the Face-to-Face Contacts of *d*-Tart Ion with Some Relevant *Λ* Complex Cations

d-tart Complex ion	O3 H(N2)	O3 H(N6)	O4 H(N6)	O4 H(N4)	O5 H(N4)	O5 H(N2)
			Distances of O··H/Å			
Λ-$[Co(en)_3]^{3+}$	2.17	2.50	2.05	2.34	2.06	2.47
Λ-$[Co(sen)]^{3+}$	2.06	2.50	2.01	2.34	2.04	2.62
Λ-$[Co(chxn)_3]^{3+}$		2.44	2.06		1.95	2.14
Λ-$[Ni(en)_3]^{2+}$	2.23		2.14		1.94	
Λ-$[Ni(chxn)_3]^{2+}$	2.19		2.10		2.34	
			Distances of O··N/Å			
Λ-$[Co(en)_3]^{3+}$	3.072(7)	3.212(8)	2.976(8)	3.050(8)	3.005(8)	3.173(8)
Λ-$[Co(sen)]^{3+}$	2.930(4)	3.289(5)	2.905(4)	3.150(4)	2.927(5)	3.391(4)
Λ-$[Co(chxn)_3]^{3+}$		3.096(9)	2.938(9)		2.870(8)	3.036(9)
Λ-$[Ni(en)_3]^{2+}$	3.120(4)		3.093(4)		2.899(4)	
Λ-$[Ni(chxn)_3]^{2+}$	3.074(5)		3.019(5)		3.270(6)	
			Angles of O··H–N/°			
Λ-$[Co(en)_3]^{3+}$	149	128	153	127	157	127
Λ-$[Co(sen)]^{3+}$	144	135	148	138	146	134
Λ-$[Co(chxn)_3]^{3+}$		122	145		155	149
Λ-$[Ni(en)_3]^{2+}$	147		158		161	
Λ-$[Ni(chxn)_3]^{2+}$	146		153		154	

Each H atom is allocated an idealized position on the basis of each H–N bond length of 1.0 Å and a tetrahedral angle around each N atom. *Λ*-$[Co(en)_3]^{3+}$: *Λ*-$[Co(en)_3]Br(d\text{-tart})\cdot 5H_2O$ (Ref. 3), *Λ*-$[Co(sen)]^{3+}$: *Λ*-$[Co(sen)]Cl(d\text{-tart})\cdot 6H_2O$ (Ref. 4), *Λ*-$[Co(chxn)_3]^{3+}$: *Λ*-$[Co(S,S\text{-chxn})_3]Cl(d\text{-tart})\cdot 2H_2O$ (Ref. 9), *Λ*-$[Ni(en)_3]^{2+}$: *Λ*, *Λ*-$[Ni(en)_3](dl\text{-tart})\cdot H_2O$ (Ref. 11), and *Λ*-$[Ni(chxn)_3]^{2+}$: **1** (this work).

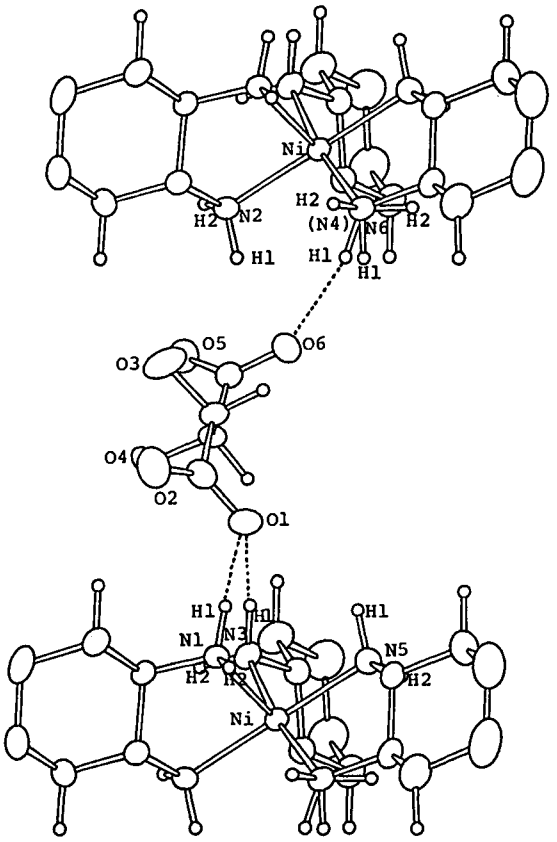

Fig. 2. Drawing of the two "deformed" contact modes found in **2**, as viewed normal to the C_3 axis of the complex. Possible hydrogen bonds are shown by broken lines and most of the CH protons are omitted for clarity.

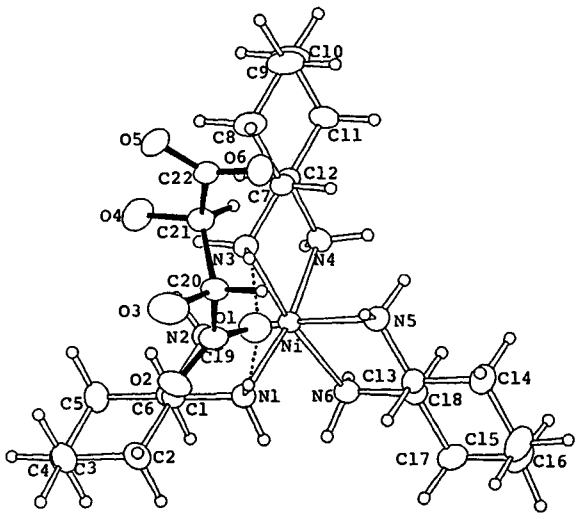

Fig. 3. Drawing of one of the "deformed" contact modes found in *Δ*-$[Ni(R,R\text{-chxn})_3](d\text{-tart})\cdot 5H_2O$ (**2**). Possible hydrogen bonds are shown by the broken lines.

but the *d*-tart ion experiences no steric repulsion from the bulky chxn ligands of the *Δ* complex in **2**.

On the other hand, the familiar face-to-face contact mode has been found in the corresponding *Δ* Co(III) complex, *Δ*-*lel*$_3$-$[Co(R,R\text{-chxn})_3]Cl(d\text{-tart})\cdot 2H_2O$ (**4**),[9] in which the *d*-tart ion is obliged to rotate its distal carboxylato group greatly so as to avoid the steric repulsion that would be otherwise imposed on it by one of the chxn ligands. That is, the *d*-tart ion maintains

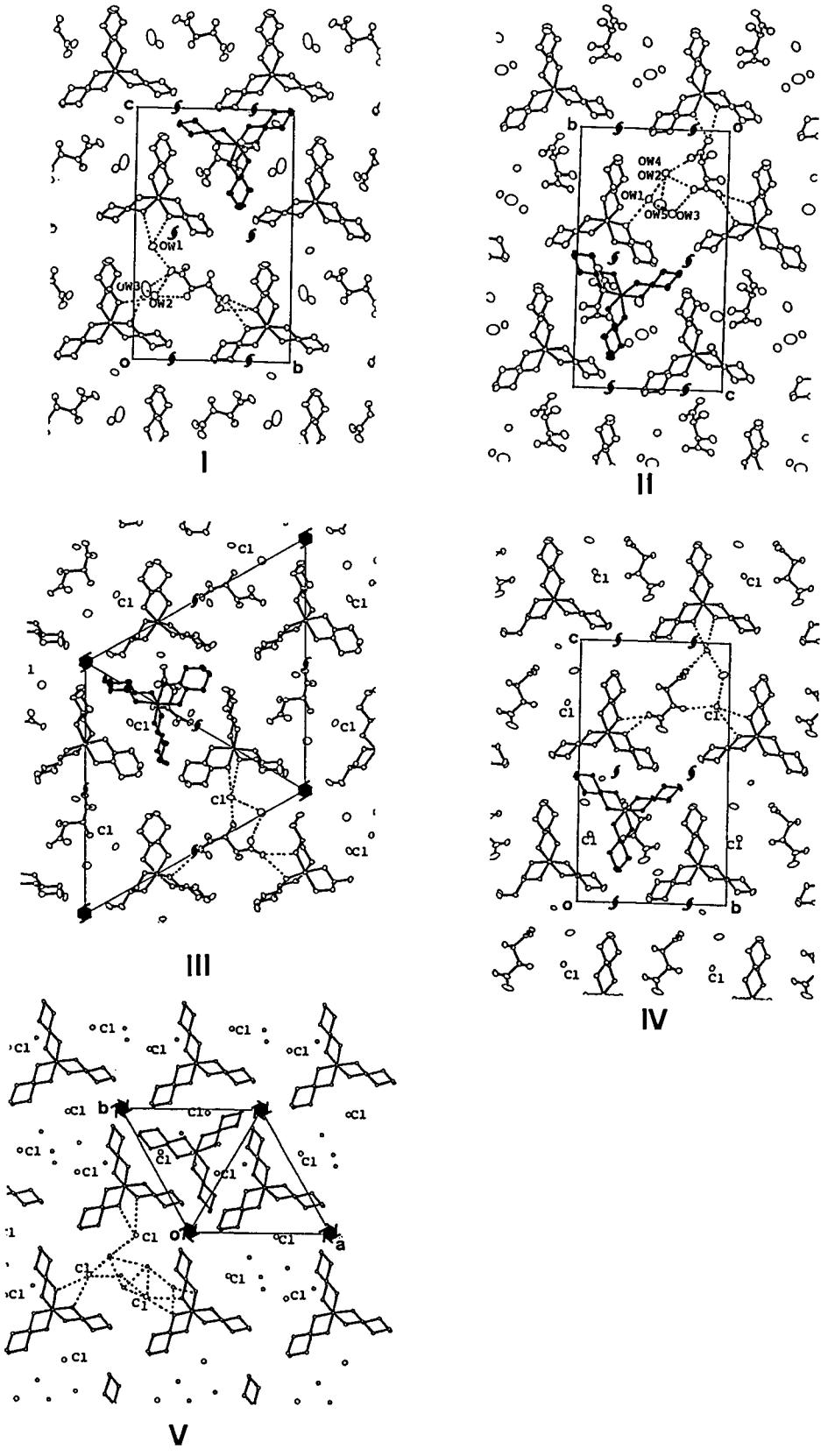

Fig. 4. Comparison of the packing modes in the relevant crystal structures. I: *Λ*-[Ni(*S,S*-chxn)$_3$](*d*-tart)·3H$_2$O (**1**), II: *Δ*-[Ni(*R,R*-chxn)$_3$](*d*-tart)·5H$_2$O (**2**), III: *Λ*-[Co(*S,S*-chxn)$_3$]Cl(*d*-tart)·2H$_2$O (**3**), IV: *Δ*-[Co(*R,R*-chxn)$_3$]Cl(*d*-tart)·2H$_2$O (**4**), and V: *Λ*-[Co(*S,S*-chxn)$_3$]Cl$_3$·5H$_2$O (**5**).

Table 5. Comparison of Space Groups and Cell Constants among Some Related Crystals

Crystals	**1**	**2**	**3**	**4**	**5**
Space group	$P2_12_12_1$	$P2_12_12_1$	$P6_3$	$P2_12_12_1$	$P6_1$
a/Å	10.093	11.197	22.068	9.666	12.34
b/Å	13.589	13.102	22.068	12.999	12.34
c/Å	22.011	22.402	10.492	22.950	33.52

1: *Λ*-[Ni(*S,S*-chxn)$_3$](*d*-tart)·3H$_2$O, **2**: *Λ*-[Ni(*R,R*-chxn)$_3$](*d*-tart)·5H$_2$O, **3**: *Λ*-[Co(*S,S*-chxn)$_3$]-Cl(*d*-tart)·2H$_2$O, **4**: *Λ*-[Co(*R,R*-chxn)$_3$]Cl(*d*-tart)·2H$_2$O, and **5**: *Λ*-[Co(*S,S*-chxn)$_3$]Cl$_3$·5H$_2$O.

the face-to-face contact even with the *Λ* complex at the expense of the conformational energy. This is because the accompanying conformational destabilization is compensated for the most part in **4** by the intimate hydrogen bonds to the neighboring complex cations,[9] and also because the face-to-face contact with the trivalent Co(III) complex cation leads to a substantial stabilization. Then, the absence of the face-to-face contact in **2** implies that the neighboring complexes are not appropriately disposed in **2** to assist the conformational change, and/or that the attractive force of the divalent Ni(II) complex is not strong enough for the *d*-tart ion to make a face-to-face contact with its *Λ* enantiomer against the accompanying steric repulsion. So, the packing modes of the composite ions in **2** need to examine and compare with those of the relevant diastereomeric salts before we proceed to settle the above problem.

Comparison of Packing Modes. Now, the packing modes in the present crystals **1** and **2** are compared with those in the relevant diastereomeric salts of the Co(III) complex cations, *Λ-lel*$_3$-[Co(*R,R*-chxn)$_3$]Cl(*d*-tart)·2H$_2$O (**3**) and *Δ-lel*$_3$-[Co(*R,R*-chxn)$_3$]Cl(*d*-tart)·2H$_2$O (**4**).[9] The space groups and the cell dimensions of the four crystals are listed in Table 5 together with those of *Λ-lel*$_3$-[Co(*S,S*-chxn)$_3$]Cl$_3$·5H$_2$O (**5**).[17] The structures of these five crystals are depicted in Fig. 4, where each structure is projected along the *a*-axis for **1**, **2**, and **4**, and along the *c*-axis for **3** and **5**. The range projected is 0—1/2 for the former three, −1/4—1/4 for **3**, and −1/12—1/12 for **5**, and each range (layer) has a thickness of ca. 5 Å. To each of these structures, one complex is added in black to demonstrate that the complex is disposed at that position both above and below the layer.

It is evident in Fig. 4 that quite similar arrangements of the complex cations are found not only in **1**, **2**, and **4**, but also in **5**; each complex cation is arranged in a similar manner in the layer of ca. 5 Å thickness with its C_3 axis directed parallel to the projection axis and with the counterion(s) and water molecules packed in a cavity thus formed. In this respect, crystal **3** has also similar arrangements of the complex cations as well as the counterions and water molecules, though the C_3 axis of each complex is directed not exactly parallel to the projection axis in **3**. Furthermore, since each layer is related to the upper and lower layers by the two- and six-fold screw axes in **1**—**4** and in **5**, respectively, it follows that the counterion(s) is packed in a cavity surrounded by the five complex cations in all of the five crystal structures. Therefore, it can be said that the five crystals bear a close resemblance to one another with respect to the spatial arrangements of the complex cations as well as the counterions, and that their packing modes are governed primarily by the bulky complex cations.

The discussions presented above indicate that the face-to-face contact mode might be adopted in **2** on the spatial grounds mentioned above. However, no such mode is present in **2**, suggesting that the divalent Ni(II) complex is not attractive enough for the *d*-tart ion to make such a contact with its *Λ* enantiomer against the accompanying steric repulsion imposed on the distal carboxylato group. In fact, the acidity of the amino protons should be much lower in the Ni(II) complex, because the central metal ion is divalent and the donation of the lone-pair electrons on the amino groups is less pronounced in the Ni(II) complex than in the low-spin Co(III) complex. Consequently, it is concluded that the contact modes with the *d*-tart ion are readily subjected to the steric demands of the composite ions in the Ni(II) complex salts, while the face-to-face contact is maintained at all costs in the Co(III) complex salts[7—10] where it leads to a substantial stabilization.

Finally, it seems noteworthy that the two "deformed" contact modes found in **2** are quite similar to those found earlier in the *Λ*-[Ni(en)$_3$]$_3$(*d*-tart)$_3$·4H$_2$O (**6**),[11] where each *d*-tart ion is sandwiched between the two triangular faces of the two *Λ* complex cations and it directs to the respective faces the two O atoms of one carboxylato group and one alcoholic O atom on the asymmetric carbon atom to which the other carboxylato group is attached, like in **2**, forming intimate hydrogen bonds to the H–N groups on them. In addition, each *d*-tart ion adopting these "deformed" contact modes in **2** also serves to connect directly the two complex cations in the same layer as it is in, through the two bifurcated hydrogen bonds (N1–H2··O2··H2–N6 and N4–H2··O5··H2–N5), as seen in II shown in Fig. 4, and similar roles are played by each *d*-tart ion in **6**. Consequently, it is fairly reasonable that the "deformed" contact modes are adopted in the Ni(II) complex salts when the face-to-face contact is prohibited by the steric repulsion, i.e., when the complex carries bulky substituents on the chelate rings and has a *Λ* configuration.

References

1) Y. Yoshikawa and K. Yamasaki, *Coord. Chem. Rev.*, **28**, 205 (1975).
2) H. Yoneda, *J. Chromatogr.*, **313**, 59 (1984).
3) Y. Kushi, M. Kuramoto, and H. Yoneda, *Chem. Lett.*, **1976**, 135. T. Tada, Y. Kushi, and H. Yoneda, *Chem. Lett.*, **1977**, 379. Y. Kushi, M. Kuramoto, and H. Yoneda, *Chem. Lett.*, **1976** 339.
4) H. Okazaki, U. Sakaguchi, and H. Yoneda, *Inorg. Chem.*, **22**, 1539 (1983).
5) D. H. Templeton, A. Zalkin, H. W. Ruben, and L. K. Templeton, *Acta Crystallogr., Sect. B*, **35**, 1608 (1979).
6) L. S. Magill, J. D. Korp, and I. Bernal, *Inorg. Chem.*, **20**, 1187 (1981).
7) I. Bernal, J. D. Korp, and I. I. Creaser, *Aust. J. Chem.*, **37**, 2365 (1984).
8) T. Mizuta, T. Tada, Y. Kushi, and H. Yonada, *Inorg. Chem.*, **27**, 3836 (1988).
9) Part XIV of this series; T. Mizuta, K. Toshitani, K. Miyoshi, and H. Yoneda, *Inorg. Chem.*, **29**, 3020 (1990).
10) Part XV of this series; T. Mizuta, K. Toshitani, and K. Miyoshi, *Bull. Chem. Soc. Jpn.*, **64**, 1183 (1991).
11) T. Mizuta, H. Yoneda, and Y. Kushi, *Inorg. Chim. Acta*, **132**, 11 (1987).
12) T. Ashida, in "The Universal Crystallographic Computation Program System," ed by T. Sakurai, The Crystallographic Society of Japan, Tokyo (1979).
13) C. K. Johnson, "Report ORNL-3794," Oak Ridge National Laboratory, Oak Ridge, TN (1976).
14) "International Tables For X-Ray Crystallography," Kynoch Press, Birmingham, U.K. (1974), Vol. IV.
15) Using all the non-hydrogen atoms, the *R* values converged for correct and inverted absolute configurations (in parentheses) were 0.062 (0.072) for **1** and 0.063 (0.071) for **2**.
16) K. Ishida, T. Tanase, T. Takahashi, Y. Sato, S. Yano, M. Hidai, K. Kobayashi, and T. Sakurai, *Acta Crystallogr., Sect. C*, **44**, 83 (1988).
17) F. Marumo, Y. Utsumi, and Y. Saito, *Acta Crystallogr., Sect. B*, **26**, 1492 (1970).

Kinetic Studies on the Quenching Reaction of the Photo-Excited $[Ru(bpy)_3]^{2+}$ with $[Co(edta)]^-$ in the Presence of EDTA, CDTA, and $C_2O_4^{2-}$

Suzuko YAMAZAKI-NISHIDA, Aiko NAGAI, Noriko MOURI, Satoko KAWASHIMA, and Masaru KIMURA*
Department of Chemistry, Faculty of Science, Nara Women's University, Nara 630
(Received February 5, 1991)

In the presence of a sacrificial donor (such as ethylenediaminetetraacetic acid, *trans*-1,2-cyclohexanediaminetetraacetic acid or oxalic acid in a deaerated aqueous solution) $[Co(edta)]^-$ is reduced to $[Co(edta)]^{2-}$ by quenching oxidatively the photo-excited $[Ru(bpy)_3]^{2+}$ ($[Ru(bpy)_3]^{2+*}$). The reduction rate for the $[Co(edta)]^-$ increases with an increase in the concentration of the sacrificial donor, and is kept constant at $[EDTA] \geqslant 0.03$ mol dm^{-3}, $[CDTA] \geqslant 0.01$ mol dm^{-3}, or $[C_2O_4^{2-}] \geqslant 0.07$ mol dm^{-3} at pH 4.6. The ratio $[[Co(edta)]^-]_{reacted}$: $[EDTA]_{reacted}$: $[[Co(edta)]^{2-}]_{formed} = 2:1:2$ is obtained at pH 5.2. The reaction rates were examined as a function of the concentrations of $[Co(edta)]^-$ and $[Ru(bpy)_3]^{2+}$ as well as the pH, ionic strength, and temperature of the solution, and the intensity of the incident light. In the presence of oxygen, the decrease of $[Co(edta)]^-$ is greatly suppressed and the formation of the hydrogen peroxide is appreciable. The reaction mechanism is presented in order to account for the obtained results.

Various redox reactions induced by $[Ru(bpy)_3]^{2+}$ (bpy= 2,2′-bipyridine) or $[Ru(bpz)_3]^{2+}$ (bpz=2,2-bipyrazine) as a photocatalyst, i.e., hydrogen evolution from water decomposition[1-8] or the reduction of carbon dioxide to methane,[9,10] have been studied from the viewpoint of the photochemical conversion of solar energy. One of the major problems in the utilization of these complexes is that the energy-saving electron-transfer reactions are accompanied by very efficient reverse electron-transfer steps which regenerate the starting materials. A simple technique most often used to prevent a reverse electron-transfer reaction is the addition of a sacrificial donor, such as ethylenediaminetetraacetic acid or triethanolamine, into the reaction system. In this paper, the effects of such sacrificial donors as EDTA,[11] CDTA,[11] and $C_2O_4^{2-}$ are discussed concerning the oxidative quenching of $[Ru(bpy)_3]^{2+*}$ with $[Co(edta)]^-$ in a deaerated aqueous solution.

Experimental

Chemicals. $[Ru(bpy)_3]Cl_2 \cdot 6H_2O$ and $K[Co(edta)] \cdot 2H_2O$ were prepared and purified as described in the literature.[12] Disodiumdihydrogenethylenediaminetetraacetate ($Na_2[H_2edta]$) and other chemicals were of guaranteed reagent grade and were used without further purification. A solution containing CDTA was prepared by dissolving in a sodium hydroxide solution. The pH of the solution was continuously adjusted with acetic acid and sodium acetate. Deionized water was further distilled both with and without the addition of permanganate in a glass still.

Procedures. The procedures are essentially the same as those described in a previous paper.[13] The $[Co(edta)]^-$ concentration was determined spectrophotometrically after removing the $[Ru(bpy)_3]^{2+}$ by adding a cation-exchange resine (1 g) (Dowex 50W-X8, 200-400 mesh, hydrogen form, washed well with distilled water) into the solution. The total concentration of the EDTA remaining and the $[Co(edta)]^{2-}$ formed in the sample solution was determined by polarography at +0.3 V vs. SCE in a solution comprised 0.05 mol dm^{-3} acetic acid, 0.05 mol dm^{-3} sodium acetate, and 0.01% gelatin at 25 °C under a nitrogen atmosphere. Polarography was performed in the dark without removing the $[Ru(bpy)_3]^{2+}$, since the cation-exchange resin adsorbs some part of the EDTA. The amount of carbon dioxide formed during the reaction was measured by a method reported previously.[14] The rate constant of the redox reaction between $[Ru(bpy)_3]^{3+}$ and EDTA, CDTA, or $C_2O_4^{2-}$ was determined with a Union RA-401 stopped-flow spectrophotometer. A solution of $[Ru(bpy)_3]^{3+}$ was prepared by oxidizing $[Ru(bpy)_3]^{2+}$ with lead dioxide (PbO_2) in 0.5 mol dm^{-3} sulfuric acid. After removing PbO_2 and $PbSO_4$ by filtration, the $[Ru(bpy)_3]^{3+}$ solution was used for the experiments.

Results and Discussion

Dependence of the Concentration of Sacrificial Donors. No appreciable formation of $[Co(edta)]^{2-}$ was observed in the quenching of $[Ru(bpy)_3]^{2+*}$ with $[Co(edta)]^-$ in the absence of sacrificial agents. However, $[Co(edta)]^-$ decreased remarkably to produce $[Co(edta)]^{2-}$ upon the addition of sacrificial donors in a deaerated aqueous solution. As Fig. 1 shows, the initial rates for a decrease in the $[Co(edta)]^-$ concentration (V_i) increase with an increase in the concentration of the sacrificial donors and are kept constant at $[EDTA] \geqslant 0.03$ mol dm^{-3}, $[CDTA] \geqslant 0.01$ mol dm^{-3}, or $[C_2O_4^{2-}] \geqslant 0.07$ mol dm^{-3}. This indicates that a reverse electron-transfer reaction between $[Ru(bpy)_3]^{3+}$ and $[Co(edta)]^{2-}$ competes with the reaction between $[Ru(bpy)_3]^{3+}$ and the sacrificial donor. It is noteworthy that the limiting rate with the excess EDTA is almost the same as that with CDTA, whereas is about 2 times as large as that with $C_2O_4^{2-}$. Otherwise (noted hereafter), the kinetic results observed with EDTA are presented in detail.

Stoichiometry. The stoichiometry of the reaction was examined in aqueous solutions containing 2×10^{-3} mol dm^{-3} $K[Co(edta)]$ and 5×10^{-5} mol dm^{-3} $[Ru(bpy)_3]Cl_2$ at pH 5.2 and 25 °C. The ratio of $[[Co(edta)]^-]_{reacted}$: $[EDTA]_{reacted}$: $[[Co(edta)]^{2-}]_{formed} = 2:1:2$ was always obtained, being independent of the initial EDTA con-

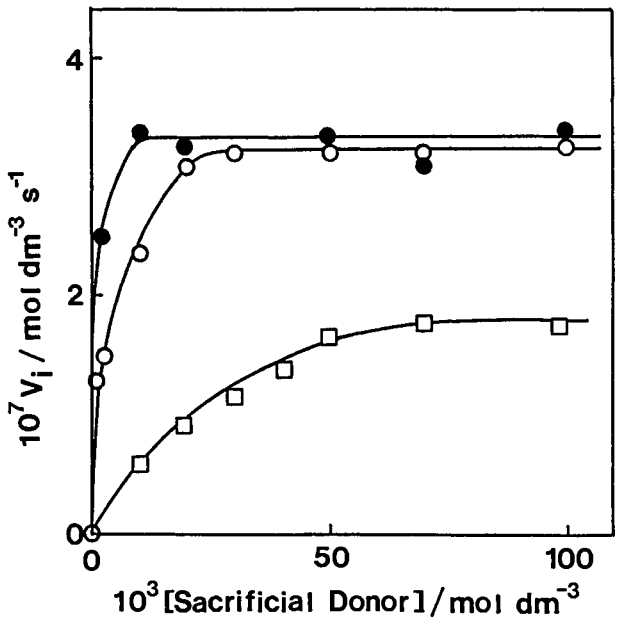

Fig. 1. Dependence of the V_i on the concentration of the EDTA (O), CDTA (●), or $C_2O_4^{2-}$ (□) in deaerated aqueous solutions containing 2×10^{-3} mol dm^{-3} K[Co(edta)] and 5×10^{-5} mol dm^{-3} $[Ru(bpy)_3]Cl_2$ at pH 4.6 and 25 °C. Irradiation was done with four lamps.

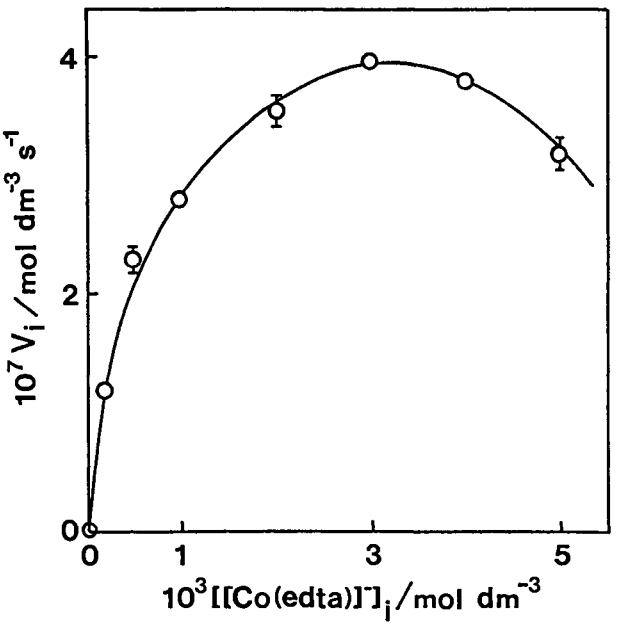

Fig. 2. Dependence of the V_i on the initial concentration of the $[Co(edta)]^-$. Conditions are the same as in Fig. 1 except for 0.05 mol dm^{-3} EDTA.

centration. Carbon dioxide was also formed in the solution; the amount produced per EDTA reacted was estimated to be 1.3—2.1. The concentration of $[Ru(bpy)_3]^{2+}$ was kept constant throughout the reaction. Thus, the stoichiometry of the photo-induced reaction can be expressed by

$$2[Co(edta)]^- + EDTA \rightarrow 2[Co(edta)]^{2-} + \text{products}(CO_2 \cdots). \quad (1)$$

Dependence of the $[Co(edta)]^-$ Concentration. Figure 2 indicates that V_i in the presence of 0.05 mol dm^{-3} EDTA increases with an increase in the initial concentrations of the $[Co(edta)]^-$ ($[[Co(edta)]^-]_i$), and has a maximum value at a $[Co(edta)]^-$ concentration of 3×10^{-3} mol dm^{-3}. A similar result was obtained with 0.05 mol dm^{-3} CDTA. Thus, the decrease of V_i at $[[Co(edta)]^-]_i > 3\times10^{-3}$ mol dm^{-3} is ascribed to an inner filter effect of $[Co(edta)]^-$ on the photoexcitation of $[Ru(bpy)_3]^{2+}$.

Effect of Light Intensity and the $[Ru(bpy)_3]^{2+}$ Concentration. The dependence of V_i on the incident light intensity was examined in an aqueous solution containing 0.05 mol dm^{-3} EDTA, 2×10^{-3} mol dm^{-3} K[Co(edta)], 5×10^{-5} mol dm^{-3} $[Ru(bpy)_3]Cl_2$, 0.05 mol dm^{-3} acetic acid and 0.05 mol dm^{-3} sodium acetate at 25 °C and pH 4.6. It was found that no appreciable formation of $[Co(edta)]^{2-}$ was observed in the dark and that V_i increased in proportion to the number of the lamps irradiated. The dependence of V_i on the $[Ru(bpy)_3]^{2+}$ concentration is presented in Fig. 3. With an increase

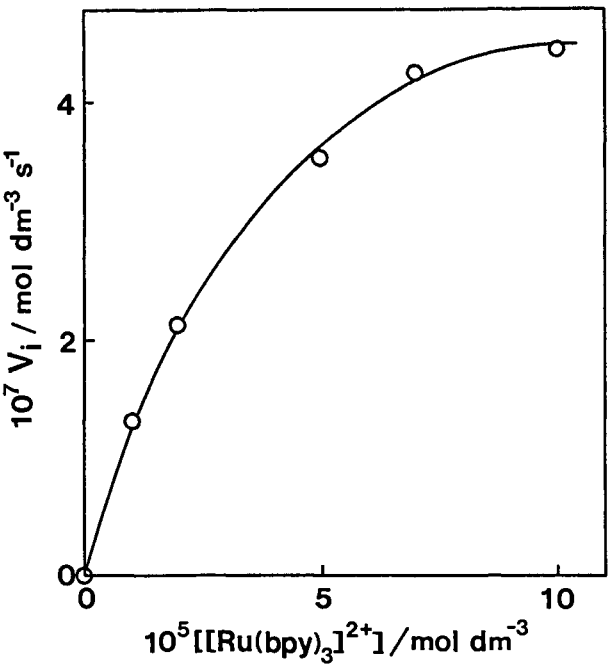

Fig. 3. Effect of the $[Ru(bpy)_3]^{2+}$ concentration. Conditions are the same as in Fig. 1 except for 0.02 mol dm^{-3} EDTA and pH 5.2.

in the $[Ru(bpy)_3]^{2+}$ concentration, V_i increases while approaching a limiting value. This finding as well as the linear relation between V_i and the incident light intensity suggests that V_i is proportional to the amount of light absorbed by $[Ru(bpy)_3]^{2+}$ (I_a), which is described by the Lambert-Beer equation:

$$I_a = I_0\{1 - \exp(-\alpha[[Ru(bpy)_3]^{2+}])\}. \quad (2)$$

Here, I_0 is the intensity of the incident light and α is a constant comprising an absorption coefficient and an optical path length.

Effect of pH. Figure 4 represents the pH effect on V_i, where the pH of the solution was adjusted with various concentrations of acetic acid and 0.05 mol dm^{-3} sodium acetate. In this paper, the term "EDTA" is used to designate all of the forms of that substance, irrespective of the protonation states.[11] As the pH increases, smaller amounts of EDTA were required for a limiting rate. It is worth noting that the V_i values under excess EDTA decrease with a decrease in pH.

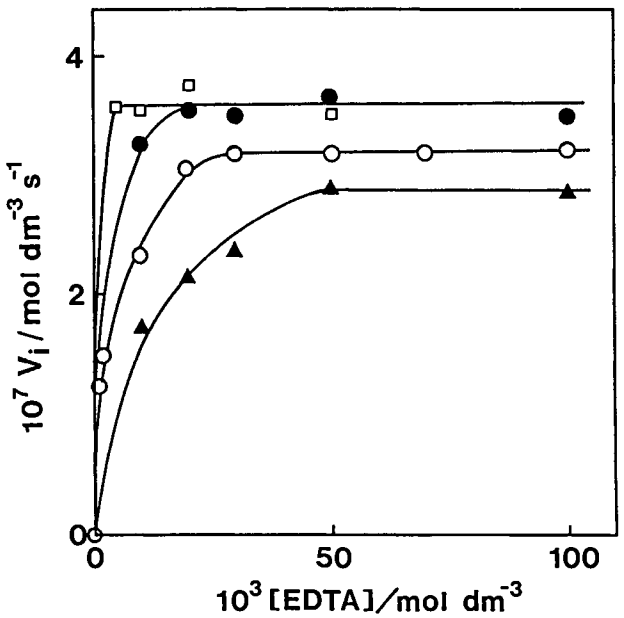

Fig. 4. Dependence of the V_i on the concentration of the EDTA at pH 6.0 (□), 5.2 (●), 4.6 (○), and 4.0 (▲). Other conditions are the same as in Fig. 1.

Effect of Ionic Strength and Temperature. The effect of the ionic strength or solution temperature is shown in Figs. 5 and 6. It was found that the reaction rate for the reduction of $[Co(edta)]^-$ decreased as the ionic strength of the solution increased. This is explainable in terms of a reaction between oppositly charged ions (Eq. 5). The rate of the reaction also increases slightly with an increase in the solution temperature.

Mechanism of Reaction. It has been reported that oxidized EDTA ($EDTA_{OX}^+$) is rapidly deprotonated to form a reducing radical (EDTA').[15–19] The stability of the EDTA' is dependent on the solution pH. In an acidic medium, EDTA' decomposes due to acid-catalyzed decarboxylation.[18,19] Glyoxylic acid, formaldehyde, and carbon dioxide were identified as being the final products for the oxidation of EDTA.[20,21] Based on the above, the following reaction mechanism is proposed to account for the obtained results:

$$[Ru(bpy)_3]^{2+} + h\nu \longrightarrow [Ru(bpy)_3]^{2+*} \quad (3)$$

$$[Ru(bpy)_3]^{2+*} \xrightarrow{k_0} [Ru(bpy)_3]^{2+} + h\nu' \text{ or } \Delta \text{ (thermal energy)} \quad (4)$$

$$[Ru(bpy)_3]^{2+*} + [Co(edta)]^- \xrightarrow{k_q} [Ru(bpy)_3]^{3+} + [Co(edta)]^{2-} \quad (5)$$

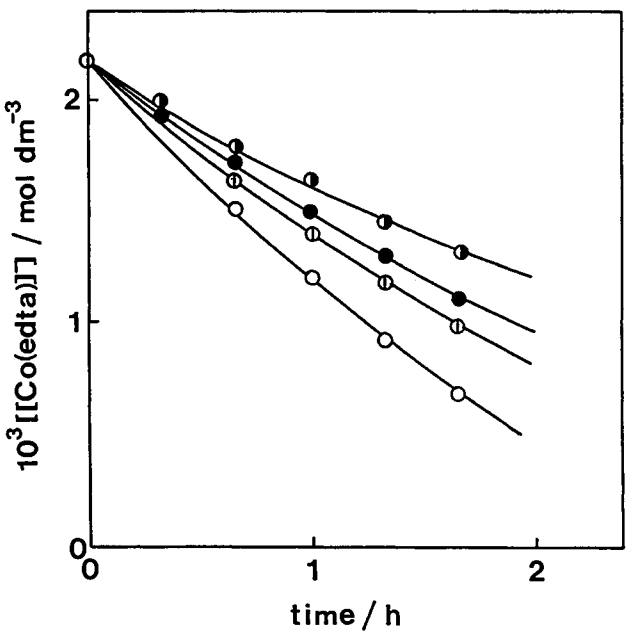

Fig. 5. Effect of the ionic strength. Conditions are the same as in Fig. 1 except for 0.02 mol dm^{-3} EDTA and various ionic strength of 0.2 (○), 0.4 (◑), 0.6 (●), and 1.0 mol dm^{-3} (◑).

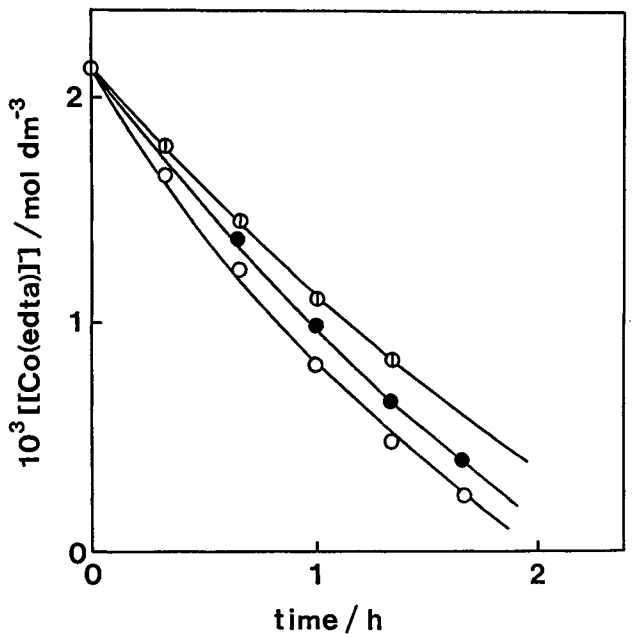

Fig. 6. Effect of temperature. Conditions are the same as in Fig. 1 except for 0.05 mol dm^{-3} EDTA, pH 5.2 and temperature of 5 °C (◑), 15 °C (●), or 25 °C (○).

$$[Ru(bpy)_3]^{3+} + [Co(edta)]^{2-} \xrightarrow{k_1} [Ru(bpy)_3]^{2+} + [Co(edta)]^{-} \quad (6)$$

$$[Ru(bpy)_3]^{3+} + EDTA \xrightarrow{k_2} [Ru(bpy)_3]^{2+} + EDTA_{ox}^{+} \quad (7)$$

$$EDTA_{ox}^{+} \xrightarrow{k_3} EDTA' + H^{+} \text{ (deprotonation)} \quad (8)$$

$$EDTA' + [Co(edta)]^{-} \xrightarrow{k_4} [Co(edta)]^{2-} + \text{products } (CO_2 \cdots) \quad (9)$$

$$EDTA' \xrightarrow{k_5} \text{products (acid-catalyzed decarboxylation).} \quad (10)$$

Assuming a steady state concentration of the $[Ru(bpy)_3]^{2+*}$, $[Ru(bpy)_3]^{3+}$, $EDTA_{ox}^{+}$ and EDTA', the reaction rate is expressed by

$$-\frac{d[[Co(edta)]^{-}]}{dt} = \frac{k_q I_a \Phi [[Co(edta)]^{-}]}{k_0 + k_q [[Co(edta)]^{-}]} \times \frac{(1+\gamma)k_2[EDTA]}{k_1[[Co(edta)]^{2-}] + k_2[EDTA]}, \quad (11)$$

where Φ is the quantum yield for the excited species $[Ru(bpy)_3]^{2+*}$; thus, $I_a\Phi$ corresponds to the formation rate of $[Ru(bpy)_3]^{2+*}$, and the γ value is defined as $k_4[EDTA'][[Co(edta)]^{-}]/\{k_4[EDTA'][[Co(edta)]^{-}] + k_5[EDTA']\}$ and is equal to unity if all of the EDTA' formed by reaction 8 reacts with $[Co(edta)]^{-}$. The second-order rate constant for reaction 6 has been estimated to be larger than $10^4\,dm^3\,mol^{-1}\,s^{-1}$. However, the reverse electron-transfer reaction between $[Ru(bpy)_3]^{3+}$ and $[Co(edta)]^{2-}$ in the solvent cage could take place quite rapidly, since no formation of $[Co(edta)]^{2-}$ was observed without adding a sacrificial donor.

In the presence of the excess EDTA, the relation $k_2[EDTA] \gg k_1[[Co(edta)]^{2-}]$ holds, and the reaction rate reduces to

$$-\frac{d[[Co(edta)]^{-}]}{dt} = \frac{(1+\gamma)k_q I_a \Phi [[Co(edta)]^{-}]}{k_0 + k_q [[Co(edta)]^{-}]}. \quad (12)$$

The obtained stoichiometry suggests that γ is equal to unity and that the decomposition of the EDTA' (Eq. 10) does not occur at pH 5.2. With a decrease in pH, γ decreases owing to reaction 10, and then the limiting rate observed at the excess EDTA decreases. Rate constant k_2 decreases with decreasing pH because of the protonation of EDTA. This is the reason why greater amounts of EDTA were required for the limiting rate at lower pH. Equation 12 indicates that the plot of V_i^{-1} vs. $[[Co(edta)]^{-}]_i^{-1}$ should be a straight line with an intercept of $1/\{(1+\gamma)I_a\Phi\}$ and an intercept/slope ratio of k_q/k_0. Figure 7 shows such a treatment of the data at $[[Co(edta)]^{-}]_i \leq 3\times10^{-3}$ mol dm^{-3} in Fig. 2. The values of $I_a\Phi$ and k_q/k_0 are calculated to be 2.4×10^{-7} mol dm^{-3} s^{-1} and 1.38×10^3 dm^3 mol^{-1}, respectively. The latter value is almost the same as that estimated separately from the Stern-Volmer plot in the quenching experiment under the same conditions. This fact indicates the validity of the reaction mechanism and the proposed rate law. The k_q value is estimated to be 2.1×10^9 dm^3 mol^{-1} s^{-1} using a k_0 value of 1.52×10^6 s^{-1}.[13] The small dependences of the reaction rate on the ionic strength and temperature suggest that both k_q and k_0 have a similar dependence on them.

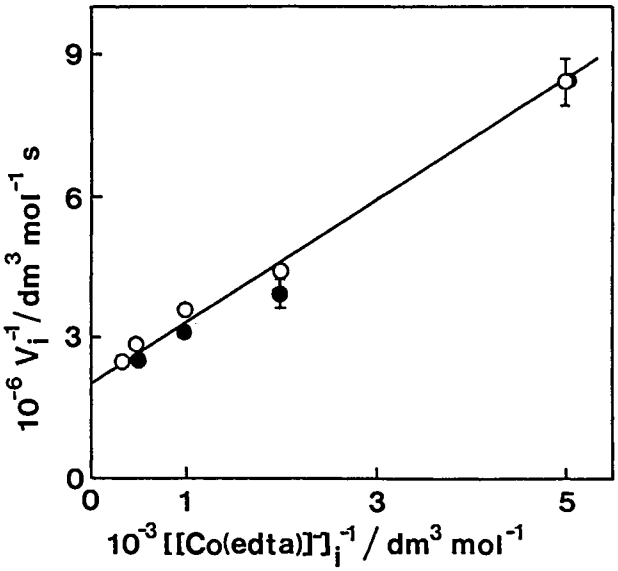

Fig. 7. Plots of V_i^{-1} vs. $[[Co(edta)]^{-}]_i^{-1}$. Conditions are the same as in Fig. 1 except for 0.05 mol dm^{-3} EDTA (○) or CDTA (●).

In the case of the CDTA or $C_2O_4^{2-}$ as a sacrificial donor, $[Ru(bpy)_3]^{3+}$ was reduced to $[Ru(bpy)_3]^{2+}$ according to the following reactions:

$$[Ru(bpy)_3]^{3+} + CDTA \xrightarrow{k_6} [Ru(bpy)_3]^{2+} + CDTA_{ox}^{+} \quad (13)$$

and

$$[Ru(bpy)_3]^{3+} + C_2O_4^{2-} \xrightarrow{k_7} [Ru(bpy)_3]^{2+} + C_2O_4^{-\cdot}. \quad (14)$$

The k_2, k_6, and k_7 were determined at pH 4.7 and 25 °C by the stopped-flow method to be 8.9×10^3, 1.7×10^4, and 1.7×10^5 dm^3 mol^{-1} s^{-1}, respectively. The reaction mechanism in the case of CDTA is supposed to be similar to that with EDTA, since the results obtained in the both systems were almost the same (Fig. 7). Smaller amounts of CDTA were required to be a limiting rate. This finding can be reasonably explained in terms of the k_2 and k_6 values. On the contrary, the dependence of V_i on the $C_2O_4^{2-}$ concentration is different from that with EDTA or CDTA, as shown in Fig. 1. This might be due to a difference in the reactivity of the reducing radicals like EDTA' and $CO_2^{-\cdot}$, since the oxidized form of $C_2O_4^{2-}$ is known to decompose promptly to $CO_2^{-\cdot}$ and CO_2. If the $CO_2^{-\cdot}$ radical is consumed by a reaction with $[Ru(bpy)_3]^{3+}$ (E°=1.26 V vs. NHE[1]), being not with $[Co(edta)]^{-}$ (E°=0.37 V vs. NHE[22]), the reaction rate is derived as Eq. 16.

$$[Ru(bpy)_3]^{3+} + CO_2^{-\cdot} \longrightarrow [Ru(bpy)_3]^{2+} + CO_2 \quad (15)$$

$$-\frac{d[[Co(edta)]^-]}{dt}=\frac{k_q I_a \Phi[[Co(edta)]^-]}{k_0+k_q[[Co(edta)]^-]}\times\frac{2k_7[C_2O_4^{2-}]}{k_1[[Co(edta)]^{2-}]+2k_7[C_2O_4^{2-}]}. \quad (16)$$

A comparison of Eq. 16 to Eq. 11 at $\gamma=1$ indicates that the limiting rate in the case of excess $C_2O_4^{2-}$ is about half that with EDTA. This is consistent with the result shown in Fig. 1. The analogous reaction to Eq. 15, i.e., the reaction between EDTA' and $[Ru(bpy)_3]^{3+}$ is also supposed to proceed. However, $[Ru(bpy)_3]^{3+}$ is reduced predominantly by EDTA since the EDTA' radical reacts with $[Co(edta)]^-$ (Eq. 9). The finding that a $C_2O_4^{2-}$ concentration greater than 0.07 mol dm^{-3} is needed to reach a limiting rate is not understandable, since the k_7 value is much greater than k_2 and k_6. This might be attributable to an interaction between $[Ru(bpy)_3]^{3+}$ and EDTA or CDTA. The equilibrium constant between $[Ru(bpy)_3]^{3+}$ and EDTA ions has been reported to be greater than 78 dm^3 mol^{-1}.[18]

The decrease rate of $[Co(edta)]^-$ is remarkably reduced in the presence of oxygen, with hydrogen peroxide being formed. The results obtained with EDTA as a sacrificial donor are presented in Fig. 8. The oxidative quenching of $[Ru(bpy)_3]^{2+*}$ with oxygen has been reported to be 5.5×10^9 dm^3 mol^{-1} s^{-1}.[23] This indicates that the quenching rate with oxygen is comparable to that with $[Co(edta)]^-$ in aqueous solutions saturated with oxygen. Therefore, the $[Co(edta)]^{2-}$ produced by the quenching reaction is supposed to be reoxidized to $[Co(edta)]^-$ (Eq. 21). In fact, the formation of $[Co(edta)]^-$ was observed upon the addition of $[Co(edta)]^{2-}$, instead of $[Co(edta)]^-$, into the solution.

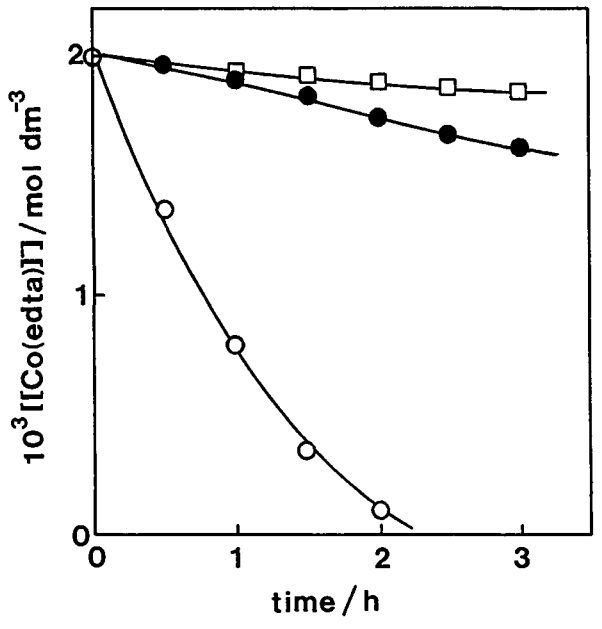

Fig. 8. Effect of oxygen. Conditions are the same as in Fig. 1 except for 0.01 mol dm^{-3} EDTA at pH 5.2 in an aqueous solution saturated with O_2 (□), air (●), or N_2 (○).

$$[Ru(bpy)_3]^{2+*}+O_2\longrightarrow[Ru(bpy)_3]^{3+}+O_2^{\cdot-} \quad (17)$$

$$O_2^{\cdot-}+H^+\rightleftarrows HO_2^{\cdot} \quad (18)$$

$$[Ru(bpy)_3]^{3+}+HO_2^{\cdot}\longrightarrow[Ru(bpy)_3]^{2+}+O_2+H^+ \quad (19)$$

$$HO_2^{\cdot}+EDTA'+H^+\longrightarrow H_2O_2+\text{products} \quad (20)$$

$$[Co(edta)]^{2-}+HO_2^{\cdot}+H^+\longrightarrow[Co(edta)]^-+H_2O_2. \quad (21)$$

The drastic retardation effect of oxygen is obviously due to reactions 19—21.

This research was partly supported by Grant-in-Aid for Scientific Research No. 01470051 from the Ministry of Education, Science and Culture.

References

1) K. Kalyanasundaram, *Coord. Chem. Rev.*, **46**, 159 (1982).

2) K. Kalyanasundaram, M. Grätzel, and E. Pelizzetti, *Coord. Chem. Rev.*, **69**, 57 (1986).

3) C. R. Bock, J. A. Connor, A. R. Gutierrez, T. J. Meyer, D. G. Whitten, B. P. Sullivan, and J. K. Nagle, *J. Am. Chem. Soc.*, **101**, 4815 (1979).

4) R. C. Young, T. J. Meyer, and D. G. Whitten, *J. Am. Chem. Soc.*, **97**, 4781 (1975).

5) G. L. Gaines, Jr., *J. Phys. Chem.*, **83**, 3088 (1979).

6) K. Takuma, M. Kajiwara, and T. Matsuo, *Chem. Lett.*, **1977**, 1199.

7) J. K. Nagle, J. S. Bernstein, R. C. Young, and T. J. Meyer, *Inorg. Chem.*, **20**, 1760 (1981).

8) J. K. Nagle, R. C. Young, and T. J. Meyer, *Inorg. Chem.*, **16**, 3366 (1977).

9) R. Maidan and I. Willner, *J. Am. Chem. Soc.*, **108**, 8100 (1986).

10) I. Willner, R. Maidan, D. Mandler, H. Dürr, G. Dörr, and K. Zengerle, *J. Am. Chem. Soc.*, **109**, 6080 (1987).

11) Although the abbreviation EDTA or CDTA is generally for H_4edta or H_4cdta, we use, in this paper, for all the forms of H_4edta, H_3edta$^-$, H_2edta^{2-}, Hedta^{3-}, and edta^{4-}, or H_4cdta, H_3cdta$^-$, H_2cdta^{2-}, Hcdta^{3-}, and cdta^{4-}, respectively.

12) S. Nishida and M. Kimura, *Bull. Chem. Soc. Jpn.*, **60**, 2367 (1987).

13) M. Kimura, M. Yamashita, and S. Nishida, *Inorg. Chem.*, **24**, 1527 (1985).

14) M. Kimura and S. Nishida, *J. Chem. Soc., Dalton Trans.*, **1985**, 355.

15) $EDTA_{OX}^+$ and EDTA' have been identified as follows by P. Keller, A. Moradpour, E. Amouyal, and H. B. Kagan (*Nouv. J. Chim.*, **4**, 377 (1980)), although the carboxyl groups are protonated, being dependent on pH of the solution.

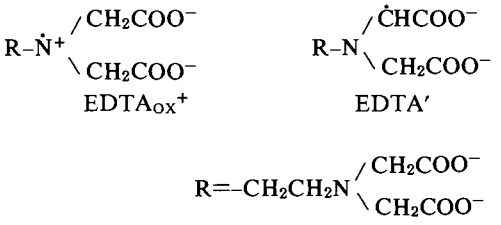

16) M. Z. Hoffman, D. R. Prasad, G. Jones, II, and V. Malba, *J. Am. Chem. Soc.*, **105**, 6360 (1983).

17) K. Mandal and M. Z. Hoffman, *J. Phys. Chem.*, **88**, 185 (1984).
18) K. Mandal and M. Z. Hoffman, *J. Phys. Chem.*, **88**, 5632 (1984).
19) Q. G. Mulazzani, M. Venturi, and M. Z. Hoffman, *J. Phys. Chem.*, **89**, 722 (1985).
20) D. Miller and G. McLendon, *Inorg. Chem.*, **20**, 950 (1981).
21) E. Amouyal and B. Zidler, *Isr. J. Chem.*, **22**, 117 (1982).
22) N. Tanaka and H. Ogino, *Bull. Chem. Soc. Jpn.*, **38**, 1054 (1965).
23) J.R. Darwent and K. Kalyanasundaram, *J. Chem. Soc., Faraday Trans. 2*, **77**, 373 (1981).

Kinetics and Mechanisms of Photo-Induced Reduction of Iodine by Diamine-*N*-polycarboxylate Ions in an Aqueous Solution

Masaru KIMURA,* Akiko OHOMURA, Fumiko NAKAZAWA, and Keiichi TSUKAHARA*
Department of Chemistry, Faculty of Science, Nara Women's University, Nara 630
(Received February 5, 1991)

Although the reduction of iodine by diamine-*N*-polycarboxylate ions such as ethylenediaminetetraacetic acid, *trans*-1,2-cyclohexanediaminetetraacetic acid, *N*-(2-hydroxyethyl)ethylenediamine-*N,N',N'*-triacetic acid, and ethylenediamine-*N,N'*-diacetic acid was negligible in the dark, it occurred greatly upon irradiation with visible light of an aqueous solution over the pH range 4—8. The rate of the photo-sensitized reaction was of half-order regarding both the light intensity irradiated and the concentrations of iodine, which correspond to those of the triiodide ion in the presence of excess iodide ions, and was proportional to the concentration of the diamine-*N*-polycarboxylate ion. Further, the rate was of half-order for concentrations of I^- below 3×10^{-4} mol dm^{-3} and was of inversely half-order for concentrations of I^- above 6×10^{-4} mol dm^{-3}. The reaction was inhibited by radical scavengers of acrylonitrile, acrylamide, and hexaamminecobalt(III) ions. Both hydrogen ion and complex-forming metal ions, such as copper(II) and zinc(II), are also strong inhibitors of the reaction. The reaction mechanism, where initiation reaction is a photo-dissociation of iodine and the reactive species is a $I_2^{\cdot-}$ radical anion, is proposed to account for the obtained results.

Previously, the photo-chemical reaction between ethylenediaminetetraacetic acid (H_4edta) and iodine (I_2) was used for the analytical chemistry determination of trace amounts of the nitrite ion.[1] The photoreduction mechanism of iodine by amine-*N*-polycarboxylic acid has been proposed based on an initial photodissociation of iodine to iodine atoms followed by chain propagation.[2] In the absence of iodide ions an induction period is present in the photoreduction of iodine by ethylenediaminetetraacetic acid; the reaction occurs with the production of I^- ions.[1,2] When high concentrations of I^- ions were used, the reduction of iodine by oxalate ions was inhibited by I^- ions.[3] Such an effect of the I^- ions on the reduction of iodine cannot be explained by the above proposed mechanism. We have reported that, under the condition that $[I_2]\ll[I^-]$, a full kinetic treatment is possible for a photo-induced reduction of iodine by oxalate ions by monitoring the decay of I_3^-.[3] To clarify the mechanisms of the oxidation of amine-*N*-polycarboxylate ions and of the reduction of iodine, we report in this study on the photo-induced reduction of iodine by amine-*N*-polycarboxylate ions in the presence of the I^- ion.

Experimental

Chemicals. Iodine, potassium iodide, Na_2H_2edta,[4] H_4cdta (=*trans*-1,2-cyclohexanediaminetetraacetic acid),[4] H_3hedta (=*N*-(2-hydroxyethyl)ethylenediamine-*N,N',N'*-triacetic acid),[4] H_2edda (=ethylenediamine-*N,N'*-diacetic acid),[4] and the other chemicals used were of guaranteed reagent grade from Wako Pure Chemical Industries, Ltd. All of the solutions were prepared from redistilled water. The pH's of the solutions were adjusted with an acetate buffer (pH 3.5—6.5), a phosphate buffer (pH 6.5—8), and sulfuric acid (below pH 3.5). No effect of anions in the buffers was observed on the kinetic results.

Procedure. The kinetic measurements employed were the same as those in the method reported previously.[3] Each sample solution was continuously irradiated with visible light from two 100-W tungsten lamps. Aliquot samples were withdrawn at appropriate time intervals after starting the reaction; the absorbance at 350 nm due to I_3^- (ε 2.5×10^4 dm^3 mol^{-1} cm^{-1})[3] was measured by Shimadzu UV-200S and UV-150-02 spectrophotometers. All of the kinetic runs were followed under the condition that the iodide ions had at least a 50-fold excess over iodine. When solutions prepared from nitrogen-saturated water were used, the kinetic results were the same as those in air-saturated solutions. Thus, all of the kinetic measurements were carried out in air-saturated solutions. The temperature was controlled within 0.1 °C. The light intensity was determined using potassium tris(oxalato)ferrate(III) trihydrate as an actinometer.[5] The iron(II) content was determined spectrophotometrically in the form of tris(1,10-phenanthroline)iron(II) ions at 510 nm with a molar absorption coefficient of 1.1×10^4 dm^3 mol^{-1} cm^{-1}.

Results and Discussion

Although the redox reaction between iodine and diamine-*N*-polycarboxylic acid was practically negligible in the dark, it occurred greatly upon irradiation with visible light of the aqueous solutions over the pH range 4—8. Iodine was rapidly converted to I_3^- in the presence of I^-:[6,7]

$$I_2 + I^- \rightleftarrows I_3^-, \quad (1)$$

where $k_f=5.6\times10^9$ dm^3 mol^{-1} s^{-1} and $K_1=7.1\times10^2$ dm^3 mol^{-1}. The absorbance of I_3^- at 350 nm, where the absorbance due to I_2 was quite negligible, was used as a monitor for the kinetic measurements in the present study. A half-order plot for the reaction based on Eq. 2 was linear up to almost completion of the reaction (Fig. 1):

$$A_t^{1/2} - A_0^{1/2} = -(1/2)(\varepsilon l)^{1/2} k_{obsd} t, \quad (2)$$

where A_0 and A_t represent the absorbance at zero time and t, respectively, ε is the molar absorption coefficient of I_3^- at 350 nm, and l is the optical path length to be 1

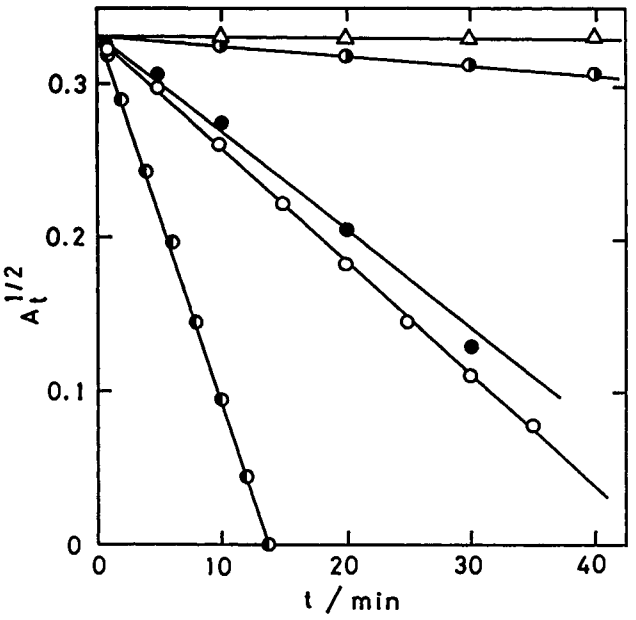

Fig. 1. The half-order plots of $A_t^{1/2}$ vs. t for the photoreaction of iodine with diamine-*N*-polycarboxylate ions and ethylenediamine. $[I_2]=1.0\times10^{-5}$ mol dm^{-3}, $[I^-]_0=1.0\times10^{-3}$, mol dm^{-3}, [diamine-*N*-polycarboxylate]$_0=1.0\times10^{-4}$ mol dm^{-3}, and $I_0=1.41\times10^{-7}$ mol dm^{-3} s^{-1} at 25 °C and pH 4.62 (a 0.1 mol dm^{-3} acetate buffer). ○: EDTA, ●: CDTA, ◐; HEDTA, ◑: EDDA, and △: ethylenediamine.

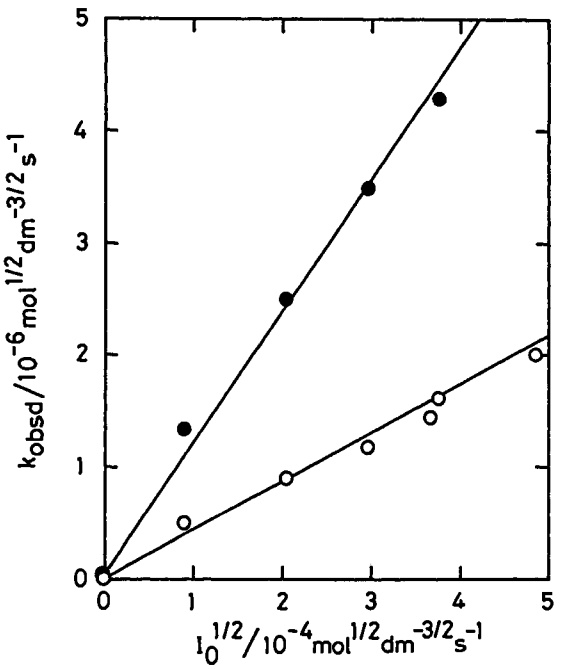

Fig. 2. Plots of k_{obsd} vs. $I_0^{1/2}$ for the photoreaction of iodine with EDTA. ○: $[EDTA]_0=1.0\times10^{-4}$ mol dm^{-3} at pH 4.62 (a 0.1 mol dm^{-3} acetate buffer) and ●: $[EDTA]_0=1.0\times10^{-5}$ mol dm^{-3} at pH 8.6 (a 0.1 mol dm^{-3} phosphate buffer). Other conditions are the same as in Fig. 1.

cm in the present study. Thus, the rate law is described as in Eq. 3:

$$-d[I_3^-]/dt = k_{obsd}[I_3^-]^{1/2}. \quad (3)$$

Effect of Light Intensity. The observed rate constant (k_{obsd}) increased with an increase in the light intensity irradiated (I_0) and plots of k_{obsd} vs. $I_0^{1/2}$ were rectilinear with zero intercept (Fig. 2). These results show that the reacting species is either I· or/and $I_2^{\cdot-}$ dissociated by light irradiation of the I_2 molecule.[3] The latter species is produced successively by a reaction between I· and I^-:

$$I_2 \overset{h\nu}{\rightleftarrows} 2I\cdot \quad [k_{-4}=8\times10^9 \text{ dm}^3\text{ mol}^{-1}\text{ s}^{-1}],^{8)} \quad (4)$$

$$I\cdot + I^- \rightleftarrows I_2^{\cdot-} \quad [K_5=1.1\times10^4 \text{ dm}^3\text{ mol}^{-1}].^{9,10)} \quad (5)$$

Concentration Dependence of Diamine-*N*-polycarboxylate. The rate of photoreduction of iodine increased proportionally to the concentrations of the diamine-*N*-polycarboxylate ions. Plots of k_{obsd} vs. the initial concentrations of EDTA ([EDTA]$_0$) are shown in Fig. 3. This fact indicates that the reaction of I· or $I_2^{\cdot-}$ with EDTA is rate determining.

Effect of the Iodide Ion Concentration. The rate of the reaction increased with increasing the concentrations of I^- ions up to about 4×10^{-4} mol dm^{-3} and then decreased (Fig. 4). This fact, together with the observation of a half-order dependence of $[I_3^-]$ on the rate, shows that the reaction of I· is negligible and that the reactive species is $I_2^{\cdot-}$, since the reaction in the absence of

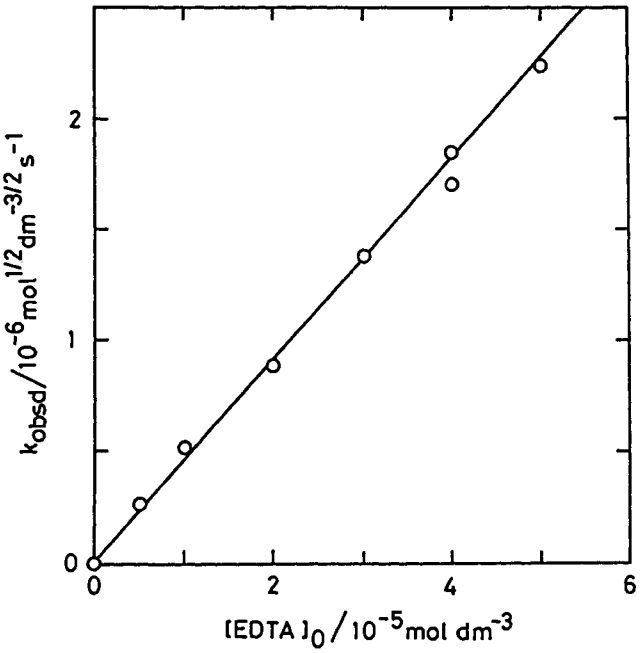

Fig. 3. Plots of k_{obsd} vs. $[EDTA]_0$ for the photoreaction of iodine with EDTA at 35 °C. Other conditions are the same as in Fig. 1.

I^- is very slow.

pH Dependence. The photoreduction of iodine by diamine-*N*-polycarboxylate ions was very slow at any pH less than 2. The reaction rate increased markedly

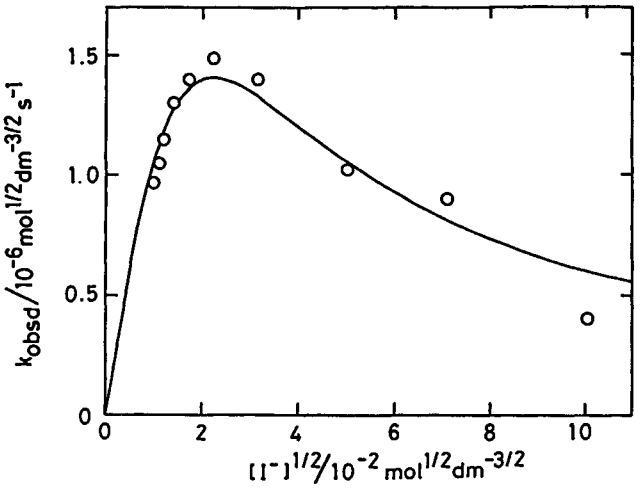

Fig. 4. Plots of k_{obsd} vs. $[I^-]_0^{1/2}$ for the photoreaction of iodine with EDTA. Conditions are the same as in Fig. 1.

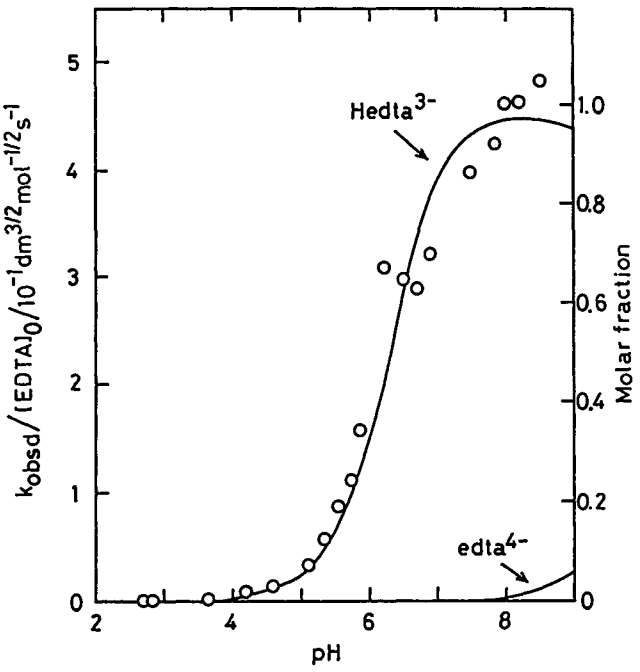

Fig. 5. Plots of k_{obsd} vs. pH for the photoreaction of iodine with EDTA and the molar fraction curve (the solid lines) for $Hedta^{3-}$ and $edta^{4-}$ against pH as indicated. Conditions are the same as in Fig. 1.

with increasing pH at 5—8. Such a pH-dependent curve for the reaction rate superimposes the molar fraction curve for the species $Hedta^{3-}$ (Fig. 5). Thus, the species of $Hedta^{3-}$ could be a main reductant for the radical $I_2^{\cdot-}$ and the other protonated species H_2edta^{2-}, H_3edta^-, and H_4edta would be quite inactive. The species of $edta^{4-}$ may be more reactive than the $Hedta^{3-}$ ion, but the $edta^{4-}$ ion is negligible below pH 8 (see Fig. 5). Consequently, the following equation can be assumed:

Table 1. Effect of Radical Scavengers for the Photoreaction of Iodine with EDTA at 1.0×10^{-4} mol dm^{-3}. Other Conditions are the Same as in Fig. 1

[Scavenger]/mol dm^{-3}	$k_{obsd}/10^{-6}$ mol$^{1/2}$ dm$^{-3/2}$ s^{-1}
0	1.30
Acrylonitrile	
0.090	1.09
0.19	0.78
0.28	0.65
Acrylamide	
0.070	1.09
0.14	0.82
0.21	0.71
$[Co(NH_3)_6]^{3+}$	
1.0×10^{-4}	1.11
2.0×10^{-4}	0.89
5.0×10^{-4}	0.64
1.0×10^{-3}	0.52

$$k_{obsd} = k[Hedta^{3-}] = k[EDTA]_0/\alpha_{HY}, \quad (6)$$

where α_{HY} is a side reaction coefficient $(1+K_{a4}/[H^+]+[H^+]/K_{a3}+[H^+]^2/K_{a2}K_{a3}+[H^+]^3/K_{a1}K_{a2}K_{a3})$ and K_{a1}, K_{a2}, K_{a3}, and K_{a4} are stepwise acid-dissociation constants of H_4edta ($pK_{a1}=2.07$, $pK_{a2}=2.75$, $pK_{a3}=6.24$, and $pK_{a4}=10.34$ at 25 °C and $I=0.1$ mol dm^{-3}).[11]

For the EDDA system the values of $k_{obsd}/[EDDA]_0$ at pH 4.62, 5.60, 6.49, and 7.20 were 1.35×10^{-3}, 6.11×10^{-3}, 2.13×10^{-2}, and 1.00×10^{-1} dm$^{3/2}$ mol$^{-1/2}$ s^{-1}, respectively. These data did not fit to the molar fraction curve for the only $Hedda^-$ species at higher pH, being different from the EDTA system. The reason is discussed later.

Effect of Radical Scavenger. The addition of a radical scavenger, acrylonitrile or acrylamide, into the reaction solution decreased the photoreduction rate of iodine. The value of k_{obsd} in the presence of 1.0—1.5% of the radical scavenger reached about half value in the absence of a radical scavenger (Table 1). In the presence of a radical scavenger and in the absence of EDTA, the absorbance of I_3^- did not decrease appreciably. Thus, it is assumed that the acrylonitrile or acrylamide monomer does not react with I_3^-, I_2, $I^{\cdot}$, and $I_2^{\cdot-}$, but reacts with the photo-oxidizing products of EDTA. Considering that the decrease in k_{obsd} is dependent on the amounts of the radical scavenger, it is also likely that the photo-oxidizing products of EDTA are able to reduce I_2 and/or I_3^-, competing with the radical scavenger.

It is found that a hexaamminecobalt(III) ion ($[Co(NH_3)_6]^{3+}$) also decreases the rate of the reaction, and that the value of k_{obsd} reaches about half in the absence of $[Co(NH_3)_6]^{3+}$ ions (Table 1). Without amine-*N*-polycarboxylate ions the photoreaction did not occur at pH 4—8, suggesting that the $[Co(NH_3)_6]^{3+}$ ions are quite inactive to the reducing radical anion $I_2^{\cdot-}$. This is reasonable on the basis of the redox potentials for these species:[12,13] $E^0([Co(NH_3)_6]^{3+/2+})=0.06$ V and $E^0(I_2/I_2^{\cdot-})=0.21$ V.

Temperature Dependence. The temperature dependence on the rate was examined under the same condi-

Table 2. Temperature Dependence on the Observed Rate Constant (k_{obsd}) for the Photoreaction of Iodine with EDTA at 4.0×10^{-5} mol dm^{-3}. Other Conditions are the Same as in Fig. 1

Temp/°C	k_{obsd}/ 10^{-6} mol$^{1/2}$ dm$^{-3/2}$ s^{-1}
10.0	0.14
15.0	0.25
25.0	0.72
30.0	1.10
35.0	1.77

tions as are shown in Fig. 1, except for $[EDTA]_0=4.0\times10^{-5}$ mol dm^{-3} with various temperatures over 10—35 °C. The results are given in Table 2. The enthalpy and entropy changes of activation were determined from the plots of $\log(k_{obsd}/T)$ vs. T^{-1} ($\Delta H^{\ddagger}=72.1\pm3.6$ kJ mol^{-1} and $\Delta S^{\ddagger}=-121\pm10$ J K^{-1} mol^{-1}).

Mechanism of Reaction. The obtained results are well accounted for by the following mechanism after Reactions 1, 4, and 5 occurred:

$$I_2^{\cdot-}+Y\xrightarrow{k_7}2I^-+Y^{\ddagger} \quad (7)$$

and

$$I_2\ (\text{or } I_3^-)+Y^{\ddagger}\xrightarrow{\text{fast}}\text{products}, \quad (8)$$

where Y represents the amine-*N*-polycarboxylate ions. Assuming a steady-state concentration for I·,

$$I_a\phi+k_{-5}[I_2^{\cdot-}]-k_{-4}[I^{\cdot}]^2-k_5[I^{\cdot}][I^-]=0, \quad (9)$$

where I_a and ϕ are the light intensity absorbed and quantum yield, respectively. Under equilibrium conditions of $k_{-5}[I_2^{\cdot-}]=k_5[I^-][I^{\cdot}]$,

$$[I^{\cdot}]=(I_a\phi/k_{-4})^{1/2}. \quad (10)$$

Under an excess concentration of I^-, $[I^{\cdot}]=[I_2^{\cdot-}]$, where

$$[I_2^{\cdot-}]=(I_a\phi/k_{-4})^{1/2}. \quad (11)$$

Under the condition $[I^{\cdot}]_{total}=[I^{\cdot}]+[I_2^{\cdot-}]$,

$$[I_2^{\cdot-}]=\frac{[I^{\cdot}]_{total}K_5[I^-]}{1+K_5[I^-]} \quad (12)$$

and

$$[I_2^{\cdot-}]=\left(\frac{I_a\phi}{k_{-4}}\right)^{1/2}\left(\frac{K_5[I^-]}{1+K_5[I^-]}\right). \quad (13)$$

Therefore, the following rate law can be derived:

$$-\frac{d[I_3^-]}{dt}=\frac{k_7}{2}\left(\frac{I_a\phi}{k_{-4}}\right)^{1/2}\left(\frac{K_5[I^-]}{1+K_5[I^-]}\right)[Y]. \quad (14)$$

From Lambert-Beer's law I_a correlates to an incident light intensity (I_0) with iodine concentrations of

$$I_a=I_0[1-\exp(-\alpha[I_2])], \quad (15)$$

where α is a constant containing an absorption coefficient and an optical path length. Under the condition $\alpha[I_2]<0.1$ employed in this study, Eq. 15 can be simplified to

$$I_a=I_0\alpha[I_2]. \quad (16)$$

Therefore, Eq. 14 can be represented as

$$-\frac{d[I_3^-]}{dt}=\frac{k_7}{2}\left(\frac{I_0\alpha\phi}{k_{-4}K_1}\right)^{1/2}\left(\frac{[I_3^-]}{[I^-]}\right)^{1/2}\left(\frac{K_5[I^-]}{1+K_5[I^-]}\right)[Y], \quad (17)$$

$$k_{obsd}=\frac{k_7}{2}\left(\frac{I_0\alpha\phi}{k_{-4}K_1}\right)^{1/2}\left(\frac{K_5[I^-]^{1/2}}{1+K_5[I^-]}\right)[Y], \quad (18)$$

The values of α and k_7 could not be obtained in this work, although the values of ϕ and k_{-4} are known ($\phi=0.11$—0.83 and $k_{-4}=8\times10^9$ dm^3 mol^{-1} s^{-1}).

The following reaction for the initial photoreaction is also possible:[9]

$$I_3^-\overset{h\nu}{\rightleftharpoons}I_2^{\cdot-}+I^{\cdot}. \quad (19)$$

The results at low concentrations of I^-, where the rate is dependent on $[I^-]^{1/2}$, could be well accounted for by Reaction 19. The solid curve in Fig. 4 was calculated by using $K_5=2\times10^3$ dm^3 mol^{-1} and $k_7(\alpha\phi)^{1/2}=8.0\times10^6$ dm$^{9/2}$ mol$^{-3/2}$ s^{-1}. The estimated value for K_5 is smaller than that reported previously.[9,10] This may be attributable to the different experimental conditions or to the contribution of the bimolecular decay of the $I_2^{\cdot-}$ ions:

$$2I_2^{\cdot-}\longrightarrow I_3^-+I^- \quad [k_{20}=4.5\times10^9\ \text{dm}^3\ \text{mol}^{-1}\ \text{s}^{-1}].[15] \quad (20)$$

The reaction of I· with EDTA and other diamine-*N*-polycarboxylate ions must be neglected on the basis of the $[I^-]$ dependence.

Effect of Diamine-*N*-polycarboxylate. The pH dependence on the reaction rate of EDTA indicates that at least one proton-free nitrogen in the molecule is required for the reduction of the radical species, $I_2^{\cdot-}$, and that the lone electron-pair on the nitrogen atom is available for electron transfer to the $I_2^{\cdot-}$ radical anion. The rate constants ($k_{obsd}/[\text{amine-}N\text{-polycarboxylate}]_0$) under completely same conditions were 1.35×10^{-3}, 1.30×10^{-2}, 1.45×10^{-2}, and 4.90×10^{-2} dm$^{3/2}$ mol$^{-1/2}$ s^{-1} at pH 4.62 for EDDA, CDTA, EDTA, and HEDTA, respectively. The trend in reactivity, EDDA$\ll$CDTA$\approx$EDTA$<$HEDTA, is the same as that for the acid-dissociation constants of these amine-*N*-polycarboxylate ions,[11] H_2edda ($pK_{a1}=6.48$)$<H_4$cdta ($pK_{a3}=6.20$)$\approx H_4$edta ($pK_{a3}=6.24$)$<H_3$hedta ($pK_{a2}=5.41$), respectively; it is noted that the EDDA system is exceptionally slow. Under the same conditions as in Fig. 1 (but at pH 7.2), the rate for EDDA increased to 70-fold in $k_{obsd}/[EDDA]_0$ (1.00×10^{-1} dm$^{3/2}$ mol$^{-1/2}$ s^{-1}). This suggests that edda^{2-} is more reactive than Hedda$^-$, the latter being less reactive than Hedta^{3-}. Chapman et al.[16] demonstrated from IR and NMR studies of Hedta^{3-} in an aqueous solution that two of the carboxylate groups of Hedta^{3-} are hydrogen-bonded to one N^+H and that the other two are free. Therefore, the free nitrogen may be reactive with $I_2^{\cdot-}$ in the Hedta^{3-} ion. The inactivity of the species, Hedda$^-$, may arise from the fact that both carboxylate groups of Hedda$^-$ are possible to be hydrogen-bonded to N^+H in solutions.

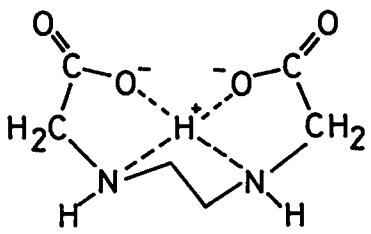

Hedda^{-}

Effect of Metal Ion. In order to confirm the importance of the lone electron-pair on the amino groups in amine-*N*-polycarboxylate ions mentioned above, we examined the effect of metal ions and found that those which were able to form chelate compounds with the diamine-*N*-polycarboxylate ions, greatly inhibited the photoreduction of iodine. The rate law of Eq. 3 was always satisfied for the coexistence of any metal ions employed. Plots of k_{obsd} vs. $[M^{2+}]_0/[EDTA]_0$ are given in Fig. 6. Strong complex-forming ions, such as copper(II) and zinc(II), inhibit quantitatively, while relatively weak complex-forming ions, such as magnesium(II) and calcium(II), can not greatly inhibit the photoreduction of iodine at pH 4.62. For example, even in a 10^3-fold excess of magnesium over EDTA, the decrease in k_{obsd} was only 20% of that in the absence of the metal ion. The trend regarding the inhibitory effect on the rate at pH 4.62 is $Mg^{2+}<Ca^{2+}\ll Zn^{2+}\approx Cu^{2+}$, the order of which is the same as that of the stability constants of the chelate complex $[M(edta)]^{2-}$; the values of $\log K_{M(edta)}$ at 25 °C and I=0.1 mol dm^{-3} are 8.7, 10.6, 16.4, and 18.7 for Mg^{2+}, Ca^{2+}, Zn^{2+}, and Cu^{2+}, respectively.[10] The results in Fig. 6 indicate that the chelated metal(II) ions cannot reduce any radicals of $I_2^{\cdot-}$ and I$^{\cdot}$ in the case of Cu(II) and Zn(II) ions. Lati and Meyerstein[17] have reported that $[Cu(edta)]^{2-}$ did not react with the $I_2^{\cdot-}$ produced by electron pulse radiolysis. Therefore, the lone electron pair on the nitrogen atom must play an important role in the oxidation and fragmentation of any amine-*N*-polycarboxylate ions.

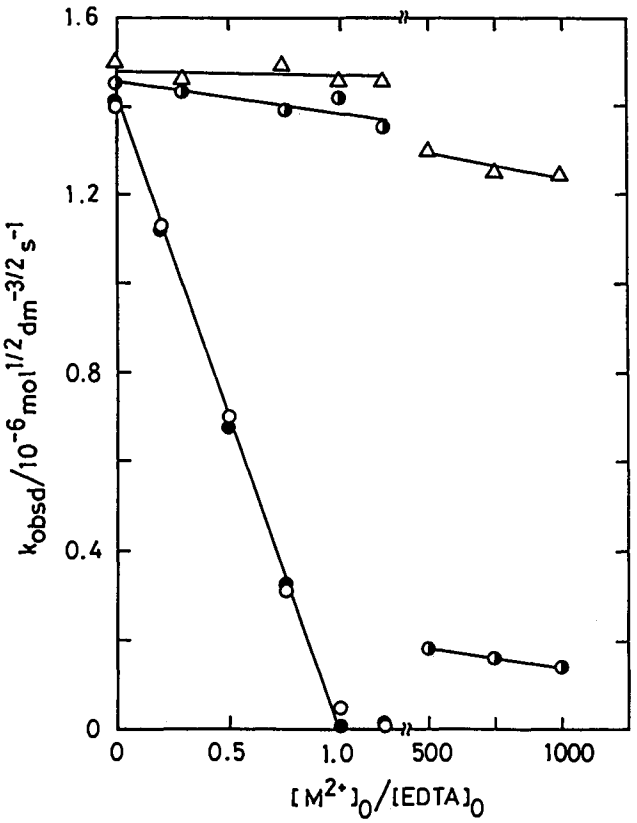

Fig. 6. Plots of k_{obsd} vs. $[M^{2+}]_0/[EDTA]_0$ for the photoreaction of iodine with EDTA. Conditions are the same as in Fig. 1. ○: Cu^{2+}, ●: Zn^{2+}, ◑; Ca^{2+}, and △: Mg^{2+} for M^{2+} ions.

The fragmentation of EDTA in thermal reactions is complicated and the reaction mechanism is still unclear. It has been reported that CO_2 and HCHO are detected as products.[18] We found CO_2 as one of the products in the photoreduction of iodine by EDTA, and also examined the stoichiometry of the reaction. Under the condition $[I_2]\gg[EDTA]_0$, the stoichiometry was not 1 : 1; more than one mole of I_2 was consumed against EDTA. An accurate stoichiometric number could not be determined, but seemed to certainly be dependent on the pH of the reacting solution. Since ethylenediamine was completely inactive under the present experimental conditions (see Fig. 1), fragmentation must occur at acetate arms of EDTA. An ESR study by Poupko et al.[19] has shown that the hydrogen abstraction from EDTA occurs at the acetate carbon atom adjacent to nitrogen atom. Under the condition $[EDTA]_0\gg[I_2]$, which was employed in the present study, fragmentation might have occurred at one acetate group. The effect of radical scavengers of acrylonitrile or $[Co(NH_3)_6]^{3+}$ for the photooxidation of EDTA is completely different from that for the oxalate system studied previously,[3] the latter having a $CO_2^{\cdot-}$ radical anion as an intermediate. This fact suggests that the intermediate radical species is not a free $CO_2^{\cdot-}$ in Reaction 7, but that the radical ion $Y^{\dagger}$ still holds the $-CO_2$ fragment.

In conclusion, we demonstrated that the photoreduction of iodine with diamine-*N*-polycarboxylate ions in an aqueous solution occurs in the order of the reaction rate, HEDTA>EDTA≈CDTA≫EDDA, and that the lone electron-pair of the nitrogen atom plays an important role in the oxidation and fragmentation of amine-*N*-polycarboxylate ions.

This research was supported by a Grant-in-Aid for Scientific Research No. 01470051 from the Ministry of Education, Science and Culture.

References

1) C. Sánchez-Pedreño, M. T. Sierra, and A. Sanz, *Analyst*, **112**, 837 (1987).

2) P. Fornier de Violet and J. Faure, *J. Chim. Phys. Phys. Chim. Biol.*, **69**, 996 (1972).

3) M. Kimura, H. Ishiguro, and K. Tsukahara, *J. Phys. Chem.*, **94**, 4106 (1990).

4) The symbols, EDTA, CDTA, HEDTA, and EDDA are abbreviated for all the forms of $H_n edta^{(4-n)-}$ (n=0—4), $H_n cdta^{(4-n)-}$ (n=0—4), $H_n hedta^{(3-n)-}$ (n=0—3), and $H_n edda^{(2-n)-}$ (n=0—2), respectively.

5) C. G. Hatchard and C. A. Parker, *Proc. R. Soc. London, Ser. A,* **235**, 518 (1956).

6) M. F. Ruasse, J. Aubard, B. Gallard, and A. Adenier, *J. Phys. Chem.*, **90**, 4382 (1986).

7) A. D. Awtrey and R. E. Connick, *J. Am. Chem. Soc.*, **73**, 1842 (1951).

8) P. Fornier de Violet, R. Bonneau, and J. Joussot-Dubien, *J. Chim. Phys.*, **70**, 1404 (1973).

9) A. Barkatt and M. Ottolenghi, *Mol. Photochem.*, **6**, 253 (1974).

10) P. Fornier de Violet, R. Bonneau, and S. R. Logan, *J. Phys. Chem.*, **78**, 1698 (1974).

11) a) A. E. Martell and L. G. Sillen, "Stability Constants of Metal-Ion Complexes," The Chemical Society, Special Publication No. 17, London (1964); b) L. G. Sillen, A. E. Martell, E. Hogfelat, and R. M. Smith, "Stability Constants of Metal-Ion Complexes, Supplement No. 1," The Chemical Society, Special Publication No. 25, London (1971).

12) J. Bjerrum, "Metal Amine Formation in Aqueous Solution," P. Haase and Son, Copenhagen (1941), p. 230.

13) H. A. Schwarz and B. H. J. Bielski, *J. Phys. Chem.*, **90**, 1445 (1986).

14) H. Okabe, "Photochemistry of Small Molecules," Wiley, New York (1978).

15) L. I. Grossweiner and M. S. Matheson, *J. Phys. Chem.*, **61**, 1089 (1957).

16) D. Chapman, D. R. Lloyd, and R. H. Prince, *J. Chem. Soc.*, **1963**, 3645.

17) J. Lati and D. Meyerstein, *J. Chem. Soc., Dalton Trans.*, **1978**, 1105.

18) K. A. Schroeder and R. E. Hamm, *Inorg. Chem.*, **3**, 391 (1964).

19) R. Poupko, B. L. Silver, and A. Lowenstein, *Chem. Commun.*, **1968**, 453.

Disposition of Ferrocenes in β- or γ-Cyclodextrin Cavity and Consideration on the Absorption Bands of Ferrocene

Nagao KOBAYASHI* and Tetsuo OSA*
Pharmaceutical Institute, Tohoku University, Aobayama, Aoba-ku, Sendai 980
(Received June 30, 1990)

By comparing the induced circular dichroism (ICD) spectrum of 1,4,7,10,13-pentaoxa[13](1,1')-ferrocenophane, **I**, in the presence of β-cyclodextrin (β-CDx) with that of ferrocenes (Fcs) in β-CDx or γ-CDx cavity, the disposition of Fcs in the CDxs is determined. Thus, the orientation of Fc in the Fc:β-CDx 1:1 complex and ferrocenecarboxylic acid (FcMA) in β-CDx at pH 2 is considered to be nearly parallel to the molecular axis of β-CDx, while that of Fc in the Fc: γ-CDx 1:1 complex, FcMA in β-CDx cavity at pH 9, and FcMA and ferrocenedicarboxylic acid (FcDA) in γ-CDx cavity appears to be close to normal to the molecular axis of the CDx. In addition, based on the ICD spectra, an intense band of Fcs at around 200 nm is assigned as a charge-transfer (CT) transition between the cyclopentadienyl (Cp) rings and iron(II). The advantage of using CDxs for the determination of the polarization direction of absorption bands of chromophore molecules is mentioned in comparison with previous methods.

Induced circular dichroism (ICD) studies on inclusion complexes between aromatic guest molecules and cyclodextrins (CDxs) have developed over the past decade.[1,2] In particular, concerning the ICD of CDx–chromophore 1:1 inclusion complexes, the following have been substantiated or shown[1] with high accuracy on the basis of the Kirkwood–Tinoco coupled oscillator expression.[3] (i) Electronic transitions parallel to the molecular axis of CDxs produce positive ICD, while those normal to the axis show negative ICD. (ii) The sign of the calculated rotational strength does not change by the movement of guest molecules along the X-, Y-, and Z-axis, although their magnitude is affected[1g] (the origin of the axes is set at the center of CDx and the Z-axis is parallel to the molecular axis of CDx). (iii) Rotation of the guest molecule in the X–Y plane has no influence on the calculated rotational strength, while that in the X–Z plane does have a great influence on it.[1g] Figure 1,

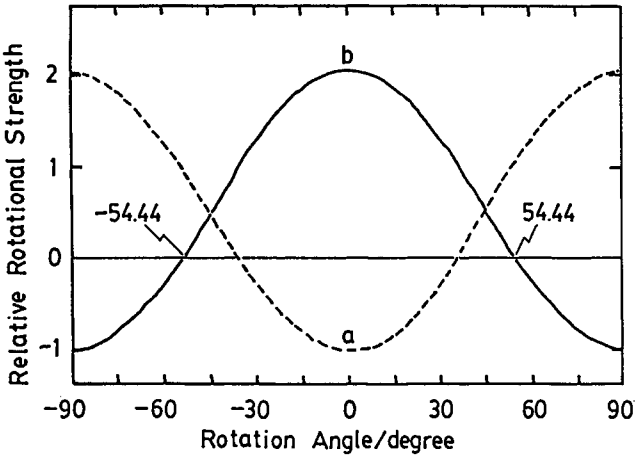

Fig. 1. The dependence of the calculated rotational strength of a CDx–chromophore complex on the rotation angle in the X–Z plane. Curves a and b are the transitions normal and parallel to the molecular axis of CDxs, respectively.

obtained by the procedure shown in Ref. 1h, depicts this dependence of calculated rotational strength on the rotation of the electric transition moment in the X–Z plane. As can be judged from curve b in this figure, electronic transitions whose directions are within 54.44 degrees from the axis of CDxs produce positive ICD sign while those more than 54.44 degrees yield negative ICD sign. Accordingly, it is now possible to determine the polarization direction of the absorption band of chromophore molecules from the sign of the ICD spectra of the chromophore: CDx 1:1 complex. Conversely, the orientation of guest molecules trapped in CDxs cavity can be inferred from the sign of the ICD spectra, if the polarization directions of the bands of the guest molecules are known. This method is valid in particular for molecules which have clear long- and short-axes, because their orientation in CDxs is likely to be fixed. However, if relatively round or square molecules are used as guest molecules, determination of the polarization direction of bands or elucidation of the orientation of guest molecules in CDxs becomes difficult, because more than one kind of orientation may exist. Typical examples are ferrocene (Fc) and its derivatives. Ferrocene is a relatively round molecule, with H atoms displaced towards the Fe atom.[4] As indicated recently by calculation,[5] Fc can bind to β-CDx in both an axial and equatorial orientation. Since the energy difference is too small to be significant (calculated value is 0.5 kcal mol^{-1}),[5] packing forces in a crystal, solvation effects in solution, or even a slight change in Fc structure and the size of the CDxs could well determine the preferred binding mode in real systems. In fact, the disposition of ferrocenecarboxylic acid (FcMA) in β-CDx cavity is altered by dissociation of its carboxyl group,[6] and the orientation of Fc in β-CDx cavity differs markedly from that in γ-CDx cavity.[7] Despite the publication of over 20 articles on Fc derivative–CDx complexes,[5–8] the orientation of Fc in CDxs cavity has not been determined to date. This difficulty is due to

the uncertainty of the assignment of the electronic absorption band of Fc and its derivatives.[9] By preparing a Fc derivative which can bind to CDxs cavity in only one binding mode, we can infer the orientation of other Fc derivatives in CDx cavity by comparing their ICD spectra. In addition, it may be possible to conjecture the polarization direction of UV bands of Fc derivatives. For these reasons we have prepared compound **I** (Fig. 2 inset) and measured its ICD spectra in the presence of β-CDx. For this molecule, only an equatorial inclusion is possible because of size limitations. As will be shown below, the orientation of other Fc derivatives in β- or γ-CDxs was conjectured based on the ICD spectrum of **I** in β-CDx.

Experimental

Measurements. UV-visible absorption and ICD spectra were recorded at 20 °C on a Shimadzu UV-250 spectrophotometer and JASCO J400X spectrodichrometer, respectively. Cells of pathlength 0.5, 1, 2, 5, 10, and 20 mm were used.

Materials. Fc, FcMA, and 1,1'-ferrocenedicarboxylic acid (FcDA) were commercially available reagents and were recrystallized from ethyl acetate, hexane, and ethanol, respectively. β-CDx and γ-CDx were donated by Japan Maize Product Co., and recrystallized from water. Fc–β-CDx and Fc–γ-CDx 1 : 1 complexes were prepared accodrding to the method reported in the literature.[7,8f] Anal. For Fc–β-CDx complex, Found: C, 45.96; H, 6.49; Fe, 4.0%. Calcd for $C_{52}H_{80}O_{35}Fe \cdot 1.5H_2O$: C, 46.26; H, 6.35; Fe, 4.14%. For Fc–γ-CDx complex, Found: C, 45.57; H, 6.45; Fe, 3.5%. Calcd for $C_{58}H_{90}O_{40}Fe \cdot 2H_2O$: C, 45.85; H, 6.24; Fe, 3.68%. Compound **I** was synthesized from 1,1'-ferrocenediol and 1,11-dichloro-3,6,9-trioxaundecane according to the literature.[10] Anal. Found: C, 57.23; H, 6.37; Fe, 14.6%. Calcd for $C_{18}H_{24}O_5Fe$: C, 57.46; H, 6.43; Fe, 14.84%. Mp 59.5—60 °C (lit, 59—61 °C).[10a]

Results

Figure 2 shows the UV-visible absorption and ICD spectra of **I** in the presence of β-CDx in ethylene glycol. The shape of the absorption spectrum is similar to that of Fc (Fig. 3), indicating that the attached crown unit does not significantly affect the electronic structure of the Fc chromophore. Corresponding to the absorption peaks at approximately 430 and 220 nm, a negative and positive ICD peak appeared, respectively. Continuous variation experiments for the determination of complex stoichiometry were not carried out through Figs. 2 to 5,

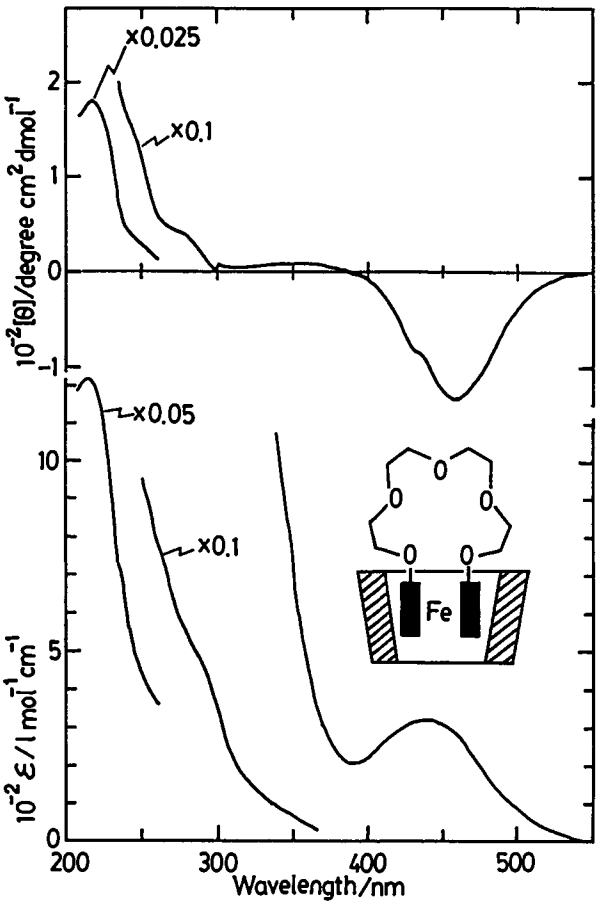

Fig. 2. ICD (top) and UV-visible (bottom) spectra of **I** in the presence of β-CDx in ethylene glycol. [**I**]/M=9.98×10^{-4} and [β-CDx]/M=0.020.

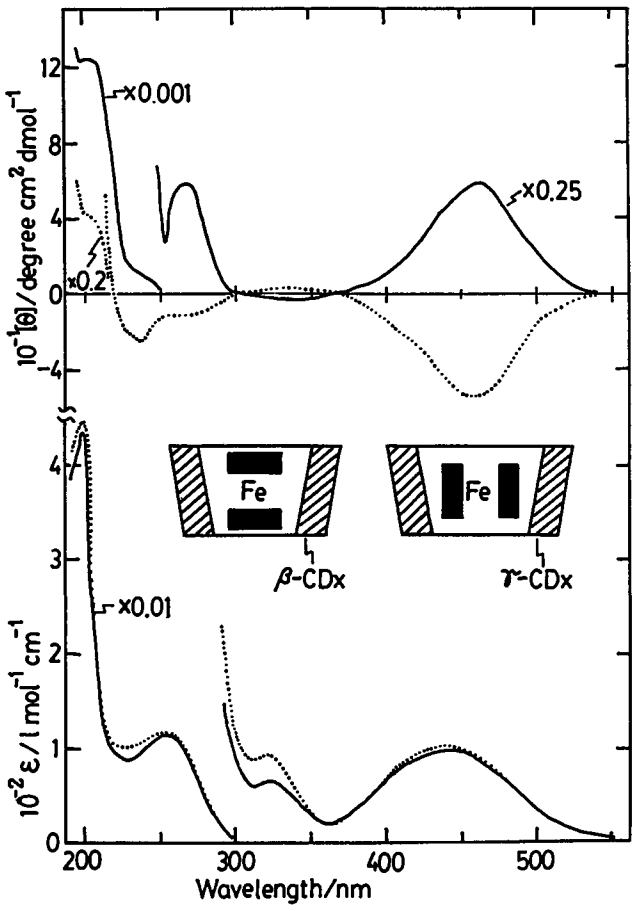

Fig. 3. ICD (top) and UV-visible (bottom) spectra of Fc–β-CDx (solid lines) and Fc–γ-CDx (dotted lines) in ethylene glycol. [Fc–β-CDx]/M=[Fc–γ-CDx]/M=0.001.

since 1 : 1 complex formation between β- or γ-CDx and Fcs has been established by many studies.[5-8]

Figure 3 shows spectra of Fc–β-CDx and Fc–γ-CDx 1 : 1 complexes in ethylene glycol. In the absorption spectra, peaks appear at around 200, 250—260, 330 and 440 nm. ICD spectra of Fc–β-CDx and Fc–γ-CDx complexes are interesting in that their signals are opposite over a wide range of wavelengths.[8p,r] Except at 300—370 nm, Fc–β-CDx complex produced positive ICD peaks or shoulders associated with each absorption peak, while Fc–γ-CDx complex showed negative ICD over a wide range of wavelengths. Note, however, that both complexes produced a positive ICD signal corresponding to the transition at approximately 200 nm.

Absorption and ICD spectra of FcMA in the presence of β-CDx or γ-CDx at pH 2 and 9 are shown in Fig. 4. The general features of the absorption spectra are similar to the spectrum of Fc (Fig. 3) but some differences occur, suggesting that the carboxyl group affects the Fc chromophore to some extent. In the presence of β-CDx at pH 9, i.e. where the carboxyl group is dissociated, the sign of the ICD spectrum is negative, except at <220 nm. On the other hand, it is positive in all regions when it is not dissociated (pH 2). The wavelengths of the absorption maxima and ICD peaks or troughs are in relatively good agreement. In the presence of γ-CDx, ICD was negative except at ca. 290—380 nm. Three troughs were observed at ca. 200—220, 270, and 470—480 nm at both pH 2 and 9.

Figure 5 shows the spectra of FcDA in the presence of β-CDx or γ-CDx at pH 2 and 9. The shape and intensity of the absorption spectrum change with dissociation of the carboxyl groups. However, the shape of the absorption spectra of FcDA is roughly similar to that of Fc without substituent groups (Fig. 3). An absorption band at around 220—230 nm is a band which lie on the tail of the higher transition band, since the absorption coefficient increases dramatically in the wavelength shorter than 200 nm (not shown). The ICD spectra in the presence of β-CDx are complex at

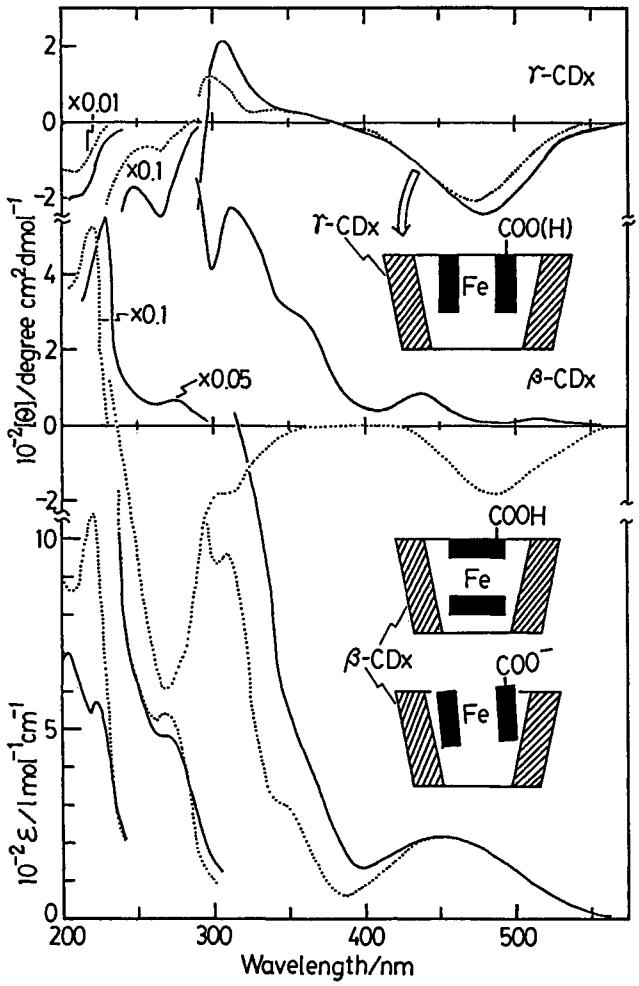

Fig. 4. ICD (middle and top) and UV-visible (bottom) spectra of FcMA in the presence of β-CDx (middle and bottom) or γ-CDx (top) at pH 2 (solid lines) and 9 (dotted lines). [β-CDx]/M=[γ-CDx]/M=0.010 and [FcMA]/M=0.001.

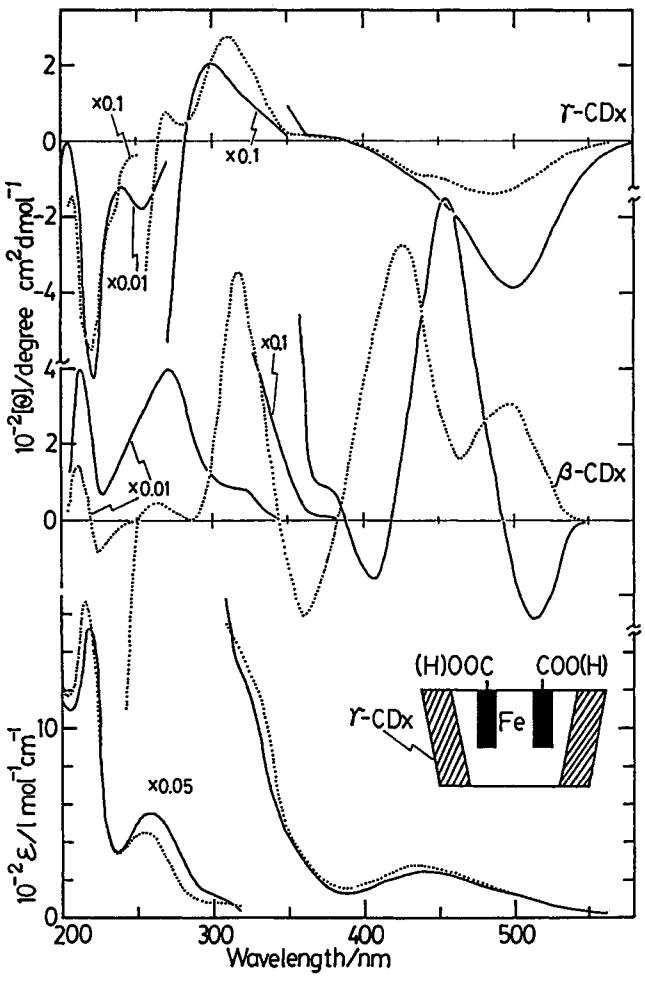

Fig. 5. ICD (middle and top) and UV-visible (bottom) spectra of FcDA in the presence of β-CDx (middle and bottom) or γ-CDx (top) at pH 2 (solid lines) and 9 (dotted lines). [β-CDx]/M=[γ-CDx]/M=0.010 and [FcDA]/M=0.001.

both pH 2 and 9, although the ICD pattern in the region <370 nm at pH 2 is relatively similar to that of FcMA at pH 2. Corresponding to an absorption maximum at around 220 nm, a positive ICD peak was observed at both pH 2 and 9. In contrast, ICD spectra in the presence of γ-CDx is relatively simple, showing negative signs in a wide range of wavelengths. The shape of the ICD curves is similar to each other at both pH 2 and 9, and resembles that of FcMA in the presence of γ-CDx (Fig. 4).

Discussion

From its shape and size, **I** can be trapped in β-CDx cavity only as an equatorial inclusion, as shown in the inset of Fig. 2. Based on the arguments (i) and (ii) mentioned in the introduction, the polarization direction of the band at the longest wavelength is not parallel to the β-CDx axis. Judging from Fig. 1 curve b, it is inclined by more than 54.44 degrees from the molecular axis of β-CDx. By argument (iii) and from the intensity change on rotation in the X–Z plane (Fig. 1), the Fc in Fc–γ-CDx complex (Fig. 3) appears to have a similar disposition to that of **I** in β-CDx cavity (equatorial inclusion), while that in Fc–β-CDx complex is completely different. In addition, since the positions of an ICD trough of Fc–γ-CDx complex and ICD peak of Fc–β-CDx complex coincide almost exactly at 460 nm, they seem to be almost normal to each other. Accordingly, the inclusion of Fc in Fc–β-CDx complex is considered to be close to axial. These results on the disposition of Fc in β- or γ-CDx cavity accord essentially with those obtained by NMR technique for solid samples. Namely, according to what one of the reviewers taught us, the Cp–Fe–Cp axis of Fc molecule declines from the axis of β-CDx by 6.5 degrees but by 72 degrees from that of γ-CDx.[11] Since the ICD pattern of FcMA in the presence of β-CDx at pH 9 (Fig. 4) is quite similar to that of Fc in Fc–γ-CDx complex (Fig. 3), the inclusion of FcMA by β-CDx also appears almost equatorial at pH 9. Although a clear ICD peak was not observed in the region >400 nm, the arrangement of this molecule at pH 2 appears to be close to axial in β-CDx cavity, since the ICD spectroscopic pattern of FcMA in the 200—400 nm region at this pH is similar to that of Fc–β-CDx complex (Fig. 3). The stoichiometry and inclusion type of CDx–chromophore host–guest complexes are determined by many factors. In the case of FcMA–β-CDx system, the pH value of the solution affects the type of inclusion. In alkaline solution, the carboxyl group dissociates and the resultant highly hydrophilic carboxylate anion may resist to be deeply accommodated into β-CDx cavity. As a result, an equatorial inclusion occurs, although FcMA may be deeply trapped by an axial inclusion when the carboxyl group is not dissociated in acidic solution, i.e. when it is less hydrophilic than carboxylate anion. Judging from the spectroscopic pattern of ICD, the inclusion of FcMA and FcDA in γ-CDx is similar at both pH 2 and 9, and it appears to be equatorial from the presence of a trough at ca. 380—550 nm. On the other hand, a zig-zag pattern in the wavelength longer than 380 nm (Fig. 5) indicates that the orientation of FcDA in β-CDx cavity is obscure both when the carboxyl groups are dissociated and undissociated. Because of steric hindrance by the two carboxyl groups, FcDA may be trapped in β-CDx cavity obliquely. In this respect, the results in FcDA–γ-CDx system suggest the possibility that the mutual positions of the two carboxyl groups may change on inclusion. That is, the two carboxyl groups would take many conformations to each other with respect to Cp–Fe–Cp axis in solution. Especially, there is no particular requirement that the two carboxyl groups of FcDA must stay in the same side of Fe atom in the absence of γ-CDx. And, if FcDA molecule is accommodated to γ-CDx cavity in the same conformations as it is in solution, it is conceivable from the consideration using the CPK molecular model that a zig-zag ICD pattern appears in >380 nm because of steric hindrance, although the cavity of γ-CDx is larger than that of β-CDx. However, no such pattern was observed in reality as shown in Fig. 5. Now that the Cp rings are much more hydrophobic than carboxyl groups, it would be most natural to think that the two Cp moieties are trapped in γ-CDx first, leaving the carboxyl groups behind (see the inset in Fig. 5).

The absorption peak in the longest wavelength region has been proposed to contain two components with absorption maxima at around 420—430 and 460—470 nm, and both are assigned as d-d transitions.[9] Interestingly, an ICD peak in the axial inclusion system (Fig. 3, Fc–β-CDx system) and ICD troughs in the equatorial inclusion system (Fig. 2, Fc–γ-CDx system in Fig. 3, FcMA–γ-CDx system in Fig. 4, and FcMA–β-CDx system at pH 9 in Fig. 4) always appear at around 460—470 nm. Hence, out of two components included in this band, the one to the red is deemed to have a polarization direction along the Cp–Fe–Cp axis, as has been found for crystals of Fc.[9f] This result appears to be in agreement with low temperature studies[9b] which indicate that the band is a symmetry-forbidden d-d transition containing charge-transfer (CT) character.

The ICD intensity of Fc–γ-CDx complex is much weaker than that of Fc–β-CDx complex. Two reasons are conceivable for this phenomenon. The first one is attributed to a difference in polarization direction. As shown in Fig. 1 curve b, when the transition dipole which is parallel to the molecular axis of CDx rotates by ca. 90 degrees in the X–Z plane, the calculated rotational strength lessens to ca. half of the original value, together with a change of ICD sign. Accordingly, for example, if a transition dipole at 460 nm which has its polarization direction along the Cp–Fe–Cp axis rotates 90 degrees in the X–Z plane (this corresponds to a change from an axial to an equatorial inclusion), its intensity becomes ca. one-half of the original value.

However, since the observed ICD intensity of Fc–γ-CDx complex is about 25% of that of Fc–β-CDx complex at 460 nm, another factor must be taken into account in order to explain the intensity difference between Fc–β-CDx and Fc–γ-CDx complexes. This factor is the distance between the Fc unit and CDx. The rotational strength is known to be proportional to the inverse of the cube of the distance.[12] Since the radius of β-CDx cavity (4.7—5.2 Å) is about 80% of that of γ-CDx cavity (6.0—6.4 Å),[13] the rotational strength in γ-CDx is estimated to be about half ($0.8^3 \fallingdotseq 0.5$) of that in β-CDx. Thus, the smaller ICD intensity at 460 nm in Fc–γ-CDx complex is quantitatively ($0.5 \times 0.5 = 0.25$, 25%) rationalized by taking the above two factors into account. If, however, the orientation of Fc in Fc–β-CDx complex is equatorial and that in Fc–γ-CDx complex is axial, the ICD intensity at 460 nm would be almost comparable by the same argument, although the sign of ICD is opposite to each other (negative and positive for Fc–β-CDx and Fc–γ-CDx systems, respectively). Thus the observed ICD sign and intensity relationship between Fc–β-CDx and Fc–γ-CDx systems can be interpreted reasonably only when the inclusion of Fc in Fc–β-CDx complex is axial while that of Fc–γ-CDx complex is equatorial. In this way, these considerations also lend support to our conclusion about the disposition of Fc in Fc–β-CDx and Fc–γ-CDx complexes.

Based on the knowledge obtained above, we are now able to resolve a question which has been disputed for a long time,[9] i.e. the assignment of an intense band of Fcs at around 200nm. Two opinions exist concerning the assignment of this band. Some[9a] groups have assigned this band as a π–π^* transition of the Cp rings, while others[9b,c] have interpreted this as a CT transition between the Cp rings and iron(II). As shown in Figs. 2 and 3, Fcs produce a positive ICD peak corresponding to this band when they are included by CDxs as both an axial and equatorial inclusion. If this band is a π–π^* transition, the sign of the ICD should be positive for an equatorial inclusion and negative for an axial inclusion based on the arguments (i)—(iii) above (note that an equatorial inclusion of Fc is equivalent to an axial inclusion of the Cp rings). Thus, the results do not agree with assignment as a "pure" π–π^* transition. Can, then, the observed ICD be reasonably interpreted as a CT transition? As depicted in Fig. 1, transitions whose polarization directions are within 54.44 degrees from the molecular axis of CDxs produce positive ICD whenever Fc is in the CDx cavity (criterion (ii)). On the other hand, the d_{xz} and d_{yz} orbitals of iron decline theoretically 45 degrees from the Cp–Fe–Cp axis of Fc. Hence, whether or not Fcs are included in CDxs cavity by an axial or equatorial inclusion, these orbitals are still declining 45 degrees from the molecular axis of CDxs. This means that if these orbitals are used in CT between the Cp rings and iron, then the sign of the ICD signal becomes positive. In this way, an intense band of Fcs at around 200 nm is reasonably assigned to a CT transition. Although negative ICD is observed at ca. 220—230 nm in FcDA–γ-CDx system, this may be due to the strong electron-withdrawing effect of the carboxyl groups attached to the Cp rings.

Previous reports[9] also discuss the polarization direction of other bands. Using crystals of Fc,[9f] the bands at ca. 260 and 320 nm are proposed to possess polarization along the Z (Cp–Fe–Cp) axis mixed with some polarization along the X or Y axis. Figures 2 and 3 indicate that the present results do not contradict this proposal concerning the 260 nm band, since the sign of ICD of this band is the same as that of the 440 nm band which is polarized along the Z (Cp–Fe–Cp) axis. The sign of ICD between 300 and 370 nm suggests that the band at ca. 320 nm is polarized more strongly along the X or Y direction rather than the Z direction. Otherwise, negative ICD is not produced in this region.

Conclusion

The proposed orientations of Fcs in CDxs are presented in each Figure. Based on the ICD spectra of **I** in β-CDx cavity, the orientations of Fcs in CDxs cavity are determined, and an answer is given for the assignment of a band of Fc which has been in dispute. We would like to stress here the importance of using CDxs for determination of the polarization direction of bands of aromatic compounds. In order to determine the polarization direction of the electronic absorption of non-crystalline compounds experimentally, measurements of dichroic spectra in stretched polymer sheet,[14] and of ICD in mesophases have been of great use.[15] However, there are limitations to these methods. Firstly, since the most essential factor is the alignment of solute molecules, it is difficult to apply these methods to relatively round or square molecules. Round molecules are, of course, not easily studied even in CDx systems. However, as shown in this paper, the orientation of round guest molecules in CDxs cavity can be regulated by modifying their structure. ICD spectra of such guest-oriented inclusion complexes then enable the polarization direction to be determined. Secondly, due to the absorption of polymers or mesophases, only a few polymers can be used for bands lying shorter than ca. 220 nm. In this respect, the CDx system appears to be superior, since water and alcohols are generally used. If water is used, this method is applicable to bands as short as ca. 190 nm.

References

1) a) K. Harata and H. Uedaira, *Bull. Chem. Soc. Jpn.*, **48**, 375 (1975). b) K. Harata, *ibid.*, **51**, 167 (1978). c) *idem., ibid.*, **52**, 1807 (1979). d) H. Yamaguchi, N. Ikeda, F. Hirayama, and K. Uekama, *Chem. Phys. Lett.*, **55**, 75 (1978). e) N. Ikeda and H. Yamaguchi, *ibid.*, **56**, 167 (1978). f) M. Ata and H. Yamaguchi, *J. Chem. Soc., Chem. Commun.*, **1981**, 3. g) H. Yamaguchi, K. Ninomiya, and R. West, *J.*

Chem. Soc., Faraday Trans. 2, **78**, 481 (1982). h) H. Shimizu, A. Kaito, and M. Hatano, *Bull. Chem. Soc. Jpn.*, **52**, 2678 (1979); **54**, 513 (1981); *J. Am. Chem. Soc.*, **102**, 7059 (1983). i) N. Kobayashi, S. Minato, and T. Osa, *Makromol. Chem.*, **184**, 2113 (1983). j) N. Kobayashi, *J. Chem. Soc., Chem. Commun.*, **1988**, 918. k) N. Kobayashi and T. Osa, *Carbohydr. Res.*, **192**, 147 (1989). l) T. Tamaki and T. Kokubu, *J. Inclusion Phenom.*, **2**, 815 (1984). m) P. Bortolus and S. Monti, *J. Phys. Chem.*, **91**, 5046 (1987).

2) a) N. Kobayashi, R. Saito, A. Ueno, T. Osa, H. Hino, and Y. Hino, *J. Chem. Soc., Perkin Trans. 2,* **1983**, 1031. b) N. Kobayashi, Y. Hino, A. Ueno, and T. Osa, *Bull. Chem. Soc. Jpn.*, **56**, 1849 (1983). c) K. Takamura, S. Inoue, and F. Kusu, *Chem. Lett.*, **1983**, 233. d) N. Kobayashi, A. Ueno, and T. Osa, *J. Chem. Soc., Chem. Commun.*, **1981**, 340. e) N. Kobayashi, A. Akiba, K. Takatori, A. Ueno, and T. Osa, *Heterocycles,* **19**, 2022 (1982). f) N. Kobayashi, R. Saito, A. Ueno, and T. Osa, *Makromol. Chem.*, **184**, 837 (1983). g) K. Fujita, T. Ueda, T. Imoto, I. Tabushi, N. Toh, and T. Koga, *Bioorg. Chem.*, **11**, 72, 108 (1982). h) N. Kobayashi, R. Saito, A. Ueno, and T. Osa, *J. Chem. Soc., Chem. Commun.*, **1982**, 706.

3) I. Tinoco, Jr., *Adv. Chem. Phys.*, **4**, 113 (1962).

4) a) R. K. Bohn and A. Haaland, *J. Organomet. Chem.*, **5**, 470 (1966). b) F. Takusagawa and T. F. Koetzle, *Acta Crystallogr., Sect. B,* **35**, 1074 (1979).

5) F. M. Menger and M. J. Sherrod, *J. Am. Chem. Soc.*, **110**, 8606 (1988).

6) N. Kobayashi and T. Osa, *Chem. Lett.*, **1986**, 421.

7) A. Harada and S. Takahashi, *J. Chem. Soc., Chem. Commun.*, **1984**, 645.

8) a) R. Breslow, M. F. Czarniecki, J. Emert, and H. Hamaguchi, *J. Am. Chem. Soc.*, **102**, 762 (1980). b) R. Breslow and G. L. Trainor, *ibid.*, **103**, 154 (1981). c) R. Breslow, G. L. Trainor, and A. Ueno, *ibid.*, **105**, 2739 (1983). d) W. J. Noble, S. Srivastava, R. Breslow, and G. L. Trainor, *ibid.*, **105**, 2745 (1983). e) H. J. Thiem, M. Brandl, and R. Breslow, *ibid.*, **110**, 8612 (1988). f) A. Harada and S. Takahashi, *J. Inclusion Phenom.*, **2**, 791 (1984). g) N. J. Clayden, C. M. Dobson, S. J. Heyes, and P. J. Wiseman, *ibid.*, **5**, 65 (1987). h) T. Matsue, U. Akiba, T. Osa, and K. Suzufuji, *Denki Kagaku,* **53**, 508 (1985). i) T. Matsue, D. H. Evans, T. Osa, and N. Kobayashi, *J. Am. Chem. Soc.*, **107**, 2745 (1985). j) A. Ueno, F. Moriwaki, T. Osa, F. Hamada, and K. Murai *Tetrahedron Lett.*, **26**, 899 (1985). k) T. Matsue, T. Kato, U. Akiba, and T. Osa, *Chem. Lett.*, **1986**, 843. l) Y. Maeda, N. Ogawa, and Y. Tahashima, *J. Chem. Soc., Dalton Trans.*, **1987**, 627. m) A. Ueno, F. Moriwaki, T. Matsue, and T. Osa, *Makromol. Chem. Rapid. Commun.*, **6**, 231 (1985). n) A. Ueno, I. Suzuki, and T. Osa, *ibid.*, **8**, 131 (1987). o) M. J. Sherrod, *Carbohydr. Res.*, **192**, 17 (1989). p) A. Harada and S. Takahashi, *Chem. Lett.*, **1984**, 2089. q) N. J. Clayden, S. J. Heyes, and P. J. Wiseman, *J. Inclusion Phenom.*, **5**, 65 (1987). r) N. Kobayashi, *J. Chem. Soc., Chem. Commun.*, **1990**, 477.

9) a) D. R. Scott and R. S. Becker, *J. Chem. Phys.*, **35**, 516 (1961), and some Refs. therein. b) A. T. Armstrong, D. G. Carroll, and S. P. McGlynn, *ibid.*, **47**, 1104 (1967). c) Y. S. Sohn, D. N. Hendrickson, and H. B. Glay, *J. Am. Chem. Soc.*, **93**, 3603 (1971). d) D. Nielson, D. Boone, and H. Eyring, *J. Phys. Chem.*, **76**, 511 (1972). e) J. W. Rabalais, L. O. Werme, T. Wergmark, L. Karlsson, M. Hussain, and K. Siegbahn, *J. Chem. Phys.*, **57**, 1185 (1972). f) S. Yamada, A. Nakahara, and R. Tsuchida, *J. Chem. Phys.*, **22**, 1620 (1954); *Bull. Chem. Soc. Jpn.*, **28**, 465 (1955).

10) a) S. Akabori, Y. Habata, Y. Sakamoto, M. Sato, and S. Ebine, *Bull. Chem. Soc. Jpn.*, **56**, 537 (1983). b) A. N. Nesmeyanov, V. A. Sazonova, and V. N. Drozd, *Chem. Ber.*, **93**, 2117 (1960).

11) We are not aware of the literature describing these facts.

12) E. Charney, "The Molecular Basis of Optical Activity," John Wiley & Sons, New York, Brisbane, and Toronto (1979).

13) W. Saenger, *Angew. Chem., Int. Ed. Engl.*, **19**, 344 (1980).

14) a) T. Hoshi and Y. Tanizaki, *Z. Phys. Chem., (Frankfurt a. Main)* **71**, 230 (1970). b) E. W. Thulstrup, J. Michl, and J. H. Eggaers, *J. Phys. Chem.*, **74**, 3868, 3878 (1970). c) E. W. Thulstrup and J. Michl, *ibid.*, **84**, 82 (1980). d) H. Inoue, T. Hoshi, J. Shiraishi, and Y. Tanizaki, *Ber. Bunsen-Ges. Phys. Chem.*, **75**, 441 (1975), and Refs. therein.

15) a) F. D. Saeva and J. J. Wysocki, *J. Am. Chem. Soc.*, **93**, 5928 (1971). b) F. D. Saeva and G. R. Olin, *ibid.*, **95**, 7872 (1973). c) E. Sackmann and H. Mohwald, *J. Chem. Phys.*, **58**, 5407 (1973). d) E. Sackmann and J. Voss, *Chem. Phys. Lett.*, **14**, 528 (1972). e) Y. Sato and H. Hatano, *Makromol. Chem.*, **183**, 971, 977 (1982).

Selective Ring-Opening Reaction of Epoxides with Sodium Borohydride in the Presence of Cyclodextrins in Aqueous Media[1)]

Ying HU, Mitsunari UNO, Akira HARADA,† and Shigetoshi TAKAHASHI*
The Institute of Scientific and Industrial Research, Osaka University, Ibaraki, Osaka 567
(Received November 26, 1990)

In the presence of cyclodextrins (CDs), the ring-opening reaction of styrene oxide with $NaBH_4$ in aqueous media proceeded smoothly to give 1-phenylethanol with high selectivity of up to 94%, and kinetic resolution of the racemic epoxide was observed. Kinetic studies suggest the resolution based on the different reaction rates between two enantiomers included in the CD's cavity. The reaction of epoxides such as 1,2-epoxyindan and 1,2-epoxy-3-phenylpropane are also affected by the addition of CDs to proceed smoothly with high regioselectivities.

Inclusion phenomenon or "host and guest chemistry" has attracted growing attention and many efforts have been done to control chemical reactions by means of inclusion phenomenon. Cyclodextrins (CDs), macrocyclic compounds consisting of α-1,4-linked D-glucopyranose, are well-known naturally-occurring host molecules characterized by definite shape and size, chirarity, and solubility in water.[2)]

We have been interested in effects of CDs on organic reactions, and attempted to utilize CDs in organic synthesis. In previous studies, we have applied CDs as inverse phase-transfer catalysts to the oxidation reactions of olefins[3)] and benzylic alcohols,[4)] and as asymmetric reaction vessels to epoxidation of olefins.[5)]

As molecular reaction vessels, CDs are expected to exert microenvironmental effects leading to acceleration of reactions, and conformational effects resulting in selectivities of reactions. Such effects of CDs have been observed in many reaction systems. Breslow reported that CDs greatly accelerated the chlorination of anisole by hypochlorous acid, and that the reaction exhibited remarkable para-selectivity in the presence of CD.[6)] Komiyama used CDs and their derivatives in the formylation, carbonylation, dihalomethylation, and allylation of phenols for rate and regioselectivity enhancement.[7)] Moreover, the effects of CDs in some photoreactions and pyrolysis have been studied in detail by Eaton and Ramamurthy,[8)] and Abelt.[9)] Recently, some efforts have been done for using CDs in asymmetric synthesis. Asymmetric epoxidation of olefins,[5,10)] asymmetric halogenation and hydrohalogenation of styrene,[11)] and asymmetric reduction of ketones[12)] have been reported. Here, we wish to report the effects of CDs on the ring-opening reaction of epoxides with $NaBH_4$ in aqueous medium.

Many methods are known about the ring opening of epoxides, including the reaction with hydrides.[13)] Although $NaBH_4$ is a readily available and mild hydride source, it has long been considered inapplicable to the ring-opening reaction of epoxides to corresponding alcohols due to slow reaction rate. It was recently reported that the reaction of epoxides with $NaBH_4$ can be carried out in alcoholic solvents, but the method seems to be inconvenient for separating products.[14)] In the present study, we have found that in the presence of cyclodextrins, the ring-opening reaction of epoxides with $NaBH_4$ in aqueous media proceeds smoothly with high regioselectivity, and racemic epoxides are kinetically resolved during the reaction.

Results and Discussion

Ring-Opening Reaction of Styrene Oxide. Styrene oxide reacted with $NaBH_4$ in aqueous solution at room temperature very slowly, and gave 1- and 2-phenylethanol with predominance of 2-phenylethanol. When CDs were applied to the reaction, the effects of CDs were found in three respects (Table 1).

Firstly, the reaction was significantly accelerated by the addition of CDs. When the reaction was carried out in the presence of 20 mol% of α-, β-, or γ-CD without changes in other conditions, the conversion of styrene oxide increased from 17% to 54, 83, and 77%, respectively.

Secondly, the regioselectivity of ring opening was changed, i.e. the product ratio of 1-phenylethanol **2a** to 2-phenyl isomer **2b** was reversed as compared with that in the absence of CDs, and the main product of the reaction involving CDs was 1-phenylethanol. When the molar ratio between β-CD and styrene oxide was 2 : 1, 1-phenylethanol reached 94% selectivity.

Thirdly, when β- or γ-CD was used, 1-phenylethanol was obtained with a majority of (*S*)-(−)-1-phenylethanol, and recovered styrene oxide was rich in (*S*)-(−)-styrene oxide. Enantiomer excesses of produced 1-phenylethanol and of recovered styrene oxide were 46 and 31%, respectively, when styrene oxide racemate and β-CD were used in the molar ratio of 1 : 2.

The good effects of CDs on the reaction may be interpreted by formation of water-soluble inclusion complexes between styrene oxide and CDs. The low solubility of styrene oxide in water prevents it from ring-opening reaction with $NaBH_4$. When CD is absent, the molecules of styrene oxide aggregate together and are difficult to come into direct contact with a reagent

† Present address: Department of Macromolecular Science, Faculty of Science, Osaka University, Toyonaka, Osaka 560.

Table 1. Effects of CDs on the Ring-opening Reaction of Styrene Oxide

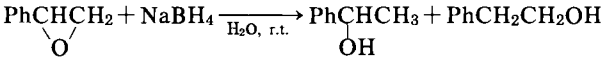

1 **2a** **2b**

5 mmol 10 mmol

CD	Time	Recovered **1**		Product			
		Recovery	e.e.	**2a**		**2b**	Selectivity
mmol	h	%	%	Yield/%	e.e./%	Yield/%	of **2a**/%
—	48	83	0	6	0	11	35
α-CD(1)	48	45	0	31	0	23	57
β-CD(1)	48	17	25(*S*)	66	15(*S*)	17	80
γ-CD(1)	48	23	0	53	2(*S*)	24	68
β-CD(10)	72	49	31(*S*)	48	46(*S*)	3	94

E.e. of styrene oxide and 1-phenylethanol were determined by HPLC and specific rotatory power.

dissolved in water. In the presence of CD, a styrene oxide molecule will be included into CD's cavity and move into water. The resulting inclusion complex will encounter easily a reagent, BH_4^-, in water. Instead of CDs, we applied methyl α-D-glucoside and dextrin, which are a sub-unit of CD and open-chain oligomers of glucopyranose, to the ring-opening reaction of styrene oxide. No effects could be observed with these compounds. This fact indicates that the effects of CDs on the reaction are inseparable from the property of inclusion complex formation. In addition, among the three kinds of CDs, β-CD showed the best effects on the reaction, also indicating that inclusion complex formation was involved, and that the shape of styrene oxide molecule is fittest to the cavity of β-CD.

Kinetic Resolution of Styrene Oxide. We confirmed that (*R*)-(+)-styrene oxide gave only (*S*)-(−)-1-phenylethanol; and (*S*)-(−)-styrene oxide gave only (*R*)-(+)-1-phenylethanol. Because the conformation of the asymmetric center should be retained during the ring-opening reaction, it is clear that the origin of the formation of the optically active products is due to kinetic resolution.

By examining the reaction of the two enantiomers, it was found that in comparison with (*R*)-(+)-styrene oxide, the reaction of (*S*)-(−)-styrene oxide was accelerated in a smaller extent and gave a lower selectivity of 1-phenylethanol (Table 2).

In which step did the the kinetic resolution occur? Two possibilities can be considered: One is that CD includes one of the enantiomers selectively. Another is that in CD's cavity the reaction rates of the two enantiomers are different. In order to answer the question, we measured dissociation constants of two enantiomers with β-CD in aqueons solution. The dissociation constants obtained are 8.3×10^{-3} M (1 M=1 mol dm^{-3}) for the inclusion complex of β-CD with (*R*)-(+)-styrene oxide and 9.8×10^{-3} M for the inclusion complex of β-CD with (*S*)-(−)-styrene oxide. The difference between the dissociation constants of two enantiomers seems too small to result in kinetic resolution. Furthermore, we isolated an inclusion complex of β-CD with styrene oxide and proved that the kinetic resolution does not

Table 2. Ring-Opening Reaction of Each Isomer of Styrene Oxide

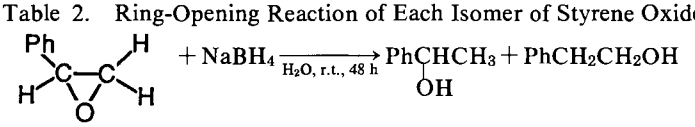

R or *S*-Isomer *R* or *S*-Isomer

5 mmol 10 mmol **2a** **2b**

Substrate	β-CD	Recovered styrene oxide		Product			
		Recovery	e.e.	**2a**		**2b**	Select. of **2a**
		%	%	Yield %	e.e. %	Yield %	%
1-*R*	—	72	~99(*R*)	11	~99(*S*)	16	41
1-*R*	1 mmol	13	~99(*R*)	73	~99(*S*)	14	84
1-*S*	—	67	~99(*S*)	14	~99(*R*)	19	41
1-*S*	1 mmol	35	~99(*S*)	48	~99(*R*)	18	72

occur in the step of inclusion complex formation. Thus, the inclusion complex was prepared by stirring an excessive amount of racemic styrene oxide with a saturated aqueous solution of β-CD at room temperature. The inclusion complex produced was collected by filtration from the mixture. By extraction with diethyl ether, the excessive styrene oxide was recovered. Styrene oxide included by β-CD was recovered by suspending the inclusion complex in water, and then extracting with diethyl ether. We found that both styrene oxide included by CD and excessive styrene oxide remained freely were racemates as measuring optical rotation of the recovered styrene oxide.

The reason of kinetic resolution therefore must rest on the different reaction rates of two enantiomers included in the cavity of CD. That is to say, both enantiomers can be included easily by CD to almost the same extent, but exhibit a different reaction rate in the cavity of CD. To confirm this, we attempted to do kinetic study on the reactions of two enantiomers. Unfortunately, the attempt has falled off success due to the complexity of the reaction.

Ring-Opening Reaction of Other Epoxides. Besides styrene oxide, the ring-opening reaction of other epoxides involving CDs was also investigated. As shown in Table 3, the accelerating effect of CDs on the ring-opening reaction of epoxides are remarkable, and the ring-opening reaction is regioselective in the presence of CDs. Especially, racemic 1,2-epoxyindan and 1,2-epoxy-3-phenylpropane were optically resolved to some extent during the reaction involving CD.

1,2-Epoxyindan reacted with $NaBH_4$ in aqueous solution and gave 2-indanol as the sole product. After the reaction involving CDs, recovered 1,2-epoxyindan showed optical rotation, indicating that 1,2-epoxyindan was kinetically resolved during the reaction. When the molar ratio of 1,2-epoxyindan to α-CD was 1 : 1, recovered 1,2-epoxyindan showed specific rotatory power of 12° corresponding to 20% enantiomer excess which was determined by ^1H NMR spectrum using $Eu(hfc)_3$ as a chiral shift reagent.

1,2-Epoxy-3-phenylpropane was another interesting substrate. In the absence of CD, 1,2-epoxy-3-phenylpropane almost did not react with $NaBH_4$ in aqueous solution. All CDs uniformly accelerated the reaction remarkablely. 1-Phenyl-2-propanol was the sole ring-opening product. Among the three kinds of CDs, the effect of α-CD was outstanding. The reaction of 1,2-epoxy-3-phenylpropane required only a catalytic amount of α-CD (Table 4). It was found that during the reaction involving α-CD, 1,2-epoxy-3-phenylpropane racemate was resolved. One thing worthy to be noted is that the effects of CDs were not modified simply by raising the amount of α-CD added. The best efficiency for optical resolution was observed when about 10 mol% of α-CD was used. Then both the reaction rate and the efficiency for optical resolution tended downwards as the increasing amount of α-CD.

By examining the inclusion mode with CPK molecular models, it seems that the decrease in the reaction rate and effeciency in optical resolution can be explained considering the formation of a 2 : 1 CD-epoxide inclusion complex (Figure 1), as the amount of α-CD is

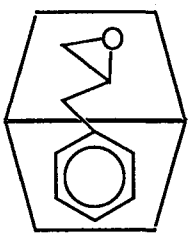

Fig. 1. 2 : 1 CD-1,2-epoxy-3-phenylpropane complexes.

Table 3. Ring-Opening of Some Epoxides

Epoxide	Product	CD	Time	Recovered epoxide		Product	
		mmol	h	Recovery/%	e.e./%	Selec./%	$[\alpha]_D$/deg.
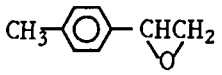	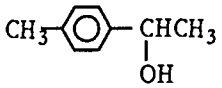	—	24	94	0	17	—
		β-CD(1)	30	63	0	68	—
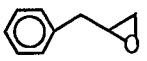	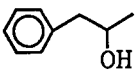	—	24	92	0	100	—
		α-CD(0.5)	5	41	26	100	−8.7
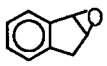	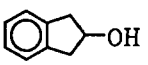	—	5	52	0	93	
		α-CD(5)	15	38	20	95	
	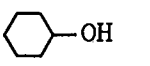	—	5	73		100	
		β-CD(1)	5	5		100	
$CH_3(CH_2)_7CHCH_2$	$CH_3(CH_2)_7CHCH_3$	—	312	100			
		γ-CD(1)	312	26		100	

Table 4. Ring-Opening Reaction of 1,2-Epoxy-3-phenylpropane

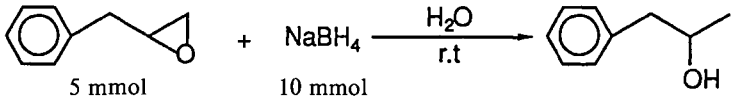

5 mmol 10 mmol

CD mmol	Time h	Conv. %	e.e.[a] of Recovered epoxide/%	$[\alpha]_D^{23}$ [b] of alcohol deg.
—	24	6	0	0
α-CD(1)	24	98	—	—
β-CD(1)	24	46	0	0
γ-CD(1)	24	81	—	−0.8
α-CD(0.3)	6	41	11	—
α-CD(0.5)	5	59	26	−8.7
α-CD(1)	5	61	18	−9.9[c]
α-CD(3)	17	49	4	−1.4
α-CD(5)	72	24	<1	—

a) E.e. of 1,2-epoxy-3-phenylpropane was determined by HPLC. b) $[\alpha]_D^{23}$ was measured in $CHCl_3$. c) $[\alpha]_D^{23}=-9.9°$ corresponds to 24% e.e. as determined by ^1H NMR spectroscopy. According to the report of Bell, the sample was rich in (*R*)-(−)-1-phenyl-2-propanol.[16]

increased. It is clear that the inclusion mode shown in Fig. 1 would undoubtedly interrupt the reaction of the epoxide.

Conclusion

It has been demonstrated by the results presented here that CDs affect the ring-opening reaction of epoxides dramatically. In comparison with the known processes for the ring-opening reaction of epoxides using organic solvents and sensitive hydrides such as lithium aluminum hydride and diborane, the present method has the advantages of easy procedure, high regioselectivity, and high yield of ring-opening product, and provides a practical method applicable for organic synthesis. In addition, although the efficiency of kinetic resolution by CDs is not satisfied at present, it has been suggested that CDs may be used to asymmetric syntheses based on the formation of inclusion complexes.

Experimental

Instruments. GLC analyses were performed on a Shimadzu GC-12A chromatograph equipped with a 3-m Thermon-1000 column. HPLC analyses of asymmetric compounds were carried out on a Shimadzu LC-6A chromatograph equipped with a 25-cm Chiralcel OF column. Optical rotations were measured on a Jasco DIP 370 polarimeter. ^1H NMR spectra were recorded on a Bruker AM 360 instrument. UV spectra were recorded with a Hitachi U-3400 spectrophotometer.

Materials. CDs, $NaBH_4$, (±)-styrene oxide, (*R*)-(+)-styrene oxide, (*S*)-(−)-styrene oxide, cyclohexene oxide, and 1,2-epoxydecane were commercially available. 1,2-Epoxyindan, 1,2-epoxy-3-phenylpropane and *p*-tolyloxirane were prepareded by KOH treatment of corresponding bromohydrins[16] which were obtained from corresponding olefins by the Guss method.[17] The chemical purities of all epoxides were checked by gas chromatography and confirmed to be higher than 98%. The optical purities of (*R*)-(+)-styrene oxide and (*S*)-(−)-styrene oxide were higher than 99% according to HPLC analysis.

Ring-Opening Reaction of Epoxides. The ring-opening reaction of all epoxides was carried out by stirring a mixture of epoxide, $NaBH_4$ and CD in water at room temperature. In the reactions involving CD, 2 ml of water per 1 mmol of CD was used, and 2 ml for all reactions in the absence of CD. The reaction mixture was extracted with ether, and crude products were analyzed by GLC and HPLC. The crude products were purified by silica gel column chromatography with hexane–ethyl acetate. All products of the reactions were identified by ^1H NMR and IR spectroscopy.

Optical purities of styrene oxide, 1-phenylethanol, 1,2-epoxy-3-phenylpropane, and *p*-tolyloxirane were determined by HPLC analysis.

Optical purities of recovered 1,2-epoxyindan and 1-phenyl-2-propanol were determined by ^1H NMR spectroscopy using $Eu(hfc)_3$ as a chiral shift reagent.

Dissociation Constants of β-CD-Styrene Oxide Inclusion Complex. Since the ultraviolet spectrum of styrene oxide is modified by binding into CD's cavity, a UV spectroscopic method was used to determine the dissociation constant K_d.[17]

To each of several 50 ml volumetric flasks containing accurately measured quantity of β-CD, 5 ml of 5.3×10^{-3} M solution of (*R*)- or (*S*)-styrene oxide in water was added. The solutions were diluted to the marks with water. The absorption at 257 nm of each of these solutions was measured at 25 °C. The reference compartment contained a solution of β-CD of identical concentration.

For the calculation of dissociation constants, following equation was used:

$$C_0S_0/\Delta Abs = K_d/\Delta\varepsilon + (C_0+S_0)/\Delta\varepsilon$$

where C_0 is the initial concentration of β-CD, S_0 is the initial concentration of styrene oxide, ΔAbs is the change in absorbance at a particular wavelength from the absorbance of styrene oxide alone at this concentration, and $\Delta\varepsilon$ is the difference in molar extinction coefficient for the complex and the pure styrene oxide. Thus, a plot of $C_0S_0/\Delta Abs$ vs. C_0+S_0 yields a straight line with intercept/slope=K_d.

Caution. (*R*)-(+)-Styrene oxide and (*S*)-(−)-styrene oxide showed plus and minus optical rotation in neat state, respectively. However, the signs of optical rotation of these two isomers reversed when the optical rotation was measured in $CHCl_3$ or CH_2Cl_2 solution at low concentrations, and the specific rotatory power significantly varied with the concentration of the solution. Calibration curves of specific rotatory power must be made for analysis.

References

1) A preliminary communication of part of this work has been published: Y. Hu, A. Harada, and S. Takahashi, *Chem. Lett.*, **1990**, 797.

2) a) M. L. Bender and M. Komiyama, "Cyclodextrin Chemistry," Springer Verlag, New York (1978); b) J. Szejlti, "Cyclodextrin and Their Inclusion Complexes," Akademiai Kiado, Budapest (1982).

3) A. Harada, Y. Hu, and S. Takahashi, *Chem. Lett.*, **1986**, 2083.

4) Y. Hu, A. Harada, and S. Takahashi, *J. Mol. Catal.*, **60**, L13 (1990).

5) Y. Hu, A. Harada, and S. Takahashi, *Synth. Commun.*, **18**, 1607 (1988).

6) R. Breslow and P. Campbell, *Bioorg. Chem.*, **1**, 140 (1971).

7) M. Komiyama and H. Hirai, *J. Am. Chem. Soc.*, **106**, 174 (1984).

8) V. Ramamurthy and D. F. Eaton, *Acc. Chem. Res.*, **21**, 300 (1988).

9) C. J. Abelt and J. M. Pleier, *J. Org. Chem.*, **53**, 2159 (1988).

10) S. Banfi, S. Colonna, and S. Julia, *Synth. Commun.*, **13**, 1049 (1983).

11) H. Sakuraba and H. Ishizaki, *J. Inclusion Phenom.*, **5**, 449 (1987).

12) H. Sakuraba, N. Inomata, and Y. Tanaka, *J. Org. Chem.*, **54**, 3482 (1989).

13) a) A. Hajos, "Complex Hydride," Elsevier Scientific Publishing Co., Budapest (1979); b) H. C. Brown and S. Krishnamurthy, *Tetrahedron*, **35**, 567 (1979).

14) A. Ookawa, M. Kitamura, and K. Soai, *Heterocycles*, **27**, 213 (1988).

15) K. H. Bell, *Aust. J. Chem.*, **32**, 2625 (1979).

16) Y. Tamura, T. Kawasaki, H. Yasuda, N. Gohda, and Y. Kita, *J. Chem. Soc., Perkin Trans. 1*, **1981**, 1577.

17) C. O. Guss and R. Rosenthal, *J. Am. Chem. Soc.*, **77**, 2549 (1955).

Photochemical Reactions of Aryl-Substituted Digermanes through a Pair of Organogermyl Radicals[1)]

Kunio MOCHIDA,* Masanobu WAKASA, Yoshio SAKAGUCHI,† and Hisaharu HAYASHI*,†
Department of Chemistry, Faculty of Science, Gakushuin University, 1-5-1 Mejiro, Tokyo 171
†The Institute of Physical and Chemical Research, Wako, Saitama 351-01
(Received January 11, 1991)

The photochemical reactions of aryl-substituted digermanes were investigated by trapping experiments and a laser flash photolysis technique. The photolysis of phenylated digermanes resulted in germanium–germanium bond homolysis to give a pair of two germyl radicals. The germyl radicals abstracted a chlorine atom from carbon tetrachloride to give chlorogermanes. The pair of germyl radicals also underwent ipso-substitution, which was a precursor of the germylenes. The mechanism for the photochemistry of phenylated digermanes is discussed.

The photochemistry of organopolysilanes having a σ(Si–Si)–π(C=C) conjugated system has been the subject of considerable attention because of their unexpected reactivities as well as in the resulting products.[2–4)]

The photolysis of an aryldisilane was first reported by Boudjouk, Roberts, Golino, and Sommer[5)] for pentaphenylmethyldisilane. The generation of a silicon–carbon double-bonded species is the characteristic feature of the reaction (type 1 in Scheme 1). Later, Ishikawa, Fuchigami, Sugaya, and Kumada[6)] have reported on another type of reaction in which a rather unusual silicon–carbon double-bonded species is postulated as a key intermediate (type 2). The generation of a silylene has also been noted (type 3). Recently, Sakurai, Nakadaira, Kira, Sugiyama, Yoshida, and Takiguchi have presented a free radical mechanism for the photolysis of aryldisilanes. Okinoshima and Weber[8)] have also reported the formation of silicon–oxygen double-bonded species by the photolysis of aryldisilanes in dimethyl sulfoxide (DMSO).

However, there has been few papers on photochemical studies of the germanium analogues.[9)] We previously reported on the photolysis of phenylpentamethyldigermane, in which the generation of a pair of germyl radicals was indicated.[10)] In this paper, we described the photoreactions of phenylated digermanes studied via trapping experiments and a laser flash photolysis technique.

Results and Discussion

Photoreaction of the Phenylated Digermanes. Four kinds of phenyl-substituted digermanes, $(Ph_nMe_{3-n}Ge)_2$ (**1**—**3**, n=1—3, respectively) and $Me_3GeGePh_3$ (**4**), in cyclohexane or in tetrahydrofuran (THF) were investigated with a 110-W low-pressure Hg arc lamp at room temperature under an argon atmosphere for 1—2 h. The photolysis of **1** and **2** in cyclohexane gave $PhMe_2GeH$ (11%), Ph_2GeMe_2 (17%), and $(Me_2Ge)_4$ (4%) for **1**, and Ph_2MeGeH (20%) and Ph_3GeMe (17%) for **2**, as main products. The photolysis of **4** in cyclohexane mainly afforded Me_3GeH (15%), Ph_3GeH (32%), and $PhGeMe_3$ (19%). High-boiling unidentified products containing germanium were also formed in the photoreactions of **1**, **2**, and **4**. The formation of octamethylcyclotetragermane $(Me_2Ge)_4$ for **1** strongly suggests the intermediacy of a dimethylgermylene.[11)] In order to detect possible reaction intermediates, cyclohexane solutions of **1**, **2**, and **4** containing a large excess of 2,3-dimethylbutadiene, a germylene trapping agent,[12)] were similarly irradiated for 1—2 h. Monogermanes ($PhMe_2GeH$ and Ph_2GeMe_2) and $(Me_2Ge)_4$ were produced for **1**, regardless of the presence of 2,3-dimethylbutadiene. No 1,1-dimethylgermacyclopent-3-ene was formed. The rate of cycloaddition of 1,1,2,2-tetramethyldigermene ($Me_2Ge{=}GeMe_2$) formed by a

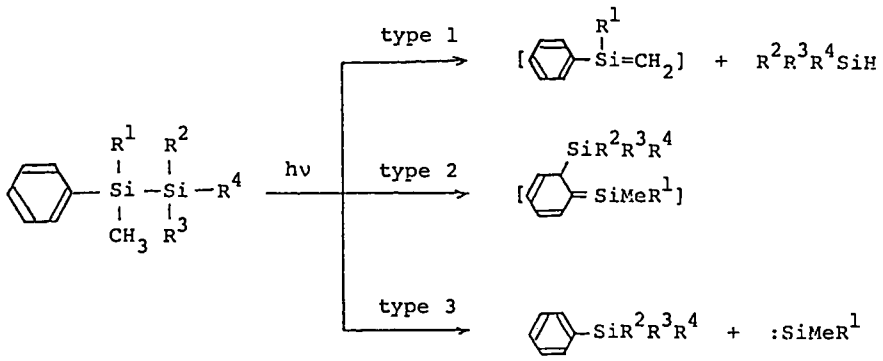

Scheme 1.

Table 1. The Results of Photochemical Reactions of the Phenylated Digermanes, **1**, **2**, and **4**

Digermane	Substrate	Main products (yield/%)
$(PhMe_2Ge)_2$	None	$PhMe_2GeH$ (11), Ph_2GeMe_2 (17), $(Me_2Ge)_4$ (4)
1	CCl_4	$PhMe_2GeCl$ (94)
		$PhMe_2GeH$ (21), Ph_2GeMe_2 (5), $(Me_2Ge)_4$ (4)
$(Ph_2MeGe)_2$	None	Ph_2MeGeH (20), Ph_3GeMe (15)
2	CCl_4	$Ph_2MeGeCl$ (95)
		PhMeGe 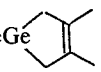 (1)
$Me_3GeGePh_3$	None	Me_3GeH (12), Ph_3GeH (32), $PhGeMe_3$ (19)
4	CCl_4	Me_3GeCl,[a] Ph_3GeCl[a]

a) The yield of products could not be determined by GLC.

dimethylgermylene may be much faster than that of the dimethylgermylene with 2,3-diemthylbutadiene under these reaction conditions. On the other hand, 1-methyl-1-phenylgermacyclopent-3-ene (1%) was formed together with mongermanes (Ph_2MeGeH and Ph_3GeMe) in the photolysis of **2** and 2,3-dimethylbutadiene. 3-Butenylgermyl derivatives were also detected by means of CC-MS in the photolysis of **1** and **2**.

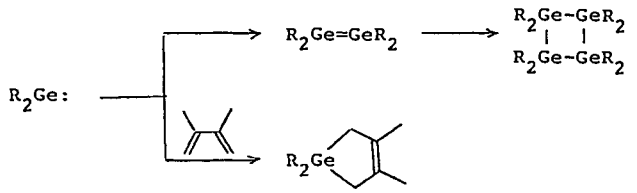

No 1,1-diphenylgermacyclopent-3-ene and octaphenylcyclotetragermane $(Ph_2Ge)_4$ derived from diphenylgermylene were formed in the photolysis of **4**.

In the presence of carbon tetrachloride, the photolysis of **1**, **2**, and **4** in cyclohexane afforded chlorogermanes quantatively, together with hexachloroethane. The formation of chlorogermanes seems to indicate the intermediacy of the germyl radicals produced by germanium–germanium bond homolysis of the phenylated digermanes. The germyl radicals are known to abstract a chlorine atom from carbon tetrachloride to give the corresponding chlorogermanes and a trichloromethyl radical:[13]

$$R_3Ge\cdot + CCl_4 \longrightarrow R_3GeCl + \cdot CCl_3.$$

The germyl radicals add to 2,3-dimethylbutadiene to produce 3-butenylgermyl derivatives.

Hydrogermanes were formed in the absence of trapping agents. Germyl radicals do not abstract a hydrogen atom from solvents, such as THF or cyclohexane. This was confirmed by the fact that THF-d_8 or cyclohexane-d_{12} solutions containing **1** upon being irradiated gave no $PhMe_2GeD$ but $PhMe_2GeH$. It is unlikely that they can abstract a hydrogen atom from precursor C–H bonds, which are even stronger. Another route to the formation of hydrogermanes may be via a disproportionation of germyl radicals.[14] Germenes are also expected to form by the disproportionation of germyl radicals. The germenes are known to react with methanol to give methoxygermanes.[15] No methoxygermanes were formed in the photolysis of cyclohexane solutions of phenylated digermanes, **1**, **2**, **4** with methanol. At present, the formation processes of hydrogermanes are unclear.

The photolysis of **3** did not proceed since **3** was very difficult to dissolve in cyclohexane or in THF. The results of photochemical reactions of **1**, **2**, and **4** in cyclohexane are summarized in Table 1. Similar results regarding the photochemical reactions of **1**, **2**, and **4** in THF were obtained.

In order to obtain more information concerning the reaction intermediates and primary photochemical processes, laser flash photolysis at 293 K studies of phenylated **1**—**3** were also carried out.

Laser Flash photolysis Studies. Nanosecond transient absorption spectra measurements were performed on degassed solutions containing **1**—**3** at 293 K using the fourth-harmonic pulse of a Nd:YAG laser as the exciting light source.[16]

The time dependence of the transient absorbance, $A(t)$, was measured using each of the THF solutions containing **1**—**3**. The $A(t)$ curves were measured in the wavelength region 300—700 nm. Appreciable signals of two well-separated transient bands were obtained, as shown in Fig. 1. The signals show a fast rise and a following slow decay. The rise time was about 10 ns, the time resolution of the present apparatus. As a typical example, the $A(t)$ curve and the $\log A(t)$ curve observed with **2** at 320 nm for kinetic studies are shown in Fig. 2. Such a curve can be computer analyzed regarding composition of two components through the decay of pseudo first-order kinetics. The $A(t)$ curve

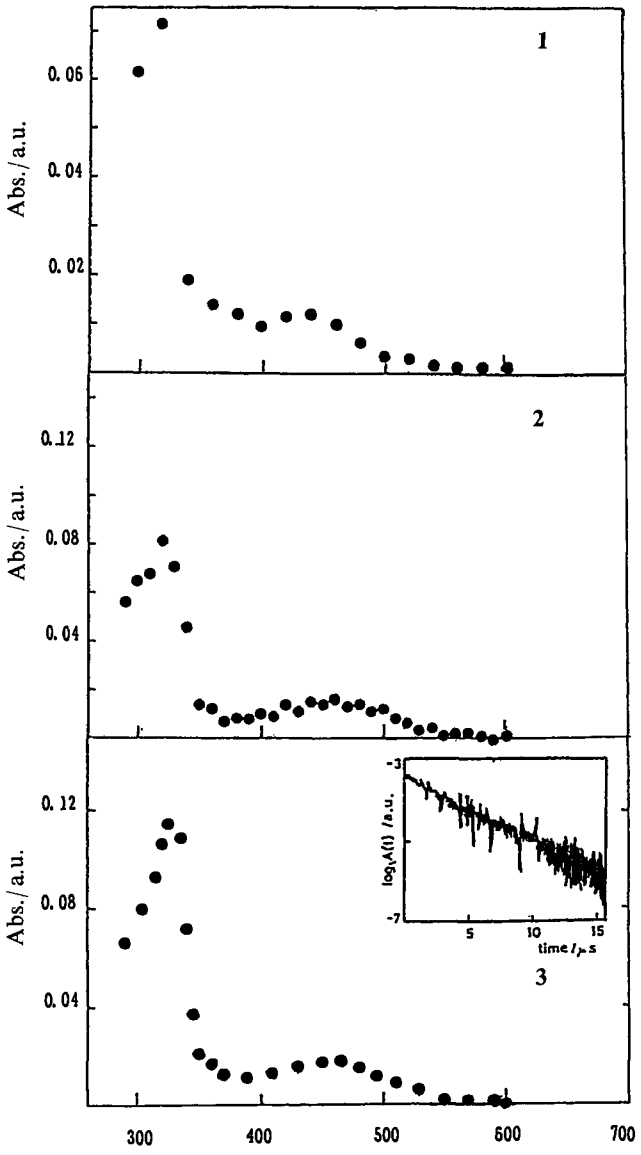

Fig. 1. Transient absorption spectra at 50 ns after photoexcitation of $(Ph_nMe_{3-n}Ge)_2$, **1**—**3** (n=1—3) (10^{-3} M) in degassed THF solutions. Insert (3): a first-order plot for decay of the absorption at 320 nm.

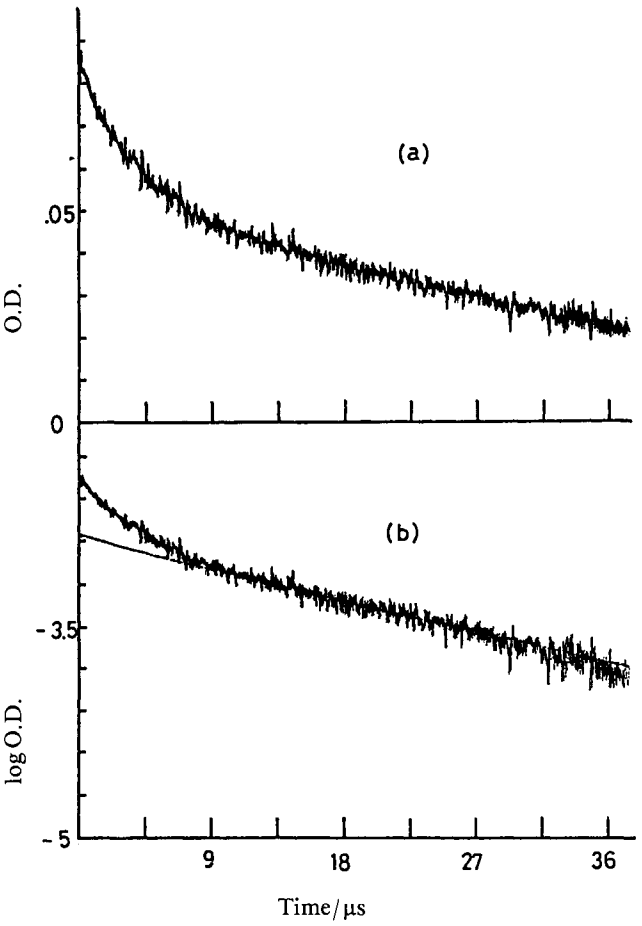

Fig. 2. Representative data displays from laser flash photolysis kinetic spectroscopy experiments: (a) absorbance at 320 nm as a function of time upon irradiation of $(Ph_2MeGe)_2$ (**2**) (2.6 mM) in degassed THF solution, (b) log absorbance at 320 nm as a function of time upon irradiation of **2** (the slope of linear plot is first-order rate constant).

and the $\log A(t)$ curve of the short-lived component, excluding those of the longer-lived one, is shown in Fig. 3. Thus, a careful examination of the transient peak at shorter wavelengths shows that it comprises two components (half lifetimes, $t_{1/2}$<5 μs and $t_{1/2}$>20 μs, respectively, for **1** and **2** in THF and hydrocarbon media). On the other hand, the transient peak at shorter wave-

Table 2. Rate Constants for Disappearance of the Shorter-Lived Transients at Shorter Wavelength in the Photolysis of **1**—**3** in THF (10^{-3} M) at 293 K

Digermane	λ_{max}/nm	Rate constant/$M^{-1}s^{-1}$			
		None[a]	CCl_4	O_2	2,3-Dimethylbutadiene
$(PhMe_2Ge)_2$ **1**	315	4.3×10^5	2.2×10^8	5.3×10^9	b)
$(Ph_2MeGe)_2$ **2**	325	3.2×10^5	4.7×10^8	4.0×10^9	b)
$(Ph_3Ge)_2$ **3**	330	1.9×10^5	5.8×10^8	3.8×10^9	b)

a) s^{-1}. b) The transient decays too fast to be observed.

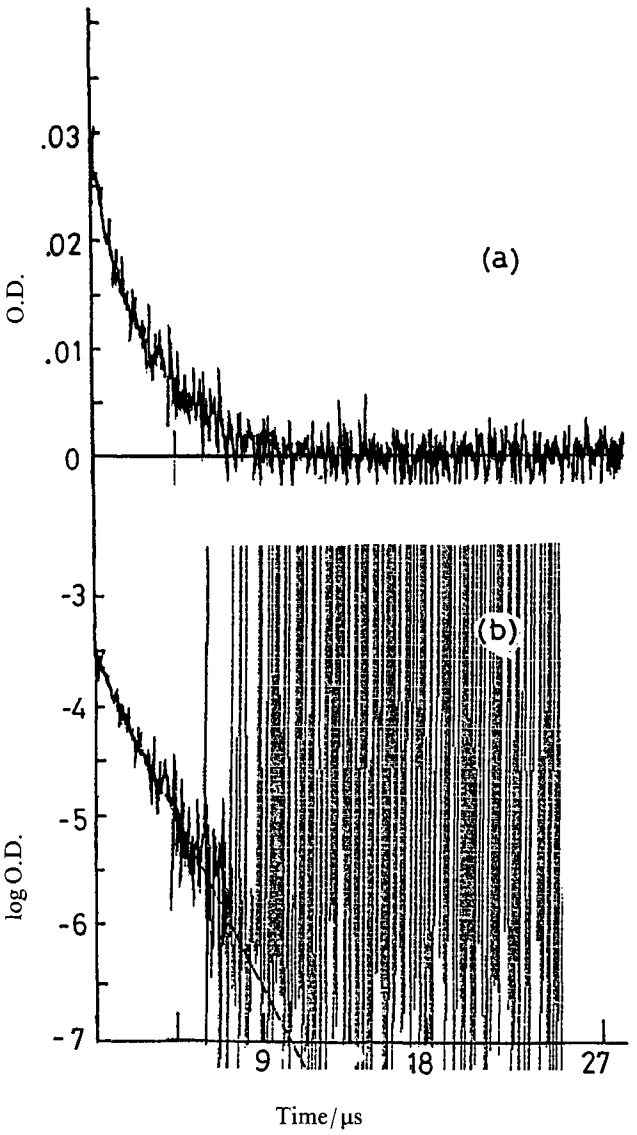

Fig. 3. Representative data displays from laser flash photolysis kinetic spectroscopy experiments: (a) absorbance of short-lived component at 320 nm as a function of time upon irradiation of $(Ph_2MeGe)_2$ (**2**) (2.6 mM) in degassed THF solution, (b) log absorbance of short-lived component at 320 nm as a function of time upon irradiation of **2** (the slope of linear plot is first-order rate constant).

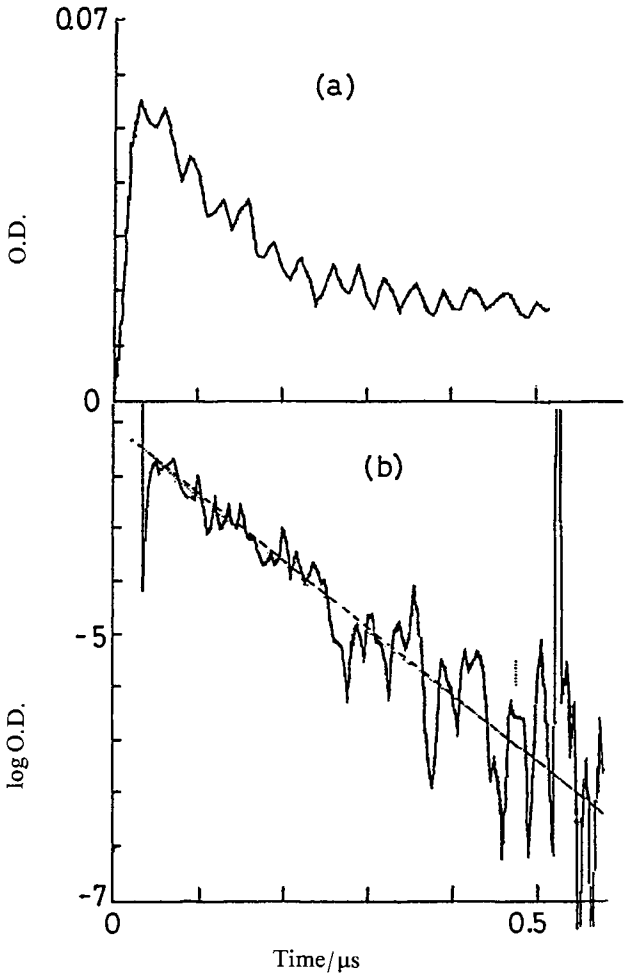

Fig. 4. Representative data displays from laser flash photolysis-kinetic spectroscopy experiments: (a) absorbance of short-lived component at 320 nm as a function of time upon irradiation of $(PhMe_2Ge)_2$ (**1**) (2.6 mM) in degassed THF solution containing CCl_4 (10 mM), (b) log absorbance of short-lived component at 320 nm as a function of time upon irradiation of **1** containing CCl_4.

lengths arising from **3** has only the short-lived component. This component has been reasonably assigned to that of the phenyl-substituted germyl radicals, $Ph_nMe_{3-n}Ge\cdot$ (n=1—3), from a comparison of the spectral characteristics with those reported for germyl radicals.[17] The experimentally determined decay constants of these transient species are summarized in Table 2. The transient arising from **1**—**3** decayed under pseudo first-order kinetics and are dependent on the concentrations of the employed phenylated digermanes. Such kinetics can be explained by the addition of the generated germyl radical to the aromatic ring on a germanium atom. This is very different from the situation reported regarding the addition of germyl radicals to aromatic compounds in solutions.[18] The assignment of a shorter-lived transient has been further substantiated by quenching experiments with carbon tetrachloride, oxygen, and 2,3-dimethylbutadiene. The addition of carbon tetrachloride, an effective germyl radical scavenger, quenched the transient absorption (Table 2). The quenching-rate constants observed nicely agree with the values reported for germyl radicals.[17] Similarly, oxygen quenched the shorter-lived transient very quickly (Table 2). Representative data displays from laser flash photolysis-kinetic spectroscopy experiments are shown in Fig. 4.

What is the latter carrier of the longer-lived transient at shorter wavelengths? The concentration of this species appeared to be correlated with that of the shorter-lived species assigned to the germyl radicals as well as that of the longer-wavelength transient arising from the

germylene described below. Furthermore, the change in the intensity of the transient was examined in isooctane as well as in more viscous solvents, such as dodecane. Figure 5 shows the intensity of the longer-lived transient in isooctane tends to increase in dodecane. This implies that this transient species may be a product of a radical which had escaped from the cage. Accordingly, the longer-lived species may be tentatively assigned to a coupling product of the germyl radicals at the ipso-position, as described in Scheme 2. The possibility of germenes and digermenes, suggested as another species, is excluded the UV data of germenes and digermenes are below 300 nm[19] and above 370 nm[20] respectively.

The experimentally determined decay constants of longer-lived transients are summarized in Table 3.

On the other hand, the transient at the longer wavelength (Fig. 1) could be assigned to that of a germylene by comparing its chemical and spectral properties with those reported.[21-23] These transients arising from **2** and **3** in THF decayed with first-order kinetics. However, the transient arising from **1** in THF is too weak to observe its decay constant. This kinetic behavior implies that the germylene reacts with THF in a similar as do the silylenes.[24] In contrast, in inert solvents, such as isooctane, the transient due to the germylene decayed with second-order kinetics, suggesting the formation of digermenes. This was further substantiated by quenching experiments with a germylene trapping agent, 2,3-dimethylbutadiene, which gives the corresponding germacyclopentenes. The transient from **2** and **3** in THF in the presence of large excess amounts of the diene decayed with pseudo first-order kinetics; the obtained rate constants are summarized in Table 4. The fact that these transients were not quenched by ethanol is in accord with the observed chemical property.

Photoreaction Mechanism of Phenylated Digermanes. The results of photochemical reactions and laser flash photolysis studies of **1**—**4** are best rationalized as a pair of germyl radicals according to the path described in Scheme 2. The photolysis of aryldigermanes cleaves the germanium–germanium bond to give a pair of germyl radicals. The generated germyl radicals readily abstract a chlorine atom from carbon

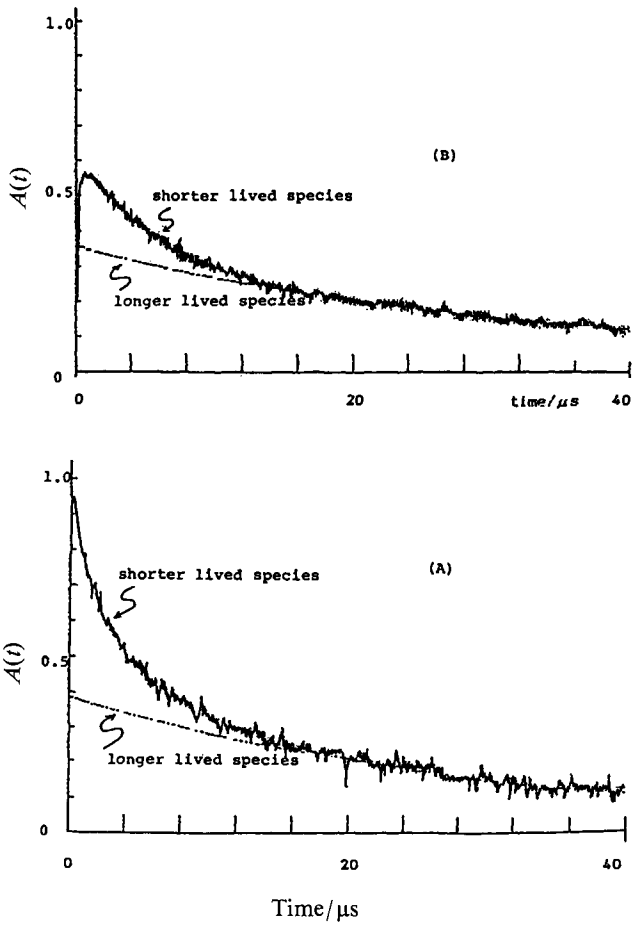

Fig. 5. Plots of the absorbance at 320 nm against t observed with the isooctane (A) and dodecane (B) of **1**.

Table 3. Rate Constants for Disappearance of the Longer-Lived Transients at Shorter Wavelength in the Photolysis of **1**—**3** in THF (10^{-3} M) at 293 K

Digermane	Rate constant/$M^{-1}s^{-1}$		
	CCl_4	O_2	2,3-Dimethylbutadiene
$(PhMe_2Ge)_2$ **1**	a)	5.8×10^8	a)
$(Ph_2MeGe)_2$ **2**	3.8×10^7	2.1×10^8	8.5×10^4
$(Ph_3Ge)_2$ **3**	a)	a)	1.5×10^5

a) The transient decays too fast to be observed.

Table 4. Rate Constants for Disappearance of the Transient at Longer Wavelength in the Photolysis of **1**—**3** in THF (10^{-3} M) at 293 K

Digermane	λ_{max}/nm	Rate constant/$M^{-1}s^{-1}$			
		None[a]	2,3-Dimethylbutadiene	O_2	EtOH
$(PhMe_2Ge)_2$ **1**	440	b)	b)	b)	c)
$(Ph_2MeGe)_2$ **2**	450	1.1×10^5	4.5×10^6	2.3×10^8	c)
$(Ph_3Ge)_2$ **3**	470	2.0×10^5	1.0×10^6	1.8×10^8	c)

a) s^{-1}. b) The absorption of **1** is too weak to determine rate constants. c) Not quenched.

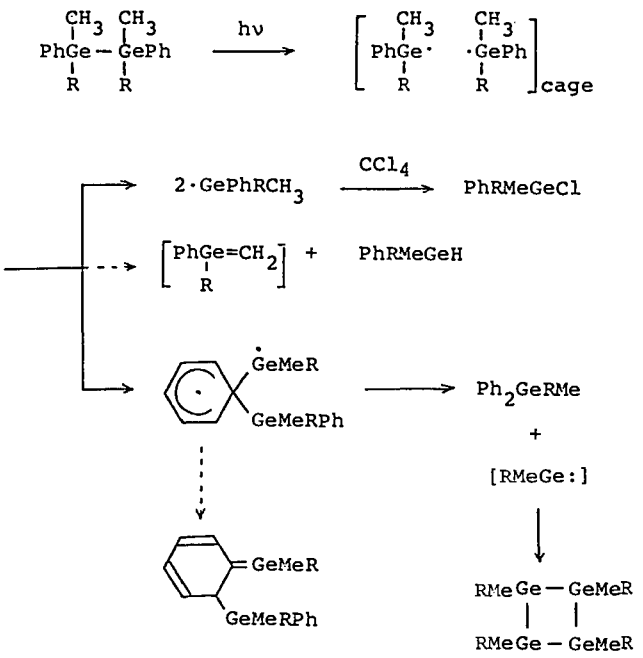

Scheme 2.

tetrachloride to give the corresponding chlorogermanes and trichloromethyl radical. The formation mechanism of hydrogermanes are unclear.

The germyl radicals couple at the ipso-position to give germyl-substituted cyclohexadienyl type radicals. The germyl-substituted cyclohexadienyl type radicals undergo further elimination to produce a gemylene and arylgermanes. The photo-generated germylene dimerize to give digermenes or react with 2,3-dimethylbutadiene to give germacyclopentenes. The arylgermanes produced by elimination processes are Ph_2GeMe_2 for **1**, Ph_3GeMe for **2**, and $PhGeMe_3$ for **4**. In contrast to the case of the aryldisilane, we have no concrete evidence for the presence of formal 1,3-germyl migration products in the photolysis of **1**, **2**, and **4**. This difference in the photochemical behavior between an arydigermane and an aryldisilane may be accounted for in terms of the following reasons. The bond dissociation energy of a germanium–carbon bond (318 kJ mol^{-1}) is less than that of a silicon–carbon bond (343 kJ mol^{-1}), and π-bonding of carbon must be formed more effectively with a silicon atom than with a germanium atom.[18]

In addition, organogermylene is more thermodynamically stable than is silylene. All of those factors favor the formation of germylene and germylene elimination products from the coupling products of germyl radicals at the ipso-position over the formation of germyl migration products.

The formation of germylenes and arylgermanes cannot necessarily be explained by a 1,2-phenyl shift of the phenylated digermanes, since the transient signal of the germylenes was observed with that of the germyl radicals immediately after photoexcitation of the phenylated digermanes. Taking the results of the trapping experiments with carbon tetrachloride, the 1,2-phenyl shift proceeds as a minor path.

Experimental

^1H NMR spectra were recorded on a Varian FT 80A, with tetramethylsilane as an internal standard. GC-MS spectra were obtained with a JEOL JMX-DX 303 mass spectrometer. Infrared spectra were recorded on a Hitachi 260-10 spectrometer. Gas chromatography was performed on a Shimadzu GC-6A and 8A with 2 m 20% SE30 and 1 m 10% SE columns.

Materials. 2,3-Dimethylbutadiene, CCl_4, and ethanol were commercially available. $PhMe_2GeGeMe_2Ph$, bp 170—174 °C/4 mmHg (1 mmHg=133,322 Pa),[25] $Ph_2MeGeGeMePh_2$, mp 132—133 °C,[25] $Ph_3GeGePh_3$, mp 335—340 °C,[25] $Me_3GeGePh_3$, mp 108—109 °C,[26] $PhMe_2GeH$, bp 65—66 °C/20 mmHg,[27] Me_3GeH, bp 26 °C,[28] Ph_2MeGeH, bp 105—106 °C/6 mmHg,[29] Ph_3GeH, mp 39.5 °C,[30] Me_3GeCl, bp 98 °C,[28] $PhMe_2GeCl$, bp 90 °C/10 mmHg,[31] $Ph_2MeGeCl$, bp 140 °C/14 mmHg,[32] Ph_3GeCl, mp 145 °C,[33] Ph_2GeMe_2, bp 145 °C/14 mmHg,[34] Ph_3GeMe, mp 71 °C,[35] $PhGeMe_3$, bp 80 °C/20 mmHg,[36] 1-methyl-1-phenylgermacyclopent-3-ene,[37] and $(Me_2Ge)_4$[11] were prepared as described in the cited references.

Solvents. Cyclohexane, isooctane, dodecane, and THF were distilled from sodium–benzophenone under an argon atmosphere.

Photochemical Reactions of the Phenylated Digermanes. The digermanes (ca. 200 mg) were dissolved in dry cyclohexane (6 cm^3) in a quartz tube. The tube was degassed in a vacuum and charged with argon. The sample was irradiated with a 110-W low-pressure Hg arc lamp at room temperature for 2 h. After irradiation, the photoproducts were verified by comparing the retention times on GLC and GC-MS with those of authentic samples.

Photochemical Reactions of the Phenylated Digermanes with Various Trapping Agents. As a representative example, photolysis of a cyclohexane solution containing 1,1-diphenyltetramethyldigermane with CCl_4 is described. Compound **1** (200 mg, 0.56 mmol) and CCl_4 (0.45 g, 30 mmol) were dissolved in dry cyclohexane (6 m^3) in a quartz tube. The sample tube was degassed in a vacuum and charged with argon. The sample was irradiated at room temperature for 20 min. After irradiation, the photoproducts were verified by comparing the retention time on GLC and GC-MS with those of authentic samples.

Time-Resolved Optical Absorption. Samples in quartz cells with an optical length of 5 mm were degassed by four freeze-pump-thaw cycles. The concentrations of the phenylated digermanes were ca. 10^{-3} M (1 M=1 mol dm^{-3}). Laser flash photolysis experiments were performed at room temperature (293 K) by using the fourth-harmonic (266 nm) of a Quanta-Ray DCR-1 Nd:YAG laser as the exciting light source. The laser pulse was about 5 ns. Details concerning the laser flash photolysis apparatus have been published elsewhere.[16] The signals were monitored by a Tektronix 485 oscilloscope (350 MHz) and recorded by an Iwatsu DM-901 digital memory (10 ns/point, 8 bit) controlled by an NEC PC 8801 microcomputer.

The authors thank Professor Yasuhiro Nakadaira of The University of Electro-Communications for valuable

discussion. This research was supported in part by a Grant-in-Aid for Scientifc Research Nos. 0649518 and 63790213 from the Ministry of Education, Science and Culture. One of the authors (M. Wakasa) thanks the Japan Chemical Society for Promotion of Science for the Fellowship for Japan Junior Scientists.

References

1) Preliminary results of the study were reported in: K. Mochida, M. Wakasa, Y. Nakadaira, Y. Sakaguchi, and H. Hayashi, *Organometallics,* **7**, 1869 (1988).

2) R. West, "Comprehensive Organometallic Chemistry," ed by G. Wilkinson, F. G. A. Stone, and E. W. Abel, Pergamon Press, New York (1982), Vol. 2, Chap. 9. 4.

3) M. Ishikawa, *Pure Appl. Chem.,* **50**, 11 (1978); M. Ishikawa and M. Kumada, *Adv. Organomet. Chem.,* **19**, 51 (1981).

4) H. Sakurai, *J. Organomet. Chem.,* **200**, 261 (1980); H. Sakurai, Y. Nakadaira, and H. Tobita, *Kagaku no Ryoiki,* **33**, 879, 973 (1979).

5) P. Boudjouk, J. R. Roberts, C. M. Gollino, and L. H. Sommer, *J. Am. Chem. Soc.,* **94**, 7926 (1975).

6) M. Ishikawa T. Fuchigami, T. Sugaya, and M. Kumada, *J. Am. Chem. Soc.,* **97**, 5926 (1975).

7) H. Sakurai, Y. Nakadaira, M. Kira, K. Yoshida, H. Sugiyama, and T. Takiguchi, *J. Organomet. Chem.,* **184**, C36 (1980).

8) H. Okinoshima and W. Weber, *J. Organomet. Chem.,* **149**, 279 (1978).

9) M. Kira, K. Sakamoto, and H. Sakurai, *J. Am. Chem. Soc.,* **105**, 7469 (1983).

10) K. Mochida, H. Kikkawa, and Y. Nakadaira, *Chem. Lett.,* **1988**, 1089.

11) H. Sakurai, K. Sakamoto, and M. Kira, *Chem. Lett.,* **1984**, 1379.

12) M. Schriewer and W. P. Neumann, *J. Am. Chem. Soc.,* **105**, 897 (1983).

13) H. Sakurai, K. Mochida, A. Hosomi, and F. Mita, *J. Organomet. Chem.,* **38**, 275 (1972).

14) K. Mochida, I. Yoneda, and M. Wakasa, *J. Organomet. Chem.,* **339**, 53 (1990).

15) J. Barrau, J. Escudié, and J. Satgé, *Chem. Rev.,* **90**, 283 (1990).

16) For example: Y. Sakaguchi, H. Hayashi, and S. Nagakura, *J. Phys. Chem.,* **86**, 3177 (1982).

17) K. Mochida, M. Wakasa, Y. Sakaguchi, and H. Hayashi, *J. Am. Chem. Soc.,* **109**, 7942 (1987).

18) H. Sakurai, "Free Radicals," ed by J. K. Kochi, Wiley, New York (1973), Vol. II, Chap. 25.

19) K. Mochida, M. Wakasa, Y. Sakaguchi, and H. Hayashi, *Nippon Kagaku Kaishi,* **1987**, 1171.

20) W. Ando, H. Itoh, T. Tsumuraya, and H. Yoshida, *Organometallics,* **7**, 1880 (1988).

21) M. Wakasa, I. Yoneda, and K. Mochida, *J. Organomet. Chem.,* **366**, C1 (1989).

22) S. Tomoda, M. Shimoda, Y. Takeuchi, Y. Kaji, K. Obi, I. Tanaka, and K. Honda, *J. Chem. Soc., Chem. Commun.,* **1988**, 910.

23) S. Konieczzy, S. J. Jacobs, J. K. B. Wilking, and P. P. Gaspar, *J. Organomet. Chem.,* **341**, C17 (1988).

24) H. Vancik, G. Raabe, M. J. Michalczyk, R. West, and J. Michl, *J. Am. Chem. Soc.,* **107**, 4097 (1985); G. R. Gillette, G. H. Noren, and R. West, *Organometallics,* **6**, 2617 (1987).

25) H. Bauer and K. Burcshkies, *Chem. Ber.,* **1934**, 2617.

26) D. B. Chambers and F. Glockling, *J. Chem. Soc. A,* **1968**, 735.

27) R. H. Fish and H. G. Kuivila, *J. Org. Chem.,* **31**, 2445 (1966).

28) A. E. Finholt, *Nucl. Sci. Abstr.,* **6**, 617 (1957).

29) J. Satgé and P. Riviere, *Bull. Soc. Chim. Fr.,* **1966**, 1773.

30) O. H. Johnson and W. H. Nebergall, *J. Am. Chem. Soc.,* **71**, 1720 (1949).

31) J. Satgé, P. Riviere, and A. Boy, *Trans. R. Acad. Sci. Ser. C,* **278**, 1309 (1974).

32) M. Kumada, S. Sakamoto, and M. Ishikawa, *J. Organomet. Chem.,* **17**, 1309 (1974).

33) E. H. Brooks and F. Glockling, *J. Chem. Soc. A,* **1966**, 1241.

34) L. A. Leites, Y. P. Egorov, G. Y. Zueva, and V. A. Ponomarenko, *Izv. Akad. Nauk SSSR,* **1961**, 2132.

35) C. Eaborn, A. Leyshon, and K. C. Pande, *J. Chem. Soc.,* **1960**, 3423.

36) H. Bauer and K. Burschkies, *Chem. Ber.,* **1933**, 1156.

37) P. Riviere, J. Satgé, and D. Soula, *J. Organomet. Chem.,* **63**, 167 (1973).

Formation of Molecular Complexes with Calixarenes as Detected by Induced Circular Dichroism

Takashi ARIMURA and Seiji SHINKAI*
Department of Organic Synthesis, Faculty of Engineering, Kyushu University, Fukuoka 812
(Received February 2, 1991)

Calix[*n*]arenes (*n*=4 and 6) bearing (*S*)-5-oxo-2-pyrrolidinylcarbonyloxyl groups on the lower rim were synthesized. In chloroform, the hexamer bearing six (*S*)-5-oxo-2-pyrrolidinylcarbonyloxyl groups could "bind" ferrocenecarboxylic acid through hydrogen-bonding interactions, the complexation being conveniently detected by induced circular dichroism (ICD) spectroscopy (λ_{max} 445 nm). On the basis of the examination of acyclic reference compounds, the appearance of the ICD band was explained as such that one pyrrolidone unit acts as a binding site and the chiral center in the neighboring pyrrolidone unit affects the transition moments in the ferrocene π-system. The association constant for the 1 : 1 complex was estimated to be 680 M^{-1}. This is a new, convenient method for detecting the formation of molecular complexes with calixarenes in organic media.

Calixarenes are cyclic oligomers which are composed of phenol units. Because of their cavity-shaped architecture, they would be expected to be useful building-blocks in the design of novel host molecules.[1—4] Although calixarenes can include several small molecules in the solid state,[1,2] there exist only a few examples for inclusion of guest molecules in solution.[5] This is because host–guest-type complexation in organic media always competes with solvation of guests by solvent molecules. Exceptional is the aqueous system: For instance, water-soluble calixarenes can associate with organic guest molecules owing to a hydrophobic force, a driving force for association specifically operating in water.[6] Thus, the host–guest chemistry of calixarenes has been studied in aqueous solutions.[3,4,7] Only one example reported so far for complexation in organic media is the binding of *t*-butylamine to 5,11,17,23-tetraallylcalix[4]arene-25,26,27,28-tetrol.[5] However, the main driving force for this complex is supposed to be acid-base neutralization between amine and phenol.[5]

In conformity with the foregoing view, we reached a conclusion that one should adopt a new concept to effect inclusion of guest molecules in organic media. Also, some new strategies should be developed to efficiently detect host–guest interactions occurring in organic media. We noticed hydrogen-bonding interactions which have frequently been used in molecular recognition may be useful.[8—11] To detect the interactions between hosts and guests we chose induced circular dichroism (ICD) which sensitively reports the interaction with chiral centers. Thus, we synthesized calix[*n*]arenes (*n*=4 and 6) as host molecules bearing (*S*)-2-pyrrolidone units which have hydrogen-bonding sites as well as a chiral center. As guest molecules, we chose ferrocene derivatives because they have a characteristic absorption band at around 450 nm.

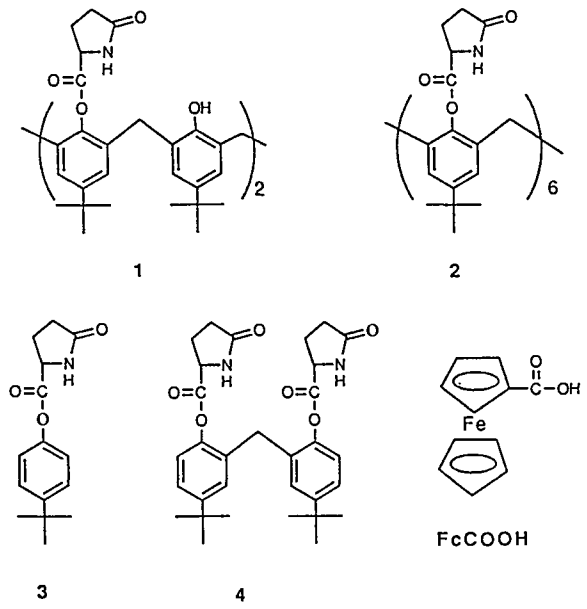

Experimental

Materials. 5,11,17,23-Tetra-*t*-butylcalix[4]arene-25,26,27,28-tetrol and 5,11,17,23,29,35-hexa-*t*-butylcalix[6]arene-37,38,39,40,41,42-hexol were prepared according to Gutsche's method.[12]# (*S*)-5-Oxo-2-pyrrolidinecarbonyl chloride was prepared from (*S*)-5-oxo-2-pyrrolidinecarboxylic acid (Aldrich, 97% purity) according to the literature.[13]

25,27-Bis[(*S*)-5-oxo-2-pyrrolidinylcarbonyloxy]-5,11,17,23-tetra-*t*-butylcalix[4]arene-26,28-diol (1). Oil-dispersed NaH (152 mg; 3.8 mmol) was added to 40 ml of THF containing tetra-*t*-butylcalix[4]arenetetrol (350 mg; 0.54 mmol). The mixture was stirred for 4 h at room temperature under a nitrogen stream. (*S*)-5-Oxo-2-pyrrolidinecarbonyl chloride (0.53 g; 4.0 mmol) was added dropwise. The reaction was continued at room temperature for 15 h. After addition of a small amount of ethanol, the mixture was concentrated to dryness under reduced pressure. The residue was dissolved in dichloromethane, the solution being washed with water and dried over Na_2SO_4. After concentration to dryness, the residue was recrystallized from hexane–toluene: White powder, mp 280—284 °C, yield 57%; ^{1}H NMR ($CDCl_3$) δ=0.92 and 1.20 (18H each, s each, *t*-Bu), 2.20—2.60 (8H, m,

The nomenclature for calix[*n*]arene is a little confused now. In this paper, we named the [1$_n$]metacyclophane structure [$\overline{(\text{CH}_2\text{-}m\text{-}\text{C}_6\text{H}_4)_n}$] "calix[*n*]arene".

CH_2CH_2 in pyrrolidone), 3.40 and 3.90 (4H each, d each (J=13 Hz), $ArCH_2Ar$), 4.28—4.32 (2H, m, CH in pyrrolidone), 6.20 (2H, broad s, NH), 6.90 and 7.15 (4H each, s each, ArH). Found: C, 74.03; H, 7.70; N, 2.94%. Calcd for $C_{54}H_{66}O_8N_2$: C, 74.45; H, 7.64; N, 3.22%. The ^{1}H NMR spectrum and elemental analysis indicate that the recovered product is 25,27-disubstituted-26,28-dihydroxy-5,11,17,23-tetra-*t*-butylcalix[4]arene. The split pattern for the $ArCH_2Ar$ protons shows that this calix[4]arene adopts a cone conformation.

37,38,39,40,41,42-Hexakis[(*S*)-5-oxo-2-pyrrolidinylcarbonyloxy]-5,11,17,23,29,35-hexa-*t*-butylcalix[6]arene (2). This compound was synthesized in a manner similar to that described for **1**: Colorless powder, mp 215—217 °C, yield 28%; ^{1}H NMR ($CDCl_3$) δ=1.20 (54H, s, *t*-Bu), 2.22—2.58 (24H, m, CH_2CH_2 in pyrrolidone), 3.80 (12H, broad s, $ArCH_2Ar$), 4.29—4.32 (6H, m, CH in pyrrolidone), 6.17 (6H, broad s, NH), 7.15 (12H, s, ArH). Found: C, 69.85; H, 6.93; N, 4.61%. Calcd for $C_{96}H_{114}O_{18}N_6$: C, 70.31; H, 7.01; N, 5.12%. The ^{1}H NMR spectrum and elemental analysis indicate that six OH groups are substituted.

***p*-*t*-Butylphenyl (*S*)-5-Oxo-2-pyrrolidinecarboxylate (3).** This compound was also synthesized from (*S*)-5-oxo-2-pyrrolidinecarbonyl chloride and *p*-*t*-butylphenol in the presence of NaH: Colorless prisms (recrystallized from acetonitrile), mp 124—127 °C, yield 60%; ^{1}H NMR ($CDCl_3$) δ=1.16 (9H, s, *t*-Bu), 2.04—2.38 (4H, m, CH_2CH_2), 4.02—4.38 (1H, m, CH), 6.12 (1H, broad s, NH), 5.73 and 7.24 (2H each, d each, (J=9 Hz), ArH). Found: C, 69.44; H, 7.70; N, 5.12%. Calcd for $C_{15}H_{19}NO_3$: C, 68.94; H, 7.33; N, 5.36%.

Bis[2-((*S*)-5-oxo-2-pyrrolidinylcarbonyloxy)-5-*t*-butylphenyl]methane (4). This compound was synthesized from (*S*)-5-oxo-2-pyrrolidinecarbonyl chloride and 4,4′-di-*t*-butyl-2,2′-methylenediphenol in the presence of NaH: Colorless prisms (recrystallized from hexane), mp 126—129 °C, yield 43%; ^{1}H NMR ($CDCl_3$) δ=1.25 (18H, s, *t*-Bu), 2.20—2.60 (8H, m, CH_2CH_2), 3.90 (2H, s, $ArCH_2Ar$), 4.30—4.35 (2H, m, CH), 6.15 (2H, broad s, NH), 6.76 and 7.10 (2H each, d each (J=8 Hz), ArH), 7.30 (2H, s, ArH). Found: C, 70.05; H, 7.20; H, 5.12%. Calcd for $C_{31}H_{38}N_2O_6$: C, 69.64; H, 7.16; H, 5.24%.

Results and Discussion

In O-acylation of 25,26,27,28-tetrahydroxy-5,11,17,23-tetra-*t*-butylcalix[4]arene with (*S*)-5-oxo-2-pyrrolidinecarbonyl chloride we found that only two OH groups can be substituted. The similar result was observed for O-alkylation of 25,26,27,28-tetrahydroxy-5,11,17,23-tetra-*t*-butylcalix[4]arene with 2-chloromethylpyridine.[14] In contrast, six OH groups in 37,38,39,40,41,42-hexahydroxy-5,11,17,23,29,35-hexa-*t*-butylcalix[6]arene are all substituted. The difference is attributed to the difference in the ring size: that is, the space on the narrow calix[4]arene ring readily becomes sterically-crowded by O-substitution.

When **2** was mixed with ferrocenecarboxylic acid (FcCOOH) in chloroform, a negative ICD band appeared at 445 nm (Fig. 1). This CD maximum is equal to the absorption maximum of FcCOOH. This band was weakened by the addition of methanol. In contrast, this band was not detected at all in DMSO under the same measurement conditions. These results indicate that FcCOOH "interacts" with **2** and the interaction is based on the formation of hydrogen-bonds.

To confirm the importance of the hydrogen-bonding interaction, we used ferrocene (Fc) and methyl ferrocenecarboxylate (FcCOOMe) as reference guest molecules. The ICD band for these compounds was not detected even in chloroform. Here, one can visualize that attraction between **2** and FcCOOH is ascribed to the hydrogen-bonding interaction between the COCHNHCO moiety in **2** and the COOH moiety in FcCOOH. Between two possible binding modes, (A) includes a seven-membered ring whereas (B) includes a six-membered ring (hydrogen atoms are not counted). We consider that binding mode (B) is more likely.

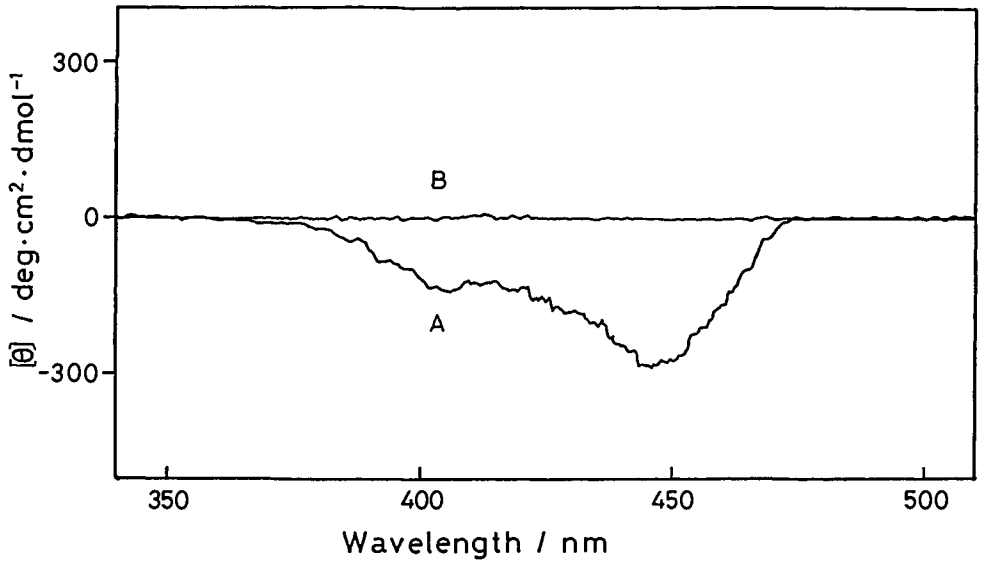

Fig. 1. ICD spectra of FcCOOH in the presence of **2**: 20 °C, [**2**]=1.00×10^{-2} M, [FcCOOH]=5.00×10^{-3} M: (A) chloroform, (B) DMSO.

Table 1. Absorption and ICD Spectra of Ferrocene Derivatives[a)]

Guest	Solvent	λ_{max} in absorption spectrum	$\lambda_{max}(\theta)$ in ICD spectrum			
		nm	Host=1	2	3	4
Fc	$CHCl_3$	440	nd	nd	nd	nd
Fc	DMSO	440	nd	nd	nd	nd
FcCOOH	$CHCl_3$	445	nd	445(−260)	nd	445(−20)
FcCOOH	DMSO	443	nd	nd	nd	nd
FcCOOMe	$CHCl_3$	446	nd	nd	nd	nd
FcCOOMe	DMSO	446	nd	nd	nd	nd

a) 20 °C, chloroform: [1]=[2]=1.00×10^{-2} M, [3]=8.00×10^{-2} M, [4]=4.00×10^{-2} M, [ferrocene derivative]=5.00×10^{-3} M. Nd denotes that the ICD band is not detected.

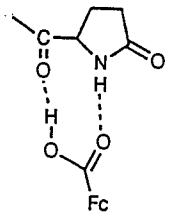

(A)

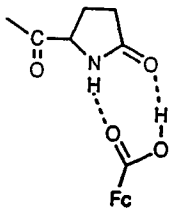

(B)

Here, we discuss how the interaction between **2** and FcCOOH becomes CD-active. Compound **1**, having two pyrrolidone units at 1,3-position, should interact with FcCOOH through the hydrogen-bonds in chloroform. Actually, however, the perceptible ICD band was not recognized. The difference suggests that two neighboring pyrrolidone units would be essential for the ICD-activity. To estimate this hypothesis, we synthesized acyclic analogs **3** and **4**. As summarized in Table 1, the ICD band of FcCOOH did not appear in the presence of monomeric **3**. In the presence of dimeric **4**, on the other hand, the weak but perceptible ICD band appeared at 445 nm. This supports the view that two neighboring pyrrolidone units act cooperatively to make the bound FcCOOH CD-active; conceivably, one pyrrolidone unit acts as a binding site and the chiral center in the neighboring pyrrolidone unit affects the transition moments in the ferrocene π-system. With this cooperative action of two neighboring units the ICD-activity is observed for the **2**·FcCOOH complex.

We determined the stoichiometry for complexation between **2** and FcCOOH on the basis of a continuous variation plot (Fig. 2). It is seen from Fig. 2 that **2** and FcCOOH form a 1 : 1 complex. Why do they form a 1 : 1 complex although **2** has six pyrrolidone units on the lower rim? The result implies that the binding of FcCOOH to one pyrrolidone unit strongly suppresses the binding to other remaining pyrrolidone units. Previously, Aoyama et al.[15)] synthesized lipophilic calix[6]arenes bearing amide groups on the lower rim. These compounds provide a polar (DMF-like) microenvironment composed of the amide linkages. Possibly, the lower rim in **2** has such a polar microenvironment.

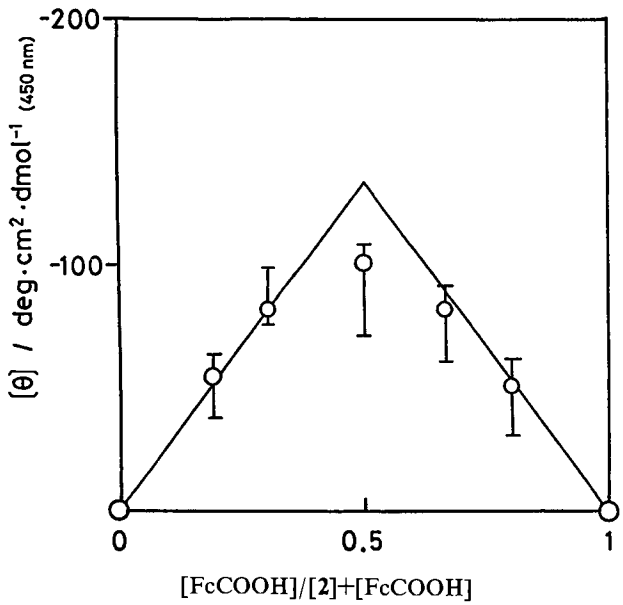

Fig. 2. Continuous variation plot for complexation of **2** and FcCOOH: 20 °C, chloroform, [2]+[FcCOOH]=5.00×10^{-3} M.

This suggests that when FcCOOH is bound to **2** through the hydrogen-bonding interaction, the ferrocene moiety is trapped in the cavity through the dipole–dipole interaction. In this binding model the lower rim is wholly occupied by the first FcCOOH, so that the binding of the second FcCOOH becomes sterically difficult. To prove this association mode, we measured the ^{1}H NMR spectrum of the **2**·FcCOOH complex ($CDCl_3$, 25 °C, [2]=5.00×10^{-2} M, ## [FcCOOH]=7.50×10^{-3} M). FcCOOH in the absence of **2** gave three peaks at 4.25 (5H), 4.45 (2H), and 4.48 (2H) ppm, which were assigned to the cyclopentadiene ring protons without COOH, C<u>H</u>(CHCCOOH), and C<u>H</u>(CCOOH) protons in the cyclopentadiene ring with COOH, respectively. In the presence of **2** the C<u>H</u>(CHCOOH) protons specially shifted to 4.81 ppm whereas the chemical shifts for other protons were scarcely affected. This result means that these protons are placed in the plane of the benzene

1 M=1 mol dm^{-3}.

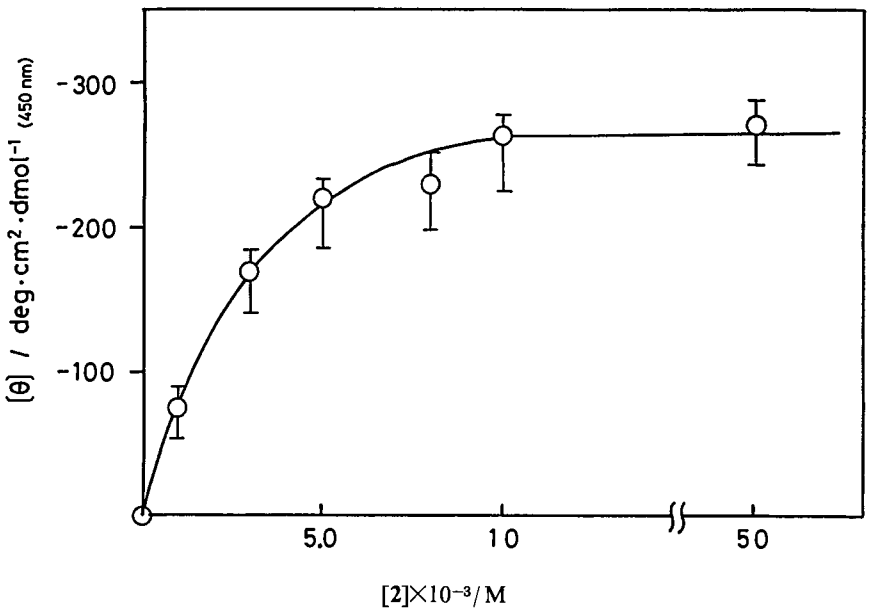

Fig. 3. Plot of θ vs. [2] in chloroform at 20 °C: [FcCOOH]=5.00×10^{-3} M.

rings in **2**; that is, the part of the ferrocene moiety is trapped in the lower rim of the calix[4]arene ring.

We measured θ as a function of [2] (Fig. 3). The plot showed a typical saturation curve. By the analysis of this plot by the Benesi-Hildebrand equation for a 1 : 1 complex, we estimated the association constant to be 680 M^{-1} (correlation coefficient 0.997). This value is comparable with those for complexes formed through two-to-three hydrogen bonds.[16]

Since the complexation between **2** and FcCOOH is based on the hydrogen-bonding interaction, FcCOOH should be substituted by other additives bearing a carboxyl group. This process is similar to the action of "competitive inhibition" in enzyme chemistry. We used trifluoroacetic acid (pK_a in water 0.23), benzoic acid (pK_a in water 4.19), adamantane-1-carboxylic acid (pK_a in water 4.50), and acetic acid (pK_a in water 4.76) as "inhibitors". To a chloroform solution containing **2** (1.00×10^{-3} M) and FcCOOH (2.00×10^{-2} M) was injected a chloroform solution containing concentrated "inhibitors". The final concentration of "inhibitors" was adjusted to 2.00×10^{-2} M. On the addition of adamantane-1-carboxylic acid and acetic acid, the ICD band on the basis of the **2**–FcCOOH interaction was scarcely affected. On the addition of trifluoroacetic acid, in contrast, the ICD band disappeared completely. Benzoic acid moderately competed with FcCOOH, the CD band being decreased with increasing benzoic acid concentration. These results support the view that the association on the basis of hydrogen-bonding interaction is primarily governed by the "acidity" of protons.

The association constant for FcCOOH (K_{FcCOOH}) is defined by Eq. 1. The substitution with benzoic acid (BA) occurring on the lower rim is expressed by Eq. 2. This gives Eq. 3 for the equilibrium constant (K_e). Thus, the association constant for BA (K_{BA}) is expressed, assuming the 1 : 1 substitution between FcCOOH and BA, by Eq. 4.

$$K_{FcCOOH}=\frac{[2\cdot FcCOOH]}{[2][FcCOOH]}, \quad (1)$$

$$2\cdot FcCOOH+BA \rightleftarrows 2\cdot BA+FcCOOH, \quad (2)$$

$$K_e=\frac{[2\cdot BA][FcCOOH]}{[2\cdot FcCOOH][BA]}, \quad (3)$$

$$K_{BA}=K_{FcCOOH}\cdot K_e. \quad (4)$$

We obtained K_e=0.22 from Eq. 3. This allows the estimation of K_{BA}=150 M^{-1}.

In conclusion, the present paper demonstrated the guest complexation through hydrogen-bonding interactions occurring in organic media. In the past, it was difficult to detect the formation of molecular complexes with calixarenes in organic media. In fact, NMR spectroscopy was the sole method.[5] It is shown here that CD spectroscopy serves as an efficent and convenient technique to detect how the guest interacts with the host calixarenes. We plan to extend this concept to chiral recognition of guest molecules.

This work was supported by the Grant-in-Aid from the Ministry of Education, Science and Culture.

References

1) C. D. Gutsche, *Acc. Chem. Res.*, **16**, 161 (1983).
2) C. D. Gutsche, "Calixarenes," Royal Society of Chemistry, Cambridge (1989).
3) S. Shinkai, *Pure Appl. Chem.*, **58**, 1523 (1986).
4) T. Arimura, S. Shinkai , and T. Matsuda, *Yuki Gosei Kagaku-Kyokaishi*, **47**, 523 (1989).

5) Bauer and Gutsche reported inclusion of *t*-butylamine in calix[4]arenes, but the driving force for inclusion is supposed to be a combination of proton transfer plus electrostatic attraction: L. J. Bauer and C. D. Gutsche, *J. Am. Chem. Soc.*, **107**, 6063 (1985).

6) C. Tanford, "The Hydrophobic Effect," Wiley Intersci., New York (1973).

7) S. Shinkai, *Bioorg. Chem. Front.*, **1**, 161 (1990).

8) J. Rebek, Jr., *Angew. Chem., Int Ed. Engl.*, **29**, 245 (1990).

9) S. Goswami and A. D. Hamilton, *J. Am. Chem. Soc.*, **111**, 3425 (1989), and references cited therein.

10) Y. Aoyama, Y. Tanaka, and S. Sugahara, *J. Am. Chem. Soc.*, **111**, 5397 (1989), and references cited therein.

11) K. Kano, K. Yoshiyasu, and S. Hashimoto, *J. Chem. Soc., Chem. Commun.*, **1988**, 801.

12) C. D. Gutsche and M. Iqbal, *Org. Synth.*, **68**, 234, 238, 243 (1989).

13) S. Wilk, T. C. Friedmann, and T. B. Kline, *Biochem. Biophys. Res. Commun.*, **130**, 662 (1985).

14) S. Shinkai, T. Otsuka, K. Araki, and T. Matsuda, *Bull. Chem. Soc. Jpn.*, **62**, 4055 (1989).

15) Y. Aoyama, Y. Nonaka, Y. Tanaka, H. Toi, and H. Ogoshi, *J. Chem. Soc., Perkin Trans. 2*, **1989**, 1025.

16) A. D. Hamilton and D. V. Engen, *J. Am. Chem. Soc.*, **109**, 5035 (1987).

Synthesis of 7-Substituted 6,7-Dihydro-5*H*-pyrrolo[3,4-*b*]pyridin-5-ones. Reaction of 7-Hydroxy Derivatives with Nucleophiles

Takehiko Goto,* Shin Utsunomiya, Hiroshi Aiba, Hirotaka Hayasaka, Mikihiro Endo, Reo Watanabe, Takeshi Ishizaki, Ryu Sato, and Minoru Saito†
Department of Resource Chemistry, Faculty of Engineering, University of Iwate, Morioka 020
(Received February 25, 1991)

Various 7-substituted 6,7-dihydro-5*H*-pyrrolo[3,4-*b*]pyridin-5-ones are synthesized by the reaction of the corresponding 7-hydroxy derivatives with nucleophiles involving active methylene compounds, aromatics, alcohols, *p*-toluenethiol, benzenesulfinic acid, triethyl phosphite, ammonia, and amines under acidic or basic conditions. Some synthetic applications of the products obtained are demonstrated to give a 7-methylene derivative and fused tricyclic derivatives.

Much effort has been devoted to the investigation of 6,7-dihydro-5*H*-pyrrolo[3,4-*b*]pyridin-5-ones and their derivatives as cyclic nicotinamide analogs or aza-analogs of phthalimidines,[1-6] some of which are known to be biologically active compounds such as antidiabetic agents,[2] central nervous agents,[3,4] and herbicides.[5] In connection with our studies of novel functionalized isoindoles,[7] we planned the synthesis of their aza-analogs and concentrated our attention on 7-substituted 6,7-dihydro-5*H*-pyrrolo[3,4-*b*]pyridin-5-ones. Though some 7-substituted derivatives are known to be interesting pharmacologically active compounds such as non-benzodiazepine anxiolytic agents,[3,4] there have been few studies on general synthetic approach to 7-substituted derivatives in the literature, partially because unsymmetrically substituted cyclic compounds pose the problem of regiochemistry. Recently, we have performed the efficient regioselective synthesis of 7-hydroxy derivative[8a] and preliminarily reported some transformations of the hydroxyl group to other substituents.[8b,c] In this paper, we describe the synthesis of a wide variety of 7-substituted derivatives **2**—**8** from 7-hydroxy derivative **1** in detail and discuss the scope and limitation of the present methodology.

Results and Discussion

In principle, hydroxylactam **1** can be considered as (a) a source of acyliminium cation which is well known to react with various types of nucleophiles[9] and (b) a masked aldehyde which is expected to react with anionic species[4,10,11] as depicted in Scheme 1. On the basis of such viewpoints, we examined the reaction of **1** with nucleophiles under various reaction conditions and

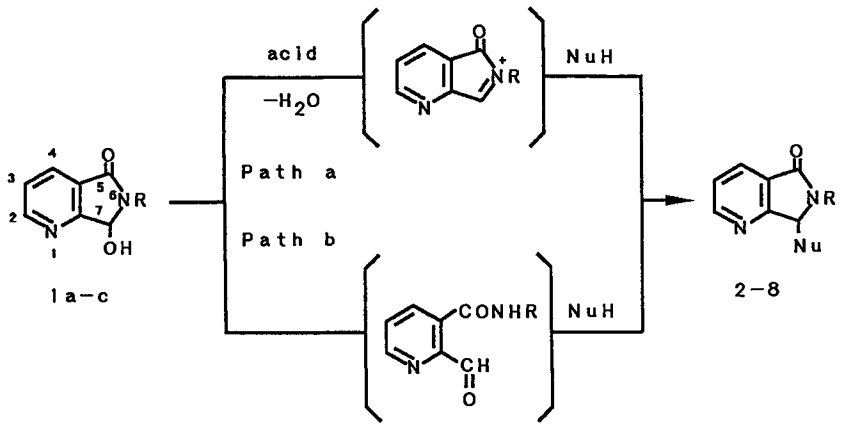

1a: R=H
1b: R=CH_3
1c: R=C_6H_5

2: Nu=active methylene
3: Nu=aryl
4: Nu=alkoxy
5: Nu=*p*-tolylthio
6: Nu=phenylsulfonyl
7: Nu=diethoxyphosphoryl
8: Nu=amino and alkylamino

Scheme 1.

† This paper is dedicated to an emeritus professor of University of Iwate, the late Minoru Saito.

Table 1. 7-Substituted Derivatives **2**—**8** Prepared

Product	R	Nu	Method[a]	React. temp °C	React. time h	Yield[b] %	mp/°C (solvent)	Molecular formula (FW)	MS (70 eV) *m/z*
2a	H	$CH(CO_2Et)COMe$	A	73	3	95[c]	125—127 (AcOEt/hexane)	$C_{13}H_{14}N_2O_4$ (262.3)	219(M^+−43)
2b	Me	$CH(CO_2Et)COMe$	A	73	6	95[c]	101—102 (AcOEt/hexane)	$C_{14}H_{16}N_2O_4$ (276.3)	233(M^+−43)
2c	Me	$CH(COMe)_2$	A	73	2.5	95	142—143 (AcOEt)	$C_{13}H_{14}N_2O_3$ (246.3)	246(M^+)
2d	Me	$CH(COPh)_2$	A	73	0.5	100	167—168 (AcOEt)	$C_{23}H_{18}N_2O_3$ (370.4)	265(M^+−105)
2e	Ph	$CH(COPh)_2$	A	73	2.5	100	166 (AcOEt/hexane)	$C_{28}H_{20}N_2O_3$ (432.5)	432(M^+)
3a	H	2,5-$(MeO)_2C_6H_3$	A	73	1	97	187—188 (EtOH)	$C_{15}H_{14}N_2O_3$ (270.3)	270(M^+)
3b	Me	2,5-$(MeO)_2C_6H_3$	A	73	1	100	115—116 (AcOEt)	$C_{16}H_{16}N_2O_3$ (284.3)	284(M^+)
3c	Ph	2,5-$(MeO)_2C_6H_3$	A	73	3	96	175 (EtOH)	$C_{21}H_{18}N_2O_3$ (346.4)	346(M^+)
3d	H	3,4-$(MeO)_2C_6H_3$	A	73	1	95	194—195 (EtOH)	$C_{15}H_{14}N_2O_3$ (270.3)	270(M^+)
3e	Ph	3,4-$(MeO)_2C_6H_3$	A	73	12	96	145 (EtOH)	$C_{21}H_{18}N_2O_3$ (346.4)	346(M^+)
3f	H	4-$MeOC_6H_4$	A	73	0.5	55	204—206 (EtOH)	$C_{14}H_{12}N_2O_2$ (240.3)	240(M^+)
3g	H	2-BrC_6H_4	B	R.T.	1	36	169—170 (EtOH)	$C_{13}H_9N_2OBr$ (289.1)	289(M^+)
3h	H	4-BrC_6H_4				53	187 (EtOH)	$C_{13}H_9N_2OBr$ (289.1)	289(M^+)
3i	Ph	2-BrC_6H_4	B	R.T.	3	28	173 (AcOEt/hexane)	$C_{19}H_{13}N_2OBr$ (365.2)	365(M^+)
3j	Ph	4-BrC_6H_4				54	207 (EtOH)	$C_{19}H_{13}N_2OBr$ (365.2)	365(M^+)
4a	Me	OMe	C	65	8	95	91 (CCl_4/hexane)	$C_9H_{10}N_2O_2$ (178.2)	178(M^+)
4b	Me	OEt	C	78	6	97	47—48 (CCl_4/hexane)	$C_{10}H_{12}N_2O_2$ (192.2)	147(M^+−45)
4c	H	OCH_2CH_2OH	C	80	5	90	106—107 (EtOH)	$C_9H_{10}N_2O_3$ (194.2)	133(M^+−61)
4d	H	OCH_2CH_2Cl	C	80	0.2	92	141 (EtOH)	$C_9H_9N_2O_2Cl$ (212.6)	212(M^+)
4e	H	$OCH_2CH_2CH_2Cl$	C	80	0.5	100	128 (EtOH)	$C_{10}H_{11}N_2O_2Cl$ (226.7)	147(M^+−79)
4f	Me	$OCH_2CH(CH_3)_2$	C	108	3	100	70—71 (CCl_4/hexane)	$C_{12}H_{16}N_2O_2$ (220.3)	147(M^+−73)
4g	Me	$OCH(CH_3)_2$	C	82	7	96	48—52 (CCl_4/hexane)	$C_{11}H_{14}N_2O_2$ (206.2)	147(M^+−59)
4h	Me	1-menthyl	C	110	6	45	138 (Et_2O/hexane)	$C_{18}H_{26}N_2O_2$ (302.4)	302(M^+)
4i	Me	1-menthyl				43	145—146 (Et_2O/hexane)	$C_{18}H_{26}N_2O_2$ (302.4)	302(M^+)
4j	H	O-*t*-Bu	F	R.T.	0.1	91	157 (AcOEt)	$C_{11}H_{14}N_2O_2$ (206.2)	206(M^+)
4k	Me	O-*t*-Bu	F	R.T.	0.1	97	106 (Et_2O/hexane)	$C_{12}H_{16}N_2O_2$ (220.3)	220(M^+)
4l	Ph	O-*t*-Bu	F	R.T.	0.1	85	133 (AcOEt)	$C_{17}H_{18}N_2O_2$ (282.3)	282(M^+)
5a	H	S(*p*-Tol)	D	82	3.5	95	185—186 (AcOEt)	$C_{14}H_{12}N_2OS$ (256.3)	256(M^+)
6a	H	$SO_2C_6H_5$	E	82	5	69	190—191 (EtOH)	$C_{13}H_{10}N_2O_3S$ (274.3)	274(M^+)
6b	Me	$SO_2C_6H_5$	E	82	5	76	153—154 (AcOEt)	$C_{14}H_{12}N_2O_3S$ (288.3)	288(M^+)

Table 1. (Continued)

Product	R	Nu	Method[a]	React. temp °C	React. time h	Yield[b] %	mp/°C (solvent)	Molecular formula (FW)	MS (70 eV) *m/z*
7a	H	$P(O)(OEt)_2$	G	R.T.	5	57	147—148 (AcOEt)	$C_{11}H_{15}N_2O_4P$ (270.2)	270(M^+)
7b	Me	$P(O)(OEt)_2$	G	R.T.	4	73	73—74 (AcOEt)	$C_{12}H_{17}N_2O_4P$ (284.3)	284(M^+)
8a	Ph	NH_2	H	110	12	99	130 (AcOEt)	$C_{13}H_{11}N_3O$ (225.3)	225(M^+)
8b	H	NH-*n*-Pr	I	101	32	98	116 ($CHCl_3$/hexane)	$C_{10}H_{13}N_3O$ (191.2)	133(M^+−58)
			J	101	1	98			
8c	Me	NH-*n*-Pr	J	101	24	96	105 (Et_2O/hexane)	$C_{11}H_{15}N_3O$ (205.3)	147(M^+−58)
8d	Ph	NH-*n*-Pr	I	101	12	84	96 ($CHCl_3$/hexane)	$C_{16}H_{17}N_3O$ (267.3)	267(M^+)
			J	101	3	91			
8e	Me	NH-*n*-Bu	J	101	18	96	116—117 (Et_2O/hexane)	$C_{12}H_{17}N_3O$ (219.3)	147(M^+−72)
8f	Me	Piperidino	J	101	24	95	122—123 ($Et_2O/CHCl_3$)	$C_{13}H_{17}N_3O$ (231.3)	147(M^+−84)
8g	Me	NH-*t*-Bu	K	R.T.	0.1	90	143—144 (EtOH)	$C_{12}H_{17}N_3O$ (219.3)	204(M^+−15)
8h	Me	NEt_2	K	R.T.	0.1	95	89 (Et_2O/hexane)	$C_{12}H_{17}N_3O$ (219.3)	147(M^+−72)

a) For Methods A—K, see Experimental section. b) Yield of the isolated product based on **1**. c) Yield of the mixture of two diastereomers.

Table 2. Spectral and Analytical Data of Compounds **2**—**8** Prepared

Compound	IR (KBr) $\nu_{C=O}$/cm^{-1}	^{1}H NMR ($CDCl_3$/TMS) δ/ppm, J/Hz	Found / Calcd/% C	H	N
2a	1720, 3180 (NH)	1.03 (3H, t, J=7, $OCH_2C\underline{H}_3$); 2.02 (3H, s, $COCH_3$); 4.06 (2H, q, J=7, $OC\underline{H}_2CH_3$); 4.23 (1H, d, J=5, H-7); 5.20 (1H, d, J=5, $COCHCO_2$); 6.92 (1H, br s H-6); 7.41 (1H, dd, J=8 and 5, H-3); 8.14 (1H, dd J=8 and 2, H-4); 8.75 (1H, dd, J=5 and 2, H-2)	59.42 59.54	5.37 5.38	10.71 10.68
2b	1720, 1740	1.17 (3H, t, J=6, $OCH_2C\underline{H}_3$); 2.09 (1H, s, $COCH_3$); 3.15 (3H, s, N-CH_3); 4.15 (2H, q, J=6, $OC\underline{H}_2CH_3$); 4.31 (1H, d, J=4, H-7); 5.18 (1H, d, J=4, $COCHCO_2$); 7.39 (1H, dd, J=8 and 5, H-3); 8.09 (1H, dd, J=8 and 2, H-4); 8.70 (1H, dd, J=5 and 2, H-2)	60.80 60.86	5.83 5.84	10.09 10.14
2c	1710, 1730	1.78 (3H, 5, $COCH_3$); 2.26 (3H, s, $COCH_3$); 3.06 (s, 3H, N-CH_3); 4.52 (1H, d, J=4, H-7); 5.33 (1H, d, J=4, COCHCO); 7.45 (1H, dd, J=8 and 5, H-3); 8.12 (1H, dd, J=8 and 2, H-4); 8.75 (1H, dd, J=5 and 2, H-2)	63.15 63.40	5.76 5.73	11.45 11.38
2d	1700	3.22 (3H, s, N-CH_3); 5.63 (1H, d, J=3, H-7); 6.21 (1H, d, J=3, COCHCO); 7.0—7.7 (m, 12H, arom+H-3+ H-4); 8.72 (1H, dd, J=5 and 2, H-2)	74.70 74.58	4.86 4.90	7.66 7.56
2e	1690, 1700	1.89 (3H, s, $COCH_3$); 3.16 (3H, s, N-CH_3); 5.38 (2H, s, H-7+COCHCO); 7.3—8.0 (6H, m, arom+H-3+H-4); 8.71(1H, dd, J=5 and 2, H-2)	78.01 77.76	4.58 4.66	6.47 6.48
3a	1710, 3310 (NH)	3.66 (3H, s, OCH_3); 3.82 (3H, s, OCH_3); 6.03 (1H, s, H-7); 6.55 (1H, s, arom); 6.82 (2H, s, J=2H, arom), 6.94 (1H, br s, H-6); 7.37 (1H, dd, J=8 and 5, H-3); 8.17 (1H, dd, J=8 and 2, H-4); 8.74(1H, dd, J=5 and 2, H-2)	66.83 66.66	5.22 5.22	10.17 10.36
3b	1710	3.00 (3H, s, N-CH_3); 3.67 (3H, s, OCH_3); 3.78 (3H, s, OCH_3); 5.91 (1H, s, H-7); 6.36 (1H, s, arom); 6.86(2H, d, J=2, arom); 7.35 (1H, dd, J=8 and 5, H-3); 8.15 (1H, dd, J=8 and 2, H-4); 8.66 (1H, dd, J=5 and 2, H-2)	67.65 67.59	5.68 5.67	9.98 9.85
3c	1700	3.59 (3H, s, OCH_3); 3.85 (3H, s, OCH_3); 6.62 (1H, s, H-7); 6.4—7.8 (9H, m, arom+H-3); 8.26 (1H, dd, J=8 and 2, H-4); 8.73 (1H, dd, J=5 and 2, H-2)	72.69 72.82	5.22 5.24	7.91 8.09

Table 2. (Continued)

Compound	IR (KBr) $\nu_{C=O}$/cm^{-1}	^{1}H NMR ($CDCl_3$/TMS) δ/ppm, J/Hz	Found / Calcd/% C	H	N
3d	1720, 3300 (NH)	3.85 (3H, s, OCH_3); 3.89 (3H, s, OCH_3); 5.66 (1H, s, H-7); 6.8—7.0 (3H, m, arom); 7.43 (1H, dd, J=8 and 5, H-3); 7.47 (1H, br s, H-6); 8.20 (1H, dd, J=8 and 2, H-4); 8.75 (dd, 1H, J=5 and 2, H-2)	66.62 66.66	5.17 5.22	10.22 10.36
3e	1690	3.75 (3H, s, OCH_3); 3.81 (3H, s, OCH_3); 6.09 (1H, s, H-7); 6.6—7.8 (9H, m, arom+H-3); 8.23 (1H, dd, J=8 and 2, H-4); 8.73 (1H, dd, J=5 and 2, H-2)	72.68 72.82	5.19 5.24	7.91 8.09
3f	1690, 3180 (NH)	3.78 (3H, s, OCH_3); 5.63 (1H, s, H-7); 6.87 (2H, d, arom); 7.17 (1H, br s, H-6); 7.24 (2H, d, arom); 7.36 (1H, dd, J=8 and 5, H-3); 8.15 (1H, dd, J=8 and 2, H-4); 8.71 (1H, dd, J=5 and 2, H-2)	70.02 69.99	5.07 5.03	11.70 11.66
3g	1690, 3250 (NH)	6.23 (1H, s, H-7); 6.9—7.7 (6H, m, arom+H-3+H-6); 8.15 (1H, dd, J=8 and 2, H-4); 8.74 (1H, dd, J=5 and 2, H-2)	54.17 54.00	3.08 3.14	9.64 9.69
3h	1730, 3220 (NH)	5.64 (1H, s, H-7); 7.25 (2H, d, J=7, arom); 7.40 (1H, dd, J=8 and 5, H-3); 7.48 (2H, d, J=7, arom); 8.13 (1H, dd, J=8 and 2, H-4); 8.34 (1H, br s, H-6); 8.70 (1H, dd, J=5 and 2, H-2)	54.27 54.00	3.09 3.14	9.72 9.69
3i	1700	6.87 (1H, s, H-7); 7.0—7.5 (9H, m, arom); 7.67 (1H, dd, J=8 and 5, H-3); 8.25 (1H, dd, J=8 and 2, H-4); 8.74 (1H, dd, J=5 and 2, H-2)	62.67 62.48	3.59 3.59	7.62 7.67
3j	1700	6.17 (1H, s, H-7); 7.1—7.6 (5H, m, arom); 7.24 (2H, d, J=7, arom); 7.49 (2H, d, J=7, arom); 7.71 (1H, dd, J=8 and 5, H-3); 8.34 (1H, dd, J=8 and 2, H-4); 8.82 (1H, dd, J=5 and 2, H-2)	62.70 62.48	3.54 3.59	7.51 7.67
4a	1720	3.14 (3H, s, N-CH_3); 3.15 (3H, s, OCH_3); 7.43 (1H, dd, J=8 and 5, H-3); 5.65 (1H, s, H-7); 8.07 (1H, dd, J=8 and 2, H-4); 8.76 (1H, dd, J=5 and 2, H-2)	60.56 60.66	5.86 5.66	15.91 15.72
4b	1700	1.22 (3H, t, J=7, $OCH_2C\underline{H}_3$); 3.13 (3H, s, N-CH_3); 3.35 (2H, m, $OC\underline{H}_2CH_3$); 5.65 (1H, s, H-7); 7.39 (1H, dd, J=8 and 5, H-3); 8.05 (1H, dd, J=8 and 2, H-4); 8.71 (1H, dd, J=5 and 2, H-2)	62.45 62.48	6.34 6.29	14.82 14.57
4c	1710, 3100 (NH and OH)	3.5—4.0 (4H, m, $OC\underline{H}_2C\underline{H}_2O$); 4.24 (1H, br s, OH); 5.95 (1H, s, H-7); 7.50 (1H, dd, J=8 and 5, H-3); 7.78 (1H, br s, H-6); 8.12 (1H, dd, J=8 and 2, H-4); 8.75 (1H, dd, J=5 and 2, H-2)	55.58 55.67	5.17 5.19	14.50 14.43
4d	1670, 1720, 3200 (NH)	3.6—4.2 (4H, m, $OC\underline{H}_2C\underline{H}_2Cl$); 6.02 (1H, s, H-7); 7.55 (1H, br s, H-6); 7.55 (1H, dd, J=8 and 5, H-3); 8.17 (1H, dd, J=8 and 2, H-4); 8.85 (1H, dd, J=5 and 2, H-2)	50.87 50.84	4.30 4.27	13.26 13.17
4e	1710, 3150 (NH)	(DMSO-d_6) 1.98 (2H, quintet, J=6, $OCH_2C\underline{H}_2CH_2Cl$); 3.4—4.0 (4H, m, $OC\underline{H}_2CH_2C\underline{H}_2Cl$); 5.87 (1H, s, H-7); 7.56 (1H, dd, J=8 and 5, H-3); 8.08 (1H, dd, J=8 and 2, H-4); 8.77 (1H, dd, J=5 and 2, H-2); 9.33 (1H, br s, H-6)	53.10 52.99	4.96 4.89	12.37 12.36
4f	1700	0.88 and 0.91 [6H, d+d, J=7, $CH(C\underline{H}_3)_2$]; 1.7—2.0 [1H, m, $C\underline{H}(CH_3)_2$]; 2.7—3.2 (m, 2H, OCH_2); 3.12 (s, 3H, N-CH_3); 5.64 (1H, s, H-7); 7.38 (1H, dd, J=8 and 5, H-3); 8.03 (1H, dd, J=8 and 2, H-4), 8.73 (1H, dd, J=5 and 2, H-2)	65.10 65.43	7.37 7.32	12.89 12.72
4g	1710	1.22 and 1.28 [6H, d+d, J=7, $CH(C\underline{H}_3)_2$]; 3.12 (3H, s, N-CH_3); 4.00 [1H, septet, J=6, $C\underline{H}(CH_3)_2$]; 5.60 (1H, s, H-7); 7.37 (1H, dd, J=8 and 5, H-3); 8.04 (1H, dd, J=8 and 2, H-4), 8.72 (1H, dd, J=5 and 2, H-2)	63.79 64.06	6.87 6.84	13.81 13.58
4h	1700	0.6—4.2 (19H, m, menthyl); 3.11 (3H, s, N-CH_3); 5.60 (1H, s, H-7); 7.36 (1H, dd, J=8 and 5, H-3); 8.03 (1H, dd, J=8 and 2, H-4); 8.66 (1H, dd J=5 and 2, H-2)	71.43 71.49	8.77 8.67	9.19 9.26
	$[\alpha]_D^{24}$=−37.9° (c=0.715, $CHCl_3$)				
4i	1710	0.6—3.7 (19H, m, menthyl); 3.16 (3H, s, N-CH_3); 5.66 (1H, s, H-7); 7.37 (1H, dd, J=8 and 5, H-3); 8.04 (1H, dd, J=6 and 2, H-4); 8.75 (1H, dd, J=5 and 2, H-2)	71.26 71.49	8.82 8.67	9.31 9.26
	$[\alpha]_D^{24}$=−91.1° (c=0.610, $CHCl_3$)				
4j	1720, 3180 (NH)	1.50 (9H, s, $C(CH_3)_3$); 6.01 (1H, s, H-7); 7.43 (1H, dd, J=8 and 5, H-3); 8.10 (1H, dd, J=8 and 2, H-4); 8.35 (1H, br, s, H-6); 8.81 (1H, dd, J=5 and 2, H-2)	64.36 64.06	6.79 6.84	13.55 13.58

Table 2. (Continued)

Compound	IR (KBr) $\nu_{C=O}$/cm^{-1}	^{1}H NMR ($CDCl_3$/TMS) δ/ppm, J/Hz	Found Calcd/% C	H	N
4k	1710	1.49 (9H, s, $C(CH_3)_3$); 3.08 (3H, s, N-CH_3); 5.71 (1H, s, H-7); 7.33 (1H, dd, J=8 and 5, H-3); 7.98 (1H, dd, J=8 and 2, H-4); 8.68 (1H, dd, J=5 and 2, H-2)	65.30 65.43	7.44 7.32	12.80 12.72
4l	1720	1.20 (9H, s, $C(CH_3)_3$); 6.16 (1H, s, H-7); 7.3—7.6 (6H, m, arom+H-3); 8.28 (1H, dd, J=8 and 2, H-4); 8.76 (1H, dd, J=5 and 2, H-2)	72.53 72.32	6.51 6.43	9.71 9.92
5a	1720	2.23 (3H, s, CH_3); 5.89 (1H, s, H-7); 6.9—7.6 (6H, m, arom+NH+H-3); 7.95 (1H, dd, J=8 and 2, H-4); 8.87 (1H, dd, J=5 and 2, H-2)	65.84 65.60	4.75 4.72	10.64 10.93
6a	1710, 3400 (NH), 1130 (S=O), 1320 (S=O)	(DMSO-d_6) 6.39 (1H, s, H-7); 7.4—7.7 (6H, m, arom+H-3), 7.94 (1H, dd, J=8 and 2, H-4); 8.82 (1H, dd, J=5 and 2, H-2); 9.96 (1H, br s, NH)	57.07 56.93	3.69 3.67	10.22 10.21
6b	1710, 1160 (S=O), 1330 (S=O)	3.46 (3H, s, CH_3), 5.62(1H, s, H-7); 7.2—7.6 (6H, m, arom+H-3); 7.80 (dd, 1H, J=8 and 2, H-4); 8.81 (1H, dd, J=5 and 2, H-2)	58.35 58.32	4.14 4.19	9.71 9.72
7a	1250 (P=O), 1710	1.28 (6H, dt, J=8 and 2, CH_3×2); 3.9—4.5 (4H, m, CH_2×2); 5.19 (1H, d, J=15, H-7); 7.50 (1H, dd, J=8 and 5, H-3); 8.24 (1H, dd, J=8 and 1, H-4); 8.76 (1H, br s, NH); 8.88 (1H, dd, J=5 and 1, H-2)	48.79 48.89	5.63 5.60	10.60 10.37
7b	1250 (P=O), 1720	1.30 (6H, dt, J=8 and 8, CH_3×2); 3.39 (3H, s, CH_3), 4.0—4.5 (4H, m, CH_2×2); 4.88 (1H, d, J=15, H-7); 7.43 (1H, dd, J=8 and 5, H-3); 8.18 (1H, dd, J=8 and 1, H-4); 8.82 (1H, dd, J=5 and 1, H-2)	50.64 50.71	6.08 6.03	10.07 9.86
8a	1690, 3320 (NH)	2.15 (2H, br s, NH_2); 5.92 (1H, s, H-7); 7.1—7.7 (6H, m, arom+H-3); 8.12 (1H, dd, J=8 and 2, H-4); 8.77 (1H, dd, J=5 and 2, H-2)	69.43 69.32	5.05 4.92	18.33 18.65
8b	1720, 3180 (NH)	0.90 (3H, t, J=7, $NCH_2CH_2C\underline{H}_3$); 1.2—1.8 (2H, m, $NCH_2C\underline{H}_2CH_3$); 2.08 (1H, br s, NH); 2.4—2.9 (2H, m, $NC\underline{H}_2CH_2CH_3$), 5.56 (1H, s, H-7); 7.48 (1H, dd, J=8 and 2, H-3); 7.93 (1H, br s, H-6); 8.17 (1H, dd, J=8 and 2, H-4); 8.83 (1H, dd, J=5 and 2, H-2)	62.77 62.80	6.85 6.85	22.22 21.97
8c	1680, 3400 (NH)	0.85 (3H, t, J=6, $NCH_2C\underline{H}_2CH_3$); 1.45 (2H, sextet, J=6, $NCH_2C\underline{H}_2CH_3$); 2.0—2.5 (3H, m, NH+$NC\underline{H}_2CH_2CH_3$); 3.13 (3H, s, N-$CH_3$); 5.23 (1H, s, H-7); 7.37 (1H, dd, J=8 and 5, H-3); 8.06 (1H, dd, J=8 and 2, H-4); 8.72 (1H, dd, J=5 and 2, H-2)	64.38 64.37	7.49 7.37	20.31 29.47
8d	1700, 3320 (NH)	0.4—3.0 (8H, m, $NHCH_2CH_2CH_3$); 6.04 (1H, s, H-7), 7.1—7.8 (6H, m, arom+H-3); 8.16 (1H, dd, J=8 and 2, H-4); 8.81 (1H, dd, J=5 and 2, H-2)	72.23 71.89	6.45 6.41	15.54 15.72
8e	1680, 3300 (NH)	0.7—1.0 (3H, m, $NCH_2CH_2CH_2C\underline{H}_3$); 1.1—1.6 (4H, m, $NCH_2C\underline{H}_2C\underline{H}_2CH_3$); 2.18 (1H, br s, NH); 2.2—2.5 (2H, m, $NC\underline{H}_2CH_2CH_2CH_3$), 3.14 (3H, s, N-$CH_3$); 5.24 (1H, s, H-7); 7.38 (1H, dd, J=8 and 5, H-3); 8.08 (1H, dd, J=8 and 2, H-4); 8.74 (1H, dd, J=5 and 2, H-2)	65.61 65.73	7.93 7.81	19.50 19.16
8f	1690	1.3—1.7 [6H, m, CH_2×3(piperidino)]; 2.3—3.0 [4H, m, CH_2×2(piperidino)]; 3.13 (3H, s, NCH_3); 5.01 (1H, s, H-7); 7.36 (1H, dd, J=8 and 5, H-3); 8.06 (1H, dd, J=8 and 2, H-4); 9.71 (1H, dd, J=5 and 2, H-2)	67.59 67.51	7.49 7.41	18.50 18.17
8g	1680, 3300 (NH)	1.34 (9H, s, $C(CH_3)_3$); 3.11 (3H, s, N-CH_3); 5.22 (1H, s, H-7); 7.34 (1H, dd, J=8 and 5, H-3); 8.02 (1H, dd, J=8 and 2); 8.70 (1H, dd, J=5 and 2, H-2, H-4)	65.53 65.73	7.84 7.81	19.34 19.16
8h	1690	1.08 [6H, t, $N(CH_2C\underline{H}_3)_2$]; 2.4—3.0 [4H, m, $N(C\underline{H}_2CH_3)_2$]; 3.11 (3H, s, N-$CH_3$), 5.22 (1H, s, H-7); 7.36 (1H, dd, J=8 and 5, H-3); 8.07 (1H, dd, J=8 and 2, H-4); 8.71(1H, dd, J=5 and 2, H-2)	65.41 65.73	7.87 7.81	19.44 19.16

representative results are shown in Tables 1 and 2.

Acyliminium cations generated from **1a**—**c** in boiling trifluoroacetic acid (Method A) smoothly reacted with active methylene compounds such as a keto ester and diketones to yield the corresponding 7-substituted derivatives **2a**—**e** quantitatively. In the case of the keto ester (ethyl acetoacetate), the ^{1}H NMR of the crude product indicated existence of two diastereomers, but only one diastereomer was obtained after recrystallization and characterized. In contrast with the diketone and keto ester, diethyl malonate was inactive under the reaction condition, probably due to the lower concentration of the enol-form compared to the keto ester and diketone. Unfortunately, our further attempts to cause the substitution reaction under severer acidic conditions with sulfuric acid[9] or aluminum trichloride[9] and a basic condition with the enolate anion[10] of diethyl malonate resulted in the formation of a complex mixture.

Although our effort to introduce a 7-alkenyl substituent by the reaction of alkenes with the acyliminium cation resulted in the formation of a complex mixture, aromatic compounds cleanly underwent an electrophilic substitution reaction with the acyliminium cation to furnish the corresponding 7-aryl substituted product **3**. Thus, when dimethoxybenzenes and anisole which are activated for the electrophilic substitution reaction were treated with **1a**—**c** under the reaction condition of Method A, the corresponding products **3a**—**f** were obtained in reasonable to excellent yields. On the other hand, a deactivated aromatics, bromobenzene required a strong acid such as concd sulfuric acid (Method B) for the preparation of products **3g**—**j** as well as the case of benzene itself.[8c] In contrast to the completely regioselective formation of the 3,4-isomer with 1,2-dimethoxybenzene, anisole, and bromobenzene afforded a mixture of ortho and para isomers. These isomers were separated by recrystallization and column chromatography and their regiochemistries were determined by ^{1}H NMR.[12]

The reaction of **1** with primary and secondary alcohols in the presence of a catalytic amount of *p*-toluenesulfonic acid (Method C) gave the corresponding 7-alkoxy products **4a**—**g** in quantitative yields. In the case of an optically active alcohol, *l*-menthol, a mixture of the corresponding diastereomers (**4h** and **4i**, diastereomeric excess=0), which was separable by column chromatography, was produced in a high chemical yield. Some 7-sulfur-atom-substituted derivatives were also prepared by the acid-catalyzed reaction in good yields. Thus, the reaction of **1** with *p*-toluenethiol in the presence of catalytic amount of *p*-toluenesulfonic acid in boiling acetonitrile (Method D) gave **5a**. Furthermore, a similar treatment with benzenesulfinic acid which was generated with sodium benzenesulfinate and *p*-toluenesulfonic acid (Method E) led to the formation of **6a,b**. However, the acid-catalyzed reaction with *t*-butyl alcohol gave only a low yield (20%) of the corresponding product because of the equilibrium between the substrate and the product in the presence of water. We could overcome this problem by the conversion of the hydroxyl group of the lactam to an excellent leaving group such as trifluoroacetate in the absence of water. Thus, the treatment of **1a**—**c** with trifluoroacetic anhydride followed by the addition of *t*-butyl alcohol (Method F) led to the formation of **4j**—**l** in high yields. This improved method was also effective for an Arbuzov type of reaction of **1a,b** with triethyl phosphite (Method G) to give the corresponding products **7a,b** which could not be obtained by the *p*-toluenesulfonic acid-catalyzed or non-catalyzed reaction. Even though the trifluoroacetylated intermediate could not be isolated due to its lability, the trifluoroacetylation procedure complements existing methods for the generation of the acyliminium cation.

N-Phenylated lactam **1c** was cleanly aminated to **8a** by heating in liquid ammonia (Method H) as shown in the previous report with *N*-unsubstituted **1a**,[8b] while *N*-methylated **1b** gave only a trace amount of the corresponding product under the same reaction conditions. Similarly, treatment of **1a**—**c** with propylamine in boiling dioxane (Method I) led to **8b**—**d** but almost all amount of **1b** was again recovered under these reaction conditions. This remarkable substituent effect suggests that an electron-donating group such as methyl group at N-6 position precludes the ring opening of the hydroxylactam depicted in Scheme 1 (Path b). The electronic effect of substituents (H, Me, and Ph) at N-6 position is consistent with chemical shifts of H-7 of **1a**—**c**; in DMSO-d_6 δ=5.72 (**1b**), 5.82 (**1a**), and 6.44 (**1c**). However, the present data can not exclude a possibility that *N*-unsubstituted lactam **1a** undergoes the elimination of water instead of the ring opening, followed by the addition of an amine (Scheme 2). As also expected from the reaction mechanism in Path b which would involve the formation of a Schiff base, secondary amines

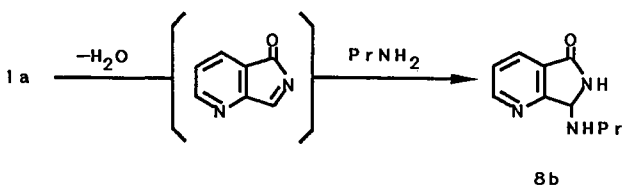

Scheme 2.

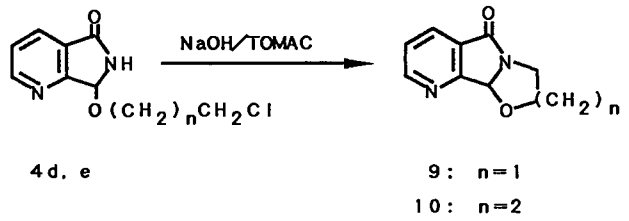

Scheme 3.

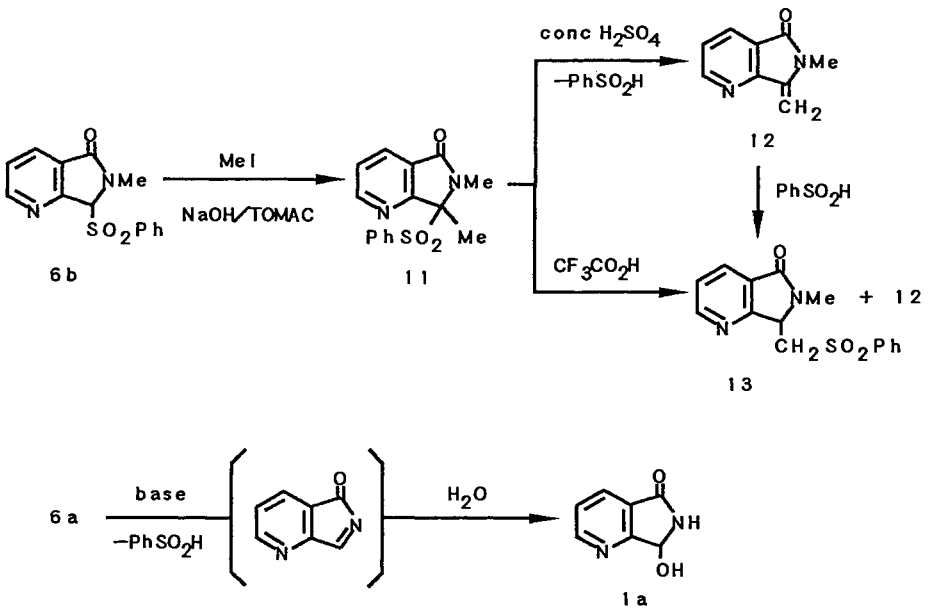

Scheme 4.

were inactive for the hydroxylactam under the basic reaction condition of Method I. Interestingly, the addition of a catalytic amount of *p*-toluenesulfonic acid in the reaction system (Method J) remarkably accelerated the rate of the reaction with primary and secondary amines to give **8b**—**f** in excellent yields, probably due to the generation of the acyliminium cation. As far as we know, it is the first example of acid-catalyzed amination of hydroxylactams. However, Method J was unsatisfactory for bulky amines such as diethylamine and *t*-butylamine resulting in low yields of the products (<36%). After examining reaction conditions, we found an effective way similar to Method G, that is the treatment of the bulky amine with the solution of **1b** in trifluoroacetic anhydride (Method K) affording **8g**,**h**, quantitatively. It is noteworthy that Methods J and K might be the fruitful methods for the preparation of alkylaminolactam **8** from hydroxylactam **1**.

Since various types of novel 7-substituted derivatives **2**—**8** have become available, we are now attracted to the synthetic application of these compounds. Previously, we reported a convenient alkylation of the 7-phenyl derivative at the 7-position in a phase transfer system, which involved synthesis of some fused cyclic derivatives, to demonstrate a synthetic utility of the 7-substituted derivative.[8b] Thus, we preliminarily tried to expand this methodology as follows: Compounds **4d** and **4e** having a terminal electrophilic carbon cleanly cyclized intramolecularly in the presence of NaOH-powder and trioctylmethylammonium chloride (TOMAC) to tricyclic products **9** and **10**, respectively (Scheme 3). 7-Sulfonylated **6b** having an active methine proton (H-7) was smoothly reacted with methyl iodide in the liquid–solid phase transfer system to give the 7-methylated product **11** in a good yield. Interestingly, compound **11** underwent the elimination of sulfinic acid in concd sulfuric acid to produce 7-methylene derivative **12** (Scheme 4). Recently, a similar elimination reaction has been observed by Hitching and Vernon with a 7-benzyl-7-hydroxy derivative.[6] Although this unstable and strongly fluorescent product could not be purified for the elemental analysis, spectroscopic data support the structure **12** and this method seems to be a useful way for the synthesis of 7-alkylidene derivatives. When compound **11** was treated with trifluoroacetic acid, 7-sulfonylmethyl derivative **13** was isolated (42%) along with **12** (36%) (Scheme 4). It is easily envisaged that this rearrangement product **13** was produced via elimination product **12**. In fact, **12** underwent the addition reaction with benzenesulfinic acid in trifluoroacetic acid to provide **13**. In contrast with 6-substituted **6b**, 6-unsubstituted **6a** could not be alkylated due to the elimination of sulfinic acid in the presence of NaOH followed by the addition of water resulting the 7-hydroxy derivative **1a** (Scheme 4).

In summary, novel 7-substituted derivatives **2**—**8** were obtained from 7-hydroxy derivative **1** by Methods A—K and some synthetic applications of the products were demonstrated.

Experimental

Measurements. Melting points are uncorrected. ^1H NMR spectra at 90 MHz were recorded with Hitachi R-22. IR spectra were recorded with Hitachi 295. Mass spectra were recorded with Hitachi M-2000. Optical rotations were measured with JASCO DPI-181. Elemental analysis were determined with Yanagimoto MT-3.

Materials. All reagents were obtained from Nacalai Tesque, Inc., Wako Pure Chemical Industries Ltd., Tokyo Kasei Co., Ltd., or Aldrich Chemical Co. The reagents were

used without further purification.

6-Substituted and Unsubstituted 6,7-Dihydro-7-hydroxy-5*H*-pyrrolo[3,4-*b*]pyridin-5-ones (1a—c). These compounds were prepared according to an earlier reported procedure.[8a]

Ethyl 2-(6-Substituted and Unsubstituted 6,7-Dihydro-5-oxo-5*H*-pyrrolo[3,4-*b*]pyridin-7-yl)-3-oxobutanoates (2a—b), 3-(6,7-Dihydro-6-methyl-5-oxo-5*H*-pyrrolo[3,4-*b*]pyridin-7-yl)-2,4-pentanedione (2c), 2-(6-Substituted 6,7-Dihydro-5-oxo-5*H*-pyrrolo[3,4-*b*]pyridin-7-yl)-1,3-diphenyl-1,3-propanediones (2d—f), and 6-Substituted and Unsubstituted 7-Aryl-6,7-dihydro-5*H*-pyrrolo[3,4-*b*]pyridin-5-ones (3a—f). General Procedure, Method A: A solution of **1** (1 mmol) and an active methylene compound or an aromatic compound (20 mmol) in trifluoroacetic acid (1 ml) was refluxed with stirring for 0.5—6 h. The reaction mixture was poured into ice-water, neutralized with solid Na_2CO_3 to pH 8 and extracted with $CHCl_3$ (10 ml×3). The organic layer was washed with water, dried over Na_2SO_4, and evaporated. The residue was further purified over a silica-gel column (Wako-gel C-200, $CHCl_3$ as eluent) to afford the product which was purified by recrystallization (Table 1). Recrystallization of a mixture of ortho and para isomers obtained by using anisole gave the pure para isomer **3f**. The ortho isomer was not isolated.

3g—3j General Procedure, Method B: To a solution of **1** (1 mmol) in concd sulfuric acid (1 ml), bromobenzene (20 mmol) was added under argon. The heterogeneous mixture was vigorously stirred at r. t. for 1—3 h. After a work-up similar to that in Method A, the mixture of the corresponding para and ortho isomer was separated by column chromatography (Wako-Gel C-200, AcOEt as eluent) to isomerically pure product which was further purified by recrystallization (Table 1).

6-Substituted and Unsbstituted 6,7-Dihydro-7-alkoxy-5*H*-pyrrolo[3,4-*b*]pyridin-5-ones (4a—i). General Procedure, Method C: A mixture of **1** (1 mmol), *p*-toluenesulfonic acid monohydrate (0.1 mmol), and an alcohol (20 mmol) was heated at 65—110 °C, if necessary under reflux, for 0.2—8 h. After evaporation of the excess alcohol under reduced pressure, water (10 ml) was added to the residue. The resulting mixture was basified with solid $NaHCO_3$ to pH 9 and extracted with $CHCl_3$ (10 ml×3). The organic layer was washed with water, dried over Na_2SO_4 and evaporated to give the product which was purified by recrystallization (Table 1). Optically pure diastereomers were obtained from the mixture of diastereomers, which were produced by the reaction with *l*-menthol, by column chromatography [Wako-gel C-200, hexane–AcOEt (5 : 4 v/v) as eluent] and recrystallization.

4j—l. General Procedure, Method F: A mixture of **1** (1 mmol) and trifluoroacetic anhydride (0.5 ml) was stirred for 20 min under nitrogen. The excess trifluoroacetic anhydride and the resulting trifluoroacetic acid were removed under reduced pressure, followed by addition of *t*-butyl alcohol (2 ml). After 5 min, the mixture was quenched with aqueous $NaHCO_3$ (saturated, 5 ml) and extracted with $CHCl_3$ (10 ml×3). The organic layer was washed with water, dried over Na_2SO_4, and evaporated to give the product which was purified by recrystallization (Table 1).

6,7-Dihydro-7-(*p*-tolythio)-5*H*-pyrrolo[3,4-*b*]pyridin-5-one (5a). Method D: A solution of **1a** (1 mmol), *p*-toluenethiol (1.1 mmol) and *p*-toluenesulfonic acid (0.05 mmol) in CH_3CN (10 ml) was refluxed for 3.5 h. After $NaHCO_3$ (0.5 g) had been added to the reaction mixture, the solvent was evaporated. The residue was treated with water (10 ml) and extracted with $CHCl_3$ (10 ml×3). The organic layer was dried over Na_2SO_4 and evaporated. The residue was chromatographed (Wako-gel C-200, $CHCl_3$ as eluent) to give the product which was purified by recrystallization (Table 1).

6-Substituted and Unsubstituted 6,7-Dihydro-7-phenylsulfonyl-5*H*-pyrrolo[3,4-*b*]pyridin-5-ones (6a,b). General Procedure, Method E: Hydroxylactam **1** (1 mmol) was added to benzenesulfinic acid generated from sodium benzenesulfinate (1 mmol) and *p*-toluenesulfonic acid (1 mmol) in acetonitrile (10 ml). The resulting mixture was heated under reflux in the reaction flask connected with a dehydration column involving Na_2SO_4. After 2 h, an additional amount of benzenesulfinic acid (0.5 mmol) was supplied and further heating was continued for 3 h. After cooling to r. t., the reaction mixture was basified with $NaHCO_3$ (0.2 g) and evaporated. The residue was treated with water (10 ml) and extracted with $CHCl_3$ (10 ml×3). The combined extract was washed with water, dried (Ns_2SO_4), and evaporated. The residue was chromatographed (Wako-gel C-200, AcOEt) to give the product which was purified by recrystallization (Table 1).

6-Substituted and Unsubstituted Diethyl 6,7-Dihydro-5-oxo-5*H*-pyrrolo[3,4-*b*]pyridin-7-ylphosphonate (7a,b). General Procedure, Method G: A mixture of **1** (1 mmol) and trifluoroacetic anhydride (2 ml) was stirred for 20 min under nitrogen. After the excess trifluoroacetic anhydride and the resulting trifluoroacetic acid were removed under reduced pressure, triethyl phosphite (2 mmol) in $CHCl_3$ (3 ml) was added to the residue and the resulting mixture was stirred for 4 h. The reaction mixture was quenched with aqueous $NaHCO_3$ (saturated, 20 ml) and extracted with $CHCl_3$ (10 ml×3). The organic layer was washed with water, dried over Na_2SO_4, and evaporated. The residue obtained was chromatographed (Wako-gel C-200, AcOEt as eluent) to give the product which was purified by recrystallization (Table 1).

7-Amino-6,7-dihydro-6-phenyl-5*H*-pyrrolo[3,4-*b*]pyridin-5-one (8a). Method H: A solution of **1c** (1 mmol) in liquid ammonia (20 ml) was heated in an autoclave at 110 °C for 12 h. After the evaporation of ammonia at r. t., the residue was chromatographed (Wako-gel C-200, $CHCl_3$ as eluent) to give the product which was purified by recrystallization (Table 1).

6-Substituted and Unsubstituted 7-Alkylamino-6,7-dihydro-5*H*-pyrrolo[3,4-*b*]pyridin-5-ones (8b—f). General Procedure, Methods I and J: A solution of **1** (1 mmol), an amine (1.5 ml), and *p*-toluenesulfonic acid [none (Method I) or 0.2 mmol (Method J)] in dioxane (3 ml) was refluxed for 3—24 h. After addition of water (5 ml), the resulting mixture was extracted with $CHCl_3$ (10 ml×3). The organic layer was washed with water and dried over Na_2SO_4. Evaporation of organic solvent from the extract gave the product which was purified by recrystallization (Table 1).

8g—h. General Procedure, Method K: To a solution of **1b** (1 mmol) in trifluoroacetic anhydride (1 ml), an amine (2 ml) was added at 0 °C under nitrogen. A work-up similar to that in Method I afforded the product which was purified by recrystallization (Table 1).

2,3,5,9b-Tetrahydro[1,3]oxazolo[3′,2′:1,2]pyrrolo[3,4-*b*]-pyridin-5-one (9) and 3,4,6,10b-Tetrahydro-2*H*-pyrido[2′,3′:3,4]pyrrolo[2,1-*b*][1,3]oxazin-6-one (10). A mixture of **4d** (0.5 mmol), trioctylmethylammonium chloride (0.05 mmol), and NaOH-powder (0.25 g) in benzene (10 ml) was stirred under nitrogen at r. t. for 40 min. After addition of dichloromethane (10 ml) and filtration, the organic layer was dried over Na_2SO_4 and evaporated to yield **9** (96%) as colorless crystals. Similar

reaction with **4e** for 5 h gave **10** (90%) as colorless crystals.

9: Mp 102 °C (from EtOH); ^{1}H NMR ($CDCl_3$) δ=3.3—4.5 (4H, m, CH_2CH_2), 5.81 (1H, s, H-7), 7.45 (1H, dd, J=8 and 5 Hz, H-3), 8.08 (1H, dd, J=8 and 2 Hz, H-4), 8.80 (1H, dd, J=5 and 2 Hz, H-2); IR (KBr) 1720 cm^{-1} (C=O); MS (70 eV) m/z 176(M^+). Found: C, 61.30; H, 4.55; N, 16.14%. Calcd for $C_9H_8N_2O_2$: C, 61.36; H, 4.57; N, 15.90%.

10: Mp 104—105 °C (from AcOEt); ^{1}H NMR ($CDCl_3$) δ=1.5—2.2 (2H, m, CH_2), 3.1—4.7 (4H, m, CH_2×2), 5.60 (1H, s, H-7), 7.48 (1H, dd, J=8 and 5 Hz, H-3), 8.17 (1H, dd, J=8 and 2 Hz, H-4), 8.80 (1H, dd, J=5 and 2 Hz, H-2); IR (KBr) 1690 cm^{-1} (C=O); MS (20 eV) m/z 176 (M^+−14). Found: C, 63.01; H, 5.35; N, 14.79%. Calcd for $C_{10}H_{10}N_2O_2$: C, 63.14; H, 5.31; N, 14.73%.

6,7-Dihydro-6,7-dimethyl-7-phenylsulfonyl-5*H*-pyrrolo[3,4-*b*]pyridin-5-one (11). Into a mixture of **6b** (2 mmol), trioctylmethylammonium chloride (3 mmol), and benzene (10 ml, saturated with argon) was added NaOH-powder (1 g) under argon with vigorous stirring. When MeI (10 mmol) was added to the resulting dark red suspension, the color disappeared and the stirring was continued for 30 min. After addition of dichloromethane (20 ml), the reaction mixture was filtered and evaporated. The residue was recrystallized from AcOEt to yield **11** (89%) as colorless crystals: Mp 145—146 °C (from AcOEt); ^{1}H NMR ($CDCl_3$) δ=2.13 (3H, s, CH_3), 3.32 (3H, s, CH_3), 7.1—7.5 (6H, m, arom+H-3), 7.70 (1H, dd, J=8 and 2 Hz, H-4), 8.80 (1H, dd, J=5 and 2 Hz, H-2); IR (KBr) 1150 (S=O), 1300 (S=O), and 1720 cm^{-1} (C=O); MS (70 eV) m/z 161 (M^+−141). Found: C, 59.69; H, 4.66; N, 9.05%. Calcd for $C_{15}H_{14}N_2O_3S$: C, 59.59; H, 4.67; N, 9.27%.

6,7-Dihydro-6-methyl-7-methylene-5*H*-pyrrolo[3,4-*b*]-pyridin-5-one (12). A mixture of **11** (1 mmol) and concd sulfuric acid was stirred at r. t. for 30 min. The reaction mixture was poured into ice-water, neutralized with solid Na_2CO_3 to pH 9, and extracted with $CHCl_3$ (10 ml×3). The extracts were washed with water, dried over Na_2SO_4 and evaporated. The residue obtained was chromatographed (Wako-gel C-200, AcOEt as eluent) to give the product **12** (86%): Mp 77 °C (decomp); ^{1}H NMR ($CDCl_3$) δ=3.31 (3H, s, CH_3), 4.94 and 5.67 (2H, d+d, J=2 Hz, =CH_2), 7.39 (1H, dd, J=8 and 5 Hz, H-3), 8.08 (1H, dd, J=8 and 2 Hz, H-4), 8.73 (1H, dd, J=5 and 2 Hz, H-2); IR (KBr) 1650 (C=C) and 1720 cm^{-1} (C=O); MS (70 eV) m/z 160 (M^+).

6,7-Dihydro-6-methyl-7-phenylsulfonyl-5*H*-pyrrolo[3,4-*b*]-pyridin-5-one (13). A solution of **1b** (0.5 mmol) in trifluoroacetic acid (2 ml) was stirred at r. t. for 1 d. The reaction mixture was quenched with ice-water, neutralized with solid Na_2CO_3, and extracted with $CHCl_3$ (10 ml×3). The organic layer was washed with water, dried over Na_2SO_4 and evaporated. The residue obtained was chromatographed (Wako-gel C-200, AcOEt as eluent) to give **12** (36%) and **13** (42%) as colorless crystals. Alternatively, into a solution of **12** (0.5 mmol) in trifluoroacetic acid (2 ml) was added sodium benzenesulfinate (4 mmol). After 4 h, a similar work-up gave **13** (62%) as colorless crystals: Mp 132—133 °C; ^{1}H NMR ($CDCl_3$) δ=3.19 (3H, s, CH_3), 3.66 (1H, dd, J=16 and 6 Hz, SO_2CH), 4.02 (1H, dd, J=16 and 5 Hz, SO_2CH), 5.93 (1H, dd, J=6 and 5 Hz, H-7), 7.5—7.9 (6H, m, H-3+arom), 8.02 (1H, dd, J=8 and 2 Hz, H-4), 8.60 (1H, dd, J=5 and 2 Hz, H-2); IR (KBr) 1140 (S=O), 1300 (S=O), and 1700 cm^{-1} (C=O); MS (20 eV) m/z 225 (M^+−77). Found: C, 59.55; H, 4.64; N, 9.35%. Calcd for $C_{15}H_{14}N_2O_3S$: C, 59.59; H, 4.67; N, 9.27%.

The present work was partially supported by a Grant-in-Aid for Scientific Research No. 63740271 from the Ministry of Education, Science and Culture.

References

1) R. A. Barnes and J. C. Godfrey, *J. Org. Chem.*, **22**, 1038 (1957); H. von Dobeneck and B. Hansen, *Chem. Ber.*, **105**, 3611 (1972); P. Fischer, J. Fleckenstein, and J. Hones, *Photochem. Photobiol.*, **47**, 193 (1988); B. Gutkowska, Z. Kabzinska, and J. Wasiak, *Acta Pol. Pharm.*, **44**, 242 (1987); Y. Sato, T. Iwashige, and T. Miyadera, *Chem. Pharm. Bull.*, **8**, 427 (1960); Y. Sato, T. Iwashige, and T. Miyadera, Jpn. Patent Kokai 21543 (196l) [*Chem. Abstr.*, **57**, 13757g (1962)]; Y. Sato, T. Iwashige, T. Miyadera, and T. Nishimura, Jpn. Patent Kokai 7346 (1963) [*Chem. Abstr.*, **59**, 11514a (1963)]; J. Hurst and D. J. Wibberley, *J. Chem. Soc.*, **1962**, 119; J. Kuthan, L. Musil, and V. Jehlica, *Collect. Czech. Chem. Commun.*, **42**, 283 (1977); S. Kakimoto and S. Tonooka, *Bull. Chem. Soc. Jpn.*, **42**, 2996 (1969); H.-J. Sattler and W. Schunack, *Chem. Ber.*, **108**, 1003 (1975); H. Takasugi, A. Kuno, H. Sakai, and T. Tanaka, Eur. Patent Appl., EP228845 (1987) [*Chem. Abstr.*, **108**, 112475p (1988)]; A. A. A. Elbannany and L. L. Ibrahim, *Heterocycles*, **26**, 2323 (1987); G. J. Hitchings and J. M. Vernon, *J. Chem. Soc., Chem. Commun.*, **1988**, 623; B. Hansen and N. von Dobeneck, *Chem. Ber.*, **105**, 3630 (1972); A. N. Kost, L. Zukauskaite, and A. Stankevicius, U. S. S. R. Patent 311913 (1971) [*Chem. Abstr.*, **75**, 151672v (1971)]; L. Zukauskaite, A. Stankevicius, and A. N. Kost, *Khim. Geterotsikl. Soedin.*, **1978**, 63; M. Wozniak, H. C. van der Plas, and S. Harkema, *J. Org. Chem.*, **50**, 3435 (1985); H. Nagao, Y. Nawata, and M. Hamana, *Chem. Pharm. Bull.*, **35**, 4068 (1987); P. J. Obrecht, P. Schoenholzer, and C. J. Jenny, *Helv. Chim. Acta*, **71**. 1319 (1988).

2) V. Hitzel, K. Geisen, R. Werner, and R. Guenter, Ger. Offen. 2948522 (1981) [*Chem. Abstr.*, **95**, 150632h (1981)].

3) J. L. Challier, C. Jeanmart, and M. N. Messer, Ger. Offen. , 2251559 (1973) [*Chem. Abstr.*, **79**, 32100e (1973)]; C. Cotrel, C. Crisan, C. Jeanmart, and M. N. Messer, Ger. Offen. 2423650 (1974) [*Chem. Abstr.*, **82**, 112103k (1975)]; C. Cotrel, C. Crisan, C. Jeanmart, and M. N. Messer, Fr. Demande 2263752 (1975) [*Chem. Abstr.*, **84**, 121901n (1976)]; C. Cotrel, C. Crisan, C. Jeanmart, and A. Leger, Ger. Offen. 2165067 (1976) [*Chem. Abstr.*, **86**, 43743n (1977)].

4) G. Goto and Y. Saji, Jpn. Pataent Kokai JP61130290 (1987) [*Chem. Abstr.*, **106**, 33014t (1987)].

5) D. Duerr, H. G. Brunner, and H. Szczepanski, U. S. Patent US4721522 (1988) [*Chem. Abstr.*, **109**, 170430b (1988)].

6) G. J. Hitchings and J. M. Vernon, *J. Chem. Soc., Perkin Trans 1*, **1990**, 1757.

7) R. Sato, T. Senzaki, Y. Shikazaki, T. Goto, and M. Saito, *Chem. Lett.*, **1984**, 1423; R. Sato, T. Senzaki, T. Goto, and M. Saito, *ibid.*, **984**, 1599; R. Sato, T. Senzaki, T. Goto, and M. Saito, *Bull. Chem. Soc. Jpn.*, **59**, 2950 (1986); R. Sato, K. Oikawa, T. Goto, and M. Saito, *Bull. Chem. Soc. Jpn.*, **61**, 2238; R. Sato, M. Ohmori, F. Kaitani, A. Kurosawa, T. Senzaki, T. Goto, and M. Saito, *Bull. Chem. Soc. Jpn.*, **61**, 2481 (1988); R. Sato, H. Endo, A. Abe, S. Yamaichi, T. Goto, and M. Saito, *Bull. Chem. Soc. Jpn.*, **63**, 1160 (1990).

8) a) T. Goto,.M. Konno, M. Saito, and R. Sato, *Bull. Chem. Soc. Jpn.*, **62**, 1205 (1989); b) T. Goto, M. Saito, and R. Sato, *Bull. Chem. Soc. Jpn.*, **60**, 4178 (1987); c) T. Goto, M. Endo, M. Saito, and R. Sato, *Bull. Chem. Soc. Jpn.*, **63**, 3047

(1990).

9) Reviews: H. E. Zaugg and W. B. Martin, "Organic Reactions," ed by A. C. Cope, John Wiley & Sons, Inc., New York (1965), Vol. 14, pp. 52—269; H. E. Zaugg, *Synthesis,* **1970**, 49; *ibid.,* **1984**, 85 and 181; W. N. Speckamp, *Recl. Trav. Chim. Pays-Bas,* **100**, 345 (1981); W. N. Speckamp and H. Hiemstra, *Tetrahedron,* **41**, 4367 (1985).

10) J. J. J. de Boer and W. N. Speckamp, *Tetrahedron Lett.,* **1975**, 4039.

11) R. S. Mari and S. N. Yeola, *Synthesis,* **1986**, 755.

12) P. L. Barili and V. Scartoni, *J. Heterocycl. Chem.,* **22,** 1199 (1985).

 © 1991 The Chemical Society of Japan Bull. Chem. Soc. Jpn., 64, 1911—1915 (1991)

Prediction of Product-Selectivity in an Electroorganic Process by Mathematical Modeling of Reaction Mechanism. A Rotating Cylinder Electrode System

Po-Chung CHENG, Tsutomu NONAKA,* and Tse-Chuan CHOU†
Department of Electronic Chemistry, Graduate School at Nagatsuta, Tokyo Institute of Technology, 4259 Nagatsuta, Midori-ku, Yokohama 227
†Department of Chemical Engineering, National Cheng-Kung University, Tainan, Taiwan, Republic of China
(Received January 27, 1991)

A mathematical mechanism model is developed for the electroreduction of carbonyl compounds in an acidic solution and shows that the formation ratio of hydrodimeric to hydromonomeric products, i.e. the product-selectivity, depends on substrate concentration, mass transfer coefficient and current density. Model calculations are in agreement with experimental results from the electroreduction of *p*-methylbenzaldehyde using a rotating cylinder cathode and explain a drastic effect of mass transport on the product-selectivity.

Product-selectivity control has been a significant subject in electroorganic synthesis. Saveant and coworkers[1-8] extensively studied modes of product distribution in preparative scale electrolysis from a theoretical aspect, but only few experimetal approaches were insufficiently made.[4-6] Wendt[9] also suggested an importance of mass transport in the product distribution of electroorganic processes with few experimental data. On the other hand, some other workers[10-13] reported experimental results that product-selectivity and/or yield were influenced by mass transport, without any theoretical considerations. For purposively designing practical electroorganic processes on the basis of prediction of product-selectivity, it is recommended that studies are harmoniously made from both theoretical and experimental aspects.

Recently we also reported that the ratio of hydrodimeric to hydromonomeric products in the electroreduction of carbonyl compounds, e.g. benzaldehyde and acetophenone, could be varied drastically by controlling mass transport conditions, such as substrate concentration, flow rate in a parallel plate flow cell and rotating speed of a rotating cylinder electrode.[14] Thus, it is aimed in this work to evaluate the product-selectivity by mathematical modeling and demonstrate how the product-selectivity can be controlled.

However, considerable hydrogen evolution[15] and formation of hydroquinonoid-dimers[16-18] in the reduction of acetophenone and benzaldehyde, respectively, might make very difficult the mathematical analysis of reaction model. In this work, therefore, *p*-methylbenzaldehyde was used as a starting compound which has an adequately low reduction potential and is blocked by a methyl group at the *p*-position to be prevented from the formation of the hydroquinonoid-type dimers.[16] In fact, using *p*-methylbenzaldehyde, current efficiencies and material balances are high enough (>90%) for mathematical analysis.

In general, mass transport conditions can be controlled using either a rotating electrode batch cell or a parallel plate flow cell. Although the availability of the latter for industrial processes, of course, is much greater than the former, in this work the former was preferably used because of easier and more accurate mathematical treatment of mass transport phenomena. Furthermore, because quantitative analysis of products was required in this work, a rotating cylinder electrode with a large area was chosen instead of a rotating disc one used commonly for voltammetric studies.

Experimental

Materials. The method of Grimshaw and Ramsey[19] was employed for preparation of the hydrodimer samples: *dl*-(mp 159—160 °C, from ethanol–water) and *meso*-1,2-bis(*p*-methylphenyl)-1,2-ethanediol(mp 143—144 °C, from benzene). All other reagents used were analytical GR grade without further purification.

Electrolytic Cell. The cathode was a Pb solid cylinder, 5 cm in length and 0.5 cm in diameter. The cylindrical Pb sheet anode, 6.5 cm in depth and 5.6 cm in diameter, was separated from the cathode by a ceramic diaphragm in a beaker type batch cell. The rotating cathode was rotated at 250 to 1500 rpm by a variable speed motor (Yanagimoto RP-3).

Procedure. The electrolyte was 0.25 M H_2SO_4 solution containing 50% v/v ethanol, unless stated otherwise. A saturated calomel electrode was used as reference electrode and the electrolyte was deaerated with nitrogen prior to the measurement of polarization curves. For preparative electrolysis, pre-electrolysis was carried out for ca. 15 min. All the electrolyses were carried out at 25±2 °C. Throughout this paper 1 M=1 mol dm^{-3}.

Analysis. The products were routinely analysed using HPLC. The mobile phase was a mixture of acetonitrile and 0.1% aqueous phosphoric acid with a volume ratio of 30:70. The column was a Utron S-C 18 reversed-phase column (Chromato Packings Center) and peaks for the products were detected by UV absorbance at 254 nm.

Results and Discussion

The reaction mechanism for the electroreduction of aromatic carbonyl compounds depends on pH, and the generally accepted scheme in acidic media is as follows:[20]

$$\mathrm{ArCOR} + \mathrm{H^+} \rightleftarrows \mathrm{Ar\overset{+}{C}(OH)R} \qquad \text{(I)}$$

$$\mathrm{Ar\overset{+}{C}(OH)R} + e \xrightarrow{k_1} \mathrm{Ar\dot{C}(OH)R} \quad \text{(II)}$$

$$\mathrm{Ar\dot{C}(OH)R} + e \xrightarrow{k_2} \mathrm{Ar\overline{C}(OH)R} \quad \text{(III)}$$

$$\mathrm{Ar\overline{C}(OH)R} + H^+ \xrightarrow{\text{fast}} \mathrm{ArCH(OH)R} \quad \text{(IV)}$$

$$2\mathrm{Ar\dot{C}(OH)R} \xrightarrow{k_D} \mathrm{ArRC(OH)C(OH)RAr} \quad \text{(V)}$$

In order to theoretically calculate the product-selectivity, a general relationship between k_2 and k_D must be mathematically written. Thus, it is our first goal to obtain Eq. 21 along with Eqs. 10 and 22. At the second stage, for a special case Eq. 27 is obtained along with Eqs. 31 and 32.

Let X_b and X_s represent substrate X in bulk solution and at electrode surface, respectively. Thus, the mass-transfer process of ArCOR(S) and $\mathrm{Ar\overset{+}{C}(OH)R(S^*)}$ from bulk solution to electrode surface can be expressed as follows:

$$S_b \xrightarrow{k_m} S_s \quad \text{(VI)}$$

$$H^+_b \rightleftarrows H^+_s \quad \text{(VII)}$$

$$S_s + H^+_s \overset{K_s}{\rightleftarrows} S^*_s \quad \text{(VIII)}$$

$$S_b + H^+_b \overset{K_b}{\rightleftarrows} S^*_b \quad \text{(IX)}$$

$$S^*_b \xrightarrow{k_m^*} S^*_s \quad \text{(X)}$$

Recognizing that reactions VIII and IX are essentially at equilibrium, we can write

$$[S^*_b] = K_b[S_b][H^+_b], \quad (1)$$

$$[S^*_s] = K_s[S_s][H^+_s], \quad (2)$$

where K_b and K_s are the equilibrium constants between ArCOR(S) and $\mathrm{Ar\overset{+}{C}(OH)R(S^*)}$ in bulk solution and at electrode surface, respectively. In strong acidic solution, $[H^+_s]$ and $[H^+_b]$ are assumed to be constant.

The steady-state material balance for S and S* is given by

$$k_1[S^*_s] = k_m([S_b]-[S_s]) + k_m^*([S^*_b]-[S^*_s]) = i_1/F, \quad (3)$$

where k_m and k_m^* are the mass transfer coefficients of S and S*, respectively, k_1 is the rate constant for the formation of radical $\mathrm{Ar\dot{C}(OH)R}$ (R_s), i_1 is the partial current density for the primary electron-transfer reaction (Eq. II), and F is the Faraday constant.

Suppose that k_m is equal to k_m^*, Eq. 3 becomes

$$k_1^*[C_s] = k_m([C_b]-[C_s]) = i_1/F \quad (4)$$

where

$$[C_b] = [S_b] + [S^*_b],$$
$$[C_s] = [S_s] + [S^*_s],$$
$$k_1^* = k_1K_s[H^+_s]/(1+K_s[H^+_s]) = k^0_1 \exp(-b_1E).$$

b_1 and k^0_1 are the characteristic constants on the assumption of Tafel relationship, and E is electrode potential. It should be noted that $[C_b]$, substrate concentration before protonation, is readily measurable rather than $[S^*_b]$.

The radical(R) formed in the primary electron-transfer reaction then undergoes the second electron-transfer reaction (Eq. III) to form the hydromonomer ArCH(OH)R(HM) or is dimerized (Eq. V) to give the hydrodimer ArRC(OH)C(OH)RAr(HD).

$$V\mathrm{d[HM]}/A\mathrm{d}t = k_2[R_s] = i_2/F, \quad (5)$$

$$k_2 = k^0_2 \exp(-b_2E), \quad (6)$$

$$2V\mathrm{d[HD]}/A\mathrm{d}t = -D_R(\mathrm{d[R]}/\mathrm{d}x)_{x=0}, \quad (7)$$

$$D_R(\mathrm{d}^2[R]/\mathrm{d}^2x) - v_x(\mathrm{d[R]}/\mathrm{d}x) - k_D[R]^2 = 0, \quad (8\text{-a})$$

$$[R] = [R_s] \quad \text{at } x = 0, \quad (8\text{-b})$$

$$[R] = 0 \quad \text{as } x \to \infty, \quad (8\text{-c})$$

where i_2 and k_2 are the partial current density and the rate constant for the second electron transfer reaction, respectively, k_D is the rate constant for the dimerization step, A is the cathode area, V is the volume of catholyte, D_R is diffusion coefficient of R, x is the distance from electrode, and v_x is the x-component of the fluid velocity vector.

Let us neglect the second term in Eq. 8-a, then we obtain Eq. 9 after satisfying the boundary conditions.[21]

$$[R] = \frac{6D_R/k_D}{(\sqrt{6D_R/(k_D[R_s])}+x)^2}. \quad (9)$$

Substituting Eq. 9 into Eq. 7, one finds

$$2V\mathrm{d[HD]}/A\mathrm{d}t = k_3[R_s]^{3/2}, \quad (10)$$

where

$$k_3 = (2k_DD_R/3)^{1/2}.$$

Since hydrogen evolution and other side reactions are negligible, we can write

$$i = i_1 + i_2, \quad (11)$$

$$k_1^*[C_s] = k_2[R_s] + k_3[R_s]^{3/2}, \quad (12)$$

where i is the total current density of electrolysis.

From these equations a simulation for predicting the product-selectivity may be accomplished if all the rate constants are available. The product-selectivity (ζ) is herein defined by

$$\zeta = \mathrm{d[HD]}/\mathrm{d[HM]} = k_3[R_s]^{1/2}/2k_2. \quad (13)$$

The Determination of k^0_1 and b_1. Equation 4 can be rearranged as

$$i_1 = k_1^*k_m[C_b]F/(k_m+k_1^*), \quad (14)$$

or

$$1/i_k = 1/i_1 - 1/i_L,$$

where the limiting current density (i_L) and kinetic current density (i_k) are defined as

$$i_L = k_m[C_b]F, \quad (15)$$

$$i_k = k^0_1 \exp(-b_1E)[C_b]F, \quad (16)$$

or

$$\ln(i_k) = \ln(k^0_1[C_b]F) - b_1E.$$

Potentiostatic electrolysis of *p*-methylbenzaldehyde at

a potential where $i<i_L$, the hydromonomer (HM) is not found and the hydrodimer is a sole product, i.e. $i \fallingdotseq i_1$. Using experimental data from polarization curves (Fig. 1), i_k can be calculated from Eq. 14. A plot of Eq. 16 is presented in Fig. 2. The slope gives a value for b_1 of 26 V^{-1} and the intercept leads to a value for k^0_1 of 5.4×10^{-14} cm s^{-1}.

Values of k^0_2, b_2 and k_3. When the total current density is larger than i_L, i_1, and i_2 can be expressed as

$$i_1 = k_1^*[C_s]F \fallingdotseq i_L, \quad (17)$$

$$i_2 \fallingdotseq i - i_L, \quad (18)$$

Substitution of Eq. 18 into Eq. 5 gives

$$k_2[R_s] = (i-i_L)/F. \quad (19)$$

Then from Eqs. 17, 19, and 12 we obtain

$$k_3[R_s]^{3/2} = (2i_L - i)/F. \quad (20)$$

Combination of Eqs. 19 and 20 leads to

$$z = k_2^3/k_3^2 = (i-i_L)^3/F(2i_L-i)^2. \quad (21)$$

From a plot of Eq. 22 (Fig. 3) b_2 is found to be 26 V^{-1} and k^0_2 can be determined from an intercept, provided k_D and D_R are known.

$$\ln(z) = \ln(k^{0}{}_2{}^3/k_3^2) - 3b_2E. \quad (22)$$

However, any rate constant (k_D) for the dimerization in electroreduction of carbonyl compounds in acidic solutions has not been reported, while k_D in hydroxide solution is known to be in a range of 10^7—10^9 mol^{-1} s^{-1} cm^3.[21,22] Here, 10^8 mol^{-1} s^{-1} cm^3 is tentatively taken as k_D.

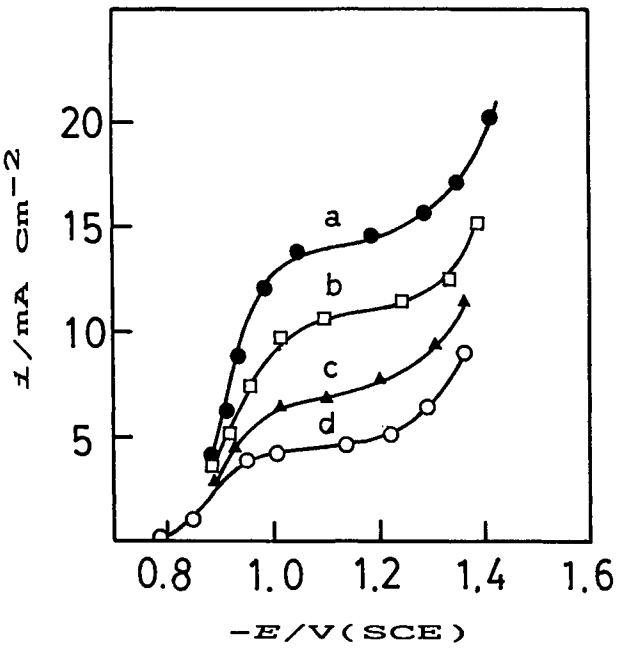

Fig. 1. Polarization curves for the reduction of *p*-methylbenzaldehyde (80 mM) at a rotating cylinder electrode in 0.25 M H_2SO_4/50% EtOH. Rotating speed, a: 1500, b: 1000, c: 500, d: 250 rpm.

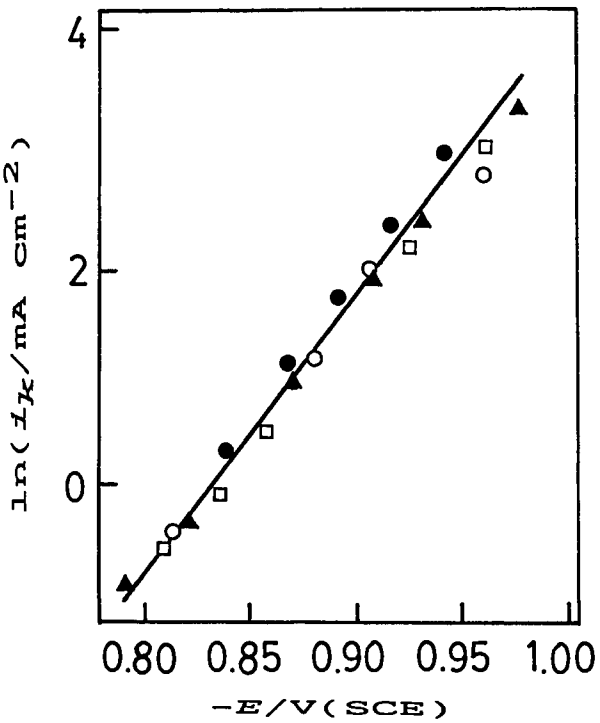

Fig. 2. The relation between i_k and E. Data from polarization curves at various rotating speed: 1500 (●), 1000 (□), 500 (△), and 250 rpm (○).

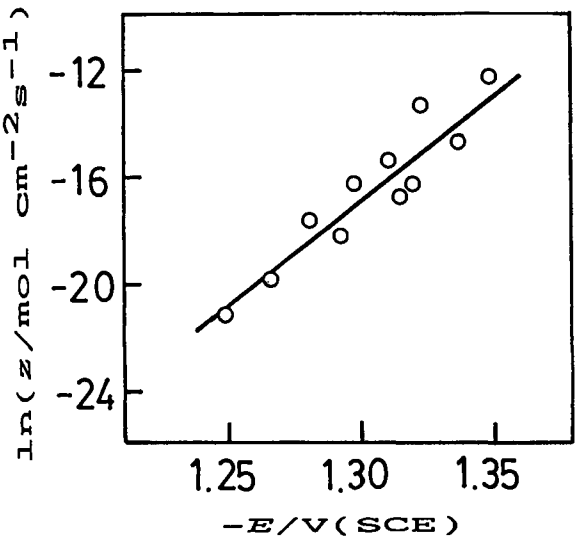

Fig. 3. The relation between $z(=k_2^3/k_3^2)$ and E. Data from polarization curves at 250 rpm.

Using Newton's method, E for a constant current operation can be solved for a set of k_m, $[C_b]$ and i, then ζ is calculated from Eqs. 4—13. Curve a in Fig. 4 shows the prediction of product-selectivity (ζ) for the galvanostatic reduction of *p*-methylbenzaldehyde at a rotating cylinder Pb electrode, using 10^{-3} cm s^{-1} as k_m, 80 mM as $[C_b]$, 10^{-5} cm^2 s^{-1} as D_R, 1.1×10^{-16} cm s^{-1} as k^0_2 and 10^8 mol^{-1} s^{-1} cm^3 as k_D. When either 10^7 or 10^9 mol^{-1}

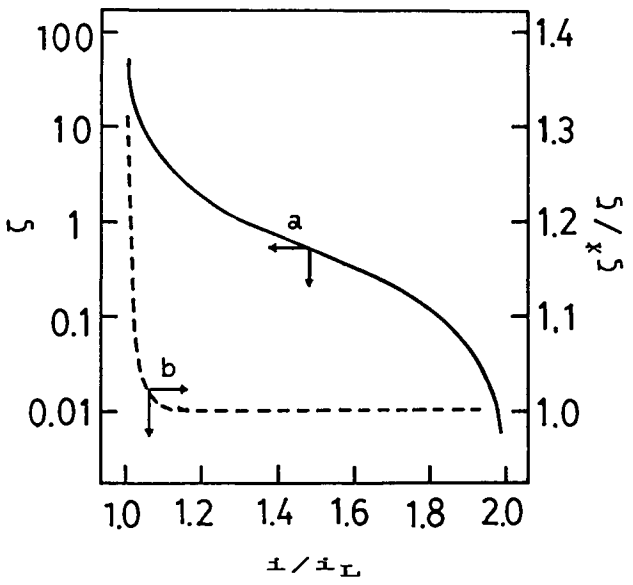

Fig. 4. Prediction of product-selectivity as a function of i/i_L. Curve a: Product-selectivity (ζ) calculated according to Eq. 4—13, using $k_1^0=5.4\times10^{-14}$ cm s^{-1}, $b_1=26$ V^{-1}, $k_2^0=1.1\times10^{-16}$ cm s^{-1}, $b_2=26$ V^{-1}, $k_D=10^8$ mol^{-1} s^{-1} cm^3, $D_R=10^{-5}$ cm^2 s^{-1}, $k_m=10^{-3}$ cm s^{-1}, $[C_b]=80$ mM. Curve b: Comparison between ζ and ζ^*.

s^{-1} cm^3 is taken as k_D, the difference of ζ from curve a is not regarded as significant for $i/i_L>1.04$.

Curve a suggests that the product-selectivity (ζ) can be drastically (ca. 10^4 times) changed by slightly (two times) varying the parameter i/i_L relating directly to mass transport. This should be noticeable from an aspect of product-selectivity control in synthetic electroorganic processes. However, an ambiguity might remain in calculation of curve a using k_D assumed. Therefore, another method, which is simpler and more convenient for predicting ζ, is developed to avoid this kind of problem. Two facts must be emphasized here: (1) When the total current density (i) is smaller than the limiting current density (i_L) of the primary electron-transfer reaction, the hydromonomer (HM) is not found and the the hydrodimer (HD) is the sole product. (2) When i exceeds the limiting current density ($2i_L$) for the two-electron reaction, the formation of HM and hydrogen evolution occur exclusively and HD is almost not formed. Hence, a mathematical evaluation for the product-selectivity is only necessary when i is between i_L and $2i_L$. In such a situation, i_1 is almost equal to i_L (Eq. 17) and Eqs. 19 and 20 are rewritten as follows:

$$V\mathrm{d[HM]}/A\mathrm{d}t=i_2/F=(i-i_L)/F, \tag{23}$$

$$V\mathrm{d[HD]}/A\mathrm{d}t=(2i_L-i)/2F. \tag{24}$$

Since i_L is a function of k_m and $[C_b]$ as presented by Eq. 15, the product-selectivity can be expressed as a function depending on the bulk concentration ($[C_b]$), total current density (i) and mass transfer coefficient (k_m),

$$\zeta^*=\mathrm{d[HD]}/\mathrm{d[HM]}=(2-i/i_L)/2(i/i_L-1)=f(k_m, [C_b], i). \tag{25}$$

Here ζ^* is used to distinguish from ζ, the product-selectivity calculated from Eq. 4—13. Curve b in Fig. 4 shows the comparison between ζ^* is and ζ. Although ζ^* is considerably larger than ζ when i/i_L is in the vicinity of unity, the difference is so small that ζ^* is almost equal to ζ when $i/i_L>1.1$. This implies that Eq. 25 can be used for predicting product-selectivity (ζ^*) in the electroreduction of carbonyl compounds, if k_m, $[C_b]$ and i are known.

For a batch electrolysis, $[C_b]$ and i_L decrease with the electrolysis time in the following ways.

$$-V\mathrm{d}[C_b]/A\mathrm{d}t=i/F \quad \text{when } i_L>i, \tag{26-a}$$

$$-V\mathrm{d}[C_b]/A\mathrm{d}t=k_m[C_b]=i_L/F \quad \text{when } i_L\leqq i. \tag{26-b}$$

Hence a relation between product-selectivity and time must be considered.

In stead of d[HD]/d[HM], the product-selectivity defined by Eq. 27 is used in the following discussion.

$$\zeta=[\mathrm{HD}]/[\mathrm{HM}]. \tag{27}$$

When $i_L>i$ at $t=0$: Let t_0 be the time that is required to decrease i_L to i, then we have

$$[C_{b,0}]=i/k_mF, \tag{28}$$

$$t_0=([C_{b,i}]-[C_{b,0}])VF/iA \tag{29}$$

where $[C_{b,i}]$ and $[C_{b,0}]$ are the substrate concentrations at $t=0$ and $t=t_0$, respectively.

Integration of Eq. 26-b gives

$$[C_b]=[C_{b,0}]\exp[-k_mA(t-t_0)/V]. \tag{30}$$

Then integration of Eq. 23 and 24, after substitution of Eq. 30 for $[C_b]$, yields:

$$[\mathrm{HM}]=iA(t-t_0)/VF-[C_{b,0}]\{1-\exp[-k_mA(t-t_0)/V]\}, \tag{31}$$

$$[\mathrm{HD}]=[C_{b,0}]\{1-\exp[-k_mA(t-t_0)/V]\}+iA(2t_0-t)/2VF. \tag{32}$$

When $i_L\leqq i$ at $t=0$: Let $t_0=0$, $[C_{b,0}]=[C_{b,i}]$, then Eqs. 31 and 32 can be applied to calculate ζ.

Prediction of ζ: Table 1 shows experimental values of the product-selectivity obtained in the galvanostatic electrolysis of *p*-methylbenzaldehyde at a rotating Pb cylinder electrode, compared with those predicted from Eqs. 27,31, and 32. Here, a dimensionless parameter, q, is used in stead of time. $q=1$ means that the charge

Table 1. Product-Selectivity (ξ) for the Reduction of *p*-Methylbenzaldehyde (Initial Concentration: 80 mM) at a Rotating Cylinder Pb Cathode

Run	ω/rpm	i/mA cm^{-2}	q[a)]	ξ_{exp}	ξ_{calcd}
1	250	5	0.2	0.9	1.0
2	250	5	0.3	0.7	0.8
3	250	5	0.4	0.6	0.7
4	500	10	0.2	0.5	0.4
5	1000	10	0.2	2.5	5.3
6	1000	10	0.4	1.9	2.1

a) $q=iAt/[C_{b,i}]VF$.

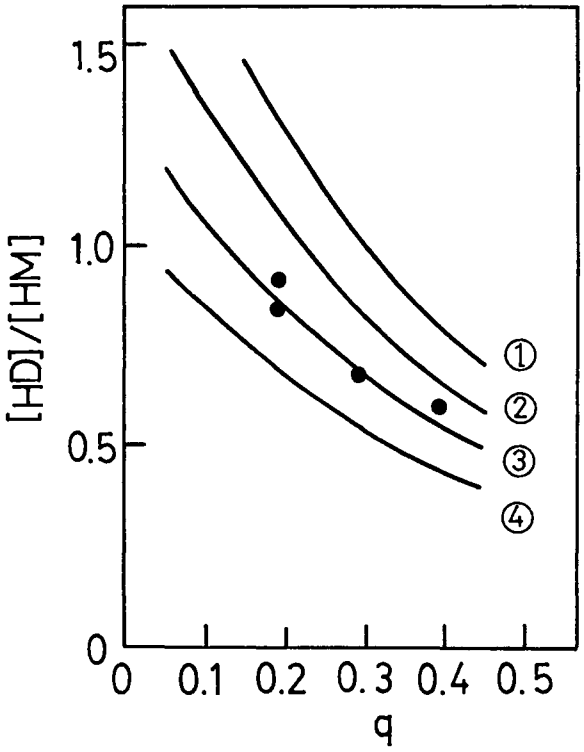

Fig. 5. Effect of charge passed ($q=iAt/[C_{b,i}]VF$) and mass transfer on product-selectivity at 5.0 mA cm^{-2} and 250 rpm. Mass transfer coefficients: ① 0.00055, ② 0.00053 (average mass transfer coefficient), ③ 0.00051, ④ 0.00049 cm s^{-1}.

passed for 1 mole of substrate is 96485 C. The relation between time and q is given by

$$t = q[C_{b,i}]VF/iA \quad (33)$$

Values of k_m's used in this model are determined from Fig. 1 at various rotating speeds. In general, both the two ζ 's are in good agreement. Bearing in mind that the model calculation is based on many assumptions, the result is encouraging. The prediction, of course, may become more accurate if we take hydrogen evolution into account.

Combination of Eqs. 27 and 31—33 gives theoretical curves of ζ vs. q as shown in Fig. 5. The mean mass transfer coefficient at 250 rpm is 0.00053 cm s^{-1} with a deviation of 5%. The theoretical curve is expected to be curve 2. Nevertheless, the measured values of ζ 's are very near to curve 3, calculated by using 0.00051 cm s^{-1} as k_m. The difference between the two k_m 's is rather small, therefore, the validity of this model is proved. It should also be noted that a slight change (5%) in mass transfer rate could lead to a considerable variation (20%) in ζ for the case in Fig. 5. Hence, this model is shown to be applicable to the electroreduction of *p*-methylbenzaldehyde and can explain why the ratio of hydrodimeric to hydromonomeric products in the electroreduction of benzaldehyde increases 20 times as the rotating speed increases from 250 to 1000 rpm.[14]

It is interesting that this model could be used in estimating k_m as implied in Fig. 5. The evaluation of mass transfer coefficient is important in designing a practical electrolytic cell, and the application of this model in a flow cell system is in progress. Finally, it must be emphasized again that the product-selectivity is itself an index of mass transport for some electrolytic systems.

References

1) C. Amatore and J. M. Saveant, *J. Electroanal. Chem. Interfacial Electrochem.*, **123**, 189 (1981).
2) C. Amatore and J. M. Saveant, *J. Electroanal. Chem. Interfacial Electrochem.*, **123**, 203 (1981).
3) C. Amatore, F. M'Halla, and J. M. Saveant, *J. Electroanal. Chem. Interfacial Electrochem.*, **123**, 219 (1981).
4) C. Amatore, J. Pinson, and J. M. Saveant, *J. Electroanal. Chem. Interfacial Electrochem.*, **123**, 231 (1981).
5) C. Amatore and J. M. Saveant, *J. Electroanal. Chem. Interfacial Electrochem.*, **125**, 1 (1981).
6) C. Amatore and J. M. Saveant, *J. Electroanal. Chem. Interfacial Electrochem.*, **125**, 23 (1981).
7) C. Amatore and J. M. Saveant, *J. Electroanal. Chem. Interfacial Electrochem.*, **126**, 1 (1981).
8) J. M. Saveant, *J. Electroanal. Chem. Interfacial Electrochem.*, **236**, 31 (1987).
9) H. Wendt, *Angew. Chem., Int. Ed. Engl.*, **21**, 256 (1982).
10) C. L. Wilson and H. V. Udupa, *J. Electrochem. Soc.*, **99**, 289 (1952).
11) D. E. Danly, *Chem. Ind. (London)*, **1979**, 439.
12) W. V. Childs and H. C. Walters, *AIChE Symp. Ser.*, **75** (185), 19 (1979).
13) Y. Kokusenya, S. Nakajima, and M. Matsuoka, *Denki Kagaku*, **55**, 235 (1987).
14) P.-C. Cheng and T. Nonaka, *J. Electroanal. Chem. Interfacial Electrochem.*, **269**, 223 (1989).
15) M. D. Birkett and A. T. Kuhn, *Electrochim. Acta*, **25**, 273 (1980).
16) L. N. Nekrasov, L. N. Vykhodtseva, A. P. Korotkov, and L. P. Yureva, *Sov. Electrochem.*, **13**, 628 (1977).
17) C. Z. Smith and J. H. P. Utley, *J. Chem. Soc., Chem. Commun.*, **1981**, 492.
18) G. Farnia, G. Sandona, R. Fornasier, and F. Marcuzzi, *Electrochim. Acta*, **35**, 1149 (1990).
19) J. Grimshaw and J. S. Ramsey, *J. Chem. Soc. C*, **1966**, 653.
20) L. G. Feoktistov and H. Lund, "Organic Electrochemistry," ed by M. M. Baizer, Marcel Dekker, New York (1973), Chap. 8.
21) I. Taniguchi, K. Yasukouchi, A. Yoshiyama, and T. Sekine, *Bull. Chem. Soc. Jpn.*, **52**, 1775 (1979).
22) L. Nadjo and J. M. Saveant, *J. Electroanal. Chem. Interfacial Electrochem.*, **33**, 419 (1971).

Raman Phonon Spectroscopic Study of Phase Transition in 4-Cyanopyridine Crystal

Subhasis CHAKRABARTI, Tridibendra Marayan MISRA,* Mahesh Kumar SARMA,† and Kanak Chandra MEDHI†
Department of Spectroscopy, Indian Association for the Cultivation of Science, Calcutta 700032, India
†Department of Physics, Gauhati University, Gawahati 781014, India
(Received July 3, 1990)

Raman phonon spectroscopy in the 10—170 cm^{-1} range has been used to study phase transition in 4-cyanopyridine crystal. At 77 K, ten distinct phonon modes and an internal mode are observed whereas at 300 K the spectrum shows only six phonon bands and an internal mode. The temperature dependence of spectral pattern and phonon band width suggest that the crystal goes through a phase transition around 120 K. Experimental result suggests that the phase transition is discontinuous with a small structural change.

Raman phonon spectroscopy is a useful technique to investigate phase transition in organic crystals.[1-4] Phonon spectroscopy is particularly suited for the purpose due to the fact that in such crystals the intermolecular forces are 10—100 times weaker than the intramolecular forces and internal and external motions of molecules fall in different domain of frequencies. The lattice vibrational frequencies in organic crystals generally lie below 200 cm^{-1}, however, some out of plane deformation and torsional mode may be active in this region. Infrared and Raman spectroscopic study and vibrational analysis of 4-cyanopyridine has been reported by Green and Harrison[5] and they have assigned the internal vibrations below 200 cm^{-1}. Medhi and Sarma[6] have reassigned some of the internal modes.

At room temperature 4-cyanopyridine crystallizes in the orthorhombic form and belongs to the space group *Pccn* with four molecules in the unit cell.[7] No studies of phase transition in 4-cyanopyridine crystal based on standard X-ray or neutron diffraction technique seem to have been reported. Recently Wong[8] has reported pressure induced phase transition in this crystal by Raman phonon spectroscopic technique. We have investigated temperature dependent phase transition in 4-cyanopyridine crystal using the same technique. In addition we have shown that temperature dependence of phonon band width study is very useful to indicate phase transition in organic crystals. Temperature dependence of some molecular internal vibrational frequencies also often indicates phase transition in organic crystals. In this paper we report the result of our studies which show that indeed there is a temperature dependent phase transition in this crystal and this transition may be structural as in the pressure induced transition.

Experimental

The compound 4-cyanopyridine was obtained from M/S Aldrich Chemical Company Ltd., U.S.A. and purified by zone refining with 200 passes. Crystals were grown in a Bridgeman furnace. Both polycrystalline samples and single crystals were used to obtain Raman spectra.

The Raman spectra were recorded using a Spex double monochromator Model 1403 equipped with a cooled photomultiplier tube and photon counting unit and the 5145 Å line of Spectra Physics Model 2020-5 Ar^+ laser was used as the excitation source. Datamate 1B was used for data acquisition and analysis. The band position measurement should be accurate within 1 cm^{-1}. A Janis research cryostat Superveritemp Model 10DT was used to cool the crystal from room temperature down to 77 K. Temperature was measured and controlled by Lake Shore Model 805 temperature controller. Some uncertainty is given to the temperature measurement. Local laser heating is expected to create a temperature gradient between the crystal and the sensor.

Results and Discussion

Temperature Dependence of Phonon Spectra. With four molecules in the unit cell of the crystal there are total 24 lattice phonon modes. Twelve zone-center phonons are Raman active. The Raman phonon spectra of 4-cyanopyridine crystal in 10—170 cm^{-1} range at a series of temperature are shown in Fig. 1. At 77 K, ten distinct low frequency modes at 20.6, 33.2, 45.0, 58.6, 71.8, 79.0, 86.2, 94.4, 114.2 and 120.6 cm^{-1} represent lattice modes and the mode at 148.0 cm^{-1} has been assigned as internal mode γ (CN) by Green and Harrison.[5] At 300 K only six phonon bands at 16.8, 29.2, 40.8, 62.0, 70.8, and 95.2 cm^{-1} persist. A close examination of these spectra reveal that some distinct changes occur at 120±1 K which can not be attributed simply to temperature change. As temperature is raised from 118 to 122 K, the 78.6 cm^{-1} (79.0 cm^{-1} at 77 K) phonon band disappears and the intensity of the band at 57.4 cm^{-1} (58.6 cm^{-1} at 77 K) increases. Intensity of this band decreases above and below 120 K. The 85.0 cm^{-1} (86.2 cm^{-1} at 77 K) phonon shows appreciable frequency shift. The 71.0 cm^{-1} (71.8 cm^{-1} at 77 K) phonon band also shows a frequency lowering by 4.4 cm^{-1} at this temperature. The 20.6 cm^{-1} frequency increases by 2.4 cm^{-1} at this temperature and then decreases gradually as temperature is raised. Much less sharp but definite shift is also observed with 120.6, 114.2, 94.2, 45.0, and 32.2 cm^{-1} phonon at this temperature. In Fig. 2 we show temperature dependence of some selected phonon frequencies. Many of the lattice

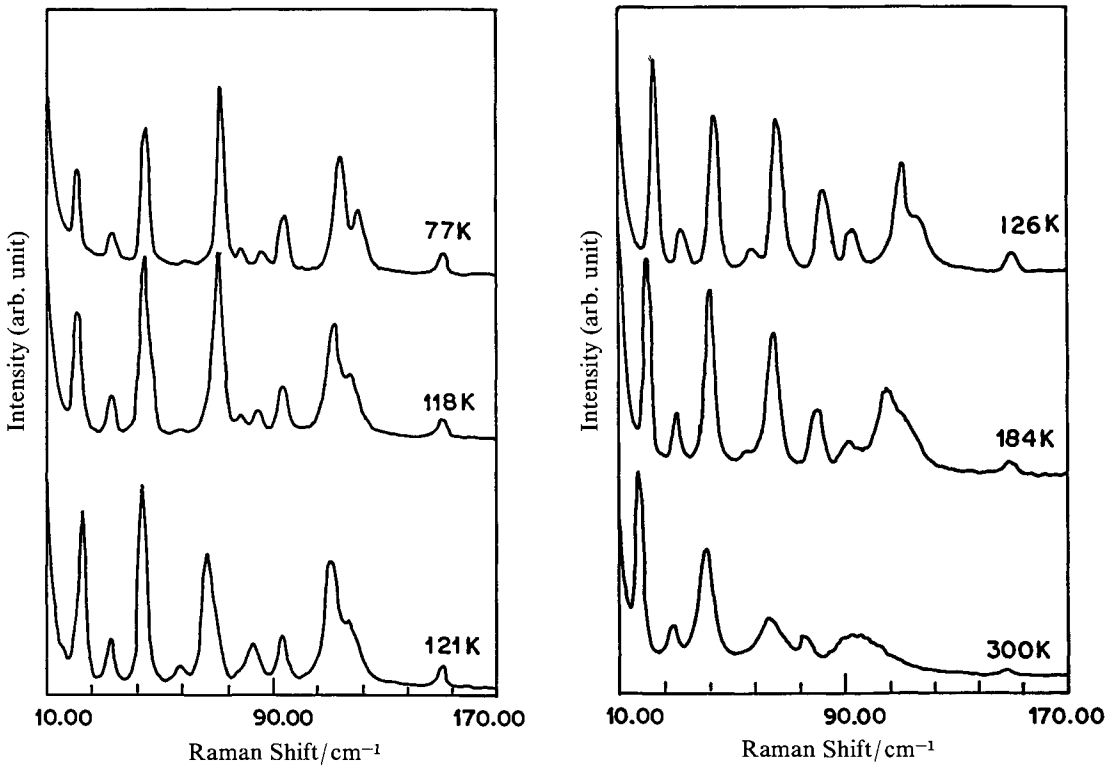

Fig. 1. Raman spectra of 4-cyanopyridine crystal in 10—170 cm^{-1} range at different temperatures.

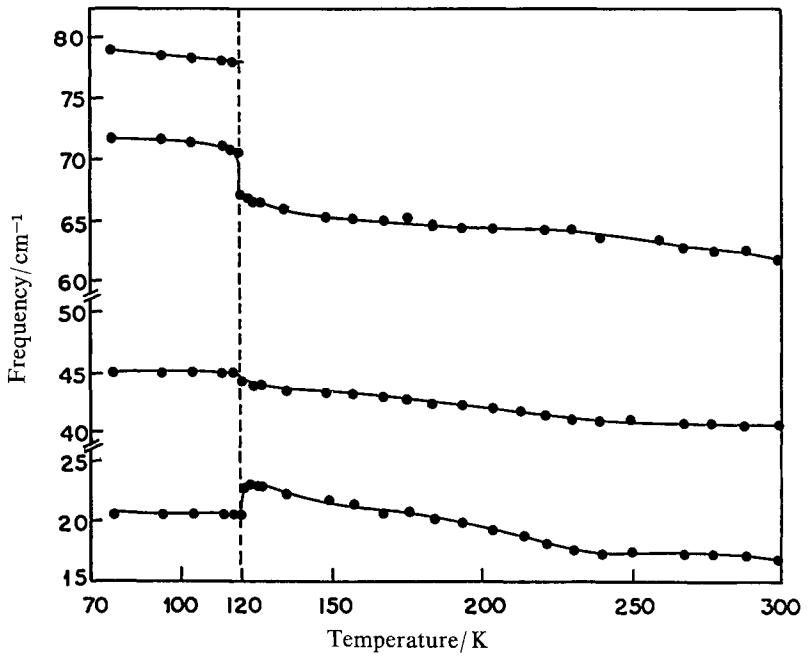

Fig. 2. Temperature dependence of some selected Raman active lattice phonon frequencies in 4-cyanopyridine crystal.

modes show discontinuous change in wavenumber as the crystal temperature is changed from 118 K to 122 K. Raman intensity decreases as the crystal is heated. This is a general observation. Around phase transition temperature there is decrease in frequency in most of the phonon modes but 20.6 cm^{-1} phonon shows reverse behavior. The frequency increases significantly during transition and then shows usual decrement with temperature.

All these results suggest that there is a definite discontinuous phase transition in 4-cyanopyridine crystal at 120±1 K.

Temperature Dependence of Internal Vibrations. We have studied the temperature dependence of internal

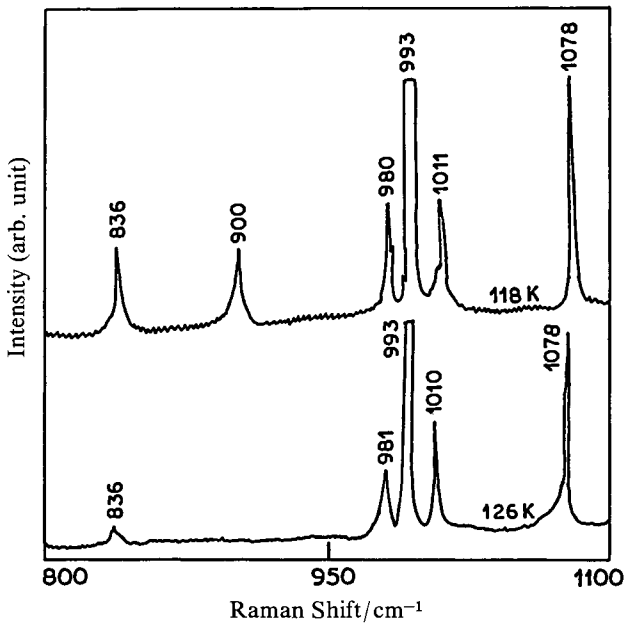

Fig. 3. Raman spectra of 4-cyanopyridine crystal in the 800—1100 cm^{-1} range below and above phase transition temperature.

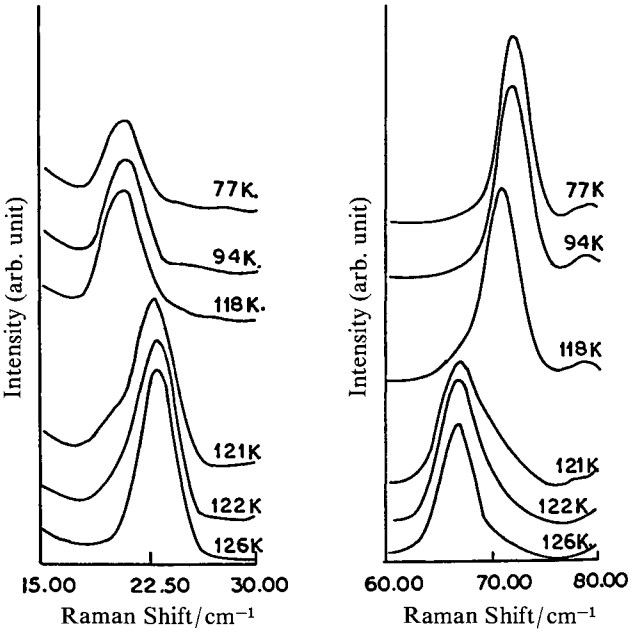

Fig. 4. 71.8 and 20.6 cm^{-1} (at 77 K) phonon bands in extended scale at several temperatures near transition region.

modes also. Though most of the spectral patterns remain unchanged below and above 120±1 K, some definite change is observed. Raman spectra in the 800 to 1100 cm^{-1} range in two phases are shown in Fig. 3. In the low temperature phase a band at 900 cm^{-1} appears. This vibration is of b_1 species and is only infrared active at room temperature.[6] Due to the structural change this vibration becomes Raman active in low temperature phase. Other changes observed are the changes in the intensity ratio of 993 and 1011 cm^{-1} bands and decreament of intensity of a band at 836 cm^{-1} in the high temperature phase.

Temperature Dependence of Phonon Bandwidth. Temperature dependence of phonon band width indicates phase transition in organic crystals.[3] In Fig. 4 we show 71.8 cm^{-1} (at 77 K) and 20.6 cm^{-1} (at 77 K) phonon bands in extended scale at several temperatures near the transition region. Indeed there is indication that new bands appear near the bands observed in one phase when the sample changes into another phase and this is shown as shoulders. Inspite of this, we have been able to measure the FWHM of these two bands. The spec-

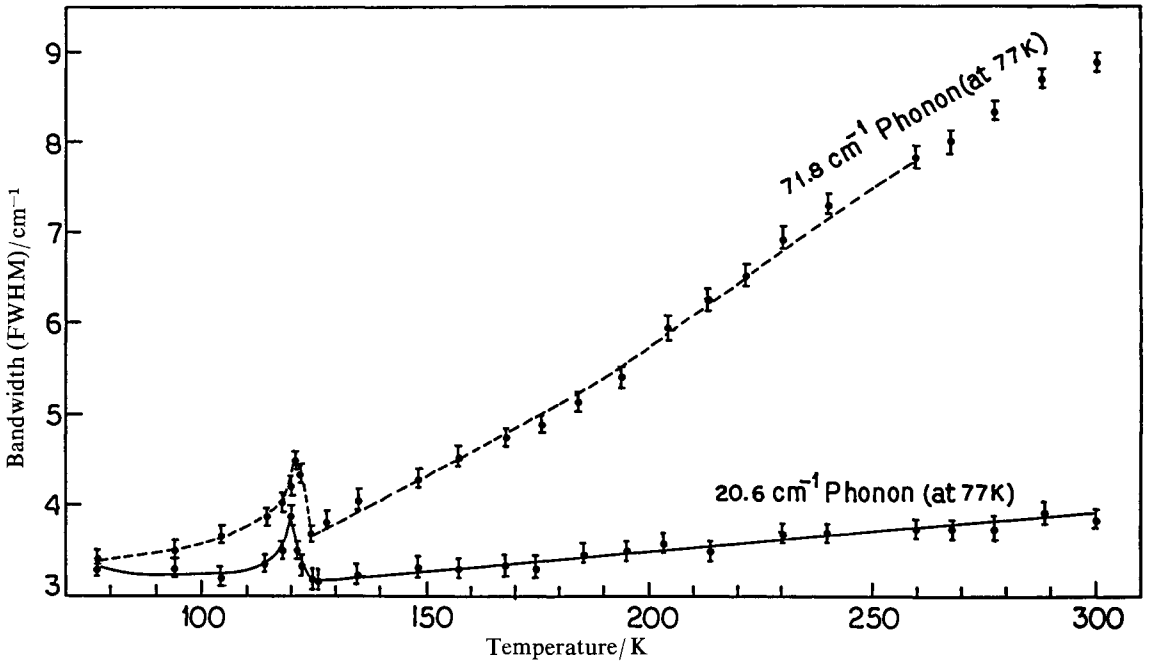

Fig. 5. Temperature dependence of band widths of Raman phonon bands of 4-cyanopyridine cryctal.

tra of Fig. 4 are considered to have been obtained because the phase transition is discontinuous and there is some temperature gradient in the sample. In Fig. 5 temperature dependence of band widths of these two bands are shown. The increase in the band widths of these two bands is large enough to be beyond the error of measurement. At 120±1 K the continuity pattern is broken and the width show some small but definite decrement with temperature rise. The temperature indeed is same as that observed in the temperature versus phonon frequency plot.

Nature of Phase Transition. Temperature dependence of phonon frequencies and band widths suggests that phase transition occurs in a small temperature interval 120±1 K. Raman study indicates that 79.0 cm^{-1} phonon disappears at these temperatures and for some other bands discontinuity as large as 4.4 cm^{-1} is also observed. Internal vibrational spectra in both the phases reveal that there is some small structural change which leads to the appearance of 900 cm^{-1} band at low temperature phase. Phase transition of 4-cyanopyridine is, therefore, a first order transition with small strutural change. The greatest change is observed in 71.8 cm^{-1} phonon band (at 77 K). The crystal lattice at low temperature phase seems to be distorted along the eigen vector of this phonon mode. This observation is similar to that reported by Wong[8] in pressure induced phase transition. However the 71.8 cm^{-1} phonon behaves differently in temperature and pressure induced phase transition. Whereas we have observed large discontinuous jumping in frequency on phase transition, Wong[8] reported only sharp discontinuity in frequency pressure plot at 10 kbar without any appreciable change in phonon frequency at higher pressure. Inspite of this, it seems probable that the phase transition we have observed at 120±1 K is the same as observed by Wong[8] at room temperature at a pressure 10 kbar.

Conclusion

We have used Raman phonon spectroscopy to study phase transition in 4-cyanopyridine crystal. The temperature dependence of spectral pattern and phonon band width suggest that there is a discontinuous phase transiton around 120 K. The lattice mode at 71.8 cm^{-1} (at 77 K) shows the greatest change (62 cm^{-1} at 300 K) while most of the other vibrations remains continuous in both the phases. The structural change is, therefore, considered small.

References

1) R. Zallen, C. H. Griffiths , M. L. Stade, H. Hayek, and O. Brafman, *Chem. Phys. Lett.*, **39**, 85 (1976).
2) B. A. Bolton and P. N. Prasad, *Chem. Phys.*, **35**, 334 (1978).
3) A. Girard, M. Sanguer, and Y. Delugeard, *Chem. Phys.*, **96**, 427 (1985).
4) Y. Ebisuzaki, L. H. Askari, and A. M. Bryan, *J. Chem. Phys.*, **87**, 6659 (1987).
5) J. H. S. Green and D. J. Harrison, *Spectrochim. Acta, Part A*, **33**, 75 (1977).
6) K. C. Medhi and M. K. Sarma, *Indian J. Phys.*, **64B**, 307 (1990).
7) M. Long, N. Sparrow, and P. Sommerville, *Acta Crystallogr., Sect. B*, **27**, 1986 (1971).
8) P. T. T. Wong, *J. Chem. Phys.*, **78**, 4840 (1983).

A Comparative Study on the Acidic Properties and Catalytic Activities of TiO_2, SiO_2, Al_2O_3, SiO_2-Al_2O_3, SiO_2-TiO_2, Al_2O_3-TiO_2, and TiO_2-SiO_2-Al_2O_3

Kuzhunellil Raghavan Pillai SABU,* Kalur Vijayachandra C. RAO, and Chandrathil Govindan Ramachandran NAIR†

Inter Disciplinary Research Group, Vikram Sarabhai Space Centre, Trivandrum 695022, India
†Department of Chemistry, University of Kerala, Trivandrum 695034, India

(Received July 16, 1990)

Investigations are carried out to have a systematic comparison of the acidic properties and catalytic activities of single oxide TiO_2, SiO_2, Al_2O_3, their binary oxides and the ternary oxide TiO_2–SiO_2–Al_2O_3. The acidity distributions are measured by using butylamine titration technique and the test reactions selected for the catalytic activity measurements are alkylation of toluene with 2-propanol and the dehydration of 2-propanol. The single oxides have only low acid strength and are not at all active in catalyzing the alkylation reaction, but are marginally active in the dehydration of 2-propanol. However the binary oxides SiO_2–TiO_2 and Al_2O_3–TiO_2 of 10% by weight of TiO_2 are found to contain very strong acid sites $H_o \leqslant -8.2$ and are highly active catalysts in both the test reactions. But TiO_2–SiO_2–Al_2O_3 of 10% by weight of TiO_2 showed the highest acid amount and the highest activity in the aikylation and dehydration reactions compared to the binary oxides. The acid amount and the catalytic activity of the ternary oxide increased with the increase of TiO_2 content upto 50 mol% of TiO_2 and then decreased. The ternary oxide containing 80 mol% of TiO_2 is rich in weak acid sites. The increase of TiO_2 content does not affect the selectivity.

The utility of supported transition metal oxide catalysts like Cr_2O_3–SiO_2, MoO_3–SiO_2–Al_2O_3, and TiO_2–SiO_2–Al_2O_3 in certain acid-catalyzed oligomerization, polymerization, and a wide range of alkylation reactions are known.[1–8] The incorporation of transition metal oxides into SiO_2–Al_2O_3 is expected to alter the acidity distribution of the latter and hence its activity in various acid-catalyzed reactions. For instance, recently it has been found that TiO_2–SiO_2–Al_2O_3 is a highly active and regenerable alkylation catalyst.[8] Further investigations undertaken to study the effect of the pH of the coprecipitating solution on the acidic and catalytic properties of the ternary oxide revealed that the ternary oxide coprecipitated from a solution of pH 4 has optimum acid amount and acid strength and it even contains nearly double the acid amount of SiO_2–Al_2O_3[9].

The acidic properties of single oxides TiO_2, SiO_2, Al_2O_3, and their binary oxides are well studied.[10–16] However a systematic comparative study on the acidic properties and catalytic activities of these single oxides, the binary oxides SiO_2–Al_2O_3, SiO_2–TiO_2, Al_2O_3–TiO_2, and the ternary oxide TiO_2–SiO_2–Al_2O_3 in the isopropylation of toluene (a reaction catalyzed by solid acids with moderately strong acid sites) and the dehydration of 2-propanol (a reaction catalyzed by solid acids with relatively weak acid sites) are not previously attempted. Hence in the present paper we discuss the results of such a study. Besides we have prepared TiO_2–SiO_2–Al_2O_3 of varying TiO_2 content and almost the same silica to alumina molar ratio and studied the effect of titania content on the acidic and catalytic properties of the ternary oxide, the results of which are also included in this paper.

Experimental

Materials: The materials used are sodium silicate (Scientific Chemicals), aluminium sulfate (A. R. grade), titanium tetrachloride (KMML Chavara), 2-propanol (BDH), toluene (BDH), butylamine (SD Chemicals), nitric acid, and ammonia of chemically pure quality. The indicators used are Neutral Red (pK_a=+6.8), Methyl Red (pK_a=+4.8), Dimethyl Yellow (pK_a=+3.3), phenylazodiphenylamine (pK_a=+1.5), Crystal Violet (pK_a=+0.8), dicinnamylideneacetone (pK_a=+3.0), benzylideneacetophenone (pK_a=−5.6), and anthraquinone (pK_a=−8.2).

Preparation of Metal Oxides: (a) Single Oxides: Single oxides such as Al_2O_3 and TiO_2 were prepared by the thermal decomposition of the respective hydroxides at 600 °C in air for 6 h. The hydroxides are precipitated from aqueous solutions of aluminium sulfate and titanium tetrachloride using 1 : 1 ammonia solution. The single oxide SiO_2 was prepared by precipitation from an aqueous solution of sodium silicate with dilute nitric acid followed by aging at 80 °C for 3 h and calcining at 600 °C for 6 h.

(b) Binary Oxides: The binary oxides SiO_2–Al_2O_3, SiO_2–TiO_2, and Al_2O_3–TiO_2 are obtained by the thermal decomposition of their hydroxides. The hydroxides were coprecipitated by adding 1 : 1 ammonia water to the mixed aqueous solutions of the metal salts, sodium silicate and aluminium sulfate for SiO_2–Al_2O_3, sodium silicate and titanium tetrachloride for SiO_2–TiO_2, and aluminium sulfate and titanium tetrachloride for Al_2O_3–TiO_2 till the pH of the final gel became 4. The precipitates were washed thoroughly to remove adhering anions such as chlorides and sulfates, extruded, dried (120 °C for 12 h) and calcined (600 °C for 6 h).

(c) TiO_2-SiO_2-Al_2O_3: The coprecipitation technique employed for the preparation of TiO_2–SiO_2–Al_2O_3 is referred elsewhere.[8] The coprecipitation was done by adding 1 : 1 ammonia water to the mixed aqueous solutions of sodium silicate, aluminium sulfate, and titanium tetrachloride till the pH of the final gel became 4. Six different samples of TiO_2–

Table 1. Amounts of Starting Materials Used for the Synthesis of Tisial with Different TiO_2 Contents and Their Physicochemical Characteristics (Calcined at 600 °C)

Sample	Amount of materials used			Composition		Surface area	Pore volume
	Sodium silicate	Titanium tetrachloride	Aluminum sulfate	SiO_2/Al_2O_3	TiO_2	$m^2 g^{-1}$	$cm^3 g^{-1}$
	g	ml	g	(mole ratio)	mol%		
Tisial-4A	270	5	105	16	2.3	120	1.05
Tisial-4B	265	10	102	15	4.3	108	0.87
Tisial-4C	260	20	100	16.4	8.4	100	0.71
Tisial-4D	220	50	85	17.3	19.8	90	0.60
Tisial-4E	175	120	70	17.4	50.0	66	0.42
Tisial-4F	120	200	40	17.0	80.0	41	0.28
SiO_2–Al_2O_3	260	—	100	16.4	—	135	1.20

SiO_2–Al_2O_3 of varying compositions viz.; Tisial-4A, Tisial-4B, Tisial-4C, Tisial-4D, Tisial-4E, and Tisial-4F were prepared by changing the starting quantities of sodium silicate, aluminium sulfate, and titanium tetrachloride as shown in Table 1. The precipitates were washed thoroughly to remove anions such as chlorides and sulfates, extruded, dried (120 °C for 12 h) and calcined (600 °C for 6 h). Tisial-4D, Tisial-4E, and Tisial-4F samples were also calcined at temperatures 150, 300, and 450 °C.

The physical characteristics such as surface area (for all the samples) and porosity (for binary oxides and ternary oxides) were measured and the chemical compositions were determined by chemical analysis.

Measurement of Acidity: The acidity distribution of different samples were measured by titrating the 100—200 mesh powder suspended in dry benzene with butylamine solution in dry benzene using the above mentioned indicators.[17]

Measurement of Catalytic Activity: The alkylation of toluene with 2-propanol was done in a fixed bed tubular reactor (LHSV 0.5 h^{-1}, toluene/2-propanol mole ratio 3, total reaction time 7 h). The dehydration of 2-propanol was also done in the same reactor (LHSV 0.5 h^{-1}, total reaction time 7 h). The reactor, experimental and analytical procedures, and the method of calculation of percentage yields of alkylaromatics were the same as those employed in the previous work.[8,9]

The products of alkylation were found to be *o*-cymene (*o*-isopropyltoluene), *p*-cymene (*p*-isopropyltoluene), and three isomers of diisopropyltoluenes (DIT).

Results and Discussion

Acidic Properties of Various Mixed Oxide Catalysts: As the TiO_2 content increased, the physical parameters such as surface area and porosity of the ternary oxide TiO_2–SiO_2–Al_2O_3 decreased considerably (Table 1).

Single oxides TiO_2, SiO_2,and Al_2O_3 showed negligible amounts of acid sites stronger than acid strength H_o= +3.3. Also they possess very low value of total acid amount (Table 2). However, the binary oxide SiO_2–Al_2O_3 is a well-known solid acid of very high acid strength ($H_o \leqslant -8.2$) and hence is used as useful catalysts for various acid-catalyzed reactions in the field of petroleum chemistry.[17-21] In good agreement with this, SiO_2–Al_2O_3 coprecipitated from a solution of pH 4 and which contains about 10% (by weight) of alumina was found to possess only strong acid sites (Table 3). Table 3 also shows that the binary oxides SiO_2–TiO_2 and Al_2O_3–TiO_2, both of which contain about 10% by weight of TiO_2 are rich in moderately strong acid sites (H_o

Table 2. The Acidity Distribution of Single Oxides (Calcined at 600 °C)

Oxide	Surface area	Acid amount (mmol g^{-1}) at different pK_a's							
	$m^2 g^{-1}$	+6.8	+4.8	+3.3	+1.5	+0.8	−3.0	−5.6	−8.2
SiO_2	264	0.181	0.175	0.115	0	0	0	0	0
Al_2O_3	166	0.211	0.193	0.121	0.022	0	0	0	0
TiO_2	31	0.052	0.042	0.042	0	0	0	0	0

Table 3. The Physicochemical Characteristics and Acidity Distribution of Binary Oxides (Calcined at 600 °C)

Binary oxide	Composition			Surface area	Pore volume	Acid amount (mmol g^{-1}) at different pK_a's							
	SiO_2, Al_2O_3	SiO_2, TiO_2	Al_2O_3, TiO_2										
	molar ratio			$m^2 g^{-1}$	$cm^3 g^{-1}$	+6.8	+4.8	+3.3	+1.5	+0.8	−3.0	−5.6	−8.2
SiO_2–Al_2O_3	16.4			135	1.21	0.35	0.35	0.35	0.35	0.35	0.35	0.35	0.35
SiO_2–TiO_2		12.0		102	0.77	0.41	0.41	0.41	0.41	0.41	0.41	0.16	0.08
Al_2O_3–TiO_2			7.1	88	0.61	0.38	0.38	0.38	0.38	0.38	0.38	0.32	0.06

Table 4. Acidity Distribution of Tisial Sample of Varying TiO_2 Content (Calcined at 600 °C)

Sample	Acid amount (mmol g^{-1}) at different pK_a's							
	+6.8	+4.8	+3.3	+1.5	+0.8	−3.0	−5.6	−8.2
Tisial-4A	0.42	0.42	0.42	0.42	0.42	0.42	0.14	0.12
Tisial-4B	0.54	0.54	0.54	0.54	0.54	0.54	0.19	0.09
Tisial-4C	0.63	0.63	0.63	0.63	0.63	0.63	0.15	0.05
Tisial-4D	0.71	0.71	0.71	0.71	0.71	0.70	0.18	0.08
Tisial-4E	0.77	0.77	0.77	0.77	0.77	0.77	0.21	0.10
Tisial-4F	0.46	0.41	0.33	0.11	0.00	0.00	0.00	0.00

between +1.5 and −5.6) and they even contain very strong acid sites ($H_o \leqslant -8.2$). Even though binary oxides containing TiO_2 are known to posses strong acid sites due to which they serve as effective catalysts in the synthesis of aniline from phenol and ammonia, acid sites of strength $H_o=-8.2$ is never observed previously in the case of Al_2O_3–TiO_2.[21] Hence it may be concluded that the pH of coprecipitation governs the acidity distribution of these binary metal oxides similar to that reported in the case of ternary oxide containing SiO_2, Al_2O_3, and TiO_2. But the total acid amount value of TiO_2–SiO_2–Al_2O_3 containing about 10% by weight each of TiO_2 and Al_2O_3 is large compared with SiO_2–TiO_2 and Al_2O_3–TiO_2 (Table 4). Si–O–Si and Al–O–Al bond formation may occur in SiO_2–TiO_2 (when SiO_2 is the major component) and Al_2O_3–TiO_2 (when Al_2O_3 is the major component) respectively and could be a probable reason for the decreased acid amount values of these binary oxides in comparison with the ternary oxide TiO_2–SiO_2–Al_2O_3. That is, the number of bonds which can generate acid sites per unit surface area may be the highest in the case of TiO_2–SiO_2–Al_2O_3. However, the acid strength of a mixed metal oxide system depends on the averaged electronegativity values of the component metal ions.[10]

The Effect of TiO_2 Content on the Acidity Distribution of TiO_2–SiO_2–Al_2O_3: The acidity distribution of TiO_2–SiO_2–Al_2O_3 of varying TiO_2 content shows that the total acid amount increased with the increase of TiO_2 content and the maximum acid amount is shown by the sample containing 50 mol% of TiO_2 (Tables 3 and 4). Further increase in TiO_2 content decreased both the acid amount and acid strength. TiO_2–SiO_2–Al_2O_3 containing 80 mol% of TiO_2 (Tisial-4F) is rich in very weak acid sites. As the silica to alumina molar ratio is the same in all these Tisial samples, it may be assumed that the probability for the formation of Si–O–Al type bonds are the same, but the probabilities for the formation of Si–O–Ti and Al–O–Ti type bonds are different. The highest acid amount shown by Tisial-4E is due to the maximum number of Si–O–Ti and Al–O–Ti bonds on the surface of the ternary oxide, which are known to generate acidic sites. But the titania rich Tisial-4F may be rich in Ti–O–Ti bonds as substantiated by the existence of acid sites with low acid strength on the surface of this sample, which is the characteristic of TiO_2. Also Fig. 1 shows that with the increase in calcination temperature, the strong acid sites do not appear in Tisial-4F whatever be the calcination temperature, as in the case of TiO_2.[11]

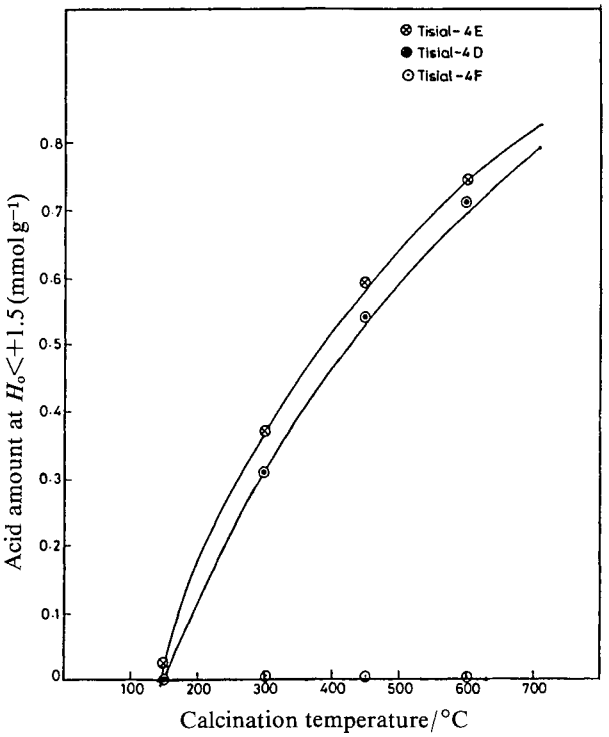

Fig. 1. The effect of calcination temperature on the acidity distribution of Tisial-4D, Tisial-4E, and Tisial-4F.

Catalytic Activity. i) Alkylation of Toluene with 2-Propanol: The single oxides SiO_2, TiO_2, and Al_2O_3 are not effective in demanding the alkylation of toluene. However, the catalytic activity in the conversion of 2-propanol to alkylaromatics is fairly high for the binary oxides SiO_2–Al_2O_3, SiO_2–TiO_2, and Al_2O_3–TiO_2 (Fig. 2). Among them, SiO_2–TiO_2 showed the highest activity and SiO_2–Al_2O_3 showed the least activity. But TiO_2–SiO_2–Al_2O_3 is more active for the conversion of 2-propanol to alkylaromatics than any of these binary oxides. The enhanced activity of TiO_2–SiO_2–Al_2O_3 catalysts could be attributed to the very large acid amount at a suitable acid strength ($H_o \leqslant +1.5$) for the alkylation.[22] This is evident from the linear activity to acidity correlation obtained by plotting the acidity at $H_o \leqslant +1.5$ of different binary oxides and the ternary oxide against their isopropylating activity (Fig. 3).

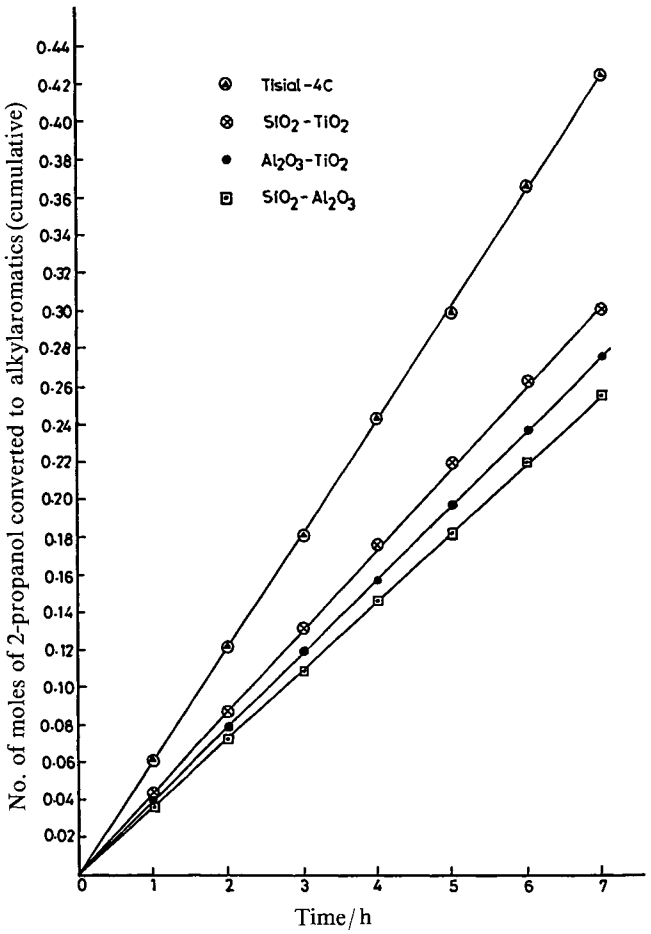

Fig. 2. Comparison of the catalytic activity of TiO_2–SiO_2–Al_2O_3 (Tisial) with that of binary oxides in the alkylation of toluene with 2-propanol. Reaction conditions; reaction temperature: 200 °C; LHSV: 0.5; toluene/2-propanol (mole ratio): 3.

With the increase in TiO_2 content, the alkylating activity of the ternary oxide system also increased (Fig. 4). But the Tisial-4F which is rich in weak acid sites are ineffective in catalyzing the alkylation of toluene.

The product mixtures obtained are rich in *p*-cymene

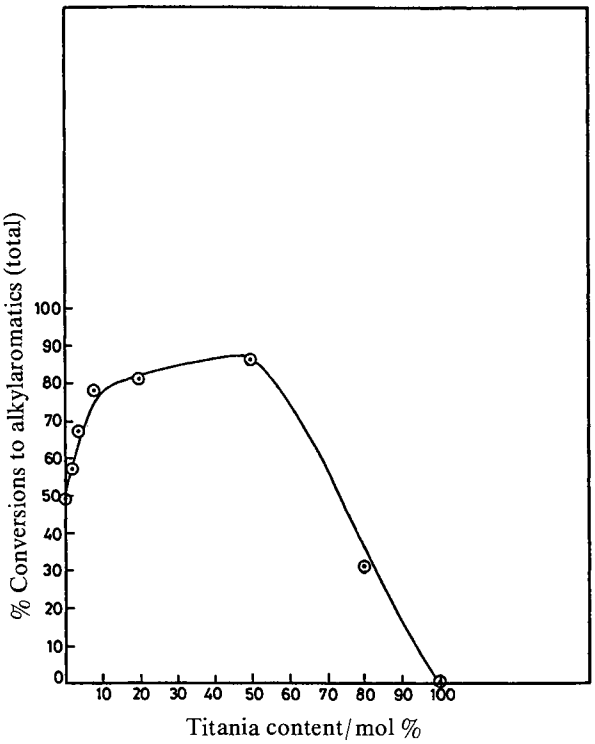

Fig. 4. Effect of titania content of Tisial on the conversion of 2-propanol to alkylaromatics. Reaction conditions; reaction temperature: 200 °C; LHSV: 0.5; toluene/2-propanol (mole ratio): 3.

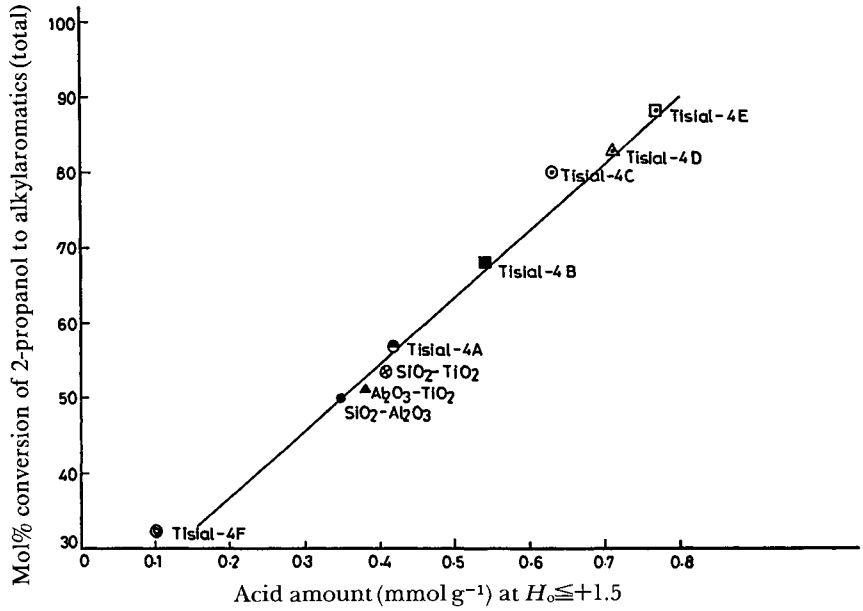

Fig. 3. Effect of acidity distribution on the conversion of 2-propanol to alkylaromatics. Reaction conditions; reaction temperature: 200 °C; LHSV: 0.5; toluene/2-propanol (mole ratio): 3.

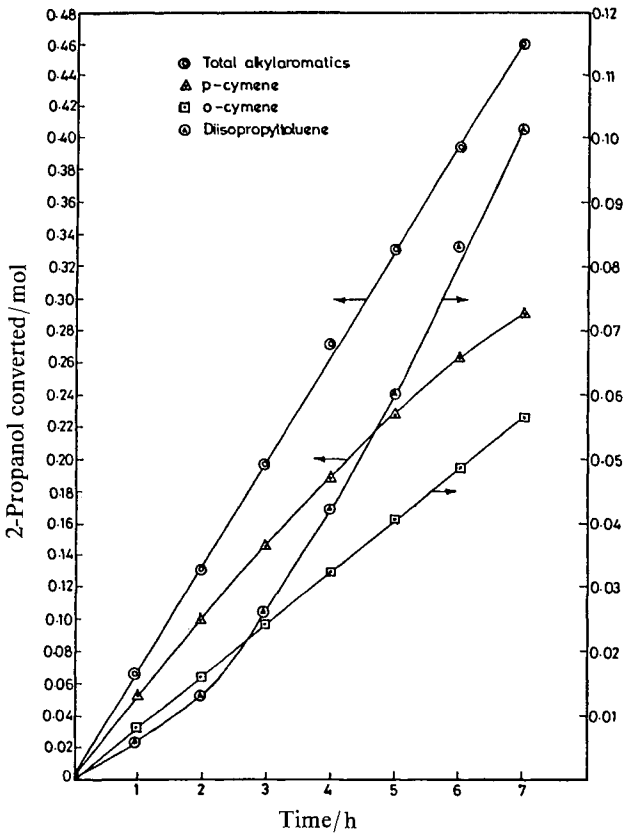

Fig. 5. Cumulative formation of *p*-cymene, *o*-cymene, and diisopropyltoluenes with reaction time over Tisial-4E. Reaction conditions; reaction temperature: 200 °C; LHSV: 0.5; toluene/2-propanol (mole ratio): 3.

content for all the catalysts studied, as illustrated in Fig. 5 for Tisial-4E, which is found to be the most active alkylation catalyst included in the present study. The conversion to *p*-cymene decreased and a corresponding increase in the formation of diisopropyltoluenes is observed with the passing of reaction time. However, the conversion to *p*-cymene remained constant throughout the reaction time.

Even though the alkylating activity of TiO_2–SiO_2–Al_2O_3 increased considerably with increase in TiO_2 content (upto 50 mol% of TiO_2), the selectivity to different products is not altered. This is evidenced from the product patterns obtained at different reaction times, (Table 5) when Tisial-4C of 8.5 mole% of TiO_2 and Tisial-4E of 50 mol% of TiO_2 are used as catalysts.

ii) Dehydration of 2-Propanol: In the dehydration of 2-propanol to propylene, the single oxides TiO_2, SiO_2, and Al_2O_3 showed marginal activity (Fig. 6), whereas the binary oxides are found to show better catalytic activity. However, the ternary oxide system is the most active catalyst for the dehydration and the enhanced activity can be due to the large acid amount values. On plotting the total acidity at $H_o \leqslant +6.8$, of single oxides, binary oxides, and ternary oxide against their dehydrating activity, a linear correlation is obtained (Fig. 7). This suggests that even the weakest acid sites are efficient in demanding the dehydration of 2-propanol.

Conclusion

The binary oxides SiO_2–TiO_2 and Al_2O_3–TiO_2 copre-

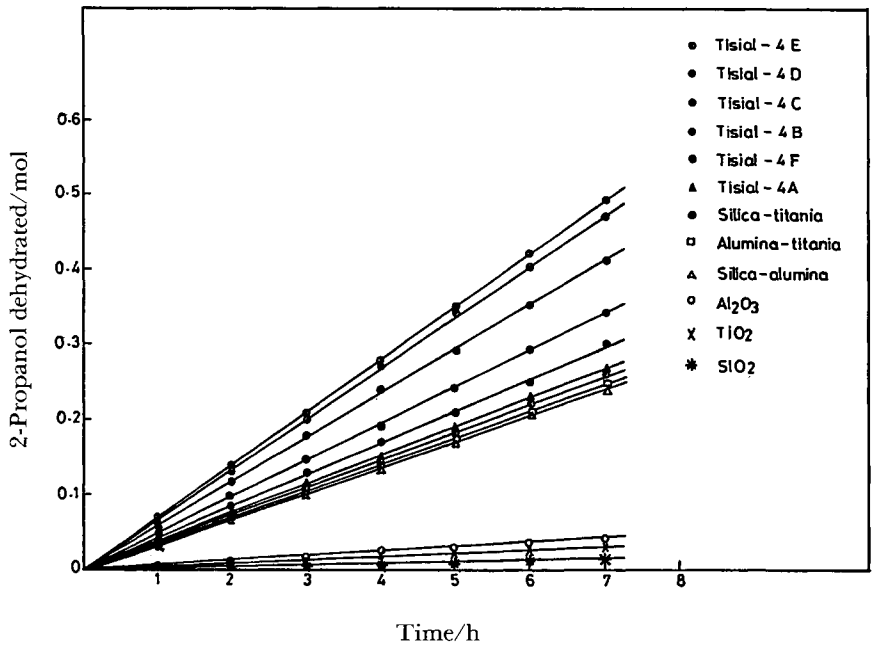

Fig. 6. Comparison of dehydrating activity of different catalysts (The cumulative number of moles of 2-propanol converted to propylene with reaction time is given). Reaction conditions; reaction temperature: 200 °C; LHSV: 0.5; toluene/2-propanol (mole ratio): 3.

Table 5. Conversions (mol%) of 2-Propanol to Alkylaromatics at Different Reaction Times over Tisial-4C (8.4 mol% of of TiO_2) and Tisial-4E (50 mol% of TiO_2)

Reaction time	Tisial-4C					Tisial-4E				
h	*o*-Cymene	*p*-Cymene	DIT	*o*/*p*	DIT/*o*+*p*	*o*-Cymene	*p*-Cymene	DIT	*o*/*p*	DIT/*o*+*p*
1	9.8	64.0	7.0	0.153	0.95	10.4	68.0	7.2	0.153	0.092
2	9.7	57.3	13.5	0.169	0.20	10.4	62.3	13.0	0.166	0.180
3	9.7	54.0	17.4	0.179	0.27	10.4	60.2	17.0	0.174	0.240
4	9.7	50.6	19.4	0.191	0.32	10.4	54.5	21.0	0.190	0.320
5	9.6	47.3	21.6	0.200	0.37	10.4	52.4	23.6	0.200	0.370
6	9.7	45.8	22.8	0.205	0.40	10.4	47.0	30.0	0.220	0.500

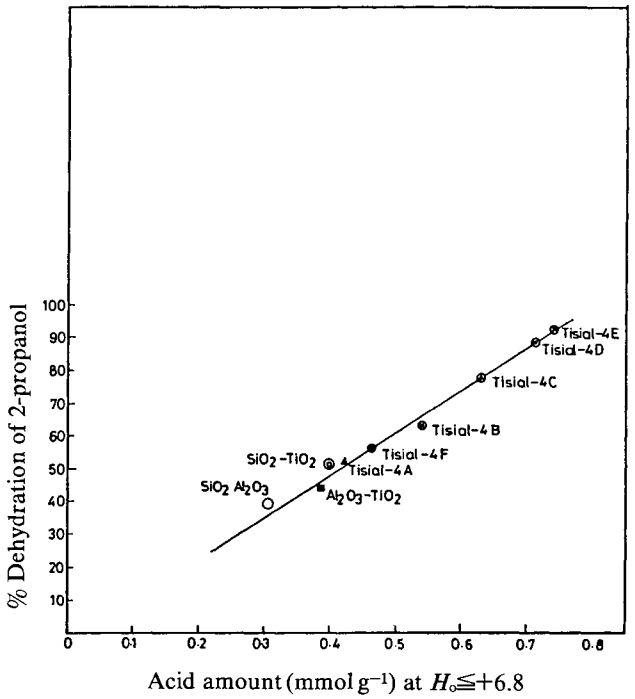

Fig. 7. Effect of acidity distribution on the dehydration of 2-propanol to propylene. Reacton conditions; reaction temperature: 200 °C; LHSV: 0.5.

cipitated from a solution of pH 4 exhibited acid strength of H_o=−8.2 and are found to be highly active catalysts in the alkylation of toluene with 2-propanol and the dehydration of 2-propanol, even though the single oxides are ineffective catalysts due to their low acid strength. However, the corresponding activity of TiO_2–SiO_2–Al_2O_3 is the highest. The acid amount of the ternary oxide system TiO_2–SiO_2–Al_2O_3 increased with the increase of TiO_2 content upto 50 mol% of TiO_2 and then decreased, without altering the selectivity.

References

1) Y. Izumi, R. Hasebe, and K. Urabe, *J. Catal.*, **84**, 402 (1983).
2) V. G. Kumar, M. Rama Rao, P. V. Ravindran, and K. V. C. Rao, *J. Polym. Sci., Polym. Chem. Ed.*, **21**, 2133 (1983).
3) V. G. Kumar, S. Venkatachalam, and K. V. C. Rao, *J. Polym. Sci., Polym. Chem. Ed.*, **22**, 2317 (1984).
4) S. Venkatachalam, V. G. Kumar, and K. V. C. Rao, *J. Polym. Sci., Polym. Chem. Ed.*, **22**, 3805 (1984).
5) C. Groenweld, P. P. M. M. Wittgen, H. R. M. Swinner, A. Wernsenn, and G. C. A. Schwitz, *J. Catal.*, **83**, 346 (1983).
6) V. G. Kumar, T. S. Shoba, and K. V. C. Rao, *Tetrahedron Lett.*, **26**, 3281 (1985).
7) V. G. Kumar, T. S. Shoba, and K. V. C. Rao, *Tetrahedron Lett.*, **26**, 6245 (1985).
8) K. V. C. Rao, K. R. Sabu, and C. G. R. Nair, *Bull. Chem. Soc. Jpn.*, **62**, 2657 (1989).
9) K. R. Sabu, K. V. C. Rao, and C. G. R. Nair, *Bull. Chem. Soc. Jpn.*, **63**, 3632 (1990).
10) K. Shibata, T. Kiyoura, J. Kitagawa, T. Sumiyoshi, and K. Tanabe, *Bull. Chem. Soc. Jpn.*, **46**, 2985 (1973).
11) K. Tanabe, C. Ishiya, I. Matsuzaki, I. Ichikawa, and H. Hattori, *Bull. Chem. Soc. Jpn.*, **45**, 47 (1972).
12) H. A. Benesi, *J. Am. Chem. Soc.*, **78**, 5490 (1956).
13) M. L. Hair and W. J. Hertl, *J. Phys. Chem.*, **74**, 91 (1970).
14) K. Marshall, G. I. Ridgewill, C. H. Rochester, and J. Simpson, *Chem. Ind. (London)*, 1974.
15) T. Morimoto, J. Imai, and M. Nagao, *J. Phys. Chem.*, **78**, 704 (1974).
16) H. A. Benesi and B. H. C. Winquist, *Adv. Catal.*, **27**, 123 (1978).
17) H. A. Benesi, *J. Phys. Chem.*, **61**, 970 (1957).
18) Heinemann, *Catal. Rev.*, **8**, 312 (1974).
19) J. Abbot, *Appl. Catal.*, 33 (1989).
20) J. S. Magee and J. J. Blazek, *ACS Monogr.*, No. 171, 615 (1976).
21) K. Tanabe, M. Ito, and M. Sato, *Chem. Commun.*, 676 (1973).
22) S. G. T. Bhat, *Indian J. Technol.*, **21**, 65 (1983).

The Acidic Property and Catalytic Activity of MoO_3-SiO_2-Al_2O_3

Kuzhunellil Raghavan Pillai SABU,* Kalur Vijayachandra C. RAO, and Chandrathil Govindan Ramachandran NAIR†
Inter Disciplinary Research Group, Vikram Sarabhai Space Centre, Trivandrum 695022, India
†Department of Chemistry, University of Kerala, Trivandrum 695034, India
(Received July 23, 1990)

The ternary oxide system MoO_3–SiO_2–Al_2O_3 was prepared by coprecipitation method. The pH of coprecipitation has been varied from pH=2 to pH=8 and its effect on the acidic properties of the ternary oxide acidic system was studied by butylamine titration. The MoO_3–SiO_2–Al_2O_3 prepared from highly acidic solution has low acid strength. The total acid amount of the ternary oxide decreased considerably at higher pH (>6) of coprecipitation. It was found that the total acid amount of MoO_3–SiO_2–Al_2O_3 containing 9.7% (by weight) of MoO_3 and silica to alumina molar ratio 16.6 is very high compared with that of SiO_2–Al_2O_3 of the same silica to alumina molar ratio. The acid strength of SiO_2–Al_2O_3 is reduced by the incorporation of MoO_3. Increase in calcination temperature increased the acid strength. The catalytic activity of MoO_3–SiO_2–Al_2O_3 was found to be very high for the alkylation of toluene with 2-propanol. The products are found to be *o*-cymene, *p*-cymene, and three isomers of diisopropyltoluenes. Reaction temperature >200 °C, higher liquid hourly space velocity, and higher alcohol content in the feed decreased the total conversion of 2-propanol to isopropyltoluenes. The acidic property and catalytic activity of MoO_3–SiO_2–Al_2O_3 are not considerably reduced up to four successive regeneration cycles.

Transition metal oxides as such are impractical acid catalysts due to their low acid strength and low value of acid amount. But binary oxides containing transition metal oxides and silica or alumina serve effective catalysts in various acid-catalyzed reactions.[1–5] Similarly many combinations of transition metal oxides viz. TiO_2–ZnO,[6] TiO_2–MoO_3,[7,8] TiO_2–V_2O_5,[8,9] ZnO–Fe_2O_3,[10] and WO_3–TiO_2[11] also have been found to show remarkable acidic properties and catalytic activities. The recent studies by K.V.C. Rao et al. on the ternary oxide sytem TiO_2–SiO_2–Al_2O_3 indicated their utility as acid catalysts in a wide range of alkylation reactions.[12] Also it has been found that the acidity distribution of this ternary oxide system depends on various parameters which include the pH of the solution from which the hydroxides of the component metals of the ternary oxides are coprecipitated, transition metal oxide content and calcination temperature.[13]

Even though MoO_3 supported on SiO_2–Al_2O_3 (Mosial) is also known to catalyze effectively certain oligomerization and polymerization reactions,[14–16] a systematic study on the synthesis of Mosial catalysts and their acidity distributions are not previously attempted. Thus in the present paper, we report the acidic and catalytic properties of a series of Mosial catalysts synthesized by changing the pH of the coprecipitating solution. The acidity distributions are evaluated using butylamine titration technique[17] and the alkylation of toluene with 2-propanol has been selected as the test reaction for comparing the activities of different Mosial catalysts. The effect of calcination temperature on the acidic and catalytic properties, and the effect of process parameters such as temperature and liquid hourly space velocity (LHSV) on the catalytic activity of alkylation are also studied. The regeneration studies on the catalyst have also been included.

Experimental

Materials: The materials used are sodium silicate (Scientific Chemicals), aluminium sulfate (A.R. grade), ammonium molybdate (BDH), 2-propanol (BDH), butylamine (SD Chemicals), nitric acid, and ammonia of chemically pure quality. The indicators used are Neutral Red (pK_a=+6.8), Methyl Red (pK_a=+4.8), Dimethyl Yellow (pK_a=+3.3), phenylazodiphenylamine (pK_a=+1.5), Crystal Violet (pK_a=+0.8), dicinnamylideneacetone (pK_a=−3.0), benzylideneacetophenone (pK_a=−5.6), and anthraquinone (pK_a=−8.2).

Preparation of MoO_3-SiO_2-Al_2O_3: To an aqueous solution of sodium silicate (260 g dm^{-3} of water), dilute nitric acid (1 : 1) is added at 90 °C under constant agitation, till the pH of

Table 1. Physicochemical Characteristics of Different Mosial Catalysts Calcined at 600 °C

Sample	pH of co-ppt	SiO_2/Al_2O_3 molar ratio	% MoO_3 (by weight)	Pore vol	Surface area
				$cm^3\ g^{-1}$	$m^2\ g^{-1}$
Mosial-2	2	48.2	11.5	0.54	52
Mosial-3	3	40.5	10.3	0.63	61.5
Mosial-4	4	16.6	9.7	0.67	83
Mosial-5	5	9.3	9.2	0.57	57
Mosial-6	6	8.8	6.4	0.36	38
Mosial-7	7	8.4	5.5	0.28	33
Mosial-8	8	8.1	5.3	0.04	8
SiO_2–Al_2O_3	4	16.3	—	1.20	135

the solution is reduced to one. Hot aluminium sulfate solution (100 g in 300 dm^3 of water) is added followed by the addition of ammonium molybdate solution (15 g in 100 dm^3 of water). Ammonia solution is added slowly, till the required pH is attained. The precipitations are carried out at different pH's (2,3,4,5,6,7,8, and 9) and are designated as Mosial-2, Mosial-3 and so on. A SiO_2–Al_2O_3 catalyst is also synthesized at pH 4 without molybdenum oxide. The precipitates are washed with distilled water till free from sulfate ion and are extruded as pellets. These are dried at 120 °C for 12 h and sintered at 600 °C. The Mosial-4 samples were also calcined at different temperatures viz. 150, 300, and 1000 °C.

The physical parameters such as surface area (BET) and pore volume, the silica to alumina molar ratio as well as molybdenum oxide contents of different Mosial catalyst (calcined at 600 °C) determined by chemical analysis are shown in Table 1.

Measurement of Acidity: The acid amounts and acid strength of samples were measured by titrating the 100—200 mesh powder, suspended in dry benzene with butylamine solution in dry benzene using the above mentioned indicators.

Measurement of Catalytic Activity: The isopropylation of toluene with 2-propanol were carried out in a fixed bed tubular reactor at 200 °C (LHSV 0.5 h^{-1}; toluene/2-propanol mole ratio 3; total reaction time 7 h) using all the catalysts synthesized. The effect of temperature on the alkylating activity of Mosial-4 catalyst has been studied at five different temperatures viz. 160, 180, 200, 220, and 240 °C (LHSV 0.5 h^{-1}; toluene/2-propanol mole ratio 3; total reaction time 3 h). Similarly the effect of LHSV on the alkylating activity of Mosial-4 is also studied at three different LHSV viz. 0.5, 1, and 2 (temperature 200 °C, toluene/2-propanol mole ratio 3; total reaction time 7 h). The reactor was fed under gravitational flow. The amount of catalyst used was 25 g which corresponds to 60 ml in volume. The reactor, experimental and analytical procedures of the product mixtures, and method of calculation of percentage yields of isopropyltoluene were the same as those employed in the previous work.[18]

To estimate the catalyst life for alkylation, the same catalyst (Mosial-4 calcined at 600 °C) is subjected to nine successive regenerations by passing air at 600 °C for 5 h, at the end of each alkylation experiment of 7 h.

The products are found to be *o*-cymene, *p*-cymene, and three isomers of diisopropyltoluenes (DIT).

Results and Discussion

The physical characteristics such as surface area and porosity are found to be optimum for the ternary oxide system coprecipitated from solution of pH 4 whereas these two parameters have been considerably reduced by the coprecipitation of the ternary oxide from highly acidic and highly alkaline solutions (Table 1). But the surface area of SiO_2–Al_2O_3 is comparatively high. The percentage of MoO_3 content decreased marginally and the silica to alumina ratio decreased drastically with the increase in the pH of coprecipitation.

Even though activated Al_2O_3 has moderately strong Lewis acid centers,[14] pure silica gel is inactive in demanding acid-catalyzed reactions as the acid strength value of surface SiOH groups is very low.[20] But several combinations of metal oxides each of which contains either SiO_2 or Al_2O_3 have been extensively used as useful catalysts in various acid-catalyzed reactions. Similarly transition metal oxides viz. TiO_2, MoO_3, etc. are impractical acid catalysts due to their low acid strength values, but serve as effective acid catalysts on combination with either SiO_2 or Al_2O_3.[1,3,4] The enhancement in the catalytic properties is attributed to increase in the acid strength and acid amount values of these binary oxides compared with the component single oxides. As reported recently, the incorporation of 10% (by weight) of TiO_2 into a SiO_2–Al_2O_3 support greately changed the acidity distribution of the latter.[13] Table 2 shows the acidity distribution of a series of MoO_3–SiO_2–Al_2O_3 samples calcined at 600 °C. The acidity distributions of all the Mosial samples differ greatly from that of SiO_2–Al_2O_3 as the latter possesses

Table 2. Acidity Distribution of Different Mosial Catalysts Calcined at 600 °C

Sample	Acid amount (mmol g^{-1}) at different pK_a's							
	+6.8	+4.8	+3.3	+1.5	+0.8	−3.0	−5.6	−8.2
Mosial-2	0.66	0.41	0.18	0.10	0.00	0.00	0.00	0.00
Mosial-3	0.61	0.48	0.32	0.14	0.05	0.00	0.00	0.00
Mosial-4	0.58	0.58	0.58	0.58	0.48	0.05	0.00	0.00
Mosial-5	0.55	0.55	0.55	0.55	0.46	0.10	0.00	0.00
Mosial-6	0.41	0.41	0.27	0.25	0.25	0.05	0.00	0.00
Mosial-7	0.37	0.34	0.22	0.21	0.21	0.02	0.00	0.00
Mosial-8	0.34	0.31	0.22	0.20	0.20	0.03	0.00	0.00

Table 3. Acidity Distribution of Mosial-4 Samples Calcined at Different Temperatures

Temperature of calcination/°C	Acid amount (mmol g^{-1}) at different pK_a's							
	+6.8	+4.8	+3.3	+1.5	+0.8	−3.0	−5.6	−8.2
150	0.64	0.48	0.24	0.15	0.00	0.00	0.00	0.00
300	0.61	0.52	0.32	0.30	0.05	0.00	0.00	0.00
600	0.58	0.58	0.58	0.58	0.48	0.05	0.00	0.00
1000	0.03	0.03	0.03	0.03	0.03	0.03	0.00	0.00

only too strong acid sites. Also it is well-known that MoO_3 is devoid of acid sites of strength $H_o<+4.8$.[5] Hence it is clear that new acidic sites which differ from those of MoO_3, SiO_2, Al_2O_3, and SiO_2–Al_2O_3 are created on the surface of the ternary oxide MoO_3–SiO_2–Al_2O_3.

However, the acidity distribution of MoO_3–SiO_2–Al_2O_3 system depends mainly on the pH of the final gel during coprecipitation. The Mosials prepared from highly acidic solutions contain mainly weak acid sites ($H_o>+1.5$) whereas a pH of 4 appears optimum in producing acid sites of fairly high acid strength and large acid amount. But further increase in pH decreased the total acid amount values even though the acid strength is not affected. The pH of the coprecipitating solution is shown to have pronounced effect on the compositions of ternary oxides prepared (Table 1). This change in composition, especially the drastic change in silica to alumina mole ratio can be a probable factor governing the acidity distribution.[13]

The acid strength of MoO_3–SiO_2–Al_2O_3 ($H_o \geqslant -3.0$) (Table 2) is comparatively lower than that of TiO_2–SiO_2–Al_2O_3 which is around $H_o=-5.6$.[13] The latter possesses even few acid sites of strength $H_o=-8.2$.[13] This can be probably due to the difference in the averaged electronegativity values of the component metal ions of these two ternary oxide systems.[21]

Effect of Calcination Temperature on Acidity Distribution: Table 3 shows that the Mosial-4 sample calcined at 150 °C is rich in weak acid site ($H_o \geqslant +3.3$) and does not contain any strong acid site. But on increasing the calcination temperature to 300 °C, moderately strong acid site appeared, which may be due to the conversion of weak acid sites to stronger Lewis sites, caused by the loss of water molecules. Mosial-4 sample calcined at 600 °C contains only moderately strong acid sites whereas further increase in calcination temperature to 1000 °C caused almost a complete destruction of acid sites.

Catalytic Activity: The enhancement in the catalytic activity of Mosial-4 and Mosial-5 compared with SiO_2–Al_2O_3 in the alkylation of toluene with 2-propanol (Fig. 1) can be due to the increased acid amount of the ternary oxide system (Table 2). Our earlier studies on TiO_2–SiO_2–Al_2O_3 have also shown that the transition metal oxide exerts a synergistic effect up on the alkylating activity of SiO_2–Al_2O_3.[18] When transition metal

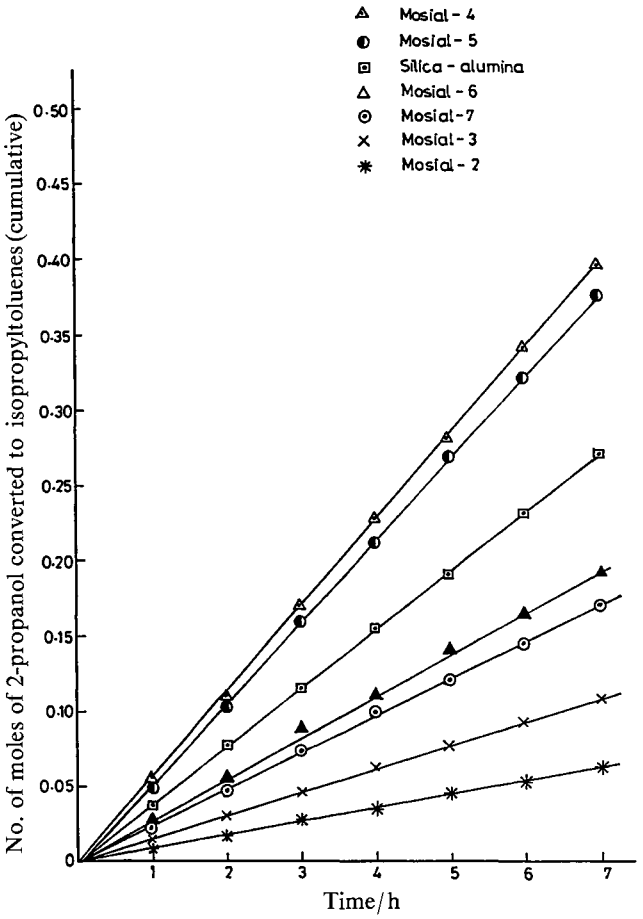

Fig. 1. Cumulative number of moles of 2-propanol converted to isopropyl toluenes over various Mosial catalysts. Reaction conditions: Reaction temperature: 200 °C; Liquid hourly space velocity: 0.5 h^{-1}; Toluene/2-propanol mole ratio: 3.

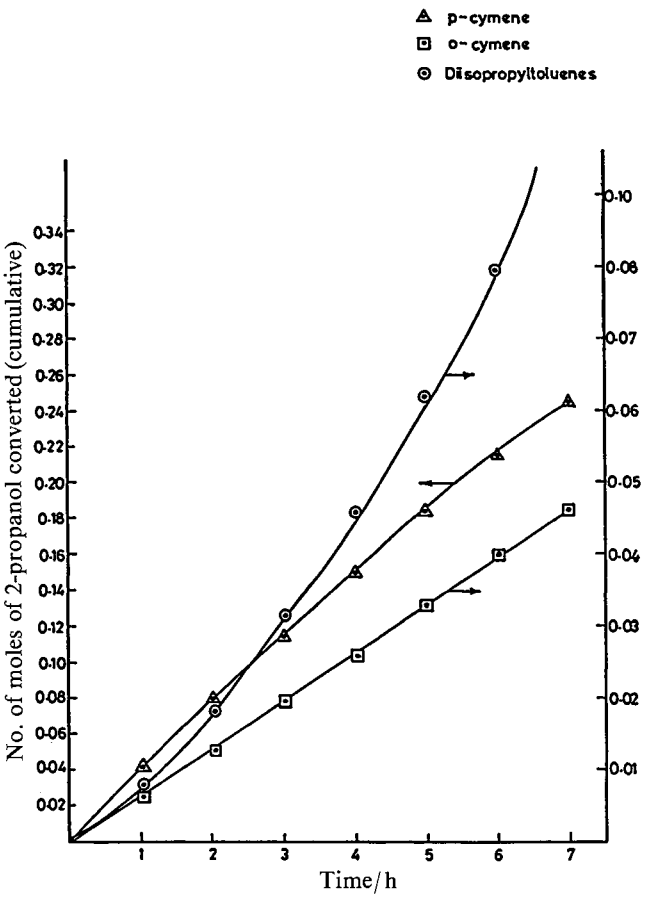

Fig. 2. Cumulative number of moles of 2-propanol converted to *o*-cymene, *p*-cymene, and diisopropyltoluenes over Mosial-4 catalyst. Reaction conditions: Reaction temperature: 200 °C; Liquid hourly space velocity: 0.5 h^{-1}; Toluene/2-propanol mole ratio: 3.

oxides are supported on SiO_2–Al_2O_3, $\overset{+}{M}$–H species are formed where M is the transition metal atom and these species are of suitable acid strength to initiate the alkylation reaction.[18] The $\overset{+}{M}$–H species interacts with the 2-propanol to produce $\overset{+}{M}$–$CH(CH_3)_2$ as shown in Scheme 1 which in turn forms a π-complex with the aromatic substrate, due to the low lying unoccupied d orbitals of the transition metal atom.[18] This π-complex on a π–σ rearrangement gives isopropyltoluenes.[18]

However Mosial-2, Mosial-3, Mosial-6, and Mosial-7 samples exhibited less alkylating activity (Fig. 1) which may be due to the low acid strength and low acid amount values respectively of the former and latter pairs (Table 2). But the rate of formation of isopropyltoluenes remained constant throughout the reaction time for all the catalysts studied (Fig. 1). Even though the product mixture is rich in *p*-cymene content which could be due to steric factors arising when the reacting species are adsorbed on adjoining sites,[22] the extent of formation of *p*-cymene decreased and a corresponding increase in the formation of diisopropyltoluenes was observed with the passing of reaction time (Fig. 2). Hence it could be depicted that the adsorbed *p*-cymene molecules are more prone to get further alkylated to produce diisopropyltoluenes.[18] However the rate of formation of *o*-cymene is unaffected by reaction time. These observations are in good agreement with the results obtained in the alkylation studies of toluene with 2-propanol over TiO_2–SiO_2–Al_2O_3.[18]

Effect of Temperature: The conversion of 2-propanol to isopropyltoluenes increased as the reaction temperature increased from 160 to 200 °C (Fig. 3). Further increase in temperature decreased the conversion. But the unreacted alcohol in the product mixtures is practically nil, irrespective of the reaction temperature (Fig. 3). This shows that the dehydration of 2-propanol is possible over Mosial-4 even at lower temperatures. As shown in Scheme 1, both the dehydrated product (propylene) as well as the alkylated product (isopropyltoluenes) may be formed from the same intermediate, $\overset{+}{M}$–isopropyl.[23] The increase in the reaction temperature from 160 °C to 200 °C may enhance the interaction between the entity $\overset{+}{M}$–isopropyl and the toluene molecule due to the effective diffusion of the latter molecules into the interior surfaces of the catalysts pellet.[23]

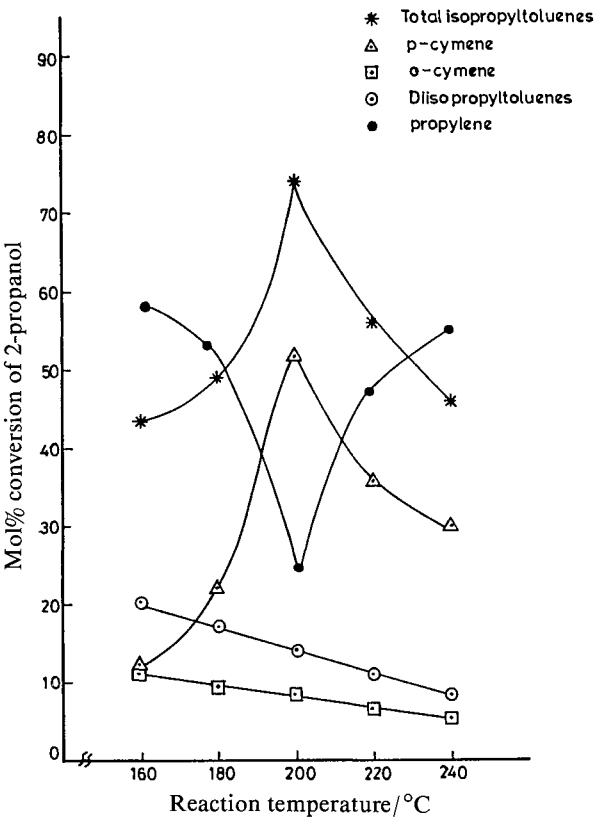

Fig. 3. Effect of reaction temperature on the conversion of 2-propanol to isopropyltoluenes over Mosial-4 catalyst. Reaction conditions: Liquid hourly space velocity: 0.5 h^{-1}; Toluene/2-propanol mole ratio: 3.

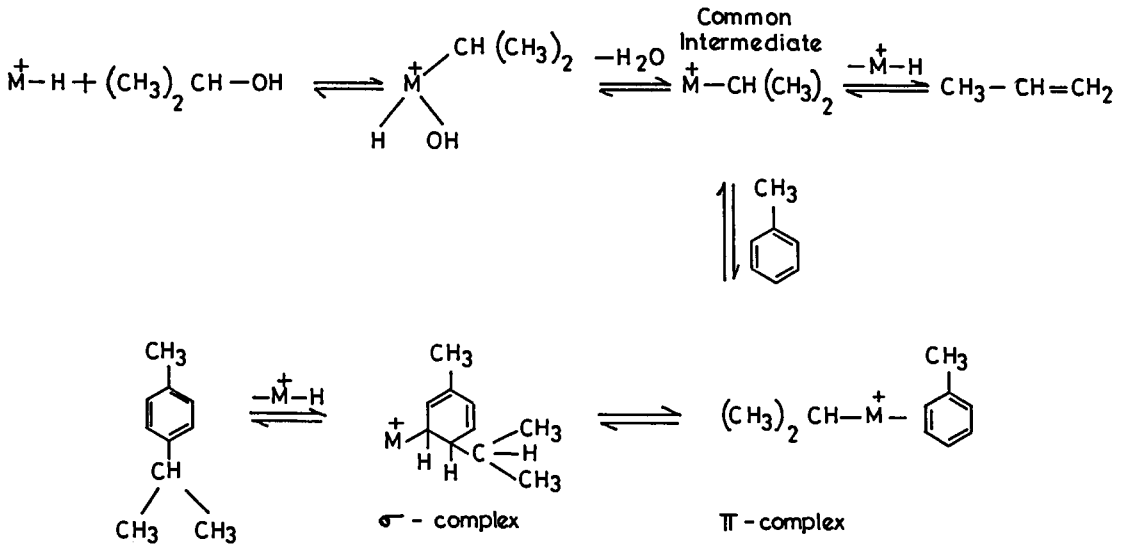

Scheme 1. The mechanism of alkylation of toluene with 2-propanol over MoO_3–SiO_2–Al_2O_3 catalyst.

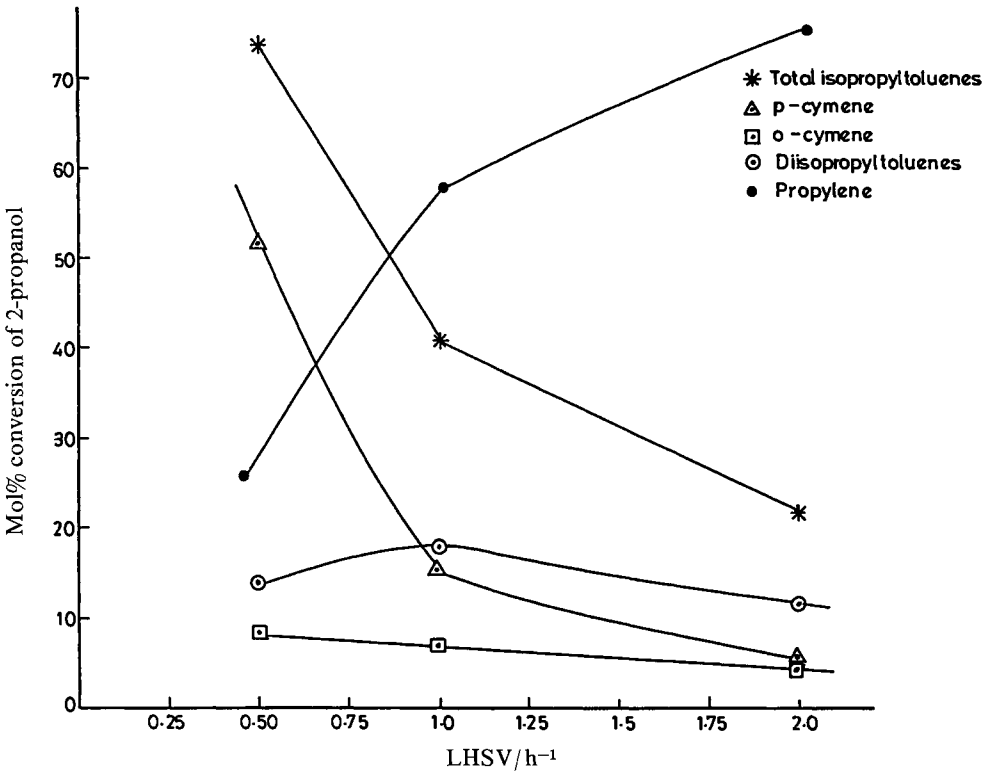

Fig. 4. Effect of liquid hourly space velocity on the conversion of 2-propanol to isopropyltoluenes over Mosial-4 catalyst. Reaction conditions: Reaction temperatures: 200 °C; Toluene/2-propanol mole ratio: 3.

However, at very high reaction temperatures (>200 °C), the formed isopropyltoluene molecules may undergo dealkylation to toluene which could be a probable reason for the decreased conversions. Similarly, the dealkylation of formed cymene molecules at reaction temperatures >200 °C has been observed by us earlier over TiO_2–SiO_2–Al_2O_3 catalyst in the alkylation of toluene with 2-propanol.[18] The *o*-cymene formation decreased marginally with the increase in reaction temperature whereas the optimum formation of *p*-cymene is observed at 200 °C. However in the product mixture, the para-isomer content is more irrespective of the reaction temperature studied, which could be due to the steric factors arising between the reacting species as discussed previously.[22] Hence it may be presumed that the interaction between an adsorbed toluene molecule and the adsorbed alkylating moiety leads to the formation of the para-isomer whereas the interaction of the latter with a free unadsorbed toluene in the gaseous state results in the formation of ortho-isomer.[18] Also it could be depicted that the formation of cymene molecules via the former route take place on the interior surface of the catalyst pellet, the rate of which is enhanced by the effective diffusion of the toluene molecules into the pores of the catalyst pellet.[23] Hence the marginal decrease in the formation of *o*-cymene and increase in the formation of *p*-cymene with increase in reaction temperature. These observations are also in line with those of alkylation reactions carried out over ion-exchanged zeolites.[24]

Increased formation of diisopropyltoluene is observed at lower reaction temperatures. This may be due to the high residence time of cymene molecules formed at lower temperatures, resulting in further alkylation.[18] Multialkylations are generally favored at lower reaction temperature.[25]

Effect of LHSV: As the LHSV increased from 0.5 to 2, the conversion of 2-propanol to isopropyltoluenes decreased drastically (Fig. 4). However unreacted 2-propanol has not been observed in the product mixture in all cases. It may be assumed that at higher LHSV, because of the less effective diffusion of the toluene molecules into the interior surface of the catalyst pellet, the $\overset{+}{M}$–isopropyl species formed there leads to propylene formation and hence the decreased conversions to *p*-cymene and marginal increase in the formation of *o*-cymene.[23] Also at higher LHSV, the formed cymene molecules may get further alkylated by $\overset{+}{M}$–isopropyl species, even before desorbing out from the reaction site, causing increase in the formation of diisopropyltoluenes.

Effect of Toluene/2-Propanol Mole Ratio in the Feed: The conversion of 2-propanol to isopropyltoluenes decreased considerably with the increase in the alcohol content in the feed (Fig. 5). However at these conditions, the dehydration of 2-propanol to propylene predominated, which suggests that large excess of toluene in the feed suppresses the formation of propyl-

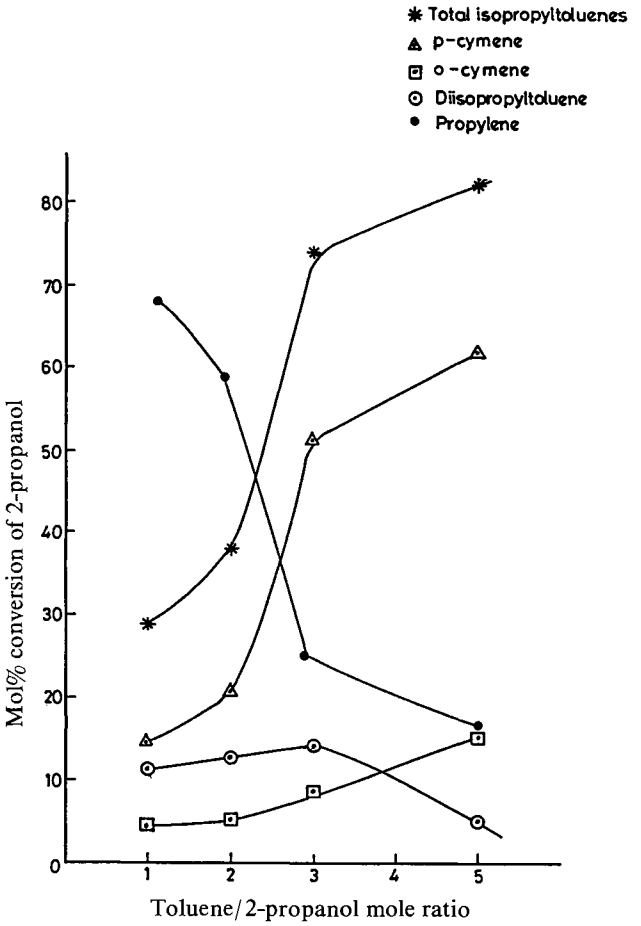

Fig. 5. Effect of toluene/2-propanol mole ratio on the conversion of 2-propanol to isopropyltoluene over Mosial-4 catalyst. Reaction conditions: Reaction temperature: 200 °C; Liquid hourly space velocity: 0.5 h^{-1}.

ene from $\overset{+}{M}$–isopropyl, causing increased conversions to isopropyltoluenes. Similarly, increased conversions to isopropylbenzene have been observed by K. H. Chandavar et al.[26] in the isopropylation of benzene at higher benzene to alcohol mole ratio.

Also the large excess of the aromatic substrate in the feed decreased the formation of diisopropyltoluene and caused marginal increase in the conversion to *o*-cymene (Fig. 5).

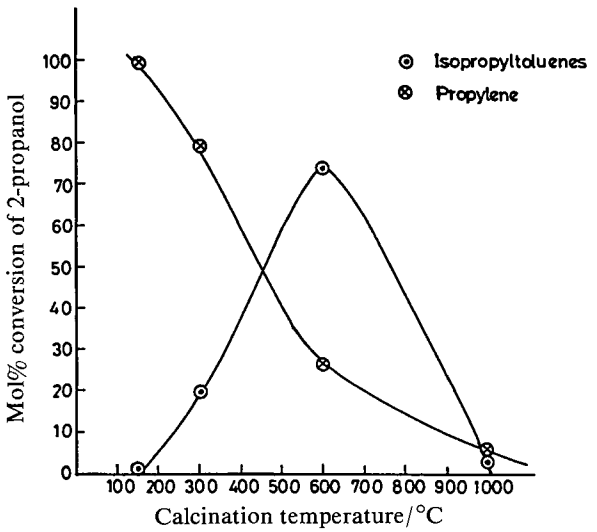

Fig. 6. Effect of calcination temperature on the alkylating activity of Mosial-4 catalyst. Reaction conditions: Reaction temperature: 200 °C; Liquid hourly space velocity: 0.5 h^{-1}; Toluene/2-propanol mole ratio: 3.

Effect of Calcination Temperature: The optimum conversion of 2-propanol to isopropyltoluenes is given by Mosial-4 samples calcined at 600 °C (Fig. 6) which has a high acid strength value and fairly large acid amount (Table 3). Even though the samples calcined at lower temperatures are less active in catalyzing the alkylation of toluene, they served as effective catlaysts in the dehydration of alcohol molecules which is evidenced by the quantity of propylene produced (Fig. 6).

The Regenerability of Mosial-4: The acidity distribution of Mosial-4 is negligibly affected by four or five successive regeneration cycles (Table 4). Correspondingly, the alkylating activity of the sample also is almost unaffected which is evidenced from (Fig. 7). However further regeneration cycles reduced alkylating activity.

Conclusion

The total acid amount of MoO_3–SiO_2–Al_2O_3 containing 9.7% by weight of MoO_3 and silica to alumina molar

Table 4. Effect of Successive Regeneration Cycles on the Acidity Distribution of Mosial-4

No. of regeneration cycle	Acid amount (mmol g^{-1}) at different pK_a's							
	+6.8	+4.8	+3.3	+1.5	+0.8	−3.0	−5.6	−8.2
0	0.58	0.58	0.58	0.58	0.48	0.05	0.00	0.00
1	0.58	0.58	0.58	0.58	0.48	0.05	0.00	0.00
2	0.57	0.57	0.57	0.57	0.48	0.04	0.00	0.00
3	0.55	0.55	0.55	0.55	0.48	0.04	0.00	0.00
4	0.53	0.53	0.53	0.53	0.46	0.04	0.00	0.00
5	0.49	0.49	0.49	0.49	0.44	0.03	0.00	0.00
6	0.44	0.44	0.44	0.44	0.40	0.02	0.00	0.00
7	0.38	0.38	0.38	0.38	0.36	0.02	0.00	0.00
8	0.32	0.32	0.32	0.32	0.10	0.00	0.00	0.00
9	0.27	0.27	0.27	0.27	0.10	0.00	0.00	0.00

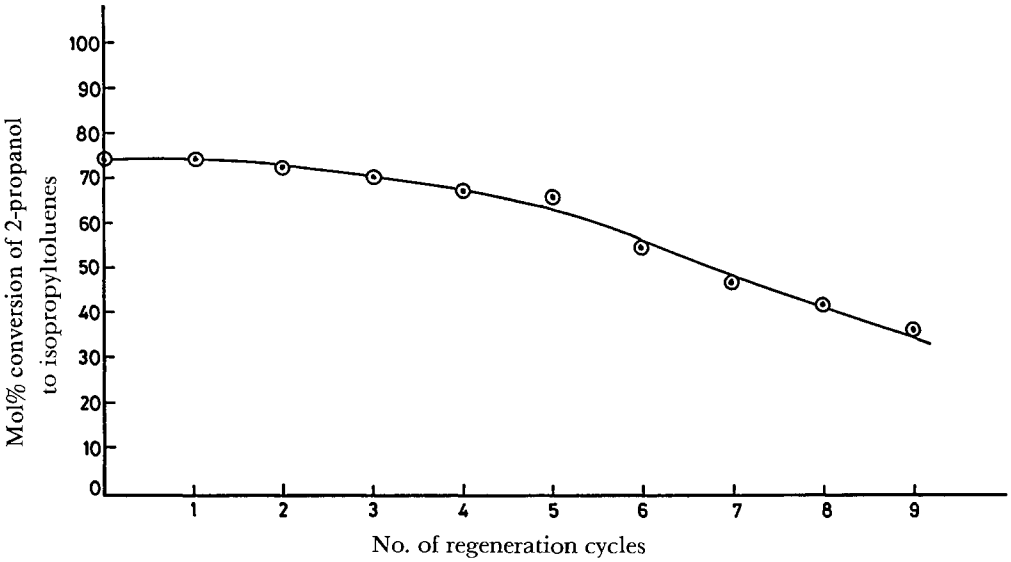

Fig. 7. Effect of successive regeneration cycles on the alkylating activity of Mosial-4 catalyst. Reaction conditions: Reaction temperature: 200 °C; Liquid hourly space velocity: 0.5 h^{-1}; Toluene/2-propanol mole ratio: 3.

ratio 16.6 is very high compared to that of SiO_2–Al_2O_3 of the same silica to alumina molar ratio. The acid strength of SiO_2–Al_2O_3 is reduced by the incorporation of MoO_3. Also the ternary oxide system coprecipitated from highly acidic solution has low acid strength and that coprecipitated from highly alkaline solution has low acid amount. The catalytic activity of MoO_3–SiO_2–Al_2O_3 for the alkylation of toluene with 2-propanol is very high compared with that of SiO_2–Al_2O_3. However reaction temperatures >200 °C, higher liquid hourly space velocity and higher alcohol content in the feed decreased the total conversion of 2-propanol to isopropyltoluenes. The acidic property and catalytic activity of MoO_3–SiO_2–Al_2O_3 are not considerably reduced up to four successive regeneration cycles.

The authors acknowledge the support and encouragement given by Director, V. S. S. C. They also acknowledge the help rendered by Dr. V. N. Krishnamurthy, Dr. M. Rama Rao, Dr. V. G. Kumar, Dr. T. S. Radhakrishnan, Dr. S. Venkatachalam, and Mr. R. Natarajan. One of the authors (K. R. Sabu) acknowledges the aid given to him by the U.G.C. in the form of a Senior Research Fellowship for carrying out this work.

References

1) R. Rodenas, T. Yamaguchi, H. Hattori, and K. Tanabe, *J. Catal.*, **69**, 434 (1981).
2) K. Tanabe, T. Sumiyoshi, and H. Hattori, *Chem. Lett.*, **1972**, 723.
3) K. Tanabe, M. Ito, and M. Sato, *Chem. Commun.*, **1973**, 676.
4) Y. Watanabe and N. Nojiri, *Nippon Kagaku Kaishi*, **1974**, 540.
5) K. Maruyama, H. Hattori, and K. Tanabe, *Bull. Chem. Soc. Jpn.*, **50**, 86 (1977).
6) K. Tanabe, C. Ishiya, I. Matsuzaki, I. Ichikawa, and H. Hattori, *Bull. Chem. Soc. Jpn.*, **45**, 47 (1973).
7) M. Ai and S. Suzuki, *Shokubai*, **15**, 159 (1973).
8) M. Ai, *Bull. Chem. Soc. Jpn.*, **49**, 1328 (1976).
9) H. Miyata, K. Fuji, and T. Ono, *J. Chem. Soc., Faraday Trans. 1*, **84**, 3121 (1988).
10) T. Kotanigawa, *Bull. Chem. Soc. Jpn.*, **47**, 950 (1974).
11) A. Andreini and J. C. Mol, *J. Chem. Soc., Faraday Trans. 1*, **81**, 1705 (1985).
12) V. G. Kumar, T. S. Shoba, and K. V. C. Rao, *Tetrahedron Lett.*, **26**, 3281 (1985).
13) K. R. Sabu, K. V. C. Rao, and C. G. R. Nair, *Bull. Chem. Soc. Jpn.*, **63**, 3632 (1990).
14) V. G. Kumar, M. Rama Rao, P. V. Ravindran, and K. V. C. Rao, *J. Polym. Soc., Polym. Chem. Ed.*, **21**, 2133 (1983).
15) V. G. Kumar, S. Venkatachalam, and K. V. C. Rao, *J. Polym. Sci., Poly. Chem. Ed.*, **22**, 2317 (1984).
16) S. Venkatachalam, V. G. Kumar, and K. V. C. Rao, *J. Polym. Sci., Polym. Chem. Ed.*, **22**, 3805 (1984).
17) H. A. Benesi, *J. Phys. Chem.*, **61**, 970 (1957).
18) K. V. C. Rao, K. R. Sabu, and C. G. R. Nair, *Bull. Chem. Soc. Jpn.*, **62**, 2657 (1989).
19) E. P. Parry, *J. Catal.*, **2**, 371 (1963).
20) H. A. Benesi and B. H. C. Winquist, *Adv. Catal.*, **27**, 120 (1978).
21) K. Shibata, T. Kiyoura, J. Kitagawa, T. Sumiyoshi, and K. Tanabe, *Bull. Chem. Soc. Jpn.*, **46**, 2985 (1973).
22) S. G. T. Bhat, *J. Catal.*, **75**, 196 (1982).
23) K. R. Sabu, K. V. C. Rao, and C. G. R. Nair, Proceedings of the 42nd Indian Chemical Engineering Congress, Trivandrum, India, 15—18 December 1989, Abstr., Vol. II, p. 233.
24) S. G. T. Bhat, *Indian J. Technol.*, **21**, 65 (1983).
25) A. V. Deo, R. M. Cursetji, M. A. Purohit, V. G. Penkar, and V. V. Deshmukh, *Indian J. Technol.*, **21**, 363 (1983).
26) K. H. Chandavar, S. G. Hedge, S. B. Kulkarni, and P. Ratnasamy, *J. Chem. Tech. Biotechnol.*, **34A**, 165 (1984).

 © 1991 The Chemical Society of Japan Bull. Chem. Soc. Jpn., 64, 1933—1937 (1991)

Photocatalytic Activities of Bi_2O_3, WO_3, and Fe_2O_3: An Assessment through Decomposition of Peroxomonosulfate in Visible Radiation

Pichai MARUTHAMUTHU,* Karuppusamy GURUNATHAN, Esaikkiappan SUBRAMANIAN, and Muthupandian ASHOKKUMAR

Department of Energy, University of Madras, A. C. College Campus, Madras 600025, India

(Received August 27, 1990)

Bi_2O_3 semiconductor powder (E_g=2.8—2.9 eV) was chosen for the first time to effect photocatalysis and was found to decompose peroxomonosulfate (PMS) with visible light of $\lambda > 400$ nm. Doping of Bi_2O_3 with Cu(II)-ion considerably enhanced the photocatalytic efficiency. The effects of variation of (i) the [dopant] in Cu(II)/Bi_2O_3, (ii) the catalyst amount, and (iii) the initial [PMS] on the rate of decomposition of PMS were investigated. It was observed that (a) 4 atomic % was the optimum [dopant] for Cu(II)/Bi_2O_3, (b) the rate increased linearly with increase in catalyst amount, and (c) the decomposition of PMS followed a Langmuir kinetics in the concentration range, $[PMS]_0$=0.5—3.0×10^{-3} mol dm^{-3}. A suitable reaction mechanism is proposed for the decomposition of PMS involving all the possible reactions. A comparative analysis of the photocatalytic activities of undoped and Cu(II)-doped Bi_2O_3, WO_3, and Fe_2O_3 indicated that Cu(II)-doping enhances the activity of Bi_2O_3 to a greater extent than those observed with the other two semiconductors. This photocatalytic decomposition of PMS is one of the examples of visible light assisted reaction which otherwise takes place under UV radiation ($\lambda \leqslant 280$ nm) only.

The search for viable means of conversion of solar energy into other forms has gained momentum during the past few years and the role of semiconductors in this aspect has occupied a prominent place.[1] The oxide semiconductors, especially in the form of powders appear to be most promising for photocatalysis because of their inherent advantages such as (1) resistance to photocorrosion,[2] (2) stability in both the acidic and alkaline media, and (3) larger surface area needed for photocatalysis. Many reports on the photocatalytic activities of several oxide semiconductors, TiO_2, ZnO, SnO_2, Fe_2O_3 etc., are already available. Using WO_3, we have recently reported the photocatalytic decomposition of peroxides[3] and the photocleavage of water.[4,5]

Although the investigations with oxide semiconductors are numerous, so far only a few studies with Bi_2O_3 have been reported, despite the fact that the band-gap energy (E_g) of this semiconductor is only 2.8—2.9 eV, which absorbs more solar radiation in the visible region compared to that of either TiO_2 or $SrTiO_3$ with which numerous investigations are available. In studies conducted over the years, Bi_2O_3 has been used as a stabilizing agent and/or as a dopant in solid electrolytes. Kruidhof et al.[6,7] have prepared, characterized, and investigated the mechanical properties of Bi_2O_3-based ceramics. Winnubst and Burggraaf[8] have also prepared and studied the electrical properties of monophasic Y_2O_3-stabilized ZrO_2 doped with Bi_2O_3. In both these studies, it has been reported that the inclusion of Bi_2O_3 enhances the stability of the solid electrolyte. Only one study[9] has been carried out in detail on the photoelectrochemical properties of anodic Bi_2O_3 films. Since investigation dealing with the photocatalytic aspects of Bi_2O_3 semiconductor powder is found absent, the present work which involves the assessment of the photocatalytic activities of undoped and Cu(II)-doped Bi_2O_3 through visible light assisted decomposition of peroxomonosulfate (PMS, HSO_5^-) and comparison of the efficiencies of the above catalysts with those of undoped and Cu(II)-doped WO_3 and Fe_2O_3, are attempted. The findings of this work are significant because they brighten the possibility of Bi_2O_3 application for photocatalysis in future. This study also serves as an example for visible light assisted decomposition of PMS which otherwise happens only by UV irradiation, $\lambda \leqslant 280$ nm.

Experimental

Bi_2O_3, WO_3, and Fe_2O_3 semiconductors (99.9%) were obtained from Fluka. PMS was from E.I. du Pont de Nemours & Co., USA and was used as such. Other chemicals used were of the purest research grade available.

In catalyst preparation, a high-temperature sintering technique was used. The Cu(II)-doped (at different atomic %) semiconductor catalysts were prepared as follows: a calculated quantity of $CuCl_2$ salt (99%) was added to the aqueous slurry of the semiconductor and it was stirred magnetically for 2 hours, dried in an air oven at 110 °C and sintered at 400—500 °C for Bi_2O_3, 700—800 °C for WO_3, and 1200—1300 °C for Fe_2O_3. The sintered samples were then ground to fine powders and stored in light-proof vials. Undoped samples of Bi_2O_3, WO_3, and Fe_2O_3 were also processed in a similar manner at temperatures mentioned above. The surface areas of the catalysts were determined by Quantasorb surface area analyzer and found to be 2.0—3.0 $m^2 g^{-1}$. The catalysts were also characterized by diffuse reflectance spectra (Hitachi, Japan) and X-ray diffraction methods (Philips, Holland).

A typical procedure followed in the photocatalytic experiment is given below. 40 ml of the PMS solution ($[PMS]_0$= 0.5—3.0×10^{-3} mol dm^{-3}) in water containing 40 mg of the catalyst was irradiated with visible light of $\lambda > 400$ nm from a 150-W xenon lamp (Applied Photophysics, London), after cutting off UV and IR radiations with appropriate glass filter

and water jacket, respectively. The experiment was carried out at room temperature (ca. 25 °C) and at natural pH (ca. 6). The [PMS] was estimated iodometrically and the rate was followed by determining [PMS] at various time intervals.

Determination of Quantum Yields. Quantum yields for the PMS decomposition were determined by employing potassium tris(oxalato)ferrate(III) actinometry as described in literature.[10] A range of wavelength (400—450 nm) rather than a single wavelength was selected for this determination, because in this range, all the catalysts have maximum absorption (nearly 60%) and this was taken as an advantage in the photocatalytic experiments. A 0.006 M $K_3[Fe(C_2O_4)_3]$ solution was irradiated with the same 150-W xenon lamp mentioned above, after passing the light through a band filter for the 400—450 nm range. From the amount of Fe^{2+} formed during irradiation, the light intensity of the lamp was determined assuming $\Phi=1.11$. This experiment was repeated by keeping the semiconductor slurry in the light path and from the difference in intensities, the light intensity absorbed by the semiconductor particles was calculated. The quantum yield (Φ) for the PMS decomposition reaction was determined from the relation,

$$\Phi = \frac{\text{Number of moles of PMS decomposed per second}}{\text{Number of Einsteins absorbed per second}} \quad (1)$$

Results and Discussion

Characterization of the Catalysts. In order to get an idea about the extent of absorption of the undoped and doped semiconductors in the visible region and to know the effect of Cu(II)-dopant on the crystallinity of the semiconductors, the catalysts were characterized by diffuse absorption spectra and X-ray diffraction methods. Figure 1 shows representatively, the absorption spectra of Bi_2O_3 and Cu(II)/Bi_2O_3 catalysts. Bi_2O_3 has 55% absorption upto 410 nm, 40—20% upto 500 nm and about 15% in the remaining part of the spectrum. But when it is doped with Cu(II), the absorption ranges are increased considerably. Similar is the case with WO_3. But with Fe_2O_3, since it is of dark brown color, both Fe_2O_3 and Cu(II)/Fe_2O_3 have relatively more absorp-

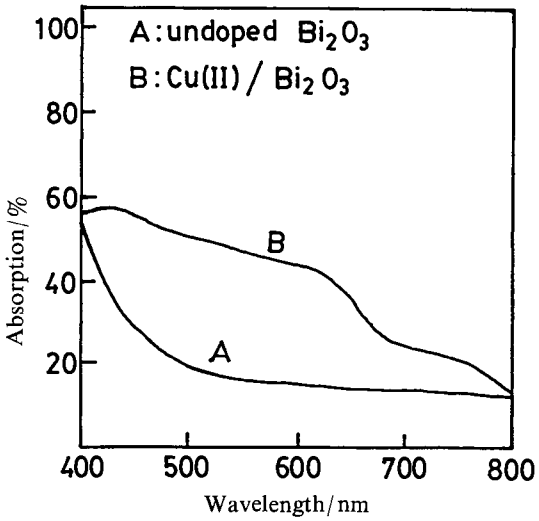

Fig. 1. Diffuse absorption spectra of undoped and doped Bi_2O_3.
A=Undoped Bi_2O_3, B=Cu(II)/Bi_2O_3.

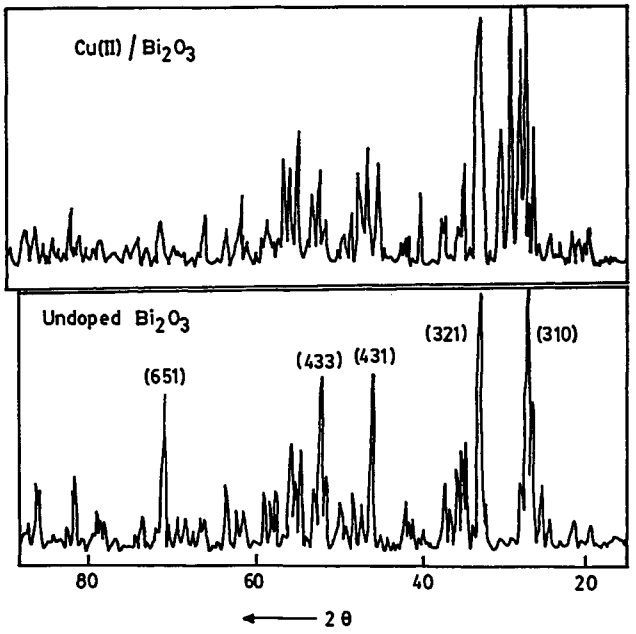

Fig. 2. XRD spectra of Cu(II)/Bi_2O_3 and undoped Bi_2O_3.

Table 1. *d*-Spacing and the Corresponding Intensity Values from the XRD Spectra

hkl Values	Literature values for γ-Bi_2O_3 (a_0=10.10 Å)		Observed values for Bi_2O_3 (a_0=10.33 Å)		Observed values for 4 at% Cu(II)/ Bi_2O_3 (a_0=10.27 Å)	
	d/Å	I/I_0	*d*/Å	I/I_0	*d*/Å	I/I_0
310	3.22	100	3.27	177	3.25	373
400	2.54	10	2.54	56	2.56	51
431	2.00	30	1.96	78	1.96	67
433	1.74	90	1.75	96	1.75	61
532	1.65	60	1.66	33	1.64	53
541	1.57	10	1.57	32	1.58	27
631	1.50	60	1.51	24	1.50	29
640	1.41	10	1.40	20	1.41	31
651	1.29	20	1.32	87	1.32	25
800	1.27	10	1.28	13	1.28	13

tion than the other two semiconductors in the entire visible region. Thus in all these semiconductors, doping of Cu(II) increases the absorption in the visible region and this has been already explained[11] as due to the introduction of 'isolated energy levels' by the dopant in the band gap of the semiconductors.

X-Ray diffraction spectra of all undoped and Cu(II)-doped semiconductors, for example, the XRD spectra of Bi_2O_3 and Cu(II)/Bi_2O_3 shown in Fig. 2 with the corresponding 'd' spacings and intensity values given in Table 1, indicate that there is no appearance of any new peaks due to Cu(II)-doping but that the intensities of the peaks are increased, even though both the doped and undoped samples were processed at the same temperature. This observation demonstrates that Cu(II)-doping increases the crystallinity of the semiconductors without affecting the original crystal structure. Thus doping with Cu(II) produces a favorable change in the catalysts by increasing the absorption as well as the crystallinity of the semiconductors.

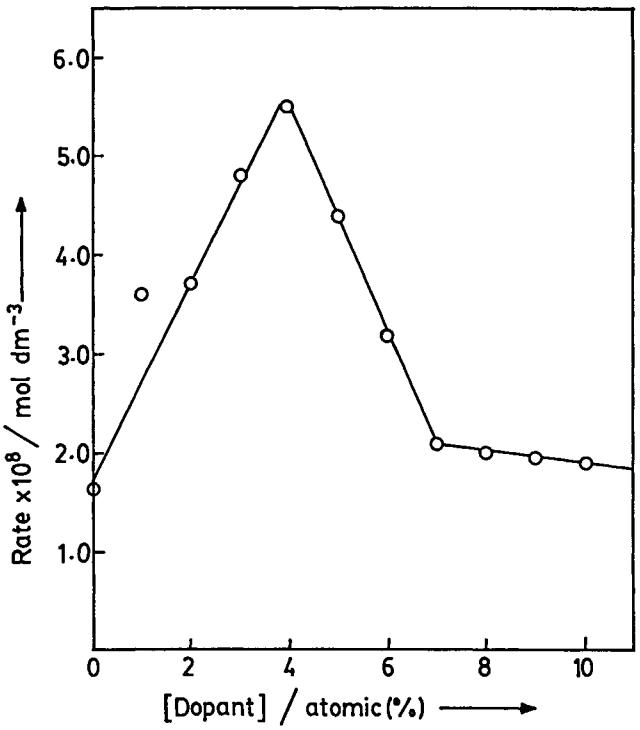

Fig. 3. Effect of variation of [dopant] on decomposition of PMS.
Catalyst (Cu(II)/Bi_2O_3)=40 mg, [PMS]=0.5×10^{-3} mol dm^{-3}, T=298 K.

Table 2. Effect of Variation of Catalyst Amount.
Catalyst=4 Atomic % Cu(II)/Bi_2O_3;
[PMS]=0.5×10^{-3} mol dm^{-3}

Catalyst amount/mg	Rate$\times10^8$ / mol dm^{-3} s^{-1}
10	5.0
20	5.2
30	5.3
40	5.5
50	5.5
60	5.5
70	5.5

Decomposition of PMS with Bi_2O_3. In the photocatalytic decomposition of PMS, both Bi_2O_3 and Cu(II)/Bi_2O_3 were used as the catalysts. The rate of decomposition of PMS was studied by varying (i) the [dopant], (ii) the catalyst amount, and (iii) the initial [PMS].

Effect of Variation of [dopant]. In our previous study with WO_3,[4] it was established that Cu(II) is an efficient dopant because of its ability to scavenge e^-_{CB} and hence to prevent e^-–h^+ recombination; therefore Cu(II)/WO_3 was found to have higher efficiency than the undoped one. In order to investigate whether the increase in [dopant] continuously enhances the photocatalytic efficiency of Bi_2O_3 or not, experiments were performed with different [dopant]. Figure 3 displays the effect of variation of [dopant] on the rate of PMS decomposition. The rate is increased with increase in [dopant] upto 4 atomic % but gets decreased beyond this limit. Therefore the optimum [dopant] at which Bi_2O_3 acquires maximum photocatalytic efficiency is 4 atomic %. This observation is explicable by the fact that Cu(II) acts as e^-_{CB} scavenger at lower [dopant] but becomes e^-–h^+ recombination centers at higher [dopant], since the distance between two Cu(II) ions becomes shorter than the distance at which the image force to both e^-_{CB} and h^+_{VB} is effective.[12] This type of observation has already been made in our earlier study.[3]

Since 4 atomic % Cu(II)-doped Bi_2O_3 is found to be the most efficient catalyst, this was chosen as the representative one for further experiments to study the effect of other factors on PMS decomposition rates.

Effect of Variation of Catalyst Amount. Table 2 shows the rates observed with different amounts of the catalyst, Cu(II)/Bi_2O_3. There is a small but linear

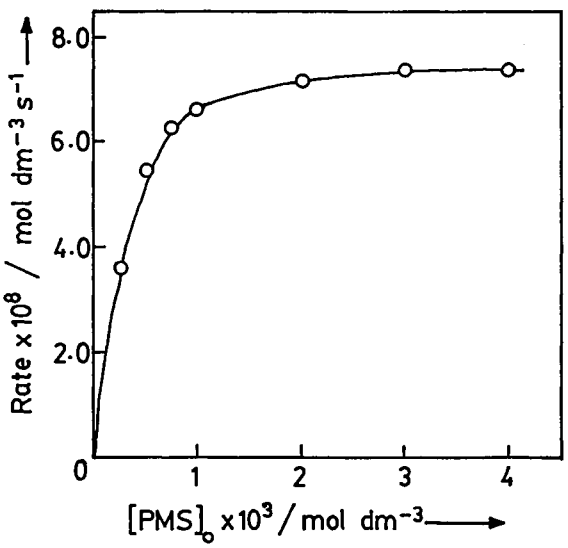

Fig. 4. Plot of rate vs. $[PMS]_0$.
Catalyst=Cu(II)/Bi_2O_3, T=298 K.

increase in the rate with increase in catalyst amount (10—40 mg) which is quite natural since with increase in catalyst amount, the number of catalyst particles coming under the irradiation region increases; in other words the effective surface area of the catalyst responsible for photocatalysis increases leading to the decomposition of more number of PMS molecules and hence the rate is increased. However, further increase of the catalyst amount only results in the saturation limit of the rates.

Effect of Initial [PMS]. The rate of decomposition of PMS was found to be affected by the initial PMS concentrations ($[PMS]_0$) employed in the experiment. From the plot of the rate vs. $[PMS]_0$ (Fig. 4), it is obvious that the rate is increased with increase in $[PMS]_0$ upto a certain range and above that it gets leveled off. This is a typical Langmuirian behavior and hence the effect of $[PMS]_0$ on rate could be described by the following relation,

$$\text{rate} = \frac{kK[PMS]_0}{1+K[PMS]_0} \quad (2)$$

Where k and K are the proportionality and equilibrium constants respectively. The reciprocal of Eq. 2 gives,

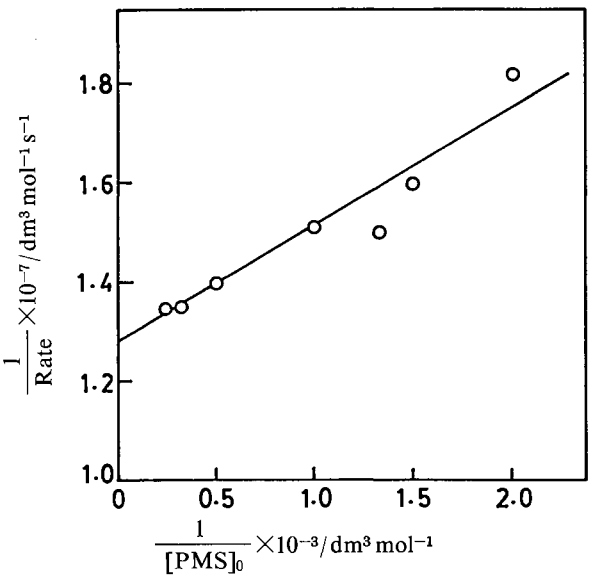

Fig. 5. Plot of $\frac{1}{\text{rate}}$ vs. $\frac{1}{[PMS]_0}$.
Catalyst=Cu(II)/Bi_2O_3, T=298 K.

$$\frac{1}{\text{rate}} = \frac{1}{kK[PMS]_0} + \frac{1}{k} \quad (3)$$

The plot of 1/rate vs. $1/[PMS]_0$ (Fig. 5) yields a straight line confirming the Eq. 3 and hence it is inferred that the reaction system under investigation obeys a Langmuir kinetics. From the intercept and slope of the plot, in Fig. 5, k and K were calculated and their values are 7.8×10^{-6} mol dm^{-3} s^{-1} and 53.4 dm^3 mol^{-1}, respectively. At lower $[PMS]_0$, since $K[PMS]_0 \ll 1$, Eq. 2 reduces to,

$$\text{rate} = kK[PMS]_0 \quad (4)$$

This is a first order equation with respect to $[PMS]_0$ and hence it explains the dependence of the rates on $[PMS]_0$ in the initial stages which is evident in Fig. 4. A similar observation on PMS decomposition has been reported.[3]

Reaction Mechanism for PMS Decomposition. PMS is a powerful oxidizing agent (E°=1.82 V). Nevertheless, it acts both as an electron acceptor and hydrogen atom donor which was confirmed by our previous study[13] on the visible-light induced decomposition of PMS with excited state $[Ru(bpy)_3]^{2+}$. Hence there is a possibility that PMS is attacked by both h^+_{VB} and e^-_{CB}. Furthermore it has been established that the hydrated electron (e^-_{aq}) reacts with PMS almost at a diffusion controlled rate.[14] Considering all the above facts, the following mechanism may be proposed for the photocatalytic decomposition of PMS in the presence of a semiconductor catalyst.

$$\text{Semiconductor} \xrightarrow[\lambda>400\text{ nm}]{h\nu} h^+_{VB} + e^-_{CB} \quad (5)$$

$$HSO_5^- \xrightarrow{\text{Catalyst}} [HSO_5^-]_{ad} \quad (6)$$

$$[HSO_5^-]_{ad} + e^-_{CB} \longrightarrow SO_4^{\cdot-} + OH^- \quad (7a)$$

$$[HSO_5^-]_{ad} + e^-_{CB} \longrightarrow SO_4^{2-} + \dot{O}H \quad (7b)$$

$$2\dot{O}H \longrightarrow 1/2\ O_2 + H_2O \quad (8)$$

$$HSO_5^- + SO_4^{\cdot-} \longrightarrow SO_5^{\cdot-} + HSO_4^- \quad (9)$$

$$HSO_5^- + \dot{O}H \longrightarrow SO_5^{\cdot-} + H_2O \quad (10)$$

$$[HSO_5^-]_{ad} + h^+_{VB} \longrightarrow SO_5^{\cdot-} + H^+ \quad (11)$$

$$2SO_5^{\cdot-} \xrightarrow{H_2O} 2HSO_4^- + 3/2\ O_2 \quad (12)$$

In these equations, $[HSO_5^-]_{ad}$ denotes the PMS molecule adsorbed onto the surface of the catalyst. The formation of $SO_5^{\cdot-}$, $SO_4^{\cdot-}$, and $\dot{O}H$ as the radical products from PMS has been identified by optical pulse radiolysis.[14] Evolution of O_2 during PMS was confirmed by oxygen sensitive electrode and this also serves

Table 3. Rates and Quantum Yields for the Decomposition of PMS with Different Catalysts.
Catalyst Amount=40 mg; [dopant]=4 Atomic % Cu(II); $[PMS]_0=1\times10^{-3}$ mol dm^{-3}

Semiconductor	Undoped Rate$\times10^8$ / mol dm^{-3} s^{-1}	Doped with Cu(II) Rate$\times10^8$ / mol dm^{-3} s^{-1}	Rate (doped) / Rate (undoped)	Φ (undoped)	Φ (doped)	Φ (doped) / Φ (undoped)
Bi_2O_3	2.3	6.6	2.86	0.9	1.7	1.8
WO_3	2.6	6.6	2.54	1.0	1.3	1.3
Fe_2O_3	3.8	8.7	2.28	0.3	0.8	2.6

as an additional proof for the above mechanism. The overall reaction could be written as:

$$HSO_5^- \xrightarrow[\lambda>400\text{ nm}]{\text{catalyst, } h\nu} 1/2\,O_2 + SO_4^{2-} + H^+ \qquad (13)$$

Efficiency Comparison with Other Catalysts: Experiments were also performed to determine the rates of decomposition of PMS with undoped and Cu(II)-doped WO_3 and Fe_2O_3. For this study, the concentration of PMS used was 1.0×10^{-3} mol dm^{-3} in all cases. Here also the Cu(II)-doped samples exhibit higher activities when compared to the undoped ones. To assign the absolute photoactivity of a particular photocatalyst, the quantum yield is a better candidate than other parameters like rate constants etc. This is because it is an activity parameter which indicates how efficiently a photocatalyst utilizes the absorbed photons for effective photochemical reaction irrespective of the light absorbing capacity of photocatalyst.

Table 3 presents the values of rates and quantum yields for the decomposition of PMS for the doped and undoped samples in the wavelength region 400—500 nm, where all the catalysts have almost equal (about 60%) absorption. By comparing the rates, we have the trend, $Bi_2O_3 \approx WO_3 < Fe_2O_3$ for both doped and undoped samples. But on comparing the quantum yields, the trend becomes, $Bi_2O_3 \approx WO_3 > Fe_2O_3$ for undoped and $Bi_2O_3 > WO_3 > Fe_2O_3$ for doped samples. On comparing the rates and quantum yields of doped and undoped samples, it is clear that both rates and quantum yields have been increased considerably by doping with Cu(II). Even though the rate is higher for Fe_2O_3 when compared with the other samples, the quantum yield seems to be lower due to the fact that the number of photons absorbed by Fe_2O_3 is greater than that absorbed by the other samples. Thus, in spite of having greater light absorbing power, Fe_2O_3 has lower quantum yield value. This is due to the fact that not all the absorbed photons are effectively utilized for PMS decomposition. But with Bi_2O_3 and WO_3, as evident from Table 3, it is the former which gets a maximum increment in activity due to Cu(II)-doping.

Since h^+_{VB} and e^-_{CB} react with PMS, the expected quantum yield for the decomposition of PMS is 2. But in all cases (Table 3) the value is less than 2, even though doping with Cu(II) considerably enhances the quantum yields of the semiconductors. The reasons may be: (i) all the photons entering into the reaction vessel are not absorbed by the catalyst and this may be due to the physical phenomena like reflection, scattering etc., (ii) recombination of a part of the e^-–h^+ pairs formed during irradiation, and (iii) the reversible formation of HSO_5^- from the $SO_4^{\cdot-}$ and $\dot{O}H$ radicals. In spite of being less than 2, the quantum yields are comparable and retain their identity.

The distinct behavior of Cu(II) with Bi_2O_3 compared to other semiconductors is interpreted as follows. The ionic radius of Cu^{2+} is closer to that of Bi^{3+} in Bi_2O_3 (ca. 0.9 Å) when compare to that of W^{6+} in WO_3 (ca. 0.6 Å). This close similarity in ionic radii of Cu^{2+} and Bi^{3+} is one more advantage which strengthens the inherent nature, i.e. the e^-_{CB} scavenging action of Cu(II). Hence the activity of Bi_2O_3 is enhanced to a greater extent by Cu(II)-doping.

The present study unequivocally reveals that although the undoped Bi_2O_3 is less efficient for photocatalysis, its activity could be improved by Cu(II)-doping to such an extent that Cu(II)/Bi_2O_3 has almost an equal activity to that of Cu(II)/WO_3 which has already found place in photocatalysis.

The authors thank the authorities of CECRI, Karaikudi and IIT. Madras for permitting to avail of the instrumental facilities. They also acknowledge the financial support from the Department of Non-conventional Energy Sources, New Delhi for this research.

References

1) "Energy Resources through Photochemistry and Catalysis," ed by M. Gratzel, Academic Press, New York (1983).
2) S. N. Frank and A. J. Bard, *J. Phys. Chem.*, **81**, 1484 (1977).
3) P. Maruthamuthu, M. Ashokkumar, and L. Venkatasubramanian, *Bull. Chem. Soc. Jpn.*, **61**, 4137 (1988).
4) P. Maruthamuthu and M. Ashokkumar, *Int. J. Hydrogen Energy*, **14**, 275 (1989).
5) P. Maruthamuthu, M. Ashokkumar, K. Gurunathan, E. Subramanian, and M.V.C. Sastri, *Int. J. Hydrogen Energy*, **14**, 525 (1989).
6) H. Kruidhof, K. Seshan, B. C. Lippens, Jr., P. J. Gellings, and A. J. Burggraaf, *Mater. Res. Bull.*, **22**, 1635 (1987).
7) H. Kruidhof, K. Seshan, G.M.H. Van de Velde, K. J. de Vries, and A. J. Burggraaf, *Mater. Res. Bull.*, **23**, 371 (1988).
8) A. J. A. Winnubst and A. J. Burggraaf, *Mater. Res. Bull.*, **19**, 613 (1984).
9) M. Metikos-Hukovic, *Electrochim. Acta*, **26**, 989 (1981).
10) C. G. Hatchard and C. A. Parker, *Proc. R. Soc. London, Ser. A*, **235**, 518 (1956).
11) P. Maruthamuthu and M. Ashokkumar, *Sol. Energy Mater.*, **17**, 433 (1988).
12) T. Sakata, K. Hashimoto, and T. Kawai, *J. Phys. Chem.*, **88**, 5214 (1984).
13) P. Maruthamuthu, L. Venkatasubramanian, and P. Dharmalingam. *Int. J. Chem. Kinet.*, **22**, 69 (1990).
14) P. Maruthamuthu and P. Neta, *J. Phys. Chem.*, **81**, 937 (1977).

Some Physico-Chemical Studies on Molecular Semiconductors Based on Charge Transfer Complexes of Substituted Phenothiazines with Iodine

Ram Adhar SINGH,* Ranjana SINGH, and Shiva Mohan VERMA*
Department of Chemistry, Faculty of Science, Banaras Hindu University, Varanasi 221005, India
(Received August 27, 1990)

The synthesis, chemical and structural characterizations, and thermal, spectral, electrical, and magnetic properties of six molecular semiconductors based on the charge transfer complexes of substituted phenothiazines namely; phenothiazine, 2-chlorophenothiazine, 2-(trifluoromethyl)phenothiazine, 2-acetylphenothiazine, *N*-acetylphenothiazine, and *N*-benzoylphenothiazine with molecular iodine have been reported in this paper. These complexes have been found to have 2:3 stoichiometries. X-Ray diffraction data show that first three complexes have orthorhombic structure whereas the other three are amorphous. Thermal analysis shows that the complexes are thermally stable upto 120 °C. The existence of monomeric and dimeric cationic species of phenothiazines has been proposed on the basis of spectral data. These complexes have been found to be molecular semiconductors having moderately high electrical conductivities and activation energies. The segregated stacking of phenothiazine and iodine moieties has been proposed to be responsible for high conductivity values and a mixed conductivity mechanism accounts for temperature dependence of electrical conductivities of these complexes.

Molecular materials with remarkable physical properties have been extensively studied in the past two decades.[1-3] Potentialities offered by these materials have been tremendous in the development of molecular level electronic devices as is evident from the number of patented compounds based on organic charge transfer solids. The observation of semiconductivity in this class of materials has opened an era of developing and testing these materials for a number of technological applications. The discoveries of organic metals and organic superconductors have resulted in an interdisciplinary approach involving synthetic and physical chemists, solid state physicists, and material scientists. This upsurge of activity has its genesis in the discovery of high electrical conductivities of bromine complex of perylenes by H. Akamatu et al.[4] However, the iodine complexes with various types of electron donors have played the key role in the development of organic electronic materials, mainly because iodine is such an acceptor, which forms charge-transfer complexes from the weakest to the strongest with various electron donors.[5] The charge-transfer complexes of iodine with phenothiazines which are fairly strong donors, were reported first by Y. Matsunaga.[6,7] This complex was found to be an organic semiconductor. The ratio of donor to the acceptor was found to be 2:3 and it had a fairly high electrical conductivity. The electrical resistivity of the complex was dependent on its composition, 2:3 being the minimum resistivity composition. Similar compositional dependence of electrical and magnetic properties of some related phenothiazine–iodine complexes were reported by Matsunaga and other workers.[8-11] A complex cation radical of phenothiazine was proposed to be responsible for high conductivity of this class of compounds in which electronic conduction takes place between phenothiazines in different oxidation states. Iida[12] proposed that the X-ray diffraction studies on phenothiazine cation radical salts will help us in determining their structure and arrangement of stacking in solid state. In a study of thermoelectric power of iodine complexes of aromatic diamines and thiazines, Akamatu et al.[13,14] reported the hole conduction for phenothiazine–iodine complexes whereas *N*-methylphenothiazine–iodine complex had temperature dependent mixed conductivity mechanism, hole conduction in higher temperature region and electron conduction in the lower temperature region. The interest in the phenothiazine–iodine complexes continued and Resonance Raman and ^{129}I Mössbauer spectroscopic study of this complex was reported very recently by Sakai et al.[15] It was shown that two iodine species in this complex were present consisting of a distorted I_3^- unit and I_2 unit strongly coordinated with this I_3^- unit in which about three electrons for five phenothiazine molecules are transferred to the iodine which are delocalized on the thirteen iodine atoms. Though the single crystal of this compound has not yet been grown, the powder X-ray diffraction may yield some information about the crystal structure of this or related complexes. Electrochemical oxidation of phenothiazine in presence of different inorganic ions yielded stoichiometric complex salts of phenothiazines having 1:1, 3:2, and 2:1 compositions.[16]

The literature survey reveals that the interest in phenothiazine–iodine complexes had mainly focussed around the parent compound and some of structurally related analogues. A few complexes of ring substituted and N-substituted phenothiazines with iodine have been reported.[8,10] However, still a large number of complexes of substituted phenothiazines with iodine have not been synthesized and studied. It is, therefore, pertinent to study the role of electronic and structural modifications on the solid state properties of these complexes. We report herein six new complexes of substituted phenothiazines with iodine on which detailed X-ray diffraction, photoacoustic, electronic, and reflec-

tance, infrared and nuclear magnetic resonance spectral studies have been performed. Electrical, magnetic, and thermal studies have also been undertaken.

Experimental

Materials and Methods. Phenothiazine (PTZ), 2-chlorophenothiazine (CPZ), 2-(trifluoromethyl)phenothiazine (TPZ), and 2-acetylphenothiazine (APZ) were commercially obtained from Aldrich Chemie (F.R.G.). Further purifications were done by vacuum sublimation and fractional crystallization using cyclohexane–chloroform–ethanol mixture. Iodine obtained from E. Merck was further purified by vacuum sublimation. *N*-Acetylphenothiazine (NAPZ) was prepared by acetylation of phenothiazine with acetic anhydride according to the literature procedure.[17] The product obtained was recrystallized from ethanol. *N*-benzoylphenothiazine (NBPZ) was prepared by the reaction of phenothiazine with benzoyl chloride in a sealed tube at 100—110 °C as reported in the literature[17] and purified by recrystallization in ethanol. The purities of the compounds were checked from their melting points, elemental analyses, electronic, infrared, and NMR spectral data which were found to agree well with the literature values.

In general, the charge-transfer complexes of these phenothiazines with iodine were prepared by taking appropriate amounts of the components for 2:3 stoichiometry in suitable solvents and by mixing their dilute solutions. The dark brown colored crystalline complexes separated out when these solutions were kept for about two weeks. The resulting precipitates were collected by filtration washed three times with solvents and dried over anhydrous calcium chloride. The detailed procedures, yields, melting points, and elemental analyses for different complexes are given below:

$(PTZ)_2$-$(I_2)_3$: A dilute solution of PTZ (0.800 g, 40 mmol) in ether (50 mL) was slowly added to the dilute solution of I_2 (1.550 g, 60 mmol) in ether (50 mL). Yield: 90%, mp 175—178 °C. Elemental analysis; Found: C, 24.60; H, 1.98; N, 2.38; S, 5.34%. Calcd for $C_{24}H_{18}I_6N_2S_2$: C, 24.83; H, 1.55; N, 2.41; S, 5.52%.

$(CPZ)_2$-$(I_2)_3$: A dilute solution of CPZ (0.940 g, 40 mmol) in ether (50 mL) was slowly added to the dilute solution of I_2 (1.550 g, 60 mmol) in ether (50 mL). Yield: 91%, mp 125—128 °C. Elemental analysis; Found: C, 23.18; H, 1.77; Cl, 5.47; N, 2.12; S, 5.01%. Calcd for $C_{24}H_{16}Cl_2I_6N_2S_2$: C, 23.44; H, 1.30; Cl, 5.78; N, 2.28; S, 5.21%.

$(APZ)_2$-$(I_2)_3$: A dilute solution of APZ (0.970 g, 40 mmol) in ether (50 mL) was slowly added to the dilute solution of I_2 (1.550 g, 60 mmol) in ether (50 mL). Yield: 92%, mp 155—158 °C. Elemental analysis; Found: C, 26.79; H, 1.92; N, 2.69; S, 5.01%. Calcd for $C_{28}H_{22}I_6N_2O_2S_2$: C, 27.02; H, 1.77; N, 2.25; S, 5.15%.

$(TPZ)_2$-$(I_2)_3$: A dilute solution of TPZ (1.100 g, 40 mmol) in ether (50 mL) was slowly added to the dilute solution of I_2 (1.550 g, 60 mmol) in ether (50 mL). Yield: 90%, mp 115—118 °C. Elemental analysis; Found: C, 23.93; H, 1.29; N, 2.66; S, 4.69%. Calcd for $C_{26}H_{16}F_6I_6N_2S_2$: C, 24.08; H, 1.23; N, 2.16; S, 4.94%.

$(NAPZ)_2$-$(I_2)_3$: A dilute solution of NAPZ (0.970 g, 40 mmol) in ether (50 mL) was slowly added to the dilute solution of I_2 (1.550 g, 60 mmol) in ether (50 mL). Yield: 92%, mp more than 320 °C. Elemental analysis; Found: C, 27.31; H, 1.68; N, 2.34; S, 4.95%. Calcd for $C_{28}H_{22}I_6N_2O_2S_2$: C, 27.02; H, 1.77; N, 2.25; S, 5.15%.

$(NBPZ)_2$-$(I_2)_3$: A dilute solution of NBPZ (1.350 g, 40 mmol) in ether (50 mL) was slowly added to the dilute solution of I_2 (1.550 g, 60 mmol) in ether (50 mL). Yield: 89%, mp 190—193 °C. Elemental analysis; Found: C, 33.60; H, 1.92; N, 2.80; S, 4.38%. Calcd for $C_{38}H_{26}I_6N_2O_2S_2$: C, 33.35; H, 1.90; N, 2.05; S, 4.68%.

Measurements. All the complexes have been obtained as powdered or polycrystalline solids and attempts to grow single crystals failed. Therefore, only powder X-ray diffraction data could be obtained. The X-ray diffraction patterns were recorded on Philips X-ray diffractometer PW 1710 using Cu $K\alpha$ radiation. The electronic absorption spectra were recorded on Cary 2390 and Shimadzu UV-160A spectrophotometers. Reflectance spectra were recorded on Cary 2390 spectrophotometer. Infrared absorption spectra were recorded on Perkin–Elmer 783 spectrophotometer. ^1H NMR spectra were recorded on a JEOL FX-90 Q FT-NMR spectrometer. Electrical measurements were made on Wayne Kerr Automatic Precision Bridge B905. For electrical measurements, the pellets were prepared at a pressure ca. 15 kbar and measurements were repeated at least twice to get reproducible values of various physical properties. AC conductivities of the samples were measured at two different frequencies 1 kHz and 10 kHz at different temperatures in the range (293—403 K). The magnetic measurements were made on a Cahn–Faraday balance at 10 K gauss magnetic field. Photoacoustic spectral measurements were made on a single beam photoacoustic spectrometer designed and fabricated in the spectroscopy section, Department of Physics, B.H.U., Varanasi. Thermogravimetric analyses were done on Stanton Red Croft STA-780 series Unit. The analytical constants were: heating rate: 5 to 10 °C min^{-1}; chart speed: 1000 mm h^{-1}; reference: Al_2O_3; thermocouple: Platinum–Rhodium. The analysis was made in the atmosphere of air between room temperature and 700 °C.

Results and Discussion

Stoichiometries of the Complexes: A Thermogravimetric Analysis. All of the phenothiazine–iodine complexes reported in this paper have been obtained as dark colored solids. When these complexes are heated on a spatula over hot plate, vigorous liberation of iodine results. Thermogravimetric analyses of these complexes show two stage decompositions. A representative thermogravimetric and differential thermogravimetric curve for phenothiazine–iodine complex has been shown in Fig. 1. The phenothiazine–iodine complex shows no weight loss upto 100 °C indicating that the air-dry compound contained no residual humidity. Between 145—290 °C, the labile molecular iodine is lost, the rate of decomposition being maximum at 170 °C as indicated by its DTG curve. DTA curve indicates an exothermic peak at 170 °C. Later, all the residual material is lost between 290—700 °C. Similar curves were obtained for other complexes as well. This data led us to calculate the stoichiometry of the complexes and their decomposition characteristics. Since elemental analyses show 2:3 stoichiometries of the complexes, the relative molecular mass of the complex was calcu-

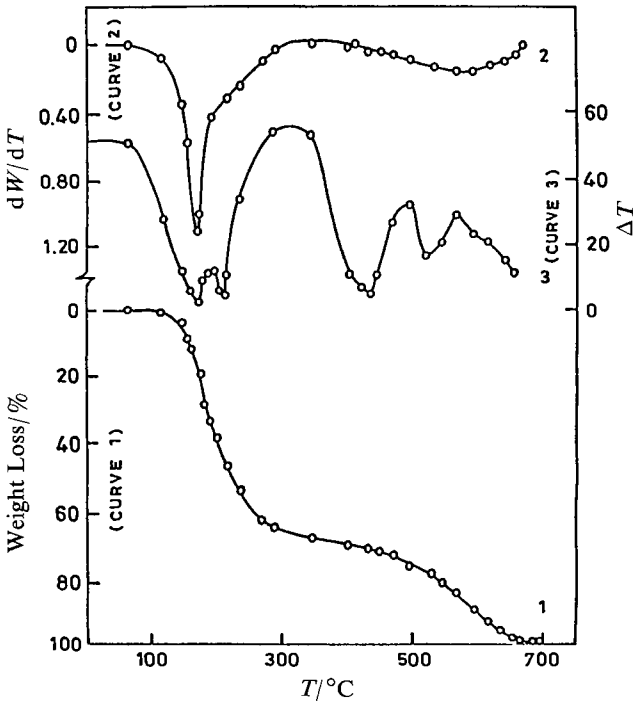

Fig. 1. Thermogravimetric (1), differential thermogravimetric (2), and differential thermal analysis (3) curves for phenothiazine–iodine complex.

lated on this basis. The decomposition steps are as follows:

$$(PTZ)_2(I_2)_3 \longrightarrow 2PTZ + 3I_2 \uparrow \quad \text{(I)}$$

$$2PTZ \longrightarrow 2(PTZ) \uparrow \quad \text{(II)}$$

Though 2:3 stoichiometries of the phenothiazine–iodine complexes have been shown to be most stable and having highest electrical conductivities, there has been a lot of controversy about the stoichiometries of this class of molecular semiconductors. Matsunaga et al.[18] proposed the structure of the complex as $(PTZ)_2^+I_5^- \cdot 1/2I_2$ in which $1/2$ I_2 is expected to be more loosely bound than those in pentaiodide. If this is so, it should result in about 10.94% loss of molecular iodine in the first stage of thermal decomposition. However, we do not observe any decomposition step corresponding to this weight loss. Similarly 2:5.2 composition proposed on the basis of Resonance Raman and Mössbauer studies can also be ruled out on the basis of thermogravimetric analysis. Thus, the phenothiazine–iodine complexes have 2:3 stoichiometries and are thermally stable upto 120 °C.

The dissociation of phenothiazine–iodine complexes in organic solvents further supports above observations. In carbon tetrachloride these complexes show intense violet color indicating the presence of molecular iodine, similar to the tetramethylammonium pentaiodides.[19] In relatively polar solvents like acetonitrile, solubility of the complexes increases indicating dative nature of these complexes. These species have been identified on the basis of their spectral data.

Spectral Data. The electronic absorption spectra of the complexes dispersed in Nujol have bands at 14.5, 20.0, 21.1, 26.7, and 30.8×10^3 cm^{-1}. The diffuse reflectance spectra showed bands at 15.1, 15.6, and 20.5×10^3 cm^{-1}. The photoacoustic spectra of solid complexes indicated bands at 12.8, 14.7, 15.6, and 18.9×10^3 cm^{-1}. The solution spectra in carbon tetrachloride and chloroform showed bands at 12.6, 19.4, 28.2, and 32.3×10^3 cm^{-1} and 11.9, 15.8, 19.7, and 33.5×10^3 cm^{-1}, respectively. Whereas in polar solvents like acetonitrile and methanol, bands at 15.5, 20.0, 21.6, 24.0, and 28.2 (sh)$\times10^3$ cm^{-1} were found. Aged solutions of the complexes in acetonitrile having lush green colors were found to have bands at 11.4, 15.2, 19.3, 24.0, and 34.5×10^3 cm^{-1}. The 11.4×10^3 cm^{-1} band on dilution by solvent, shifted to 11.9×10^3 cm^{-1}. These spectral data indicate that the phenothiazine–iodine complexes have a number of molecular species of phenothiazines in solution, which may possibly be present in solid state as well on the basis of their electronic spectra. The intense violet color of the complexes kept in nonpolar solvents having bands at 19.4×10^3 cm^{-1} indicates the presence of molecular iodine, which in polar solvents gets complexed and thus blue shifted to 21.6 and 24.0×10^3 cm^{-1}. The solvent assisted dimerization of phenothiazine cation radicals, as proposed by Foster et al.,[20] may possibly be true nature of molecular species present in polar solvents. Similar results have been obtained for DDQ complexes.[21]

The above observations are further supported from the vibrational spectra of the complexes which are identical with those reported by Matsunaga et al.[18] The sharp N–H peaks of phenothiazines between 3320—3380 cm^{-1} are replaced by broad bands in this region in the complex indicating the existence of weakly acidic N–H in the cation radical of phenothiazine, but the bands at 1560, 1590, 1050, 930, 890, and 780 cm^{-1} indicate the existence of some neutral phenothiazines in solid state. Thus, these complexes are expected to have mixed valence structures, which help in electronic conduction.

The ^1H NMR spectra of phenothiazines in $CDCl_3$ at room temperature shows two peaks at δ=1.55 and 5.84 ppm vs. TMS exchangeable with D_2O. These peaks have been attributed to two conformations of N–H protons; 'H-intra' (75%) δ=5.84, 'H-extra' (25%) δ=1.55 as reported.[22] The ^1H NMR spectra of complexes in $CDCl_3$ give exchangeable protons at δ=1.57 and 10.20. The former confirms the existence of 'H-extra' conformation as such in zero oxidation state while the later confirms the existence of acidic N–H protons. Therefore, the NMR spectra of the complexes in solution indicate the existence of mixed valence structures possibly present in solid state. The X-ray diffraction data for these complexes have been given below:

X-Ray Diffraction Data. The powder X-ray diffraction data of three complexes were indexed by Ito's method.[23] The observation of diffraction patterns in

the present set of complexes rules out the possibility of any interference by heavy halogen contents in the complexes. The lattice constants of the complexes are as follows:

(i) $(PTZ)_2$–$(I_2)_3$: *a* 4.87 Å, *b* 9.18 Å, *c* 18.51 Å.
(ii) $(CPZ)_2$–$(I_2)_3$: *a* 6.90 Å, *b* 9.07 Å, *c* 19.56 Å.
(iii) $(TPZ)_2$–$(I_2)_3$: *a* 6.93 Å, *b* 9.52 Å, *c* 24.64 Å.

The indexing of the data showed that all the phenothiazine–iodine complexes have orthorhombic crystal structures as for the parent compounds with almost similar lattice parameters.[24] Similar results have been obtained for PTZ–DDQ complexes.[25] *N*-Methylphenothiazine–iodine complex has been reported to have the orthorhombic crystal structures with lattice constants as *a* 11.4 Å, *b* 21.4 Å, *c* 21.1 Å.[11] Our values of *a*, *b*, and *c* are quite different from the above but they all have the same crystal structure. No data on crystal structure of any other complex of iodine with phenothiazines is available for comparison. The lattice constants of the parent compounds and the iodine complexes being comparable indicate that the unit cells of the complexes contain arrays of phenothiazine species in which pentaiodides occupy vacant lattice sites as speculated by Sakai et al.[15] Face to face stacking of folded phenothiazine cation radicals resulting in linear extended chain as proposed by Iida[12] may possibly be structure of high conductivity complexes.

Electrical and Magnetic Data: The electrical properties of iodine complexes of phenothiazines have been extensively studied.[26] However, the electrical conductivities of the iodine complexes of present set of substituted phenothiazines have not yet been reported. Both N-substitution and ring substitution with both electron withdrawing and electron donating group has been studied to learn about the electronic, structural, and conformational aspects of these complexes.

The logarithms of the conductivities of the complexes, plotted against the reciprocal temperatures have been shown in Figs. 2—4. The plots were nonlinear showing marked decrease at higher temperatures than at lower temperatures. Bandrauk et al.[26] proposed that the deviation from linearity was indicative of changes in conductivity mechanisms. The electrical and magnetic data of the complexes have been presented in Table 1.

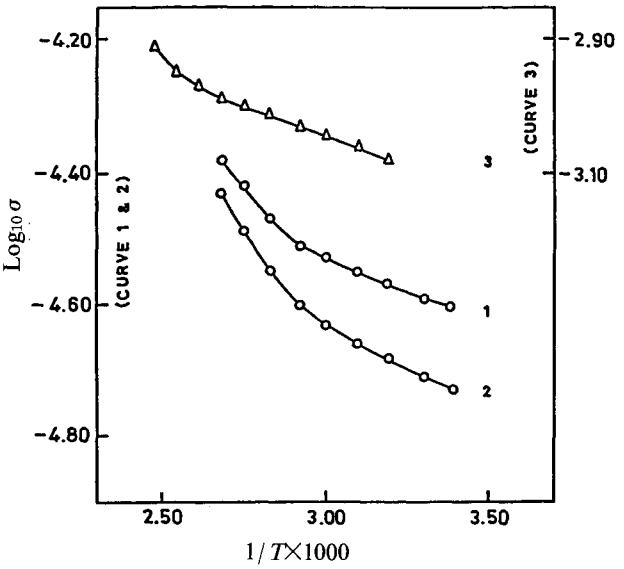

Fig. 3. The plot of logarithm of conductivities vs. T^{-1} for complexes of (1) 2-chlorophenothiazine–iodine at 10 kHz, (2) 2-chlorophenothiazine–iodine at 1 kHz, and (3) 2-acetylphenothiazine–iodine at 10 kHz.

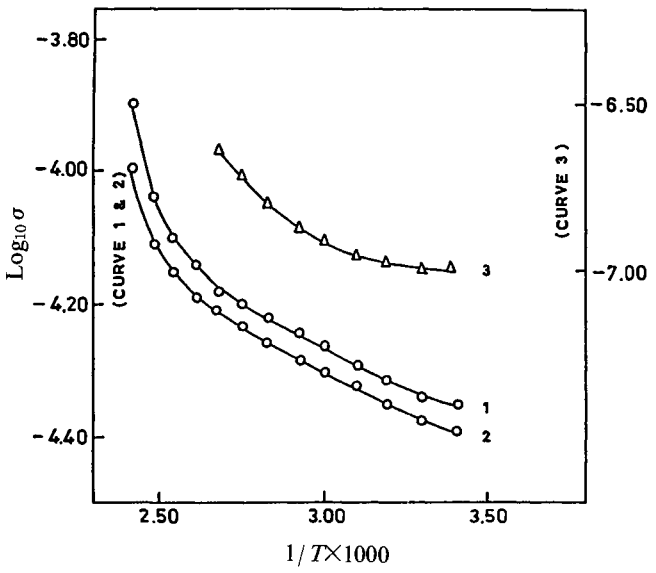

Fig. 2. The plot of logarithm of conductivities vs. T^{-1} for complexes of (1) phenothiazine–iodine at 10 kHz, (2) phenothiazine–iodine at 1 kHz, and (3) 2-(trifluoromethyl)phenothiazine–iodine at 10 kHz.

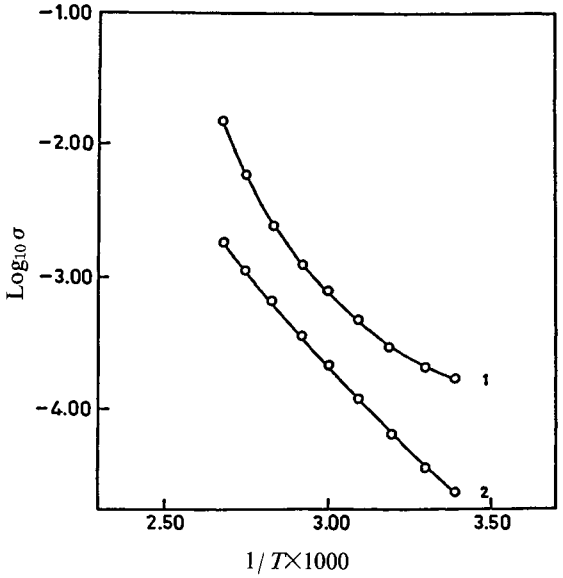

Fig. 4. The plot of logarithm of conductivities vs. T^{-1} for complexes of (1) *N*-acetylphenothiazine–iodine at 10 kHz and (2) *N*-benzoylphenothiazine–iodine at 10 kHz.

Table 1. Electrical and Magnetic Properties of Charge-Transfer Complexes of Iodine with Some Substituted Phenothiazines

Compounds	Electrical conductivity at r.t./μS cm^{-1}			Energy of activation for electrical conductivity (eV) at frequency 10 kHz		Corrected magnetic susceptibility	Magnetic moment
	10 kHz	1 kHz	100 Hz	E_{a_1}	E_{a_2}	(ml mol^{-1})$\times 10^{-6}$	BM
$(PTZ)_2$–$(I_2)_3$	44.67	40.74	—	0.15	0.04	3626.16	2.93
$(CPZ)_2$–$(I_2)_3$	24.98	18.71	15.92	0.12	0.04	3394.83	2.83
$(APZ)_2$–$(I_2)_3$	336.00	—	—	0.06	0.07	1338.73	1.78
$(TPZ)_2$–$(I_2)_3$	0.10	0.03	—	0.20	0.06	3422.41	2.84
$(NAPZ)_2$–$(I_2)_3$	174.98	144.37	127.40	0.99	0.20	—	Diamagnetic
$(NBPZ)_2$–$(I_2)_3$	24.25	19.88	17.55	0.44	—	—	Diamagnetic

Room temperate electrical conductivities of the complexes vary in the order;

$$(APZ)_2\text{–}(I_2)_3 > (NAPZ)_2\text{–}(I_2)_3 > (PTZ)_2\text{–}(I_2)_3 > (CPZ)_2\text{–}(I_2)_3 \approx (NBPZ)_2\text{–}(I_2)_3 > (TPZ)_2\text{–}(I_2)_3.$$

These values are much lower than reported for other phenothiazine–iodine complexes. This may be due to different structural factors, such as the size of crystallites, amorphous nature of some of them, and the changes due to different functional groups. The energy of activation determined from the slopes of two linear portions have also been presented in Table 1, they have been labelled as E_{a_1} and E_{a_2}. E_{a_1} has been found to be higher than E_{a_2} but both the values are characteristic of organic semiconductors. These values have been found to vary in order;

$$(NAPZ)_2\text{–}(I_2)_3 > (NBPZ)_2\text{–}(I_2)_3 > (TPZ)_2\text{–}(I_2)_3 > (PTZ)_2\text{–}(I_2)_3 > (CPZ)_2\text{–}(I_2)_3 > (APZ)_2\text{–}(I_2)_3.$$

It has been well established that the charge-transfer interaction between the ion radicals leads to a marked decrease paramagnetic susceptibilities of ion radical salts.[12] Magnetic susceptibilities and magnetic moments of the charge-transfer salts of iodine with substituted phenothiazines at room temperatures have been determined and given in Table 1. The small rise in weight of the samples of $(PTZ)_2$–$(I_2)_3$, $(CPZ)_2$–$(I_2)_3$, $(APZ)_2$–$(I_2)_3$, $(TPZ)_2$–$(I_2)_3$ on application of magnetic field of strength 10 K gauss shows that these compounds are weakly paramagnetic. The corrected molar magnetic susceptibilities yield magnetic moments of the order of about 1.78, 2.83, and 2.93 BM respectively, indicating the presence of some unpaired spins in the complexes, either on molecular or impurity sites of these partially ionized solids. $(NAPZ)_2$–$(I_2)_3$ and $(NBPZ)_2$–$(I_2)_3$ show no change in weight on application of magnetic field, therefore these compounds are diamagnetic possibly due to strong antiferromagnetic interactions.

Summary

The phenothiazine–iodine complexes reported in this paper have been found as molecular semiconductors having quite different physical properties. This highlights the importance of both electronic and structural factors on which physical properties of this class of complexes depend. Segregated stacking and mixed conductivity mechanisms have been proposed to account for electrical properties of these complexes.

We are thankful to CSIR for sanctioning a research scheme on this topic. We are grateful to Professor Suresh Chandra and Dr. S. A. Hashmi of Physics Department, B.H.U. for helping us with electrical measurements and Professor O. N. Srivastava of the same department for X-ray diffraction data. We also thank Mr. J. P. Pandey of Chemical Engineering, I.T., B.H.U. for his help in TGA measurements. We thank the referee for his fruitful comments.

References

1) R. C. Haddon, M. L. Kaplan, and F. Wudl, "Encyclopedia of Semiconductor Technology," ed by M. Grayson, Wiley-Interscience, New York (1984).
2) F. Gutmann and L. E. Lyons, "Organic Semiconductors," John Wiley and Sons Inc., New York (1967).
3) M. R. Bryce, *Chem. Br.*, **24**, 781 (1988).
4) H. Akamatu, H. Inokuchi, and Y. Matsunaga, *Nature*, **173**, 168 (1954).
5) M. Tamres, "Spectroscopy and Structure of Molecular Complexes," ed by J. Yarwood, Plenum Press (1971).
6) F. H. Herbstein, "Perspectives in Structural Chemistry," ed by J. D. Dunitz and J. A. Ibers, John Wiley & Sons, New York (1971), Vol. IV.
7) Y. Matsunaga, *Helv. Phys. Acta*, **36**, 800 (1963).
8) Y. Matsunaga, *J. Chem. Phys.*, **41**, 1609 (1964).
9) F. Gutmann and H. Keyzer, *J. Chem. Phys.*, **46**, 1969 (1967).
10) S. N. Bhat and C. N. R. Rao, *Can. J. Chem.*, **47**, 3899 (1969).
11) S. Doi, T. Inabe, and Y. Matsunaga, *Bull. Chem. Soc. Jpn.*, **50**, 837 (1977).
12) Y. Iida, *Bull. Chem. Soc. Jpn.*, **44**, 663 (1971).
13) M. Sano, K. Ohno, and H. Akamatu, *Bull. Chem. Soc. Jpn.*, **44**, 3269 (1971).
14) K. Kan and Y. Matsunaga, *Bull. Chem. Soc. Jpn.*, **45**, 2096 (1972).
15) H. Sakai, S. Muraishi, and Y. Maeda, *Bull. Chem. Soc. Jpn.*, **60**, 857 (1987).

16) K. Yakushi, M. Yoshitake, and H. Kuroda, *Bull. Chem. Soc. Jpn.*, **60**, 1519 (1987).
17) "Beilstein Organischen Chemie, Band XXVII, System nymme, Heterocyclische Reihe," ed by B. Prager and P. Jacobson, (1937), pp. 65—66.
18) Y. Matsunaga and Y. Suzuki, *Bull. Chem. Soc. Jpn.*, **45**, 3375 (1972).
19) R. A. Singh and S. N. Bhat, *Can. J. Chem.*, **59**, 1212 (1981).
20) R. Foster and P. Hanson, *Biochim. Biophys. Acta*, **112**, 482 (1966).
21) R. A. Singh, R. Singh, and S. M. Verma, *Indian J. Technol.*, **29**, 000 (1991).
22) C. Bodea and I. Silberg, "Advances in Heterocyclic Chemistry," ed by A. R. Katritzky and A. J. Boulton, Academic Press, New York (1968), Vol. 9.
23) L.V. Azaroff and M. J. Buerger, "The Powder Method in X-Ray Crystallography," McGraw-Hill, New York (1958).
24) D. Feil, M. H. Linck, and J. J. H. McDowell, *Nature*, **207**, 285 (1965).
25) R. A. Singh, R. Singh, and S. M. Verma, *Cryst. Res. Technol.*, **26**, 201 (1991).
26) A. D. Bandrauk, K. Ishii, K. D. Truong, M. Aubin, and A. W. Hanson, *J. Phys. Chem.*, **89**, 1478 (1985).

Study of the Vibrational Spectra and Determination of Thermodynamic Functions of 2-Pyridone and 2-Pyridone-*N*-*d*

Kanak Chandra MEDHI
Department of Physics, Gauhati University, Guwahati 781014, India
(Received November 8, 1990)

The infrared spectra in the polycrystalline state (4000—50 cm^{-1}), in melt and in solution and the Raman spectra in the solid state and in melt of the substances have been studied for 2-pyridone and 2-pyridone-*N*-*d*. A vibrational assignment of the observed frequencies is given. Ideal gas state thermodynamic functions of the two isotopic molecules based on the observed fundamental frequencies have been determined in the temperature range 200—1500 K.

Continuing the earlier investigations on the vibrational spectra of substituted pyridines[1-4] the infrared and Raman spectra of 2-pyridone and 2-pyridone-*N*-*d* have been reported. The infrared spectrum of 2-pyridone in the solid state or in solution was measured by Gibson et al.,[5] Mason,[6] Katritzky and Jones,[7] and Albert and Spinner[8] in a limited range, and only a few bands were assigned. The incomplete simple Raman spectrum of 2-pyridone in aqueous solution was reported by Albert and Spinner.[8] No polarization of the Raman lines was studied previously. It also appears that there is no earlier report on the infrared and Raman spectra of 2-pyridone-*N*-*d*.

The present investigation was aimed at making a detailed study of the infrared and Raman spectra of 2-pyridone and 2-pyridone-*N*-*d* in the polycrystalline, liquid and solution phases. Assignments of the observed vibrational frequencies based on the polarization of the Raman lines and also on the comparison with the assignments proposed for the related molecules[4,9-12] are presented. The ideal gas state thermodynamic functions of the two isotopic molecules have been determined on the basis of the assigned fundamental frequencies.

Experimental

2-pyridone was supplied by Schuchardt, Germany. The compound was purified by repeated sublimation under reduced pressure. A sample of 2-pyridone-*N*-*d* was prepared by the exchange reaction of 2-pyridinol with D_2O. The final product used in the experiment was collected after four such

Table 1. Observed Fundamental Frequencies of 2-Pyridone and 2-Pyridone-*N*-*d*

2-Pyridone					2-Pyridone-*N*-*d*				Assignment
Infrared/cm^{-1}			Raman/cm^{-1}		Infrared/cm^{-1}			Raman/cm^{-1}	
Nujol or HCB mull	Melt	Solution[a]	Pellet	Melt	Nujol or HCB mull	Melt	Solution[a]	Pellet	
3197 (mw)					3197 (mw)				$\nu_6+\nu_8$ (A′)
		3134 (ms)							$\nu_6+\nu_{10}$ (A′)
		3116 (ms)							$\nu_6+2\nu_{26}$ (A′)
		3085 (ms)	3090 (5)	3091 (p)				3096 (4) 3085 (4)	ν_2 (a′) and ν_3 (a′), 20b, 2
		3028 (ms)	3042 (1)	3040 (p)				3043 (2)	ν_4 (a′) and ν_5 (a′), 20a, 7b
2982 (ms)		2977 (ms)			2982 (ms)				$\nu_9+\nu_{10}$ (A′)
2942 (ms)					2942 (ms)				$3\nu_{23}$ (A″)
2873 (ms)		2886 (w)			2873 (ms)				$\nu_{10}+\nu_{11}$ (A′)
2842 (ms)		2862 (w)			2843 (ms)				$2\nu_{11}$ (A′)
~2817 (ms)		2826 (w)			2814 (ms)				$\nu_{10}+\nu_{12}$ (A′)
2785 (ms)		2795 (w)			2783 (ms)				$\nu_6+\nu_{14}$ (A′)
2677 (w)					2673 (w)				$\nu_{11}+\nu_{13}$ (A′)
2602 (w)					2612 (w)				$\nu_{10}+\nu_{14}$ (A′)
2549 (w)									$\nu_{10}+\nu_{22}$ (A″)
2527 (w)					2537 (w)				$\nu_9+\nu_{17}$ (A′)
2462 (mw)					2459 (mw)				$\nu_9+\nu_{24}$ (A″)
					2282 (s)				ν_1 (a′), N–D Stretching
					2230 (s)				$\nu_7+\nu_{22}+\nu_{27}$ (A′)
1978 (w)					1978 (w)				$2\nu_{17}$ (A′)
1850 (mw)		1866 (w)			1841 (w)				$2\nu_{24}$ (A′)
1815 (w)		1835 (w)			1806 (w)				$\nu_{15}+\nu_{26}$ (A″) $\nu_{25}+2\nu_{27}$ (A″)

Table 1. (Continued)

2-Pyridone					2-Pyridone-*N*-*d*				Assignment
Infrared/cm^{-1}			Raman/cm^{-1}		Infrared/cm^{-1}			Raman/cm^{-1}	
Nujol or HCB mull	Melt	Solution[a)]	Pellet	Melt	Nujol or HCB mull	Melt	Solution[a)]	Pellet	
1766 (w)		1766 (w)			1758 (w)				$\nu_{23}+\nu_{25}$ (A′)
1683 (ms)		1676 (ms)			1683 (ms)		1650 (sh)	1663 (1)	$2\nu_{26}+\nu_{30}$ (A″)
1643 (vs)	1663 (vs)	1659 (vs)	1654 (3)	1680	1637 (vs)	1661 (vs)	1645 (vs)	1645 (1)	ν_6 (a′), C=O Stretching
1608 (vs)	1605 (vs)	1619 (s)	1610 (3)	1599 (p)					ν_7 (a′), N–H in-plane deformation.
1567 (s)			1567 (5)		1560 (s)			1574 (6)	ν_8 (a′), 8a
1537 (s)	1538 (s)	1543 (ms)	1543 (11)	1539 (p)	1531 (s)	1538 (s)	1563 (vs)	1532 (22)	ν_9 (a′), 8b
1453 (s)	1465 (ms)	1472 (ms)	1458 (9)	1459 (p)	1450 (s)	1468 (ms)	1454 (mw)	1451 (5)	ν_{10} (a′), 19a
1433 (s)	1430 (ms)	1442 (ms)	1434 (1)	1427 (p)	1433 (s)	1432 (s)			ν_{11} (a′), 19b
	1370 (mw)	1375 (w)	1366 (9)	1369 (p)		1371 (w)	1385 (mw)	1388 (2)	ν_{12} (a′), 14
1305 (w)	1305 (w)				1307 (mw)	1308 (s)	1307 (mw)	1310 (29)	$\nu_{25}+\nu_{27}$ (A′)
1239 (ms)	1239 (ms)	1248 (s)	1244 (45)	1248 (p)	1239 (ms)	1240 (ms)	1248 (ms)	1242 (15)	ν_{13} (a′), 3
1230 (sh)		1237 (sh)	1234 (sh)		1231 (ms)		1236 (sh)	1235 (88)	$\nu_{16}+\nu_{30}$ (A″)
1217 (sh)	1216 (s)	1214 (sh)	1219 (7)		1217 (sh)	1216 (ms)	1214 (sh)		$\nu_{17}+\nu_{30}$ (A″)
1173 (mw)			1174 (3)		1170 (mw)			1172 (4)	$\nu_{25}+\nu_{29}$ (A′)
1156 (ms) 1149 (sh)	1155 (s)	1154 (s)	1159 (1) 1148 (3)	1157 (p)	1156 (s) 1143 (sh)	1151 (s)	1158 (s)	1151 (10)	ν_{14} (a′), 9a
1099 (ms)	1093 (ms)	1097 (ms)	1099 (3)	1096 ρ=0.77	1098 (mw)	1094 (mw)	1096 (w)		ν_{15} (a′) and ν_{22} (a″), 15 and N–H out-of-plane deformation
					1031 (mw)	1026 (mw)	1036 (mw)	1031 (2)	ν_7 (a′), N–D in-plane deformation
1009 (ms)		1007 (ms)	1013 (7)	1011 (p)	1007 (mw)	1010 (sh)	1006 (w)		ν_{16} (a′), 18a
993 (mw)	992 (s)	990 (s)	991 (2)	996 (p)	992 (mw)	985 (s)	989 (s)	994 (2)	ν_{17} (a′), 1
981 (s)		982 (sh)	982 (3)		982 (s)		980 (s)	984 (8)	ν_{23} (a″), 17a
926 (ms)		923 (ms)			934 (s)	930 (mw)	916 (ms)	933 (2)	ν_{24} (a″), 5
864 (w)			854 (5)		865 (mw)		857 (ms)	855 (3) 842 (9)	$\nu_{28}+\nu_{29}$ (A′)
845 (w)	851 (mw)	843 (mw)	844 (39)	847 (p)	845 (w)	849 (ms)	844 (sh)	833 (61)	ν_{18} (a′), 12
835 (w)			835 (11)	831	832 (w)			825 (12)	$\nu_{19}+\nu_{30}$ (A″)
780 (vs)	769 (s)	768 (vs)	784 (3)		782 (vs)	771 (s)	783 (vs)	782 (2)	ν_{25} (a″), 10b
731 (s)	723 (ms)	724 (s)			731 (ms)	726 (ms)	724 (ms)		ν_{26} (a″), 4
					667 (ms)		682 (ms)		ν_{22} (a″), N–D out-of-plane deformation
609 (mw)	611 (mw)	612 (w)	614 (4)	617 (p)	612 (mw)	610 (mw)	610 (mw)	615 (5)	ν_{19} (a′), 6b
559 (ms) 553 (ms)	557 (ms)	559 (s)	561 (9) 552 (3)	555 (p) ρ=0.61	556 (ms) 548 (ms)	555 (ms)	558 (s)	557 (10) 548 (5)	ν_{20} (a′) and ν_{21} (a′) C=O in-plane bending and 6a
525 (s)	511 (ms)	513 (ms)	526 (3)		522 (s)	510 (mw)	508 (ms)	525 (2)	ν_{27} (a″), 11
473 (s)	487 (mw)	495 (s)			471 (s)	488 (sh)	491 (s)		ν_{28} (a″), C=O out-of-plane deformation
449 (mw)	455 (mw)	454 (mw)	450 (1)	464 (p)	443 (mw)	456 (mw)	454 (mw)	445 (1)	$2\nu_{30}$ (A′)
392 (mw)			393 (4)	393 (dp)	392 (ms)			389 (6)	ν_{29} (a″), 16a
228 (sh)					228 (sh)				$\nu_{16}-\nu_{25}$ (A″)
220 (ms)			221 (3)		220 (ms)			221 (3)	ν_{30} (a″), 16b
			208 (5)					209 (5)	$\nu_{10}-\nu_{13}$ (A′)
142 (ms)			142 (23)	141 (ms)	141 (ms)			142 (22)	Lattice mode
128 (sh)			125 (41)		129 (sh)			124 (44)	
								112 (34)	
101 (ms)			101 (47)		101 (ms)			102 (50)	
86 (mw)			86 (67)		86 (mw)			87 (84)	
68 (mw)			65 (100)					65 (110)	
			35 (100)					35 (100)	

a) Solution in CS_2, CH_2Cl_2, CCl_4, or D_2O.

exchanges.

The infrared spectra of 2-pyridone and 2-pyridone-*N*-*d* in the range 4000—400 cm^{-1} were measured on a Carl-Zeiss Specord IR 75 spectrometer in the polycrystalline state as nujol or hexachlorobutadiene (HCB) mull, in the liquid state just above the melting point and in solutions in different solvents, e.g., CCl_4, CS_2, CH_2Cl_2, and D_2O. The far infrared spectra of the two compounds in the region 500—50 cm^{-1} were recorded in nujol mull on a Perkin-Elmer Model 180 spectrophotometer.

The Raman spectra were obtained in the polycrystalline state in the case of both the molecules and also in the melt of the substance in the case of 2-pyridone using a Spex 1403 Ramalog spectrometer and the 514.5 nm line as the exciting wavelength from a Spectra Physics argon ion laser. The polarization of the Raman lines of 2-pyridone was also measured using an analyser and a scrambler as described elsewhere.[1)]

Results and Discussion

The observed infrared frequencies and Raman shifts of the two isotopic molecules, their approximate relative intensities and probable assignments are given in Table 1. Tables 2 and 3 list the calculated values of the thermodynamic functions. In Fig. 1 is reproduced the laser Raman spectrum of 2-pyridone-*N*-*d* in the polycrystalline state.

Assuming the amide form for 2-pyridone[6,8,13,14)] and 2-pyridone-*N*-*d* the two isotopic molecules belong to the point group C_s and the thirty normal modes of vibration, which are active both in the infrared and Raman

Table 2. Thermodynamic Functions of 2-Pyridone[a,b)]

Temp	C_p°	$(H^\circ-E_o^\circ)/T$	S°	$-(F^\circ-E_o^\circ)/T$
K	$cal_{th}\ K^{-1}\ mol^{-1}$	$cal_{th}\ K^{-1}\ mol^{-1}$	$cal_{th}\ K^{-1}\ mol^{-1}$	$cal_{th}\ K^{-1}\ mol^{-1}$
200	15.04	10.13	66.15	56.03
250	18.63	11.46	69.88	58.42
273.15	20.32	12.14	71.61	59.47
298.15	22.15	12.91	73.47	60.56
300	22.29	12.96	73.60	60.64
400	29.19	16.17	80.98	64.81
500	35.03	19.38	88.14	68.76
600	39.77	22.40	94.96	72.57
700	43.61	25.16	101.40	76.23
800	46.75	27.67	107.40	79.76
900	49.35	29.94	113.10	83.15
1000	51.54	31.99	118.40	86.41
1100	53.39	33.86	123.40	89.55
1200	54.97	35.55	128.10	92.57
1300	56.31	37.10	132.60	95.48
1400	57.48	38.51	136.80	98.28
1500	58.48	39.81	140.80	101.00

a) Ideal gas state at standard pressure of 1 atm. b) cal_{th}=4.184 J.

Table 3. Thermodynamic Functions of 2-Pyridone-*N*-*d*[a,b)]

Temp	C_p°	$(H^\circ-E_o^\circ)/T$	S°	$-(F^\circ-E_o^\circ)/T$
K	$cal_{th}\ K^{-1}\ mol^{-1}$	$cal_{th}\ K^{-1}\ mol^{-1}$	$cal_{th}\ K^{-1}\ mol^{-1}$	$cal_{th}\ K^{-1}\ mol^{-1}$
200	15.48	10.22	66.36	56.14
250	19.34	11.66	70.23	58.57
273.15	21.16	12.38	72.02	59.64
298.15	23.09	13.20	73.95	60.76
300	23.23	13.26	74.10	60.84
400	30.38	16.67	81.79	65.12
500	36.29	20.03	89.22	69.20
600	41.03	23.15	96.27	73.13
700	44.84	25.98	102.90	76.91
800	47.95	28.54	109.10	80.55
900	50.50	30.84	114.90	84.05
1000	52.63	32.92	120.30	87.41
1100	54.42	34.80	125.40	90.64
1200	55.93	36.50	130.20	93.74
1300	57.22	38.04	134.80	96.72
1400	58.32	39.45	139.00	99.59
1500	59.26	40.74	143.10	102.40

a) Ideal gas state at standard pressure of 1 atm. b) cal_{th}=4.184 J.

spectra, are distributed among the symmetry species as follows:

$$\Gamma = 21\ a' + 9a''$$

The species a′ gives polarized Raman lines and the species a″ depolarized Raman lines.

Species a′. The polarized Raman lines at 3091 and 3040 cm^{-1} in the case of 2-pyridone and the Raman shifts observed at 3096, 3085, and 3043 cm^{-1} in the case of 2-pyridone-*N-d* are assigned to the four C–H stretching modes. The infrared spectra of both the isotopic molecules in the liquid state show absorption at 1538 cm^{-1}, but in the polycrystalline state it is split up into two components. The Raman counterpart behaves similarly. These are attributed to both the components of the highest C–C stretching mode. The remaining ring stretching modes are identified with the polarized Raman lines at 1459, 1427, 1369, and 996 cm^{-1} in 2-pyridone and the Raman shifts observed at 1451, 1388, 994 cm^{-1} and the infrared band at 1433 cm^{-1} in 2-pyridone-*N-d*. The Raman spectrum of 2-pyridone gives polarized lines at 1248, 1157, and 1011 cm^{-1} and the infrared spectrum shows absorption of medium strength at 1099 cm^{-1}, while in the deuterated compound the Raman lines at 1242 and 1151 cm^{-1} and the infrared bands at 1098 and 1007 cm^{-1} are observed. These are assigned to the four C–H in-plane deformation modes.

Polarized Raman lines are observed at 847, 617, and 555 cm^{-1} in 2-pyridone while its deuterated analogue

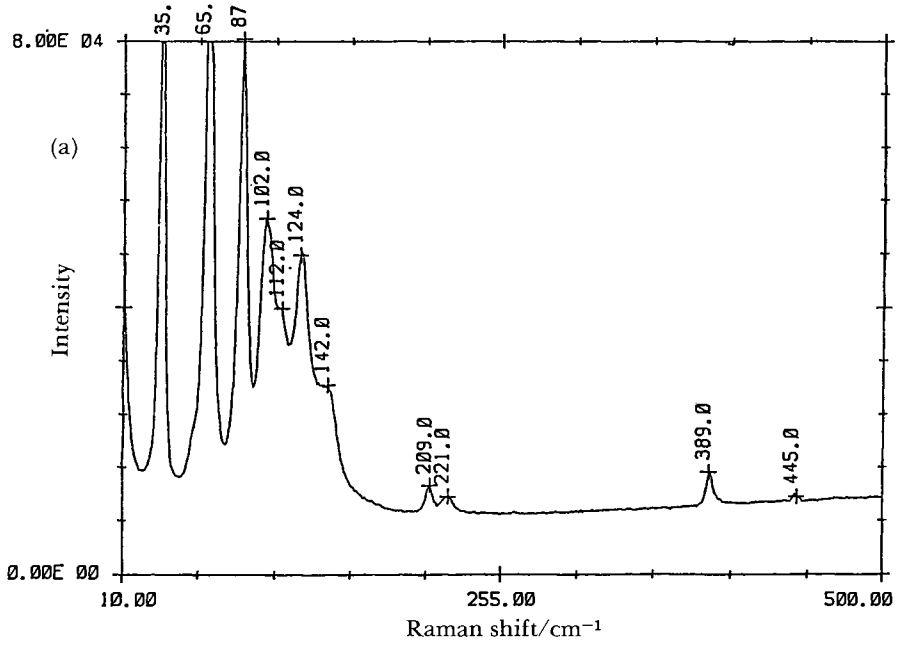

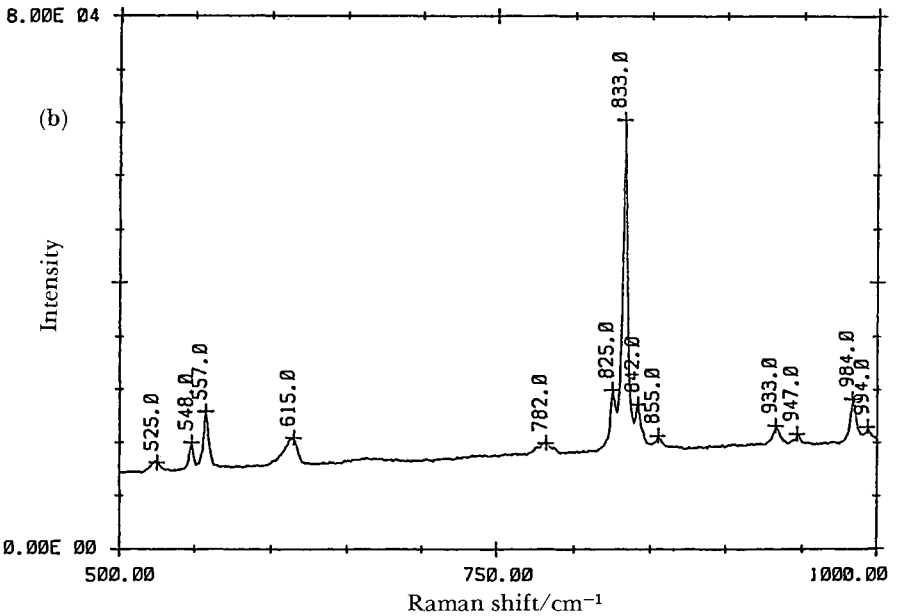

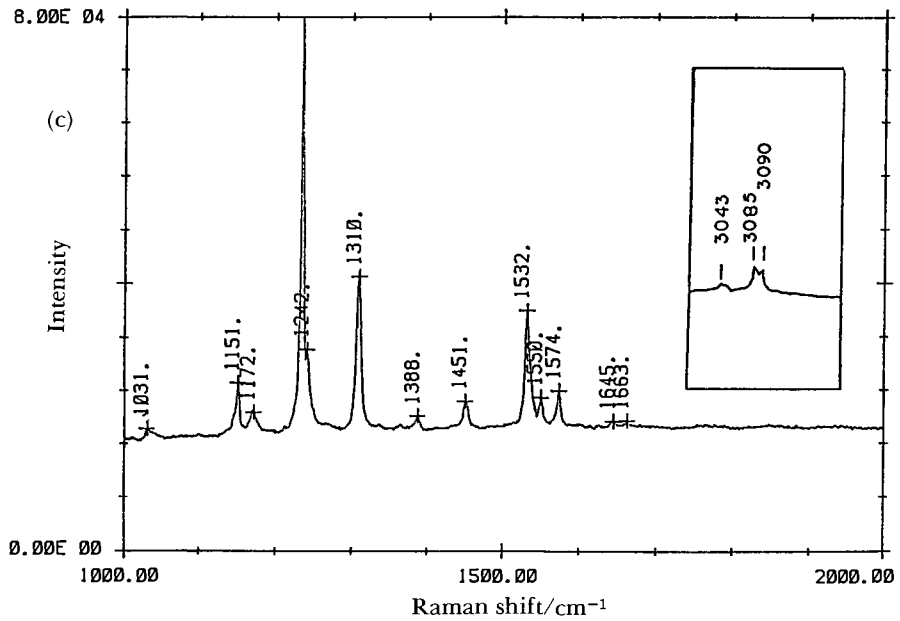

Fig. 1. (a), (b), and (c). Laser Raman spectrum of 2-pyridone-*N*-*d* in the polycrystalline state.

shows Raman shifts at 833, 615, and 548 cm^{-1}. These may be unambiguouly identified with the modes being derived primarily from the planar ring deformation.

Species a″. A depolarized Raman line is observed at 393 cm^{-1} in 2-pyridone in the liquid state, while the corresponding Raman shift is observed at 389 cm^{-1} in the case of 2-pyridone-*N*-*d*. This may be associated with one component of the nonplanar ring angle deformation, the other component being substituent sensitive may be identified with the infrared band of medium intensity observed at 220 cm^{-1} in the case of both the isotopic molecules. The other fundamental frequencies belonging to a″ class may be assigned to the infrared bands at 981, 926, 780, 731, and 525 cm^{-1} in 2-pyridone and 982, 934, 782, 731, and 522 cm^{-1} in 2-pyridone-*N*-*d*. These assignments are in close agreement with those proposed for other monosubstituted pyridines.[1,3,4,9,10]

The Internal Vibrations of the NH and CO Group. If the molecule of 2-pyridone exists in the amide form[15] due to tautomerism, it should exhibit the N–H stretching band near 3400 cm^{-1} in the infrared spectrum. Since there is strong intermolecular hydrogen bonding which exists not only in the crystalline state[16] but also in the liquid and solution phases (as evident from the

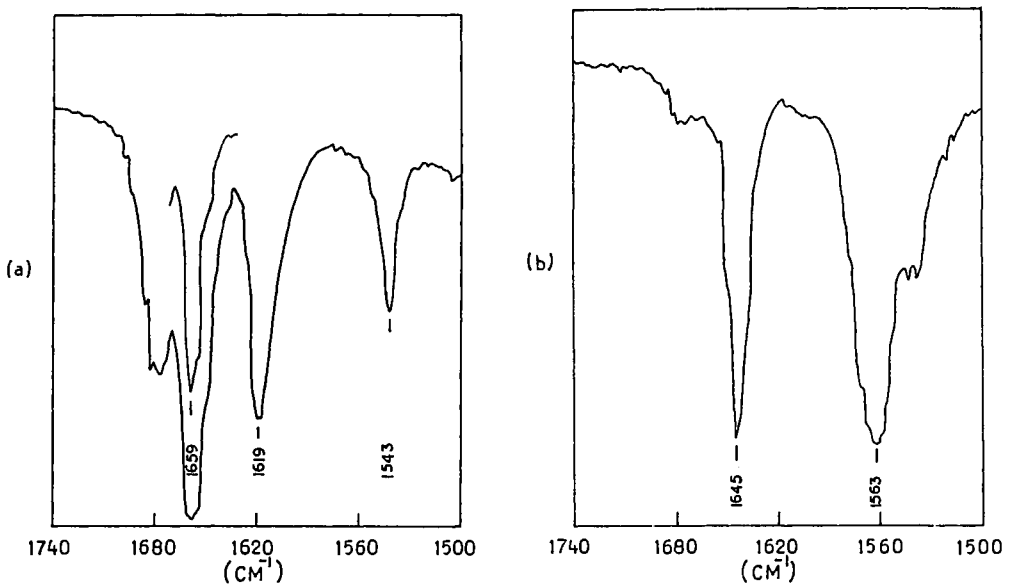

Fig. 2. Portions of the infrared spectra of (a) 2-pyridone in methylene chloride, and (b) 2-pyridone-*N*-*d* in D_2O.

spectrum) the N–H stretching frequency may decrease to about 3200 cm^{-1} and it is, therefore, probably submerged in the broad absorption region covering the range 3300—2500 cm^{-1}, and as such this frequency cannot be located with certainty. Mason[6] reported the N–H stretching band at 3404 cm^{-1} in a very dilute solution in CCl_4 and at 3198 cm^{-1} in the solid state in the case of 2-pyridone. The present study shows that the infrared band at 3197 cm^{-1} (present value) persists in solid 2-pyridone-*N*-*d*. So the band at 3197 cm^{-1} cannot be assigned to the N–H stretching mode. But in the case of 2-pyridone-*N*-*d* a strong infrared band is observed at 2282 cm^{-1} which is absent in the spectrum of the normal 2-pyridone molecule. It is, therefore, assigned to the N–D stretching mode.

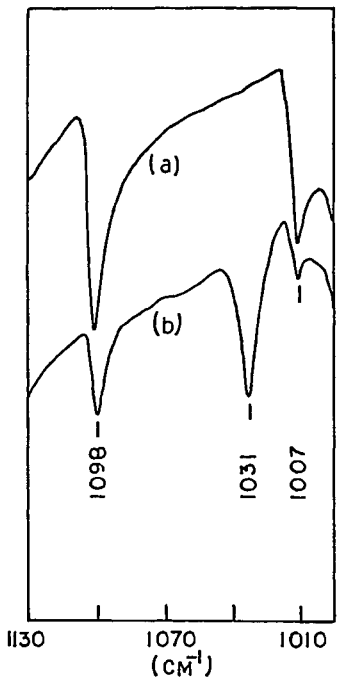

Fig. 3. Portions of the infrared spectra of (a) 2-pyridone in nujol, and (b) 2-pyridone-*N*-*d* in nujol.

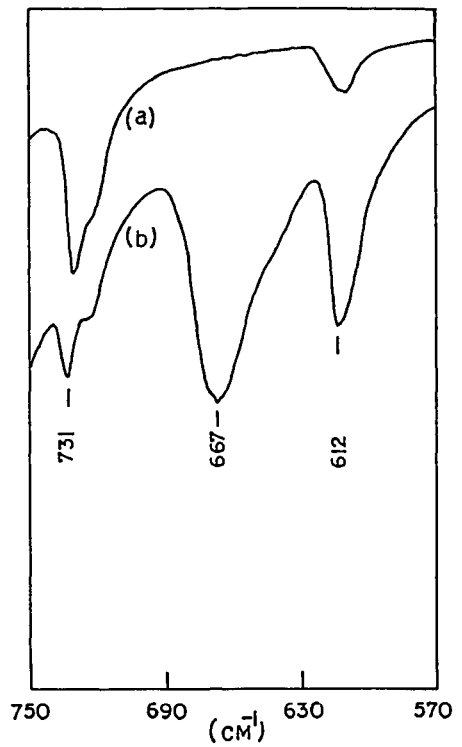

Fig. 4. Portions of the infrared spectra of (a) 2-pyridone in nujol, and (b) 2-pyridone-*N*-*d* in nujol.

A polarized Raman line at 1599 cm^{-1} with a very strong infrared counterpart at 1605 cm^{-1} is observed in 2-pyridone. This band is found to disappear on N–H deuteration (Fig. 2) and a new band of medium strength at 1031 cm^{-1} is observed in both the infrared (Fig. 3) and Raman spectra of 2-pyridone-*N*-*d*. The former band must therefore be assigned to the N–H in-plane deformation mode[1] against the previous assignment of this frequency to a C–C stretching mode[7] and the latter (1031 cm^{-1}) to the N–D in-plane bending mode.

It is observed that in 2-pyridone an infrared band of medium intensity at 1099 cm^{-1}, which has already been assigned to a C–H in-plane deformation mode, decreases in intensity on N–H deuteration. This is indicative of the fact that two fundamentals are overlapping at this position. Moreover, the Raman line at the same frequency which appears to be depolarized in 2-pyridone is missing in the Raman spectrum of 2-pyridone-*N*-*d*. This shows that the band at 1099 cm^{-1} must have some contribution from the N–H out-of-plane deformation mode. On the other hand, an infrared band of medium intensity at 667 cm^{-1} is observed on N–H deuteration (Fig. 4). This band is attributed to the N–D out-of-plane deformation mode.

The highly intense infrared bands at 1643 and 1637 cm^{-1} in 2-pyridone and 2-pyridone-*N*-*d*, respectively, are assigned to the C=O stretching frequency.[1] The C=O in-plane and out-of-plane deformation frequencies are identified with the observed infrared bands at 559 and 473 cm^{-1} respectively in 2-pyridone and at 556 and 471 cm^{-1} respectively in the case of 2-pyridone-*N*-*d*.[17]

Teller–Redlich product rule applied to the present assignment gives the following result:

$$\text{For the a' species} \quad \Gamma'_{exp} = \prod_i \frac{\nu_i^D}{\nu_i^H} = 0.445, \quad \Gamma'_{cal} = 0.510$$

$$\text{For the a'' species} \quad \Gamma''_{exp} = \prod_i \frac{\nu_i^D}{\nu_i^H} = 0.613, \quad \Gamma''_{cal} = 0.728$$

Thermodynamic Functions: Assuming a rigid rotator and harmonic oscillator approximation ideal gas state thermodynamic functions of 2-pyridone and 2-pyridone-*N*-*d* have been calculated in the temperature range 200—1500 K using the standard expressions[18] and the wavenumbers of the fundamental frequencies.

Remarks

It is seen from the vibrational analysis given above

that the spectral behavior of the two isotopic molecules corroborates to the fact that 2-pyridone and 2-pyridone-*N-d* exist predominantly in the amide form due to tautomerism in the solid, liquid, and solution phases.

The author is thankful to Professor I. Haque for his kind permission to use the infrared spectrophotometer. Thanks are also due to the Department of Science and Technology, Government of India for financial support to the project work.

References

1) K. C. Medhi, *Indian J. Phys.*, **51A**, 399 (1977).
2) K. C. Medhi, *Proc. Indian Acad. Sci., Sect. A, (Chem. Sci.)*, **91**, 137 (1982).
3) K. C. Medhi, *Bull. Chem. Soc. Jpn.*, **56**, 3486 (1983).
4) K. C. Medhi, *Bull. Chem. Soc. Jpn.*, **57**, 261 (1984).
5) J. A. Gibson, W. Kynaston, and A. S. Lindsey, *J. Chem. Soc.*, **1955**, 4340.
6) S. F. Mason, *J. Chem. Soc.*, **1957**, 4874.
7) A. R. Katritzky and R. A. Jones, *J. Chem. Soc.*, **1960**, 2947.
8) A. Albert and E. Spinner, *J. Chem. Soc.*, **1960**, 1221.
9) J. H. S. Green, W. Kynaston, and H. M. Paisley, *Spectrochim. Acta*, **19**, 549 (1963).
10) D. A. Long and W. C. George, *Spectrochim. Acta*, **19**, 1777 (1963).
11) V. I. Berezin and M. D. Elkin, *Opt. Spectrosc.*, **34**, 395 (1973).
12) V. I. Berezin and M. D. Elkin, *Opt. Spektrosk.*, **35**, 49 (1973).
13) D. J. Brown and L. N. Short, *J. Chem. Soc.*, **1953**, 331.
14) D. J. Brown, E. H. Hoerger, and S. F. Mason, *J. Chem. Soc.*, **1955**, 211.
15) R. C. Elderfield, "Heterocyclic Compounds," Wiley, New York (1950).
16) B. R. Penfold, *Acta Cryst.*, **6**, 591 (1953).
17) C. Dellepaine and J. Overend, *Spectrochim. Acta*, **22**, 593 (1966).
18) G. Herzberg, "Molecular Spectra and Molecular Structure," Vol. II, "Infrared and Raman Spectra of Polyatomic Molecules," D. Van Nostrand Company, Inc., New York (1960), p. 501.

A Combined Solvent Extraction-Spectrophotometry for the Determination of Bismuth(III)

Ganesh Shantilal DESAI and Vijay Malhar SHINDE*
Analytical Laboratory, The Institute of Science, 15 Madam Cama Road, Bombay 400032, India
(Received September 5, 1990)

A method has been proposed for the extraction of bismuth(III) at microgram level from bromide media using mesityl oxide as an extractant. The bismuth–bromo complex formed in the concentration range of 0.05—0.3 mol dm^{-3} hydrobromic acid showed quantitative extraction into mesityl oxide. Various experimental conditions such as acid concentration, mesityl oxide concentration, period of equilibration, stripping agents, and diverse ions have been studied. Bismuth ion after stripping is determined by thiourea spectrophotometrically. The method is applicable to the analysis of pharmaceutical samples, alloy samples, and synthetic mixtures.

Bismuth is an important element because of its intermediate or metalloid character. It is chiefly employed for the preparation of hard and easily fusible alloys which are useful as safety plugs in boilers, electrical fuses, solders, and type metal for printing. Trivalent bismuth salts are used medicinally to control diarrhoea and other gastrointestinal distresses. Bismuth salts are also used as radio-contrast agents. In view of this separation of bismuth from associated elements for the determination is desired.

Literature survey reports a very few extraction methods for bismuth(III). Amongst the ion-association systems, polar solvents such as tributyl phosphate (TBP), methyl isobutyl ketone (MIBK), isopentyl alcohol, isopentyl acetate, and diethyl ether have been used for the extraction of bismuth from iodide, perchlorate and thiocyanate media.[1–5] High molecular weight amines have also been used for extraction of bismuth from iodide, chloride, thiocyanate, bromide, and succinate media.[6–11] *N*-*m*-Tolyl-*p*-chlorobenzohydroxamic acid has been used to extract bismuth.[12] However the existing methods suffer from limitations such as longer extraction time,[3,12] critical pH,[12] centrifugation,[11] and large number of interferences.[2,3,6] The proposed method is free from these limitations and affords separation for the determination of bismuth in some samples. The method is reproducible and rapid.

Experimental

Apparatus and Reagents. Mesityl oxide (bp 128 °C, Fluka) was used after double distillation.

Thiourea; 10% solution was used for the determination of bismuth.[13]

The stock solution of bismuth(III) was prepared by dissolving 0.58 g of bismuth nitrate (AR grade) in distilled water containing 2 cm^3 of concentrated nitric acid and diluting to 250 cm^3. The solution was standardised by known method[14] and diluted as required for working solution. All other reagents used were of analytical reagent grade.

Absorbance measurements were made on a Unicam SP 500 spectrophotometer with 1 cm (silica) cells.

General Extraction Procedure. To an aliquot of solution containing 200 μg of bismuth(III), hydrobromic acid was added so that its concentration is 0.2 mol dm^{-3} in a total volume of 10 cm^3. The solution was transferred into a separatory funnel and extracted with 5 cm^3 of undiluted mesityl oxide for 30 s. After separating the aqueous layer, bismuth from the organic layer was stripped with two 5 cm^3 portions of 0.2 mol dm^{-3} nitric acid and determined with thiourea spectrophotometrically at 460 nm.[12]

Results and Discussion

Extraction Conditions. The concentration of hydrobromic acid was varied from 0.05 to 1.0 mol dm^{-3} and that of mesityl oxide from 50 to 100% (v/v) by dilution

Table 1. Extraction of Bismuth(III) as a Function of Hydrobromic Acid Concentration and Mesityl Oxide Concentration. Bi(III)=200 μg

Mesityl oxide concn/%	[HBr] mol dm^{-3}	Extraction %	Distribution ratio, D
50	0.2	13.8	0.32
60	0.2	25.0	0.67
70	0.2	42.6	1.48
80	0.2	58.7	2.84
90	0.2	72.6	5.30
100	0.05—0.3	99.9	1998
100	0.4	83.7	10.26
100	0.5	73.1	5.43
100	1.0	57.5	2.70

with toluene. The results (Table 1) showed that the quantitative extraction of bismuth occurs with undiluted mesityl oxide from the solution containing 0.05 to 0.3 mol dm^{-3} hydrobromic acid. Variation of shaking time from 5 to 60 s showed that an equilibration for 30 s was enough for complete extraction of bismuth into organic phase. However prolonged shaking had no adverse effect on the extraction of bismuth.

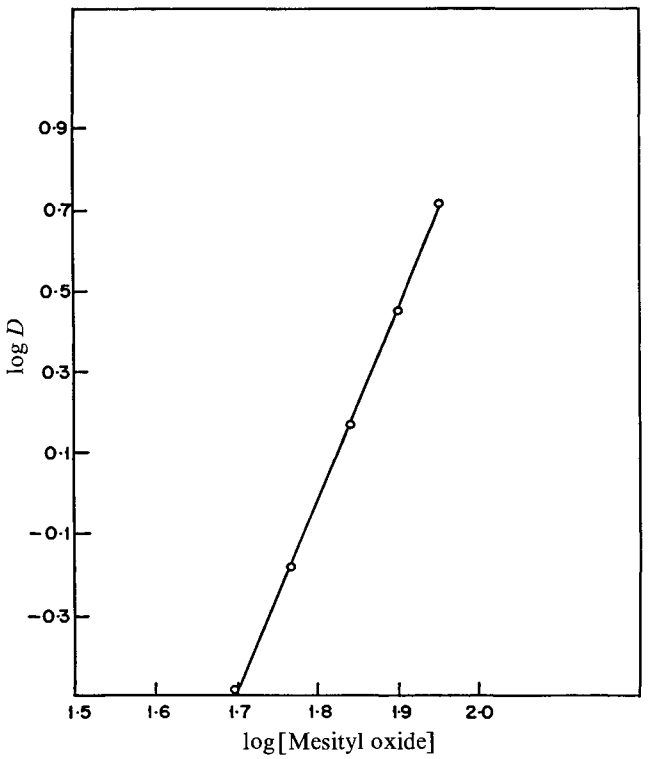

Fig. 1. Plot of log(distribution ratio, D) vs. log(Mesityl oxide concentration, %) at 0.2 mol dm^{-3} hydrobromic acid concentration.

Nature of the Extracted Species. The nature of the extracted species was established using log–log plot. A plot of log of distribution ratio (D) versus log of mesityl oxide concentration (at 0.2 mol dm^{-3} hydrobromic acid concentration) gave a slope of 2.3 indicating a molar ratio of 1 : 2 with respect to the extractant (Fig. 1).

Effect of Strippng Agents. Different stripping agents were tried for back extraction of bismuth. Nitric acid was suitable stripping agent because with other agents such as hydrochloric acid, perchloric acid, sulphuric acid, ammonium hydroxide, and sodium hydroxide the recovery of bismuth was not quantitative. Water do not strip bismuth from the organic phase. The results are reported in Table 2.

Effect of Foreign Ions. Varying amounts of foreign ions were added to a fixed amount of bismuth (200 μg) to study interference in the recommended procedure. The tolerance limit was set at the amount required to cause ±1% error in bismuth recovery. There was no interference from 8000 μg each of Cu(II), Zn(II), Fe(III), Mn(II), and Ni(II); 6000 μg each of Mo(VI), Co(II), Mg(II), citrate, and tartrate; 4000 μg each of Be(II), Pb(II), Th(IV), As(III), and fluoride; 2000 μg each of W(VI), Sb(III), V(V), Ba(II), Ti(IV), U(VI), thiourea, oxalate, sulfate, nitrate, nitrite, phosphate, chloride, and ascorbic acid; 1000 μg each of Cd(II), Hg(II), Sn(II), Cr(VI), Au(III), Ag(I), and Pd(II); 400 μg of thiosulfate and 200 μg of EDTA.

Analysis of Synthetic Mixture. The proposed method was applied for the extraction and determination of

Table 2. Effect of Stripping Agents.[a] Bi(III)=200 μg

Stripping agent	Concentration / mol dm^{-3}	Extraction / %	Distribution ratio, D
HNO_3	0.1	77.8	7.01
	0.15—0.5	99.9	1998
	2.0	92.3	23.97
HCl	0.01	7.4	0.16
	0.1	74.1	5.72
	0.2	70.4	4.76
	2.0	40.7	1.37
H_2SO_4	0.01	59.3	2.91
	0.05—0.4	98.1	103.26
	1.0	92.3	23.97
$HClO_4$	0.05	59.3	2.91
	0.1	70.4	4.76
	0.2	96.3	52.05
	0.3—0.8	97.8	88.91
	2.0	88.9	16.02
NaOH	0.1	60.5	3.06
	0.2	70.4	4.76
	1.0—2.0	Interference[b]	
NH_4OH	0.2	37.0	1.17
	2.0	40.7	1.37
	4.0	Interference[b]	

a) Water do not strip bismuth from the organic phase. b) Interference in the color development.

Table 3. Analysis of Synthetic Mixture

Composition	Bismuth found[a)]	Relative error
μg	μg	±,%
Bi, 200.0; Ti, 1000.0; Mo, 1000.0; V, 1000.0; Fe, 1000.0	200.0	0.0
Bi, 200.0; As, 600.0; Sb, 600.0; Sn, 600.0; Pb, 600.0	198.0	1.0

a) Average of triplicate analysis.

bismuth in different synthetic mixtures. The results showed that the recovery of bismuth was $\geqslant$99%. The results are reported in Table 3.

Analysis of Alloys. A known amount of bismuth was added to leaded brass (BCS 385), leaded bronze (BCS 364), and leaded gunmetal (BCS 183/4) and bismuth was recovered by the proposed method. The procedure is detailed below.

Weigh accurately 100 mg each of leaded brass, leaded bronze, and leaded gunmetal, add 3 cm^3 of concentrated nitric acid and evaporate to almost dryness. The residue is taken up with water and the precipitate of metastannic acid is filtered off. The precipitate is first washed with hot dilute nitric acid and then thoroughly with hot water. To the filtrate add solution containing 2.5 mg of bismuth and dilute to 25 cm^3. 2 cm^3 of this solution is taken for extraction and determination of bismuth by the proposed method. The results are reported in Table 4.

40 mg of Woods alloy was taken and dissolution was carried out as described above. Then the filtrate was diluted to 100 cm^3 and 1 cm^3 of this solution was taken for extraction and determination of bismuth by the proposed method. The result is reported in Table 4.

Analysis of Pharmaceutical Samples. Bismuth containing drugs such as Denol were analysed by the proposed method. A Denol tablet was dissolved in 10 cm^3 of perchloric acid, evaporated to almost dryness, taken up in water, filtered and the filtrate was diluted to 500 cm^3. Agrawal and Bhatt have determined bismuth in

Table 4. Analysis of Standard Alloys for Extraction of Bismuth(III)

Alloy	Composition	Bismuth found[a)]/mg	Relative error
	%		±,%
Leaded brass (BCS[b)] 385)	Cu, 58.7; Pb, 2.24; Fe, 0.15; Zn, 38.5; Sn, 0.27; Ni, 0.13; Al, 0.005; Mn, 0.005; Sb, 0.005+2.5 mg Bi	2.49	0.4
Leaded bronze (BCS 364)	Cu, 80.6; Sn, 9.35; Pb, 9.25; Ni, 0.28; Sb, 0.18; Zn, 0.13; As, 0.065; P, 0.056; Al, 0.002 Si, 0.002+2.5 mg Bi	2.48	0.8
Leaded gunmetal (BCS 183/4)	Cu, 84.06; Pb, 3.15; Sn, 7.27; Zn, 3.47; Ni, 1.0; P, 0.090; Fe, 0.056; Sb, 0.23; As, 0.13; S, 0.11+2.5 mg Bi	2.48	0.8
Woods alloy (Indalloy 158) Indium Corporation of America	Bi, 50.0; Pb, 26.7; Sn, 13.3; Cd, 10.0	19.99	0.1

a) Average of triplicate analysis. b) BCS=British Chemical Standard.

Table 5. Analysis of Drugs

Name of drug	Composition	Certified value or added value of Bi	Bismuth found[a)]
Denol (Elder Pharmaceuticals, India)	Colloidal bismuth subcitrate, calculated as Bi_2O_3 120 mg	107.64 mg	107.63 mg
Pectomycin suspension (Lyka Labs. Limited, India)	Each 15 cm^3 contains, light kaolin. I.P. 2.5 mg Pectin I.P. 50 mg Streptomycin sulphate I.P. $\cong$0.5 mg streptomycin Flavoured syrupy base q.s.+2.5 mg Bi	2.5 mg	2.5 mg

a) Average of triplicate analysis.

Pectomycin suspension[12] (Manufactured by Lyka Labs, India). The sample of Pectomycin available in the Bombay market, however does not contain bismuth and hence 2.5 mg of bismuth was added to 5 cm^3 of Pectomycin suspension and dissolved in 10 cm^3 of 2.5 mol dm^{-3} H_2SO_4 the solution was filtered and diluted to 50 cm^3. 1 cm^3 and 4 cm^3 aliquot of Denol and Pectomycin suspension were respectively taken for extraction and determination of bismuth by the proposed method. The results are reported in Table 5.

The method is selective and permits a rapid separation and determination of a microgram amount of bismuth. The average recovery of bismuth was 99.0±1%. Each determination took a total of 20—25 min.

The authors are grateful to the University of Bombay for awarding "The Pandit Bhagwandin Dube and Mrs. Ramdulari Dube Scholarship in Science" to one of them. (G.S.D.)

References

1) E. Jackwerth and H. Speaker, *Z. Anal. Chem.*, **177**, 327 (1960).
2) F. Aoki and H. Tomioka, *Bull. Chem. Soc. Jpn.*, **38**, 1557 (1965).
3) H. A. Mottola and E. B. Sandell, *Anal. Chim. Acta*, **24**, 301 (1961).
4) T. Kono and A. Nemori, *Bunseki Kagaku*, **24**, 419 (1975).
5) C. Rozycki, *Chem. Anal.*, **14**, 755 (1969).
6) S. D. Shete and V. M. Shinde, *Mikrochim. Acta*, **I(1—2)**, 63 (1984).
7) B. Ya. Spivakov, V. I .Lebedev, N. P. Krivenkova, T. S. Plotnikova, I. P. Kharlamov, and Yu. A. Zolotov, *Zh. Anal. Khim.*, **31**, 757 (1976).
8) I. A. Shevchuk, T. N. Simonova, Z. N. Kravtsova, T. I. Pluzhnik, and N. I. Gorshkova, *Ukr. Khim. Zh.*, **41**, 959 (1975).
9) G. Nakagawa, *Ukr. Khim. Zh.*, **81**, 750 (1960).
10) T. Suzuki, *Bunseki Kagaku*, **15**, 667 (1966).
11) J. R. Clark and J. G. Viets, *Anal. Chem.*, **53**, 61 (1981).
12) Y. K. Agrawal and V. J. Bhatt, *Analyst*, **109**,1287 (1984).
13) E. B. Sandell, "Colorimetric Determination of Traces of Metals," 3rd ed, Interscience, New York (1958), p. 337.
14) A. I. Vogel, "A Textbook of Quantitative Inorganic Analysis," 3rd ed, Longmans, London (1961), p. 442.

Dynamics of Autoxidation of Aqueous Sulfur Dioxide in Aqueous Suspensions of Cadmium Oxide

Ashu RANI, D. S. N. PRASAD, Rachna BHARGAVA, and Krishna Swarup GUPTA*
Atmospheric Chemistry Laboratory, Department of Chemistry, University of Rajasthan, Jaipur 302004, India
(Received September 12, 1990)

Autoxidation of S(IV), in buffered solutions,conforms the rate law (1). The increase in buffer concentration has a

$$R_{obsd} = k_5[CdO][S(IV)]^2[H^+]^{-1.22} \quad (1)$$

rate decreasing effect. On the other hand, in unbuffered solutions the kinetics obey a different rate law (2).

$$R_{obsd} = (k_{10} + k_{11}[CdO])[S(IV)][H^+]^{-0.5} \quad (2)$$

In both situations, the dissolution of CdO accompanies the autoxidation. A heterogeneous catalytic mechanism involving adsorption of both dioxygen and sulfur(IV) on the surface of CdO particle has been proposed.

While investigating heterogeneous photocatalytic oxidation of sulfite in aqueous suspensions of semiconductor powders, Frank and Bard (1977)[1] observed that zinc oxide, in dark, displayed a significant catalysis in suspensions containing 1×10^{-2} mol dm^{-3} acetic acid although the autoxidation was accompanied by a dissolution of ZnO and as a sequel neutralization of the solution also took place, and the experiments with ZnO were not persued further. In view of the fact that cadmium belongs to Zn-subgroup and CdO is more basic than ZnO, it may be expected that surface-pH of CdO particles would be higher than the former and as a consequence CdO would exhibit a stronger catalytic activity, as surface pH is reported to be a dominant factor in determining rates and capacities of SO_2 removal by several metal oxides in systems; aerosol–SO_2(g)–water (Judeikis et al., 1978).[2]

Additional points of interest in studying CdO catalysis were as follows. CdO is found, to a small extent, in suspended particulate matter.[3,4] In an earlier study, the photocatalytic autoxidation of S(IV) in CdS-suspensions has been reported by Gutierrez and Henglein (1983).[5] In this paper, the kinetics of the autoxidation of S(IV), in aqueous suspensions of CdO, is being reported.

Experimental

Materials and Methods. Cadmium oxide in powder form was of Arbha IM make and of 99.5% purity. All other chemicals were of reagent grade and used as received. For obtaining aqueous S(IV) solution, sodium sulfite was used. For study at constant pH, CH_3COOH–CH_3COONa buffer was used. In case of study in unbuffered solutions, the desired initial pH was obtained by adding dilute perchloric acid.

The experimental procedure was essentially the same as used by Brodzinsky et al.[6] The reactions were conducted in an open Erlenmayer flask, which was maintained at desired temperature by circulating thermostated water around it. The reaction was initiated by first adding temperature equilibrated sodium sulfite solution to the buffer solution maintained at the same temperature, followed by the addition of weighed CdO. The reaction mixture was stirred continuously at 1600±100 rpm using a magnetic bar. At this stirring speed, the reaction was shown not to be oxygen mass transfer controlled.

Table 1. Estimation of Sulfate in Final Product Solution, [CdO]=0.3 mol dm^{-3}, pH=5.06

[S(IV)]×10^3 mol dm^{-3}	[Sulfate]×10^3 mol dm^{-3}	[Sulfate]/[S(IV)]	% Recovery as sulfate
2.0	1.94	0.97	97
3.0	2.89	0.96	96
4.0	3.91	0.98	98

The kinetics were followed by withdrawing 5 ml aliquot, filtering of the solid rapidly with glass wool and analyzing the filterate iodometrically.

The initial rates for kinetics runs were calculated and as the reaction is accompanied by a dissolution of CdO, the initial rates had a slightly higher uncertainty, nevertheless, the rate measurements were reproducible within ±15%. All calculations were done on Apple IIe Computer using Curve Fitter and Scientific Plotter programmes of Interactive Microwave Inc. U.S.A. In the presentation of rate data later, the statistical parameters have been abbreviated as follows: correlation coefficient=CC; coefficient of determination=CD; standard error of estimate=SEE.

Product Analysis. The quantitative analysis, performed on the final product solution, showed sulfate to be the only product. It was quantitatively estimated in solutions having different initial sulfite concentrations using the standard procedure. The results are given in Table 1. Thus, the stoichiometry of the reaction could be written as,

$$\text{Sulfur(IV)} + 1/2O_2 \xrightarrow{CdO} \text{Sulfate}.$$

Results

To begin with, the effect of stirring speed on the reaction rate was examined by varying rpm from 300—1800. It was found that the rate increased with increase in rpm attaining a maximal value around 1200 rpm. Hence, all the experiments were carried out at 1600±100 rpm, as at this rpm, reaction is not oxygen mass transfer-controlled.

The initial kinetics experiments, both in buffered and in unbuffered solutions, indicated that CdO has a significant catalytic activity and the standard S(IV) disappearance curves are normal in this case. However, a disturbing and complicating factor, that the reaction is accompanied by a dissolution of CdO powder, also came to light. The same observation was made by Frank and Bard[1] in case of ZnO-catalyzed reaction. The dissolution was apparent from a visual examination of the reaction mixture and it was observed to be higher in buffered solution than in unbuffered reaction mixtures, presumably owing to the reaction of CdO with CH_3COOH in the former. In case of unbuffered solutions, some CdO was left undissolved at the end of a kinetics run (60% completion). Despite CdO dissolution, the pH in buffered solutions remained effectively constant throughout the course of a kinetics run. This is probably due to interplay of two opposing factors. CdO dissolution tends to increase the pH, while sulfite ion oxidation into sulfate tends to decrease pH and thus, these two factors counter-balance each other leaving pH of the reaction mixtures almost unchanged.

The dissolution of CdO and consequent production of Cd^{2+} ions made us to look for the cause of the catalysis; whether it was due to homogeneous catalysis perpetuated by Cd^{2+} ions or due to CdO particles or due to both. For this reason, influence of 1—2.4×10^{-3} mol dm^{-3} cadmium acetate, $Cd(OAc)_2$, and 2—5×10^{-3} mol dm^{-3} cadmium chloride, in the absence of CdO, was examined. For comparison, the uncatalyzed reaction was also studied under exactly similar conditions. The results given in Table 2 indicate that the rate of autoxidation, in presence of added Cd-salts, is no different than the rate in their absence. This rules out Cd^{2+} being the cause of catalysis.

It may be mentioned that the cadmium acetate used in aforesaid experiments was prepared by dissolving same CdO in acetic acid, as was used in preparing aqueous suspensions for kinetics work. In view of the dissolution of the CdO, the treatment of kinetics results obtained in this study, was based on initial rates, as the initially most of CdO will remain undissolved.

Kinetics in Buffered Suspensions. Influence of Buffer Concentration: The effect of buffer concentration on the reaction rate was studied with twin objectives of finding out a suitable buffer concentration required for maintaining pH for the range of CdO employed, and for examining its influence on the rate itself. The rate increases with decreasing buffer concentrations, while maintaining the ratio $[CH_3COONa]/[CH_3COOH]$ and hence, pH same. However, at buffer concentrations less than $[CH_3COOH]=6\times10^{-2}$ mol dm^{-3} and $[CH_3COONa]=1.4\times10^{-1}$ mol dm^{-3}, the pH could not be maintained constant. This led us to select these concentrations of acetic acid and sodium acetate for buffering reaction mixtures. When it was desired to vary pH, $[CH_3COONa]$ was held constant at 1.4×10^{-1} mol dm^{-3}, and $[CH_3COOH]$ was varied.

Table 2. The Influence of $Cd(OAc)_2$ and $CdCl_2$ on S(IV) Autoxidation. $[S(IV)]=2\times10^{-3}$ mol dm^{-3}, pH=5.16, t=30 °C

Salt	$[Cd^{2+}]\times10^3$ / mol dm^{-3}	$R_{obsd}\times10^8$ / mol dm^{-3}/s^{-1}
$Cd(OAc)_2$	1.0	1.6
$Cd(OAc)_2$	1.7	1.5
$Cd(OAc)_2$	2.3	1.6
$CdCl_2$	2.5	1.5
$CdCl_2$	3.5	1.4
$CdCl_2$	5.0	1.4
Uncatalyzed	—	2.0

CdO-Dependence: Using initial rates, R_{obs}, for CdO variation an order of 0.98±0.02 was determined for CdO. The plots of R_{obsd} vs. [CdO] (Fig. 1) are linear with small intertepts in agreement with the rate law (1). R_{buff} and k_1 values obtained from this figure are collected in Table 3.

$$R_{obsd} = R_{buff} + k_1[CdO], \quad (1)$$

where R_{buff} is the rate of uncatalyzed reaction in buffered suspensions. k_1 values are seen to vary with S(IV) in accordance with Eq. 2.

$$k_1 = k_2[S(IV)]^2. \quad (2)$$

From a plot of k_1 and $[S(IV)]^2$, k_2 was determined to be

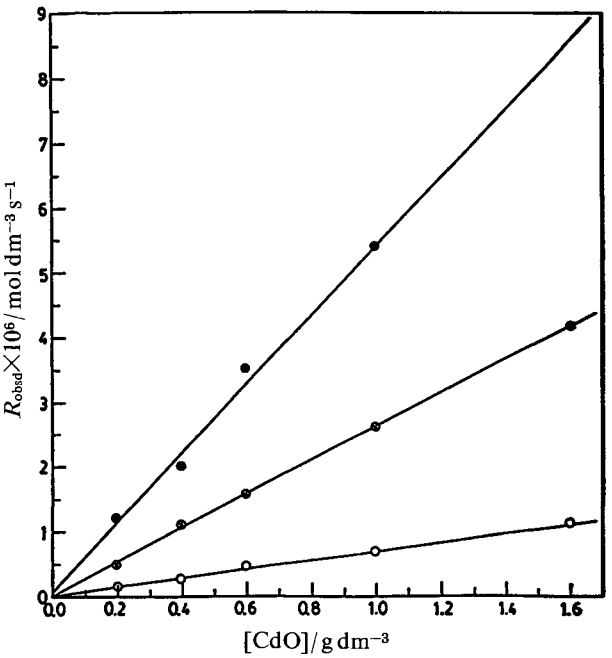

Fig. 1. Variation of CdO at three different S(IV) in buffered solutions at pH 5.06 and 30 °C. [S(IV)]; ○=2.5×10^{-3}, ⊗=5×10^{-3}, ●=7.5×10^{-3} mol dm^{-3}.

Table 3. The Values of R_{buff} and k_1 at Different [S(IV)] at pH=5.06 and 30 °C

$[S(IV)]\times10^3$/mol dm^{-3}	2.5	5.0	7.5
$k_1\times10^7$/mol g^{-1} s^{-1}	7.1	26.2	53.8
$R_{buff}\times10^8$/mol dm^{-3} s^{-1}	0.2	0.4	6.2

$(8.6\pm0.2)\times10^{-2}$ $dm^6\,mol^{-1}\,g^{-1}\,s^{-1}$. The uncatalyzed rate, R_{buff}, is negligible in comparison to catalyzed rate and contribution of the former to the total rate does not exceed more than 6% at the highest [S(IV)], which is well within the uncertainty of present rate measurements and R_{buff} can, therefore, be neglected. In the light of Eq. 2, Eq. 1 then can be modified as Eq. 3.

$$R_{obsd} = k_2[CdO][S(IV)]^2. \quad (3)$$

Sulfur(IV)-Dependence: R_{obsd} values for sulfur(IV) variations yielded an order of 2.05 ± 0.07, in conformity with the rate law (4).

$$R_{obsd} = k_4[S(IV)]^2. \quad (4)$$

The values of k_4, given in Table 4, were determined at various [CdO] from R_{obsd} vs. $[S(IV)]^2$ plots which are given in Fig. 2. A comparison of Eqs. 4 and 3 shows,

$$k_4 = k_2[CdO]. \quad (5)$$

Thus, the results of variation of S(IV) also conform Eq. 3. Using Eq. 2, the values of k_2 from sulfur(IV) variations at 0.2, 0.6, and 1.0 $g\,dm^{-3}$ [CdO] were determined to be 0.12 ± 0.02, 0.08 ± 0.01, and 0.07 ± 0.01 $dm^6\,mol^{-1}\,g^{-1}\,s^{-1}$ respectively at pH 5.06 and 30 °C. Similarly, at same pH and temperature, k_2 values of 0.11 ± 0.01, 0.11 ± 0.01, and 0.10 ± 0.01 $dm^6\,mol^{-1}\,g^{-1}\,s^{-1}$ were determined by varying [CdO] at 2.5×10^{-3}, 5.0×10^{-3}, and 7.5×10^{-3} $mol\,dm^{-3}$ [S(IV)], respectively. Some variation is seen in these values which fall in the range 0.07—0.12 $dm^6\,mol^{-1}\,g^{-1}$.

It must be admitted that under varying reaction conditions, such as [S(IV)], [CdO] and pH, the rate of dissolution of CdO will not be same and is likely to vary from one reaction condition to another. Perhaps, this is the reason for variation in k_2 values, although the values fit the same rate law (11) and one gets nearly same values if extracted from a particular variation. We, therefore, ascribe the variation in k_2 values to the phenomenon of differential dissolution.

pH-Dependence: The results of pH variation in the range 4.8—5.9, given in Table 5, show the rate to increase with increase in pH. From a log-log plot between R_{obsd} and $[H^+]$, an order of -1.22 in $[H^+]$ was obtained. The complete rate law, including [CdO], [S(IV)] and $[H^+]$-dependences can, therefore, be written as Eq. 6.

$$R_{obsd} = k_5[CdO][S(IV)]^2[H^+]^{-1.22}. \quad (6)$$

Rate laws (3) and (6) are equivalent through $k_2 = k_5[H^+]^{-1.22}$.

Temperature-Dependence: The values of R_{obsd}, determined at 25, 30, and 35 °C (Table 6), yielded an energy of activation of 322 kJ mol^{-1}.

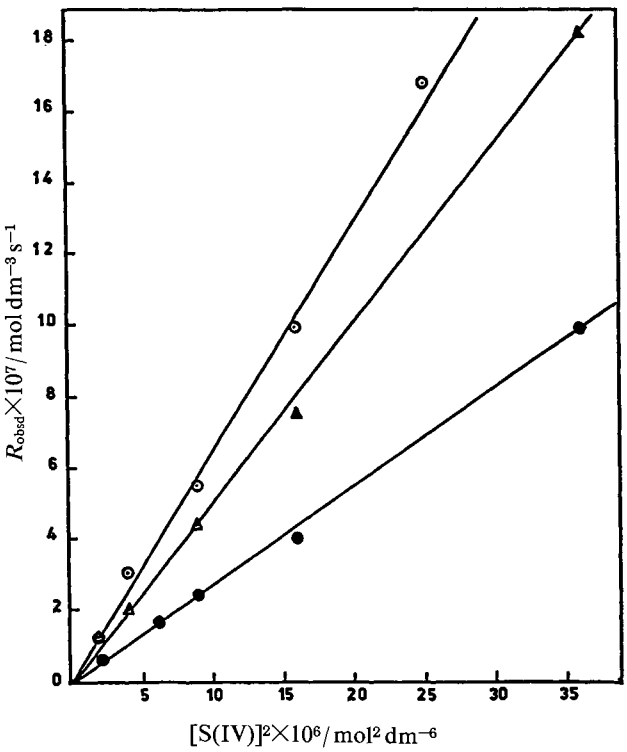

Fig. 2. Dependence of R_{obsd} on [S(IV)] in CdO-catalyzed [S(IV)] autoxidation in buffered solutions at 30 °C and pH=5.06. ●; [CdO]=0.2 g dm^{-3}, △; [CdO]=0.6 $g\,dm^{-3}$; ⊙; [CdO]=1.0 $g\,dm^{-3}$.

Table 4. k_4 Values at Different [CdO] at pH=5.06 and 30 °C

[CdO]/$g\,dm^{-3}$	0.2	0.6	1.0
$k_4\times10^2/dm^3\,mol^{-1}\,s^{-1}$	2.9	5.0	6.7

Table 5. Values of R_{obsd} and k_2 at Different pH and at 30 °C

Expt. No.	[S(IV)]$\times10^3$ / $mol\,dm^{-3}$	[CdO] / $g\,dm^{-3}$	pH	$R_{obsd}\times10^6$ / $mol\,dm^{-3}\,s^{-1}$	k_2 / $dm^6\,mol^{-1}\,g^{-1}\,s^{-1}$
1	2.5	0.6	5.71	3.33	0.89
2	2.5	0.6	5.46	1.65	0.44
3	2.5	0.6	5.30	0.77	0.21
4	2.5	0.6	4.96	0.46	0.12
5	2.5	0.6	4.88	0.29	0.08
6	2.5	0.3	5.71	1.67	0.89
7	2.5	0.3	5.46	0.83	0.45
8	2.5	0.3	5.30	0.38	0.20
9	2.5	0.3	4.96	0.23	0.13
10	2.5	0.3	4.88	0.15	0.08

Table 6. R_{obsd} Values at Temperatures and [S(IV)]=5×10^{-3} mol dm^{-3}, [CdO]=0.20 g dm^{-3}, pH=5.06

Temp/°C	25	30	35
$R_{obsd}\times10^{7}$/mol dm^{-3} s^{-1}	0.50	5.00	36.4

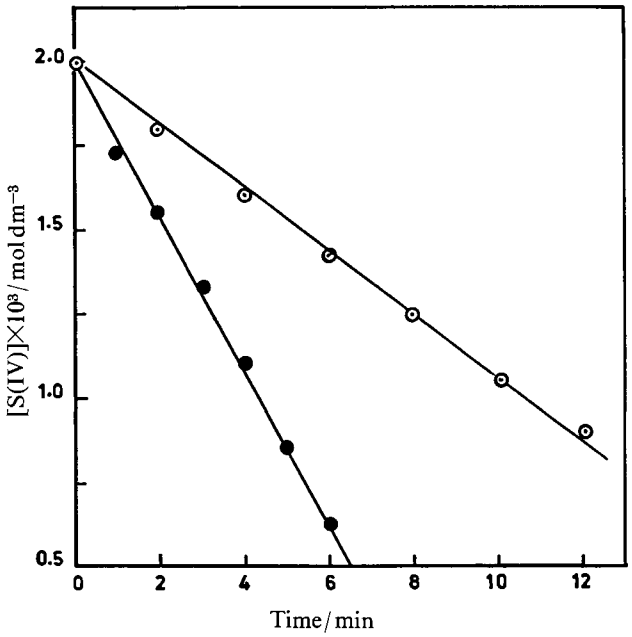

Fig. 3. Rate profiles for CdO-catalyzed [S(IV)] autoxidation in unbuffered solutions at 30 °C. [S(IV)]= 2×10^{-3} mol dm^{-3}, [CdO]=0.2 g dm^{-3}, t=30 °C. ⊙; pH=4.93, ●; pH=5.80.

Kinetics in Unbuffered Suspensions. for studying kinetics in unbuffered solutions, initial pH was adjusted to desired value with the help of dilute perchloric acid. In all these experiments, pH varied with the progress of the reaction. The reaction profiles at different pH values are shown in Fig. 3. For investigating [CdO] and [S(IV)] dependences, a pH value of 5.06±0.02 was selected.

CdO-Dependence: [CdO] was varied from 0.05 to 0.30 g dm^{-3} at [S(IV)]=2×10^{-3} mol dm^{-3}, pH=5.06 and 30 °C and order in CdO was determined to be 0.6. The fractional order in CdO probably indicates the presence of a term independent of [CdO] in the rate law. In all likelihood, this term corresponds to uncatalyzed reaction. Indeed, the rate measurements, in the absence of CdO, yielded an uncatalyzed rate of 6×10^{-7} mol dm^{-3} s^{-1} under similar reaction conditions. On this premise, a plot between R_{obsd} and [CdO] was drawn and found to be linear (Fig. 4) in agreement with the rate law (7).

$$R_{obsd} = R_{un} + k_6[CdO], \quad (7)$$

where R_{un} is the rate of uncatalyzed reaction in unbuffered suspensions. R_{un} and k_6 values were found to be (6.8±2.1)×10^{-7} mol dm^{-3} s^{-1} and (8.0±1)×10^{-6} mol g^{-1} s^{-1} (CC=0.99; CD=0.99; SEE=3.18×10^{-8}). The presence of uncatalyzed rate term in unbuffered suspensions and its near absence in buffered suspensions deserves an

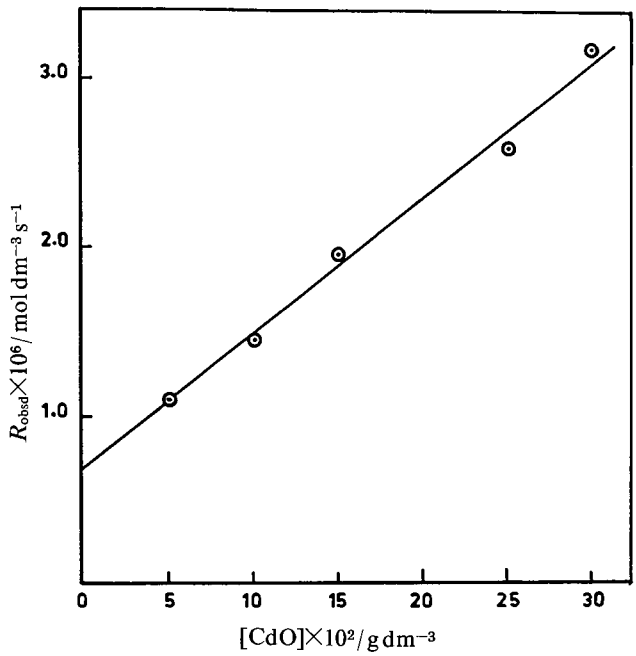

Fig. 4. Variation of R_{obsd} with CdO in unbuffered solutions at [S(IV)]=2×10^{-3} mol dm^{-3}, pH=5.06, t=30 °C.

explanation. The uncatalyzed rate has its origin in trace metal ion catalysis.[7,8] In buffered solutions, the acetate ions render these metal ions less reactive by forming complexes with them and, therefore, suppress the uncatalyzed path. Indeed, Cohen et al. (1981)[9] found the autoxidation of S(IV) in fly ash slurries, which incidentally is catalyzed by trace metal ions, is completely seized in acetate buffers, presumably due to masking of trace metal ion catalysts.[9] Moreover, trace organics are also known to inhibit the S(IV) autoxidation and their presence in acetic acid sample used by us can not be denied.[9,10]

S(IV)-Dependence: At a fixed [CdO] of 0.1 g dm^{-3}, pH 5.06 and 30 °C, [S(IV)] was varied from (1—5)×10^{-3} mol dm^{-3} (Table 7) and order in S(IV) was found to be 0.97 in agreement with Eq. 8,

$$R_{obsd} = k_7[S(IV)]. \quad (8)$$

In view of the fact that a first order dependence of uncatalyzed reaction is well established,[11] it shows the catalyzed reaction to be also of first order in [S(IV)]. On combining Eqs. 7 and 8, one obtains Eq. 9. Comparison of rate laws (7) and (9), and (8) shows,

$$R_{obsd} = (k_8 + k_9[CdO])[S(IV)], \quad (9)$$
$$k_7 = k_8 + k_9[CdO], \quad (10)$$
$$R_{un} = k_8[S(IV)], \quad (11)$$
$$k_6 = k_9[S(IV)]. \quad (12)$$

The values of R_{un}, k_6, and k_7 are collected in Table 8 and these values were used for obtaining k_9. The validity of the proposed rate law was tested by calculating the values of k_7 at [CdO]=0.1 g dm^{-3} using Eq. 10. The calculated value of 7.4×10^{-4} s^{-1} is in good agreement

with the experimental value of $(9.7\pm2.6)\times10^{-4}$ s^{-1} obtained from Fig. 5, based on Eq. 10 under similar conditions.

pH-Dependence: A variation in initial pH showed the rate to increase on increasing pH (Table 7). From a log–log plot between rate and $[H^+]$, an order of -0.5 in $[H^+]$ was extracted. On including $[H^+]$-dependence, the rate law (11) is modified to

$$R_{obsd}=(k_{10}+k_{11}[CdO])[S(IV)][H^+]^{-0.5}, \quad (13)$$

where,

$$k_8=k_{10}[H^+]^{-0.5} \text{ and } k_{11}=k_9[H^+]^{-0.5}.$$

Table 7. Values of R_{obsd} at Different [S(IV)], [CdO], and pH at 30 °C in Unbuffered Suspensions

Expt. No.	$[S(IV)]\times10^3$ / mol dm^{-3}	[CdO] / g dm^{-3}	pH	$R_{obsd}\times10^6$ / mol dm^{-3} s^{-1}
1	2.0	0.05	5.06	1.11
2	2.0	0.10	5.06	1.43
3	2.0	0.15	5.06	1.94
4	2.0	0.20	5.06	2.35
5	2.0	0.25	5.06	2.58
6	2.0	0.30	5.06	3.16
7	1.0	0.10	5.06	1.04
8	2.0	0.10	5.06	1.43
9	3.0	0.10	5.06	2.70
10	4.0	0.10	5.06	3.39
11	5.0	0.10	5.06	4.89
12	2.0	0.20	4.93	1.33
13	2.0	0.20	5.15	1.75
14	2.0	0.20	5.50	2.33
15	2.0	0.20	5.80	3.80

Table 8. Values of R_{un}, k_6, k_8, and k_9 at pH=5.06 and 30 °

$R_{un}\times10^7$ / mol dm^{-3} s^{-1}	$k_6\times10^6$ / mol g^{-1} s^{-1}	$k_7\times10^4$ / s^{-1}	$k_8\times10^4$ / s^{-1}	$k_9\times10^3$ / dm^3 g^{-1} s^{-1}
6.8	8.0	9.7	3.4	4.0

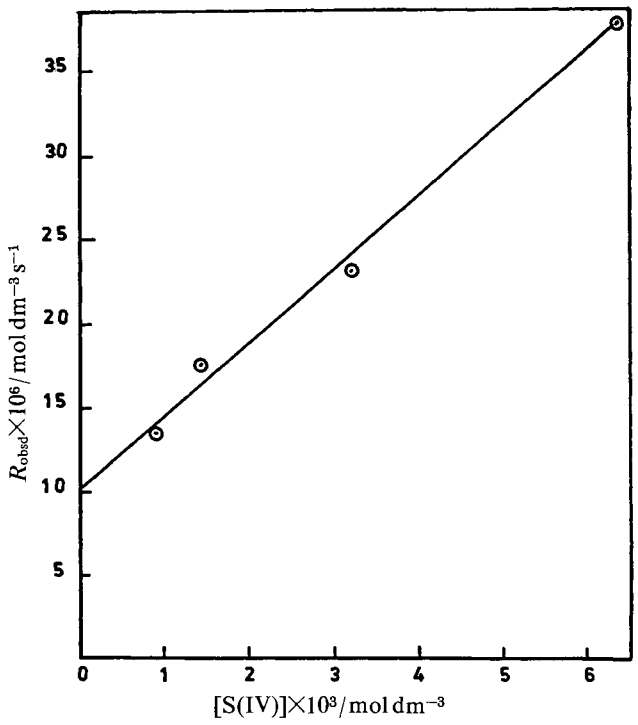

Fig. 5. Variation of [S(IV)] in unbuffered solutions at [CdO]=0.1 g dm^{-3}, pH=5.06 and t=30 °C.

Discussion

The most complicating aspect of this study is the dissolution of cadmium oxide, which accompanies the autoxidation of sulfur(IV), as the reaction progresses. However, the observation, that $CdCl_2$ and $Cd(OAc)_2$ do not possess any catalytic activity, is a redeeming feature which renders the system amenable to explanation. It should be mentioned here that the $Cd(OAc)_2$ solution, used for detecting any homogeneous catalysis by Cd^{2+} ions, was prepared by dissolving the same CdO in acetic acid, as was used in aqueous suspensions for studying heterogeneous catalysis. This firmly rules out the possibility of the impurities present in the CdO-sample as a possible cause of catalysis.

Having ruled out the possibility of catalytic activity of CdO-suspensions being due to Cd^{2+} ion, it is attractive to apportion it to the surface provided by CdO-particles. There are two strong points in favor of the heterogeneous nature of the catalysis in the present case. First is the order of two in [S(IV)], as has been found in glass,[12] silica,[13] and ceramic[13] catalyzed reactions. Second is the lack of an alternative explanation.

However, before presenting a mechanism, it is necessary to discuss the apparent difference in $[H^+]$ dependencies in buffered (Eq. 6) and unbuffered (Eq. 13) suspensions. Since, the uncatalyzed reaction, for

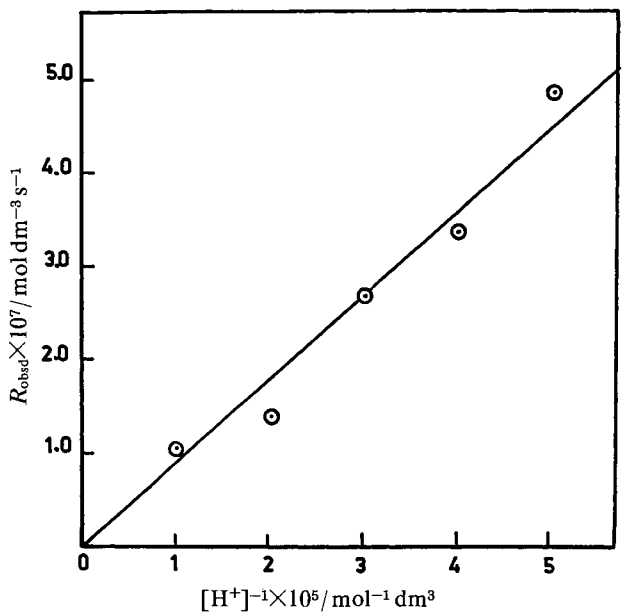

Fig. 6. Variation of R_{obsd} with $[H^+]$ in unbuffered solutions at [S(IV)]=2×10^{-3} mol dm^{-3}, [CdO]=0.2 g dm^{-3}, t=30 °C.

which rate is known to vary as $[H^+]^{-1}$ makes a substantial contribution to overall rate, it is likely that the order of −0.5 in $[H^+]$ in unbuffered study is largely due to this path and the CdO-catalyzed might be $[H^+]$-independent. On this premise, the rate law (13) if written as Eq. 14 fully accounts for observed $[H^+]$-dependence. The plot of R_{obsd} vs. $[H^+]^{-1}$ is straight line with a non-zero intercept (Fig. 6),

$$R_{obsd} = k_{12}[S(IV)][H^+]^{-1} + k_{13}[S(IV)][CdO]. \quad (14)$$

It yielded k_{12} and k_{13} values of $(2.2\pm0.4)\times10^{-9}$ s^{-1} and $(2.5\pm0.5)\times10^{-3}$ dm^3 g^{-1} s^{-1} respectively at 30 °C.

In buffered study, the uncatalyzed rate is negligible and, therefore, $[H^+]$-dependence can not be ascribed to this path, except nominally. An interpretation in terms of reaction mechanism via involvement of HSO_3^- and SO_3^{2-} ions would be vitiated and obscurred by the fact that the variation in $[H^+]$ also entails a variation in the ratio $[CH_3COONa]/[CH_3COOH]$. Obviously, with increase in pH, $[H^+]$ and $[CH_3COOH]$ both decrease and there is no way to discern whether the rate increases on increasing pH is due to decrease in $[H^+]$ or due to decrease in $[CH_3COOH]$ or both. It should be mentioned that a decrease in $[CH_3COOH]$ would result in decreasing the rate of dissolution of CdO (loc cit) and will thus have a rate increasing effect. CH_3COOH may affect the reaction in another way by getting adsorbed onto particle surface and thus by inhibiting the heterogeneous reaction. In view of this it is best not to consider the $[H^+]$-dependence in the construction of the reaction mechanism.

The kinetics order of unity in bulk [CdO] would result in an order of 1.5 in surface CdO provided all particles are of same radius and the situation would be much more complicated if the particles are not of uniform size as is usually the case.# The interpretation of kinetics results obtained in this study is based on bulk concentration of CdO, which is similar to mechanistic treatment resorted to by earlier workers in respect of similar systems.[6]

Now, the results obtained in the present study can be explained by proposing that both S(IV) and O_2 are adsorbed on CdO surface. Subsequently, the reaction is accomplished via interaction between these. Although oxygen dependence could not be studied, it is implicated to account for the observation that no reaction occurs in the absence of O_2 and that if O_2 is not allowed to diffuse rapidly in the suspension, as is evident from the influence of stirring speed on the reaction rate, the rate of autoxidation is quite slow. The kinetics orders of one in bulk [CdO], of two in [S(IV)] in buffered study and of one in unbuffered study would require the formation of at least two activated complexes having the gross compositions—$CdO\cdot O_2\cdot S(IV)$ and $CdO\cdot O_2\cdot(S(IV))_2$ for an unified treatment. The observed kinetics in both types of studies can be explained by the following general mechanism for the CdO-catalyzed path.

$$CdO + O_2 \underset{}{\overset{K_1}{\rightleftharpoons}} CdO\cdot O_2, \quad (15)$$

$$CdO\cdot O_2 + S(IV) \overset{K_2}{\rightleftharpoons} CdO\cdot O_2\cdot S(IV), \quad (16)$$

$$CdO\cdot O_2\cdot S(IV) + S(IV) \overset{K_3}{\rightleftharpoons} CdO\cdot O_2\cdot (S(IV))_2, \quad (17)$$

$$CdO\cdot O_2\cdot S(IV) \xrightarrow{k_{14}} \text{Products}, \quad (18)$$

$$CdO\cdot O_2\cdot (S(IV))_2 \xrightarrow{k_{15}} \text{Products}. \quad (19)$$

Assuming that the equilibria (Eqs. 15—17) are rapidly established and that the values of K_1, K_2, and K_3 are low, the rate expression (Eq. 20), at constant atmospheric pressure, can be derived.

$$R_{CdO} = A[CdO][S(IV)]^2 + B[CdO][S(IV)], \quad (20)$$

where R_{CdO} is the rate of CdO-catalyzed path and $A=k_{15}K_1K_2K_3[O_2]$ and $B=k_{14}K_1K_2[O_2]$. It appears that in buffered suspensions path A is dominant and B makes a negligible contribution. The reverse appears to be true in unbuffered suspensions. It is interesting to recall that in carbon-catalyzed sulfur(IV) autoxidation[6] and in nitrite–sulfur(IV)[14] reactions, order in sulfur(IV) was found to vary from zero to two.

An alternative mechanism may also be proposed. CdO due to its basic nature is likely to become hydrated to form $Cd(OH)_2$ and this species may react further with S(IV) and O_2. It may be mentioned here that in Fe(III)-catalyzed reaction above pH 5, and in Cu(II)-catalyzed reaction in alkaline solutions, the possibility of involvement of $Fe(OH)_3$[15] and $Cu(OH)_2$[16] has been indicated. Dyson and Quon,[17] while studying the reaction between ZnO fume and SO_2, found that in presence of water vapors $Zn(OH)_2$ is formed. Based on reactive $Cd(OH)_2$, a mechanism similar to (Eq. 15—19) can be written which will reproduce the observed kinetics. The autoxidation in surficial complexes,[18] $CdO_2\cdot O_2\cdot S(IV)$ and $CdO_2\cdot O_2\cdot(S(IV))_2$, is likely to proceed through the formation of peroxomonosulfate[19] and disulfate[20] species. It should be pointed out that in the present study an initial rapid drop in [S(IV)] has not been observed as was the case with carbon particles.[6] This phenomenon was taken as an evidence of adsorption of O_2 on particle surface in a primary step i.e. in Eq. 15 by Brodzinsky et al.[6] So, in the absence of any initial rapid fall in S(IV) in this case, it is possible to formulate the proposed mechanism in an alternative way, which involves the adsorption of S(IV) on CdO first, followed by adosrption or reaction with O_2. At pH=5.06, $[S(IV)]=2\times10^{-3}$ mol dm^{-3}, $[CdO]=0.2$ g dm^{-3}, and $t=30$ °C. R_{obsd} values of 1.3×10^{-7} and 2.35×10^{-6} mol dm^{-3} s^{-1} have been determined in buffered and unbuffered suspensions respectively. This shows the rate in unbuffered solution to be much faster than in buffered solutions. This could possibly be linked to the difference in the solubility of CdO in two situations. In unbuffered solutions, the solubility of CdO is compara-

This was pointed by the referee.

tively low and a large amount of solid CdO particles is available for surface catalysis and probably this explains the higher rate in unbuffered solutions.

It is interesting to speculate the possible cause of CdO-catalysis. In our laboratory several transition metal oxides such as CuO,[12] CoO,[13] Co_2O_3,[13] and Ni_2O_3[13] have been found to be effective catalyst for S(IV) autoxidation. However, in all these cases it is possible to ascribe the catalytic activity to the ease of availability of multiple oxidation states and their easy interconvertibility (for example Co(II)/Co(III) in CoO) and adsorption of S(IV) and O_2. In case of CdO, such an explanation does not seem plausible. On the basis of the fact that like CdO, other basic oxides like MgO and ZnO also catalyze the S(IV) autoxidation, the most probable reason for the catalytic activity possessed by CdO particles is its relatively high surface-pH due to its basis nature, which helps in accomplishment of the reaction between sulfur(IV) and O_2.[21]

In the light of the present work, it is desirable that the catalytic activity of other metal oxides, which are found in suspended particulate matter, should also be investigated.

The authors are grateful to Dr. R. E. Huie, National Institute of Standards and Technology, Gaithersburg, MD, USA. The work was supported by Indo-US Subcommission Research Project CE-2.

References

1) S. N. Frank and A. J. Bard, *J. Phys. Chem.*, **81**, 1484 (1977).

2) H. S. Judeikis, B. S. Thomas, and A. G. Wren, *Atmos. Environ.*, **12**, 1633 (1978).

3) A. K. De, "Environmental Chemistry," Wiley Eastern, New Delhi (1989), p. 160.

4) Ashu Rani, "Analysis of Air Borne Particulate Matter in Environs of Jhalana Area." A case study submitted to Indira Gandhi Centre for HEEPS, University of Rajasthan, Jaipur 302004, India.

5) M. Gutierrez and A. Henglein, *Ber. Bunsen-Ges. Phys. Chem.*, **87**, 474 (1983).

6) R. Brodzinsky, S. G. Chang, S. S. Markowitz, and T. Novakov, *J. Phys. Chem.*, **84**, 3254 (1980).

7) L. R. Martin, "SO_2, NO, and NO_2 Oxidation Mechanisms: Atmospheric Considerations," ed by J. G. Calvert, 1984, pp. 70—71.

8) A. Huss, Jr., P. K. Lim, and C. A. Eckert, *J. Am. Chem. Soc.*, **100**, 6252 (1978).

9) S. Cohen, S. G. Chang, S. S. Markowitz, and T. Novakov, *Environ. Sci. Technol.*, **15**, 1498 (1981).

10) L. A. Barrie and H. W. Georgii, *Atmos. Environ.*, **10**, 743 (1976).

11) S. Beilke, D. Lamb, and J. Muller, *Atmos. Environ.*, **9**, 1083 (1975).

12) A. Rani and K. S. Gupta, unpublished work.

13) D. S. N. Prasad, R. Bhargava, and K. S. Gupta, unpublished work.

14) a) S. B. Oblath, S. B. Markowitz, T. Novakov, and S. G. Chang, *J. Phys. Chem.*, **85**, 1017 (1981); b) S. Yamamoto and T. Kaneda, *Nippon Kagaku Zasshi*, **80**, 1908 (1959); c) D. S. N. Prasad and K. S. Gupta, *Bull. Soc. Kin. Ind.*, **12(2)**, 1 (1990).

15) S. Fuzzi, *Atmos. Environ.*, **12**, 1439 (1978).

16) E. C. Fuller and R. H. Crist, *J. Am. Chem. Soc.*, **63**, 1644 (1941).

17) W. L. Dyson and J. E. Quon, *Environ. Sci. Technol.*, **10**, 476 (1976).

18) B. C. Faust and M. R. Hoffmann, *Environ. Sci. Technol.*, **20**, 9 and 943 (1986).

19) R. D. Srivastava, A. F. Mcmillan, and I. J. Harris, *Can. J. Chem. Eng.*, **46**, 181 (1968).

20) E. A. Betterton and M. R. Hoffmann, *J. Phys. Chem.*, **92**, 5962 (1988).

21) H. Guesten, "Chemistry of Multiphase Atmospheric Systems," ed by W. Jaeschke, Springer Verlag, Berlin and Heidelberg (1986), p. 567.

Separation of Scandium Using Liquid-Liquid Extraction with Macrocyclic Polyether(s) from Picrate Media

N. V. DEORKAR and Shnpad M. KHOPKAR*
Department of Chemistry, Indian Institute of Technology, Bombay 400076, India
(Received October 11, 1990)

Scandium was quantitatively extracted at pH 2.5—4.5 with 4.0×10^{-2} mol dm^{-3} 18-crown-6 in dichloromethane from 4.0×10^{-2} mol dm^{-3} solution of picric acid. It was stripped with 0.1 mol dm^{-3} nitric acid and determined spectrophotometrically at 650 nm as its complex with Arsenazo-III. It was separated from yttrium, lanthanides, zirconium, hafnium, vanadium, niobium, and uranium in multicomponent mixtures. Scandium from rock sample was also analysed.

Solvent extraction of scandium(III) with oxygenated solvents[1] is not quantitative, although, in the presence of salting out agent scandium can be extracted completely with tributyl phosphate.[2-5] Long chain amines were effective for its extraction.[6-7] The study of 15-crown-5, DB-18-crown 6, and DB-24-crown-8 indicated complexation is due to weak ion-dipole interaction.[8-11] However, systematic investigations on solvent extraction separation of scandium with crown ethers are lacking. Such studies are reported in this paper.

Experimental

Apparatus and Reagents: Apparatus used was similar to one described earlier.[12]

A stock solution of scandium was prepared by dissolving 0.850 g of its oxide (Merck, Germany) in 25 cm^3 of concentrated nitric acid and made upto 250 cm^3 with deionized water. The solution was standardized[13] complexometrically. It contained 2.20 mg cm^{-3} of scandium. A dilute solution containing 25 μg cm^{-3} of scandium was prepared by appropriate dilution. Picric acid (0.05 mol dm^{-3}) solution, benzo-15-crown-5 (B15C5), 12-crown-4 (12C4), 15-crown-5 (15C5), 18-crown-6 (18C6), dibenzo-18-crown-6 (DB18C6), and dicyclohexyl-18-crown-6 (DC18C6) (Merck, Germany) were used without further purification.

General Procedure: To an aliquot of solution containing scandium (25 μg) picric acid was added so as to have its concentration as 4.0×10^{-2} mol dm^{-3} in total volume of 10 cm^3. Then pH of the solution was adjusted to 2.5—4.5 with 0.05 mol dm^{-3} picric acid or lithium hydroxide solution. The solution was transferred to a separatory funnel and 10 ml of 4.0×10^{-2} mol dm^{-3} of 18C6 in dichloromethane was added to it and it was shaken on wrist action shaker for 10 min. The two phases were allowed to settle and separate. Scandium from the organic phase was stripped with 0.1 mol dm^{-3} nitric acid and it was determined spectrophotometrically as its complex with Arsenazo-III.[14] The concentration of scandium was calculated from the calibration curve.

Results and Discussion

Extraction as the Function of pH: Scandium was extracted at different pH to ascertain optimum pH for quantitative extraction. The phase volume ratio was maintained as 1 : 1. The extraction commenced at pH 1.5 and was complete at pH 2.5—4.5 only with 18C6. With other extractants it was not quantitative. Hence, 18C6 was used in subsequent studies (Fig. 1).

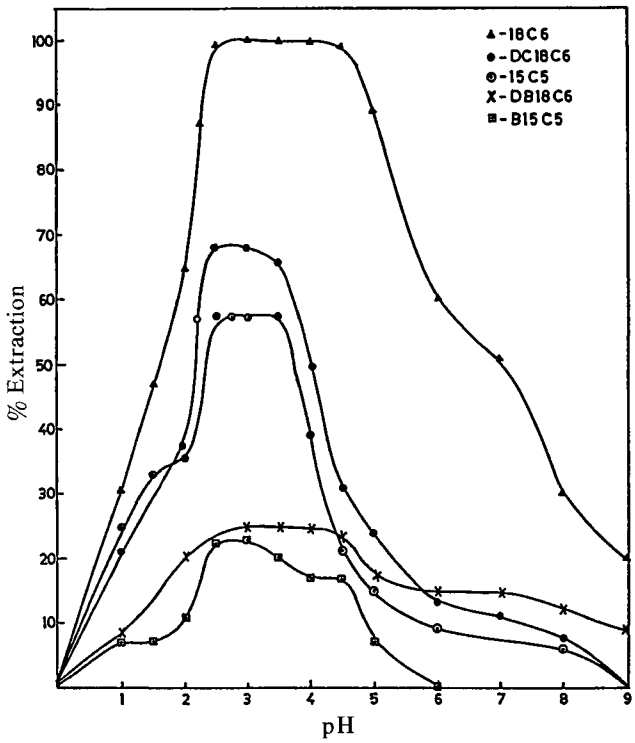

Fig. 1. Extraction of the scandium as the function of pH.

Extraction as the Function of 18C6 Concentration: Scandium was extracted at pH 2.5—4.5 with varying concentration of crown ether in dichloromethane (Table 1). The extraction was incomplete below 3.5×10^{-2} mol dm^{-3} 18C6 while it was quantitative with 4.0×10^{-2}

Table 1. Effect of 18-Crown-6 Concentration on Extraction of Scandium(III)

[18C6]/10^{-2} mol dm^{-3}	% E	D
0.5	9.1	0.10
1.0	32.0	0.47
1.5	50.3	1.01
2.0	64.2	1.79
2.5	75.0	3.0
3.0	88.0	7.33
3.5	95.0	19.0
4.0—10	>99.9	999

Table 2. Effect of Picric Acid Concentration on Extraction of Scandium(III)

[Picric acid]/10^{-2} mol dm^{-3}	% E	D
0.5	5.0	0.05
0.70	15.2	0.17
1.5	33.2	0.49
2.0	55.0	1.22
3.0	81.0	4.26
3.3	90.2	9.2
3.8—5.0	99.9	999

mol dm^{-3} 18C6 in dichloromethane.

Extraction as the Function of Picric Acid Concentration: Among the various counter ions such as eosin, tropeolin 00, dipicrylamine, Metanil Yellow, and picric acid, only picric acid was most suitable as it was capable of forming stable ion pair complex. Scandium was extracted with various concentrations of picric acid in concentration range of 0.5×10^{-2}—5.0×10^{-2} mol dm^{-3}. The extraction was quantitative above 4.0×10^{-2} mol dm^{-3} picric acid (Table 2).

Effect of on Diluent on Extraction: Benzene, toluene, xylene, carbon tetrachloride, chloroform, dichloromethane, dichloroethane, nitrobenzene, and cyclohexane were tested as the diluents (Table 3). Dichloromethane, dichloroethane, and nitrobenzene were effective as the diluents whereas all other diluents showed incomplete extraction.

Effect of Stripping Agents: Scandium was stripped with hydrochloric, nitric, sulfuric, perchloric, and acetic acid. Hydrochloric and acetic acid were effective from 2.0—7.0 mol dm^{-3} while other stripping agents were good from 0.1—0.7 mol dm^{-3}. 0.1 mol dm^{-3} nitric acid was used as the stripping agent in this work (Table 4).

Table 3. Effect of Diluents

Solvents	Dielectric constant E	% E	D
Cyclohexane	2.0	87.0	6.69
Benzene	2.28	17.5	0.21
Toluene	2.30	8.7	0.10
Xylene	2.38	5.6	0.06
Carbon tetrachloride	2.24	21.0	0.265
Chloroform	5.8	89.1	8.17
Dichloromethane	9.08	100.0	∞
Dichloroethane	10.5	100.0	∞
Nitrobenzene	34.8	100.0	∞

Table 4. Effect of Stripping Agents[a)]

Stripping agent	Scandium stripped/%				
	0.01 M	0.025 M	0.05 M	0.1 M	2—7 M
HCl	17.0	31.0	47.3	82.1	100
HNO_3	21.0	52.1	83.1	100	100
H_2SO_4	27.0	47.3	81.2	100	100
$HClO_4$	30.9	59.0	76.1	100	100
CH_3COOH	23.1	37.0	53.0	76.1	100

a) 1 M=1 mol dm^{-3}.

Effect of Shaking Period on Extraction: The extraction was carried out for various time of shaking from 2 to 20 min. Beyond 8 min shaking the extraction attained equilibrium. In order to ensure complete extraction 10 min shaking was employed.

Nature of Extracted Species: The composition of extracted species was ascertained by plotting a log D vs. log[18C6] at fixed picric acid concentration and a graph of log D vs. log[picric acid] at fixed 18C6 concentration. The corresponding slopes were 1.96 and 2.87 respectively. Hence the probable composition of extracted species was scandium : 18C6 : picric acid=1 : 2 : 3 i.e. $[Sc(pic)_3\cdot(18C6)_2]$. These findings were in agreement with those of earlier workers.[10)]

Separation from Binary Mixtures: Scandium was extracted in the presence of several ions. The tolerance limit was set as the amount of foreign ion and not salt which is causing an error of less than ±0.5% in the recovery of scandium. Since pH for extraction of scandium and alkali metals are different under condition of extraction of scandium, alkali and alkaline earths are not extracted. Alkali and alkaline earths were tolerated in the ratio of 1 : 6 to 1 : 80 except lithium tolerated in the ratio of 1 : 200. Yttrium, titanium, zirconium, hafnium, and uranium were tolerated in the ratio of 1 : 40 while thorium was tolerated in the ratio of 1 : 4.

Table 5. Separation of Scandium from Binary Mixtures Sc=25 μg, picric acid=4.0×10^{-2} M, 18C6=4.0×10^{-2} M, pH=2.5

Foreign ions	Added as	Tolerance limit/μg
Li(I)	LiCl	5000
Na(I)	NaCl	300
K(I)	KCl	150
Cs(I)	CsCl	300
Be(II)	$BeCl_2$	2000
Mg(II)	$MgSO_4\cdot7H_2O$	1500
Ca(II)	$CaCl_2\cdot6H_2O$	1000
Sr(II)	$Sr(NO_3)_2\cdot2H_2O$	500
Ba(II)	$Ba(NO_3)_2\cdot4H_2O$	300
Y(II)	$Y(NO_3)_3$	1000
Ti(IV)	$Ti(SO_4)_2$	1000
ZrO(II)	$Zr(NO_3)_4\cdot4H_2O$	1000
HfO(II)	$Hf(SO_4)_2\cdot4H_2O$	1200
Th(IV)	$Th(NO_3)_4\cdot6H_2O$	100
UO_2(II)	$UO(NO_3)_2\cdot6H_2O$	800
VO(II)	$VOSO_4\cdot H_2O$	1500
Nb(V)	Nb_2O_5	900
Cr(III)	$Cr(NO_3)_3$	900
Mo(VI)	$(NH_4)_2MoO_4\cdot4H_2O$	1000
Mn(II)	$MnSO_4\cdot4H_2O$	700
Fe(III)	$FeCl_3$	1500
Co(II)	$Co(NO_3)_2\cdot6H_2O$	1200
Ni(II)	$NiSO_4\cdot6H_2O$	900
Zn(II)	$ZnSO_4\cdot7H_2O$	1000
Cd(II)	$3CdSO_4\cdot8H_2O$	1200
Cl^-	LiCl	5000
NO_3^-	$LiNO_3$	4000
ClO_4^-	$HClO_4$	4000
Acetate	CH_3COOH	3500

The common anions were tolerated in the ratio of 1 : 200 (Table 5).

Separation from Multicomponent Mixtures: A mixture of scandium, cerium(III), and yttrium was separated by first extracting scandium with 4.0×10^{-2} mol dm^{-3} 18C6 from 4.0×10^{-2} mol dm^{-3} picric acid at pH 2.5. Then cerium(III) was extracted with 5.0×10^{-2} mol dm^{-3} 15C5 at pH 6.0. Scandium and cerium were stripped with 0.1 mol dm^{-3} nitric acid and 1 mol dm^{-3} perchloric acid respectively. Since yttrium was not extracted, it was determined directly from the aqueous phase. Since size of the hydrated scandium species is large, it readily reacts with 18-crown-6 to form complex in comparison with that of yttrium in the presence of picrate anion.

Scandium was separated from mixture of scandium, lanthanum, and yttrium by extracting it with 4.0×10^{-2} mol dm^{-3} 18C6 followed by extraction of lanthanum at pH 4.5 with 1.0×10^{-1} mol dm^{-3} 18C6 from 4.0×10^{-2} mol dm^{-3} picric acid. Since yttrium was not extracted, it was determined directly from the aqueous phase.

A mixture of lead, scandium, and aluminium was resolved by first extracting lead with 2.0×10^{-2} mol dm^{-3} DB18C6 at pH 3.0 from 1.0×10^{-2} mol dm^{-3} picric acid followed by extraction of scandium with 4.0×10^{-2} mol dm^{-3} 18C6 from 4.0×10^{-2} mol dm^{-3} picric acid when aluminium was not extracted and it remained unextracted in the aqueous phase.

A mixture of scandium, iron(III), zirconium, and titanium was separated by first extracting scandium with 4.0×10^{-2} mol dm^{-3} 18C6 from 4.0×10^{-2} mol dm^{-3} picric acid. Iron(III) was latter extracted with 1.0×10^{-2} mol dm^{-3} DB18C6 from 7.0 mol dm^{-3} hydrochloric acid followed by extraction of zirconium with 2.5×10^{-2} mol dm^{-3} DC18C6 from 8.5 mol dm^{-3} hydrochloric acid. Titanium remained in the aqueous phase as unextracted species.

Similarly scandium was separated from niobium(V)/uranium(VI), hafnium, and vanadium(IV) by extracting first scandium with 4.0×10^{-2} mol dm^{-3} 18C6 from 4.0×10^{-2} mol dm^{-3} picric acid. The niobium/uranium was extracted with 2.0×10^{-2} mol dm^{-3} DC18C6 from 7.0 mol dm^{-3} hydrochloric acid, finally, hafnium was extracted with 7.0×10^{-2} mol dm^{-3} DC18C6 from 9.0 mol dm^{-3} hydrochloric acid. The unextracted vanadium remained in the aqueous phase (Table 6).

Analysis of Scandium from Real Samples: About 0.5 g of rock sample was dissolved in a mixture of hydrofluoric and nitric acid (1 : 1) and was evaporated to dryness. The solution after filtration was diluted to 250 ml. An aliquat of solution containing barium, iron, zirconium, hafnium, yttrium, vanadium and aluminium was taken and first barium was extracted with 1.0×10^{-2} mol dm^{-3} DB18C8 in nitrobenzene from 1.0×10^{-2} mol dm^{-3} picric acid at pH 6.0 then scandium was extracted with 4.0×10^{-2} mol dm^{-3} 18C6 from 4.0×10^{-2} mol dm^{-3} picric acid at pH 2.5. From the organic phase scandium was stripped with 0.1 mol dm^{-3} nitric acid and determined spectrophotometrically. All other elements did not interfere during the extraction of scandium. The amount of scandium in the rock sample was 3.43% against the standard value of 3.5% which was determined by atomic absorption spectrometer.

The proposed method is simple, rapid, and selective. The total time required for extractive separation and determination is about 2 h. The relative standard deviation was ±1.9%. The separation of scandium from yttrium, lanthanum, cerium, uranium, zirconium, hafnium, and niobium was significant.

Thanks are due to the Council of Scientific and Industrial Research for sponsoring this project and awarding a senior research fellowship to one of the authors (NVD).

Table 6. Separation of Scandium from Multicomponent Mixtures

Sr. No.	Mixture	Extractant	Counter anion	pH	Amount taken (μg)	% Recovery	Stripping agent
1	Sc	0.04 M 18C6	0.04 M Picrate	2.5	25	99.7	0.1 M HNO_3
	Ce(III)	0.05 M 15C5	0.04 M Picrate	6.0	15	99.0	1.0 M $HClO_4$
	Y	Unextracted	—	—	50	100	Aq phase
2	Sc	0.04 M 18C6	0.04 M Picrate	2.5	25	99.1	0.1 M HNO_3
	La(III)	0.1 M 18C6	0.04 M Picrate	4.5	25	97.6	0.05 M H_2SO_4
	Y	Unextracted	—	—	50	99.8	Aq phase
3	Pb(II)	0.02 M DB18C6	0.01 M Picrate	3.0	25	99.7	1.0 M $HClO_4$
	Sc	0.04 M 18C6	0.04 M Picrate	2.5	25	99.0	0.1 M HNO_3
	Al	Unextracted	—	—	50	99.8	Aq phase
4	Sc	0.04 M 18C6	0.04 M Picrate	2.5	25	99.0	0.1 M HNO_3
	Fe(III)	0.01 M DB18C6	7.0 M Chloride	—	50	99.7	0.5 M H_2SO_4
	Zr(IV)	0.025 M DC18C6	8.5 M Chloride	—	25	99.1	0.5 M HCl
	Ti(IV)	Unextracted	—	—	50	99.7	Aq phase
5	Sc	0.04 M 18C6	0.04 M Picrate	2.5	25	99.6	0.1 M HNO_3
	Nb/UO_2(II)	0.02 M DC18C6	7.0 M Chloride	—	25	99.1	0.5 M HCl
	Hf(IV)	0.07 M DC18C6	9.0 M Chloride	—	25	98.7	0.1 M $HClO_4$
	V(IV)	Unextracted	—	—	50	100	Aq phase

References

1) R. Bock and E. Bock, *Z. Anorg. Allg. Chem.*, **246**, 146 (1950), *Chem. Abstr.*, **46**, 7453 (1950).

2) D. F. Peppard, G. W. Mason, and J. L. Maier, *J. Inorg. Nucl. Chem.*, **3**, 215 (1956).

3) D. F. Peppard, J. P. Faris, P. R. Gray, and G. W. Mason, *J. Phys. Chem.*, **57**, 294 (1953).

4) D. F. Peppard, G. Asanovich, R. W. Attebarry, O. DuTemple, M. V. Gergel, A. W. Gnaedinger, G. W. Mason, V. H. Meschko, E. S. Nachtman, and I. O. Winsch, *J. Am. Chem. Soc.*, **75**, 4576 (1953).

5) A. M. Reznik, S. A. Senrenov, and L. D. Zurehenko, *Zh. Neorg. Khim.*, **31**, 738 (1986).

6) Wang, Lengwei, Liu Xuanicon, and Yang Xeuqun, *Xiangton Dame Ziran Kexue Xeubao,* **11**, 74 (1986). *Chem. Abstr.*, **106**, 26989 (1987).

7) M. B. Dalvi and S. M. Khopkar, *Talanta,* **26**, 892 (1979).

8) D. J. Olszanski and G. A. Melson, *Inorg. Chim. Acta,* **26**, 263 (1976).

9) Gan Xinmin, Tang Ning, Shu Yin, Sai Yingli, and Ton Minyll, *Zhongguo Xitu Xuebao,* **7**, 13 (1989). *Chem. Abstr.*, **112**, 150561 (1990).

10) Jin Zhongsheng, Liu Yongsheng, Sang Shugon, and Yu Fengian, *Xuexue Xuebao,* **45**, 1048 (1987). *Chem. Abstr.*, **108**, 105242 (1988).

11) Qi Youxum, Tan Minyu, and Zhai Yingli, *Goodeng Xuexia Huaxue Huebao,* **8**, 199 (1987). *Chem. Abstr.*, **107**, 146237 (1987).

12) N. V. Deorkar and S. M. Khopkar, *Analyst,* **114**, 105 (1989).

13) F. J. Welcher, "Analytical Uses of Ethylenediaminetetraacetic Acid," D. Van Nostrand Inc., New York (1958), p. 175.

14) F. D. Snell, "Photometric and Fluorometric Methods of Analysis," John Wiley and Sons, New York (1978), Part I.

Reaction of Amidine Phenylogous with *p*-Benzoquinones

Ahmed M. Nour EL-DIN,* Aboul-Fetouh E. MOURAD, Alaa A. HASSAN, and Mohsen A. GOMAA
Department of Chemistry, Faculty of Science, El-Minia University, El-Minia, A.R. Egypt
(Received October 20, 1990)

N-(4-Dimethylaminobenzylidene)anilines and N^1-(4-dimethylaminophenyl)-N^1,N^2-diphenylformamidine reacted with tetrachloro-, tetrabromo,- and tetrafluoro-*p*-benzoquinones via charge-transfer complexes formation giving 2-monoarylamino-3,5,6-trihalo-*p*-benzoquinones and 2,5-bis(arylamino)-3,6-dihalo-*p*-benzoquinones. The course of the reaction leading to the formation of the products has been interpreted.

Recently, we have shown that azomethines,[1] azomethine *N*-oxides[2] (nitrones), as well as heteroaromatic *N*-oxides[3] form charge-transfer complexes (CTC) with different electron-deficient π-systems as *p*-benzoquinones, tetracyanoethylene, and tetracyanoquinodimethane.

In the previous work[1] concerning the study of the CTC of aryl substituted azomethines with electron-poor *p*-benzoquinones, tetrachloro-*p*-benzoquinone (chloranil, CHL), tetrabromo-*p*-benzoquinone (bromanil, BRL), and 2,3-dichloro-5,6-dicyano-*p*-benzoquinone (DDQ), we found that, the presence of dimethylamino group on the benzylidene ring increases the donor ability of the azomethine compound enough for immediate reaction with the *p*-benzoquinones. This behavior prompted us to study the chemical interaction between different *N*-(4-dimethylaminobenzylidene) anilines (**1a—i**) (Fig. 1), and the electron-deficient *p*-benzoquinones CHL, BRL and tetrafluoro-*p*-benzoquinone (fluoranil, FRL).

On addition of equimolar amounts of *p*-benzoquinones CHL, BRL, and FRL to azomethines (**1a—i**) in ethyl acetate, with admission of air at room temperature, a green color of the transient CTC was observed, which immediately changed to brown color and a solid product precipitated. When the reaction was followed spectrophotometrically, absorption maxima were observed in the range 620—728 nm, and were assigned to the CTC, since both the azomethines (**1a—i**) and the

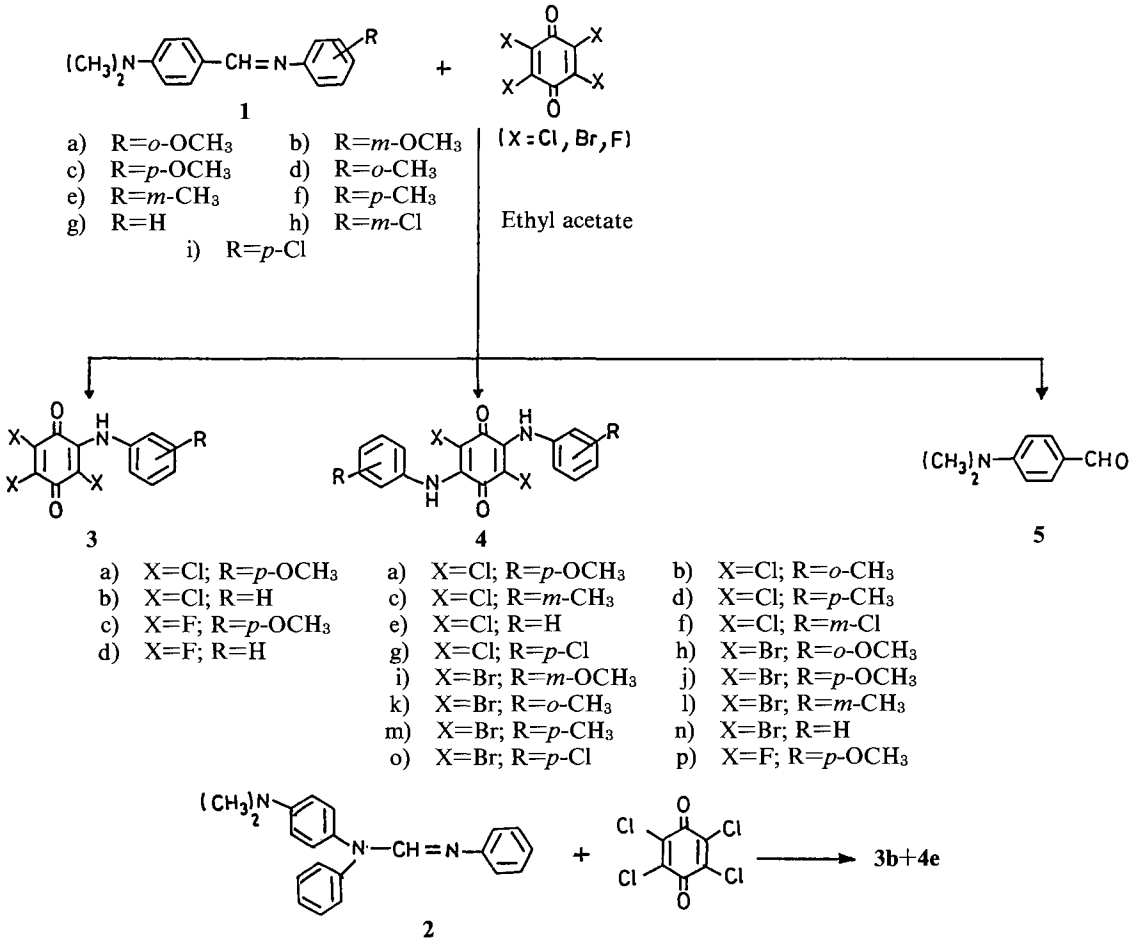

Fig. 1.

p-benzoquinones alone did not absorb in this region[4] (Table 1). The chromatographic separation of the reaction mixtures yielded the 2-arylamino-3,5,6-trihalo-*p*-benzoquinones (**3a—d**) as minor products (10—16%), the 2,5-bis(arylamino)-3,6-dihalo-*p*-benzoquinones (**4a—p**) (41—61%) as major products,[5] and 4-dimethylaminobenzaldehyde (**5**) (Fig. 1).

However, the reactions of other azomethines, which bear methoxy or methyl substituents instead of a dimethylamino group on the benzylidene ring led to the formation of relatively stable CTC and did not give the expected mono- and/or di-arylaminohalo-*p*-benzoquinone products. This result indicates that the presence of dimethylamino group on the benzylidene ring plays an important role in this reaction and is essential for the azomethine **1a—i** to be capable of undergoing this chemical reaction. On the other hand, the structures of the products **3a—d** and **4a—p** show that the active center of the azomethines **1a—i** is the nitrogen atom of the imino group. Thus, it may be assumed that the presence of the good electron-donating dimethylamino group in para position on the benzylidene ring, and consequently in conjugation with it, makes Schiff's bases (**1a—i**) to behave like amidines[6] (⩾N–CH=N–) or phenylogous amidines. This assumption could be rationalized through the formation of both the 2-arylamino- (**3b**) and the 2,5-bis-arylamino- (**4e**) derivatives (Fig. 1) from the reaction of the amidine **2** with chloranil under the same conditions.

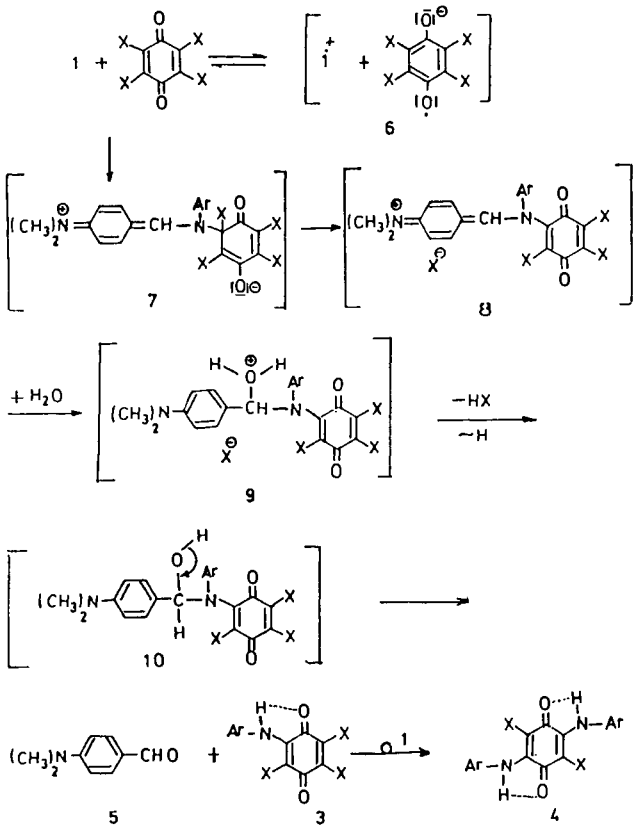

Fig. 2.

Table 1. Absorption (λ_{max}) of the Charge-Transfer Complexes of *p*-Benzoquinones with Various Donors in Dichloromethane at Room Temperature (25 °C)

Donor	Acceptor	λ_{max}/nm	Donor	Acceptor	λ_{max}/nm
1a	CHL	670	**1a**	BRL	710
1b	CHL	695	**1b**	BRL	714
1c	CHL	711	**1c**	BRL	728
1d	CHL	695	**1d**	BRL	717
1e	CHL	693	**1e**	BRL	710
1f	CHL	705	**1f**	BRL	721
1g	CHL	690	**1g**	BRL	707
1h	CHL	686	**1h**	BRL	700
1i	CHL	688	**1i**	BRL	705
1a	FLR	648(sh)	**1b**	FLR	632
1c	FLR	650	**1d**	FLR	641(sh)
1e	FLR	628	**1f**	FLR	640
1g	FLR	625	**1i**	FLR	620
2	CHL	586			

These findings can be interpreted according to Fig. 2. The mixing of the electron-deficient *p*-benzoquinones CHL, BRL, or FRL with each of the donors **1a—i** would lead initially to the formation of CTC **6**, which exists in equilibrium with the two reactants: Then the activation of the nitrogen atom of the imino group through the electron-pair of the dimethylamino group enables their nucleophilic attack on the *p*-benzoquinone forming **7**, which gives the salt **8**. The addition of H_2O molecule to the intermediate **8** followed by dehydrohalogenation, deprotonation on oxygen and protonation on the arylated nitrogen affords the 2-arylamino-*p*-benzoquinones (**3**) and 4-dimethylaminobenzaldehyde (**5**). Hydrolysis of the Schiff's base (which should generate the aldehyde and the free amine Ar–NH_2, which in turn would attack the quinone) prior to reaction with the quinone is considered unlikely, because there is no change in the Schiff's base under the similar conditions where a *p*-benzoquinone is absent. On the other hand, the salt **8** may be attacked by moisture faster than the free Schiff's base. The reaction of **3** with another molecule of amidine phenylogous **1** should lead to the formation of the major product **4** (Fig. 2). Proofs of the structures of the products were based firmly on elemental analysis, UV, IR, ^{1}H NMR, and the mass spectra, chemical reactions, or comparison with authentic samples (Tables 1—4).

Experimental

Melting points are uncorrected. UV-vis spectra were measured on a Perkin-Elmer Lambda 2 spectrophotometer using 1.0 cm stoppered silica cells. IR spectra were measured on a Shimadzu 408 spectrophotometer (KBr). The ^{1}H NMR spectra were recorded on Bruker Wp 80 (80 MHz), and the chemical shifts were expressed as δ (ppm) with TMS as the internal standard. The MS spectra were recorded on Finnigan MAT 8430 spectrometer at 70 eV. Elemental analyses were performed by microanalytical unit at Duisburg University, FRG, using Carlo ERBA strumentazione elemental analyzer Model 1106.

Table 2. Analytical and Physical Data of **3a—d** and **4a—p**

Compd	Yield %	Mp °C	Lit[a] mp	Color of crystal	Solvent of recryst	Molecular formula (M. Wt)	Analysis % found (calcd) C	H	N
3a	12	188—189		Blue	A	$C_{13}H_8Cl_3NO_3$ (332.569)	46.83 (46.95)	2.31 (2.42)	4.29 (4.20)
3b	16	>300	—	Blue	A	$C_{12}H_6Cl_3NO_2$ (302.526)	47.58 (47.63)	2.01 (1.99)	4.67 (4.63)
3c	14	140—142	—	Blue	A	$C_{13}H_8F_3NO_3$ (283.200)	55.51 (55.14)	2.87 (2.84)	4.87 (4.95)
3d	10	119—121	—	Brown		$C_{12}H_6F_2NO_2$ (253.146)	56.97 (56.93)	2.41 (2.39)	5.49 (5.53)
4a	44	295—296	298	Black	B	—	—	—	—
						—	—	—	—
4b	48	275—277	—	Brown	B	$C_{20}H_{16}Cl_2N_2O_2$ (387.264)	61.94 (62.00)	4.21 (4.15)	7.19 (7.25)
4c	46	285d	—	Black	B	$C_{20}H_{16}Cl_2N_2O_2$ (387.264)	62.07 (62.00)	4.19 (4.15)	7.31 (7.25)
4d	53	306d	310d	Black	C	—	—	—	—
						—	—	—	—
4e	51	314—316	315d	Brown	C	—	—	—	—
						—	—	—	—
4f	41	305—306	—	Brown	B	$C_{18}H_{10}Cl_4N_2O_2$ (427.100)	50.41 (50.45)	2.39 (2.35)	6.49 (6.55)
4g	43	>330	350	Black	B	—	—	—	—
						—	—	—	—
4h	54	240	—	Deep green	B	$C_{20}H_{16}Br_2N_2O_4$ (508.148)	46.99 (47.25)	3.14 (3.15)	5.48 (5.50)
4i	49	206—208	—	Brown	B	$C_{20}H_{16}Br_2N_2O_4$ (508.148)	47.23 (47.25)	3.12 (3.15)	5.52 (5.50)
4j	57	263d	267	Black	B	—	—	—	—
						—	—	—	—
4k	51	220—221	—	Reddish brown	B	$C_{20}H_{16}Br_2N_2O_2$ (476.148)	50.28 (50.40)	3.31 (3.35)	5.93 (6.00)
4l	55	221—222	—	Brown	B	$C_{20}H_{16}Br_2N_2O_2$ (476.148)	50.41 (50.43)	3.42 (3.35)	5.84 (6.00)
4m	59	358d	360	Brown	—	—	—	—	—
						—	—	—	—
4n	48	283—284	285	Brown	B	—	—	—	—
						—	—	—	—
4o	41	318	320	Black	B	—	—	—	—
						—	—	—	—
4p	61	272—273	—	Reddish brown	B	$C_{20}H_{16}F_2N_2O_4$ (386.360)	62.25 (62.18)	4.06 (4.17)	7.16 (7.25)

A=Cyclohexane
B=Acetone
C=Ethyl acetate
The percentage of yield of the aldehyde $(CH_3)_2N$-C_6H_4CHO is 20%.
a) Refs. 5 and 12.

Table 3. IR and ^1H NMR Spectra of the 2-Arylamino-3,5,6-trihalo-*p*-benzoquinone **3a—d** and 2,5-Bis(arylamino)-3,6-dihalo-*p*-benzoquinone **4a—p**

Compound	IR (KBr, cm^{-1})	^1H NMR[a] (δ, TMS)
3a	3250 (NH), 2900 (aliph. CH), 1690 (CO), 3010, 1605 (Ar-CH), 1585 (Ar-C=C).	
3b	3220 (NH), 1680 (CO), 1605 (Ar-CH), 1580 (Ar-C=C).	6.95—7.60 (m, 5H) Ar-H, 9.25 (br. s, 1H) NH.
3c	3360 (NH), 2885 (aliph. CH), 1680 (CO), 1620 (Ar-CH), 1500—1530 (Ar-C=C).	
3d	3310 (NH), 1695 (CO), 1610 (Ar-CH), 1525 (Ar-C=C).	6.80—7.60 (m, 5H) Ar-H, 9.20 (br. s, 1H) NH.
4a	3210 (NH), 2900 (aliph. CH), 1645 (CO), 1605 (Ar-CH), 1560—1580 (Ar-C=C).	
4b	3210 (NH), 1650 (CO), 3010, 1610 (Ar-CH), 1560-1570 (Ar-C=C).	2.20 (s, 6H) CH_3, 7.10—7.30 (m, 8H) Ar-H, 9.30 (br. s, 2H) NH.
4c	3210 (NH), 2900 (aliph. CH), 1645 (CO), 3010 (Ar-CH), 1560 (Ar-C=C).	2.31 (s, 6H) CH_3, 6.99—7.22 (m, 8H) Ar-H, 9.25 (br. s, 2H) NH.

Table 3. (Continued)

Compound	IR (KBr, cm^{-1})	^1H NMR[a] (δ, TMS)
4d	3250 (NH), 1645 (CO), 3010, 1610 (Ar-CH), 1560 (Ar-C=C).	2.28 (s, 6H) CH_3, 7.00—7.20 (m, 8H) Ar-H, 9.58 (br. s, 2H) NH.
4e	3240 (NH), 1645 (CO), 1600 (Ar-CH), 1575 (Ar-C=C).	7.14—7.40 (m, 10H) Ar-H, 9.78 (br. s, 2H) NH.
4f	3250 (NH), 1650 (CO), 1605 (Ar-CH), 1560 (Ar-C=C).	7.05—7.45 (m, 8H) Ar-H, 9.45 (br. s, 2H) NH.
4g	3250 (NH), 1645 (CO), 1610 (Ar-CH), 1560 (Ar-C=C).	7.00—7.10 (m, 8H) Ar-H, 9.25 (br. s, 2H) NH.
4h	3240 (NH), 1645 (CO), 1600 (Ar-CH), 1555 (Ar-C=C).	3.85 (s, 6H) OCH_3, 6.85—7.35 (m, 8H) Ar-H, 8.35 (br. s, 2H) NH.
4i	3250 (NH), 1645 (CO), 1610 (Ar-CH), 1570 (Ar-C=C).	3.78 (s, 6H) OCH_3, 6.70—7.35 (m, 8H) Ar-H, 9.40 (br. s, 2H) NH.
4j	3240 (NH), 1640 (CO), 1600 (Ar-CH), 1560 (Ar-C=C).	3.82 (s, 6H) OCH_3, 6.80—7.35 (m, 8H) Ar-H, 8.40 (br. s, 2H) NH.
4k	3210 (NH), 1655 (CO), 1610 (Ar-CH), 1585 (Ar-C=C).	2.30 (s, 6H) CH_3, 6.95—7.30 (m, 8H) Ar-H, 8.30 (br. s, 2H) NH.
4l	3240 (NH), 1645 (CO), 1600 (Ar-CH), 1560 (Ar-C=C).	2.35 (s, 6H) CH_3, 6.90—7.30 (m, 8H) Ar-H, 8.35 (br. s, 2H) NH.
4m	3250 (NH), 1645 (CO), 1610 (Ar-CH), 1565 (Ar-C=C).	2.35 (s, 6H) CH_3. 6.95—7.30 (m, 8H) Ar-H, 8.35 (br. s, 2H) NH.
4n	3250 (NH), 1645 (CO), 3010, 1600 (Ar-CH), 1565 (Ar-C=C).	7.10—7.40 (m, 10H) Ar-H, 8.50 (br. s, 2H) NH.
4o	3200 (NH), 1640 (CO), 1600 (Ar-CH), 1555 (Ar-C=C).	7.10—7.45 (m, 8H) Ar-H, 9.25 (br. s, 2H) NH.
4p	3250 (NH), 1665 (CO), 1610 (Ar-cH), 1585 (Ar-C=C).	3.77 (s, 6H) OCH_3, 6.80—7.20 (m, 8H) Ar-H, 8.75 (br. s, 2H) NH.

a) The solvent of ^1H NMR is DMSO-d_6 except **3b** and **3d** ($CDCl_3$).

Table 4. Mass Spectroscopy of 2-Arylamino-3,5,6-trihalo-*p*-benzoquinone **3a—d** and 2,5-Bis(arylamino)-3,6-dihalo-*p*-benzoquinone **4a—f, n—p**

Compound	MS *m/z* (rel intensity %)
3a	332½ (M^+, 100), 297 (73), 281 (17), 175 (50), 92 (26), 77 (30), 65 (50), 51 (22).
3b	302½ (M^+, 33), 267 (29), 175 (18), 77 (100), 51 (90).
3c	283 (M^+, 100), 268 (84), 248 (5), 212 (7), 192 (8), 92 (16), 77 (9), 65 (31).
3d	253 (M^+, 100), 206 (24), 108 (32), 77 (61), 51 (56).
4a	419 (M^+, 100), 403 (3), 383 (24), 367 (13), 348 (16), 347 (51), 331 (4), 174 (80), 123 (10), 77 (32), 65 (19).
4b	387 (M^+, 100), 351½ (64), 316 (39), 286 (13), 246 (12), 158 (41), 91 (64), 77 (24), 65 (52), 44 (18).
4c	387 (M^+, 58), 371 (8), 351½ (46), 315 (41), 91 (100), 77 (21), 65 (71).
4d	387 (M^+, 100), 371 (16), 351½ (47), 336 (12), 315 (49), 91 (100), 77 (25), 65 (70).
4e	359 (M^+, 90), 323 (77), 287 (38), 77 (100).
4f	427 (M^+, 10), 391½ (54), 356 (26), 320½ (4), 178 (100).
4n	448 (M^+, 46), 368 (24), 340 (18), 288 (22), 77 (100), 51 (40).
4o	516 (M^+, 37), 436 (17), 402 (14), 356 (7), 321 (16), 223 (34), 178 (100).
4p	386 (M^+, 100), 368 (10), 355 (69), 348 (41), 324 (7), 264 (5), 107 (4), 77 (10), 65 (9).

Preparative Layer Chromatography. Air dry 1.0 mm layers of silica gel Merck pf 254 on plates were employed for preparative TLC and bands were detected by indicator fluorescence quenching upon exposure to 254 mm UV-light.

Compounds: 2,3,5,6-Tetrachloro-*p*-benzoquinone (chloranil, CHL, Aldrich) and 2,3,5,6-tetrabromo-*p*-benzoquinone (bromanil, BRL, Merck) were recrystallized several times from benzene before use. 2,3,5,6-Tetrafluoro-*p*-benzoquinone (Fluoranil, FRL, Aldrich) was used without purification. Azomethines **1a—i** were prepared by the usual condensation reaction of 4-dimethylaminobenzaldehyde with substituted aromatic amines.[7,8] The amidine **2** was prepared according to the literature.[9] Ethyl acetate used as a solvent, was purified according to Vogel[10] and Organikum,[11] dried and distilled.

The Reaction of *p*-Benzoquinones, (BRL, CHL, FRL) with Azomethines 1a—i and Amidine[#] 2. General Procedure: To a solution of tetrahalo-*p*-benzoquinone (0.001 mol) in 20 ml dry ethyl acetate, the azomethine (0.001 mol) which was dissolved in 10 ml dry ethyl acetate was added dropwise with stirring at room temperature. The reaction mixture became deep green which turned immediately into brown color. The stirring was continued for 48 h with admission of air to complete the reaction.

The reaction mixture was filtered and the precipitate was washed several times with cold ethyl acetate until the mother liquor became clear. The filtrate was concentrated and the residue was chromatographed on thin-layer plates using toluene as eluent to give two zones; the first contained compound **3** which is characterized by a deep blue color, and the second the 4-dimethylaminobenzaldehyde.

The two zones were extracted with acetone and the products recrystallized from the suitable solvent to afford the pure compounds (see Table 2).

The precipitate was recrystallized from acetone to give a pure compounds of 2,5-bis(arylamino)-3,6-dihalo-*p*-benzoquinone **4**.

We thank DAAD (F.R.G) for the financial support of this work. Thanks are also due to Professor Dr. D. Döpp, Fachbereich Organische Chemie, Duisburg Uni-

[#] In the case of reaction with amidine **2**, the corresponding aldehyde could not be isolated in apure form.

versität, F.R.G, for providing laboratory facilities and for valuable discussions.

References

1) A. M. Nour El-Din, *Z. Phys. Chem. (Leipzig)*, **267**, 980 (1986).
2) A. M. Nour El-Din and D. Döpp, *Bull. Soc. Chim. Belg.*, **93**, 891 (1984).
3) A. M. Nour El-Din, *Spectrochim. Acta, Part A*, **41**, 1101 (1985).
4) R. Foster, "Organic Charge Transfer Complexes," Academic Press, London (1969).
5) H. Hishi, Y. Hatada, and K. Kitahara, *Bull. Chem. Soc. Jpn.*, **56**, 1482 (1983).
6) S. Patai, "The Chemistry of Amidines and Imidates," John Wiley & Sons, London (1975).
7) A. Roe and J. A. Montgomery, *J. Am. Chem. Soc.*, **75**, 910 (1952).
8) H. Gilman, *Org. Synth.*, Coll. Vol. I, 80 (1956).
9) A. M. Nour El-Din, *J. Chem. Res. (M)*, **79**, 3019 (1984).
10) A. I. Vogel, "A Textbook of Practical Organic Chemistry," 3rd ed, Longman, London (1957).
11) H. Becker et al., "Organikum," Deut. Verl. Wiss., Berlin (1973).
12) R. L. Mital and S. K. Jain, *J. Chem. Soc. C*, **1971**, 1875.

Crystalline 1:1 Inclusion Complexes between a Roof-Shaped Diamide Host and Methanol or Propionic Acid. Crystal Structures and Modes of Interaction

Ingeborg CSÖREGH,* Stephan FINGE,† and Edwin WEBER*,†
Department of Structural Chemistry, Arrhenius Laboratory, Stockholm University, S-106 91 Stockholm, Sweden
†Institut für Organische Chemie und Biochemie der Universität Bonn, Gerhard-Domagk-Straße 1, D-5300 Bonn-1, FR-Germany
(Received November 26, 1990)

The crystal structures of two inclusion complexes between *anti-N,N'*-di-*t*-butyl-9,10-dihydro-9,10-ethanoanthracene-11,12-dicarboxamide host and methanol [a=11.8893(4), b=18.0943(7), c=12.6322(4) Å, β=108.47(3)°, $P2_1/c$, Z=4] or propionic acid [a=11.4580(8), b=11.7614(9), c=12.4675(8) Å, α=95.37(3), β=109.70(3), γ=113.26(3)°, $P\bar{1}$, Z=2] as guests have been studied by X-ray diffraction. Closed loops of different sizes, formed via hydrogen-bond interactions between host and guest or between the hosts only, characterize both structures. The crystals with the propionic acid guest consist of hydrogen-bonded host : guest associates with 2 : 2 stoichiometry, while the methanol inclusion gives rise to infinite hydrogen-bonded chains.

Carboxylic acids have been noted as powerful crystalline hosts.[1] Due to their distinct hydrogen bonding properties,[2,3] they make possible crystalline complex formation with a wide range of guests.[4–6] Amides corresponding to the carboxylic acids are also crystalline hosts[7] but show different complexation behavior. An example is the diamide **1** which yielded a crystalline 1 : 1 inclusion compound with methanol (**2**) in a highly selective manner,[8] while the corresponding diacid[9] gave crystalline inclusion complexes with higher alcohols only.[8] Apart from this difference, the inclusion ability of the diacid is much more pronounced.[8] Nevertheless, **1** also yields a crystalline inclusion compound with propionic acid (**3**) which has the same stoichiometric ratio (1 : 1) as the corresponding propionic acid complex

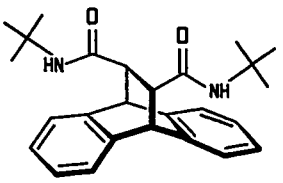

1

2 = **1** · MeOH (1:1)

3 = **1** · EtCOOH (1:1)

Table 1. Crystal Data and Some Details of the Refinement Calculations (esd's, where given, are in Parentheses)

Compound	2	3
Formula unit	$C_{26}H_{32}N_2O_2 \cdot CH_4O$	$C_{26}H_{32}N_2O_2 \cdot C_3H_6O_2$
Formula weight	436.59	478.63
Unit cell dimensions		
a/Å	11.8893(4)	11.4580(8)
b/Å	18.0943(7)	11.7614(9)
c/Å	12.6322(4)	12.4675(8)
α/deg	90	95.37(3)
β/deg	108.47(3)	109.70(3)
γ/deg	90	113.26(3)
V_c/Å^3	2577.6(5)	1402.4(7)
Space group	$P2_1/c$	$P\bar{1}$
Z	4	2
$D_{c,\,X\text{-ray}}$/g cm^{-1}	1.125	1.133
$\mu_{c,\,Cu\,K\alpha}$/cm^{-1}	5.44	5.66
F(000)	944	516
Radiation (λ/Å)	Cu $K\alpha$ (1.5418)	Cu $K\alpha$ (1.5418)
θ_{max}/deg	70	60
N_{obs} (unique, non-zero)	4225	3750
N_{ref} with $I>3\sigma(I)$	2595	2322
$N_{variables}$	315	375
Final agreement factors		
$R=\sum\|\Delta F\|/\sum\|F_o\|$	0.048	0.051
$R_w=[\sum w\cdot\|\Delta F\|^2/\sum w\cdot\|F_o\|^2]^{1/2}$	0.073	0.078
Weighting: g in SHELX[a]	0.00886	0.0091

a) Weights of the structure factors in SHELX[12] are estimated as $w=\text{const}/(\sigma^2(F)+g\cdot F^2)$

formed by the mentioned diacid host.[8] Analogs of **1** with less bulky groups than *t*-butyl are inefficient.[8]

For a better understanding of the inclusion properties of **1**, and to learn the general modes of interaction between host amide and different guest functions,[9] we studied the crystal structures of the 1 : 1 complexes of **1** with methanol (**2**) and propionic acid (**3**).

Experimental

Crystals of the inclusion complexes **2** [**1**·methanol (1 : 1)] and **3** [**1**·propionic acid (1 : 1)] were obtained as described earlier.[8] In order to protect the crystals from possible solvent evaporation during the measurements, each selected single crystal of both **2** and **3** was sealed in a glass capillary.

X-Ray Data Collection and Processing. X-Ray diffraction data were collected on a STOE/AED2 diffractometer at room temperature, using the ω–2θ scan technique. Five reference reflections for the crystal of **2** were measured at intervals of about 1 h. No systematic variation of intensity was detected. The six monitor reflections, measured approximately every 45 min for **3**, however, showed a decrease in intensity of about 7%. Moreover, despite the low absorption coefficients of the present crystals (cf. Table 1), significant absorption effects were detected in the case of compound **3**, in all probability due to the mother liquor content of the capillary. Accordingly, the net intensities were corrected for Lorentz and polarization effects, and in the case of **3** also for decay and absorption effects. The absorption correction was based upon ψ scans of eight reflections within the limits $76<\chi<85°$ and $25<2\theta<71°$. The transmission factor varied between 50 and 83%.

The unit cell parameters, listed in Table 1, were refined by least-squares fit to θ values of 57 [$37<2\theta<57°$] and 58 [$16<2\theta<53°$] accurately centered reflections.

Structure Analysis and Refinement

The positions of the non-hydrogen atoms were derived by direct methods [SHELXS][11] and refined by full-matrix least-squares treatment according to Sheldrick.[12] The carbon-bonded hydrogen positions

Table 2. Fractional Atomic Coordinates of Non-Hydrogen Atoms and of the Hydrogens Involved in the Hydrogen Bonds of Compounds **2** and **3**, Respectively (esd's, where given, are in Parentheses)

Atom	*x*/*a*	*y*/*b*	*z*/*c*	B_{eq}[a]/*B*/Å²	Atom	*x*/*a*	*y*/*b*	*z*/*c*	B_{eq}[a]/*B*/Å²
Compound **2** [**1**·MeOH (1 : 1)]					C(1)	0.3405(5)	0.7020(4)	0.0854(3)	6.0(2)
C(1a)	0.7146(3)	0.3273(2)	−0.1505(3)	4.4(1)	C(2)	0.2477(5)	0.5868(5)	0.0015(4)	7.2(2)
C(1)	0.6147(3)	0.2853(2)	−0.1984(3)	5.6(1)	C(3)	0.1593(6)	0.4857(5)	0.0288(4)	8.0(3)
C(2)	0.5715(3)	0.2778(2)	−0.3138(3)	6.6(1)	C(4)	0.1637(5)	0.4975(4)	0.1417(4)	6.6(2)
C(3)	0.6266(4)	0.3129(2)	−0.3800(3)	6.4(1)	C(4a)	0.2570(4)	0.6140(4)	0.2261(3)	5.2(2)
C(4)	0.7279(3)	0.3559(2)	−0.3324(3)	5.0(1)	C(5a)	0.4263(4)	0.6899(3)	0.4296(3)	4.8(2)
C(4a)	0.7709(3)	0.3627(2)	−0.2178(2)	4.1(1)	C(5)	0.4809(5)	0.6398(4)	0.5202(3)	6.0(2)
C(5a)	0.9586(3)	0.3559(2)	−0.0686(3)	4.3(1)	C(6)	0.6236(6)	0.6951(5)	0.5831(4)	6.8(2)
C(5)	1.0776(3)	0.3434(2)	−0.0563(3)	5.5(1)	C(7)	0.7098(5)	0.7998(5)	0.5590(4)	6.8(2)
C(6)	1.1396(4)	0.2918(2)	0.0226(4)	7.2(2)	C(8)	0.6563(4)	0.8511(4)	0.4697(4)	5.6(2)
C(7)	1.0847(4)	0.2537(2)	0.0866(4)	7.4(2)	C(8a)	0.5152(4)	0.7949(3)	0.4045(3)	4.7(2)
C(8)	0.9664(3)	0.2674(2)	0.0755(3)	6.1(1)	C(9)	0.4389(4)	0.8332(3)	0.3022(3)	4.6(2)
C(8a)	0.9035(3)	0.3183(2)	−0.0025(3)	4.6(1)	C(10)	0.3390(3)	0.8736(3)	0.3390(3)	4.0(1)
C(9)	0.7755(3)	0.3399(2)	−0.0271(2)	4.3(1)	C(11)	0.2410(3)	0.7597(3)	0.3688(3)	4.0(1)
C(10)	0.7721(2)	0.4258(2)	−0.0074(2)	3.6(1)	C(12)	0.2746(4)	0.6453(3)	0.3532(3)	4.8(2)
C(11)	0.8294(2)	0.4660(2)	−0.0846(2)	3.4(1)	C(13)	0.2588(4)	0.9157(3)	0.2400(3)	4.4(2)
C(12)	0.8778(2)	0.4077(2)	−0.1518(2)	3.9(1)	O(14)	0.1321(3)	0.8561(3)	0.1837(2)	6.0(1)
C(13)	0.8329(2)	0.4421(2)	0.1162(2)	3.7(1)	N(15)	0.3375(3)	1.0196(3)	0.2160(2)	5.1(1)
O(14)	0.9397(2)	0.4556(1)	0.1542(2)	4.8(1)	C(16)	0.2903(5)	1.0704(4)	0.1126(3)	6.2(2)
N(15)	0.7592(2)	0.4386(2)	0.1770(2)	4.3(1)	C(17)	0.2305(7)	0.9674(5)	0.0004(4)	9.0(3)
C(16)	0.7934(3)	0.4447(2)	0.3000(3)	5.6(1)	C(18)	0.1795(6)	1.1108(5)	0.1160(4)	8.2(3)
C(17)	0.6766(4)	0.4408(3)	0.3274(3)	8.2(2)	C(19)	0.4187(6)	1.1882(6)	0.1251(6)	10.0(3)
C(18)	0.8703(4)	0.3791(3)	0.3534(4)	8.8(2)	C(20)	0.2507(4)	0.7933(3)	0.4939(3)	4.2(2)
C(19)	0.8567(5)	0.5174(3)	0.3385(4)	9.4(2)	O(21)	0.3615(3)	0.8600(3)	0.5792(2)	5.3(1)
C(20)	0.7408(2)	0.5173(2)	−0.1658(2)	3.5(1)	N(22)	0.1274(3)	0.7366(3)	0.5014(2)	4.6(1)
O(21)	0.6350(2)	0.5192(2)	−0.1720(2)	5.0(1)	C(23)	0.1009(4)	0.7446(4)	0.6097(3)	5.5(2)
N(22)	0.7839(2)	0.5571(2)	−0.2326(2)	3.9(1)	C(24)	−0.0540(5)	0.6578(5)	0.5698(4)	7.4(2)
C(23)	0.7130(3)	0.5996(2)	−0.3316(3)	4.6(1)	C(25)	0.1340(6)	0.8808(4)	0.6609(5)	8.2(3)
C(24)	0.6473(3)	0.6634(2)	−0.2973(3)	6.3(1)	C(26)	0.1852(6)	0.6963(7)	0.6976(5)	9.4(4)
C(25)	0.6240(4)	0.5488(2)	−0.4117(3)	6.4(1)	O(A1)	−0.1209(2)	0.6494(3)	0.2701(3)	7.1(2)
C(26)	0.8008(4)	0.6293(3)	−0.3853(4)	8.2(2)	O(A2)	−0.1210(3)	0.7994(3)	0.1762(3)	8.1(2)
O(M)	0.4985(2)	0.5929(2)	−0.0645(3)	7.6(1)	C(A1)	−0.1805(4)	0.7042(4)	0.2184(4)	5.9(2)
C(M)	0.5688(4)	0.6085(3)	0.0428(4)	7.8(2)	C(A2)	−0.3304(5)	0.6711(6)	0.1896(5)	8.5(3)
H(15)	0.6604	0.4402	0.1542	12(2)	C(A3)	−0.4031(6)	0.5624(5)	0.2316(6)	9.1(3)
H(22)	0.8629	0.5560	−0.2202	4.4(6)	H(15)	0.4342	1.0649	0.2663	6.6(9)
H(M1)	0.5440	0.5681	−0.0918	10(2)	H(22)	0.0387	0.6885	0.4295	7.5(10)
					H(A2)	−0.0220	0.8234	0.1886	11(2)
Compound **3** [**1**·EtCOOH (1 : 1)]									
C(1a)	0.3450(4)	0.7157(4)	0.1991(3)	4.7(2)					

a) $B_{eq}=1/3\sum_i\sum_j a^*_i a^*_j B_{ij}\boldsymbol{a}_i\cdot\boldsymbol{a}_j$.

Table 3. Bond Lengths (Å) and Bond Angles (deg) of Possible Hydrogen Bonds in Compounds **2** and **3**. (esd's, where given,[a] are in Parentheses)

Atoms involved	Symmetry	Distance			Angle
		Donor ··· Acceptor	D–H	H ··· A	∠D–H ··· A
Compound **2** [**1** · MeOH (1 : 1)]					
O(M)–H(1M) ··· O(21)	x, y, z	2.766(4)	0.86	1.92	172
N(15)–H(15) ··· O(M)	$1-x, 1-y, -z$	2.995(3)	1.11	1.96	152
N(22)–H(22) ··· O(14)	$2-x, 1-y, -z$	3.125(3)	0.90	2.24	168
Compound **3** [**1** · EtCOOH (1 : 1)]					
O(A2)–H(A2) ··· O(14)	x, y, z	2.673(5)	1.00	1.68	170
N(22)–H(22) ··· O(A1)	x, y, z	3.012(4)	0.97	2.05	161
N(15)–H(15) ··· O(21)	$1-x, 2-y, 1-z$	3.154(4)	0.95	2.23	163

a) The H atom positions are not refined (cf. text).

were calculated after each refining cycle, using geometric evidence. The amide H atoms in both structures, together with the hydroxyl H in **2** and the carboxylic one in **3**, were located from difference electron density maps and were held riding on their respective 'mother' atoms during the subsequent calculations.

In the last stage of the refinements, the C, O, and N atoms were allowed to vibrate anisotropically, while isotropic temperature factors were refined for the H positions. The methyls were treated as rigid groups with three rotation parameters refined for each of them. The final R values together with the crystal data and some details of the refinement calculations are shown in Table 1.

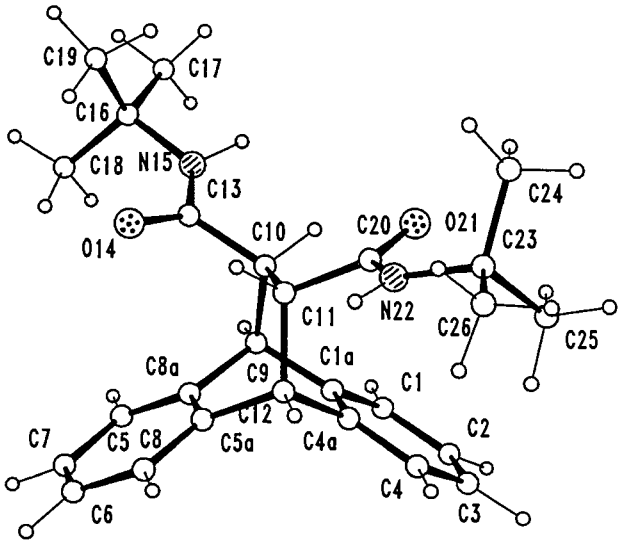

Fig. 1. Perspective view and atom labelling of host molecule **1**.

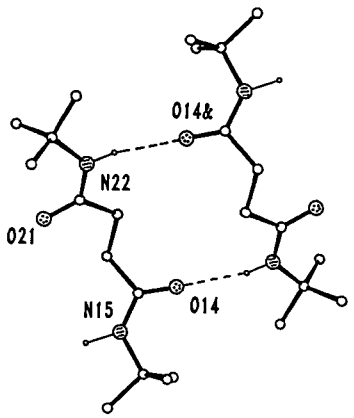

Fig. 2. Diagram of the hydrogen-bonded host–host unit present in the inclusion compounds **2** and **3**. Excerpts of the host molecules including the bridge C-atoms and functional groups only. Hydrogen bonds are indicated by broken lines.

Results and Discussion

The final fractional coordinates and the hydrogen bond dimensions for **2** and **3** are listed in Tables 2 and 3, respectively. The crystallographic labelling of the atoms of the host is shown in Fig. 1. Figure 2 is a schematic representation of the H-bonded host-host interaction found in the complexes. Figures 3 and 4 illustrate the H-bonded host-guest units in **2** and **3**, while the respective crystal packings are shown in Figs. 5 and 6. Intramolecular bond distances and angles and the thermal parameters of the non-hydrogen atoms are collected in Tables 4, 5, and 6.[13]

Molecular Structures. The dihydroanthracene moiety of the diamide host **1**, in both structures, shows the expected roof-shaped form with bond lengths and bond angles in agreement with the data published earlier for related carboxylic host molecules.[8,14,15] Accordingly, the elongated C(9)–C(10) and C(11)–C(12) bonds

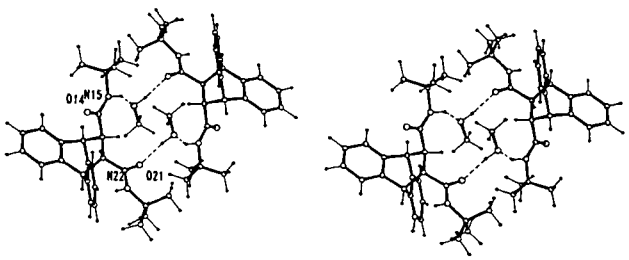

Fig. 3. Stereoscopic view of the hydrogen-bonded host–guest unit in **2** (methanol inclusion complex of **1**). Hydrogen bonds are indicated by broken lines.

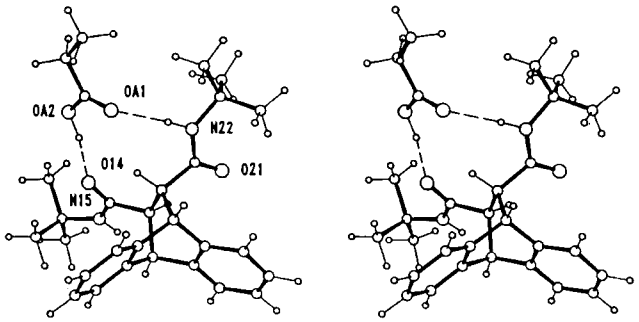

Fig. 4. Stereoscopic view of the hydrogen-bonded host–guest unit in **3** (propionic acid inclusion complex of **1**). Hydrogen bonds are indicated by broken lines.

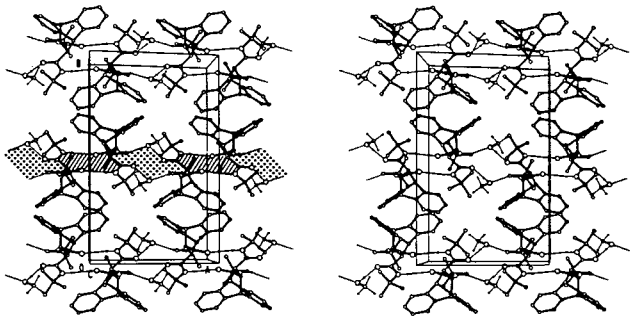

Fig. 5. Stereoscopic view of the crystal packing of **2** (inclusion complex with methanol). The nonrelevant hydrogen atoms of the host are omitted for clarity. Hydrogen bonds as thin lines. Individual cases of zones with host–host and host–guest hydrogen bond contacts are indicated by hatched and dotted areas, respectively.

of the ethano bridge in the present structures have the average length values of 1.577 and 1.562 Å, respectively; the mean C(10)–C(11) bond distance is 1.540 Å, and the dihedral angles[16] between the two aromatic ring planes are 121.0(1)° in **2** and 122.8(2)° in **3**. The bond dimensions in the amide groups, with the calculated mean values of 1.336 Å for N–$C_{(sp^2)}$, 1.486 Å for N–$C_{(sp^3)}$ and 1.231 Å for C=O, also conform to the common values for such bonds.[17] The guest molecules, (methanol in **2** and propionic acid in **3**) have ordered structures with acceptable bond dimensions.

Packing Relations and Host-Guest Interactions. The host **1** as well as the guests (methanol and propionic acid) in the present inclusion complexes are equipped with functional groups (carbamoyl, hydroxyl or carboxyl) possessing both proton donor and proton acceptor ability. Consequently, hydrogen bonds are expected to play an important role in these structures. There are hydrogen bonds between the amide moieties of symmetry-related host molecules (Table 3). These relatively weak N(–H)···O bonds form 14-membered (including the hydrogen atoms) closed loops when linking the hosts pairwise in both compounds (Fig. 2). The 1 : 1 clusters of hosts comprise two proton donor (NH)

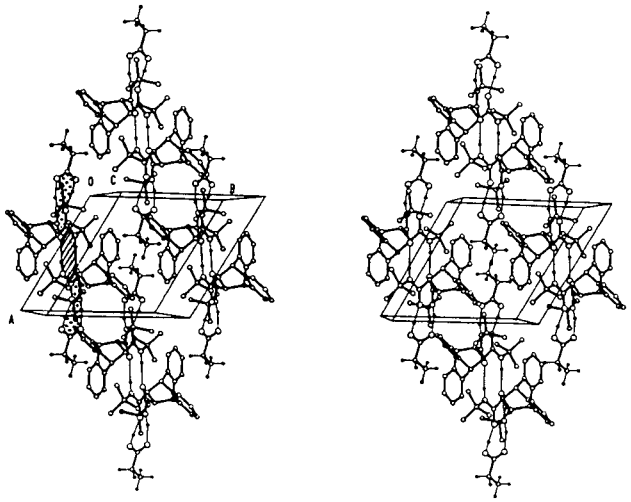

Fig. 6. Stereoscopic view of the crystal packing of **3** (inclusion complex with propionic acid). The nonrelevant hydrogen atoms of the host are omitted for clarity. Hydrogen bonds as thin lines. Individual cases of zones with host–host and host–guest hydrogen bond contacts are indicated by hatched and dotted areas, respectively.

and two proton acceptor sites (C=O) for potential H bond interaction with the guests (see Fig. 2).

Although both guest molecules have typical proton donor and acceptor functions, the H bond interactions between host and guest show different topologies in the present two complexes. In **2**, each methanol is H-bonded to two different host molecules (or host–host clusters), and the two amide moieties of the host are involved in H-bonding with two different guests. Accordingly, a large, 18-membered (including the H atoms) loop is formed around the center of symmetry via two O–H···O and two N–H···O interactions (Fig. 3). In the case of **3**, however, an 11-membered loop is closed via H-bond interactions involving the two amide moieties of one host and the carboxyl group of the guest molecule (Fig. 4).

Thus, in the methanol inclusion crystal, the total hydrogen bonding scheme results in a framework which is infinite in one dimension. It includes 'double chains' of opposite O–H···O and N–H···O hydrogen-bonded strings, running in the crystallographic *a* direction (Fig. 5). By way of contrast, in the propionic acid inclusion, discrete hydrogen-bonded host–guest associates with 2 : 2 stoichiometry are created (Fig. 6). They include a large 24-membered ring with O–H···O and N–H···O hydrogen bonds. Both the supramolecular strings in **2** and the discrete clusters of host–guest units in **3** are shielded by a smooth cover of lipophilic groups, which makes possible a quite dense packing in the crystal. The host–guest associates are held together by van der Waal's forces.

Conclusions

Elucidations of the crystal structures in the present

study provides a rationale for the host properties of **1** and analogous compounds. Normally, amide molecules use their self-complementary hydrogen bonding functionality to form dimers (8-membered hydrogen-bonded rings) in the crystal.[10] Obviously, this causes severe sterical problems for the bulky molecules **1**, both in the intra- and intermolecular sense, except for the extended dimer formation specified in Fig. 2. On the other hand, it is a general rule[10] that good proton donors and acceptors, such as provided by the amide function, are always involved in hydrogen bonding in a crystal structure. Consequently, **1** makes use of suitably shaped proton donor and acceptor guest molecules to accomplish hydrogen bonding in a densely packed host–guest co-crystal. The analogues of **1** with substituents less bulky than *t*-butyl are different.[8] They do not need the aid of a guest molecule for crystallization, and they make no space available for guest molecules. Thus, the present inclusion structures are determined primarily by the bonding characteristics between host and guest and steric requirements in the crystal structure. On the same line, other host molecules with amide functions for selective crystal inclusion may be designed, and the observed interaction patterns are also a promising approach for engineering organic solids.[18]

I.C. is indebted to Professor P. Kierkegaard (Stockholm University) for his continuous interest and encouragement. Financial support from the Swedish Natural Research Council (NFR), and the Deutsche Forschungsgemeinschaft (SFB 334), and the Fonds der Chemischen Industrie is gratefully acknowledged.

References

1) E. Weber, *J. Mol. Graphics,* 7, 12 (1989).
2) L. Leiserowitz, *Acta Crystallogr., Sect. B,* **32**, 775 (1976).
3) X. Zhao, Y.-L. Chang, F. W. Fowler, and J. W. Lauher, *J. Am. Chem. Soc.,* **112**, 6627 (1990).
4) E. Weber and M. Czugler, "Molecular Inclusion and Molecular Recognition—Clathrates II," (Topics in Current Chemistry, Vol. 149), ed by E. Weber, Springer-Verlag, Berlin-Heidelberg-New York (1988), p. 45.
5) E. Weber, M. Hecker, E. Koepp, W. Orlia, M. Czugler, and I. Csöregh, *J. Chem. Soc., Perkin Trans. 2,* **1988**, 1251.
6) E. Weber, M. Hecker, I. Csöregh, and M. Czugler, *J. Am. Chem. Soc.,* **111**, 7866 (1989).
7) F. Toda, "Molecular Inclusion and Molecular Recognition—Clathrates I," (Topics in Current Chemistry, Vol. 140), ed by E. Weber, Springer-Verlag, Berlin-Heidelberg-New York (1987), p. 43.
8) E. Weber, I. Csöregh, J. Ahrendt, S. Finge, and M. Czugler, *J. Org. Chem.,* **53**, 5831 (1988).
9) M. Czugler, E. Weber, and J. Ahrendt, *J. Chem. Soc., Chem. Commun.,* **1984**, 1632.
10) M. C. Etter, *Acc. Chem. Res.,* **23**, 120 (1990).
11) G. M. Sheldrick, SHELXS 84: Program for Crystal Structure Solution, University of Göttingen, FR-Germany (1984) (personal communication).
12) G. M. Sheldrick, SHELXS 76: Program for Crystal Structure Determination, University of Cambridge, England (1976).
13) Tables 4—6 and structure factors have been deposited as Document No. 9107 at the Office of the Editor of Bull. Chem. Soc. Jpn.
14) I. Csöregh M. Czugler, A. Ertan, E. Weber, and J. Ahrendt, *J. Inclusion Phenom. Mol. Recogn. Chem.,* **8**, 275 (1990).
15) I. Csöregh, M. Czugler, E. Weber, and J. Ahrendt, *J. Inclusion Phenom. Mol. Recogn. Chem.,* **8**, 309 (1990).
16) M. Nardelli, A. Musatti, P. Domiano, and G. Andreetti, *Ric. Sci.,* **15**, 807 (1965).
17) O. Kennard, "Tables of Bond Lengths between Carbon and Other Elements," in "International Tables for X-Ray Crystallography," Kynoch Press, Birmingham, England (1968), Vol. III, pp. 275—276 (Distributed by Kluwer Academic Publishers, Dordrecht, The Netherlands).
18) G. R. Desiraju, "Crystal Engineering," (Materials Science Monographs, Vol. 54), Elsevier, Amsterdam (1989).

Spin-Trapping of Selenium-Containing Inorganic Radicals in Aqueous Solutions

Toshihiko OZAWA* and Akira HANAKI
National Institute of Radiological Sciences, 9-1, Anagawa-4-chome, Chiba 260
(Received January 9, 1991)

Synopsis. The selenite radical anion, $SeO_3^{\cdot-}$, can be detected by ESR spectroscopy using water-soluble spin-traps, *N*-(4-pyridylmethylene)-*t*-butylamine *N,N'*-dioxide (POBN) and 3,5-dibromo-4-nitrosobenzenesulfonate (DBNBS), but selenate radical anion, $SeO_4^{\cdot-}$, cannot be trapped by POBN or DBNBS.

In continuation of our works[1-4] on the spin-trapping of short-lived inorganic radicals, we have investigated the spin-trapping of selenium-containing inorganic radicals. Selenium is being increasingly recognized as biochemical importance.[5] It is now recognized to be an essential nutrient and is present, for example, in glutathione peroxidase, an enzyme important in the metabolism of hydroperoxides. It also has come out as a significant anticarcinogen. However, the chemistry *per se* is still not understood.[6] Selenium can exist as selenide (Se^{2-}), elemental selenium (Se^0), selenite (SeO_3^{2-}), and selenate (SeO_4^{2-}). Each oxidation state exhibits different chemical behavior. Metal selenides, Se-sulfides, and elemental Se are insoluble, and therefore biologically unavailable. For the pH and redox conditions of aquatic environments, SeO_3^{2-} and SeO_4^{2-} should be dominant forms of Se. Consequently, it is imperative to know the chemical reactivities of these ions. If these ions are oxidized by one electron oxidation, these may produce radical intermediates. However, at present there have been no reports concerning the spin-trapping of radical intermediates formed during the oxidation of the selenium-containing inorganic compounds, the lifetime of which is too short to be detected by conventional ESR measurements. It has been reported that spin-trapping is a technique to detect short-lived free radicals in solutions. That is, this technique involves the ability of spin-trap to react with short-lived free radicals to yield a spin adduct having a longer lifetime, the ESR spectrum of which gives information specially identifying the original radical species.

It is known that Ce(IV) is a strong oxidizing agent in acidic aqueous solutions. Then, using this ion as an oxidizing agent, we have examined the spin-trapping of selenium-containing inorganic radicals. We now first report herein selenium-containing inorganic radicals trapped by water-soluble spin-trap.

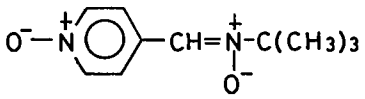

POBN(1)

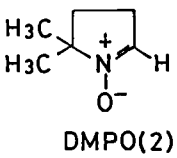

DMPO(2)

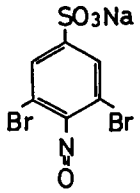

DBNBS(3)

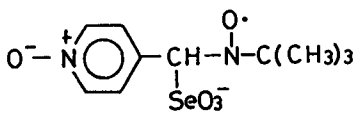

POBN-SeO_3^- (4)

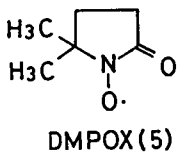

DMPOX(5)

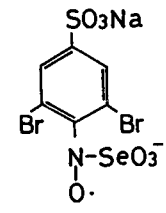

DBNBS-SeO_3^- (6)

Experimental

Materials. Water-soluble spin-traps, *N*-(4-pyridylmethylene)-*t*-butylamine *N,N'*-dioxide (POBN, **1**) and 5,5-dimethyl-1-pyrroline *N*-oxide (DMPO, **2**), were purchased from Sigma Chemical Co. and used without further purification, because no ESR signal was observed when these spin-traps were dissolved in an acidic aqueous solution. Other water-soluble spin-trap, sodium 3,5-dibromo-4-nitrosobenzenesulfonate (DBNBS, **3**) was synthesized as described previously.[7] The selenium compounds, sodium selenite (Na_2SeO_3) and sodium selenate (Na_2SeO_4) were obtained from Wako Pure Chemical Ind., Ltd. and used as received. $Ce(NO_3)_4 \cdot 2NH_4NO_3$ was purchased from Wako Pure Chemical Ind., Ltd. and used as a source of Ce(IV). Other reagents were commercially available. All reaction solutions were prepared from deionized and triply distilled water and their pHs were adjusted to be 2.0 by sulfuric acid.

Measurements. ESR measurements were carried out on a JEOL JES-RE-1X ESR spectrometer (X-band) with 100 kHz field modulation. ESR spectra were recorded at room temperature in a JEOL flat quartz cell. ESR parameters were calibrated by comparison with a standard Mn^{2+}/MgO marker and 1,1-diphenyl-2-picrylhydrazyl (DPPH, g=2.0036). Further, magnetic field was calibrated with NMR field meter (JEOL ES-FC5).

Results and Discussion

Spin-Trapping with POBN. When Ce(IV) solution (1 mmol dm^{-3}) was mixed with the aqueous solution of selenite ion (SeO_3^{2-}) (10 mmol dm^{-3}) containing POBN (10 mmol dm^{-3}), ESR spectrum as shown in Fig. 1 was

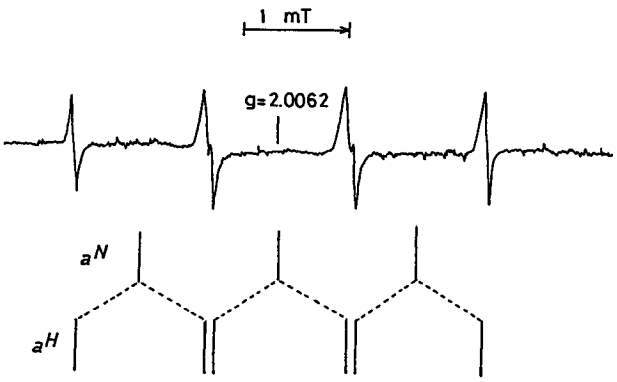

Fig. 1. ESR spectrum observed during the oxidation of SeO_3^{2-} with Ce(IV) in the presence of POBN. Conditions: Ce(IV), 1 mmol dm^{-3}; SeO_3^{2-}, 10 mmol dm^{-3}; POBN, 10 mmol dm^{-3}.

observed. The ESR spectrum could be analyzed as shown by the stick diagram in Fig. 1 and ESR parameters obtained were as follows: $a^N(1)=1.49$ mT, $a^H(1)=1.39$ mT, $g=2.0062$. When either Ce(IV) or SeO_3^{2-} ion was omitted from the solution, no ESR spectrum was observed. Further, Ce(IV) is used as an one-electron oxidant. The potential of Ce(IV)/Ce(III) couple in 1 M H_2SO_4 (1 M=1 mol dm^{-3}) solution is as follows:[8]

$$Ce(IV)+e=Ce(III) \qquad E^0=+1.44\ V \qquad (1)$$

Therefore, the observed radical species is assigned to SeO_3^- adduct of POBN (**4**). The formation of (**4**) can be expressed as follows:

$$Ce(IV)+SeO_3^{2-} \longrightarrow Ce(III)+SeO_3^{\cdot-} \qquad (2)$$

$$SeO_3^- + POBN \longrightarrow (\mathbf{4}) \qquad (3)$$

In this case, hyperfine splitting from ^{75}Se ($I=1/2$, natural abundance 7.50%) was not observed.

On the other hand, no ESR spectrum was observed from selenate ion (SeO_4^{2-}) by oxidation with Ce(IV). The yellow color of aqueous Ce(IV) solutions, however, changed to colorless immediately after additon of selenate solutions, suggesting that Ce(IV) was reduced to Ce(III). Therefore, this result may be considered that POBN cannot form the stable adduct with selenate anion radical, $SeO_4^{\cdot-}$.

Spin-Trapping-with DMPO. ESR spectrum was observed as shown in Fig. 2, when Ce(IV) solution (1 mmol dm^{-3}) was mixed with aqueous solutions of selenite ion (10 mmol dm^{-3}) containing DMPO (10 mmol dm^{-3}). The ESR spectrum could be analyzed as shown by the stick diagram in Fig. 2 and ESR parameters obtained were as follows: $a^N(1)=0.74$ mT, $a^H(2)=0.41$ mT, and $g=2.0070$. ESR spectrum shown in Fig. 2 could not be observed, when either Ce(IV) or selenite ion was omitted from the reaction solution. This ESR spectrum was identical with that of 5,5-dimethyl-2-oxol-1-pyrrolidinyloxyl (DMPOX, **5**)[9] which was generated by the oxidation of DMPO with α-cumyl hydroperoxide–hematin system. Thus, the radical species giving ESR spectrum shown in Fig. 2 can be assigned to DMPOX. The same ESR spectrum as

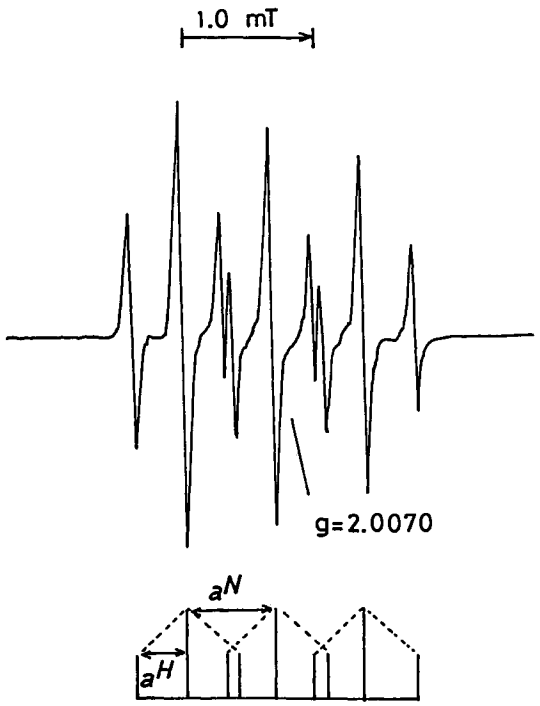

Fig. 2. ESR spectrum obtained during the oxidation of SeO_3^{2-} by Ce(IV) in the presence of DMPO. Conditions: Ce (IV), 1 mmol dm^{-3}; SeO_3^{2-}, 10 mmol dm^{-3}; DMPO, 10 mmol dm^{-3}.

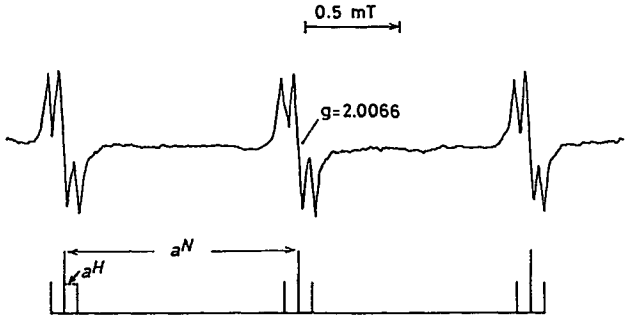

Fig. 3. ESR spectrum observed from the oxidation of SeO_3^{2-} by Ce(IV) in the presence of DBNBS. Conditions: Ce(IV), 1 mmol dm^{-3}; SeO_3^{2-}, 10 mmol dm^{-3}; DBNBS, 10 mmol dm^{-3}.

shown in Fig. 2 was observed when the selenate ion was oxidized by Ce(IV) in the presence of DMPO. Rosen et al. suggsted that DMPOX arises by spin-trapping α-cumyldioxyl radicals followed by base-catalyzed rearrangement.[10] Thus, according to their suggestion, DMPOX may arise by spin-trapping selenite anion radical or selenate anion radical followed by base-catalyzed rearrangement. However, since it is known that the formation mechanism of DMPOX is very complicated,[11] at present the exact reaction scheme is not explained.

Spin-Trapping with DBNBS. When Ce(IV) solution (1 mmol dm^{-3}) was mixed with the aqueous solution of selenite ion (SeO_3^{2-}) (10 mmol dm^{-3}) including DBNBS (10 mmol dm^{-3}), ESR spectrum was observed as shown in Fig. 3. The ESR spectrum could be analyzed as

shown by the stick diagram in Fig. 3 and ESR parameters obtained were as follows: $a^{N}(1)=1.24$ mT, $a^{H}(2)=0.07$ mT, $g=2.0066$. This ESR spectrum could not be observed, when either Ce(IV) or selenite ion was ommited from the reaction solution. Further, the hyperfine splitting constants are similar to the spin adducts of DBNBS with sulfur-containing inorganic radicals such as $SO_3^{\bar{\cdot}}$,[1] $S_2O_3^{\bar{\cdot}}$, and $S^{\bar{\cdot}}$.[4] These results suggest that the radical species observed here are assignable to the spin adduct of DBNBS with $SeO_3^{\bar{\cdot}}$ radical (**6**). In this case, hyperfine splitting due to ^{75}Se was not observed.

On the other hand, no ESR spectrum was obtained from selenate ion (SeO_4^{2-}) by oxidation with Ce(IV). Since Ce(IV) is reduced by SeO_4^{2-} to Ce(III) as described previously, $SeO_4^{\bar{\cdot}}$ radical may be formed. Thus, DBNBS may not give a stable spin adduct with $SeO_4^{\bar{\cdot}}$.

In our experiments, $SeO_4^{\bar{\cdot}}$ radical could not be trapped by water-soluble spin-traps used here. In this case, it is very difficult to distinguish whether $SeO_4^{\bar{\cdot}}$ radical was not generated from the oxidation of SeO_4^{2-} ion with Ce^{4+} or the spin adducts of $SeO_4^{\bar{\cdot}}$ radical was too unstable to be detected by ESR. To elucidate this problem it will be needed to use the some radical scavenger for $SeO_4^{\bar{\cdot}}$ radical, although we can not find out such radical scavenger at present time.

In conclusion, selenite anion radical, $SeO_3^{\bar{\cdot}}$, was first observed by ESR using water-soluble spin-traps, POBN and DBNBS. But, $SeO_4^{\bar{\cdot}}$ cannot be trapped by both spin-traps. Using DMPO as a spin-trap for both $SeO_3^{\bar{\cdot}}$ and $SeO_4^{\bar{\cdot}}$ radicals, oxidation product, DMPOX was formed instead of spin adduct of DMPO.

References

1) T. Ozawa and A. Hanaki, *Biochem. Biophys. Res. Commun.*, **142**, 410 (1987).
2) T. Ozawa and A. Hanaki, *Chem. Lett.*, **1987**, 1885.
3) T. Ozawa and A. Hanaki, *Nippon Kagaku Kaishi*, **1989**, 1408.
4) T. Ozawa and A. Hanaki, *Biochem. Int.*, **20**, 649 (1990).
5) T. Jukes, *Nature*, **316**, 673 (1985).
6) J. M. McNeal and L. S. Balistrieri, "Selenium in Agriculture and the Environment," SSSA Special Publication No. 23, 1989, pp. 1—13.
7) a) T. Ozawa and A. Hanaki, *Biochem. Biophys. Res. Commun.*, **136**, 657 (1986): b) T. Ozawa and A. Hanaki, *Bull. Chem. Soc. Jpn.*, **60**, 2304 (1987).
8) F. A. Cotton and G. Wilkinson, "Advanced Inorganic Chemistry," 5th ed, John Wiley & Sons, New York (1988), pp. 975—976.
9) R. A. Floyd and L. M. Soong, *Biochem. Biophys. Res. Commun.*, **74**, 79 (1977).
10) G. M. Rosen and E. J. Rauckman, *Mol. Pharmacol.*, **17**, 233 (1980).
11) K. Makino, T. Hagiwara, A. Hagi, M. Nishi, and A. Murakami, *Biochem. Biophys. Res. Commun.*, **172**, 1073 (1990).

Association of *p*-Halofluorobenzenes with α- and β-Cyclodextrins in Aqueous Medium

Tatsuyoshi TAKUMA, Toshio DEGUCHI, and Isao SANEMASA*
Department of Chemistry, Faculty of Science, Kumamoto University, Kurokami 2-39-1, Kumamoto 860
(Received January 14, 1991)

Synopsis. The complex formation of α- and β-cyclodextrins (CyDs) with *p*-(chloro, bromo, and iodo)fluorobenzenes has been studied in aqueous medium at 25 °C. Formation constants are compared with those of CyD–monohalobenzene systems.

The concept of microscopic binding constant (MBC concept) has been proposed by Connors and Pendergast.[1] They applied the concept to α-cyclodextrin (CyD) complex formations with various 1,4-disubstituted benzenes. In a system consisting of a guest substrate having two sites, X and Y, and a host with a single binding site (α-CyD), two isomeric 1 : 1 complexes can exist, X′Y and XY′, where the superscript prime indicates the binding site. The observed 1 : 1 formation constant, K_{11}^{XY}, is related to microscopic binding constants, $K_{X'Y}$ and $K_{XY'}$, as $K_{11}^{XY}=K_{X'Y}+K_{XY'}$. If the two substrate sites are identical, the equation becomes $K_1^{XX}=2K_{X'X}$.

We studied host–guest associations using α-, β-, and γ-CyDs as hosts and four monohalobenzenes,[2] X–C_6H_5, where X refers to a halogen atom, and four symmetrical *p*-dihalobenzenes,[3] X–C_6H_4–X, as guests. Based on a comparison of their 1 : 1 formation constants, we discussed the validity of the MBC concept.[3] It turned out that the equation, $K_{11}^{XX}=2K_{X'X}$, holds for chloro- and bromobenzene, but this is not the case for fluoro- and iodobenzene. We concluded therefore that the concept does not necessarily apply to α-CyD complex formations with all of symmetrical *p*-disubstituted benzenes.

The present work is concerned with α- and β-CyD complex formations with *p*-dihalobenzenes, X–C_6H_4–Y, where X and Y refer to different halogen atoms. One of the aimes of the present study is to discuss the validity of the MBC concept. There are many possible XY combinations. The formation constants of α- and β-CyD with monohalobenzenes and symmetrical *p*-dihalobenzenes increase with an increase in the size of the halogen atom.[2,3] It is therefore preferable to use either fluoro- or iodobenzene derivatives in order to make clear the difference of another halogen atom. Here we chose *p*-halofluorobenzenes.

In the case of β-CyD complex formations, where the MBC concept cannot be applied, it is of interest to see if there is any relationship between the 1 : 1 association constant of X–C_6H_4–Y and that of X–C_6H_5 and Y–C_6H_5. This is another incentive of the present study.

The method used in this work to determine the association constant is the same as that employed in our previous works,[2–4] and is based on the volatility of guest in aqueous solutions. Volatile guest molecules are driven out to the gas phase by introducing an inert gas at a constant flow rate into the aqueous solution. The volatilization rate is measured with and without addition of CyD; the rate decreases as a result of the association with CyD.

Experimental

Materials and Preparation of Sample Solutions. Deionized distilled water was used throughout the experiments. An appropriate amount of α- or β-CyD of guaranteed grade (Nakarai Chemical Co.), dried over phosphorus pentoxide under vacuum, was weighed and dissolved in water to prepare CyD stock solutions of desired concentrations. Three guest substances, (*p*-chloro-, *p*-bromo-, and *p*-iodo-)fluorobenzenes, were used as received; the minimum purities are 99.0, 98.0, and 98.0%, respectively, as claimed by the manufacturer (Tokyo Kasei Kogyo Co.). An aqueous stock solution of each guest was prepared by adding an excess of each *p*-dihalobenzene to water and stirring for at least 24 h in the dark. After leaving the mixture standing for at least 24 h, a portion of the saturated guest solution was transferred to a separatory funnel and the absorbance of its cyclohexane extract was measured to determine the guest concentration at the following wavelengths: *p*-chloro- at 270 (or 263), *p*-bromo- at 270, and *p*-iodo-fluorobenzene at 271.8 nm.

A portion of the saturated guest solution was transferred into a 2.5φ×25 cm cylindrical glass tube. An appropriate fraction of the CyD stock solution was then added, and the solution was diluted with water to 80 cm³. The concentration ranges of host and guest are given in the footnote of Table 1.

Apparatus and Procedures. The apparatus and the experimental procedure were the same as those described in previous papers.[2,3] Nitrogen gas was bubbled into the aqueous guest solution with or without CyD placed in the cylindrical glass tube immersed in a bath thermostated at 25.0±0.1 °C, at a constant flow rate suitable for each guest volatility: *p*-chloro- at 50, *p*-bromo- at 80, and *p*-iodofluorobenzene at 100 cm³ min⁻¹. The N_2 gas leaving the sample solution was passed through a glass column of 0.5 φ×23 cm filled to 8 cm in length with XAD-2 resin beads (80—150 mesh). The guest adsorbed on the resin within a fixed time was eluted out with 4 cm³ of cyclohexane, and the amount of guest, ΔQ_ϕ, was determined by UV absorption measurements.

Results and Discussion

Determination of Formation Constants. The equation derived in a previous paper[4] was used to estimate the 1 : 1 and 2 : 1 (host : guest) association constants, K_1 and K_2:

$$\ln(C_\phi - Q_\phi V^{-1}) = -kt/(1+K_1C_{CyD}+K_1K_2C^2_{CyD}) + \ln C_\phi = -k't + \ln C_\phi, \quad (1)$$

where C_{CyD} and C_ϕ refer to the total concentration of host and that of guest, respectively, Q_ϕ is the sum of ΔQ_ϕ from time 0 to t, V is the volume of the aqueous solution, k is the rate constant for transfer of guest molecules from the aqueous to gas phase, and

$$K' = k/(1+k_1C_{CyD}+K_1K_2C^2_{CyD}). \quad (2)$$

Rearrangement of Eq. 2 yields

$$1/k' = K_1K_2C^2_{CyD}/k + K_1C_{CyD}/k + 1/k. \quad (3)$$

The plots according to Eq. 1 for all the *p*-halofluorobenzene–CyD systems examined in this work gave straight lines over the whole aeration time, during which ca. 70% of the guest molecules present initially in the sample solutions were purged. Slopes of the resulting straight lines, k' (and k), were evaluated by the least-squares method. Typical $1/k'$ vs. C_{CyD} plots are shown in Figs. 1 and 2. The plots exhibit upward curvatures for α- and β-CyDs, indicating formations of both 1 : 1 and 2 : 1 (host : guest) complexes. The K_1 and K_2 values were determined by the curve-fitting method and are summarized in Table 1. Concerning the present host–guest systems, there are no data available in the literature.

α-Cyclodextrin Complex Formation. According to the MBC concept,[1] the 1 : 1 formation constant is to be 134 for *p*-chlorofluorobenzene (abbreviation; Cl–F), 544 for *p*-bromofluorobenzene (Br–F), and 1134 M^{-1} for *p*-iodofluorobenzene (I–F), where 1 M=1 mol dm^{-3}. The expected value for each guest, however, is not in agree-

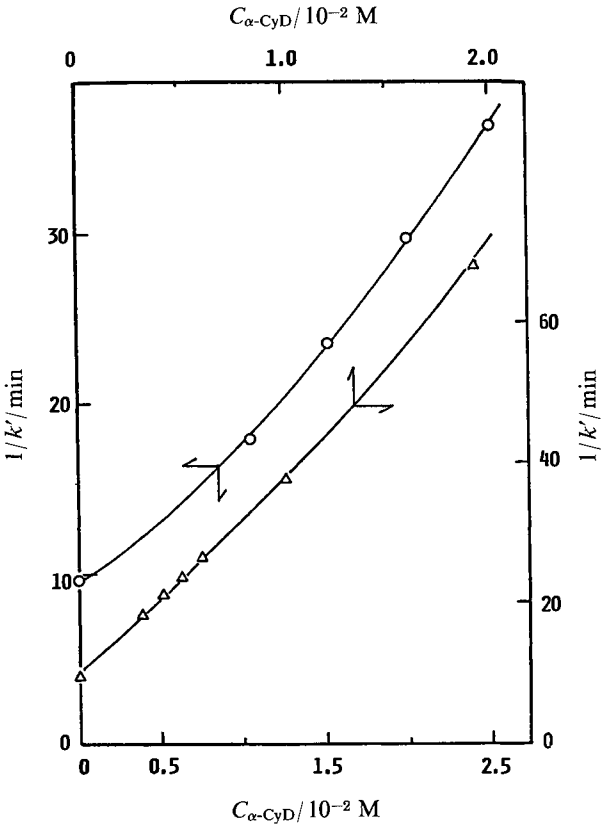

Fig. 1. Plots of $1/k'$ vs. C_{CyD}. α-CyD–*p*-chlorofluorobenzene (○). –*p*-bromofluorobenzene (△).

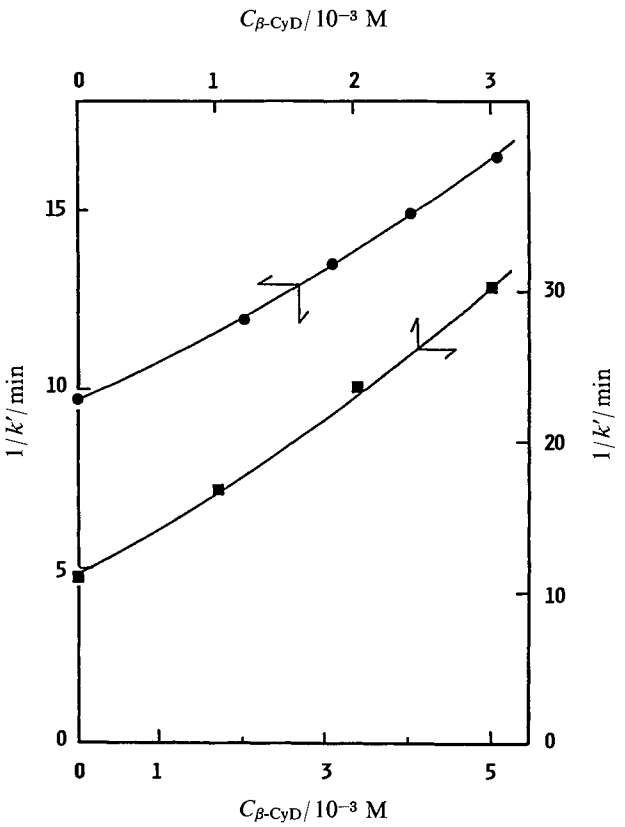

Fig. 2. Plots of 1/k' vs. C_{CyD}. β-CyD–*p*-chlorofluorobenzene (●), –*p*-iodofluorobenzene (■).

Table 1. Formation Constants, K_1 (1 : 1) and K_2 (2 : 1) of (Cyclodextrin: *p*-Halofluorobenzene) Complexes at 25 °C[a]

Guest (*p*-Halofluorobenzene)	Host (Cyclodextrin)	Formation constant	
		K_1	K_2
		M^{-1}	M^{-1}
p-Chlorofluorobenzene	α-CyD	65±4	29±6
	β-CyD	120±2	30±10
p-Bromofluorobenzene	α-CyD	250±7	9±2
	β-CyD	180±40	50±50
p-Iodofluorobenzene	α-CyD	980±30	50±30
	β-CyD	510±20	50±10

a) The total concentration of guest and that of host are as follows: *p*-chlorofluorobenzene ((4.53—4.68)×10^{-4} M) –α-CyD ((1.06—2.51)×10^{-2} M) and –β-CyD ((2.01—5.09)×10^{-3} M); *p*-bromofluorobenzene (2.70—2.82)×10^{-4} M) –α-CyD ((3.01—19.2)×10^{-3} M) and –β-CyD ((1.00—8.03)×10^{-3} M); *p*-iodofluorobenzene ((1.69—2.32)×10^{-6} M) –α-CyD ((0.258—2.04) ×10^{-3} M) and –β-CyD ((1.01—3.02)×10^{-3} M).

ment with the corresponding experimental value.

Of halogen atoms, iodine with the van der Waals radius of 2.2 Å best fits to the cavity of α-CyD. The van der Waals contact area within the cavity decreases in going from iodine to fluorine atom. This is the reason that the K_1 of iodobenzene is much larger than that of fluorobenzene.[2] When α-CyD associates with the I–F guest, the host molecule is expected to associate preferentially with the iodine atom of this guest. Under the present experimental conditions where CyD molecules are always in large excess of guest molecules, there are many chances for CyD molecules to come into contact with the fluorine atom side of I–F. Nevertheless, it does not seem that the association with the fluorine atom contributes to the K_1 of I–F, because this value is almost equal to the K_1 of iodobenzene itself.

It is noteworthy that the K_1 of Cl–F or Br–F is considerably smaller than that of chlorobenzene or bromobenzene itself. This is in conflict with the MBC concept and is difficult to explain even if the association with the fluorine atom of Cl–F or Br–F is assumed not to occur. Here we postulate that the fluorine atom has a negative contribution to α-CyD complex formations, that is, the presence of this atom reduces the K_1 of Cl–F or Br–F (or I–F) that would be expected from the corresponding mono(chloro, bromo, or iodo)benzene. This assumption is made based on the fact that symmetrical *p*-difluorobenzene has a much smaller K_1 value than that of monofluorobenzene itself. The addition of an F atom to the para-position of the benzene ring might render the guest molecule somewhat hydrophilic (not the guest molecule as a whole, but locally, probably at around the F atom), which is unfavorable to the association with CyD.

When a substituent is the methyl group, a typical hydrophobic group, the MBC concept holds. For instance, as was pointed out in a previous paper,[3] the toluene (K_1=33±3)–*p*-xylene (K_1=72±7 M^{-1})[4] system supports the concept.

Connors and Pendergast derived an equation which correlates 2:1 (host:guest) formation constants to microscopic binding constants.[1] In the present paper, however, we are not concerned with this point, because K_2 values are in general less reliable than K_1 values.

β-Cyclodextrin Complex Formation. Since β-CyD can include a benzene ring as a whole, the MBC concept is not applicable to 1,4-disubstituted benzenes unless the substituent groups are not so large as to hinder the approach of a β-CyD molecule to the benzene ring.

We see an interesting relationship between the K_1 of Cl–F, Br–F, or I–F and that of the corresponding monohalobenzene. Namely, the K_1 of Cl–F, Br–F, or I–F is neary equal to half the sum of the K_1 of fluorobenzene and that of chloro-, bromo-, or iodobenzene, respectively. It should be mentioned here that this relationship does not hold for the toluene (K_1=140±10) –*p*-xylene (K_1=240±10 M^{-1})[4] system; in this case, the K_1 of *p*-xylene is approximately twice that of toluene. A further study is necessary using various kinds of both symmetrical and unsymmetrical 1,4-disubstituted benzenes as guests to see whether this arithmetic mean is a general rule for unsymmetrical guests or only applicable to the *p*-dihalobenzene series.

References

1) K. A. Connors and D. D. Pendergast, *J. Am. Chem. Soc.*, **106**, 7607 (1984).
2) T. Takuma, T. Deguchi, and I. Sanemasa, *Bull. Chem. Soc. Jpn.*, **63**, 1246 (1990).
3) T. Takuma, T. Deguchi, and I. Sanemasa, *Bull. Chem. Soc. Jpn.*, **64**, 480 (1991).
4) I. Sanemasa and Y. Akamine, *Bull. Chem. Soc. Jpn.*, **60**, 2059 (1987).

Complexations of New Pyridylazo Ligands with Ni(II), Zn(II), and Cd(II)

Hu HUANG, Fumiaki KAI,* Chiemi URAGAMI,† Masaaki HIROHATA,† Hiroaki CHIKUSHI,†
Hisae YANAKA,† Mayumi HONDA,† and Masaaki NAKAMURA†
Department of Environmental Science, Graduate School of Natural Science and Technology,
Kumamoto University, Kumamoto 860
†Department of Chemistry, Faculty of Science, Kumamoto University, Kumamoto 860
(Received January 28, 1991)

Synopsis. New ligands, 1-(3,5-dichloro-2-pyridyl-azo)-2-naphthol, 2-(3,5-dichloro-2-pyridyl-azo)-5-(dimethylamino) phenol, and 2-(3,5-dichloro-2-pyridyl-azo)-5-(dimethylamino)benzoic acid, were synthesized. Changes in the reduction potentials and electronic spectra of the ligands upon complexation with Ni(II), Zn(II), and Cd(II) were studied. The dissociation constants of the ligands and the stability constants of their metal(II) complexes are discussed.

It is well known for pyridylazo compounds that introduction of halogen or dimethylamino groups on appropriate aromatic ring enhances the sensitivity of photometric determination of a given metal ion, and these substituents are advantageous for metal determination because the absorption peak wavelengths of ligands themselves and those of the complexes are shifted from the ultraviolet to visible region.[1] In view of this, 1-(3,5-dichloro-2-pyridyl-azo)-2-naphthol (abbr. as $Cl_2\beta$PAN), 2-(3,5-dichloro-2-pyridyl-azo)-5-(dimethylamino)phenol (Cl_2DMPAP) and 2-(3,5-dichloro-2-pyridyl-azo)-5-(dimethylamino)benzoic acid (Cl_2PAMB) were newly synthesized in the present work, and their complexing equilibria with Ni(II), Zn(II), and Cd(II) were studied both polarographically and spectrophotometrically.

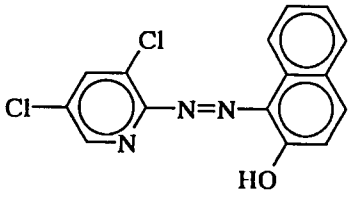

$Cl_2\beta$PAN

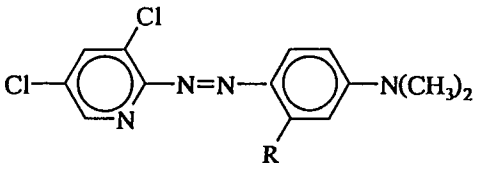

R=OH : Cl_2DMPAP
R=COOH : Cl_2PAMB

Experimental

Preparation of Ligands. $Cl_2\beta$PAN was prepared by coupling 2-naphthol with 3,5-dichloro-2-pyridyldiazonium salt synthesized according to a previous paper.[1c] Yield, 10.8%; mp 191—192 °C. Found: C, 56.83; H, 3.08; N, 13.49%. Calcd for $C_{15}H_9N_3OCl_2$: C, 56.63; H, 2.85; N, 13.21%. IR ($\nu_{N=N}$) 1365 cm^{-1}. ^{1}H NMR ($CDCl_3$) δ=6.60 (1H, d, J=9.90 Hz, H-8), 7.40—7.63 (3H, m, H-4, H-5, H-6), 7.66 (1H, d, J=9.90 Hz, H-7), 7.76 (1H, d, J=1.8 Hz, H-4'), 8.41 (1H, d, J=1.8 Hz, H-8'), 8.53 (1H, dd, J=6.3 and 1.4 Hz, H-3), 16.32 (1H, br, s, OH). Cl_2DMPAP was synthesized in a similar manner. Yield, 12.1%; mp 189—191 °C. Found: C, 49.90; H, 4.00; N, 17.80%. Calcd for $C_{13}H_{12}N_4OCl_2$: C, 50.18; H, 3.99; N, 18.01%. IR ($\nu_{N=N}$) 1300 cm^{-1}. ^{1}H NMR ($CDCl_3$) δ=3.32 (6H, s, 2×CH_3), 6.05 (1H, d, J=2.4 Hz, H-6), 6.60 (1H, dd, J=10.2 and 2.4 Hz, H-4), 7.62 (1H, d, J=10.2 Hz, H-3), 7.86 (1H, d, J=3.0 Hz, H-4'), 8.47 (1H, d, J=3.0 Hz, H-6'), 16.11 (1H, br, s, OH). Cl_2PAMB was obtained by a similar procedure. Yield, 5.9%; mp 198—202 °C. Found: C, 49.48; H, 3.45; N, 16.20%. Calcd for $C_{14}H_{12}N_4O_2Cl_2$: C, 49.58; H, 3.57; N, 16.52%. IR ($\nu_{N=N}$) 1296 cm^{-1}. ^{1}H NMR ($CDCl_3$) δ=3.23 (6H, s, 2×CH_3), 6.85 (1H, dd, J=9.0 and 3.0 Hz, H-4), 7.68 (1H, d, J=3.0 Hz, H-6), 7.87 (1H, d, J=2.4 Hz, H-4'), 8.06 (1H, d, J=9.0 Hz, H-3), 8.40 (1H, d, J=2.4 Hz, H-6'), 14.35 (1H, br, s, OH). These compounds are slightly soluble in water, methanol, and ethanol, and readily soluble in dioxane, benzene, and chloroform. All the solutions of the ligands and the metal (II) complexes were prepared with aqueous 60% (v/v) dioxane.

Measurements. ^{1}H NMR spectra were recorded on a JEOL JNM-EX90 FT NMR spectrometer. IR spectra were recorded on a JASCO A-102 spectrometer (KBr disk). Electronic spectra were recorded on a Hitachi 220A recording spectrophotometer. Polarograms were obtained on a Yanaco Polarographic Analyzer P-1100 as described previously,[2] in an aqueous 60% (v/v) dioxane solution.

Results and Discussion

Protonation Constants of Ligands. All of the dissociation constants of the ligands were obtained by the Hildebrand-Reilly's method.[3] The values are summarized in Table 1 together with those of analogous ligands for comparison. The larger pK_{ai} values of hydroxyl groups in $Cl_2\beta$PAN and Cl_2DMPAP than

Table 1. Dissociation Constants of the Ligands

Ligand	pK_{a1}	pK_{a2}	pK_{a3}	Ref
$Cl_2\beta$PAN	<0[a]	10.91[b]		This work
Cl_2DMPAP	<0[a]	1.05[c]	11.29[d]	This work
Cl_2PAMB	<0[a]	0.21[c]	4.59[e]	This work
βN	9.31[b]			Ref. 8
AP	9.83[d]			Ref. 8
MAB	2.57[c]	5.00[e]		Ref. 8

Aq 60% (v/v) dioxane soln, μ=0.1 (KNO_3), 25.0± 0.5 °C. All the experimental errors are within ±0.05 in pK_a unit in this work. The dissociations of proton are from: a) nitrogen atom in pyridine moiety; b) HO- in naphthol moiety; c) nitrogen atom in dimethylamino group; d) HO- in phenol moiety; e) HOOC-. βN=2-naphthol; AP=3-aminophenol; MAB=4-dimethylaminobenzoic acid.

those of βNS and AP indicate the presence of strong intramolecular hydrogen bonding[2] between the azo and hydroxyl groups in Cl_2βPAN and Cl_2DMPAP. The ^{1}H NMR data for these ligands are in line with this speculation, namely, the signal of the proton of the hydroxyl groups in these ligands appears in very low magnetic fields (δ=16.32 for Cl_2βPAN and 16.11 for Cl_2DMPAP). On the other hand, the pK_{ai} value of the carboxyl group in Cl_2PAMB is lower than that of MAB. This may reflect a strong electron-attractive ability of the dichloropyridylazo group rather than weak intramolecular hydrogen bonding between the azo and carboxyl group in Cl_2PAMB, which has a highly distorted six-membered ring by forming the intramolecular hydrogen bonding as speculated from a molecular model.

Coordination Modes in Metal (II) Complexes. Figure 1 shows the relation between the pH and the reduction potential of the azo group. For Cl_2βPAN and Cl_2DMPAP, it is particularly noteworthy that the half-wave potentials are markedly shifted toward positive potentials region at pH=10.9 and 11.3, respectively, where the proton in the hydroxyl group at an ortho position to the azo group will be dissociated (see Table 1). This means that a very strong hydrogen bond formed between the proton of the hydroxyl group and the N atom in the azo group is abruptly destroyed at this pH; the azo group is thus easily reduced at this pH by a positive shift effect.[4] In Cl_2PAMB, however, the reduction potential of the azo group is only dependent on pH, but independent of the kinds of the ligand species, since the hydrogen bonding is very weak. The reduction potentials of the ligands in Ni(II) complexes are markedly negative of those of free ligands at the same pH, showing stabilization by a negative shift effect.[5,6] This means that, for these complexes, stable chelate rings involving the azo group are formed. The magnitude of the shift for the metal (II) complexes was in the order of Ni(II)>Zn(II)>Cd(II).

It is seen in Fig. 2 that the absorption for the $\pi\rightarrow\pi^*$ transition[7] in the metal (II) complexes markedly shift to lower wavenumbers compared with those of the HL species. In addition, the absorption band of the complexes is split into two peaks, although this splitting is not very clear for the Cl_2PAMB complexes. Similar shifts upon complexation were reported in metal (II) complexes of analogous ligands forming *N,N,O*-terdentate chelate rings.[7] Accordingly, the above mentioned changes in the reduction potentials and absorption spectra of the azo group by complexation strongly suggest that these ligands coordinate to metal (II) ions with *N,N,O*-(N atom in the pyridine ring, N atom in the

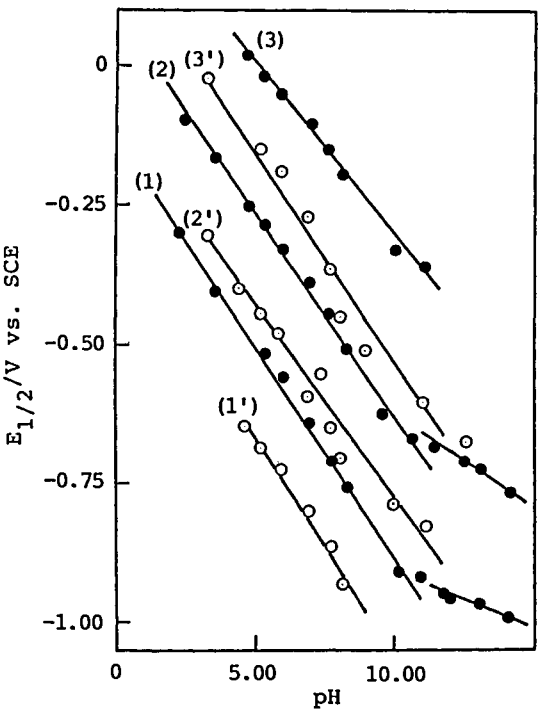

Fig. 1. Relation between pH and half-wave potential of ligands and their Ni(II) complexes.
(1): Cl_2βPAN, (1'): Cl_2βPAN+Ni(II), (2): Cl_2DMPAP, (2'): Cl_2DMPAP+Ni(II), (3): Cl_2PAMB, (3'): Cl_2PAMB+Ni(II), C_L=C_{Ni}=1.25×10^{-4} mol dm^{-3}, μ=0.1 (KNO_3), 0.01% gelatin, 24±2°C. Curves (1) and (1') are shifted 0.20 unit downward, and (3) and (3') are shifted 0.10 unit upward for clarity.

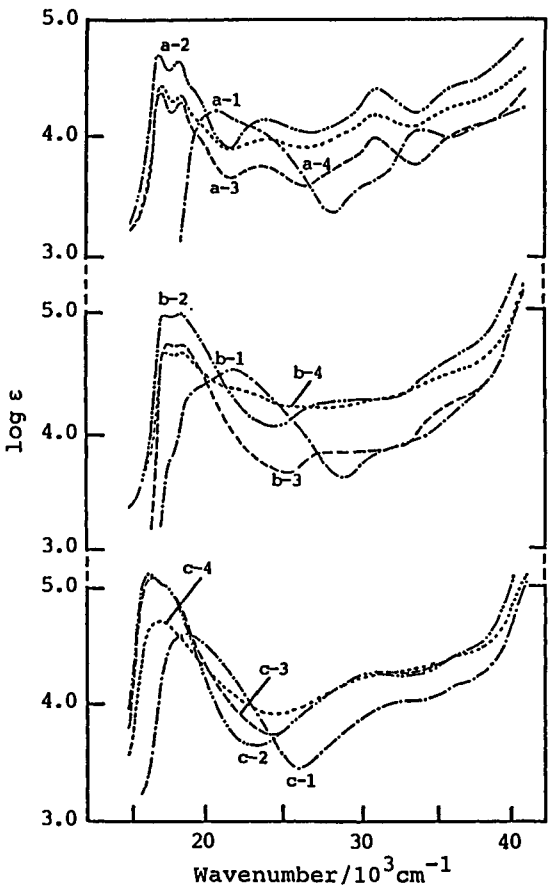

Fig. 2. Absorption spectra of Cl_2βPAN (a-series), Cl_2DMPAP (b-series) and Cl_2PAMB (c-series), and their metal(II) complexes.
a-1: HL (pH 8.18); a-2: NiL(7.67); a-3: ZnL(9.28); a-4: CdL(9.65); b-1: HL (7.16); b-2: NiL (9.07); b-3: ZnL (9.70); b-4: CdL (9.21); c-1: HL (1.67); c-2: NiL (7.40); c-3: ZnL (6.52); c-4: CdL (7.08). C_L=1.00×10^{-5} mol dm^{-3}, C_{Me}=1.00×10^{-4} mol dm^{-3}, 25.0±0.5 °C.

Table 2. Composition, Maximum Wavenumber (Molar Absorptivity), and Stability Constant of the Ni(II), Zn(II), and Cd(II) Complexes[a]

Metal ion		$Cl_2\beta$PAN	Cl_2DMPAP	Cl_2PAMB
	b)	NiL_2	NiL_2	NiL_2
Ni (II)	c)	17.4, 18.6 (6.0, 5.3)	17.7, 18.7 (11.1, 11.4)	16.5, 17.5_{sh} (13.2, 10.1)
	d)	$\log\beta_2$=35.33	$\log\beta_2$=35.48	$\log\beta_2$=16.99
	b)	ZnL	ZnL	ZnL_2
Zn(II)	c)	17.4, 18.7 (2.9, 2.4)	17.7, 18.9 (6.3, 6.0)	16.7, 17.5_{sh} (12.3, 11.0)
	d)	$\log\beta_1$=19.80	$\log\beta_1$=20.07	$\log\beta_2$=13.34
	b)	CdL	CdL	CdL
Cd(II)	c)	17.4, 18.7 (3.3, 2.8)	17.7, 18.9 (5.3, 5.2)	17.2 (5.3)
	d)	$\log\beta_1$=16.09	$\log\beta_1$=17.00	$\log\beta_1$=6.28

a) Aq 60% (v/v) dioxane soln, μ=0.1 (KNO_3), 25.0±0.5 °C. b) Chemical form of complex (L: fully deprotonated ligand.). c) Maximum wavenumber/10^3 cm^{-1} (maximum molar absorptivity, $\varepsilon_{max}/10^4$). sh: shoulder. d) $\beta_{1,2}$ mean over-all stability constants. Experimental errors are within ±0.10 in log β unit.

azo group adjacent to the naphthol, phenol, or benzoic acid ring, O atom of the naphtholate, phenolate, or benzoate)terdentate. In these ligands, no formation of tetrahedral complexes is anticipated in view of the steric restriction since the three coordination sites (*N,N,O*) lie on the same plane. The structure of these complexes may be a six-coordinated octahedron. In the case of 1 : 1 complexes three water molecules as solvent would be coordinated as $ML(H_2O)_3$, and in 1 : 2 complexes two *N,N,O*-terdentate ligands coordinated to a metal (II) ion.

Stability Constants of Metal (II) Complexes. For all the metal (II)-ligand combinations, pH variation of the complex solution led to a spectral change with a clear isosbestic point due to the presence of an equilibrium. The complexing equilibria could thus be analyzed as described previously.[2]

Table 2 summarizes the results. The complexes formed were very stable in a wide pH range up to about pH=12. The maximum molar absorptivity exceeds 10^5 for the Ni(II) complexes with Cl_2DMPAP and Cl_2PAMB, and the Zn(II) complex with Cl_2PAMB. Therefore Cl_2DMPAP and Cl_2PAMB are useful as highly sensitive spectrophotometric reagents. The stability constants, after a final correction for the side-reaction coefficients of ligands using the values in Table 1 and the values for metal (II) ions,[8] are listed in Table 2. The β_1 values of Zn(II) and Cd(II), having filled *d* shells, with $Cl_2\beta$PAN and Cl_2DMPAP are significantly larger than those of other complexes with inorganic or amino acid ligands[8] having no π conjugated system. Namely, this can be contributed to the strong π back-donation in these complexes, since all the ligands have conjugated system which is formed between the pyridine ring and the phenol, naphthol, or benzoic acid ring via the azo group. On the other hand, the magnitude of β for the Cl_2PAMB complex is very small. This probably reflects the situation that Cl_2PAMB forms a metal (II) complex involving a five-membered ring and a highly distorted six-membered ring as suggested by molecular model. As noted in Table 1, the pK_a (4.59) of Cl_2PAMB is much smaller than those of the other two ligands (10.91 for $Cl_2\beta$PAN and 11.29 for Cl_2DMPAP).

References

1) a) T. Katami, T. Hayakawa, M. Furukawa, S. Shibata, and T. Hara, *Anal. Sci.*, **2**, 169 (1986); b) M. Villarreal, L. Porta, E. Marchevsky, and R. Olsina, *Talanta*, **33**, 375 (1986); c) F. Kai, Y. Sakanashi, S. Sato, and S. Uchikawa, *Anal. Lett.*, **16**, 1013 (1983); d) M. Nakamura, Y. Sakanashi, H. Chikushi, F. Kai, S. Sato, T. Sato, and S. Uchikawa, *Talanta*, **34**, 369 (1987).

2) H. Huang, H. Chikushi, M. Nakamura, and F. Kai, *Bull. Chem. Soc. Jpn.*, **63**, 1985 (1990).

3) G. P. Hildebrand and C. N. Reilly, *Anal. Chem.*, **29**, 258 (1957).

4) T. Iijima and M. Sekido, *J. Soc. Dyers Colour.*, **76**, 354 (1960).

5) T. M. Florence and Y. J. Farrar, *Aust. J. Chem.*, **17**, 1085 (1964).

6) a) T. Takahashi and N. Tanaka, *Nippon Kagaku Zasshi*, **91**, 339 (1970); b) L. Holleck, J. M. Abd El Kader, and A. M. Shams El Din, *J. Electroanal. Chem.*, **20**, 287 (1969).

7) a) J. P. Hart and W. F. Smith, *Spectrochim. Acta, Part A*, **36**, 279 (1980); b) F. Gerson and E. Heilbronner, *Helv. Chim. Acta*, **45**, 42 (1962); c) Y. Kudo, N. Yoshida, and M. Fujimoto, *Bull. Chem. Soc. Jpn.*, **59**, 795 (1986).

8) R. M. Smith and A. E. Martell, "Critical Stability Constants," Plenum Press, New York (1989).

Effects of Six-Membered Chelate Rings in the Oxidant Cobalt(III) Complexes on the Stereoselective Oxidation of $[Co(en)_3]^{2+}$

Akira TATEHATA* and Hiromi AKITA
Department of Chemistry, Faculty of Science, Shizuoka University, Ohya, Shizuoka 422
(Received January 28, 1991)

Synopsis. The stereoselectivities in the oxidation of $[Co(en)_3]^{2+}$ by chiral cobalt(III) complexes containing six-membered chelate ligands, such as malonate, β-alaninate, and acetylacetonate ions, were examined. All of the oxidant complexes with the Δ-configuration studied here, like the corresponding oxalato and glycinato complexes containing five-membered chelate rings, led to an excess of Λ-$[Co(en)_3]^{3+}$, with the exception of Δ-$[Co(ox)(acac)_2]^-$.

There have been some studies on stereoselective electron-transfer reactions between cobalt(II) and cobalt(III) complexes.[1-4] Most of them, however, were limited to the oxidation of cobalt(II) amine complexes by $[Co(edta)]^-$ and its derivatives. Then, as shown for the $[Co(en)_3]^{2+}$-$[Co(edta)]^-$ system (en=ethylenediamine and edta=ethylenediaminetetraacetate ion), it was thought that the ion-pairing stereoselectivity must play a dominant role in the electron-transfer stereoselectivity. Recently, we reported that even the Δ-$[Co(ox)_2(en)]^-$, Δ-C_2-*cis(N)*- and Δ-*trans(N)*-$[Co(ox)(gly)_2]^-$ (ox=oxalate ion and gly=glycinate ion), which form favorable pairs with Λ-$[Co(en)_3]^{3+}$, oxidized $[Co(en)_3]^{2+}$ to produce an excess of Λ-$[Co(en)_3]^{3+}$.[5] This indicates that there exist systems in which the observed stereoselectivity in the electron-transfer reaction is different from the ion-pairing stereoselectivity. Thus, in order to obtain more detailed information about the stereoselective reaction mechanisms, it is important to know what kinds of factors affect the electron-transfer stereoselectivity between metal complexes. In this paper, the influence of six-membered chelate rings in the chiral oxidant cobalt(III) complexes are examined.

Experimental

Preparation of Complexes. $K_3[Co(mal)_3]\cdot 3H_2O$ (mal=malonate ion) was prepared and resolved according to a method by Butler and Snow,[6] with Λ-lel$_3$-$[Co(+pn)_3]Cl_3$ (+pn=(S)-1,2-propanediamine) used as a resolving agent. Several Δ anionic complexes ($[Co(mal)_2(gly)]^{2-}$,[7] $[Co(mal)_2(\beta\text{-ala})]^{2-}$,[7] $[Co(ox)_2(\beta\text{-ala})]^{2-}$,[7] $[Co(ox)_2(acac)]^{2-}$,[8] $[Co(ox)(acac)_2]^-$,[8] $[Co(mal)_2(en)]^-$,[9] and C_1-*cis(N)*-,[10] C_2-*cis(N)*-,[10] and *trans(N)*-[11]$[Co(ox)(\beta\text{-ala})_2]^-$ (β-ala=β-alaninate ion and acac=acetylacetonate ion)) were prepared according to methods described in the literature, and were isolated as their sodium or potassium salts. *fac*-[12] and *mer*-[13]$[Co(\beta\text{-ala})_3]$ were resolved by the chromatographic methods of Yoneda and co-workers. All of the complexes presently obtained were confirmed by the absorption and circular dichroism (CD) spectra, and were then used as the oxidant in electron-transfer reactions with $[Co(en)_3]^{2+}$.

Electron-Transfer Stereoselectivity. Measurements of electron-transfer stereoselectivity were made in the same manner as in a previous study.[5] The maximum absorbance and CD spectrum in the first absorption region of the $[Co(en)_3]^{3+}$ product collected in 1.5 M HCl (1 M=1 mol dm^{-3}) were measured by a Jasco Uvidec-320 spectrophotometer and a Jasco J-500 spectropolarimeter, respectively, using 2 cm cells. The stereoselectivity was expressed in terms of enantiomeric excess (%ee) by evaluating the optical purity of the $[Co(en)_3]^{3+}$ product. Each standard deviation of %ee in this study was smaller than ±0.2%ee for at least triplicate runs.

Ion-Pairing Stereoselectivity. A column (φ 1.0 cm×55 cm) of SP-Sephadex C-25 cation exchanger, saturated with chiral $[Co(en)_3]^{3+}$, was prepared. When the anionic or neutral complex (3 cm^3 of 10—15 mmol dm^{-3}) was passed through the column with water, a partial resolution took place. The enantiomer which interacts favorably with the chiral $[Co(en)_3]^{3+}$ anchored to the ion exchanger can be expected to be eluted later from the column. Thus, favorable pairs between $[Co(en)_3]^{3+}$ and the complexes used as the oxidant were chromatographically determined by examining the late-eluted enantiomer.

Results and Discussion

In Table 1 are summarized the enantiomeric excesses of $[Co(en)_3]^{3+}$ produced by electron-transfer reactions of $[Co(en)_3]^{2+}$ with Δ-anionic or neutral complexes containing six-membered chelate rings and the enantiomers of $[Co(en)_3]^{3+}$ which form favorable pairs with the Δ-oxidant complexes, together with previous results for complex systems containing the corresponding five-membered chelate rings. It has been pointed out that the oxidation of $[Co(en)_3]^{2+}$ by chiral $[Co(mal)_3]^{3-}$ leads to a much lower stereoselectivity than that by chiral $[Co(ox)_3]^{3-}$.[4,5] A similar trend has been observed for bis(malonato) complexes such as $[Co(mal)_2gly]^{2-}$ and $[Co(mal)_2(\beta\text{-ala})]^{2-}$, although the differences in magnitude of stereoselectivity between bis(malonato) and the corresponding bis(oxalato) complexes are considerably smaller than that between the tris complexes. The complexes of the type $[Co(ox\text{ or }mal)_2(gly\text{ or }\beta\text{-ala})]^{2-}$ possess a pseudo-C_3 carboxylate face capable of forming hydrogen bonds with N–H protons of $[Co(en)_3]^{3+}$ and, therefore, were classified as the C_3^- group by Miyoshi and Yoneda.[14] This group of anionic complexes shows the same stereoselectivity in the electron-transfer reaction as that in ion-pairing reaction (ΛΔ preference). On the other hand, $[Co(mal)_2en]^-$ showed a more enhanced electron-transfer stereoselectivity than did $[Co(ox)_2en]^-$, and the electron-transfer (ΛΔ preference) and the ion-pairing stereoselectivities (ΔΔ preference) by $[Co(mal)_2en]^-$ were opposite to each other, unlike the above C_3^- group complexes, in direction in the same manner as those by $[Co(ox)_2en]^-$. These anionic complexes were expected to interact with $[Co(en)_3]^{3+}$ along their C_2 axes and, thus, were classified as the C_2^- group;[14] the above results, therefore, indicate that bis(malonato) chelates lead to either a lower or higher electron-transfer stereoselectivity than do the corresponding bis(oxalato) chelates according as they belong

Table 1. Electron-Transfer and Ion-Pairing Stereoselectivities

Oxidant	$[Co(en)_3]^{3+}$		Oxidant	$[Co(en)_3]^{3+}$	
	%ee	Favorable pair[a]		%ee[b]	Favorable pair[a,b]
Δ-$[Co(mal)_3]^{3-}$	1.9Λ, 0.6Λ[c]	Λ	Δ-$[Co(ox)_3]^{3-}$	10.0Λ, 7.6Λ[c]	—[d]
Δ-$[Co(mal)_2gly]^{2-}$	6.2Λ	Λ	Δ-$[Co(ox)_2gly]^{2-}$	9.0Λ	Λ[g]
Δ-$[Co(mal)_2(\beta\text{-ala})]^{2-}$	4.3Λ	Λ			
Δ-$[Co(ox)_2(\beta\text{-ala})]^{2-}$	8.7Λ	Λ			
Δ-$[Co(mal)_2en]^-$	5.6Λ	Λ[c]	Δ-$[Co(ox)_2en]^-$	3.6Λ	Λ[g]
Δ-$[Co(ox)(\beta\text{-ala})_2]^-$			Δ-$[Co(ox)(gly)_2]^-$		
C_1-*cis(N)*	10.5Λ	Λ	C_1-*cis(N)*	9.4Λ	Λ[g]
C_2-*cis(N)*	10.0Λ	Λ	C_2-*cis(N)*	2.1Λ	Λ[g]
trans(N)	—[f]	—[f]	*trans(N)*	0.5Λ	Λ
Δ-$[Co(\beta\text{-ala})_3]$					
fac	7.9Λ	Λ[g]			
mer	3.6Λ	Λ[c]			
Δ-$[Co(ox)_2acac]^{2-}$	2.6Λ	Λ[g]			
Δ-$[Co(ox)(acac)_2]^-$	3.1Δ	Λ			

a) The enantiomer of $[Co(en)_3]^{3+}$ which forms favorable pair with Δ-complexes used as the oxidant. b) Ref. 5. c) Ref. 4. d) Precipitation (less soluble diastereomer is a Δ-Δ pair). Erroneously given in Ref. 5 and thus corrected here. e) Very small stereoselectivity. f) Virtually no detectable stereoselectivity. g) Also reported in Ref. 14.

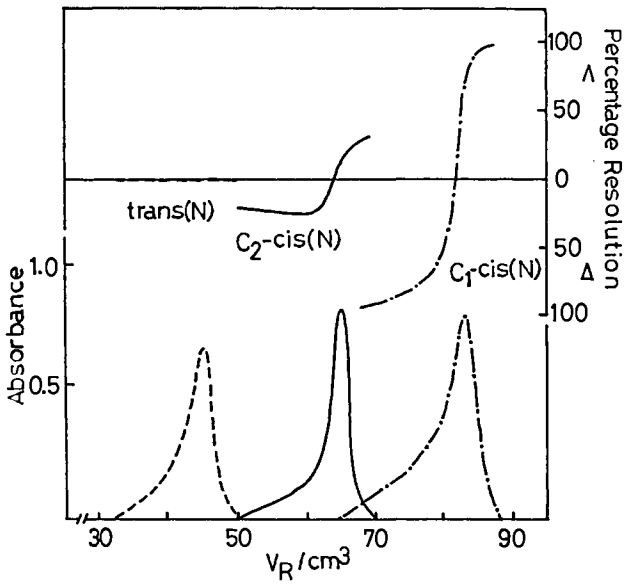

Fig. 1. Elution curves and percentage resolutions for *trans(N)*-, C_2-*cis(N)*-, and C_1-*cis(N)*-$[Co(ox)(\beta\text{-ala})_2]^-$ by Δ-$[Co(en)_3]^{3+}$ form SP-Sephadex column using H_2O as an eluent.

to either the C_3^-or C_2^- group. This suggests that the interaction mode of malonato complexes with $[Co(en)_3]^{2+}$ plays an important role regarding the magnitude of electron-transfer stereoselectivity.

For β-alaninato complexes, apart from *trans(N)*-$[Co(ox)(\beta\text{-ala})_2]^-$, which show virtually no detectable stereoselectivities in both the electron-transfer and the ion-pairing reactions (Fig. 1), all of the β-alaninato complexes with the Δ-configuration used here produced excess Λ-$[Co(en)_3]^{3+}$, although the electron-transfer and ion-pairing stereoselectivities by tris(β-alaninato) complexes were inverted in same manner as those by $[Co(ox)_2en]^-$ and $[Co(mal)_2en]^-$. Thus, in spite of large size and conformational lability of the six-membered chelate ring, it may be concluded that the observed electron-transfer stereoselectivity by the malonato and β-alaninato complexes was the same in direction as that by the corresponding oxalato and glycinato complexes containing five-membered chelate rings.

Finally, for the acetylacetonato complexes, the mono(acetylacetonato) complex, $[Co(ox)_2(acac)]^{2-}$ showed essentialy the same electron-transfer stereoselectivity as did $[Co(ox)_2gly]^{2-}$ and $[Co(ox)_2(\beta\text{-ala})]^{2-}$. However, the bis(acetylacetonato) complex, Δ-$[Co(ox)(acac)_2]^-$, was the only oxidant complex which produced an excess of Δ-$[Co(en)_3]^{3+}$ in the present study. The favorable ion pair of $[Co(en)_3]^{3+}$ with $[Co(ox)(acac)_2]^-$ was $\Lambda\Delta$, similar to that with $[Co(ox)_2acac)]^{2-}$. At present, it is difficult to explain the unique phenomenon caused by $[Co(ox)(acac)_2]^-$. The selectivities in the oxidation reactions by various acetylacetonato complexes need to be examined further.

References

1) D. A. Geselowitz and H. Taube, *J. Am. Chem. Soc.*, **102**, 4525 (1980).
2) P. Osvath and A. G. Lappin, *Inorg. Chem.*, **26**, 195 (1987). A. G. Lappin, R. A. Marusak, and P. Osvath, *Inorg. Chem.*, **26**, 4292 (1987).
3) D. A. Geselowitz, A. Hammershoi, and H. Taube, *Inorg. Chem.*, **26**, 1842 (1987).
4) R. A. Marusak, P. Osvath, M. Kemper, and A. G. Lappin, *Inorg. Chem.*, **28**, 1542 (1989).
5) A. Tatehata and T. Mitani, *Chem. Lett.*, **1989**, 1167.
6) K. R. Butler and M. R. Snow, *J. Chem. Soc., Dalton Trans.*, **1976**, 251.
7) K. Yamasaki, J. Hidaka, and Y. Shimura, *Bull. Chem. Soc. Jpn.*, **42**, 119 (1969).
8) F. P. Dwyer, I. K. Reid, and A. M. Sargeson, *Aust. J. Chem.*, **18**, 1919 (1965).
9) F. P. Dwyer, I. K. Reid, and F. L. Garvan, *J. Am. Chem. Soc.*, **83**, 1285 (1961).
10) T. Ama, M. Higa, N. Koine, and T. Yasui, *Bull. Chem.*

Soc. Jpn., **50**, 2632 (1977).
11) J. Hidaka and Y. Shimura, *Bull. Chem. Soc. Jpn.*, **40**, 2312 (1967).
12) H. Yoneda and T. Yoshizawa, *Chem. Lett.*, **1976**, 707.
13) S. Yamazaki and H. Yoneda, *Inorg. Nucl. Chem. Lett.*, **15**, 195 (1979).
14) K. Miyoshi, Y. Sakamoto, A. Ohguni, and H. Yoneda, *Bull. Chem. Soc. Jpn.*, **58**, 2239 (1985).

Solvent Bulkiness Effect on *N,N*-Dimethylformamide Exchange of the *o*-Phenylenediamine-*N,N,N',N'*-tetraacetatoferrate(III) Complex as Studied by a High-Pressure NMR Method

Masafumi MIZUNO, Shigenobu FUNAHASHI,* Noriyuki NAKASUKA, and Motoharu TANAKA
Laboratory of Analytical Chemistry, Faculty of Science, Nagoya University, Chikusa, Nagoya 464-01
(Received February 1, 1991)

Synopsis. Activation parameters for solvent exchange of the title complex in *N,N*-dimethylformamide (DMF) have been determined as follows: k (25 °C)=(3.4±0.2)×10^7 s^{-1}, $\Delta H^{\ddagger}$=18±3 kJ mol^{-1}, $\Delta S^{\ddagger}$=−40±10 J K^{-1} mol^{-1}, and $\Delta V^{\ddagger}$=10±2 cm^3 mol^{-1}. The positive value of $\Delta V^{\ddagger}$ indicates that the DMF exchange proceeds via a dissociative interchange mechanism.

Rates for the complexation of d^5 iron(III) ion have been found to be greatly affected by the electron donecity of the bound ligand and the bulkiness of coordinated solvent molecules in several solvents.[1-3] The purpose of this work is to demonstrate the effects of the bound multidentate ligand and the solvent bulkiness on the solvent exchange of iron(III) complexes in terms of activation parameters. Recently we have reported the bound ligand effect on the water exchange of the iron(III) complex with *o*-phenylenediamine-*N,N,N',N'*-tetraacetate (phdta^{4-}) in aqueous solution.[4] In order to investigate the solvent bulkiness effect on solvent exchange rate, we selected *N,N*-dimethylformamide (DMF) as a bulky solvent.

Experimental

Oxygen-17-enriched DMF was synthesized according to the reference method.[5] The ^{17}O-enriched DMF was purified by distillation over the 4A Molecular Sieves. PhDTA and its iron(III) complex were prepared by the procedures previously described.[4] The preparation of the sample solution for variable-temperature NMR measurement was carried out by the freeze-thaw technique under vacuum. Transfer of the sample solution into a high-pressure NMR tube (o.d. 7 mm) was performed under nitrogen gas in a dry box.[6,7] The concentration of Fe(III)-PhDTA in sample solutions ($C_{\mathrm{Fe(III)\text{-}PhDTA}}$) is given in the Figure caption.

Variable-temperature Fourier-transform ^{17}O NMR spectra were measured with JEOL JNM-FX100 and JNM-GX270 NMR instruments operating at 13.50 and 36.63 MHz, respectively. Variable-pressure FT oxygen-17 NMR spectra were obtained with a JEOL-FX100 NMR spectrometer equipped with a high-pressure NMR probe.[6] Temperature and pressure were measured by the same methods as reported previously.[4]

The structure of Fe(III)-PhDTA in the DMF solution should be similar to that in water: The central iron(III) ion is seven-coordinate, with one DMF molecule being solvated.[4] Thus the DMF exchange at the iron(III) complex is expressed by Eq. 1.

$$[\mathrm{Fe(dmf^*)(phdta)}]^- + \mathrm{dmf} \rightleftarrows [\mathrm{Fe(dmf)(phdta)}]^- + \mathrm{dmf^*}. \quad (1)$$

The exchange rate of solvent molecules between the bulk and the coordination site of a paramagnetic metal ion has been estimated from the transverse relaxation time (T_{2P}) of the bulk solvent nuclei. The solvent ^{17}O NMR line broadening, $(T_{2P}P_M)^{-1}$, due to the paramagnetic iron(III) complex is expressed as $(T_{2P}P_M)^{-1}=\pi(\Delta\nu_{obsd}-\Delta\nu_{solv})P_M^{-1}$, where $\Delta\nu_{obsd}$ and $\Delta\nu_{solv}$ are the half-height widths of the ^{17}O NMR spectra of DMF in the bulk in the presence and absence, respectively, of Fe(III)-PhDTA. P_M is the ratio of the number of DMF molecule bound to the iron(III) complex to that of DMF molecules in the bulk. NMR line broadening data were analyzed on the basis of the modified Swift-Connick equation.[4,8]

Results and Discussion

Figure 1 shows the temperature dependence of $(T_{2P}P_M)^{-1}$ for the Fe(III)-PhDTA complex in DMF over the range from −58 to 72 °C. Since the transverse relaxation rate due to the bound DMF in the absence of exchange, T_{2M}^{-1}, is small enough compared with the other relaxation terms over the observable temperature region for the present system, the modified Swift-Connick equation is reduced to Eq. 2:

$$(T_{2P}P_M)^{-1} = 1/(\tau_M^{-1}\Delta\omega_M^{-2} + \tau_M), \quad (2)$$

where τ_M is the residence time of the solvent molecule in the inner sphere of the iron(III) complex and $\Delta\omega_M$ is the shift between bulk and bound DMF resonances when no exchange occurs. The temperature dependence of $\Delta\omega_M$ is assumed to be $\Delta\omega_M=-C_\omega/T$.[9,10] A nonlinear least-squares analysis of the data led to the following parameters by fitting to Eq. 2: $\Delta H^{\ddagger}$/kJ mol^{-1}, $\Delta S^{\ddagger}$/

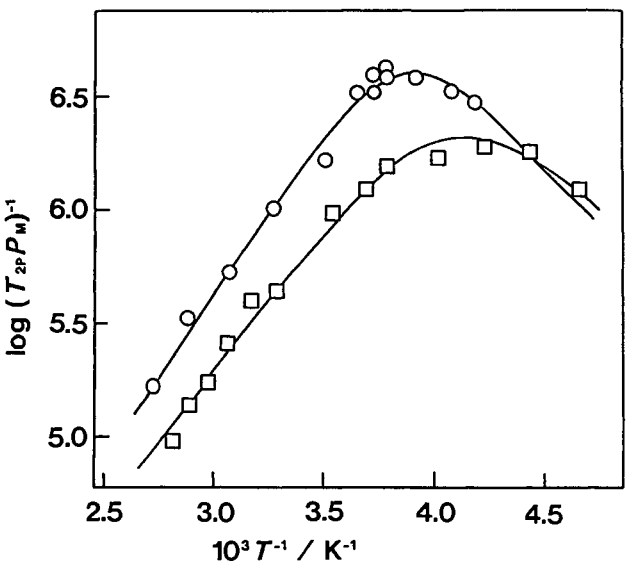

Fig. 1. Variation of the solvent DMF oxygen-17 relaxation rates $(T_{2P}P_M)^{-1}$ with temperature for Fe(III)-PhDTA in DMF solution. $C_{\mathrm{Fe(III)\text{-}PhDTA}}$= 4.50×10^{-3}, 7.03×10^{-3}, and 1.85×10^{-2} mol kg^{-1}. ○: 36.63 MHz ^{17}O; □: 13.50 MHz ^{17}O.

Table 1. Kinetic Parameters for Solvent Exchange on Fe(III) Complexes

	k (25 °C)	$\Delta H^{\ddagger}$	$\Delta S^{\ddagger}$	$\Delta V^{\ddagger}$	Ref.
	s^{-1}	kJ mol^{-1}	J K^{-1} mol^{-1}	cm^3 mol^{-1}	
[Fe(dmf)(phdta)]$^-$	3.4×10^7	18±3	−40±10	10±2	This work
$[Fe(dmf)_6]^{3+}$	6.1×10	42.3±4.0	−69.0±13	−0.9±0.2	14
$[Fe(OH_2)(phdta)]^-$	1.2×10^7	26±3	−22±9	4.6±0.2	4
$[Fe(OH_2)_6]^{3+}$	1.6×10^2	64.0±2.5	12.1±6.7	−5.4±0.4	15, 16

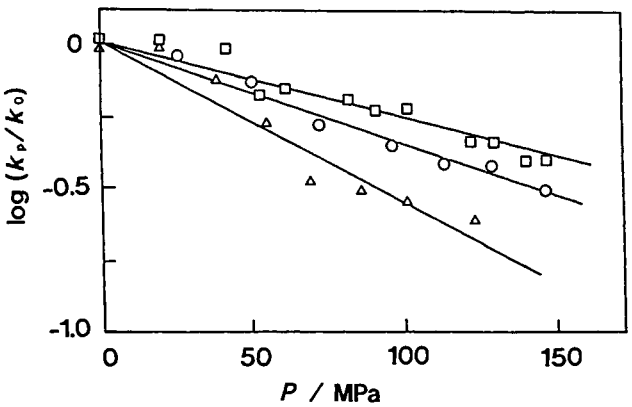

Fig. 2. Pressure dependence of logk_P for DMF exchange of the Fe(III)–PhDTA complex at −23.4 °C (△), 27.0 °C (○), and 61.3 °C (□). $C_{Fe(III)\text{-}PhDTA}=2.16\times10^{-2}$ mol kg^{-1}.

J K^{-1} mol^{-1}, and C_ω/K rad s^{-1} are 16.1±0.8, −51±3, and (1.03±0.06)×10^9 for 13.50 MHz and 20.9±0.9, −33±3, and (2.05±0.09)×10^9 for 36.63 MHz, respectively. These values obtained were used for drawing the solid curves in Fig. 1. The enthalpy and entropy of activation for DMF exchange on Fe(III)–PhDTA were determined to be 18±3 kJ mol^{-1} and −40±10 J K^{-1} mol^{-1}, respectively, taking experimental errors into account.

Since the definite chemical exchange region was not observed, we estimated the activation volume according to the following procedure. The solvent electrostriction acting on the primary coordination sphere may result in a large compression, typically of the order of gigapascals,[11] so that an externally applied pressure of about 150 MPa will not produce any noticeable changes in bond lengths. Therefore, the scalar coupling constant (A)[12] which depends on the distance between the iron(III) ion and the oxygen nucleus is not expected to vary to an appreciable extent in the present pressure experiments. Consequently, we calculated the k_P values at various pressures at three different temperatures, assuming that $\Delta\omega_M$ is independent of pressure as has been demonstrated by Merbach et al.[13] Values of ln (k_P/k_0) are plotted against P in Fig. 2. The activation volume at the respective temperature was obtained as follows: $\Delta V^{\ddagger}$=11.9±2.6 (−23.4 °C), 8.7±1.0 (27.0 °C), and 8.6±1.1 cm^3 mol^{-1} (61.3 °C). Taking into account experimental errors, the mean value of $\Delta V^{\ddagger}$ should be 10±2 cm^3 mol^{-1}.

The exchange of DMF on the Fe(III)–PhDTA complex is much faster than the solvent exchange on the hexa(solvento)iron(III) ion in water and DMF (see Table 1). This fact comes mainly from the difference in activation enthalpy. The values of $\Delta V^{\ddagger}$ for the solvent exchange on the hexa(solvento)iron(III) ion are negative, while those of the Fe(III)–PhDTA complex are positive both in water and DMF: The solvent exchange proceeds via an associative interchange mechanism for the former, while a dissociative interchange mechanism is operative for the latter. Since a ligand with electron donecity such as phdta^{4-} binds to the iron(III) ion, the electron density of the iron(III) atom should increase and the bond between the metal ion and a coordinated DMF molecule may be weakened (the bound ligand effect). The solvent exchange of the Fe(III) complex with electron-donating ligand proceeds much faster and more dissociatively than that on the hexa(solvento)-iron(III) ion. The more positive activation volume for the DMF exchange may be attributed to the bulkiness of a DMF molecule compared with a water molecule. In bulkier solvents, a coordinated leaving solvent molecule may be forced to leave partly the inner sphere of the central metal ion due to steric hindrance before an entering solvent starts to coordinate (solvent bulkiness effect). In conclusion, this study has clearly demonstrated that both the bound ligand effect and the solvent bulkiness effect make the activation mode less associative for the solvent exchange of Fe(III)–PhDTA in DMF.

This work was supported by Grants-in-Aid for Scientific Research No. 62470041 and for Scientific Research on the Priority Area of "Non-equilibrium Processes" (No. 02245106) from the Ministry of Education, Science and Culture.

References

1) K. Ishihara, S. Funahashi, and M. Tanaka, *Inorg. Chem.*, **22**, 194 (1983).
2) S. Funahashi, K. Ishihara, and M. Tanaka, *Inorg. Chem.*, **22**, 2070 (1983).
3) K. Ishihara, S. Funahashi, and M. Tanaka, *Inorg. Chem.*, **22**, 3589 (1983).
4) M. Mizuno, S. Funahashi, N. Nakasuka, and M. Tanaka, *Inorg. Chem.*, **30**, 1550 (1991).
5) R. R. Koganty and G. A. Digenis, *J. Labeled Compd.*, **10**, 419 (1973).
6) M. Ishii, S. Funahashi, and M. Tanaka, *Inorg. Chem.*, **27**, 3192 (1988).
7) M. Ishii, S. Funahashi, K. Ishihara, and M. Tanaka, *Bull. Chem. Soc. Jpn.*, **62**, 1852 (1989).
8) J. Granot and D. Fiat, *J. Magn. Reson.*, **15**, 540 (1974).
9) L. L. Rusnak and R. B. Jordan, *Inorg. Chem.*, **15**, 709 (1976).
10) N. Bloembergen, *J. Chem. Phys.*, **27**, 572, 595 (1957).
11) T. W. Swaddle, *Inorg. Chem.*, **22**, 2663 (1983).

12) According to Bloembergen's equation,[10] $\Delta\omega_M=-\omega_I[S(S+1)]\gamma_e A/3\gamma_I k_B T$, where ω_I is the Larmor frequency of the nucleus, S is the electron spin quantum number, γ_e and γ_I are the magnetogyric ratios of the electron and the nucleus, and A is the scalar coupling constant.

13) A. D. Hugi, L. Helm, and A. E. Merbach, *Inorg. Chem.*, **26**, 1763 (1987).

14) F. K. Meyer, A. R. Monnerat, K. E. Newman, and A. E. Merbach, *Inorg. Chem.*, **21**, 774 (1982).

15) M. Grant and R. B. Jordan, *Inorg. Chem.*, **20**, 55 (1981).

16) T. W. Swaddle and A. E. Merbach, *Inorg. Chem.*, **20**, 4212 (1981).

Effects of Halide Ions on Micelle-Enhanced Chemiluminescence Reaction of Lucigenin with Adrenaline

Tamio KAMIDATE,* Tetsutoshi KANEYASU, Tadashi SEGAWA, and Hiroto WATANABE
Faculty of Engineering, Hokkaido University, Kita-ku, Sapporo 060
(Received February 13, 1991)

Synopsis. A remarkable lowering of chemiluminescence (CL) emitted from the CL reaction of lucigenin (Luc) with adrenaline (AD) was observed in cationic micellar assemblies containing halide ions, when their concentrations were above 5×10^{-3} mol dm^{-3}. These results could be explained in terms of the quenching of the Luc CL reaction by halide ions. The quenching by chloride ions was dependent on the carbon number in the alkyl group of surfactant reagents.

The use of appropriate aqueous micellar solutions has been shown to enhance the chemiluminescence (CL) intensity from CL reaction systems involving lucigenin (10,10′-dimethyl-9,9′-biacridinium dinitrate, Luc). Micelle-enhanced Luc CL reactions have been employed in order to improve the sensitivity of the determination of hydrogen peroxide and biological reductants.[1,2]

We previously proposed the Luc CL method for the determination of such catecholamines (CAs) as dopamine, noradrenaline and adrenaline (AD).[3] In addition, we have shown that cationic surfactant micelles are superior to nonionic and anionic surfactant micelles with respect to the enhancement effect on the CL intensity.[4] In this paper we describe the effects of such halide ions as bromide and chloride on the CL intensity emitted from the Luc CL reaction with AD in cationic micellar solutions.

Experimental

Reagents. Hexadecyltrimethylammonium hydroxide (CTAOH), hexadecyltrimethylammonium chloride (CTAC), hexadecyltrimethylammonium bromide (CTAB), tetradecyltrimethylammonium chloride(TTAC) and dodecyltrimethylammonium chloride (DTAC) were used without further purification. All of the solutions used were prepared as described previously.[4]

Apparatus. All CL measurements were performed by use of a fluorometer (Farrand Optical Co., Type Ratio-2) equipped with an automatic injector which had two flow lines (Ohtsuka Denshi Co., Type MX-7). A strip-chart recorder was used to record the CL intensity–time profiles.

Procedure. A 250 μl portion of surfactant solution and a 250 μl portion of a 0.2 M (1 M=1 mol dm^{-3}) NaOH solution were added using an Eppendorf pipet into a 1-cm glass cell in the fluorometer. Next, a 250 μl portion of 6.0×10^{-5} M Luc solution and a 250 μl portion of 1.0×10^{-4} M AD solution were injected simultaneously through Teflon tubing into the cell by using an automatic injector. Thus, the CL reaction was initiated and light emission was detected by a photomultiplier tube. The resultant photocurrent was converted to a voltage and displayed on a chart recorder. The maximum light emission was corrected using the light emission of a blank containing no AD. These background-corrected CL values were referred to as the CL intensities.

Results and Discussion

The CL measurements were carried out using different counterion-types of such cationic surfactants as CTAOH, CTAC, and CTAB. Figure 1 shows the CL intensity-surfactant concentration profiles. When the surfactant concentrations were well below the critical micelle concentrations (cmc) (results not shown), the CL intensity was about the same as that in water. The increase in the CL intensity commenced at surfactant concentrations near cmc, which were 9×10^{-4} M for CTAOH, 1.3×10^{-3} M for CTAC and 9.2×10^{-4} M for CTAB, respectively.[5] The CL intensities were maximal at 5×10^{-3} M and were about the same, regardless of the cationic micellar assemblies used. However, the CL intensities were dependent on the counterion types and concentrations of cationic surfactants used, when their concentrations were above 5×10^{-3} M. The relative effectiveness of these cationic micelles at enhancing the CL intensity followed the order CTAOH>CTAC> CTAB, thus indicating that the micelle-enhanced Luc CL reaction was affected by the concentrations of halide ions.

In order to elucidate the effect of halide ions on the Luc CL reaction, a 250 μl portion of NaCl solution or that of NaBr solution was added to the reaction mixture instead of surfactant micellar solutions. The results

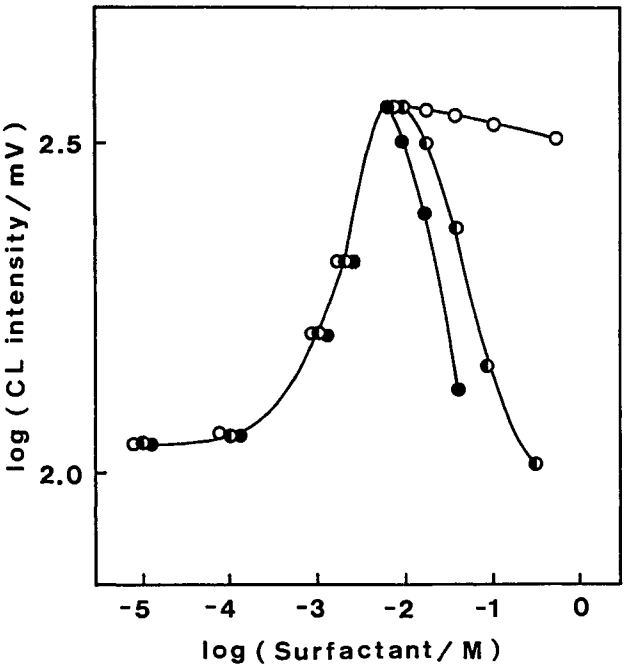

Fig. 1. Variation in the chemiluminescence intensity with surfactant concentration.
○: CTAOH, ◐: CTAC, and ●: CTAB.
Conditions: 9.0×10^{-4} M AD, 6.0×10^{-5} M Luc, and 0.2 M NaOH.

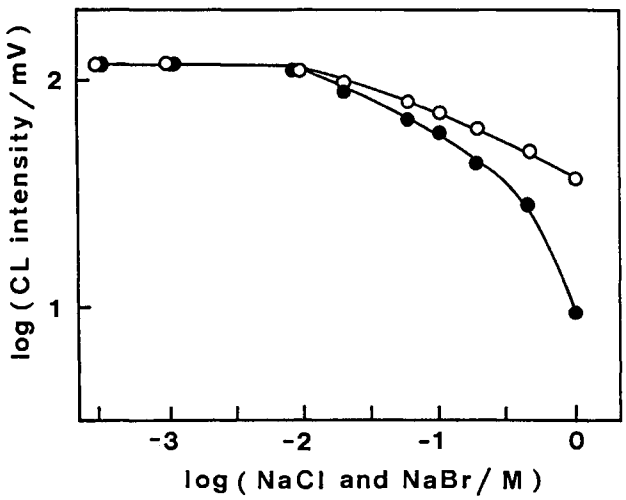

Fig. 2. Effect of halide concentration on the chemiluminescence intensity.
○: NaCl and ●: NaBr.
Conditions: 9.0×10^{-4} M AD, 6.0×10^{-5} M Luc, and 0.2 M NaOH.

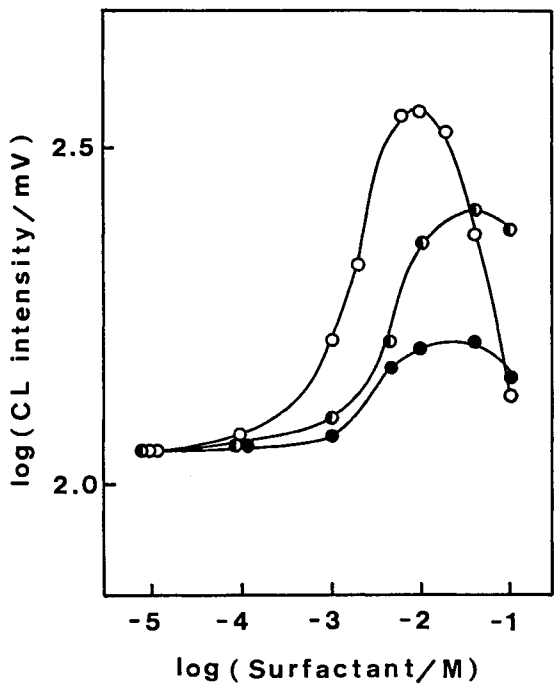

Fig. 3. Variation in the chemiluminescence intensity with surfactant concentration.
○: CTAC, ◐: TTAC, and ●: DTAC.
Conditions: 9.0×10^{-4} M AD, 6.0×10^{-5} M Luc, and 0.2 M NaOH.

shown in Fig. 2 indicate that halide ions play the roll as a quencher for the Luc CL reaction with AD when their concentration are above 1×10^{-2} M. Quenching by bromide ions was greater than that by chloride ions. Therefore, the remarkable decrease of the CL intensity in the micellar assemblies containing halide ions is probably attributable to quenching of the Luc CL reaction by halide ions. However, the degree of lowering the CL intensity in micellar assemblies was greater than that in water alone at the same concentration of haliden ions. These results may be interpreted as follows. Halide ions interact electrostatically with and bind to a cationic micelle pseudophase. Consequently, the local halide concentration on the micelle surface is greater than the stoichiometric concentration in bulk water alone. Thus, quenching by halide ions is greater in micellar assemblies compared to that in water alone.

We then examined the effect of chloride ions on the micelle-enhanced CL using DTAC, TTAC, and CTAC with different carbon numbers in an alkyl group of surfactant reagents. Figure 3 shows the CL intensity–surfactant concentration profiles for the respective surfactants. The CL intensity increased with an increase in the carbon number of the alkyl group. The degree of quenching by chloride ions was dependent on the carbon number in the alkyl group of the surfactant reagents used. This is ascribable to their cmc, which are 1.3×10^{-3} M for CTAC, 4.5×10^{-3} M for TTAC,[6] and 2.0×10^{-2} M for DTAC,[7] respectively. Along with a decrease in the carbon number of the alkyl group, the cmc, and thus the concentration of surfactant micelles, increased, resulting in an effective enhancement of the CL intensity in micellar assemblies. The concentration of chloride ions increases simultaneously under these conditions.

Consequently, the degree of the quenching by chloride ions may increase with a decrease in the carbon number of the alkyl group of surfactant reagents. On the other hand, the maximum CL intensities in such C_{16} surfactants as CTAOH, CTAC, and CTAB, were not affected by the counterions of the surfactant reagents. This result may be interpreted by taking into acount their cmc. That is, the CL intensity reached a maximum value without suffering from the quenching effect of halide ions on the CL intensity, since the cmc for CTAC and CTAB are well below the concentrations required for quenching by halide ions.

As described above, CTAOH is very useful as a micellar medium for enhancing the CL intensity of Luc CL with AD. On the other hand, the optimum concentrations of CTAC and CTAB are within a very limited range, thus precluding their use.

References

1) W. L. Hinze, T. E. Riehl, H. N. Singh, and Y. Baba, *Anal. Chem.*, **56**, 2180 (1984).
2) T. E. Riehl, C. L. Malehorn, and W. L. Hinze, *Analyst*, **111**, 931 (1986).
3) T. Kamidate, K. Yoshida, T. Segawa, and H. Watanabe, *Anal. Sci.*, **5**, 359 (1989).
4) T. Kamidate, K. Yoshida, T. Kaneyasu, T. Segawa, and H. Watanabe, *Anal. Sci.*, **6**, 645 (1990).
5) A. Ingvarsson, C. L. Flurer, T. E. Riehl, K. N. Thimmaiah, J. M. Williams, and W. L. Hinze, *Anal. Chem.*, **60**, 2047 (1988).
6) H. W. Hoyer and A. Marmo, *J. Phys. Chem.*, **65**, 1807 (1961).
7) J. Osugi, M. Sato, and N. Ifuku, *Rev. Phys. Chem. Jpn.*, **35**, 32 (1965).

Epoxidation of 2-Butene-1,4-diones with Hydrogen Peroxide in the Presence of a Catalytic Amount of Quaternary Ammonium Iodide

Shinsei SAYAMA* and Yutaka INAMURA
Department of Chemistry, Fukushima Medical College, Hikarigaoka, Fukushima 960-12
(Received December 13, 1990)

Synopsis. The epoxidation of 1,4-disubstituted 2-butene-1,4-diones with 30% aq H_2O_2 in the presence of a catalytic amount of quaternary ammonium iodide afforded 2,3-epoxy-1,4-butanediones in high yield.

The epoxidation of α,β-unsaturated ketones was carried out with nucleophilic reagents, such as hydrogen peroxide or *t*-butyl hydroperoxide, in alkaline solution.[1-3] These available methods are not applicable to base-sensitive substrates.[7] There have therefore been many studies of an epoxidation reaction to overcome the problem without employing a strong base.[4-9] It was reported that the epoxidation reaction of α,β-unsaturated ketones using 30% aq H_2O_2–Bu_4NF gave the corresponding epoxy ketones.[7] Also reported was a direct and stereospecific epoxidation of 2-butene-1,4-diones with $MoO_5 \cdot H_2O \cdot HMPA$, based on approaches to the synthesis of antibiotic cerulenin.[8-10] Although 30% aq H_2O_2 was a convenient and inexpensive reagent for the oxidation reactions, in comparison with other peroxides, the epoxidation of 1,4-disubstituted 2-butene-1,4-diones with H_2O_2 under the non-basic reaction conditions, has not been examined. We would like to report on the results of studies concerning the chemoselective epoxidation of 1,4-disubstituted 2-butene-1,4-diones with H_2O_2 in the presence of a catalytic amount of quaternary ammonium iodides.

The epoxidation of *trans*-1,4-diphenyl-2-butene-1,4-dione (**1**), chosen as a representative 2-butene-1,4-dione for this study, with 30% aq H_2O_2–quaternary ammonium halides in various stoichiometric ratios, was carried out. The results are summarized in Table 1. At an appropriate ratio of enedione **1**, H_2O_2, and Bu_4NI (1 : 26 : 1, 1 : 28 : 0.5, or 1 : 29 : 0.1), *cis*-2,3-epoxy-1,4-diphenyl-1,4-butanedione (**1b**) was predominantly obtained (Entries 1—3).[15] The yield of *trans*- and *cis*-epoxides **1a** and **1b** was determined by the recrystallization of crude products from ethyl acetate as follows.

trans-2,3-Epoxy-1,4-diphenyl-1,4-butanedione (**1a**) was obtained in 10—18% yield as the first crop of crystals; *cis*-epoxide **1b** was then afforded by recrystallization of the filtrates. The stereochemistries of *trans*- and *cis*-epoxides (**1a** and **1b**) were determined by a direct comparison of the spectral data with that of *trans*-epoxide **1a**, which was alternatively prepared by the epoxidation of **1** with alkaline hydrogen peroxide. The spectral data of **1a** and **1b** were also identical with those of known compounds reported in the literature.[8,9] In addition, the catalytic amount of Bu_4NI (0.1 equiv) and a slight excess molar equivalent of H_2O_2 (5 equiv) gave a similar result (Entry 5). On the other hand, the epoxidation of enedione **1** with H_2O_2 and other common quaternary ammonium halides (Bu_4NF, Me_4NCl, Bu_4NBr, and $PhCH_2N(Et)_3Br$) did not give *trans*- and *cis*-epoxides **1a** and **1b** in high yield (less than 15%), and a complex mixture of hydroxy derivatives was obtained

Table 1. Epoxidation of *trans*-1,4-Diphenyl-2-butene-1,4-dione **1** with 30% aq H_2O_2–R_4NI in THF at 0—23 °C[a]

Entry	Molar ratio			R_4NX	Products yield/%[b]		
	Enedione **1**	H_2O_2	R_4NX		2,3-Epoxy-1,4-butanedione[c]		Recovered enedione **1**
					trans **1a**	*cis* **1b**	
1	1	26	1.0	Bu_4NI	15	73	—
2	1	28	0.5	Bu_4NI	15	71	—
3	1	29	0.1	Bu_4NI	18	70	—
4	1	28	0.5	Bu_4NI[d]	10	75	—
5	1	5	0.1	Bu_4NI	28	63	—
6	1	32	0.1	Bu_4NI[e]	12	38	28
7	1	—[f]	0.1	Bu_4NI	—	—	96
8	1	29	—	—	—	—	75
9	1	28	0.6	Bu_4NF[g]	15	15	—
10	1	28	0.8	$(CH_3)_4NCl$[g]	—	—	66
11	1	29	0.7	Bu_4NBr[g]	—	—	—
12	1	29	0.5	$PhCH_2N(Et)_3Br$[g]	—	—	—
13	1	26	0.2	$PhCH_2N(Me)_3I$	20	68	—

a) Enedione **1**; 0.5—1.0 mmol. THF; 10-15 ml. Reaction time; 20—78 h. b) Yield is based on enedione **1** used. c) Purified by recrystallization from ethyl acetate.[8,9] d) THF–DMF (4/1 v/v) was used as solvent. e) CH_2Cl_2 was used as solvent. f) H_2O (270 mol equiv) was used instead of 30% aq H_2O_2. g) Complex mixture of hydroxy derivatives was obtained.

Table 2. Epoxidation of 2-Butene-1,4-diones with 30% aq H_2O_2–Bu_4NI in THF at 0—23 °C[a]

Substrate (S)		Molar ratio S : H_2O_2 : Bu_4NI			Products	Yield/%[b]	
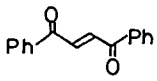	**1**	1	29	0.1	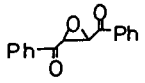	**1a**[8,9]	18[c]
					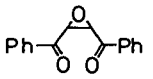	**1b**[8,9]	70[c]
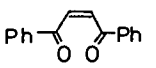	**2**	1	29	0.5	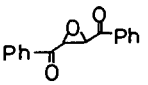	**1a**	30[c]
					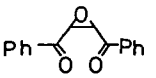	**1b**	54[c]
PhCOCH=CHCO$_2$Et	**3**	1	22	0.5	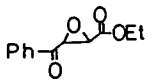	**3a**	60[d]
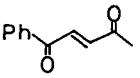	**4**	1	18	0.1	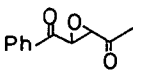	**4a**[8,9]	58[d]
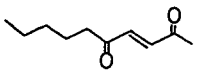	**5**	1	14	0.1	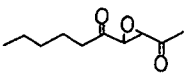	**5a**	56[d]
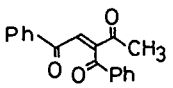	**6**	1	30	1.0	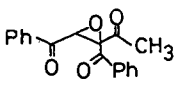	**6a**[14]	55[d]

a) 2-Butene-1,4-dione; 0.5—1.0 mmol. THF; 10—15 ml. Reaction time; 20—45 h. b) Yield is based on 2-butene-1,4-dione used. c) Purified by recrystallization from ethyl acetate.[8,9] d) Purified by column chromatography on silica gel.

Table 3. Epoxidation of 2-Butene-1,4-diones with 30% aq H_2O_2–$PhCH_2N(CH_3)_3I$ in THF at 0—23 °C[a]

Substrate (S)	Molar ratio S : H_2O_2 : BTMAI[c]			Time h	Products Yield/%[b]	
1	1	26	0.2	48	**1a**[8,9]	20[d]
					1b[8,9]	68[d]
2	1	23	0.1	25	**1a**	15[d]
					1b	60[d]
3	1	18	0.1	96	**3a**	60[e]
4	1	22	0.1	68	**4a**[8,9]	69[e]
5	1	14	0.1	66	**5a**	61[e]
6	1	23	0.1	47	**6a**[14]	53[e]

a) 2-Butene-1,4-dione; 0.5—1.0 mmol. THF; 10—15 ml. b) Yield is based on 2-butene-1,4-dione used. c) BTMAI; $PhCH_2N(CH_3)_3I$. d) Purified by recrystallization from ethyl acetate.[8,9] e) Purified by column chromatography on silica gel.

under various ratios of H_2O_2 and quaternary halides (Entries 9—12). These results suggest that the iodide ion acts as a base while promoting the conjugate addition of hydroperoxide to the carbon–carbon double bond of enedione **1**.[7,11,12] The epoxidation of enedione **1** with H_2O_2 in the presence of another quaternary ammonium iodide ($PhCH_2N(Me)_3I$) also gave epoxides in good yield (Entry 13).

The results of the epoxidation of other 2-butene-1,4-diones with 30% aq H_2O_2–quaternary ammonium iodide (Bu_4NI or $PhCH_2N(CH_3)_3I$) are shown in Tables 2 and 3. *cis*-1,4-Diphenyl-2-butene-1,4-dione (**2**) also afforded *cis*-epoxide **1b** predominantly as well as *trans*-enedione **1**. *trans*-1-Phenyl-2-pentene-1,4-dione (**4**), *trans*-3-decene-2,5-dione (**5**), and ethyl 4-oxo-4-phenyl-2-butenoate (**3**) afforded the corresponding *trans*-2,3-epoxy derivatives (**3a**, **4a**, and **5a**). The stereochemistries of *trans*-epoxides of **3a**, **4a**, and **5a** were assigned based on the ^1HNMR spin–spin coupling constants between the epoxy ring protons; **3a**—**5a** showed coupling constants of 2 Hz. This coupling constant was in good agreement with the reported value for *trans*-vicinal coupling in epoxides.[8,9] 3-Benzoyl-1-phenyl-2-pentene-1,4-dione (**6**) also afforded the corresponding epoxide (**6a**)[14] in good yield.

On the other hand, the epoxidation of α,β-unsaturated ketones such as 5-isopropenyl-2-methyl-2-cyclohexen-1-one, 4-(2,6,6-trimethyl-2-cyclohexen-1-yl)-3-buten-2-one, 3-methyl-2-cyclohexen-1-one, 4,4-dimethyl-2-cyclohexen-1-one, and chalcone with H_2O_2–Bu_4NI did not give corresponding epoxides in high yield (less than 10%). α,β-Unsaturated ketones were recovered unchanged in 61—98% yield.

Thus, the reagent 30% aq H_2O_2-quaternary ammonium iodides provides a new convenient method for mild and chemoselective epoxidation of 2-butene-1,4-diones without using a strong base. Further application of epoxidation with this method to *cis*-2-butene-1,4-diones and other functional unsaturated compounds is now in progress.

Experimental

IR spectra were recorded on a JASCO FT-IR 5000 spec-

trometer. ^{1}H NMR spectra were taken on a Hitachi R-24B spectrometer with TMS as an internal standard. MS spectra were taken on a JEOL-HX 110 spectrometer at 70 eV. The products were identified by spectroscopic data.

General Procedure. To a solution of 2-butene-1,4-dione (1 mmol) and Bu_4NI or $PhCH_2N(Me)_3I$ (0.1 mmol) in THF (10 ml) at 0 °C was added dropwise 30% aq H_2O_2 (5—30 mmol) dissolved in THF (3 ml). After stirring for 20—96 h at 0—23 °C, the reaction mixture was poured into 0.5 M aq KI. The resulting mixture was treated with 0.5 M aq $Na_2S_2O_3$ and extracted with ethyl acetate. The organic layer was washed by 0.5 M aq $Na_2S_2O_3$ and successively saturated aq NaCl and dried by $MgSO_4$. After removal of solvent in vacuo, the residue was purified by recrystallization or column chromatography on silica gel (Wakogel C-200) with CCl_4 and $CHCl_3$ (1 : 1, v/v). Epoxy diketones **1a**—**6a** were obtained in 53—91% yield.

2-Butene-1,4-diones were prepared according to the literature procedure.[13]

trans-1,4-Diphenyl-2-butene-1,4-dione (**1**) was prepared by Friedel-Crafts acylation of benzene with fumaroyl dichloride. *cis*-1,4-Diphenyl-2-butene-1,4-dione (**2**) and 3-benzoyl-1-phenyl-2-pentene-1,4-dione (**6**) were prepared by oxidation of corresponding furan derivatives with HNO_3 in acetic acid.

trans-1-Phenyl-2-pentene-1,4-dione (**4**) and *trans*-3-decene-2,5-dione (**5**) were prepared by pyridinium chlorochromate (PCC) oxidation of corresponding 2,5-dialkylfuran derivatives.

***trans*-2,3-Epoxy-1,4-diphenyl-1,4-butanedione (1a):** Mp 130—131 °C (from ethyl acetate) (lit,[8,9] Mp 129—130 °C); IR (KBr) 1686 cm^{-1}; ^{1}H NMR ($CDCl_3$) δ=4.48 (2H, s), 7.30—7.76 (6H, m), 7.95—8.21 (4H, m); MS *m/z* (rel intensity) 252 (M^+ 0.3), 147 (64), 105 (100), and 77 (34).

***cis*-2,3-Epoxy-1,4-diphenyl-1,4-butanedione (1b):** Mp 129—130 °C (from ethyl acetate) (lit,[8,9] Mp 127.5—128.5 °C); IR (KBr) 1696 cm^{-1}; ^{1}H NMR ($CDCl_3$) δ=4.48 (2H, s), 7.33—7.78 (6H, m), 7.91—8.28 (4H, m); MS *m/z* (rel intensity) 252 (M^+, 0.3), 147 (66), 105 (100), and 77 (35).

Ethyl *trans*-2,3-Epoxy-4-oxo-4-phenylbutanoate (3a): IR (neat) 1748 and 1694 cm^{-1}; ^{1}H NMR ($CDCl_3$) δ=1.31 (3H, t, *J*=7.0), 3.68 (1H, d, *J*=2.0), 4.30 (2H, q, *J*=7.0), 4.41 (1H, d, *J*=2.0), 7.31—7.70 (3H, m), 7.90—8.16 (2H, m); MS *m/z* (rel intensity) 220 (M^+, 1), 147 (29), 105 (100), and 77 (25).

***trans*-2,3-Epoxy-1-phenyl-1,4-pentanedione (4a):** Mp 50—51 °C (from ether) (lit,[8,9] Mp 48—49 °C); IR (KBr) 1723 and 1692 cm^{-1}; ^{1}H NMR ($CDCl_3$) δ=2.18 (3H, s), 3.61 (1H, d, *J*=2.0), 4.30 (1H, d, *J*=2.0), 7.25—7.68 (3H, m), 7.81—8.08 (2H, m); MS *m/z* (rel intensity) 147 (99), 105 (100), 85 (19), and 77 (78).

***trans*-3,4-Epoxy-2,5-decanedione (5a):** Mp 60—61 °C (from pentane); IR (KBr) 1707 cm^{-1}; ^{1}H NMR ($CDCl_3$) δ=0.86 (3H, t, *J*=6.0), 2.08 (3H, s), 1.06—1.83 (6H, m), 2.23—2.56 (2H, m), 3.51 (2H, m); MS *m/z* (rel intensity) 184 (M^+, 9), 141 (23), 128 (18), 99 (100), 85 (28), and 71 (61).

3-Benzoyl-2,3-epoxy-1-phenyl-1,4-pentanedione (6a):[14] IR (neat) 1715 and 1688 cm^{-1}; ^{1}H NMR ($CDCl_3$) δ=2.26 (3H, s), 4.64 (1H, s), 7.30—7.76 (6H, m), 7.93—8.26 (4H, m); MS *m/z* (rel intensity) 294 (M^+, 0.8), 251 (9), 189 (28), 147 (100), 105 (95), and 77 (39).

We wish to express our thanks to Professor Masanori Sakamoto for the information concerning NMR and IR data of *trans*- and *cis*-2,3-epoxy-1,4-butanediones. We also thank Professors Masaaki Yoshifuji and Masafumi Yasunami for their help in the measurements of ^{1}H NMR spectra. We wish to thank Mr. Toshio Sato of Instrumental Analysis Center for Chemistry Faculty of Science of Tohoku University for the measurements of MS spectra.

References

1) H. O. House, "Modern Synthetic Reactions," W. A. Benjamin, Inc., Menlo Park, California (1972), Chap. 6, p. 306.
2) a) G. B. Payne, *J. Org. Chem.*, **26**, 250 (1961); b) G. B. Payne and P. H. Williams, *J. Am. Chem. Soc.*, **26**, 651 (1961); c) G. B. Payne, P. H. Deming, and P. H. Williams, *ibid.*, **26**, 659 (1961).
3) R. E. Lutz and F. N. Wilder, *J. Am. Chem. Soc.*, **56**, 1987 (1934).
4) P. F. Corey and F. E. Ward, *J. Org. Chem.*, **51**, 1925 (1986).
5) R. Bloch, J. Abecassis, and D. Hassan, *J. Org. Chem.*, **50**, 1544 (1985).
6) C. Venturello, E. Alneri, and M. Ricci, *J. Org. Chem.*, **48**, 3831 (1983).
7) M. Miyashita, T. Suzuki, and A. Yoshikoshi, *Chem. Lett.*, **1987**, 285.
8) C.-S. Chien, T. Kawasaki, M. Sakamoto, Y. Tamura, and Y. Kita, *Chem. Pharm. Bull.*, **33**, 2743 (1985).
9) C.-S. Chien, Ph. D. Thesis, Meiji College of Pharmacy, Tokyo, Japan, 1985.
10) a) A. Matsumae, S. Nomura, T. Hata, and S. Ōmura, *J. Antibiot.*, **25**, 365 (1972); b) A. A. Jakubowski, F. S. Guziec, Jr., M. Sugiura, C. C. Tam, M. Tishler, and S. Ōmura, *J. Org. Chem.*, **47**, 1221 (1982), and references cited therein.
11) J. A. Parker, *Adv. Org. Chem.*, **5**, 1 (1965).
12) T.-L. Ho, "Hard and Soft Acids and Bases Principle in Organic Chemistry," Academic Press, New York (1977), p. 4.
13) S. Sayama and Y. Inamura, *Bull. Chem. Soc. Jpn.*, **64**, 306 (1991), and references cited therein.
14) Though the stereochemistry of **6a** was proposed as shown the figure in Table 2 on the basis of the reaction manners of enediones **1** and **4**, it could not be exactly determined by the assignment of ^{1}H NMR and IR spectral data of **6a**.
15) The structure of crude products was determined as *cis*-epoxide by its FT-IR spectral data (KBr; *cis*-epoxide **1b**: $\nu_{C=O}$ 1696 cm^{-1}) after washing with CCl_4.

Synthesis of Azonia Derivatives of Benzoperylene and Benzocoronene by Photocyclization

Sadao ARAI,* Norikazu NAKAMURA, Hiromichi YAMAGUCHI,
Masa-aki OKAZAKI, and Mitsuhiko HIDA*
Department of Industrial Chemistry, Faculty of Technology, Tokyo Metropolitan University,
1-1, Minami-Osawa, Hachioji, Tokyo 192-03
(Received January 24, 1991)

Synopsis. The 2-styrylbenzo[*a*]quinolizinium salt was photocyclized to afford 12a-azoniabenzo[*ghi*]perylene salt in 66% yield. The 2a-azoniabenzo[*a*]coronene salt was obtained by the photocyclization of 2-[2-(4-biphenylyl)vinyl]benzo[*a*]-quinolizinium salt and 2-styryl-10-phenylbenzo[*a*]quinolizinium salt in 80% and 75% yields, respectively.

Recently we reported that the photocyclization of *N*-styrylpyridinium-type molecules provided a good route to construct new fused polycyclic azonia aromatic compounds.[1] In these reactions it was demonstrated that the bond formation via a conrotatory photocyclization is possible when the bond order (*Prs**) between the atoms *r* and *s*, involved in the cyclization in the excited state, has a negative value.[1] Compounds 2-(2-arylvinyl)-benzo[*a*]quinolizinium salts (**2**), which was obtained by the reaction of 2-methylbenzo[*a*]quinolizinium salt (**1a**) with benzaldehyde derivatives in the presence of piperidine,[2,3] would be an ideal precursor of fused polycyclic azonia aromatic compounds. We report herein the synthesis of azonia derivatives of benzoperylene and benzocoronene by oxidative photocyclization of compounds **2**.

Results and Discussion

The Knoevenagel condensation of 2-methylbenzo-[*a*]quinolizinium salt (**1a**) or 2-methyl-10-phenylbenzo-[*a*]quinolizinium salt (**1b**) with benzaldehyde derivatives in the presence of piperidine afforded the corresponding *trans*-arylvinyl derivatives **2a**—**g** in good yields. Compound **2a** was irradiated with a Pyrex-filtered light (λ>280 nm) in ethanol in the presence of iodine. The photocyclization of **2a** could, hypothetically, give 6a-azoniadibenzo[*a*,*h*]anthracene salt (**3a**) and 2a-azoniadibenzo[*c*,*g*]phenanthrene salt (**4a**). The values of *Prs**, however, predicted that out of the two possible cyclization products **3a** (*Prs**=0.018) and **4a** (*Prs**=−0.032) only **4a** should be formed. The fast-atom bombardment (FAB) mass spectrum of the isolated product (66% yield) using *m*-nitrobenzyl alcohol as a matrix showed that the ion at highest *m*/*z* value (278) did not correspond to the intact cation (C^+) of **4a** (*m*/*z* 280) predicted but to that of 12a-azoniabenzo[*ghi*]-perylene salt (**5a**) (C^+, *m*/*z* 278), formed by further photocyclization of **4a**. This structure was confirmed by the fact that the spectral data were identical with those of the photocyclization product[1] of 2-[2-(2-naphthyl)vinyl]isoquinolinium salt (**6**). The *Prs** value (−0.075) shows that the photocyclization of **4a** is possible to give **5a**.[1] The methyl derivative **2b**[3] was also photocyclized to afford 7-methyl-12a-azoniabenzo[*ghi*]-perylene salt **5b** in 40% yield.

The *Prs** value predicted that **2c** could be photocyclized by two succesive oxidative photocylization via 9-aza-2a-azoniabenzo[*c*,*g*]phenanthrene salt (**4c**) to afford 7-aza-12a-azoniabenzo[*ghi*]perylene salt **5c**. The irradiation of **2c** in ethanol or methanol, however, caused decomposition. Compound **2c** was successfully photocyclized to give **5c** in acetonitrile in 42% yield.

The cyanine-type compounds **2d**[2] and **2e**,[3] however, failed to undergo photocyclization: the irradiation with or without iodine in ethanol or acetonitrile leads to only

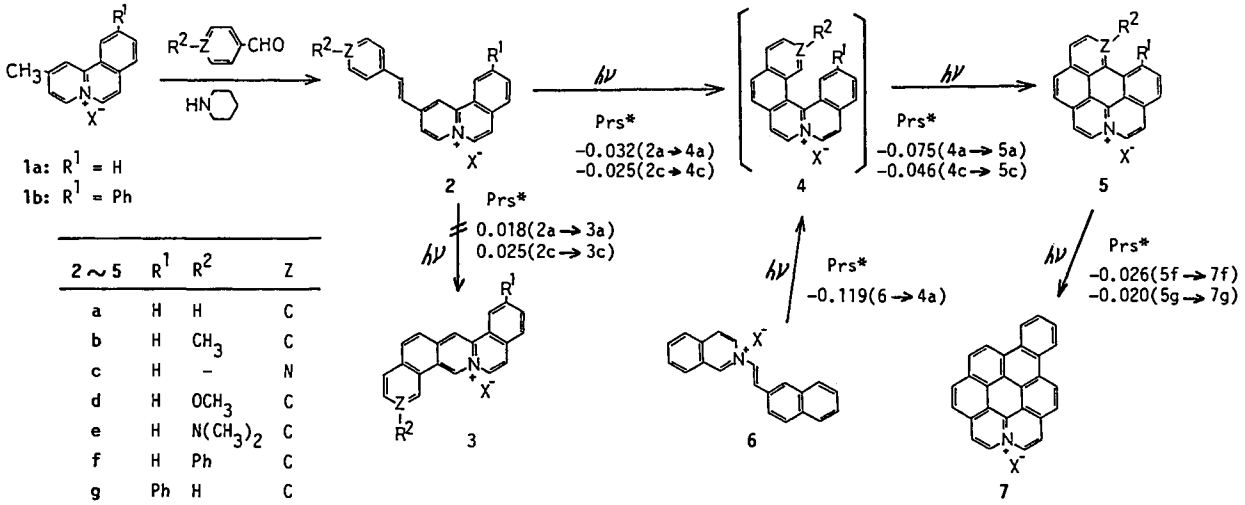

2～5	R^1	R^2	Z
a	H	H	C
b	H	CH_3	C
c	H	-	N
d	H	OCH_3	C
e	H	$N(CH_3)_2$	C
f	H	Ph	C
g	Ph	H	C

Scheme.

decomposition.

In the photocyclization of **2f**, the values of *Prs** predicted that three succesive photocyclizations should take place to give 2a-azoniabenzo[*a*]coronene salt (**7**). A methanol solution of **2f** in the presence of iodine was irradiated with a Pyrex-filtered light. The FAB mass spectrum of the product (80% yield) showed the presence of a peak at *m/z* 352 (C^+): this pointed to the loss of six mass units from **2f** (C^+ 358). The FAB mass spectrum of the photocyclization-product (75% yield) from **2g** also exhibited the intact cation at *m/z* 352. The ^1H NMR and UV spectral data of the photoproduct from **2f** was identical with those of the photoproduct from **2g**. These results indicate that photocyclization of both **2f** and **2g** afforded **7** as predicted from *Prs** values.

Experimental

Melting points were determined with a Yamato melting point apparatus (MP21) and are uncorrected. IR spectra were recorded on a JASCO IRA-1 spectrometer. ^1H NMR spectra were recorded on a Hitachi R-24 (60 MHz) or a JEOL FX90Q (90 MHz) spectrometer with Me_4Si as an internal standard. ^1H NMR (400 MHz) and ^{13}C NMR (100.40 MHz) spectra were obtained on a JEOL GSX-400 spectrometer. UV spectra were obtained with a Hitachi 220A spectrophotometer. Fast-atom bombardment (FAB) mass spectra were obtained with a JEOL JMS-DX 300 using *m*-nitrobenzyl alcohol as a matrix. Elemental analyses were performed by Mr. Hirokatsu Suzuki at Department of Chemistry, Tokyo Metropolitan University. An Eikosha 300 W high-pressure mercury lamp was used as the irradiation source.

The bond orders (*Prs**) were obtained by Hückel MO calculations using the parameters suggested by Streitwieser, Jr.[4]

2-Methylbenzo[*a*]quinolizinium salt (**1a**) was prepared by photocyclization of 1-styryl-4-methylpyridinium salt according to our previous paper.[2] **1a** (X=Br): Found: C, 61.14; H, 4.47; N, 4.99%. **1a** (X=ClO_4): Found: C, 57.23; H, 3.94; N, 4.64%. **1a** (X=PF_6): Found: C, 49.51; H, 3.71; N, 4.15%.

2-Methyl-10-phenylbenzo[*a*]quinolizinium Perchlorate (1b: X=ClO_4): Compound **1b** was prepared in a four-step process according to the method[2] described for **1a**. The reaction of 4-methylpyridine with 1-(4-biphenylyl)-2-bromoethanone gave 2-(4-methyl-1-pyridinio)-1-(4-biphenylyl)ethanone bromide (79% yield): Pale yellow crystals from ethanol; mp 240—242 °C (decomp); ^1H NMR (60 MHz, CF_3CO_2H) δ=2.79 (3H, s, CH_3), 6.32 (2H, s, CH_2), and 7.2—8.7 (13H, m, ArH). Found: C, 64.98; H, 4.81; N, 3.78%. Calcd for $C_{20}H_{18}NOBr$: C, 65.23; H, 4.98; N, 3.80%.

The pyridinium salt was reduced with $NaBH_4$ in water to afford 1-[2-hydroxy-2-(-4-biphenylyl)ethyl]-4-methylpyridinium bromide (54%): Pale yellow crystals from ethanol–benzene; mp 226—228 °C (decomp); ^1H NMR (60 MHz, CF_3CO_2H) δ=2.66(3H, s, CH_3), 4.7—5.2 (2H, m, CH_2), 5.25—5.6 (1H, m, CH), and 7.2—8.6 (13H, m, ArH). Found: C, 64.94; H, 5.39; N, 3.66%. Calcd for $C_{20}H_{20}NOBr$: C, 64.87; H, 5.44; N, 3.78%. The reaction between the alcohol with phosphorus tribromide gave 1-[2-(4-biphenylyl)vinyl]-4-methylpyridinium bromide (51%): Yellow crystals from 1-pentanol; mp 215—218 °C (decomp); ^1H NMR (60 MHz, CF_3CO_2H) δ=2.56 (3H, s, CH_3) and 7.1—8.8 (15H, m, CH=CH and ArH). Found: C, 68.33; H, 5.30; N, 3.76%. Calcd for $C_{20}H_{18}NBr$: C, 68.19; H, 5.15; N, 3.98%.

2-Methyl-10-phenylbenzo[*a*]quinolizinium perchlorate (**1b**: X=ClO_4) was obtained by photocyclization of the olefin, followed by anion exchange (33% yield): White crystals from ethanol–acetonitrile; mp 290—293 °C (decomp); IR (KBr) 1643, 1480, 1312, 1122, 850, and 764 cm^{-1}; ^1H NMR (90 MHz, DMSO-d_6) δ=2.81 (3H, s, CH_3) and 7.4—9.7 (15H, m, ArH); FABMS *m/z* 270 $(M-ClO_4)^+$. Found; C, 65.23; H, 4.27; N, 3.91%. Calcd for $C_{20}H_{16}NClO_4$; C, 64.96; H, 4.36; N, 3.79%

2-(2-Arylvinyl)benzo[*a*]quinolizinium salts **2a—g** were prepared by the reaction of **1a** or **1b** with benzaldehyde derivatives in the presence of piperidine in methanol, according to our previous paper.[2,3]

2-Styrylbenzo[*a*]quinolizinium Hexafluorophosphate (2a: X=PF_6; 69%): Yellowish green crystals from methanol–acetone; mp 239.7—240.5 °C; UV (C_2H_5OH) 401 nm (log ε 4.58); IR (KBr) 3040, 1660, 1640, 1482, 1210, 1162, and 980 cm^{-1}; ^1H NMR (60 MHz, CF_3CO_2H) δ=7.3—9.6 (m, ArH); FABMS *m/z* 282 $(M-PF_6)^+$. Found: C, 59.02; H, 3.78; N, 3.28%. Calcd for $C_{21}H_{16}NPF_6$: C, 59.02; H, 3.89; N, 3.32%.

2-[2-(4-Methylphenyl)vinyl]benzo[*a*]quinolizinium Perchlorate (2b: X=ClO_4 74%):[3] Found: C, 66.55; H, 4.53; N, 3.72%.

2-[2-(4-Pyridyl)vinyl]benzo[*a*]quinolizinium Hexafluorophosphate (2c: X=PF_6; 68%): Yellowish green crystals from methanol; mp 244—247 °C; UV (C_2H_5OH) 388 nm (log ε 4.57); IR (KBr) 3080, 1660, 1640, 1481, and 981 cm^{-1}; ^1H NMR (90 MHz, 7.6—9.7 (m, ArH); FABMS *m/z* 283 $(M-PF_6)^+$. Found: C, 55.99; H, 3.56; N, 6.69%. Calcd for $C_{20}H_{15}N_2PF_6$: C, 56.08; H, 3.54; N, 6.54%.

2-[2-(4-Methoxyphenyl)vinyl]benzo[*a*]quinolizinium Perchlorate (2d: X=ClO_4; 99%):[2] Found: C, 64.25; H, 4.30; N, 3.23%.

2-[2-(4-Dimethylaminophenyl)vinyl]benzo[*a*]quinolizinium Bromide (2e: X=Br; 62%):[3] Found: C, 68.06; H, 5.34; N, 6.87%.

2-[2-(4-Biphenylyl)vinyl]benzo[*a*]quinolizinium Bromide (2f: X=Br; 88%): Yellowish green needles from methanol: mp >300 °C; UV (C_2H_5OH) 272 (log ε 4.41), 290 (4.34), 338 (4.16), 354 (4.29), and 407 nm (4.82); IR (KBr) 1620, 1484, 1195, 1162, 979, and 782 cm^{-1}; ^1H NMR (90 MHz, DMSO-d_6) δ=7.4—9.6 (m, ArH); FABMS *m/z* 283 $(M-Br)^+$. Found: C, 73.81; H, 4.56; N, 3.23%. Calcd for $C_{27}H_{20}NBr$: C, 73.98; H, 4.60; N, 3.20%.

2-Styryl-10-phenylbenzo[*a*]quinolizinium Perchlorate (2g: X=ClO_4; 65%): Yellow crystals from methanol; mp 260—263 °C (decomp); UV (CH_3OH) 290 (4.51), 336 (4.30), 348 (4.46), and 410 nm(4.58); IR (KBr) 1618, 1472, 1445, 1120, 975, and 690 cm^{-1}; ^1H NMR (90 MHz, DMSO-d_6) δ=7.4—9.7 (m, ArH); FABMS *m/z* 358 $(M-ClO_4)^+$. Found: C, 71.06; H, 4.36; N, 3.10%. Calcd for $C_{27}H_{20}NClO_4$: C, 70.82; H, 4.40; N, 3.06%.

Photocyclization of compounds **2a—g** was carried out according to our previous paper.[1]

12a-Azoniabenzo[*ghi*]perylene Hexafluorophosphate (5a: X=PF_6; 66%): Yellowish green crystals from methanol–acetone; mp >320 °C; IR (KBr) 1650, 1440, and 1315 cm^{-1}; ^1H NMR (90 MHz, CD_3CN) δ=8.3—9.4 (m, ArH); FABMS *m/z* 278 $(M-PF_6)^+$. Found; C, 59.45; H, 2.83; N, 3.50%. Calcd for $C_{21}H_{12}NPF_6$: C, 59.59; H, 2.86; N, 3.31%.

7-Methyl-12a-azoniabenzo[*ghi*]perylene Perchlorate (5b: X=ClO_4; 40%): Pale orange crystals from acetonitrile; mp >300 °C; UV (CH_3OH) 316 (log ε 4.41), 402 (4.09), and 431 nm (4.24); IR (KBr) 1655, 1608, 1404, 1350, 1095, 870, and 742 cm^{-1}; ^1H NMR (90 MHz, DMSO-d_6) δ=3.01 (3H, s, CH_3) and 7.9—9.5 (m, 11H, ArH); FABMS *m/z* 292 $(M-PF_6)^+$. Found; C, 67.21; H, 3.50; N, 3.37%. Calcd for $C_{22}H_{14}NClO_4$; C, 67.44 ; H, 3.60; N, 3.58%.

7-Aza-12a-azoniabenzo[*ghi*]perylene Hexafluoroposphate (5c: X=PF_6; 43%): Brown crystals from methanol–acetonitrile; mp >320 °C; UV (C_2H_5OH) 435 (log ε 4.25), 410 (3.99), 388 (3.57), and 373 nm (3.83); IR (KBr) 1640, 1430, and 1340 cm^{-1}; ^1H NMR (90 MHz, CD_3CN) δ=8.4—9.9 (m, ArH);

FABMS m/z 280 $(M-PF_6)^+$. Found; C, 56.76; H, 2.63; N, 6.59%. Calcd for $C_{20}H_{11}N_2PF_6$; C, 56.62; H, 2.61; N, 6.60%.

2a-Azoniabenzo[*a*]coronene Bromide (7: X=Br; 80%): An orange powder from *N,N*-dimethylformamide–ethanol; mp >300 °C; UV (CH_3OH) 279 (log ε 4.46), 339 (4.56), 420 (3.99), and 446 nm (3.98); IR (KBr) 1640, 1342, 856, and 752 cm^{-1}; ^1H NMR (400 MHz, DMSO-d_6) δ=7.55 (1H, s, ArH), 7.6—7.7 (3H, m, ArH), 7.87 (1H, s, ArH), 7.9—8.1 (5H, m, ArH), 8.2—8.4 (2H, m, ArH), 8.99 (1H, d, J=4.9 Hz, ArH), and 9.19 (1H, d, J=5.4 Hz, ArH); ^{13}C NMR (100.40 MHz, DMSO-d_6) 113.8—133.7 (27 lines); FABMS m/z 352 $(M-Br)^+$. Found; C, 74.75; H, 3.00; N, 2.98%. Calcd for $C_{27}H_{14}NBr$; C, 75.01; H, 3.26; N, 3.24%.

2a-Azoniabenzo[*a*]coronene Perchlorate (7: X=ClO_4; 75%): An orange powder from *N,N*-dimethylformamide–ethanol; mp >300 °C; UV (CH_3OH) 278 (log ε 4.45), 338 (4.55), 420 (4.00), and 446 nm (3.99); FABMAS m/z 352 $(M-ClO_4)^+$. Found; C, 71.50; H, 3.00; N, 2.85%. Calcd for $C_{27}H_{14}NClO_4$; C, 71.77; H, 3.12; N, 3.10%.

The authors are grateful to Dr. Masashi Kikuchi of Shiseido Laboratories for obtaining the NMR spectra (400 MHz).

References

1) S. Arai, T. Takeuchi, M. Ishikawa, T. Takeuchi, M. Yamazaki, and M. Hida, *J. Chem. Soc., Perkin Trans. 1,* **1987**, 481.

2) S. Arai, M. Yamazaki, and M. Hida, *J. Heterocycl. Chem.,* **27**, 1073 (1990).

3) S. Arai, K. Nagakura, M. Ishikawa, and M. Hida, *J. Chem. Soc., Perkin Trans. 1,* **1990**, 1915.

4) A. Streitwieser, Jr., "Molecular Orbital Theory for Organic Chemists," John Wiley & Sons, New York (1961).

Palladium-Catalyzed Carbonylative Cross-Coupling Reaction of 1-Halo-1-alkenes with 9-Alkyl-9-BBN Derivatives. A Direct Synthesis of α,β-Unsaturated Ketones

Tatsuo ISHIYAMA, Norio MIYAURA, and Akira SUZUKI*
Department of Applied Chemistry, Faculty of Engineering, Hokkaido University, Sapporo 060
(Received February 12, 1991)

Synopsis. The synthesis of α,β-unsaturated ketones by means of the palladium-catalyzed cross-coupling reaction between 9-alkyl-9-borabicyclo[3.3.1]nonanes (9-R-9-BBN) and 1-halo-1-alkenes under carbon monoxide atmosphere is described.

Carbonylative cross-coupling of organic halides with organometallic compounds, such as organotin,[1] boron,[2] aluminum,[3] and zinc[4] compounds has been extensively studied and reported to provide a good method for the synthesis of unsymmetrical ketones. Among a variety of organometallic reagents, organoboron compounds were first examined by Kojima and his co-workers[2a] for the synthesis of alkyl aryl ketones. Due to the low nucleophilicity of alkyl group on boron, the transmetallation between organoboranes and acylpalladium(II) species generated in catalytic cycles is anticipated to be a step of retarding for the coupling of organoboron compounds. They found that bis(acetylacetonato)zinc(II) accelerates the transmetallation and the palladium-catalyzed carbonylative coupling of organoboranes with aryl and benzyl halides to give the corresponding ketones. However, when we applied the procedure in the reaction with 1-halo-1-alkenes, it was found that no expected α,β-unsaturated ketones are obtained. Thus, we have reinvestigated such a carbonylative cross-coupling reaction of organoboranes, and observed that the cross-coupling reaction of 9-R-9-BBN, with carbon monoxide and 1-iodo-1-alkenes is effectively induced with K_3PO_4 at room temperature in the presence of Pd-catalyst (Eq. 1). The reactions with aryl or benzyl halides proceed nicely under similar conditions to give the corresponding products, respectively.

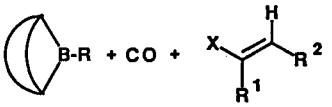

1

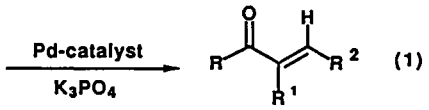

(1)

2

The effects of such conditions on the reaction of 9-octyl-9-BBN with (*E*)-1-hexenyl, phenyl, and benzyl halides are listed in Table 1. The addition of bis(acetylacetonato)zinc(II) never accelerates the reaction with 1-iodo-1-alkene (Entry 1). When we use K_3PO_4 as a base, 1-iodo-1-hexene is effectively carbonylated and couples with 9-octyl-9-BBN in the presence of 5 mol% of $Pd(PPh_3)_4$ to give (*E*)-5-pentadecen-7-one in almost quantitative yields (Entries 2—4). Both $Pd(PPh_3)_4$ and $PdCl_2(PPh_3)_2$ are effective as catalysts for the present carbonylative coupling reaction (Entries 4 and 5). However, dichloro[1,1′-bis(diphenylphosphino)ferrocene]palladium(II), $PdCl_2$(dppf), gives a lower yield of ketone (Entry 6) whereas this catalyst has been reported to be a good catalyst for the carbonylative coupling reaction of aryl triflates[1e] with organostannanes. The carbonylation of 1-bromo-1-octene gives a mixture of products, (*E*)-7-heptadecen-9-one and (*E*)-7-hexa-

Table 1. Carbonylative Cross-Coupling Reaction of 9-Octyl-9-BBN with Organic Halides[a]

Entry	Organic halide	Catalyst	Solvent	Additive	CO/atm	Temp/°C	Yield[b]/%
1	(*E*)-C_4H_9CH=CHI	$Pd(PPh_3)_4$	HMPA/THF[e] =1/4	$Zn(acac)_2$	1	50	0
2	(*E*)-C_4H_9CH=CHI	$Pd(PPh_3)_4$	Dioxane	K_3PO_4	1	25	98
3	(*E*)-C_4H_9CH=CHI	$Pd(PPh_3)_4$	Dioxane	K_3PO_4	3	25	92
4	(*E*)-C_4H_9CH=CHI	$Pd(PPh_3)_4$	Benzene	K_3PO_4	1	25	99
5	(*E*)-C_4H_9CH=CHI	$PdCl_2(PPh_3)_2$	Benzene	K_3PO_4	1	25	98
6	(*E*)-C_4H_9CH=CHI	$PdCl_2$(dppf)	Dioxane	K_3PO_4	1	25	51
7	(*E*)-$C_6H_{13}CH$=CHBr	$Pd(PPh_3)_4$	Dioxane	K_3PO_4	3	65	31[c]
8	(*E*)-$C_6H_{13}CH$=CHBr	$Pd(PPh_3)_4$	Dioxane	K_3PO_4/KI[d]	1	25	69
9	PhI	$PdCl_2(PPh_3)_2$	Benzene	K_3PO_4	1	25	(82)
10	PhI	$Pd(PPh_3)_4$	Dioxane	K_3PO_4	1	25	51
11	$PhCH_2Br$	$PdCl_2(PPh_3)_2$	Benzene	K_3PO_4	1	25	(72)

a) All reactions were carried out in 6 ml of solvent for 5 h using catalyst (5 mol%), organic halides (1 mmol), 9-octyl-9-BBN (1.1 mmol), and $Zn(acac)_2$ (1.1 mmol) or K_3PO_4 (3 mmol). b) GLPC yields based on organic halides and isolated yields were in parentheses. c) (*E*)-7-Hexadecene (16%) was also obtained. d) 3 equiv of KI. e) HMPA; hexamethylphosphoric triamide, THF; tetrahydrofuran.

Table 2. Carbonylative Cross-Coupling Reaction of 9-Alkyl-9-BBN with Alkenyl Iodides[a]

Organic halide 1		Alkene	Product	Method[b]	Yield[c]/%
R^1	R^2				
H	C_4H_9	1-Octene	(*E*)-$C_4H_9CH{=}CHCOC_8H_{17}$	A	99
H	*t*-C_4H_9	$CH_2{=}CH(CH_2)_8CO_2Me$	(*E*)-*t*-$C_4H_9CH{=}CHCO(CH_2)_{10}CO_2Me$	B	(78)
H	Ph	$CH_2{=}CH(CH_2)_8CN$	(*E*)-$PhCH{=}CHCO(CH_2)_{10}CN$	B	(68)
H	TBDMSO[e] $C_5H_{11}CH$–	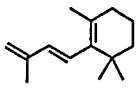	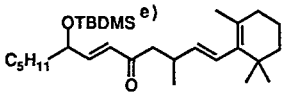	B	(53)
–$(CH_2)_4$–		1-Octene	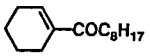	B	90
H	C_4H_9	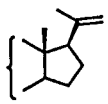	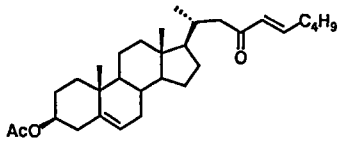	A	(48)
		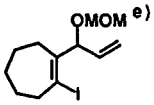	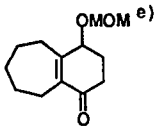	A[d]	(74)

a) The 9-alkyl-9-BBN derivatives obtained by hydroboration of alkenes (1.1 equiv) with 9-BBN (1.1 equiv) were directly used for the next coupling reaction with haloalkenes (1.1 equiv). b) Method A: The reaction was conducted in benzene at room temperature for 5 h under 1 atm CO in the presence of K_3PO_4 (3 equiv) and $Pd(PPh_3)_4$ (5 mol%); Method B: The same conditions with A, except in dioxane under 3 atm CO. c) GLC yields based on organic iodides and isolated yields are in parentheses. d) $PdCl_2(PPh_3)_2$ (5 mol%) was used as a catalyst. e) TBDMS; *t*-butyldimethylsilyl, MOM; methoxymethyl.

decene, in a ratio of 2:1 even under 3 atmospheric pressure of carbon monoxide (Entry 7), the yield of which can be improved to 69% by running the reaction in the presence of powdered potassium iodide (Entry 8). Iodobenzene and benzyl bromide are also carbonylated and coupled with 9-octyl-9-BBN in good yields under the same reaction conditions (Entries 9 and 11).

In Table 2, the representative results obtained by a sequence of hydroboration of alkenes, followed by coupling with 1-iodo-1-alkenes under carbon monoxide atmosphere in the presence of $Pd(PPh_3)_4$ (5 mol%) and K_3PO_4 (3 equiv) are summarized. In Method A, the reaction is carried out under relatively mild conditions by using 1 atm of carbon monoxide at room temperature, whereas Method B is performed under 3 atm of carbon monoxide. Although the carbonylative coupling proceeds especially smoothly when iodoalkenes substituted with alkyls are used, the presence of electron-withdrawing substituents[5] leads to a mixture of carbonylated and uncarbonylated coupling products. For example, the carbonylation of 3-iodo-2-cyclohexenone and 1-iodo-1-octen-3-one mainly gives direct coupling products without the CO insertion, together with small amounts of the desired α,β-unsaturated ketones.

As shown in the last column of Table 2, the hydroboration-carbonylative coupling sequence can be readily extended to intramolecular reaction to afford cyclic ketones.

The reaction may proceed by a pathway similar to that of the palladium-catalyzed carbonylative coupling reaction of organometallics[1-4] which involves (a) oxidative addition of haloalkene to Pd(0) complex, (b) insertion of carbon monoxide to give acylpalladium(II) halide, (c) transfer of alkyl group on boron to acylpalladium(II) halide with the aid of K_3PO_4, and (d) reductive elimination to ketone. Although the carbonylation[6] of 9-alkyl-9-BBN with carbon monoxide to provide ketones is known, we have not observed any evidence that acylboron species are participated in a catalytic cycle.

In a course of our study on the palladium-catalyzed reaction[7a] of organoboranes, we reported the direct coupling reactions of aryl,[7b] 1-alkenyl,[7a,c] and alkylboron[7d] compounds with organic halides. The present reaction can make it possible for the extension of such coupling reactions to the synthesis of ketones.

Experimental

IR spectra were recorded on a Hitachi Perkin-Elmer Model 125 spectrometer. ^1H NMR spectra were obtained with a Hitachi-R-90H Fourier transform NMR spectrometer (90 MHz) and are recorded in δ values using tetramethylsilane as an internal standard. Mass spectra were taken on a JEOL JMS-D300 for a high resolution analysis and Finnigan ITD 800. GLC analyses were performed on a Hitachi 163 instrument using Silicone OV-17 on Uniport B (2 m).

Material and Reagents. Benzene and dioxane were dried and distilled before use. 9-Borabicyclo[3.3.1]nonane (9-BBN) in THF from Aldrich Chemical Co. was used directly. $Pd(PPh_3)_4$ and $PdCl_2(PPh_3)_2$ were commercial products. $PdCl_2(dppf)$ was prepared by the reported procedure.[8] (*E*)-

1-Iodo-1-hexene,[9] (*E*)-1-bromo-1-octene,[10] (*E*)-3,3-dimethyl-1-iodo-1-butene,[9] (*E*)-β-iodostyrene,[9] 1-iodocyclohexene,[11] and (*E*)-3-(*t*-butyldimethylsiloxy)-1-iodo-1-octene[12] were prepared by reported procedures. 1-(2,6,6-Trimethyl-1-cyclohexenyl)-3-methyl-1,3-butadiene[13] and 3β-acetoxy-20-methylene-5-pregnene[14] were prepared from the corresponding ketones by Wittig olefination. 1-Iodo-2-(1-methoxy-methoxy-2-propenyl)-1-cycloheptene was prepared[7d] as follows. Treatment of 2-chloro-1-cycloheptenecarbaldehyde obtained by Vilsmeier reaction of cycloheptanone with NaI in acetonitrile in the presence of 1 equivalent of chlorotrimethylsilane at room temperature for 24 h gave 2-iodo-1-cycloheptenecarbaldehyde in a yield of 54% (bp 95—100 °C/0.1 mmHg; 1 mmHg=133.322 Pa). This was treated with vinylmagnesium bromide (1 equiv) in THF, followed by the reaction with chloromethyl methyl ether (1.2 equiv) to afford the compound in an 83% yield.

General Procedure for the Carbonylative Cross-Coupling Reaction. A 50 ml pressure bottle equipped with a magnetic stirring bar was charged with an alkene (1.1 mmol) in THF (0.5 ml). A 0.5 M (1M=1 mol dm^{-3}) solution of 9-BBN in THF (1.1 mmol) was added slowly at 0 °C, and then the reaction mixture was warmed up slowly to room temperature. After stirring for 5 h, dioxane or benzene (6 ml), $Pd(PPh_3)_4$ (5 mol%), K_3PO_4 (3 mmol), and iodoalkene (1 mmol) were added. The flask was flushed with carbon monoxide (1 or 3 atmospheric pressure) and the mixture was stirred for 5 h at room temperature. Water (20 ml) was added and stirred for 30 min. The product was extracted with benzene, washed with brine, and finally dried over $MgSO_4$. Chromatography over silica gel with hexane–ethyl acetate gave the ketone.

The following ketones were obtained by this procedure.

(*E*)-5-Pentadecen-7-one: n_D 1.4531; IR (film) 1700, 1680, 1635, 1470, and 985 cm^{-1}; ^{1}H NMR ($CDCl_3$) δ=0.92 (t, 6H, *J*=6.0 Hz), 1.28 (m, 16H), 2.22 (dt, 2H, *J*=7.2 Hz), 2.52 (t, 2H, *J*=7.4 Hz), 6.08 (d, 1H, *J*=15.6 Hz), and 6.82 (dt, 1H, *J*=15.8 and 6.6 Hz); MS *m/z* (rel intensity) 28 (27), 41 (53), 55 (97), 111 (53), 126 (22), 167 (13), and 225 (100); High resolution MS, Found: *m/z*, 224.2163. Calcd for $C_{15}H_{28}O$: M, 224.2140.

Methyl (*E*)-15,15-Dimethyl-12-oxo-13-hexadecenoate: n_D 1.4853; IR (film) 1740, 1700, 1680, 1625, 1460, 1440, 1360, 1165, and 980 cm^{-1}; ^{1}H NMR ($CDCl_3$) δ=1.09 (s, 9H), 1.28 (m, 16H), 2.30 (t, 2H, *J*=7.2 Hz), 2.53 (t, 2H, *J*=7.2 Hz), 3.66 (s, 3H), 6.00 (d, 1H, *J*=16.0 Hz), and 6.81 (d, 1H, *J*=16.0 Hz); MS *m/z* (rel intensity) 41 (47), 55 (52), 111 (100), 126 (26), 221 (11), 253 (20), 279 (25), and 311 (33); High resolution MS, Found: *m/z*, 310.2510. Calcd for $C_{19}H_{34}O_3$: M, 310.2508.

(*E*)-12-Oxo-14-phenyl-13-tetradecenonitrile: Mp 64 °C; IR (Nujol) 2250, 1695, 1610, 1580, 1470, 1380, and 1080 cm^{-1}; ^{1}H NMR ($CDCl_3$) δ=1.31 (m, 16H), 2.32 (t, 2H, *J*=6.6 Hz), 2.66 (t, 2H, *J*=6.9 Hz), 6.72 (d, 1H, *J*=16.3 Hz), and 7.49 (m, 6H); MS *m/z* (rel intensity) 41 (13), 55 (10), 77 (18), 103 (35), 131 (100), 146 (79), 159 (7), 188 (3), and 297 (4); High resolution MS, Found: *m/z*, 297.2083. Calcd for $C_{20}H_{27}ON$: M, 297.2093.

(1*E*,6*E*)-8-(*t*-Butyldimethylsiloxy)-3-methyl-1-(2,6,6-trimethyl-1-cyclohexenyl)-1,6-tridecadien-5-one: n_D 1.4805; IR (film) 1705, 1685, 1640, 1470, 1365, 1260, 1100, 980, 840, and 780 cm^{-1}; ^{1}H NMR ($CDCl_3$) δ=−0.03 (s, 6H) , 0.88 (s, 18H), 1.04 (d, 3H, *J*=6.4 Hz), 1.23 (m, 8H), 1.44 (m, 4H), 1.58 (s, 3H), 1.91 (m, 2H), 2.56 (s, 2H), 2.73 (m, 1H), 4.25 (m, 1H), 5.24 (dd, 1H, *J*=15.8 and 7.0 Hz), 5.81 (d, 1H, *J*=16.0 Hz), 6.19 (d, 1H, *J*=15.8 Hz), and 6.73 (dd, 1H, *J*=15.8 and 4.8 Hz); MS *m/z* (rel intensity) 73 (74), 95 (37), 107 (34), 121 (45), 161 (31), 177 (73), 215 (46), 269 (25), 337 (10), 403 (8), and 460 (26); High resolution MS, Found: *m/z* 460.3731. Calcd for $C_{29}H_{52}O_2Si$: M, 460.3736.

1-(1-Cyclohexenyl)nonan-1-one: n_D 1.4777; IR (film) 1670, 1640, 1460, 1440, 1385, 1205, and 1185 cm^{-1}; ^{1}H NMR ($CDCl_3$) δ=0.88 (t, 3H, *J*=5.6 Hz), 1.28 (m, 12H), 1.62 (m, 4H), 2.23 (m, 4H), 2.61 (t, 2H, *J*=6.7 Hz), and 6.87 (s, 1H); MS *m/z* (rel intensity) 29 (22), 41 (47), 53 (22), 81 (74), 109 (100), 124 (57), and 222 (89); High resolution MS, Found: *m/z* 222.1974. Calcd for $C_{15}H_{26}O$: M, 222.1948.

Steroid: Mp 83 °C; IR (Nujol) 1745, 1715, 1690, 1640, 1260, and 1055 cm^{-1}; ^{1}H NMR ($CDCl_3$) δ=0.73 (s, 3H), 0.94 (d, 3H, *J*=4.6 Hz), 0.96 (t, 3H, *J*=4.8 Hz), 1.02 (s, 3H), 2.02 (s, 3H), 0.9—2.5 (m, 29H), 4.3—4.8 (m, 1H), 5.35 (d, 1H, *J*=4.1 Hz), 6.01 (d, 1H, *J*=15.8 Hz), and 6.75 (dt, 1H, *J*=15.8 and 6.8 Hz); MS *m/z* (rel intensity) 43 (65), 55 (100), 81 (50), 105 (38), 145 (29), 161 (23), 282 (86), 390 (4), 434 (2), and 469 (2); High resolution MS, Found: *m/z*, 468.3623. Calcd for $C_{31}H_{48}O_3$: M, 468.3604.

11-(Methoxymethoxy)bicyclo[5.4.0]undec-1(7)-en-8-one: n_D 1.5045; IR (film) 1660, 1440, 1280, 1140, 1080, 1020, 910, 870, and 840 cm^{-1}; ^{1}H NMR ($CDCl_3$) δ=1.60 (m, 8H), 2.10 (m, 2H), 2.47 (m, 4H), 3.43 (s, 3H), 4.18 (m, 1H), 4.67 (d, 1H, *J*=6.8 Hz), and 4.81 (d, 1H, *J*=7.0 Hz); MS *m/z* (rel intensity) 45 (100), 79 (12), 91 (9), 120 (5), 133 (5), 163 (13), and 224 (3); High resolution MS, Found: *m/z*, 224.1402. Calcd for $C_{13}H_{20}O_3$: M, 224.1413.

References

1) a) M. Tanaka, *Tetrahedron Lett.*, **20**, 2601 (1979); b) T. Kobayashi and M. Tanaka, *J. Organomet. Chem.*, **205**, C27 (1981); c) H. Yamashita, T. Kobayashi, T. Sakakura, and M. Tanaka, *ibid.*, **356**, 125 (1988); d) W. F. Grove, M. E. Wright, P. D. Davis, S. S. Labadie, and J. K. Stille, *J. Am. Chem. Soc.*, **106**, 6417 (1984); e) A. M. Echavarren and J. K. Stille, *ibid.*, **110**, 1557 (1988).

2) a) Y. Wakita, T. Yasunaga, M. Akita, and M. Kojima, *J. Organomet. Chem.*, **301**, C17 (1986); b) T. Kondo, Y. Tsuji, and Y. Watanabe, *ibid.*, **345**, 387 (1988).

3) Y. Wakita, T. Yasunaga, and M. Kojima, *J. Organomet. Chem.*, **288**, 261 (1985).

4) Y. Tamaru, H. Ochiai, Y. Yamada, and Z. Yoshida, *Tetrahedron Lett.*, **24**, 3869 (1983).

5) An electron withdrawing group decreases the rate of insertion of carbon monoxide into palladium–carbon bond; F. R. Hartley, "The Chemistry of the Metal-Carbon Bond," ed by S. Patai, Wiley, New York (1985).

6) H. C. Brown, E. F. Night, and R. A. Coleman, *J. Am. Chem. Soc.*, **91**, 2144 (1969).

7) a) A. Suzuki, *Pure Appl. Chem.*, **57**, 1749 (1985); b) N. Miyaura, T. Yanagi, and A. Suzuki, *Synth. Commun.*, **11**, 513 (1981); c) N. Miyaura, K. Yamada, H. Suginome, and A. Suzuki, *J. Am. Chem. Soc.*, **107**, 972 (1985); d) N. Miyaura, T. Ishiyama, H. Sasaki, M. Ishikawa, M. Satoh, and A. Suzuki, *ibid.*, **111**, 314 (1989).

8) T. Hayashi, M. Konishi, Y. Kobori, M. Kumada, T. Higuchi, and K. Hirotsu, *J. Am. Chem. Soc.*, **106**, 158 (1984).

9) G. Zweifel and G. C. Whitney, *J. Am. Chem. Soc.*, **89**, 2753 (1967).

10) R. B. Miller and T. Reichenbach, *Tetrahedron Lett.*, **15**, 543 (1974).

11) A. Pross and S. Stevnhell, *Aust. J. Chem.*, **23**, 989 (1970).

12) F-T. Luo and E. Negishi, *J. Org. Chem.*, **50**, 4762 (1985).

13) E. Pievs and I. Nagakura, *Synth. Commun.*, **5**, 193 (1975).

14) F. Sondheimer and R. Mechoulam, *J. Am. Chem. Soc.*, **80**, 3087 (1958).

Molecular Structure and Carbonylation of Ethyl(benzenethiolato)-palladium(II) Complex, *trans*-PdEt(SPh)(PMe_3)$_2$

Kohtaro OSAKADA,* Youichi OZAWA, and Akio YAMAMOTO*,†
Research Laboratory of Resources Utilization, Tokyo Institute of Technology,
4259 Nagatsuta, Midori-ku, Yokohama 227
(Received February 22, 1991)

Synopsis. X-Ray crystallography of ethylpalladium thiolato complex, *trans*-PdEt(SPh)(PMe_3)$_2$, shows the detailed features of the Pd–C and Pd–S bonding. Reaction of the complex with CO at 5 atm gives *S*-phenyl thiopropionate. The NMR spectrum of the reaction mixture under 1 atm of CO shows the presence of *trans*-Pd(COEt)(SPh)(PMe_3)$_2$ formed through CO insertion into the Pd–C bond.

Recently attention has been paid to organotransition metal thiolato complexes which are regarded as key intermediates in the metal complex-catalyzed synthetic organic reactions such as desulfurization of organosulfur compounds[1–4] and coupling reaction of organic halides with thiolate anion to give dialkyl sulfides.[5–7] In the course of our study on chemical properties of organonickel and -palladium thiolato complexes[8] we found that the palladium complexes, *trans*-PdEt(SAr)(PMe_3)$_2$ (Ar=Ph, *p*-MeC_6H_4, and *p*-$MeOC_6H_4$), reacted with various organic halides to give sulfides through selective coupling of the thiolato ligand with the alkyl or acyl group of the substrates.[9]

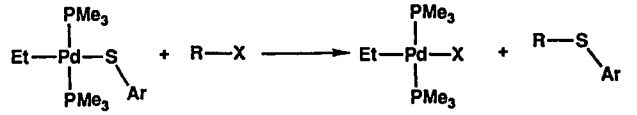

(R–X = MeCOCl, MeI, CH_2=$CHCH_2Cl$, $PhCH_2Br$)

Although various interesting properties of thiolato complexes of transition metals were already revealed, there have been few reports on the alkylpalladium thiolato complexes. We carried out further investigation on the structure and reactivities of *trans*-PdEt(SPh)(PMe_3)$_2$. Here we report the results of the X-ray crystallography and of the study on the reaction with CO.

Results and Discussion

Structure. Figure 1 shows the molecular structure of *trans*-PdEt(SPh)(PMe_3)$_2$ (**1**) determined by X-ray crystallography. The bond distances and angles of the non-hydrogen atoms are summarized in Table 1. The molecule has a square-planar coordination around the palladium center. The phenyl plane of the thiolato ligand is almost perpendicular to the coordination plane similarly to the phenoxide ligand of the already reported methylpalladium phenoxide complexes with PMe_3 ligands.[10] The methyl carbon atoms of the two PMe_3 ligands are staggered with respect to the P–Pd–P axis. The molecule of the already reported *trans*-PdEt(Br)(PMe_3)$_2$ has an eclipsed conformation regarding with the carbon atoms in the PMe_3 ligands, and has a pseudo-mirror plane that includes Pd, Br, and the car-

† Present address: Department of Applied Chemistry, School of Science and Engineering, Waseda University, 3-4-1, Ohkubo, Shinjuku-ku, Tokyo 169.

Table 1. Bond Distances and Bond Angles for Non-H Atoms with esd's in Parentheses

	Bond distance/Å		
Pd1–S2	2.384(2)	Pd1–P3	2.307(3)
Pd1–P4	2.309(3)	Pd1–C5	2.098(9)
C5–C6	1.491(15)	S2–C13	1.737(9)
C13–C14	1.408(11)	C14–C15	1.380(15)
C15–C16	1.357(15)	C16–C17	1.376(13)
C17–C18	1.440(14)	C18–C13	1.412(12)
P3–C7	1.799(14)	P3–C8	1.811(14)
P3–C9	1.845(11)	P4–C10	1.794(12)
P4–C11	1.800(11)	P4–C12	1.819(13)
	Bond angle/°		
S2–Pd1–P3	87.04(9)	S2–Pd1–P4	91.83(9)
S2–Pd1–C5	172.7(3)	P3–Pd1–P4	174.4(1)
P3–Pd1–C5	92.0(3)	P4–Pd1–C5	89.8(3)
Pd1–C5–C6	107.6(6)	Pd1–S2–C13	109.2(3)
S2–C13–C14	119.8(7)	C13–C14–C15	121.9(9)
C14–C15–C16	120.3(8)	C15–C16–C17	120.8(1.0)
C16–C17–C18	120.5(9)	C17–C18–C13	118.3(7)
Pd1–P3–C7	113.7(5)	Pd1–P3–C8	113.3(4)
Pd1–P3–C9	120.7(5)	C7–P3–C8	104.3(7)
C8–P3–C9	101.8(6)	C7–P3–C9	101.0(6)
Pd1–P4–C10	117.6(5)	Pd1–P4–C11	120.3(4)
Pd1–P4–C12	110.5(5)	C10–P4–C11	99.9(6)
C11–P4–P12	103.0(6)	C10–P4–C12	103.3(6)

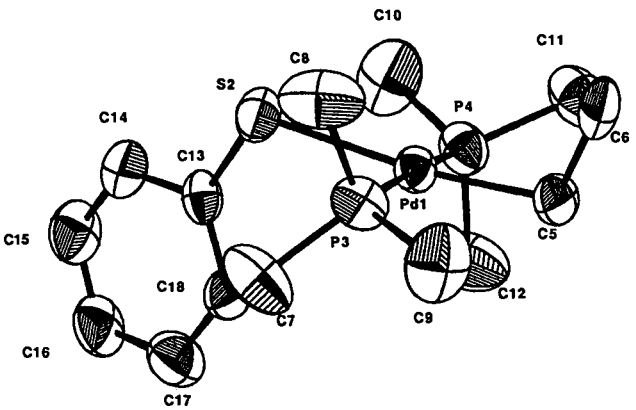

Fig. 1. The molecular structure of *trans*-PdEt(SPh)-(PMe_3)$_2$ (**1**) with the atomic numbering scheme. Non-hydrogen atoms are shown by thermal ellipsoids at 50% probability levels. Hydrogen atoms are omitted for simplicity.

bon atoms in the ethyl ligand.[9] The Pd–C bond distance [2.098(9) Å] in the present ethylpalladium thiolato complex is longer than that in *trans*-PdEt(Br)(PMe_3)$_2$ [2.063(5) Å], suggesting a larger trans influence of the thiolato ligand than the bromo ligand. The Pd–S bond distance [2.384(2) Å] is somewhat longer than the Pd–S bond of the terminal thiolato ligand in [Pd(SC_6F_5)-(PPh_3)(μ-SC_6F_5)]$_2$.[11]

A recent review on the structures of transition metal thiolato complexes indicated that the M–S–C bond angles of the benzenethiolato complexes are in the range 103—118°.[12] The Pd–S–C angle in the title compound (109.2(3)°) is within the range.

Reaction of 1 with CO. Reaction of complex **1** with CO at 5 atm for 3 h gives *S*-phenyl thiopropionate in 62% yield accompanied by formation of small amounts of diethyl ketone and diphenyl sulfide. The resulting palladium complexes consisted of a mixture of several palladium(0) carbonyl complexes Pd(CO)$_m$(PMe_3)$_n$[13] as deduced on the basis of the IR spectrum. The NMR

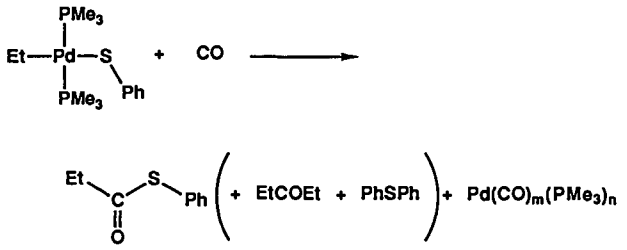

study of the reaction mixture was carried out in CD_2Cl_2 under 1 atm of CO. NMR spectra (^{1}H, ^{13}C, and ^{31}P) indicated the presence of *trans*-Pd(COEt)(SPh)(PMe_3)$_2$ as the major palladium complex. Signals due to unreacted **1** are also observed, while the signals due to the *S*-thioester are not observed under the conditions. The above carbonylation of **1** under 5 atm of CO seems to proceed through formation of a propionyl palladium complex through CO insertion into the Pd–C bond in **1** followed by reductive elimination of the propionyl and thiolate ligands.[14]

Previously we have reported carbonylation of similar organonickel and -palladium alkoxide complexes. PdMe($OCH(CF_3)_2$)(dppe) (dppe=1,2-[bis(diphenylphosphino)ethane]) reacts with CO easily to give PdMe($COOCH(CF_3)_2$)(dppe) through selective CO insertion into the Pd–O bond.[15] On the other hand, *trans*-PdMe(OAr)L_2 (L=PEt_3) undergoes CO insertion into the Pd–C bond to give Pd(COMe)(OAr)L_2.[16] In the present case it is noted that CO insertion occurs into the Pd–C bond rather than into the Pd–S bond.

Experimental

trans-PdEt(SPh)(PMe_3)$_2$ (**1**) was prepared by the method reported previously.[9] GC-MS measurement was preformed on a Hitachi M-80 mass spectrometer. GC was measured on a Shimadzu 3BT gas-chromatograph using a 1-m column packed with Silicone OV-1. NMR spectra were recorded at −40 °C on a JEOL FX-100 spectrometer.

Crystallography. The single crystals suitable for crystallography were grown in acetone at −20 °C.

Crystald Data: $C_{14}H_{28}P_2SPd$, M=396.55, triclinic, $P\bar{1}$, a=9.613(7), b=12.204(6), c=8.419(4) Å, α=91.10(4), β=101.85(5), γ=94.82(5)°, U=962.5(9) Å^3, Z=2, D_c=1.369 g cm^{-3}, μ(Mo$K\alpha$)=12.1 cm^{-1}, F(000)=408.

Data Collection and Structure Refinement: A crystal with approximate dimensions of 0.45×0.50×0.50 mm sealed in a glass capillary under argon was mounted on a Rigaku AFC-5 automated four-cycle diffractometer. Unit cell parameters were determined by the least-squares calculation of 2θ values of 25 reflections with 19°<2θ<22°. Intensity data collection was carried out using Mo$K\alpha$ radiation (λ=0.71069 Å) by the ω–2θ mode. The scan speed and range were 4° min^{-1} in 2θ and $\Delta(2\theta)$=(1.40+0.7 tanθ)°, respectively. Among 2516 unique reflections (3°<2θ<45° and $-10 \leqslant h \leqslant 10$, $-13 \leqslant k \leqslant 13$, $0 \leqslant l \leqslant 8$), 2407 reflections with $F_o \geqslant 3\,\sigma(F_o)$ were used in the structure calculation. No absorption correction was applied.

Calculations were carried out on a FACOM A-70 computer. The position of palladium was determined by a direct method (SAPI85).[17] The other non-hydrogen atoms were found in the subsequent Fourier procedure. A full-matrix least-squares refinement was carried out applying anisotropic thermal factors for the non-hydrogen atoms. Hydrogen atoms were located in the difference Fourier map or at the idealized positions, and included in least-squares calculations without refinement of their parameters. Atomic coordinates are listed in Table 2. The weighting scheme, $w=1/\{\sigma^2(F_o)+[0.009(F_o)]^2\}$, with $\sigma(F_o)$ from counting statistics, gave satisfactory agreement analyses. Final R and R_w values were 0.059 and 0.064, respectively.**

Reaction of 1 with CO. To a tetrahydrofuran (3 cm^3) solution of **1** (36 mg, 0.091 mmol) in a glassware autoclave was introduced CO at 5 atm at room temperature. The orange yellow solution soon changed into deep red. After stirring for 3 h GC and GC-MS analyses of the solution indicated formation of *S*-phenyl thiopropionate (9.4 mg, 62%); MS (70 eV) m/z (rel intensity) 166 (M^+; 29), 110 (81), 109 (36), 57 (100), and 29 (87). Formation of small amounts (<10%) of diethyl ketone and diphenyl sulfide was also observed in the reaction mixture. IR spectrum of the reaction mixture after removal of the solvent showed strong broad peaks near 1700

Table 2. Fractional Atomic Coordinates and Equivalent Isotropic Thermal Parameters of Non-H Atoms with esd's in Parentheses

Atom	x	y	z	B_{eq}/Å^2
Pd1	0.63172(6)	0.72191(5)	0.04074(6)	3.39
S2	0.4785(3)	0.6863(2)	−0.2203(3)	4.35
P3	0.8095(3)	0.7767(2)	−0.0953(3)	4.70
P4	0.4453(3)	0.6838(2)	0.1716(3)	4.46
C5	0.7757(10)	0.7333(8)	0.2666(11)	4.7
C6	0.8270(12)	0.6217(9)	0.2942(11)	6.5
C7	0.7626(13)	0.8828(11)	−0.2375(17)	7.7
C8	0.8565(14)	0.6667(10)	−0.2169(18)	8.0
C9	0.9864(12)	0.8344(12)	0.0179(16)	7.7
C10	0.2846(13)	0.6126(11)	0.0557(15)	7.8
C11	0.4702(12)	0.6036(9)	0.3514(13)	6.3
C12	0.3848(13)	0.8106(10)	0.2402(17)	7.8
C13	0.3611(8)	0.7885(7)	−0.2579(10)	3.6
C14	0.2307(10)	0.7676(8)	−0.3709(11)	4.6
C15	0.1358(10)	0.8471(9)	−0.4084(12)	5.3
C16	0.1686(10)	0.9501(9)	−0.3400(12)	5.3
C17	0.2927(11)	0.9755(8)	−0.2259(13)	5.5
C18	0.3940(9)	0.8946(8)	−0.1828(11)	4.4

** The complete F_o—F_c data, temperature factors of the non-hydrogen atoms, and bond distances and angles of the hydrogen atoms are deposited as Document No. 9117 at the Office of the Editor of Bull. Chem. Soc. Jpn.

cm^{-1} which are assigned to the CO stretching vibrations of palladium carbonyl complexes with the phosphine ligands.

A CD_2Cl_2 (ca. 0.3 cm^3) solution of **1** (32 mg, 0.081 mmol) was introduced to an NMR tube (5 mmϕ) which was then capped with a rubber septum under argon atmosphere. After removal of the argon in the system with a needle connected with a vacuum line, CO (1 atm) was charged with a syringe. After setting the solution at room temperature for 6 h the NMR spectra indicated formation of *trans*-Pd(COEt)(SPh)-$(PMe_3)_2$ in ca. 80% yield. Signals due to unreacted **1** were also observed. ^1H NMR (CD_2Cl_2) δ=0.99 (t, CH_3, J(HH)=7 Hz), 1.21 (t, $P(CH_3)_3$, J=4Hz),[18] 2.55 (q, CH_2, J(HH)=7 Hz), and 6.8—7.5 (m, C_6H_5); $^{13}C\{^1H\}$ NMR (CD_2Cl_2) δ=149.7 (s, C_6H_5), 132.0 (s, C_6H_5), 127.3 (s, C_6H_5), 120.3 (s, C_6H_5), 49.6 (t, CH_2, J(PC)=16 Hz), 13.9 (t, $P(CH_3)_3$, J=15 Hz),[18] 8.4 (s, CH_3); $^{31}P\{^1H\}$ NMR (CD_2Cl_2, chemical shift referred to external H_3PO_4) −20.4 ppm.

Reaction of **1** with ^{13}CO in an NMR tube was carried out similarly. $^{13}C\{^1H\}$ NMR spectrum of the reaction mixture showed a singlet at 250.1 ppm due to the carbonyl carbon atom of *trans*-Pd(COEt)(SPh)$(PMe_3)_2$. The signals of the ethyl ligand in the ^1H and $^{13}C\{^1H\}$ NMR spectra showed splitting due to the C–C and C–H coupling. The obtained coupling constants ^1J(CC), ^2J(CH), and ^3J(CH) are 33, 5, and 7 Hz, respectively.

This work was partially supported by the Grant-in-Aid for Scientific Research Nos. 63470079 and 02855210 from the Ministry of Education, Science and Culture.

References

1) J. J. Eisch, L. E. Hallenbeck, and K I. Han, *J. Org. Chem.*, **48**, 2963 (1983).

2) H. Alper and C. Blais, *J. Chem. Soc., Chem. Commun.*, **1980**, 169; S. Antebi and H. Alper, *Organometallics,* **5**, 596 (1986).

3) N. N. Sauer and R. J. Angelici, *Organometallics,* **6**, 1146 (1987); G. H. Spies and R. J. Angelici, *ibid.*, **6**, 1897 (1987); J. W. Hachgenei and R. J. Angelici, *ibid.*, **8**, 14 (1989).

4) M. R. DuBois, *Chem. Rev.*, **89**, 1 (1989).

5) M. Kosugi, T. Shimizu, and T. Migita, *Chem. Lett.*, **1978**, 13; T. Migita, T. Shimizu, Y. Asami, J. Shiobara, Y. Kato, and M. Kosugi, *Bull. Chem. Soc. Jpn.*, **53**, 1385 (1980).

6) S. Murahashi, M. Yamamura, K. Yanagisawa, N. Mita, and K. Kondo, *J. Org. Chem.*, **44**, 2408 (1979).

7) H. Okamura and H. Takei, *Tetrahedron Lett.*, **1979**, 3425.

8) K. Osakada, M. Maeda, Y. Nakamura, T. Yamamoto, and A. Yamamoto, *J. Chem Soc., Chem. Commun.*, **1986**, 442; K. Osakada, H. Hayashi, M. Maeda, T. Yamamoto, and A. Yamamoto, *Chem. Lett.*, **1986**, 597; K. Osakada, T. Chiba, Y. Nakamura, T. Yamamoto, and A. Yamamoto, *J. Chem. Soc., Chem. Commun.*, **1986**, 1589; K. Osakada, T. Chiba, Y. Nakamura, T. Yamamoto, and A. Yamamoto, *Organometallics,* **8**, 2602 (1989); K. Osakada, Y. Ozawa, and A. Yamamoto, *J. Organomet. Chem.*, **399**, 341 (1991).

9) K. Osakada, Y. Ozawa, and A. Yamamoto, *J. Chem. Soc., Dalton Trans.*, **1991**, 759.

10) Y.-J. Kim, K. Osakada, A. Takenaka, and A. Yamamoto, *J. Am. Chem. Soc.*, **112**, 1096 (1990).

11) R. H. Fenn and G. R. Segrott, *J. Chem. Soc. A,* **1970**, 3197.

12) M. T. Ashby, *Comments Inorg. Chem.*, **10**, 297 (1990).

13) P. M. Maitlis, "The Organic Chemistry of Palladium," Academic Press, New York (1971), Vol. 1.

14) Since direct reductive elimination of the *S*-thioester from *trans* acylpalladium thiolato complex is not feasible, prior change in the configuration of the two coordinating ligands seems to occur during the reaction.

15) Y.-J. Kim, K. Osakada, K. Sugita, T. Yamamoto, and A. Yamamoto, *Organometallics,* **7**, 2182 (1988).

16) T. Yamamoto, J. Ishizu, T. Kohara, S. Komiya, and A. Yamamoto, *J. Am. Chem. Soc.*, **102**, 3758 (1980); T. Yamamoto, T. Kohara, and A. Yamamoto, *Bull. Chem. Soc. Jpn.*, **54**, 2161 (1981); S. Komiya, Y. Akai, K. Tanaka, T. Yamamoto, and A. Yamamoto, *Organometallics,* **4**, 1130 (1985).

17) F. Fan, SAPI85, Chinese Academy of Science, Beijing (1985).

18) The signal appears like a triplet due to virtual coupling. Apparent coupling constant is shown. See: P. S. Pregosin and R. W. Kunz, "^{31}P and ^{13}C NMR Spectroscopy of Transition Metal Complexes," Springer, Heidelberg (1979), p. 65.

Association Behavior of Protoporphyrin IX in Water and Aqueous Poly(*N*-vinylpyrrolidone) Solutions. Interaction between Protoporphyrin IX and Poly(*N*-vinylpyrrolidone)

Isamu INAMURA* and Kazutomo UCHIDA
Department of Chemistry, Faculty of Science, Shimane University, Matsue 690
(Received December 25, 1990)

Synopsis. The association behavior of protoporphyrin IX was investigated at different pH by absorption spectroscopy and gel chromatography. Protoporphyrin IX existed as monomer in acidic water, as aggregate in neutral water, and as dimer in basic water. Poly(*N*-vinylpyrrolidone) tended to suppress dimerization and aggregation of protopophyrin IX.

Protoporphyrin IX is a metal-free porphyrin of the same structure as hemin. It has both the acid and base properties due to two pyrrole nitrogens capable of accepting protons and two propionic acid residues. In addition to these ionizable groups, this molecule contains a wide hydrophobic region. Tough hemin has been widely studied by many investigators,[1,2] there are only a few reports on the association behavior of protoporphyrin IX. Savitski et al.[3] reported that protoporphyrin IX was solubilized as monomer in the micelles of Triton X-100. Gallagher et al.[4] observed spectral changes of hematoporphyrin and protoporphyrin IX reflecting the dimer-to-monomer conversion. Except for these works, the association behavior of protoporphyrin IX has not been elucidated.

We recently succeeded in solubilizing hemin as monomer in both neutral and acidic water by complexing with poly(*N*-vinylpyrrolidone)] (PVP).[5] In view of this, we got interested in clarifying the interaction between PVP and protoporphyrin IX, and its influence on the association behavior of protoporphyrin IX.

In the present work, we measured at different pH the absorption spectra of protoporphyrin IX both in water and in aqueous PVP solutions. Some of the solution were examined by gel chromatography. Three types of absorption spectra were observed, and assigned to monomer, dimer, and aggregate of protoporphyrin IX. The effects of pH and PVP on the association behavior of protopophyrin IX are discussed on the basis of the structure of protoporphyrin IX.

Experimental

Materials. Protoporphyrin IX disodium salt was purchased from Nacalai Tesque, Inc. PVP (molecular weight 40000) was from Kishida Chemical Co., Ltd, and was purified by reprecipitation in water–acetone.

Preparation of Aqueous Protoporphyrin IX/PVP Solution. Protoporphyrin IX disodium salt (2 mg) and PVP (1.32 g) were dissolved in water to obtain 80 ml of an aqueous solution (pH 4.8). The pH of the solution was adjusted with HCl or NaOH. Aqueous protoporphyrin IX solutions were prepared in a similar way.

Gel Chromatography. Gel chromatography of aqueous protoporphyrin IX and protoporphyrin IX/PVP solutions was performed as follows. Two milliliters of the sample (pH 4.8 or 10) was applied onto a column (0.8×40 cm) of Toyopearl HW-55 equilibrated with water adjusted to pH of the sample. Then it was eluted with water (pH 4.8 or 10) at a flow rate of 0.13 ml min^{-1}. Concentrations of samples applied to the column were 2.5×10^{-4} mol dm^{-3} for protoporphyrin IX, and 10% wt/vol-solution for PVP. The content of protoporphyrln IX in the eluted fraction (4 ml) was monitored by measuring the maximum absorbance in a wavelength range of 350 nm to 800 nm. The amount of PVP was monitored by weighing the fraction after evaporation, which usually contained a negligible content of protoporphyrin IX.

Analytical Method. Absorption spectra at room temperature were measured with a double beam spectrophotometer UVIDEC-510 (Japan Spectroscopic Co., Ltd.).

Results

Figure 1 shows the absorption spectra of protoporphyrin IX in different states. At pH 1.0, protopor-

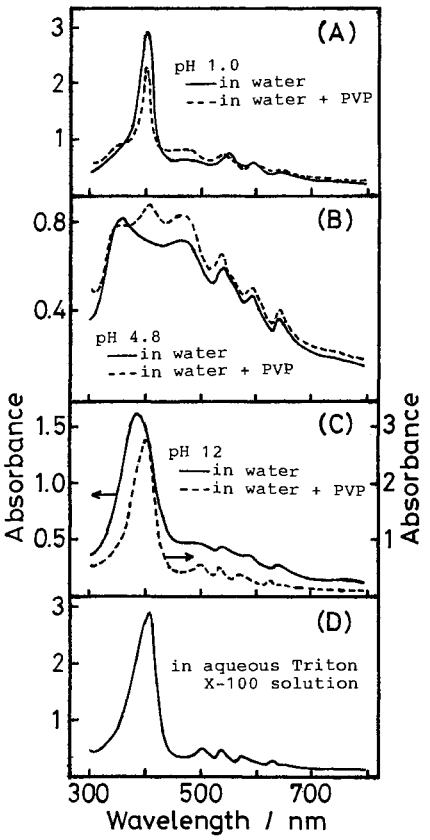

Fig. 1. Absorption spectra of protoporphyrin IX in different states.
Protoporphyrin IX in water (——) and in aqueous PVP solution (------) at pH 1.0 (A), 4.8 (B) and 12 (C). Protoporphyrin IX in aqueous Triton X-100 (1.5%) solution at pH 5.4 (D). Concentrations of protoporphyrin IX and PVP are 4.12×10^{-5} mol dm^{-3} and 1.65×10^{-2} g cm^{-3}, respectively.

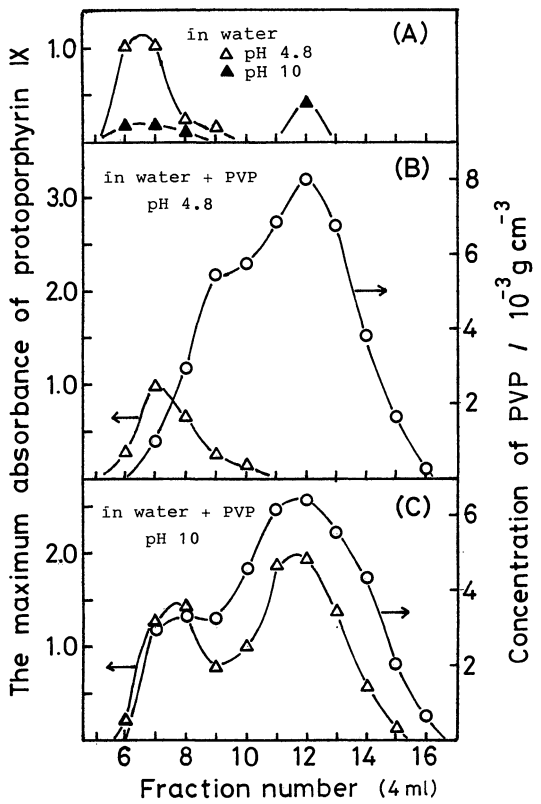

Fig. 2. Elution patterns of gel chromatography.
(A) aqueous protoporphyrin IX solution at pH 4.8 and 10, (B) aqueous protoporphyrin IX/PVP solution at pH 4.8, (C) aqueous protoporphyrin IX/PVP solution at pH 10.

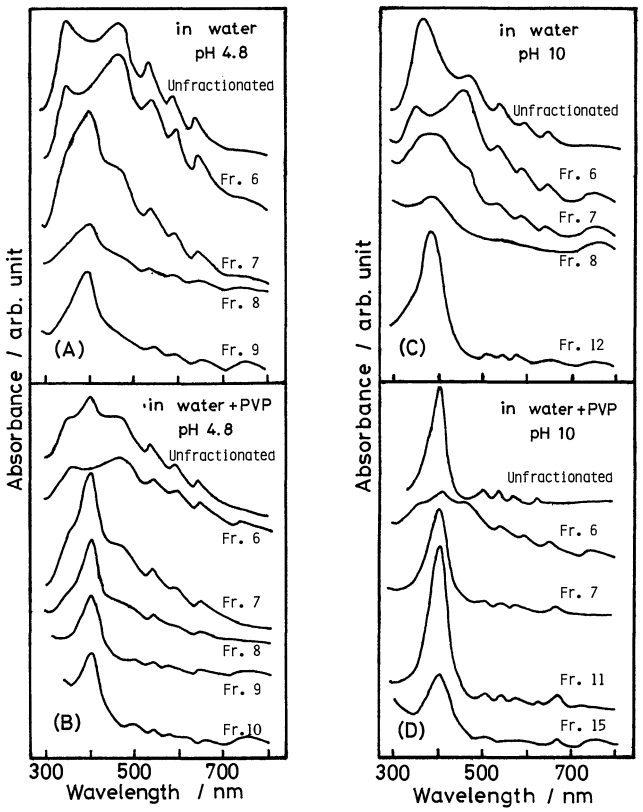

Fig. 3. Absorption spectra of protoporphyrin IX in unfractionated and fractionated solutions in gel chromatography.
(A) protoporphyrin IX in water at pH 4.8, (B) protoporphyrin IX in aqueous PVP solution at pH 4.8, (C) protoporphyrin IX in water at pH 10, (D) protoporphyrin IX in aqueous PVP solution at pH 10. Fraction numbers are the same as those in Fig. 2. The absorption spectra of fractions 8—10 and 12—14 for sample (D) are not shown, because they changed successively as the fraction number grew.

phyrin IX in water and in aqueous PVP solution had a sharp Soret band at 405 nm and four weak Q-bands. Protoporphyrin IX in water at pH 4.8 exhibited a weak Soret band at about 350 nm and four weak Q-bands; on interacting with PVP, a new Soret band appeared at 406 nm. Protoporphyrin IX in water at pH 12 showed a sharp Soret band at 388 nm and four weak Q-bands; on interacting with PVP, the Soret band shifted to 404 nm and its intensity increased about 1.7 times, resulting in the same intensity as the Soret band at pH 1.0.

Thus, the following three types of absorption spectra were observed for protoporphyrin IX in water and aqueous PVP solutions. Type 1—a weak Soret band at about 350 nm and four weak Q-bands, Type 2—a sharp Soret band at 388 nm and four weak Q-bands, Type 3—a sharp Soret band at about 405 nm and four weak Q-bands.

Figure 2 shows the elution patterns of gel chromatography. Each plot in this figure gives the amount of protoporphyrin IX or PVP contained in each fraction. The elution curves of protoporphyrin IX and PVP were remarkably dependent on pH.

Figure 3 shows the absorption spectra of protoporphyrin IX in unfractionated (sample applied onto the column) and fractionated solutions. For each sample, Fr. 6 showed the Type 1 absorption spectrum. As the fraction number increased, the Soret bands shifted from about 350 nm to 398 nm (Fig. 3-A), 403 nm (Fig. 3-B), 381 nm (Fig. 3-C), or 405 nm (Fig. 3-D), and their intensities became much higher as compared with Q-bands. These absorption spectra were classified into Types 2 and 3 as follows. The absorption spectra of later fractions in water at pH 4.8 (Fig. 3-A), and in aqueous PVP solutions at pH 4.8 (Fig. 3-B) and at pH 10 (Fig. 3-D) belonged to Type 3, since the Soret bands were at 398—405 nm. On the other hand, the absorption spectrum of a later fraction, Fr. 12, in water at pH 10 (Fig. 3-C) belonged to Type 2 with the Soret maximum at 381 nm.

Discussion

Effect of pH. Since protoporphyrin IX is an amphoteric electrolyte, it is considered to dissociate into ions in acidic and basic water. This explains the result that the intensity of the Soret band of protoporphyrin IX in water increased in the order at pH 4.8< at pH 12< at pH 1.0 (Fig. 1). At pH 4.8, the solubility of protoporphyrin IX was substantially small due to the low degree of electrolytic dissociation.

Assignment of Three Types of Absorption Spectra. In

gel chromatography, it is expected that as the fraction number increased, the molecular weight was lower. Therefore, Type 1 observed in the earliest fraction, Fr. 6, may represent a bulky species of protoporphyrin IX. On the other hand, Types 2 and 3 observed in later fractions may be due to a small species. Based on these, we assigned the three types of absorption spectra of protoporphyrin IX as follows.

Type 1 was supposed to arize from a large species. The molecular weight of this species was inferred to be larger than 700000, because as specified by the manufacturer, Toyopearl HW-55 excludes proteins of molecular weight larger than 700000. A most probable candidate for Type 1 is thus an aggregate of protoporphyrin IX. The lowest intensity of the Soret band of Type 1 in water at pH 4.8 (Fig. 1-B) was consistent with this assignment. Savitski et al.[3] reported a similar absorption spectrum for protoporphyrin IX in water at pH 8.0.

Type 2 was observed in basic water of pH 10 and 12 (Figs. 1-C and 3-C), and the gel chromatographic elution time suggested that it was a small species. The spectral feature of Type 2 was similar to that of a hematoporphyrin dimer in 0.02 M NaOH (1 M=mol dm^{-3}), reported by Gallagher et al.[4] The dimer of hematopophyrin had a Soret band at about 375 nm and four weak Q-bands, and on dilution the Soret band shifted to 395 nm and its intensity increased about 1.5 times, due to disintegration of dimer to monomer. They also described that a similar spectral change was observed for protoporphyrin IX under the same conditions.[4] Therefore, Type 2 was assigned to a dimer of protoporphyrin IX.

Type 3 was also suggested to reflect a small species from gel chromatography. It should be noted that this type was also observed in an aqueous Triton X-100 solution (Fig. 1-D). Savitski et al.[3] reported that protoporphyrin IX was solubilized as monomer in Triton X-100 micelles, on the basis of fluorescence spectra. Therefore, Type 3 was assigned to the monomer of protoporphyrin IX. The highest intensity of the Soret band of type 3 (Fig. 1) supports this assignment.

From the assignments of three types of absorption spectra, it can be concluded that protoporphyrin IX was dissolved as monomer in acidic water, as aggregate in neutral water, and as dimer in basic water, though a small amount of other species was involved in some cases.

Model for Dimerization and Aggregation. It is interesting to note that protoporphyrin IX is dissolved as monomer in acidic water whereas as dimer in basic water, though the ionization occurs in both media. This fact seems to suggest that ionization of two pyrrole nitrogens at nearly the center of the porphyrin ring under acidic conditions, is more effective in inhibiting dimerization than that of two propionic acid residues outside the ring under basic conditions. This interpretation is in line with the "face-to-face" or "ring stacking" model[2] for dimerization and aggregation of protoporphyrin IX. Furthermore, the blue shift of the Soret band of protoporphyrin IX due to conversion of monomer to dimer (Fig. 1-C) also supports this model for dimerization.[2,6,7]

Interaction between PVP and Protoporphyrin IX. When PVP was present, protoporphyrin IX tended to show Type 3 assigned to a monomer, even in neutral and basic water (Figs. 1—3). Therefore, we could conclude that PVP tends to suppress dimerization and aggregation of protoporphyrin IX. This effect of PVP was more conspicuously observed at pH 10 and 12 than at pH 4.8. Since the protoporphyrin IX molecule has a wide hydrophobic region, PVP probably binds the molecule within its random coil chain through a hydrophobic interaction, thereby preventing dimerization and aggregation of protoporphyrin IX.

The present work was partially supported by a Grant-in-Aid for Scientific Research No. 02650651 from the Ministry of Education, Science and Culture.

References

1) K M. Smith, "Porphyrins and Metalloporphyrirns," Elsevier, Amsterdam (1975).

2) W. I. White, "The Porphyrins," ed by D. Dolphin, Academic Press, New York (1978), Vol. 5, Chap. 7, pp. 303—339.

3) A. P. Savitski, E. V. Vorobyova, I. V. Berezin, and N. N. Ugarova, *J. Colloid Interface Sci.*, **84**, 175 (1981).

4) W. A. Gallagher and W. B. Elliott, *Ann. N. Y. Acad. Sci.*, **206**, 463 (1973).

5) I. Inamura, M. Isshiki, and T. Araki, *Bull. Chem. Soc. Jpn.*, **62**, 2413 (1989).

6) A. E. Alexander, *J. Chem. Soc.*, **1937**, 1813.

7) H. Kobayashi, "Seitai-ryoshi-kagaku," ed by K. Fukui, Kyoritsu Shuppan, Tokyo (1967), Chap. 5, pp. 121—123.

Synthesis of 2,2,2-Trifluoroethylated Onium Salts of Nitrogen, Sulfur, and Phosphorus with (2,2,2-Trifluoroethyl)phenyliodonium Triflate

Teruo UMEMOTO* and Yoshihiko GOTOH
Sagami Chemical Research Center, Nishi-Ohnuma 4-4-1, Sagamihara, Kanagawa 229
(Received January 25, 1991)

Synopsis. Various 2,2,2-trifluoroethyl onium triflates were synthesized by treating tertiary amines, pyridines, quinoline, a triazole, sulfides, and a phosphine with (2,2,2-trifluoroethyl)phenyliodonium triflate. Sulfoxides and N-oxide were converted to the corresponding trifluoroethylated salts. As an application, CsF-treatment of (2,2,2-trifluoethyl)triphenylphosphonium triflate with an aldehyde was shown to produce a trifluoromethylated olefin.

Much attention has been directed to trifluoromethyl or 2,2,2-trifluoroethyl-containing organic compounds for developing new medicines, agricultural chemicals and other materials since trifluoromethyl and trifluoroethyl groups are considered to be importantly involved in biological activity and physical properties of materials in consideration of their own unique features.[1] The onium salts of nitrogen, sulfur, and phosphorus are important particularly for their use as reagents in synthetic organic chemistry.[2] No effective methods are presently available for preparing trifluoroethylated onium salts and only a few 2,2,2-trifluoroethylated salts are known.[3] We successfully developed (2,2,2-trifluoroethyl)phenyliodonium triflate (**1**), the smallest in a series of (1*H*,1*H*-perfluoroalkyl)phenyliodonium triflates (FMITS reagents), as the most reactive source of 2,2,2-trifluoroethyl cation.[4,5] The present study was conducted to establish an effective means for preparing 2,2,2-trifluoroethylammonium, pyridinium, quinolinium, sulfonium, and phosphonium triflates with **1**. One application of the phosphonium salt obtained is discussed.

Results and Discussion

Table 1 shows modes for the synthesis of various kinds of 2,2,2-trifluoroethyl onium triflates using **1**. Salt **1** reacted readily with tertiary amines, pyridine and its derivatives, quinoline and benzothiazole in dichloromethane at room temperature to give 2,2,2-trifluoroethyl onium triflates **2**—**10** in high yields. Both bulky 2,4,6-collidine or 2,6-lutidine and the less nucleophilic ethyl nicotinate were well-trifluoroethylated with **1** under the same conditions. Salt **1** was clearly shown as the most reactive in a series of (1*H*,1*H*-perfluoroalkyl)phenyliodonium triflates, since (1*H*,1*H*-perfluoropropyl, -perfluorobutyl and -perfluorooctyl)-phenyliodonium triflates (**15**, **16**, and **17**) failed to react with 2,4,6-collidine, due possibly to bulkiness about the pyridine nitrogen. Pyridine reacted with **15**, **16**, and **17** in dichloromethane to give the corresponding pyridinium triflates[6] in 93, 92, and 74% yields, respectively, but this required increase in reaction temperature and/or time. The high reactivity of **1** greatly facilitated converting sulfides to trifluoroethylsulfonium salts so that diphenyl and dimethyl sulfides smoothly reacted with **1** at room temperature to give the trifluoroethylsulfonium triflates, **11** and **12**, in high yields. The reaction of dibenzothiophene, however, was quite slow and the yield of **13** was low, owing possibly to the great decrease in the reactivity of the latter sulfide. Salts **11** and **13** are stable crystals, while those of **12** are unstable due to their highly hygroscopic nature. The reaction of triphenylphosphine with **1** was successfully conducted using benzene as the solvent to obtain trifluoroethylphosphonium triflate **14**, nonhygroscopic and stable crystals, in 95% yield. Previously, (2,2,2-trifluoroethyl)triphenylphosphonium iodide could be obtained only in 9% yield by treating triphenylphosphine with 2,2,2-trifluoroethyl iodide for 9 months at room temper-

Table 1. Syntheses of Various 2,2,2-Trifluoroethyl Onium Triflates with **1**

Run[a]	Substrate	Time[b] / min	Product	Yield/%
1	$PhCH_2NMe_2$	30	$PhCH_2N^+(CH_2CF_3)Me_2\ ^-OTf$ (**2**)	89
2	$PhNMe_2$	30	$PhN^+(CH_2CF_3)Me_2\ ^-OTf$ (**3**)	89
3	Pyridine	10	*N*-(CF_3CH_2)-Pyridinium triflate (**4**)	83
4	3,5-Lutidine	10	*N*-(CF_3CH_2)-3,5-Lutidinium triflate (**5**)	83
5	2,6-Lutidine	10	*N*-(CF_3CH_2)-2,6-Lutidinium triflate (**6**)	77
6	2,4,6-Collidine	10	*N*-(CF_3CH_2)-Collidinium triflate (**7**)	63
7	Ethyl nicotinate	10	*N*-(CF_3CH_2)-3-Ethoxycarbonylpyridinium triflate (**8**)	93
8	Quinoline	10	*N*-(CF_3CH_2)-Quinolinium triflate (**9**)	87
9	Benzothiazole	10	*N*-(CF_3CH_2)-Benzothiazolinium triflate (**10**)	84
10	Ph_2S	120	Ph_2S^+–$CH_2CF_3\ ^-OTf$ (**11**)	90
11	Me_2S	120	Me_2S^+–$CH_2CF_3\ ^-OTf$ (**12**)	92
12	Dibenzothiophene	5 days	*S*-(CF_3CH_2)-Dibenzothiophenium triflate (**13**)	31
13	Ph_3P	60	Ph_3P^+–$CH_2CF_3\ ^-OTf$ (**14**)	95

a) Dichloromethane was used as a solvent for Runs 1—12 and benzene for Run 13. All the reactions were carried out at room temperature. b) Minute, unless otherwise noted.

ature with northern exposure.[3b]

Diphenyl sulfoxide and dimethyl sulfoxide were each found to react smoothly with **1**. Isolating the resulting salts in pure form, however, was difficult owing to their extremely hygroscopic nature. The ^{19}F NMR spectra of the crude products showed a peak of the trifluoroethyl group at −72.8 ppm for the product from diphenyl sulfoxide and at −73.9 ppm for dimethyl sulfoxide. These chemical shifts appeared in considerably high magnetic fields compared with those of sulfonium salts **11** (−60.0) and **12** (−61.1). However, structural assignments for *O*- or *S*-trifluoroethyl salts **18** or **19** could not

$R_2S{=}O + \mathbf{1} \longrightarrow R_2S^+{-}OCH_2CF_3\ {}^-OTf$

a; R=Ph **18, b**

b; R=Me

or $R_2S^+{-}CH_2CF_3\ {}^-OTf$ (O double-bonded to S)

19a,b

be determined. Pyridine *N*-oxide smoothly reacted with **1** under the same conditions to give *N*-(2,2,2-trifluoroethoxy)pyridinium triflate (**20**) in a quantitative yield.

As an application of trifluoroethyl onium salts in synthetic organic chemistry, phosphonium triflate **14** was treated with benzaldehyde using cesium fluoride as a base in *N,N*-dimethylformamide at room temperature to give β-(trifluoromethyl)styrene in 43% yield (*E*-/*Z*-isomer=46/54). When sodium hydride was used as the base, there was no product formation.

Experimental

Melting points were uncorrected. ^{1}H and ^{19}F NMR spectra were recorded with a Varian EM 390 NMR and a Hitachi R-20 B NMR spectrometer, respectively. Unless otherwise noted, acetone-d_6 was used as a solvent. ^{19}F NMR chemical shifts were reported in ppm downfield from trichlorofluoromethane as an internal standard. The IR spectra were measured on a JASCO A-202 diffraction grating infrared spectrometer. Mass spectra were recorded on a Hitachi RMU-6MG spectrometer at 70 eV. (2,2,2-Trifluoroethyl)-phenyliodonium triflate (**1**) was prepared according to a reported method.[4c] Cesium fluoride was dried at 140 °C for 3—12 h in vacuo.

Preparation, of 2,2,2-Trifluoroethyl Onium Triflates with 1. General Procedure; Into a solution of 1 mmol of a substrate (shown in Table 1) in 2 ml of dry dichloromethane was added 436 mg (1 mmol) of **1** under an argon atmosphere. The reaction mixture was stirred for the time shown in Table 1 at room temperature. The results are summarized in Table 1. In the case of triphenylphosphine as a substrate, benzene was used as a solvent. Isolation of products **2**—**10** was carried out by preparative thin-layer chromatography on silica gel. Products **11**—**14** each appeared as crystals upon adding pentane to the reaction mixture, and were collected by filtration. Analytically pure samples of **2** and **4** could not be obtained, probably due to changing hydrate formation for the former and the oily nature for the latter. For **12**, only ^{1}H and ^{19}F NMR were measured, since pure crystals of **12** were not obtained because of lability.

Benzyldimethyl(2,2,2-trifluoroethyl)ammonium triflate (**2**): mp 99—100 °C; ^{1}H NMR δ=3.48 (6H, s, 2×CH_3), 4.65 (2H, q, *J*=9 Hz, CH_2CF_3), 5.00 (2H, s, CH_2), 7.43—7.86 (5H, m); ^{19}F NMR δ=−60.8 (3F, t, *J*=9 Hz, CF_3), −77.6 (3F, s, SCF_3); Mass *m/z* 218 (M^+ −OTf). *N,N*-Dimethyl-*N*-(2,2,2-trifluoroethyl)anilinium triflate (**3**): mp 82—84 °C; ^{1}H NMR δ=4.10 (6H, s, 2×CH_3), 5.25 (2H, q, *J*=9 Hz, CH_2), 7.56—7.83 (3H, m), 8.06—8.26 (2H, m); ^{19}F NMR δ=−62.3 (3F, t, *J*=9 Hz, CF_3), −78.0 (3F, s, SCF_3); Mass *m/z* 204 (M^+ −OTf). Found; C, 36.84; H, 3.87; N, 4.14%. Calcd for $C_{11}H_{13}F_6NO_3S \cdot 1/2H_2O$; C, 36.47; H, 3.89; N, 3.87%. *N*-(2,2,2-Trifluoroethyl)pyridinium triflate (**4**):[7] oil; ^{1}H NMR δ=5.81 (2H, q, *J*=8 Hz, CH_2), 8.28—8.53 (2H, m), 8.80—9.40 (3H, m); ^{19}F NMR δ=−70.7 (3F, t, *J*=8 Hz, CF_3), −77.9 (3F, s, SCF_3); IR (neat) 3070, 1640, 1500, 1400, 1260, 1170, 1030, 840, 780, 695, 640, 600, 520 cm^{-1}; Mass *m/z* 162 (M^+ −OTf). *N*-(2,2,2-Trifluoroethyl)-3,5-lutidinium triflate (**5**): mp 162—164 °C (1,2-dichloroethane); ^{1}H NMR δ=2.70 (6H, s, 2×CH_3 5.72 (2H, q, *J*=8 Hz, CH_2), 8.60 (1H, br.s), 9.02 (2H, br.s); ^{19}F NMR δ=−70.4 (3F, t, *J*=8 Hz, CF_3), −77.9 (3F, s, SCF_3); Mass *m/z* 190 (M^+ −OTf). Found: C, 35.31; H, 3.33, N, 4.07%. Calcd for $C_{10}H_{11}F_6NO_3S$: C, 35.40; H, 3.27; N, 4.13%. *N*-(2,2,2-Trifluoroethyl)-2,6-lutidinium triflate (**6**): mp 188—189 °C (1,2-dichloroethane); ^{1}H NMR δ=2.97 (6H, s, 2×CH_3), 5.68 (2H, q, *J*=8 Hz, CH_2), 7.8—8.6 (3H, m); ^{19}F NMR δ=−65.4 (3F, t, *J*=8 Hz, CF_3), −77.6 (3F, s, CF_3S); Mass *m/z* 190 (M^+ −OTf). Found: C, 35.31; H, 3.33, N, 4.07%. Calcd for $C_{10}H_{11}F_6NO_3S$; C, 35.40; H, 3.27; N, 4.13%. Found; C, 35.30; H, 3.33; N, 4.02%. *N*-(2,2,2-Trifluoroethyl)-2,4,6-collidinium triflate (**7**): mp 146—148 °C (chloroform); ^{1}H NMR δ=2.59 (3H, s, CH_3), 2.96 (6H, s, 2×CH_3), 5.68 (2H, q, *J*=8 Hz, CH_2);7.89 (2H, br.s); ^{19}F NMR δ=−65.6 (3F, t, *J*=8 Hz, CF_3), −77.3 (3F, s, SCF_3); Mass *m/z* 204 (M^+ −OTf). Found: C, 37.10; H, 3.62; N, 3.86%. Calcd for $C_{11}H_{13}F_6NO_3S$: C, 37.40; H, 3.71; N, 3.96%. *N*-(2,2,2-Trifluoroethyl)-3-(ethoxycarbonyl)pyridinium triflate (**8**): mp 88—89 °C (1,2-dichloroethane); ^{1}H NMR δ=1.47 (3H, t, *J*=7 Hz, CH_3), 4.45 (2H, q, *J*=7 Hz, CH_2), 6.04 (2H, q, *J*=8 Hz, CH_2CF_3), 8.50—8.77 (1H, m), 9.30—9.66 (2H, m), 9.89 (1H, br.s, 2-H); ^{19}F NMR δ=−70.5 (3F, t, *J*=8 Hz, CF_3), −78.0 (3F, s, SCF_3); IR (KBr) 1740 (COO) cm^{-1}; Mass *m/z* 234 (M^+ −OTf). Found; C, 34.34; H, 2.89; N, 3.57%. Calcd for $C_{11}H_{11}F_6NO_5S$; C, 34.47; H, 2.89; N, 3.65%. *N*-(2,2,2-Trifluoroethyl)quinolinium triflate (**9**): mp 103—105 °C (1,2-dichloroethane); ^{1}H NMR δ=6.35 (2H, q, *J*=8 Hz, CH_2), 8.05—8.98 (5H, m), 9.52—9.86 (2H, m); ^{19}F NMR δ=−68.6 (3F, t, *J*=8 Hz, CF_3), −77.9 (3F, s, SCF_3); Mass *m/z* 212 (M^+ −OTf). Found: C, 39.69; H, 2.32; N, 3.71%. Calcd for $C_{12}H_9F_6NO_3S$: C, 39.89; H, 2.51; N, 3.88%. *N*-(Trifluoroethyl)benzothiazolinium triflate (**10**): mp 133—135 °C (1,2-dichloroethane); ^{1}H NMR δ=6.06 (2H, q, *J*=8 Hz, CH_2), 8.0—8.4 (2H, m), 8.7—8.9 (2H, m), 10.9 (1H, br.s, 2-H); ^{19}F NMR δ=−69.0 (3F, t, *J*=8 Hz, CF_3), −77.9 (3F, s, SCF_3); Mass *m/z* 218 (M^+ −OTf). Found: C, 32.40; N, 1.75; N, 3.65%. Calcd for $C_{10}H_7F_6NO_3S$: C, 32.70; H, 1.92; N, 3.81%. (2,2,2,-Trifluoroethyl)diphenylsulfonium triflate (**11**): mp 138—140 °C (acetonitrile–ether); ^{1}H NMR (acetonitrile-d_3) δ=5.21 (2H, q, *J*=9 Hz, CH_2), 7.66—7.98 (6H, m), 7.98—8.23 (4H, m); ^{19}F NMR (acetonitrile-d_3) δ=−60.0 (3F, t, *J*=9 Hz, CF_3), −78.0 (3F, s, SCF_3); Mass *m/z* 186 (Ph_2S^+). Found: C, 42.93; H, 2.93%. Calcd for $C_{15}H_{12}F_6O_3S_2$: C, 43.06; H, 2.89%. (2,2,2-Trifluoroethyl)dimethylsulfonium triflate (**12**): ^{1}H NMR (acetonitrile-d_3) δ=3.10 (6H, s, 2×CH_3), 4.30 (2H, q, *J*=9 Hz, CH_2); ^{19}F NMR (acetonitrile-d_3) δ=−61.1 (3F, t, *J*=9 Hz, CF_3), −78.1 (3F, s, SCF_3). (2,2,2-Trifluoroethyl)dibenzothiophenium trilfate (**13**): mp 168 °C (acetonitrile–ether); ^{1}H NMR (acetonitrile-d_3) δ=4.80 (2H, q, *J*=9 Hz, CH_2), 7.78—8.11 (4H, m), 8.34—8.48 (4H, m); ^{19}F NMR (acetonitrile-d_3) δ=−59.4 (3F, t, *J*=9 Hz, CF_3), −78.4 (3F, s, SCF_3); Mass (SIMS method) *m/z* 267 (M^+ −OTf), 184 (267−CH_2CF_3). Found: C, 43.05; H, 2.69%. Calcd for $C_{15}H_{10}F_6O_3S_2$: C, 43.27; 2.42%. (2,2,2-Trifluoroethyl)-

triphenylphosphonium trilfate (**14**): mp 208 °C (acetonitrile–ether); ^{1}H NMR (acetonitrile-d_3) δ=4.42—4.96 (2H, m, CH_2), 7.60—8.00 (15H, m, 3×Ph); ^{19}F NMR (acetonitrile-d_3) δ=−52.5 (3F, dt, J=7, 9 Hz, CF_3), −78.0 (3F, s, SCF_3); ^{31}P NMR (acetonitrile+acetonitrile-d_3, Ph_3P as an standard) δ=22.6 (q, J=7 Hz); Mass m/z 220 (M^+ −OTf). Found: C, 51.05; H, 3.46%. Calcd for $C_{21}H_{17}F_6O_3PS$: C, 51.02; H, 3.47%.

Reaction of Pyridine with (1*H*,1*H*-Perfluoropropyl, -Perfluorobutyl, or -Perfluorooctyl)phenyliodonium Triflate (15, 16, or 17). The procedure was the same as that mentioned above. The reaction time and temperature were as follows: 30 min, room temperature for **15** and **16**; 1 h, reflux temperature for **17**. After each reaction, the solvent was evaporated and the residue recrystallized from 1,2-dichloroethane. Spectral data and elemental analysis of new compounds are as follows. *N*-(1*H*,1*H*-Perfluoropropyl)pyridinium triflate: mp 84—86 °C; ^{1}H NMR δ=6.05 (2H, t, J=15 Hz, CH_2), 8.30—8.66 (2H, m), 8.90—9.50 (3H, m); ^{19}F NMR δ=−77.6 (3F, s, SCF_3), −82.7 (3F, s, CF_3), −119.3 (2F, t, J=15 Hz, CF_2); Mass m/z 262, 242. Found: C, 29.89; H, 1.77; N, 3.80%. Calcd for $C_9H_7F_8NO_3S$: C, 29.93; H, 1.95; N, 3.88%. *N*-(1*H*,1*H*-Perfluorobutyl)-pyridinium triflate: mp 126—127 °C; ^{1}H NMR δ=6.02 (2H, t, J=15 Hz, CH_2), 8.33—8.60 (2H, m), 8.90—9.50 (3H, m); ^{19}F NMR; δ=−77.6 (3F, s, SCF_3), −79.7 (3F, t, J=15 Hz, CH_2CF_2), −116.3 (2F, m, CF_2), −125.3 (2F, m, CF_2); Mass m/z 212, 192. Found: C, 29.07; H, 1.73, N, 3.28%. Calcd for $C_{10}H_7F_{10}NO_3S$: C, 29.21; H, 1.72; N, 3.41%.

Preparation of 18a,b or 19a,b and 20. The procedure was the same as that described above using diphenyl sulfoxide, dimethyl sulfoxide, and pyridine N-oxide as substrates. The reaction time and temperature were as follows: 4 h, room temperature for **18a** or **19a**; 5 h, room temperature for **18b** or **19b**; 3 h, room temperature for **20**. The spectral data and elemental analyasis are shown in the following: **18a** or **19a**: ^{1}H NMR (acetonitrile-d_3) δ=5.15 (2H, q, J=9 Hz, CH_2), 7.35—8.13 (10H, m, 2×Ph); ^{19}F NMR (acetonitrile-d_3) δ=−72.8 (3F, t, J=9 Hz, CF_3), −78.0 (3F, s, SCF_3). **18b** or **19b**: ^{1}H NMR (acetonitrile-d_3) δ=3.41 (6H, s, 2×CH_3), 4.82 (2H, q, J=9 Hz, CH_2); ^{19}F NMR (acetonitrile-d_3) δ=−73.9 (3F, t, J=9 Hz, CF_3), −78.0 (3F, s, SCF_3). Salt **20** was purified by washing the oily product, which was obtained by adding pentane to the reaction solution, with pentane. **20**: oil; ^{1}H NMR (acetonitrile-d_3) δ=5.26 (2H, q, J=9 Hz, CH_2), 8.06—8.40 (2H, m, 4-H), 8.58—8.80 (1H, m, 3-H), 9.00—9.28 (2H, m, 2-H); ^{19}F NMR (acetonitrile-d_3) δ=−72.0 (3F, t, J=9 Hz, CF_3), −78.0 (3F, s, SCF_3); Mass m/z 178 (M^+ −OTf). Found: C, 28.36; H, 2.23; N, 4.16%. Calcd for $C_8H_7F_6NO_4S \cdot 1/2H_2O$: C, 28.58; H, 2.40; N, 4.17%.

Reaction of 14 with Benzaldehyde. Into a mixture of 5 mmol of dry cesium fluoride in 5 ml of dry *N,N*-dimethylformamide were added 1 mmol of **14** and 1 mmol of benzaldehyde. The reaction mixture was stirred at room temperature for 8 h, poured into water, and extracted with pentane. The pentane layer was washed with water, dried with magnesium sulfate, and concentrated. The product yields were determined by ^{19}F NMR analyses of the concentrated solution. Structural assignments were carried out by spectral analyses of the isolated products. β-(Trifluoromethyl)styrene: ^{19}F NMR (chloroform-*d*) δ=−58.3 (d, J=9.0 Hz, CF_3, *Z*-isomer), −64.1 (dd, J=7.0, 2.0 Hz, CF_3, E-isomer).

References

1) a) "90 Nendai No Fussokei Seirikassei Bussitu No Kaihatu To Oyo," ed by N. Ishikawa, CMC Co., Ltd., Tokyo (1990). b) "Fusso Kagobutu No Gosei To Kino," ed by N. Ishikawa, CMC Co., Ltd., Tokyo (1987). c) "Biomedicinal Aspects of Fluorine Chemistry," ed by R. Filler and Y. Kobayashi, Kodansha Ltd., Tokyo (1982). d) N. Kokubu, "Fusso No Kagaku," Shokabo Co., Ltd., Tokyo (1989), pp. 95—97.

2) For example: a) I. Gosney and A. G. Rowley, "Organophosphorus Reagents in Organic Synthesis," ed by J. I. G. Cadogan, Academic Press (1979), Chap. 2. b) B. M. Trost and L. S. Melvin, Jr., "Sulfur Ylides," Academic Press (1975). c) E. Block, "Reactions of Organosulfur Compounds," Academic Press (1978), Chap. 3.

3) a) J. Bardon and V. C. R. McLoughlin, *Tetrahedron,* **21**, 1 (1965). b) R. A. Henry, *J. Chem. Eng. Data,* **21**, 503 (1976). c) M. Kuwabara, H. Miura, K. Fukunishi, M. Nomura, and H. Yamanaka, *Nippon Kagaku Kaishi,* **1986**, 681. d) H. Yamanaka, M. Kuwabara, M. Okudo, K. Fukunishi, and M. Nomura, *ibid.,* **1985**, 1988.

4) a) T. Umemoto and Y. Gotoh, *J. Fluorine Chem.*, **28**, 235 (1985). b) *idem., ibid.*, **31**, 231 (1986). c) *idem., Bull. Chem. Soc. Jpn.,* **60**, 3307 (1987). d) *idem., ibid.,* **60**, 3823 (1987).

5) Recently, Yagupol'skii et al. reported the synthesis and reactivity of (1*H*,1*H*,ω*H*-perfluoroalkyl)phenyliodonium tetrafluoroborate, but in their paper they mentioned that the smallest one, (2,2,2-trifluoroethyl)phenyliodonium tetrafluoroborate could not be prepared; A. A. Mironova, I. V. Soloshonok, I. I. Maletina, V. V. Orda, and L. M. Yagupol'skii, *J. Org. Chem., USSR,* **1988**, 530.

6) D. M. Updegraff, D. C. Kvam, and J. E. Robertson, *J. Pharm. Sci.,* **59**, No. 2, 188 (1970).

7) It was described that salt **4** was formed when 2,2,2-trifluoroethanol was treated with trifluoromethanesulfonyl fluoride in the presence of pyridine, but **4** was not fully assigned.[3a]

Formation of Acyclic *cis*-Azobenzene without Light

Nobuyuki TAMAOKI,* Sawako YOSHIMURA, and Tsuguo YAMAOKA
Department of Image Science and Technology, Faculty of Engineering, Chiba University, 1-33 Yayoi-cho, Chiba 260
(Received February 2, 1991)

Synopsis. Reduction mixture of bis(4-nitrobenzyl) ether contained a considerable amount of *cis*-4,4′-dimethylazobenzene.

Although several chemical syntheses of *trans*-azobenzene derivatives are known,[1] chemical syntheses of *cis* isomers are known only in the case of cyclic azobenzene derivatives.[2] The only method to synthesize acyclic *cis*-azobenzene derivatives ever known is a photochemical one, namely, exposing the corresponding *trans*-azobenzene derivatives to UV light.[3] This is probably due to the fact that the intermediates in the chemical formations of azo linkages energetically favor *trans* conformations about the N–N bonds. In this note we describe the one-pot chemical formation of *cis*-4,4′-dimethylazobenzene, **3**, without using light.

Bis(4-nitrobenzyl) ether, **1**, was reduced with $LiAlH_4$ in dry THF by a high-dilution method. It was found by TLC that the reaction mixture contained several orange products. The mixture was then separated by column chromatography. Two main orange compounds which were eluted together during the early stage of chromatography were further separated by preparative GPC and crystallized by slow evaporation of the solvent under atmospheric pressure at room temperature. One of the fractions was identified as being *trans*-4,4′-dimethylazobenzene by comparing the ^{1}H NMR and retention time on reversed-phase HPLC with an authentic sample# which was synthesized by the reduction of 4-nitrotoluene. Identification of the fraction was further confirmed by FD-MS. The detected mass was 210, which corresponds to 4,4′-dimethylazobenzene. The other fraction of the preparative GPC showed two peaks on reversed-phase HPLC after crystallization. This means that the compound in this fraction of GPC is slowly changed to another compound in the dark. On the ^{1}H NMR chart there exist four kinds of doublets (each two peaks of which is coupled) and two kinds of singlets. By a comparison of ^{1}H NMR and the retention time on reversed-phase HPLC with an authentic mixture prepared by the UV irradiation of *trans*-4,4′-dimethylazobenzene in solvent, the second isolated fraction was identified as being a mixture of *trans*- and *cis*-4,4′-dimethylazobenzene.

Since we performed the entire process under yellow light (<500 nm), it is certain that *cis*-4,4′-dimethylazobenzene is formed chemically, not photochemically. This interesting phenomenon is explained as below (scheme). Bis(4-nitrobenzyl) ether was first reduced to form 2-oxa-10,11-diaza[3.2]paracyclophan-10-ene, **2** in which the azo linkage is fixed to the *cis* form due to a ring restriction. The cyclophane is destabilized by ring strain and is thus very easily further reduced to form an acyclic azobenzene derivative, **3**, while maintaining the azo configuration in the *cis* form. Another possible route, in which the ether linkage of **1** is first decomposed to form 4-nitrotoluene and then converted to **3**, is excluded by the following observation. A reduction of 4-nitrotoluene under similar conditions did not produce *cis*-4,4′-dimethylazobenzene, but produced *trans*-4,4′-dimethylazobenzene only.

This proposed reaction process to form the *cis*-azobenzene derivative is also interesting fields involving the synthesis of cyclophanes which contain hetero atoms. The synthesis of 10,11-diaza[3.2]paracyclophane-10-enes has not yet succeeded, in spite of the intensive efforts by Funke and Grützmacher.[4] Although we have not yet isolated 10,11-diaza[3.2]paracyclophane-10-enes, we believe that 1,3-bis(4-nitrophenyl)propane will be stably converted to 10,11-diaza[3.2]paracyclophan-10-ene under the same reduction conditions as described in this study.

Experimental

Synthesis of Bis(4-nitrobenzyl) Ether, 1: **1** was synthesized by a bimolecular condensation of 4-nitrobenzyl alcohol, **4**. 6 ml of concd H_2SO_4 was added to 25 g of **4** in 150 ml of benzene. The solution was heated under reflux for 4 h. After that, H_2SO_4 was further added until **4** completely disappeared. After 25 h the solution was cooled to room temperature and washed four times with 100 ml (each) of water. A small portion of **1** appeared as a white solid two or three days after removing the benzene from the solution by evaporation. Additional **1** appeared after removing (4-nitrophenyl)-

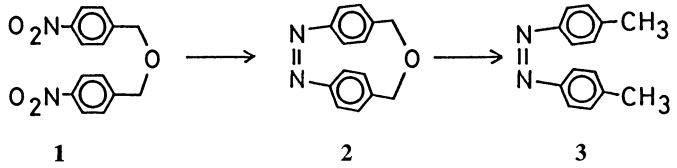

1 **2** **3**

Scheme 1.

#^{1}H NMR (270 MHz) *trans*-4,4-dimethylazobenzene ($CDCl_3$) δ=2.43 (s, 6H), 7.30 (d, J=8.2 Hz, 4H, Ar), 7.81 (d, J=8.2 Hz, 4H, Ar); *cis*-4,4′-dimethylazobenzene ($CDCl_3$) δ=2.30 (s, $-CH_3$), 6.77 (d, J=7.2 Hz, 4H, Ar), 7.05 (d, J=7.2 Hz, 4H, Ar).

phenylmethane[5] from the remaining solution by distillation. The product was combined and recrystallized from ethanol. 3.82 g (16.2%), mp 97—98 °C (lit,[6] 97—98 °C), ^{1}H NMR ($CDCl_3$) δ=4.72 (s, 4H, CH_2OCH_2), 7.55 (d, 4H, Ar), 8.24 (d, 4H, Ar).

Reduction of 1: A solution of 5.0 g of **1** in 100 ml of dry THF was added dropwise for 3 h to a suspension of 3.4 g of $LiAlH_4$ in 140 ml of dry THF under a nitrogen atmosphere. After 20 h of stirring, a small amount of water was carefully added to the reaction mixture in order to destroy the remaining any $LiAlH_4$. O_2 was then passed through the reaction mixture for 4.5 h in order to oxidize any hydrazo compounds to the corresponding azo compounds. The solid was filtered off and the filtrate evaporated. The residue was extracted by chloroform. A condensed chloroform solution was transferred to a silica gel column and eluted with hexane–chloroform (1:1 v/v). The first eluent was further purified by preparative GPC (Waters, ULTRASTYRAGEL 500 Å+100 Å/chloroform). *cis*- and *trans*-4,4′-Dimethylazobenzene was eluted at retention volumes of 95.5 and 99.6 ml, respectively. By slowly evaporating of chloroform parts of the first fraction (8.07 mg, 0.21%) and second fraction (0.196 g, 5.1%) were isolated.

We are grateful to Mr. Madoka Yasuike and Mr. Yasumasa Toba of Toyo Ink M.F.D. Co., Ltd., Japan for FD mass spectra.

References

1) H. E. Bigelow and D. B. Robinson, *Org. Synth.*, Coll. Vol. III, 103 (1955), and references sited in.

2) a) H. Dural, *Bull. Soc. Chim. Fr.*, **4**, 727 (1910). b) G. M. Badger, J. H. Seidler, and B. Thomson, *J. Chem. Soc.*, **1951**, 3207. c) U. Funke and H.-F. Grützmacher, *Tetrahedron*, **43** (16), 3787 (1987). d) H.-F. Grützmacher and J. Schmiegel, *Chem. Ber.*, **122**, 1929 (1989).

3) A. H. Cook, *J. Chem. Soc.*, **1938**, 876.

4) U. Funke and H.-F. Grützmacher, *Chem. Ber.*, **122**, 1503 (1989).

5) A. Basler, *Ber.*, **16**, 2714 (1883).

6) P. F. G. Praill, *J. Chem. Soc.*, **1957**, 3162.

Efficient Transformation of Methyl Propargyl Ethers into α,β-Unsaturated Ketones

Yukitoshi FUKUDA† and Kiitiro UTIMOTO*
Department of Industrial Chemistry, Faculty of Engineering, Kyoto University, Sakyo-ku, Yoshida, Kyoto 606
(Received February 13, 1991)

Synopsis. Methyl propargyl ethers, obtained from carbonyl compounds by successive treatment with an acetylide and MeI, were easily converted to the corresponding α,β-unsaturated ketone by regioselective hydration of acetylenic moiety followed by elimination of methanol under the catalytic action of Au(III).

Hydration of an acetylenic moiety has been utilized for the preparation of ketones from easily accessible alkynes. Various transition metal catalysts have been employed for the hydration of unactivated alkynes.[1-14] As a propargylic alcohol **1** is a suitable precursor of α-hydroxy ketone **2** or α,β-unsaturated ketone **4** by the regiocontrolled hydration, generally applicable methodologies have been needed. We have disclosed the regioselective formation of **2** (R=Ac) from acetate **1** (R=Ac) under the catalytic action of Au(III).[15] As for selective formation of **4**, Hg(II) catalysts are applied in strongly acidic conditions, other effective catalysts are needed for the transformation in mild conditions.

During the continuous studies on selective hydration of the derivatives of propargyl alcohols **1**, we have observed the highly regioselective hydration of methyl ethers to give **4** exclusively. This paper describes Au(III) catalyzed regioselective hydration of **1** (R=Me) under mild conditions.

Internal methyl propargyl ethers **1** (R=Me, R^1 and/or $R^2 \neq H$, $R^3 \neq H$) were treated with $NaAuCl_4$ (5 mol%) in refluxing aqueous methanol to give α,β-unsaturated ketones by regioselective hydration followed by elimination of methanol. A propargyl methyl ether **1f** (R=Me, $R^1=R^2=H$, $R^3=n$-C_5H_{11}), on the other hand, afforded β-methoxy ketone **3f** (R=Me, $R^1=R^2=H$, $R^3=n$-C_5H_{11}) in an excellent yield. Results are summarized in Table 1.

Although the hydration of internal propargyl methyl ethers afforded α,β-unsaturated ketone **4** mainly, small amount of methoxy ketone **3** was obtained as a by-product. Pure **4** was obtained by column chromatography. An attempt to obtain **4** in pure state by employing nonalcoholic solvent was unsuccessful; the reaction of 4-methoxy-2-nonyne (**1b**) in aqueous tetrahydrofuran or acetonitrile resulted in quantitative recovery of the starting material.

The stereochemistry around the double bond was exclusively *trans* in the cases of disubstituted olefins (Entry 1—3). It should be noted that alkynes bearing a methoxyl substituent on the propargylic position were regioselectively hydrated as described above, whereas no regioselectivity was observed in the hydration of simple alkynes catalyzed by Au(III) salt.[12,15] This regioselectivity might be realized both by electron withdrawing effect of the methoxyl group or by the interaction of oxygen with Au(III) at transition state; the reverse regioselectivity was observed for acetoxy alkynes where anchimeric interaction of carbonyl oxygen with Au(III) could control the regioselectivity.[10,12,13]

In contrast to the regioselective hydration giving **3** or **4** from methyl propargyl ethers (**1**, R=Me, $R^3 \neq H$), a methyl ether of α-ethynyl alcohol (**1g**, R=Me, $R^1=n$-

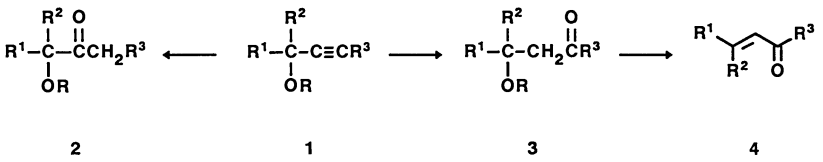

2 **1** **3** **4**

Scheme 1. Hydration of propargyl alcohol derivatives.

Table 1. Au(III) Catalyzed Hydration of Methyl Propargyl Ether **1** (R=Me)

Entry	Starting material	R^1	R^2	R^3	Reaction time[a]/h	Product	Yield/%[b]
1	**1a**	n-C_5H_{11}	H	n-C_4H_9	2	**4a**	79
2	**1b**	n-C_5H_{11}	H	CH_3	2	**4b**	75
3	**1c**	C_2H_5	H	Ph	10	**4c**	21
4	**1d**	CH_3	CH_3	n-C_6H_{13}	10	**4d**	70
5	**1e**	$-(CH_2)_5-$		CH_3	10	**4e**	30
6	**1f**	H	H	n-C_5H_{11}	5	**3f**	91
7	**1g**	n-C_5H_{11}	H	H	1	**2g**	91

a) Refluxed in MeOH containing 10% H_2O. b) Isolated yield after column chromatography.

† On leave from Kyowa Yuka Co., Ltd., Yokkaichi, Mie.

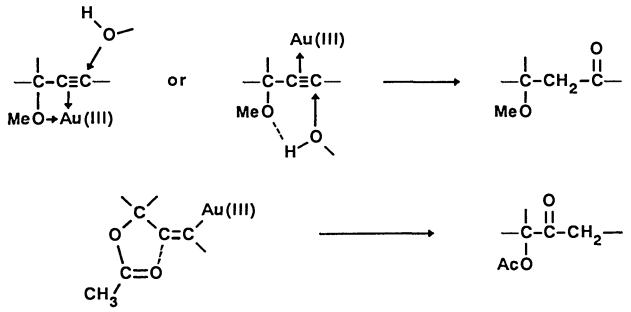

Scheme 2. Regioselective hydration.

C_5H_{11}, R^2=R^3=H) afforded α-methoxyketone **2g** (Table 1, Entry 7).

The conversion of propargyl alcohols into, α,β-unsaturated ketones has been known as Meyer–Schuster rearrangement.[16] This rearrangement, however, requires strongly acidic conditions, and aliphatic propargyl alcohols were not applicable to the reaction.

Compared with reported procedures, the Au(III) catalyzed reaction described above produces α,β-unsaturated ketones in good yields under mild and neutral conditions. Since methyl propargyl ethers are easy accessible by the etherification of propargyl alcohols,[17,18] the above described hydration would find practical uses in organic synthesis.

Experimental

IR spectra were obtained on a JASCO IR-810 spectrometer. ^{1}H NMR (200 MHz) were measured on a Varian XL-200. Elemental analyses were performed at Elemental Analysis Center of Kyoto University.

Preparation of Methyl Propargyl Ethers 1: Methyl propargyl ethers were prepared from 1-alkyne, aldehyde or ketone, and methyl iodide described in the literature.[18] Alternatively, they were synthesized by the reaction of propargyl alcohols, whose easy synthesis is known as Favorskii–Babayan synthesis,[19] with methyl iodide in the presence of solid potassium hydroxide in DMSO (dimethyl sulfoxide).[17]

Hydration of Methyl Propargyl Ethers 1 to α,β-Unsaturated Ketones 4 (General Procedure): Methyl propargyl ether (**1**, 1 mmol) was dissolved in a mixture of methanol (10 ml) and water (1 ml) and $NaAuCl_4 \cdot 2H_2O$ (20 mg, 0.05 mmol, 5 mol%) was added to this solution. The reaction mixture was heated at reflux for 2—10 h and then concentrated under reduced pressure. The residue was diluted with ether and washed with 1 : 1 mixture of brine and aqueous ammonia. The ethereal solution was dried over Na_2SO_4 and concentrated to give the crude product, which was purified by column chromatography (silica gel; hexane–ethyl acetate).

7-Methoxy-5-dodecyne (1a): ^{1}H NMR ($CDCl_3$), δ=0.89 (3H, t, *J*=7.0 Hz), 0.92 (3H, t, *J*=7.0 Hz), 1.22—1.74 (12H, m), 2.23 (2H, td, *J*=6.8, 2.0 Hz), 3.39 (3H, s), 3.91 (1H, tt, *J*=6.3, 2.0 Hz); IR (neat) 2220, 1378, 1337, 1186, 1143, 1121, 1097, 984, 925, 899, 728 cm^{-1}; Found: C, 79.35; H, 12.42%. Calcd for $C_{13}H_{24}O$: C, 79.53; H, 12.32%.

4-Methoxy-2-nonyne (1b): ^{1}H NMR ($CDCl_3$), δ=0.89 (3H, t, *J*=6.4 Hz), 1.23—1.52 (8H, m), 1.87 (3H, d, *J*=2.0 Hz), 3.39 (3H, s), 3.89 (1H, tq, *J*=6.9, 2.0 Hz); IR (neat) 2250, 1021, 1095, 927, 900 cm^{-1}; Found: C, 77.60; H, 11.96%. Calcd for $C_{10}H_{18}O$: C, 77.86; H, 11.76%.

3-Methoxy-1-phenyl-1-pentyne (1c): ^{1}H NMR ($CDCl_3$), δ=1.08 (3H, t, *J*=7.2 Hz), 1.84 (2H, quint, *J*=7.2 Hz), 3.49 (3H, s), 4.12 (1H, t, *J*=7.2 Hz), 7.34 (3H, m), 7.46 (2H, m); IR (neat) 3075, 3050, 2220, 1595, 1490, 1464, 1444, 1338, 1128, 1105, 1085, 755, 690 cm^{-1}; Found: C, 82.58; H, 8.17%. Calcd for $C_{12}H_{14}O$: C, 82.72; H, 8.10%.

2-Methoxy-2-methyl-3-decyne (1d): ^{1}H NMR ($CDCl_3$), δ=0.90 (3H, t, *J*=6.7 Hz), 1.24—1.58 (8H, m), 1.42 (6H, s), 2.19 (2H, t, *J*=6.9 Hz), 3.35 (3H, s); IR (neat) 2225, 1376, 1359, 1225, 1172, 1150, 1079 cm^{-1}; Found: C, 78.85; H, 12.27%. Calcd for $C_{12}H_{22}O$: C, 79.06; H, 12.16%.

1-Methoxy-1-(1-propynyl)cyclohexane (1e): ^{1}H NMR ($CDCl_3$), δ=1.18—1.93 (10H, m), 1.88 (3H, s), 3.35 (3H, s); IR (neat) 1294, 1185, 1146, 1094, 926 cm^{-1}; Found: C, 78.71; H, 10.84%. Calcd for $C_{10}H_{16}O$: C, 78.89; H, 10.59%.

6-Dodecen-5-one (4a): ^{1}H NMR ($CDCl_3$), δ=0.90 (3H, t, *J*=6.7 Hz), 0.93 (3H, t, *J*=7.2 Hz), 1.29—1.67 (10H, m), 2.23 (2H, tdd, *J*=7.3, 7.3, 1.6 Hz), 2.53 (2H, t, *J*=7.5 Hz), 6.10 (1H, dt, *J*=16.0, 1.6 Hz), 6.83 (1H, dt, *J*=16.0, 7.3 Hz); IR (neat) 3050, 1699, 1676, 1631, 1378, 1192, 983 cm^{-1}; Found: C, 78.86; H, 12.35%. Calcd for $C_{12}H_{22}O$: C, 79.06; H, 12.16%.

Pure **3a** was obtained in 6% yield: ^{1}H NMR ($CDCl_3$), δ=0.90 (3H, t, *J*=6.9 Hz), 0.92 (3H, t, *J*=7.0 Hz), 1.25—1.72 (12H, m), 2.44 (1H, dd, *J*=16.1, 5.1 Hz), 2.46 (2H, t, *J*=7.3 Hz), 2.68 (1H, dd, *J*=16.1, 7.7 Hz), 3.32 (3H, s), 3.45 (1H, m); IR (neat) 1714, 1128, 1093 cm^{-1}; Found: C, 72.69; H, 12.44%. Calcd for $C_{13}H_{26}O_2$: C, 72.84; H, 12.23%.

3-Nonen-2-one (4b): ^{1}H NMR ($CDCl_3$), δ=0.89 (3H, t, *J*=6.8 Hz), 1.24—1.55 (6H, m), 2.22 (2H, tdd, *J*=6.2, 6.2, 1.6 Hz), 2.23 (3H, s), 6.02 (1H, dt, *J*=16.0, 1.6 Hz), 6.83 (1H, dt, *J*=16.0, 7.0 Hz); IR (neat) 3050, 3000, 1698, 1675, 1624, 1360, 1254, 980 cm^{-1}; Found: C, 76.82; H, 11.80%. Calcd for $C_9H_{16}O$: C, 77.09; H, 11.50%.

1-Phenyl-2-penten-1-one (4c): ^{1}H NMR ($CDCl_3$), δ=1.16 (3H, t, *J*=7.2 Hz), 2.36 (2H, qdd, *J*=7.2, 6.2, 1.6 Hz), 6.87 (1H, dt, *J*=16.0, 1.6 Hz), 7.12 (1H, dt, *J*=16.0, 6.2 Hz), 7.50 (3H, m), 7.95 (2H, m); IR (neat) 3050, 1671, 1648, 1621, 1283, 1215, 990, 972, 691 cm^{-1}; Found: C, 82.31; H, 7.52%. Calcd for $C_{11}H_{12}O$: C, 82.46; H, 7.55%.

2-Methyl-2-decen-4-one (4d): ^{1}H NMR ($CDCl_3$), δ=0.88 (3H, t, *J*=6.7 Hz), 1.22—1.71 (8H, m), 1.89 (3H, d, *J*=2.0 Hz), 2.14 (3H, d, *J*=2.0 Hz), 2.40 (2H, t, *J*=7.4 Hz), 6.08 (1H, septi, *J*=2.0 Hz); IR (neat) 1689, 1622, 1378, 1132, 730 cm^{-1}; Found: C, 78.69; H, 12.01%. Calcd for $C_{11}H_{20}O$: C, 78.51; H, 11.98%.

1-Cyclohexylidene-2-propanone (4e): ^{1}H NMR ($CDCl_3$), δ=1.52—1.75 (6H, m), 2.12 (2H, m), 2.13 (3H, s), 2.81 (2H, br-t, *J*=6.0 Hz), 6.02 (1H, s); IR (neat) 3000, 1687, 1620, 1173, 960 cm^{-1}; Found: C, 77.99; H, 10.05%. Calcd for $C_9H_{14}O$: C, 78.21; H, 10.21%.

Hydration of 1-Methoxy-2-octyne (1f): **1f** was prepared from commercially available 2-octyn-1-ol by the reaction with methyl iodide according to the procedure described above.

1-Methoxy-2-octyne (1f): ^{1}H NMR ($CDCl_3$), δ=0.90 (3H, t, *J*=7.0 Hz), 1.25—1.63 (6H, m), 2.23 (2H, tt, *J*=7.2, 2.4 Hz), 3.37 (3H, s), 4.08 (2H, t, *J*=2.4 Hz); IR (neat), 2170, 1184, 1131, 1096, 1000, 905 cm^{-1}; Found: C, 77.02; H, 11.44%. Calcd for $C_9H_{16}O$: C, 77.09; H, 11.50%.

1-Methoxy-3-octanone (3f): ^{1}H NMR ($CDCl_3$), δ=0.88 (3H, t, *J*=6.8 Hz), 1.20—1.72 (6H, m), 2.44 (2H, t, *J*=7.2 Hz), 2.65 (2H, t, *J*=6.4 Hz), 3.34 (3H, s), 3.65 (2H, t, *J*=6.4 Hz); IR (neat) 1716, 1119 cm^{-1}; Found: C, 68.01; H, 11.55%. Calcd for $C_9H_{18}O_2$: C, 68.31; H, 11.47%.

3-Methoxy-1-octyne (1g): **1g** was obtained by the methylation of commercially available 1-octyne-3-ol. ^{1}H NMR ($CDCl_3$), δ=0.90 (3H, t, *J*=6.5 Hz), 1.25—1.80 (8H, m), 2.46 (1H, d, *J*=2.0 Hz), 3.40 (3H, s), 3.95 (1H, td, *J*=6.3, 2.0 Hz); IR (neat) 3300, 2100, 1120, 1096, 940, 917 cm^{-1}; Found: C, 76.80; H, 11.69%. Calcd for $C_9H_{16}O$: C, 77.09; H, 11.50%.

Hydration of Methyl Ether of α-Ethynyl Alcohol (1g): 3-Methoxy-1-octyne (**1g**, 140 mg, 1 mmol) was dissolved in a mixture of methanol (10 ml) and water (1 ml) and

$NaAuCl_4 \cdot 2H_2O$ (8 mg, 0.025 mmol, 2 mol%) was added to this solution. The reaction mixture was heated at reflux for 1 h, concentrated in vacuo and then diluted with ether. The ethereal solution was washed with 1:1 mixture of brine and aqueous ammonia, dried (Na_2SO_4) and concentrated. Column chromatographical purification gave 3-methoxy-2-octanone (**2g**, 143 mg, 0.91 mmol, 91% yield).

3-Methoxy-2-octanone (2g): ^1H NMR ($CDCl_3$), δ=0.89 (3H, t, J=6.2 Hz), 1.18—1.67 (8H, m), 2.15 (3H, s), 3.36 (3H, s), 3.59 (1H, t, J=7.0 Hz); IR (neat) 1717, 1354, 1123, 1100 cm^{-1}; Found: C, 68.32; 11.63%. Calcd for $C_9H_{18}O_2$: C, 68.31; H, 11.47%.

References

1) P. F. Hudrlik and A. M. Hudrlik, "The Chemistry of Carbon–Carbon Triple Bond," John Wiley and Sons, New York (1978), Part I.
2) V. Jager and H. G. Viehe, "Methoden der Organishen Chemie (Houben–Weyl)," 4th ed, ed by E. Muller, (1977), Vol. V/2a.
3) T. F. Rutledge, "Acetylenes and Allenes," Reinhold, New York (1969).
4) G. A. Olah and D. Meidar, *Synthesis,* **1978**, 671.
5) G. Chandra, D. Devaprahakara, and M. S. Muthana, *Curr. Sci.,* **40**, 400 (1971).
6) G. W. Stacy and R. A. Mikulec, *Org. Synth.,* Coll. Vol. IV, 13 (1963).
7) M. S. Newman, *J. Am. Chem. Soc.,* **75**, 4740 (1953).
8) M. A. Islam and R. A. Raphael, *J. Chem. Soc.,* **1952**, 4086.
9) A. Janout and S. L. Regen, *J. Org. Chem.,* **47**, 3331 (1982).
10) G. Stork and R. Borch, *J. Am. Chem. Soc.,* **86**, 935, 936 (1964).
11) W. D. Harman, J. C. Dobson, and H. Taube, *J. Am. Chem. Soc.,* **111**, 3061 (1989).
12) K. Imi, K. Imai, and K. Utimoto, *Tetrahedron Lett.,* **28**, 3127 (1987).
13) K. Utimoto, *Pure Appl. Chem.,* **55**, 1845 (1983).
14) W. C. Hiscox and P. W. Jennings, *Organometallics,* **9**, 1997 (1990).
15) Y. Fukuda and K. Utimoto, *J. Org. Chem.,* **56** (1991), in press.
16) K. Meyer and K. Schuster, *Ber,* **55**, 819 (1922).
17) R. A. W. Johnstone and M. E. Rose, *Tetrahedron,* **35**, 2169 (1979).
18) L. Bransma and H. D. Verkruijsse, "Synthesis of Acetylenes, Allenes and Cumulenes," Elsevier, Amsterdam (1981), p. 231.
19) A. W. Johnson, "The Chemistry of Acetylenic Compounds," London (1946), Vol. 1, p. 14.

Reduction of Carbon Dioxide to Give Unstable Carbon Oxides. An Attempt of Capture of Unstable Carbon Oxides Formed by the Reduction of Carbon Dioxide with Benzoin Carbanion Using Phenyliodonium Bis(phenylsulfonyl)methylide

Fuminori AKIYAMA
Chemical Research Institute of Nonaqueous Solutions, Tohoku University, Sendai 980
(Received March 11, 1991)

Synopsis. Capture of unstable carbon oxides formed by the reduction of carbon dioxide (CO_2) with benzoin carbanion using phenyliodonium bis(phenylsulfonyl)methylide (**1**) was tried. In this reaction decomposition of the ylide **1** by the unstable carbon oxides was observed to give phenylsulfonylcarbene : $CH(SO_2Ph)$.

The reaction of CO_2 is receiving much attention in view of the use of resources. In most of many reactions of CO_2 reported, CO_2 combines with organic compounds keeping CO_2 unit to give carboxylic acids, carbonates, lactones, carbamates, substituted 5(2*H*)-oxazolones, and substituted 2-oxazolidinones as described in the preceding papers.[1] In a previous paper[2] of this study, a hypothesis that CO_2 can be converted to unstable carbon oxides by the reduction with mild reducing reagent such as benzoin carbanion and that the unstable carbon oxides formed have special reactivities, has been proposed. The preceding papers have shown that the reduction products of CO_2 with benzoin carbanion, which was formed using LDA, had special reactivities with sydnones,[3] and that carbon atom of unstable carbon oxides was captured by sodium dithionites.[1]

Unstable carbon oxides formed by the reduction of CO_2 with benzoin carbanion was considered to have the structure : $C\frac{}{n}C=O$.[1] Various sorts of unstable carbon oxides such as C_2O,[4] C_3O,[5] C_4O,[6] and C_6O[6] have been reported to have the structure : $C\frac{}{n}C\frac{}{n}C=O$.[1] Since unstable carbon oxides are considered to have carbene and cumulene structures, it seems to be preferable to use substances having ability to eject carbene in order to capture such carbon oxides. Recently, it has been reported that phenyliodonium bis(phenylsulfonyl)-methylide $PhI^+-C^-(SO_2Ph)_2$ (**1**) are able to eject carbene under mild conditions.[7] In the present report it will be shown that unstable carbon oxides formed by the reduction of CO_2 with benzoin carbanion show specific reaction behavior to phenyliodonium bis(phenylsulfonyl)methylide (**1**).

Results and Discussion

Benzoin carbanion was formed by the reaction of benzoin with lithium metal (see Experimental).[8] After treating of the THF solution of benzoin carbanion with CO_2 gas, the ylide **1** was added to this solution and the products were separated as described in Experimental. In this reaction mixture, besides benzoin, benzil, hydrobenzoin, and lithium benzoate, the insertion products of the carbene derived from the ylide **1** to benzoin were observed. The insertion products consisted of two isomers. Because of close R_f values of two isomers, relatively low solubilities, and a little instabilities of these isomers,[1] separation of two isomers were unsuccessful. However, analyses of a mixture of two isomers and trimethylsilylation and acetylation of these two isomers showed that the mixture consisted of isomer **2** and **3** (vide infra).

Mass spectroscopy indicated following peaks; m/z 366 (M^+, rel intensity 3), 259 ($M^+ - CH(OH)Ph$, 58), 125 (PhSO, 13), 118 (CHC(O)Ph, 31), and 105 (PhCO, 100). Measurement of molecular weight by means of vapor phase osmometry also showed that molecular weight of the mixture was 366. IR spectrum of the mixture indicated the absorptions at 3475 (OH), 1683 (C=O), 1302 and 1153 (SO_2), 1083 (C–O), 746 and 700 cm^{-1} (Ph).

^1H NMR spectrum of the mixture of two isomers indicated that the isomer **2** had signals at 7.0—8.0 ppm (Ph), 5.85—5.89 ppm (two doublets combined to give a triplet, HC(OH)(Ph) for two diastereomers of **2**), 4.30—4.51 ppm (two doublets, $HC(SO_2Ph)$ for two diastereomers of **2**). Double irradiation at 5.85—5.89 ppm converted two doublets at 4.30—4.51 ppm into two singlets. ^1H NMR spectrum of the mixture also indicated that isomer **3** had signals at 7.0—8.0 ppm (Ph) and 4.25—4.29 ppm (s,[10], CH_2SO_2Ph). Double irradiation technique for this case did not give any change in this apectrum.

^{13}C NMR of the two isomers were assigned reasonably as following (absorptions for phenyl groups appear at 124—141 ppm)

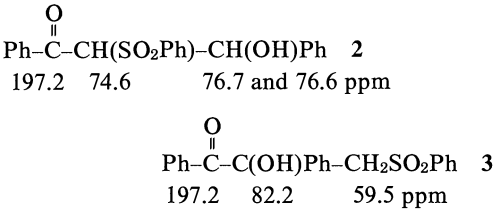

Trimethylsilylation of a mixture of **2** and **3** using trimethylchlorosilane, hexamethyldisilazane, and pyridine gave a rearranged silylated compound and a small amount of decomposition product, in addition to silylated products of **2** and **3**. R_f values of two silylated products of **2** and **3** were almost same and that of a rearranged silylated compound was slightly smaller than those of two silylated products of **2** and **3**. It was impossible to isolate the silylated product of **2** and **3** from a mixture of these compounds having similar R_f values by TLC or HPLC. Acetylation of a mixture of **2** and **3** by a mixture of acetic anhydride and pyridine showed disappearance of ^1H NMR absorption at 4.30—4.51 and 5.85—5.89 ppm, which are attributed to those

of isomer **2** (vide ante), and appearrance of ^{1}H NMR absorption (singlet) at 6.72 ppm. Presumably the isomer **2** was dehydrated to give an olefin. By this acetylation the isomer **3** was converted to an acetylated product which showed ^{1}H NMR absorption at 4.29 ppm (2H, CH_2SO_2Ph) and 2.2 ppm (3H, CH_3CO). Unfortunately R_f values of an acetylated product of **3** and this decomposition product of **2** were almost same. Therefore, isolation of the acetylated product of **3** from this mixture by means of TLC or HPLC was impossible. However, this acetylation experiment indicated that ^{1}H NMR absorptions at 4.30—4.51 and 5.85—5.89 ppm can be attributed to one isomer **2** and a singlet at 4.25—4.29 ppm can be attributed to another isomer **3**.

Yields of **2** and **3** were 10 and 8 mol% based on ylide **1** used, respectively. Although the yields of the products **2** and **3** are relatively low, formation of **2** and **3** indicates that unstable carbon oxides formed by the reduction of CO_2 with benzoin carbanion decomposes ylide **1** to give a carbene and the carbene formed inserts to benzoin to give **2** and **3**.

One might suppose that ylide **1** is decomposed by the compounds which is present in the solution. In order to exclude this possibility, six sorts of control experiments were undertaken. The reactions of ylide **1** with following six mixtures were carried out at room temperature for 0.5 h. (a) Benzoin and THF; (b) Benzoin, Li, and THF; (c) Benzoin, benzaldehyde, and THF; (d) Benzoin, hydrobenzoin (see Experimental), THF; (e) Benzoin, benzil, and THF; (f) Benzoin, lithium benzoate, lithium carbonate, and THF. These six experiments gave only disulfone $CH_2(SO_2Ph)_2$ but did not give product **2** and **3**. Presumably ylide **1** abstracts hydrogen atom from THF to give disulfone. In the control expertiments the ylide **1** was remained as a powder at first and gradually dissolved in the THF solution by the reaction with THF in 0.5 h. On the other hand, ylide **1** decomposed in a few minutes when **1** was added to the solution containing reduction products of CO_2. These control experiments exclude the possibility that compounds in the solution other than reduction products of CO_2 (C_xO_y) decompose the ylide **1**. Therefore, it is probable that C_xO_y decompose the ylide **1**.

Reaction scheme is tentatively shown as following.

$$\mathrm{Ph{-}\overset{O}{\overset{\|}{C}}{-}CH(OH)Ph} + 2\mathrm{Li} \longrightarrow \mathrm{Ph{-}\overset{O}{\overset{\|}{C}}{-}\overset{OLi}{\overset{|}{C}}{-}Ph} \xrightarrow{CO_2} C_xO_y \quad (1)$$

$$C_xO_y + \underset{\mathbf{1}}{PhI^+{-}C^-(SO_2Ph)_2} \longrightarrow PhI^+{-}C^{\mp}(SO_2Ph) \quad (2)$$

$$PhI^+{-}C^{\mp}(SO_2Ph) \xrightarrow[\text{from THFor -OH}]{+H} \longrightarrow :CH(SO_2Ph) \quad (3)$$

$$\text{Benzoin} + :CH(SO_2Ph) \xrightarrow{\text{C-H insertion}} \mathbf{3} \quad (4)$$

$$\text{Benzoin} + :CH(SO_2Ph) \longrightarrow \mathrm{Ph{-}\overset{O^-}{\overset{|}{C}}{-}CH(OH)Ph} \longrightarrow \mathbf{2} \quad (5)$$

$$\mathrm{HC(SO_2Ph)}$$

Such a characteristic decomposition reaction of **1** has not been reported.[7] Forbus et al. have reported the preference of C_2O for attack on oxygen over C–H insertion.[4h] In preceding paper carbon atom of unstable carbon oxide was captured by sulfur atom.[1] The fact that C_xO_y showed characteristic behavior to sydnones[3] can be explained by similar tendency of them. Presumably such a tendency of a preferential attack of C_xO_y on heteroatom such as sulfur atom over carbon atom of the ylide brings about elimination of a sulfonyl group as shown in the reaction (2). Although phenylsulfonylcarbene is considered to be formed as shown in reaction (3), detailed interpretation of this reaction can not be given in the present stage of this study. Insertion of phenylsulfonylcarbene to C–H bond of benzoin gives the isomer **3** as is shown in reaction (4). Attack of carbene to a carbon atom of C=O bond of ketones has been proposed to give dipolar intermediate[11] as is shown in reaction (5). Rearrangement of an alkyl group in such a dipolar adduct does not seem to occur to so much extent in the reaction of simple ketones. However, rearrangement of CH(OH)Ph group to carbon atom of $CH(SO_2Ph)$ group seems to occur to some extent to give isomer **2**.

Although capture of carbon atom from unstable carbon oxides by ylides **1** was unsuccessful in the present report, the present results indicated that benzoin carbanion formed using Li metal reduced CO_2 to give C_xO_y, and that C_xO_y formed had special reactivity.

Experimental

General Procedures. The ^{1}H NMR spectra were recorded on JEOL Fourier transform NMR spectrometer operating at 89.55 MHz and Brooker AC 250T NMR spectrometer operating at 250 MHz. The ^{13}C NMR were recorded on a Brooker AC 250T NMR spectrometer. Mass spectra were recorded on JEOL JMS-DX-300 mass spectrometer. Other procedures and instruments were described in the previous paper.[2]

Formation of Benzoin Carbanion and the Reaction of the Carbanion Formed with CO_2. Into the nitrogen containing 100 ml two-necked flask, in which 0.009 g atom of lithium powder was placed, 10 ml of THF, which was refluxed over $LiAlH_4$ under nitrogen atmosphere and distilled just before use, was injected through a serum cap using a syringe. To this mixture 16 ml of THF solution containing 0.0045 mol of benzoin was injected through a serum cap using a syringe, and the resulting mixture was stirred for 3 h at room temperature. The resulting dark red mixture was immersed in a cooling bath maintained at −78 °C. To this solution CO_2 was bubbled as gas through a delivery tube for 20 min. During the introduction of CO_2 a part of CO_2 escapes from a needle which is attached to a serum cap. After the reaction THF was evaporated and the residue was analyzed by same procedure as described in the previous paper.[2] Yields of the reaction products were benzoin 55, benzil 20, hydrobenzoin 11,[12] and lithium benzoate 3% based on benzoin used.[13]

Reaction of the Reduction Products of CO_2 with Ylide 1. After the reaction of benzoin carbanion with CO_2 was finished as described above, a serum cap was put off and 0.0018 mol of ylide **1** was added at −78 °C as a powder through one neck of the flask. The resulting mixture was warmed to room temperature. A few minutes after warming up to room temperature the ylide seemed to decompose. The mixture was stirred for one hour at room temperature. THF was evaporated and the residue was separated by means of TLC using chloroform as an eluent. Crude mixture of **2** and **3** was again separated by means of TLC using a mixture of chloroform and ethyl acetate as an eluent. Yields of **2** and **3** were determined to be 10 and 8 mol% based on the ylide used from ^{1}H NMR spectrum. Although a mixture of **2** and **3** was slightly contaminated with decomposition products or hydro-

benzoin because of difficulty of separation as mentioned above, satisfactory analytical result was obtained. Calcd for $C_{21}H_{18}O_4S$; M^+, 366.0926. Found: m/z 366.0930. This molecular formula of **2** and **3** and the fact shown by acetylation experiment that one isomer **2** has ^1H NMR absorptions at 4.30—4.51 and 5.85—5.89 ppm and another isomer **3** has a singlet at 4.25—4.29 ppm, together with fact shown by double irradiation technique that one isomer **2** consists of two diastereomers and another isomer **3** consists of one structure, indicate that structures of **2** and **3** are correct. Although disulfone was formed, quantitative analysis of it was not undertaken.

Author thanks to Dr. Hisahiro Hagiwara of this institute for measurement of mass spectra and helpful discussion.

References

1) F. Akiyama, *Bull. Chem. Soc. Jpn.*, **63**, 2131 (1990).
2) F. Akiyama, *Bull. Chem. Soc. Jpn.*, **61**, 3951 (1988).
3) F. Akiyama, *Chem. Lett.*, **1989**, 2009.
4) a) K. D. Bayes, *J. Am. Chem. Soc.*, **83**, 3712 (1961); b) K. D. Bayes, *ibid.*, **84**, 4077 (1962); c) C. Willis and K. D. Bayes, *ibid.*, **83**, 3203 (1966); d) R. T. Mullen and A. P. Wolf, *ibid.*, **84**, 3214 (1962); e) C. Devillers, *C. R. Acad. Sci. (Paris), Ser. C*, **262**, 1485 (1966); f) R. T. Baker, J. A. Kerr, and A. F. Trotman-Dickenson, *J. Chem. Soc., A*, **1967**, 1641; g) G. R. Smith and W. Weltner, Jr, *J. Chem. Phys.*, **62**, 4592 (1975); h) T. R. Forbus, P. A. Birdsong, and P. B. Shevlin, *J. Am. Chem. Soc.*, **100**, 6425 (1978); i) G. Parker, D. Wiseman, C. Winter, and C. Mackay, *J. Org. Chem.*, **49**, 4494 (1984); j) O. Horie, W. Bauer, R. Meuser, V. H. Schmidt, and K. H. Becker, *Chem. Phys. Lett.*, **100**, 251 (1983); k) W. Bauer, R. Meuser, and K. H. Becker, *J. Photochem.*, **24**, 99 (1984); l) W. Bauer, K. H. Becker, and R. Meuser, *Ber. Bunsen-Ges. Phys. Chem.*, **89**, 340 (1985); m) C. Yamada, H. Kanamori, H. Horiguchi, S. Tsuchiya, and E. Hirota, *J. Chem. Phys.*, **84**, 2573 (1986); n) C. F. Chabalowski, R. T. Buenker, and S. D. Peyerimhoff, *J. Chem. Phys.*, **84**, 268 (1986).
5) a) R. L. Dekock and W. Weltner, Jr, *J. Am. Chem. Soc.*, **93**, 7106 (1971); b) R. D. Brown, F. W. Eastwood, P. S. Elmes, and P. D. Godfrey, *J. Am. Chem. Soc.*, **105**, 6496 (1983); c) R. D. Brown and E. N. Rice, *J. Am. Chem. Soc.*, **106**, 6475 (1954); d) T. B. Tang, H. Inokuchi, S. Saito, and E. Hirota, *Chem. Phys. Lett.*, **116**, 83 (1985).
6) a) R. J. Van Zee, G. R. Smith, and W. Weltner, Jr., *J. Am. Chem. Soc.*, **110**, 609 (1988); b) D. W. Ewing, *J. Am. Chem. Soc.*, **111**, 8809 (1989).
7) L. Hatjarapoglou, A. Varvoglis, N. W. Alcock, and G. A. Pike, *J. Chem. Soc., Perkin Trans. 1*, **1988**, 2839.
8) When ylide **1** was added to the reaction mixture of CO_2 with benzoin carbanion formed using LDA, totally decomposition of the ylide **1** was observed to give disulfone. Presumably diisopropylamine decomposes ylide to give disulfone. Therefore, lithium was used to make benzoin carbanion.
9) During the separation procedure of a mixture of **2** and **3** by means of TLC or HPLC, decomposition of the isomers was observed to occur to some extent. During the separation procedure by means of HPLC elution time became very longer because of stuffing of the column.
10) Although this signal was observed as a singlet in the measurement by 90 MHz ^1H NMR this signal separated to a multiplet in the measurement by 250 MHz ^1H NMR. Presumably this separation can be attributed to a slight barrier for rotation around C–C bond since OH group locates between carbony and sulfonyl groups.
11) W. Kirmse, "Carbene Chemistry," 2nd ed, Academic Press, New York (1971), Chap. 11, p. 434.
12) Hydrobenzoin has been reported to be prepared by the reaction of benzoin with basic compound. For example, see A. Breuer and T. Zinke, *Liebigs Ann. Chem.*, **198**, 151 (1879). Therefore, hydrobenzoin is presumably formed during the reaction of benzoin with lithium at room temperature (vide ante).
13) Small amounts of benzaldehyde was formed. Since benzaldehyde was lost during evaporation procedure of THF, quantitative analyses of it was not undertaken. An unknown compound, which was found in near R_f range with hydrobenzoin, was obtained in a few wt% yield. It showed very low solubility, high melting point (220 °C). NMR spectra indicated that this compound had PhCH(OH) and PhC(OH) groups. Since this compound showed very peculiar behavior in NMR analyses including 2D NMR, which has not ever been reported in the literatures, structure can not be determined at present. Since this compound has same functional group with benzoin and it exists in small amount, it certainly has nothing to do with decomposition of the ylide **1**. Therefore, determination of the structure of this compound was postponed.

Urea Sensitive Field Effect Transistors Based on Dithio Group-Containing Langmuir-Blodgett Membranes

Shouryu LEE, Jun-ichi ANZAI, and Tetsuo OSA*
Pharmaceutical Institute, Tohoku University, Aobayama, Sendai 980
(Received December 21, 1990)

Synopsis. 2-(Octadecyldithio)pyridine (**1**) and 5-(octadecyldithio)-2-nitrobenzoic acid (**2**) were synthesized in order to prepare Langmuir–Blodgett (LB) membranes which possess reactive dithio groups on the surface for further modification with enzymes. The monolayer membrane, composed of **1** or **2**, was deposited successfully on an ion-sensitive field effect transistor, and the membrane surface was modified with urease covalently by a thiol–disulfide exchange reaction. The LB membrane-based sensor **2** showed a better potentiometric response to urea than that of the membrane-based sensor **1**. The results are discussed on the basis of the reactivity of the dithio groups to urease at the membrane surface.

Recently, much attention has been devoted to the development of biosensors based on Langmuir–Blodgett (LB) membranes, because of the advantages they offer in the form of thinness, uniform thickness, and controlled molecular orientation.[1] We have already reported that a penicillin sensor can be constructed by immobilizing penicillinase through adsorption on the surface of LB membrane deposited on the gate surface of an H^+-ion-sensitive field effect transistor (pH-ISFET).[2,3] Penicillinase, fortunately, can be tightly adsorbed, through electrostatic and/or hydrophobic force of attraction, to the surface of the LB membrane. However, it is not always possible for enzymes to be adsorbed to the LB membrane surface without deactivation. In fact, we have observed poor reproducibility in potentiometric responses of the pH-ISFETs covered with LB membranes adsorbing urease, trypsin, and α-chymotrypsin, presumably on account of the desorption or deactivation of the enzymes. For these reasons, we have developed the reactive LB membranes which can bind enzymes covalently.[4,5] Watanabe et al. also used reactive LB membranes for enzyme sensor preparation.[6]

The present paper reports the preparation of dithio group-containing reactive LB membranes and their application to the ISFET urea sensors.

Experimental

Materials. 1-Octadecanethiol, di-(2-pyridyl)disulfide, and 6,6-dinitro-3,3′-dithiodibenzoic acid were purchased from the Tokyo Kasei Co. Urease (EC 3.5.1.5) was obtained from the Sigma Co. The amphiphile **1** was prepared by a coupling reaction of 1-octadecanethiol (2 g) and di-(2-pyridyl)disulfide (1.6 g) in dichloromethane (20 ml) at room temperature for 16 h. The crude product was washed twice with water and then applied to a silica-gel column chromatograph with dichloromethane as the eluent. It was finally purified by repeated recrystallization from methanol–water. Yield: 1.2 g (44%). Mp 42—43 °C. Found: C, 69.73; H, 10.40; N, 3.47; S, 16.36%. Calcd for $C_{23}H_{41}NS_2$: C, 69.83; H, 10.54; N, 3.54; S, 16.18%. For the synthesis of **2**, a chloroform solution (30 ml) of 1-octadecanethiol (3 g), 6,6′-dinitro-3,3′-dithiodibenzoic acid (4.2 g), and triethylamine (5 ml) was stirred for 5 h. The amphiphile **2** was purified by column chromatograph and recrystallization. Yield: 2.4 g (47%). Mp 62—63 °C. Found: C, 62.08; H, 8.55; N, 2.90; S, 13.23%. Calcd for $C_{25}H_{41}NO_4S_2$: C, 61.85; H 8.49; N, 2.83; S, 13.20%.

Sensor Fabrication. A benzene solution (0.1 w/v%) of **1** or **2** was spread on a pure water subphase in a Langmuir trough (Kyowa Kaimenkagaku Co.) at 17 °C, and the surface monolayer was compressed at the rate of 0.4 $cm^2 min^{-1}$ up to a surface pressure of 20 $mN m^{-1}$ for **1** or 30 $mN m^{-1}$ for **2**. Monolayer **1** or **2** was deposited on the gate surface of the pH-ISFET precoated with an octadecanoic acid LB membrane (1, 3, or 5 layers), according to the reported procedure,[3] by dipping the probe vertically through the monolayer at a rate of 0.4 $cm min^{-1}$. After the remaining surface monolayer had been removed from the water subphase, the probe was raised. By this kind of treatment, the dithio groups should be located at the uppermost surface of the deposited LB layer. Thus, the surface will be reactive to protein containing free mercapto groups such as urease (Fig. 1). The deposition ratios of **1** and **2** LB membranes were elucidated by the use of glass plates precoated with a 1-layer octadecanoic acid LB membrane, since the small size of the pH-ISFET inhibited precise measurement of the deposition ratio.

The LB membrane-coated pH-ISFET prepared in the above manner, was immersed in a 0.01 mM (1 M=1 mol dm^{-3}) urease solution (100 mM tris(hydroxymethyl)aminomethane–HCl buffer containing 100 mM KCl and 1 mM EDTA, pH 7.2) for 1 h at 23 °C, in order to immobilize urease on the LB membrane surface. The ISFET urea sensors so prepared were rinsed thoroughly with the working buffer before use.

The procedures for the fabrication and the electric property of the bare pH-ISFET used in this study are described elsewhere.[7]

Results and Discussion

Figure 2 shows surface pressure/area isotherms (π–A isotherms) of **1** and **2** spread on a pure water subphase at 17 °C. Both **1** and **2** gave condensed phase monolayers at the air/water interface, with the occupied area of ca. 29 Å²/molecule for **1** and ca. 35 Å²/molecule for **2**. The bulky head group (nitrobenzoic acid) in **2** may be responsible for the larger value of its occupied area. The monolayer **2** gave a higher collapse pressure than

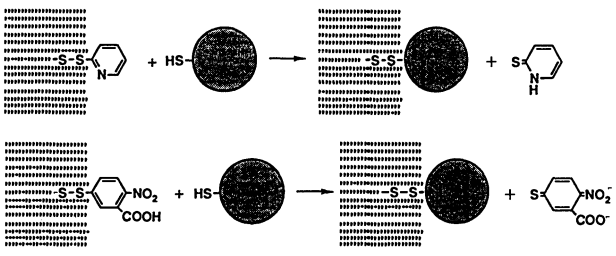

Fig. 1. A schematic illustration of enzyme immobilization on the surface of LB membranes composed of disulfide amphiphiles.

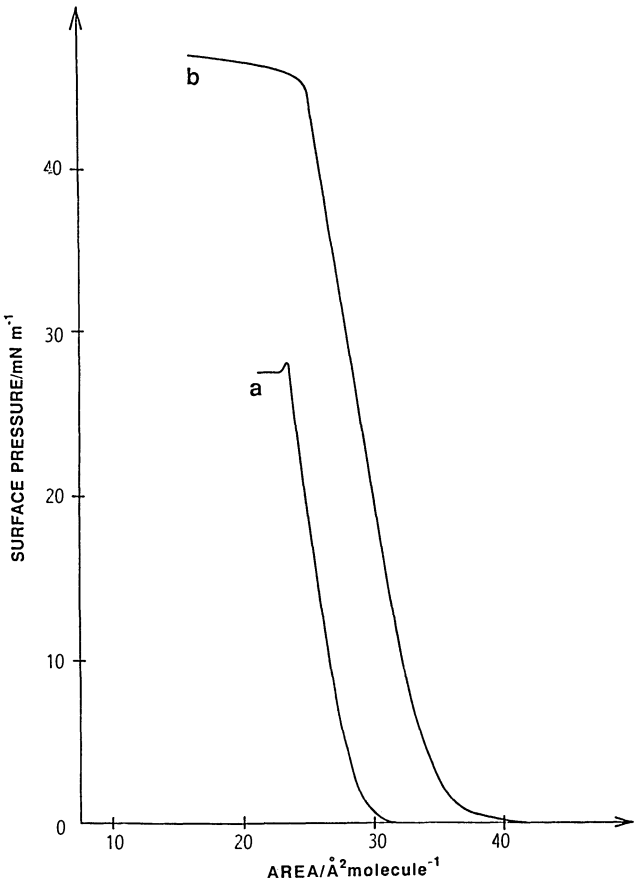

Fig. 2. The π–A isotherms of the **1** (a) and **2** (b) monolayers on pure water at 17 °C.

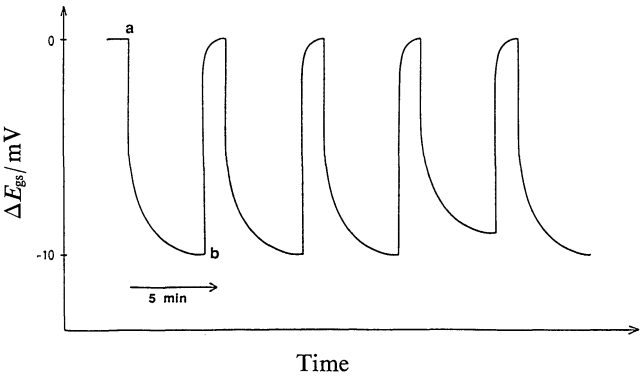

Fig. 3. A typical response curve of the urea sensor prepared with the LB membrane **2**. The prove was immersed in the urea solution (10 mM) at (a) and in the buffer solution at (b). 2 mM KH_2PO_4 buffer containing 1 mM EDTA (pH 6.0) was used.

monolayer **1**, probably as a result of the stabilizing effect of hydrogen bonding between carboxyl groups in the nitrobenzoic acid moieties.

The deposition ratios of the monolayers **1** and **2** were measured by dipping the glass plate with hydrophobic surface into the pure water subphase through the monolayer at 20 mN m^{-1} for **1** and 30 mN m^{-1} for **2**. The deposition ratios, thus measured, were ca. 1.0 for both the monolayers **1** and **2**. This result suggests that the monolayers **1** and **2** can be deposited successfully with the dithio groups located at the uppermost surface on the gate of the pH-ISFET precoated with the octadecanoic acid LB membrane.

Figure 3 shows a typical response curve for the ISFET urea sensor prepared with the LB membrane **2** by the use of an ISFET precoated with a 1-layer octadecanoic acid LB membrane. The sensor exhibited a potentiometric response, ΔE_{gs}, to urea, confirming that the urease was immobilized without deactivation and catalyzed the hydrolysis of urea, while changing the pH value at the gate surface of the pH-ISFET as follows:

$$(NH_2)_2CO + 2H_2O + H^+ \xrightarrow[\text{urease}]{} 2NH_4^+ + HCO_3^-$$

During five successive measurements, the potentiometric response was fairly reproducible, demonstrating clearly the effectiveness of the thiol–disulfide exchange reaction to immobilize urease covalently. However, the sensor response was deteriorated gradually after ten successive measurements.

The ISFET probes precoated with 3- and 5-layer octadecanoic acid LB membranes were also used for urea sensor fabrication. The potentiometric response was suppressed by increasing the thickness of the LB layer. The response of the sensor depended significantly on the buffer capacity of the sample solution. The useful calibration graphs could be obtained in the buffers of lower than 10 mM KH_2PO_4. These properties of the LB membrane-based sensors are the common case for the potentiometric enzyme sensors reported so far.[1,3,8]

It is interesting to clarify the effects of the different chemical structures of the hydrophilic head groups in **1** and **2** on the potentiometric and enzyme-binding properties of the LB membranes. Firstly, it was checked

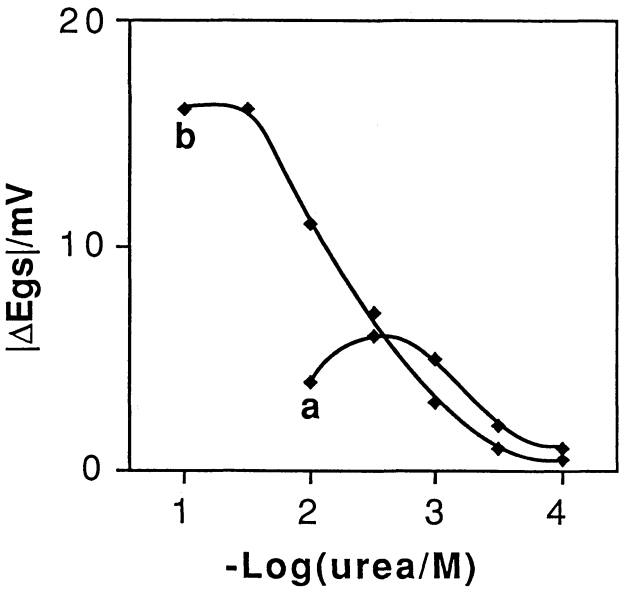

Fig. 4. Typical calibration graphs of the urease-immobilized pH-ISFETs to urea. The sensors were prepared with LB membranes **1** (a) or **2** (b), deposited on the 1-layer octadecanoic acid LB membrane. 2 mM KH_2PO_4 buffer containing 1 mM EDTA (pH 6.0) was used.

that the LB membrane-coated ISFETs with both **1** and **2** show almost the same pH response with each other (45—50 mV/pH). Figure 4 shows the typical calibration graphs for the ISFET urea sensors based on LB membranes **1** and **2**. The potentiometric response of the sensor prepared with LB membrane **2** was higher than that for **1**-based sensor. The dynamic range of the **2**-based sensor was 0.3—30 mM urea. This range is comparable to those of the urea sensors based on a urease–albumin crosslinked membrane.[8,9] The low response of the membrane sensor **1** may stem from the low enzyme loading on the gate surface, which, in turn, probably results from the limited reactivity of LB membrane **1** with mercapto groups in urease.

Thus, we have shown that 5-(octadecyldithio)-2-nitrobenzoic acid is a useful material for the preparation of a reactive LB membrane and it can bind an enzyme covalently to its surface, and so is useful as a biosensor application.

This work was supported in part by Grant-in-Aid for International Joint Research "SUPRAMOL" from New Energy and Industrial Technology Development Organization.

References

1) J. Anzai and T. Osa, *Selective Electrode Rev.*, **12**, 3 (1990).
2) J. Anzai, K. Furuya, C-W. Chen, T. Osa, and T. Matsuo, *Anal. Sci.*, **3**, 271 (1987).
3) J. Anzai, J. Hashimoto, T. Osa, and T. Matsuo, *Anal. Sci.*, **4**, 247 (1988).
4) J. Anzai, S. Lee, and T. Osa, *Chem. Pharm. Bull.*, **37**, 3320 (1989).
5) J. Anzai, S. Lee, and T. Osa, *Bull. Chem. Soc. Jpn.*, **62**, 3018 (1989).
6) H. Tsuzuki, T. Watanabe, Y. Okawa, S. Yoshida, S. Yano, K. Koumoto, M. Komiyama, and Y. Nihei, *Chem. Lett.*, **1988**, 1265.
7) T. Matsuo and M. Esashi, *Sens. Actuators*, **1**, 77 (1981).
8) J. Anzai, T. Kusano, T. Osa, H. Nakajima, and T. Matsuo, *Bunseki Kagaku*, **33**, E131 (1984).
9) J. Anzai, S. Tezuka, T. Osa, H. Nakajima, and T. Matsuo, *Chem. Pharm. Bull.*, **35**, 693 (1987).

Preparation and Crystal Data of the New Compounds Ag_7MS_6 (M=Ta and Nb)

Hiroaki WADA
National Institute for Researches in Inorganic Materials, Namiki 1-1, Tsukuba, Ibaraki 305
(Received December 14, 1990)

Synopsis. The compounds Ag_7TaS_6 and Ag_7NbS_6 were prepared by a sealed silica tube method at 500 °C for 4 d. They crystallize in the face-centered cubic system with the unit-cell dimensions of a=10.5139±0.0003 Å and a=10.5001 ±0.0006 Å, respectively. From the density measurements, it has been clarified that the unit cell contains four formula units.

In recent years there has been great interest in ternary silver sulfides with the general formula $Ag^{+}_{(12-n)}M^{n+}S_6$ (M=Al, Ga, Si, Ge, Sn, P, As, and Sb) which are usually called 'Argyrodite' compounds. Many works have been done on their crystal structures and physical properties.[1-13] A common feature of these compounds is the presence of tetrahedrally closed-packed S sublattice forming the interpenetraiting, centered, distorted icosahedra, and the highly ionic motion of Ag atoms in a 'liquid-like manner' within the rigid framework of S lattice. Hitherto, however, preparative studies reported of this type have been limited only to the compounds associated with M=group 3 (IIIB), group 4 (IVB), and group 5 (VB) cations. A similar $Ag^{+}_{(12-n)}M^{n+}S_6$ compound could be expected for other metal systems. In this connection group 5 (VA) transition metals were selected as candidates for M cations and the possibility of preparing analogous compounds was examined. In the course of the investigation of the Ag–Ta–S system, the new compound Ag_7TaS_6 whose crystal structure is face-centered cubic has been recently discovered besides $AgTaS_3$.[14] Furthermore, the analogous new compound Ag_7NbS_6 has been obtained successfully. This note is concerned with the X-ray powder diffraction studies of the compounds, Ag_7TaS_6 and Ag_7NbS_6.

Results and Discussion

For the preparation of Ag_7MS_6 (M=Ta and Nb), tantalum (3N6), niobium (3N6), sulfur (6N), and Ag_2S (3N) powders were used as starting materials. Initially TaS_2 and NbS_2 were produced from these elements at 600 °C. The title compounds were prepared by using TaS_2, NbS_2, Ag_2S, and S in the stoichiometric proportions. The materials were mixed in an agate mortar in the glove box under pure N_2 atmosphere, pressed into pellets (radius: 7 mm), and sealed in evacuated silica tubes. The heat treatments were performed at 500 °C for 4 d. At the end of runs the tubes were quenched into water. The final volume of pellet became about 2 times larger than the initial one owing to the expansion through the reaction process.

Black-colored products obtained were identified by means of X-ray powder diffraction methods. A Rigaku diffractometer (Geigerflex, RAD-B system) with graphite-monochromated Cu $K\alpha$ radiation was used. The lattice constants were calculated by least-squares method. All peaks in X-ray diffraction patterns of Ag_7TaS_6 and Ag_7NbS_6 could be indexed by means of the cubic lattice with the unit cell dimension of

Table 1. Low-Angle Powder Data of X-Ray Diffraction of Ag_7TaS_6 and Ag_7NbS_6

Cu $K\alpha$ radiation								
Ag_7TaS_6						Ag_7NbS_6		
d_o/Å	d_c/Å	I/I_0	h	k	l	d_o/Å	d_c/Å	I/I_0
6.074	6.070	50	1	1	1	6.070	6.062	58
5.257	5.257	57	2	0	0	5.254	5.250	26
3.717	3.717	4	2	2	0	3.711	3.712	2
3.169	3.170	96	3	1	1	3.166	3.166	55
3.034	3.035	100	2	2	2	3.029	3.031	100
2.628	2.628	30	4	0	0	2.625	2.625	25
2.412	2.412	51	3	3	1	2.409	2.409	31
2.351	2.351	21	4	2	0	2.348	2.348	8
2.146	2.146	51	4	2	2	2.143	2.143	32
2.023	2.023	22	5	1	1	2.020	2.021	36
1.8588	1.8586	59	4	4	0	1.8560	1.8562	56
1.7771	1.7772	24	5	3	1	1.7742	1.7748	10
1.7524	1.7523	18	6	0	0	1.7508	1.7500	10
1.6623	1.6624	12	6	2	0	1.6603	1.6602	5
1.6034	1.6034	6	5	3	3	1.6011	1.6012	2
1.5848	1.5850	10	6	2	2	1.5828	1.5829	3
1.4723	1.4723	17	5	5	1	1.4704	1.4703	10
1.4580	1.4580	7	6	4	0	1.4561	1.4560	2
1.4052	1.4050	8	6	4	2	1.4030	1.4031	4
1.3688	1.3688	11	7	3	1	1.3672	1.3670	6

a=10.5137±0.0003 Å and a=10.5001±0.0006 Å, respectively. Both X-ray patterns were very similar except for the slight difference in diffraction intensities. The systematic extinction (*hkl*: $h+k=2n+1$, $k+l=2n+1$, $l+h=2n+1$) is indicative of the face centered cubic and leads to the possible space groups $F23$, $Fm3$, $Fm3m$, $F\bar{4}3m$, and $F432$. In order to determine the number of formula units per cell, density measurements were carried out by immersion method, using CCl_4. The values d_m=6.55 g cm^{-3} and d_m=5.90 g cm^{-3} were obtained for Ag_7TaS_6 and Ag_7NbS_6, respectively. These results suggest clearly that the unit cell contains four formula units (Z=4). In the analogy of other cubic Argyrodites compounds the space group $F\bar{4}3m$ could be considered to be most probable. The *d*-spacings, *hkl* indecies and relative intensities of both compounds are listed in Table 1. Based on the close similarity of data it can be concluded that Ag_7TaS_6 and Ag_7NbS_6 are isotypic to each other. In order to examine the transporting phenomena of these compounds, conductivity measurements were carried out on disk-shaped, cold pressed polycrystalline samples (thickness: 1.0—1.6 mm). Direct current methods were employed with Solartron 1286 electrical interface. The cell arrangement was $Ag/RbAg_4I_5/Ag_7MS_6/RbAg_4I_5/Ag$ (M=Ta or Nb), in which $RbAg_4I_5$ served as an electron blocking layer. The experiment was made by sending a constant current (less than 30 μA) and measuring the voltage drop across the specimen. The silver ionic conductivity $\log \sigma_{Ag^+}$ of Ag_7TaS_6 is −4.9 at 27 °C and rises linearly to −3.5 at 144 °C with an activation energy of 0.33 eV. This compound becomes more conductive above 144 °C based on some of the phase transition and the curvature changes rapidly. The value of $\log \sigma_{Ag^+}$ reaches −1.8 at 200 °C with an activation energy of 1.13 eV. Similarly the silver ionic conductivity of Ag_7NbS_6 is −4.6 at 27 °C and increases linearly to −3.6 at about 119 °C with an activation energy of 0.25 eV. After that the value of $\log \sigma_{Ag^+}$ rises rapidly to +0.1 at 135 °C. However, the results of preliminary experiments on the ionic transport number indicated clearly that both compounds are the mixed conductors like Ag_2S.[15] Detailed studies on their crystal structure and physical properties are now in progress.

References

1) H. Hahn, H. Schulze, and L. Sechser, *Naturwissenschaften,* **52**, 451 (1965).
2) O. Gorochov and J. Flahaut, *C. R. Acad. Sci., Paris, Ser. C.*, **264**, 2153 (1967).
3) G. Brandt and V. Kramer, *Mater. Res. Bull.*, **11**, 1381 (1976).
4) N. Rysanek, P. Laruelle, and A. Katty, *Acta Crystallogr., Sect. B,* **32**, 692 (1976).
5) B. Krebs and J. Mandt, *Z. Naturforsch., B,* **32**, 373 (1977).
6) P. Toffoli and P. Khodadad, *C. R. Acad. Sci., Ser. C,* **286**, 349 (1978).
7) J. P. Deloume, R. Faure, H. Loiseleur, and M. Roubin, *Acta Crystallogr., Sect. B,* **34**, 3189 (1978).
8) C. Carcaly, R. Ollitrault-Fichet, D. Houphouet, R. Eholie, and J. Flahaut, *Mater. Res. Bull.*, **14**, 1497 (1979).
9) W. F. Kuhs, R. Nitsche, and K. Scheunemann, *Mater. Res. Bull.*, **14**, 241 (1979).
10) S. Geller, *Z. Kristallogr.*, **149**, 31 (1979).
11) R. Blachnik and U. Wickel, *Z. Naturforsch., B,* **35**, 1268 (1980).
12) E. E. Hellstrom and R. A. Huggins, *J. Solid State Chem.*, **35**, 207 (1980).
13) J. P. Deloume and R. Faure, *J. Solid State Chem.*, **36**, 112 (1981).
14) H. Wada and M. Onoda, *Chem. Lett.*, **1990**, 705.
15) C. Tubandt and N. Reinhold, *Z. Phys. Chem., Abt. B,* **24**, 22 (1934).

Partition Coefficient of 21*H*,23*H*-Porphine and Its Metal(II) Complexes between Heptane and Nonaqueous Polar Solvents

Yoshito WAKUI,*,† Hisanori IMURA,†† and Nobuo SUZUKI
Department of Chemistry, Faculty of Science, Tohoku University, Sendai 980
(Received January 5, 1991)

Synopsis. The partition coefficients of 21*H*,23*H*-porphine (H_2por) and its copper(II) (Cu(por)) and zinc(II) (Zn(por)) complexes were determined in nonaqueous two-phase systems. A linear free-energy relationship was observed between the partition coefficients of H_2por and Cu(por). The partition coefficient of Zn(por) was suppressed by coordination bonding with the polar solvent molecules.

Porphyrin and its related compounds are important substances in biochemistry and geochemistry. Porphyrin and metal-porphyrin compounds occur extensively in nature as well-known chlorophylls, hemoglobins, and petroporphyrins, which usually contain magnesium, iron, vanadium, and nickel as central metals. In relation to chemical separation and natural migration of these porphyrin compounds, a systematic study on the solution behavior of porphyrins, and their metal complexes is desirable. However, little is known about the solubility and the liquid–liquid partition of these porphyrin compounds. The liquid–liquid partition coefficient is an important equilibrium constant which governs the behavior of organic substances and metal complexes in both solvent extraction and liquid chromatography.

In previous work[1] we prepared a mother compound of porphyrins, 21*H*,23*H*-porphine, and investigated the liquid–liquid partition behavior between various nonpolar organic solvents and an acidic aqueous solution. In the present work we determine the liquid–liquid partition coefficients of 21*H*,23*H*-porphine (H_2por) and its copper(II) (Cu(por)) and zinc(II) (Zn(por)) complexes in a nonaqueous partition system, i.e., heptane as a nonpolar solvent and acetonitrile (AN), nitromethane (NM), dimethyl sulfoxide (DMSO), and methanol (MeOH) as polar solvents. The solvent effect and role of the central metals in the partition coefficient is discussed.

Experimental

Materials. 21*H*,23*H*-Porphine was synthesized and purified in the same manner as that described previously.[1] Porphinatocopper(II) was synthesized by refluxing 0.014 mmol of purified 21*H*,23*H*-porphine and 0.042 mmol of bis(acetylacetonato)copper(II) in chloroform (200 cm^3) for 270 min. The chloroform solution obtained was passed through an alumina column (Merck, 200—400 mesh). The porphinatocopper(II) was eluted with chloroform and recrystallized from chloroform–methanol.

Porphinatozinc(II) was synthesized by mixing 0.014 mmol of purified 21*H*,23*H*-porphine in chloroform (50 cm^3) with 0.10 mmol of anhydrous zinc(II) acetate in methanol (20 cm^3) and heating for 45 min at 60 °C. The porphinatozinc(II) was purified in a similar manner as that for the copper(II) complex.

The purity of the metal complexes synthesized was ascertained by high-performance liquid chromatography (column, LiChrosorb RP-18, 250 mm×4 mm (i.d.); mobile phase, acetonitrile: acetone=70:30; detection wavelength, 388 nm for the copper(II) complex and 397 nm for the zinc(II) complex). Each metal complex gave a single peak on the chromatogram.

Heptane and polar organic solvents such as acetonitrile, nitromethane, dimethyl sulfoxide, and methanol were purified by fractional distillation after appropriate chemical treatment and dehydration.[2]

Procedure. Heptane and a polar organic solvent were presaturated with each other before use. A certain volume of the solution of porphine, or its metal(II) complex, was shaken with the other phase for 5—60 min and centrifuged. The partition coefficient, P, which is defined as the ratio of the concentration in the heptane phase to that in the polar phase, was determined from the absorbance of the initially prepared phase and the equilibrated phase.

The wavelengths used for the absorbance measurements in different solvents are shown in Table 1.

The quartz cuvette and such glasswares as extraction vials, volumetric flasks, and pipettes were treated with dimethyldichlorosilane prior to use in order to prevent the adsorption of porphine and its metal(II) complexes onto the wall. All of the experiments were carried out in a thermostated room at 25 °C.

Table 1. Wavelength(nm) Used for the Absorbance Measurement of Porphine and Its Copper(II) and Zinc(II) Complex

Solvent	H_2por		Cu(por)	Zn(por)	
	λ_{max} [a]	λ_{max} [b]	λ_{max} [a]	λ_{max} [a]	λ_{max} [b]
Heptane	391.5		389.5		
AN	389.5	486.3	387.8	396.9	529.6
NM	391.3	487.3	389.4	396.2	526.2
DMSO	393.9	488.4	392.1	404.0	533.6
MeOH	388.8	486.4	388.2	397.4	530.3

a) Soret band. b) Q band.

Results and Discussion

Partition equilibrium was completely attained within 5 min. A constant partition coefficient was obtained within the experimental error when the porphine concentration was altered in the concentration range 10^{-6} to 10^{-5} M (1 M=1 mol dm^{-3}). This demonstrates that a single species of porphine is present in both the heptane and polar phases under the experimental conditions. Measurements of the partition coefficient of porphinatocopper(II) and porphinatozinc(II) were also performed in a similar manner as that for porphine. The mean values and the standard deviations of the obtained partition coefficients are summarized in Table 2.

† Present address: Government Industrial Research Institute, Tohoku, Nigatake, Sendai 983.
†† Present address: Department of Chemistry, Faculty of Science, Ibaraki University, Mito 310.

Table 2. Partition Coefficients[a] of Porphine and Its Copper(II) and Zinc(II) Complex between Heptane and a Polar Solvent at 25 °C

Polar solvent	H_2por	Cu(por)	Zn(por)
AN	$(1.01\pm0.04)\times10^{-1}$	$(2.65\pm0.08)\times10^{-1}$	$(2.23\pm0.02)\times10^{-2}$
NM	$(5.54\pm0.20)\times10^{-2}$	$(1.38\pm0.03)\times10^{-1}$	$(4.74\pm0.12)\times10^{-2}$
DMSO	$(3.06\pm0.42)\times10^{-3}$	$(6.46\pm0.12)\times10^{-3}$	$(5.17\pm0.31)\times10^{-5}$
MeOH	$(2.65\pm0.20)\times10^{-1}$	$(7.04\pm0.12)\times10^{-1}$	$(9.11\pm0.23)\times10^{-2}$

a) Mean value±standard deviation.

The Gibbs free energy for the partition of a solute (denoted by the subscript 2) from a polar solvent to heptane is represented by the difference in the Gibbs free energy ($\Delta\bar{G}_s$) for the dissolution of the solute in both phases,

$$-RT\ln P_2=\Delta\bar{G}_{s,n}-\Delta\bar{G}_{s,p}, \quad (1)$$

where subscripts p and n denote the polar and nonpolar solvent, respectively. The dissolution process can be divided into two steps: the formation of a cavity to accommodate the solute molecule in the solvent, followed by an interaction of the surrounding solvent molecules with the solute introduced into the cavity. Equation (1) can be rewritten as

$$RT\ln P_2=(\bar{G}_{c,p}-\bar{G}_{c,n})+(\bar{G}_{i,p}-\bar{G}_{i,n})$$
$$=\Delta\bar{G}_c+\Delta\bar{G}_i, \quad (2)$$

where $\Delta\bar{G}_c$ and $\Delta\bar{G}_i$ denote the cavity-formation energy and interaction energy, respectively. The solute–solvent interaction of porphine is probably dominated by the van der Waals interaction, since a specific solute–solvent interaction is not notable for porphine with not only nonpolar solvents (such as heptane, carbon tetrachloride, and benzene), but somewhat polar hydrogen bonding solvents (such as chloroform and 1-octanol), as we pointed out previously.[1)]

By applying Eq. 2 to the partition of both porphine and its metal complex, the following relation is obtained:

$$RT\ln P_M-RT\ln P_H=(\Delta\bar{G}_{c,M}-\Delta\bar{G}_{c,H})$$
$$+(\Delta\bar{G}_{i,M}-\Delta\bar{G}_{i,H}), \quad (3)$$

where subscripts H and M denote porphine and its metal complex, respectively. It would be reasonable that the molecular diameter of porphine is approximately equal to that of porphinatometal(II) and, hence, the cavity formation energy ($\Delta\bar{G}_c$) for those compounds can be considered to be equal to each other. Therefore, the following equation is given:

$$\log P_M=\log P_H+\frac{(\Delta\bar{G}_{i,M}-\Delta\bar{G}_{i,H})}{2.303\,RT}. \quad (4)$$

Plots of $\log P_M$ against $\log P_H$ for porphinatocopper(II) and porphinatozinc(II) are shown in Fig. 1. Almost

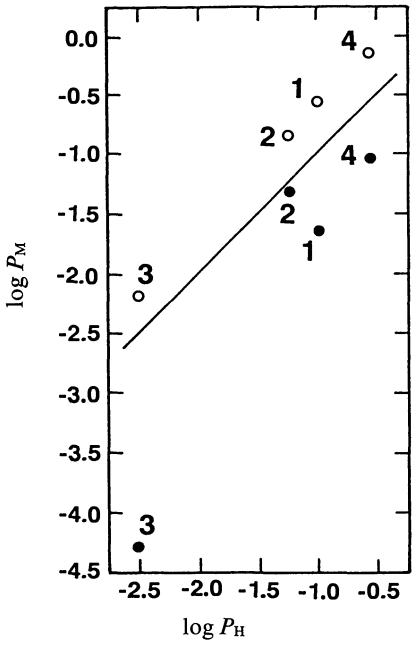

Fig. 1. Relationship between the partition coefficient of the copper(II) and zinc(II) complex and that of porphine.
○, Cu(por); ●, Zn(por).
1, heptane/acetonitrile; 2, heptane/nitromethane; 3, heptane/dimethyl sulfoxide; 4, heptane/methanol.

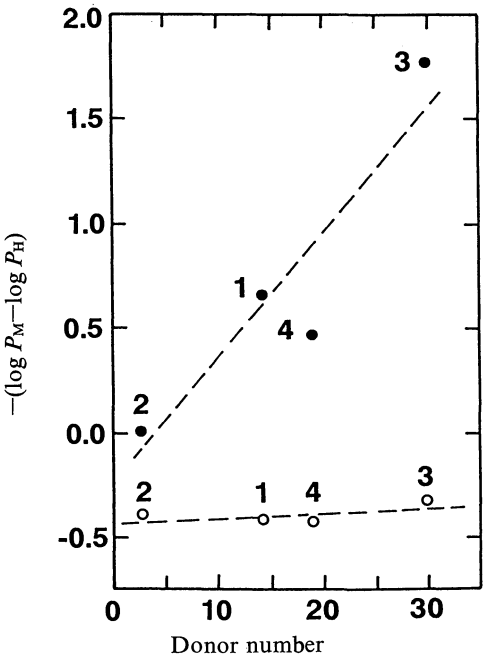

Fig. 2. Correlation between $-(\log P_M-\log P_H)$ and donor number of the solvents.
○, Cu(por); ●, Zn(por).
The numbers correspond to those in Fig. 1.

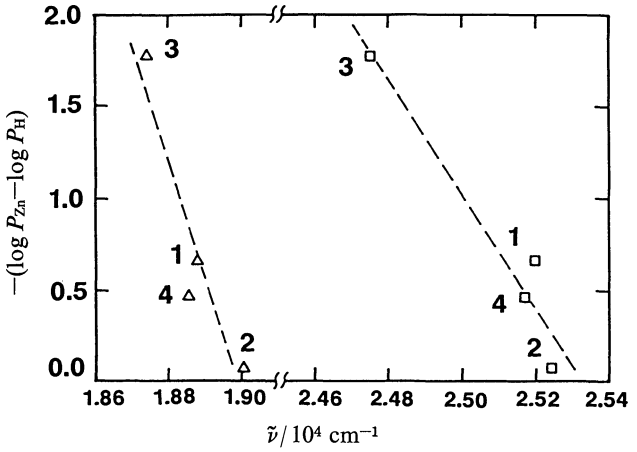

Fig. 3. Correlation between $-(\log P_{Zn}-\log P_H)$ and the wavenumber at the absorption peak of Zn(por) in each polar solvent.
□, Soret band; △, Q band.
The numbers correspond to those in Fig. 1.

linear plots were observed for the copper(II) complex; they fall almost along a straight line with a slope of unity passing through the origin. The observed linear free-energy relationship (LFER) indicates that the value of the interaction term, $\Delta\bar{G}_{i,M}-\Delta\bar{G}_{i,H}$, in Eq. 4 should be small and nearly constant. This result means that the solute–solvent interaction for the copper(II) complex is quite similar to that for the ligand, itself. Accordingly, the central copper(II) ion in the complex can be concluded to have no specific interaction with the polar solvents used.

On the other hand, the plot of the zinc(II) complex is located in a region lower than the solid line, except for the nitromethane system. Additionally, the degree of deviation from the solid line is very different for each polar solvent; LFER is not observed. This means that the interaction term, $\Delta\bar{G}_{i,M}-\Delta\bar{G}_{i,H}$, in Eq. 4 has negative values and is fairly different with the polar solvents used.

Figure 2 shows the correlation between $-(\log P_M-\log P_H)$ and the donor number of the polar solvents, which is a measure of the coordination efficiency of solvent molecules. The value of $-(\log P_M-\log P_H)$, corresponding to the interaction term in Eq. 4, for the zinc(II) complex increases with an increase in the donor number; that for the copper(II) complex, however, is nearly constant. This result suggests that the partition coefficient of the zinc(II) complex is strongly influenced by specific interactions, such as the coordination bond with the polar solvents.

In studies of the solvent effect on the absorption spectrum of tetraphenylporphinatozinc(II),[3–6] the red shift of the absorption peak at the Soret and Q bands has been reported and ascribed to the axial coordination of solvent molecules to the central metal in the zinc(II) complex. Figure 3 shows plots of $-(\log P_{Zn}-\log P_H)$ against the wavenumber $\tilde{\nu}$ at the absorption peak of porphinatozinc(II) (Table 1). A good correlation is observed; the absorption peak is shifted to the lower energy region as the interaction term for the zinc(II) complex becomes larger. Therefore, the specific interaction of porphinatozinc(II) with the polar organic solvents should be attributed to the axial coordination of the solvent molecules to the central metal in the zinc(II) complex.

References

1) Y. Wakui, H. Imura, and N. Suzuki, *Bull. Chem. Soc. Jpn.*, **62**, 2520 (1989).
2) J. A. Riddick and W. B. Burger, "Techniques of Chemistry, Organic Solvents," Wiley, New York (1970).
3) M. Nappa and J. S. Valentine, *J. Am. Chem. Soc.*, **100**, 5075 (1978).
4) G. C. Vogel and J. R. Stahlbush, *Inorg. Chem.*, **16**, 950 (1977).
5) O. W. Kolling, *Anal. Chem.*, **50**, 1581 (1978).
6) J. V. Nardo and J. H. Dawson, *Inorg. Chim. Acta*, **123**, 9 (1986).

Equilibrium and Kinetic Studies on Complex Formation Reaction between Crown Ethers and Bivalent Transition Metal Ions

Hideto MATSUYAMA,* Takeo ARIMURA, Yoshikazu MIYAKE, and Masaaki TERAMOTO
Department of Chemistry and Materials Technology, Faculty of Engineering and Design, Kyoto Institute of Technology, Matsugasaki, Sakyo-ku, Kyoto 606
(Received January 5, 1991)

Synopsis. The complex formation reaction between crown ethers and bivalent transition metal ions was investigated. Although the obtained equilibrium constants were generally small, there was a case where the constant was larger than that for the crown ether–alkali metal system. From kinetic studies the reactions were found to obey the Eigen's mechanism.

It is well known that crown ethers can stably capture various metal ions in their cavities. A number of studies on such complex formations were carried out for an interest in the reaction itself, or for the purpose of metal separation or analysis.[1] However, the target metal has been restricted mostly to alkali and alkaline earth metals so far. Further, relatively few studies have been reported on the kinetics of complex formation reaction although they are important to elucidate the reaction mechanism.

In this work we attempted to investigate both equilibria and kinetics of the complex formation reaction between crown ethers, not containing N or S, and bivalent transition metal ions, for which little information is available in the literature.

Experimental

Materials. Benzo-15-crown-5 (B15C5) and dibenzo-18-crown-6 ($B_2$18C6), purchased from Nacalai Tesque, Inc., were employed in this work. The metal ions used were Co^{2+}, Ni^{2+}, Cu^{2+}, and Zn^{2+}. Metal solutions were prepared by dissolving their perchlorates in acetonitrile or methanol.

Equilibrium and Kinetic Experiments. Equilibrium constants were determined spectrophotometrically. An example of the metal-induced spectral change is shown in Fig. 1. In the case of reactions of Zn^{2+} or Co^{2+} with B15C5 in acetonitrile, the equilibrium constants were directly determined by using the molar absorption coefficients of the complexes since the equilibrium constants were large enough to evaluate these coefficients accurately. In other cases where the equilibrium constants were small, they were determined as follows. The metal concentration was adjusted to be much higher than the crown ether concentration so that the former was approximately constant before and after the complex formation. Thus, the absorbance (Abs) obtained by substracting the metal ion absorbance from the total absorbance is given by

$$Abs=\varepsilon_1[C]+\varepsilon_2[MC^{2+}] \quad (1)$$

Here [C] and $[MC^{2+}]$ are the concentrations of crown ether and the complex, respectively, and ε_1 and ε_2 are molar absorption coefficients. The total concentration of crown ether, $[C]_t$, and the equilibrium constant, K_M, are given by Eqs. 2 and 3.

$$[C]_t=[C]+[MC^{2+}] \quad (2)$$

$$K_M=[MC^{2+}]/([C][M^{2+}]) \quad (3)$$

where M^{2+} denotes a metal ion. Combination of Eqs. 1—3 gives the following formula:

$$\frac{-1}{Abs/[C]_t-\varepsilon_1}=\frac{1}{\varepsilon_1-\varepsilon_2}+\frac{1}{K_M(\varepsilon_1-\varepsilon_2)}\cdot\frac{1}{[M^{2+}]} \quad (4)$$

K_M can hence be determined from a plot of $-1/(Abs/[C]_t-\varepsilon_1)$ against $1/[M^{2+}]$. An example of such plots is shown in Fig. 2. Linear relations were observed in all cases: this ensures the formation of 1 : 1 complexes assumed in Eq. 3. Almost the same equilibrium constants were obtained at two or three wavelengths near 280 nm in every case.

The rate of complex formation was measured with a stopped flow apparatus (Otsuka Electronics Co., Ltd., RA-401) by following the temporal change in absorbance at 280 nm. To simplify the analysis, the metal concentration was

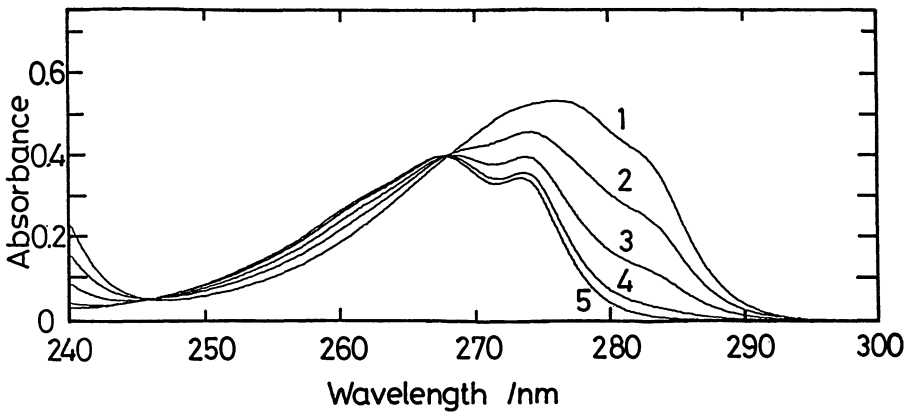

Fig. 1. UV absorption spectra of B15C5 in the absence and presence of Zn^{2+}.
Solvent: acetonitrile. [B15C5]=2.0×10^{-4} mol dm^{-3}.
1: $[Zn^{2+}]$=0, 2: $[Zn^{2+}]$=8.8×10^{-5} mol dm^{-3}, 3 : 1.8×10^{-4} mol dm^{-3}, 4 : 3.5×10^{-4} mol dm^{-3}, 5 : 3.5×10^{-3} mol dm^{-3}.

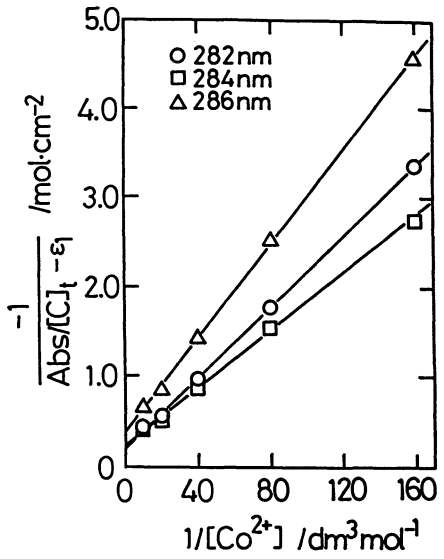

Fig. 2. Relation between $-1/(Abs/[C]_t-\varepsilon_1)$ and $1/[Co^{2+}]$ at various wavelengths. Crown ether: $B_2$18C6, Solvent: acetonitrile, $[C]_t=2.0\times10^{-4}$ mol dm^{-3}.

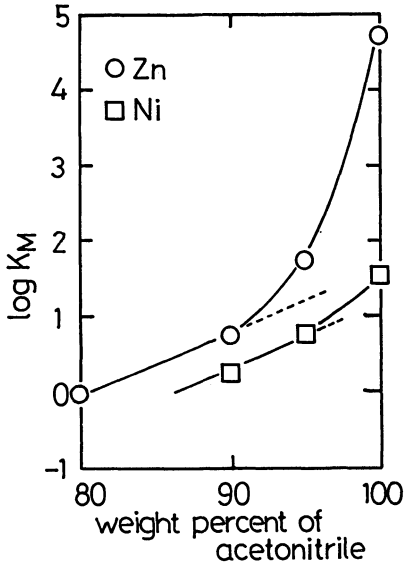

Fig. 3. Equilibrium constant in various acetonitrile–water mixtures. Crown ether: B15C5.

always sufficiently higher than that of crown ether. All the experiments were carried out at 298 K.

Results and Discussion

Equilibrium Constant. The equilibrium constants obtained are listed in Table 1. The values of K_M with B15C5 in methanol are three orders-of-magnitude smaller than that for the Na^+–B15C5 system in methanol.[2] One of the reasons for this result is that "soft" transition metal ions do not easily form a complex with "hard" crown ether.[3] The sequence of K_M, $Co^{2+}<Ni^{2+}<Cu^{2+}>Zn^{2+}$, follows the Irving–Williams order,[4] which generally holds for the equilibrium constants of transition metals. A similar tendency was observed also with $B_2$18C6 in acetonitrile.

However, the sequence of K_M for B15C5 in acetonitrile is quite different from those in the above two systems. The value of K_M for Zn^{2+} is especially large and is larger than that of Na^+–B15C5 system (3.5×10^4 at 295 K[5]). The ionic radius of Zn^{2+} is the largest among the four metal ions[6] and is closest to the 15C5 cavity radius.[1] One of the causes for the unusual K_M sequence in this solvent may be the metal–crown ether size fitting. However, further investigation is necessary to settle this problem.

Figure 3 shows the values of K_M in various acetonitrile–water mixtures. The value of K_M decreases as the water content increases. This suggests that an increase in the water content leads to an increase in the hydration number of the metal ion, thereby enhancing the total strength of the metal ion solvation and suppressing the complex formation. In the region of higher water content, the variation of $\log K_M$ for Zn^{2+} was found to parallel that for Ni^{2+}, though the number of data points is limited. This indicates that the linear free energy relationship[7] holds between the complex formation of Zn^{2+} and that of Ni^{2+}. On the other hand, as the water content decreases, the $\log K_M$ value for Zn^{2+} gradually deviates from the parallel relation, probably in accordance with the anomaly for the complex formation of Zn^{2+} in pure acetonitrile mentioned above.

Rate of Complex Formation. The reaction between a crown ether and a metal ion is expressed as Eq. 5.

$$M^{2+}+C \underset{k_{-1}}{\overset{k_1}{\rightleftarrows}} MC^{2+} \quad (5)$$

The pseudo-first-order rate constant, k_p with respect to [C] is given by

$$k_p=k_1[M^{2+}]+k_1/K_M \quad (6)$$

The relations between k_p and the metal concentration are shown in Fig. 4. In line with Eq. 6, linear relations were obtained. The obtained complex formation rate constants, k_1, and K_M thus obtained are listed in Table 2. Good agreement is seen between the K_M values obtained from this kinetic study and those from the equilibrium study mentioned above.

If the reaction obeys the Eigen's mechanism,[8] the complex formation rate constant, k_1, is given by $K_{os}k_{sol}$ (K_{os}: equilibrium constant of the outer complex, k_{sol}: rate constant of solvent exchange). Since the value of

Table 1. Equilibrium Constants, K_M/dm³ mol⁻¹

Crown ether	Solvent	Co^{2+}	Ni^{2+}	Cu^{2+}	Zn^{2+}
B15C5	Methanol	3.4±0.5	7.8±0.8	$4.9\pm0.3\times10^1$	1.9±0.3
B15C5	Acetonitrile	$1.1\pm0.1\times10^3$	$3.5\pm0.4\times10^1$	$4.8\pm0.3\times10^2$	$5.4\pm0.6\times10^4$
$B_2$18C6	Acetonitrile	$1.4\pm0.1\times10^1$	$3.8\pm0.6\times10^1$	$2.9\pm0.1\times10^2$	$2.2\pm0.2\times10^1$

Table 2. Rate and Equilibrium Constants

	k_1	K_M [a]	K_M [b]	k_1/K_{os} [c]	k_{sol} [d]
	$dm^3\ mol^{-1}\ s^{-1}$	$dm^3\ mol^{-1}$	$dm^3\ mol^{-1}$	s^{-1}	s^{-1}
Ni	7.0×10^2	4.1×10^1	3.5×10^1	2.2×10^3	2.0×10^3 [e]
Zn	1.7×10^6	4.9×10^4	5.4×10^4	5.3×10^6	3.0×10^7 [f]

Crown ether: B15C5, Solvent: acetonitrile
a) Obtained from kinetic studies. b) Obtained from equilibrium studies. c) Equilibrium constant of outer complex, estimated from Fouss's equation[12] by using 5×10^{-10} m as minimum separation distance between molecules. d) Rate constant of solvent exchange. e) Rate constant of acetonitrile exchange, cited from Ref. 9. f) Rate constant of water exchange, cited from Ref. 10.

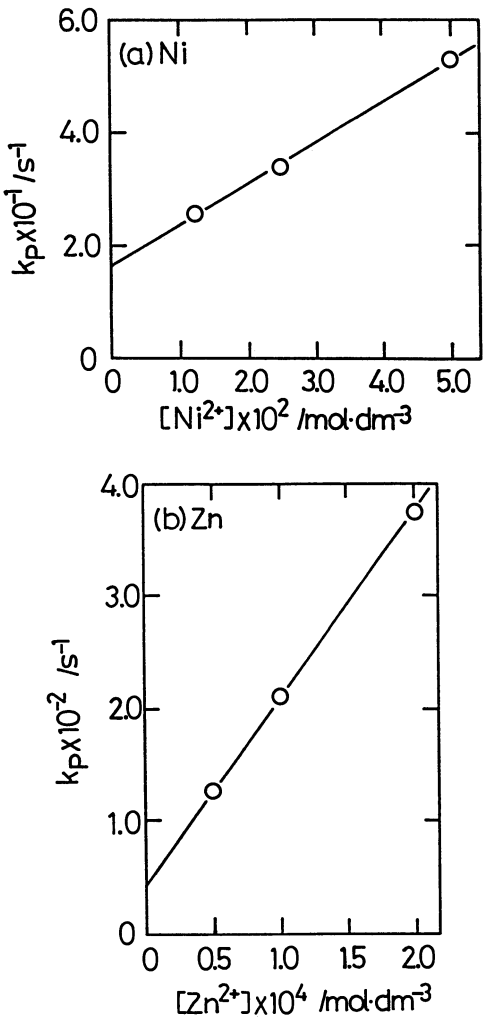

Fig. 4. Relation between k_p and metal concentration. Crown ether: B15C5, Solvent: acetonitrile.
(a) [B15C5]$=2.0\times10^{-3}$ mol dm^{-3}, (b) [B15C5]$=7.0\times10^{-6}$ mol dm^{-3}.

k_1/K_{os} for Ni^{2+} is almost in accord with the rate constant for acetonitrile exchange,[9] we conclude that the reaction obeys the Eigen's mechanism. As far as we know, the rate of exchange of acetonitrile molecules coordinated to Zn^{2+} in the bulk of the solution has not been reported. Although the value of k_1/K_{os} for Zn^{2+} is somewhat smaller than the rate constant of water exchange,[10] it is presumed that the reaction for Zn^{2+} also obeys the Eigen's mechanism because the rates of water exchange are 3—16 times those of acetonitrile exchange for other bivalent transition metals.[11]

Maynard et al.[13] studied the 18-crown-6 ether complexation of alkali metal ions in nonaqueous solvents, and speculated that the reactions consisted of succesive steps involving both ion desolvation and ligand rearrangement, and also that the rearrangement of the macrocyclic ligand was the slowest step. However, the reaction in the present case obeyed the Eigen's mechanism and therefore an ion desolvation should be the rate-determining step. Because the ion desolvation rates for bivalent transition metals are much slower than those for alkali metals, the rate of ligand rearrangement may become faster relatively.

References

1) R. M. Izatt, J. S. Bradshaw, S. A. Nielsen, J. D. Lamb, and J. J. Christensen, *Chem. Rev.*, **85**, 271 (1985).
2) D. G. Parsons, M. R. Truter, and J. N. Wingfield, *Inorg. Chim. Acta*, **47**, 81 (1980).
3) R. G. Pearson, *J. Am. Chem. Soc.*, **85**, 3533 (1963).
4) H. Irving and R. J. P. Williams, *J. Chem. Soc.*, **1953**, 3192.
5) A. Hofmanova, J. Koryta, M. Brezina, and M. L. Mittal, *Inorg. Chem. Acta*, **28**, 73 (1978).
6) "Landolt-Börstein Zahlenwerte und Funktionen," I. Band, Atom—und Molekularphysik, 4. Teil, Kristalle, Springer-Verlag (1955).
7) P. R. Wells, "Linear Free Energy Relationships," Academic Press, New York (1968).
8) M. Eigen and K. Tamm, *Z. Elektrochem.*, **66**, 107 (1962).
9) S. F. Lincoln and R. J. West, *Aust. J. Chem.*, **26**, 255 (1973).
10) F. Fittipaldi and S. Petrucci, *J. Phys. Chem.*, **71**, 3414 (1967).
11) H. Ohtaki, M. Tanaka, and S. Funahashi, "Youekihannou no Kagaku," Gakkai Syuppan Senta (1977).
12) R. M. Fouss, *J. Am. Chem. Soc.*, **80**, 5059 (1958).
13) K. J. Maynard, D. E. Irish, E. M. Eyring, and S. Petrucci, *J. Phys. Chem.*, **88**, 729 (1984).

Dielectric Relaxation Studies of Oligether of Ethylene Glycol at Microwave Frequencies

Hari Dutt PUROHIT and Ram Jeewan SENGWA*
Microwave Research Laboratory, Department of Physics, University of Jodhpur, Jodhpur 342001, India
(Received September 19, 1990)

Synopsis. Dielectric relaxation studies of dialkyl ethers of ethylene glycol and of diethylene glycol have been carried out at microwave frequencies in benzene solutions. Dipole moment and relaxation times corresponding to overall and group rotations and their weight factors have been determined. The configuration of these molecules and the mechanism of the rotation of end alkoxyl groups have been discussed.

Several[1-3] attempts have been made to study the configuration of oligethers of ethylene glycol by carrying out measurements of dipole moments in solutions. So far these studies have been made with ethers, R-$(OCH_2CH_2)_m$-OR with different values of m but keeping same end alkoxyl groups. All these studies concluded the preference of the trans positions in the chain.

In this paper dipole moments of dialkyl ethers of ethylene glycol and of diethylene glycol with different end alkoxyl groups in benzene solutions have been determined, using Higasi[4] equation (Table 1). The dielectric measurements of these molecules in benzene solutions have also been carried out at microwave frequencies with a view to study the group rotations of the end alkoxyl groups and configurations of these molecules.

Experimental

The dielectric permittivity ε' and dielectric loss ε'' at four microwave frequencies viz. 9.83, 18.26, 24.50, and 30.20 GHz and static permittivity ε_0 at 1 MHz and permittivity at high frequency $\varepsilon_\infty = n_D^2$ in benzene solutions were determined using the method described in an earlier paper.[5] All measurements were made at 35 °C.

Linear slopes a_0, a', a'', and a_∞ (ε_0, ε', ε'', and ε_∞ vs. wt fraction of solute) have been used for complex plane plots (a'' vs. a') and analysis of data. Average relaxation time τ_0 and distribution parameter α have been calculated from these plots.[6] Data have been analyzed for the relaxation time of overall rotation τ_1, group rotation τ_2 and their corresponding weight factors, using Budo[7] equation (Table 2).

The compounds were obtained from Riedel-de Haën, E. Merck, Germany and Messrs Fluka A.G., Switzerland of purum grade and used as such. Benzene Analar (B.D.H., India) was used as solvent after double distillation.

Results and Discussion

The dipole moment of these compounds are in good agreement with those reported earlier[1-3] (Table 1). The dipole moment of the molecule decreases with increase in the size of two end alkoxyl groups. This is the characteristic behavior of all homologous series in which increase in the size of the alkoxyl groups decreases the polarity at the two ends of the chain, hence there is a decrease in the dipole moment. The dipole moment of dialkyl ether of diethylene glycol is greater than the corresponding dialkyl ether of ethylene glycol because of the increase in the separation of the end polar alkoxyl groups resulting in an increase in the dipole moment. Dipole moment of monoalkyl ether[8,9] is greater than the corresponding dialkyl ether because of the higher group moment of the hydroxyl group in comparison to that of the alkoxyl group (Table 1).

The complex plane plots obeyed the Cole-Cole arcs which show the symmetrical distribution of relaxation time in these molecules. The value of τ_0 increases with increase in the size of the molecule which is in agreement with that of the other homologous series.[8,9] Small values of τ_0 and large values of α indicate that besides

Table 2. Relaxation Times τ_0, τ_1, and τ_2, Distribution Parameter α, and Weight Factor C_2 for Group Rotation in Benzene Solutions at 35 °C

Compound	τ_0/ps	α	τ_1/ps	τ_2/ps	C_2
	Dialkyl ethers of ethylene glycol				
Dimethyl	1.8	0.25	24.8	1.6[a]	0.90
Diethyl	3.0	0.23	16.8	2.3	0.82
	Dialkyl ethers of diethylene glycol				
Dimethyl	2.0	0.34	21.7	1.5[a]	0.80
Diethyl	3.5	0.29	18.1	2.0	0.75
Dibutyl	4.5	0.25	14.6	2.7	0.66

a) 1,4-Dimethoxybenzene[10,11] in benzene, τ_1=11.55 τ_2=1.65 C_2=0.20. Anisole[10,11] in benzene, τ_1=9.90 τ_2=1.65 C_2=0.16. Ethylene glycol monomethyl ether[8] in benzene, τ_1=16.26 τ_2=1.54 C_2=0.75.

Table 1. Values of Dipole Moments in Benzene Solutions at 35 °C[e]

Ethers of ethylene glycol				Ethers of diethylene glycol			
Compound	μ/Debye	Compound	μ/Debye	Compound	μ/Debye	Compound	μ/Debye
Monomethyl	2.24	Dimethyl[a]	1.81	Monomethyl	2.75	Dimethyl[c]	2.09
Monoethyl	2.26	Diethyl[b]	1.76	Monoethyl	2.78	Diethyl[d]	1.98
Monobutyl	2.24			Monobutyl	2.65	Dibutyl	1.88

a) 1.71 Debye[1] at 25 °C. b) 1.61 Debye[3] at 20 °C. c) 1.97 Debye[1] at 25 °C. d) 1.99 Debye[2] at 20 °C, 1.93 Debye[3] at 25 °C. e) 1 Debye=3.3356×10^{-30} C m.

the overall rotation, there is considerable contribution of group rotations. It has been observed that the presence of polar end alkoxyl groups in the polymers of lower molecular weight results in proportionately higher rigidity in the polymer chain, consequently there is practically no twisting or coiling of the chain. In case of these molecules central portion may be regarded as a rigid rod, at the two ends of which the alkoxyl groups rotate. The situation can be compared with 1,4-dimethoxybenzene[10] in which there is internal rotation of the alkoxyl groups about the C–O axes, the angle of rotation of two groups at the upper and lower end being different and hence these molecules have two distinct relaxation processes viz., due to overall rotation as well as to internal rotations. The weight factor for group rotations C_2 is considerably large indicating the possibility of the trans positions of the end groups. In this model if the two alkoxyl groups would have been in gauche form with respect to the central portion of the chain, the freedom of rotation of end groups would have been restricted. Value of C_2 decreases with increase in the size of the alkoxyl group in the same series which indicates that the freedom of the rotation of alkoxyl groups decreases and hence τ_2 increases. The values of C_2 for dialkyl ethers of diethylene glycol are less as compared to the dialkyl ethers of ethylene glycol because with the increase in the size of the chain, the flexibility of the chain increases causing the end alkoxyl groups to be closer thereby decreasing the freedom of rotation of the end alkoxyl groups. The values of τ_2 of methoxyl group presented in this paper compares favorably with that reported earlier.[8,10,11] The value of τ_1 is found to decrease with the increase in the size of the alkoxyl groups because of the decrease in the dipole moment with increase in the size of the alkoxyl group.

The authors wish to express their appreciation to Professor N. K. Mathur, Department of Chemistry of this University for many fruitful discussions. One of the authors (R. J. S.) is also thankful to Council of Scientific and Industrial Research, New Delhi for providing financial assistance.

References

1) K. Kimura and R. Fujishiro, *Bull. Chem. Soc. Jpn.*, **39**, 608 (1966).
2) J. Marchal and H. Bénoit, *J. Chim. Phys.*, **52**, 818 (1955); *J. Polym. Sci.*, **23**, 223 (1957).
3) A. Kotera, K. Suzuki, K. Matsumura, T. Nakano, T. Oyama, and U. Kambayashi, *Bull. Chem. Soc. Jpn.*, **35**, 797 (1962).
4) K. Higasi, *Denki Kenkyusho Iho*, **4**, 231 (1952).
5) H. D. Purohit, H. S. Sharma, and A. D. Vyas, *Bull. Chem. Soc. Jpn.*, **48**, 327 (1975).
6) K. S. Cole and R. H. Cole, *J. Chem. Phys.*, **9**, 341 (1941).
7) A. Budo, *Z. Physik.*, **39**, 706 (1938).
8) H. D. Purohit and R. J. Sengwa, *J. Mol. Liq.*, **39**, 43 (1988).
9) H. D. Purohit and R. J. Sengwa, *J. Mol. Liq.*, **40**, 237 (1989).
10) K. Chitoku, K. Higasi, M. Nakamura, Y. Koga, and H. Takahashi, *Bull. Chem. Soc. Jpn.*, **44**, 992 (1971).
11) K. Higasi, Y. Koga, and M. Nakamura, *Bull. Chem. Soc. Jpn.*, **44**, 988 (1971).

Synthesis and Reactions of Some New Pyridazinones

Essam Abdel GHANI†
Chemistry Department, Faculty of Science, Zagazig University, Zagazig, Egypt
(Received August 1, 1990)

Synopsis. 3-(*p*-Ethoxybenzoyl)acrylic acid (**1**) reacts with 3-methyl-1-phenyl-2-pyrazolin-5-one to give an addition compound **2**. The condensation of **2** with hydrazine hydrate affords 4,5-dihydro-3(2*H*)-pyridazinone (**3a**). Reaction of **3a** with dimethyl sulfate, diethyl sulfate, ethyl bromoacetate, $POCl_3$, and P_2S_5 gave the N-substituted pyridazinones **3b**—**d**, a dichloro derivative **5a**, and a dithione **7**. The behavior of the dichloro and the dithione derivatives was studied toward different reagents. The *in vitro* antibacterial screening reveals moderate activity against Gram-positive for compounds **3a** and **3c** while **4** and **7** are inactive.

A large number of pyridazinones are reported to exhibit bactericidal activities.[1-4] Direct methods for introduction of oxygenated substituents into aromatic rings are often quite limited. Anodic oxidation is potentially an excellent procedure for direct introduction of oxygen functionalities into aromatics.[5] In addition, efficiency of the anodic oxidation of para-substituted aromatic ethers[6] prompted the author to synthesize a new series of pyridazinones, through the nucleophilic addition of 3-methyl-1-phenyl-2-pyrazolin-5-one to 3-(*p*-ethoxybenzoyl)acrylic acid followed by cyclization of the adduct to give the corresponding dihydropyridazinone. The synthesis of various compounds (**2**—**9**) are outlined in Scheme 1.

Thus, the reaction of 3-(*p*-ethoxybenzoyl)acrylic acid[7] (**1**) with 3-methyl-1-phenyl-2-pyrazolin-5-one[8] in dry benzene gave 4,5-dihydro-α-[2-(4-ethoxyphenyl)-2-oxoethyl]-3-methyl-5-oxo-1-phenyl-1*H*-pyrazole-4-acetic acid (**2**). Structure[a] of the acid **2** was derived from its infrared spectrum which showed ν C=O (acid) at 1700, ν C=O at 1675 and ν C=N at 1605. The reaction of the acid **2** with hydrazine hydrate in boiling ethanol yielded 6-(*p*-ethoxyphenyl)-4-(5-oxo-2-pyrazolin-4-yl)-4,5-dihydro-3(2*H*)-pyridazinone (**3a**). The IR spectrum of **3a** showed ν C=O at 1655, ν C=N at 1605 and ν NH at 3430. Reaction of **3a** with dimethyl sulfate, diethyl sulfate, and ethyl bromoacetate gave the N-substituted products **3b**—**d**. The IR spectra of **3b**—**d** showed ν C=O at 1660—1630, ν C=N 1600—1585, and additional band at 1740 for **3d** attributable to ν C=O (ester). Condensation of **3a** with *p*-anisaldehyde in the presence of ethanolic KOH took place at the 5-position[9] to give 4,5,6-trisubstituted pyridazin-3(2*H*)-one (**4**). The IR specrum of **4** showed bands at 1650 (ν C=O), 1600 (ν C=N), and 3390 (ν NH).

This work reports on the behavior of the pyridazinone derivative towards nucleophilic reagents like phosphoryl chloride. Treatment of **3a** with $POCl_3$ gave the dichloro derivative **5a**. The IR spectrum of **5a** was devoid of ν C=O and showed ν C=N at 1605. The ^{1}H NMR (DMSO-d_6) of **5a** showed signals at δ=8.1—6.9 (9H, m, Ar-H), 3.9—2.7 (5H, m, CH_2CH+CH_2 of ethyl), 2.30 (3H, s, CH_3) and 1.32 (3H, t, CH_3 of ethyl). The dichloro derivative **5a** reacted with sodium methoxide to give the dimethoxy derivative **5b**. The IR spectrum showed ν C=N at 1610. Reaction of **5a** with hydrazine hydrate in ethanol gave the dihydrazino derivative **5c**. The IR spectrum showed ν C=N at 1600 and ν NH at 3170. Compound **5c** condensed with aromatic aldehydes namely benzaldehyde, *p*-anisaldehyde, and *p*-tolualdehyde and yielded the bis (hydrazone) derivatives **5d**—**f** which showed ν C=N at 1605—1600 and ν NH at 3420—3400. The reaction of the dichloro derivative **5a** with sodium azide gave compound **6**. The IR spectrum of **6** showed ν C=N at 1590. ^{1}H NMR (DMSO-d_6) of **6** showed signals at δ=8.08—7.2 (9H, m, Ar-H), 3.8—2.7 (5H, m, CH_2-, CH, $+CH_2$ of ethyl), 2.20 (3H, s, CH_3), and 1.32 (3H, t, CH_3 of ethyl). An alternative route for the preparation of compound **6** was the reaction of the dihydrazino derivative **5c** with nitrous acid to give the same compound **6**. The similarity of these compounds were identified by IR spectra and by mixed melting point determination with the sample prepared before.

Compound **3a** reacted with P_2S_5 in dry xylene to give the dithioxo derivative **7**. Compound **7** evidently exists in the mercapto–thioxo equilibrium. The IR spectrum exhibited bands for ν N–C=S at 1470, ν C=S at 1385, ν C=N at 1600 and band at 3420 evidently for ν SH. The ^{1}H NMR (DMSO-d_6) of **7** showed signals at δ= 8.0—7.7 (10H, m, Ar-H+pyridazine proton), 3.43 (2H, q, CH_2 of ethyl), 3.30 (1H, s, pyrazolethione proton), 2.29 (3H, s, CH_3), and 1.34 (3H, t, CH_3 of ethyl). Treatment of **7** with dimethyl sulfate, diethyl sulfate, and/or methyl acrylate in dry acetone yielded the corresponding S-substituted derivatives **8a**—**c**, respectively. The IR spectra of **8** showed bands at 1605 (ν C=N) in addition to a strong band at 1725 of the ν C=O (ester) for compound **8c**. Compound **7** was easily oxidized to the cyclic disulfide **9** by iodine solution and the IR spectrum of **9** showed ν C=N at 1600.

Screening for an Antibacterial Activity. The prepared compounds **3a**, **3c**, **4**, and **7** were tested for *in vitro* antibacterial activity using the method described by Heatly.[6] The medium for screening was composed of (g 11000 ml) "Lab-lemco" beef extract, 1.0; yeast extract (Oxoid 120), 20; peptone (Oxoid L 37), 5.0; sodium chloride, 2.0, and agar, 15.0 (pH 7.0). Cylinders of known volume (0.1 ml) were placed on the solid medium seeded with a Gram-positive and Gram-negative test organism. A known constant volume (0.05 ml) of the compounds **3a**, **3c**, **4**, and **7** dissolved in SDS was introduced into each cylinder and allowed to diffuse through the agar at room temperature for 1 h and finally incubated at 37 °C for about 18—20 h. Clear circular zones of inhibition of the test organisms were formed around the holes containing compounds **3a** and **3c**. It

† Present address: University Post Office, P. O. Box 11602, Sana'a, Yemen Republic.

a) IR_{max} here and elsewhere in the paper in cm^{-1}.

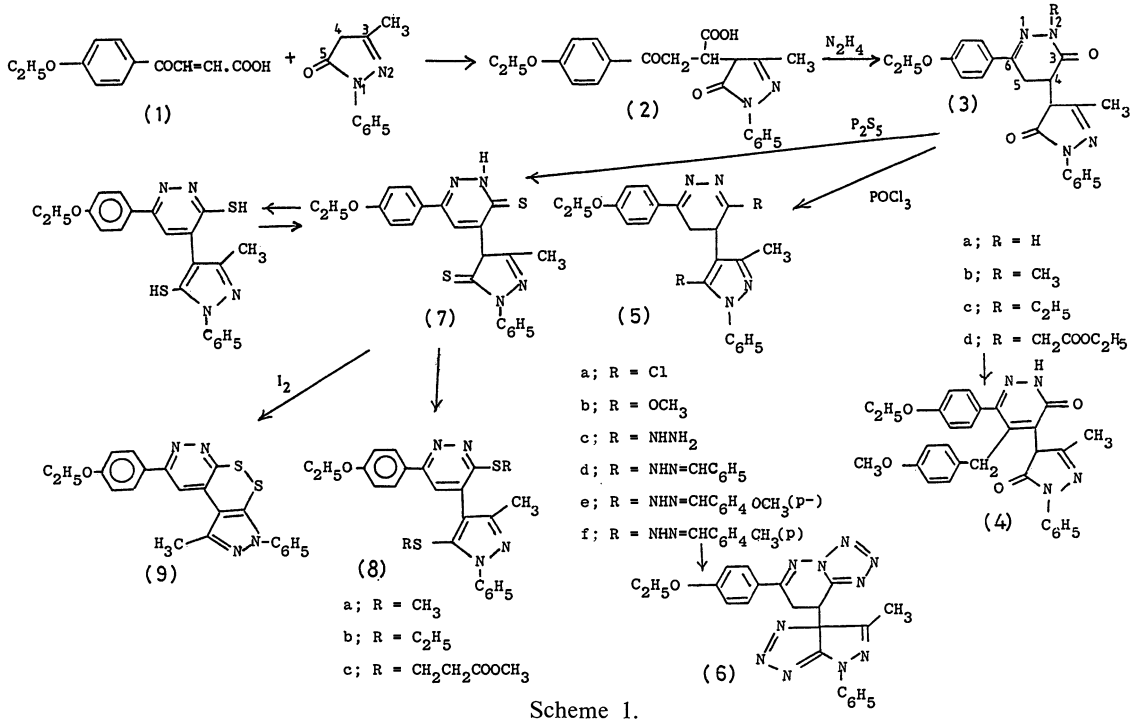

Scheme 1.

Table 1. *In Vitro* Antibacterial Activities of Some of the Prepared Compounds[a)]

Compound	*Staphylococcus aureus*	*Echerichia Coli*	*Pseudomonas auregonosa*
3a	++	++	++
3c	++	++	+
4	−	−	−
7	−	−	−

a) (−) No antibacterial activity of the zone equal to 1 cm. (+) Mild activity with the diameter of the zone equal to 1 cm. (++) Moderate activity with the diameter of the zone equal to 1.8 cm.

is suggested that compounds **3a** and **3c** possess moderate activities against Gram-positive as shown in Table 1.

Experimental

All melting points are uncorrected. The IR spectra (KBr discs) were recorded on a Unicam SP 1200 spectrophotometer. The ^{1}H NMR spectra were obtained on a JEOL FX-100 Fourier transform instrument using tetramethylsilane as internal standard. Physical data of **2**—**9** are summarized in Table 2.

Preparation of Compound 2. To a solution of **1**[7] (0.01 mol) in dry benzene (20 ml), 3-methyl-1-phenyl-2-pyrazolin-5-one[8] (0.01 mol) was added and the reaction mixture refluxed for 10 h. The solid that separated on cooling was crystallized from ethanol to give **2**.

Preparation of Compounds 3a, 5c, and 5d—f. To a solution of **2**, **5a**, or **5c** (0.01 mol) in ethanol (20 ml), hydrazine hydrate, benzaldehyde, *p*-anisaldehyde, or *p*-tolualdehyde (0.01 or 0.02 mol) was added and the reaction mixture refluxed for 5 h. The solid that separated on cooling was crystallized from a suitable solvent to give **3a**, **5c**, and **5d**—**f**, respectively.

Preparation of Compounds 3b—d and 8a,b. A mixture of **3a** or **7** (0.01 mol), anhydrous potassium carbonate (0.03 mol), dimethyl sulfate, diethyl sulfate, or ethyl bromoacetate (0.03 mol), and dry acetone (50 ml) was refluxed for 20 h. After removing the excess solvent the products were crystallized from the proper solvent to give compounds **3b**—**d** and **8a,b**.

Preparation of Pyridazinone 4. A warm solution of **3a** (0.01 mol) in ethanol (20 ml) was treated with an ethanolic KOH solution (25 ml, 4%) and *p*-anisaldehyde (0.01 mol) was added portionwise with continuous shaking. The reaction mixture was refluxed for 2 h, cooled, poured into cold water and the solid obtained crystallized from the proper solvent to give **4**.

Preparation of Dichloro Derivative 5a. A mixture of **3a** (0.01 mol) and $POCl_3$ (10 ml) was gently refluxed for 30 min, cooled, and treated with crushed ice. The precipitated solid was filtered and crystallized from a suitable solvent to give **5a**.

Preparation of Dimethoxy Derivative 5b. The dichloro compound **5a** (0.01 mol) was added to sodium methoxide solution [from sodium (0.02 mol) in absolute methanol (50 ml)]. The mixture was refluxed for 2 h, then evaporated under reduced pressure. To the residue was added water (10 ml) and insoluble matter was filtered off and crystallized from suitable solvent to give **5b**.

Formation of Compound 6. (a) A mixture of **5a** (1.0 g), sodium azide (2.0 g), water (5 ml), and *N*,*N*-dimethylformamide (20 ml) was boiled for 2 h and cooled. The solid obtained upon dilution with water was filtered and crystallized from a suitable solvent to give **6** (in 55% yield).

(b) An aqueous solution of $NaNO_2$ (0.03 mol in 10 ml H_2O) was added dropwise with stirring to a solution of **5c** (0.01 mol) in 4 M (M=mol dm^{-3}) acetic acid (10 ml) and stirring was continued for 1 h. The solid formed was filtered and crystallized from a suitable solvent to give **6** (in 49% yield).

Preparation of Dithione 7. A solution of **3a** (0.01 mol) and P_2S_5 (0.03 mol) in dry xylene (50 ml) was boiled under reflux for 6 h. The reaction mixture was filtered while hot and then concentrated. The product which separated on cooling was crystallized from a suitable solvent to give **7**.

Preparation of Compound 8c. A solution of **7** (0.01 mol) and methyl acrylate (0.02 mol) in ethanol (20 ml) was treated with a few drops of 10% aqueous sodium hydroxide solution and the mixture heated under reflux for 12 h. The solid formed after cooling was crystallized from a suitable solvent to

Table 2. Physical Data of Various Compounds Prepared

Compound	Mp/°C (Solvent)	Yield/%	Mol formula	Analysis/% Found/Calcd		
				C	H	N
2	210 (Ethanol)	46	$C_{22}H_{22}N_2O_5$	F 67.20 C 66.99	5.40 5.62	6.90 7.10
3a	188 (Acetic acid)	60	$C_{22}H_{22}N_4O_3$	F 67.80 C 67.68	5.71 5.68	14.30 14.35
3b	183 (Benzene)	68	$C_{23}H_{24}N_4O_3$	F 68.40 C 68.30	6.11 5.98	13.75 13.85
3c	202 (Benzene)	59	$C_{24}H_{26}N_4O_3$	F 68.90 C 68.88	6.40 6.26	13.52 13.39
3d	180 (Benzene)	57	$C_{26}H_{28}N_4O_5$	F 65.62 C 65.53	5.78 5.92	11.83 11.76
4	199 [Benzene: Ethanol(1 : 1)]	50	$C_{30}H_{28}N_4O_4$	F 70.94 C 70.85	5.53 5.55	10.82 11.02
5a	160 (Methanol)	45	$C_{22}H_{20}Cl_2N_4O$	F 61.63 C 61.83	4.82 4.72	12.97 13.11
5b	135 (Pet.ether 80—100)	73	$C_{24}H_{26}N_4O_3$	F 68.91 C 68.88	6.30 6.26	13.52 13.39
5c	160 [Benzene: Ethanol(1 : 1)]	70	$C_{22}H_{26}N_8O$	F 63.40 C 63.14	6.32 6.26	26.51 26.78
5d	283 (Acetic acid)	68	$C_{36}H_{34}N_8O$	F 72.79 C 72.71	5.70 5.76	18.83 18.84
5e	260 (Acetic acid)	73	$C_{38}H_{38}N_8O_3$	F 69.84 C 69.71	5.63 5.85	16.89 17.11
5f	270 (Acetic acid)	70	$C_{38}H_{38}N_8O$	F 73.52 C 73.29	5.93 6.15	18.12 17.99
6	185 (Ethanol)	55	$C_{22}H_{20}N_{10}O$	F 59.83 C 59.99	4.52 4.58	31.87 31.80
7	241 (DMF)	69	$C_{22}H_{20}N_4OS_2$	F 62.92 C 62.83	4.83 4.79	13.52 13.32
8a	138 (Pet.ether 80—100)	63	$C_{24}H_{24}N_4OS_2$	F 64.43 C 64.26	5.62 5.39	12.50 12.49
8b	125 (Pet.ether 80—100)	57	$C_{26}H_{28}N_4OS_2$	F 65.83 C 65.51	5.92 5.92	11.81 11.75
8c	100 (Pet. ether 80—100)	71	$C_{30}H_{32}N_4O_5S_2$	F 60.60 C 60.79	5.29 5.44	9.73 9.45
9	239 (DMF)	76	$C_{22}H_{18}N_4OS_2$	F 63.43 C 63.13	4.32 4.34	13.58 13.39

give **8c**.

Formation of 1,2-Dithiin Derivative 9. A solution of iodine (0.02 mol) in 5% aqueous KI solution (100 ml) was added dropwise with stirring to a solution of **7** (0.01 mol) in 10% aqueous sodium hydroxide (10 ml) until the color of iodine persisted. The solid formed was filtered off and crystallized from a suitable solvent to give **9**.

References

1) S. Kamiya, A. Nakamura, T. Itai, K. Koshinuma, and G. Okusa, *Yakugaku Zasshi,* **86**, 1099 (1966).
2) G. H. Sayed, A. A. Ismail, and Z. Hashem, *Egypt J. Chem.,* **27**, 757 (1984).
3) G. H. Sayed, A. A. Ismail, and Z. Hashem, *J. Chem. Soc. Pak.,* **6**, 95 (1984).
4) G. H. Sayed, A. A. Ismail, S. El-Nagdy, and S. M. Mohamed, *Egypt J. Chem.,* **29**, 433 (1986).
5) L. Eberson and K. Nyberg, *Tetrahedron,* **32**, 2185 (1976). Z. Blum, L. Cedheim, and K. Nyberg, *Acta Chem. Scand., Ser. B,* **29**, 715 (1975). Y. So and L. L. Miller, *Synthesis,* **1976**, 468.
6) M. P. Capparelli, R. E. De Schepper, and J. S. Swenton, *J. Org. Chem.,* **52**, 4953 (1987).
7) D. Papa, E. Schwenk, F. Villani, and E. Klingsberg, *J. Am. Chem. Soc.,* **70**, 3356 (1948).
8) Kh. V. Bal'yan and A. L. Shtangeev, *Zh. Obshch. Khim.,* **24**, 238 (1954).
9) G. H. Sayed, M. Y. El-Kady, I. Abd-El-Mawgoud, and M. Hamdy, *J. Chem. Soc. Pak.,* **7**, 263 (1985).
10) N. G. Heatly, *Analyst,* **73**, 244 (1948).

Synthesis of Phosphorus-Containing Polymers with Aziridine Ring

Dimitrina TRENDAFILOVA-GERCHEVA, Koljo TROEV,*,† and Milka GEORGIEVA
Department of Plastics, Higher Institute for Chemical Technology,
Kliment Ohridski Ave. 8, Sofia 1756, Bulgaria
†Institute for Polymers, Bulgarian Academy of Sciences, Sofia 1040, Bulgaria
(Received September 4, 1990)

Synopsis. It has been established that phosphorus containing alkylammonium salts obtained by alkylation of primary amines with bis(2-chloroethyl) phosphonate or alkyl 2-chloroethyl phosphonate can be transformed into corresponding compounds with aziridine ring.

Physiologically active polymers replace successfully in recent years well known low-molecular therapeutic compounds. Advantages of such drug forms, lower toxicity, prolongated action, higher selectivity etc.[1,2] are due to the unique combination between the polymer character of the drug carrier and the physiological action of the low-molecular medicine.

This work is a continuation of our previous studies on the reaction of *N*-alkylation of compounds containing amino groups with esters of phosphorous acids.[3]

Polycations are effective anticancer agents. They create some level of selectivity regard to malignant cells, which possess greater negative charge and greater endocytic ability compared to normal cells.

The purpose of the present research is the synthesis of polymers with potential biological activity containing an ethyleneimine ring in its side chain.

Results and Discussion

It is well known[4,5] that ethyleneimine is obtained by treating 2-bromoethylamine with potassium hydroxide:

$$H_2N\text{-}CH_2CH_2Br + KOH \longrightarrow \underset{\diagdown\ \diagup}{\overset{}{CH_2\text{-}CH_2}} + KBr + H_2O$$
$$\qquad\qquad\qquad\qquad\qquad\qquad\quad NH$$

This reaction is fundamental in our studies on the synthesis of phosphorus containing polymers with aziridine ring.

We used two polymers containing amino groups—a glucomacropeptide (GMP), and a vinylpyrrolidone—vinylamine copolymer (VP-VA). The fragments containing amino groups with reaction ability are different for them.

In the GMP the amino group is included in the amino acid lysine (ε-amino group) $-HN-\underset{\displaystyle (CH_2)_4}{\overset{\displaystyle |}{\underset{\displaystyle |}{CH}}}-CO-$ while in the $\qquad\qquad\qquad\qquad\qquad\qquad

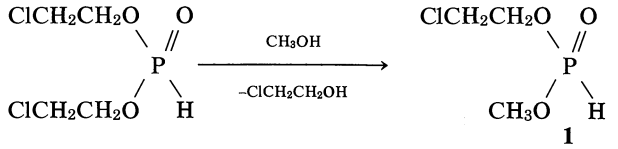

The reaction of transesterification at that temperature 50 °C, is possible as it takes place in a base environment which accelerates the reaction. The obtained methyl 2-chloroethyl phosphonate alkylates the copolymer following the scheme:

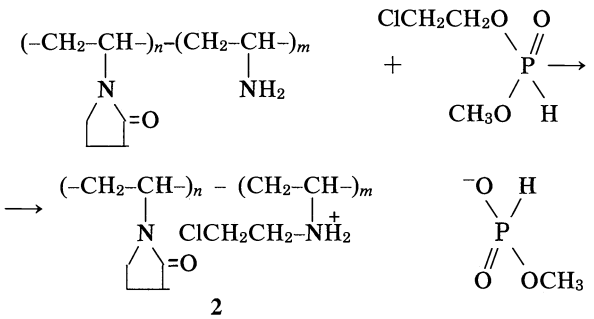

In the IR spectra of product **2** (Table 2) the bands for P=O and P–H groups are bathochromically shifted. This proves the ionic character of the bonds.[6]

A. II. Treating of Product 2 with NaOH. Further treatment of the reaction mixture by equimolar amount of 0.1 M NaOH leads to the final product **3** containing an aziridine ring.

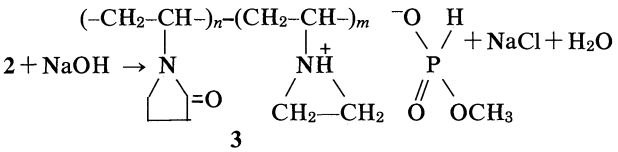

The structure is proven by the disappearance of both triplets in the ^{1}H NMR spectra. The singlet at δ=2.71 for the aziridine ring can not be observed (Table 1) because of overlapping with the polymer signals.

B. Reaction of GMP with Bis(2-chloroethyl) Phosphonate. Dimethyl sulfoxide was used as a solvent in this case. The reaction takes place without the isolation of the intermediate product **4** and follows the equation:

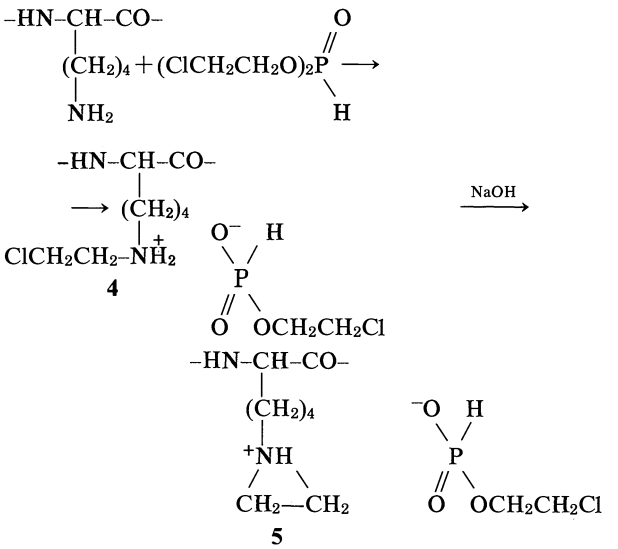

Table 2. IR Spectral Data for Products **2** and **5**

Compound	P=O/cm^{-1}		P–H/cm^{-1}	
	Starting ester	Product	Starting ester	Product
2	1268	1213	2444	2348
5	1268	1214	2444	2319

There is a singlet at δ=2.72 for the aziridine ring in the ^{1}H NMR spectrum of product **4**. The bathochromic shift of P–H and P=O group bands in the IR spectrum is a further proof for the ionic character of the bonds.

The structure of product **3** obtained from the reaction of the VP–VA copolymer with bis(2-chloroethyl) phosphonate is confirmed also by the model reaction between *n*-BuNH$_2$ and bis(2-chloroethyl) phosphonate. Methanol is used as a solvent.

In the first stage of the reaction a transesterification of the phosphonate takes place. It is followed by the *N*-alkylation of the amine by the methyl 2-chloroethyl phosphonate:

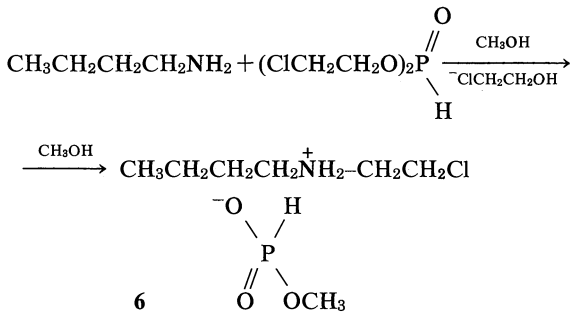

The process is followed by means of ^{1}H NMR spectroscopy. The characteristic doublets for P–H and P–OCH$_3$ protons at δ=6.66 and $^1J_{P-H}$=634.6 Hz, and δ=3.554 $^3J_{P-OCH}$=11.9 Hz, respectively are observed. At δ=3.67 and δ=3.84 two triplets appear for $\overset{+}{N}$–CH$_2$ and CH$_2$Cl protons.

In the second stage, after the treatment of product **6** with NaOH these triplets disappear while a singlet at δ=2.71 for the aziridine ring protons is observed.

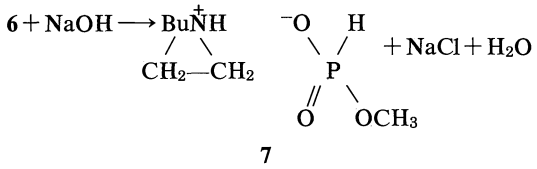

Together with these signals the spectra of products **6** and **7** display another doublet at δ=6.78 with J=641.9 Hz and a singlet at δ=2.68 of very low intensity. It may be that under the conditions of the reaction part of bis(2-chloroethyl) phosphonate is transesterified to di methyl phosphonate which takes part further in the *N*-alkylation of butylamine:

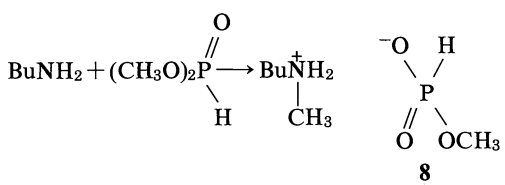

The ratio between this component **8** and the main product **7** is 1 : 8.5 or 11.8% : 88.2% calculated from the integral intensity of the peaks.

These two signals are absent in the case of the reaction between the VP-VA copolymer and bis(2-chloroethyl) phosphonate in the presence of CH_3OH. It is probable that the ability for transesterification also of the *s*-alkoxyl group is a function of the basicity of the amines in use.

Experimental

Materials. We used two type of polymers:

A. Synthetic polymer—a copolymer of vinylpyrrolidone with vinylamine (VP-VA) was prepared according the literature[7] with molar ratio of 9:91 and molecular weight 80000±1000.

B. Natural polymer—a glucomacropeptide (GMP) isolated from milk[8] with molecular weight 6000. Galactose, galactosamine, neuraminic acid and 58 anino acids take part in its composition.

Bis(2-chloroethyl) phosphonate (Fluka product) purified by distillation under vacuum was used as an alkylating agent.

The solvents—methanol and dimethyl sulfoxide were purified and dried according the literature.[9]

Procedure. A. Reaction between the Copolymer VP-VA and Bis(2-chloroethyl) Phosphonate. The reaction is carried out in a flask equipped with a stirrer and a capillary for purging with argon. The copolymer is solved in methanol and the phosphonate is added. The temperature of the reaction is t=50 °C. After reaching pH=7 an equimolar amount of 0.1 M NaOH is added and the mixture is heated at 50 °C for 11 h. The product is isolated by precipitation in ether and is dried under vacuum. Elem. Anal. P=2.10%.

B. Reaction between GMP and Bis(2-chloroethyl) Phosphonate. The reaction is carried out in a flask equipped with a stirrer and a capillary for purging with argon. The GMP is solved in DMSO and the bis(2-chloroethyl) phosphonate is added. The mixture is stirred for 4 h at t=50 °C after which an equimolar amount of 0.1 M NaOH is added. After the reaction has taken place the polymer is precipitated in acetone (0 °C) and is dried under vacuum. Elem. Anal. P=3.14%.

C. Reaction between *n*-Butylamine with Bis(2-chloroethyl) Phosphonate. In a flask equipped with a stirrer and a capillary for purging with argon equimolar quantities of *n*-$BuNH_2$ and bis(2-chloroethyl) phosphonate are mixed. The mixture is heated at t=50 °C until reaching pH=7 after which 0.1 M NaOH is added. The reaction takes place at t=50 °C until once again pH=7 is reached. The final product is isolated by evaporating the methanol under vacuum.

The structure of the final products is proved by IR spectroscopy (PE 983) and ^{1}H NMR spectroscopy (BRUKER WP 250).

Conclusion

The presence of positive charge at the quaternary nitrogen atom probably will accelerate the reaction of forming an aziridine ring because the synthesis is accompanied by release of HCl. The positive charge at the nitrogen atom will provide for higher acidity of the proton associated with it and in this way will accelerate the acid-base reaction:

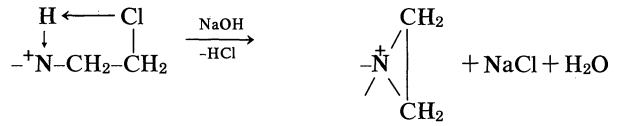

These results show that polymers containing amino groups *N*-alkylated by bis(2β-chloroethyl) phosphonate may be transformed into *N*-alkylated polymers with aziridine ring.

References

1) H. Ringsdorf, *J. Polym. Sci., Polym. Symp.*, **51**, 135 (1975).

2) N. A. Plate and A. E. Vassiliev, "Physiologically Active Polymers," Khimia, Moscow (1988), (in Russian).

3) D. Trendafilova-Gercheva, V. Vassileva, M. Georgieva, K. Troev, and E. F. Panarin, *Angew. Chem.*, 1990, submitted.

4) W. Marckwald, *Ber.*, **33**, 764 (1900).

5) W. Marckwald and O. Frobenius, *Ber.*, **34**, 3544 (1901).

6) J. Brand and G. Ellington, "Application of Spectroscopy in Organic Chemistry," Mir, Moscow, (1967), p. 128, (in Russian).

7) R. I. Grus, T. Iv. Verhogljadova, and E. F. Panarin, *Vissokomol. Soed.*, **13A**, 647 (1971) (in Russian).

8) P. Velcheva, I. Abrashev, J. Kurteva, P. Nikolov, and T. Donev, *Acta Microbiol. Bulg.*, **9**, 1981.

9) H. Becker et al., "Organikum Organisch-Chemishes Grundpractikum," B. II, VEB, Berlin (1976).

 © 1991 The Chemical Society of Japan Bull. Chem. Soc. Jpn., 64, 2039—2044 (1991)

Classification of Phenothiazine Complexes by Structure and Electronic Properties

Kozo Kozawa,* Taketoshi Hoshizaki, and Tokiko Uchida
Department of Industrial and Engineering Chemistry, Faculty of Science and Technology, Science University of Tokyo, Noda, Chiba 278
(Received September 21, 1990)

Donor-acceptor complexes were prepared, and their structures and electronic properties were observed. Donors were phenothiazine and its four derivatives, and acceptors were metallic chlorides (Lewis acids), iodine, and two π-type acceptors. By the absorption edge of diffuse reflection spectra (λ_E) and crystal structure, the complexes were classified into four groups. Groups I, II, and III correspond to the complexes with Lewis acids or iodine, and group IV consists of complexes with π-type acceptors. The summarized characteristics of each group are as follows. Group I: $\lambda_E \leqslant 950$ nm, complete charge transfer, insulator, and alternate arrangement of cations and anions. Group II: 1200 nm$\leqslant\lambda_E\leqslant$1700 nm, complete charge transfer, semiconductive behavior, and oligomeric or columnar arrangement of cation radicals. Group III: $\lambda_E > 2500$ nm, partial charge transfer, metallic conductor or semiconductor with small activation energy, and columnar arrangement. Group IV: $\lambda_E \geqslant 1700$ nm, and semiconductive behavior. Based on these classifications, we have proposed a mechanism for controlling the aggregate manner of cation radicals.

Recently, functional organic solid materials have attracted attention due to their potential for practical applications. These materials include organic conductors (or superconductors), photosensitive materials used for information recording, and substances having nonlinear optical properties. In designing these organic functional materials, it should be noted that not only their molecular structure but also their aggregate manner (i.e., crystal structure) plays a very important role, since the interactions (such as electron transfer or energy transfer) between neighboring molecules closely depend on their arrangements in the crystal. For instance, the magnitude of the electrical conductivity of organic conductors is greatly affected by the arrangement of the molecules in the crystal.[1] However, it has not been elucidated what rules determine the arrangement of molecules in the solid state, especially the formation of segregated stacks of molecules, though several authors have tried to define these rules.[2]

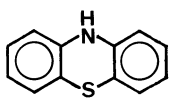
1

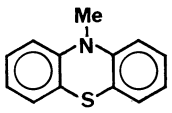
2

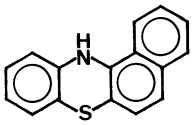
3

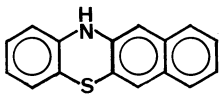
4

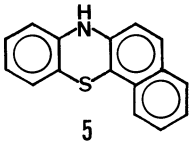
5

We have been studying solid complexes of the electron donor–acceptor type, relating their electronic properties to their crystal structures. This report describes the results of our studies of phenothiazine (hereafter PT) and its derivatives (hereafter PT derivatives) as electron donors.

PT derivatives used in this study were the following five substances: phenothiazine (PT, **1**), 10-methylphenothiazine (MPT, **2**), benzo[*a*]phenothiazine (B[*a*]PT, **3**), benzo[*b*]phenothiazine (B[*b*]PT, **4**), and benzo[*c*]phenothiazine (B[*c*]PT, **5**). Acceptors used in this study were various metal chlorides (Lewis acids): $SbCl_3$ (**6**), $SbCl_5$ (**7**), $SnCl_4$ (**8**), $TeCl_4$ (**9**), and $CuCl_2$ (**10**), iodine (**11**) and two typical π-acceptors: 2,3-dichloro-5,6-dicyano-*p*-benzoquinone (DDQ, **12**) and 7,7,8,8-tetracyanoquinodimethane (TCNQ, **13**). Many complexes, possessing a variety of both structures and electronic properties, were prepared by the combination of these donors and acceptors. The purpose of this research was to describe the determining factor of molecular arrangements in the solid state through the classification of the complexes obtained, and to search for a method to control the molecular arrangement.

Experimental

Materials. PT (Wako Junyaku Co.) was purified by sublimation in vacuo after repeated recrystallization from benzene. MPT was prepared by the method described in the literature,[3] and purified by recrystallization from hexane. B[*a*]PT, B[*b*]PT, and B[*c*]PT were also synthesized according to the literature[4] and purified by sublimation in vacuo. $SbCl_3$ and $TeCl_4$ were purified by sublimation in vacuo and I_2 was sublimed by the usual method.

Each complex was prepared by slow evaporation of solvent from a solution of a suitable donor and an acceptor. Single

Table 1. Numbering and Preparative Conditions of Complexes with Some Characteristics

No.[a]	Donor	Acceptor	Mole ratio[b]	Solvent[c]	Features
1-6a	PT	$SbCl_3$	1 : 2	DCE	$PT^{+\cdot}$–$SbCl_4^-$, triclinic
1-6b		$SbCl_3$	1 : 2	DCE	$PT^{+\cdot}$–$SbCl_4^-$, monoclinic
1-7a		$SbCl_5$	1 : 1	DCE	$PT^{+\cdot}$–$SbCl_6^-$
1-7b		$SbCl_5$	1 : 3	DCE	$PT^{+\cdot}$–$SbCl_6^-$·H_2O
1-7c		$SbCl_5$	1 : 5	DCE	$DCPT^{+\cdot}$–$SbCl_6^-$[d]
1-9		$TeCl_4$	1 : 1	DCE	
1-11		I_2	2 : 3	BZ	
1-12		DDQ	1 : 1	BZ	
1-13		TCNQ	1 : 1	DCM	
2-6	MPT	$SbCl_3$, $SbCl_5$	2 : 6 : 1	DCE	
2-7		$SbCl_5$	1 : 1	DCE	$MPT^{+\cdot}$–$SbCl_6^-$
2-9		$TeCl_4$	1 : 1	DCE	
2-11		I_2	2 : 3	ETH	
2-12		DDQ	1 : 1	BZ	
2-13		TCNQ	1 : 1	AN	
3-6	B[*a*]PT	$SbCl_3$	1 : 5	DCE	
3-7		$SbCl_5$	1 : 20	DCE	
3-9		$TeCl_4$	1 : 1	DCE	$(B[a]PT^{+\cdot})_2$–Te_2Cl_{10}[e]
3-10		$CuCl_2$	1 : 1	AN	
3-11		I_2	2 : 3	BZ	
3-12		DDQ	1 : 1	BZ	
3-13		TCNQ	1 : 1	AN	
4-7	B[*b*]PT	$SbCl_5$	1 : 1	DCE	
4-8		$SnCl_4$	1 : 2	DCE	
4-11		I_2	1 : 2—6	BZ	$B[b]PT^{+\cdot}$–$I_{2.5}$
4-13		TCNQ	1 : 1	AN	
5-6a	B[*c*]PT	$SbCl_3$	1 : 4	DCE	$B[c]PT^{+\cdot}$–$SbCl_4^-$·0.5DCE
5-6b		$SbCl_3$	1 : 1	DCE	
5-7		$SbCl_5$	1 : 1	DCE	
5-9		$TeCl_4$	1 : 1	DCE	
5-10		$CuCl_2$	1 : 1	AN	
5-11		I_2	2 : 3	BZ	
5-12		DDQ	1 : 1	BZ	
5-13		TCNQ	1 : 1	DCE	

a) Complexes are presented by their numbering hereafter. The first and second numbers indicate the donor and acceptor, respectively. A letter represents a different crystal from the same combination of donor and acceptor. b) Mole ratio of a solution. c) DCE: 1,2-dichloroethane; BZ: benzene; DCM: dichloromethane; ETH: diethyl ether; AN: acetonitrile. d) DCPT: 3,7-dichlorophenothiazine (PT was substituted). e) Ref. 18.

crystals were also obtained by a similar method. Table 1 shows the preparative conditions of the complexes along with their numbering.

Electrical Resistivity. For a single crystal of **4-11**, resistivity was measured along its three axes by direct current with the four probe method from −170 °C to room temperature.[5] Resistivities of other single crystals of **1-6b**, **5-6a**, and **2-7** were measured by direct current with the two probe method from room temperature to 100 °C, from −65 °C to room temperature, and only at room temperature, respectively. For other complexes, direct current with the two probe method was applied to a compressed polycrystalline pellet of 3 mm diameter. The electric potential generator used was a Takedariken (Advantest) TR6142 or a Yokogawa Electric Co. 2853, 2861. A Takedariken TR8651 was used for current measurements. Probes were 100 μmϕ Pt wires. Specimens and probes were connected with Dotite XC-12 paint (Fujikurakasei carbon series). Measurements were carried out in a dry nitrogen atmosphere.

Diffuse reflectance spectra of powder crystalline complexes were measured with a Hitachi 330 spectrometer with a 60 mmϕ integral sphere and an Al_2O_3 plate as a reference. Although the nominal measurable ranges of this sphere were 250—800 nm and 900—1500 nm, absorption was observed in the ranges 800—900 nm and 1500—2500 nm. Hence, measurements were carried out in the range 250—2500 nm.

In order to determine the oxidation state of the PT derivatives in the solid state, solution spectra of the complexes, dissolved in 1,2-dichloroethane, were measured with a Hitachi 330 spectrometer. Although the donors do not always remain in the same oxidation state when dissolved, a stable oxidized state might be confirmable by this procedure.

The X-ray structure determinations were carried out for several complexes, of which appropriate single crystals were obtained.

Results and Discussion

Classification of the PT Complexes. PT is readily oxidized to a cation radical which is fairly stable in solution and in the solid state.[6,7] Figure 1 shows a typical solution spectra of neutral PT and $PT^{+\cdot}$. The characteristic λ maxima of each cation radical are presented in Table 2.

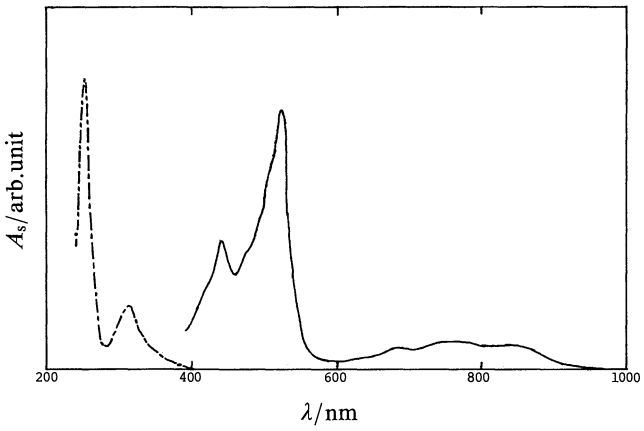

Fig. 1. Absorption spectra of PT (——·——) and PT–$SbCl_6$ (**1–7a**) (———), in 1,2-dichloroethane solution.

Table 2. Characteristic Absorption Maxima of the Cation Radical of Phenothiazine Derivatives

Cation radical	Absorption maximum λ/nm					
$PT^{+\cdot}$ [a]		271,	435,	480, 500,	515,	
$MPT^{+\cdot}$ [b]		271,	450,		518	
B[*a*]$PT^{+\cdot}$ [c]	230,	299,				597
B[*b*]$PT^{+\cdot}$ [c]		305,	425,		540	
B[*c*]$PT^{+\cdot}$ [c]	234,	302,				608

a) Ref. 6. b) This work. c) Ref. 19.

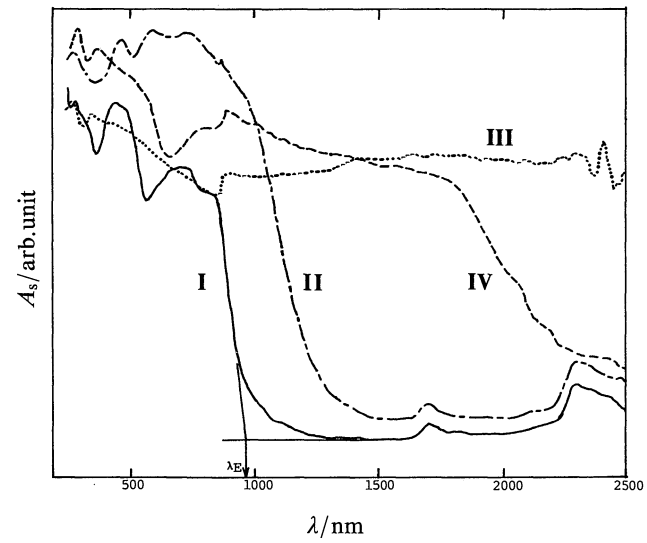

Fig. 2. Diffuse reflection spectra of **2–7**(I), **5–6a**(II). **4–11**(III), and **1–13**(IV). The manner for evaluation of λ_E is shown in the curve of **2–7**.

Figure 2 shows four typical diffuse reflectance spectra, in which reflectance is converted to absorbance by Kubelka–Munk's equation. The wavelengths of the absorption edge (λ_E) are defined by the intersection of tangent lines of the absorption edge and the baseline, as shown in Fig. 2.

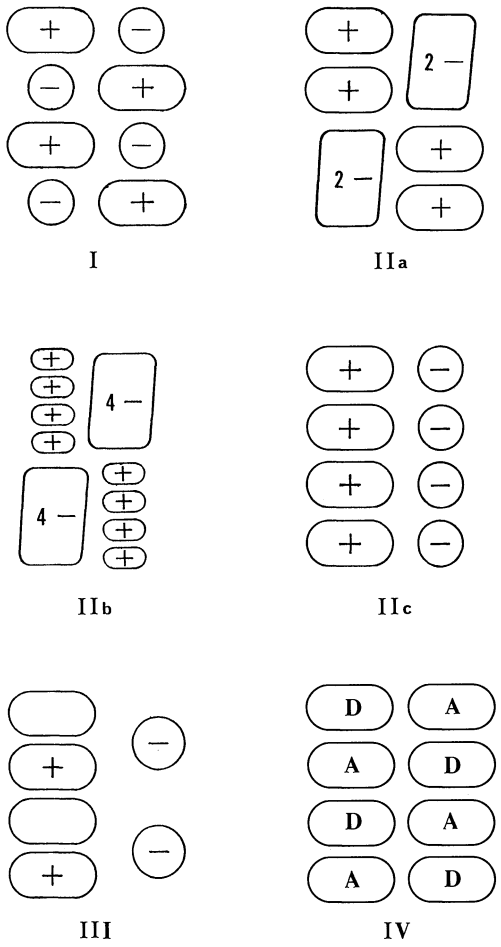

Fig. 3. Classification of crystal structure of the complexes of PT derivatives. I: Simple ionic crystal type; IIa: dimer; IIb: tetramer; IIc: segregated stack of donors with unit charge per molecule; III: segregated stack of donors with fractional charge per molecule; IV: mixed stack of π–π type CT complex.

We found that the physical properties and crystal structures of PT complexes were closely correlated if we classified them into four groups. The classification was made based on the value of λ_E as defined above. Namely, Group I: $\lambda_E \leqslant 950$nm, Group II: 1200 nm$\leqslant \lambda_E \leqslant$1700 nm, Group III: $\lambda_E > 2500$ nm, those complexes mainly between PT derivatives and iodine, and Group IV: complexes between PT derivatives and π-acceptors. Table 3 presents the physical properties of the complexes along with the crystal structures so far determined. Schematic structures for each group of complexes are shown in Fig. 3.

Group I: Substances classified in this group possess very high electrical resistivity (actually unobservable), and their absorption edges are in a shorter wavelength range than those of the other three groups. The commonly observable absorption band with its edge at 900 nm can be assigned to the intramolecular transition of the corresponding cation radical by reference to its

Table 3. Physical Properties, Crystal Structures, and Oxidation States of PT Derivative Complexes in Crystals

Group	No.	λ_E/nm	$\rho_{25°C}$/Ω cm	E_a/eV	Cryst. struct.	Cation radical[a]
I	**1-7a**	900	—	—	Ionic monomer[b]	○
	1-7b	850	—	—	Ionic monomer[c]	○
	1-7c	900	—	—	Ionic monomer[c]	○
	2-7	950	$>10^{11}$[d]	—	Ionic monomer[e]	○
	3-7	690	$>10^{11}$	—	—	○
II	**1-6a**	—	—	—	Tetramer[f]	○
	1-6b	1400	$>10^5$ (// *c*)	0.3—0.2	Column[f]	○
	1-9	1200	10^7	0.5—0.6	—	○
	2-6	1200	10^9	0.6—0.8	—	○
	2-9	1300	10^9	0.7	—	○
	3-6	1500	10^5	0.2	—	○
	3-9	1450	10^5	0.3—0.4	Dimer[c]	○
	3-10	1200	10^4	0.4	—	○
	4-7	1700	10^4	0.2	—	○
	4-8	1700	10^4	0.2	—	○
	5-6a	1250	10^6 (s.c.)	0.2	Column[c]	○
	5-7	1350	10^{10}—10^{11}	0.7	—	○
	5-9	1400	10^5	0.3—0.4	—	○
	5-10	1200	10^5	0.4	—	○
III	**1-11**	>2500	19 (20°C)	0.19[g]	—	—
	2-11	>2500	10^{-2} (s.c.)	0.20[h]	—	—
	3-11	>2500	34 (20°C)	0.16[g]	—	—
	4-11	>2500	10^{-2} (// *c*)	Metallic	Column[i]	—
			30 (// *a*)	0.02		
			60 (// *b*)	0.03		
	5-6b	>2500	40	0.14	—	—
	5-11	>2500	18 (20°C)	0.14[g]	—	○
IV	**1-12**	>2500	2×10^4	0.36[j]	—	—
	1-13	2200	7×10^7	0.67[k]	Mixed stack[l]	—
	2-12	>2500	2×10^5	0.33[j]	—	—
			6×10^8[l]			
	2-13	1900	2×10^9	0.83[k]	Mixed stack[m]	—
			7×10^9	0.48[n]		
	3-12	>2500	10^9	1.0	—	—
	3-13	2200	10^{10}	0.3—0.4	—	—
	4-13	1700	2×10^9	0.6	—	—
	5-12	>2500	2×10^4	0.35[k]	—	—
	5-13	2100	10^6	0.3	—	—

a) A circle in this column means that the cation radical peaks were observed in its solution spectrum. A hyphen means that the peaks were not observed there. b) Ref. 7. c) Ref. 18. d) Ref. 20. e) Ref. 21. f) Ref. 8. g) Ref. 22. h) Ref. 23. i) Ref. 5. j) Ref. 24. k) Ref. 25. l) Ref. 13. m) Ref. 14. n) Ref. 26.

solution spectra (Table 2).[7] All the crystal structures so far determined of the substances belonging to this group are simple ionic crystal types similar to NaCl. They are almost spherical anions and plate-like cation radicals arranged alternately without any overlap between the donor planes (see Fig. 3). This is the reason why the substances belonging to Group I are good insulators.

A typical example of this group is **1-7a**. Polarized absorption spectra, observed with its single crystal, and observation of ESR absorption clearly indicate the existence of stable cation radicals in the crystal.[7]

Group II: As illustratively shown in Fig. 3, there are various kinds of crystal structures in this group, namely, dimers(IIa), tetramers(IIb), or segregated stacks of donors(IIc). In these solids, plate-like cation radicals overlap each other in a face-to-face manner. However, attractive interactions between donors can not be very large because of the Coulomb repulsion between fully ionized donors. It is obvious that the mean interplanar distance of 3.47 Å in **1-6b** is rather large in spite of its structure of segregated stacks.[8]

Anions in Group II crystals also exist as dimers, tetramers or polyanions, having a unit negative charge per one chemical unit (see Fig. 3). Since all the complexes so far studied in this group had a donor/acceptor mole ratio of 1:1, donors also should have a unit positive charge per molecule. Consequently, the absorption bands ranging from 950 nm to 1700 nm,

between the λ_E's of Group I and Group II, can be interpreted as a charge transfer absorption band between the cation radicals.

Measurement of electrical resistivity, performed with single crystals of **1-6b** and **5-6a**, proved that they were semiconductors with anisotropy. The observed rather high resistivity and comparatively large spacing in the column, in spite of its one-dimensional structure, can be understood by considering that the amount of charge transfer is very close to unity. Since other complexes of this group possess electrical resistivity of a similar magnitude, their structures should be similar to those already determined.

Group III: As shown in Table 3, most iodine complexes of PT derivatives belong to this group. The crystal structure determination of the complexes of this group has been successful with only one complex: **4-11**, though it is not yet complete.[5] Its structure (Fig. 4) and characteristics are briefly described below.

The crystal structure of **4-11**, $(B[b]PT)_2(I_3^-)(I)_2$, consists of infinite stacks of B[*b*]PT molecules (stack direction is parallel to the *c* axis), separated by univalent I_3^- anions, and linear polyiodide chains (also parallel to the *c* axis). Though the electronic state of the polyiodide has not yet been precisely determined, the amount of charge transfer from B[*b*]PT to the iodine species is probably less than unity. This presumption is supported by the observation of metallic conduction along the *c* axis, and a plasma-edge-like dispersion of reflection spectra in the near-IR region with polarized light parallel to the *c* axis. The observations of ESR spectra and electronic absorption spectra indicate the existence of B[*b*]PT cation radicals.

All the Group III complexes, except **4-11**, are semiconductors. Though they have not yet been structurally analyzed, their structures and electronic states in the solid state are thought to be very similar to those of **4-11**. The structural feature common to Group III complexes is probably an infinite stack of PT derivatives with a fractional charge as shown in Fig. 3 III. Our observations, such as an absorption band extending to the near infrared range, fairly good electrical conductivity with small activation energy, positive Seebeck coefficients etc., support this assumption. Moreover, we propose that all of the Group III iodine complexes have the possibility of possessing metallic conduction, which is hidden by the semiconductive behavior in the observable room temperature range, namely, by the existence of the metal–insulator transition point at a higher range than room temperature.

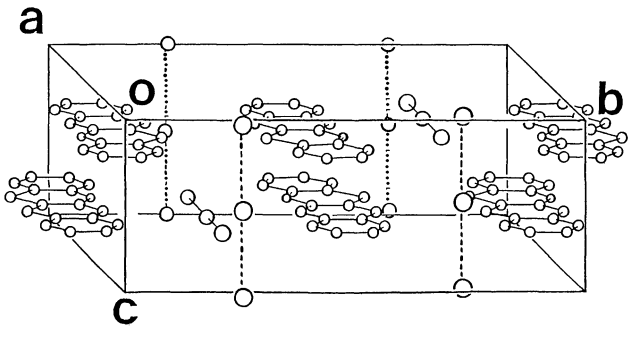

Fig. 4. Perspective view of the crystal structure of **4-11**.

Next, we compare the infinite donor stacks of Group II and Group III. Since the charge on PT derivatives per molecule is fractional in Group III, they have a smaller Coulomb repulsion than those of Group II. In fact, an observed interplanar distance of 3.22 Å between B[*b*]PT moieties in **4-11** is smaller than the value of the Group II complex cited above.

Group IV: Since both donor and acceptor molecules have a π-electron system in this group, both mixed column structure and segregated column structure are possible in the solid state. In the former structure, charge transfer interaction occurs between the donor and acceptor species, and in the latter structure, charge transfer interactions are of the donor–donor or acceptor–acceptor type. Several structural studies have been published describing the complexes between PT and π-acceptors: PT–pyromellitic dianhydride (PMDA),[9] PT–$(PMDA)_2$,[10] PT–trinitrobenzene,[11] and PT-*cis*-bis(trifluoromethylene-1,2-dithiolato)nickel.[12] All of these structures, including **1-13**[13] and **2-13**,[14] are made up of mixed stacks, as shown in Fig. 3 IV, in which PT molecules and flat acceptors stack alternately. The observed absorption band in the near infrared region is probably caused by some intermolecular interaction as cited above, though its precise assignment was not performed at this stage of our research.

The electrical resistivities of this group are in the range of "organic semiconductors". However, the variety of ρ values suggests that there are some possible crystal structures other than a 1:1 mixed column or a simple segregated column; for example, $(perylene)_3(DDQ)_2$,[15] $(perylene)_3(TCNQ)$,[16] and TTF·TCNQ.[17] More structural information should be accumulated for further investigation of this group.

Configuration and Arrangement of PT Derivatives. Since a thiazine ring has an S atom as a member of the ring, PT and its derivative molecules are consequently folded in two planes with creasing through the N and S atoms, in their neutral state. However, we found that these molecules were easily flattened by incorporating their thiazine rings into conjugated systems, such as being oxidized to their cation radicals. Such enlargement of a conjugated system onto the whole molecule is favorable for stabilizing the cation radicals in the solid state, and the flattened molecules can be stacked easily to make dimers or tetramers or segregated columns. In Groups I and II, where all the PT derivatives are flattened cation radicals, their aggregate manner probably depends on the characteristics of the anions. Namely, PT derivatives combined with hexa-coordinated globular anions, such

as $SbCl_6^-$ in Group I, exist as monomers. In Group II, the aggregate manner of PT derivatives are the same as those of the anions; dimeric pairs with dimer anions (**3-9**), tetrameric stacks with tetramer anions (**1-6a**), and infinite stacks with infinite polyanions (**1-6b**). By analogy with **4-11**, we presume that the crystals in Group III are composed of segregated columns of fractionally charged donors, which are also flattened.

In conclusion, the aggregate manner of PT derivatives in solids can be somewhat controlled by choosing Lewis acids which form polyanions.

References

1) J. Tanaka, M. Tanaka, T. Kawai, T. Takabe, and O. Maki, *Bull. Chem. Soc. Jpn.*, **49**, 2358 (1976); K. Bechgaard, C. S. Jacobsen, K. Mortensen, H. J. Pedersen, and N. Thorup, *Solid State Commun.*, **33**, 119 (1980).

2) G. Saito and J. P. Ferraris, *Bull. Chem. Soc. Jpn.*, **53**, 2141 (1980); J. B. Torrance, "Low-Dimensional Conductors and Superconductors," ed by D. Jerome and L. G. Caron, Plenum Press, New York (1987), pp. 113—133.

3) H. I. Bernstein and L. R. Rothstein, *J. Am. Chem. Soc.*, **66**, 1886 (1944).

4) E. Knoevenagel, *J. Prakt. Chem.*, **89**, 14 (1914); J. A. VanAllan, G. A. Reynolds, and R. E. Adel, *J. Org. Chem.*, **27**, 1659 (1962).

5) T. Someno, T. Hoshizaki, K. Kozawa, T. Uchida, H. Hayashi, T. Sugano, and M. Kinoshita, *Bull. Chem. Soc. Jpn.*, **64**, 921 (1991).

6) H. J. Shine and E. E. Mach, *J. Org. Chem.*, **30**, 2130 (1965).

7) T. Uchida, M. Ito, and K. Kozawa, *Bull. Chem. Soc. Jpn.*, **56**, 577 (1983).

8) T. Uchida, H. Seki, M. Ito, C. K. Nakano, T. Hoshizaki, and K. Kozawa, *Chem. Lett.*, **1986**, 999; K. Kozawa and T. Uchida, *Acta Crystallogr., Sect. C*, **46**, 1006 (1990).

9) R. Anthonj, N. Karl, B. E. Robertson, and J. J. Stezowski, *J. Chem. Phys.*, **72**, 1244 (1980).

10) C. Brierley, R. Barton, B. Robertson, R. Anthonj, and N. Karl, *J. Chem. Phys.*, **82**, 1522 (1985).

11) C. J. Fritchie, Jr., *J. Chem. Soc. A*, **1969**, 1328.

12) A. Shinghabhandhu, P. D. Robinson, J. H. Fang, and W. E. Geiger, Jr., *Inorg. Chem.*, **14**, 318 (1975).

13) H. Kobayashi, *Acta Crystallogr., Sect. B*, **30**, 1010 (1974).

14) H. Kobayashi, *Bull. Chem. Soc. Jpn.*, **46**, 2945 (1973).

15) K. Kozawa, T. Okada, S. Shikanai, and T. Uchida, 49th National Meeting of the Chemical Society of Japan, Tokyo, April 1984, Abstr., No. 3A14.

16) A. W. Hanson, *Acta Crystallogr., Sect. B*, **34**, 2339 (1978).

17) T. J. Kistenmacher, T. E. Phillips, and D. O. Cowan, *Acta Crystallogr., Sect. B*, **30**, 763 (1974).

18) T. Uchida and K. Kozawa, 53rd National Meeting of the Chemical Society of Japan, Nagoya, October 1986, Abstr., No. 2T20.

19) N. Urasaki, K. Kozawa, and T. Uchida, 55th National Meeting of the Chemical Society of Japan, Fukuoka, October 1987, Abstr., No. 1U19.

20) V. G. Koshechko, V. A. Krylov, and V. D. Pokhodenko, *Elektrokhimiya*, **16**, 1812 (1980).

21) Q. Wang, Y. Liu, Y. Ding, and Z. Liu, *Jiegou Huaxue*, **7**, 153 (1988).

22) Y. Matsunaga and Y. Suzuki, *Bull. Chem. Soc. Jpn.*, **45**, 3375 (1973); Y. Matsunaga and Y. Suzuki, *ibid.*, **46**, 719 (1973).

23) G. Dix, *Phys. Status Solidi A*, **24**, 139 (1974).

24) Y. Matsunaga, *Nippon Kagaku Zasshi*, **89**, 905 (1968).

25) S. N. Bhat, V. P. Shedbalkar, and H. Kuroda, *Indian J. Chem., Sect. A*, **21**, 1015 (1982).

26) J. W. Summers and M. H. Litt, *J. Polym. Sci., Polym. Chem. Ed.*, **11**, 1379 (1973).

Observation of Propagation Speed of Conductive Front in Electrochemical Doping Process of Polypyrrole Films

Yoshihiko TEZUKA,* Shigeru OHYAMA, Tadahiro ISHII, and Koichi AOKI†
Department of Applied Chemistry, Faculty of Science, Science University of Tokyo, Kagurazaka, Shinjuku-ku, Tokyo 162
† Department of Applied Physics, Faculty of Engineering, Fukui University, 9-1, Bunkyo 3-Chome, Fukui 910
(Received January 21, 1991)

According to the propagation theory of a conductive zone for the electrochemical doping process of conducting polymer films, an oxidized conductive zone works as an electrode for oxidizing the reduced non-conductive region and is propagated throughout the film under charge transfer control. This theory was verified for polypyrrole films by tracing the temporal and spatial variations of conductive regions in a film. An exhaustively reduced polypyrrole film was laid on an insulating glass plate and connected electrically to an ITO electrode at the marginal part. The film absorbance to a monochromatic light beam was monitored with a photodiode array detector at 14 segments of the film. When the potential of the ITO electrode was stepped to an oxidation potential of the film, an electrochemically oxidized conductive zone was propagated through the film with a manifest phase boundary. The distance from the edge of the ITO electrode to the front of the conductive zone increased linearly with time. The logarithmic slope of the propagation speed exhibited a linear relation to the applied potential.

A conducting polymer film deposited on an electrode can be switched between a highly conductive oxidized (doped) state and a resistive (or insulating) reduced (undoped) state by controlling the electrode potential. This electrochemical conversion involves mass and charge transport in the film and heterogeneous charge transfer at the underlying electrode. Therefore, the composition of the film is non-uniform and varies with time during the process of conversion.

In order to predict the temporal and spatial variations in composition, we have proposed the propagation model of a conductive zone under charge transfer control.[1-4] This model is available when supporting electrolytes permeate sufficiently into the film and so mass transport of the supporting electrolyte does not limit the conversion rate. This model consists of the following processes: Initially the film is resistive or in the reduced state. When the potential of the underlying electrode was set more anodic than the oxidation potential of the film, first the film is oxidized only in a region very close to the underlying electrode and becomes locally conductive. This conductive region works as a new electrode for oxidizing the reduced non-conductive region on it. Then a reduced region very close to this new 'electrode' is subsequently oxidized and converted into the conductive to yield an additional new electrode. Through the repetition of this process, the conductive zone is propagated up to the top of the polymer film. The conversion rate is controlled by charge transfer at the interface between the conductive zone and the reduced region. This concept has been introduced by Lacroix and Diaz.[5]

We have verified this model for the electrochemical doping process of polypyrrole films by analyzing linear sweep voltammograms,[1] in situ spectroscopic voltammograms,[2] and chronoamperometric responses.[3] This model differs on the time dependence of current from the reported models; models for charge transport due to diffusion-like electron hopping[6-10] and due to both diffusion and migration,[11] a model analogous to a porous electrode which yields charging current,[12] a capacity model including deeply and shallowly trapped ions,[13] an RC time constant model,[14] and a film resistance model.[15]

An aspect of the propagation of the conductive zone can be seen from the temporal and spatial analysis of a distribution of conductive species in the film. In our previous paper,[4] a polypyrrole film was coated onto an addressable microband array electrode in the reduced state, and oxidized from the margin of the film by applying an oxidation potential only to the marginal electrode. The potentials of the other microband electrodes were expected to reflect the distribution of the conductive species on the basis of the Nernst equation. Unfortunately, these potentials were overlapped by the applied potential because the electrochemically generated conductive zone conducted the potential of the marginal electrode. In order to obtain the precise distribution of the conductive species, a non-electric measurement is required.

Polypyrrole shows great spectral change in visible and near-infrared regions with the conversion between the reduced and the oxidized states.[2,16] Therefore, the extent of oxidation or the concentration of the conductive species can be estimated from the absorbance at a wavelength at which it is sufficiently different between the two states. The distribution of such species which absorb the light with a particular wavelength can be measured with a photodiode array detector, a linear arrangement of small photodiode elements with a multichannel detector.[17,18] In this study, an exhaustively reduced polypyrrole film was laid on an insulating glass plate and connected electrically to an ITO electrode at the margin of the film. The film was

oxidized by applying an oxidation potential to the ITO electrode, and variations in absorbance at 14 segments of the film were measured with the photodiode array detector. The relation between the distance from the ITO electrode to each segment and the time at which each absorbance begin to change gives the intuitive evidence of the propagation of the conductive zone.

Experimental

Chemicals. Pyrrole (Tokyo Kasei Ltd.) was distilled under reduced pressure (at 1.07×10^4 Pa) and stored in a sealed vessel at N_2 atmosphere. Acetonitrile was distilled successively with molecular sieves, 4A 1/16 (Wako, Tokyo), and with calcium hydride (Tokyo Kasei Ltd.) at N_2 atmosphere and stored in a sealed vessel at N_2 atmosphere. Lithium perchlorate anhydrous (Wako, Tokyo) was of analytical grade and was used as received.

Apparatus and Procedure. Polypyrrole was formed by applying a potential of 1.2 V (vs. SCE) to an ITO electrode (15 mm×8 mm) for 40 s in an acetonitrile solution containing 0.06 mol dm^{-3} pyrrole, 0.1 mol dm^{-3} $LiClO_4$ and 1% H_2O at N_2 atmosphere at 25 °C. The ITO electrode was a glass plate coated on one side with In-Sn oxide (ITO) and supplied by ULCOAT (Saitama, Japan). The resistance of the electrode was 12 Ω cm^{-2}. A potentiostat was HA-301 (Hokuto Denko Ltd., Tokyo). Current vs. time curves for the polymerization were recorded with a *x–t* recorder, RW-21T (Rikadenki, Tokyo). The charge, *Q*, consumed in the polymerization was evaluated by integrating the current vs. time curve and was 0.133 C cm^{-2}. From the equivalence of 1 C cm^{-2} to 6.85 μm,[2] the film was 0.91 μm thick. The film was covered with a platinum plate so that is was sandwiched between the platinum and the ITO electrodes. The film was reduced exhaustively by applying a potential of −1.0 V (vs. SCE) to both the electrodes for 15 min in an N_2 saturated acetonitrile solution containing 0.1 mol dm^{-3} $LiClO_4$. Then the film turned uniformly yellow. Without the platinum plate, the film was not completely reduced and looked green. The reduced film was stripped

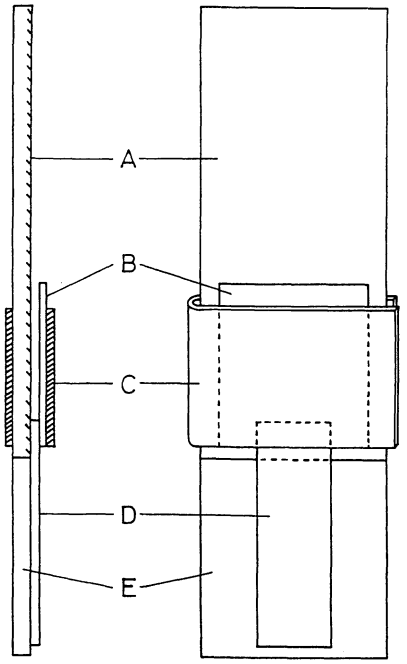

Fig. 1. Schematic diagram of the working electrode. (A) ITO electrode; (B) thin glass plate; (C) stainless steel holder; (D) polypyrrole film; (E) glass plate.

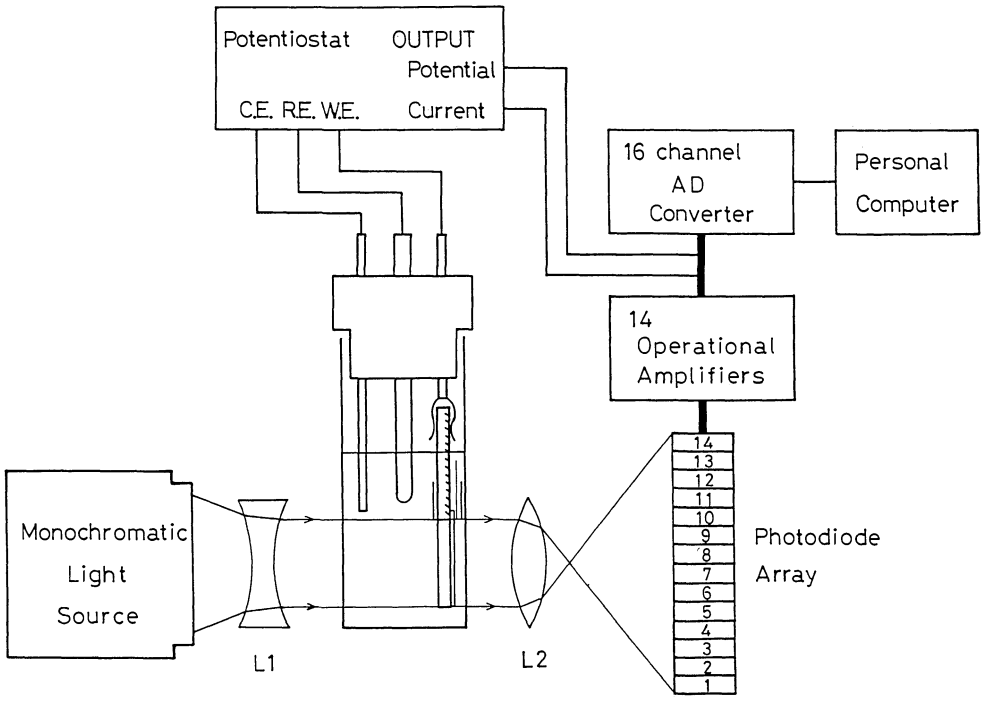

Fig. 2. Schematic diagram of optical apparatus. L1 is a concave lens (*f*=29 mm). L2 is a convex lens (*f*=28 mm).

from the ITO substrate and cut into a rectangle (6 mm×2 mm). It was laid on an insulating glass plate which was joined to an ITO electrode, so that the marginal part of the film (1 mm long) was on the ITO electrode (see Fig. 1). For electrical contact, the marginal part was pressed to the ITO electrode with a thin glass plate and a stainless steel holder. All these procedures were done at N_2 atmosphere in a glove box.

An optical apparatus is shown in Fig. 2. A rectangular (1 cm×1 cm) quartz cell with a teflon holder was used as an electrochemical cell. The top of the ITO electrode was clipped with a stainless steel holder so that the polypyrrole film was immersed into an N_2 saturated acetonitrile solution containing 0.1 mol dm^{-3} $LiClO_4$. A counter electrode was a platinum plate. A reference electrode was a saturated calomel electrode (SCE) which was connected to the electrochemical cell through a salt bridge filled with acetonitrile containing 0.1 mol dm^{-3} $LiClO_4$. Excitation light of a fluorescence spectrophotometer, Hitachi 650-40, was used as a monochromatic light source. A beam from the monochromatic light source was collimated with a concave lens L1 and passed through the polypyrrole film on the glass plate perpendicularly. The beam was then magnified by 2.8 times with a convex lens L2 and imaged onto 14 elements of a photodiode array, S2311-35Q (Hamamatu, Shizuoka, Japan), located on the image plane of the film. The photodiode elements were 0.94 mm wide and lined up at intervals of 0.05 mm. Since the image of the film was magnified by 2.8 times, the spatial resolution to the film was 0.36 mm. The 14 photodiode elements were connected to operational amplifiers through which photocurrent signals were converted to voltage signals. Deterioration in the spatial resolution by scattering of the excitation beam was negligible, which was confirmed by measuring the 14 photocurrents with attaching a narrow grid to the polymer film.

The polypyrrole film was oxidized by stepping the potential of the ITO electrode from −1.0 to 0.2 V (vs. SCE) or more anodic potentials. According to the result from the conductivity measurements of polypyrrole films reported by Feldman et al., polypyrrole is insulating at potentials more cathodic than −0.4 V (vs. SSCE) and highly conductive at potentials more anodic than 0.0 V.[19] Therefore, the films exhaustively reduced at −1.0 V (vs. SCE) and the films oxidized at 0.2 V or more anodic potentials can be considered as resistive and highly conductive, respectively. The stepped potential was limited up to the polymerization potential of the film, 1.2 V (vs. SCE), in order to avoid irreversible over-oxidation of the film which lead to the destruction of the polymer structure. The films oxidized at potentials between 0.2 V and 1.2 V (vs. SCE) could be reversed to the exhaustively reduced state by sandwiching the film between an ITO and a platinum electrodes and applying a potential of −1.0 V (vs. SCE) to both the electrodes.

After the potential of the ITO electrode was stepped, the 14 photocurrents measured with the photodiode array detector were recorded every 25 ms on a personal computer, PC-9801 (NEC, Tokyo), with potential and current outputs of the potentiostat through a 12 bits A/D converter, AZI-204 (Interface, Tokyo). Each photocurrent, i_p, was converted to the absorbance, A, at the corresponding segment of the film through the following equation:

$$A = -\log(i_p/i_p^\circ) \quad (1)$$

where i_p° is the photocurrent measured without setting the film on the glass plate.

Absorption spectra of the polypyrrole film at various potentials were measured with a multichannel photodetector system, MCPD-1000 (Photal, Tokyo), sufficiently after the potential of the ITO electrode was stepped to each potential.

Time-sequence photographs were taken every 0.4 s with a single-lens reflex camera, Olympus OM-2, equipped with a lens, Zuiko Auto Macro 50 mm F3.5, and a motor-drive unit, Winder 2.

Results and Discussion

Figure 3 shows absorption spectra of the polypyrrole film in the exhaustively reduced state (at −1.0 V vs. SCE) and in the oxidized states (at 0.0, 0.4, and 0.8 V). The spectrum at −1.0 V showed a prominent absorption band centered at 420 nm. There was no peak at wavelengths longer than 500 nm, indicating that the film was in the completely reduced state. When the film was oxidized at 0.0 V, the band at 420 nm decreased and two broad bands appeared around 520 nm and in the near-infrared region (700—1000 nm). As the oxidation of the film proceeds (at 0.4 and 0.8 V), the band around 520 nm slightly decreased with shifting to the shorter wavelength and the band in the near-infrared region increased monotonically.

Figure 4 shows a chronoamperometric curve for the oxidation of the polypyrrole film when the potential of the ITO electrode was stepped from −1.0 to 0.8 V (vs. SCE). Immediately after the potential was stepped, large current flowed for a short period (t<0.1 s). After this pulsed current, the curve showed a plateau up to 5.8 s. Exhibition of the plateau is consistent with the theoretical chronoamperometric curve for a very rapid heterogeneous rate at the underlying electrode.[3] After showing the plateau, the curve decreased exponentially.

The absorbance vs. time curves simultaneously measured with the chronoamperometric curve (Fig. 4)

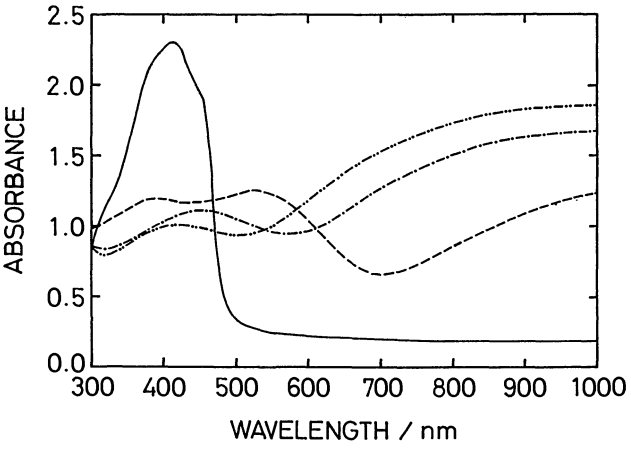

Fig. 3. Absorption spectra of a polypyrrole film at −1.0 (———), 0.0 (– – –), 0.4 (–·–·–), and 0.8 V (vs. SCE) (–··–··–··–).

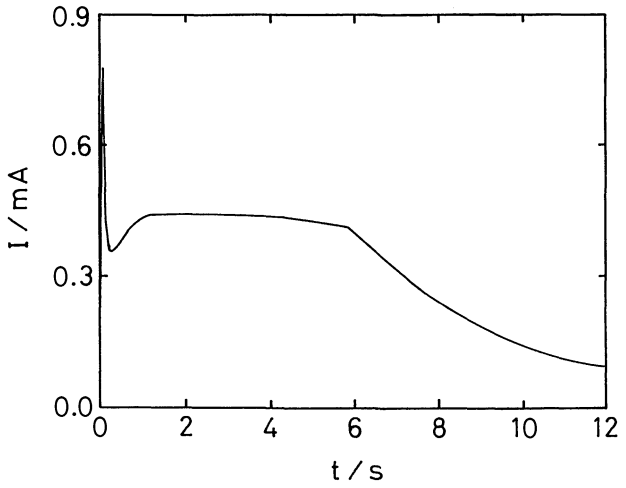

Fig. 4. Chronoamperometric curve of the polypyrrole film when the potential of the ITO electrode was stepped from −1.0 to 0.8 V (vs. SCE).

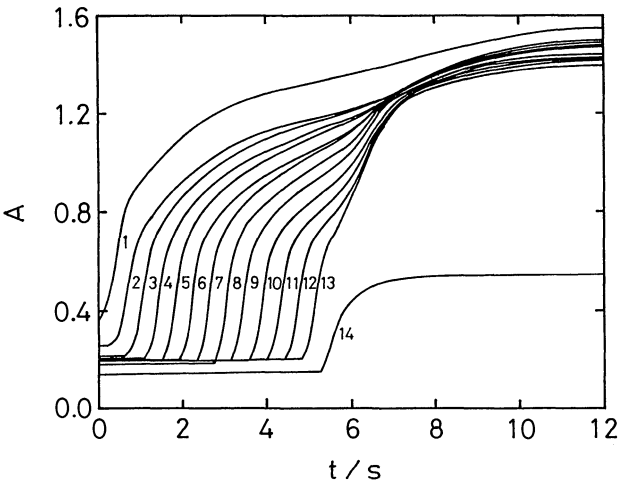

Fig. 5. Variations in the absorbance at 800 nm with time. The number marked beside the curves corresponds to the number of the photodiode element in Fig. 2.

are shown in Fig. 5. The monitored wavelength was 800 nm. Curve 1 represents the absorbance at the segment closest to the ITO electrode, and curve 14 represents the furthest segment. The higher absorbance in curve 1 was caused by scattering of the excitation beam at the joint between the glass plate and the ITO electrode. The lower absorbance in curve 14 was due to a shortage in length of the film. The further from the ITO electrode the segment was, the slower the absorbance began to change, indicating that the conversion proceeded from the electrode/film interface towards the end of the film.

The amount of charge, q, evaluated by integrating the chronoamperometric curve in Fig. 4, was 40 mC cm^{-2}. The efficiency of the oxidation, q/Q, was 0.30, being much greater than the value, 0.17, calculated from the maximum doping level (0.33) of polypyrrole perchlorate on the assumption that both q and Q did not include non-faradaic components. This large q/Q value suggests that the chronoamperometric cuve includes large capacitive components as observed in ordinary potential step experiments.

The initial pulsed current (t<0.1 s) in Fig. 4 can be ascribed to a capacitive current at the interface between the ITO electrode and the reduced film. The other source of the capacitive current is the interface between the conductive zone and the solution or the reduced region in the film. The conductive zone can be considered as a series connection of a resistor, R, and a capacitor, C. When a potential is applied to such a series connection of R and C, the capacitive current shows an exponential decay according to the product, RC (RC time constant). As the conductive zone is propagated in the film, both R and C should increase because they are proportional to the length (amount) of the conductive zone. Unfortunately, these capacitive components have not been separated mathematically from the faradaic current.[3] When the chronoamperometric curve began to decrease from the plateau (t=5.8 s), the absorbance vs. time curve 14 (in Fig. 5) had passed a half of the transition, namely, the top of the oxidized zone had reached the end of the film. Thus, the decreasing portion of chronoamperometric curve is mainly attributed to the capacitive current with a large RC time constant rather than the faradaic current.

Every absorbance vs. time curve in Fig. 5 changed at two stages; a steep rise from the initial value (0.18—0.25 for curves 2—13) to the intermediate value (0.67—0.68) and the following gradual increase to the final steady state value (1.4—1.5). Absorbance vs. time curves at 400 nm showed a precipitous fall from the initial value to the final steady state value. At 550 nm, they showed a steep rise from the initial value to a intermediate value followed by a gradual decrease to the final steady-state value.

The change at two stages observed at 800 and 550 nm indicates the presence of an intermediate state between the exhaustively reduced state and the final oxidized state. The intermediate state in polypyrrole has been found by in situ spectroscopic voltammetry[2] and ESR measurements.[20-23] Simultaneous ESR and electrochemical measurements[21-23] have demonstrated the participation of polaron (radical cation) as an intermediate between the neutral form in the reduced state and bipolaron (dication) in the sufficiently oxidized state. Therefore, the intermediate state may correspond to the polaron, and the final oxidized state to the bipolaron. The intermediate state is not observed when the conversion from the intermediate to the final state is much faster than that from the initial to the intermediate state. Therefore, the conversion from the polaron to the bipolaron is considered to be slower than that from the neutral form to the polaron.

Both the regions in the intermediate state and in the

final oxidized state can be considered as conductive because both polaron and bipolaron have been considered as conductive species.[23,24] Therefore, the rapid change in the absorbance vs. time curves from the initial value to the intermediate value indicates the presence of a distinctive conductive zone rather than a vague boundary as observed in diffusion. A diffusional process such as charge transfer by electron hopping or electron exchange in the film might provide more gradual change with an increase in distance from the ITO electrode.

Since the film absorbance increased monotonically with the extent of oxidation at a wavelength in the near-infrared region, we can estimate the concentration of oxidized species, C_O, (and reciprocally the concentration of reduced species, C_R,) from it. When it is assumed that $C_O=0$ in the exhaustively reduced state and $C_R=0$ in the final oxidized state, the ratio of C_O to C_O+C_R is estimated from the absorbance, A, through the following equation:

$$C_O/C^* = (A - A_0)/(A_\infty - A_0), \quad (2)$$

where $C^*=C_O+C_R$, A_0 is the absorbance in the exhaustively reduced state, and A_∞ is that in the final oxidized state. If we apply Eq. 2 to the result of the spatially resolved spectral measurement, we obtain concentration vs. distance profiles of the oxidized species in the film.

Figure 6 shows the concentration vs. distance profiles of the oxidized species in the film at various times calculated from the absorbance vs. time curves in Fig. 5. A representative distance from the ITO electrode to the each monitored segment is the distance, d, from the edge of the ITO electrode to the center of the each segment. The small circles in Fig. 6 represent the center of the 14

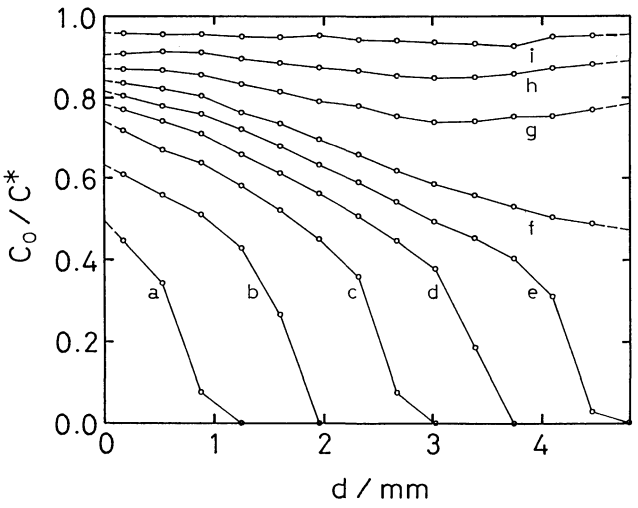

Fig. 6. Concentration vs. distance profiles of the oxidized species in the film at t=(a) 1.0, (b) 2.0, (c) 3.0, (d) 4.0, (e) 5.0, (f) 6.0, (g) 7.0, (h) 8.0, (i) 10.0 s. Dashed lines represents the extrapolation.

monitored segments of the film. Both C_O/C^* at a given d and d at a given C_O/C^* increased with time. These concentration profiles are similar to the theoretical ones derived from the propagation theory.[3] Since the intermediate state, at which A=0.67—0.68 for curves 2—13 in Fig. 5, corresponds to C_O/C^*=0.37, the segment in which $C_O/C^*>0.37$ can be considered as the conductive region. Therefore, the steep concentration gradients below C_O/C^*=0.37 indicate the presence of a manifest phase boundary between the conductive zone and the resistive region.

Figure 6 obviously shows that the conversion proceeded from the electrode/film interface towards the end of the film. For conducting polymer films deposited on ordinary solid electrodes, the relation between the rate-limiting process and the conversion direction has been considered as follows: When the conversion rate is limited by charge transfer in the film, the conversion occurs from the electrode/film interface towards the solution/film interface:[25] When the conversion rate is limited by mass transport of supporting electrolytes in the film, the conversion occurs in the reverse direction.[26] In our experimental condition, the direction of the ion transport is perpendicular to the direction of the film length. Therefore, if conversion proceeded with the mass transport being the rate-limiting process, the conversion has occurred from the upper layer of the film and seemed to occur from the whole of the film without depending on the distance from the electrode. Therefore, the conversion from the electrode/film interface indicates that the conversion proceeded with the charge transfer being the rate-limiting process.

In some previous papers, however, conversion with the mass transport being the rate-limiting process has been reported for polypyrrole films.[26-29] The reason why different rate-limiting processes have been observed for the same kind of polymer film may be attributed to the difference in permeability and porosity of the film which effects mobility of dopant ions in the film. Slow conversion from the fringe (solution/film interface) was also observed in our experimental condition when the film was sandwiched with two glass plates, in which the supporting electrolyte was supplied only by capillary action through the gap between the two glass plates and so the conversion might occur with the mass transport being the rate-limiting process.

The distance, d_{CF}, from the edge of the ITO electrode to the front of the conductive zone is an intercept of the abscissa in the concentration vs. distance profiles. However, they sometimes deviate from the real profiles especially at the conductive front, because the 14 measuring points is insufficient to describe the steep concentration gradient at the conductive front. Consequently, curves a, c, and d in Fig. 6 seemed to lean back in $C_O/C^*<0.1$. Therefore, the d_{CF} was estimated approximately with d at C_O/C^*=0.1. In Fig. 7, the d_{CF} was plotted against t at various stepped potentials, E's.

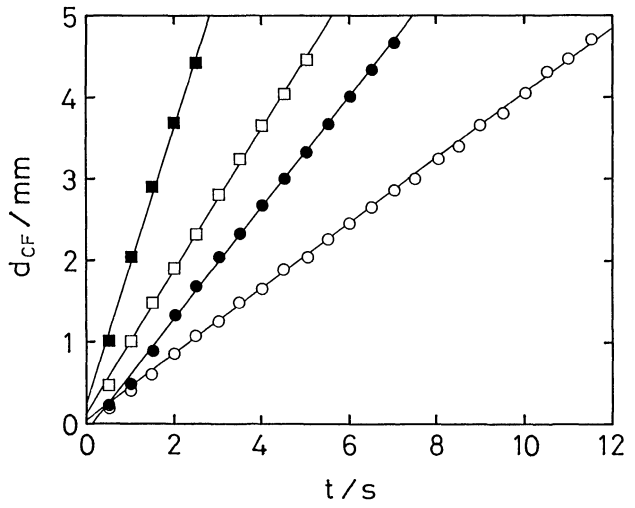

Fig. 7. Plots of d_{CF} against t at E=(○) 0.2, (●) 0.4, (□) 0.8, and (■) 1.2 V (vs. SCE).

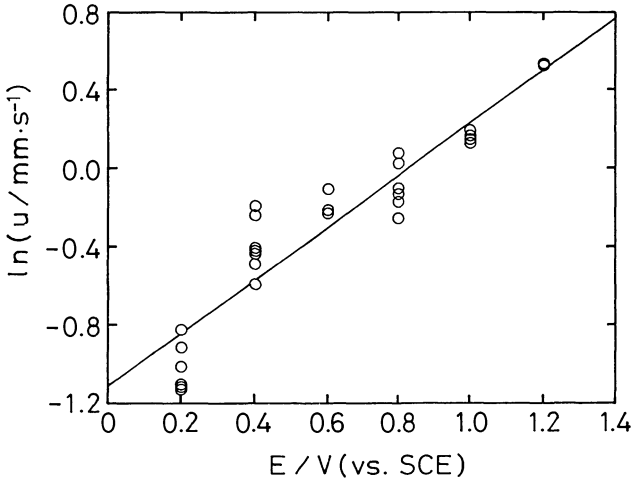

Fig. 8. Dependence of u on E. Values of u are the slope in Fig. 7.

These plots fell on the each straight line, indicating that the conductive zone was propagated in the film at a constant speed according to the applied potential. The propagation speed, u, is the slope of each line. A typical speed was 1.0 mm s^{-1} at E=0.8 V (vs. SCE). The linear relation of d_{CF} with t has been predicted from the propagation theory of a conductive zone in which the charge transfer at the interface between the conductive zone and the resistive region being the rate-limiting process.[3] This linear relation does not support any diffusional charge transfer process such as charge transport by electron hopping or electron exchange in the film. In such diffusional process, d_{CF}, which corresponds to the thickness of the diffusion layer, should have increased with $\sqrt{t}$.

The logarithm of the propagation speed (u) was plotted against E in Fig. 8. They exhibit a linear relation, i.e. the propagation speed varies exponentially with the applied potential. This exponential relation indicates that the propagation is controlled by a charge transfer process of the Tafel type.

An aspect of the propagation could be seen in time-sequence photographs (Fig. 9) taken after the potential of the ITO electrode was stepped from −1.0 to 0.8 V (vs. SCE). Initially, the polypyrrole film was in the exhaustively reduced state and was uniformly yellow (Fig. 9a). After stepping the potential, the purple conductive zone grew, invading the yellow reduced domain (Figs. 9b and c). The distinctive phase boundary does not support the diffusive propagation but suggests the propagation under the charge transfer control as at a conventional electrode/solution interface. The distinctness of the boundary was independent of applied potentials in the range from 0.2 to 1.2 V (vs. SCE). It has been reported that a rapid charge transfer rate makes the boundary vague.[30] Thus the rate constant belongs to the totally irreversible case.[30] The purple zone was followed by a blue-black zone with a vague phase boundary (Figs. 9 c and d). The purple and

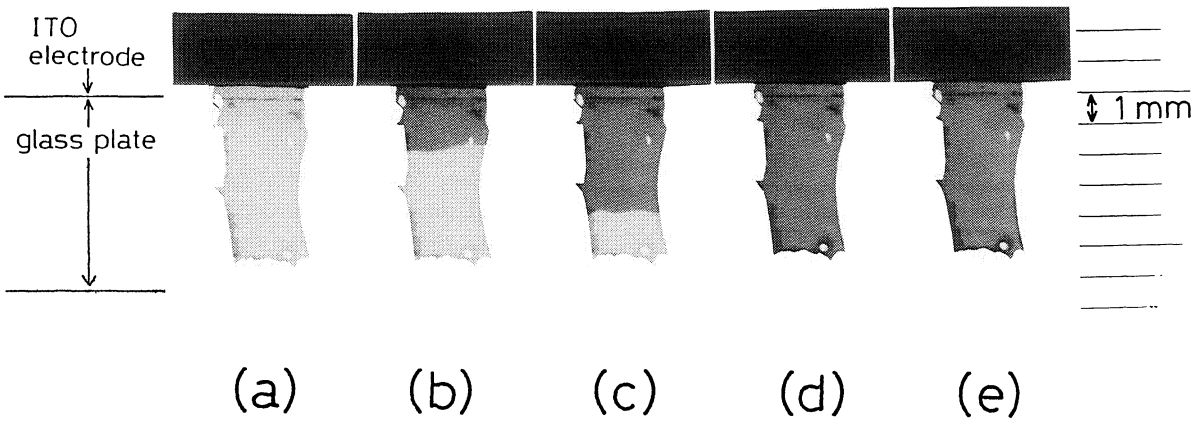

Fig. 9. Time-sequence photographs of a polypyrrole film at t=0 (a), 1.6 (b), 3.2 (c), 4.8 (d), 9.6 (e) s.

the blue-black zones were observed when the potential was more anodic than 0.2 V (vs. SCE). The film finally turned uniform in the blue-black state (Fig. 9 e).

Apparently, the purple zone corresponds to the intermediate state and the blue-black zone to the final oxidized state, therefore, they may correspond to the polaron and the bipolaron, respectively. The transient appearance of the intermediate state (polaron) is consistent with the transient ESR responses in polypyrrole films reported by Zhong et.al.,[23] in which the intensity of the ESR signal initially increased to a maximum and afterwards decreased to a steady state when the potential was stepped to 0.2 V (vs. SCE) or more anodic potentials.

In conclusion, the oxidation of resistive polypyrrole films obeyed the propagation theory of a conductive zone under charge transfer control in that (1) the distinctive phase boundary was observed; (2) the propagated distance was linear to the time of the electrolysis; (3) the propagation speed exhibited the exponential dependence on the applied potential.

References

1) K. Aoki, Y. Tezuka, K. Shinozaki, and H. Sato, *Denkikagaku (J. Electrochem. Soc. Jpn.),* **57**, 397 (1989).

2) Y. Tezuka, K. Aoki, and K. Shinozaki, *Synth. Met.*, **30**, 369 (1989).

3) K. Aoki and Y. Tezuka, *J. Electroanal. Chem.*, **267**, 55 (1989).

4) Y. Tezuka and K. Aoki, *J. Electroanal. Chem.*, **273**, 161 (1989).

5) J. C. Lacroix and A. F. Diaz, *Makromol. Chem., Macromol. Symp.*, **8**, 17 (1987).

6) N. Oyama, T. Ohsaka, K. Chiba, and K. Takahashi, *Bull. Chem. Soc. Jpn.*, **61**, 1095 (1988).

7) E. M. Genies and J. M. Pernaut, *Synth. Met.*, **10**, 117 (1984/1985).

8) T. Osaka, K. Naoi, and S. Ogano, *J. Electrochem. Soc.*, **124**, 2096 (1987).

9) N. Oyama and T. Ohsaka, *Synth. Met.*, **18**, 375 (1987).

10) S. Panero, P. Prosperi, and B. Scrosati, *Synth. Met.*, **28**, C133 (1989).

11) K. Naoi and T. Osaka, *J. Electrochem. Soc.*, **134**, 2479 (1987).

12) W. T. Yap, R. A. Durst, E. A. Blubaugh, and D. D. Blabaugh, *J. Electroanal. Chem.*, **144**, 69 (1983).

13) J. Tanguy, N. Mermilliod, and M. Hoclet, *Synth. Met.*, **18**, 7 (1987).

14) J. Lacroix, K. Kanazawa, and A. Diaz, *J. Electrochem. Soc.*, **136**, 1308 (1989).

15) S. Gottesfeld, A. Redondo, I. Rubinstein, and S. W. Feldberg, *J. Electroanal. Chem.*, **265**, 15 (1989).

16) J. L. Bredas, J. C. Scott, K. Yakushi, and G. B. Street, *Phys. Rev. B,* **30**, 1023 (1984).

17) C. C. Jan, R. L. McCreery, and F. T. Gamble, *Anal. Chem.*, **57**, 1763 (1985).

18) C. C. Jan and R. L. McCreery, *Anal. Chem.*, **58**, 2771 (1986).

19) B. J. Feldman, P. Burgmayer, and R. W. Murray, *J. Am. Chem. Soc.*, **107**, 872 (1985).

20) F. Devreux, F. Genoud, M. Nechtschein, and B. Villeret, *Synth. Met.*, **18**, 89 (1987).

21) J. F. Oudard, R. D. Allendoerfer, and R. A. Osteryoung, *J. Electroanal. Chem.*, **241**, 231 (1988).

22) Shaojun Dong, Jie Ding, and Ruiyun Zhan, *J. Chem. Soc., Faraday Trans. 1,* **85**, 1599 (1989).

23) C. J. Zhong, Z. Q. Tian, and Z. W. Tian, *J. Phys. Chem.*, **94**, 2171 (1990).

24) A. M. Waller and R. G. Compton, *J. Chem. Soc., Faraday Trans. 1,* **85**, 977 (1989).

25) C. Lee, J. Kwak, L. J. Kepley, and A. J. Bard, *J. Electroanal. Chem.*, **282**, 239 (1990).

26) C. Lee, J. Kwak, and A. J. Bard, *J. Electrochem. Soc.*, **136**, 3720 (1989).

27) C. D. Paulse and P. G. Pickup, *J. Phys. Chem.*, **92**, 7002 (1988).

28) M. Salmon, A. F. Diaz, A. J. Logan, M. Krounbi, and J. Bargon, *Mol. Cryst. Liq. Cryst.*, **83**, 1297 (1983).

29) J. R. Reynolds, N. S. Sundaresan, M. Pomerantz, S. Basak, and C. K. Baker, *J. Electroanal. Chem.*, **250**, 355 (1988).

30) K. Aoki, *J. Electroanal. Chem.*, **292**, 53 (1990).

Pressure-Induced Neutral-Ionic Phase Transition of a Tetrathiafulvalene-Iodanil Crystal

Susumu MATSUZAKI,* Toshihiro HIEJIMA, and Mizuka SANO†
Department of Chemistry, Faculty of Science, Kumamoto University, Kumamoto 860
† Division of Natural Sciences, International Christian University, Mitaka, Tokyo 181
(Received March 4, 1991)

The pressure dependence of IR spectra measured for a mixed-stack neutral charge-transfer (CT) crystal, tetrathiafulvalene–iodanil (TTF-IA), showed an occurrence of a neutral–ionic (N–I) transition at 1.9 GPa. The N–I transition is accompanied by gradual dimerization of the crystal lattice and a small ionicity jump, in contrast to the case of TTF–chloranil (TTF–CA). Such a quasi-continuous N–I transition is attributable to stronger electron–lattice interaction in TTF–IA than that in TTF–CA.

Organic charge-transfer (CT) crystals with mixed-stack structures are classified into two types with a neutral and an ionic ground electronic states. The occurrence of either ground state is determined by a balance between energy gain by the electrostatic Madelung energy (E_M) of an ionic crystal lattice and energy cost on ionization of a donor–acceptor pair ($I_D - E_A$) in a neutral crystal lattice, where I_D is ionization potential of a donor (D) and E_A is electron affinity of an acceptor (A). When a transfer integral "t" determined by an orbital overlap between the D–A pairs is negligibly small, the neutral–ionic interface is sharp; i.e., degree of ionicity (ρ) takes one of the extreme values, zero or one.[1] The interface diffuses with an increase in "t", and ρ comes to take a value between zero and one. In such a case, the CT crystals are labeled as quasi-neutral ($\rho<0.5$) and quasi-ionic ($\rho>0.5$) compounds.[2]

It has recently been found[3] that application of pressure or lowering of temperature generates a phase transition accompanying an increase in ρ from quasi-neutral to quasi-ionic i.e., N–I transition, for several mixed-stack CT crystals near the neutral–ionic interface. In particular, a mixed-stack CT crystal of tetrathiafulvalene (TTF) and chloranil (CA), TTF–CA, has attracted much attension of physicists and chemists for the pressure-induced[4,5] and temperature-induced[6,7] N–I transitions. Many experimental and theoretical works on TTF–CA have revealed that an increase in E_M with a contraction of the crystal lattice and electron–lattice interaction play important roles in the N–I transition. On the other hand, there are only a few reports on the N–I transition of other CT crystals.[8,9] Experimental studies on various CT crystals are necessary to draw a complete scheme of N–I transitions.

TTF–tetrahalo-*p*-benzoquinones are known to give several CT crystals with segregated- or mixed-stack structure and neutral or ionic ground state;[10,11] e.g., mixed-stack crystals of TTF–FA[12] (FA, fluoranil), TTF–CA,[12] and TTF–IA[11] (IA, iodanil) are neutral, and the crystal of TTF–BA[13] (BA, bromanil) is ionic. We are interested in an effect of halogen-substitution on the ionicity and N–I transition in the TTF–tetrahalo-*p*-benzoquinone crystals. Here, we report a pressure-induced N–I transition in a mixed-stack CT crystal of TTF and iodanil (TTF–IA) and compare the results with those of TTF–CA.

Experimental

Tetrathiafulvalene (Tokyo Kasei Co.) was purified by sublimation in vacuo. Iodanil (tetraiodo-*p*-benzoquinone) synthesized from bromanil and potassium iodide by the method of Torrey and Hunter[14] was purified by repeated recrystalizations from ethyl acetate to give deep purple needle-like crystals. They were identified by elemental analyses and IR spectra.

Charge-transfer complexes of TTF and IA were prepared by mixing of the hot ethyl acetate solutions of each component. When the mixed solution was cooled, two kinds of crystals were simultaneously obtained: One is an orange needle and another is a dark brown plate. The former is a 1:1 CT complex (TTF–IA) and the latter is a 2:1 CT complex, $(TTF)_2IA$. Compositions of these complexes were determined by elemental analyses and X-ray crystal-structure analyses.[15] The results for $(TTF)_2IA$ will be published elsewhere. A potassium salt of IA, K·IA, was prepared from IA and potassium iodide in acetone. Crystals of TTF–CA and TTF–BA were prepared by mixing of the hot acetonitrile solutions of each component.

IR spectra of powder samples were recorded on a JASCO FT/IR-7000 Fourier-transform infrared spectrometer in the pressure region up to 6.3 GPa by use of a diamond anvil cell (DAC). A stainless steel foil 0.03 mm thick was used as a gasket which had a hole of 0.6 mm in diameter. Nujol was used as a pressure medium and the applied pressure was calibrated by use of the R_1 fluorescence line of ruby. Raman spectra of powder samples were recorded on a JASCO R-800 spectrometer equipped with an NEC GLG-3200 Ar^+ laser as an excitation light source at ambient pressure to determine frequencies of totally symmetric vibrations. The fluorescence line of ruby was also recorded on the Raman spectrometer. All the measurements were performed at ambient temperature.

Results and Discussion

Ionicity at Ambient Pressure. Figure 1a shows an IR-spectrum of a TTF–IA powder sample at ambient pressure. A spectrum of TTF–CA obtained in this study is shown in Fig. 1b for comparison. Frequencies and assignment of the IR bands are given in Table 1 with those of IA^0 and IA^-.[11] The frequencies of K·IA are

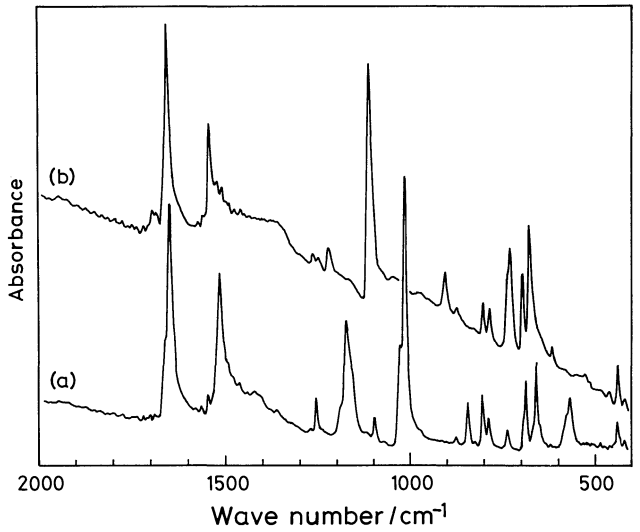

Fig. 1. IR spectra of power samples at ambient pressure. (a) TTF–IA; (b) TTF–CA.

Table 1. IR Frequencies of TTF–IA at Ambient Pressure

TTF–IA	Wave number[a)]/cm^{-1}				Assignment		
	IA^0	IA^-	TTF^0	TTF^+			
3080			3073		TTF	b_{2u}	ν_{22}
1647	1662	1498			IA	b_{1u}	ν_{10}
1518	1519	1519			IA	b_{2u}	ν_{18}
1510			1530	1478	TTF	b_{1u}	ν_{14}
1255			1254	1237	TTF	b_{2u}	ν_{23}
1172	1177				IA	b_{2u}	ν_{19}
1096			1090	1072	TTF	b_{1u}	ν_{15}
1013	1018	1065			IA	b_{1u}	ν_{11}
841	840	849			IA	b_{1u}	ν_{12}
803			794	825	TTF	b_{2u}	ν_{25}
785			781	836	TTF	b_{1u}	ν_{16}
735			734	751	TTF	b_{1u}	ν_{17}
687	692	688			IA	b_{3u}	ν_{28}
659			639	705	TTF	b_{3u}	ν_{34}
567	567				IA	b_{2u}	ν_{20}
437			427	460	TTF	b_{1u}	ν_{18}

a) Frequencies of TTF^0 and TTF^+ are from Ref. 16.

used as those of IA^-, and frequencies and assignment of TTF^0 and TTF^+ have been reported in the literature.[16] The spectrum of TTF–IA (Fig. 1a) is reasonably explained as a superposition of the spectra of neutral donor (TTF^0) and neutral acceptor (IA^0), as in the case of TTF–CA (Fig. 1b);[17] i.e., TTF–IA is a neutral CT crystal. The degree of ionicity at ambient pressure (ρ_0) is estimated at 0.08 for TTF–IA from the C=O stretching IR frequency (1647 cm^{-1}) of IA on the assumption of a linear relation between the frequency and ρ.[17]

Metzger and Torrance[18] and Girlando, et al.[13] discussed on the difference in ionicity between two mixed stack CT crystals, TTF–CA and TTF–BA: the former is neutral and the latter is ionic. They claimed that BA has larger polarizability than CA and the resulting large polarization energy plays an important role in stabilizing the ionic ground state in TTF–BA. However, their claim appears to be inconsistent with the fact found in this study that TTF–IA has a neutral ground state. Iodanil has larger polarizability than BA as reported by Sato, et al.[19]. They have estimated that the molecular polarizability of IA is about twice as large as that of BA, on the basis of the difference in ionization energy between the gaseous and solid states. The electron affinity of IA, on the other hand, is not so different from the electron affinities of CA and BA.[20] These factors are expected to advantage the ionic ground state also in the case of TTF–IA. Therefore, the neutral ground state found in this study suggests that other factors should be considered to explain the difference in the ionicity of TTF–tetrahalo-*p*-benzoquinone crystals.

Large polarizability of the component molecules in CT crystals stabilizes the energy of D^+ and A^-. This effect decreases the energy difference, I_D-E_A, and is favorable for the ionic ground state. On the other hand, the large polarizability simultaneously increases dielectric constant (ε) of the crystals, according to Clausius–Mossotti relation. The increased dielectric constant reduces the Madelung energy, $E_M=\alpha e^2/\varepsilon r$, where α, e, and r are Madelung constant, electron charge, and intermolecular distance, respectively; therefore, this effect is favorable for the neutral ground state. Ionicity of the CT crystals is expected to be dominated by the relative importance of these two effects, so that large polarizability of the component molecules does not necessarily produce the ionic ground state.

There is another factor to be taken into consideration, i.e., a packing motif of donor and acceptor molecules in the crystal. The packing motif is expected to affect the ionicity through a change of E_M. Among all the CT crystals of TTF–tetrahalo-*p*-benzoquinones with the mixed stack structure, only TTF–BA is ionic and the others are neutral. The neutral CT crystals, TTF–FA,[12] TTF–CA,[12] and TTF–IA,[15] have packing motifs similar to each other: The crystals are composed of a single mixed stack. On the other hand, the crystal of TTF–BA is composed of two mutually orthogonal mixed stacks; i.e., the packing motif is quite different from those of the three neutral CT crystals. The results suggest that the difference in the molecular packing motif must also play an important role in the occurrence of the ionic ground state of TTF–BA in addition to the polarization effect.

The value of ρ_0 is estimated at 0.18 for TTF–CA[5,17] by use of the C=O stretching frequencies of the complex (1657 cm^{-1}), CA^0 (1693 cm^{-1}), and CA^{-1} (1518 cm^{-1}). The ionicity estimated for TTF–IA (0.08) is considerably smaller than that of TTF–CA. The small value is attributed to the effect of the substitution of large iodine atoms into the acceptor. An interplanar distance between TTF and IA (3.57 Å)[15] is 0.18 Å longer than that of TTF–CA (3.39 Å),[12] because of the larger atomic

radius of iodine than that of chlorine. The large interplanar distance in TTF–IA should be responsible for the small value of ρ_0. The ionicity is approximately expressed by the relation, $\rho \propto t^2/(h\nu_{CT})^2$, where t is a transfer integral and $h\nu_{CT}$ is energy of charge-transfer absorption. The value of $h\nu_{CT}$ observed for TTF–IA in a KBr disk is 6300 cm^{-1}, which is not so different from the value for TTF–CA (5300 cm^{-1}).[21] Therefore, the small ρ_0 value of TTF–IA is attributed to a small transfer integral, which results from the large interplanar distance, i.e., a small overlap between π molecular orbitals of donors and acceptors in comparison with TTF–CA.

Pressure Dependence of Ionicity and N–I Transition. Figure 2 shows pressure dependence of the IR spectra for TTF–IA. The IR band A of an IA C=O stretching vibration (b_{1u} ν_{10}) shows a large low-frequency shift with increasing pressure. At 1.9 GPa (Fig. 2c), a new band A′ appears as a shoulder on the low-frequency side of band A. On further compression, intensity of band A′ increases and band A disappears as shown in Fig. 2e. The crystals of TTF–IA were found to decompose gradually when storaged in a desiccator to give neutral iodanil. The decomposition is probably attributed to sublimation of TTF molecules which leaves IA^0 molecules on the crystal surface. An IR band of the IA^0 molecules is marked with an asterisk in the figure. The rate of decomposition was so slow that no spectral change induced by the decomposition was observed during the measurements of pressure dependence.

Pressure dependence of the IR frequencies (Fig. 3) shows that band A changes to band A′ at 1.9 GPa with a slight frequency jump. The degrees of ionicity are estimated at 0.36 and 0.42 for bands A and A′, respectively, at 1.9 GPa. With further compression, the frequency of band A′ gradually decreases and the degree of ionicity increases up to 0.57 at 6.3 GPa which is the highest pressure in this study. The C=O stretching frequencies of IA and K·IA are practically independent of applied pressure as shown in Fig. 3. Therefore, ionicity at every pressure was estimated by use of the frequencies of IA and K·IA at ambient pressure.

Even at the highest pressure, the R_1 fluorescence line of ruby showed only small inhomogeneous broadening. The broadening is known as a measure of non-hydrostatic compression in a pressure medium.[22] Small inhomogeneous broadening observed shows negligible pressure distribution in the gasket hole of the DAC. Such negligible pressure distribution is also demonstrated by absence of inhomogeneous broadening of bands A and A′ of which widths are expected to be sensitive to the non-hydrostatic compression because of the large frequency shifts by pressure. (See Fig. 2.)

An increase in ρ at P_c is also indicated by frequency

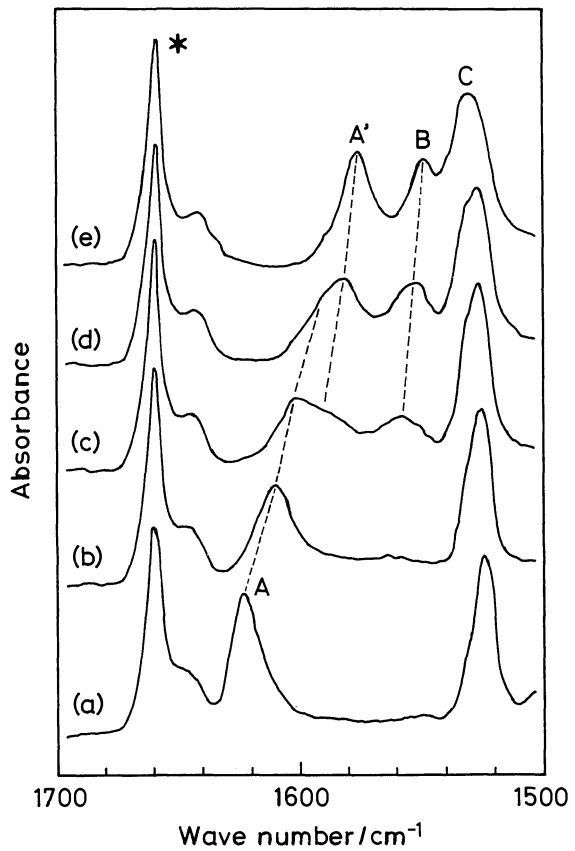

Fig. 2. IR spectra of TTF–IA in the region of C=O stretching vibrations at high pressures. (a) 1.2; (b) 1.7; (c) 1.9; (d) 2.3; (e) 2.7 GPa. *; a band of IA^0.

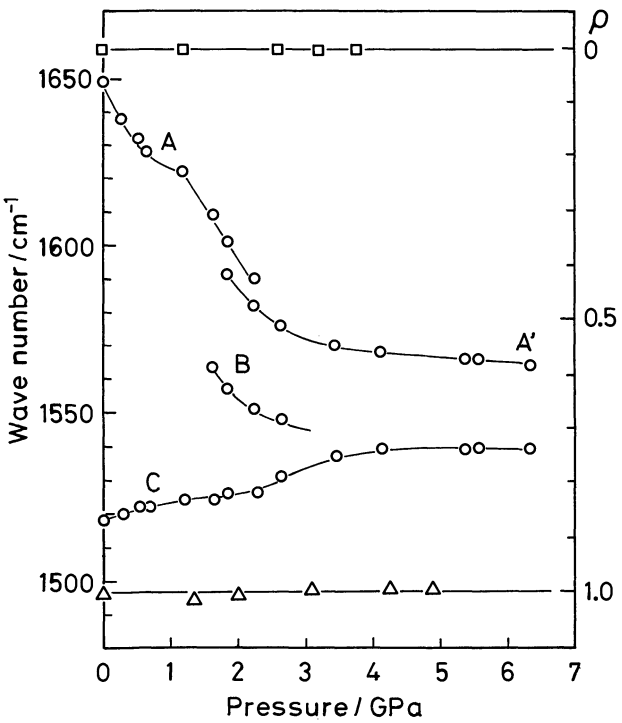

Fig. 3. Pressure dependence of IR frequencies of TTF–IA in the region of C=O stretching vibrations. (○) TTF–IA; (□) IA^0; (△) IA^-.

shifts of TTF C–S stretching vibrations (bands E, F, and G) in Fig. 4. Bands E, F, and G are assigned to b_{2u} ν_{25}, b_{1u} ν_{16} and b_{1u} ν_{17}, respectively, as given in Table 1.

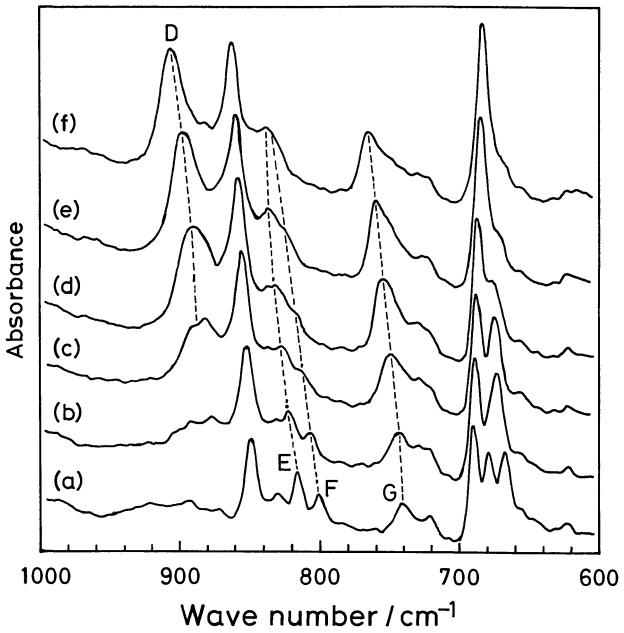

Fig. 4. IR spectra of TTF–IA in thee region of C–S stretching vibrations at high pressures. (a) 1.2; (b) 1.7; (c) 1.9; (d) 2.3; (e) 2.7; (f) 3.5 GPa.

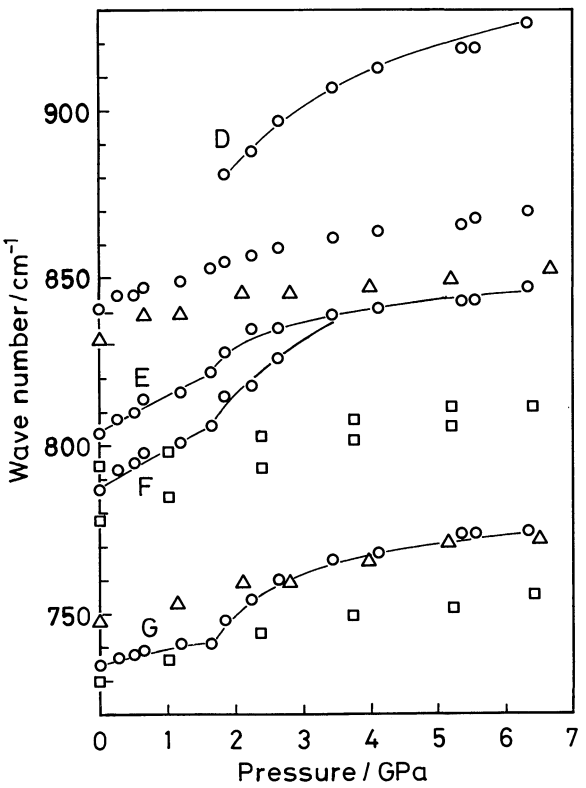

Fig. 5. Pressure dependence of IR frequencies of TTF–IA in the region of C–S stretching vibrations. (○) TTF–IA; (□) TTF^0; (△) TTF^+.

These bands show considerable high-frequency shifts (20—40 cm^{-1}) on ionization of TTF as shown in the table, and can be used as indicators for ionicity of TTF. Figure 5 shows the pressure dependence of the three bands. The corresponding frequencies of TTF^0 and TTF^+ are also plotted versus applied pressure in the figure: frequencies of TTF–BA are used as those of TTF^+. The figure shows that the pressure dependence of the frequencies clearly changes at P_c and the frequencies gradually approach to those of TTF^+ above P_c: band F comes to be concealed by band E. However, ionicity of TTF could not be precisely estimated because of the nonlinear relations between the frequencies and ionicity, which were found by use of the frequencies of TTF^0, $TTF{\cdot}Br_{0.76}$ and TTF^+.

A new band B appears around 1560 cm^{-1} at P_c, as shown in Fig. 2c. This band is assigned to the totally-symmetric C=O stretching vibration of IA (a_g ν_1) from its frequency value. Band B shows a low-frequency shift with an increase in pressure as shown in Fig. 3 and is concealed by the band C of an IA C=C stretching vibration (b_{2u} ν_{18}) at ca. 3 GPa. Another new band D appears around 880 cm^{-1} at P_c, as shown in Fig. 4c. This band is assigned to a totally-symmetric ring-deformation vibration of IA (a_g ν_3) from its frequency value. Figure 5 shows that the frequency of band D increases with an increase in pressure. This is consistent with an observed high-frequency shift of the a_g ν_3 Raman band of IA on ionization: 870 cm^{-1} for IA^0 and 935 cm^{-1} for IA^-.

IR activation of these bands B and D, which are intrinsically IR-inactive, is attributed to a kind of vibronic interaction, i.e., electron–molecular vibration (e–mv) interaction, between TTF and IA.[23] The appearance of vibronically-activated IR bands demonstrates dimerization of a crystal lattice, because such IR activation is not expected to occur in CT crystals with regular mixed-stack structures.[23] Such dimerization of a crystal lattice is the same as that observed in the N–I transition of TTF–CA,[5] and is produced by electron–lattice interaction. Consequently the anomaly observed for the IR spectra of TTF–IA at 1.9 GPa is attributed to a pressure-induced N–I transition accompanied by dimerization of the crystal lattice. Upon this transition, a yellow sample of TTF–IA was found to turn red, which is attributable to a change in the electronic state of the complex at P_c. The state of the high-pressure phase should rather be labeled as "quasi-ionic" in spite of the result that ionicity of the high-pressure phase is less than 0.5 at P_c as mentioned above. Such a "quasi-ionic" phase is theoretically suggested to exist in the case of strong electron–lattice interaction.[24]

There is another possible assignment of the C=O stretching IR bands A′ and B: band A′ is assigned to a_g ν_1 and band B to b_{1u} ν_{10}. The frequencies of bands A′ and B are 1591 and 1557 cm^{-1} at P_c, respectively. If this assignment is accepted, the phase transition of TTF–IA should be accompanied by a large ionicity jump from

0.36 to 0.64, which is almost equal to that of TTF-CA. However, this assignment is unacceptable because of the following reason. The two C=O stretching vibrations of IA^0 are almost equal to one another: 1656 cm^{-1} (a_g ν_1) and 1659 cm^{-1} (b_{1u} ν_{10}). Furthermore, magnitudes of the low frequency shifts on ionization are also almost equal to one another: 171 cm^{-1} (a_g ν_1) and 161 cm^{-1} (b_{1u} ν_{10}). Therefore, frequencies of the two vibrations are expected to be almost equal to one another at every ionicity if the frequencies are not affected by the e-mv interaction. In fact, frequencies of totally-symmetric vibrations are decreased by the e-mv interaction. On the other hand, non-totally symmetric vibrations are free from any influence by the interaction.[23] Consequently, the frequency of a_g ν_1 must be less than that of b_{1u} ν_{10}.

Comparison of N-I Transitions between TTF-IA and TTF-CA. In the pressure-induced N-I transition of TTF-CA at room temperature, IR bands as well as visible bands of the ionic species appear at pressures considerably lower than P_c. The bands of the neutral and ionic phases are both observed in the pressure region between 0.7 and 1.1 GPa.[5] On the other hand, in the temperature-induced N-I transition of TTF-CA at 81 K, such coexistence of the two phases is not observed.[7]

Table 2. Comparison of N-I Transitions in TTF-IA and TTF-CA

Complex	ρ_0	P_c / GPa	$\Delta\rho$	IR intensity of totally symmetric vibrations above P_c
TTF-IA	0.08	1.9	0.06 (0.36→0.42)	Gradual increase
TTF-CA[a]	0.18	1.1	0.30 (0.34→0.64)	Abrupt increase

a) Refs. 5 and 6.

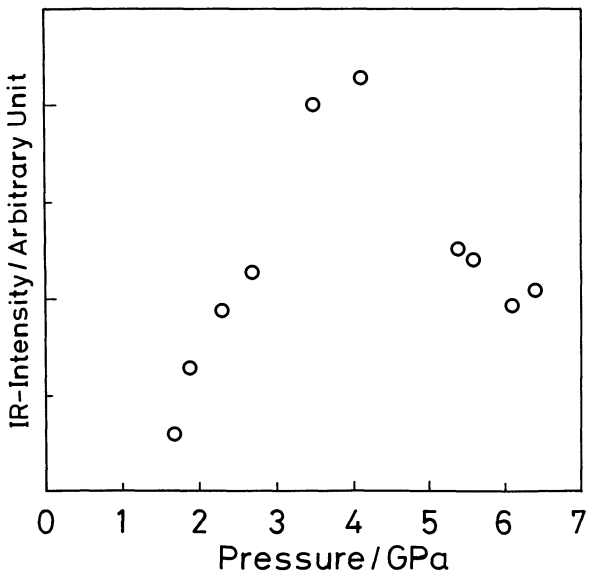

Fig. 6. Pressure dependence of IR intensity observed for a totally-symmetric vibration (IA a_g ν_3) of TTF-IA.

The coexistence is attributed to thermal excitation of the ionic state which has an energy not far off the neutral state near the transition point.[24] Also in the case of TTF-IA, such coexistence is observed as shown in Figs. 2 and 3. The N-I transitions of TTF-IA and TTF-CA are similar to one another on this point but there are a few remarkable differences between the two CT crystals.

Characteristic features of the N-I transition in the two systems are shown in Table 2. In the case of TTF-CA, a large ionicity jump of 0.3 (from 0.34 to 0.64) is observed at the transition pressure (1.1 GPa): The average of ρ for the neutral and ionic phases at P_c is almost equal to 0.5. On the other hand, in the case of TTF-IA, the ionicity shows only a slight jump of 0.06 (from 0.36 to 0.42) at the transition pressure (1.9 GPa): The average of ρ is clearly less than 0.5. There is a difference also in the IR activation of the totally symmetric vibrations between the two CT crystals. An abrupt increase is observed for the IR intensity of CA (a_g ν_3) in TTF-CA at P_c.[5] In the case of TTF-IA, on the other hand, intensity of the corresponding IR band of IA (a_g ν_3) gradually increases with an increase in pressure above P_c, as shown in Fig. 6. The intensity of the vibronically-activated totally symmetric vibrations is known as a measure of dimerization of crystal lattice,[23] so that Fig. 6 demonstrates gradual dimerization in TTF-IA.

According to a quantum Monte Carlo simulation by Nagaosa,[24] the N-I transition of the mixed-stack CT crystal changes from the discontinuous transition of the first order to the continuous one of the second order with an increase in the electron-lattice interaction, which is due to a variaton of a transfer integral with a change in the interplanar distance between the donor and acceptor. The quasi-continuous transition observed for TTF-IA, i.e., the small ionicity jump and the gradual dimerization of the crystal lattice, are characteristic to the case of large electron-lattice interaction in comparison with TTF-CA. The simulation, on the other hand, predicts a decrease in the transition pressure for the case of large electron-lattice interaction if other conditions are unchanged. This disagrees with the increased transition pressure in TTF-IA compared with TTF-CA as shown in Table 2. This disagreement may be due to the large interplanar distance between TTF and IA[15] and the large polarizability of IA.[19] These two factors decrease the electrostatic Madelung energy and are expected to push up the transition pressure.

This work was partially supported by a Grant-in-Aid for Scientific Research No.01540381 from the Ministry of Education, Science and Culture.

References

1) H. M. McConnell, B. M. Hoffman, and R. M. Metzger, *Proc. Natl. Acad. Sci. U.S.A.*, **53**, 46 (1963).

2) Z. G. Soos and S. Mazumdar, *Phys. Rev. B*, **18**, 1991 (1978).

3) J. B. Torrance, J. E. Vasquez, J. J. Mayerle, and V. Y. Lee, *Phys. Rev. Lett.*, **46**, 253 (1981).
4) A. Girlando, C. Pecile, A. Brillante, and K. Syassen, *Solid State Commun.*, **57**, 891 (1986).
5) H. Okamoto, T. Koda, Y. Tokura, T. Mitani, and G. Saito, *Phys. Rev. B*, **39**, 1339 (1989).
6) J. B. Torrance, A. Girlando, J. J. Mayerle, J. I. Crowley, V. Y. Lee, P. Batail, and S. J. La Placa, *Phys. Rev. Lett.*, **47**, 1747 (1981).
7) Y. Tokura, T. Koda, G. Saito, and T. Mitani, *J. Phys. Soc. Jpn.*, **53**, 4445 (1984).
8) A. Girlando, C. Pecile, A. Brillante, and K. Syassen, *Synth. Met.*, **19**, 503 (1987).
9) Y. Iwasa, T. Koda, Y. Tokura, A. Kobayashi, N. Iwasawa, and G. Saito, *Phys. Rev. B*, **42**, 2374 (1990).
10) J. B. Torrance, J. J. Mayerle, V. Y. Lee, and K. Bechgaad, *J. Am. Chem. Soc.*, **101**, 4748 (1979).
11) S. Matsuzaki, T. Moriyama, M. Onomichi, and K. Toyoda, *Bull. Chem. Soc. Jpn.*, **56**, 369 (1983).
12) J. J. Mayerle, J. B. Torrance, and J. I. Crowley, *Acta Crystallogr., Sect. B*, **35**, 2988 (1979).
13) A. Girlando, C. Pecile, and J. B. Torrance, *Solid State Commun.*, **54**, 753 (1985).
14) H. A. Torrey and W. H. Hunter, *J. Am. Chem. Soc.*, **34**, 702 (1912).
15) M. Murase, M. Konno, S. Matsuzaki, T. Hiejima, and M. Sano, 59th National Meeting of the Chemical Society of Japan, Yokohama, March 1990, Abstr., 2F212.
16) R. Bozio, I. Zanon, A. Girlando, and C. Pecile, *J. Chem. Phys.*, **71**, 2282 (1972).
17) A. Girlando, F. Marzola, C. Pecile, and J. B. Torrance, *J. Chem. Phys.*, **79**, 1075 (1983).
18) R. M. Metzger and J. B. Torrance, *J. Am. Chem. Soc.*, **107**, 117 (1985).
19) N. Sato, K. Seki, and H. Inokuchi, *J. Chem. Soc., Faraday Trans. 2*, **77**, 1621 (1981).
20) E. C. M. Chen and W. E. Wentworth, *J. Chem. Phys.*, **63**, 3183 (1975); E. C. M. Chen and W. E. Wentworth, *Mol. Cryst. Liq. Cryst.*, **171**, 271 (1989).
21) C. S. Jacobsen and J. B. Torrance, *J. Chem. Phys.*, **78**, 112 (1983).
22) G. J. Piermarini, S. Block, and J. S. Barnett, *J. Appl. Phys.*, **44**, 5377 (1973).
23) A. Painelli and A. Girlando, *J. Chem. Phys.*, **84**, 5655 (1986).
24) N. Nagaosa, *J. Phys. Soc. Jpn.*, **55**, 2754 (1986).

Elucidation of Solvatochromism for the Ligand Field Absorption Bands of Polyamine-*N*-polycarboxylato Cobaltate(III) and Chromate(III) Complexes of $[M(N)_2(O)_4]$ Type

Sumio KAIZAKI,* Norio KOINE,† and Narumi SAKAGAMI††,§
Department of Chemistry, Faculty of Science, Osaka University, Toyonaka, Osaka 560
† Department of Industrial Chemistry, Faculty of Engineering, Ehime University, Bunkyou-chyo, Matsuyama 790
†† Department of Chemistry, Faculty of Science, Nara Women's University, Nara 630
(Received January 14, 1991)

The solvatochromism of the first ligand field absorption bands and/or the solvent dependence of ^{13}C and ^{59}Co NMR shifts for *trans*- and *cis*-$[M(N)_2(O)_4]$ type complexes of cobalt(III) or chromium(III) with various kinds of polyamine-*N*-polycarboxylato ligands was elucidated in terms of the angular overlap model (AOM) parametrization. On the basis of the difference in the solvent-dependence of spectroscopic data of the complexes studied in various solvents, it was found that the solvatochromism could result from variations of the metal-ligand σ and/or π bond interactions (expressed by the $e_\sigma(O)$, $e_\sigma(N)$, and anisotropic $e_\pi(O)$ AOM parameter values) due to the preferential solvation toward the oxygen p_π orbitals coplanar with the $M(O)_2$ coordinate planes.

There have been a few reports on the solvent dependence of the ligand field d–d transitions of inert complexes with the saturated coordination numbers in comparison with a number of investigations on remarkable solvatochromism in the charge transfer transitions of metal complexes.[1] For Co(III) and Cr(III) complexes with ethylenediaminetetraacetate (edta) type ligands, the first d–d absorption band maxima were found to shift to the shorter wavelength with increasing acceptor numbers,[2] which were defined as a quantitative empirical electron pair acceptor number for solvents by Gutmann et al.[3] on the basis of the ^{31}P NMR chemical shifts of triethylphosphine oxide in various kinds of solvents. Nevertheless, there has been no systematic study on the elucidation for the solvent dependence of the ligand field bands of this type of complexes. Though Taura proposed the preferential solvation model toward the σ electrons of the carboxylato oxygens for *cis*-$[Co(ox)_2(NH_3)_2]^-$ in terms of EHMO calculations,[2d] this approach could not necessarily account for the blue shift of the first ligand field band. For the higher symmetry complexes of *trans*-$[CrX_2(N)_4]$ type, on the other hand, it has recently been reported that the solvent dependent ligand field band and ^2H NMR shifts can be elucidated in terms of the ligand field or the angular overlap model (AOM) parametrization.[4] A notable ligand field variability and the interligand cooperative effect due to the selective solvation toward electronegative ligating atoms has been revealed. These findings might make feasible to account for the solvatochromism of the edta type complexes with multiple (at most triple) d–d transition components due to much lower symmetry than tetragonal or octahedral, and could provide a basis for more plausible solvation models than Taura's one.[2d]

In this article, we will examine the solvent-dependence of the ligand field absorption spectra for *trans*- and *cis*-$[M(N)_2(O)_4]$ type complexes of Co(III) and Cr(III) together with ^{13}C and ^{59}Co NMR spectra for the Co(III) complexes and analyze them on the basis of the AOM parametrization. Assuming that the polyamine-*N*-polycarboxylato ligands are nonlinear ligators with the anisotropic π interaction between metal d orbitals and ligating oxygen p_π orbitals perpendicular to the chelate plane, it has been revealed that preferential (additional) solvations toward a pair of two neighboring oxygen p_π orbitals coplanar with the $M(O)_2$ plane play an important role in the solvatochromism and that the solvatochromic behavior reflects the difference in the topological arrangements of the ligating oxygen p_π orbitals in the carboxylato groups.

Experimental

Materials. The complexes used in this study are given in Table 1 together with numbering (**1**—**37**) for short. The ligands' abbreviations are as follows: ida=iminodiacetate; mida=*N*-methyliminodiacetate; eida=*N*-ethyliminodiacetate; bida=*N*-butyliminodiacetate; nta=nitrilotriacetate; β-alada=β-alanine-*N*,*N*-diacetate; edta=ethylenediaminetetraacetate; (*S*)-pdta=(*S*)-1,2-propanediaminetetraacetate; 1,3-pdta=1,3-propanediaminetetraacetate; eddda=ethylenediamine-*N*,*N*′-diacetate-*N*,*N*′-dipropionate; (*S*,*S*)-edds=(*S*,*S*)-ethylenediamine-*N*,*N*′-disuccinate; edtp=ethylenediaminetatrapropionate; (*S*)-pdtp=(*S*)-1,2-propanediaminetetrapropionate; dmedda=*N*,*N*′-dimethylethylenediamine-*N*,*N*′-diacetate; edda=ethylenediamine-*N*,*N*′-diacetate; aeida=*N*-(2-aminoethyl)iminodiacetate or ethylenediamine-*N*,*N*-diacetate.

Preparation of Complexes. Most complexes except **11**, **12**, **16**, **32**, **33**, and **36** complexes in Table 1 were prepared by the literature methods; **1**,[5] **2**,[6] **3**,[7] **4**,[7] **5**,[7], **6**,[8] **7**,[9] **8**,[9] **9**,[10] **10**,[11] **13**,[12] **14**,[13] **15**,[12] **17**,[14] **18**,[15] **19**,[15] **20**,[16] **21**,[17] **22**,[18a] **23**,[19] **24**,[20] **25**,[19b] **26**,[21] **27**,[17] **28**,[22] **29**,[23] **30**,[22] **31**,[23] **34**,[8] **35**,[9] **37**.[25] These complexes were identified by the absorption spectra.

***trans*(*N*)-K[Co(mal)(gly)$_2$]·2H$_2$O.** The reaction mixture was obtained by the same method as that for the corresponding oxalato complex[10] by using potassium malonate instead of potassium oxalate. The separation of three isomers, *trans*(*N*),

§ Present address: Department of Chemistry, Faculty of Science, Osaka University, Toyonaka, Osaka 560.

Table 1. Solvatochromic Data of $[M(N)_2(O)_4]$ Type Complexes

	Complexes	Absorption			^{59}Co NMR	
		Slope	Intercept	Correlation factor	Slope	Intercept
		cm^{-1}	$10^3\ cm^{-1}$		ppm	ppm
	trans(*N*) Type					
1	$[Co(ida)_2]^-$	2.85	20.0	0.94	0.77	10552
2	$[Co(mida)_2]^-$	1.11	19.0	0.91	−1.79	11011
3	$[Cr(mida)_2]^-$	1.01	20.2	0.86		
4	$[Cr(eida)_2]^-$	3.05	19.9	0.99		
5	$[Cr(bida)_2]^-$	1.92	19.9	0.93		
6	[Co(nta)(gly)]$^-$	2.72	19.5	0.86		
7	*sym*-[Co(β-alada)(gly)]$^-$	3.80	19.2	0.88	−0.73	11091
8	*unsym*-[Co(β-alada)(gly)]$^-$	3.09	19.2	0.88	0.29	10958
9	$[Co(ox)(gly)_2]^-$	8.93	18.5	0.96		
10	$[Co(ox)(\beta\text{-ala})_2]^-$	5.20	18.5	0.93	−4.72	10833
11	$[Co(mal)(gly)_2]^-$	8.37	18.5	0.99		
12	$[Co(mal)(\beta\text{-ala})_2]^-$	5.99	18.4	0.97		
	cis(*N*) Type					
13	$[Co(ox)_2(en)]^-$	8.17	18.1	0.99	−3.46	10683
14	$[Cr(ox)_2(en)]^-$	8.53	18.3	0.97		
15	$[Co(mal)_2(en)]^-$	12.66	17.9	0.98	−5.70	11322
16	$[Cr(mal)_2(en)]^-$	13.12	18.2	0.90		
17	[Co(edta)]$^-$	9.46	18.2	0.97	−6.36	10626
18	[Cr(edta)]$^-$	12.91	17.8	0.89		
19	[Cr{(*S*)-pdta}]$^-$	13.25	17.8	0.85		
20	[Co(1,3-pdta)]$^-$	8.33	17.8	0.93		
21	[Cr(1,3-pdta)]$^-$	11.09	19.1	0.79		
22	[Co(eddda)]$^-$*	13.70	17.8	0.97	−8.80	11410
23	[Cr(eddda)]$^-$*	22.36	17.8	0.97		
24	[Co{(*S,S*)-edds}]$^-$*	13.76	18.8	0.98		
25	[Cr{(*S,S*)-edds}]$^-$*	23.84	18.4	0.86		
26	[Co(edtp)]$^-$	15.18	17.3	0.95	−8.61	11755
27	[Cr{(*S*)-pdtp}]$^-$	20.09	17.5	0.95		
28	*sym*-[Co(edda)(ox)]$^-$	9.96	17.5	0.99		
29	*sym*-[Cr(edda)(ox)]$^-$	12.57	18.1	0.92		
30	*sym*-[Co(edda)(mal)]$^-$	9.35	17.4	0.98		
31	*sym*-[Cr(edda)(mal)]$^-$	12.12	18.0	0.97		
32	*sym*-[Co(dmedda)(ox)]$^-$	4.82	17.5	0.85		
33	*sym*-[Co(dmedda)(mal)]$^-$	9.29	17.0	0.97	−5.50	11319
34	[Co(nta)(gly)]$^-$	11.07	17.0	0.98		
35	*unsym*-[Co(β-alada)(gly)]$^-$	9.97	17.1	0.88	−6.85	11475
36	*sym*-[Co(aeida)(ox)]$^-$	6.91	17.6	0.86		
37	*unsym*-[Co(aeida)(ox)]$^-$	9.57	18.5	0.97	−4.02	10519

The symbols, *sym*- and *unsym*-, denote symmetrical and unsymmetrical geometrical structures, respectively. The asterisked (*) complexes (**22**—**25**) take a *trans*-(O_5) geometrical structure in which the five-membered acetate rings occupy *trans*-axial sites while the propionate rings lie in the equatorial plane with two nitrogen atoms.

C_1-*cis*(*N*), C_2-*cis*(*N*), was chromatographically performed by a method similar to that for the oxalato complex. The *trans*(*N*) isomer was first eluted and was isolated as crystals from its eluate. The geometrical structure of the *trans*(*N*) isomer was determined on the basis of the presence of a shoulder at the lower energy region in the first absorption band as found for the corresponding oxalato complex.[10] Found: C, 22.02; H, 3.76; N, 7.21%. Calcd for $K[Co(mal)(gly)_2]\cdot 2H_2O$:C, 21.88; H, 3.67; N, 7.29%.

***trans*(*N*)-K[Co(mal)(β-ala)$_2$]·2.5H$_2$O·KCl.** This complex was prepared and characterized by a similar method to that for the corresponding glycinato complex. Found: C, 22.10; H, 3.80; N, 5.68%. Calcd for $K[Co(mal)(\beta\text{-ala})_2]\cdot 2.5H_2O\cdot KCl$: C, 21.80; H, 3.86; N, 5.65%.

Na[Cr(mal)$_2$(en)]·0.5H$_2$O. Five grams of *cis*-$Na[Cr(mal)_2(H_2O)_2]\cdot 3H_2O$ was dissolved in 400 cm^3 of hot *N*,*N*-dimethylformamide (DMF) at 90 °C. To the resulting dark blue solution was added 1.2 g of ethylenediamine in 25 cm^3 of DMF. The color of the mixture changed to be light violet. After this solution was allowed to stand for a while at 90 °C, it was cooled to room temperature. By the addition of a large amount of ether to the reaction solution, red precipitate was obtained. The aqueous solution of this precipitate was poured onto a QAE-Sephadex C-25 anion-exchange column (ϕ 3.5×40 cm). After washing the column with water, the chromatography was carried out by eluting with 0.04 M (1 M=1 mol dm^{-3}) aqueous NaCl solution. The column gave three bands. The first eluate was collected and evaporated to dryness. By the repetition of the extraction of the red complex with methanol, sodium chloride was removed. This was recrystallized from water and acetone. Calcd for $Na[Cr(mal)_2(en)]\cdot 0.5H_2O$: C, 27.58; H, 3.73; N, 8.04%. Found: C, 27.59; H, 3.55; N, 7.95%.

***sym-cis*-K[Co(dmedda)(ox)]·0.5H$_2$O.** This complex was

prepared according to the literature method for the corresponding sodium salt[24] by using potassium oxalate instead of sodium oxalate. Found: C, 30.20; H, 3.69; N, 7.14%. Calcd for K[Co(ox)(dmedda)]·0.5H_2O: C, 30.23; H, 3.44; N, 7.05%.

***sym-cis*-K[Co(dmedda)(mal)]·1.5H_2O.** This complex was prepared by the same method as that for the corresponding oxalato complex by using potassium malonate instead of potassium oxalate. Found: C, 30.90; H, 4.35; N, 6.54%. Calcd for K[Co(dmedda)(mal)]·1.5H_2O: C, 30.78; H, 4.46; N, 6.53%. The *sym-cis* structure with a C_2 symmetry was confirmed by the ^{13}C NMR spectroscopy.

***sym*-K[Co(aeida)(ox)].** This complex could be prepared using *unsym*-K[Co(NO_2)$_2$(aeida)]·H_2O as a starting material. Potassium salt of the dinitro complex was prepared according to the literature method for the corresponding sodium salt[26] by using potassium nitrite instead of sodium nitrite. Found: C, 18.95; H, 3.24; N, 14.45%. Calcd for K[Co(NO_2)$_2$(aeida)]·H_2O: C, 18.85; H, 3.16; N, 14.65%.

To a solution containing 5 g of the dinitro complex and 5.32 g of potassium oxalate in 50 cm^3 of water was added 0.3 g of activated charcoal. The mixture was stirred at 60 °C for 1 h. Then, the dinitro complex was almost quantitatively converted to a mixture of the *sym* and *unsym* isomers of the oxalato complex. After the charcoal was removed, the *unsym* and *sym* isomers were separately obtained by means of fractional crystallization; the former complex being less soluble than the latter one. Found: C, 26.65; H, 2.90; N, 7.75%. Calcd for *sym*-K[Co(aeida)(ox)]: C, 26.68; H, 2.80; N, 7.78%.

Measurements. The ligand field absorption spectra were obtained by a Shimadzu UV-240 spectrophotometer at room temperature. ^{13}C and ^{59}Co NMR spectra were measured by a JEOL GX-270 FT-NMR spectrometer at 20 °C and 25 °C, respectively, at Nara Women's University. ^{13}C NMR shifts were determined by using dioxane (66.6 ppm) as an external standard, whereas [Co(edta)]$^-$, *fac*-[Co(β-ala)$_3$], *cis*(*N*)-[Co(nta)(gly)]$^-$, and [Co(ox)$_3$]$^{3-}$ were taken as the external standards for ^{59}Co NMR shifts according to the chemical shift range of the complexes with the down field positive convention. The chemical shifts of the complexes were converted as δ(Co)=10300 ppm for the edta complex relative to external aqueous [Co(CN)$_6$]$^{3-}$ (δ(Co)=0). In order to obtain the sufficient concentrations for these spectroscopic measurements (0.001—0.01 M, 0.2 M, and 0.005—0.02 M for absorption, ^{13}C and ^{59}Co NMR, respectively) in aprotic solvents, cryptand 222 was used as a solubilizing agent.

The solvents used for the measurements were of spectrograde or reagent grade. The abbreviations for the solvents in parentheses and their acceptor numbers in square brackets as found in the literature[3] are as follows: *N*,*N*-dimethylacetamide (DMA) [13.6]; *N*,*N*-dimethylformamide (DMF) [16.0]; dimethyl sulfoxide (DMSO) [19.3]; *N*-methylformamide (NMF) [31.0]; formamide (FA) [39.8]; methanol (MeOH) [41.3]; H_2O [54.8].

Results and Discussion

Since the present complexes are so stable or inert to be isolated from aqueous solutions as described in the Experimental section, it is unlikely that the solvatochromism is associated with the ligand dissociation. There exists to be fairly good linear correlation between the ligand field band maxima and the solvents' acceptor numbers for the present complexes including those bearing the N–H protons. This fact indicates that the solvatochromism is accompanied by the acceptor properties of the solvents, but not by the donor properties. In view of the extent of the solvatochromism and/or the solvation sites, the trans and cis type complexes are classified into two and three groups, respectively, as below.

***trans*-[M(N)$_2$(O)$_4$] Type Complexes.** In general, *trans*-[Co(N)$_2$(O)$_4$] type complexes give two components in the first ligand field absorption band region. These components are assigned to the holohedrized tetragonal (D_4) $^1A_2$ and ^1E state in the $^1T_1 \leftarrow {}^1A_1$ transition region from the longer wavelength side. As found for [Co(edta)]$^-$ and the analogous complexes,[2] the absorption band maxima corresponding to the transition $^1E \leftarrow {}^1A_1$ of the trans type complexes also give linear correlations with Gutmann's acceptor numbers[3] as

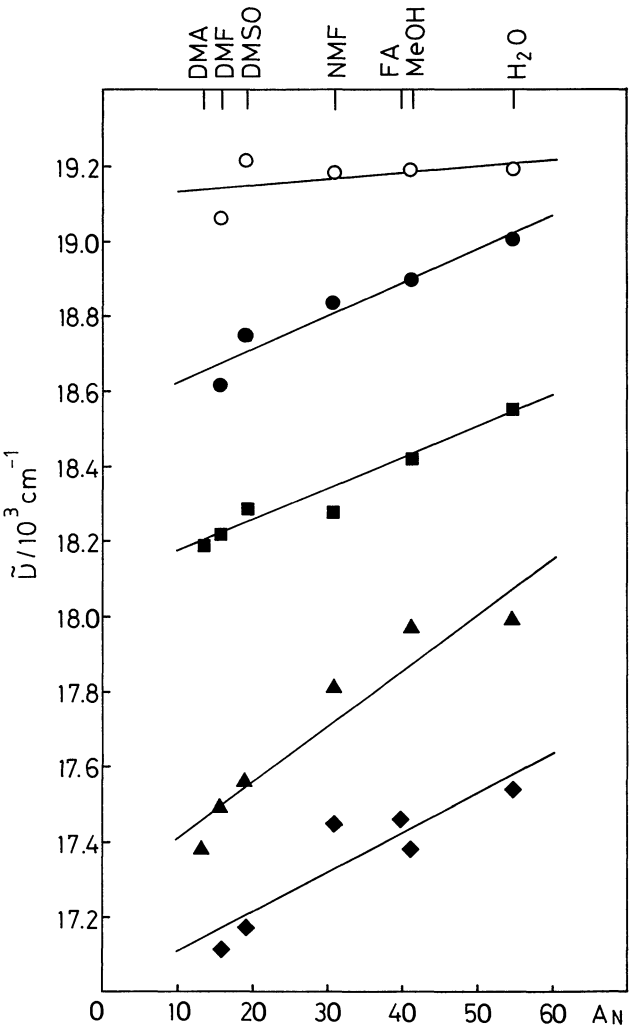

Fig. 1. Plots of the absorption band maxima ($\nu/10^3$ cm^{-1}) vs. the acceptor numbers (A_N): ○ *trans*(*N*)-[Co(mida)$_2$]$^-$ (A group); ● *trans*(*N*)-[Co(ox)(gly)$_2$]$^-$ (B group); ■ [Co(ox)$_2$(en)]$^-$ (C group); ▲ [Co(edtp)]$^-$ (D group); ◆ *cis*(*N*)-[Co(nta)(gly)]$^-$ (E group).

shown in Fig. 1. However, the extent of the solvent-dependence varies from one group of the complexes to the other. That is, for *trans*(*N*)-[Co(ida)$_2$]$^-$ type complexes which are classified as the A group (**1**—**8**), the slopes of the plots of the shorter wavelength absorption band maxima (the ^{1}E component near 20000 cm^{-1}) with the acceptor numbers are smaller by about one half than those for *trans*(*N*)-[Co(ox)(gly)$_2$]$^-$ type complexes which are classified as the B group (**9**—**12**) as shown in Fig. 1 and Table 1. In other words, the former A group complexes show negligible solvent-dependence, whereas the latter B group complexes exhibit considerable solvatochromism. Such solvatochromic behavior of the ^{1}E component together with that for the ^{1}A$_2$ one is also substantiated by the ^{59}Co NMR shifts as in Table 1. The A group complexes give little dependence of the ^{59}Co NMR shifts on the acceptor numbers, whereas the ^{59}Co NMR shifts of the B group complexes are more dependent on the acceptor number. These ^{59}Co NMR shifts behave in a manner similar to the solvatochromism for the ^{1}E component and reflect the solvent change of both the tetragonal split components in the first band region more directly than the solvatochromism, since the ^{59}Co NMR shifts are related with the sum of the reciprocal of the transition energy of each split component in the ^{1}T$_1$←^{1}A$_1$ transition.[27] Such a remarkable difference in the solvatochromism can be accounted for by considering the AOM parametrization including the anisotropic π interaction between metal d orbitals and the ligating oxygen p_π orbitals perpendicular to the chelate planes rather than the isotropic one as in Fig. 2. The transition energies of the first ligand field band components for two groups of *trans*-[Co(N)$_2$(O)$_4$] type complexes with holohedrized tetragonal (D$_4$) symmetry are given in terms of the AOM parameters on the assumption of the orthoaxial coordination by taking account of only the anisotropic π metal–oxygen p_π interaction perpendicular to the chelate planes for the carboxylato groups as follows:

$$E(^1\mathrm{E}) = 3/2e_\sigma(\mathrm{N}) + 3/2e_\sigma(\mathrm{O}) + 4B \quad (1)$$

$$E(^1\mathrm{A}_2) = 3e_\sigma(\mathrm{O}) - 4e_\pi(\mathrm{O}) + 4B \quad (2)$$

for *trans*(*N*)-[Co(ida)$_2$]$^-$ type complexes of the A group. The same formulations of the transition energies are given for *trans*(*N*)-[Co(nta)(gly)]$^-$ type complexes assuming the identical topological arrangements of the ligating oxygen p_π orbitals of the carboxylato groups unless three kinds of the ligating oxygen atoms of the different carboxylato groups were discriminated.

$$E(^1\mathrm{E}) = 3/2e_\sigma(\mathrm{N}) + 3/4e_\sigma(\mathrm{O}) + 3/4e_\sigma(\mathrm{O}') - e_\pi(\mathrm{O}') + 4B \quad (3)$$

$$E(^1\mathrm{A}_2) = 3/2e_\sigma(\mathrm{O}) + 3/2e_\sigma(\mathrm{O}') - 2e_\pi(\mathrm{O}) + 4B \quad (4)$$

for *trans*-[Co(ox)(gly)$_2$]$^-$ type complexes of the B group

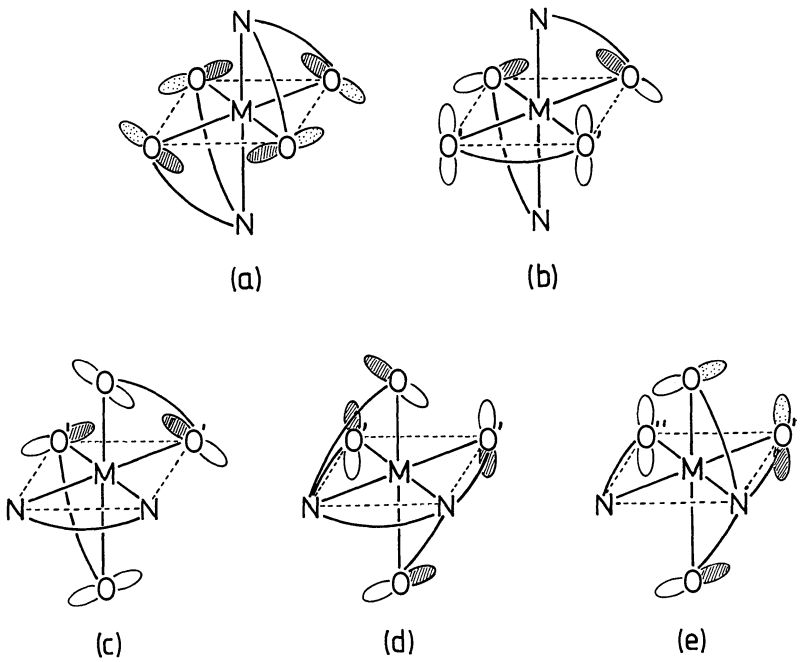

Fig. 2. Topological arrangements of the ligating oxygen p_π orbitals for which a pair of the shaded and/or dotted lobes at the octahedral edge is directed toward the solvents; implying the preferential (additional) solvation for the following types of complexes: (a) *trans*(*N*)-[M(ida)$_2$]; (b) *trans*(*N*)-[M(ox)(gly)$_2$]; (c) [M(ox)$_2$(en)]; (d) [M(edta)]; (e) *cis*(*N*)-[M(nta)(gly)].

where O and O′ denote the coordinated oxygen atoms of the amino acidato and oxalato ligands, respectively, as in Fig. 2(b). The last term B in Eqs. 1—4 is the Racah interelectronic repulsion parameter. It is plausible that this parameter is almost solvent independent as mentioned previously.[4]

Although the absorption bands and ^{59}Co NMR shifts of the A group complexes are little altered with variation of the solvents' acceptor numbers as in Fig. 1 and Table 1, ^{13}C NMR signals of the carboxylato carbons shift to the lower field with increasing the acceptor numbers; the slope of the plots with the acceptor numbers is +0.1. This suggests the solvation toward the ligating oxygens of the carboxylato groups as claimed from the ^{13}C NMR behavior of [Co(edta)]$^-$ by Taura,[28] leading to the change of the AOM parameter values in each energy term in Eqs. 1 and 2. It is likely that the highly preferential (additional) solvation occurs toward pairs of the ligating oxygen p_π orbitals coplanar with the $M(O)_4$ plane of the A group complexes as shown in Fig. 2(a). This may give the decrease in the AOM e_π(O) parameters. As a result, both the AOM e_π(O) and e_σ(O) values decrease with increasing the acceptor numbers. This variation in the AOM parameter values results in the negligible change of the $^1A_2$ transition energy; the term $3e_\sigma(O)-4e_\pi(O)$ keeping almost constant with change of the solvents as found for $3e_\sigma(F)-4e_\pi(F)$ of *trans*-[CrF_2(3.2.3-tet)]$^+$ complex.[4] On the other hand, the e_σ(N) value increases with increasing the acceptor numbers due to a cis electronic effect, followed by the decrease in the e_σ(O) or e_π(O) value as revealed for *trans*-[CrF_2(3.2.3-tet)]$^+$ complex.[4] The solvent dependent ^{13}C NMR shifts of the methyl carbons in *trans*(*N*)-[Co(mida)$_2$]$^-$ lend support to the solvent variation of the e_σ(N) values, since the slope (−0.025) of the plots of these shifts with the acceptor numbers is opposite to that (+0.1) of the carboxylato carbons. Thus, the ^{1}E transition energy is little affected by the solvents' acceptor properties owing to the cancellation between the e_σ(N) and e_σ(O) values within the energy terms, whereas the parallel change of the e_σ(O) and e_π(O) values gives a small alternation of the $^1A_2$ transition energy. This is the finding for the solvatochromism of the A group complexes (**1**—**8**), though the solvatochromism cannot clearly be seen for the latter $^1A_2$ component of most *trans*(*N*) type complexes, because this component is usually observed only as the shoulders or poorly defined band maxima at the longer wavelength side of the ^{1}E component.

For *trans*(*N*)-[Co(ox)(gly)$_2$]$^-$ (the B group), however, ^{13}C NMR chemical shifts of the carboxylato carbons for the glycinato ligands is more largely solvent dependent than that for the oxalato ones; the slopes of the plots for ^{13}C NMR shifts with the acceptor numbers of the solvents are +0.12 and +0.065 for the carboxylato carbons of the glycinato and oxalato ligands, respectively. This suggests the preferential (additional) solvation toward a pair of the p_π orbitals of the glycinato oxygens coplanar with the $M(O)_4$ plane in support of the proposed solvation mode for the A group complexes as shown in Fig. 2(b). In this case, the observed solvatochromism may be explained by grouping the AOM parameters into the braces in the following equations for the transition energies (Eqs. 3 and 4) of each component:

$$E(^1E) = 3/4e_\sigma(N) + 3/4\{e_\sigma(N) + e_\sigma(O)\} + 1/4\{3e_\sigma(O') - 4e_\pi(O')\} + 4B \quad (5)$$

$$E(^1A_2) = 3/2e_\sigma(O') + 1/2\{3e_\sigma(O) - 4e_\pi(O)\} + 4B \quad (6)$$

The terms $\{e_\sigma(N)+e_\sigma(O)\}$ and $\{3e_\sigma(O)-4e_\pi(O))\}$ and/or $\{(3e_\sigma(O')-4e_\pi(O')\}$ are almost solvent independent as revealed for the A group complexes, whereas the remaining e_σ(N) and e_σ(O) parameters may be more susceptible to the solvent dependence as revealed from the following consideration. The preferential solvation toward a pair of the p_π orbitals for two glycinato coordinated oxygens (O in Fig. 2(b)) causes shortening both the Cr–N and Cr–O′ bond or increasing both the e_σ(N) and e_σ(O′) values, followed by the lengthening of the Cr–O bonds or the decrease in the e_σ(O) or e_π(O) owing to a cis electronic effect or the electroneutrality principle. Accordingly, it is plausible that the band maxima of two components in the first band region shift to the higher frequency side with increasing the acceptor numbers. This indeed accounts for the fact that the solvatochromism for the B group complexes is significantly larger than that for the A group complexes.

For the corresponding Cr(III) complexes, the transition energies of two tetragonal split components in the $^4T_2 \leftarrow {}^4A_2$ transition are given by the same AOM parametrization as for the Co(III) complexes except for the use of the irreducible representation $^4B_2$ instead of the $^1A_2$ and the exclusion of the Racah parameter B. Therefore, it is expected that the solvatochromism for *trans*(*N*)-[Cr(mida)$_2$]$^-$, -[Cr(eida)$_2$]$^-$, and -[Cr(bida)$_2$]$^-$ complexes occurs as similarly to the corresponding cobalt(III) complexes. This is the finding as in Table 1.

***cis*-[M(N)$_2$(O)$_4$] Type Complexes.** On the basis of the AOM parametrization, the cis type complexes are also classified into three groups. That is, the C group is represented by [M(ox)$_2$(en)] type complexes (**13**—**16**) and the others D and E are the edta type (**17**—**33**) and the *cis*(*N*)-(nta)(gly) type complexes (**34**—**37**), respectively.

The transition energies of each tetragonal split component in the first ligand field transition of the C and D group complexes of Co(III) are given by the AOM parameters as follows:

$$E(^1A_2) = 3/2e_\sigma(N) + 3/2e_\sigma(O') - 2e_\pi(O') + 4B \quad (7)$$

$$E(^1E) = 3/4e_\sigma(N) + 3/4e_\sigma(O') + 3/2e_\sigma(O) - e_\pi(O) + 4B \quad (8)$$

for the C group complexes, and

$$E(^1A_2) = 3/2e_\sigma(N) + 3/2e_\sigma(O') + 4B \quad (9)$$

$$E(^1E) = 3/4e_\sigma(N) + 3/2e_\sigma(O) - e_\pi(O) + 3/4e_\sigma(O') - e_\pi(O') + 4B \quad (10)$$

for the D group complexes. For both cases, the O and O′ denote the carboxylato ligating oxygens cis and trans to the amine nitrogens, respectively, as shown in Fig. 2. The same situation of the AOM parameters is encountered with Cr(III) complexes where the Racah parameter is excluded. The absorption band maxima of both the Co(III) and Cr(III) complexes and ^{59}Co NMR chemical shifts of the Co(III) complexes are linearly correlated with the acceptor numbers as shown in Table 1.

For the C group complexes, the preferential solvation is expected to occur toward a pair of two oxygen p_π orbitals on the $M(N)_2(O)_2$ plane (Fig. 2(c)), as in the cases of the A and B group complexes. Then, the Co–N and Co–O bond distances become shorter or the $e_\sigma(N)$ and $e_\sigma(O)$ values increase, followed by the decrease in the $e_\sigma(O')$ and $e_\pi(O')$ values or the lengthening of the Co–O′ bonds. On the other hand, the transition energies in terms of the AOM parameters (Eqs. 7 and 8) are reformulated by grouping almost solvent-independent terms into the braces in Eqs. 11 and 12.

$$E(^1A_2) = 3/2e_\sigma(N) + 1/2\{3e_\sigma(O') - 4e_\pi(O')\} + 4B \quad (11)$$

$$E(^1E) = 3/4e_\sigma(N) + 3/4\{e_\sigma(O) + e_\sigma(O')\} + 1/4\{3e_\sigma(O) - 4e_\pi(O)\} + 4B \quad (12)$$

The first terms $3/2e_\sigma(N)$ and $3/4e_\sigma(N)$ for the $^1A_2$ and ^1E components are solvent dependent, respectively. Thus, the $e_\sigma(N)$ values or both the tetragonal split components are predicted to increase the transition energies or to shift to the higher frequency side with increasing the acceptor numbers. This predicted tendency is in accordance with the finding for the C group complexes (**13**—**16**) as in Fig. 1 and Table 1, although the observed band maxima correspond to the position of either one of the split components or the weighted average of two components.

For the D group complexes including the *sym-cis*-[M(edda)(ox)] type, each transition energy of two tetragonal components contains only almost solvent independent terms in the braces as in Eqs. 13 and 14.

$$E(^1A_2) = 3/2\{e_\sigma(N) + e_\sigma(O')\} + 4B \quad (13)$$

$$E(^1E) = 3/4\{e_\sigma(N) + e_\sigma(O)\} + 1/4\{3e_\sigma(O) - 4e_\pi(O)\} + 1/4\{3e_\sigma(O') - 4e_\pi(O')\} + 4B \quad (14)$$

In contrast with the C group complexes, there are two preferential solvation sites for the D group complexes as in Fig. 2(d). It is assumed that the extent of the bond length variation due to the solvation per one solvation site does not change so much on going from the C group complexes with one solvation site to the D group complexes with two solvation sites in view of the similarity of the slopes of the plots for the ^{13}C NMR shifts of the carboxylato carbons with the acceptor numbers; +0.083 for $[Co(edta)]^-$ [28] and +0.08 for $[Co(mal)_2(en)]^-$. This situation is analogous to the case for ruthenium(III) ammine complexes where the correlation of the donor solvent dependent solvatochromism with the numbers of the ammine protons has been claimed.[29] Thus, the increase in the $e_\sigma(N)$ value due to the solvation for the D group complexes may be about twice as large as that for the C group complexes and the decrease in the $e_\sigma(O')$ and $e_\sigma(O)$ values owing to the electroneutrality principle. As a result, $3/2\{e_\sigma(N)+e_\sigma(O')\}$ and $3/2\{e_\sigma(N)+e_\sigma(O)\}$ terms in Eqs. 13 and 14 are not necessarily solvent independent as for the A, B, and C group complexes, but are expected to change in a similar manner to the variation of the $e_\sigma(N)$ which increase with increasing the acceptor numbers. Since the other remaining terms are almost solvent independent, the transition energies of two components increase with increasing the acceptor numbers. This is the finding for the D group complexes (**17**—**33**) as in Fig. 1 and Table 1.

For the E type complexes exemplified by *cis*(*N*)-$[Co(nta)(gly)]^-$ with two solvation sites, three components in the holohedrized D_2 field of the $^1T_1 \leftarrow {}^1A_1$ transition are different in energy from each other. The following transition energies for *cis*(*N*)-$[Co(nta)(gly)]^-$ are given in terms of the AOM parameters.

$$E(^1A_2) = 3/4e_\sigma(N) + 3/2e_\sigma(O) + 3/4e_\sigma(O'') - e_\pi(O'') + 4B \quad (15)$$

$$E(^1B_1) = 3/4e_\sigma(N) + 3/2e_\sigma(O) + 3/4e_\sigma(O') - e_\pi(O') - 2e_\pi(O) + 4B \quad (16)$$

$$E(^1B_2) = 3/2e_\sigma(N) + 3/4e_\sigma(O') + 3/4e_\sigma(O'') + 4B \quad (17)$$

where O, O′, and O″ denote two equivalent in-plane carboxylato oxygens (O), one out-of-plane carboxylato oxygen (O′) of the nta, and glycinato oxygen (O″), respectively, as in Fig. 2(e). For *sym*- and *unsym*-$[Co(aeida)(ox)]^-$, the same expressions for the transition energies are given by disregarding the difference in the carboxylato oxygens in view of the identical topological arrangements of the ligating oxygen p_π orbitals in the carboxylato groups. By grouping $3e_\sigma(X)-4e_\pi(X)$ (X=O, O′, and O″) and comparing the increasing $e_\sigma(N)$ and $e_\sigma(O'')$ values with the decreasing $e_\lambda(X)$ values($\lambda=\sigma$ and π; X=O and O′) as a result of the preferential solvation toward the O and O′ ligating oxygens, three components for the E group complexes are expected to shift to the higher frequency side with increasing the acceptor numbers, assuming that $e_\sigma(N)$ and $e_\sigma(O'')$ variation due to the solvation is about twice as large as

the e_σ(O) and e_σ(O′) ones as in the case of the D group complexes with two solvation sites. This is the finding for the E group complexes (**34**—**37**) as in Table 1.

These elucidations of the solvatochromism seem to be in accordance with the difference in the observed solvent dependence of the absorption band maxima from complex to complex, depending on the topological arrangements of the ligating oxygen p_π orbitals perpendicular to the chelate plane. The slopes of the plots of the absorption band maxima with the solvents' acceptor numbers for the C and D group complexes with six-membered malonato or amino acidato chelates are larger than those with five-membered ones as shown in Table 1. This behavior may arise from the difference in the displacement from the regular octahedral vertices; i.e., the ligating oxygens of the six-membered chelate rings are in general located closer to the regular octahedral vertices (90°) than those of the five-membered ones. Such a displacement may result in the mismatch of the coordinated oxygen p_π orbitals with the donor sites of the solvents. This appears to be responsible for the difference in the extent of the solvent dependence between the complexes with five- and six-membered rings.

In the edta type complexes of the D group, the solvent dependence is larger by more than 30% for the chromium(III) complexes than for the cobalt(III) complexes with the identical ligands as shown in Table 1 (**17**—**31**). Thus, the ligand field for the chromium(III) complexes may be more susceptible with variation of solvents than that for the cobalt(III) complexes; suggesting the more ligand field variability or the higher electronegativity of the coordinated oxygen in the chromium(III) complexes than in the cobalt(III) complexes as claimed from a comparison of the solvatochromism for *trans*-[CrX_2(3.2.3-tet)]$^+$ complexes with various halide ligands.[4)]

References

1) K. Sone and Y. Fukuda, "Inorganic Thermochromism," Springer-Verlage, Berlin (1987), p. 94, and references therein.

2) a) T. Taura, *Chem. Lett.*, **1984**, 2011; b) N. Miura, M. Shimura, and H. Ogino, *Bull. Chem. Soc. Jpn.*, **60**, 1349 (1987); c) M. Fujiwara, M. Yoshitake, Y. Fukuda, and K. Sone, *Bull. Chem. Soc. Jpn.*, **61**, 2967 (1988); d) T. Taura, *Inorg. Chim. Acta*, **163**, 133 (1989).

3) a) U. Mayer, V. Gutmann, and W. Gerger, *Monatsh. Chem.*, **106**, 1235 (1975); b) V. Gutmann, G. Resch, and W. Linert, *Coord. Chem. Rev.*, **43**, 133 (1982).

4) S. Kaizaki and H. Takemoto, *Inorg. Chem.*, **29**, 4960 (1990).

5) J. Hidaka, Y. Shimura, and R. Tsuchida, *Bull. Chem. Soc. Jpn.*, **35**, 567 (1962).

6) T. Ama, H. Kawaguchi, and T. Yasui, *Chem. Lett.*, **1981**, 323.

7) R. Wernicke, H.-H. Schmidtke, and P. E. Hoggard, *Inorg. Chim. Acta*, **24**, 145 (1977).

8) N. Koine, N. Sakota, J. Hidaka, and Y. Shimura, *Bull. Chem. Soc. Jpn.*, **42**, 1583 (1969).

9) N. Koine, N. Sakota, J. Hidaka, and Y. Shimura, *Inorg. Chem.*, **12**, 859 (1973).

10) N. Matsuoka, J. Hidaka, and Y. Shimura, *Bull. Chem. Soc. Jpn.*, **40**, 1868 (1967).

11) J. Hidaka and Y. Shimura, *Bull. Chem. Soc. Jpn.*, **40**, 2312 (1967).

12) F. P. Dywer, I. K. Reid, and F. L. Garvan, *J. Am. Chem. Soc.*, **83**, 1285 (1961).

13) S. Kaizaki, J. Hidaka, and Y. Shimura, *Bull. Chem. Soc. Jpn.*, **42**, 988 (1969).

14) S. Kirschner, *Inorg. Synth.*, **5**, 186 (1957).

15) S. Kaizaki and H. Mizu-uchi, *Inorg. Chem.*, **25**, 2732 (1986).

16) N. Tanaka and H. Ogino, *Bull. Chem. Soc. Jpn.*, **37**, 877 (1964).

17) a) S. Kaizaki and H. Mori, *Chem. Lett.*, **1981**, 567; b) S. Kaizaki and M. Hayashi, *J. Chem. Soc., Chem. Commun.*, **1988**, 613.

18) W. Byers and B. E. Douglas, *Inorg. Chem.*, **11**, 1470 (1972).

19) a) S. Kaizaki and H. Mori, *Bull. Chem. Soc. Jpn.*, **54**, 3562 (1981); b) D. J. Radanovic and B. E. Douglas, *J. Coord. Chem.*, **4**, 191 (1975).

20) J. A. Neal and N. J. Rose, *Inorg. Chem.*, **7**, 2405 (1968).

21) C. W. Van Saun and B. E. Douglas, *Inorg. Chem.*, **8**, 1145 (1969).

22) P. F. Coleman, J. I. Legg, and J. Steele, *Inorg. Chem.*, **9**, 937 (1970).

23) D. J. Radanovic, D. S. Veselinovic, and S. A. Grujic, *Bull. Soc. Chim., Beograd*, **44**, 503 (1979).

24) C. W. Maricondi and B. E. Douglas, *Inorg. Chem.*, **11**, 688 (1972).

25) G. A. Sigel and J. A. Weyh, *Inorg. Chem.*, **23**, 3246 (1984).

26) K. Kuroda, S. Ohtsuka, and N. Matsumoto, *Bull. Chem. Soc. Jpn.*, **48**, 1055 (1975).

27) N. Juranic, *Coord. Chem. Rev.*, **96**, 253 (1989).

28) T. Taura, *Inorg. Chem.*, **27**, 2845 (1988).

29) J. C. Curtis, B. P. Sullivan, and T. S. Meyer, *Inorg. Chem.*, **22**, 224 (1983).

Synthesis and Reactions of Titanoxycarbene-Metal Carbonyl Complexes

Kazushi MASHIMA, Kouki JYODOI,† Akira OHYOSHI,† and Hidemasa TAKAYA*
Department of Industrial Chemistry, Faculty of Engineering, Kyoto University, Yoshida, Kyoto 606
† Department of Synthetic Chemistry, Faculty of Engineering, Kumamoto University, Kurokami, Kumamoto 860
(Received February 7, 1991)

A family of titanoxycarbene-metal carbonyl complexes of formula $Cp^*_2TiOC(=ML_n)CH_2CH_2$ (**3**), where $Cp^*=\eta^5$-C_5Me_5 and ML_n=$Cr(CO)_5$, $Mo(CO)_5$, $W(CO)_5$, $Mn_2(CO)_9$, and $Re_2(CO)_9$, has been prepared by the treatment of titanocene-ethylene complex **1** with metal carbonyls of group 6 and 7. Complex **3b** crystallizes in space group $P2/a$ (Z=8) with cell constants a=30.401(1), b=9.251(1), c=27.561(5) Å, β=105.73(1)°, and V=7460(2) Å^3 (data taken at −40 °C, 6715 reflections, R=0.069). Two independent molecules of **3b** in crystal make an enantiomorphic pair. A notable feature of the structure is the long distance of Ti–O bond coupled with the short distance of C(2)–O bond, which is characterized by a large contribution of zwitterionic canonical form **7**. Thermal decomposition of **3** affords ethylene and the corresponding metal carbonyls, indicating that the C(carbenic)–C(3) bond fission occurred selectively, which is rather unusual for conventional Fischer-type carbene complexes. Complexes **3** react rapidly with atmospheric pressure of carbon monoxide below −30 °C to produce cyclic acyltitanium complexes **12**. The reverse reactions occur even below −30 °C upon replacement of carbon monoxide by argon. Complex **3b** also reacts with *t*-butyl isocyanide with a cleavage of the Ti–O bond to give 1:2 adduct **17**, whose molecular structure has been elucidated by X-ray crystallography [$P2_1/n$ with cell constants a=14.964(2), b=26.207(4), c=14.719(3) Å, β=100.30(1)°, and V=5679(2) Å^3 (measured at −120 °C, 5311 reflections, R=0.068)], revealing that it has a novel zwitterionic structure possessing (η^2-imidoyl)titanium cation and anionic acyldirhenium carbonyl moieties linked by an ethylene bridge. The controlled experiments show that complex **16** in which acyl ligand is trans to the Re–Re bond is the precursor of complex **17**. Complex **18**, a tungsten analogue of **17**, has also been prepared. Reactions of **3b** and **3e** with acetylenes are also described.

Activation of carbon monoxide by coordination to transition metals has been actively investigated.[1] Fischer and his co-workers in their pioneering works accomplished synthesis of so-called Fischer-type carbene-metal complexes by the reaction of carbon monoxide coordinated to transition metals of group 6 and 7 with nucleophiles followed by alkylation.[2,3] Recently a new entry to a synthesis of Fischer-type carbene complexes has been developed, which is based on the reaction of early transition metal or actinoid metal complexes such as (1,3-diene)zirconocene, (η^2-aryne)zirconocene, (dinitrogen)zirconocene, and so on with a variety of metal carbonyls to form carbene-metal complexes.[4,5] We have found that titanocene-ethylene complex **1** reacts readily with metal carbonyl complexes of group 6 and 7 to afford new cyclic titanoxycarbene-metal carbonyl complexes and revealed their characteristic features in molecular structures and chemical properties.[6]

Results and Discussion

Preparation of Cyclic Titanoxycarbene-Metal Carbonyl Complexes 3. The reaction of titanocene-ethylene complex **1** with decacarbonyldirhenium (**2b**) in toluene-d_8 was monitored by ^{1}H NMR measurement. Above −30 °C, resonances due to complex **1** disappeared slowly and a new set of two triplets assignable to complex **3b** appeared reaching to 84% yield. Above −10 °C, however, amount of **3b** decreased gradually and ethylene was formed, which indicates that the product **3b** starts to decompose even at −10 °C. Therefore, a mixture of complexes **1** and **2b** in toluene was stirred at −20 °C for 48 h and then the reaction mixture was diluted with hexane to afford after cooling to −80 °C titanoxycarbene-dirhenium carbonyl complex **3b** as orange red prisms in 57% yield (Eq. 1). The isolated **3b** is relatively stable and decomposes at 95—99 °C. Similar reaction of **1** with decacarbonyldimanganese (**2a**) gave complex **3a** in 30% isolation yield. This approach can also be applied to the reaction of **1** with metal carbonyls of group 6 transition metals. Thus, complexes **3c** and **3e** were isolated as orange solids in 26% and 34% yields, respectively. The molybdenum derivative **3d** was also formed

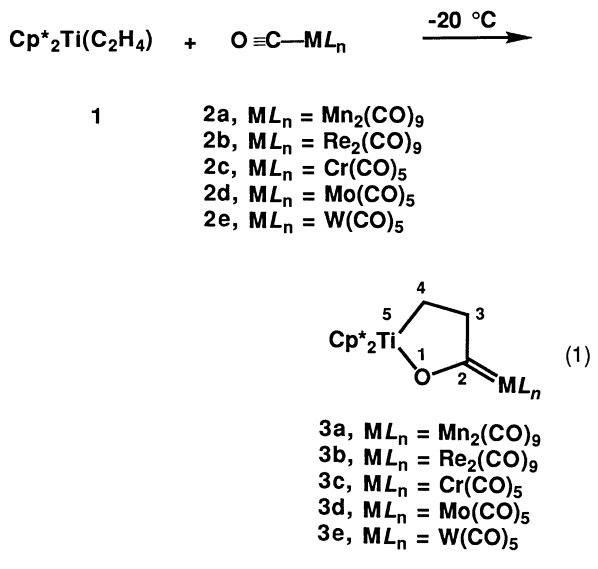

Table 1. ^{1}H and ^{13}C NMR Spectral Data of Complexes **3**[a]

Complex		Chemical shift[b]/ppm				
		C (3)	C (4)	C (carbene)	Cp*	CO
3a	^{1}H	4.20	1.53 (6.8)		1.74	
	^{13}C	80.34 (124)	65.99 (130)	333.97	11.93 (127)	226.45 225.60 218.58
3b	^{1}H	4.02	1.60 (7.1)		1.78	
	^{13}C	85.02 (124)	66.35 (128)	289.76	11.96 (127)	200.95 199.04
3c	^{1}H	4.35	1.62 (6.9)		1.78	
	^{13}C	81.01 (124)	67.44 (129)	349.79	11.99 (127)	220.19 225.2 (broad)
3d	^{1}H	4.20	1.65 (7.0)		1.78	
	^{13}C	82.10 (122)	67.87 (129)	344.94	12.09 (128)	209.30
3e	^{1}H	4.10	1.60 (7.1)		1.78	
	^{13}C	83.59 (124)	67.56 (127)	328.36	12.02 (127)	201.07[c] 205.2 (broad)

a) All spectra were recorded in toluene-d_8 at −30 °C using solvent absorptions at δ=2.31 (^{1}H) and δ=137.70 (^{13}C) as internal standards. b) Coupling constants are given in parentheses (Hz). c) $J_{C\text{-}W}$=125 Hz.

from **1** and $Mo(CO)_6$, but it was too unstable to be isolated in pure form and characterized based solely on NMR spectra. Similar tendency in stability has been observed for the carbene complexes of the type $(CO)_5M{=}C(OCH_3)R$ (M=Cr, Mo, W; R=CH_3 and C_6H_5).[3]

The structures of titanoxycarbene-metal carbonyl complexes **3a**—**e** were assigned based mainly on the elemental analyses and spectroscopic data. The NMR spectral data of complexes **3** are summarized in Table 1. The absorptions due to C(3) methylene protons (δ= 4.02—4.35) appear at a little lower field than those due to methylene protons α to the carbenic carbon of Fischer-type carbene complexes [e.g. δ=3.22 for $(CO)_5W{=}C(OCH_3)CH_2CH_3$].[7] $^{13}C\{^{1}H\}$ NMR spectra exhibited absorptions due to carbenic carbons in the range of 290—350 ppm which are comparable with the chemical shift values of carbenic carbons reported for Fischer-type carbene complexes.[8] The chemical shift values of C(4) methylene protons and ^{13}C resonances due to C(4) are also comparable with those of titanacyclopentanes.[9-11]

The trans structure of dinuclear metal carbonyl moieties in **3a** and **3b** were determined based on $^{13}C\{^{1}H\}$ NMR spectra, which exhibited three absorptions for **3a** and two for **3b** due to coordinated carbon monoxide. In the ordinary syntheses of Fischer-type carbene complexes of dinuclear group 7 metal carbonyls, nucleophiles are known to attack initially equatorial CO which has lower electron density than axial ones, while, in the present reaction, electrophilic titanium atom reacts with axial CO having a higher electron density. Moreover, in the trans complexes **3a** and **3b**, the steric interaction between CO on rhenium atom and Cp* ligands on titanium is minimized.

When NMR spectra of complexes **3a**—**c** and **3e** were monitored over a temperature range of 0—30 °C, quantitative formations of ethylene and the corresponding metal carbonyls were observed. The fate of titanocence moiety has not been revealed. Clear first-order disappearance of these complexes was observed. Plots of these observed first-order rate constants were made as shown in Fig. 1 for complex **3a**, which gave activated parameters summarized in Table 2. The results show that the complexes **3a** and **3b** derived from **1** and group 7 metal carbonyls are more stable than those obtained from group 6 transition metal carbonyls. The C(2)–C(3) bond of 1-oxa-5-titanacyclopentane moiety in complex **3** was selectively cleaved during the thermolysis. This corresponds to the reverse reaction of the formation of **3** [Eq. 1], where a concerted pericyclic $[2_s+2_s]$-type

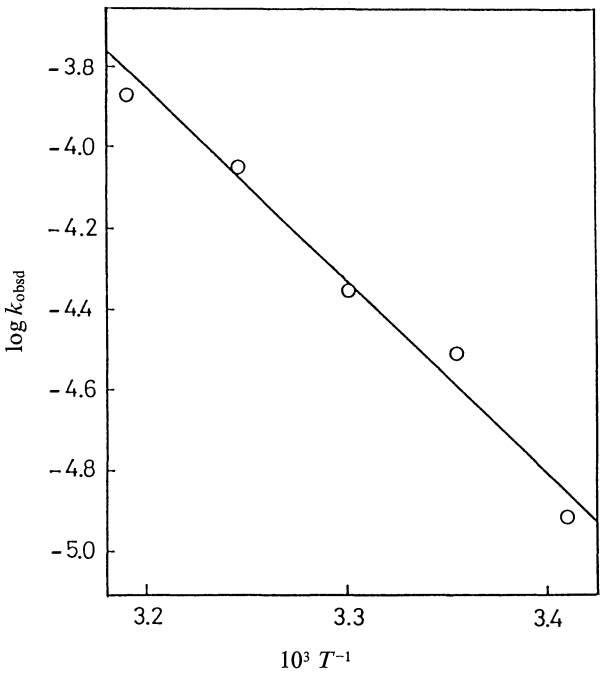

Fig. 1. An Arrhenius plot for the thermal decomposition of **3a**.

Table 2. Activation Parameters (at 303 K) of Thermolysis of Complexes 3

Complex	$\Delta G^{\ddagger}$	$\Delta H^{\ddagger}$	$\Delta S^{\ddagger}$	$t_{1/2}$
	kcal	kcal	cal K^{-1} mol^{-1}	min
3a	23.8	20.8	−5.0	116 (30°C)
3b	24.2	11.6	−21.1	223 (30°C)
3c	21.2	16.8	−8.2	73 (0°C)
3e	23.4	18.5	−8.2	64 (30°C)

reaction via a transition state **4** is proposed.[12] Such fission of C(carbenic)–C bond is rarely observed for conventional Fischer-type carbene complexes,[13] while this fission is rather common in the thermolysis of 5-membered titanacycles such as titanacyclopentane **5**[9-12] and 1-oxa-5-titanacyclopentane complexes **6**.[14] This shows that the complexes **3** have thermal behaviors characteristic of five-membered metallacycles, rather than those of Fischer-type carbene complexes.

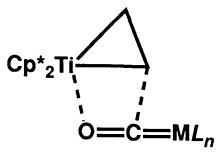

4

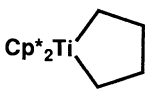

5

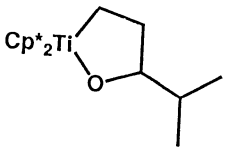

6

Crystal Structure of Titanoxycarbene-Dirhenium Complex 3b. For further elucidation of the molecular structure of **3**, a single crystal X-ray diffraction study has been done for the most stable complex **3b**. Selected data on the molecular geometry are listed in Table 3. The molecular structure of **3b** with numbering scheme is shown in Fig. 2. Two molecules of **3b–I** and **3b–II** with

Table 3. Selected Bond Distances (Å) and Angles (Degree) of Complex **3b–I** and **3b–II**[a]

	3b–I	**3b–II**
	Bond distances	
Re1–Re2	3.057 (2)	3.054 (2)
Re1–C2	2.12 (3)	2.12 (2)
Ti–O	2.02 (2)	2.04 (2)
Ti–C4	2.25 (2)	2.26 (2)
O–C2	1.26 (3)	1.28 (3)
C2–C3	1.57 (4)	1.56 (4)
C3–C4	1.52 (4)	1.60 (3)
	Angles	
Re2–Re1–C2	176.7 (7)	176.5 (7)
O–Ti–C4	79.1 (9)	79.5 (8)
Ti–O–C2	121.6 (18)	120.4 (17)
Re1–C2–O	125.2 (22)	124.1 (21)
O–C2–C3	116.6 (22)	119.1 (21)
Re1–C2–C3	118.2 (16)	116.7 (16)
C2–C3–C4	110.1 (21)	107.4 (20)
Ti–C4–C3	106.0 (18)	105.9 (16)

a) Two molecules **3b–I** and **3b–II** are crystallographically independent and make an enantiomorphic pair.

different conformations of the metallacyclic five-membered ring are crystallographically independent and make an enantiomorphic pair. A stereoview of crystal packing of **3b–I** and **3b–II** is shown in Fig. 3.

The Ti–C(4) bond distances, 2.25(2) Å for molecule **I** and 2.26(2) Å for molecule **II**, are normal as a single covalent Ti–C bond. The C(2)–O bond distances of 1.26(3) Å for molecule **I** and 1.28(3) Å for molecule **II** are considerably shorter than that of usual covalent C–O bond (1.43 Å), while Ti–O bond distances of 2.02(3) Å for **I** and 2.04(2) Å for **II** are much longer than those of

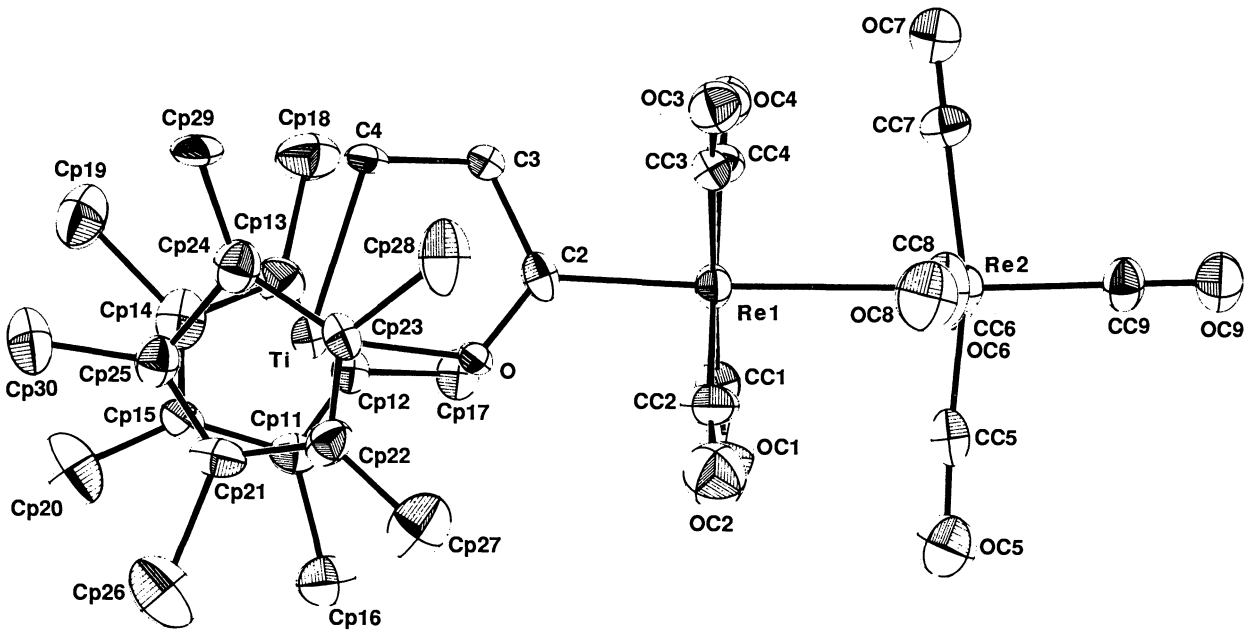

Fig. 2. ORTEP drawing of a molecule of complex **3b–I** showing the atom-labeling scheme. Ellipsoids represent 30% probability. Hydrogen atoms are omitted.

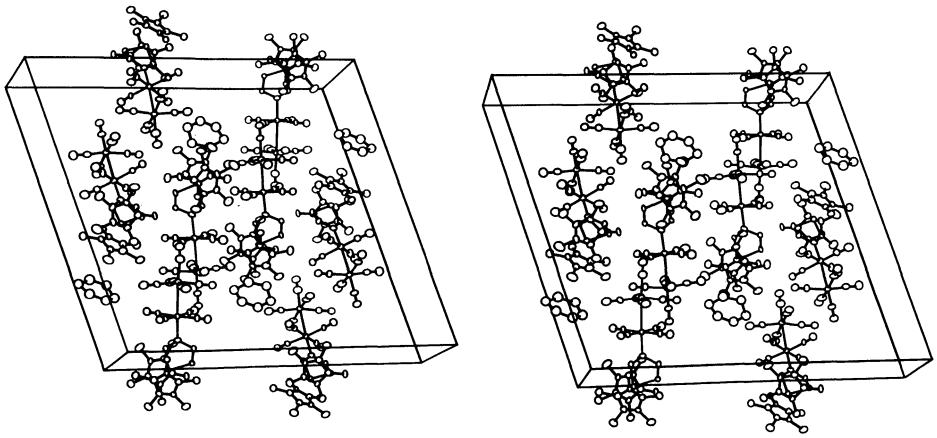

Fig. 3. Stereoview of crystal packing of complex **3b**. Two molecules are crystallographically independent and make an enantiomorphic pair. Methyl carbon of crystalline solvent toluene was not located.

$Cp_2TiCl(OC_2H_5)$ [1.855(2) Å][15] and complex **6** [1.866 (3) Å].[14a] These results contrast with the fact that Ti–O bond of titanacyclopentanes such as **6** has a double bond character due to the considerable degree of donation from the pπ orbital of oxygen to the laterally-directed dπ acceptor orbital of titanocene. The C(2)–C(3) bond distances, 1.57(4) Å for **I** and 1.56(4) Å for **II**, are almost comparable with 1.493(11) Å reported for *cis*-$Mn(CO)_5$-$Re(CO)_4$=$C(OCH_3)CH_3$.[16] Thus, complex **3b** has a characteristic Fischer-type carbene structure[17] and there is an important contribution of a dipolar resonance structure **7**. Such contribution of dipolar resonance structures has been already pointed out for many zirconoxy-carbene complexes.[5]

Titanium atom in complex **3b** has a monomeric pseudo tetrahedral configuration defined by two η^5-C_5Me_5, methylene carbon, and an oxygen ligands. The angles C(4)–Ti–O, 79.1(9)° for molecule **I** and 79.5(8)° for molecule **II**, are comparable with that of **6** [80.9(2)°].[14a]

Angles of C(2)–Re(1)–Re(2) for **I** and **II** are 176.7(7)° and 176.5(7)°, respectively. The carbenic ligand is *trans* to Re–Re bond which contrasts with the complexes derived from $Re_2(CO)_{10}$ by conventional Fischer method where the carbene is *cis* to the Re–Re bond as is seen in complex **8**.[18] The Re(1)–C(2) bond distances of 2.12(3) and 2.12(2) Å for molecules **I** and **II**, respectively, are comparable with the reported values of 2.094(7) Å for *cis*-$Mn(CO)_5Re(CO)_4$=$C(OCH_3)CH_3$[16] and 2.09(2) Å for **8**,[18b] but longer than that of *trans* C(carbenic)–Re bond of 1.85(3) Å.[18b] Carbonyl groups on one rhenium atom occupy the staggered position relative to those on the another rhenium metal. Similar staggered geometry is commonly observed for the complexes such as $Re_2(CO)_{10}$[19] and $Re_2(CO)_9(CNCMe_3)$.[20] The Re–Re bond distances of 3.057(2) Å for **I** and 3.054(2) Å for **II** are comparable with those of carbene complexes such as **8** [3.052(1) Å] and *cis*-$Re(CO)_5Re(CO)_4$=$C(SiPh_3)(OEt)$ [3.050(3) Å],[18b] but are longer by 0.013—0.016 Å than that of $Re_2(CO)_{10}$ [3.041(1) Å].[19]

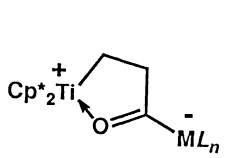

7

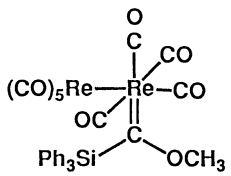

8

Reactions of 3b and 3e with Alkynes. Reaction of complex **3b** with diphenylacetylene was monitored by NMR spectroscopy. The addition of diphenylacetylene to a solution of **3b** in toluene-d_8 at room temperature induced rapid change in color from orange to deep red. ^1H and $^{13}C\{^1H\}$ NMR spectra indicated the formation of ethylene, $Re_2(CO)_{10}$ (**2b**), and titanocene–diphenylacetylene complex **10**[9b] (Scheme 1). Reaction of **3e** with diphenylacetylene afforded the same complex **10**, ethylene, and $W(CO)_6$. On the other hand, reaction of **3b** with 2-butyne afforded $Re_2(CO)_{10}$ and titanacyclopentene complex **11**.[9b] By contrast, reaction of **3e** with 2-butyne afforded no metallacyclic compounds, but ethylene, $W(CO)_6$, and unidentified titanocene species as detected by NMR. The complex **9** in which carbon monoxide of metal carbonyl coordinates to titanium may be an intermediate. In fact, similar complexes, $Cp^*_2Ti(CH_3)OCW(CO)_2Cp$,[21a] $Cp_2Ti(THF)OCMo(CO)_2Cp$,[21b] $Cp_2Zr(\eta^2\text{-}COCH_3)OCMo(CO)_2Cp$,[21c,21d] and $Cp^*_2Yb(THF)OCCo(CO)_3$[21e] have been prepared and characterized. No products arising from the reaction of carbene moiety and alkynes have been detected.

Reaction of 3 with Carbon Monoxide. Complex **3b**

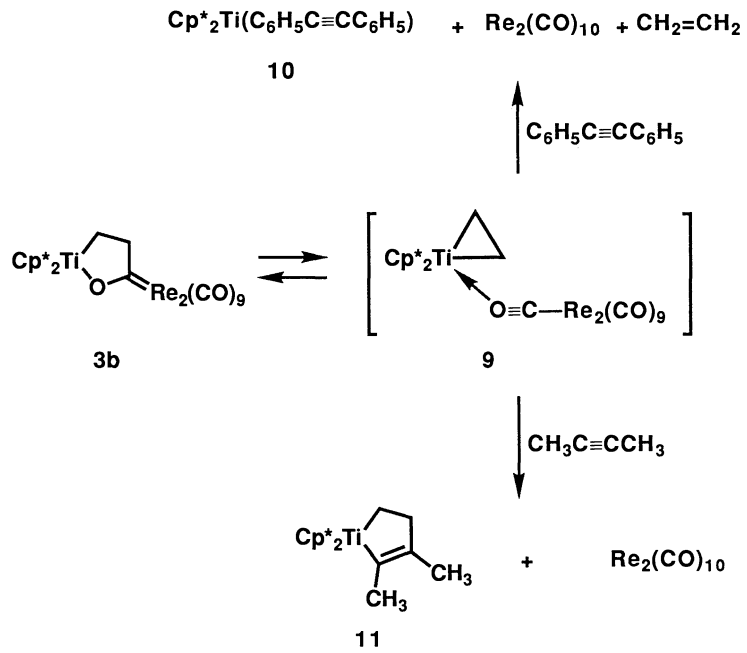

Scheme 1.

was allowed to react with atmospheric pressure of CO in a sealed NMR tube, and the reaction was monitored by ^{1}H NMR spectroscopy, showing that the carbonylation reaction was completed in a few minutes at −30 °C. Absorptions due to **3b** were rapidly replaced by those due to acyltitanium complex **12b**, which indicates that the yield is quantitative. On allowing the solution to warm up to room temperature, however, complex **12b** decomposed gradually to give ethylene, $Re_2(CO)_{10}$, and unidentified titanocene species, the same product obtained by the thermal reaction of **3b**. Interestingly when the CO was replaced by argon, complex **12b** liberated CO to give **3b**. Similar decarbonylation has been found in the reaction of dialkyl derivatives of zirconocene and hafnocene, but not reported for titanium analogues.[22] The carbonylations of other titanoxycarbene complexes **3a**, **3c**, and **3e** afforded the corresponding acyltitanium complexes **12a**, **12c**, and **12e** in quantitative yields, though they are too unstable to be isolated. These results contrast with the reported fact that 1-oxa-5-oxo-6-titanacyclohexanes, structurally related complexes to **12**, are thermally stable.[14a] For stabilization of cyclic η^1-acyltitanium(IV) complexes, π-donation from the p_π orbital of O(1) to the acceptor $1a_1$ orbital of titanocene is considered to be important. As can be easily deduced from the molecular structure of carbene complex **3** determined by X-ray analysis, such π-donation from O(1) will not be significant for complex **12** due to the presence of electron-accepting carbene moiety adjacent to the O(1) atom.

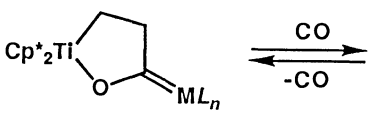

3

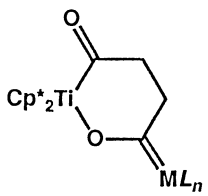

(2)

12a, $ML_n = Mn_2(CO)_9$
12b, $ML_n = Re_2(CO)_9$
12c, $ML_n = Cr(CO)_5$
12e, $ML_n = W(CO)_5$

The structures of **12a—e** were determined on the basis of spectral data. The ^{13}C NMR resonances due to acyl carbons were observed around 294 ppm (Table 4) which are comparable with those of η^1-acyltitanium complexes $Cp^*_2\overline{TiOCH(R)CH_2CH_2CO}$ (**13**).[14a] The IR spectrum of **12b** exhibited an absorption at 1600 cm^{-1} which is consistent with acyltitanium structure. When ^{13}C enriched CO was allowed to react with complexes **3b** and **3e**, the products exhibited signals with ^{13}C–^{13}C coupling constants of 9.2 and 7.3 Hz for $J_{CO\text{-}C(4)}$, respectively. These values contrast with those of acyl complexes such as **14** and **15** which showed coupling constants of 19 Hz[23] and 28 Hz,[24] respectively, and comparable with the values 4.9 Hz and 11.9 Hz for **13**[14a] and titanacyclopentanone, $Cp_2\overline{TiCMe=CMeCH_2C(=O)}$,[25] respectively.

Table 4. NMR Spectral Data of Carbonylated Complexes

Complex	Nucleus	Chemical shift[a,b]/ppm					
		C (4)	C (3)	C (2)	Cp*	Ti-acyl	M (CO)
12a	^{1}H	1.57	3.22 (6.2)		1.73		
	^{13}C	44.07 (127)	58.55 (129)	329.66	12.30 (127)	293.70	225.96 225.4 (broad)
12b	^{1}H	1.61	3.07 (6.4)		1.74		
	^{13}C	44.23 (127)	64.04 (128)	283.32	12.36 (127)	293.91	201.29 198.3 (broad)
12c	^{1}H	1.47	3.32 (6.4)		1.75		
	^{13}C	42.59 (128)	58.25 (127)	343.41	12.33 (127)	294.19	224.02 219.34
12e	^{1}H	1.44	3.14 (6.4)		1.74		
	^{13}C	42.37 (126)	61.19 (127)	320.32	12.39 (128)	294.37	204.38 200.68[c]

a) Measured in toluene-d_8 at −30 °C under CO atmosphere. b) Coupling constants are given in parentheses (Hz). c) $J_{C\text{-}W}$=129 Hz.

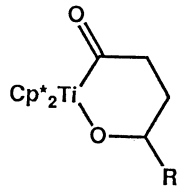

13

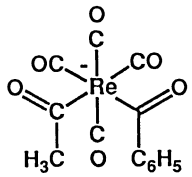

14

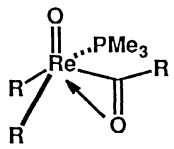

15 R = $CH_2Si(CH_3)_3$

Reaction of 3b and 3e with *t*-Butyl Isocyanide. Reaction of titanoxycarbene–dirhenium carbonyl complex **3b** with excess *t*-butyl isocyanide completed in 1 h at −15 °C in toluene to give a 1:1 mixture of **16** and **17** in 81% yield. Complex **17** crystallized as yellow plates at −20 °C. When the solution of **17** in toluene-d_8 was allowed to warm to 20 °C, the complex gradually decomposed and formations of ethylene, free *t*-butyl isocyanide, and unidentified species with titanocene moiety were detected by NMR spectroscopy. The first order disappearance of **17** was observed by ^{1}H NMR spectroscopy to give $\Delta G^{\neq}$ value at 30 °C of 25 kcal mol^{-1}.

The spectroscopic data of **17** are consistent with the structure assigned. ^{1}H NMR spectrum of **17** consists of two singlets at δ=1.50 and 1.80, indicating the presence of

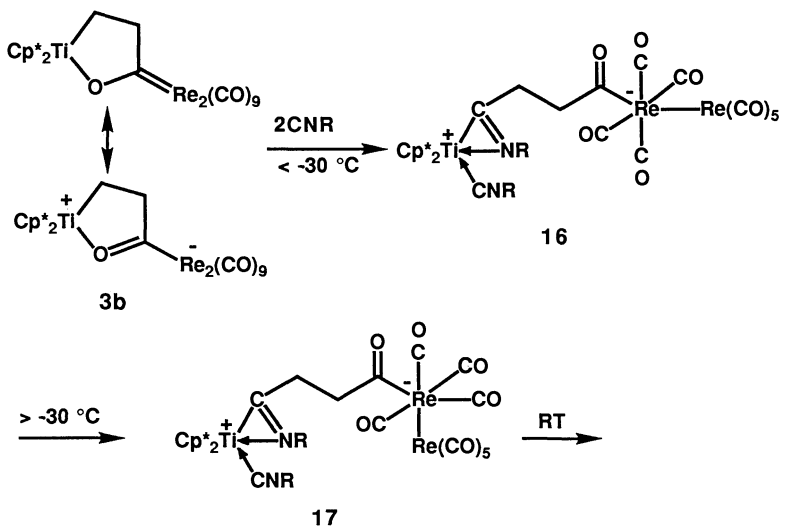

$CH_2{=}CH_2$ + $Re_2(CO)_9L$

R = $C(CH_3)_3$
L = CO or $CNC(CH_3)_3$

Scheme 2.

two magnetically nonequivalent *t*-butyl groups. Four kinds of carbon monoxide coordinated to rhenium were displayed by $^{13}C\{^1H\}$ NMR spectrum which supported the *cis* geometry between acyl group and dirhenium moiety. The low $\nu_{C=N}$ of 1586 cm^{-1} suggested the presence of iminoacyl moiety and the other $\nu_{C\equiv N}$ of 2162 cm^{-1} is due to an isocyanide coordinated to titanium. A weak absorption at 1650 cm^{-1} was tentatively assigned to acyl-rhenium moiety. The molecular geometry of **17** has been determined by a single-crystal X-ray analysis (vide infra).

When the above reaction was carried out at −55 °C for 4 h and then the liquid phase was decanted below −30 °C, another 1:2 complex **16** could be obtained as yellow crystals in 77% yield. ^1H NMR spectrum of the complex resembles with that of **17** which indicates that the complex is stereoisomer of **17**. $^{13}C\{^1H\}$ NMR spectrum is consistent with the structure **16** in which acyl ligand is trans to the Re–Re bond.

The compound **16** in THF-d_8 gradually isomerized to **17** even at −10 °C, as monitored by ^1H NMR spectroscopy. The half life of **17** in THF at 0 °C is 41 min. This indicates that the formation of *cis*-product **17** proceeds sequentially by way of the *trans*-isomer **16**. Although the driving force of the isomerization from **16** to **17** is not clear at present, *cis* structures are common to anionic acyl-$M(CO)_4M(CO)_5$ species (M=Mn and Re).[16]

Reaction of **3e** with *t*-butyl isocyanide gave the analogous tungsten derivative **18**, whose structural determination is based on spectroscopic data. Therefore, these reactions can be regarded as general for the cyclic titanoxycarbene–metal carbonyl complexes of type **3**. In spite of the strong oxophilic nature of the central titanium atom, dissociation of oxygen ligand from titanium occurred. This may be attributed to the important contribution from the dipolar resonance structure **7** in the starting complex **3**.

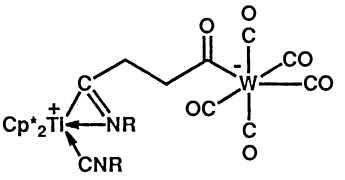

18 R = $C(CH_3)_3$

Molecular Structure of Zwitterionic Complex 17. In order to get more insights into the molecular structure of **17**, an X-ray crystal structure determination was performed. Figure 4 shows an ORTEP drawing of the molecule with the atom numbering scheme. Selected bond distances and angles are listed in Table 5. No unusually short intermolecular contacts are observed. The Ti–C(6) and Ti–N(2) bond distances are 2.14(3) and 2.17(2) Å, respectively. The bond distances 2.17(2) Å for Ti–C(1) and 1.14(3) Å for C(1)–N(1) in complex **17** are comparable with those of η^2-iminoacyl complexes of Y,[26] U,[27] Ti,[28-30] Zr,[30,31] and Mo.[32] Contribution from the carbene resonance form **19** can be considered to

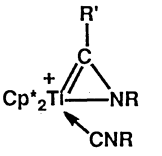

19 R = $C(CH_3)_3$

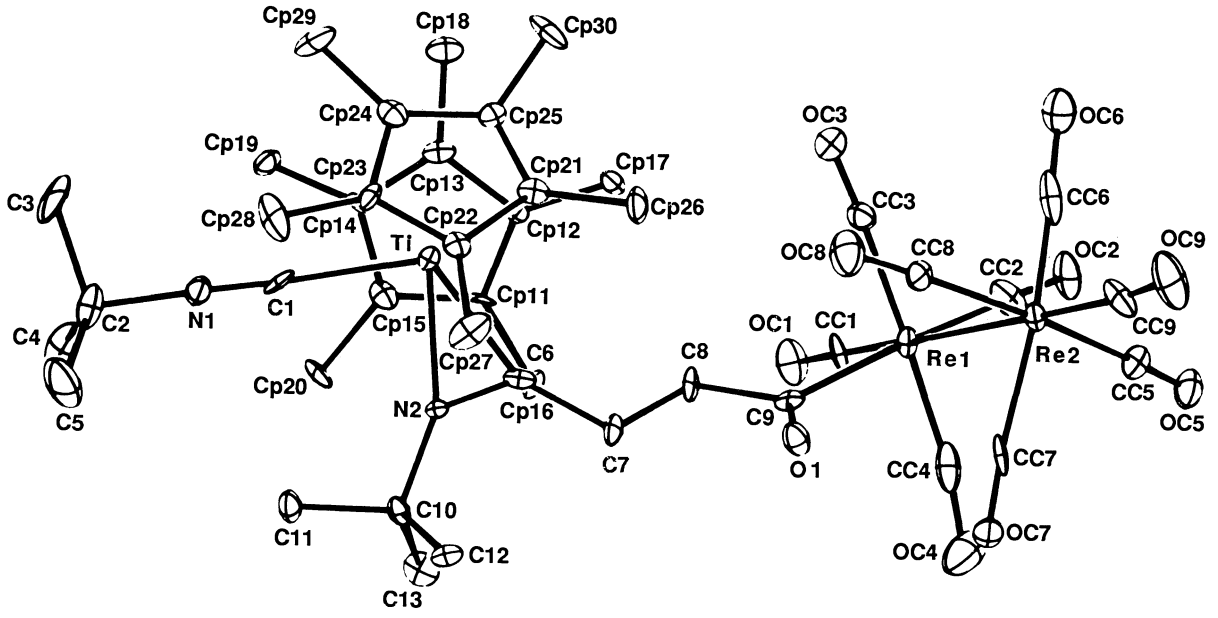

Fig. 4. ORTEP drawing of a molecule of complex **17** with the numbering scheme. Ellipsoids represent 30% probability. Hydrogen atoms are omitted.

Table 5. Selected Bond Distances (Å) and Angles (Degree) of Complex **17**

	Bond distances		
Re1–Re2	3.060 (2)	Re1–C9	2.27 (2)
Ti–N2	2.17 (2)	Ti–C1	2.17 (2)
Ti–C6	2.14 (3)		
O1–C9	1.20 (3)		
N1–C1	1.16 (3)	N1–C2	1.51 (3)
N2–C6	1.26 (3)	N2–C10	1.56 (3)
C2–C3	1.55 (5)	C2–C4	1.56 (5)
C2–C5	1.43 (5)	C6–C7	1.51 (3)
C7–C8	1.52 (3)	C8–C9	1.57 (3)
C10–C11	1.54 (3)	C10–C12	1.51 (4)
C10–C13	1.49 (4)		
	Angles		
Re2–Re1–C9	91.7 (6)	N2–Ti–C1	83.6 (9)
N2–Ti–C6	33.9 (7)	C1–Ti–C6	117.4 (9)
C1–N1–C2	177.0 (26)	Ti–N2–C6	72.1 (14)
Ti–N2–C10	157.4 (14)	C6–N2–C10	130.5 (20)
Ti–C1–N1	176.8 (23)	N1–C2–C3	102.3 (24)
N1–C2–C4	106.0 (22)	N1–C2–C5	109.9 (26)
C3–C2–C4	108.1 (26)	C3–C2–C5	118.2 (30)
C4–C2–C5	111.4 (31)	Ti–C6–N2	74.1 (15)
Ti–C6–C7	155.0 (16)	N2–C6–C7	130.8 (22)
C6–C7–C8	116.0 (21)	C7–C8–C9	113.2 (21)
Re1–C9–O1	127.4 (17)	Re1–C9–C8	113.3 (16)
O1–C9–C8	119.4 (20)	N2–C10–C11	107.1 (20)
N2–C10–C12	111.2 (19)	N2–C10–C13	107.8 (19)
C11–C10–C12	111.0 (20)	C11–C10–C13	109.1 (22)
C12–C10–C13	110.5 (24)		

be little, if any. Titanium atom has only three anionic ligands, but the coordination of an isocyanide on titanium brings about a closed 18-electron valence shell, and this might be the reason for the observed stability of **17**. Thus, intramolecular charge separation occurred upon reaction with isocyanides to afford a zwitterionic complex, where positive charge is on the titanium moiety, while negative charge is on the rhenium carbonyl residue. Such charge separation within a molecule has been reported recently.[13]

The acyl ligand in **17** is *cis* to Re–Re bond, which contrasts with the fact that in the starting complex **3b** the carbenic carbon is *trans* to Re–Re bond. The Re(1)–C(9)–O(1) bond angle of 127(2)° shows that the acyl ligand has η^1 coordination mode. To our knowledge, the present study provides the first structural data for anionic acyldirhenium carbonyl complex determined by a single-crystal X-ray analysis.

Conclusion

A direct synthesis of new Fischer-type carbene complexes has been developed by the reaction of titanocene–ethylene complex with various group 6 and 7 metal carbonyls and their molecular structures have been determined by spectroscopic techniques and X-ray crystallography. The structural characteristics of cyclic titanoxycarbene–metal carbonyl complexes **3** thus obtained have been shown to be reflected in their chemical properties. The modes of thermal reaction of **3** and of the reactions of **3** with CO are closely related to those of 1-oxa-5-titanacyclopentanes, though the carbonylation products **12** are much less stable than those derived from the latter complexes. Reactions of **3** with *t*-butyl isocyanide give rise to novel zwitterionic 1:2 adducts. These characteristic features of **3** could be attributed to an important contribution from the dipolar resonance structure **7**.

Experimental

General: All manipulations involving air- and moisture-sensitive organometallic compounds were carried out by the use of standard Schlenk techniques under argon atmosphere purified by passing through a hot column packed with BASF-Catalyst R3-11. All solvents were purified by distillation under argon after drying over calcium hydride or sodium benzophenone ketyl. All NMR spectra were recorded in toluene-d_8 at −30 °C using a Varian EM-390 (90 MHz) spectrometer or a JEOL GX400 (^{1}H, 400 MHz; ^{13}C, 100 MHz) spectrometer. Chemical shifts were determined using solvent absorption at δ=2.31 (^{1}H) and δ=137.70 (^{13}C) as internal standards. Other spectra were recorded by the use of the following instruments: IR, Hitachi 295; low and high resolution mass spectra, JEOL D300 (70 eV). Gas chromatographic (GLC) analyses were conducted on a Hitachi 263-30 equipped with a flame ionization detector. Elemental analyses were performed by the Wako Pure Chemical Ind. Ltd. All melting points were measured in sealed tubes and uncorrected. $Cp^*_2Ti(C_2H_4)$ was prepared according to the published procedure.[9a] The metal carbonyls **2a**—**e** were obtained from Strem Chem. Inc. *t*-Butyl isocyanide was obtained from Aldrich Chem. Co. 2-Butyne and diphenylacetylene were obtained from Tokyo Kasei Kogyo Co., Ltd. Carbon monoxide was obtained from Takachiho Chem. Ind. Co. ^{13}CO (99.3 atom %) was used as obtained from MDS Isotopes.

Titanoxycarbene-Dimanganese Complex 3a. To decacarbonyldimanganese (**2a**) (0.31 g, 0.80 mmol) and titanocene–ethylene complex **1** (0.28 g, 0.81 mmol) placed in a Schlenk tube at −50 °C was added toluene (25 mL) via a syringe. The mixture was stirred at −20 °C for a period of 120 h and the deep red solution was obtained. The liquid phase was separated from the residual manganese carbonyl, concentrated to 10 mL under reduced pressure at −30 °C, and to this hexane (15 mL) was layered. The solution was kept at −80 °C overnight to afford **3a** as orange red crystalline solid (0.18 g, 30% yield), mp 115—118 °C (decomp). ^{1}H and ^{13}C NMR data are listed in Table 1. IR (KBr) 2085 (vw), 2001 (sh), 1950 (vs), 1923 (vs) cm^{-1}. Mass spectrum (^{100}Mn^{48}Ti) *m*/*z* 391 (M^+ −345, base peak), 337 (M^+ −399), 318 (Cp^*_2Ti), 251 [$Mn_2(CO)_5$], 223 [$Mn_2(CO)_4$], 196 (M^+ −540), 167 [$Mn(CO)_4$]. Anal.Found: C, 52.06; H, 4.89%. Calcd for $C_{32}H_{34}O_{10}Mn_2Ti$: C, 52.20; H, 4.65%.

Titanoxycarbene-Dirhenium Complex 3b. To a solution of dirhenium decacarbonyl (**2b**) (0.52 g, 1.5 mmol) in toluene (10 mL) at −40 °C was added a solution of **1** (0.25 g, 0.38 mmol) in toluene (5 mL) via a syringe. The solution was stirred for 48 h at −20 °C until the color became deep red. The residual **2b** was separated by decantation, the solution was concentrated to 5 mL under reduced pressure in the temperature range of −30—−20 °C, and then hexane (15 mL) was layered. After

12 h at −80 °C, orange red crystals were isolated (0.41 g, 57% yield), mp 95—99 °C (decomp). IR (KBr) 2089 (w), 2011 (s), 1969 (vs), 1951 (vs), 1914 (vs) cm^{-1}. IR (toluene) 2091 (w), 2016 (m), 1985 (vs), 1951 (m), 1919 (m) cm^{-1}. Mass spectrum ($^{187}Re^{48}Ti$) m/z 654 [$Re_2(CO)_{10}$], 626 (M^+ −374), 596 [$Re_2(CO)_8$], 570 [$Re_2(CO)_7$, base peak], 542 [$Re_2(CO)_6$], 514 [$Re_2(CO)_5$], 337 (M^+ −663), 318 (Cp^*_2Ti), 299 [$Re(CO)_4$]. Anal. Found: C, 40.39; H, 3.74%. Calcd for $C_{32}H_{34}O_{10}Re_2Ti \cdot 1/2(C_7H_8)$: C, 40.80; H, 3.67%.

Titanoxycarbene–Chromium Complex 3c. To a solution of chromium hexacarbonyl (**2c**) (0.14 g, 0.64 mmol) in toluene (8 mL) cooled at −50 °C was added a solution of **1** (0.21 g, 0.61 mmol) in toluene (8 mL) via a syringe. After the mixture was stirred at −20 °C for a period of 120 h, the deep red solution was separated from the white solid of unreacted **2c**. Hexane (8 mL) was layered on the solution and the mixture was kept at −80 °C overnight to afford **3c** as deep red crystalline solid (0.09 g, 26% yield), mp 98—103 °C (decomp). IR (KBr) 2041 (vw), 1966 (sh), 1876 (vs) cm^{-1}. Mass spectrum ($^{52}Cr^{48}Ti$) m/z 337 (M^+ −229), 318 (Cp^*_2Ti), 220 [$Cr(CO)_6$, base peak]. Anal. Found: C, 59.76; H, 6.25%. Calcd for $C_{28}H_{34}O_3CrTi$: C, 59.37; H, 6.05%.

Titanoxycarbene–Molybdenum Complex 3d. To molybdenum hexacarbonyl (**2d**) (6.9 mg, 2.6×10^{-5} mol) and **1** (6.6 mg, 1.9×10^{-5} mol) placed in NMR tube (5ϕ) was added toluene-d_8 (0.5 mL) by trap-to-trap distillation and then the tube was sealed. ^1H and ^{13}C NMR data are summarized in Table 1, which showed the formation of titanoxycarbene–molybdenum complex **3d**. Attempted isolation of **3d** failed due to the thermal instability of the product even below −20 °C.

Titanoxycarbene–Tungsten Complex 3e. To a mixture of tungsten hexacarbonyl (**2e**) (0.31 g, 0.64 mmol) and complex **1** (0.22 g, 0.88 mmol) placed in a Schlenk tube was added toluene (15 mL) at −50 °C. The mixture was stirred at −20 °C for 90 h. To the deep red solution separated from the remaining white solid of tungsten hexacarbonyl was layered hexane (10 mL). The mixture was kept at −80 °C overnight and the product **3e** was obtained as deep orange crystalline solid (0.15 g, 34% yield), mp 106—110 °C (decomp). IR (KBr) 2051 (w), 1974 (m), 1904 (vs), 1887 (vs) cm^{-1}. IR (toluene) 2051 (vw), 1984 (vs), 1919 (s) cm^{-1}. Mass spectrum ($^{184}W^{48}Ti$) m/z 352 [$W(CO)_6$], 318 (Cp^*_2Ti), 296 [$W(CO)_4$], 268 [$W(CO)_3$, base peak], 240 [$W(CO)_2$], 212 [W(CO)]. Anal. Found: C, 47.84; H, 5.09%. Calcd for $C_{28}H_{34}O_6TiW$: C, 48.16; H, 4.91%.

Thermal Decomposition of Titanoxycarbene–Metal Complexes 3a—e. A solution of complex **3b** (10 mg) in toluene-d_8 (0.5 mL) was sealed in an NMR tube under argon. The disappearance of complex **3b** was measured at specified constant temperatures. The half lives (min) of **3a**, **3b**, **3c**, and **6e** in toluene-d_8 are 116 (30 °C), 223 (30 °C), 73 (0 °C), and 64 (30 °C), respectively. The thermodynamic parameters thus obtained are listed in Table 2.

Reaction of 3b or 3e with Diphenylacetylene. A solution of complex **3b** (15 mg, 1.5×10^{-2} mmol) and diphenylacetylene (2 equiv) in toluene-d_8 (0.5 mL) was placed in an NMR tube at room temperature. Color of the solution darkened. The formation of **10** was confirmed by the comparison of ^1H and ^{13}C NMR spectral data with those reported.[9b] Reaction of **3e** with diphenylacetylene in a similar manner gave the same complex **10** in quantitative yield.

Reaction of 3b or 3e with 2-Butyne. A solution of complex **3b** (10 mg, 1.0×10^{-5} mol) and 2-butyne (excess) in toluene-d_8 (0.5 mL) was placed in an NMR tube. Color of the solution gradually darkened. The formation of **11** was confirmed by the comparison of ^1H and ^{13}C NMR spectral data with the reported ones.[9b] Similar treatment of **3e** with excess 2-butyne did not give **11**, but afforded ethylene, tungsten hexacarbonyl (**2e**), and unidentified species containing titanocene residue.

Reaction of 3a—e with Carbon Monoxide. To complex **3b** (0.06 g, 0.06 mmol) placed in an NMR tube (10ϕ) was added toluene-d_8 (2.5 mL) by the trap-to-trap distillation technique. Atmospheric pressure of carbon monoxide was introduced into the tube and the tube was sealed. A yellow-green solution was obtained after a few min at −50 °C. ^1H and ^{13}C NMR data were taken which are listed in Table 4.

Reactions of **3a**, **3c**, and **3e** with carbon monoxide were carried out in similar manners as described above and the ^1H and ^{13}C NMR spectral data obtained are summarized in Table 4.

Reaction of 3b with *t*-Butyl Isocyanide. To a solution of **3b** (47 mg, 0.047 mmol) in toluene (12 mL) at −35 °C was added *t*-butyl isocyanide (0.05 μL, 0.44 mmol). The reaction mixture was slowly warmed up to −15 °C and then stirred at this temperature for 1 h in which pale yellow crystalline solid (43 mg, 81% yield) deposited. The product is a 1:1 mixture of **16** and **17**, from which **17** was separated by recrystallization of the product from toluene at −20 °C, mp 119—122 °C (decomp). ^1H NMR (22 °C, THF-d_8) δ=1.50 (s, CMe_3), 1.80 (s, CMe_3), 1.87 (s, $2C_5Me_5$), 3.29—3.33 (m) and 3.44—3.48 (m) [C(7)H_2 and C(8)H_2]. ^{13}C NMR (−30 °C, THF-d_8) δ=13.34 (J_{C-H} 125 Hz, C_5Me_5), 30.42 (129 Hz, CMe_3), 31.15 [127 Hz, C(7) or C(8)], 31.97 (127 Hz, CMe_3), 60.29 (CMe_3), 63.84 (CMe_3), 118.36 (C_5Me_5), 189.81, 195.76, 197.49, 200.22 (rel intensities 1.0:2.4:2.7:4.9, CO), 205.45 ($CNCMe_3$), 226.91 (C=N), 250.70 (C=O). When ^{13}C NMR was measured in CD_2Cl_2 (the absorption at δ=53.60 due to the solvent was used as internal standard), signals due to C(7) and C(8) were observed at δ=29.59 (J_{C-H} 127 Hz) and 66.16 (127 Hz). IR (KBr) 2162 (m, CN), 2084 (m), 2008 (s), 1973 (vs), 1955 (sh), 1932 (s), 1918 (s), 1876 (s) (CO), 1650 (m, acyl), 1586 (m, C=N) cm^{-1}. Anal. Found: C, 43.41; H, 4.78; N, 2.50%. Calcd for $C_{42}H_{52}N_2O_{10}Re_2Ti$: C, 43.29; H, 4.50; N, 2.40%.

Reaction of 3b with *t*-Butyl Isocyanide at Low Temperature. To a solution of **3b** (40 mg, 0.040 mmol) in toluene (8 mL) at −55 °C was added *t*-butyl isocyanide (0.05 μL, 0.44 mmol). The reaction mixture was stirred at this temperature for a period of 4 h. The pale yellow crystalline solid was isolated by decantation to give complex **16** (36 mg, 77% yield), mp 124—126 °C (decomp). NMR measurement at −50 °C showed that **16** was the only product. ^1H NMR (−50 °C, THF-d_8) δ=1.54 (s, CMe_3), 1.81 (s, CMe_3), 1.89 (s, $2C_5Me_5$), 3.45—3.49 (m) and 3.58—3.60 (m) [C(7)H_2 and C(8)H_2]. ^{13}C NMR (−50 °C, THF-d_8) δ=13.34 (J_{C-H} 127 Hz, C_5Me_5), 30.34 (129 Hz, CMe_3), 31.84 (129 Hz, CMe_3), 31.24 (127 Hz) and 72.49 (129 Hz) [C(7) and C(8)], 60.30 (CMe_3), 63.80 (CMe_3), 118.29 (C_5Me_5), 191.43, 203.21, 203.65 (rel intensity 1.0:7.8:5.6, CO), 205.52 ($CNCMe_3$), 226.89 (C=N), 235.60 (C=O). IR (KBr) 2162 (w) (CN), 2085 (m), 1960 (vs), 1935 (sh), 1883 (s) (CO), 1648 (w) (tentatively assigned to acyl), 1565 (vw) (C=N) cm^{-1}. Mass spectrum ($^{187}Re^{48}Ti$) m/z 1165 (M^+ −1), 1138 (M^+ −CO), 895 (M^+ −271), 707, 652, 624, 596, 570 (base peak), 135 (Cp*). Anal. Found: C, 43.28; H, 4.52; N, 2.23%. Calcd for $C_{42}H_{52}N_2O_{10}Re_2Ti$: C, 43.29; H, 4.50; N, 2.40%.

Reaction of Titanoxycarbene–Tungsten Complex with *t*-

Butyl Isocyanide. To a solution of **3e** (78.5 mg, 0.11 mmol) in toluene (10 mL) at −60 °C was added *t*-butyl isocyanide (0.05 mL, 0.44 mmol). The mixture was stirred at −50 °C for 1.5 h, and to this was added hexane (10 mL). The yellow precipitates formed were separated by filtration to give **18** (66.7 mg, 70% yield), mp 66—70 °C (decomp). ^{1}H NMR (−50 °C, THF-d_8) δ=1.52 (s, CMe_3), 1.81 (s, CMe_3), 1.87 (s, $2C_5Me_5$), 3.35—3.39 (m) and 3.45—3.48 (m) [C(7)H_2 and C(8)H_2]. ^{13}C NMR (−50 °C, THF-d_8) δ=12.00 ($J_{C\text{-}H}$=127 Hz, C_5Me_5), 12.05 (J=127 Hz, C_5Me_5), 28.05 [J=126 Hz, C(7) or C(8)], 29.46 (J=129 Hz, CMe_3), 30.53 (J=126 Hz, CMe_3), 58.21 (CMe_3), 62.00 (CMe_3), 68.41 [J=127 Hz, C(7) or C(8)], 116.30 ($2C_5Me_5$), 191.34 (CO, $J_{C\text{-}W}$=122 Hz), 202.95 (CO, $J_{C\text{-}W}$= 129 Hz), 207.90 ($CNCM_3$), 224.78 (C=N), 274.58 (C(9), $J_{C\text{-}W}$= 88 Hz). IR (KBr) 2162 (m) (NC), 2041 (m), 1986 (w), 1947 (w), 1894 (s), 1874 (sh) (CO), 1642 (w) (tentatively assigned to acyl), 1553 (w) (C=N) cm^{-1}. Anal. Found: C, 51.26; H, 5.69; N, 2.98%. Calcd for $C_{38}H_{52}N_2O_6TiW$: C, 52.79; H, 6.06; N, 3.24%.

X-Ray Structure Determination of 3b. Deep red crystals were grown from a saturated toluene–hexane solution of **3b** at −20 °C overnight. Crystals were placed in thin-walled glass capillaries under argon at −20 °C and then sealed. Preliminary measurements of several crystals yielded rough cell dimensions and peak profiles. A suitable crystal with dimensions 0.21×0.32×0.53 mm was finally mounted on Rigaku AFC-5 diffractometer at −40 °C and centered in the beam. Below this temperature the crystal cracked. Automatic peak search and indexing procedure yielded the primitive cell. The pertinent datails of data collection and the final cell dimensions, which were obtained from a least-squares refinement of 2θ values of 50 independent reflections in the range of $20°<2\theta<30°$, are given in Table 6.

The 6715 unique raw intensity data with $|F_o|>3\sigma(F_o)$ were corrected for absorption, Lorentz and polarization effects. Three standard reflections measured after every 50 reflections showed no systematic variation in intensity. In unit cell, two independent molecules of titanoxycarbene–dirhenium complex are involved and make an enantiomorphic pair. The location of four rhenium and two titanium atoms were determined by the direct method (MULTAN 78 program). A series of standard least-squares refinement and Fourier synthesis revealed the remaining carbon and oxygen atoms as anisotropic temperature factors. Aromatic carbons of the solvated toluene were located also by the following difference Fourier synthesis, but the methyl carbon of toluene was not located, which might be attributed to the disorder. Final difference Fourier synthesis did not locate all hydrogen atoms. Molecular and crystal structures of **3b** are shown in Figs. 2 and 3. Atomic coordinates have been deposited.[6a)]

X-Ray Structure Determination of 17. Pale yellow crystals were grown from the saturated toluene–hexane solution of **17** at 4 °C overnight. Selected crystals were mounted in thin-walled glass capillaries under argon at −40 °C, and a suitable crystal (0.10×0.15×0.45 mm) was selected as for **17**. Data were collected at −120 °C by using Rigaku AFC-5 diffractometer. The data collection procedure and the cell parameters, obtained from a least-squares refinement of 2θ values of 50 independent

Table 6. Crystal Data and Data Collection Parameters of Complexes **3b** and **17**

	3b	**17**
Formula	$C_{32}H_{34}O_{10}Re_2Ti\cdot 1/2(C_7H_8)$	$C_{42}H_{52}O_{10}N_2Re_2Ti\cdot C_7H_8$
FW	1044.98	1257.32
Crystal system	Monoclinic	Monoclinic
Space group	$P2/a$	$P2_1/n$
a/Å	30.401(1)	14.964(2)
b/Å	9.251(1)	26.207(4)
c/Å	27.561(5)	14.719(3)
β/deg	105.73(1)	100.30(1)
V/Å^3	7460(2)	5679(2)
Z	8	4
D_{calcd}/g cm^{-3}	1.86	1.47
Crystal size	0.21×0.32×0.53	0.10×0.15×0.45
μ(Mo $K\alpha$)/cm^{-1}	71.14	46.88
Diffractometer	Rigaku AFC-5	Rigaku AFC-5
Monochrometer	Graphite	Graphite
Temperature/°C	−40	−120
Scan type	ω scan ($2.0<2\theta<20.0°$) θ–2θ scan ($20.0<2\theta$)	θ–2θ scan
bkgd/s	8	8
Scan range/deg	0.9+0.5tan θ	1.1+0.5tan θ
Scan speed/deg min^{-1}	3	3
stds	3 every 50 reflections	3 every 50 reflections
Data collected	$\pm h$, k, l	$\pm h$, k, l
$2\theta_{max}$/deg	50.0	55.0
No. of total reflections	9494	6520
No. of unique reflections	6715	4852
No. of variables	866	578
Weighting scheme	$w=[\sigma_c^2+(0.015\|F_o\|)^2]^{-1}$	$w=[\sigma_c^2+(0.015\|F_o\|)^2]^{-1}$
R	0.069	0.068
R_w	0.082	0.089
Goodness of fit	5.68	5.69

reflections in the range of $20° < 2\theta < 30°$, are listed in Table 6.

The 4852 intensity data with $|F_o| > 3\sigma(F_o)$ were converted to the structure factor amplitudes by correction for absorption, Lorentz and polarization effects. No correction for systematic variation in intensity is necessary. The structure of **17** was solved by Patterson method to locate two rhenium atoms in unit cell. A series of standard least-squares refinement and Fourier synthesis revealed the remaining titanium, oxygen, nitrogen, and carbon atoms as anisotropic temperature factors. Aromatic carbons of the solvated toluene were also located by the following difference Fourier synthesis. Final difference Fourier synthesis did not locate any hydrogen atoms. Molecular structure of **17** is shown in Fig. 4. Atomic coordinates have been deposited.[6b]

We gratefully acknowledge financial support from the Ministry of Education, Science and Culture for a grant in support of this work No. 01300011.

References

1) P. C. Ford, "Catalytic Activation of Carbon Monoxide," ACS Series 152 (1981).

2) K. H. Dötz, H. Fischer, P. Hofmann, F. R. Kreissl, U. Schubert, and K. Weiss, "Transition Metal Carbene Complexes," Verlag Chemie, Weinheim (1983).

3) E. O. Fischer and A. Maasböl, *Chem. Ber.*, **100**, 2445 (1967).

4) D. H. Berry, J. E. Bercaw, A. Jircitano, and K. B. Mertes, *J. Am. Chem. Soc.*, **104**, 4712 (1982).

5) a) G. Erker, U. Dorf, R. Benn, R. -D. Reinhardt, and J. L. Petersen, *J. Am. Chem. Soc.*, **106**, 7649 (1984). b) G. Erker, U. Dorf, R. Mynott, Y. -H. Tsay, and C. Krüger, *Angew. Chem., Int. Ed. Engl.*, **24**, 584 (1985). c) G. Erker, T. Mühlenbernd, R. Benn, and A. Rufinska, *Organometallics*, **5**, 402 (1986). d) G. Erker, R. Lecht, Y. -H. Tsay, and C. Krüger, *Chem. Ber.*, **120**, 1763 (1987). e) G. Erker and R. Lecht, *J. Organomet. Chem.*, **311**, 45 (1986). f) G. Erker, R. Lecht, J. Petersen, and H. Bönnemann, *Organometallics*, **6**, 1962 (1987). h) G. Erker, R. Lecht, C. Krüger, Y. -H. Tsay, and H. Bönnemann, *J. Organomet. Chem.*, **326**, C75 (1987). i) G. Erker, R. Lecht, R. Schlund, K. Angermund, and C. Krüger, *Angew. Chem., Int. Ed. Engl.*, **26**, 666 (1987). j) R. Beckaus and K. -H. Thiele, *J. Organomet. Chem.*, **368**, 315 (1989). k) G. Erker, U. Dorf, R. Lecht, M. T. Ashby, M. Aulbach, R. Schlund, C. Krüger, and R. Mynott, *Organometallics*, **8**, 2037 (1989). l) G. Erker, U. Hoffmann, R. Zwettler, P. Betz, and C. Krüger, *Angew. Chem., Int. Ed. Engl.*, **28**, 630 (1989). m) G. Erker, F. Sosna, J. L. Petersen, R. Benn, and H. Grondey, *Organometallics*, **9**, 2462 (1990).

6) a) K. Mashima, K. Jyodoi, A. Ohyoshi, and H. Takaya, *J. Chem. Soc., Chem. Commun.*, **1986**, 1145. b) K. Mashima, K. Jyodoi, A. Ohyoshi, and H. Takaya, *Organometallics*, **6**, 885 (1987).

7) C. P. Casey, R. A. Boggs, and R. L. Anderson, *J. Am. Chem. Soc.*, **94**, 8947 (1972).

8) a) G. M. Bodner, S. B. Kahl, K. Bork, B. N. Storhoff, J. E. Wuller, and L. Todd, *Inorg. Chem.*, **12**, 1071 (1973). b) J. A. Connor, E. M. Jones, E. W. Randall, and E. Rosenberg, *J. Chem. Soc., Dalton Trans.*, **1972**, 2419. c) C. G. Kreiter and V. Formacek, *Angew. Chem., Int. Ed. Engl.*, **11**, 141 (1972). d) D. J. Ciappenelli, F. A. Cotton, and L. Kruczynski, *J. Organomet. Chem.*, **50**, 171 (1973).

9) a) S. A. Cohen, P. R. Auburn, and J. E. Bercaw, *J. Am. Chem. Soc.*, **105**, 1136 (1983). b) S. A. Cohen and J. E. Bercaw, *Organometallics*, **4**, 1006 (1985).

10) K. Mashima and H. Takaya, *Organometallics*, **4**, 1464 (1985).

11) a) J. X. McDermott, M. E. Wilson, and G. M. Whitesides, *J. Am. Chem. Soc.*, **98**, 6529 (1976). b) R. H. Grubbs and A. Miyashita, *J. Chem. Soc., Chem. Commun.*, **1977**, 864.

12) M. L. Steigerwald and W. A. Goddard III, *J. Am. Chem. Soc.*, **107**, 5027 (1985).

13) J. S. Drage and K. P. C. Vollhardt, *Organometallics*, **5**, 280 (1986).

14) a) K. Mashima, H. Haraguchi, A. Ohyoshi, N. Sakai, and H. Takaya, *Organometallics*, in press. b) A similar ring fission has also been observed for 5-zircona-1-oxacyclopentanes: H. Takaya, M. Yamakawa, and K. Mashima, *J. Chem. Soc., Chem. Commun.*, **1983**, 1283.

15) J. C. Huffman, K. G. Moloy, J. A. Marsella, and K. G. Caulton, *J. Am. Chem. Soc.*, **102**, 3009 (1980).

16) C. P. Casey, C. R. Cyr, R. L. Anderson, and P. F. Marten, *J. Am. Chem. Soc.*, **97**, 3053 (1975).

17) H. Nakatsuji, J. Ushio, S. Han, and T. Yonezawa, *J. Am. Chem. Soc.*, **105**, 426 (1983).

18) a) E. O. Fischer and P. Rustemeyer, *J. Organomet. Chem.*, **225**, 265 (1982). b) U. Schubert, K. Ackermann, and P. Rustemeyer, *J. Organomet. Chem.*, **231**, 323 (1982). c) E. O. Fischer, P. Rustemeyer, O. Orama, D. Neugebauer, and U. Schubert, *J. Organomet. Chem.*, **247**, 7 (1983). d) E. O. Fischer, P. Rustemeyer, and K. Ackermann, *Chem. Ber.*, **115**, 3851 (1982).

19) M. R. Churchill, K. N. Amoh, and H. J. Wasserman, *Inorg. Chem.*, **20**, 1609 (1981).

20) a) M. O. Albers, J. C. A. Boeyens, N. J. Coville, and G. W. Harris, *J. Organomet. Chem.*, **260**, 99 (1984). b) G. W. Harris, C. A. Boeyens, and N. J. Coville, *Organometallics*, **4**, 914 (1985).

21) a) D. M. Hamilton, Jr., W. S. Willis, and G. D. Stucky, *J. Am. Chem. Soc.*, **103**, 4255 (1981). b) J. S. Merola, R. A. Gentile, G. B. Ansell, M. A. Modrick, and S. Zentz, *Organometallics*, **1**, 1731 (1982). c) B. Longato, J. R. Norton, J. C. Huffman, J. A. Marsella, and K. G. Caulton, *J. Am. Chem. Soc.*, **103**, 209 (1981). d) J. A. Marsella, J. C. Huffman, K. G. Caulton, B. Longato, and J. R. Norton, *J. Am. Chem. Soc.*, **104**, 6360 (1982). e) T. D. Tilley and R. A. Andersen, *J. Chem. Soc., Chem. Commun.*, **1981**, 985.

22) G. Fachinetti, G. Fochi, and C. Floriani, *J. Chem. Soc., Dalton Trans.*, **1977**, 1946.

23) C. P. Casey and L. M. Baltusis, *J. Am. Chem. Soc.*, **104**, 6347 (1982).

24) S. Cai, D. M. Hoffman, D. Lappas, H. -G. Woo, and J. C. Huffman, *Organometallics*, **6**, 2273 (1987).

25) J. D. Meinhart, B. D. Santarsiero, and R. H. Grubbs, *J. Am. Chem. Soc.*, **108**, 3318 (1986).

26) K. H. den Haan, G. A. Luinstra, A. Meetsma, and J. H. Teuben, *Organometallics*, **6**, 1509 (1987).

27) P. Zanella, G. Paolucci, G. Rossetto, F. Benetollo, A. Polo, R. D. Fischer, and R. G. Bombieri, *J. Chem. Soc., Chem. Commun.*, **1985**, 96.

28) a) M. Bochmann, L. M. Wilson, M. B. Hursthouse, and R. L. Short, *Organometallics*, **6**, 2556 (1987). b) M. Bochmann and L. M. Wilson, *J. Chem. Soc., Chem. Commun.*, **1986**, 1610.

29) F. van Bolhuis, E. J. M. de Boer, and J. H. Teuben, *J. Organomet. Chem.*, **170**, 299 (1979).
30) L. R. Chamberlain, L. D. Durfee, P. E. Fanwick, L. Kobriger, S. L. Latesky, A. K. McMullen, I. P. Rothwell, K. Folting, J. C. Huffman, W. E. Streib, and R. Wang, *J. Am. Chem. Soc.*, **109**, 390 (1987).
31) F. S. Bristow, M. F. Lappert, J. L. Atwood, and W. E. Hunter, unpublished result. See, D. J. Cardin, M. F. Lappert, and C. L. Raston, "Chemistry of Organo-Zirconium and -Hafnium Compounds," Ellis Horwood Ltd., Chichester (1986), Chaps. 8 and 10.
32) R. D. Adams and D. F. Chodosh, *Inorg. Chem.*, **17**, 41 (1978).

Stability Constants of Imidazole- and Alkylimidazole-Copper(II) Complexes

Hiromu IMAI* and Hiroshi TAMURA
Faculty of Engineering, Kansai University, Yamate-cho, Suita 564
(Received February 28, 1991)

The stability constants of imidazole (HIm)- and alkylimidazoles-copper(II) acetate complexes were calculated from the potentiometric titration data with the aid of the SUPERQUAD computer program. The stability constants of ionic species of $[CuAL_r]^+$ type (A: CH_3COO, L: HIm **a**, 1-CH_3·Im **b**, 2-CH_3·HIm **c**, 4-CH_3·HIm **d**, 2-C_2H_5·HIm **e**, 2-$(CH_3)_2CH$·HIm **f**, r=1, 2, 3, and 4) detected from the complexes were ascertained to be decreased in the order of **b**(1-substituted)≥**d**(4-substituted)>**c**(2-substituted) relating to the position of methyl group bonded to the imidazole ring, and **c**(2-CH_3)>**e**(2-C_2H_5)>**f**(2-$(CH_3)_2CH$) relating to the kinds of alkyl group substituted on 2-position, respectively. The stability of these ionic species was discussed from the neutralization effect of the charge and the steric effect of alkyl group or acetate ion. The stability constants of the hydroxo species of $[CuL_2(OH)_2]$ type indicated the extremely small values, and its order did not indicate a similar tendency with those of ionic species of $[CuAL_r]^+$ types. The distribution of these complex species was investigated as a function of pH.

It has been well-known that the metalloproteins, such as plastocyanin,[1] azurin,[2] and hemocyanin[3] formed the active center by the coordination of Cu(II) to imidazole N of histidine residue, play an important roles, biologically. Since we were interested in the situation of coordination of such active center, imidazole-copper(II) acetate complex $[Cu(CH_3COO)_2(HIm)_2]$ (HIm; imidazole), which is similar to the structure of the active center in metalloprotains, was synthesized by the reaction of imidazole and copper(II) acetate monohydrate. It has been already reported by us that this compound is decomposed slowly by refluxing in ethanol.[4] On the other hand, the stability constants of the ionic species detected from imidazole- and alkylimidazoles-copper(II) acetate complexes ($[Cu(CH_3COO)_2L_r]$, L: HIm **a**, 1-CH_3·Im **b**, 2-CH_3·HIm **c**, 4-CH_3·HIm **d**, 2-C_2H_5·HIm **e**, 2-$(CH_3)_2CH$·HIm **f**, r=1 and 2) were determined by the potentiometric titration method.[5] The order of stability constants for the ionic species of $[Cu(CH_3COO)L]^+$ was favorably explicable from the relation of the steric hindrance between alkyl groups and acetate ion. However, that for the ionic species of $[Cu(CH_3COO)L_2]^+$ type could not be explained from the influence of steric hindrance. This cause is considered to be due to the calculation which neglected the presence of ionic species other than $[Cu(CH_3COO)L_r]^+$ (r=1 and 2) types.

To solve this question, the acetic acid solutions of imidazole- and alkylimidazoles-copper(II) acetate systems were potentiometrically titrated with sodium hydroxide, and the stability constants from the obtained data were calculated with the aid of the SUPERQUAD computer program.[6] The stability of ionic species detected was discussed from the influence of the kinds and the substituted position of alkyl group bonded to imidazole ring. Further, the distribution of these ionic species was investigated as the function of pH.

Experimental

Reagents. Imidazole (HIm) **a**, 2-methylimidazole (2-CH_3·HIm) **c**, 4-methylimidazole (4-CH_3·HIm) **d**, 2-ethylimidazole (2-C_2H_5·HIm) **e**, and 2-isopropylimidazole (2-$(CH_3)_2CH$·HIm) **f** of reagent grade were purchased from Kanto Chemical Co., Inc. and Tokyo Kasei, Co., Ltd., and used after recrystallization from benzene, respectively. 1-methylimidazole(1-CH_3·Im) **b** of reagent grade was purchased from Tokyo Kasei Kogyo Co., Ltd., and used after distillation under reduced pressure (51.5 °C/3 mmHg, 1 mmHg=133.322 Pa).

Copper(II) acetate monohydrate of special grade was purchased from Wako Pure Chemical Industries Ltd., and used without further purification. The stock solution of Cu(II) was standardized by the chelatometric titration with 0.01 M solution of EDTA (1 M=1 mol dm^{-3}).

The other reagents of special grade employed were purchased from Wako Pure Chemical Industries Ltd., and used without further recrystallization.

Preparation of Sample Solution. All the sample solution were prepared with distilled water decarbonated.

The sample solutions of 5.017×10^{-3} M acetic acid were prepared to measure the apparent activity coefficient of hydrogen ion (γ_H) and the ionic product of water (k_w).

The sample solution dissolved about 1×10^{-3} M of copper(II) acetate and $(4—12)\times10^{-3}$ M of imidazoles in about 5×10^{-3} M acetic acid were prepared to measure the stability constants of the complex species.

Potentiometric Titration. The sample solution of 50 ml was pipetted in the vessel of 100 ml, and titrated with sodium hydroxide standardized at about 0.1 M under a nitrogen atmosphere. The temperature was maintained at 25±0.1 °C, and the ionic strength was adjusted to 0.1 M with potassium nitrate. The combination glass electrode of Orion 81-20 was calibrated with pH 4.008 and 6.865 buffer solution at 25± 0.1 °C. All pH values were estimated with an Orion Research ion Analyser EA-920.

Calculation

The calculation of stability constants were performed by the use of a FACOM M-780/10 computer at Kansai University Information Processing Center.

(1) Apparent Activity Coefficient of Hydrogen Ion and Ionic Product of Water. On the bases of the procedure described in previous paper,[5,7] γ_H and K_w were calculated from pH value (α_H) obtained by the potentiometric acid-base titration. In this case, the 2.95×10^{-5} was used as the acid dissociation constant of acetic acid at 25 °C.[8]

$$\gamma_H = \alpha_H/[H] \qquad K_w = \alpha_H[OH] \tag{1}$$

(2) Stability Constants. The overall stability constants (β_{pqrs}) of complex species are represented as follows.

$$pCu + qA + rL + sH \rightleftharpoons Cu_pA_qL_rH_s$$

$$\beta_{pqrs} = \frac{[Cu_pA_qL_rH_s]}{[Cu]^p[A]^q[L]^r[H]^s} \tag{2}$$

Where, A and H denote acetate ion and hydrogen ion, and p, q, r, and s denote the numbers of Cu, A, L, and H, respectively. The coordinated water and the charge numbers of each ionic species were omitted to simplify the expression.

Hypothesizing the best model which is close to the equilibrum system in aqueous solution, the successive stability constants were calculated by the use of the SUPERQUAD computer program[6] inputted the titration data together with the values of γ_H, K_w, and K_L. (The acid dissociation constants of the protonated imidazoles cation, K_L, used the values reported in the previous paper.[5])

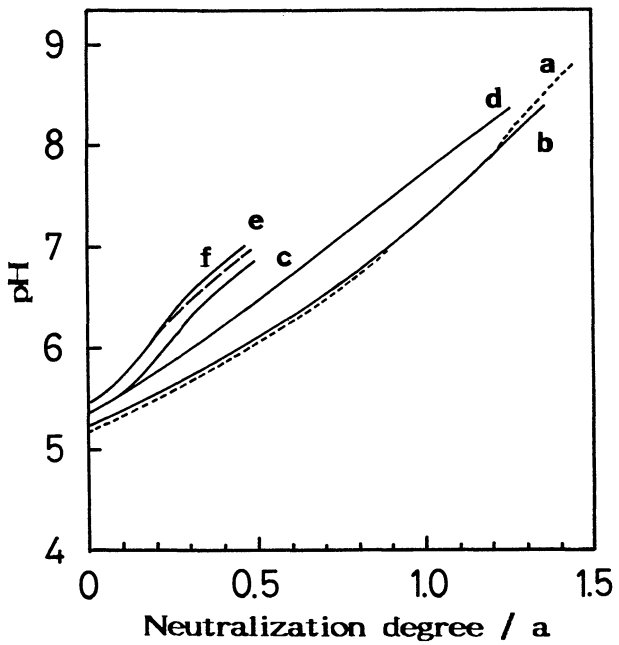

Fig. 1. Potentiometric titration curves of the $Cu(CH_3COO)_2$: L=1:4 system. L: HIm **a**, 1-CH_3·Im **b**, 2-CH_3·HIm **c**, 4-CH_3·HIm **d**, 2-C_2H_5·HIm **e**, 2-$(CH_3)_2CH$·HIm **f**. Concn of $Cu(CH_3COO)_2$: 9.546×10^{-4} M. Concn of L: $(3.820—4.004)\times10^{-3}$ M. Concn of CH_3COOH: 4.396×10^{-3} M. Concn of NaOH: 9.676×10^{-2} M.

Results

(1) Activity Coefficient of Hydrogen Ion and Ionic Product of Water. The average values of γ_H and K_w were 0.8073 (in the pH 3 to 5 region) and 1.334×10^{-14} (in the pH 10 to 12 region) in acetic acid solution, respectively. Hereinafter, the values of $[H^+]$ and $[OH^-]$ for some pH reading were calculated from Eq. 1 by the use of γ_H and K_w measured from the acetic acid solutions.

(2) Stability Constants. The representative titration curves shown in Fig. 1 were obtained from the solution of the 1:4 mole ratio of copper(II) acetate and imidazoles.

The titration was impossible to run because of the formation of copper(II) hydroxide at higher pH more than 8.5 for **a**, **b**, and **d**, and 6.5 for **c**, **e**, and **f**.

To calculate the stability constant of the complexes, the titration data obtained from the 1:4 mole ratio was inputted into the program together with those data obtained from the 1:8 and 1:12 mole ratios. In this case, the 2.10 was used as the stability constant (log K_{CuA}) of CuA^+.[5]

The stability constants shown in Table 1 are the average value obtained from the range of pH 5.0 to 8.5.

As the ionic species of $[CuAL_r]^+$ type, the four kinds corresponding to r=1, 2, 3, and 4 were detected from the complexes of **a**, **b**, and **d**, and the three kinds corresponding to r=1, 2, and 3, from the complexes of **c**, **e**, and **f**, respectively. From the results as mentioned above, the ionic species is conveniently classified into two groups such as Group(I) consisted of **a**, **b**, and **d**, and Group(2) consisted of **c**, **e**, and **f**.

The stability constants of the ionic species for r=1 were in good agreement with the values reported in the previous paper.[5] The stability constants of the other ionic species except for $[CuAL_4]^+$ of Group(1) indicated a slightly large value compared with those of the analogous species for Group(2).

On the other hand, the species of $[CuL_2H_s]^{(2+s)+}$ type

Table 1. Stability Constants of the Ionic Species Detected from $[Cu_pA_qL_rH_s]^{(2-q+s)+}$

L		Stability constant log β_{pqrs}				
		1110	1120	1130	1140[a)]	102—2
HIm	**a**	6.75 (0.06)	10.35 (0.07)	13.32 (0.06)	16.00 (0.08)	−7.83 (0.08)
1-CH_3·Im	**b**	6.48 (0.07)	10.03 (0.06)	12.92 (0.07)	15.65 (0.08)	−8.17 (0.09)
2-CH_3·HIm	**c**	6.31 (0.06)	9.71 (0.04)	12.83 (0.08)		−6.91 (0.12)
4-CH_3·HIm	**d**	6.44 (0.02)	9.91 (0.05)	12.89 (0.05)	15.27 (0.05)	−8.00 (0.06)
2-C_2H_5·HIm	**e**	6.15 (0.03)	9.30 (0.05)	12.18 (0.07)		−7.12 (0.10)
2-$(CH_3)_2CH$·HIm	**f**	5.73 (0.06)	8.62 (0.04)	11.35 (0.07)		−7.58 (0.11)

a) This ionic species seems to be the $[CuL_4]A^+$ type. The values in parenthesis are the standard deviations.

which indicated the value of s=−2, that is, hydroxo species which can be expressed by $[CuL_2(OH)_2]$ is considered to be formed by the hydrolysis of ionic species consisted of **a**—**f**. The stability constants were in the range of −6.9 to −8.2 as log β_{102-2}.

Discussion

(1) Stability of Ionic Species. 1) Influence of Acetate Ion. The stability constants for the ionic species of $[CuAL_r]^+$ type indicated the higher values in the range of 2—3 as log β_{11r0} than those of $[CuL_r]^{2+}$ (r=1, 2, 3, and 4) type reported by Nozaki et al.[9] and Sjöberg.[10] Therefore, the stability of ionic species for $[CuAL_r]^+$ type was found to be increased than those of $[CuL_r]^{2+}$ type because of the neutralization effect of charge by the coordination of acetate ion to copper(II).

2) Influence of Alkyl Groups. According to the X-ray crystal analysis of $[Cu(HIm)_4]^{2+}$, it has been reported that the imidazole ring is inclined at angle of 72.4° from the CuN_4 plane.[11] Then, the imidazole ring of ionic species consisted of the alkylimidazoles is presumed to be inclined at more than 72.4° because of the steric hindrance between alkyl group and acetate ion or between each alkyl group. Therefore, the stability constants of ionic species for the alkylimidazoles–copper(II) complexes shown in Table 1 indicated a slightly small value than those of ionic species for a imidazole–copper(II) complex.

The stability constants of these ionic species decreased in the order of **b**(1-substituted)≧**d**(4-substituted)>**c**(2-substituted) relating to the position of methyl group, and **c**(2-CH_3)>**e**(2-C_2H_5)>**f**(2-$(CH_3)_2CH$) relating to the kinds of alkyl group substituted at 2-position, respectively. The former is considered to be agreed with the order of the increase of steric hindrance. The latter is in agreement with the order of the polar substituent constant for the aliphatic series,[12] and is also considered to be agreed with the order of bulkiness for the alkyl groups.

The order of stability constants for the hydroxo species could not to be found the similar tendency with that for the ionic species. This reason is considered to be due to the different of the steric hindrance on hydroxide ion and acetate ion.

To investigate the stability of ionic species, we were discussed from the term of $\Delta\log K_r$ shown in Eq. 3.

$$\begin{aligned} \Delta\log K_r &= \Delta\log \beta_{11r0} - \log K_{CuA} \quad (r=1) \\ \Delta\log K_r &= \Delta\log \beta_{11r0} - \log K_{11(r-1)0} \quad (r=2, 3, \text{and } 4) \end{aligned} \tag{3}$$

These values are given in Table 2.

The $\Delta\log K_r$ of these ionic species for Group(1) indicated a slightly large value as compared with those of ionic species of the same type for Group(2). The magnitude of $\Delta\log K_r$ suggests the difficulty or facility of introduction of the rth ligand into the $[CuAL_{(r-1)}]^+$ species. The $\Delta\log K_r$ of each ionic species tend to decrease in the order of the r=1, 2, 3, and 4. Such result suggests that the introduction of ligand of rth into $[CuAL_{(r-1)}]^+$ species is made gradually difficult with the increase of numbers of r.

From the stability constants and the $\Delta\log K_r$, the stability of ionic species is summarized as follows.

(1) The ionic species consisted of **a** no having the substituent on the imidazole ring indicate the slightly high stability than those of **b**—**f**.

(2) As the ionic species consisted of **b**, **c**, and **d** do not suffer excessively the influence of steric hindrance on the position of methyl group bonded to the imidazole ring, the stability of these ionic species is similar to each other.

(3) The stability of the ionic species consisted of **c**, **e**, and **f** having the alkyl group on the 2-position of imidazole ring tends to decrease with the increase of bulkiness of the alkyl group.

(4) The ionic species consisted of **f** having the bulky alkyl group indicate the low stability than those consisted of **a**—**e**.

As mentioned above, the stability of imidazoles–copper(II) complexes is explained from the steric effect caused by the alkyl group.

(2) Distribution Curves of Complex Species. The distribution state of the ionic species and hydroxo species were investigated from the stability constants as a function of pH. These results are shown in Fig. 2.

The ionic species of $[CuAL_r]^+$ types were found to form in the order of r=1, 2, 3, and 4 with the increase of pH. The hydroxo species of $[CuL_2(OH)_2]$ type, which formed by the hydrolysis of these ionic species, was detected at pH more than 6.5, and its amounts increased rapidly with pH.

The distribution curves of these ionic species are classified into the two patterns of Group(1) and Group(2) as described already. On the basis of this classification,

Table 2. Values of $\Delta\log K_r$ for Each Ionic Species

r	Group (1)			Group (2)		
	HIm **a**	1-CH_3·Im **b**	4-CH_3·HIm **d**	2-CH_3·HIm **c**	2-C_2H_5·HIm **e**	2-$(CH_3)_2CH$·HIm **f**
1	4.65	4.38	4.34	4.21	4.05	3.63
2	3.60	3.55	3.74	3.40	3.15	2.89
3	2.97	2.89	2.98	3.12	2.88	2.73
4	2.68	2.73	2.38			

Table 3. The pH and the Percentage of Ionic Species at the Maximum Point of Distribution Curves

Ionic species	Group		Maximum point			
			r			
			1	2	3	4
$[CuAL_r]^+$	(1) **a**, **b**, **d**	pH	5.6—6.3	6.4—7.1	7.3—7.7	7.6—7.9
		%	42—50	42—47	32—36	8—22
	(2) **c**, **e**, **f**	pH	6.7—6.9	7.1—7.2	7.3—7.4	
		%	25—38	7—25	4—12	

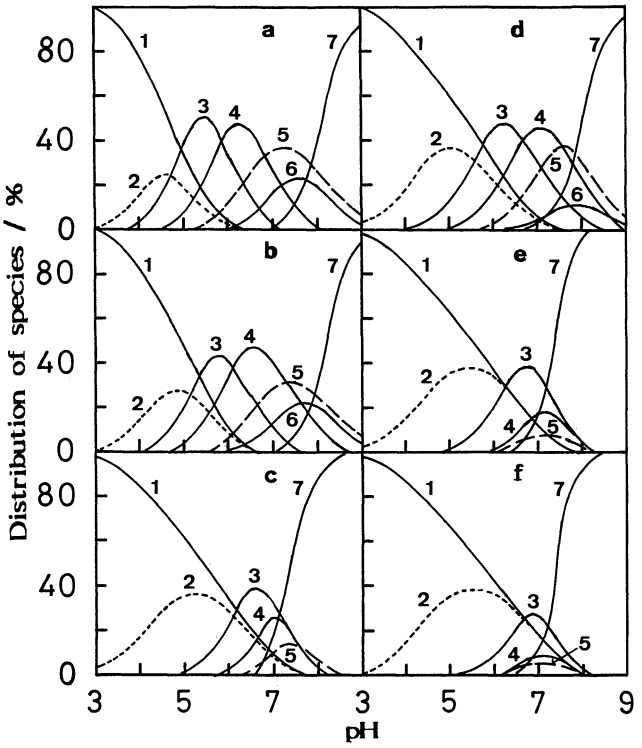

Fig. 2. Distribution curves of the $[CuA_qL_rH_s]^{(2-q+s)+}$ species obtained from the $Cu(CH_3COO)_2$:L=1:4 system. L: Same as Fig. 1. Concn of $Cu(CH_3COO)_2$, L and CH_3COOH: Same as Fig. 1. 1: $q=r=s=0$, 2: $q=1$ $r=s=0$, 3: $q=r=1$, $s=0$, 4: $q=1$ $r=2$ $s=0$, 5: $q=1$ $r=3$ $s=0$, 6: $q=1$ $r=4$ $s=0$, 7: $q=0$ $r=2$ $s=-2$.

the relationship between the pH and the percentage at the maximum point of each ionic species were summarized in Table 3.

The ionic species of $r=1$ and 2 detected from the complexes belong to Group(1), and $r=1$ detected from the complexes belong to Group(2) were ascertained to be preferentially formed in the acidic regions. Additionally, the ionic species of $[CuA]^+$ was present over a wide range of pH, and its maximum point of distribution was 24—35% at pH 4.7—5.6. On the other hand, the ionic species of $r=3$ and 4 detected from the complexes belong to Group(1), and $r=2$ and 3 detected from the complexes belong to Group(2) were ascertained mainly to be formed in the basic regions, respectively.

These ionic species were hydrolyzed with increase of pH, and were found to be changed to the hydroxo species of $[CuL_2(OH)_2]$ type.

References

1) P. M. Colman, H. C. Freeman, J. M. Guss, M. Murata, V. A. Norris, J. M. A. Ramshaw, and M. P. Venkatappa, *Nature*, **272**, 319 (1978).
2) E. T. Adman, R. E. Stenkamp, L. C. Sieker, and L. H. Jensen, *J. Mol. Biol.*, **123**, 35 (1978).
3) E. J. M. van Schaick, W. G. Shutter, W. G. Gaykema, A. M. H. Schepman, and W. G. J. Hol, *J. Mol. Biol.*, **158**, 457 (1982).
4) H. Imai, H. Ohno, and H. Tamura, *Nippon Kagaku Kaishi*, **1987**, 667.
5) H. Imai, H. Ochiai, and H. Tamura, *Nippon Kagaku Kaishi*, **1989**, 2022.
6) P. Gans, A. Sabatini, and A. Vacca, *J. Chem. Soc., Dalton Trans.*, **1985**, 1195.
7) H. Imai, Y. Yaehashi, and Y. Mizuno, *Nippon Kagaku Kaishi*, **90**, 1048 (1969).
8) M. Yasuda, K. Yamasaki, and H. Ohtaki, *Bull. Chem. Soc. Jpn.*, **33**, 1067 (1960).
9) Y. Nozaki, F. R. N. Gurd, R. F. Chen, and J. T. Edsall, *J. Am. Chem. Soc.*, **79**, 2123 (1957).
10) S. Sjöberg, *Acta Chem. Scand.*, **25**, 2149 (1971).
11) G. Ivarsson, *Acta Chem. Scand.*, **27**, 3523 (1973).
12) M. S. Newman and R. W. Taft, "Steric Effects in Organic Chemistry," John Wiley & Sons, New York (1956), p. 618.

Synthesis of Benzo[1,2:4,5]dicycloheptene-1,9-dione via 6,7,12,13-Tetrahydro-7,12-methano-3*H*-cycloheptacyclodecene-3,14-dione and Its Protonation Behavior

Masahiko KATO,* Masaru MITSUDA, Takuji SHIBUYA, and Kimiaki FURUICHI
Faculy of Science, Osaka City University, Sumiyoshi-ku, Osaka 558
(Received January 18, 1991)

6,7,12,13-Tetrahydro-7,12-methano-3*H*-cycloheptacyclodecene-3,14-dione has been synthesized starting from the [4+6]-cycloaddition product of the reaction of 3,4-bis(methylene)-7,7-dibromobicyclo-[4.1.0]heptane with tropone. The adducts were transformed to their epoxides, which were treated with trifluoroacetic acid to give the 3,14-dione. This was transformed to benzo[1,2:4,5]dicycloheptene-1,9-dione, bis(tropono)benzene, by two different methods: (1) by heating it with trichloroacetic acid and DDQ in toluene or (2) through bromination followed by heating in DMF. The 1,9-dione is protonated in concd sulfuric acid to give bis(hydroxytropylium) dication, while it is protonated mainly (>80%) on the C-9 carbonyl oxygen and less (<40%) on the C-1 carbonyl oxygen in deuteriochloroform containing trifluoroacetic acid.

In a previous paper,[1] we reported the scope and limitations for one pot synthesis of substituted tropones starting from 7,7-dihalo-2,3- (or 3,4-) epoxybicyclo-[4.1.0]heptane derivatives.

Using this procedure with the epoxides obtained from cycloaddition products of 3,4-bis(methylene)-7,7-dibromobicyclo[4.1.0]heptane (**1**)[1] with tropone, we obtained 6,7,12,13-tetrahydro-7,12-methano-3*H*-cycloheptacyclodecene-3,14-dione (**2**).

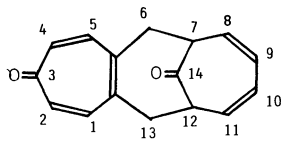

2

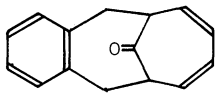

3

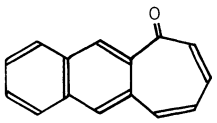

4

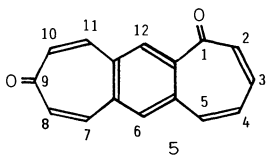

5

Fujise et al. observed the oxidative rearrangement of 5,6,12,13-tetrahydro-6,11-methanobenzocyclodecen-13-one (**3**) to 6*H*-cyclohepta[*b*]naphthalen-6-one (**4**) by heating with DDQ in DMF or with trityl tetrafluoroborate.[2] If this rearrangement is accomplished in dione **2**, we may obtain a new bis(tropono)benzene (**5**).

Results and Discussion

Synthesis of Benzo[1,2:4,5]dicycloheptene-1,9-dione (5). 6,7,12,13-Tetrahydro-7,12-methano-3*H*-cycloheptacyclodecene-3,14-dione (2). When 3,4-bis(methylene)-7,7-dibromobicyclo[4.1.0]heptane (**1**) was used as a diene in the [6+4] cycloaddition reaction with tropone in refluxing toluene, tetracyclic compounds **6a** and **6b** were obtained in a ratio of 3.8:1. This reaction proceeded more regioselectively in benzene solution in a sealed tube at 100 °C (yield, 90%; **6a**:**6b**=9:1). Because it is known that tropone adds anti to cyclopentadiene or furan in a sense of $[_6\pi_s+_4\pi_s]$cycloaddition preventing secondary orbital repulsion,[3,4] it seems reasonable to assume that the main product of the cycloaddition to **1** might be **6a**,

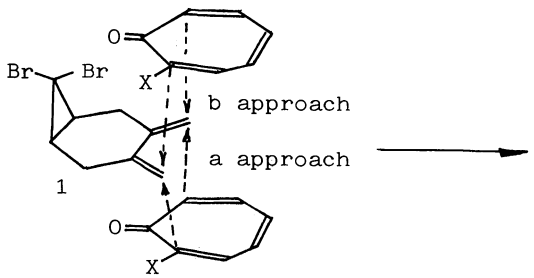

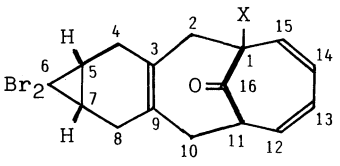

6a X = H
6c X = Cl

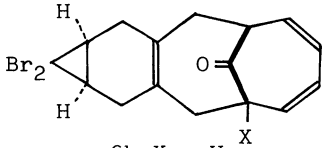

6b X = H

Scheme 1.

formed by the approach from the less hindered side (a) of **1**, and the minor product might be **6b**, formed by the attack from the more hindered side (b) of **1** (Scheme 1).

Though compound **1** did not react with 2-chlorotropone in refluxing toluene, they produced the [6+4] adduct **6c** in benzene solution in a sealed tube at 100 °C (yield 52%; solely *anti*).

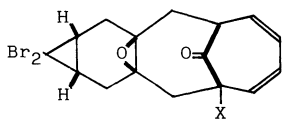

7a X = H
7c X = Cl

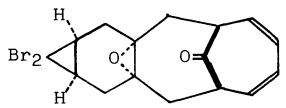

7b

Epoxidation of a mixture of **6a** and **6b** with *m*-chloroperbenzoic acid (mCPBA) resulted in a mixture of **7a** and **7b** in the same ratio as that of the starting material. We have already seen that the epoxidation is usually prohibited or only proceeds with difficulty from the *syn*-face of the dibromomethylene bridge in the 3,4-annelated 7,7-dibromobicyclo[4.1.0]hept-3-ene moiety,[1,5] therefore, the major product is expected to be *anti*-7 (**7a**) and the minor one to be *syn*-7 (**7b**). Compound **6c** was also converted to an epoxide (**7c**) as a single product.

Treatment of the epoxides, **7a** or a mixture of **7a** and **7b**, with 20 equimolar amounts of trifluoroacetic acid (TFA) either in refluxing chloroform or preferably in toluene at 100 °C, gave tropone **2** in 41—55% yields.[6] On the other hand, when **7a** was treated with 4 equimolar amounts of trichloroacetic acid (TCA) in refluxing toluene for 4 h, it gave benzo[1,2:4,5]dicycloheptene-1,9-dione (**5**) in a 27% yield. As it is reasonable to assume that compound **5** might be formed via tropone **2**, this was treated with TCA in toluene at 100 °C in the presence or absence of 2,3-dichloro-4,5-dicyano-*p*-benzoquinone (DDQ) (Table 1). From Table 1, it is clear that the presence of DDQ did not much improve the yield of bistropone **5** and, on the other hand, in the presence of 1 or 2 equimolar amounts of TCA and DDQ, a new rearranged product, benzoheptalene derivative **8**, was isolated in a 10% yield in addition to **5**.

Structures of Tropones 2, 5, and 8. 6,7,12,13-Tetrahydro-7,12-methano-3*H*-cycloheptacyclodecene-3,14-dione (2). From ^{1}H and ^{13}C NMR spectra, it is clear that compound **2** has a plane of symmetry. Thus, it shows seven kinds of proton signals and nine kinds of carbon signals. The IR spectrum shows two strong absorptions at 1631 and 1595 cm^{-1} characteristic of tropone[7] in addition to a normal carbonyl absorption at 1703 cm^{-1}. These spectral data are compatible with structure **2** resulting from the normal ring opening of **7a** and **7b**.

Benzo[1,2:4,5]dicycloheptene-1,9-dione (5). In the ^{13}C NMR spectrum, two carbonyl carbon signals are seen at 187.9 and 187.2 ppm attributed to the tropone carbonyl,[8] in addition to twelve olefinic carbon signals in which four are assigned to quaternary carbons. Signals attributed to C_8/C_{10} or C_7/C_{11} are unresolved. In ^{1}H NMR spectra, all ten kinds of protons are detected, in which two singlets (8.75 and 7.94 ppm) are assigned to the aromatic protons on the benzene ring, and one in the lowest field is assigned to a proton on C_{12} as it is expected to be deshielded by the ortho carbonyl group. A series of signals, 6.99(bd), 7.13(ddd), 6.82(ddd), and 7.38 (bd) ppm are assigned to H_2, H_3, H_4, and H_5, respectively, and are coupled vicinally to each other with bond order alteration as shown by the coupling constants: $J_{2,3}$=12.2, $J_{3,4}$=7.8, $J_{4,5}$=11.6 Hz. Two pairs of signals coupled to each other (6.83(d), 7.63(d) and 6.86(dd), 7.52(d)) are assigned to H_8, H_7 and H_{10}, H_{11}. In the IR spectrum, two sets of characteristic tropone absorption are seen at 1634, 1610, 1594, and 1584 cm^{-1}.[7] In the mass spectrum, in addition to the molecular ion peak (m/z=234), peaks due to M^+—CO and M^+—2CO were observed, in which the latter constitutes the base peak. These spectral data support a structure in which the benzene ring is fused at its 1,2 and 4,5 positions with two tropone rings, one symmetrically (at the 4,5 position of the tropone ring) and the other unsymmetrically (at the 2,3 position) as in **5**.

6,12-Dihydrobenzo[*b*]heptalene-5,9-dione (8). In the ^{13}C NMR spectrum, in addition to two carbonyl carbon signals (204.0(ketone) and 186.2 ppm (tropone)), twelve aromatic and two aliphatic carbon signals were observed. In the ^{1}H NMR spectrum, characteristic AA'BB' proton signals for 4,5-annelated tropones were seen at δ=7.02 (1H, dd, J=12.7, 2.7 Hz), 7.05 (1H, dd, J=12.7, 2.7 Hz), and 7.21 (2H, bd, J=12.7 Hz). The

Table 1. Oxidative Rearrangement of **2**

Entry	Acid[a] equiv	DDQ[a] equiv	Solvent	Temperature/°C	Time h	Yield/%[b] **5**	**8**
1	TCA/5	Nil	Toluene	100	50	21	0
2	TCA/1	2	Toluene	100	30	18	10
3	TCA/2	2	Toluene	100	30	19	10
4	TCA/1	6	Toluene	100	30	23	0
5	AcOH/1	4	Toluene	100	50	17	0
6	Nil	5	CH_3CN	Reflux	30	7	0

a) Quantities of acid and 2,3-dichloro-5,6-dicyano-*p*-benzoquinone (DDQ) used are shown in equivalet(s) per mole of **2**. b) Isolated yields are shown.

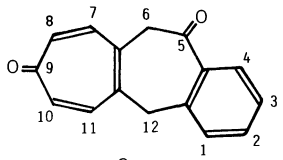

8

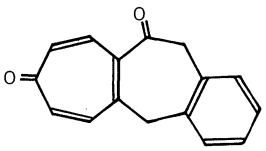

9

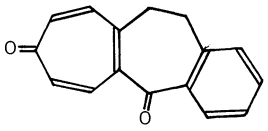

10

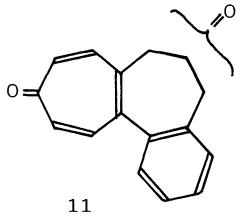

11

aromatic signals at 7.39, 7.65, 7.51, and 7.60 ppm in this order showed similar vicinal coupling constants, $J_{1,2}=J_{2,3}=J_{3,4}=7.8$ Hz, and meta coupling, $J_{1,3}=J_{2,4}=1.0—1.5$ Hz, which predicted a complete double bond delocalization. This supports the presence of an *o*-annelated benzene ring. Aliphatic proton signals were also seen as a broad singlet at 2.90—3.10 ppm (4H). Among four possible structures, (**8**)—(**11**), structure **8** may well predict the identical chemical shifts of H_7 and H_{11} (both are not adjacent to a carbonyl group or an aromatic ring), and the relatively low chemical shift of H_4.

The Reaction Mechanism for Formation of 5. Formation of **5** (and **8**) from **2** may be explained by the three mechanisms shown in Scheme 2: (1) Initial dehydrogenation of **2** to bistropone (**12**), followed by a 6π-electrocyclic reaction to **13**, then a [1,5]sigmatropic

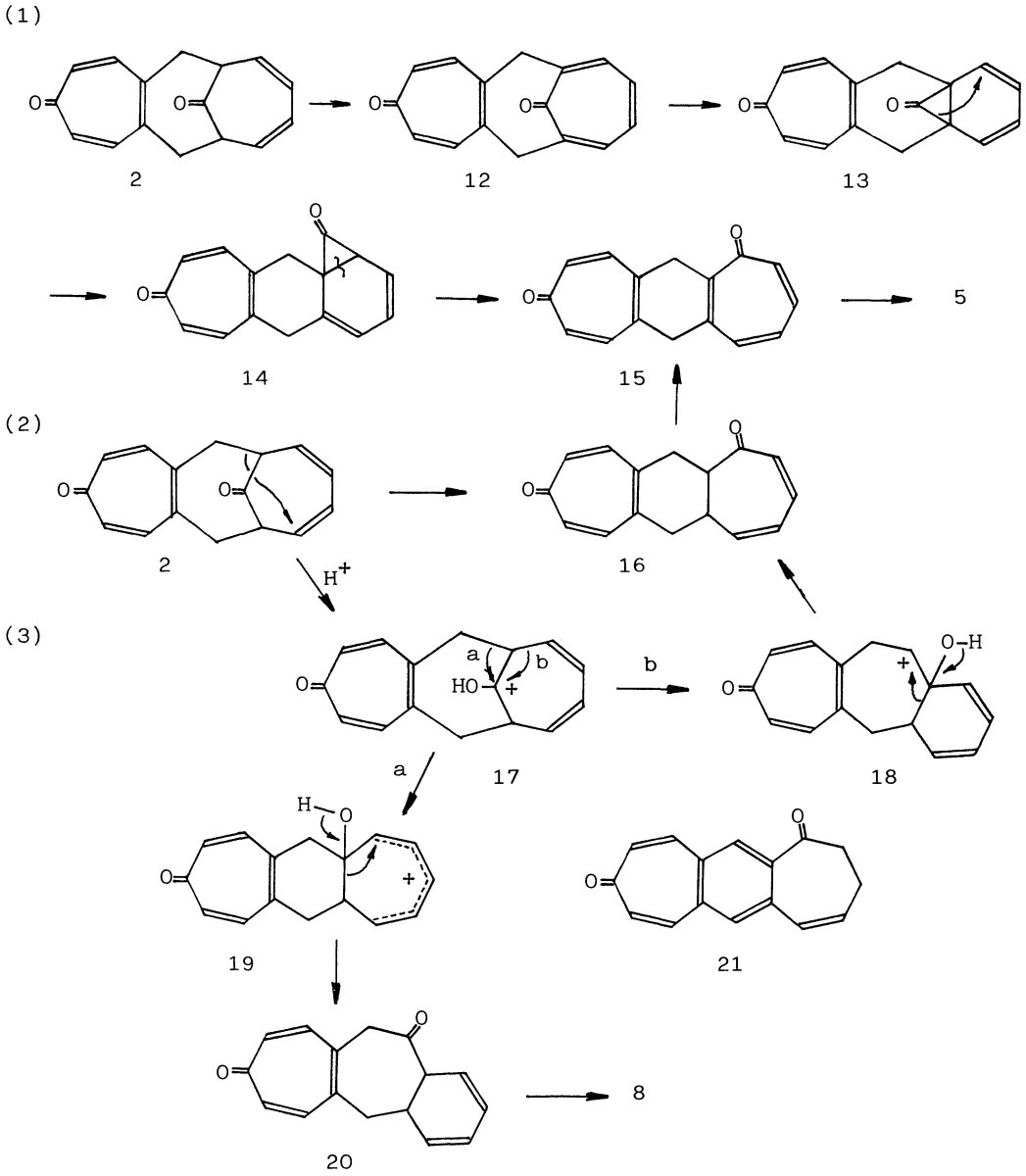

Scheme 2.

shift of the carbonyl carbon[2] results in a norcaradienone derivative (**14**), which undergoes 6π-retrocyclization to a 6,12-dihydro compound of **5** (**15**). (2) A thermal [1,5]-sigmatropic shift of **2** controlled by orbital symmetry gives a tetrahydro compound of **5** (**16**). Dehydrogenation of **16** may give **5** via **15**. (3) The protonated form (**17**) of **2** may undergo two successive 1,2-cationic rearrangements[9,10] to **16** via **18**. The last mechanism can only explain the formation of **8** through **19**. The NMR spectra of **2** in DMSO-d_6 revealed that compound **5** and its dihydro derivative (**21**) were formed at elevated temperatures (>155 °C), but these products were not detected below 145 °C.

Another Route to 5 Starting from 2. Next, the bromination/dehydrobromination procedure of **2** was studied. We found that this procedure gave an improved yield (56%) of **5**. Thus, tropone **2** was treated with 1 equimolar amount of bromine to give a dibromide (**22**), which was transformed to **5** by heating at 100 °C in *N*,*N*-dimethylformamide (DMF). This reaction can be predicted by the following two mechanisms as shown in Scheme 3: (1) two successive dehydrobrominations of **22** may give bis(tropono)phane **12**, which follows the sequence (1) in Scheme 2 leading to **5**. (2) If deprotonation occurs on the brominated carbon of allylic cation **23** formed from **22** by Br^-- elimination in DMF, diene **24** may be formed. This can then undergo a [1,5]sigmatropic shift assisted by bromine to give **25**, which may be transformed to **5** via **15**. At present, it is left to be discovered which mechanism is involved.

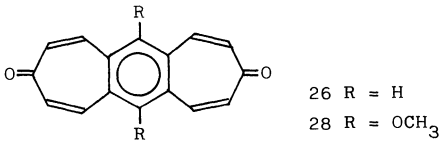

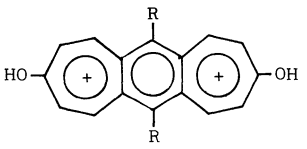

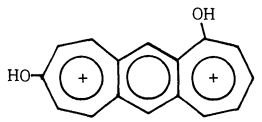

Protonation of Benzo[1,2:4,5]dicycloheptene-1,9-dione (5). In 1969, Föhlisch et al. synthesized benzo-[1,2:4,5]dicycloheptene-3,9-dione (**26**) and suggested the formation of the corresponding bis(hydroxytropylium) dication (**27**) in concentrated sulfuric acid on the basis of a bathochromic shift (Δ+30 nm) of the absorption maximum compared with that in methanol (λ_{max} 296 nm).[11] We also compared the spectrum of the 6,12-dimethoxy derivative (**28**)[12] in ethanol (λ_{max} 313 nm) with the one in concd sulfuric acid (λ_{max} 347 nm) and found a similar bathochromic shift (Δ+34 nm), suggesting the formation of dication **29**. The same tendency (Δ+36 nm) was observed in the electronic spectra for **5** in ethanol (λ_{max} 284 nm) and in concd sulfuric acid (λ_{max} 320 nm). This fact supports the existence of dication (**30**) in concd

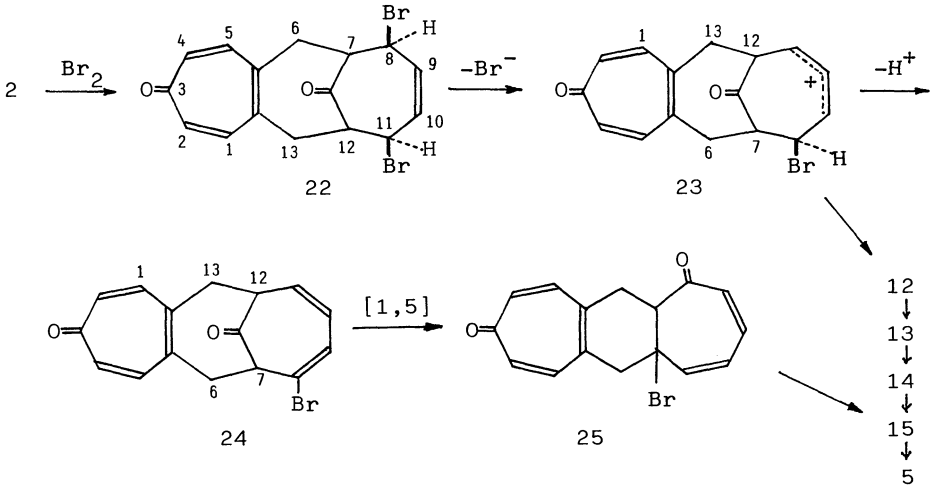

Scheme 3.

Table 2. ^{1}H NMR Chemical Shifts (δ in ppm) of Compounds **5** and **28** in the Presence or Absence of TFA[a]

Solvent	Compound **28**		Compound **5**							
	H_2, H_4, H_8, H_{10}	H_1, H_5, H_7, H_{11}	H_8 and H_{10}		H_7 and H_{11}		H_2	H_3	H_4	H_5
$CDCl_3$	6.92	8.08	6.83	6.86	7.52	7.63	6.99	7.13	6.82	7.38
$CDCl_3$ (TFA)	8.12	9.60	7.80	7.95	8.75	8.83	7.54	7.34	7.39	7.98
	−1.29	−1.52	−0.97	−1.09	−1.23	−1.20	−0.55	−0.21	−0.57	−0.60

a) 5 Drops of TFA and 1 drop of trifluoroacetic anhydride were added to a 5% solution of the sample in $CDCl_3$.

sulfuric acid.

Additionally, the ^{1}H NMR spectra of **5** and **28** in $CDCl_3$ in the presence of a large excess of TFA containing one drop of trifluoroacetic anhydride were examined. From Table 2, though the deshielding shifts of the signals due to protons H_7, H_8, H_{10}, and H_{11} of **5** are 80% of those due to the respective protons in **28**, signals due to protons H_2, H_3, H_4, and H_5 in **5** showed only a moderate deshielding shift, which means protonation occured mostly (>80%) on the C_9 carbonyl oxygen and less on the C_1 carbonyl oxygen (<40%) in **5** under the same conditions.

The reduction potential of **5** was examined by a cyclic voltammograph. An irreversible reduction curve was obtained. The reduction started at −1.03 V and the first peak was observed at −1.2 V, but the second peak varied considerably in the second and the later cycles. We have observed the corresponding peaks of the reduction wave for benzo- or naphtho-annelated tropones to range from −1.6 to −1.8 V.[13] Enhancement of the electron affinity of compound **5** is clearly recognized. The systematic study of the electron affinities of various troponobenzenes and bis(tropono)benzenes is now under investigation and will be reported in a separate paper.

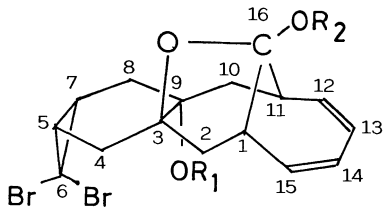

31 a R_1= $COCF_3$, R_2= H

b R_1= H, R_2= $COCF_3$

Experimental

General Procedure. The NMR spectra were taken on JEOL Models GX400 (^{1}H; 400 MHz, ^{13}C; 100 MHz) and FX100 (1H; 100 MHz, ^{13}C; 25 MHz), or a Hitachi Model R90H (1H; 90 MHz) FT-NMR spectrometer. Deuteriochloroform was used as solvent in every case unless otherwise specified. The existence of spin–spin coupling was confirmed by double irradiation experiments. The IR spectra were recorded on a JASCO Model A-102 spectrometer and the UV spectra on a Hitachi Recording spectrometer Model 323. The reduction potential of **5** was recorded on a BAS voltammetry control unit Model CV-1B in acetonitrile containing tetrabutylammonium perchlorate (10^{-1} mol dm^{-3}) as the supporting electrolyte. Ferrocene was used as an internal standard (+0.40 V).

[4+6]Cycloaddition of Diene 1 to Tropone. Method A. A solution of diene **1** (550 mg, 2.0 mmol) and tropone (284 mg, 2.7 mmol) dissolved in toluene was refluxed for 17 h. The residue, obtained after evaporation of the solvent under reduced pressure, was purified by chromatography on silica gel to give products **6a** and **6b** (591 mg, 77%; 3.8:1). The main product **6a**; mp 166—168 °C. ^{1}H NMR (400 MHz): See Table 3. ^{13}C NMR (100 MHz) δ=26.2 (C5, C7), 28.7 and 34.7 (C2, C10 and C4, C8), 38.3 (C6), 55.1 (C1, C11), 127.4 (C3, C9), 125.2 and 127.6 (C12, C15 and C13, C14), 207.4 (C16). IR (nujol mull) ν_{max} 1695, 1680 cm^{-1}. Found: C, 50.01; H, 4.24%. Calcd for $C_{16}H_{16}OBr_2$: C, 50.03; H, 4.20%. Compound **6b** was not obtained in a pure state. The content of **6b** in a mixture was estimated by ^{1}H NMR spectra. **6b**: ^{1}H NMR (400 MHz): See Table 3. ^{13}C NMR (100 MHz) δ=26.1 (C_5, C_7), 29.1 and 34.4 (C_2, C_{10} and C_4, C_8), 36.7 (C_6), 55.7 (C_1, C_{11}), 127.4 (C_3, C_9), 124.9 and 126.7 (C_{12}, C_{15} and C_{13}, C_{14}), 207.4 (C_{16}).

Method B. A mixture of diene **1** (0.90 g, 3.24 mmol) and tropone (519 mg, 4.89 mmol) dissolved in benzene (2.7 mL) was sealed in a glass tube and heated at 100 °C for 16 h. The mixture was then concentrated in vacuo and chromatographed on silica gel to give a mixture of **6a** and **6b** (9:1)(1.13 g, 90%).

[6+4]Cycloaddition of 1 to 2-Chlorotropone. A mixture of diene **1** (992 mg, 3.57 mmol) and 2-chlorotropone (600 mg, 4.27 mmol) dissolved in benzene (6 mL) was heated in a sealed tube at 100 °C for 37 h. The usual workup as above gave

Table 3. ^{1}H NMR Chemical Shifts (δ in ppm) and Their Coupling Constants (J in Hz) of Compounds **6a**, **6b**, **7a**, and **7b** in Deuteriochloroform (400 MHz)

Proton	6a	6b	7a	7b
H_{13} H_{14}	5.83 (A_2) of $A_2B_2X_2$	5.813 (A_2) of $A_2B_2X_2$	5.962 (d)	5.88 (m)
H_{12} H_{15}	5.51 (B_2) of $A_2B_2X_2$	5.470 (B_2) of $A_2B_2X_2$	5.605 (t)	5.60 (m)
H_1 H_{11}	3.43 (m)	3.5—3.42 (m)	3.391 (dd)	3.48 (m)
H_2 H_{10}	2.445 (dd)	2.49—2.38	2.453 (dd)	2.42 (dd)
$H_{2'}$ $H_{10'}$	2.352 (dd)	2.25 (dd)	2.215 (dd)	2.24 (dd)
H_4 H_8	2.450 (dd)	2.49—2.38	2.357 (ddm)	2.43 (d)
$H_{4'}$ $H_{8'}$	2.01 (d)	2.09 (d)	1.778 (d)	1.81 (dm)
H_5 H_7	1.94—1.86	1.94—1.86	1.68—1.73	1.70 (m)
$J_{12,13}$	11.8 (Hz)	11.9 (Hz)	11.5 (Hz)	—
$J_{11,12}$	6.0	—	—	6.6 Hz
$J_{1,2}$	6.0	—	6.8	8.1
$J_{1,2'}$	6.0	6.4	7.8	10.3
$J_{2,2'}$	14.5	14.4	15.6	14.7
$J_{4,4'}$	16.8	16.4	16.8	15.4
$J_{4,5}$	5.0	—	6.6	—
$J_{4',5}$	0.0	0.0	0.0	—

Table 4. The Chemical Shifts (δ in ppm) and the Coupling Constants (J in Hz) of Compounds **6c** and **7c**

Protons	6c	7c
H_{13}	5.915 (ddd) (ppm)	5.974 (ddd) (ppm)
H_{14}	5.865 (dd)	5.898 (dd)
H_{12}	5.573 (dd)	5.620 (dd)
H_{15}	5.778 (d)	5.798 (d)
H_{11}	3.762 (m)	3.50—3.57 (m)
H_2	3.372 (d)	3.290 (d)
H_{10}	2.550 (dd)	2.630 (dd)
$H_{2'}$	2.425 (d)	2.327 (d)
$H_{10'}$	2.3—2.43 (b)	2.271 (dd)
H_4	2.764 (bd)	2.45—2.54
H_8	2.3—2.43 (b)	2.28—2.38
$H_{4'}$ $H_{8'}$	1.97—2.11	1.72—1.8
H_5 H_7	1.87—1.97 (m)	
$J_{13,14}$	6.6 (Hz)	6.4 (Hz)
$J_{14,15}$	11.5	11.2
$J_{12,13}$	11.5	11.1
$J_{11,13}$	1.7	1.8
$J_{11,12}$	5.0	4.8
$J_{2,2'}$	15.4	16.1
$J_{10,11}$	9.0	9.9
$J_{10,10'}$	15.8	15.6
$J_{10',11}$	0.0	4.2

colorless crystals of **6c** (755 mg, 52%), mp 176—177.5 °C. ^{1}H NMR (400 MHz): See Table 4. ^{13}C NMR (100 MHz) δ=197.4 (s), 132.4 (d), 131.1 (s), 128.2 (d), 126.1 (s), 124.8 (d), 123.4 (d), 81.4 (s), 53.0 (d), 41.7 (t), 37.7 (s), 36.4 (t), 29.7 (t), 28.6 (t), 26.2 (d), 26.1 (d). IR (nujol mull) ν_{max} 1716, 1420, 1320, 1200, 1125, 1155 cm^{-1}. Found: C, 45.95; H, 3.59%. Calcd for $C_{16}H_{15}OBr_2Cl$: C, 45.91; H, 3.61%.

Epoxidation of Adduct 6. A solution of *m*-CPBA (779 mg, 4.51 mmol) in dichloromethane (11 mL) was added dropwise at −10 °C to a mixture (3:1) of adducts **6a** and **6b** (1.17 g, 3.05 mmol) dissolved in dichloromethane (10 mL) and stirred for 4 h below 0 °C. More dichloromethane was added in order to dissolve precipitated *m*-chlorobenzoic acid and the solution was washed successively with 10% aq sodium hydrogensulfite (twice), 5% aq sodium hydrogencarbonate (twice), and saturated brine, and then dried. After concentration, the residue was chromatographed on silica gel to give epoxides **7a** (715 mg, 59%) and **7b** (202 mg, 17%). **7a**: Mp 97.5—101 °C (CH_2Cl_2–hexane). ^{1}H NMR (400 MHz): See Table 3. ^{13}C NMR (100 MHz) δ=191.1 (s), 129.1 (d), 126.0 (d), 61.6 (s), 51.9 (d), 38.5 (s), 34.1 (t), 28.7 (t), 24.6 (d). IR ($CHCl_3$) ν_{max} 3000, 2910, 1700, 995, 840 cm^{-1}. Found: C, 48.03; H, 4.05%. Calcd for $C_{16}H_{16}O_2Br_2$: C, 48.03; H, 4.03%. **7b**: Mp 101—104 °C. ^{1}H NMR (400 MHz): See Table 3. IR ($CHCl_3$) ν_{max} 3000, 2930, 1700, 1080, 860 cm^{-1}. Found: C, 48.06; H, 4.05%. Calcd for $C_{16}H_{16}O_2Br_2$: C, 48.03; H, 4.03%.

Tropone 2 from Epoxide 7a. TFA (1.67 mL, 5 molar equiv) was added to a solution of **7a** (1.74 g, 4.34 mmol) in toluene (17 mL) and heated at 80 °C for 1.5 h. At this point, an additional TFA (6.69 mL, 20 molar equiv) was introduced and the mixture was refluxed for an additional 27 h. After cooling, it was diluted with chloroform and washed successively with water, 5% aq sodium hydrogencarbonate, and saturated brine, and then dried. After concentration to dryness, the residue was triturated with ethyl acetate to give pale yellow crystals (509 mg) of **2**. The filtrate of the crystals gave a 2nd crop (58 mg) of **2** after chromatographic separation (total yield, 55%). **2**: Mp 226—231 °C (CH_2Cl_2–AcOEt). ^{1}H NMR (400 MHz) δ=3.00 (2H, dd, J=14.4, 7.2 Hz; H_6, H_{13}), 3.14 (2H, dd, J=14.4, 4.2 Hz; $H_{6'}$, $H_{13'}$), 3.68 (2H, m; H_7, H_{12}), 5.57 (2H, m; H_8, H_{11}), 5.78 (2H, m; H_9, H_{10}), 6.89 (2H, dm, J=12.5 Hz; H_2, H_4), 6.98 (2H, dm, J=12.5 Hz; H_5, H_1). ^{13}C NMR (100 MHz) δ=205.8 (s), 186.3 (s), 145.1 (s), 141.3 (d), 139.6 (d), 126.6 (d), 125.5 (d), 56.0 (d), 39.7 (t). IR ($CHCl_3$) ν_{max} 1703, 1631, 1595 cm^{-1}. Found: C, 80.48; H, 5.90%. Calcd for $C_{16}H_{14}O_2$: C, 80.65; H, 5.92%.

Direct Formation of Bis(tropono)benzene 5 from Tropone 2 (Table 1; Entry 3). DDQ (294 mg, 1.27 mmol) in toluene (7.5 mL) was added to a solution of tropone **2** (150 mg, 0.630 mmol) and TCA (208 mg, 1.27 mmol) in toluene (2.5 mL) and the resulting solution was stirred for 30 h at 100 °C. After cooling, the mixture was diluted with chloroform and then washed successively with water, 5% aq sodium hydrogencarbonate, and saturated brine, and then dried. After concentration, the residue was separated by chromatography to give **5** (27.5 mg, 19%) and **8** (15.5 mg, 10%). The procedures for other entries in Table 1 are similar to this one. **5**: Mp 206.5—209.0 °C. ^{1}H NMR (400 MHz) δ=6.82 (1H, ddd, J=11.6, 7.8, 1.0 Hz; H_4), 6.83 (1H, d, J=12.7 Hz) and 6.86 (1H, dd, J=12.9, 2.6 Hz)(H_8, H_{10}), 6.99 (1H, d, J=12.2 Hz; H_2), 7.13 (1H, ddd, J=12.2, 7.8 Hz; H_3), 7.38 (1H, bd, J=11.6 Hz; H_5), 7.52 (1H, d, J=12.9 Hz) and 7.63 (1H, d, J=12.7 Hz)(H_7, H_{11}), 7.94 (1H, s; H_6), 8.75 (1H, s; H_{12}). ^{13}C NMR (100 MHz) δ=187.9 (s), 187.2 (s), 140.7 (d), 139.6 (d), 139.5 (d), 138.8 (s), 138.2 (d), 138.0 (s), 137.6 (s), 136.8 (d), 136.7 (d), 136.5 (s), 135.8 (d), 135.7 (d), 128.6 (d, 2C). IR ($CHCl_3$) ν_{max} 3040, 1634, 1610, 1594, 1584, 1338 cm^{-1}. MS m/z (%) 234 (47, M^+), 206 (15, M^+−CO), 178 (100, M^+−2CO), 152 (10). UV λ_{max} (log ε) 237 (4.31), 284 (4.68), 351 (4.07). **8**: ^{1}H NMR (400 MHz); see in the text. ^{13}C NMR (100 MHz) δ=204.1, 186.2, 145.6, 143.5, 141.6, 140.5, 140.1, 139.8, 139.4, 138.6, 132.2, 129.4, 129.2, 127.9, 47.2, 33.9. IR ($CHCl_3$) ν_{max} 1680, 1624, 1594, 1570, 900 cm^{-1}.

Bis(tropono)benzene 5 from Epoxide 7a. A solution of **7a** (143 mg, 0.356 mmol) and TCA (140 mg, 0.51 mmol) in toluene (5.0 mL) was refluxed for 28 h. After cooling, the mixture was diluted with chloroform and washed successively with water, 5% aq sodium hydrogencarbonate, and saturated brine, and then dried. After concentration, the residue was chromatographed on silica gel to give **5** (27.4 mg, 27%).

Bis(tropono)benzene 5 from 2 via Bromination and Dehydrobromination. Bromination of 2. A solution of bromine (0.77 molar solution, 8.6 mL) in chloroform was added dropwise to a solution of **2** (158 mg, 0.66 mmol) in chloroform (6.0 mL) on ice in a period of 20 min. Stirring was continued for 30 min at the same temperature and the precipitates formed (**22**; 134 mg, 77%) were collected by filtration. This compound was used directly without further purification. The symmetrical nature of the ^{1}H NMR spectrum suggests that two bromine atoms add to **2** symmetrically from less-hindered *exo*-directions. **22**: ^{1}H NMR (90 MHz, DMSO-d_6 δ=2.8—3.1 (4H, m; $2H_6$, $2H_{13}$), 3.21—3.5 (2H, m; H_7, H_{12}), 5.0 (2H, bs; H_8, H_{11}), 6.1 (2H, bs; H_9, H_{10}), 6.7 (2H, d, J=12.0 Hz; H_2, H_4), 7.13 (2H, d, J=12.0 Hz; H_1, H_5). IR (nujol mull) ν_{max} 1710, 1600 cm^{-1}.

Bis(tropono)benzene 5 from Dibromide 22. A solution of dibromide **22** (151 mg, 0.38 mmol) in DMF (7.5 mL) was heated at 100 °C for 3 h with stirring. After cooling, the

solvent was evaporated under aspirator vacuum and the residue was purified with silica-gel chromatography to give **5** (65 mg, 73%).

Thermal Rearrangement of Epoxide 2 to Bis(tropono)benzene 5 via 6,12-Dihydro Compound of 5 (15). A 10% solution of **2** in DMSO-d_6 was heated to the appropriate temperature and the reaction was monitored by ^{1}H NMR measurement (90 MHz). Below 145 °C for 2 h, no change in the ^{1}H NMR spectrum of the starting material was observed. However, after 2 h at 155 °C, compound **2** was transformed to a product believed to be **21** in a 40% yield. This was isolated using chromatography and its NMR spectrum was taken. ^{1}H NMR (400 MHz) of the product, δ=2.56—2.64 ($2H_3$, m), 2.99—3.31 ($2H_2$, m), 6.35 (H_4, dt, J=11.8, 5.5 Hz), 6.58 (H_5, d, J=11.8 Hz), 6.78 (H_8 or H_{10}, dd, J=12.3, 2.6 Hz), 6.83 (H_{10} or H_8, dd, J=12.3, 2.6 Hz), 7.36 (H_{11} or H_7, d, J=12.3 Hz), 7.49 (H_7 or H_{11}, d, J=12.3 Hz), 7.54 (H_6, s), 8.18 (H_{12}, s). This compound does not seem to be the primary product resulting from a simple [1,5]shift but the product formed by dehydrogenation and migration of double bonds. It was observed that compound **2** was partially transformed to **5** concomitant with some decomposition by heating at 170 °C for 2 h.

This work was supported by the Grant-in-Aid for Scientific Reserch on Priority Areas No. 02230225 from the Ministry of Education, Science and Culture.

The authors wish to thank Mr. Jun-ichi Goda and Mr. Tetsuya Shimada of our University for the elementary analyses and measurements of mass spectra.

References

1) M. Kato, S. Yamamoto, S, Nomura, and T. Miwa, *Bull. Chem. Soc. Jpn.*, **63**, 64 (1990).

2) Y. Fujise, H. Saito, and S. Ito, *Tetrahedron Lett.*, **1976**, 1117.

3) R. C. Cookson, B. V. Drake, J. Hudec, and A. Morrison, *J. Chem. Soc., Chem. Commun.*, **1966**, 15.

4) S. Ito, Y. Fujise, T. Okuda, and Y. Inoue, *Bull. Chem. Soc. Jpn.*, **39**, 1351 (1966).

5) M. Kato, S. Nomura, H. Kobayashi, and T. Miwa, *Chem. Lett.*, **1986**, 281.

6) When a solution of epoxide **7a** (32.2 mg, 0.083 mmol) dissolved in chloroform (1.0 mL) was heated at 65 °C with TFA (0.13 mL, 1.66 mmol) for 2 h, a single product (R_f=0.18) different from the starting compound **7a** (R_f=0.34) on TLC (silica gel/benzene–ethyl acetate (9:1)) was observed. The product was isolated by column chromatography as an oil (21 mg; 60%). ^{1}H NMR (400 MHz) δ=5.919 (H_{14}, dd), 5.849 (H_{13}, ddd), 5.709 (H_{12}, bdd), 5.683 (H_{15}, dd), 3.094 (H_1, m), 2.77 (H_{11}, m), 2.748 (H_{8a}, d), 2.565 (H_{10b}, dd), 2.401 (H_{8b}, ddd), 2.282 (H_{4b}, dd), 2.164 (H_{2b}, t), 2.07 (H_7, m), 2.04 (H_5, m), 1.99 (H_{10a}, m), 1.945 (H_{2a}, dd), 1.776 (H_{4a}). $J_{1,2a}$=7.8 Hz, $J_{1,2b}$=13.4 Hz, $J_{1,11}$=2.2 Hz, $J_{1,15}$=4.6 Hz, $J_{2,2b}$=13.4 Hz, $J_{4a,4b}$=15.3 Hz, $J_{4a,5}$=5.6 Hz, $J_{4b,5}$=10.0 Hz, $J_{7,8a}$=0 Hz, $J_{7,8b}$=9.5 Hz, $J_{8a,8b}$=17.3 Hz, $J_{10a,10b}$=13.7 Hz, $J_{10b,11}$=9.5 Hz, $J_{11,12}$=8.5 Hz, $J_{12,13}$=12.0 Hz, $J_{13,14}$=6.8 Hz, $J_{14,15}$=11.0 Hz. ^{13}C NMR (100 MHz) δ=129.7, 127.7, 127.3, and 123.1 (C_{12}, C_{13}, C_{14}, C_{15}), 105.7 (s, C_{16}), 81.9 (d, J_{CH}=7.3 Hz) and 79.2 (d, J_{CH}=7.3 Hz)(C_3, C_9), 50.8 (d, J_{CH}=125 Hz) and 45.1 (d, J_{CH}=131 Hz)(C_1, C_{11}), 38.5 (s, C_6), 37.1 (t, J_{CH}=135 Hz), 33.7 (t, J_{CH}=134 Hz), 29.0 (t, J_{CH}=130 Hz), and 26.5 (t, J_{CH}=127 Hz)(C_2, C_4, C_8, C_{10}), 26.9 (d, J_{CH}=166 Hz) and 26.3 (d, J_{CH}=169 Hz)(C_5, C_7). IR ($CHCl_3$) ν_{max} 3600 (s), 1780 (vs), 1365 (m), 1160 (vs), 1132 (m), 1185 (m), 1160 (m), 1100 (m) cm^{-1}.

This compound seems to be a hemiacetal (**31**) and was transformed to tropone **2** by prolonged heating with TFA in toluene.

7) a) A. Krebs and B. Schrader, *Ann. Chem.*, **709**, 46 (1969); b) H. Junge, *Spectrochim. Acta, Part A*, **24**, 1951 (1968).

8) J. F. Bagli and M. St. Jacques, *Can. J. Chem.*, **56**, 578 (1978).

9) M. Larcheveque, P. Mulot, and T. Cuvigny, *C. R. Acad. Sci., Ser. C*, **280**, 309 (1975).

10) L. Lombardo and D. Wege, *Tetrahedron Lett.*, **1975**, 115.

11) B. Föhlisch and E. Widmann, *Z. Naturforsch., B*, **24**, 464 (1969).

12) M. Kato, M. Kasai, K. Shiraki, K. Furuichi, and T. Miwa, *Chem. Lett.*, **1987**, 669.

13) We have observed the following reduction potentials in a cyclic voltammogram: 1,4-dimethoxy-7*H*-benzocyclohepten-7-one,[12] −1.78 V; 1,4- and 5,11-dimethoxy-8*H*-cyclohepta[b]-naphthalen-8-one,[12] −1.66 and −1.60 V, respectively, and 7*H*-benzocyclohepten-7-one, −1.7 V (reduction peak maximum).

Archaebacterial Lipids: Surface Pressure–Surface Area Isotherms of 1,1′-(1,32-Dotriacontanediyl)bis[2-[(3*RS*,7*R*,11*R*)-3,7,11,15-tetramethylhexadecyl]-*sn*-glycero-3-phosphocholine]

Kiyoshi YAMAUCHI,* Katsu YAMADA, Masayoshi KINOSHITA, and Tadao KAMIKAWA†
Department of Bioapplied Chemistry, Faculty of Engineering, Osaka City University, Sumiyoshi-ku, Osaka 558
† Department of Chemistry, Faculty of Science and Technology, Kinki University, Kowakae, Higashiosaka 577
(Received February 15, 1991)

1,1′-(1,32-Dotriacontanediyl)bis[2-[(3*RS*,7*R*,11*R*)-3,7,11,15-tetramethylhexadecyl]-*sn*-glycero-3-phosphocholine] (the tetramethylhexadecyl group=phytanyl) was synthesized conveniently by reactions involving etherification of 1,1′-(1,32-dotriacontanediyl)bis(3-benzyl-*sn*-glycerol) (**1**) with (7*R*,11*R*)-3,7,11,15-tetramethyl-2-hexadecenyl bromide and hydrogenation of the resulting unsaturated ether with *p*-tolylsulfonylhydrazine; a total yield from **1**, 7—10%. Unlike usual monopolar double-chain-amphiphiles, the bipolar lipid bent into a U-form in a water–air interface to produce the Langmuir membrane, exhibiting peculiar surface pressure–surface area isotherms.

Previously we mentioned the highly thermostable liposomes made of 1,1′-(1,32-dotriacontanediyl)bis[2-[(3*RS*,7*R*,11*R*)-3,7,11,15-tetramethylhexadecyl]-*sn*-glycero-3-phosphocholine] (the tetramethylhexadecyl group=phytanyl) (**L-32-Phy**).[1] The membrane, despite its low gel-to-liquid crystalline phase temperature (T_m; 8 °C), could retain well not only small molecules such as 5-(and 6-)-carboxyfluorescein (MW 376) but also large phospholipase A_2 (MW 14000) at high temperature as 80 °C. The bipolar lipid, however, was obtained via a multistage synthetic pathway in a total yield of 3—8%. In this paper we wish to describe an improved preparation of **L-32-Phy** and surface pressure–surface area isotherms of the amphiphile in an interface between water and air.

Experimental

1,2-Distearyl-*sn*-glycero-3-phosphocholine (DSPC) was prepared previously[2]; cf., the "stearyl" means "octadecyl". Thin-layer, column and gel permeation chromatographies were performed using the supports mentioned previously.[1] Compound spots in TLC were visualized by spraying with 0.0012% Rhodamine 6G and the Dittmer–Lester reagent.[3] IR spectra were measured by the use of a JASCO A-100 spectrometer. ^{1}H NMR spectra were recorded on JEOL PS-100 and GX-400 spectrometers using a dilute solution in $CDCl_3$ and tetramethylsilane as an internal standard. Fast atom bombardment mass spectra (FABMS) were obtained using a JEOL HX-100, whereby a sample in a matrix was subjected to a beam of xenon atoms produced at 8 kV and 2 mA. Optical rotation was determined by means of a JASCO DIP-360 digital polarimeter. A microprocessor-controlled film balance, Sun-etsu FDS-20, was utilized for the monolayer study.

(7*R*,11*R*)-3,7,11,15-Tetramethyl-2-hexadecenyl bromide (2). Phosphorus tribromide (1.35 g) in anhydrous hexane (2 ml) was added dropwise to the solution of isophytol (2.97 g, 0.01 mol), pyridine (0.4 ml) and hexane (6 ml), which was stirred and cooled to −7—−10 °C. After addition, the mixture was stirred at the temperature for 3 h, then poured into ice-water and extracted with diethyl ether. The organic extract was washed with 1 M hydrochloric acid (1 M=1 mol dm^{-3}), then with aqueous sodium hydrogencarbonate and dried by anhydrous magnesium sulfate. Upon removal of the solvent, the bromide (**2**) was obtained as oil, 3.56 g (99%); mobility (R_f) in TLC (hexane) 0.6; IR (neat) 2960 (s), 1655 (w), 1465 (s), 1380 (m), and 1200 (m) cm^{-1}; ^{1}H NMR (100 MHz) δ=0.87 (d, 12H, *J*= 7 Hz, 4CH_3), 1.25 (m, 19H, CH and CH_2), 1.70 (d, 3H, *J*= 1 Hz, *trans*-CH_3), 2.00 [t, 2H, *J*= 7 Hz, $C\underline{H}_2(CH_3)CH{=}CH$], 4.05 (d, 2H, *J*= 8 Hz, CH_2Br), and 5.56 (t, 1H, *J*= 8 Hz, $C{=}C\underline{H}CH_2Br$). Although the ^{1}H NMR spectrum showed also the minor signals attributable to impurities, the bromide was used for the next reaction without further purification since it changed to unknown(s) when distillation was attempted under reduced pressure (bp about 145—155 °C/3 mmHg, 1 mmHg= 133.322 Pa).

1,1′-(1,32-Dotriacontanediyl)bis[2-[(7*R*,11*R*)-3,7,11,15-tetramethyl-2-hexadecenyl]-3-benzyl-*sn*-glycerol] (3). 1,1′-(1,32-Dotriacontanediyl)bis(3-benzyl-*sn*-glycerol)[4] (**1**; 1.78 g, 2.07 mmol) and sodium hydride (60% in oil, 0.34 g, 8.1 mmol) in anhydrous tetrahydrofuran (25 ml) were stirred at room temperature for 1 h. Compound (**2**, 3.0 g, 8.2 mmol) was added to the resulting alkoxide solution. After heating to reflux for 20 h, the reaction mixture was concentrated, fractionated between water and chloroform. The organic extract was subjected to a silica-gel column chromatography using hexane–ethyl acetate (25/1 v/v). The fraction, which showed a homogeneous spot in TLC under the UV-light and with the Rhodamine 6G spraying, gave **3** as colorless viscous liquid, 2.0 g (71%); R_f (hexane–ethyl acetate, 10/1 v/v) 0.40; 100 MHz ^{1}H NMR δ=0.83—0.87 (a mixture of s and d, 30H, 10CH_3), 4.15 (d with a complex line pattern, 4H, $=CHC\underline{H}_2$), 4.5 (s, 4H, $C\underline{H}_2C_6H_5$), 5.35 (s with a complex line pattern, 2H, $C\underline{H}{=}CH_2O$) and 7.32 (s, 10H, 2C_6H_5); positive FABMS (matrix: 3-nitrobenzyl alcohol and NaCl) *m*/*z* (rel intensity) 1389 ($M+Na$, 3%), 1366 (M^+, 1%).

1,1′-(1,32-Dotriacontanediyl)bis[2-[(3*RS*,7*R*,11*R*)-3,7,11,15-tetramethylhexadecyl]-3-benzyl-*sn*-glycerol] (4). A diglyme solution (15—20 ml) of **3** (1.79 g, 1.3 mmol) and *p*-tolylsulfonylhydrazine (2.5 g, 13 mmol) was heated to reflux under nitrogen for 3 h. The reaction mixture was concentrated to about 10 ml, diluted with hexane and, after removal of the resulting precipitates, was subjected into silica-gel column chromatography. Elution with hexane–ethyl acetate (15/1

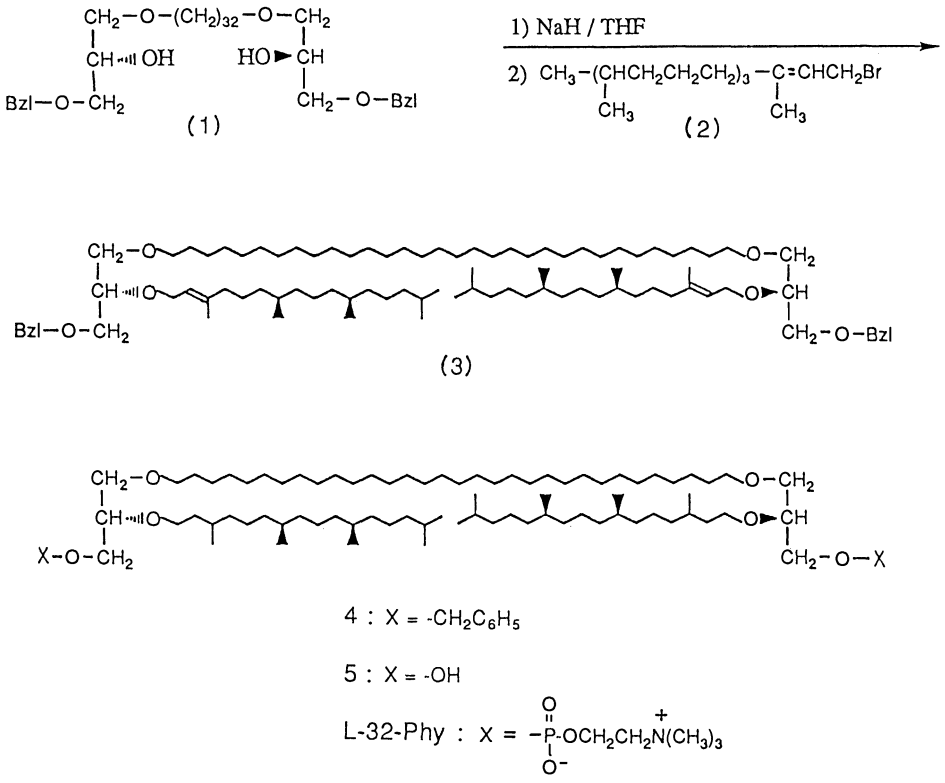

Fig 1.

v/v) gave the diglycerol (**4**) which was further purified by means of a Sephadex LH-20 column using chloroform–methanol (2/1 v/v) as an analytically pure compound, 1.3 g (73%); colorless oil; R_f (hexane–ethyl acetate, 10/1 v/v) 0.56; $[\alpha]_D^{25}$ +1.1° (*c* 1.0, chloroform); 100 MHz ^{1}H NMR and IR spectra were identical with that of the authentic sample;[1] FABMS (matrix: glycerol/3-mercapto-1,2-propanediol, 1/1 v/v) *m/z* (rel intensity) 1371 (M+H, 10%).

L-32-Phy. The dipolar lipid was obtained from **4** via the debenzylation and phosphocholination reactions which were described previously;[1] an overall yield from **4**, 13—18%; mp 152—158 °C (lit,[1] 152—160 °C); a mobility in TLC as well as ^{1}H NMR and IR spectra were identical with those of an authentic sample.

Surface Pressure-Surface Area Isotherms. The film balance system consisted of a Teflon-coated trough of 506 mm (length)×150 mm (width) and a microprocessor (NEC, PC-9801). Temperature of the subphase (water) was thermostated with circulating water within the aluminum trough. A benzene–ethanol solution of **L-32-Phy** (45 µl; 2.66 mg ml^{-1} of the solution) was placed gently on the surface of the subphase, then, a Teflon barrier was swept to compress the film at speed (1 point s^{-1} or 60 mm^2 s^{-1}). The pressure (π) was calibrated by the π–area curve of stearic acid monolayer. The typical results are shown in Fig. 1.

Results and Discussion

In the previous preparation of **L-32-Phy**, phytanyletherification of **1** at the *sn*-2- and -3-O atoms was the most inefficient step; viz., **3** was obtained in a yield of only 15—20% after refluxing a THF-suspension of the sodium salt of **1** and phytanyl bromide for 84 h. The present procedure utilized, instead of the saturated bromide, (7*R*,11*R*)-3,7,11,15-tetramethyl-2-hexadecenyl bromide (**2**). The allylic bromde was reactive to the alkoxide of **1** to produce **3** in a yield of as much as 72%. The reaction time was also shortened considerably. ^{1}H NMR as well as EIMS and FABMS spectra were in accordance with the assigned structure displaying the signals for the C(CH$_3$)=CH–CH$_2$O moiety.

Conversion of **3** into **4** was attempted using various reducing reactions. Palladium-catalyzed hydrogenation of **3** was not fruitful. Heating of **3** with *p*-tolylsulfonylhydrazine[5] in diglyme was efficient to afford **4** in a yield of 73%. Conversion of **4** into **L-32-Phy** was performed according to the previous procedure;[1] namely, (i) debenzylation of **4** by the use of BF_3·$O(C_2H_5)_2$/ethanethiol, (ii) phosphocholination of the resulting diglycerol (**5**) with 2-bromoethyl phosphorodichloridate and trimethylamine. A total yield from **1**: 7—10% in the present method.

Now, the bipolar **L-32-Phy** was different in surface pressure (π)–surface area isotherm from DSPC, one of typical monopolar amphiphiles (Fig. 2). Namely, DSPC gave a stable Langmuir membrane with a limiting area of about 50 Å^2/molecule (curves 1—3). The surface pressure raised sharply upon compressing the spreading area and collapsed at a high lateral pressure as 63 mN m^{-1}. The breakdown occurred instantaneously at an apparent surface area about 36 Å^2/molecule. By

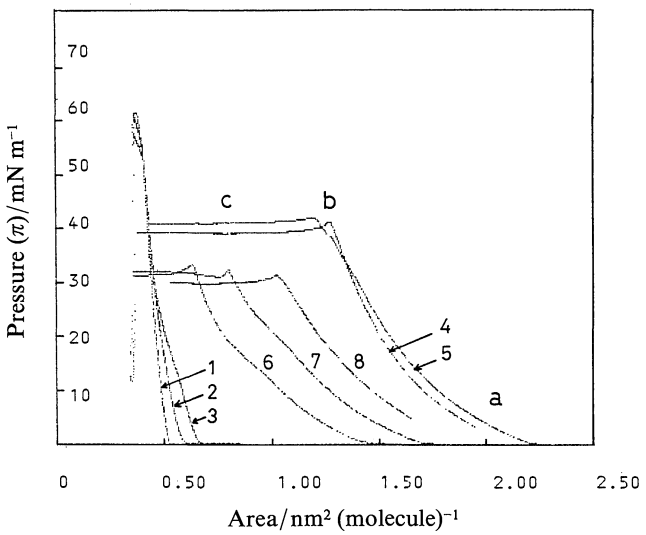

Fig. 2. Surface pressure (π)-surface area isotherms; subphase=water. **DSPC**: curve 1 (5 and 10°C), 2 (15°C), and 3 (20°C); **L-32-Phy**: curve 4 (5°C), and 5 (15°C) (the isotherm curve of 10°C was omitted); **L-32-16**: curve 6 (5°C), 7 (10°C), and 8 (20°C).

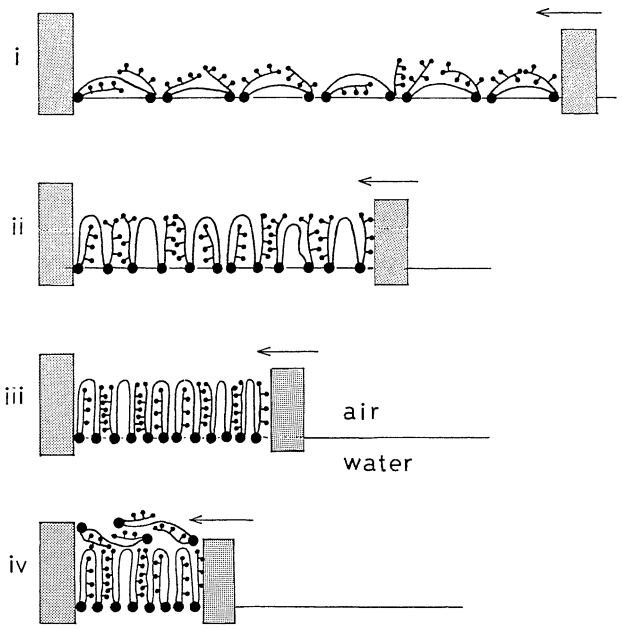

Fig. 3. Schematic representations of formation and collapse of **L-32-Phy** in an interface between water and air.

contrast, **L-32-Phy** did not exhibit a highly cooperative compression; viz., the surface pressure increased gradually upon compressing the spreading area (curves 4 and 5). The limiting area was as large as 160 Å^2/molecule. It appeared also that the monolayer did not collapse, holding constant pressure as inferred by the parallel lines with the abscissa (from point b through c). The peculiar isotherms of **L-32-Phy** may be rationalized as follows. At the low pressure, the bipolar lipids lie sporadically on a water/air interface with the polar heads in water and the hydrophobic residues in air (Fig. 2, point a; Fig. 3-i). With a continuing sweep of the barrier of a film balance, the bipolar lipids are bent gradually to a U-form interacting with neighboring bipolar lipids until the limiting area is closed to the value calculated for two phosphocholine heads (Fig. 2, point b; Fig. 3-ii and iii); cf. DSPC, and DOPC; 50 (this study) and 72 Å^2/molecule,[6] respectively. Upon further compression, the U-shaped **L-32-Phy** may be extruded from the monolayer to pile up on the membrane; the process may permit the constant surface pressure (Fig. 3-iv).

On the other hand, we dealt previously with a Langmuir membrane of 1,1′-(1,32-dotriacontanediyl)-bis(1,2-hexadecyl-*sn*-glycero-3-phosphocholine) (**L-32-16**).[4] The bipolar lipid bearing slim hexadecyl groups gave the π–area isotherms (Fig. 2, curves 6—8) which were characterized by (*a*) significant temperature-dependency as seen in the varying limiting area (90, 120, and 160 Å^2/molecule at 5, 10, and 20 °C, respectively; cf., T_m=61.5 °C; ΔS=0.8 eu/methylene unit) and (*b*) low maximum collapsing pressure (about 30 mN m^{-1}). By contrast, **L-32-Phy**, despite of the low T_m (8 °C),[1] showed that (*a′*) the π–area isotherm or the limiting area was relatively insensitive to temperature (5—15 °C), and (*b′*) the Langmuir membrane was more stable mechanically than the **L-32-16** membrane as judged from the relatively large collapsing pressure (about 40 mN m^{-1} in Fig. 2). Though the above aspects (*a′* and *b′*) have not been fully explained, the temperature-insensitivity might be explained by the ΔS in the phase transition which was as small as 0.4—0.6 eu/methylene unit or high fluidity of the phytanyl groups,[7] and the mechanical stability might be ascribed to the branched structure which would offer high frictional resistance between hydrophobic chains in the membrane. It, however, was apparent from the maximum collapsing pressure that a double-chain-monopolar amphiphile such as DSPC produce a more stable Langmuir membrane than **L-32-Phy**.

References

1) K. Yamauchi, Y. Sakamoto, A. Moriya, K. Yamada, T. Hosokawa, H. Higuchi, and M. Kinoshita, *J. Am. Chem. Soc.*, **112**, 3188 (1990).

2) K. Yamauchi, F. Une, and M. Kinoshita, *Bull. Chem. Soc. Jpn.*, **60**, 2169 (1987).

3) J. D. Dittmer and R. L. Lester, *J. Lipid Res.*, **5**, 126 (1964).

4) K. Yamauchi, A. Moriya, and M. Kinoshita, *Biochim. Biophys. Acta*, **1003**, 151 (1989).

5) R. S. Dewey and E. E. van Tamelen, *J. Am. Chem. Soc.*, **83**, 3720 (1961).

6) M. K. Jain and R. C. Wagner, "Introduction to Biological membranes," John Wiley & Sons, New York (1980), Chap. 4.

7) L. L. Yang and A. Haug, *Biochim. Biophys. Acta*, **573**, 308 (1979).

Syntheses and Properties of Dimethyl and Tetramethyl Anthra[1,9-*cd*:4,10-*c'd'*]-bis[1,2]dichalcogenoles and Their Charge-Transfer Complexes

Kazuo TAKIMIYA, Yoshio ASO, Tetsuo OTSUBO, and Fumio OGURA*
Department of Applied Chemistry, Faculty of Engineering, Hiroshima University, Kagamiyama, Higashi-Hiroshima 724
(Received February 18, 1991)

The dimethyl and tetramethyl derivatives of a series of anthra[1,9-*cd*:4,10-*c'd'*]bis[1,2]dithiole, diselenole, and ditellurole have been prepared as a new type of electron donor. The introduced methyl groups serve to enhance not only the donor strength, but also the solubility, enabling a ready formation of their charge-transfer complexes with various electron acceptors such as 7,7,8,8-tetracyanoquinodimethane (TCNQ), its 2,3,5,6-tetrafluoro derivative, 2,5-dimethyl derivative (DMTCNQ), 2,5-dimethoxy derivative (DMOTCNQ), 2,6-bis(dicyanomethylene)-2,6-dihydronaphthalene (TNAP), 3,3'-dichloro-5,5'-bis(dicyanomethylene)-$\Delta^{2,2'}$-bi(3-thiolene) (DCBT), and 3,3'-dibromo-5,5'-bis(dicyanomethylene)-$\Delta^{2,2'}$-bi(3-selenolene) (DBBS). Although the resulting complexes are mostly 1:1 stoichiometrical, the TCNQ complexes tend to favor a composition rich in acceptors; on the contrary, the DMTCNQ and DMOTCNQ complexes tend to favor a composition rich in donors. Their electrical conductivities range widely from 8 to 10^{-9} S cm^{-1}, being apparently dependent on appropriate combinations of the donors and the acceptors. In general, the present donors have a tendency to form highly conductive complexes with TCNQ, TNAP, DCBT, and DBBS. These highly conductive complexes mostly show a broad electron absorption in the infrared region, being characteristic of a segregated stacked structure in a mixed valence state. On the other hand, the X-ray analyses of DMTCNQ complexes of 3,4-dimethyl, 8,9-dimethyl, and 3,4,8,9-tetramethylanthra[1,9-*cd*:4,10-*c'd'*]diselenoles and 3,4,8,9-tetramethylanthra[1,9-*cd*:4,10-*c'd'*]dithiole have revealed that all of the crystal structures have mixed stack columns of donor–donor–acceptor type. Of them, the 3,4-dimethyl derivative complex shows an unusually high conductivity (0.53 S cm^{-1}) for a mixed stacked structure, which is considered to be due to strong heteroatomic interactions of the intra- and inter-columns.

Polyacenes bearing peri-dichalcogen bridges are known as prototypes of superior electron donors. A representative is naphthaceno[5,6-*cd*:11,12-*c'd'*]bis-[1,2]dithiole, abbreviated as tetrathiotetracene or TTT; it has a stronger donating ability than does tetrathiafulvalene (TTF).[1] However, it has a very low solubility in common solvents, limiting any wide study concerning its molecular complexes. Although the selenium isologue (TST)[1] and the tellurium isologue (TTeT)[2] have also aroused interest concerning the introduction of interactive heavy chalcogens, they are intractable because of their poorer solubilities. The lower polyacene homologues, anthra[1,9-*cd*:4,10-*c'd'*]bis[1,2]dithiole (tetrathioanthracene or TTA),[3] naphtho[1,8-*cd*:4,5-*c'd'*]bis-[1,2]dithiole (tetrathionaphthalene or TTN),[4] and their selenium isologues (TSA[5] and TSN[6]), have thus been studied as more tractable materials. However, their donor characters considerably decrease, and their solubilities are not so much improved as expected. In addition, their tellurium isologues still remain unknown. We previously investigated the 2,3,6,7-tetramethyl derivatives of tetrachalcogenonaphthalenes.[7] This structural modification allowed the formation of all of the chalcogen derivatives (TMTTN, TMTSN, and TMTTeN) involving the tellurium isologue. In addition, the introduced methyl groups served to enhance not only the donor strength, but also the solubility, enabling a detailed study of their complexes. We have further designed the same modification in other peri-dichalogenide polyacenes. We here report on the syntheses and properties of 2,3-dimethyl, 6,7-dimethyl, and 2,3,6,7-tetramethyl derivatives of tetrachalcogenoanthracenes and their charge-transfer complexes.[8]

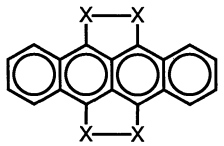
TTT, X=S
TST, X=Se
TTeT, X=Te

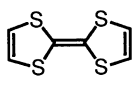
TTF

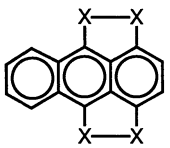
TTA, X=S
TSA, X=Se

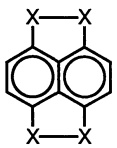
TTN, X=S
TSN, X=Se

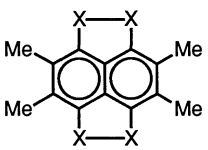
TMTTN, X=S
TMTSN, X=Se
TMTTeN, X=Te

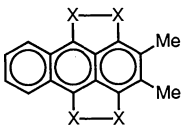
2,3-DMTTA, X=S
2,3-DMTSA, X=Se
2,3-DMTTeA, X=Te

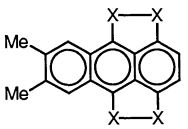
6,7-DMTTA, X=S
6,7-DMTSA, X=Se

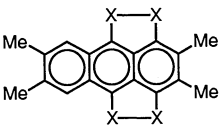
TMTTA, X=S
TMTSA, X=Se
TMTTeA, X=Te

Results and Discussion

Syntheses. Syntheses of dimethyl and tetramethyl tetrachalcogenoanthracenes were carried out according

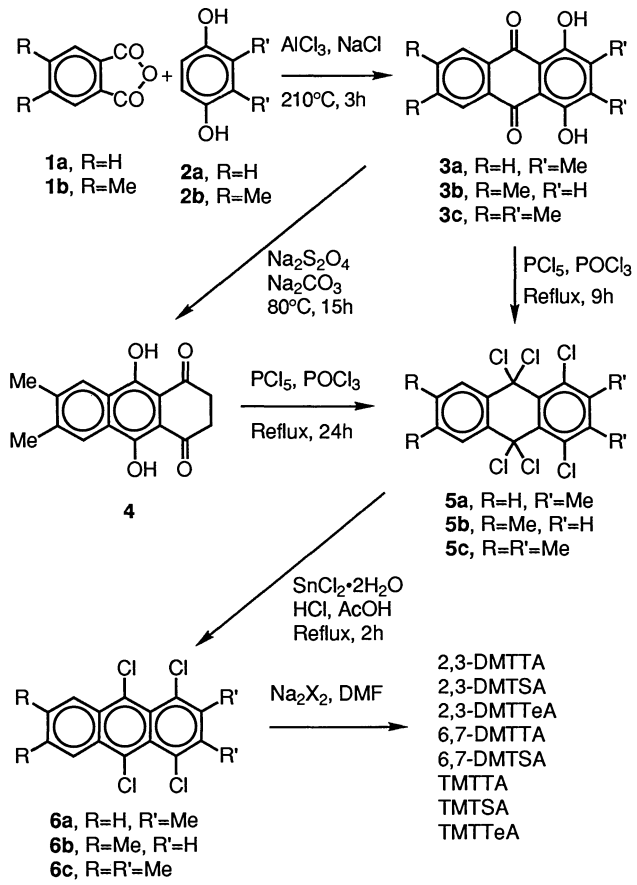

Scheme 1.

to Scheme 1. Thus 1,4-dihydroxy-2,3-dimethylanthraquinone (**3a**), prepared from a one-step condensation of phthalic anhydride (**1a**) with 2,3-dimethylhydroquinone (**2b**),[9] was allowed to react with phosphorus pentachloride to give 1,4,9,9,10,10-hexachloro-2,3-dimethyl-9,10-dihydroanthracene (**5a**) in 59% yield which, upon subsequent dechlorination with tin(II) chloride dihydrate, afforded 1,4,9,10-tetrachloro-2,3-dimethylanthracene (**6a**) in 75% yield. The treatment of **6a** with sodium disulfide, freshly prepared from sodium and sulfur, in refluxing *N*,*N*-dimethylformamide gave 2,3-dimethyltetrathioanthracene (2,3-DMTTA) in 43% yield. A similar reaction of **6a** with sodium diselenide gave the selenium isologue (2,3-DMTSA) in 31% yield. In contrast to an unsuccessful synthesis of the parent tetratelluroanthracene (TTeA), the tellurium isologue (2,3-DMTTeA) was obtained in 15% yield from a reaction of **6a** with sodium ditelluride at a lower temperature of 100 °C. The same approach to 6,7-dimethyl isomers from a combination of 4,5-dimethylphthalic anhydride (**1b**) and hydroquinone (**2a**) were unexpectedly troublesome regarding the following two steps. The first problem was that the treatment of 1,4-dihydroxy-6,7-dimethylanthraquinone (**3b**) with phosphorus pentachloride did not afford any amount of 1,4,9,9,10,10-hexachloro-6,7-dimethyl-9,10-dihydroanthracene (**5b**). Then, **3b** was reduced with sodium dithionite to 6,7-dimethylanthracene-1,4,9,10-tetrol, which mainly exists as the keto form, 2,3-dihydro-9,10-dihydroxy-6,7-dimethyl-1,4-anthracenedione (**4**) (88% yield). An alternative reaction of **4** with phosphorus pentachloride gave the desired hexachloro compound (**5b**) in 30% yield. The other problem arose in the last substitution reaction of the tetrachloro compound (**6b**) with sodium dichalcogenide. Although 6,7-dimethyltetraselenoanthracene (6,7-DMTSA) was obtained in 38% yield by the reaction, in spite of much effort 6,7-dimethyltetrathioanthracene (6,7-DMTTA) was obtained in only a trace yield and was hardly reproducible. Furthermore, no 6,7-dimethyltetratelluroanthracene was formed. On the other hand, a set of 2,3,6,7-tetramethyl derivatives (TMTTA, TMTSA, and TMTTeA) were smoothly completed by the same reaction sequence starting with a combination of **1b** and **2b**, as described for the 2,3-dimethyl derivatives.

Table 1. Half-Wave Oxidation Potentials of Peri-Dichalcogenide Donors[a]

Compound	$E_{1/2}(1)$/V	$E_{1/2}(2)$/V	ΔE/V
TTA	0.36	0.75	0.39
TSA	0.35	0.71	0.36
2,3-DMTTA	0.32	0.73	0.41
2,3-DMTSA	0.31	0.72	0.41
2,3-DMTTeA	0.20	0.63	0.43
6,7-DMTTA	0.31	0.72	0.41
6,7-DMTSA	0.30	0.68	0.38
TMTTA	0.26	0.69	0.43
TMTSA	0.26	0.68	0.42
TMTTeA	0.16	0.55	0.39
TTT	0.19	0.56	0.37
TTF	0.34	0.72	0.38

a) Cyclic voltammetry was measured at 100 mV s^{-1} scan rate with Pt working and counter electrodes and Ag/AgCl reference electorde in 10^{-3} mol dm^{-3} benzonitrile solution containing 0.1 mol dm^{-3} tetrabutylammonium perchlorate as supporting electrolyte.

Oxidation Potentials. Cyclic voltammograms of all of the tetrachalcogenoanthracenes show two reversible one-electron redox waves; their half-wave oxidation potentials are summarized in Table 1. The first and second oxidation potentials of the parent TTA are almost comparable to the corresponding ones of TTF. The introduction of methyl groups actually lowers these values in the order of dimethylation and tetramethylation. The effect is more eminent in the first oxidation than in the second one. There is no essential difference between the enhanced effects due to dimethylation at the 2,3-positions and at the 6,7-positions. Substitution of selenium for sulfur in any series of the parent, dimethyl, and tetramethyl derivatives has little influence on the oxidation potentials. However, substitution of tellurium results in a considerable lowering of both the first and second potentials. As a result, 2,3-DMTTeA and TMTTeA have very strong donating abilities which are either comparable or superior to that of TTT.

Table 2. Charge-Transfer Complexes of Peri-Dichalcogenide Anthracenes

Complex	D:A	Appearance[a]	Dp	Found (Calcd)[b]/%			ν_{CN}	CT Band[c]	ΔE_{redox}[d]	σ[e]
			°C	C	H	N	cm^{-1}	$\times 10^3\ cm^{-1}$	V	$S\ cm^{-1}$
2,3-DMTTA·TCNQ	2:3	Black needles	214	64.66 (64.13	2.56 2.57	13.92 13.20)	2206	3.1, 10.1	0.13	9.6×10^{-1}
2,3-DMTSA·TCNQ	1:2	Black needles	238	52.56 (51.85	1.95 1.96	11.40 12.09)	2203	2.8, 9.9, 11.4	0.12	1.2
2,3-DMTTeA·TCNQ	1:1	Black needles	>300	36.58 (36.68	1.49 1.54	5.55 6.11)	2186	10.2	0.01	5.3×10^{-6}
6,7-DMTSA·TCNQ	1:1	Blue-black powder	245	47.49 (46.56	1.95 1.95	7.31 7.75)	2202	3.2, 11.5	0.11	2.0
TMTTA·TCNQ	1:2	Black needles	220	65.50 (65.78	3.10 2.89	13.81 14.61)	2204	3.3, 11.5, 13.0	0.07	5.0×10^{-2}
TMTSA·TCNQ	1:2	Black needles	237	53.32 (53.03	2.58 2.11	11.00 10.71)	2207	6.1, 10.0, 11.5	0.07	2.7×10^{-1}
TMTTeA·TCNQ	1:1	Black fine needles	>300	39.04 (38.13	2.11 1.92	5.33 5.93)	2187	10.0	−0.03	1.8×10^{-6}
2,3-DMTTA·TCNQF$_4$	1:1	Black powder	>300	55.78 (55.44	1.55 1.66	9.31 9.24)	2200	11.2	−0.28	2.2×10^{-6}
2,3-DMTSA·TCNQF$_4$	1:1	Purple powder	>300	42.05 (42.34	1.17 1.27	7.00 7.05)	2199	11.2	−0.29	5.4×10^{-6}
2,3-DMTTeA·TCNQF$_4$	1:1	Black powder	>300	34.80 (34.01	1.02 1.02	6.11 5.67)	2198	10.5	−0.40	1.8×10^{-7}
6,7-DMTSA·TCNQF$_4$	1:1	Black needles	>300	42.17 (42.34	1.33 1.27	6.06 7.05)	2200	11.0	−0.30	8.8×10^{-5}
TMTTA·TCNQF$_4$	1:1	Purple powder	240	56.53 (56.77	2.00 2.22	9.72 8.83)	2202	11.3	−0.34	5.0×10^{-7}
TMTSA·TCNQF$_4$	1:1	Purple powder	270	43.52 (43.82	1.62 1.72	6.82 6.81)	2201	11.1	−0.34	5.2×10^{-7}
TMTTeA·TCNQF$_4$	1:1	Dark blue powder	>300	35.43 (35.44	1.41 1.39	5.43 5.51)	2201	11.4	−0.44	4.4×10^{-6}
2,3-DMTTA·DMTCNQ	2:1	Black needles	219	62.37 (61.85	3.41 3.16	6.49 6.27)	2198	3.3, 11.2	0.20	9.5×10^{-1}
2,3-DMTSA·DMTCNQ	2:1	Black needles	236	44.25 (43.56	2.32 2.22	4.49 4.42)	2172	4.6, 11.3, 12.6	0.19	5.3×10^{-1}
2,3-DMTTeA·DMTCNQ	2:1	Black needles	>300	33.29 (33.13	2.29 1.70	3.85 3.58)	2186	10.2	0.08	1.2×10^{-3}
6,7-DMTSA·DMTCNQ	2:1	Black needles	262	44.09 (43.55	2.18 2.22	4.25 4.42)	2190	5.4, 11.6	0.18	2.7×10^{-8}
TMTTA·DMTCNQ	2:1	Black needles	241	63.72 (63.26	3.88 3.82	6.57 5.90)	2214	Non	0.14	7.4×10^{-7}
TMTSA·DMTCNQ	2:1	Black needles	>300	46.29 (45.34	2.94 2.74	4.25 4.23)	2210	11.5	0.14	1.2×10^{-5}
TMTTeA·DMTCNQ	2:1	Black powder	>300	35.56 (35.04	2.37 2.12	3.68 3.26)	2183	10.2	0.04	4.6×10^{-2}
2,3-DMTTA·DMOTCNQ	1:1	Black needles	266	46.17 (46.06	2.80 2.32	6.74 7.16)	2204	3.7, 10.3	0.31	2.2
2,3-DMTSA·DMOTCNQ	1:1	Black needles	269	60.91 (60.59	3.43 3.05	9.32 9.42)	2208	6.9	0.32	5.0×10^{-7}
2,3-DMTTeA·DMOTCNQ	1:1	Black needles	>300	37.18 (36.89	1.86 1.86	5.57 5.74)	2190	10.3	0.19	3.2×10^{-2}

Table 2. (Continued)

Complex	D:A	Appearance[a]	Dp	Found (Calcd)[b]/%			ν_{CN}	CT Band[c]	ΔE_{redox}[d]	σ[e]
			°C	C	H	N	cm^{-1}	$\times 10^3\ cm^{-1}$	V	$S\ cm^{-1}$
6,7-DMTSA·DMOTCNQ	2:1	Black needles	270	43.12	2.03	4.33	2222	Non	0.29	1.9×10^{-9}
				(42.49	2.17	4.31)				
TMTTA·DMOTCNQ	2:1	Brown needles	283	61.36	4.08	6.52	2220	Non	0.25	4.0×10^{-9}
				(61.20	3.70	5.71)				
TMTSA·DMOTCNQ	2:1	Black needles	295	45.18	2.60	4.12	2219	Non	0.25	1.0×10^{-8}
				(44.27	2.67	4.13)				
TMTTeA·DMOTCNQ	2:1	Black powder	>300	35.00	2.10	3.13	2183	Non	0.15	1.1×10^{-7}
				(34.40	2.07	3.21)				
2.3-DMTTA·TNAP	1:1	Black fine needles	232	66.05	2.64	9.42	2200	2.3, 8.8	0.11	7.9
				(65.73	2.76	9.58)				
2,3-DMTSA·TNAP	1:1	Black fine needles	250	49.93	2.16	7.30	2205	3.5, 8.9	0.10	2.6×10^{-2}
				(49.76	2.09	7.25)				
2,3-DMTTeA·TNAP	1:1	Black power	>300	40.40	1.63	5.55	2187	8.5, 10.2	−0.01	4.9×10^{-2}
				(39.75	1.67	5.79)				
TMTTA·TNAP	1:1	Black powder	231	66.88	3.23	8.90	2202	2.4, 8.8	0.05	1.7
				(66.64	3.29	9.14)				
TMTSA·TNAP	1:1	Purple plates	>300	50.02	2.59	6.73	2184	8.8, 10.0	0.05	9.2×10^{-3}
				(51.02	2.52	7.00)				
TMTTeA·TNAP	1:1	Black powder	>300	41.59	2.03	5.70	2190	8.8, 10.3	−0.05	6.0×10^{-1}
				(41.04	2.03	5.63)				
2,3-DMTTA·DCBT	1:1	Dark green fine needles	>300	51.17	2.02	7.86	2216	5.9	0.16	1.5×10^{-6}
				(52.09	1.75	8.10)				
2,3-DMTSA·DCBT	1:1	Dark green fine needles	>300	40.94	1.41	6.32	2206	3.6	0.15	3.7
				(40.98	1.38	6.37)				
2,3-DMTTeA·DCBT	1:1	Dark green fine needles	>300	33.51	1.21	5.03	2196	3.5, 10.1	0.04	6.0
				(33.55	1.13	5.22)				
TMTTA·DCBT	1:1	Green fine needles	254	54.09	2.16	6.78	2201	5.1, 8.7	0.10	6.0×10^{-3}
				(53.40	2.24	7.78)				
TMTSA·DCBT	1:1	Green needles	280	42.18	1.91	5.94	2208	5.5, 8.7	0.10	3.1×10^{-3}
				(42.36	1.78	6.17)				
TMTTeA·DCBT	1:1	Black powder	>300	34.46	1.51	4.80	2199	3.5, 8.5, 10.1	0	2.3
				(34.88	1.46	5.08)				
2,3-DMTTA·DBBS	1:1	Dark green fine needles	>300	42.16	1.62	6.20	2216	3.5, 8.3	0.20	7.1×10^{-1}
				(41.21	1.38	6.41)				
2,3-DMTSA·DBBS	1:1	Dark green plates	>300	33.95	1.29	5.23	2198	3.4, 8.3	0.19	8.0
				(33.93	1.14	5.27)				
2,3-DMTTeA·DBBS	1:1	Dark green powder	>300	28.81	1.19	4.40	2200	3.4, 10.0	0.08	5.8
				(28.68	0.96	4.46)				
TMTTA·DBBS	1:1	Dark green needles	>300	42.94	2.17	5.48	2212	5.0, 8.7	0.14	1.0×10^{-3}
				(42.59	1.79	6.21)				
TMTSA·DBBS	1:1	Dark green needles	>300	35.71	1.45	4.38	2208	5.5, 8.7	0.14	8.1×10^{-4}
				(35.26	1.48	5.14)				
TMTTeA·DBBS	1:1	Black powder	>300	30.08	1.25	4.34	2202	3.3, 9.9	0.04	3.6
				(29.92	1.26	4.36)				

a) Obtained from chlorobenzene. b) Calculated as stoichiometry indicated for the complex. c) Measured with a KBr disk method. d) $\Delta E_{redox}=E_{1/2}(D)-E_{1/2}(A)$. e) Measured on compressed pellets at RT with a two-probe or four-probe method.

Molecular Complexes. The methyl group of the present tetrachalcogenoanthracenes actually contributes to enhance their solubilities. This effect, however, is more remarkable in dimethylation than in tetramethylation. For example, the molar solubilities of a series of tetraselenoanthracenes in chloroform are as follows: TSA 2.1×10^{-4} mol dm^{-3}, 2,3-DMTSA 3.1×10^{-3} mol dm^{-3}, 6,7-DMTSA 8.5×10^{-4} mol dm^{-3}, and TMTSA 3.2×10^{-4} mol dm^{-3}. The stronger donating abilities and better solubilities of the dimethyl and tetramethyl derivatives than parent tetrachalcogenoanthracenes facilitated a study of their complexation. They thus gave a number of charge-transfer complexes, as summarized in Table 2. The acceptors used in this experiment involve not only those of well-known classes such as 7,7,8,8-tetracyanoquinodimethane (TCNQ), its 2,3,5,6-tetrafluoro derivative ($TCNQF_4$), 2,5-dimethyl derivative (DMTCNQ), 2,5-dimethoxy derivative (DMOTCNQ), and 2,6-bis(dicyanomethylene)-2,6-dihydronaphthalene (a common name: 9,9,10,10-tetracyano-2,6-naphthoquinodimethane or TNAP) but also of new types such as 3,3'-dichloro-5,5'-bis(dicyanomethylene)-$\Delta^{2,2'}$-bi(3-thiolene) (DCBT)[10] and 3,3'-dibromo-5,5'-bis(dicyanomethylene)-$\Delta^{2,2'}$-bi(3-selenolene) (DBBS).[11] The half-

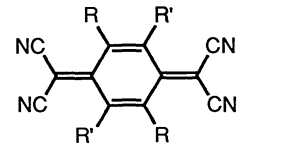

TCNQ: R=R'=H
$TCNQF_4$: R=R'=F
DMTCNQ: R=Me, R'=H
DMOTCNQ: R=MeO, R'=H

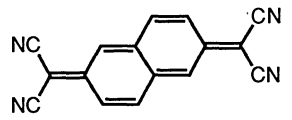

TNAP

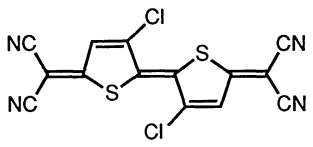

DCBT

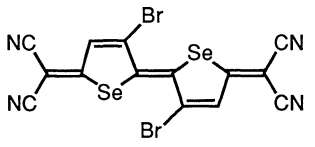

DBBS

wave reduction potentials and infrared nitrile frequencies of these acceptors are given in Table 3. The reduction potentials, except for that of $TCNQF_4$, are just appropriate to form conductive complexes with the present donors; the differences ΔE_{redox} between the oxidation potentials of the donors and the reduction potentials of the acceptors are in the range from −0.05 V to 0.32 V, which has a high probability of being organic metals.[12] The resulting complexes are mostly 1 : 1 stoichiometrical, but some complexes favor a composition rich in either donors or acceptors, even when both components are mixed in equimolar amounts. In addition, their electrical conductivities widely range from 8 to 10^{-9} S cm^{-1}, being independent of the stoichiometry. The stoichiometry and conductivities are apparently dependent on appropriate combinations of the donors

Table 3. Half-Wave Reduction Potentials[a] and Nitrile Vibrational Frequencies of Electron Acceptors

Compound	$E_{1/2}(1)$/V	$E_{1/2}(2)$/V	ΔE/V	ν_{CN}/cm^{-1}
TCNQ	0.19	−0.43	0.62	2232
$TCNQF_4$	0.60	−0.05	0.65	2234
DMTCNQ	0.12	−0.42	0.54	2230
DMOTCNQ	0.01	−0.52	0.53	2225
TNAP	0.21	−0.21	0.42	2225
DCBT	0.16	−0.09	0.25	2217
DBBS	0.12	−0.10	0.22	2220

a) Cyclic voltammetry was measured at 100 mV s^{-1} scan rate with Pt working and counter electrodes and Ag/AgCl reference electorde in 10^{-3} mol dm^{-3} benzonitrile solution containing 0.1 mol dm^{-3} tetrabutylammonium perchlorate as supporting electrolyte.

and acceptors, but can be somewhat systematized according to the used acceptors rather than the donors, as follows. The TCNQ complexes of the TTA and TSA derivatives tend to favor a composition rich in acceptor species, and the electrical conductivities measured on compressed pellets at room temperature are in the high range of 0.05—2.0 S cm^{-1}. These complexes, except for the TMTSA complex, show a broad electron absorption in the infrared region, being characteristic of a segregated stacked structure in a mixed valence state.[13] The incomplete charge transfer was also supported by nitrile vibrational frequencies, which are intermediate between those of neutral TCNQ (2232 cm^{-1}) and Na^+TCNQ^- (2174 cm^{-1}).[14] In contrast, the TCNQ complexes of stronger tellurium-containing donors, DMTTeA and TMTTeA, have the 1 : 1 composition and low conductivities. All of the complexes with a stronger acceptor, $TCNQF_4$, are also 1 : 1 stoichiometrical and exhibit a low conductivity. These low conductivity complexes must correspond to Mott insulators, since the increasing donor or acceptor character causes a complete charge transfer, as indicated by the low frequencies of the infrared nitrile vibrations. On the other hand, a weaker acceptor DMTCNQ takes complexes of a 2 : 1 composition rich in donor, reflecting increasing bulkiness of the acceptors. These complexes mostly exhibit a low conductivity, and the electronic spectra indicate segregated stacking only for a complex with 2,3-DMTTA. A similar result was observed for the DMOTCNQ complexes. Some of the DMTCNQ complexes were actually confirmed by X-ray crystallographic analyses to take mixed stacking, which is further discussed later in connection with their conductivities. The other acceptors (TNAP, DCBT, and DBBS) are strong electron acceptors comparable to TCNQ and have additional advantages of high polarization and reduced Coulomb repulsion due to their extensive conjugation. Their complexes are all 1 : 1 stoichiometrical and mostly high-conductive, indicating mutual fitness of the donors and the acceptors. The enhanced intermolecular interactions of the individual components due to the

Table 4. Crystal Data of DMTCNQ Complexes

	2,3-DMTSA	6,7-DMTSA	TMTSA	TMTTA
Formula	$C_{46}H_{28}N_4Se_8$	$C_{46}H_{28}N_4Se_8$	$C_{50}H_{36}N_4Se_8$	$C_{50}H_{36}N_4S_8$
Fw	1268.44	1268.44	1324.54	949.37
Crystal system	Monoclinic	Monoclinic	Monoclinic	Monoclinic
Space group	$P2_1/n$	$P2_1/n$	$P2_1/n$	$P2_1/n$
a/Å	8.869(1)	16.561(4)	10.027(1)	9.942(1)
b/Å	20.322(2)	11.532(3)	20.852(2)	20.542(2)
c/Å	11.132(2)	10.901(3)	10.613(1)	10.500(1)
β/°	91.14(1)	99.22(2)	99.06(1)	98.65(1)
V/Å^3	2005.9(4)	2054.9(9)	2191.4(4)	2120.1(4)
Z	2	2	2	2
Crystal size/mm^3	0.24×0.04×0.01	0.33×0.13×0.08	0.41×0.06×0.01	0.50×0.10×0.08
Abs correction	Analytical[a)]	None	None	Analytical[a)]
No. of data	2423	2538	2333	2623
R	0.045	0.068	0.070	0.069

a) Ref. 18.

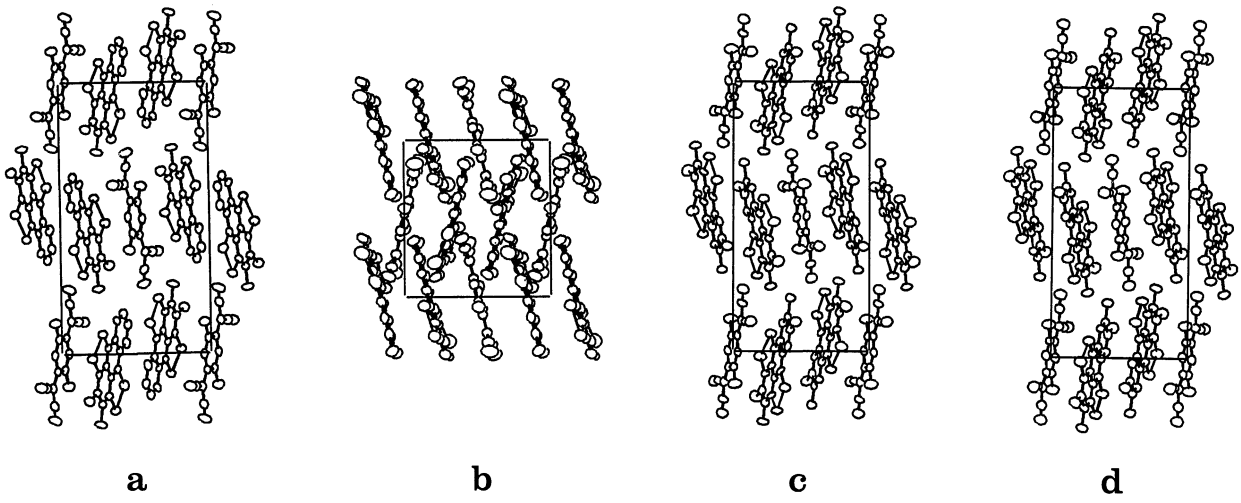

Fig. 1. Crystal structures of DMTCNQ complexes with 2,3-DMTSA (a), 6,7-DMTSA (b), TMTSA (c), and TMTTA (d) projected along the a axis.

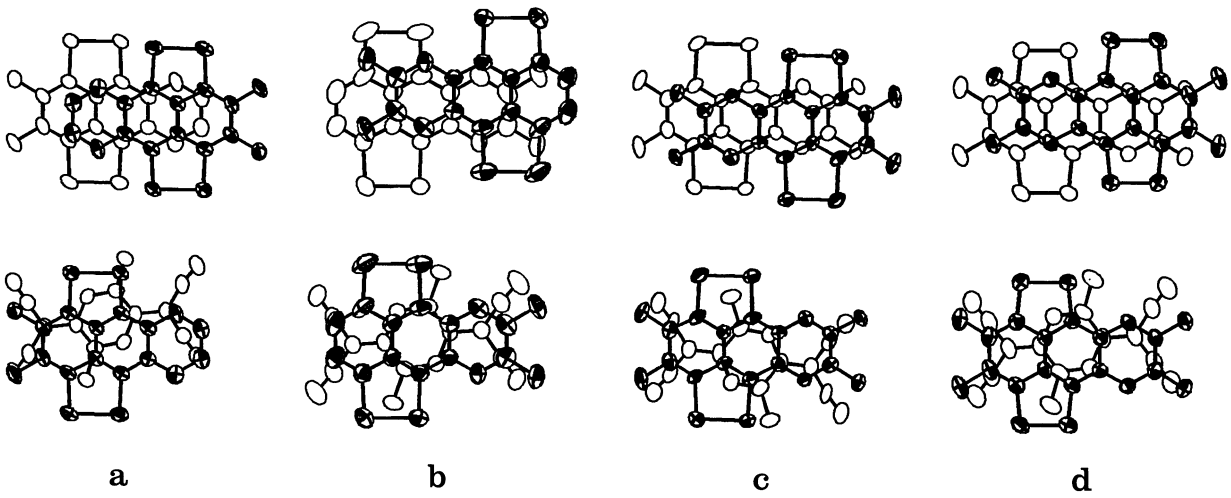

Fig. 2. Molecular overlapping modes of DMTCNQ complexes with 2,3-DMTSA (a), 6,7-DMTSA (b), TMTSA (c), and TMTTA (d) viewed perpendicular to the molecular planes.

Table 5. Intramolecular Bond Distances and Angles for DMTCNQ Complexes

Bond distance/Å	2,3-DMTSA	6,7-DMTSA	TMTSA	TMTTA
X1–X2	2.319(1)	2.342(1)	2.331(2)	2.091(2)
X1–C16	1.885(7)	1.909(8)	1.904(11)	1.746(5)
X2–C3	1.894(7)	1.901(10)	1.930(11)	1.762(6)
C3–C4	1.379(10)	1.350(13)	1.344(16)	1.378(8)
C3–C17	1.426(10)	1.440(13)	1.462(16)	1.424(8)
C4–C5	1.398(11)	1.448(18)	1.430(17)	1.441(9)
C4–C19	1.520(11)	—	1.525(18)	1.512(9)
C5–C6	1.369(11)	1.383(17)	1.391(17)	1.372(8)
C5–C20	1.533(10)	—	1.506(17)	1.528(9)
C6–X7	1.904(8)	1.890(12)	1.926(12)	1.762(6)
C6–C18	1.437(10)	1.427(14)	1.387(15)	1.423(7)
X7–X8	2.328(1)	2.353(2)	2.335(2)	2.090(2)
X8–C9	1.896(7)	1.899(9)	1.923(12)	1.760(6)
C9–C10	1.421(10)	1.402(13)	1.384(15)	1.403(8)
C9–C18	1.377(10)	1.384(14)	1.431(16)	1.386(7)
C10–C11	1.436(11)	1.419(14)	1.412(15)	1.409(7)
C10–C15	1.436(10)	1.442(12)	1.447(15)	1.456(7)
C11–C12	1.379(11)	1.383(15)	1.347(17)	1.376(8)
C12–C13	1.401(12)	1.418(16)	1.436(16)	1.448(8)
C12–C21	—	1.544(16)	1.542(16)	1.504(8)
C13–C14	1.370(12)	1.388(14)	1.381(16)	1.368(8)
C13–C22	—	1.505(15)	1.502(16)	1.504(8)
C14–C15	1.461(10)	1.403(12)	1.424(16)	1.428(7)
C15–C16	1.413(10)	1.412(12)	1.422(15)	1.409(7)
C16–C17	1.382(9)	1.377(12)	1.374(15)	1.391(7)
C17–C18	1.422(10)	1.451(13)	1.418(15)	1.412(7)
C23–C24	1.417(11)	1.445(12)	1.491(18)	1.447(9)
C23–C25'	1.405(10)	1.462(12)	1.430(17)	1.435(8)
C23–C26	1.438(10)	1.347(12)	1.388(17)	1.383(8)
C24–C25	1.369(11)	1.357(12)	1.340(17)	1.340(8)
C24–C31	1.547(11)	1.540(12)	1.529(18)	1.521(10)
C26–C27	1.445(11)	1.443(15)	1.417(18)	1.428(9)
C26–C29	1.395(12)	1.462(13)	1.416(20)	1.454(11)
C27–N28	1.120(11)	1.155(17)	1.125(17)	1.132(10)
C29–N30	1.145(13)	1.130(14)	1.126(20)	1.155(11)
Bond angle/°	**2,3-DMTSA**	**6,7-DMTSA**	**TMTSA**	**TMTTA**
X2–X1–C16	92.0(2)	91.1(3)	91.8(3)	95.9(2)
X2–X1–C3	92.0(2)	92.7(3)	93.2(3)	95.8(2)
X2–C3–C4	121.7(6)	122.4(8)	122.2(9)	124.5(4)
X2–C3–C17	116.2(5)	115.5(7)	113.2(7)	112.9(4)
C4–C3–C17	122.1(7)	122.1(9)	124.5(11)	122.6(5)
C3–C4–C5	119.6(7)	120.2(10)	120.5(11)	118.3(5)
C3–C4–C19	119.8(7)	—	118.4(11)	120.3(6)
C5–C4–C19	120.5(6)	—	121.2(11)	121.5(6)
C4–C5–C6	119.7(6)	119.2(10)	116.0(11)	119.8(5)
C4–C5–C20	121.2(7)	—	123.0(11)	120.3(6)
C6–C5–C20	119.1(7)	—	120.9(11)	119.9(6)
C5–C6–X7	121.5(5)	122.0(9)	119.3(8)	125.2(4)
C5–C6–C18	122.9(7)	122.2(11)	124.6(11)	122.0(5)
X7–C6–C18	115.6(5)	115.6(8)	116.1(9)	112.8(4)
C6–X7–X8	92.1(2)	91.8(4)	92.3(3)	95.9(2)
X7–X8–C9	92.2(2)	91.1(3)	92.3(3)	95.9(2)
X8–C9–C10	121.0(5)	120.8(7)	120.8(9)	124.3(4)
X8–C9–C18	117.3(5)	116.7(7)	115.3(8)	113.8(4)
C10–C9–C18	121.8(6)	122.4(8)	123.9(10)	121.9(5)
C9–C10–C11	122.5(7)	122.8(8)	123.5(10)	123.1(5)
C9–C10–C15	117.7(6)	118.8(8)	118.4(10)	118.2(5)
C11–C10–C15	119.8(7)	118.5(8)	118.2(10)	118.7(5)
C10–C11–C12	119.7(7)	121.1(9)	122.1(11)	122.5(5)
C11–C12–C13	121.0(8)	120.5(10)	120.9(11)	119.3(5)
C11–C12–C21	—	118.5(10)	121.3(10)	119.8(5)
C13–C12–C21	—	121.0(9)	117.8(11)	120.9(5)

Table 5. (Continued)

Bond angle/°	2,3-DMTSA	6,7-DMTSA	TMTSA	TMTTA
C12–C13–C14	121.9(7)	119.0(9)	119.0(10)	119.3(5)
C12–C13–C22	—	121.3(10)	121.9(10)	119.8(5)
C14–C13–C22	—	119.7(10)	119.0(10)	120.9(5)
C13–C14–C15	119.6(7)	122.2(9)	121.1(10)	122.7(5)
C10–C15–C14	118.0(7)	118.8(8)	118.7(10)	117.5(5)
C10–C15–C16	119.6(6)	118.4(8)	117.9(10)	119.1(5)
C14–C15–C16	122.4(7)	122.8(8)	123.4(10)	123.4(5)
X1–C16–C15	121.1(5)	119.8(6)	120.5(8)	125.0(4)
X1–C16–C17	117.7(5)	118.0(7)	117.6(8)	114.3(4)
C15–C16–C17	121.2(7)	122.2(8)	122.0(10)	120.7(5)
C3–C17–C16	121.9(6)	122.5(8)	123.9(10)	121.0(5)
C3–C17–C18	118.7(6)	118.3(8)	114.4(9)	118.6(5)
C16–C17–C18	119.4(6)	119.2(8)	121.7(10)	120.5(5)
C6–C18–C9	122.8(7)	123.2(9)	124.0(10)	121.6(5)
C6–C18–C17	117.0(6)	118.0(9)	120.0(10)	118.8(5)
C9–C18–C17	120.2(6)	118.9(8)	116.0(10)	119.7(5)
C24–C23–C25′	118.1(6)	117.7(7)	117.1(10)	117.5(5)
C24–C23–C26	123.8(7)	124.8(8)	123.3(11)	122.9(5)
C25′–C23–C26	118.2(7)	117.5(8)	119.6(11)	119.7(6)
C23–C24–C25	118.1(7)	119.3(8)	118.8(11)	119.4(5)
C23–C24–C31	124.9(7)	121.7(8)	122.7(11)	126.6(5)
C25–C24–C31	117.1(7)	118.8(8)	118.5(11)	114.1(6)
C23–C25–C24	123.9(7)	122.9(7)	124.1(11)	123.2(5)
C23–C26–C27	126.1(7)	129.0(9)	127.3(12)	126.8(6)
C23–C26–C29	118.9(7)	121.5(9)	119.7(11)	121.9(6)
C27–C26–C29	115.0(7)	109.5(8)	113.0(11)	111.3(6)
C26–C27–N28	172.6(9)	173.8(11)	172.7(16)	174.7(7)
C26–C29–N30	177.4(11)	179.0(13)	175.1(15)	176.6(7)

extended π-systems as well as interactive heteroactoms are considered to lead to a ready formation of segregated columns. In particular, it is worth noting that the tellurium-containing donors can form highly conductive complexes with these acceptors.

Crystal Structures of DMTCNQ Complexes. The four DMTCNQ complexes with 2,3-DMTSA, 6,7-DMTSA, TMTSA, and TMTTA offered good single crystals for X-ray analysis. Table 4 shows their crystal data, in which all crystals belong to the monoclinic space group. Of these complexes, only the 2,3-DMTSA complex has a high conductivity (0.53 S cm^{-1}) and an electronic absorption band at 4.6×10^3 cm^{-1}. Although it is expected to have a different crystal structure, all of the DMTCNQ complexes are isostructural with mixed stacked columns of a donor–donor–acceptor sequence along the *c*-axis (Fig. 1). In addition, overlapping modes for donor–donor and donor–acceptor are quite similar (Fig. 2). Their infrared nitrile vibrations as compared with that (2230 cm^{-1}) of neutral DMTCNQ indicate a complete charge-transfer for the 2,3-DMTSA complex (2172 cm^{-1}) but some charge-transfer for the 6,7-DMTSA complex (2190 cm^{-1}), the TMTTA complex (2214 cm^{-1}), and the TMTSA complex (2210 cm^{-1}). The actual charge-transfer of the 2,3-DMTSA complex is also supported by a detailed consideration of the molecular structures of the components (Fig. 3, Table 5).

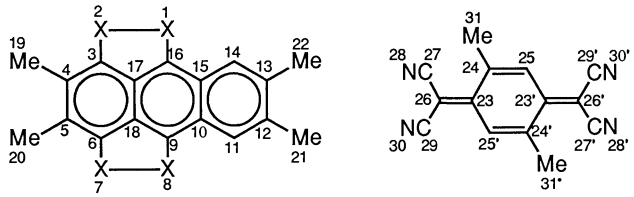

Fig. 3. Atomic numbering scheme for X-ray crystal structure analysis.

Because the strong donating character of the peri-dichalcogenide polyacenes is based on aromatization of the heterocyclic ring in the resulting cationic species, a charge-transfer in their complexes might bring about a change in the ring dimensions: that is, a shortening of the Se–Se and Se–C bond lengths.[15] For a comparison the molecular structures of neutral 2,3-DMTSA, 6,7-DMTSA, and 2,3-DMTTA were determined. 2,3-DMTSA was analyzed for a single crystal including one benzene per two molecules. The crystal data and the molecular structures are given in Tables 6 and 7, respectively. Since TMTTA and TMTSA did not offer good crystals for X-ray analyses, neutral 2,3-DMTTA and 2,3-DMTSA were used as substitutes for examining any dimensional change. Both the Se–Se and C–Se bond lengths of the 2,3-DMTSA complex are shorter

Table 6. Crystal Data of 2,3-DMTSA, 6,7-DMTSA, and 2,3-DMTTA

	$(2,3\text{-DMTSA})_2C_6H_6$	6,7-DMTSA	2,3-DMTTA
Formula	$C_{38}H_{26}Se_8$	$C_{16}H_{10}Se_4$	$C_{16}H_{10}S_4$
Fw	1114.30	518.10	330.51
Crystal system	Monoclinic	Monoclinic	Triclinic
Space group	$P2_1/n$	$P2_1/c$	$P\bar{1}$
a/Å	18.354(1)	7.509(1)	10.343(2)
b/Å	16.199(2)	22.028(2)	12.496(2)
c/Å	5.679(1)	9.471(1)	7.456(2)
α/°	90.0	90.0	90.15(2)
β/°	93.51(1)	111.41(1)	108.14(2)
γ/°	90.0	90.0	129.37(1)
V/Å^3	1685.3(4)	1458.4(3)	681.2(3)
Z	2	4	2
Crystal size/mm^3	0.64×0.08×0.06	0.35×0.10×0.02	0.35×0.13×0.10
Abs correction	Analytical[a)]	Analytical[a)]	Analytical[a)]
No. of data	2274	1874	1853
R	0.041	0.041	0.059

a) Ref. 18.

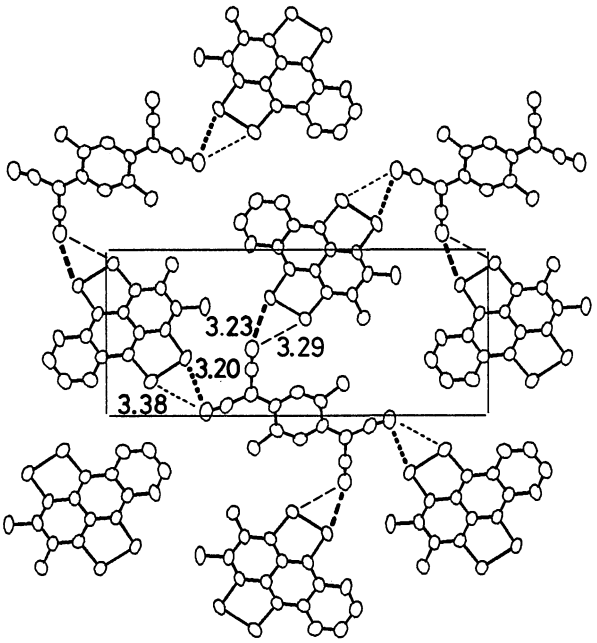

Fig. 4. Crystal structure of 2,3-DMTSA·DMTCNQ projected along the c axis.

than the corresponding ones of neutral 2,3-DMTSA, while the other complexes do not show such appreciable variations. In addition, the molecular geometry of DMTCNQ becomes more benzenoid in character for the 2,3-DMTSA·DMTCNQ complex (Table 5), supporting a complete charge transfer.[16] A question is why only the 2,3-DMTSA·DMTCNQ complex shows so large charge-transfer and high conductivity. As already pointed out, although its crystal structure is very similar to those of the other complexes, there is a small difference in overlapping distances. Thus the 2,3-DMTSA·DMTCNQ complex has a rather longer interplanar distance between the donor and acceptor than do the other omplexes, being in conflict with the actual degree of charge transfer. On the other hand, the interplanar distance between paired donors is shorter, and a short Se–Se contact (3.62 Å) is observed. In addition, there are observed some intercolumnar Se–N contacts between 2,3-DMTSA and the neighboring DMTCNQ, constituting a net-work sheet (Fig. 4). It is thus concluded that the large charge transfer and high conductivity of the 2,3-DMTSA·DMTCNQ complex are induced by strong heteroatomic interactions of Se–Se and Se–N.

Experimental

General. Melting points are uncorrected. All chemicals and solvent are of reagent grade. Elemental analyses were measured by Mr. Hideaki Iwatani, Microanalytical Laboratory in Department of Applied Chemistry, Faculty of Engineering, Hiroshima University. NMR spectra were recorded on a JEOL PMX-60 spectrometer (60 MHz) using deuteriochloroform as a solvent and tetramethylsilane as an internal standard. IR spectra were taken on a Hitachi 260-30 spectrometer with a KBr disk method. MS spectra were measured at 70 eV on a Shimadzu QP-1000A spectrometer using a direct insertion technique. Electronic spectra were recorded on a Shimadzu UV-160 spectrometer or on a Hitachi 330 spectrophotometer. Cyclic voltammetry was carried out on a Hokuto Denko HA-301 potentiostat and a Hokuto Denko HB-104 function generator.

1,4-Dihydroxy-2,3-dimethylanthraquinone (3a). Compound (**3**) was prepared by modifying the synthetic method of Kerdersky et al.[9] A mixture of anhydrous aluminium chloride (50 g) and sodium chloride (10 g) was well ground together in a mortor, and heated at 210 °C to melt. Into a stirred solution was added a mixture of phthalic anhydride (**1a**) (7.4 g, 50 mmol) and 2,3-dimethylhydroquinone (**2b**) (6.9 g, 50 mmol); heating at the temperature was continued for further 4 h. Concd hydrochloric acid (50 cm^3) and water (200 cm^3) were successively added into a mixture cooled to ca. 100 °C, which was then gently boiled for 2 h. The resulting solid, while still hot, was collected by filtration and dissolved in chloroform (2 dm^3). After the solution was filtered, the filtrate was concen-

Table 7. Intramolecular Bond Distances and Angles for 2,3-DMTSA, 6,7-DMTSA, and 2,3-DMTTA

Bond distance/Å	2,3-DMTSA	6,7-DMTSA	2,3-DMTTA
X1–X2	2.336(1)	2.344(1)	2.102(3)
X1–C16	1.912(6)	1.906(6)	1.760(4)
X2–C3	1.913(6)	1.913(6)	1.755(5)
C3–C4	1.382(8)	1.352(9)	1.388(10)
C3–C17	1.421(8)	1.429(9)	1.400(7)
C4–C5	1.417(8)	1.440(9)	1.442(7)
C4–C19	1.521(9)	—	1.520(8)
C5–C6	1.380(8)	1.364(10)	1.378(8)
C5–C20	1.508(8)	—	1.520(12)
C6–X7	1.915(6)	1.899(6)	1.763(4)
C6–C18	1.440(8)	1.441(9)	1.409(10)
X7–X8	2.345(1)	2.339(1)	2.090(3)
X8–C9	1.922(5)	1.898(6)	1.748(5)
C9–C10	1.405(8)	1.424(9)	1.421(10)
C9–C18	1.369(8)	1.372(10)	1.390(7)
C10–C11	1.433(9)	1.414(10)	1.420(8)
C10–C15	1.440(8)	1.430(8)	1.433(7)
C11–C12	1.393(9)	1.373(9)	1.388(13)
C12–C13	1.411(10)	1.422(10)	1.401(9)
C12–C21	—	1.527(11)	—
C13–C14	1.382(9)	1.399(10)	1.379(10)
C13–C22	—	1.513(10)	—
C14–C15	1.426(8)	1.415(9)	1.420(12)
C15–C16	1.414(8)	1.413(9)	1.405(8)
C16–C17	1.381(8)	1.393(8)	1.393(10)
C17–C18	1.443(8)	1.436(8)	1.419(6)
Bond angle/°	**2,3-DMTSA**	**6,7-DMTSA**	**2,3-DMTTA**
X2–X1–C16	91.6(2)	91.8(2)	95.7(3)
X1–X2–C3	92.3(2)	92.1(2)	95.3(2)
X2–C3–C4	120.9(4)	121.3(5)	124.2(4)
X2–C3–C17	115.7(4)	115.4(4)	114.1(5)
C4–C3–C17	123.4(5)	123.3(6)	121.7(4)
C3–C4–C5	119.6(5)	119.3(7)	119.0(5)
C3–C4–C19	120.2(5)	—	120.6(5)
C5–C4–C19	120.2(5)	—	120.4(6)
C4–C5–C6	118.3(5)	119.5(6)	118.8(7)
C4–C5–C20	121.4(5)	—	120.7(5)
C6–C5–C20	120.2(5)	—	120.6(5)
C5–C6–X7	121.0(4)	121.7(5)	124.2(5)
C5–C6–C18	124.1(5)	122.3(6)	122.6(4)
X7–C6–C18	114.9(4)	116.0(5)	113.3(4)
C6–X7–X8	92.4(2)	92.1(2)	95.4(2)
X7–X8–C9	91.5(2)	91.7(2)	96.0(2)
X8–C9–C10	120.5(4)	120.3(5)	125.1(3)
X8–C9–C18	116.9(4)	117.9(5)	113.9(5)
C10–C9–C18	122.6(5)	121.7(5)	121.0(4)
C9–C10–C11	122.6(5)	122.9(6)	121.8(5)
C9–C10–C15	118.5(5)	118.7(6)	118.7(5)
C11–C10–C15	118.9(5)	118.3(5)	119.5(7)
C10–C11–C12	119.8(6)	121.9(6)	119.8(5)
C11–C12–C13	120.7(6)	120.4(7)	120.8(6)
C11–C12–C21	—	119.8(6)	—
C13–C12–C21	—	119.7(6)	—
C12–C13–C14	121.2(6)	118.8(6)	120.6(9)
C12–C13–C22	—	120.5(6)	—
C14–C13–C22	—	119.7(6)	—
C13–C14–C15	119.8(6)	121.3(6)	120.6(6)
C10–C15–C14	119.6(5)	119.2(6)	118.8(5)
C10–C15–C16	118.3(5)	118.8(5)	118.9(6)
C14–C15–C16	122.1(5)	121.9(6)	122.3(5)
X1–C16–C15	120.5(4)	121.3(4)	124.3(6)
X1–C16–C17	117.2(4)	116.8(5)	113.6(4)
C15–C16–C17	122.3(5)	121.8(5)	122.0(4)
C3–C17–C16	123.2(5)	123.3(5)	121.4(4)
C3–C17–C18	117.9(5)	117.7(5)	120.0(6)
C16–C17–C18	118.9(5)	119.0(6)	118.9(5)
C6–C18–C9	123.9(5)	122.3(5)	121.4(4)
C6–C18–C17	116.6(5)	117.8(6)	118.3(5)
C9–C18–C17	119.4(5)	119.9(6)	120.4(6)

trated to ca. 200 cm³ and purified by column chromatography on silica gel using chloroform as an eluent to give a reddish-orange solid of **3a** (11.3 g, 84.6%). An analytical sample was obtained as reddish-orange needles upon recrystallization from benzene–hexane: Mp 259—260 °C (lit,[9] mp 252—253 °C); ^{1}H NMR δ=2.40 (s, 6H, CH_3), 7.73 (AA'BB' m, 2H, ArH), 8.24 (AA'BB' m, 2H, ArH), and 13.48 (s, 2H, OH); IR 1590 cm^{-1} (C=O); MS *m/z* 268 (M^+); Anal. Calcd for $C_{16}H_{12}O_4$: C, 71.64; H, 4.51%. Found: C, 71.63; H, 4.51%.

1,4-Dihydroxy-6,7-dimethylanthraquinone (3b): 74% yield; reddish orange needles from chloroform; mp 228 °C; ^{1}H NMR δ=2.30 (s, 6H, CH_3), 7.20 (s, 2H, ArH), 7.95 (s, 2H, ArH), and 12.75 (s, 2H, OH); IR 1630 and 1590 cm^{-1} (C=O); MS *m/z* 268 (M^+); Anal. Calcd for $C_{16}H_{12}O_4$: C, 71.64; H, 4.51%. Found: C, 71.60; H, 4.49%.

1,4-Dihydroxy-2,3,6,7-tetramethylanthraquinone (3c): 69% yield; reddish orange needles from chloroform; mp 276 °C; ^{1}H NMR δ=2.25 (s, 6H, CH_3), 2.40 (s, 6H, CH_3), 7.96 (s, 2H, ArH), and 13.40 (s, 2H, OH); IR 1580 cm^{-1} (C=O); MS *m/z* 296 (M^+); Anal. Calcd for $C_{18}H_{16}O_4$: C, 72.96; H, 5.44%. Found: C, 72.84; H, 5.40%.

2,3-Dihydro-9,10-dihydroxy-6,7-dimethyl-1,4-anthracenedione (4). Into a suspension of **3b** (5.3 g, 19.8 mmol) and anhyd. sodium carbonate (5 g) in water (100 cm³) was added sodium dithionite (10 g); the mixture was heated at 80 °C for 15 h. After cooling, the resulting yellow solid was collected by filtration and dried. Chromatography on silica gel using dichloromethane as an eluent followed by recrystallization from benzene–hexane gave yellow needles of **4** (4.8 g, 88%): Mp 182 °C; ^{1}H NMR δ=2.45 (s, 6H, CH_3), 2.96 (s, 4H, CH_2), 8.00 (s, 2H, ArH), and 13.60 (s, 2H, OH); IR 1610 cm^{-1} (C=O); MS *m/z* 270 (M^+); Anal. Calcd for $C_{16}H_{14}O_4$: C, 71.11; H, 5.22%. Found: C, 71.40; H, 5.05%.

1,4,9,9,10,10-Hexachloro-2,3-dimethyl-9,10-dihydroanthracene (5a). A mixture of **3a** (4.2 g, 15.7 mmol), phosphorus pentachloride (23 g, 110 mmol), and phosphoryl oxychloride (40 cm³) was refluxed for 9 h. Concentration in a reduced pressure followed by thorough washing of the residue with hexane and then with methanol left a white solid of **5a** (3.8 g, 59%); mp 140 °C (decomp); ^{1}H NMR δ=2.55 (s, 6H, CH_3), 7.42 (AA'BB' m, 2H, ArH), and 7.95 (AA'BB' m, ArH); IR 710 cm^{-1} (C–Cl); MS *m/z* 414 (M^+) with an isotopic pattern hexachlorine. Anal. Calcd for $C_{16}H_{10}Cl_6$: C, 46.31; H, 2.43%. Found: C, 45.71; H, 2.36%.

1,4,9,9,10,10-Hexachloro-6,7-dimethyl-9,10-dihydroanthracene (5b): 30% yield from **4**; a white solid; mp 232 °C (decomp); ^{1}H NMR δ=2.45 (s, 6H, CH_3), 7.52 (s, 2H, ArH), and 7.73 (s, 2H, ArH); IR 740 cm^{-1} (C–Cl); MS *m/z* 414 (M^+) with an isotopic pattern of hexachlorine. Anal. Calcd for $C_{16}H_{10}Cl_6$: C, 46.31; H, 2.43%. Found: C, 45.72; H, 2.24%.

1,4,9,9,10,10-Hexachloro-2,3,6,7-tetramethyl-9,10-dihydroanthracene (5c): 44% yield from **3c**; a white solid; mp 139 °C (decomp); ^{1}H NMR δ=2.37 (s, 6H, CH_3), 2.58 (s, 6H, CH_3), and 7.73 (s, 2H, ArH); IR 750 cm^{-1} (C–Cl); MS *m/z* 440 (M^+) with an isotopic pattern of hexachlorine. Anal. Calcd for $C_{18}H_{14}Cl_6$: C, 48.80; H, 3.19%. Found: C, 48.37; H, 3.00%.

1,4,9,10-Tetrachloro-2,3-dimethylanthracene (6a). A mixture of **5a** (3.8 g, 9.2 mmol), tin(II) chloride dihydrate (29.2 g), acetic acid (40 cm³), and concd hydrochloric acid (36 cm³) was refluxed for 1.5 h. After cooling, the resulting yellow solid of **6a** was collected by filtration, washed, and purified by column chromatography on active alumina using

benzene as eluent (2.4 g, 75%). An analytical sample was obtained as yellow needles by recrystallization from chloroform–hexane; mp 119—120 °C (decomp); ^{1}H NMR δ=2.56 (s, 6H, CH_3), 7.52 (AA'BB' m, 2H, ArH), and 8.45 (AA'BB' m, 2H, ArH); IR 660 cm^{-1} (C–Cl); MS m/z 344 (M^+) with an isotopic pattern of tetrachlorine. Anal. Calcd for $C_{16}H_{10}Cl_4$: C, 55.85; H, 2.93%. Found: C, 55.84; H, 2.89%.

1,4,9,10-Tetrachloro-6,7-dimethylanthracene (6b): 80% yield; yellow needles from chloroform–hexane; mp 172 °C; ^{1}H NMR δ=2.48 (s, 6H, CH_3), 7.32 (s, 2H, ArH), and 8.45 (s, 2H, ArH); IR 810 and 605 cm^{-1}; MS m/z 344 (M^+) with an isotopic pattern of tetrachlorine. Anal. Calcd for $C_{16}H_{10}Cl_4$: C, 55.85; H, 2.93%. Found: C, 55.82; H, 3.06%.

1,4,9,10-Tetrachloro-2,3,6,7-tetramethylanthracene (6c): 75% yield; yellow needles from benzene; mp 187—188.5 °C; ^{1}H NMR δ=2.47 (s, 6H, CH_3), 2.53 (s, 6H, CH_3), and 8.23 (s, 2H, ArH); IR 670 cm^{-1} (C–Cl); MS m/z 370 (M^+) with an isotopic pattern of tetrachlorine. Anal. Calcd for $C_{18}H_{14}Cl_4$: C, 58.10; H, 3.79%. Found: C, 58.07; H, 3.58%.

3,4-Dimethylanthra[1,9-*cd*:4,10-*c'd'*]dithiole (2,3-DMTTA). In a nitrogen atmosphere, sodium metal (165 mg, 7.2 mmol) was allowed to react with sulfur (236 mg, 7.2 mmol) in dry DMF (30 cm^3) at 100 °C for 2 h, forming fresh sodium disulfide. Into the mixture was added a solution of **6a** (516 mg, 1.5 mmol) in dry DMF (30 cm^3). It was refluxed for 8 h, stirred overnight at room temperature with exposure to air, and then poured into brine (200 cm^3). The resulting brown solid was collected by filtration, dried, and extracted with hexane and then with carbon disulfide by use of a Soxhlet apparatus. The carbon disulfide extract was recrystallized from benzene to give black purple needles of 2,3-DMTTA (211 mg, 43%); mp 271 °C; IR 1610, 1300, and 740 cm^{-1}; MS m/z 330 (M^+); UV (CS_2) 450.5 (log ε 3.79), 531 (3.87), and 566.5 nm (3.90). Anal. Calcd for $C_{16}H_{10}S_4$: C, 58.15; H, 3.05%. Found: C, 58.41; H, 2.87%.

3,4-Dimethylanthra[1,9-*cd*:4,10-*c'd'*]diselenole (2,3-DMTSA). 2,3-DMTSA was prepared from a similar reaction of **6a** with sodium diselenide at 150 °C and recrystallized from benzene to give black crystals. The elemental analysis and X-ray crystallographic analysis showed that it consists of 2,3-DMTSA and benzene of 2:1 ratio. Its heating at 150 °C under a reduced pressure left the free 2,3-DMTSA: 31% yield; mp 289 °C; IR 1270 and 740 cm^{-1}; MS m/z 520 (M^+); UV (CS_2) 439.5 (log ε 3.75) and 568.5 nm (4.09). Anal. Calcd for $C_{16}H_{10}Se_4$: C, 37.09; H, 1.95%. Found: C, 37.21; H, 1.93%.

3,4-Dimethylanthra[1,9-*cd*:4,10-*c'd'*]ditellurole (2,3-DMTTeA). 2,3-DMTTeA was prepared from a similar reaction of **6a** with sodium ditelluride at 100 °C. Recrystallization from chlorobenzene gave black needles; 15% yield; mp >300 °C; IR 1250 cm^{-1}; MS m/z 714 (M^+); UV (CS_2) 598.5 nm (log ε 4.05). Anal. Calcd for $C_{16}H_{10}Te_4$; C, 26.97; H, 1.41%. Found: C, 26.96; H, 1.40%.

8,9-Dimethylanthra[1,9-*cd*:4,10-*c'd'*]dithiole (6,7-DMTTA): 2% yield; black purple powder from benzen mp >300 °C; IR 1340, 1290, 1165, and 790 cm^{-1}; MS m/z 330 (M^+); UV (CS_2) 451 (log ε 3.66), 529 (3.92), and 562 nm (3.98). Anal. Calcd for $C_{16}H_{10}S_4$: C, 58.14; H, 3.05%. Found: C, 58.08; H, 3.04%.

8,9-Dimethylanthra[1,9-*cd*:4,10-*c'd'*]diselenole (6,7-DMTSA): 38% yield; black plates from chlorobenzene; mp >300 °C; IR 1320, 1280, 1150, and 795 cm^{-1}; MS m/z 520 (M^+); UV (CS_2) 446.5 (log ε 3.66) and 568.5 nm (4.10). Anal. Calcd for $C_{16}H_{10}Se_4$: C, 37.09; H, 1.95%. Found: C, 37.19; H, 1.95%.

3,4,8,9-Tetramethylanthra[1,9-*cd*:4,10-*c'd'*]dithiole (TMTTA): 41% yield; black needles from chlorobenzene; mp >300 °C; IR 2990, 2850, and 1310 cm^{-1}; MS m/z 358 (M^+); UV (CS_2) 447.5 (log ε 3.82), 525.5 (3.89), and 557 nm (3.94). Anal. Calcd for $C_{18}H_{14}S_4$: C, 60.29; H, 3.94%. Found: C, 60.23; H, 3.85%.

3,4,8,9-Tetramethylanthra[1,9-*cd*:4,10-*c'd'*]diselenole (TMTSA): 29% yield; black powder from gradient sublimation; mp >300 °C; IR 3000, 2930, and 1290 cm^{-1}; MS m/z 548 (M^+); UV (CS_2) 559 nm (log ε 4.11). Anal. Calcd for $C_{18}H_{14}Se_4$: C, 39.59; H, 2.58%. Found: C, 39.55; H, 2.51%.

3,4,8,9-Tetramethylanthra[1,9-*cd*:4,10-*c'd'*]ditellurole (TMTTeA): 14% yield; black powder from carbon disulfide; mp >300 °C; MS m/z 740 (M^+); UV (CS_2) 586.5 nm (log ε 4.07). Anal. Calcd for $C_{18}H_{14}Te_4$: C, 29.19; H, 1.91%. Found: C, 29.48; H, 1.82%.

Charge-Transfer Complexes. All of the complexes described in this report were prepared by mixing two hot saturated solutions of the donor and acceptor in chlorobenzene. The resulting complexes precipitated out upon cooling, which were collected by filtration, washed with cold dichloromethane, and dried.

Crystal Structures. The X-ray diffraction data were collected with a Rigaku automated diffractometer using Cu $K\alpha$ radiation monochromatized with a graphite plate. Independent reflections within 2θ=126° ($|F_o| \geqslant 3.0\sigma(F_o)$) were used for analyses. The structures were solved by a direct method combined with the Monte-Carlo method for the selection of the initial set of phase,[17] and refined by a full-matrix least squares method.[18] Atomic scattering factors were taken from International Tables for X-ray Crystallography.[19] The anisotropic temperature factors were used for the refinement; hydrogen atoms were not included in the refinement. Tables of final atomic parameters, structure factors, and anisotropic thermal parameters are deposited as Document No. 9116 at the Office of the Editor of Bull. Chem. Soc. Jpn.

The present work was in part supported by the Grant-in-aid of Scientific Research on Priority Areas No. 02230222 from the Ministry of Education, Science and Culture. The authors thank Dr. K. Kawabata and Dr. M. Mizutani of Central Research Laboratories, Idemitsu Kosan Co., Ltd. for helpful discussions.

References

1) For an excellent review on TTT and TST, see I. F. Shchegolev and E. B. Yagubskii, "Extended Linear Chain Compounds," ed by J. S. Miller, Plenum Press, New York (1982), Vol. 2, pp. 385—434.

2) D. J. Sandman and J. C. Stark, *Organomet.*, **1**, 739 (1982).

3) S. Ohnishi, T. Nogami, and H. Mikawa, *Tetrahedron Lett.*, **1983**, 2401; T. Nogami, H. Tanaka, S. Ohnishi, Y. Tasaka, and H. Mikawa, *Bull. Chem. Soc. Jpn.*, **57**, 22 (1983).

4) F. Wudl, D. E. Schafer, and B. Miller, *J. Am. Chem. Soc.*, **98**, 252 (1976).

5) S. Ohnishi, T. Nogami, and H. Mikawa, *Chem. Lett.*, **1982**, 1841.

6) A. Yamahira, T. Nogami, and H. Mikawa, *J. Chem. Soc.*,

Chem. Commun., **1983**, 904; J. C. Stark, R. Reed, L. A. Acampora, D. J. Sandman, S. Jansen, M. T. Jones, and B. M. Foxman, *Organomet.*, **3**, 732 (1984).

7) T. Otsubo, N. Sukenobe, Y. Aso, and F. Ogura, *Chem. Lett.*, **1987**, 315; *Synth. Met.*, **27**, B509 (1988).

8) A preliminary account on a part of the present work has appeared: K. Takimiya, H. Miyamoto, Y. Aso, T. Otsubo, and F. Ogura, *Chem. Lett.*, **1990**, 567.

9) F. A. J. Kerdesky and M. P. Cava, *J. Am. Chem. Soc.*, **100**, 3635 (1978); F. A. J. Kerdesky, R. J. Ardecky, M. V. Lakshmikantham, and M. P. Cava, *ibid.*, **103**, 1992 (1981).

10) K. Yui, Y. Aso, T. Otsubo, and F. Ogura, *Bull. Chem. Soc. Jpn.*, **62**, 1539 (1989).

11) K. Yui, Y. Aso, T. Otsubo, and F. Ogura, *Chem. Lett.*, **1988**, 1179.

12) J. B. Torrance, *Acc. Chem. Res.*, **12**, 79 (1979); G. Saito and J. P. Ferraris, *Bull. Chem. Soc. Jpn.*, **53**, 2141 (1980).

13) J. B. Torrance, B. A. Scott, and F. B. Kaufman, *Solid State Commun.*, **17**, 1369 (1975); J. Tanaka, M. Tanaka, T. Kawai, T. Takabe, and O. Maki, *Bull. Chem. Soc. Jpn.*, **49**, 2358 (1976); E. M. Engler, V. V. Patel, J. R. Andersen, R. R. Schumaker, and A. A. Fukushima, *J. Am. Chem. Soc.*, **100**, 3769 (1978); K. Nakasuji and I. Murata, *Synth. Met.*, **27**, B289 (1988).

14) J. S. Chappell, A. N. Bloch, W. A. Bryden, M. Maxfield, T. O. Poehler, and D. O. Cowan, *J. Am. Chem. Soc.*, **103**, 2442 (1981).

15) R. P. Shibaeva, "Extended Linear Chain Compounds," ed by J. S. Miller, Plenum Press, New York (1982), Vol. 2, pp. 435—467.

16) T. J. Kristenmacher, T. J. Emge, A. N. Bloch, and D. O. Cowan, *Acta Crystallogr., Sect. B*, **38**, 1193 (1982).

17) A. Furusaki, *Acta Crystallogr., Sect. A*, **35**, 220 (1979).

18) C. Katayama, N. Sakabe, and K. Sakabe, *Acta Crystallogr., Sect. A*, **28**, S207 (1972).

19) "International Tables for X-ray Crystallography," Kynoch Press, Birmingham, England (1974), Vol. IV.

Structural Studies of a Liquid Crystalline Compound, 2-(4-Cyanophenyl)-5-(4-butylphenyl)-1,3,2-dioxaborinane, by Means of Nuclear Magnetic Resonance and X-Ray Analyses

Hiroshi MATSUBARA, Takanori TANAKA, Yoshio TAKAI, Masami SAWADA, Koji SETO,† Hideyuki IMAZAKI,† and Shigetoshi TAKAHASHI*
The Institute of Scientific and Industrial Research, Osaka University, Mihogaoka, Ibaraki, Osaka 567
† Research & Development Division, Nitto Kasei Co., Ltd., 3 Nishiawaji, Higashiyodogawa, Osaka 533
(Received February 21, 1991)

The crystal and molecular structure of the title nematogen (**1**), has been determined by an X-ray analysis. Compound **1** belongs to the triclinic system with space group $P\bar{1}$, a=9.798(2), b=11.579(2), c=9.716(2) Å, α=74.081(13), β=117.766(14), γ=108.179(13)°, and with two molecules in the unit cell. The geometry around the boron atom is planar, and the plane defined by O2BC is parallel to the phenyl ring bonded to the boron atom. The angle between two phenyl rings is 74.3°. The molecules are in their most extended conformation, with nearest neighbors oriented antiparallel to each other. The ^{1}H NMR studies have indicated that the half-chair conformation of the dioxaborinane is kept in a solution even at 125 °C where **1** forms a nematic phase, and the rigidity is essential for the formation of mesophases.

Relation between molecular structure and property of liquid crystalline materials are of current interest. In order to understand molecular arrangements in mesophases on the basis of the molecular structure, direct analyses of nematic or smectic phases by spectroscopic and X-ray methods have been made,[1] but only a little information has been obtained to date. Thus at present in many cases it may be obliged to infer the molecular structure and arrangement in a liquid crystalline state from those in a crystalline one.[2]

Previously we have shown[3] that 2-aryl-1,3,2-dioxaborinane derivatives (I) provide a new series of liquid crystalline materials and form nematic, smectic A and C, and chiral smectic C phases depending on their structures. Since they contain a metalloid atom, boron, in the

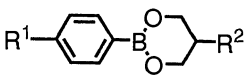

(I)

six-membered ring, it is supposed that they have a unique structural feature. In order to discuss the characteristics of the dioxaborinane compounds, especially in terms of the influence of the boron atom on the molecular structure and liquid crystalline property, we have performed structural analyses of a representative nematogen among them both in a solution and in a crystalline state. Here we report the NMR and X-ray analyses of 2-(4-cyanophenyl)-5-(4-butylphenyl)-1,3,2-dioxaborinane (**1**)[4] which forms a stable nematic phase in the temperature range of 120—128 °C as shown in Fig. 1.

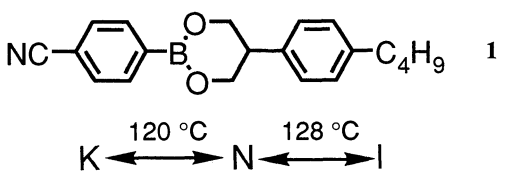

Fig. 1. Structure and phase sequence of **1**.

Experimental

Materials. 2-(4-Cyanophenyl)-5-(4-butylphenyl)-1,3,2-dioxaborinane (**1**) and 2-(4-butoxyphenyl)-5-octyl-1,3,2-dioxaborinane (**6a**) were prepared by the method[4] reported previously and the single crystals of **1** were obtained by slow evaporation from a solution of **1** in hexane.

2-(4-Butoxyphenyl)-5-octyl-4,4,6,6-tetradeuterio-1,3,2-dioxaborinane (**6b**) was similarly prepared by dehydrocondensation in toluene between 4-butoxyphenylboronic acid and 2-octyl-1,1,3,3-tetradeuterio-1,3-propanediol which was obtained by the reduction of diethyl octylmalonate with lithium alminum deuteride. Recrystallization from hexane gave colorless crystals of **6b** in 40% yield. IR (KBr) 2920 (ν_{CH}), 2220 and 2110 (ν_{CD}), 1340 cm^{-1} (ν_{BO}); MS m/z 350 (M^+).

Collection of X-ray Diffraction Data and Structure Determination. Crystal data and experimental conditions are summarized in Table 1. Three dimensional intensity data were collected on a Rigaku AFC-5FOS automated four circle diffractometer at room temperature. Mo K_α (λ=0.71069 Å) radiation with a graphite crystal monochrometor in the incident beam was used. Unit cell constants were determined by a least-squares fit of 25 reflections in the range of $21°<2\theta<27°$. Three standard reflections were checked every 55 reflections during the course of the intensity-collection and no intensity-decrease was observed. Intensity data were reduced to structure factors without any absorption corrections.

Structure was solved by direct methods (MULTAN84), refined by block-diagonal least-squares methods and RASA software was employed for the entire structure analyses. Non-hydrogen atoms were assigned with anisotropic temperature factors. Hydrogen atoms were found by difference Fourier calculations and refined with isotropic thermal parameters. The structure has been refined to R=0.070 (R_w=0.056) for 2121 observed reflections.

Computations were carried out on a FACOM S3500 superminicomputer at Material Analysis Center, ISIR, Osaka University.

NMR Measurement. High resolution ^{1}H NMR spectra of **1**

Table 1. Crystal and Experimental Data

Empirical formula	$C_{20}H_{22}NBO$
Crystal system	Triclinic
Space group	$P\bar{1}$
a/Å	9.798
b/Å	11.579
c/Å	9.716
α/°	74.081
β/°	117.766
γ/°	108.179
V/Å^3	915.700
Z	2
D/g cm^{-3}	1.1581
μ(Mo $K\alpha$)/Å	0.71069
Scan method	θ–2θ
Scan range d(2θ)	1.4+tanθ°
Scan speed in 2θ/° min^{-1}	4
$2\theta_{max}$/°	50
Background/s^{-1}	2×5.0
Refl. measd	2625
Refl. used ($F>2\sigma(F)$)	2121
Final R (R_w)	0.070 (0.056)

were recorded on a Bruker WM360 spectrometer. Deuteriochloroform and 1,2-dideuterio-1,1,2,2-tetrachloroethane were used as solvents on the measurements at a room temperature and at a higher temperature, respectively.

Results and Discussion

Description of Structure. The crystal and molecular structures of **1** have been determined by a single-crystal X-ray analysis. This is the first X-ray structural analysis of the 1,3,2-dioxaborinane derivatives. The molecular structure of **1** is illustrated in Fig. 2. The final positional and thermal parameters of all the non-hydrogen atoms are listed in Table 2, and Tables 3 and 4 list the bond length and the angles, respectively.

It can be seen from the projection that the geometry around the boron atom is planar and the plane defined by O2BC is coplanar with the phenyl ring bonded to the boron atom. The conformation of the dioxaborinane ring is characterized to be in a half-chair form.

The bond length between boron and carbon is 1.562 Å, shorter than those of borates, compounds **2** (1.590 Å)[5] and **3** (1.628, 1.630 Å).[6] The length is somewhat shorter than that of triphenylborane **4** (1.571, 1.589 Å),[7] because

Table 2. Final Atomic Coordinates and Isotropic Thermal Parameters with esd's in Parentheses for the Non-Hydrogen Atoms of **1**

Atom	x	y	z	B_{eq}[a]
O(1)	0.7477(3)	0.2660(2)	0.1809(3)	6.6
O(2)	0.7905(3)	0.3672(3)	0.3850(3)	7.4
N(1)	−0.0649(4)	0.4237(3)	−0.1698(5)	7.9
B(1)	0.6987(5)	0.3259(4)	0.2463(5)	5.4
C(1)	1.1363(5)	0.2199(4)	0.5256(5)	6.1
C(2)	0.5266(4)	0.3475(3)	0.1544(4)	4.9
C(3)	0.2693(5)	0.3140(4)	−0.0633(5)	6.4
C(4)	0.0614(5)	0.4068(4)	−0.0987(5)	5.9
C(5)	0.9069(5)	0.2468(4)	0.2596(5)	6.5
C(6)	0.3212(5)	0.4395(4)	0.1222(5)	6.2
C(7)	0.4721(5)	0.4190(4)	0.2036(4)	6.0
C(8)	0.9480(5)	0.3443(4)	0.4763(5)	7.6
C(9)	0.4208(5)	0.2955(4)	0.0193(4)	5.9
C(10)	0.2189(4)	0.3859(3)	−0.0112(4)	5.1
C(11)	1.3138(5)	0.0931(4)	0.7187(5)	6.2
C(12)	1.2635(5)	0.3069(4)	0.5073(5)	6.9
C(13)	0.9655(5)	0.2384(4)	0.4336(5)	7.1
C(14)	1.1631(5)	0.1142(4)	0.6324(5)	6.2
C(15)	1.4432(5)	0.1792(4)	0.7030(5)	6.5
C(16)	1.4173(5)	0.2863(4)	0.5960(5)	7.2
C(17)	1.6084(5)	0.1541(5)	0.7973(6)	8.7
C(18)	1.6346(6)	0.0630(5)	0.7265(6)	9.9
C(19)	1.8051(8)	−0.0644(6)	0.7475(8)	11.6
C(20)	1.7925(7)	0.0295(6)	0.8182(8)	11.1

a) $B_{eq}=(4/3)\sum_{ij}\beta_{ij}(\boldsymbol{a}_i\cdot\boldsymbol{a}_j)$.

Table 3. Bond Length (l/Å) of **1**

Atoms	l/Å	Atoms	l/Å
C(1)–C(12)	1.387(7)	B(1)–C(2)	1.562(7)
C(2)–C(9)	1.392(6)	C(1)–C(14)	1.375(6)
C(3)–C(10)	1.383(6)	C(3)–C(9)	1.373(6)
C(6)–C(10)	1.383(6)	C(4)–C(10)	1.436(6)
O(1)–B(1)	1.360(6)	C(5)–C(13)	1.496(7)
O(2)–B(1)	1.345(6)	C(11)–C(15)	1.390(7)
O(2)–C(8)	1.446(6)	C(12)–C(16)	1.405(8)
C(1)–C(13)	1.540(7)	C(15)–C(16)	1.388(7)
C(2)–C(7)	1.389(6)	C(11)–C(14)	1.380(7)
C(6)–C(7)	1.377(6)	C(15)–C(17)	1.520(7)
C(8)–C(13)	1.477(7)	C(17)–C(18)	1.544(9)
O(1)–C(5)	1.442(5)	C(18)–C(20)	1.496(10)
N(1)–C(4)	1.152(6)	C(19)–C(20)	1.497(11)

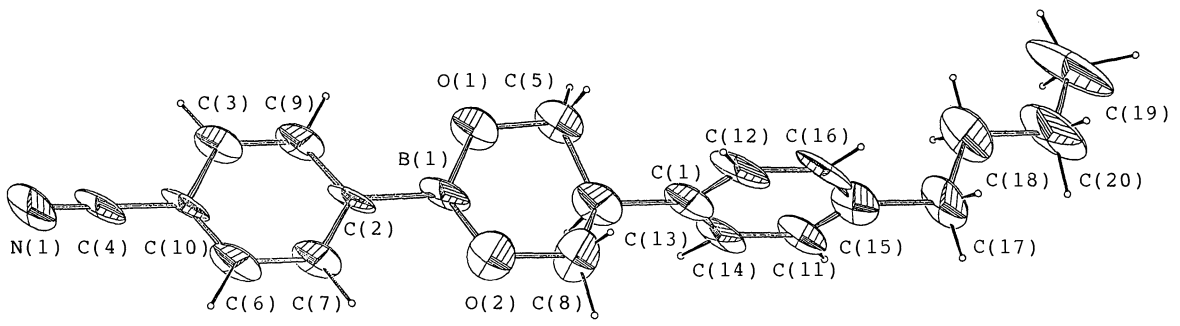

Fig. 2. ORTEP view of **1** with 50% probability thermal ellipsolids.

Table 4. Bond Angles (ϕ/°) of **1**

Atoms	ϕ/°	Atoms	ϕ/°
B(1)–O(1)–C(5)	119.73(35)	B(1)–O(2)–C(8)	120.21(37)
O(1)–B(1)–C(2)	117.81(41)	O(2)–B(1)–C(2)	118.77(41)
C(12)–C(1)–C(14)	119.25(44)	C(13)–C(1)–C(14)	118.35(40)
B(1)–C(2)–C(9)	121.31(39)	C(7)–C(2)–C(9)	116.95(39)
O(1)–C(5)–C(13)	110.09(36)	C(3)–C(10)–C(6)	120.05(40)
C(7)–C(6)–C(10)	119.39(42)	C(1)–C(13)–C(8)	110.79(39)
C(2)–C(7)–C(6)	122.05(42)	C(11)–C(15)–C(17)	120.48(43)
O(2)–C(8)–C(13)	111.59(39)	O(1)–B(1)–O(2)	123.42(43)
C(2)–C(9)–C(3)	122.04(41)	C(12)–C(1)–C(13)	122.38(42)
C(3)–C(10)–C(4)	119.56(40)	B(1)–C(2)–C(7)	121.73(39)
C(14)–C(11)–C(15)	120.98(43)	C(9)–C(3)–C(10)	119.51(42)
C(1)–C(12)–C(16)	120.11(48)	N(1)–C(4)–C(10)	179.52(49)
C(1)–C(13)–C(5)	113.03(39)	C(4)–C(10)–C(6)	120.37(40)
C(5)–C(13)–C(8)	112.37(40)	C(16)–C(15)–C(17)	120.93(44)
C(1)–C(14)–C(11)	120.85(43)	C(17)–C(18)–C(20)	113.99(54)
C(11)–C(15)–C(16)	118.55(44)	C(18)–C(20)–C(19)	110.70(61)
C(12)–C(16)–C(15)	120.25(48)		
C(15)–C(17)–C(18)	111.16(46)		

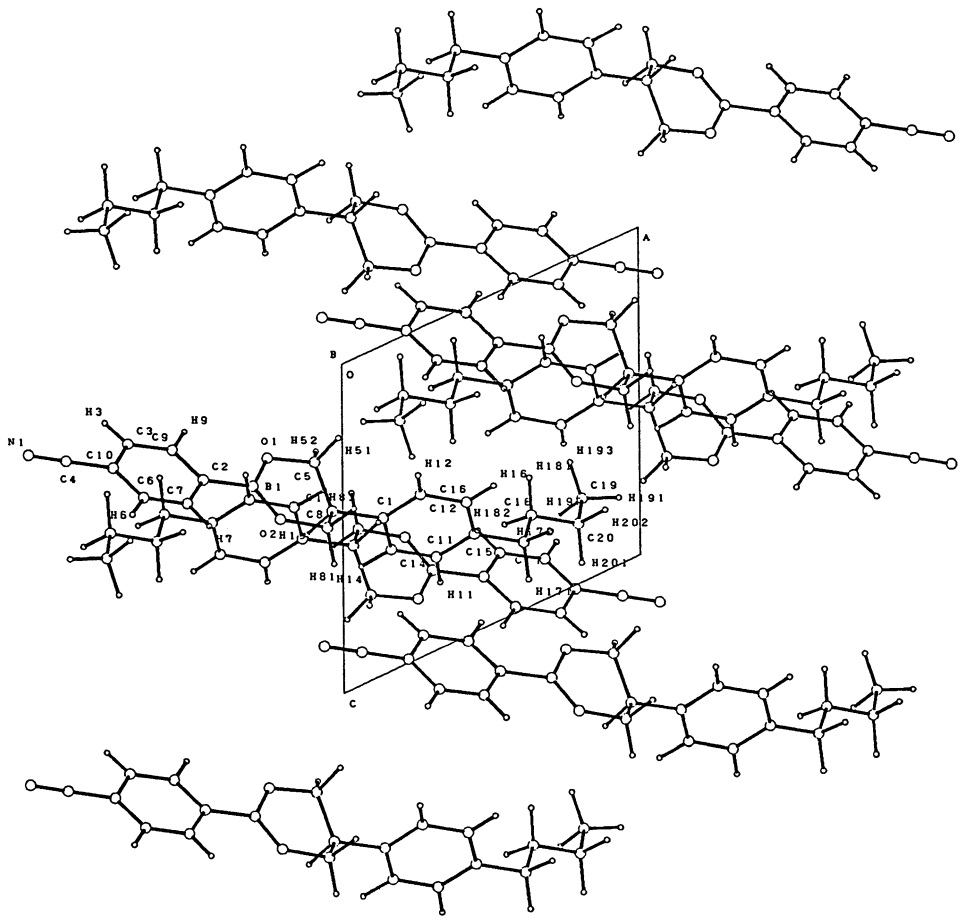

Fig. 3. Crystal structure of **1** viewed along *b* axis.

the boron atom in **4** is not in conjugation with the phenyl rings. The bond length between boron and oxygen are also shorter than those of compounds **2** and **3**. The amine adduct of boronic acid trimer **5** has rather longer B–O (1.400 Å) and B–C (1.574 Å) bonds,[8] which may be due to a borate character.

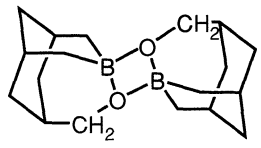

2

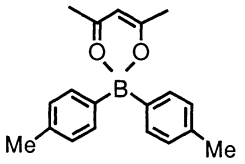

3

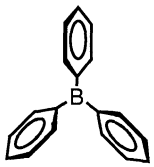

4

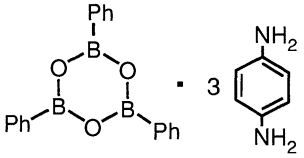

5

The two phenyl rings in compound **1** lie nearly perpendicular, i.e. the torsion angle between them is 74.3°, which compares well with the angles of 81.5° in the molecule of 4-(4-propylcyclohexyl)benzonitrile[9] and 64.5° of 4-(4-octylcyclohexyl)benzonitrile[10] which are well-known to form mesophases. The butyl chain is extended in a trans conformation and the molecule adopts a widely stretched and nearly linear form.

Molecular Packing. In Fig. 3 a projection along the *b*-axis is depicted, which shows the molecules of **1** are arranged in a head-to-tail manner parallel to each other. Such antiparallel arrangement is usually observed in the cases of cyano-substituted mesomorphic molecules (e.g. cyanobiphenyl and cyclohexylbenzonitrile[10,11]) and it is believed that the antiparallel imbricated molecular arrangement in the crystalline state would be kept in the nematic phase. As reported previously for dioxaborinane derivatives[4] the cyano terminal is actually effective for the formation of a nematic phase. The antiparallel dimer structure due to the cyano group effectively contributes to the thermal stability of nematic phases formed by the cyano derivatives of dioxaborinane compounds.

The distance between the cyano groups of neighboring molecules is 3.65 Å, which is within the distance (3.5—4.3 Å) reported on the nematogens having a cyano group by Haase et al.[10-12] The nearest atoms of the neighboring molecules are H3–H81: 2.447 Å, H14–H52:

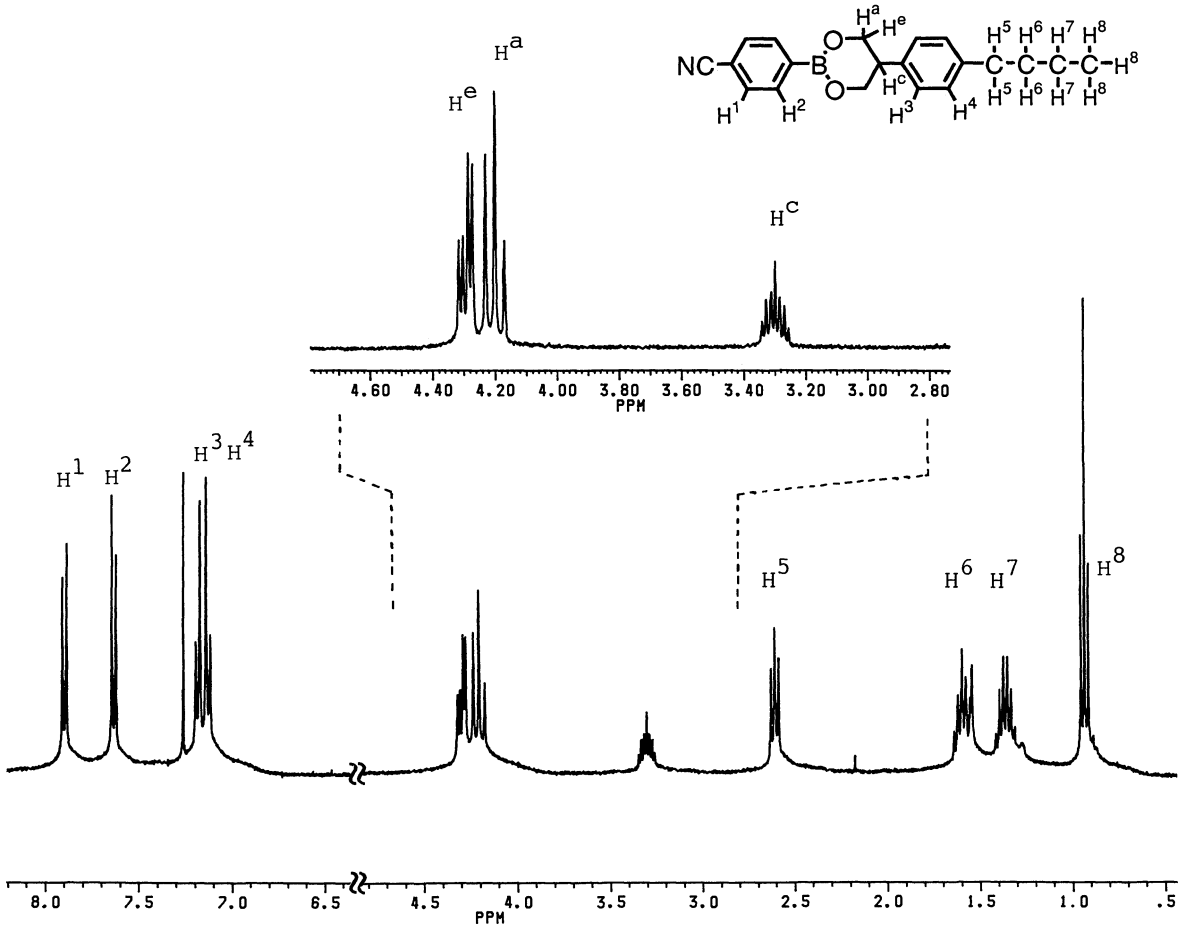

Fig. 4. ^{1}H NMR spectrum of **1** in deuterochloroform at 360 MHz and 25°.

2.448 Å, the dioxaborinane ring is relatively close to a benzene ring, suggesting an interaction between these two rings.

Structure in a Solution. In order to obtain information on the molecular structure, in particular on the dioxaborinane ring of compound **1** in a solution, we have performed detailed investigations by an NMR method. In the $^{11}B\{^1H\}$ NMR spectrum of **1** in acetone-d_6 at ambient temperature showed a relatively broad singlet at 8.3 ppm down field from triethoxyborane as an internal standard. The chemical shift is comparable with that (10.4 ppm) of diethyl phenylboronate.[13] The ^1H NMR spectrum at room temperature is shown in Fig. 4 along with the expanded spectrum in the region of δ=5—3 ppm. Assignment of the signals observed at 4.20 and 4.29 ppm have been made by comparison between ^1H NMR spectra of 2-(4-butoxyphenyl)-5-octyl-1,3,2-dioxaborinane (**6a**) and its 4,4,6,6-tetradeuterio derivative (**6b**). The spetrum of **6a** exhibited three signals at

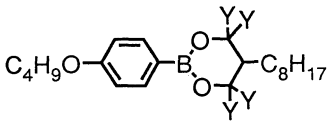

6a: Y=H
6b: Y=D

3.73, 3.97, and 4.14 ppm in the region of δ=3—5 ppm, whereas in the spectrum of deuterio derivative **6b** two of them completely disappeared and only the signal at 3.97 ppm remained, clearly indicating that the signals at 3.73 and 4.14 ppm can be assigned to the methylene protons attached to 4- and 6-carbons of the dioxaborinane ring and the signal at 3.97 ppm to the methylene protons (-O-CH_2-) of the butoxyl group. Thus we can assign the signals observed for compound **1** at 4.20 and 4.29 ppm to the methylene protons of the dioxaborinane ring which were shifted, as compared with **6a**, to a down field due to the phenyl substituent. The signals at 4.29 ppm appeared as a double doublet and at 4.20 ppm apparently as a triplet. The latter is expected to appear as a triplet by accidental superposition of a double doublet.

On the basis of the chemical shifts and the coupling constants observed for them the signal at 4.29 ppm is assigned to the equatorial hydrogens (H^e, $J_{H^e\text{-}H^a}$=11, $J_{H^e\text{-}H^c}$=5 Hz), and at 4.20 ppm to the axial ones (H^a, $J_{H^a\text{-}H^e}$=11, $J_{H^a\text{-}H^c}$=11 Hz) attached to the C4 and C6 of the dioxaborinane ring as shown in Fig. 4 and Table 5. Consequently observation of such the fine structure in the NMR spectra indicates that the half-chair conformation of the dioxaborinane ring is tightly fixed even in a solution. Moreover the spectra measured in 1,1,2,2-tetrachloroethane-d_2 at 125 °C showed the essentially same fine structure in which the geminal-geminal and geminal-axial proton couplings were observed, that is the rigidity of the ring is still kept at the

Table 5. NMR Data for the Methylene (H^e and H^a) and the Methine (H^c) Protons of the 1,3,2-Dioxaborinane Ring

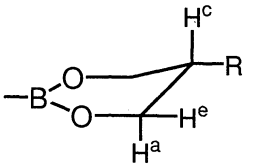

Compounds	H^e	H^a	H^c
1	δ=4.29 2H, dd $J_{H^e\text{-}H^a}$=11 Hz $J_{H^e\text{-}H^c}$=5 Hz	4.20 2H, dd $J_{H^a\text{-}H^a}$=11 Hz $J_{H^a\text{-}H^c}$=11 Hz	3.30 1H, m
6a	δ=4.14 2H, dd $J_{H^e\text{-}H^a}$=11 Hz $J_{H^e\text{-}H^c}$=5 Hz	3.73 2H, dd $J_{H^a\text{-}H^a}$=11 Hz $J_{H^a\text{-}H^c}$=11 Hz	2.06 1H, m
7	δ=4.18 4H, d J=4 Hz		3.74 1H, t J=4 Hz
8	δ=4.17 2H, dd $J_{H^e\text{-}H^a}$=11 Hz $J_{H^e\text{-}H^c}$=5 Hz	3.78 2H, dd $J_{H^a\text{-}H^a}$=11 Hz $J_{H^a\text{-}H^c}$=11 Hz	2.09 1H, m

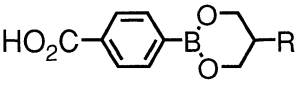

7: R=$OC_{12}H_{25}$ K $\overset{130\ °C}{\longleftrightarrow}$ I

8: R=$C_{12}H_{25}$ K $\overset{151\ °C}{\longleftrightarrow}$ S_C $\overset{163\ °C}{\longleftrightarrow}$ N $\overset{185\ °C}{\longleftrightarrow}$ I

Fig. 5. Structure and phase sequence of **7** and **8**.

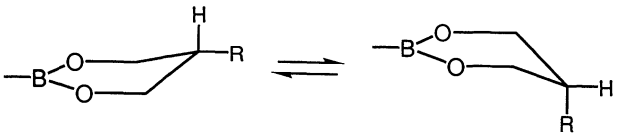

Scheme 1.

temperature where compound **1** forms a nematic phase.

On the other hand, compound **7**, which bears an alkoxyl group on 5-carbon of the dioxaborinane ring, showed a signal attributable to the methylene protons at 4.18 ppm as a doublet (J=4 Hz) and a siganal due to the methyne at 3.74 ppm as a triplet (J=4 Hz) in the NMR spectrum recorded at room temperature, and no geminal-geminal proton couplings were observed, indicating a rapid interconversion between two conformers within the NMR time scale for **7** in solution (Scheme 1). The similar phenomenon has recently been observed for a dioxane derivative.[14] When the alkoxyl group is replaced by an alkyl group, the dioxaborinane derivative **8**

clearly showed a geminal-geminal coupling (11 Hz). Though compound **8** exhibited smectic and nematic phases, **7** did no mesophases, strongly suggesting that the rigidity of the dioxaborinane ring is essential for the formation of mesophases.

In conclusion the rigid half-chair form of the dioxaborinane ring in crystalline state is kept in solution, thus suggesting a similar conformation in liquid crystalline state as well. Loss of the rididity does not lead to the formation of mesophases. The rigid dioxaborinane ring may constitute, in connection with phenyl nuclei, a suitable principal structure required for liquid crystalline compounds.

This work was partially supported by a Grant-in-Aid for Scientific Research No.02205085 from the Ministry of Education, Science and Culture.

References

1) For example, Ph. Martinot-Lagarde, R. Dunk, and G. Durand, *Mol. Cryst. Liq. Cryst.*, **75**, 249 (1981); K. Hayamizu, M. Yanagisawa, and O. Yamamoto, *Liq. Cryst.*, **4**, 273 (1989); A. Yoshizawa, H. Kikuzaki, T. Hirai, and M. Yamane, *Jpn. J. Appl. Phys.*, **29**, L1153 (1990).

2) K. Hori and Y. Ohashi, *Bull. Chem. Soc. Jpn.*, **61**, 3859 (1988); K. Hori, M. Takamatsu, and Y. Ohashi, *ibid.*, **62**, 1751 (1989); K. Hori and Y. Ohashi, *ibid.*, **62**, 3216 (1989).

3) K. Seto, S. Takahashi, and T. Tahara, *J. Chem. Soc., Chem. Commun.*, **1985**, 122; K. Seto, H. Matsubara, S. Takahashi, T. Tahara, M. Murakami, S. Miyake, T. Masumi, T. Ando, and A. Fukami, *J. Chem. Soc., Chem. Commun.*, **1988**, 56.

4) H. Matsubara, K. Seto, T. Tahara, and S. Takahashi, *Bull. Chem. Soc. Jpn.*, **62**, 3896 (1989).

5) G. L. Vorontzova, O. S. Chijov, L. S. Vasilev, V. V. Veselovckii, and M. B. Mihailov, *Izv. Akad. Nauk SSSR, Ser. Chem.*, **1980**, 353.

6) R. Boese, R. Koster, and M. Yalpani, *Chem. Ber.*, **118**, 670 (1985).

7) "Comprehensive Organometallic Chemistry," ed by G. Wilkinson, F. G. A. Stone, and E. W. Abel, Pergamon Press, New York (1982), Vol. 1, p. 443.

8) R. Boese and M. Yalpani, *Chem. Ber.*, **116**, 3347 (1983).

9) J. K. Foitzik. H. Paulus, and W. Haase, *Mol. Cryst. Liq. Cryst., Lett. Sect*, **1**, 1 (1985).

10) H. Paulus and W. Haase, *Mol. Cryst. Liq. Cryst., Lett.*, **92**, 237 (1983).

11) P. Mandel and S. Paul, *Mol. Cryst. Liq. Cryst.*, **131**, 223 (1985); G. V. Vani, *ibid.*, **99**, 21 (1983).

12) W. Haase, H. Paulus, and H. T. Huller, *Mol. Cryst. Liq. Cryst.*, **97**, 131 (1983).

13) R. Schaeffer, "Progress in Boron Chemistry," ed by H. Steingerg and A. L. McClosky, Pergamon Press, New York (1964), Vol. 1, p. 417.

14) E. Kleinpeter, H. Kohler, A. Lunow, C. Tshierske, and H. Zaschke, *Tetrahedron*, **44**, 1609 (1988).

Direct Epoxidation of Olefins Catalyzed by Nickel(II) Complexes with Molecular Oxygen and Aldehydes

Tohru YAMADA,* Toshihiro TAKAI, Oliver RHODE, and Teruaki MUKAIYAMA†
Basic Research Laboratories for Organic Synthesis, Mitsui Petrochemical Industries, Ltd., Nagaura, Sodegaura-shi, Chiba 299-02
† Department of Applied Chemistry, Faculty of Science, Science University of Tokyo, Kagurazaka, Shinjuku-ku, Tokyo 162
(Received February 27, 1991)

In the presence of a bis(1,3-diketonato)nickel(II) complex, various olefins are directly monooxygenated into the corresponding epoxides on treatment with atmospheric pressure of oxygen or air and aldehydes. Especially, it is noted that bis[1,3-bis(*p*-methoxyphenyl)-1,3-propanedionato]nickel(II) behaves as an excellent catalyst in the present epoxidation.

Epoxides are one of the most useful synthetic intermediates for the preparation of oxygen-containing natural products or the production of epoxy resins, etc. Much effort has been made to develop the direct and selective epoxidation of olefins by use of molecular oxygen. However, it is difficult to control the reaction because of over-oxidations or side reactions under conventional severe reaction conditions, such as high pressure of oxygen or high reaction temperature. Then, it is desired to search milder reaction conditions to suppress these reactions for development of an efficient epoxidation method. Only several effective catalysts have been reported for the epoxidation with molecular oxygen under milder reaction conditions, for example, (tetramesitylporphinato)ruthenium(II),[1] or oxoethoxo(tetra-*p*-tolylporphinato)molybdenum(V).[2] We also reported that oxovanadium(IV) complexes[3] and nickel(II) complexes[4] coordinated with 1,3-diketone type ligands behave as fairly good catalysts when treated together with molecular oxygen (Oxidant) and primary or secondary alcohols (Reductant), and it was shown there that reductants are essential for the above catalytic epoxidation. Through our continued studies on the aerobic epoxidation of olefins catalyzed by nickel(II) complexes, it was found that an aldehyde acts as an excellent reductant when used with molecular oxygen at room temperature.[5]

Similar reactions have been reported in the literature. Propylene was monooxygenated into propylene oxide with molecular oxygen in the coexistence of metal complexes and aldehyde, such as acetaldehyde[6] or crotonaldehyde,[7] but the conversion of olefin and the selectivity of epoxide were never reached to satisfactory levels.

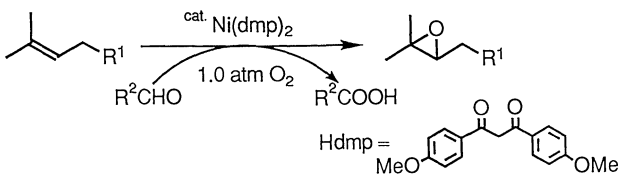

Scheme 1.

Recently, praseodymium(III) acetate was also shown to be an effective catalyst for the aerobic epoxidation of olefins in the presence of aldehyde.[8] In our previous communication, it was reported that both trisubstituted and *exo*-terminal olefins were smoothly monooxygenated into the corresponding epoxides in high to quantitative yields by combined use of atmospheric pressure of oxygen and aldehydes in the presence of catalytic amount of nickel(II) complexes.[5] However, the epoxidation of 1,2-disubstituted or terminal olefins stopped halfway, and conversions and yields were not reached satisfactory levels, because a part of aldehyde, being employed as a reductant, seemed to be consumed independently of the epoxidation.

Herein, we would like to discuss in detail the highly efficient method for epoxidation of various olefins catalyzed by nickel(II) complexes with molecular oxygen (Oxidant) and aldehydes (Reductant).

Results and Discussion

Epoxidation of Trisubstituted and *exo*-Terminal Olefins. First, several aldehydes, reductants, were screened by taking the epoxidation of 2-methyl-2-decene

Table 1. Epoxidation of 2-Methyl-2-decene (**1**) by Using Several Aldehydes[a]

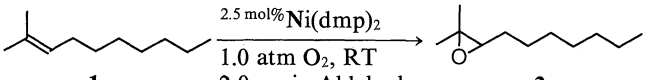

1 **2**

Entry	Aldehyde	Conversion/%[b]	Yield/%[b]
1		10	7
2		100	Quant.
3		100	Quant.
4		100	Quant.

a) Reaction conditions; 2-Methyl-2-decene (**1**) 2.5 mmol in 2.0 ml of 1,2-dichloroethane, 1.0 atm of oxygen for 12 h. b) Determined by GC.

Table 2. Effect of Ligand on Epoxidation of 2-Methyl-2-decene (**1**)[a]

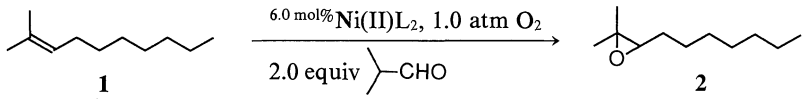

Entry	Ligand (LH)		Conversion/%[b]	Yield/%[b]
1	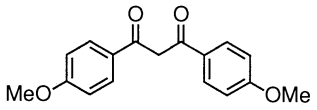	**3b** Hdmp	100	Quant.
2	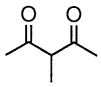	**4b** Hmac	100	Quant.
3	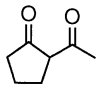	**5b** Hacp	100	Quant.
4	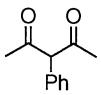	**6b** Hpac	100	Quant.
5	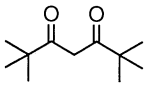	**7b** Hdpm	100	Quant.
6	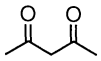	**8b** Hacac	100	Quant.
7	Hdmg[c]	**9b**		14
8	H_2salen[d]	**10b**		Trace

a) Reaction conditions; 2-Methyl-2-decene (**1**) 2.5 mmol in 2.0 ml of 1,2-dichloroethane, 1.0 atm of oxygen for 12 h. b) Determined by GC. c) Dimethylglyoxime. d) *N,N'*-Disalicylideneethylenediamine.

(**1**) catalyzed by bis[1,3-bis(*p*-methoxyphenyl)-1,3-propanedionato]nickel(II) (Ni(dmp)$_2$, **3a**) as a model reaction. In the case of employing butyraldehyde, both conversion of olefin and yield of the epoxide were low (Entry 1 in Table 1), while the corresponding epoxide **2** was obtained in quantitative yields, respectively (Entries 2—4) when aldehydes having secondary or tertiary carbon next to the carbonyl carbon, such as isobutyraldehyde, cyclohexanecarbaldehyde or pivalaldehyde were employed. The reaction afforded the corresponding carboxylic acids, co-products as confirmed by GC analysis. Therefore, it is reasonable to assume that an aldehyde behaves as an effective reductant to accept one oxygen atom from molecular oxygen in the present epoxidation.

Next, several 1,3-diketone type ligands were examined for the epoxidation of 2-methyl-2-decene (**1**) using isobutyraldehyde under an atmospheric pressure of oxygen (see Table 2). It was found that nickel(II) complexes having 1,3-diketone type ligands behave as excellent catalysts for the present epoxidation of trisubstituted olefins (Entries 1—6, (**A**) **Standard Method**), while Ni(II)(salen) (**9b**)[9] or Ni(II)(dmg)$_2$ (**10b**)[10] is not effectively employed at all (Entries 7 and 8).

Epoxidation of 1,2-Disubstituted Olefins. According to the above procedure (**Method (A)**), the epoxidation of 1,2-disubstituted or terminal olefins was interrupted halfway, and the conversions and the yields were not reached satisfactory levels. Taking the epoxidation of *cis*-2-octene (**11**) as a model reaction, nickel(II) complexes having several 1,3-diketone type ligands were examined. As shown in Table 3, Ni(dmp)$_2$ (**3a**), Ni(mac)$_2$ (**4a**), and Ni(dpm)$_2$ (**7a**) behaved as efficient catalysts for the epoxidation of *cis*-2-octene (**11**) (Entries 2—4). On the contrary, Ni(acac)$_2$ (**8a**), which was an excellent catalyst for the epoxidation of trisubstituted olefin (Entry 6 in Table 2) or Ni(tfa)$_2$ (**13a**) was not effective for the epoxidation of 1,2-disubstituted olefin at all (Entries 1 and 2). Based on the measurements of the oxidation potentials of nickel(II) complexes,[4] it was suggested that Ni(dmp)$_2$ (**3a**, E_{ox} 1.14 V), Ni(mac)$_2$ (**4a**, E_{ox} 0.97 V), and Ni(dpm)$_2$ (**7a**, E_{ox} 1.05 V) would be more readily oxidized with molecular oxygen to form active species of the present epoxidation compared with Ni(acac)$_2$ (**8a**, E_{ox} 1.24 V) or Ni(tfa)$_2$ (**13a**, E_{ox} 1.89 V). Subsequently, the concentration of aldehyde or nickel(II) catalyst in the above reaction was examined in detail to improve yield of the epoxide **12** (see Table 4). In our previous letter,[11] it was reported that Ni(II) complexes, such as Ni(dmp)$_2$ (**3a**), are also employed as excellent

Table 3. Effect of 1,3-Diketone Ligand on Epoxidation of *cis*-2-Octene (**11**)[a]

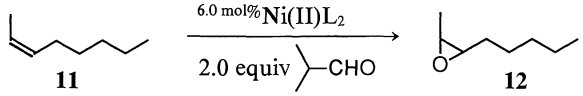

Entry	Ligand (LH)		E_{ox}/V vs. Ag/Ag$^+$[b]	Conversion/%[c]	Yield/%[c]
1	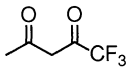	**13b** Htfa	1.89	1	1
2	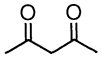	**8b** Hacac	1.24	5	5
3	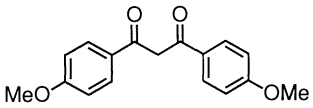	**3b** Hdpm	1.14	78	68[d]
4	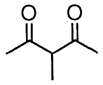	**4b** Hmac	0.97	78	68[d]
5	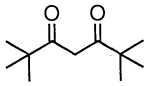	**7b** Hdmp	1.05	69	65[d]

a) Reaction conditions; *cis*-2-Octene (**11**) 2.5 mmol, isobutyraldehyde 2.0 equiv, $Ni(dmp)_2$ 6.0 mol%, in 1,2-dichloroethane 2.0 ml, 1.0 atm O_2, RT, 13 h. b) Oxidation potentials (E_{ox}) were measured in CH_3CN solution. c) Determined by GC analysis. d) Mixture of *cis*- and *trans*-epoxides (*cis*:*trans*=28:72).

Table 4. Effect of Concentration on Epoxidation of *cis*-2-Octene (**11**)[a]

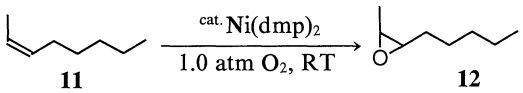

Entry	Aldehyde (equiv)	Catalyst/mol%	Solvent/ml	Conversion/%[b]	Yield/%[b]
1	(2.0)	6.0	2.0	78	68[c]
2	(3.0)	6.0	2.0	89	77[c]
3	(2.0)	0.3	2.0	88	86[c]
4	(3.0)	0.3	10.0	94	89[c]

a) Reaction conditions; *cis*-2-Octene (**11**) 2.5 mmol in 1,2-dichloroethane, 1.0 atm O_2, RT, 13 h. b) Determined by GC analysis. c) Mixture of *cis*- and *trans*-epoxides.

catalysts for the oxidation of aldehydes into the corresponding carboxylic acids in the absence of olefins. Therefore, it is reasonable to assume that a part of aldehyde was consumed to form carboxylic acid independent of epoxidation.

When 3.0 equivalent of isobutyraldehyde against olefin **11** was employed, both conversion and yield increased up to 89% and 77%, respectively, as expected (Entry 2 in Table 4). It was also found that the use of smaller amount of nickel(II) complex was effective to improve yield of the epoxide **12** (86%, Entry 3). Further, under highly diluted conditions, the corresponding epoxide **12** was obtained in 89% yield as a mixture of *cis*- and *trans*-epoxides. It is reasonable to assume that under highly diluted conditions, oxidation of aldehyde itself into the corresponding acid could be suppressed and then aldehyde would be effectively consumed for the epoxidation to improve both conversion of olefin and

Table 5. Effect of Aldehydes on Epoxidation of 1-Decene (**13**)[a]

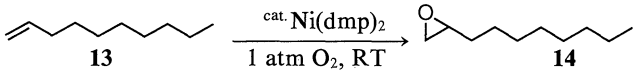

Entry	Aldehyde	Conversion/%	Yield/%
1		61	42
2		41	33
3	CH_3CHO	72	51
4	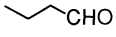	71	57
5	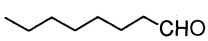	64	44
6	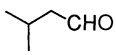	95	75

a) Reaction conditions; 1-Decene (**13**) 3.0 mmol, aldehyde 6.0 equiv, $Ni(dmp)_2$ **3a** 0.3 mol%, in 1,2-dichloroethane 10.0 ml, 1.0 atm O_2, RT, 24 h.

Table 6. Epoxidation of Various Olefins[a] ((A) **Standard Method**)

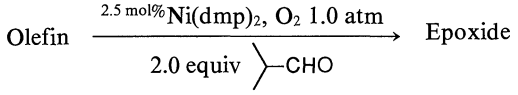

Entry[a]	Olefin		Time/h	Epoxide		Yield/%	Note
1	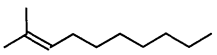	**1**	3	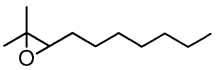	**2**	Quant.[b]	
2[d]			12			Quant.[b]	
3	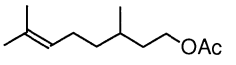	**15**	3	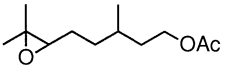	**16**	95[b]	
4	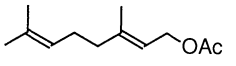	**17**	13	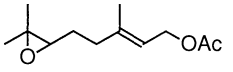	**18**	68[c]	Total yield 87%
				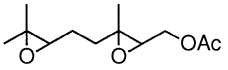	**19**	19[c]	
5	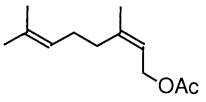	**20**	43	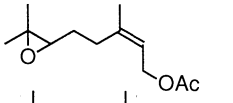	**21**	61[c]	Total yield 73%
				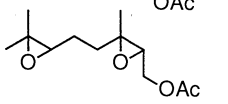	**22**	12[c]	
6	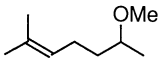	**23**	3	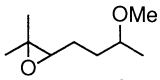	**24**	95[b]	
7	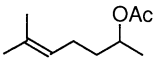	**25**	6	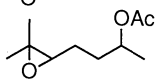	**26**	Quant.[b]	
8	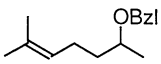	**27**	13	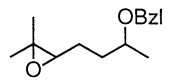	**28**	95[c]	Bzl =
9	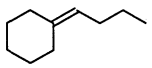	**29**	3	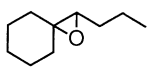	**30**	89[b]	
10		**31**	3		**32**	80[b]	
11	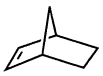	**33**	3	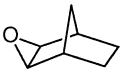	**34**	Quant.[b]	
12	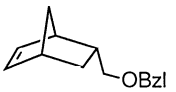	**35**	13	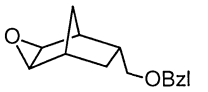	**36**	84[c]	
13	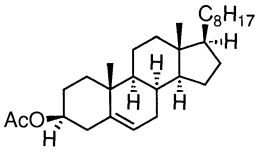	**37**	5	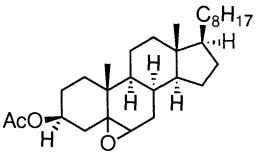	**38**	84[c]	$\alpha:\beta$ 24:76[e]
14	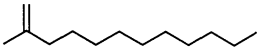	**39**	13	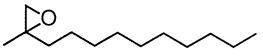	**40**	93[b]	
15	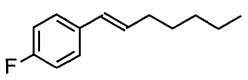	**41**	43	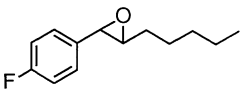	**42**	85[b]	

a) Reaction conditions; Olefin 2.5 mmol in 1,2-dichloroethane. b) Determined by GC analysis. c) Isolated yield. d) Under an atmospheric pressure of air. e) Diastereomer ratio was determined by NMR, see Ref. 1.

yield of epoxide (**(B) Dilution Method**).

Epoxidation of Terminal Olefin. Next, when the present procedure (**Method B**) was applied to the epoxidation of terminal olefin, such as 1-decene (**13**), the corresponding epoxide **14** was obtained only in 42% yield (Entry 1 in Table 5). And then, several aldehydes were examined taking the above reaction as a model.

As shown in Table 5, it is interesting to note that normal aliphatic aldehydes were quite effective for the epoxidation of 1-decene (**13**) (Entries 3—6), whereas these aldehydes were less effective for the epoxidation of trisubstituted olefins (Entry 1 in Table 1). Especially, isovaleraldehyde was found to be remarkably effective for the epoxidation of 1-decene (**13**), and 1,2-epoxydecane (**14**) was obtained in 75% yield and 95% conversion (Entry 6, **(C) Isovaleraldehyde Method**).

Epoxidation of Various Olefins. The above procedures were successfully applied to the nickel(II)-catalyzed epoxidation of various trisubstituted or *exo*-terminal olefins, norbornene analogues, 1,2-disubstituted and terminal olefins.

According to the above procedure (**Method (A) Standard Method**), various trisubstituted or *exo*-terminal olefins and norbornene analogues were smoothly monooxygenated into the corresponding epoxides in high to quantitative yields under an atmospheric pressure of oxygen at room temperature as shown in Table 6. It was observed that epoxidation of isolated carbon–carbon double bonds was faster than that of allyl esters (Entries 4 and 5). It should be pointed out here that, in every case, no over-oxidation at allylic position nor cleavage reaction of carbon–carbon double bonds took place to any extent. *exo*-Terminal olefin **39** and styrene derivative **41** were also monooxidized into corresponding epoxides **40** and **42** in high yields, respectively (Entries 14 and 15). In the case of the epoxidation of trisubstituted olefin **1**, the corresponding epoxide **2** was obtained in quantitative yield even under air (Entry 2).

Various 1,2-disubstituted olefins were monooxygenated into the corresponding epoxides in high yields by **Method (B) (Dilution Method)**, and also in the case of terminal olefin by **Method (C) (Isovaleraldehyde Method)**, respectively (see Table 7).

As shown in Table 7, when **Method (B)** was applied to *cis*-olefin (*cis*-2-octene (**11**)) and *trans*-olefin (*trans*-2-octene (**43**)), the corresponding epoxides **12** and **44** were obtained in 97% and 92% yields, respectively, as mixture of *cis*- and *trans*-epoxides (Entries 1 and 2). It is noted

Table 7. Epoxidation of Various Olefins

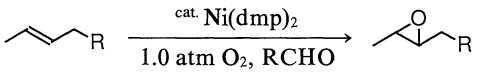

Entry	Olefin		Time/h	Epoxide		Yield/%	Note
(B) Dilution method							
1	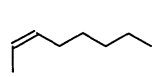	**11**	13	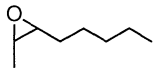	**12**	97[a,c]	*cis*:*trans*=51:49
2	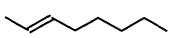	**43**	13	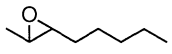	**44**	92[a,c]	*cis*:*trans*=13:87
3	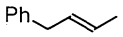	**45**	13	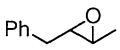	**46**	75[a,c]	
4		**47**	13		**48**	84[a,c]	
(C) Isovaleraldehyde method							
5	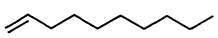	**13**	24	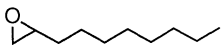	**14**	75[b,c]	
6	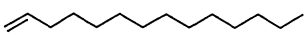	**49**	47	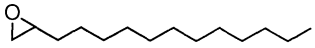	**50**	89[b,d]	
7	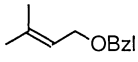	**51**	24	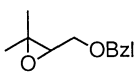	**52**	97[b,d]	Bzl =
8	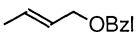	**53**	24	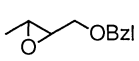	**54**	62[b,d]	

a) (B) Dilution method; Reaction conditions; Olefin 2.5 mmol, isobutyraldehyde 3.0 equiv, $Ni(dmp)_2$ **3a** 0.3 mol%, in 1,2-dichloroethane 10.0 ml, 1.0 atm O_2, RT. b) **(C) Isovaleraldehyde method**; Reaction conditions; Olefin 3.0 mmol, isovaleraldehyde 6.0 equiv, $Ni(dmp)_2$ **3a** 0.3 mol%, in 1,2-dichloroethane 10.0 ml, 1.0 atm O_2, RT. c) Determined by GC analysis. d) Isolated yield.

Table 8. Effect of Amount of Ni(II) Complex on the Yield of Epoxide 2

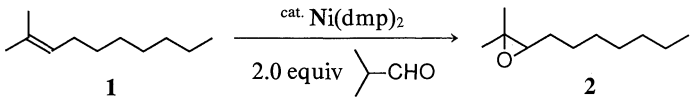

Entry	Amount of catalyst/mol%	Yield/%[b]	Yield based on catalyst/%[b]
1	4.0	100.0	2500
2	0.256	100.0	39000
3	0.0096[a]	98.1	1020000

a) Reaction conditions; 2-Methyl-2-decene (**1**) 10.0 mmol, isobutyraldehyde 20.0 mmol, Ni(dmp)$_2$ **3a** 0.6 mg in 6.0 ml of 1,2-dichloroethane 1.0 atm of oxygen for 12 h. b) Determined by GC.

that cyclohexene (**47**) was also smoothly monooxygenated into 1,2-epoxycyclohexane (**48**) in high yield (Entry 4) accompanied by less than 5% yields of by-product, such as allylic oxidation product, 2-cyclohexen-1-ol or 2-cyclohexen-1-one. With regard to the epoxidation of terminal olefins, isovaleraldehyde was quite effective (**Method C**), and 1-decene (**13**) and 1-tetradecene (**49**) were converted into the corresponding 1,2-epoxyalkanes **14** and **50** in 75% and 89% yields, respectively (Entries 5 and 6).

Table 9. Stereochemistry in Epoxidation of *cis*-2-Octene (**11**)

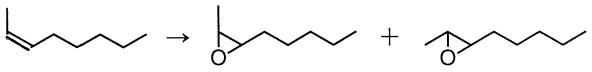

11 *cis*-2-Octene — **12** *cis*-Epoxide — **44** *trans*-Epoxide

Entry	Epoxidation conditions	Ratio of epoxide (*cis*:*trans*)[a]
1	1.0 atm O_2, 0.3 mol% Ni(dmp)$_2$ **3a**, 2.0 equiv	51:49[b]
2	*m*CPBA	98:2
3	*m*CPBA, 0.3 mol% Ni(dmp)$_2$ **3a**	97:3

a) Determined by GC analysis. b) During the reaction, isomerization of *cis*-olefin into *trans*-olefin was not observed by GC analysis.

Efficiency of Nickel(II) Complex Catalyst. The efficiency of nickel(II) complexes in the present epoxidation was demonstrated by taking epoxidation of 2-methyl-2-decene (**1**) as a model reaction. Through three experiments carried out in the presence of 4.0 mol%, 0.256 mol%, and 0.0096 mol% of Ni(dmp)$_2$ (**3a**) against olefin **1**, respectively (see Table 8), it was found that, even in the case of employing only 0.0096 mol% of Ni(dmp)$_2$, the epoxidation proceeded smoothly and the corresponding epoxide **2** was obtained in 1020000% yield based on Ni(dmp)$_2$ (**3a**) (Entry 3).

Stereochemistry of the Present Epoxidation.

a) Epoxidation of *cis*-Olefin. According to the

Table 10. Stereoselective Epoxidation of Cholesteryl Benzoate(**55**) Catalyzed by Ni(dmp)$_2$ **3a**

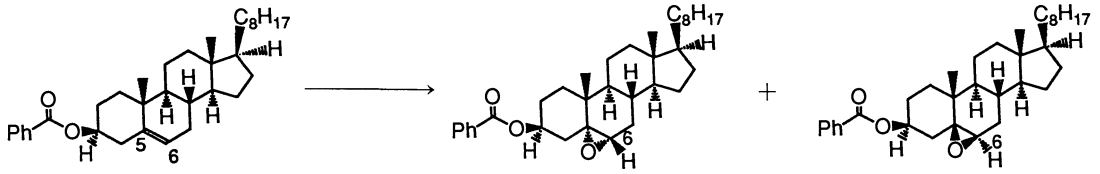

55 — **56** α-Epoxide — **57** β-Epoxide

Entry	Epoxidation reagent	α-Epoxide **56**:β-Epoxide **57**[c]
1[a]	cat. Ni(dmp)$_2$ **3a**, O_2,	31:69
2[b]	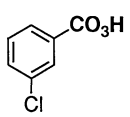 (*m*CPBA)	71:29
3[b]	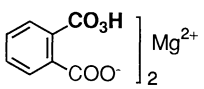 (MMPP)	85:15

Reaction Conditions: a) Cholesteryl Benzoate (**55**) 245 mg (0.5 mmol), isobutyraldehyde (2.0 mmol), catalyst (0.0047 mmol, 0.94 mol%) in 1,2-dichloroethane (5.0 ml), RT, 1.0 atm O_2, 2.0 h. b) Ref. 10. c) Determined by HPLC analysis.

present procedure, *cis*-olefin **11** was converted into a mixture of *cis*- and *trans*-epoxides (**12** and **44**), whereas *cis*-epoxide was formed predominantly when generally known peroxy acid such as *m*-chloroperbenzoic acid (*m*CPBA) was employed (see Table 9).

b) Epoxidation of Cholesterol Derivatives. Stereochemistry of the epoxidation of double bond on 5,6-position in cholesteryl benzoate (**55**) was examined by using $Ni(dmp)_2$ (**3a**) as a catalyst together with molecular oxygen and isobutyraldehyde (see Table 10). It was found that epoxidation catalyzed by nickel(II) complex afforded the *hindered* 5,6β-epoxide **57** as major product (Entry 1). On the contrary, it was reported that by using peroxy acids, such as *m*CPBA or magnesium monoperoxyphthalate hexahydrate (MMPP), cholesteryl benzoate was converted into the corresponding mixture of 5,6α- and 5,6β-epoxides in the ratio of 71:29 or 85:15 indicating that 5,6α-epoxide **56** is formed as a major product, respectively (Entries 2 and 3).[12] It is interesting to point out that the *less hindered* 5,6α-epoxide **56** was obtained as major product in above mentioned peracid epoxidation.[13]

Remarkably opposing stereoselection shown in the above two epoxidations clearly indicates that the active oxidant of the present nickel(II) complex-catalyzed epoxidation is not a simple peroxy carboxylic acid generated from aldehydes by autoxidation manner.

Conclusion

It is concluded that bis(1,3-diketonato)nickel(II) complexes effectively catalyzes the epoxidation of various olefins with an atmospheric pressure of oxygen (Oxidant) and an aldehyde (Reductant) at room temperature to afford the corresponding epoxides in high to quantitative yields. It was shown that $Ni(dmp)_2$ (**3a**) is an effective catalyst, and when $Ni(dmp)_2$ (**3a**) as employed as a catalyst, the epoxide was obtained in more than 1000000% yield based on the catalyst. Further, it is suggested that the active species in the present epoxidation reaction is not a simple carboxylic peracid generated from aldehyde by autoxidation manner. The present procedure thus provides a highly efficient and useful method for the preparation of a variety of epoxides from trisubstituted, 1,2-disubstituted and terminal olefins under mild conditions.

Experimental

General: Melting points were measured on a Mettler FP62 apparatus and uncorrected.

(a) Spectrometers: IR spectra were obtained by using a JASCO Model IR-700 infrared spectrometer on KBr pellets or liquid film on KBr. ^1H NMR spectra were recorded with a JEOL Model FX270 spectrometer using $CDCl_3$ as solvent and with tetramethylsilane as internal standard.

(b) Chromatography: Column chromatography was conducted under silica gel (Daiso gel IR-60). Preparative TLC was carried out on silica gel (E. Merck, 5714). HPLC analysis were performed on a Shimadzu LC-6A chromatograph using a Shimadzu Shimpack-Sil, and the peak area were calculated on a Shimadzu chromatopack CR-4A. GC-analyses were performed on a Shimadzu GC-15A or GC-14A chromatograph using a glass capirally column (Shimadzu CBP-10, 25 m), and the peak areas were obtained with a Shimadzu chromatopack CR-5A.

(c) Cyclic Voltammetry: All cyclic voltammograms were recorded with a BAS Model CV1B-120 in acetonitrile solution containing 0.1 M (M=mol dm^{-3}) tetrabutylammonium perchlorate (TBAP) and 0.001 M nickel(II) complex. The working and auxiliary electrodes were platinum and the reference electrode was Ag/AgCl (Model RE-1B). Tetrabutylammonium perchlorate and acetonitrile (HPLC-grade) were purchased from TCI (Tokyo Kasei Kogyo, Inc) and Kanto Chemical Co. Ltd., respectively.

Preparation of 1,3-Diketones and Bis(1,3-diketonato)nickel-(II) Complexes. Bis(acetylacetonato)nickel(II) (**8a**, $Ni(acac)_2$) and bis(1,1,1-trifluoro-2,4-pentanedinonato)nickel(II) (**13a**, $Ni(tfa)_2$) were purchased from TCI Co., Ltd. Bis(3-methyl-2,4-pentanedionato)nickel(II) (**4a**, $Ni(mac)_2$),[16] bis-(2,2,6,6-tetramethyl-3,5-heptanedionato)nickel(II) (bis(dipivaloylmethanato)nickel(II), **7a**, $Ni(dpm)_2$),[16] bis(2-acetylcyclopentanonato)nickel(II) (**5a**, $Ni(acp)_2$),[16] and bis(3-phenyl-2,4-pentanedionato)nickel(II) (**6a**, $Ni(pac)_2$)[16] were prepared according to the reported methods, respectively, and the ligands were purchased from TCI Co., Ltd. (**5b** and **7b**), Dojindo laboratories (**6b**), and Aldrich Chemical Company, Inc. (**4b**), respectively.

1,3-Bis(*p*-methoxyphenyl)-1,3-propanedione (3b, Hdmp):[15,17] A refluxing suspension of sodium hydride (0.39 mol) in cyclohexane (400 ml), a solution of *p*-methoxyacetophenone (0.33 mol) and ethyl *p*-methoxybenzoate (0.33 mol) in cyclohexane (200 ml) was added over 1 h, and reflux was continued for another 2 h. After cooling, reaction was quenched with 1.0 mol dm^{-3} aqueous HCl, then crude product was extracted with THF–Et_2O. The organic extract was washed with brine, and dried over anhydrous sodium sulfate, then solvent was removed in vacuo. Recrystallization from hexane–ethyl acetate gave slightly colored needle (58% yield). Mp 131—138 °C; ^1H NMR ($CDCl_3$) δ=3.90 (6H, s), 6.80 (1H, s), 7.00 (4H, m), 7.95 (4H, m); IR(KBr) 2938, 2840, 1687, 1605, 1507, 1429, 1305, 1263, 1230, 1170 cm^{-1}.

Bis[1,3-bis(*p*-methoxyphenyl)-1,3-propanedionato] nickel-(II) (3a):[15] A vigorously stirred mixture of Hdmp (0.1 mol) in ether (300 ml), a solution of nickel(II) acetate (0.05 mol) in 10% aqueous ammonia (800 ml) was added in one portion. Precipitated pale green solid was filtered and washed with water. After dried in vacuo for 6 h (110 °C/0.1 mmHg, 1 mmHg= 133.322 Pa), $Ni(dmp)_2$ was yielded as yellow solid. Found: C, 65.45; H, 4.87%. Calcd for $C_{34}H_{30}O_8Ni$: C, 65.31; H, 4.84%.

Bis(3-methyl-2,4-pentanedionato)nickel(II) (4a):[14,16] To the stirred mixture of nickel(II) acetate (0.1 mol) in water (150 ml), 3-methyl-2,4-pentanedione (Hmac, 0.2 mol) in methanol (5 ml) was added. After stirring for 5 min, aqueous sodium acetate (0.2 mol) in water (10 ml) was added over 10 min. Precipitated yellowish green solid was filtered and washed with water. After drying in vacuo for 6 h (90 °C/ 0.1 mmHg), $Ni(mac)_2$ was yielded as purple solid.

Melting Points and IR Spectra of Nickel(II) Complexes. Bis[1,3-bis(*p*-dimethoxyphenyl)-1,3-propanedionato]nickel-(II) (3a, $Ni(dmp)_2$): Yellow solid; mp 279—284 °C; IR (KBr)

2932, 2834, 1604, 1529, 1492, 1431, 1391, 1304, 1256, 1227, 1174 cm^{-1}.

Bis(3-methyl-2,4-pentanedionato)nickel(II) (4a, Ni(mac)$_2$): Purple solid; mp 180 °C (decomp); IR (KBr) 2920, 1599. 1570, 1424, 1388 cm^{-1}.

Bis(2,2,6,6-tetramethyl-3,5-heptanedionato)nickel(II) (bis-(dipivaloylmethanato)nickel(II), 7a, Ni(dpm)$_2$): Purple solid; mp 221—223 °C; IR (KBr) 2956, 1570, 1542, 1502, 1401, 1360 cm^{-1}.

Bis(2-acetylcyclopentanonato)nickel(II) (5a, Ni(acp)$_2$): Light green solid; mp >250 °C (decomp); IR (KBr) 2950, 1602, 1478, 1401, 1272 cm^{-1}.

Bis(3-phenyl-2,4-pentanedionato)nickel(II) (6a, Ni(pac)$_2$): Purple solid; mp 204—207 °C; IR (KBr) 2922, 1583, 1420, 1377, 1301 cm^{-1}.

Epoxidation of 1,5-Dimethyl-4-hexenyl Benzoate (27) (Method (A), Standard Method, see Entry 8 in Table 6). A mixture of olefin (3.0 mmol), Ni(dmp)$_2$ (40.0 mg, 0.064 mmol, 2.1 mol%) an isobutyraldehyde (6.25 mmol) in 1,2-dichloroethane(2.0 ml)[3,4] was stirred at room temperature under an atmospheric pressure of oxygen overnight. The crude product was purified by column chromatography on silica gel (hexane–ethyl acetate) to afford the corresponding epoxide[7] (713.0 mg, 95% yield).

Epoxidation of *trans*-4-Phenyl-2-butene (45) (Method (B), Dilution Method, see Entry 3 in Table 7). A mixture of olefin (2.0 mmol), Ni(dmp)$_2$ (4.0 mg, 0.006 mmol, 0.3 mol%) and isobutyraldehyde (6.0 mmol) in 1,2-dichloroethane (10.0 ml)[3,4] was stirred at room temperature under an atmospheric pressure of oxygen overnight. After the reaction, organic layer was washed with sat. $NaHCO_3$ and brine. Purification with TLC on silica gel to afford the corresponding epoxide (223 mg, 75% yield).

Epoxidation of 1-Tetradecene (49) (Method (C), Isovaleraldehyde Method, see Entry 6 in Table 7). A mixture of olefin (10.0 mmol), Ni(dmp)$_2$ (12.0 mg, 0.019 mmol, 0.19 mol%) and isovaleraldehyde (60.0 mmol) in 1,2-dichloroethane (30 ml)[3,4] was stirred at room temperature under an atmospheric pressure of oxygen for 47 h. After the reaction, organic layer was washed with sat.$NaHCO_3$ (4 times) and brine. Purification with silica-gel column chromatography afforded the corresponding epoxide (1.89 g, 89.2% yield).

^{1}H NMR and IR Spectra of the Epoxides (in Table 6 and Table 7). **1,2-Epoxydecane (14), *exo*-2,3-Epoxybicyclo[2.2.1]-heptane (34), 1,2-Epoxycyclohexane (48).** ^{1}H NMR spectra, IR spectra, and retention time in GC analysis agreed with those of the authentic sample.

2,3-Epoxy-2-methyldecane (2); ^{1}H NMR ($CDCl_3$) δ=0.88 (3H, t, J=6.92 Hz), 1.26 (3H, s), 1.28 (10H, m), 1.31 (3H, s), 1.50 (2H, m), 2.71 (1H, t, J=6.27 Hz); IR(neat) 2925, 2850, 1465 cm^{-1}.

***cis*-2,3-Epoxyoctane (12);** ^{1}H NMR ($CDCl_3$) δ=0.93 (3H, t, J=7.09 Hz), 1.27 (3H, d, J=5.28 Hz), 1.35—1.45 (4H, m), 1.48—1.55 (4H, m), 2.90 (1H, m), 3.06 (1H, m); IR(neat) 2958, 2928, 2856, 1466, 1381 cm^{-1}.

6,7-Epoxy-3,7-dimethyloctyl Acetate (16); ^{1}H NMR ($CDCl_3$) δ=0.94 (3H, d, J=6.27 Hz), 1.27 (3H, s), 1.31 (3H, s), 1.40—1.60 (7H, m), 2.05 (3H, s), 2.70 (1H, t, J=6.06 Hz), 4.11 (2H, m); IR(neat) 2960, 2924, 2872, 1741, 1461, 1379, 1367, 1241 cm^{-1}.

***trans*-6,7-Epoxy-3,7-dimethyl-2-octenyl Acetate (18);** ^{1}H NMR ($CDCl_3$) δ=1.26 (3H, s), 1.31 (3H, s), 1.60—1.80 (5H, m), 2.05 (3H, s), 2.10—2.30 (2H, m), 2.70 (1H, t, J=6.26 Hz), 4.59 (2H, d, J=7.25 Hz), 5.40 (1H, m); IR(neat) 2960, 2926, 1740, 1454, 1380, 1234 cm^{-1}.

2,3:6,7-Diepoxy-3,7-dimethyloctyl Acetate (19); ^{1}H NMR ($CDCl_3$) δ=1.30 (6H, m), 1.50—1.80 (7H, m), 2.10 (3H, s), 2.70 (1H, m), 3.05 (1H, m), 4.05 (1H, m), 4.30 (1H, m); IR(neat) 2970, 2929, 1743, 1455, 1380, 1232 cm^{-1}.

***cis*-6,7-Epoxy-3,7-dimethyl-2-octenyl Acetate (21);** ^{1}H NMR ($CDCl_3$) δ=1.27 (3H, s), 1.31 (3H, s), 1.63 (2H, dt, J_1=7.75 Hz, J_2=6.27 Hz), 1.78 (3H, s), 2.05 (3H, s), 2.26 (2H, t, J=7.75 Hz), 2.71 (1H, t, J=6.27 Hz), 4.58 (2H, d, J=6.60 Hz), 5.41 (1H, t, J=6.60 Hz); IR(neat) 2964, 2930, 1739, 1670, 1453, 1379, 1234 cm^{-1}.

2,3:6,7-Diepoxy-3,7-dimethyloctyl Acetate (22); ^{1}H NMR ($CDCl_3$) δ=1.28 (3H, s), 1.32 (3H, s), 1.35 (3H, s), 1.60—1.80 (4H, m), 2.72 (1H, m), 3.00 (1H, m), 4.09 (1H, m), 4.35 (1H, m); IR(neat) 2970, 2931, 1744, 1454, 1378, 1234 cm^{-1}.

2,3-Epoxy-6-methoxy-2-methylheptane (24); Bp 84—85 °C (20 mmHg); ^{1}H NMR ($CDCl_3$) δ=1.15 (3H, d, J=6.26 Hz), 1.27 (3H, s), 1.31 (3H, s), 1.45—1.80 (4H, m), 2.75 (1H, m), 3.25—3.40 (1H, m), 3.30 (3H, s); IR(neat) 2968, 1462, 1377, 1090 cm^{-1}.

4,5-Epoxy-1,5-dimethylhexyl Acetate (26); ^{1}H NMR ($CDCl_3$) δ=1.25 (9H, s), 1.45—1.85 (4H, m), 2.00 (3H, s), 2.70 (1H, m), 4.90 (1H, m); IR(neat) 2974, 1737, 1376, 1243 cm^{-1}.

4,5-Epoxy-1,5-dimethylhexyl Benzoate (28); ^{1}H NMR ($CDCl_3$) δ=1.20—1.40 (9H, m), 1.55—2.00 (4H, m), 2.75 (1H, m), 5.20 (1H, m), 7.40—7.60 (3H, m), 8.05 (2H, m); IR(neat) 2974, 1716, 1276, 1111, 714 cm^{-1}.

2-Propyl-1-oxaspiro[2.5]octane (30); Bp 82 °C (10 mmHg); ^{1}H NMR ($CDCl_3$) δ=0.95 (3H, m), 1.40—1.80 (14H, m), 2.70 (1H, t, J=5.94 Hz); IR(neat) 2930, 1449, 913 cm^{-1}.

1-Methyl-1,2-epoxycyclohexane (32); ^{1}H NMR ($CDCl_3$) δ=1.30—1.40 (2H, m), 1.60—1.70 (2H, m), 1.80—2.00 (4H, m), 2.95 (1H, s); IR(neat) 2982, 2936, 2858, 1555, 1538 cm^{-1}.

5,6-Epoxybicyclo[2.2.1]hept-2-ylmethyl Benzoate (36); ^{1}H NMR ($CDCl_3$) δ=0.90 (2H, m), 1.40 (2H, m), 1.80 (1H, m), 2.26 (1H, m), 3.25 (2H, m), 4.30 (2H, m), 7.45 (2H, m), 7.55 (1H, m), 8.05 (2H, m); IR(neat) 3030, 2964, 2870, 1719, 1602, 1452, 1314, 1276, 1113 cm^{-1}.

5,6-Epoxycholesteryl Acetate (38); ^{1}H NMR ($CDCl_3$) δ=0.60 (3H, m), 0.80—1.60 (6H, m), 1.80—2.20 (34H, m), 2.00 (3H, s), 2.90 (0.24H, d, J=2.90 Hz), 3.10 (0.76H, d, J=2.00 Hz), 4.70—5.00 (1H, m); IR(KBr) 2950, 1734, 1470, 1368, 1247, 1041 cm^{-1}.

1,2-Epoxy-2-methylundecane (40); ^{1}H NMR ($CDCl_3$) δ= 0.88 (3H, t, J=6.80 Hz), 1.27 (3H, s), 1.29 (14H, m), 1.50 (2H, t, J=10.9 Hz), 2.57 (1H, d, J=10.9 Hz); IR(neat) 2924, 2852, 1465 cm^{-1}.

1,2-Epoxy-1-(*p*-fluorophenyl)heptane (42); ^{1}H NMR ($CDCl_3$) δ=0.80 (3H, s), 1.10—1.60 (8H, m), 2.90 (0.15H, m), 3.15 (0.85H, m), 3.60 (0.15H, d, J=1.98 Hz), 4.05 (0.85H, d, J=3.95 Hz), 7.05 (2H, m), 7.25 (2H, m); IR(neat) 2928, 1511, 1222, 837 cm^{-1}.

***trans*-2,3-Epoxyoctane (44);** ^{1}H NMR ($CDCl_3$) δ=0.89 (3H, t, J=6.93 Hz), 1.29 (3H, d, J=5.27 Hz), 1.33 (4H, br), 1.45—1.52 (4H, m), 2.62 (1H, m), 2.75 (1H, m); IR(neat) 2960, 2930, 2854, 1464, 1378 cm^{-1}.

2,3-Epoxy-1-phenylbutane (46); ^{1}H NMR ($CDCl_3$) δ=1.30 (3H, d, J=5.30 Hz), 2.70—2.90 (4H, m), 7.20—7.40 (5H, m); IR(neat) 2980, 1495, 1453, 1381, 737, 699 cm^{-1}.

2,3-Epoxy-3-methylbutyl Benzoate (52); ^{1}H NMR ($CDCl_3$) δ=1.40 (6H, s), 3.15 (1H, m), 4.30 (1H, m), 4.60 (1H, m), 7.40—7.60 (3H, m), 8.05 (2H, m); IR(neat) 2964, 1721, 1272, 1114, 712 cm^{-1}.

2,3-Epoxybutyl Benzoate (54); ^{1}H NMR ($CDCl_3$) δ=1.36 (3H, d, J=5.94 Hz), 3.00 (2H, m), 4.20 (1H, dd, J_1=5.94 Hz, J_2=12.2 Hz), 4.60 (1H, dd, J_1=3.30 Hz, J_2=12.2 Hz); IR(neat) 1722, 1273, 712 cm^{-1}.

5,6-Epoxycholesteryl Benzoate (Mixture of 56 and 57); ^{1}H NMR ($CDCl_3$) δ=0.60 (3H, m), 0.80—1.60 (6H, m), 1.80—2.20 (34H, m), 2.90 (0.31H, d, J=2.90 Hz), 3.10 (0.69H, d, J=2.00 Hz), 4.70—5.00 (1H, m), 7.20—7.40 (5H, m); IR(KBr) 2950, 1734, 1470, 1368, 1247, 1041 cm^{-1}.

Measurement of Cyclic Voltammetry. The acetonitrile solution containing 0.1 M TBAP and 0.001 M nickel(II) complex was degassed by bubbling of argon for 15 min and the measurements were performed at the scan rate of 200 mV s^{-1}. The range of measurement was between −2.0 V and +2.0 V.

References

1) J. -C. Marchon and R. Ramasseul, *Synthesis,* **1989**, 389.

2) Y. Matsuda, H. Koshima, K. Nakamura, and Y. Murakami, *Chem. Lett.,* **1988**, 625.

3) T. Takai, T. Yamada, and T. Mukaiyama, *Chem. Lett.,* **1990**, 1657.

4) T. Mukiyama, T. Takai, T. Yamada, and O. Rhode, *Chem. Lett.,* **1990**, 1661.

5) T. Yamada, T. Takai, O. Rhode, and T. Mukaiyama, *Chem. Lett.,* **1991**, 1.

6) Nippon Soda Co., Ltd., JP Patent Tokkaisho 46-26063 (1971).

7) Y. Maeda, M. Ai, and S. Suzuki, *Kogyo Kagaku Zasshi,* **73**, 99 (1970).

8) Shell International Research, JP Patent Tokkaisho 59-231077 (1984).

9) B. Kirson and H. Sechter, *Bull. Soc. Chim. Fr.,* **1978**, 2236.

10) J. E. Caton, Jr. and C. V. Banks, *Inorg. Chem.,* **6**, 1670 (1967).

11) T. Yamada, O. Rhode, T. Takai, and T. Mukaiyama, *Chem. Lett.,* **1991**, 5.

12) P. Brougham, M. S. Cooper, D. A. Cummerson, H. Heaney, and N. Thompson, *Synthesis,* **1987**, 1015.

13) Similar stereoselection in the epoxidation of cholesterol derivatives were reported in several reactions. By using molybdenum(V) chloride as a catalyst and *t*-pentyl hydroperoxide as an oxidant, β-epoxide of steroid derivative was afforded with 80% selectivity. G. A. Tolstikov, U. M. Dzhemilev, and V. P. Yur'ev, *J. Org. Chem.,* USSR, *Engl. Transl.,* **8**, 2253 (1972). Recently, it was also reported that aerobic epoxidation catalyzed by (tetramesitylporphinato)-ruthenium(II) converted cholesterol derivatives into the corresponding β-epoxides selectively, see Ref. 1.

14) P. G. Charles and M. A. Pawlikowski, *J. Phys. Chem.,* **62**, 440 (1958).

15) H. Okawa, K. Ueda, and S. Kida, *Inorg. Chem.,* **21**, 1594 (1982).

16) A. W. Addison and D. P. Graddon, *Aust. J. Chem.,* **21**, 2003 (1968).

17) K. Kurosawa and A. Moriyama, *Bull. Chem. Soc. Jpn.,* **47**, 2717 (1974).

Synthesis of Optically Active Substituted Cyclohexenones from Carbohydrates by Catalytic Ferrier Rearrangement

Noritaka CHIDA, Masami OHTSUKA, Katsuyuki OGURA, and Seiichiro OGAWA*
Department of Applied Chemistry, Faculty of Science and Technology, Keio University, Hiyoshi, Kohoku-ku, Yokohama 223
(Received March 6, 1991)

Conversion of hex-5-enopyranosides into substituted cyclohexanones (Ferrier rearrangement) was found to proceed efficiently with a catalytic amount of various mercury(II) salts at room temperature in a neutral solvent system. Among the mercury(II) salts tested, mercury(II) trifluoroacetate showed the highest activity. Four optically active cyclohexenones were prepared from hex-5-enopyranosides utilizing this method.

In 1979, Ferrier disclosed the efficient synthesis of chiral substituted cyclohexanones (2-deoxyinsoses) from hex-5-enopyranosides by the action of stoichiometric amount of mercury(II) chloride in hot aqueous acetone.[1] After this discovery, many reports concerning the mechanistic study,[2] application for syntheses of natural products,[3-8] and improved reaction conditions[5,9,10] have appeared so far. Lukacs and co-workers have reported that the Ferrier rearrangement proceeds with a catalytic amount (2 mol%) of mercury(II) sulfate in aqueous 1,4-dioxane containing sulfuric acid.[11] Recently, Adam has reported $PdCl_2$ or $Pd(OAc)_2$ also catalyzes conversion of hex-5-enopyranoside with an amino function at C-2 into 4-amino-2,4-dideoxyinososе in the solvent containing sulfuric acid.[12] Although this reaction is very useful and convenient for preparations of optically active cyclohexanones and/or cyclohexenones, sometimes difficulty is encountered in isolating the pure products due to the presence of excess Hg salts,[10] or in suppressing side reactions which might be caused by the acidic reaction conditions.[11,13]

During our study for the synthesis of natural products containing cyclohexane rings utilizing the Ferrier rearrangement,[14] we have investigated milder and simpler reaction conditions to avoid undesired side reactions such as β-elimination and aromatization. We report here our findings that the Ferrier rearrangement proceeds in high yields with a catalytic amount of various Hg(II) salts at room temperature in the neutral solvent system (acetone–water, without sulfuric acid), and the preparation of optically active cyclohexanones and cyclohexenones using this methodology.

The results of the catalytic Ferrier rearrangement of several hex-5-enopyranosides are shown in Table 1.

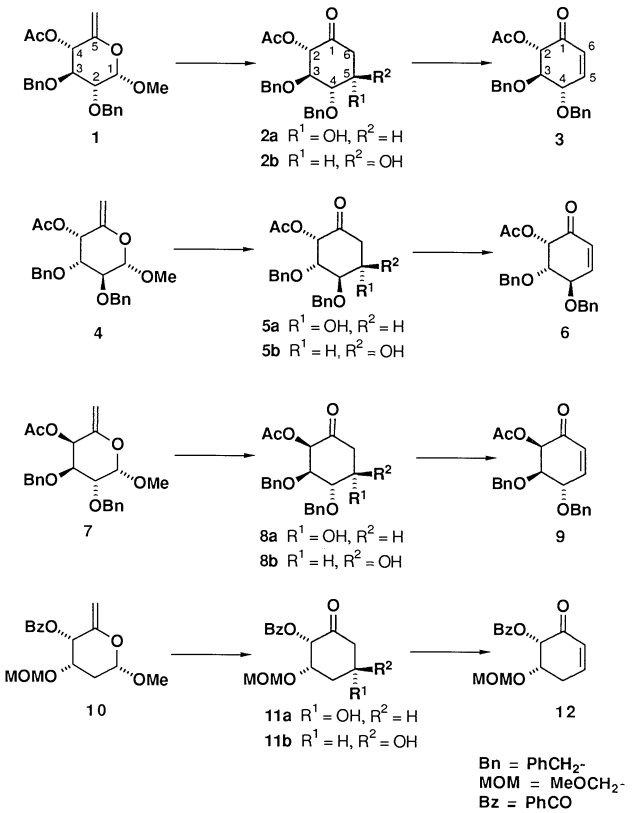

Scheme 1.

Table 1. Catalytic Ferrier Rearrangement of Some Hex-5-enopyranosides[a]

Run	Enopyranoside	Catalyst mol%	Time h	Products	Yield %	a/b[b]
1	**1**	$HgCl_2$ (10)	72	**2a, 2b**	97	6/1
2	**1**	HgO (10)	180	**2a, 2b**	94	6/1
3	**1**	$Hg(OAc)_2$ (10)	72	**2a, 2b**	96	8/1
4	**1**	$Hg(OCOCF_3)_2$ (10)	6	**2a, 2b**	96	8/1
5	**1**	$Hg(OCOCF_3)_2$ (5)	15	**2a, 2b**	96	8/1
6	**4**	$Hg(OCOCF_3)_2$ (10)	1	**5a, 5b**	79	1/4
7	**7**	$Hg(OCOCF_3)_2$ (10)	5	**8a, 8b**	91	4/1
8	**10**	$Hg(OCOCF_3)_2$ (10)	1.5	**11a, 11b**	86	1/19

a) All reactions were carried out at room temperature. b) Determined with 270 MHz ^{1}H NMR spectra.

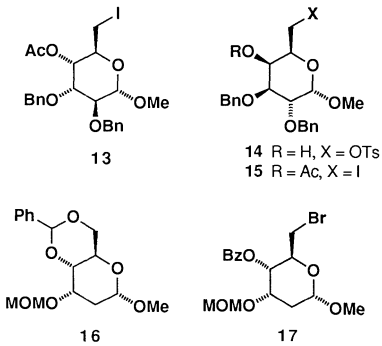

Scheme 2.

Although reactions of methyl 4-*O*-acetyl-2,3-di-*O*-benzyl-α-D-*xylo*-5-enopyranoside (**1**)[7] with 10 mol% of $HgCl_2$, HgO, and $Hg(OAc)_2$ in acetone–water (2 : 1) at room temperature were sluggish, they afforded the cyclized products (**2a**) and (**2b**)[7] in high yields (Runs 1—3). On the other hand, use of $(CF_3CO_2)_2Hg$[15] as the catalyst (5 or 10 mol%) accelerated the reaction and gave (**2a**) and (**2b**) in high yield as well as in much shorter time (Runs 4 and 5). Reaction of hex-5-enopyranosides having D-*arabino* configuration (**4**, Run 6), prepared from compound **13** in one step, with 10 mol% of $(CF_3CO_2)_2Hg$ at room temperature also provided the corresponding cyclohexanones (**5a** and **5b**) in 79% yield. Similar reaction of compounds **7** possessing L-*arabino* configuration (Run 7), synthesized from compound **14** in 3 steps, afforded the products (**8a** and **8b**) which were enantiomers of **5b** and **5a**, in 91% yield. Treatment of 2-deoxy-D-*erythro*-hex-5-enopyranoside derivative (**10**, Run 8), obtained from compound **16** in 2 steps via compound **17**, under the same reaction condition gave the desired products (**11a** and **11b**).

These β-hydroxycylohexanones, (**2a**, **2b**), (**5a**, **5b**), (**8a**, **8b**), and (**11a**, **11b**) were effectively converted into the corresponding cyclohexenones (**3**,[16] **6**, **9**, and **12**) by the action of methanesulfonyl chloride and triethylamine in moderate-to-good yields, respectively. The compounds thus obtained would be useful precursors for syntheses of optically active cyclitols, aminocyclitols, and other natural products.

Therefore, use of $(CF_3CO_2)_2Hg$ as the catalyst is found to be very effective for the Ferrier rearrangement. The mild reaction conditions as well as the short reaction time using a small amount (5—10 mol%) of $(CF_3CO_2)_2Hg$ should allow us to apply this reaction to the synthesis of complex natural products having acid labile functions. Use of the catalytic amount of mercury(II) salt also makes the work-up procedure of this reaction quite easy.

Experimental

Melting points were determined on a Mitamura Riken micro hot stage and are uncorrected. ^1H NMR spectra were taken on JEOL GX 270 (270 MHz) or JEOL EX 90 (90 MHz) spectrometers in chloroform-*d* with tetramethylsilane as an internal standard. Specific rotations were measured in a 0.1 dm tube with a JASCO DIP-370 Digital Polarimeter. Mass spectra were taken on a JEOL JMS-DX 302 spectrometer with EI (70 eV) mode. IR spectra were recorded with a JASCO IR-810 spectrometer.

Organic solutions were dried over anhydrous sodium sulfate and concentrated below 40 °C under reduced pressure.

General Procedure for Catalytic Ferrier Rearrangement: To a stirred mixture of hex-5-enopyranoside (**1**, **4**, **7**, and **10**; 1 mmol) in acetone–water (2:1, 10 ml) at room temperature was added Hg(II) salt (0.05 or 0.1 mmol) and the mixture was stirred at room temperature for the period indicated in Table 1. The mixture was partially evaporated to remove acetone and extracted with ethyl acetate, and the extract was dried. Removal of the solvent left a residue, which was purified on a column of silica gel (ethyl acetate–toluene) to afford the products.

2L-(2,4,5/3)- and 2L-(2,4/3,5)-2-*O*-Acetyl-3,4-di-*O*-benzyl-2,3,4,5-tetrahydroxycyclohexanone (2a) and (2b). Treatment of methyl 4-*O*-acetyl-2,3-di-*O*-benzyl-α-D-*xylo*-5-enopyranoside (**1**)[7] (398 mg) with mercury(II) trifluoroacetate (43 mg) in acetone–water afforded 370 mg (96%) of a mixture of **2a** and **2b** (8:1): $[\alpha]_D^{27}$ −24° (*c* 2.2, $CHCl_3$). The ^1H NMR data for the major isomer (**2a**) were identical with those reported in the literature.[7]

2L-(2,4/3)-2-*O*-Acetyl-3,4-di-*O*-benzyl-2,3,4-trihydroxy-5-cyclohexen-1-one (3). A mixture of **2a** and **2b** (8:1, 161 mg) was converted into compound **3** by the same procedure reported in the reference[14] to give 140 mg (91%) of **3** as a colorless syrup. The physical and spectral properties were all identical with those of the authentic sample.[14]

Methyl 4-*O*-Acetyl-2,3-di-*O*-benzyl-α-D-*arabino*-5-enopyranoside (4). A mixture of **13** (530 mg) and 1,8-diazabicyclo[5.4.0]undec-7-ene (DBU, 0.30 ml) in toluene (6 ml) was heated at 80 °C for 3 h. The mixture was diluted with ethyl acetate and washed successively with diluted hydrochloric acid solution, saturated aqueous sodium hydrogencarbonate solution and brine, and dried. Evaporation of the solvent left a residue, which was purified on a column of silica gel (10 g) with acetone–hexane (1:6) to give 364 mg (91%) of compound **4** as a colorless syrup. $[\alpha]_D^{27}$+21° (*c* 0.25, $CHCl_3$); IR (neat) 1740 and 1660 cm^{-1}; ^1H NMR (270 MHz) δ=2.12 (3H, s, OAc), 3.60 (3H, s, OMe), 3.64 (1H, dd, $J_{2,3}$=9.2 Hz, $J_{3,4}$=3.3 Hz, H-3), 3.78 (1H, dd, $J_{1,2}$=6.2 Hz, H-2), 4.45 (1H, d, H-1), 4.58 (1H, d, *J*=11.7 Hz, benzyl), 4.67 (1H, bs, H-6), 4.70 (1H, d, *J*=11.7 Hz, benzyl), 4.73 (1H, d, *J*=11.0 Hz, benzyl), 4.80 (1H, bs, H-6′), 4.82 (1H, d, *J*=11.0 Hz, benzyl), 5.73 (1H, d, H-4), and 7.26—7.36 (10H, m, phenyl). Found: *m*/*z* 399.1808 ($M+H^+$). Calcd for $C_{23}H_{27}O_6$: 399.1808 (M+H).

2L-(2,3,5/4)- and 2L-(2,3/4,5)-2-*O*-Acetyl-3,4-di-*O*-benzyl-2,3,4,5-tetrahydroxycyclohexanone (5a) and (5b). Treatment of compound **4** (398 mg) with mercury(II) trifluoroacetate (43 mg) in acetone–water gave 303 mg (79%) of a mixture of **5a** and **5b** (1:4) as a colorless syrup. $[\alpha]_D^{27}$ −37° (*c* 0.95, $CHCl_3$); IR (neat) 3450 and 1750 cm^{-1}; ^1H NMR (270 MHz) for the major isomer (**5b**) δ=2.19 (3H, s, OAc), 2.20—2.30 (1H, m, H-6), 2.71—2.75 (2H, m, H-6′ and OH), 3.90 (1H, dd, $J_{3,4}$=4.0 Hz, $J_{4,5}$=3.7 Hz, H-4), 4.09 (1H, dd, $J_{2,3}$=3.3 Hz, H-3), 4.20—4.40 (1H, m, H-5), 4.51 and 4.60 (each 1H, 2d, *J*=12 Hz, benzyl), 4.70 (2H, d, *J*=12 Hz, benzyl), 5.60 (1H, d, H-2), and 7.30—7.35

(10H, m, phenyl). Found: m/z 384.1585 (M^+). Calcd for $C_{22}H_{24}O_6$: M, 384.1573.

2L-(2,3/4)-2-*O*-Acetyl-3,4-di-*O*-benzyl-2,3,4-trihydroxy-5-cyclohexen-1-one (6). To a solution of a mixture of **5a** and **5b** (1:4, 39 mg) in dichloromethane (1.5 ml) were added triethylamine (0.15 ml) and methanesulfonyl chloride (0.023 ml). After stirring at room temperature for 15 min, the mixture was diluted with dichloromethane and washed successively with 0.25 mol dm^{-3} aqueous sulfuric acid and water, and dried. Evaporation of the solvent left a syrup, which was purified on a column of silica gel (1 g) with ethyl acetate–toluene (1:15) to afford **6** (29 mg, 79%) as a colorless syrup. $[\alpha]_D^{27}$ −92° (c 1.36, $CHCl_3$); IR (neat) 1750 and 1700 cm^{-1}; ^{1}H NMR (270 MHz) δ=2.19 (3H, s, OAc), 4.12—4.18 (2H, m, H-3 and 4), 4.55, 4.57, 4.64, and 4.70 (each 1H, 4d, J=12.1 Hz, benzyl), 5.84 (1H, d, $J_{5,6}$=2.6 Hz, H-6), 6.10 (1H, d, $J_{2,3}$=10.3 Hz, H-2), 6.74 (1H, ddd, $J_{3,4}$=4.6 Hz, $J_{3,5}$=1.8 Hz H-5), and 7.29—7.33 (10H, m, phenyl). Found: C, 72.07; H, 6.11%. Calcd for $C_{22}H_{22}O_5$: C, 72.12; H, 6.05%.

Methyl 4-*O*-Acetyl-2,3-di-*O*-benzyl-6-deoxy-β-L-*arabino*-hex-5-enopyranoside (7). A mixture of **15** (31 mg) and DBU (0.035 ml) in toluene (1 ml) was heated at 80 °C for 2 d. The mixture was worked up similarly as described for a preparation of compound **4** to give **7** (13 mg, 57%) as a colorless syrup. $[\alpha]_D^{27}$ +28° (c 0.79, $CHCl_3$); IR (neat) 1740 and 1660 cm^{-1}; ^{1}H NMR (270 MHz) δ=2.10 (3H, s, OAc), 3.42 (3H, s, OMe), 3.94 (1H, dd, $J_{1,2}$=3.3 Hz, $J_{2,3}$=9.9 Hz, H-2), 4.06 (1H, dd, $J_{3,4}$=3.7 Hz, H-3), 4.61 (1H, d, J=11.7 Hz, benzyl), 4.68 and 4.71 (each 1H, 2d, J=9.2 Hz, benzyl), 4.72 (2H, bs, H-6 and 6′), 4.75 (1H, d, H-1), 4.87 (1H, d, J=11.7 Hz, benzyl), 5.80 (1H, d, H-4), and 7.33 (10H, m, phenyl). Found: C, 69.17; H, 6.61%. Calcd for $C_{23}H_{26}O_6$: C, 69.33; H, 6.58%.

2D-(2,3/4,5)- and 2D-(2,3,5/4)-2-*O*-Acetyl-3,4-di-*O*-benzyl-2,3,4,5-tetrahydroxycyclohexanone (8a) and (8b). Treatment of compound **7** (398 mg) with mercury(II) trifluoroacetate (43 mg) in acetone–water gave 349 mg (91%) of a mixture of **8a** and **8b** (4:1) as a colorless syrup: $[\alpha]_D^{28}$ +45° (c 0.48, $CHCl_3$). The IR and ^{1}H NMR spectra were identical with those of compound **5b** and **5a**. Found: C, 69.02; H, 6.49%. Calcd for $C_{22}H_{24}O_6$: C, 68.74; H, 6.29%.

2D-(2,3/4)-2-*O*-Acetyl-3,4-di-*O*-benzyl-2,3,4-trihydroxy-5-cyclohexen-1-one (9). A mixture of **8a** and **8b** (4:1, 14 mg) was treated similarly as described for a preparation of compound **6** to afford **9** (9.6 mg, 71%) as a colorless syrup. $[\alpha]_D^{27}$ +91° (c 0.48, $CHCl_3$). The IR and ^{1}H NMR spectra of **9** were all identical with those of compound **6**. Found: C, 71.79; H, 6.07%. Calcd for $C_{22}H_{22}O_5$: C, 72.12; H, 6.05%.

Methyl 4-*O*-Benzoyl-2,6-dideoxy-3-*O*-methoxymethyl-α-D-*erythro*-hex-5-enopyranoside (10). A mixture of **17** (522 mg) and DBU (0.50 ml) in toluene (15 ml) was heated at 90 °C for 8 h. The mixture was worked up similarly as described for a preparation of compound **4** to afford **10** (378 mg, 91%) as a colorless syrup. $[\alpha]_D^{29}$ +79° (c 0.73, $CHCl_3$); IR (neat) 1740 and 1670 cm^{-1}; ^{1}H NMR (270 MHz) δ=2.14—2.56 (2H, m, H-2 and 2′), 3.33 and 3.58 (each 3H, 2s, OMe), 4.06 (1H, ddd, $J_{2,3}$=4.8 Hz, $J_{2',3}$=9.5 Hz, $J_{3,4}$=3.5 Hz, H-3), 4.66 and 4.75 (each 1H, 2d, J=7.0 Hz, methylene), 4.68 (1H, dd, $J_{1,2}$=3.7 Hz, $J_{1,2'}$=10.6 Hz, H-1), 4.79 (1H, s, H-6), 4.83 (1H, bs, H-6′), 5.75 (1H, d, H-4), and 7.44—8.11 (5H, m, phenyl). Found: C, 62.46; H, 6.35%. Calcd for $C_{16}H_{20}O_6$: C, 62.33; H, 6.54%.

2L-(2,3,5/0)- and 2L-(2,3/5)-2-*O*-Benzoyl-3-*O*-methoxymethyl-2,3,5-trihydroxycyclohexanone (11a) and (11b). Treatment of compound **10** (308 mg) with mercury(II) trifluoroacetate (43 mg) in acetone–water gave 253 mg (86%) of a mixture of **11a** and **11b** (1:19) as a colorless syrup. $[\alpha]_D^{27}$ −37° (c 1.1, $CHCl_3$); IR (neat) 3450, 1750, and 1730 cm^{-1}; ^{1}H NMR (270 MHz) for the major isomer (**11b**) δ=2.02 (1H, ddd, $J_{3,4}$=2.2 Hz, $J_{4,5}$=11.2 Hz, $J_{4,4'}$=13.4 Hz, H-4), 2.14 (1H, b, OH), 2.54 (1H, m, H-4′), 2.60 (1H, dd, $J_{5,6}$=10.7 Hz, $J_{6,6'}$=13.7 Hz, H-6), 2.95 (1H, ddd, $J_{5,6'}$=4.9 Hz, $J_{4',6'}$=2.4 Hz, H-6′), 3.39 (3H, s, OMe), 4.36—4.47 (2H, m, H-3 and 5), 4.74 and 4.79 (each 1H, 2d, J=6.5 Hz, methylene), 5.52 (1H, d, $J_{2,3}$=2.9 Hz, H-2), and 7.43—8.08 (5H, m, phenyl). Found: m/z 294.1104 (M^+). Calcd for $C_{15}H_{18}O_6$: M, 294.1104.

2L-(2,3/0)-2-*O*-Benzoyl-3-*O*-methoxymethyl-2,3-dihydroxy-5-cyclohexen-1-one (12). To a mixture of **11a** and **11b** (1:19, 48 mg) in dichloromethane (2 ml) at 0 °C were added methanesulfonyl chloride (33 μl) and triethylamine (0.158 ml). After stirring at room temperature for 90 min, the reaction mixture was treated similarly as described for a preparation of compound **6** to afford **12** (43 mg, 95%) as a crystalline residue. Mp 118—119 °C (from ethanol); $[\alpha]_D^{25}$ −12° (c 0.97, $CHCl_3$); IR (KBr) 1730 and 1695 cm^{-1}; ^{1}H NMR (270 MHz) δ=2.86 (2H, m, H-4 and 4′), 3.35 (3H, s, OMe), 4.53 (1H, dddd, $J_{3,4}$=4.4 Hz, $J_{3,4'}$= 2.9 Hz $J_{2,3}$=2.6 Hz, $J_{3,5}$=1.8 Hz, H-3), 4.73 and 4.78 (each 1H, 2d, J=7.0 Hz, methylene), 5.76 (1H, d, H-2), 6.19 (1H, ddd, $J_{4,6}$=$J_{4',6}$=1.8 Hz, $J_{5,6}$=9.9 Hz, H-6), 6.86 (1H, dddd, $J_{4,5}$=$J_{4',5}$=4.3 Hz, H-5), and 7.46—8.12 (5H, m, phenyl). Found: C, 64.92; H, 5.87%. Calcd for $C_{15}H_{16}O_5$: C, 65.21; H, 5.84%.

Methyl 4-*O*-Acetyl-2,3-di-*O*-benzyl-6-deoxy-6-iodo-α-D-altropyranoside (13). To a solution of methyl 2,3-di-*O*-benzyl-6-deoxy-6-iodo-α-D-altropyranoside[14] (200 mg) in pyridine (1.5 ml) was added acetic anhydride (1.5 ml), and the mixture was stirred at room temperature overnight. The reaction mixture was concentrated and co-distilled with toluene several times to give a residue, which was purified on a column of silica gel (10 g) with acetone–toluene (1:40) to afford **13** (210 mg, 97%) as a colorless syrup. $[\alpha]_D^{27}$ +21° (c 0.25, $CHCl_3$); IR (neat) 1740 cm^{-1}; ^{1}H NMR (90 MHz) δ=2.02 (3H, s, OAc), 3.17 (1H, dd, $J_{5,6}$=9.8 Hz, $J_{6,6}$=13.0 Hz, H-6), 3.36 (1H, dd, $J_{5,6}$=4.0 Hz, H-6′), 3.49 (3H, s, OMe), 3.65 (1H, dd, $J_{1,2}$=2.5 Hz, $J_{2,3}$=5.2 Hz, H-2), 3.88 (1H, dd, $J_{3,4}$=4.0 Hz, H-3), 4.10 (1H, ddd, $J_{4,5}$=8.6 Hz, H-5), 4.42 and 4.59 (each 1H, 2d, J=12.0 Hz, benzyl), 4.57 (2H, s, benzyl), 4.68 (1H, d, H-1), 5.00 (1H, dd, H-4), and 7.20—7.43 (10H, m, phenyl). Found: m/z 527.0925 ($M+H^+$). Calcd for $C_{23}H_{28}O_6I$: 527.0931 (M+H).

Methyl 2,3-Di-*O*-benzyl-6-*O*-tosyl-α-D-galactopyranoside (14). A mixture of methyl 2,3-di-*O*-benzyl-α-D-galactopyranoside[17] (255 mg), *p*-toluenesulfonyl chloride (470 mg) and 4-dimethylaminopyridine (8 mg) in pyridine (4.5 ml) was stirred at room temperature for 16 h. The mixture was diluted with ethyl acetate and then washed successively with diluted hydrochloric acid and brine, and dried. Removal of the solvent gave a residue, which was purified on a column of silica gel (10 g) with ethyl acetate–toluene (1:5) to afford **14** (365 mg, 100%) as a colorless syrup. $[\alpha]_D^{24}$ +37° (c 1.9, $CHCl_3$); IR (neat) 3500 and 1360 cm^{-1}; ^{1}H NMR (90 MHz) δ=2.42 (3H, s, $PhC\underline{H}_3$), 3.32 (3H, s, OMe), 3.72—4.24 (6H, m, H-2,3,4,5,6 and 6′), 4.59 (1H, d, $J_{1,2}$=3.0 Hz, H-1), 4.60 and 4.63 (each 1H, 2d, J=12.0 Hz, benzyl), 4.80 (2H, d, J=12 Hz, benzyl), and 7.33—7.38 (14H, m, phenyl). Found: C, 63.39; H, 5.86%. Calcd for $C_{28}H_{32}O_8S$: C, 63.62; H, 6.10%.

Methyl 4-*O*-Acetyl-2,3-Di-*O*-benzyl-6-deoxy-6-iodo-α-D-

galactopyranoside (15). A mixture of **14** (202 mg) and sodium iodide (172 mg) in *N,N*-dimethylformamide (1 ml) was heated at 80 °C for 4 d. The mixture was diluted with ethyl acetate and washed with water, and dried. Evaporation of the solvent left a residue, which was then treated with acetic anhydride (1.8 ml) and pyridine (3.6 ml) at room temperature overnight. The mixture was concentrated and diluted with ethyl acetate, and washed successively with diluted hydrochloric acid, saturated aqueous sodium hydrogencarbonate solution and brine, and dried. Evaporation of the solvent gave a syrup, which was purified on a column of silica gel (4.2 g) with ethyl acetate–hexane (1:9) to afford **15** (139 mg, 70%) as a colorless syrup. $[\alpha]_D^{25}$ +65° (*c* 0.54, $CHCl_3$); IR (neat) 1740 cm^{-1}; ^1H NMR (270 MHz) δ=2.13 (3H, s, OAc), 3.11 (2H, m, H-6 and 6′), 3.46 (3H, s, OMe), 3.75 (1H, dd, $J_{1,2}$=3.7 Hz, $J_{2,3}$=9.9 Hz, H-2), 3.96 (1H, dd, $J_{3,4}$=4.0 Hz, H-3), 4.00 (1H, ddd, $J_{5,6}$=2.9 Hz, $J_{5,6'}$=8.1 Hz, $J_{4,5}$=1.8 Hz, H-5), 4.57 (1H, d, *J*=11.4 Hz, benzyl), 4.64 (1H, d, *J*=12.1 Hz, benzyl), 4.67 (1H, d, H-1), 4.73 (1H, d, *J*=11.4 Hz, benzyl), 4.84 (1H, d, *J*=12.1 Hz, benzyl), 5.59 (1H, dd, H-4), and 7.26—7.35 (10H, m, phenyl). Found: 526.0857 (M^+). Calcd for $C_{23}H_{27}O_6I$: M, 526.0853.

Methyl 4,6-*O*-Benzylidene-2-deoxy-3-*O*-methoxymethyl-α-D-ribopyranoside (16). A mixture of methyl 4,6-*O*-benzylidene-2-deoxy-α-D-ribopyranoside[18] (1.00 g), chloromethyl methyl ether (0.57 ml) and *N,N*-diisopropylethylamine (2.62 ml) in dichloromethane (20 ml) was heated under reflux overnight. The mixture was diluted with dichloromethane and washed successively with diluted hydrochloric acid, saturated aqueous sodium hydrogencarbonate solution and brine, and dried. Concentration of the mixture afforded a residue, which was purified on a column of silica gel (30 g) with ethyl acetate–toluene (1:8) to give **16** (1.15 g, 86%) as needles. Mp 53—53.5 °C (from ether–petroleum ether); $[\alpha]_D^{27}$ +95° (*c* 1.0, $CHCl_3$); ^1H NMR (270 MHz) δ=2.00 (1H, ddd, $J_{1,2}$=4.4 Hz, $J_{2,3}$=4.0 Hz, $J_{2,2'}$=15.0 Hz, H-2), 2.19 (1H, ddd, $J_{1,2'}$=0.7 Hz, $J_{2',3}$=2.6 Hz, H-2′), 3.39 (6H, s, OMe), 3.65 (1H, dd, $J_{3,4}$=2.9 Hz, $J_{4,5}$=8.4 Hz, H-4), 3.70 (1H, dd, $J_{5,6}$=$J_{6,6'}$=12.1 Hz, H-6), 4.19 (1H, ddd, H-3), 4.26—4.37 (2H, m, H-5 and 6′), 4.71 (1H, dd, H-1), 4.76 and 4.85 (each 1H, 2d, *J*=7.0 Hz, methylene), 5.55 (1H, s, PhCH), and 7.31—7.56 (5H, m, phenyl). Found: C, 62.07; H, 6.96%. Calcd for $C_{16}H_{22}O_6$: C, 61.92; H, 7.15%.

Methyl 6-Bromo-4-*O*-benzoyl-2,6-dideoxy-3-*O*-methoxymethyl-α-D-ribopyranoside (17). A mixture of **16** (1.0 g), *N*-bromosuccinimide (599 mg), 1,1,2,2-tetrachloroethane (1.6 ml), and barium carbonate (332 mg) in carbon tetrachloride (20 ml) was heated at 90 °C for 4 h. After cooling, the insoluble matter was removed by filtration and washed with chloroform. The filtrate was concentrated to give a residue, which was dissolved in ethyl acetate and washed with water, and dried. Evaporation of the solvent left a residue, which was purified on a column of silica gel (80 g) with acetone–hexane (1:16) to afford **17** (1.13 g, 90%) as a colorless syrup. $[\alpha]_D^{27}$ +129° (*c* 1.5, $CHCl_3$); IR (neat) 1720 cm^{-1}; ^1H NMR (90 MHz) δ=1.87—2.40 (2H, m, H-2 and 2′), 3.24 and 3.46 (each 3H, 2s, OMe), 3.36—3.73 (2H, m, H-6 and 6′), 4.22—4.58 (2H, m, H-3 and 5), 4.57 and 4.73 (each 1H, 2d, *J*=7.0 Hz, methylene), 4.84 (1H, m, H-1), 5.02 (1H, dd, $J_{3,4}$=3.4 Hz, $J_{4,5}$=10.0 Hz, H-4), and 7.39—8.12 (5H, m, phenyl). Found: C, 49.60; H, 5.28%. Calcd for $C_{16}H_{21}O_6Br$: C, 49.37; H, 5.44%.

References

1) R. J. Ferrier, *J. Chem. Soc., Perkin Trans. 1,* **1979**, 1455.

2) R. Blattner, R. J. Ferrier, and S. R. Hains, *J. Chem. Soc., Perkin Trans. 1,* **1985**, 2413; M. Mádi-Puskás, I. Pelyvás, and R. Bognár, *J. Carbohydr. Chem.,* **4**, 323 (1985).

3) R. Blattner, R. J. Ferrier, and P. Prasit, *J. Chem. Soc., Chem. Commun.,* **1980**, 944.

4) N. Sakairi, M. Hayashida, A. Amino, and H. Kuzuhara, *J. Chem. Soc., Perkin Trans. 1,* **1990**, 1301, and references therein.

5) D. H. R. Barton, S. Augy-Dorey, J. Camara, P. Dalko, J. M. Delaumény, S. D. Gero, B. Quiclet-Sire, and P. Stutz, *Tetrahedron,* **46**, 215 (1990), and references therein.

6) D. Semeria, M. Philippe, J. M. Delaumény, A. M. Sepulchre, and S. D. Gero, *Synthesis,* **1983**, 710.

7) A. Köhn and R. R. Schmidt, *Liebigs Ann. Chem.,* **1987**, 1045.

8) K. Sato, S. Sakuma, Y. Nakamura, J. Yoshimura, and H. Hashimoto, *Chem. Lett.,* **1991**, 17.

9) R. J. Ferrier and S. R. Haines, *Carbohydr. Res.,* **130**, 135 (1984).

10) F. Chretien and Y. Chapleur, *J. Chem. Soc., Chem. Commun.,* **1984**, 1268.

11) A. S. Machado, A. Olesker, and G. Lukacs, *Carbohydr. Res.,* **135**, 231 (1985); A. S. Machado, A. Olesker, S. Castillon, and G. Lukacs, *J. Chem. Soc., Chem. Commun.,* **1985**, 330.

12) S. Adam, *Tetrahedron Lett.,* **29**, 6589 (1988).

13) I. Pelyvás, F. Sztaricskai, and R. Bognár, *J. Chem. Soc., Chem. Commun.,* **1984**, 104.

14) N. Chida, M. Ohtsuka, K. Nakazawa, and S. Ogawa, *J. Chem. Soc., Chem. Commun.,* **1989**, 436; N. Chida, M. Ohtsuka, K. Nakazawa, and S. Ogawa, *J. Org. Chem.,* **56**, 2976 (1991).

15) Stoichiometric amount of $(CF_3CO_2)_2$ Hg was first used in Ferrier rearrangement by Chretien and Chapleur (see Ref. 10).

16) This compound had been converted into the aminocyclitol moiety of antibiotic hygromycin A (see Ref. 14).

17) J. Kiss and F. Burlkhardt, *Helv. Chim. Acta,* **53**, 1000 (1970).

18) D. A. Prins, *J. Am. Chem. Soc.,* **70**, 3955 (1948).

Asymmetric Reactions of Enamines with Methyl (*E*)-4-Oxo-4-(2-oxo-1,3-oxazolidin-3-yl)-2-butenoate by the Use of a Chiral Titanium Reagent

Yujiro HAYASHI, Ken OTAKA, Nobuo SAITO, and Koichi NARASAKA*
Department of Chemistry, Faculty of Science, The University of Tokyo, Hongo, Bunkyo-ku, Tokyo 113
(Received March 6, 1991)

Asymmetric Michael and [2+2] cycloaddition reactions between enamines and methyl (*E*)-4-oxo-4-(2-oxo-1,3-oxazolidin-3-yl)-2-butenoate proceed with a chiral titanium reagent generated in situ from dichlorodiisopropoxytitanium and a tartrate-derived chiral 1,4-diol. In the presence of excess amounts of the chiral titanium reagent, good to moderate enantioselectivity is attained. The reactions are also well catalyzed even with a catalytic amount of the titanium reagent.

Michael reaction, one of the most versatile carbon–carbon bond forming reactions, is an indispensable tool in organic synthesis and the asymmetric version of this reaction has been intensively examined.[1] A variety of asymmetric Michael reactions have been devised by the use of chiral Michael acceptors or donors such as chiral enamines[2] or chiral vinyl sulfoxides.[3] Furthermore, in this decade, several good results have been reported on the enantioselective Michael reaction of prochiral substrates,[4] but only a few examples are known for the asymmetric Michael reactions by the use of a catalytic amount of chiral auxiliaries.[5]

We have reported the preparation and properties of a chiral titanium reagent which is prepared in situ from dichlorodiisopropoxytitanium and optically active 1,1,4,4-tetraphenyl-2,3-(1-phenylethylidene)dioxy-1,4-butanediol (**1**) derived from dimethyl tartrate.[6] This reagent promotes the inter- and intra-molecular Diels–Alder reactions,[7] the [2+2] cycloaddition reaction,[8] the intramolecular ene reaction[9] and the hydrocyanation,[10] in which very high enantioselectivities are attained. For another application of this chiral titanium reagent, the Michael reaction of enamines[11] was investigated by employing the chiral titanium reagent as a reaction promoter.

Results and Discussion

Methyl (*E*)-4-oxo-4-(2-oxo-1,3-oxazolidin-3-yl)-2-butenoate (**2**) which was a suitable dienophile in the above asymmetric Diels–Alder reaction[7a] was chosen as a Michael acceptor, and the reaction with enamines was examined in the presence of the chiral titanium reagent prepared by mixing dichlorodiisopropoxytitanium and the chiral (2*R*, 3*R*)-1,4-diol **1**. When **2** and 4-(1-phenylethenyl)morpholine (**3**) was treated with an equimolar amount of the chiral titanium reagent at 0 °C for 24 h in the presence of Molecular Sieves 4A (MS 4A) in CH_2Cl_2, the Michael adduct **4** was obtained in 61% yield in 22% ee after hydrolysis of the reaction mixture. The reference reaction of **2** and **3** without the Lewis acid proceeded very slowly under the same reaction conditions to give the product **4** in only 6% yield.

After screening the amino moiety of acetophenone enamines and the reaction solvents, **4** was found to be obtained in 51% yield with 58% ee when the morpholino enamine **3** reacted with **2** in ether in the presence of an equimolar amount of the titanium reagent. The enantioselectivity was further improved to 73% ee by the use of excess amounts (2 molar amounts) of the chiral titanium reagent (54% yield). Moreover, even by a catalytic use (20% molar amount) of the chiral titanium reagent, the reaction proceeded with slight loss of the optical purity (68% yield, 55% ee), which indicates that the catalyst is regenerated during the course of the reaction. The product before hydrolysis[12] is considered to be the enamine **5**,[12b] the dihydropyran **6**,[12c,d] or the cyclobutane derivative **7**.[12e,f]

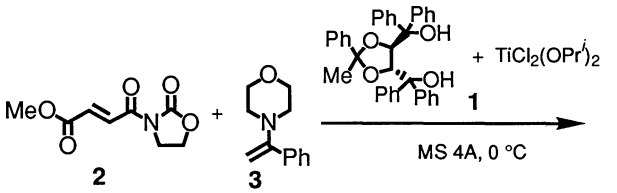

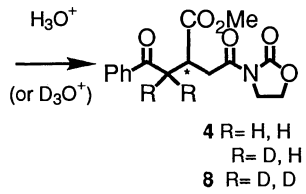

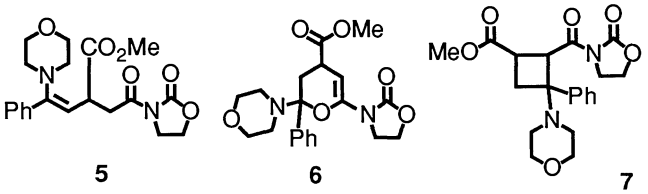

To determine which is the real intermediate, the reaction was quenched with D_2O–CH_3COOD. The Michael product was obtained in 30% yield, which consisted of d_0(**4**, 4%), d_1(24%), and d_2(**8**, 72%) deriva-

tives. The major d_2-product **8** is considered to be generated by the rapid equilibrium between the enamine and the iminium salt during the hydrolysis.[13] The selective deuteration at the α-position of the phenacyl group clearly indicates that the enamine **5** is the intermediate before hydrolysis.

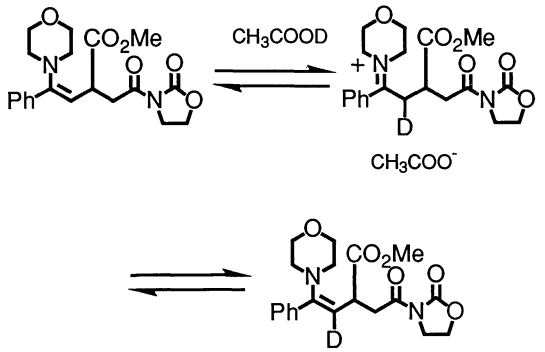

The reaction of **2** and 4-(1-*t*-butylethenyl)morpholine (**9**) was also examined by varying the amount of the chiral titanium reagent. By the use of excess amount of the chiral Lewis acid, good enantioselectivity was attained (78% ee). And, in the cases of a catalytic and an equimolar use of the chiral titanium reagent, the adduct **10** was obtained with moderate optical purity (53 and 57% ee, respectively).

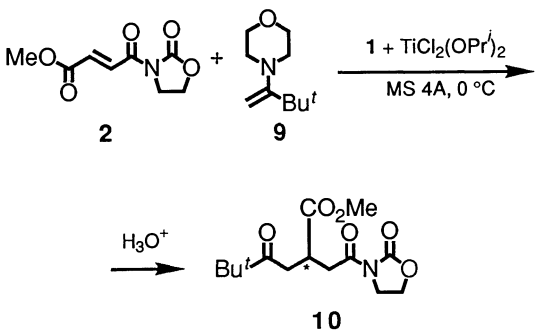

Morpholino enamine of cyclohexanone **11** also reacted in the presence of an equimolar amount of the chiral titanium reagent to afford the addition product **12** in 78% yield as a mixture of two diastereomers in a ratio of 2 : 1. Although the mixture exhibited optical rotation ($[\alpha]_D$ +17.8 (*c* 1.6, CH_2Cl_2)), the optical purity of each isomer could not be determined because of the difficulty of the separation. Accordingly, 3-acryloyl-1,3-oxazolidin-2-one (**13**), the product of which has a single chiral center, was employed as a Michael acceptor. When an ether solution of **11** and **13** was treated with an equimolar amount of the chiral reagent, the Michael product **14** was obtained in 38% yield as an optically active form (28% ee). The asymmetric induction at the chiral center is the clear evidence of the generation of a different type of intermediate from the former one **5** which should give the racemic product after hydrolysis. D_2O–CH_3COOD quenching of the reaction mixture afforded the 6-deuterated and nondeuterated cyclohexanone derivatives **16** and **14** in the ratio of 70 : 30, indicating the formation of the alternative enamine intermediate **17**. The present reaction using an enamine **11** with an α-substituent having a hydrogen is considered to proceed via the ene reaction or/and the Michael reaction followed by the successive proton transfer.[12b]

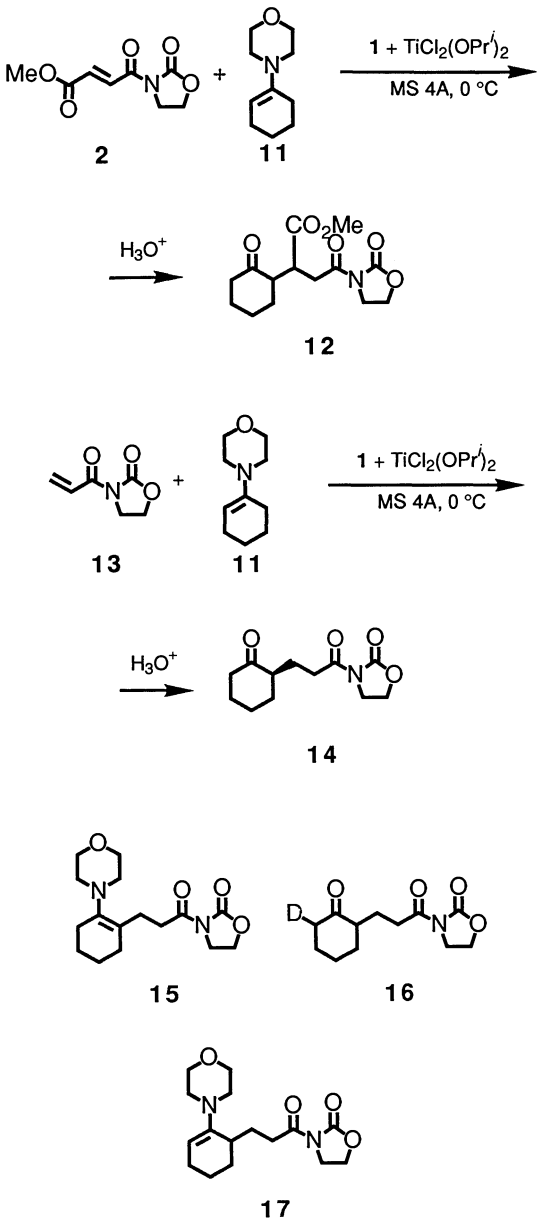

Contrary to the Michael reaction of the above enamines, the reactions of 2,2-disubstituted enamines with **2** were found to afford cyclobutanes. That is, 4-(2-methyl-1-propenyl)morpholine (**18**) reacted with **2** at 0 °C in ether by the use of an equimolar or a catalytic amount of the chiral titanium reagent to give the cyclobutane derivative **19** as a single stereoisomer in 86% and 78% yield with 53% ee and 56% ee, respectively, in which morpholino and oxazolidinylcarbonyl groups are

trans. By the usage of the excess amount of the catalyst, the *trans* isomer **19** was obtained in higher optical purity (48%, 77% ee), but a small amount (22%) of the *cis* isomer **20** was also isolated.

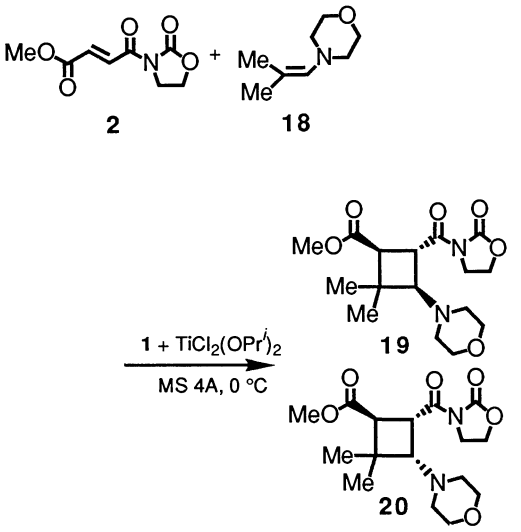

Since the reaction of the 2,2-disubstituted enamine **18** afforded the optically active cyclobutane, the preparation of optically active spiro compounds was next examined by employing enamines **21** and **22** prepared from cyclohexanecarbaldehyde and cyclopentanecarbaldehyde. The reactions were carried out with a catalytic amount (20% mol) of the chiral titanium reagent and the results are shown in the following equations. Two diastereomers **23** and **24** were obtained in the reaction of **21**. The optical purity of the *trans* and *cis* isomers **23**, **24** were found to be 69 and 64% ee, respectively. In the case of **22**, the *trans* isomer **25** was obtained exclusively in 71% yield with 38% ee.

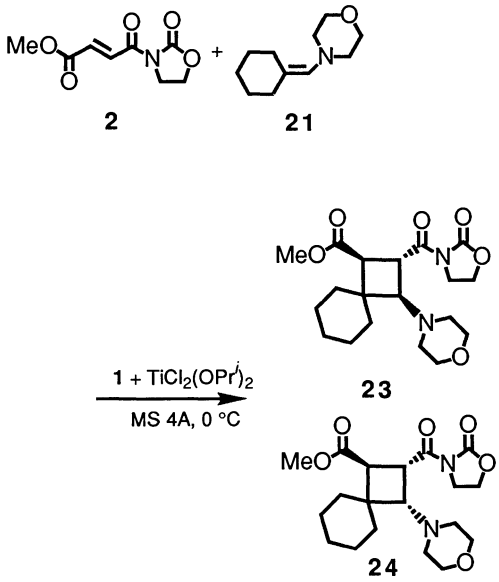

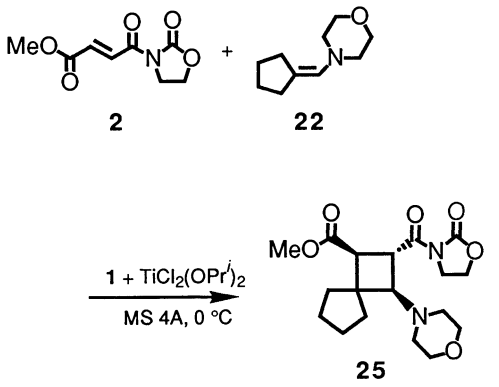

Thus, in the chiral titanium catalyzed reaction, enamines react with unsaturated carboxylic acid derivatives **2** in various courses depending on their structures, which is almost the same tendency observed in the noncatalyzed reactions.[12b] As for the enantioselectivity, good asymmetric induction is attained by the use of excess amount of the chiral titanium reagent, and moderate enantioselectivity is observed in the reaction with a catalytic and an equimolar amount of the reagent. The absolute configurations of the adducts have not been determined except for **14**. In the Diels–Alder reaction[7] and the [2+2] cycloaddition reaction[8] using **2** and the chiral titanium reagent prepared from the (2*R*, 3*R*)-diol **1**, the *re*-face of the β-carbon of α,β-unsaturated acyl moiety is attacked without exception. The same sence of the enantioselection would be anticipated in these reactions with enamines.

Experimental

General. (a) NMR spectra were recorded on Hitachi R24B, and Bruker AM500 spectrometers using tetramethylsilane as the internal standard and $CDCl_3$ as a solvent. IR spectra were recorded on Hitachi 260-30 or Horiba FT-300S spectrometers. Optical rotations were measured with JASCO DIP-180 or DIP-370 digital polarimeters. Mass spectra were obtained with JEOL JMS-D300 mass spectrometer operating at 70 eV. Melting points were uncorrected.

(b) Chromatography: Flash column chromatography was conducted on silica gel (E. Merck, 7734, 70—230 mesh) and the medium pressure column chromatography was performed with the YFLC-254 system of Yamazen Corp. Preparative thin-layer chromatography (TLC) was carried out on silica gel (Wakogel B-5F).

(c) Solvents and Reagents: Toluene and petroleum ether were distilled and stored over Molecular Sieves 4A (MS 4A). Ether was freshly distilled from sodium diphenylketyl. Dichlorodiisopropoxytitanium was prepared from titanium(IV) chloride and titanium(IV) isopropoxide according to the literature method.[14] (2*R*, 3*R*)-1,1,4,4-Tetraphenyl-2,3-(1-phenylethylidene)dioxy-1,4-butanediol (**1**) was prepared according to the method in our previous paper.[7a] Methyl (*E*)-4-oxo-4-(2-oxo-1,3-oxazolidin-3-yl)-2-butenoate (**2**) and 3-acryloyl-1,3-oxazolidin-2-one (**13**) were prepared according to the procedure of Evans.[15] Enamines **3**,[16] **9**,[16] **11**,[17] **18**,[18] **21**,[19] and **22**[19] were prepared according to the methods in the

literatures. All the operations were performed under an argon atmosphere.

Typical Procedure for the Reaction of 2 and Enamines Using a Catalytic Amount of the Chiral Titanium Catalyst. To an ether solution (3 ml) of dichlorodiisopropoxytitanium (30.9 mg, 0.13 mmol) was added the chiral diol **1** (74.5 mg, 0.14 mmol) at room temperature. After stirring for 20 min, MS 4A (powder, 100 mg) was added and the mixture was cooled to 0 °C. Then **2** (129.6 mg, 0.65 mmol) and an ether solution (1.5 ml) of 4-(1-phenylethenyl)morpholine (**3**) (135.0 mg, 0.71 mmol) was added, and the reaction mixture was stirred for 24 h at 0 °C. The reaction was quenched with pH 7 phosphate buffer and inorganic materials were removed by filtration. The organic materials were extracted three times with ethyl acetate and the combined extracts were washed with brine and dried over anhydrous Na_2SO_4. After evaporation of the solvent, the crude product was purified by preparative TLC (hexane : ethyl acetate, 1 : 1) to afford the Michael product **4** (140.9 mg, 0.44 mmol, 68% yield).

The procedure of the reactions using one or two equimolar amounts of the chiral titanium catalyst was identical with that described above, excepting the amount of the catalyst. Reaction conditions, chemical and optical yields are summarized in Table 1.

Spectral data and physical properties of the adducts and the determination of the optical purities were as follws.

Methyl (*R*)-2-Phenacyl-4-oxo-4-(2-oxo-1,3-oxazolidin-3-yl)butyrate (4). IR (neat) 1775, 1725, 1680 cm^{-1}; ^1H NMR (500 MHz) δ=3.20—3.27 (m, 2H), 3.42 (dd, J=7.4, 18.2 Hz, 1H), 3.48—3.55 (m, 1H), 3.57—3.62 (m, 1H), 3.69 (s, 3H), 3.98 (t, J=8.1 Hz, 2H), 4.41 (t, J=8.1 Hz, 2H), 7.44 (t, J=7.4 Hz, 2H), 7.55 (t, J=7.4 Hz, 1H), 7.93 (d, J=7.4 Hz, 2H); ^{13}C NMR (125 MHz) δ=35.72, 36.52, 39.50, 42.31, 52.10, 62.18, 127.94, 128.54, 133.28, 136.30, 153.43, 171.22, 174.47, 197.15; $[\alpha]_D^{21}$ +2.07° (*c* 1.4, CH_2Cl_2), $[\alpha]_{435}^{21}$ +5.68° (*c* 1.4, CH_2Cl_2):55% ee; HRMS Found: m/z 319.1003. Calcd for $C_{16}H_{17}NO_6$: M, 319.1056.

The Michael product **4** was converted to the bis-(+)-3,3,3-trifluoro-2-methoxy-2-phenylpropionic acid (MTPA) ester[20] **26** by the following procedure shown in Scheme 1, and the opitical purity was determined by the intergration of the signals at 30.09 (major) and 29.91 (minor) ppm of the ^{13}C NMR (125 MHz) spectrum.

Methyl (*R*)-5,5-Dimethyl-4-oxo-2-[(2-oxo-1,3-oxazolidin-3-yl)carbonylmethyl]hexanoate (10). Mp 87 °C; IR (neat) 1790, 1740, 1710 cm^{-1}; ^1H NMR (60 MHz) δ=1.1 (s, 9H), 2.7—3.0 (m, 5H), 3.6 (s, 3H), 3.8—4.6 (m, 4H); $[\alpha]_D^{24.5}$ +4.07° (*c* 1.17, CH_2Cl_2): 57% ee; Found: C, 56.06; H, 7.08; N, 4.61%. Calcd for $C_{14}H_{21}NO_6$: C, 56.18; H, 7.07; N, 4.68%.

The enantiomeric excess of the Michael adduct **10** was determined by the ^1H NMR analysis of the compound **10** with the existence of a chiral reagent, Eu(hfc)$_3$,[21] in which *t*-Bu group was sufficiently separated.

(*R*)-3-[(3-(2-Oxocyclohexyl)propanoyl]-1,3-oxazolidin-2-one (14). IR (neat) 1775, 1705 cm^{-1}; ^1H NMR (500 MHz) δ=1.32—1.41 (m, 1H), 1.47—1.54 (m, 1H), 1.58—1.67 (m, 2H), 1.78—1.84 (m, 1H), 1.97—2.11 (m, 3H), 2.21—2.28 (m, 1H), 2.30—2.37 (m, 2H), 2.82—2.92 (m, 2H), 3.94 (t, J=8.2 Hz, 2H), 4.35 (t, J=8.2 Hz, 2H); ^{13}C NMR (125 MHz) δ=24.08, 25.01, 27.95, 32.92, 34.15, 42.10, 42.47, 49.70, 62.00, 153.50, 173.22,

Table 1. Asymmetric Reaction between **2** and Enamines

Enamine	Product	Amount of the catalyst/mol%	Time/h	Yield/%	Optical purity/%ee
3	**4**	200[a]	23	54	73
		110[a]	29	51	58
		20[a]	24	68	55
9	**10**	200[a]	41	16	78
		110[a]	30	37	57
		20[a]	108	36	53
18	**19, 20**	200[b]	19	48, 22	77[e]
		110[a]	15	86[d]	53[e]
		20[a]	72	78[d]	56[e]
21	**23, 24**	20[b]	70[c]	41, 23	69, 64
22	**25**	20[b]	70[c]	71	38

a) Ether was used as solvent. b) Toluene-petroleum ether (1:1) was used as solvent. c) The reaction time is 70 h at 0 °C, then 24 h at r.t. d) **20** was not obtained. e) The optical purity is that of **19**.

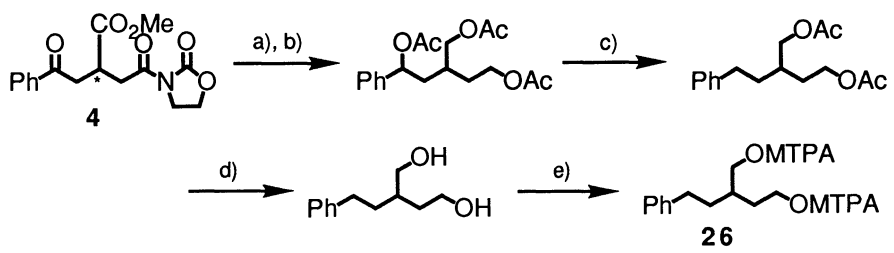

Scheme 1. a) $LiAlH_4$, b) Ac_2O, Pyridine, c) H_2, Pd/C, d) LiOH/H_2O-MeOH, e) (+)-MTPACl, Pyridine.

212.60; $[\alpha]_D^{26}$ +1.38° (*c* 0.755, CH_2Cl_2); HRMS Found: *m/z* 239.1178. Calcd for $C_{12}H_{17}NO_4$: M, 239.1158. The optical yield and the absolute configuration was determined by the comparison of the optical rotation of methyl 3-(2-oxocyclohexy)propionate derived from **14** with that of the literature; $[\alpha]_{435}^{27}$ +4.65° (*c* 1.55, MeOH), 27% ee (lit, $[\alpha]_{436}^{20}$ +17.13° (*c* 5.1, MeOH), 97% ee).[22]

Methyl (1*S*, 3*R*, 4*S*)-2,2-Dimethyl-3-morpholino-4-(2-oxo-1,3-oxazolidin-3-ylcarbonyl)cyclobutanecarboxylate (19). IR (neat) 1775, 1735, 1690 cm^{-1}; ^1H NMR (500 MHz) δ=1.08 (s, 3H), 1.33 (s, 3H), 2.22—2.28 (m, 2H), 2.29—2.35 (m, 2H), 2.75 (d, *J*=9.7 Hz, 1H), 2.76 (d, *J*=8.8 Hz, 1H), 3.67 (s, 3H), 3.63—3.70 (m, 4H), 4.03 (t, *J*=8.2 Hz, 2H), 4.35—4.44 (m, 2H), 4.75 (dd, *J*=8.8, 9.7 Hz, 1H); $[\alpha]_D^{23}$ −8.71° (*c* 0.81, CH_2Cl_2): 56% ee; Found: C, 58.70; H, 8.07; N, 4.81%. Calcd for $C_{14}H_{23}NO_5$: C, 58.93; H, 8.13; N, 4.91%.

The relative stereochemistry of morpholino and oxazolidinylcarbonyl groups was determined after conversion of the latter to the methoxycarbonyl group. The procedure is as follows; dry methanol (2 ml) and a drop of carbon tetrachloride was added to metal magnesium (15.75 mg, 0.648 mmol) at 0 °C to generate magnesium methoxide. After the magnesium dissolved completely, a THF solution (1.5 ml) of **19** (52.45 mg, 0.154 mmol) was added and stirred for 1 h. The reaction was quenched with saturated aqueous ammonium chloride solution and the organic materials were extracted with ethyl acetate. The combined organic layers were washed with brine and dried over Na_2SO_4. After evaporation of the solvent, the crude product was purified by TLC (hexane:ethyl acetate, 1 : 1) to afford dimethyl (1*S*, 2*S*, 3*R*)-4,4-dimethyl-3-morpholino-1,2-cyclobutanedicarboxylate 24.25 mg (55%).

IR (neat) 1735 cm^{-1}; ^1H NMR (500 MHz) δ=0.99 (s, $3H^e$), 1.30 (s, $3H^f$), 2.23—2.36 (m, 2H), 2.36—2.43 (m, $2H^d$), 2.61 (d, *J*=9.4 Hz, H^a), 2.74 (d, *J*=9.6 Hz, H^c), 3.17 (dd, *J*=9.4, 9.6 Hz, H^b), 3.65—3.68 (m, 4H), 3.69 (s, 3H), 3.70 (s, 3H).

The relative stereochemistry was determined as shown below by the NOESY spectrum, because NOEs were observed between H^a and H^d, H^b and H^d, H^b and H^e, H^a and H^c, H^a and H^f, H^c and H^f.

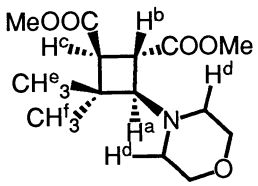

The determination of the optical purity is as follows; the cyclobutane derivative **19** was converted to the bis-(+)-MTPA esters[20] by the following sequence; 1) $Mg(OMe)_2$, 2) $LiAlH_4$, 3) (+)-MTPA-Cl, pyridine, cat. DMAP. The two sets of two singlet signals due to the methyl group appeared at 0.953, 0.934 (major) and 0.940, 0.910 (minor) ppm by 500 MHz ^1H NMR, and the optical yield was determined by the integration of these signals.

Methyl (1*S*, 2*S*, 3*R*)-3-Morpholino-2-(2-oxo-1,3-oxazolidin-3-ylcarbonyl)spiro[3.5]nonane-1-carboxylate (23) and Methyl (1*S*, 2*S*, 3*S*)-3-Morpholino-2-(2-oxo-1,3-oxazolidin-3-ylcarbonyl)spiro[3.5]nonane-1-carboxylate (24). **23** and **24** were obtained as a mixture. IR (neat) 1785, 1730, 1695 cm^{-1}; Found: C, 59.71; H, 7.50; N, 7.16%. Calcd for $C_{19}H_{28}N_2O_6$: C, 59.99; H, 7.42; N, 7.36%. ^1H NMR of the major isomer **23**; (500 MHz) δ=0.98—1.86 (m, 9H), 1.96—2.02 (m, 1H), 2.28—2.51 (m, 4H), 2.70 (d, *J*=9.5 Hz, 1H), 2.75 (d, *J*=9.2 Hz, 1H), 3.63—3.69 (m, 4H), 3.67 (s, 3H), 3.99 (t, *J*=8.1 Hz, 2H), 4.24—4.46 (m, 2H), 4.87 (dd, *J*=9.2, 9.5 Hz, 1H). The distinguishable peaks of the minor isomer **24** were as follows; δ=3.19 (d, *J*=9.7 Hz, 1H), 3.48 (d, *J*=9.7 Hz, 1H), 3.66 (s, 3H).

The mixture of spirononanes **23** and **24** was treated with $Mg(OMe)_2$ in THF to afford the corresponding dimethyl esters, which were separated by TLC (hexane:ethyl acetate, 3:2). The physical data of these dimethyl esters are as follows.

Dimethyl (1*S*, 2*S*, 3*R*)-3-morpholinospiro[3.5]nonane-1,2-dicarboxylate; IR (neat) 1729 cm^{-1}; ^1H NMR (500 MHz) δ=0.91—1.02 (m, 1H), 1.08—1.18 (m, 1H), 1.37 (dt, *J*=4.0, 13.6 Hz, 1H), 1.48—1.63 (m, 5H), 1.74—1.81 (m, H^e), 1.88-1.94 (m, H^f), 2.33—2.46 (m, $4H^d$), 2.58 (d, *J*=9.4 Hz, H^a), 2.69 (d, *J*=10.0 Hz, H^c), 3.32 (dd, *J*=9.4, 10.0 Hz, H^b), 3.65—3.71 (m, 4H), 3.67 (s, 3H), 3.71 (s, 3H); ^{13}C NMR (125 MHz) δ=22.06, 22.44, 25.84, 26.25, 40.18, 41.51, 45.93, 46.42, 51.88, 52.00, 66.69, 68.96, 172.46, 173.70; $[\alpha]_D^{27}$ −6.58° (*c* 1.02, CH_2Cl_2).

The relative stereochemistry was determined as shown below by the NOESY spectrum, because NOEs were observed between H^b and H^e, H^b and H^d, H^a and H^f, H^a and H^d, H^c and H^f, and H^a and H^c.

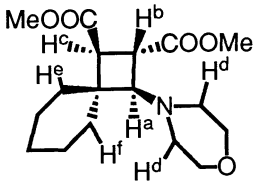

Dimethyl (1*S*, 2*S*, 3*S*)-3-morpholinospiro[3.5]nonane-1,2-dicarboxylate; IR (neat) 1733 cm^{-1}; ^1H NMR (500 MHz) δ=1.07—1.76 (m, 10H), 2.33—2.50 (m, 4H), 3.05 (dd, *J*=9.6, 9.8 Hz, 1H), 3.13 (d, *J*=9.6 Hz, 1H), 3.17 (d, *J*=9.8 Hz, 1H), 3.64—3.73 (m, 4H), 3.64 (s, 3H) 3.68 (s, 3H); $[\alpha]_D^{27}$ −1.18° (*c* 1.18, CH_2Cl_2).

The dimethyl ester derived from cycloadduct **23** was converted to the corresponding bis-(+)-MTPA ester[20] and the optical purity was determined by the integration of the signals (CH_2OMTPA) at 3.98 (dd, *J*=3.4, 11.7 Hz, major) and 4.13 (dd, *J*=3.8, 11.6 Hz, minor) ppm by the 500 MHz ^1H NMR.

The dimethyl ester derived from cycloadduct **24** was converted to the corresponding (+)-MTPA ester[20] and the optical purity was determined by the integration of the signals at 2.47 (m, 1H, major) and 2.58 (m, 1H, minor) ppm by the 500 MHz ^1H NMR.

Methyl (1*S*, 2*S*, 3*R*)-3-Morpholino-2-(2-oxo-1,3-oxazolidin-3-ylcarbonyl)spiro[3.4]octane-1-carboxylate (25). IR (neat) 1780, 1725, 1690 cm^{-1}; ^1H NMR (500 MHz) δ=1.43—1.97 (m, 8H), 2.22—2.35 (m, 4H), 2.87 (d, *J*=9.9 Hz, 1H), 2.98 (d, *J*=8.9 Hz, 1H), 3.66 (s, 3H), 3.62—3.71 (m, 4H), 3.97—4.07 (m, 2H), 4.35—4.46 (m, 2H), 4.63 (dd, *J*=8.9, 9.9 Hz, 1H); $[\alpha]_D^{24}$ −1.53° (*c* 0.806, CH_2Cl_2). 38% ee. The elemental analysis was performed after conversion to the corresponding dimethyl ester. Found: C, 61.58; H, 8.06; N, 4.47%. Calcd for $C_{16}H_{25}NO_5$: C, 61.72; H; 8.09, N; 4.50%.

The cycloadduct **25** was converted to the corresponding (+)-MTPA ester.[20] By the 500 MHz ^1H NMR, one of the four ester methylene protons (CH_2OMTPA) of the major distereomer appeared at 4.07 (dd, *J*=3.6, 11.7 Hz) ppm with the integration of 0.69 proton, which indicated the optical purity to

be 38% ee.

The D_2O Quenching of the Reactions 2 with 3, and 13 with 11. The reactions between **2** and **3**, and **13** and **11** were performed by the use of a catalytic amount of the chiral titanium reagent as described previously and were quenched by adding a mixture of D_2O (1 ml) and CH_3COOD (0.5 ml) at 0 °C. After stirring for 30 min at 0 °C, pH 7 phosphate buffer was added and the inorganic materials were filtered off. The organic materials were extracted with ethyl acetate and the purification was carried out by the same procedure as described before. Methyl 4-oxo-4-(2-oxo-1,3-oxazolidin-3-yl)-2-[α,α-$^2H_2$]phenacylbutanoate (**8**) was obtained by the reaction between **2** and **3** as a mixture with the mono- and nondeuterated adduct (d_2:d_1:d_0=72:24:4). The products ratio was determined by the mass spectrum of the mixture.

Spectral data of **8** is as follows; ^1H NMR (500 MHz) δ=3.24 (dd, J=5.5, 18.1 Hz, 1H), 3.44 (dd, J=7.3, 18.1 Hz, 1H), 3.60 (dd, J=5.5, 7.3 Hz, 1H), 3.69 (s, 3H), 3.98 (t, J=8.1 Hz, 2H), 4.41 (t, J=8.1 Hz, 2H), 7.44 (t, J=7.7 Hz, 2H), 7.55 (t, J=7.4 Hz, 1H), 7.93 (d, J=7.2 Hz, 2H); ^{13}C NMR (125 MHz) δ=35.62, 36.50, 39.20 (quintet), 42.32, 52.13, 62.18, 127.94, 128.57, 133.30, 136.35, 153.43, 171.25, 174.49, 197.24; HRMS Found: m/z 321.1151. Calcd for $C_{16}H_{15}D_2NO_6$: M, 321.1181.

The quintet of the carbon at 39.2 ppm indicates that the two deuteriums were attached at the same carbon, which was a secondary carbon by the DEPT measurement and it was also assigned as an α position of the phenacyl group because deuterium effect was observed at the carbonyl carbon of the benzoyl group.

(*R*)-3-[(2-Oxo[3-^{2}H]cyclohexyl)propanoyl]-1,3-oxazolidin-2-one (**16**) was obtained by the reaction of **13** and **11** as a mixture with the nondeuterated product **14** (**16**:**14**=70:30). Spectral data of **16** is as follows; ^1H NMR (500 MHz) δ=1.32—1.41 (m, 1H), 1.47—1.54 (m, 1H), 1.58—1.67 (m, 2H), 1.78—1.84 (m, 1H), 1.97—2.11 (m, 3H), 2.21—2.28 (m, 1H), 2.30—2.37 (m, 1H), 2.82—2.92 (m, 2H), 3.94 (t, J=8.2 Hz, 2H), 4.35 (t, J=8.2 Hz, 2H); ^{13}C NMR (125 MHz) δ=24.07, 25.01, 27.86, 32.90, 34.15, 41.77 (t, J=10.3 Hz), 42.45, 49.70, 62.00, 153.50, 173.21, 212.64.

The position of deuterium was assigned as follows; the carbon at 41.77 ppm, which was connected with deuterium, was assigned as a secondary carbon and α to the carbonyl group of cyclohexanone by the chemical shift of ^{13}C NMR, DEPT measurement, and the deuterium effect observed at the carbonyl carbon of cyclohexanone.

References

1) Reviews; K. Tomioka and K. Koga, "Noncatalytic Additions to α,β-Unsaturated Carbonyl Compounds," in "Asymmetric Synthesis," ed by J. D. Morrison, Academic Press, Inc., New York (1983), Vol. 2, Chap. 7; M. Norgradi, "Stereoselective Synthesis," VCH Verlagsgesellschaft, Weinheim (1987), p. 221.

2) D. Seebach, R. Imwinkelried, and T. Weber, "EPC Synthesis with C, C Bond Formation via Acetals and Enamines," in "Modern Synthetic Methods 1986," ed by R. Scheffold, Springler-Verlag, Berlin (1986); Y. Hirai, T. Terada, and T. Yamazaki, *J. Am. Chem. Soc.*, **110**, 958 (1988); S. L. Schreiber and H. V. Meyers, *ibid.*, **110**, 5198 (1988); and the references cited therein.

3) Review; G. H. Posner, "Addition of Organometallic Reagents to Chiral Vinylic Sulfoxides," in "Asymmetric Synthesis," ed by J. D. Morrison, Academic Press, Inc., New York (1983), Vol. 2, Chap. 8.

4) Review; K. Tomioka, *Synthesis*, **1990**, 541.

5) H. Wynberg and R. Helder, *Tetrahedron Lett.*, **1975**, 4057; D. J. Cram and G. D. Y. Sogah, *J. Chem. Soc., Chem. Commun.*, **1981**, 625; T. Yura, N. Iwasawa, K. Narasaka, and T. Mukaiyama, *Chem. Lett.*, **1988**, 1025; K. Soai, T. Hayasaka, and S. Ugajin, *J. Chem. Soc., Chem. Commun.*, **1989**, 516.

6) N. Iwasawa, Y. Hayashi, H. Sakurai, and K. Narasaka, *Chem. Lett.*, **1989**, 1581.

7) a) K. Narasaka, N. Iwasawa, M. Inoue, T. Yamada, M. Nakashima, and J. Sugimori, *J. Am. Chem. Soc.*, **111**, 5340 (1989); b) N. Iwasawa, J. Sugimori, Y. Kawase, and K. Narasaka, *Chem. Lett.*, **1989**, 1947; c) K. Narasaka, H. Tanaka, and F. Kanai, *Bull. Chem. Soc. Jpn.*, **64**, 387 (1991).

8) Y. Hayashi and K. Narasaka, *Chem. Lett.*, **1989**, 793; **1990**, 1295; Y. Hayashi, S. Niihata, and K. Narasaka, *ibid.*, **1990**, 2091; Y. Ichikawa, A. Narita, A. Shiozawa, Y. Hayashi, and K. Narasaka, *J. Chem. Soc., Chem. Commun.*, **1989**, 1919.

9) K. Narasaka, Y. Hayashi, and S. Shimada, *Chem. Lett.*, **1988**, 1609.

10) H. Minamikawa, S. Hayakawa, T. Yamada, N. Iwasawa, and K. Narasaka, *Bull. Chem. Soc. Jpn.*, **61**, 4379 (1988).

11) Lewis acid catalyzed Michael reaction of enamines, see; Y. Hashimoto, S. Machida, K. Saigo, J. Inoue, and M. Hasegawa, *Chem. Lett.*, **1989**, 943.

12) a) As for the mechanism of the α,β-unsaturated carbonyl compounds and enamines, see; H. O. House, "Modern Synthetic Reactions," 2nd ed, W. A. Benjamin, Inc., Menlo Park (1972), p. 616; b) G. Stork, A. Brizzolara, H. Landesman, J. Szmuskovicz, and R. Terrell, *J. Am. Chem. Soc.*, **85**, 207 (1963); c) G. Opitz and I. Loschmann, *Angew. Chem.*, **72**, 523 (1960); d) W. Schroth and G. Fischer, *Angew. Chem., Int. Ed. Engl.*, **2**, 394 (1963); e) I. Fleming and J. Harley-Mason, *J. Chem. Soc.*, **1964**, 2165; f) D. E. Heitmeier, J. T. Hortenstine, Jr., and A. P. Gray, *J. Org. Chem.*, **36**, 1449 (1971), and the references cited therein.

13) S. K. Malhotra and F. Johnson, *Tetrahedron Lett.*, **1965**, 4027; J. P. Scaefer and D. S. Weinberg, *ibid.*, **1965**, 1801.

14) C. Dijkgraaf and J. P. G. Rousseau, *Spectrochim. Acta, Part A.*, **24**, 1213 (1968).

15) D. A. Evans, K. T. Chapman, and J. Bisaha, *J. Am. Chem. Soc.*, **110**, 1238 (1988).

16) W. A. White and H. Weingarten, *J. Org. Chem.*, **32**, 213 (1967).

17) S. Hünig, E. Lucke, and W. Brenninger, *Org. Synth.*, Coll. Vol. V, 808 (1973).

18) E. Benzing, *Angew. Chem.*, **71**, 521 (1959).

19) L. Citerio, D. Pocar, R. Stradi, and B. Gioia, *J. Chem. Soc., Perkin Trans. 1*, **1978**, 309.

20) J. A. Dale, D. L. Dull, and H. S. Mosher, *J. Org. Chem.*, **34**, 2543 (1969).

21) Eu(hfc)$_3$=tris[3-heptafluoropropylhydroxymethylene)-*d*-camphorato]europium(III).

22) C. Stetin, B. D. Jeso, and J-C, Pommier, *J. Org. Chem.*, **50**, 3863 (1985).

One-Step Hydroamidation of a Schiff Base with Trichlorosilane

Hidenori OKAMOTO* and Shozo KATO
Tsukuba Research Lab., Tokuyama Soda Co., Ltd., 40 Wadai, Tsukuba, Ibaraki 300-42
(Received January 5, 1991)

We have found that the treatment of a Schiff base (**2**) with trichlorosilane and chloroacetyl chloride results in a highly active chloroacetamide herbicide (**1**) in an excellent yield. This one-step hydroamidation reaction of a Schiff base is a useful synthetic method.

Recently, we have reported on a highly active chloroacetamide herbicide (**1**) for paddy field rice.[1] The compound (**1**) has previously been synthesized in two steps (a reducing step and a chloroacetylating step) from a Schiff base (**2**) as shown in Scheme 1.

During the course of our studies, we found that treatment of a Schiff base (**2**) with trichlorosilane and chloroacetyl chloride produces the chloroacetamide (**1**) in one step with an excellent yield. Further studies have revealed this method to be quite general and versatile for the synthesis of amides from Schiff bases.

Results and Discussion

One-Step Hydroamidation of a Schiff Base (2). The reduction of a Schiff base (**2**) has previously been accomplished by two steps as shown in Scheme 2. The *N*-trichlorosilyl adduct (**4**) can be converted to the amide without hydrolysis by treatment with chloroacetyl chloride. These results are summarized in Table 1. As we expected, the trichlorosilylation of **2** in the presence of BF_3·Et_2O, followed by the chloroacetylation of the intermediary silyl adduct, resulted in the chroloacetamide (**1**) (Entry 2). Further work established that the amide could be obtained without the BF_3·Et_2O catalyst (Entry 3).

We have examined the chloroacetamidation of **2** in the presence of trichlorosilane. Chloroacetyl chloride (1.1 equiv) and trichlorosilane (1.6 equiv) in benzene were added to **2** in benzene at room temperature and the mixture was heated at 40 °C for 3 h to give **1** in 97% yield. Consequently, by reacting **2** with chloroacetyl chloride in the presence of trichlorosilane in benzene, we could prepare **1** easily in an almost quantitative yield (Scheme 3).

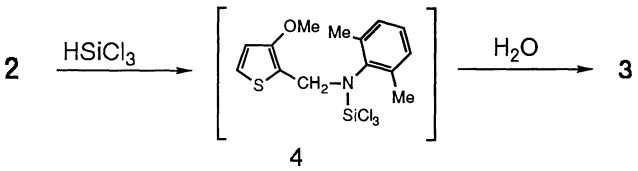

Scheme 2.

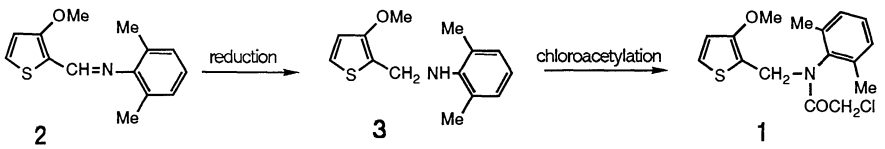

Scheme 1.

Table 1. Hydroamidation of a Schiff Base (2)

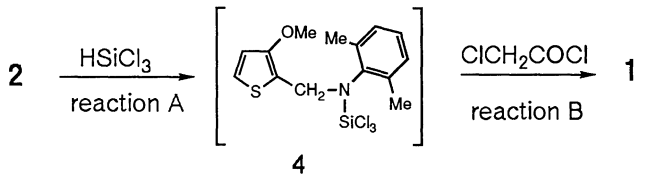

Entry	Reaction A[a]			Reaction B[b]		Yield of **1**[c]
	$HSiCl_3$/**2**	Cat.	Time/h	Temp/°C	Time/h	%
1	1.5	BF_3·Et_2O	6	50	1	23
2	3.0	BF_3·Et_2O	6	r.t.	12	69
3[d]	1.5	None	10	50	1	74

a) Reaction was carried out at 70°C. b) The ratio of chloroacetyl chloride to **2** was 1.1:1. c) The yield was determined by ^{1}H NMR. d) Reaction was carried out in an autoclave.

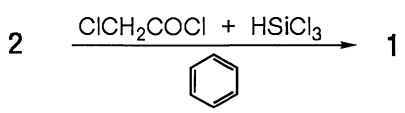

Scheme 3.

Reaction Mechanism. In order to study the mechanism of this reaction, we have measured the ^{1}H NMR spectra of the reactants in C_6D_6. When the Schiff base (**2**) was treated with trichlorosilane in C_6D_6 at room temperature, the spectral pattern of the Schiff base did not change; it showed only an additional signal originating from trichlorosilane (at 5.59 ppm). No interaction between **2** and trichlorosilane could be observed in the benzene solution. When **2** was treated with chloroacetyl chloride in C_6D_6 at room temperature, the signal at 8.40 ppm (CH=N) disappeared and a signal at 3.49 ppm, attributable to the $NCOCH_2Cl$ group (δ=3.72 in **1**), was observed. This indicates that chloroacetyl chloride reacts or interacts with **2**. When trichlorosilane was added to this mixture, a new signal at 4.89 ppm (CH_2–N) appeared. The spectrum of this product was the same as that of **1**. From these observations, it has been concluded that **2** and chloroacetyl chloride react to form an iminium salt-type compound (**5**) or its chlorine adduct (**6**) as an intermediate which further reacts with trichlorosilane to form the desired amide compound **1** as shown in Scheme 4.

Generalization of the One-Step Hydroamidation of Schiff Bases. We have extensively studied a new preparative method of an amide from a Schiff base. The results are summarized in Table 2. A Schiff base prepared by the reaction of an aldehyde or a ketone with an amine was treated with an acyl chloride and trichlorosilane in benzene. The amide was obtained in a good yield. According to the ^{1}H NMR spectra, the products formed were highly pure before purification. When an acyl chloride was treated with a Schiff base at room temperature, a slight exothermic reaction occured with the formation of either an iminium salt or its chlorine adduct. This was demonstrated by ^{1}H NMR studies of compound **8a.** The signal from the methine proton (CH=N) at 8.33 ppm disappeared and a new signal at 7.88 ppm appeared after the addition of chloroacetyl chloride in $CDCl_3$. In the case of **8i**, no exothermic reaction took place. When the reaction was carried out in acetonitrile instead of benzene, **8a** was obtained in 53% yield accompanied by some decomposed products, such as chloroacetanilide. When trifluoroacetic anhydride was employed as an acid derivative, trifluoroacetamide (**8j**) was produced in 76% yield.

Previously, several reports have been published on the

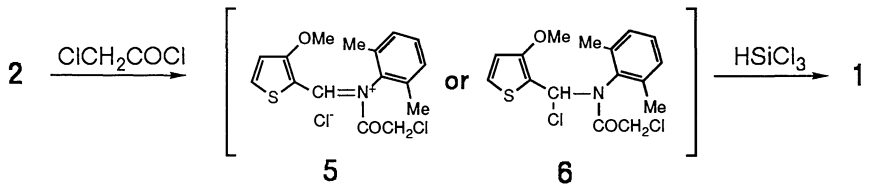

Scheme 4.

Table 2. One-Step Hydroamidation of a General Schiff Base (**7**)

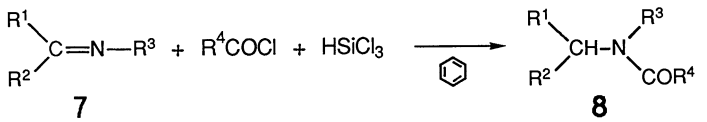

Reaction	R^1	R^2	R^3	R^4	Conditions		Yield[a]
					Temp/°C	Time/h	%
a	C_6H_5	H	C_6H_5	CH_2Cl	30	0.5	97
b	C_6H_5	H	$CH_2CH_2OC_2H_5$	CH_2Cl	40	1	80
c	2-$MeOC_6H_4$	H	2,6-$Me_2C_6H_3$	CH_2Cl	35	1	83
d	2-Thienyl	H	C_4H_9	CH_2Cl	30	1	91
e	2-Furyl	H	C_2H_5	CH_2Cl	40	2	72
f	C_4H_9	H	$C_{10}H_{21}$	CH_2Cl	30	1	77
g	C_6H_5	H	C_6H_5	CH_3	r.t.	3	78
h	3-MeO-2-thienyl	H	2,6-$Me_2C_6H_3$	CH_3	r.t.	5	92
i	C_6H_5	H	C_6H_5	C_6H_5	50	6	91
j[b]	C_6H_5	H	C_6H_5	CF_3	45	3	76
k	C_6H_5	Me	C_6H_5	CH_2Cl	50	6	92
l	C_6H_5	Me	C_6H_5	CH_3	60	2	82

a) The yield was determined by ^{1}H NMR after the product was dried. b) Trifluoroacetic anhydride was used as an acyl derivative.

Table 1. ^{1}H NMR Data of Amides

Compound	^{1}H NMR ($CDCl_3$, δ)
8a	3.80 (2H, s, $COCH_2$), 4.85 (2H, s, CH_2N), 6.85—7.40 (10H, m, aromatic H)
8b	1.11 (3H, t, J=8 Hz, CH_3), 3.15—3.60 (6H, m, $NCH_2CH_2OCH_2$), 4.05 and 4.28 (2H, $COCH_2$), 4.61 (2H, s, CH_2N), 7.18 (5H, s, aromatic H)
8c	1.90 (6H, s, CH_3×2), 3.42 (3H, s, OCH_3), 3.61 (2H, s, $COCH_2$), 4.86 (2H, s, CH_2N), 6.55—7.42 (7H, m, aromatic H)
8d	0.75—1.75 (7H, br, $CH_2CH_2CH_3$), 3.05—3.50 (2H, br, NCH_2), 4.06 (2H, s, $COCH_2$), 4.63 (2H, s, CH_2N), 6.75—7.25 (3H, m, aromatic H)
8e	1.05 and 1.16 (3H, t, J=7 Hz, CH_3), 3.39 (2H, q, J=7 Hz, NCH_2), 4.10 and 4.22 (2H, $COCH_2$), 4.51 (2H, s, CH_2N), 6.25 (2H, s, aromatic H), 7.31 (1H, s, aromatic H)
8f	0.70—1.90 (26H, br, CH_2×10 and CH_3×2), 3.10—3.50 (4H, br, CH_2NCH_2), 4.06 (2H, s, $COCH_2$)
8g	1.83 (3H, s, CH_3), 4.81 (2H, s, CH_2N), 6.60—7.40 (10H, m, aromatic H)
8h	1.17 (3H, s, CH_3), 2.01 (6H, s, CH_3×2), 3.46 (3H, s, OCH_3), 4.80 (2H, s, CH_2N), 6.65 (1H, d, J=6 Hz, thienyl H), 7.07 (1H, d, J=6 Hz, thienyl H), 7.06 (3H, s, aromatic H)
8i	5.10 (2H, s, CH_2N), 6.70—7.40 (15H, m, aromatic H)
8j	4.88 (2H, s, CH_2N), 6.80—7.40 (10H, m, aromatic H)
8k	1.42 (3H, d, J=7 Hz, CH_3), 3.68 (2H, s, $COCH_2$), 6.20 (1H, q, J=7 Hz, CHN), 7.16 (10H, br, aromatic H)
8l	1.41 (3H, d, J=7 Hz, CH_3), 1.77 (3H, s, CH_3), 6.30 (1H, q, J=7 Hz, CHN), 7.18 (10H, br, aromatic H)

preparation of amides from Schiff bases using hydrosilanes.[2,3] However, these reactions required a catalyst, such as a rhodium compound, and required several steps.

This one-step reaction is applicable to the reaction of a wide range of Schiff bases with a variety of carboxylic acid derivatives.

Experimental

The IR spectra were measured with a Hitachi I-2000 spectrometer. The ^{1}H NMR spectra were measured in a $CDCl_3$ solution with a Hitachi R-1500 spectrometer using tetramethylsilane as an internal standard. The mass spectra were obtained on a Hitachi M-80 spectrometer.

Synthesis of the Schiff Base (2). 3-Methoxy-2-thiophenecarbaldehyde (18.4 g, 0.13 mol), 2,6-dimethylaniline (15.6 g, 0.13 mol), benzene (30 ml), and a catalytic amount of BF_3·Et_2O were added to a flask equipped with a Dean–Stark trap. The mixture was refluxed in an oil bath until the water had distilled out. The resulting yellow liquid (31.1 g, 99% yield) was composed of *N*-[(3-methoxy-2-thienyl)methylene]-2,6-dimethylaniline which boiled at 144 °C/0.1 mmHg (1 mmHg= 133.322 Pa). ^{1}H NMR ($CDCl_3$) δ=2.13 (6H, s, CH_3), 3.78 (3H, s, OCH_3), 6.77—7.31 (5H, aromatic H), and 8.29 (1H, s, CH=N); IR (KBr) 1640 cm^{-1} (CH=N); MS m/z 245 (M^+). Other Schiff bases were prepared from aldehydes or ketones by reaction with amines according to an established method similar to that described above.

Reduction of 2 with Trichlosilane Followed by Chloroacetamidation. To a flask were added **2** (2.48 g, 10 mmol), trichlorosilane (4.00 g, 30 mmol), benzene (20 ml), and a catalytic amount of BF_3·Et_2O. The mixture was stirred for 1 h at room temperature and then heated in an oil bath (70 °C) for 6 h. A solution of chloroacetyl chloride (1.19 g, 11 mmol) in benzene (10 ml) was then gradually added dropwise with stirring at room temperature. This mixture was stirred overnight at room temperature. The low-boiling components were evaporated, and the resulting viscous liquid was dissolved in benzene, cooled to 5 °C, and neutralized with aqueous potassium carbonate. The organic layer was extracted with benzene and dried over sodium sulfate. The benzene was then distilled out and the resulting viscous liquid was dried under reduced pressure to give a brown solid (2.29 g, 69% yield) composed of **1**.

One-Step Hydroamidation of 2. Compound **2** (3.80 g, 15 mmol) and benzene (25 ml) were combined in a flask. A solution of trichlorosilane (3.58 g, 26 mmol) and chloroacetyl chloride (1.90 g, 17 mmol) in benzene (10 ml) was gradually added dropwise while stirring at 5 °C. The mixture was heated in an oil bath (40 °C) for 3 h, then stirred for 1 h at room temperature. The low-boiling components were evaporated and the resulting liquid was dried under reduced pressure to give a brown solid (5.03 g, 97% yield) composed of **1**. ^{1}H NMR ($CDCl_3$) δ=1.95 (6H, s, CH_3), 3.50 (3H, s, OCH_3), 3.72 (2H, s, $COCH_2Cl$), 4.75 (2H, s, CH_2N), 6.55 (2H, q, thienyl H), and 7.00—7.45 (3H, m, aromatic H); IR (KBr) 1670 cm^{-1} (C=O); MS m/z 323 (M^+), 288 (M^+—Cl), and 246 (M^+—$COCH_2Cl$).

One-Step Hydroamidation of a Schiff Base. The general procedure is as follows. A Schiff base (10 mmol) and benzene (15 ml) were combined in a flask. A solution of trichlorosilane (15—20 mmol) in benzene and a carboxylic acid derivative (11—12 mmol) in benzene were gradually added dropwise while stirring at 5—10 °C. The mixture was heated in an oil bath for several hours, and then stirred for 1 h at room temperature. The low-boiling components were evaporated, and the resulting viscous liquid was dissolved in benzene, cooled to 5 °C, and neutralized with aqueous potassium carbonate. The organic layer was extracted with benzene and dried over sodium sulfate. The benzene was then distilled out and the resulting viscous liquid was dried under reduced pressure to give the desired amide. The ^{1}H NMR data of the amides obtained by this procedure are summarized in Table 3.

References

1) M. Ogasawara, M. Konnai, T. Takematsu, S. Kato, and M. Ishizaki, *Weed Res., Jpn.*, **34**, 131 (1989).

2) I. Ojima, T. Kogure, and Y. Nagai, *Tetrahedron Lett.*, **27**, 2175 (1973).

3) R. Becker, H. Brunner, S. Mahboobi, and W. Wiegrebe, *Angew. Chem., Int. Ed. Engl.*, **24**, 995 (1985).

 © 1991 The Chemical Society of Japan Bull. Chem. Soc. Jpn., 64, 2131—2139 (1991)

Benzo[*b*]cyclohept[*e*][1,4]oxazines§ IV.[1] Synthesis and Properties of All Possible Benzoxazinotropones[2]

Hidetsugu WAKABAYASHI,* Teruo KURIHARA,* Sumio ISHIKAWA, Joji OKADA,† and Tetsuo NOZOE††
Department of Chemistry, Faculty of Science, Josai University,
1-1 Keyakidai, Sakado-shi, Saitama 350-02
† Tochigi Research Laboratories, Kao Corporation,
2606, Akabane, Ichikaimachi, Tochigi 321-34
†† Tokyo Research Laboratories, Kao Corporation,
2-1-3 Bunka, Sumida-ku, Tokyo 131
(Received January 24, 1991)

Five isomeric benzo[*b*]cyclohept[*e*][1,4]oxazin-6~10-ones (hereafter refered to as benzoxazinotropones) and bromobenzoxazinotropones were prepared almost quantitatively by the hydrolysis of the corresponding mono-, di-, and tribromobenzo[*b*]cyclohept[*e*][1,4]oxazines with refluxing acetic acid. On the basis of spectral data and theoretical calculations, benzo[*b*]cyclohept[*e*][1,4]oxazin-6~9(11*H*)-ones are believed to exist in the keto form. These compounds gave respective methoxy- and acetoxybenzo[*b*]cyclohept[*e*][1,4]oxazines when reacted with diazomethane and acetic anhydride. On the other hand, benzo[*b*]cyclohept[*e*][1,4]oxazin-10(11*H*)-one was found to exist in a stable, intermolecularly hydrogen-bonded form and did not form acetoxylated or methylated compounds. Possible reaction pathways for the formation of these products are discussed.

One of the authors (T.N.) and his co-worker reported[3] that a small amount (less than 1%) of isomeric isopropylbenzo[*b*]cyclohept[*e*][1,4]oxazin-10(11*H*)-ones (**1a—c**) were produced along with the main products 7-, 8-, and 9-isopropylbenzo[*b*]cyclohept[*e*][1,4]oxazines (**2a—c**), when isomeric 2-chloro-4-, 5-, and 6-isopropyltropones (**3a—c**) were refluxed in acetic acid with *o*-aminophenol (**4**). We later reported[4] that the condensation of 3-bromo-2-methoxytropone (**5a**) with an excess of **4** in refluxing acetic acid gave a small amount of benzo[*b*] cyclohept[*e*][1,4]oxazin-6(11*H*)-one (**6**), and its 10(11*H*)-one isomer (**10**) as 1:1-condensation products, along with various interesting 1:2-condensation products. Although some possible reaction pathways for the formation of **6** and **10** (and for **1**) were presented, we did not have enough experimental evidence to distinguish between them.[1] In this paper we wish to describe the details of the synthesis, structures, and keto-enol tautomerism of all possible isomers of the benzo[*b*]cyclohept[*e*][1,4]oxazin-6~10(11*H*)-ones (hereafter refered to as benzoxazinotropones, **6—10**), as well as a possible mechanism for the formation of these compounds.

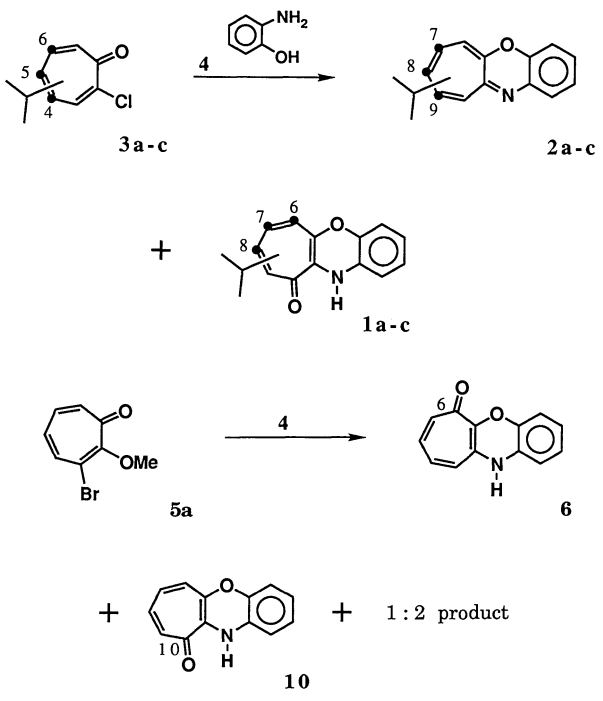

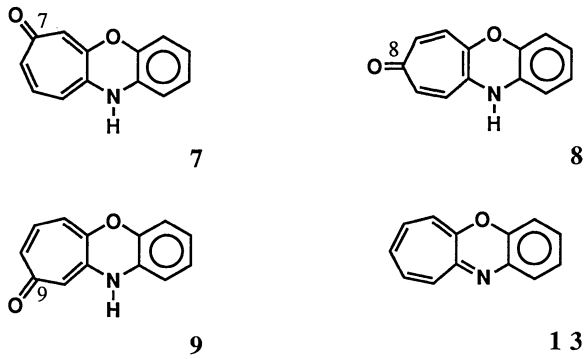

Results and Discussion

Synthesis of Various Bromobenzo[*b*]cyclohept[*e*]-[1,4]oxazines (11a—e). 6-Bromo- (**11a**)[5] and 8-bromobenzo[*b*]cyclohept[*e*][1,4]oxazine (**11c**)[6] were respectively prepared by the condensation of 7-bromo- (**5d**) and 5-bromo-2-methoxytropone (**5c**) with **4**, via the respective bromo-2-(2-hydroxyanilino)tropones (**12a, b**). The 10-bromo compound (**11e**) was obtained from **11a** by an intermolecular heterocycle exchange reaction[7] with **4** in

§ Benzo[*b*]cyclohept[*e*][1,4]oxazine was refered to as cyclohepta[*b*][1,4]benzoxazine in the preceding paper.

methanol (Scheme 1).

The reaction of 5-bromotropolone *p*-toluenesulfonate (**14**) with **4** in pyridine gave anilinotropone **12c** (84% yield) through cine substitution.[8] Compound **12c** underwent cyclization in hot acetic acid containing a trace amount of concd sulfuric acid to give **11d** (82% yield, Scheme 2). The structures of **12c** and **11d** were determined to be 4-bromo-2-(2-hydroxyanilino)tropone and 9-bromobenzo[*b*]cyclohept[*e*][1,4]oxazine, respectively, on the basis of the spectral data (see the Experimental section).

The reaction of **11d** with 2 equiv of **4** in MeOH at room temperature was studied by time-dependent HPLC. It was determined that **11d** and **11b** attained an approximately 1:1 equilibrium within 1 h by an intermolecular heterocycle exchange reaction (Scheme 2).[7] The reaction mixture was separated by silica-gel chromatography and **11b** (45% yield) was identified as 7-bromobenzo[*b*]cyclohept[*e*][1,4]oxazine on the basis of NMR spectra and comparison of its UV spectra with **11d**.

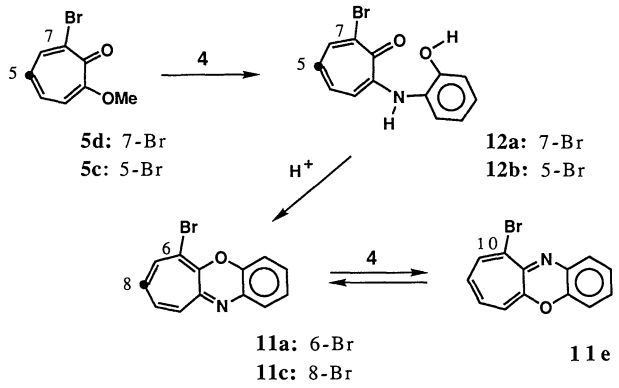

Scheme 1.

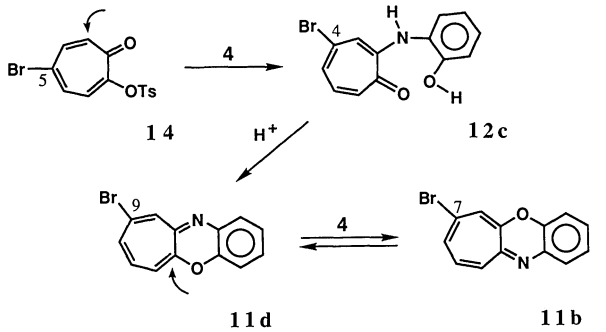

Scheme 2.

Synthesis of Benzoxazinotropones. Heating of bromo compounds **11a—e** in acetic acid at 110 °C for 20 min to 2 h (depending on the position of the Br atom) gave the corresponding benzoxazinotropones (**6—10**) in nearly quantitative yields. Compounds **6** and **10** were identified as benzo[*b*]cyclohept[*e*][1,4]oxazin-6(11*H*)-one and -10(11*H*)-one, respectively, by direct comparison with the authentic samples.[4] The structure of **7** was shown spectroscopically to be benzo[*b*]cyclohept[*e*]-[1,4]oxazin-7(11*H*)-one. Compounds **8** and **9** were also shown to be benzo[*b*]cyclohept[*e*][1,4]oxazin-8(11*H*)-one and -9(11*H*)-one, respectively, on the basis of the spectral data (see the Experimental section).

Similarly, 6,8-dibromobenzo[*b*]cyclohept[*e*][1,4]-oxazine (**15**)[6] produced two bromobenzoxazinotropones (**16** (5% yield) and **17** (80% yield)) as well as a small amount of **12d**. The structures of **16** and **17** were determined to be 8-bromobenzo[*b*]cyclohept[*e*][1,4]-oxazin-6-(11*H*)-one and 6-bromobenzo[*b*]cyclohept[*e*]-[1,4]oxazin-8(11*H*)-one, respectively, on the basis of high resolution mass spectral data and comparison of their UV spectra with those of **6** and **8**, as well as the results of acylation (see below). On the other hand, 6,8,10-tribromobenzo[*b*]cyclohept[*e*][1,4]oxazine (**18**)[9] gave, under similar conditions, isomeric dibromobenzoxazinotropones **19** (60% yield) and **20** (20% yield). Zinc dust reduction of compounds **19** and **20** resulted in the same benzoxazinotropone **10**. Compound **19** was also prepared by the reaction of 2,4,6-tribromo-7-methoxytropone (**21**) with **4**. This evidence along with the spectral data mentioned above showed the structures of **19** and **20** to be 7,9-dibromo- and 6,8-dibromobenzo-[*b*]cyclohept[*e*][1,4]oxazin-10(11*H*)-one, respectively (Scheme 3).

Hydrolysis of **18** with AcOH gave only the dibromo derivatives of benzo[*b*]cyclohept[*e*][1,4]oxazin-10(11*H*)-one (**10**), but neither 6(11*H*)-one nor 8(11*H*)-one deriva-

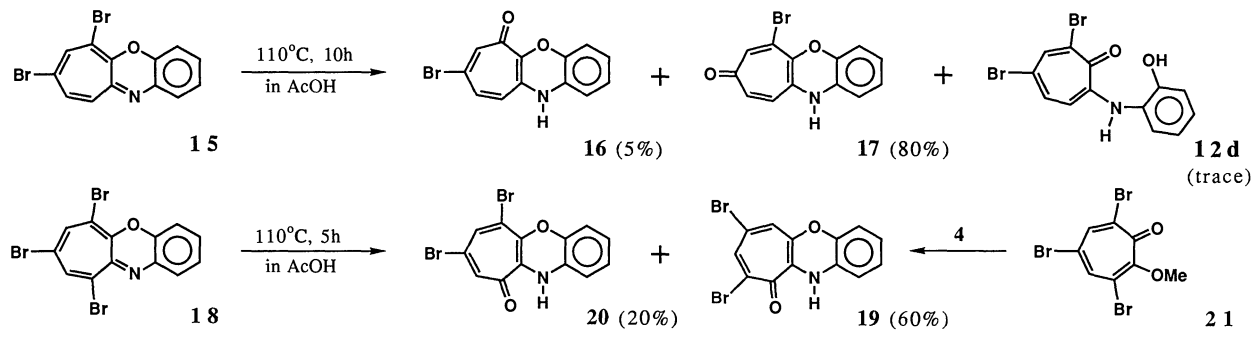

Scheme 3.

tives were produced, whereas the same treatment of **15** gave a mixture of 6(11*H*)-one derivative **16** and 8(11*H*)-one derivative **17** in a 1:16 ratio. These results suggest that the facility of the hydrolytic cleavage is in order C-10>C-8>C-6.

The bonding energies between the Br-attached carbon and Br of **11a—e** were calculated by the MINDO/3 method to be −11.38, −11.27, −11.32, −11.31, and −11.34 eV, respectively. In the case of **15**, the binding energy between C-6 and Br was calculated to be −11.45 eV, while that between C-8 and Br was −11.35 eV. Therefore, the bond between C-8 and its Br atom is hydrolyzed more readily than the bond between C-6 and its Br atom. In the case of **18**, the binding energies between a Br-attached carbon and its Br atom are in order C-6 (−11.47 eV) < C-8 (−11.42 eV) < C-10 (−11.40 eV). These results agree with the order of the facility of the hydrolytic cleavage.

Keto-Enol Tautomerism of Benzoxazinotropones. Keto-enol tautomerism is believed to exist in compounds **6—10**. In order to clarify the tautomerism, the acetylation and methylation of benzoxazinotropones **6—10** were studied. Moreover, HMO[10] and MINDO/3[11] molecular orbital theoretical calculations were performed and the theoretical results were compared with the experimental results.

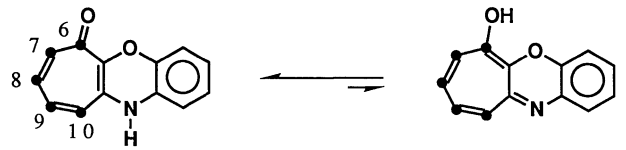

6-10 **6a-10a**

a) Acylation and Methylation. No products were obtained when **6—10** were combined with acetic anhydride in pyridine at 80 °C. However, acetates **22a—d** were produced in ca. 80% yields when **6—9** were mixed with acetic anhydride in acetic acid containing a trace amount of concd sulfuric acid at room temperature. Compound **22a** was determined to be 6-acetoxybenzo[*b*]cyclohept[*e*][1,4]oxazine from the high resolution mass spectral determination of molecular weight (*m/z* M^+, 253.0769) and other spectral data. The IR spectrum showed an *O*-acetyl carbonyl absorption peak near 1770 cm^{-1}. The electronic spectrum is very similar to that of the parent compound **13**. The structures of **22b—d** were also identified as 7-, 8-, and 9-acetoxybenzo[*b*]cyclohept[*e*][1,4]oxazine, respectively, on the basis of their NMR and other spectral data (see the Experimental section). Similarly, **16** and **17** were reacted as above to form acetoxyl derivatives **23** and **24**, respectively. Acetylated compounds **22a—d**, **23**, and **24** reverted to the corresponding benzoxazinotropones **6—9**, **16**, and **17** when treated with refluxing acetic acid for about 5 min.

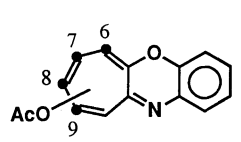

22a-d

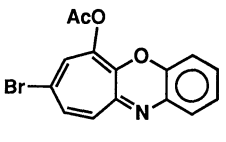

23

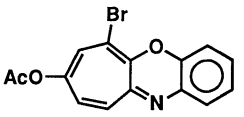

24

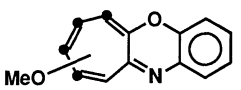

25a-d

Compounds **6—9** reacted slowly with diazomethane to give the corresponding methylated products **25a—d** as brown needles. However, **10** did not result in acetylated and methylated compounds under similar conditions. The structures of **25a—d** were assigned to 6-, 7-, 8-, and 9-methoxybenzo[*b*]cyclohept[*e*][1,4]oxazines, respectively, on the basis of their NMR and other spectral data (see the Experimental section). Methylated compounds **25a—d** gradually reverted to the corresponding benzoxazinotropones **6—9** on standing in methanol at room temperature.

b) Theoretical Calculations. The resonance energies and bond currents of the keto forms **6—10** and the enol forms **6a—10a** have been calculated by means of Aihara's graph theory of aromaticity.[12] The HMO theory is assumed to be in its simplest form. Streitwieser[10] evaluated the heteroatom parameters for the amine nitrogen, the

Table 1. Resonance Energies, Heats of Formation, and Circuit Resonance Energies for Keto Forms (**6—10**) and Enol Forms (**6a—10a**)

Compd	RE	ΔH_f	CRE		Compd	RE	ΔH_f	CRE	
		kcal mol^{-1}	r_1	r_3			kcal mol^{-1}	r_1	r_3
6	0.401	−25.1	0.152	0.216	**6a**	0.312	−22.2	0.126	0.201
7	0.404	−35.4	0.142	0.213	**7a**	0.319	−31.8	0.117	0.197
8	0.402	−29.1	0.151	0.216	**8a**	0.314	−28.4	0.125	0.200
9	0.403	−35.0	0.142	0.213	**9a**	0.318	−30.7	0.117	0.197
10	0.402	−30.0	0.152	0.216	**10a**	0.315	−27.2	0.130	0.201

RE: Resonance energy (in β units). CRE: Circuit resonance energy (in β units). ΔH_f: Heats of formation calculated by the MINDO/3 method.

imine nitrogen, the ether oxygen, and the ketone oxygen. We have used these values in this paper.

MINDO/3[11] is a reasonably reliable method for the prediction of heats of formation. The molecular geometries of **6**—**10** and its enol forms **6a**—**10a** were calculated by MINDO/3 optimizations. In all cases, the MINDO/3 optimized geometries were planar and exhibited appreciable bond alternation. As shown in Table 1, the heats of formation of the keto forms are more stable than those of the enol forms by 0.7—4.3 kcal mol^{-1}.

All the keto and enol compounds are predicted to be aromatic with positive resonance energies.[12a] The keto form species have larger resonance energies than those of the enol forms. With a view to clarifying the origin of the aromaticity, we calculated the circuit resonance energies[12c] of the keto forms by means of Aihara's graph theory of aromaticity. The π-electron ring system in the keto forms consists of six π-ring components, from r_1 to r_6, as shown in Fig. 1. Geometrically unidentical π-electron circuits are shown and numbered in Fig. 1. The results are listed in Table 1. The circuit resonance energies of r_1 and r_3 are positive, while those of r_2, r_4, r_5, and r_6 are near zero or negative. Consequently, the keto form compounds are stabilized as the 6-π-tropylium-6-π-benzenoid form.

Since **6**—**10** are only slightly soluble in less polar solvents, the NMR spectra were measured in DMSO-d_6. In all cases, the ^{13}C NMR spectra exhibited a peak at about δ=180 resulting from a carbonyl group. These results match the keto form but not the enol form in a polar solvent such as DMSO. In the ^1H NMR spectra, the chemical shifts of the seven-membered ring protons for **6**—**10** differ from those of parent compound **13**. This can also be explained by assuming the compounds are in the keto form. This causes the signals of the β proton of the carbonyl groups to appear at a lower field compared with those of compounds **13**, **22**, and **25**. The observed values of the average chemical shifts of the seven-membered ring protons and benzene ring protons of **6**—**10** are at δ=6.61 and 6.70, respectively. In contrast, the chemical shifts of the seven-membered ring protons of the enol forms and **13** are expected to be much higher than those of the benzene ring protons.[13] Furthermore, ring currents of the keto forms of **6**—**10** and their enol forms **6a**—**10a** have been calculated by Aihara's method,[12b] and the results are shown in Fig. 1. The average ring currents of the seven-membered rings (r_1) and benzene rings (r_3) of **6**—**10** are 0.930 I_0 and 1.000 I_0, respectively, whereas those of **6a**—**10a** are 0.710 I_0 and 1.040 I_0 respectively. We therefore conclude that benzoxazinotropones **6**—**10** exist mainly in the keto form on the basis of the experimental facts, NMR spectral data, and theoretical calculations.

Though compounds **6**—**9** were almost the same yellow-brown color and had very similar electronic absorption bands, **10** had a red color. The electronic spectra of **10**, in methanol solution, showed the longest

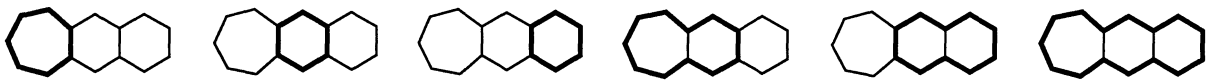

	r_1	r_2	r_3	r_4	r_5	r_6
6	0.956 I_0	-0.026 I_0	0.974 I_0	-0.064 I_0	-0.044 I_0	0.064 I_0
7	0.895 I_0	-0.001 I_0	0.956 I_0	-0.061 I_0	-0.005 I_0	0.060 I_0
8	0.952 I_0	-0.023 I_0	0.973 I_0	-0.064 I_0	-0.041 I_0	0.063 I_0
9	0.895 I_0	-0.001 I_0	0.957 I_0	-0.061 I_0	-0.005 I_0	0.060 I_0
10	0.957 I_0	-0.026 I_0	0.973 I_0	-0.064 I_0	-0.043 I_0	0.063 I_0

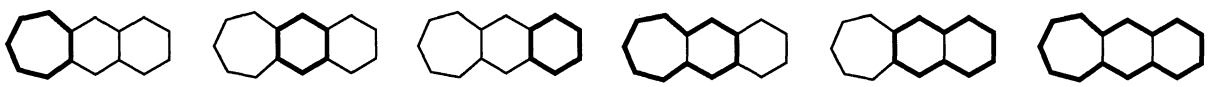

	r_1	r_2	r_3	r_4	r_5	r_6
6a	0.792 I_0	0.045 I_0	0.904 I_0	-0.194 I_0	0.004 I_0	0.107 I_0
7a	0.734 I_0	0.066 I_0	0.885 I_0	-0.182 I_0	0.043 I_0	0.100 I_0
8a	0.788 I_0	0.031 I_0	0.902 I_0	-0.192 I_0	0.007 I_0	0.106 I_0
9a	0.734 I_0	0.051 I_0	0.887 I_0	-0.184 I_0	0.042 I_0	0.101 I_0
10a	0.818 I_0	0.007 I_0	0.904 I_0	-0.146 I_0	0.040 I_0	0.169 I_0

Fig. 1. Ring currents of **6**—**10** and **6a**—**10a**. (I_0=Ring currents of benzene).

wavelength band centered at 480 nm. We have also calculated the electronic transitions for **6**—**10** by the CNDO/S-CI method. For example, the spectra of **7** showed an absorption band, deriving from the HOMO–LUMO transition, lying in the UV region at 3.13 eV (395 nm). The electronic transitions calculated by adopting the MINDO/3 geometries of **10** are predicted to have $\pi\pi^*$ λ_{max} of 2.73 eV (454 nm, f=0.000), 2.75 eV (450 nm, f=0.000), 2.98 eV (416 nm, f=0.094), and 3.05 eV (406 nm, f=0.072) in the long wavelength region. The calculated results, however, do not conform to the electronic spectra of **10**.

To elucidate the molecular structure of **10**, an X-ray diffraction analysis was carried out.[14] The molecular framework is illustrated in Fig. 2. The definitive structure determination of **10** was particularly interesting, because this compound was shown to exist in an intermolecularly hydrogen-bonded form in the solid state.

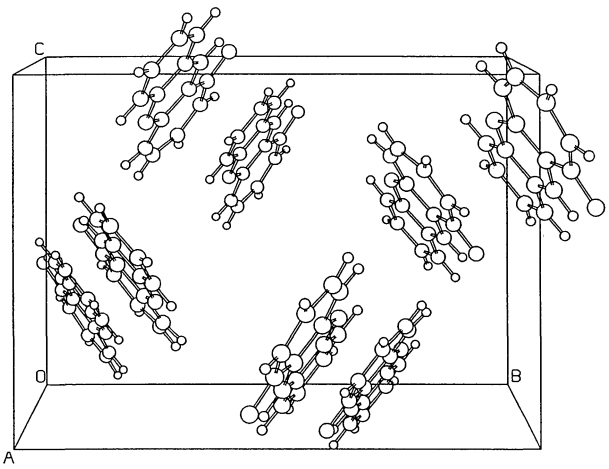

Fig. 2. A perspective view of **10**.

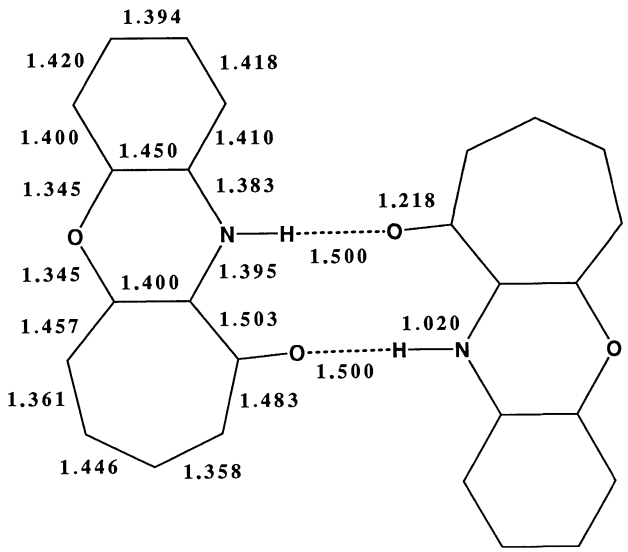

Fig. 3. Assumed structure of Model A. Bond lengths are expressed in Angstroms (Å).

The *H*-bond is between the ketone oxygen in one molecule and the imine hydrogen in another molecule. We therefore propose two dimeric model structures on the basis of the above X-ray experimental geometry and MINDO/3 optimized values. Model A is a planar molecule with an assumed N···O bond length of 2.718 Å (Fig. 3), whereas Model B is a nonplanar molecule. The geometries of Model B are the same as those of Model A, except that the separation of two molecular planes is assumed to be 1.9 Å and the N···O bond length is 2.2 Å. The calculated electronic transitions of Model A are predicted to have $\pi\pi^*$ λ_{max} of 2.57 eV (481 nm, f=0.000), 2.80 eV (442 nm, f=0.000), 2.85 eV (435 nm, f=0.166), and 2.96 eV (418 nm, f=0.238) in the long wavelength region and are very close to the calculated transitions of monomeric compound **10**. The calculated electronic transitions of Model B are predicted to have $\pi\pi^*$ λ_{max} of 2.48 eV (500 nm, f=0.002), 2.53 eV (490 nm, f=0.215), 2.84 eV (436 nm, f=0.012), 2.92 eV (424 nm, f=0.151), 2.93 eV (423 nm, f=0.180), and 3.06 eV (405 nm, f=0.051) in the same region. In the calculated results of Model B, its next longest absorption band can be attributed to an intermolecular charge-transfer transition from one molecule to another molecule because this absorption band was assigned to a HOMO–LUMO transition, and π charges in HOMO or LUMO orbitals were distributed on each molecule of the assumed dimer. The electronic transitions calculated for Model B agree with the expeprimental electronic spectra of **10**. The agreement between calculated and experimental data is satisfactory, especially if we bear in mind that theoretical values refer to the gas phase and experimental values to the solution state.

Possible Reaction Pathways for the Formation of Benzoxazinotropones. As mentioned above, bromo compounds **11a**—**e** gave an almost quantitative yield of benzoxazinotropones **6**—**10**, respectively, upon heating in 97% acetic acid. However, upon heating in ethanol, **11a**—**d** did not result in benzoxazinotropones **6**—**9**, while **11e** gave **10** almost quantitatively. Additionally, by periodically checking the reaction with reversed-phase HPLC we observed the formation of **22d** when **11d** was heated in anhydrous acetic acid at 110 °C. As shown in Fig. 4, a peak corresponding to acetoxyl compound **22d** appears first, then the peak corresponding to **9** increases as the peaks corresponding to **22d** and **11d** decrease in the chromatogram. In this transformation, as shown in Scheme 4, intermediate **a** may be produced first by the attack of an acetoxyl anion (not by moisture in the acetic acid) at the bromine-substituted C-9 position of **11d**. Compound **a** may then give **9** via acetoxyl derivative **22d**. Similarly, **11a**—**c** are likely to produce **6**—**8** via acetoxyl compounds **22a**—**c**, respectively, and **15** is likely to produce **16** and **17** via acetoxyl compounds **23** and **24**, respectively.

As we reported earlier,[7] position C-5a in the benzo[*b*]cyclohept[*e*][1,4]oxazine nucleus is most easily

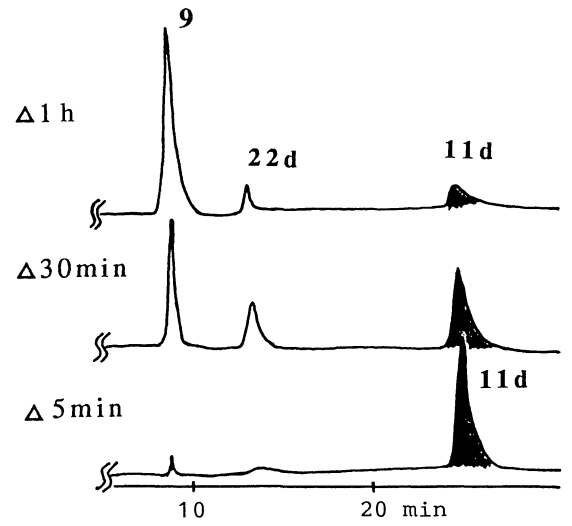

Fig. 4. Time-dependent HPLC chromatograms of the hydrolysis of **11d** in dry AcOH at 110°C.

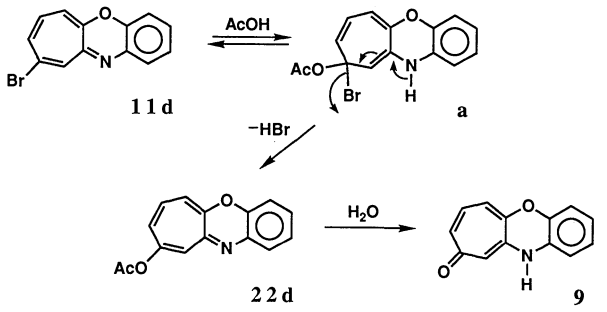

Scheme 4.

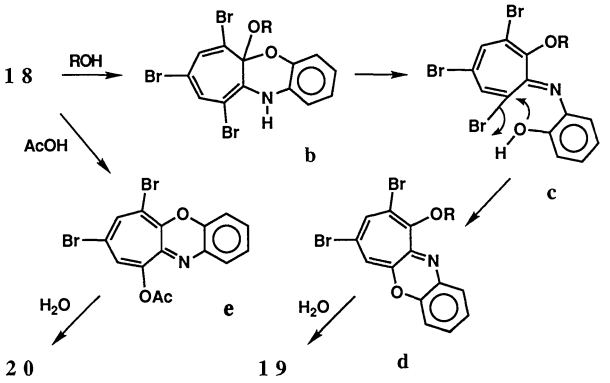

Scheme 5.

attacked by nucleophiles, and when the C-10 position is substituted with a group such as a bromine atom, that group acts as a good leaving group. Therefore, it is quite understandable that the 10-bromo compound **11e** is readily transformed to **10** even in MeOH (containing a small amount of water), and the tribromo compound **18** gives 7,9-dibromobenzoxazinotropone **19** as the main product along with the 6,8-dibromo compound **20**, as illustrated in Scheme 5.

Experimental

Melting points were determined with a Yanagimoto MP-3S melting point apparatus and were uncorrected. The IR and electronic spectra were measured by using a Shimadzu IR-450 and a Shimadzu UV-265FS spectrometer, respepctively; the UV spectra in acid and alkali solutions were taken after adding a few drops of 6 M HCl or 6 M NaOH (1 M=1 mol dm^{-3}) to the sample solution. The NMR spectra were measured in $CDCl_3$ (unless otherwise specified) with a JEOL JNM-PS/PET (100 MHz) or a JEOL JNM-GX270 (270 MHz for 1H and 67.8 MHz for ^{13}C) spectrometer using TMS as the internal standard. The assignments of all signals were made by employing a first-order analysis with the aid of a decoupling technique. The mass spectra were taken on a JEOL JMS-DX300 mass spectrometer and a Shimadzu LKB 9000 GC-mass spectrometer at 70 eV. The HPLC was carried out on Hitachi gel #3011 with MeOH–hexane (9:1) as the solvent. The centrifugal chromatography was performed with a Hitachi CLC-5 instrument in a Fuji silica-gel layer (KT-2151, 3 mm thickness) using benzene as an eluent. The TLC analyses were carried out with Merck Kieselgel 60F-254 plates.

4-Bromo-2-(2-hydroxyanilino)tropone (12c). A mixture of 5-bromotropolone *p*-toluenesulfonate[15] (**14**, 506 mg, 1.42 mmol) and *o*-aminophenol (**4**, 310 mg, 2.82 mmol) in pyridine (5 cm^3) was heated at 60 °C for 5 h. The solvent was evaporated in vacuo and the residue was chromatographed on a column of silica gel with benzene–MeOH (50:1), giving **12c** (345 mg, 84% yield):Orange needles (from MeOH); mp 170—172 °C (decomp); UV_{max} (MeOH) 240 (log ε 4.20), 262 (4.31), 347 (4.04), and 407 nm (4.18), (MeOH+ 6 M NaOH) 244 (log ε 4.29), 272 (4.17), 346 (3.89), and 413 nm (4.11); IR (KBr) 3430 (OH) and 3250 cm^{-1} (NH); ^1H NMR (270 MHz, CD_3OD) δ=6.96 (1H, td, *J*=8.0 and 2.0 Hz, H-5′), 7.00 (1H, dd, *J*=8.0 and 2.0 Hz, H-3′), 7.05—7.10 (4H, m, H-3,5,6,7), 7.20 (1H, td, *J*=8.0 and 2.0 Hz, H-4′), and 7.28 (1H, dd, *J*=8.0 and 2.0 Hz, H-6′). Found: C, 53.26; H, 3.57; N, 4.60%; M^+, 292. Calcd for $C_{13}H_{10}NO_2Br$: C, 53.45; H, 3.45; N, 4.79%; M, 292.

9-Bromobenzo[*b*]cyclohept[*e*][1,4]oxazine (11d). A solution of **12c** (210 mg) in acetic acid (5 cm^3) containing a trace amount of concd sulfuric acid was heated at 120 °C for 2 h under nitrogen. The solvent was then evaporated in vacuo. The residue was neutralized with aq $NaHCO_3$ and extracted twice with benzene. The extracts were combined, dried (Na_2SO_4) and evaporated in vacuo. The residue was chromatographed centrifugally on a layer of silica gel with benzene as the eluent, giving **11d** (161 mg, 82% yield): Brown needles; mp 145—147 °C (from benzene); UV_{max} (MeOH) 263 (log ε 4.47), 270 (4.47), 305 (4.03), and 414 nm (4.10), (MeOH +6M HCl) 267 (log ε 4.37), 287 (4.27), 320 (4.15), and 449 nm (3.99); ^1H-NMR (270 MHz) δ=5.29 (1H, d, *J*=9.8 Hz, H-6), 5.70 (1H, dd, *J*=11.5 and 9.8 Hz, H-7), 5.90 (1H, dd, *J*=11.5 and 2.0 Hz, H-8), 6.40 (1H, m, H-4), 6.54 (1H, d, *J*=2.0 Hz, H-10), and 6.78 (3H, m, H-1,2,3). Found: C, 57.00; H, 3.08; N, 4.99%; M^+, 274. Calcd for $C_{13}H_8NOBr$: C, 56.96; H, 2.94; N, 5.11%; M, 274.

7-Bromobenzo[*b*]cyclohept[*e*][1,4]oxazine (11b). A mixture of **11d** (30 mg, 0.11 mmol) and **4** (24 mg, 0.22 mmol) in methanol (5 cm^3) was allowed to stand for 1 h at room

temperature. The reaction contents were checked by means of time-dependent HPLC. The solvent was evaporated in vacuo. The residue was chromatographed on silica-gel thin-layer plates with benzene as the eluent. The product was recrystallized from benzene, giving **11b** (13 mg, 45% yield)(along with 50% recovered **11d**): Brown needles; mp 130—132 °C; UV_{max} (MeOH) 222 (log ε 4.31), 262 (4.39), 272 (4.36), 309 (4.15 sh), 322 (3.76 sh), and 415 nm (4.05), (MeOH+6 M HCl) 230 (log ε 4.35), 267 (4.30), 285 (4.17 sh), 317 (4.01), 439 (3.98), and 427 nm (3.87 sh); ^{1}H NMR (270 MHz) δ=5.69 (1H, d, *J*=1.5 Hz, H-6), 5.82 (1H, dd, *J*=12.4 and 8.8 Hz, H-9), 6.00 (1H, d, *J*=12.4 Hz, H-10), 6.12 (1H, dd, *J*=8.8 and 1.5 Hz, H-8), 6.43 (1H, m, H-4), and 6.73—6.85 (3H, m, H-1,2,3). Found: C, 56.74; H, 3.05; N, 4.89%; M$^+$, 274. Calcd for $C_{13}H_8NOBr$: C, 56.96; H, 2.94; N, 5.11%; M, 274.

Similarly, when a methanolic solution of **11b** and **4** was allowed to stand at room temperature, an additional peak due to compound **11d** began to appear in the HPLC chromatogram and an equilibrium was reached within a few hours. The isomerized **11d** was isolated in pure crystalline form.

Hydrolysis of 11a—e. A solution of **11c** (55 mg) in acetic acid (10 cm^3) was heated at 110 °C for 1 h, followed by the same procedures as those described above for **12c**. The residual solid was recrystallized from MeOH to give **8** (40 mg, 95% yield). Similarly, **6**[4] (95% yield), **7** (95% yield), **9** (90% yield), and **10**[4] (95% yield) were obtained from **11a, 11b, 11d,** and **11e**, respectively.

Benzo[*b*]cyclohept[*e*][1,4]oxazin-6(11*H*)-one (6): Mp 270—271 °C (lit,[4] mp 270 °C); UV_{max} (DMSO) 264, 305, 315, 330 (sh), and 393 nm, ($CHCl_3$) 259, 300, 310, 326 (sh), and 388 nm; ^{1}H NMR (270 MHz, DMSO-d_6) δ=6.42 (1H, dd, *J*=8.0 and 1.8 Hz, H-4), 6.49 (1H, dd, *J*=12.2 and 2.6 Hz, H-7), 6.56 (1H, dd, *J*=8.0 and 1.8 Hz, H-1), 6.64 (1H, td, *J*=8.0 and 1.8 Hz, H-2), 6.72 (1H, td, *J*=8.0 and 1.8 Hz, H-3), 6.81 (3H, m, H-8,9,10), and 8.57 (1H, br, NH); ^{13}C NMR (67.8 MHz, DMSO-d_6) δ=113.4 (d), 114.9 (d), 123.1 (d), 124.6 (d), 126.9 (d), 130.9 (s), 131.0 (d), 131.6 (d), 139.9 (s), 140.9 (d), 143.2 (s), 145.2 (s), and 173.3 (s).

Benzo[*b*]cyclohept[*e*][1,4]oxazin-7(11*H*)-one (7): Orange needles; mp 294—296 °C (from MeOH); UV_{max} (MeOH) 221 (log ε 4.27), 237 (4.14), 295 (4.29), 325 (3.70 sh), and 427 nm (4.02), (MeOH+6 M HCl) 225 (log ε 4.30), 256 (4.14), 287 (4.20), 309 (3.99 sh), and 452 nm (3.91),(MeOH+6 M NaOH) 258 (log ε 4.28), 300 (4.25), 465 (4.17), and 497 nm (4.08), (DMSO) 265, 289, 396 (sh), and 423 nm, ($CHCl_3$) 242, 288, 296, 390 (sh), and 413 nm; IR (KBr) 3250 and 1640 cm^{-1}; ^{1}H NMR (270 MHz, DMSO-d_6) δ=5.99 (1H, d, *J*=9.7 Hz, H-10), 6.13 (1H, dd, *J*=11.8 and 2.7 Hz, H-8), 6.33 (1H, d, *J*=2.7 Hz, H-6), 6.70 (1H, dd, *J*=8.0 and 1.8 Hz, H-4), 6.75 (1H, td, *J*=8.0 and 1.8 Hz, H-2), 6.81 (1H, dd, *J*=11.8 and 9.7 Hz, H-9), 6.84 (1H, dd, *J*=8.0 and 1.8 Hz, H-1), 6.89 (1H, td, *J*=8.0 and 1.8 Hz, H-3), and 9.93 (1H, br, NH). Found: *m*/*z* 211.0656. Calcd for $C_{13}H_9NO_2$: M, 211.0633.

Benzo[*b*]cyclohept[*e*][1,4]oxazin-8(11*H*)-one (8): Brown needles; mp>300 °C (from MeOH); UV_{max} (MeOH) 222 (log ε 4.12), 266 (4.34), 275 (4.32), 318 (3.39 sh), and 420 nm (4.02), (MeOH+6 M HCl) 227 (log ε 4.25), 266 (4.29), 275 (4.31), 330 (3.60), 443 (3.81), and 466 nm (3.79 sh), (DMSO) 268, 277, 315, and 408 nm, ($CHCl_3$) 264, 274, 320 (sh), and 402 nm; IR (KBr) 3250—2800 and 1644 cm^{-1}; ^{1}H NMR (270 MHz, DMSO-d_6) δ=6.36 (1H, dd, *J*=12.7 and 2.0 Hz, H-7), 6.43 (1H, dd, *J*=8.0 and 2.0 Hz, H-4), 6.52 (1H, dd, *J*=8.0 and 2.0 Hz, H-1), 6.64 (1H, td, *J*=8.0 and 2.0 Hz, H-3), 6.69 (2H, m, H-9,10), 6.73 (1H, td, *J*=8.0 and 2.0 Hz, H-2), 6.75 (1H, d, *J*=12.7 Hz, H-6), and 8.70 (1H, br, NH); ^{1}H NMR (270 MHz, CD_3OD) δ=6.57 (1H, dd, *J*=13.1 and 2.5 Hz, H-7), 6.77 (1H, d, *J*=13.1 Hz, H-10), 6.84 (1H, dd, *J*=13.1 and 2.5 Hz, H-9), and 6.89 (1H, d, *J*=13.1 Hz, H-6); ^{13}C NMR (67.8 MHz, DMSO-d_6) δ=114.3 (d), 114.9 (d), 123.7 (d), 124.9 (d), 129.5 (d), 129.6 (d), 130.0 (s), 131.1 (d), 138.8 (d), 139.7 (s), 143.2 (s), 143.4 (s), and 179.5 (s). Found: C, 73.76; H, 3.99; N, 6.28%; M$^+$, 211. Calcd for $C_{13}H_9NO_2$: C, 73.92; H, 4.29; N, 6.63%; M, 211.

Benzo[*b*]cyclohept[*e*][1,4]oxazin-9(11*H*)-one (9): Yellow needles; mp 243—245 °C (from MeOH); UV_{max} (MeOH) 239 (log ε 4.19), 294 (4.48 sh), 307 (4.55), 338 (4.00 sh), 373 (3.77), and 394 nm (3.77), (MeOH+6 M HCl) 226 (log ε 4.14), 251 (4.22), 257 (4.24), 289 (4.36), 308 (4.54), and 426 nm (3.94), (MeOH+6 M NaOH) 240 (log ε 3.99), 305 (4.54), 324 (4.27 sh), 340 (4.07 sh), 423 (4.09), and 453 nm (3.91 sh), (DMSO) 298, 308, 340 (sh), and 380 nm (sh), ($CHCl_3$) 296, 307, 340 (sh), and 394 nm (sh); IR (KBr) 3250 and 1614 cm^{-1}; ^{1}H NMR (270 MHz, DMSO-d_6) δ=6.05 (1H, d, *J*=2.5 Hz, H-10), 6.32 (1H, dd, *J*=12.4 and 2.5 Hz, H-8), 6.39 (1H, d, *J*=10.3 Hz, H-6), 6.70 (1H, dd, *J*=12.4 and 10.3 Hz, H-7), 6.71 (1H, dd, *J*=8.0 and 1.5 Hz, H-4), 6.78 (1H, td, *J*=7.5 and 1.5 Hz, H-2), 6.83 (1H, dd, *J*=8.0 and 1.5 Hz, H-1), 6.88 (1H, td, *J*=7.5 and 1.5 Hz, H-3), and 9.80 (1H, br, NH); ^{13}C NMR (67.8 MHz, DMSO-d_6) δ=114.0 (d), 114.2 (d), 114.8 (d), 115.2 (d), 121.8 (d), 124.2 (d), 127.1 (s), 132.2 (d), 136.3 (d), 140.8 (s), 141.5 (s), 151.0 (s), and 183.1 (s). Found: C, 73.61; H, 4.38; N, 6.30%; M$^+$, 211. Calcd for $C_{13}H_9NO_2$: C, 73.92; H, 4.29; N, 6.63%; M, 211.

Benzo[*b*]cyclohept[*e*][1,4]oxazin-10(11*H*)-one (10): Mp 171—172 °C (lit,[4] mp 170 °C); UV_{max} (DMSO) 265, 273, 312, 330, 406, and 487 nm, ($CHCl_3$) 261, 271, 305, 324, 404, and 483 nm; ^{1}H NMR (270 MHz, DMSO-d_6) δ=6.57 (1H, dd, *J*=8.0 and 2.0 Hz, H-4), 6.68 (2H, m, H-3,7), 6.73 (1H, td, *J*=8.0 and 2.0 Hz, H-2), 6.78 (1H, dd, *J*=11.1 and 1.2 Hz, H-6), 6.93 (1H, dd, *J*=8.0 and 2.0 Hz, H-1), 6.94 (1H, dd, *J*=11.4 and 1.5 Hz, H-9), 7.03 (1H, ddd, *J*=11.4, 8.3, and 1.5 Hz, H-8), and 8.85 (1H, br, NH); ^{13}C NMR (67.8 MHz, DMSO-d_6) δ=114.4 (d), 115.5 (d), 123.8 (d), 124.6 (d), 125.2 (d), 128.2 (d), 129.3 (s), 133.9 (d), 134.2 (d), 141.4 (s), 143.7 (s), 146.5 (s), and 171.9 (s).

Acetylation of 6—10. A mixture of **9** (10 mg, 0.05 mmol) and acetic anhydride (0.6 cm^3) in acetic acid (1 cm^3) containing a trace amount of concd sulfuric acid was stirred for 2 h at room temperature, followed by the same procedures as those described above for **11b**. The residual solid was recrystallized from MeOH to give **22d** (10 mg, 83% yield). Similarly, **22a** (80% yield), **22b** (80% yield), and **22c** (80% yield) were obtained from **6**, **7**, and **8**, respectively. Compound **10** was recovered unchanged under similar conditions.

6-Acetoxybenzo[*b*]cyclohept[*e*][1,4]oxazine (22a): Brown needles; mp 120—122 °C (from MeOH); UV_{max} (MeOH) 259 (log ε 4.33), 267 (4.30), 300 (3.80), 316 (3.70 sh), 330 (3.54 sh), and 405 nm (3.99), (MeOH+6 M HCl) 225 (log ε 4.35), 263 (4.29), 271 (4.33), 319 (3.84), 431 (3.91), and 453 nm (3.88 sh); IR (KBr) 1770 cm^{-1} (C=O); ^{1}H NMR (270 MHz, CD_3CN) δ=2.19 (3H, s, Me), 5.89 (1H, ddd, *J*=12.4, 6.4, and 2.5 Hz, H-8), 5.98 (1H, dd, *J*=12.4 and 2.0 Hz, H-7), 6.19 (1H, dd, *J*=12.5 and 2.5 Hz, H-10), 6.23 (1H, ddd, *J*=12.5, 6.4, and 2.0 Hz, H-9), 6.50 (1H, m, H-4), and 6.82 (3H, m, H-1,2,3). Found: C, 70.92; H, 4.65; N, 5.34%; M$^+$, 253. Calcd for $C_{15}H_{11}NO_3$: C, 71.14; H, 4.38; N, 5.53%; M, 253.

7-Acetoxybenzo[*b*]cyclohept[*e*][1,4]oxazine (22b); Brown

needles; mp 95—97 °C (from MeOH); UV_{max} (MeOH) 259 (log ε 4.17), 268 (4.12), 294 (3.95), and 410 nm (3.94), (MeOH+6 M HCl) 225 (log ε 4.27), 261 (4.17), 272 (4.12), 311 (3.82), 429 (3.77), and 457 nm (3.75 sh); IR (KBr) 1755 cm^{-1} (C=O); ^1H NMR (270 MHz, CD_3CN) δ=2.14 (3H, s, Me), 5.60 (1H, d, *J*=2.0 Hz, H-6), 5.84 (1H, dd, *J*=10.0 and 2.0 Hz, H-8), 6.37 (1H, dd, *J*=12.0 and 10.0 Hz, H-9), 6.47 (2H, m, H-4,10), and 6.80 (3H, m, H-1,2,3). Found: *m/z* 253.0737. Calcd for $C_{15}H_{11}NO_3$: M, 253.0737.

8-Acetoxybenzo[*b*]cyclohept[*e*][1,4]oxazine (22c): Brown needles; mp 139—141 °C (from MeOH); UV_{max} (MeOH) 260 (log ε 4.36), 269 (4.32), 300 (3.82), 320 (3.70 sh), 334 (3.66 sh), and 415 nm (4.05), (MeOH+6 M HCl) 225 (log ε 4.35), 263 (4.38), 272 (4.41), 323 (3.87), 441 (3.97), and 467 nm (3.93 sh); IR (KBr) 1750 cm^{-1} (C=O); ^1H NMR (270 MHz, CD_3CN) δ=2.10 (3H, s, Me), 5.40 (1H, d, *J*=10.1 Hz, H-6), 5.77 (1H, dd, *J*=10.1 and 2.7 Hz, H-7), 6.00 (1H, dd, *J*=12.7 and 2.7 Hz, H-9), 6.10 (1H, d, *J*=12.7 Hz, H-10), 6.42 (1H, m, *J*=8.0 and 2.0 Hz, H-4), and 6.77 (3H, m, H-1,2,3). Found: *m/z* 253.0721. Calcd for $C_{15}H_{11}NO_3$: M, 253.0737.

9-Acetoxybenzo[*b*]cyclohept[*e*][1,4]oxazine (22d): Brown needles; mp 149—151 °C (from MeOH); UV_{max} (MeOH) 260 (log ε 4.49), 268 (4.39), 295 (3.94), and 410 nm (4.07), (MeOH+6 M HCl) 226 (log ε 4.29), 262 (4.32), 272 (4.37), 315 (4.00), 432 (3.95), and 457 nm (3.91 sh); IR (KBr) 1743 cm^{-1} (C=O); ^1H NMR (270 MHz, CD_3CN) δ=2.12 (3H, s, Me), 5.40 (1H, d, *J*=9.6 Hz, H-6), 5.57 (1H, dd, *J*=11.6 and 2.6 Hz, H-8), 5.79 (1H, d, *J*=2.6 Hz, H-10), 6.02 (1H, dd, *J*=11.6 and 9.6 Hz, H-7), 6.44 (1H, dd, *J*=8.0 and 2.0 Hz, H-4), and 6.66—6.88 (3H, m, H-1,2,3). Found: C, 70.85; H, 4.55; N, 5.29%; M^+, 253. Calcd for $C_{15}H_{11}NO_3$: C, 71.14; H, 4.38; N, 5.53; M, 253.

Methylation of 6—10. Ethereal diazomethane (0.5 mmol) was added to a solution of **9** (10 mg, 0.05 mmol) in ether (2 cm^3) and the mixture was stirred for 24 h at room temperature. After removal of the ether, the residue was recrystallized from benzene to give **25d** (10 mg, 80% yield). Similarly, **25a** (70% yield), **25b** (70% yield), and **25c** (80% yield) were obtained from **6**, **7**, and **8**, respectively. Compound **10** was recovered unchanged under similar conditions.

6-Methoxybenzo[*b*]cyclohept[*e*][1,4]oxazine (25a): Brown needles; mp 94—96 °C (from benzene); UV_{max} (MeOH) 263, 269, 312, and 415 nm, (MeOH+6 M HCl) 230, 275, 310, and 436 nm; ^1H NMR (270 MHz, CD_3CN) δ=3.68 (3H, s, OMe), 6.08 (1H, ddd, *J*=12.0, 6.5, and 3.0 Hz, H-8), 6.34 (2H, m, H-7,9), 6.39 (1H, d, *J*=12.0 Hz, H-10), 6.49 (1H, m, H-4), and 6.74—6.85 (3H, m, H-1,2,3). Found: *m/z* 225.0771. Calcd for $C_{14}H_{11}NO_2$: M, 225.0790.

7-Methoxybenzo[*b*]cyclohept[*e*][1,4]oxazine (25b): Brown needles; mp 87—89 °C (from benzene); UV_{max} (MeOH) 222, 260, 268, 325, and 414 nm, (MeOH+6 M HCl) 226, 261, 271, 310, 430, and 467 nm (sh); ^1H NMR (270 MHz) δ=3.66 (3H, s, OMe), 5.65 (1H, d, *J*=1.5 Hz, H-6), 5.92 (1H, dd, *J*=12.5 and 9.7 Hz, H-9), 6.10 (1H, d, *J*=12.5 Hz, H-10), 6.25 (1H, dd, *J*=9.7 and 1.5 Hz, H-8), 6.49 (1H, m, H-4), and 6.74—6.86 (3H, m, H-1,2,3); MS (70 °C) *m/z* 225 (M^+, 64%), 210 (M^+—Me, 24%), and 182 (M^+—Me—CO, 100%). Found: *m/z* 225.0763. Calcd for $C_{14}H_{11}NO_2$: M, 225.0790.

8-Methoxybenzo[*b*]cyclohept[*e*][1,4]oxazine (25c): Brown needles; mp 105—107 °C (from benzene); UV_{max} (MeOH) 220, 263, 272, 320, and 427 nm, (MeOH+6 M HCl) 228, 265, 271, 300, 325, 440, and 510 nm (sh); ^1H NMR (270 MHz) δ=3.58 (3H, s, OMe), 5.35 (1H, dd, *J*=10.3 and 2.0 Hz, H-7), 5.51 (1H, d, *J*=10.3 Hz, H-6), 6.12 (1H, dd, *J*=13.0 and 2.0 Hz, H-9), 6.28 (1H, d, *J*=13.0 Hz, H-10), 6.34 (1H, dd, *J*=7.5 and 1.5 Hz, H-4), and 6.64—6.81 (3H, m, H-1,2,3). Found: *m/z* 225.0793. Calcd for $C_{14}H_{11}NO_2$: M, 225.0790.

9-Methoxybenzo[*b*]cyclohept[*e*][1,4]oxazine (25d): Brown needles; mp 89—91 °C (from benzene); UV_{max} (MeOH) 224 (log ε 4.09), 258 (4.39), 267 (4.44), 350 (3.99 sh), 412 (4.08), and 448 nm (3.72 sh), (MeOH+6 M HCl) 225 (log ε 4.13), 252 (4.25), 259 (4.30), 287 (4.32), 305 (4.21), and 432 nm (3.94); ^1H NMR (270 MHz) δ=3.64 (3H, s, OMe), 5.44 (1H, d, *J*=9.7 Hz, H-6), 5.69 (2H, m, H-8,10), 5.99 (1H, dd, *J*=12.3 and 9.7 Hz, H-7), 6.47 (1H, m, H-4), and 6.72—6.86 (3H, m, H-1,2,3). Found: C, 74.35; H, 5.06; N, 5.93%; M^+, 225. Calcd for $C_{14}H_{11}NO_2$: C, 74.65; H, 4.92; N, 6.22%; M, 225

Hydrolysis of 22a—d. Similar procedures as those described above for compounds **11a—e** were followed. Thus, the treatment of **22a—d** (ca. 5 mg) with AcOH (2 cm^3) at 100 °C for 5—15 min gave **6—9**, respectively, in an almost quantitative yield.

Hydrolysis of 25a—d. Solutions of **25a—d** (ca. 2 mg) in methanol (5 cm^3) were allowed to stand for 48 h at room temperature. After removal of the solvent in vacuo, the residue was recrystallized from methanol, giving **6—9** in an almost quantitative yield.

Hydrolysis of 15. A solution of **15**[6] (50 mg) in acetic acid (10 cm^3) was heated at 110 °C for 10 h. The reaction mixture was chromatographed over thin-layer plates with benzene–MeOH (10:1) as the eluent, giving **16** (2 mg, 5% yield), **17** (34 mg, 80% yield), and **12d**[6] (trace).

8-Bromobenzo[*b*]cyclohept[*e*][1,4]oxazin-6(11*H*)-one (16): Brown solid; UV_{max} (MeOH) 230, 260, 300, 320 (sh), and 400 nm; MS (70 °C): *m/z* 291 (M^+, 15%), 289 (M^+, 17%), 263 (M^+—CO, 71%), 261 (M^+—CO, 65%), 182 (67%), and 154 (100%). Found: *m/z* 290.9741 and 288.9739 (1:1). Calcd for $C_{13}H_8NO_2Br$: M, 290.9718 and 288.9738.

6-Bromobenzo[*b*]cyclohept[*e*][1,4]oxazin-8(11*H*)-one (17): Brown solid; UV_{max} (MeOH) 250, 275, 315, and 410 nm, (MeOH+6 M HCl) 236, 264, 270, 320, and 435 nm, (MeOH+6 M NaOH) 238, 265, 275, 320, 463, and 495 nm (sh). Found: *m/z* 290.9759 and 288.9741 (1:1). Calcd for $C_{13}H_8NO_2Br$: M, 290.9718 and 288.9738.

Acetylation of 16 and 17. Acetylation of **16** and **17** was conducted in a manner similar to that described above for **6—10**, and gave **23** and **24**, respectively, in an almost quantitative yield.

6-Acetyloxy-8-bromobenzo[*b*]cyclohept[*e*][1,4]oxazine (23): Brown needles; mp 139—140 °C (from benzene); UV_{max} (MeOH) 220 (log ε 4.33), 258 (4.40), 269 (4.32), 294 (3.94), 305 (3.94), 319 (3.89 sh), and 409 nm (4.08), (MeOH+6 M HCl) 232 (log ε 4.29), 263 (4.40), 270 (4.42), 325 (3.95), 445 (4.03), and 472 nm (3.98 sh); IR (KBr) 1770 cm^{-1} (C=O); ^1H NMR (270 MHz) δ=2.22 (3H, s, Me), 6.05 (1H, d, *J*=13.0 Hz, H-10), 6.27 (1H, d, *J*=2.0 Hz, H-7), 6.28 (1H, dd, *J*=13.0 and 2.0 Hz, H-9), 6.41 (1H, m, H-4), and 6.76—6.90 (3H, m, H-1,2,3). Found: *m/z* 330.9792 and 332.9832 (1:1). Calcd for $C_{15}H_{10}NO_3Br$: M, 330.9844 and 332.9824.

8-Acetyloxy-6-bromobenzo[*b*]cyclohept[*e*][1,4]oxazine (24): Brown needles; mp 110—111 °C (from benzene); UV_{max} (MeOH) 259 (log ε 4.25), 268 (4.23), 307 (3.76), 320 (3.71 sh), and 410 nm (3.90), (MeOH+6 M HCl) 227 (log ε 4.27), 263 (4.42), 270 (4.24), 321 (3.81), 441 (3.82), and 471 nm (3.77 sh); IR (KBr) 1750 cm^{-1} (C=O); ^1H NMR (270 MHz) δ=2.17 (3H, s,

Me), 5.89 (1H, dd, J=13.0 and 2.2 Hz, H-9), 6.18 (1H, d, J=13.0 Hz, H-10), 6.22 (1H, d, J=2.2 Hz, H-7), 6.60 (1H, dd, J=8.0 and 2.0 Hz, H-4), 6.78—6.94 (3H, m, H-1,2,3). Found: C, 54.50; H, 3.27; N, 3.95%; M^+, 332. Calcd for $C_{15}H_{10}NO_3Br$: C, 54.24; H, 3.03; N, 4.22%; M, 332.

Hydrolysis of 18. A solution of **18**[9] (25 mg) in acetic acid (5 cm^3) was heated at 110 °C for 5 h, followed by the same procedures as those described above for **15**, and produced **19** (13 mg, 60% yield) and **20** (4 mg, 20% yield).

7,9-Dibromobenzo[*b*]cyclohept[*e*][1,4]oxazin-10(11*H*)-one (19): Reddish-violet needles; mp 256—257 °C (from benzene); UV_{max} (MeOH) 256 (log ε 4.42), 272 (4.26 sh), 302 (4.20), 339 (3.79 sh), 418 (3.51 sh), and 520 nm (4.08), (MeOH+6 M NaOH) 260 (log ε 4.31), 274 (4.25), 304 (4.16), and 503 nm (4.16); IR (KBr) 3270 and 1557 cm^{-1}; ^{1}H NMR (100 MHz) δ=6.43—6.82 (4H, m, H-1,2,3,4), 7.62 (1H, d, J=2.0 Hz, H-6), and 8.08 (1H, d, J=2.0 Hz, H-8); MS (140 °C): m/z 370 (M^+, 50%), 368 (M^+, 100%), and 366 (M^+, 51%). Found: C, 42.41; H, 2.12; N, 3.59%. Calcd for $C_{13}H_7NO_2Br_2$: C, 42.31; H, 1.91; N, 3.80%. Compound **19** was also obtained (90 mg, 90% yield) by heating **21**[16] (100 mg, 0.27 mmol) with **4** (50 mg, 0.46 mmol) in ethanol (3 cm^3) at 60 °C for 2 h, followed by the same procedures as those described above for **12c**.

6,8-Dibromobenzo[*b*]cyclohept[*e*][1,4]oxazin-10(11*H*)-one (20): Reddish-violet solid; UV_{max} (MeOH) 225, 260, 270 (sh), 320, 420, and 510 nm; ^{1}H NMR (270 MHz) δ=6.54 (2H, m, H-2,4), 6.77 (2H, m, H-1,3), 7.12 (1H, d, J=1.8 Hz, H-9), 7.84 (1H, br, NH), and 8.08 (1H, d, J=1.8 Hz, H-7). Found: m/z 370.8789, 368.8847, and 366.8838 (1:2:1). Calcd for $C_{13}H_7NO_2Br_2$: M, 370.8804, 368.8824, and 366.8844.

Reduction of 19 and 20 Zinc dust (20 mg) was added to a solution of **19** (30 mg, 0.08 mmol) in acetic acid (5 cm^3), and the mixture was stirred at room temperature for 2 h. The reaction mixture was filtered and evaporated to dryness in vacuo. The residue was then chromatographed on silica-gel thin layer plates with benzene–MeOH (50:1) as the eluent, giving compound **10**[4] (40% yield). Compound **10** was also obtained from **20** by following an identical procedure.

We thank professor Hiroshi Yamamoto (Okayama Univ.) for helpful discussions. We also thank Professor Jun-ichi Aihara (Shizuoka Univ.) for helpful discussions on the resonance energy and ring currents. We are grateful to Dr. Chizuko Kabuto, Instrumental Analysis Center for Chemistry, Faculty of Science, Tohoku University, for helpful discussions concerning the X-ray crystallograph analysis. We also thank Mr. Hiroshi Isa and Miss Rie Taguchi for their assistance with some of the experiments.

References

1) Part III: T. Nozoe, H. Okai, H. Wakabayashi, and S. Ishikawa, *Bull. Chem. Soc. Jpn.*, **62**, 2307 (1989).

2) Part of these results have been preliminarily reported: H. Wakabayashi, S. Ishikawa, H. Okai, and T. Nozoe, The 50th National Meeting of the Chemical Society of Japan, Tokyo, April 1985, Abstr., 1T16 and 1T17.

3) T. Nozoe and T. Someya, *Bull. Chem. Soc. Jpn.*, **51**, 3316 (1978).

4) T. Someya, H. Okai, H. Wakabayashi, and T. Nozoe, *Bull. Chem. Soc. Jpn.*, **56**, 2756 (1983).

5) T. Nozoe, T. Someya, and H. Okai, *Bull. Chem. Soc. Jpn.*, **52**, 1156 (1979).

6) H. Wakabayashi, S. Ishikawa, H. Okai, and T. Nozoe, *Bull. Chem. Soc. Jpn.*, **58**, 2840 (1985); T. Nozoe, H. Wakabayashi, and S. Ishikawa, *Heterocycles*, **29**, 1005 (1989).

7) T. Nozoe, H. Okai, H. Wakabayashi, and S. Ishikawa, *Chem. Lett.*, **1988**, 1589.

8) T. Nozoe, K. Takase, H. Matsumura, T. Asao, K. Kikuchi, and S. Itô, "Dai Yuki Kagaku," ed by M. Kotake, Asakura Shoten, Tokyo (1960), Vol. XIII.

9) T. Nozoe, K. Shindo, H. Wakabayashi, and S. Ishikawa, *Heterocycles*, **29**, 1459 (1989).

10) A. Streitwieser, Jr., "Molecular Orbital Theory for Organic Chemists," Wiley, New York (1961).

11) J. J. P. Stewart and F. J. Seiler, MOPAC QCPE #549.

12) a) J. Aihara, *J. Am. Chem. Soc.*, **98**, 2750 (1976); b) *ibid.*, **107**, 298 (1985); c) *ibid.*, **99**, 2048 (1977).

13) T. Nozoe, H. Okai, and T. Someya, *Bull. Chem. Soc. Jpn.*, **51**, 2185 (1978).

14) The crystal data of **10** were as follows: $C_{11}H_9NO_2$, monoclinic with the space group $P2_1/c$, a=10.320(1), b=16.333(5), c=11.937(4) Å, β=97.71(3)°, V=1994(1) Å^3, Z=8, Dc=1.411 g cm^{-3}. 3334 independent reflections ($2\theta<126°$; $|F_o|>3\sigma|F_o|$) were collected with a Rigaku AFC-5 automatic diffractometer, using graphite-monochromated Cu $K\alpha$ radiation. The final R value was 0.0620. The molecular framework was illustrated; C. Kabuto, J. Okada, A. Kawamata, H. Wakabayashi, S. Ishikawa, and T. Nozoe, to be published elsewhere.

15) W. von E. Doering and C. F. Hiskey, *J. Am. Chem. Soc.*, **74**, 5688 (1952).

16) K. Kikuchi, *Bull. Chem. Soc. Jpn.*, **33**, 628 (1960).

Benzophenone-Sensitized Photolysis of *N*,*N*-Dibenzyl-*O*-acylhydroxylamines. Mechanism of the Imine-Forming Radical Elimination Reaction

Tadamitsu SAKURAI,* Hisashi MIZUNO, Tsuneari KUBOTA, and Hiroyasu INOUE
Department of Applied Chemistry, Faculty of Technology, Kanagawa University, Kanagawa-ku, Yokohama 221
(Received January 28, 1991)

Title hydroxylamines (**1**) undergo benzophenone-sensitized photolysis to give *N*-benzylidenebenzylamine (**2**), *p*-substituted benzoic acids (**3**), and monosubstituted benzenes (**4**) derived from decarboxylation of *p*-substituted benzoyloxyl radicals. Analysis of the linear Stern–Volmer plots, both for the sensitized photolysis of **1** and for the phosphorescence quenching of benzophenone by **1**, demonstrates the participation of triplet **1** in this photolysis. The logarithm of the ratio (k_r/k_d), where k_r is the rate constant for homolytic cleavage of the N–O bond in triplet **1** and k_d is that for its deactivation, used as a measure of the triplet-state reactivities of **1**, exhibited a good Hammett-type relationship against the substituent constant (σ) with a slope (ρ) of −0.75. This indicates the exclusive occurrence of homolysis of the N–O bond in the first excited triplet state of **1**. Thus the decomposition of **1** activated by triplet benzophenone is classified as an imine-forming radical elimination. The results of deuterium isotope and micellar effects on the sensitized photolysis suggest that the "out-of-cage" products **4** are obtained by decarboxylation and subsequent hydrogen abstraction of *p*-substituted benzoyloxyl radicals which escaped from the triplet cage in competition with spin inversion to the singlet cage. In this singlet cage, hydrogen abstraction giving **2** and **3** and recombination affording the starting **1** were found to take place exclusively.

Much effort has been devoted to synthetic, mechanistic, and theoretical studies on olefin-forming eliminations and has contributed to the establishment of one of the chemical paradises.[1] A detailed mechanistic investigation of these unimolecular and bimolecular eliminations has unraveled the delicate transition-state structure for the reactions.[2] Base-promoted imine-forming eliminations have recently been found[3] and a detailed comparison has been made between mechanisms of olefin- and imine-forming eliminations, with attention focusing primarily upon the effects of the nitrogen atom in a molecule on the transition-state structure.[4] On the other hand, there are some interesting reports describing the stereochemistry of olefin-forming radical eliminations.[5]

In contrast with ionic imine-forming eliminations there has been no study on imine-forming radical eliminations as far as we know. As an extension of our systematic study of the direct and sensitized photolyses of hydroxamic acid derivatives,[6a-e] we prepared *N*,*N*-dibenzyl-*O*-acylhydroxylamines (**1a**—**c**) and investigated benzophenone (BP)-sensitized photolysis of these compounds, hoping to find an imine-forming radical elimination and to gain an insight into its mechanism. In this paper we present the first observation of imine-forming radical eliminations of **1a**—**c** and discuss their mechanism.

$(PhCH_2)_2N-OC(=O)C_6H_4R\text{-}p$

1a: R= OMe 1b: R= F 1c: R= CF_3

Results

Products Derived from the Sensitized Photolysis. An oxygen-free acetonitrile solution of **1a** (0.020 M, 1 M=1 mol dm^{-3}) containing BP (0.020 M) was irradiated for a given period of time with light of wavelengths longer than 320 nm on a merry-go-round irradiation apparatus. The products were identified by comparing their HPLC or GLC behavior with that of commercially available authentic samples. As shown in Fig. 1, *N*-benzylidenebenzylamine (**2**), *p*-anisic acid (**3a**), and anisole (**4a**, data

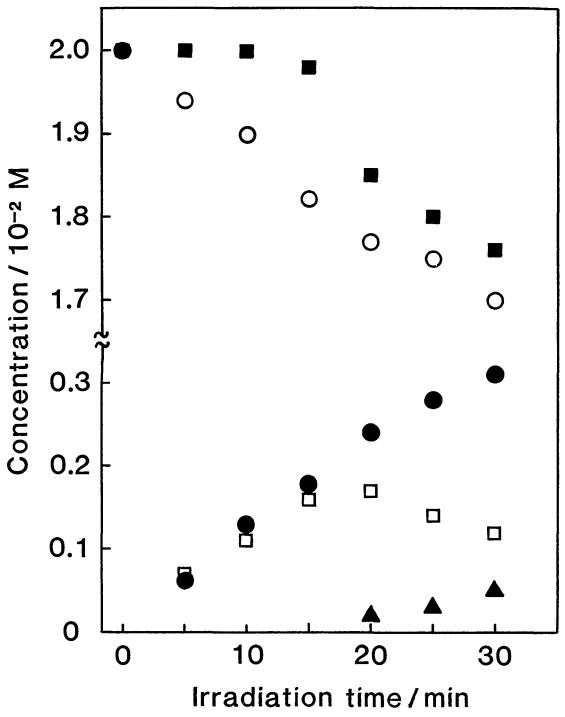

Fig. 1. Plots of reactant and product concentrations against irradiation time for the BP (0.020 M)-sensitized photolysis of **1a** (0.020 M) with light of wavelengths longer than 320 nm in oxygen-free acetonitrile. ○: **1a**, ●: **3a**, □: **2**, ■: BP, ▲: benzopinacol.

not presented) were obtained as the only detectable products at conversions lower than 9%, while BP remained unchanged during the irradiation. On the other hand, a secondary photoreaction between **2** and BP in excited states occurred to give benzopinacol as one of the products at conversions higher than 12%. This secondary photoreaction is reflected in a decrease in both **2** and BP concentrations (Fig. 1) and was confirmed by independent irradiation of **2** in the presence of BP under identical conditions. Control experiments revealed that there was no decomposition of **1a** without BP under the same irradiation conditions. The detectable formation of **4a**, derived from decarboxylation of *p*-anisoyloxyl radical, suggests the involvement of homolytic cleavage of the N–O bond in **1a**. Similar results were obtained by BP-sensitized photolysis of **1b** and **1c** (Scheme 1).

Quenching of the BP Phosphorescence by 1a—c. The room-temperature phosphorescence of BP (the first triplet excitation energy, E_{T_1}=69 kcal mol^{-1}; 1 kcal=4.184 kJ)[7] was quenched by **1a—c** according to the Stern–Volmer equation (Fig. 2). The E_{T_1} values of **1a—c** (69, 67, and 67 kcal mol^{-1} for **1a**, **1b**, and **1c**, respectively) were estimated from the 0–0 peaks of their phosphorescence spectra in methanol–ethanol (1:1 v/v) at 77 K. Although the fluorescence of **1a—c** is too weak to be detected, it is evident from a comparison of the UV spectra of **1a—c** with that of BP that the first singlet excitation energy of **1a—c** is much higher than that of BP. Thus the BP-phosphorescence quenching is due to triplet-triplet energy transfer from BP to **1a—c** but not due to singlet–singlet energy transfer. The quenching constants ($k_t\tau_T$, where k_t and τ_T refer to the rate constant for triplet–triplet energy transfer and the lifetime of triplet BP without **1a—c**, respectively) were determined from the slopes of linear Stern–Volmer plots (Fig. 2) to be 62, 48, and 56 M^{-1} for **1a**, **1b**, and **1c**, respectively. A comparison of these constants demonstrates that the triplet energy transfer efficiency undergoes substituent effects, if any, to only a small extent.

Quantum Yields for the Sensitized Photolysis. The results of BP-phosphorescence quenching as well as product analysis suggest that the BP-sensitized photolyses of **1a—c** proceed according to Scheme 2 which allows us to derive Eqs. 1 and 2 under the steady-state approximation:

$$1/\Phi_{-1}=1/\Phi_2=(1+k_d/k_r)(1+1/k_t\tau_T[\mathbf{1a—c}]) \quad (1)$$

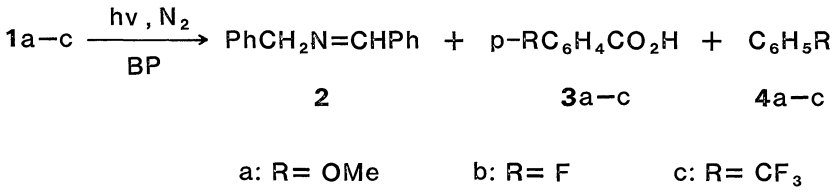

Scheme 1.

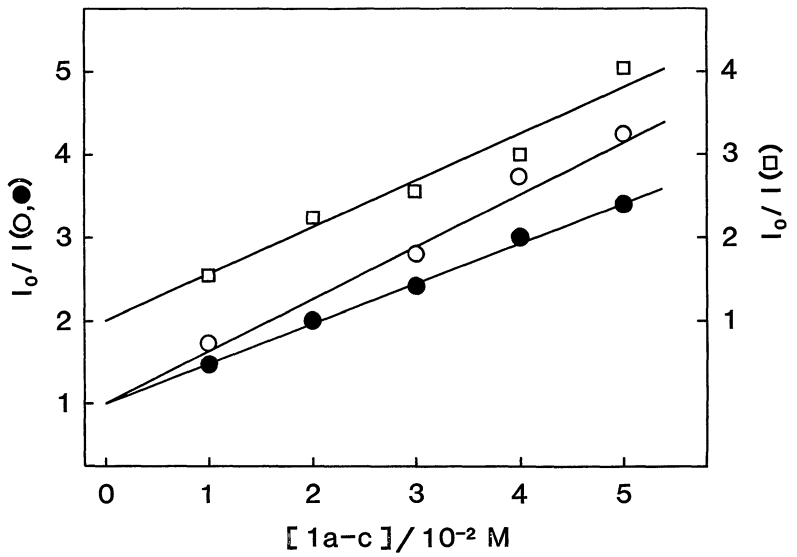

Fig. 2. Stern–Volmer plots for the quenching of BP (0.050 M) phosphorescence by **1a** (○), **1b** (●), and **1c** (□) under nitrogen in acetonitrile at room temperature (26±1°C). I and I_0 are the phosphorescence intensity of BP with and without **1a—c**, respectively.

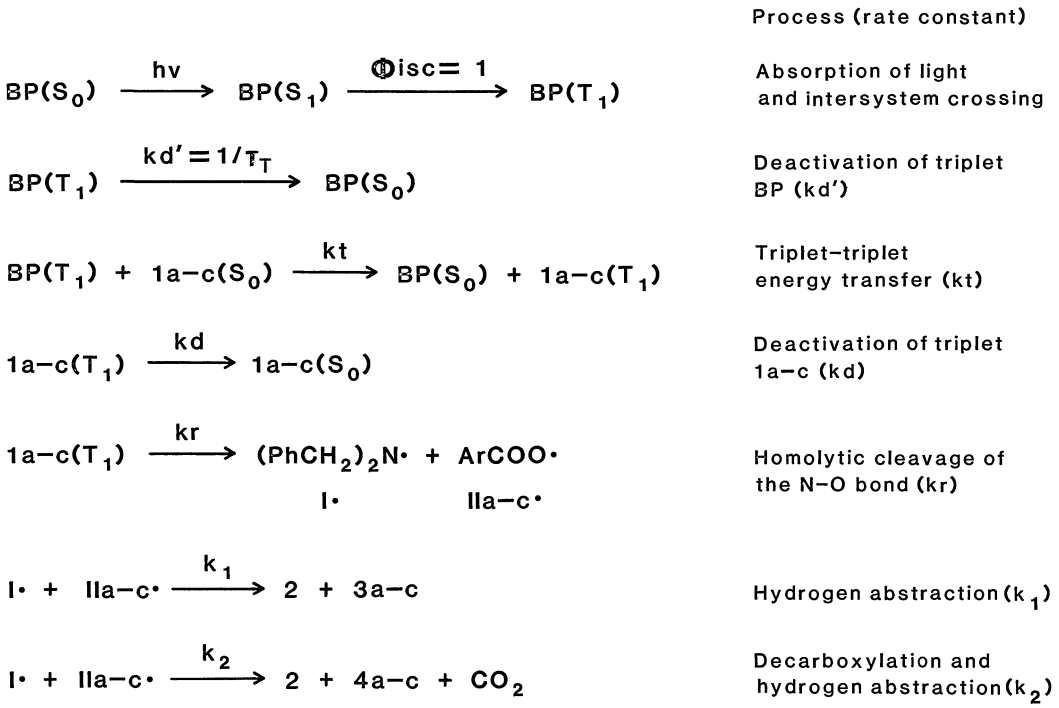

Scheme 2.

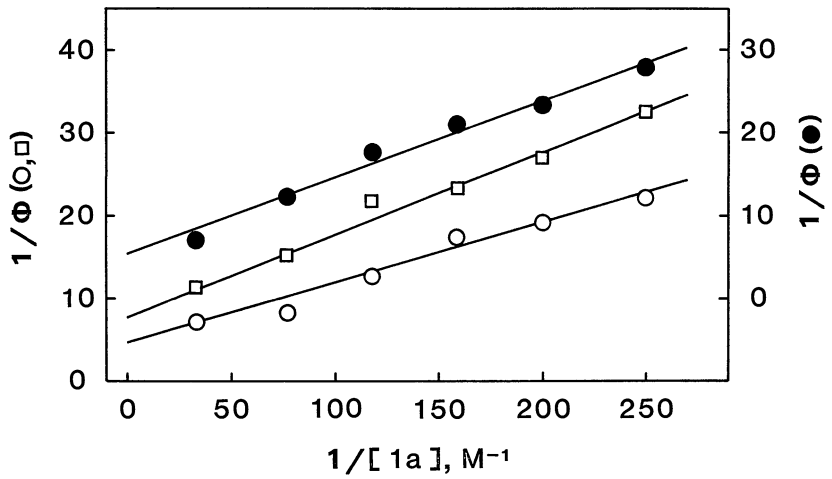

Fig. 3. Stern-Volmer plots of $1/\Phi_{-1a}$ (○), $1/\Phi_2$ (●), and $1/\Phi_{3a}$ (□) versus 1/[**1a**] for the BP (0.050 M)-sensitized photolysis of **1a** with 366-nm light in oxygen-free acetonitrile.

$$1/\Phi_3=(1+k_d/k_r)(1+k_2/k_1)(1+1/k_t\tau_T[\mathbf{1a}—\mathbf{c}]) \quad (2)$$

where Φ_{-1}, Φ_2, and Φ_3 are the quantum yields for the disappearance of **1a**—**c** and for the appearance of **2** and **3**, respectively. These quantum yields were determined by using a potassium trioxalatoferrate (III) actinometer at low conversions (3—4%) of the starting **1a**—**c**. If our Scheme for the sensitized photolysis is valid, then we expect a linear relationship between $1/\Phi$ and the reciprocal of **1a**—**c** concentrations (1/[**1a**—**c**]). In Fig. 3 are shown typical double reciprocal plots for the BP-sensitized photolysis of **1a** in acetonitrile. Similar plots were obtained also for **1b** and **1c**.

The good linear correlation between $1/\Phi$ and 1/[**1a**—**c**], therefore, justifies the validity of Scheme 2. These linear Stern-Volmer plots of $1/\Phi_{-1}$, $1/\Phi_2$, and $1/\Phi_3$ vs. 1/[**1a**—**c**] allow us to estimate the limiting quantum yields for the disappearance of **1a**—**c** ($\Phi_{-1,\mathrm{lim}}$) and for the appearance of **2** ($\Phi_{2,\mathrm{lim}}$) and **3a**—**c** ($\Phi_{3,\mathrm{lim}}$). In addition, the intercept/slope ratios of these linear plots provide the $k_t\tau_T$ values, while the k_r/k_d values can be evaluated based on Eq. 1. All of these values (Φ_{lim}, $k_t\tau_T$, and k_r/k_d) are

Table 1. Limiting Quantum Yields and Related Parameters for the BP (0.050 M)-Sensitized Photolysis of **1a—c** (0.0040—0.030 M) with 366-nm Light under Nitrogen at 28±2°C

Compound	Solvent	$\Phi_{-1,\lim}$	$\Phi_{2,\lim}$	$\Phi_{3,\lim}$	Φ_4	$\Phi_{4,\lim}$[a]	k_r/k_d	$k_t\tau_T$[b] / M^{-1}	$k_t\tau_T$[c] / M^{-1}
1a	CH_3CN	0.22	0.19	0.13	0.03[d]	0.08	0.26	62	67
1b	CH_3CN	0.13	0.12	0.10	—[e]	0.03	0.14	48	49
1c	CH_3CN	0.06	0.06	0.03	—[e]	0.03	0.064	56	90
1a-d_4	CH_3CN	0.11	0.10	0.07	—[f]	0.04	0.12	60	63
1a	CH_2ClCH_2Cl	0.22	0.23	0.18	—[f]	0.05	0.29	56	53
1a	Benzene	0.28	0.29	0.29	≈0[d]	0	0.40	36	27

a) Calculated by assuming $\Phi_{4,\lim}=1/2(\Phi_{-1,\lim}+\Phi_{2,\lim})-\Phi_{3,\lim}$. b) Determined from the BP-phosphorescence quenching experiments. c) Average of the $k_t\tau_T$ values determined from the quantum yield (Φ_{-1}, Φ_2, and Φ_3) measurements. d) Determined for **[1a]**=0.030 M (GLC analysis). e) Could not be determined. f) Not determined.

collected in Table 1 which also includes the results of solvent and deuterium isotope effects on the quantum yields for the BP-sensitized photolysis of **1a**. The latter effects were examined in acetonitrile by use of *N,N*-di(benzyl-α-d_2)-*O*-(*p*-anisoyl)hydroxylamine (**1a-d_4**). An additional supporting evidence for Scheme 2 comes from the finding that the $k_t\tau_T$ value determined from the BP-phosphorescence quenching corresponds well to that obtained from the linear plot of $1/\Phi$ against $1/[\mathbf{1}]$ for any starting **1** as well as in any solvent studied.

Discussion

Substituent and Deuterium Isotope Effects. Because the $k_t\tau_T$ values obtained for **1a**, **1b**, and **1c** in acetonitrile may be taken as consistent with each other within the experimental error, we can discuss a difference in the reactivity among these compounds from the standpoint of substituent effects on the triplet-state reactivities (k_r/k_d). One expects that an increased electron-withdrawing ability of the substituent R should accelerate heterolytic cleavage of the N–O bond in **1**[3] whereas it may suppress homolytic cleavage of this bond because of an electrophilic character of the aroyloxyl radical formed by this type of N–O bond cleavage.[8] A comparison of the k_r/k_d values obtained for **1a—c** in acetonitrile establishes that the triplet-state reactivity decreases with increasing electron-withdrawing ability of the substituent R; this strongly evidences that homolytic cleavage of the N–O bond occurs in triplet **1a—c**. An important problem is whether the substituent R affects the triplet-state deactivation (k_d) or the N–O bond cleavage (k_r) process. Figure 4 shows that there is a nice Hammett-type linear relationship with a slope (ρ) of −0.75 between $\log(k_r/k_d)$ and the substituent constant σ values. This ρ value suggests a relatively large contribution of the ionic structure to the transition-state structure **III** for homolytic N–O bond cleavage in triplet **1a—c**.

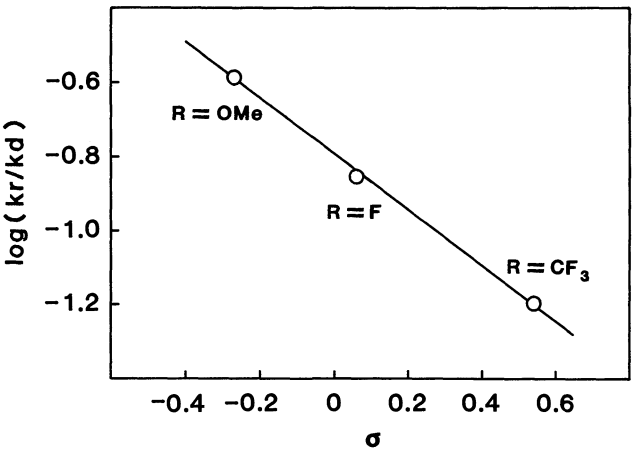

Fig. 4. Correlation of $\log(k_r/k_d)$ and σ values for the BP-sensitized photolysis of **1a—c** with 366-nm light in acetonitrile.

On the other hand, the Hammett ρ–σ correlation has been applied in order to scrutinize the transition-state structure for the homolysis of the benzylic C–H bond. The ρ values in a range of −0.4 to −1.0 have been obtained from this correlation depending on the structures of both substrates and attacking radicals, and explained in terms of a similar transition-state structure.[9] Thus the fact that our ρ value is comparable to these ρ values suggests that the N–O bond cleavage process rather than the triplet-state deactivation is mainly subject to polar substituent effects.

Inspection of Scheme 2 provides us another important problem: Is the benzylic hydrogen atom of dibenzylaminyl radical (**I**·) abstracted by aroyloxyl radical (**II**·)? To solve this problem we prepared **1a-d_4** and examined

$^3[\ BzI_2N\text{----}OC(=O)Ar \longleftrightarrow BzI_2N\text{----}OC(=O)Ar\ ]^{\neq}$ (δ• δ• ↔ δ− δ+)

III

BzI= $PhCH_2$ Ar= p-RC_6H_4

$(PhCD_2)_2N\text{–}OC(=O)C_6H_4OMe\text{-}p$

1a-d_4

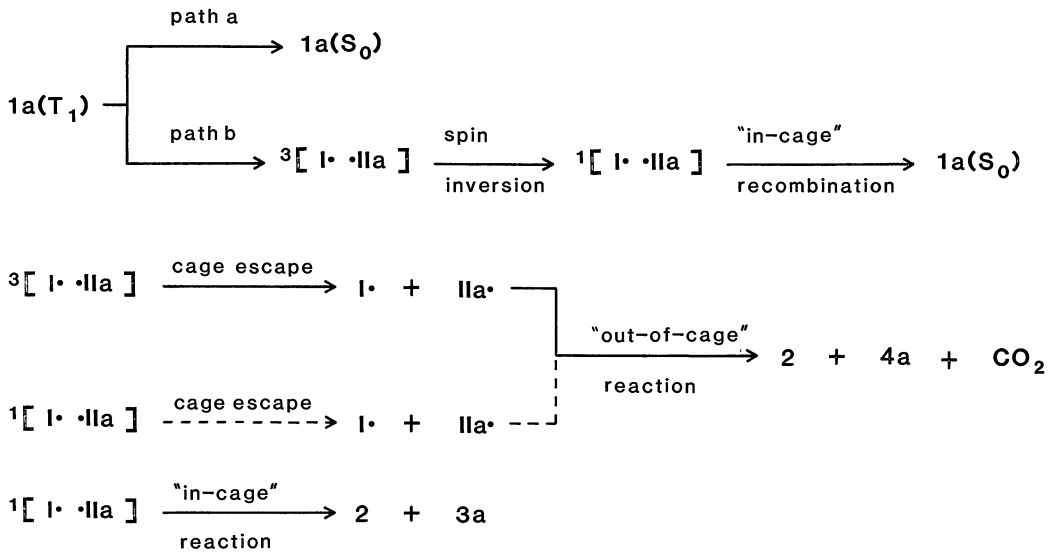

Scheme 3.

deuterium isotope effects on the reaction of **1a** with triplet BP. The deuterium substitution decreases both the Φ_{lim} and k_r/k_d values by a factor of about 2, whereas the $k_t\tau_T$ value is not affected by deuteration (Table 1). In order to discuss the mechanism of our imine-forming radical eliminations in more detail, we present Scheme 3 which takes into account the spin-correlated (singlet or triplet) radical pair in a solvent cage as already successfully applied to the BP-sensitized photolysis of *N*-(1-naphthoyl)-*O*-(*p*-toluoyl)-*N*-phenylhydroxylamine (NT).[6b] A comparison of Schemes 2 and 3 shows that the rate constants k_r and k_d in Scheme 2 correspond to the rate of the N–O bond cleavage in triplet **1a**—**c** giving the triplet radical pair and to the total rate of physical (path a) and chemical (path b) deactivations of triplet **1a**—**c** affording eventually the starting **1a**—**c**, respectively. In addition, the rate constants k_1 and k_2 in Scheme 2 conform to the total rate of triplet→singlet cage spin inversion and subsequent "in-cage" hydrogen abstraction yielding **2** and **3a**—**c** and to the total rate of diffusive escape from the triplet cage, decarboxylation of "out-of-cage" aroyloxyl radicals, and subsequent hydrogen abstraction forming eventually **2**, **4a**—**c**, and CO_2, respectively.

The observation that the relative phosphorescence quantum yield $[\Phi_p(\mathbf{1a})/\Phi_p(\mathbf{1a}\text{-}d_4)]$ of **1a** and **1a**-d_4 (E_{T_1}= 69 kcal mol^{-1}) at 77 K is nearly equal to unity makes it reasonable to assume that in addition to the N–O bond cleavage process of triplet **1a**, its physical deactivation process (path a in Scheme 3) also undergoes deuterium isotope effects to a negligible extent. Thus a decrease in Φ_{lim} as well as k_r/k_d observed by deuteration implies that hydrogen abstraction from **I**· by **IIa**· takes place in competition with recombination of these two radicals to generate the starting **1a**. The latter process (path b in Scheme 3) contributes to accelerating the deactivation process of triplet **1a** and, hence, the deuteration of **1a** should enhance the chemical deactivation process of this triplet to reduce k_r/k_d as observed. In view of the fact that hydrogen abstraction to give **2** and **3a**—**c** (k_1 in Scheme 2) competes with decarboxylation to form eventually **2** and **4a**—**c** (k_2 in Scheme 2), the retardation of hydrogen abstraction by the deuterium incorporation is expected to be reflected in an increase in the relative rate of this decarboxylation and, thus, in the enhanced k_2/k_1 value. From Eqs. 1 and 2 we can estimate the k_2/k_1 values using the Φ_{lim} values listed in Table 1: k_2/k_1 =0.57 (**1a**), 0.49 (**1a**-d_4), 0.25 (**1b**), and 1.0 (**1c**) in acetonitrile. A comparison of these values for **1a** and **1a**-d_4 clearly indicates that decarboxylation of **IIa**· cannot compete with hydrogen abstraction from **I**· by this radical. This means that diffusive separation of **I**· and **IIa**· from the caged singlet radical pair must be slow enough to allow the exclusive hydrogen abstraction and recombination in this cage (Scheme 3). It is thus very likely that anisole (**4a**), one of the "out-of-cage" products, originates from decarboxylation of **IIa**· which escaped from the triplet cage in competition with spin inversion from the triplet to the singlet pair. Because diffusive separation of the caged radical pair is thought to undergo negligible deuterium isotope and polar substituent effects, our k_2/k_1 value may reflect the relative ease of this spin inversion, which is in the following order: R=F (k_2/k_1=0.25)>R=OMe (0.57)>R=CF_3 (1.0). Although this order seems to be consistent with that of the magnitude of heavy-atom effects of these substituents on the rate of spin inversion, we cannot discuss it in detail at the present stage.

Solvent and Micellar Effects. Our previous study on the BP-sensitized photolysis of NT indicated that the triplet-state reactivity (k_r/k_d) of this diacylhydroxylamine increases with decreasing solvent polarity.[6a,b] On

the other hand, a study of the micellar effects on the photolysis of NT provided us an interesting result that the "out-of-cage" reaction of the resulting radicals is almost completely suppressed in the micelle cage.[6b] In order to discuss further the reaction course of imine-forming radical eliminations, we examined solvent and micellar effects on the BP-sensitized photolysis of **1a** chosen for this purpose.

The $k_t\tau_T$ values obtained by the above-mentioned two methods are in good agreement with each other also for 1,2-dichloroethane and benzene (Table 1), indicating that the reaction proceeds according to Scheme 2 in any solvent employed. In addition the triplet-state reactivity tends to increase with decreasing solvent polarity, although this reactivity is little affected by a change in solvent polarity. Interestingly the sensitized photolysis of **1a** in benzene does not give any **4a** derived from decarboxylation of **IIa·**. Because benzene is not so viscous (viscosity at 30 °C=0.5621 cP),[10] it is very unlikely that only the "in-cage" reaction occurs in this nonpolar solvent. Ingold and co-workers have recently reported that in a nonpolar solvent, carbon tetrachloride, the rates of unimolecular decarboxylation and bimolecular hydrogen abstraction of **IIa·** increase by a factor of about 20 and 2—3, respectively, compared with those in a polar solvent, acetonitrile.[11] Their results suggest that the reactivities of **IIa·** should increase to more extent in the nonpolar solvent, benzene, than in acetonitrile, and thus allow us to expect that we obtain a larger $\Phi_{4,\mathrm{lim}}$ value in benzene than in acetonitrile since solvent changes can have a dramatic effect on the rate of decarboxylation of **IIa·**. However, the result (Table 1) is not in line with this expectation. Aromatic solvents including benzene are known to form a charge-transfer-type π-complex with an electrophilic chlorine atom.[12] The fact that aroyloxyl radicals add easily to alkenes suggests that these radicals also have an electrophilic character.[8] Thus it is reasonable to assume that the radical **IIa·** forms a similar type of π-complex with benzene to stabilize this radical and, hence, to reduce the relative rate of decarboxylation of the "out-of-cage" radical **IIa·** to hydrogen abstraction from **I·** by **IIa·**. If benzene can enhance the reactivity of **I·** toward hydrogen abstraction to an extent similar to or more than that of **IIa·**, then the existence of such a π-complex provides a good explanation for the negligible formation of **4a** in benzene.

It is well established that micelles offer a large energy barrier to diffusive separation of a radical pair generated within the micellar phases, so that the efficiency of "in-cage" reaction of the triplet-derived radical pair is enhanced in a micellar solution to a larger extent than that in a homogeneous solution.[13] Based on this characteristic of micelles we expect in the sensitized photolysis of **1a** in micelles that the quantum yield for the formation of **4a**, one of the "out-of-cage" products, becomes negligibly small.

The sensitized photolysis of **1a** (1.3×10^{-2} M) by BP (2.0×10^{-2} M) in hexadecyltrimethylammonium chloride (HTAC) micelles (1.8×10^{-3} M) under nitrogen at 28±1 °C gave the following results: Φ_{-1a}=0.03, Φ_2=0.03, Φ_{3a}=0.03, and $\Phi_{4a}\approx0$. For comparison these quantum yields were determined in acetonitrile under identical conditions except for the omission of HTAC micelles: Φ_{-1a}=0.10, Φ_2=0.09, Φ_{3a}=0.08, and Φ_{4a}=0.01. The finding that the ratio (I_0/I=1.9) of BP-phosphorescence intensity with (I) and without (I_0) **1a** in micelles is consistent with that (I_0/I=1.8) obtained in acetonitrile under the same conditions allows us to discuss the differences in the quantum yields on the basis of micellar effects not on the triplet–triplet energy transfer efficiency but solely on the "in-cage" reaction efficiency. As we would expect, the formation of **4a** in HTAC micelles is negligible, whereas the quantum yields Φ_{-1a}, Φ_2, and Φ_{3a} for the reaction in this micelle decreased by a factor of about 3 compared with those in acetonitrile. Owing to the relatively large intramicellar viscosity of HTAC (18 cP at 30 °C),[14] translational movement of the paired radicals **I·** and **IIa·** in this micelle should be restricted to a large extent to result in a more efficient recombination of **I·** and **IIa·** giving the starting **1a** than hydrogen abstraction from **I·** by **IIa·** forming **2** and **3a**, as observed. These observations, therefore, constitute further evidence for the occurrence of recombination in competition with hydrogen abstraction within the singlet solvent cage.

Experimental

General Methods. HPLC analysis of the photoproducts was performed on a Shimadzu Model LC-6A high-performance liquid chromatograph equipped with a 4.6×250-mm ODS (Zorbax) column and a Shimadzu Model SPD-2A UV detector (240 nm). IR spectra were taken with a Hitachi Model 270-30 infrared spectrometer. ^{1}H NMR spectra were recorded on a JEOL Model FX-200 spectrometer. GLC analysis was carried out on a Shimadzu Model GC-8AP gas chromatograph using a 3.0×3000-mm glass column packed with 10% Silicone SE-30 on Uniport B (60/80 mesh, Gasukuro Kogyo). Room-temperature phosphorescence of benzophenone with and without quencher was measured under nitrogen with a Shimadzu Model RF-5000 spectrofluorimeter. UV spectra at room temperature and phosphorescence spectra at 77 K were taken on a Shimadzu Model UV-210A spectrophotometer and a Shimadzu Model RF-500 spectrofluorimeter equipped with a cylindrical rotating sector, respectively.

Materials and Solvents. *N*,*N*-Dibenzylhydroxylamine was prepared according to the method of Jones and Sneed, mp 123—124 °C (lit,[15] 124 °C). *O*-Aroylation of this hydroxylamine with *p*-substituted benzoyl chlorides in the presence of pyridine in dichloromethane gave *N*,*N*-dibenzyl-*O*-(*p*-substituted benzoyl)hydroxylamines in good yields. The crude products were purified by column chromatography over silica gel (70—230 mesh, Merck) using chloroform as eluent followed by repeated recrystallization from hexane to give colorless needles with the following physical properties.

N,*N*-Dibenzyl-*O*-(*p*-anisoyl)hydroxylamine (**1a**), mp 84.5—85.5 °C (lit,[3] 83—84 °C); IR (KBr) 1730 cm^{-1} (ester C=O); ^{1}H NMR ($CDCl_3$) δ=3.83 (3H, s), 4.20 (4H, s), 6.87 (2H, d,

J=8 Hz), 7.24—7.48 (10H, m), and 7.82 (2H, d, J=8 Hz).

N,N-Dibenzyl-*O*-(*p*-fluorobenzoyl)hydroxylamine (**1b**), mp 99—100 °C; IR (KBr) 1740 cm^{-1} (ester C=O); ^1H NMR ($CDCl_3$) δ=4.20 (4H, s), 7.04 (2H, dd, J=8 and 8 Hz), 7.22—7.48 (10H, m), and 7.86 (2H, dd, J=8 and 5 Hz). Found: C, 75.32; H, 5.47; N, 4.16%. Calcd for $C_{21}H_{18}NO_2F$: C, 75.20; H, 5.41; N, 4.18%.

N,N-Dibenzyl-*O*-(*p*-trifluoromethylbenzoyl)hydroxylamine (**1c**), mp 98—99 °C; IR (KBr) 1745 cm^{-1} (ester C=O); ^1H NMR ($CDCl_3$) δ=4.22 (4H, s), 7.22—7.48 (10H, m), 7.59 (2H, d, J=8 Hz), and 7.91 (2H, d, J=8 Hz). Found: C, 68.59; H, 4.61; N, 3.69%. Calcd for $C_{22}H_{18}NO_3F_3$: C, 68.56; H, 4.71; N, 3.64%.

N,N-Di(benzyl-α-d_2)-*O*-(*p*-anisoyl)hydroxylamine (**1a**-d_4), mp 85—86 °C, was obtained from the reaction of *p*-anisoyl chloride with *N,N*-di(benzyl-α-d_2)hydroxylamine, which was prepared according to the previous method,[3] under the same conditions as those used for syntheses of **1a**—**c**. The content of deuterium in **1a**-d_4 was determined to be 98 atom% by ^1H NMR spectroscopy. Benzophenone was purified by repeated recrystallization from ethanol. Fractional distillation of *N*-benzylidenebenzylamine (**2**), anisole (**4a**), fluorobenzene (**4b**), and trifluoromethylbenzene (**4c**) gave analytically pure samples. *p*-Methoxy (**3a**)-, *p*-fluoro (**3b**)-, and *p*-trifluoromethyl (**3c**)-benzoic acids were recrystallized twice from aqueous ethanol. Benzene and 1,2-dichloroethane were of spectroscopic grade and were used without further purification. Purification of acetonitrile was done by standard methods. Hexadecyltrimethylammonium chloride (HTAC) was recrystallized twice from acetone–methanol and dried in vacuo.

Quantum Yields. A potassium trioxalatoferrate(III) actinometer[16] was employed to determine quantum yields for the benzophenone-sensitized photolysis at low conversions (3—4%) of the starting **1a**—**c**. A 450 W high-pressure Hg lamp was used as the light source from which 366-nm light for the photolysis was selected with Corning 0-52, Corning 7-37, and Toshiba IRA-25S glass filters. Linear calibration curves for each compound, made under the same analytical conditions, were utilized to quantify both the disappearance of **1a**—**c** and the appearance of **2** and **3a**—**c**. Quantum yields for the photolysis in HTAC micelles were determined similarly. All the quantum yields are average of more than six determinations. Quantitative GLC analysis of **4a** was done by using its calibration curve. Any attempt to separate the GLC peak of **4b** or **4c** from that of the solvent was unsuccessful so that quantum yields for these products could not be estimated.

The micelle concentration was evaluated on the basis of the equation [micelle]=([HTAC surfactant]−cmc)/N, where [HTAC surfactant]=0.20 M, critical micelle concentration, cmc=1.3×10^{-3} M, and aggregation number, N=113.[17] Both benzophenone and **1a** were stable in micellar solutions for a long period of time so that undesired dark reactions including hydrolysis of **1a** can be ignored during quantum yield determinations.

Parallel Irradiations. Ten milliliters of an acetonitrile solution of **1a**—**c** (0.020 M) and benzophenone (0.020 M) was placed in a Pyrex tube, degassed by bubbling oxygen-free nitrogen through it for 10 min, and sealed. The sealed tubes were irradiated in parallel for a given period of time on a merry-go-round apparatus (Riko Model RH400-10W) with a 400 W high-pressure Hg lamp through a Pyrex-cylindrical solution filter, which was an aqueous solution of Copper(II) sulfate pentahydrate (250 g dm^{-3}) and isolated light of wavelengths longer than 320 nm. All the irradiations were carried out in a water bath thermostated by circulating water.

References

1) C. K. Ingold, "Structure and Mechanism in Organic Chemistry," 2nd ed, Cornell University Press (1969), Chaps. 7 and 9; W. H. Saunders, Jr. and A. F. Cockerill, "Mechanisms of Elimination Reactions," Wiley-Interscience, New York (1973), Chaps. 1 and 2; A. F. Cockerill and R. G. Harrison, "The Chemistry of Double-Bonded Functional Groups," Part I, ed by S. Patai, Wiley-Interscience, New York (1977), pp. 155—189.

2) F. G. Bordwell, *Acc. Chem. Res.*, **5**, 374 (1972); W. H. Saunders, Jr., *ibid.*, **9**, 19 (1976); R. A. Bartsch and J. Závada, *Chem. Rev.*, **80**, 453 (1980).

3) S. Oae and T. Sakurai, *Bull. Chem. Soc. Jpn.*, **49**, 730 (1976).

4) R. V. Hoffman and R. J. Cadena, *J. Am. Chem. Soc.*, **99**, 8226 (1977); R. V. Hoffman and E. L. Belfoure, *ibid.*, **104**, 2183 (1982); B. R. Cho, S. K. Namgoong, and R. A. Bartsch, *J. Org. Chem.*, **51**, 1320 (1986); B. R. Cho, S. Y. Pyun, and T. R. Kim, *J. Am. Chem. Soc.*, **109**, 8041 (1987); R. V. Hoffman and J. M. Shankweiler, *ibid.*, **110**, 4019 (1988); R. V. Hoffman, R. A. Bartsch, and B. R. Cho, *Acc. Chem. Res.*, **22**, 211 (1989).

5) T. E. Boothe, J. L. Greene, Jr., and P. B. Shevlin, *J. Am. Chem. Soc.*, **98**, 951 (1976); B. Lythgoe and I. Waterhouse, *Tetrahedron Lett.*, **1977**, 4223; T. E. Boothe, J. L. Greene, Jr., P. B. Shevlin, M. R. Willcott, III, R. R. Inners, and A. Cornelis, *J. Am. Chem. Soc.*, **100**, 3874 (1978); T. E. Boothe, J. L. Greene, Jr., and P. B. Shevlin, *J. Org. Chem.*, **45**, 794 (1980); N. Ono, H. Miyake, R. Tamura, I. Hamamoto, and A. Kaji, *Chem. Lett.*, **1981**, 1139; N. Ono, A. Kamimura, and A. Kaji, *J. Org. Chem.*, **52**, 5111 (1987); M. K. Eberhardt and K. Soto, *Tetrahedron Lett.*, **28**, 3439 (1987); D. Crich and L. Quintero, *Chem. Rev.*, **89**, 1413 (1989).

6) a) T. Sakurai, H. Yamamoto, S. Yamada, and H. Inoue, *Bull. Chem. Soc. Jpn.*, **58**, 1174 (1985). b) T. Sakurai, H. Sukegawa, and H. Inoue, *ibid.*, **58**, 2875 (1985). c) T. Sakurai, K. Inomata, T. Ishikawa, H. Inoue, T. Hoshi, and J. Okubo, *ibid.*, **60**, 4099 (1987). d) T. Sakurai, T. Obana, T. Inagaki, and H. Inoue, *J. Chem. Soc., Perkin Trans. 2*, **1989**, 535. e) T. Sakurai, Y. Murakata, and H. Inoue, *ibid.*, **1990**, 499.

7) S. L. Murov, "Handbook of Photochemistry," Marcel Dekker, New York (1973), p. 3.

8) J. K. Kochi, "Free Radicals," ed by J. K. Kochi, Wiley-Interscience, New York (1973), Vol. 2, Chap. 23, pp. 698—701.

9) M. M. Martin and G. J. Gleicher, *J. Org. Chem.*, **28**, 3266 (1963); K. H. Lee, *Tetrahedron*, **24**, 4793 (1968); G. J. Gleicher, *J. Org. Chem.*, **33**, 332 (1968); H. Sakurai, A. Hosomi, and M. Kumada, *ibid.*, **35**, 993 (1970); T. P. Low and K. H. Lee, *J. Chem. Soc.B*, **1970**, 535; S. S. Friedrich, L. J. Andrews, and R. M. Keefer, *J. Org. Chem.*, **35**, 944 (1970).

10) J. A. Riddick, W. B. Bunger, and T. K. Sakano, "Organic Solvents," 4th ed, Wiley-Interscience, New York (1986), p. 135.

11) J. Chateauneuf, J. Lusztyk, and K. U. Ingold, *J. Am. Chem. Soc.*, **110**, 2877, 2886 (1988).

12) G. A. Russell, *J. Am. Chem. Soc.*, **79**, 2977 (1957); G. A. Russel, *ibid.*, **80**, 4987, 4997 (1958); N. J. Bunce, K. U. Ingold, J. P. Landers, J. Lusztyk, and J. C. Scaiano, *ibid.*, **107**, 5464

(1985); K. U. Ingold, J. Lusztyk, and K. D. Raner, *Acc. Chem. Res.*, **23**, 219 (1990).

13) N. J. Turro and B. Kraeutler, *Acc. Chem. Res.*, **13**, 369 (1980); N. J. Turro and G. C. Weed, *J. Am. Chem. Soc.*, **105**, 1861 (1983); I. R. Gould, M. B. Zimmt, N. J. Turro, B. H. Baretz, and G. F. Lehr, *ibid.*, **107**, 4607 (1985).

14) J. Emert, C. Behrens, and M. Goldenberg, *J. Am. Chem. Soc.*, **101**, 771 (1979); N. J. Turro, M. Aikawa, and A. Yekta, *ibid.*, **101**, 772 (1979).

15) L. W. Jones and C. N. Sneed, *J. Am. Chem. Soc.*, **39**, 674 (1917).

16) C. G. Hatchard and C. A. Parker, *Proc. R. Soc. London, Ser. A*, **235**, 518 (1956).

17) A. Malliaris, J. Le Moigne, J. Sturm, and R. Zana, *J. Phys. Chem.*, **89**, 2709 (1985).

Amidoselenation of Olefins Using *p*-Toluenesulfonamide as a Nitrogen Nucleophile

Akio Toshimitsu,* Takehiro Kusumoto, Tatsuo Oida, and Shigeo Tanimoto
Institute for Chemical Research, Kyoto University, Uji, Kyoto 611
(Received March 4, 1991)

The reaction of olefins, benzeneselenenyl chloride, and *p*-toluenesulfonamide in the presence of zinc(II) chloride affords *N*-[2-(phenylseleno)alkyl]-*p*-toluenesulfonamides in good to excellent yields. When combined with alkylation on the carbon atom bearing the phenylseleno group thus introduced and subsequent oxidative or reductive removal of the selenium moiety, this reaction can be utilized in the preparation of a wide range of allylic or saturated amides.

We have already reported the organoselenium-induced Ritter-type amide syntheses which resulted in the introduction of arylseleno and acylamino groups into the olefins.[1] These reactions were utilized in the preparation of allylic and saturated amides by oxidative and reductive removal of the arylseleno group thus introduced.[1b,2] For the application of selenium chemistry to organic syntheses, introduction of various nitrogen functional groups would be desirable. We now found that *p*-toluenesulfonamide, usually considered as poor nucleophile, reacts cleanly with episelenonium ion to afford *N*-[2-(phenylseleno)alkyl]-*p*-toluenesulfonamides in good to excellent yields. We also tried and succeeded in the lithiation and subsequent alkylation of the carbon atom bearing the phenylseleninyl group generated by the in situ oxidation of the phenylseleno group. In the combination of these procedures, suitable choice of an olefin and an alkylating reagent would allow the preparation of any kind of β-tosylamino-substituted selenide which is a good precursor of allylic or saturated amide by oxidative or reductive removal of phenylseleno group.

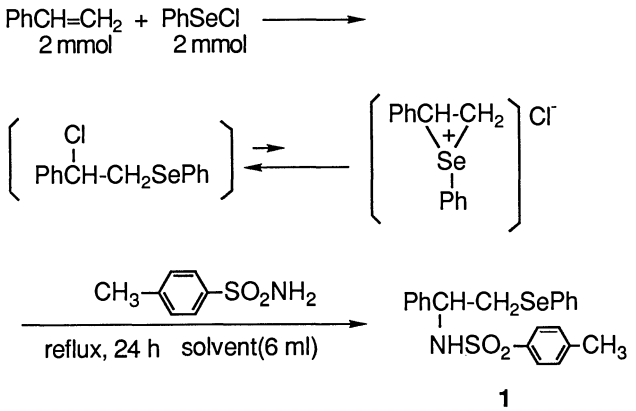

1

Scheme 1.

p-Toluenesulfonamide mmol	Solvent	1 Yield[a] %
2	CH_3CN	45
2	1,4-Dioxane	64
2	$ClCH_2CH_2Cl$	79
3	$ClCH_2CH_2Cl$	96

a) Isolated yield by colomn chromatography.

Results and Discussion

p-Toluenesulfonamide (1 equiv) was added to the adduct of benzeneselenenyl chloride to styrene (prepared in situ) and the resulting mixture was heated under reflux to afford *N*-[1-phenyl-2-(phenylseleno)ethyl]-*p*-toluenesulfonamide (**1**). The effect of solvent was examined briefly and summarized in Scheme 1 which showed that 1,2-dichloroethane was the suitable solvent for this reaction. By the increase of the amount of sulfonamide to 1.5 equivalent, the yield of **1** was improved up to 96%.

When applied to cyclohexene, the yield of β-tosylamino-substituted selenide (**2**) was 66% under the analogous conditions (Scheme 2). We tried to improve the yield by the addition of a catalyst. Typical results are summarized in Scheme 2. Among various acids ex-

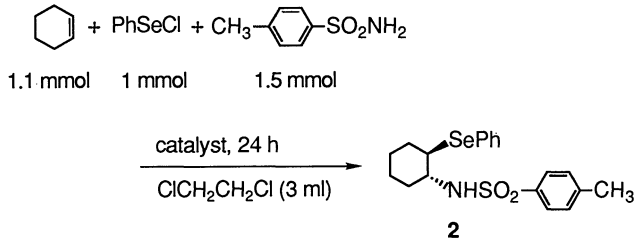

2

Scheme 2.

Catalyst	(equiv)	Temp	2, Yield[a]/%
—	—	Reflux	66
SiO_2	(0.8)	Reflux	60
50% CF_3SO_3H aq	(0.5)	R.T.	53
Dow X	(0.01)	Reflux	89
$ZnCl_2/Et_2O$	(0.2)	R.T.	85

a) Isolated yield by column chromatography.

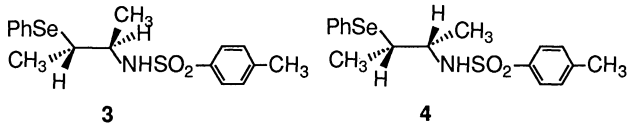

3 4

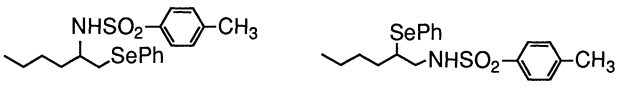

5 6

amined, zinc(II) chloride and cation-exchange resin Dow X showed the remarkable effect to produce **2** in satisfactory yields. It is interesting that trifluoromethanesulfonic acid, which was a good catalyst in the amidoselenation using nitriles as the nitrogen source (Ritter-type reaction),[1] did not facilitate the present reaction. The role of the catalyst may be ascribed to the interaction with chlorine atom in 2-chlorocyclohexyl phenyl selenide to form an episelenonium ion intermediate, but the detail is not yet clear.

To confirm the stereospecificity of this reaction, *cis*- and *trans*-2-butene were employed as substrates. In the case of *trans*-2-butene, the yield of **3** (18%) was much worse than that of **2** in the absence of catalyst. The addition of Dow X improved the yield of **3** to moderate (53%), and a satisfactory result was obtained by the use of zinc(II) chloride as catalyst (92%). In all cases, the *erythro*-isomer was found to be the sole product. On the other hand, the *threo*-isomer (**4**) was produced selectively from *cis*-2-butene in quantitative yield ($ZnCl_2$ as catalyst). This stereospecificity can be explained by trans addition of benzeneselenenyl chloride to olefins[3] and subsequent substitution of chlorine atom by *p*-toluenesulfonamide with an anchimeric assistance of phenylseleno group.

When applied to 1-hexene under the same conditions, a mixture of regioisomers (**5** and **6**) was produced in 76% total yield. The Markovnikov-type adduct (**5**) was the major product and the ratio (78:22) was similar to those in the previously reported selenium-induced Ritter-type reactions.[1] This result suggests that the nature of episelenonium ion is similar in both reactions despite the difference of the catalysts and solvents.

It is interesting that **1** was produced in an excellent yield without catalyst while the addition of catalyst was required for the formation of **2**, **3**, **4**, and **5** and **6** in good yields. This difference seems to reflect the activation energy for the formation of episelenonium ion from β-chloroalkyl phenyl selenide. It is reasonable to assume that the episelenonium ion stabilized by phenyl group can be generated more easily than those stabilized by one or two alkyl group(s).

As we succeeded in the introduction of tosylamino and phenylseleno groups into various types of olefins, our interest was focused on the lithiation and subsequent alkylation of the carbon atom bearing the phenylseleno group thus introduced. We adopted the one-pot procedure reported by Reich.[4] As summarized in Scheme 3, this procedure consists of four steps; 1) the oxidation of selenide to selenoxide (**8**) at −78 °C; 2) hydrogen abstraction by lithium diisopropyl amide (LDA) on the carbon atom bearing the seleninyl group in **8**; 3) replacement of the lithium by carbon electrophile (**9**→**10**); 4) reduction of the alkylated selenoxide to selenide (**11**) or to allow the selenoxide to eliminate to afford olefinic compounds (**12**) by raising the reaction temperature. Reaction conditions were examined using unsubstituted selenide **7**. Typical results are summarized in Table 1 using various carbon electrophiles. When the lithiation (**8**→**9**) was carried out in the absence of hexamethylphosphoric triamide (HMPA)(Run 1), the yield of **11a** was a little lower than that in Run 2. Although sodium iodide reduced the selenoxides to selenides effectively in the cases of R^3=H and CH_3 (Runs 2 and 3), it could not reduce the selenoxides **10c** and **10d** efficiently and considerable amounts of elimination products (**12c** and **12d**) were obtained in the cases of R = CH_2=CH and Ph (Runs 4 and 7). This difference seems to be due to the

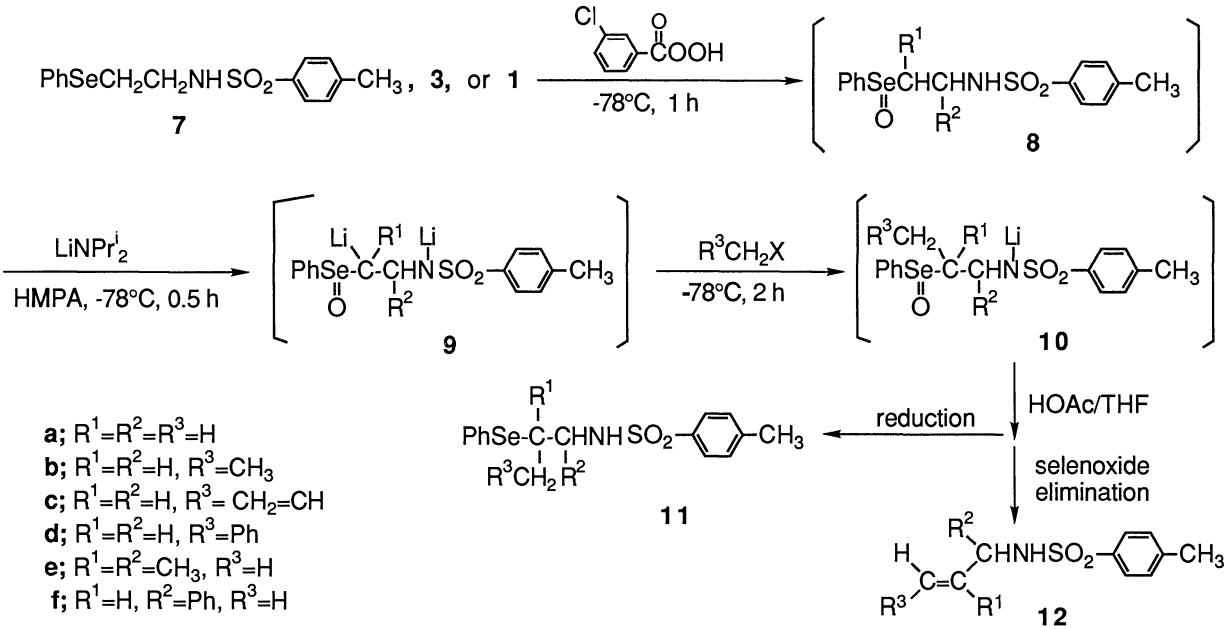

Scheme 3.

Table 1. Yields of **11** and/or **12** Using Various Electrophiles and Reducers[a]

Run	Selenide	R^3	X	mmol	Reducer	mmol	Time/h	Product(s) and yield(s) (%)[b]
1	**7**	H	I	2	NaI aq	2	0.25	**11a** (61)[c]
2	**7**	H	I	2	NaI aq	2	0.25	**11a** (75)
3	**7**	CH_3	I	2	NaI aq	2	0.25	**11b** (80)
4	**7**	CH_2=CH	Br	2	NaI aq	2	0.25	**12c** (88)
5	**7**	CH_2=CH	Br	2	$(MeO)_3P$	1.1	12	**11c** (63)+**12c** (13)
6	**7**	CH_2=CH	Br	4	$(MeO)_3P$	2.2	12	**11c** (72)+**12c** (16)[d]
7	**7**	Ph	Br	2	NaI aq	2	0.25	**11d** (13)+**12d** (58)
8	**7**	Ph	Br	4	$(MeO)_3P$	2.2	12	**11d** (65)+**12d** (35)
9	**3**	H	I	2	—	—	0.5	**12e** (62)[d]
10	**3**	H	I	4	$(MeO)_3P$	4.4	12	**12e** (55)[d]
11	**1**	H	I	2	NaI aq	2	2	**12f** (45)[d]
12	**1**	H	I	4	$(MeO)_3P$	4.4	12	**11f** (50)+**12f** (21)[d]

a) Carried out using selenide (1 mmol), *m*-CPBA (1.1 mmol), LDA (3.6 mmol), HMPA (5 mmol) in THF (5 ml) and AcOH/THF (1/10; 3.5 ml). b) Isolated yield by column chromatography. c) Carried out without HMPA. d) LDA (4.8 mmol) was used.

conjugation of the forming double bond with the vinyl or phenyl group, which would facilitate the selenoxide elimination reaction. We searched for more powerful reducers and found that selenides **11c** and **11d** were obtained as the major products by the use of trimethyl phosphite (Runs 5,6, and 8). We also studied the methylation of substituted selenides (**3** and **1**) under the analogous conditions. To our surprise, reduced selenide (**11e**) was not obtained even by the use of trimethyl phosphite as reducer in the dimethyl-substituted case (**3**) (Run 10). This seems to reflect the rate enhancement of the elimination reaction by the presence of methyl group (R^1) on the carbon atom bearing the seleninyl group.[7] The yield of **12e** was a little better when the reaction mixture was allowed to warm up to room temperature without the addition of any reducer (Run 9). The structure of the elimination product was allylic amide (**12e**) and we could not detect the regioisomer (vinylic amide) which would result from the selenoxide elimination with the hydrogen atom attached to the carbon bearing the nitrogen functional group. Similar to the acetamide case,[1b,2] selenoxide elimination "away from" the nitrogen functional group was confirmed in this sulfonamide case. Even in the phenyl-substituted case (**1**), allylic amide (**12f**) was the product of the selenoxide elimination reaction and vinylic amide, double bond in which would conjugate with phenyl ring, was not detected in the producuts.[5] In good agreement with the fact that R^1=H in **10f**, selenide (**11f**) was the major product accompanied with the elimination product (**12f**) when trimethyl phosphite was employed as reducer (Run 12).

Finally, we confirmed that reductive removal of phenylseleno group by nickel boride[6] to afford saturated compounds is applicable to our β-tosylamino-substituted selenides. Thus, the reaction of **3** with nickel chloride and sodium borohydride afforded *N*-(1-methylpropyl)-*p*-toluenesulfonamide in a satisfactory yield (Scheme 4).

As a conclusion, our methodology would allow the introduction of phenylseleno and tosylamino groups into various types of olefins with predicted regioselectivity and also allow the further introduction of various carbon electrophiles into the carbon atom bearing the phenylseleno group. Subsequent reductive or oxidative removal of the phenylseleno group will afford saturated or allylic amide selectively. Thus, the preparation of a wide range of saturated or allylic amides is now possible by the present methodology by a suitable choice of olefins and carbon electrophiles.

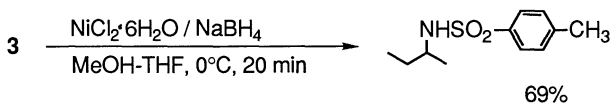

Scheme 4.

Experimental

The IR spectra were taken with a JASCO IR-810 spectrometer. ^{1}H and ^{13}C NMR spectra were recorded with JEOLCO JNM-FX-100 (100 MHz), JNM-GX-400 (400 MHz), and Varian VXR-200 (200 MHz) instruments in $CDCl_3$ using TMS as internal standard. Melting points were determined with a Shimadzu MM-2 micro melting point determination apparatus and were uncorrected. Liquid chromatographic analyses were carried out with a Waters HPLC system equipped with a 6000A solvent delivery system, a Model 440 absorbance detector (at 254 nm), and a Cosmosil packed column (4.6 mm×10 mm). GLC analyses were carried out on a Shimadzu 4CMPF apparatus using EGSS-X (15%)–Chromosorb W (3 m) column. Mass spectra were measured on a JEOL JMS-DX-300 mass spectrometer.

Materials. Tetrahydrofuran (THF) and diethyl ether were dried over benzophenone ketyl and were distilled just before use. All other organic solvents were purified before use by distillation. Zinc(II) chloride was purified by sublimation and was stored and used as saturated solution in diethyl ether (0.69 mol dm^{-3}). LDA was prepared by the addition of a solution of butyllithium in hexane (1.5 mol dm^{-3}) to a solution of diisopropylamine in THF at −78 °C and subsequent stirring at 0 °C for 30 min. Dow X (50 w×8, Na type, 20—50 mesh, Dow

Chemical Company) were treated with aqueous HCl before use. All other organic and inorganic materials were commercial products and were used without further purification.

Preparation of *N*-[2-(Phenylseleno)cyclohexyl]-*p*-toluenesulfonamide (2). Typical Procedure. Cyclohexene (0.12 ml; 1.1 mmol) was added to a solution of benzeneselenenyl chloride (97%, 0.20 g; 1.0 mmol) in 1,2-dichloroethane (3.0 ml) and the resulting colorless solution was stirred at ambient temperature for 15 min. After the addition of *p*-toluenesulfonamide (0.26 g, 1.5 mmol) and stirring for 0.5 h, a saturated solution of zinc(II) chloride in diethyl ether (0.29 ml; 0.20 mmol) was added and the resulting mixture was stirred at ambient temperature for 24 h. The reaction mixture was added to saturated aqueous $NaHCO_3$ (60 ml) and the products were extracted with dichloromethane (20 ml×3). The organic layer was washed with brine (30 ml), dried over $MgSO_4$, and evaporated in vacuo to leave a pale yellow oil. Column chromatography [silica gel (200 mesh), hexane–ethyl acetate (2:1) as eluant] of this oil afforded **2** (0.35 g, 0.85 mmol; 85%) as white crystals; mp 133—134 °C [from hexane–ethyl acetate (5:1)]. IR (KBr disc) 3270 cm^{-1}. ^1H NMR (400 MHz) δ=1.2—1.7 (m. 8H), 2.44 (s. 3H), 2.9—3.1 (m. 2H), 5.10 (br. d. 1H, J=3.4 Hz), 7.2—7.4 (m. 7H), and 7.75 (d. 2H, J=8.3 Hz). ^{13}C NMR (25 MHz) δ=21.5 (q), 23.3 (t), 25.2 (t), 32.2 (t), 32.5 (t), 47.6 (d), 55.8 (d), and phenyl signals. Found: C, 56.07; H, 5.65; N, 3.40%. Calcd for $C_{19}H_{23}NO_2SSe$: C, 55.87; H, 5.69; N, 3.43%.

Spectral and analytical data other β-tosylamino-substituted selenides are as follows.

***N*-[1-Phenyl-2-(phenylseleno)ethyl]-*p*-toluenesulfonamide (1):** White crystals, mp 92—93 °C [from hexane–ethyl acetate (5:1)]. IR (KBr disc) 3270 cm^{-1}. ^1H NMR (100 MHz) δ=2.34 (s. 3H), 3.09 (dd. 1H, J=12.7 and 6.8 Hz), 3.27 (dd, 1H, J=12.7 and 6.8 Hz), 4.36 (q. 1H, J=6.7 Hz), 5.65 (d. 1H, J=6.3 Hz), and 6.8—7.7(m. 14 H). ^{13}C NMR (25 MHz) δ=21.5 (q), 35.1 (t), 57.3 (d), and phenyl signals. Found: C, 58.64; H, 4.73; N, 3.18%. Calcd for $C_{21}H_{21}NO_2SSe$: C, 58.60; H, 4.93; N, 3.26%.

***N*-[*erythro*-1-Methyl-2-(phenylseleno)propyl]-*p*-toluenesulfonamide (3):** White crystals, mp 117—118 °C (from hexane). IR(KBr disc) 3275 cm^{-1}. ^1H NMR (400 MHz) δ=1.08 (d. 3H, J=6.8 Hz), 1.37 (d. 3H, J=7.3 Hz), 2.36 (s. 3H), 3.20 (dq. 1H, J=3.6 and 7.3 Hz), 3.4—3.5 (m. 1H), 5.33 (d. 1H, J=8.8 Hz), 7.2—7.4 (m. 7H), and 7.72 (d. 2H, J=8.3 Hz). ^{13}C NMR (25 MHz) δ=18.3 (q), 19.5 (q), 21.4 (q), 47.7 (d), 53.8 (d), and phenyl signals. Found: C, 53.16; H, 5.43; N, 3.57%. Calcd for $C_{17}H_{21}NO_2SSe$: C, 53.39; H, 5.55; N, 3.66%.

***N*-[*threo*-1-Methyl-2-(phenylseleno)propyl]-*p*-toluenesulfonamide (4):** White crystals, mp 123—124 °C (from hexane). IR (KBr disc) 3260 cm^{-1}. ^1H NMR (400 MHz) δ=1.04 (d. 3H, J=6.8 Hz), 1.30 (d. 3H, J=6.8 Hz). 2.39 (s. 3H), 3.3—3.5 (m. 2H), 5.26 (d. 1H, J=7.3 Hz), 7.2—7.5 (m. 7H), and 7.64 (d. 2H, J=8.3 Hz). ^{13}C NMR (25 MHz) δ=15.9 (q), 16.8 (q), 21.4 (q), 44.0 (d), 53.2 (d), and phenyl signals. Found: C. 53.35; H, 5.56; N, 3.68%. Calcd for $C_{17}H_{21}NO_2SSe$: C, 53.39; N, 5.55; N, 3.66%.

***N*-[1-[(Phenylseleno)methyl]pentyl]-*p*-toluenesulfonamide (5) and *N*-[2-(phenylseleno)hexyl]-*p*-toluenesulfonamide (6)** (identified as a mixture, 78:22 by ^{13}C NMR): IR (liq. film) 3280 cm^{-1}. ^1H NMR (400 MHz) δ=0.75 (t. 3H, J=7.1 Hz; **5**), 0.86 (t. 3H, J=7.1 Hz; **6**), 1.0—1.6 (m. 6H), 2.40 (s. 3H; **5**), 2.44 (s. 3H; **6**), 2.77 (dd. 1H, J=12.7 and 6.4 Hz; **5**), 2.91 (ddd. 1H, J=13.9, 8.7, and 5.8 Hz; **6**), 3.0—3.1 (m. 2H; **6**), 3.10 (dd. 1H, J=12.7 and 3.9 Hz; **5**), 3.3—3.4 (m. 1H; **5**), 4.74 (d. 1H, J=8.3 Hz; **5**), 5.03 (br. t. 1H, J=5.8 Hz; **6**), 7.1—7.5 (m. 7H), 7.62 (d. 2H, J=8.3 Hz; **5**), and 7.69 (d. 2H, J=8.3 Hz; **6**). ^{13}C NMR (25 MHz) δ (**5**)=13.7 (q), 21.4 (q), 22.1 (t), 27.3 (t), 29.6 (t), 33.8 (t), 53.5 (d), and phenyl signals: δ (**6**)=13.7 (q), 21.4 (q), 22.1 (t), 22.2 (t), 32.0 (t), 45.2 (d), 46.5 (t), and phenyl signals. Found: C, 55.57; H, 6.23; N, 3.30%. Calcd for $C_{19}H_{25}NO_2SSe$: C, 55.59; H, 6.15; N, 3.41%.

***N*-[2-(Phenylseleno)ethyl]-*p*-toluenesulfonamide (7):** White crystals, mp 59—60 °C (from hexane). IR (KBr disc) 3270 cm^{-1}. ^1H NMR (200 MHz) δ=2.42 (s. 3H), 2.90 (t. 2H, J=6.8 Hz), 3.14 (q. 2H, J=6.3 Hz), 4.98 (t, 1H, J=5.9 Hz), 7.1—7.4 (m. 7H), and 7.69 (d. 2H, J=8.2 Hz). ^{13}C NMR (25 MHz) δ=21.4 (q), 27.0 (t), 42.5 (t), and phenyl signals. Found: C, 50.77; H, 4.88; N, 3.89%. Calcd for $C_{15}H_{17}NO_2SSe$: C, 50.84; H, 4.85; N, 3.95%.

Methylation of β-Position on *N*-Ethyl Group of 7. General Procedure. To a solution of **7** (0.35 g, 1.0 mmol) in THF (2.0 ml) was added a solution of *m*-chloroperbenzoic acid (*m*-CPBA) (80%; 0.24 g, 1.1 mmol) in THF (1.0 ml) under nitrogen atmosphere at −78 °C and the resulting mixture was stirred at the same temperature for 1 h. A solution of LDA (3.6 mmol) in THF (2.0 ml) and then HMPA (0.87 ml, 5.0 mmol) were added slowly to the mixture and the resulting mixture was stirred at −78 °C for 0.5 h. Methyl iodide (98%; 0.13 ml, 2.0 mmol) was added and the reaction mixture was further stirred at −78 °C for 2 h. Afterward it was not necessary to keep the reaction under nitrogen atmosphere. A mixture of acetic acid and THF (1:10, 3.5 ml) and then sodium iodide (0.30 g, 2.0 mmol) in water (1.0 ml) were added and the resulting mixture was stirred vigorously at ambient temperature for 0.25 h. Saturated aqueous $Na_2S_2O_3$ was added in small portions until pale yellow and the reaction mixture was further stirred at the same temperature for 0.25 h. The reaction mixture was added to saturated aqueous $Na_2S_2O_3$ (10 ml) and the products were extracted with chloroform (15 ml×3). The organic layer was washed with saturated aqueous $NaHCO_3$ and brine, dried ($MgSO_4$), and evaporated in vacuo to leave a brown oil. Column chromatography [silica gel (200 mesh), hexane–ethyl acetate (3:1) as eluant] afforded *N*-[2-(phenylseleno)propyl]-*p*-toluenesulfonamide (**11a**)(0.275 g, 0.75 mmol; 75%) as a brown oil. IR (liq. film) 3280 cm^{-1}. ^1H NMR (400 MHz) δ=1.33 (d. 3H, J=6.8 Hz), 2.40 (s. 3H), 2.96 (dt. 1H, J=19.0 and 6.3 Hz), 2.99 (dt. 1H, J=19.0 and 6.3 Hz), 3.23 (sextet, 1H, J=6.7 Hz), 5.37 (t. 1H, J=6.4 Hz), 7.1—7.4(m. 7H), and 7.69(d. 2H, J=8.3 Hz). ^{13}C NMR(25 MHz) δ=19.1 (q), 21.5 (q), 38.3 (d), 48.2 (t), and phenyl signals. Found: C, 52.13; H, 5.24; N, 4.10%. Calcd for $C_{16}H_{19}NO_2SSe$: C, 52.16; H, 5.21; N, 3.80%.

Spectral and analytical data of other alkylated products are as follows.

***N*-[2-(Phenylseleno)butyl]-*p*-toluenesulfonamide (11b):** Brown oil. IR (liq. film) 3280 cm^{-1}. ^1H NMR(400 MHz) δ=0.98 (t. 3H, J=7.3 Hz), 1.53 (d.quint. 1H, J=13.7 and 7.3 Hz), 1.66 (d.quint. 1H, J=13.7 and 7.3 Hz), 2.40 (s. 3H), 2.9—3.1 (m. 3H), 5.53 (br. t. 1H, J=5.9 Hz), 7.1—7.4 (m. 7H), and 7.69 (d. 2H, J=8.3 Hz). ^{13}C NMR (25 MHz) δ=12.2 (q), 21.5 (q), 25.6 (t), 46.2 (d), 46.2 (t), and phenyl signals. Found: C, 53.57; H, 5.58; N, 3.79%. Calcd for $C_{17}H_{21}NO_2SSe$: C, 53.39; H, 5.55; N, 3.66%.

***N*-[2-(Phenylseleno)-4-pentenyl]-*p*-toluenesulfonamide (11c):** Pale yellow oil. IR(liq. film) 3290 cm^{-1}. ^1H NMR (400 MHz) δ=2.37 (t. 2H, J=6.8 Hz), 2.42 (s. 3H), 2.95 (quint.

1H, J=6.8 Hz), 3.07 (dt. 1H, J=19.3 and 6.8 Hz), 3.14 (dt. 1H, J=19.3 and 6.8 Hz), 5.0—5.1 (m, 2H), 5.15 (t. 1H, J=6.1 Hz), 5.76 (ddt. 1H, J=17.1, 10.3, and 6.8 Hz), 7.1—7.4 (m. 7H), and 7.68 (d. 2H, J=8.3 Hz). ^{13}C NMR (25 MHz), δ=21.4 (q), 36.5 (t), 43.7 (d), 46.0 (t), 117.7 (t), 134.7 (d), and phenyl signals. Found: C, 54.39; H, 5.37; N, 3.45%. Calcd for $C_{18}H_{21}NO_2SSe$: C, 54.81; H, 5.38; N, 3.55%.

***N*-[2-(phenylseleno)-3-phenylpropyl]-*p*-toluenesulfonamide (11d):** Pale yellow oil. IR (liq. film) 3280 cm^{-1}. ^{1}H NMR (400 MHz) δ=2.40 (s. 3H), 2.88 (dd. 1H, J=14.2 and 7.8 Hz), 2.93 (dd. 1H, J=14.2 and 7.3 Hz), 2.97 (dt. 1H, J=19.4 and 6.4 Hz), 3.01 (dt. 1H, J=19.4 and 6.4 Hz), 3.31 (quint. 1H, J=6.6 Hz), 5.17 (t. 1H, J=6.1 Hz), 7.0—7.4 (m. 12H), and 7.60 (d. 2H, J=8.3 Hz). ^{13}C NMR (25 MHz) δ=21.3 (q), 38.7 (t), 45.7 (d), 45.7 (t), and phenyl signals. High-resolution mass spectrum, M$^+$. Found: m/z 445.06217. Calcd for $C_{22}H_{23}NO_2SSe$: M, 445.06210.

***N*-[1-Phenyl-2-(phenylseleno)propyl]-*p*-toluenesulfonamide (11f)** (identified as a mixture of *threo* and *erythro*[8] isomers, *threo*:*erythro*=80:20 by ^{13}C NMR): White solid. IR (KBr disc) 3270 cm^{-1}. ^{1}H NMR (200 MHz) δ=1.20 (d. 3H, J=7.2 Hz; *threo*), 1.32 (d. 3H, J=7.0 Hz; *erythro*), 2.34 (s. 3H), 3.39 (quint. 1H, J=7.2 Hz), 4.21 (dd. 1H, J=7.5 and 5.1 Hz; *threo*), 4.44 (dd. 1H, J=7.2 and 4.3 Hz; *erythro*), 5.50 (d. 1H, J=4.3 Hz; *erythro*), 5.74 (d. 1H, J=5.1 Hz; *threo*), and 7.0—7.5 (m. 14H). ^{13}C NMR (25 MHz) (*threo*) δ=19.0 (q), 21.3 (q), 44.8 (d), 62.2 (d), and phenyl signals. (*erythro*) δ=18.1 (q), 21.3 (q), 46.2 (d), 61.7 (d), and phenyl signnals. Found: C, 59.73; H, 5.24; N, 3.18%. Calcd for $C_{22}H_{23}NO_2SSe$: C, 59.44; H, 5.23; N, 3.15%.

***N*-(trans-2,4-pentadienyl)-*p*-toluenesulfonamide (12c):** White crystals, mp 89—90 °C [from hexane–ethyl acetate (5:1)]. IR (KBr disc) 3270 cm^{-1}. ^{1}H NMR (400 MHz) δ=2.42 (s. 3H), 3.60 (t. 2H, J=6.1 Hz), 4.93 (t. 1H, J=6.1 Hz), 5.06 (d. 1H, J=10.3 Hz), 5.13 (d. 1H, J=16.6 Hz), 5.53 (dt. 1H, J=15.0 and 6.5 Hz), 6.09 (dd. 1H, J=15.0 and 11.0 Hz), 6.21 (dt. 1H, J=16.6 and 10.3 Hz), 7.30 (d. 2H, J=8.3 Hz), and 7.76 (d. 2H, J=8.3 Hz). ^{13}C NMR (25 MHz) δ=21.5 (q), 44.8 (t), 117.9 (t), 128.1 (d), 133.4 (d), 135.8 (d), and phenyl signals. Found: C, 60.71; H, 6.43; N, 5.82%. Calcd for $C_{12}H_{15}NO_2SSe$: C, 60.72; H, 6.38; N, 5.90%.

***N*-(trans-3-Phenyl-2-propenyl)-*p*-toluenesulfonamide (12d):** White crystals, mp 106—107 °C [from hexane–ethyl acetate (5:1)] (lit,[9] mp 110 °C). IR (KBr disc) 3290 cm^{-1}. ^{1}H NMR (100 MHz) δ=2.34 (s. 3H), 3.70 (t. 2H, J=6.1 Hz), 5.28 (t. 1H, J=6.1 Hz), 5.94 (dt. 1H, J=15.9 and 6.1 Hz), 6.39 (d. 1H, J=15.9 Hz), 6.8—7.4 (m. 7H), and 7.77 (d. 2H, J=8.3 Hz). ^{13}C NMR (25 MHz) δ=21.4 (q), 45.4 (t), 124.3 (d), 132.8 (d), and phenyl signals.

***N*-(1,2-Dimethyl-2-propenyl)-*p*-toluenesulfonamide (12e):** Pale yellow oil. IR(liq. film) 3280 cm^{-1}. ^{1}H NMR (400 MHz) δ=1.15 (d. 3H, J=7.3 Hz), 1.57 (s. 3H), 2.41 (s. 3H), 3.83 (quint. 1H, J=7.3 Hz), 4.68 (s. 1H), 4.80 (s. 1H), 5.40 (d. 1H, J=7.3 Hz), 7.27 (d. 2H, J=8.3 Hz), and 7.78 (d. 2H, J=8.3 Hz). ^{13}C NMR (25 MHz) δ=18.1 (q), 20.5 (q), 21.5 (q), 54.8 (d), 111.9 (t), 145.1 (s), and phenyl signals. High-resolution mass spectrum, M$^+$. Found: m/z 239.09506. Calcd for $C_{12}H_{17}NO_2S$: M, 239.09535.

***N*-(1-Phenyl-2-propenyl)-*p*-toluenesulfonamide (12f):** Pale yellow oil (lit,[9] mp 103 °C). IR (liq. film) 3290 cm^{-1}. ^{1}H NMR (200 MHz) δ=2.43 (s. 3H), 4.93 (t. 1H, J=6.7 Hz), 5.0—5.2 (m. 3H), 5.86 (ddd. 1H, J=16.6, 10.8, and 6.7 Hz), 7.0—7.4 (m. 7H), and 7.66 (d. 2H, J=8.2 Hz). ^{13}C NMR (25 MHz) δ=21.4 (q), 59.8 (d), 116.6 (t), 137.1 (d), and phenyl signals.

The authors are grateful to the Ministry of Education, Science and Culture for the financial support to this work [Grant-in-Aid for Scientific Research (C) 01550648].

References

1) a) A. Toshimitsu, T. Aoai, S. Uemura, and M. Okano, *J. Chem. Soc., Chem. Commun.*, **1980**, 1041; b) A. Toshimitsu, T. Aoai, H. Owada, S. Uemura, and M. Okano, *J. Org. Chem.*, **46**, 4727 (1981); c) A. Toshimitsu, G. Hayashi, K. Terao, and S. Uemura, *J. Chem. Soc., Perkin Trans. 1*, **1986**, 343; d) A. Toshimitsu, G. Hayashi, K. Terao, and S. Uemura, *ibid.*, **1988**, 2113.

2) A. Toshimitsu, H. Owada, T. Aoai, S. Uemura, and M. Okano, *J. Chem. Soc., Chem. Commun.*, **1981**, 546.

3) D. Liotta and G. Zima, *Tetrahedron Lett.*, **1978**, 4977.

4) H. J. Reich, S. K. Shah, and F. Chow, *J. Am. Chem. Soc.*, **101**, 6648 (1979).

5) In the cases of *N*-acylpiperidine and δ-lactam, the course of selenoxide elimination was changed by the presence of phenyl group to afford vinylic amide derivatives: A. Toshimitsu, K. Terao, and S. Uemura, *J. Org. Chem.*, **51**, 1724 (1986); A. Toshimitsu, K. Terao, and S. Uemura, *ibid.*, **52**, 2018 (1987).

6) T. G. Back, V. I. Birss, M. Edwards, and M. V. Krishna, *J. Org. Chem.*, **53**, 3815 (1988).

7) H. J. Reich, "Oxidation in Organic Chemistry," ed by W. S. Trahanovsky, Academic Press, New York (1978), Part C, pp. 1—130.

8) Authentic sample of the *erythro* isomer was prepared by the amidoselenation of *trans*-1-phenylpropene.

9) P. A. Briscoe, F. Challenger, and P. S. Duckworth, *J. Chem. Soc.*, **1956**, 1755.

1-Chloroalkyl *p*-Tolyl Sulfoxides as Acetylide Anion Equivalent: A Novel Synthesis Including Asymmetric Synthesis of Propargylic Alcohols from Carbonyl Compounds

Tsuyoshi SATOH, Yasumasa HAYASHI, and Koji YAMAKAWA*
Faculty of Pharmaceutical Sciences, Science University of Tokyo,
Ichigaya-funagawara-machi, Shinjuku-ku, Tokyo 162
(Received March 7, 1991)

Addition of the carbanion of 1-chloroalkyl *p*-tolyl sulfoxide to carbonyl compounds gave the adducts, which were heated in refluxing toluene or xylene to give vinyl chlorides in high overall yield. Dehydrochlorination of the vinyl chlorides with excess *n*-BuLi afforded propargylic alcohols in high yields. Asymmetric synthesis of both enantiomers of the propargylic alcohols was realized using optically active 1-chloroalkyl *p*-tolyl sulfoxide and aldehyde.

Acetylenes are very important compounds in synthetic organic chemistry.[1] In the acetylenes, propargylic alcohols, including optically active ones, are now recognized to be quite useful building blocks in natural product synthesis.[2] Many methods for synthesizing propargylic alcohols have been reported; however, in view of the usefulness of propargylic alcohols in organic synthesis, new methods are eagerly sought.

We recently reported some new synthetic methods using 1-chloroalkyl *p*-tolyl sulfoxides **1**.[3] For example, ozonolysis of vinyl chlorides **3**, which were synthesized from **1** and carbonyl compounds **2** through chloro alcohols, gave α-hydroxy carboxylic acids and their derivatives **4** in high yields.[4] In this method **1** acted as a hydroxycarbonyl-, alkoxycarbonyl-, and formamide anion equivalent (Scheme 1). In continuation of our study concerning the use of 1-chloroalkyl aryl sulfoxides in organic synthesis, we report here a novel synthesis of propargylic alcohols (**5**, **7**, and **8**) form **1** and carbonyl compounds through vinyl chloride **3**. In this method **1** acts as an acetylide anion and acetylide dianion equivalent.

Results and Discussion

A Synthesis of Propargylic Alcohols from Carbonyl Compounds and 1-Chloroalkyl *p*-Tolyl Sulfoxides. The synthesis of 1-(1-butynyl)-1-cycloheptanol **5a** from cycloheptanone and 1-chlorobutyl *p*-tolyl sulfoxide (**1**: R=Et) as acetylide anion equivalent is reported as a representative example. 1-Chlorobutyl *p*-tolyl sulfoxide, easily prepared from butyl *p*-tolyl sulfide,[5] was treated with lithium diisopropylamide (LDA) in THF at

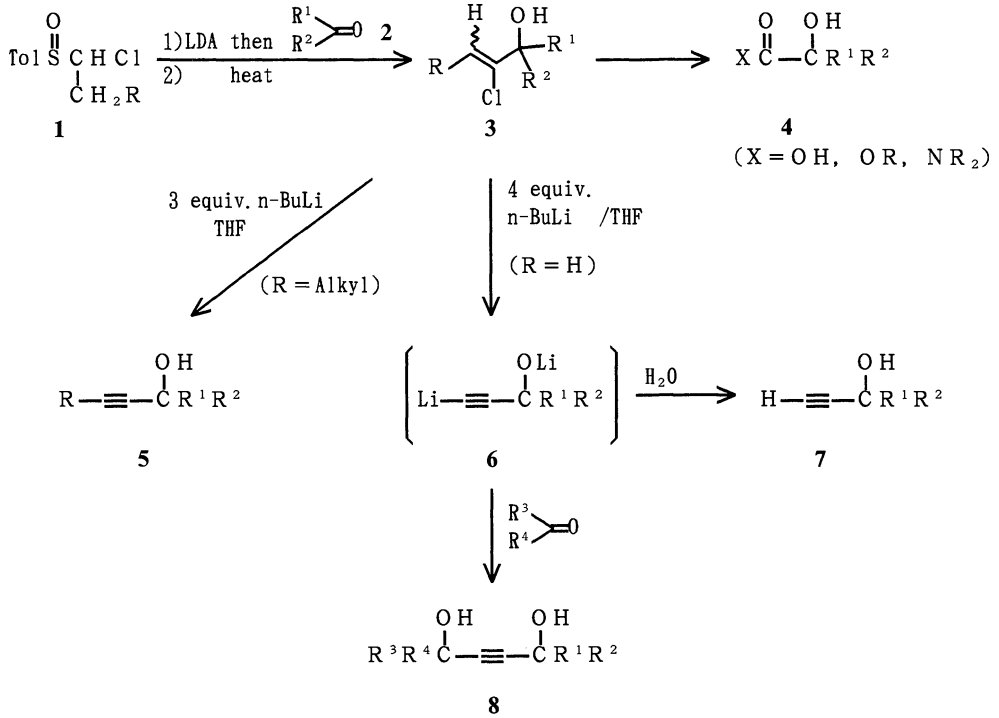

Scheme 1.

Table 1. Synthesis of Propargylic Alcohols **5** and **7** from **1** and Carbonyl Compound **2** through Vinyl Chlorides **3**

	1 R	**2** R^1	**2** R^2	**3** (Yield/%)[a]	*n*-BuLi (equiv)	Conditions[b]	**5** or **7** (Yield/%)	
a	Et	$-(CH_2)_6-$		**3a** (77)	(3)	A	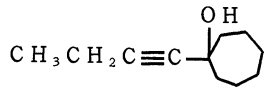 **5a**	(92)
b	Et	$CH_3(CH_2)_8$	H	**3b-L** (34)[c]	(3)	A	$CH_3CH_2C{\equiv}C-CH(CH_2)_8CH_3$ (OH) **5b**	(99)
				3b-P (46)[c]	(3)	B		(51)
c	H	$-(CH_2)_2CH(CH_2)_2-$		**3c** (80)	(4)	A	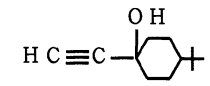 **7c**	(85)
d	H	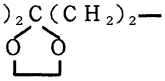		**3d** (92)	(4)	C	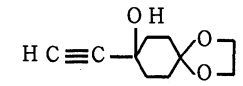 **7d**	(95)
e	H	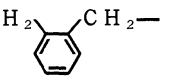		**3e** (90)	(4)	D	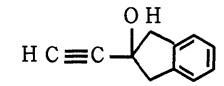 **7e**	(92)
f	H	$CH_3(CH_2)_8$	H	**3f** (91)	(4)	E	$HC{\equiv}CCH(CH_2)_8CH_3$ (OH) **7f**	(93)

a) Two-step overall yield from **1** and carbonyl compound **2** through chloro alcohol. Isolated yield. b) Conditions: A, −35 to 0 °C (2 h) then 0 °C (0.5 h); B, −35 °C to room temperature (4 h) then at room temperature (0.75 h); C, −45 to −35 °C (0.7 h); D, −50 to −40 °C (0.7 h); E, −40 to −10 °C (2 h). c) L: less polar isomer, P: more polar isomer.

−60 °C followed by addition of cycloheptanone to give the adduct, which was then heated in refluxing toluene for 5 min to afford cleanly the vinyl chloride **3a** (R=Et, R^1=R^2=$-(CH_2)_6-$) in 77% overall yield.

As vinylic hydrogen is relatively more acidic than that of saturated carbon, it might be expected that on treatment of vinyl chloride **3** with a strong base elimination of hydrogen chloride takes place to afford propargylic alcohol **5**.[6] The vinyl chloride **3a** was treated with a variety of bases (such as LDA, *t*-BuOK, *n*-BuLi etc.) under various conditions, and three-equivalents of *n*-BuLi in THF at low temperature (below 0 °C) was found to be the best conditions to give **5a** (Table 1) in 92% yield. Interestingly, treatment of **3a** with *n*-BuLi in hexane gave a quite sluggish and incomplete reaction even at room temperature.

Representative examples of the synthesis of propargylic alcohols **5** and **7** from carbonyl compounds are summarized in Table 1. As shown in the Table 1, various kinds of propargylic alcohols are synthesized in good overall yield. In the step of the elimination of hydrogen chloride, some difference in the reaction was found between the stereoisomers (Entry b). Generally speaking, the elimination giving monosubstituted acetylenes (**7c**–**7f**) is more reactive than that giving disubstituted acetylenes (**5a**, **5b**).

The elimination of hydrogen chloride from vinyl chloride (**3**: R=H) derived from 1-chloroethyl *p*-tolyl sulfoxide (**1**: R=H) gave propargylic alcohol dianion **6**. This dianion **6** was trapped with carbonyl compounds at −15 °C to afford acetylenic diol **8** in good yields. As shown in Table 2, this reaction gave almost quantitative yields with aldehydes; however, the yields was 72% with cyclohexanone because of its high enolizability. It is worth noting that 1-chloroethyl *p*-tolyl sulfoxide (**1**: R=H) acts as dianion of acetylene.

Asymmetric Synthesis of Both Enantiomers of Propargylic Alcohols. Asymmetric synthesis is one of the most important subjects in modern organic synthesis. We recently reported some new methods for synthesis of optically active 1-chloroalkyl *p*-tolyl sulfoxide.[3a,3b,4] Here we describe an asymmetric synthesis of both enantiomers of propargylic alcohols (**12a** and **12b**) using the above-mentioned method from (−)-**9** (Scheme 2).[7]

Treatment of (−)-1-chloro-2-phenylethyl *p*-tolyl sulfoxide **9** (over 98% ee) with LDA in THF at −60 °C followed by addition of propanal afforded two adducts, which were easily separated by silica-gel column chromatography to give the less polar adduct **10a** (41%) and the more polar adduct **10b** (53%). The absolute stereo-

Table 2. Synthesis of Acetylenic Diol **8** from Vinyl Chloride **3**

Entry	Vinyl chloride **3**	Carbonyl compound	**8** (Yield/%)
1	**3c**		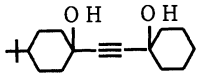 **8a** (72)
2		$CH_3(CH_2)_8CHO$	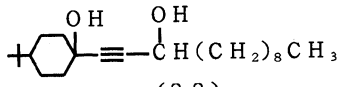 **8b** (88)
3		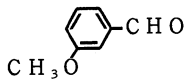	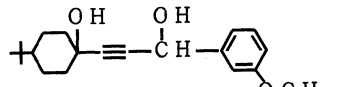 **8c** (98)
4	**3f**	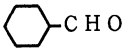	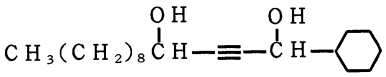 **8d** (91)
5		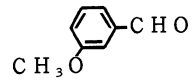	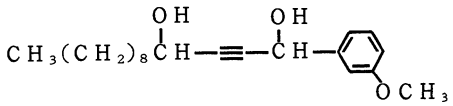 **8e** (96)

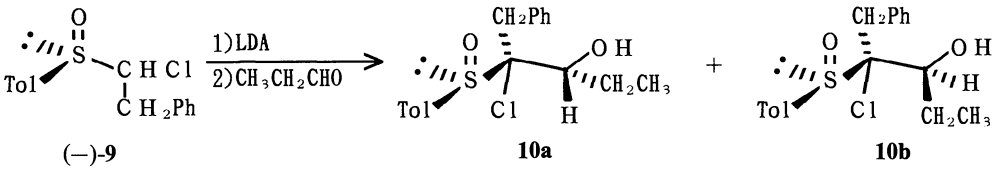

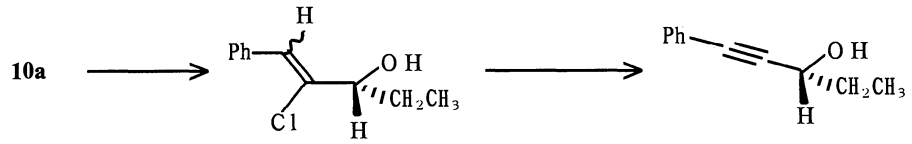

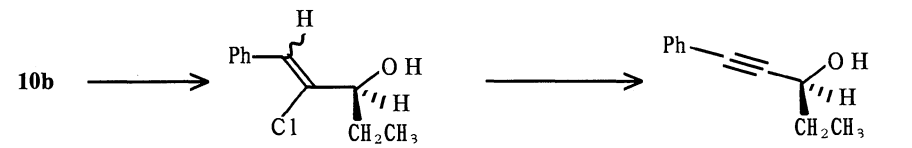

Scheme 2.

chemistry of **10a** and **10b** were presumed as depicted in Scheme 2 based on the experiences gained from the study with α,β-epoxy sulfoxides.[3a] Thermal elimination of the sulfinyl group in **10a** and **10b** in refluxing toluene under N_2 for 20 min afforded cleanly the desired vinyl chlorides **11a** (single isomer) and **11b** (*E*/*Z*-mixture), both in 99% yield. Elimination of hydrogen chloride from **11b** was carried out with three equivalents of *n*-

BuLi at −35 to 0 °C for 2 h to afford (*S*)-(−)-1-phenyl-1-pentyn-3-ol **12b** in 92% yield. The specific rotation of (−)-**12b** ($[\alpha]_D^{24}$ −20.0° (*c* 2.6, Et_2O) was consistent with that of the reported value ($[\alpha]_D^{25}$ −13.7° (*c* 2.0, Et_2O); 70% ee).[7g] Similar treatment of **11a** with *n*-BuLi gave (*R*)-(+)-**12a** ($[\alpha]_D^{26}$ +19.3° (*c* 2.3, Et_2O)) in 96% yield.

Unfortunately, as the addition of the carbanion of 1-chloroethyl *p*-tolyl sulfoxide with aldehyde gave an inseparable diastereomeric mixture of the adducts, this method could not be used for the asymmetric synthesis of the propargylic alcohols of type **7**. However, because of its overall simplicity and high overall yields, we believe that the presented method will prove valuable in the synthesis of propargylic alcohols in racemic and optically active form.

Experimental

All melting points are uncorrected. ^1H NMR spectra were measured in a $CDCl_3$ solution with a JEOL FX-100 spectrometer. Electron-impact mass spectra (MS) were obtained at 70 eV by direct insertion. Silica gel BW-127 ZH (Fuji-Devison) containing 2% fluorescence reagent 254 and quartz column were used for column chromatography, and products having UV absorption were detected by UV irradiation. In experiments requiring dry solvents, THF was distilled from diphenylketyl; toluene, xylene, and diisopropylamine were dried over CaH_2 and distilled.

1-(1-Chloro-1-butenyl)-1-cycloheptanol (3a). A solution of 1-chlorobutyl *p*-tolyl sulfoxide **1** (R=CH_2CH_3; 1.15 g; 5 mmol) in 2 ml of THF was added dropwise to a solution of LDA (6 mmol) in 6 ml of THF under N_2 at −60 °C with strring. The reaction mixture was stirred at −60 °C for 10 min, then cycloheptanone (6 mmol) was added to the mixture. The reaction mixture was stirred for 10 min, then the reaction was quenched with sat. aqueous NH_4Cl. The whole was extracted with ether–benzene and the organic layer was washed once with sat. aqueous NH_4Cl. The solution was dried over $MgSO_4$ and then the solvent was evaporated under vacuum to give the residue, which was purified by silica-gel column chromatography to afford 1.51 g (88%) of chloro alcohol.

A solution of the chloro alcohol (1.46 g; 4.26 mmol) in 15 ml of toluene was refluxed under N_2 for 5 min. The toluene was evaporated under vacuum to leave a residue, which was purified by flash chromatography (hexane:AcOEt=10:1) to give 0.75 g (87%) of **3a** (single isomer; *E*/*Z* not determined) as a colorless oil. Ir (neat) 3380 (OH), 1645 (C=C) cm^{-1}; ^1H NMR δ=1.01 (3H, t, *J*=7 Hz), 1.2–2.2 (13H, m), 2.17 (2H, quintet, *J*=7 Hz), 5.79 (1H, t, *J*=7 Hz); MS *m*/*z* (%) 202 (M^+, 26), 173 ($[M-C_2H_5]^+$, 84), 145 (100). Found: *m*/*z* 202.1131. Calcd for $C_{11}H_{19}ClO$: M, 202.1124.

4-Chloro-3-tetradecen-5-ol (3b). Addition of the carbanion of 1-chlorobutyl *p*-tolyl sulfoxide to decanal gave less polar adduct and more polar adduct; these were easily separated by silica-gel column chromatography. The less polar adduct: 42% yield; mp 66–67 °C (AcOEt–Hexane); IR (KBr) 3470 cm^{-1}; ^1H NMR δ=3.80 (1H, t, *J*=5 Hz); Found: C, 65.14; H, 9.42; Cl, 9.19; S, 8.08%. Calcd for $C_{21}H_{35}ClO_2S$: C, 65.12; H, 9.12; Cl, 9.16; S, 8.28%. The more polar adduct: 51% yield; colorless oil; IR (neat) 3400 cm^{-1}; ^1H NMR δ=3.76 (1H, dd, *J*=8, 2 Hz). Thermal elimination of the sulfinyl group of the less polar adduct in refluxing xylene for 15 min gave **3b-L** as a colorless oil in 80% yield (*E*/*Z*-mixture; ratio about 10:1). IR (neat) 3350 (OH), 1655 (C=C) cm^{-1}; ^1H NMR δ=0.87 (3H, t, *J*=7 Hz), 1.01 (3H, t, *J*=7 Hz), 1.1–1.9 (16H, m), 2.21 (2H, quintet, *J*=7 Hz), 4.11 (0.9H, t, *J*=7 Hz), 4.54 (0.1H, t, *J*=7 Hz), 5.71 (1H, t, *J*=7 Hz); MS *m*/*z* (%) 246 (M^+, 2), 211 ($[M-Cl]^+$, 8), 119 (100). Found: *m*/*z* 246.1751. Calcd for $C_{14}H_{27}ClO$: M, 246.1749. In a similar way, the more polar adduct gave **3b-P** as a colorless oil in 96% yield (*E*/*Z*-mixture; ratio about 2:1). IR (neat) 3350 (OH), 1655 (C=C) cm^{-1}; ^1H NMR δ=4.11 (2/3H, t, *J*=7 Hz), 4.54 (1/3H, t, *J*=7 Hz), 5.70 (1/3H, t, *J*=7 Hz), 5.72 (2/3H, t, *J*=7 Hz); MS and high resolution mass spectral data are quite similar to those of **3b-L**.

1-(1-Chlorovinyl)-4-*t*-butyl-1-cyclohexanol (3c). Addition of the carbanion of 1-chloroethyl *p*-tolyl sulfoxide to 4-*t*-butylcyclohexanone gave the adduct in 83% yield as colorless crystals; mp 215–216 °C (AcOEt–hexane). IR (KBr) 3360 (OH) cm^{-1}; ^1H NMR δ=0.89 (9H, s), 1.44, 2.43 (each 3H, s). Found: C, 63.56; H, 8.47; Cl, 10.13, S, 8.87%. Calcd for $C_{19}H_{29}ClO_2S$: C, 63.93; H, 8.19; Cl, 9.93; S, 8.98%. Thermal elimination of the sulfinyl group of this adduct in refluxing xylene for 20 min gave **3c** as a colorless crystals, mp 51–52 °C (AcOEt–hexane). IR (KBr) 3375 (OH), 1630 (C=C) cm^{-1}; ^1H NMR δ=0.89 (9H, s), 1.0–1.9 (10H, m), 5.24, 5.46 (each 1H, d, *J*=2 Hz); MS *m*/*z* (%) 216 (M^+, 1), 181 (5), 142 (12), 107 (20), 57 (100). Found: *m*/*z* 216.1288. Calcd for $C_{12}H_{21}ClO$: M, 216.1279.

Vinyl Chloride (3d, 3e, 3f). These vinyl chlorides were reported in the Ref. 8.

1-(1-Butynyl)-1-cycloheptanol (5a). To a solution of vinyl chloride **3a** (61 mg; 0.3 mmol) in 3 ml of dry THF under N_2 was added *n*-BuLi (0.9 mmol) dropwise with stirring at −35 °C. The reaction mixture was stirred and allowed to warm to 0 °C in 2 h, and finally stirred at 0 °C for 30 min. The reaction was quenched with sat. aqueous NH_4Cl. The whole was extracted with ether–benzene and the organic layer was dried over $MgSO_4$. The product was purified by silica-gel column chromatography to afford 46 mg (92%) of **5a** as a colorless oil. IR (neat) 3370 (OH), 2230 (C≡C) cm^{-1}; ^1H NMR δ=1.13 (3H, t, *J*=7 Hz), 1.3–2.1 (13H, m), 2.21 (2H, q, *J*=7 Hz); MS *m*/*z* (%) 166 (M^+, 3), 151 ($[M-CH_3]^+$, 4), 137 ($[M-C_2H_5]^+$, 42), 109 (100). Found: *m*/*z* 166.1357. Calcd for $C_{11}H_{18}O$: M, 166.1357.

Propargylic Alcohol (5b, 7c—7f). These propargylic alcohols were synthesized from corresponding vinyl chlorides with three or four equivalents of *n*-BuLi in a similar way as described above for the synthesis of **5a**. The conditions and the yields are summarized in Table 1.

3-Tetradecyn-5-ol (5b). Colorless oil; IR (neat) 3340 (OH), 2225 (C≡C) cm^{-1}; ^1H NMR δ=0.88 (3H, t, *J*=7 Hz), 1.13 (3H, t, *J*=7 Hz), 1.2–1.8 (13H, m), 2.22 (2H, dq, *J*=7, 2 Hz), 4.31 (1H, m); MS *m*/*z* (%) 210 (M^+, trace), 181 ($[M-C_2H_5]^+$, 7), 83 (100). Found: *m*/*z* 210.1972. Calcd for $C_{14}H_{26}O$: M, 210.1981.

1-Ethynyl-4-*t*-butyl-1-cyclohexanol (7c). Low melting solid; IR (KBr) 3530, 3420, 3320, 3260 (OH), 2100 (C≡C) cm^{-1}; ^1H NMR δ=0.86 (9H, s), 1.0–2.2 (10H, m), 2.41 (1H, s); MS *m*/*z* (%) 180 (M^+, trace), 165 (1.5), 106 (44), 57 (100). Found: *m*/*z* 180.1515. Calcd for $C_{12}H_{20}O$: M, 180.1513.

4-Ethynyl-4-hydroxyl-1-cyclohexanone Ethylene Acetal (7d). Colorless oil; IR (neat) 3450, 3320, (OH), 2125 (C≡C) cm^{-1}; ^1H NMR δ=1.6–2.1 (8H, m), 2.48 (1H, s), 3.94 (4H, s); MS *m*/*z* (%) 182 (M^+, 0.4), 154 (2), 125 (2), 99 (100). Found:

m/z 182.0942. Calcd for $C_{10}H_{14}O_3$: M, 182.0942.

2-Ethynyl-2-indanol (7e). Colorless crystals; mp 91–92.5 °C (AcOEt–hexane); IR (KBr) 3450, 3290 (OH), 2125 (C≡C) cm^{-1}; ^1H NMR δ=2.52 (1H, s), 3.26, 3.40 (each 2H, d, J=17 Hz), 7.17 (4H, s); MS m/z (%) 158 (M^+, 51), 129 (18), 105 (100). Found: C, 83.35; H, 6.27%. Calcd for $C_{11}H_{10}O$: C, 83.51; H, 6.37%.

1-Dodecyn-3-ol (7f). Colorless oil; IR (neat) 3330 (OH), 2130 (C≡C) cm^{-1}; ^1H NMR δ=0.87 (3H, t, J=7 Hz), 1.0–2.0 (17H, m), 2.45 (1H, d, J=2 Hz), 4.35 (1H, dq, J=7, 2 Hz); MS m/z (%) 182 (M^+, trace), 181 (0.3), 121 (14), 43 (100). Found: m/z 182.1660. Calcd for $C_{12}H_{22}O$: 182.1669.

1-[2-(1-Hydroxycyclohexyl)ethyl]-4-*t*-butyl-1-cyclohexanol (8a). To a solution of the vinyl chloride **3c** (54 mg; 0.25 mmol) in 3 ml of dry THF at −25 °C under N_2 was added *n*-BuLi (1 mmol) with stirring. The reaction mixture was stirred and allowed to warm to −15 °C in 1 h. To this reaction mixture was added cyclohexanone (0.3 mmol) and the mixture was stirred at −15 °C for 10 min. The reaction was quenched with sat. aqueous NH_4Cl and the whole was extracted with ether–benzene. The product was purified by silica-gel column chromatography to give 50 mg (72%) of **8a** as colorless crystals; mp 164.5–165 °C (AcOEt–hexane). IR (KBr) 3390 (OH) cm^{-1}, the signal due to C≡C stretching vibrations could not be observed; ^1H NMR δ=0.85 (9H, s), 1.0–2.3 (20H, m); MS m/z (%) 278 (M^+, 14), 260 (14), 232 (19), 203 (45), 162 (63), 57 (100). Found: C, 77.66; H, 10.97%. Calcd for $C_{18}H_{30}O_2$: C, 77.65; H, 10.86%.

1-(3-Hydroxy-1-dodecynyl)-4-*t*-butyl-1-cyclohexanol (8b). Colorless crystals; mp 73–74 °C (hexane); IR (KBr) 3370 (OH) cm^{-1}; ^1H NMR δ=0.85 (9H, s), 0.88 (3H, t, J=7 Hz), 1.0–2.2 (27H, m), 4.35 (1H, t, J=7 Hz); MS m/z (%) 336 (M^+, 0.8), 318 ([$M-H_2O$]$^+$, 3), 303 (5), 57 (100). Found: C, 78.70; H, 12.24%. Calcd for $C_{22}H_{40}O_2$: C, 78.51; H, 11.98%.

1-[3-Hydroxy-3-(3-methoxyphenyl)-1-propynyl]-4-*t*-butyl-1-cyclohexanol (8c). Colorless crystals; mp 104–105 °C (AcOEt–hexane) IR (KBr) 3360 (OH) cm^{-1}; ^1H NMR δ=0.85 (9H, s), 0.9–2.2 (10H, m), 3.79 (3H, s), 5.41 (1H, d (+D_2O singlet), J=6 Hz), 6.7–7.4 (4H, m); MS m/z (%) 316 (M^+, 100), 298 ([$M-H_2O$]$^+$, 5), 283 (4), 241 (15), 200 (48). Found: C, 75.97; H, 8.87%. Calcd for $C_{20}H_{28}O_3$: C, 75.91; H, 8.92%.

1-Cyclohexyl-2-tridecyne-1,4-diol (8d). Colorless oil; IR (neat) 3310 (OH) cm^{-1}; ^1H NMR δ=0.88 (3H, t, J=7 Hz), 1.0–2.0 (27H, m), 4.16 (1H, d, J=4 Hz), 4.38 (1H, t, J=5 Hz); MS m/z (%) 294 (M^+, 0.3), 276 ([$M-H_2O$]$^+$, 1.5), 233 (1.5), 194 (60), 83 (100). Found: m/z 294.2553. Calcd for $C_{19}H_{34}O_2$: M, 294.2556.

1-(3-Methoxyphenyl)-2-tridecyne-1,4-diol (8e). Colorless oil; IR (neat) 3340 (OH) cm^{-1}; ^1H NMR δ=0.87 (3H, t, J=7 Hz), 1.1–1.9 (16H, m), 3.79 (3H, s), 4.40 (1H, dt, J=6, 1 Hz), 5.44 (1H, s), 6.7–7.4 (4H, m); MS m/z (%) 318 (M^+, 15), 138 (100). Found: m/z 318.2199. Calcd for $C_{20}H_{30}O_3$: M, 318.2193.

(2*R*, 3*R*, R_s)-2-Chloro-1-phenyl-2-(*p*-tolylsulfinyl)-3-pentanol (10a) and (2*R*, 3*S*, R_s)-Isomer (10b). The carbanion of (−)-1-chloro-2-phenylethyl *p*-tolyl sulfoxide (**9**; 98% ee) was reacted with propanal in a similar way as described above to give two adducts **10a** (41%) and **10b** (53%). These products were easily separated by silica-gel column chromatography.

10a: Colorless oil; IR (neat) 3400 (OH), 1080, 1040, 1015 (SO) cm^{-1}; ^1H NMR δ=0.93 (3H, t, J=7 Hz), 1.4–1.8 (4H, m), 2.44 (3H, s), 3.36 (1H, d, J=15 Hz), 3.82 (1H, dd, J=8, 4 Hz), 4.13 (1H, d, J=15 Hz), 7.2–7.7 (5H, m); $[\alpha]_D^{27}$ −128.1° (*c* 0.2, acetone).

10b: Colorless crystals; mp 156–157 °C (AcOEt–hexane); IR (KBr) 3430 (OH), 1080, 1050, 1030 (SO) cm^{-1}; ^1H NMR δ=0.90 (3H, t, J=7 Hz), 1.3–1.8 (2H, m), 1.8–2.3 (2H, m), 2.41 (3H, s), 3.34 (1H, d, J=15 Hz), 3.38 (1H, dd, J=8, 2 Hz), 3.41 (1H, d, J=15 Hz), 7.1–7.7 (5H, m). Found: C, 64.03; H, 6.03; Cl, 10.59; S, 9.25%. Calcd for $C_{18}H_{21}ClO_2S$: C, 64.18; H, 6.28; Cl, 10.52; S, 9.52%. $[\alpha]_D^{25}$−68.0° (*c* 1.0, acetone).

(3*R*)-2-Chloro-1-phenyl-1-penten-3-ol (11a) and (3*S*)-Isomer (11b). Thermal elimination of **10a** in refluxing toluene for 20 min gave **11a** in 99% yield as a colorless oil (single isomer; *E*/*Z* not determined). IR (neat) 3380 (OH), 1645 (C=C) cm^{-1}; ^1H NMR δ=0.96 (3H, t, J=7 Hz), 1.79 (2H, m), 4.21 (1H, t, J=7 Hz), 6.70 (1H, s), 7.2–7.7 (5H, m); MS m/z (%) 196 (M^+, 29), 167 (100), 31 (85). Found: m/z 196.0652. Calcd for $C_{11}H_{13}ClO$: M, 196.0654. $[\alpha]_D^{23}$+10.4° (*c* 0.7, acetone). Similar treatment of **10b** in refluxing toluene for 10 min gave **11b** in 99% yield as a colorless oil (a mixture of geometrical isomers; ratio about 2:1; *E*/*Z* not determined). IR (neat) 3380 (OH), 1650 (C=C) cm^{-1}; ^1H NMR δ=0.89 (1H, t, J=7 Hz), 0.96 (2H, t, J=7 Hz), 1.79 (2H, m), 4.21 (2/3H, t, J=7 Hz), 4.59 (1/3H, t, J=7 Hz), 6.71 (2/3H, s), 6.85 (1/3H, s), 7.1-7.7 (5H, m); MS m/z (%) 196 (M^+, 31), 167 (100), 131 (80). Found: m/z 196.0646. Calcd for $C_{11}H_{13}ClO$: M, 196.0654. $[\alpha]_D^{25}$ +15.3° (*c* 0.9, acetone).

(3*R*)-1-Phenyl-1-pentyn-3-ol (12a) and (3*S*)-Isomer (12b). To a solution of **11a** (60 mg; 0.3 mmol) in 3 ml of dry THF at −50 °C under N_2 was added *n*-BuLi (0.9 mmol) dropwise with stirring. The reaction mixture was then stirred at −35 °C and allowed to warm to 0 °C in 2 h, and finally at 0 °C for 30 min. The reaction was quenched with sat. aqueous NH_4Cl, and the usual workup gave **12a** (46 mg; 96%) as a colorless oil. IR (neat) 2350 (OH), 2240 (C≡C) cm^{-1}; ^1H NMR δ=1.07 (3H, t, J=7 Hz), 1.82 (2H, m), 4.53 (1H, t, J=6 Hz), 7.1–7.5 (4H, m); MS m/z (%) 160 (M^+, 15), 131 (100), 103 (26). Found: m/z 180.0893. Calcd for $C_{11}H_{12}O$: M, 180.0888. $[\alpha]_D^{26}$+19.3° (*c* 2.3, Et_2O).

Vinyl chloride **11b** gave (−)-(3*S*)-isomer **12b** in 92% yield. $[\alpha]_D^{24}$−20.0° (*c* 2.6, Et_2O). The IR and NMR spectra were superimposable on those of **12a**.

We are grateful to Dr. Mikio Takeda, Tanabe Seiyaku Co., Ltd., for elemental analysis, and to Noriko Sawabe and Fukiko Hasegawa of this laboratory for NMR and MS measurements. This work was supported by a Grant-in-Aid for Scientific Research No. 01571168 from the Ministry of Education, Science and Culture, which is gratefully acknowledged.

References

1) J. F. Stoddart, "Comprehensive Organic Chemistry," Pergamon Press, Oxford (1979), Vol. 1, pp. 193–208; G. Zweifel and J. A. Miller, *Org. React. N. Y.*, **32**, 375 (1984).

2) Some recent papers: W. H. Pirkle and W. C. Boeder, *J. Org. Chem.*, **43**, 2091 (1978); K. Mori and H. Akao, *Tetrahedron Lett.*, **1978**, 4127; J. P. Vigneron and V. Bloy, *ibid.*, **1980**, 1735; J. P. Vigneron and J. M. Blanchard, *ibid.*, **1980**, 1739; T. Mukaiyama and K. Suzuki, *Chem. Lett.*, **1980**, 255; W. S. Johnson, B. Frei, and A. S. Gopalan, *J. Org. Chem.*, **46**, 1512 (1981); A. K. Kluge, D. J. Kertesz, C. O-Yang, and H. Y. Wu,

ibid., **52**, 2860 (1987); S. Y. Mhaskar and G. Lakshminarayana, *Tetrahedron Lett.*, **31**, 7227 (1990).

3) a) T. Satoh, T. Oohara, Y. Ueda, and K. Yamakawa, *J. Org. Chem.*, **54**, 3130 (1989); b) T. Satoh, T. Sato, T. Oohara, and K. Yamakawa, *ibid.*, **54**, 3973 (1989); c) T. Satoh and K. Yamakawa, *Yuki Gosei Kagaku Kyokaishi*, **47**, 734 (1989).

4) T. Satoh, K. Onda, and K. Yamakawa, *Tetrahedron Lett.*, **31**, 3567 (1990).

5) T. Satoh, Y. Kaneko, T. Izawa, K. Sakata, and K. Yamakawa, *Bull. Chem. Soc. Jpn.*, **58**, 1983 (1985).

6) T. Ito, S. Okamoto, and F. Sato, *Tetrahedron Lett.*, **30**, 7083 (1989).

7) Some recent papers for asymmetric synthesis of propargylic alcohols: a) M. M. Midland, D. C. McDowell, R. L. Hatch, and A. Tramontano, *J. Am. Chem. Soc.*, **102**, 867 (1980); b) M. Nishizawa, M. Yamada, and R. Noyori, *Tetrahedron Lett.*, **22**, 247 (1981); c) M. M. Midland and A. Kazubski, *J. Org. Chem.*, **47**, 2814 (1981); d) H. C. Brown and G. G. Pai, *ibid.*, **50**, 1384 (1985); e) H. C. Brown, J. Chandrasekharan, and P. V. Ramachandran, *J. Am. Chem. Soc.*, **110**, 1539 (1988); f) M. M. Midland, *Chem. Rev.*, **89**, 1553 (1989); g) K. Soai and S. Niwa, *Chem. Lett.*, **1989**, 481; h) S. Takano, K. Samizu, T. Sugihara, and K. Ogasawara, *J. Chem. Soc., Chem. Commun.*, **1989**, 1344; i) S. Niwa and K. Soai, *J. Chem. Soc., Perkin Trans. 1*, **1990**, 937; j) J. S. Yadav, P. K. Deshpande, and G. V. M. Sharma, *Tetrahedron*, **46**, 7033 (1990).

8) T. Satoh, K. Onda, and K. Yamakawa, *J. Org. Chem.*, **56**, (1991), in press.

 © 1991 The Chemical Society of Japan Bull. Chem. Soc. Jpn., 64, 2159—2168 (1991)

Crystal Structures and Electrical Conductivities of TXC_n-TTF (X=Sulfur, Selenium, Tellurium; n=2,3)·TCNQ Charge-Transfer Complexes

Kenichi IMAEDA,* Takehiko MORI, Chikako NAKANO, Hiroo INOKUCHI, Naoko IWASAWA,† and Gunzi SAITO†,††

Institute for Molecular Science, Myodaiji, Okazaki 444

† Institute for Solid State Physics, The University of Tokyo, Roppongi, Minato-ku, Tokyo 106

(Received October 25, 1990)

The crystal structures and the electrical conductivities have been studied for tetrakis(alkylchalcogeno)tetrathiafulvalene (TXC_n-TTF (X=sulfur, selenium, tellurium; n=2,3)) complexes with tetracyanoquinodimethane (TCNQ). All the complexes with a composition of 1 : 1 had the same crystal system (triclinic) and the same space group ($P\bar{1}$). The donor and acceptor molecules were alternately stacked in their crystals. (TSeC$_2$-TTF)TCNQ was obtained as plate and needle crystals. The molecular structure of TSeC$_2$-TTF and the overlapping mode between TSeC$_2$-TTF and TCNQ molecules of the two complexes were subtly different. All the complexes were semiconductors because of their mixed-stack structures. (TTeC$_2$-TTF)TCNQ showed the lowest resistivity (5 Ω cm at room temperature). Its good conductivity was brought about by the effective degree of charge-transfer and the favorable overlap between TTeC$_2$-TTF and TCNQ molecules. An overall discussion on the structural and physical properties of a series of TCNQ complexes with TXC_n-TTF (X=sulfur, selenium, tellurium; n=1,2,3) is presented.

Tetrakis(alkylchalcogeno)tetrathiafulvalene (TXC_n-TTF) has exhibited novel electronic properties as a consequence of the intermolecular interactions between the tetrachalcogeno-TTF conjugated π systems and the alkyl side chains. TTC_n-TTF compounds with long alkyl chains had relatively low resistivities because of a reduction of the interplanar distances between the TTF skeletons through the van der Waals interactions of the alkyl side chains between molecules. This was termed "a molecular fastener effect".[1-4] This finding was significant since high conductivities in single-component organic solids are produced not by an external pressure but by an internal pressure derived from attractive forces between attached organic functional groups. TTeC$_1$-TTF is a new organic semiconductor with high electrical conductivity and high carrier mobility, which does not belong to the category of molecular fasteners. The unusual properties of TTeC$_1$-TTF are caused by a formation of regular Te chains through quasi-covalent Te–Te interatomic contacts between neighboring TTeC$_1$-TTF stacks.[5]

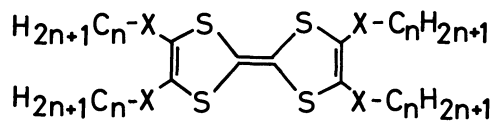

X=S : TTC_n-TTF
Se : $TSeC_n$-TTF
Te : $TTeC_n$-TTF

Scheme 1.

TXC_n-TTF compounds are also attractive donors used in the formation of charge-transfer (CT) complexes.[6-9] TXC_1-TTF complexes with various acceptors have been actively investigated and a metallic conductivity has been found in $(TTC_1\text{-TTF})(I_3)_{0.823}$.[10-13] TXC_n-TTF compounds with long alkyl side chains may form highly conductive CT complexes since they are expected to generate charge carriers in addition to their fastener effect. The present system allows us to systematically study how the chain length of alkyl groups and the variation of chalcogen atoms affect the physical properties of the complexes.

Various (TXC_1-TTF)–TCNQ complexes have been previously studied: the crystal structures and the physical properties of (TTC_1-TTF)TCNQ and (TTC_1-TTF)$_2$TCNQ were reported by Mori et al.[14] and those of ($TSeC_1$-TTF)TCNQ and ($TTeC_1$-TTF)TCNQ were reported by Iwasawa et al.[9,15,16] In this work, we prepared single crystals of TXC_n-TTF (X=S, Se, Te; n=2,3) complexes with TCNQ. We present the experimental results of their crystal structure determinations and electrical conductivity measurements. The correlation between the structure and the conductivity is discussed on the basis of the degree of charge-transfer (ionicity) and the molecular overlap between the donor and the acceptor.

Experimental

Black single crystals of TXC_n-TTF (X=S, Se, Te; n=2,3)·TCNQ were prepared by mixing hot CH_3CN solutions of each component and then keeping the solutions cool in a refrigerator (5 °C) or a freezer (−20 °C) for several days. (TTC_2-TTF)-TCNQ, ($TSeC_3$-TTF)TCNQ, ($TTeC_2$-TTF)TCNQ, and ($TTeC_3$-TTF)TCNQ crystallized in needles, while (TTC_3-TTF)TCNQ crystallized in plates. In the case of ($TSeC_2$-TTF)TCNQ, two kinds of crystals were obtained depending on

†† Present address: Department of Chemistry, Faculty of Science, Kyoto University, Sakyo-ku, Kyoto 606.

Table 1. Crystallographic Data of (TXC_n-TTF)TCNQ

	(TTC$_2$-TTF)TCNQ	(TTC$_3$-TTF)TCNQ	(TSeC$_2$-TTF)TCNQ	(TSeC$_3$-TTF)TCNQ	(TTeC$_2$-TTF)TCNQ	(TTeC$_3$-TTF)TCNQ
Chemical formula	$C_{26}H_{24}N_4S_8$	$C_{30}H_{32}N_4S_8$	$C_{26}H_{24}N_4S_4Se_4$	$C_{30}H_{32}N_4S_4Se_4$	$C_{26}H_{24}N_4S_4Te_4$	$C_{30}H_{32}N_4S_4Te_4$
FW	649.02	705.13	836.60	892.71	1031.16	1087.27
Crystal shape	Needle	Plate	Plate	Needle	Needle	Needle
Crystal system	Triclinic	Triclinic	Triclinic	Triclinic	Triclinic	Triclinic
Space group	$P\bar{1}$	$P\bar{1}$	$P\bar{1}$	$P\bar{1}$	$P\bar{1}$	$P\bar{1}$
a/Å	9.143(1)	9.107(1)	9.168(1)	9.140(1)	9.203(2)	9.243(2)	10.285(2)
b/Å	11.374(2)	13.197(2)	11.418(1)	11.430(2)	12.918(2)	11.287(2)	13.245(2)
c/Å	8.052(1)	8.168(1)	8.382(1)	8.181(1)	8.494(3)	8.458(1)	8.467(2)
α/°	95.37(1)	98.29(2)	92.14(1)	95.29(1)	96.91(2)	90.80(1)	81.96(2)
β/°	105.83(1)	109.19(1)	110.66(1)	105.31(1)	111.52(2)	107.90(1)	121.48(1)
γ/°	100.93(1)	101.58(1)	100.68(1)	99.83(1)	101.88(2)	101.25(1)	108.09(2)
V/Å^3	781.5(2)	884.4(3)	801.8(2)	803.7(2)	897.7(4)	821.0(2)	934.6(4)
Z	1	1	1	1	1	1	1
D_x/g cm^{-3}	1.379	1.324	1.733	1.729	1.651	2.086	1.932
R	0.048	0.078	0.057	0.050	0.060	0.038	0.039
μ(Mo $K\alpha$)/cm^{-1}	5.71	5.10	48.03	47.91	42.95	37.96	33.39
$(\sin\theta/\lambda)_{max}$	0.7014	0.7009	0.7035	0.7035	0.7026	0.7056	0.6965
No. of reflections	1205	1730	2516	1587	2180	4074	1445

the temperature; plates formed at 5 °C and needles formed at −20 °C.

X-Ray diffraction data were collected at room temperature with a Rigaku AFC-5 automated four circle diffractometer with monochromatized Mo $K\alpha$ (λ=0.71069 Å) radiation in the range of $2\theta<60°$ using a θ–2θ scan technique. The unit cell parameters were determined by a least-squares fit of 50 reflections with $20°<2\theta<30°$. The crystallographic data are summarized in Table 1. The independent reflections ($|F_o|>3\sigma(|F_o|)$) were used for structure analyses. The crystal structures were solved by the Patterson method for (TTeC$_3$-TTF)TCNQ and the direct method using the MULTAN 78 program system[17] for the other complexes, and were refined by the block diagonal least-square method after an absorption correction. Anisotropic thermal parameters were adopted for non-hydrogen atoms and the hydrogen atoms were refined isotropically. The atomic scattering factors were taken from the International Tables for X-ray Crystallography.[18] All the calculations were carried out on a HITAC M-680H computer with the UNICS III program system.[19] The atomic parameters are listed in Table 2.[20]

The electrical conductivity along the long axis of the crystals, which corresponds to the a-axis, was measured between room temperature and 200 K with a four-probe method for (TTeC$_2$-TTF)TCNQ and a two-probe method for the other complexes using a gold paste as electrical contacts.

Results and Discussion

Crystal Structure. The TXC_n-TTF (X=S, Se, Te; n=2,3) complexes with TCNQ crystallized in the triclinic system and the $P\bar{1}$ space group, as listed in Table 1. (TTC$_2$-TTF)TCNQ and (TSeC$_3$-TTF)TCNQ crystals were isomorphous to the (TSeC$_2$-TTF)TCNQ needle-shaped crystal (abbreviated as n-(TSeC$_2$-TTF)TCNQ). (TTC$_3$-TTF)TCNQ and (TTeC$_2$-TTF)TCNQ crystals were isomorphous to the (TSeC$_2$-TTF)TCNQ plate-shaped crystal (abbreviated as p-(TSeC$_2$-TTF)TCNQ). The crystal structure of (TTeC$_2$-TTF)TCNQ was identical to that reported by Ahalon-Shalom et al.[21] Therefore, we have described the crystal structures of p-(TSeC$_2$-TTF)TCNQ and n-(TSeC$_2$-TTF)TCNQ only.

The molecular structures with atomic numbering schemes for p-(TSeC$_2$-TTF)TCNQ and n-(TSeC$_2$-TTF)TCNQ are illustrated in Figs. 1 and 2, respectively. The tetraseleno-TTF ($C_6S_4Se_4$) moieties in both complexes are nearly planar, in contrast to the nonplanar structure in the crystal of uncomplexed TSeC$_2$-TTF.[22] The ethyl groups attached to Se(2) of p-(TSeC$_2$-TTF)TCNQ lie almost coplanar to the $C_6S_4Se_4$ plane. The other ethyl groups attached to Se(1) are perpendicular to the $C_6S_4Se_4$ plane. This configuration of the molecule is denoted as the p-form. In constrast, the four ethyl groups of n-(TSeC$_2$-TTF)TCNQ are perpendicular to the $C_6S_4Se_4$ plane. This configuration of the molecule is denoted as the n-form. The comparatively large temperature factors of the terminal carbon atoms of the ethyl groups in both complexes may be caused by large thermal vibrations. The molecular structure of TCNQ in these complexes is planar with a

Table 2. Positional Parameters ($\times 10^4$) and Equivalent Isotropic Thermal Parameters ($Å^2$) of (TXC_n-TTF)TCNQ

Atom	x	y	z	B_{eq}	Atom	x	y	z	B_{eq}
	(TTC_2-TTF)TCNQ					($TSeC_2$-TTF)TCNQ Needle Crystal			
S1	7501(2)	−2321(2)	8709(3)	6.6	Se1	7527(1)	−2231(1)	8941(1)	5.7
S2	5586(2)	−3383(2)	4543(3)	6.4	Se2	5636(1)	−3482(1)	4718(1)	5.6
S3	9510(2)	−461(1)	7407(2)	5.2	S1	9506(2)	−397(2)	7403(3)	4.7
S4	7897(2)	−1421(1)	3700(2)	4.7	S2	7973(2)	−1442(1)	3802(3)	4.3
C1	9471(6)	−398(5)	5236(8)	4.3	C1	9487(8)	−381(6)	5269(9)	3.8
C2	7981(7)	−1762(5)	6929(8)	4.7	C2	8009(8)	−1685(6)	6.993(9)	4.2
C3	7246(6)	−2192(5)	5250(8)	4.4	C3	7321(8)	−2147(6)	5374(9)	3.9
C4	9202(9)	−2843(7)	9680(9)	7.7	C4	9373(12)	−2847(9)	9787(12)	8.2
C5	9504(9)	−3829(7)	8540(11)	12.2	C5	9587(13)	−3814(10)	8593(14)	9.3
C6	5656(8)	−4132(6)	2508(9)	7.8	C6	5642(11)	−4070(9)	2489(12)	8.7
C7	6856(9)	−4795(7)	2667(12)	9.7	C7	6864(13)	−4770(10)	2476(16)	10.6
CC1	6184(6)	847(5)	6263(8)	4.7	CC1	6157(8)	865(7)	6205(9)	4.6
CC2	6002(6)	869(5)	4427(8)	4.4	CC2	6002(8)	835(6)	4444(9)	4.1
CC3	4754(7)	−19(5)	3207(8)	4.8	CC3	4791(9)	−62(7)	3246(9)	4.7
CC4	6965(7)	1711(5)	3866(8)	4.8	CC4	6965(8)	1658(7)	3829(10)	4.9
CC5	8203(7)	2609(5)	5062(8)	5.5	CC5	8160(9)	2570(7)	4980(11)	5.5
CC6	6810(7)	1762(5)	2058(9)	6.2	CC6	6806(9)	1661(8)	2038(10)	6.1
N1	9181(7)	3327(5)	6038(8)	7.7	N1	9111(8)	3281(7)	5918(10)	7.5
N2	6679(8)	1799(6)	633(8)	9.4	N2	6698(10)	1674(8)	641(10)	9.1
	(TTC_3-TTF)TCNQ					($TSeC_3$-TTF)TCNQ			
S1	8771(3)	1963(2)	9721(3)	7.1	Se1	7178(1)	−2041(1)	8234(1)	6.3
S2	7877(3)	3041(2)	6222(3)	7.5	Se2	5159(1)	−3166(1)	3657(1)	6.4
S3	9706(2)	366(2)	7563(3)	6.3	S1	9420(2)	−403(2)	7174(3)	4.9
S4	8889(2)	1287(2)	4416(3)	6.0	S2	7788(2)	−1313(2)	3436(3)	4.7
C1	9713(8)	338(5)	5412(9)	5.5	C1	9415(8)	−368(5)	5127(10)	4.4
C2	9010(8)	1504(5)	7723(9)	5.6	C2	7789(8)	−1558(5)	6472(10)	4.2
C3	8640(8)	1936(5)	6315(9)	5.5	C3	7056(8)	−1985(5)	4796(10)	4.2
C4	10835(11)	2534(7)	11164(10)	9.7	C4	9236(10)	−2310(6)	9631(10)	5.8
C5	11617(13)	3525(12)	10730(13)	19.1	C5	9646(10)	−3238(7)	8818(11)	5.6
C6	12835(22)	4187(12)	11747(18)	21.5	C6	8482(12)	−4317(7)	8531(13)	7.5
C7	7877(13)	3325(7)	4105(12)	10.8	C7	6003(12)	−4155(7)	2447(13)	8.5
C8	7424(16)	4221(8)	3761(14)	14.2	C8	6899(15)	−4733(9)	3573(17)	10.8
C9	7264(17)	4448(8)	2027(15)	14.8	C9	7430(15)	−5585(8)	2610(16)	10.1
CC1	5155(8)	−68(5)	6747(8)	5.1	CC1	6268(8)	828(5)	6325(9)	3.9
CC2	4549(7)	762(5)	5978(8)	4.8	CC2	6054(7)	747(5)	4569(9)	3.8
CC3	4427(7)	788(5)	4191(8)	5.0	CC3	4753(8)	−113(5)	3237(9)	4.0
CC4	4114(8)	1504(5)	6958(8)	5.5	CC4	7097(9)	1462(5)	4098(9)	4.3
CC5	4193(8)	1493(5)	8753(9)	6.2	CC5	8377(9)	2340(6)	5372(10)	4.9
CC6	3528(9)	2341(5)	6301(9)	6.4	CC6	6938(9)	1388(6)	2341(11)	5.3
N1	4528(8)	1467(5)	10168(8)	8.3	N1	9410(8)	3027(6)	6370(9)	7.2
N2	3053(8)	3019(5)	5761(9)	8.8	N2	6810(9)	1332(6)	951(9)	7.5
	($TSeC_2$-TTF)TCNQ Plate Crystal					($TTeC_2$-TTF)TCNQ			
Se1	8557(1)	2166(1)	9394(1)	5.7	Te1[a)]	83735(3)	21556(2)	95134(3)	4.1
Se2	7802(1)	3657(1)	5759(1)	5.7	Te2[a)]	77926(3)	38785(2)	57381(3)	3.7
S1	9605(2)	345(1)	7392(2)	4.8	S1	9505(1)	302(1)	7332(1)	3.8
S2	8897(2)	1537(1)	4252(2)	4.7	S2	8946(1)	1570(1)	4286(1)	3.7
C1	9703(6)	392(4)	5363(6)	4.2	C1	9679(4)	392(3)	5347(5)	3.4
C2	8881(6)	1657(4)	7384(6)	4.1	C2	8777(4)	1614(3)	7327(4)	3.1
C3	8567(6)	2210(4)	5971(6)	4.0	C3	8530(4)	2216(3)	5943(4)	3.0
C4	10790(9)	2762(7)	10824(8)	7.8	C4	10802(6)	2840(5)	10834(6)	6.1
C5	11649(9)	3744(7)	10241(10)	8.7	C5	11602(6)	3767(5)	10048(8)	6.7
C6	8001(12)	4117(8)	3428(14)	12.5	C6	7667(7)	4076(5)	3186(6)	6.2
C7	6666(15)	3704(12)	2494(17)	19.0	C7	6117(9)	3921(8)	2043(8)	10.8
CC1	5062(6)	−131(5)	6681(6)	4.2	CC1	4995(4)	−169(3)	6635(4)	3.4
CC2	4461(5)	839(4)	5822(6)	4.0	CC2	4395(4)	807(3)	5788(4)	3.3
CC3	4424(6)	932(5)	4102(6)	4.3	CC3	4435(4)	935(3)	4115(5)	3.4
CC4	3919(6)	1656(5)	6611(6)	4.5	CC4	3798(4)	1597(3)	6561(5)	3.7
CC5	3906(7)	1550(5)	8300(7)	5.5	CC5	3747(5)	1474(4)	8221(5)	4.4
CC6	3352(7)	2649(5)	5797(7)	5.9	CC6	3236(5)	2599(4)	5764(6)	4.5
N1	3879(7)	1455(5)	9641(6)	7.9	N1	3691(6)	1359(4)	9539(5)	6.5
N2	2892(8)	3430(5)	5140(7)	8.5	N2	2777(6)	3389(4)	5098(6)	6.3

Table 2. (Continued)

Atom	x	y	z	B_{eq}	Atom	x	y	z	B_{eq}
				(TTeC$_3$-TTF)TCNQ					
Te1	13007(1)	2064(1)	11344(1)	5.9	C8	13140(24)	4690(16)	6840(28)	15.3
Te2	15039(1)	3224(1)	8396(1)	6.0	C9	12332(21)	5563(12)	5240(23)	11.3
S1	10667(3)	420(2)	7796(4)	4.5	CC1	4799(12)	−113(8)	11532(14)	3.9
S2	12170(3)	1285(2)	5582(4)	4.4	CC2	6088(11)	698(7)	11538(13)	3.4
C1	10584(11)	355(8)	5699(13)	4.0	CC3	6237(11)	796(7)	9933(13)	3.7
C2	12287(11)	1528(8)	8689(13)	3.9	CC4	7158(11)	1405(8)	13047(13)	3.9
C3	12984(11)	1933(8)	7700(14)	3.9	CC5	7049(13)	1321(9)	14641(15)	5.2
C4	10757(13)	2306(9)	10442(15)	5.4	CC6	8427(12)	2235(8)	13089(16)	5.0
C5	10373(14)	3231(9)	9215(16)	5.7	N1	6990(12)	1259(8)	15973(13)	6.9
C6	11408(16)	4302(11)	10058(20)	8.1	N2	9450(12)	2930(8)	13136(15)	7.2
C7	13756(22)	4335(13)	6176(24)	13.4					

a) Positional parameters ($\times 10^5$).

maximum deviation of only 0.033 Å for CC(1). The planar structure is commonly observed in many TCNQ complexes.

Figures 3(a) and 3(b) show the intermolecular overlap between the donor and the acceptor of p-(TSeC$_2$-TTF)TCNQ and n-(TSeC$_2$-TTF)TCNQ, respectively. In the case of p-(TSeC$_2$-TTF)TCNQ, a six-membered ring of TCNQ overlaps one of the two five-membered rings of TSeC$_2$-TTF. This overlapping manner is denoted as the p-mode. On the other hand, n-(TSeC$_2$-TTF)TCNQ has a disadvantageous donor–acceptor overlap with a smaller overlap between a six-membered ring of TCNQ and a five-membered ring of TSeC$_2$-TTF. This overlapping manner is denoted as the n-mode.

Figures 4(a) and 4(b) show the crystal structures of p-(TSeC$_2$-TTF)TCNQ and n-(TSeC$_2$-TTF)TCNQ, respectively. In both complexes, the donor and acceptor molecules alternately stack along the a-axis. The molecular short axis of the C$_6$S$_4$Se$_4$ molecular plane is nearly parallel to the c-axis.

The molecular structure of TTeC$_3$-TTF in the (TTeC$_3$-TTF)TCNQ complex is analogous to that of TSeC$_2$-TTF in n-(TSeC$_2$-TTF)TCNQ and the donor-acceptor overlapping mode is analogous to that of p-(TSeC$_2$-TTF)TCNQ. The characteristic difference between (TTeC$_3$-TTF)TCNQ and the other complexes is that in the (TTeC$_3$-TTF)TCNQ complex the stacking axis is [101] which is different from the growing axis [100] of the crystal.

We have observed interchain atomic contacts in the (TXC$_2$-TTF)TCNQ complexes which are shorter than the sum of the van der Waals radii. n-(TSeC$_2$-TTF)-TCNQ possesses a contact between the outer chalcogen atoms, while (TTeC$_2$-TTF)TCNQ possesses a contact between the outer chalcogen atom and the nitrogen atom. The shortest distances are 3.58 Å (Se(2)–Se(2) in n-(TSeC$_2$-TTF)TCNQ) and 3.28 Å (Te(2)–N(2) in (TTeC$_2$-TTF)TCNQ). In contrast, (TXC$_3$-TTF)TCNQ complexes do not possess any interchain atomic contacts due to a disturbance of the longer propyl groups elongated in the interchain direction.

Degree of Charge-Transfer. The degree of CT (γ) for the TCNQ complexes was estimated from the bond lengths of TCNQ by the procedure developed by Kistenmacher et al.[23] Table 3 presents the calculated values of γ for the present TCNQ complexes.

Table 3. Bond Lengths of TCNQ and Degree of Charge-Transfer for (TXC$_n$-TTF)TCNQ

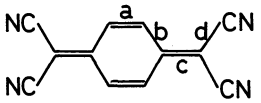

	a/Å	b[a]/Å	c/Å	d[a]/Å	$c/(b+d)$	γ	
(TTC$_2$-TTF)TCNQ	1.331(9)	1.439(8)	1.369(9)	1.429(8)	0.477	0.04	
(TTC$_3$-TTF)TCNQ	1.327(10)	1.443(10)	1.377(10)	1.433(11)	0.479	0.13	
(TSeC$_2$-TTF)TCNQ							
Plate	1.350(8)	1.436(8)	1.383(8)	1.430(8)	0.483	0.29	
Needle	1.343(11)	1.426(10)	1.397(11)	1.435(11)	0.488	0.50	
(TSeC$_3$-TTF)TCNQ	1.363(11)	1.434(9)	1.393(11)	1.435(10)	0.486	0.42	
(TTeC$_2$-TTF)TCNQ	1.340(6)	1.434(6)	1.386(6)	1.428(6)	0.484	0.33	
(TTeC$_3$-TTF)TCNQ	1.352(13)	1.426(17)	1.395(12)	1.404(18)	0.493	0.71	
TCNQ	1.346(3)	1.448(4)	1.374(3)	1.441(3)	0.476	0	Ref. 23
TCNQ$^-$	1.373(4)	1.423(4)	1.420(4)	1.416(4)	0.500	1	Ref. 23

a) The average value of the two equivalent bond lengths.

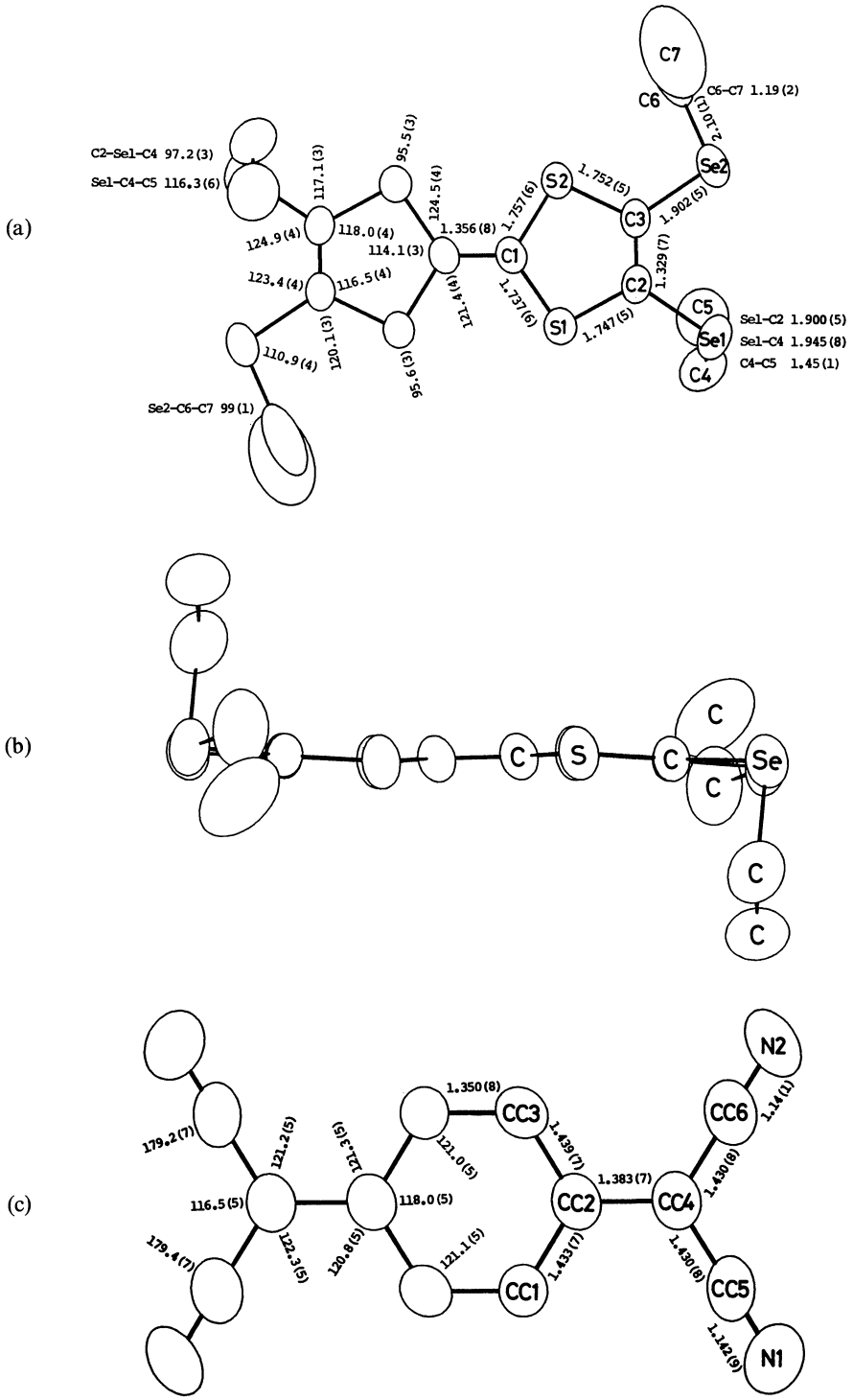

Fig. 1. Molecular structures and atomic numbering schemes of the donor (top view (a) and side view (b)) and the acceptor (c) of p-(TSeC$_2$-TTF)TCNQ.

Furthermore, γ was also estimated by the IR procedure established by Chappell et al.[24] The calculated γ from the CN stretching vibration frequencies in the nujol samples are listed in Table 4.

The electronic spectra in the KBr pellets showed the charge-transfer bands. These CT absorption energies are also listed in Table 4. The charge-transfer transition energy (E_{CT}) in a neutral complex with a mixed-stack can be expressed by the following equation:[25]

$$E_{CT} = I_p - E_A - E_M,$$

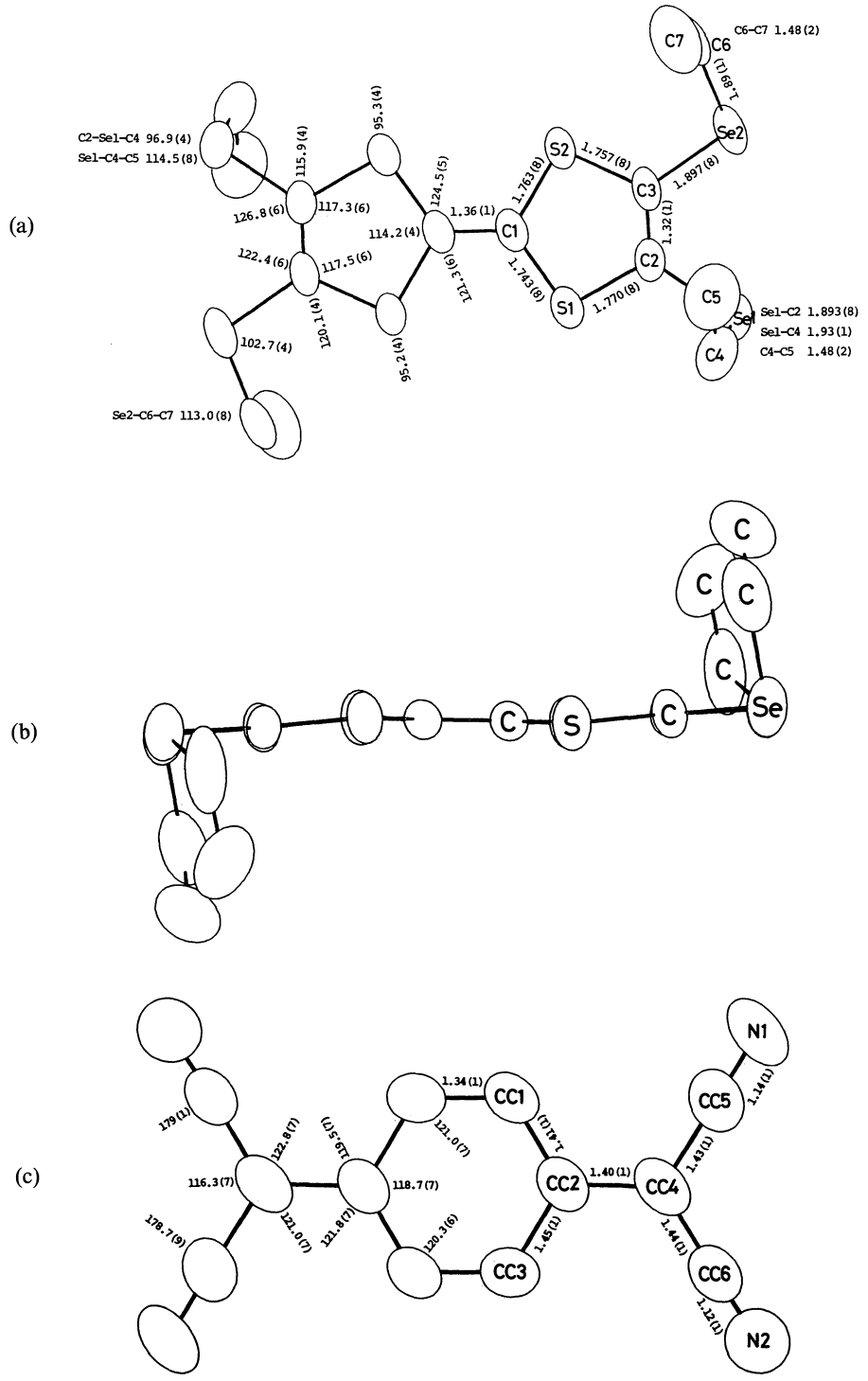

Fig. 2. Molecular structures and atomic numbering schemes of the donor (top view (a) and side view (b)) and the acceptor (c) of n-($TSeC_2$–TTF)TCNQ.

where I_p is the ionization potential of a donor, E_A is the electron affinity of an acceptor, and E_M is a crystal Madelung energy value. A large E_{CT} gives a small γ, while a small E_{CT} gives a large γ.

The X-ray and IR methods gave somewhat different estimated values of γ. However, TTC_n-TTF(n=2,3)·TCNQ, $TSeC_n$-TTF(n=2,3)·TCNQ, and $TTeC_n$-TTF(n=2,3)·TCNQ had about the same CT absorption energies (6100—5200 cm^{-1}, 4700—4600 cm^{-1}, and 4200—3900 cm^{-1}, respectively). This fact suggested that γ of

Table 4. Degree of Charge-Transfer (γ) Calculated by the IR Method, Charge-Transfer Absorption Energy (E_{CT}), and Electrical Properties of (TXC_n-TTF)TCNQ

	ν_{CN}/cm^{-1}	γ	E_{CT}/cm^{-1}	ρ_{RT}/Ω cm	E_a/eV
(TTC_2-TTF)TCNQ	2214	0.30	6100	3.6×10^{7}	0.35
(TTC_3-TTF)TCNQ	2214	0.30	5200	1.2×10^{6}	0.33
($TSeC_2$-TTF)TCNQ					
Plate	2212	0.34	4700	3.5×10^{3}	0.09
Needle	2216	0.25	4700	2.3×10^{5}	0.29
($TSeC_3$-TTF)TCNQ	2214	0.30	4600	2.2×10^{6}	0.39
($TTeC_2$-TTF)TCNQ	2206	0.48	4200	5.0	0.06
($TTeC_3$-TTF)TCNQ	2204	0.52	3900	7.5×10^{3}	0.18

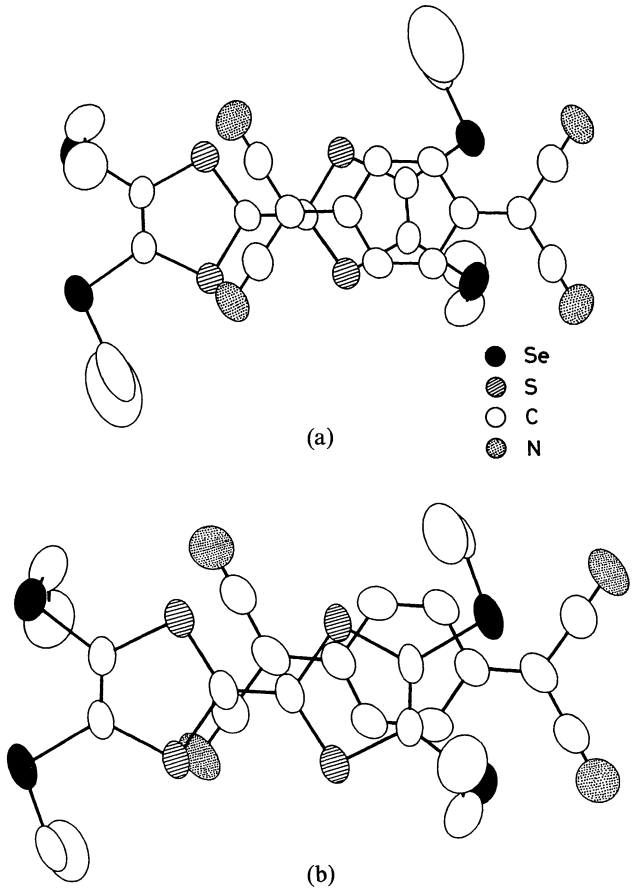

Fig. 3. Overlapping modes between the donor and acceptor molecules; (a) p-($TSeC_2$-TTF)TCNQ, (b) n-($TSeC_2$-TTF)TCNQ.

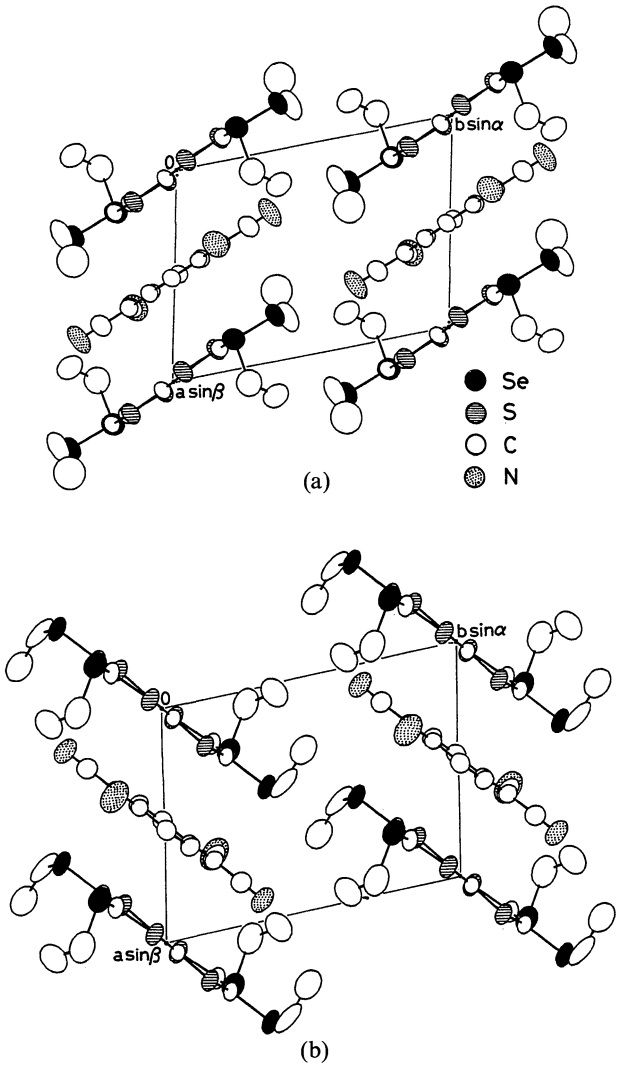

Fig. 4. Crystal structures projected along the c-axis; (a) p-($TSeC_2$-TTF)TCNQ, (b) n-($TSeC_2$-TTF)TCNQ.

TTC_n-TTF(n=2,3)·TCNQ, $TSeC_n$-TTF(n=2,3)·TCNQ, and $TTeC_n$-TTF(n=2,3)·TCNQ were in the ranges of 0.04—0.30, 0.25—0.50, and 0.33—0.71, respectively.

In the present system, γ increased in the order TTC_n-TTF(n=2,3)·TCNQ<$TSeC_n$-TTF(n=2,3)·TCNQ<$TTeC_n$-TTF(n=2,3)·TCNQ. According to the cyclic voltammetry studies of TXC_n-TTF (X=S, Se, Te; n=1—18),[9] the first redox potentials of TXC_n-TTF compounds were independent of n and decreased in the order TTC_n-TTF>$TSeC_n$-TTF>$TTeC_n$-TTF. Thus, the tendency of the ionicity observed in the present system could be explained by the decrease of (I_p-E_A).

Electrical Conductivity. The electrical resistivity at room temperature (ρ_{RT}) and the activation energy (E_a) are given in Table 4. ($TTeC_2$-TTF)TCNQ showed a markedly low resistivity of 5 Ω cm, which was smaller than the value (ca. 10^2 Ω cm) reported by Aharon-Shalom et al.[21] The measurement by Aharon-Shalom et al. may have included a contact resistance. p-($TSeC_2$-TTF)TCNQ and ($TTeC_3$-TTF)TCNQ also showed

relatively low resistivities of 3.5×10^3 and 7.5×10^3 Ω cm, respectively. The other complexes showed comparatively high resistivities of 10^5—10^7 Ω cm. The temperature dependence of the resistivities for all the complexes was simply semiconductive, which resulted from the alternate stacks of the donor and acceptor molecules in their crystal structures. (TTeC$_2$-TTF)-TCNQ, which had the lowest resistivity, had the lowest E_a (0.06 eV).

The electrical conductivity is universally expressed by a simple relation: $\sigma=ne\mu$. The carrier number n and the carrier mobility μ are believed to depend on γ and the magnitude of the molecular orbital overlap of the donor and the acceptor in the crystal, respectively. According to the band calculation by the extended Hückel method,[26] the intermolecular overlap integrals between the highest occupied molecular orbital (HOMO) of TSeC$_2$-TTF and the lowest unoccupied molecular orbital (LUMO) of TCNQ along the stacking direction were -8.78×10^{-3} and 7.36×10^{-3} for p-(TSeC$_2$-TTF)TCNQ and n-(TSeC$_2$-TTF)TCNQ, respectively. The p-mode had an overlap integral larger than of the n-mode.

The high resistivities of (TTC$_2$-TTF)TCNQ and (TTC$_3$-TTF)TCNQ are easily understood in terms of the smaller γ values. n-(TSeC$_2$-TTF)TCNQ and (TSeC$_3$-TTF)TCNQ also showed high resistivities due to the n-mode overlap with a smaller overlap integral (as shown in Fig. 3(b)) in spite of having a larger γ than the S analogues.

The best planes for the C$_6$S$_4$X$_4$(X=S, Se, Te) moieties of the donor and TCNQ were parallel to each other. The interplanar distances were 3.45, 3.44, 3.51, 3.49, 3.43, 3.57, and 3.47 Å for (TTC$_2$-TTF)TCNQ, (TTC$_3$-TTF)-TCNQ, p-(TSeC$_2$-TTF)TCNQ, n-(TSeC$_2$-TTF)TCNQ, (TSeC$_3$-TTF)TCNQ, (TTeC$_2$-TTF)TCNQ, and (TTeC$_3$-TTF)TCNQ, respectively. These complexes had nearly the same interplanar spacings, which meant that the complexes including Se and Te atoms with larger van der Waals radii had stronger intermolecular interactions than the S analogues. The lower resistivities of p-(TSeC$_2$-TTF)TCNQ, (TTeC$_2$-TTF)TCNQ, and (TTeC$_3$-TTF)TCNQ compared with the S analogues are qualitatively explained in terms of the difference of the van der Waals radii of the chalcogen atoms. (TTeC$_2$-TTF)TCNQ had the lowest resistivity among the present complexes, owing to the p-mode overlap with a larger overlap integral (as shown in Fig. 3(a)) and the effective γ.

(TTeC$_3$-TTF)TCNQ possessed the p-mode overlap shown in Fig. 3(a) and the highest γ. However, (TTeC$_3$-TTF)TCNQ showed a higher resistivity than (TTeC$_2$-TTF)TCNQ, because of a mismatch between the measuring direction of the conductivity and the stacking direction of the donor and acceptor molecules. If we can measure along the stacking axis, a lower resistivity of (TTeC$_3$-TTF)TCNQ is expected to be observed.

Finally, we compared the crystal structures and the electrical properties of the TXC$_1$-TTF(X=S, Se, Te)-TCNQ complexes,[9,14-16] The structural and physical properties of TXC$_n$-TTF(X=S, Se, Te; n=1,2,3)-TCNQ complexes are presented in Table 5. The molecular structure of the donor and the donor(D)-acceptor(A) overlapping mode in TXC$_1$-TTF(X=S, Se, Te)·TCNQ were analogous to those of p-(TSeC$_2$-TTF)TCNQ. (TTeC$_1$-TTF)TCNQ made simple DA type stacks, similar to TXC$_n$-TTF (X=S, Se, Te; n=2,3)·TCNQ. In contrast, (TTC$_1$-TTF)TCNQ and (TSeC$_1$-TTF)TCNQ formed DDAA mixed-stacks, and (TTC$_1$-TTF)$_2$TCNQ formed a DDA mixed-stack.

(TTC$_1$-TTF)TCNQ and (TSeC$_1$-TTF)TCNQ had interchain atomic contacts between the outer chalcogen atom and the nitrogen atom, similar to (TTeC$_2$-TTF)TCNQ. In particular, (TTeC$_1$-TTF)TCNQ had a unique crystal structure with three-dimensional intermolecular interactions through two kinds of DA stacks along the [110] and [1$\bar{1}$0] direction and strong interchain Te-N contacts. These chalcogen-N interactions modulated the CN stretching vibration frequency and caused an overestimation of γ by the IR method for (TXC$_1$-TTF)TCNQ.

Judging from the value of γ calculated by the X-ray method and E_{CT}, (TTC$_1$-TTF)TCNQ, (TTC$_1$-TTF)$_2$-TCNQ, and (TSeC$_1$-TTF)TCNQ were in the neutral CT state, similar to TTC$_n$-TTF(n=2,3)·TCNQ. It was difficult to determine the ionicity of (TTeC$_1$-TTF)TCNQ by the IR and X-ray methods.

Summary

TXC$_n$-TTF (X=S, Se, Te; n=2,3) formed semiconductive 1 : 1 CT complexes with TCNQ, in which donor and acceptor molecules alternately stacked with a uniform spacing. This situation was in contrast to (TXC$_1$-TTF)-TCNQ complexes with a variety of stoichiometries and donor-acceptor stacks. It was of interst that (TSeC$_2$-TTF)TCNQ crystallized in plates and needles. These two phases had different crystal structures and showed different electrical properties. The crystal structures of the other complexes were isomorphous to either p-(TSeC$_2$-TTF)TCNQ or n-(TSeC$_2$-TTF)TCNQ.

The ionicity of TXC$_n$-TTF (X=Se, Te; n=2,3)·TCNQ was at the boundary between the neutral (N) and ionic (I) states. These complexes may exhibit an N-I phase transition induced by temperature and/or pressure.

(TXC$_1$-TTF)TCNQ and (TXC$_2$-TTF)TCNQ had two- or three-dimensional networks in the crystals through intrachain and interchain atomic contacts less than the van der Waals distance. On the other hand, (TXC$_3$-TTF)TCNQ was one-dimensional. TXC$_n$-TTF($n\geq4$) did not form CT complexes with TCNQ. The reason was speculated to be a decrease of lattice energy by further weakened interchain interactions, in addition to a size mismatch between the donor and TCNQ molecules.

Table 5. Summary of Structural and Physical Properties of (TXC_n-TTF)–TCNQ Complexes

n		X=T (Sulfur)[a]		X=Se[a]		X=Te[a]
1	D:A	1:1	2:1	1:1		1:1
	Stacking	DDAA	DDA	DDAA		DA
	Spacing	Non-uniform	Non-uniform	Non-uniform		Uniform
		D··D A··A D··A	D··D D··A	D··D	A··A D··A	
	/Å	3.48 3.41 3.58	3.51 3.60	3.51	3.38 3.28	3.38
	Molecular structure	p-Form[b]	p-Form	p-Form		p-Form
	Mode of DA overlap	p-Mode[b]	p-Mode	p-Mode		p-Mode
	γ (X-ray)	0.04	0.25	0.29		>1
	γ (IR)	0.57	0.43	0.61		>1
	E_{CT}/cm^{-1}	6000	5100	6000		4800
	ρ_{RT}/Ω cm	3.8×10^5	5.5×10^4	1.5×10^5		1.0×10^2
	E_a/eV	0.30	0.17	0.35		0.11
	Melting point/°C	111—112	105	131—132		312—315
2				Plate	Needle	
	D:A	1:1		1:1	1:1	1:1
	Stacking	DA		DA	DA	DA
	Spacing	Uniform		Uniform	Uniform	Uniform
	/Å	3.45		3.51	3.49	3.57
	Molecular structure	n-Form[b]		p-Form	n-Form	p-Form
	Mode of DA overlap	n-Mode[b]		p-Mode	n-Mode	p-Mode
	γ (X-ray)	0.04		0.29	0.50	0.33
	γ (IR)	0.30		0.34	0.25	0.48
	E_{CT}/cm^{-1}	6100		4700	4700	4200
	ρ_{RT}/Ω cm	3.6×10^7		3.5×10^3	2.3×10^5	5.0 (~10^2[c])
	E_a/eV	0.35		0.09	0.29	0.06
	Melting point/°C	108—109		108—109	107—108	151—154
3	D:A	1:1		1:1		1:1
	Stacking	DA		DA		DA
	Spacing	Uniform		Uniform		Uniform
	/Å	3.44		3.43		3.47
	Molecular structure	p-Form		n-Form		n-Form
	Mode of DA overlap	p-Mode		n-Mode		p-Mode
	γ (X-ray)	0.13		0.42		0.71
	γ (IR)	0.30		0.30		0.52
	E_{CT}/cm^{-1}	5200		4600		3900
	ρ_{RT}/Ω cm	1.2×10^6		2.2×10^6		7.5×10^3
	E_a/eV	0.33		0.39		0.18
	Melting point/°C	95—96		100—101		87—89

a) The first redox potential ($E^1_{1/2}$) vs. SCE 0.1 M TBA·BF_4/CH_2ClCH_2Cl, Pt electrode: 0.64 V (TTC_n-TTF), 0.58 V ($TSeC_n$-TTF), 0.51 V ($TTeC_n$-TTF). b) The abbreviation is described in the text. c) The value reported by Aharon-Shalom et al. (Ref. 21).

The authors wish to thank Dr. Susumu Matsuzaki of Kumamoto University for his measurements of the IR spectra. They are also grateful to Professor Kazuhiro Nakasuji of the Institute for Molecular Science for his helpful discussions.

References

1) H. Inokuchi, G. Saito, P. Wu, K. Seki, T. B. Tang, T. Mori, K. Imaeda, T. Enoki, Y. Higuchi, K. Inaka, and N. Yasuoka, *Chem. Lett.*, **1986**, 1263.

2) K. Seki, T. B. Tang, T. Mori, P. Wu, G. Saito, and H. Inokuchi, *J. Chem. Soc., Faraday Trans. 2*, **82**, 1067 (1986).

3) K. Imaeda, T. Enoki, Z. Shi, P. Wu, N. Okada, H. Yamochi, G. Saito, and H. Inokuchi, *Bull. Chem. Soc. Jpn.*, **60**, 3163 (1987).

4) Z. Shi, T. Enoki, K. Imaeda, K. Seki, P. Wu, H. Inokuchi, and G. Saito, *J. Phys. Chem.*, **92**, 5044 (1988).

5) H. Inokuchi, K. Imaeda, T. Enoki, T. Mori, Y. Maruyama, G. Saito, N. Okada, H. Yamochi, K. Seki, Y. Higuchi, and N. Yasuoka, *Nature*, **329**, 39 (1987).

6) G. Saito, *Physica B, Amsterdam*, **143**, 296 (1986).

7) N. Okada, H. Yamochi, F. Shinozaki, K. Oshima, and G. Saito, *Chem. Lett.*, **1986**, 1861.

8) H. Yamochi, N. Iwasawa, H. Urayama, and G. Saito, *Chem. Lett.*, **1987**, 2265.

9) N. Iwasawa, Ph. D. Thesis, The University of Tokyo, Tokyo, Japan, 1987.

10) P. Wu, G. Saito, K. Imaeda, Z. Shi, T. Mori, T. Enoki, and H. Inokuchi, *Chem. Lett.*, **1986**, 441.

11) P. Wu, T. Mori, T. Enoki, K. Imaeda, G. Saito, and H. Inokuchi, *Bull. Chem. Soc. Jpn.*, **59**, 127 (1986).

12) G. Saito, H. Kumagai, C. Katayama, C. Tanaka, J. Tanaka, P. Wu, T. Mori, K. Imaeda, T. Enoki, H. Inokuchi, Y.

Higuchi, and N. Yasuoka, *Isr. J. Chem.*, **27**, 319 (1986).
13) K. Imaeda, T. Enoki, T. Mori, P. Wu, M. Kobayashi, H. Inokuchi, and G. Saito, *Synth. Met.*, **19**, 721 (1987).
14) T. Mori, P. Wu, K. Imaeda, T. Enoki, H. Inokuchi, and G. Saito, *Synth. Met.*, **19**, 545 (1987).
15) N. Iwasawa, H. Urayama, H. Yamochi, G. Saito, K. Imaeda, T. Mori, Y. Maruyama, H. Inokuchi, T. Enoki, Y. Higuchi, and N. Yasuoka, *Synth. Met.*, **27**, B463 (1988).
16) N. Iwasawa, F. Shinozaki, G. Saito, K. Oshima, T. Mori, and H. Inokuchi, *Chem. Lett.*, **1988**, 215.
17) P. Main, S. E. Hull, L. Lessinger, G. Germain, J. P. Declercq, and M. M. Woolfson, MULTAN 78, Univ. of York, England and Louvain, Belgium (1978).
18) "International Tables for X-Ray Crystallography," Kynoch Press, Birmingham (1974), Vol. IV.
19) T. Sakurai and K. Kobayashi, *Rep. Inst. Phys. Chem. Res.*, **55**, 69 (1978).
20) Tables of atomic parameters of H-atoms, anisotropic thermal parameters, the F_o-F_c lists, bond distances, bond angles, and equations of the planes are deposited as Document No. 9200 at the Office of the Editor of Bull. Chem. Soc. Jpn.
21) E. Aharon-Shalom, J. Y. Becker, J. Bernstein, S. Bittner, and S. Shaik, *Synth. Met.*, **11**, 213 (1985). Their final R value is 0.051 for 2291 reflections, while R=0.038 for 4074 reflections in our work. Thus, we report crystallographic data as a well-refined structure for (TTeC$_2$-TTF)TCNQ.
22) P. Wang, T. Mori, C. Nakano, Y. Maruyama, H. Inokuchi, N. Iwasawa, H. Yamochi, H. Urayama, and G. Saito, *Bull. Chem. Soc. Jpn.*, **61**, 3455 (1988).
23) T. J. Kistenmacher, T. J. Emge, A. N. Bloch, and D. O. Cowan, *Acta Crystallogr., Sect. B*, **38**, 1193 (1982).
24) J. S. Chappell, A. N. Bloch, W. A. Bryden, M. Maxfield, T. O. Poehler, and D. O. Cowan, *J. Am. Chem. Soc.*, **103**, 2442 (1981).
25) J. B. Torrance, J. E. Vazquez, J. J. Mayerle, and V. Y. Lee, *Phys. Rev. Lett.*, **46**, 253 (1981).
26) T. Mori, A. Kobayashi, Y. Sasaki, H. Kobayashi, G. Saito, and H. Inokuchi, *Bull. Chem. Soc. Jpn.*, **57**, 627 (1984).

 © 1991 The Chemical Society of Japan Bull. Chem. Soc. Jpn., 64, 2169—2173 (1991)

Mechanism of Production of Singlet Oxygen on Photoexcitation of Drugs Inducing Photosensitivity

Tatsuo ARAI, Yoshinobu NISHIMURA, Masako SASAKI,*,† Hitoshi FUJITA,††
Itsuro MATSUO,†† Hirochika SAKURAGI, and Katsumi TOKUMARU*
Department of Chemistry, University of Tsukuba, Ibaraki 305
† Institute of Research and Development, Tokai University,
Hiratsuka, Kanagawa 259-12
†† Tokai University, School of Medicine, Isehara, Kanagawa 259-11
(Received December 25, 1990)

The mechanism and active species of drug-induced photosensitive reactions were investigated by measuring the absorption spectra of the transient species on photoexcitation as well as by determining the efficiency of singlet oxygen production on quenching by oxygen of the excited state of drugs. The quantum yields of singlet oxygen production were determined for chlorpromazine hydrochloride, mequitazine, and afloqualone as 0.27, 0.28, and 0.14, respectively. These rather high yields of singlet oxygen suggest its important role in photosensitivity of the drugs. On the basis of the transient-spectroscopic investigations the quenching mechanism of excited-state drugs by oxygen was discussed.

Much attention has been focused on the real active species in photosensitive reactions of drugs. Among drugs benoxaprofen[1] and chlorpromazine[2-6] are reported to undergo photodecarboxylation and photodechlorination, respectively, yielding radical species which can add to DNA or cause disruption of cell membrane. Furthermore, it was reported that benoxaprofen[1b] and chlorpromazine[7] produce singlet oxygen while piroxicam[8,9] produces no detectable amount of singlet oxygen on photoexcitation. In this respect, we investigated the mechanism and active species of drug-induced photosensitive reactions by measuring the absorption spectra of the transient species on photoexcitation and by determining the efficiency of singlet oxygen production on quenching by oxygen of the excited state of drugs which are shown in Chart 1. Among these drugs chlorpromazine hydrochloride (CPZ), mequitazine (MQZ), afloqualone (AQ), and piroxicam (PRX) are known to induce skin photosensitivity, and 5- (5-MOP) and 8-methoxypsoralen (8-MOP) are phototoxic.

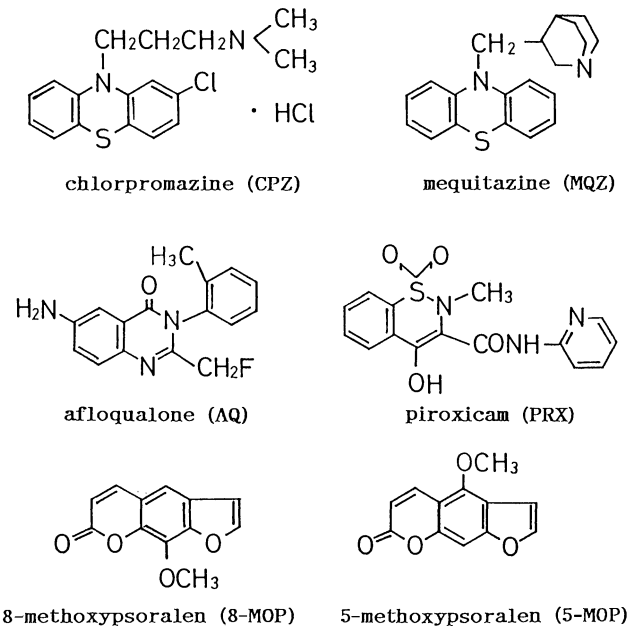

Chart 1.

Experimental

Materials. CPZ was supplied by Sionogi & Co., MQZ by Nippon Shoji Co., AQ by Tanabe Seiyaku Co., PRX by Pfizer Taito Co., 8-MOP by Tokyo Chemical Industry Co. 5-MOP was a gift from Kanebo Cosmetic Laboratory. These drugs were used as received. Solvent benzene (Luminazol) was obtained from Dojin Chem Co.

Laser Flash Photolyses. Laser flash photolyses and singlet oxygen detections were performed as described previously[10,11] by using 308-nm laser pulses of 10-ns fwhm from an excimer laser (Lambda Physik EMG 101, XeCl) as an exciting light source.

The efficiency of the singlet oxygen production was determined as follows. The decay curves of singlet oxygen ($^1\Delta_g$) emission at 1.27 μm were measured for the solutions optically matched at 308 nm for drugs and benzophenone using a germanium diode as a detector.[10-12] The initial intensities of the singlet oxygen emission were obtained from the decay curves, and the quantum yields for singlet oxygen production (Φ_{SO}) were obtained by comparing the initial intensities with that of benzophenone (BP, Φ_{SO}=0.29) as a standard.[13] The detection limit of the present instrument is 0.02 as the quantum yield of singlet oxygen production.

Results

Determination of the Singlet Oxygen Yields. Figure 1a shows a decay profile of the near-infrared emission of singlet oxygen on excitation of benzophenone in benzene at ambient temperature by a 308-nm laser pulse. Excitation of either CPZ, MQZ, or AQ afforded a similar decay curve. The decay curve observed for MQZ is shown in Figure 1b as an example. The singlet oxygen lifetime (28—32 μs) thus obtained is in good agreement with the value reported.[13] The quantum yields of singlet oxygen production (Φ_{SO}) from the drugs are

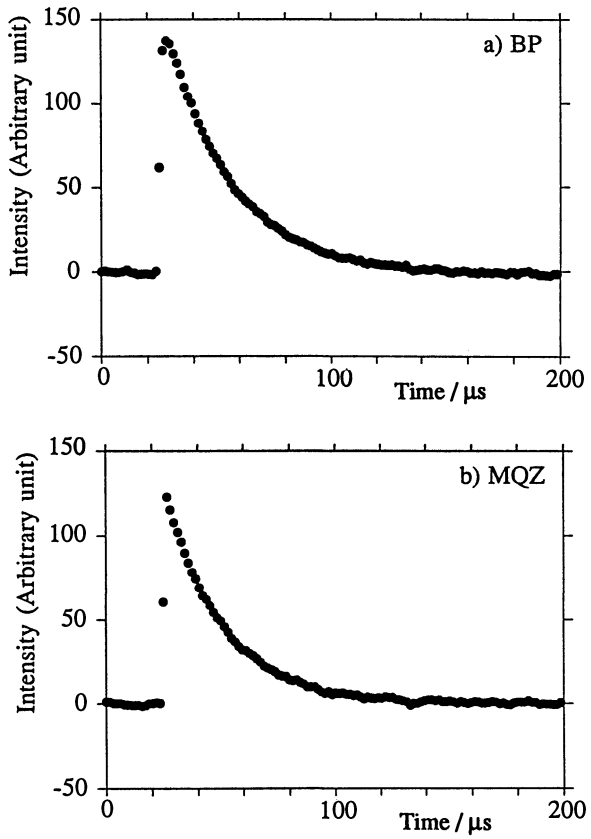

Fig. 1. Decay profiles of singlet oxygen luminescence at 1.27μm in the presence of BP (a) or MQZ (b) in aerated benzene.

obtained using the initial intensities of the emission compared with that of BP (0.29).[13] The quantum yields for CPZ, MQZ, and AQ are 0.27, 0.28, and 0.14, respectively. However, the emission could not be detected for PRX,[9] 5-MOP, and 8-MOP under our experimental conditions, indicating that Φ_{SO} for these compounds must be lower than 0.02. These low values for 5-MOP and 8-MOP are in accordance with the values reported.[14]

T_1-T_n Absorption Spectra and Their Quenching Rate Constants by Oxygen. Figure 2 shows the transient absorption spectra of CPZ, MQZ, and AQ in benzene. CPZ exhibited its transient spectrum at 360—700 nm (λ_{max}: 480 nm) which decayed by first-order kinetics (τ_T=5.8 μs) under argon atmosphere and was efficiently quenched by oxygen (k_q=1.4×10^{10} M^{-1} s^{-1}, M=mol dm^{-3}). The maximum wavelength in the present observation in benzene is shifted to the longer wavelength compared with that reported[15,16] in mixed solvents of alcohols and water (λ_{max}: 460—465 nm). The observed lifetime and the oxygen quenching rate constant suggest that this spectrum is attributed to the T_1–T_n absorption. MQZ also exhibited the T_1–T_n absorption spectrum at 360—700 nm (λ_{max}: 480 nm, τ_T=4.2 μs) and was quenched by oxygen (k_q=1.6×10^{10} M^{-1} s^{-1}). AQ exhibited an intense

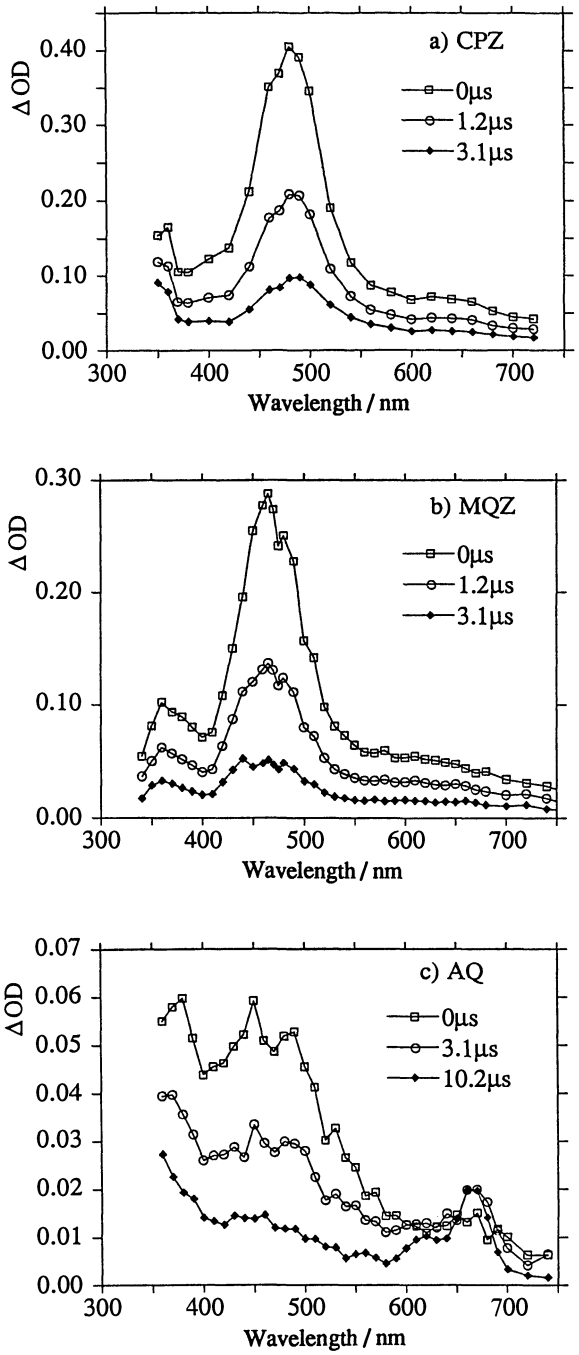

Fig. 2. Transient absorption spectra observed on 308 nm excitation of CPZ (a), MQZ (b), and AQ (c) in benzene.

absorption band at 360—600 nm (λ_{max}: 450 nm) accompanied by a weak band at 600—720 nm; the former band decayed with a lifetime of 6.7 μs (Fig. 3a and b) under argon and was quenched by oxygen at a nearly diffusion-controlled rate (k_q=6.4×10^9 M^{-1} s^{-1}), and the latter band around 670 nm increased in intensity with the μs time scale (Fig. 3c). This behavior indicates occurrence of chemical reactions at the excited state of AQ.

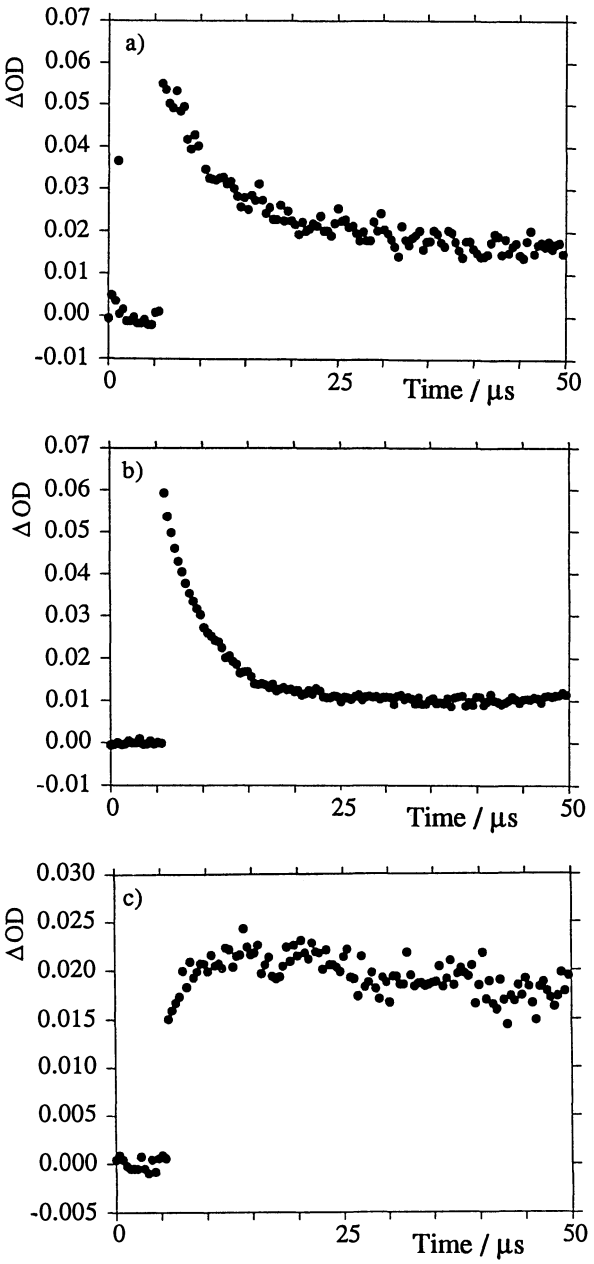

Fig. 3. Time profiles of transient absorptions monitored at 360 nm (a), 450 nm (b), and 670 nm (c) following 308 nm laser photolysis of AQ in benzene.

Discussion

Possible Quenching Mechanism by Oxygen. The quenching of excited triplet states by oxygen proceeds as shown by Eqs. 1—3, where spin statistical factors in triplet-triplet annihilation play an important role. If the triplet state of a substrate has an energy higher than that of singlet oxygen, 95 kJ mol^{-1}, the quenching proceeds through energy transfer (Eq. 1). The probability for this process is only 1/9 for every collisional encounter, and thus, the rate constant for this process must be 1/9 of the diffusion-controlled rate constant (3×10^9 M^{-1} s^{-1}).[17] On the other hand, quenching by acceleration of intersystem crossing to the ground state (Eq. 2) becomes more important as the energy difference between the ground S_0 and triplet T_1 states becomes smaller than 95 kJ mol^{-1}. The triplet energies of CPZ, MQZ, AQ, 5-MOP, and 8-MOP were determined as 246, 247, 238, 252, and 259 kJ mol^{-1}, respectively, by phosphorescence measurements.[18] From these values the oxygen quenching is presumed to proceed through energy transfer (Eq. 1).

$$^3S^*+{}^3O_2 \underset{}{\overset{k_d/9}{\rightleftarrows}} {}^1[S\cdots O_2]^* \longrightarrow {}^1S+{}^1O_2^* \quad (1)$$

$$\overset{3k_d/9}{\rightleftarrows} {}^3[S\cdots O_2]^* \longrightarrow {}^1S+{}^3O_2 \quad (2)$$

$$\overset{5k_d/9}{\rightleftarrows} {}^5[S\cdots O_2]^* \quad (3)$$

Mechanism of Singlet Oxygen Production.

$$S \xrightarrow{h\nu} {}^1S^* \quad (4)$$

$$^1S^* \xrightarrow{k_5} S \quad (5)$$

$$^1S^* \xrightarrow{k_6} S+h\nu \quad (6)$$

$$^1S^* \xrightarrow{k_7} {}^3S^* \quad (7)$$

$$^1S^*+O_2 \xrightarrow{k_8} {}^3S^*+{}^1O_2^* \quad (8)$$

$$^1S^*+O_2 \xrightarrow{k_9} {}^3S^*+O_2 \quad (9)$$

$$^3S^*+O_2 \xrightarrow{k_{10}} S+{}^1O_2^* \quad (10)$$

$$^3S^*+O_2 \xrightarrow{k_{11}} S+O_2 \quad (11)$$

$$^3S^* \xrightarrow{k_{12}} S \quad (12)$$

$$\Phi_{SO}=\frac{\{k_8[O_2]+\dfrac{k_{10}[O_2]\{k_7+(k_8+k_9)[O_2]\}}{\{(k_{10}+k_{11})[O_2]+k_{12}\}}\}}{\{k_5+k_6+k_7+(k_8+k_9)[O_2]\}} \quad (13)$$

$$\Phi_{SO}=k_7k_{10}/(k_5+k_6+k_7)(k_{10}+k_{11})=\Phi_{isc}\Phi_\Delta \quad (14)$$

The quenching of excited drugs by oxygen should take place as shown in Eqs. 4—12, where S denotes a drug. The quantum yield of singlet oxygen production (Φ_{SO}) is described as Eq. 13. If the quenching of excited singlet drugs by oxygen is not important ($(k_5+k_6+k_7)\gg$

$(k_8+k_9)[O_2])$, Φ_{SO} can be reduced to Eq. 14, where Φ_{isc} $(=k_7/(k_5+k_6+k_7))$ and Φ_Δ $(=k_{10}/(k_{10}+k_{11}))$ mean the quantum yields of intersystem crossing from the singlet excited states to the triplet excited states and the efficiency of singlet oxygen production in the quenching of the triplet molecules by oxygen, respectively.

Therefore, the efficiency of singlet oxygen production is related to the quantum yield of intersystem crossing of the excited singlet state of drugs. The quantum yields of intersystem crossing were reported to be as low as 0.067 and 0.011[19] for 5-MOP and 8-MOP, respectively. Thus, these low Φ_{ISC} values might be the reason why no singlet oxygen emission was detected from 5-MOP and 8-MOP. Actually, Φ_{SO}'s are reported as 0.021 and 0.0044 for 5- and 8-MOP,[14] respectively, which are below our detection limit.

Quenching of a singlet excited state by oxygen can give directly singlet oxygen together with the triplet excited state, if the energy difference between the singlet and triplet excited states is higher than the excitation energy of singlet oxygen (95 kJ mol^{-1}). However, this is not the case since the energies of the singlet excited state of CPZ and AQ are measured as 271 and 276 kJ mol^{-1},[18] respectively, and accordingly, they cannot produce singlet oxygen on their quenching by oxygen (E_T: 246 and 238 kJ mol^{-1} for CPZ and AQ, respectively).[18]

Therefore, the efficiency of singlet oxygen production observed for the drugs examined mainly reflects those of intersystem crossing and singlet oxygen production in the quenching of their triplet state. The quenching of the triplet molecules having enough energies to produce singlet oxygen is usually assumed to produce singlet oxygen with a nearly unit efficiency, and thus, we can tentatively assume the efficiency of singlet oxygen production as a lower limit of the intersystem crossing efficiency for these drugs.

The observed quenching rate constants for ^{3}CPZ*, ^{3}MQZ*, and ^{3}AQ* by oxygen are 2—5 times larger than the assumed value (3×10^9 M^{-1} s^{-1}) from Eq. 1. Therefore, there must be some other interactions resulting in the efficient production of singlet oxygen.

For some molecules, participation of the electron transfer mechanism[20] is proposed in the quenching of their triplet states by oxygen. For example, the observed rate constats of oxygen quenching for substituted benzophenone triplets exceed a limit imposed by the spin-statistical restriction (3×10^9 M^{-1} s^{-1}); the quenching rate constant for 4,4′-bis(dimethylamino)benzophenone (DAB, $k_q=12.3\times10^9$ M^{-1} s^{-1}) is more than 5 times higher than that for benzophenone (2.3×10^9 M^{-1} s^{-1}). However, the singlet oxygen is produced with the same efficiency in the quenching of triplet DAB as from triplet benzophenone. The aforementioned large rate constants determined for the present drugs might suggest an intervention of the electron transfer interaction in addition to the usual energy transfer mechanism in the quenching process to produce singlet oxygen.

It should be noted that singlet oxygen ($^1\Delta_g$) is often claimed as an acting species of photosensitivity of drugs based only on the observation of their triplet states and their quenching by oxygen. However, as has been revealed recently, the efficiency of singlet oxygen production is very much dependent on the properties of the triplet excited state. For example, aromatic ketones such as benzophenone produce singlet oxygen not with a unit efficiency but with a rather low value, 0.29.[13] In this case the quenching is supposed to proceed not only by energy transfer but also by addition of oxygen on the carbonyl moiety producing biradical species.[21] Measurements of intersystem crossing yields of durgs will be useful to elucidate the quenching mechanism and the relation between quenching rates and singlet oxygen yields. However, the present determination of the singlet oxygen yields by the direct observation of emission gives an important information for the elucidation of real active species in the photosensitive reactions of drugs.

Conclusion

Quenching of the triplet state of CPZ, MQZ, and AQ by oxygen efficiently produces singlet oxygen, which seems to be responsible for the photosensitive reactions induced by these drugs. Furthermore, AQ also undergoes photoreactions even without oxygen, and can cause additional photosensitive reactions.

The authors thank the Ministry of Education, Science and Culture for partial support by Grant-in-Aid for Special Project Research Nos. 61123001, 62113001, and 63104001 (KT), Nos. 61223023, 62213029, and 63104001 (MS), and by Grant-in-Aid for Scientific Research No. 01740255 (TA).

References

1) a) K. Reszka and C. F. Chignell, *Photochem. Photobiol.*, **38**, 281 (1983); b) S. J. Navaratnam, L. Hughes, B. J. Parsons, and G. O. Phillips, *Photochem. Photobiol.*, **41**, 375 (1985).

2) F. Laterrier, A. Mendyk, and J. Viret, *Biochem. Pharmacol.*, **25**, 2469 (1976).

3) I. E. Kochevar, *J. Invest. Dermatol.*, **76**, 59 (1981).

4) H. Fujita, F. Yanagisawa, A. Endo, and K. Suzuki, *J. Radiat. Res.*, **21**, 279 (1980).

5) G. Testylier, G. Clement, and F. Leterrier, *Photochem. Photobiol.*, **39**, 277 (1984).

6) A. G. Motten, G. R. Buttener, and C. Chignell, *Photochem. Photobiol.*, **42**, 9 (1985).

7) R. D. Hall, G. R. Buettner, A. G. Motten, and C. F. Chignell, *Photochem. photobiol.*, **46**, 295 (1987).

8) I. E. Kochevar, W. L. Morison, J. L. Lamm, D. J. Mc Auliffe, A. Wester, and A. F. Hood, *Arch. Dermatol.*, **122**, 1283 (1986).

9) A. Western, J. R. Van Camp, R. Bensasson, E. J. Land, and I. E. Kochevar, *Photochem. Photobiol.*, **46**, 469 (1987).

10) T. Arai, T. Karatsu, M. Tsuchiya, H. Sakuragi, and K. Tokumaru, *Chem. Phys. Lett.*, **149**, 161 (1988).

11) H. Okamoto, T. Arai, H. Sakuragi, and K. Tokumaru, *Bull. Chem. Soc. Jpn.*, **63**, 2881 (1990).
12) M. A. J. Rodgers and P. T. Snowden, *J. Am. Chem. Soc.*, **104**, 5541 (1982).
13) A. A. Gorman, I. Hamblett, and M. A. J. Rodgers, *J. Am. Chem. Soc.*, **106**, 4679 (1984).
14) C. N. Knox, E. J. Land, and T. G. Truscott, *Photochem. Photobiol.*, **43**, 359 (1986).
15) T. Iwaoka and M. Kondo, *Bull. Chem. Soc. Jpn.*, **50**, 1 (1977).
16) S. B. Navaratnam, J. Parsons, and G. O. Phillips, *J. Chem. Soc., Faraday Trans. 1*, **74**, 1811 (1978).
17) O. L. Gijzeman, J. F. Kaufman, and G. Porter, *J. Chem. Soc., Faraday Trans. 2*, **69**, 708 (1973).
18) M. Sasaki, H. Fujita, and I. Matsuo, unpublished results.
19) R. V. Bensasson, E. J. Land, and C. Salet, *Photochem. Photobiol.*, **27**, 273 (1978).
20) S. K. Chattopadhyay, C. V. Kumar, and P. K. Das, *J. Photochem.*, **30**, 81 (1985).
21) A. A. Gorman and M. A. J. Rodgers, *J. Am. Chem. Soc.*, **108**, 5074 (1986).

 © 1991 The Chemical Society of Japan Bull. Chem. Soc. Jpn., 64, 2174—2182 (1991) [Vol. 64, No. 7

Structural Transition Behavior of Potassium Salts of Saturated Fatty Acids, $CH_3(CH_2)_nCO_2K$ (n=14, 16, 18, 20)

Tsutomu ISHIOKA
Department of Material Systems Engineering, Faculty of Technology,
Tokyo University of Agriculture and Technology, Koganei, Tokyo 184
(Received January 16, 1991)

The structural transition behavior of potassium soaps (99% purity), $CH_3(CH_2)_nCO_2K$ (n=14, 16, 18, 20), having low water contents of less than 10 wt% was investigated by both DSC and vibrational spectroscopies. Nine phases from crystal (I<80 °C) to liquid crystal (260 °C<IX) were observed for n=14 and 16 by thermal measurements. An additional phase I′ (I<I′<II) was found for n=18 and 20. The structural changes of the alkyl chains accompanied by these transitions were investigated by using IR and Raman methods. With increase in temperature, the itensities of the IR methylene progressive bands which were characteristic of all-trans conformation decreased and conformational defect bands ascribed to *gt*-, *gg*-, and *gtg′* conformations, were observed in phases I′, II, and III for n=14—20. These indicate the onset of a partial melting of the chains in these phases. At the transition from phase III to IV, the chains entered liquid-like conformations. The result was also confirmed by the Raman spectra.

Even-numbered anhydrous potassium soaps, $CH_3(CH_2)_nCO_2K$ (where n is the number of the methylene groups), take successive phase transitions from the crystalline phase to the liquid crystalline phase with an increase in temperature.[1] The lowest temperature crystalline phase of n=10—16 is ascribed to the triclinic B-form (space group $P\bar{1}$). The unit cell contains two molecules having an all-trans conformation. The molecules are parallel to each other and are packed with a triclinic $T_{//}$ subcell. With an elevation in temperature, the B-form is transformed to the monoclinic C-form ($P2_1/a$) at 50—80 °C. The molecule in the C-form is supposed to have a partially conformational disorder at the methyl end. A further increase in the temperature causes the transition from the crystalline phase to the two-dimensional rectangular or oblique lattice at 170—195 °C for n=12—16. The lattice is changed into the lamellar liquid crystalline phase at 270—280 °C.

Several experimental techniques, such as x-ray diffraction or NMR methods, have been applied in order to characterize the molecular structure in these phases, while the detailed molecular transition behavior, especially the melting process of the alkyl chains during these successive transitions, has not yet been clearly shown. In this study, we tried to clarify the melting behavior of the alkyl chains in soaps with n=14, 16, 18, and 20 using differential scanning calorimetry (DSC), infrared, and Raman methods.

Experimental

Potassium soaps of n=14—20 were synthesized from even-numbered saturated fatty acids (Σ company, 99%) by the titration of potassium carbonate in ethanol solution kept at 70 °C. The products were purified by reprecipitation with diethyl ether from the solutions and dried at 100 °C in vacuo for 24 h. Neutralization was confirmed by the IR spectrum. The contents of water were evaluated as a few wt% by a elementary analysis.

DSC measurements were carried out with a Rigaku DSC using sealed pans at a heating rate 10 K min^{-1}. The transition temperatures and enthalpy changes were calibrated using seven standards: carbon tetrachloride, benzene, naphthalene, benzoic acid, indium, tin, and lead. Infrared measurement was made with a JASCO IR-810 spectrophotometer. The wavenumbers were calibrated with an indene standard. The sample for IR measurements was pressed into a KBr disk. Raman measurements were made with a JASCO R-800 double monochromator using a 514.5 nm exciting beam from an Ar^+ laser. A powder sample sealed in a glass capillary was subjected to a Raman measurement. The heating rate for the IR and Raman measurements was 10 K min^{-1}. In order to achieve thermal equilibrium, the measurements were carried out after 1 h of temperature setting.

Results and Discussion

The results of DSC measurements for n=14, 16, 18, and 20 are shown in Fig. 1. With increasing temperature from room temperature to 280 °C, eight endothermic peaks were observed for n=14 and 16 and nine peaks for n=18 and 20. According to Cingolani et al.,[2] these transitions are described with symbols from b′ to F, as shown in Fig. 1. Their temperatures, enthalpy, and entropy changes were the same as those obtained by Cingolani et al.[2] for n=14, 16, and 18 within the experimental error. Those for n=20 are listed in Table 1. Nine phases were designated as from phase I

Table 1. Transition Temperatures, Enthalpy, and Entropy Changes for n=20

	t	ΔH	ΔS
	K	kJ mol^{-1}	J K^{-1} mol^{-1}
I→I′	342.0	2.5	7.2
I′→II	361.1	14.9	41.2
II→III	403.2	1.8	4.5
III→IV	427.7	2.3	5.4
IV→V	450.2	12.3	27.2
V→VI	488.8	0.5	1.1
VI→VII	501.3	0.6	1.2
VII→VIII	519.4	1.0	1.9
VIII→IX	538.6	9.4	17.5

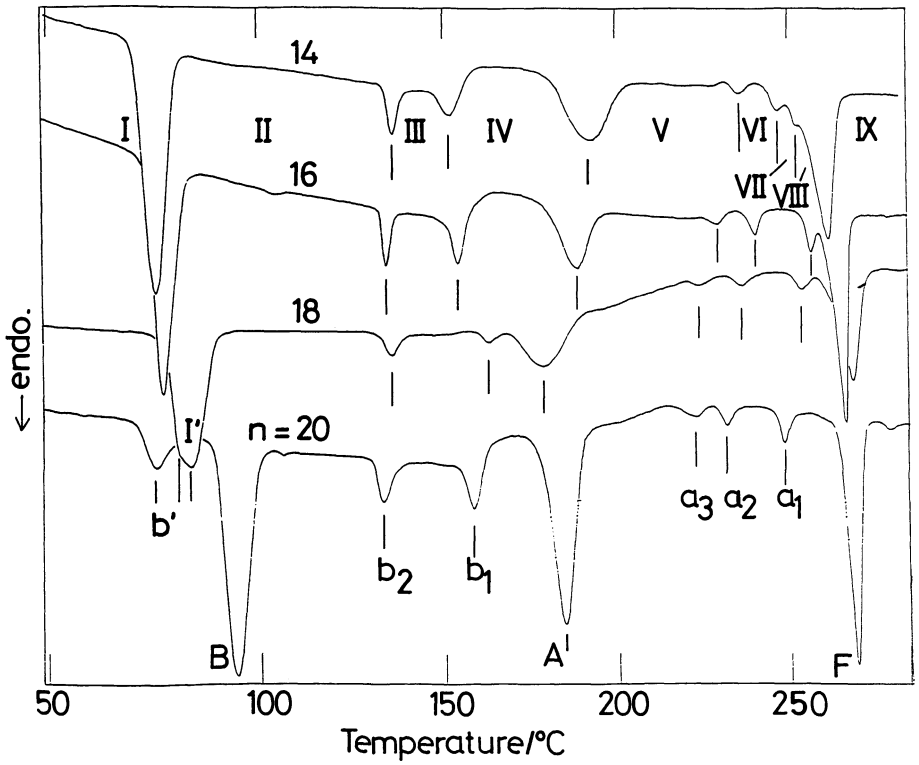

Fig. 1. DSC curves for n=14—20.

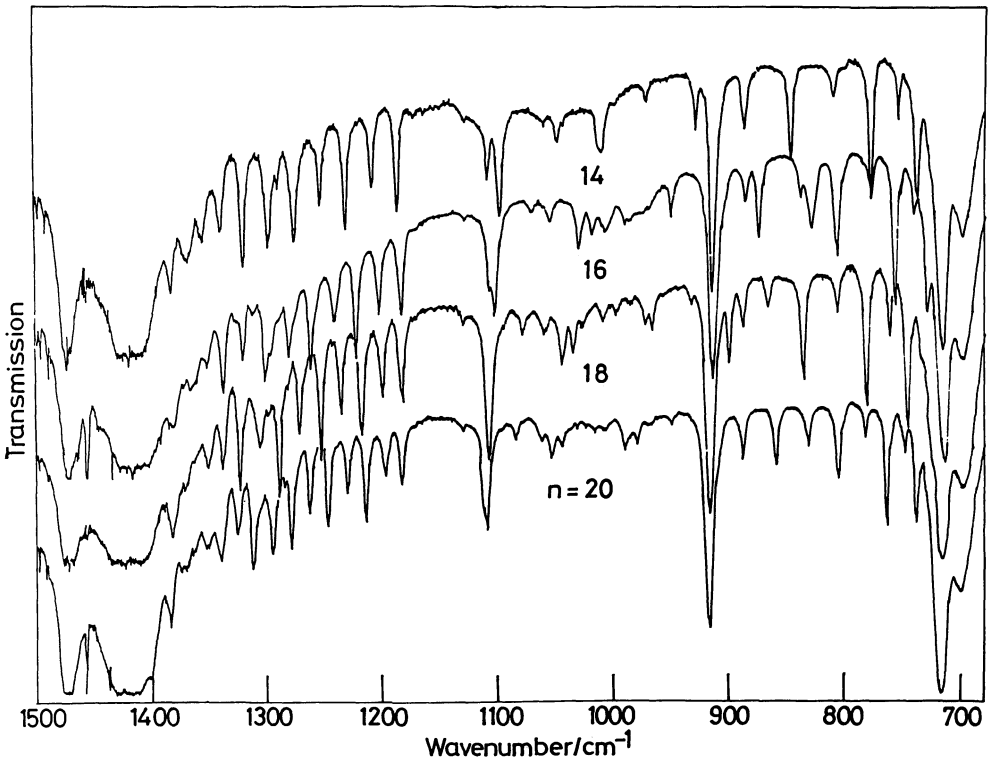

Fig. 2. IR spectra for n=14—20 in the 700—1400 cm^{-1} region at room temperature.

Table 2. Observed and Calculated Frequencies (cm^{-1}) for $n=14$

ν_{obsd}	Relative intensity[a]	ν_{calcd}	P. E. D. (%)[b]			
A′ mode						
1417	s	1414	δ(44),	W(22),	R(15),	ν_s(COO)(14)
		1410	W(54),	R(30),	δ(13)	
		1404	W(60),	R(30)		
		1394	W(60),	R(27),	δ(11)	
1385	m	1383	W(61),	R(25),	δ(10)	
		1373	U(70),	W(15),	R(11)	
1367	m	1367	W(59),	R(17),	U(16)	
1357	m	1351	W(73),	R(16)		
1340	m	1332	W(80),	R(11)		
1322	m	1312	W(86)			
1299	m	1294	W(89)			
1276	m	1276	W(87)			
1253	m	1257	W(83)			
1232	m	1235	W(78),	ω(11)		
1209	m	1208	W(76),	ω(10)		
1188	m	1181	W(83)			
1130	w	1129	R(39),	ω(33),	W(13)	
1099	m	1093	R(41),	ω(27),	W(21)	
		1069	R(81),	W(17)		
		1067	R(78),	W(15)		
		1065	R(76),	W(17)		
1061	w	1061	R(82),	W(17)		
		1058	R(80),	W(17)		
		1054	R(82),	W(11)		
1049	w	1050	R(66),	W(15),	ω(15)	
		1033	R(75),	W(10),	ω(10)	
1014	m	1017	R(80),	W(10)		
998	vw	1000	R(72),	ω(13)		
		983	R(80),	ω(11)		
		973	R(78),	ω(12)		
917	m	891	R(47),	β(33)		
889	m	888	R(49 ,	δ(COO)(39)		
A″ mode						
		1302	T(96)			
		1302	T(97)			
		1300	T(98)			
		1299	T(95)			
		1297	T(97)			
		1296	T(100)			
		1294	T(90)			
1289	w	1286	T(85),	P(12)		
		1274	T(79),	P(17)		
1258	vw, sh	1259	T(72),	P(23)		
		1241	T(62),	P(32)		
		1219	T(49),	P(43)		
		1196	P(59),	T(30)		
1174	vw	1177	P(82)			
1109	m	1103	T(64),	P(32)		
1043	vw, sh	1036	T(88),	P(10)		
1011	m	1005	T(70),	P(24)		
973	w	968	T(56),	P(35)		
931	m	930	P(45),	T(45)		
889	m	890	P(54),	T(36)		
849	m	851	P(62),	T(28)		
812	w	813	P(69),	T(21)		
779	m	778	P(76),	T(15)		
755	m	745	P(82),	T(11)		
739	m	718	P(88)			
727	w, sh	695	P(92)			
		679	P(96)			
		667	P(98)			
716	s	661	P(100)			

a) s, m, w, v, sh mean strong, medium, weak, very, and shoulder. b) P. E. D.=potential energy distribution where W, R, P, T, U, β, ω, δ, ν_s(COO), and δ(COO) indicate methylene wagging, C–C stretching, methylene rocking-twisting, twisting-rocking, methyl symmetric bending, rocking, C–C–C bending, methylene bending, carboxylate symmetric stretching, and bending, respectively.

Table 3. Observed and Calculated Frequencies (cm^{-1}) for n=16

ν_{obsd}	Relative intensity	ν_{calcd}	P. E. D. (%)			
A′ mode						
		1416	W(45),	R(27),	δ(17)	
1419	s	1413	W(40),	δ(28),	R(23)	
		1408	W(53),	R(28),	δ(16)	
		1401	W(57),	R(28),	δ(13)	
		1391	W(60),	R(26),	δ(11)	
1385	w	1380	W(60),	R(23)		
1371	vw, sh	1372	U(77),	W(11)		
1364	w	1364	W(66),	R(18)		
1355	w	1348	W(75),	R(15)		
1340	m	1331	W(81),	R(10)		
1323	m	1314	W(86),			
1303	m	1298	W(88)			
1283	m	1282	W(88)			
1263	m	1266	W(86)			
1244	m	1245	W(82),	ω(10)		
1224	m	1227	W(78),	ω(11)		
1205	m	1203	W(77),	ω(10)		
1185	m	1178	W(86)			
1130	w	1127	R(39),	ω(34),	W(11),	β(10)
1104	m	1096	R(40),	ω(28),	W(20)	
1072	w	1072	R(74),	W(18)		
		1071	R(80),	W(18)		
		1069	R(74),	W(20)		
		1066	R(81),	W(17)		
		1063	R(76),	W(16)		
		1062	R(75),	W(17)		
1056	w	1061	R(78),	W(16)		
		1048	R(69),	ω(13),	W(13)	
1030	w	1037	R(78),	W(10)		
		1019	R(84)			
1003	vw	1009	R(65),	ω(17),	W(13)	
991	w	992	R(82)			
		975	R(73),	ω(15),	W(10)	
970	vw	969	R(80),	ω(11)		
917	m	890	R(48),	β(32)		
888	w	888	R(48),	δ(COO)(40)		
A″ mode						
		1302	T(92)			
		1302	T(96)			
		1300	T(97)			
		1300	T(96)			
		1298	T(95)			
1297	m, sh	1297	T(99)			
		1296	T(100)			
1291	w	1294	T(90)			
		1287	T(86),	P(12)		
1280	w, sh	1278	T(81),	P(16)		
		1265	T(75),	P(22)		
1259	w, sh	1250	T(67),	P(28)		
		1232	T(57),	P(37)		
1219	vw, sh	1212	P(49),	T(43)		
		1192	P(64),	T(25)		
1173	vw	1176	P(85)			
		1102	T(64),	P(32)		
1042	vw	1039	T(90),			
1020	w	1014	T(75),	P(21)		
987	w	982	T(62),	P(32)		
951	w	948	T(51),	P(41)		
914	vw, sh	914	P(49),	T(41)		
877	m	879	P(57),	T(34)		
841	m	844	P(64),	T(27)		
809	m	811	P(70),	T(21)		
780	m	779	P(76),	T(16)		
759	m	750	P(82),	T(12)		
743	m	725	P(87)			
732	m	704	P(91)			
		687	P(94)			
		674	P(97)			
		665	P(99)			
716	s	660	P(100)			

(crystalline phase) to phase IX (lamellar liquid crystalline phase) for n=14 and 16. An additional phase I′ was observed for n=18 and 20. The crystal structure of phase I of n=14—20 was ascribed to the triclinic B-form by analysis of the X-ray powder pattern, while that of phase I′ of n=18 and 20 is uncertain at the present stage. Transition A was attributed to that from the crystalline phase to the two-dimensional lattice and F from the lattice to the lamellar liquid-crystalline phase.

In order to reveal any structural changes in the alkyl chains accompanied by these transitions, the temperature dependence of the IR and Raman spectra was measured. First, the spectra of n=14—20 at room temperature (phase I) were measured (Fig. 2) and their assignments were made with a normal coordinate calculation. The calculation was carried out by the Wilson GF matrix method using an NEC computer (ACOS 1000) at this university. The molecules were assumed to have an all-trans conformation and to belong to the C_s point group. A tetrahedral geometry was assumed for C–C–C, C–C–H, and H–C–H angles with C–C and C–H bond lengths equal to 1.54 and 1.093 Å, respectively. The C–C–O and O–C–O angles were assumed to be 120° with a C–O length equal to 1.27 Å.[3] The force constants regarding $CH_3(CH_2)_n$ group were transformed from the valence force constants derived by Snyder for normal paraffins (calculation V).[4] For the constants of the $C_\alpha H_2$ group and the torsional constants around all of the C–C bonds, those derived by Umemura were used.[5] For the COO^- group, the Urey-Bradley force constants derived by Nakamura[3] were transformed into the valence force constants[6] as initial values, and then adjusted to fit both

Table 4. Observed and Calculated Frequencies (cm^{-1}) for n=18

A′ mode						A″ mode					
ν_{obsd}	Relative intensity	ν_{calcd}	P. E. D. (%)			ν_{obsd}	Relative intensity	ν_{calcd}	P. E. D. (%)		
1417	s	1414	δ(49),	W(18),	R(13)			1302	T(96)		
		1410	W(61),	R(33)				1302	T(96)		
		1406	W(59),	R(31)				1301	T(96)		
		1400	W(60),	R(29),	δ(10)	1300	w	1300	T(97)		
		1393	W(61),	R(27),	δ(10)			1298	T(98)		
		1384	W(62),	R(25)				1298	T(95)		
1385	m	1374	W(41),	U(34),	R(18)			1297	T(98)		
1373	w	1371	U(50),	W(33),	R(12)			1296	T(99)		
		1360	W(70),	R(18)				1294	T(90)		
1352	w	1346	W(76),	R(14)		1283	vw, sh	1288	T(86),	P(12)	
1340	m	1331	W(81),	R(10)				1280	T(81),	P(16)	
1324	m	1315	W(86)					1270	T(76),	P(20)	
1307	m	1301	W(88)					1257	T(70),	P(26)	
1289	m	1287	W(89)					1242	T(62),	P(33)	
1272	m	1272	W(87)					1225	T(52),	P(41)	
1253	m	1257	W(83)					1206	P(53),	T(39)	
1236	m	1240	W(79),	ω(11)				1188	P(69),	T(22)	
1219	m	1221	W(76),	ω(12)		1172	vw	1176	P(87)		
1201	m	1199	W(76),	ω(11)		1095	vw	1103	T(64),	P(32)	
1185	m	1176	W(86)			1044	w	1041	T(92)		
1131	w	1131	R(40),	ω(35),	W(10)			1020	T(78),	P(18)	
1108	m	1104	R(39),	ω(29),	W(21)			993	T(66),	P(29)	
1078	w	1074	R(50),	ω(21),	W(21)	967	w	963	T(56),	P(38)	
		1067	R(81),	W(16)		933	vw	932	T(47),	P(46)	
		1067	R(79),	W(17)		900	m	901	P(53),	T(39)	
		1065	R(80),	W(16)		868	w	870	P(59),	T(32)	
1060	w	1063	R(82),	W(17)		836	m	839	P(65),	T(26)	
		1059	R(82),	W(17)		807	w	809	P(71),	T(21)	
		1057	R(78),	W(16)		781	m	780	P(77),	T(16)	
		1056	R(79),	W(15)		761	m	754	P(82),	T(12)	
		1054	R(81),	W(11)		746	m	731	P(86)		
1035	w	1037	R(84)			735	w, sh	711	P(90)		
1026	vw	1031	R(61),	ω(18),	W(16)	726	m, sh	694	P(93)		
1009	w	1015	R(85)					681	P(96)		
998	w	1000	R(69),	ω(16),	W(11)			671	P(97)		
986	vw	991	R(81)					664	P(99)		
		974	R(77),	ω(13)		716	s	660	P(100)		
972	w	971	R(80),	ω(12)							
917	m	891	R(47),	β(33)							
888	w	888	R(49),	δ(COO)(40)							

Table 5. Observed and Calculated Frequencies (cm^{-1}) for n=20

ν_{obsd}	Relative intensity	ν_{calcd}	P. E. D. %)			
A′ mode						
1420	s	1414	δ(49),	W(18),	ν_s(COO)(15),	R(13)
		1411	W(61),	R(34)		
		1407	W(60),	R(32)		
		1403	W(60),	R(30)		
		1396	W(60),	R(28)		
		1389	W(62),	R(26)		
1385	vw	1380	W(60),	R(24)		
1372	vw	1373	U(58),	W(25),	R(13)	
		1368	W(54),	U(22),	R(16)	
1362	vw	1357	W(71),	R(17)		
1352	w	1344	W(76),	R(14)		
1340	w	1330	W(82),	R(10)		
1326	w	1316	W(86)			
1311	m	1303	W(88)			
1293	m	1290	W(89)			
1277	m	1278	W(88)			
1261	m	1265	W(85)			
1246	m	1250	W(82),	ω(10)		
1229	m	1234	W(78),	ω(11)		
1214	m	1216	W(76),	ω(12)		
1197	m	1195	W(76),	ω(10)		
1183	m	1175	W(87)			
1130	w	1131	R(41),	ω(36)		
1111	m, sh	1107	R(39),	ω(30),	W(21)	
		1079	R(46),	ω(24),	W(22)	
		1068	R(80),	W(16)		
		1068	R(81),	W(17)		
		1065	R(80),	W(17)		
		1064	R(78),	W(16)		
1063	w	1062	R(80),	W(13)		
		1061	R(80),	W(16)		
		1058	R(81),	W(17)		
1054	w	1056	R(83),	W(17)		
		1050	R(84)			
1045	w	1045	R(64),	ω(16),	W(15)	
1031	vw	1033	R(75),	ω(10),	W(10)	
1026	vw	1021	R(81)			
1008	vw	1009	R(67),	ω(15),	W(12)	
		996	R(83)			
980	w	986	R(73),	ω(14)		
		973	R(81),	ω(11)		
968	vw	969	R(78),	ω(12)		
917	m	889	R(49),	β(31)		
888	m	888	R(49),	δ(COO)(40)		
A″ mode						
		1303	T(95)			
1305	w	1302	T(96)			
		1302	T(95)			
		1301	T(96)			
		1300	T(97)			
		1299	T(95)			
		1298	T(96)			
		1297	T(99)			
		1296	T(100)			
		1294	T(89),	P(10)		
		1289	T(85),	P(13)		
1284	w	1281	T(81),	P(17)		
		1271	T(77),	P(21)		
		1259	T(71),	P(27)		
		1246	T(65),	P(33)		
		1230	T(56),	P(42)		
		1212	P(53),	T(46)		

Table 5. (Continued)

ν_{obsd}	Relative intensity	ν_{calcd}	P. E. D. %)		
		1194	P(67),	T(31)	
		1179	P(86),	T(12)	
1108	m	1103	T(64),	P(32)	
1184	w	1086	T(75),	P(24)	
1037	vw	1040	T(90),	P(10)	
1018	vw	1018	T(75),	P(24)	
		993	T(43),	β(31),	P(24)
990	w	988	β(50),	T(30),	P(16)
950	vw	962	T(54),	P(43)	
920	m, sh	932	P(51),	T(46)	
		902	P(58),	T(39)	
859	m	872	P(64),	T(33)	
832	m	842	P(69),	T(28)	
806	m	815	P(75),	T(23)	
782	m	787	P(79),	T(18)	
763	m	762	P(83),	T(14)	
749	w	739	P(87),	T(11)	
739	m	719	P(90)		
731	w, sh	702	P(93)		
		688	P(95)		
		677	P(97)		
		669	P(98)		
		663	P(99)		
716	s	660	P(100)		

the observed and calculated frequencies by a trial-and-error method. The calculated frequencies in the methylene progressive region from 700 to 1400 cm^{-1}, which were sensitive to the conformational change of the chain, are listed in Table 2—5 for n=14—20, respectively. The frequencies of the observed progressive bands were satisfactorily assigned according to the all-trans conformation, although the above-mentioned force constants gave slightly higher calculated frequencies for the CH_2 wagging modes.[7] The assignment was almost the same as that derived by Gotoh and Takenaka[8] for n=14 and 16, except for that of the CH_3 rocking band.

Second, the conformational change with an increase in the temperature was considered. With increasing temperature, the intensities of the progressive bands ascribed to the all-trans conformation decreased at the transition from phase I to II for n=16, as shown in Fig. 3. New bands appeared at 1348, 1077, 932, 867, 855, 772, and 752 cm^{-1} (marked with asterisks in Fig. 3). At the transition from phase II to III, the intensities of the progressive bands further decreased and those of the new bands observed in phase II decreased and became slightly detectable. At temperatures above phase IV, all of these bands were smeared out. Similar spectral changes were also observed for n=14, 18, and 20. The new bands observed in phases I′, II, and III for n=14—20 are summarized in Table 6.

Comparing the new bands observed in phases I′, II, and III with the conformationally disordered bands of normal alkanes, we considered the structural transition behavior. Because of the localized character of the defect modes in normal alkanes, they may be well transferable among the molecules of the same class, as in the present cases. The frequencies of the defect modes have been evaluated for the end gauche (*gt-* where *g* and *t* represented trans and gauche conformations, respectively, and the dash meant the remainder of the chain was in all-trans or nearly all-trans conformation), double gauche (*gg-*), and kink (*gtg′*) conformations by normal-mode analysis for normal alkanes.[9-11] According to the analysis, the new bands observed in phases I′, II, and III were assigned as listed in Table 6, indicating that there was a conformational defect at the methyl-end. With an increase in the chain length, there appeared *gtg′* conformation for n=20. There remained several bands which could not be assigned at the present stage. Based

Table 6. Frequencies (cm^{-1}) of Conformational Defect Bands Observed in Phases I′, II, and III for n=14—20

n=14	16	18	20	Assignment	Ref.
1348	1348	1348	1347	*gt-*	9
			1289	(*gtg′*)	10
1116				*	
			1095	(*gtg′*)	10
			1081	*	
1075	1077	1072	1075	*gt-*	9
943				*	
	932	928	933	(*gt-*)	10
	867			(*gt-*)	10
	855			*gg-*	11
770	772	774	776	*gt-*	10
			760	*	
748	752	754		*	

( ): uncertain. *: not assigned at the present stage.

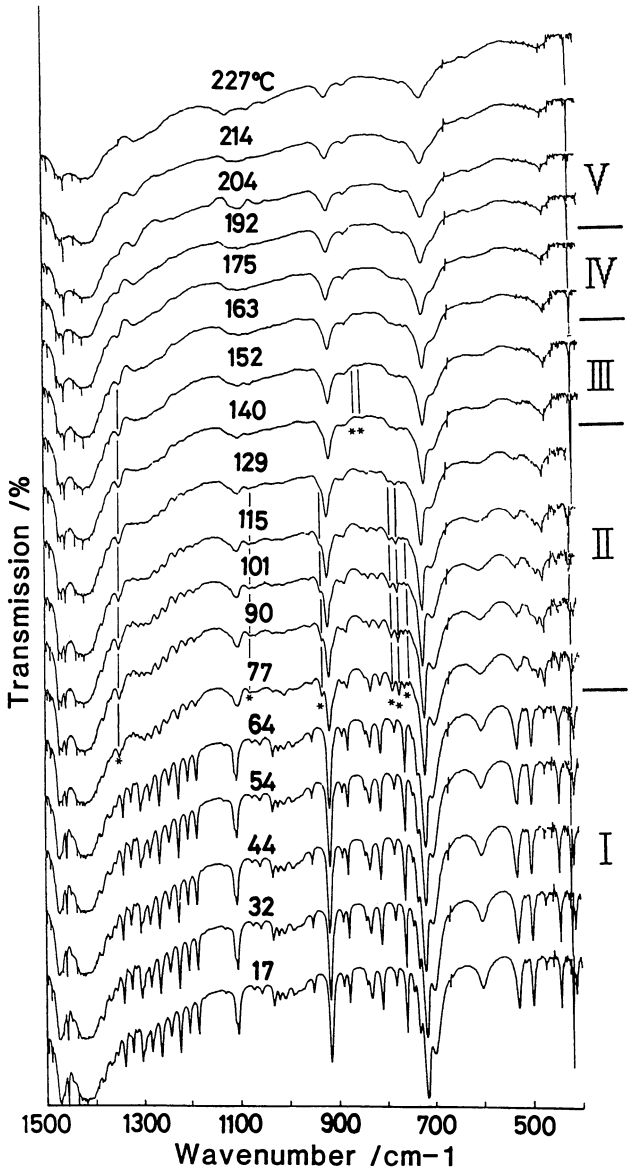

Fig. 3. Temperature dependence of IR spectrum for n=16 in the 400—1500 cm^{-1} region.

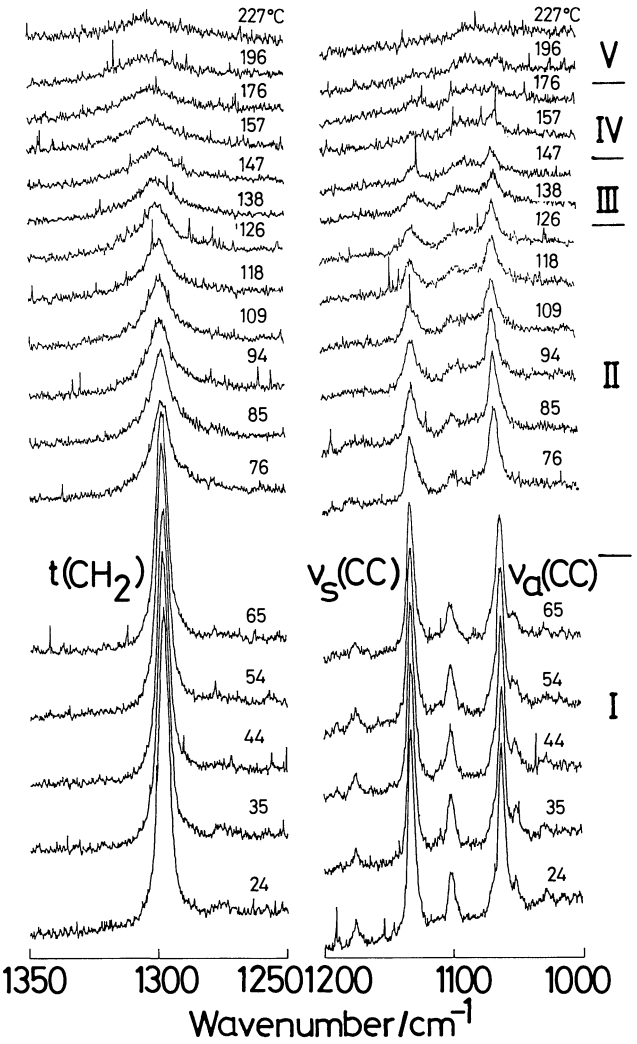

Fig. 4. Temperature dependence of Raman spectra for n=14.

on the result of a decrease in the intensities of the progressive bands and the appearance of defect bands, it was concluded that the conformational disordering proceeded in phases I′, II, and III, and the disappearance of these bands indicated that the chains went into a liquid state above phase IV for n=14—20.

In order to confirm the structural transition, the temperature dependence of the Raman spectra was observed, as shown in Fig. 4. The Raman spectra of the alkyl chains in the 1000—1500 cm^{-1} region are sensitive to the conformational order of the chains. The intensities of the bands at 1295 cm^{-1} [the CH_2 twisting $t(CH_2)$], and 1170 cm^{-1} [the CH_2 rocking $r(CH_2)$], as well as 1130, 1062 cm^{-1} [the symmetric and antisymmetric C–C stretchings ν_s(CC) and ν_a(CC)] are proportional to the amount of all-trans segments longer than a certain length characteristic of each vibrational mode. For example, the 1295 cm^{-1} band is due to all-trans sequences of 6 or more methylene units, the 1130 cm^{-1} band to those of 16—20 or more units, and the 1062 cm^{-1} band to those of 8 or more units.[12] The temperature dependence of the peak intensities of the Raman $t(CH_2)$, ν_s(CC), and ν_a(CC) modes relative to the peak intensity of the $t(CH_2)$ mode[13] at room temperature for n=14—20 is plotted in Fig, 5. With an increase in the temperature, at the transition from phase I to I′ or II, the intensity of the 1130 cm^{-1} band (which is characteristic of the long methylene sequences) decreased selectively. At the temperatures in phase II and III, the intensities of all of bands (including those characteristic of short trans sequences) decreased. At temperatures above phase IV, these bands were smeared out. Therefore, the result of the IR measurements was confirmed by the Raman measurements.

In conclusion, from the IR and Raman methods it was revealed for n=14—20 that the conformational disordering of the alkyl chains proceeded in phases I′, II,

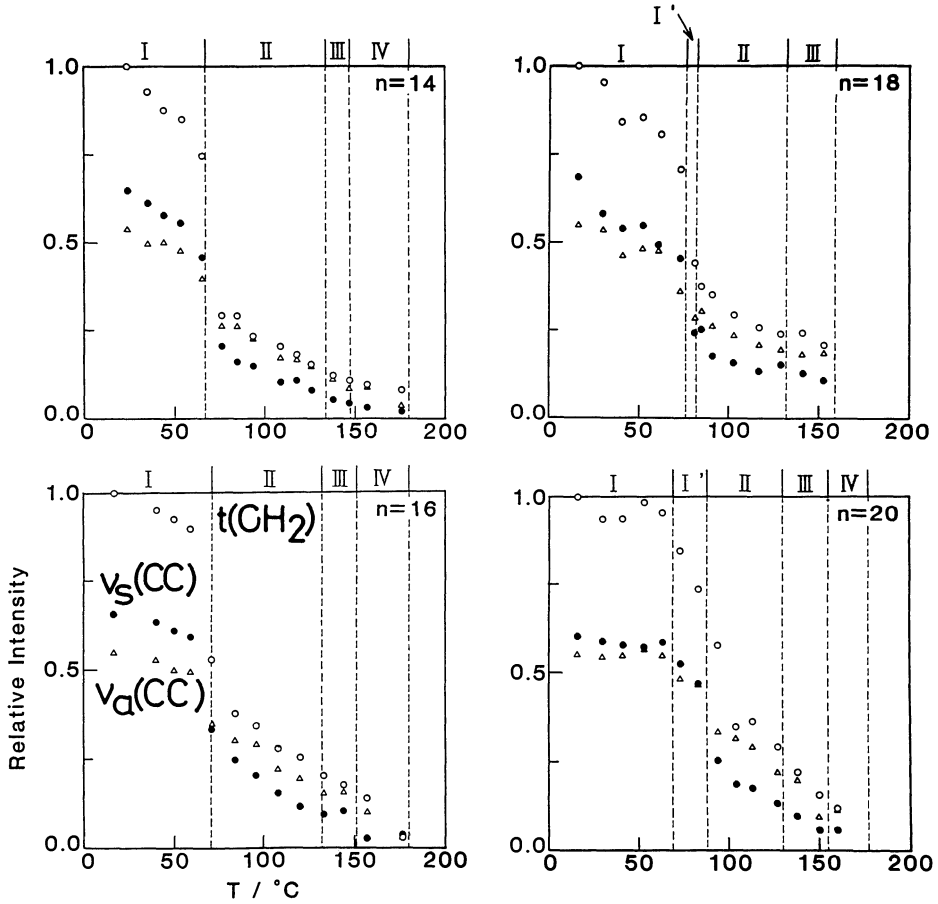

Fig. 5. Temperature dependence of relative peak intensities of Raman spectra for n=14—20.

and III. At temperatures above phase IV, the chains entered a liquid-like conformation.

References

1) D. M. Small, "Handbook of Lipid Research," Plenum Press, New York and London (1986), Vol. 4.
2) A. Cingolani, G. Spinolo, M. Sanesi, and P. Franzosini, *Z. Naturforsch., A,* **35**, 757 (1980).
3) K. Nakamura, *Nippon Kagaku Zasshi,* **79**, 1411 (1958).
4) J. H. Schachtschneider and R. G. Snyder, *Spectrochim. Acta,* **19**, 117 (1963).
5) J. Umemura, *J. Chem. Phys.,* **68**, 42 (1978).
6) T. Miyazawa, *Nippon Kagaku Zasshi,* **74**, 915 (1953).
7) R. G. Snyder, *J. Mol. Spectrosc.,* **23**, 224 (1967).
8) R. Gotoh and T. Takenaka, *Nippon Kagaku Zasshi,* **84**, 392 (1963).
9) M. Maroncelli, S. P. Qi, H. L. Strauss, and R. G. Snyder, *J. Am. Chem. Soc.,* **104**, 6237 (1982).
10) P. Jona, M. Gussoni, and G. Zerbi, *J. Appl. Phys.,* **57**, 834 (1985).
11) Y. Kim, H. L. Strauss, and R. G. Snyder, *J. Phys. Chem.,* **93**, 485 (1989).
12) M. Kobayashi, *J. Mol. Struct.,* **126**, 193 (1985).
13) G. R. Strobl and W. Hagedorn, *J. Polym. Sci., Polym. Phys. Ed.,* **16**, 1181 (1978).

 © 1991 The Chemical Society of Japan Bull. Chem. Soc. Jpn., 64, 2183—2187 (1991)

β-α Photoisomerization of Cobaloxime Complexes in the Solid State. III. Accelerated Reaction Rate by Hydrogen Bond

Akiko SEKINE* and Yuji OHASHI
Department of Chemistry, Faculty of Science, Tokyo Institute of Technology,
O-okayama, Meguro-ku, Tokyo 152
(Received January 18, 1991)

The crystal structures of two cobaloxime complexes with different axial base ligands have been determined by X-ray analysis at room temperature. I: (3-Aminopyridine)(2-cyanoethyl)bis(dimethylglyoximato)cobalt(III); the cystal is monoclinic, the space group being $C2/c$, $Z=8$ with $a=28.849(8)$, $b=7.746(2)$, $c=18.429(5)$ Å, and $\beta=105.71(3)°$. II: (Aniline)(2-cyanoethyl)bis(dimethylglyoximato)cobalt(III) aniline solvate; the crystal is monoclinic, the space group being $P2_1/c$, $Z=4$ with $a=14.228(7)$, $b=11.426(4)$, $c=14.178(3)$ Å, and $\beta=91.92(3)°$. Both structures were refined by a full-matrix least-squares method to final R values of 0.070 and 0.074 for 3886 and 3311 observed reflections, respectively. Their photoisomerization rates in the solid state obtained from changes in the IR spectra, 3.2 and 4.2×10^{-4} s^{-1}, respectively, are significantly greater than those of the related compounds. The hydrogen bonds between the reactive 2-cyanoethyl groups and the atoms of the neighboring molecules in the two crystals should be responsible for the greater reaction rates. Taking into account the role of the hydrogen bonds, a probable isomerization mechanism is proposed.

The 2-cyanoethyl group bonded to the cobalt atom in the bis(dimethylglyoximato)cobalt(III), cobaloxime, complex was found to be isomerized to the 1-cyanoethyl group upon exposure to visible light.[1] The photoreaction, β–α isomerization, proceeds only in the solid state, and the reverse reaction has not yet been observed.

Since the reactive group is very similar to that in crystalline-state racemization, we expected that the reaction rate would be well explained by the reaction cavity for the reactive group, as observed in the crystalline-state reaction.[2] A series of cobaloxime complexes with different axial base ligands has been prepared and the relation between the reaction rate and the reaction cavity examined.

For a complex with 3-methylpyridine as an axial base ligand (3mp), two crystal forms (I and II) were obtained under the same conditions. The powdered sample of form II revealed a significantly greater rate than that of form I. The reaction cavity around the 2-cyanoethyl group of form II is greater than that of the form I, indicating that the cavity size is one factor controlling the reaction rate.[3] For a complex with pyridine used as an axial base ligand (py), two forms were also crystallized under the same conditions. Although the reaction cavity of form II was significantly smaller than that of form I, form II revealed a significantly greater reaction rate than did form I. The 2-cyanoethyl group in form II takes a nearly parallel conformation to the cobaloxime plane, whereas that of form I takes a perpendicular conformation. The 2-cyanoethyl group with a parallel conformation would be more easily transformed to the α-cyanoethyl group than that with a perpendicular conformation, since the former has a closer resemblance in shape to the 1-cyanoethyl group than does the latter. Therefore, such a topochemical factor should be the second factor controlling the reaction rate in the case of the complex (py).[4]

It was recently reported that for four complexes with 3-ethylpyridine (3ep),[5] 4-ethylpyridine (4ep),[5] 3-cyanopyridine (3cp),[6] and 4-aminopyridine (4ap)[6] the reaction rates could be well-explained in terms of the above two factors. However, the two complexes with 3-aminopyridine (3ap) and aniline (1ab) as axial base ligands revealed significantly greater reaction rates than those expected from the above two factors.

The present paper deals with the two complexes, 3ap and 1ab, and proposes a third factor.

Experimental

Crystal Structures. The complexes were synthesized by a previously reported method.[7] The crystals were obtained from hot methanol solutions. The approximate dimensions of the crystals used were 0.3×0.3×0.1 (3ap) and 0.3×0.3×0.1 mm (1ab). X-Ray measurements were performed with a Rigaku four-circle diffractometor (AFC-4). Mo $K\alpha$ radiation monochromated by graphite ($\lambda=0.71069$ Å) was used. The cell parameters were refined by least-squares on the basis of 16 and 15 independent 2θ values ($20°<2\theta<30°$) for 3ap and 1ab, respectively. Three-dimensional intensity data were collected up to $2\theta=55°$ (3ap) and 50° (1ab); the ranges of hkl were −36 to 36, 0, to 10, and 0 to 22 (3ap), and −16 to 16, 0 to 13, and 0 to 16 (1ab). The intensities were measured using an ω–2θ scan technique and a scan speed $4°(2\theta)$ min^{-1}. The background counts were accumulated for 5 s both before and after each scan. Three standard reflections were monitored for every 50 reflections, and no significant variations in the intensities were observed. The reflections for $|F_o|>3\sigma(|F_o|)$ were considered as being observed and used for structural determinations. Although corrections for the Lorentz and polarization factors were made, no correction for the absorption was applied.

The structure of 3ap was solved by the direct method with a program called MULTAN 78,[8] refined by full-matrix least-squares with the program called SHELX 76.[9] All of the hydrogen atoms were found on the difference map. The final refinement was made with the anisotropic temperature factors for non-hydrogen atoms and the isotropic ones for hydrogen atoms. The quantities minimized were $\sum w(|F_o|-|F_c|)^2$ and $w=[\sigma^2(|F_o|+0.004|F_o|^2]^{-1}$. The final R and R_w values became 0.070 and 0.084 for 3886 observed reflections. No peaks higher than 0.3 $eÅ^{-3}$ were found on the final difference map.

Table 1. Final Atomic Coordinates ($\times10^5$ for Co, and $\times10^4$ for C, N, and O) and Equivalent Isotropic Thermal Parameters for 3ap

Atom	x	y	z	B_{eq}
Co(1)	39751(2)	17774(7)	60516(3)	2.9
N(1)	3570(1)	3720(5)	5794(2)	3.5
N(2)	3437(1)	949(5)	6328(2)	3.6
N(3)	4380(1)	−155(5)	6326(2)	3.5
N(4)	4521(1)	2652(5)	5806(2)	3.7
O(1)	3711(1)	5163(4)	5521(2)	4.8
O(2)	3429(1)	−642(5)	6644(2)	4.8
O(3)	4250(1)	−1574(4)	6629(2)	4.7
O(4)	4551(1)	4280(5)	5548(2)	5.2
C(1)	3144(2)	3591(6)	5883(3)	4.0
C(2)	3066(2)	1928(7)	6205(3)	4.2
C(3)	4805(2)	−41(6)	6206(3)	4.0
C(4)	4887(2)	1614(6)	5897(3)	3.8
C(5)	2783(3)	5038(10)	5723(4)	6.7
C(6)	2610(2)	1449(12)	6403(4)	6.6
C(7)	5159(2)	−1490(10)	6388(4)	6.0
C(8)	5342(2)	2104(10)	5713(4)	5.6
N(5)	3399(3)	4963(8)	7630(3)	7.9
C(9)	4261(2)	2560(7)	7114(3)	3.9
C(10)	4207(3)	4444(7)	7310(3)	5.4
C(11)	3748(3)	4761(7)	7480(3)	5.8
N(6)	3714(1)	828(4)	4974(2)	3.1
C(12)	3574(2)	−804(6)	4869(3)	3.4
C(13)	3403(2)	−1564(6)	4151(3)	3.8
C(14)	3379(2)	−503(7)	3533(3)	4.5
C(15)	3524(2)	1187(7)	3636(3)	4.5
C(16)	3689(2)	1815(7)	4356(3)	4.1
N(7)	3250(2)	−3206(7)	4083(3)	6.0

$B_{eq}=(8/3)\pi^2\sum_i\sum_j U_{ij}a_i^*a_j^*\boldsymbol{a}_i\cdot\boldsymbol{a}_j$.

Table 2. Final Atomic Coordinates ($\times10^5$ for Co, and $\times10^4$ for C, N, and O) Equivalent Isotropic Thermal Parameters for 1ab

Atom	x	y	z	B_{eq}
Co(1)	67767(5)	2186(6)	15038(5)	3.4
N(1)	7774(3)	1247(4)	1804(3)	4.2
N(2)	6075(3)	1602(4)	1632(3)	4.3
N(3)	5779(3)	−804(4)	1187(3)	3.9
N(4)	7483(3)	−1164(4)	1408(3)	3.8
O(1)	8676(3)	919(5)	1867(3)	5.2
O(2)	5122(3)	1646(4)	1546(3)	5.6
O(3)	−5111(3)	−447(4)	1110(3)	5.0
O(4)	8426(3)	−1197(4)	1551(3)	5.2
C(1)	7548(4)	2343(6)	1893(4)	5.0
C(2)	6542(5)	2557(5)	1801(4)	5.0
C(3)	6007(4)	−1892(5)	1029(4)	4.6
C(4)	7019(4)	−2099(5)	1151(4)	4.4
C(5)	8264(7)	3287(8)	2075(7)	7.8
C(6)	6100(7)	3730(7)	1885(7)	7.5
C(7)	5296(6)	−2815(7)	786(6)	6.9
C(8)	7495(6)	−3247(6)	1004(6)	6.2
N(5)	7257(5)	1820(7)	4466(6)	10.3
C(9)	6554(5)	−226(7)	2849(4)	5.5
C(10)	7341(6)	−96(7)	3556(5)	6.1
C(11)	7303(5)	987(7)	4083(6)	6.4
N(6)	6887(3)	639(5)	69(3)	3.6
C(12)	7563(3)	22(5)	−488(3)	3.6
C(13)	7323(5)	−960(6)	−978(4)	4.5
C(14)	7977(7)	−1558(8)	−1490(5)	6.0
C(15)	8881(6)	−1173(9)	−1487(6)	6.8
C(16)	9139(5)	−194(10)	−1000(5)	6.7
C(17)	8475(4)	422(7)	−492(4)	5.0
C(2B)[a]	10235(9)	4672(21)	934(10)	11.6
C(3B)[a]	10046(10)	5813(17)	633(13)	11.8
N(1B)[a]	10186(13)	6616(17)	1369(12)	11.8
C(1B)[a]	9826(8)	6122(20)	−299(18)	13.3

a) Occupancy factors of C(2B), C(3B), N(1B), and C(1B) are 0.5. $B_{eq}=(8/3)\pi^2\sum_i\sum_j U_{ij}a_i^*a_j^*\boldsymbol{a}_i\cdot\boldsymbol{a}_j$.

The procedure of a structure determination for the lab was similar to that for 3ap. An aniline molecule appeared in the difference map, which occupies an inversion center with disordered orientations. Some of the hydrogen atoms were found on the difference map. The others were calculated geometrically and refined with C–H distances constrained to 1.00 Å. The final refinement was made with the anisotropic temperature factors for non-hydrogens atoms and isotropic ones for hydrogen atoms. The weighting scheme was $w=[\sigma^2(|F_o|)+0.004|F_o|^2]^{-1}$. The final R and R_w values became 0.074 and 0.074 for 3311 reflections. No peaks higher than 0.5 e Å^{-3} were found on the final difference map. The atomic scattering factors were taken from International Tables for X-ray Crystallography.[10] The final atomic coordinates and equivalent isotropic temperature factors for non-hydrogen atoms are given in Tables 1 and 2. Lists of the anisotropic temperature factors for non-hydrogen atoms, atomic coordinates and temperature factors for hydrogen atoms, all the bond distances and angles, as well as the observed and calculated structure factors are kept in the office of Chemical Society of Japan. Computations were carried out on M-280H and M-680H computers at the Computer Centre of the University of Tokyo.

β–α Isomerization. KBr disks which contained 1% of the 2-cyanoethyl complex were exposed to a 500 W Xe lamp. The IR spectra of the KBr disk were measured at intervals of 5 min and 10 min for 3ap and 1ab, respectively. The absorption assigned to the stretching vibration mode of the cyano group, ν_{CN} in 2-cyanoethyl complex, was at 2250 cm^{-1}. The peak decreased with the irradiation time and ν_{CN} of the 1-cyanoethyl complex appeared at 2200 cm^{-1}, and increased. Since the change during the early stages, within 40 min, was represented by first-order kinetics, the rate constant was obtained by least-squares fitting.

Results

The crystal structures of 3ap and 1ab are shown in Figs. 1 and 2, respectively. For 3ap, N(5) in the cyanoethyl group is hydrogen-bonded to N(7) of the amino group in the neighboring molecule at (x,$-y$, $0.5+z$)[N(5)···N(7) 3.135(10) Å]. The molecules are connected along the c axis as a ribbon by hydrogen bonds. For 1ab, a unit cell contains two free aniline molecules, which occupy the inversion centers. The N(5) atom in the cyanoethyl group is hydrogen-bonded to N(6) of the amino group of the neighboring molecule at (x, $0.5-y$, $0.5+z$) [N(5)···N(6) 3.076(10) Å], and O(3) is hydrogen-bonded to N(6) of the adjacent molecule at ($1-x$, $-y$, $-z$). The molecules form a ribbon comprising two rows along the c axis. Free aniline mole-

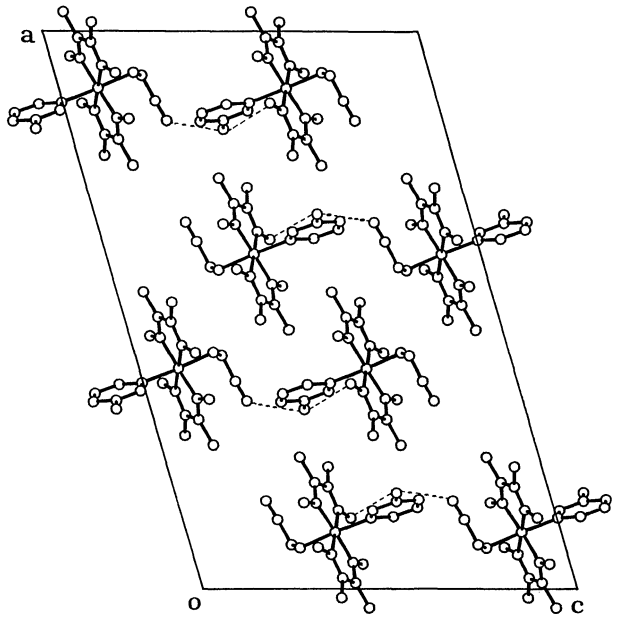

Fig. 1. Crystal structure of 3ap viewed along the *b* axis. Broken lines indicate the hydrogen bonds.

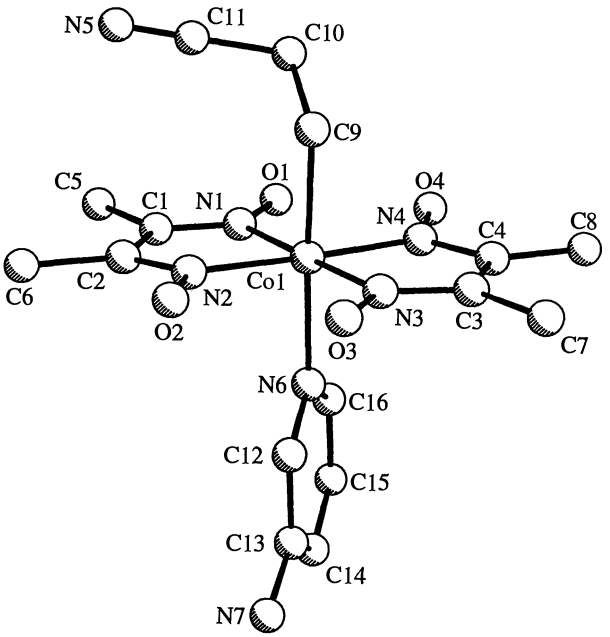

Fig. 3. Molecular structure of 3ap.

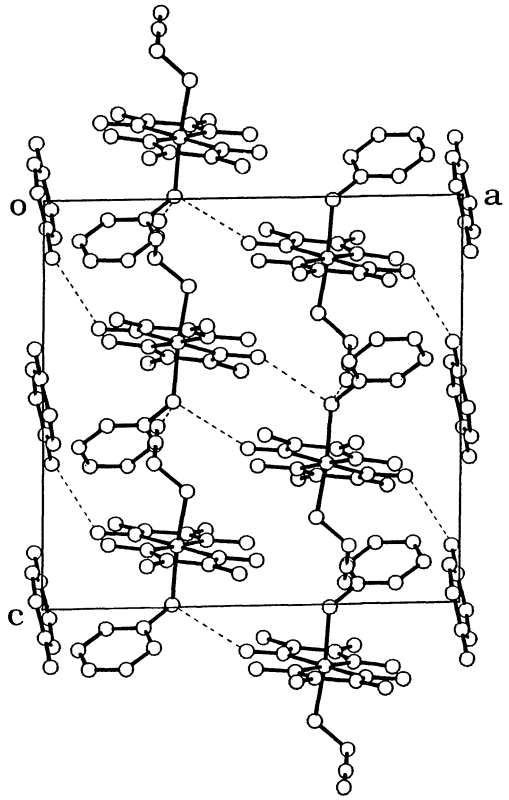

Fig. 2. Crystal structure of 1ab viewed along the *b* axis. Broken lines indicate the hydrogen bonds.

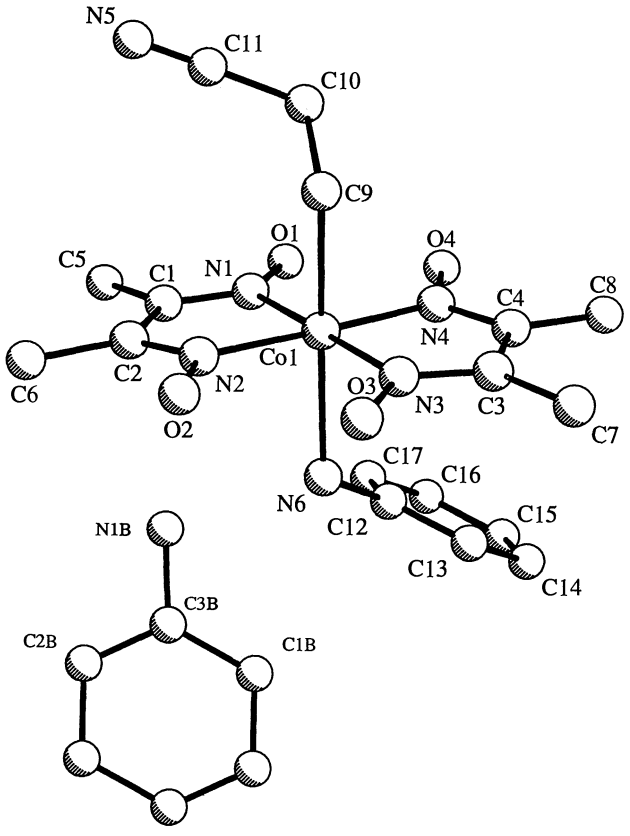

Fig. 4. Molecular structure of 1ab.

cules are hydrogen-bonded to the O(1) of the neighboring cobaloxime molecule, forming walls between the ribbons.

The molecular structures of 3ap and 1ab are shown in Figs. 3 and 4, respectively. The selected bond distances and angles of 3ap and 1ab are shown in Tables 3. Torsional angles of Co(1)–C(9)–C(10)–C(11) in 3ap and 1ab are +84.7(6)° and +96.9(4)°, respectively. This means the 2-cyanoethyl groups in both complexes are approximately parallel to their cobaloxime planes. The

Table 3. Selected Bond Distances (l/Å) and Bond Angles (ϕ/°)

	3ap	1ab
Co(1)–N(1)	1.885(4)	1.882(5)
Co(1)–N(2)	1.874(4)	1.880(5)
Co(1)–N(3)	1.882(4)	1.879(5)
Co(1)–N(4)	1.880(4)	1.881(5)
Co(1)–C(9)	2.001(5)	2.009(8)
Co(1)–N(6)	2.059(4)	2.102(6)
N(1)–Co(1)–N(2)	80.7(2)	81.5(2)
N(1)–Co(1)–N(3)	179.1(2)	178.6(2)
N(1)–Co(1)–N(4)	98.9(2)	98.4(2)
N(1)–Co(1)–C(9)	93.9(2)	91.1(3)
N(1)–Co(1)–N(6)	90.1(2)	87.6(2)
N(2)–Co(1)–N(3)	98.9(2)	98.1(2)
N(2)–Co(1)–N(4)	178.0(2)	179.3(2)
N(2)–Co(1)–C(9)	89.5(2)	94.9(3)
N(2)–Co(1)–N(6)	91.5(2)	89.8(2)
N(3)–Co(1)–N(4)	81.4(2)	82.1(2)
N(3)–Co(1)–C(9)	85.2(2)	87.6(3)
N(3)–Co(1)–N(6)	90.8(2)	93.7(2)
N(4)–Co(1)–C(9)	88.6(2)	85.9(3)
N(4)–Co(1)–N(6)	90.5(2)	89.5(2)
C(9)–Co(1)–N(6)	176.0(2)	174.9(3)

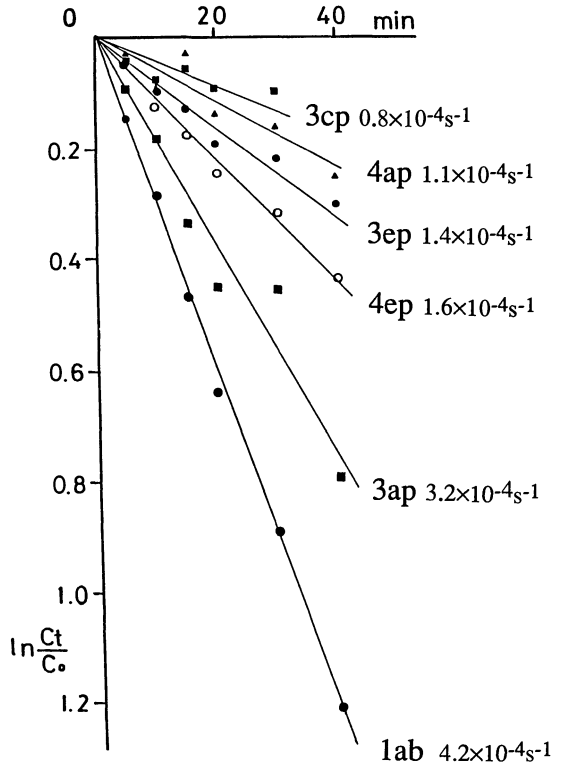

Fig. 5. Reaction rate for β–α isomerization for 3ep, 4ep, 3cp, 4ap, 3ap, and 1ab. Solid lines are obtained by least-squares fitting, assuming the first-order kinetics.

molecular structure of 3ap is similar to those of the other cobaloxime complexes with pyridine derivatives; pyridine,[4] 3-methylpyridine,[3] 3-ethylpyridine, and 4-ethylpyridine.[5] For 1ab, the Co(1)–N(6)–C(12) angle is 119.3(4)°. Approximately the same angle was observed in bis(aniline)bis(dimethylglyoximato)cobalt(III)chloride,[11] 119.5(7)°. Such expanded angles would be caused by short contacts between the aniline and cobaloxime moieties. The shortest distances between the nitrogen atom of the cobaloxime moieties and the benzene ring of aniline ligand are 3.016(7) Å and 2.920(8) Å for 1ab and the bis(aniline) complex.

Table 4. Cavity Size (V/Å^3) and Rate Constant (k/s^{-1}, $\times 10^4$)

	V	k	Conformation
3cp	12.24	0.8	Perpendicular
4ap	14.99	1.1	Perpendicular
3ep	13.12	1.4	Parallel
4ep	14.00	1.6	Parallel
3ap	10.06	3.2	Parallel
1ab	14.97	4.2	Parallel

The rate of isomerization during the early stages follows first-order kinetics (Fig. 5), in which the rates of 3-cyanopyridine (3cp), 4-aminopyridine (4ap), 3-ethylpyridine (3ep), 4-ethylpyridine (4ep), 3-aminopyridine (3ap), aniline (1ab) are given. The 3ap and 1ab crystals have significantly greater values than do the other four crystals.

Discussion

Table 4 gives the cavity size,[12] the rate constant during the early stages and the conformation of the 2-cyanoethyl group for six complex crystals: 3ep, 4ep, 3cp, 4ap, 3ap, and 1ab. The crystals with a parallel conformation have greater rate constants than do those with the perpendicular type. The second topochemical factor observed in the two crystal forms of the pyridine complex[4] plays an important role, even if the crystals have different base ligands. Moreover, in the two crystals with a perpendicular conformation, 3cp and 4ap, the crystal with a greater cavity has a greater rate constant. The first cavity factor observed in the two crystal forms of 3mp[3] controls the reaction rate when the reactive group takes the perpendicular conformation. For crystals with a parallel conformation, however, the first factor has no effect on the reaction rate. Although the cavity of 3ap is smaller than those of 3ep and 4ep, the rate constant of 3ap is greater than those of 3ep and 4ep. This fact indicates that the third factor should be taken into account.

It appears that solvent molecules may cause the greater reaction rate, since the 1ab crystal has another aniline as a crystalline solvent. However, the 3ap crystal, which has a greater reaction rate too, has no solvent and the 3cp has a water molecule used as a solvent in spite of the smallest reaction rate. This suggests that the solvation may have no significant effect on the reaction rate.

Only in the 3ap and 1ab crystals, the nitrogen atoms of the 2-cyanoethyl groups have hydrogen bonds with the

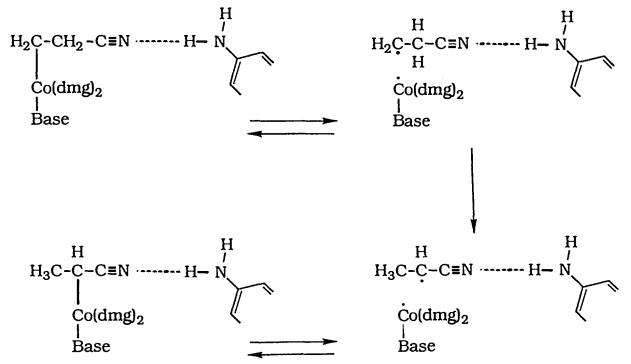

Fig. 6. Mechanism of β–α isomerization. The hydrogen bonds are indicated by broken lines.

amino groups of the neighboring molecules. Although hydrogen bonds are also observed in the 3cp crystal, they connect the solvent water molecules with the neighboring cobaloxime moieties; the nitrogen atom of the 2-cyanoethyl group does not take part in the hydrogen bonding.

A probable mechanism of the β–α photoisomerization associated with the hydrogen bond is shown in Fig. 6. When the Co–C bond is cleaved by visible light, the 2-cyanoethyl radical is produced. Such a homolyitic Co–C bond cleavage of the cobaloxime complexes has been extensively reported.[13,14] Since the produced radicals may be unstable, and cannot move so easily in the crystalline lattice, most part of the radicals would return to the original 2-cyanoethyl group. However, a small parts of the radicals may be transformed to the 1-cyanoethyl radicals by virtue of lattice vibration; the rate-determining step is probably the 2→1 radical transformation in this photoisomerization.

If the nitrogen atom of the 2-cyanoethyl group is hydrogen bonded to the amino group in a neighboring molecule, the produced 2-cyanoethyl radical may be stabilized and the prolonged lifetime of the 2-cyanoethyl radical would cause an increased extent of the 2→1 radical transformation. The four crystals with a parallel-type conformation, therefore, can be divided into two classes depending on whether or not the reactive group has a hydrogen bond with the neighboring molecule. The first factor, the cavity factor, controls the reaction rate in both classes.

In conclusion, the reaction rate is well explained by three factors in the solid state β–α photoisomerization of cobaloxime complexes; the size of the cavity, the conformation of the reactive group and the hydrogen bond with the reactive group. Although the structure in which the 2-cyanoethyl group with a perpendicular conformation is hydrogen-bonded to the neighboring molecule has not yet been observed, the third factor seems to be most important among the three factors, considering the significantly greater reaction rate of 3ap and 1ab crystals. As a matter of course, the second factor is more important than the first. Table 4 indicates that the reaction rate is affected by the first factor only if the second and third factors are equivalent.

This work was supported by a Grant-in-Aid for Scientific Research from the Ministry of Education, Science and Culture.

References

1) Y. Ohgo and S. Takeuchi, *J. Chem. Soc., Chem. Commun.*, **1985**, 21.

2) Y. Ohashi, *Acc. Chem. Res.*, **21**, 268 (1988).

3) A. Uchida, M. Danno, Y. Sasada, and Y. Ohashi, *Acta Crystallogr., Sect. B*, **43**, 528 (1987).

4) A. Uchida, Y. Ohashi, and Y. Ohgo, *Acta Crystallogr., Sect. C*, in press.

5) A. Sekine, Y. Ohashi, E. Shimizu, and K. Hori, *Acta Crystallogr., Sect. C*, **47**, 53 (1991).

6) A. Sekine, Y. Ohashi, and K. Hori, *Acta Crystallogr., Sect. C*, **47**, 525 (1991).

7) Y. Ohgo, S. Takeuchi, Y. Natori, J. Yoshimura, Y. Ohashi, and Y. Sasada, *Bull. Chem. Soc. Jpn.*, **54**, 3095 (1981).

8) P. Main, S. E. Hull, L. Lessinger, G. Germain, J. P. Declercq, and M. M. Woolfson, MULTAN 78. A System of Computer Program for the Automatic Solution of Crystal Structures from X-ray Diffraction Data, Univ. of York, England, and Louvain, Belgium. (1978).

9) G. M. Sheldrick, SHELX 76. Program for crystal structure determination. Univ. of Cambridge, England (1976).

10) "International Tables for X-Ray Crystallography," Kynoch Press, Birmingham, (Present distributor Kluwer Academic Publishers, Dordrecht), Vol. IV.

11) L. P. Battaglia, A. B. Corradi, C. G. Palmieri, M. Nardelli, and M. E. V. Tani, *Acta Crystallogr., Sect. B*, **30**, 1114 (1974).

12) Y. Ohashi, A. Uchida, Y. Sasada, and Y. Ohgo, *Acta Crystallogr., Sect. B*, **39**, 54 (1983).

13) Y. Ohgo, K. Orisaku, E. Hasegawa, and S. Takeuchi, *Chem. Lett.*, **27**, (1986).

14) J. Halpern, S. H. Kim, and T. W. Leung, *J. Am. Chem. Soc.*, **106**, 8317 (1984).

ESR Studies at High Pressures. III.[1] Spin-Exchange Reactions of Some Nitroxide Radicals in Acetone and Hexane

Yoshimi Sueishi,* Masahiro Kuzukawa, Shunzo Yamamoto, and Norio Nishimura
Department of Chemistry, Faculty of Science, Okayama University,
Tsushima Naka 3-1-1, Okayama 700
(Received February 7, 1991)

Pressure effects on the rate of spin–spin exchange of some nitroxide radicals in acetone and hexane at 298.2 K have been studied by means of a high-pressure ESR technique. It was found that this exchange reaction is diffusion-controlled. The rate of the spin exchange is related to that of diffusion, the probability of the spin exchange, $P = f(J, \tau_1)$, and steric factor f_s. The values of P and hence τ_1 were estimated as a function of pressure. A method for evaluating the steric factor and the exchange integral is proposed.

It has been recognized over the past half a century that kinetic studies at high pressures are informative for characterizing reaction processes in condensed systems. When investigations at high pressures are undertaken, we often face some difficulties that should be surpassed. For high-pressure NMR and ESR experiments in particular, sophisticated techniques are required. At present, high pressure/high temperature NMR probse have been designed, and this has enabled us to know detailed information about the dynamic structure of liquids.[2] On the contrary, only a few high-pressure ESR studies have been done; among them, papers concerning the effects of pressure on spectral linewidth[3,4] and hyperfine splittings[5] besides chemical equilibria[6,7] and reaction rates[8] have been put forward.

In previous papers,[1,9] we have reported the pressure effects on the rate of spin–spin exchange of 2,2,6,6-tetramethyl-4-oxo-1-piperidinyloxyl (TANONE) in various solvents. The rate constant for the spin-exchange process was found to be strongly correlated to solvent viscosity η, indicating that a diffusion-controlled process is involved. Since viscosity variation with temperature inevitably involves unfavorable energetic problems, the viscosity was changed by applying pressure p. It was found that in aprotic solvents except acetone, the activation volumes for the spin-exchange process ($\Delta V_{ex}^{\neq}$) coincided well with the apparent activation volumes for diffusive processes ($\Delta V_{diff}^{\neq}$).

In the present work, we used acetone and hexane as low viscosity solvents to utilize available η–p data together with compressibility data. In order to obtain further information about the effect of pressure on the rate of the spin–spin exchange, we investigated the spin-exchange reaction of three kinds of nitroxides: 2,2,6,6-tetramethyl-4-oxo-1-piperidinyloxyl (TANONE), 2,2,6,6-tetramethyl-1-piperidinyloxyl (TEMPO), and di-*t*-butyl nitroxide (DTBN) in acetone and hexane.

Experimental

TANONE, TEMPO, and DTBN were purchased from Wako Pure Chemicals Co., Ltd., and used without further purification. Reagent grade acetone and hexane were used after distillation. The instrumentation of a high-pressure ESR cell has already been described elsewhere.[9] A sample solution was deaerated by bubbling nitrogen and was transferred into the cell under nitrogen atmosphere. After a required pressure had been attained, the stop valve on the cell was closed and then cell was separated from the pump system. By doing that, troublesome instrumentations[6–8] have been overcome.

ESR signals were monitored by using a JEOL JES-FE3XG ESR spectrometer with a 100 kHz field modulator. The peak-to-peak width of the central signal was measured at 298.2 K within a precision of ±1.5%.

Theoretical Background

The rate constant of spin-exchange reaction k_{ex} is related to the line broadening of an ESR signal by Eq. 1.[10]

$$\Delta H = (k_{ex}/A)C + \Delta H_0, \quad (1)$$

where ΔH and ΔH_0 are the linewidth in the presence and absence of spin exchange, respectively; A is a constant characteristic of each radical, and is equal to 2.28×10^8 mT^{-1} s^{-1} for the Lorentzian type of ESR signals of nitroxides.[10] Since no activation energy will be needed for the exchange process, the exchange rate constant can be given by the rate constant for a diffusive process k_{diff} multiplied by P:

$$k_{ex} = Pk_{diff}, \quad (2)$$

where P is the probability of spin exchange upon "collision". The probability (P) is related to the exchange integral J and collision time τ_1 by Eq. 3,[10]

$$P = J^2\tau_1^2/(1 + J^2\tau_1^2). \quad (3)$$

The term collision is used here in the sense that a pair of reacting molecules are encountering in a solvent cage. According to the Stokes–Einstein–Smoluchowski equation, k_{diff} for spherical molecules in a medium-incontinuum of bulk viscosity η is given by:

$$k_{diff} = 8000RT/3\eta. \quad (4)$$

In real solution, the shape, mutual orientation and solvation of reacting molecules would affect k_{ex}. Hereafter such composite effects will be called comprehensive-

ly the steric factor f_s. Then, Eq. 2 can be modified as:

$$k_{ex} = Pf_s k_{diff}. \quad (5)$$

According to Plachy and Kivelson,[11] the collision time τ_1 can be given by Eq. 6

$$\tau_1 = \pi b\lambda^2\eta/kT, \quad (6)$$

where b is the effective hydrodynamic radius of a molecule moving in a liquid, and $\lambda=\lambda(p, T)$ is the jump length which may be, according to the hole theory, inversely proportional to the cube root of the liquid density.[11] Thus, the following relationship will approximately hold.

$$\lambda_p^3 = \lambda_0^3\rho_0/\rho_p, \quad (7)$$

where λ_0 and ρ_0 denotes the jump length and the (liquid) density at the freezing point under atmospheric pressure, respectively and λ_p and ρ_p represent them at pressure p and 298.2 K. By combining Eqs. 3, 5, 6, and 7, and eliminating P and λ_p, we finally obtain Eq. 8 which enables us to estimate the steric factor f_s and exchange integral J:

$$k_{diff}/k_{ex} = 1/f_s + (k^2T^2/J^2\pi^2\lambda_0^4\rho_0^{4/3}b^2f_s)(\rho_p^{4/3}/\eta^2). \quad (8)$$

Another equation that will be useful for our discussion is obtained by the combination of Eqs 4 and 5:

$$k_{ex}\eta \propto P. \quad (9)$$

Results

Figure 1 shows that ΔH increases linearly with the radical concentration at each pressure (correlation coefficient $r\geqslant 0.9985$) in accordance with Eq. 1. From the linewidth of the central peak of the triplet signals, the spin-exchange rate constants k_{ex} at various pressures were estimated by means of Eq. 1, and are given in Table 1. From the pressure dependence of k_{ex}, the activation volumes $\Delta V_{ex}^{\neq}$ at 1 bar for the spin exchange have been estimated. These are given in Table 2. Using available

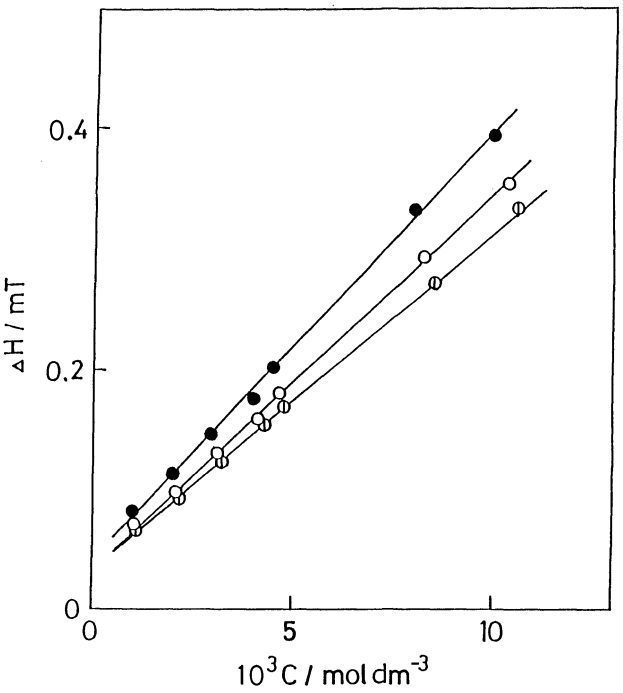

Fig. 1. Concentration dependence of ESR linewidth for TANONE radical in acetone at 1 (●), 343 (○), and 637 (◫) bar.

η–p data[12] the apparent activation volumes for diffusion $\Delta V_{diff}^{\neq}$ extrapolated to 1 bar have been calculated to be 15.8 cm^3 mol^{-1} in acetone and 23.2 cm^3 mol^{-1} in hexane. The differences between $\Delta V_{ex}^{\neq}$ and $\Delta V_{diff}^{\neq}$ are about -5 and -11 cm^3 mol^{-1} in acetone and hexane, solvents of low viscosity, but are near zero in toluene, benzene, and *o*-xylene. The physical meaning of the activation volume for a diffusive process has already been discussed.[9]

Discussion

Pressure Dependence of the Probability *P*. It is seen in Table 1 that k_{ex}-values clearly decrease inversely to the applied pressure and that they are smaller in toluene than in acetone and hexane. The above findings may simply

Table 1. Rate Constants for the Spin Exchange of Nitroxide Radicals at Various Pressures and at 298.2 K

Compd	Solvent	$10^{-9}\,k_{ex}$/mol^{-1} dm^3 s^{-1} ($10^{-9}\,k_{diff}$/mol^{-1} dm^3 s^{-1})[a]								
		p/bar								
		1	98	196	294	343	392	490	588	637
TANONE	Toluene[b]	5.27	5.08	4.74	4.22		4.06	3.81	3.74	
	Benzene[b]	5.31	4.73	4.57		4.04		3.43		
	o-Xylene[b]	4.17	3.94	3.69	3.21		3.28	3.10	2.71	
	Acetone	8.07	7.79	7.44		7.04		6.69		6.38
	Acetone	(23.2)	(21.7)	(20.3)		(18.6)		(17.1)		(15.9)
	Hexane	11.5	10.8	10.3		9.28		8.54		7.92
	Hexane	(22.3)	(20.1)	(18.3)		(16.1)		(14.3)		(13.0)
DTBN	Acetone	9.44	8.98	8.65		8.27		7.85		7.41
TEMPO	Acetone	7.78	7.41	7.03		6.56		6.21		5.85

a) The rate constants calculated by Eq. 4 are given in parentheses. b) Cited from Refs. 1 and 9.

Table 2. Activation Volumes and Exchange Integrals at 1 bar for the Spin-Exchange Reactions of Nitroxides

Compd	Solvent	$\Delta V_{ex}^{\neq}$ / $cm^3\ mol^{-1}$	$\Delta\Delta V^{\neq}$ [a] / $cm^3\ mol^{-1}$	f_s	$10^{-10}J$ / s^{-1}
TANONE	Acetone	8.7	−7.1	0.48	6.9
	Hexane	12.1	−11.1	0.68	5.3
	Toluene[b]	13.7	−0.5		
	Benzene[b]	18.4	0.7		
	o-Xylene[b]	15.3	−0.2		
TEMPO	Acetone	10.7	−5.1	0.41	9.5
DTBN	Acetone	7.4	−8.4	0.56	8.4

a) $\Delta V_{ex}^{\neq}-\Delta V_{diff}^{\neq}$. b) Cited from Refs. 1 and 9.

Table 3. Collision Time (in s) and Probability for the Spin Exchange of Nitroxides at Various Pressures at 298.2 K

Pressure	TANONE in acetone		DTBN in acetone		TEMPO in acetone		TANONE in hexane	
bar	$10^{11}\tau_1$	P	$10^{11}\tau_1$	P	$10^{11}\tau_1$	P	$10^{11}\tau_1$	P
1	2.35	0.72	1.93	0.71	2.23	0.81	3.39	0.76
98	2.50	0.75	2.05	0.74	2.37	0.83	3.69	0.79
196	2.65	0.78	2.17	0.76	2.51	0.84	4.03	0.83
343	2.87	0.80	2.36	0.79	2.73	0.86	4.36	0.85
490	3.09	0.82	2.54	0.82	2.94	0.89	4.68	0.88
637	3.30	0.84	2.71	0.83	3.13	0.90	5.01	0.90

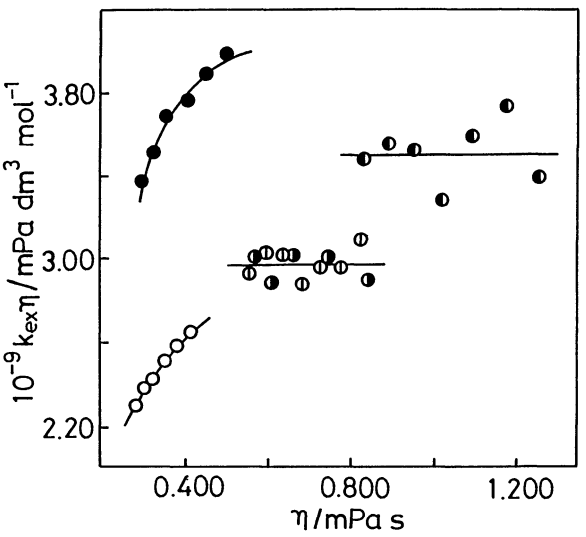

Fig. 2. Relationship between $k_{ex}\eta$ and η for spin exchange of TANONE radical in acetone (○), hexane (●), toluene (◫), benzene (◑), and *o*-xylene (◐).

be interpreted in terms of viscosity dependence of k_{ex}. As stated in the introductory section, acetone behaves differently from other aprotic solvents of comparatively high viscosity. The reason is as follows. In Fig. 2, $k_{ex}\eta$ is plotted against η. It could safely be said that $k_{ex}\eta$ and hence P is independent of η in toluene, benzene, and *o*-xylene. Judging from Eq. 3, the condition $J^2\tau_1^2\gg1$ and hence $P\approx1$ must hold in this case. In acetone and hexane, $k_{ex}\eta$ increases with viscosity, suggesting that P is susceptible to η. By means of Eqs. 4 and 5, the P-values for spin exchange of some nitroxide radicals in acetone and hexane were calculated as a function of pressure assuming the steric factor (vide infra) is independent of pressure and they are given in Table 3. No significant difference among P-values of the some nitroxide radicals listed in Table 3 was observed. In acetone and hexane, the P-values become progressively larger and approach unity, as the external pressure increases. The pressure dependence of P-value in acetone and hexane is ascribed to that of the collision time τ_1 in agreement with the prediction of Eqs. 3 and 6. The discussion on τ_1 will be made below. In any case, it is obvious that the difference $\Delta V_{ex}^{\neq}-\Delta V_{diff}^{\neq}$ in acetone and hexane is a result of the pressure dependence of the probability in accordance with Eq. 5.

Estimation of the Steric Factor and the Exchange Integral. According to Eq. 8, a plot of k_{diff}/k_{ex} against $\rho_p^{4/3}/\eta^2$ will give a straight line with the slope $(k^2T^2/J^2\pi^2\lambda_0^4\rho_0^{4/3}b^2f_s)$ and the intercept $1/f_s$. The plots are shown in Fig. 3. It follows that each plot constitutes a straight line, and this strongly suggests that the f_s- and J-values are independent of pressure or viscosity. It is difficult to estimate the numerical value of b and λ_0 exactly. Plachy and Kivelson[11] measured the diffusion coefficient of DTBN in pentane and estimated the radius b as 0.32 nm. Here, this value was used as the standard of estimating the b-values (TANONE and TEMPO) and λ_0 (acetone and hexane) referring the size of their CPK models. The estimated b-values are 0.39 nm for TANONE and 0.37 nm for TEMPO, and λ_0=0.50 nm for acetone and λ_0=0.59 nm for hexane. The liquid density extrapolated to its freezing point ρ_0 was estimated as 0.920 g cm^{-3} for acetone[12] and 0.757 g cm^{-3} for hexane.[13] After these numerical values were substituted in Eq. 8, f_s-

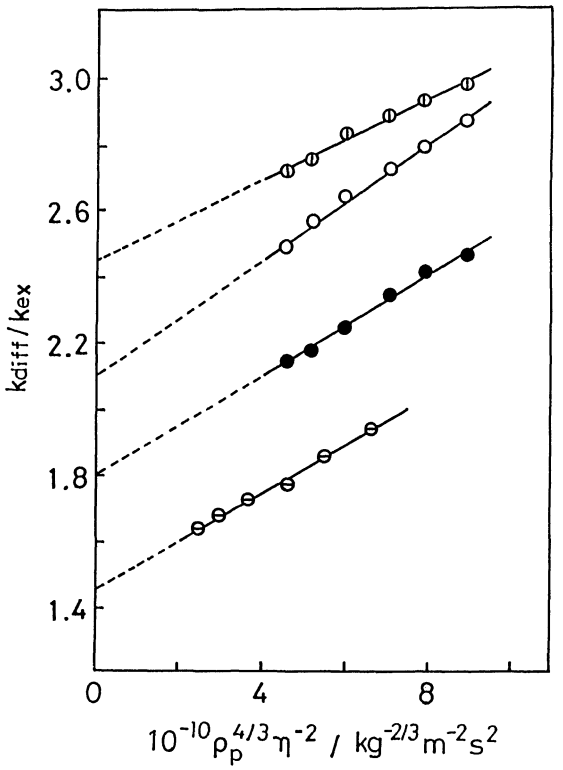

Fig. 3. Plots of k_{diff}/k_{ex} against $\rho_p^{4/3}\eta^{-2}$ for spin exchange: TANONE (○) in acetone, TEMPO (◫) in acetone, DTBN (●) in acetone, TANONE (⊖) in hexane.

and J-values for the spin exchange of the nitroxide radicals were calculated from the slope of the linear plot of Eq. 8, and they are given in Table 2. The f_s-values of some nitroxide radicals listed in Table 2 are about 0.5 and the J-values are of the order of 10^{10} s^{-1}.

According to Kivelson,[14] J should be a rapidly varying function of the radical-radical separation r, but approximately be regarded as constant if $r \leqslant r_c$, and zero if $r > r_c$, where r_c is a critical distance. The straight line of the above plot indicates the constancy of J. This means that the radicals are remaining within a distance r_c to each other during the collision time.

The J- and f_s-values seem to depend somewhat on the nature of radical species (Table 2). Studies are under way using various types of nitroxides. As the numerical values agree fairly well with the reported J-value for DTBN in pentane ($J=6\times10^{10}$ s^{-1}),[11] these values could be regarded as reasonable. It is notable that the exchange integral which is a very important quantity for radical-radical reactions can be simply estimated.

Estimation of Collision Time. The jump length at pressure p and at 298.2 K can be estimated by means of Eq. 7, using available ρ-p data.[12] If the numerical values of b, ρ_p, and ρ_0 are substituted into Eqs. 6 and 7, one obtains the collision time τ_1. They are listed in Table 3. The viscosity η raises while the jump length λ decreases with increasing pressure. We can see that the product $\lambda^2\eta$ increases proportionately with pressure resulting in the net increase in τ_1. The collision times τ_1 for the spin exchange of the nitroxide radicals in acetone and hexane are of the order of 10^{-11} s (Table 3). These values are nearly equal to the rotational correlation time ($\tau_{rot}=1.7\times10^{-11}$ s TANONE in acetone) estimated from the following equation:[15]

$$\tau_{rot} = 4\pi\eta b^3/3kT. \quad (10)$$

This suggests that the collision time in acetone and hexane is deeply correlated to the rotational correlation time, which is responsible for $P<1$. Meanwhile for toluene, if the numerical values of b, λ, and η (b=0.39 nm TANONE, λ=0.86 nm, η=0.556 mPa s at 1 bar and λ_p= 0.84 nm, η_p=0.853 mPa s at 637 bar) are substituted in Eq. 6, we have $\tau_1=1.22\times10^{-10}$ and 1.79×10^{-10} s at 1 and 637 bar, respectively. With these values and $J=6.9\times10^{10}$ s^{-1}, $J^2\tau_1^2$ becomes 71 and 153 at 1 and 637 bar, respectively, in agreement with our foregoing prediction from Fig. 2.

References

1) Part II. Y. Sueishi, N. Nishimura, K. Hirata, and K. Kuwata, *Bull. Chem. Soc. Jpn.*, **63**, 252 (1990).
2) J. Jonas, *Rev. Phys. Chem. Jpn.*, **50**, 19 (1980), and references cited therein.
3) N. Edelstein, A. Kwok, and A. H. Maki, *J. Chem. Phys.*, **41**, 179, 3473 (1964).
4) J. Hwang, D. Kivelson, and W. Plachy, *J. Chem. Phys.*, **58**, 1753 (1973).
5) D. Griller, *J. Am. Chem. Soc.*, **100**, 5240 (1978).
6) K. J. le Noble and P. Staub, *J. Organomet. Chem.*, **156**, 25 (1978).
7) K. W. Böddeker, G. Lang, and U. Schindewolf, *Angew. Chem., Int. Ed. Engl.*, **8**, 138 (1969).
8) P. R. Marriott and D. Griller, *J. Am. Chem. Soc.*, **103**, 1521 (1981).
9) Y. Sueishi, N. Nishimura, K. Hirata, and K. Kuwata, *Bull. Chem. Soc. Jpn.*, **61**, 4253 (1988).
10) Yu N. Molin, K. M. Salikhov, and K. I. Zammaraev, "Spin Exchange," Springer-Verlag, New York (1980).
11) W. Plachy and D. Kivelson, *J. Chem. Phys.*, **47**, 3312 (1967).
12) "International Critical Table," McGraw-Hill, New York (1928), Vols. III and VII. N. B. Bargaftik, "Physical and Thermodynamic Properties of Gas and Liquid," Nauka, Moscow (1972).
13) F. D. Rossini, "Selected Values of Physical and Thermodynamic Properties of Hydrocarbons and Related Compounds," NBS, Pittsburg (1953).
14) D. Kivelson, *J. Chem. Phys.*, **33**, 1094 (1960).
15) A. Abragam, "The Principle of Nuclear Magnetism," Oxford University Press, Oxford (1961).

Mesomorphic Properties of 4-[3,4-Bis(4-alkoxybenzoyloxy)benzylideneamino]azobenzenes and Related Compounds

Tatsuya MASUDA and Yoshio MATSUNAGA*
Department of Chemistry, Faculty of Science, Hokkaido University, Sapporo 060
(Received February 16, 1991)

The mesomorphic properties of a homologous series of 4-[3,4-bis(4-alkoxybenzoyloxy)benzylideneamino]azobenzenes have been studied by differential scanning calorimetry and microscopy. While the nematic phases exhibited by the ethoxy and propoxy homologues are metastable, those exhibited by all of the butoxy-to-hexadecyloxy homologues exhibit the temperature range of stable existence. A metastable smectic A-phase is observed for the tetradecyloxy and hexadecyloxy homologues. Among the examined 4-[2,4-bis(4-alkoxybenzoyloxy)benzylideneamino]azobenzenes, only the dodecyloxy and tetradecyloxy members are nematogenic. Their clearing points are located at more than 30 °C below the melting points. 4-(Benzylideneamino)azobenzene and its 3-(4-dodecyloxybenzoyloxy) derivative are nonmesogenic; however, the phase diagrams of binary systems with 4-(4-nonyloxybenzylideneamino)azobenzene revealed that the addition of a 3-(4-dodecyloxybenzoyloxy) group to the former molecule depresses the virtual nematic behavior, but promotes the smectic A behavior. A further addition of the same group at the 4-position drastically raises the nematic-isotropic transition temperature.

Systematic studies on the influence of lateral substitutents on the mesomorphic properties of rod-like molecules indicated that only relatively small ones allow the persistence of the liquid crystalline state.[1-3] However, Weissflog and Demus discovered that some molecules with a long alkyl group, and even with an aromatic branch bound to the middle moiety of a rod-like molecule, can form mesophases.[4-7] The compounds of the latter type include 4-nitrophenyl 2,5-bis(4-octyloxybenzoyloxy)benzoate and 4′-ethoxy-3-[*N*-(4-ethoxyphenyl)iminomethyl]-4-(4-methoxybenzoyloxy)azobenzene. The former compound exhibits a stable smectic A-phase covering the temperature range from 96 to 164 °C, whereas the latter exhibits a metastable nematic phase, the transition into an isotropic liquid of which is located far below the melting point (73 °C vs. 160 °C). A single-crystal X-ray analysis performed on the azobenzene derivative disclosed that the molecule is in a bifurcated shape. The phenyliminomethyl branch is markedly bent from the nearly linear three-ring basic fragment, but is almost coplanar with the azobenzene moiety.

More extensive synthetic studies concerning closely-related compounds were carried out by Takenaka et al.[8-10] Tris(4-alkoxyphenyl) 1,2,4-benzenetricarboxylates were shown to exhibit a metastable nematic phase when the alkyl group is heptyl or octyl and a smectic A-phase as well as a nematic phase when the alkyl group is nonyl or decyl.[8] 4-Cyanophenyl 3,4-bis(4-alkoxybenzoyloxy)benzoates, in which the alkyl group is from pentyl to octyl, are nematogenic. Among these members only the hexyl compound gives a nematic phase with a temperature range of stable existence. A metastable smectic A-phase was observed for the heptyl-to-decyl homologues.[9] The 4-alkoxylphenyl esters of the same acid are also nematogenic when the alkyl group is butyl-to-nonyl. The nematic–isotropic transitions in the hexyl compound and the higher homologous members are enantiotropic. The nonyl compound shows a metastable smectic-A phase in addition to a nematic phase. Thus, many 1,2,4-benzene derivatives comprising four-rings are mesogenic; however, the mesophase–isotropic transitions are known to be mostly monotropic. Consequently, we prepared a series of 4-[3,4-bis(4-alkoxybenzoyloxy)benzylideneamino]azobenzene (**1**) and the related compounds (**2**), both of which have a linear four-ring basic fragment, and studied their liquid-crystalline behavior. In order to clarify the effects of an aromatic branch on the mesomorphic properties, the thermal behavior of 4-[3-(4-alkoxybenzoyloxy)benzylideneamino]azobenzenes (**3**) were also examined.

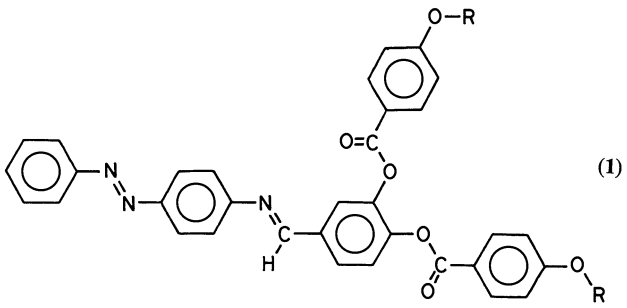

(1)

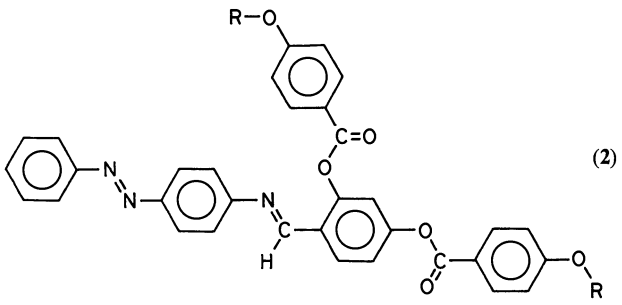

(2)

Experimental

Materials. Equimolar amounts of 4-aminoazobenzene and

3-hydroxybenzaldehyde or 2,4- or 3,4-dihydroxybenzaldehyde were dissolved in ethanol, and then a few drops of acetic acid were added. The precipitated orange-colored 4-(benzylideneamino)azobenzene derivative was collected by filtration and washed first with ethanol and then with hexane. Compounds **1** were obtained by the reaction of 4-(3,4-dihydroxybenzylideneamino)azobenzene with 4-alkoxybenzoic acids in chloroform, following a procedure of Hassner and Alexanian.[11] Found: C, 76.61; H, 8.10; N, 4.79%. Calcd for $(C_{12}H_{25}OC_6H_4CO_2)_2C_6H_3$–CH=N–$C_6H_4$–N=N–$C_6H_5$: C, 76.56; H, 8.00; N, 4.70%. Compounds **3** were similarly prepared. In order to synthesize compounds **2**, the esterification of 4-(2,4-dihydroxybenzylideneamino)azobenzene had to be carried out by the reaction with 4-alkoxybenzoyl chloride in boiling benzene by the addition of pyridine.

Measurements. The transition temperatures and associated enthalpy changes were measured by means of a Rigaku Denki Thermoflex differential scanning calorimeter. Phase diagrams were determined by the calorimetric curves of mixtures.

Results and Discussion

The mesomorphic transition temperatures and associated enthalpy changes of compounds **1** are summarized in Table 1. Here, K, S_A, N, and I stand for crystalline, smectic A, nematic, and isotropic liquid phases, respectively. In spite of the presence of an aromatic lateral branch, all of the ethoxy-to-hexadecyloxy homologues were found to be mesogenic. The N–I transition temperature gradually decreases with increasing the alkyl chain length throughout this series. The mesophases given by the ethoxy and propoxy compounds are metastable, whereas those given by the butoxy-to-hexadecyloxy compounds have a temperature range of stable existence. Thus, the presence of the 4-(phenylazo)phenyliminomethyl group in the molecule greatly enhances the thermal stability of the mesophases, compared with those reported by other workers.[5-10] They show a marble texture characteristic of nematic phases formed by rod-like molecules. The temperature ranges of stable existence given by the octyloxy homologue and the later members of the series are about 30 °C. In addition, a metastable smectic phase exhibiting a fan texture is observable with the tetradecyloxy and hexadecyloxy homologues.

As is shown in Fig. 1, the nematic phase of the dodecyloxy compound is completely miscible with the nematic phase of 4-(4-nonyloxybenzylideneamino)azobenzene, indicating that the mesophase is classical nematic, in spite of the molecular shape being far from rod-like. The latter compound has been reported to give the following transitions: K 109.5 S_B 126 S_A 156 N 162 I.[12] The present conclusion is in a sharp contrast with our previous finding that *N*,*N*′-dialkanoyl-2,5,6-trimethyl-4-alkanoyloxy-1,3-benzenediamines (the molecular shape of which is supposed to resemble, to some degree, that of the present series) is discotic nematic.[13] The smectic A- and B-phases of the reference mesogen are considerably destabilized upon mixing. The S_A–N transition point curve intersects with the melting point curve of the reference compound at 108 °C and 68 mol% and the S_B–S_A transition point curve at 111 °C and 92 mol%. Fitting Van Hecke's equation, $T=\Delta H_{AV}/\Delta S_{AV}$, to the diagram using the entropy ratio as a parameter suggests that the virtual S_A–

Table 1. Transition Temperatures (°C) and Enthalpy Changes (kJ mol^{-1}) of Compounds **1**[a]

n[b]	K	S_A	N	I
2	· 181(43)		[· 160(0.4)]	·
3	· 176(52)		[· 141(0.4)]	·
4	· 145(40)		· 147(0.4)	·
5	· 126(51)		· 135(0.4)	·
6	· 107(55)		· 136(0.4)	·
7	· 110(61)		· 132(0.4)	·
8	· 102(59)		· 131(0.4)	·
9	· 99(68)		· 127(0.4)	·
10	· 91(67)		· 125(0.5)	·
11	· 82(65)		· 121(0.5)	·
12	· 82(73)		· 121(0.6)	·
14	· 91(78)	[· 76(0.4)]	· 115(0.7)	·
16	· 100(80)	[· 88(0.5)]	· 113(0.8)	·

a) The enthalpy changes are in parentheses. Brackets indicate monotropic transitions. b) The number of carbon atoms in the alkyl group.

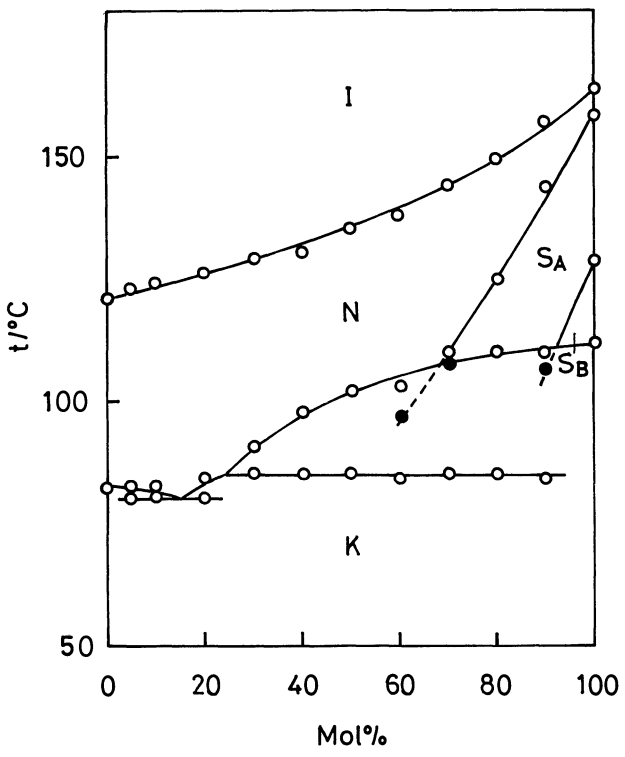

Fig. 1. Phase diagram of the binary system consisting of 4-[3,4-bis(4-dodecyloxybenzoyloxy)benzylideneamino]azobenzene and 4-(4-nonyloxybenzylideneamino)azobenzene. The latter compound is located on the right-hand side. The open and shaded circles are transitions recorded in the processes of heating and cooling respectively.

Table 2. Transition Temperatures (°C) and Enthalpy Changes (kJ mol^{-1}) of Compounds **2** and **3**[a]

n[b]	K	N			I
		Compounds **2**			
10	·	109(61)			·
11	·	98(65)			·
12	·	105(64)	[·	73(0.5)]	·
14	·	106(70)	[·	71(0.6)]	·
16	·	108(72)			·
		Compounds **3**			
6	·	131(71)			·
10	·	114(75)			·
12	·	107(82)			·

a) The enthalpy changes are in parentheses. Brackets indicate monotropic transitions. b) The number of carbon atoms in the alkyl group.

N transition of the dodecyloxy compound is located at about 35 °C.[14] It may be noted that the destabilization of the ordered smectic phase is more drastic than that of the non-ordered one.

Table 2 presents the thermal properties of series **2** and **3**. For the former series, only the decyloxy, undecyloxy, dodecyloxy, tetradecyloxy, and hexadecyloxy members were studied. The melting point tends to be higher than that of the corresponding member of series **1**. A metastable mesophase is detectable only with dodecyloxy and tetradecyloxy compounds. Judging from the magnitude of the enthalpy change at the clearing point, the mesophase is undoubtedly nematic. The transition is located more than 30 °C below the melting point. In other words, the N–I transition temperature is depressed by 41 or 48 °C by the shift of the 4-alkoxybenzoyloxy branch from the 3-position to the 2-position of the benzylideneamino moiety. This mesomorphic behavior of compound **2** may be ascribed to the difference in the rigidity between the specific moieties of the linear four-ring basic fragment located close to the 4-alkoxybenzoyloxy branch. While the more-or-less planar 4-(phenylazo)phenyliminomethyl group is favorable for an enhancement of the thermal stability of the mesophase (as seen earlier), the 4-alkoxybenzoyloxy branch at the 2-position in compound **2** is not allowed to adopt configurations relaxed well from the Y-shape because of the rigidity of the afore-mentioned group. On the other hand, the two 4-alkoxybenzoyloxy groups at the 3- and 4-positions may easily take configurations less deviated from the rod-like shape by rotating rather freely around the C–O and C–C single bonds.

All of the three examined members of compounds **3**, the molecule of which has a bent, is not mesogenic at all. In order to explore the potential mesogenic properties, we studied the phase diagrams of binary systems comprising the dodecyloxy homologue and the corresponding member of series **1**, as well as the afore-mentioned reference compound, 4-(4-nonyloxybenzylideneamino)-azobenzene. In the former system, which shows a eutectic point at 75 °C and 37 mol% of compound **3**, the thermal stability of the mesophases given by the reference compound is so diminished that the N–I transition point curve meets the melting point curve of compound **1** at 78 °C and 27 mol%.

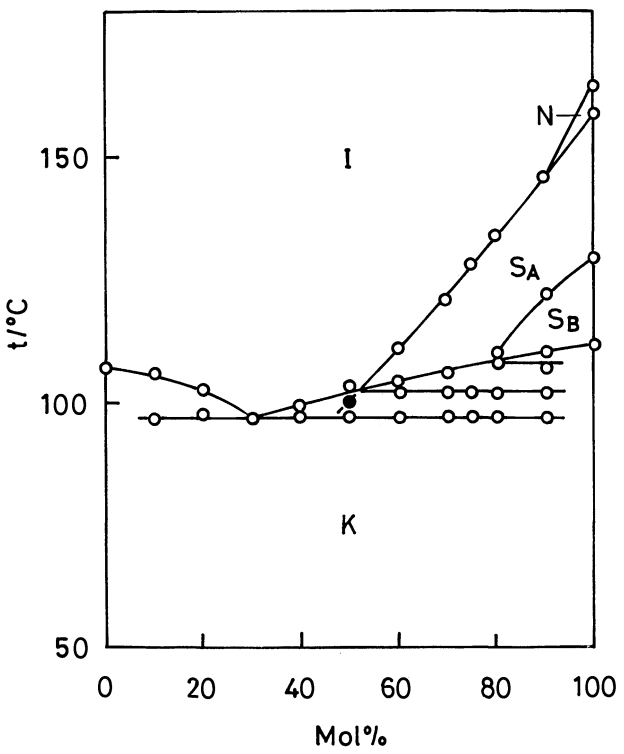

Fig. 2. Phase diagram of the binary system consisting of 4-[3-(4-dodecyloxybenzoyloxy)benzylideneamino]azobenzene and 4-(4-nonyloxybenzylideneamino)azobenzene. The latter compound is located on the right-hand side. As to the open and shaded circles, see the caption of Fig. 1.

The phase diagram given by the latter system is presented in Fig. 2. The nematic phase disappears upon the addition of 10 mol% of compound **3**; therefore, the N–I transition point curve is only our eye guide drawn so as to be consistent with the curve in the former system. The S_A–I transition point curve intersects with the melting point curve of the reference compound at 102 °C and 52 mol% and the S_B–S_A transition point curve at 108 °C and 79 mol%. The virtual S_A–I transition of compound **3** may be located at about 60 °C by the extrapolation of the transition point curve, which is slightly concave upwards, observable down to 50 mol% of the reference compound to 0 mol%.[14] This temperature is undoubtedly higher than the S_A–N transition temperature estimated for the corresponding member of series **1**. In contrast to the S_A–I transitions, the S_A–S_B transitions seem to form a curve that is slightly convex upwards. Thus, the introduction of a 4-(4-dodecyloxybenzoyloxy) group to the molecule of compound **3** leads to very significant stabilization of the

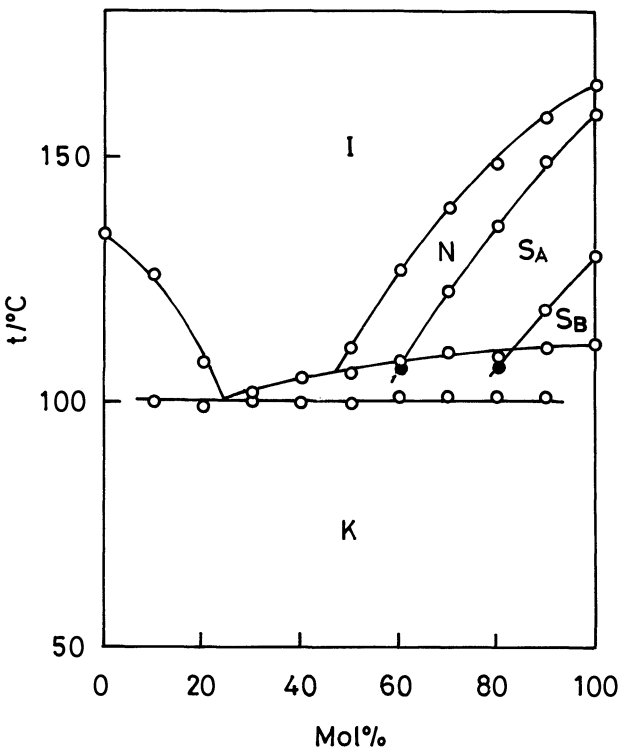

Fig. 3. Phase diagram of the binary system consisting of 4-(benzylideneamino)azobenzene and 4-(4-nonyloxybenzylideneamino)azobenzene. The latter compound is located on the right-hand side. As to the open and shaded circles, see the caption of Fig. 1.

nematic phase and a relatively small destabilization of the smectic A-phase. If we consider that the dodecyloxy homologue of series **1** is formed by the introduction of a (4-dodecyloxybenzoyloxy) group to the 3-position of 4-[4-(4-dodecyloxybenzoyloxy)benzylideneamino]-azobenzene, the depression of the N–I transition by the branching is as much as 157 °C, since this linear four-ring compound exhibits transitions, K 142 N 277 I.

Fig. 3 presents a phase diagram of a binary system comprising nonmesogenic 4-(benzylideneamino)azobenzene, the common moiety of all the compounds studied here, and 4-(4-nonyloxybenzylideneamino)azobenzene. The N–I transition is enantiotropic above 47 mol%, the S_A–N transition above 61 mol%, and the S_B–S_A transition above 83 mol%. The maximum temperatures of both the virtual nematic and smectic phases of 4-(benzylideneamino)azobenzene may be located near or below 0 °C.[14] A comparison of the present diagram with the one in Fig. 2 strongly suggests a depression of the N–I transition temperature, as well as a promotion of the S_A–N or S_A–I transition temperature by the introduction of a 3-(4-dodecyloxybenzoyloxy) group to this common moiety. Therefore, if a mesogenic compound could be obtained employing molecules with an obtuse-angled configuration one would speculate that it tends to be smectogenic rather than nematogenic. The mesomorphic properties of 1,3-phenylene bis[4-(4-alkoxybenzylideneamino)benzoates] and their related compounds will be the subject of a forthcoming paper.[15]

References

1) J. Byron, G. W. Gray, and B. M. Worrall, *J. Chem. Soc.*, **1965**, 3706.
2) W. R. Young, I. Haller, and D. C. Green, *J. Org. Chem.*, **23**, 3707 (1972).
3) M. A. Osman, *Mol. Cryst. Liq. Cryst.*, **128**, 45 (1985).
4) W. Weissflog and D. Demus, *Mol. Cryst. Liq. Cryst.*, **129**, 235 (1985).
5) S. Diele, W. Weissflog, G. Pelzl, H. Manke, and D. Demus, *Liq. Cryst.*, **1**, 101 (1986).
6) W. Weissflog and D. Demus, *Liq. Cryst.*, **3**, 275 (1988).
7) U. Baumeister, Z. Kosturkiewicz, H. Hartung, D. Demus, and W. Weissflog, *Liq. Cryst.*, **7**, 241 (1990).
8) S. Takenaka, Y. Masuda, and S. Kusabayashi, *Chem. Lett.*, **1986**, 751.
9) S. Takenaka, H. Morita, M. Iwano, S. Kusabayashi, T. Ikemoto, Y. Sakurai, and H. Miyake, *Mol. Cryst. Liq. Cryst.*, **166**, 157 (1989).
10) S. Takenaka, Y. Masuda, M. Iwano, H. Morita, S. Kusabayashi, H. Sugiura, and T. Ikemoto, *Mol. Cryst. Liq. Cryst.*, **168**, 111 (1989).
11) A. Haussner and V. Alexanian, *Tetrahedron Lett.*, **1978**, 4475.
12) D. Demus and H. Sackmann, *Z. Phys. Chem.* (*Leipzig*), **238**, 215 (1968).
13) H. Kawada and Y. Matsunaga, *Bull. Chem. Soc. Jpn.*, **63**, 1691 (1990).
14) G. R. Van Hecke, *J. Phys. Chem.*, **89**, 2058 (1985).
15) T. Akutagawa, Y. Matsunaga, and K. Yasuhara, to be published elsewhere.

The Number of Organic Radicals on a Decationated Y-Type Zeolite before, during, and after Irradiating with Ultraviolet Light or Heating

Hiroshi KASHIWAGI
Faculty of Pharmaceutical Sciences, Toyama Medical and Pharmaceutical University, Sugitani, Toyama 930-01
(Received March 18, 1991)

A decationated Y-type zeolite (HY) was adsorbed by a single organic compound from a heptane solution, and dried in vacuo. The numbers of the radicals in these binary systems before, during, and after irradiating with ultraviolet (UV) light or heating were followed by electron paramagnetic resonance spectroscopy and then compared. During UV irradiation, the number of radicals increased from the constant number of spins before illumination (C_1) to the second constant number of spins (C_2). After stopping the illumination, the C_2 decreased up to the third constant number of spins (C_3). The C_3 value was smaller than C_2, but was significantly greater than C_1. The enhancement of radicals induced by UV light, expressed quantitatively in terms of the C_3/C_1 ratio, was pronounced when either a weak donor or a weak acceptor was adsorbed on HY calcined at a low temperature. C_1 was proportional to the amount of adsorption up to the maximal amount of adsorption, whereas C_2 and C_3 were proportional only at a considerably decreased amount of adsorption. A similar tendency was observed when the binary systems were heated at 40 or 80 °C. A quantitative determination of the mechanically induced enhancement of radicals would prompt either an improvement in the reproducibility of physicochemical data or an elucidation of the solid acidity or basicity.

Organic radical formation on the surface of an aluminosilicate due to a charge-transfer interaction has frequently been studied.[1] In order to find some new factors available for improving the reproducibility of the physicochemical data concerning relatively complicated systems, or for correlatively and comprehensively elucidating the solid acidity or basicity, we followed in a preceding paper the time course of the number of spins (NOS) in either a binary system comprising a decationated Y-type zeolite (HY) and a single organic compound or a ternary system comprising HY and two organic compounds after removing a solvent (heptane).[2] The NOS values and their time courses were dependent on the calcination temperature of HY (T_{ca}) as well as the electron-donating or -accepting characteristics of the organic molecules. The NOS values of the binary system were reversible and linear up to the amount of adsorption,[2,3] whereas those of the solvent-free ternary (HY–two organic) systems, which were irreversible and nonlinear to the amount of adsorption, were dependent on the order of adsorption.[2]

The NOS values of the solvent-free ternary systems were suitable for quantitative consideration of this kind of irreversibility. However, vigorous stirring of the HY–organic binary system in heptane caused another qualitative irreversible dependence of NOS on the amount of adsorption. Furthermore, this kind of irreversibility was also induced in solvent-free binary systems either by ultraviolet (UV) irradiation or by heating.

The radical species produced at solid (Lewis) acid sites induced by photoillumination were identified based on analyses of the hyperfine structures of the electron paramagnetic resonance (EPR) spectra.[4] In addition, the stoichiometric formation of complexes between the Lewis acids and the radicals induced by photoirradiation was confirmed.[4]

In the present study, we followed by EPR spectroscopy the NOS values of the solvent-free HY–organic binary systems before, during, and after UV irradiation or before, during, and after the application of heat. The results obtained with binary systems comprising both HY calcined at 400 or 650 °C and perylene (PE, a strong donor), naphthalene (NA, a weak donor), tetracyanoethylene (TCNE, a strong acceptor), or 1,3-dinitrobenzene (DNB, a weak acceptor) were compared with one another. The NOS values obtained after illumination or heating were significantly greater than those obtained before the treatment. The enhancement of radicals was related to the T_{ca} and electron-donating or -accepting characteristics of the organic molecules. Furthermore, nonlinear dependence of the NOS values on the amount of adsorption was determined quantitatively. We thought that a quantitative consideration of the mechanically induced enhancement of radicals would prompt the finding of some new factors necessary either for improving the reproducibility of physicochemical data of relatively complicated systems or for elucidating the mechanically induced solid acidity or basicity.

Experimental

Materials. An HY was obtained by calcining an NH_4^+-exchanged Y-type zeolite (Si/Al=1.90) at 400 or 650 °C. The purification of PE, NA, TCNE, and DNB has been previously described.[2]

Procedure. HY was brought into contact with a heptane solution (0.01—0.1 mol dm^{-3}) of PE, NA, TCNE, or DNB, dried under reduced pressure (ca. 3 Pa), and stored in an EPR cell in dry nitrogen at 25 °C until the first constant number of spins (C_1) was attained. This binary system, being stored in

the EPR cell, was then irradiated with UV light or heated at 40 or 80 °C with occasional shaking until the second constant number of spins (C_2) was reached. After stopping either the illumination or heating, the sample was permitted to stand at 25 °C until the third constant number of spins (C_3) was attained. The EPR spectra were followed throughout all of these processes.

The heating temperature was adjusted by using a thermostat. A JEOL ES-05 H-type UV irradiation unit fitted with a 500-W mercury lamp was used for illumination.

Spectral Measurement. The EPR spectrometer, experimental conditions, and method for determinating both NOS and amount of adsorption have been described previously.[2] The experimental errors in NOS and the amount of organic molecules adsorbed on HY were less than 10%.[2]

Results and Discussion

Time Courses of NOS before, during, and after UV Irradiation or Heating. As described previously, a fairly well-resolved hyperfine structure was obtained in the EPR spectrum of the PE or NA cation radicals on solid acid sites or of the DNB anion radicals on solid base sites; the spectrum of the TCNE anion radicals, however, was unresolved.[3,5]

The time courses of the NOS before, during, and after UV irradiating or before, during, and after heating were examined using a solvent-free binary system comprising a maximal amount of adsorption (A_{max}) of PE, NA, TCNE, or DNB and HY calcined at 400 or 650 °C. As descrived previously,[2] the NOS for the binary system before illumination was initially small, gradually increased with the passage of time, and finally reached C_1.

The time courses of NOS during or after UV irradiation are demonstrated in Figs. 1 and 2, respectively.[6] As shown from Fig. 1, the NOS increases with the passage of time from C_1 to C_2 after the start of UV irradiation. As illustrated in Fig. 2, NOS is the greatest (C_2) immediately after stopping the illumination; it gradually decreases with the passage of time, finally reaching C_3. As described below, the NOS values and their time courses are dependent on T_{ca} and the electron-donating or -accepting characteristics of the organic molecules.

The time courses of the values of NOS obtained before, during, or after heating at 40 or 80 °C were analogous to

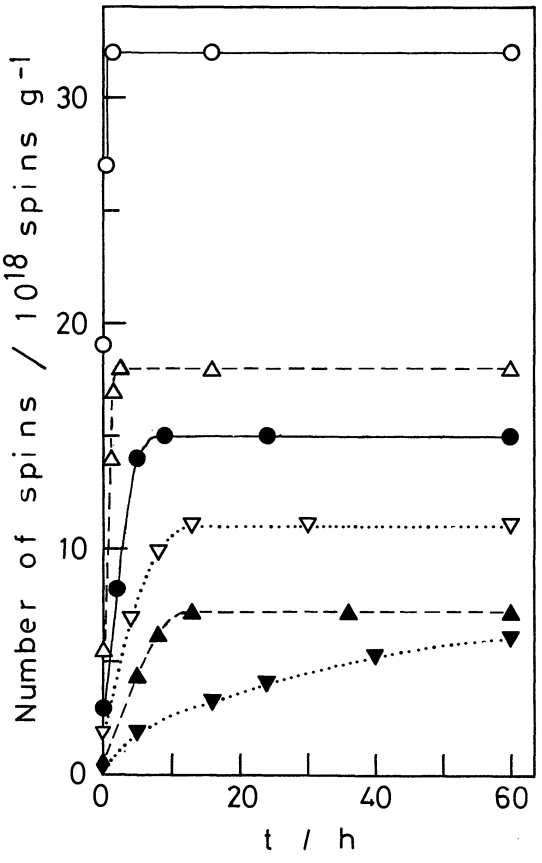

Fig. 1. Time course of the number of PE cation radicals on HY calcined at 650 (○) or 400 (●)°C, TCNE anion radicals on HY calcined at 650 (△) or 400 (▲)°C, or DNB anion radicals on HY calcined at 650 (▽) or 400 (▼)°C during UV irradiation. The amount of the organic molecules adsorbed on HY was A_{max}.

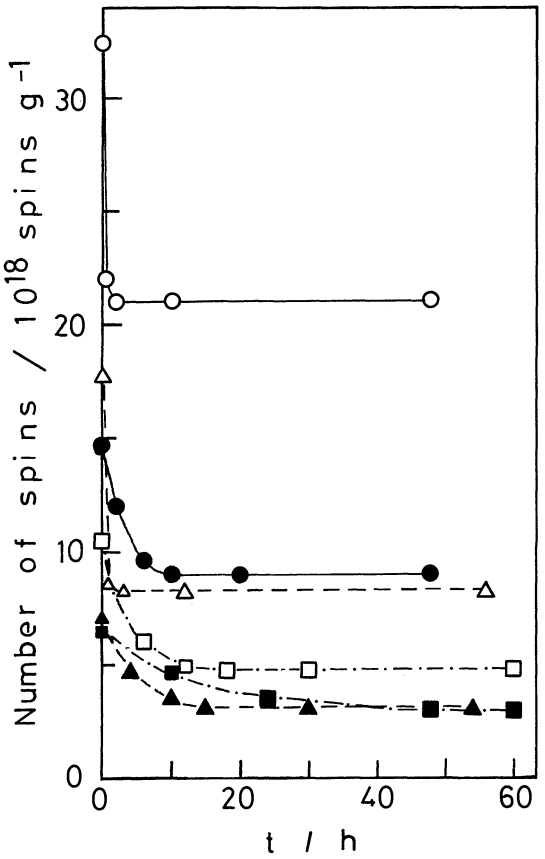

Fig. 2. Time course of the number of PE cation radicals on HY calcined at 650 (○) or 400 (●)°C, NA cation radicals on HY calcined at 650 (□) or 400 (■)°C, or TCNE anion radicals on HY calcined at 650 (△) or 400 (▲)°C after stopping illuminating. The amount of adsorption was A_{max}.

Table 1. Constant Number of Spins and the Time Required for Attaining the Constant upon UV Irradiation[a)]

Organic compound	T_{ca}	C_1	C_2	C_3	C_3/C_1	t_{C1}	t_{C2}	t_{C3}
	°C	10^{18} spins g^{-1}				h		
PE	650	19	32	21	1.1	1	1.5	2
	400	2.9	15	9.0	3.1	8	9	10
NA	650	4.4	11	5.8	1.3	8	9	10
	400	0.92	7.0	3.4	3.7	40	45	50
TCNE	650	5.5	18	8.3	1.5	2	2.5	3
	400	0.61	7.2	3.2	5.2	12	13	15
DNB	650	1.8	11	4.8	2.7	10	13	18
	400	0.22	6.5	2.7	12	120	130	140

a) The amount of adsorption on HY was A_{max}.

Table 2. Constant Number of Spins and the Time Required for Attaining the Constant upon Heating at 80°C[a)]

Organic compound	T_{ca}	C_1	C_2	C_3	C_3/C_1	t_{C1}	t_{C2}	t_{C3}
	°C	10^{18} spins g^{-1}				h		
PE	650	19	28	19	1.0	1	1.5	2
	400	2.9	11	5.8	2.0	8	9	10
NA	650	4.4	9.8	4.8	1.1	8	10	11
	400	0.92	5.4	1.8	2.0	40	45	50
TCNE	650	5.5	13	6.5	1.2	2	2.5	3
	400	0.61	4.9	2.1	3.4	12	14	15
DNB	650	1.8	6.6	3.0	1.7	10	14	20
	400	0.22	2.5	1.1	5.0	120	135	150

a) The amount of adsorption on HY was A_{max}.

those obtained upon UV irradiation.

Enhancement of Radicals by Illuminating or by Heating. Table 1 summarizes the values of C_1, C_2, C_3, the time required for attaining the C_1 (t_{C1}), the time required for attaining C_2 (t_{C2}), and the time required for attaining C_3 (t_{C3}), as well as the ratio C_3 to C_1 (C_3/C_1) obtained upon UV irradiation of the HY–organic system at a given amount of adsorption (A_{max}). Tables 2 and 3 list the corresponding values obtained upon heating at 80 or 40 °C, respectively. Although not shown in Table 3, the values of t_{C1}, t_{C2}, and t_{C3} obtained by heating at 40 °C were close to those obtained by heating at 80 °C (Table 2).

In general, C_3 is significantly greater than C_1, indicating that an enhancement of the radicals is induced by either heating or photoillumination applied after HY is adsorbed by the organic molecules. The C_1, C_2, and C_3 are small, while the t_{C1}, t_{C2}, t_{C3}, and C_3/C_1 are large when either a weak donor (NA) or a weak acceptor (DNB) is adsorbed on HY calcined at a low temperature (400 °C).

Dependence of the C_2 and C_3 Values on the Amount of Adsorption. As described previously,[2)] the C_1 value of the solvent-free HY–organic binary system before photoillumination increased linearly with an increase in the amount of adsorption, finally reaching a maximum number of spins at the amount of adsorption of A_{max}. Independent of T_{ca}, the A_{max} value for PE, NA, TCNE, or DNB was determined to be 3.1, 6.2, 3.6, or 2.2×10^{20} molecules/g-HY, respectively.[2)] The maximum numbers of spins/g–HY, shown as the C_1 in Table 1, however, were significantly dependent on T_{ca}.

Table 3. Constant Number of Spins upon Heating at 40°C[a)]

Organic compound	T_{ca}	C_1	C_2	C_3	C_3/C_1
	°C	10^{18} spins g^{-1}			
PE	650	19	21	19	1.0
	400	2.9	5.3	3.7	1.3
NA	650	4.4	5.9	4.5	1.0
	400	0.92	1.8	1.2	1.3
TCNE	650	5.5	7.0	5.7	1.0
	400	0.61	1.6	0.94	1.5
DNB	650	1.8	2.8	2.0	1.1
	400	0.22	0.75	0.40	1.8

a) The amount of adsorption was A_{max}.

The dependence of the C_2/C_1 or C_3/C_1 obatined upon photoillumination on the amount of adsorption/A_{max} (A) from 0.1 to 1.0 is demonstrated in Table 4 or 5, respectively. The C_2 and C_3 values at A=0 were, of course, nil. On the surface of HY calcined at 650 °C, as can be seen from Table 5, the C_3 value for PE, NA, TCNE, or DNB is identical with the corresponding C_1 value at an A value of less than 0.6, 0.3, 0.5, or 0.1, respectively. With a further increase in the A value, C_3 gradually becomes greater than the corresponding C_1. On the surface of HY calcined at 400 °C, C_3 becomes greater than C_1, even at a decreased A value (less than 0.1); it further increases with an increase in the A value.

Table 4. Dependence of the C_2/C_1 Ratio on the Amount of Adsorption upon UV Irradiation

Organic compound	T_{ca}	C_2/C_1 at $A^{a)}$=									
	°C	0.1	0.2	0.3	0.4	0.5	0.6	0.7	0.8	0.9	1.0
PE	650	1.6	1.6	1.6	1.6	1.6	1.6	1.7	1.7	1.7	1.7
	400	3.9	4.0	4.1	4.2	4.4	4.6	4.8	5.0	5.1	5.2
NA	650	2.0	2.0	2.1	2.1	2.2	2.2	2.3	2.3	2.4	2.5
	400	4.1	4.4	4.9	5.4	5.9	6.4	6.8	7.2	7.4	7.6
TCNE	650	3.0	3.0	3.0	3.0	3.1	3.1	3.2	3.2	3.3	3.3
	400	8.0	8.1	8.5	8.9	9.3	9.8	10	11	12	12
DNB	650	4.9	5.0	5.1	5.3	5.4	5.5	5.7	5.8	5.9	6.1
	400	12	13	14	15	17	19	21	24	28	30

a) The amount of adsorption/A_{max}.

Table 5. Dependence of the C_3/C_1 Ratio on the Amount of Adsorption upon UV Irradiation

Organic compound	T_{ca}	C_3/C_1 at $A^{a)}$=									
	°C	0.1	0.2	0.3	0.4	0.5	0.6	0.7	0.8	0.9	1.0
PE	650	1.0	1.0	1.0	1.0	1.0	1.0	1.1	1.1	1.1	1.1
	400	1.3	1.4	1.5	1.6	1.7	1.8	2.0	2.4	2.8	3.1
NA	650	1.0	1.0	1.0	1.1	1.1	1.2	1.2	1.3	1.3	1.3
	400	1.9	2.1	2.3	2.5	2.7	2.8	3.0	3.3	3.6	3.7
TCNE	650	1.0	1.0	1.0	1.0	1.0	1.1	1.3	1.5	1.5	1.5
	400	1.6	1.8	2.1	2.5	2.9	3.5	4.0	4.6	5.0	5.2
DNB	650	1.0	1.1	1.2	1.4	1.6	1.9	2.2	2.5	2.7	2.7
	400	2.8	3.2	3.8	4.6	5.4	6.8	8.1	9.9	11	12

a) The amount of adsorption/A_{max}.

In the vicinity of A=1.0, however, the slope of the increase curve of C_3 decreases. Therefore, different from the C_1, C_3 is proportional to the amount of adsorption only at a decreased amount of adsorption.

The C_2/C_1 depends on the amount of adsorption, similarly to C_3/C_1. It can be seen from Table 4 that the C_2 values are much greater than C_1 and C_3. However, C_2/C_1 is constant at a decreased A value. It increases with a further increase in the A value. Therefore, C_2 is linear with respect to the amount of adsorption for a small amount of adsorption. The range of the A values providing a linear dependence of C_2 on the amount of adsorption is somewhat wider than that of C_3. Moreover, the ratio of C_2/C_1 at A=0.1 to that at A=1.0 is much smaller than the corresponding ratio for C_3/C_1.

Both C_3/C_1 and the C_2/C_1 are great, while the range of A values providing the linear dependence of C_2 and C_3 on the amount of adsorption is small when a weak donor (NA) or a weak acceptor (DNB) is adsorbed on HY calcined at 400 °C. At an identical A value, the C_2/C_1 or C_3/C_1 obtained at T_{ca}=650 °C is remarkably smaller than that obtained at T_{ca}=400 °C. Although not shown in Tables 4 and 5, the t_{C2} and t_{C3} values increased very slightly with an increase in the amount of adsorption.

The values of C_2/C_1 or C_3/C_1 obtained upon heating (40 or 80 °C) depended on the amount of adsorption in a manner similar to those shown in Table 4 or 5, respectively.

The C_2 and C_3 Values Obtained upon Heating Twice at Different Temperatures. The solvent-free HY–organic binary system was at first heated at a low temperature (40 °C) until attaining C_2; heating was then stopped and left at 25 °C until attaining C_3. This binary system was again heated at a sufficiently high temperature (80 °C) until attaining another C_2; heating was then stopped and left at 25 °C until attaining another C_3. In this case, the C_2 and C_3 values obtained upon the second heating at 80 °C was little influenced by the first heating at 40 °C. On the contrary, when the binary system was treated at first at 80 °C and subsequently at 40 °C, the final C_3 was identical with that obtained without the second heating at 40 °C.

Heating with a Slow Raise in Temperature. The C_2 and C_3 values shown in Tables 2 and 3 were obtained by placing the HY–organic system, having been stored at 25 °C, directly into a thermostat of 40 or 80 °C. On the other hand, when the temperature of the binary system was slowly raised from 25 to 40 or 80 °C (less than 0.3 °C h^{-1}), the C_2 and C_3 values at an increased amount of adsorption became smaller than those shown in Tables 2 and 3. By way of heating with a slow temperature rise, the C_2 and C_3 obtained at a heating temperature of 40 °C became proportional to the amount of adsorption up to A=1.0. Although the range of the A values providing the linear dependence on the amount of adsorption increased, the C_2 and C_3 obtained by heating at 80 °C were still nonlinear to the amount of adsorption.

Comparison of the Results Obtained by Continuous and Discontinuous Photoirradiation. Although not shown in Table 1, the C_3 obtained at a decreased

irradiation duration ($<t_{C2}$) was smaller than that shown in Table 1. The C_3 obtained by continuous irradiation was smaller than that obtained by discontinuous irradiation of the same total duration. For example, the C_3 for NA or DNB (A_{max}) on HY calcined at 400 °C induced by continuous irradiation for 20 h was 2.9 or 0.75×10^{18} spins/g-HY, respectively, while the corresponding value induced by 20-times irradiation for 1 h was 3.0 or 0.91×10^{18} spins/g-HY, respectively. This difference in the C_3 value was pronounced when NA or DNB was adsorbed on HY calcined at 400 °C. In general, the C_3 values and their nonlinear dependence on the amount of adsorption became pronounced in the case of discontinuous photoirradiation. Similarly, the C_3 induced by continuous heating was somewhat smaller than that induced by discontinuous heating of the same total duration.

As shown from Tables 1 and 2, t_{C1} is the smallest, while t_{C3} is greatest among the t_{C1}, t_{C2}, and t_{C3} values. Generally, the time required for attaining a constant number of spins increased with an increase in the number of operations (discontinuous heating or illumination).

Enhancement of Radicals Induced by General Mechanical Energy. General mechanical energy (e.g., shaking or compressing) applied after the adsorption of the organic molecules on HY qualitatively increased the C_2/C_1 and C_3/C_1 ratios and decreased the range of A values providing the linear dependence of the C_2 and C_3 values on the amount of adsorption.

Strong and Weak Acid or Base Sites. According to the preceding paper,[2] there coexist two kinds of active sites on the surface of HY: A strong active site is related to an induction of PE cations or TCNE anion radicals on HY calcined at 650 °C, whereas a weak active site is related to the formation of radicals from a weak donor (NA) or a weak acceptor (DNB) on HY calcined at a low temperature (400 °C). Since weak active sites may be related to a slow increase in the NOS values,[2] they may play some important roles in the mechanically induced enhancement of radicals, especially in a binary system comprising NA or DNB and HY calcined at 400 °C.

Improvement of the Reproducibility of Physicochemical Data of Relatively Complicated Systems. By using the physicochemical properties of complicated systems it is quite difficult to reproduce the same phenomena constantly. In the case of HY–organic systems, the NOS values of the binary systems were proportional,[2,3] while those of the ternary systems were not proportional to the amount of adsorption.[2] As described above, a similar nonlinearity (irreversibility) was induced by either heating or irradiating the HY–organic systems. A quantitative determination of the mechanically induced enhancement of radicals, and of the nonlinear dependence of NOS on both the amount of adsorption and the method of applying the mechanical energy, may be available for finding some new factors necessary for improving the reproducibility of physicochemical data of relatively complicated systems.

Radical Formation Induced by Mechanical Energy Applied after the Adsorption of Organic Molecules on HY. The results described above may also provide some new factors necessary for constructing a model of solid acid or base sites. The spin-generating sites on the surface of an aluminosilicate have been attributed to Lewis acid sites,[1,3] which are known to be produced from Brönsted acid sites at an elevated T_{ca} (over 500 °C).[1,3] However, radicals were induced by mechanical energy, such as UV light or heat, and applied after the adsorption of organic molecules on HY calcined at 400 °C. Extremely, the PE cations or TCNE anion radicals were induced by either heating or illuminating an NH_4^+-exchanged zeolite without any calcination which had been adsorbed by the organic molecules. A pronounced increase in the NOS obtained with a binary system comprising either a weak donor (NA) or a weak acceptor (DNB) and HY calcined at a low temperature (400 °C) as well as great t_{C1}, t_{C2}, and t_{C3} values might indicate some important roles of weak acid sites on the surface of HY.[2]

Conclusion

The NOS values of the HY–organic binary systems were proportional,[2,3] while those of the HY–two organic systems were only partly proportional to the amount of adsorption.[2] The nonlinearity of the NOS to the amount of adsorption was also induced by heating or irradiating the solvent-free binary systems. These findings may provide some new factors necessary for improving the reproducibility of physicochemical data.

Although the charge-transfer interaction, mechanochemistry, and properties of polymers appear in large and relatively complicated systems, they may disappear when a large, complicated system is divided into subsystems possessing appropriately equal sizes. In the present study we dealt quantitatively with the mechanically (UV light or heat) induced enhancement of radicals and the nonlinear dependence of NOS on the amount of adsorption, regarding not only the surface of HY, but also adsorbate molecules, the experimental conditions (e.g., temperatures and UV light), and the methods and processes of heating or illuminating as constituents of a large system. Such a correlative, comprehensive approach would prompt an elucidation of solid acidity or basicity. The other factors necessary for constructing a model of solid acidity or basicity will be described in a subsequent publication.

References

1) K. Tsutsumi and H. Takahashi, "Zeoraito," ed by N. Hara and H. Takahashi, Kodansha Scientific Publishers, Tokyo (1975), pp. 72—78, and references therein.

2) H. Kashiwagi, *Chem. Lett.*, **1990**, 1063; H. Kashiwagi, *Bull. Chem. Soc. Jpn.*, **64**, 423 (1991).

3) D. N. Stamires and J. Turkevich, *J. Am. Chem. Soc.*, **86**, 749 (1964).

4) For example: B. M. Hoffman and T. B. Eames, *J. Am. Chem. Soc.*, **91**, 5168 (1969); P. H. Kasai and R. J. Bishop, Jr., "Zeolite Chemistry and Catalysis," ed by J. A. Rabo, ACS Monograph (1976), Vol. 171, p. 350.

5) B. D. Flockhart, L. McLoughlin, and R. C. Pink, *J. Catal.*, **25**, 305 (1972); K. Hirota, K. Kuwata, and Y. Akagi, *Bull. Chem. Soc. Jpn.*, **38**, 2209 (1965).

6) Even during irradiating with UV light or during heating at 80 °C, the shape and intensity of an EPR spectrum of the HY–organic system after attaining the C_2 was unchanged. After stopping illuminating or heating, the organic molecules adsorbed on HY were recovered unchanged by desorbing them with a large excess of the solvent. Since HY (Si/Al=1.9) was composed of relatively weak acid sites (Refs. 1 and 2), no further reaction of the ion radicals produced on HY occurred even during irradiating or heating.

Discrimination of Rotational Isomers of Jet-Cooled Acetophenone Derivatives as Studied by Sensitized Phosphorescence Excitation Spectroscopy

Seiji YAMAMOTO, Nobuhisa HASHIMOTO, and Mitsuo ITO*
Department of Chemistry, Faculty of Science, Tohoku University,
Sendai 980
(Received March 20, 1991)

The $S_1(n,\pi^*)\leftarrow S_0$ and $T(n,\pi^*)\leftarrow S_0$ sensitized phosphorescence excitation spectra of jet-cooled *o*- and *m*-substituted (fluoro- and methyl-) acetophenones have been measured. The two rotational isomers (*O-cis* and *O-trans* isomers) of each molecule arising from the orientation of the acetyl group with respect to *o*- or *m*-substituent have been discriminated. The energy difference in the 0–0 transition between the two isomers is less than 100 cm^{-1} for *m*-substituted acetophenone but more than 300 cm^{-1} for *o*-substituted acetophenone. The characteristic energy difference can be explained from the fact that the electronic excitation is localized on the C=O group.

In a series of papers, we have reported the studies on discrimination of the rotational isomers of *o*- and *m*-substituted phenols, anisoles, and benzaldehydes using the electronic transition in a supersonic free jet.[1-6] In molecules such as phenols and anisoles, the $S_1(\pi,\pi^*)\leftarrow S_0$ excitation energy difference between the rotational isomers amounts to 100—300 cm^{-1} for both *m*- and *o*-substituted compounds. On the other hand, it was found that the $S_1(n,\pi^*)\leftarrow S_0$ and $T(n,\pi^*)\leftarrow S_0$ transition energy differences between the rotational isomers are quite different for *m*- and *o*-substituted benzaldehydes (several tens cm^{-1} for the former and 400—500 cm^{-1} for the latter). The characteristic difference in the transition energy between phenol derivatives and benzaldehyde derivatives is caused by their difference in the nature of the electronic excited state.

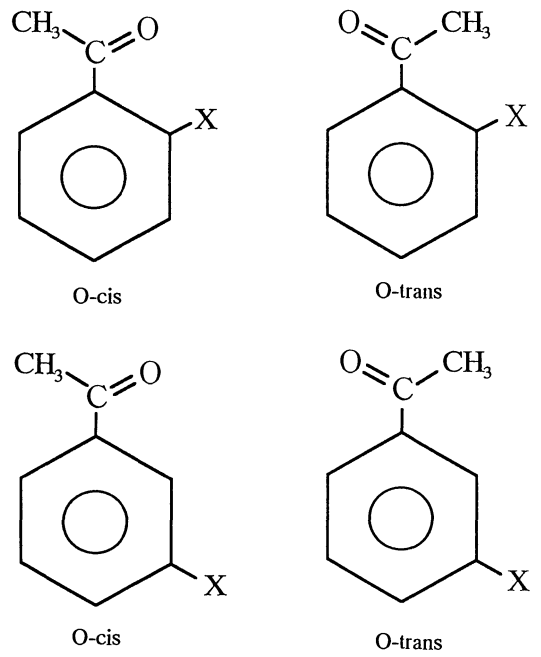

Fig. 1. The molecular structures of *O-cis* (*sp*) and *O-trans* (*ap*) rotational isomers of *o*- and *m*-substituted acetophenones. X indicates substituent.

In the present work, we extended the study to the rotational isomers of *o*- and *m*-substituted acetophenones. There exist two rotational isomers for each molecule. They are *O-cis(sp)* and *O-trans (ap)* isomers arising from orientation of the oxygen atom of the acetyl group with respect to the *o*- or *m*-substituent (Fig. 1). Similar to the case of substituted benzaldehydes, it is expected that the rotational isomers of subsitituted acetophenone are easily discriminated by the electronic spectrum of the jet-cooled molecule. In general, acetophenone derivatives are nonfluorescent and have a low efficiency of ionization. It is difficult therefore to apply the technique such as laser induced fluorescence (LIF) and multiphoton ionization (MPI) to these molecules. However, they are usually highly phosphorescent, and we can measure the electronic spectrum by phosphorescence excitation spectroscopy. However, the application of this technique to jet-cooled molecules is not easy because of a very weak phosphorescence signal gained by a space fixed photomultiplier from the molecules having a long phosphorescence lifetime and moving with a high speed in the jet. The difficulty had been solved by the development of a new spectroscopy called sensitized phosphorescence excitation spectroscopy, which uses sensitized phosphorescence emitted by a solid phosphor to which the triplet-state molecules in the jet collide.[7,8] We used this spectroscopy for the measurements of the electronic spectra of the substituted acetophenones.

By using this spectroscopy, we observed the $S_1(n,\pi^*)\leftarrow S_0$ transitions of *o*-, *m*-, and *p*-fluoroacetophenones, and *o*-, *m*-, and *p*-methylacetophenones. For each molecule except for *p*-derivatives, the existence of the two rotational isomers was confirmed. The difference in the electronic excitation energy between the two isomers is large for *o*-substituted acetophenone, but very small for *m*-substituted acetophenone, indicating the electronic excitation localized on the C=O group in the $S_1(n,\pi^*)$ state. Similar results were also obtained for the $T_1(n,\pi^*)\leftarrow S_0$ transitions. These results are consistent with those of benzaldehyde derivatives.

In our recent work, a remarkable difference was found

for photochemical behaviors of the rotational isomers of *o*-methylbenzaldehyde in their $S_1(n,\pi^*)$ and $T(n,\pi^*)$ states.[6] The *O-cis* isomer was found to undergo a photochemical reaction involving intramolecular hydrogen abstraction (photoenolization). A similar reaction was also suggested for *o*-methylacetophenone.

Experimental

The sensitized phosphorescence excitation spectra of jet-cooled molecules were measured with the same apparatus as that reported elsewhere.[7] The sample was heated up to about 320 K to obtain sufficient vapor pressure and was seeded in 3 atm He gas. The gas mixture was expanded into a vacuum chamber through a pulsed nozzle with an orifice of 800 μm diameter. The UV output of a dye laser (Lambda Physik FL 3002) pumped by a XeCl excimer laser (Lambda Physik LPX100) was used as an exciting light source. The laser light crossed the jet 15 mm down stream of the nozzle. The triplet state molecules produced by the intersystem crossing from the S_1 state or by the direct laser excitation travel for about 40 μs further down stream from the excitation position and collides with a liquid-nitrogen-cooled copper surface which is covered with the solid sample serving as a sensitized phosphor. When the triplet state molecules collide with the phosphor surface, the energy transfer occurs and the sensitized phosphorescence is emitted. The sensitized phosphorescence was detected by a photomultiplier (HTV R585) and the signal was processed by a gated photon counting system (Ortec 9302, 9315, 9325 and a home made gate generator).

The samples, *o*-, *m*-, and *p*-fluoroacetophenones and *o*-, *m*-, and *p*-methylacetophenones (Tokyo Kasei) were used without further purification.

Results

A. *p*-Substituted Acetophenones. First of all, the results of *p*-substituted acetophenones having no rotational isomer are shown. Figure 2(a) shows the $S_1(n,\pi^*)\leftarrow S_0$ sensitized phosphorescence excitation spectrum of jet-cooled *p*-fluoroacetophenone. The longest wavelength, prominent band at 27591 cm^{-1} is assigned to the band origin. On the higher frequency side of the 0–0 band, several low frequency bands appear with displacements of 34, 64, and 88 cm^{-1} from the origin. These bands can be assigned to the levels of the internal rotation of the methyl group in the S_1 state similar to the case of acetophenone.[8] The frequencies of 34, 64, and 88 cm^{-1} represent the 2e, $3a_1$, and 4e levels in the conventional notation of the internal rotation levels. It is suggested from the observed intensity pattern that the most stable conformation of the methyl group with respect to the molecular framework is quite different between the S_0 and S_1 states.

Figure 2(b) shows the $S_1(n,\pi^*)\leftarrow S_0$ sensitized phosphorescence excitation spectrum of jet-cooled *p*-methylacetophenone. The 0–0 band is located at 27445 cm^{-1}. The spectral feature is almost the same as that of *p*-fluoroacetophenone. The frequencies of 43, 75, and 96 cm^{-1} represent the internal rotation levels.

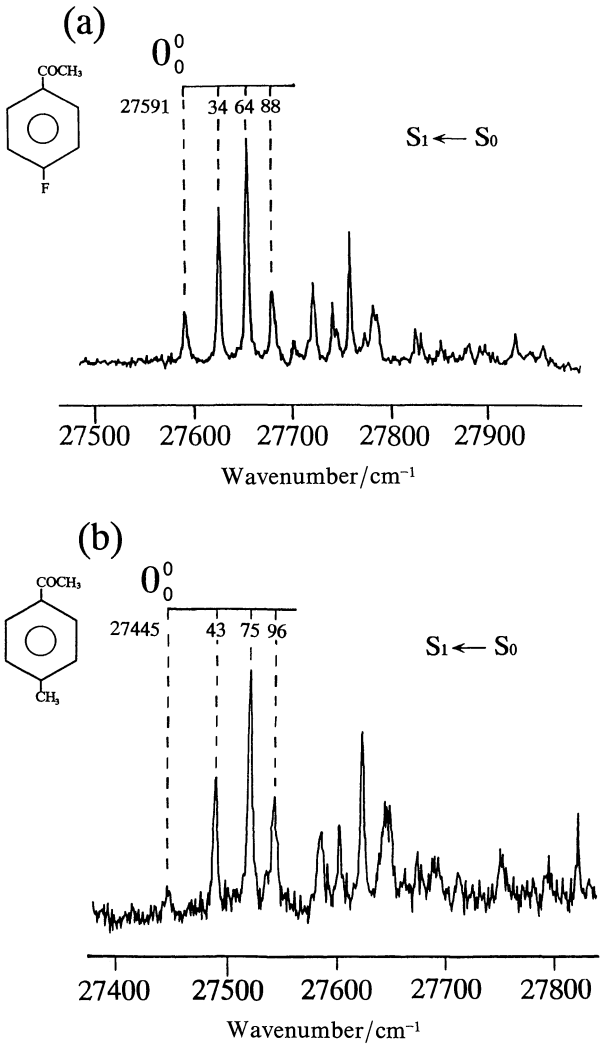

Fig. 2. (a) The $S_1(n,\pi^*)\leftarrow S_0$ sensitized phosphorescence excitation spectrum of jet-cooled *p*-fluoroacetophenone. (b) The $S_1(n,\pi^*)\leftarrow S_0$ sensitized phosphorescence excitation spectrum of jet-cooled *p*-methylacetophenone.

The $T(n,\pi^*)\leftarrow S_0$ transition was also observed. The energy of the 0–0 transition of *p*-fluoroacetophenone is 26104 cm^{-1}. The 0–0 band is exclusively strong in the spectrum but its absolute intensity is about 1/20 of that of the $S_1\leftarrow S_0$ transition. For *p*-methylacetophenone, the transition could not be observed because of the very low signal intensity.

From these results, the $S_1(n,\pi^*)$—$T(n,\pi^*)$ energy gap is 1341 cm^{-1} for *p*-fluoroacetophenone.

B. *m*-Substituted Acetophenones. Figure 3(a) shows the $S_1(n,\pi^*)\leftarrow S_0$ sensitized phosphorescence excitation spectrum of jet-cooled *m*-fluoroacetophenone. As seen from the figure, it has a complex structure. The structure can be decomposed to two progressions due to methyl torsion. The two band origins are located at 27047 and 27111 cm^{-1}, the energy difference being 64 cm^{-1}. The frequencies of 31, 60, and 85 cm^{-1} for the former, and 31, 60, and 82 cm^{-1} for the latter represent 2e,

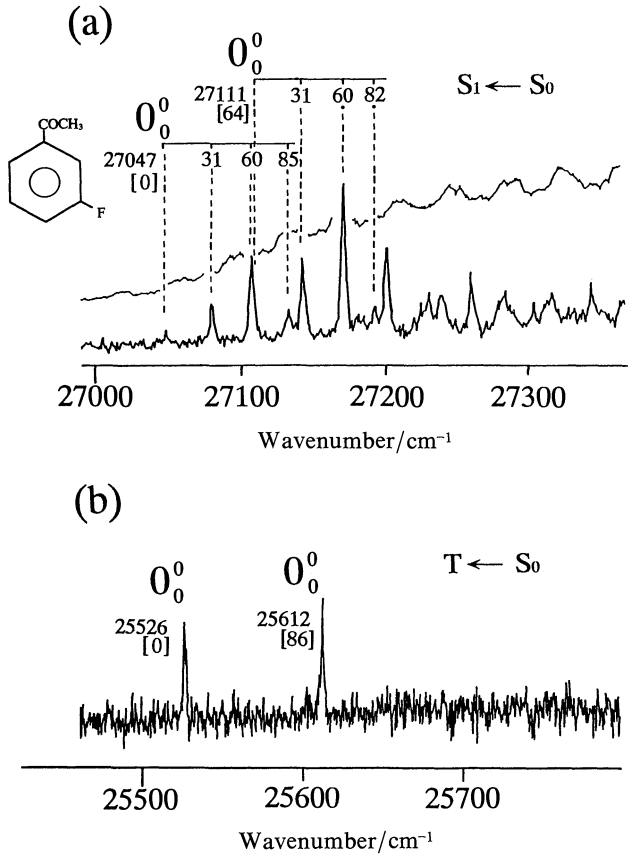

Fig. 3. (a) The $S_1(n,\pi^*) \leftarrow S_0$ sensitized phosphorescence excitation spectrum of jet-cooled *m*-fluoroacetophenone. (b) The $T(n,\pi^*) \leftarrow S_0$ sensitized phosphorescence excitation spectrum of jet-cooled *m*-fluoroacetophenone. The upper trace in (a) represents the laser power.

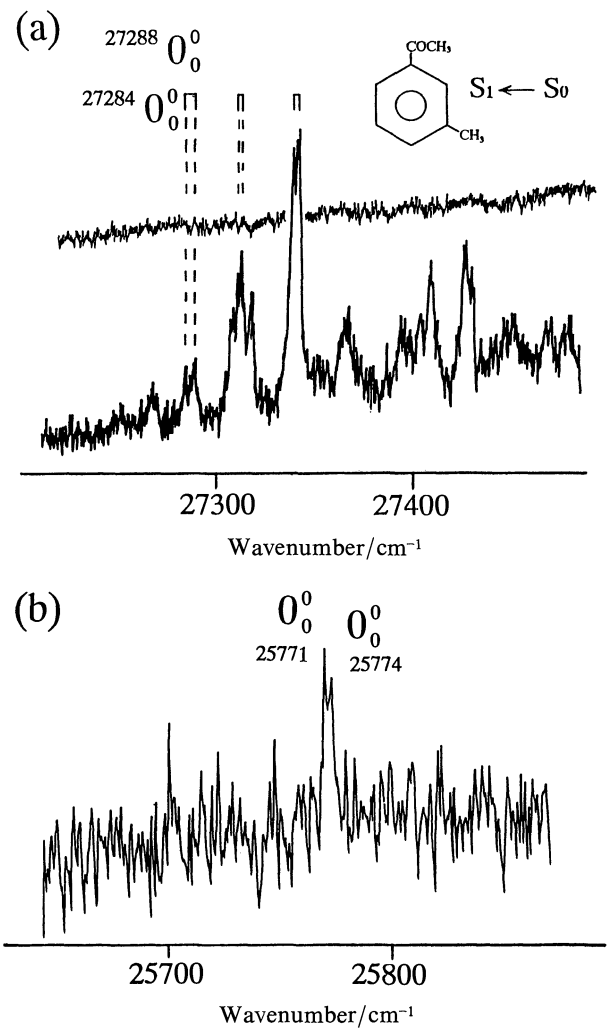

Fig. 4. (a) The $S_1(n,\pi^*) \leftarrow S_0$ sensitized phosphorescence excitation spectrum of jet-cooled *m*-methylacetophenone. (b) The $T(n,\pi^*) \leftarrow S_0$ sensitized phosphorescence excitation spectrum of jet-cooled *m*-methylacetophenone. The upper trace in (a) represents the laser power.

$3a_1$, and 4e levels, respectively. The $3a_1$ band of the former accidentally overlaps with the 0–0 band of the latter. The two band origins are ascribed to the two rotational isomers, namely *O-cis* and *O-trans* isomers of *m*-fluoroacetophenone. If this assignment is right, we also expect the appearance of two origin bands in the spectrum due to $T(n,\pi^*) \leftarrow S_0$ transition.

Figure 3(b) shows the $T(n,\pi^*) \leftarrow S_0$ sensitized phosphorescence excitation spectrum of jet-cooled *m*-fluoroacetophenone. As expected, two 0–0 bands are observed at 25526 cm^{-1} and 25612 cm^{-1}, which are assigned to the two rotational isomers. The energy difference between the two rotational isomers is 86 cm^{-1}. The intensities of the two bands are comparable, indicating that the two isomers have almost equal stabilities.

Figures 4(a) and 4(b) show the $S_1(n,\pi^*) \leftarrow S_0$ and $T(n,\pi^*) \leftarrow S_0$ sensitized phosphorescence excitation spectra of jet-cooled *m*-methylacetophenone. All the bands appear in pair of a small frequency separation. The pair bands can be ascribed to two rotational isomers. For the $S_1(n,\pi^*) \leftarrow S_0$ transition, the band origins of the two isomers are located at 27284 and 27288 cm^{-1}, the energy difference being 4 cm^{-1}. The situation is similar for the $T(n,\pi^*) \leftarrow S_0$ transition. The 0–0 bands are located at 25771 and 25774 cm^{-1}, the energy difference being only 3 cm^{-1}. Such a small energy difference was seen also in the case of *m*-methylbenzaldehyde.[6]

C. *o*-Substituted Acetophenones. Figures 5(a) and 5(b) show the $S_1(n,\pi^*) \leftarrow S_0$ and $T(n,\pi^*) \leftarrow S_0$ sensitized phosphorescence excitation spectra of jet-cooled *o*-fluoroacetophenone, respectively. It is seen in Fig. 5(b) that two 0–0 bands appear at 25746 and 26074 cm^{-1}, the frequency difference being 328 cm^{-1}. These bands are attributed to the 0–0 bands of the $T(n,\pi^*) \leftarrow S_0$ transitions of the two rotational isomers. The $S_1 \leftarrow S_0$ spectrum also consists of two components. One origin is located at 27188 cm^{-1} and the other origin at 27522 cm^{-1}. The energy difference amounts to 334 cm^{-1}, which is nearly equal to the difference in the $T \leftarrow S_0$ transition energy. The progression developing from the origin is assigned to the internal rotation of the methyl

group. The frequencies of the internal rotation shown in the figure are slightly different from those of *m*- and *p*-substituted acetophenones. This suggests that the internal rotation of the methyl group is considerably affected by the *o*-substituent. In the case of *o*-methylacetophenone, the signal of sensitized phosphorescence could not be detected. But a spectrum having a complicated structure could be observed by multiphoton ionization spectroscopy. The complicated MPI spectrum and the absence of the sensitized phosphorescence suggest the existence of a fast nonradiative relaxation process (probably, intramolecular reaction) in the triplet state.

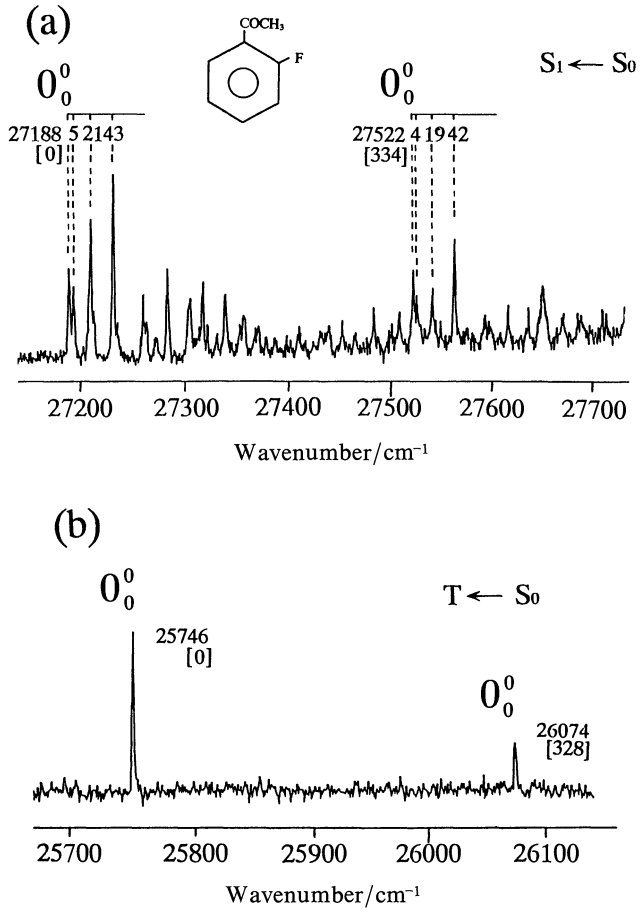

Fig. 5. (a) The $S_1(n,\pi^*) \leftarrow S_0$ sensitized phosphorescence excitation spectrum of jet-cooled *o*-fluoroacetophenone. (b) The $T(n,\pi^*) \leftarrow S_0$ sensitized phosphorescence excitation spectrum of jet-cooled *o*-fluoroacetophenone.

Discussion

The spectroscopic data obtained in the present work are summarized in Tables 1 and 2. It is seen from the tables that both the $S_1(n,\pi^*) \leftarrow S_0$ and $T(n,\pi^*) \leftarrow S_0$ transitions are shifted to blue in *p*-substituted acetophenone relative to those of acetophenone. On the other hand, red shift is seen for all the isomers of *m*-substituted acetophenones except for the $S_1 \leftarrow S_0$ transition of the isomers of *m*-methylacetophenone. In *o*-fluoroacetophenone, the band origin of one isomer is red-shifted but the other blue-shifted. It is interesting to compare the direction of the shift with that of the $S_1(n,\pi^*) \rightarrow S_0$ transition of substituted benzaldehyde. For example, in *p*-fluorobenzaldehyde, the $S_1(n,\pi^*) \leftarrow S_0$ transition exhibits a large blue shift relative to benzaldehyde, and all the rotational isomers of *o*- and *m*-fluorobenzaldehydes except for the $T_1 \leftarrow S_0$ transition of the isomers of *m*-fluorobenzaldehyde show red shift.[6] So the direction of shift is parallel between substituted benzaldehyde and substituted acetophenone. It is noted that the direction of the shift is entirely different between substituted phenol and substituted benzaldehyde or acetophenone. In phenols, *o*- and *p*-substituted phenol exhibits red shift while *m*-substituted phenol shows blue shift. The difference reflects the difference in the nature of the S_1 state, that is, the (π,π^*) states for substituted phenol and the (n,π^*) state for substituted benzaldehyde or acetophenone.

The characteristic nature of the $S_1(n,\pi^*)$ or $T(n,\pi^*)$ state of substituted acetophenone is also reflected in the difference in the excitation energy between the two rotational isomers, that is, the difference is very small for *m*-substituted acetophenone but very large for *o*-substituted acetophenone. This can be explained from the fact that the electronic excitation is essentially localized on C=O of the acetyl group in the $S_1(n,\pi^*)$ or $T(n,\pi^*)$ state. In *m*-substituted acetophenone, the

Table 1. Spectroscopic Data of the $S_1(n,\pi^*)$ and $T(n,\pi^*)$ States of Fluoroacetophenones. The Data of Acetophenone is Also Listed for Comparison.[8] All Frequencies are in cm^{-1}

Molecule	*o*-Fluoro		*m*-Fluoro		*p*-Fluoro	Acetophenone
$S_1 \leftarrow S_0$ 0_0^0	27188	27522	27047	27111	27591	27279
Δ[a]	334		64			
Shift[b]	−91	+243	−232	−168	+312	0
$T \leftarrow S_0$ 0_0^0	25746	26074	25526	25612	26104	25791
Δ[a]	328		86			
Shift[b]	−45	+283	−265	−179	+313	0
$S_1 - T$ gap	1442	1448	1521	1499	1487	1488

a) Δ indicates the frequency difference of the 0–0 transition between the two rotational isomers. b) The frequency difference of the 0–0 band from that of acetophenone. The − and + signs indicate red and blue shifts, respectively.

Table 2. Spectroscopic Data of the $S_1(n,\pi^*)$ and $T(n,\pi^*)$ States of Methylacetophenones. The Data of Acetophenone is Also Listed for Comparison.[8] All Frequencies are in cm^{-1}

Molecule	*o*-Methyl	*m*-Methyl		*p*-Methyl	Acetophenone
$S_1 \leftarrow S_0$ 0_0^0	27284		27288	27445	27279
Δ[a]		4			
Shift[b]	+5		+9	+166	0
$T \leftarrow S_0$ 0_0^0	25771		25774		25791
Δ[a]		3			
Shift[b]	−20		−17		0
S_1-T gap	1513		1514		1488

a) Δ indicates the frequency difference of the 0–0 transition between the two rotational isomers. b) The frequency difference of the 0–0 band from that of acetophenone. The − and + signs indicate red and blue shifts, respectively.

distance between the C=O group and the substituent at *m*-position is far for both rotational isomers. Therefore, the electronic excitation energy is not greatly affected by the orientation of the C=O group. Contrary, in *o*-substituted acetophenone, the excitation energy changes greatly by the orientation because of a close distance between the C=O group and the substituent. In the case of the $S_1(\pi,\pi^*)$ of substituted phenol, the difference in the excitation energy between the rotational isomers is comparable between the *o*- and *m*-substituted phenols, showing the spread of the π-electronic excitation over the whole molecule.

The $S_1(n,\pi^*)$—$T(n,\pi^*)$ energy gap is almost constant at ca. 1490 cm^{-1} for all the molecules and isomers, although a slightly smaller value is found for *m*-fluoroacetophenone. The constant energy gap implies that the electronic structures of the $S_1(n,\pi^*)$ and $T(n,\pi^*)$ states of each molecule are very similar except for spin, and the energies of the both states are perturbed by almost equal amounts irrespective of the nature of the perturbation.

The remaining problem is the assignment of the two 0–0 bands to individual rotational isomers. In the case of *o*-fluoroacetophenone, the intensity ratio of the two origin bands is about 3:1, the lower energy 0–0 band being more intense. The reported population ratio is 1:9 for *O-cis* isomer to *O-trans* isomer.[9] Therefore, we tentatively assigned the 0–0 band of 27188 cm^{-1} to *O-trans* isomer and that of 27522 cm^{-1} to *O-cis*. In the case of *m*-substituted acetophenone, the intensities of two 0–0 bands are almost the same, suggesting nearly equal population. Therefore, the assignment is difficult only from the intensity ratio.

Finally, we have to mention the case of *o*-methylacetophenone for which the measurement of the phosphorescence excitation spectrum failed. *o*-Methylacetophenone is known to be a typical molecule undergoing the intramolecular photoenolization reaction like *o*-methylbenzadehyde or *o*-methylbenzophenone.[10-16] The oxygen atom of the acetyl group abstracts the hydrogen atom of the methyl group at *o*-position after photoexcitation. The reaction will selectively occur in the *O-cis* isomer. This explains the nonphosphorescence of the *O-cis* isomer. It was reported that the ratio of *O-cis* to *O-trans* is 7:3[17] or 84:16[18] in the solution and 93:7[19] from calculation. The intramolecular enolization reaction for the abundant *O-cis* isomer and a small amount of the *O-trans* isomer explain the failure of the measurement of the phosphorescence excitation spectrum for this molecule.

References

1) A. Oikawa, H. Abe, N. Mikami, and M. Ito, *J. Phys. Chem.*, **88**, 5180 (1984).
2) M. Ito and A. Oikawa, *J. Mol. Spectrosc.*, **126**, 133 (1985).
3) A. Oikawa, H. Abe, N. Mikami, and M. Ito, *Chem. Phys. Lett.*, **116**, 50 (1985).
4) S. Yamamoto, K. Okuyama, N. Mikami, and M. Ito, *Chem. Phys. Lett.*, **125**, 1 (1986).
5) a) H. Mizuno, K. Okuyama, T. Ebata, and M. Ito, *J. Phys. Chem.*, **91**, 5589 (1987).
b) T. Aota, T. Ebata, and M. Ito, *J. Phys. Chem.*, **93**, 3519 (1989).
6) S. Yamamoto, T. Ebata, and M. Ito, *J. Phys. Chem.*, **94**, 5786 (1990).
7) S. Kamei, H. Abe, N. Mikami, and M. Ito, *J. Phys. Chem.*, **89**, 3636 (1985).
8) N. Ohmori, T. Suzuki, and M. Ito, *J. Phys. Chem.*, **92**, 1086 (1988).
9) E. Bock, R. Wasylishen, B. E. Gaboury, and E. Tomchuk, *Can. J. Chem.*, **51**, 1906 (1973).
10) R. Haag, J. Wirz, and P. J. Wagner, *Helv. Chim. Acta*, **60**, 2595 (1977).
11) P. J. Wagner and C. P. Chen, *J. Am. Chem. Soc.*, **98**, 239 (1976).
12) G. Porter and M. F. Tchir, *J. Chem. Soc. A*, 3772 (1971).
13) P. G. Sammes, *Tetrahedron*, **32**, 405 (1976).
14) D. M. Findlay and M. F. Tchir, *J. Chem. Soc., Faraday Trans. 1*, **72**, 1096 (1976).
15) R. K. Das, M. V. Encinas, R. D. Small, Jr., and J. C. Scaiano, *J. Am. Chem. Soc.*, **101**, 6965 (1979).
16) T. Ikoma, K. Akiyama, S. Tero-Kubota, and Y. Ikegami, *J. Phys. Chem.*, **93**, 7087 (1989).
17) R. Benassi, D. Iarossi, U. Folli, L. Schenetti and F. Taddei, *J. Chem. Soc., Perkin Trans. 2*, **1980**, 228.
18) M. Grimaud and Pfister-Guillouzo, *Org. Magn. Reson.*, **7**, 386 (1975).
19) H. Lumbroso, C. Liegeois, G. Goethals, and R. Uzan, *Z. Phys. Chem.*, **138**, 167 (1983).

 © 1991 The Chemical Society of Japan Bull. Chem. Soc. Jpn., 64, 2207—2213 (1991)

VUV Photoionization Efficiency Curves and Appearance Energies of *N*, *N*-Dimethylformamide Ion and Its Fragment Ions

Masana ARIMURA* and Yozaburo YOSHIKAWA
Institute of Chemistry, College of General Education, Osaka University,
1-1 Machikaneyama, Toyonaka, Osaka 560
(Received December 28, 1990)

Ionization efficiency curves of *N*,*N*-dimethylformamide (DMF) ion and of its fragment ions, $C_3H_6NO^+$, $C_2H_4NO^+$, and $C_2H_6N^+$ were obtained by use of vacuum ultraviolet photoionization method. The appearance energy of the parent ion was 9.12±0.06 eV. The appearance energies of $C_3H_6NO^+$, $C_2H_4NO^+$, and $C_2H_6N^+$ were very close (10.77±0.08 eV for $C_3H_6NO^+$ and $C_2H_4NO^+$, 10.59±0.08 eV for $C_2H_6N^+$). The relative intensity curve of $C_2H_6N^+$ normalized by the sum of fragment ions vs. photon energy has the second rise at 12.2±0.3 eV, which implies that another fragmentation process appears at the photon energy above 12.2 eV. The second fragmentation process is ascribed to a channel through DMF cation in an excited electronic state.

Determination of the ionization energy of a parent molecule and appearance energies of its fragment ions is most important to elucidate the fragmentation mechanism and their reactions with other molecules. Several methods have been carried out to determine the ionization energy of a molecule and appearance energies of its fragment ions.[1] By using a photoionization technique, ionization energies of molecules are determined from the photon energy at which the ion current vanishes. This method is also useful for the estimation of appearance energies of the fragment ions which are produced through processes faster than ca. 10^4 sec^{-1} in the vicinity of critical energies.

Most of unimolecular reactions of the parent and fragment ions have been examined mainly in term of statistical partitioning of the whole energy to the vibration and rotation modes. Fragmentation rates are successfully understood by means of the statistical RRKM theory.[2] It has been reported that the statistical theory, however, can not be applied to the fragmentations of small molecular ions and fragmentations via the stable isomers of parent ion.[3] On the high energy excitation, another kind of unimolecular reactions, which the statistical theory failed to explain, occurs from electronic excited states before converting the electronic energy to the vibrational energy of ground state.[4]

Participation of another process is expected to emerge as another rise in the relative intensity curve normalized by the sum of the fragment ions (RI curve) which is derived from the ionization efficiency curves. We have found by using vacuum ultraviolet (VUV) photoionization technique that the CHO· elimination reaction of DMF cation exhibits plural thresholds at 10.59 eV and 12.2 eV of photon energy and that the fragmentations eliminating $C_3H_6NO^+$, $C_2H_4NO^+$, and $C_2H_6N^+$ appear at nearly the same energy. Ionization efficiency curves of DMF and the RI curves of the fragment ions were utilized to elucidate the fragmentation mechanisms.

Experimental

Photoionization efficiency curves were obtained by using a quadrupole mass spectrometer (QMS; Extranucler Co.). The mass resolution (ΔM) of QMS was ca. 1 (about 10 channels per mass unit for measurement).[5] An H_2 discharge lamp was used as the VUV light source for the ionization. The H_2 discharge lamp was operated at about 1 kW with 20—25 A cm^{-2} of current. The wavelength resolution of a monochrometor (McPherson model 234) is 8 Å full width at half maximum (FWHM), or ca. 0.07 eV in the energy range covered when the width and length of both entrance and exit slits are 100 μm and 3 mm respectively. The wavelength of light beam was calibrated by Lyman α line (1216 Å). The light beam strikes a thin layer of sodium salicylate as phosphor after traversing the ionization chamber. The fluorescence was led through an optical fiber to a photonmultiplier to obtain the photon intensity. The ions were counted by using a secondary electron multiplier (Ceratoron, Murata Seisakusyo). Values of ion-counting were given as the sum of the counted number of ions at three points (the peak top, before and behind the peak top of the resolved mass peak). The measurements of the ionization efficiency curves were fully operated by using a microcomputer. The light wavelength was scanned by 3 Å step for the measurements. The sample gas was introduced into the ion source without temperature control through a variable leak valve (the sample stagnation pressure was its vapor pressure at 0 °C).

The pressure of the vaccum chamber was measured intermittently by an ionization gauge just above the QMS and was held lower than 8×10^{-6} Torr (1 Torr=133.322 Pa).

The ionization energy 9.24±0.06 eV of benzene obtained here (Fig. 1) agrees very closely with the data obtained by others.[6]

The fragment ions were assigned by using a high resolution electron impact mass spectrometer (JMS-01SG-2, JEOL Co) at ca. 15 eV electron energy.

Results

Photoionization efficiency curves of DMF ion, m/z 73, and of its fragment ions, m/z 72, 58, and 44, were obtained in the photon energy range of 8.85—13.0 eV (Fig. 2). The other fragment ion in this energy region is mainly m/z 30.

The RI curves for the four fragment ions were obtained from the ionization efficiency curves, as are shown in Fig. 3. The RI curves give the relative fragmentation rates which are the convoluted rate from the critical photon

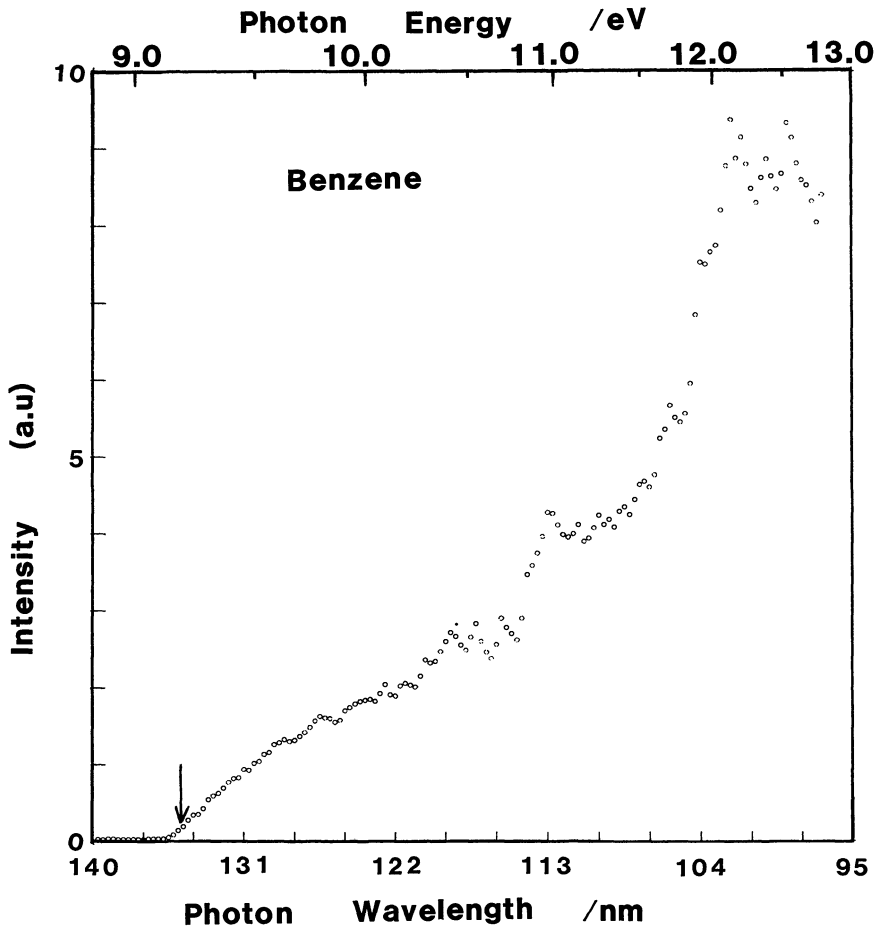

Fig. 1. The photoionization efficiency curve of benzene. The arrow shows the vertical ionization energy, 9.24±0.06 eV.

Table 1. Ionization and Appearance Energy of *N,N*-Dimethylformamide and Its Fragments (eV)

	This work (PI)	Reference
$C_3H_7NO^+$	9.12±0.06	9.12±0.02 (PI)[a] 9.14 (PE)[b]
$C_3H_6NO^+$	10.77±0.08	—
$C_2H_4NO^+$	10.77±0.08	—
$C_6H_6N^+$	10.59±0.08	11.6±0.1 (EI)[c]
	12.2 ±0.3 (2nd)	
CH_4N^+	11.9 ±0.02	—

PI, PE, and EI denote the methods of photoionization mass spectrometry, electron impact mass spectrometry, and photoelectron spectroscopy, respectively. a) Ref. 15. b) Ref. 12. c) Ref. 8.

energy up to the marked photon energy.

The ionization energy of the parent ion and the appearance energies of the four fragment ions were determined from the ionization efficiency curves (Fig. 2) and are listed in Table 1 with the reference data.

Metastable peak at m/z ca. 26.5 due to slow fragmentation of m/z 73→44[16] was observed in the 30 eV electron impact ionization. The other metastable peak implying a successive reaction, m/z 73→58→30, is also observed at m/z ca. 15.5 due to m/z 58→30.

Discussion

The appearance energy (9.12±0.06 eV) of the parent ion, m/z 73, is agreed well with the value of an adiabatic ionization energy determined by PES.[7] Mass numbers of the fragment ions, m/z 72, 58, and 44, are assigned to $C_2H_6NO^+$, $C_2H_4NO^+$, and $C_2H_6N^+$, respectively (see Fig. 4). All of three fragment ions except for m/z 30 are produced in the unimolecular decompositions of the parent ion m/z 73, Eqs. 1—3.

$$C_3H_7NO^{+\cdot} \rightarrow C_2H_6N^+(44) + {\cdot}CHO \quad (1)$$

$$\rightarrow C_2H_4NO^+(58) + {\cdot}CH_3 \quad (2)$$

$$\rightarrow C_2H_6NO^+(72) + H \quad (3)$$

***m/z*=44.** The m/z 44 appears at 10.59±0.07 eV of photon energy and grows rapidly from ca. 1.5 eV above the appearance energy. The intensity ratios of m/z 44 against m/z 72 and 58 did not change so much up to ca. 12 eV of photon energy. The appearance of $C_2H_6N^+$ at 10.59 eV was not detected previously by mean of electron impact ionization. Meanwhile, the second rise at

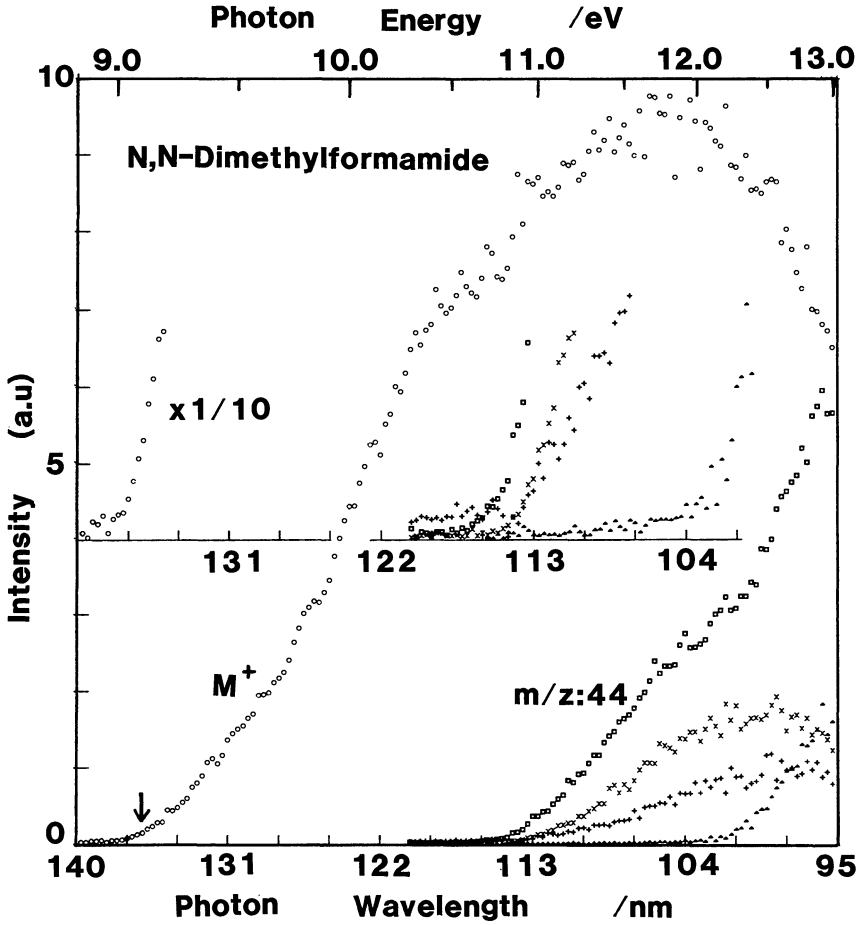

Fig. 2. The photo-ionization efficiency curves of *N,N*-dimethylformamide ion and three fragment ions. Each ions are denoted by ○: the parent ion m/z 73$^+$, +: m/z 72 ($C_3H_6NO^+$), ×: m/z 58 ($C_2H_4NO^+$), □: m/z 44 ($C_2H_6N^+$), ▲: m/z 30 (CH_4N^+).

12.2±0.3 eV is rather close to the previously reported appearance energy of $C_2H_6N^+$ by electron impact.[8] The second rise for m/z 44 in the RI curve (Fig. 3) indicates the appearance of another process at the photon energy above 12.2 eV. Four kinds of process are candidates or another fragmentation to m/z 44; (i) the fragments in Eq. 1 have high KER, (ii) the fragment ion is in an electronically excited state as given in Eq. 4, (iii) the fragment neutral is in an electronically excited state as is given in Eq. 5, (iv) the total enthalpy of the products by the successive reaction is so large as is given in Eq. 6.

$$C_3H_7NO^{+\cdot}* \rightarrow C_2H_6N^+(m/z\ 44)+CHO\cdot \quad (4)$$

$$\rightarrow C_2H_6N^+ + CHO\cdot* \quad (5)$$

$$\rightarrow C_2H_6N^+ + H + CO \quad (6)$$

Here, the asterisk denotes the species in an excited state. The processes Eqs. 4—6 are not clear from the energetic point of view. Alternative assignment of m/z 44 as $C_2H_4^+$ having the same mass number as $C_2H_6N^+$ is not coincided with the high resolution mass spectrum (electron impact) obtained. The fragments produced by electron impact are assumed not to be so different from those produced by photoionization. The sum of enthalpy ($\Sigma\Delta H_f$) of the products is not estimated for Eq. 4, because the excitation energies of $C_2H_6N^{+}*$ are unknown. The product CHO·* in Eq. 5 has excited electronic states at 1.15 eV and 3.0 eV[9] above the ground state. The first excitation energy of CHO·, 1.15 eV, is lower than ca. 1.5 eV which is the energy difference between the appearance energy and the second rise of m/z 44. The sum of enthalpy for CO and H[17] (1.11 eV), which are the products in Eq. 3, is larger than the ΔH_f of CHO· by 0.94 eV. This difference in energy is smaller than the difference of ca. 1.5 eV obtained.

Formations of high energetic products such as CHO·* in the excited electronic state or a pair of CO and H substantially reduce their kinetic energy released (KER) of $C_2H_6N^+$ compared with the formation of $C_2H_6N^+$ via the first decomposition channel. Effects of the ion repeller voltage on the intensity of $C_2H_6N^+$ and of the parent ion were measured as are shown in Figs. 5 (a) and (b) in place for direct measurement of KER. For the

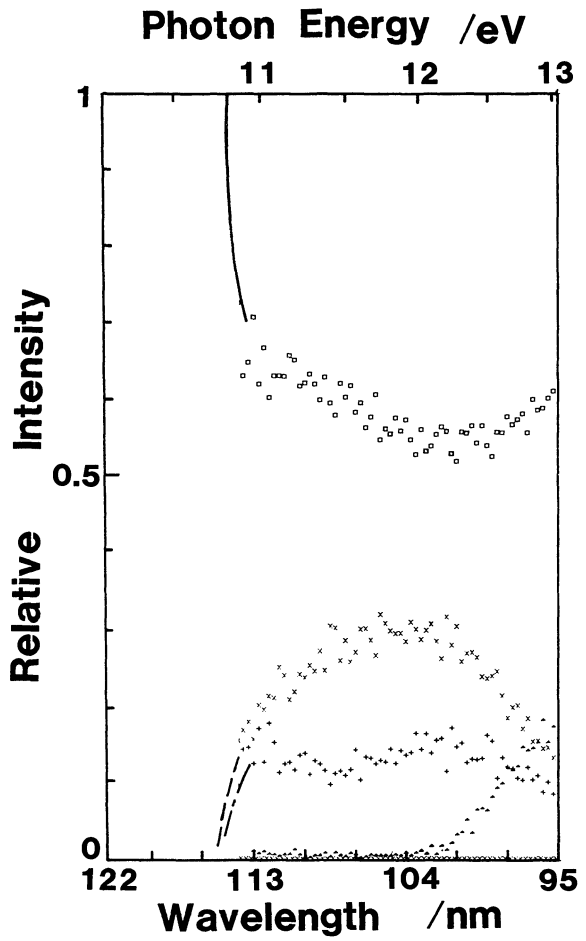

Fig. 3. The relative intensity curve normalized by the sum of four fragment ions (breakdown curves). Each ions are denoted by +: m/z 72 ($C_3H_6NO^+$), ×: m/z 58 ($C_2H_6NO^+$), □: m/z 44 ($C_2H_6N^+$), ▲: m/z 30 (CH_4N^+).

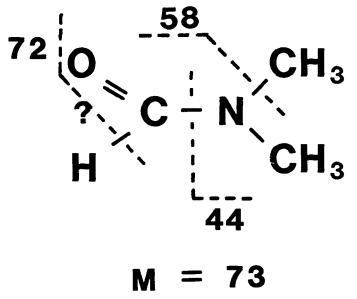

Fig. 4. The molecular structure of *N,N*-dimethylformamide. The dotted lines show the scheme of bonds rupture to produce the fragment ions.

sake of comparison, the dependence of ion repeller voltage on the intensities of $C_2H_5Br^{+\cdot}$ and of $C_2H_5^+$ are shown in Figs. 5 (c) and (d) for a fragmentation, $C_2H_5Br^{+\cdot} \rightarrow C_2H_5^+ + \cdot Br$, where $C_2H_5^+$ is known to have a higher KER than that partitioned statistically above 12.0 eV excitation.[10] At lower repeller voltages, the higher relative intensity of $C_2H_6N^+$ than the parent ion obtained on the 13.0 eV excitation implies a higher KER of $C_2H_6N^+$ as in the case of $C_2H_5^+$. The high KER of $C_2H_6N^+$ is inconsistent with Eqs. 4—6. Therefore, m/z 73 on the excitation above 12.2 eV decomposes along a repulsive potential to give $C_2H_6N^+$ with a high KER.

High energy electron impact ionization (30 eV) produces a metastable peak at m/z 26.5 due to fragmentation, M^+ (73)→44^+ as is shown in Fig. 6. The slow fragmentation giving the metastable peak at m/z 26.5 can not be ascribed to DMF^+ formed on the lower excitation energy than 12.2 eV, because the rate of the fragmentation to m/z 44 is the greatest among those to m/z 44, 58, and 72 assuming from the greatest intensity. Most probably, the slow fragmentation rises from an electronically excited DMF^+ formed on the high excitation energy. The metastable peak at m/z 26.5 suggests that the DMF^+ in the excited electronic state having a high vibrational energy takes the long way round before crossing the potential to dissociate. The second process producing $C_2H_6N^+$ presumably takes place along a repulsive potential after the slow crossing.

Fig. 7 shows a schematic energy diagram of $C_3H_7NO^{+\cdot}$ with its PES and the ionization efficiency curve of $C_2H_6N^+$. The point D indicates the lowest energy level of $C_3H_7NO^{+\cdot}$ dissociating to $C_2H_6N^+$ and CHO·. The parent ion excited above the threshold energy B stretches the N–C bond to dissociate. The transition probability to a hatched part above level B is very small, which is in agreement with the efficiencies of photoelectron and the photoionization efficiency curves. The transition probability to a repulsive energy level is also very small. The parent ion is efficiently excited to an energy level C by a vertical transition shown by a big arrow in PES. The formation of $C_2H_6N^+$ and CHO· in the ground state occurs at an intersystem-crossing point (C) between a bonding and an antibonding potential curve. After some vibrational relaxation the parent ion in the excited electronic state decomposes along the repulsive potential. The major part of the energy difference between the intersystem-crossing point and the dissociation limit D is converted to the kinetic energies of the dissociation products.

***m/z*=30.** The RI curve for m/z 30 arises in place of m/z 58 coming down. The m/z 30 is assigned to CH_4N^+ over NO^+ (m/z 30 produced from CH_3NO_2 by help of high resolution mass spectrum.)

$$C_3H_7NO^{+\cdot *} \rightarrow (C_2H_4NO^+) \rightarrow CH_4N^{+\cdot} + CO + \cdot CH_3 \quad (7)$$

This CH_4N^+ produced from DMF^+ is also discriminated from both CH_2O^+ and $C_2H_6^+$ having the same m/z 30. This assignment is supported by the $\Sigma\Delta H_f$ of the decomposition products in the following alternative reactions.

The formation of $CH_4N^{+\cdot}$ together with CO (Eq. 7) is supported by the $\Sigma\Delta H_f$ of the decomposition products. The sum of enthalpy is calculated to be 8.0 eV, which is

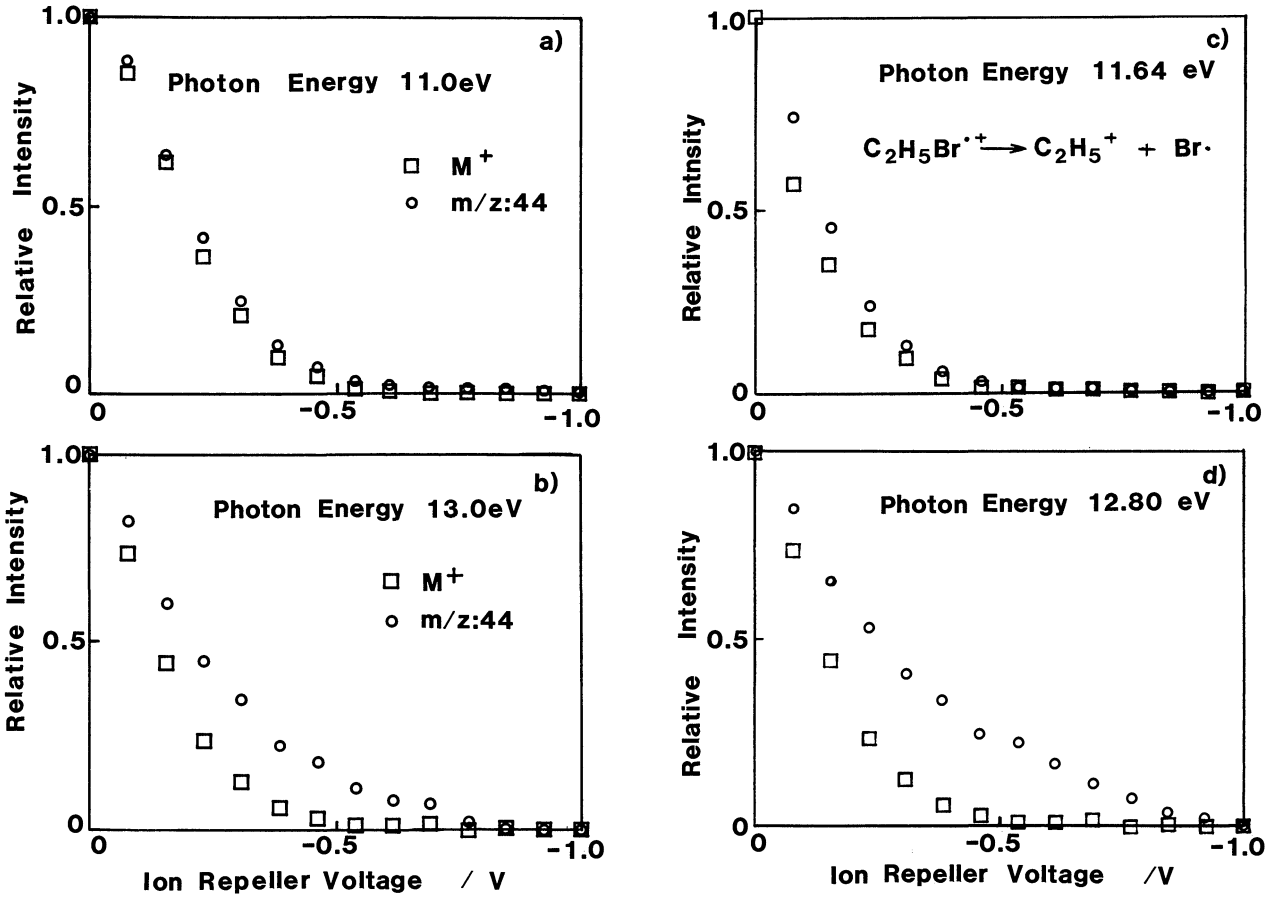

Fig. 5. The dependence of m/z 44 (○) and parent ion (□) on the reverse ion repeller voltages at the photon energy 11.0 eV (a) and 13.0 eV (b). The dependence of $C_2H_5^+$ (○) eliminated from ethyl bromide ion (□) at the photon energy 12.8 eV (c) and 11.64 eV (d) on the reverse ion repeller voltages. Since the ionization still occurs via the first channel in the higher photon energy region than ca. 12.2 eV, even if the new channel occurs through one of the processes such as Eqs. 1—3, the average KER of $C_2H_6NO^+$ will not drop significantly.

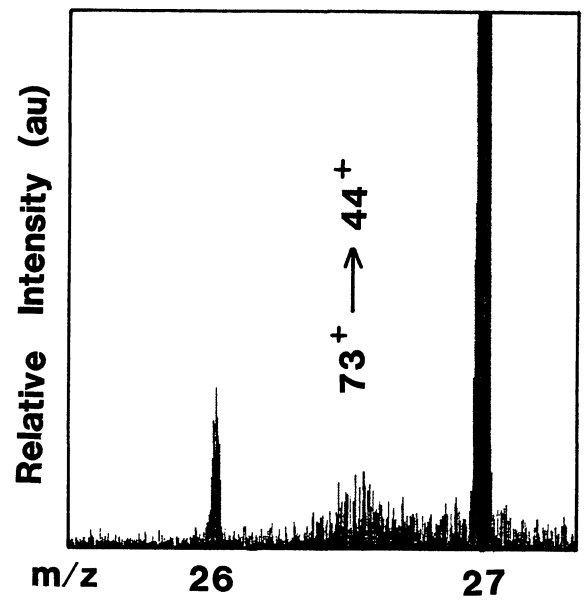

Fig. 6. A metastable peak at m/z ca. 26.5 corresponds to the fragmentation, $73^+ \rightarrow 44^+$, by 30 eV electron impact.

lower than the activation potential (9.9 eV[18]) estimated from the appearance energy (11.9 eV) for m/z 30. For alternative fragmentation processes, Eqs. 8—10 are followings.

$$C_3H_7NO^{+\cdot *} \rightarrow (C_2H_4NO^+) \rightarrow NO^{+\cdot} + C_2H_4 + \cdot CH_3 \quad (8)$$

$$\rightarrow CH_2O^{+\cdot} + CH_2N + \cdot CH_3 \quad (9)$$

$$\cdots\cdots\cdots \rightarrow C_2H_6^{+\cdot} + CHNO \quad (10)$$

The $\Sigma\Delta H$ are estimated to be 12.2,>11.2, and >10.8 eV, respectively, which are larger than the activation potential of the process giving m/z 30.

The appearance of fragment ions, $C_3H_6NO^+$, $C_2H_4NO^+$, and $C_2H_6N^+$, at the similar energies (Table 1) may be realized by ionization mechanism (kinetics and/or energetics). The small transition probability at the appearance energies makes the onsets of the ionization efficiency curves ambiguous. A tentative explanation is as follows. DMF is ionized above 9.12 eV via the

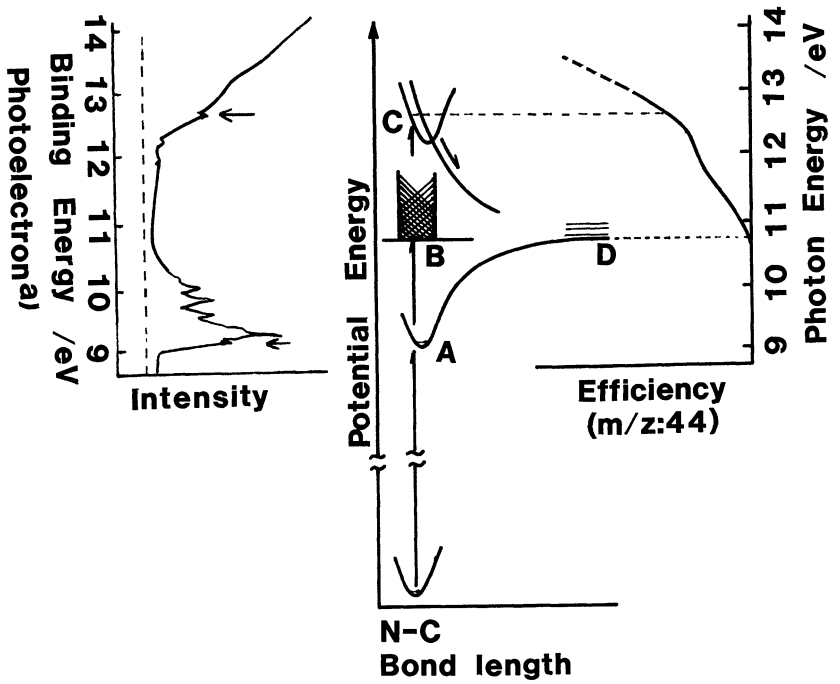

Fig. 7. The schematic energy diagram of fragmentation of *N,N*-dimethylformamide ion with the PES and the breakdown curve of m/z 44. The arrow in the PES points the vertical ionization energy A. *N,N*-dimethylformamide is excited vertically in the higher energy region than 10.7 eV of its continuum energy level B in producing CHO· and $C_2H_6N^+$ at D. A predissociative ionization producing CHO· occurs at C (ca. 12.2 eV) corresponding to a peak in the PES which is pointed by the big arrow.

removal of nonbonding electron of the nitrogen and/or the oxygen atom.[11] The ionization mechanism suggests that the removal of a nonbonding electron causes a change in the molecular orbital hybridization from sp^3 to sp^2 on the nitrogen atom of $C_3H_7NO^{+\cdot}$[12] accompanied by reduction of the length of C–N and the bond angle of C–N–C and C–N–O. This brings about a conversion of the electronic energy to the internal vibrational and rotational energy for the parent ion. The increased internal energy of $C_3H_7NO^{+\cdot}$ exceeds the activation energy of the decompositions to $C_3H_6NO^+$, $C_2H_4NO^+$, or $C_2H_6N^+$. This seems to be one of the reasons why the appearance energies of three fragment ions are nearly the same, though the bond energies may be different from each other.

We thank Professor Takesi Ohno of Osaka University for his discussions on the kinetics.

References

1) H. M. Rosenstock, K. Draxl, B. W. Steiner, and J. T. Herron, "J. P. Chem. Ref. Data," NBS, (1976), Vol. 6.

2) W. Forst, "Theory of Unimolecular Reactions," Academic Press, New York (1973).

3) C. W. Tsang and A. G. Harrison, *Org. Mass Spectrom.*, **7**, 377 (1973). A. N. H. Yeo and D. H. Williams, *J. Am. Chem. Soc.*, **93**, 395 (1971).

4) M. T. Bowers et al., "Gas Phase Ion Chemistry," Academic Press, New York (1974), Vol. 1.

5) M. Arimura and Y. Yoshikawa, *Mass Spectrom. Jpn.*, **32**, 375 (1984).

6) J. Momigny, C. Goffart, and L. d'Or, *Int. J. Mass Spectrom. Ion Phys.*, **1**, 53 (1968).

7) G. W. Mines and H. W. Tompson, *Spectrochim. Acta, Part A*, **31**, 137 (1975).

8) B. G. Gowenlock, P. P. Jones, and J. R. Majer, *Trans. Faraday Soc.*, **57**, 23 (1961).

9) G. Herzberg, "Molecular Spectra and Molecular Structure, III. Electronic Spectra and Electronic Structure of Polyatomic Molecules," Van Nostrand-Reinhold, New York (1966).

10) M. T. Bowers, "Advanced Mass Spectrometry, A," p. 533 (1985).

11) D. A. Sweigart and D. W. Turner, *J. Am. Chem. Soc.*, **94**, 5592 (1972).

12). D. W. Turner, C. Baker, A. D. Baker, and C. R. Brundle, "Molecular Photoelectron Spectroscopy," John Wiley & Sons, New York (1970).

13) R. G. Cooks, J. H. Beynon, R. M. Capriol, and R. G. Lester, "Metastable Ions," Elsevier, New York (1973).

14) "Kagaku Binran," 3rd ed, ed by Chem. Soc. Jpn., Maruzen, Tokyo (1984).

15) K. Watanabe, T. Nakayama, and J. Mottl, *J. Quant. Spectrosc. Radiat. Transfer*, **2**, 369 (1962).

16) The mass number of metastable peak m due to the reaction $m_1 \rightarrow m_2^+ + n$ before the magnetic sector of mass spectrometer is given as follows.[a]

$m^*=m_2^2/m_1$

[a] Ref. 13.

17) The ΔH_f of respective species[a] are the followings in kcal mol^{-1}.

Species	$C_3H_7NO^{+\cdot}$	$NO^{+\cdot}$	CH_4N^+	$CH_2O^{+\cdot}$	$C_2H_6^{+\cdot}$
ΔH_{f298}	165	235	178	224	249
Species	C_2H_4	CO	$\cdot CH_3$	H	HCO
ΔH_{f298}	12.5	−26.4	34.0	52.1	8

The ΔH_f of $C_2H_4NO^+$, which is unknown, can be estimated from the appearance energy of $C_2H_4NO^+$ by using the following relation.

$$\Delta H_f(C_2H_4NO^+)+\Delta H_f(\cdot CH_3)\leqslant AE(C_2H_4NO^+) - IE(C_3H_7NO^{+\cdot})+\Delta H_f(C_3H_7NO^{+\cdot})$$

Where AE and IE are an appearance energy and an ionization energy, respectively. The enthalpy of $C_2H_4NO^+$ is estimated to $\leqslant$169 kcal mol^{-1}.

[a] Ref. 1, Ref. 14, Ref. 11.

18) Under the conservation of energy and momentum, the released energy from the parent ion is partitioned into the fragmentation products in a decomposition. The fragment ions, $C_2H_6N^+$ and $C_2H_5^+$, get about 40 and 73% of the respective whole released kinetic energy.

Additional Formation of Brønsted Acid Sites on Silica-Alumina Catalyst Surfaces by Depositing Silica Component

Satoshi SATO,* Masahiro HIRATSUKA, Toshiaki SODESAWA, and Fumio NOZAKI
Department of Applied Chemistry, Faculty of Engineering, Chiba University,
Yayoi-cho, Chiba 260
(Received January 21, 1991)

The chemical vapor deposition (CVD) of silica onto an amorphous silica–alumina was investigated using tetraethoxysilane in order to create Brønsted acid sites on the surface of original silica–alumina. Silica loading could be readily controlled by the CVD time at 160 °C; the silica covered an internal wall of mesopore of the support of silica–alumina. The resulting CVD silica–alumina was catalytically more active than the original silica–alumina support for such test reactions as the cracking of cumene and the isomerization of 1-butene. The characteristic changes in the amount of Brønsted acid sites were clarified by means of the temperature-programmed desorption of adsorbed 2,6-dimethylpyridine. Strong Lewis acid sites of the original silica–alumina were converted into strong Brønsted acid sites upon depositing the silica component.

Chemical vapor deposition (CVD) techniques are effective for attaining the high dispersion of a deposit on the surface of a catalyst support, and have recently been investigated regarding both the modification and preparation of solid acid catalysts.[1-9] We previously reported a supported type of silica–alumina catalyst prepared by depositing silica on an alumina surface.[5,9] Silica was effectively deposited onto the alumina by using tetraethoxysilane at 240 °C in the presence of oxygen; silica loading was readily controlled by the deposition time. The obtained alumina-supported silica catalyst was found to have predominantly Brønsted acid sites which are transformed from the Lewis acid sites of an alumina surface. The silica–alumina catalyst exhibited catalytic activities for several reactions such as cracking, isomerization, and dehydration.

Silica–alumina is an important catalyst for manufacturing various petrochemical products, and is commercially prepared by wet methods, such as co-precipitation and co-gelation. Although the conventional preparation methods are suitable for obtaining a "bulk" level dispersion of the binary oxide component, the respective oxide species do not disperse atomically. Thus, amorphous silica–alumina usually has both Brønsted and Lewis acid sites. In contrast to the wet methods, CVD techniques are attractive for surface modifications used to attain atomical dispersions of other oxide species on the surface of a catalyst support.

If the Lewis acid sites of amorphous silica–alumina are able to be converted into Brønsted acid sites by the deposition of silica, the catalytic properties must be improved. In this paper we describe various experimental results concerning the CVD of silica onto an amorphous silica–alumina support commercially produced by the co-gelation preparation method. In addition, we describe the acidic character of the CVD silica–alumina catalyst, which has been clarified by means of temperature-programmed desorption (TPD) using 2,6-dimethylpyridine as an adsorbate, together with the pore characteristics.

Experimental

Commercial silica–alumina (N631-L) with a specific surface area of 420 $m^2 g^{-1}$, an alumina content of 13 wt%, and a granule size of 24—60 mesh was supplied by Nikki Chemical Co., Ltd. A CVD silica–alumina catalyst was prepared at the prescribed temperatures by bringing tetraethoxysilane vapor together with a carrier gas into contact with the silica–alumina support in a CVD reactor made up of a Pyrex glass tube rotating in an electrical furnace inclined at 45°;[9] the flow rates of tetraethoxysilane and the carrier gas were 2.7 and 400 mmol h^{-1}, respectively. After CVD operation, the sample was calcined at 550 °C for 3 h in an air atmosphere. The silica loading was calculated by measuring the weight increase of the CVD samples after calcination.

The cracking of cumene was tested at 350 °C using a fixed-bed continuous-flow apparatus under atmospheric pressure at a W/F of 28 g h mol^{-1}, where W is the weight of the catalyst and F is the molar flow rate of cumene, together with a nitrogen carrier gas (15 ml min^{-1}). The reactor effluent was analyzed by on-line GLC using a column of Bentone 34 and dinonyl phthalate (1 m).

The isomerization of 1-butene was performed in a closed circulation reactor comprising a circulation volume of 200 ml. After a catalyst (55 mg) had been evacuated at 200 °C for 1 h, the reaction was carried out at 50 °C at an initial pressure of 22 kPa. The products were analyzed by on-line GLC with a VZ-7 column (4.5 m). The isomerization activity was evaluated by the first-order rate constant during the initial reaction period.

A BET surface area and pore characteristics were obtained by nitrogen physisorption at −196 °C. The pore volume distribution was calculated using the method of Cranston and Inkley[10] and the desorption isotherm of nitrogen. A T-plot, giving an information about micropores with radii less than 0.35 nm, was also obtained from the desorption isotherm according to the articles by Boer and co-workers.[11-13]

A TPD measurement of the adsorbed pyridine or 2,6-dimethylpyridine was performed in order to evaluate the acidic property. After a sample (10 mg) had been evacuated at 500 °C for 1 h, pyridine was injected at 200 °C; the sample was then evacuated at 200 °C for 1 h. The TPD measurement was run from 200 to 700 °C at a heating rate of 5 °C min^{-1}. The

desorbed pyridine was bubbled into a conductivity cell containing 0.5 mmol dm^{-3} of a sulfuric acid solution (30.0 g) together with nitrogen flow (70 ml min^{-1}); the amount of desorbed pyridine was monitored by the change in the solution conductivity.[14] The obtained cumulative curve differentiates to give an acid strength distribution as a function of desorption temperature.

Results and Discussion

Catalyst Preparation. Figure 1 shows the influence of the CVD temperature and time upon silica loading. In a stream of air, silica loading was increased with the CVD temperature at temperatures below 200 °C, and maximized at nearly 200 °C. Above this temperature, the silica loading decreased with the CVD temperature; above 280 °C the obtained catalyst had a color which varied from brown to black, due to coking. Thus, the optimum CVD temperature was found to be below 200 °C. At CVD temperature of 160 °C, the silica loading increased monotonously with the CVD time up to 2 h, and then leveled off. The silica loadings were 0.20 and 0.39 g/g-support for 2 and 8 h, respectively. In a stream of nitrogen, the silica loading also changed with the CVD time at 160 °C in the same manner as in the presence of oxygen. It can consequently be said that silica loading is readily controlled by the CVD time at 160 °C. No oxygen was needed for to accelerate the deposition rate at 160 °C, although oxygen was effective for the acceleration of silica deposition onto an alumina support at 240 °C.[9] Silica deposition onto silica–alumina occurred at lower temperatures (about 80 degree) compared to that for silica deposition onto an alumina support. In a stream of nitrogen above 200 °C, silica loading was almost unchanged with the CVD temperature, whereas it varied with the CVD temperature below 200 °C in a similar way as in air. This observation is presumed to be related to the deposition rate, as will be discussed later.

Physical Properties. Changes in the surface area of CVD catalysts with silica loading are shown in Fig. 2. For CVD catalysts prepared at 160 °C, the surface area (based on the unit weight of the original silica–alumina support) slightly decreased with an increase in silica loading up to a loading of 0.2 g/g-support; it then decreased steeply. For an alumina support which has relatively large mesopores (ranging from 4 to 20 nm in diameter[9]), the deposited silica is uniformly dispersed on the support, since the surface area (based on the unit weight of the support) is almost unchanged, irrespective of the silica loading. For the present silica-alumina, the deposition of silica is considered to be affected by the pore structure of the support. Figure 3 shows the pore volume distribution of CVD catalysts together with the original silica–alumina support. The silica–alumina support had 0.47 ml g^{-1} of total pore volume and a maximum pore volume at a diameter of about 3.8 nm, which was smaller than that of the alumina support mentioned above. The CVD catalysts had the maximum pore volume at a diameter close to 3.8 nm, although the total pore volume was significantly decreased with silica loading. Furthermore, for CVD catalysts prepared at

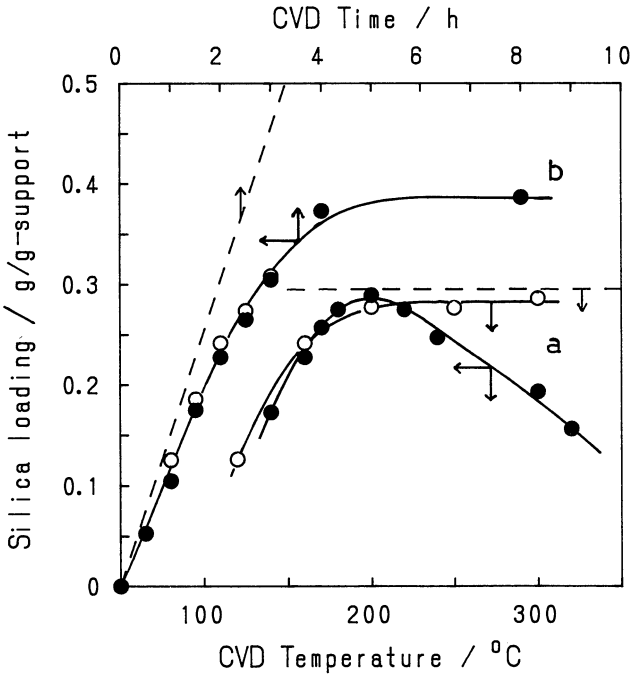

Fig. 1. Effect of CVD temperature and time. a, CVD was operated for 2 h; b, CVD was operated at 160 °C; ●, CVD was operated in air; ○, in nitrogen. Dashed line denotes the critical deposition amount limited by an amount of fed tetraethoxysilane.

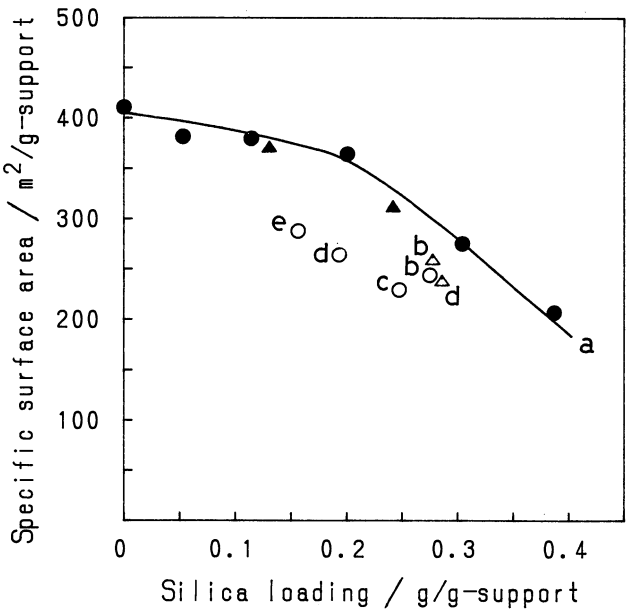

Fig. 2. Change in the surface area of a CVD catalyst with silica loading. ●, ○, CVD was operated in air; ▲, △, in nitrogen. a (solid line), prepared at 160 °C; b, 200 °C; c, 240 °C; d, 300 °C; e, 320 °C,

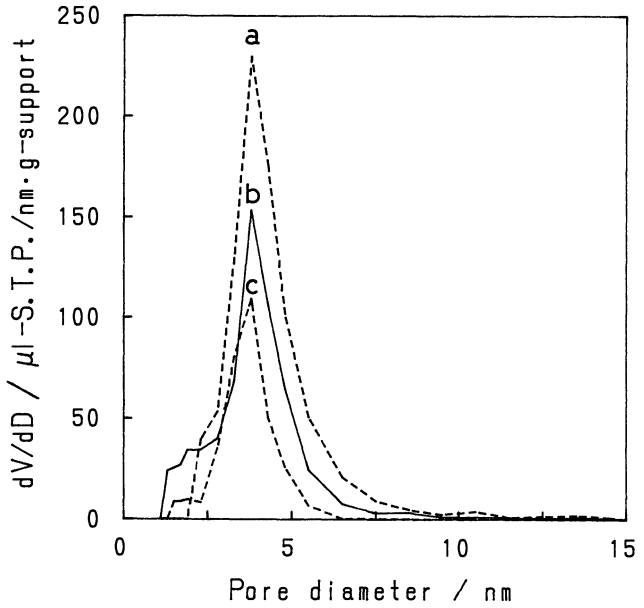

Fig. 3. Pore volume distribution of CVD catalysts. a, Original silica–alumina support; b, CVD catalyst (silica loading, 0.20 g/g-support); c, CVD catalyst (silica loading, 0.39 g/g-support).

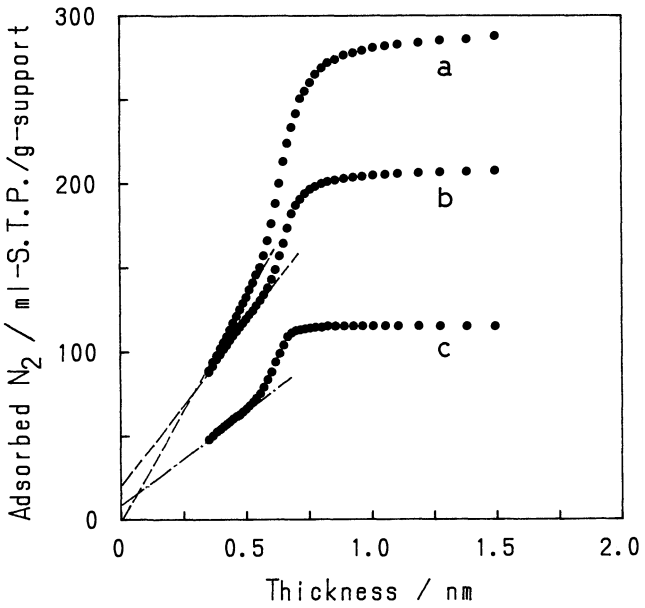

Fig. 4. T-plot for CVD catalysts. Symbols as those in Fig. 3.

temperatures higher than 200 °C in air, the surface area was much smaller than those prepared at 160 °C (Fig. 2). This indicates that aggregated deposition occurred in the neighborhood of the entrance of the micropores of the support; it then followed by the closure of the micropores at higher temperatures in air owing to a too-fast deposition. For a catalyst prepared at 300 °C in nitrogen, however, the surface area was not so small as those prepared in air. Since oxygen results in an aggregated deposition of silica at high temperatures (above 200 °C), the surface area steeply decreased.

In order to elucidate the existence of micropores under a diameter of 0.7 nm, a T-plot was examined according to the procedure proposed by Boer et al.[11-13] T-plots for CVD catalysts are shown in Fig. 4. A T-plot passes through the origin for a sample having no micropores, whereas it has an intercept which expresses the micropore volume for a sample having micropores.[13] Thus, an original silica–alumina support has no micropores because of the passing through the origin in the T-plot. For a CVD catalyst with a silica loading of 0.20 g/g-support, micropores (21 ml-STP) were generated with a small decrease in the BET surface area (Fig. 4b). Further silica deposition (0.39 g/g-support) led to a decrease in the micropore volume (10 ml-STP) together with a large decrease in the surface area (Figs. 2 and 4c). The deposition of silica resulted in the formation of micropores in the silica–alumina support. These results indicate that silica deposition develops on the interior wall of mesopore in such a characteristic way that the pore size decreases with silica deposition.

Acidic Properties. It has been known that 2,6-dimethylpyridine (2,6-DMP) selectively adsorbs on Brønsted acid sites, but not on Lewis acid sites because of a steric hindrance of two methyl groups, whereas sterically nonhindered pyridine adsorbs on both Brønsted and Lewis acid sites.[15,16] 2,6-DMP has been used for the characterization of acid surfaces with pulse adsorption,[15] IR spectroscopy,[16] and gravimetric titration.[17] We recently applied the TPD measurement of adsorbed 2,6-DMP to the elucidation of the acidic nature of an alumina-supported silica catalyst.[14] This investigation has elucidated that silica deposition creates Brønsted acid sites on the surface of alumina together with the disappearance of Lewis acid sites.

The TPD spectra of adsorbed pyridine and 2,6-DMP are illustrated in Fig. 5. The original silica–alumina support had a large desorption peak of pyridine and a somewhat smaller peak of 2,6-DMP than that of pyridine at peak tops of about 300 °C. Since curve b shows the acid strength distribution of Brønsted acid sites, the difference between curves a and b is a measure of Lewis acid sites. The silica–alumina support dominates Brønsted acid sites with a small amount of Lewis acid sites. This fact is also supported by the ^{31}P NMR of trimethylphosphine adsorbed on it.[9] In contrast, for a CVD catalyst loaded 0.20 g/g-support of silica, it had no significant difference between two distribution curves of pyridine and 2,6-DMP. This indicates that the CVD catalyst has dominantly Brønsted acid sites. In addition, the total numbers of acid sites, represented by the amount of desorbed pyridine, were reduced, as can be seen from a comparison of curves c and a. Moreover, the amount of desorbed 2,6-DMP decreased in the low-

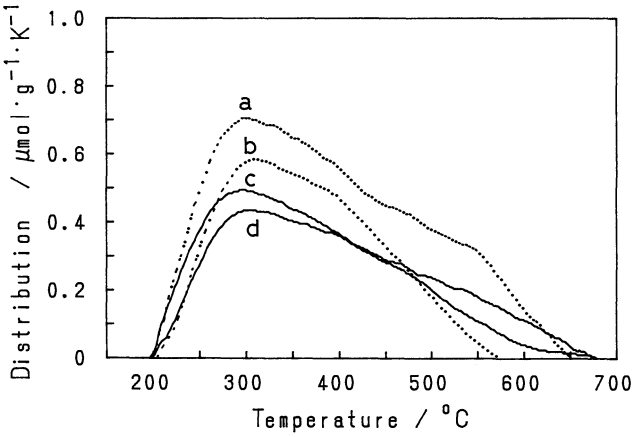

Fig. 5. TPD profiles of adsorbed pyridine and 2,6-dimethylpyridine. Original silica–alumina support (dotted line): a, pyridine; b, 2,6-DMP; CVD catalyst (silica loading, 0.20 g/g-support): c, pyridine; d, 2,6-DMP.

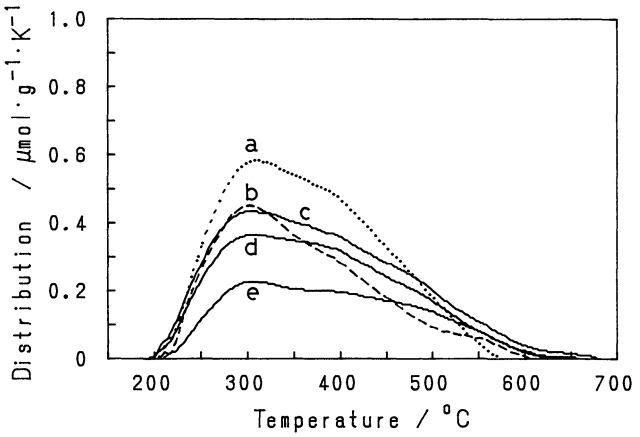

Fig. 6. TPD profiles of 2,6-dimethylpyridine. a, Original silica–alumina support (dotted line); b, CVD catalyst (dashed line): silica loading, 0.10; c, 0.20; d, 0.30; e, 0.39 g/g-support.

Table 1. Amounts of Pyridine and 2,6-Dimethylpyridine Desorbed from Catalysts

Catalyst (loading)[a]	Adsorbate	Amount μmol/g-support		
		Total	400—500[b]	>500[b]
Support	Pyridine	190	44	35
(0)	2,6-DMP	126	33	7
CVD	Pyridine	102	18	12
(0.11)	2,6-DMP	84	17	5
CVD	Pyridine	130	28	25
(0.20)	2,6-DMP	108	29	13
CVD	Pyridine	99	30	17
(0.30)	2,6-DMP	84	26	10
CVD	Pyridine	62	14	11
(0.39)	2,6-DMP	58	17	10

a) Silica loading (g/g-support). b) Desorption temperature (°C).

temperature region, but increased in the high-temperature region, as can be understood from a comparison of curves d and b. This indicates that strong Brønsted acid sites, represented by the desorption of 2,6-DMP at temperatures above 500 °C, were increased together with a decrease in the total number of Brønsted acid sites.

Figure 6 illustrates the changes in the Brønsted acidity, measured by the desorption of 2,6-DMP, with a variation of silica loading; Table 1 summarizes the amounts of disorbed pyridine and 2,6-DMP. A small silica loading of 0.11 g/g-support decreased the total amounts of desorbed pyridine and 2,6-DMP. Interestingly, a further silica loading increased the total amounts, and enhanced the Brønsted acid strength. Especially, the number of strong Brønsted acid sites (expressed by the desorption of 2,6-DMP at temperatures above 400 °C) was maximized at silica loadings near 0.20 g/g-support. Above this loading, the total numbers of desorbed pyridine and 2,6-DMP monotonically decreased with increasing the silica loading. Another catalyst, such as a K^+ ion-exchanged silica–alumina, which gave no desorption of 2,6-DMP in the temperature region above 400 °C, exhibited no catalytic activity for 1-butene isomerization.[14] The effective Brønsted acid sites for 1-butene isomerization held 2,6-DMP, even at high temperatures above 400 °C. The present TPD results indicate that strong Brønsted acid sites were generated upon depositing silica onto strong Lewis acid sites.

Catalytic Activities. The catalytic activities were examined for CVD catalysts prepared at 160 °C. Figure 7 shows the change in the cumene-cracking activity with process time at 350 °C. Cumene conversion was significantly improved by depositing silica on the

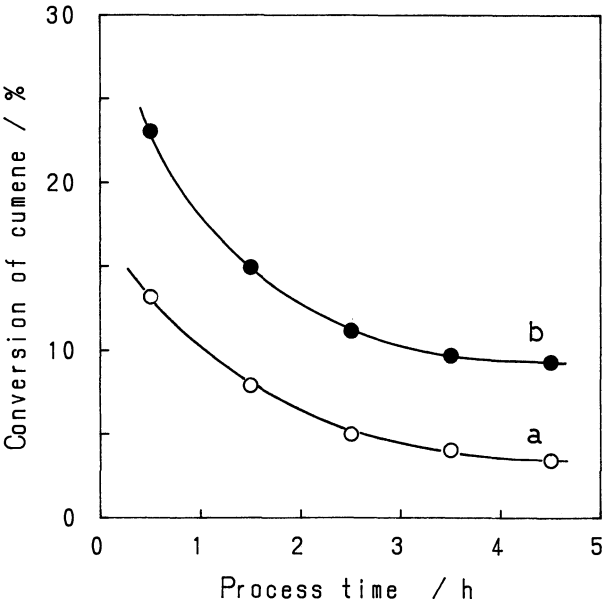

Fig. 7. Cumene conversion with process time. a, Original silica–alumina support; b, CVD catalyst (silica loading, 0.20 g/g-support).

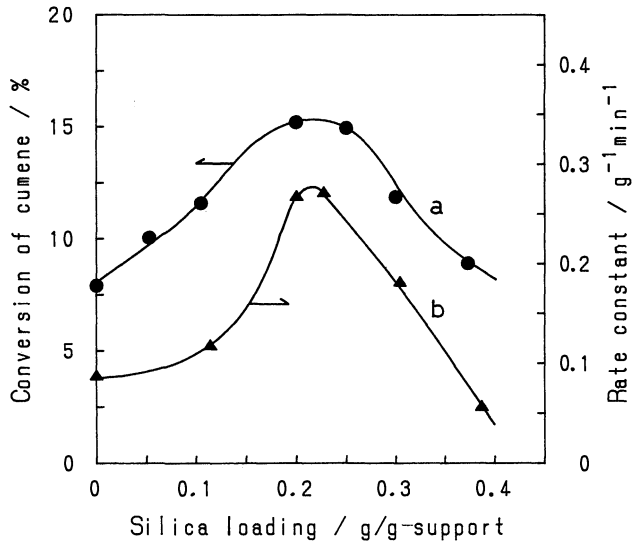

Fig. 8. Changes in the catalytic activities with silica loading. a, Cumene cracking at 350 °C; b, 1-butene isomerization at 50 °C.

original silica–alumina support. Figure 8 depicts the change in the catalytic activity for the cracking of cumene with silica loading, together with the results concerning the isomerization of 1-butene at 50 °C. Since the conversion of cumene decreased with the process time, the cracking activity was evaluated in terms of the average conversion during process times of 1—2 h. Cumene conversion increased with increasing silica loading, and attained a maximum at a silica loading of about 0.2 g/g-support. Above this loading, the cracking activity decreased with silica loading. For 1-butene isomerization, the initial first-order rate constant exhibited a maximum at a silica loading of about 0.2 g/g-support. This activity-pattern was similar to that for cumene conversion. Although the original silica–alumina support has essential activities for the reactions, the deposition of silica made it possible to increase the catalytic activities to twice the value for cumene cracking, and three times that for 1-butene isomerization, compared with the activity levels of the original silica–alumina support. In addition, with regard to the product distribution of 1-butene isomerization, the ratio of *cis*-/*trans*-2-butene was slightly decreased (from 0.95 to 0.83) with an increase in the silica loading, compared to the values at 1-butene conversion of 50%.

It is worth noting that the silica loading of a 0.2 g/g-support, at which catalytic activities were maximized, is equal to the loading at which the rate of silica deposition decelerated (Fig. 1), the loading at which the strong Brønsted acid sites were maximized (Fig. 6 and Table 1), and the loading at which the surface area steeply decreased (Fig. 2). Below this critical loading, the catalytic activity for 1-butene isomerization was apparently unchanged (Fig. 8b). For the cracking of cumene, however, the cumene conversion increased with increasing silica loading (Fig. 8a). Since the pretreatment conditions for the cracking of cumene were different from those for the isomerization of 1-butene, the surface acidities are presumed to be different from each other. On the other hand, above the critical loading, the decreasing features in both the deposition rate and the catalytic activities are in fair agreement with the decreasing pattern in strong Brønsted acidity of the CVD silica–alumina catalyst.

In view of practical usage, the present CVD catalyst was compared with an alumina-supported silica catalyst that has been previously reported.[9,14] For the isomerization of 1-butene, the alumina-supported silica catalyst was active, even at a low temperature of 0 °C,[14] and superior to the present CVD catalyst. This shows no discrepancy with the fact reported by Imizu and Tada.[8] In contrast, for the cracking of cumene, the present CVD silica–alumina catalyst was much preferable because even the original support was superior to the alumina-supported silica catalyst.[9] It is interesting that the enhanced activities vary regarding reaction type.

Formation of Active Site on Silica–Alumina Surface. Although the original silica–alumina support, itself, has Brønsted acidity, an optimal silica deposit results in an increase in the number of strong Brønsted acid sites as well as enhancements in catalytic activity. The superiority of CVD catalysts for catalytic reactions is presumably caused by an increase in the number of Brønsted acid sites for CVD catalysts. When alumina is used as a support, these features are much clearer.[5,9,14] Since an alumina surface almost comprises Lewis acid sites, Brønsted acid sites are effectively generated by the deposition of silica. The resulting alumina-supported silica shows significant catalytic activities for various reactions, whereas the alumina support showed few activities by itself. An excess of the silica deposit, however, weakened strong Brønsted acid sites.[14]

The present silica–alumina support originally had not only strong Brønsted acid sites, but also Lewis acid sites.[9] A small amount of silica loading decreased the number of strong Brønsted acid sites (Fig. 6b). Prior to CVD operation, a support was heated at a low temperature of 160 °C in a stream of carrier gas, so that strong Lewis acid sites could be hydrated to form hydroxyl groups. Silica deposits proceed via an ester exchange of tetraethoxysilane with the surface hydroxyl groups. During the initial stage of deposition, a silica deposit is mainly initiated on strong Brønsted acid sites, and contributes to a weakening of the acid strength. After the original Brønsted acid sites are weakened, further silica deposition induces a transformation of Lewis acid sites into Brønsted acid sites. Furthermore, an excess of silica deposits weaken Brønsted acid sites. Consequently, strong Brønsted acid sites were maximized at silica loadings close to 0.2 g/g-support, as shown in Table 1. Such Lewis acid sites are probably localized

not on isolated alumina in the original silica–alumina, but on the boundary between silica and alumina. If Lewis acid sites exist on isolated alumina, the *cis*/*trans* ratio of produced 2-butene for 1-butene isomerization should be increased from 1 to close to about 3, which has been reported for silica overlayers deposited on alumina.[8] The ratio actually decreased to less than 1 for the present CVD silica–alumina. The difference in Lewis acidity of support materials results in variations of the catalytic properties for the above-mentioned reactions.

In conclusion, an enhancement of catalytic efficiency was achieved by depositing silica onto amorphous silica–alumina. This favorable nature should be attributed to an additional formaton of Brønsted acid sites which are ascribable to the transformation of Lewis acid sites through the CVD process.

References

1) M. Niwa, S. Kato, T. Hattori, and Y. Murakami, *J. Chem. Soc., Faraday Trans. 1,* **80**, 3135 (1984).
2) S. Sato, K. Urabe, and Y. Izumi, *J. Catal.,* **102**, 99 (1986).
3) S. Sato, S. Hasebe, H. Sakurai, K. Urabe, and Y. Izumi, *Appl. Catal.,* **29**, 107 (1987).
4) T. Okuhara and J. M. White, *Appl. Surf. Sci.,* **29**, 223 (1987).
5) S. Sato, M. Toita, Y. Q. Yu, T. Sodesawa, and F. Nozaki, *Chem. Lett.,* **1987**, 1535.
6) Y. Imizu, A. Tada, and I. Toyoshima, *Shokubai (Catalyst)*, **30**, 388 (1988).
7) M. Niwa, T. Hibino, H. Murata, N. Katada, and Y. Murakami, *J. Chem. Soc., Chem. Commun.,* **1989**, 289.
8) Y. Imizu and A. Tada, *Chem. Lett.,* **1989**, 1793.
9) S. Sato, M. Toita, T. Sodesawa, and F. Nozaki, *Appl. Catal.,* **62**, 73 (1990).
10) R. W. Cranston and F. A. Inkley, *Adv. Catal.,* **9**, 143 (1957).
11) B. C. Lippens, B. G. Linsen, and J. H. de Boer, *J. Catal.,* **3**, 32 (1964).
12) B. C. Lippens and J. H. de Boer, *J. Catal.,* **4**, 319 (1965).
13) J. H. de Boer, B. G. Linsen, Th. van der Plas, and G. J. Zondervan, *J. Catal.,* **4**, 649 (1965).
14) S. Sato, M. Tokumitsu, T. Sodesawa, and F. Nozaki, *Bull. Chem. Soc. Jpn.,* **64**, 1005 (1991).
15) H. A. Benesi, *J. Catal.,* **28**, 176 (1973).
16) A. Corma, C. Rodellas, and V. Fornes, *J. Catal.,* **88**, 374 (1984).
17) L. L. Murrell and N. C. Dispenziere, Jr., *J. Catal.,* **117**, 275 (1989).

Characterization of Molecular-Sieving Carbon for CO_2-Adsorbers in Controlled Atmosphere Storage System

Ichiro TANAHASHI,* Hiroto NAKAMA,† Atsushi NISHINO,†† and Jun TAKEDA†
Central Research Laboratories, Matsushita Electric Industrial Co., Ltd.,
Yagumo-Nakamachi, Moriguchi, Osaka 570
† Engineering Center, Matsushita Refrigeration Co., Takaida-Hondori, Higashi-Osakashi, Osaka 577
††Living System Research Center, Matsushita Electric Industrial Co., Ltd.,
Yagumo-Nakamachi, Moriguchi, Osaka 570
(Received February 8, 1991)

Molecular sieving carbon (MSC) has been characterized for CO_2-adsorbers in a controlled atmosphere storage (CA storage) system by a gas-adsorption method. Experimental data were analyzed by means of the Dubinin–Astakhov equation, the *t*-method, and the micropore analysis method. The BET surface area of MSC was 592 $m^2 g^{-1}$. In the pore size distribution curve of MSC, the most common pore diameter was 0.68 nm. The temperature and the space velocity dependence of adsorbers with MSC have been investigated. The CO_2 adsorption capacity of adsorbers was determined by the gas-flow method. The capacity of the adsorbers at 60 °C decreased to 55%, compared with that at 20 °C; it decreased with increasing space velocity.

It has been known that the decay of fruits and vegetables can be reduced under atmospheres of highly concentrated CO_2 (2—15%) and low concentrations of O_2 (2—10%) during storage at low temperatures of 0—10 °C.[1,2]

The controlled atmosphere storage (CA-storage) system has been used practically for reducing the decay of fruits and vegetables. Several types of CA-storage have been proposed.[3] They mainly comprise of three parts; a storeroom, a CO_2-generator, and a CO_2-adsorber. In a previous paper we reported that the reliability of CO_2-adsorbers with molecular sieving carbon (MSC) is better than that of an adsorber with an X-type zeolite.[4] The difference in reliability of the two types of adsorbers was probably attributed to a difference in the micropore structure between MSC and X-type zeolite. The temperature and space velocity (flow rate/volume of the adsorbent) dependence of CO_2-adsorbers with MSC are also influenced by the micropore structure. However, the characterization of MSC by the gas-adsorption method using different analysis approaches has not yet been carried out.

Adsorption methods are frequently used and several adsorbates have been proposed to analyze the micropores of activated carbons.[5-7] Micropores are defined as pores that do not exceed 2 nm, according to the IUPAC classification of pore size. Recent experimental measurements have revealed that micropores influence the adsorption properties of adsorbents.[8,9]

In this report, experimental data concerning adsorption isotherms are analyzed using three different approaches. The first one is the Dubinin–Astakhov (DA) equation (1),[10] which is a general expression of the Dubinin–Radushkevich (DR) equation,[11]

$$W=W_0\{\exp-(A/E)^n\}. \quad (1)$$

Here, W is the volume of the gas adsorbed at a relative pressure, P/P_0, considered to be a characteristic similar to a bulk liquid at the experimental temperature, W_0 the micropore volume, n an additional parameter, and E the characteristic free energy of adsorption for the given system. At the relative pressure, P/P_0, the adsorption potential, or the differential free energy of adsorption, A, is given by

$$A=RT\ln(P_0/P). \quad (2)$$

The second approach is the so-called "*t*-method",[12-14] which is an empirical procedure used for the analysis of adsorption isotherms. This method is based on a comparison between the isotherm on a specimen (porous carbon) and the standard isotherm on a nonporous reference carbon. The amount of adsorbed gas on a porous carbon is plotted against the statistical film thickness, t, for a nonporous reference carbon.

The third approach is the so-called "MP-method" (micropore analysis method).[15] The MP-method is based on the de Boer V–t plot obtained from an adsorption isotherm on nonporous carbons.[15] In the de Boer plot, V is the volume of adsorbed gas. The pore-size distribution and the specific surface area of porous carbon are obtained from this method. Details of the analytical procedure were reported in Ref. 15.

In the present study, MSC was characterized by the gas adsorption method and analyzed by the above-mentioned three methods. The temperature and space velocity dependences of the CO_2-adsorber with MSC were also investigated.

Experimental

1. Materials. The molecular sieving carbon (MSC) used is a product of Takeda Chemical Industries Co., Ltd., (X_2M), the size being about 3 mm in diameter and 3 to 8 mm in length. The nonporous carbon black of Spheron 6 was supplied by Cabot Carbon Co., Ltd. The isotherm of the carbon black was used as the standard adsorption isotherm in the "*t*-method".

2. Apparatus and Procedure. Adsorption experiments for

characterizing MSC were carried out in a conventional volumetric apparatus of BEL Japan, Inc. (BELSORP28) equipped with a high-precision Baratron capacitance manometer. Before the experiments, the samples were out-gassed at 423 K for 2 h. N_2 and CO_2 adsorption isotherms were measured at 77 and 195 K, respectively.

The CO_2 adsorption capacity of the adsorber was measured by the flow method using the same apparatus reported in a previous paper.[4] The apparatus comprises three parts: an adsorber, gas-mixing equipment, and gas-analyzing equipment. The adsorber was 55 mm in diameter and 700 mm in height. To carry out the adsorption experiment, gas of 3.4—14.0% CO_2 was introduced from the bottom of the adsorber at a space velocity of 140—700 h^{-1}. The adsorption temperature was controlled by heating the adsorber with a tape-heater. During adsorption, small portions of the leaked gas were withdrawn from the adsorber, and the concentration of CO_2 was measured by a combustion gas analyzer (Shimadzu, CGT-10-1A).

Results and Discussion

1. Properties of MSC. Figure 1 shows the adsorption (a) and desorption (b), N_2 isotherms of MSC at 77 K and CO_2 adsorption (c) at 195 K. The hysterisis of the N_2 isotherm is small. Brunauer et al. proposed to classify the adsorption isotherms into five different groups.[16] According to their classification, the isotherms of N_2 and O_2 belong to type I. From the N_2 isotherm, the BET surface area (S_{BET}) was calculated to be 592 $m^2 g^{-1}$ by using the well-known BET equation. The S_{BET} of MSC is not so large as that of conventional activated carbons.[7]

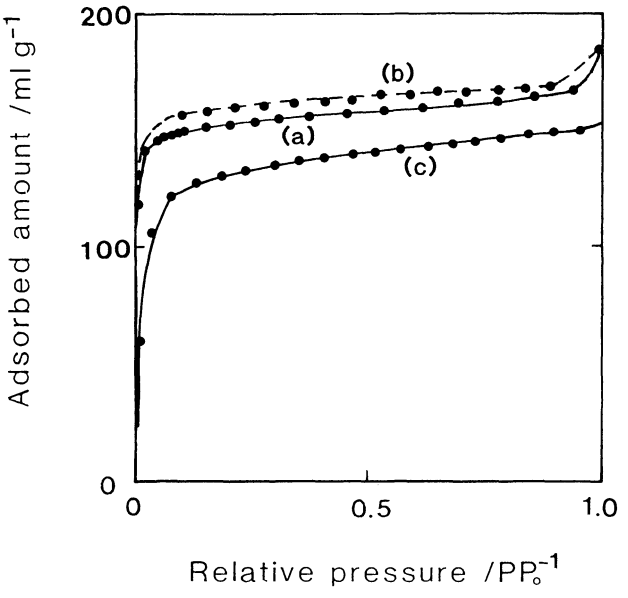

Fig. 1. Adsorption-desorption isotherm of MSC for N_2 at 77 K and for CO_2 at 195 K. (a): adsorption of N_2, (b): desorption of N_2, and (c): adsorption of CO_2.

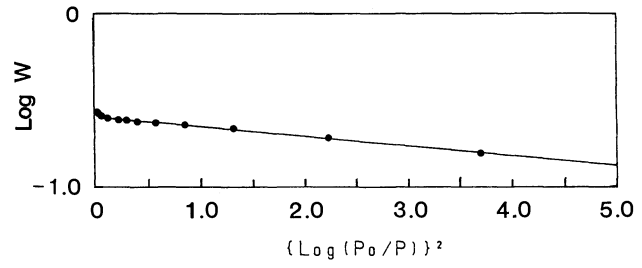

Fig. 2. DA-plots of MSC.

The CO_2 adsorption data were fitted to the DA equation (1). In Fig. 2, $\log W$ is plotted against $\log^2 (P_0 / P)$. The DA plot of MSC lies on a straight line in the case of n=2. According to Eq. 1, the intercept of the linear DA plot should equal to $\log W_0$; from the slope, the value E is obtained. It is known that decreases in the characteristic free energy of the DA equation, E, are correlated with increases in the micropore sizes.[9] The value of n was determined by the relative size between adsorbate and adsorbent. In fact, the value of n on MSC was 3 due to the adsorption of benzene.[17] In this experiment, the value seemed to be 2. This is because the volume of CO_2 was smaller than that of benzene. The E and W_0 values of MSC were 10.43 kJ mol^{-1} and 0.254 ml g^{-1}, respectively. The E value of MSC was larger than that of carbon black and activated carbon.[10] The larger E value suggested that the size of the micropore is smaller than that of carbon black and activated carbon.

Figure 3 shows a t-plot of MSC obtained from the N_2 adsorption isotherm shown in Fig. 1. Carrott et al.[8] has proposed that back extrapolation of the linear portion of the plot to the ordinate yields the total micropore volume, V; the slope of the linear section provides the external area, S_{EXT}, of the adsorbent; and extrapolation to the origin of the initial part of the plot provides the total surface area, S_t. From the figure, S_t and S_{EXT} were calculated to be 711 and 16.4 $m^2 g^{-1}$, respectively. The

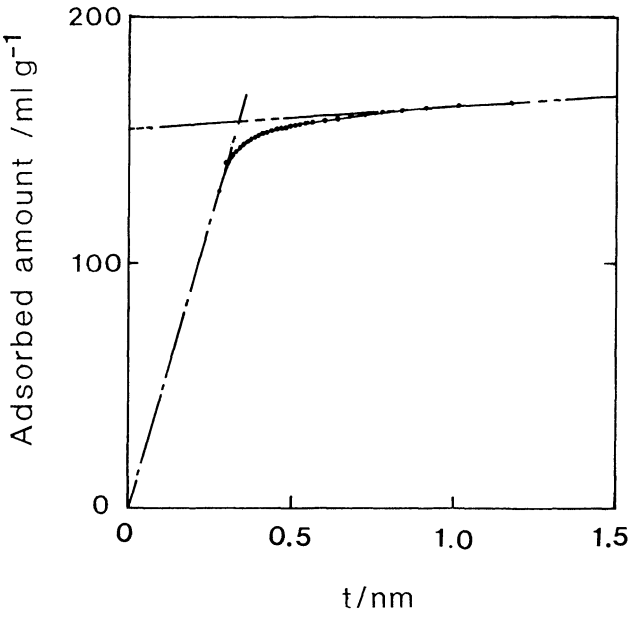

Fig. 3. t-plots of MSC.

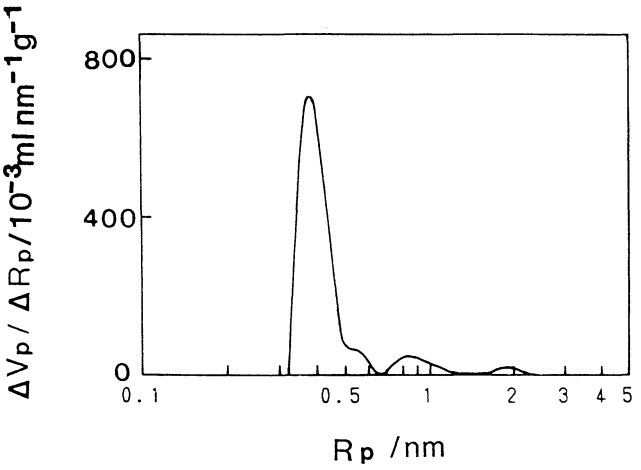

Fig. 4. Pore size distribution of MSC.

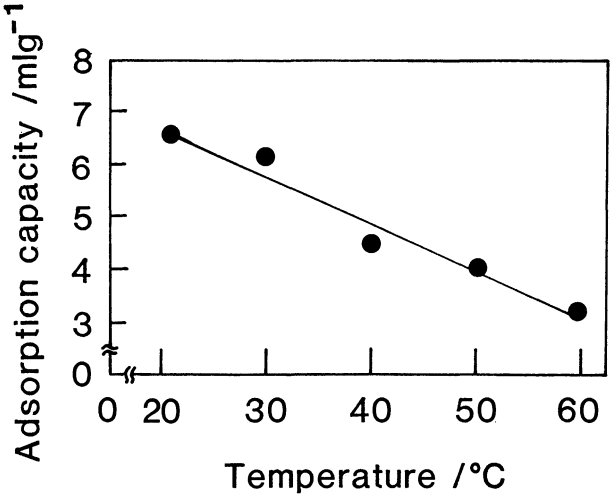

Fig. 5. Temperature dependence of CO_2-adsorber with MSC.

S_{BET} was smaller than S_t. The difference seems to be due to the fact that the t-method is based on a standard adsorption isotherm of nonporous carbon.

The pore-size distribution of MSC obtained from N_2 adsorption isotherms by using the MP-method is shown in Fig. 4. In the figure, R_p shows the micropore radius, and V_p the pore volume. The maximum of $\Delta V_p/\Delta R_p$ (differential value of V_p/R_p) is located at R_p=0.34 nm. Assuming that the walls of the pores are parallel plates, the most common pore diameter is 0.68 nm. The MSC is, thus, concluded to contain only micropores.

2. Characteristics of Adsorber. In a CA storage system, the adsorption of CO_2 was usually carried out in a temperature range of 5 to 60 °C. The concentration and the space velocity of adsorbed CO_2 varied with the concentration of CO_2 in the storeroom. It is therefore important to study both the temperature and the space velocity dependence of adsorbers with MSC.

The CO_2 adsorption capacity was estimated as follows: The concentration of leaked CO_2 was plotted against the time of adsorption and the amount of adsorbed CO_2 was accumulated until the time when CO_2 began to leak (break point).

Figure 5 shows the temperature dependence of the CO_2 adsorption capacity of adsorbers with MSC. The gas used in this experiment was a mixture of 9% CO_2 and 91% N_2. The adsorption capacity of adsorbers at 20 °C is 6.5 ml g^{-1}. In this experiment, the adsorption pressure of CO_2 was not clear; therefore, the estimated amount of adsorbed CO_2 by the flow method could not be compared with that by the conventional volumetric method. The CO_2 adsorption capacity decreases with increasing the temperature of adsorption. This result indicates that the physical adsorption of CO_2 onto MSC occurred. The adsorption capacity of CO_2 at 60 °C decreased to 55% in comparison with that at 20 °C. Almost all of the adsorbed CO_2 was desorbed from MSC by blowing air into the adsorber over a temperature range of 20 to 60 °C. It is known that the pore shape of MSC was a parallel

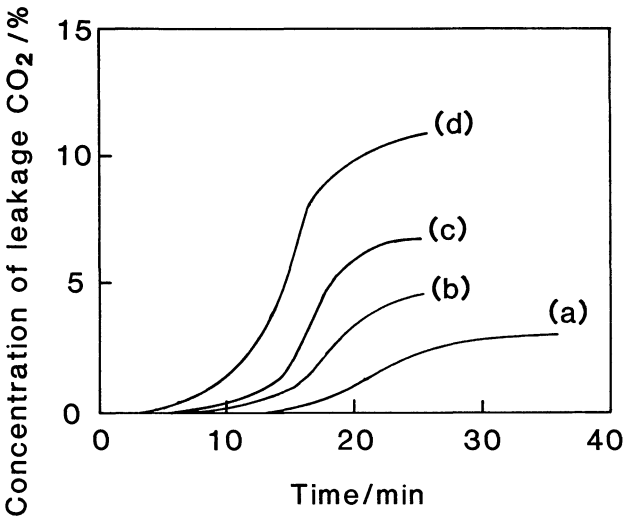

Fig. 6. Leaked CO_2 concentration vs. adsorption time for various concentration of introduced CO_2. (a): 3.4; (b): 5.7, (c): 8.0, and (d): 12.4%.

plate slit;[17] the desorption of gases from MSC was therefore easy. In accordance with this fact, the hysterisis of the adsorption isotherm for MSC was small, as is shown in Fig. 1.

The CO_2 breakthrough curves for CO_2 adsorbers with MSC at various concentrations of introduced CO_2 are shown in Fig. 6. The concentrations of introduced CO_2 were 3.4% (curve a), 5.7% (curve b), 8.0% (curve c), and 12.4% (curve d). In this experiment, the space velocity was 270 h^{-1} and the adsorption was carried out at 17 °C. In the figure, the break points are inversely proportional to the concentration of introduced CO_2. In the CO_2 adsorption isotherm of MSC shown in Fig. 1, the adsorbed amount of CO_2 increases rapidly within the low relative pressure region. It is reported[17] that gas adsorption on MSC within the low relative pressure

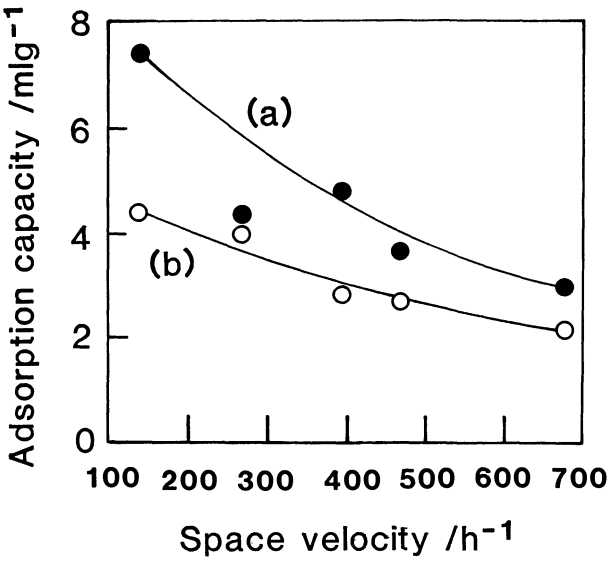

Fig. 7. Space velocity dependence of CO_2-adsorber with MSC for different concentration of introduced CO_2. (a): 12.4 and (b): 3.4%.

region can be attributed to adsorption by micropores. Therefore, MSC was a suitable adsorbent for CO_2 adsorbers in a CA storage system.

Figure 7 shows the space-velocity dependence of CO_2 adsorbers with MSC for different concentrations of introduced CO_2. The experiment was carried out at 17 °C. The concentration of introduced CO_2 was 12.4% (curve a) and 3.4% (curve b). In the case of (b), the CO_2 adsorption capacity gradually decreases with increasing space velocity. In the cass of (a), the capacity decreses largely with increasing space velocity. Thus, the CO_2 adsorption capacity in this experiment seems to be smaller than that of the volumetric method (saturated adsorption amount of CO_2). In order to operate the adsorber effectively, it was important to study the dependence on both the temperature and space velocity of the adsorbers.

Only MSC with micropores showed a large CO_2 adsorption capacity over a wide range of temperature, concentration, and space velocity. It is, thus, a suitable adsorbent for CO_2-adsorbers in a CA storage system.

Conclusion

1) The BET surface area of MSC was 592 $m^2 g^{-1}$. In the pore size distribution curve of MSC, the most common pore diameter was 0.68 nm. From the *t*-plot of MSC obtained from the N_2 adsorption isotherm, the specific surface area (S_t) and external surface area (S_{EXT}) of the MSC were calculated to be 711 and 16.4 $m^2 g^{-1}$, respectively. The S_{BET} was smaller than S_t.

2) The adsorption capacity of CO_2-adsorber with MSC was determined by the gas-flow method. The capacity of the adsorbers at 60 °C decreased to 55% in comparison with that at 20 °C; it decreased with increasing the space velocity.

The authors would like to acknowledge Professor T. Minami of the University of Osaka Prefecture for his helpful discussion and critical reading of the manuscript.

References

1) R. Saijo, *Refrigeration (Tokyo)*, **64**, 1215 (1989).
2) J. M. Wells and M. Uota, *Phytopathology*, **60**, 50 (1970).
3) K. Kato, *Refrigeration (Tokyo)*, **64**, 149 (1989).
4) I. Tanahashi, H. Nakama, A. Nishino, and J. Takeda, *Chem. Express*, **6**, 237 (1991).
5) H. Marsh, *Fuel*, **44**, 253 (1965).
6) M. Molina-Sabio, C. Salinas-Martinez de Lecea, F. Rodriguez-Reinoso, C. Puente-Ruiz, and A. Linares Solano, *Carbon*, **23**, 91 (1985).
7) J. de D. Casquero-Ruiz, J. M. Guil, J. de D. Lorez-Gonzalez, and A. Ruiz-Paniego, *Carbon*, **26**, 647 (1988).
8) P. J. M. Carrott, R. A. Roberts, and K. S. W. Sing, *Carbon*, **25**, 59 (1987).
9) B. McEnaney, *Carbon*, **25**, 69 (1987).
10) M. M. Dubinin, *Russ. J. Phys. Chem. Engl. Transl.*, **39**, 697 (1965).
11) V. A. Astakhov, M. M. Dubinin, and P. G. Romankov, *Teor. Osn. Khim. Tekhnol.*, **3**, 292 (1969).
12) B. C. Lippens, B. G. Linsen, and J. H. de Boer, *J. Catal.*, **3**, 32 (1964).
13) J. H. de Boer and B. C. Lippens, *J. Catal.*, **3**, 38 (1964).
14) B. C. Lippens and J. H. de Boer, *J. Catal.*, **4**, 319 (1965).
15) R. Sh. Mikhall, S. Brunauer, and E. E. Bodor, *J. Colloid Interface Sci.*, **26**, 45 (1968).
16) S. Brunauer, L. S. Deming, W. S. Deming, and E. Teller, *J. Am. Chem. Soc.*, **62**, 1723 (1940).
17) Y. Eguchi and K. Itoga, *Kagaku-Kogaku*, **35**, 1306 (1971).

Solvent Polarity Parameters of Supercritical Carbon Dioxide as Measured by Infrared Spectroscopy

Yutaka IKUSHIMA,* Norio SAITO, Masahiko ARAI,† and Kunio ARAI††

Government Industrial Research Institute, Tohoku,
Nigatake 4-chome, Miyagino-ku, Sendai 983
† Institute for Chemical Reaction Science, Tohoku University,
Katahira, Aoba-ku, Sendai 980
†† Department of Biochemistry and Chemical Engineering, Tohoku University,
Aramaki, Aoba-ku, Sendai 980
(Received February 27, 1991)

The solvent polarity parameters of supercritical carbon dioxide were determined as a function of the temperature and pressure within the ranges 318—353 K and 5.85—28.5 MPa. An infrared (IR) spectroscopic technique has been employed to determine the values of π^* dipolarity/polarizability and the Lewis basicity parameter B_{MeOD} by measuring the transitions in the IR absorption wavelength of functional groups (such as C=O and O–H···BA, where BA is a hydrogen-bond acceptor), in supercritical carbon dioxide. Ultraviolet/visible (UV/vis) spectroscopy was used to determine the value of the Kamlet–Taft's solvatochromic acidity partameter, α. The B_{MeOD}-value was enhanced with density, but was very small at the temperatures and pressures examined, almost the same as that for hexane. The α-value tended to be dependent on density at lower pressures, but was remarkably smaller compared with those for alcohols. The π^*-value significantly increased with an increase in the density, becoming more negative at higher temperatures above 10 MPa. Furthermore, the $E_T(30)$-value was estimated by using the determined π^*-value. A reliable $E_T(30)$-value for supercritical carbon dioxide has been obtained.

Supercritical carbon dioxide and some other supercritical fluids have recently been attracting much attention concerning their interesting properties for extraction solvents and reaction media.[1-5] When we use cabon dioxide at supercritical conditions, the desired extractions and chemical reactions are expected to be attained at around the ambient temperatures by adjusting the pressures and/or using proper entrainers.[6] In particular, in the near-critical region, the solvent stength varies widely with both the pressure and temperature; this sensitivity in solvent strength could be applied to controling the chemical reaction processes, as well as that of extraction. It is, therefore, be very important to know the solvent strength of supercritical fluids as a function of the pressure, temperature, and/or other variables of state.

For the above-mentioned use of supercritical carbon dioxide to be well effected, its solvent strength should be quantitatively evaluated. The solvent strength has so far been represented by the dipole monent, dielectric constant, refractive index, and solubility parameter.[7-9] When one is interested in the solvent strength at molecular levels, however, these are not adequate, since in these evaluations solvents are regarded as being nonstructured types; solute/solvent interactions, such as hydrogen-bond donor (HBD)/acceptor (HBA) interactions, are not considered, even though they often play dominant roles in many chemical processes.

The variation of the absorption wavelength of a chromophore in IR, NMR, ESR, or UV/vis spectroscopy represents the intermolecular solute–solvent interaction forces,[10-14] and can be used as a good measure of the solvent strength. A few spectroscopic studies have been applied to fluids under supercritical conditions. For example, Johnston et al. measured the solvent strength with the transition energy of a phenol blue indicator in a given solvent by the UV/vis method.[15] Leffler et al. estimated the π^* dipolarity/polarizability of supercritical carbon dioxide using several indicators by the UV/vis method as well.[16] For supercritical carbon dioxide, as well as others, however, the spectroscopic solvent strength is not widely available, since either no convenient polarity parameters could be determined or the precision in measurements and evaluations of its solvent strength was low; the spectroscopic approach is therefore still very much limited at present.

The present work has been aimed at determining the HBD acidity parameter, α; the HBA basicity parameter, B_{MeOD}; and the dipolarity/polarizability parameter, π^*, of carbon dioxide within the range 5.85—28.5 MPa and 318—353 K. In order to consider two or more aspects of solvation, the following multiparameter approach has been presented and shown to be useful:[17]

$$A = A_o + s\pi^* + a\alpha + bB_{MeOD}, \quad (1)$$

where A is a solvent-dependent physicochemical property in a given solvent; A_o is a quantity corresponding to this property in an inert solvent; and the coefficients s, a, b describe the sensitivity to property A. The present study has used FTIR spectroscopy methods to determine the values of B_{MeOD} and π^* as well as UV/vis spectroscopy for the α-value. According to the literature the FTIR method has been only slightly used so far,[18] while many studies have used UV/vis methods.[19-23] In addition, we have attempted to estimate the $E_T(30)$ parameter by using the determined π^*-values. The $E_T(30)$ parameter is one of the polarity parameters

used most widely and possesses great advantages.[24–28] Little is presently known about the $E_T(30)$-values for supercritical fluids.

Experimental

The solvatochromic indicator molecules chosen for the measurements of the π^*-values were methyl acetate (Tokyo Kasei Co., Inc.), cyclohexanone (Merck), acetone (Merck), and *N*,*N*-dimethylformamide (Tokyo Kasei Co., Inc.). As indicators, methanol-*d* CH_3OD (Merck) for Lewis basicity B_{MeOD} and 1-ethyl-4-methoxycarbonylpyridinium iodide (Tokyo Kasei Co., Inc.) and 4-nitroanisole (Tokyo Kasei Co., Inc.) for Lewis acidity α measurements were used. Commercial-grade carbon dioxide (above 99.999%) was used. All chemicals were used without further purification.

Details concerning the experimental apparatus used have been described elsewhere.[6-c] Liquid carbon dioxide was charged into a JASCO Model 880-PU syringe pump through a 1/16-in. tube (1 in.=2.54 cm) and a check valve, and then compressed to the desired pressures. Pressure control was achieved by a back-pressure regulator (Model 880-81, JASCO), which can perform a high-speed flow switching and also control the outlet pressure, irrespective of the mass flow rate of SCF. Then, a 0.2-μL of an indicator was injected using an injection valve (Pheodyne Inc.) which contained a 10-μL sample loop; this made it easy to introduce an indicator into the cell.

The infrared spectrometer used in this study was a JASCO Model FTIR-7300 instrument (Japan Spectroscopic Co., Ltd.) equipped with a narrow-bandwidth mercury cadmium telluride (MCT) detector cooled by liquid nitrogen. The low-frequency cut-off was approximately 800 cm^{-1}. Spectra were acquired at 1 cm^{-1} nominal resolution and interferrograms were accumulated at a rate of 1 scan per 1.2 s. Details concerning the high-pressure IR flow cell used (nominal volume of 16-μL, optical path length of 5 mm, and cross section area of 3 mm^2 were described previously.[6-c] The IR flow cell which was placed in a JASCO Model HC-12 cell heating unit was maintained at temperatures of 318—353±0.5 K. The UV/vis absorption spectra were measured by a Model JASCO MULTI-340 recording spectrometer. The high-pressure cell used for UV/Vis was constructed from stainless steel with quartz windows 1 mm i.d., having a 1-cm path length and a 8 μL nominal total volume. The flow cell was wrapped with heating tape and maintained at a temperature of 318±1 K.

An indicator was passed into the high-pressure flow cell, trapped there by stopping the flow, and the absorption spectrum of the indicator in supercritical carbon dioxide was recorded. Only the spectrum of supercritical carbon dioxide was measured in advance in order to provide a background spectrum. No data manipulation, such as spectral subtraction or base line corrections, was used.

Results and Discussion

Density-Dependence of the HBD Acidity, α. We examined Kamlet–Taft α-value[29] for supercritical carbon dioxide by using the wavenumber (ν_{max}) of the maximum absorbance of 4-nitroanisole in the UV/vis spectrum through the following relationship:

$$Z = 79.6(1 + S) \tag{2}$$

and

$$Z = 2.859 \times 10^{-3}\nu, \tag{3}$$

where S is Brownstein's polarity parameter,[30] Z is Kosower's Z-value,[31] and ν is the charge-transfer band in the UV/vis spectrum of 1-ethyl-4-methoxycarbonylpyridinium iodide. These relations were obtained for a number of solvents and will be applied to supercritical carbon dioxide. This S-value from Eq. 2 is here defined as S_{obs}.

Plots of the S-values for non-hydrogen-bonding solvents against the corresponding ν_{max}-values yielded linear relationship, as expressed by[17]

$$S = -0.0846\nu_{max} + 2.569,$$
$$r = 0.9925,\ \mathrm{SD} = 0.0052,\ \text{and}\ n = 8. \tag{4}$$

Here, r is the correlation coefficient, SD the standard deviation, and n the number of solvents examined. The S-value determined using Eq. 4 is here expressed as S_{cal}, and is evaluated to be

$$\Delta\Delta S = S_{obs} - S_{cal}. \tag{5}$$

The $\Delta\Delta S$-values represent the deviations of the HBD solvents from the correlation line for non-hydrogen-bonding solvents. Furthermore, the solvatochromic displacement ($\Delta\Delta\nu$) attributable to enhanced hydrogen bonding by HBD solvents to the strong HBA Dimroth' betaine dye[32] is related to $\Delta\Delta S$ as follows:

$$\Delta\Delta S = 0.0403\cdot\Delta\Delta\nu + 0.002,$$
$$r = 0.9962,\ \mathrm{SD} = 0.0036,\ \text{and}\ n = 8. \tag{6}$$

Using $\Delta\Delta S$, Kamlet and Taft determined the α-value using the following equation:

$$\alpha = (\Delta\Delta S - 0.002)/(0.0403\cdot 6.24). \tag{7}$$

Figure 1 shows the dependence of the α-value for supercritical carbon dioxide on the density at 318 K. The α-value ranges from the negative values at densities above 0.44 g cm^{-3} to 0.195 at 0.25 g cm^{-3}. The negative α-values at higher densities are assumed to be zero by taking into account errors in the present calculations. The α-value of 0.19 for supercritical carbon dioxide at 0.25 g cm^{-3} is larger than that for acetone (α=0.08),[29] and is comparable to that for acetonitrile (α=0.23).[17] Although the α-values at lower densities show a certain strength of acidity, the α-values are remarkably smaller than those of formamide and alcohols.

Temperature- and Pressure-Dependence of the HBA Basicity, B_{MeOD}. The large solvent-induced shifts of the IR stretching vibrations, $\nu_{X=H}$, do not occur in HBD solvents, but do in the HBA solvents of the Lewis-base type, as shown in Eq. 8:[33,34]

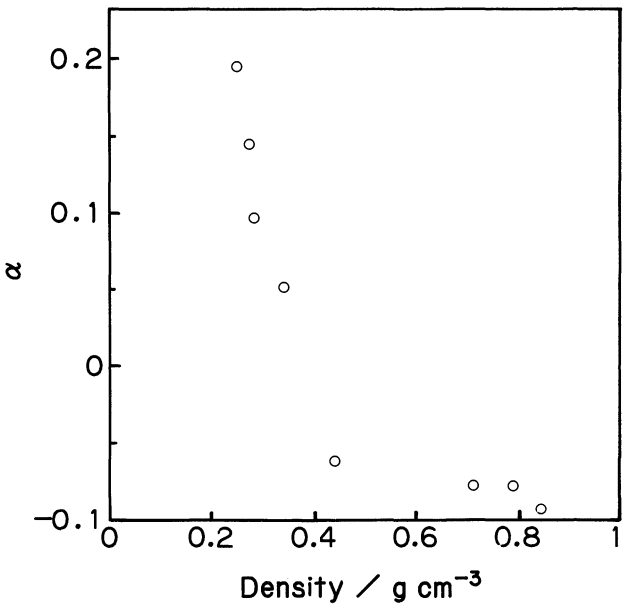

Fig. 1. Plot of α versus density of supercritical carbon dioxide at 318 K.

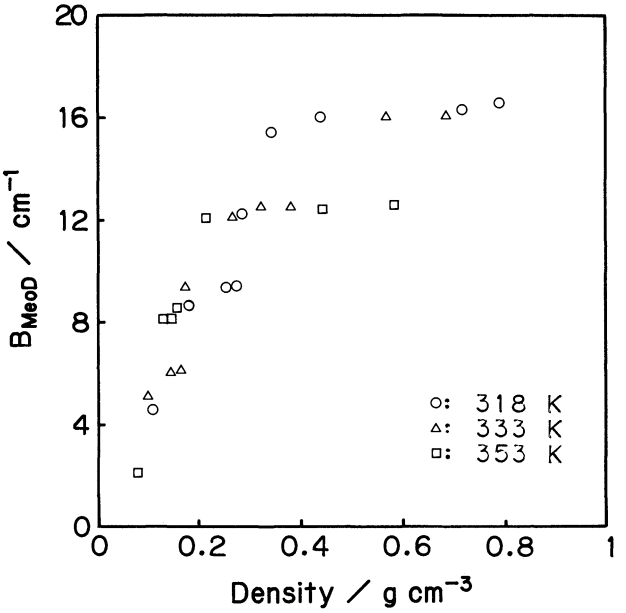

Fig. 2. Plots of B_{MeOD} versus density of supercritical carbon dioxide at (○) 318, (△) 333, and (□) 353 K.

$$R\text{-}O^{\delta\ominus}\text{-}H^{\delta\oplus} + |X\text{-}H \rightleftarrows R\text{-}O^{\delta\ominus}\text{-}H^{\delta\oplus}\cdots X\text{-}H. \quad (8)$$

Here, X=B, C, N, S, etc. In accordance with Eq. 8, the $\nu_{O\text{-}D}$ IR stretching absorption band of methanol-*d* (CH_3OD) undergoes larger bathochromic shifts in less dipolar HBA solvents, compared with those observed in dipolar non-HBA solvents.[35] Thus, a Lewis basicity parameter, B_{MeOD}, has been introduced based on measurements of the O-D IR stretching frequency of CH_3OD, as follows:[36,37]

$$B_{MeOD} = \nu^{\circ}{}_{MeOD} - \nu_{MeOD\cdots B}, \quad (9)$$

where $\nu^{\circ}{}_{MeOD}$ and $\nu_{MeOD\cdots B}$ are the O-D IR stretching frequencies of CH_3OD in the gas phase ($\nu^{\circ}{}_{MeOD}$[36]=2720 cm^{-1}) and in a given solvent, B, respectively. This Lewis basicity parameter, B_{MeOD}, can be linearly correlated well with the Kamlet-Taft parameter, β,[38] with $r>0.98$.[16,29,34] The β- and B_{MeOD}-values for supercritical carbon dioxide can bear the same linear relationship together with a number of organic solvents. Figure 2 indicates the values of B_{MeOD} for supercritical carbon dixide at 318, 333, and 353 K as a function of the density. The B_{MeOD}-value is gradually enhanced as the density increases and reaches 16 cm^{-1} in the range of higher densities above 0.4 g cm^{-3} at 318 and 333 K; the Lewis basicity of supercritical carbon dioxide is found to increase with density. In addition, the B_{MeOD}-value does not seem to show a distinct temperature dependence, except that the values at 353 K are somewhat lower than those at 318 and 333 K at higher densities. The B_{MeOD}-value of hexane is 24 cm^{-1}, the lowest among the organic solvents examined.[35] The B_{MeOD}-value of supercritical carbon dioxide is maximally 16 cm^{-1} under the above-mentioned conditions and is comparable to that of hexane; supercritical carbon dioxide can be regarded as being a non-HBA solvent. The values of β of supercritical carbon dioxide at various densities under constant temperatures of 309—315 K were determined by Leffler et al.[16] based on solvent shifts of the absorption of 4-nitroaniline and *N*,*N*-diethyl-4-nitroaniline. It was reported that since all of the values are either zero or near to zero, the Lewis basicity of supercritical carbon dioxide is negligibly small. However, the density-dependence of the Lewis basicity (as described above) could not be confirmed by the UV/vis method.

Temperature- and Pressure-Dependence of the Dipolarity/Polarizability Parameter, π^*. As shown above, the α-value of supercritical carbon dioxide is very small at densities larger than 0.3 g cm^{-3}. The B_{MeOD}-value is also small at densities lower than 0.2 g cm^{-3} and, even at higher densities, is smaller compared to that of hexane, a low HBA basic solvent.[34] In the following treatment, therefore, the contribution of the HBD acidity and HBA basicity to the solvent properties of supercritical carbon dioxide will not be taken into consideration. Strict treatment is now in progress, including those two parameters, evaluating coefficients *a* and *b* for them in Eq. 1. Eq. 1 can be thus be approximated by Eq. 10 (with $A=\nu$), reducing to

$$\nu = \nu_o + s\pi^*. \quad (10)$$

Here, ν is the frequency of a chromophore in supercritical carbon dioxide. The *s*-values for several indicators have previously been determined.[39-43] The *s*-values for

the C=O stretching frequencies of cyclohexanone, acetone, *N*,*N*-dimethylformamide, and methyl acetate chosen as indicators in the present work are −18.90±0.50, −12.15±0.38, −22.80±0.75, and −15.36±0.73, respectively. The values of ν_0 can also be quoted from the literature.[40-43] One can determine the change in the π^*-value of supercritical carbon dioxide as a function of the temperature and pressure by using Eq. 10 along with the *s*- and ν_0-values.

Figure 3 shows the dependence of the π^*-values on the density of supercritical carbon dioxide at temperatures of 318, 333, and 353 K. The mean values of the π^*-values measured for the four indicators are plotted in those figures. Figure 3 includes the value obtained by Essfar et al.[44] for a vacuum at temperatures between 278 and 345 K. The π^* vs. density plot at each temperature is extrapolated to the intercept with the vacuum system. The intercept at 318, 333, and 353 K calculated by a first-order least-squares method give values of −1.03, −0.95, and −1.17, respectively; the mean is −1.05 and agrees closely with a π^*-value of −1.06±0.10 for a vacuum, obtained by Essfar et al.[44] Furthermore, the extrapolated π^*-values determined at different temperatures are the same within the experimental errors, indicating the insensitivity of π^* to the temperature. The π^*-values for supercritical carbon dioxide from shifts of the absorption maxima of several kinds of indicators in the UV/vis spectra have been reported in the literature; the π^*-values for carbon dioxide at 6.89 MPa and 315 K estimated by Hyatt[45] using dyes as indicators are −0.52 to −0.60, and are close to our π^*-value of −0.40 at 6.86 MPa and 318 K. With regard to the effect of the temperature on π^*, the values at 317 and 335 K and 10 MPa measured by Yonker and Smith[46] using 2-nitroanisole are −0.18 and −0.42, respectively; our values at 318 and 333 K and at 9.81 MPa are −0.15 and −0.38, respectively, in good agreement with their results within experimental errors. These show a high reliability in the measurements of the π^*-values for supercritical carbon dioxide by our IR method. The average π^*-values for carbon dioxide at different pressures, and around 313 K using ten indicators, were reported by Leffler;[16] these are also plotted with error ranges in Fig. 3. It has been found that the discrepancy in π^* due to the indicators in this UV/vis method is remarkably larger compared with that in our IR method. This might be because, in this work, the shifts for the C=O stretching vibrations of indicators are used for determining the π^*-values, and the diffence in the degree of C=O dipolarity among the indicators (which reflects the relative contribution of the two mesomeric forms) is less than that in the UV/vis method using entirely different types of indicator molecules.

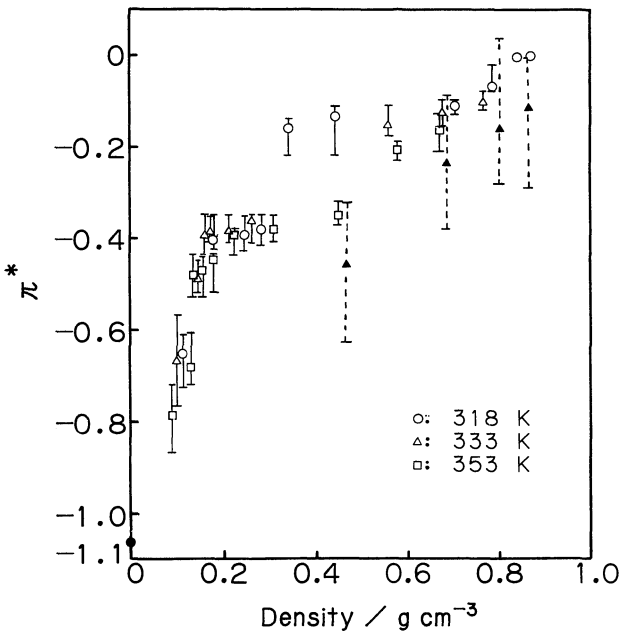

Fig. 3. Plots of π^* versus density for supercritical carbon dioxide at (○) 318, (△) 333, and (□) 353 K. The mean values of the data are plotted by the symbols ○, △, □ and the bars given are the data ranges: ●, π^* for vacuum at temperatures between 298 and 345 K determined by Essfar.[44] ⊢−▲−⊣, the mean π^*-values with error ranges measured at 309—315 K by Leffler.[16]

As shown in Fig. 3, the π^*-value decreases from a value near to zero (or zero) to a more negative value as the density decreases; it becomes more negative at higher temperatures in the range above about 10 MPa. From Fig. 3, irrespective of the temperature, the π^*-value decreases with a decrease in the density. The π^*-values of supercritical fulids have previously been reported to be dependent on the density, but not on temperature;[47] this agrees with the present result given in Fig. 3.

Estimation of the $E_T(30)$-Value. The $E_T(30)$ parameter has been shown to be related to the polarization of solvent molecules through linear relationships using the Kirkwood function and the Onsager reaction field function,[48] while the transition energy for the dissolved betaine dye has been demonstrated to have a linear dependence on the Kamlet-Taft's parameters.[29] According to Bekárek,[48] the $E_T(30)$-values for a set of 24 solvents including nonpolar liquids can be correlated with the π^* parameter, the Kirkwood function $[f(\varepsilon)=(\varepsilon-1)/(2\varepsilon+1)]$, and the Onsager reaction field function $[f(n^2)=(n^2-1)/(2n^2+1)]$ by Eq. 11:

$$E_T(30) = 31.84 + 10.61\pi^* f(\varepsilon)/f(n^2) - 10.85\pi^*,$$
$$r = 0.984, \text{ and } SD = 0.86. \quad (11)$$

Using the π^*-values determined in the present work in the above relationship, one can calculate the value of $E_T(30)$ of supercritical carbon dioxide as a function of the temperature and pressure. The refractive index and the dielectric constant for supercritical carbon dioxide as a function of the temperature and pressure can be determined from the Lorents-Lorenz equation and a virial expansion of the Clausius-Mossotti function with

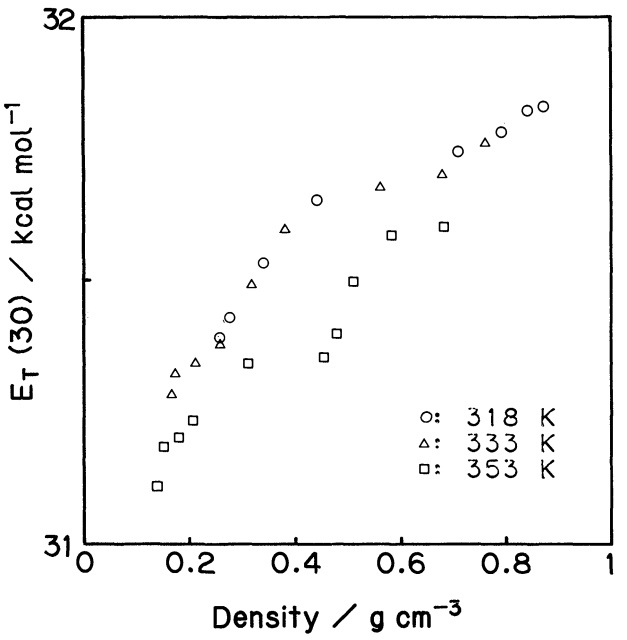

Fig. 4. Relationship between $E_T(30)$-values estimated by Eq. 11 and density of supercritical carbon dioxide at (○) 318, (△) 333, and (□) 353 K.

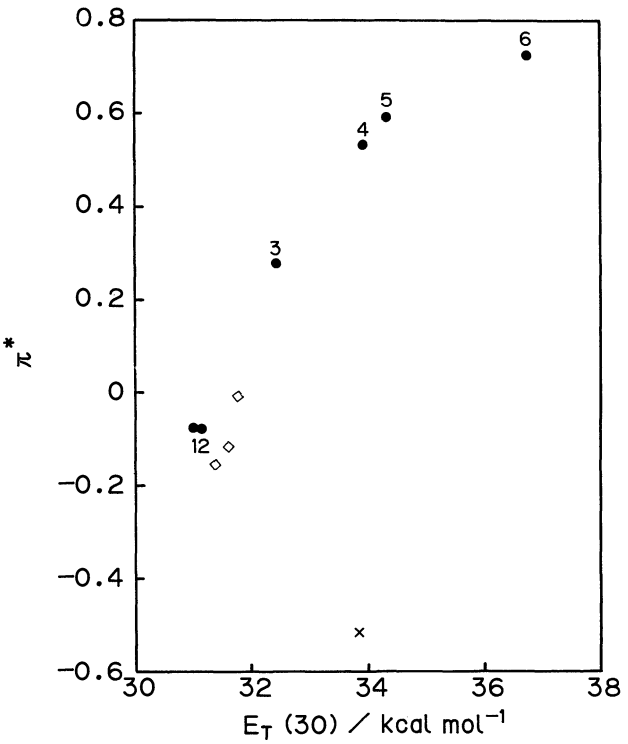

Fig. 5. Relationship between $E_T(30)$- and π^*-values[29] for 1, hexane; 2, heptane; 3, tetrachloromethane; 4, toluene; 5, benzene; 6, chlorobenzene; ◇, supercritical carbon dioxide at 318 K estimated in this work; ×, supercritical carbon dioxide at 297 K and 6.9 MPa reported by Hyatt.[45]

respect to density, respectively:

$$(n^2 - 1)/(n^2 + 2) = A_R\rho_m + B_R\rho_m^2 + \cdots \quad (12)$$

and

$$(\varepsilon - 1)/(\varepsilon + 2) = A_E\rho_m + B_E\rho_m^2 + \cdots, \quad (13)$$

where ρ_m is the molar density; A_R and B_R the first and second refractivity virial coefficients, respectively; and A_E and B_E the first and second dielectric virial coefficients, respectively.[49,50] The refractivity (A_R, B_R) and dielectric virial coefficients (A_E, B_E) for carbon dioxide have been reported by Bose and St-Arnaud[49] and Johnston and Cole.[50] The refractive index and the dielectric constant determined by substituting the corresponding virial coefficients into Eqs. 12 and 13 are used for calculating $f(n^2)$ and $f(\varepsilon)$ for supercritical carbon dioxide.

Figure 4 shows the $E_T(30)$-values for supercritical carbon dioxide at 313, 333, and 353 K as a function of the density. The $E_T(30)$-value increases with an increase in the density, and seems to be not much dependent on the temperature, although in the range of about 0.4—0.6 g cm^{-3} the $E_T(30)$-values at 353 K are only slightly lower, compared with those at 318 and 333 K.

Figure 5 shows the relationship between the π^*- and $E_T(30)$-values for solvents that have very low HBD acidities and HBA basicities (α, $\beta<0.1$), including supercritical carbon dioxide. The $E_T(30)$-values for supercritical carbon dioxide are linked to the relationship for the other solvents, as shown in Fig. 5; the $E_T(30)$-values for supercritical carbon dioxide estimated by the present method are believed to be both reasonable and reliable results. Although the $E_T(30)$-value for supercritical carbon dioxide at 6.9 MPa and 297 K (estimated by Hyatt[45]) is 33.8 kcal mol^{-1}, supercritical carbon dioxide scarcely contains a hydrogen-bonding contribution; in Figure 5 the $E_T(30)$-value (given as symbol (×)) seems to be only slightly greater than that expected from the π^*-values of −0.07[46]—−0.20[16] of supercritical carbon dioxide determined at around 6.9 MPa and 297 K. The reason for this discrepancy is unknown.

Conclusions

Although the B_{MeOD}-value increases with density, the value is very small and almost the same as that for hexane. The α-value is also relatively small, although it tends to increase with a decrease in the density in the range below 0.44 g cm^{-3}. The π^*-values of supercritical carbon dioxide at 5.85—28.5 MPa and 318—353 K are determined using the displacements of the IR stretching frequencies of the same chromophore of the four indicators based on the assumption that the B_{MeOD}- and α^*-values are negligibly small. The π^*-value become more negative as the pressure decreases. The π^*-value decreases with temperature above 10 MPa, but is scarcely dependent on the temperature at lower pressures. The

π^*-value deterrmined by the IR method is found to be highly reliable and the discrepancy in the π^*-values due to the indicators in this IR method have the advantage of being smaller than that in the UV/vis method. The $E_T(30)$-values for supercritical carbon dioxide have been estimated by using the π^*-values determined in this study as well as the $f(\varepsilon)$ and the $f(n^2)$ functions. The $E_T(30)$-value increases with an increase in density. The $E_T(30)$-value can be well-correlated with the π^*-value together with other nonpolar organic solvents, and the estimated $E_T(30)$-values are believed to be reliable.

References

1) S. Kim and K. P. Johnston, *Chem. Eng. Commun.*, **63**, 49 (1988).
2) K. Arai and S. Saito, *J. Jpn. Oil Chem. Soc.*, **35**, 267 (1986).
3) N. Saito, Y. Ikushima, and T. Goto, *Bull. Chem. Soc. Jpn.*, **63**, 1532 (1990).
4) M. E. Paulaitis and G. C. Alexander, *Pure Appl. Chem.*, **59**, 61 (1987).
5) T. G. Squires, C. G. Venier, and T. Aida, *Fluid Phase Equilib.*, **10**, 261 (1983).
6) a) Y. Ikushima, N. Saito, and M. Arai, *Bull. Chem. Soc. Jpn.*, **64**, 282 (1991). b) Y. Ikushima, S. Ito, T. Asano, T. Yokoyama, N. Saito, K. Hatakeda, and T. Goto, *J. Chem. Eng. Jpn.*, **23**, 96 (1990). c) Y. Ikushima, N. Saito, K. Hatakeda, S. Ito, and T. Goto, *Chem. Lett.*, **1989**, 1707. d) Y. Ikushima, N. Saito, and T. Goto, *Ind. Eng. Chem. Res.*, **28**, 1364 (1989).
7) E. G. McRae, *J. Phys. Chem.*, **61**, 562 (1957).
8) A. F. M. Barton, *Chem. Rev.*, **75**, 731 (1975).
9) G. Allen, G. Gee, and G. J. Wilson, *Polymer*, **1**, 456 (1960).
10) A. E. Lutskii, V. V. Prezhdo, L. I. Degtereva, and V. G. Gordienko, *Usp. Khim.*, **51**, 1398 (1982).
11) C. N. R. Rao, S. Singh, and V. P. Senthilnathan, *Chem. Soc. Rev.*, **5**, 297 (1976).
12) M. C. R. Symons, *Chem. Soc. Rev.*, **12**, 12 (1983).
13) H. E. Hallam, "Infrared Spectroscopy and Molecular Structure," Elsevier, Amsterdam (1963), Chap. XII.
14) M. D. Joesten and L. J. Schaad, "Hydrogen Bonding," Dekker, New York (1974).
15) S. Kim and K. P. Johnston, *Ind. Eng. Chem. Res.*, **26**, 1206 (1987).
16) M. E. Sigman, S. M. Lindley, and J. E. Leffler, *J. Am. Chem. Soc.*, **107**, 1471 (1985).
17) R. W. Taft and M. J. Kamlet, *J. Am. Chem. Soc.*, **98**, 2886 (1976).
18) J. P. Blitz, C. R. Yonker, and R. D. Smith, *J. Phys. Chem.*, **93**, 6661 (1989).
19) E. W. Kosower and M. Mohammad, *J. Am. Chem. Soc.*, **93**, 2713 (1971).
20) H. Langhals, *Tetrahedron Lett.*, **27**, 339 (1986).
21) M. C. Rezende, D. Zanette, and C. Zucco, *Tetrahedron Lett.*, **25**, 3423 (1984).
22) M. J. Kamlet, R. M. Doherty, M. H. Abraham, P. W. Carr, R. F. Doherty, and R. W. Taft, *J. Phys. Chem*, **91**, 1996 (1987).
23) P. Nicolet and C. Laurence, *J. Chem. Soc., Perkin Trans. 2*, **1986**, 1071.
24) C. Reichardt and E. Harbusch-Gornert, *Liebigs Ann. Chem.*, **1983**, 721.
25) C. Laurence, P. Nicolet, M. Lucon, and C. Reichardt, *Bull. Soc. Chim. Fr.*, **1987**, 1001.
26) T. M. Krygowski, P. K. Wrona, U. Zielkowska, and C. Reichardt, *Tetrahedron*, **41**, 4519 (1985).
27) B. P. Johnson, M. G. Khaledi, and J. G. Dorsey, *J. Chromatogr.*, **384**, 221 (1987).
28) H. Elias, G. Gumbel, S. Neitzel, and H. Z. Volz, *Anal. Chem.*, **52**, 240 (1981).
29) M. J. Kamlet, J. L. Abboud, M. H. Abraham, and R. W. Taft, *J. Org. Chem.*, **48**, 2844 (1983).
30) S. Brownstein, *Can. J. Chem.*, **38**, 1690 (1960).
31) E. M. Kosower, "An Introduction to Physical Organic Chemistry," Wiley, New York (1968), p. 293.
32) K. Dimroth, C. Reichardt, T. Siepmann, and F. Bohlmann, *Liebigs Ann. Chem.*, **1**, 661 (1963).
33) L. J. Bellamy, H. E. Hallam, and R. L. Williams, *Trans. Faraday Soc.*, **54**, 1120 (1958).
34) H. E. Hallam, *J. Mol. Struct.*, **3**, 43 (1969).
35) A. G. Burden, G. Collier, and J. Shorter, *J. Chem. Soc., Perkin Trans. 2*, **1976**, 1627.
36) I. A. Koppel and J. B. Koppel, *Org. React. (Tartu)*, **20**, 523 (1983).
37) J. Shorter, "Advances in Linear Free Energy Relationships," Plenum Press, London and New York (1972), Chap. 5.
38) M. J. Kamlet, J. L. Abboud, and R. W. Taft, *J. Am. Chem. Soc.*, **99**, 6027 (1977).
39) A. Allerhard and P. V. R. Schleyer, *J. Am. Chem. Soc.*, **85**, 374 (1963).
40) L. J. Bellamy, C. P. Conduit, R. J. Pace, and R. L. Williams, *Trans. Faraday Soc.*, **55**, 1677 (1959).
41) N. Oi and J. F. Coetzee, *J. Am. Chem. Soc.*, **91**, 2473 (1969).
42) K. C. James and M. Ramgoolan, *Spectrochim. Acta, Part A*, **31**, 599 (1975).
43) L. J. Bellamy and R. L. Williams, *Trans. Faraday Soc.*, **55**, 14 (1959).
44) M. Essfar, G. Cuiheneaf, and J. C. M. Abboud, *J. Am. Chem. Soc.*, **104**, 6786 (1982).
45) J. A. Hyatt, *J. Org. Chem.* **49**, 5097 (1984).
46) C. R. Yonker and R. D. Smith, *J. Phys. Chem.*, **92**, 2374 (1988).
47) C. R. Yonker, S. C. Frye, P. R. Kalkuaf, and R. D. Smith, *J. Phys. Chem.*, **90**, 3022 (1986).
48) V. Bekárek and J. Jurina, *J. Collect. Czech. Chem. Commun.*, **47**, 1060 (1982).
49) J. M. St-Arnaud and T. K. Bose, *J. Chem. Phys.*, **68**, 2129 (1978).
50) D. R. Johnston and R. H. Cole, *J. Chem. Phys.*, **36**, 318 (1961).

Computational Studies of the Isomerization Pathways of Isocyanic Acid HNCO

Keiichi YOKOYAMA, Shin-ya TAKANE, and Takayuki FUENO*
Department of Chemistry, Faculty of Engineering Science, Osaka University, Toyonaka, Osaka 560
(Received April 18, 1991)

Paths of isomerizations of isocyanic acid HNCO into various chain isomers via ring intermediates have been investigated by ab initio MO calculations with the MRD-CI procedure employing the 6-31G** basis sets. Geometry optimizations were accomplished at the RHF, UHF, or CASSCF level of theory. It is found that the isomerization from HNCO to cyanic acid HOCN is energetically the most favorable and that it should proceed via successive 1,2-hydrogen migrations rather than by a single 1,3-hydrogen migration. The overall barrier height is calculated to be 423 kJ mol^{-1}, which is ca. 60 kJ mol^{-1} higher than the critical energy for the main decomposition channel, HNCO→NH($^3\Sigma$)+CO. Implications of the results to the kinetics of the thermal decompostion of HNCO at high temperatures are discussed.

Isocyanic acid HNCO decomposes mainly into NH ($^3\Sigma$)+CO in the temperature region above 2000 K.[1-3] Another bond dissociation channel to produce H+NCO has been reported to contribute by less than 5% to the total HNCO consumption.[3] In addition to these two dissociation channels, we observed an indication of the occurrence of an apparent "direct" decomposition leading to CN+OH at higher temperatures.[4]

	$\Delta H°_0$/kJ mol^{-1}	
HNCO + M → NH($^3\Sigma^-$) + CO + M	361	(1a)
→ H + NCO + M	474	(1b)
→ CN + OH + M	574	(1c)

This last process must involve an initial isomerization of HNCO into HOCN or HONC. Characteristics of the saddle points for the isomerizations are of particular interest in this connection.

Potential energy surfaces for various isomers of the four-atomic HCNO entity were first studied by Poppinger, Radom, and Pople[5] using ab initio MO calculations at the RHF/4-31G level of theory. Their study has revealed that the surfaces are complicated with many potential wells corresponding to various chain isomers and ring isomers. Thus, a number of isomerization pathways would have to be considered in order to clarify the dynamical mechanism of reaction (1c).

The isomerizations we will consider in the present work include the following:

HNCO → $\overline{\text{HCON}}$ → HOCN	(2a)
→ HONC	(2b)
→ HCNO	(2c)
HNCO → $\overline{\text{HNCO}}$ → HOCN	(2d)

where both $\overline{\text{HCON}}$ and $\overline{\text{HNCO}}$ denote ring structures while the remaining species are chain isomers. Theoretical assessments of the relative eases of the various isomerization processes at the split-valence+polarization+correlation level are the principal concern of this work.

Method

Geometry optimizations for the minimum energy structures and the saddle points were carried out by the SCF procedure with the energy gradient technique. For a ring intermediate and the relevant transition states(TS), the complete-active-space (CAS) SCF procedure was utilized.

At all the stationary points located, the multi-reference single- and double-excitation (MRD) configuration-interaction (CI) calculations were carried out to obtain the electronic correlation energy. For singlet state the configurations whose contributions $|c_i|^2$ to a state exceed 0.25% were all regarded as the main (reference) configurations. In the case of triplet states, however, we were obliged to loosen the weight limit to $|c_i|^2$=1.0% because of otherwise too many configurations selected for handling properly. Triplet state energies might thus be somewhat inaccurate. At any rate, the lowest configuration-selection threshold T was deliberately assigned a value between 1 and 30 μhartree, so that the maximal dimension of the configurational space fell in the region 7000—9000. Four successive threshold values increasing stepwise by 5 μhartree each were used to obtain the CI energy extrapolated to T=0 hartree. Further, the generalized Langhoff-Davidson approximation[6,7] was used to correct for possible errors which might arise from the use of a limited number of reference configurations. The CI energies thus corrected are regarded as estimates of full CI values,[7,8] which will be denoted as E_{CI}. The iterative natural-orbital CI method was applied occasionally with two or three cycles at each state.

All calculations were done by using the 6-31G** basis set. The Gaussian 86[9] and HONDO7[10] programs were used for SCF optimization calculations, and the TABLE

MRD-CI program furnished by Buenker[11,12] was used for CI calculations.

Results

(A) Chain Isomers. For molecular entities constituted of one each of the H, C, N, and O atoms, several isomeric structures are conceivable. Under the constraint that the H atom is attached to the terminal heavy atom (C, N, or O), one can anticipate six chain structures as follows:

HNCO	HOCN	HCNO
1	**2**	**3**
HNOC	HONC	HCON
6	**4**	**5**

Preliminary STO-3G calculations have shown that the entities **1**—**4** indeed possess the restricted Hartree–Fock (RHF) SCF minima at their respective chain structures. By contrast, the entity **6** is liable to dissociate into NH+CO, and the entity **5** tends to cyclize into the form HCON upon geometry optimizations. Although the four chain isomers have already been the matter of thorough investigations by Teles et al.,[14] we also treat these molecules here for the sake of quantitative considerations of the potential energy profiles for isomerizations.

Geometries of the four chain isomers **1**—**4** optimized by the restricted Hartree–Fock (RHF) SCF procedure employing the 6-31G** functions are shown in Fig. 1. Their energies at the RHF and MRD-CI levels are listed in Table 1. HNCO (**1**, isocyanic acid) is a well-known stable entity, and HCNO (**3**, fulminic acid) has been recognized as an isomer that can exist in the gas phase. However, HOCN (**2**, cyanic acid) and HONC (**4**, isofulminic acid) have been observed only in the rare gas matrices.[14,15] The relatively low total energy calculated for **2** suggests the possibility that it could be detected in the gas phase. The quasi-degeneracy noted between **3** and **4** at the RHF SCF level is released at the CI level. The relative energies deduced by the present CI calculations agree reasonably well with the coupled-

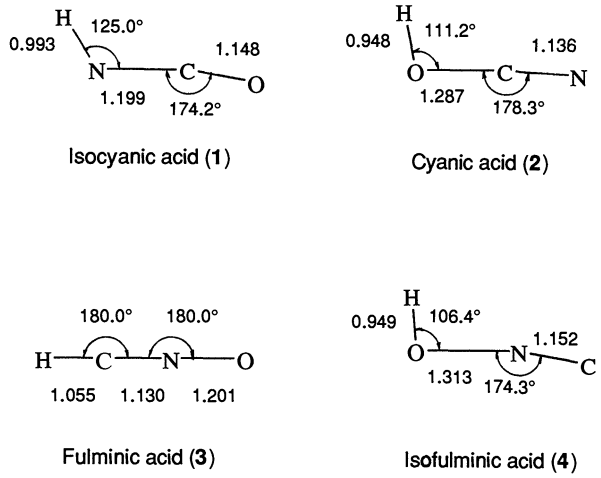

Fig. 1. Optimized geometries of the chain isomers. The bond lengths are given in units of Å.

Table 1. Total and Relative Energies of the HNCO Chain Isomers

Isomer	Energy / hartree		Relative energy / kJ mol^{-1}		
	E_{RHF}+167	E_{CI}+168	ΔE_{RHF}	ΔE_{CI}	ΔE_{CCD}[a]
HNCO (**1**)	−0.76602	−0.24780	0	0	0
HOCN (**2**)	−0.72902	−0.21125	97	96	88
HCNO (**3**)	−0.63260	−0.12193	350	331	308
HONC (**4**)	−0.63273	−0.10221	350	382	340

a) The CCD (coupled-cluster, double-excitation) energy reported by Teles et al.[14]

Table 2. Comparisons of the Dissociation Energies (kJ mol^{-1}) of HNCO Calculated by the MRD-CI Method with the Thermochemical Data

Products	Calcd			Expt[a]	
	E_{CI}+167 / hartree	ΔE_{CI} / kJ mol^{-1}	D_0[b] / kJ mol^{-1}	ΔH_0° / kJ mol^{-1}	ΔH_{3000}° / kJ mol^{-1}
NH($^3\Sigma^-$)+CO	−1.11296	354	332	361	359
H+NCO	−1.06639	476	447	474	496
NH($^1\Delta$)+CO	−1.04531	532	510	512	510
CN+OH	−1.02094	596	576	574	366
CH+NO	−0.93877	811	785	779	786

a) Based on the "JANAF Thermochemical Tables."[16] b) Corrected for the vibrational zero-point energy.

cluster double-excitation (CCD) energies reported by Teles et al.[14]

The dissociation energies D_0 calculated for HNCO (**1**) in particular are listed in Table 2, together with the experimental enthalpy change, ΔH°_0.[16] Zero-point energy corrections were made by use of the experimental vibrational frequencies.[16] Theoretical dissociation energies D_0 are in fairly good agreement with the experimental ΔH°_0 values.

(B) Ring and Branched Isomers. For the entities **5** and **6**, we took a step further to carry out the perfect-pairing multi-configuration (PPMC) SCF calculations[13] with the STO-3G basis set. The active space included eight orbitals accommodating six electrons (8,6) with only double excitations permitted.

In the PPMC/STO-3G optimization for the entity HCON (**5**), use of the initial RHF MO's gave an apparent ring structure, whereas use of the initial guess molecular orbital (MO) coefficients prepared from a UHF solution (diradical type MO's) resulted in a curious ring-like structure in which the OCN angle exceeded 90°. The latter form may be visualized as a "branched" structure. The discrepancy is probably because of an unavoidable incompleteness in the configuration space utilized rather than due to the presence of two hardly distinguishable electronic states.

In the RHF/6-31G** optimization of **5**, no ring isomer has been found. All initial guess geometries we tried led to the potential well of HNCO (**1**). The tendency is similar to that reported by Poppinger et al. using the 4-31G basis set.[5] On the other hand, the UHF/6-31G** optimization has given a branched structure with the OCN angle being 123.5°. The branched isomer is strongly spin-polarized and its eigenvalue of the $\hat{S}^2$ operator is $S^2=1.16$, indicative of a strong diradical character. The two odd electrons are localized mainly on the in-plane orbitals of the O and N atoms.

In order to settle this problem, we performed CASSCF/6-31G** optimization in which four frontier orbitals were invoked for four electrons (4,4) to be accommodated. Both the diradical and the closed-shell type MO coefficients were used as initial guess. As a result, the optimized geometries have proved to be identical, showing a structure intermediate between the ring the the branched forms. The electronic structure found is such as described with two major configurations, one being of the diradical type while the other, the closed-shell type:

$$\cdots(1a'')^2(8a')^2(2a'')^2(9a')^1(10a')^1,$$

$$\cdots(1a'')^2(8a')^2(2a'')^2(9a')^2.$$

Their CI coefficients are 0.84 and −0.46, respectively.

Figure 2 shows the structure for HCON (**5**) in its electronic ground state optimized by the CASSCF(4,4) procedure assuming Cs symmetry. The remarkable feature is that its OCN angle is 94.1°, with the O–N bond index of ca. 0.5. These values indicate that **5** in its ground state takes a "half-ring structure". The normal ring species called oxazirine, which was proposed as a reaction intermediate in matrix experiments,[17,18] has still been unknown. We will here refer to the half-ring isomer as "oxazirine" and simply regard it as a ring isomer.

Table 3 lists the geometric parameters and the CI energies for the ground-state oxazirine (**5**) and its three excited states. All these excited states are low-lying and have branched structures with the OCN angle of ca. 120°. Both the $^3A''$ and $^1A''$ states to be regarded as formylnitrene have their odd electrons in the nearly degenerate in-plane and out-of-plane p orbitals of the N atom.

The ring isomer in which the H atom is attached to the N atom, HNCO (**7**, oxaziridinylidene), was suggested by

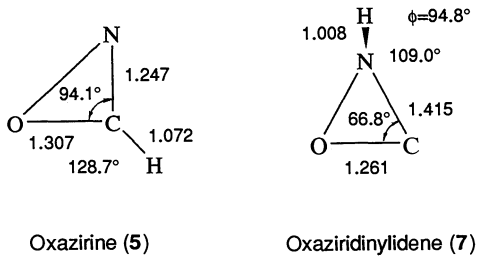

Oxazirine (**5**) Oxaziridinylidene (**7**)

Fig. 2. Optimized geometries of the isomers. The bond lengths are given in units of Å. ϕ indicates the dihedral angle ϕ_{HNCO}.

Table 3. Geometries and Energies of the Cyclic HNCO Isomers

State	Geometry					Energies		
	R_{OC}	R_{CN}	R_{CH}	A_{OCN}	A_{OCH}	$E_{UHF}+167$	$E_{CI}+168$	ΔE_{CI}[a]
	Å	Å	Å	degree	degree	hartree	hartree	kJ mol^{-1}
HCON (**5**)								
$^1A'$	1.307	1.247	1.072	94.1	128.7	−0.70142[b]	−0.11767	342
$^3A''$	1.236	1.354	1.085	120.8	121.8	−0.69776	−0.09085	412
$^1A''$	1.253	1.326	1.083	121.2	121.2	−0.66954	−0.08716	422
$^3A'$	1.333	1.251	1.086	126.2	111.7	−0.66866	−0.06582	478
HNCO (**7**)	1.261	1.415	1.008[c]	66.8	109.0[d]	−0.58786[e]	−0.05575	504

a) Relative to HNCO (**1**). b) CAS(4,4) energy. c) R_{NH}. d) A_{HNC}. e) RHF energy.

Poppinger et al.[5] We have confirmed that it lies in a potential well on the RHF/6-31G** surface as well. It has a nonplanar structure with the HNCO dihedral angle ϕ=94.8°, as can be seen in Fig. 2. Its CI energy is listed in Table 3. The high energy value (504 kJ mol^{-1} relative to HNCO) makes us suspect that the potential well will be shallow. The situation will be clarifed with the results of MRD-CI calculation for the transition state of its ring opening reaction to form HNCO (**1**).

(C) Isomerizations. We examined four isomerization pathways (2a)—(2d). All these pathways from HNCO (**1**) consist of two steps involving a cyclic intermediate **5** or **7**. We denote the transition state of the cyclization of **1** to **5** as TS1. The transition states from **5** to **2**, **3**, and **4** will be denoted as TS2, TS3, and TS4, respectively. TS5 stands for the transition state for the ring-closure of **1** giving **7**, and TS6 for that of the path from **7** to **2**. All these elementary steps involved are diagrammatically illustrated in Fig. 3.

Since neither UHF nor RHF calculation can describe the electronic state of **5** properly, we have carried out CASSCF(6,10) optimizations to determine the geometries of TS1 and TS2. The geometries obtained are shown in Fig. 4. TS2 on the UHF surface was also examined for the sake of comparison with the CASSCF geometry. It can be seen that the goemetry of TS2 is sensitive to the extent of assessment of correlation energy. Either way, TS2 is structurally more HOCN(**2**)-like than is TS1. TS1 is more HNCO(**1**)-like, as it should be.

Strictly speaking, TS2 was found to be slightly nonplanar at the CASSCF level, the dihedral angle ϕ (HNCO) being 0.5°. Since vibrational analysis at the CASSCF level is a formidable task, we carried out the analysis by the UHF procedure at the planar TS2 (UHF) geometry, to confirm a single imaginary frequency being 2362i cm^{-1}. Assumption of the Cs symmetry for TS2 will cause no serious error.

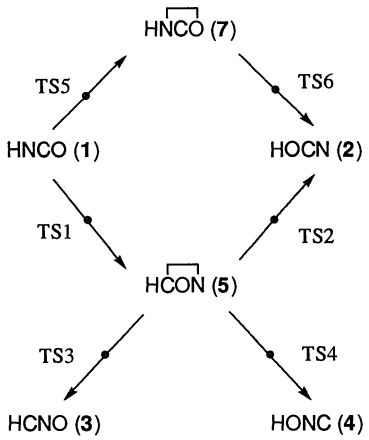

Fig. 3. Isomerization pathways of HNCO (**1**). TS 1—6 denote the SCF saddle points on the isomerization pathways indicated with arrows.

TS3 and TS4 are responsible for the formations of **3** and **4**, respectively, from the cyclic intermediate **5**. Their geometries obtained by the RHF SCF procedure are shown in Fig. 4.

The remaining transition states, TS5 and TS6, are related to the isomerization of **1** to **2** via the cyclic intermediate **7**. The first saddle point, TS5, was found only on the UHF surface and its geometry (Fig. 4) proved to closely resemble that of **7**. On the contrary, TS6 was found on the RHF surface. Its geometry is also shown in Fig. 4. Both TS5 and TS6 were confirmed to have a single imaginary frequency of vibration.

All the transition state structures, TS1 through TS6, were then subjected to the MRD-CI calculations. The CI energies obtained are summarized in Table 4. The relative energies ΔE_{CI} are the values expressed by taking HNCO (**1**) as the common standard.

Figure 5 diagrammatically illustrates the calculated potential energy profiles for all the isomerization pathways considered here. It is apparent that the most favorable isomerization pathway of HNCO (**1**) is reaction (2a), which proceeds through the cyclic intermediate HCON (**5**) to give HOCN (**2**). In a sense, it is a suc-

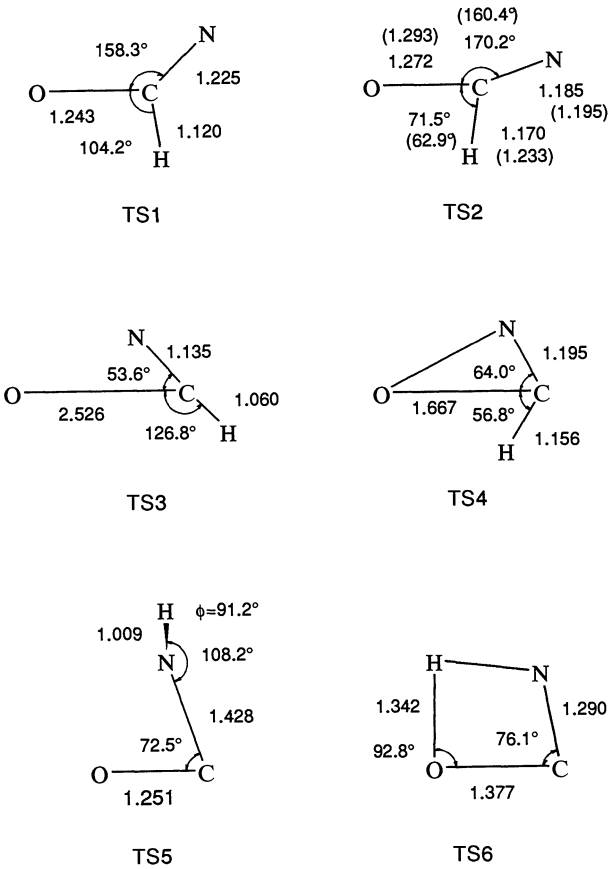

Fig. 4. Optimized geometries of the transition states for isomerizations. The bond lengths are given in units of Å. The figures given in parentheses for TS2 are the bond lengths and angles obtained by the UHF SCF procedure.

Table 4. MRD-CI Energies for the Transition States of Various Isomerizations

TS	Reaction	Method	E_{SCF}+167 / hartree	E_{CI}+167 / hartree	ΔE_{CI}[a] / kJ mol^{-1}
TS1	**1**→**5**	CAS (6,10)	−0.63668	−1.11305	354
TS2	**5**→**2**	CAS (6,10)	−0.62758	−1.08653	423
TS3	**5**→**3**	RHF	−0.54022	−0.98838	681
TS4	**5**→**4**	RHF	−0.50022	−1.00423	639
TS5	**1**→**7**	UHF	−0.58488	−1.05843	497
TS6	**7**→**2**	RHF	−0.51115	−1.00929	626

a) Relative to HNCO (**1**).

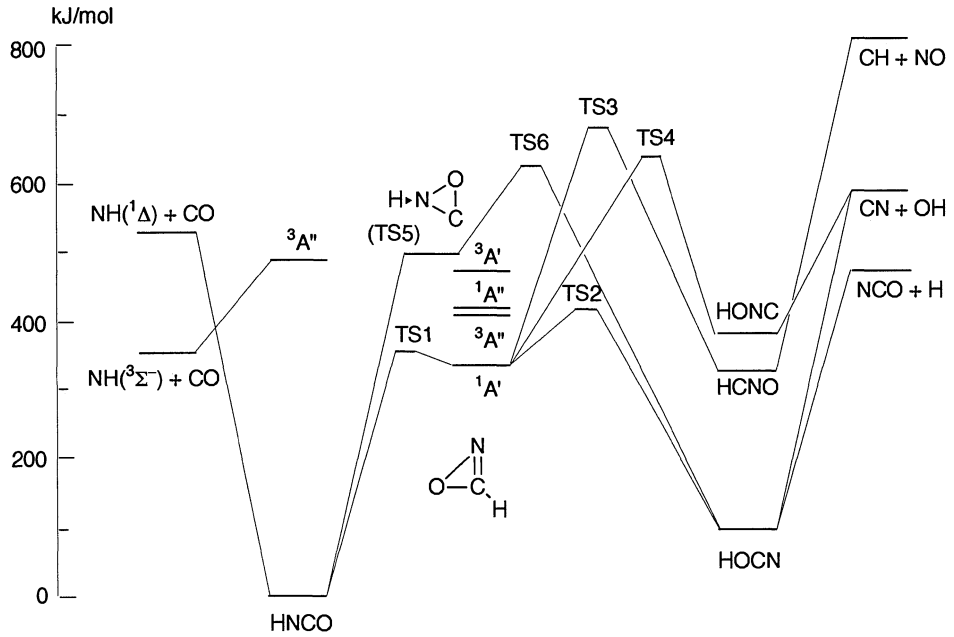

Fig. 5. Potential energy profiles of the HNCO systems calculated by the MRD-CI/6-31G** computations.

cession of two 1,2-hydrogen migrations. Its overall TS is TS2, the net barrier height being 423 kJ mol^{-1}.

Another pathway of isomerization of **1** to **2** is reaction (2d), which involves the cyclic intermediate HNCO (**7**). According to the present CI calculations, however, the TS for the initial cyclization, i.e., TS5, is more stable than **7**. Hence, the existence of **7** as an intermediate is dubious, in contradiction to the conclusion reached by Poppinger et al.[5] on the basis of the SCF/4-31G calculations. The overall reaction should thus be regarded as a one-step 1,3-hydrogen migration passing over TS6. Because TS6 lies much higher (626 kJ mol^{-1}) than does TS2, the 1,3-hydrogen migration (2d) will be far less important than reaction (2a).

In both reactions (2b) and (2c), the second steps seem to be rate-controlling. Since the net barriers TS3 and TS4 lie at much higher energy levels (681 and 639 kJ mol^{-1}, respectively) as compared to TS2, reactions (2b) and (2c) will both be much less favorable than reaction (2a).

Discussion

All the isomerization reactions considered in this work have been presumed to proceed through a cyclic intermediate, **5** or **7**. Oxazirine (**5**) is calculated to lie in energy minimum even though the barrier (TS1) preventing its transfomation into HNCO (**1**) is low (only 12 kJ mol^{-1}). On the other hand, oxaziridinylidene (**7**) does not seem to be a stable entity; it is liable to be led to the HNCO (**1**) minimum with no activation barrier at all. It should be noted that both these conclusions based on CI calculations are just opposite to the views presented by Poppinger et al.[5] at the SCF level.

Direct isomerizations may deserve attention as well. Among others, the HONC (**4**)–HOCN (**2**) isomerization is likely to be an elementary reaction of the well-documented isonitrile-nitrile rearrangement type.[19,20] Practically, however, formation of **4** from **1** requires a high activation energy, so that the direct isomerization in question will have little significance in the present context.

The most important point to be noted in this work is the demonstration that the two-step isomerization reaction of HNCO (**1**) to HOCN (**2**), i.e., reaction (2a), is energetically the most favorable process. The net activation barrier (TS2) lies 423 kJ mol^{-1} above HNCO (**1**). Corrected for the vibrational zero-point energy, the barrier height is slightly lowered to 411 kJ mol^{-1}, which is only modestly higher than the experimental activation energy (355±4 kJ mol^{-1}) reported recently by Wu et al.[3] for the main decomposition reaction (1a) of HNCO. Thus, reaction (2a) could well be an unignorable side reaction of reaction (1a) particularly at high temperatures. HOCN (**2**) thus formed will be liable to decompose into H+NCO, just as HNCO (**1**) is partly led to the same fragments beside the principal decomposition products NH($^3\Sigma^-$)+CO.[3] At still higher temperatures, formation of CN from **2** may be feasible. Our observation of a sizable amount of CN radicals in the shock-heated decomposition of HNCO in the high temperature region (2500—3500 K) could only be rationalized from this view. The anomalously low heat of formation of the CN radical at high temperatures (ΔH°_f at 3000 K being 221.3 kJ mol^{-1} as compared to 436.8 kJ mol^{-1} at 0 K)[16] may assist this formation of CN in the high temperature region.

Conclusion

Ab initio MO calculations based on the MRD-CI method reveal that the isomerization reaction HNCO→HOCN can compete with the primary decomposition channel HNCO→NH($^3\Sigma$)+CO. The isomerization consists of two 1,2-hydrogen migrations with an intermediacy of oxazirine, a half-ring isomer HC(O)N. The transition state of the second step HC(O)N→HOCN constitutes the overall barrier top. Both the intermediate and the transition state are sensitive to the degree of assessment of the correlation energy involved.

This work was supported by the Grants-in-Aid Nos. 62303002 and 02303002 from the Ministry of Education, Science and Culture. The authors are grateful to Professor R. J. Buenker for supplying his Table MRD-CI program to them. All calculations were carried out on a HITAC M-680 at the Computer Center of the Institute for Molecular Science. The authors thank the Center for an allocation of CPU time.

References

1) O. Kajimoto, O. Kondo, K. Okada, J. Fujikane, and T. Fueno, *Bull. Chem. Soc. Jpn.*, **58**, 3469 (1985).
2) J. D. Mertens, A. Y. Chang, R. K. Hanson, and C. T. Bowman, *Int. J. Chem. Kinet.*, **21**, 1049 (1989).
3) C. H. Wu, H.-t. Wang, M. C. Lin, and R. A. Fifer, *J. Chem. Phys.*, **94**, 3344 (1990).
4) K. Yokoyama, Doctoral Dissertation, Osaka University (1991).
5) D. Poppinger, L. Radom, and J. A. Pople, *J. Am. Chem. Soc.*, **99**, 7806 (1977).
6) S. R. Langhoff and E. R. Davidson, *Int. J. Quantum Chem.*, **8**, 61 (1974).
7) R. J. Bruna and S. D. Peyerimhoff, "Ab initio Methods in Quantum Chemistry," ed by K. P. Lawley, Wiley-Interscience, New York (1987), Part 1, pp. 1—97.
8) R. J. Buenker, *Int. J. Quantum Chem.*, **29**, 435 (1986).
9) M. J. Frisch, J. S. Binkley, H. B. Schlegel, K. Raghavachari, C. F. Melius, R. L. Martin, J. J. P. Stewart, F. W. Bobrowicz, C. M. Rohlfing, L. R. Kahn, D. J. DeFrees, R. Seeger, R. A. Whiteside, D. J. Fox, E. M. Fleuder, S. Topiol, and J. A. Pople, GAUSSIAN 86, Carnegie-Mellon Quantum Chemistry Publishing Unit. Pittsburgh (1984), IMS version registered by N. Koga, S. Yabushita, K. Sawabe, and K. Morokuma.
10) a) M. Dupuis, J. Rys, and H. F. King, *J. Chem. Phys.*, **65**, 111 (1976). b) M. Dupuis, J. D. Watts, H. O. Villar, and G. J. B. Hurst, HONDO 7, QCPE #544, Indiana University, IMS version converted by M. Aoyagi and S. Obata.
11) R. J. Buenker, "Studies in Physical and Theoretical Chemistry," ed by R. Carbo, Elsevier, Amsterdam (1982), Vol. 21, pp. 17—34.
12) R. J. Buenker and R. A. Phillips, *J. Mol. Struct. (Theochem)*, **123**, 291 (1985).
13) K. Morokuma, S. Kato, K. Kitaura, I. Ohmine, S. Sakai, and S. Obara, IMSPAK, Institute for Molecular Science (1989).
14) J. H. Teles, G. Maier, B. A. Hess, Jr., L. J. Schaad, M. Winnewisser, and B. P. Winnewisser, *Chem. Ber.*, **122**, 753 (1989).
15) V. E. Bondybey, J. H. English, C. W. Mathews, and R. J. Contolini, *J. Mol. Spectrosc.*, **92**, 431 (1982).
16) M. W. Chase, Jr., C. A. Davies, J. R. Downey, Jr., D. J. Frurip, R. A. McDonald, and A. N. Syverud, "JANAF Thermochemical Tables," 3rd ed, National Bureau of Standards, Washington, D. C. (1985).
17) B. K. Carpenter, N. Goldstein, A. Kam, and J. R. Wiesenfeld, *J. Chem. Phys.*, **81**, 1785 (1984).
18) J. N. Crowley and J. R. Sodeau, *J. Phys. Chem.*, **93**, 3100 (1989).
19) D. H. Liskow, C. F. Bender, and H. F. Schaefer, *J. Am. Chem. Soc.*, **94**, 5178 (1972).
20) P. K. Pearson, H. F. Schaefer, and U. Wahlgren, *J. Chem. Phys.*, **62**, 350 (1975).

Selective Isomerization of 1,5-Cyclooctadiene to 1,4-Cyclooctadiene Catalyzed by Bis(acetylacetonato)nickel–Triethyldialuminum Trichloride–Phosphorus Ligand

Yasumasa SAKAKIBARA,* Isao YAMAMOTO, Ken SASAKI, Mutsuji SAKAI, and Norito UCHINO
Department of Polymer Science and Engineering, Kyoto Institute of Technology, Matsugasaki, Sakyo-ku, Kyoto 606
(Received January 29, 1991)

The isomerization of 1,5-cyclooctadiene (1,5-COD) with Ni(acac)$_2$–$Et_3Al_2Cl_3$–phosphorus ligand (Ni : Al_2 : P= 1 : 10 : 3) was first examined with varying P ligands in toluene in order to find suitable conditions for the formation of 1,4-COD. The product distribution depended largely on the P ligands. For several phosphites possessing very strong π-acceptor properties, the main product was 1,4-COD. In particular, the less-bulky bicyclic phosphite, 4-ethyl-2,6,7-trioxa-1-phosphabicyclo[2.2.2]octane (L-**3**) was very effective and gave 1,4-COD in a high selectivity of 93% at 66% conversion (1,5-COD/Ni=500, molar ratio) by employing a low temperature of −30 °C. However, the reaction stopped before reaching completion because the catalyst was deactivated by the accumulation of 1,4-COD product. The conversion, depending on the 1,5-COD/toluene ratio (volume) rather than the 1,5-COD/Ni ratio, increased with a decrease in the 1,5-COD/toluene ratio and was 66—69% at a ratio of 0.19. On the other hand, the catalyst (P: L-**3**) was much less active for 1,4-COD than for 1,5-COD and was deactivated quickly under the same reaction conditions. This appeared to result in a high selectivity of 1,4-COD in the isomerization of 1,5-COD. The mechanistic implications of the experimental results are discussed.

The ordinary methods of preparation of 1,4-cyclooctadiene (1,4-COD) are either tedious[1] or use rather expensive starting materials.[2] Recently, selective isomerization of 1,5-COD to 1,4-COD with homogeneous transition-metal catalysts has been noted and investigated as a method of large-scale synthesis of 1,4-COD.[3] In the isomerization, from the standpoints of the selectivity of 1,4-COD and its separation by fractional distillation, it is desirable to suppress the formation of the 1,3-isomer, which has a boiling point near that of 1,4-COD.

The isomerization of 1,5-COD to 1,4-COD and 1,3-COD has previously been attempted with homogeneous transition-metal catalysts, such as $PtCl_2(PPh_3)_2$–$SnCl_2 \cdot 2H_2O$,[4,5] $PtCl_2(PPh_3)_2$–Ph_3SnCl,[6] $Ru_2(1,5\text{-COD})_2(O_2CCF_3)_2(\mu\text{-}O_2CCF_3)_2(\mu\text{-}OH_2)$,[7] $(\eta^5\text{-}C_5H_5)_2TiCl_2$–*i*-PrMgBr,[8] $Ti(OBu)_4$–Et_3Al,[3] or $Ru_3(CO)_{12}$[9] (vide infra). A satisfactory yield of 1,4-COD, however, has not been obtained because of a subsequent rapid isomerization of 1,4-COD to 1,3-COD under the reaction conditions used. We have observed previously that Ni(acac)$_2$–$Et_3Al_2Cl_3$–phosphorus ligand, which forms an active nickel species, catalyzed the isomerization of 1,5-COD to bicyclo[3.3.0]oct-2-ene (BCO, transannular product), 1,4-COD, and 1,3-COD (double-bond isomerization product) and that the latter two products, especially 1,4-COD, increased with a decrease in the electron-donating ability of the phosphorus ligands.[10] This observation prompted us to study the selective isomerization of 1,5-COD to 1,4-COD with this catalyst system. This paper details the results of our investigation.

Experimental

Materials. Toluene was purified by the ordinary method. 1,5-COD was distilled after drying over metallic natrium. Bis(acetylacetonato)nickel (anh.) and triethyldialuminum trichloride were obtained commercially.

Several phosphorus ligands, tris(*p*-chlorophenyl) phosphite,[11] 2-phenoxy-1,3,2-dioxaphospholane,[12] tri-*o*-tolyl phosphite,[11] and diphenyl phenylphosphonite,[13] were prepared according to the literature methods. Other phosphorus ligands were obtained commercially.

Reaction Procedure. A typical example is detailed below. In a 100 cm^3 flask fitted with a three-way stopcock and a thermometer were placed bis(acetylacetonato)nickel (25.7 mg, 0.10 mmol) and 4-ethyl-2,6,7-trioxa-1-phosphabicyclo-[2.2.2]octane (48.6 mg, 0.30 mmol). Liquid phosphorus ligands were added with 1,5-COD as a toluene solution. After replacing the air with nitrogen, a solution of 1,5-COD (5.41 g, 50 mmol) and propylbenzene (GLC internal standard) in toluene (30 cm^3) was added by syringe while stirring. The reaction was started by adding triethyldialuminum trichloride (1.0 mmol: 2.0 cm^3 of a 0.5 M (1 M=1 mol dm^{-3}) toluene solution) by syringe at −30 °C. The reaction mixture was kept at this temperature for 6 h. Small aliquots of the mixture were withdrawn, if necessary, during the course of the reaction and treated with a methanol–aqueous hydrochloric acid mixture. The organic layer was then separated and subjected to GLC analysis.

Analysis. The gas chromatographic analysis was made by a Shimadzu-GC-4AIT with a TC detector and He carrier gas using a 9-m PEG-20M column at 80 °C.

Results and Discussion

Effect of the Phosphorus Ligands. The isomerization of 1,5-COD with Ni(acac)$_2$–$Et_3Al_2Cl_3$–P ligand (Ni: Al_2 : P=1 : 10 : 3 molar ratio) was carried out at −30 °C and 10 °C in toluene. Various phosphites having π-acceptor properties were used as phosphorus ligands in view of the results of our previous work.[10] The results

Table 1. Effect of Phosphorus Ligands[a]

Ligand	ν_{CO}[b]/cm^{-1}	θ[b]/deg	Temp/°C	Time/h	Conversion[c]/%	Selectivity[d]/%		
						1,4-COD	1,3-COD	BCO
$P(OCH_2CF_3)_3$ (L-**1**)	2095.4[e]	110[e]	20	6	50 (22)	68	7	25
			−30	6	48 (3)	89	7	5
$P(O\text{-}p\text{-}C_6H_4Cl)_3$ (L-**2**)	2089.3	128	10	6	34[h] (21)	61	3	35
			−30	6	32 (1)	91	5	4
$P(OCH_2)_3CEt$ (L-**3**)	2086.8	101	10	1.5	54[h] (48)	90	5	6
			−30	6	66[h] (24)	93	6	1
$P(OCH_2)_2OPh$ (L-**4**)	2086.5	114[f]	10	6	45[h] (7)	30	3	66
			−30	6	68 (2)	78	12	11
$P(OPh)_3$ (L-**5**)	2085.3	128	10	1.5	23[h] (16)	67	3	30
			−30	6	24 (3)	81	5	14
$P(O\text{-}o\text{-}C_6H_4Me)_3$ (L-**6**)	2084.1	141	10	1.5	26[h] (18)	70	3	27
$PPh(OPh)_2$ (L-**7**)	2079.8	129[g]	10	1	89 (10)	12	2	86
$P(OEt)_3$ (L-**8**)	2076.3	109	10	1.5	97 (18)	2	0	98
			−30	6	7(1)	5	0	95
PPh_3 (L-**9**)	2068.9	145	10	1.5	97 (7)	1	0	99
None			10	1.5	100(8)	1	0	99

a) 1,5-COD, 50 mmol; $Ni(acac)_2$, 0.1 mmol (Ni:Al_2:P=1:10:3); Toluene, 32 cm^3, including 2 cm^3 of 0.5 M toluene solution of $Et_3Al_2Cl_3$. b) From Ref. 14 unless otherwise noted. c) Values in parentheses are conversions at 5 min. d) Selectivity of 1,4-COD is defined as 100×[1,4-COD]/([1,4-COD]+[1,3-COD]+[BCO]). e) P. W. N. M. van Leeuwen and C. F. Roobeek, *Tetrahedron*, **37**, 1973 (1981). f) Value for $P(OMe)_2OPh$. g) P. Heimbach, J. Kluth, H. Schenkluhn, and B. Weimann, *Angew. Chem., Int. Ed. Engl.*, **19**, 569 (1980). h) The reaction stopped practically at the conversions.

are shown, together with $\nu_{CO}(A_1)$ of $Ni(CO)_3L$ and the cone angle (θ) of the P ligands,[14] in Table 1. The effect of the P ligands on the product distribution was remarkable at both temperatures of −30 and 10 °C. Of the various P ligands used, a bicyclic phosphite, 4-ethyl-2,6,7-trioxa-1-phosphabicyclo[2.2.2]octane (L-**3**), which has the smallest cone angle (θ=101°) and comparatively weak electron-donating ability (ν_{CO}=2086.8 cm^{-1}), gave the best result. At −30 °C, the selectivities of 1,4-COD, 1,3-COD, and BCO were 93, 6, and 1%, respectively, with 66% conversion. It was particularly noteworthy that the subsequent isomerization of 1,4-COD to 1,3-COD was suppressed satisfactorily.

Judging from the ν_{CO} values, strong π-acceptor ligands L-**1**—**6**, which have ν_{CO} values higher than 2084 cm^{-1}, gave 1,4-COD at the major product, while weaker π-acceptor ligands L-**7**—**9** and no ligand gave BCO as the major product.[15] On the other hand, the small cone angle of the ligand favors the formation of 1,4-COD, as indicated by the results with ligands L-**3** (ν_{CO}=2086.8 cm^{-1}, θ=101°) and L-**4** (ν_{CO}=2086.5 cm^{-1}, θ=114°) which have almost the same ν_{CO} values. In conclusion, P ligands such as L-**1** and L-**3**, which are less bulky and have strong π-acceptor abilities, appear to facilitate the formation of 1,4-COD.

With ligands L-**1**—**6**, however, the reaction stopped before reaching completion, e.g., only 66% conversion with ligand L-**3** at −30 °C. Although the rate of the isomerization to 1,4-COD was generally fast at the initial stage, as seen by the values of the conversion at 5 min (Table 1, Footnote c), it dropped rapidly and the reaction stopped prematurely. This termination was found to occur at especially low conversions in the cases of triaryl phosphite-type ligands L-**2**, **5**, and **6** which have relatively large cone angles.

Effect of Temperature and Time. The isomerization was carried out at temperatures ranging from 10 °C to −50 °C in toluene using L-**3** as the P ligand. These results are shown in Table 2. The reaction proceeded more rapidly in the early stages at higher temperatures, as indicated by the variations of conversion with time, but stopped before reaching completion in all runs. For example, the conversion at −30 °C (Run 3) stopped at about 65% for the times ranging from 4 to 6 h, though reaching 62% in just 2 h. In the temperature range of 10 to −30 °C, the conversion of 1,5-COD increased with a decrease in the temperature from 52% at 10 °C to 66% at −30 °C. At the lower temperature of −50 °C, however, the conversion was less than 50% (Run 4). Additionally, the selectivity of 1,4-COD at about 50% conversion increased with a decrease in the temperature from 90% at 10 °C to 96% at −50 °C. This was due largely to the decrease in the formation of BCO. With respect to the values of both the conversion and the selectivity, −30 °C appeared to be the most suitable temperature. The variation of the conversion of 1,5-COD and the selectivity of 1,4-COD with time at −30 °C showed that the isomerization of 1,4-COD to 1,3-COD proceeded much more slowly compared with that of 1,5-COD to 1,4-COD, and that both the isomerizations stopped at almost the same time. It was noteworthy that the Ni–Al_2–L-**3** catalyst favorably suppressed the isomerization of 1,4-COD to 1,3-COD even at a fairly high conversion of 66%, in contrast to several transition-metal complex catalysts previously reported[3-9] (See Table 4). Allinger et al.,[16] who investigated the isomer-

Table 2. Effect of Temperature and Time[a)]

Run	Temp/°C	Time/min	Conversion/%	Selectivity/%		
				1,4-COD	1,3-COD	BCO
1	10	30	51	90	5	6
		60	52	90	5	6
2	−10	30	57	92	5	3
		120	58	92	5	3
3	−30	5	24	98	1	1
		30	43	97	3	1
		120	62	94	5	1
		240	65	93	5	1
		360	66	93	6	1
4	−50	240	42	96	3	1
		360	46	96	4	1
5[b)]	−30	120	69	77	17	6
		360	75	73	20	7

a) 1,5-COD, 50 mmol; $Ni(acac)_2$, 0.1 mmol (Ni:Al_2:L-**3**=1:10:3); Toluene, 32 cm^3. b) Dichloromethane (30 cm^3) was used as solvent.

Table 3. Effect of Amounts of 1,5-COD and Catalyst[a)]

Run	1,5-COD / mmol	Ni / mmol	Toluene / cm^3	1,5-COD / Ni	1,5-COD[b)] / Toluene	Conversion/%	Selectivity of 1,4-COD[c)]/%	Catalyst turnover[d)]
3	50	0.1	32	500	0.19	66	93	307
6	50	0.2	32	250	0.19	69	92	159
7	100	0.1	32	1000	0.38	52	93	484
8	100	0.2	32	500	0.38	54	95	257
9	100	0.2	14	500	0.88	37	95	176
10	100	0.2	3.5[e)]	500	3.5	16	95	76
11	6	0.1	32	60	0.023	80	81	39

a) Ni:Al_2:L-**3**=1:10:3; Temp, −30 °C; Time, 6 h. b) Volume ratio. c) See Note c) in Table 1. d) Defined as [1,4-COD]/[Ni]. e) From 4 cm^3 of a 0.5 M toluene solution of $Et_3Al_2Cl_3$.

ization equilibrium of the cyclooctadienes, reported that the equilibrium composition in dimethyl sulfoxide at 70 °C is <0.01% 1,5-COD, 0.5% 1,4-COD, and 99.5% 1,3-COD. We have found that the nickel catalyst is not very active in the isomerization of 1,4-COD to 1,3-COD and , in addition, is probably deactivated by the accumulation of 1,4-COD to result in a practical stop of the isomerization of 1,5-COD to 1,4-COD. As an apparent phenomenon concerning the deactivation, it was observed that the color of the reaction mixture changed from its initial reddish-brown to pale yellow as the reaction approached termination.

The use of other solvents was also investigated. With dichloromethane as solvent, the conversion of 1,5-COD increased to 75%, but the selectivity of 1,4-COD decreased to 73%, the selectivities of 1,3-COD and BCO being 20 and 7%, respectively (Table 2, Run 5). With THF as solvent, the isomerization did not occur.

Effect of the Amounts of 1,5-COD and Catalyst. The P ligand L-**3** gave a high selectivity of 1,4-COD, but the reaction stopped at a certain degree of conversion, as described above. In an attempt to increase the degree of conversion, the isomerization was performed at various 1,5-COD/Ni molar ratios and 1,5-COD/toluene volume ratios at −30 °C (Table 3). In all cases, the reaction stopped after several hours without reaching completion, though 1,4-COD was formed in selectivities higher than 92% (except for Run 11 which was carried out in a very dilute solution). When the reaction was performed using 50 mmol of 1,5-COD in 32 cm^3 of toluene (1,5-COD/toluene=0.19), the conversions and catalyst turnovers were 66% and 307 with 0.1 mmol Ni (Run 3), and 69% and 159 with 0.2 mmol of Ni (Run 6), respectively. It is noteworthy that irrespective of the catalyst amount, the conversions are almost the same and the catalyst turnover in the former reaction was about twice that in the latter. A similar result was also observed in the case in which the amount of 1,5-COD was increased from 50 to 100 mmol (1,5-COD/toluene ratio=0.38). The conversions and catalyst turnovers were 52% and 484 with 0.1 mmol of Ni (Run 7), and 54% and 257 with 0.2 mmol of Ni (Run 8), respectively. Thus, it was concluded that the conversion of 1,5-COD did not greatly increase with an increase in the catalyst amount.

On the other hand, the conversion appears to be influenced largely by the dilution of 1,5-COD with toluene, namely, the 1,5-COD/toluene ratio. In fact,

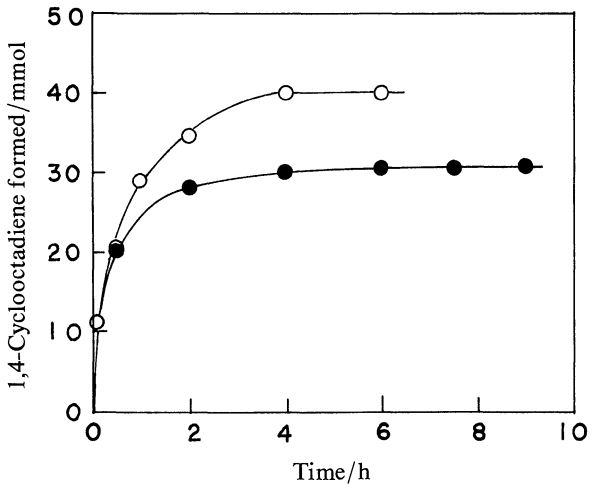

Fig. 1. Addition of 1,5-cyclooctadiene during the course of reaction. Reaction conditions: 1,5-COD, 50 mmol; $Ni(acac)_2$, 0.1 mmol ($Ni:Al_2:L\text{-}3=1:10:3$); Toluene, 32 cm^3; Temp, −30°C. ○: After 0.5 h 50 mmol of additional 1,5-COD was added. ●: After 6 h 50 mmol of additional 1,5-COD was added.

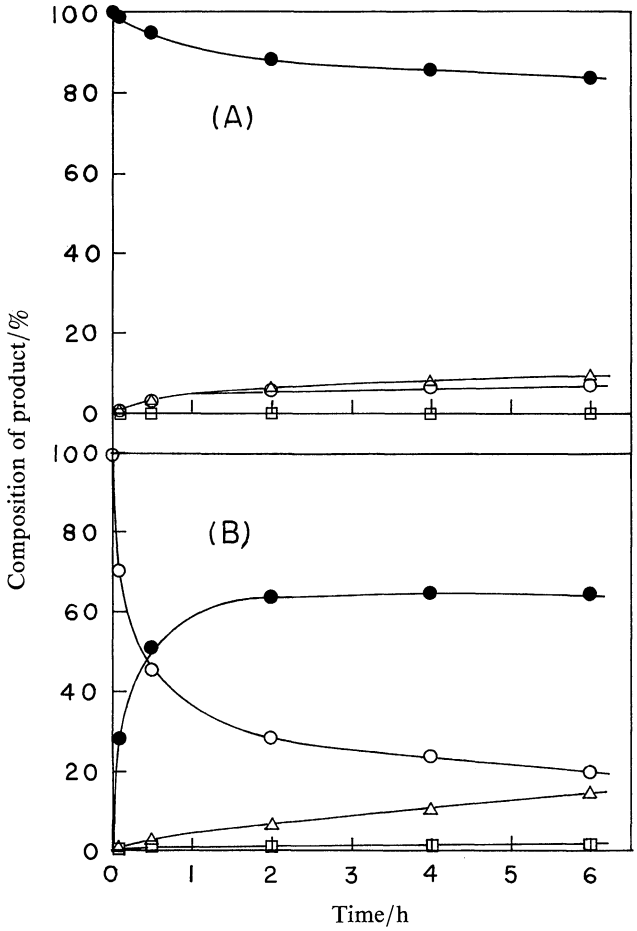

Fig. 2. Isomerization of 1,4- and 1,5-cyclooctadienes. (A): From 1,4-COD; (B): From 1,5-COD. Reaction conditions: COD, 6 mmol; $Ni(acac)_2$, 0.1 mmol ($Ni:Al_2:L\text{-}3=1:10:3$); Toluene, 32 cm^3; Temp, −30°C. ●: 1,4-COD; ○: 1,5-COD; △: 1,3-COD; □: BCO.

the conversion decreased with an increase in the 1,5-COD-toluene ratio, being 66, 54, and 37% at ratios of 0.19, 0.38, and 0.88, respectively, in the case of 1,5-COD/Ni=500 (Runs 3, 8, and 9). Furthermore, when the ratio was 3.5 (no additional toluene was added, only the 0.5 M toluene solution of $Et_3Al_2Cl_3$ was used), the conversion remained at only 16% (Run 10). Conversely, a very dilute solution with a ratio of 0.023 gave a high conversion of 80% (Run 11). From the above results, we have concluded that toluene as solvent contributes to the stabilization of the catalytically active nickel species (vide infra) to result in a higher conversion at a lower 1,5-COD/toluene ratio and that the accumulation of 1,4-COD product deactivates the catalyst. In order to confirm the deactivation of the catalyst, an attempt was made to add additional 1,5-COD to the reaction. The reaction was started under the same conditions as those for Run 3 (Fig. 1). When additional 1,5-COD was introduced after 6 h, at which time the reaction had practically stopped, no further isomerization was observed. On the other hand, when additional 1,5-COD was added after 30 min of reaction, 1,4-COD was obtained in a larger amount than that obtained in the former additional reaction. We interpret this to mean that after 6 h, the catalytically active species are no longer present. Thus, the termination of the reaction is not due to an equilibrium between 1,5-COD and 1,4-COD,[17] but to the deactivation of the catalyst.

The Characteristics of the Catalyst. The isomerization of 1,4-COD with the Ni–Al_2–L-**3** catalyst was investigated in comparison with the isomerization of 1,5-COD (Fig. 2). In both cases, the reaction had stopped practically after 6 h. The conversion of 1,4-COD at that time was only 16% in contrast to 80% cnversion for 1,5-COD. The ratio of the relative initial rates of 1,4-COD to 1,5-COD, calculated based on the conversions at 5 min, was about 0.04. These data, together with the results of the isomerization of 1,5-COD, indicated that the catalytically active species was much less active for 1,4-COD than for 1,5-COD and was rapidly destroyed by the accumulation of the 1,4-COD product.[18] In addition, it was noteworthy that 1,4-COD isomerized to the better-chelating 1,5-COD at almost the same initial rate as that of its isomerization to 1,3-COD (Fig. 2-(A)). As a result, the catalyst suppressed the isomerization of 1,4-COD to 1,3-COD to result in a highly selective isomerization of 1,5-COD to 1,4-COD. Several investigations on the isomerization of 1,5-COD to 1,4-COD are summarized in Table 4. Since the 1,4-COD product isomerizes rapidly to 1,3-COD with catalysts other than ours, the selectivities of 1,4-COD at 45—66% conversions are shown for comparison. With our catalyst, the selectivity was especially high compared with the selectivities of the others. Furthermore, good suppres-

Table 4. Summary of Several Investigations

Catalyst system	Solvent	1,5-COD[a] / Catalyst	Temp / °C	Time / min
$Ni(acac)_2$–$Et_3Al_2Cl_3$–$P(OCH_2)_3CEt$	PhMe	500	−30	240
$PtCl_2(PPh_3)_2$–$SnCl_2 \cdot 2H_2O$–H_2	CH_2Cl_2	1000	75	240
$PtCl_2(PPh_3)_2$–Ph_3SnCl–H_2	CH_2Cl_2	150	120	30
$Ru_2(1,5\text{-COD})_2(O_2CCF_3)_2(\mu\text{-}O_2CCF_3)_2(\mu\text{-}OH_2)$	THF	100	45	20
$(\eta^5\text{-}C_5H_5)_2TiCl_2$–*i*-PrMgBr	(Et_2O)[e]	200	25	15
$Ti(OBu)_4$–Et_3Al	None	800	100	70
$Ru_3(CO)_{12}$	*n*-C_8H_{18}	200	125	30
$Ru_3(CO)_{12}/SiO_2$[f]	*n*-C_8H_{18}	200	70	45

Catalyst system	Composition of Product[b]/% 1,5-COD	1,4-COD	1,3-COD	BCO	Selectivity of 1,4-COD[c]	Reference
$Ni(acac)_2$–$Et_3Al_2Cl_3$–$P(OCH_2)_3CEt$	35	60	4	1	93	This paper
$PtCl_2(PPh_3)_2$–$SnCl_2 \cdot 2H_2O$–H_2	36	42	22	0	66	4, 5)
$PtCl_2(PPh_3)_2$–Ph_3SnCl–H_2	54	34	11	0[d]	76	6)
$Ru_2(1,5\text{-COD})_2(O_2CCF_3)_2(\mu\text{-}O_2CCF_3)_2(\mu\text{-}OH_2)$	51	20	29	0	41	7)
$(\eta^5\text{-}C_5H_5)_2TiCl_2$–*i*-PrMgBr	50	30	20	0	60	8)
$Ti(OBu)_4$–Et_3Al	55	30	15	0.5	66	3)
$Ru_3(CO)_{12}$	50	23	27	0	46	9)
$Ru_3(CO)_{12}/SiO_2$[f]	34	35	31	0	53	9)

a) Molar ratio. b) Taken at 45—66% conversions. c) See Note c) in Table 1. d) Cyclooctene was formed in a trace amount. e) From a small amount of *i*-PrMgBr-ether. f) Heterogenized catalyst.

sion of the formation of 1,3-COD is favorable for the isolation of 1,4-COD by distillation,[3,19] because the boiling points of 1,5-COD (150.8 °C/755 mmHg (1 mmHg=133.322 Pa)), 1,4-COD (145.1 °C/758 mmHg), and 1,3-COD (142.7 °C/754 mmHg),[20] (and especially of the latter two), are close to each other.

Mechanistic Implications. In general, the catalyst $Ni(acac)_2$–$Et_3Al_2Cl_3$–P ligand, which in situ generates a specific square planar nickel hydride complex **1**, operates by the addition and elimination of a Ni–H function in double-bond migration.[21] A reaction mechanism, being essentially the same as that described in our previous paper,[10] is proposed to account for the experimental results (Scheme 1). The Ni–H species **1** may coordinates 1,5-COD[22] which then undergoes insertion into the Ni–H bond and subsequent coordination of the second double bond to give a σ, π-cyclooctenyl nickel complex **3**. In complex **3**, a β-H elimination reaction and an intramolecular insertion reaction take place competitively to result in double-bond isomerization (complex **4**) and cyclization (complex **5**) of 1,5-COD, respectively. The isomerization/cyclization ratio depends primarily on the P ligands.[10] The η^2-1,4-COD complex **4** gives 1,4-COD and **1**, and the catalytic cycle recurs.

The Ni–H species **1** with weak σ-donor P ligands may be normally unstable and ineffective for the isomerization of common olefins. In practice, 1,4-COD was only slightly isomerized with the Ni–Al_2–L-**3** catalyst, as shown in Fig. 2-(A), but 4-methyl-1-pentene was not isomerized at all.[18] With 1,5-COD, however, complex **3** would be stabilized by coordination of the second

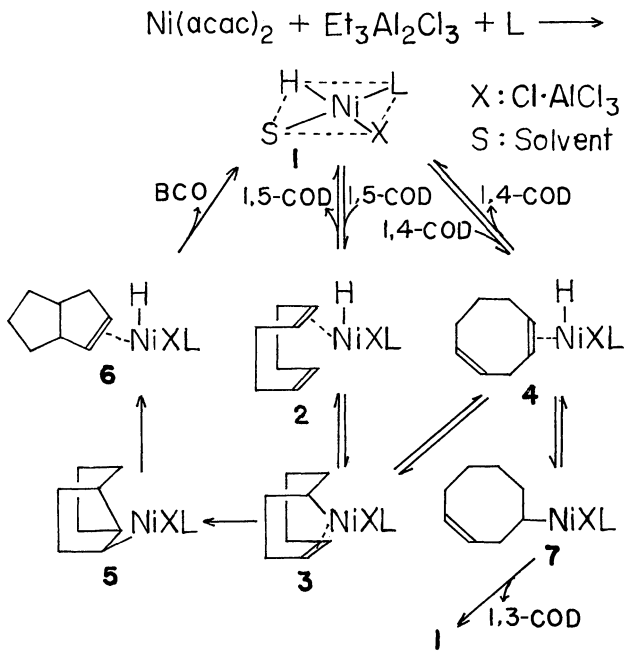

Scheme 1. Reaction mechanism.

double bond to act as an intermediate in the isomerization of 1,5-COD. In view of the high selectivity of 1,4-COD, it seems likely that the coordinate double bond in **3** is not adequately activated with strong π-acceptor P ligands and therfore **3** undergoes Ni–H elimination in preference to intramolecular insertion. In addition, the less bulky phosphite L-**3** appears to favor the formation of complex **4**, which has a more crowded environment

around the nickel than does complex **5**, compared with bulky phosphites such as L-**4** and L-**5** having almost the same ν_{CO} values. Then, complex **4** would give complex **2** rapidly via the dissociation of 1,4-COD if 1,5-COD exists in large amounts and the double bond in **4** coordinates weakly to the nickel. Thus, the use of strong π-accepting and less bulky phosphites may lead to the highly selective isomerization of 1,5-COD to 1,4-COD.

Next, the deactivation of the catalyst caused by the accumulation of 1,4-COD will be discussed in some detail. In the isomerization of 1,5-COD, while the 1,5-COD/1,4-COD ratio is large, complex **4** may transfer to the stabilized complex **3**, via complex **2** rather than complex **7**. As 1,4-COD is produced with subsequent 1,5-COD depletion, however, the ratios of complexes **4** and **7** to total active nickel species would increase. This seems to relate to the deactivation of the catalytic species in view of the fact that the isomerization of 1,4-COD with the Ni–Al_2–L-**3** catalyst stops at a very low conversion, as described above. However, the deactivation process is not clear at the present time. As a possible process, it may be proposed that, besides undergoing normal β-elimination, complex **7** is converted to the inactive nickel species Ni[L-**3**]$_n$, 1,3-COD, and HX by the action of L-**3**.[23] Consequently, this conversion could result in the termination of the reaction and the suppression of 1,3-COD formation.

Concerning solvents, suitable ones such as toluene and dichloromethane may participate in stabilizing the catalytically active species, in contrast to THF in which the isomerization does not proceed. Therefore, high dilution of 1,5-COD with toluene along with low reaction temperature would bring about its high conversion to 1,4-COD.

References

1) S. Moon and C. R. Ganz, *J. Org. Chem.*, **34**, 465 (1969).

2) L. E. Craig, R. M. Elofson, and I. J. Ressa, *J. Am. Chem. Soc.*, **75**, 480 (1953); W. O. Jones, *J. Chem. Soc.*, **1954**, 312.

3) W. Holtrup, R. Streck, W. Zaar, and D. Zerpner, *J. Mol. Catal.*, **36**, 127 (1986).

4) H. A. Tayim and M. Kharboush, *Inorg. Chem.*, **10**, 1827 (1971).

5) H. A. Tayim and J. C. Bailar, Jr., *J. Am. Chem. Soc.*, **89**, 3420 (1967).

6) A. Vassilian and J. C. Bailar, Jr., *J. Catal.*, **62**, 389 (1980).

7) M. O. Albers and E. Singleton, *J. Mol. Catal.*, **31**, 211 (1985).

8) Q. Yanlong, L. Jiaqui, and X. Weihua, *J. Mol. Catal.*, **34**, 31 (1986).

9) J. Kaspar, M. Graziani, G. Dolcetti, A. Trovarelli, and R. Ganzerla, *J. Mol. Catal.*, **48**, 29 (1988).

10) Y. Sakakibara, K. Oheda, M. Sakai, and N. Uchino, *Nippon Kagaku Kaishi*, **1986**, 805.

11) E. N. Walsh, *J. Am. Chem. Soc.*, **81**, 2023 (1959).

12) L. Hechenbleikner, C. W. Pause, and F. C. Lanoue, U. S. Patent 2834798 (1958); *Chem. Abstr.*, **52**, 17297b (1958).

13) A. E. Arbuzov, G. Kamai, and L. V. Nesterov, *Tr. Kazan. Khim. Tekhnol. Inst.*, **1951**, 17; *Chem. Abstr.*, **51**, 5720f (1957).

14) C. A. Tolman, *Chem. Rev.*, **77**, 313 (1957).

15) In this connection, it has been reported that the isomerization of 1,5-COD can be directed to almost complete formation of 1,3- and 1,4-COD by employing trimethylphosphine (ν_{CO}=2064 cm^{-1}, θ=118°) as P ligand and that it is possible, by terminating the reaction before completion, to isolate 1,4-COD in up to 40% yield (B. Bogdanović, "Selectivity Control in Nickel-Catalyzed Olefin Oligomerization," in "Advances in Organometallic Chemistry," ed by F. G. A. Stone and R. West, Academic Press, New York (1979), Vol. 17, p. 105). Therefore, the use of PMe_3 was attempted under our conditions. The result was considerably different from that reported by Bogdanović, but it was observed that PMe_3 gave 1,4-COD in a moderate selectivity of 49%, together with BCO in 45% selectivity, at 48% conversion at 10 °C, in contrast with other trialkylphosphines such as PEt_3 and PBu_3.[10]

16) N. L. Allinger, J. F. Viskocil, Jr., U. Burkert, and Y. Yuh, *Tetrahedron*, **32**, 33 (1976).

17) It has been reported that the isomerization of 1,5-COD to 1,4-COD catalyzed by $Ir_2H_2Cl_2$(1,5-COD) is reversible (M. Gargano, P. Giannoccaro, and M. Rossi, *J. Organomet. Chem.*, **84**, 389 (1975)).

18) Furthermore, the isomerization of an alkene, 4-methyl-1-pentene, with the catalyst Ni–Al_2–L-**3**, was attempted for reference. We found that the catalyst did not have the ability to isomerize the olefin, in contrast with the Ni–Al_2–PPh_3 (L-**9**) catalyst (Y. Sakakibara, M. Mukai, M. Sakai, and N. Uchino, *Nippon Kagaku Kaishi*, **1972**, 1457).

19) In many cases, 1,4-COD is separated from the mixture of 1,3- and 1,4-COD by the method of $AgNO_3$ adduct formation, because the boiling points are close to each other (Ref. 1).

20) K. Ziegler and H. Wilms, *Justus Liebigs Ann. Chem.*, **567**, 1 (1950).

21) a) P. W. Jolly and G. Wilke, "The Organic Chemistry of Nickel," Academic Press, New York (1975), Vol. 2, p. 1. b) P. W. Jolly, "Nickel Catalyzed Oligomerization of Alkenes and Related Reactions," in "Comprehensive Organometallic Chemistry," ed by G. Wilkinson, F. G. A. Stone, and E. W. Abel, Pergamon Press, Oxford (1982), Vol. 8, p. 615.

22) In the 1,5-COD complex **2**, the nickel may also be able to coordinate the second double bond of 1,5-COD (C. A. Tolman and W. C. Seidel, *J. Am. Chem. Soc.*, **96**, 2780 (1974)). In this connection, the relative stability of the various conformations of 1,5-COD was reported to be the following order: twist-boat>chair>boat>twist (N. L. Allinger and J. T. Sprague, *Tetrahedron*, **31**, 21 (1975)).

23) The reaction of acetylacetonato(4-cyclooctenyl)nickel with triphenyl phosphite forms Ni[$P(OPh)_3$]$_4$, 1,3-COD, and Hacac (B. Bogdanović, M. Kröner, and G. Wilke, *Justus Liebigs Ann. Chem.*, **699**, 1 (1966)). In view of the formation of 1,3-COD, it can be assumed that the above reaction proceeds via the isomerization of the 4-cyclooctenylnickel complex to the 3-cyclooctenylnickel complex.

Selenation of 1,5-Naphthoquinones: Novel Synthesis of Naphthopyridoselenazines

Makoto SAKAKIBARA, Tetsuya ISHIDA, Yoshihiko WATANABE, Takeshi TORU, and Yoshio UENO*
Department of Applied Chemistry, Nagoya Institute of Technology, Gokiso, Showa-ku, Nagoya 466
(Received February 15, 1991)

Selenation of 2-chloro- and 2,6-dichloro-1,5-naphthoquinones with benzeneselenolate ion, generated from diphenyl diselenide and tributylphosphine in an alkaline medium, afforded 2-phenylseleno- and 2,6-bis(phenylseleno)-1,5-naphthoquinones in excellent yields. Reaction of halo-1,4-naphthoquinones with 3-amino-2-pyridineselenolate ion generated from bis(3-amino-2-pyridyl) diselenide gave naphtho[2,1-*b*]pyrido[3,2-*e*][1,4]-selenazines and pyrido[2,3-*b*]pyrido[3″,2″:5′,6′][1,4]selenazino[2′,3′:3,4]naphtho[1,2-*e*][1,4]selenazines in high yields.

Phenothiazinones[1] and phenoselenazinones[2] are known as potent dyes for semiconductor lasers used for optical information recording media. We previously synthesized 4*H*-benzo[*a*]phenothiazin-4-ones[3] and 4*H*-benzo[*a*]phenoselenazin-4-ones[4] and found that they show absorptions in the near infrared. In a previous report[5] we described a new efficient selenation method for conversion of 2-halo-1,4-naphthoquinones into 2-phenylseleno-1,4-naphthoquinones. We herein describe the application of this new selenation to the synthesis of naphthopyridoselenazines using bis(3-amino-2-pyridyl) diselenide as a selenating reagent. We also report the selenation of 2-chloro- and 2,6-dichloro-4,8-bis(alkylamino)-1,5-naphthoquinones.

Results and Discussion

Preparation of Seleno-Substituted 1,5-Naphthoquinones. We were interested in the reaction site of benzeneselenolate ion to 2-chloro-1,5-naphthoquinones and examined the selenation of 2,6-dichloro- and 2-chloro-4,8-bis(2-propylamino)-1,5-naphthoquinones (**3** and **5**), and 2-chloro-4,8-bis(methylamino)-1,5-naphthoquinone (**6**). We found that 2,6-dichloro- and 2-chloronaphthoquinones **3** and **5** were obtainable by the reaction of 4,8-bis(2-propylamino)-1,5-naphthoquinone[6] (**1**) with bromine in hydrochloric acid in 45 and 26% yield, respectively. Chlorination of 4,8-bis(methylamino)-1,5-naphthoquinone[6] (**2**) in the same manner affored chloronaphthoquinone **6** in 36% yield, together with 2,6-dichloronaphthoquinone **4** (yield 22%) (Scheme 1).

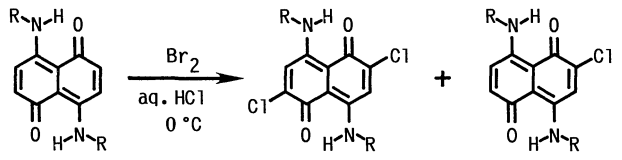

1 R=i-Pr
2 R=Me
3 R=i-Pr
4 R=Me
5 R=i-Pr
6 R=Me

Scheme 1.

With chloronaphthoquinones **3**, **5**, and **6** in hand, we then attempted the selenation. A solution of benzeneselenolate ion was prepared as follows. To a vigorously stirred tetrahydrofuran (THF) solution of 1.10 molar equiv of diphenyl diselenide and 1.20 molar equiv of tributylphosphine, was added 2.20 molar equiv of an aqueous NaOH solution. The mixture was vigorously stirred for 15 min during which time the yellow two-phase solution became colorless and homogeneous, a mixture containing benzeneselenolate ion being formed. The mechanism for the generation of selenolate ion can be postulated as we described earlier:[5] A selenophosphonium ion **I** and/or a pentavalent phosphorus species **II** are initially formed in the reaction of diphenyl diselenide and a phosphine, and addition of NaOH liberates benzenselenolate ion and the phosphonium ion **III**, from which is

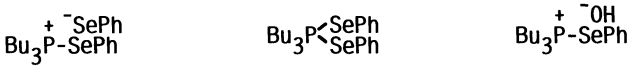

I **II** **III**

further generated selenolate ion together with phosphine oxide by the action of NaOH. In line with this mechanism, tributylphosphine oxide was be isolated quantitatively. Treatment of dichloronaphthoquinone **3** with a solution of benzeneselenolate ion thus obtained at room temperature yields bisphenylselenated naphthoquinone in 88% yield. The regioselectivity of the phenylseleno group, however, could not be determined directly on the basis of the spectral data. The structure was eventually assigned as 4,8-bis(2-propylamino)-2,6-bis(phenylseleno)-1,5-naphthoquinone (**7**) by X-ray analysis (see Fig. 1 and Tables 2 and 3). Consequently, the selenation presumably starts with the attack of benzeneselenolate ions on both carbons α to the carbonyl groups, i.e., on each carbon attached to the chloro group, of 2,6-dichloro-1,5-naphthoquinone **3**, followed by β-elimination of chloride ions to form 2,6-bis(phenylseleno)-1,5-naphthoquinone **7**.

The selenation of **5** and **6** using diphenyl diselenide

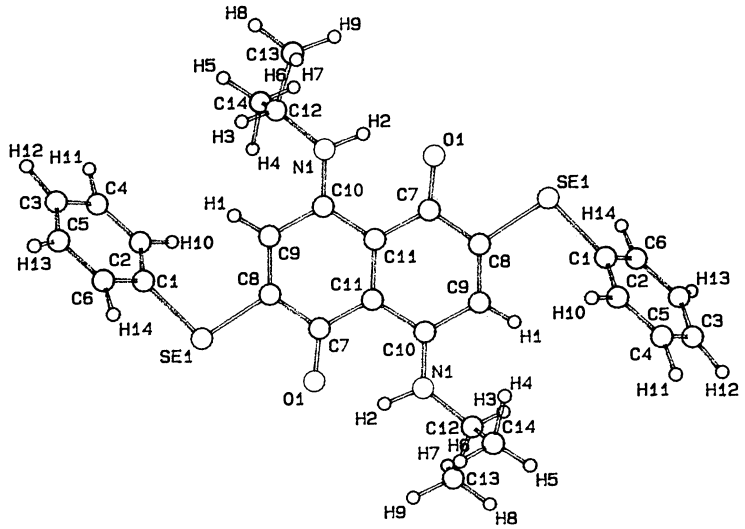

Fig. 1. An ORTEP view of **7** together with the atom numbering system.

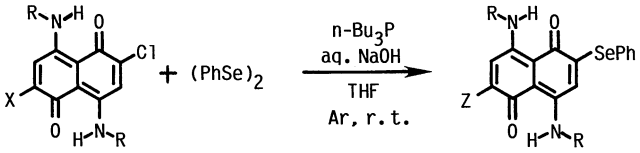

Scheme 2.

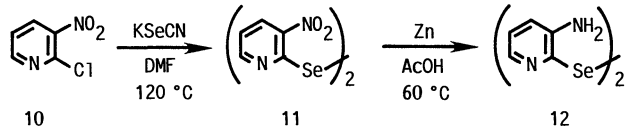

Scheme 3.

(0.55 molar equiv), tributylphosphine (0.60 molar equiv), and an aqueous NaOH (1.10 molar equiv) solution afforded phenylselenated 4,8-bis(2-propylamino)- and 4,8-bis(methylamino)-1,5-naphthoquinones **8** and **9** in 94 and 89% yield, respectively. In the ^{1}H NMR spectrum, the protons on C-3 and C-7 of **7** appeared at δ=6.39. The protons on C-3 of **8** and **9** appeared at δ=6.46 and 6.51, respectively. From the mechanistic point of view, as shown above in the selenation of **3** as well as the ^{1}H NMR data, **8** and **9** were tentatively assigned as 4,8-bis(2-propylamino)- and 4,8-bis(methylamino)-2-phenylseleno-1,5-naphthoquinones, respectively (Scheme 2).

Preparation of Naphthopyridoselenazines. Recently we found that the reaction of naphthoquinones with zinc 2-aminobenzeneselenenate, prepared from bis(2-nitrophenyl) diselenide and zinc in acetic acid, gave phenoselenazinones in high yield.[4] In order to prepare naphthopyridoselenazine derivatives in a similar manner as above, we first attempted to prepare zinc 3-amino-2-pyridineselenenate by the reaction of bis(3-nitro-2-pyridyl) diselenide (**11**) with zinc. The reaction, however, did not give zinc 3-amino-2-pyridineselenenate but instead gave bis(3-amino-2-pyridyl) diselenide (**12**) in good yield. Thus, dipyridyl diselenide **12** was obtained in 53% yield by the reaction of 2-chloro-3-nitropyridine (**10**) with potassium selenocyanate in DMF at 120 °C followed by reduction with zinc and acetic acid (Scheme 3). Fortunately, the 3-amino-2-pyridineselenolate ion was found to be generated from the dipyridyl diselenide **12** on treatment with triphenyl- or tributylphosphine in an alkaline medium. An acetonitrile solution of dipyridyl diselenide **12** (0.58 molar equiv) and triphenylphosphine (1.25 molar equiv) was vigirously stirred under argon at room temperature. To this was added an aqueous NaOH (1.08 molar equiv) solution, and the mixture was vigorously stirred for 15 min to give a mixture containing 3-amino-2-pyridineselenolate ion. Treatment of 2-bromo-3-methyl-1,4-naphthoquinone (**13**) with a solution of 3-amino-2-pyridineselenolate ion at room temperature gave 6-methyl-5*H*-naphtho[2,1-*b*]pyrido[3,2-*e*][1,4]selenazin-5-one (**14**) in 91% yield, which would have been formed via selenation and subsequent condensation between the quinone carbonyl and aromatic amino group (or vice versa). 3-Amino-2-pyridineselenolate ion formed from diselenide **12** (0.58 molar equiv) and tributylphosphine (1.25 molar equiv) in place of triphenylphosphine in an alkaline medium (1.08 molar equiv) was also effective, giving **14** in 93% yield. The reaction of 2,3-dichloro-1,4-naphthoquinone (**15**) with 3-amino-2-pyridineselenolate ion generated from diselenide **12** (0.69 molar equiv) and triphenylphosphine (1.46 molar equiv) afforded 6-chloro-5*H*-naphtho[2,1-*b*]pyrido[3,2-*e*][1,4]selenazin-5-one (**16**) and pyrido[2,3-

b]pyrido[3″,2″:5′,6′][1,4]selenazino[2′,3′:3,4]naphtho[1,2-*e*][1,4]selenazine (**17**) in 61 and 18% yield, respectively. When tributylphosphine was used instead of triphenylphosphine, **16** and **17** was formed in 20 and 54% yield, respectively. The bisselenated product **17** was formed predominantly when tributylphosphine was used. This is presumably because of higher reducing ability of Bu_3P compared to Ph_3P, which caused a rapid formation and thus higher concentration of selenolate ion in the reaction mixture (reaction time: 20 min for Bu_3P vs. 1 h for Ph_3P), resulting in the formation of a larger amount of the bisselenated product **17**. A similar result was obtained in the following reaction. Treatment of 2,3-dichloro-5-nitro-1,4-naphthoquinone[7] (**18**) with 3-amino-2-pyridineselenolate ion gave two regioisomeric nitro-5*H*-naphtho[2,1-*b*]pyrido[3,2-*e*][1,4]-selenazin-5-ones (**19** and **20**), and a bisselenated product, 6-nitropyrido[2,3-*b*]pyrido[3″,2″:5′,6′][1,4]selenazino[2′,3′:3,4]naphtho[1,2-*e*][1,4]selenazine (**21**), in 47, 19, and 17% yield, respectively, when triphenylphosphine was used, and in 30, 18, and 40% yield, respectively, when tributylphosphine used (Scheme 4).

Though two regioisomeric products **19** and **20** could not be distinguished from each other by examining their spectral data, they were unambiguously assigned to be a 6-chloro-1-nitro compound **19** and a 6-chloro-4-nitro compound **20**, respectively, by the correlation with known compounds 6-chloro-4-nitro-5*H*-benzo[*a*]phenothiazin-5-one[8] (**24**) and the corresponding 6-chloro-1-nitro isomer[8] **26**. Two reference compounds **24** and **26** were respectively subjected to selenation with dipyridyl diselenide **12** and tributylphosphine in a mixture of acetonitrile, dimethyl sulfoxide and an aqueous NaOH solution (160 °C), giving 6-nitrobenzo[*b*]pyrido-[3″,2″:5′,6′][1,4]selenazino[2′,3′:3,4]naphtho[1,2-*e*]-[1,4]thiazine (**23**) and the 9-nitro isomer **25** in 32% and 52% yield. The reaction of the above-mentioned product **19** with 2-aminobenzenethiol (**22**) and Na_2CO_3 in DMF–toluene at 120 °C gave naphthothiazine, which was readily identified as the 6-nitro compound **23** in terms of the spectral data. On the other hand, the naphthothiazine obtained from the reaction of **20** with **22** was shown to be identical to the 9-nitro isomer **25** (Scheme 5). Thus, two isomeric products **19** and **20**

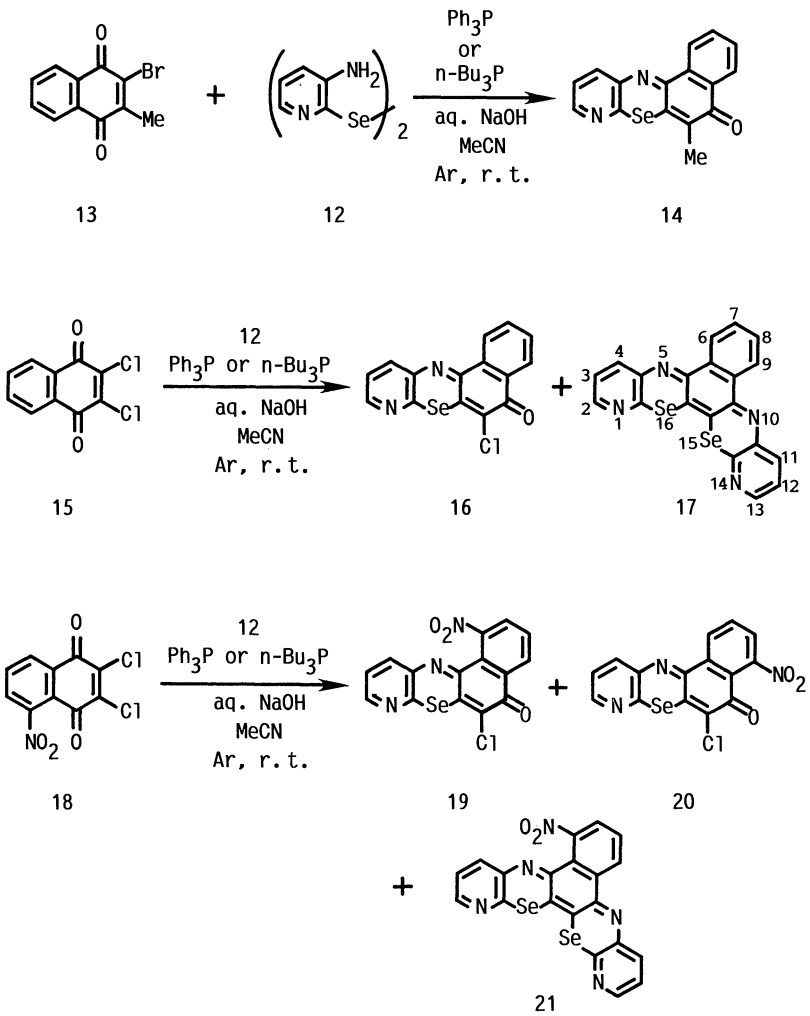

13 12 14

15 16 17

18 19 20

21

Scheme 4.

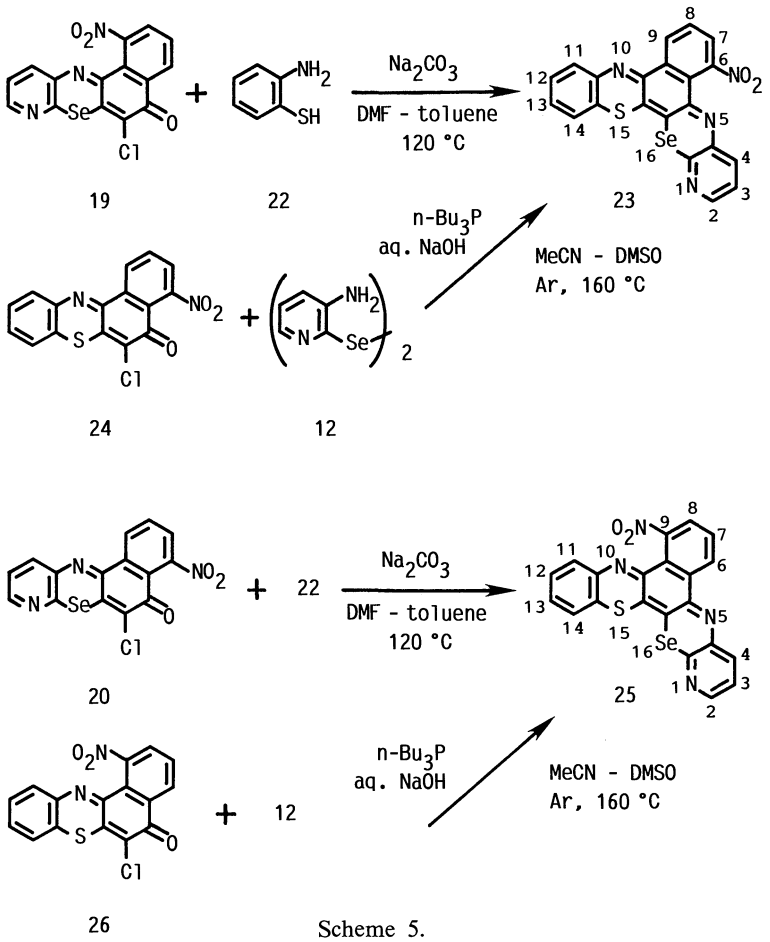

Scheme 5.

were identified to have 6-chloro-1-nitro and 6-chloro-4-nitro structures, respectively.

Since gallium arsenide, a semiconductor for optical recording media, emits a laser light at 800—830 nm, optical absorption in the near infrared region is required for dyes used in optical recording. In previous reports we described that 4*H*-benzo[*a*]phenothiazin-4-ones[3] and 4*H*-benzo[*a*]phenoselenazin-4-ones[4] absorbed at 750—770 nm. The naphthopyridoselenazines and phenylselenated 1,5-naphthoquinones prepared in the present work unfortunately do not show satisfactory absorptions compatible with semiconductor lasers: The naphthopyridoselenazines and naphthopyridoselenazine derivatives absorb at wavelengths in a region of 470—573 nm, whereas phenylseleno- and bis(phenylseleno)-1,5-naphthoquinones absorb at 664—666 nm. The λ_{max} values of these compounds are given in Table 1.

Table 1. UV and Visible Spectra Data[a]

Product	λ_{max} / nm	ε	Product	λ_{max} / nm	ε
7	666	50900	**17**	559	12500
	611	21200		529	11000
	421	13000		371	9800
	249	45900		348	9000
				277	18500
8	664	26100			
	610	11700	**19**	489	10100
	441	3000		318	12600
	347	3900		275	18500
	250	22200		258	21100
9	665	28800	**20**	489	24400
	611	13000		350	16400
	446	3300		317	19000
	347	4300		279	30200
	249	25300		256	34300
14	469	26100	**21**	573	19700
	360	19100		337	20900
	291	41000		281	40100
	273	43700			
			23	556	16800
16	475	11900		341	15900
	366	8100		279	34100
	291	23000		275	24800
	268	22400			

a) In chloroform.

Experimental

General. Mps were recorded on a Yanaco micro-melting point apparatus and are uncorrected. IR spectra were measured on KBr discs on a JASCO A-102 spectrometer. ^{1}H NMR spectra were taken with a JEOL JNM-PMX 60SI NMR spectrometer for solutions in deuteriochloroform with TMS as internal standard. Mass spectra were obtained with a Hitachi M-2000 spectrometer. Elemental analyses were

performed by the Microanalytical Laboratory of Kyoto University.

Preparation of 2,6-Dichloro- and 2-Chloro-4,8-bis(2-propylamino)-1,5-naphthoquinone (3 and 5). To a solution of 4,8-bis(2-propylamino)-1,5-naphthoquinone[6] (**1**) (400 mg, 1.47 mmol) in 27% hydrochloric acid (30 ml) was added bromine (0.30 ml, 5.82 mmol) in 27% hydrochloric acid (10 ml) at 0 °C slowly over 2 h. After stirring for 30 min, the mixture was neutralized with a 5% aqueous $NaHCO_3$ solution, thereby the dark-brown color of the solution turned to blue. The solution was extracted with chloroform (3×15 ml). The combined extracts were washed successively with water (2×5 ml) and brine (2×5 ml). The solution was dried over $MgSO_4$ and evaporated. Column chromatography on silica gel with chloroform–ethyl acetate (9:1) as eluent yielded dichloronaphthoquinone **3** (226 mg, 45%) and chloronaphthoquinone **5** (117 mg, 26%).

3: Mp 200—210 °C (decomp) (from hexane–CH_2Cl_2); IR (KBr) 1593 and 1558 cm^{-1}; ^1H NMR ($CDCl_3$) δ=1.40 (12H, d, J=6.0 Hz), 3.71—4.40 (2H, m), 7.46 (2H, s), and 12.78—13.14 (2H, m); MS m/z 342 (M^+; 47), 340 (M^+; 63), 338 (M^+; 11), 327 (61), 325 (100), and 323 (33). Found: C, 56.12; H, 5.08%. Calcd for $C_{16}H_{18}Cl_2N_2O_2$: C, 56.32; H, 5.32%.

5: Mp 145—150 °C (decomp) (from hexane–CH_2Cl_2); IR (KBr) 1598 and 1542 cm^{-1}; ^1H NMR ($CDCl_3$) δ=1.40 (12H, d, J=6.0 Hz), 3.88—4.42 (2H, m), 7.00 (1H, d, J=10.0 Hz), 7.24 (1H, d, J=10.0 Hz), 7.45 (1H, s), and 12.45—13.46 (2H, m); MS m/z 307 (M^+; 28), 305 (M^+; 62), 291 (42), and 289 (100). Found: C, 62.65; H, 6.32%. Calcd for $C_{16}H_{19}ClN_2O_2$: C, 62.64; H, 6.24%.

Preparation of 2,6-Dichloro- and 2-Chloro-4,8-bis(methylamino)-1,5-naphthoquinone (4 and 6). Chlorination of 4,8-bis(methylamino)-1,5-naphthoquinone[6] (**2**) (300 mg, 1.39 mmol) with bromine (0.20 ml, 3.88 mmol) in 27% hydrochloric acid (10 ml) afforded **4** (87 mg, 22%) and **6** (125 mg, 36%).

4: Mp 220—230 °C (decomp) (from hexane–CH_2Cl_2); IR (KBr) 1600 cm^{-1}; ^1H NMR ($CDCl_3$) δ=3.24 (6H, d, J=6.0 Hz), 7.51 (2H, s), and 12.63—12.86 (2H, m); MS m/z 286 (M^+; 41), 284 (M^+; 87), 282 (M^+; 58), and 207 (100). Found: C, 50.14; H, 3.47%. Calcd for $C_{12}H_{10}Cl_2N_2O_2$: C, 50.55; H, 3.54%.

6: Mp 190—200 °C (decomp) (from hexane–CH_2Cl_2); IR (KBr) 1595 and 1532 cm^{-1}; ^1H NMR ($CDCl_3$) δ=3.17 (3H, d, J=6.0 Hz), 3.24 (3H, d, J=6.0 Hz), 6.92 (1H, d, J=10.0 Hz), 7.18 (1H, d, J=10.0 Hz), 7.37 (1H, s), and 12.07—13.30 (2H, m); MS m/z 252 (M^+; 37), 250 (M^+; 100), 235 (17), and 233 (42). Found: C, 57.39; H, 4.28%. Calcd for $C_{12}H_{11}ClN_2O_2$: C, 57.50; H, 4.42%.

Selenation of 2,6-Dichloro-4,8-bis(2-propylamino)-1,5-naphthoquinone (3). A solution of diphenyl diselenide (68 mg, 0.22 mmol) and tributylphosphine (60 µl, 0.24 mmol) in THF (0.5 ml) was vigorously stirred ultrasonically under argon atmosphere at room temperature for 5 min. To this was added a 10% aqueous NaOH solution (160 µl, 0.44 mmol), and the mixture was ultrasonically stirred further for 15 min, during which time the two-phase mixture became homogeneous and the starting yellow solution turned to colorless. Then, the mixture was added dropwise to a solution of **3** (68 mg, 0.20 mmol) in THF (0.5 ml) at room temperature under argon atmosphere and stirred for 15 min. The mixture was then poured into a mixture of brine (10 ml) and dichloromethane (10 ml), and the aqueous layer was extracted with dichloromethane (2×5 ml). The combined extracts were washed with brine (5 ml), dried over $MgSO_4$, and evaporated. Column chromatography on silica gel with hexane–ethyl acetate (7:3) as eluent yielded 4,8-bis(2-propylamino)-2,6-bis(phenylseleno)-1,5-naphthoquinone (**7**) (102 mg, 88%). Mp 220—223 °C (from hexane–CH_2Cl_2); IR (KBr) 1585 and 1532 cm^{-1}; ^1H NMR ($CDCl_3$) δ=1.12 (12H, d, J=6.0 Hz), 3.09—3.74 (2H, m), 6.39 (2H, s), 7.21—7.83 (10H, m), and 12.33—12.60 (2H, m); MS m/z 584 (M^+; 35), 582 (M^+; 33), 580 (M^+; 15), 427 (94), 425 (45), 411 (100), and 409 (53). Found: C, 58.02; H, 4.76%. Calcd for $C_{28}H_{28}N_2O_2Se_2$: C, 57.74; H, 4.85%.

Selenation of 2-Chloro-4,8-bis(2-propylamino)-1,5-naphthoquinone (5). Selenation of **5** (61 mg 0.20 mmol) using diphenyl diselenide (34 mg, 0.11 mmol), tributyphosphine (30 µl, 0.12 mmol), and a 10% aqueous NaOH solution (80 µl, 0.22 mmol) gave 4,8-bis(2-propylamino)-2-phenylseleno-1,5-naphthoquinone (**8**) (80 mg, 94%). Mp 141—143 °C (from hexane–CH_2Cl_2); IR (KBr) 1588 and 1540 cm^{-1}; ^1H NMR ($CDCl_3$) δ=1.12 (6H, d, J=6.0 Hz), 1.38 (6H, d, J=6.0 Hz), 3.05—3.77 (1H, m), 3.77—4.30 (1H, m), 6.46 (1H, s), 6.98—7.33 (2H, m), 7.33—7.78 (5H, m), and 12.37—12.98 (2H, m); MS m/z 428 (M^+; 100), 426 (M^+; 56), 411 (43), 409 (20), 272 (34), and 270 (15). Found: C, 61.80; H, 5.71%. Calcd for $C_{22}H_{24}H_2O_2Se$: C, 61.82; H, 5.67%.

Selenation of 2-Chloro-4,8-bis(methylamino)-1,5-naphthoquinone (6). Selenation of **6** (50 mg 0.20 mmol) using diphenyl diselenide (34 mg, 0.11 mmol), tributylphosphine (30 µl, 0.12 mmol), and a 10% aqueous NaOH solution (80 µl, 0.22 mmol) gave 4,8-bis(methylamino)-2-phenylseleno-1,5-naphthoquinone (**9**) (66 mg, 89%). Mp 185—187 °C (from hexane–CH_2Cl_2); IR (KBr) 1583 and 1544 cm^{-1}; ^1H NMR ($CDCl_3$) δ=2.63 (3H, d, J=5.4 Hz), 3.30 (3H, d, J=5.4 Hz), 6.51 (1H, s), 7.01—7.35 (2H, m), 7.35—7.82 (5H, m), and 12.27—12.93 (2H, m); MS m/z 372 (M^+; 100) and 370 (M^+; 56). Found: C, 57.98; H, 4.20%. Calcd for $C_{18}H_{16}N_2O_2Se$: C, 58.23; H, 4.34%.

Preparation of Bis(3-amino-2-pyridyl) diselenide (12). A solution of 2-chloro-3-nitropyridine (**10**) (5.0 g, 31.5 mmol) and potassium selenocyanate (7.5 g, 52.1 mmol) in DMF (40 ml) were heated at 120 °C for 8 h. To this was added a 10% aqueous NaOH solution (100 ml, 277.5 mmol). After stirring for 2 h at room temperature, the mixture was poured into water to form precipitates, which were filtered. The precipitates were dissolved in acetic acid (250 ml), and to this solution was added powder zinc (10.0 g, 153.0 mmol) at 60 °C. The mixture was stirred for 40 min at the same temperature. A 20% hydrochloric acid (80 ml) was then and stirred for 10 min. The mixture was filtered and the filtrate was neutralized with a 5% aqueous $NaHCO_3$ solution to form precipitates, which were filtered, washed with water, and dried under reduced pressure. Recrystallization from EtOH gave **12** (2.88 g, 53%). Mp 193—195 °C (from $CHCl_3$); IR (KBr) 3420 and 3260 cm^{-1}; ^1H NMR ($CDCl_3$) δ=5.60—5.85 (4H, m), 6.83—7.20 (4H, m), and 7.60—7.83 (2H, m); MS m/z 346 (M^+; 100) and 344 (M^+; 91). Found: C, 34.81; H, 2.74; N, 16.46%. Calcd for $C_{10}H_{10}N_4Se_2$: C, 34.90; H, 2.93; N, 16.28%.

Preparation of 6-Methyl-5*H*-naphtho[2,1-*b*]pyrido[3,2-*e*]-[1,4]selenazin-5-one (14). Method A: solution of **12** (25 mg, 0.07 mmol) and triphenylphosphine (40 mg, 0.15 mmol) in acetonitrile (3 ml) was ultrasonically stirred under argon atmosphere at room temperature for 5 min. To this was added a 5% aqueous NaOH solution (100 µl, 0.13 mmol) and stirred for 15 min. Then, 2-bromo-3-methyl-1,4-naphthoquinone

(**13**) (30 mg, 0.12 mmol) was added and stirred for 40 min. The mixture was poured into a water (20 ml) to form precipitates, which were filtered washed with water (10 ml), dried under reduced pressure. Column chromatography on silica gel with toluene–ethyl acetate (8:2) as eluent yielded **14** (36 mg, 91%).

Method B: The reaction of **13** (30 mg, 0.12 mmol) with 3-amino-2-pyridineselenolate ion generated from **12** using tributylphosphite (38 μl, 0.15 mmol) gave **14** (37 mg, 93%). Mp 237—238 °C (from benzene); IR (KBr) 1620 cm^{-1}; ^1H NMR (DMSO-d_6, 90 °C) δ=2.10 (3H, s), 7.54—7.66 (1H, m), 7.76—7.92 (2H, m), 8.14—8.30 (2H, m), 8.51—8.60 (1H, m), and 8.72—8.82 (1H, m); MS *m/z* 326 (M^+; 100) and 324 (M^+; 56). Found: C, 59.34; H, 3.10; N, 8.51%. Calcd for $C_{16}H_{10}N_2OSe$: C, 59.09; H, 3.10; N, 8.61%.

Reaction of 2,3-Dichloro-1,4-naphthoquinone (15) with 3-Amino-2-pyridineselenolate Ion Generated from 12. Method A: The reaction of **15** (30 mg, 0.13 mmol) with selenolate ion generated from **12** (30 mg, 0.09 mmol), triphenylphosphine (50 mg, 0.19 mmol), and a 5% aqueous NaOH solution (112 μl, 0.15 mmol), gave 6-chloro-5*H*-naphtho[2,1-*b*]pyrido[3,2-*e*]-[1,4]selenazin-5-one (**16**) (28 mg, 61%) and pyrido[2,3-*b*]-pyrido[3″,2″:5′,6′][1,4]selenazino[2′,3′:3,4]naphtho[1,2-*e*][1,4]selenazine (**17**) (11 mg, 18%).

Method B: The reaction of **15** (30 mg, 0.13 mmol) with 3-amino-2-pyridineselenolate ion generated from **12** using tributylphosphine (48 μl, 0.19 mmol) gave **16** (9 mg, 20%) and **17** (33 mg, 54%).

16: Mp 282—285 °C (from benzene); IR (KBr) 1628 cm^{-1}; ^1H NMR (DMSO-d_6, 90 °C) δ=7.64—7.72 (1H, m), 7.87—7.99 (2H, m), 8.22—8.33 (1H, m), 8.36—8.45 (1H, m), 8.62—8.68 (1H, m), and 8.84—8.91 (1H, m); MS *m/z* 348 (M^+; 42), 346 (M^+; 100), and 344 (M^+; 50). Found: C, 52.40; H, 1.99; N, 8.18%. Calcd for $C_{15}H_7ClN_2OSe$: C, 52.12; H, 2.04; N, 8.10%.

17: Mp 280—281 °C (from EtOH); IR (KBr) 1562 cm^{-1}; ^1H NMR ($CDCl_3$) δ=7.36—7.46 (2H, m), 7.74—7.82 (2H, m), 8.04—8.14 (2H, m), 8.43—8.50 (2H, m), and 8.88—8.99 (2H, m); MS *m/z* 466 (M^+; 100) and 464 (M^+; 96). Found: C, 51.80; H, 2.08; N 11,85%. Calcd for $C_{20}H_{10}N_4Se_2$: C, 51.74%; H, 2.17; N, 12.07%.

Reaction of 2,3-Dichloro-5-nitro-1,4-naphthoqionone[7] (18) with 3-Amino-2-pyridineselenolate Ion Generated from 12. Method A: The reaction of **18** (60 mg, 0.22 mmol) with selenolate ion generated from **12** (50 mg, 0.15 mmol), triphenylposphine (84 mg, 0.32 mmol), and a 5% aqueous NaOH solution (190 μl, 0.25 mmol), gave 6-chloro-1-nitro-5*H*-naphtho[2,1-*b*]pyrido[3,2-*e*][1,4]selenazin-5-one (**19**) (40 mg, 47%), 6-chloro-4-nitro-5*H*-naphtho[2,1-*b*]pyrido[3,2-*e*][1,4]-selenazin-5-one (20) (16 mg, 19%), and 6-nitropyrido[2,3-*b*]-pyrido[3″,2″:5′,6′][1,4]selenazino[2′,3′:3,4]naphtho[1,2-*e*]-[1,4]selenazine (**21**) (19 mg, 17%).

Method B: The reaction of **18** (60 mg, 0.22 mmol) with 3-amino-2-pyridineselenolate ion generated from **12** using tributylphosphine (80 μl, 0.32 mmol) gave **19** (26 mg, 30%), **20** (15 mg, 18%), and **21** (45 mg, 40%).

19: Mp 277 °C (from EtOH); IR (KBr) 1635, 1523, and 1372 cm^{-1}; ^1H NMR ($CDCl_3$) δ=7.56—7.68 (1H, m), 7.84—8.11 (3H, m), 8.36—8.44 (1H, m), and 8.50—8.66 (1H, m); MS *m/z* 393 (M^+; 40), 391 (M^+; 100), nad 389 (M^+; 47). Found: C, 46.28; H, 1.51; N, 10.82%. Calcd for $C_{15}H_6ClN_3O_3Se$: C, 46.12; H, 1.55; N, 10.76%.

20: Mp 313 °C (from EtOH); IR (KBr) 1620, 1522, and 1362 cm^{-1}; ^1H NMR (DMSO-d_6, 90 °C) δ=7.70—7.80 (1H, m), 8.09—8.16 (2H, m), 8.44—8.52 (1H, m), 8.68—8.74 (1H, m), and 9.08—9.16 (1H, m); MS *m/z* 393 (M^+; 45), 391 (M^+; 100), and 389 (M^+; 47). Found: C, 46.09; H, 1.48; N, 10.71%. Calcd for $C_{15}H_6ClN_3O_3Se$: C, 46.12; H, 1.55; N, 10.76%.

21: Mp 332 °C (from benzene); IR (KBr) 1514 and 1352 cm^{-1}; ^1H NMR (DMSO-d_6, 90 °C) δ=7.39—7.53 (1H, m), 7.74—7.82 (1H, m), 7.86—8.00 (2H, m), 8.08—8.18 (1H, m), 8.42—8.52 (2H, m), and 9.02—9.10 (1H, m); MS *m/z* 511 (M^+; 100) and 509 (M^+; 89). Found: C, 47.18; H, 1.70; N, 13.50%. Calcd for $C_{20}H_9N_5O_2Se_2$: C, 47.17; H, 1.78; N, 13.75%.

Condensation of 6-Chloro-1-nitro-5*H*-naphtho[2,1-*b*]pyrido[3,2-*e*][1,4]selenazin-5-one (19) with 2-Aminobenzenethiol (22). A mixture of **22** (16 mg, 0.13 mmol), Na_2CO_3 (28 mg, 0.26 mmol), and **19** (40 mg, 0.10 mmol) in DMF (1 ml) and toluene (1 ml) was heated at 120 °C for 6 h. The mixture was poured into water (20 ml) to form precipitates, which were filtered, washed with water (10 ml), and dried under reduced pressure. Column chromatography on silica gel with toluene–ethyl acetate (8:2) as eluent yielded 6-nitrobenzo[*b*]pyrido[3″,2″:5′,6′][1,4]selenazino[2′,3′:3,4]naphtho[1,2-*e*][1,4]thiazine (**23**) (26 mg, 57%). Mp 308—309 °C (from benzene); IR (KBr) 1530 and 1377 cm^{-1}; ^1H NMR ($CDCl_3$) δ=7.40—7.54 (3H, m), 7.68—7.90 (5H, m), 8.33—8.44 (1H, m), and 9.10—9.19 (1H, m); MS *m/z* 462 (M^+; 79), 460 (M^+; 43), 430 (100), and 428 (55). Found: C, 54.84; H, 2.11; N, 11.91%. Calcd for $C_{21}H_{10}N_4O_2SSe$: C, 54.67; H, 2.18; N, 12.14%.

Condensation of 6-Chloro-4-nitro-5*H*-naphtho[2,1-*b*]pyrido[3,2-*e*][1,4]selenazin-5-one (20) with 22. The condensation of **20** (15 mg, 0.04 mmol) carried out as above using **22** (6 mg, 0.05 mmol), Na_2CO_3 (11 mg, 0.10 mmol) yielded 9-nitrobenzo[*b*]pyrido[3″,2″:5′,6′][1,4]selenazino[2′,3′:3,4]-naphtho[1,2-*e*][1,4]thiazine (**25**) (15 mg, 81%). Mp 337—339 °C (from benzene); IR (KBr) 1532 and 1375 cm^{-1}; ^1H NMR ($CDCl_3$) δ=7.37—7.47 (2H, m), 7.52—7.60 (2H, m), 7.69—7.79 (3H, m), 7.96—8.03 (1H, m), 8.39—8.43 (1H, m), and 9.09—9.16 (1H, m); MS *m/z* 462 (M^+; 100), 460 (M^+; 52), 430 (53), and 428 (25). Found: C, 54.41; H, 2.58; N, 11.71%. Calcd for $C_{21}H_{10}N_4O_2SSe$: C, 54.67; H, 2.18; N, 12.14%.

Reaction of 6-Chloro-4-nitro-5*H*-benzo[*a*]phenothiazin-5-one (24) with 3-Amino-2-pyridineselenolate Ion Generated from 12. To a mixture containing 3-amino-2-pyridineselenolate ion generated from **12** (20 mg, 0.06 mmol), tributylphosphine (30 μl, 0.12 mmol), and a 5% aqueous NaOH solution (76 μl, 0.10 mmol) as described in the preparation of **14** was added a solution of **24** (30 mg, 0.09 mmol) in DMSO (1 ml). The mixture was heated at 160 °C for 4 h. The mixture was poured into a water (20 ml) to form precipitates, which were filtered, washed with water (10 ml), and dried under pressure. Column chromatography on silica gel with toluene as eluent yielded **23** (13 mg, 32%).

Reaction of 6-Chloro-1-nitro-5*H*-benzo[*a*]phenothiazin-5-one (26) with 3-Amino-2-pyridineselenolate Ion Generated from 12. The reaction of **26** (30 mg, 0.09 mmol) with 3-amino-2-pyridineselenolate ion generated from **12** (20 mg, 0.06 mmol), tributylphosphine (30 μl, 0.12 mmol), and a 5% aqueous NaOH solution (76 μl. 0.10 mmol) gave **25** (22 mg, 52%).

Crystallographic Study. A crystal was obtained by slow crystallization from CH_2Cl_2–hexane. A Rigaku automated four-circle diffractometer AFC-5R was used with graphite monochromated Cu radiation (CuK=1.5418 Å).

Table 2. Final Position Parameters and B_{eq} in Crystal Structure of 7[a)]

Atom	x/a	y/b	z/c	B_{eq}/Å^2
C1	0.1176(8)	−0.0604(7)	−0.2441(8)	3.6(2)
C2	0.2011(9)	−0.1499(8)	−0.282(1)	4.5(3)
C3	−0.068(1)	−0.2864(9)	−0.535(1)	5.4(3)
C4	0.106(1)	−0.2610(9)	−0.427(1)	5.2(3)
C5	−0.151(1)	−0.1957(9)	−0.495(1)	5.0(3)
C6	−0.0581(8)	−0.0839(7)	−0.3486(9)	3.9(2)
C7	0.4432(8)	0.1239(6)	0.3271(8)	3.1(2)
C8	0.3396(8)	0.0210(7)	0.1626(8)	3.6(2)
C9	0.3046(8)	−0.1214(7)	0.1569(8)	3.2(2)
C10	0.3795(7)	−0.1728(6)	0.3295(8)	3.0(2)
C11	0.4845(8)	−0.0736(6)	0.5013(8)	2.9(2)
C12	0.2580(9)	−0.4235(7)	0.167(1)	4.0(2)
C13	0.195(1)	−0.5538(8)	0.225(1)	5.1(3)
C14	0.372(1)	−0.449(1)	0.093(1)	6.1(3)
N1	0.3506(7)	−0.3104(5)	0.3291(7)	3.5(2)
O1	0.4680(6)	0.2528(4)	0.3157(5)	4.0(2)
Se1	0.2482(1)	0.10442(8)	−0.0532(1)	4.20(3)

a) Atoms are labeled as shown in Fig. 1. Estimated standard deviations, in parentheses, occur in the last figures for each parameter. $B_{eq}=(8\pi^2/3)\sum_i\sum_j U_{ij}a^*_i a^*_j \boldsymbol{a}_i \boldsymbol{a}_j$.

Table 3. Selected Bond Lengths and Bond Angles for 7[a)]

	Bond lengths (Å)		
C8–C7	1.417(8)	C11–C11	1.43(1)
C9–C8	1.373(9)	N1–C10	1.331(8)
C9–H1	0.96(4)	N1–C12	1.460(7)
C10–C9	1.488(8)	O1–C7	1.267(7)
C11–C7	1.435(8)	Se1–C1	1.920(6)
C11–C10	1.438(7)	Se1–C8	1.911(6)
	Bond angles (deg)		
C6–C1–C2	120.9(6)	C10–C9–H1	120(3)
Se1–C1–C2	120.2(5)	C11–C10–C9	119.2(5)
Se1–C1–C6	118.8(5)	N1–C10–C9	120.4(5)
C11–C7–C8	116.8(6)	N1–C10–C11	120.4(5)
O1–C7–C8	119.3(5)	C10–C11–C7	119.4(5)
O1–C7–C11	123.9(5)	C11–C11–C7	121.0(6)
C9–C8–C7	124.7(60	C11–C11–C10	119.5(7)
Se1–C8–C7	111.8(5)	C10–N1–C12	126.7(5)
Se1–C8–C9	123.5(4)	C10–N1–H2	112(4)
C8–C9–H1	120(3)	C12–N1–H2	119(4)
C10–C9–C8	118.7(5)	C1–Se1–C8	100.7(3)

a) Labeling corresponds to that indicated in Fig. 1. Estimated standard deviations in parentheses.

$C_{28}H_{28}N_2O_2Se_2$, M_r=582.46; triclinic, $P\bar{1}$, a=9.273 (1) Å, b=9.849 (1) Å, c=8.468 (1) Å, α=93.90 (1)°, β=119.83°, γ=100.64 (1)°, V=647.7 (1) Å^3, D_C=1.493 g cm^{-3}; Crystal size, 0.10×0.20×0.30 mm; 2081Intensities were collected, $2\theta_{max}$=126°.

Structures were solved with the aids of Texsan program system, and refined by the full-matrix least squares program using 1816 greater than $3\sigma(F)$. Non-H atoms were assigned anisotropic temperature factors. Hydrogen atoms were located from a difference Fourier map and refined with the equivalent isotropic temperature factor to that for the bonded carbon atoms.

$$R=0.057,\ R_W=[\sum_W(|F_o|^2-|F_c|^2)^2/\sum_W|F_o|^2]^{1/2}$$

$$W=1/\sigma^2(F^2),\ \Delta\rho_{max}=2.8/\text{eÅ}^3.$$

Atomic scattering factors were employed from "International Table for X-Ray Crystallography". ORTEP was employed for drawing the molecular structures (Fig. 1). All calculations were made on a microVax 3500. Listing of atomic parameters, thermal parameters, selected bond lengths and bond angles are included in the supplementary material Tables 2 and 3.[9)]

We thank Mr. Shigeru Takaoka and Mr. Takuya Seko, Ono Pharmaceutical Co., Ltd., for performing the X-ray structural analysis.

References

1) S. H. Kim, S. Minami, M. Matsuoka, and T. Kitao, *Chem. Express,* **2**, 73 (1987); K. Takagi, S. Kanamoto, K. Itoh, M. Matsuoka, S.H. Kim, and T. Kitao, *Dyes Pigm.,* **8**, 71 (1987); I. Shiratani, N. Sato, H. Nishi, K. Fukuhara, T. Kajiwara, and H. Inokuchi, *Nippon Kagaku Kaishi,* **1986**, 485; K. Kitahara, T. Murakami, T. Mitamura, and H. Nishi, *ibid.,* **1986**, 1329.

2) M. Matsuoka, S. H. Kim, and T. Kitao, *J. Chem. Soc., Chem. Commun.,* **1985**, 1195; S. H. Kim, M. Matsuoka, and T. Kitao, *Chem. Lett.,* **1985**, 1351; H. Nishi, T. Mitamura, K. Kitahara, T. Furukawa, and K. Shinjo, *Nippon Kagaku Kaishi,* **1985**, 1506.

3) K. Hasegawa, M. Sakakibara, T. Ishida, and Y. Ueno, *Bull. Chem. Soc. Jpn.,* **63**, 1467 (1990).

4) T. Ishida, M. Sakakibara, Y. Ueno, and K. Hasegawa, *J. Heterocycl. Chem.,* **26**, 785 (1989).

5) M. Sakakibara, Y. Watanabe, T. Toru, and Y. Ueno, *J. Chem. Soc., Perkin Trans. 1,* in press.

6) S. M. Bloom and G. O. Dudek, *Tetrahedron,* **26**, 1267 (1969).

7) T. Kasai, R. Kurabayashi, Y. Suzuki, A. Yoshida, and S. Tsuruoka, *Yuki Gousei Kagaku Kyokai Shi,* **27**, 162 (1969); *Chem. Abstr.,* **70**, 96456x (1969).

8) S. Nan'ya, E. Maekawa, W-B. Kang, and Y. Ueno, *J. Heterocycl. Chem.,* **23**, 589 (1986).

9) Tables of complete $|F_o-F_c|$ data, anisotropic thermal parameters, and coordinates of hydrogen atoms are deposited as Document No. 8946 at the Office of the Editor of Bull. Chem. Soc. Jpn.

Silicon Effects. II.[1] Structure and Stability of 1-Phenyl-2-(trimethylsilyl)ethyl Cation in Solution

Nobujiro SHIMIZU,* Shin-ichiro WATANABE, and Yuho TSUNO
Department of Chemisty, Faculty of Science, Kyushu University,
Hakozaki 6-10-1, Higashi-ku, Fukuoka 812
(Received March 2, 1991)

Solvolysis rates have been measured in various solvents at 25 °C for 1-(substituted phenyl)-2-(trimethylsilyl)ethyl trifluoroacetates (**1a**—**1g**; R=H, 4-Me, 4-Cl, 4-Br, 3-Cl, 3,4-Cl_2, and 3,5-Cl_2, respectively) and structurally related compounds, 1-phenylethyl-, 3,3-dimethyl-1-phenylbutyl-, and 1-(4-methylphenyl)ethyl trifluoroacetates (**3a**, **4**, and **5**). In dioxane/water mixtures **1g** solvolyzes with the same sensitivity to the change in solvent ionizing power as that for a k_c substrate **5**. The solvolyses of **1e** and **5** exhibit almost identical α-deuterium kinetic isotope effects (k_H/k_D) of 1.18—1.19 in aq dioxane. Substituent effect on the solvolysis of **1** in 90% aq dioxane is expressed by an LArSR equation: $\log k^X/k^H=-3.05$ ($\sigma^\circ+1.05\Delta\bar{\sigma}_R^+$) ($R$=0.9997). These findings are consistent with k_c mechanism for the solvolysis of **1**. Relative rates for the solvolysis of **1a**, **3a**, and **4** in 30% aq dioxane are 2.99×10^5 : 2.84 : 1.0 indicating solvolytic generation of α-(trimethylsilylmethyl)benzyl cation to be about 7 kcal mol^{-1} energetically more favorable than that of the corresponding α-alkylbenzyl cations.

Previously[2] we have shown in a preliminary report that α-(pentamethyldisilanyl)benzyl bromide solvolyzes 2×10^5 times more rapidly than does α-trimethysilybenzyl bromide indicative of a marked β-silicon effect of the disilanyl group. It is of interest to compare the effect of the Si–Si bonds on stability of adjacent carbocations with the effect of the corresponding carbon–silicon bonds. Lambert and co-workers have shown that an anti β-$SiMe_3$ group exerts a rate-acceleration effect of 2.4×10^{12} relative to hydrogen in the solvolysis of cyclohexyl derivatives suggesting a β-$SiMe_3$ group to stabilize cyclohexyl cation by about 17 kcal mol^{-1} (1 cal=4.184 J) relative to hydrogen.[3] Seemingly, the β-silicon effect appears much less effective in a $R^1R^2C^+$–Si–$SiMe_3$ system than in a $R^1R^2C^+$–C–$SiMe_3$ system, although the Si–Si single bonds possess low ionization potentials as compared to the C–Si bonds.[4] However, a direct comparison of the β-silicon effects in the benzylic and cyclohexyl solvolyses is not justified. There is a marked difference in the electronic demands at the carbenium carbon in the two systems. Theoretical study[5] indicates marked dependence of the β-silicon effect on the electronic demands of the carbocations as well as on the stereoelectronic restraint for the β-silicon group. In order to discuss the effect of the disilanyl group, it is therefore desirable to estimate the β-silicon effect of the corresponding silylmethyl group in the same benzylic system. This paper describes kinetic details on the solvolysis of 1-aryl-2-(trimethylsilyl)ethyl trifluoroacetates (**1a**—**1g**) and related α-alkylbenzyl trifluoroacetates **3**—**5**, and discusses mechanistic implications on the β-silicon effect in the benzylic solvolysis.

Results

The trifluoroacetates **1a**—**1g** were prepared by treatment of the corresponding alcohols **2** with trifluoroacetic anhydride in the presence of pyridine.[3] The trifluoroacetates **1** were labile at room temperature and a crude

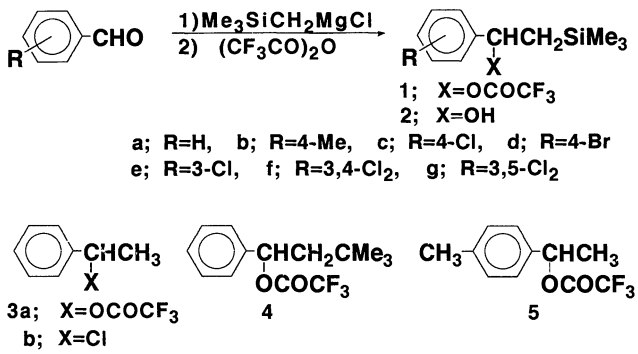

product was directly used for kinetic measurements. We used three α-alkylbenzyl trifluoroacetates as alkyl reference standards. They were 1-phenylethyl trifluoroacetate (**3a**), 3,3-dimethyl-1-phenylbutyl trifluoroacetate (**4**), and 1-(4-methylphenyl)ethyl trifluoroacetate (**5**). Oxidation of **2e** followed by reduction with $LiAlD_4$ gave corresponding α-deuterated alcohol, which was converted into its trifluoroacetate **1e**-α-d_1.

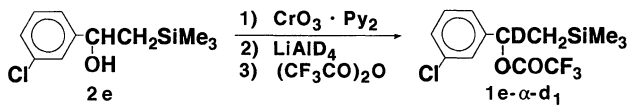

Solvolysis reactions were followed spectrometrically at 25.0±0.05 °C by measuring either increase in produced trifluoroacetic acid as its acridinium salt[1] or increase in styrene derivatives which were formed practically as a single product under solvolytic conditions. All the solvolyses followed good first-order kinetics over 3 to 4 half-lives (correlation coefficient R>0.9999) and both methods gave identical rate constants within experimental error (±3%). We also compared spectrometric rates with conductimetric rates in several cases; for example, a spectrometric rate for the solvolysis of **1e** in

Table 1. Solvolysis Rates for **1**, **3a**, **4**, and **5** at 25.0±0.05°C

Substrate	Solvent[a]	10^{-5} k/s^{-1}[b]	$\Delta H^{\neq}_{298}$ kcal mol^{-1}	$\Delta S^{\neq}_{298}$ cal K^{-1} mol^{-1}
1a	90D	752 ±11[c]	17.8[d]	−8.5[d]
	95D	128 ±0.5		
1b	90D	7450[e]	17.1[f]	−6.3[f]
	95D	1200±0.3		
1c	90D	371 ±3[g]		
1d	90D	306 ±0.1		
1e	90D	52.6 ±0.8[h]		
	80D	374 ±5.1[c]		
	90A	277 ±0.1		
	EtOH	225 ±0.2		
1f	90D	41.6 ±0.02		
1g	90D	5.45 ±0.02[g]	20.4[i]	−9.6[i]
	80D	35.2 ±0.02		
	70D	154 ±0.1		
	60D	618 ±0.2		
	50D	2570±23[j]	16.1[k]	−11.6[k]
	90A	31.3 ±0.1		
	80A	135 ±0.2		
	70A	413 ±0.3		
	60A	1210±1.0		
	EtOH	24.9 ±0.06		
	80E	355 ±0.8		
	MeOH	171 ±0.05		
3a	30D	35.2 ±0.3[g]		
4	30D	12.3 ±0.2[g]		
5	60D	4.40 ±0.002		
	50D	19.1 ±0.02	18.9[l]	−12.3[l]
	40D	59.8 ±0.8[g]	18.4[m]	−11.3[m]
	30D	200 ±0.5		
	20D	567 ±1.0[g]		
	97T	91.5 ±0.02		
	60A	5.80 ±0.02		
	40A	75.8 ±0.1		
	30A	236 ±0.5		
	20A	657 ±1.0		
	50E	37.3 ±0.3[g]		
	40E	130 ±0.1		
	30E	495 ±0.4		

a) A: acetone/water (v/v), D: dioxane/water (v/v), E: ethanol/water (v/v), and 97T: 97/3 (w/w) trifluoroethanol/water mixtures. b) Single run except otherwise noted. c) Average of four runs. d) Calculated from the following rates: 10^5 k/s^{-1} (temp/°C) 113 (7.6), 189 (11.7), 296 (16.0), 494 (20.5), and 752 (25.0). e) Extrapolated value from other temperatures. f) Calculated from the following rates: 10^5 k/s^{-1} (temp/°C) 4680 (20.5), 2890 (16.0), 1920 (11.7), 1130 (7.6), and 687 (2.9). g) Average of two runs. h) Average of six runs. i) Calculated from the following rates: 10^5 k/s^{-1} (temp/°C) 5.45 (25.0), 60.3 (46.2), and 451 (67.4). j) Average of three runs. k) Calculated from the following rates: 10^5 k/s^{-1} (temp/°C) 696 (11.7), 1071 (16.0), 1733 (20.5), and 2570 (25.1). l) Calculated from the following rates: 10^5 k/s^{-1} (temp/°C) 19.1 (25.0), 47.5 (33.8), and 127 (43.2). m) Calculated from the following rates: 10^5 k/s^{-1} (temp/°C) 14.4 (11.7), 23.8 (16.0), 59.8 (25.0), 161 (34.3), and 418 (43.2).

90% aq acetone at 25.0°C measured by the acridine method, k=(2.765±0.003)×10^{-3} s^{-1}, was identical to a conductimetric rate, k=(2.772±0.001)×10^{-3} s^{-1}. The conductimetric method could not be successfully applied to the solvolyses in 90% aq dioxane because of a poor conductimetrical response of trifluoroacetic acid. Table 1 summarizes solvolysis rates for **1a**—**1g**, **3a**, **4**, and **5** in various solvents including 20/80 to 95/5 (v/v) dioxane/water (D series), 20/80 to 90/10 (v/v) acetone/water (A series), 30/70 to 100/0 (v/v) ethanol/water (E series), 97/3 (w/w) 2,2,2-trifluoroethanol (TFE)/water (T series) binary mixtures and methanol. Table 2 shows the β-silicon effect in the α-alkylbenzyl solvolysis.

α-Deuterium kinetic isotope effects (KIE) were measured for the solvolysis of **1e** in 80D and in 90D. We also measured KIE for the solvolysis of the reference compound **5** in 40D for comparison. The results are given in Table 3.

Solvent effects were examined for **1g**. Unfortunately, a solvent ionizing power scale for the trifluoroacetoxy

Table 2. β-Silicon Effect in Benzylic Solvolysis[a]

ArCHCH$_2$R OCOCF$_3$		Solvent	k/s^{-1}	k_{rel}
Ar	R			
4-CH$_3$C$_6$H$_4$	SiMe$_3$	50D	35.2[b]	1.84×10^5
	H	50D	1.91×10^{-4}	1.0
C$_6$H$_5$	SiMe$_3$	30D	36.8[c]	2.99×10^5
	H	30D	3.52×10^{-4}	2.86
	t-Bu	30D	1.23×10^{-4}	1.0

a) At 25.0°C. b) Extrapolated value from k(**1g**) in 50D and a rate ratio k(**1b**)/k(**1g**)=1.37×10^3 in 90D. c) Extrapolated value from k(**1g**) in 50D and rate raios k(**1a**)/k(**1g**)=138 in 90D and k_{30D}/k_{50D}=10.4 for **4**.

Table 3. α-Deuterium Kinetic Isotope Effects[a]

Substrate	Solvent	10^5k/s^{-1}	k_H/k_D
1e	80D	347.5 ±2.6[b]	
1e-α-d_1		293.2 ±2.3[c]	1.185±0.018
1e	90D	52.63±0.76[d]	
1e-α-d_1		44.57±1.00[e]	1.181±0.044
5	40D	59.81±0.78[e]	
5-α-d_1		50.76±0.07[e]	1.178±0.017

a) At 25.0±0.05°C. b) Average of seven runs. c) Average of six runs. d) Average of four runs. e) Average of two runs.

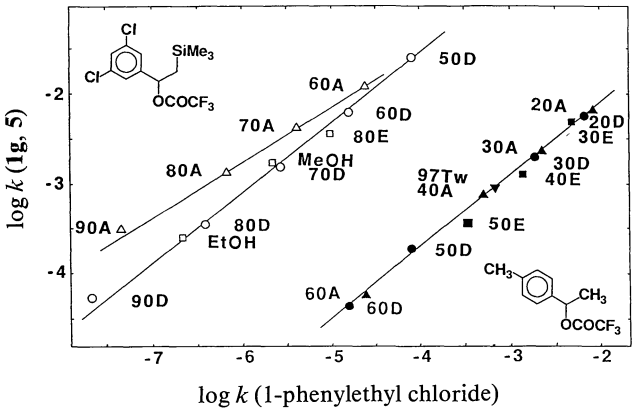

Fig. 1. Plots of log k for **1g** (open circles, triangles, and squares) and **5** (closed circles, triangles, and squares) vs. log k (1-phenylethyl chloride **3b**) in various solvents.

leaving group is not available; so we chose 1-phenylethyl chloride (**3b**) as a standard benzylic substrate undergoing k_c solvolysis.[6,7] Figure 1 represents a plot of the rates (log k) for **1g** against log k for **3b**[6] in various solvents. Aq dioxane and alcoholic solvents show a single linear response with a slope (m') of 0.78, while acetone/water mixtures exhibit a separate line (m'=0.61). Figure 1 includes a log k–log k plot for **5** for comparison. Judging from a comparable nucleofugality of the trifluoroacetoxy leaving group to that of Cl,[8] we can

Table 4. Comparison of Solvent Effect

Substrate	m'[a]	
	For aq dioxane	For all solvents
1g	0.80 (n=4, R=0.999)[b]	0.78 (n=7, R=0.999)[c]
5	0.79 (n=4, R=0.999)	0.80 (n=12, R=0.999)

a) Slope for a plot of log k vs. log k (1-phenylethyl chloride) (Ref. 6). b) Except for 90D. c) Except for aq acetone and 90D.

assume k_c mechanism for the solvolysis of **5**. This is consistent with the fact that the solvolysis rates for **5** exhibit a linear response to those for **3b** for a range of solvents of varying solvent nucleophilicity and ionizing power including aq dioxane, aq acetone, aq ethanol, and aq trifluoroethanol. A significantly reduced slope for **5**, m'=0.80 relative to the chloride **3b**, should be ascribed to the leaving group effect. Since trifluoroacetate ion is a highly delocalized species, it must be less strongly solvated hence less sensitive to the change in solvent ionizing power than chloride ion. Table 4 shows a comparison of the solvent effect between the solvolyses of **1g** and **5**.

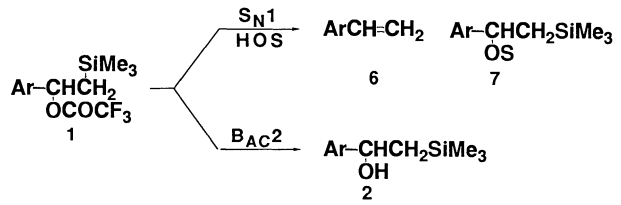

Solvolytic reactions of **1** in aq dioxane and ethanol gave the corresponding styrenes (**6**) exclusively. In the case of the reaction of **1e** in methanol, a significant amount (14%) of a methanolysis product **7** was also formed. Under basic conditions, however, was produced the alcohol **2** as the major product instead. For example, a reaction of **1e** in methanol containing sodium methoxide (0.09 M; 1 M=1 mol dm^{-3}) gave **2e** in 93% yield. The formation of **2** undoubtedly arises from a $B_{AC}2$ reaction of the trifluoroacetates. Amines promoted this process and hence accelerated the rate of reaction; the presence of 0.01 M triethylamine accelerated the reaction rate of **1g** in 70D by a factor of 4.85. Thus, the amine-induced $B_{AC}2$ reaction may become a serious problem in the rate measurement for the solvolysis of the trifluoroacetates **1** when acridine is used as a monitoring base. Fortunately, however, we found that acridine did not affect significantly the rate of the solvolysis under solvolytic conditions at acridine concentrations around 10^{-4} M; for instance, the solvolyses of **1g** in 70D in the presence of 1.0×10^{-3} M acridine showed an identical rate constant to that measured in the absence of acridine within experimental error: k=1.58×10^{-3} and 1.54×10^{-3} s^{-1} at 25°C, respectively.

Discussion

Table 2 indicates that a β-$SiMe_3$ group exerts a rate-acceleration effect of (1—3)$\times 10^5$ relative to hydrogen or *t*-Bu in the α-alkylbenzyl solvolysis. Although the solvolysis of α-alkylbenzyl derivatives is subjected to the steric effect of the α-alkyl groups,[2,9,10] a rate ratio of **1a** and a structurally related compound **4** provides a reasonable estimate for the β-silicon effect in the benzylic solvolysis. The rate acceleration by the β-silicon can be interpreted either by a σ-participation mechanism (k_Δ) via a bridged siliconium ion intermediate **8** or by a simple ionization mechanism (k_c) via an open 1-aryl-2-(trimethylsilyl)ethyl cation **9**.[3,11-15]

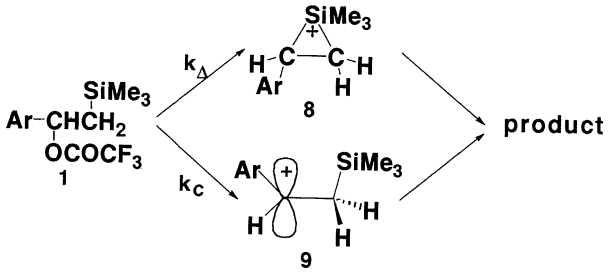

The following kinetic features are informative on the structure of the transition state. First, the KIE for **1g**, i.e., k_H/k_D=1.18—1.19 in aq dioxane, is comparable to the KIE, k_H/k_D=1.18, for the reference compound **5** which can be assumed to be a k_c substrate (Table 3). These isotope effects can be compared with KIE values for the typical k_c solvolysis of α-alkylbenzyl derivatives e.g., k_H/k_D=1.157 for the solvolysis of 1-(4-methoxyphenyl)ethyl chloride in aq ethanol.[16] Apparently, the isotope effect indicates a striking resemblance in the structures of the transition state for the solvolysis of **1g** and **5**.

Second, solvolytic reactivities of a series of 1-aryl-2-(trimethylsilyl)ethyl trifluoroacetates **1a**—**1g** were well linearly correlated with σ^+ [17] affording a ρ^+ value of -3.07 (R=0.9997). The application of the LArSR equation (Eq. 1)[18] gave an almost identical expression with a resonance parameter close to unity, r=1.05, and a reaction constant ρ=-3.05 (R=0.9997, SD=0.029).[19]

$$\log k^X/k^H = \rho(\sigma^\circ + r\Delta\bar{\sigma}_R^+) \quad (1)$$

The limited number of π-donor substituents may not give us a precise r value; nevertheless, a rather high r value around 1.0 is apparently inconsistent with the bridged siliconium ion intermediate **8**. The result is interestingly compared with the substituent effect for the α-alkylbenzyl solvolysis which has been characterized by r close to 1.15 and ρ around -5.[20] A reduced r value for **1** is quite reasonable judging from the anticipated high stability of the cation **9a** as compared to 1-phenylethyl cation. It has been shown that r decreases with increasing stability of the benzylic cations $ArC^+R^1R^2$.[20] The rate ratio, k(**1a**)/k(**3a**)=1.1$\times 10^5$, would suggest the electronic demand of the carbenium carbon in the cation **9a** to be comparable to that in the α,α-dimethylbenzyl cation which is characterized by r=1.0 by definition.[18]

It is also instructive to note that **1g** and **5** showed very similar activation entropies in their solvolyses in a common solvent. For example, it is clear from Table 1 that a rate ratio of **1g** to **5** observed in 50D at 25 °C of a factor of 135 is entirely attributable to a 2.8 kcal mol^{-1} low enthalpy of activaion for **1g** relative to **5**. Again the result is more in accord with thr k_c mechanism than with the k_Δ mechanism which must involve substantial restraint of rotational motions at the transition state.

Finally it should be noted that in a log k–log k (**3b**) plot (Fig. 1), **1g** showed an identical slope to that for **5** (Table 4). This means that **1g** solvolyzes with the same susceptibility to the change in solvent ionizing power as that for **5** indicative of a marked resemblance in mechanism for ionization of the two substrates. Obviously, the solvent effect support the k_c solvolysis for **1**, although we do not understand quite well the origin for deviations of aq acetone at present.

Thus, the combined results lead us to conclude that **1** solvolyzes via rate-determining formation of a classical 1-aryl-2-(trimethylsilyl)ethyl cation **9**. The cation must be effectively stabilized by the β-$SiMe_3$ group through hyperconjugation.[5,21] It is worth stating that the k_c mechanism has been proposed also for the solvolysis of α-(pentamethyldisilanyl)benzyl halides which cleanly give 1,2-$SiMe_3$ rearranged products seemingly suggestive of σ-participation.[2] Extensive hyperconjugative interactions between the β-C–$SiMe_3$ σ-bond and the carbenium carbon would naturally involve changes in bond angles and bond lengths associated with the β-silicon atom.[5] However, the absence of compelling evidence suggesting bond-forming interactions between the β-silicon and the benzylic carbon leads us at present to prefer a simple k_c mechanism to a σ-participated ionization. The k_c mechanism for **1** is compatible with the recent theoretical[5] and experimental results in the gas phase[22] that an open structure of β-silyl-substituted alkyl cations is energetically more favorable than a bridged form except for the primary cation which preferably takes a bridged form. It can thus be said that the solvolytic generation of 1-phenyl-2-(trimethylsilyl)ethyl cation is about 7 kcal mol^{-1} energetically more favorable than that of the corresponding α-alkylbenzyl cations.

Noteworthy is a marked reduction in ρ value for the k_c solvolysis of **1** indicative of substantial dispersion of the positive charge on the benzylic carbon to the β-C–$SiMe_3$ σ-bond in the transition state without significant bridging of the β-silicon. This would undoubtedly result from the electronic interaction between the empty 2p orbital and the β-C–Si bond, although it is not clear at present whether such the interaction is purely hyperconjugative or includes intramolecular charge or elec-

tron transfer interaction as illustrated by the structure **10**.

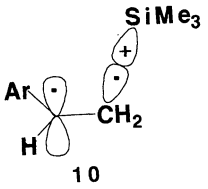

10

The β-silicon effects in the present α-alkylbenzyl system as well as in the α-silylbenzyl system[2] are obviously much smaller than would be expected from a reported rate-acceleration of 2.4×10^{12} in the cyclohexyl solvolysis corresponding to a reduction of activation energy by 17 kcal mol^{-1} by a β-$SiMe_3$ group relative to hydrogen.[3] The reduced β-silicon effect would undoubtedly arise from the low electronic demands at the carbenium carbon for benzylic cations as compared to cyclohexyl cation. Li and Stone[22] have shown from the gas-phase experiments that the stabilization of the carbocations afforded by a β-$SiMe_3$ group relative to hydrogen markedly decreases with increasing stability of the parent carbocations from 38 kcal mol^{-1} for isopropyl cation to 22 kcal mol^{-1} for 1-phenylethyl cation. The difference in the β-silicon effect between the secondary alkyl and 1-phenylethyl cations by 16 kcal mol^{-1} in the gas phase reasonably accounts for the observed ca. 10 kcal mol^{-1} difference in the β-silicon effect between the α-alkylbenzyl and cyclohexyl solvolyses.

Experimental

IR spectra were recorded on a Hitachi R-215 spectrophotometer. NMR spectra were taken on a Hitachi R-20B spectrometer in carbon tetrachloride using TMS as internal standard. GLC were performed with a Hitachi 163 gas chromatograph using a 4 mm×2 m column packed with 5% Silicone GE SE-30 on Chamelite CS. UV spectra were recorded on a Hitachi 220A spectrophotometer equipped with a programmed data printer.

Dioxane was refluxed first with potassium hydroxide for 3 days, then with sodium for 3 days, and distilled. Acetone was refluxed with potassium permanganate and the distillate was dried over potassium carbonate and fractionated. Ethanol was distilled twice over sufficient amounts of magnesium ethoxide.

1-Aryl-2-(trimethylsilyl)ethyl Trifluoroacetates (1a—1g). These trifluoroacetates were prepared from the corresponding alcohols **2** according to the literature method.[3] The alcohols **2** were prepared by the Grignard reaction between the corresponding benzaldehyde and (trimethylsilyl)methylmagnesium chloride. A typical example is shown below:

To a stirred solution of (trimethylsilyl)methylmagnesium chloride prepared from trimethylsilylmethyl chloride (4.88 g, 40 mmol) and Mg (1.07 g) in ether (50 cm^3) was added a solution of 3-chlorobenzaldehyde (5.07 g, 36 mmol) in ether (25 cm^3) at room temperature. The mixture was stirred for 3 h at ambient temperature. A crude oil obtained after workup was distilled to give 4.75 g (93%) of 1-(3-chlorophenyl)-2-(trimethylsilyl)-ethanol (**2e**) as a colorless oil: Bp 121—121.5 °C (1.5 Torr; 1 Torr=133.3 Pa); IR (neat) 3350, 1250, 860, 840, 785 cm^{-1}; ^{1}H NMR δ=0.0 (9H, s), 1.03—1.17 (2H, m), 2.32 (1H, broad s, OH), 4.72 (1H, t, J=7.2 Hz), 7.20—7.29 (4H, m). Found: C, 57.66; H, 7.46%. Calcd for $C_{11}H_{17}ClOSi$: C, 57.75; H, 7.49%. To a stirred solution of **2e** (286 mg, 1.3 mmol) and pyridine (2.5 mmol) in ether (4 cm^3) precooled in an ice-salt bath was added slowly trifluoroacetic anhydride (525 mg, 2.5 mmol) in ether (2 cm^3) and the mixture was stirred for 30 min at that temperature. Pentane (15 cm^3) was added. Organic layer was decanted, washed first with 10% hydrochloric acid, then with aq $NaHCO_3$, and dried. Solvent was removed under reduced pressure affording a crude oil which was shown to be a practically pure 1-(3-chlorophenyl)-2-(trimethylsilyl)ethyl trifluoroacetate (**1e**; 353 mg, 87%) by ^{1}H NMR analysis: IR 1780, 1255, 1220, 1150, 860, 840, 780 cm^{-1};^{1}H NMR δ=—0.06 (9H, s), 1.33—1.47 (2H, m), 5.89 (1H, t, J=7.8 Hz), 7.27 (4H, broad s). Found: C, 48.33; H, 4.97%. Calcd for $C_{13}H_{16}ClF_3O_2Si$: C, 48.07; H, 4.97%.

In a similar procedure, the following alcohols and their trifluoroacetates were prepared.

1-Phenyl-2-(trimethylsilyl)ethanol (**2a** in 98% yield): IR 3350, 1250 cm^{-1}; ^{1}H NMR δ=—0.09 (9H, s), 1.00—1.13 (2H, m), 1.74 (1H, s, OH), 4.68 (1H, t, J=7.8 Hz), 7.18 (5H, broad s). Found: C, 67.81; H, 9.19%. Calcd for $C_{11}H_{18}Si$: C, 67.98; H, 9.38%. **1a**: ^{1}H NMR δ=—0.11 (9H, s), 1.45 (2H, d, J=7.8 Hz), 5.93 (1H, t, J=7.8 Hz), 7.33 (5H, broad s).

1-(4-Methylphenyl)-2-(trimethylsilyl)ethanol (**2b**; 98%): IR 3350, 1250, 860, 820 cm^{-1}; ^{1}H NMR δ=—0.06 (9H, s), 1.08 (2H, d, J=6.6 Hz), 1.50 (1H, s, OH), 4.70 (1H, t, J=6.6 Hz), 7.08 (4H, broad s). Found: C, 69.11; H, 9.80%. Calcd for $C_{12}H_{20}OSi$: C, 69.17; H, 9.67%. **1b**: ^{1}H NMR δ=—0.11 (9H, s), 1.44 (2H, d, J=7.8 Hz), 2.35 (3H, s), 5.89 (1H, t, J=7.8 Hz), 7.18 (4H, broad s).

1-(4-Chlorophenyl)-2-(trimethylsilyl)ethanol (**2c**, 95%): ^{1}H NMR δ=—0.04 (9H, s), 1.03—1.17 (2H, m), 1.68 (1H, s, OH), 4.73 (1H, t, J=7.2 Hz), 7.22 (4H, broad s). Found: C, 57.96; H, 7.49%. Calcd for $C_{11}H_{17}ClOSi$: C, 57.75; H, 7.49%. **1c**: ^{1}H NMR δ=—0.07 (9H, s), 1.33—1.47 (2H, m), 5.90 (1H, t, J=8.4 Hz), 7.31 (4H, broad s).

1-(4-Bromophenyl)-2-(trimethylsilyl)ethanol (**2d**, 96%): IR 3350, 1250, 860, 825 cm^{-1}; ^{1}H NMR δ=0.03 (9H, s), 1.00—1.13 (2H, m), 1.71 (1H, s, OH), 4.72 (1H, t, J=7.2 Hz), 7.06—7.48 (4H, m). Found: C; 48.20, H; 6.27%. Calcd for $C_{11}H_{17}BrOSi$: C; 48.35, H; 6.27%. **1d**: ^{1}H NMR δ=—0.07 (9H, s), 1.32—1.47 (2H, m), 5.89 (1H, t, J=7.8 Hz), 7.16—7.58 (4H, m).

1-(3,4-Dichlorophenyl)-2-(trimethylsilyl)ethanol (**2f**, 93%): IR 3350, 1250, 1130, 860, 840 cm^{-1}; ^{1}H NMR δ=—0.02 (9H, s), 0.97—1.11 (2H, m), 1.97 (1H, s, OH), 4.70 (1H, at, J=7.2 Hz), 6.97—7.42 (3H, m). **1g**: IR 1775, 1250, 1220, 1175, 855, 840, 795 cm^{-1}; ^{1}H NMR δ=—0.03 (9H, s), 1.31—1.48 (2H, m), 5.88 (1H, m), 7.10—7.53 (3H, m). Found: C, 43.54; H, 4.20%. Calcd for $C_{13}H_{15}Cl_2F_3O_2Si$: C, 43.46; H, 4.21%.

1-(3,5-Dichlorophenyl)-2-(trimethylsilyl)ethanol (**2g**, 92%): IR 3350, 1250, 850, 835, 795 cm^{-1}; ^{1}H NMR δ=0.0 (9H, s), 0.98—1.12 (2H, m), 1.70 (1H, s, OH), 4.70 (1H, t, J=7.8 Hz), 7.18 (3H, broad s). **1g**: IR 1765, 1250, 1140, 860, 840 cm^{-1}; ^{1}H NMR δ=0.0 (9H, s), 1.30—1.49 (2H, m), 5.87 (1H, t, J=7.8 Hz), 7.23—7.36 (3H, m). Found: C, 43.49; H, 4.23%. Calcd for $C_{13}H_{15}Cl_2F_3O_2Si$: C, 43.46; H, 4.21%.

1-Phenylethyl Trifluoroacetate (3a): Bp 33-33.5 °C (1 Torr) [lit,[8] bp 32 °C (0.5 Torr)]; IR 1785, 1230, 1160 cm^{-1}; ^1H NMR δ=1.68 (3H, d, J=6.6 Hz), 5.99 (1H, q, J=6.6 Hz), 7.33 (5H, broad s).

3,3-Dimethyl-1-phenylbutyl Trifluoroacetate (4): Bp 50—55 °C (1 Torr); IR 1780, 1225, 1170, 1150 cm^{-1}; ^1H NMR δ= 0.97 (9H, s), 1.76—2.07 (2H, m), 5.84—6.05 (1H, m), 7.29 (5H, broad s). Found: C, 61.44, H, 6.28%. Calcd for $C_{14}H_{17}F_3O_2$: C, 61.31; H, 6.25%.

1-(4-Methylphenyl)ethyl Trifluoroacetate (5): Bp 30—31 °C (0.5 Torr); IR 1780, 1220, 1160, 810 cm^{-1}; ^1H NMR δ=1.64 (3H, d, J=6.6 Hz), 2.34 (3H, s), 5.95 (1H, q, J=6.6 Hz), 7.16 (4H, broad s). Found: C, 56.94; H, 4.78%. Calcd for $C_{11}H_{11}F_3O_2$: C, 56.90; H, 4.78%.

Kinetic Procedure. Solvolyses were followed spectrophotometrically by measuring increase in trifluoroacetic acid as its acridinium ion at 402.5 nm[1] or increase in producing styrenes at 252 nm by using (0.5—2)$\times 10^{-4}$ M solutions. In the former case, the solvolysis was carried out in the presence of (1—3)$\times 10^{-4}$ M acridine and 1.0×10^{-4} M of acridinium trifluoroacetate. The initial addition of the acridinium salt was necessary for linear response of absorbance to concentration of acridinium ion under solvolysis conditions.[1]

Product Studies. Solvolysis reactions were performed with 0.02—0.04 M solutions of a substrate in a given solvent at 25 °C and a crude product obtained after workup was directly analyzed by GLC using an appropriate internal standard. A reaction of **1d** in ethanol qunatitatively gave *p*-bromostyrene (**6d**). A reaction of **1e** in 90% aq dioxane gave *m*-chlorostyrene (**6e**) in 95% yield. A reaction of **1e** in methanol gave **6e** and *m*-chloro-α-ethoxy-α-(trimethylsilylmethyl)toluene (**7e**) in 86 and 14% yield, respectively. **7e**: IR 1250, 1100, 860 cm^{-1}; ^1H NMR δ=−0.04 (9H, s), 0.94—1.15 (2H, m), 3.10 (3H, s), 4.10 (1H, dd, J=8.5 and 6.6 Hz), 7.17 (4H, broad s). A reaction of **1e** in methanol containing sodium methoxide (0.087 M) gave a mixure of **2e**, **6e**, and **7e** in the ratio 1.0 : 0.04 : 0.03. A reaction of **1e** in methanol in the presence of equimolar amounts of lutidine gave a mixture of **6e**, **7e**, and **2e** in the ratio 1.0 : 0.37 : 0.02.

The present work was supported by a Grant-in-Aid for Scientific Research No. 01470025 from the Ministry of Education, Science and Culture.

References

1) Part I. N. Shimizu, E. Osajima, and Y. Tsuno, *Bull. Chem. Soc. Jpn.*, **64**, 1145 (1991).

2) N. Shimizu, C. Kinoshita, and Y. Tsuno, *Chem. Lett.*, **1990**, 1937.

3) J. B. Lambert, G.-t. Wang, R. B. Finzel, and D. H. Teramura, *J. Am. Chem. Soc.*, **109**, 7838 (1989).

4) H. Bock and B. Solouki, "The Chemistry of Organic Silicon Compounds," ed by S. Patai and Z. Rappoport, John Wiley & Sons, New York (1989), Part I, Chap. 9, p. 555.

5) S. G. Wierschke, J. Chandrasekhar, and W. L. Jorgensen, *J. Am. Chem. Soc.*, **107**, 1496 (1985); M. R. Ibrahim and W. L. Jorgensen, *ibid.*, **111**, 819 (1989).

6) A. H. Fainberg and S. Winstein, *J. Am. Chem. Soc.*, **79**, 1597 (1957).

7) Y. Tsuno, Y. Kusuyama, M. Sawada, T. Fujii, and Y. Yukawa, *Bull. Chem. Soc. Jpn.*, **48**, 3337 (1975); Y. Tsuji, M. Fujio, and Y. Tsuno, *Mem. Fac. Sci., Kyushu Univ., Ser. C*, **17(1)**, 139 (1989).

8) D. S. Noyce and J. A. Virgilio, *J. Org. Chem.*, **37**, 2644 (1972).

9) G. Baddeley, J. Chadwick, and H. T. Taylor, *J. Chem. Soc.*, **1954**, 2405.

10) H. Tanida and H. Matsumura, *J. Am. Chem. Soc.*, **95**, 1586 (1972).

11) Y. Apeloig, "The Chemistry of Organic Silicon Compounds," ed by S. Patai and Z. Rappoport, John Wiley & Sons, Chichester (1989), Part 1, Chap. 2.

12) L. H. Sommer and G. A. Baughman, *J. Am. Chem. Soc.*, **83**, 3346 (1961).

13) A. W. P. Jarvie, A. Holt, and J. Thompson, *J. Chem. Soc. B*, **1970**, 746 and **1969**, 852.

14) M. A. Cook, C. Eaborn, and D. R. M. Walton, *J. Organomet. Chem.*, **24**, 301 (1970).

15) J. Vencl, J. Hetflejš, J. Čermák, and V. Chvalovský, *Collect. Czech. Chem. Commun.*, **38**, 1256 (1973).

16) V. J. Shiner, Jr., W. E. Buddenbaum, B. L. Murr, and G. Lamaty, *J. Am. Chem. Soc.*, **90**, 418 (1968).

17) H. C. Brown and Y. Okamoto, *J. Am. Chem. Soc.*, **80**, 4979 (1958).

18) Y. Yukawa and Y. Tsuno, *Bull. Chem. Soc. Jpn.*, **32**, 971 (1959); *idem., Nippon Kagaku Zasshi*, **86**, 873 (1965); Y. Yukawa, Y. Tsuno, and M. Sawada, *Bull. Chem. Soc. Jpn.*, **39**, 2274 (1966).

19) A similar result on the substituent effect has been reported for the solvolysis of 1-aryl-1-trifluoromethyl-2-(trimethylsilyl)ethyl 3,5-dinitrobenzoates: R. Fujiyama, K. Nagao, K. Moriwaki, and S. Kiyooka, 59th National Meeting of the Chemical Society of Japan, Yokohama, March 1990, Abstr., No. 1E408.

20) T. G. Traylor, W. Hanstein, H. J. Berwin, N. A. Clinton, and R. S. Brown, *J. Am. Chem. Soc.*, **93**, 5715 (1971).

21) M. Fujio, M. Goto, A. Murata, Y. Tsuji, M. Mishima, and Y. Tsuno, *Mem. Fac. Sci., Kyushu Univ., Ser. C*, **16(2)**, 271 (1988), and references cited therein.

22) X. Li and J. A. Stone, *J. Am. Chem. Soc.*, **111**, 5586 (1989).

Photochemical Trifluoromethylation of 1-Methylimidazoles and 1-Methylpyrroles Containing Methylthio Groups

Masakazu NISHIDA,* Hiroshi KIMOTO, Shozo FUJII, Yoshio HAYAKAWA, and Louis A. COHEN†

Government Industrial Research Institute, Nagoya, Kita-ku, Nagoya 462

† Laboratory of Bioorganic Chemistry, National Institute of Diabetes, Digestive and Kidney Diseases, National Institutes of Health, Bethesda, Maryland 20892, USA

(Received March 27, 1991)

The title reaction was achieved by UV (254 nm) irradiation with CF_3I. The methylthio group was introduced to increase electron density and to limit available reactive sites in the rings. Following trifluoromethylation, the methylthio groups were readily removed by hydrogenolysis (Raney Ni) to give the desired trifluoromethyl heterocycles.

Heterocyclic compounds containing the trifluoromethyl group are of considerable interest because of their utility as drugs and agricultural chemicals. Trifluoromethyl groups on imidazoles and pyrroles possess the additional property of undergoing facile transformations to other functional groups.[1)]

Regiospecific introduction of this group has been achieved by reaction of the carboxyl group with SF_4,[2a)] by reaction of hetaryl halides with trifluoromethyl organometallics,[2b)] by ring closure of 1,2-bis(acylamino)-ethylenes with trifluoroacetic anhydride[3)] and by ring closure involving various ketones.[4)] Of these methods, only the latter two can be performed under reaction conditions mild enough for use in polyfunctional or biologically significant systems. Comparably mild are methods involving photochemical[1d,5)] or electrochemical[6)] generation of trifluoromethyl radicals, or generation from trifluoroacetyl peroxide.[7)] These methods often yield isomer mixtures or, when regioselective, may give mainly undesired isomers. In order to provide better routes to specific isomers, we considered the introduction of reversible blocking groups on ring carbons prior to photochemical trifluoromethylation, and demonstrate here the utility of methylthio groups for this purpose. Such groups are introduced and removed with relative ease. In addition, the mildly electron-donating methylthio group would be expected to help reverse the deactivation of heteroaromatic rings by electronegative substituents,[5a)] and offers the further possibility of conversion to potentially bioactive sulfoxides and sulfones. In views of our particular interest in (perfluoroalkyl)imidazoles and pyrroles, these heteroaromatic systems received our first attention. In this study, the ring NH functions are blocked as *N*-methyl but other photostable protective groups, which are readily removed by acid hydrolysis or by hydrogenolysis, should be equally applicable. Furthermore, our previous results[5a)] have shown that trifluoromethylation is representative of perfluoroalkylation in general.

Results and Discussion

The methylthio group was introduced by selective deprotonations of **1a**[8)] and **1b**[9)] (Scheme 1) with butyllithium and reaction of the resulting carbanions with dimethyl disulfide. The use of an equivalent of butyllithium provided mono(methylthio) derivatives **2** in high yield. Two equivalents of butyllithium led to the bis(methylthio) derivatives **3** but, even in the presence of excess base or with **2** as the starting material, formation of **3** was never complete. Fortunately, **2** and **3** are readily separated by fractional vacuum distillation. In contrast to our results, **2a** (containing *N*-methoxymethyl in place of methyl) has been reported to undergo deprotonation at $S-CH_3$ rather than at a ring position.[10)] The preferential formation of the carbanion at C-2 in *N*-methylimidazole (**1a**)[11)] and in *N*-methylpyrrole (**1b**)[9,12)] is governed by the inductive effects of the ring nitrogen atoms. The generation of the second carbanion in **1a** occurs exclusively at C-5 and leads to the single bis(methylthio) product **3a**.[8)] This selectivity is determined by the strong repulsion that would exist between adjacent sp^2 lone pairs at N-3 and a C-4 carbanion (the ALP effect).[13)]

Photochemical trifluoromethylation was performed according to our published procedure,[5a)] samples being irradiated in quartz ampules for 7 d at ambient temperature. According to the solubility of the starting compound, either methanol or acetonitrile was used as solvent and triethylamine was added to neutralize the hydrogen iodide evolved. As seen from the results in Table 1, the choice of solvent has relatively little effect on yield or isomer distribution.

The photochemical trifluoromethylation of 1-methyl-2-(methylthio)imidazole (**2a**) gave mixtures of **4a** and **5a**, the latter being the major isomer (Table 1).[14)] A bis(trifluoromethyl) product was not observed. Several criteria were used to assign isomer structure: (a) coupling patterns of the ^{13}C NMR signal for C-4 and C-5 with CF_3 group;[15)] (b) the ^{19}F NMR signal for 4-CF_3 appears at higher field than for 5-CF_3;[5b)] (c) the ring proton in **5a** (meta-like) is found at higher field than that in **4a** (para-like);[16)] (d) weak coupling is observed between the $N-CH_3$ and the adjacent CF_3 group; (e) products were compared with authentic samples following reductive

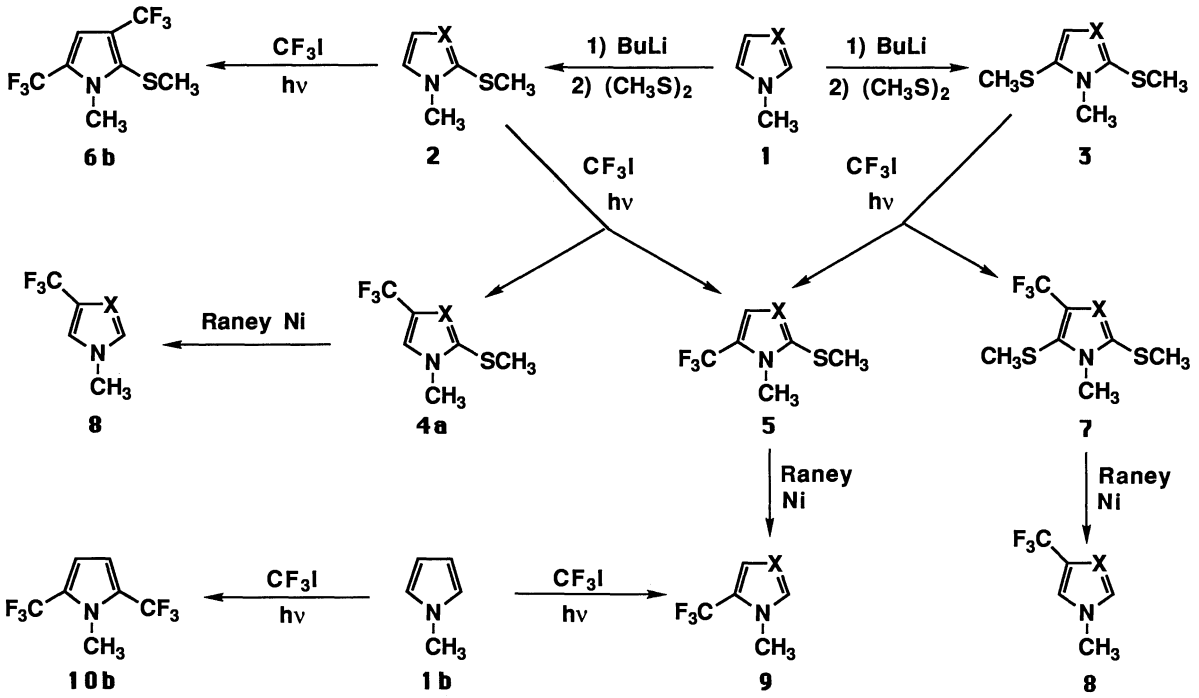

Scheme 1.

Table 1. Yields and Conversions in Trifluoromethylation by UV Irradiation of 1-Methyl-2-methylthioimidazole (**2a**)

CF_3I (equiv)	Solvent	Yields[a]/%		
		4a	**5a**	**2a**
0.5	CH_3CN	0.8	11.9	31.2
0.5	CH_3OH	2.7	14.1	30.3
1.2	CH_3CN	1.5	25.0	12.7
1.2	CH_3OH	2.8	20.7	47.4
2.5	CH_3CN	2.6	29.3	0.7
2.5	CH_3OH	3.2	30.8	26.1

a) Isolated yields based on the imidazole, not adjusted for recovered **2a**.

Table 2. Yields and Conversions in Trifluoromethylation by UV Irradiation of 1-Methyl-2,5-bis(methylthio)imidazole (**3a**)

CF_3I (equiv)	Solvent	Yields[a]/%		
		5a[b]	**7a**[c]	**3a**[c]
0.5	CH_3CN	1.3	6.3	43.3
1.2	CH_3CN	2.9	7.8	32.0
1.2	CH_3OH	—	7.2	12.3
2.5	CH_3CN	2.3	8.3	31.1

a) Based on the imidazole, not adjusted for recovered **3a**. b) Determined by ^{19}F NMR. c) Isolated yields.

removal of the methylthio group. The direct trifluoromethylation of 1-methylimidazole had given three isomeric products (2-CF_3 : 4-CF_3 : 5-CF_3) in the ratio 43 : 8 : 50, separation requiring the use of both preparative gas and column chromatography.[5a] On the other hand, isomers **4a** and **5a** were formed in the ratio 10 : 90, the increased degree of substitution at C-5 probably being due to the electron-releasing effect of the methylthio group.

The 4-CF_3 isomer is the most difficult to obtain by photochemical trifluoromethylation of either **1a** or **2a**. Although C-4 is the only vacant ring position in **3a**, yields of **7a** never exceeded 6—8% (Table 2), even with 2.5 equiv of CF_3I. Interestingly, **7a** was accompanied by smaller amounts of **5a**, which may have arisen due to a slow photochemical conversion of **3a** to **2a**.

Photochemical trifluoromethylation of 1-methylpyrrole (**1b**) has been reported to yield the 2-trifluoromethyl derivative (**9b**) in 35% yield.[1d] We have confirmed this result, but found that excess CF_3I also provides a small yield (Table 3) of the 2,5-bis(trifluoromethyl) derivative (**10b**). Unfortunately, the boiling points of **9b** and **10b** are too close to permit clean separation and yields given in Table 3 are based on GC analysis. Although *N*-methylpyrrole undergoes efficient α-perfluoroalkylation with higher bis(perfluoroalkanoyl) peroxides, introduction of the CF_3 group could not be achieved.[7] The results of trifluoromethylation of **2b** are given in Table 4. Significant yields of **5b** require the use of at least 2.5 equiv of CF_3I, but small amounts of a bis(trifluoromethyl) derivative, presumably **6b**, are also formed. Fortunate-

Table 3. Yields in Trifluoromethylation by UV Irradiation of 1-Methylpyrrole (**1b**)

CF_3I (equiv)	Solvent	Yields[a]/%		
		9b	**10b**	**1b**
1.2	CH_3CN	36.5	—	10.5
2.5	CH_3CN	32.2	7.4	—

a) Determined by GC analysis based on the pyrrole, not adjusted for recovered **1b**.

Table 4. Yields and Conversions in Trifluoromethylation by UV Irradiation of 1-Methyl-2-methylthiopyrrole (**2b**)

CF_3I (equiv)	Solvent	Yields[a]/%		
		6b[b]	**5b**[c]	**2b**[c]
0.5	CH_3CN	—	4.2	18.4
1.2	CH_3CN	—	17.7	4.7
2.0	CH_3CN	0.14	18.8	5.0
2.5	CH_3CN	1.24	33.3	5.3

a) Based on the pyrrole, not adjusted for recovered **2b**. b) Determined by GC analysis. c) Isolated yields.

Table 5. Yields and Conversions in Trifluoromethylation by UV Irradiation of 1-Methyl-2,5-bis(methylthio)pyrrole (**3b**)

CF_3I (equiv)	Solvent	Yields[a]/%		
		5b[b]	**7b**[c]	**3b**[c]
0.5	CH_3CN	6.7	2.3	29.5
1.2	CH_3CN	10.2	3.9	38.1
2.5	CH_3CN	23.6	7.0	7.0

a) Based on the pyrrole, not adjusted for recovered **3b**. b) Determined by ^{19}F NMR. c) Isolated yields.

ly, the methylthio group facilitates the separation of mixtures by increasing boiling points and R_f differences in silica-gel chromatography.

Introduction of the trifluoromethyl group at the β-position of the pyrrole ring has not been achieved by direct or indirect methods. The reaction of 5-methyl-2-pyrrolecarbaldehyde with bis(heptafluorobutyryl) peroxide provided the 3-heptafluoropropyl derivative,[7] but this method failed to provide the trifluoromethyl derivative. Photochemical trifluoromethylation of **3b** provided the desired product **7b**. Even at a level of 2.5 equiv of CF_3I, the yield of **7b** was only 7% and was accompanied by 17% of **5b** (Table 5). Detection of a trace of **2b** suggested that the apparent replacement of the methylthio group by trifluoromethyl, both in the conversion of **3a** to **5a** and **3b** to **5b**, may actually be due to a prior loss of the methylthio group by irradiation. On the other hand, products devoid of the methylthio group were not detected in the photochemical trifluoromethylation of **2a** or **2b**.

Methylthio groups were removed by hydrogenolysis with Raney nickel in refluxing ethanol.[17] The imidazole derivatives provided the expected products in yields of 50—90%, and these products were readily isolated and purified by vacuum distillation in a microtube oven. In each case, properties of the sulfur-free imidazole coincided with those of authentic samples.[5a] On the other hand, the lower boiling points of (trifluoromethyl)pyrroles (and their closeness to that of ethanol) rendered isolation and purification difficult. Even the use of higher boiling alcohols as reaction solvents did not eliminate this problem. Thus, spectral properties were determined in mixtures containing some solvent. Yields were determined by GC analysis and were found comparable to those of the imidazoles. Reduction at 90—100 °C gave somewhat higher yields than at the temperature of refluxing ethanol. For certain (trifluoromethyl)pyrroles, therefore, it may be necessary to use the materials for further synthetic procedures without recovery of the pure product.

In these test cases, the overall yields of trifluoromethylated products were found to be comparable (or even inferior) to those obtained by direct photochemical trifluoromethylation. On the other hand, laborious isomer separations have been eliminated. Finally, this method provides a route to β-(trifluoromethyl)pyrroles, isomers which have not yet been obtained by direct trifluoromethylation.

Experimental

Analytical Methods and Instrumentation. All boiling and melting points are uncorrected. ^1H NMR spectra were measured on a Hitachi R-90H (90 MHz) instrument with tetramethylsilane as internal reference. ^{19}F NMR spectra were measured on a Hitachi R-90F (84.67 MHz) instrument with trifluoroacetic acid as external reference. Gas chromatographic analyses were performed on a Shimadzu GC-4A instrument (column KF-96, 3m). Mass spectra were obtained on a Hitachi M-80 instrument with 20 eV electron impact ionization.

Materials. Trifluoromethyl iodide was prepared by reaction of silver trifluoroacetate and iodine.[18] The following methylthio compounds were prepared according to literature methods: 1-methyl-2-(methylthio)imidazole, **2a**, 55% yield, bp 124—125 °C/30 Torr (1 Torr=133.322 Pa) (lit,[8] 65—70 °C/0.5 Torr); 1-methyl-2,5-bis(methylthio)imidazole, **3a**, 34% yield, bp 104—105 °C/5 Torr (lit,[8] 100—110 °C/0.5 Torr); 1-methyl-2-(methylthio)pyrrole, **2b**, 73% yield, bp 90—91 °C/30 Torr (lit,[9] 144—145 °C/12 Torr). Raney nickel (Aldrich) was used as a suspension in ethanol after thorough washing of the commercial material with water and ethanol.

2,5-Bis(methylthio)pyrrole (3b). To a solution of 2-(methylthio)pyrrole (**2b**, 2.77 g, 21.8 mmol) and *N,N,N',N'*-tetramethylethylenediamine (3.33 g, 28.7 mmol) in hexane (20 mL), was added dropwise a hexane solution of butyllithium (1.6 M, 18 mL, 1.2 equiv) at 30 °C under nitrogen. The reaction mixture became dark red instantly, and the suspension was stirred for 1 h. To the reaction mixture, cooled in an ice bath, was added dimethyl disulfide (2.70 g, 28.7 mmol) in hexane (5 mL). The reaction mixture was stirred at 0 °C for 1 h, and was then poured into water (50 mL). The organic layer was separated, washed with water and dried ($MgSO_4$). The water

layer was extracted with ethyl acetate (2×100 mL) and the organic layer was treated in a similar manner. Vacuum distillation of the combined organic layers afforded 2,5-bis(methylthio)pyrrole (**3b**, 1.58 g, 31.8% yield) as a colorless oil, bp 94—95 °C/7 Torr; ^{1}H NMR ($CDCl_3$) δ=2.26 (s, 6H, SCH_3), 3.72 (s, 3H, NCH_3), 6.30 (s, 2H, ring); MS *m/z* 173 (M^+ 100%), 158 (84), 117 (70). Found: C, 48.78; H, 6.23; N, 8.35%. Calcd for $C_7H_{11}NS_2$: C, 48.52; H, 6.40; N, 8.08%.

UV-Induced Trifluoromethylation of 1-Methyl-2-(methylthio)imidazole (2a). Into a solution of **2a** (2.56 g, 20.0 mmol) and triethylamine (2.43 g, 24.0 mmol) in acetonitrile (10 mL), was bubbled gaseous trifluoromethyl iodide until the weight had increased by 4.70 g (24.0 mmol). The solution was placed in a quartz tube and the remaining upper space was filled with argon. The tube was sealed with a glass stopper and then the solution was irradiated for 7 d at ambient temperature, using a 60 W low-pressure mercury lamp equipped with a Vycor filter.

The dark orange reaction mixture was poured into water and the products were extracted with ethyl acetate (3×100 mL). The combined organic layers were washed with water, dried (Na_2SO_4) and evaporated under reduced pressure. The residual oil was subjected to silica-gel chromatography with CH_2Cl_2 and ether as successive eluents to provide, in order, **4a** (1.5%), **5a** (25.0%), and **2a** (12.7%). The eluting solvent was removed and the product purified by vacuum distillation using a glass tube oven. Additional runs are summarized in Table 1.[19]

1-Methyl-2-methylthio-4-(trifluoromethyl)imidazole (4a): White needles, mp 44—46 °C; ^{1}H NMR (acetone-d_6) δ=26.0 (s, 3H, SCH_3), 3.66 (br s, 3H, NCH_3), 7.63 (q, 1H, *J*=1.1 Hz, H-5); ^{13}C NMR ($CDCl_3$) δ_C=15.8 (s, SCH_3), 33.3 (s, NCH_3), 121.7 (q, *J*=267 Hz, CF_3), 121.8 (q, *J*=4.1 Hz, C-5), 131.9 (q, *J*=39 Hz, C-4), 145.8 (s, C-2); ^{19}F NMR (acetone-d_6) δ_F=14.8 (s); MS *m/z* 196 (M^+ 100%), 163 (54) Found: C, 36.65; H, 3.57; N, 14.40%. Calcd for $C_6H_7N_2F_3S$: C, 36.73; H, 3.60; N, 14.28%.

1-Methyl-2-methylthio-5-(trifluoromethyl)imidazole (5a): Colorless oil, bp 98—99 °C/30 Torr; ^{1}H NMR (acetone-d_6) δ=2.64 (s, 3H, SCH_3) 3.65 (br s, 3H, NCH_3), 7.42 (q, *J*=1.5 Hz, H-4); ^{13}C NMR ($CDCl_3$) δ_C=15.3 (s, SCH_3), 31.6 (d, *J*=1.4 Hz, NCH_3), 121.0 (q, *J*=266 Hz, CF_3), 123.2 (q, *J*=39 Hz, C-5), 130.9 (q, *J*=4.2 Hz, C-4), 149.1 (br s, C-2); ^{19}F NMR (acetone-d_6) δ_F=17.3 (s); MS *m/z* 196 (M^+ 100%), 163 (59). Found: C, 36.30; H, 3.68; N, 14.77%. Calcd for $C_6H_7N_2F_3S$: C, 36.73; H, 3.60; N, 14.28%.

UV-Induced Trifluoromethylation of 1-Methyl-2,5-bis(methylthio)imidazole (3a). Trifluoromethylation of **3a**, by the procedure described above, gave **7a** (7.8%), **5a** (2.9%), and unreacted **3a** (32.0%). The mixture of imidazoles was separated by silica-gel chromatography with 50% hexane/50% CH_2Cl_2 and 100% CH_2Cl_2 as successive eluents and products were eluted in the order given. Additional runs are summarized in Table 2.

1-Methyl-2,5-bis(methylthio)-4-(trifluoromethyl)imidazole (7a): White needles, mp 39—40 °C; ^{1}H NMR (acetone-d_6) δ=2.33 (s, 3H, SCH_3), 2.63 (s, 3H, SCH_3), 3.65 (br s, 3H, NCH_3); ^{19}F NMR (acetone-d_6) δ_F=16.6 (s); MS *m/z* 242 (M^+ 100%), 227 (46), 209 (45), 186 (37). Found: C,34.38; H, 3.77; N, 11.52%. Calcd for $C_7H_9N_2F_3S_2$: C, 34.70; H, 3.74; N, 11.56%.

UV-Induced Trifluoromethylation of 1-Methylpyrrole (1b). Following the procedure used with **2a**, **1b** gave **9b** and **10b** or **9b** and recovered **1b**. The results are given in Table 3. It was difficult to separate **9b**, **10b**, and **1b** because the boiling points are very close to one another, therefore, these materials were identified in a mixture and the yields are based on GC analysis.

1-Methyl-2-(trifluoromethyl)pyrrole (9b): ^{1}H NMR (acetone-d_6) δ=3.73 (s, 3H, SCH_3), 6.07 (m, 1H, ring), 6.53 (m, 1H, ring), 6.88 (m, 1H, ring); ^{19}F NMR (acetone-d_6) δ_F=18.6 (s); MS *m/z* 149 (M^+ 100%), 130 (36).

1-Methyl-2,5-bis(trifluoromethyl)pyrrole (10b): ^{1}H NMR (acetone-d_6) δ=3.83 (s, 3H, SCH_3), 6.66 (s, 2H, ring); ^{19}F NMR (acetone-d_6) δ_F=17.6 (s); MS *m/z* 217 (M^+ 100%), 198 (40), 156 (21).

UV-Induced Trifluoromethylation of 1-Methyl-2-(methylthio)pyrrole (2b). Following the procedure used with **2a**, **2b** gave **5b** (17.7%) and **2b** (4.7%). The mixture of pyrroles was separated by silica-gel chromatography with 90% hexane/10% CH_2Cl_2 and 100% CH_2Cl_2 as successive eluents. The results of additional runs are given in Table 4. At higher ratios of CF_3I, small amounts of a bis(trifluoromethyl)derivative, probably **6a**, were also obtained. The material was identified by mass spectrum (M^+ 263) and yields are based on GC analysis; however, no effort was made to isolate **6b**.

1-Methyl-2-methylthio-5-(trifluoromethyl)pyrrole (5b): Colorless oil, bp 80—81 °C/30 Torr; ^{1}H NMR (acetone-d_6) δ=2.32 (s, 3H, SCH_3), 3.77 (q, 3H, *J*=0.7 Hz, NCH_3), 6.31 (AB, 1H, *J*=4.0 Hz, H-3), 6.57 (AB-q, 1H, *J*=4.0 Hz and 0.9 Hz, H-4); ^{19}F NMR δ_F=17.9 (s); MS *m/z* 195 (M^+ 100%), 180 (61). Found: C, 43.02; H, 4.17; N, 7.09; S, 16.36%. Calcd for $C_7H_9NF_3S$: C, 43.07; H, 4.13; N, 7.18; S, 16.42%.

UV-Induced Trifluoromethylation of 1-Methyl-2,5-bis(methylthio)pyrrole (3b). Following the procedure used with **2a**, **3b** gave **7b** (3.9%), **5b** (10.2%), and unreacted **3b** (38.1%). The mixture of pyrroles was separated by silica-gel chromatography with 100% hexane; the pure products were obtained following removal of solvent in a glass tube oven. The results of additional runs are given in Table 5.

1-Methyl-2,5-bis(methylthio)-3-trifluoromethylpyrrole (7b): Colorless oil, bp 164—168 °C; ^{1}H NMR (acetone-d_6) δ=2.29 (s, 3H, SCH_3), 2.36 (s, 3H, SCH_3), 3.83 (br s, 3H, NCH_3), 6.56 (br s, 1H, H-4); ^{19}F NMR (acetone-d_6) δ_F=20.9 (s); MS *m/z* 241 (M^+ 100%), 226 (73) 185 (74). Found: C, 39.88; H, 4.21; N, 5.72%. Calcd for $C_7H_9N_2F_3S_2$: C, 39.82; H, 4.18; N, 5.80%.

Hydrogenolysis of Methylthio Groups of Imidazoles. To an ethanol solution (30 mL) of 1-methyl-2-methylthio-5-(trifluoromethyl)imidazole (**5a**) (1.34 g, 6.81 mmol) was added Raney nickel dampened with ethanol (ca. 10 g), and the reaction mixture was vigorously stirred under reflux for 5 h. The nickel was removed by filtration, the filtrate was poured into water (100 mL) and the mixture was extracted with dichloromethane (3×100 mL). The combined organic layers were washed with water and dried (Na_2SO_4). The solvent was evaporated and the residue was vacuum distilled in a glass tube oven to give **9a** in 57.3% yield.

1-Methyl-5-(trifluoromethyl)imidazole (7a): White needles, mp 38—41 °C; ^{1}H NMR (acetone-d_6) δ=3.83 (s, 3H, NCH_3), 7.41 (br s, 1H, H-4), 7.76 (br s, 1H, H-2) (lit,[5a] δ=3.83, 7.40, 7.75); ^{19}F NMR δ_F=17.8 (s); MS *m/z* 150 (M^+).

Hydrogenolysis of methylthio groups in other imidazoles was carried out by a similar procedure.

1-Methyl-4-(trifluoromethyl)imidazole (8a): 54.5% yield from **4a**, 86.6% yield from **7a**; colorless oil, bp 222—225 °C; ^{1}H NMR (acetone-d_6) δ=3.82 (br s, 3H, NCH_3), 7.58 (br s, 1H, H-2), 7.66 (br s, 1H, H-5) (lit,[5a] δ=3.88, 7.58, 7.64); ^{19}F NMR

δ_F=15.3 (s); MS *m*/*z* 150 (M^+).

Hydrogenolysis of Methylthio Groups in Pyrroles. To an ethanol solution (25 mL) of 1-methyl-2-methylthio-5-(trifluoromethyl)pyrrole (**5b**) (1.68 g, 8.60 mmol), was added Raney nickel dampened with ethanol (ca. 15 g), and the reaction mixture was vigorously stirred under reflux for 1 h. The nickel was removed by filtration, the filtrate was poured into water (100 mL), and the mixture was extrated with dichloromethane (2×100 mL). The organic layers were combined, washed with water and dried (Na_2SO_4). The solvent was removed and the estimated yield of **9b** was 60%, determined by GC analysis. Properties of **9b** were determined using a sample (90% purity) obtained in a microdistillation apparatus.

1-Methyl-2-(trifluoromethyl)pyrrole (9b): Colorless oil, bp. 114 °C; ^{1}H NMR (acetone-d_6) δ=3.75 (br s, 3H, NCH_3), 6.08 (m, 1H, ring) 6.55 (m, 1H, ring), 6.91 (m, 1H, ring) (lit,[1d] ($CDCl_3$) δ=3.60, 5.90, 6.36, 6.48); ^{19}F NMR δ_F=18.8 (s); MS *m*/*z* 149 (M^+).

Hydrogenolysis of the methylthio groups of **7b** was carried out by a similar procedure, and the estimated yield of **8b** was 41% determined by GC analysis. A sample of **8b** could not be obtained by preparative GC and microdistillation led to a dark tarry product; properties of **8b** were determined using a dichloromethane solution.

1-Methyl-3-(trifluoromethyl)pyrrole (8b): ^{19}F NMR (acetone-d_6) δ_F=21.0 (s); *m*/*z* 149 (M^+).

References

1) a) H. Kimoto and L. A. Cohen, *J. Org. Chem.*, **44**, 2902 (1979); b) *ibid.*, **45**, 3831 (1980); c) S. Fujii, Y. Maki, H. Kimoto, and L. A. Cohen, *J. Fluorine Chem.*, **35**, 437 (1987); d) Y. Kobayashi, I. Kumadaki, A. Ohsawa, S.-I. Murakami, and T. Nakano, *Chem. Pharm. Bull.*, **26**, 1247 (1978).

2) a) D. Owen, R. G. Plevey, and J. C. Tatlow, *J. Fluorine Chem.*, **17**, 179 (1981); b) Citations in footnotes 7 and 8 of Ref. 5a.

3) H. Kimoto, K. L. Kirk, and L. A. Cohen, *J. Org. Chem.*, **43**, 3403 (1978).

4) a) J. G. Lombardino and E. H. Wiseman, *J. Med. Chem.*, **17**, 1182 (1974); b) J. J. Baldwin, P. A. Kisinger, F. C. Novello, and J. M. Sprague, *J. Med. Chem.*, **18**, 895 (1975).

5) a) H. Kimoto, S. Fujii, and L. A. Cohen, *J. Org. Chem.*, **47**, 2867 (1982); b) *ibid.*, **49**, 1060 (1984).

6) a) M. Medebielle, J. Pinson, and J.-M. Saveant, *Tetrahedron Lett.*, **1990**, 1279; b) J. H. P. Utley and R. J. Holman, *Electrochim. Acta*, **21**, 987 (1976).

7) M. Yoshida, T. Yoshida, M. Kobayashi, and N. Kamigata, *J. Chem. Soc., Perkin Trans. 1*, **1989**, 909.

8) A. J. Carpenter, D. J. Chadwick, and R. I. Ngochindo, *J. Chem. Res., Synop.*, **1983**, 196; *Miniprint*, **1983**, 1913.

9) S. Gronowitz and R. Kada, *J. Heterocycl. Chem.*, **21**, 1041 (1984).

10) C. C. Tang, D. Davalian, P. Huang, and R. Breslow, *J. Am. Chem. Soc.*, **100**, 3918 (1978).

11) a) D. P. Davis, K. L. Kirk, and L. A. Cohen, *J. Heterocycl. Chem.*, **19**, 253 (1982); b) K. L. Kirk, *J. Org. Chem.*, **43**, 4381 (1978); c) K. L. Kirk, *J. Heterocycl. Chem.*, **22**, 57 (1985).

12) A. I. Shatenshtein, A. G. Kamrad, I. O. Shapiro, Y. I. Ranneva, and E. N. Zvyagintseva, *Dokl. Akad. Nauk SSSR*, **168**, 364 (1966).

13) a) Y. Takeuchi, H. J. C. Yeh, K. L. Kirk, and L. A. Cohen, *J. Org. Chem.*, **43**, 3565 (1978); b) Y. Takeuchi, K. L. Kirk, and L. A. Cohen, *J. Org. Chem.*, **43**, 3570 (1978).

14) A plausible explanation for preferential substitution at C-5 is discussed in Ref. 5a.

15) a) G. Assef, J. Kister, J. Metzger, R. Faure, and E. J. Vincent, *Tetrahedron Lett.*, **1976**, 3313; b) R. Faure, E. J. Vincent, G. Assef, J. Kister, and J. Metzger, *Org. Magn. Reson.*, **9**, 688 (1977).

16) C. Rav-Acha and L. A. Cohen, *J. Org. Chem.*, **46**, 4717 (1981).

17) H. Hauptmann and W. F. Walter, *Chem. Rev.*, **62**, 347 (1962).

18) A. L. Henne and W. G. Finnegen, *J. Am. Chem. Soc.*, **72**, 3806 (1950).

19) Material balance is not achieved in any of the photochemical reactions. The formation of dark, tarry side products suggests competitive radical polymerizations.

Synthesis of Optically Active Polyamides Having Axially Dissymmetric 1,1′-Binaphthalene-2,2′-dicarboxylic Acid Component and Their Optical Resolution Ability as Chiral Adsorbent for HPLC

Yasufumi TAMAI, Yutaka MATSUZAKA, Shuichi ÔI, and Sotaro MIYANO*
Department of Biochemistry and Engineering, Faculty of Engineering, Tohoku University, Aramaki-Aoba, Aoba-ku, Sendai 980

(Received April 4, 1991)

Optically active polyamides **4a**—**4c** were synthesized from the polycondensation of axially dissymmetric 1,1′-binaphthalene-2,2′-dicarbonyl dichloride (**2**) with 1,4-benzenediamine, 1,6-hexanediamine, and 1,10-decanediamine, respectively. CD spectra of the polyamides **4a**—**4c** are essentially the same as those of the corresponding model diamides **6a**—**6c** prepared from **2** and benzenamine, 1-hexanamine, and 1-decanamine, respectively. This similarity indicates that the conformation of the 1,1′-binaphthalene-2,2′-dicarboxamide moieties of the polyamides **4a**—**4c** in solution state are rather similar to those of the corresponding model diamides **6a**—**6c**. Several axially chiral biaryl compounds and 3,5-dinitrophenylcarbamates (3,5-DNPCs) derived from 1-aryl-1-alkanols were resolved by HPLC equipped with the columns packed the chiral stationary phases (CSPs) prepared from **4a**—**4c** adsorbed on spherical silica gel. A main control factor for the chiral discrimination seems to be the hydrogen bonding between the amide groups of the CSPs and the hydrogen-bonding sites of the atropisomeric biaryls. The donor–acceptor interaction between the binaphthalene moiety of the CSPs and the 3,5-dinitrobenzene moiety of the 3,5-DNPCs may also be important for the chiral discrimination of the 3,5-DNPCs.

A wide variety of polymeric chiral stationary phases (CSPs) have recently been developed for the separation of enantiomers by means of high-performance liquid chromatography (HPLC).[1] Some kinds of optically active polyamides have been reported to show the chiral recognition ability as the chiral adsorbents for the CSPs.[2] It is well-known that axially dissymmetric 1,1′-binaphthalene derivatives serve as highly efficient chiral inducers for a wide range of asymmetric reactions.[3] Therefore, the optically active polyamide having axially dissymmetric 1,1′-binaphthalene component in the main chain is expected to serve as the efficient chiral adsorbent of the CSP for HPLC. Although the chiroptical properties of some axially chiral polyamides have been investigated,[4] no report has dealt with the chiral recognition ability of the axially chiral polyamide. Previously, we reported a practical method for the synthesis of optically pure 1,1′-binaphthalene-2,2′-dicarboxylic acid (**1**) derivatives and their usefulness as the chiral modifiers of the packing material for HPLC.[5] In this paper, we wish to report the synthesis of polyamides **4a**—**4c** from optically pure **1** and 1,4-benzenediamine (**3a**), 1,6-hexanediamine (**3b**), and 1,10-decanediamine (**3c**). Further reported are the chiroptical properties of these polyamides and their optical resolution ability as the chiral adsorbents for the CSPs.

Results and Discussion

Synthesis of Polyamides 4a—4c and Model Diamides 6a—6c. The syntheses of the polyamides **4a**—**4c** were carried out by the method of solution polycondensation at ambient temperature in *N*,*N*-dimethylacetamide (DMAc) as shown in Scheme 1. Diamines **3a**—**3c** were reacted with the dicarbonyl dichloride **2** derived from optically pure (*S*)-**1** to yield the optically active polyamides **4a**—**4c**, respectively (Table 1). For the synthesis of **4b** and **4c**, concomitant formation of linear and/or cyclic oligomers was observed.

All the polyamides were soluble in 1,1,1,3,3,3-hexafluoro-2-propanol (HFIP) and aprotic polar solvents such as *N*,*N*-dimethylformamide (DMF), DMAc, and dimethyl sulfoxide (DMSO), but insoluble in chloroform, tetrahydrofuran (THF), and usual nonpolar solvents.

Model diamides **6a**—**6c** were prepared by condensation of **2** with benzenamine (**5a**), 1-hexanamine (**5b**), and 1-decanamine (**5c**) in benzene at reflux temperature, respectively (Table 1).

Comparison of the Chiroptical Properties of the Polyamides 4a—4c to the Corresponding Diamides 6a—6c. As shown in Table 1, the mean residue rotations ($[m]_D$) of **4b** and **4c** were comparable to the molar rotations ($[\phi]_D$) of the corresponding model diamides **6b** and **6c** in DMAc solution. CD spectra of **4b** and **4c** in both DMAc and HFIP were almost comparable to those of **6b** and **6c**, respectively, as shown in Figs. 2 and 3. In contrast, the mean residue rotation of **4a** was rather

Table 1. Synthesis of Polyamides (**4a**—**4c**) and Diamides (**6a**—**6c**)

	Yield / %	$\bar{M}_n$ [a]	$\bar{M}_w/\bar{M}_n$ [a]	$[m]_D$ [b] for **4a**—**4c** ($[\phi]_D$ [c] for **6a**—**6c**)
4a	84	20000	1.92	−2.1°
6a	95			−70.5°
4b	59	27000	1.49	−48.9°
6b	83			−71.7°
4c	27	26000	1.48	−59.4°
6c	94			−64.0°

a) Determined by GPC calibrated with polystylene standards. b) Mean residue rotation. Measured at ca. 0.024 (repeating unit mol) dm^{-3} in DMAc at ambient temperature. c) Molar rotation. Measured at ca. 0.024 mol dm^{-3} in DMAc at ambient temperature.

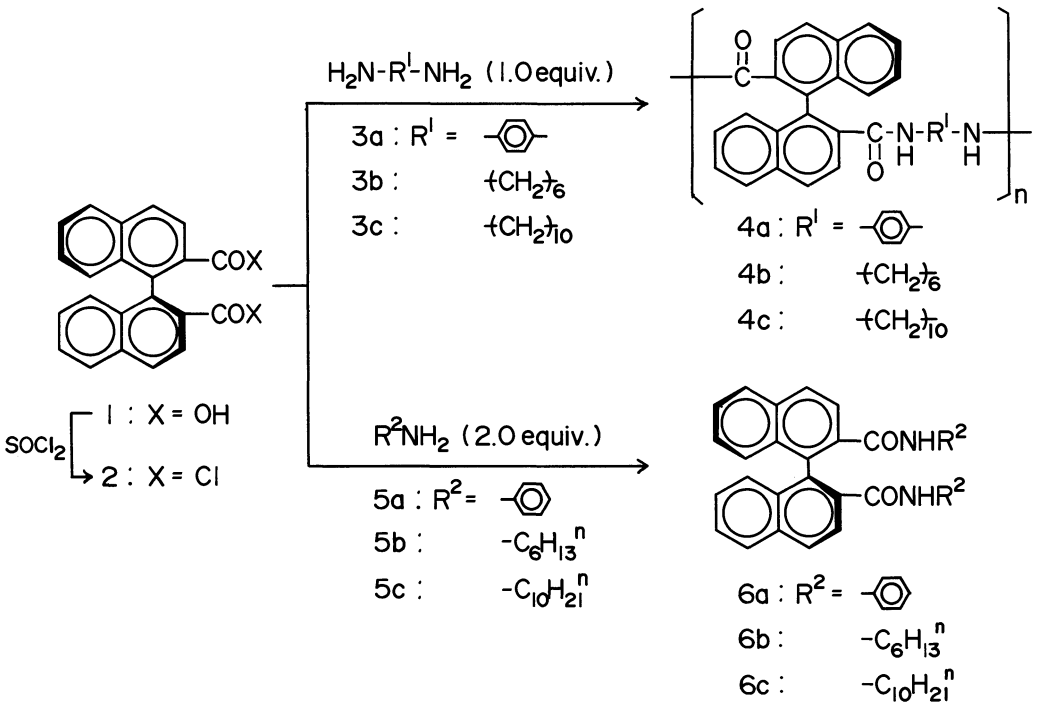

Scheme 1.

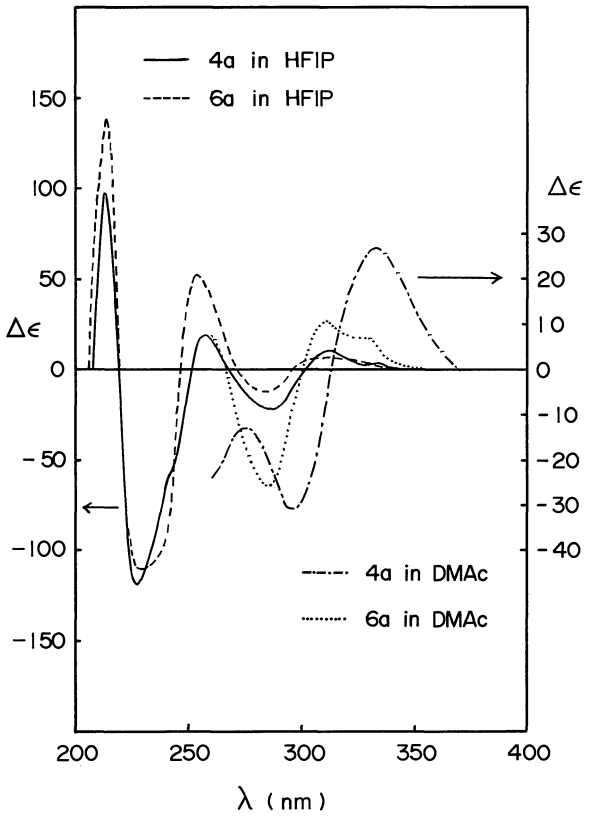

Fig. 1. CD spectra of polyamide **4a** and model diamide **6a**.

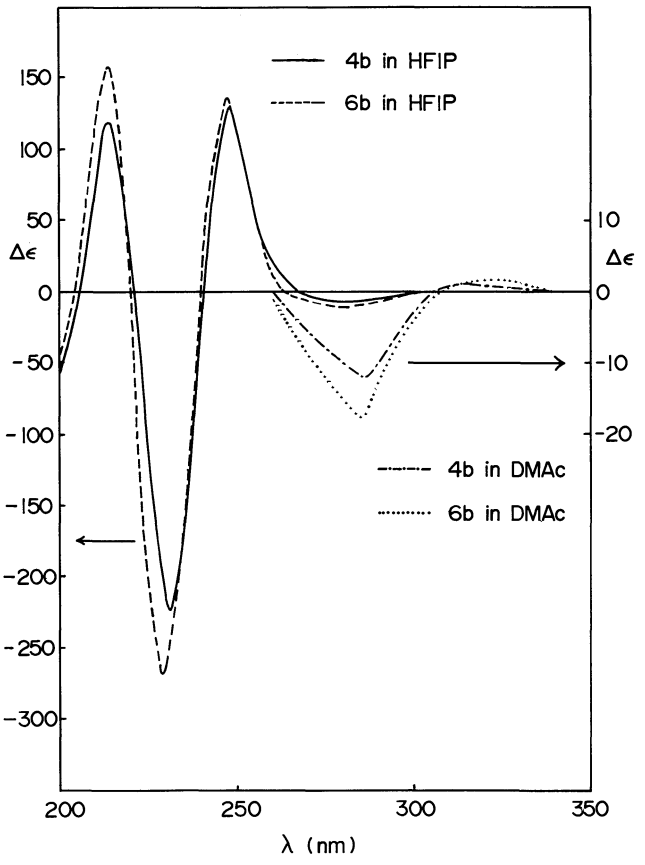

Fig. 2. CD spectra of polyamide **4b** and model diamide **6b**.

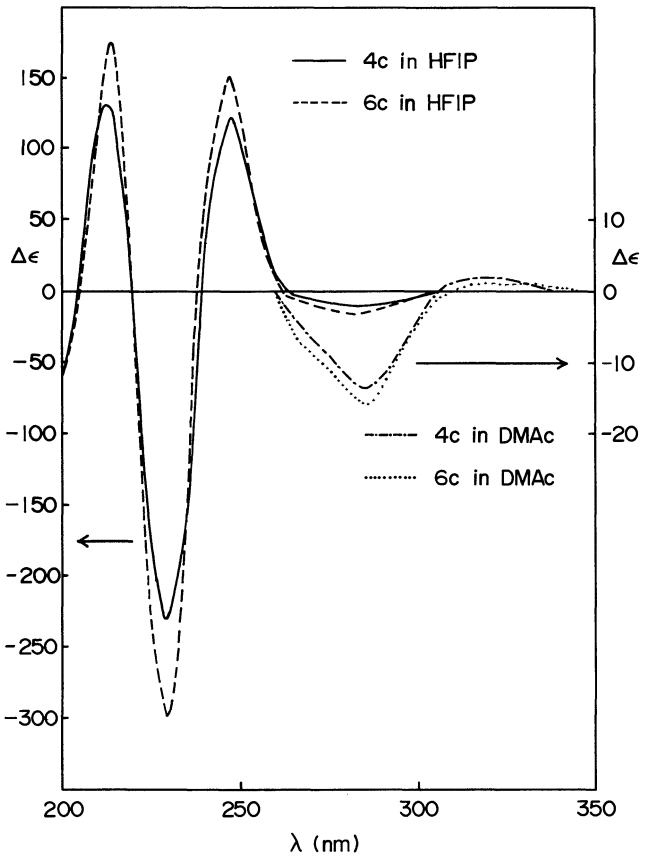

Fig. 3. CD spectra of polyamide **4c** and model diamide **6c**.

smaller than the molar rotation of **6a**. CD spectrum of **4a** at wavelength longer than 260 nm in DMAc was somewhat different from that of **6a**, while the spectrum at wavelength shorter than 260 nm in HFIP was almost comparable to that of **6a** (Fig. 1).

It is known that the Cotton effects derived from the ^1B_b transition of the naphthalene chromophores in 1,1′-binaphthalene derivatives appear at wavelength shorter than 260 nm; the Cotton effects are supposed to reflect the conformation of the binaphthalene skeletons more closely than those derived from other transitions of the naphthalene chromophores.[6] Thus, the similarity of the CD spectra of **4a**—**4c** at wavelength shorter than 260 nm to those of the corresponding model diamides **6a**—**6c** suggests that the conformations of the 1,1′-binaphthalene-2,2′-dicarboxamide moieties of the polyamides in the solution state are similar to those of the model diamides. It seems that the differences of the chiroptical properties between **4a** and **6a** at wavelength longer than 260 nm are attributed to the differences of transition properties between the 1,4-bis(acylamino)benzene chromophore of the polyamide **4a** and the (acylamino)benzene chromophore of the model diamide **6a**.

Chiral Recognition Ability of Polyamides 4a—4c as the Chiral Adsorbents for the CSPs. To investigate the chiral recognition ability of the polyamides **4a**—**4c**, CSP-4a—CSP-4c were prepared by coating spherical, macroporous silica gel with DMAc solutions of **4a**—**4c** using a conventional technique.[7] Polyamides **4a**—**4c** are constituted of amide linkages which can function as hydrogen-bonding site and bulky binaphthalene moieties which can serve as π-electron-donor group. Thus, dia-

Table 2. Chromatographic Resolution of Racemates **7**—**16** by CSP-4a—CSP-4c Packed Columns

Racemate	Eluent[a]	CSP-4a			CSP-4b			CSP- 4c		
		k_1'[b]	α[c]	R_s[d]	k_1'	α	R_s	k_1'	α	R_s
7	A	2.76(*S*)[e]	1.76	0.40	0.97	1.56	0.94	0.98(*S*)[e]	1.55	0.96
	B	—[f]			—[f]			5.92	1.86	2.36
8[g]	A	1.86	1.0		0.78	1.0		0.65	1.0	
9	A	0.33	1.48	0.17	0.18	1.34	0.29	0.16	1.46	0.33
	B	—[f]			1.03	1.52	0.88	0.80	1.54	1.26
10	A	2.18	1.0		0.34	1.0		0.38	1.0	
	B	—[f]			1.74	1.15	0.29	0.91(*S*)[e]	1.17	0.55
11[g]	A	0.47	1.0		0.15	1.0		0.17	1.0	
12	A	1.08	1.58	0.39	0.49	1.40	0.67	0.52	1.36	0.53
	B	—[f]			5.42	1.74	0.96	2.52[h]	1.57	1.46
13	A	1.39	1.0		0.44	1.20	0.35	0.44(*S*)[e]	1.17	0.25
	B	—[f]			5.42	1.44	0.78	2.67[h]	1.29	0.78
14	A	1.46	1.0		0.49	1.0		0.60(*S*)[e]	1.20	0.27
	B	—[f]			8.09	1.32	0.41	5.15	1.32	0.71
15	A	1.06	1.0		0.24	1.0		0.54	1.32	0.56
	B	—[f]			8.38	1.41	0.86	4.98	1.43	0.94
16[g]	A	0.48	1.0		0.19	1.0		0.26	1.0	

a) A, 2-propanol/hexane=10/90, Flow rate=1.0 ml min^{-1}; B, 2-propanol/hexane=1/99, Flow rate=1.0 ml min^{-1}. b) Capacity factor of the enantiomer eluting first=(retention volume of enantiomer—void volume of column)/(void volume of column). c) Separation factor=(k' of more retained enantiomer)/(k' of less retained enantiomer). d) Resolution factor=2×(distance between the peaks of more and less retained enantiomers)/(sum of band width of two peaks). e) Absolute configuration of the enantiomer eluting first. f) The capacity factor of the racemate was so large that no clear peak of the racemate was observed. g) This racemate couldn't be resolved even by use of eluent B. h) Flow rate=0.5 ml min^{-1}.

stereomeric interactions via π–π interaction and hydrogen bonding are expected between the CSPs and racemates which have an electron-accepting aromatic group and a hydrogen-bonding site. Table 2 shows the results of the HPLC analyses of such racemates **7**—**16**. Figure 4

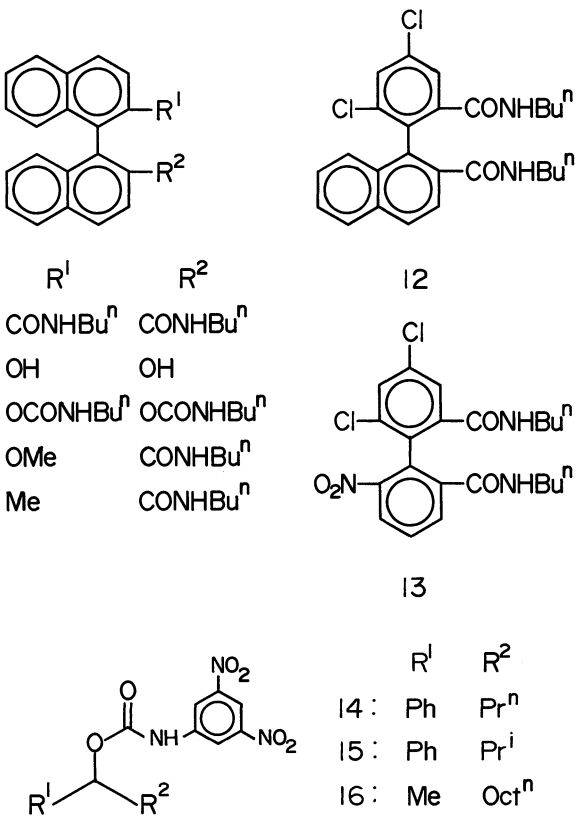

Structure of racemates.

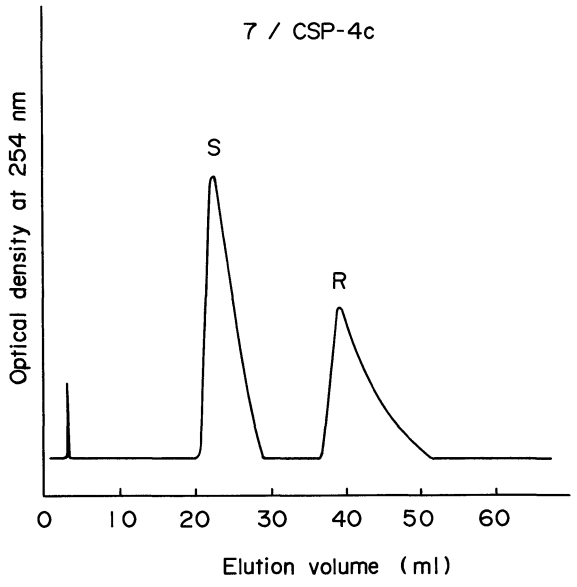

Fig. 4. Chromatographic resolution of racemate **7** on CSP-**4c** column. Column: 25×0.46 (i.d.) cm, eluent: 1% 2-propanol in hexane, flow rate: 1.0 ml min^{-1} at room temperature.

shows the chromatogram of the resolution of **7** on a CSP-4c column using 1% 2-propanol in hexane as the eluent. CSP-4b and CSP-4c could resolve the axially chiral 1,1'-biaryl compounds **7**, **9**, **12**, and **13**, which possessed two amide or carbamate groups, respectively. Racemate **10** which had an amide group and a methoxyl group could be resolved by CSP-4b and CSP-4c. CSP-4a could also resolve the racemates **7**, **9**, and **12**, but couldn't resolve **10** and **13**. On the other hand, none of the CSPs could resolve racemate **11** which had only an amide group as the hydrogen-bonding site. These results indicate that the presence of two hydrogen-bonding sites in a racemate is necessary for efficient chiral discrimination of these biaryl compounds. Thus, a main control factor for the chiral discrimination of biaryl atropisomers seems to be the hydrogen bonding between the amide groups of the polyamides and the hydrogen-bonding sites of the racemates. The capacity factor (k_1') and the separation factor (α) of all of the racemates decreased with a increase in the content of 2-propanol in the eluent. This result also supports the importance of the hydrogen bonding for the chiral discrimination; hydrogen bonding between the polyamides and 2-propanol in competition with the racemates should decrease the interaction between the polyamide CSPs and the racemates.

Racemate **8** couldn't be resolved by all of the CSPs despite bearing two phenolic hydroxyl groups as the hydrogen-bonding sites. This result indicates that a suitable alignment of the two hydrogen-bonding sites of a racemate is also important for efficient chiral discrimination.

Although having only one hydrogen-bonding site, 3,5-dinitrophenylcarbamates (3,5-DNPCs) **14** and **15** derived from the corresponding 1-aryl-1-alkanols were also resolved efficiently (α>1.3) by CSP-4b and CSP-4c. An important control factor of the chiral discrimination should be donor–acceptor interaction between the binaphthalene moiety of the polyamides and the 3,5-dinitrobenzene moiety of the 3,5-DNPCs.

In conclusion, we have shown here that optically active polyamides **4a**—**4c**, obtained by solution polycondensation of 1,1'-binaphthalene-2,2'-dicarbonyl dichloride (**2**) with diamines **3a**—**3c**, have chiral discriminating ability for atropisomeric biaryls **7**,**9**—**13**, and 3,5-DNPCs **14** and **15**.

Experimental

Measurements. Melting points were measured on a Yamato MP-21 and uncorrected. Microanalyses were carried out in the Microanalytical Laboratory of the Chemical Research Institute of Non-aqueous Solutions, Tohoku University. Optical rotations were obtained at room temperature (23—25 °C) using a Union Giken PM-101 polarimeter. CD spectra were measured in an 0.10 cm cell at room temperature on a JASCO J-400X spectropolarimeter. HPLC measurements were carried out on a Shimadzu LC-6A, with UV detection at 254 nm. IR spectra were measured on a Shimadzu IR-460

infrared spectrophotometer. ^{1}H NMR spectra were recorded on a JEOL JNM-FX60 instrument. GPC measurements were carried out at 40 °C on a Tosoh HLC-8020 instrument equipped with TSK gel GMH$_{XL}$ (×2) and G2000H$_{XL}$ columns using a 5 mM LiBr solution of DMF as an eluent.

Materials. Homochiral (*S*)-1,1′-binaphthalene-2,2′-dicarboxylic acid (**1**) was prepared by a previously reported procedure[5] and converted to the bis(acid chloride) **2** by the usual method using thionyl chloride. Diamines **3a**—**3c** and amines **5a**—**5c** were purchased from Tokyo Kasei Kogyo Co., Ltd. and purified by distillation under reduced pressure (**3b**, **3c**, and **5a**—**5c**) or by recrystallization from benzene (**3a**) before use. DMAc was purified by distillation under reduced pressure over calcium hydride before use. Triethylamine was purified by distillation over calcium hydride before use. Other solvents were purified by distillation.

Preparation of Polyamides. The synthetic procedure for **4a** is representative. To a stirred solution of diamine **3a** (181 mg, 1.68 mmol) and triethylamine (343 mg, 3.39 mmol) in DMAc (14 ml) was added finely powdered dicarbonyl dichloride **2** (636 mg, 1.68 mmol) portionwise at room temperature under a nitrogen atmosphere. After stirring for 30 min, the reaction mixture was dropped into 200 ml of methanol with stirring. The resultant precipitate was collected by filtration and washed with methanol and then with acetone. Polyamide **4a** thus obtained was purified by reprecipitation from methanol and dried at 90 °C for 20 h. The polyamide weighed 580 mg (83%). **4b** and **4c** were similarly prepared (Table 1).

4a: IR (KBr) 1636, 1303, 827, and 757 cm^{-1}; ^{1}H NMR (DMSO-d_6) δ=7.0—8.1 (16H, m, Ar–H) and 10.8 (2H, br, N–H). Found: C, 79.02; H, 4.49; N, 6.86%. Calcd for $(C_{28}H_{18}N_2O_2)_n$: C, 81.14; H, 4.38; N, 6.76%.

4b: IR (KBr) 1619, 1541, 1280, 819, and 749 cm^{-1}; ^{1}H NMR (DMSO-d_6) δ=−0.1—0.9 (8H, br, CH_2), 2.4—3.2 (4H, br, CH_2–N), 6.8—8.3 (12H, m, Ar–H), and 8.6—9.2 (2H, br, N–H). Found: C, 78.40; H, 6.20; N, 6.39%. Calcd for $(C_{28}H_{26}N_2O_2)_n$: C, 79.59; H, 6.20; N, 6.63%.

4c: IR (KBr) 1643, 1538, 824, and 756 cm^{-1}; ^{1}H NMR (DMSO-d_6) δ=0.3—1.5 (16H, br, CH_2), 2.4—3.2 (4H, br, CH_2–N), 6.9—8.1 (12H, m, Ar–H), and 8.7—9.2 (2H, br, N–H). Found: C, 77.83; H, 7.17; N, 6.18%. Calcd for $(C_{32}H_{34}N_2O_2)_n$: C, 80.30; H, 7.16; N, 5.85%.

The discrepancies in these carbon analyses may be attributed to the carbonization of the binaphthalene moieties of the polyamides.[8]

Synthesis of Model Diamides. The synthetic procedure for **6a** is representative. To a stirred solution of the dicarbonyl dichloride **2** (212 mg, 0.558 mmol) in dry benzene (10 ml) were added benzenamine (**5a**) (125 mg, 1.34 mmol) and triethylamine (136 mg, 1.34 mmol) at room temperature under a nitrogen atmosphere. The solution was refluxed with stirring for 1 h and then cooled to room temperature. The reaction mixture was washed (2 M HCl (1 M=1 mol dm^{-3}), 10% Na_2CO_3, and distilled water) and dried over Na_2SO_4. Solvents were removed under reduced pressure, and the residue was purified by silica-gel column chromatography (eluent: 50% ethyl acetate in hexane) to afford the diamide **6a** in 95% yield (260 mg) as amorphous powder. Diamides **6b** and **6c** were similarly prepared as colorless glass (Table 1).

6a: IR (KBr) 1643, 1545, 1332, 755, and 690 cm^{-1}; ^{1}H NMR ($CDCl_3$) δ=6.80—8.10 (22H, m, Ar–H) and 8.90—9.30 (2H, br, N–H). Found: C, 82.90; H, 5.00; N, 5.70%. Calcd for $C_{34}H_{24}N_2O_2$: C, 82.90; H, 4.91; N, 5.69%.

6b: IR (neat) 1624, 1543, 1326, 1299, 824, and 756 cm^{-1}; ^{1}H NMR ($CDCl_3$) δ=0.85—1.00 (22H, m, CH_2 and CH_3), 2.82—3.14 (4H, m, CH_2–N), and 7.05—8.08 (14H, m, Ar–H and N–H). Found: C, 80.63; H, 8.06; N, 5.47%. Calcd for $C_{34}H_{40}N_2O_2$: C, 80.27; H, 7.93; N, 5.51%.

6c: IR (neat) 1631, 1563, 1331, 1301, 825, and 756 cm^{-1}; ^{1}H NMR ($CDCl_3$) δ=0.80—1.24 (38H, m, CH_2 and CH_3), 2.82—3.14 (4H, m, CH_2–N), and 6.96—8.04 (14H, m, Ar–H and N–H). Found: C, 81.04; H, 9.30; N, 4.41%. Calcd for $C_{42}H_{56}N_2O_2$: C, 81.24; H, 9.09; N, 4.51%.

Preparation of Packing Material and Column Packing. Macroporous silica gel (Merck, LiChrospher SI 1000: mean particle size, 10 μm; pore size, 100 nm) was silanized with dichlorodiphenylsilane according to the literature method.[7] A polyamide (ca. 0.15 g) was dissolved in 7 ml of DMAc and the silanized silica gel (3.0 g) was wetted with the polymer solution. The resultant mixture was irradiated with ultrasound for 1 min. Then the solvent was evaporated in vacuo. Obtained polymer-coated silica gel was dried in vacuo at 80 °C for 5 h and then dispersed in 30 ml of methanol with sonication during 5 min. After filtration and washing with methanol, the silica gel was dried in vacuo at 80 °C for 5 h. The chiral packing material thus obtained was packed in a stainless steel HPLC column (i. d.: 0.46 cm, length: 25 cm) by a slurry method. The plate number of the columns packed CSP-4a—CSP-4c were about 4500, 2900, and 2500, respectively, for benzene using 10% 2-propanol in hexane as the eluent at ambient temperature.

We thank Professor Hisashi Uda and Professor Nobuyuki Harada of the Chemical Research Institute of Non-aqueous Solutions of our university for CD measurement. We also thank Mr. Katsuo Komiya and Dr. Ryuichi Kitayama of Tosoh Co., Ltd. for GPC measurements and analyses. A part of this work was supported by a Grant-in-Aid for Scientific Research No. 02555177 from the Ministry of Education, Science and Culture.

References

1) For example, Y. Okamoto, *CHEMTECH,* **1987**, 176; N. Kunieda, H. Chakihara, and M. Kinoshita, *Chem. Lett.,* **1990**, 317.

2) K. Saigo, Y. Chen, K. Fujioka, N. Yonezawa, and M. Hasegawa, *Chem. Lett.,* **1988**, 647; Y. Chen, K. Saigo, N. Yonezawa, K. Tachibana, and M. Hasegawa, *Bull. Chem. Soc. Jpn.,* **60**, 3341 (1987); Y. Okamoto, T. Fukumoto, R. Aburatani, and K. Hatada, *Polym. Prepr., Jpn.,* **37**, 3700 (1988).

3) S. Miyano and H. Hashimoto, *Yuki Gosei Kagaku Kyokai Shi,* **44**, 713 (1986).

4) C. G. Overberger, T. Yoshimura, A. Ohnishi, and A. S. Gomes, *J. Polym. Sci., Polym. Chem. Ed.,* **8**, 2275 (1970); C. G. Overberger, A. Ohnishi, and A. S. Gomes, *ibid.,* **9**, 1139 (1971); R. C. Schulz and R. H. Jung, *Makromol. Chem.,* **116**, 190 (1968).

5) S. Ôi, Y. Matsuzaka, J. Yamashita, and S. Miyano, *Bull. Chem. Soc. Jpn.,* **62**, 956 (1989); S. Ôi, M. Shijo, J. Yamashita, and S. Miyano, *Chem. Lett.,* **1988**, 1545; J. Yamashita, H. Satoh, S. Ôi, T. Suzuki, S. Miyano, and N. Takai, *J. Chromatogr.,* **464**, 411 (1989).

6) N. Harada and K. Nakanishi, "Circular Dichroic Spectroscopy—Exiton Coupling in Organic Stereochemistry—,"

University Science Books, Mill Valley, California (1983), and references cited therein.

7) Y. Okamoto, E. Yashima, M. Ishikura, and K. Hatada, *Bull. Chem. Soc. Jpn.*, **61**, 255 (1988).

8) The similar phenomenon was reported by Saigo et al. for the polyamides having cyclobutane rings in the main chain; see K. Saigo, Y. Chen, N. Yonezawa, T. Kanoe, K. Tachibana, and M. Hasegawa, *Macromolecules,* **19**, 1552 (1986).

A Synthesis of 5′-*O*-Acryloyl-5-fluorouridine by Use of *p*-Methoxybenzyl Group as an N^3-Imide Protecting Group of 5-Fluorouridine[1)]

Takahiko Akiyama, Yasuhiro Takesue, Masahiro Kumegawa, Hiroyuki Nishimoto, and Shoichiro Ozaki*
Department of Resources Chemistry, Faculty of Engineering, Ehime University, Bunkyo-cho, Matsuyama 790
(Received February 18, 1991)

5′-*O*-Acryloyl-5-fluorouridine was prepared by use of *p*-methoxybenzyl (PMB) group as an N^3-imide protecting group of 5-fluorouridine. PMB group was introduced chemoselectively by use of *N*,*N*-diisopropylethylamine or DBU as a base. A new deprotection method was developed by means of $AlCl_3$–anisole system at room temperature.

In our laboratory, as part of a continuing synthetic program designed to develop antitumor agents with high antitumor activity and low toxicity, we have synthesized various kinds of 5-fluorouracil (5-FU) derivatives such as 1-carbamoyl-,[2)] 1-acyloxyalkyl-,[3)] 1-alkylthiocarbamoyl-,[4)] 1-alkoxyalkyl-5-fluorouracils,[5)] and also functional polymers bearing 5-FU as a side chain.[6)] Recently, functional polymers containing 5-FU have attracted considerable attention from the standpoint of polymeric drugs. Polymeric drugs bearing 5-fluorouridine (FUR) as a side chain, however, have not been developed so far. In previous papers,[1,7)] we reported syntheses and antitumor activity of 5′-*O*-acyl-5-fluorouridines, which showed high antitumor activity against L-1210 leukemia in mice. These results prompted us to synthesize functional polymers containing FUR as a side chain. We focused on 5′-*O*-acryloyl-5-fluorouridine (**3a**) as a promising ester monomer containing FUR and attempted to synthesize it. Unexpectedly, **3a** was not obtained by the usual method (5′-*O*-acylation of 2′,3′-*O*-isopropylidene-5-fluorouridine (**1**) followed by acidic hydrolysis). In order to synthesize it efficiently, protection of the N^3-imide function was necessary. Protection of N^3-imide function in uridine moiety has attracted considerable attention in nucleotide chemistry and various kinds of protecting groups such as benzoyl,[8)] 2-(4-nitrophenyl)ethyl,[9)] 2-(4-nitrophenylsulfonyl)-ethyl,[10)] phenyl,[11)] and 2-(methoxy)ethoxymethyl[12)] groups have been developed. Because N–glycosidic bonds are acid labile and *O*-acryloyl moiety is unstable in basic conditions, an N^3-imide protecting group removable under mild conditions is desirable. We have found that *p*-methoxybenzyl (PMB) group meets above requirements. The PMB group has following features; 1) selective introduction is possible in the presence of free OH group with DBU (1,8-diazabicyclo[5.4.0]undec-7-ene) as a base, 2) deprotection was effected smoothly by the action of $AlCl_3$ in anisole at room temperature under mild conditions.[13)] In this paper we wish to describe a synthesis of **3a** by use of PMB group as a N^3-imide protecting group removable under weakly acidic conditions by means of $AlCl_3$–anisole system.[14)]

Results and Discussion

A variety of 5′-*O*-acyl-5-fluorouridines were synthesized by 5′-*O*-acylation of **1** followed by acidic hydrolysis of the isopropylidene moiety.[1)] However, when **1** was treated with acryloyl chloride in the presence of tertiary amine, corresponding 5′-*O*-acylated compound **2a** was obtained in a very low yield and was too labile to purify by column chromatography. All our attempts to synthesize **2a** in a pure form failed. We therefore speculated that **2a** could be obtained by protecting N^3-imide function in advance and sought a protecting group for the N^3-imide function. We have found that a PMB group meets above requirements.

Introduction of a PMB group was carried out as follows. Treatment of **1** with *p*-methoxybenzyl bromide (1.5 equiv) in the presence of *N*,*N*-diisopropylethylamine (2.0 equiv) as a base in CH_3CN at room temperature for 3 h gave 2′,3′-*O*-isopropylidene-3-(4-methoxybenzyl)-5-fluorouridine (**4**) quantitatively. The PMB group was introduced more conveniently by use of commercially available *p*-methoxybenzyl chloride in the presence of DBU as a base in CH_3CN without protecting 5′-OH group to afford **4** in a good yield. No formation of 5′-*O*-alkylated compound was observed under these conditions. Next, acylation of N^3-protected derivative **4** with acryloyl chloride proceeded smoothly to obtain 5′-*O*-acryloyl-2′,3′-*O*-isopropylidene-3-(4-methoxybenzyl)-5-fluorouridine (**5a**) in a good yield. Acidic hydrolysis of the isopropylidene moiety afforded 5′-*O*-acryloyl-3-(4-methoxybenzyl)-5-fluorouridine (**6a**).

An $AlCl_3$–anisole system has been utilized in the deprotection of benzyl esters.[15)] We employed the $AlCl_3$–anisole system for the deprotection of N^3-benzyl moieties of FUR. Deprotection of the PMB group was achieved by treatment of **6a** with $AlCl_3$ (10 equiv) in anisole at room temperature overnight to obtain 5′-*O*-acryloyl-5-fluorouridine (**3a**) in 96% yield. When ammonium cerium(IV) nitrate was used for the deprotection of PMB moiety,[13)] **3a** was not obtained at all presumably due to the decomposition of **3a** or **6a** under the reaction conditions. This result demonstrates mild conditions of our deprotection methods.

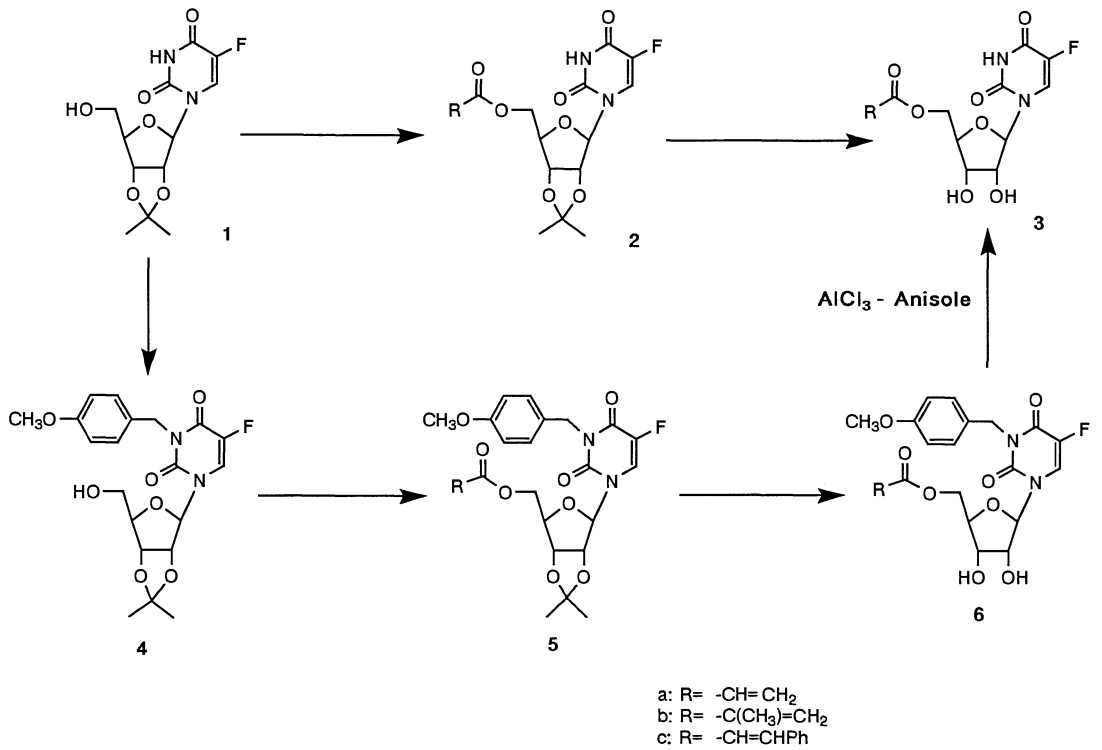

Scheme 1.

Table 1. Deprotection of the *p*-Methoxybenzyl Group[a)]

Run	R_1	R_2	R_3	Product	Yield/%
1	**6a** $-COCH=CH_2$	H	H	**3a**	96
2	**6b** $-COC(CH_3)=CH_2$	H	H	**3b**	81
3	**6c** $-COCH=CHPh$	H	H	**3c**	93
4	**5c** $-COCH=CHPh$	$C(CH_3)_2$		**2c**	81

a) 10 equiv of $AlCl_3$ was used in anisole at room temperature.

The present method was successfully applied to other PMB-protected 5-fluorouridine derivatives as shown in Table 1. In the case of cinnamoyl (**6c**), methacryloyl (**6b**) derivatives, PMB groups were also cleaved without harming N-glycosidic bond to afford the NH free compounds in good yields. It is noted that PMB group was cleaved in preference to the 2′,3′-*O*-isopropylidene moiety (Run 4).

Finally, we tested an unsubstituted benzyl group. When 5′-*O*-cinnamoyl-3-benzyl-5-fluorouridine (**9**) was treated with $AlCl_3$ (10 equiv) in anisole at room temperature, no reaction took place. Deprotection of the benzyl group proceeded at a higher temperature (80 °C, 4 h) with concurrent cleavage of the N-glycosidic bond to afford **3c** in a low yield (<10%). Thus, presence of the *p*-methoxy substituent is essential for the smooth cleavage of N^3-benzyl moiety in the present method.

Experimental

Melting points were determined on a Yamato melting point apparatus and are uncorrected. ^1H NMR spectra were recorded on a JEOL GSX-270 spectrometer with tetramethylsilane as an internal standad. IR spectra were recorded on a Hitachi EPI G-3 spectrometer. $AlCl_3$ was ground into fine powder and stored under N_2 atmosphere. Anisole was distilled over CaH_2 and stored over Molecular Sieves 4A. *p*-Methoxybenzyl bromide[17)] was prepared by NBS-mediated bromination[18)] of *p*-methoxytoluene and used immediately. Purification of products was performed by column chromatography on silica gel (Wako gel C-300) or preparative TLC on silica gel (Wako gel B-5F).

2′,3′-*O*-Isopropylidene-3-(4-methoxybenzyl)-5-fluorouridine (4). To a solution of 2′,3′-*O*-isopropylidene-5-fluorouridine[19)] (**1**) (1.35 g, 4.47 mmol) in CH_3CN (15 ml) was added *p*-methoxybenzyl chloride (1.12 ml, 8.94 mmol) and DBU (1.34 ml, 8.94 mmol). The mixture was allowed to reflux at 50—60 °C for 3 h. After the mixture was cooled to room temperature, H_2O was added. The mixture was extracted with ethyl acetate. The combined organic layers were successively washed with 1 M HCl (1 M=1 mol dm^{-3}) and brine, and then concentrated to dryness to give an oil, which was purified by column chromatography on silica gel (CH_2Cl_2 : ethyl acetate=5.5 : 1, v/v) to afford an oil. Recrystallization of it from a mixture of hexane and ethyl acetate (v/v=1 : 1) gave **4** as crystals (1.85 g, 98%): Mp 118—119 °C; ^1H NMR ($CDCl_3$) δ=1.36 (3H, s, CH_3), 1.58 (3H, s, CH_3), 2.46—2.51 (1H, m, OH), 3.78 (3H, s, OCH_3), 3.81 (1H, ddd, $J_{5',5''}$=11.9 Hz, $J_{4',5'}$=2.7 Hz, $J_{5',OH}$=6.1 Hz, H-5′), 3.94 (1H, dt, $J_{4',5''}$=2.7 Hz, H-5″), 4.33 (1H, q, $J_{3'4'}$=2.7 Hz, H-4′), 4.88—4.95 (2H, m, H-2′,3′), 5.02, 5.08 (2H, ABq, J=13.6 Hz, CH_2), 5.68 (1H, d, $J_{1',2'}$= 2.4 Hz, H-1′), 6.80—6.86 (2H, m, aromatic), 7.42—7.48 (2H, m, aromatic), and 7.59 (1H, d, J=5.8 Hz, H-6); IR (nujol) 3420, 1690, 1660, and 1640 cm^{-1}. Found: C, 56.81; H, 5.51; N,

6.41%. Calcd for $C_{20}H_{23}N_2O_7F$: C, 56.87; H, 5.49; N, 6.63%.

General Procedure for the 5′-*O*-Acylation of 4. A typical procedure is described for 5′-*O*-acryloyl-2′,3′-*O*-isopropylidene-3-(4-methoxybenzyl)-5-fluorouridine (**5a**). To a solution of **4** (1.53 g, 3.63 mmol) in CH_3CN (2 ml) was added successively *N*,*N*-diisopropylethylamine (1.26 ml, 7.25 mmol) and acryloyl chloride (0.884 ml, 10.9 mmol) at room temperature. The mixture was stirred at that temperature for 4 h, and 5% $KHSO_4$ solution was added. Organic phase was separated and aqueous layers were extracted with ethyl acetate. The combined orgaic layers were successively washed with brine, 2.5% $NaHCO_3$ solution, and brine, dried over anhydrous Na_2SO_4, and concentrated to leave an oil, which was purified by column chromatography on silica gel (CH_2Cl_2 : ethyl acetate=2 : 1, v/v) to give **5a** (1.66 g, 96%): ^{1}H NMR ($CDCl_3$) δ=1.36 (3H, s, CH_3), 1.58 (3H, s, CH_3), 3.77 (3H, s, OCH_3), 4.32—4.51 (3H, m, H-4′,5′), 4.79 (1H, dd, $J_{3',4'}$=2.1 Hz, $J_{2',3'}$=6.4 Hz, H-3′), 4.89 (1H, dd, $J_{1',2'}$=2.1 Hz, H-2′), 4.99, 5.10 (2H, ABq, J=13.6 Hz, CH_2), 5.74 (1H, d, H-1′), 5.84 (1H, dd, J=10.4 Hz, 1.4 Hz, vinyl-H), 6.08 (1H, dd, J=10.4 Hz, 17.3 Hz, =CHCO), 6.41 (1H, dd, J=1.4 Hz, 17.3 Hz, vinyl-H), 6.87 (2H, d, J=8.9 Hz, aromatic), 7.39 (2H, d, J=5.5 Hz, H-6), and 7.47 (2H, d, J=8.9 Hz, aromatic); IR (nujol) 3000, 1700, 1680, and 1650 cm^{-1}. Found: C, 57.75; H, 5.31; N, 5.77%. Calcd for $C_{23}H_{25}N_2O_8F$: C, 57.98; H, 5.29; N, 5.88%.

2′,3′-*O*-Isopropylidene-5′-methacryloyl-3-(4-methoxybenzyl)-5-fluorouridine (5b): ^{1}H NMR ($CDCl_3$) δ=1.37 (3H, s, CH_3), 1.58 (3H, s, CH_3), 1.91 (3H, s, =CCH_3), 3.78 (3H, s, OCH_3), 4.28—4.50 (3H, m, H-4′,5′), 4.79 (1H, dd, $J_{3',4'}$=3.4 Hz, $J_{2',3'}$=6.4 Hz, H-3′), 4.86 (1H, dd, $J_{1',2'}$=2.1 Hz, H-2′), 5.01, 5.09 (2H, ABq, J=13.4 Hz, CH_2), 5.51—5.55 (1H, m, vinyl-H), 5.72 (1H, d, H-1′), 6.03 (1H, brs, vinyl-H), 6.80—6.85 (2H, m, aromatic), 7.36 (1H, d, J=5.8 Hz, H-6), 7.42—7.49 (2H, m, aromatic; IR ($CHCl_3$) 2990, 1700, 1645, 1490, and 1400 cm^{-1}. Found: C, 58.98; H, 5.78; N, 5.63%. Calcd for $C_{24}H_{27}N_2O_8F$: C, 58.77; H, 5.55; N, 5.71%.

5′-*O*-Cinnamoyl-2′,3′-*O*-isopropylidene-3-(4-methoxybenzyl)-5-fluorouridene (5c): ^{1}H NMR ($CDCl_3$) δ=1.37 (3H, s, CH_3), 1.59 (3H, s, CH_3), 3.75 (3H, s, OCH_3), 4.42—4.51 (3H, m, H-4′,5′), 4.82—4.85 (1H, m, H-3′), 4.89 (1H, dd, $J_{1',2'}$=1.8 Hz, $J_{2',3'}$=6.4 Hz, H-2′), 4.99, 5.05 (2H, ABq, J=13.4 Hz, CH_2), 5.79 (1H, d, H-1′), 6.42 (1H, d, J=15.8 Hz, PhCH=), 6.79—6.84 (2H, m, aromatic), 7.37—7.52 (7H, m, aromatic), and 7.72 (1H, d, =CHCO); IR ($CHCl_3$) 2950, 1700, 1650, 1500, 1440, 1360, 1260, and 1240 cm^{-1}. Found: C, 62.79; H, 5.34; N, 5.00%. Calcd for $C_{29}H_{29}N_2O_8F$: C, 63.04, H, 5.29; N, 5.07%.

General Procedure for the Cleavage of Isopropylidene Moiety. A typical procedure is described for 5′-*O*-acryloyl-3-(4-methoxybenzyl)-5-fluorouridine (**6a**). A solution of **5a** (1.65 g, 3.45 mmol) in an 80% methanolic solution of trifluoroacetic acid (4.0 ml) was stirred at room temperature for 10 min. The reaction mixture was concentrated in vacuo to leave an oil, which was purified by column chromatography on silica gel (hexane : ethyl acetate=1 : 2, v/v) to give **6a** (1.32 g, 88%) as an amorphous solid: ^{1}H NMR ($CDCl_3$: CD_3OD=95 :5, v/v) δ=2.70 (2H, brs, OH), 3.79 (3H, s, OCH_3), 4.00—4.10 (2H, m, H-2′,3′), 4.22—4.30 (1H, m, H-4′), 4.50 (1H, brs, H-5′), 4.51 (2H, brs, H-5″), 5.03, 5.09 (2H, ABq, J=13.7 Hz, CH_2), 5.79 (1H, brs, H-1′), 5.93 (1H, dd, J=1.2 Hz, J=10.4 Hz, vinyl-H), 6.14 (1H, dd, J=10.4 Hz, 17.2 Hz, =CHCO), 6.46 (1H, dd, J=1.2 Hz, J=17.2 Hz, vinyl-H), 6.78—6.88 (2H, m, aromatic), 7.35—7.48 (2H, m, aromatic), and 7.73 (1H, d, J=6.1 Hz, H-6); IR (nujol) 3400, 3000, 1690, 1660, and 1630 cm^{-1}. Found: C, 54.93; H, 4.91; N, 6.08%. Calcd for $C_{20}H_{21}N_2O_8F$: C, 55.05, H, 4.85; N, 6.42%.

5′-*O*-Methacryloyl-3-(4-methoxybenzyl)-5-fluorouridine (6b): ^{1}H NMR ($CDCl_3$: CD_3OD=95 : 5, v/v) δ=1.95 (3H, brs, CH_3), 2.46 (2H, brs, OH), 3.79 (3H, s, OCH_3), 4.02—4.15 (2H, m, H-2′,3′), 4.23—4.52 (1H, m, H-4′), 4.46 (1H, dd, $J_{4',5'}$=3.4 Hz, $J_{5',5''}$=12.5 Hz, H-5′), 4.51 (1H, dd, $J_{4',5''}$=2.7 Hz, H-5″), 5.03, 5.08 (2H, ABq, J=13.7 Hz, CH_2), 5.63—5.67 (1H, m, vinyl-H), 5.75—5.81 (1H, m, H-1′), 6.09 (1H, brs, vinyl-H), 6.77—6.88 (2H, m, aromatic), 7.39—7.49 (2H, m, aromatic), and 7.62 (1H, d, J=5.8 Hz, H-6); IR (nujol) 3350, 1700, 1630, and 1260 cm^{-1}. Found: C, 56.13; H, 5.15; N, 5.92%. Calcd for $C_{21}H_{23}N_2O_8F$: C, 56.00; H, 5.15; N, 6.22%.

5′-*O*-Cinnamoyl-3-(4-methoxybenzyl)-5-fluorouridine (6c): ^{1}H NMR ($CDCl_3$: CD_3OD=95 : 5, v/v) δ=3.76 (3H, s, OCH_3), 4.10—4.16 (2H, m, H-2′,3′), 4.32 (1H, m, H-4′), 4.48—4.51 (2H, m, H-5′, 5″), 5.01, 5.06 (2H, ABq, J=13.7 Hz, CH_2), 5.85 (1H, brs, H-1′), 6.46 (1H, d, J=15.9 Hz, =CHCO), 6.81 (2H, d, J=8.5 Hz, aromatic), 7.39—7.42 (5H, m, aromatic), 7.50—7.54 (2H, m, aromatic), 7.75 (1H, d, PhCH=), and 7.89 (1H, d, J=6.1 Hz, H-6); IR (nujol) 3450, 1700, 1620, 1290, 1230, 1160, and 1090 cm^{-1}. Found: C, 60.10; H, 5.31; N, 5.15%. Calcd for $C_{26}H_{25}N_2O_8F \cdot 0.5H_2O$: C, 59.88, H, 5.03, N, 5.37%.

General Procedure for the Cleavage of PMB Group. A typical procedure is described for 5′-*O*-acryloyl-5-fluorouridine (**3a**). To a solution of **6a** (208 mg, 0.477 mmol) in anisole (1 ml) and $AlCl_3$ (636 mg, 4.77 mmol) in anisole (1 ml). After stirring at that temperature overnight, methanol (1.0 ml) was added to the reaction mixture at 0 °C, the mixture was evaporated by rotary evaporator at a bath temperature below 40 °C. The resultant anisole solution was subjected to short column chromatography on silica gel (methanol: CH_2Cl_2=1 : 10 (v/v)) to afford an oil, which was further purified by TLC on silica gel (methanol : CH_2Cl_2=1 : 10 (v/v)) to give **3a** (144 mg, 96%): ^{1}H NMR ($CDCl_3$: DMSO-d_6=95 : 5, v/v) δ=3.33 (2H, s, H-2′,3′), 4.09—4.17 (1H, m, H-5′), 4.17—4.28 (1H, m, H-4′), 4.39—4.53 (2H, m, H-2′,3′), 5.93 (1H, dd, J=1.5 Hz, 10.4 Hz, vinyl-H), 6.21 (1H, dd, J=17.0 Hz, 10.4 Hz, =CHCO), 6.46 (1H, dd, J=1.5 Hz, 17.0 Hz, vinyl-H), 7.65 (1H, d, J=6.4 Hz, H-6), and 11.51 (1H, brs, H-3); IR (nujol) 3450, 3370, 3330, 1700, 1680, and 1660 cm^{-1}. Found: C, 45.52; H, 4.44; N, 8.51%. Calcd for $C_{12}H_{13}N_2O_7F$: C, 45.58; H, 4.14; N, 8.86%.

3-Benzyl-2′,3′-*O*-isopropylidene-5-fluorouridine (7). This was obtained by the similar procedure as described for the preparation of **4** in a quantitative yield: Mp 124—125 °C; ^{1}H NMR ($CDCl_3$) δ=1.36 (3H, s, CH_3), 1.58 (3H, s, CH_3), 2.45—2.49 (1H, m, OH), 3.81 (1H, ddd, $J_{5',5''}$=12.0 Hz, $J_{4',5'}$=2.6 Hz, $J_{5',OH}$=5.8 Hz, H-5′), 3.94, (1H, dt, $J_{4',5''}$=2.6 Hz, H-5″), 4.33 (1H, q, $J_{3',4'}$=2.6 Hz, H-4′), 4.87—4.95 (2H, m, H-2′3′), 5.08, 5.15 (2H, ABq, J=13.9 Hz, CH_2), 5.69 (1H, d, $J_{1',2'}$=2.5 Hz, H-1′), 7.23—7.35 (3H, m, aromatic), 7.45—7.55 (2H, m, aromatic), and 7.62 (1H, d, J=5.8 Hz, H-6); IR (nujol) 3400, 1700, 1675, and 1640 cm^{-1}. Found: C, 58.18; H, 5.33; N, 6.95%. Calcd for $C_{19}H_{21}N_2O_6F$: C, 58.16; H, 5.39; N, 7.14%.

3-Benzyl-5′-*O*-cinnamoyl-2′,3′-*O*-isopropylidene-5-fluorouridine (8). This was obtained by the similar procedure as described for the preparation of **5a** in 75% yield: ^{1}H NMR ($CDCl_3$) δ=1.37 (3H, s, CH_3), 1.56 (3H, s, CH_3), 4.42—4.55 (3H, m, H-4′,5′), 4.80—4.86 (1H, m, H-3′), 4.88 (1H, dd, $J_{1',2'}$=1.8 Hz, $J_{2',3'}$=6.4 Hz, H-2′), 5.05, 5.12 (2H, ABq,

J=13.7 Hz, CH_2), 5.79 (1H, d, H-1′), 6.42 (1H, d, J=15.9 Hz, PhCH=), 7.20—7.75 (10H, m, aromatic), and 7.72 (1H, d, =CHCO); IR ($CHCl_3$) 1700, 1650, 1250, 1150, and 1040 cm^{-1}. Found: C, 63.75; H, 5.06; N, 5.47%. Calcd for $C_{24}H_{27}N_2O_7F$: C, 63.52; H, 5.33; N, 5.49%.

3-Benzyl-5′-*O*-cinnamoyl-5-fluorouridine (9). This was obtained by the similar procedure as described for the preparation of **6a** in 93% yield: ^1H NMR ($CDCl_3$: CD_3OD (v/v=95/5)) δ=2.62 (2H, s, OH), 4.03—4.17 (2H, m, H-2′,3′), 4.23—4.33 (1H, m, H-4′), 4.51 (1H, dd, $J_{4',5'}$=2.4 Hz, $J_{5',5''}$=12.8 Hz, H-5′), 4.60 (1H, dd, $J_{4',5''}$=3.1 Hz, H-5″), 5.09, 5.14 (2H, ABq, J=13.7 Hz, CH_2), 5.81 (1H, brs, H-1′), 6.47 (1H, d, J=15.9 Hz, PhCH=), 7.20—7.60 (10H, m, aromatic), 7.76 (1H, d, =CHCO), and 7.93 (1H, d, J=6.1 Hz, H-6); IR ($CHCl_3$) 3600, 1720, 1650, and 1200 cm^{-1}. Found: C, 61.24; H, 4.81; N, 5.68%. Calcd for $C_{24}H_{23}N_2O_7F$: C, 61.27; H, 4.93; N, 5.95%.

The authors wish to thank the Advanced Center for Chemical Analysis, Ehime University, for elemental analyses.

References

1) 5-Fluorouracil derivatives. Part XXI. Part XX of this series: S. Ozaki, T. Akiyama T. Morita, M. Kumegawa, T. Nagase, N. Uehara, and A. Hoshi, *Chem. Pharm. Bull.*, **38**, 3164 (1990).

2) S. Ozaki, Y. Ike, H. Mizuno, K. Ishikawa, and H. Mori, *Bull. Chem. Soc. Jpn.*, **50**, 2406 (1977).

3) S. Ozaki, Y. Watanabe, T. Hoshiko, H. Mizuno, K. Ishikawa, and M. Hori, *Chem. Pharm. Bull.*, **32**, 733 (1984).

4) S. Ozaki, Y. Watanabe, T. Ogasawara, Y. Yamauchi, K. Fujiwara, A. Hoshi, and M. Iigo, *Chem. Pharm. Bull.*, **33**, 2832 (1985).

5) S. Ozaki, Y. Watanabe, T. Hoshino, T. Nagase, T. Ogasawara, H. Furukawa, A. Uemura, K. Ishikawa, H. Mori, A. Hoshi, M. Iigo, and R. Tokuzen, *Chem. Pharm. Bull.*, **34**, 150 (1986).

6) S. Ozaki, J. Ohnishi, Y. Watanabe, T. Nohda, T. Nagase, T. Akiyama, N. Uehara, and A. Hoshi, *Polym. J.*, **21**, 955 (1989); S. Ozaki, J. Ohnishi, T. Akiyama, T. Nagase, N. Uehara, and A. Hoshi, *ibid.*, **22**, 689 (1990).

7) S. Ozaki, T. Akiyama, Y. Ike, H. Mori, and A. Hoshi, *Chem. Pharm. Bull.*, **37**, 3405 (1989).

8) T. Kamimura, T. Masegi, and T. Hata, *Chem. Lett.*, **1982**, 965; T. Kamimura, T. Masegi, K. Urakami, S. Honda, M. Sekine, and T. Hata, *ibid.*, **1983**, 1051; M. Sekine, *J. Org. Chem.*, **54**, 2321 (1989).

9) B. S. Schultz and W. Pfleiderer, *Tetrahedron Lett.*, **24**, 3587 (1983).

10) C. A. A. Claeson, A. M. P. Pistorius, and G. I. Tesser, *Tetrahedron Lett.*, **26**, 3859 (1985).

11) S. S. Jones, C. B. Reese, S. Sibanda, and A. Ubasawa, *Tetrahedron Lett.*, **22**, 4755 (1981).

12) H. Takaku, S. Ueda, and T. Ito, *Tetrahedron Lett.*, **24**, 5363 (1983).

13) Independent from our work, Danishefsky already employed PMB group as a protecting group for the N^3-imide function of uridine in a synthesis of tunicamycin subunit, whereby the protecting group was deprotected by use of ammonium cerium(IV) nitrate. See, S. J. Danishefsky, S. L. DeNimno, S. Chen, L. Boisvert, and M. Barbachyn, *J. Am. Chem. Soc.*, **111**, 5810 (1989).

14) A part of this work was reported; T. Akiyama, M. Kumegawa, Y. Takesue, H. Nishimoto, and S. Ozaki, *Chem. Lett.*, **1990**, 339.

15) T. Tsuji, T. Kataoka, M. Yoshioka, Y. Sendo, Y. Nishitani, S. Hirai, T. Maeda, and W. Nagata, *Tetrahedron Lett.*, **1979**, 2793.

16) T. Akiyama, H. Nishimoto, and S. Ozaki, *Bull. Chem. Soc. Jpn.*, **63**, 3356 (1990).

17) R. P. Pinnell, E. S. Huyster, and J. Kleinberg, *J. Org. Chem.*, **30**, 38 (1965).

18) T. F. Corbin, R. C. Hahn, and H. Shechter, *Org. Synth.*, Coll. Vol. V, 328 (1973).

19) K. A. Watanabe, A. Matsuda, M. J. Halat, D. H. Hollenberg, J. S. Nisselbaum, and J. J. Fox, *J. Med. Chem.*, **24**, 893 (1981).

CO Hydrogenation over TiO_2-Supported Ultrafine Fe_3O_4 Particle Catalysts Prepared by a Colloid Chemical Method

Byong-tae CHANG* and Sung-jin KIM
Department of Chemistry, Faculty of Science, Korea University, Kodaira, Tokyo 187
(Received January 16, 1991)

The properties of TiO_2 supports and the H_2 reduction temperature of Fe_3O_4/TiO_2 catalysts were found to play imortant roles in determining their activity and light olefin selectivity. For each catalyst, a good linear relationship was observed between the CO conversion and the light olefin selectivity. The sequence of the latter under identical conditions was JRC-TIO-5>TIO-3>TIO-4.

In recent years, much attention has been focused on the interactions between metal and support in various supported catalysts.[1-3] Previously we found that the catalytic activity of ultrafine particles of metallic Fe (10—20 nm), prepared by a gas evaporation method, depends largely on the nature of support (TiO_2, SiO_2, Al_2O_3, NaZSM-5 and HZSM-5), and that the physical and chemical properties of TiO_2 supports exert considerable influence on the activity, particularly the light olefin selectivity.[4,5]

According to Ito,[6] ultrafine particles (smaller than 10 nm) of several metal oxides can be prepared by a colloid chemical method. The purpose of this work was to study the catalytic properties of TiO_2-supported Fe_3O_4 prepared by this method; effects of TiO_2 support, H_2 reduction temperature and potassium-promoter on the CO hydrogenation activity and the product distribution.

Experimental

Ultrafine Particle Fe_3O_4 (UFP-Fe_3O_4) were supplied from

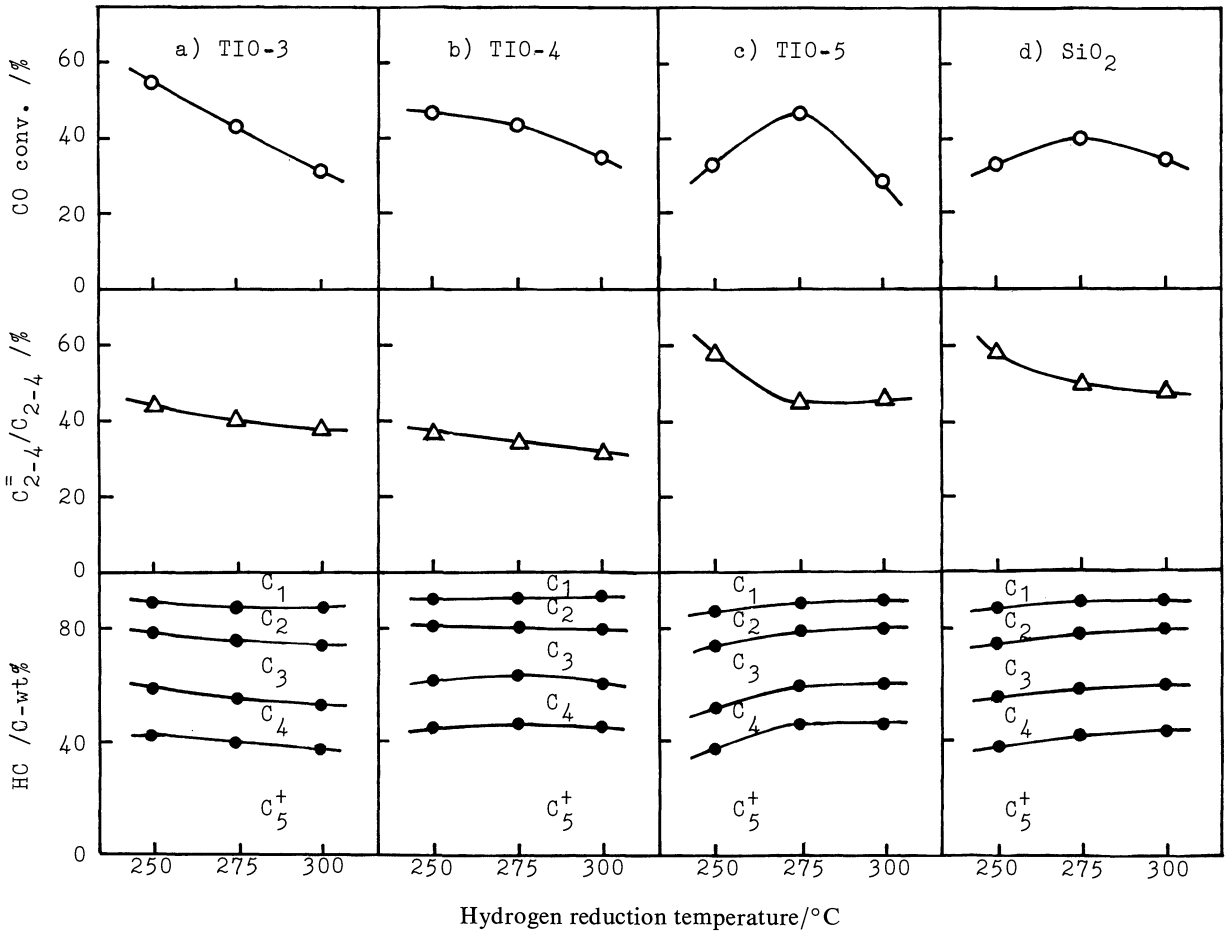

Fig. 1. Effects of hydrogen reduction temperature on the CO conversion, the light olefin selectivity, and the distribution of hydrocarbons produced over UFP-Fe_3O_4/support catalysts. CO hydrogenation conditions; t=250°C, P=5 kg cm^{-2}, and W/F=24±3 g h mol^{-1}.

Okamura Oil Co. By chemical analysis UFP-Fe_3O_4 was found to contain Fe at 55.2 wt% together with several organics. The X-ray diffraction pattern was in good agreement with that of Fe_3O_4, and the particle size determined by X-ray broadening analysis was 9.6±0.2 nm.

Three kinds of TiO_2 (JRC-TIO-3, 4, and 5) and, for comparison, SiO_2 (Aerosil 300) were used as supports. Catalysts were prepared by mechanically mixing UFP-Fe_3O_4 (20 wt%) with one of the supports in an agate mortar, then adding a K_2CO_3 solution (K_2CO_3/Fe=6 wt%) to the Fe_3O_4/support and subsequent drying at 60 °C. Prior to the CO hydrogenation, each catalyst was reduced in situ by hydrogen at a temperature of 225—300 °C, a pressure of 2 kg cm^{-2} and a flow rate of 60 ml min^{-1} for 13 h.

The CO hydrogenation was conducted with a flow type fixed-bed stainless steel reactor, using a feed gas of CO : H_2 : Ar=47.5 : 47.5 : 5 (vol%) under the common condition of t=250 °C, P=5 kg cm^{-2}, and W/F (contact time)=19—33 g h mol^{-1} (W=weight of catalyst, F=molar flow rate of CO and H_2). The products were analyzed by gas chromatography as detailed elsewhere.[5] The conversion of CO (η_{CO}) was calculated on the basis of Ar as an internal standard.

Results and Discussion

UFP-Fe_3O_4/Support Catalysts. Figure 1 shows the effects of hydrogen reduction temperature on the CO conversion (stationary values at time on stream of 5—6 h), the distribution of hydrocarbons produced (HC, carbon-wt%) and the light olefin selectivity ($C^{=}_{2-4}$/total C_{2-4}). As seen in Figs. 1-(a) and (b), in the cases of TIO-3 (rutile type, 40 m^2 g^{-1}) and TIO-4 (anatase type, 50 m^2 g^{-1}), the CO conversion decreases as the reduction temperature increases. On the other hand, the TIO-5 (rutile type, 2.6 m^2 g^{-1})-supported catalyst exhibits a maximum value of η_{CO} at 275 °C (Fig. 1-(c)). A similar temperature dependence of η_{CO} was observed for the SiO_2-supported catalyst, as shown in Fig. 1-(d).

The carbon number distribution of the products, except for CO_2 with yields of 40±5% in η_{CO}, does not depend so much on the nature of support used. The probability of carbon chain growth (α) was in a range of 0.66±0.3. On the other hand, the value of $C^{=}_{2-4}/C_{2-4}$ slightly decreases with a rise of the reduction temperature regardless of the nature of support. The sequence of $C^{=}_{2-4}/C_{2-4}$ under identical conditions was TIO-5> SiO_2>TIO-3>TIO-4. The rutile type and small surface area of TiO_2 seem advantageous for the formation of light olefins, as observed for TiO_2-supported ultrafine Fe

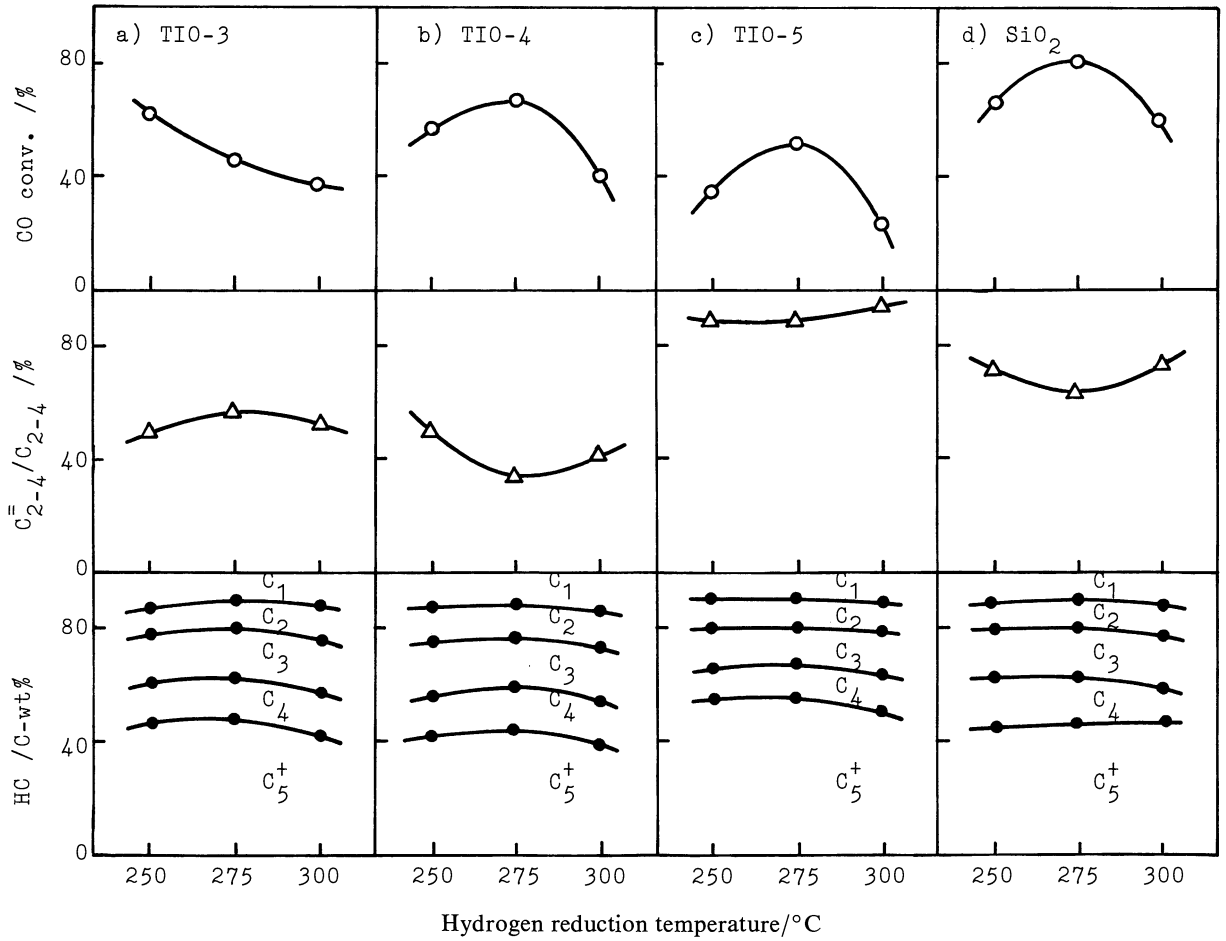

Fig. 2. Effects of hydrogen reduction temperature on the CO conversion, the light olefin selectivity, and the distribution of hydrocarbons produced over the K-promoted UFP-Fe_3O_4/support catalysts. CO hydrogenation conditions; t=250 °C, P=5 kg cm^{-2}, and W/F=23±4 g h mol^{-1}.

metal particles prepared by the gas evaporation method.[5] This tendency becomes more conspicuous when the potassium promoter is added to Fe_3O_4, as will be described below.

K-Promoted UFP-Fe_3O_4/Support Catalysts. Potassium is well known as one of the most effective promoters for CO hydrogenation on iron catalysts.[7,8] Figure 2 shows the effects of K-promoter on η_{CO}, $C_{2-4}^{=}/C_{2-4}$, and the carbon number distribution. In general, the addition of K-promoter to Fe results in an increase in the electron density on Fe through electron donation from potassium. This in turn leads to electron donation to the bonding orbital of Fe–C and to the antibonding orbital of C–O in the adsorbed CO molecules, thereby weakening the C–O bond and suppressing the H_2 adsorption. Thus the catalytic activity, the olefin selectivity, and the average molecular weight of the products are enhanced. Also the water shift reaction is accelerated by a similar mechanism.[7,8] As is obvious from Fig. 2, such discussions are in principle valid for the effects of K-promoter on the catalytic properties of UFP-Fe_3O_4, although the increase in the average molecular weight of the products cannot be clearly depicted except for the case of TIO-5.

The light olefin selectivity depends clearly on the support. TIO-5 gave the highest value (ca. 90%) of $C_{2-4}^{=}/C_{2-4}$ and larger amounts of C_5^+ (carbon number $\geqslant 5$) than TIO-3 or TIO-4. The α values (0.73—0.74) of TIO-5 are neatly higher than those for TIO-3 or TIO-4. These results are consistent with a view that, in the CO hydrogenation process, chemisorbed hydrogen is involved in both chain termination and addition to olefin to form paraffin.

Changes in Fe Particle Size. To clarify the effect of H_2 reduction temperature, changes in the phase of Fe_3O_4 and the particle size of metallic Fe formed during the reduction process have been examined by X-ray diffraction analysis (XRD). As given in Table 1, the reduction at 225 °C does not result in the formation of metallic Fe thick enough to be detectable by XRD. Practically no change was noted in the particle size. An extremely low value of η_{CO} indicated that catalyst has not been sufficiently activated. On the other hand, reduction at 250 °C leads to a neat increase in η_{CO}, accompanied by partial reduction of Fe_3O_4 to Fe, and a slight increase in the particle size.

On an assumption that the Fe particles are uniform and spherical, the specific activity (a_{CO}) of the catalysts can be evaluated from the particle size, the space velocity of CO, and η_{CO}. For each catalyst (except TIO-3), the a_{CO} value is maximal at 275 °C. The specific activity seems to depend on the degree of the reduction to metallic Fe and its particle size; probably the smaller the particle size, the higher the a_{CO} value.

Correlation between η_{CO} and $C_{2-4}^{=}/C_{2-4}$. In Fig. 3 are plotted the light olefin selectivity against the CO con-

Table 1. Changes in the Phase of Fe_3O_4, the Particle Size of Metallic Fe, and the Specific Activity of UFP-Fe_3O_4/Support Catalysts

Support	K_2CO_3	H_2 red. temp	Phase[a]	Particle size of Fe	W/F	η_{CO}[b]	a_{CO}
	wt%	°C		nm	g h mol^{-1}	%	μmol s^{-1} m^{-2}
TIO-3	0	225	O	10[c]	33	4.0	0.023[d]
		250	M+O	11	21	56.0	0.55[d]
		275	M	14	24	42.9	0.47
		300	M	19	25	31.6	0.45
	6	250	M+O	13	23	62.1	0.66[d]
		275	M	16	24	45.6	0.57
		300	M	22	27	36.8	0.56
TIO-4	0	250	M+O	11	23	46.6	0.42[d]
		275	M	15	23	43.5	0.53
		300	M	19	25	34.3	0.49
	6	250	M+O	13	23	56.8	0.60[d]
		275	M	16	20	66.3	1.00
		300	M	22	26	41.1	0.65
TIO-5	0	250	M+O	11	27	32.5	0.25[d]
		275	M	15	23	46.9	0.58
		300	M	19	26	29.5	0.41
	6	250	M+O	13	28	35.9	0.31[d]
		275	M	17	27	51.7	0.61
		300	M	19	31	36.2	0.42
SiO_2	0	250	M+O	10	26	33.0	0.24[d]
		275	M	10	24	40.4	0.32
		300	M	11	24	34.6	0.30
	6	250	M+O	11	22	67.4	0.63[d]
		275	M	12	19	80.4	0.95
		300	M	14	24	56.1	0.62

a) O; oxide (Fe_3O_4), M; metal (Fe). b) t=250 °C and P=5 kg cm^{-2}. c) Particle size of Fe_3O_4. d) a_{CO} was calculated for total (M+O).

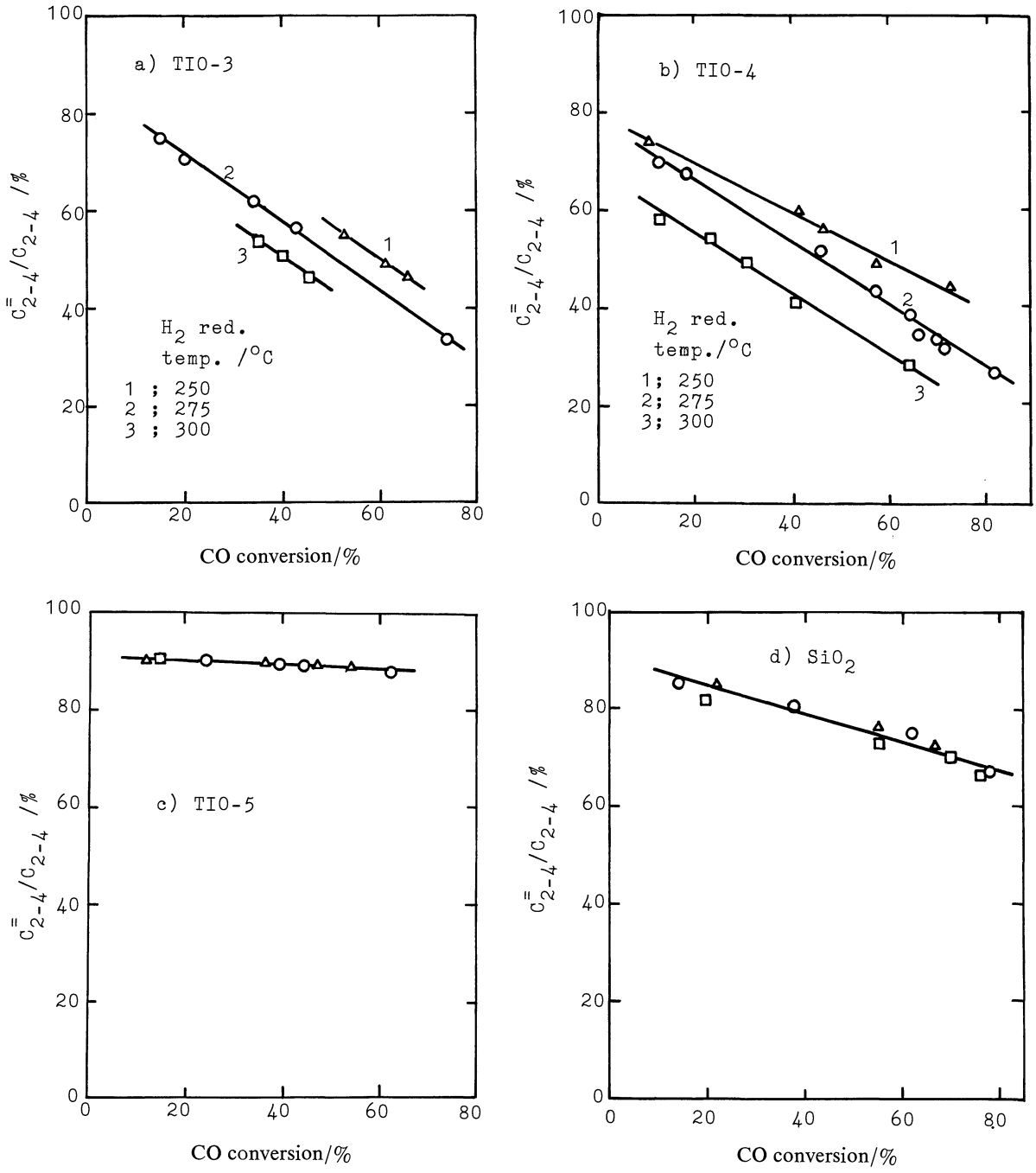

Fig. 3. Correlations between the CO conversion and the light olefin selectivity for the K-promoted UFP-Fe_3O_4/support catalysts under various reduction and CO hydrogenation conditions.

version over the K-promoted catalysts, observed under the reaction conditions in a range of t=225—275 °C, P=5—10 kg cm^{-2}, and W/F=10—33 g h mol^{-1}. For each catalyst a good linear relationship is seen, with a slope characterstic of the support used. In the cases of TIO-3 and TIO-4, the light olefin selectivity abruptly decreases with an increase in η_{CO}, so that it is impossible to carry out the reaction with high activity and high light olefin selectivity at the same time. The clear shift of the correlation line by a change in the H_2 reduction temperature could be attributed mainly to a change in the Fe particle size and consequently in the magnitude of a_{CO}.

In contrast, TIO-5 always exhibits very high values of $C_{2-4}^{=}/C_{2-4}$ almost independently of η_{CO}. Under the same conditions, the sequence of $C_{2-4}^{=}/C_{2-4}$ is TIO-5>SiO_2>TIO-3>TIO-4, as is the case for the unpromoted catalysts. In comparison with SiO_2, which is expected to

interact weekly with metallic Fe, TIO-3 and TIO-4 render the Fe active sites more hydrogenating, while TIO-5 does so to a lesser extent. These findings strongly suggest that TiO_2 supports exert significant influence on the CO hydrogenation process on Fe metal. According to Vannice,[9] the rate-determining step of CO hydrogenation on Fe catalysts is the adsorption and dissociation of H_2 on Fe surface. Also the properties (amount, activity etc.) of adsorped hydrogen play an important role in controlling the formation ratio of olefin to paraffin.[10] In view of this, the support effects observed in this work could be ascribed to promotion (TIO-3 and TIO-4) or suppression (TIO-5) of the H_2 adsorption and dissociation by the TiO_2 support.

References

1) H. Arakawa, K. Kunimori, and T. Uchijima, *Petrotech (Tokyo)*, **6**, 859 (1983).
2) M. Ichikawa, *Shokubai,* **26**, 68 (1984).
3) K. Kunimori and T. Uchijima, *Shokubai,* **28**, 508 (1986).
4) B.-T. Chang, S.-J. Kim, and P.-B. Hong, *Chem. Lett.,* **1989**, 805.
5) B.-T. Chang and S.-J. Kim, *Chem. Lett.,* **1989**, 1353.
6) S. Ito, *Hyomen,* **25**, 562 (1987).
7) M. Roper, "Catalysis in C_1 Chemistry," ed by W. Keim, D. Reidel Publishing (1983), pp. 56—57.
8) K. Fujimoto, "Kogyoshokubaihanno II, Shokubaikoza No. 9," ed by Catalysis Society of Japan, Kodansha, Tokyo (1985), pp. 110—111.
9) M. A. Vannice, *Catal. Rev.,* **14**, 153 (1976).
10) R. X. Brady, III and R. Pettit, *J. Am. Chem. Soc.,* **102**, 6181 (1980); **103**, 1287 (1981).

On the Role of Gallium for the Aromatization of Lower Paraffins with Ga-Promoted ZSM-5 Catalysts

Kaoru FUJIMOTO,* Ikusei NAKAMURA,† Kohshiroh YOKOTA, and Kohjiroh AIMOTO

Department of Synthetic Chemistry, Faculty of Engineering, The University of Tokyo, Bunkyo-ku, Hongo, Tokyo 113
(Received January 30, 1991)

H-ZSM-5 showed a high selectivity of propane and low selectivity of aromatic hydrocarbons in butane conversion at 450 °C, whereas Ga-supportd ZSM-5 (Ga-ZSM-5) showed higher selectivities of aromatic hydrocarbons and hydrogen. A small amount of oxygen in the feed promoted butane conversion to aromatic hydrocarbons on H-ZSM-5. Hybrid catalysts composed of the physical mixture of Ga/Al_2O_3 and H-ZSM-5 showed comparable activities and aromatic selectivities to those of the Ga-supported ZSM-5 zeolite (Ga-ZSM-5). Hydrogen was adsorbed quickly on the Ga-ZSM-5 and on the hybrid catalyst at 400 °C and the adsorbed hydrogen was desorbed at around 450 °C during the temperature programmed desorption experiment from both catalysts. However, little hydrogen was adsorbed on H-ZSM-5 and was desorbed from it. It was pointed out that the supported Ga promoted the zeolite-catalyzed aromatization of lower paraffins by promoting hydrogen desorption via the "reverse spillover" effecct.

Conversion of lower paraffins into aromatic hydrocarbons is of great interest because of its potential application for producing transportation fuel or chemicals from natural gas. Cattanach has claimed that H-ZSM-5 type or Zn-supported ZSM-5 zeolites are effective catalysts for this reaction.[1] Recently, it has been found that a Ga-supported ZSM-5 type zeolite is an exceptionally effective catalyst for this type of reaction.[2] Ga and Zn are effective in promoting the reaction in the impregnated form,[3,4] in the ion exchanged form,[5,6] in the physically mixed form[7] or even when they are incorporated in the zeolite framework.[8]

There are many interpretations postulated as to why Ga or Zn are so effecctive in promoting the formation of aromatic hydrocarbons. Anderson and Mole suggested that the dehydrogenation of propane was promoted by Zn on H-ZSM-5.[9] Ono et al. has concluded from the study of pentane conversion that the Ga-loading does not affect the cracking ability of the zeolite, but enhances the activity of aromatization of olefins.[10] They also observed that Ga-loading promotes propane conversion and suggested that the Ga-promoted aromatization suppresses the formation of propane from intermediate products.[10] Inui et al. showed that Pt-ion-exchanged Ga-silicate exhibited excellent performance for the conversion of C_2—C_5 paraffins and claimed that Pt promotes the paraffin dehydrogenation to olefins and Ga promotes aromatization of olefins.[8] On the other hand, Yashima et al. claimed that Ga on ZSM-5 promotes the dehydrogenation of cycloparaffins or cycloolefins which are formed on zeolite.[3] Recently, Gnep et al. pointed out that Ga_2O_3 showed a catalytic activity for propane dehydrogenation and claimed that Ga on ZSM-5 exists as Ga_2O_3 and promotes the naphthene dehydrogenation.[11] The present authors have found that added oxygen gas in the propane or butane conversion on H-ZSM-5 selectively oxidizes hydrogen on the zeolite to promote the conversion of the feed and especially the formation of aromatic hydrocarbons. We claimed that H-ZSM-5 exhibits an excellent ability for paraffin conversion and aromatics formation if the hydrogen atom on the zeolite surface is effectively removed. Also, the authors have found that the hybrid catalyst composed of the compressed physical mixture of finely powdered H-ZSM-5 and alumina-supported Ga_2O_3 exhibits the activity of butane conversion and the selectivity of aromatics which are comparable to those of Ga-supported H-ZSM-5 and have postulated a concept that hydrogen atoms on the zeolite surface come out through the Ga-site (to result in the promoted aromatics formation[12-14]. Recently, Mao et al. found that an H-ZSM-5 to which a small quantity of zinc oxide/aluminum oxide co-precipitate was admixed mechanically could convert selectively light olefins and/or paraffins to aromatic hydrocarbons and claimed that the high aromatic selectivity should be attributed to hydrogen "back-spillover" from the zeolite to ZnO/Al_2O_3.[16]

The present work tries to clarify the role of gallium on ZSM-5 in the conversion of lower paraffins from the stand point of hydrogen spillover and reverse spillover.

Experimental

The ZSM-5 zeolite was supplied by Tosoh Chem. Ind. Ltd. (Si/Al atom ratio: 50, 850 NAA). X-ray diffraction confirmed that the material was Na-ZSM-5. A protonic ZSM-5 (H-ZSM-5) was prepared by repeated ion exchange of the Na-ZSM-5 with aqueous ammonium nitrate solution (5 times) followed by calcination in air at 500 °C. Ga was supported on the H-ZSM-5 (Ga-ZSM-5) or a commercially available γ-alumina (Ga/Al_2O_3) by impregnating them with gallium nitrate from its aqueous solution and then calcining the precursors in air at 500 °C for 3 h. Ga contents were 1.5 wt%, and 5 wt% for Ga-ZSM-5 and Ga/Al_2O_3, respectively. Hybrid catalysts were prepared by co-grinding the two type of catalysts into a

† Present address: Central Research Laboratories, Idemitsu Kosan Co., Ltd., 1280, Kamiizumi, Sodegaura, Kimitsu, Chiba 299-02.

fine powder and then pressure-molding the mixture to granules (20—40 mesh).

Conversion of butane was conducted with a flow type fixed bed reaction apparatus operated under atmospheric pressure. Catalysts were packed in a stainless steel tube with an inner diameter of 4 mm. Products were analyzed by gas chromatography. Adsorption of hydrogen and its desorption were measured using a flow through cell connected to a conventional glass vacuum system. The adsorption measurement was crried out at 400 °C and the temperature programmed desorption (TPD) was carried out from room temperature to 800 °C with a heating rate of 400 °C h^{-1}. The desorbed hydrogen was determined by mass spectrometry.

Results and Discussion

Effect of Oxygen. In Table 1 are shown some of the results of butane conversion over H-ZSM-5 and Ga-ZSM-5 in the presence and absence of oxygen. The product was propane with a small amount of isomerized butane, C_2—C_4 olefins and aromatic hydrocarbons. The composition of the aromatics was scarcely affected by the oxygen and was quite similar to those reported in other papers.[4,8,9] As it has been already pointed out, the protonic ZSM-5 (H-ZSM-5) producted propane and C_2—C_4 olefins as the main products, with only a small amount of aromatic hydrocarbons.[13] However, when the feed gas contained 5% oxygen, the butane conversion on the H-ZSM-5 catalyst increased considerably and the selectivity of the aromatic hydrocarbons increased drastically from 4.1 to 16.4%. Since the yield of dehydrogenated products or oxygenated products was less than 1% in the non-catalyzed reaction, the higher conversion for the reaction in the presence of oxygen should never be attributed to the oxidation of butane. Also, since the non-catalyzed oxidation of hydrogen under the same reaction condition was less than 10%, the low hydrogen production should be attributed to the direct oxidation of hydrogen on the zeolite surface.[13] Results shown in Table 1 suggest that if hydrogen atoms on the zeolite surface are removed effectively, H-ZSM-5 exhibits a high selectivity for aromatic hydrocarbons.

Effect of Additives. Figure 1 shows the results of butane conversion on H-ZSM-5, Ga-ZSM-5 and Pt-ZSM-5 as a function of reaction temperature. The catalytic activity of Pt-ZSM-5 was much higher than those of the other two catalysts. Also, the selectivity of aromatics over Pt-ZSM-5 was higher than those of the other catalysts. However, the aromatic selectivity on Ga-ZSM-5 increased markedly with increasing reaction temperature and reached a level comparable to that of Pt-ZSM-5 at around 500 °C, whereas the selectivity of the aromatics on H-ZSM-5 stayed at a much lower level than the other two catalysts. Also, the mole ratio of hydrogen to reacted butane on Ga-ZSM-5 catalyzed reaction increased with increasing temperature finally reaching that on Pt-ZSM-5.

Table 1. Conversion of Butane on ZSM-5 Catalysts[a]

Catalyst	H-ZSM-5			Ga-ZSM-5	
O_2 (mol% in feed)	0.0	0.0[b]	5.0	0.0	5.0
n-C_4 conversion (%)	39.5	41.0	50.9	49.0	54.2
H_2/converted n-C_4	0.40	—	0.16	1.4	0.94
Product distribution (carbon %)					
C_1+C_2 paraffins	9.8	9.7	8.5	10.7	10.4
C_3H_8	59.7	60.8	55.6	58.0	50.5
C_2–C_4 olefins	22.7	22.0	15.4	15.8	12.1
C_5^+ aliphatics	3.7	3.6	2.3	2.4	1.9
Aromatics	4.1	3.9	16.1	13.1	22.8
CO+CO_2	0.0	0.0	2.1	0.0	1.9

a) Reaction temperature 450 °C, W/F=10 g h mol^{-1}, $P_{C_4H_{10}}$=20 kPa. b) Hydrogen was introduced instead of oxygen.

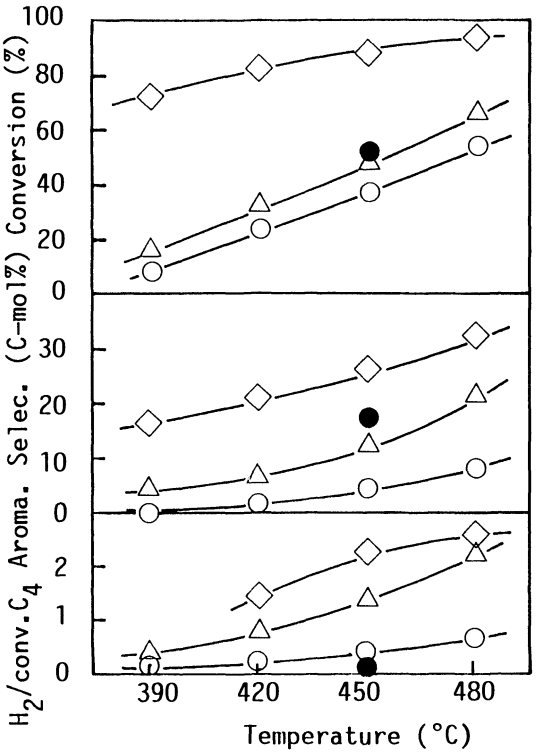

Fig. 1. Comparison of ZSM-5 catalysts for conversion of n-C_4. n-C_4 20%, N_2 80%, W/F; 10 g h mol^{-1}. ◇ Pt-ZSM-5, △ Ga-ZSM-5, ○ H-ZSM-5, ● H-ZSM-5 (5% O_2).

It has been well known that supported platinum on H-ZSM-5 promotes the dehydrogenation of lower paraffins to olefins,[8] which are much more reactive in dehydroaromatization.[14] The slight increase in the conversion activity and the drasic increace in the aromatics selectivity caused by adding Ga on H-ZSM-5 has been also reported in other papers,[2-8] which will be discussed in a later chapter.

Catalytic Performances of Ga-containing Hybrid Catalysts. Table 2 shows some of the results of the butane conversion on a variety of Ga-containing catalysts. The first point which should be noted is that the hybrid catalyst containing Ga/Al_2O_3, which was finely powdered and pressed in to granules with H-ZSM-5,

Table 2. Conversion of Butane on a ZSM-5 Catalysts (1)[a)]

Catalyst	H–ZSM-5	Ga–ZSM-5	Ga/Al_2O_3	H–ZSM-5+ Ga/Al_2O_3[b)]	H–ZSM-5+ Ga/Al_2O_3[c)]	Ga/Al_2O_3[d)]
Conversion of butane/%	41.6	47.9	0.7	47.7	46.8	1.6
H_2/converted butane (mol ratio)	0.3	1.4	—	1.3	0.8	—
Product distribution (carbon %)						
C_1+C_2 paraffins	9.6	9.5	3.0	11.0	10.8	3.9
C_3H_8	58.6	52.5	3.5	51.7	56.5	20.1
C_4H_{10} isomer	3.7	3.5	0.0	3.2	3.0	0.0
C_2–C_4 olefins	16.3	10.0	88.1	13.0	16.2	17.2
C_5^+ aliphatics	3.0	2.5	0.5	1.7	2.3	1.3
Aromatics	8.8	22.0	4.9	19.4	11.2	21.0

a) Reaction temperature 450 °C, $P_{C_4H_{10}}$ =20 kPa, P_{N_2}=80 kPa, W/F=10 g h mol^{-1}. b) Powdery mixture, Content of Ga/γ-Al_2O_3 was 20 wt%. c) Granular mixture, Content of Ga/γ-Al_2O_3 was 20 wt%. d) Propene was reacted instead of butane.

exhibited high aromatic selectivity which was comparable to those of the Ga–ZSM-5 catalyst, whereas the Ga/Al_2O_3 itself exhibited little catalytic activity for the butane conversion and olefin aromatization. It should be also noted that the content of the ZSM-5 zeolite in the hybrid was only 80% and thus the catalytic activity of the H–ZSM-5 hybrid catalyst is estimated to be 1.4 times higher than that of only H–ZSM-5. The second important point is that the physical mixture of granular Ga/Al_2O_3 and granular H–ZSM-5 showed catalytic performances much inferior to the powdery mixed hybrid catalyst with the same composition.

The former studies indicated that the higher aromatic selectivity of the Ga–ZSM-5 catalyst than that of H–ZSM-5 should be attributed to the dehydrogenation or dehydroaromatization of olefins[4,7,15] or the dehydrogenation of naphthenic hydrocarbons.[3,11] However, the data in Table 2 show that Ga/Al_2O_3 showed little catalytic activity for both olefin aromatization and paraffin dehydrogenation, whereas it exhibited an excellent promotional effect for the aromatics formation when it was intimately contacted with H–ZSM-5. Thus, the promotional effect of gallium should be attributed to functions other than its dehydrogenation activity. If the promotional effect of the gallium is attributed to its dehydrogenation activity, Ga/Al_2O_3 should exhibit catalytic activity for the dehydrogenation of butane or the dehydroaromatization of propene and also the granular mixture of Ga/Al_2O_3 and H–ZSM-5 should exhibit comparable performances to that of the hybrid catalyst.

Hydrogen Effect. In Fig. 2 are shown the results of the Temperature Programmed Reaction (TPRE) of C_2H_4 in a hydrogen atmosphere on H–ZSM-5, Ga–ZSM-5, and Pt–ZSM-5. On Pt–ZSM-5, C_2H_4 was converted completely at any temperature producing mostly ethane. On H–ZSM-5, on the other hand, the conversion of C_2H_4 started at 150 °C and reached 100% at around 300 °C. Neither the ethane formation nor the hydrogen consumption occurred below 450 °C, which means that H–ZSM-5 exhibits little catalytic activity for the olefin hydrogenation under the reaction conditions previously

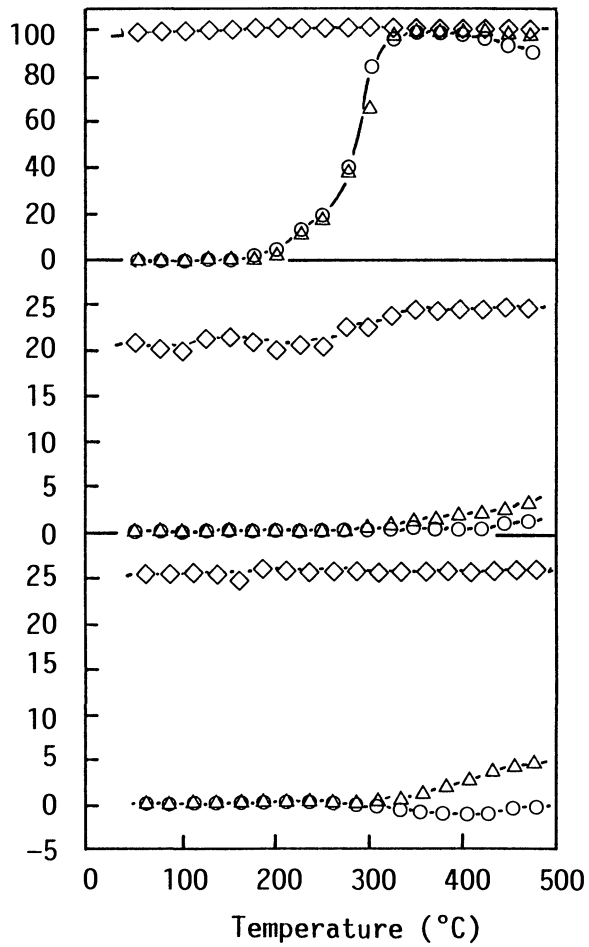

Fig. 2. TRPE of C_2H_4 with hydrogen. C_2H_4 25%, H_2 75%, 5 °C min^{-1}, W/F; 10 g h mol^{-1}. ◇ Pt–ZSM-5, △ Ga–ZSM-5, ○ H–ZSM-5.

mentioned. Ga–ZSM-5 showed similar catalytic character to those of H–ZSM-5 except that a slight hydrogenation of ethylene proceeded above 350 °C, pointing out that the hydrogenation activity of Ga–ZSM-5 was quite low, while its activity for olefin conversion is similar to that of H–ZSM-5. Thus, ethylene was mostly polymerized to higher hydrocarbons. The low hydrogenation activity of Ga–ZSM-5 should contribute

Table 3. Effects of Hydrogen on the Conversion of Butane[a)]

Catalyst	H-ZSM-5		Ga-ZSM-5		Pt-ZSM-5	
Atmosphere	N_2	H_2	N_2	H_2	N_2	H_2
Conversion of butane/%	59.0	60.0	57.7	56.3	91.2	96.3
Product distribution (carbon %)						
C_1+C_2 paraffins	7.8	8.0	9.4	11.7	37.9	21.6
C_3H_8	57.6	59.3	47.2	53.4	29.5	69.3
C_4H_{10} isomer	6.5	6.6	7.2	10.6	4.3	3.8
C_2–C_4 olefins	10.3	10.8	8.9	7.0	7.2	0.8
C_5^+ aliphatics	2.3	2.3	3.1	3.1	0.9	0.3
Aromatics	15.6	13.5	26.5	14.2	20.2	4.2

a) Reaction temperature 455 °C, $P_{C_4H_{10}}$=20 kPa, $P_{N_2(H_2)}$= 80 kPa, W/F=10 g h mol^{-1}.

to the high aromatic selectivity during the paraffin conversion.

Table 3 shows the effects of hydrogen on the conversion of butane over the 3 types of catalysts previously mentioned. In the case of the H-ZSM-5, hydrogen in the gas phase affected neither the butane conversion nor product selectivity. This phenomenon is consistent with the fact the H-ZSM-5 has no hydrogenation activity. The catalytic activity of the Pt-ZSM-5 was promoted slightly by hydrogen while the selectivities of aromatic hydrocarbon and C_2—C_4 olefins were markedly suppressed. The phenomena should be attributed to its excellent hydrogenation activity. In the case of the Ga-ZSM-5, the selectivity of aromatic hydrocarbons and C_2—C_4 olefins were much lower in the presence of hydrogen than that in the presence of nitrogen. This should not be attributed to the hydrogenation of olefins, because the Ga-ZSM-5 exhibits little hydrogenation activity but should be explained in terms of the spillover of hydrogen. This inconsistency will be discussed later in this report.

Adsorption and Desorption of Hydrogen. Figure 3 shows the adsorptions of H_2 at 400 °C on H-ZSM-5, Ga-ZSM-5, and hybrid samples composed of H-ZSM-5 and Ga/Al_2O_3. Apparently from the figure, a fairly large amount of hydrogen was adsorbed quickly on Ga-ZSM-5, while little hydrogen was adsorbed on H-ZSM-5. The difference between H-ZSM-5 and Ga-ZSM-5 is explained as follows. In the case of Ga-ZSM-5, Ga has the function to adsorb hydrogen molecule and to dissociate hydrogen molecule to hydrogen atom and then the hydrogen atom on Ga particle moves to ZSM-5 zeolite by spillover effect. On the other hand, H-ZSM-5 has no entrance of hydrogen such as Ga, so only little hydrogen was adsorbed to H-ZSM-5. The data in Fig. 3 shows that on the physical mixture of H-ZSM-5 and Ga/Al_2O_3 more hydrogen was adsorbed than on Ga/Al_2O_3 only.

Figure 4 shows the spectra of temperature programmed desorption (TPD) of adsorbed hydrogen from Ga-ZSM-5 and H-ZSM-5. The desorption of hydrogen was prominent at two temperature ranges around 400 °C and at higher than 700 °C, while H-ZSM-5 showed only one prominent desorption temperature at higher than 700 °C.

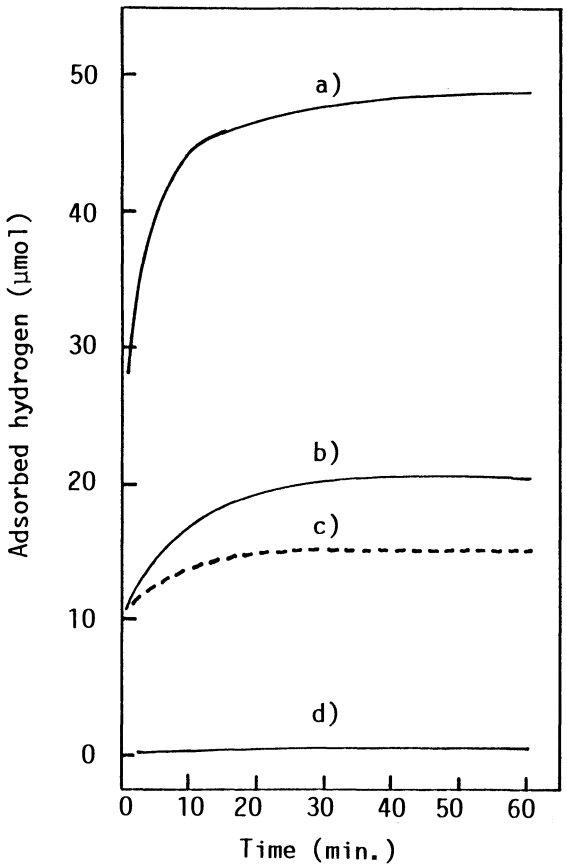

Fig. 3 Hydrogen spillover on ZSM-5 catalysts. Pretreatment; 600 °C 1 h evacuated, adsorption temperature; 400 °C. a) Ga-ZSM-5 1.0 g, b) (Ga/Al_2O_3 0.2 g+H-ZSM-5 0.8 g) hybrid catalyst, c) (Ga/Al_2O_3 0.2 g)+(H-ZSM-5 0.8 g) calculated value, d) H-ZSM-5 1.0 g.

The desorption of hydrogen at lower temperature range was in the molecular state whereas that at higher temperature range was in the atomic state. This suggests that desorption in the lower temperature range is of the "reverse spillover" type. The process is composed of (1) the transfer of hydrogen atoms on the solid surface to the gallium site, (2) the combination of two hydrogen atoms to form one hydrogen molecule, and (3) the desorption of the hydrogen molecule into gas phase. This is just the reverse process of hydrogen spillover. On the other hand, the desorption of hydrogen in the atomic state at higher temperature range may be attributed to the direct dissociation of zeolite-hydrogen bonds by thermal energy. Although the hydrogen atoms in the gas phase usually recombine quickly to molecules, the ultra high vacuum ($<10^{-8}$ Torr, 1 Torr=133.322 Pa) may prevent the collision between hydrogen atoms of the removal of excess energy from hot hydrogen molecules produced by the collision of two hydrogen atoms. Also this desorption of atomic hydrogen at high temperature was observed in the case of

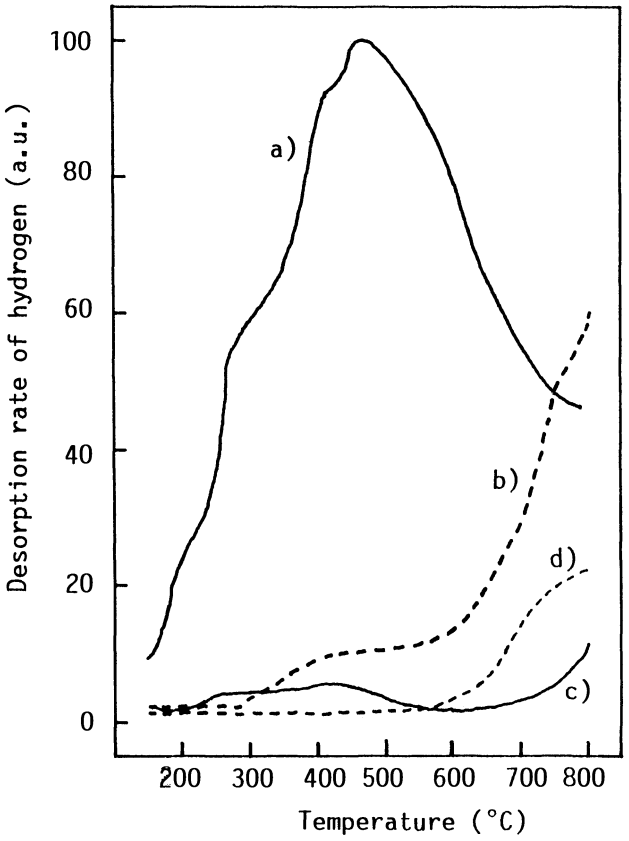

Fig. 4. Temperature programmed desorption spectra of hydrogen on ZSM-5 catalysts. Heating rate; 400°C h^{-1}, a) Ga–ZSM-5 1.0 g mass number 2, b) Ga–ZSM-5 1.0 g mass number 1, c) H–ZSM-5 1.0 g mass number 2, d) H–ZSM-5 1.0 g mass number 1.

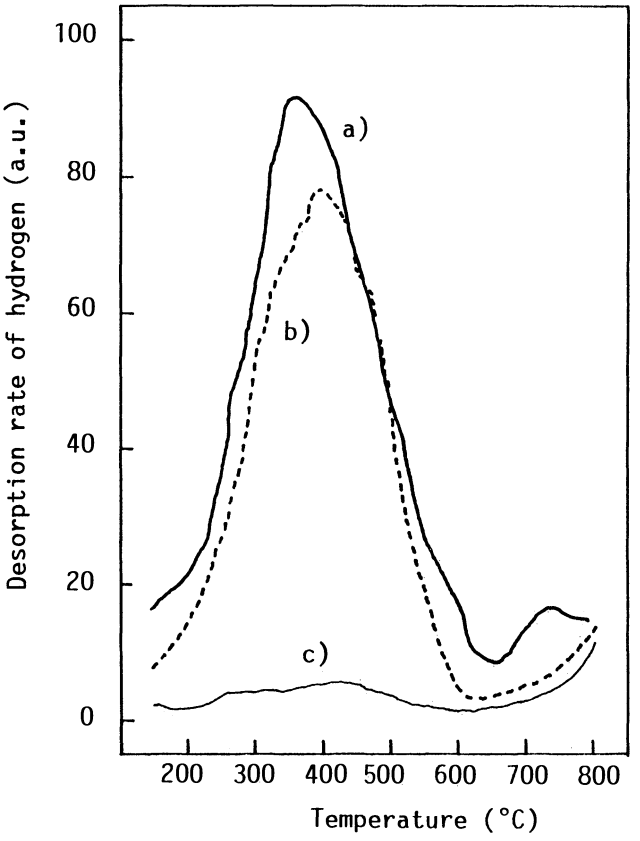

Fig. 5. Temperature programmed desorption spectra of hydrogen on ZSM-5 hybrid catalyst. Heating rate; 400°C h^{-1}, mass number 2, a) (Ga/Al_2O_3 0.2 g+H–ZSM-5 0.8 g) hybrid catalyst, b) (Ga/Al_2O_3 0.2 g)+(H–ZSM-5 0.8 g) calculated value, c) H–ZSM-5 1.0 g.

hybrid catalyst. The more important process of hydrogen desorption for catalytic dehydrogenation is convinced to be the reverse spillover process.

Figure 5 shows the TPD spectra of molecular hydrogen. From H–ZSM-5 hydrogen molecule desorbed mostly at higher than 700 °C. The TPD spectra of H_2 desorption from Ga–ZSM-5 is characterized by its much larger peak between 300 and 600 °C and the peak at 700 °C. The TPD spectrum from Ga/Al_2O_3 is rather close to that from Ga–ZSM-5 but the peak top is shifted to lower temperature (by about 100 °C). The character of H_2 desorption from the Ga/Al_2O_3/H–ZSM-5 hybrid is quite close to that from Ga/Al_2O_3 but its amount is considerably larger than the former. These phenomena clearly suggest that hydrogen molecules are desorbed much more easily from Ga on Al_2O_3 than on zeolite, and that even the hydrogen on H–ZSM-5 is desorbed at much lower temperature when the zeolite is hybridized with Ga/Al_2O_3. The desorption of H_2 below 600 °C from the hybrid catalyst should be attributed to the reverse spillover of hydrogen including inter-particle hydrogen transfer (Fig. 7).

Reaction Model. The most probable explanation of the promotional effect of gallium should be attributed to the "reverse spillover" effect whose model is shown in Fig. 6.[21] In the model, gallium acts as the exit of hydrogen on the zeolite surface. It has been reported in many studies that the conversion of lower paraffins on H–ZSM-5 gives a small amount of aromatic hydrocarbons or hydrogen but a large amount of lower paraffins such as propane and ethane.[4,9] It means that hydrogen atoms generated upon aromatization reaction do not come out of the zeolite surface into the gas phase but hydrogenate ethylene or propene which are intermediates in paraffin-to-aromatic conversion.

On the gallium-supported ZSM-5 zeolite, on the other hand, hydrogen atoms on the zeolite surface migrate to Ga site where they recombine to form hydrogen molecules and then desorb into the gas phase.

When hydrogen atoms on a zeolite surface are effectively removed, their concentration in the zeolite surface should be reduced. As is the case of the reaction in the presence of oxygen, H–ZSM-5 itself exhibits a high conversion activity and aromatic selectivity, if the surface hydrogen is effectively removed. The desorbed hydrogen is rather inactive for a hydrogenation reaction in the

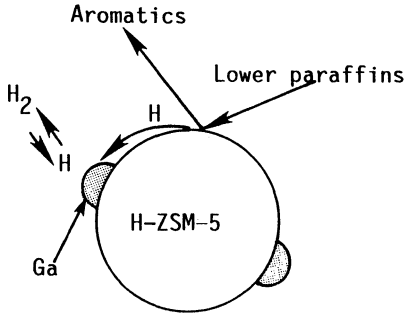

Fig. 6. Model of hydrogen reverse spillover.

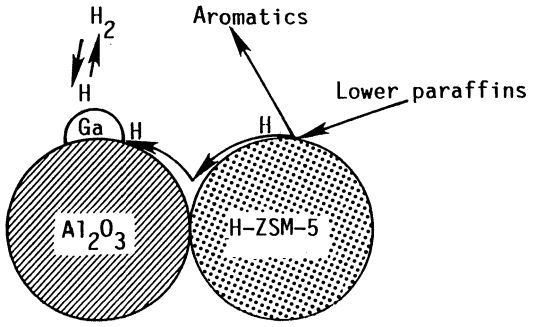

Fig. 7. Model of interparticle hydrogen reverse spillover.

Ga–ZSM-5 catalyzed system as shown in Fig. 2. In the case of hybrid catalysts, their high catalytic performances should be attributed to inter-particle hydrogen transfer and reverse spillover as demonstrated in Fig. 7. The hydrogen atom on H–ZSM-5 moves to the alumina surface and then goes into the gas phase through the Ga sites (reverse spillover). It is reasonable that the granular mixture of Ga/Al_2O_3 and H–ZSM-5 exhibited a significantly inferior ability for butane conversion as compared to the hybrid catalyst. In the granular system the poor contact between the two components impede hydrogen transfer from the H–ZSM-5 to the Ga/Al_2O_3.

The concept of spillover also reasonably explain the fact that the selectivity of aromatic hydrocarbons on the Ga–ZSM-5 was suppressed by hydrogen in the gas phase in spite of its low hydrogenation activity. When hydrogen exists in the gas phase, the desorption of hydrogen atoms from the zeolite is suppressed by the spillover effect. If the hydrogen desorption is slow, it will react with olefins or carbonium ions to form paraffins, suppressing the formation of aromatic hydrocabons.

Conclusion

1) Gallium on ZSM-5 promotes the formation of aromatic hydrocarbons in the conversion of lower paraffins through the reverse spillover of hydrogen atoms on the zeolite surface.

2) H–ZSM-5 is sufficiently active and selective for the conversion of butane to aromatic hydrocarbons if the hydrogen atoms on its surface are effectively removed during the reaction.

References

1) Jpn. Patent Kokai Tokkyo 56-42639 (1981).
2) Jpn. Patent Kokai Tokkyo 62-61569 (1987).
3) T. Yashima, T. Sasaki, K. Takahashi, S. Watanabe, and S. Namba, *Sekiyu Gakkai-shi,* **31**, 154 (1988).
4) C. Tan, C. Cheng, L. Zhou, and S. Peng, *Proc. Int. Congr. Catal., 9th.,* **1**, 445 (1988).
5) T. Mole and J. R. Anderson, *Appl. Catal.,* **17**, 141 (1985).
6) G. Sirokman, Y. Sendoda, and Y. Ono, *Zeolites,* **6**, 299 (1986).
7) N. S. Gnep, J. Y. Doyemet, and M. Guisnet, *J. Mol. Catal.,* **45**, 281 (1988).
8) T. Inui, Y. Makino, F. Okazumi, S. Nagano, and A. Miyamoto, *Int. Eng. Chem. Res.,* **26**, 647 (1987).
9) H. Kitagawa, Y. Sendoda, and Y. Ono, *J. Catal.,* **101**, 12 (1986).
10) T. Yashima, T. Sasaki, K. Takahashi, S. Watanabe, and S. Namba, *Sekiyu Gakkai-shi,* **31**, 154 (1988).
11) N. S. Gnep, J. Y. Doyemet, A. M. Seco, F. Ramoa Ribeiro, and M. Guisnet, *Appl. Catal.,* **43**, 155 (1988).
12) K. Fujimoto and I. Nakamura, *Proc China-Jpn.-U.S. Trilateral Semin., 3rd.,* (1988).
13) K. Fujimoto, I. Nakamura, and K. Yokota, *Zeolites,* **9**, 120 (1989).
14) N. S. Gnep, J. Y. Doyemet, A. M. Seco, F. Ramoa Ribeiro, and M. Guisnet, *Appl. Catal.,* **35**, 93 (1987).
15) M. Shibata, H. Kitagawa, Y. Sendoda, and Y. Ono, *Proc. Int. Zeolite Conf., 7th,* 717 (1987).
16) R. Le Van Mao and L. Dufresne, *Appl. Catal.,* **52**, 1 (1989).
17) P. A. Sermon and G. C. Bond, *Catal. Rev.,* **8**, 211 (1973).
18) M. A. Vannice and W. C. Neikman, *J. Catal.,* **20**, 260 (1971).
19) W. C. Neikman and M. A. Vannice, *J. Catal.,* **27**, 207 (1972).
20) K. Fujimoto and S. Toyoshi, *Proc. Int. Congr. Catal., 7th,* (1980).
21) S. Asaoka, S. Masamizu, K. Fujimoto, and T. Kunugi, *Nihon Kagakukai-shi,* **1976**, 388.

Optical Properties of CdS Microcrystallite-Doped Al_2O_3 Thin Films Prepared by Rf-Sputtering

Ichiro TANAHASHI,* Masaru YOSHIDA, and Tsuneo MITSUYU
Central Research Laboratories, Matsushita Electric Industrial Co., Ltd.,
Yagumo-Nakamachi, Moriguchi, Osaka 570
(Received February 6, 1991)

Synopsis. Al_2O_3 thin films containing CdS microcrystallites were successfully prepared by an rf-magnetron sputtering technique. Photoluminescence spectra of films exhibited blue band-edge emission at a higher energy than that of bulk CdS. The spectral change seems to arise from a zero-dimensional confinement of electrons and holes in CdS microcrystallites.

Semiconductor microcrystallites doped in solid matrices, such as glasses and polymers, exhibit a large optical nonlinearity due to the quantum size effect.[1-3] In fact, the diameter of semiconductor microcrystallites in bulk glasses was less than 100 Å, where the microcrystallites could be considered as "quantum dots".

In order to improve the uniformity of the crystallite size, the doping of semiconductors to glasses is carried out by alternative preparation processes such as melt-quenching,[1,2] sol-gel,[4-5] and sputtering methods.[6-8] Sputtering is one of the promising technique for the preparation of various types of semiconductor-doped glass thin-films. Most of the matrices investigated for the films were SiO_2. However, the effects of the matrices on the chemical bond of a doped semiconductor and on the optical properties of the films have not yet been investigated. To clarify the nature of the quantum size effect, it is important to study the relation between the chemical bond of doped semiconductors and the matrices.

In this paper, we report on the preparation of Al_2O_3 thin films containing CdS microcrystallites by the rf-magnetron sputtering technique. The optical properties of the films have also been investigated.

Experimental

Al_2O_3 thin films containing CdS microcrystallites were prepared by a conventional rf-magnetron sputtering systems. The targent used was an Al_2O_3 plate (100 mm in diameter with 5 mm in thickness) with a number of CdS tablets (10 mm in diameter with 1.5 mm in thickness). The concentration of CdS was controlled by changing the number of tablets. The substrates used were SiO_2 glass or GaAs. Sputtering was carried out for 5 h in Ar gas of 5.32 Pa while applying an rf power of 200 W. The substrate was not intentionally heated.

X-Ray photoelectron spectra (XPS) analyses were performed using a Mg$K\alpha$ X-ray source. Details of the measurements were described previously.[8] For calculating the binding energies of each peak, the peak position of the main component in the 1s core level spectrum of carbon was assumed to be 284.6 eV.

The composition of the films was determined by electro-probe microanalysis (EPMA) using the films on GaAs substrates. X-Ray diffraction measurements (XRD) were carried out in order to examine the crystallinity of the films.

The optical absorption spectra were measured in the range from 200 to 700 nm by a spectrometer. The photoluminescence spectra were measured at room temperature by using a spectrofluorophotometer with filters to eliminate the excitation light.

Results and Discussion

Figure 1 shows the Al2p electron spectra of a film with 25.4 cadmium wt%. In this figure, the arrows indicate the standard peak position for Al2p of Al metal[9] and Al_2O_3.[10] The peak of the film coincides with that of Al_2O_3. The Ols electron spectra of the film also coincided with that of Al_2O_3.[10] Thus, Al_2O_3 was

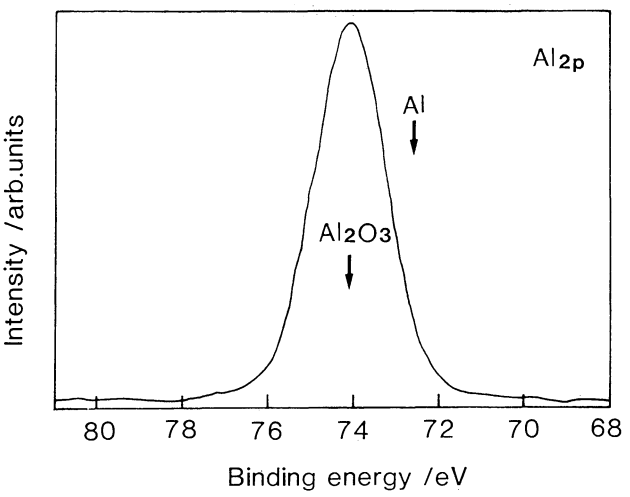

Fig. 1. A12p electron spectra of the film containing 25.4 cadmium wt%. Al indicates the standard peak position of A12p electron spectra of Al metal, Al_2O_3; A12p of Al_2O_3.

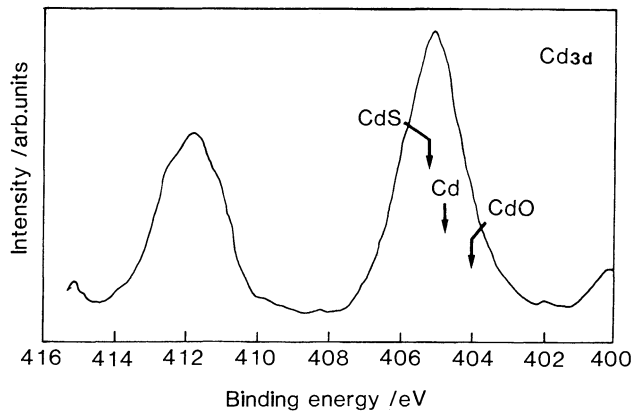

Fig. 2. Cd3d electron spectra of the film containing 25.4 cadmium wt%. CdS indicates the standard peak position of Cd3d electron spectra of CdS, Cd; Cd3d of Cd metal, CdO; Cd3d of CdO.

successufully formed by rf-magnetron sputtering.

Figure 2 shows the Cd3d electron spectra of the film. The film examined was the same as that shown in Fig. 1. The spin-doublet of $Cd3d_{3/2}$ and $Cd3d_{5/2}$ is given in Fig. 2. In this figure, the arrows indicate the peak position of the Cd3d electron spectra for CdS, Cd metal, and CdO.[11] These experimental peak positions are close to those of the standard CdS. The Cd and S atoms were reasonably doped in the Al_2O_3 matrix as CdS. In conclusion, CdS was successfully doped into Al_2O_3.

The XRD patterns of the films showed no reflection lines, suggesting that the Al_2O_3 thin film was amorphous. The crystal system of the doped CdS could not be identified in this expepriment. The doped CdS was too small to identify its crystal system by the XRD patterns.

By means of the EPMA measurements, the ratio of S to Cd atoms (S/Cd) of a film containing 25.4 cadmium wt% was estimated to be 0.83. This is because the reevaporation of S atoms from the substrates was larger than that of Cd atoms under the experimental condition. Although the Cd and S atoms were reasonably doped as CdS by XPS analyses, it seemed that part of the Cd atoms were doped as Cd metal and CdO.

Figure 3 shows the transmission spectra measured at room temperature for Al_2O_3 thin films containing CdS: (a) film with 10.9 cadmium wt%, (b) 20.0 wt%, and (c) 25.4 wt%. The thickness of the films was 0.4—0.6 μm. The films, thus, show interference oscillations (the waves in the spectra) in the transparent region. The three spectra are different in the region below 500 nm. From the figure, the power of the absorption coefficient, α, was plotted against the photon energy, $h\nu$. The α^2 varied linearly with $h\nu$, indicating that the direct interband transition took place. The optical band-gap energy, E_g, of the film (a) was estimated to be 2.66 eV from the α^2 vs. $h\nu$ plot. The E_g of the film (a) is clearly blue-shifted by about 0.25 eV, compared with that of the bulk CdS (2.41 eV). With increasing the concentration of CdS, E_g decreased. This is because the diameter of CdS microcrystallites became large.

In spherical semiconductor quantum dots enclosed by the insulating matrix, the blue shift, ΔE_g, is expressed by

$$\Delta E_g = h^2/8a^2\mu \quad (2)$$

where a and μ are the radius of the spherical dots and the reduced effective mass of an electron-hole pair, respectively; h is Planck's constant. This equation is valid when the radius, a, is smaller than the Bohr radius of the bulk exciton.[12] The diameter of the CdS-microcrystallites in the film (a) was 57 Å, as calculated by Eq. 2. The blue shift of an Al_2O_3 thin film with 25.4 cadmium wt% was 0.04 eV larger than that of SiO_2 thin films with 35.9 cadmium wt%.[8] The reasons for the larger blue shift of the films have not been clarified. However, the larger shift seems to represent the difference in the size between the CdS in an Al_2O_3 thin film and that in a SiO_2 thin film. Direct observations of CdS in Al_2O_3 thin films is the next problem.

The effect of the dielectric constant of the matrix on the blue shift has also been reported by Brus et al.[13] They calculated the blue shift for CdS microcrystallite in vacuum using an equation with three energy terms; kinetic, coulomb, and polarization. The polarization term was influenced by the dielectric constant of the matrices. According to the calculation: 1) the blue shift became small with increasing the value of the dielectric constant of matrices and 2) the contribution of the polarization term to the blue shift was rather small in comparison with the other two terms. The dielectric

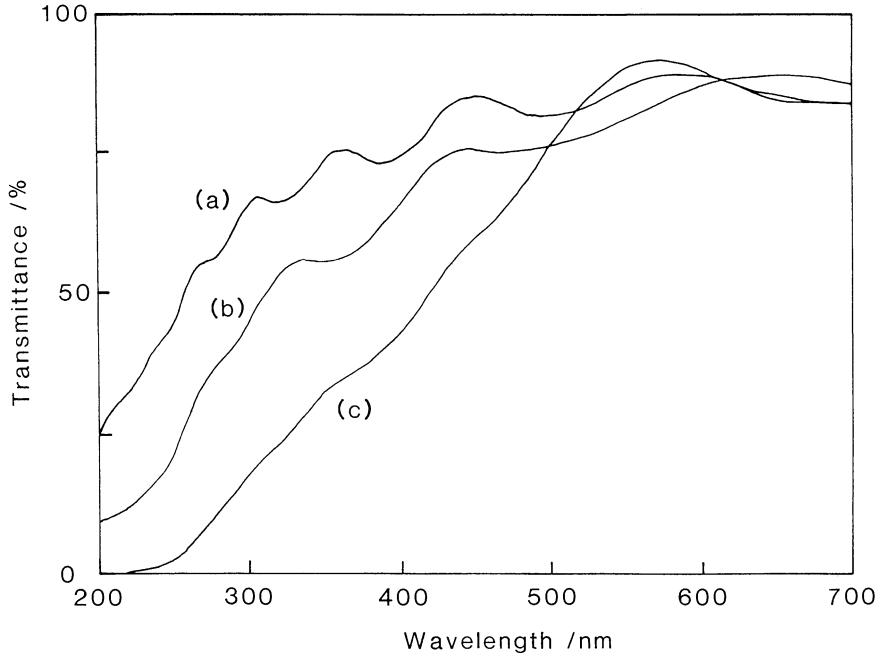

Fig. 3 Optical transmission spectra of the films at room temperature. (a) the films with 10.9 cadmium wt%, (b) 20.0wt%, and (c) 25.4 wt%.

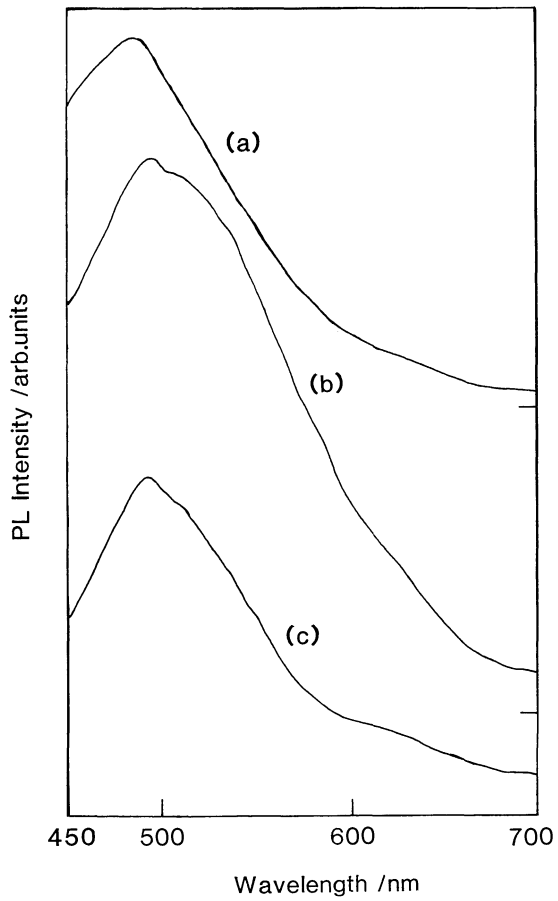

Fig. 4. Photoluminescence spectra of the films at room temperature. (a) the film with 10.9 cadmium wt%, (b) 20.0 wt%, and (c) 25.4 wt%.

constants of Al_2O_3 and SiO_2 were 8.6 and 4.5, respectively. Therefore, the larger blue shift of the Al_2O_3 thin films with CdS seems to be due to the smaller size of CdS.

Figure 4 shows the photoluminescence (PL) spectra at room temperature measured for films (a), (b), and (c). The emission of the films appears below 500 nm. It is reported that CdS deposited in porous vycor glass showed emission associated with a sulfur vacancy at 680 nm and band-edge emission at 520 nm.[14] The PL spectrum of CdS deposited in porous vycor glass was close to that of bulk CdS. The band-edge emission of the films examined were clearly blue-shifted in comparison with that of bulk CdS. The emission of the films is broad, suggesting that the size distribution of doped CdS was rather large. With increasing concentration of CdS, the PL peak position of the films shift to lower energy. In accordance with the results of the optical transmission spectra, the energy of the band-edge emission of the films is higher than that of bulk CdS. The shift to higher energy is attributed to a low-dimensional quantum size effect due to the confinement of electrons and holes in CdS microcrystallites.

The authors would like to thank Drs. T.Nitta and A.Nishino for their continuous encouragement. A part of this work was performed under the management of Japan High Polymer Center as a part of the R&D of Nonlinear photonics materials supported by NEDO (New Energy and Industrial Technology Development Organization).

References

1) R. K. Jain and R. C. Lind, *J. Opt. Soc. Am.*, **73**, 647 (1983).
2) N. F. Borrelli, D. W. Hall, H. J. Holland, and D. W. Smith, *J. Appl. Phys.*, **61**, 5399 (1987).
3) M. F. Finlayson, K. H. Park, N. Kakuta, A. J. Bard, A. Campion, M. A. Fox, S. E. Webber, and J. M. White, *J. Lumin.*, **39**, 205 (1988).
4) M. Nogami, K. Nagasawa, and M. Takata, *J. Non-Cryst. Solids*, **122**, 101 (1990).
5) N. Touge, M. Asuka, and T. Minami, *Chem. Express*, **5**, 521 (1990).
6) H. Jerominek, M. Pigion, S. Patela, Z. Jakubczyk, C. Delisle, and R. Tremblay, *J. Appl. Phys.*, **63**, 957 (1988).
7) H. Nasu, K. Tsunetomo, Y. Tokumitsu, and Y. Osaka, *Jpn. J. Appl. Phys.*, **28**, L862 (1989).
8) I. Tanahashi, A. Tsujimura, T. Mitsuyu, and A. Nishino, *Jpn. J. Appl. Phys.*, **29**, 2111 (1990).
9) J. A. Taylor, *J. Vac. Sci. Technol.*, **20**, 751 (1982).
10) V. I. Nefedor, *J. Electron Spectrosc. Relat. Phenom.*, **25**, 29 (1982).
11) S. W. Gaarenstroom and N. Winograd, *J. Phys. Chem.*, **67**, 3500 (1977).
12) Y. Kayanuma, *Solid State Commun.*, **59**, 405 (1986).
13) L. E. Brus, *J. Chem. Phys.*, **80**, 4403 (1984).
14) J. Kuczynski and J. K. Thomas, *J. Phys. Chem.*, **89**, 2720 (1985).

A Theorem on *p*-Densities in the Hückel Model of Linear Chains

Makoto ISIHARA
Department of General Education, Shotoku-Gakuen Women's Junior College,
Nakauzura 1-38, Gifu 500
(Received February 18, 1991)

Synopsis. The hyperivial condition upon *p*-densities is applied to the simple Hückel model of linear chains. The invariance of the modified *p*-density is derived in fully generalized form. Any bond order between nonadjacent sites is shown expressible in terms of two electron densities or two bond orders between adjacent sites.

The author has manifested the significance and the usefulness of the hypervirial condition upon *p*-densities[1] in the Hückel model in the previous paper,[2] where he has mentioned a few consequences of the condition in the simple Hückel model[3] of linear chains as an illustrative example. In this note, the invariance of the modified electron density and that of the modified bond order between adjacent sites are fully generalized in a systematic way. The resulting theorem enables us to express any bond order between nonadjacent sites in terms of two electron densities or two bond orders between adjacent sites. In particular, for the neutral ground state, this means that an analytic expression is given to the bond order between nonadjacent sites. A few remarks are added last on the treatment of linear chain parts.

The following mathematical notation is used throughout. The symbol $[z_s,z_l]$ stands for the set of integers that contains z_s and z_l as the smallest and the largest elements, respectively; understand the set to be empty if $z_l<z_s$. The symbol $[z]$ means the largest integer not more than z.

Suppose the linear chain of m sites in the simple Hückel model. Number the sites consecutively from 1 to m and denote $[1,m]$ by M. Each stationary state has its *p*-densities $\{p_{rs}\}$ $(r,s\in M)$, which fulfil the hypervirial relationships[2]

$$p_{r+1,s}+p_{r-1,s}-p_{r,s-1}-p_{r,s+1}=0 \qquad (r<s\in M). \tag{1}$$

Here, understand the term having an improper subscript as being absent. Although the inherent symmetry

$$p_{sr}=p_{rs} \qquad (r,s\in M) \tag{2}$$

is assumed, we need not consider the symmetry of the system for the present purpose.

Introduce the index b taking the two values 0 and 1, and define p_{bvi} by

$$p_{bvi}=p_{v-i,v+b+i} \tag{3}$$

for vi of the range expressed as follows. Let M_b be $[1,m-b]$ and d_{bv} be the largest i for each $v\in M_b$;

$$d_{bv}=\begin{cases} v-1 & (v\in[1,c_b]) \\ m-b-v & (v\in[c_b+1,\,m-b]) \end{cases} \tag{4}$$

with

$$c_b=[(m-b+1)/2]. \tag{5}$$

Denoting $[0,d_{bv}]$ by D_{bv}, we have $i\in D_{bv}$ with $v\in M_b$. The other expression of the range is often useful. Let d_b be the largest of d_{bv}'s $(v\in M_b)$ given by

$$d_b=[(m-b-1)/2] \tag{6}$$

and denote $[0,d_b]$ by D_b and $[1+i,m-b-i]$ by M_{bi}. Then, we have $v\in M_{bi}$ with $i\in D_b$. Any site pair index rs $(r\leqq s\in M)$ can be transformed by

$$b=\begin{cases} 0 & (s-r \text{ even}) \\ 1 & (s-r \text{ odd}), \end{cases} \tag{7}$$

$$v=(r+s-b)/2, \tag{8}$$

and

$$i=(s-r-b)/2 \tag{9}$$

into the present triple index bvi uniquely.

Now, let us define the modified *p*-density ξ_{bvi} for each $i\in D_b$ as

$$\xi_{bvi}=\begin{cases} p_{bvi}-p_{bv,i+1} & (v\in M_{b,i+1}) \\ p_{bvi} & (v=1+i,\,m-b-i). \end{cases} \tag{10}$$

Then, the hypervirial relationships can be rewritten as

$$\xi_{bvi}=\xi_{b,v+1,i} \qquad (v,\,v+1\in M_{bi})\ (i\in D_b). \tag{11}$$

Successive applications of these lead immediately to[4]

$$\xi_{bvi}=\xi_{bwi} \qquad (v,\,w\in M_{bi})\ (i\in D_b), \tag{12}$$

which can be further generalized as shown below.

Let $D_b(f)$ be $[0,d_b-f]$ for each $f\in D_b$ and redefine the modified *p*-density $\xi_{bvi}(f)$ for each $i\in D_b(f)$ as

$$\xi_{bvi}(f)=\begin{cases} p_{bvi}-p_{bv,i+f+1} & (v\in M_{b,i+f+1}) \\ p_{bvi} & (v=1+f+i,\,m-b-f-i), \end{cases} \tag{13}$$

which contains the preceding modified p-density as the particular case of f=0. Because $\xi_{bvi}(f)$ can be written as

$$\xi_{bvi}(f) = \sum_{k=i}^{i+f} \xi_{bvk}, \tag{14}$$

we attain the theorem

$$\xi_{bvi}(f) = \xi_{bwi}(f) \quad (v, w \in M_{b,i+f}) \ (i \in D_b(f)) \ (f \in D_b), \tag{15}$$

namely, "The modified p-density is an invariant every fi." The theorem is ready to yield readable relationships:

(1) Let both of v and w belong to $M_{b,i+f+1}$ and rewrite $i+f+1$ as j. Then, for $i<j$, we have

$$p_{bvj} - p_{bwj} = p_{bvi} - p_{bwi} \qquad (v, w \in M_{bj}). \tag{16}$$

(2) Let v be $1+f+i$ and d_{bw} be larger than d_{bv}. Then, we have

$$p_{bwv} = p_{bwi} - p_{bvi} \qquad (i \in D_{bv}). \tag{17}$$

(3) Let v be $1+f+i$ and w be $m-b-f-i$. Then, the symmetry condition

$$p_{bvi} = p_{b,m-b+1-v,i} \qquad (v \in [1,c_b]) \tag{18}$$

follows.

Important is the i=0 case of the second. Arranging the letters relevantly, we find that

$$p_{bvi} = p_{bv0} - p_{bi0} \qquad (0 < i \in D_{bv}) \ (v \in M_b), \tag{19}$$

which connects bond orders between nonadjacent sites with two electron densities (b=0) or with two bond orders between adjacent sites (b=1).[5] In particular, for the m-electron ground state, using an analytic expression of the bond order between adjacent sites,[6] we obtain

$$p_{1vi} = (A_m(v) - A_m(i))/(m+1) \tag{20}$$

with

$$A_m(t) = \begin{cases} (-1)^{t-1}\mathrm{cosec}((2t+1)\pi/(2m+2)) & (m \text{ even}) \\ (-1)^{t-1}\cot((2t+1)\pi/(2m+2)) & (m \text{ odd}) \end{cases} \tag{21}$$

from the b=1 case. The b=0 case connects the two well-known consequences[7] of the alternant symmetry with each other.

The above theorem is essentially valid for any linear chain part aside from bifurcation sites. For the linear chain part having an end site, number the sites from 1 to m with the end site as 1 and the bifurcation site as m. Considering the hypervirial relationships for $r<s\in[1,m-1]$, we find that the theorem holds with the range for v and w restricted to $M_{b,i+f+1}$ plus $1+f+i$. On the other hand, for the linear chain part between bifurcation sites, number the sites from 1 to m with the bifurcation sites as 1 and m. The hypervirial relationships for $r,s\in[2,m-1]$ leave p_{1m} extraneous, so that we have

$$d_{bc_b} = c_b - 2 \qquad (c_b \text{ odd}), \tag{22}$$

which affects d_b. The range for v and w is further restricted to $M_{b,i+f}$. The expressions obtained by utilizing the property at the terminal $1+f+i$ of $M_{b,i+f}$ remain valid only if the linear chain part has an end site.

References

1) Electron densities and bond orders are called generically p-densities.

2) M. Isihara, *Bull. Chem. Soc. Jpn.*, **62**, 2284 (1989).

3) The simple Hückel model assumes a sole Coulomb integral for all sites and a sole resonance integral for all adjacent sites.

4) Putting i=0, we have the invariance of the modified electron density (b=0) and that of the modified bond order between adjacent sites (b=1) previously derived (Ref. 2).

5) The previous result (Ref. 2) on the bond order between the two end sites is particular cases of this.

6) C. A. Coulson and H. C. Longuet-Higgins, *Proc. R. Soc. London, Ser. A*, **193**, 447 (1948); C. A. Coulson, *Proc. R. Soc. London, Ser. A*, **169**, 413 (1939).

7) One is that all the electron densities are unity, the other being that all the bond orders between starred sites and between unstarred sites vanish.

Synthesis and X-Ray Crystal Structure of the Dicopper(I) Complex of 2-(Diphenylphosphino)pyridine (Ph_2Ppy). $[Cu_2(\mu\text{-}Ph_2Ppy)_2(CH_3CN)_2](PF_6)_2$

Masahiko MAEKAWA, Megumu MUNAKATA,*,† Susumu KITAGAWA,† and Teijiro YONEZAWA
Research Institute for Science and Technology, Kinki University, Kowakae, Higashi-Osaka 577
† Department of Chemistry, Kinki University, Kowakae, Higashi-Osaka 577
(Received November 2, 1990)

Synopsis. The dicopper(I) complex with 2-(diphenylphosphino)pyridine (Ph_2Ppy), $[Cu_2(\mu\text{-}Ph_2Ppy)_2(CH_3CN)_2](PF_6)_2$ has been prepared. The crystal structure has been determined crystallographically: Space group $P\bar{1}$, a=10.807(6), b=11.756(8), c=8.606(7) Å, α=90.36(6), β=95.98(5), γ=92.90(5)°, Z=1, R=0.067. The two copper atoms are bridged by two Ph_2Ppy molecules in a head-to-tail arrangement, resulting in a rare staggered conformation of the eight-membered ring $Cu_2P_2N_2C_2$, whose factor is concerned with the coordination numbers of the central metal atoms. ^1H NMR studies show that the ligand of a CH_3CN in the titled compound undergoes dissociation in acetone solution.

2-(diphenylphosphino)pyridine (Ph_2Ppy) can form dimetal complexes[1-4] having an eight-membered ring $M_2P_2N_2C_2$, because of its ability to act as a bidentate bridging ligand. The two sort donor atoms in Ph_2Ppy stabilize metals in the lower oxidation state. However, there is sparse literature on its copper(I) and silver(I) complexes. Recently the dicopper(I) complex containing three Ph_2Ppy molecules as bridging ligands was reported.[5] The framework of the eight-membered ring gives an eclipsed[1-4,6-11] and a staggered conformation.[12] The latter seldom occurs in metal complxes, whereas the former often occurs in various metal complexes.

We have synthesized the dicopper(I) complex bridged by two Ph_2Ppy molecules which form a eight-membered ring and have determined the crystal structure in order to clarify the factors governing the eclipsed and staggered conformations.

Table 1. Crystal Data for $[Cu_2(\mu\text{-}Ph_2Ppy)_2(CH_3CN)_2](PF_6)_2$

Formula	$Cu_2C_{38}N_4H_{34}P_2F_{12}$
Formula weight	1025.68
Crystal system	Triclinic
Space group	$P\bar{1}$
Cell constants	
a/Å	10.807(6)
b/Å	11.756(8)
c/Å	8.606(7)
α/°	90.36(6)
β/°	95.98(5)
γ/°	82.90(5)
V/Å^3	1079.1
Z	1
Density/g cm^{-3}	3.935
Crystal size/mm	0.3×0.3×0.3
Radiation	Mo $K\alpha$
λ (Mo $K\alpha$)/Å	0.71073
μ (Mo $K\alpha$)/cm^{-1}	11.42
Scan mode	ω-2θ
Scan rate/° min^{-1}	8
Scan range/°	1.4194+0.5tan θ
2θ range/°	2—60
Number of observed reflections	5354
Reflections used in refiment	3753 (F_o>3σ(F_o))
F(000)	486
R	0.067
R_w	0.067

$R=\Sigma(|F_o|-|F_c|)/\Sigma|F_o|$. $R_w=\{\Sigma w(|F_o|-|F_c|)^2/\Sigma w|F_o|^2\}^{1/2}$, where $w=1/\sigma^2(F_o)$.

Experimental

Preparation of $[Cu_2(\mu\text{-}Ph_2Ppy)_2(CH_3CN)_2](PF_6)_2$. All operations were carried out under an atmosphere of purified argon. The reaction of Ph_2Ppy[13] (52.7 mg, 0.2 mmol) with $[Cu(CH_3CN)_4]PF_6$[14] (74.5 mg, 0.2 mmol) in dry methanol (10 ml) gave a clear solution, which was allowed to stand for

Table 2. Atomic Parameters for Non-Hydrogen Atoms in $[Cu_2(\mu\text{-}Ph_2Ppy)_2(CH_3CN)_2](PF_6)_2$

Atom	x	y	z	B_{eq}
Cu	−0.1030(1)	−0.1074(1)	0.0106(1)	4.28(4)
P(1)	−0.1512(1)	0.0659(1)	0.1031(2)	3.55(6)
P(2)	−0.3141(2)	−0.4507(2)	0.3033(2)	5.6(1)
F(1)	−0.4300(6)	−0.4220(8)	0.1924(9)	17.4(6)
F(2)	−0.2668(7)	−0.5346(5)	0.1740(7)	12.7(4)
F(3)	−0.2472(7)	−0.3589(5)	0.2343(7)	12.2(4)
F(4)	−0.3580(7)	−0.3675(6)	0.4295(8)	13.9(5)
F(5)	−0.3734(10)	−0.5432(7)	0.3753(9)	19.9(8)
F(6)	−0.1929(7)	−0.4822(8)	0.4110(9)	16.9(6)
N(1)	0.0617(4)	−0.2023(4)	−0.9091(5)	3.9(2)
N(2)	−0.2150(5)	−0.2145(4)	−0.0714(6)	4.6(2)
C(1)	0.0624(6)	−0.2802(5)	0.2046(8)	5.1(3)
C(2)	0.1734(7)	−0.3333(6)	0.2782(9)	6.2(3)
C(3)	0.2839(6)	−0.3101(6)	0.2335(8)	5.9(3)
C(4)	0.2845(6)	−0.2324(5)	0.1123(8)	4.7(2)
C(5)	0.1700(5)	−0.1797(4)	0.0453(6)	3.7(2)
C(11)	−0.0325(5)	0.1160(5)	0.2443(6)	3.7(2)
C(12)	0.0572(5)	0.0345(5)	0.3210(7)	4.0(2)
C(13)	0.1449(6)	0.0694(6)	0.4342(7)	5.1(3)
C(14)	0.1446(6)	0.1818(6)	0.4725(7)	5.4(3)
C(15)	0.0566(6)	0.2638(6)	0.3978(8)	5.4(3)
C(16)	−0.0327(6)	0.2303(5)	0.2836(7)	4.6(2)
C(21)	−0.2960(5)	0.0828(5)	0.1966(7)	4.0(2)
C(22)	−0.3713(6)	−0.0022(7)	0.1808(9)	6.1(3)
C(23)	−0.4800(8)	0.0058(9)	0.2530(11)	7.9(5)
C(24)	−0.5108(6)	0.0964(8)	0.3432(9)	6.9(4)
C(25)	−0.4362(6)	0.1808(7)	0.3638(9)	6.3(4)
C(26)	−0.3289(6)	0.1742(6)	0.2897(9)	5.7(3)
C(31)	−0.2687(6)	−0.2873(5)	−0.1107(8)	4.9(3)
C(32)	−0.3380(9)	−0.3816(6)	0.8376(11)	8.1(5)

$B_{eq}=(4/3)\{\Sigma_i\Sigma_{ij}B_{ij}\boldsymbol{a}_i\boldsymbol{a}_j\}$.

two days at 0 °C. A small colorless crystal, $[Cu_2(\mu\text{-}Ph_2Ppy)_2(CH_3CN)_2](PF_6)_2$ (**1a**) was obtained together with many pale yellow-green crystals (**1b**).[15] The structure of **1a** was determined by X-ray crystallography, but that of **1b** could not determined because of the decay of the reflection intensities during data collection of the X-ray diffraction. ^{1}H NMR ($(CD_3)_2CO$) **1a** δ=9.45 (d, 6-H), 8.16 (t, 4-H), 7.93 (t, 5-H), 7.00 (d, 3-H), 7.34—7.49 (m, ph), and 2.03(s, CH_3CN); ^{31}P NMR ($(CH_3)_2CO$) **1a** 4.02. Yield **1a** 5 mg (3%).

X-Ray Data Analysis for $[Cu_2(\mu\text{-}Ph_2Ppy)_2(CH_3CN)_2](PF_6)_2$. The colorless crystal suitable for X-ray diffraction study was mounted on a Rigaku AFC-6B diffractometer with graphite monochromated Mo $K\alpha$ radiation (λ=0.71073 Å). The conditions of data collection and the crystal data are listed in Table 1. A total of 3753 independent reflections having $F_o > 3\sigma(F_o)$ were used. The structure was solved by a direct method (MULTAN 78)[16] and refined by Block diagonal least-squares calculations with anisotropic thermal parameters including isotropic H atoms located on a difference Fourier synthesis, using the program system KPPXRAY.[17] Reliability factors are defined as $R=\sum(|F_o|-|F_c|)/\sum|F_o|$ and $R_w=\{\sum w(|F_o|-|F_c|)^2/\sum w|F_o|^2\}^{1/2}$, where $w=1/\sigma^2(F_o)$. Atomic scattering factors and anomalous dispersion terms were taken from the International Tables for X-ray Crystallography, Vol. IV. The final R and R_w values were 0.067. Atomic coordinates of nonhydrogen atoms are given in Table 2.[18]

Results and Discussion

This section describes only the structure of **1a** because that of **1b** could not be determined by X-ray crystal analysis. The X-ray crystal structure of the complex **1a** is shown in Fig. 1. The complex consists of a centrosymmetric cation and noninteracting PF_6^- anions. Each copper atom is coordinated to one nitrogen atom of one Ph_2Ppy molecule and the nitrogen of CH_3CN, and one phosphorus atom of the other Ph_2Ppy molecule, resulting in a distorted trigonal geometry. The two copper atoms are bridged by two Ph_2Ppy molecules to form an eight-membered ring $Cu_2P_2N_2C_2$. The bridging mode of each Ph_2Ppy molecule is head-to-tail.[1-3,5,9] The most striking feature of the complex is that the eight-membered ring has a staggered conformation. To our knowledge, there is only one report of the conformation for $[Au_2(\mu\text{-dppm})_2Cl_2]$[12] in which the gold(I) atoms are three-coordinate. On the other hand, the dimetal complexes having a four-coordinate copper(I) atom[6,7,9] and silver(I) atom[8] give an eclipsed conformation. The complex **1a** and the Au(I) complex $[Au_2(\mu\text{-dppm})_2Cl_2]$ in which the central ions are three-coordinate give staggered conformations as described above. It was reported that the conformation of an eight-membered ring depends on the size and mode of binding of the other ligands which don't form part of the eight-membered ring.[8] In addition, the coordination numbers of the central metal ions are considered to be one of the most important factors governing the eight-membered ring conformation.

The Cu–N(1′)(pyridyl) distance of 2.038(4) Å is slightly shorter than those (2.048(4)—2.114(4) Å) reported for three-coordinate copper(I) complexes.[5,9,19] It is interesting to note that the Cu–N(2)(CH_3CN) distance of 1.933(5) Å is between those (1.843(8)—1.846(10) Å) of three-coordinate copper(I) complexes[19] with CH_3CN and those (1.999(9)—2.161(3) Å) of four-coordinate copper(I) complexes[5,6] with CH_3CN. The Cu–P(1) distance of 2.204(2) Å is close to those (2.231(3)—2.296(8) Å) of copper(I) complexes with 1,1′-bis(diphenylphosphino)methane[6,20-22] and Ph_2Ppy.[5] The Cu···Cu′ distance of 3.584(3) Å is much longer than that (2.721(3) Å) of the analogous dicopper(I) complex[5] $[Cu_2(\mu\text{-}Ph_2Ppy)_3(CH_3CN)]^{2+}$.

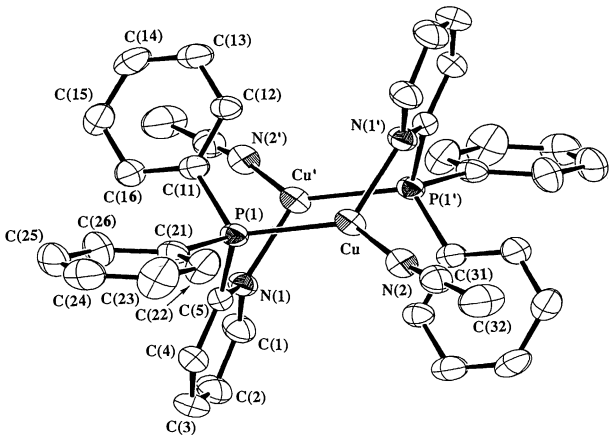

Fig. 1. ORTEP drawing of $[Cu_2(\mu\text{-}Ph_2Ppy)_2(CH_3CN)_2]^{2+}$ cations with 30% probability plots for thermal ellipsoids and atomic numbering. Half the atoms are labeled: the others are related by a center of inversion at the midpoint of the Cu···Cu′ vector. Only Cu′, P(1′), N(1′) and N(2′) in the coordination sphere are labeled. Selected bond distances (Å) and bond angles (°); Cu···Cu′=3.584(3), Cu–P(1)=2.204(2), Cu–N(2)=1.933(5), Cu–N(1′)=2.038(4), C(18)–N(2)=1.123(8), P(1)–Cu–N(2)=128.3(2), P(1)–Cu–N(1′)=120.0(1), N(2)–Cu–N(1′)=106.7(2), Cu–P(1)–C(5)=113.9(2), Cu–P(1)–C(11)=115.4(2), Cu–P(1)–C(21)=113.7(2), Cu–N(2)–C(31)=171.1(5).

The angles around copper(I) are P(1)–Cu–N(1′)=120.0(1), P(1)–Cu–N(2)=128.3(2), and N(2)–Cu–N(1′)=106.7(2)°, summing to 355.0°, since the copper atom lies 0.2661 Å from the plane defined by one phosphorus and two nitrogen atoms. The P(1)–Cu–N(1′) angle of 120.0(1)° is much smaller than the corresponding P–Au–P angle (155.9(1)°) of $[Au_2(\mu\text{-dppm})_2Cl_2]$[12] (the only complex reported to have a staggered conformation), while it is similar to those of eclipsed copper(I) complexes.[6,7]

^{1}H and ^{31}P NMR chemical shifts[23] of complex **1a** are shown in the experimental section. The ^{1}H NMR coordination shifts ($\Delta\delta=\delta_{complex}-\delta_{free}$) of the pyridine ring protons are 0.09—0.78 ppm, indicating the coordination of the nitrogen atom of Ph_2Ppy to Cu(I). On the other hand, the coordination shift of the CH_3 signal of CH_3CN was not observed within experimental error. This fact reveals the dissociation of a CH_3CN in acetone solution in contrast to the crystal structure. The ^{31}P NMR coordination shift of 7.70 ppm indicates the coordination of the phosphorus atom of the Ph_2P group to Cu(I). This value is significantly large when compared with other dinuclear complexes[2-4] with Ph_2Ppy and slightly larger than those of dinuclear complexes[6,12] with dppm.

We thank Mr. Hisao Shimono and Mr. Shinji Matsuyama for their assistance with the X-ray measurements. This work was partially supported by a Grant-in-Aid for Scientific Research No. 63540465 from the Ministry of Education, Science and Culture.

References

1) J. P. Farr, M. M. Olmstead, and A. L. Balch, *J. Am. Chem. Soc.*, **102**, 6654 (1980).
2) J. P. Farr, M. M. Olmstead, C. H. Hunt, and A. L. Balch, *Inorg. Chem.*, **20**, 1182 (1981).
3) J. P. Farr, M. M. Olmstead, and A. L. Balch, *Inorg. Chem.*, **22**, 1229 (1983).
4) J. P. Farr, M. M. Olmstead, N. M. Rutherford, F. E. Wood, and A. L. Balch, *Organometallics*, **2**, 1758 (1983).
5) E. Lastra, M. P. Gamasa, J. Gimeno, M. Lanfranchi, and A. Tiripicchio, *J. Chem. Soc., Dalton Trans.*, **1989**, 1499.
6) J. Diez, M. P. Gamasa, J. Gimeno, A. Tiripicchio, and M. T. Camellini, *J. Chem. Soc., Dalton Trans.*, **1987**, 1275.
7) A. M. M. Lanfredi, F. Ugozzoli, A. Camus, and N. Marsich, *Inorg. Chim. Acta*, **99**, 111 (1985).
8) D. M. Ho and R. Bau, *Inorg. Chem.*, **22**, 4073 (1983).
9) M. Munakata, S. Kitagawa, S. Shimono, T. Emori, and H. Masuda, *J. Chem. Soc., Chem. Commun.*, **1987**, 1798.
10) H. C. Jaw, M. M. Savas, R. D. Rogers, and W. R. Mason, *Inorg. Chem.*, **28**, 1028 (1989).
11) R. G. Holloway, B. R. Penfold, R. Colton, and M. J. McCormick, *J. Chem. Soc., Chem. Commun.*, **1976**, 485.
12) H. Schmidbauer, A. Wohlleber, U. Schubert, A. Frank, and G. Huttner, *Chem. Ber.*, **110**, 2751 (1977).
13) A. Maisonnent, J. P. Farr, M. M. Olmstead, C. T. Hunt, and A. L. Balch, *Inorg. Chem.*, **21**, 3961 (1982).
14) D. F. Shriver, "Inorganic Syntheses," Wiley-Interscience, New York (1979),Vol. 19, p. 90.
15) The structure of **1b** was identified as $[Cu_2(\mu\text{-}Ph_2Ppy)_3(CH_3CN)](PF_6)_2$ by elemental analysis and the NMR method. ^1H NMR ($(CD_3)_2CO$) δ=9.43 (d, 6-H), 8.15 (t, 4-H), 7.92 (t, 5-H), 7.00 (d, 3-H), 7.33—7.48 (m, Ph), and 2.09 (s, CH_3CN); ^{31}P NMR ($(CH_3)_2CO$) 4.13. Found: C, 50.63; H, 4.44; N, 4.51%. Calcd for $Cu_2C_{53}H_{45}N_4P_5F_{12}$ (**1b**): C, 51.00; H, 3.63; N, 4.48%. Yield: 32.5 mg (21%).
16) P. Main, S. E. Hull, L. Lessinger, G. Germain, J. -P. Declercq, and M. M. Woolfson, "MULTAN 78. A System of Computer Programs for the Automatic Solution of Crystal Structures from X-Ray Diffraction Data," Universities of York, England and Louvain, Belgium (1978).
17) T. Taga, T. Higashi and H. Iizuka, KPPXRAY (Kyoto Program for X-Ray Crystal Structure Analysis), University of Kyoto, Japan (1985).
18) Tables of atomic parameters for non-hydrogen atoms, fractional coordinates, isotropic thermal parameters for hydrogen atoms, anisotropic thermal parameters for nonhydrogen atoms, bond distances, bond angles, and torsion angles and observed and calculated structure factors are deposited as Document No. 9118 at the Office of the Editor of Bull. Chem. Soc. Jpn.
19) M. Munakata, M. Maekawa, S. Kitagawa, S. Matsuyama, and H. Masuda, *Inorg. Chem.*, **28**, 4300 (1989).
20) A. M. M. Lanfredi, A. Tiripicchio, A. Camus, and N. Marsich, *J. Chem. Soc., Chem. Commun.*, **1983**, 1126.
21) N. Marsich, G. Nardin, and L. Randaccio, *J. Am. Chem. Soc.*, **95**, 4053 (1973).
22) D. M. Ho and R. Bau, *Inorg. Chem.*, **22**, 4079 (1983).
23) ^1H and ^{31}P NMR chemical shifts ($(CD_3)_2CO$) of free Ph_2Ppy and free CH_3CN: ^1H NMR δ=8.67 (d, 6-H), 7.69 (t, 4-H), 7.29 (t, 5-H), 7.09 (d, 3-H), and 7.40 (m, Ph) for Ph_2Ppy, and 2.02 (CH_3) for CH_3CN; ^{31}P NMR δ=−3.68 for Ph_2Ppy.

Demetalation of (5,10,15,20-Tetraphenylporphyrinato)iron Complexes: Effect of Substituents at the *o*-Positions of Phenyl Groups

Etsuo HASEGAWA, Eriko MATSUBUCHI, and Eishun TSUCHIDA*
Department of Applied Chemistry, Waseda University, Tokyo 169
(Received November 26, 1990)

Synopsis. The demetalation of a series of (5,10,15,20-tetraphenylporphyrinato)iron(III) complexes having bulky substituents at the *o*-positions of phenyl rings was studied in acetic acid in the presence of iron(II) chloride and HCl. The reaction occurred simultaneously with the reduction of Fe(III) porphyrin to Fe(II) porphyrin, since no demetalation was observed without iron(II) chloride. The pseudo-first-order rate constants, which were determined spectrophotometrically, decreased with an increase in the bulkiness of the *o*-substituents on the phenyl rings. The atropisomeric structures of the products were determined by high-resolution NMR measurements.

The metal insertion reaction was studied kinetically and thermodynamically in order to understand the mechanism of how porhyrins form the metalloporphyrin complexes in nature.[1,2] An intermediate complex (sitting-atop model) was proposed.[3] Still, less attention has been pain to the demetalation process, although the reaction is closely related to metalation.[4] It is expected that the introduction of bulky substituents to a porphyrin induces not only a decrease in intermolecular metal-metal interaction (dimerization), but also affects the reactivities of the porphyrin group. A preliminary report appeared concerning the effect of such bulky substituents on copper incorporation into tetraphenylporphyrins.[5]

In this paper we describe the demetalation of a series of (5,10,15,20-tetraphenylporphyrinato)iron(III) complexes with bulky ortho-substituents at the phenyl groups in a $FeCl_2$–HCl–acetic acid system at 20 °C and the rate of demetalation in order to discuss the effect of the ortho-substituents on the intramolecular reaction. In addition, a method to determine the atropisomeric structure was established by the use of high-resolution ^1H NMR measurements on the demetalated products prepared by the present method.

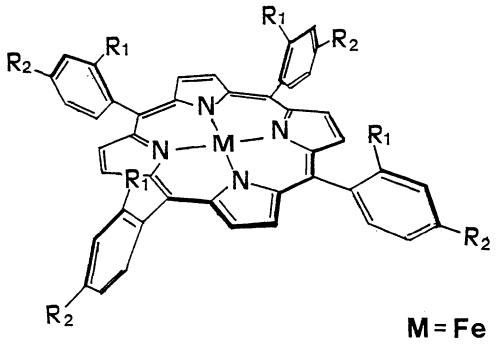

1 R_1=H, R_2=H

2 R_1=H, R_2=NHCOC$(CH_3)_3$

3 R_1=NHCOC$(CH)_3$, R_2=H

4 R_1=NHCOC$(CH_3)_2(CH_2)_{18}$OH, R_2=H

5 R_1=NHCOC$(CH_3)_2(CH_2)_{18}$OP(=O)(O$^-$)O$(CH_2)_2$N$^+(CH_3)_3$, R_2=H

Experimental

Materials. Reagent-grade iron(II) chloride, concd HCl and acetic acid were purchased from Wako Chem. Co. and used without further purification. (5,10,15,20-Tetrapheylporphyrinato)iron(II) chloride (**1**) was purchased from Aldrich Chemical Co. and purified by silicagel column chromatography. [5,10,15,20-*Tetrakis*(α,α,α,α-*o*-pivalamidophenyl)-porphyrinato] iron(III) chloride (**3**) was prepared according to methods described in the literature.[6,7] Fe(III) porphyrin chloride (**4**) and Fe(III) porphyrin chloride (**5**) were prepared according to previous papers.[8,9][5,10,15,20-*Tetrakis*(*p*-pivalamidophenyl)porphyrinato]iron(III) chloride (**2**) was propared by the reaction of pivaloyl chloride with 5,10,15,20-tetrakis (*p*-aminophenyl)porphyrin.[10]

Kinetic Measurements. The rate constants of demetalation were determined spectrophotometrically by measuring the UV and VIS adsorption spectra of a porphyrin. A double-beam UV and VIS absorption spectrophotometer (Shimadzu MPS-2000) was used. The kinetic runs were conducted under pseudo-first-order conditions, i.e. in the presence of a large excess of HCl and $FeCl_2$ over porphyrinatoiron(III). The reaction temperature was 20 °C. A solution of a Fe(III) porphyrin (20 μmol dm^{-3}) in acetic acid (5 cm^3) was mixed under argon with 0.02 ml of concd HCl. The reaction was started by adding a $FeCl_2$-saturated aqueous solution under an argon atmosphere in a sealed quartz cell (path length: 10 mm). The final concentrations of HCl, $FeCl_2$, and water were 0.33 mol dm^{-3}, 3.9 mmol dm^{-3}, and 1.8 mol dm^{-3}, respectively.

Preparative Demetalation for ^1H NMR Spectral Measurements. Measurements of the ^1H NMR spectra of demetalated products were carried out with derivatives **3** and **5**. Sample preparations were as follows. Fe(III) porphyrin **3** (30 mg, 26 μmol) was dissolved in a mixed solution of acetic acid (150 ml) and concd HCl (30 ml). To the porphyrin solution was added solid $FeCl_2$ (30 mg, 0.42 mmol) under an argon atmosphere at 20 °C. After 1 h of stirring, the solvent was removed under reduced pressure. The residue dissolved in chloroform was washed with 5% $NaHCO_3$, dried over Na_2SO_4 and then evaporated to dryness. The residue was chromatographed on silica gel eluted with benzene–diethyl ether (4/3 by volume) to give the metal-free porphyrin **3′**. The yield was 23 mg (87%). Anal. Found: C, 74.27; H, 7.28; N, 9.23%. Calcd for $C_{64}H_{66}N_8O_4 \cdot 1H_2O$: C, 74.68; H, 6.54; N, 9.89%. IR (KBr) 1690 and 1580 cm^{-1}. VIS ($CHCl_3$) λ_{max} 643, 587, 545, 511, 480(sh), and 418 nm.

Fe(III) porphyrin **5** (100 mg, 35 μmol) was demetalated by the same procedure described for **3**. The product, however, was purified by column chromatography on Toyopearl HW-40F (Tosoh Co.) eluted with methanol. During column

purifivation, porphyrin dication was spontaneously converted to the correponding porphyrin. The yield was 76 mg (80%). Anal. Found: C, 61.76; H, 9.35; N, 5.23; P, 3.97%. Calcd for $C_{152}H_{248}N_{12}O_{20}P_4 \cdot 15H_2O$: C, 61.69; H, 9.53; N, 5.68; P, 4.19%. IR (KBr) 1690, 1580, 1240, 1080, and 960 cm^{-1}. VIS (MeOH) λ_{max} 644, 589, 547, 513, 480(sh), and 418 nm.

The ^1H NMR spectra of the products were obtained by JEOL GSX-400 FTNMR spectrometer in $CDCl_3$ or CD_3OD with Me_4Si used as an internal standard.

Results and Discussion

It is well-known that the metalloporphyrins can be divided into five 'stability classes' which indicate their resitance towards protic acids.[11] A porphyrinatoiron(III) complex belongs to class-III in demetalation,[12] and the reduced one (porphyrinatoiron(II)) is much more susceptible to demetalation. From this view a demetalation reaction of an iron(III) porphyrin was studied with the concomitant reduction to iron(II) by various reductants.[13] The mechanism of iron(III) demetalation in the presence of iron(II) chloride and HCl as a 'catalytic' reductant has been studied kinetically and the following mechanism was postulated:[13]

$$ClFe(III)P + Fe(II) + HCl \rightleftarrows HFe(III)Cl_4 + Fe(II)P \quad (1)$$

and

$$Fe(II)P + n\ HCl \rightarrow Fe(II) + H_4P^{2+}, \quad (2)$$

where P indicates a porphyrinato ligand. The reaction follows pseudo-first-order kinetics:

$$-d[ClFe(III)P]/dt = k_{obsd}\,[ClFe(III)P], \quad (3)$$

where k_{obsd} indicates a pseudo-first-order rate constant for demetalation.

In the present paper, the demetalation of a series of iron(III) porphyrins was conducted in acetic acid containing concd HCl in the presence of an excess amount of iron(II) chloride, as described in the Experimental section. For example, the original spectrum of **5** (absorption maxima at 506, 589, and 645 nm) disappeared and changed to that of the metal-free porphyrin dication (absorption maxima at 585 and 636 nm). The isosbestic points (472, 560, and 661 nm) were maintained during the reaction. This indicates that the reaction is apparently from Fe(III)P to H_4P^{2+}. No demetalation reaction occurred in the absence of iron(II) chloride under the HCl concentration employed in the present study; in the absence of HCl no reaction could be induced by iron(II) chloride. This fact indicates that the demetalation is caused by a concurrent reaction accompanying both a reduction process and a removal process of an iron ion, shown by the ternary reaction (1). Other iron(III) porphyrins also showed the same reaction behavior.

The pseudo-first-order rate constants (k_{obsd}) were determined by pseudo-first order plots. The linearity of the plots revealed the first-order kinetics, and the determined rate constants were independent of employed wavelength (480—680 nm). Table 1 summarizes the rate constants, under the same experimental conditions, for the demetalation reactions of a series of (5,10,15,20-tetraphenylporphyrinato)iron(III) having different substituents at the ortho positions of phenyl rings (complexes **1**—**5**). Table 1 clearly shows that the rate constants are remarkably dependent on the substituents at ortho-positions.

Table 1. Values of Pseudo-First-Order Rate Constants (k_{obsd}) of Demetalation Reactions

Compound	k_{obsd}/s^{-1} [a]
1	1.5×10^{-2}
2	1.0×10^{-2}
3 (α_4) [b]	1.4×10^{-3}
3 ($\alpha_n\beta_{4-n}$) [b]	1.3×10^{-3}
4	3.1×10^{-4}
5 (α_4) [b]	1.8×10^{-4}
5 ($\alpha_n\beta_{4-n}$) [b]	4.3×10^{-4}

a) Pseudo-first-order rate constants at 20°C, in acetic acid–H_2O. [Fe(III)porphyrin]=20 μmol dm^{-3}, [HCl]= 0.33 mol dm^{-3}, [$FeCl_2$]=3.9 mmol dm^{-3}. b) α_4 and $\alpha_n\beta_{4-n}$ (n=4, 3, 2) mean a $\alpha,\alpha,\alpha,\alpha$-atropisomer and a mixture of four atropisomers, respectively.

The rate of a demetalation reaction is considered to be affected largely by the following three factors: (1) the basicity of a porphyrinato ligand, (2) the deformability of a porphyrin ring plane, and (3) the solvation on a porphyrin ring plane.

The basicity of these tetraphenylporphyrin ligands having various ortho-substituents is considered to be almost the same, since the Hammet sigma coefficient of the alkanamido groups is practically zero.[14]

An X-ray diffraction analysis revealed that the porphyrin dications (diacids), that is, products of demetalation, form a domed structure by a van der Waals repulsion of the inner hydrogen atoms of the porphyrin ring.[15] During a demetalation reaction, it can be postulated that an intermediate complex having a domed structure of a porphyrin ring, like a sitting-atop model,[3] is formed. It has been reported concerning a kinetic study of the thermal atropisomerization and photomerization study of [5,10,15,20-*tetrakis*($\alpha,\alpha,\alpha,\alpha$-*o*-substituted phenyl)porphyrinato]metal complexes that the planality of a porphyrin ring is closely related to the steric repulsion of the bulky groups and regulates the rotation of the phenyl rings.[16] That is, the bulky substituents restrict the tilting of pyrrole rings, resulting in less deformability of a porphyrin ring. The fact that the bulky groups (pivalamido groups) at the para positions, as in the case of the complex **2**, showed a rate constant similar to that of **1** also suggests that a steric interation of the bulky groups at the ortho positions is important. Our results are consistant with the conclusion that the ruffling of the porphyrin may results in an enhancement of the reactivity on the electrophilic meso-substitution in metalloporphyrins.[17]

The porphyrin ring is considered to be less solvated on the side of bulky ortho-substituents and desolvated irons are expected to be more easily removed. However, this is inconsistent with the experimental results.

The demetalation of **3** and **5** was carried out in preparative scales in order to give the corresponding

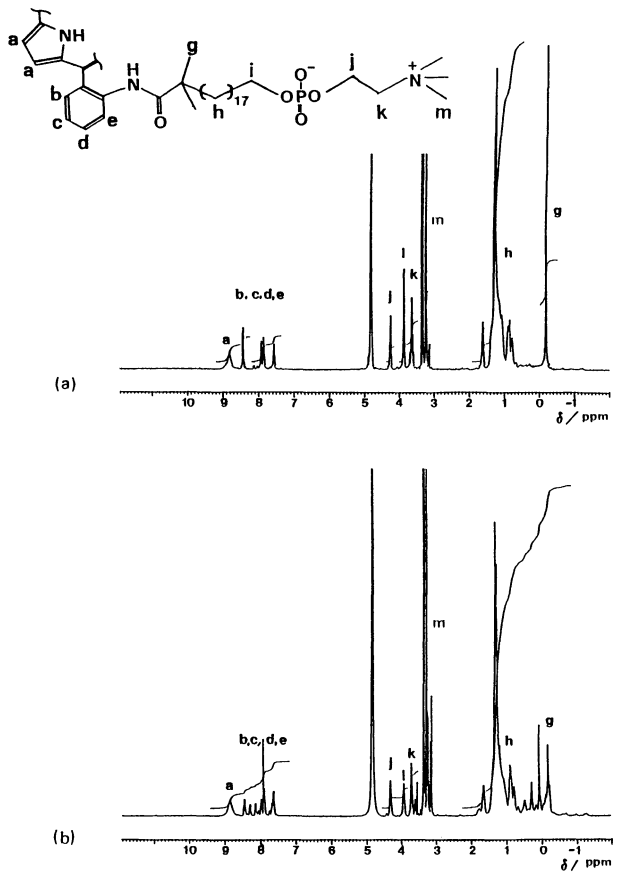

Fig. 1. 400 MHz ^{1}H NMR spectra of the demetalated products of **5**(α_4) (a) and a mixture of four atropisomers (**5**($\alpha_n\beta_{4-n}$)) (b) in CD_3OD.

demetalated products in high yields (>80%). The structures of the products were confimed by various analyses, as described in the experimental section. Figure 1 shows the 400 MHz ^{1}H NMR spectra of the demetalated products of **5**(α_4) and a mixture of four atropisomers **5**($\alpha_n\beta_{4-n}$). The structure of the α_4 atropisomer of **5** was supported by the single peak at δ=−0.2 ppm due to the methyl protons of the 2,2-position of the acyl chains of the same chemical environment (Fig. 1(a)), while the Fe(III) porphyrin comprising of a mixture of four atropisomers,**5**($\alpha_n\beta_{4-n}$), gave a product having multiple signals near δ=0.0 ppm due to the multiple methyl protons of chemically different environments (Fig. 1(b)). It is therefore obvious that no atropisomerization was induced during the demetalation reaction under the conditions used in the present study.

References

1) J. H. Buchler, "Porphyrins and Metalloporphyrins," ed by K. M. Smith, Elsevier Publ., Amsterdam (1975), p. 157; *idem.*, "The Porphyrins," ed by D. Dolphin, Academic Press, New York (1978), Vol. IA, p. 389.
2) D. K. Lavallee, *Comments Inorg. Chem.*, **5**, 155 (1986).
3) E. B. Fleisher and J. H. Wang, *J. Am. Chem. Soc.*, **82**, 3498 (1960).
4) P. Hambright, "Porphyrins and Metalloporphyrins," ed by K. M. Simth, Elsvier Publ., Amstendam (1975), p. 233.
5) J. Turay and P. Hambright, *Inorg. Chim. Acta*, **53**, L147 (1981).
6) J. P. Collman, R. R. Gagne, C. A. Reed, T. R. Halbert, G. Lang, and W. T. Robinson, *J. Am. Chem. Soc.*, **93**, 1247 (1975).
7) T. H. Sorrell, *Inorg. Synth.*, **20**, 161 (1980).
8) Y. Matsushita, E. Hasegawa, K. Eshima, and E. Tsuchida, *Chem Lett.*, **1983**, 1387; E. Tsuchida, H. Nishide, M. Yuasa, E. Hasegawa, Y. Matsushita, and K. Eshima, *J. Chem. Soc., Dalton Trans.*, **1985**, 275.
9) E. Tsuchida and H. Nishide, *Top. Curr. Chem.*, **132**, 64 (1986).
10) A. Bettelheim, B. A. White, S. A. Raybuck, and R. W. Murray, *Inorg. Chem.*, **26**, 1009 (1987).
11) J. W. Buchler, L. Puppe, K. Rohbok, and H. H. Schneehage, *Ann. N. Y. Acad. Sci.*, **206**, 116 (1973).
12) J. N. Phillips, *Rev. Pure Appl. Chem.*, **10**, 35 (1960).
13) J. H. Espenson and R. J. Christensen, *Inorg. Chem.*, **16**, 2561 (1977).
14) P. Zuman, "Substituent Effects in Organic Polarography," Plenum Press, New York (1967), p. 46.
15) A. Stone and E. B. Fleisher, *J. Am. Chem. Soc.*, **90**, 2735 (1968).
16) R. A. Fritag and D. G. Whitten, *J. Phys. Chem.*, **87**, 3918 (1983).
17) E. Watanabe, S. Nishimura, H. Ogoshi, and Z. Yoshida, *Tetrahedron*, **31**, 1385 (1975).

Intercalation of Enzymes in γ-Titanium(IV) Phosphate

Yasushi KANZAKI*,† and Mitsuo ABE
Department of Chemistry, Faculty of Science, Tokyo Institute of Technology,
2-12-1 Ohokayama, Meguro-ku, Tokyo 152
† Laboratory of Analytical Chemistry, Showa College of Pharmaceutical Sciences,
3 Higashi-Tamagawagakuen, Machida, Tokyo 194
(Received February 16, 1991)

Synopsis. The intercalation of enzymes with molecular weights of 23000—240000 was examined for layered inorganic compounds. The intercalation of papain and catalase into γ-type titanium(IV) phosphate was achieved by coexisting propylamine in an aqueous medium. The intercalation compound of papain was enzyme active for *N*-benzoyl-L-arginine ethyl ester and a catalase intercalation compound for H_2O_2 decomposition.

A great variety of methods for the preparation of immobilized enzymes have been reported and practically applied in many quarters. Inorganic materials, such as clay minerals, have been used as supports of immobilized enzymes.[1] However, such immobilized enzymes are prepared by simple adsorption or ion-exchange reaction of enzymes on the surface of clay minerals. Intercalation occurs in layered inorganic compounds in which each lamella is combined by weakly interacting forces, such as van der Waals force. Enzymes which are intercalated between such weakly interacting lamellae are expected to be utilized as immobilized enzymes. Such an approach may develop different conceptions regarding the immobilization of enzymes.

This paper deals with the intercalation of some common enzymes in layered γ-type titanium(IV) phosphate ($Ti(HPO_4)_2 \cdot 2H_2O$: γ-TiP). The enzyme activity of the intercalation compounds was also examined.

Experimental

Layered Materials. The H^+ form γ-TiP was prepared according to the procedure reported by Kobayashi and Yamazaki[2] as follows. Amorphous titanium(IV) phosphate was heated hydrothermally in 10 M (M=mol dm^{-3}) phosphoric acid for 24 h at 280 °C. Well crystallized γ-TiP with an average diameter of 10—20 μm was prepared.[3] The crystal thus prepared was carefully washed with deionized water and air-dried.

Procedure. The direct intercalation of enzymes into inorganic layered compounds seemed to be improbable because of the tremendously large size of the enzymes. The following procedures were employed according to the intercalation reaction of α-zirconium(IV) phoshate with propylamine reported previously.[4] It was found that delamination occurred in the reaction of α-zirconium(IV) phosphate with an aqueous propylamine solution, and gave a colloidal solution of α-zirconium phosphate. Relamination, which gave a transparent film, was found to occur when the solvent was removed from the colloidal soluion. If delamination and the following relamination occurred in the presence of enzymes, the intercalation of enzymes with large moleculr weights could be achieved by coexisting enzymes in such a colloidal solution.

We have found that γ-TiP gave similar colloidal (delaminated) materials in an aqueous propylamine solution.[5] Two procedures for the intercalation were examined in this study according to the above-mentioned findings.

Table 1. Enzymes and Their Molecular Weight

Enzymes	Mol. weight
Papain (Protein decomposition)	23000
Lipase (Triglyceride decomposition)	38000
Peroxidase (H_2O_2 decomposition)	40000
α-Amylase (Starch hydrolysis)	51000
Gluco-Amylase (Starch-Glucose)	70000
Glucose-Oxidase (Glucose oxidation)	153000
Catalase (H_2O_2 decomposition)	240000

Procedure (1): Enzymes were reacted with a colloidal solution of γ-TiP which was prepared in an aqueous propylamine solution.

Procedure (2): γ-TiP was reacted with an enzyme–propylamine mixed solution (cointercalation).

Enzymes. Seven commonly available enzymes were selected for the intercalation, and are listed in Table 1. They were used without any pretreatment. Intercalation was carried out at 30 °C for 1 week unless otherwise stated. The reaction product was developed on a glass plate and the X-ray diffraction spectrum was measured using Mn-filtered Fe-$K\alpha$ radiation. The X-ray diffractometer used could measure down to $2\theta=0.9°$ which corresponds to the *d*-value of about 12 nm.

Assay. An enzme assay for the intercalation compounds was examined by contacting the substrate solutins (*N*-benzoyl-L-arginine ethyl ester (BAEE) for papain and H_2O_2 for catalase) with those corresponding intercalation compounds which were developed on glass plates and were fixed by air-drying.

Results and Discussion

Procedure (1): Few systematic results were obtained although a variety of reaction products were observed in the reaction of enzymes with colloidal solution of γ-TiP. The only result that implied the success of enzyme intercalation was observed in a reaction with papain. Figure 1a shows the X-ray diffraction pattern of the reaction products with respect to the added amount of papain. The peak for the propylamine intercalation compound[6] ($2\theta=5.9°$; *d*-value=1.9 nm,) which was observed in a dilute papain solution, completely disappeared at a papain content of 30 mg, suggesting the perfect conversion of γ-TiP into the papain intercalation compound. The first two sequences of the baseal plane reflection ($n\lambda$: n=1,2,3...) were observed. Such sequential reflections generally imply the formation of an intercalation compound. The average interlayer spacing of the product calculated from the peak angle was 5.6 nm, which was compared with 1.2 nm for the host γ-TiP or 1.9 nm for propylamine intercalated γ-TiP. The line width of the peak was 1.7°—2.3°, corresponding to the interlayer spacing of 6.5—4.8 nm. The large line

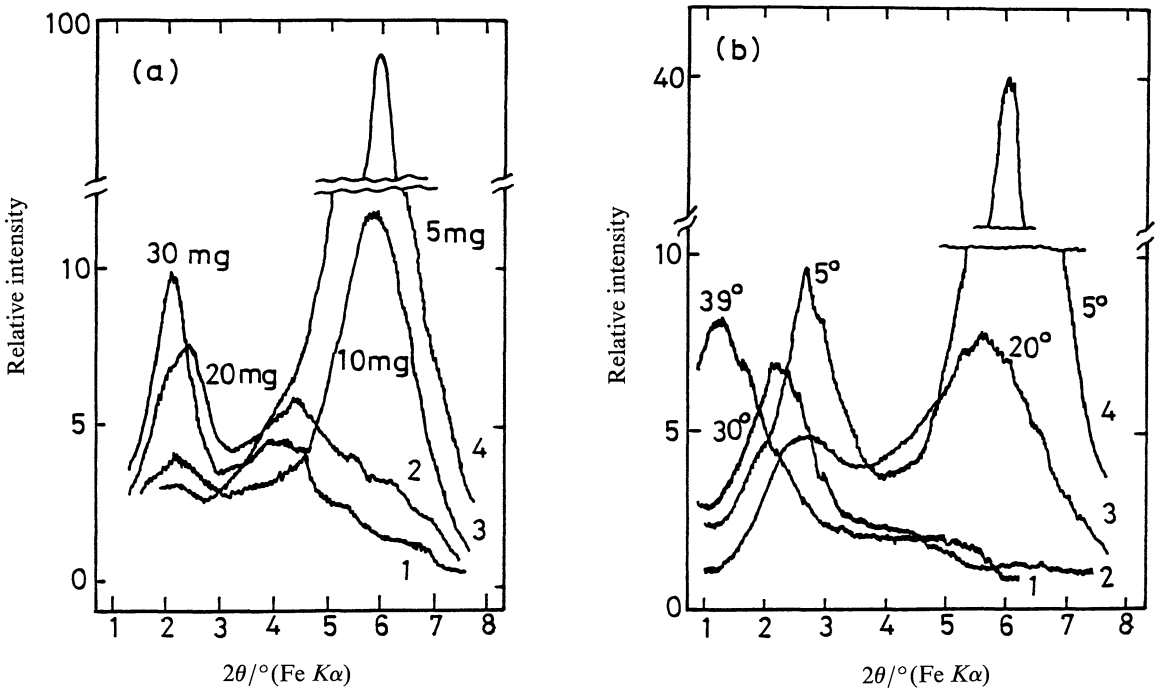

Fig. 1a. X-Ray diffraction patterns of papain intercalation compound of γ-TiP. Solution: 10 ml-aq, propylamine: 25 μL (0.04 mol dm^{-3}), γ-TiP: 0.1 g, Temp 30°C. Papain: (1): 30 mg, (2): 20 mg, (3): 10 mg, (4): 5 mg.

Fig. 1b. X-Ray diffraction patterns of catalase intercalation compound of γ-TiP. Solution: 10 ml-aq, γ-TiP: 0.1 mg, propylamine: 25 μl. Intercalation was carried out at (1): 39°C, (2): 30°C, (3): 20°C, (4): 5°C.

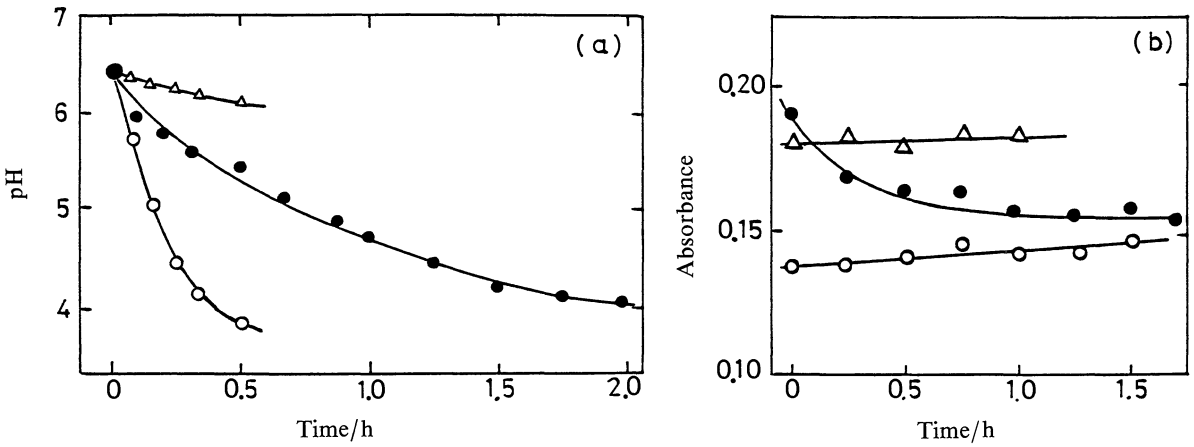

Fig. 2a Activity measurement for papain intercalation compound of γ-TiP (on decomposition of BAEE). Absorbance at 270 nm for buffer solutions containing; (○): aqueous papain solution, (●): papain intercalated γ-TiP, (△): supernatant solution of Fig. 1a-1.

Fig. 2b. Activity measurement for catalase intercalation compound of γ-TiP (on decomposition of H_2O_2). Absorbance at 240 nm for buffer solutions containing, (○): H_2O_2, (△): Catalase intercalated γ-TiP, (●): H_2O_2+catalase intercalated γ-TiP.

width might reflect the irregular arrangement of enzymes in the layered material.

An enzyme assay for the intercalation compound was carried out through the time dependence of the absorbance at 270 nm for BAEE according to the standard procedure.[7] The results are shown in Fig. 2b. A decay in absorbance was observed (closed circles), and indicating that the intercalated papain retained enzyme activity against BAEE. The decay was slow in comparison with that observed in a papain solution. Such slowness may be ascribable to the difficulty in contacting BAEE with papain in layered lattices. In addition, the

reaction was heterogeneous while the reaction of papain solution was homogeneous. The activity of papain in the supernatant solution was rather low since the intercalation reaction was carried out in a basic medium (propylamine solution). The activity of papain decreased rapidly in such a basic solution. (Papain must be kept in a buffer solution at pH=6.2.)

Procedure (2) Cointercalation of enzymes with propylamine was examined according to the success concerning the intercalation of phosphatidyl-ethanolamine.[8] No systematic results was obtained similar to that for Procedure (1). However, intercalation was found to occur in a catalase solution. The X-ray diffraction pattern strongly depended on the temperature in this reaction. At 5 °C, little evidence for the intercalation was observed, and most of the products were propylamine intercalation compound.[6] A product with a large interlayer spacing appeared at higher temperatures. The peak for the propylamine intercalation compound completely disappeared at around 39 °C (Fig. 1b) and a single-phase product with an average interlayer spaing of 8.5 nm (2θ=1.3°) was obtained. The line width was estimated to be 12 nm (0.9°)—5.5 nm (2.0°). The sequence of the basal plane reflection was not observed because of the large width of the spectrum.

It seems improbable that the γ-TiP formed a colloidal solution of single lamellae, which was cleaved from γ-TiP crystals in a propylamine solution. Thus the catalase intercalation compound with an interlayer spacing of around 8.5 nm must be formed through the delamination-relamination reaction of colloidal thin lamellae[4] of γ-TiP. A similar mechanism has been proposed in the intercalation of *t*-alkylamines into clay minerals.[9]

An enzyme assay of the catalase intercalation compound was carried out according to the standard procedure[10] (oxidation of H_2O_2). The enzyme activity was examine through the decrease in the absorbance at 240 nm due to H_2O_2 decomposition. Figure 2b shows the result. Catalase as well as its decomposition products show a strong absorbance at this wavelength, which often disturbs the measurements. A blank solution in the absence of H_2O_2 containing a catalase intercalation compound showed a certain residual absorbance due to catalase which might be released from the glass plates on which intercalation product was fixed. The solution of (H_2O_2+catalase intercalation compound) showed a rapid decay at this wavelength (closed circles). The infinite value did not reach zero because of the absorbance due to either catalase or its decomposition products which were released from the glass plate.

The supernatant solution which was used for the intercalation changed its original color (from brown to yellow) and did not show any enzyme activity against H_2O_2. On the other hand, the catalase intercalation compound kept its original color, suggesting that catalase was still alive. It can be concluded from the present results that the catalase intercalated in γ-TiP retained activity against H_2O_2 decomposition.

The intercalation of large-size enzymes was achieved in this study; the intercalation products exhibited enzyme activity even in an alkaline medium. Althogh the intercalation procedures adopted here seem to be somewhat tricky and no systematic results were obtained, the success of our methods offer some guiding priniciples regarding the intercalation of enzymes or new immobilizing methods for enzymes.

The authors wish to thank Professor M. Aizawa and Dr. H. Shinohara, Tokyo Institute of Technology, for their helpful suggestions and discussion concerning enzymes.

References

1) A. D. McLaren and E. F. Esterman, *Arch. Biochem. Biophys.*, **61**, 158 (1958), C. Schwabe, *Biochemistry*, **8**, 795 (1969), etc.
2) E. Kobayashi and S. Yamazaki, *Bull. Chem. Soc. Jpn.*, **56**, 1632 (1983).
3) Y. Kanzaki and M. Abe, *Bull. Chem. Soc. Jpn.*, **64**, 1846 (1991).
4) G. Alberti, M. Casciola, and U. Costantino, *J. Colloid Interface Sci.*, **107**, 256 (1985).
5) Y. Kanzaki and M. Abe, to be submitted.
6) U. Costantino, *J. Inorg. Nucl. Chem.*, **43**, 1985 (1981).
7) R. Arnon, "Methods in Enzymology," ed by G. E. Perlamnn and L. Lorand, Academic Press, New York (1970), Vol. XIX, p. 226.
8) Y. Kanzaki and M. Abe, *Bull. Chem. Soc. Jpn.*, in press.
9) Y. Okahata and A. Shimizu, *Langmuir*, **5**, 954 (1989).
10) B. Chance and A. C. Maehley, "Methods in Enzymology," ed by S. P. Colowick and N. O. Kaplan, Academic Press, New York (1955), Vol. II, p. 764.

Ortho Lithiation of 2-Hydroxymethyl-1,4,5,6,8-pentamethoxynaphthalene, a Supplement[1)]

Yasuhiro TANOUE* and Akira TERADA*,†
Department of Food Science and Technology, Shimonoseki University of Fisheries, Nagatahonmachi, Shimonoseki, Yamaguchi 759-65
† Department of Chemistry, Kyushu Institute of Technology, Tobata, Kitakyushu, Fukuoka 804
(Received August 9, 1990)

Synopsis. The structures of the products in our previous report "One-Pot Ortho Hydroxylations of 2-(1-Hydroxyalkyl)-naphthalenes and (1-Hydroxyalkyl)benzenes"[2)] were reexamined by ^{13}C NMR spectra and part of our previous interpretation will be corrected here. The lithiations of 2-(1-hydroxyalkyl)-1,4,5,6,8-pentamethoxynaphthalenes occurred at the 7-position, and not at the 3-position as we reported.

During our synthetic study of fusarubin (**1**)[3)] (see Scheme 1), we found an error in our previous report titled "One-Pot Ortho Hydroxylations of 2-(1-Hydroxyalkyl)-naphthalenes and (1-Hydroxyalkyl)benzenes" published in this Journal.[2)] We therefore used ^{13}C NMR spectroscopy to reexamin the hydroxylation products in further detail.

In this paper, we wish to correct part of our previous explanation.

Results and Discussion

We have already reported that the lithiation of 2-hydroxymethyl-1,4,5,6,8-pentamethoxynaphthalene (**3b**) with butyllithium and subsequent oxidation by oxygen gave 3-hydroxymethyl-1,4,5,7,8-pentamethoxy-2-naphthol (**2b**).[2)] However, a question during our synthetic study of fusarubin led us to reexamine the structure of the product. The ^{13}C NMR spectrum of **3b** showed the C-2,3, and 7-signals at δ=128.30, 108.20, and 98.91, respectively. If the structure of our product was **2b**, the 6-position carbon would be slightly affected by the hydroxyl group and the C-6 signal would have been found near δ=96 (i.e., shifted upfield by 2—3 ppm relative to that (δ=98.91) of **3b**). However, the aromatic carbon signal bearing no substituent in our product was found at δ=104.38, not near δ=96. If we presume the formation of 7-hydroxymethyl-1,3,4,5,8-pentamethoxy-2-naphthol (**2B**) instead of **2b**, these ^{13}C NMR results could be reasonably interpreted. That is to say, the C-6 signal (δ=104.38) in **2B** was shifted upfield by 3.8 ppm relative to that (δ=108.20) of **3b** by the introduction of a hydroxyl group (see Chart 1).

This explanation was also supported by the following reaction result. The lithiation of **3b** with butyllithium and subsequent treatment with propylene oxide gave 2-hydroxymethyl-7-(2-hydroxypropyl)-1,4,5,6,8-pentamethoxynaphthalene (**10**) in 62% yield, and no 2-hydroxymethyl-3-(2-hydroxypropyl)-1,4,5,6,8-pentamethoxynaphthalene (**9**) (Scheme 1). The ^{13}C NMR spectrum of **10** is shown in Chart 1.

In the cases of **3d** and **3f**, the hydroxyl group was also introduced at the 7-position between two methoxyl groups. We have concluded, therefore, that the lithiation of **3b**, **3d**, and **3f** with butyllithium occurred at the 7-position.

A similar hydroxylation of 3-methoxybenzylalcohol (**6c**) gave a mixture of 2-hydroxy-3-methoxybenzylalcohol (**7c**) and 4-hydroxy-3-methoxybenzylalcohol (**8C**). The product mixture could be separated by silica gel column chromatography. The ^{13}C NMR spectra of these products are shown in Chart 1. The IR and ^{1}H NMR spectra of **7c** and **8C** agreed with those of the authentic samples obtained by reduction of *o*-vanillin and vanillin, respectively.

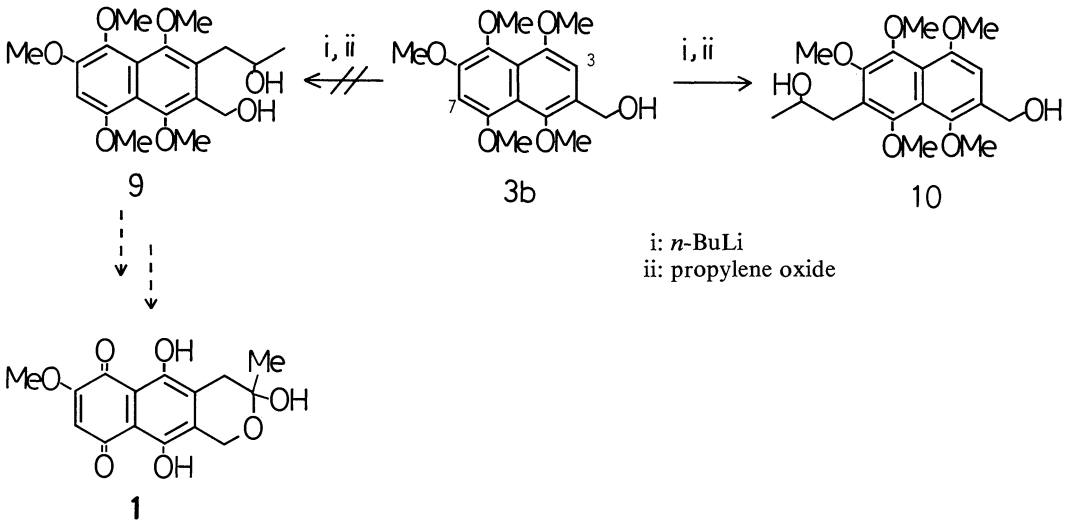

Scheme 1.

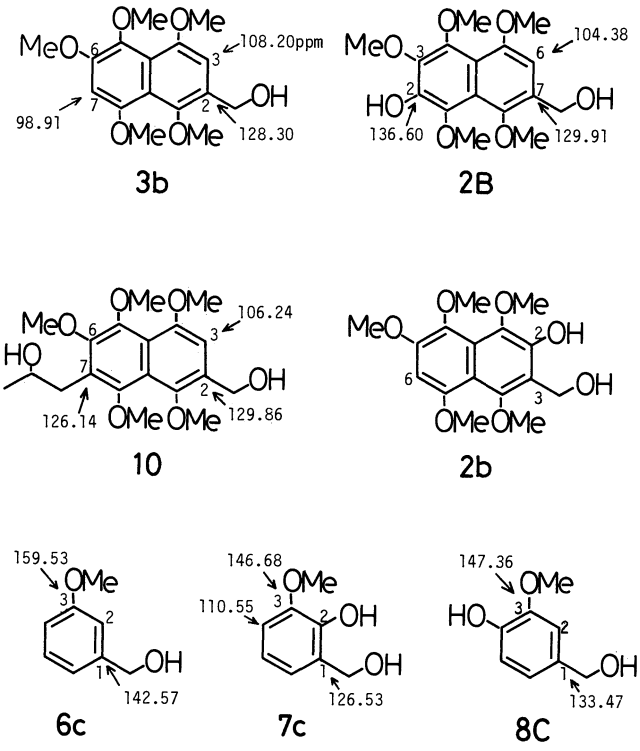

Chart 1.

Table 1. Hydroxylation of 2-(1-Hydroxyalkyl)-1,4,5,6,8-pentamethoxynaphthalene and (1-Hydroxyalkyl)-3-methoxybenzene

Substrate	Product and Yield/%
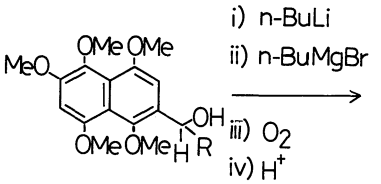	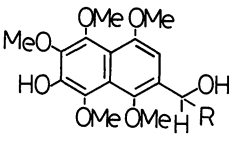
3b: R=H	**2B**, 59[98][a]
3d: R=C_4H_9	**2D**, 73
3f: R=$CH_2CH{=}CH_2$	**2F**, 78
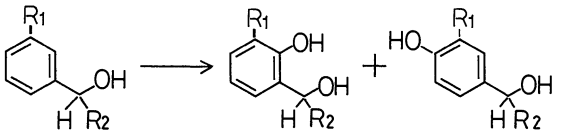	
6c: R_1=OMe, R_2=H	**7c**, 12[23] **8C**, 21[40]
6d: R_1=OMe, R_2=C_4H_9	**7d**, 23[37] **8D**, 35[56]
6e: R_1=R_2=H	**7e**, 26[66]
6f: R_1=H, R_2=C_4H_9	**7f**, 19[93]

a) Conversion yield.

Correcting Tables 1 and 3 in our previous report,[2] we present our new results in Table 1 of this text. The C-4 chemical shift of δ=128.83 in the ^{13}C NMR spectrum of 2-hydroxymethylnaphthalene (**4a**) noted in the previous report should be corrected to δ=128.98.

Experimental

Melting points were determined with a Yanagimoto micro-melting point apparatus and were uncorrected. ^1H and ^{13}C NMR spectra were taken on a JEOL JNM-60 in $CDCl_3$ solutions, using Me_4Si and $CDCl_3$ as internal standards, respectively. Mass spectra and IR spectra were obtained with a JEOL DX-300 spectrometer and a Hitachi 260-30 spectrometer, respectively. Column chromatography was carried out on silica gel (Wakogel C-200) eluting with chloroform. The procedure for the hydroxylation of **3b**, **3d**, **3f**, and **6c**—**6f** is described in Ref. 2. The spectra (IR, ^1H NMR, MS, and HRMS) of **2B**, **2D**, and **2F** were the same as those of **2b**, **2d**, and **2f** in the previous report.[2]

2B: Viscous oil; ^{13}C NMR δ=56.47 (CH_2OH), 61.02, 61.46, 62.09, 62.34, and 62.73 (OCH_3), 104.38 (C-6), 116.56 (C-4a), 121.30 (C-8a), 129.91 (C-7), 136.60 (C-2), 141.05, 142.42, 145.45, 145.65, and 152.84 (C–OCH_3).

2D: Viscous oil; ^{13}C NMR δ=14.08 (CH_3), 22.69, 28.41, and 38.23 (CH_2), 56.47, 61.41, 62.09, 62.34, and 62.97(OCH_3), 68.69 (CH), 102.23 (C-6), 116.37 (C-4a), 121.01 (C-8a), 133.52 (C-7), 136.70 (C-2), 140.95, 142.42, 144.47, 145.70, and 152.98 (C–OCH_3).

2F: Viscous oil; ^{13}C NMR δ=43.07 (CH_2), 56.42, 61.36, 62.05, 62.29, and 62.92 (OCH_3), 67.71 (CH), 104.14 (C-6), 116.37 (C-4a), 117.93 (=CH_2), 120.96 (C-8a), 132.54 (C-7), 134.94 (–CH=), 136.65 (C-2), 140.95, 142.38, 144.43, 145.65, and 152.88 (C–OCH_3).

7c: Viscous oil; IR (neat) 3350 (OH), 1615, 1590, 1480, 1270, 1230, 1080, 1035, and 1000 cm^{-1}; ^1H NMR δ=2.40 (broad, 1H, OH), 3.88 (s, 3H, OCH_3), 4.74 (s, 2H, CH_2), 6.83 (s, 4H, OH, ArH); ^{13}C NMR δ=56.08 (OCH_3), 61.65 (CH_2OH), 110.55 (C-4), 119.64 (C-6), 120.81 (C-5), 126.53 (C-1), 143.84(C-2), and 146.68 (C-3); MS *m/z* 154 (M^+), 136, 107, and 65; HRMS, Found: *m/z* 154.0612. Calcd for $C_8H_{10}O_3$: M, 154.0630.

8C: Mp 115—116 °C (hexane)(lit,[4] 115 °C); IR (KBr) 3340 (OH), 3150 (OH), 1610, 1270, 1240, 1038, 998 cm^{-1}; ^1H NMR δ=1.82 (broad, 1H, OH), 3.90 (s, 3H, OCH_3), 4.60 (s, 2H, CH_2), 5.50 (broad, 1H, OH), 6.86(s, 2H, ArH), and 6.91 (s, 1H, ArH); ^{13}C NMR δ=55.59 (OCH_3), 63.07 (CH_2OH), 111.13 (C-2), 115.09 (C-5), 119.15 (C-6), 133.47 (C-1), 145.31 (C-4), and 147.36 (C-3); MS, *m/z* 154 (M^+), 137, 93, and 65. Found: C, 62.37; H, 6.66%. Calcd for $C_8H_{10}O_3$: C, 62.33; H, 6.54%.

7d: Viscous oil; IR (neat) 3400 (OH), 1615, 1595, 1493, 1278, 1080, 1045, and 1010 cm^{-1}; ^1H NMR δ=0.89 (t, *J*=5.0 Hz, 3H, CH_3), 1.1—1.9 (m, 6H, CH_2), 2.20 (broad, 1H, OH), 3.88 (s, 3H, OCH_3), 4.88 (t, *J*=6.7 Hz, 1H, CH), 6.37 (broad, 1H, OH), and 6.81(s, 3H, ArH); ^{13}C NMR δ=14.03 (CH_3), 22.59, 28.06, and 36.96 (CH_2), 55.98 (OCH_3), 72.02 (CH), 109.86 (C-4), 119.15 (C-6), 119.49 (C-5), 129.86 (C-1), 143.25 (C-2), and 146.87 (C-3); MS *m/z* 210 (M^+), 192, 163, 137, 131, and 103; HRMS, Found: *m/z* 210.1227. Calcd for $C_{12}H_{18}O_3$: M, 210.1255.

8D: Mp 79—80 °C (hexane–benzene (10:1)); IR (KBr) 3380 (OH), 1613, 1440, 1270, 1245, 1057, and 1038 cm^{-1}; ^1H NMR δ=0.88 (t, *J*=5.4 Hz, 3H, CH_3), 1.1—1.9 (m, 7H, OH, CH_2), 3.89 (s, 3H, OCH_3), 4.58 (t, *J*=6.9 Hz, 1H, CH), 5.65 (s, 1H, OH), 6.83 (s, 2H, ArH), and 6.87 (s, 1H, ArH), ^{13}C NMR δ=13.98 (CH_3), 22.54, 28.02, and 38.63 (CH_2), 55.84 (OCH_3), 74.51 (CH), 108.54 (C-2), 114.16 (C-5), 118.86 (C-6), 136.90 (C-1), 144.86 (C-4), 146.62 (C-3); MS, *m/z* 210 (M^+), 153, 125, 93. Found: C, 68.61; H, 8.80%. Calcd for $C_{12}H_{18}O_3$: C, 68.55; H, 8.63%.

2-Hydroxymethyl-7-(2-hydroxypropyl)-1,4,5,6,8-pentamethoxynaphthalene (10). A solution of 2-hydroxymethyl-1,4,5,6,8-pentamethoxynaphthalene **3b**[5] (1.62 g, 5.26 mmol) in

THF (70 ml) was cooled to −10 °C and allowed to react with *n*-BuLi (16.8 ml, 26.3 mmol, 10% (w/v) in hexane) for 1.5 h. Propylene oxide (2.02 ml, 28.9 mmol) in THF (10 ml) was then added to this solution at −10 °C and stirred for 5 h. The reaction mixture was stored in a refrigerator overnight, then quenched with aqueous ammonium chloride, and extracted with chloroform. The chloroform solution was washed with brine, dried over Na_2SO_4, and concentrated. The residue was chromatographed on silica gel to give **10** (1.06 g, 62% yield) and **3b** (0.59 g, 36% yield) was recovered.

10: Viscous oil: IR (neat) 3370 (broad, OH), 1610, 1595, 1355, 1045 cm^{-1}; ^1H NMR δ=1.29 (d, J=6.2 Hz, 3H, CH_3), 2.35 (broad, 2H, 2×OH), 3.0 (m, 2H, CH_2), 3.75 (s, 6H, 2×OCH_3), 3.84, 3.98 (each s, 3H, OCH_3), 3.90 (m, 1H, CH), 4.00 (s, 3H, OCH_3), 4.85 (s, 2H, CH_2OH), and 6.85 (s, 1H, ArH); ^{13}C NMR δ=23.71 (CH_3), 33.88 (CH_2), 56.42 (CH_2OH), 60.72, 61.12, 61.56, 62.29, and 62.53 (OCH_3), 69.13 (CH), 106.24 (C-3), 121.11, 121.94, 126.14 (C-7), 129.86 (C-2), 145.26, 145.90, 149.66 (2C), and 152.55 (C–OCH_3); MS, m/z 366 (M^+), 319, and 289. HRMS, Found: m/z 366. 1690. Calcd for $C_{19}H_{26}O_7$: M, 366.1689.

References

1) Paper X, on Synthesis of Naphthoquinone Derivatives. Paper IX, Y. Tanoue, A. Terada, and Y. Matsumoto, *Bull. Chem. Soc. Jpn.*, **62**, 2736 (1989).

2) Y. Tanoue, A. Terada, I. Seto, Y. Umezu, and O. Tsuge, *Bull. Chem. Soc. Jpn.*, **61**, 1221 (1988).

3) R. H. Thomson, "Naturally Occurring Quinones," 2nd ed, Academic Press, London (1971), p. 291.

4) W. H. Carothers and R. Adams, *J. Am. Chem. Soc.*, **46**, 1080 (1924).

5) Y. Tanoue, A. Terada, T. Tsuboi, T. Hayashida, and O. Tsuge, *Bull. Chem. Soc. Jpn.*, **60**, 2927 (1987).

Reaction of Tris(*t*-butylthio)cyclopropenylium Perchlorate with Arylmagnesium Bromides

Hideo KOJIMA, Kazuyoshi OZAKI, Noboru MATSUMURA, and Hiroo INOUE*
Department of Applied Chemistry, College of Engineering,
University of Osaka Prefecture, Sakai, Osaka 591
(Received January 14, 1991)

Synopsis. The reaction of tris(*t*-butylthio)cyclopropenylium perchlorate with phenyl-, *o*-tolyl-, or 1-naphthylmagnesium bromide in tetrahydrofuran at room temperature gave *t*-butylthio-substituted allenes and indenes. The reaction with 2,6-xylylmagnesium bromide gave only the corresponding allene derivative.

The cyclopropenyl cations are interesting from the viewpoint of their applications to synthetic reactions. Recently, we reported that tris(isopropylthio)cyclopropenyl cation reacts with pyrrole and indoles in the presence of sodium hydride in dimethyl sulfoxide to give pyrrolizine and fluorazene derivatives, respectively, in good yields.[1] On the other hand, recent studies have shown that the 1-(methylthio)- and 1-(diphenylamino)-2,3-diphenylcyclopropenyl cations react with phenylmagnesium bromide in tetrahydrofuran (THF) at room temperature to give 1-(methylthio)- and 1-(diphenylamino)-2,3,3-triphenylcyclopropenes, and the resulting cyclopropenes are converted into the 1-(methylthio)- and 1-(diphenylamino)-2,3-diphenylindenes, respectively, on heating at 50-70 °C.[2,3] In the course of our studies on the reactivity of the tris(alkylthio)cyclopropenyl cations, we examined the reactions of tris(*t*-butylthio)cyclopropenylium perchlorate (**1**) with phenyl-, *o*-tolyl-, 1-naphthyl-, and 2,6-xylylmagnesium bromides (**2a—d**). The reaction was carried out under argon in dry THF at room temperature for 4 h. In the cases of **2a—c**, *t*-butylthio-substitutd allenes (**3a—c**) and indenes (**4a—c**) were obtained (reaction 1 and Table 1). The reaction with **2d** gave only the allene **3d**. Thus, we found that the cyclopropenyl cation **1** reacts with arylmagnesium bromides to bring about the formation of *t*-butylthio-substituted allenes. The reactions proceeded more readily than those using 1-(methylthio)- and 1-(diphenylamino)-2,3-diphenylcyclopropenyl cations,[2,3] indicating that the cyclopropene ring with three *t*-butylthio groups undergoes ring opening much more readily than the ring with two phenyl groups. It has been reported that the conversion of 1-(methylthio)-2,3,3-triphenylcyclopropene into the corresponding indene derivative proceeds through the formation of a vinylcarbene intermediate, followed by the C-H insertion of the carbene into the benzene ring.[2] From these results, it is reasonable to believe that the reaction proceeds through the formation of a vinylcarbene intermediate (**5a—d**) to give allenes (**3a—d**) by rearrangement of the *t*-butylthio group and indenes (**4a—c**) by intramolecular cyclization, as shown in Scheme 1.

Table 1. Reaction of **1** with Arylmagnesium Bromides[a]

ArMgBr[b]	Yield[c]/%	
	Allenes	Indenes
2a	**3a** (29)	**4a** (47)
2b	**3b** (20)	**4b** (65)
2c	**3c** (14)	**4c** (67)
2d	**3d** (77)	—[d]

a) THF, r.t., and 4 h. b) The ArMgBr/**1** molar ratio= 3:1. c) Isolated yields based on **1**. d) Not detected.

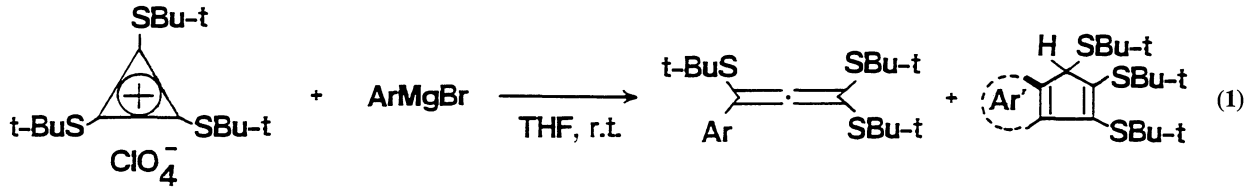

1 2a-d 3a-d 4a-c

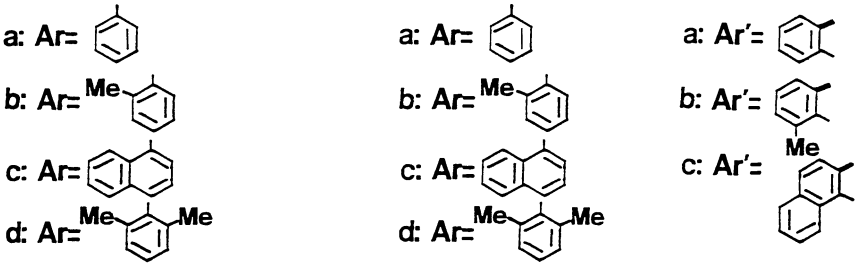

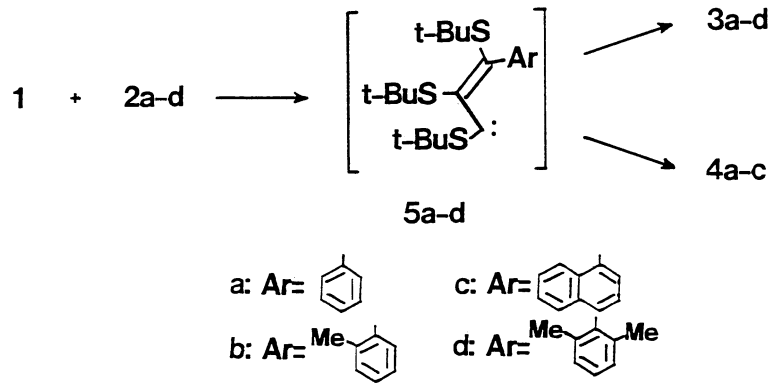

Scheme 1.

Experimental

IR spectra were measured on a Hitachi 215 spectrophotometer. All ^{1}H NMR spectra (270 MHz) and ^{13}C NMR spectra (68 MHz) were determined on a JEOL JNM-GX 270 FT NMR spectrometer in $CDCl_3$ using TMS as an internal standard. Mass spectra were recorded on a Shimadzu LKB-9000 spectrometer operating at an ionization potential of 70 eV. Elemental analysis data (C and H) agreed within ±0.3% with the calculated values.

General Procedure for the Reaction of Tris(*t*-butylthio)cyclopropenylium Perchlorate (1) with Arylmagnesium Bromides. To a solution of arylmagnesium bromides (**2a**—**d**) (1.5 mmol) in dry THF (5 ml) was added the compound **1** (0.5 mmol) in one portion. The mixture was stirred under argon at room temperature for 4 h. A saturated aqueous ammonium chloride solution was then added, and the mixture was extracted with dichloromethane (100 ml). The organic layer was washed with water (100 ml) and dried over anhydrous sodium sulfate. The solvent was removed under reduced pressure, and the residual oil was chromatographed over silica gel using hexane-dichloromethane (5:1) as the eluent to give the products (**3a**—**d** and **4a**—**c**). The structures of all products described above were determined by ^{1}H and ^{13}C NMR, IR, mass spectra, and elemental analyses.

3a: Colorless oil; IR (neat) 2970, 2930, 2870, 1900, 1495, 1450, 1395, 1370, 1160, 825, 770, and 700 cm^{-1}; ^{1}H NMR ($CDCl_3$) δ=1.40 (s, 18H), 1.41 (s, 9H), 7.24—7.38 (m, 3H), and 7.67—7.70 (m, 2H); ^{13}C NMR ($CDCl_3$) δ=31.4, 31.8, 48.6, 48.7, 94.9, 100.1, 122.7, 127.7, 128.0, 128.3, 136.7, and 213.8; MS *m*/*z* 380 (M^+).

3b: Colorless oil; IR (neat) 3075, 2970, 2930, 2870, 2350, 1920, 1460, 1370, 1165, 835, 760, and 725 cm^{-1}; ^{1}H NMR ($CDCl_3$) δ=1.30 (s, 9H), 1.38 (s, 18H), 2.47 (s, 3H), 7.15—7.17 (m, 3H), and 7.47—7.49 (m, 1H); ^{13}C NMR ($CDCl_3$) δ=20.8, 31.1, 31.6, 48.1, 48.4, 93.8, 99.4, 125.5, 127.8, 129.4, 130.7, 135.8, 136.3, and 211.1; MS *m*/*z* 394 (M^+).

3c: Colorless oil; IR (neat) 3050, 2960, 2925, 1920, 1475, 1460, 1395, 1370, 1165, 840, 805, and 780 cm^{-1}; ^{1}H NMR ($CDCl_3$) δ=1.32 (s, 9H), 1.36 (s, 18H), 7.42—7.56 (m, 3H), 7.72—7.85 (m, 3H), and 8.49 (d, 1H); ^{13}C NMR ($CDCl_3$) δ=31.2, 31.7, 48.5 (2C), 94.6, 98.4, 125.1, 126.0, 126.2 (2C), 127.2, 128.3, 128.5, 134.0, 134.5, 137.6, and 211.8; MS *m*/*z* 430 (M^+).

3d: Colorless oil; IR (neat) 3060, 2930, 2720, 1910, 1460, 1395, 1365, 1220, 1160, 875, 830, and 765 cm^{-1}; ^{1}H NMR ($CDCl_3$) δ=1.38 (s, 18H), 1.44 (s, 9H), 2.48 (s, 6H), and 6.98—7.10 (m, 3H); ^{13}C NMR ($CDCl_3$) δ=20.8, 31.1, 31.4, 47.4, 48.2, 97.5, 100.0, 127.8, 127.9, 134.2, 136.8, and 207.0; MS *m*/*z* 408 (M^+).

4a: Colorless oil; IR (neat) 3070, 2950, 2900, 2860, 1475, 1455, 1395, 1365, 1250, 1220, 1160, 1020, 975, 760, and 720 cm^{-1}; ^{1}H NMR ($CDCl_3$) δ=1.34 (s, 9H), 1.38 (s, 18H), 1.47 (s, 9H), 4.53 (s, 1H), 7.26—7.34 (m, 2H), and 7.55—7.64 (m, 2H); ^{13}C NMR ($CDCl_3$) δ=32.2 (2C), 32.4, 44.9, 50.1 (2C), 56.5, 122.7, 124.1, 126.5, 127.2, 144.6, 144.7, 147.3, and 152.9; MS *m*/*z* 380 (M^+).

4b: Yellow crystals, mp 117.5—118.0 °C (decomp); IR (KBr) 3050, 2950, 2900, 1595, 1500, 1470, 1455, 1395, 1365, 1265, 1220, 1170, 1150, 1075, 1035, and 790 cm^{-1}; ^{1}H NMR ($CDCl_3$) δ=1.20 (s, 9H), 1.38 (s, 9H), 1.40 (s, 9H), 2.62 (s, 3H), 4.58 (s, 1H), 7.03 (d, 1H), 7.26 (t. 1H), and 7.51 (d, 1H); ^{13}C NMR ($CDCl_3$) δ=19.2, 32.2, 32.3, 32.4, 46.2, 49.2, 50.1, 56.8, 120.3, 127.6, 128.3, 134.0, 142.3, 142.9, 144.9, and 154.8; MS *m*/*z* 394 (M^+).

4c: Yellow crystals, mp 146.0—146.5 °C; IR (KBr) 3050, 2960, 2920, 1475, 1460, 1400, 1375, 1165, 1095, 830, and 760 cm^{-1}; ^{1}H NMR ($CDCl_3$) δ=1.10 (s, 9H), 1.41 (s, 9H), 1.44 (s, 9H), 4.89 (s, 1H), 7.42—7.59 (m, 2H), 7.86—7.89 (m, 3H), and 8.72 (d, 1H); ^{13}C NMR ($CDCl_3$) δ=32.3, 32.4 (2C), 47.0, 49.4, 50.4, 56.7, 121.2, 124.6, 125.3, 126.0, 128.5, 128.8, 129.6, 132.6, 140.2, 142.7, 143.0, and 155.9; MS *m*/*z* 430 (M^+).

References

1) H. Kojima, K. Ozaki, N. Matsumura, and H. Inoue, *Chem. Lett.*, **1989**, 1499.

2) H. Yoshida, H. Sano, M. Kato, T. Ogata, and K. Matsumoto, *Bull. Chem. Soc. Jpn.*, **59**, 2833 (1986).

3) H. Yoshida, H. Sano, T. Ogata, and K. Matsumoto, *Bull. Chem. Soc. Jpn.*, **61**, 4341 (1988).

Vinyl Polymers Bearing a Pyrrole Ring. II. 5,10,15,20-Tetraphenylporphyrins with a Substituent-Bearing Vinyl Group at the Pyrrole Residue and Their Zinc Complexes

Hiroyoshi KAMOGAWA,* Takuharu NAKATA, and Sei KOMATSU
Department of Applied Chemistry, Yamanashi University, Takeda 4, Kofu 400
(Received February 2, 1991)

Synopsis. 5, 10, 15, 20-Tetraphenylporphyrins (**Por**) with a styrenic double bond-bearing substituent attached at the pyrrole residue with an amide or ester spacer were synthesized starting with 3-substituted pyrroles. Free radical copolymerization of **ZnPor**, prepared from **Por**, with 1-vinyl-2-pyrrolidone gave more favorable results than did **Por**.

Numerous studies on the preparation of polymers bearing porphyrin or metalloporphyrin units have been reported.[1-5] The present note discusses the preparation of novel water-soluble vinyl polymers with pendant porphyrin and zinc porphyrin units. 5, 10, 15, 20-tetraphenylporphyrins with a substituent-bearing vinyl group (**Por**) attached at the pyrrole residue and their zinc complexes (**ZnPor**) were synthesized. Subsequent copolymerizations of these vinyl monomers with 1-vinyl-2-pyrrolidone (VP) produced copolymers soluble in aqueous solvents. For the **Por** monomer synthesis, 3-substituted pyrroles, synthesized as in a previous study,[6] were employed as starting materials, as shown in **Methods A** and **B**.

Method A

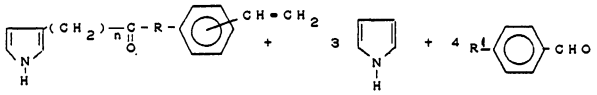

n=0, 1, 3; R=O-CH_2, NH; R′=CH_3, H
1a—1f

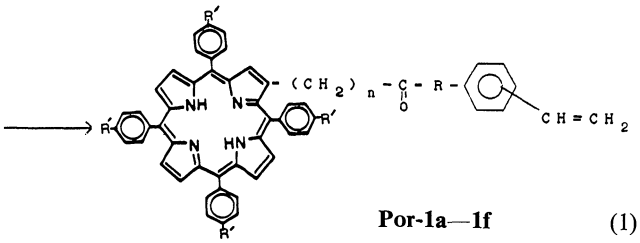

Por-1a—1f (1)

		n	R	R′	p- or m-
1a:	**Por-1a**:	0	-NH-	-H	p-
1a′:	**Por-1a′**:	0	-NH-	-H	m-
1b:	**Por-1b**:	1	-NH-	-H	p-
1b′:	**Por-1b′**:	1	-NH-	-H	m-
1c:	**Por-1c**:	3	-NH-	-H	p-
1c′:	**Por-1c′**:	3	-NH-	-H	m-
1d:	**Por-1d**:	0	-OCH_2-	-CH_3	p-
1e:	**Por-1e**:	1	-OCH_2-	-CH_3	p-
1f:	**Por-1f**:	3	-OCH_2-	-CH_3	p-

Method B

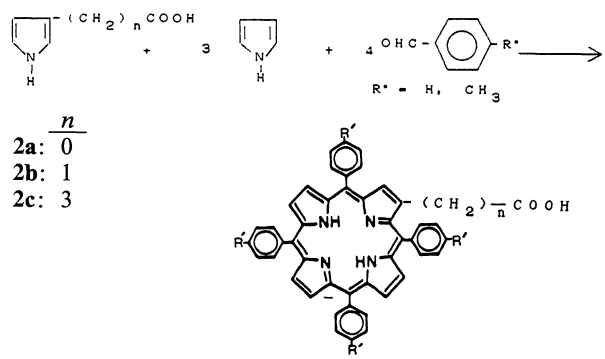

	n
2a:	0
2b:	1
2c:	3

	n	R′
Por-2a:	0	-H
Por-2b:	1	
Por-2c:	3	
Por-2d:	0	-CH_3
Por-2e:	1	
Por-2f:	3	

(2)

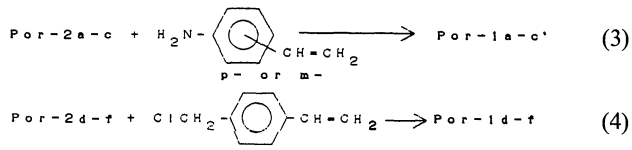

(3)

(4)

Results and Discussion

Method A consisted of the application of a conventional procedure[7] for the preparation of 5, 10, 15, 20-tetraphenylporphyrins from **1a—f**, and easily produced the desired products, **Por-1a—f** (Eq. 1), which were purified by silica-gel column chromatography.

In **Method B**, carboxyl group-bearing **Por-2a—f** were first synthesized using **2a—c** (Eq. 2) and then converted to **Por-1a—c**, **Por-1a′—c′**, and **Por-1d—f** with p- and m-anilines and p-vinylbenzyl chloride, respectively, also without any difficulty (Eqs. 3 and 4).

An advantage of **Method B**, compared to **Method A**, was that **Por-2a—f** could be separated easily from the by-product porphyrins bearing no COOH group. Addition of triethylamine (TEA) to the benzene solutions of the crude products neutralized the COOH group and precipitated the resulting salts, thereby facilitaing the purification of the final products **Por-1a—f**. The analytical data for the **Por-1a—f** synthesized according to **Method B** are given in Table 1. The absorption spectra of **Por-1a—f** in chloroform indicated the Soret

Table 1. Analytical Results for **Por-1a—f**[a]

Por	Yield %	Element. analysis[b] C %	H %	N %	IR[c] cm^{-1}	NMR[d] δ
1a	21	83.22 (83.79)	4.83 (4.87)	9.19 (9.22)	1650 (Amide), 990, 900 (Vinyl)	5.5 (q), 6.7 (q) (vinyl); 8.9 (s, por.)
1a′	39	83.34 (83.79)	5.06 (4.87)	9.25 (9.22)	1660 (Amide), 990, 900 (Vinyl)	5.6 (q), 6.5 (q) (vinyl); 8.9 (s, por.)
1b	11	83.51 (83.83)	5.12 (5.05)	9.16 (9.06)	1650 (Amide), 990, 910 (Vinyl)	3.4 (s, CH_2); 5.5 (q), 6.7 (q) (vinyl); 9.0 (s, por.)
1b′	32	83.81 (83.83)	4.96 (5.05)	9.35 (9.06)	1660 (Amide), 990, 910 (Vinyl)	3.4 (s, CH_2); 5.4 (q), 6.7 (q) (vinyl); 8.9 (s, por.)
1c	33	83.65 (83.90)	5.44 (5.37)	8.92 (8.74)	1640 (Amide), 990, 900 (Vinyl)	1.0—3.5 (m, CH_{22}); 5.4 (q), 6.7 (q) (vinyl); 8.9 (s, por.)
1c′	28	83.68 (83.90)	5.49 (5.37)	8.35 (8.74)	1650 (Amide), 990, 900 (Vinyl)	1.0—3.5 (m, CH_2); 5.5 (q), 6.8 (q) (vinyl); 8.8 (s, por.)
1d	47	83.40 (83.61)	4.92 (5.03)	7.00 (7.23)	1740 (Ester), 990, 910 (Vinyl)	5.3 (s, CH_2); 5.5 (q), 6.8 (q) (vinyl); 8.9 (s, por.)
1e	44	83.24 (83.65)	5.48 (5.20)	7.08 (7.10)	1740 (Ester), 980, 900 (Vinyl)	3.5 (s, CH_2); 5.3 (s, CH_2); 5.5 (q), 6.6 (q) (vinyl); 8.9 (s, por.)
1f	51	83.51 (83.72)	5.43 (5.51)	7.03 (6.85)	1740 (Ester), 990, 910 (Vinyl)	1.0—3.5 (m, CH_2); 5.1 (s, CH_2); 5.5 (q), 6.7 (q) (vinyl); 8.9 (s, por.)

a) Prepared according to Method B. b) Figures in parentheses indicate calcd values. c) KBr. d) $CDCl_3$; por.=porphyrin ring.

Table 2. Copolymerization Behavior of **Por** and **ZnPor** with VP[a]

Por or ZnPor	Conversion %	Polymer Soret band nm	Content of **Por** or[b] **ZnPor**/%	$[\eta]$[c]
Por-1a	26	424.0	3.1	0.12
Por-1a′	31	420.5	0.4	0.09
Por-1b	25	423.0	3.0	0.12
Por-1b′	33	418.5	0.8	0.09
Por-1c	20	418.0	3.5	0.09
Por-1c′	29	419.0	0.6	0.09
ZnPor-1c	84	420.0	13.4	0.23
ZnPor-1c′	67	420.0	15.8	0.27

a) **Por** or **ZnPor**, 0.1 mmol; VP, 5.0 mmol; AIBN, 2%/total monomers; 20% total monomers concentration in DMF; at 80°C for 4 h under N_2. b) Determined spectrophotometrically employing the Soret band. c) Intrinsic viscosity (dLg^{-1}) in DMF at 25°C.

band at 418.5—421 nm and had several longer λ_{max} with decreasing, ε_{max}, which was characteristic of a porphyrin structure. The introduction of a Zn atom caused the reversal of the order of λ_{max} around 515 and 550 nm together with slight red λ_{max}-shifts [e. g. λ_{max} (ε_{max}): 515.0 (2.50×10^4 mol^{-1} dm^3 cm^{-1})) and 549.5 (1.09) for **Por-1c**; 517.5 (1.71) and 552.5 (2.13) for **ZnPor-1c**].

The results obtained by subjecting **Por-1a—c′** and **ZnPor-1c,c′** to conventional free-radical copolymerization with VP are summarized in Table 2. As Table 2 shows, copolymerization of **Por-1a—c′** without Zn gave poor results; both the conversions and the values of the intrinsic viscosity of the polymer were low and **Por**-contents in the polymer were also much lower than those (>10%) in the initial monomer mixture.

IR-spectra indicated, however, that the vinyl absorptions around 990—980 and 910—900 cm^{-1} (Table 1) no longer existed and a strong C=O absorption around 1650 cm^{-1} (attributable to the VP portion) appeared, indicating that water-soluble polymers of low molecular weights were obtained by this procedure.

ZnPor-1c and **-1c′** gave, on the other hand, larger values of conversion, **ZnPor**-content, and intrinsic viscosity, indicating a satisfactory process of copolymerization. Particularly, the values of the **ZnPor**-content in the copolymer were close to that (13.5%) in the initial monomer mixture. Visible absorption spectra for polymers made from **Por-1a—c′** were somewhat deformed, whereas those for polymers made from **ZnPor-1c** and **-1c′** indicated no signs of deformity. From these observations, especially as regards **Por-1a—c′**, we suppose that the porphyin ring may participate in free-radical polymerization. The applications of these polymers, e. g. as redox catalysts, will be the subject of another study.

Experimental

N-[*p*- and *m*-Vinylphenyl)-1*H*-pyrrole-3-carboxamides (**1a,a'**), -3-acetamides (**1b,b'**), and -3-butyramides (**1c,c'**), and *p*-vinylbenzyl 1*H*-pyrrole-3-carboxylate (**1d**), -3-acetate (**1e**), and -3-butyrate (**1f**) were synthesized via the respective carboxylic acids (**2a**—**c**) according to the methods described in a previous study.[6]

5,10,15,20-Tetraphenylporphyrins (Por-1a—f). Method A: Pyrroles bearing the vinylphenyl group [**1a**—**f** (2 mmol)], pyrrole (0.40 g, 6 mmol), and benzaldehyde or *p*-tolualdehyde (8 mmol) were dissolved in propionic acid (5 mL). The resulting solution was added to refluxing propionic acid (50 mL), followed by further refluxing for 30 min, with hydroquinone (0.1 g) added. Upon standing at room temperature overnight, the resulting crystals were washed thoroughly with hot water and subjected to silica-gel column chromatography.

Method B: Pyrroles bearing a carboxyl group [**2a**—**c** (5 mmol)], pyrrole (1.0 g, 15 mmol), and benzaldehyde or *p*-tolualdehyde (20 mmol) were refluxed in propionic acid (50 mL) for 30 min, as in **Method A**. Upon cooling, the resulting crystals were dissolved in benzene (50 mL). TEA (10 mL) was added to the benzene solution to precipitate out the TEA-salts of **Por-2a**—**f**, which were washed thoroughly with benzene. Methyl chloroformate (0.2 g, 2 mmol) was added with vigorous shaking to a solution of the salt (2 mmol) in tetrahydrofuran (THF; 15 mL) at −15—15 °C. After stirring for 20 min, the mixture was cooled to below 0 °C and a solution of *p*- or *m*-vinylaniline (0.24 g, 2 mmol) and TEA (0.3 mL) in $CHCl_3$ (15 mL) was added dropwise. Stirring was continued for one hour at this temperature and then overnight at 20 °C. The reaction mixture was extracted with H_2O (200 mL) and $CHCl_3$ (500 mL). The organic layer was washed successively with aq $NaHCO_3$ and H_2O and worked up. Silica-gel column chromatography ($CHCl_3$–acetone; 5:1 v/v) gave purified products (**Por-1a**—**c'**). To prepare **Por-1d**—f, *p*-vinylbenzyl chloride (0.6 g, 4 mmol) was added to solutions of the TEA-salts of **Por-2d**—**f** (2 mmol) and TEA (0.3 g, 3 mmol) in DMF (10 mL) and the mixtures were stirred at 20 °C for 24 h and kept moisture-free. The reaction mixtures were poured into water and extracted with ether (150 mL). The organic layers were worked up and silica-gel column chromatography gave purified products. The analytical data for **Por-1a**—f prepared by **Method A** were almost identical to the data for **Por-1a**—**f** prepared by **Method B**.

Introduction of a Zn-Atom into Por-1a—**f.** The application of the conventional procedure[8] provided crude products, which were purified by SiO_2 column chromatography.

Copolymerization of Por or ZnPor with 1-Vinyl-2-pyrrolidone (VP). In a typical example, a solution of **Por** or **ZnPor** (0.1 mmol), VP (0.5 g, 5.0 mmol), and α,α-azobisisobutyronitrile (AIBN; 1 mg) in DMF (2.5 mL) was put into a glass ampule, which was sealed under N_2 in a conventional manner and kept at 80 °C for 4 h. The contents of the ampule were then poured into ether to precipitate the polymerization product. All polymers produced by this method were soluble in aqueous solvents. IR (KBr) 1650, [1700 (for polymers of **Por**- and **ZnPor-1d**—**f**)] $cm.^{-1}$

References

1) W. Lautsch, W. Broser, W. Biedermann, and S. Gnichtel, *J. Polym. Sci.*, **17**, 479 (1955).

2) H. Kamogawa, *Polym. Lett.*, **10**, 711 (1972); H. Kamogawa, *J. Polym. Sci.*, **12**, 2317 (1974); H. Kamogawa, H. Inoue, and M. Nanasawa, *ibid.*, **18**, 2209 (1980); H. Kamogawa, S. Miyama, and S. Minoura, *Macromolecules*, **22**, 2123 (1989).

3) K. Kamachi, H. Akimoto, and S. Nozakura, *Polym. Lett.*, **21**, 693 (1983); M. Kamachi, X. S. Cheng, T. Kida, A. Kajiwara, M. Shibasaka, and S. Nagata, *Macromolecules*, **20**, 2665 (1987); H. Aota, H. Fujii, A. Harada, and M. Kamachi, *Chem. Lett.*, **1990**, 823.

4) D. Woehrle, G. Krawezyk, and M. Patiuras, *Makromol. Chem.*, **189**, 1001 (1988).

5) E. Tsuchida, H. Nishide, M. Yuasa, T. Baba, and M. Fukuzumi, *Macromolecules*, **22**, 66 (1989).

6) H. Kamogawa, T. Nakata, S. Ohori, and S. Komatsu, *Bull. Chem. Soc. Jpn.*, **64**, 1066 (1991).

7) A. D. Adler, F. R. Rongo, J. D. Finarelli, J. Goldmacher, J. Assour, and L. Korsakoff, *J. Org. Chem.*, **32**, 476 (1967).

8) J. E. Falk, "Porphyrins & Metalloporphyrins," Elsevier, Amsterdam (1964).

X-Ray Crystallographic Analysis of Methyl (1*S*,2*R*,5*R*,6*S*,7*R*)-5,6-Dimethyl-2-(ω-camphanoyloxy)bicyclo[4.3.0]nonane-7-carboxylate. Revision of the Absolute Configurations of the Liverwort Sesquiterpenoids (−)-Chiloscyphone and (+)-Chiloscypholone

Motoo Tori, Takeshi Hasebe, Yoshinori Asakawa,* Keiichiro Ogawa,*,† and Shin Yoshimura†

Faculty of Pharmaceutical Sciences, Tokushima Bunri University, Yamashiro-cho, Tokushima 770

† Department of Chemistry, The College of Arts and Science, The University of Tokyo, Komaba, Meguro-ku, Tokyo 153

(Received February 15, 1991)

Synopsis. The X-ray analysis of the title compound has been carried out to give unambiguous assignment of the absolute configurations of the liverwort sesquiterpenoids (−)-chiloscyphone and (+)-chiloscypholone, each for which the enantiomerically opposite configurations had been assigned in the previous report.

Determination of the absolute structure of the terpenoids isolated from the liverworts is a matter of interest, since it is closely related to their biological activities. In the previous work,[1] the absolute structures of **1** and **6** were elucidated on the basis of the analysis of the CD spectra of the synthetic intermediates in the total synthesis of **1**. In the present work, the absolute configuration of the title compound (**2**), one of the intermediates in the total synthesis of **1**,[1] was determined by X-ray analysis. The results gave the revision of our previous assignment of the absolute configurations of **1** and **6**.

Among the four ω-camphanic esters prepared,[1] **2**, $[\alpha]_D$ −1.4° (*c* 4.9 $CHCl_3$); mp 159—160 °C, was nicely recrystallized from chloroform–methanol, whose X-ray analysis has been carried out. The final atomic coordinates are listed in the Table 1.[2] Perspective view of the molecule is given in Fig. 1. This clearly shows that **2** has 1*S*, 2*R*, 5*R*, 6*S*, 7*R* configurations, since the absolute configurations of the camphanic ester part are known. That is, the absolute configuration of **2** is expressed as in the structure formula. This figure also shows that the conformation of the six-membered ring of the hydrindan system is chair and that the hydrindan system adopts nonsteroidal conformation.

In the total synthesis of **1**, we used the diastereomeric ω-camphanic ester **3** ($[\alpha]_D$ −7.8°), whose absolute configurations were clear, because both **2** and **3** were prepared from the corresponding alcohol (±)-**4** by camphanoylation and HPLC separation. The alcohol

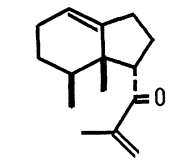

(−)- Chiloscyphone (1)

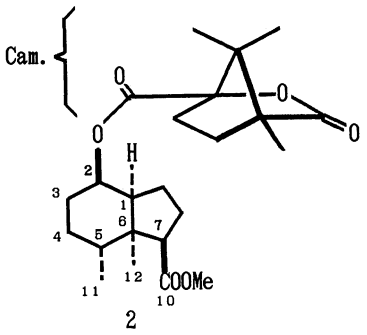

2

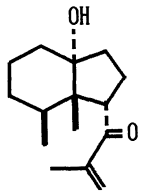

(+)-Chiloscypholone (6)

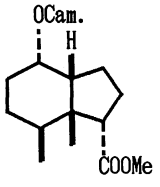

3

Table 1. Non-Hydrogen Positional and Isotropic Displacement Parameters (Å²) for **2**, with esd's in Parentheses

	x/*a*	*y*/*b*	*z*/*c*	U_{eq}
C(1)	0.4083(2)	0.1998(5)	0.2287(2)	0.0406(6)
C(2)	0.4660(2)	0.07300	0.3145(2)	0.0445(7)
C(3)	0.4818(2)	−0.1189(5)	0.2669(3)	0.0520(8)
C(4)	0.3834(2)	−0.2041(5)	0.2231(3)	0.0534(8)
C(5)	0.3238(2)	−0.0854(5)	0.1326(2)	0.0427(7)
C(6)	0.3089(2)	0.1163(5)	0.1767(2)	0.0374(6)
C(7)	0.2855(2)	0.2563(5)	0.0734(2)	0.0449(7)
C(8)	0.3854(2)	0.2993(6)	0.0242(3)	0.0575(8)
C(9)	0.4652(2)	0.2579(5)	0.1221(3)	0.0528(8)
C(10)	0.2091(2)	0.1971(5)	−0.0228(2)	0.0517(7)
C(11)	0.2272(3)	−0.1895(6)	0.0968(3)	0.0648(9)
C(12)	0.2292(2)	0.1249(6)	0.2658(3)	0.0579(8)
C(13)	0.0392(3)	0.1728(9)	−0.0791(5)	0.110(1)
C(14)	0.7169(2)	0.2044(5)	0.4335(2)	0.0402(6)
C(15)	0.7257(2)	0.4109(5)	0.4031(3)	0.0464(7)
C(16)	0.8369(2)	0.4292(5)	0.3854(3)	0.0489(7)
C(17)	0.8778(2)	0.2274(5)	0.4035(2)	0.0424(7)
C(18)	0.8683(2)	0.1964(5)	0.5330(2)	0.0479(7)
C(19)	0.7889(2)	0.1074(5)	0.3524(2)	0.0383(6)
C(20)	0.6152(2)	0.1194(5)	0.4383(2)	0.0473(7)
C(21)	0.9797(2)	0.1933(6)	0.3613(3)	0.0619(8)
C(22)	0.7649(2)	0.1357(5)	0.2208(2)	0.0502(7)
C(23)	0.8018(3)	−0.1000(5)	0.3789(3)	0.0576(8)
O(1)	0.5621(1)	0.1650(4)	0.3397(2)	0.0502(5)
O(2)	0.2269(2)	0.1292(5)	−0.1144(2)	0.0727(7)
O(3)	0.1169(2)	0.2318(5)	0.0067(2)	0.0801(8)
O(4)	0.9299(2)	0.1875(5)	0.6137(2)	0.0684(7)
O(5)	0.5881(2)	0.0227(5)	0.5150(2)	0.0749(7)
O(6)	0.7694(1)	0.1829(4)	0.5495(1)	0.0487(5)

a) $U_{eq}=\frac{1}{3}\sum_i\sum_j U_{ij}a_i^*a_j^*\boldsymbol{a}_i\boldsymbol{a}_j$.

(+)-**4** was derived from **3** by alkaline treatment.[1] The sign of the specific rotation of the corresponding ketone **5** was (−) and the sign of the Cotton effect was (−). The back octant of (−)-**5** shown in Fig. 2 suggests that the expected sign of the Cotton effect should be (−), which was erroneously assigned previously.[1] Since the results of the X-ray analysis of **2** are unambiguous and natural (−)-chiloscyphone (**1**) had been synthesized from the diastereomeric isomer **3**,[1] the absolute configuration of (−)-**1** as well as (+)-chiloscypholone (**6**), which was converted to (−)-**1**,[1] should be formulated as depicted in the scheme.

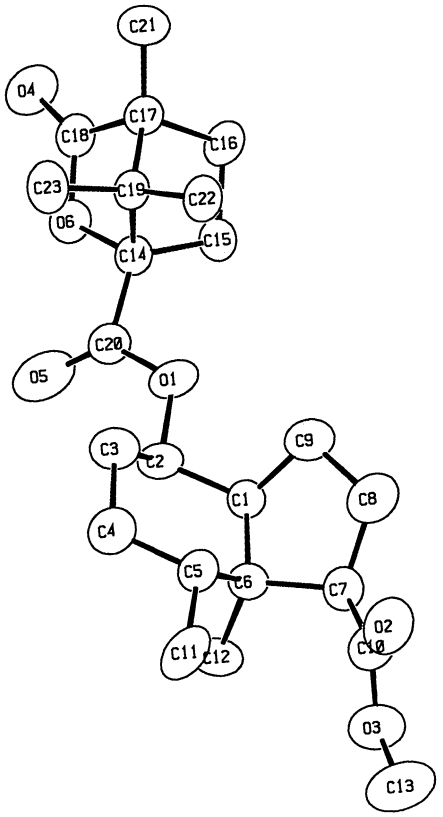

Fig. 1. Computer generated perspective view of **2**.

Experimental

General. See Ref. 1.

Single-Crystal X-Ray Structure Analysis. Crystals of **2** were recrystallized from chloroform–methanol. A truncated rectangular prism of approximately 0.5×0.5×0.5 mm was chosen for X-ray measurements. The crystals are monoclinic, space group $P2_1$ (No. 4), with a=13.516 (1), b=7.1924 (7), c=11.398 (1) Å, β=93.94 (1)°, V=1105.4 (2) Å^3, and d_{calcd}=1.221 g cm^{-3} for Z=2 ($C_{23}H_{34}O_6$, M=406.52). Intensity data were measured at 298 K on a Rigaku AFC-5 diffractometer with graphite monochromated Mo $K\alpha$ radiation (λ=0.71073 Å). The cell dimensions were obtained from the least-squares refinement of 50θ values in the range of $25<2\theta<40°$. The data were collected using the ω–2θ scan technique at an ω rate of 3.0° min^{-1} with a 2θ range from 3.0—60.0°. Data having $-19\leqq h\leqq 19$, $-10\leqq k\leqq 0$, $0\leqq l\leqq 16$ were measured. Three reflections (200, 040, 004) were remeasured every 100 reflections to monitor instrument and crystal stability, and the intensity monotonically decreased 17% during the measurement. All the intensity data were empirically corrected on the basis of the intensity variation of the three standard reflections using UNICS3.[3] Of 2928 reflections with $F_o\geqq 3\sigma(F_o)$, 2491 were unique, with R_{int}=0.0071 from averaging symmetry-equivalent reflections. The data were corrected for Lp effects, but not for absorption.

The structure was solved by direct methods with SHELXS86[4] and refined by full-matrix least squares with SHELX76.[5] The number of the parameters refined was 397. The non-H atoms were refined with anisotropic displacement parameters. All of the H-atoms were initially calculated in idealized positions but were refined under the C–H bond length constraint during the final refinement cycles. The function $\Sigma(|F_o|-|F_c|)^2$ was optimized, where $w=[\sigma^2(F_o)+0.0004(F_o)^2]^{-1}$. In the final least-squares refinement, R=0.045, R_w=0.051, S=1.544, and $(\Delta/\sigma)_{max}$=0.396. The maximum and the minimum height in the final difference Fourier synthesis were 0.15 and −0.26 eÅ^{-3}, respectively. Atomic scattering factors were taken from International Tables for X-Ray Crystallography.[6] Calculations of the geometrical parameters and drawing of the ORTEP diagrams were performed using XTAL3.0 software.[7]

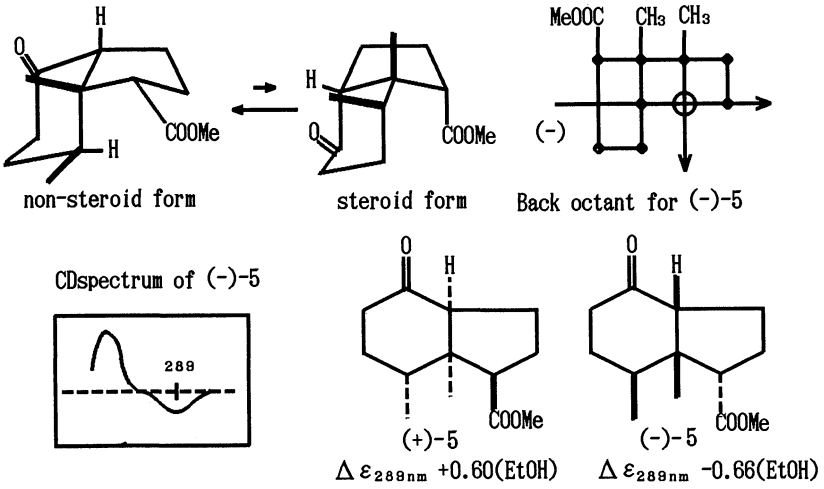

Fig. 2. The CD spectrum and back octant for (−)-(5).

References

1) M. Tori, T. Hasebe, and Y. Asakawa, *J. Chem. Soc., Perkin Trans. 1,* **1989**, 1552; *Bull. Chem. Soc. Jpn.,* **63**, 1706 (1990).

2) The complete F_o-F_c data are deposited as Document No. 8947 at the Office of the Editor of Bull. Chem. Soc. Jpn.

3) T. Sakurai and K. Kobayashi, *Rigaku Kenkyusho Houkoku,* **55**, 69 (1979).

4) G. M. Sheldrick, SHELXS86, Program for crystal structure determination, University of Göttingen, Federal Republic of Germany (1986).

5) G. M. Sheldrick, SHELX76, Program for crystal structure determination. Univ. of Cambridge, England.

6) "International Tables for X-Ray Crystallography," Kynoch Press, Birmingham (1974), Vol. IV.

7) "XTAL3.0," ed by S. Hall and J. Stewart, Universities of Western Australia and Maryland (1990).

Synthesis of Pyrazole Nucleosides Using Acylketene Dithioacetal Derivatives

Masataka YOKOYAMA,* Toshihiro IKUMA, Sadataka SUGASAWA, and Hideo TOGO
Department of Chemistry, Faculty of Science, Chiba University,
Yayoi-cho, Chiba 260
(Received March 1, 1991)

Synopsis. Several nucleosides bearing pyazole ring as the base moiety were synthesized by the reaction of D-ribofuranosylhydrazine or 2-deoxy-D-ribosuranosylhydrazine with easily available acylketene ditioacetal derivatives.

In a part of our study directed toward the synthesis of pharmaceutically important compounds,[1] we found that several kinds of pyrazole nucleosides could be easily synthesized by the reaction of ketene dithioacetals de rived from cyanoacetamide or malononitrile with pro tected D-ribofuranosylhydrazine.[2] In this paper the work was extended to acylketene dithioacetal derivatives as ketene dithioacetals and to protected 2-deoxy-D-ribofuranosylhydrazine as a sugar moiety. The acylketene dithioacetal derivatives could be easily synthesized by the reaction of the corresponding ketones and carbon disulfide followed by methylation. The protected 2-deoxy-D-ribofuranosylhydrazine could be synthesized by the reaction of protected 2-deoxy-D-ribose with hydrazine.

This report presents a simple synthetic method for 5-substituted or 4,5-disubstituted 3-(methylthio)pyrazole nucleosides. The nucleosides obtained by this method are β-anomer or a mixture of α- and β-anomers, which can be separated by usual preparative TLC on silica gel.

Results and Discussion

The reaction of 3,3-bis(methylthio)-1-phenyl-2-propen-1-one (**1a**) with 2,3-*O*-isopropylidene-D-ribofuranosylhydrazine **2a′(H)** gave an expected nucleoside **3a″(H)** as only β-form. However **1a** reacted with 2,3-*O*-isopropylidene-5-*O*-trityl-D-ribofuranosylhydrazine **2a′(T)** to afford the corresponding nucleoside **3a″(T)** in 77% yield (α/β=51/26). The steric hindrance of bulky trityl group seems to have effect on the increase of the α-anomer. In the reaction of 4,4-bis(methylthio)-3-buten-2-one (**1b**) with **2a′(H)**, 1-(2,3-*O*-isopropylidene-β-D-ribofuranosyl)-5-methyl-3-(methylthio)pyrazole **3b″** and its regioisomer **4b″** were isolated in 13% and 22% yields, respectively. The reaction of 2-[bis(methylthio)methylene]-cyclohexanone (**1c**) with **2a′(H)** gave 1-(2,3-*O*-isopropylidene-D-ribofuranosyl)-3-methylthio-4,5,6,7-tetrahydro-1*H*-indazole **3c″** as β-form.

Further, the present reaction was extended to the synthesis of 2-deoxy-D-ribonucleosides. 3,5-Di-*O*-benzyl-2-deoxy-D-ribofuranosylhydrazine (**5**) was prepared by the reaction of 3,5-di-*O*-benzyl-2-deoxy-D-ribofuranose with hydrazine. Its ^{1}H NMR observation shows that **5** comprises an equilibrium mixture of the hydrazone form **5a** and the hydrazino form **5b**, in which the former predominates (ca. 90%). This result is the same as in the

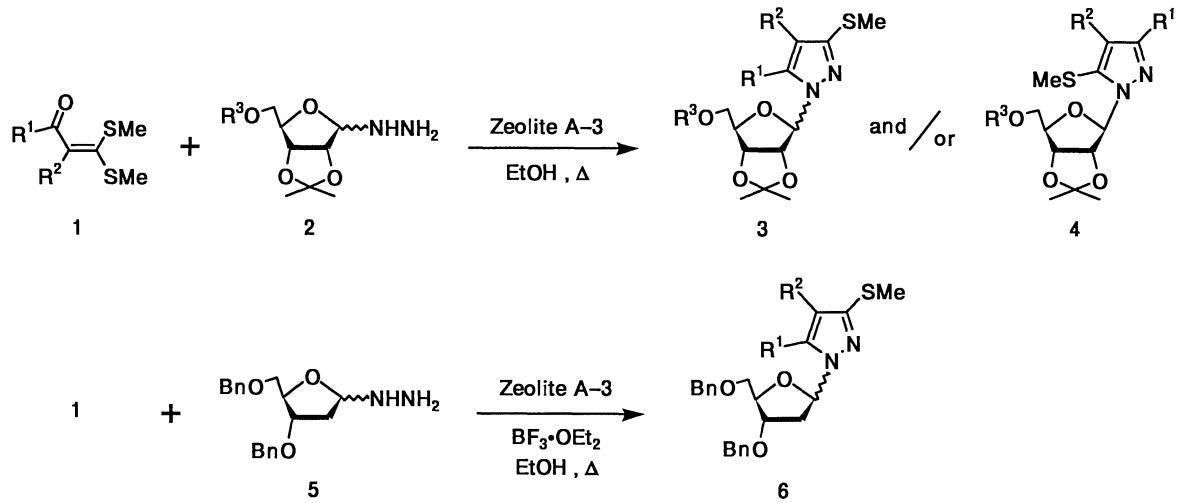

1 2 3 4

1 5 6

a : R^1 = Ph ; R^2 = H
b : R^1 = Me ; R^2 = H
c : R^1, R^2 = -$(CH_2)_4$-

a′(H) : R^3 = H
a′(T) : R^3 = Tr

a″(H) : R^1 = Ph ; R^2 = H ; R^3 = H
a″(T) : R^1 = Ph ; R^2 = H ; R^3 = Tr
b″ : R^1 = Me ; R^2 = H ; R^3 = H
c″ : R^1, R^2 = -$(CH_2)_4$- ; R^3 = H

Scheme 1.

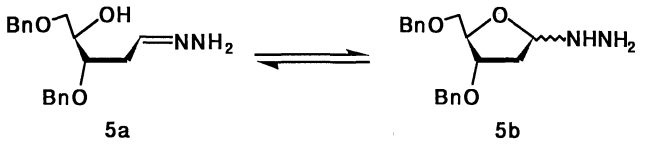

Scheme 2.

Table 1. Isolated Yields of Pyrazole Nucleosides

Compd	R^1	R^2	R^3	Yield[a]/%
3a′(H)	Ph	H	H	25(10)
3a′(T)	Ph	H	Tr	77(51)
3b′	Me	H	H	13(0)
3c′	$-(CH_2)_4-$		H	15(0)
4b′	Me	H	H	22(0)
6a	Ph	H	—	30(12)
6b	Me	H	—	38(10)

a) The value in the parenthesis shows the yield of α-anomer.

case of 2,3-*O*-isopropylidene-D-ribofuranosylhydrazine.[3]

The reaction of **1a** with **5** in the presence of boron trifluoride etherate gave 1-(3,5-di-*O*-benzyl-2-deoxy-D-ribofuranosyl)-3-methylthio-5-phenylpyrazole **6a** in 30% yield. Thus obtained **6a** was a mixture of α- and β-anomers, which could be separated easily by low-pressure chromatography (α-anomer 12%; β-anomer 18%). Several nucleosides prepared by this procedure are summarized in Table 1.

The structures of α- and β-anomers of **3** were determined on the basis of a difference of chemical shift values for the two methyl protons of the isopropylidene moiety in the ^{1}H NMR.[4] Regioisomers, **3b″** and **4b″** could be differentiated by the splitting pattern of $^3J_{C-H}$ of the ^{13}C NMR[5] [**3b″**: quartet splitting (C-3 and C-4), doublet splitting (C-5); **4b″**: singlet splitting (C-3), quartet splitting (C-4), multiplet splitting (C-5)]. The structures of α- and β-anomers for **6** were tentatively assigned by the characteristic splitting pattern of **1′-H**[6] (dd, $J_{1',2'A}$=8.0 Hz, $J_{1',2'B}$=4.0 Hz for the α-anomer; t, $J_{1',2'A}=J_{1',2'B}$=5.5 Hz for the β-anomer).

The deblocking of **3** and **6** could be easily carried out in the usual way (stir at r.t. with AcOH for **3**; Ac_2O/BF_3, followed by NH_3–MeOH for **6**).

Experimental

Microanalysis was performed with a Perkin–Elmer elemental 240 analyser at the Chemical Analysis Center of Chiba University. IR, MS, UV, and ^{1}H NMR spectra were measured with Hitachi 215, RMU 6MC, EPS-3T, JOEL MH-100, and JMN-GX-270 spectrometers, respectively. Optical rotation was measured on a JASCO-DIP-370 polarimeter. Wakogel C-200 was used for low-pressure liquid chromatography and Wakogel B-5F was used for TLC. 3,3-Bis(methylthio)-1-phenyl-2-propen-1-one (**1a**),[7] 4,4-bis(methylthio)-3-buten-2-one (**1b**),[8] and 2-[bis(methylthio)methylene]cyclohexanone (**1c**),[9] were prepared according to the literature. 2,3-*O*-Isopropylidene-D-ribofuranosylhydrazine **2a′(H)** was prepared by our previous method.[2]

2,3-*O*-Isopropylidene-5-*O*-trityl-D-ribofuranosylhydrazine 2a′(T). 2,3-*O*-Isopropylidene-5-*O*-trityl-D-ribofuranose was prepared according to the literature,[10] and then allowed to react with anhydrous hydrazine by the same method for the preparation of **2a′(H)** (R^3=H). The colorless crystals thus obtained (mp. 59—60 °C in sealed tube) were used without purification in the next step.

1-(2,3-*O*-Isopropylidene-β-D-ribofuranosyl)-3-methylthio-5-phenylpyrazole 3a″(H). A mixture of **2a′(H)** (0.57 g, 3 mmol), dry ethanol (5 ml), Zeolite A-3 (400 mg), and **1a** (224 mg, 1 mmol) was refluxed under stirring for 3 d. The reaction mixture was filtered through Celite and then the filtrate was evaporated to give an oil, which was purified by TLC on silica gel (eluent: $CHCl_3$–MeOH, 9:1) to form colorless crystals **3a″(H)** (91 mg, 25%), mp 84—85 °C; IR (KBr) 3220 (OH), 3020 (Ph), and 2980, 2920 cm^{-1} (CH); ^{1}H NMR ($CDCl_3$) δ=1.36 (s, 3H, Me), 1.49 (s, 3H, Me), 2.55 (s, 3H, SMe), 3.77, 3.98 (AB pattern, J_{gem}=14 Hz, $J_{4',5'}$=7 Hz, 2H, CH_2OH), 4.49 (s, 1H, OH), 5.06 (dd, $J_{4',5}$=7 Hz, $J_{3',4'}$=2 Hz, 1H, 4′-H), 5.26 (dd, $J_{2',3'}$=3 Hz, $J_{1',2'}$=2 Hz, 1H, 2′-H), 5.70 (dd, $J_{2',3'}$=3 Hz, $J_{3',4'}$=2 Hz, 1H, 3′-H), 5.90 (d, $J_{1',2'}$=2 Hz, 1H, 1′-H), 6.22 (s, 1H, 4-H), and 7.26—7.50 (m, 5H, Ph); MS *m/z* 362 (M$^+$); UV (99% EtOH) 208 (ε 27000) and 242 nm (21000); $[\alpha]_D$ −126° (*c* 0.55, EtOH); Found: C, 59.6; H, 6.14; N, 7.66%. Calcd for $C_{18}H_{22}N_2O_4S$: C, 59.6; H, 6.12; N, 7.73%.

Compounds **3b″** and **3c″** were prepared from **1b** and **1c** by the same method as above.

1-(2,3-*O*-Isopropylidene-β-D-ribofuranosyl)-5-methyl-3-(methylthio)pyrazole 3b″. Syrup; IR (neat) 3280 (OH) and 2990, 2860 cm^{-1} (CH); ^{1}H NMR ($CDCl_3$) δ=1.37 (s, 3H, Me), 1.60 (s, 3H, Me), 2.31 (s, 3H, Me), 2.48 (s, 3H, SMe), 3.66, 3.88 (AB pattern, J_{gem}=13 Hz, $J_{4',5'}$=7 Hz, 2H, CH_2OH), 4.52 (s, 1H, OH), 5.10 (m, 2H, 2′-H and 4′-H), 5.82 (m, 2H, 1′-H and 3′-H), and 5.94 (s, 1H, 4-H); MS *m/z* 300 (M$^+$); UV (99% EtOH) 210 (ε 7000), 230 (6460), and 250 nm (sh, 3420); $[\alpha]_D$ −52 ° (*c* 0.07, EtOH); Found: C, 51.6; H, 6.72; N, 9.30%. Calcd for $C_{13}H_{20}N_2O_4S$: C, 51.9; H, 6.71; N, 9.32%.

1-(2,3-*O*-Isopropylidene-β-D-ribofuranosyl)-3-(methylthio)-4,5,6,7-tetrahydro-1*H*-indazole 3c″. Syrup; IR (neat) 3250 (OH) and 2960, 2920, 2840 cm^{-1} (CH); ^{1}H NMR ($CDCl_3$) δ=1.36 (s, 3H, Me), 1.59 (s, 3H, Me), 1.78 (m, 4H, CH_2×2), 2.33 (s, 3H, SMe), 2.50 (m, 4H, CH_2×2), 3.73, 3.94 (AB pattern, J_{gem}=12 Hz, $J_{4',5'}$=8 Hz, 2H, CH_2OH), 4.52 (s, 1H, OH), 5.10 (m, 2H, 2′-H and 4′-H), 5.75 (d, $J_{1',2'}$=2 Hz, 1H, 1′-H), and 6.16 (m, 1H, 3′-H); MS *m/z* 340 (M$^+$); UV (99% EtOH) 242 (3900), and 309 nm (7200); $[\alpha]_D$ −21 ° (*c* 0.12, EtOH); Found: C, 56.0; H, 7.10; N, 8.17%. Calcd for $C_{16}H_{24}N_2O_4S$: C, 56.4; H, 7.11; N, 8.23%.

1-(2,3-*O*-Isopropylidene-β-D-ribofuranosyl)-3-methyl-5-(methylthio)pyrazole 4b″. Syrup; IR (neat) 3280 (OH) and 2980, 2840, 2710 cm^{-1} (CH); ^{1}H NMR ($CDCl_3$) δ=1.36 (s, 3H, Me), 1.62 (s, 3H, Me), 2.24 (s, 3H, Me), 2.40 (s, 3H, SMe), 3.69, 3.92 (AB pattern, J_{gem}=13 Hz, $J_{4',5'}$=7 Hz, 2H, CH_2OH), 4.53 (s, 1H, OH), 5.05 (m, 2H, 2′-H and 4′-H), 6.15 (m, 2H, 1′-H and 3′-H), and 6.25 (s, 1H, 4-H); MS *m/z* 300 (M$^+$); UV (99% EtOH) 207 (ε 5620), 238 (sh, 5420), and 260 nm (6250); $[\alpha]_D$ −85° (*c* 1.24, EtOH); Found: C, 51.6; H, 6.72; N, 9.30%. Calcd for $C_{13}H_{20}N_2O_4S$: C, 51.9; H, 6.71; N, 9.32%.

3,5-Di-*O*-benzyl-2-deoxy-D-ribofuranosylhydrazine 5. A mixture of methyl 3,5-di-*O*-benzyl-2-deoxy-D-ribofuranoside[11] (5.1 g, 16 mmol) and 80% aqueous acetic acid (50 ml) was refluxed for 15 min. The reaction mixture was evaporated to give an oil, which was purified by column chromatography on silica gel (eluent: AcOEt–hexane, 1:2) to afford colorless crystals (3.19 g, 66%). 3,5-Di-*O*-benzyl-2-deoxy-D-ribofuranose obtained thus (0.63 g, 2 mmol), dry methanol (3 ml), and anhydrous hydrazine (0.64 ml, 20 mmol) was stirred for 17 h at room temperature. The solvent was removed under reduced

pressure. The residue was evaporated with dry methanol (4 ml×4) and then under vacuum pump (133.3 Pa) below 50 °C to remove excess hydrazine. A pale yellow syrup was used without purification for next step.

1-(3,5-Di-*O*-benzyl-2-deoxy-D-ribofuranosyl)-3-methylthio-5-phenylpyrazole 6a. A mixture of **5** (2 mmol), dry ethanol (5 ml), Zeolite A-3 (400 mg), **1a** (449 mg, 2 mmol), and boron trifluoride etherate (0.3 ml, 2 mmol) was refluxed for 18 h. The reaction mixture was filtered through Celite and the filtrate was evaporated to give a light brown oil, which was purified by TLC on silica gel (eluent: AcOH–hexane, 1:4): A lower band gave α-anomer (113 mg, 12%) and an upper band gave β-anomer (170 mg, 18%); MS *m/z* 487 $(M+1)^+$; Found: C, 71.8; H, 6.10; N, 5.70%. Calcd for $C_{29}H_{30}N_2O_3S$: C, 71.6; H, 6.17; N, 5.76%.

α-Anomer: IR (neat) 3050, 3020 (Ph) and 2900, 2850 cm^{-1} (CH); ^1H NMR ($CDCl_3$) δ=2.4 (s, 3H, SMe), 3.1 (m, 2H, 2′-H), 3.6 (m, 2H, 5′-H), 4.3—4.4 (m, 2H, 3′-H and 4′-H), 4.6 (bs, 4H, CH_2Ph×2), 6.0 (dd, $J_{1',2'A}$=8.0, $J_{1',2'B}$=4.0 Hz, 1H, 1′-H), 6.2 (s, 1H, 4-H), 7.2 (bs, 10H, CH_2Ph×2), and 7.3—7.4 (m, 5H, 5-Ph); UV (99% EtOH) 208 (ε 36000) and 248 nm (16000); $[\alpha]_D$ +81° (*c* 0.93, EtOH).

β-Anomer: IR (neat) 3050, 3020 (Ph) and 2920, 2850 cm^{-1} (CH); ^1H NMR ($CDCl_3$) δ=2.3, 3.1 (m, 2H, 2′-H), 2.4 (s, 3H, SMe), 3.6 (m, 2H, 5′-H), 4.3 (m, 1H, 3′-H), 4.4 (m, 1H, 4′-H), 4.5—4.6 (m, 4H, CH_2Ph×2), 6.0 (t, $J_{1',2'A}$=$J_{1',2'B}$=5.5 Hz, 1H, 1′-H), 6.2 (s, 1H, 4-H), 7.2—7.3 (m, 10H, CH_2Ph×2), and 7.4—7.5 (m, 5H, 5-Ph); UV (99% EtOH) 211 (ε 22600) and 245 nm (12500); $[\alpha]_D$−70° (*c* 0.06, EtOH).

Compound **6b** was prepared from **1b** by the same method as above.

1-(3,5-Di-*O*-benzyl-2-deoxy-D-ribofuranosyl)-5-methyl-3-(methylthio)pyrazole 6b. Purification by TLC on silica gel (eluent: AcOEt–hexane, 1:4); α-anomer (66 mg, 14%) in a lower band; β-anomer (114 mg, 24%) in an upper band. Found: C, 67.8; H, 6.53; N, 6.70%. Calcd for $C_{24}H_{28}N_2O_3S$: C, 67.9; H, 6.60; N, 6.60%.

α-Anomer: IR (neat) 3050, 3020, (Ph) and 2900, 2850 cm^{-1} (CH); ^1H NMR ($CDCl_3$) δ=2.3 (s, 3H, 5-Me), 2.4 (s, 3H, SMe), 2.4, 3.1 (m, 2H, 2′-H), 3.6 (m, 2H, 5′-H), 4.3 (m, 1H, 3′-H), 4.4 (m, 1H, 4′-H), 4.5—4.6 (m, 4H, CH_2Ph×2), 5.9 (s, 1H, 4-H), 6.0 (dd, $J_{1',2'A}$=8.0, $J_{1',2'B}$=4.0 Hz, 1H, 1′-H), and 7.3—7.4 (bs, 10H, CH_2Ph×2); UV (99% EtOH) 211 (ε 8100), 235 (2300), and 248 nm (sh, 2100); MS 424 (M^+); $[\alpha]_D$+54° (*c* 0.08, EtOH).

β-Anomer: IR (neat) 3050, 3020, (Ph) and 2920, 2850 cm^{-1} (CH); ^1H NMR ($CDCl_3$) δ=2.2 (s, 3H, 5-Me), 2.4 (s, 3H, SMe), 2.4, 3.0 (m, 2H, 2′-H), 3.6 (m, 2H, 5′-H), 4.3 (m, 1H, 3′-H), 4.4 (m, 1H, 4′-H), 4.5—4.6 (m, 4H, CH_2Ph×2), 6.1 (s, 1H, 4-H), 6.3 (t, $J_{1',2'A}$=$J_{1',2'B}$=6.3 Hz, 1H, 1′-H), and 7.3—7.4 (bs, 10H, CH_2Ph×2); UV (99% EtOH) 211 (ε 18400), 229 (4500), and 247 nm (2100); MS 424 (M^+); $[\alpha]_D$−3.7° (*c* 0.10, EtOH).

1-(β-D-Ribofuranosyl)-3-methylthio-5-phenylpyrazole. A mixture of **3a″(H)** (26.5 mg, 0.07 mmol) and 10% acetic acid (1 ml) was stirred under refluxing for 4 h. The reaction mixture was evaporated under reduced pressure and then purified by TLC on silica gel using AcOEt as eluent to give a colorless oil (21 mg, 93%); IR (neat) 3500—3200 (OH) 3020 (Ph), and 2840 cm^{-1} (CH); ^1H NMR ($CDCl_3$–CCl_4) δ=2.3 (s, 3H, SMe), 3.2—4.2 (br, 3H, OH×3), 3.68 (m, 2H, CH_2OH), 4.2 (m, 1H, 4′-H), 4.4 (m, 1H, 2′-H), 4.8 (m, 1H, 3′-H), 5.6 (d, $J_{1',2'}$=4 Hz, 1H, 1′-H), 6.0 (s, 1H, 4-H), and 7.2 (s, 5H, Ph); MS 332 (M^+); UV(99% EtOH) 209 (ε 18600) and 243 nm (16600); $[\alpha]_D$−97.4° (*c* 0.09, EtOH); Found: C, 55.8; H, 5.56; N, 8.72%. Calcd for $C_{15}H_{18}N_2O_4S$: C, 55.9; H, 5.63; N, 8.69%.

1-(2-Deoxy-β-D-ribofuranosyl)-3-methylthio-5-phenylpyrazole. The reported procedure[12] was modified as follows: Boron trifluoride etherate (0.05 ml, 0.4 mmol) was added to a stirred solution of **6a** (β-isomer, 94.4 mg, 0.2 mmol) in acetic anhydride (3 ml). The resulting solution was kept at room temperature for 16 h and then evaporated in vacuo. The residue was subjected to TLC on silica gel (eluent: AcOEt–hexane, 1:1) to give 1-(3,5-di-*O*-acetyl-2-deoxy-β-D-ribofuranosyl)-3-methylthio-5-phenylpyrazole as a colorless syrup, which was then stirred with methanolic ammonia (saturated at 0 °C, 10 ml) in a closed flask at room temperature for 16 h and then evaporated. The usual work-up by TLC on silica gel gave a colorless oil (32 mg, 53%); IR (neat) 3300—3400 (OH), 3020 (Ph), and 2900—2850 cm^{-1} (CH); ^1H NMR ($CDCl_3$) δ=2.0 (m, 2H, 2′-H), 2.4 (s, 3H, SMe), 3.6—6.0 (m, 5H, 1′,3′,5′-H), 6,2 (s, 1H, 4-H), and 7.1 (m, 5H, Ph); MS 306 (M^+); Found: C, 58.8; H, 5.90; N, 9.04%. Calcd for $C_{15}H_{18}N_2O_3S$: C, 58.8; H, 5.91; N, 9.14%.

References

1) M. Yokoyama, K. Tsuji, and T. Imamoto, *Bull. Chem. Soc. Jpn.*, **57**, 2954 (1984); M. Yokoyama, K. Tsuji, and M. Kushida, *J. Chem. Soc., Perkin Trans. 1*, **1986**, 67; M. Yokoyama, S. Watanabe, and T. Seki, *Synthesis*, **1988**, 879; M. Yokoyama and N. Yamada, *Tetrahedron Lett.*, **30**, 3675 (1989); M. Yokoyama, N. Yamada, and H. Togo, *Chem. Lett.*, **1990**, 753; Y. A. Maurinsh, K. Sujino, H. Togo, and M. Yokoyama, *Heterocycles*, **31**, 1089 (1990); M. Yokoyama, E. Nakao, K. Sujino, S. Watanabe, and H. Togo, *Heterocycles*, **31**, 1669 (1990); M. Yokoyama, T. Ikuma, N. Obara, and H. Togo, *J. Chem. Soc., Perkin Trans. 1*, **1990**, 3243.

2) M. Yokoyama, K. Kumata, N. Yamada, H. Noro, and Y. Sudo, *J. Chem. Soc., Perkin Trans. 1*, **1988**, 2309.

3) R. R. Schmidt, J. Karg, and W. Guilliard, *Angew. Chem., Int. Ed. Engl.*, **14**, 64 (1975).

4) B. Rayner, C. Tapiero, and J. L. Imbach, *Carbohydr. Res.*, **47**, 195 (1976).

5) T. Somorai, G. Jerkovich, and P. Dvortsak, *J. Heterocycl. Chem.*, **19**, 1157 (1982).

6) E. M. Schubert, R. G. Bass, and R. A. Glennon, *Nucleosides & Nucleotides*, **2**, 127 (1983).

7) K. T. Potts, M. J. Cipullo, P. Ralli, and G. Theodoridis, *J. Org. Chem.*, **47**, 3027 (1982).

8) A. Thuillier and J. Vialle, *Bull. Soc. Chim. Fr.*, **1962**, 2182. 2182.

9) E. J. Corey and R. H. K. Chen, *Tetrahedron Lett.*, **1973**, 3817.

10) H. Ohrui and J. J. Fox, *Tetrahedron Lett.*, **1973**, 1951.

11) W. Wierenga and H. I. Skulnick, *Carbohydr. Res.*, **90**, 41 (1981).

12) D. P. C. McGee, J. C. Martin, D. F. Smee, T. R. Matthews, and J. P. H. Verheyden, *J. Med. Chem.*, **28**, 1242 (1985).

Synthesis of D-Altrose via D-Altrosan from Levoglucosenone

Katsuya MATSUMOTO,* Takashi EBATA,* Koshi KOSEKI, Hiroshi KAWAKAMI, and Hajime MATSUSHITA
Life Science Research Laboratory, Japan Tobacco Inc., 6-2 Umegaoka, Midori-ku, Yokohama, Kanagawa 227
(Received March 16, 1991)

Synopsis. The stereoselective reduction and *cis*-dihydroxylation of levoglucosenone (1,6-anhydro-3,4-dideoxy-β-D-*glycero*-hex-3-enopyranos-2-ulose), gave D-altrosan (1,6-anhydro-β-D-altropyranose), which could be converted to D-altrose in high yield.

Levoglucosenone (1,6-anhydro-3,4-dideoxy-β-D-*glycero*-hex-3-enopyranos-2-ulose, **1**)[1] is a pyrolytic product of cellulose.[2] The structure of **1** is attractive as a starting material for a variety of organic syntheses, since it includes convertible functional groups and one chiral center. We have synthesized various useful compounds from **1** to date and have demonstrated its great utility as a chiral building block.[3] In this paper, we describe a novel synthesis of D-altrose (**4**) via D-altrosan (1,6-anhydro-β-D-altropyranose, **3**)[4] from **1**. D-Altrose (**4**) is a rare sugar which cannot be obtained from natural products. Besides, the conventional syntheses of **4** are complicated due to the many steps required, or low selectivity.[5] Thus, a synthesis of **4** using fewer reaction steps with a high overall yield is required.

1,6-Anhydro-3,4-dideoxy-β-D-*threo*-hex-3-enopyranose (**2**) was synthesized by the reduction of **1**, according to the method of previous papers.[2,6,7] The *cis*-dihydroxylation of the carbon–carbon double bond of **2** stereoselectively gave D-altrosan (**3**) with catalytic osmium tetroxide in 86.0% yield, and with stoichiometric potassium permanganate in 32.7% yield. These facts arise due to an attack of osmium tetroxide and potassium permanganate on the carbon–carbon double bond from the less-hindered side, thus avoiding any steric hindrance by the 1,6-anhydro bond of the acetal ring. This observation is similar to that in the reduction of **1**. D-Altrose (**4**) was obtained by an acid hydrolysis of **3**.

In conclusion, we have developed a simple method for the preparation of D-altrose (**4**) in 3 steps in 29.1% overall yield, via D-altrosan (**3**) from levoglucosenone (**1**).

Experimental

Spectral Measurements. The IR spectra were measured with a JASCO FT/IR-5000 Spectrometer. The ^{1}H NMR spectra (300 MHz) and ^{13}C NMR spectra (75 MHz) were measured with a Bruker AM-300.

D-Altrosan (1,6-Anhydro-β-D-altropyranose, 3). *cis*-Dihydroxylation of the double bond between C-3 and C-4 of **2** was carried out by osmium tetroxide or potassium permanganate.

***cis*-Dihydroxylation by Osmium Tetroxide:** A solution (23 cm^3) of osmium tetroxide in *t*-butyl alcohol (osmium tetroxide/*t*-butyl alcohol=1/30; w/v) was added to a mixture of **2** (3.84 g, 30.0 mmol) and *N*-methylmorpholine *N*-oxide (7.03 g, 60.0 mmol) in acetone–water (150 cm^3, 8/1; v/v), and stirred for 13 h at room temperature. Na_2SO_3 (81.0 g, 643 mmol) was added to the reaction mixture with ice-cooling, and was then vigorously stirred for 10 min at room temperature. The reaction mixture was evaporated under reduced pressure. Purification of the residue by column chromatography on silica gel (eluent: dichloromethane/acetone=1/2—4; v/v) and recrystallization from 2-propanol afforded 4.19 g (86.0%) of **3** as white powder: Mp 129—130 °C; $[\alpha]_D^{25}$ −219° (*c* 1.00, H_2O) [lit,[4a,8] mp 134—135 °C; $[\alpha]_D^{20}$ −215° (*c* 1, H_2O)]; IR (KBr) 3400 (br), 1450 (br), 1137 (s), and 1073 cm^{-1} (s); ^{1}H NMR (CD_3OD, ppm from CD_3OD, 3.40 ppm) δ=3.75—3.83 (2H, m, H-6), 3.61 (1H, dd, *J*=1.7 and 8.6 Hz, H-2), 3.69 (1H, dd, *J*=4.4 and 8.6 Hz, H-3), 3.89 (1H, dd, *J*=2.5 and 4.4 Hz, H-4), 4.61 (1H, ddd, *J*=2.1, 2.5 and 4.6 Hz, H-5), 5.30 (1H, d, *J*=1.7 Hz, H-1); ^{13}C NMR (D_2O, ppm from 1,4-dioxane; 67.4 ppm) δ=102.0, 77.8, 72.9, 70.4, 70.0, 66.1. Found: C, 44.46; H, 6.26%. Calcd for $C_6H_{10}O_5$: C, 44.45; H, 6.22%.

***cis*-Dihydroxylation by Potassium Permanganate:** A 0.6% aqueous sodium hydroxide (16 cm^3) was added to a solution of **2** (128 mg, 1.00 mmol) in 2 cm^3 of water. Potassium permanganate (190 mg, 1.20 mmol) was then gradually added to the ice-cooled reaction mixture. After stirring for 20 min at room temperature, the reaction mixture was neutralized by 1 mol dm^{-3} hydrochloric acid, and filtered through a Celite pad. The residue was washed with water. The filtrate was evaporated under reduced pressure. Purification of the residue by

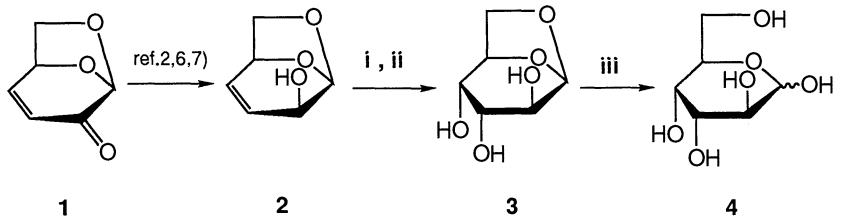

1 2 3 4

Scheme 1. i) OsO_4, *N*-methylmorpholine *N*-oxide, acetone, H_2O, ii) Na_2SO_3, iii) 1 mol dm^{-3} HCl, 1,4-dioxane.

column chromatography on silica gel (eluent: dichloromethane/acetone=1/2—4; v/v) afforded 53 mg (32.7%) of **3** as a white powder, which was identified with the **3** obtained above by a ^{1}H NMR spectral comparison.

D-Altrose (4). A solution of **3** (1.62 g, 10.0 mmol) in 1 mol dm^{-3} hydrochloric acid (100 cm^3) and 1,4-dioxane (50 cm^3) was heated at 100 °C for 5 h. The reaction mixture was neutralized by passing it through Amberlite IRA-410 (OH^- form); the aqueous eluent was evaporated under reduced pressure. The residue was purified by column chromatography on silica gel (eluent: chloroform/methanol=5—1; v/v). The first fraction, having R_f=0.4 (eluent: chloroform/methanol=4/1; v/v), was evaporated and dried under reduced pressure, and 1.09 g (6.7 mmol) of the starting material **3** was recovered. The second fraction, having R_f=0.2 (eluent: chloroform/methanol=4/1; v/v), was evaporated and dried under reduced pressure. 0.40 g of **4** was obtained.[9] The recovered **3** was hydrolyzed by the procedure described above. As a result, 0.70 g of **4** was obtained and 0.32 g of **3** was recovered (the procedures were rapeated three times). The obtained compound **4** was identified by comparing its IR spectra data and ^{13}C NMR spectra data with those of an authentic sample.[10] IR (nujol) 3300 (br) and 1065 cm^{-1} (br); ^{13}C NMR (D_2O, ppm from 1,4-dioxane; 67.4 ppm): α-Pyranose form;[11] δ=61.4 (C-6), 66.0 (C-4), 71.0 (C-3), 71.1 (C-5), 72.1 (C-2), 94.5 (C-1), β-pyranose form;[11] δ=62.4 (C-6), 65.1 (C-4), 71.4 (C-3), 71.6 (C-2), 74.9 (C-5), 92.6 (C-1), α-furanose form;[11] δ=63.2 (C-6), 72.5 (C-5), 76.7 (C-3), 82.2 (C-2), 84.1 (C-4), 102.0 (C-1), β-furanose form;[11] δ=63.2 (C-6), 73.5 (C-5), 75.9 (C-3), 77.4 (C-2), 81.9 (C-4), 96.1 (C-1).

References

1) This compound is available from Yuki Gosei Kogyo Co., Ltd.

2) F. Shafizadeh and P. P. S. Chin, *Carbohydr. Res.*, **58**, 79 (1977), and references cited therein.

3) a) K. Koseki, T. Ebata, H. Kawakami, H. Matsushita, Y. Naoi, and K. Itoh, *Heterocycles*, **31**, 423 (1990). b) H. Kawakami, T. Ebata, K. Koseki, H. Matsushita, Y. Naoi, and K. Itoh, *Chem. Lett.*, **1990**, 1459. c) T. Ebata, K. Matsumoto, H. Yoshikoshi, K. Koseki, H. Kawakami, and H. Matsushita, *Heterocycles*, **31**, 1585 (1990). d) H. Kawakami, T. Ebata, K. Koseki, K. Matsumoto, H. Matsushita, Y. Naoi, and K. Itoh, *ibid.*, **31**, 2041 (1990).

4) Conventional methods for synthesis of **3** are described on; a) N. K. Richtmyer and C. S. Hudson, *J. Am. Chem. Soc.*, **61**, 214 (1939). b) *idem., ibid.*, **62**, 961 (1940). c) F. H. Newth and L. F. Wiggins, *J. Chem. Soc.*, **1950**, 1734. d) K. Bock and C. Pedersen, *Acta Chem. Scand.*, **27** (8), 2701 (1973). e) K. Heyns and P. Köll, *Chem. Ber.*, **106**, 611 (1973). f) P. L. Durette and H. Paulsen, *Carbohydr. Res.*, **35**, 221 (1974).

5) a) P. A. Levene and W. A. Jacobs, *Ber.*, **43**, 3141 (1910). b) N. K. Richtmyer, "Methods in Carbohydrate Chemistry," ed by R. L. Whistler and M. L. Wolfrom, Academic Press, New York and London (1962), Vol. I, p. 107.

6) In Ref. 2, F. Shafizadeh and P. P. S. Chin have erroneously reported on the configurational assignments of two epimers obtained by reduction of **1** with $LiAlH_4$. The correct assignment has been reported in, J. S. Brimacombe, F. Hunedy, and L. C. N. Tucker, *Carbohydr. Res.*, **60**, C11 (1978).

7) J. S. Brimacombe, F. Hunedy, A. M. Mather, and L. C. N. Tucker, *Carbohydr. Res.*, **68**, 231 (1979).

8) I. Johansson and N. K. Richtmyer, *Carbohydr. Res.*, **10**, 322 (1969).

9) **3** and **4** are equilibrated in acid solution. See Ref. 4b, and references cited therein.

10) D-Altrose (97%, mixture of anomers) purchased from Aldrich Chemical Company, Inc.

11) These assignments were based on; "Carbon-13 NMR Spectroscopy," ed by E. Breitmaier and W. Voelter, VCH, Weinheim (1987), Third completely revised edition, pp. 380—383.

Reductive Deacetoxylation of Allylic Acetates Using Hexacarbonylmolybdenum(0)

Yoshiro MASUYAMA,* Kazunobu MAEKAWA, Toshiyuki KURIHARA, and Yasuhiko KURUSU
Department of Chemistry, Faculty of Science and Technology, Sophia University,
7-1 Kioicho, Chiyoda-ku, Tokyo 102
(Received March 22, 1991)

Synopsis. Aliphatic allylic acetates were reduced to alkenes with hexacarbonylmolybdenum(0) in refluxing dioxane under nitrogen atmosphere. These reactions were accelerated by the addition of H_2O. 1-Aryl- or 3-arylallyl acetates caused deacetoxylative allylic homocoupling under the same conditions.

Hexacarbonylmolybdenum [$Mo(CO)_6$] seems to have both oxidizing and reducing ability, since molybdenum has a variety of oxidation states between −2 and +6. In particular, the reducing ability can be presumably applied to organic synthesis. We have recently reported that hexacarbonylmolybdenum is a useful reducing agent for reductive chalcogenization of allylic sulfides, sulfones, and selenides.[1-3] The reductive desulfonylation of allylic sulfones with $Mo(CO)_6$ should proceed via the formation of π-allylmolybdenum complexes.[2-4] Allylic acetates have also reacted with $Mo(CO)_6$ to form π-allylmolybdenum complexes, which have been utilized to nucleophilic substitution by carbon nucleophiles.[5] If carbon nucleophiles were absence in the reaction system, allylic acetates would be reduced to alkenes by electron transfer from molybdenum atom to η^3-allyl ligand π-allylmolybdenum intermediates,[6] similarly to reductive desulfonylation of allylic sulfones.[2,3]Here we report a reductive deacetoxylation of various allylic acetates with $Mo(CO)_6$ under the same conditions as π-allylmolybdenum complex has been formed.

The reaction of methyl 9-acetoxy-10-undecenoate with $Mo(CO)_6$ was investigated under various conditions. Reductive deacetoxylation proceeded in refluxing THF or dioxane (Entries 1—4 in Table 1). Addition of H_2O accelerated the reductive deacetoxylation similarly to reductive dechalcogenization of allylic sulfides, sulfones, and selenides with $Mo(CO)_6$ (Entries 2 and 3). In refluxing THF (Entry 3), an elimination of acetic acid occurred to give a diene, in contrast with the reaction in refluxing dioxane (Entry 2). The reaction of various allylic acetates with $Mo(CO)_6$ was carried out in the presence of H_2O (5 equiv) in refluxing dioxane (Table 1). Aliphatic allylic acetates caused only the reductive deacetoxylation to produce the corresponding alkene isomers (Entries 1—11, and 16, Scheme 1). Allylic acetates bearing an aryl substituent on an allylic position of the π-allylmolybdenum intermediates, caused reductive allylic homocoupling with the reductive deacetoxylation without adding a reducing agent such as zinc powder (Entries 13, 14, and 17, Scheme 1).[7] In the case having a proton on an α-position of 1-aryl-π-allylmolybdenum intermediate, a diene was obtained as a single product without base, as shown in Scheme 2 (Entries 18 and 19).[8] The reductive deacetoxylation smoothly proceeded with even a half equimolar amount of $Mo(CO)_6$ (Entries 15 and 16).[9] Hexacarbonylmolybdenum(0) proved to have such a reducing ability that more than two electrons apparently transfered from molybdenum(0) to allylic acetates. Addition of D_2O instead of H_2O produced a quantitatively deuterated product, and use of dioxane-d_8 as a solvent did not cause the deuteration (Entries 7 and 8). Hence, a proton or radical hydrogen source is presumably H_2O.[10]

Experimental

General Procedure of Reductive Deacetoxylation of Allylic Acetates with $Mo(CO)_6$. To a solution of allylic acetate (1 mmol) and H_2O (5 mmol) in dioxane (3—5 ml) was added hexacarbonylmolybdenum(0) (0.5—1 mmol). The mixture was refluxed for 14—25 h under nitrogen atmosphere. The reaction mixture was diluted with ether (50 ml), washed with water (20×3 ml), and dried over $MgSO_4$. Evaporation of ether followed by purification of a residue by column chromatography on silica gel (Merck 60) using hexane or hexane/ethyl acetate as an eluent gave reductively deacetoxylated products and/or allylic homocoupling products. The structures were determined by IR (Hitachi 260-50), ^1H NMR (JEOLCO GX-270), and mass spectra (JEOLCO JMS-D300). The isomer ratios were determined by ^1H NMR.

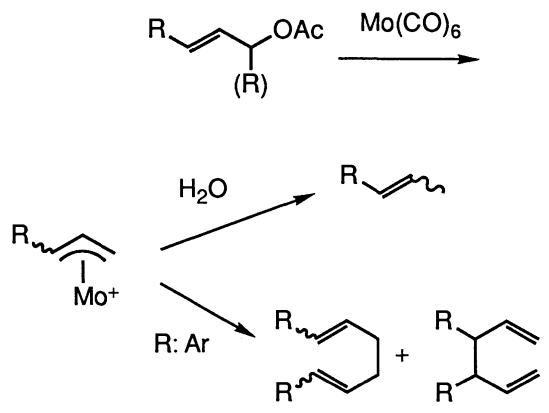

Scheme 1.

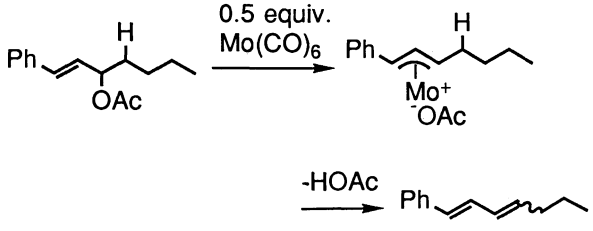

Scheme 2.

Table 1. Reductive Deacetoxylation of Allylic Acetates with $Mo(CO)_6$

Entry	Allylic acetate	H^+ (or H·) source	Time/h	Product	Yield[a]/%
1	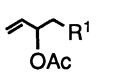	—	20	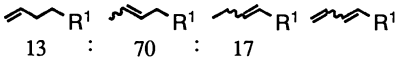 13 : 70 : 17	40
2	R^1: $(CH_2)_6COOMe$	H_2O	15	15 : 54 : 31	58
3		H_2O	19	16 : 39 : 18 : 27	31[b]
4		CH_3COOH	18	15 : 63 : 15 : 7	64[b]
5	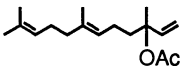	—	15	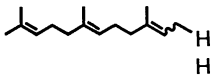 H	47
6		H_2O	15	H	55
7		D_2O	15	D	49[c]
8		—	19	H	49[c,d]
9	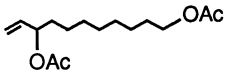	—	24	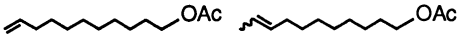	39
10		H_2O	20	20 : 80	50
11	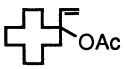	H_2O	22		60
12		H_2O	17		35
13	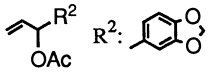	H_2O	23	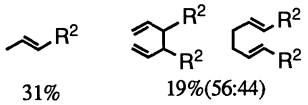 31% 19%(56:44)	50[e]
14	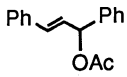	H_2O	21	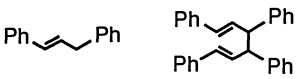 19% 37%	56[e]
15		H_2O	25	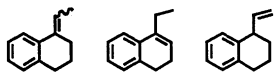 67 : 20 : 13	70[e]
16	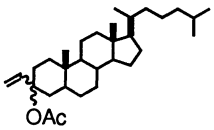	H_2O	19	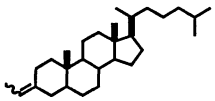	82[e]
17	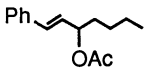	—	14	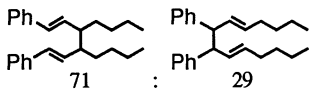 71 : 29	48
18		H_2O	20		50[e]
19		—	22	cis:trans=50:50	50[e]

a) Yields of mixtures of regio- and/or stereoisomers. The ratio was determined by ^1H NMR (JEOLCO GX-270). b) THF as a solvent was used. c) The deuteration was confirmed by ^1H NMR and GC-MS (JEOLCO JMS-D300). d) Dioxane-d_8 as a solvent was used. e) A half equimolar amount of $Mo(CO)_6$ was used.

A Mixture of Methyl 8-Undecenoate, Methyl 9-Undecenoate, and Methyl 10-Undecenoate (Entry 1 in Table 1): IR (neat) 3000, 2920, 2845, 1735, 1430, 1160 cm^{-1}. ^1H NMR ($CDCl_3$) δ=0.95, 0.96 (2t, J=7.33 Hz, 0.5H), 1.22—1.42 (br, 8H), 1.54—1.70 (m, 4.1H), 1.90 (m, 2.3H), 2.30 (t, J=7.36 Hz, 2H), 3.66 (s, 3H), 4.89—5.03 (m, 0.25H), 5.30—5.50 (m, 1.7H), 5.80 (ddt, J=17.1, 10.3, 6.65 Hz, 0.13H). MS (70 eV) m/z (rel intensity) 198 (M^+, 6), 166 (21), 124 (28), 97 (21), 96 (27), 87 (46), 84 (34), 83 (37), 82 (25), 81 (23), 74 (83), 69 (55), 68 (24), 67 (25), 59 (23), 55 (100). Found: m/z 198.1622. Calcd for $C_{12}H_{22}O_2$: M, 198.1619.

2,6,10-Trimethyl-2,6,10-dodecatriene (Entry 5 in Table 1): IR (neat) 2950, 2900, 2850, 1435, 1370 cm^{-1}. ^1H NMR ($CDCl_3$) δ=1.56 (d, J=6.72 Hz, 3H), 1.59 (br.s, 6H), 1.62 (br.s, 2H), 1.67 (br.s, 4H), 1.93—2.13 (m, 8H), 5.05—5.16 (m, 2H), 5.20 (q, J=6.68 Hz, 1H). MS (70 eV) m/z (rel intensity) 206 (M^+, 3.7), 137 (12), 136 (11), 123 (12), 95 (27), 82 (11), 81 (40), 69 (100), 67 (13), 55 (14). Found: m/z 206.2027. Calcd for $C_{15}H_{26}$: M, 206.2033.

11-Acetoxy-2-undecene (Entry 9 in Table 1): IR (neat) 2920, 2860, 1730, 1440, 1365, 1235, 1035, 960 cm^{-1}. ^1H NMR ($CDCl_3$) δ=1.20—1.45 (br, 10H), 1.56—1.67 (m, 5H), 1.91—

2.01 (m, 2H), 2.04 (s, 3H), 4.06 (t, J=6.60 Hz, 2H), 5.37—5.44 (m, 2H). MS (70 eV) m/z (rel intensity) 212 (M^+, 1.2), 109 (20), 97 (28), 96 (31), 95 (34), 84 (32), 83 (22), 82 (51), 81 (66), 69 (63), 68 (90), 67 (66), 61 (21), 55 (100), 54 (40). Found: m/z 212.1773. Calcd for $C_{13}H_{24}O_2$: M, 212.1775.

Ethylidenecyclododecane (Entry 11 in Table 1): IR (neat) 2920, 2840, 1455 cm^{-1}. ^1H NMR (CCl_4) δ=1.00—1.70 (br, 18H), 1.57 (d, J=7.0 Hz, 3H), 1.80—2.23 (m, 4H), 4.93—5.37 (m, 1H). MS (70 eV) m/z (rel intensity) 194 (M^+, 44), 165 (24), 110 (23), 109 (46), 96 (62), 95 (61), 83 (56), 82 (70), 81 (69), 71 (32), 70 (88), 69 (55), 68 (50), 67 (81), 55 (100), 54 (32). Found: m/z 194.2034. Calcd for $C_{14}H_{26}$: M, 194.2033.

1-(3,4-Methylenedioxyphenyl)propene (Entry 12 in Table 1): IR (neat) 2900, 2850, 1485, 1440, 1245, 1120, 1035 cm^{-1}. ^1H NMR ($CDCl_3$) δ=1.84 (dd, J=6.52, 1.49 Hz, 3H). 5.93 (s, 2H), 6.06 (dq, J=15.6, 6.44 Hz, 1H), 6.31 (dq, J=15.6, 1.45 Hz, 1H), 6.73 (s, 2H), 6.87 (s, 1H). MS (70 eV) m/z (rel intensity) 162 (M^+, 100), 161 (31), 135 (46), 131 (40), 104 (42), 103 (33), 97 (36), 85 (30), 83 (37), 81 (32), 77 (34), 71 (46), 69 (46), 57 (77), 55 (59). Found: m/z 162.0678. Calcd for $C_{10}H_{10}O_2$: M, 162.0680.

1,3-Diphenylpropene (Entry 14 in Table 1): IR (neat) 3010, 2910, 2850, 1595, 1485, 1445, 960, 735, 690 cm^{-1}. ^1H NMR ($CDCl_3$) δ=3.54 (d, J=6.30 Hz, 2H), 6.34 (dt, J=15.7, 6.30 Hz, 1H), 6.45 (d, J=15.7 Hz, 1H), 7.14—7.37 (m, 10H). MS (70 eV) m/z (rel intensity) 194 (M^+, 100), 193 (54), 179 (37), 116 (36), 115 (58), 91 (35). Found: m/z 194.1096. Calcd for $C_{15}H_{14}$: M, 194.1095.

1,3,4,6-Tetraphenyl-1,5-hexadiene (Entry 14 in Table 1): IR (neat) 3030, 2930, 1600, 1490, 1450, 965, 745, 705 cm^{-1}. ^1H NMR ($CDCl_3$) δ=3.84—3.93 (m, 2H), 6.16—6.58 (m, 4H), 7.03—7.33 (m, 20H). MS (70 eV) m/z (rel intensity) 194 (21), 193 (100), 178 (12), 115 (51), 91 (17). Found: C, 92.93; H, 6.64%. Calcd for $C_{30}H_{26}$: C, 93.21; H, 6.78%.

A Mixture of 1-Ethylidenetetralin, 1-Ethyl-3,4-dihydronaphthalene, and 1-Vinyltetralin (Entry 15 in Table 1): IR (neat) 3010, 2920, 2850, 1475, 1445, 745 cm^{-1}. ^1H NMR (CCl_4) δ=1.14 (t, J=7.36 Hz, 0.60H), 1.76 (d, J=6.92 Hz, 2.0H), 1.64—1.97 (m, 1.9H), 2.17—2.54 (m, 2.1H), 2.64—2.82 (m, 2.1), 4.96—5.09 (m, 0.3H), 5.78—5.96 (m, 0.30H), 5.99—6.16 (m, 0.70H), 7.00—7.15 (m, 4H). MS (70 eV) m/z (rel, intensity) 158 (M^+, 48), 141 (23), 131 (49), 130 (69), 129 (100), 128 (49), 127 (20), 118 (20), 115 (41), 91 (25). Found: m/z 158.1095. Calcd for $C_{12}H_{14}$: M, 158.1095.

3-Ethylidenecholestane (Entry 16 in Table 1): IR (neat) 2930, 2860, 1455, 1380, 910 cm^{-1}. ^1H NMR ($CDCl_3$) δ=0.65 (s, 3H), 0.87 (d, J=6.89 Hz, 9H), 0.92 (s, 3H), 0.95—2.20 (m, 31H), 1.55 (d, J=6.61 Hz, 3H), 4.96—5.15 (m, 1H). MS (70 eV) m/z (rel intensity) 398 (M^+, 30), 396 (33), 243 (30), 161 (38), 149 (34), 147 (41), 135 (52), 134 (45), 133 (41), 123 (43), 122 (55), 121 (62), 120 (31), 119 (44), 109 (66), 108 (36), 107 (71), 105 (51), 97 (31), 95 (96), 93 (65), 91 (36), 83 (42), 81 (100), 79 (46), 71 (38), 69 (66), 67 (53), 57 (80), 55 (94). Found: m/z 398.3898. Calcd for $C_{29}H_{50}$: M, 398.3910.

A Mixture of 3,4-Dibutyl-1,6-diphenyl-1,5-hexadiene and 7,8-Diphenyl-5,9-tetradecadiene (Entry 17 in Table 1): IR (neat) 3020, 2940, 2920, 2850, 1485, 1445, 960, 735, 690 cm^{-1}. ^1H NMR (CCl_4) δ=0.93 (br, 6H), 1.10—2.80 (m, 13.4H), 3.17—3.43 (0.60H), 5.17—5.57 (m, 1.2H), 5.96(dd, J=15.0, 5.6 Hz, 1.4H), 6.36 (d, J=15.0 Hz, 1.4H), 6.93—7.33 (m, 10H). MS (70 eV) m/z (rel intensity) 174 (35), 131 (15), 118 (15), 117 (100), 116 (10), 115 (29), 105 (28), 104 (89), 92 (13), 91 (63), 81 (13), 77 (19), 69 (26), 57 (11), 55 (23). Found: C, 89.75; H, 10.12%. Calcd for $C_{26}H_{34}$: C, 90.10; H, 9.90%.

1-Phenyl-1,3-heptadiene (Entry 18 and 19 in Table 1): IR (neat) 3020, 2960, 2870, 1490, 1460, 990, 745, 690 cm^{-1}. ^1H NMR ($CDCl_3$) δ=0.92 (t, J=7.04 Hz, 1.5H), 0.95 (t, J=7.04 Hz, 1.5H), 1.36—1.53 (m, 2H), 2.11 (br.q, J=7.23 Hz, 1H), 2.26 (br.q J=7.42 Hz, 1H), 5.52 (dt, J=9.89, 7.42 Hz, 0.5H), 5.80 (dt, J=15.0, 7.04 Hz, 0.5H), 6.10 (m, 1H), 6.42 (d, J=15.6 Hz, 0.5H), 6.50 (d, J=15.6 Hz, 0.5H), 6.74 (dd, J=15.6, 10.3 Hz, 0.5H), 7.06 (ddd, J=15.6, 10.8, 1.33 Hz, 0.5H), 7.12—7.42 (m, 5H). MS (70 eV) m/z (rel intensity) 172 (M^+, 42), 143 (63), 131 (22), 130 (24), 129 (100), 128 (69), 117 (42), 115 (56), 91 (60), 77 (23), 71 (27). Found: m/z 172.1252. Calcd for $C_{13}H_{16}$: M, 172.1251.

References

1) Y. Masuyama, K. Yamada, and Y. Kurusu, *Tetrahedron Lett.*, **28**, 443 (1987).

2) Y. Masuyama, K. Yamada, and Y. Kurusu, *Chem. Express*, **2**, 687 (1987).

3) Y. Masuyama, K. Yamada, S. Shimizu, and Y. Kurusu, *Bull. Chem. Soc. Jpn.*, **62**, 2913 (1989).

4) B. M. Trost, *Bull. Chem. Soc. Jpn.*, **61**, 107 (1988).

5) B. M. Trost and M. Lautens, *J. Am. Chem. Soc.*, **104**, 5543 (1982); **105**, 3343 (1983); **109**, 1469 (1987).

6) For reductive deacetoxylation via π-allylmetal complexes using reducing agents, see: J. Tsuji and T. Yamakawa, *Tetrahedron Lett.*, **1979**, 613; R. O. Hatchins, K. Learn, and R. P. Fulton, *ibid.*, **21**, 27 (1980); H. Matsushita and E. Negishi, *J. Org. Chem.*, **47**, 4161 (1982); E. Keinan and N. Greenspoon, *ibid.*, **48**, 3545 (1983); J. Tsuji, I. Minami, and I. Shimizu, *Synthesis*, **1986**, 623.

7) Allylic homocoupling may occur via the formation of bis(η^1-γ-arylallyl)molybdenum intermediates; the transformation of initially prepared η^3-allyl complexes to η^1-allyl complexes may create a vacant coordination site on the molybdenum, and then second η^1-allylation may easily occur on the molybdenum, since olefins bearing an electron-withdrawing aryl group are hard to coordinate to the molybdenum. For reductive allylic homocoupling with $Mo(CO)_6$-Zn, see: Y. Masuyama, K. Otake, and Y. Kurusu, *Bull. Chem. Soc. Jpn.*, **60**, 1527 (1987).

8) B. M. Trost, M. Lautens, and B. Peterson, *Tetrahedron Lett.*, **24**, 4525 (1983).

9) The reductive deacetoxylation scarcely occurred in the use of a 0.1—0.2 equimolar amount of $Mo(CO)_6$ to allylic acetate.

10) The reductive deacetoxylation of allylic acetates may occur via the reductive elimination of hydrido(π-allyl)molybdenum intermediates derived from initially prepared π-allylmolybdenum complexes with H_2O. In order to detect the hydrido(π-allyl)molybdenum intermediate, ^1H NMR spectroscopic investigation was carried out in the reaction of allyl acetate with $Mo(CO)_6$ and H_2O in dioxane-d_8. The formation of the hydrido(π-allyl)molybdenum complex was not confirmed, since the reductive deacetoxylation probably occurred rapidly at high reaction temperature (100 °C), which needed in the formation of initial π-allylmolybdenum complex. For reductive elimination of hydrido(η^1-allyl)molybdenum complexes, see: T. Ito, T. Matsubara, and Y. Yamashita, *J. Chem. Soc., Dalton Trans.*, **1990**, 2407.

 © 1991 The Chemical Society of Japan Bull. Chem. Soc. Jpn., 64, 2315—2322 (1991)

Resonance Raman Study on Photoreduction of Iron-Porphyrins. A Novel Insight into the Ligand-Aided Process

Vlastimil FIDLER,†† Takashi OGURA, Shin-ichiro SATO, Katsuhiro AOYAGI,† and Teizo KITAGAWA*
Institute for Molecular Science, Okazaki National Research Institutes, Myodaiji, Okazaki 444
†Department of Industrial Chemistry, Fukushima National College of Technology, Taira, Iwaki, Fukushima 970
(Received March 14, 1991)

Photoreduction of Fe(OEP) (OEP: octaethylporphyrin) in organic solvents by visible light was demonstrated to be a ligand-aided process in which simultaneous coordinations of a base such as 2-methylimidazole (2MeIm) and of an aliphatic alcohol to two axial positions of the iron ion were required. Coordination of an alcohol was evidenced from the observation of the Fe–alcohol stretching ($\nu_{Fe\text{-}alcohol}$) resonance Raman (RR) band. Since this band exhibited an appreciable frequency shift between ROH and ROD, coordination of the alcohol in a protonated form was suggested. When a primary or secondary alcohol was added to the CH_2Cl_2 solution of Fe^{III} (OEP)Cl in the presence of 2MeIm, a new absorption band appeared around 560—590 nm and the $\nu_{Fe\text{-}alcohol}$ RR band was most intense for excitation at the maximum of the new absorption band. The new absorption was therefore assigned to the alcohol to Fe^{III} charge transfer (CT) band. A tertiary alcohol gave neither the CT band nor the $\nu_{Fe\text{-}alcohol}$ RR band, although some spectral changes were noticed after long laser illumination at 441.6 nm, and the photoreduction as seen for other alcohol solutions did not take place. This photoreduction was not apparently recognized in the presence of oxygen. However, flash photolysis experiments demonstrated that the photoreduction occurs irrespective of the presence or absence of oxygen but rapid reoxidation results in apparent no effect.

Photoreduction of iron-porphyrins has been attracting chemists' interest since the initial finding of photoreduction on cytochrome oxidase by visible light.[1–3] Afterwards the photoreduction has been extensively observed for various heme proteins[4–8] and metalloporphyrins.[9–16] While a mechanism of photoreduction of Pd-, Zn-, and a few water soluble porphyrins has been studied in detail,[9,16] little is known about the photoreduction mechanism of iron porphyrins as well as heme proteins. Ozaki et al.[17] recognized occurrence of photoreduction of an iron porphyrin during resonance Raman (RR) measurements of 2-methylimidazole (2MeIm) complex of Fe^{III}(OEP)Br in CH_2Cl_2 (OEP: octaethylporphyrin). It was shown that any ring reduction to a porphyrin anion radical or chlorin did not take place and that the photoreduction was a ligand-aided process.

Recently, we noticed that the photoreduction observed by Ozaki et al.[17] was catalyzed by a trace amount of alcohol contained as a stabilizer of solvent.[18,19] In this paper we report detailed results on isotope substitution experiments which show that the catalytic alcohol binds to the sixth coordination position of Fe^{III}(OEP)(2MeIm) in the ROH form and gives rise to a charge transfer (CT) band around 560—590 nm. Although apparently the photoreduction does not seem to occur in the presence of oxygen, the flash photolysis experiments revealed that the photoreduction occurred but it was promptly reoxidized. It is most surprising that the laser illumination within the CT band induces no photoreduction.

†† Present address: Department of Physical Chemistry, Faculty of Science, Charles University, 128-40 Praha 2, Czechoslovakia.

Experimental

Fe^{III}(OEP)X (X=Cl, Br, and I) were synthesized by the procedure described elsewhere.[20,21] Since no difference was observed by using X=Cl, Br or I for Fe^{III}(OEP)X, Fe^{III}(OEP)Cl was used unless otherwise stated. 2MeIm was recrystallized from benzene and its ^1H NMR spectrum did not show any detectable impurity. CH_2Cl_2 of spectroscopic grade from different suppliers were found to contain different stabilizers. We analyzed CH_2Cl_2 from Wako, Kanto-kagaku, Cica-MERCK, Aldrich, and Dojin companies with gas chromatography and their influence on photoreduction of Fe^{III}(OEP)(2MeIm). Since the Cica-MERCK product contained the smallest amount of stabilizer and/or impurities (less than 0.1%) and had no side-effect on photoreduction, it was used without further purification. The standard concentration of the sample was 2 mM of Fe^{III}(OEP)X, 50—100 mM of 2MeIm, and a few % (v/v) of added alcohol. Fresh solution was prepared for each experiment.

Raman spectra were measured with a JEOL-400D Raman spectrometer equipped with a cooled RCA-31034a photomultiplier and a home-made computer-controlled data aquisition system based on NEC 9801 computer. As an excitation source of Raman scattering were used Kr^+ laser (Spectra Physics, 164), He/Cd laser (Kinmon Electrics, CDR80MGE), Ar^+ laser (NEC, GLG3200), and Ar^+ laser-pumped dye laser (Spectra Physics, 164/175) with rhodamine 6G. Laser power was measured at the sample point with a hand power-meter (Advantest TA-8210). Raman shifts were calibrated with indene for individual excitation lines. Uncertainties in wavenumbers of well-defined band are less than ± 1 cm^{-1}. During the Raman measurements the sample was kept at 10 °C by circulating temperature-controlled water through the cell holder. For the measurements under anaerobic conditions, the sample solution in the air-tight cell was degassed through three freeze/thaw cycles and stopped by a cock.

Conventional absorption spectra were recorded with a Hitachi 220S spectrophotometer. For the test of photoreduc-

tion the sample in the anaerobic cell was illuminated by a projector lamp through the short cut filter (L-38, Hoya Corp.) for 5 min. During illumination the sample cell was placed in a water bath at 20 °C. Time profiles of absorption changes of the sample after pulse illumination were measured by a home-made apparatus described elsewhere.[22]

Results

At the beginning of this study we encountered some problems regarding reproducibility of the previous results.[17] The RR spectrum of Fe^{III}(OEP)(2MeIm) (Fig. 1A) was the same as that reported previously[17] but Fe^{III}(OEP)(2MeIm) in pure CH_2Cl_2 did not exhibit any photoreduction even after careful degassing and long-lasting illumination by white light or laser. Figure 1(B) shows the spectrum obtained for Fe^{III}(OEP)Cl in a CH_2Cl_2–CH_3OH mixed solvent (1 : 1 in v/v). This is again the same as that of Fe^{III}(OEP)Cl. Following systematic tests of all components of the system revealed that photoreduction of Fe^{III}(OEP)(2MeIm) went on only when the solvent CH_2Cl_2 contained alcohol as a stabilizer. Figure 1(C) shows the RR spectrum observed for Fe^{III}(OEP)(2MeIm) in CH_2Cl_2 in the presence of MeOH. The resultant spectrum remained unaltered by the concentration change of MeOH from 0.5 to 20% (v/v) and is the same as that of Fe^{II}(OEP)(2MeIm) as noted previously.[17] In the presence of oxygen, however, the spectrum was the same as Fig. 1(A). It became evident, therefore, that both 2MeIm and MeOH are required for photoreduction to occur and apparently the photoreduction seems not to occur in the presence of oxygen. A similar phenomenon was seen for Fe^{III}(OEP)(1,2-Me_2Im) but not at all for Fe^{III}(OEP)$(Im)_2$ and Fe^{III}(OEP)$(1MeIm)_2$.

Figure 2 shows the effect of alcohol on absorption spectra. The spectra in the upper panel were obtained in the presence of oxygen. Although Soret band is little affected by the presence of alcohol except its slight weakening, Q band of Fe^{III}(OEP)(2MeIm) at 535 nm disappears and a new band appears at 584 nm in the presence of MeOH (B). The 584 nm band did not appear when MeOH was added to Fe^{III}(OEP)Cl in CH_2Cl_2. A similar spectral change was observed when ethanol (EtOH), or 1-propanol (*n*-PrOH) was used for

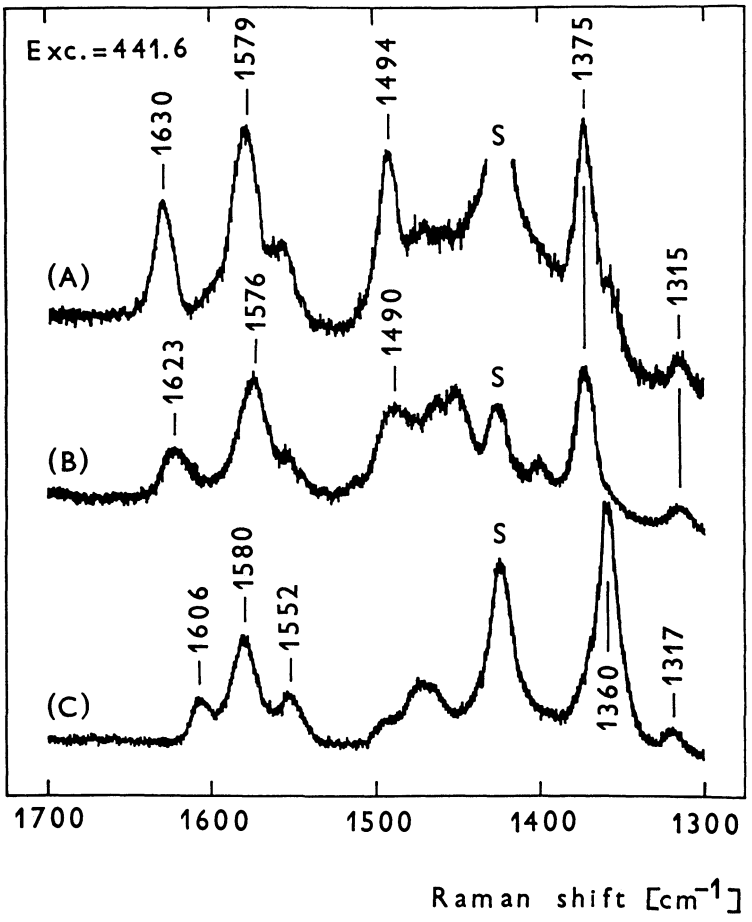

Fig. 1. Typical RR spectra of Fe(OEP) complexes under different solvent conditions. A) Fe^{III}(OEP) (2MeIm) in CH_2Cl_2, B) Fe^{III}(OEP)Cl in MeOH: CH_2Cl_2=1 : 1 (v/v), C) Fe^{III}(OEP)-(2MeIm)(MeOH) in CH_2Cl_2. Excitation: 441.6 nm. All spectra were observed under anaerobic conditions.

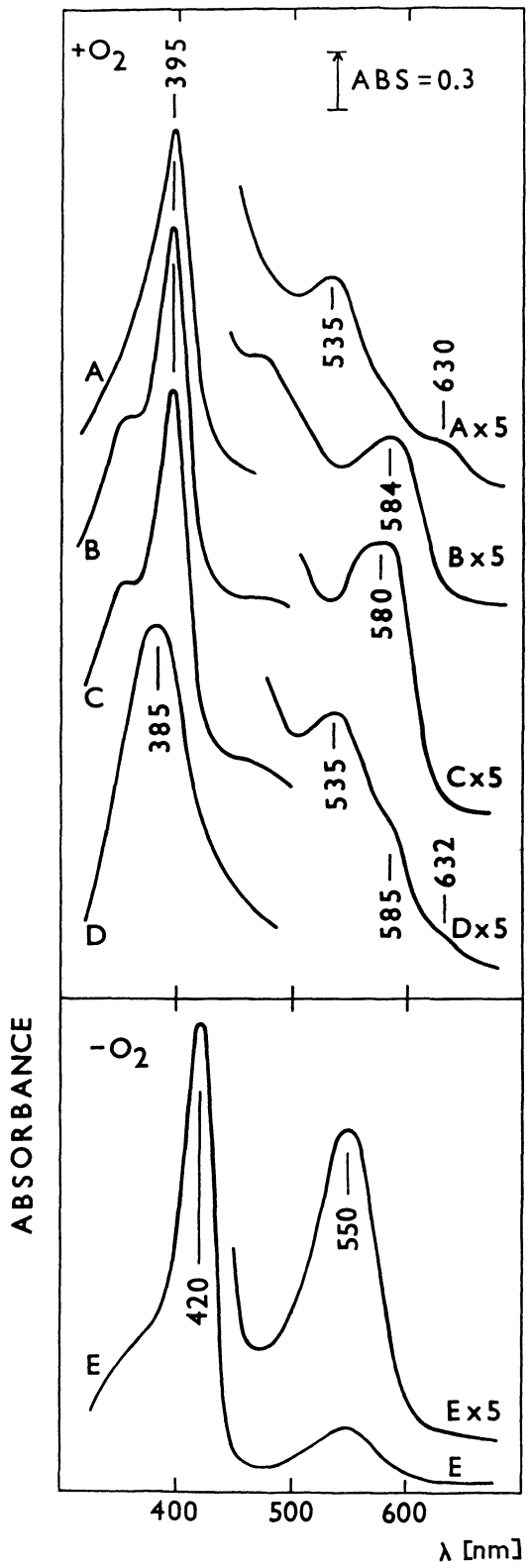

Fig. 2. Visible absorption spectra of Fe^{III}(OEP)(2MeIm) in various alcohol-containing CH_2Cl_2 solutions. A) without alcohol, B) MeOH (EtOH and *n*-PrOH are the same as this), C) *i*-PrOH, D) *t*-BuOH, E) MeOH (EtOH, *n*-PrOH, and *i*-PrOH are the same as this). Spectra A through D (upper panel) were obtained in the presence of oxygen but spectrum E (lower panel) was obtained under anaerobic conditions.

Fe^{III}(OEP)(2MeIm) (Fig. 2B). In the case of 2-propanol (*i*-PrOH) the new band was appreciably broader at 580 nm (Fig. 2C). A spectral change recognized for *t*-butyl alcohol (*t*-BuOH) was quite small in the 500—600 nm region as shown by Fig. 2D, but the shape of the Soret band was altered. When these solutions were brought to anaerobic conditions and subjected to light illumination at 380—450 nm, the spectrum shown in the lower panel (Fig. 2E) was obtained. It gave strong Soret band at 420 nm and weak Q band at 550 nm and the whole spectrum was almost the same as that of Fe^{II}(OEP)(2MeIm) prepared separately. Note that MeOH, EtOH, *n*-PrOH, or *i*-PrOH did not yield any difference in the resultant absorption spectra but *t*-BuOH did not induce the light-illumination effect. With this it changed only after long illumination of laser light at 441.6 nm; bands at 635 and 535 nm became pronounced and the Soret band shifted to red by a few nm. Consequently, it became evident that alcohols active to photoreduction cause a distinctive spectral change in the oxidized state, implying their coordination to the iron ion, but different alcohols bring no difference after photoreduction.

Since the active alcohols yield a new absorption band around 584—590 nm, RR spectra were excited at 590 nm. In contrast with the excitation at 441.6 nm, the RR spectra excited at 590 nm obtained in the absence of oxygen were the same as those obtained when it was present. The polarized RR spectra of Fe^{III}(OEP)(2MeIm)(MeOH) and its *meso*-(5, 10, 15, 20-) deuterated and ^{15}N-substituted derivatives are shown in Fig. 3 (1700—1300 cm^{-1}) and Fig. 4 (1300—900 cm^{-1}). The ν_4 band, which exhibits a downward shift by 6 cm^{-1} upon ^{15}N-substitution, appears at a typical frequency of iron(III) porphyrins (1376 cm^{-1}). Two anomalously polarized (ap) bands are seen at 1564 and 1315 cm^{-1} which are little shifted upon ^{15}N-substitution but greatly upon *meso*-deuteration; they are assigned to ν_{19} and ν_{21}, respectively.[23-25] The strong enhancement of the two ap bands is general characteristic of the Q-band excited RR spectra of metalloporphyrins.[26,27]

The highest frequency depolarized (dp) band, which exhibits a downshift by 16 cm^{-1} upon *meso*-deuteration and 5 cm^{-1} upon ^{15}N-substitution, is assigned to ν_{10}.[23-25] This band is sensitive to the coordination number;[28,29] in typical cases the five coordinate iron(III) high-spin complexes give it around 1629—1631 cm^{-1} while the six-coordinate iron(III) high-spin complexes do it around 1615—1625 cm^{-1}. Since Fe^{III}(OEP)$(CH_3OH)_2$ and Fe^{III}(OEP)$(Im)_2$ give ν_{10} at 1624 and 1640 cm^{-1}, respectively,[30] the present compounds are clearly different. For six-coordinate complexes with an oxygen of ClO_4^- and a nitrogen of pyridine derivative, which have the intermediate spin state,[28] this band is observed around 1634—1636 cm^{-1}. Therefore, the ν_{10} frequency is not unreasonable if the present compound is a six-coordinate intermediate spin complex. Its difference from the five-coordinate high-spin state is seen in the

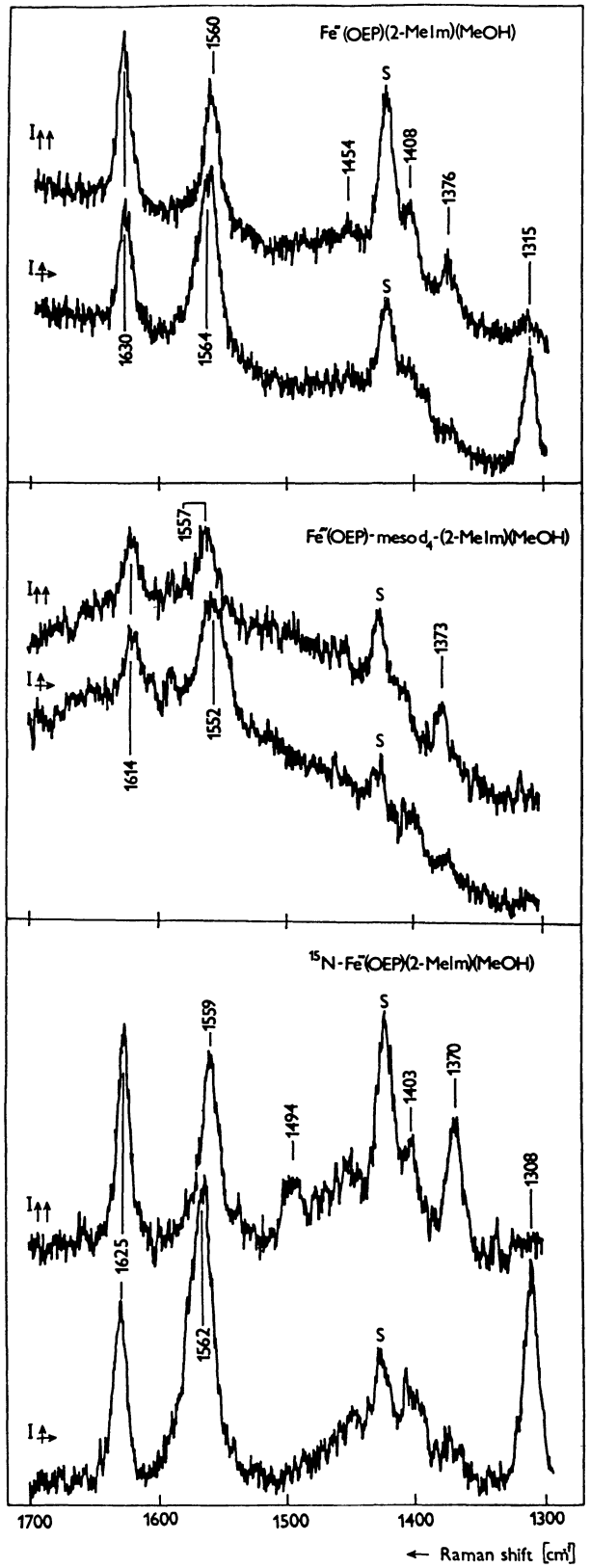

Fig. 3. Polarized RR spectra of Fe^{III}(OEP)(2MeIm)(MeOH) and its isotopic substitutes in the 1700—1300 cm^{-1} region; Fe^{III}(OEP-d_4) (2MeIm)(MeOH) (middle) and Fe^{III}(OEP-$^{15}N_4$)(2MeIm)(MeOH) (bottom). All spectra were excited at 590 nm (100 mW) under aerobic conditions. $I_{\parallel}$ and $I_{\perp}$ mean the parallel and perpendicular components, respectively.

size of deuteration shift; ^{15}N-isotope shift is much smaller (1 cm^{-1}) for five-coordinate complex[31] than for the present complex (5 cm^{-1}).

In Figure 4 an ap band is observed at 1132 cm^{-1} and is

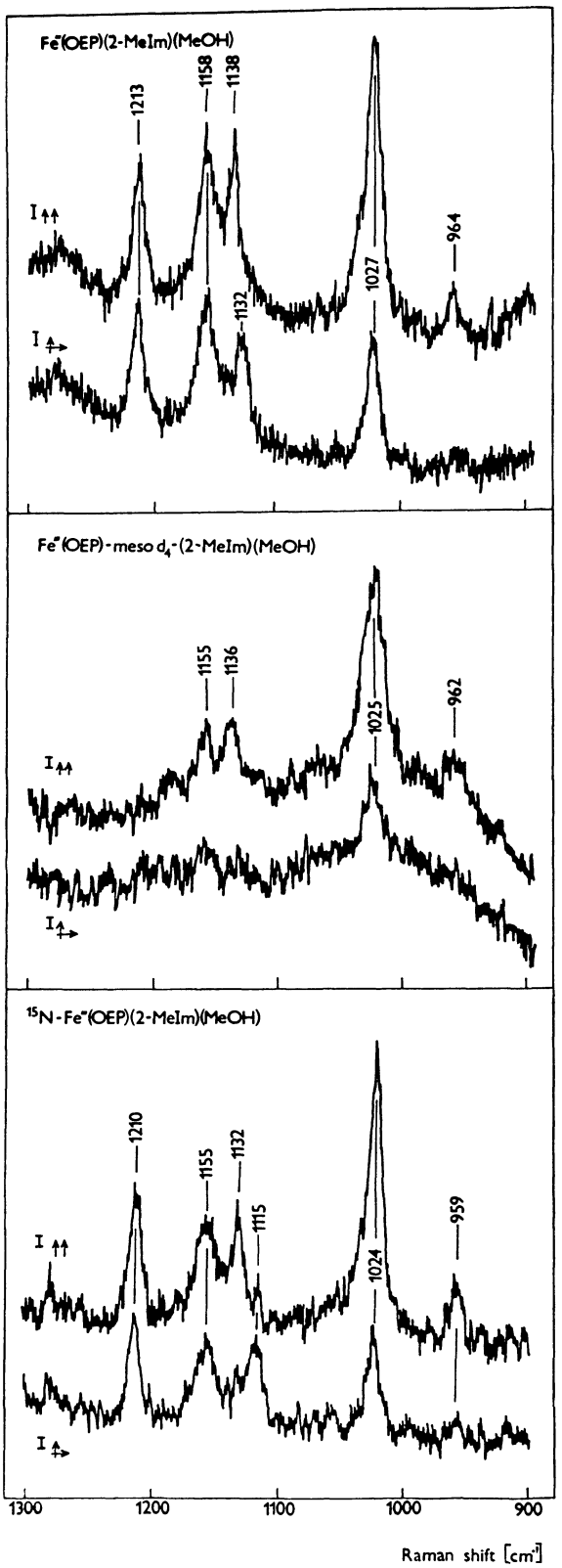

Fig. 4. The same set of spectra as in Fig. 3 but in the 1300—900 cm^{-1} region.

assigned to ν_{22}. This band is downshifted by 17 cm^{-1} upon ^{15}N-substitution for expectation of 13 cm^{-1},[24] and is thought to largely upshift to ca. 1200 cm^{-1} upon *meso*-deuteration. Two p bands at 1138 and 1027 cm^{-1} were originally assigned to a combination and ν_5 modes, respectively,[24] but recently Li et al.[25] reassigned them to ν_5 and the ethyl C–C stretching vibrations. Two dp bands at 1213 and 1158 cm^{-1} are assigned to ν_{13} and ν_{30}; ν_{13} is expected to show little shift upon ^{15}N-substitution but a large down-shift (to ca. 950 cm^{-1}) upon *meso*-deuteration, while ν_{30} is expected to show little shift upon *meso*-deuteration and appreciable down-shift (9—10 cm^{-1}) upon ^{15}N-substitution.[24,25]

The observed frequencies and isotope shifts of the alcohol complex are compared with those of Fe^{III}(OEP)(2MeIm) and Fe^{III}(OEP)Cl[31,32] in Table 1. The ν_2, ν_{21}, and ν_{22} frequencies are lower and the size of *meso*-deuteration shift of ν_{19} is distinctly larger for Fe^{III}(OEP)Cl. Therefore, even within the five coordinate ferric high-spin complexes, Fe^{III}(OEP)(2MeIm) is slightly different from Fe^{III}(OEP)Cl. The magnitude of the isotopic frequency shifts reflects the vibrational displacement of the isotope-replaced atoms in the vibration in question and accordingly it is sensitive to the vibrational mode. On the basis of the observed isotopic shifts, the vibrational modes of Fe^{III}(OEP)(2MeIm)(MeOH) are closer to those of Fe^{III}(OEP)(2MeIm) than to those of Fe^{III}(OEP)Cl. It may imply the similarity of their geometrical structure and raise a question about the coordination of MeOH to the sixth coordination position.

The evidence for alcohol coordination was obtained from the 590 nm-excited RR spectra in the lower frequency region shown in Figure 5. In the absence of MeOH, there are no prominent RR bands in the 600—400 cm^{-1} region as shown by spectrum E. When CH_3OH was added to the CH_2Cl_2 solution of Fe^{III}(OEP)(2MeIm), a new band appeared at 524 cm^{-1} as shown by spectrum B and it is shifted to a higher frequency by 4 cm^{-1} upon replacement of ^{56}Fe with ^{54}Fe as shown by spectrum A. Isotope replacement of CH_3OH with CH_3OD and CD_3OD gave rise to spectra C and D, respectively. The peak frequencies for CH_3OH and CH_3OD derivatives are definitely different, indicating that MeOH is bound in the protonated form but not in the alkoxide form. When we assume that MeOH is a single dynamic unit, a simple harmonic approximation for the Fe–MeOH stretching vibration provides the isotopic frequency shifts as follows; +3.5 cm^{-1} for ^{54}Fe, −5.0 cm^{-1} for CH_3OD, and −18.7 cm^{-1} for CD_3OD. The observed value for ^{54}Fe agrees with the expected one but those for MeOH are smaller than expected values, implying the vibrational coupling of the Fe–alcohol stretching mode with internal vibrations of MeOH. Anyway, the 524 cm^{-1} band is assigned to the Fe–MeOH stretching vibration. This band did not appear in the MeOH–CH_2Cl_2 (1 : 1 in v/v) mixed solution of Fe^{III}(OEP)Cl. It means that the 524 cm^{-1} band appears from the six-coordinated complex with MeOH and 2MeIm as axial ligands.

The excitation profile of the 524 cm^{-1} band is illustrated in Fig. 6, where relative intensities of the 524 cm^{-1} band to the solvent band at 1158 cm^{-1} are plotted against the excitation wavelengths. The relative intensities were corrected for different transmittances at 524 and 1158 cm^{-1} for each excitation wavelength on the basis of the observed transmission spectrum. The broken line in Fig. 6 indicates the background subtracted absorption spectrum for the 585-nm band which is normalized at the maximum absorption to the Raman excitation profile. The peak of Raman excitation profile is noticeably coincident with the absorption curve, suggesting strongly that the 585 nm absorption has a charge transfer character from MeOH to the Fe^{III} ion.

The Raman excitation at 585 nm within the CT band did not exhibit a trace of Raman spectrum of the reduced species; this was unexpected. This is not due to poor resonance but to nonphotoreduction. Indeed,

Table 1. Comparison of the Observed Frequencies and Isotopic Frequency Shifts of Fe^{III}(OEP)(2MeIm)(MeOH) with Those of Fe^{III}(OEP)(2MeIm) and Fe^{III}(OEP)Cl

Mode	P[a]	Fe^{III}(OEP)(2MeIm)(MeOH)			Fe^{III}(OEP)(2MeIm)			Fe^{III}(OEP)Cl		
		ν	$\Delta\nu(^{15}N)$[b]	$\Delta\nu(D)$[c]	ν	$\Delta\nu(^{15}N)$	$\Delta\nu(D)$	ν	$\Delta\nu(^{15}N)$[d]	$\Delta\nu(D)$[e]
ν_{10}	dp	1630	−5	−16	1629	−1	−13	1629	−1	−12
ν_{19}	ap	1564	−2	−12	1564	+1	−8	1568	−1	−21
ν_2	p	1560	−1	−3	1559	+2	0	1582	−1	−1
ν_{29}	dp	1408	−5					1405	−1	−2
ν_4	p	1376	−6	−3				1374	−5	−1
ν_{21}	ap	1315	−7		1315	−5		1306	−2	
ν_{13}	dp	1213	−3		1218	+3		1210	0	
ν_5	p	1138	−6	−2				1135	−3	+1
ν_{22}	ap	1132	−17					1125	−17	
C_1–C_2	p	1027	−3	−2	1025	0	0	1025	−1	+2
		964	−5	−2				964	−4	+3

a) Polarization property; p. polarized, dp. depolarized; ap, anomalously polarized. b) Isotopic shift upon ^{15}N-substitution. c) Isotopic shift upon *meso*-deuteration. d) From Ref.18. e) From Ref. 19.

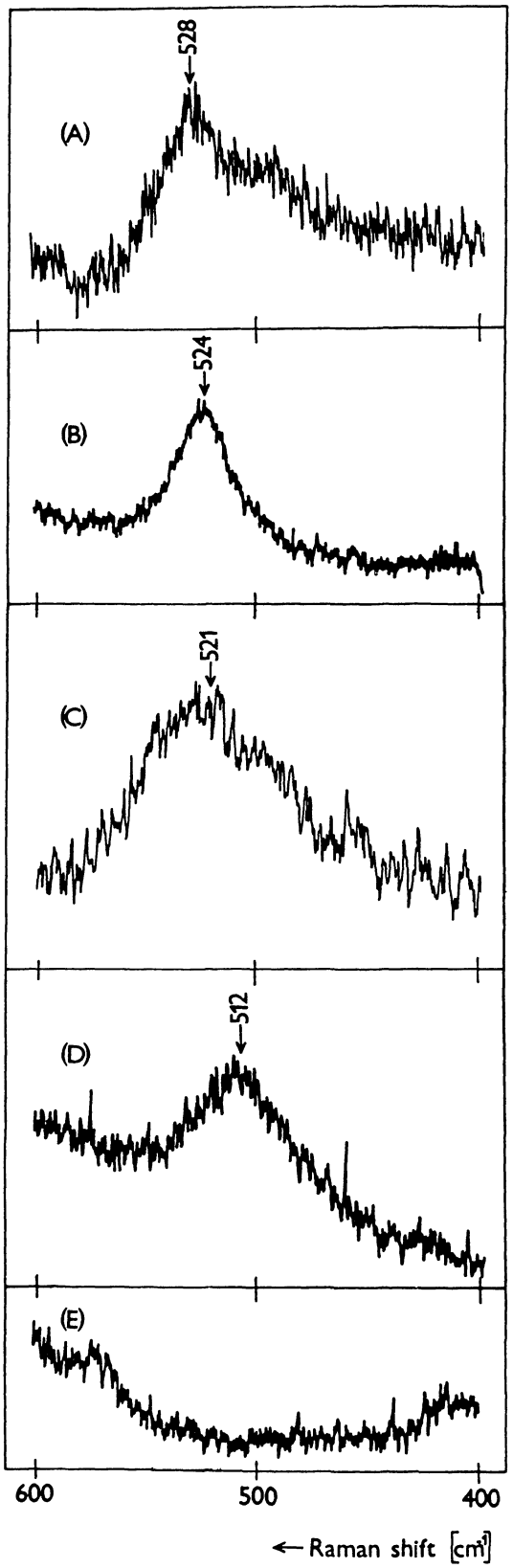

Fig. 5. Dependence of the 524 cm^{-1} RR band on isotopic substitutions. A) $^{54}Fe(OEP)(2MeIm)(CH_3OH)$, B) $Fe^{III}(OEP)(2MeIm)(CH_3OH)$, C) $Fe^{III}(OEP)(2MeIm)(CH_3OD)$, D) $Fe^{III}(OEP)(2MeIm)(CD_3OD)$, E) $Fe^{III}(OEP)(2MeIm)$ without methanol. All spectra were obtained with the 590 nm excitation line (100 mW) under aerobic conditions.

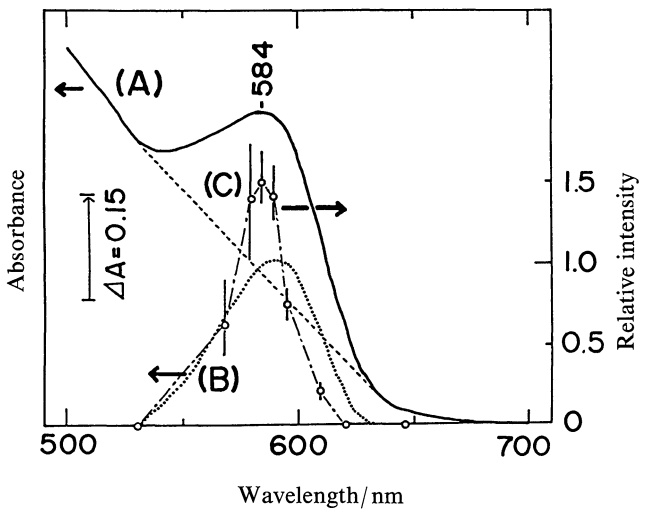

Fig. 6. Comparison of the excitation profile of the 524 cm^{-1} RR band of $Fe^{III}(OEP)(2MeIm)(MeOH)$ with the absorption profile of the new band. A) Observed absorption curve, B) Approximate absorption profile of the new band that was obtained by subtracting an extrapolated tail (indicated by a broken line) of absorption from curve (A). The ordinate scale is illustrated by an arrow. C) Excitation profile of the 524 cm^{-1} RR band represented in terms of its relative intensity to the solvent band at 1158 cm^{-1}.

the anaerobic sample illuminated by laser light around 570—610 nm did not yield a change of visible absorption spectrum. Therefore, the mechanism of the photoreduction of $Fe^{III}(OEP)(2MeIm)(MeOH)$ is distinct from a trivial photoreduction in which the electron transfer takes place via a CT excited state.

Since no photoreduction was observed by a Raman spectrum in the presence of oxygen, we pursued the time course of the phenomenon by using transient absorption spectroscopy. The results are shown in Fig. 7(A), where a change of absorption at 420 nm is drawn against time; (a) and (b) were obtained in the absence and presence of oxygen, respectively, for the MeOH containing solution while (c–e) were obtained in the presence of oxygen for various alcohol-containing solutions; EtOH (c), *i*-PrOH (d) and *n*-PrOH (e). Since the reduced species has the absorption maximum at 420 nm, the increase of absorption at $t=0$, when the laser pulse at 355 nm with 10 ns duration was fired, indicates that photoreduction has occurred. It is apparent that the photoreduction takes place irrespective of the presence or absence of oxygen. In the presence of oxygen (b–e), however, it is reoxidized in 50 ms, while the reduced state lasts in its absence (a). The rate of oxidation depends on the O_2 concentration. The individual curves shown in Fig. 7A(b–e) are well reproduced by a single exponential decay curve with an arbitrary time constant (the determined values are cited in the figure captions) as illustrated by thin solid lines in Fig. 7A. The curve displayed in Fig. 7(B) was observed for the

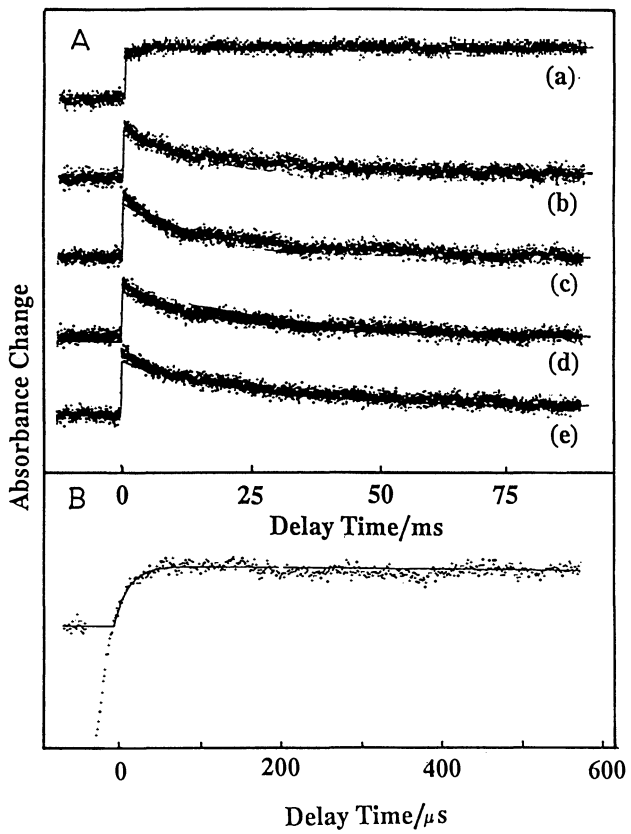

Fig. 7. Time profile of the absorbance at 420 nm after photolysis by the 355 nm pulse (10 ns width). A) (a) Fe^{III}(OEP)(2MeIm)(MeOH) under anaerobic conditions. (b) Fe^{III}(OEP)(2MeIm)(MeOH), (c) Fe^{III}(OEP)(2MeIm)(EtOH), (d) Fe^{III}(OEP)(2MeIm)-(*n*-PrOH), (e) Fe^{III}(OEP)(2MeIm)(*i*-PrOH). All spectra for (b—e) were obtained under the same aerobic conditions. The thin solid lines were calculated by assuming the single exponential decay; the decay constants are 17.9 ms for MeOH, 16.5 ms for EtOH, 20.7 ms for *n*-PrOH, and 25.0 ms for *i*-PrOH under an atmospheric pressure. B) Time profile in the shorter delay time region of (A-a). The solid line indicates the calculated curve obtained by assuming that both the rise and decay are single exponential; τ_{rise}=14.1 μs and τ_{decay}=15.8 ms.

MeOH containing solution on shorter time scale. The thin solid line was obtained by assuming that both the rise and decay are single exponential. This suggests that the photoreduction occurs with a time constant of 17 μs. The apparently slow photoreaction implicates that it involves ligand replacement besides simple electron transfer.

Discussion

The photoreduction described here has two characteristics; cooperative action of axial ligands and no photoreducibility under the CT excitation. When Im or 1-MeIm are present besides alcohol, it forms a biscoordinate complex and alcohol cannot bind to the axial position due to its weak ligand field. Accordingly, photoreduction does not occur. On the other hand, when Fe^{III}(OEP)Cl is dissolved in CH_2Cl_2–MeOH mixed solvent, MeOH is considered to bind to the iron ion but photoreduction was not seen. Therefore, simultaneous coordinations of a N base and an alcohol are required for photoreduction to occur. The next question is what is an electron donor?

The primary and secondary alcohols were effective but a tertiary alcohol was not. One interpretation assumes a role of C_α-hydrogen of alcohol, which occasionally serves as a reductant.[10,33] This would be likely if *t*-BuOH were bound to the sixth coordination position but photoreduction did not occur. Actually, however, *t*-BuOH gave neither the CT absorption band nor the Fe–alcohol stretching RR band, and therefore it is more reasonable to deduce that *t*-BuOH was not bound to the iron ion. The coordination of *t*-BuOH to the iron ion is probably inhibited by steric hindrance between CH_3 hydrogen and pyrrole nitrogen. An alternative interpretation is to regard an N base as an electron donor as postulated in the previous study.[17] In order to determine the alternative we carried out gas chromatographic analysis of the photoreduced solution. The product was not a simple compound like formaldehyde and acetone. Unfortunately, however, we failed to identify the product by this analysis. The requirement is to prepare an enough of the product to determine its NMR spectrum.

Upon excitation of Raman scattering within the new absorption band around 590 nm, both the Fe–alcohol stretching RR band and the ordinary porphyrin bands characteristic for the Q band excitation[26,27] were observed. Therefore, the 585 nm absorption band should have a CT character besides the porphyrin $\pi\pi^*$ character. The fact that the laser illumination in the 550—600 nm region did not induce photoreduction may imply alcohol is not an electron donor.

The Fe–2MeIm stretching RR band for Fe^{II}(OEP)(2MeIm) was observed at 206 cm^{-1} upon excitation at 441.6 nm[17] but not upon red excitations. We failed to observe the Fe^{III}-2MeIm stretching RR band and therefore it is not clear where a CT band from 2MeIm to Fe^{III} is located. If it were present below 450 nm, the occurrence of photoreduction would be reasonably explained in terms of the CT excited state from 2MeIm to the Fe^{III} ion. Anyway, elucidation of photoreduction mechanism of iron porphyrin as well as heme proteins requires further study and the pump/probe time-resolved RR experiments for determining the structure of photoreduction intermediates are currently under investigation in this laboratory.

The authors thank Professor Y. Ozaki of Kwansei Gakuin Univ. for stimulating discussion and Dr. T. Ohta of chemical material center of this institute for the gas chromatographic analysis of solvents and products. V. F. is indebted to IMS for financial support during his stay in IMS at Okazaki.

References

1) F. Adar and T. Yonetani, *Biochim. Biophys. Acta,* **502**, 80 (1978).
2) I. Salmeen, L. Rimai, and G. T. Babcock, *Biochemistry,* **17**, 800 (1978).
3) T. Kitagawa and Y. Orii, *J. Biochem. (Tokyo),* **84**, 1245 (1978).
4) T. Ogura, N. Sone, K. Tagawa, and T. Kitagawa, *Biochemistry,* **23**, 2826 (1984).
5) T. Kitagawa and K. Nagai, *Nature (London),* **281**, 503 (1979).
6) T. Kitagawa, S. Chihara, K. Fushitani, and H. Morimoto, *J. Am. Chem. Soc.,* **106**, 1860 (1984).
7) S. Yoshikawa, H. Mochizuki, S. Chihara, B. Hagihara, and T. Kitagawa, *Biochim. Biophys. Acta,* **786**, 267 (1984).
8) J. T. Sage, D. Morikis, and P. M. Champion, *J. Chem. Phys.,* **90**, 3015 (1989).
9) A. Harriman and G. Porter, *J. Chem. Soc., Faraday Trans.,* **75**, 1543 (1979).
10) C. Bartocci, F. Scandola, A. Ferri, and V. Carassiti, *J. Am. Chem. Soc.,* **102**, 7067 (1980).
11) C. Bartocci, A. Maldotti, O. Traverso, C. A. Bignozzi, and V. Carassiti, *Polyhedron,* **2**, 97 (1983).
12) A. Maldotti, C. Bartocci, R. Amadelli, and V. Carassitti, *Inorg. Chim. Acta,* **74**, 275 (1983).
13) C. Bizet, P. Morliere, D. Brault, O. Delgado, M. Bazin, and R. Santus, *Photochem. Photobiol.,* **34**, 315 (1981).
14) M. Hoshino, S. Konishi, and M. Imamura, *Bull. Chem. Soc. Jpn.,* **57**, 1713 (1984).
15) T. Imamura, T. Jin, T. Suzuki, and M. Fujimoto, *Chem. Lett.,* **1985**, 847.
16) K. Kalyanasundaram, *J. Photochem. Photobiol., A Chem.,* **42**, 87 (1988).
17) Y. Ozaki, K. Iriyama, H. Ogoshi, and T. Kitagawa, *J. Am. Chem. Soc.,* **109**, 5583 (1987).
18) T. Ogura, V. Fidler, Y. Ozaki, and T. Kitagawa, *Chem. Phys. Lett.,* **169**, 457 (1990).
19) V. Fidler, T. Ogura, S. Sato, and T. Kitagawa, in Proceedings of the VIth Intl. Conf. on Energy and Electron Transfer, Prague, **2**, 170 (1989).
20) H. Ogoshi, E. Watanabe, Z. Yoshida, J. Kincaid, and K. Nakamoto, *J. Am. Chem. Soc.,* **95**, 2845 (1973).
21) H. Ogoshi, H. Sugimoto, and Z. Yoshida, *Bull. Chem. Soc. Jpn.,* **54**, 3414 (1984).
22) T. Ogura and T. Kitagawa, to be published.
23) T. Kitagawa, M. Abe, and H. Ogoshi, *J. Chem. Phys.,* **69**, 4516 (1978).
24) M. Abe, T. Kitagawa, and Y. Kyogoku, *J. Chem. Phys.,* **69**, 4526 (1978).
25) X-Y. Li, R. S. Czernuszewicz, J. R. Kincaid, P. Stein, and T. G. Spiro, *J. Phys. Chem.,* **94**, 47 (1990).
26) T. Kitagawa and Y. Ozaki, *Struct. Bonding,* **64**, 71 (1987).
27) T. G. Spiro and X-Y. Li, in "Biological Application of Raman Spectroscopy," ed by T. G. Spiro, John Wiley & Sons, New York (1987), Vol. 3, Chap. 1.
28) J. Teraoka and T. Kitagawa, *J. Phys. Chem.,* **84**, 1928 (1980).
29) T. G. Spiro, J. D. Stong, and P. Stein, *J. Am. Chem. Soc.,* **101**, 2648 (1979).
30) Y. Ozaki, K. Iriyama, H. Ogoshi, T. Ochiai, and T. Kitagawa, *J. Phys. Chem.,* **90**, 6105 (1986).
31) T. Kitagawa, M. Abe, Y. Kyogoku, H. Ogoshi, H. Sugimoto, and Z. Yoshida, *Chem. Phys. Lett.,* **48**, 55 (1977).
32) T. Kitagawa, H. Ogoshi, E. Watanabe, and Z. Yoshida, *Chem. Phys. Lett.,* **30**, 451 (1975).
33) K. Hatano, K. Usui, and Y. Ishida, *Bull. Chem. Soc. Jpn.,* **54**, 413 (1981).

 © 1991 The Chemical Society of Japan Bull. Chem. Soc. Jpn., 64, 2323—2327 (1991)

Emission Spectra of Fluorobenzenes by Controlled Electron Impact

Takahiro FUKUZUMI, Keiji NAKASHIMA, and Teiichiro OGAWA*
Department of Molecular Science and Technology, Kyushu University, Kasuga-shi, Fukuoka 816
(Received May 15, 1991)

The fluorescence emission spectra of fluorobenzene, *p*-difluorobenzene and hexafluorobenzene excited in collisions with electrons were measured for the study of the dynamics of the exciting aromatic system. These spectra showed a band assignable to the $S_1 \rightarrow S_0$ transition of the parent molecule. The bands of fluorobenzene and *p*-difluorobenzene were intense and showed a pronounced vibrational structure and the intense vibrational transitions were optically allowed. Whereas, that of hexafluorobenzene was broad and weak and did not show any clear vibrational structure.

An electron impact method has a distinctive advantage over a photoexcitation method in the excitation to highly-excited states, to optically-forbidden states and to triplet states. An interaction between an electron and a molecule is the simplest case of a chemical reaction and the elementary process in the plasma. Many organic compounds have been investigated by means of the electron impact method. Aromatic compounds have shown an intense optical emission of the S_1–S_0 transition of the parent molecule as well as bands of the fragment species such as H*, CH*, and C_2*.[1,2] Their exciting processes have been investigated and differences between the spectra excited by electrons and those by photons were revealed.[1]

Electrons can induce both optically allowed and forbidden transitions when the energy of the incident electron is close to the threshold energy of an excitation process.[3] The emission spectrum of benzene by controlled electron impact was different from the one by the photoexcitation;[4] the vibrational structure due to the $6^0 1^n$ series, which was symmetry forbidden for optical excitation, was clearly observed in the former at the electron energy of 25 eV.[5] However, comparisons of the spectra of other aromatic compounds by electron impact with those by photoexcitation remain as a subject of research.

Fluorobenzene (C_6H_5F) and *p*-difluorobenzene (*p*-$C_6H_4F_2$) have both a large optical absorption cross section and fluorescence quantum yield, and the vibrational structure of their absorption[6,7] and the fluorescence[8,9] spectra has been discussed in detail. Hexafluorobenzene (C_6F_6) showed no vibrational structure in both the absorption[10] and the fluorescence[11] spectra, although the excitation process of C_6F_6 would be expected to be identical with benzene since C_6F_6 has the same symmetry (D_{6h}). Though the emission spectrum of C_6H_5F by controlled electron impact has already been measured at 200 eV,[12] no detailed investigation on the excitation process has been reported.

In the present paper the optical emission spectra of C_6H_5F, *p*-$C_6H_4F_2$ and C_6F_6 were measured in the 250—450 nm region under the electron impact excitation as an extension of our investigation[2,12] on aromatic compounds. The electron energy dependence of the emission spectrum was also measured since the optically forbidden bands will become intense as the electron energy is decreased.[3] The vibrational structure of the S_1–S_0 transition of the parent molecule was also measured at 24 eV in order to compare it with that obtained by photoexcitation.

Experimental

The apparatus is almost identical with that described previously.[2,13] In brief, the collision chamber (20 cm) was evacuated with a 10 cm oil-diffusion pump (650 $dm^3 s^{-1}$) having a liquid nitrogen trap. The sample gas was introduced into a gas cell, and was collided with an electron beam from a tungsten filament. The base pressure was of the order of 10^{-6} Torr (1 Torr=133 Pa) and the operating pressure in the gas cell was kept at about 3×10^{-3} Torr for a single collision condition to be valid.

The optical emission was observed through a quartz window at an angle of 90° with respect to the electron beam. The overall spectrum was obtained with a SPEX MINIMATE 1670 monochromator and the high-resolution spectrum with a SPEX 1269 monochromator equipped with a 1200 grooves/mm grating blazed at 300 nm and a Hamamatsu R585 photomultiplier. Photons were counted with a Hamamatsu C1230 photon counter. When the optical emission was very weak, the electron beam was pulsed so that stray radiation from the tungsten filament could be subtracted (a digital boxcar technique). A JASCO CT-50 monochromator equipped with a 1200 grooves/mm grating blazed at 300 nm and an NF PC545 photon counter were used in such cases so as to obtain a medium-resolution spectrum with a high detection efficiency.

The instrumental response of the optical system was calibrated with a Hamamatsu L591 standard deuterium lamp. The electron energy was calibrated with the peak of N_2* (337.1 nm) at 14.02 eV and its energy resolution was about ±1—2 eV at 11eV.

C_6H_5F was obtained from the Nakarai Chemicals, Ltd. and *p*-$C_6H_4F_2$ and C_6F_6 were obtained from the Wako Pure Chemical Industries, Ltd. Each sample was frozen and pumped repeatedly to remove any dissolved gases.

Results and Discussion

Mono and Difluorobenzene. Typical emission spectra of C_6H_5F and *p*-$C_6H_4F_2$ in the 250—450 nm region with an optical resolution of 1.0 nm are shown in Fig. 1

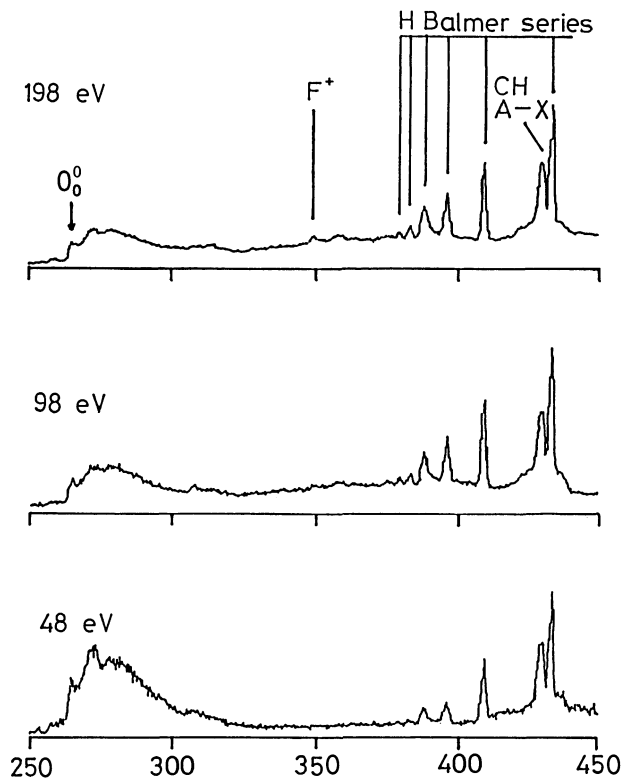

Fig. 1. Emission spectra of fluorobenzene by controlled electron impact measured by a SPEX MINIMATE 1670 monochromator. Optical resolution: 1.0 nm, electron beam current: 2—10 μA.

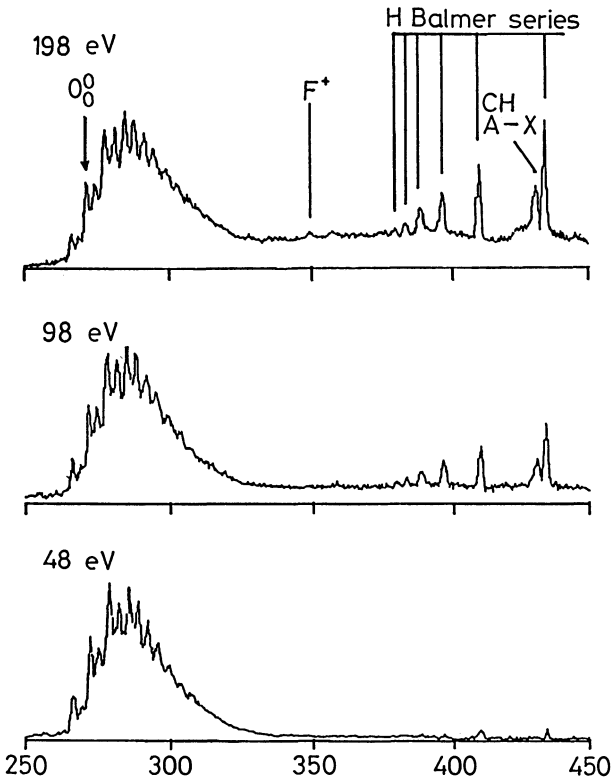

Fig. 2. Emission spectra of *p*-difluorobenzene by controlled electron impact measured by a SPEX MINIMATE 1670 monochromator. Optical resolution: 1.0 nm, electron beam current: 2—10 μA.

and Fig. 2, respectively. An intense band at 260—320 nm was assigned to the transition from the lowest-excited singlet state (S_1) to the ground state (S_0), since an optical fluorescence spectrum was located in the same region.[8,9] The excitation functions of these bands were also measured and the threshold energies were found at 4.4 eV and 4.1 eV, respectively; they agree well with the absorption edge[6,7] of the two molecules within experimental errors.

In the wavelength region longer than 350 nm, there are several lines and bands of excited fragment species as in the case of other aromatic molecules.[2] They have been assigned to H (the Balmer lines), F^+ ($3p^5\,P$–$3d^5\,D$), and CH (the A–X transition), as shown in the figures. No CF* (A–X) emission at 220—280 nm was observed; whereas, it was intense in the spectra of CF_4 excited by $He(2^3S)$, He^+, and He_2^+.[14] At higher incident electron energy, a continuous emission becomes clear in the region longer than 320 nm. This may be due to the excited fragment species made of 3—4 atoms such as C_2H^* and C_2F^*; C_6F_6 shows this continuous emission as will be mentioned later.

As the electron energy increases, the dipole Born approximation becomes valid, the optically allowed transition becomes dominant, and finally the process would be equivalent to the photoexcitation process.[3] For example, the $S_0(^1A_{1g})$–$S_1(^1B_{2u})$ excitation of benzene is the symmetry-forbidden transition; this band almost disappears at 100 eV.[2,15] On the other hand, the corresponding transitions of toluene and *p*-xylene are no longer optically forbidden because of their descending symmetry (C_{2v} or D_{2h}), and they are intense even at higher energy.[16] The spectra of C_6H_5F and *p*-$C_6H_4F_2$ would be similar to those of toluene and *p*-xylene. Indeed, the S_1–S_0 emission of these molecules is intense at higher energy as shown in Figs. 1 and 2. A rough estimate of the S_1–S_0 emission intensity can be done in comparison with the intensity of the Balmer line.[17] At the electron beam energy of 50 eV, the relative S_1–S_0 emission intensity of C_6H_5F and *p*-$C_6H_4F_2$ is about 2 times and 40 times as large as that of benzene, respectively.

Hexafluorobenzene. Typical emission spectra of C_6F_6 in the 250—470 nm region are shown in Fig. 3. At an excitation energy of 9 eV, the emission spectrum of C_6F_6 shows a broad band in the 290—470 nm region; this spectrum is noisy in the region longer than 450 nm owing to an intense stray radiation from the tungsten filament. This broad band was assigned to the S_1–S_0 transition since its fluorescence spectrum was located in the same region.[11] The threshold energy could not be measured owing to its small intensity. The fluores-

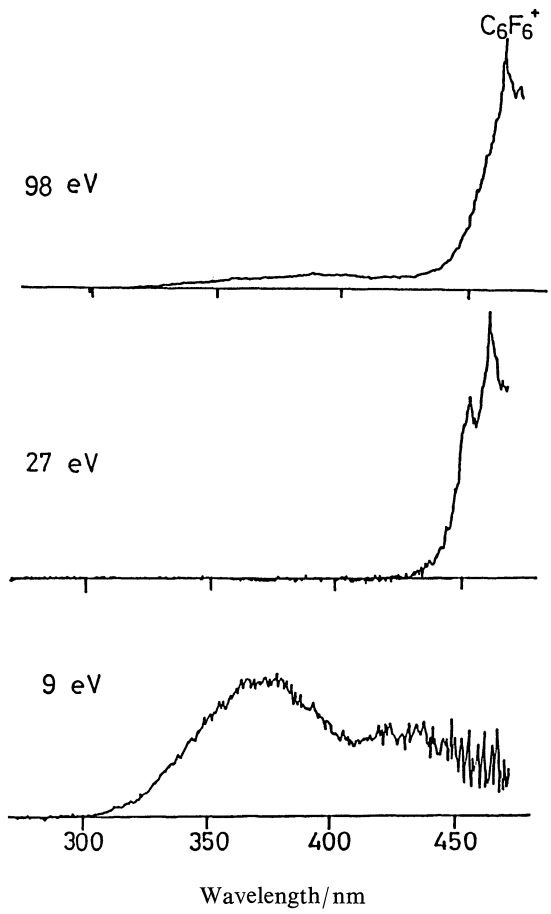

Fig. 3. Emission spectrum of hexafluorobenzene by controlled electron impact. 9 eV: The electron beam was pulsed to subtract the stray radiation. Optical resolution: 3.0 nm, monochromator used: JASCO CT-50, electron beam current: 8—10 μA. 27 eV and 98 eV: The electron beam was direct. Optical resolution: 1.0 nm, monochromator used: SPEX MINIMATE 1670, electron beam current: 2—5 μA.

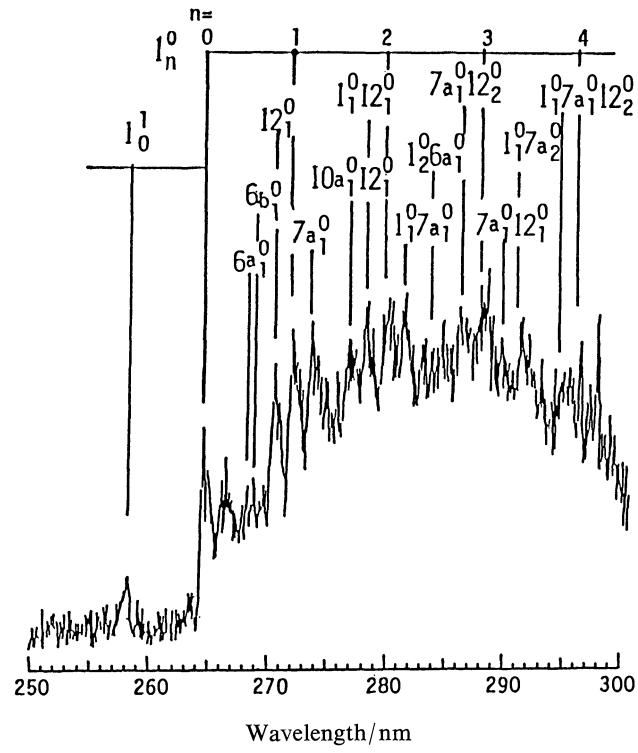

Fig. 4. High-resolution emission spectrum of fluorobenzene by controlled electron impact measured by a SPEX 1269 monochromator. Optical resolution: 0.20 nm, electron energy: 24 eV, electron beam current: 3 μA.

cence quantum yield of C_6F_6 is 1.4×10^{-3} (excited by a medium-pressure mercury arc at 235 nm).[11] Such a small value is consistent with the observed weakness of the emission of the parent molecule. The observation of this band of C_6F_6 was made possible by lowering the electron beam energy to 9 eV so as to remove all bands of the fragment species and of the parent ion which has a threshold energy of 12.56 eV.[18] There are, however, some contributions of the parent ion in the spectrum due to a low energy resolution of the electron beam at 9 eV.

At excitation energies of 27 and 98 eV, in contrast with C_6H_5F and *p*-$C_6H_4F_2$, C_6F_6 shows no detectable optical emission of the S_1–S_0 transition but shows intense bands of the parent molecule ion ($C_6F_6^+$).[18] A continuous band, which has a peak at about 400 nm, is also shown in the region longer than 320 nm at the electron energy of 98 eV. This band can be assigned to the emission of the excited fragment species made of 3—4 atoms as in the case of the other two molecules, since a fluorescence spectrum by photoexcitation was located nearly in the same region (ca. 290—470 nm) with a peak at 365 nm[11] and the threshold energy of this band is considerably higher. No CF* emission was also observed as in the case of the other two molecules.

Vibrational Structure. The high-resolution emission spectra of the S_1–S_0 transition of these molecules were also measured and are compared with those obtained by photoexcitation. A typical spectrum of C_6H_5F and that of *p*-$C_6H_4F_2$ with an optical resolution of 0.20 nm are shown in Figs. 4 and 5. The vibrational structure was well resolved and assigned by referring to the fluorescence spectra by the photoexcitation[8,9] as partly described in the figures with the Wilson notation.[19] However, no vibrational structure was resolved for C_6F_6 in the spectrum taken at a resolution of 0.60 nm.

C_6H_5F shows the following bands:[20] 6a (517 cm^{-1} at S_0), 6b (612), 16a (411), 12 (808), 1 (1012), 18a (1030), 9a (1153), 7a (1220), and C–F stretching (824), and combinations of these bands such as 1_n^0, $12_1^0 1_n^0$, $6a_1^0 1_n^0$, $6b_1^0 1_n^0$, $6b_1^0 12_1^0 1_n^0$, $7a_1^0 1_n^0$, $6b_1^1 1_n^0$, $6b_2^1 12_1^0 1_n^0$, $6b_1^1 7a_0^1 1_n^0$, and $6b_2^1 1_n^0$. *p*-$C_6H_4F_2$ shows the following bands:[21] 6a (451), 6b (507), 16a (370), 1 (859), and 7a (1245), and combinations of these bands such as 1_n^0, $7a_1^0 1_n^0$, $7a_1^0 16a_1^1 1_n^0$, $16a_1^1 7a_n^0$, $16a_1^1 1_n^0$, and $1_1^0 7a_n^0$. Since *p*-$C_6H_4F_2$ has higher symmetry than C_6H_5F, its vibrational structure is simpler than that of C_6H_5F. The bands due to the skeletal vibration are

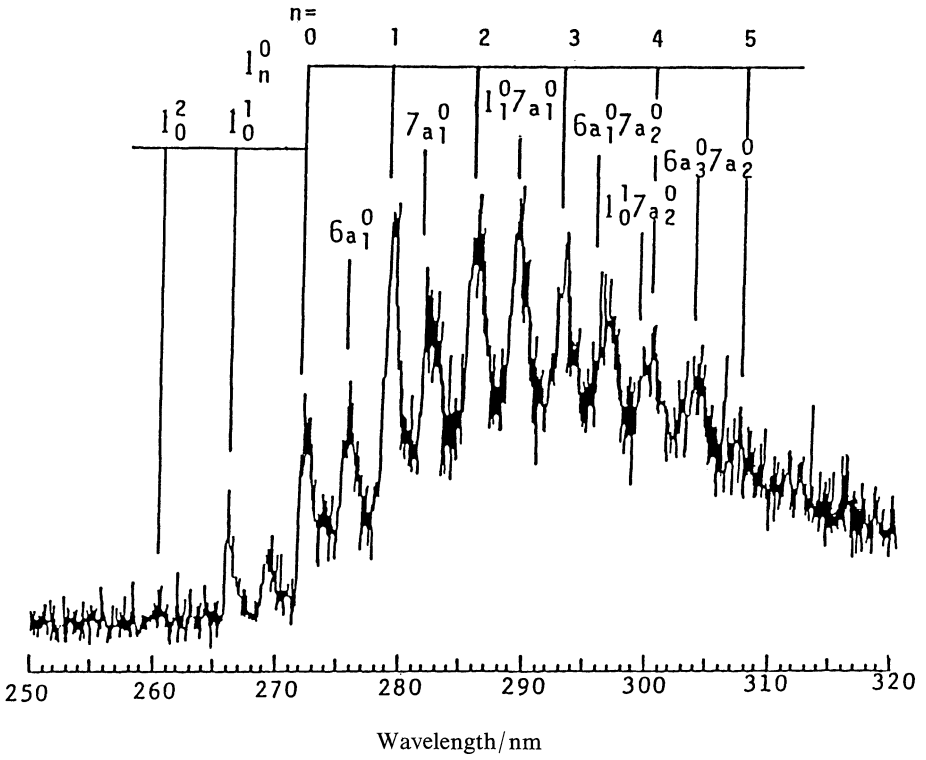

Fig. 5. High-resolution emission spectrum of *p*-difluorobenzene by controlled electron impact measured by a SPEX 1269 monochromator. Optical resolution: 0.20 nm, electron energy: 24 eV, electron beam current: 3 μA.

intense in both molecules. Furthermore, the bands from the vibrationally excited states of the S_1 state (1^n_0 series and combinations with them) are also shown although these hot bands did not appear in the spectra excited by monochromatic light even at a low operating pressure.[8,9] This finding is characteristic of the excitation process by electron impact.

Although benzene showed the optically forbidden ($6^0 1^n$ series) vibrational bands,[5] major bands observed for C_6H_5F and *p*-$C_6H_4F_2$ are due to optically allowed transitions; they were also found in the fluorescence spectra[8,9] and/or the SVL spectra[19] by photoexcitation. The optically-forbidden transitions of C_6H_5F and *p*-$C_6H_4F_2$ are the out-of-plane vibrations, and their Franck–Condon factors are small, thus, the transitions from the S_0 state to these modes in the S_1 state would be very weak. Indeed, benzene also showed no band assignable to an out-of-plane mode.[5]

On the other hand, C_6F_6 does not show any vibrational bands though it has the same symmetry with benzene. None of the optical absorption,[10] the fluorescence[11] and the electron energy loss[22] spectra of C_6F_6 shows vibrational structure. It has been suggested that upon fluorination $\pi \rightarrow \pi^*$ transitions will not show any substantial shift and $\pi \rightarrow \sigma^*$ transitions will be red shifted.[10] As a result of this shift, the $^1A_{1g} \rightarrow {}^1B_{2u}$ transition and the $\pi \rightarrow \sigma^*$ transition (the C band[22]) would overlap[10,22] and the band becomes broad and structureless.

The authors thank Professor Yukio Nishimura for the use of his standard deuterium lamp and Dr. Masaaki Fujii of Tohoku University for his useful discussion on the excited states of C_6F_6. The present work was partially supported by a Grant-in-Aid for Scientific Research on Priority Area Nos. 62606519, and 63606512 from the Ministry of Education, Science and Culture.

References

1) T. Ogawa, *Eng. Sci. Repts. Kyushu Univ.*, **7**, 231 (1986).
2) T. Ogawa, N. Yamami, M. Tsuji, and Y. Nishimura, *Bull. Chem. Soc. Jpn.*, **54**, 1203 (1981).
3) K. Takayanagi, "Electron-Molecule Collisions," ed by I. Shimamura and K. Takayanagi, Plenum Press, New York (1984), Chap. 1.
4) W. H. Smith, *J. Chem. Phys.*, **54**, 4169 (1971).
5) H. Kawazumi, T. Oomori, N. Yamami, and T. Ogawa, *Chem. Phys. Lett.*, **106**, 351 (1984).
6) S. H. Wollman, *J. Chem. Phys.*, **14**, 123 (1946).
7) C. D. Cooper, *J. Chem. Phys.*, **22**, 503 (1954).
8) A. M. Bass and H. Sponer, *J. Opt. Soc. Am.*, **40**, 389 (1950).
9) A. H. Delsemme and J. Duchene, *Compt. Rend.*, **234**, 612 (1952).
10) J. Philis, A. Bolovinos, G. Andritsopoulos, E. Pantos, and P. Tsekeris, *J. Phys. B*, **14**, 3621 (1981).
11) D. Phillips, *J. Chem. Phys.*, **46**, 4679 (1967).
12) T. Ogawa, M. Tsuji, M. Toyoda, and N. Ishibashi, *Bull. Chem. Soc. Jpn.*, **46**, 1063 (1973).
13) T. Ogawa, H. Tomura, K. Nakashima, J. Kurawaki,

and H. Kawazumi, *J. Spectrosc. Soc. Jpn.*, **35**, 303 (1986).
14) T. Mizuguti, Master Thesis, Kyushu University, Fukuoka, Japan, 1982.
15) K. C. Smyth, J. A. Schiavon, and R. S. Freund, *J. Chem. Phys.*, **61**, 4747 (1974).
16) T. Ogawa, M. Tsuji, M. Toyoda, and N. Ishibashi, *Bull. Chem. Soc. Jpn.*, **46**, 2637 (1973).
17) D. A. Vroom and F. J. de Heer, *J. Chem. Phys.*, **50**, 573 (1969).
18) M. Allan and J. P. Maier, *Chem. Phys. Lett.*, **34**, 442 (1975).
19) R. A. Coveleskie and C. S. Parmenter, *J. Mol. Spectrosc.*, **86**, 86 (1981).
20) D. C. Smyth, E. E. Ferguson, R. L. Hudson, and J. R. Nielsen, *J. Chem. Phys.*, **21**, 1475 (1953).
21) E. E. Ferguson, R. L. Hudson, J. R. Nielsen, and D. C. Smyth, *J. Chem. Phys.*, **21**, 1457 (1953).
22) R. P. Frueholz, W. M. Flicker, O. A. Mosher, and A. Kuppermann, *J. Chem. Phys.*, **70**, 3057 (1979).

Combustion Reactions in Silane-Air Flames I. Flat Premixed Flames

Seishiro FUKUTANI,* Yasuhiro UODOME, Nílson KUNIOSHI, and Hiroshi JINNO†
Department of Industrial Chemistry, Faculty of Engineering, Kyoto University, Yoshida-honmachi, Sakyo-ku, Kyoto 606
†Department of Chemistry, Faculty of Science and Engineering, Sophia University, Kioicho 7-1, Chiyoda-ku, Tokyo 102
(Received April 1, 1991)

In this work the combustion mechanism of silane–air flames is elucidated through a simulation employing a detailed chemical scheme. Two different pathways for the consumption of silane were found: $SiH_4 \rightarrow SiH_3 \rightarrow SiH_2O \rightarrow HSiO$, which proceeds in low-temperature regions, and $SiH_4 \rightarrow SiH_2 \rightarrow HSiO$, occurring at high temperatures; this supports results previously reported in the literature. It was also found that some reactions occur over wide ranges of temperature and that the governing step for the whole silane combustion is the reaction of silane with hydroxyl radicals. A least square fitting to the burning velocities and adiabatic flame temperatures obtained for the four investigated mixtures, with equivalence ratios of 2.0, 1.43, 1.0, and 0.5, indicated that a mixture with equivalence ratio of about 1.2 would have the largest burning velocity and the highest flame temperature.

The oxidation of silicon tetrachloride or silane yields silicon dioxide in condensed states. The production of solid or liquid phases from gases is a complicated phenomenon comprising chemical reactions and physical processes such as nucleation and crystal growth; it is interesting and, at the same time, important to investigate these processes from standpoints of both fundamental and applied researches on production of clusters and fine particles or on the CVD methods.

Silane is widely used as a silicon-containing material in semiconductor industries, for instance. This species is, however, spontaneously explosive in the air or sometimes causes production of undesirable products because of its high reactivity. The reaction between silane and oxygen should be investigated in detail to treat them safely and to maintain their efficient reactions. This work aims to simulate flat premixed silane–air flames using a model which neglects the physical processes to avoid complexities, and to elucidate the mechanisms of silane–oxygen combustion reactions under various conditions.

Recently some experimental and theoretical works have been done on the chemistry of silane. McLain et al.[1,2] have proposed the most reliable reaction schemes at present for the combustion of silane, which has been derived on the basis of the similarity to that of methane, and compared the predicted ignition delay times with the corresponding experimental values. Koda et al.[3–7] have studied experimentally silane combustion reactions by use of counterflow diffusion flames, and Tokuhashi et al.[8] have experimentally and theoretically investigated premixed silane flames. The explosion behavior of silane–oxygen mixtures has been investigated by Hartman et al.[9] in thermochemical discussion on the reaction mechanism. In spite of these pioneering works, the mechanism of silane combustion is still left unknown in many points. At present it is inevitable to accumulate the information in this field by both experimental and theoretical approaches.

Simulation Model

We used the same assumptions as those made in a previous work[10] in constructing the simulation model. Additional assumptions applicable only for this investigation are that (1) silicon dioxide exists in condensed phases over the temperature range considered here: high-temperature cristobalite phase below 1996 K and liquid phase above it; (2) only chemical processes are considered in the formation of silicon dioxide and hence the processes of condensation or crystallization such as nucleation and crystal growth are neglected. According to these two assumptions the produced silicon dioxide is removed from the gaseous reaction system but its amount is evaluated in terms of molar concentration and not of the size or number of silica particles. As thermochemical data for silicon dioxide, the data for high-temperature cristobalite were used below 1996 K and those corresponding to the liquid state were employed above the melting point.

The governing equations are expressed as follows:

$$\frac{\partial \rho}{\partial t} + \frac{\partial}{\partial x}(\rho v) = 0 \tag{1}$$

$$\frac{\partial}{\partial t}(c_p \rho T) + \frac{\partial}{\partial x}(c_p \rho T v) = \frac{\partial}{\partial x}\left(\lambda \frac{\partial T}{\partial x}\right) + \sum_i D_i \rho \frac{\partial h_i}{\partial x}\frac{\partial \omega_i}{\partial x} - \sum_i h_i \varphi_i \tag{2}$$

$$\frac{\partial}{\partial t}(\rho \omega_i) + \frac{\partial}{\partial x}(\rho \omega_i v) = \frac{\partial}{\partial x}\left(D_i \rho \frac{\partial \omega_i}{\partial x}\right) + \varphi_i \tag{3}$$

$$p = \rho R T \sum_i \frac{\omega_i}{m_i} \tag{4}$$

where ω_i and φ_i are the mass fraction and chemical production rate of the i-th species. The other symbols have their usual meanings.

The partial differential terms were discretized into the corresponding finite difference terms according to the

Table 1. SiH_4–H_2–O_2 Reaction Scheme[a)]
$k=AT^n\exp(-E/T)$

No.	Reaction	A	n	E	Ref.
R1	$H_2+O_2 \longrightarrow OH+OH$	2.50E06	0.0	19630	12
R2	$H+O_2 \longrightarrow OH+O$	1.20E11	−0.91	8310	13
R3	$O+H_2 \longrightarrow OH+H$	1.50E01	2.0	3800	13
R4	$OH+OH \longrightarrow O+H_2O$	1.50E03	1.14	0	13
R5	$OH+H_2 \longrightarrow H+H_2O$	1.00E02	1.6	1660	13
R6	$H+H+M \longrightarrow H_2+M$	9.70E04	−0.6	0	13
R7	$O+O+M \longrightarrow O_2+M$	2.86E05	−1.0	0	13
R8	$H+O+M \longrightarrow OH+M$	3.60E06	−1.0	0	14
R9	$OH+H+M \longrightarrow H_2O+M$	2.15E10	−2.0	0	13
R10	$H+O_2+M \longrightarrow HO_2+M$	2.00E06	−0.8	0	13
R11	$H+HO_2 \longrightarrow H_2+O_2$	2.50E07	0.0	350	13
R12	$H+HO_2 \longrightarrow OH+OH$	1.50E08	0.0	500	13
R13	$H+HO_2 \longrightarrow O+H_2O$	5.00E07	0.0	500	12
R14	$OH+HO_2 \longrightarrow H_2O+O_2$	2.00E07	0.0	0	13
R15	$O+HO_2 \longrightarrow OH+O_2$	2.00E07	0.0	0	13
R16	$HO_2+H_2 \longrightarrow H+H_2O_2$	7.30E05	0.0	9390	13
R17	$HO_2+HO_2 \longrightarrow H_2O_2+O_2$	2.00E06	0.0	0	13
R18	$OH+H_2O_2 \longrightarrow HO_2+H_2O$	7.00E06	0.0	720	13
R19	$H+H_2O_2 \longrightarrow OH+H_2O$	1.00E07	0.0	1800	13
R20	$O+H_2O_2 \longrightarrow OH+HO_2$	2.80E07	0.0	3220	13
R21	$OH+OH+M \longrightarrow H_2O_2+M$	3.25E10	−2.0	0	13
R22	$SiH_4 \longrightarrow SiH_2+H_2$	3.30E12	0.0	25720	2
R23	$SiH_4+O_2 \longrightarrow SiH_3+HO_2$	2.00E05	0.0	22150	2
R24	$SiH_4+HO_2 \longrightarrow SiH_3+H_2O_2$	3.00E06	0.0	2820	2
R25	$SiH_4+H \longrightarrow SiH_3+H_2$	1.50E07	0.0	1260	2
R26	$SiH_4+O \longrightarrow SiH_3+OH$	4.20E06	0.0	810	2
R27	$SiH_4+OH \longrightarrow SiH_3+H_2O$	8.40E06	0.0	50	2
R28	$SiH_3+H \longrightarrow SiH_2+H_2$	1.50E07	0.0	1260	2
R29	$SiH_3+O \longrightarrow SiH_2O+H$	1.30E08	0.0	1010	2
R30	$SiH_3+OH \longrightarrow SiH_2O+H_2$	5.00E06	0.0	0	2
R31	$SiH_3+O_2 \longrightarrow SiH_2O+OH$	8.60E08	0.0	5750	2
R32	$SiH_2+O_2 \longrightarrow HSiO+OH$	1.00E08	0.0	1860	2
R33	$SiH_2O+M \longrightarrow HSiO+H+M$	5.00E10	0.0	38570	2
R34	$SiH_2O+H \longrightarrow HSiO+H_2$	3.30E08	0.0	5290	2
R35	$SiH_2O+O \longrightarrow HSiO+OH$	1.80E07	0.0	1550	2
R36	$SiH_2O+OH \longrightarrow HSiO+H_2O$	7.50E06	0.0	90	2
R37	$SiH_2O+HO_2 \longrightarrow HSiO+H_2O_2$	1.00E06	0.0	4030	2
R38	$HSiO+M \longrightarrow SiO+H+M$	5.00E08	0.0	14600	2
R39	$HSiO+H \longrightarrow SiO+H_2$	2.00E08	0.0	0	2
R40	$HSiO+O \longrightarrow SiO+OH$	1.00E08	0.0	0	2
R41	$HSiO+OH \longrightarrow SiO+H_2O$	1.00E08	0.0	0	2
R42	$HSiO+O_2 \longrightarrow SiO+HO_2$	1.20E08	0.0	2000	2
R43	$SiO+O+M \longrightarrow SiO_2+M$	2.50E03	0.0	2200	2
R44	$SiO+OH \longrightarrow SiO_2+H$	4.00E06	0.0	2870	2
R45	$SiO+O_2 \longrightarrow SiO_2+O$	1.00E07	0.0	3270	2

a) The rate constants are expressed in m, mol, s units.

control-volume method;[11] the meshes have unequal sizes being roughly proportional to the product of the temperature and its gradient so that even fast reactions occurring there can be simulated with accuracy.

The boundary conditions at the unburned side are that the gas mixture is at 298 K and has given composition and velocity, and those at the burned side are that all the gradients of the dependent variables are zero.

A reaction scheme composed of forty-five pairs of elementary reactions was used for silane combustion; the first twenty-one pairs of reactions belong to hydrogen combustion, and the rest are reactions of silicon-containing species, which are SiH_4, SiH_3, SiH_2, SiH_2O, HSiO, SiO, and SiO_2, and were selected from the most reliable scheme at present (Table 1).

Since produced silicon dioxide is extinguished from the system the reverse reactions of (R43), (R44), and (R45) are neglected; in the actual system, however, the chemical equilibrium is reached between the gaseous and the condensed phases of silicon dioxide at high temperatures, and these reactions have their reverse partners.

Results and Discussion

Stoichiometric Flame. Figure 1 shows the profiles

of the temperature and the stable species mole fractions in a stoichiometric silane-air premixed flame and Figs. 2 and 3 show those of active species. The abscissas of these figures are, strictly speaking, the distance from an arbitrary origin. As described above, silicon dioxide is not a gaseous component, but, for convenience' sake, it is referred to with the mole fraction defined as the quotient of its concentration over the total concentration of the gaseous phase.

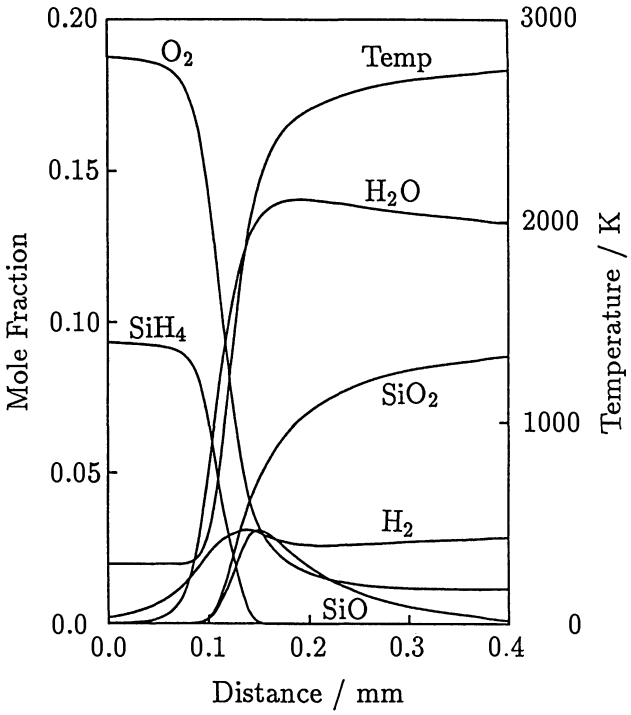

Fig. 1. Profiles of the temperature and the concentrations of stable species in the stoichiometric silane flame.

The reaction zone is about 0.05 mm thick and very thin in comparison with those of hydrogen and methane premixed flames; the combustion reaction is confined within this thin area. The second last and the last oxidation products of silane, that is, SiO and SiO_2, appear at fairly high temperatures, but hydrogen and water are present even at room temperature; their presence at low temperatures suggests that these species are produced at an early stage of silane combustion though hydrogen, in particular, has a large diffusion coefficient and diffuses from the high-temperature region to extremely upstream zones.

The intermediate species of silane combustion reactions, SiH_3, SiH_2, SiH_2O, and HSiO, are not distributed in a common region; SiH_3 appears in a low-temperature region, both SiH_2 and HSiO in a high-temperature region, and SiH_2O over a wide temperature range.

The three active species of the hydrogen–oxygen system, OH radicals and H and O atoms, increase above 1000 K. Hydroxyl radicals are particularly present in a large amount even in the low-temperature region comparing with that in hydrogen premixed flames.[10] Hydroperoxyl radicals are scattered widely and clearly have a shoulder in their profile suggesting that different reaction mechanisms contribute to their production depending on temperature.

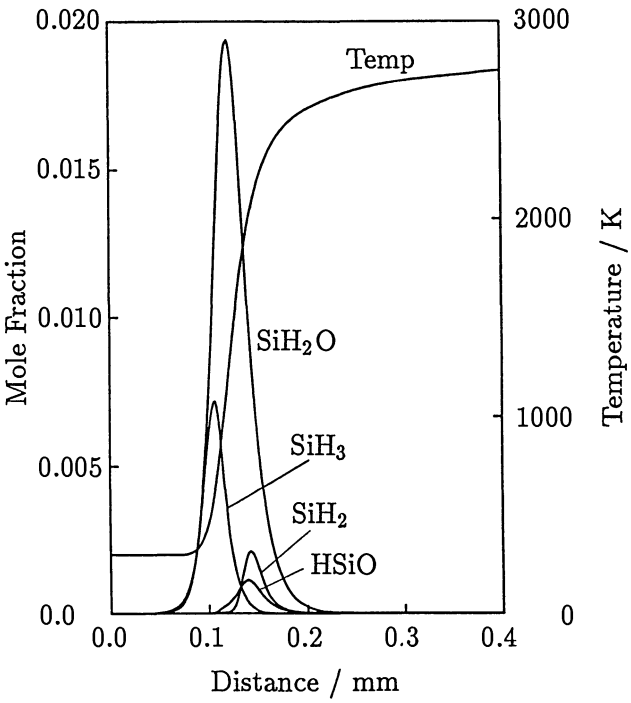

Fig. 2. Profiles of the temperature and the concentrations of intermediate silicon-containing species in the stoichiometric silane flame.

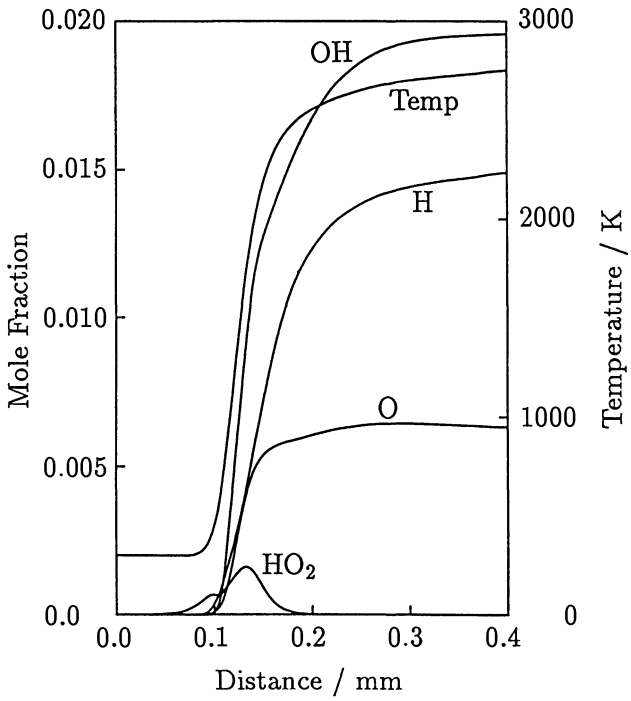

Fig. 3. Profiles of the temperature and the concentrations of intermediate hydrogen–oxygen-containing species in the stoichiometric silane flame.

Koda et al.[7] has already pointed out that the reaction scheme proposed by McLain gives two alternative pathways in the silane reaction from SiH_4 to HSiO: one via SiH_3 and the other via SiH_2. Our simulation also supports their result.

Figures 4 and 5 show, respectively, the reaction rates and the heat release rates for the predominant silicon-containing species reactions as functions of temperature. The profiles indicate that those reactions can be classified into three different groups based on the temperature range of their activation: low-temperature reactions, high-temperature reactions and wide-temperature-range reactions.

Reactions

$$SiH_4 + OH \rightarrow SiH_3 + H_2O, \quad \text{(R27)}$$

$$SiH_4 + H \rightarrow SiH_3 + H_2, \quad \text{(R25)}$$

$$SiH_3 + O_2 \rightarrow SiH_2O + OH, \quad \text{(R31)}$$

$$SiH_3 + O \rightarrow SiH_2O + H, \quad \text{(R29)}$$

and

$$SiH_2O + OH \rightarrow HSiO + H_2O \quad \text{(R36)}$$

are low-temperature reactions. They oxidize silane following the sequence $SiH_4 \rightarrow SiH_3 \rightarrow SiH_2O \rightarrow HSiO$. Hydroxyl radicals hold a particularly important role at the first step of this series of reactions due to their cyclic consumption and production by reactions (R27) and (R31). Since reaction (R27) is already activated and also begins to release considerable amounts of heat at temperatures as low as 500 K, it can be considered the most important of the governing elementary steps for the low-temperature combustion mechanism. At temperatures higher than 700 K, SiH_3 is oxidized by oxygen to SiH_2O through reaction (R31) with formation of hydroxyl radicals, and the SiH_2O is dehydrogenated with hydroxyl radicals by reaction (R36); reactions (R31) and (R36) are also exothermic, leading to a steep temperature increase and allowing the activation of reactions with higher activation energies, like the silane decomposition.

The activation of the silane decomposition reaction is the origin of an alternative reaction pathway, that is, $SiH_4 \rightarrow SiH_2 \rightarrow HSiO$, which predominates at temperatures higher than 1500 K. The overall silane consumption rate has then two peaks, one being located at about 1000 K and other at about 2000 K, and the fuel remaining from the low-temperature region is completely exhausted at the second pathway. The initiation reaction of the high-temperature route,

$$SiH_4 \rightarrow SiH_2 + H_2, \quad \text{(R22)}$$

is a spontaneous unimolecular dissociation which, however, cannot occur at low temperatures because of its large activation temperature (see Table 1) and endothermic character, as shown by Fig. 5. This is actually the only route for the production of SiH_2 though the assumed reaction scheme gives another possible step for the production of SiH_2 (R28). The formed SiH_2 is

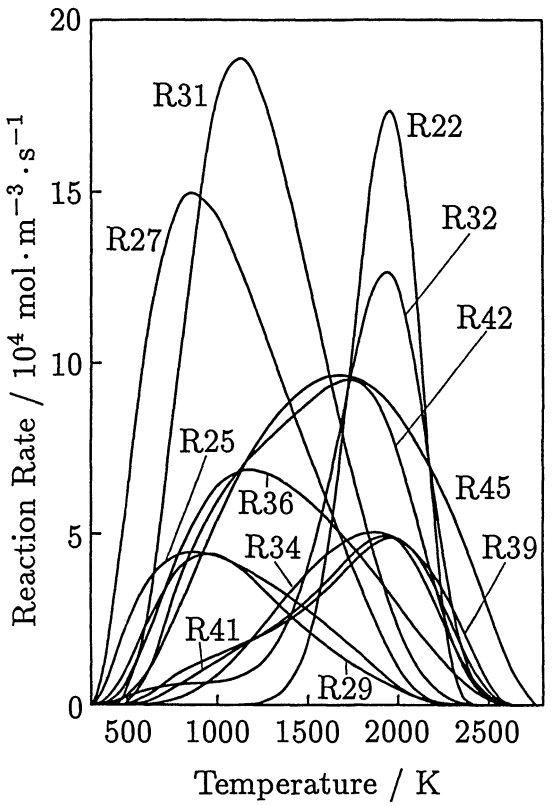

Fig. 4. Reaction rates in the stoichiometric silane flame as functions of temperature. The numbers in the figure correspond to those in Table 1.

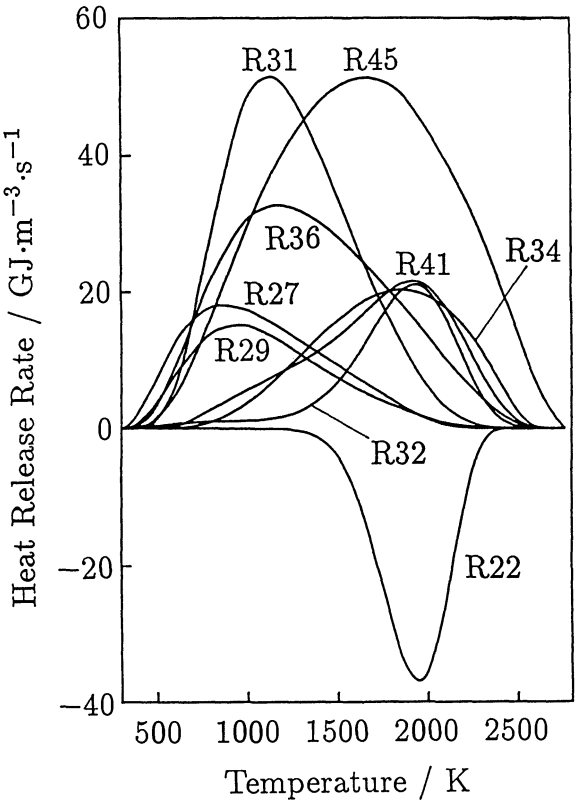

Fig. 5. Rates of heat release due to reactions in the stoichiometric silane flame.

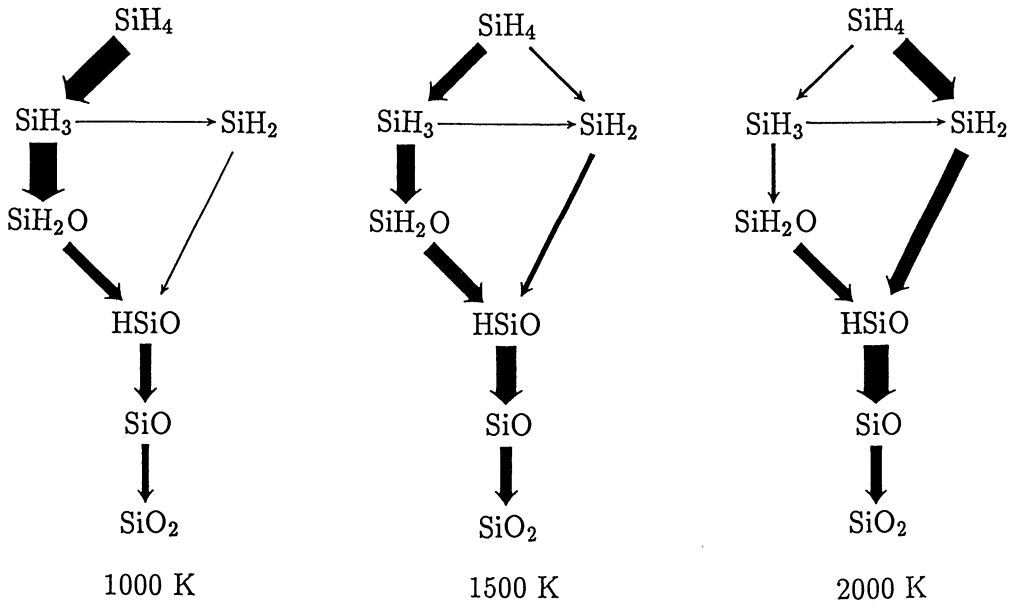

Fig. 6. Predominant reaction pathways in the stoichiometric silane flame at three temperatures. The widths of the arrows are proportional to the rates of the corresponding routes.

immediately oxidized by reaction

$$SiH_2 + O_2 \rightarrow HSiO + OH \quad (R32)$$

so that this species is not considerably accumulated in the system.

The final product SiO_2 is produced by two reactions:

$$HSiO + O_2 \rightarrow SiO + HO_2 \quad (R42)$$

and

$$SiO + O_2 \rightarrow SiO_2 + O. \quad (R45)$$

Both reactions, corresponding to the last steps of the oxidation, are activated through a wide range of temperature and constitute direct oxidation with oxygen; therefore an insufficient amount of oxygen would hinder the progression of these steps. Above 1000 K, two additional reactions,

$$HSiO + H \rightarrow SiO + H_2 \quad (R39)$$

and

$$HSiO + OH \rightarrow SiO + H_2O, \quad (R41)$$

contribute to the consumption of HSiO so that HSiO does not remain in appreciable amounts, as shown in Fig. 2.

Although the reaction scheme gives many possible ways for the silane dehydrogenation, only the reactions (R27) and (R22) are promoted around 1000 K and 2000 K, respectively. Thus, the silane consumption clearly occurs by two alternative routes, each one being well identified by the temperature activation and the intermediate species. Figure 6 illustrates the obtained reaction pathways at three temperatures in the stoichiometric silane–air flame.

Since hydroxyl radicals contribute to a great extent to the initial step of the low-temperature mechanism of silane combustion, the chemical behavior of the species which contain hydrogen and/or oxygen will be discussed. Change in a species concentration is deter-

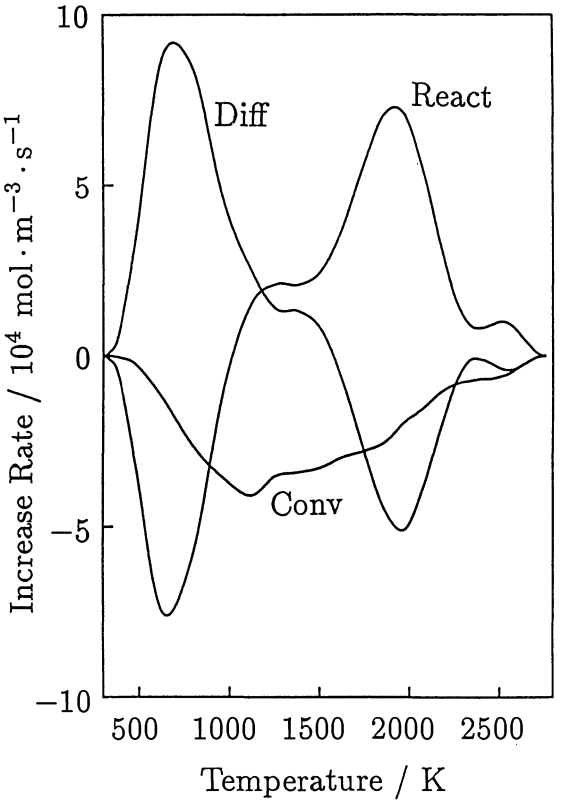

Fig. 7. Increase rates of hydroxyl radicals due to reactions (React), diffusion (Diff), and convection (Conv).

mined according to the governing equation for each species, Eq. 3. Figure 7 shows the rates of the individual terms constituting Eq. 3 for hydroxyl radicals. The reaction term expresses the net rate for the elementary reactions in which that species participates. According to the figure, hydroxyl radicals are supplied by diffusion to the low-temperature region and decrease mostly by reactions; reaction (R27) keeps the largest contribution to their consumption.

On the other hand, the reactions

$$H + O_2 + M \rightarrow HO_2 + M \qquad (R10)$$

and

$$H + HO_2 \rightarrow OH + OH \qquad (R12)$$

proceed with fairly large rates among hydrogen–oxygen reactions, particularly at low temperatures, though their rates are only about 1/5 of that of reaction (R27), for instance. Hydroxyl radicals are thus produced via hydroperoxyl radicals by this pair of reactions, which start from diffused hydrogen atoms supplied with a rate similar to the diffusion rate of hydroxyl radicals. Hydroperoxyl radicals, which have an interesting profile at low temperatures as shown in Fig. 3, are produced by reaction (R10) and then consumed by reaction (R12), and above 800 K are also produced by reaction (R42).

The starting point of the hydrogen–oxygen reactions in this flame is the liberation of hydrogen by reaction (R22) at high temperatures. The hydrogen is transformed into hydroxyl radicals and hydrogen atoms by the chain-branching reaction (R3) at temperatures around 2000 K, and then is oxidized by reaction (R5) also producing hydrogen atoms. The hydrogen atoms are oxidized into hydroxyl radicals by reaction (R12) reacting with the hydroperoxyl radicals. These hydroxyl radicals and hydrogen atoms are carried toward the low-temperature region by diffusion and used as the reactant of the initiation reaction (R27). Water, on the other hand, is produced in a large amount by reaction (R5) and also by the dehydrogenation reactions of the silicon-containing species with hydroxyl radicals over a wide range of temperature so that it exists widely in the flame, as shown in Fig. 1.

Rich and Lean Flames. We simulated also rich and lean silane premixed flames with equivalence ratios (ϕ) equal to 2.0, 1.43, and 0.5 to discuss the reaction mechanisms under various conditions. The calculated burning velocities are 1.8 m s^{-1} for the flame with ϕ=2.0, 2.2 m s^{-1} for ϕ=1.43, 2.2 m s^{-1} for ϕ=1.0, and 0.9 m s^{-1} for ϕ=0.5. The least square method approximating them with a cubic function of the silane content gives the maximum burning velocity of 2.6 m s^{-1} at 11%, which corresponds to an equivalence ratio of 1.2. The adiabatic flame temperature changes similarly to the burning velocity.

The oxidation of Si and H takes place in parallel in silane flames; therefore it is important to determine which oxidation takes precedence particularly under the conditions of insufficient oxygen.

Concentration profiles of silicon-containing species indicated clearly that SiH_2 remains in rich flames, and at the richest investigated condition SiH_2 increases monotonically up to 2.8% in mole fraction showing no overshoot; this species holds 19% of the silicon atoms at the final state. The rest of them are shared by SiO (59%) and SiO_2 (22%). Hydrogen atoms, on the contrary, are shared by H_2O (50%), H_2 (41%), and SiH_2 (9%). At the final state of the flame with ϕ=1.43, unburned SiH_2 still remains in a small amount, and 62% and 60% of the silicon and hydrogen atoms are kept in SiO_2 and H_2O, respectively. In the stoichiometric flame, all the silicon atoms are contained in silicon dioxide and water shares 82% of the hydrogen atoms at the final state.

Water is produced already at very early stages of combustion by reactions such as (R27) and (R31) throughout the four flames so that the oxidation of H proceeds fast at first. In the highest temperature region of the rich and stoichiometric flames, however, the produced water is reduced by the reverse reactions of (R5) and

$$OH + OH \rightarrow O + H_2O, \qquad (R4)$$

and the formed hydroxyl radicals are used by the final oxidation toward SiO_2

$$SiO + OH \rightarrow SiO_2 + H. \qquad (R44)$$

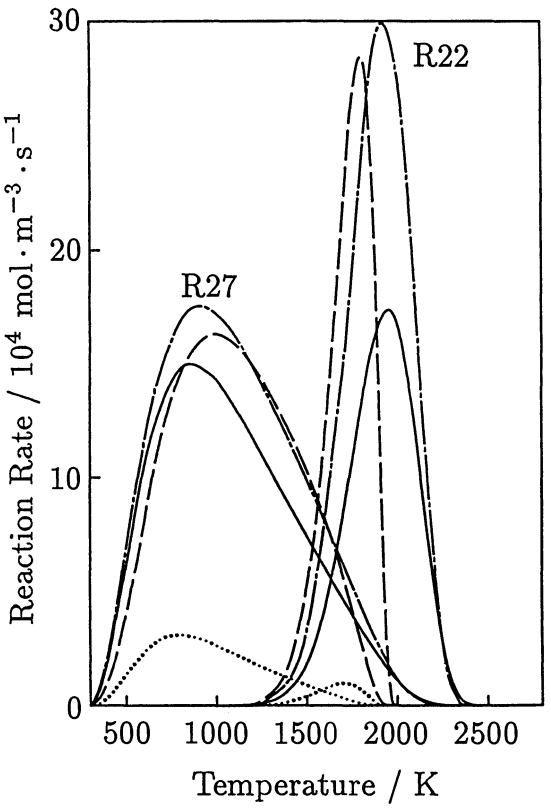

Fig. 8. Rates of reactions (R27) and (R22) in four silane premixed flames with equivalence ratio of 2.0 (dashed lines), 1.43 (dashed-dotted lines), 1.0 (solid lines), and 0.5 (dotted lines).

Formation of SiO_2 through free oxygen (reaction (R45)) is also promoted in this stage.

The rich and stoichiometric flames possess a similar low-temperature reaction mechanism, indicating that the product between the concentrations of silane and hydroxyl radicals, which determine the rate of the initiation reaction of this mechanism (R27), are almost equal one another: the maximum rates of reaction (R27) are 1.63×10^5 mol m^{-3} s^{-1} in the flame with $\phi=2.0$ (at 1000 K), 1.77×10^5 mol m^{-3} s^{-1} at $\phi=1.43$ (at 930 K) and 1.51×10^5 mol m^{-3} s^{-1} at $\phi=1.0$ (at 870 K); and those of reaction (R31) are 1.89×10^5 mol m^{-3} s^{-1} at $\phi=2.0$ (at 1210 K), 2.15×10^5 mol m^{-3} s^{-1} at $\phi=1.43$ (at 1190 K) and 1.89×10^5 mol m^{-3} s^{-1} at $\phi=1.0$ (at 1130 K). In the leanest flame, both rates are only about 1/5 of those in the above flame because of insufficient amounts of silane and hydroxyl radicals.

As for the high-temperature mechanism, on the contrary, the rates of reaction (R22) are remarkably different since this is a unimolecular reaction and its rate is simply proportional to the concentration of silane. Its maximum rate, however, becomes the largest at $\phi=1.43$ but not at $\phi=2.0$. The reason is that the flame temperature of the latter flame is much lower than that of the former one.

The rates of reactions (R27) and (R22) are consequently a good index for the reaction mechanisms in silane flames as shown in Fig. 8.

Conclusions

The simulation of silane–air flat premixed flames using a detailed reaction scheme and the analyses of the obtained results led to the following conclusions:

(I) In the flames with equivalence ratio around 1.0 the combustion reactions take place very intensely, and consequently are confined within thin areas of about 0.05 mm thick. The burning velocity of the stoichiometric flame is 2.2 m s^{-1}, Which is a little smaller than that of the hydrogen flame.

(2) Two mechanisms are provided for the reaction from SiH_4 to HSiO: one proceeds along $SiH_4\rightarrow SiH_3\rightarrow SiH_2O\rightarrow HSiO$ and the other along $SiH_4\rightarrow SiH_2\rightarrow HSiO$. These pathways are activated in different temperature ranges. The former starts even at low temperatures because it progresses as chain reactions having hydroxyl radicals as chain carriers, which are produced in a large amount even at low temperatures. The latter is activated at high temperatures because the initiation reaction of this route has a large activation temperature. The second mechanism is also accelerated under rich conditions since it starts with dissociation of silane.

References

1) C. J. Jachimowski and A. G. McLain, *NASA Tech. Rep.*, **1983**, 2129.
2) A. G. McLain, C. J. Jachimowski, and R. C. Rogers, *NASA Tech. Rep.*, **1985**, 2415.
3) S. Koda, O. Fujiwara, and T. Ohnishi, *Combust. Flame,* **65**, 121 (1986).
4) S. Koda and O. Fujiwara, "Twenty-first Symposium (International) on Combustion," The Combustion Institute, Pittsburgh (1986), p. 1861.
5) S. Koda and O. Fujiwara, *Combust. Flame,* **73**, 187 (1988).
6) S. Suga and S. Koda, *Jpn. J. Appl. Phys.*, **27**, L1966 (1988).
7) S. Koda and O. Fujiwara, "ISPC-8 Tokyo," Tokyo (1987), p. 2022.
8) K. Tokuhashi, S. Horiguchi, Y. Urano, M. Iwasaki, H. Ohtani, and S. Kondo, *Combust. Flame,* **82**, 40 (1990).
9) J. R. Hartman, J. Famil-Ghiriha, H. A. Ring, and H. E. O'Neal, *Combust. Flame,* **68**, 43 (1987).
10) S. Fukutani, N. Kunioshi, and H. Jinno, *Bull. Chem. Soc. Jpn.*, **63**, 2191 (1990).
11) S. V. Patankar, "Numerical Heat Transfer and Fluid Flow," Hemisphere Publishing Co., New York (1980), Chap. 3.
12) D. L. Baulch, D. D. Drysdale, D. G. Horne, and A. C. Lloyd, "Evaluated Kinetic Data for High Temperature Reactions," Butterworths, London (1972), Vol. 1.
13) J. Warnatz, "Combustion Chemistry," ed by W. C. Gardiner, Jr., Springer-Verlag, New York (1984), pp. 197—360.
14) D. E. Jensen and G. A. Jones, *Combust. Flame,* **32**, 1 (1978).

Combustion Reactions in Silane-Air Flames II. Counterflow Diffusion Flame

Seishiro FUKUTANI,* Nílson KUNIOSHI, Yasuhiro UODOME, and Hiroshi JINNO†
Department of Industrial Chemistry, Faculty of Engineering, Kyoto University, Yoshida-honmachi, Sakyo-ku, Kyoto 606
†Department of Chemistry, Faculty of Science and Engineering, Sophia University, Kioicho 7-1, Chiyoda-ku, Tokyo 102
(Received April 1, 1991)

A detailed chemical reaction scheme and a full set of governing equations for fluid dynamics were used to elucidate the chemical and physical phenomena involved in a silane–air counterflow diffusion flame, where the fuel and air issue from the lower and upper nozzles, respectively. It was found that a stagnation surface, where the axial velocities fall down to zero, is kept in a position slightly shifted to the upper side, dividing the system into two zones: the upper air side and the lower fuel side; after leaving the nozzle silane begins to dissociate itself into SiH_2 and H_2 when it reaches the region of rising temperature; oxygen penetrates into the fuel side by diffusion and reacts with H_2 forming OH radicals and H atoms. The produced SiH_2 is further dehydrogenated to SiO via HSiO; comparing with premixed flames, the diffusion flames have large local equivalence ratios, so that the combustion reactions in the latter flames occur through a different mechanism.

Opposite flow of gaseous fuel and air originates a stagnation point at an intermediate position between the two nozzles on the center line. The fuel and air are mixed each other within a narrow region near the stagnation point mainly due to diffusion and can hold stably a diffusion flame as shown in Fig. 1 if the flow velocities of the fuel and air do not exceed certain critical values. The flame maintained in the stagnation area is called a counterflow diffusion flame and has the simplest structure among the various types of diffusion flames.

Silane–air mixtures are very reactive and hence the gas mixtures should be treated carefully to avoid eventual explosions. In diffusion flames, on the contrary, the characteristic time of the diffusion process which mixes the fuel and air is usually longer than that of the chemical reactions, so that the former process controls the rate of the whole combustion phenomenon. Diffusion flames of silane are, therefore, preferred to premixed flames in both academic and industrial fields.

The mechanisms of chemical reactions occurring in diffusion flames, however, are not necessarily the same as those in the corresponding premixed flames. This investigation aims to elucidate the mechanism of combustion reaction of a silane–air counterflow diffusion flame and also its structure by means of computer simulation.

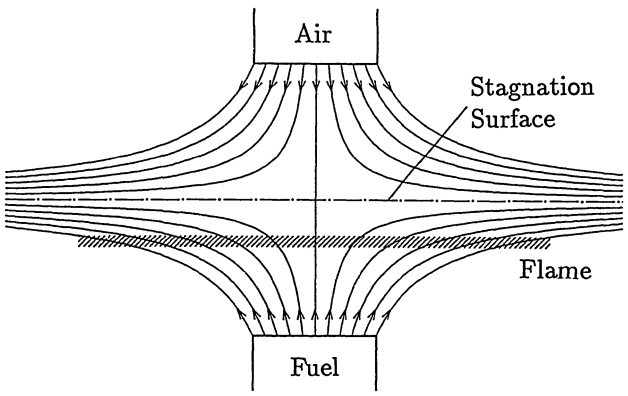

Fig. 1. Schematic figure of a counterflow diffusion flame.

Since diffusion flames have more complicated structures than premixed flames, their theoretical investigations have been predominantly based on the simple model called Burke–Schumann flame sheet model.[1] This model is constructed upon the following assumptions; (1) fuel and air react with a rate much larger than their diffusion rates so that the reaction zone is thin enough to be considered as a geometrical plane; (2) the ratio between the diffusion rates of fuel and air into the reaction zone equals the stoichiometry of the combustion reaction of both components or, in other words, the reaction zone is located at a position so that the above condition is satisfied. The Burke–Schumann model has been applied to various kinds of diffusion flames and derived many useful results.[2–6] However, most of those researches have necessarily represented their combustion reactions with overall reactions or replaced them with correspondent exothermic processes to simplify the analyzing algorithms.

The application of one-step reaction approximations is not appropriate, in particular, for diffusion flames where combustion reactions take place step by step such as methane[7] and silane flames.[8] A model containing a full reaction scheme can describe precisely the reaction mechanism and details of the flame structure such as the distributions of temperature, reaction rates and chemical species.

Theoretical studies have been done on counterflow diffusion flames by various workers;[9,10] in most of their studies the flames are treated as hypothetical one-dimensional flames by simulating only along the center line. The one-dimensional treatment of such diffusion

flames, however, is not satisfactory because the flames do not strictly possess homogeneous structures along any radial axis. Both full reaction scheme and detailed fluid mechanics are included in the model used in this investigation.

Simulation Model

The simulation model for the silane–air counterflow diffusion flame treated here was formulated under the same assumptions made in the previous work of this series[8] plus the additional condition of axial symmetry of the flame. The governing equations can be written as:

$$\frac{\partial \rho}{\partial t}+\frac{1}{r}\frac{\partial}{\partial r}(\rho u r)+\frac{\partial}{\partial z}(\rho v)=0 \tag{1}$$

$$\frac{\partial \rho u}{\partial t}+\frac{\partial \rho u^2}{\partial r}+\frac{\partial \rho uv}{\partial z}=\frac{\partial}{\partial r}\left[\mu\left\{2\frac{\partial u}{\partial r}-\frac{2}{3}\left(\frac{1}{r}\frac{\partial}{\partial r}(ur)+\frac{\partial v}{\partial z}\right)\right\}\right]+\frac{\partial}{\partial z}\left[\mu\left(\frac{\partial u}{\partial z}+\frac{\partial v}{\partial r}\right)\right]+\frac{2\mu}{r}\left(\frac{\partial u}{\partial r}-\frac{u}{r}\right)-\frac{\partial p}{\partial r} \tag{2}$$

$$\frac{\partial \rho v}{\partial t}+\frac{\partial \rho uv}{\partial r}+\frac{\partial \rho v^2}{\partial z}=\frac{\partial}{\partial z}\left[\mu\left\{2\frac{\partial v}{\partial z}-\frac{2}{3}\left(\frac{1}{r}\frac{\partial}{\partial r}(ur)+\frac{\partial v}{\partial z}\right)\right\}\right]+\frac{1}{r}\frac{\partial}{\partial r}\left[\mu r\left(\frac{\partial u}{\partial z}+\frac{\partial v}{\partial r}\right)\right]-\frac{\partial p}{\partial z}-\rho g \tag{3}$$

$$\frac{\partial c_p \rho T}{\partial t}+\frac{\partial c_p \rho Tu}{\partial r}+\frac{\partial c_p \rho Tv}{\partial z}=\frac{1}{r}\frac{\partial}{\partial r}\left(\lambda r\frac{\partial T}{\partial r}\right)+\frac{\partial}{\partial z}\left(\lambda\frac{\partial T}{\partial z}\right)+\sum_i D_i\rho\frac{\partial h_i}{\partial r}\frac{\partial \omega_i}{\partial r}+\sum_i D_i\rho\frac{\partial h_i}{\partial z}\frac{\partial \omega_i}{\partial z}-\sum_i h_i\varphi_i \tag{4}$$

$$\frac{\partial \rho\omega_i}{\partial t}+\frac{\partial \rho\omega_i u}{\partial r}+\frac{\partial \rho\omega_i v}{\partial z}=\frac{1}{r}\frac{\partial}{\partial r}\left(D_i\rho r\frac{\partial \omega_i}{\partial r}\right)+\frac{\partial}{\partial z}\left(D_i\rho\frac{\partial \omega_i}{\partial z}\right)+\varphi_i \tag{5}$$

$$p=\rho RT\sum_i\frac{\omega_i}{m_i} \tag{6}$$

where t is the time, r and z the radial and axial distances, u and v the radial and axial flow velocities; and h_i, ω_i, and φ_i are the enthalpy, the mass fraction and the production rate due to chemical reactions of the i-th species. The viscosity μ, the thermal conductivity λ and the diffusion coefficient D of the components were estimated, respectively, using Hirschfelder's, Eucken's, and Hirschfelder's approximated equations.[11] The other thermodynamic data, including the equilibrium constants were obtained from JANAF data.[12]

The partial differential equations were transformed into the corresponding finite difference equations based on the control-volume method.[13] The resulting finite difference equations were solved iteratively until time-independent solutions were obtained.

The reaction scheme used in this investigation is the same as that in the previous work, and composed of forty-five pairs of elementary reactions among SiH_4, SiH_3, SiH_2, SiH_2O, HSiO, SiO, SiO_2, OH, H, O, HO_2, H_2O_2, H_2O, H_2, O_2, and N_2. Silicon dioxide is present in the solid or liquid phase and hence the produced SiO_2 is assumed to disappear from the gaseous reaction system; therefore the steps producing SiO_2 from SiO do not have their reverse reactions. Nitrogen is assumed to be inert and any NO_x production reactions are not included in the reaction scheme.

The following conditions were imposed on the system as the boundary conditions:

1. A mixture of 5% of silane and 95% of nitrogen and air issue in the opposite directions from lower and upper nozzles, respectively, with uniform flow velocity of 0.3 $m\,s^{-1}$ at 298 K. The two nozzles are 8 mm in diameter, and located oppositely with a displacement of 10 mm.
2. Nitrogen flows with constant velocity of 0.3 $m\,s^{-1}$ outside both nozzles in order to stabilize the flow of the fuel and air.
3. The gradients of all dependent variables are zero at the lateral boundaries.

Results and Discussion

Flame Structure. The combustion conditions given above can provide a stable diffusion flame without any turbulence nor vortexes.

Figure 2 shows the flow velocity and temperature distributions over the whole calculation area. The points where the axial flow velocity becomes zero define the stagnation surface; on the center line, the stagnation point is located at 5.4 mm above the fuel nozzle. The axial velocity temporarily increases by about 0.05 $m\,s^{-1}$ at the lower edge of the high-temperature region because of the sharp temperature rise; the momentary increase in the axial velocity observed at the edges of the high-temperature region is characteristic of this type of diffusion flames.[10] The radial component of the flow velocity increases as the gas flows away from the nozzles and becomes 0.61 $m\,s^{-1}$ at the lateral boundary.

The high-temperature region is confined into a fairly narrow zone of about 2 mm wide and is unevenly distributed to the side lower than the stagnation surface.

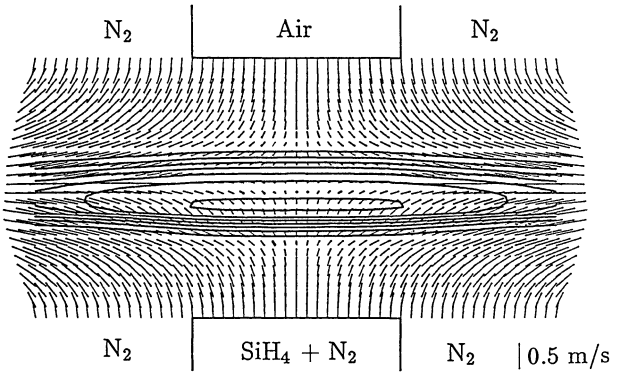

Fig. 2. Distributions of the flow velocity and temperature. The two nozzles are 8 mm in diameter and separated by a distance of 10 mm. The contour lines of the temperature are drawn for every 250 K from 500 K to 2000 K.

The temperature reaches about 2000 K, which is the highest temperature in this flame, at 4.0 mm in height on the center line; the maximum value is much lower than that found in premixed flames[8] due to the excess dilution of the combustion gas with nitrogen. The averaged temperature gradient in the axial direction is about 1420 K mm^{-1} at the lower side and larger than that at the upper side suggesting that exothermic reactions occur intensely at the lower side. The radial gradients of the temperature are almost zero within the cylindrical region between the nozzles.

The concentrations of the reactants and products are shown with contour lines in Fig. 3. As described above silicon dioxide is assumed to exist in the condensed states and is removed out from the gaseous reaction system. Its amount should be expressed with the number and the size of deposited silicon dioxide particles but it is expressed here, for convenience' sake, with the mole fraction defined as the molar concentration over the total molar concentration of the gaseous components.

The fuel and oxygen are both exhausted at about 4 mm in height. The following two points should be noted on their profiles; (1) oxygen penetrates deeply into the lower side across the stagnation surface; (2) a gap of about 0.2 mm wide is observed between the disappearing positions of the fuel and oxygen even on the center line and such a displacement is much wider than the reaction zone of silane–air premixed flames.[8]

The location and thickness of the fuel-and-air mixing region depend on the chemical and transport properties of the gases such as reactivity and diffusivity. The binary diffusion coefficient between oxygen and nitrogen is about 1.6×10^{-4} $m^2 s^{-1}$ at 1000 K, for instance, and about 1.6 times as large as that between silane and nitrogen. The diffusional flux of oxygen overwhelms that of silane and this species penetrates into the lower side transgressing the stagnation surface. In a hydrogen–air counterflow diffusion flame, on the contrary, hydrogen enters deeply into the air side over the stagnation surface.[10] Hereafter the regions below and above the stagnation surface will be called fuel side and air side, respectively.

As for the second point, the empty region of both fuel and air indicates that the Burke–Schumann assumption of the diffusion-rate ratio equal to the stoichiometry of reaction between the two components is not valid in this flame and that the fuel and oxygen do not directly react each other.

Silicon dioxide is present in a narrow region lying between the stagnation surface and the fuel-and-oxidizer exhaustion layer; the confinement suggests that the SiO_2 formation occurs just below the stagnation surface and, in addition, the species is carried by the upstream flow toward the stagnation surface. The other final product, water, however, extends widely due to its movability.

Figure 4 shows the distributions of silicon-containing intermediate species having important roles. The rest three species are present in small amounts. The maximum mole fractions are 2.9×10^{-3} for SiH_3, 6.9×10^{-4} for SiH_2O, and 2.1×10^{-5} for HSiO; the amounts of the last two species, in particular, are more than 100 times as small as those in the premixed flame. The presence of this group of species is concentrated in the fuel side, while SiH_2O and HSiO are distributed in regions with radius larger than 6 mm.

The hydrogen–oxygen-containing species, however, extend over fairly wide regions even in the air side crossing over the stagnation surface as shown in Fig. 5. Hydroperoxyl radicals distribute mainly in the region above the stagnation surface though the amount is much smaller than the three active species OH, H, and O.

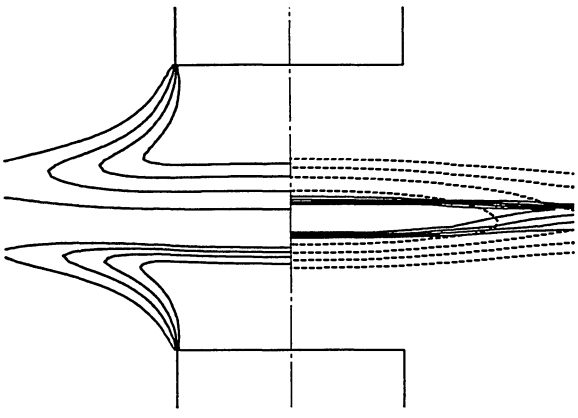

Fig. 3. Distributions of the stable species mole fractions. The contour lines for each species correspond to four values of equal intervals from the minimum to the maximum mole fraction (x_{max}). The mole fractions of SiH_4 ($x_{max}=5.0\times10^{-2}$) and O_2 ($x_{max}=2.1\times10^{-1}$) are shown in the left half of the figure, and those of SiO_2 ($x_{max}=1.3\times10^{-1}$) and H_2O ($x_{max}=4.5\times10^{-2}$) are shown in the right half with the solid and the dashed lines, respectively.

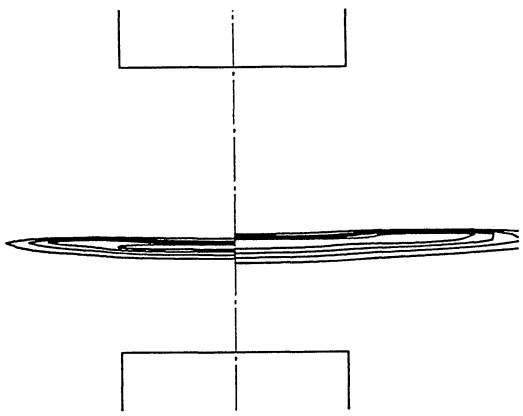

Fig. 4. Distributions of the mole fractions of silicon-containing intermediate species. The four contour lines are defined as those in Fig. 3. The mole fraction of SiH_2 ($x_{max}=8.9\times10^{-3}$) is shown in the left half and that of SiO ($x_{max}=4.1\times10^{-3}$) in the right half.

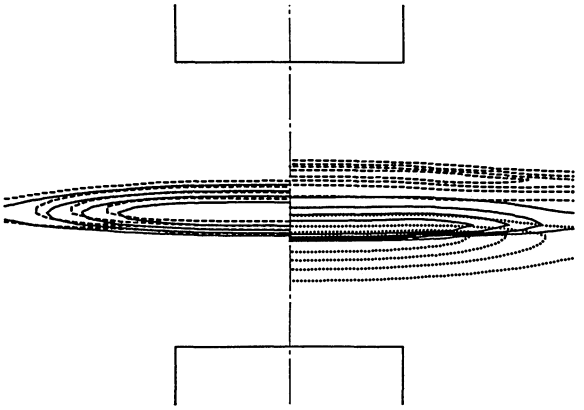

Fig. 5. Distributions of the mole fractions of hydrogen–oxygen-containing intermediate species. The four contour lines are defined as those in Fig. 3. The mole fractions of OH ($x_{max}=3.4\times10^{-3}$) and O ($x_{max}=1.9\times10^{-3}$) are shown with the solid and dashed lines, respectively, in the left half and those of H_2 ($x_{max}=8.3\times10^{-3}$), H ($x_{max}=1.9\times10^{-3}$), and HO_2 ($x_{max}=2.0\times10^{-5}$) are shown with the dotted, solid and dashed lines, respectively, in the right half of the figure.

According to Figs. 4 and 5 the silicon-containing and hydrogen–oxygen-containing species are present in two regions clearly divided at about 4 mm in height, which just coincides with the exhaustion zone of the fuel and air suggesting that the reactions of silicon-containing species and those of hydrogen–oxygen-containing species take place separately in the fuel and the air sides, respectively.

Combustion Reaction. Figure 6 shows the distributions of the predominant reactions occurring at the early silane combustion and the species participating in that step. Silane is dehydrogenated by hydrogen atoms at a height as low as 3.5 mm through reaction

$$SiH_4 + H \longrightarrow SiH_3 + H_2, \qquad (R25)$$

and the produced SiH_3 further reacts also with hydrogen atoms through reaction

$$SiH_3 + H \longrightarrow SiH_2 + H_2. \qquad (R28)$$

About 35% of SiH_4 is transformed into SiH_2 by the above pair of reactions even at very low positions of the fuel side, where the temperature is about 1400 K. The rest of the fuel is directly decomposed to SiH_2 by reaction

$$SiH_4 \rightarrow SiH_2 + H_2 \qquad (R22)$$

in a region located 0.2 mm above that for reactions (R25) and (R28). It is noticeable that the reactions converting SiH_4 to SiH_2 do not require O_2 or any oxygen-containing species.

Figure 7 shows the distributions of the other silicon-containing species and the reactions yielding the products up to SiO_2. The SiH_2 formed by either of the above reaction pathways is oxidized through

$$SiH_2 + O_2 \longrightarrow HSiO + OH. \qquad (R32)$$

Then, the produced HSiO is immediately dehydrogenated by reactions

$$HSiO + H \longrightarrow SiO + H_2 \qquad (R39)$$

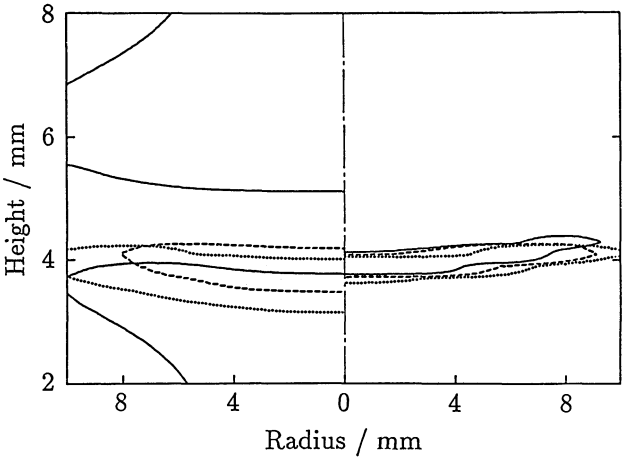

Fig. 6. In the left-hand side: distributions of SiH_4 (lower solid contour line for the mole fraction of $x=9.0\times10^{-3}$), SiH_3 (dotted line, $x=5.9\times10^{-4}$), SiH_2 (dashed line, $x=1.8\times10^{-3}$), and O_2 (upper solid line, $x=3.9\times10^{-2}$); in the right-hand side: distributions of reactions (R22) (solid contour line for the reaction rate of $\varphi=57$ mol m^{-3} s^{-1}), (R25) (dotted line, $\varphi=43$ mol m^{-3} s^{-1}), and (R28) (dashed line, $\varphi=33$ mol m^{-3} s^{-1}). The reaction numbers correspond to those in the text. The mole fractions and the reaction rates designated by the contour lines are 80% of the corresponding maximum values.

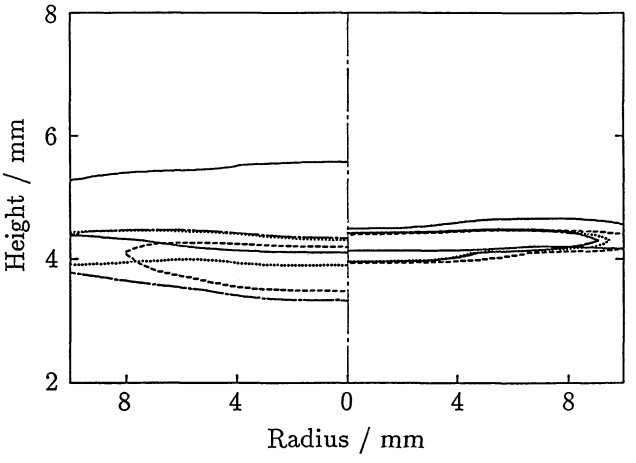

Fig. 7. In the left-hand side: distributions of SiH_2 (dashed line, $x=1.8\times10^{-3}$), HSiO (dotted line, $x=4.3\times10^{-6}$), SiO (dotted-dashed line, $x=8.2\times10^{-4}$), and SiO_2 (solid line, $x=2.7\times10^{-2}$); in the right-hand side: distributions of reactions (R32) (dotted line, $\varphi=66$ mol m^{-3} s^{-1}), (R38) and (R44) (the two dotted-dashed lines, for $\varphi=23$ mol m^{-3} s^{-1} and $\varphi=29$ mol m^{-3} s^{-1}, respectively, lie upon each other), (R39) (dashed line, $\varphi=34$ mol m^{-3} s^{-1}), and (R45) (solid line, $\varphi=39$ mol m^{-3} s^{-1}).

or

$$HSiO + M \longrightarrow SiO + H + M. \quad (R38)$$

According to Fig .7 the SiO-producing reactions are intensely activated from about 4 mm in height but the produced SiO appears even at 3 mm on the center line. The conservation equation of chemical species requires, in the steady state, that each species must keep the balance among the five terms of Eq. 5, that is, axial and radial convection and diffusion, and reaction terms; only one steady state should be realized due to given boundary conditions but independently of initial conditions. Silicon monoxide in the mesh located at 3 mm in height and on the center line, for instance, increases with a rate of 1.9×10^{-1} mol m^{-3} s^{-1} by diffusion in the axial direction, decreases with a rate of 1.6×10^{-1} mol m^{-3} s^{-1} by axial convection and is compensated with the other three terms. The reaction term is negligible as described above, and the two radial terms, particularly radial diffusion, are also small.

The final oxidation predominantly consists of reactions

$$SiO + OH \longrightarrow SiO_2 + H \quad (R44)$$

and

$$SiO + O_2 \longrightarrow SiO_2 + O. \quad (R45)$$

The former reaction occurs in lower positions.

Consequently SiH_4 is oxidized step by step according to the sequence $SiH_4 \rightarrow SiH_2 \rightarrow HSiO \rightarrow SiO \rightarrow SiO_2$; the first step is composed of two routes, the direct dehydrogenation and the route via SiH_3.

The hydrogen–oxygen-containing species required by the above reactions as reactants are hydrogen atoms at the early stages, hydroxyl radicals at the final stage and oxygen at the middle and final stages. Those species and the main reactions related to them are shown in Fig. 8. The comparison of Figs. 7 and 8 indicates that the reactions among the hydrogen–oxygen-containing species take place at higher positions than those occurring among the silicon-containing species.

Hydrogen liberated by reaction (R22) reacts with oxygen at positions higher than 4 mm by reactions

$$O + H_2 \longrightarrow OH + H \quad (R3)$$

and

$$H + O_2 \longrightarrow OH + O. \quad (R2)$$

These are the predominant chain-branching reactions which are of great importance in almost all flames of hydrogen-containing fuel, and produce hydroxyl radicals with exponentially increasing rate. The hydroxyl radicals oxidize hydrogen to water and further produce hydrogen atoms by reaction

$$OH + H_2 \longrightarrow H + H_2O. \quad (R5)$$

Reactions (R2) and

$$OH + OH \longrightarrow O + H_2O \quad (R4)$$

proceed backward between 4 and 4.5 mm in height.

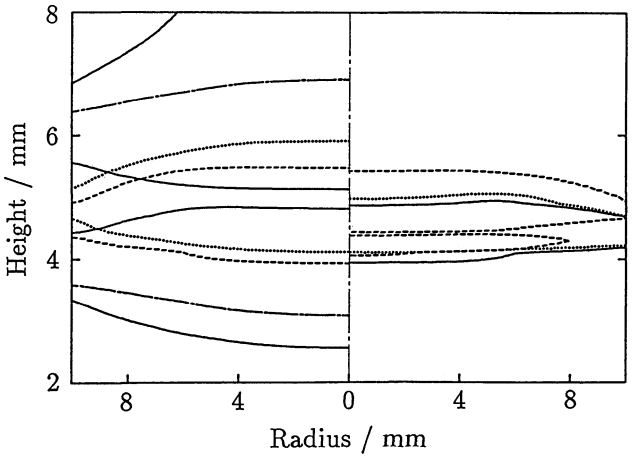

Fig. 8. In the left-hand side: distributions of H_2 (lower solid line, $x=1.7\times10^{-3}$), H (dashed line, $x=3.8\times10^{-4}$), OH (dotted line, $x=6.2\times10^{-4}$), H_2O (dotted-dashed line, $x=8.9\times10^{-3}$), and O_2 (upper solid line, $x=3.9\times10^{-2}$); in the right-hand side: distributions of reactions (R2) (upper dashed line, $\varphi=66$ mol m^{-3} s^{-1} for forward reaction and lower dashed line, $\varphi=18$ mol m^{-3} s^{-1} for backward reaction), (R3) (dotted line, $\varphi=18$ mol m^{-3} s^{-1}), and (R5) (solid line, $\varphi=39$ mol m^{-3} s^{-1}).

Oxygen and hydroxyl radicals are produced so that their insufficient supply to the lower region is compensated by those reactions. Hydrogen atoms are produced at heights above 4 mm and diffuse toward lower positions because of their large diffusion coefficient and are consumed by reactions (R25) and (R28).

In the previous paper on the combustion mechanism of silane–air premixed flames[8] two different pathways between SiH_4 and HSiO have been reported under a wide range of equivalence ratios: $SiH_4 \rightarrow SiH_3 \rightarrow SiH_2O \rightarrow HSiO$, which proceeds in low-temperature regions, and $SiH_4 \rightarrow SiH_2 \rightarrow HSiO$, occurring at high temperatures. These two routes can be clearly distinguished by the parameters of temperature and equivalence ratio. Hydroxyl radicals are the most important oxidizer in those pathways and in the former mechanism, in particular, they promote the dehydrogenation

$$SiH_4 + OH \longrightarrow SiH_3 + H_2O \quad (R27)$$

and

$$SiH_3 + O_2 \longrightarrow SiH_2O + OH \quad (R31)$$

with the cooperation of oxygen. The direct dehydrogenation of SiH_4 to SiH_2 by reaction (R22) is not accelerated until about 2000 K.

The two dehydrogenation pathways of SiH_4 are also observed in the counterflow diffusion flame; however, the one via SiH_3 does not proceed toward SiH_2O and, in addition, the reaction partners of SiH_4 and SiH_3 are hydrogen atoms instead of hydroxyl radicals. The main reason for those differences is that the local equivalence ratio in the region where the silicon-containing

species reactions occur is remarkably small in the diffusion flame so that SiH_3 is not oxidized into SiH_2O.

Conclusions

A silane–air counterflow diffusion flame was simulated using a detailed reaction scheme and complete fluid-dynamic governing equations, and the following conclusions were obtained:

(1) Oxygen which issues from the upper nozzle transgresses the stagnation surface, and hence reaction zone is formed in the fuel side. The temperature becomes maximum near the fuel-side edge of the reaction zone. Silane is preferentially oxidized in the fuel side of the reaction zone, and then the liberated hydrogen is oxidized producing active species necessary for silane combustion such as hydroxyl radicals and hydrogen atoms.

(2) Silane reacts through the sequence: $SiH_4 \rightarrow SiH_2 \rightarrow HSiO \rightarrow SiO \rightarrow SiO_2$. The first step is composed of two alternative routes: the direct dehydrogenation of SiH_4 to SiH_2 and the route $SiH_4 \rightarrow SiH_3 \rightarrow SiH_2$; the direct hydrogenation is predominant though the activation energy of unimolecular dissociation (R22) is much larger than the initiation reaction of the indirect dehydrogenation. In the premixed flames a large variety of species are present even at early stages of the reactions, but in the diffusion flame the initiation reaction, in particular, inevitably proceed in the state of insufficient oxygen-containing species relatively to premixed flames. The fuel oxidation up to silicon dioxide, therefore, occurs only in small amounts in the fuel side.

References

1) S. P. Burke and T. E. W. Schumann, *Ind. Eng. Chem.*, **20**, 998 (1928).
2) F. G. Roper, *Combust. Flame,* **29**, 219 (1977).
3) R. E. Mitchell, A. F. Sarofim, and L. A. Clomburg, *Combust. Flame,* **37**, 227 (1980).
4) R. A. Allison and J. F. Clarke, *Combust. Sci. Tech.,* **23**, 113 (1980).
5) R. A. Allison and J. F. Clarke, *Combust. Sci. Tech.,* **25**, 97 (1981).
6) M. Klajn and A. K. Oppenheim, "Nineteenth Symposium (International) on Combustion," The Combustion Institute, Pittsburgh (1982), p. 223.
7) S. Fukutani, K. Sakaguchi, N. Kunioshi, and H. Jinno, *Bull. Chem. Soc. Jpn.,* **64**, 1623 (1991).
8) S. Fukutani, Y. Uodome, N. Kunioshi, and H. Jinno, *Bull. Chem. Soc. Jpn.,* **64**, 2328 (1991).
9) G. Dixon-Lewis, T. David, P. H. Gaskell, S. Fukutani, H. Jinno, J. A. Miller, R. J. Kee, M. D. Smooke, N. Peters, E. Effelsberg, J. Warnatz, and F. Behrendt, "Twentieth Symposium (International) on Combustion," The Combustion Institute, Pittsburgh (1984), p. 1893.
10) S. Fukutani, *Nenshokenkyu,* **75**, 1 (1987).
11) R. H. Perry and C. H. Chilton, "Chemical Engineer's Handbook," 5th ed, McGraw-Hill, New York (1973).
12) M. W. Chase, Jr., C. A. Davies, J. R. Downey, Jr., D. J. Frurip, R. A. McDonald, and A. N. Syverud, "JANAF Thermochemical Tables," Part I and II, 3rd ed, The American Chemical Society and the American Institute of Physics (1985).
13) S. V. Patankar, "Numerical Heat Transfer and Fluid Flow," Hemisphere Publishing Co., New York (1980), Chap. 3.

 © 1991 The Chemical Society of Japan Bull. Chem. Soc. Jpn., 64, 2341—2348 (1991)

Luminescence and Circularly Polarized Luminescence of Mononuclear and Binuclear Chromium(III) L-Alaninato Complexes

Taro TSUBOMURA,* Iwao OHKOUCHI, and Makoto MORITA*
Department of Industrial Chemistry, Faculty of Engineering, Seikei University, Musashino, Tokyo 180
(Received December 28, 1990)

Luminescence and circularly polarized luminescence (CPL) spectra were investigated at low temperatures in order to clarify the chiroptical and electronic structures of monomeric and dimeric chromium(III) alaninato complexes. In the monomeric complexes, [Cr(L-(or D-)ala)$_3$]·H_2O, R_1 and R_2 lines of opposite spectral signs were found in the CPL spectra. The signs and relative intensities of the peaks were found to be comparable with circular dichroism (CD) spectra by employing theoretical arguments based on a strong crystal field theory. In the case of hydroxo-bridged dimeric complexes, [$Cr_2(OH)_2$(L-(or D-)ala)$_4$]·$3H_2O$, although the luminescence spectra of exchange-coupled pair states were clearly observed with a deduction of reasonable exchange interaction parameters, the CPL spectral components were not discernible because of the *meso*-type structure.

The luminescence properties of a large number of chromium(III) complexes have been thoroughly investigated over several decades.[1] A series of chromium complexes having amino acid ligands was carefully synthesized and the crystallographical as well as electronic structural data of the complexes were accumulated.[2] We have synthesized various series of monomeric and dimeric chromium amino acid complexes, and have found that they show a wide variety of luminescence spectra, although the energy and the intensity of the spin-allowed transitions are quite similar.[3]

We have been studying the chiroptical properties of chromium(III) complexes by using circularly polarized luminescence (CPL) spectroscopy.[4] Recently, we have reported that complexes with L-(or D-)alaninato (ala) ligands showed very sharp and split-line spectra, from which much interesting chiroptical information can be obtained. In this paper we precisely describe the luminescence properties of some chromium alaninato complexes: namely, monomeric *Λ-fac*-[Cr(L-ala)$_3$],[5] and dimeric [$Cr_2(OH)_2$(L-ala)$_4$],[6] whose structures are shown in Fig. 1. The complexes of the enantiomer containing D-ala ligands were also used to confirm the results. Powdery samples of the chromium(III) complexes showed reproducible luminescence and CPL spectra at low temperatures. We would represent clearly resolved R_1 and R_2 lines of opposite signs for the circularly polarized luminescence (CPL) of the [Cr(L- (and D-) ala)$_3$]·H_2O complex. A conventional crystal field theory regarding chirality is employed in order to explain some experimental foundations in the CPL spectra of the monomeric chromium(III) complexes. Then, fine structures due to exchange-coupled chromium pair are examined in the luminescence spectra of the binuclear complex.

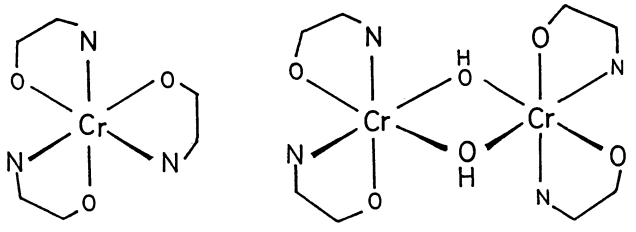

Fig. 1. Schematic drawings of the chromium complexes. (left) [Cr(L-ala)$_3$]·H_2O (right) [$Cr_2(OH)_2$(L-ala)$_4$]·$3H_2O$.

Experimental

Preparation of Mononuclear and Binuclear Chromium Complexes. The complexes were prepared by the reaction of [$Cr(NH_3)_6$](NO_3)$_3$ and L-alanine, according to Oki's method,[7] but with a slight modification. The molar ratio of the hexaammine complex to the L-alanine ligand was intentionally varied in greater amounts in order to obtain good yields of mononuclear or binuclear chromium alaninato complexes separately.

[Cr(L-(or D-)ala)$_3$]·H_2O. To a solution of [$Cr(NH_3)_6$](NO_3)$_3$ (6 mmol) in 70 mL of water was added 60 mmol of L- (or D-) alanine. This solution was heated to 70 °C for 90 min. Fine red needles of *fac-Λ*-[Cr(L-ala)$_3$]·H_2O or *fac-Δ*-[Cr(D-ala)$_3$]·H_2O were deposited and then separated and washed thoroughly with cold water. Anal. Calcd for $CrC_9H_{20}N_3O_7$: C, 33.51; H, 6.02; N, 12.66%. Found for L-ala complex: C, 33.84; H, 5.84; N, 13.06%. Found for D-ala complex: C, 33.48; H, 5.68; N, 13.09%.

[$Cr_2(OH)_2$(L-(or D-)ala)$_4$]·$3H_2O$. To obtain the binuclear metal complex, 50 mL of an aqueous solution containing 6 mmol of [$Cr(NH_3)_6$](NO_3)$_3$ and 6 mmol of L- (or D-) alanine was heated to 70 °C for 90 min. The solution was kept for several days at room temperature. [$Cr_2(OH)_2$(L-(or D-)ala)$_4$]·$3H_2O$ was obtained as violet crystals. Anal. Calcd for $Cr_2C_4H_{32}N_4O_{13}$: C, 26.47; H, 5.92; N, 10.29%. Found for L-ala complex: C, 26.49; H, 6.05; N, 9.99%. Found for D-ala complex: C, 25.97, H, 5.56; N, 10.44%.

Spectroscopic Measurements. Since the obtained samples were almost insoluble in water, the absorption spectra were obtained using the complex (2—2.5 mg) in KBr (150 mg) pellets on a Hitachi U-3200 spectrophotometer. The magnitudes of the molar absorption coefficients ε in KBr pellets were estimated on the basis of Lambert–Beer's law. The CD spectra of the same sample were recorded on a JASCO J-40 spectropolarimeter.

The luminescence spectra were measured on an instrumental system constructed in this laboratory.[8] Finely ground

powder samples were excited by the 514.5 nm line of an argon-ion laser (Spectra Physics, model 2025-05). The luminescent light was analyzed by a Spex 1401 double monochrometer set at 0.5 nm spectral resolution, and detected by a cooled Hamamatsu R943-02 photomultiplier tube. The luminescence signal was monitored by a Keithley model 614 electrometer. These instruments were totally controlled by an Apple II GS microcomputer. The emission spectra were corrected for monochrometer and photomultiplier photoefficiency by using a standard tungsten lamp.

Several optical devices were inserted into this system in order to detect CPL signals. The excitation light was chopped by an optical chopper at 30 Hz, and the luminescent light was passed through a photoelastic modulator (Morvue PEM-1) operated at 50 kHz with a polarizer sheet. The output signal of the photomultiplier tube was fed to a PAR 181 current-sensitive preamplifier; the AC signals were processed simultaneously by a NF Circuit Design LI-573 lock-in amplifier for the total luminescent (TL) current at 30 Hz, and by a EG&G PAR 5206 lock-in amplifier for the CPL current at 50 kHz. The two output signals were digitized and sent to an Apple II GS computer.

Optical glass cryostats for liquid-nitrogen and liquid-helium temperatures were used for the low-temperature luminescence measurements. An Air Products "Displex" model 202 helium closed cycle refrigerator was used for the experiments between 12 and 77 K.

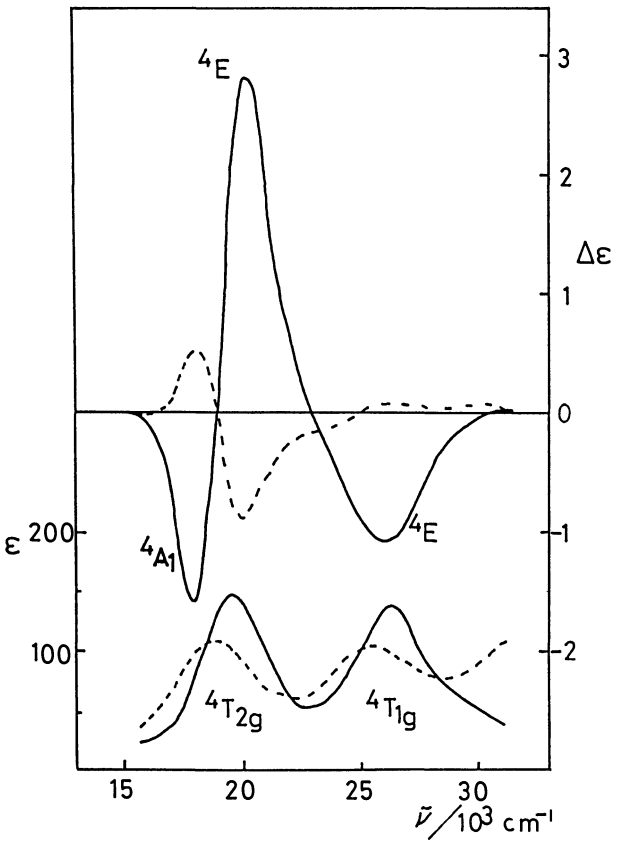

Fig. 2. Circular dichroism (upper part) and absorption spectra (lower part) of (——) [Cr(L-ala)$_3$]·H_2O and (– – –) [$Cr_2(OH)_2$(L-ala)$_4$]·$3H_2O$ in KBr pellets at room temperature.

Results

Absorption and Luminescence Spectra of [Cr(L-ala)$_3$]·H_2O. The room-temperature absorption spectra are displayed in Fig. 2 to give the spin-allowed transitions of the monomeric and dimeric chromium L-alaninato complexes in KBr pellets. The two broad bands are indicated as corresponding to the $^4A_{2g}\rightarrow{}^4T_{2g}$, $^4T_{1g}$ transition, respectively.

The 77 K absorption spectrum in the 14400 cm^{-1} energy region in a KBr pellet is shown in Fig. 3. The two peaks separated by 40 cm^{-1} correspond to the R lines; these have been assigned to the transition from the $^4A_{2g}$ state to the trigonal components of the $^2E_g(O_h)$ level. Two other peaks were observed at 15108 cm^{-1} and 15051 cm^{-1} at 77 K (not shown in the figure) and assigned to the $^4A_{2g}\rightarrow{}^2T_{1g}$ transition.

The low-temperature luminescence spectrum of a powdered sample is shown in Fig. 4. At 77 K, two prominent peaks were observed at 14386 cm^{-1} (R_1) and 14424 cm^{-1} (R_2), separated by 38 cm^{-1} in energy. A strong peak was further observed at 14185 cm^{-1}. The luminescence spectrum of the enantiomer, [Cr(D-ala)$_3$]·H_2O, was confirmed to be identical in both shape and position with that of L-ala complex. The integrated relative R_2/R_1 intensity ratio of these peaks is 0.42 at 77 K. The highest-energy peak was found to lose its intensity at 4 K, though the spectral resolution at 4 K was not significantly improved at 4 K, as compared to 77 K.

Therefore, the two distinct peaks, R_1 and R_2, should be assigned to transitions which occur from the split states of $^2E_g(O_h)$ in a trigonal field.

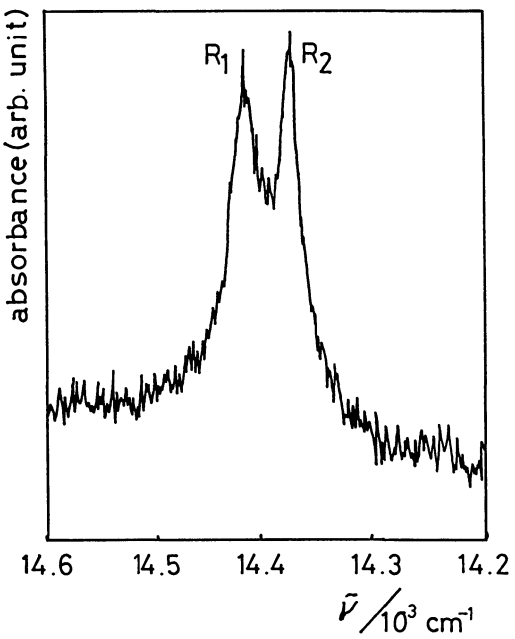

Fig. 3. Absorption spectrum of [Cr(L-ala)$_3$]·H_2O in KBr pellets at 77 K in the R line spectral region.

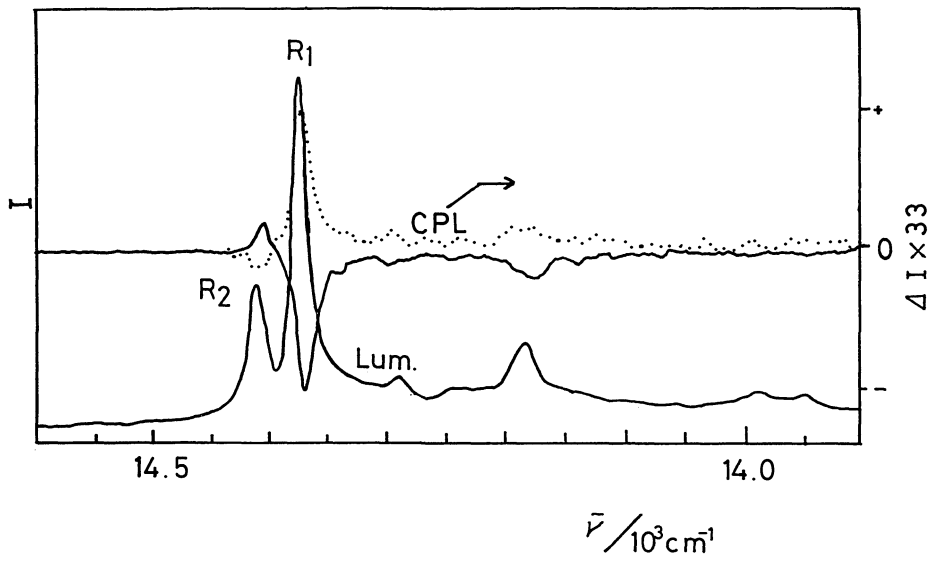

Fig. 4. Luminescence (I) and CPL (ΔI) spectra of tris alaninato chromium(III) complexes at 77 K. (——) $[Cr(L\text{-ala})_3]\cdot H_2O$, (– – –) $[Cr(D\text{-ala})_3]\cdot H_2O$. The intensity of ΔI is multipied by 33 compared to that of I.

CD and CPL Spectrum of $[Cr(D\text{-ala})_3]\cdot H_2O$. The room-temperature CD spectrum is also shown for the spin-allowed transition of $[Cr(L\text{-ala})_3]\cdot H_2O$ in KBr pellets in Fig. 2. A similar spectrum pattern (but of opposite CD sign) was obtained for $[Cr(D\text{-ala})_3]\cdot H_2O$ (but not displayed for clarity). The absolute values of $\Delta\varepsilon_{max}$ of a pair of enantiomers coincide with each others within 15% experimental discrepancies. In the CD spectrum of $[Cr(L\text{-ala})_3]\cdot H_2O$, a pair of bands of (+) and (−) signs was observed at 20,000 cm^{-1} in the $^4A_{2g}\rightarrow{}^4T_{2g}$ transition, and a single (−) band at 26,000 cm^{-1} in the $^4A_{2g}\rightarrow{}^4T_{1g}$ transition region.

Circularly polarized luminescence spectra of the powdered samples were recorded at 77 K. Figure 4 clearly shows two prominent R_1 and R_2 peaks of opposite CPL sign as well as some vibronic bands associated with the R_1 peak. The ordinate in the CPL spectrum indicates the (I_L—I_R) component of luminescence, where I_L and I_R refer to left-handed and right-handed circularly polarized luminescence, respectively. It is well-known that artificial CPL signals are often observed if the emitted light is partially linearly polarized under some conditions.[9] To reduce artifacts in the CPL measurement of a powdered sample, the following precautions were carefully taken. The exciting beam was aligned at 90° angle with respect to the emission direction, and the exciting Argon laser light was aligned so that its linearly polarized **E** vector was aligned in directions parallel to the detective direction of emission.[9] Furthermore, in order to examine the genuiness of the observed CPL spectra, both of the enantiomeric samples (i.e., $[Cr(L\text{-ala})_3]\cdot H_2O$ and $[Cr(D\text{-ala})_3]\cdot H_2O$) were measured, and the luminescent dissymmetry factor g_{em} ($g_{em}=2\times(I_L-I_R)/(I_L+I_R)$) was evaluated for comparisons. The absolute values of g_{em} of the two enantiomers should, in principle, be equal. For the L-ala complex, the g_{em} value of the R_1 line was estimated to be −0.024 and that of R_2 line to be +0.0040. For the D-ala complex, the g_{em} of R_1 was +0.025, while that of R_2 line was −0.0038. These g values agreed in repeated experiments within ca. 10% errors. From these results it was confirmed that these CPL spectra were not caused by any artificial factors but were genuine.

A negative CPL peak was observed at 14185 cm^{-1} in $[Cr(L\text{-ala})_3]\cdot H_2O$, with $g_{em}=-0.021$. This peak may be a vibronic sideband of the R_1 line, since R_1 was found to have a negative sign. The vibrational progression was calculated to be 201 cm^{-1}.

Luminescence and Absorption Spectral Results of $[Cr_2(OH)_2(L\text{-ala})_4]\cdot 3H_2O$. The luminescence spectra of the powdered sample of the binuclear complex are shown at low temperature in Fig. 5. At 43 K (solid curve), there are six peaks at around 14200 cm^{-1}. The peak locations are as follows: 14290, 14258, 14248, 14230, 14200, and 14164 in units of cm^{-1}. The luminescence intensity of these peaks was found to be very weak in comparison with the monomeric L-alaninato complex. A series of similar structures was also found in the 14000 cm^{-1} energy region. They were assigned to the vibronic peaks of 200 cm^{-1} energy relative to a group of 14200 cm^{-1} peaks. As the temperatures were lowered, the luminescence intensities of peaks **1** and **2** became reduced in intensity; at 4 K they completely disappeared.

The absorption spectrum of $[Cr_2(OH)_2(L\text{-ala})_4]\cdot 3H_2O$ is also shown in Fig. 2. Two spin-allowed bands, $^4A_{2g}\rightarrow{}^4T_{2g}$ and $^4T_{1g}$, are red-shifted in comparison with the monomeric complex. This corresponds to the fact that the dimeric complex (N_2O_4 coordination) has a weaker crystal field strength than the monomeric com-

plex (N_3O_3 coordination).

CD and CPL Spectra of $[Cr_2(OH)_2(L\text{-ala})_4]\cdot 3H_2O$. The room-temperature CD spectrum of the dimeric complexes is also shown in Fig. 2. The CD intensity of the dimeric complex is considerably weak in contrast to the CD spectra of the monomeric complexes, and a higher energy CD band ($^4A_{2g}\rightarrow{}^4T_{1g}$) can scarcely be seen. This spectral result can be rationalized by the fact that the dimer has a "*meso*"-type structure, i.e. the absolute configuration around two chromium ions are opposite to each other. Some discussions are given later concerning these results.

Although we have attempted CPL measurements of this complex at 77 K several times, a reproducible CPL signal could not be obtained. The CPL intensity should be too small to be observed within our detection limits.

Discussion

I. Mononuclear Complex, *fac*-$[Cr(L\text{-ala})_3]\cdot H_2O$. The absolute configuration of this almost insoluble pink isomer was determined to be Λ by Gillard et al.[5] According to their report, this chromium complex was found to be isomorphous with *fac*-$[Co(L\text{-ala})_3]$ of the Λ structure.

Spin-Allowed Transitions. The broad bands (Fig. 2), assigned to the transitions $^4A_{2g}\rightarrow{}^4T_{2g}$ and $^4T_{1g}$ (in O_h notation) split in a trigonal crystal field, i.e., the $^4T_{2g}$ (O_h) electronic level must split into two components, ^4E and $^4A_1$. Actually, two CD bands of opposite signs are seen in the $^4T_{2g}$ absorption band in Fig. 2. According to a static crystal field model, Shinada[10] theoretically discussed the CD spectra of trigonally-distorted bidentate Cr(III) and Co(III) complexes in general. The Λ-$[Cr(ox)_3]^{3-}$ (ox=oxalato ion) complex is already known to show a positive CD band at higher energy, and a negative CD band at lower energy in the $^4A_{2g}\rightarrow{}^4T_{2g}$ transition regions. The CD data were reported to be as follows: ν ($\Delta\varepsilon$), 18.1×10^3 cm^{-1} (+2.83), 16.1×10^3 cm^{-1} (−0.12).[11] The higher- and lower-energy bands were assigned to transitions due to the ^4E and $^4A_1$ components. This analysis assumes, in turn, a positive trigonal splitting parameter, K. Considering the second-order rotatory strength, the net rotatory strength of the $^4A_{2g}\rightarrow{}^4T_{2g}$ band was estimated to have a positive value.[10] This theoretical result agrees with the observed spectrum.

A similar assignment can be made for the CD spectrum of $[Cr(L\text{-ala})_3]\cdot H_2O$. Although the actual point symmetry of this molecule is C_3, we analyzed the electronic levels of this complex by assuming a D_3 chromophore. Richardson has extended the static crystal field model[12] so that it can be applied to distorted octahedral complexes. As a result, he concluded theoretically that both the net rotatory strength of the $^4A_{2g}\rightarrow{}^4T_{2g}$ band and the trigonal splitting parameter K are positive for trigonally compressed and azimuthally contracted O_h chromium(III) complexes. This alaninato complex can be reasonably classified to have this type of structure. According to these considerations, it is concluded that the trigonal splitting parameter K of $[Cr(L\text{-ala})_3]\cdot H_2O$ is positive, i.e. the ^4E electronic level lies above the $^4A_1$ level. The observed fact that the net rotatory strength of the $^4A_{2g}\rightarrow{}^4T_{2g}$ transition is positive, i.e. (+) CD component is larger than the (−) CD component, is also consistent with his theory.

It is notable that a comparatively large CD band is observed in the $^4A_{2g}\rightarrow{}^4T_{1g}$ region (in O_h notation). This is attributed to the ^4E component of the $^4T_{1g}$ level, since the $^4A_{2g}\rightarrow{}^4E$ transition is magnetically allowed, but the other transition ($^4A_{2g}\rightarrow{}^4T_2$) is forbidden under D_3 symetry. According to another theory,[13] the $^4A_2\rightarrow{}^4E$ ($^4T_{1g}$) transition borrows CD intensity from $^4A_{2g}\rightarrow{}^4E$ ($^4T_{2g}$) by configuration interaction. The CD sign of this $^4A_{2g}\rightarrow{}^4E$ ($^4T_{1g}$) transition is opposite to that of $^4A_{2g}\rightarrow{}^4E$ ($^4T_{2g}$) if K is positive. The observation of a negative CD sign in the $^4T_{1g}$ band is in accordance with this prediction. However, the matrix element of the configuration interaction, which equals $3K/2$, is too small to interpret the CD intensity. Another mechanism[14] must contribute in addition to the configuration interaction with ^4E ($^4T_{2g}$).

Spin Forbidden Transitions. Two sharp peaks were detected in luminescence at 14424 and 14386 cm^{-1}. The peak locations and the energy separation (38 cm^{-1}) of these two luminescent peaks are in good agreement with the absorption peaks at 77 K. They have been assigned to the split components of the $^2E_g\rightarrow{}^4A_{2g}$ transition by a contribution of trigonal crystal field and spin-orbit coupling. According to Tanabe and Sugano's strong ligand field theory,[15] the splitting of Kramers doublet λ can be expressed as

$$\lambda = E(2\bar{A}) - E(\bar{E}) = 4K\zeta_{so}/(E(^2E_g) - E(^2T_{2g})), \qquad (1)$$

where ζ_{so} denotes the spin-orbit coupling constant. The denominator, $E(^2E_g)-E(^2T_{2g})$, must be negative, and the trigonal splitting parameter, K, being positive (as described in the previous section) is such that the splitting energy, λ, should be negative. The energy difference, $E(^2E_g)-E(^2T_{2g})$, in $[Cr(L\text{-ala})_3]$ was estimated to be −6900 cm^{-1} by considering the position of the $^4T_{2g}$ and $^4T_{1g}$ absorption bands using a conventional Tanabe and Sugano diagram with C/B=4.5. If the K parameter is assumed to be +300 cm^{-1}, we obtain a ζ_{so} parameter of 220 cm^{-1} in energy for λ=−38 cm^{-1}.

It is interesting to quote a large splitting of the ^2E_g state of other amino acid complexes, i.e., λ of *fac*-$[Cr(gly)_3]\cdot 3H_2O$ is 89 cm^{-1}, where gly=glycine.[16] The analysis of a large ^2E splitting is still controversial.[17] However, in the case of the L-alaninato complex, λ is comparable to 29 cm^{-1} in ruby. We conclude that λ should be negative in sign and that the 14424 (R_2) and 14386 (R_1) peaks should be assigned to the transition from the $\bar{E}$ and $2\bar{A}$ states, respectively.

CPL Spectrum of $[Cr(L\text{-ala})_3]\cdot H_2O$. Both positive

and negative CPL peaks were detected in the R line region. For the $[Cr(L\text{-ala})_3]\cdot H_2O$ complex, the R_1 and R_2 peaks show a strong negative peak and a weak positive peak, respectively. Kaizaki et al. have presented theoretical arguments[18] to deduce the rotatory strength of the R lines based on Tanabe and Sugano's perturbation theory. The spin-forbidden transitions acquire both electric and magnetic dipole strengths through spin-orbit coupling from the spin-allowed transitions. In their calculation, only an electronic coupling between the ^2E_g and $^4T_{2g}$ states were taken into consideration, because, in trigonal symmetry, the $^4A_{2g}\rightarrow{}^4T_{2g}$ transitions are allowed in CD absorption, whereas the $^4A_{2g}\rightarrow{}^4T_{1g}$ transitions are forbidden. According to their theory, the rotatory strength of the R lines in trigonal symmetry can be calculated from the rotatory strength of the $^4A_{2g}\rightarrow{}^4E(^4T_{2g})$, $^4A_1(^4T_{2g})$ transitions, as follows:

$$R(\bar{E}) = 8R(^4A_1) + 20R(^4E) \quad (2)$$

and

$$R(2\bar{A}) = 24R(^4A_1) + 12R(^4E), \quad (3)$$

where $R(2\bar{A})$ and $R(\bar{E})$ are the rotatory strength of the R_1 and R_2 lines.

The low-temperature CD or CPL spectra of the R lines of $[Cr(en)_3]^{3+}$ (en=ethylenediamine) doped in a single crystal have already been reported.[19] Since only the axial spectra were measured, the R-line transitions borrow their intensity only from the ^4E component of the $^4T_{2g}(O_h)$ state. According to Eqs. 2 and 3, the axial rotatory strength ratio, $R_{ax}(\bar{E})/R_{ax}(2\bar{A})$, is estimated to be 5/3. Geiser and Güdel observed[19a] an axial circular dichroism of $[Cr(en)_3]^{3+}$ doped in a $2[Ir(en)_3]Cl_3\cdot KCl\cdot 6H_2O$ single crystal. They reported that the CD intensity of the $^4A_2\rightarrow\bar{E}$ transition is slightly larger than that of $^4A_2\rightarrow 2\bar{A}$ transition. The optical activity of single crystals of the spin-forbidden transitions of $[Cr(en)_3]^{3+}$ complex seems to be interpreted by Kaizaki's treatment.

In our case, the complex molecules are randomly dispersed in KBr pellets. We therefore have to take into account the contribution of the $^4A_1(^4T_{2g})$ components. From Eqs. 2 and 3, one can deduce that the signs and magnitudes of $R(\bar{E})$ and $R(2\bar{A})$ are mainly determined by the values of $R(^4E)$ and $R(^4A_1)$, respectively. In the observed spectra, indeed, the signs of the R_1 and R_2 lines in the CPL spectrum coincide with the signs of the $^4A_1$ and ^4E CD bands.

The relative CPL intensity ratios of the two peaks of ^2E are given by

$$\Delta I(\bar{E})/\Delta I(2\bar{A}) = (2+5\alpha)/(6+3\alpha)\times\exp(-\Delta E/k_BT), \quad (4)$$

where $\Delta I(\bar{E})$ and $\Delta I(2\bar{A})$ are CPL intensities of the two peaks, and $\alpha=R(^4E)/R(^4A_1)$ is the rotatory strength ratio of the $^4T_{2g}$ transition, ΔE the splitting of the ^2E_g level, and the k_B the Boltzmann constant. The CPL intensity ratio, $I(\bar{E})/I(2\bar{A})$, was evaluated from the observed 77 K CPL spectra to be −0.15. By employing this value, the calculated α ratio is −0.63. The room-temperature CD spectrum (Fig. 2), however, gives an α ratio of −2.0. This quantity seems not to be agreeable with this treatment.

We now consider some reasons why the theoretical predictions differ from the observations. First of all, we must reconsider the validity of Eqs. 2 and 3, as follows. In the theoretical considerations described so far, only the spin-orbit coupling between the ^2E_g and $^4T_{2g}$ (O_h) levels were considered for calculations of the rotatory strength. Under strict octahedral symmetry, indeed, the ^2E_g level can only mix with the $^4T_{2g}$ level, not with the $^4T_{1g}$ level (theoretically) through a spin-orbit interaction. Furthermore, most chromium complexes have a very small rotatory strength in the $^4A_{2g}\rightarrow{}^4T_{1g}$ region, as compared with the $^4A_{2g}\rightarrow{}^4T_{2g}$ region, so that the contribution from the $^4A_{2g}\rightarrow{}^4T_{1g}$ transition to the CPL intensity in the R lines can be reasonably ignored for ordinary cases. However, for the $[Cr(L\text{-ala})_3]\cdot H_2O$ complex, a large negative CD band, the rotatory strength of which is comparable to that of $^4T_{2g}$, was observed at the $^4A_{2g}\rightarrow{}^4E(^4T_{1g})$ transition (as described before). It should therefore be quite reasonable that the CPL transition of the R lines in trigonal symmetry acquire an additional negative rotatory strength by an introduction of the ^4E component of the $^4T_{1g}$ state. However, in perturbation theory, mixing of the ^4E state with the ^2E state is in inverse proportion to the energy difference, $\Delta E(^4E—^2E)$, the contribution of $^4E(^4T_{1g})$ being about half that of $^4E(^4T_{2g})$. Such a comparatively small negative contribution of the $^4E(^4T_{1g})$ state to the CPL intensity reduces the α value substantially; the observed α value approaches the theoretical value, −0.64. This contribution, however, may not be sufficient to understand the entire CPL intensity.

Secondary, one more assumption concerning Eqs. 2 and 3 must be pointed out. Eqs. 2 and 3 were obtained on the assumption that the trigonal splitting of $^4T_{1g}$ is small. The apparent trigonal splitting of the state, however, is very large (about 20000 cm^{-1}) in the CD spectrum. The actual splitting parameter must be smaller than this (as described in the next paragraph) and the difference between $\Delta E(^2E—^4E(^4T_{2g}))$ and $\Delta E(^2E—^4A_1(^4T_{2g}))$ must be considered. For the alaninato complex, since the energy of the $^4A_1(^4T_{2g})$ state is lower than that of $^4E(^4T_{2g})$, the coefficients of $R(^4A_1)$ become larger and those of $R(^4E)$ become smaller for Eqs. 2 and 3. Consequently, the theoretical value approaches the experimental value.

Thirdly, we examine the experimental value of α obtained from CD data. Since the rotatory strength of the $^4A_1$ and ^4E components of the $^4T_2$ band should have different signs, it is very difficult to correctly resolve the $^4T_2$ band into two components. An apparent splitting of the $^4T_2$ band in Fig. 2 is estimated to be 2000 cm^{-1}; this gives a trigonal splitting parameter of K=1300 cm^{-1}. The obtained K value is too large in comparison

with that of ordinary chromium(III) complexes. Clearly, an overlapping of two components of the $^4T_2$ band must occur; it is therefore difficult to estimate the correct α value from the spectrum.

No further quantitative discussion can be presented because of theoretical and experimental ambiguities. We think that the quantitative disagreement of the theoretical and experimental values results from a combination of the above-mentioned causes. However, it should be mentioned here that the signs of the CPL peaks of the R lines correspond to those of the CD bands. Therefore, Eqs. 2 and 3 are very useful expressions to qualitatively explain the CPL spectra of trigonal chromium(III) complexes.

We consider the g_{em} value of a vibronic peak. A single vibronic peak was clearly observed in the CPL spectrum. In general, it is hard to predict the rotatory strength of a vibronically induced transition which strongly depends on the nature of the vibration modes. According to the Herzberg–Teller mechanism, it is shown that if the vibronic band is coupled with e-mode vibrations, the dissymmetry factor, g, is smaller in vibronics than in their electronic origin.[19a] Geiser and Güdel[19a] have considered the vibronic CD intensity of $[Cr(en)_3]^{3+}$ at low temperatures. They obtained very small g_{abs} values for almost all of the peaks which are coupled with e-mode vibrations. Still, they found some interesting vibronic levels, the g_{abs} values of which are 0.5—4 times larger in magnitude with respect to their electronic origins. These prominent vibronic peaks are assigned to correspond to totally symmetric vibration. Peacock and Stewart[19b] reported that the g_{em} values for the R lines are 0.19 in the CPL of $[Cr(en)_3]^{3+}$. The g_{em} values of the vibronic bands seemed not to be as large as those of the electronic origin.

In the CPL spectra of $[Cr(L\text{-ala})_3]\cdot H_2O$, the g_{em} value of a peak seen at 14185 cm^{-1} was found to be −0.021, which is almost equal in magnitudes to −0.024 at the electronic origin. Considering the above-mentioned arguments, this peak is assigned to be a vibronic peak of R_1 coupled with a symmetric vibrational mode.

II. Binuclear Complex, $[Cr_2(OH)_2(L\text{-ala})_4]\cdot 3H_2O$. Electronic Eenergy Levels of Chromium Pair States. A series of peaks observed at low temperature (Fig. 5) can be interpreted as being due to the luminescence of a pair of chromium(III) ions. The ground state $|^4A_{2g}{}^4A_{2g}>$ are usually well described by the eigenvalues of the Hamiltonian,[20]

$$H = JS_1\cdot S_2 - j(S_1\cdot S_2)^2, \tag{5}$$

where J denotes an isotropic exchange parameter, j is the biquadratic contribution and S_1, S_2 are the spin quantum numbers of the Cr(1) and Cr(2) ions, respectively. The exchange interactions lead to a splitting of the ground state into four spin sub-levels, denoted by S_t=0, 1, 2, and 3, where S_t is total spin quantum number,

$$S_t = S_1 + S_2, \tag{6}$$

At 4.2 K, four peaks were detected in luminescence (peak number **3**, **4**, **5**, and **6** in Fig. 5). They have been assigned to a transition from the lowest excited electronic levels to the ground pair states. According to Eq. 5, the theoretical energy splitting between the neighboring pair levels are calculated to be $J+13j/2$, $2J+7j$, and $3J-9j/2$ for the S_t=0, 1, 2, and 3, respectively. From the observed peak separations (18, 30, and 36 cm^{-1}) the exchange parameters were calculated to be J=13.3 cm^{-1} and j=0.6 cm^{-1}. These energy levels are illustrated in Fig. 6. The J value of this complex is consistent with that of 17.1 cm^{-1}, which was deduced from magnetic susceptibility measurements while neglecting the j terms.[21] At higher temperatures, some

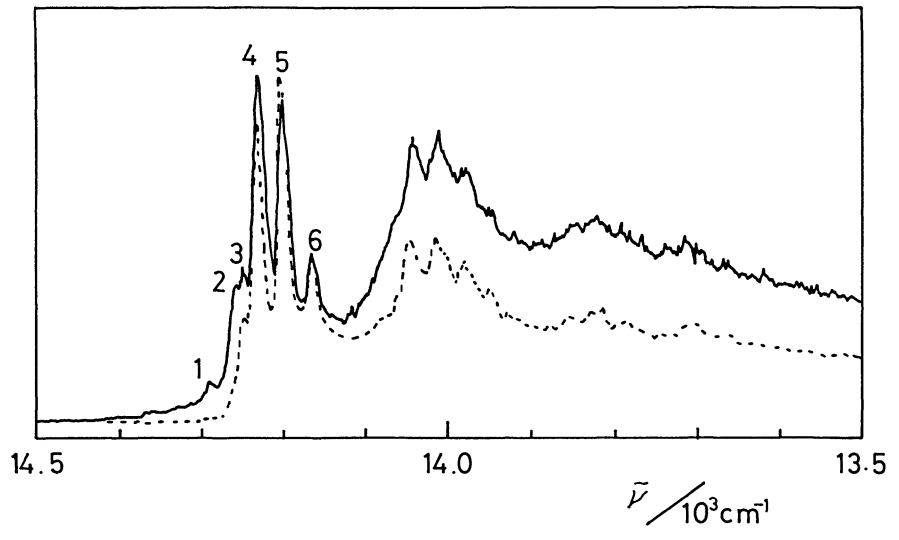

Fig. 5. Luminecsence spectra of $[Cr_2(OH)_2(L\text{-ala})_4]\cdot 3H_2O$. (——) at 43 K and (– – –) at 16 K.

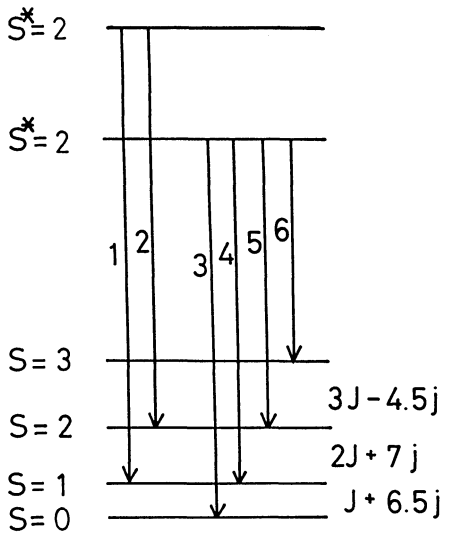

Fig. 6. Energy level diagram of exchange-coupled pair states in $[Cr_2(OH)_2(L\text{-ala})_4]\cdot 3H_2O$.

high-energy peaks (peak number **1** and **2**) grow in intensity; these have been assigned to the transition from the next higher excited state. The interval between the lowest and the next-higher excited states was determined to be 42 cm^{-1}. The total spin numbers of the excited pair states were supposed from the peak intensity, as follows. The $|^4A_{2g}{}^2E_g>$ pair state comprises four triplet (S_t*=1) and four quintet (S_t*=2) states. The observed transitions occur from these excited states and ground pair states (S_t=0, 1, 2, and 3). Two mechanisms[22] are possible to obtain the optical intensity in the pair system. They are a single ion mechanism and an exchange mechanism. The ΔS=0 transition is allowed by both mechanisms; thus, this ΔS=0 transition generally gives the most intense luminescence. Since the luminescence spectrum at 4 K (Fig. 5) shows that peak **5**, which is assigned to the S_t=2 state, is the most intense, the total spin number of the lowest excited state is determined to be 2 (see Fig. 6). A small peak, **3**, is assigned to the transition from S_t*=2 to S_t=0. Although both mechanisms cannot explain a ΔS=2 transition, a weak ΔS=2 transition had already been reported for μ-$(OH)_2$-$[Cr_2(OH)_2(en)_2]^{2+}$.[23] Since, no distinct peak assigned to the transition from the next lower excited state to the S_t=0 ground state could be observed, the next excited state may also be assigned to S_t*=2.

Optical Activity of $[Cr_2(L\text{-ala})_4(OH)_2]\cdot 3H_2O$. We were not successful in detecting the CPL spectra for this binuclear complex. It has already been shown[6] that the structure of this complex is of the "*meso*" type, i.e., one chromium moiety has a *Λ* configuration and the other has *Δ* (Fig. 1). Accordingly, the entire optical activity was smaller than that of the monomeric complex, $[Cr(L\text{-ala})_3]\cdot H_2O$. The CD intensity of the dimeric complex is, indeed, one third of the monomer (see Fig. 4). Furthermore, the total luminescence intensity of this dimer was found to be considerably lower than that of the corresponding monomer. It is reasonable to think that no CPL spectrum could be obtained at the present stage.

Conclusion. We have obtained the following results from the luminescence and CPL spectra of chromium alaninato complexes:

(1) Sharp luminescence and CPL spectra were obtained at low temperatures in the R-line energy regions for $[Cr(L\text{-(or D-)ala})_3]\cdot H_2O$. The CPL spectral features are qualitatively well explained if we assume that the rotatory strength of the R lines are mainly determined by contributions from the trigonally split components of the allowed $^4A_{2g}\rightarrow{}^4T_{2g}$ transitions. However, both theoretical and experimental difficulties prevent us from obtaining any quantitative discussion regarding the limit of crystal-field theory.

(2) Highly structured luminescence spectra of $[Cr_2(OH)_2(L\text{-ala})_4]\cdot 3H_2O$ were observed and interpreted by a Heisenberg-type of an exchange-coupled system. The exchange parameters were determined as being J=13.3 cm^{-1} and j=0.6 cm^{-1}. The CPL spectrum, however, was not observed, since this complex is considered to be a *meso*-type dimer complex.

This work was partly supported by the Japan Private School Promotion Foundation, 1984—1986.

References

1) L. S. Forster, *Transition Met. Chem. (N. Y.), Ser. Advances,* **5**, 1 (1969).
2) M. Morita, K. Eguchi, M. Shishikura, H. Nishikawa, and M. Inoue, *J. Lumin.,* **31—32**, 558 (1984).
3) H. Oki and Y. Takahashi, *Bull. Chem. Soc. Jpn.,* **50**, 2288 (1988), and the references there in.
4) T. Tsubomura, I. Ohkouchi, and M. Morita, *J. Lumin.,* **41—42**, 268 (1988), and unpublished results.
5) R. D. Gillard, S. H. Laurie, D. A. Price, and C. F. Weick, *J. Chem. Soc.,* **1974**, 1385.
6) G. Ranger and A. L. Beauchamp, *Acta Crystallogr., Sect. B,* **37**, 1063, (1981).
7) H. Oki, *Bull. Chem. Soc. Jpn.,* **50**, 680 (1977).
8) M. Morita and K. Eguchi, *Pap. Inst. Phys. Chem. Res.,* **78**, 157 (1984).
9) J. P. Riehl and F. S. Richardson, *Chem. Rev.,* **86**, 1 (1986).
10) M. Shinada, *J. Phys. Soc. Jpn.,* **19**, 1607, (1964).
11) A. J. McCaffery, S. F. Mason, and R. E. Ballard, *J. Chem. Soc.,* **1965**, 2883.
12) F. S. Richardson, *J. Phys. Chem.,* **7**, 692 (1971).
13) T. S. Piper and A. Karipides, *Mol. Phys.,* **5**, 339 (1962).
14) a) M. J. Harding, *J. Chem. Soc., Faraday Trans. 2,* **68**, 234 (1972); b) L. D. Barron, *Mol. Phys.,* **21**, 241 (1971).
15) S. Sugano and Y. Tanabe, *J. Phys. Soc. Jpn.,* **13**, 880 (1958).
16) A. G. Baca and W. F. J. Coleman, *J. Lumin.,* **22**, 29 (1980).
17) H.-H. Schmidtke, H. Adamski, and T. Schoenherr, *Bull. Chem. Soc. Jpn.,* **61**, 59 (1988).
18) S. Kaizaki, J. Hidaka, and Y. Shimura, *Inorg. Chem.,*

12, 142 (1973).

19) a) U. Geiser and H. U. Güdel, *Inorg. Chem.*, **20**, 3013 (1981); b) R. D. Peacock and B. Stewart, *J. Chem. Soc., Chem. Commun.*, **1982**, 295.

20) M. Morita and S. Sionoya, *J. Phys, Soc. Jpn.*, **28**, 144 (1970). Since there are several different forms of the exchange Hamiltonian, attention must be paid to compare the *J* parameters reported from different laboratories. See Ref. 18.

21) D. J. Hodgson, "Magneto-Structural Correlations in Exchange Coupled Systems," ed by R. D. Willet, D. Gatteschi, and O. Kahn, Reidel Publishing, Dordrecht, Holland (1985), p. 501.

22) H. Riesen and H. U. Güdel, *Inorg. Chem.*, **25**, 3566 (1986).

23) S. Decurtins and H. U. Güdel, *Inorg. Chem.*, **21**, 3598 (1982).

X-Ray Crystal Structures of Octahedral Diaquabis(*N,N*-dialkylethylenediamine)nickel(II) Complexes Possessing Elongated Nickel(II)-Nitrogen Bonds along Axial Direction

Yoshinori IHARA, Yasuhiro SATAKE,† Yumi FUJIMOTO, Hitoshi SENDA,††
Masatatsu SUZUKI,† and Akira UEHARA*,†
Laboratory of Chemistry, Faculty of Education, Kanazawa University, Kanazawa 920
†Department of Chemistry, Faculty of Science, Kanazawa University, Kanazawa 920
††Laboratory of Chemistry, Faculty of Liberal Arts, Kanazawa University, Kanazawa 920
(Received January 9, 1991)

The structures of two diaquabis(*N,N*-dialkylethylenediamine)nickel(II) chlorides ($[Ni(H_2O)_2(diamine)_2]Cl_2 \cdot nH_2O$) were determined by X-ray crystallographic studies, where diamine is *N,N*-dimethylethylenediamine(*NN*-dmen) or *N,N*-diethylethylenediamine (*NN*-deen). Both complexes are trans and crystallize in the monoclinic space group $P2_1/n$. The unit cell parameters of the *NN*-dmen complex, $NiCl_2C_8N_4O_4H_{32}$, are a=7.531(1), b=13.092(1), c=9.591(1) Å, β=107.76(1)°, and Z=2, and those of the *NN*-deen complex, $NiCl_2C_{12}N_4O_2H_{36}$, are a=9.154(1), b=8.692(1), c=12.395(2) Å, β=104.46(1)°, and Z=2. In *trans*-$[Ni(H_2O)_2(NN\text{-dmen})_2]Cl_2 \cdot 2H_2O$ and *trans*-$[Ni(H_2O)_2(NN\text{-deen})_2]Cl_2$, the Ni–$NMe_2$ and Ni–NEt_2 bond distances (2.183 and 2.271 Å) are much longer than the Ni–NH_2 distances (2.078 and 2.064 Å), forming tetragonally distorted octahedrons with four close in-plane neighbors(N_2O_2) and two remote axial ones(N_2). It is apparent that this distortion originates from the steric requirement of N-substituted groups. Such a distortion significantly affects the electronic spectra of these complexes.

We have studied on the coordination structures of various octahedral diaquabis(N- or C-substituted ethylenediamine)nickel(II) complexes and the products of their thermal reactions, and also on the effects of N- or C-substituent group(s) upon their structural changes during thermal treatments.[1-5] In general, the diaqua complexes could readily be characterized to be trans from the feature of their electronic spectra in near IR region, and they changed to the corresponding dianiono species upon thermal deaquation-anation, retaining trans configuration as shown below.[1,2]

$$\textit{trans}\text{-}[Ni(H_2O)_2(diamine)_2]X_2 \xrightarrow{-2H_2O} \textit{trans}\text{-}[NiX_2(diamine)_2]$$

The diaqua complexes with *N,N*-dialkylated ethylenediamines, however, showed a somewhat obscure splitting or a red shift of the two bands in near IR region, compared with a typical trans spectrum. In addition, some of these complexes peculiarly produced cis dianiono complexes by thermal treatment.[6] Accordingly, to understand the unusual spectra and thermal behaviors of these asymmetric diamine complexes, the structures of the octahedral diaqua complexes with *NN*-dmen (*N,N*-dimethylethylenediamine) and *NN*-deen (*N,N*-diethylethylenediamine) were determined by X-ray crystallographic studies in the present study.

Experimental

The complexes, *trans*-$[Ni(H_2O)_2(NN\text{-dmen})_2]Cl_2 \cdot 2H_2O$ (**A**) and *trans*-$[Ni(H_2O)_2(NN\text{-deen})_2]Cl_2$ (**B**) were prepared by the known methods.[7,8] The single crystals of the former grew as violet blocks upon slow evaporation from the ethanolic solution containing stoichiometric amounts of the diamine and nickel(II) chloride hexahydrate, and those of the latter were obtained as blue blocks by recrystallization from methanol.

The unit-cell parameters and intensities were measured on a Rigaku AFC-5R automated four-circle diffractometer using graphite-monochromatized Mo $K\alpha$ (λ=0.71073 Å) radiation at room temperature. The 2θ–ω scan mode at a rate of 6° min^{-1} was employed to record the intensities. The intensity data were corrected for Lorentz-polarization and absorption effects. Both structures were solved by the heavy atom method and refined by the block-diagonal least-squares method. Calculations were performed with the TEXSAN Structure Analysis software package on microVax II and with the UNICS III programs[9,10] on a FACOM 760/10 computer at the Kanazawa University Information Processing Center. Tables giving the positional parameters for all atoms, the anisotropic thermal parameters, the observed and calculated

Table 1. Crystal Data of *trans*-$[Ni(H_2O)_2(NN\text{-dmen})_2]Cl_2 \cdot 2H_2O$ (**A**) and *trans*-$[Ni(H_2O)_2(NN\text{-deen})_2]Cl_2$ (**B**)

Complex	A	B
Formula	$NiCl_2C_8N_4O_4H_{32}$	$NiCl_2C_{12}N_4O_2H_{36}$
Fw	377.97	398.05
Crystal system	Monoclinic	Monoclinic
Space group	$P2_1/n$	$P2_1/n$
a/Å	7.531(1)	9.154(1)
b/Å	13.092(1)	8.692(1)
c/Å	9.591(1)	12.395(2)
β/deg	107.76(1)	104.46(1)
V/Å^3	900.1	955.0
Z	2	2
D_c/g cm^{-3}	1.395	1.382
D_m/g cm^{-3}	1.390	1.381
No. of data	2334	2503
No. unique data[a]	1757	1557
No. parameters	223	173
R	0.0275	0.0327
R_w	0.0257[b]	0.0254[c]
μ/cm^{-1}	13.84	12.99
2θ limits/deg	3—55	3—55

a) $I_o > 3\sigma(I_o)$. b) $w=1/\sigma(F)$. c) $w=1/(\sigma(F))^2$.

structure factors, the intramolecular bond distances, the intramolecular bond angles, the interatomic distances in crystal, the intramolecular torsion angles, the least squares planes and deviations therefrom, and Figures showing stereoviews of full cell are deposited as Document No. 8949 at the Office of the Editor of Bull. Chem. Soc. Jpn.

The electronic spectra in solid phase were measured by the diffuse reflectance method with a Hitachi U-3400 spectrophotometer.

Results and Discussion

Crystal data of *trans*-$[Ni(H_2O)_2(NN\text{-dmen})_2]Cl_2 \cdot 2H_2O$ (**A**) and *trans*-$[Ni(H_2O)_2(NN\text{-deen})_2]Cl_2$ (**B**) are given in Table 1. The final atomic coordinates and thermal parameters of non-hydrogen atoms with their estimated deviations are given in Table 2. Figure 1 shows the perspective views of the two complex cations.

Table 2. Atomic Coordinates ($\times 10^4$) and Thermal Parameters of Non-Hydrogen Atoms with Their Estimated Standard Deviations in Parentheses

	Atom	x	y	z	B/Å^2
Complex **A**	Ni	0(0)	0(0)	0(0)	2.21(0)
	Cl	4248(1)	2057(1)	−553(1)	4.33(1)
	O(1)	487(2)	1586(1)	38(2)	4.13(5)
	O(2)[a]	3289(2)	2133(1)	5984(2)	4.92(4)
	N(1)	1690(2)	−97(2)	2295(2)	3.32(9)
	N(2)	−2150(2)	231(1)	905(2)	2.98(12)
	C(1)	645(4)	503(3)	3055(3)	4.08(31)
	C(2)	−1420(3)	241(2)	2516(3)	4.12(0)
	C(3)	168(13)	−354(7)	3020(9)	3.88(0)
	C(4)	3588(4)	354(3)	2583(4)	5.40(0)
	C(5)	1979(6)	−1151(3)	2893(4)	6.00(0)
	C(6)	2557(14)	893(9)	2880(10)	5.04(0)
	C(7)	3094(14)	−870(9)	2565(11)	5.08(0)
Complex **B**	Ni	0(0)	0(0)	0(0)	1.69(1)
	Cl	−4051(1)	2380(1)	−1915(1)	2.93(1)
	O	1355(2)	−141(3)	1629(2)	2.61(5)
	N(1)	1734(3)	1571(3)	−459(2)	2.13(8)
	N(2)	1262(3)	−1702(3)	−499(2)	2.31(9)
	C(1)	2970(3)	470(4)	−438(3)	2.72(8)
	C(2)	2380(4)	−1005(4)	−1024(3)	3.01(0)
	C(3)	2281(4)	2786(4)	399(3)	3.20(0)
	C(4)	3558(4)	3803(5)	232(4)	4.23(0)
	C(5)	1283(4)	2272(4)	−1595(3)	3.18(0)
	C(6)	163(5)	3570(5)	−1712(4)	4.80(0)

a) Lattice water.

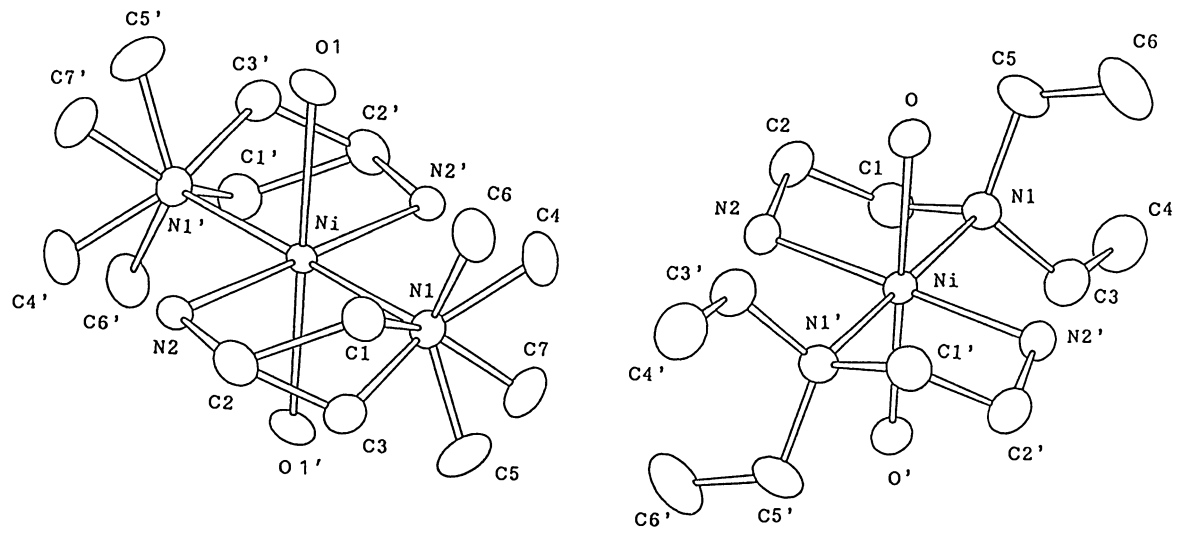

(A) (B)

Fig. 1. Crystal structures of the complex cations; (A) *trans*-$[Ni(H_2O)_2(NN\text{-dmen})_2]^{2+}$, which involves disorder, and (B) *trans*-$[Ni(H_2O)_2(NN\text{-deen})_2]^{2+}$.

The nickel(II) ion lies at a center of symmetry. Two coordinated waters of the complexes occupy trans positions of the N_4O_2 octahedrons and the two alkylated nitrogen atoms (N(1)) occupy axial sites apart from each other to minimize their mutual steric hindrance. Complex **A** shows a disorder of gauche and eclipsed five-membered chelate rings: C(4) and C(5) methyl carbon atoms belong to C(1) methylene one of gauche form. The relative occupancy of the dislocated atoms C(1) (C(4), and C(5)) and C(3) (C(6) and C(7)) is 0.75 : 0.25:[11] namely gauche form is predominant in the crystal. All chloride ions (not shown) fall within a distance of hydrogen bonding with adjacent amino group and either coordinated water or lattice water.[12]

The selected bond distances and angles are listed in Tables 3 and 4 for the *NN*-dmen and *NN*-deen complexes, respectively. It can be seen that the common striking characteristic in these structures is the elongated nickel(II)-nitrogen(N(1)) bonds along axial direction: the Ni–N(1) bond distances (2.183(2) Å for the *NN*-dmen and 2.271(3) Å for the *NN*-deen complexes) are much longer than the Ni–N(2) ones (2.078(2) Å for the former and 2.064(3) Å for the latter), so that tetragonally distorted octahedrons with four in-plane neighbors (N(2)N(2′)OO′ or N(2)N(2′)O(1)O(1′)) and two remote axial ones (N(1)N(1′)) are formed rather than familiar N_4(plane)O_2(axial) octahedrons.[13,14] Such distortion is noticeable in the *NN*-deen complex. The relevant bond distances in analogous nickel(II) complexes are collected in Table 5 along with our results. Similar elongated Ni–NR_2 bonds are observed in complexes **1**—**3**, which also contain either *NN*-dmen or *NN*-deen. It is additionally found that the distances of Ni–N bonds increase in the order of Ni–NH_2<Ni–NHR<Ni–NR_2.

Table 3. Selected Interatomic Distances and Angles of *trans*-[Ni(H_2O)$_2$(*NN*-dmen)$_2$]$Cl_2 \cdot 2H_2O$

Distances/Å		Angles/deg	
Ni–O(1)	2.108(2)	O(1)–Ni–N(1)	89.7(1)
Ni–N(1)	2.183(2)	O(1)–Ni–N(2)	90.2(1)
Ni–N(2)	2.078(2)	N(1)–Ni–N(2)	82.9(1)
N(1)–C(1)	1.455(4)	Ni–N(1)–C(1)	103.6(1)
N(1)–C(3)	1.547(11)	Ni–N(1)–C(3)	100.5(3)
N(1)–C(4)	1.492(4)	Ni–N(1)–C(4)	113.2(2)
N(1)–C(5)	1.486(4)	Ni–N(1)–C(5)	114.5(2)
N(1)–C(6)	1.484(11)	Ni–N(1)–C(6)	112.6(4)
N(1)–C(7)	1.429(11)	Ni–N(1)–C(7)	113.3(4)
N(2)–C(2)	1.473(3)	Ni–N(2)–C(2)	110.5(1)
C(1)–C(2)	1.520(4)	N(1)–C(1)–C(2)	111.2(2)
C(2)–C(3)	1.385(10)	N(1)–C(3)–C(2)	113.5(6)
		N(2)–C(2)–C(1)	112.0(2)
		N(2)–C(2)–C(3)	111.5(4)

Table 4. Selected Interatomic Distances and Angles of *trans*-[Ni(H_2O)$_2$(*NN*-deen)$_2$]Cl_2

Distances/Å		Angles/deg	
Ni–O	2.093(2)	O–Ni–N(1)	89.7(1)
Ni–N(1)	2.271(3)	O–Ni–N(2)	90.4(1)
Ni–N(2)	2.064(3)	N(1)–Ni–N(2)	83.0(1)
N(1)–C(1)	1.478(4)	Ni–N(1)–C(1)	100.7(2)
N(1)–C(3)	1.493(4)	Ni–N(1)–C(3)	112.2(2)
N(1)–C(5)	1.495(4)	Ni–N(1)–C(5)	115.8(2)
N(2)–C(2)	1.473(5)	Ni–N(2)–C(2)	109.9(2)
C(1)–C(2)	1.505(5)	N(1)–C(1)–C(2)	111.2(2)
C(3)–C(4)	1.520(6)	N(1)–C(3)–C(4)	116.5(3)
C(5)–C(6)	1.507(6)	N(1)–C(5)–C(6)	114.6(3)
		N(2)–C(2)–C(1)	110.0(3)

Table 5. Summary of Relevant Bond Distances

Complex[a]	Bond distance/Å		Reference
t-[Ni(H_2O)$_2$(*NN*-dmen)$_2$]$Cl_2 \cdot 2H_2O$ (**A**)	Ni–NH_2=2.08 Ni–OH_2=2.11	Ni–NMe_2=2.18	This work
t-[Ni(ONO)$_2$(*NN*-dmen)$_2$] (**1**)	Ni–NH_2=2.08 Ni–ONO=2.11	Ni–NMe_2=2.22	16
c-[Ni(NO_2)(H_2O)(*NN*-dmen)$_2$]ClO_4 (**2**)	Ni–NH_2=2.09—2.10 Ni–OH_2=2.07	Ni–NMe_2=2.19—2.20 Ni–NO_2=2.12	17
t-[Ni(H_2O)$_2$(*NN*-deen)$_2$]Cl_2 (**B**)	Ni–NH_2=2.06 Ni–OH_2=2.09	Ni–NEt_2=2.27	This work
t-[Ni(NCS)$_2$(*NN*-deen)$_2$] (**3**)	Ni–NH_2=2.09 Ni–NCS=2.08	Ni–NEt_2=2.30—2.33	18
t-[Ni(NO_2)$_2$(*NN*′-dmen)$_2$]$\cdot H_2O$ (**4**)	Ni–NHMe=2.11—2.12 Ni–NO_2=2.13		16
c-[Ni(ONO)(*NN*′-deen)$_2$]BF_4 (**5**)	Ni–NHEt=2.10—2.16 Ni–ONO=2.10—2.12		19
t-[Ni(NCS)$_2$(en)$_2$] (**6**)	Ni–NH_2=2.09—2.11 Ni–NCS=2.15		20
t-[Ni(NO_2)$_2$(en)$_2$] (**7**)	Ni–NH_2=2.09—2.10 Ni–NO_2=2.13		21
t-[Ni(H_2O)$_2$(*m*-stien)$_2$](Cl_2CHO_2)$_2 \cdot 2H_2O$ (**8**)	Ni–NH_2=2.03—2.05 Ni–OH_2=2.12		13
t-[Ni(H_2O)$_2$(*dl*-chxn)$_2$]Cl_2 (**9**)	Ni–NH_2=2.10 Ni–OH_2=2.13		14

a) *NN*′-dmen=*N,N*′-dimethylethylenediamine; *NN*′-deen=*N,N*′-diethylethylenediamine; *m*-stien=*meso*-1,2-diphenyl-1,2-ethanediamine; *dl*-chxn=*dl*-1,2-cyclohexanediamine.

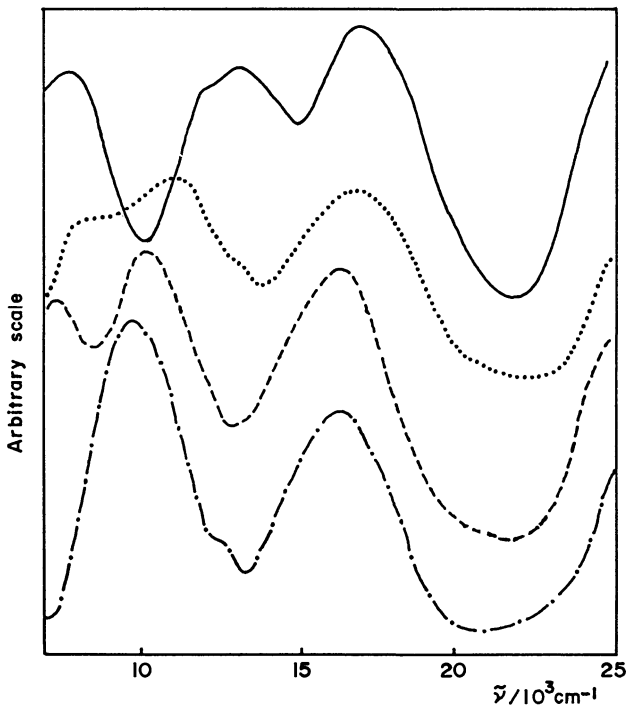

Fig. 2. Electronic spectra of *trans*-$[Ni(H_2O)_2(diamine)_2]Cl_2 \cdot nH_2O$, where diamine is *NN'*-dmen (——), *NN*-dmen (·····), or *NN*-deen (——), and of *cis*-$[Ni(H_2O)_2(NN\text{-dmen})_2]I_2$ (— - —). (*NN'*-dmen is *N,N'*-dimethylethylenediamine.)

It is thus apparent that these tetragonal distortions of complexes **A** and **B** originate from the steric requirement of N-substituted groups.

The electronic spectra of the two complexs are shown in Fig. 2, together with those of *trans*-$[Ni(H_2O)_2(NN'\text{-dmen})_2]Cl_2$ and *cis*-$[Ni(H_2O)_2(NN\text{-dmen})_2]I_2$ which are typical of trans and cis configurations, respectively.[15] Compared with the typical trans spectrum, it can be seen that complex **A** shows a somewhat obscure splitting of the two bands in near IR region, and complex **B** shows a red shift of all the bands in their spectra. These spectra can now be interpreted in terms of the above structural results: in comparison with the symmetric diamine complexes, it is anticipated that (1) the difference between ligand field strength along O–O axis and that in N_4 rhombus becomes small because of the elongation of the $Ni–NMe_2$ (or $–NEt_2$) bond length, and (2) the overall ligand field strength becomes weak (cf. the data of complexes **4** and **5** in Table 5). The effects of (1) and (2) should be responsible for the somewhat obscure splitting and the red shift of the bands in their spectra, respectively.

Both *trans*-diaqua complexes were transformed into the *cis*-dichloro complexes upon thermal deaquation-anation.[6] This is contrary to the complexes with the symmetric diamines which show simple deaquation-anation retaining a trans configuration. The differences in their reactivities seem to be related to the finding that the bonds between nickel(II) and the alkylated nitrogen atom are much weaker than the other coordination bonds in the asymmetric diamine complexes: it appears reasonable to assume that, in the case of the complexes with the asymmetric diamines, the rupture of a $Ni–NR_2$ bond precedes the liberation of the coordinated water, providing a driving force for these peculiar reactions.

References

1) R. Tsuchiya, S. Joba, A. Uehara, and E. Kyuno, *Bull. Chem. Soc. Jpn.*, **46**, 1454 (1973).
2) Y. Ihara, E. Izumi, A. Uehara, R. Tsuchiya, S. Nakagawa, and E. Kyuno, *Bull. Chem. Soc. Jpn.*, **55**, 1028 (1982).
3) Y. Ihara, T. Kamishima, and R. Tsuchiya, *Thermochim. Acta*, **67**, 23 (1983).
4) Y. Ihara, A. Wada, Y. Fukuda, and K. Sone, *Bull. Chem. Soc. Jpn.*, **59**, 2309 (1986).
5) Y. Ihara, Y. Fukuda, and K. Sone, *Inorg. Chem.*, **26**, 3745 (1987).
6) Details on this topic will shortly be reported.
7) D. M. L. Goodgame and L. M. Venanzi, *J. Chem. Soc.*, **1963**, 616.
8) D. M. L. Goodgame and L. M. Venanzi, *J. Chem. Soc.*, **1963**, 5909.
9) T. Sakurai and K. Kobayashi, *Rikagaku Kenkyusho Hokoku*, **55**, 69 (1979).
10) S. Kawano, *Rep. Comp. Cent. Kyushu Univ.*, **16**, 113 (1983).
11) These populations gave a minimum *R* value.
12) The distances are 3.357(2) Å for N(2)–Cl and 3.133(2) Å for O(2) (lattice water)–Cl in complex **A**, and 3.431(2) Å for N(2)–Cl and 3.081(2) Å for O–Cl in complex **B**.
13) S. C. Nyburg and J. S. Wood, *Inorg. Chem.*, **3**, 468 (1964).
14) A. V. Capilla, R. A. Aranda, and F. G. Beltran, *Cryst. Struct. Chem.*, **9**, 147 (1980).
15) A. B. P. Lever, "Inorganic Electronic Spectroscopy," 2nd ed, Elsevier, Amsterdam (1985).
16) A. J. Finney, M. A. Hitchman, C. L. Raston, G. L. Rowbottom, and A. H. White, *Aust. J. Chem.*, **34**, 2047 (1981).
17) A. J. Finney, M. A. Hitchman, C. L. Raston, G. L. Rowbottom, and A. H. White, *Aust. J. Chem.*, **34**, 2085 (1981).
18) A. B. P. Lever, I. M. Walker, P. J. McCarthy, K. B. Mertes, A. Jircitano, and R. Sheldon, *Inorg. Chem.*, **22**, 2252 (1983).
19) R. Birdy, D. M. L. Goodgame, J. C. McConway, and D. Rogers, *J. Chem. Soc., Dalton Trans.*, **1977**, 1730.
20) B. W. Brown and E. C. Lingafelter, *Acta Crystallogr.*, **16**, 753 (1963).
21) L. K. Minacheva, M. A. Porai-Koshits, and A. S. Antsyshkina, *J. Struct. Chem.*, **10**, 72 (1969).

Effect of Water Vapor on the Formation of Lithium *cyclo*-Hexaphosphate

Hiroyuki NARIAI,* Itaru MOTOOKA, and Mitsutomo TSUHAKO†
Department of Chemistry, Faculty of General Education, Kobe University, Tsurukabuto, Nada-ku, Kobe 657
†Kobe Women's College of Pharmacy, Kitamachi, Motoyama, Higashinada-ku, Kobe 658
(Received February 4, 1991)

The effect of water vapor on the formation of lithium *cyclo*-hexaphosphate $Li_6P_6O_{18}(P_{6m})$ from trilithium hydrogenpyrophosphate monohydrate $Li_3HP_2O_7 \cdot H_2O$ was investigated by means of DTA-TG, X-ray diffraction analysis, isothermal heating with electric furnace, and HPLC. $Li_3HP_2O_7 \cdot H_2O$ lost the water of crystallization at about 180 °C to give anhydrous $Li_3HP_2O_7$. At 300 °C the disproportionation of $Li_3HP_2O_7$ anhydride to $Li_4P_2O_7$ and $Li_4P_4O_{12}$ (P_{4m}) proceeded faster under humid conditions than under dry air, and subsequently P_{4m} increased with a decrease in P_2 and soluble polyphosphates (P_{poly}). At 400 °C, P_{4m} changed largely to P_{6m} under humid conditions. In these reaction processes, water plays an important role as catalyst in the cyclization by dehydration of the end group and in ring opening by attacking the P–O–P bond. At 450 °C, the amounts of P_2 and P_{6m} were almost equal under both humid and dry conditions, because all of P_{4m} thermally changed to P_{6m}.

It is well known that phosphates hydrolyze or condense on heating to form various kinds of phosphates.[1–4] Some types of them, linear and cyclic phosphates, have been investigated from the viewpoint of their thermal behavior.[5–21] These phosphates have been used for water treatment, as food additives, detergents, catalysts, and components of laser materials, and in phosphate glasses, and so forth.[22–26] The practical importance of these phosphates has been reviewed.[27]

In the syntheses of these phosphates, several factors including the nature of the metal, the temperature, the atmosphere, the time and rate of heating, and the state of the starting material, influence the structure and composition of the products. However, many works have been carried out on the thermal behavior of these phosphates without adequate consideration of the above-mentioned factors.

In a previous paper[28] we reported that, when lead *cyclo*-tetraphosphate decomposed to lead *cyclo*-octaphosphate, the cyclic phosphates were prepared optimally at a low water-vapor pressure, while linear phosphates were produced at a high water-vapor pressure.

The synthesis and thermal behavior of formation of lithium *cyclo*-hexaphosphate was investigated by Griffith and Buxton in 1965.[29] Schülke and Kayser reported a detailed formation mechanism in 1985.[30]

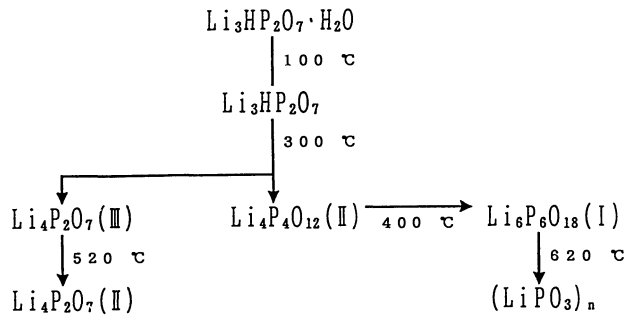

Fig. 1. Thermal dehydration processes of $Li_3HP_2O_7 \cdot H_2O$ as described by Schülke and Kayser.

Figure 1 shows the formation process of *cyclo*-hexaphosphate proposed by Schülke and Kayser.[30] $Li_3HP_2O_7$ changes to $Li_4P_2O_7$(III) and $Li_4P_4O_{12}$(II) by disproportionation at around 300 °C, followed by the transformation of $Li_4P_4O_{12}$(II) to $Li_6P_6O_{18}$(I) at around 400 °C. In spite of extensive works on the formation mechanism of *cyclo*-hexaphosphate, the yield of product exhibits a heavy scatter among the published results. A dominant cause for such a scatter appears to be a difference in the heating atmosphere from one experiment to another. In view of this, the effect of water vapor on the formation of lithium *cyclo*-hexaphosphate from trilithium hydrogenpyrophosphate monohydrate on heating was investigated in the present work.

Experimental

Chemicals. Trilithium hydrogenpyrophosphate monohydrate $Li_3HP_2O_7 \cdot H_2O$ was prepared by the method given in the literature.[30] Guaranteed reagent sodium pyrophosphate decahydrate ($Na_4P_2O_7 \cdot 10H_2O$) was used after double recrystallization. Other chemicals were of guaranteed reagent from Wako Chemical Industries, Ltd. and were used without further purification.

Determination of Lithium, Phosphorus, and the Water of Crystallization. Atomic absorption analysis was used for the determination of lithium ion in the sample solution with a Hitachi atomic absorption spectrophotometer Model 207. The total amount of phosphorus in phosphates was determined by absorptiometry after hydrolyzing the condensed phosphates with dilute hydrochloric acid. The condensed phosphates obtained by calcination were separated by HPLC, and then each phosphate was determined by the Molybdenum Blue Method.[18,20,21,28,31] The amount of the water of crystallization was calculated from the weight loss in TG curves. Other analytical procedures and apparatus were essentially the same as those used in previous works.[18,28]

Results and Discussion

Thermal Decomposition of the Phosphates Examined by DTA-TG. Figure 2 shows the DTA-TG curves for

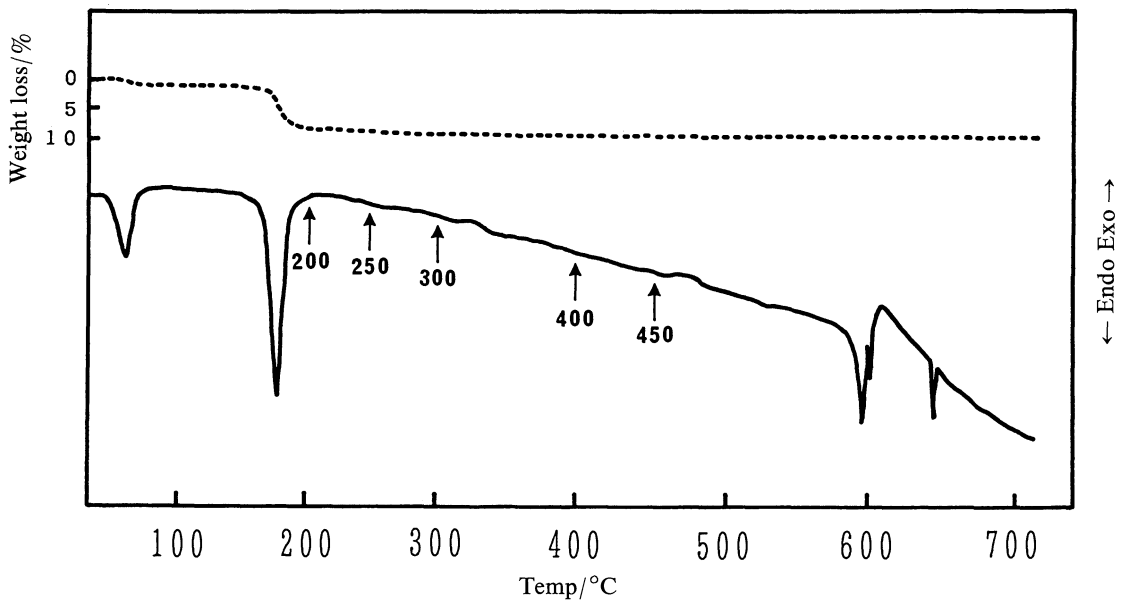

Fig. 2. DTA-TG curves for $Li_3HP_2O_7 \cdot H_2O$. Solid line: DTA, dotted line: TG.

$Li_3HP_2O_7 \cdot H_2O$ at atmospheric pressure. Endothermic peaks are noted at about 50, 180, 600, and 640 °C. From the HPLC analytical results, the first endothermic peak accompanying a small weight loss at 50 °C seemed to be due to liberation of absorbed acetone, and/or methanol, and/or water, since no change took place in the X-ray diffraction pattern of $Li_3HP_2O_7 \cdot H_2O$. The second endothermic peak with a large weight loss at 180 °C was attributed to elimination of the water of crystallization. HPLC analysis showed that anhydrous $Li_3HP_2O_7$ alone was present in the sample heated at 200 °C. No change in the TG curve occurred at temperatures above 300 °C. From the HPLC analysis, the products were found to be P_2, P_{4m}, and P_{poly} at 300 °C, P_2, P_{4m}, and P_{6m} at 400 °C, and P_2 and P_{6m} at 500 °C. The sample melted at around 600 °C. HPLC results indicated that P_{6m} and P_2, and P_{4m} and P_2 were present before and after the endothermic peak at 600 °C, respectively. Lithium metaphosphate (polymetaphosphate) was observed after the endothermic peak at 640 °C.

Isothermal Change. Although the DTA-TG curves do not exhibit definite peaks in the 200—500 °C region in Fig. 2, P_2 gradually changed to P_{4m} and/or P_{6m} and/or P_{poly}. Therefore, the influence of water vapor on the thermal decomposition was examined by heating $Li_3HP_2O_7 \cdot H_2O$ at 200, 250, 300, 400, or 450 °C for 1 h in air of 0 or 90% (at 25 °C) relative humidity. Figure 3 shows the X-ray diffraction patterns of the sample heated in dry air. In the 200—300 °C region, the diffraction lines of $Li_3HP_2O_7$ anhydride are dominant. At 400 °C, the characteristic diffraction lines of P_2(III) at 2θ=21.2°, and P_{4m}(II) at 2θ=17.5, 26.8, and 30.3° began to appear. At 450 °C, the diffraction lines of P_{4m}(II) disappeared, and those of P_{6m}(I) at 2θ=18.6, 19.2, 22.4, 23.7, and 33.6°, and P_2(II) at 21.2, 27.4, 28.5, 35.6, and

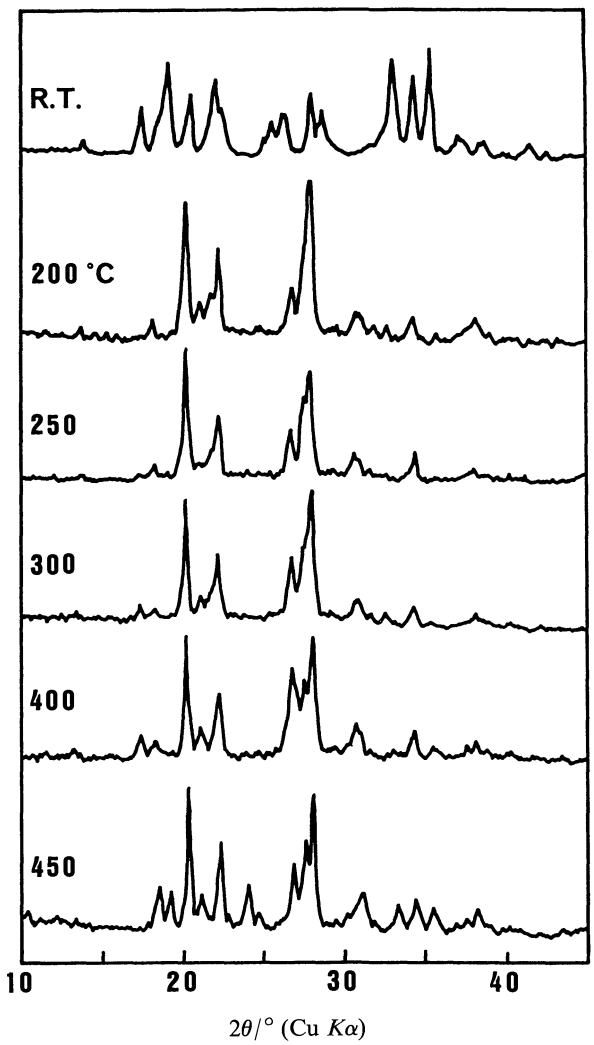

Fig. 3. X-Ray diffraction patterns of products in the course of heating. Sample: $Li_3HP_2O_7 \cdot H_2O$, relative humidity: 0%. R.T. is room temperature.

Table 1. Changes in the Amounts of Phosphates (Starting Material: $Li_3HP_2O_7 \cdot H_2O$)

Temp/°C	Compound[a] R.H.[b]/%	P_2 %	P_{4m} %	P_{6m} %	P_{poly} %
200	0%	93.5			6.5
	90%	96.5			3.5
250	0%	88.0	7.9		4.1
	90%	90.1	8.7		1.2
300	0%	79.4	15.9		4.7
	90%	69.7	28.4	1.9	
400	0%	66.3	30.8	2.9	
	90%	65.7	17.9	16.4	
450	0%	65.0		35.0	
	90%	65.1		34.9	

a) P_{4m}, P_{6m}, and P_{poly} represent *cyclo*-tetra-, *cyclo*-hexa-, and polyphosphates, respectively. P_2 represents the sum of diphosphates of $Li_3HP_2O_7$ and $Li_4P_2O_7$. P% denotes the percentage of phosphorus atoms present in these phosphate anions. b) Relative humidity at 25 °C.

38.0° began to appear. The persistence of the diffraction lines of $Li_3HP_2O_7$ anhydride at 450 °C in Fig. 3 indicates that the starting material remains even at this temperature.

Table 1 summarizes the changes in the amounts of phosphorus compounds in the samples. At 200—250 °C, a decrease in the amount of P_2 is accompanied by a 5-% level formation of P_{poly}. The condensation reaction was somewhat faster in dry air than in humid air. At 250 °C, P_{4m} was formed at about 8% in both dry air and humid air: the influence of atmosphere is hence negligible at this temperature. At 300 °C, P_{4m} increased with a decrease in P_2. In 90% relative humidity this trend was significant, and further P_{6m} was formed in a slight amount and P_{poly} was lost. At 400 °C, a fairly large amount of P_{4m} was convented into P_{6m}, particularly in 90% relative humidity. At 450 °C, the amounts of P_2 and P_{6m} were almost equal under both atmospheric conditions, since all the P_{4m} formed by the disproportionation changed to P_{6m}.

These results clearly show that a dry atmosphere is more favorable for the dehydration reaction at temperatures below about 300 °C, while a humid atmosphere is more favorable for the thermal process at above 300 °C where P_2 and P_{poly} change to P_{4m} and further to P_{6m}. In the processes at above 300 °C, water most probably plays a role of catalyst; the water molecule accelerates the ring opening by attacking the P–O–P bond, and promotes the difussion and recombination of the radicals formed by the ring opening.

References

1) R. N. Bell, L. F. Audrieth, and O. F. Hill, *Ind. Eng. Chem.*, **44**, 568 (1952).
2) J. R. Van Wazer and E. Karl-Kroupa, *J. Am. Chem. Soc.*, **78**, 1772 (1956).
3) J. F. McCullough, J. R. Van Wazer, and E. J. Griffith, *J. Am. Chem. Soc.*, **78**, 4528 (1956).
4) R. P. Langguth, R. K. Osterheld, and E. Karl-Kroupa, *J. Phys. Chem.*, **60**, 1335 (1956).
5) E. Thilo and I. Grunze, *Z. Anorg. Allg. Chem.*, **290**, 209 and 223 (1957).
6) E. Thilo, *Adv. Inorg. Chem. Radiochem.*, **4**, 1 (1962).
7) E. Thilo and U. Schülke, *Z. Anorg. Allg. Chem.*, **341**, 293 (1965).
8) J. D. Lee and A. H. Bond, *J. Appl. Chem.*, **18**, 345 (1968).
9) U. Schülke, *Z. Anorg. Allg. Chem.*, **360**, 231 (1968).
10) M. Watanabe, S. Sato, and H. Saito, *Bull. Chem. Soc. Jpn.*, **48**, 896 (1975).
11) H. Worzala, *Z. Anorg. Allg. Chem.*, **445**, 27 (1978).
12) E. V. Lazarevski, L. V. Kubasova, N. N. Chudinova, and I. V. Tananaev, *Izv. Akad. Nauk SSSR, Neorg. Mater.*, **16**, 120 (1980).
13) M. Watanabe, M. Matsuura, and T. Yamada, *Bull. Chem. Soc. Jpn.*, **54**, 738 (1981).
14) E. V. Lazarevski, *Izv. Akad. Nauk SSSR, Neorg. Mater.*, **18**, 1550 (1982).
15) E. V. Lazarevski, L. V. Kubasova, N. N. Chudinova, and I. V. Tananaev, *Izv. Akad. Nauk SSSR, Neorg. Mater.*, **18**, 1544 (1982).
16) I. Grunze and H. Grunze, *Z. Anorg. Allg. Chem.*, **512**, 39 (1984).
17) Th. R. Hinsch, W. Guse, and H. Saalfeld, *J. Cryst. Growth*, **79**, 205 (1986).
18) H. Nariai, I. Motooka, and M. Tsuhako, *Bull. Chem. Soc. Jpn.*, **61**, 2811 (1988).
19) M. Watanabe, K. Murata, and M. Maeda, *Bull. Chem. Soc. Jpn.*, **61**, 3877 (1988).
20) A. Takenaka, I. Motooka, and H. Nariai, *Bull. Chem. Soc. Jpn.*, **62**, 2819 (1989).
21) A. Takenaka, H. Kobayashi, K. Tsuchie, I. Motooka, and H. Nariai, *Bull. Chem. Soc. Jpn.*, **62**, 3808 (1989).
22) J. R. Van Wazer, "Phosphorus and Its Compounds," Interscience Publishers, Inc., New York (1961), Vol. II.
23) M. Trojan and D. Brandova, *Thermochim. Acta*, **88**, 415 (1985).
24) D. Brandova, *Thermochim. Acta*, **92**, 49 (1985).
25) D. Brandova and M. Trojan, *J. Therm. Anal.*, **30**, 159 (1985).
26) M. Trojan, D. Brandova, and Z. Solc, *Thermochim. Acta*, **110**, 343 (1987).
27) T. Kanazawa, "Inorganic Phosphate Materials," Kodansha Ltd., Tokyo (1989).
28) H. Nariai, I. Motooka, Y. Kanaji, and M. Tsuhako, *Bull. Chem. Soc. Jpn.*, **60**, 1337 (1987).
29) E. J. Griffith and R. L. Buxton, *Inorg. Chem.*, **4**, 549 (1965).
30) U. Schülke and R. Kayser, *Z. Anorg. Allg. Chem.*, **531**, 167 (1985).
31) G. Kura, *Bull. Chem. Soc. Jpn.*, **56**, 3769 (1983).

Chromatographic Optical Resolution Based on the Chiral Discrimination between Ions of the Same Sign, Anionic Cobalt(III) Complex Racemates and Anionic Selector $[Sb_2(d\text{-tart})_2]^{2-}$

Norio KOINE
Department of Industrial Chemistry, Faculty of Engineering,
Ehime University, Bunkyo-cho, Matsuyama 790
(Received December 10, 1990)

Column chromatographic optical resolutions of twenty-six typical univalent anionic cobalt(III) complexes, e.g., $[Co(edta)]^-$ and *fac*-$[Co(NO_2)_3(edma)]^-$, were carried out, using as a chiral eluent an aqueous solution of $[Sb_2(d\text{-tart})_2]^{2-}$ on a strongly basic anion exchanger, where edta=ethylenediamine-*N,N,N',N'*-tetraacetate(4-), edma=ethylenediamine-*N*-acetate(1-), and *d*-tart=*d*-tartrate(4-). The racemates were resolved with separation factors comparable to those obtained in conventional resolutions by use of cationic selectors. From a comparison of elution orders of enantiomers and separation factors obtained for the racemates, a chiral discrimination mechanism without direct contact between the racemate and selector was proposed.

Chromatographic complete resolution of anionic metal complexes is difficult to achieve compared with that of cationic ones, although many attempts have been made from of old.[1–3] The first complete resolution of anionic complexes was achieved for $[Co(ox)_2(gly)]^{2-}$[4] by use of Λ-$[Co(en)_3]^{3+}$ as a selector (resolving agent) by Tatehata et al.[5] in 1981. Since then complete resolutions of several anionic cobalt(III) complexes have been attained by Tatehata et al.[6] and Yoneda et al.,[3,7–9] but the selectors used have been limited to cations, cationic metal complexes and alkaloid cations. In such systems, the resolution is governed by the chiral discrimination between ions of opposite signs. We have recently reported of a complete resolution based on the chiral discrimination between ions of the same sign: anionic racemates, *cis*(*N*)-$[Co(ida)_2]^-$ and $[Co(edta)]^-$, were resolved by an anionic selector $[Sb_2(d\text{-tart})_2]^{2-}$ on a strongly basic anion exchanger.[10] This resolution technique was first adopted on a DEAE-Sephadex (DEAE=2-(diethylamino)ethyl) column by Yoshikawa and Yamasaki[2] but resulted in unseparated elution curves with partial resolution. The efficiency of our resolutions is comparable to that obtained by the chiral discrimination between ions of opposite signs.[3,5–9] Such an unexpectedly high ability of discrimination is of interest for the stereoselective interaction in general between charged species, particularly in connection with weak chemical interactions important in biological systems.[11]

Chiral discrimination phenomena dependent on diastereomeric interactions have been recognized between ions of the same sign, in spite of the occurrence of interference with the mutual approach of ions by the inevitable electrostatic repulsion. Discriminatory interactions in cation–cation systems have been recognized as phenomena such as the Pfeiffer effect (the displacement of enantiomer equilibrium of a labile racemic complex caused by an optically active "environment substance")[9,12–14] and optical resolution.[15] On the other hand, phenomena in anion-anion systems have rarely been reported[16] except for the above observation.[2,10] Although the mechanism of chiral discrimination for the phenomena observed has been widely examined, its nature has not yet been clearly elucidated.[12–19] Furthermore, the phenomena have strangely been manifested only for systems containing racemic complexes with N-heterocyclic unsaturated ligands, such as 1,10-phenanthroline and 2,2'-bipyridine. Under these circumstances, further investigation on the present phenomenon, which occurs between anions having no unsaturated ligands, can be expected to provide important information regarding the origin of chiral discrimination.

The present work deals with chromatographic optical resolutions of a series of typical anionic cobalt(III) complexes by our method.[10] The mechanism of chiral discrimination will be discussed on the basis of the relation between the resolution behavior of enantiomers and the structure of complexes.

Experimental

Materials. The twenty-six racemic cobalt(III) complex anions (**1a**—**11**) used in this work are listed in Table 1, where the complexes are numbered with the same numeral for the same type of complexes. All these anions have been isolated as their sodium or potassium salts and their structures have been well characterized. Optical resolution has been achieved except for *unsym*-$[Co(ox)(aeida)]^-$ (**5a**). Absolute configurations have been determined on the basis of X-ray crystallographic, circular dichroism (CD) spectral, or stereochemical analysis, except for the aeida (**5a**[20] and **5b**[21]) and edma (**7**)[22] complexes: **1a**, **1b**, **1d**—**4**, and **6a** in a review by Radanović,[23] **1c**,[8] **6b**—**6e**,[24] **8a**, **9a**, **10a**,[25] **8b**, **9b**, **10b**,[26] and **11**.[27] Three (**1a**, **1b**, and **11**) of these complexes were determined X-ray crytallographically.

The optical resolution of the racemic *unsym*-K[Co(ox)(aeida)]·H_2O (**5a**)[20] was achieved by an up-scaled present type chromatography and the resolved complex was isolated as a potassium salt, $(+)^{CD}_{567}$-*unsym*-K[Co(ox)(aeida)]·$3H_2O$, from an eluate containing the early eluted enantiomer. Found: C, 23.33; H, 3.97; N, 6.66%. Calcd for K[Co(ox)(aeida)]·

$3H_2O$=$KCoC_8H_{16}N_2O_{11}$: C, 23.20; H, 3.89; N, 6.76%. $[\alpha]_D$= +300°. $\Delta\varepsilon_{max}$=+1.82 (at 567 nm), −0.71 (497), and +0.23 (375).

The selector potassium bis(*d*-tartrato)diantimonate(III) trihydrate, $K_2[Sb_2(d\text{-tart})_2]\cdot 3H_2O$, was commercially available.

Chromatographic Resolution. The strongly basic anion-exchanger used was derived from Toyopearl (Fractogel TSK) HW50s gel (20—40 μm on swelling in water) in this laboratory.[10] The exchanger of form $[Sb_2(d\text{-tart})_2]^{2-}$ was packed in a glass column (1.0 cm×80 cm) and about 5 mg of a racemic cobalt(III) complex was loaded on the top of the column. The adsorbed band was eluted with 0.02 mol dm^{-3} aqueous solution of $K_2[Sb_2(d\text{-tart})_2]\cdot 3H_2O$. The elution rate was regulated to 0.25—0.27 cm^3 min^{-1} by a Pharmasia LKB 2132 type peristaltic pump. The elution curve was recorded at the wavelength of the first absorption maximum of the complex on a Shimadzu SPD-6AV spectrophotometric detector. The elution order of the enantiomers was determined by measuring CD spectra of fractional eluates.

Measurements. Elemental analysis was carried out at the Advanced Instrumentation Center for Chemical Analysis, Ehime University. The CD spectra were recorded on a JASCO J-20 spectropolarimeter using a 1.0 cm cell at room temperature.

Results and Discussion

Absolute Configuration of the Cobalt(III) Complexes. As described in the Experimental section, the absolute configurations of the three complexes, *unsym*-$[Co(ox)(aeida)]^-$ (**5a**), *unsym*-$[Co(NO_2)_2(aeida)]^-$ (**5b**), and *fac*-$[Co(NO_2)_3(edma)]^-$ (**7**), are unknown. The ring-pairing method cannot be applied to the absolute configurations of these complexes, because the complexes lack the net ring-pairing chirality.[28,29] Fortunately, the absolute configuration of *fac*-$[Co(edma)(NH_3)_3]^{2+}$, which has the same chromophore (CoN_5O) as *fac*-$[Co(NO_2)_3(edma)]^-$, has been determined: $(+)^{CD}_{512}$-*fac*-$[Co(edma)(NH_3)_3]^{2+}$ has an (*S*)-configuration with respect to the secondary nitrogen atom of the coordinated edma.[30] The CD curve of the early eluted enantiomer of *fac*-$[Co(NO_2)_3(edma)]^-$ ($\Delta\varepsilon_{max}$=+1.095 (at 485 nm) and −0.822 (at 427 nm))[22] shows the same general shape and sign pattern in the first absorption region as that of the (*S*)-isomer of *fac*-$[Co(edma)(NH_3)_3]^{2+}$ ($\Delta\varepsilon_{max}$=+1.641 (at 512 nm) and −0. 811 (at 444 nm)).[30] By comparison of the CD curves, thus, the absolute configuration of the early eluted enantiomer, $(+)^{CD}_{485}$-*fac*-

Table 1. Data of the Chromatographic Optical Resolution

No.	Racemic complex ion	Retention volume/cm^3 [a]	Separation factor (α)[b]	Early eluted enantiomer		
				Sign of CD extremum	Absolute configuration	Configuration of NNO-facet
1a	$[Co(edta)]^-$	115	1.08	$(-)_{582}$	*Λ*	LL
b	$[Co(trdta)]^-$	96	1.09	$(-)_{588}$	*Λ*	LL
c	$[Co(tdta)]^-$	86	1.06	$(-)_{623}$	*Λ*	LL
d	$[Co(pdta)]^-$ [c]	100	1.09	$(-)_{584}$	*Λ*	LL
e	$[Co(cydta)]^-$ [c]	95	s[d]	$(-)_{595}$	*Λ*	LL
2a	$[Co(NO_2)(ed3a)]^-$	137	1.10	$(+)_{582}$	—[e]	LL
b	$[Co(NO_2)(med3a)]^-$	114	1.06	$(-)_{575}$	—	LL
c	$[Co(NO_2)(hed3a)]^-$	118	1.07	$(-)_{578}$	—	LL
3a	*cis*-α-$[Co(ox)(edda)]^-$	97	1.16	$(+)_{560}$	*Λ*	LL
b	*cis*-α-$[Co(ox)(dmedda)]^-$	80	1.04	$(+)_{558}$	*Λ*	LL
4	*cis*-β-$[Co(ox)(edda)]^-$	95	1.04	$(+)_{544}$	*Λ*	R
5a	*unsym*-$[Co(ox)(aeida)]^-$	128	1.15	$(+)_{567}$	—	(L)[f]
b	*unsym*-$[Co(NO_2)_2(aeida)]^-$	271	1.08	$(+)_{502}$	—	(L)[f]
6a	*cis*(*N*)-$[Co(ida)_2]^-$	134	1.17	$(+)_{588}$	*Λ*[g]	RR
b	*cis*(*N*)-$[Co(ida)(mida)]^-$	110	1.13	$(-)_{592}$	*Λ*	LL
c	*cis*(*N*)-$[Co(mida)_2]^-$	86	1.07	$(-)_{613}$	*Λ*	LL
d	*cis*(*N*)-$[Co(ida)(eida)]^-$	95	1.04	$(-)_{592}$	*Λ*	LL
e	*cis*(*N*)-$[Co(eida)_2]^-$	77	1.05	$(-)_{620}$	*Λ*	LL
7	*fac*-$[Co(NO_2)_3(edma)]^-$	453	1.07	$(+)_{485}$	(*S*)[h]	L
8a	*trans*(*N*)-$[Co(ox)(gly)_2]^-$	78	s	$(-)_{530}$	*Λ*	—
b	*trans*(*N*)-$[Co(ox)(\beta\text{-ala})_2]^-$	59	s	$(-)_{637}$	*Λ*	—
9a	C_1-*cis*(*N*)-$[Co(ox)(gly)_2]^-$	141	s	$(+)_{565}$	*Λ*	R
b	C_1-*cis*(*N*)-$[Co(ox)(\beta\text{-ala})_2]^-$	88	s	$(+)_{588}$	*Λ*	R
10a	C_2-*cis*(*N*)-$[Co(ox)(gly)_2]^-$	143	1.10	$(+)_{555}$	*Λ*	LL
b	C_2-*cis*(*N*)-$[Co(ox)(\beta\text{-ala})_2]^-$	87	1.10	$(+)_{607}$	*Λ*	LL
11	$[Co(ox)_2(en)]^-$	116	1.03	$(-)_{581}$	*Λ*	—

a) The mean value for the enantiomers. b) The void volume is not considered for the estimation of factor. c) Racemic $[Co(pdta)]^-$ and $[Co(cydta)]^-$ are an equimolar mixture of the enantiomers *Λ*-$[Co\{(R)\text{-pdta}\}]^-$ ··· *Λ*-$[Co\{(S)\text{-pdta}\}]^-$ and *Λ*-$[Co\{(R,R)\text{-cydta}\}]^-$ ··· *Λ*-$[Co\{(S,S)\text{-cydta}\}]^-$, respectively. d) Single elution curve. e) Not characterized by the IUPAC nomenclature concerned with the octahedral complexes (Ref. 29). f) Tentative assignment; see text. g) Erroneously determined in Ref. 10 and thus corrected here. h) Absolute configuration of the secondary nitrogen atom of coordinated edma.

$[Co(NO_2)_3(edma)]^-$, can be assigned to (*S*).

Chromatographic Resolution and Chiral Discrimination Mechanism. The representative elution curves in the present optical resolutions are shown in Fig. 1. The mean retention volumes and separation factors (α) are summarized in Table 1. The α value greater than about 1.07 corresponds to the virtual complete resolution in the present resolutions. Single elution curves were obtained for the five complexes (**1e**, **8a**—**9b**), but in every case partial resolution was confirmed by measuring CD spectra of fractional eluates. The α value is regarded approximately as the difference in free energy of distribution between for the enantiomers which results from the diastereomeric interaction of enantiomers with a selector in the ion-exchange process: $\Delta(\Delta G^\circ)=-RT\ln\alpha$.[31] In the present estimation of α values, the void volume of column used is not contained in the retention volumes, so that the true α values are larger than those shown in Table 1; for example, the value for *cis*(*N*)-$[Co(ida)_2]^-$ (**6a**) has been found to be 1.23 in a preliminary experiment. It is noted that the α values in the present resolutions are, on the whole, comparable to those obtained by use of cationic selectors, which are smaller than 1.28 except for two special examples[9] in many resolutions.[3,5–9]

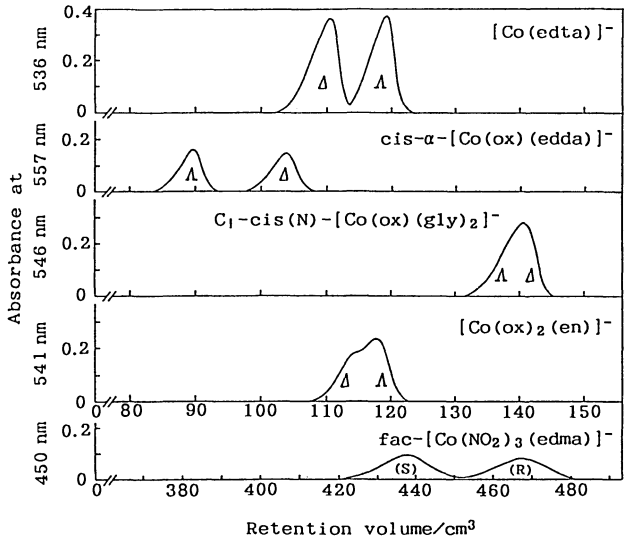

Fig. 1. Representative elution curves in the chromatographic resolution of the cobalt(III) complexes.

The signs of the CD extrema and absolute configurations of the early eluted enantiomers are shown in the forth and the fifth column, respectively, in Table 1. The absolute configurations of the ed3a type (**2a**—**2c**), aeida type (**5a** and **5b**), and edma (**7**) complexes cannot be characterized by the current IUPAC nomenclature concerned with octahedral complexes, because of the lack of net ring-pairing chirality.[29] The absolute configuration of the edma complex is designated with that of the secondary nitrogen atom. The structures of the enantiomers eluted early in each type are illustrated with chelate skeletons in Fig. 2. In each of the types with the plural complexes (**1**, **2**, **3**, **8**, **9**, and **10**), except for the bis(ida) type (**6**), the elution orders of the enantiomers are the same for all the complexes, as seen in Table 1. In the bis(ida) type, the elution order of *cis*(*N*)-$[Co(ida)_2]^-$ (**6a**) and that of the other complexes (**6b**—**6e**) are opposite; the structure in Fig. 2 is for the latter complexes. The absolute configurations of the aeida type complexes (**5a** and **5b**) are tentatively assigned in the present work (vide infra) and the structure for *unsym*-[Co(ox)(aeida)]$^-$ (**5a**) is illustrated in Fig. 2. As described above, the elution order of enantiomers can be correlated to the absolute configuration for the com-

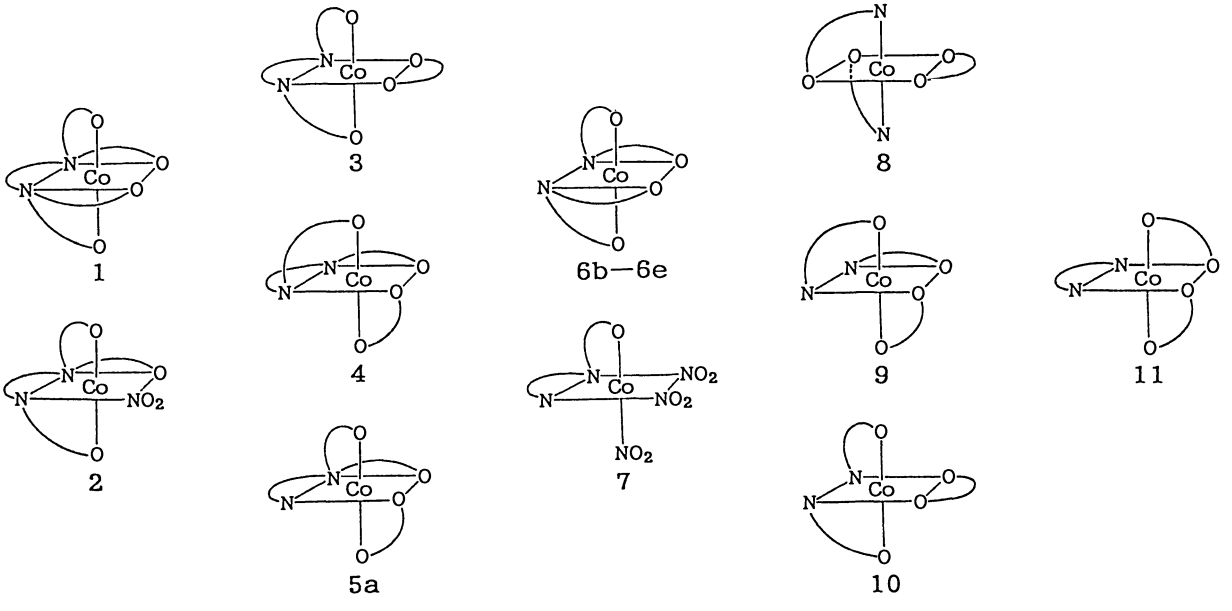

Fig. 2. Absolute configurations of the early eluted enantiomers.

plexes belonging to the same type, with the exception of *cis*(*N*)-[Co(ida)$_2$]$^-$ (**6a**). Such a correlation, however, is by no means recognized for the whole complexes used; namely, the *Δ*-isomers are early eluted for about half of the complexes and the *Λ*-isomers for the others. Accordingly, the chiral discrimination mechanism in the present systems is difficult to explain in relation with the absolute configuration, which is associated with the number of helical chelate pairs (*Δ* and *Λ*) in a complex.[29]

All the univalent anionic complexes used are coordinated by the two neutral nitrogen atoms of the amino carboxylato ligand(s) and the four anionic groups, carboxyl and/or nitro ones. It is reasonable to consider that the moiety near the two nitrogen atoms of the amino carboxylato ligand(s), where a relatively positive charge is produced owing to charge localization in a complex, favorably interacts with the anionic selector. The complexes have one or two triangular "NNO-facets" in a complex as a common structural unit, except for *trans*(*N*)-[Co(ox)(gly)$_2$]$^-$ (**8a**), *trans*(*N*)-[Co(ox)(*β*-ala)$_2$]$^-$ (**8b**), and [Co(ox)$_2$(en)]$^-$ (**11**). The NNO-facet consists of the two nitrogen atoms of the amino carboxylato ligand(s) and the glycinato or *β*-alaninato chelate ring (N–O) toward the apical position from either of the two nitrogen atoms. The enantiomeric forms are possible for the NNO-facet and illustrated in Fig. 3. The configurations of NNO-facets are defined here as L (left) and R (right) to indicate the direction of the nitrogen atom contained in the N–O chelate ring, when the NNO-facet is viewed as in Fig. 3.

The configurations of the NNO-facets in the early eluted enantiomers are shown in the last column in Table 1. In the complexes having two NNO-facets in a complex, the NNO-facets share the moiety of two nitrogen atoms. In the complexes having the NNO-facet, except for the aeida complexes (**5a** and **5b**), the early eluted enantiomers for the seventeen complexes contain the NNO-facet of L- or LL-configuration, while those for the four complexes, *cis*-*β*-[Co(ox)(edda)]$^-$ (**4**), *cis*(*N*)-[Co(ida)$_2$]$^-$ (**6a**), C_1-*cis*(*N*)-[Co(ox)(gly)$_2$]$^-$ (**9a**), and C_1-*cis*(*N*)-[Co(ox)(*β*-ala)$_2$]$^-$ (**9b**), contain the NNO-facet of R- or RR-configuration. Thus, it is reasonable to expect that the elution order of enantiomers can be correlated to the configuration of NNO-facet. On the other hand, all the complexes (**8a**, **8b**, and **11**) that have no NNO-facets give small *α* values (single—1.03). These facts suggest that the chirality of NNO-facet plays a dominant role in the chiral discrimination in the present resolution systems.

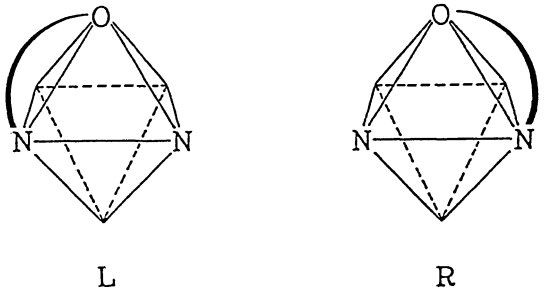

Fig. 3. L and R configurations of the NNO-facet.

It is to be noted as a simplified model for the chiral discrimination that *fac*-[Co(NO$_2$)$_3$(edma)]$^-$ (**7**) was completely resolved (Fig. 1), in spite of having no helical chelate arrangement (Fig. 2). This fact indicates that the helical chelate system is not essentially required for the chiral discrimination and that a significant unit in the discriminatory interactions exist in the facially coordinated edma moiety. The fact also is a strong support for the above suggestion concerning the role of NNO-facet for the discrimination, because the structure of edma is very close to that of the NNO-facet. It should also be noted for *cis*(*N*)-[Co(ida)$_2$]$^-$ (**6a**) that not only, the elution order is exceptional as described above but the *α* value is largest in the present resolutions (Table 1). This specific behavior in the bis(ida) type complexes (**6a**—**6e**) is particularly noteworthy, because it is caused only by the difference in *N*-substituent. This fact seems to hold a key to elucidate the chiral discrimination mechanism in the present resolutions. Although it cannot clearly be explained at present (vide infra), the fact at least adds support for the importance of NNO-facet for the chiral discrimination.

In most experimental studies on chiral discrimination phenomena between ions of the same sign, the direct contact mechanism has been proposed, where the racemic complex and environment substance (or selector) interact directly.[12–16] On the other hand, a non-contact mechanism has also been postulated experimentally[17] and theoretically.[18] In all systems for which the direct contact mechanism was proposed, one or both of the racemic (e.g., [Zn(phen)$_3$]$^{2+}$ (1,10-phenanthroline)) and environment (*d*-cinchoninium) ions contain groups with aromaticity (N-heterocyclic unsaturated groups in most cases). The mechanism has been explained in terms of a sequence that the hydrogen bonding or the hydrophobic interactions in a wide sense lead to direct contact between ions of the same sign against their mutual electrostatic repulsion inevitably expected, and that this contact provides a main driving force for the chiral discrimination.

In the present resolution systems, in contrast, both the racemate and selector are hydrophilic. The selector has acceptor oxygen atoms but no donor hydrogen atoms. Accordingly, a probable attractive force is brought about by the hydrogen bonding between the donor hydrogen atom of racemate and the acceptor oxygen atom of selector. Nine of the present racemates, edta type (**1a**—**1e**), med3a (**2b**), dmedda (**3b**), bis(mida) (**6c**), and bis(eida) (**6e**), have no donor hydrogen atoms, indicating the absence of attractive force. Nevertheless, the *α* values for these complexes are fairly large on the average, although they are somewhat smaller than those for the other complexes having N–H

bonds available for the hydrogen bonding (Table 1). By the way, it may be possible that direct contact is electrically allowed under special conditions at exchanging sites on the anion exchanger. Even if this is so, however, it appears to be difficult to explain the present results that the four edta type complexes (**1a**—**1d**) give α values (1.06—1.09) similar to one another; namely, it is difficult to construct such an interacting model as suggests the direct contact of the NNO-facet with the selector, because the N–N backbone chelates are distinctly different in their bulkiness.

The C_1- and C_2-cis(N) isomers of [Co(ox)(gly or β-ala)$_2$]$^-$ (**9a**—**10b**) have four N–H bonds in the NNO-facet. From X-ray structural studies, it has been found that the five-membered glycinato chelate is almost planar,[32] whereas the six-membered β-alaninato chelate exists in a puckered conformation with two kinds of N–H bonds, axial and equatorial.[33] In spite of such a clear difference of the N–H geometries in the NNO-facet, the glycinato and β-alaninato complexes show practically the same resolution behavior in the same geometrical isomer (Table 1). This fact is also difficult to explain in terms of direct and concrete interactions through hydrogen bonding to the selector, even if the N–H bonds participate in the chiral discrimination.

From these considerations, we conclude that the ability of the present discrimination has nothing to do with direct contact between the racemate and selector. Bosnich and Watts[17] have speculated such a noncontact mechanism, where the chiral discrimination is induced by the diastereomeric interaction between chiral solvent sheaths formed about enantiomers and selector. This mechanism can favorably explain the present discrimination phenomenon, because the presence of some waters intervening between ions of the same sign will effectively reduce the electrostatic repulsion between ions.

The alkyl substitution of the N–H proton of [Co(NO$_2$)(ed3a)]$^-$ (**2a**), forming [Co(NO$_2$)(med3a)]$^-$ (**2b**), significantly lowers the α value (from 1.10 to 1.06). Such is the case with the other pairs, *cis*-α-[Co(ox)(edda)]$^-$ (**3a**)···*cis*-α-[Co(ox)(dmedda)]$^-$ (**3b**) (1.16 to 1.04) and *cis*(N)-[Co(ida)(mida)]$^-$ (**6b**)···*cis*(N)-[Co(mida)$_2$]$^-$ (**6c**) (1.13 to 1.07), but the α values of *cis*(N)-[Co(ida)(eida)]$^-$ (**6d**) and *cis*(N)-[Co(eida)$_2$]$^-$ (**6e**) (1.04 to 1.05) are comparable to each other. This behavior is in contrast to the fact that the four edta type complexes (**1a**—**1d**) show similar α values (1.06—1.09) in spite of the variation in alkyl N–N backbone, as pointed out above. This fact, therefore, indicates a participation of the N–H proton in the chiral discrimination. According to our proposal, this may imply that the N–H proton(s) contribute to the formation of water sheaths about the racemate. It may first be considered that the number and direction of N–H bonds in an NNO-facet effectively affect the formation of water sheath. Molecular model considerations show that the two N–H bonds of cis(N)-[Co(ida)$_2$]$^-$ (**6a**) roughly face to each other. There are no complexes which have such a geometry of two N–H bonds in the present complexes, except for the four complexes (**9a**—**10b**), C_1- and C_2-*cis*(N)-[Co(ox)(gly or β-ala)$_2$]$^-$. The excluded complexes have two N–H bonds of a geometry similar to those of *cis*(N)-[Co(ida)$_2$]$^-$, but additionally two more N–H bonds. Thus, *cis*(N)-[co(ida)$_2$]$^-$ has the characteristic donor hydrogen atoms in the present complexes. This is a possible explanation for the exceptional behavior of *cis*(N)-[Co(ida)$_2$]$^-$ described above.

The α value for [Co(cydta)]$^-$ (**1e**) is markedly small compared with those for the other edta type complexes (**1a**—**1d**). This may be ascribed to the high hydrophobicity of the large-sized cyclohexane ring, by which the formation of water sheath about the complex is depressed. The *cis*-β-[Co(ox)(edda)]$^-$ (**4**), C_1-*cis*(N)-[Co(ox)(gly)$_2$]$^-$ (**9a**), and C_1-*cis*(N)-[Co(ox)(β-ala)$_2$]$^-$ (**9b**) complexes show the exceptional behavior in elution order, as mentioned above. In addition to this fact, these complexes give small α values (single—1.04), out of proportion to the structure that the complexes have both the NNO-facet and some N–H bonds. The complexes have the same chelate skeleton, except for the presence or absence of the ethylene bridge spanned between two nitrogen atoms. Although it is presumed that the reason for the behavior observed is concealed in the common chelate structure in these complexes, its detail is not clear.

Under the situation described above, the elution order of enantiomers cannot confidently be correlated to the configuration of NNO-facet. The aeida complexes, *unsym*-[Co(ox)(aeida)]$^-$ (**5a**) and *unsym*-[Co(NO$_2$)$_2$(aeida)]$^-$ (**5b**), of which the absolute configurations are unknown, do not have such a structure as brings about the exceptional relation as described above. Accordingly, the regular relation may be applicable to these complexes; namely, their early eluted enantiomers are tentatively considered to have the NNO-facet of L-configuration and the absolute configuration which is self-evidently derived from it (Table 1 and Fig. 2). The *unsym*-[Co(NO$_2$)$_2$(aeida)]$^-$ (**5b**) complex is another example which has been completely resolved in spite of the lack of helical chelate arrangement.

In the present chromatographic resolution systems, the [Sb$_2$(*d*-tart)$_2$]$^{2-}$ selector participates in the chiral discrimination in both the stationary phase and the mobile phase. If it is assumed that the mode of diastereomeric interaction between the selector and racemate is the same in both phases, the selector exerts an opposite effect upon the elution order of the enantiomers, and the elution order depends on the relative concentrations of the selector in the phases. The concentration of the selector in the stationary phase (0.24 mmol cm^{-3} on the basis of the ion-exchange capacity of the exchanger used)[10] is more than ten times as high as that in the mobile one (0.02 mol dm^{-3}). Thus, the elution order is governed by the selector in the stationary phase,

that is, one of the enantiomers which interacts more favorably with the selector is late eluted than the other. A further study is now in progress.

The author wishes to thank Professor Takaji Yasui and his co-workers of Kochi University for helpful supports in the preparation of cobalt(III) complexes. This work was supported by a Grant-in-Aid for Scientific Research No. 01540513 from the Ministry of Education, Science and Culture.

References

1) D. R. Buss and T. Vermeulen, *Ind. Eng. Chem.*, **60**, 12 (1968).

2) Y. Yoshikawa and K. Yamasaki, *Coord. Chem. Rev.*, **28**, 205 (1979).

3) H. Yoneda, *J. Chromatogr., Chromatogr. Rev.*, **313**, 59 (1985).

4) Abbreviations of the ligands: *d*-tart=*d*-tartrate(4-), edta=ethylenediamine-*N,N,N',N'*-tetraacetate(4-), trdta=trimethylenediamine-*N,N,N',N'*-tetraacetate(4-), tdta=tetramethylenediamine-*N,N,N',N'*-tetraacetate(4-), pdta=1, 2-propanediamine-*N,N,N',N'*-tetraacetate (4-), cydta=*trans*-1,2-cyclohexanediamine-*N,N,N',N'*-tetraacetate(4-), ed3a=ethylenediamine-*N,N,N'*-triacetate(3-), med3a=*N*-methylethylenediamine-*N,N',N'*-triacetate(3-), hed3a=*N*-(2-hydroxyethyl)ethylenediamine-*N,N',N'*-triacetate(3-), edda=ethylenediamine-*N,N'*-diacetate(2-), dmedda=*N,N'*-dimethylethylenediamine-*N,N'*-diacetate(2-), aeida=*N*-(2-aminoethyl)-iminodiacetate(2-), ida=iminodiacetate(2-), mida=*N*-methyliminodiacetate(2-), eida=*N*-ethyliminodiacetate(2-), edma=ethylenediamine-*N*-acetate(1-), gly=glycinate(1-), β-ala=β-alaninate(1-), ox=oxalate(2-), en=ethylenediamine.

5) A. Tatehata, M. Iiyoshi, and K. Kotsuji, *J. Am. Chem. Soc.*, **103**, 7391 (1981).

6) A. Tatehata, M. Fujita, K. Ando, and Y. Asaba, *J. Chem. Soc., Dalton Trans.*, **1987**, 1977; A. Tatehata and Y. Asaba, *Bull. Chem. Soc. Jpn.*, **61**, 3145 (1988).

7) S. Izumoto, U. Sakaguchi, and H. Yoneda, *Bull. Chem. Soc. Jpn.*, **56**, 1646 (1983); K. Miyoshi, M. Natsubori, N. Dohmoto, S. Izumoto, and H. Yoneda, *ibid.*, **58**, 1529 (1985); K. Miyoshi, Y. Sakamoto, A. Ohguni, and H. Yoneda, *ibid.*, **58**, 2239 (1985).

8) U. Sakaguchi, I. Yamamoto, S. Izumoto, and H. Yoneda, *Bull. Chem. Soc. Jpn.*, **56**, 153 (1983).

9) K. Miyoshi, N. Dohmoto, and H. Yoneda, *Inorg. Chem.*, **24**, 210 (1985).

10) N. Koine, *Chem. Lett.*, **1988**, 1547.

11) For example: J. D. Watson, N. H. Hopkins, J. W. Roberts, J. A. Steitz, and A. M. Weinen, "Molecular Biology of the Gene," 4th ed, the Benjamin/Cumming Publishings Co., Inc., California (1987), p. 126.

12) S. Kirschner and N. Ahmad, "Coordination Chemistry," ed by S. Kirschner, Prenum Press, New York (1969), p. 42; R. C. Brasted, V. J. Landis, E. J. Kuhajek, P. E. R. Nordiquist, and L. Mayer, *ibid.*, p. 64; R. D. Gillard, "Optical Activity and Chiral Discrimination," ed by S. F. Mason, D. Reidel Publishing Co., Dordrecht (1979), p. 353.

13) K. Ogino and T. Kumagai, *Bull. Chem. Soc. Jpn.*, **47**, 855 (1974).

14) K. Miyoshi, Y. Kuroda, and H. Yoneda, *J. Phys. Chem.*, **80**, 270 (1976); K. Miyoshi, Y. Kuroda, H. Okazaki, and H. Yoneda, *Bull. Chem. Soc. Jpn.*, **50**, 1476 (1977).

15) A. Yamagishi, *Inorg. Chem.*, **21**, 1778 (1982); A. Yamagishi, *J. Chromatogr.*, **262**, 41 (1983); D. Kotbar and P. K. Ghosh, *Inorg. Chem.*, **26**, 208 (1987).

16) H. G. Brittain, *Inorg. Chem.*, **20**, 3007 (1981).

17) B. Bosnich and D. W. Watts, *Inorg. Chem.*, **14**, 47 (1975).

18) P. E. Shipper, *J. Am. Chem. Soc.*, **100**, 1079 (1978).

19) D. P. Craig and D. P. Mellor, *Top. Curr. Chem.*, **63**, 1 (1976); D. P. Craig, "Optical Activity and Chiral Discrimination," ed by S. F. Mason, D. Reidel Publishing Co., Dordrecht (1979), p. 293; S. F. Mason, *ibid.*, p. 319.

20) G. A. Sigel and J. A. Weyh, *Inorg. Chem.*, **23**, 3246 (1984).

21) K. Kuroda, S. Ohtsuka, and N. Matsumoto, *Bull. Chem. Soc. Jpn.*, **48**, 1055 (1975).

22) K. Akamatsu, T. Komorita, and Y. Shimura, *Bull. Chem. Soc. Jpn.*, **55**, 140 (1982).

23) D. J. Radanović, *Coord. Chem. Rev.*, **54**, 159 (1984).

24) T. Yasui, H. Kawaguchi, N. Koine, and T. Ama, *Bull. Chem. Soc. Jpn.*, **56**, 127 (1983).

25) N. Matsuoka, J. Hidaka, and Y. Shimura, *Bull. Chem. Soc. Jpn.*, **48**, 458 (1975).

26) T. Ama, M. Higa, N. Koine, and T. Yasui, *Bull. Chem. Soc. Jpn.*, **50**, 2632 (1977).

27) T. Yasui, K. Okamoto, J. Hidaka, T. Ama, and H. Kawaguchi, *Bull. Chem. Soc. Jpn.*, **60**, 2573 (1987).

28) J. I. Legg and B. E. Douglas, *J. Am. Chem. Soc.*, **88**, 2697 (1966).

29) Tentative proposals for nomenclature of absolute configurations concerned with octahedral complexes by IUPAC: *Inorg. Chem.*, **9**, 1 (1970).

30) T. Yasui, T. Shikiji, N. Koine, T. Ama, and H. Kawaguchi, *Bull. Chem. Soc. Jpn.*, **60**, 595 (1987).

31) B. L. Karger, "Modern Practice of Liquid Chromatography," ed by J. J. Kirkland, John-Wiley and Sons, New York (1971), p. 8.

32) H. C. Freeman, *Adv. Protein Chem.*, **22**, 257 (1967).

33) H. Soling, *Acta Chem. Scand., Ser. A*, **32**, 361 (1978).

Spectrochemical Series for the Outersphere Coordination of Carboxylatocobaltate(III) Complexes with Solvent Molecules[1)]

Toshiaki TAURA
Department of Chemistry, University of Aichi Prefecture, Takadacho 3-28, Mizuho-ku, Nagoya 467
(Received March 2, 1991)

The d–d transition spectra of K[Co(edta)]·2H_2O, K[Co(mal)$_2$en]·H_2O, K[Co(ox)$_2$en]·1.5H_2O, K$_2$[Co(ox)$_2$gly]·3H_2O, and K$_3$[Co(ox)$_3$]·3H_2O (edta=ethylenediaminetetraacetate, mal=malonate, en=ethylenediamine, ox=oxalate, and gly=glycinate) were measured in a variety of solvents: H_2O, $HOCH_2CH_2OH$, CH_3OH, $HCONH_2$, C_2H_5OH, *i*-C_3H_7OH, $CHCl_3$, CH_3NO_2, CH_2Cl_2, $(CH_3)_2SO$, CH_3CN, $HCON(CH_3)_2$, C_6H_5CN, $C_6H_5NO_2$, $CH_3CON(CH_3)_2$, $(CH_3)_2CO$, and $[(CH_3)_2N]_3PO$. The ^{59}Co NMR spectra of K[Co(edta)]·H_2O and K$_3$[Co(ox)$_3$]·3H_2O were also recorded at 25 °C in these solvents. It was found that the peak positions (λ_{max}) of the first and second d–d transition bands were greatly influenced by solvent molecules; the peak positions (λ_{max}) of all the cobalt(III) complexes were linearly correlated to the electrophilic ability (Gutmann's acceptor number) of the solvent and those of K[Co(edta)]·2H_2O and K$_3$[Co(ox)$_3$]·3H_2O were linearly correlated to the ^{59}Co NMR chemical shifts in the corresponding solvents. This suggests that the d–d transition energy (ΔE) is influenced by solvent molecules as electron acceptors since ^{59}Co NMR chemical shifts are theoretically correlated linearly to the peak positions in the first d–d transition (A_{1g}–T_{1g}). The ^{13}C NMR measurements indicated that solvent molecules directly interact with the carboxyl groups of cobalt(III) complexes. Therefore, the influence of the solvent on the d–d transition energy of the carboxylatocobaltate(III) complex is due to the electron-withdrawing effect of solvent molecules on the carboxyl oxygens of the cobalt(III) complex. A spectrochemical series for the outersphere coordination of the cobalt(III) complex with solvent molecules is proposed.

It was reported that potassium ethylenediaminetetraacetatocobaltate(III) dihydrate, K[Co(edta)]·2H_2O, was solubilized by macrocyclic polyethers, crown ethers and cryptand 222, in a variety of organic solvents including low-polarity chloroform (dielectric constant=4.8).[2)] In the course of this work, it was discovered that the color of this cobalt(III) complex changed from reddish violet in water to bluish violet in acetone. This complex was quite stable and inert against ligand substitution or redox reaction in these solvents, and thus this color change has been due to the outersphere interaction of $[Co(edta)]^-$ with solvent molecules.

In a previous paper,[3)] it was suggested that the peak positions (λ_{max}) of the first d–d transition band (corresponding to the color of the complex) were linearly correlated with the acceptor numbers of solvents, which were proposed by Mayer, et al.[4)] as a measure of the electrophilic ability of solvents. The solvent influence on the peak position and the interaction between $[Co(edta)]^-$ and solvent molecules could then be quantitatively estimated by using the acceptor number of the solvent. Using this procedure, the solvent influence of some cobalt(III) or chromium(III) complexes has been studied.[1,5–7)]

The present work is an attempt to elucidate what kind of interaction between solvent molecules and $[Co(edta)]^-$ or some related carboxylatocobaltate(III) complexes plays an important role in the solvent influence on the d–d transition spectra. The solvent influence on the electronic and ^{59}Co NMR spectra of K[Co(edta)]·2H_2O, K[Co(mal)$_2$en]·H_2O, K[Co(ox)$_2$en]·1.5H_2O, K$_2$[Co(ox)$_2$gly]·3H_2O, and K$_3$[Co(ox)$_3$]·3H_2O, where edta=ethylenediaminetetraacetate, mal=malonate, en=ethylenediamine, ox=oxalate, and gly=glycine, was investigated, and was compared with the influence of the solvent on the ^{13}C NMR spectra which has already been reported.[5)]

Experimental

Materials. The cobalt(III) complexes used in this work (K[Co(edta)]·2H_2O,[8)] K[Co(mal)$_2$en]·H_2O,[9)] K[Co(ox)$_2$en]·1.5H_2O,[10)] K$_2$[Co(ox)$_2$gly]·3H_2O,[11)] K$_3$[Co(ox)$_3$]·3H_2O,[12)] [Co(en)$_3$](ClO$_4$)$_3$,[13)] and [Co(NH$_3$)$_6$](ClO$_4$)$_3$[14)]) were prepared by the usual methods. The anhydrous salt of K[Co(edta)]·2H_2O was prepared by heating the complex at 110 °C in an oven. The purities of these complexes were checked by elemental analysis and spectroscopic methods. The organic solvents and cryptand 222 (Merck: Kryptofix 222) were of the purest commercial grade available and were used without further purification. The solvents used in this study were; water (H_2O), ethylene glycol (EG), methanol (CH_3OH), formamide (FA), ethanol (C_2H_5OH), 2-propanol (*i*-C_3H_7OH), chloroform ($CHCl_3$), nitromethane (CH_3NO_2), dichloromethane (CH_2Cl_2), dimethyl sulfoxide (Me_2SO), acetonitrile (CH_3CN), *N,N*-dimethylformamide (DMF), benzonitrile (C_6H_5CN), nitrobenzene ($C_6H_5NO_2$), *N,N*-dimethylacetamide (DMA), acetone (Me_2CO), and hexamethylphosphoric triamide (HMPA).

Measurements. Electronic Spectra: The electronic absorption spectra of the cobalt(III) complexes in solutions of appropriate concentrations (0.001—0.005 mol dm^{-3}) were measured at room temperature. The complex salts were dissolved in organic solvents by the addition of an excess of cryptand 222 (amounts 1.5 times larger than the concentration of the K^+ ion). The spectra were recorded on a Shimadzu UV-240 recording spectrophotometer. The spectra were not influenced by the addition of various amounts of cryptand 222, by a change in the concentration of the cobalt(III) complex, or by a change in the temperature. Water of crystallization in the complexes was not found to change the peak positions of the absorption spectra.[15)]

The reflection spectra of the cobalt(III) complexes and the anhydrous salt of K[Co(edta)] were measured on a JASCO UVIDEC-410 spectrophotometer with a TIS-241 reflectance attachment.

^{59}Co NMR. The ^{59}Co NMR spectra of K[Co(edta)]·2H_2O and K_3[Co(ox)$_3$]·3H_2O were measured at 25 °C in solutions of the complex anion for water, and for organic solvents containing cryptand 222 (amounts 1.5 times larger than the concentration of the K^+ ion). The ^{59}Co chemical shift is influenced by the concentration of the complex. Therefore, measurements were carried out in solutions of various concentrations. A JEOL JNM-GX400 NMR spectrometer was operated in Fourier transform mode at 95.856 MHz for K[Co(edta)]·2H_2O and 96.095 MHz for K_3[Co(ox)$_3$]·3H_2O. The 10-mm NMR tube used here contained a sample solution of 2.5 ml; D_2O in a 2-mm tube was fixed inside a sample 10-mm tube during spectra accumulation. The reference was not used, but the signal of the complex appeared quite broad and the peak position in water was set at 0 ppm before the other ^{59}Co NMR measurements were taken. The position of the signal in water did not change after the measurements of the other samples. The spectra were recorded after 256—4096 accumulations of 0.1 s pulse intervals.

Results and Discussion

Electronic Spectra in a Variety of Solvents. The electronic spectra of K[Co(edta)]·2H_2O and K[Co(mal)$_2$en]·H_2O in water, methanol, ethanol, and chloroform are shown in Fig. 1. The spectral bands in the longer wavelength region correspond to the first d–d transition[16] of the cobalt(III) center. The second d–d transition bands appear in the shorter wavelength region. It is clear that the peak positions of the first and second d–d transition bands appear in the shorter wavelength regions in water, and shift to longer wavelengths in the other solvents.[17] As the [Co(edta)]$^-$ and [Co(mal)$_2$en]$^-$ anions are inert and stable in these solvents under the conditions of the measurements, the differences in the peak positions are due to the outersphere interaction between the complex anion and solvent molecules.

As for the other complex anions, the peak positions also appear in the shorter wavelength regions in water and shift to longer wavelengths in the other solvents. The data of the observed peak positions (λ_{max} : λ_1 and λ_2) of the first and second d–d transition bands are presented in Table 1 for the solvents listed in the Experimental section. This table also includes some solvent parameters: Gutmann's acceptor number (*AN*) and Kosower's parameter (*Z*).[18]

Correlation between the Peak Positions in the d-d Transition Spectrum and the Acceptor Numbers of Solvents. As the solvent influence should be generated by the outersphere interaction between the complex anion and solvent molecules, we have considered the solvent influence on the peak position (λ_{max}) on the basis of the acceptor numbers (*AN*) which were proposed by Mayer, Gutmann, and Gerger as a measure of estimating the electrophilic ability of solvents.[4] The *AN* values of the solvents were determined on the basis of ^{31}P NMR chemical shifts of triethylphosphine oxide ((C_2H_5)$_3$P=O) in the solvents. A large acceptor number indicates that a solvent is a good electron acceptor. Therefore, solvent molecules could interact strongly with an anion like [Co(edta)]$^-$ if the solvent has a large acceptor number.

In Fig. 2, the λ_{max} (λ_1) values of the first d–d transition bands of the complex anions are plotted versus the acceptor numbers of the solvents: H_2O, CH_3OH, FA,

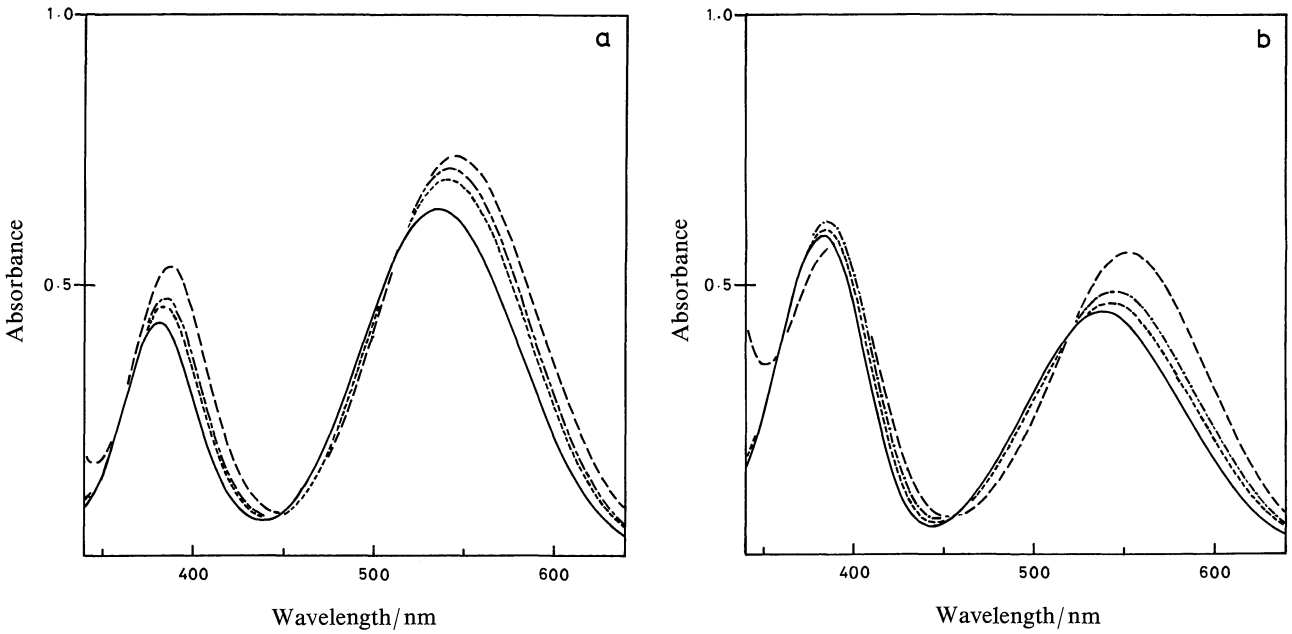

Fig. 1. The electronic absorption spectra of K[Co(edta)]·2H_2O (0.002 mol dm^{-3}) (a) and K[Co(mal)$_2$en]·H_2O (0.005 mol dm^{-3}) (b) in water (——), methanol (------), ethanol (— - —), and chloroform (——).

Table 1. The Peak Positions (λ_1 and λ_2) of the First and Second d–d Transition Bands of the Carboxylatocobaltate(III) Complexes in a Variety of Solvents

Solvent	AN[a]	Z[a]	K[Co(edta)]·2H$_2$O		K[Co(mal)$_2$en]·H$_2$O		K[Co(ox)$_2$en]·1.5H$_2$O		K$_2$[Co(ox)$_2$gly]·3H$_2$O		K$_3$[Co(ox)$_3$]·3H$_2$O	
			λ_1/nm	λ_2/nm	λ_1/nm	λ_2/nm	λ_1/nm	λ_2/nm	λ_1/nm	λ_2/nm	λ_1/nm	λ_2/nm
1 H_2O	54.8	94.6	536.0	381.5	540.0	384.0	540.5	382.5	566.5	403.5	602.0	424.0
2 EG		85.1	540.5	382.5	543.0	385.5	543.0	384.5	568.5	405.5	603.0	425.0
3 CH_3OH	41.3	83.6	541.5	383.5	544.5	385.5	544.5	386.0	569.5	405.5	603.5	425.0
4 FA	39.8	83.3	539.5	383.0	544.0	387.0	543.0	385.0	568.5	405.0	603.5	424.5
5 C_2H_5OH	37.1	79.6	542.5	384.0	546.0	386.0	546.0	387.0	572.0	407.0	603.0	425.0
6 *i*-C_3H_7OH	33.5	76.3	544.0	385.0	547.5	386.5	548.5				606.5	427.0
7 $CHCl_3$	23.1	63.2	547.5	388.0	553.5	388.5			577.0	409.5	609.0	427.0
8 CH_3NO_2	20.5	71.2	544.5		552.0		549.5		574.0		606.0	424.5
9 CH_2Cl_2	20.4	64.7	547.5	388.0	555.0	389.5			577.0	410.0	609.0	427.0
10 Me_2SO	19.3	71.1	545.5	387.0	552.5	390.0	549.5	390.5	576.0	409.0	609.0	427.0
11 CH_3CN	18.9	71.3	545.5	386.5	553.0	389.0			574.0	408.5	606.0	426.5
12 DMF	16.0	68.5	547.5	388.0	554.5	391.0			576.5	410.0	607.0	427.5
13 C_6H_5CN	15.5	65.0	547.5	387.5	552.5	388.0					607.5	427.0
14 $C_6H_5NO_2$	14.8		547.5									
15 DMA	13.6	66.9	548.0	387.5	554.0	389.5					609.5	428.5
16 Me_2CO	12.5	65.5	547.0	388.0							609.5	428.5
17 HMPA	10.6	62.8	548.0	387.0								
		A[b] =	551.3	390.0	560.1	391.9	555.2	394.9	581.0	412.7	610.9	428.5
			±0.6	±0.5	±0.8	±0.6	±1.6	±1.0	±1.2	±0.6	±0.8	±0.6
		B[b] =	0.259	0.154	0.373	0.146	0.264	0.226	0.271	0.171	0.171	0.086
			±0.023	±0.016	±0.028	±0.020	±0.043	±0.025	±0.038	±0.019	±0.029	±0.019
		r[b] =	−0.947	−0.941	−0.970	−0.918	−0.940	−0.982	−0.931	−0.961	−0.865	−0.794

a) AN and Z refer to the acceptor number of the solvent and Kosower's solvent parameter, respectively. b) A, B, and r refer to the intercept, the slope, and the correlation coefficient in Eq. 2, respectively.

C_2H_5OH, *i*-C_3H_7OH, $CHCl_3$, CH_3NO_2, CH_2Cl_2, Me_2SO, CH_3CN, DMF, C_6H_5CN, $C_6H_5NO_2$ DMA, Me_2CO, and HMPA. The λ_1 value shifts to the longer wavelength regions as the acceptor number becomes smaller. For example, the λ_1 value (Fig. 2a, Table 1) for K[Co(edta)]·2H$_2$O is 536 nm in water (AN=54.8) and shifts to 547 nm in acetone (AN=12.5) (the color changes from reddish violet in water to bluish violet in acetone). According to the literature,[19] protic solvents such as ethanol, methanol, and water having large AN values can strongly solvate the anion through hydrogen bonding, while dipolar aprotic solvents such as acetone, dimethyl sulfoxide, and acetonitrile having small AN values solvate the anion weakly. Therefore, the λ_1 values in aprotic solvents correspond to those of weakly solvated $[Co(edta)]^-$ anions and the values in protic solvents seem to be greatly influenced by solvating molecules as outersphere ligands.

Therefore, the colors (corresponding to the λ_1 values) of the $[Co(edta)]^-$ anions are caused by the ligands (edta) and the solvating molecules. A plot of the λ_1 values in Table 1 versus the acceptor numbers of the

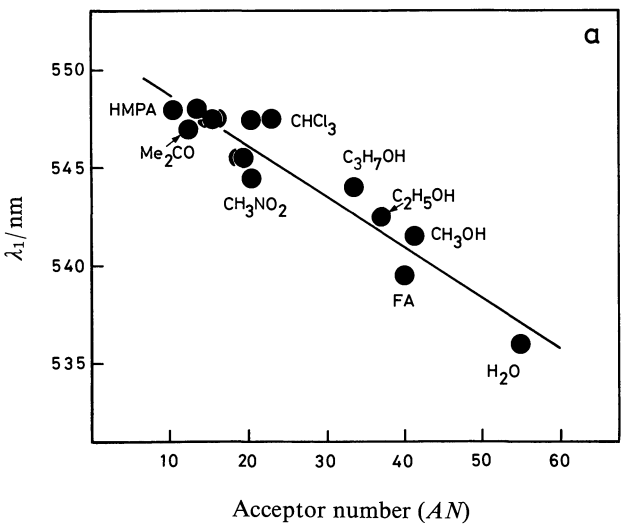

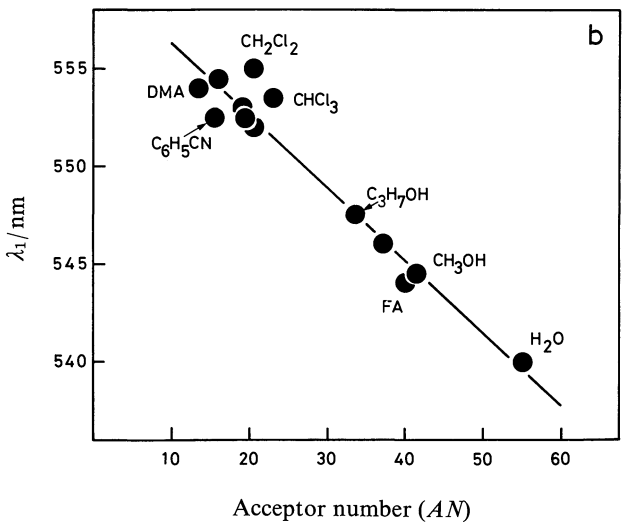

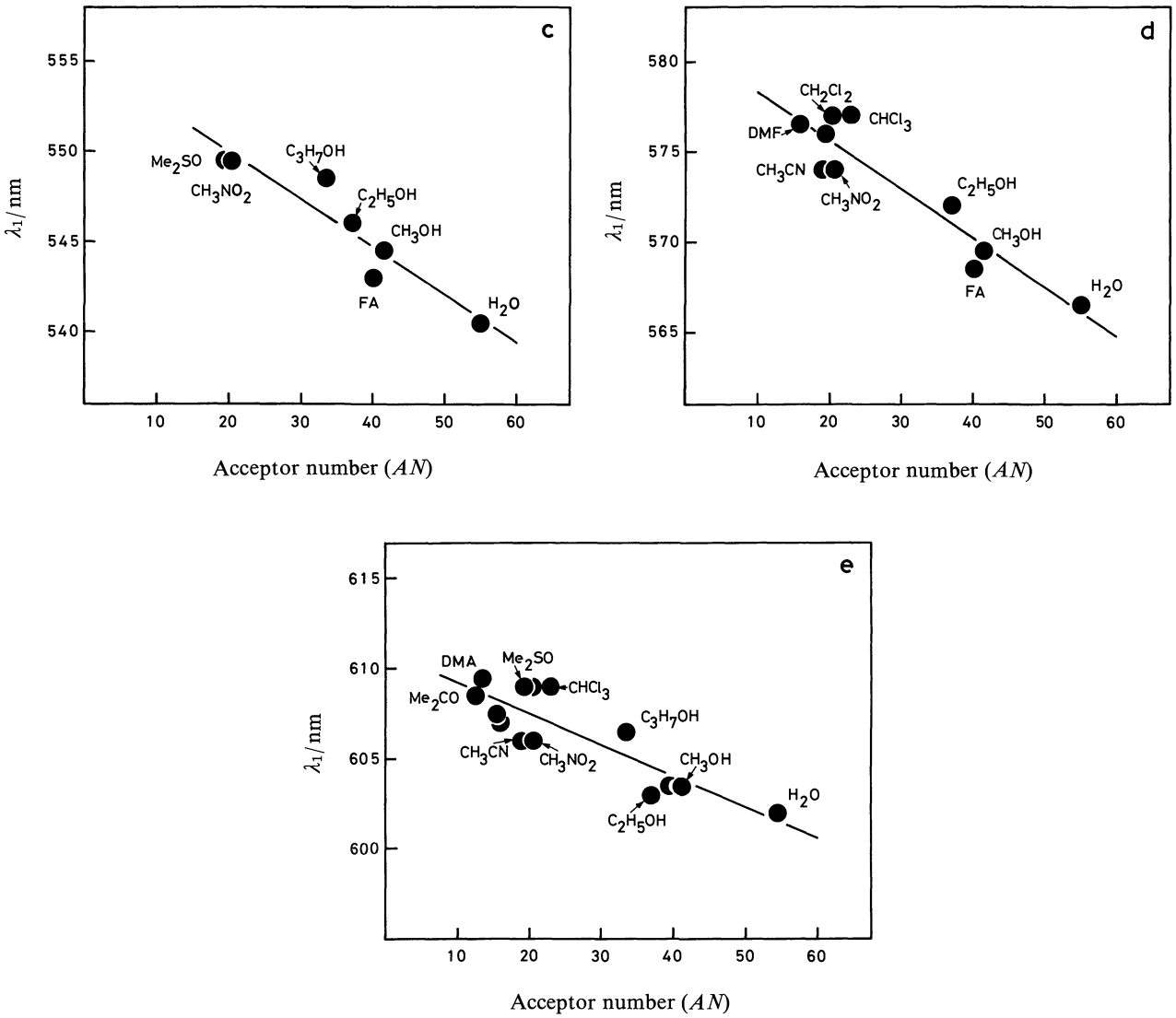

Fig. 2. The correlation between the peak positions (λ_1 in Table 1) of the first d–d transition bands of K[Co(edta)]·2H$_2$O (a), K[Co(mal)$_2$en]·H$_2$O (b), K[Co(ox)$_2$en]·1.5 H$_2$O (c), K$_2$[Co(ox)$_2$gly]·3H$_2$O (d), and K$_3$[Co(ox)$_3$]·3H$_2$O (e) and the acceptor numbers (*AN*) of the solvents.

solvents gives a straight line as shown in Fig. 2a.[20] The linearity of the line suggests that the contribution of the solvent molecules to the peak position is linearly correlated to the *AN* values of the solvents. The peak position in the solvent is calculated by the following equation (error bars are one standard deviation):

$$\lambda_1 = \lambda_1^\circ - (0.259 \pm 0.023) \times AN \quad (1)$$

where λ_1° refers to the peak position (λ_1°=551.3±0.6 nm determined by a least-squares analysis) in hexane as a standard solvent (*AN*=0), and *AN* is the acceptor number of the solvent. The first term in this equation corresponds to the inherent peak position of the [Co(edta)]$^-$ anion which is not solvated and the second term to the outersphere-ligand effect which is caused by solvating molecules.

We have concluded that the color (or λ_1) of the cobalt(III) complex is changed by the outersphere coordination of solvent molecules and that this color (or λ_1) change can be predicted by using the acceptor number of the solvent.

The linear correlation[20] between the peak positions and the acceptor numbers was observed for the other anionic cobalt(III) complexes: K[Co(mal)$_2$en]·H$_2$O (Fig. 2b), K[Co(ox)$_2$en]·1.5H$_2$O (Fig. 2c), K$_2$[Co(ox)$_2$gly]·3H$_2$O (Fig. 2d), and K$_3$[Co(ox)$_3$]·3H$_2$O (Fig. 2e). The correlation is generally represented by the following equation:

$$\lambda_1 = A - B \times AN \quad (2)$$

The intercepts (*A*) and slopes (*B*), which refer to the inherent peak positions and the contribution of the solvent molecules, respectively, were also obtained by least-squares calculations, and are listed in Table 1.

The slopes (B) were slightly different from each other, but were independent of the charge of the complex anion (−, 2−, or 3−). The highly-charged anion could generally be strongly solvated by the solvent molecules. Therefore, this slight difference in the slopes (B) is attributed to an other factor; for example, the probability of the d–d transition for the 1:1 solvation of the anion and solvent molecules. The magnitude of the slope is smaller for $K_3[Co(ox)_3]\cdot 3H_2O$ than for $K_3[Co(CN)_6]$, which has already been obtained.[6] Therefore, the magnitude of the solvent influence depends on the ligand which is coordinated with the cobalt(III) ion.

On the other hand, Fig. 3 presents the correlation between the peak positions of the first d–d transition of $K[Co(edta)]\cdot 2H_2O$ (λ_1) and Kosower's solvent parameters (Z).[18] This plot also gives a straight line. The linearity of the plot is higher than that of the plot versus the acceptor number (AN): the correlation coefficient (−0.980) is greater in the plot versus Z than in the plot versus AN (Table 1: −0.947). For other carboxylato complexes described here, the linearity is also higher in the plots versus Z than the plots versus AN, though the data are not presented in this paper. Kosower's parameters were determined on the basis of the peak positions in the UV absorption spectra (CT: charge transfer) of 1-ethylpyridium iodide in the solvents.[18] Therefore, the influence of the solvent on the d–d transition seems to be correlated more with the parameter from the CT transition than that from the NMR chemical shifts.[21]

In order to confirm that the blue shift of the peak position of $[Co(edta)]^-$ in H_2O was due to the interaction between the complex anion and solvent molecules, the reflection spectra of solid $K[Co(edta)]\cdot 2H_2O$ and $K[Co(edta)]$ were obtained. It was found that the peak positions of solid $K[Co(edta)]\cdot 2H_2O$ were 552 nm for the first d–d transition and 387 nm for the second d–d transition, and its anhydrous salt showed peaks at 556 nm and 387 nm for the first and second d–d transitions, respectively. If, in the solid state, the $[Co(edta)]^-$ anion does not interact with H_2O, these peak positions can be seen to be quite similar to the hypothetical positions (551 nm and 390 nm) in hexane in which the complex does not interact with solvent molecules. In contrast to the edta complexes, the λ_{max} values of other hydrates: $K[Co(mal)_2en]\cdot H_2O$, $K[Co(ox)_2en]\cdot 1.5H_2O$, $K_2[Co(ox)_2gly]\cdot 3H_2O$, and $K_3[Co(ox)_3]\cdot 3H_2O$ are 535, 541, 561, and 596 nm for the first d–d transition and 385, 384, 402, and 423 nm for the second d–d transition, respectively. These values are similar to those in water (540.5, 540.0, 566.5, and 602.0 nm for the first transition and 382.5, 384.0, 403.5, and 424.0 nm for the second transition). An interaction such as hydrogen bonding may exist in those complexes in the solid state, though it could not be confirmed by X-ray analysis.

Spectrochemical Parameter Δ and Interelectronic Repulsion Parameter B. The λ_{max} (λ_2) values of the second d–d transition are also correlated linearly to the AN values of the solvents, as shown in Fig. 4. Therefore, the spectrochemical parameter Δ and Racah parameter B can be evaluated by the λ_1 and λ_2 values of the first and second d–d transition bands. We have used these two parameters to clarify the mechanism of the change in the d–d transition spectra. The parameters Δ and B are approximately calculated by the equations of Schäffer.[22]

$$\Delta = 1/\lambda_1 + (1/\lambda_2 - 1/\lambda_1)[0.1824(\lambda_1/\lambda_2)^2 - 0.5531(\lambda_1/\lambda_2) + 0.6165], \quad (3)$$

$$B = (1/\lambda_2 - 1/\lambda_1)[4.077\times 10^{-2}(\lambda_1/\lambda_2)^2 - 7.090\times 10^{-2}(\lambda_1/\lambda_2) + 9.352\times 10^{-2}]. \quad (4)$$

The peak positions of the first and second d–d transition

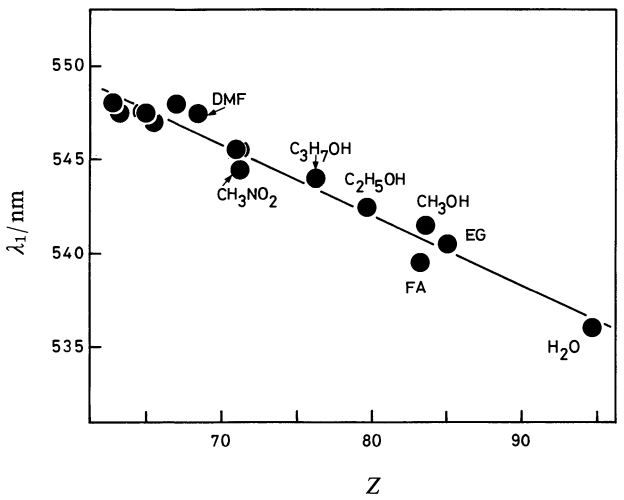

Fig. 3. The correlation between the peak positions (λ_1 in Table 1) of $K[Co(edta)]\cdot 2H_2O$ and Kosower's solvent parameters (Z).

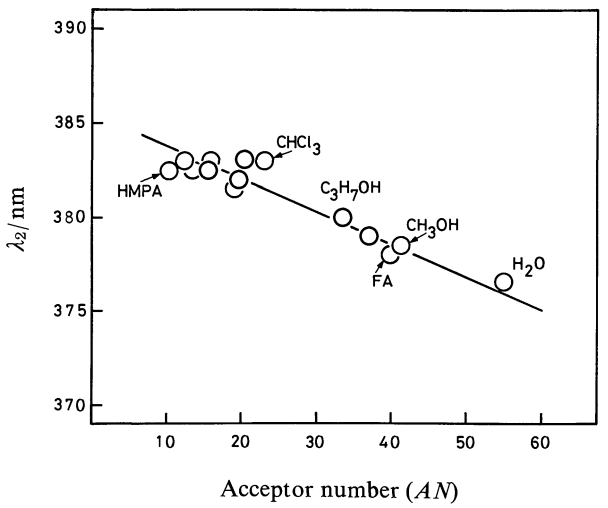

Fig. 4. The correlation between the peak positions (λ_2 in Table 1) of the second d–d transition band of $K[Co(edta)]\cdot 2H_2O$ and the acceptor numbers (AN).

Table 2. The Spectrochemical Parameters (Δ) and the Interelectronic Repulsion Parameters (B) of the Carboxylatocobaltate(III) Complexes in a Variety of Solvents

Solvent[a]	$K[Co(edta)]\cdot 2H_2O$		$K[Co(mal)_2en]\cdot H_2O$		$K[Co(ox)_2en]\cdot 1.5H_2O$		$K_2[Co(ox)_2gly]\cdot 3H_2O$		$K_3[Co(ox)_3]\cdot 3H_2O$	
	Δ	B	Δ	B	Δ	B	Δ	B	Δ	B
1	20116	561.5	20020	559.7	20021	571.0	19072	530.1	17996	523.0
2	20021	571.0	19919	560.5	19932	570.0	19001	525.0	17962	521.3
3	19986	568.4	19878	565.5	19872	562.7	18976	528.0	17954	522.4
4	20049	564.2	19868	555.2	19924	563.2	19007	528.0	17960	525.2
5	19946	568.7	19831	567.7	19818	561.2	18894	527.6	17962	521.3
6	19892	567.2	19774	570.0					17868	520.2
7	19756	560.7	19594	577.2			18743	528.7	17811	527.3
8									17902	532.4
9	19756	560.7	19540	575.7			18737	525.9	17811	527.4
10	19827	560.2	19601	564.7	19677	551.9	18773	528.5	17811	527.4
11	19832	563.0	19597	573.3			18828	525.3	17882	522.0
12	19756	560.7	19532	566.2			18754	523.9	17846	519.4
13	19755	565.4	19624	576.9					17844	523.2
14										
15	19755	565.4	19565	572.6					17788	520.8
16	19773	558.7							17813	523.5
17	19755	565.4								

a) The number of the solvent corresponds to the number assigned in Table 1.

bands shifted to shorter wavelengths as the acceptor number became larger. The spectrochemical parameter Δ, the energy splitting of d orbitals in the O_h field, also became larger as the acceptor number increased (Table 2). Therefore, we have concluded that the solvent influence on the electronic absorption spectra is attributed to an influence on the d–d transition energy (the energy splitting of the d orbital).

Table 2 indicates that the Racah parameter B of $K[Co(mal)_2en]\cdot H_2O$ in a variety of solvents becomes small as the electrophilic ability (AN value) of the solvents (outersphere ligand) becomes larger. It is well known that a decrease of the B value indicates a decrease in the interelectronic repulsion, and is generated by the expansion of the d electron cloud. This expansion of the d electron cloud is due to the electron-withdrawing effect of solvent molecules on the d electrons of $[Co(mal)_2en]^-$ through the ligand atoms (oxygen and carbon). This cloud expanding (nephelauxetic) effect roughly corresponds to the electrophilic ability of the solvents. The expansion of d electron clouds is known to be due to the increase of the covalency of the Co–L bond. We suggest that the solvent influence on the d–d transition energy of $[Co(mal)_2en]^-$ is based on the change of the covalency between the cobalt ion and the innersphere ligand, though the parameter B is similar in a variety of solvents for the other complexes. The spectrochemical series and the nephelauxetic series of outersphere coordination with solvent molecules could be proposed: for the spectrochemical series of $[Co(mal)_2en]^-$,

H_2O, EG, CH_3OH~FA, C_2H_5OH, i-C_3H_7OH, $CHCl_3$~Me_2SO~CH_3CN~C_6H_5CN, DMA, CH_2Cl_2~DMF,

and for the nephelauxetic series of $[Co(mal)_2en]^-$,

FA, H_2O, EG, Me_2SO, CH_3OH, DMF, C_2H_5OH, i-C_3H_7OH, DMA, CH_3CN, CH_2Cl_2, C_6H_5CN, $CHCl_3$.

Correlation between the Peak Positions in the Electronic Spectra and the Chemical Shifts in the ^{59}Co NMR Spectra. If the energy of the d–d electronic transition of the cobalt(III) ion could be changed by the interaction between the solvent molecules and this complex anion, the ^{59}Co NMR chemical shifts should also vary according to changes in the electronic spectrum. This is because the chemical shift of ^{59}Co NMR is correlated to the peak position in the electronic spectrum, as shown in the following equation (which is abbreviated):[23]

$$\delta(^{59}Co) \propto 1/\Delta E \quad (5)$$

where $\delta(^{59}Co)$ and ΔE are the ^{59}Co chemical shift and the energy difference for the first d–d transition band of the cobalt(III) complex, respectively.

Figure 5 shows the ^{59}Co NMR spectra of $K[Co(edta)]\cdot 2H_2O$ and $K_3[Co(ox)_3]\cdot 3H_2O$ in H_2O,

Table 3. The Chemical Shifts of the ^{59}Co NMR Spectra of $K[Co(edta)]\cdot 2H_2O$ and $K_3[Co(ox)_3]\cdot 3H_2O$ in a Variety of Solvents

Solvent	$K[Co(edta)]\cdot 2H_2O$ $\delta(^{59}Co)$/ppm	$K_3[Co(ox)_3]\cdot 3H_2O$ $\delta(^{59}Co)$/ppm
H_2O	0	0
CH_3OH	146	71
C_2H_5OH	197	127
CH_3NO_2	190	98
CH_2Cl_2	230	114
Me_2SO	221	134
CH_3CN	219	122
DMF	262	184
C_6H_5CN	252	141
DMA	274	204

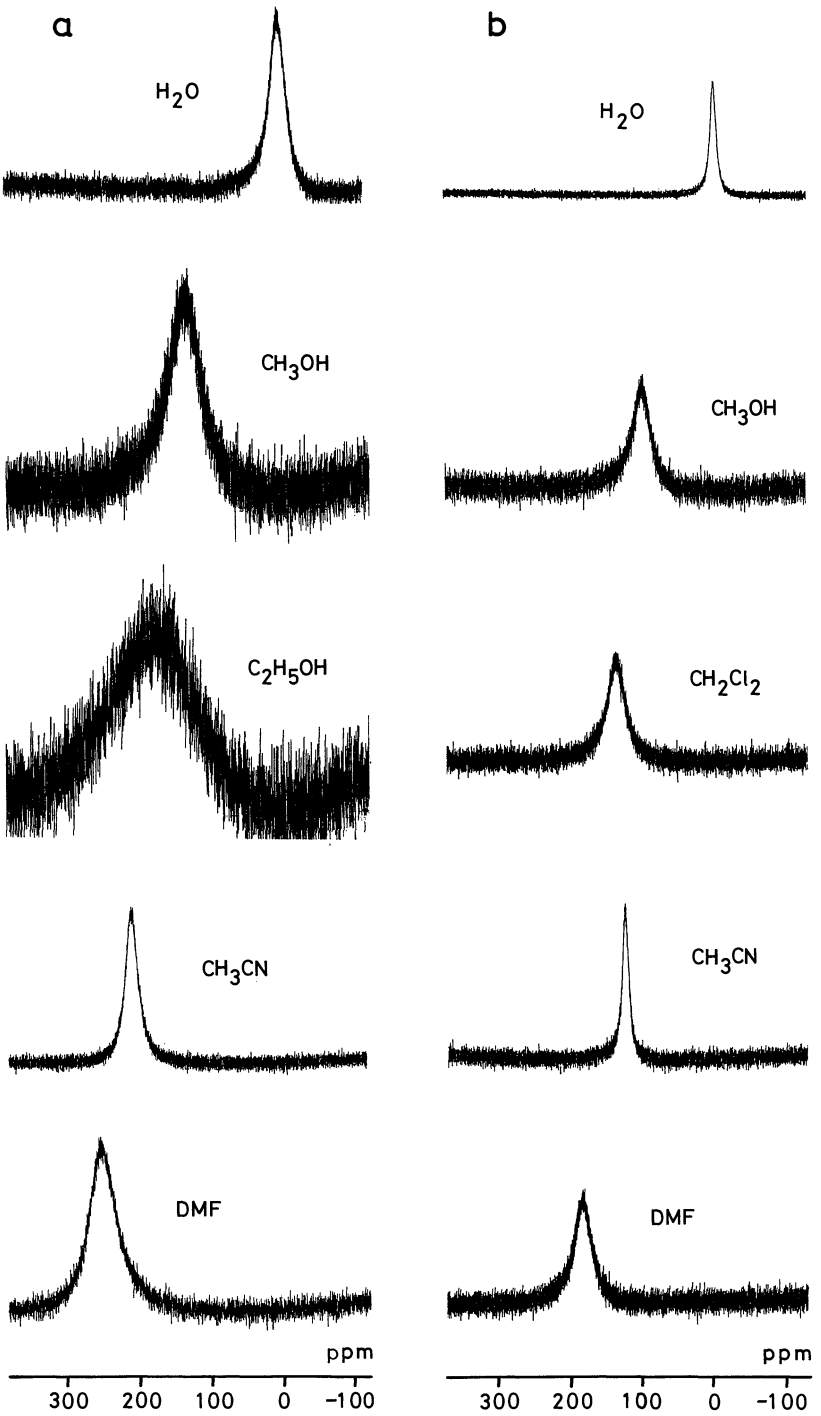

Fig. 5. ^{59}Co NMR spectra of K[Co(edta)]·2H$_2$O (a) and K$_3$[Co(ox)$_3$]·3H$_2$O (b) in a variety of solvents (0.1 mol dm^{-3}).

CH_3OH, C_2H_5OH, (or CH_2Cl_2), CH_3CN, and DMF. In all solvents, the signal appeared quite broad, but the chemical shifts of the ^{59}Co NMR were fairly solvent-dependent. The chemical shifts obtained are shown in Table 3; the solvents used were H_2O, CH_3OH, C_2H_5OH, CH_3NO_2, CH_2Cl_2, Me_2SO, CH_3CN, DMF, C_6H_5CN, and DMA. The chemical shifts also changed as the concentration of the complex decreased. This may have been due to the ion association between the complex anion and K^+ with cryptand 222. The chemical shifts, which were obtained by extrapolation to be the concentration zero, should be the value without any influence of the counter cation. Therefore, the extrapolated values are listed in Table 3 instead of the observed values.

It seemed that the ^{59}Co chemical shifts were linearly correlated to the λ_1 values listed in Table 1. In order to confirm this correlation, the chemical shifts ($\delta(^{59}Co)$)

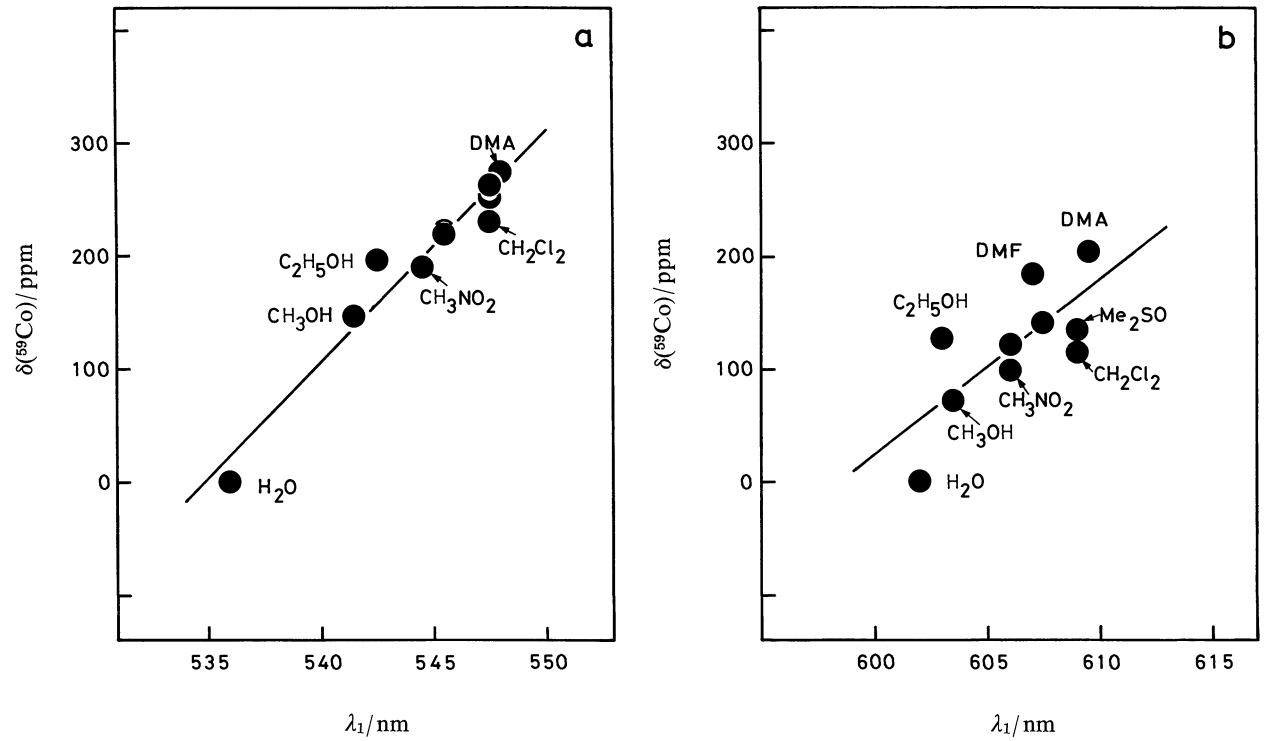

Fig. 6. The correlation between the ^{59}Co chemical shifts ($\delta(^{59}Co)$ in Table 3) and the peak positions (λ_1 in Table 1) of K[Co(edta)]·2H$_2$O (a) and K$_3$[Co(ox)$_3$]·3H$_2$O (b).

were plotted versus the λ_1 values of the first d–d transition band (A_{1g}—T_{1g}) in the corresponding solvents: H_2O, CH_3OH, C_2H_5OH, CH_3NO_2, CH_2Cl_2, Me_2SO, CH_3CN, DMF, C_6H_5CN, and DMA (Fig. 6a and 6b). It was clear that the $\delta(^{59}Co)$ values were linearly correlated to the λ_1 value (the intercepts were −11002.68 ppm for $[Co(edta)]^-$ and −9299.24 ppm for $[Co(ox)_3]^{3-}$, and the slopes were 20.57 for $[Co(edta)]^-$ and 15.54 for $[Co(ox)_3]^{3-}$).[24] This result indicated that the d–d transition energy (ΔE in Eq. 5) was influenced by the solvent molecules, and this influence changed the electronic spectrum and the ^{59}Co NMR of the cobalt(III) complex anion. The intercepts for $[Co(edta)]^-$, $[Co(ox)_3]^{3-}$, and $[Co(CN)_6]^{3-}$ (−9968.75 ppm: obtained in the previous study[6]) were similar to each other, but the slopes for $[Co(edta)]^-$, $[Co(ox)_3]^{3-}$, and $[Co(CN)_6]^{3-}$ (32.01[6]) were quite different. Thus, the solvent influence depended on the nature of the coordinated ligand atoms.

The influence of the solvent on the d–d transition energy (ΔE) has been speculatively interpreted as a change in the contribution of the empty π-orbital of the ligand oxygen to a complex that is composed of σ- and π-bonding between Co and the ligand.[6,25] If the contribution of the π-orbital in this case increases, the orbital split should become great, leading to blue shifts in hydrogen-bonding solvents. This model was preliminarily tested by EHMO calculation of the $[Co(ox)_2(NH_3)_2]^-$ and H_2O system. The result of the calculation showed that H_2O interacts with carboxyl oxygens along the direction of the angle ranging from about 40 °C to −40 ° for the σ-electron lobes, and not only with the π-electron lobes.[26]

Solvation Site. We now consider the correlation between the solvent influence on the d–d absorption spectrum and the solvation site. Prior to the work described here, we found that $[Co(en)_3]^{3+}$ and $[Co(NH_3)_6]^{3+}$, which have no carboxyl groups, did not show a solvent influence on the d–d transition spectra: for $[Co(en)_3]^{3+}$, λ_1=466.5, 466.5, 467.5, 467.0, 468.0, 468.0, 467.0, 467.0, and 468.0 nm and λ_2=338.0, 338.5, 339.0, 338.5, 339.0, 339.0, 339.0, 338.5, and no peak (in H_2O, EG, CH_3OH, FA, Me_2SO, CH_3CN, DMF, DMA, and Me_2CO, respectively); for $[Co(NH_3)_6]^{3+}$, λ_1=474.0, 474.0, 475.0, 475.0, and 475.5 nm and λ_2=339.0, 339.0, 340.0, 340.0, and 340.0 (in H_2O, FA, Me_2SO, DMF, and DMA, respectively). Therefore, the interaction between solvent molecules and carboxyl groups of complex anions could play an important role in the solvent influence on the d–d transition spectra. In a previous paper,[5] we reported that the ^{13}C NMR chemical shifts of the $[Co(edta)]^-$ anion were correlated to the electrophilic ability of the solvents (Gutmann's acceptor number). In order to elucidate the solvent influence on the d–d absorption, the peak positions (λ_1) in the first d–d transition were plotted versus the ^{13}C NMR chemical shifts of this complex anion in several solvents (Fig. 7). It is clear that the peak positions (λ_1) of the first d–d transition bands of the $[Co(edta)]^-$ anion were correlated linearly with the ^{13}C NMR chemical shifts (δ values) of the carboxyl carbon. The downfield shift of

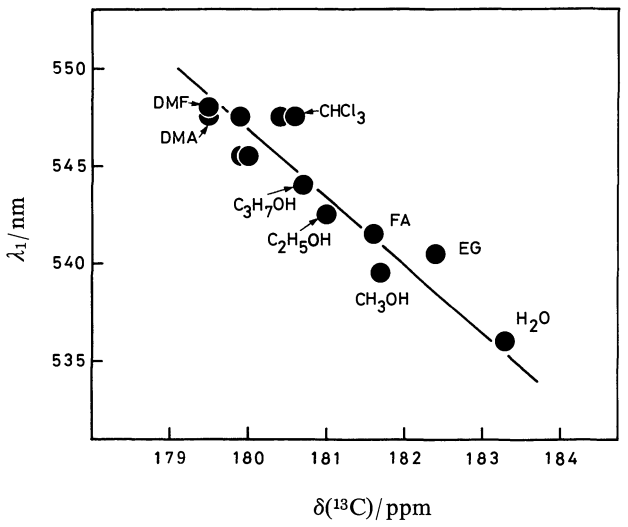

Fig. 7. The correlation between the peak positions (λ_1 in Table 1) and the ^{13}C chemical shifts (Ref. 5) of $K[Co(edta)]\cdot 2H_2O$.

carboxylate ^{13}C signals was due to the electron-withdrawing effect of solvent molecules on the carboxyl groups (specially, perhaps, the carboxyl oxygens) of the cobalt(III) complexes,[27] and thus this effect produced a change in the electronic state for the d–d transition band of the $[Co(edta)]^-$ anion.

We attempted to measure the ^{17}O NMR spectrum of $[Co(edta)]^-$ in the solvents, but no signals were detected. Therefore, we can not confirm the exact site of the interaction of solvation. However, the EHMO calculation of the solvation model, $[Co(ox)_2(NH_3)_2]^- \text{-} H_2O$, shows that H_2O interacts with carboxyl oxygens along the direction of the angle ranging from about 40° to −40° for the σ-electron lobes. A detailed examination of the correlation between the solvation mode and the change of the d–d transition state of the complex anion is now being carried out by ab initio calculations.

Conclusions

The color of the $[Co(edta)]^-$ anion was changed by the outersphere coordination of solvent molecules. This color change could be predicted by using the acceptor number of the solvent. The ^{59}Co NMR chemical shifts and the peak positions in the electronic spectra suggested that the color change was due to the change in the d–d transition energy of the cobalt(III) center. From a comparison with the solvent influence on the ^{13}C NMR, it was found that the $[Co(edta)]^-$ anion interacts with protic solvents through an interaction such as hydrogen bonding between solvent hydrogens and carboxyl oxygens of the cobalt(III) complex anion, and this interaction caused the color change of this complex anion in a variety of solvents. In this work, we have established the method by which the solvent influence on the UV, ^{59}Co NMR, and ^{13}C NMR spectra and the interaction between some carboxylatocobaltate(III) complex anions and solvent molecules can be quantitatively estimated by using the acceptor number of the solvent.

The author thanks the Instrument Center, Institute for Molecular Science, for the use of the NMR spectrometer (JEOL Model JNM-GX400). The author also thanks Dr. Y. Ihara for the measurements of reflection spectra in Kanazawa University. This work was partially supported by a Grant-in-Aid for Scientific Research No. 60740337 from the Ministry of Education, Science and Culture.

References

1) A preliminary communication on part of this work has appeared: *Chem. Lett.*, **1984**, 2011; other of this article were partially reported at the 34th Symposium on Coordination Chemistry, Nagaoka, Japan, October 1984 (Abstr., 1B22); the 35th Symposium on Coordination Chemistry, Hiroshima, Japan, October 1985 (Abstr., 1B20); the 52nd Annual Meeting of the Chemical Society of Japan, Tokyo, April 1986 (Abstr., 4TOKU406); the 24th International Conference on Coordination Chemistry, Athens, Greece, August 1986 (Abstr., A3-219); and the 37th Symposium on Coordination Chemistry, Tokyo, Japan, October 1987 (Abstr., 3B08).

2) T. Taura, *Inorg. Chim. Acta,* **98**, L15 (1985); T. Taura, *Inorg. Chim. Acta,* **162**, 105 (1989).

3) T. Taura, *Chem. Lett.*, **1984**, 2011.

4) U. Mayer, V. Gutmann, and W. Gerger, *Monatsh. Chem.*, **106**, 1235 (1975); V. Gutmann, "The Donor–Acceptor Approach to Molecular Interactions," Plenum Press, New York (1978), translated into Japanese by H. Ohtaki and I. Okada, Gakkai Shuppan Center, Tokyo (1983).

5) T. Taura, *Inorg. Chem.*, **27**, 2845 (1988).

6) T. Taura, *Bull. Chem. Soc. Jpn.*, **63**, 1105 (1990).

7) a) T. Taura, *Bull. Chem. Soc. Jpn.*, **62**, 2541 (1989); b) N. Miura, M. Shimura, and H. Ogino, *Bull. Chem. Soc. Jpn.*, **60**, 1349 (1987); c) M. Fujiwara, M. Yoshitake, Y. Fukuda, and K. Sone, *Bull. Chem. Soc. Jpn.*, **61**, 2967 (1988); d) S. Kaizaki and H. Takemoto, *Inorg. Chem.*, **29**, 4960 (1990).

8) F. P. Dwyer, E. C. Gyarfas, and D. P. Mellor, *J. Phys. Chem.*, **59**, 296 (1955).

9) F. P. Dwyer, I. K. Reid, and F. L. Garvan, *J. Am. Chem. Soc.*, **83**, 1285 (1961).

10) The potassium salt was prepared by using $K_2C_2O_4\cdot H_2O$ instead of $Na_2C_2O_4$ as in Ref. 9 where the preparation of the Na salt was described.

11) K. Yamasaki, J. Hidaka, and Y. Shimura, *Bull. Chem. Soc. Jpn.*, **42**, 119 (1969).

12) J. C. Bailar, Jr. and E. M. Jones, *Inorg. Synth.*, **1**, 37 (1938).

13) J. B. Work, *Inorg. Synth.*, **2**, 221 (1938).

14) J. Bjerrum and J. P. McReynolds, *Inorg. Synth.*, **2**, 216 (1938).

15) In order to check the influence of water of crystallization, we measured the absorption spectra of the sample solution of anhydrous K[Co(edta)]. The peak positions were the same as those of the dihydrate salt ($K[Co(edta)]\cdot 2H_2O$) within experimental error. For other complexes, the peak positions

did not change, though 1 vol% H_2O was added to the sample solution. As the volume of included water in the solution measured was less than that of the added water, there could be no influence of water of crystallization.

16) The first d–d transition band could contain some components since the complexes used here did not exhibit O_h symmetry. However, the band width was not influenced by the solvents. Therefore, the solvent influence on each component in the complex is similar.

17) The solvent influence on the extinction coefficient of the carboxylatocobaltate(III) anions were also checked in the solvents, and there was less than 20% change.

18) E. M. Kosower, *J. Am. Chem. Soc.*, **80**, 3253 (1958).

19) A. J. Parker, *Q. Rev., Chem. Soc.*, **16**, 163 (1962).

20) A plot of the wavenumbers (cm^{-1}) of the peak positions versus the acceptor number also gave a straight line. The intercepts and correlation coefficients were quite similar to those obtained from the plots of the wavelength (nm).

21) The CT bands which appeared in the UV region also shifted from solvent to solvent (226.5, 228.5, and 230.0 nm H_2O, CH_3OH, and C_2H_5OH, respectively, for $[Co(edta)]^-$).

22) R. Bramley, M. Brorson, A. M. Sargeson, and C. E. Schäffer, *J. Am. Chem. Soc.*, **107**, 2780 (1985).

23) J. S. Griffith and L. E. Orgel, *Trans. Faraday Soc.*, **53**, 601 (1957); J. S. Griffith, "The Theory of the Transition Metal Ion," Cambridge University Press, London (1961).

24) The ^{59}Co NMR chemical shift also correlated linearly to the electrophilic ability of the solvents. The chemical shift of the ^{59}Co NMR in the solvent was calculated by the following equations (error bars were one standard deviation):

$$\delta(^{59}Co) = \delta(^{59}Co)^\circ - (5.33\pm0.77) \times AN,$$

where $\delta(^{59}Co)^\circ$=336±22 ppm (the correlation coefficient was −0.924) for $K[Co(edta)] \cdot 2H_2O$, and

$$\delta(^{59}Co) = \delta(^{59}Co)^\circ - (3.51\pm0.77) \times AN,$$

where $\delta(^{59}Co)^\circ$=210±22 ppm (the correlation coefficient was −0.848) for $K_3[Co(ox)_3] \cdot 3H_2O$.

25) J. E. Huheey, "Inorganic Chemistry: Principle of Structure, and Reactivity," 2nd ed, Harper & Row, New York (1978).

26) T. Taura, *Inorg. Chim. Acta*, **163**, 133 (1989).

27) In the literature (O. W. Howarth, P. Moore, and N. Winterton, *J. Chem. Soc., Dalton Trans.*, **1974**, 2271) where the [Co(edta)X] (X: H_2O, Cl, Br, OH, and NO_2)-type complexes were studied, it was proposed that a lower-frequency absorption gave rise to a bigger paramagnetic contribution and to a downfield shift in the case of a positive slope of the line (λ_1 vs. $\delta(^{13}C)$). However, the slope was negative in this work. Therefore, the solvent influence on the ^{13}C chemical shift was not mainly related to the paramagnetic contribution which should be correlated with the mixing of the excited states of the cobalt(III) ion.

Preparation and Characterization of Cobalt(III) Complexes Containing 4,7-Diphenyl-4,7-diphosphadecane-1,10-diamine and 4,8-Diphenyl-4,8-diphosphaundecane-1, 11-diamine, $NH_2(CH_2)_3P(C_6H_5)$-$(CH_2)_nP(C_6H_5)(CH_2)_3NH_2$ (n=2,3)

Kazuo KASHIWABARA, Minho JUNG, and Junnosuke FUJITA*
Department of Chemistry, Faculty of Science, Nagoya University, Chikusa-ku, Nagoya 464-01
(Received March 14, 1991)

Twelve new cobalt(III) complexes of the types, *cisα*-[Co(L)(*rac*(*P*)-323 or 333NPPN)]$^{p+}$ (L=2,4-pentanedionate (acac) and oxalate (ox) ions) (four complexes) and *cisβ*-[Co(L)(*rac*(*P*)- or *meso*(*P*)-323 or 333NPPN)]$^{p+}$ (eight complexes) were prepared and characterized by ^{1}H NMR and absorption spectra, where *rac*(*P*)- and *meso*(*P*)-323NPPN denote *rac*(*P*)- and *meso*(*P*)-$NH_2(CH_2)_mP(C_6H_5)(CH_2)_nP(C_6H_5)(CH_2)_mNH_2$ with m=3 and n=2, and 333NPPN the ligand with m=3 and n=3. Reactivities of the complexes towards hydrochloric acid were examined and compared with those of the corresponding 222NPPN (m=2, n=2) and 232NPPN (m=2, n=3) complexes. All the *cisα* isomers yield the *cisα*-dichloro complexes, the 333NPPN and 222NPPN complexes being more reactive than the 232NPPN and 323NPPN complexes in which five- and six-membered chelate rings of NPPN are involved. For the *cisβ* isomers, the acac complexes afford [Co(acac)(Cl)(mnmNPPNH$^+$)]$^{2+}$ except the *rac*(*P*)- and *meso*(*P*)-333NPPN complexes which give the *trans*-dichloro complexes, while all the ox complexes liberate the ox ion to yield the dichloro complex of the *cisα*, *cisβ*, or *trans* configuration. For both *cisβ*-acac and -ox isomers, the 222NPPN and 232NPPN complexes are more reactive than those of 323NPPN and 333NPPN, and the *meso*(*P*)-complexes are more reactive than the *rac*(*P*)-complexes.

In a previous paper,[1] we reported the preparation of stereoisomers of 2,4-pentanedionato (acac) and oxalato (ox) cobalt(III) complexes containing a linear quadridentate ligand with two chiral phosphorus donor atoms, $NH_2(CH_2)_2P(C_6H_5)(CH_2)_nP(C_6H_5)(CH_2)_2NH_2$ (n=2: 222NPPN, n=3: 232NPPN), and their novel reactivities towards hydrochloric acid. For example, the *cisβ* isomers of the acac complexes dissociate the amino group trans to the phosphorus donor atom of NPPN reversibly depending on the acidity of solution to form [Co(acac)-(H_2O)(NPPNH$^+$)]$^{2+}$, while the *cisα* isomers yield *cisα*-dichloro complexes in hydrochloric acid. These properties are quite different from those of analogous tetramine complexes[2] which are stable under the same conditions. In order to examine whether such chemical properties depend on the size of chelate rings of NPPN ligands, we have prepared 4,7-diphenyl-4,7-diphosphadecane-1,10-diamine (323NPPN) and 4,8-diphenyl-4,8-diphosphaundecane-1,11-diamine (333NPPN) complexes of cobalt(III) (Fig. 1).

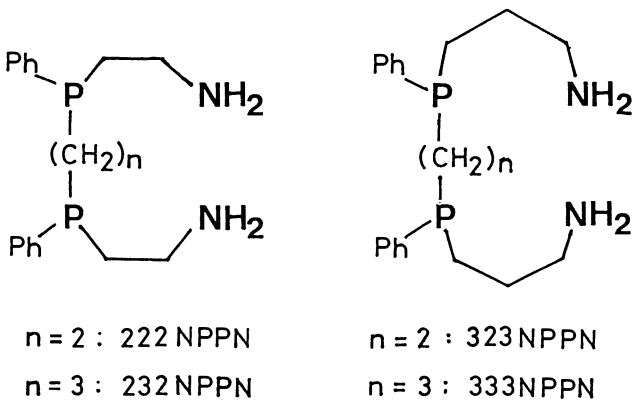

Fig. 1. Linear quadridentate phosphine ligands of the NPPN-type.

Experimental

The phosphine ligands were prepared and handled under an atmosphere of nitrogen until they formed cobalt(III) complexes. All solvents used for the preparation were made oxygen-free by bubbling nitrogen for 20 min immediately before use. Absorption spectra were recorded on a Hitachi U3400 spectrophotometer, and ^{1}H and ^{13}C NMR spectra on a Hitachi R-90H spectrometer.

Preparation of Ligands. 323NPPN and 333NPPN were prepared by a method similar to that for 333NPPN reported by Meek et al.,[3] except that (3-aminopropyl)phenylphosphine was obtained from (3-aminopropyl)diphenylphosphine and sodium.

(3-Aminopropyl)diphenylphosphine, $NH_2CH_2CH_2CH_2P(C_6H_5)_2$. The reported method for $NH_2CH_2CH_2CH_2P(C_6H_5)_2$ was reduction of $NCCH_2CH_2P(C_6H_5)_2$ with $LiAlH_4$.[4] In the present paper, it was prepared from $NH_2CH_2CH_2CH_2Cl$ and $NaP(C_6H_5)_2$. A liquid ammonia solution (300 cm^3) containing $P(C_6H_5)_3$ (65 g, 0.247 mol) and sodium metal (13 g, 0.565 mol) was stirred for 3 h at −78 °C. To the resulting red-orange solution were added $NH_2CH_2CH_2CH_2Cl \cdot HCl$ (Tokyo Kasei Kogyo Co., Ltd.) (32.5 g, 0.25 mol) and tetrahydrofuran (THF) (300 cm^3) by portions. After stirring for 2 h at −78 °C, liquid ammonia was allowed to evaporate slowly. The THF solution was refluxed for 8 h at 60—70 °C, and then the solvent was evaporated under reduced pressure. The residue was distilled at 150—160 °C/ca. 60 Pa to give a colorless viscous liquid. Yield: 48 g (80%).

(3-Aminopropyl)phenylphosphine, $NH_2CH_2CH_2CH_2PH(C_6H_5)$. To a liquid ammonia solution (300 cm^3) of sodium metal (8 g, 0.348 mol) was added (3-aminopropyl)diphenylphosphine (40 g, 0.164 mol) dropwise with stirring at −78 °C. The solution was stirred for 2 h to give an yellow-orange solution. Water (10 cm^3) was added by portions with care,

yielding a colorless solution. Liquid ammonia was evaporated, and the residue was stirred with a mixture of water (200 cm^3) and diethyl ether (200 cm^3). The ethereal layer was separated from water and dried over Na_2SO_4 (5 g) overnight. The solvent was evaporated and the residue was distilled at 95—100°/ca. 60 Pa to yield a colorless liquid. Yield: 22 g (80%).

4,7-Diphenyl-4,7-diphosphadecane-1,10-diamine (323NPPN), $NH_2(CH_2)_3P(C_6H_5)(CH_2)_2P(C_6H_5)(CH_2)_3NH_2$. A THF solution (50 cm^3) of (3-aminopropyl)phenylphosphine (10 g, 59.8 mmol) was added dropwise with stirring at 0 °C to sodium metal (1.5 g, 65.2 mmol) in THF (50 cm^3). After a while the orange solution was warmed at 20 °C, stirred for 6 h and cooled to 0 °C. To the solution was added a THF solution of 1,2-dichloroethane (2.9 g, 29.3 mmol) dropwise with stirring at 0 °C, and then the colorless solution was stirred at 25 °C for 5 h. The solvent THF was evaporated, and diethyl ether was added to precipitate NaCl, which was filtered off. The filtrate was evaporated under vacuum, yielding a colorless oily product. Yield: 15 g (70%). This was used for preparing Co(III) complexes without further purification.

4,8-Diphenyl-4,8-diphosphaundecane-1,11-diamine (333NPPN), $NH_2(CH_2)_3P(C_6H_5)(CH_2)_3P(C_6H_5)(CH_2)_3NH_2$. This ligand was prepared by the same method as that for 323NPPN using 1,3-dichloropropane instead of 1,2-dichloroethane. Yield: 16 g (73%).

Preparation of Cobalt(III) Complexes. *cis*α-[Co(acac)(*rac*(*P*)-323NPPN)]{$B(C_6H_5)_4$}$_2$·1/2$(CH_3)_2CO$ (A-I), *cis*β-[Co(acac)(*rac*(*P*)-323NPPN)]{$B(C_6H_5)_4$}$_2$·H_2O (A-II), and *cis*β-[Co(acac)(*meso*(*P*)-323NPPN)]{$B(C_6H_5)_4$}$_2$ (A-III). A methanol solution (100 cm^3) containing [$Co(acac)_3$] (590 mg, 1.66 mmol) and 323NPPN (600 mg, 1.67 mmol) was stirred at room temperature overnight. The dark orange solution was diluted with water (2 dm^3) and applied on a column (ϕ 4 cm×70 cm) of SP-Sephadex C-25. The adsorbed products were eluted with a 0.1 mol dm^{-3} NaCl aqueous solution. Three large orange bands (**A-I**, **A-II**, **A-III** in the order of elution) and two small red bands developed. Each eluate of **A-I** and **A-II** was evaporated to dryness under reduced pressure at 40 °C. The orange complex in the residue was extracted with ethanol, and the extract was evaporated again to dryness under reduced pressure. The residue was dissolved in water (10 cm^3). On addition of an aqueous solution of $NaB(C_6H_5)_4$, complexes **A-I** and **A-II** were precipitated and recrystallized from a mixture of acetone and water (2:1, 15 cm^3). Yield: **A-I**, 430 mg (33%); **A-II**, 150 mg (8%). The eluate of **A-III** was diluted ten times with water, and rechromatographed using a column (ϕ 3 cm×70 cm) of SP-Sephadex C-25 and a 0.1 mol dm^{-3} Na_2SO_4 aqueous solution. After elution of a small reddish orange band, the eluate of a large orange band (**A-III**) was collected and worked up by the same manner as for **A-I** and **A-II**. Yield: 350 mg (18%). Found for **A-I**: C, 75.54; H, 7.11; N, 2.28%. Calcd for [Co(acac)(323NPPN)]{$B(C_6H_5)_4$}$_2$·1/2$(CH_3)_2CO$=$C_{74.5}H_{80}N_2P_2O_{2.5}B_2Co$: C, 75.45; H, 6.80; N, 2.36%. Found for **A-II**: C, 74.40; H, 6.96; N, 2.27%. Calcd for [Co(acac)(323NPPN)]{$B(C_6H_5)_4$}$_2$·H_2O=$C_{73}H_{79}N_2P_2O_3B_2Co$: C, 74.63; H, 6.78; N, 2.38%. Found for **A-III**: C, 75.70; H, 6.81; N, 2.33%. Calcd for [Co(acac)(323NPPN)]{$B(C_6H_5)_4$}$_2$=$C_{73}H_{77}N_2P_2O_2B_2Co$: C, 75.79; H, 6.71; N, 2.42%. These three complexes are soluble in acetone and acetonitrile, but insoluble in water, methanol and ethanol.

***cis*α-[Co(acac)(*rac*(*P*)-333NPPN)]{$B(C_6H_5)_4$}$_2$·$2H_2O$ (B-I), *cis*β-[Co(acac)(*rac*(*P*)-333NPPN)]{$B(C_6H_5)_4$}$_2$·1/$2H_2O$ (B-II), and *cis*β-[Co(acac)(*meso*(*P*)-333NPPN)]{$B(C_6H_5)_4$}$_2$·1/$2H_2O$ (B-III).** A methanol solution (150 cm^3) containing [$Co(acac)_3$] (810 mg, 2.27 mmol) and 333NPPN (850 mg, 2.27 mmol) was stirred at 50 °C for 30 min, and then at room temperature for 6 h. The resulting brown solution was diluted with water (3 dm^3) and applied on a column (ϕ 4 cm×70 cm) of SP-Sephadex C-25. By elution with a 0.1 mol dm^{-3} NaCl aqueous solution, three large orange bands (**B-I**, **B-II**, **B-III** in the order of elution) and a small red one appeared. From eluates of the orange bands, complexes **B-I**, **B-II**, and **B-III** were isolated as tetraphenylborates by methods similar to those for complexes **A-I** and **A-II**. Yields: **B-I**, 370 mg (14%); **B-II**, 640 mg (24%); **B-III**, 620 mg (23%). Found for **B-I**: C, 73.95; H, 6.97; N, 2.31%. Calcd for [Co(acac)(333NPPN)]{$B(C_6H_5)_4$}$_2$·$2H_2O$=$C_{74}H_{83}N_2P_2O_4B_2Co$: C, 73.64; H, 6.93; N, 2.32%. Found for **B-II**: C, 75.63; H, 6.99; N, 2.19%. Found for **B-III**: C, 75.25; H, 6.96; N, 2.34%. Calcd for [Co(acac)(333NPPN)]{$B(C_6H_5)_4$}$_2$·1/$2H_2O$=$C_{74}H_{80}N_2P_2O_{2.5}B_2Co$: C, 75.33; H, 6.83; N, 2.34%. Solubilities of the complexes are quite similar to those of the 323NPPN analogues.

***cis*α-[Co(ox)(*rac*(*P*)-323NPPN)]$B(C_6H_5)_4$·H_2O·$(CH_3)_2CO$ (C-I), *cis*β-[Co(ox)(*rac*(*P*)-323NPPN)]$B(C_6H_5)_4$·$(CH_3)_2CO$ (C-II), and *cis*β-[Co(ox)(*meso*(*P*)-323NPPN)]$B(C_6H_5)_4$ (C-III).** A methanol solution (15 cm^3) of 323NPPN (695 mg, 1.93 mmol) was added to a solution of $K_3[Co(ox)_3]$·$3H_2O$ (953 mg, 1.93 mmol) in a mixture of water (20 cm^3) and methanol (120 cm^3). The resulting brown solution was stirred overnight and filtered. The filtrate was diluted with water (2 dm^3), and applied on a column (ϕ 3 cm×120 cm) of SP-Sephadex C-25. By elution with a 0.05 mol dm^{-3} NaCl aqueous solution, three large orange bands (**C-I**, **C-II**, **C-III** in the order of elution) and several slow-moving small reddish bands developed. Each eluate of the three orange bands was evaporated to dryness under reduced pressure at 40 °C. The orange complex in the residue was extracted with ethanol. The extract was evaporated again to dryness under reduced pressure, and the residue was dissolved in water (10 cm^3). On addition of an aqueous $NaB(C_6H_5)_4$ solution, the aqueous solution yielded a precipitate of the complex. Complexes **C-I** and **C-II** were recrystallized from a mixture of acetone and water (2:1, 10 cm^3), while complex **C-III** was not recrystallized because of its insolubility in solvents useful for recrystallization. Yields: **C-I**, 90 mg (6%); **C-II**, 400 mg (25%); **C-III**, 270 mg (17%). Found for C-I: C, 65.41; H, 6.43; N, 2.98%. Calcd for [Co(ox)(323NPPN)]$B(C_6H_5)_4$·H_2O·$(CH_3)_2CO$=$C_{49}H_{58}N_2P_2O_6BCo$: C, 65.20; H, 6.48; N, 3.10%. Found for **C-II**: C, 66.48; H, 6.55; N, 3.09%. Calcd for [Co(ox)(323NPPN)]$B(C_6H_5)_4$·$(CH_3)_2CO$=$C_{49}H_{56}N_2P_2O_5BCo$: C, 66.52; H, 6.38; N, 3.17%. Found for **C-III**: C, 66.70; H, 6.27; N, 3.36%. Calcd for [Co(ox)(323NPPN)]$B(C_4H_5)_4$=$C_{46}H_{50}N_2P_2O_4BCo$: C, 66.84; H, 6.10; N, 3.39%. Complexes **C-I** and **C-II** are soluble in acetone and acetonitrile, but insoluble in water and methanol. Complex **C-III** is soluble in dimethyl sulfoxide, slightly soluble in acetone and acetonitrile, and insoluble in water and methanol.

***cis*α-[Co(ox)(*rac*(*P*)-333NPPN)]$B(C_6H_5)_4$·$2(CH_3)_2CO$ (D-I), *cis*β-[Co(ox)(*rac*(*P*)-333NPPN)]$B(C_6H_5)_4$·$2(CH_3)_2CO$ (D-II), and *cis*β-[Co(ox)(*meso*(*P*)-333NPPN)]$B(C_6H_5)_4$ (D-III).** These complexes were prepared by the same method as that for the 323NPPN complexes. Yields: **D-I**, 7%; **D-II**, 36%; **D-III**, 30%. Found for **D-I**: C, 66.67; H, 6.52; N, 2.66%. Found for **D-II**: C, 66.93; H, 6.63; N, 2.85%. Calcd for

[Co(ox)(333NPPN)]$B(C_6H_5)_4 \cdot 2(CH_3)_2CO$=$C_{53}H_{64}N_2P_2O_6BCo$: C, 66.53; H, 6.74; N, 2.93%. Found for **D-III**: C, 67.07; H, 6.32; N, 3.35%. Calcd for [Co(ox)(333NPPN)]$B(C_6H_5)_4$=$C_{47}H_{52}N_2P_2O_4BCo$: C, 67.15; H, 6.24; N, 3.33%. The complexes show similar solubilities to those of the corresponding isomers of the 323NPPN complex.

Reactions of the Complexes with Hydrochloric Acid. All the complexes were converted to the chlorides, which were readily soluble in water, by treating with Dowex 1×8 (Cl^- form) in a mixture of acetone and water (2 : 1). The resin was filtered off, and the filtrate was evaporated to dryness under reduced pressure. The residue was used for studying the reactivity of the complex in water or hydrochloric acid without further purification.

Results and Discussion

The [Co(acac or ox)(mnmNPPN)]$^{p+}$ (*m*, *n*=2, 3) complexes can have three possible geometrical isomers, *cisα-rac(P)*, *cisβ-rac(P)*, and *cisβ-meso(P)* (Fig. 2). The *meso(P)*-ligand can not form the *cisα* isomer, since the two terminal P–N chelate arms point to the same apical site with respect to the P–Co–P plane. These three isomers of [Co(acac or ox)(323NPPN or 333NPPN)]$^{p+}$ were obtained by reactions of [Co(acac)$_3$] or [Co(ox)$_3$]$^{3-}$ with 323NPPN or 333NPPN according to methods for the 232NPPN complexes described in a previous paper.[1] The structures of the acac complexes were assigned on the basis of ^{1}H NMR spectral data (Table 1). Complexes **A-I** and **B-I** show only one methyl signal of acac and are assigned to the *cisα-rac(P)* isomer, while other acac complexes **A-II**, **A-III**, **B-II**, and **B-III** are *cisβ* isomers, since they give two kinds of methyl signal. Of these complexes, **A-III** and **B-III** exhibit one of the two methyl signals at a remarkably high field, δ=0.93 and 1.04, respectively, compared with other methyl signals (δ=1.55—2.19). One methyl group in the *cisβ*-[Co(acac)(*meso(P)*-NPPN)]$^{2+}$-type complexes is located over the phenyl ring bonded to the phosphorus atom trans to the oxygen atom of acac (Fig. 2(c)), and is shielded by this phenyl group as reported for the corresponding 232NPPN complex.[1] Thus complexes **A-III** and **B-III** are assigned to the *cisβ-meso(P)* isomer, and the other **A-II** and **B-II** complexes to the *cisβ-rac(P)* isomer. Both *cisβ-rac(P)* and *cisβ-meso(P)* isomers have a phenyl group over the acac chelate ring, and show the methine proton signal of acac at a higher field than those of the *cisα* isomers (Table 1 and Fig. 2).

For the ox complexes, the *cisα* isomers (**C-I** and **D-I**) can be assigned from a similarity of the visible absorption spectra to those of the acac complexes. The *cisα* isomers show a nearly symmetrical first d–d band, while the *cisβ* isomers give a band with a shoulder in this region (Fig. 3). The spectra of the *cisβ-rac(P)* and *cisβ-*

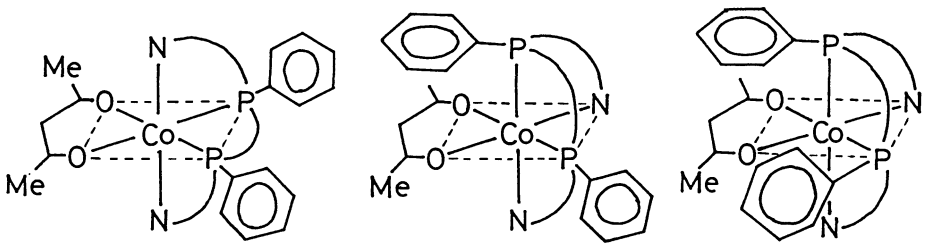

(a) *cisα-rac(P)* (b) *cisβ-rac(P)* (c) *cisβ-meso(P)*

Fig. 2. Three possible isomers of [Co(acac)(*mnm*NPPN)]$^{2+}$.

Table 1. ^{1}H NMR and Absorption Spectral Data

Complex		^{1}H NMR (acac)[a]			Absorption[b]	
		$-CH_3$		=CH–		
cisα-[Co(acac)(*rac(P)*-323NPPN)]$^{2+}$	(**A-I**)	2.29		5.85	21.83 (2.70)	
cisβ-[Co(acac)(*rac(P)*-323NPPN)]$^{2+}$	(**A-II**)	1.55	1.99	4.85	22.46 (3.04)	
cisβ-[Co(acac)(*meso(P)*-323NPPN)]$^{2+}$	(**A-III**)	0.93	2.19	4.97	18.9 (2.4)[c]	22.85 (3.06)
cisα-[Co(acac)(*rac(P)*-333NPPN)]$^{2+}$	(**B-I**)	2.18		5.77	20.73 (2.62)	
cisβ-[Co(acac)(*rac(P)*-333NPPN)]$^{2+}$	(**B-II**)	1.57	1.95	5.20	19.7 (2.5)[c]	22.27 (2.79)
cisβ-[Co(acac)(*meso(P)*-333NPPN)]$^{2+}$	(**B-III**)	1.04	2.16	4.99	19.2 (2.4)[c]	22.27 (2.79)
cisα-[Co(ox)(*rac(P)*-323NPPN)]$^{+}$	(**C-I**)				22.06 (2.50)	
cisβ-[Co(ox)(*rac(P)*-323NPPN)]$^{+}$	(**C-II**)				22.38 (2.82)	
cisβ-[Co(ox)(*meso(P)*-323NPPN)]$^{+}$	(**C-III**)				18.8 (2.2)[c]	22.77 (2.96)
cisα-[Co(ox)(*rac(P)*-333NPPN)]$^{+}$	(**D-I**)				21.15 (2.48)	
cisβ-[Co(ox)(*rac(P)*-333NPPN)]$^{+}$	(**D-II**)				19.6 (2.3)[c]	22.07 (2.58)
cisβ-[Co(ox)(*meso(P)*-333NPPN)]$^{+}$	(**D-III**)				19.6 (2.4)[c]	22.12 (2.67)

a) δ, solvent $(CD_3)_2SO$. b) First absorption band $\tilde{\nu}/10^3$ cm^{-1} (log ε), solvent CH_3CN except for **C-III** and **D-III** (solvent $(CH_3)_2SO$). c) Shoulder.

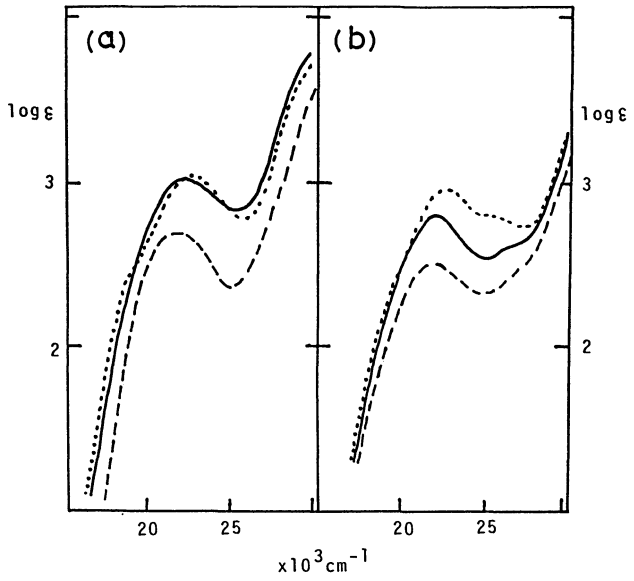

Fig. 3. Absorption spectra of (a) isomers **A-I** (——), **A-II** (——), **A-III** (·····), and (b) isomers **C-I** (——), **C-II** (——), **C-III** (·····).

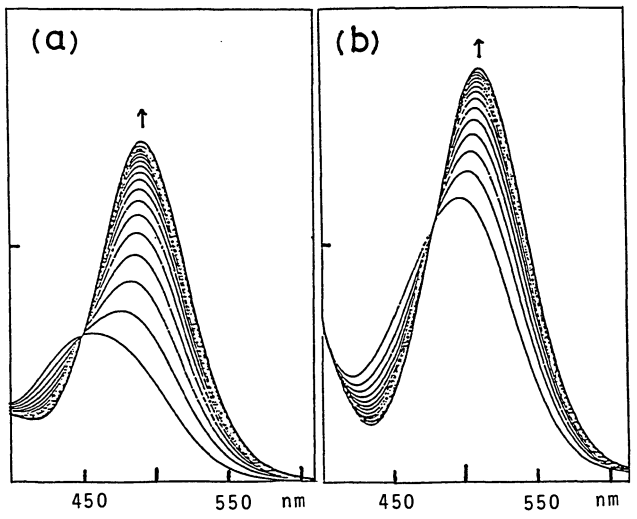

Fig. 4. Changes in absorption spectra of (a) isomer **A-I** in concd HCl recorded at 30 min intervals at 25 °C, and (b) isomer **B-I** in concd HCl recorded at 2 min intervals at 15 °C.

meso(*P*) isomers have a similar pattern, and no assignment can be made for the two *cisβ* isomers. Hence we derived the acac complexes from the ox complexes by treating with Li(acac), and assigned complexes **C-II** and **D-II** as the *cisβ-rac*(*P*) isomer and complexes **C-III** and **D-III** as the *cisβ-meso*(*P*) isomer.

The data of absorption spectra are given in Table 1. The spectra of the 333NPPN complexes are very similar to those of the corresponding 323NPPN and the previously reported 232NPPN[1] complexes. The first d–d bands of the *cisα* isomers shift to the higher energy side in the order of complexes, 333NPPN<232NPPN< 323NPPN<222NPPN. The complexes where the central P–Co–P chelate forms a five-membered ring show the band at higher energy than those containing a six-membered P–Co–P chelate ring. The *cisβ* isomers have all a broad d–d band, and their peak positions do not differ appreciably among the complexes.

The water-soluble chlorides of *cisα*-[Co(acac)(323 or 333NPPN)]$^{2+}$ are stable in water and dil HCl (ca. 1 mol dm^{-3}), but react gradually with concd HCl, changing the color of solutions from orange to red. Figure 4 shows the spectral changes with time. The spectra change with an isosbestic point, and the changes are very similar to those observed for the corresponding 232NPPN and 222NPPN complexes in concd HCl.[1] The products isolated by reactions of the 232NPPN and 222NPPN complexes with concd HCl were *cisα*-[$CoCl_2$(232 or 222NPPN)]$^+$.[1] The spectral changes of the 323NPPN and 333NPPN complexes in concd HCl indicate the formation of *cisα*-[$CoCl_2$(323 or 333NPPN)]$^+$, since their final spectra are very similar to those of the 232NPPN and 222NPPN complexes under the same conditions. The half-life times of the reactions are 390 min at 20 °C for the 323NPPN complex and 6 min at 15 °C for the 333NPPN complex, while those of the 222NPPN and 232NPPN complexes were 87 min and 364 min at 20 °C, respectively.[1] The reactivity of *cisα*-[Co(acac)(*mnm*NPPN)]$^{2+}$ towards concd HCl decreases in the order of the 333NPPN>222NPPN >232NPPN≈323NPPN complexes. The differences in reactivity of the complexes seem to result from steric factors as indicated by molecular models. The 333NPPN complex is the most crowded structure, and the 222NPPN complex involves strain arising from the NPPN skeleton formed by three small five-membered chelate rings. These crowded 333NPPN and strained 222NPPN complexes would be less stable than the 232NPPN and 323NPPN complexes in which such unfavorable conditions are reduced to some extent.

The *cisα*-[Co(ox)(323 or 333NPPN)]Cl complexes in HCl solutions show similar spectral changes, and the final spectra coincide with those of the corresponding acac complexes in concd HCl, indicating the formation of the same *cisα*-dichloro complexes. The ox complexes are more reactive towards HCl than the acac complexes. The half-life times of the reactions in 2 mol dm^{-3} HCl at 30 °C are 43 min for the 323NPPN complex and 3 min for the 333NPPN complex, while it was 220 min for the 232NPPN complex.[1] Thus the reactivity towards HCl decreases in the order of the 333NPPN>323NPPN>232NPPN complexes. The 333NPPN complex is also the most reactive towards HCl as well as the acac analog. For the ox complexes, there is a fairly large difference in reactivity between the 323NPPN and 232NPPN complexes, in contrast to their acac complexes with similar reactivity described above.

The chlorides of *cisβ*-[Co(acac)(*rac*(*P*)- or *meso*(*P*)-323NPPN)]$^{2+}$ are stable in water and fairly strong HCl (ca. 5 mol dm^{-3}) solutions, but react slowly with concd

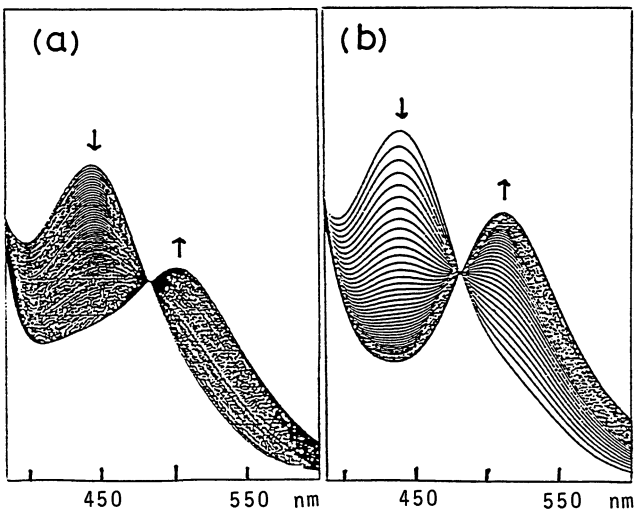

Fig. 5. Changes in absorption spectra of isomers **A-II** (a) and **A-III** (b) in concd HCl at 25 °C recorded at 60 min and 30 min intervals, respectively.

HCl. Figure 5 shows that the spectra of these *rac*(*P*) and *meso*(*P*) complexes change with an isosbestic point at 482 nm and 480 nm, respectively. The colors of solutions change from orange to red. The spectra of the red solutions show the first d–d band at 502 nm for the *rac*(*P*) and 509 nm for the *meso*(*P*) complexes. These values and spectral patterns are quite similar to those of [Co(acac)Cl(*rac*(*P*)- or *meso*(*P*)-232NPPNH$^+$)]$^{2+}$ (505 and 513 nm, respectively) reported in a previous paper.[1] The liberated amino group of the 232NPPN complexes in HCl solutions was found to be the one at the position trans to phosphorus, as shown in Fig. 6, from the ^{1}H NMR spectra of the complexes in DCl.[1] The red concd HCl solutions of the *rac*(*P*)- and *meso*(*P*)-323NPPN complexes turned orange by dilution with water. From the dilute solutions the original complexes were recovered by column chromatography, although some decomposition to Co(II) species occured for both complexes. These observations are also the same as those for the 232NPPN complexes. Therefore, the spectral changes of *cisβ*-[Co(acac)(*rac*(*P*)- or *meso*(*P*)-323NPPN)]$^{2+}$ in concd HCl are also attributable to the dissociation of the amino group trans to phosphorus to form [Co(acac)Cl(*rac*(*P*)- or *meso*(*P*)-323NPPNH$^+$)]$^{2+}$ shown in Fig. 6, although the ^{1}H NMR

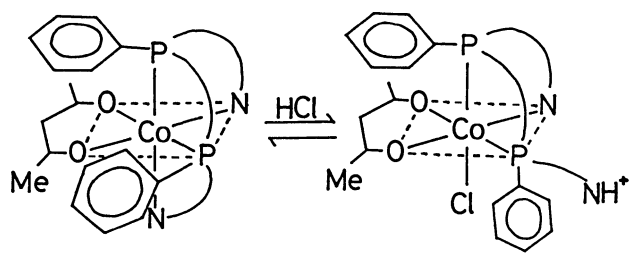

Fig. 6. Dissociation of one amino group of *cisβ*-[Co(acac)(323NPPN)]$^{2+}$ in concd HCl.

spectra in DCl did not show the liberated amino group because of the insufficient acidity of DCl for the 323NPPN complexes. The half-life times at 40 °C in concd HCl are 720 and 75 min for the *rac*(*P*)- and *meso*(*P*)-323NPPN complexes, respectively. The corresponding 232NPPN complexes are more reactive and dissociate the amino group fairly rapidly in 0.1 mol dm^{-3} HCl at room temperature.[1] The remarkable reactivity of the 232NPPN complexes may be attributed to the larger strain of the five-membered chelate ring of the leaving amino group linked meridionally with the P–Co–P chelate ring. The half-life time of 720 min for the reaction of *cisβ*-[Co(acac)(*rac*(*P*)-323NPPN)]$^{2+}$ in concd HCl at 40 °C is much longer than that of the reaction of the *cisα* isomer to *cisα*-[CoCl$_2$(*rac*(*P*)-323NPPN)]$^+$ (21 min at 40 °C in concd HCl), while the corresponding 232NPPN complexes are more stable in the *cisα* isomer than the *cisβ* isomer.

The *cisβ*-[Co(acac)(*rac*(*P*)- or *meso*(*P*)-333NPPN)]$^{2+}$ complexes show different reactivity from the other *cisβ*-acac complexes. The complexes, which are stable in water, react slowly with concd HCl to give a green-brown solution. These solutions exhibit a band around 630 nm, which can be assigned to the split component (Ia) of the first d–d band of the *trans*-[CoCl$_2$(NPPN)]$^+$-type complex.[5] The *trans*-dichloro complexes seem to decompose gradually in concd HCl, since the bands show weak structures characteristic of [CoCl$_4$]$^{2-}$ with passage of time. The reactivity of [Co(acac)(333NPPN)]$^{2+}$ towards HCl is *cisα*-*rac*(*P*) isomer$\gg$*cisβ*-*meso*(*P*) isomer$>$*cisβ*-*rac*(*P*) isomer. The 333NPPN complexes are also more stable in the *cisβ* form than the *cisα* form.

All the isomers of *cisβ*-[Co(ox)(323 or 333NPPN)]Cl are stable in water, but react with concd HCl. Both spectra of *rac*(*P*)- and *meso*(*P*)-323NPPN complexes in concd HCl change in a similar rate with isosbestic points. The final spectrum of the *rac*(*P*) isomer coincides with that of *cisα*-[CoCl$_2$(*rac*(*P*)-323NPPN)]$^+$ yielded from *cisα*-[Co(acac)(*rac*(*P*)-323NPPN)]$^{2+}$ in concd HCl, while that of the *meso*(*P*) isomer shows the first d–d band at 511 nm. The reaction product could not be isolated because of poor crystallization and a small amount. However, the product was tentatively assigned to *cisβ*-[CoCl$_2$(*meso*(*P*)-323NPPN)]$^+$ from the peak position of the d–d band. No starting oxalato complex was detected from the reaction product by column chromatography. The *cisβ* isomers of *rac*(*P*)- and *meso*(*P*)-333NPPN complexes are more reactive than those of the 323NPPN complexes. The orange solutions of the two 333NPPN complexes in 8 mol dm^{-3} HCl slowly turn dark green, and the spectra exhibit a band around 620 nm, which is characteristic of the *trans*-dichloro complex. The *meso*(*P*) isomer is more reactive than the *rac*(*P*) isomer, and its spectral change in a HCl solution has isosbestic points. For the *rac*(*P*) isomer, there is no isosbestic point in the spectra, indicating the presence of a rather stable intermediate

during the reaction of the *cisβ*-oxalato to *trans*-dichloro complexes. However, no further studies were made in this paper.

From the present and the previous papers,[1] the following features are pointed out for the [Co(acac or ox)(*mnm*NPPN)]$^{p+}$-type complexes. (1) The [Co(acac or ox)(*mnm*NPPN)]$^{p+}$ (*m*, *n*=2, 3) complexes yielded all of the three possible isomers (*cisα-rac*(*P*), *cisβ-rac*(*P*), and *cisβ-meso*(*P*)) except that the 222NPPN complex formed no *cisβ-rac*(*P*) isomer. On the other hand, the analogous tetramine (*mnm*NNNN) complexes of the type, [Co(bidentate)(*mnm*NNNN)]$^{p+}$ often afford particular isomers. For example, the 232NNNN complex yields only the *cisβ-rac*(*N*) isomer,[6] and the 323NNNN complex two isomers, *cisβ-rac*(*N*) and *cisβ-meso*(*N*), no *cisα-rac*(*N*) isomer being known.[7] Only known complex of 333NNNN is *cisβ*-[Co(sal)(333NNNN)]$^{+}$ (sal=salycilate ion),[8] and it is reported that [Co(ox)-(333NNNN)]$^{+}$ is too unstable to be isolated,[9] in contrast to the stable 333NPPN complex. The formation of all possible isomers in the *mnm*NPPN complexes may be related in part to the optical stability of a phosphorus donor atom. In the *mnm*NNNN complexes, inversion of the secondary amine group takes place rather easily, and the complexes tend to be stabilized in particular isomers. (2) All *cisα*-[Co(acac or ox)(*rac*(*P*)-NPPN)]$^{p+}$ react with hydrochloric acid to yield *cisα*-[$CoCl_2$(*rac*(*P*)-NPPN)]$^{+}$, and the 222NPPN and 333NPPN complexes are more reactive than the 232NPPN and 323NPPN complexes where the NPPN skeletal structures are formed by a combination of five- and six-membered chelate rings. The *cisα*-[Co(acac)(222NNNN)]$^{2+}$ complex is quite stable under the same conditions.[1] (3) Except the 333NPPN complexes, all *cisβ*-[Co(acac)-(NPPN)]$^{2+}$ in HCl solutions dissociate the amino group trans to phosphorus of NPPN reversibly depending on the acidity of solution, yielding [Co(acac)(Cl or H_2O)(NPPNH^{+})]$^{p+}$. Such a reversible dissociation of an amino end group of chelate has never been reported for cobalt(III) complexes. The *cisβ*-[Co(acac)(*rac*(*P*)- or *meso*(*P*)-333NPPN)]$^{2+}$ complexes yield the *trans*-dichloro complex by reaction with concd HCl. (4) All *cisβ*-[Co(ox)(NPPN)]$^{+}$ release the oxalate ion in hydrochloric acid to form the *cisα*-, *cisβ*-, or *trans*-dichloro complex. No dissociation of the amino group of NPPN was observed. (5) In hydrochloric acid solutions, the 222NPPN and 232NPPN complexes are more stable in the *cisα* isomer than the *cisβ* isomer, while the 323NPPN and 333NPPN complexes are more stable in the *cisβ* isomer than the *cisα* isomer. For each NPPN, the *cisβ-rac*(*P*) isomer is more stable than the *cisβ-meso*(*P*) isomer.

References

1) M. Jung, M. Atoh, K. Kashiwabara, and J. Fujita, *Bull. Chem. Soc. Jpn.*, **63**, 2051 (1990).

2) D. A. House, "Comprehensive Coordination Chemistry," ed by G. Wilkinson, R. D. Gillard, and J. A. McCleverty, Pergamon Press, Oxford (1987), Vol. 2, Chap. 13.1.

3) L. G. Scanlon, Y. Tsao, K. Toman, S. C. Cummings, and D. W. Meek, *Inorg. Chem.*, **21**, 1215, 2707 (1982).

4) L. Sacconi, G. P. Speron, and R. Morrassi, *Inorg. Chem.*, **7**, 1521 (1968).

5) M. Atoh, H. Sugiura, Y. Seki, K. Kashiwabara, and J. Fujita, *Bull. Chem. Soc. Jpn.*, **60**, 1699 (1987).

6) G. R. Brubaker and D. P. Schaefer, *Inorg. Chem.*, **10**, 968, 2170 (1971).

7) B. Bosnich, J. MacB. Harrowfield, and H. Boucher, *Inorg. Chem.*, **14**, 815 (1975).

8) Y. Yamamoto, H. Kudo, and E. Toyota, *Bull. Chem. Soc. Jpn.*, **56**, 1051 (1983).

9) G. R. Brubaker and D. P. Schaefer, *Inorg. Chem.*, **10**, 968 (1971).

Kinetics and Mechanism of Reduction of Metmyoglobins by Dithionite. Role of the Heme Propionates

Keiichi TSUKAHARA* and Kazuyo ISHIDA
Department of Chemistry, Faculty of Science, Nara Women's University, Nara 630
(Received March 25, 1991)

The kinetics of the reduction by dithionite ions of metmyoglobins reconstituted with porphinatoiron(III) complexes containing the protoporphyrin IX dimethyl ester, the deuteroporphyrin IX dimethyl ester, and octaethylporphyrin were studied at 25 °C and pH 6.3—9.2 in aqueous solution. Esterification of the heme propionate groups accelerated the reduction rate by $SO_2^{\cdot-}$, as well as the case of octaethylporphyrin (which does not contain the propionate groups); it also affected the redox potential of metmyoglobin, but much less so the rate of the self-exchange reaction. The reaction mechanisms are discussed.

Myoglobin is an oxygen-storage heme protein found in the muscles of vertebrates. Although oxymyoglobin is quite stable under physiological conditions, it undergoes slow autoxidation to form iron(III) metmyoglobin (metMb), which is inactive to molecular oxygen. The reduction of metMb to deoxymyoglobin (deoxyMb) is therefore an important reaction used for recovering deoxyMb. The reduction kinetics of metMb have been extensively studied using both inorganic and organic reducing agents.[1] The modification of the heme environment is a useful technique for elucidating the mechanism of the electron-transfer reactions of hemoproteins. We have reported that modifying the heme distal histidine, heme propionates, and peripheral substituents of the heme affects the reduction rate of metMb and that the geometry change at the iron site upon reduction of metMb(H_2O) to deoxyMb is an especially important factor.[1,2]

The native metMb has protoporphinatoiron(III) ($Fe^{III}PP$) as a prosthetic group. The heme propionates in sperm whale metMb make a salt bridge with Arg 45 and a hydrogen bond to His 97, thereby stabilizing the structure of the heme pocket.[3] We previously suggested that the salt bridge as well as the hydrogen bond between these residues and the heme propionates are important regarding the reactivity differences in the redox reactions of sperm whale and horse heart metmyoglobins, the latter having a Lys residue in place of Arg 45 in the former.[4]

Dithionite ions are widely used as a reducing agent for the reductions of not only metal complexes, but also biological redox systems;[5] the reactive species is a $SO_2^{\cdot-}$ radical anion which is produced by a dissociation of the $S_2O_4^{2-}$ ion. In this work we report on a dithionite reduction of the reconstituted metmyoglobins with three artificial hemes containing methyl esters of propionate groups, or without propionic acid chains, which cannot make the salt bridge with Arg 45 and/or the hydrogen bond to His 97; it is therefore expected to clarify the role of the heme propionates on the reduction of metmyoglobin.

Experimental

Materials. Sperm whale skeletal muscle metmyoglobin (type II, Sigma) was purified as previously described.[4] The recombination of chloro(porphinato)iron(III) complexes containing protoporphyrin IX dimethyl ester (PPDME), deuteroporphyrin IX dimethyl ester (DPDME), and octaethylporphyrin (OEP) with apomyoglobin, as well as the purification, were carried out by a method which has already been published.[6,7] The purity of the reconstituted metmyoglobins was checked spectrophotometrically. Sodium dithionite (Fluka AG) was used without further purification. The concentration was determined spectrophotometrically by reactions with

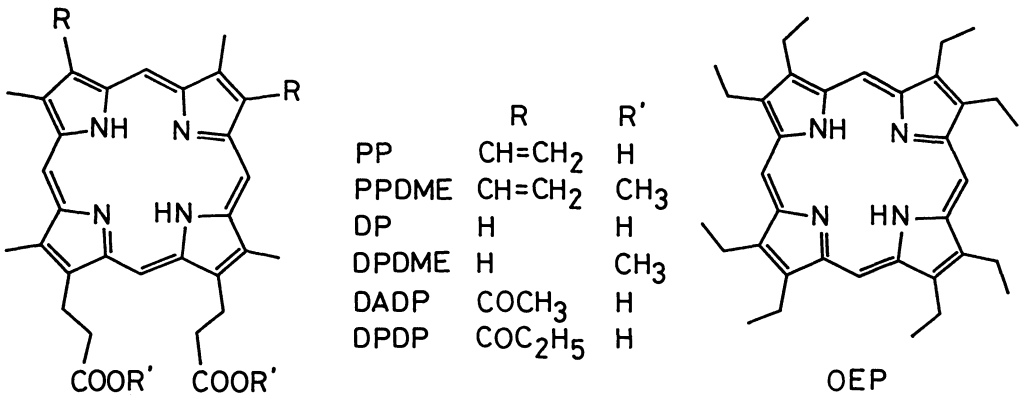

Fig. 1. Structures of porphyrins.

the hexacyanoferrate(III) ion (ε_{418}=1.01×10³ $M^{-1}cm^{-1}$; 1 M= 1 mol dm^{-3}).[8] Hexaammineruthenium(III) chloride ([Ru(NH_3)$_6$]Cl_3) was purchased from Aldrich Chemical Co. and purified by a method described in the literature.[9] The corresponding ruthenium(II) ion was prepared in situ by dithionite reduction. All other chemicals used were of guaranteed grade. All of the solutions used for measurements were prepared by using redistilled water.

Kinetic Measurements. All of the reactions were carried out in argon-saturated solutions at 25 °C. The solutions of the dithionite ion ((0.43—3.50)×10⁻³ M) and metmyoglobins ((2.0—4.0)×10⁻⁶ M) in a 0.1 M MES (2-morpholinoethanesulfonic acid) or a 0.1 M phosphate buffer at pH 6.3—9.2 and the ionic strength (I) of 0.1 M or 0.2 M (adjusted with NaCl) were mixed in Photal RA-401 stopped-flow and RA-415 rapid-scanning spectrophotometers. The reactions were followed by the decrease in absorbance at 407 nm (PPDMEmetMb(H_2O)), 393 nm (DPDMEmetMb(H_2O)), and 395 nm (OEPmetMb(H_2O)). The appearance of deoxyMb was also followed at 434 nm (PPDMEdeoxyMb), 422 nm (DPDMEdeoxyMb), and 420 nm (OEPdeoxyMb). The electron-transfer reaction between PPDMEmetMb(H_2O) and native deoxyMb produced by a dithionite ion was carried out at 25 °C, pH 6.3 (a 0.1 M MES buffer), and I=0.1 M. The reaction was followed at both 502 and 550 nm by the use of a Shimadzu UV-200S spectrophotometer. The concentrations of PPDMEmetMb(H_2O) and native deoxyMb were 3.00×10⁻⁵ M and (1.70—4.20)×10⁻⁴ M, respectively.

Equilibrium Measurements. The acid-dissociation constant for the heme-linked water molecule of DPDMEmetMb(H_2O) (1.00×10⁻⁵ M) was determined spectrophotometrically (380—395 nm) at 25 °C and I=0.1 M (a phosphate buffer). The redox potential of PPDMEmetMb(H_2O) was determined spectrophotometrically by using the [Ru(NH_3)$_6$]$^{2+}$ ion as a redox partner. Redox titration was carried out in an argon atmosphere at 25 °C, pH 6.3 (a 0.1 M MES buffer), I=0.1 M, [metMb]=4.40×10⁻⁵ M, [Ru(II)]=0—1.98×10⁻⁴ M, and [Ru(III)]=3.50×10⁻⁴ M. The spectral change was monitored in the 450—700 nm region by using a Shimadzu UV-200S spectrophotometer. The molar absorption coefficients used in this work were as follows: ε_{505}=8.80×10³ $M^{-1}cm^{-1}$ and ε_{555}=4.30×10³ $M^{-1}cm^{-1}$ for PPDMEmetMb(H_2O); ε_{505}= 6.00×10³ $M^{-1}cm^{-1}$ and ε_{555}=1.30×10⁴ $M^{-1}cm^{-1}$ for PPDMEdeoxyMb.

The pH's of the solutions were measured on a Hitachi-Horiba F-14RS pH meter.

Results and Discussion

Redox Potential of PPDMEmetMb(H_2O). The redox potential of PPDMEmetMb(H_2O) was determined spectrophotometrically in combination with the [Ru(NH_3)$_6$]$^{3+/2+}$ redox couple by a previously described method.[2] The [Ru(NH_3)$_6$]$^{2+}$ ion was prepared by a dithionite reduction of the [Ru(NH_3)$_6$]$^{3+}$ ion, since the Zn(Hg) reduction[2] of Ru(III) induced the denaturation of PPDMEmetMb(H_2O) in contrast to reconstituted metmyoglobins with hemins containing propionic acids. Four isosbestic points were observed in the 450—700 nm region during titration (Fig. 2). The equilibrium constant for the reaction

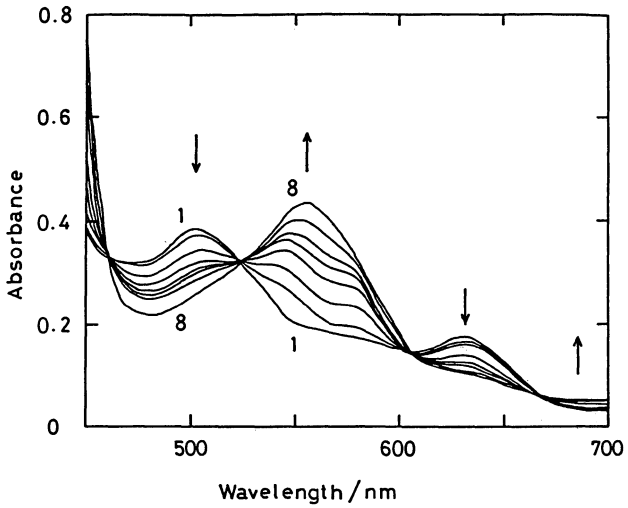

Fig. 2. Redox titration of PPDMEmetMb(H_2O) (4.40×10⁻⁵ M) in the presence of [Ru(NH_3)$_6$]$^{3+}$ ions (3.50×10⁻⁴ M) with various amounts of [Ru(NH_3)$_6$]$^{2+}$ ions at 25 °C, pH 6.3 (0.1 M MES buffer), and I=0.1 M. (1) 0, (2) 2.0×10⁻⁵, (3) 4.0×10⁻⁵, (4) 6.0×10⁻⁵, (5) 8.0×10⁻⁵, (6) 1.19×10⁻⁴, (7) 1.79×10⁻⁴, and (8) 1.98×10⁻⁴ M.

$$\text{PPDMEmetMb}(H_2O) + [Ru(NH_3)_6]^{2+} \rightleftarrows \text{PPDMEdeoxyMb} + [Ru(NH_3)_6]^{3+} \quad (1)$$

was determined from the slope of plots of [deoxyMb]/[metMb] against [Ru(II)]/[Ru(III)]. When the value of 0.05 V was used for the redox potential of the [Ru(NH_3)$_6$]$^{3+/2+}$ couple,[10] a value of 0.090±0.010 V was obtained for the redox potential of PPDMEmetMb(H_2O). The redox potential of PPDMEmetMb(H_2O) is higher than that of the native metMb(H_2O) by about 30 mV (E^0=0.059 V for the latter[11]). The shift of the E^0 value by esterification of the heme propionate groups is similar to that for cytochrome b_5.[12] The pK_a for the acid dissociation of the coordinated water molecule of PPDMEmetMb(H_2O) is 8.0, being smaller than that for native metMb(H_2O) (pK_a=9.16[1]). These results strongly suggest that the electron density of the Fe(III) center decreases upon esterification of the heme propionate groups.

Reduction of Reconstituted Metmyoglobins by Dithionite. Rapid scanning difference absorption spectra taken during the reduction of PPDMEmetMb(H_2O) by dithionite ions are shown in Fig. 3. Three isosbestic points were observed in the 380—540 nm region for each system. The plots of $-\ln(A_\infty - A_t)$ vs. time were linear for at least 90% completion of both the decay of metMb and the formation of deoxyMb, where A_∞ and A_t represent the absorbance at infinity and time t, respectively. The observed first-order rate constants (k_{obsd}) obtained from the slopes of the straight lines showed a half-order dependence on the initial concentrations of the dithionite ion ([$S_2O_4^{2-}$]$_0$), as is shown in Fig. 4. Therefore, the rate law for the dithionite reduction is given by

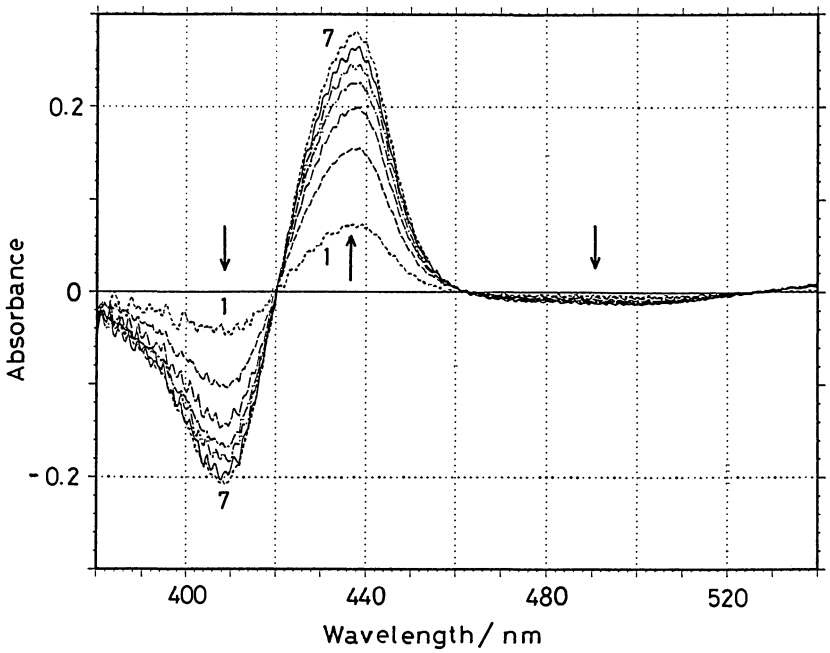

Fig. 3. Rapid-scanning spectra for the reduction of PPDME-metMb(H_2O) (3.9×10^{-6} M) by dithionite ions (1.10×10^{-3} M) at 25 °C and pH 6.7 (0.1 M phosphate buffer). (1) 18 ms, (2) 22 ms, (3) 26 ms, (4) 30 ms, (5) 34 ms, (6) 38 ms, and (7) 46 ms. The times given are for the start of scan at 380 nm.

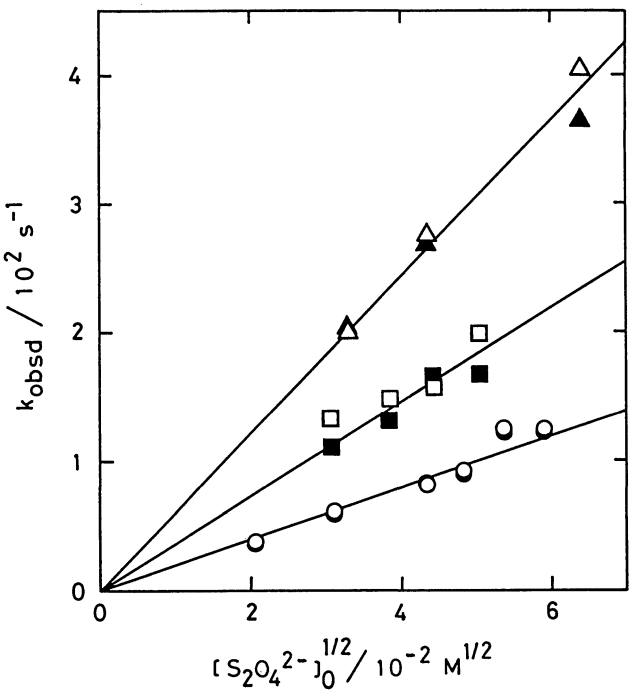

Fig. 4. Plots of k_{obsd} vs. $[S_2O_4^{2-}]_0^{1/2}$ for the dithionite reductions of reconstituted metmyoglobins at 25 °C, pH 6.3 (0.1 M MES buffer), and I=0.1 M. ○: PPDMEmetMb(H_2O) at 407 nm, ●: PPDME-metMb(H_2O) at 434 nm, □: DPDMEmetMb(H_2O) at 393 nm, ■: DPDMEmetMb(H_2O) at 422 nm, △: OEPmetMb(H_2O) at 395 nm, and ▲: OEP-metMb(H_2O) at 420 nm.

$$-d[Fe(III)]/dt = kK_D^{1/2}[S_2O_4^{2-}]_0^{1/2}[Fe(III)], \quad (2)$$

where K_D is the dissociation constant for the dithionite ion (K_D=1.4×10^{-9} M at 25 °C).[5a]

$$S_2O_4^{2-} \overset{K_D}{\rightleftarrows} 2SO_2^{\cdot-} \quad (3)$$

The second-order rate constant (k) obtained from the slopes of the straight lines in Fig. 4 decreased with an increase in pH (Fig. 5). The reduction of metMb can be accommodated by the following scheme:

$$metMb(H_2O) \overset{K_a}{\rightleftarrows} metMb(OH) + H^+ \quad (4)$$

$$metMb(H_2O) + SO_2^{\cdot-} \xrightarrow{k_{H_2O}} deoxyMb + SO_2 \quad (5)$$

$$metMb(OH) + SO_2^{\cdot-} \xrightarrow{k_{OH}} deoxyMb + SO_2 \quad (6)$$

Since the intercept in Fig. 4 is near zero, reduction by the $S_2O_4^{2-}$ species is negligible in the present systems. According to Reactions 4—6, the second-order rate constant (k) is represented as

$$k = \frac{k_{OH}K_a + k_{H_2O}[H^+]}{K_a + [H^+]}. \quad (7)$$

The k_{OH} path is at least 10-times slower than the k_{H_2O} path (k_{H_2O}=6.5×10^7 $M^{-1}s^{-1}$ and $k_{OH} \leqq 6.5\times10^6$ $M^{-1}s^{-1}$ for the PPDME system). This behavior is consistent with the results for the other dithionite reduction of metmyoglobins.[2,5] Since the electron density of the Fe(III) center increased upon the ligation of OH^-, more so than the water molecule, the rate of reduction by $SO_2^{\cdot-}$ is considered to decrease. The rate constants for Reaction 5 are listed in Table 1 along with the values of

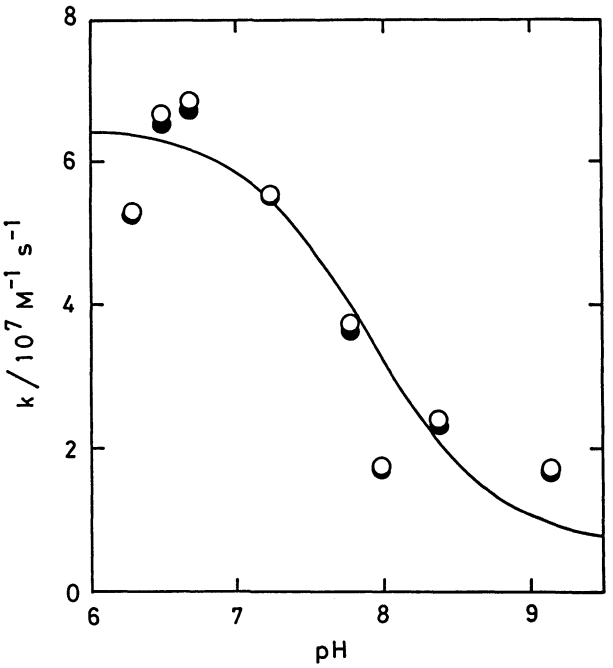

Fig. 5. pH Dependence of the second-order rate constants (k) for the reduction of PPDMEmetMb(H_2O) by $SO_2^{\cdot-}$ at 25 °C and I=0.2 M. The solid curve is on the basis of Eq. 7 by the use of pK_a=7.90, k_{H_2O}= 6.5×10^7 $M^{-1}s^{-1}$, and $k_{OH}=6.5\times10^6$ $M^{-1}s^{-1}$. ○: 407 nm and ●: 434 nm.

Table 1. Rate Constants of the Reduction of Metmyoglobins by $SO_2^{\cdot-}$ at 25 °C and I=0.1 M

metMb(H_2O)	k_{H_2O}/$M^{-1}s^{-1}$	pK_a
OEPmetMb(H_2O)	$(1.6\pm0.1)\times10^8$	7.83[a]
DPDMEmetMb(H_2O)	$(9.8\pm0.5)\times10^7$	8.0
PPDMEmetMb(H_2O)	$(6.5\pm0.5)\times10^7$	7.90[b]
PPmetMb(H_2O)	$(2.2\pm0.1)\times10^6$ [c]	9.16[d]
DPmetMb(H_2O)	$(1.5\pm0.1)\times10^6$ [c]	9.25[d]
DPDPmetMb(H_2O)	$(1.4\pm0.2)\times10^7$ [c]	7.87[d]
DADPmetMb(H_2O)	$(6.1\pm0.9)\times10^6$ [c]	7.80[b]

a) Ref. 7. b) Ref. 1. c) Refs. 2a and 5. d) Ref. 4.

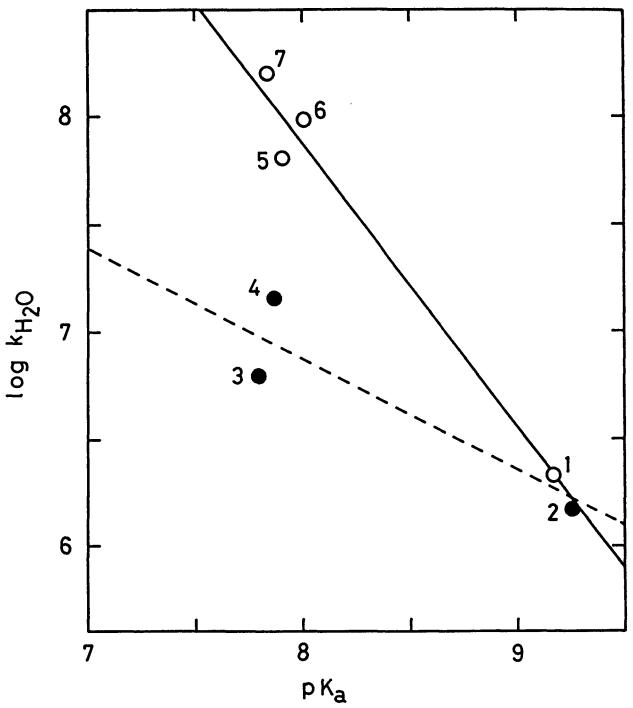

Fig. 6. Plots of log k_{H_2O} vs. pK_a of metMb(H_2O) for the reduction of metmyoglobins by $SO_2^{\cdot-}$. (1) native PPmetMb(H_2O), (2) DPmetMb(H_2O), (3) DADPmetMb(H_2O), (4) DPDPmetMb(H_2O), (5) PPDMEmetMb(H_2O), (6) DPDMEmetMb(H_2O), and (7) OEPmetMb(H_2O).

Table 2. Rate Constants of the Electron-Transfer Reaction between PPDMEmetMb(H_2O) (3.00×10^{-5} M) and Native deoxyMb at 25 °C, pH 6.3, and I=0.1 M

$[deoxyMb]_0$	k_{obsd}	k
10^{-4} M	$10^{-4}s^{-1}$	$M^{-1}s^{-1}$
1.69	1.05	0.62
2.48	1.07	0.43
3.07	1.38	0.45
3.43	1.76	0.51
4.14	1.50	0.36

pK_a regarding the dissociation of the coordinated water molecule at the heme iron site of metMb(H_2O). Plots of log k_{H_2O} vs. pK_a of metMb(H_2O) are shown in Fig. 6. The values of log k_{H_2O} increase with a decrease in the pK_a values of metMb(H_2O). Since the decrease in pK_a corresponds to that in the electron density at the Fe(III) center, the electron of $SO_2^{\cdot-}$ may be easily transferred to the Fe(III) center. The slopes of the plots of log k_{H_2O} vs. pK_a for both the dimethyl esters and OEP are quite different from those of systems containing propionic acid side chains (−1.32 for the former and −0.51 for the latter). Although the redox potential of PPDMEmetMb(H_2O) is lower than that of either DADPmetMb(H_2O) or DPDPmetMb(H_2O), the reduction of the former by $SO_2^{\cdot-}$ is faster than that for the latter. It is known that the heme environmental structures of the DP-, DADP-, and DPDP-metmyoglobins are similar to that of the native metMb(H_2O).[1] Therefore, the acceleration in the reduction of the dimethyl esters cannot be explained by only electronic effects. A steric alteration in the heme environment due to esterification must be concerned. Esterification of the heme propionate groups breaks the salt bridge between Arg 45 and the heme propionic acids and the hydrogen bond with His 97. The heme pocket is thereafter expected to expand, allowing the $SO_2^{\cdot-}$ ion to easily attack the heme iron center and/or the heme edge. Neya et al.[7] have demonstrated by an NMR study of OEP-myoglobin that OEP iron(III) serves as a prosthetic group for myoglobin with normal function, despite the structural difference from native myoglobin, especially at the heme distal side.

Estimation of Self-Exchange Rate Constant for PPDMEmetMb(H_2O)/deoxyMb System. To estimate the self-exchange rate constants for the PPDME-

Table 3. Rate Constants of the Electron-Transfer Reaction between Myoglobins at 25 °C

System	k/M^{-1} s^{-1}	E^0 (metMb)/V
S.W.metMb(H_2O)+H.H.deoxyMb[a]	1.0±0.2[b]	0.059±0.002[c]
DADPmetMb(H_2O)+native deoxyMb	0.94±0.13[d,e]	0.16±0.01[d]
PPDMEmetMb(H_2O)+native deoxyMb	0.50±0.12	0.09±0.01

a) S.W.=sperm whale and H.H.=horse heart. b) Ref. 13. c) Ref. 11. d) Ref. 2a. e) Ref. 14.

metMb(H_2O)/deoxyMb system, the reaction of PPDMEmetMb(H_2O) with native deoxyMb was examined at 25 °C, pH 6.3, and I=0.1 M. The differences in the molar absorption coefficients between metMb(H_2O) and deoxyMb are 3.1×10^3 M^{-1} cm^{-1} at 502 nm and -6.7×10^3 M^{-1} cm^{-1} at 505 nm for PPDME-myoglobins and 5.0×10^3 M^{-1} cm^{-1} at 502 nm and -9.3×10^3 M^{-1} cm^{-1} at 550 nm for native myoglobins, respectively. An increase in the absorbance at 502 nm and a decrease in the absorbance at 550 nm were observed during reactions under the condition [native deoxyMb]$_0$> [PPDMEmetMb(H_2O)]$_0$. Therefore, the following reaction occurs:

$$\text{PPDMEmetMb}(H_2O) + \text{native deoxyMb} \rightarrow \text{PPDMEdeoxyMb} + \text{native metMb}(H_2O). \quad (8)$$

This is also expected from the redox potentials for these myoglobins (0.090 V for PPDMEmetMb(H_2O) and 0.059 V for native metMb(H_2O)). The rate constants of Reaction 8 are given in Table 2. The rate constants of the electron-transfer reactions between myoglobins are about 1 M^{-1} s^{-1}, as is given in Table 3. This value is similar to the self-exchange rate constant estimated from the Marcus theory for the electron-transfer reactions of myoglobins containing heme propionic acids with inorganic and organic redox reagents.[2,13] The slowness of the self-exchange reaction of these myoglobins may be ascribable to a geometry change at the heme iron site from hexacoordinated metMb(H_2O) to pentacoordinated deoxyMb, where the release of the water molecule must occur upon reduction.[2] Contrary to the dithionite reduction of metmyoglobins, the electron-transfer reaction between PPDMEmetMb(H_2O) and native deoxyMb was not accelerated. This is probably due to a reaction between large molecules in the latter system.

We are grateful to Itoh Science Foundation for financially supporting this work. This research was partially supported by a Grant-in-Aid for Scientific Research No. 03453049 from the Ministry of Education, Science and Culture.

References

1) K. Tsukahara, T. Okazawa, H. Takahashi, and Y. Yamamoto, *Inorg. Chem.*, **25**, 4756 (1986), and references therein.

2) a) K. Tsukahara, *J. Am. Chem. Soc.*, **111**, 2040 (1989); b) K. Tsukahara, *Chem. Lett.*, **1987**, 1291; c) K. Tsukahara, *J. R. Neth. Chem. Soc.*, **106**, 291 (1987).

3) a) J. C. Kendrew, R. E. Dickerson, B. E. Strandberg, R. G. Hart, D. R. Davies, D. C. Phillips, and V. C. Shore, *Nature*, **185**, 422 (1960); b) T. Takano, *J. Mol. Biol.*, **110**, 537 (1977).

4) a) K. Tsukahara and Y. Yamamoto, *J. Biochem.*, **93**, 15 (1983); b) K. Tsukahara, *Inorg. Chim. Acta*, **124**, 199 (1986).

5) a) D. O. Lambeth and G. Palmer, *J. Biol. Chem.*, **248**, 6095 (1973); b) R. P. Cox and M. R. Hollaway, *Eur. J. Biochem.*, **74**, 575 (1977); c) E. Olivas, D. J. A. de Waal, and R. G. Wilkins, *J. Biol. Chem.*, **252**, 4038 (1977).

6) M. Tamura, T. Asakura, and T. Yonetani, *Biochim. Biophys. Acta*, **295**, 467 (1973).

7) S. Neya, N. Funasaki, and K. Imai, *J. Biol. Chem.*, **263**, 8810 (1988).

8) F. Aziz and G. A. Mirza, *Talanta*, **11**, 889 (1964).

9) T. J. Meyer and H. Taube, *Inorg. Chem.*, **7**, 2369 (1968).

10) H. S. Lim, D. J. Barclay, and F. C. Anson, *Inorg. Chem.*, **11**, 1460 (1972).

11) R. J. Crutchley, W. R. Ellis, Jr., and H. B. Gray, *J. Am. Chem. Soc.*, **107**, 5002 (1985).

12) L. S. Reid, M. R. Mauk, and A. G. Mauk, *J. Am. Chem. Soc.*, **106**, 2182 (1984).

13) Z. Bradic, K. Tsukahara, P. C. Wilkins, and R. G. Wilkins, "Frontiers in Bioinorganic Chemistry," ed by A. V. Xavier, VCH Publishers, Weinheim, Germany (1986), p. 336.

14) K. Tsukahara, The 1989 International Chemical Congress of Pacific Basin Societies, Honolulu, Hawaii, U. S. A., Book of Abstracts, INORG 146 (1989).

 © 1991 The Chemical Society of Japan Bull. Chem. Soc. Jpn., 64, 2383—2387 (1991)

Unique Condensation Reactions of Tropones with Bis(benzoylthio)trithiafulvene Leading to 10a*H*-Cyclohepta[*c*]-1,3-dithiolo[*e*][1,2]dithiin-2-thione

Katsuhiro SAITO,* Kazuaki ITO, Chizuko KABUTO,† and Kensuke TAKAHASHI
Department of Applied Chemistry, Nagoya Institute of Technology, Gokiso-cho, Showa-ku, Nagoya 466
†Department of Chemistry, Faculty of Science, Tohoku University, Aoba-ku, Aramaki, Sendai 980
(Received December 5, 1990)

Reactions of tropone derivatives with 4,5-bis(benzoylthio)-1,3-dithiole-2-thione (2,3,6-trithiafulvene derivative) afforded 1,3,5-cycloheptatriene derivatives doubly substituted by trithiafulvene and S–S groups (10a*H*-cyclohepta[*c*]-1,3-dithiolo[*e*][1,2]dithiin-2-thione). The structure of the 1,3,5-cycloheptatriene derivative and its crystal structure were investigated by single crystal X-ray analysis to show the existence of a unique three-dimensional network of the molecules through S···S contacts.

Not only from the viewpoint of pharmacological utilities, but also from chemical and physical interests in their reactivities and electronic natures, the chemistry of sulfur-containing heterocyclic compounds have attracted much attention from chemists.[1] A trithiafulvene derivative, 4,5-bis(benzoylthio)-1,3-dithiole-2-thione (**2**)[2] has been used to prepare donor components of several types of organic superconductors such as bis(ethylenedithio)tetrathiafulvalene (BEDT-TTF).[3] While many studies have been published on the reactivities of sulfur-containing heterocyclic compounds to show facile occurences of cleavages and recombinations of C–S and S–S bonds,[4] only a few have been researched the reaction of trithiafulvene derivatives. The trithiafulvene derivative (**2**) has two benzoylthio groups per molecule, forming a tetrathio-substituted ethylene moiety, which is expected to show characteristic reactivities.

Tropones are known to have dipolar components constructing 6π-electron aromatic structures.[5] Despite their aromaticities, tropones are fairly active in addition reactions. Tropones not only react easily with halogens or hydrogenes,[6] but they also behave as 4π- or 8π-electron units in [4+2]- or [8+2]-type cycloaddition reactions, respectively.[7] Although many types of addition reactions of tropones and olefins or heterocyclic compounds have been researched extensively, studies of reactions with sulfur-containing compounds seem to be relatively few in number. This is curious, considering that tropothione and 2-mercatotropone have been attracting the attention of chemists because of their unique and characteristic reactivities caused by the introduction of sulfur atoms.[8]

As part of our research on the addition reactions of troponoid compounds,[9] we have studied the reactions of **2** with various tropones (**1**) to obtain condensation products leaving benzoic anhydride. We present our results in this report.

Results and Discussion

A solution of **2** and an excess amount of tropone (**1a**) was allowed to react at room temperature for 3 d. Separation and purification of the reaction mixture with silica-gel chromatography gave a crystalline product **3a** in a 39% yield (Scheme 1).[10] The analogous reaction using 2-phenyltropone (**1b**) in benzene resulted in a quantitative recovery of the starting materials. At an elevated temperature of 60 °C for 3 d, however, **3b** was obtained in a 14% yield. The reactions with 2-(*p*-methoxyphenyl)- (**1c**) and 2-methyltropones (**1d**) at 60 °C gave **3c** (26% yield) and **3d** (26% yield), respectively.

The structures of the products were deduced on the basis of their spectral properties. The molecular ion peaks in the high-resolution MS spectra demonstrated

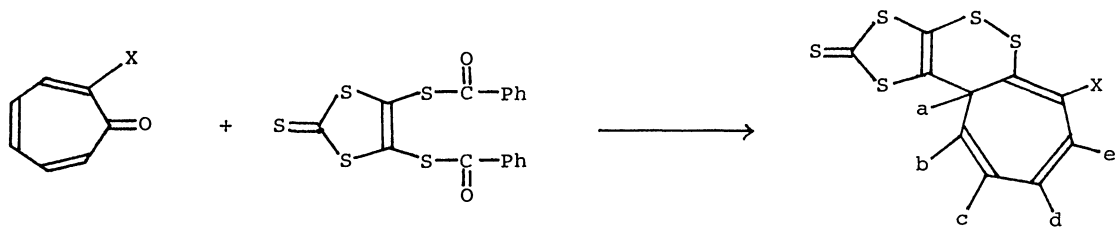

1
a: X=H,
b: X=Ph,
c: X=$C_4H_6OMe(p$-),
d: X=Me,
e: X=Cl,
f: X=CN

2

3a—d

Scheme 1.

that the products were derived from the condensation reactions of **1** and **2** followed by the elimination of benzoic anhydride. ^{1}H NMR spectra and ^{13}C NMR spectra indicated the existence of a 1,3,5-cycloheptatriene moiety with a continued array of ring protons H_a, H_b, H_c, H_d, and H_e in that order, with H_a as a methine proton. The position of the substituents were determined by the use of NOE measurements.[11] The existence of thioxo groups was clearly demonstrated by characteristic absorptions at ca. 1060 cm^{-1} in the IR spectra.[2,3]

Finally, the structure of **3a** was determined unambiguously by X-ray analysis, indicating the existence of a disulfide bond (Fig. 1). The bond lengths and angles obtained were all normal (Table 1). The analysis of molecular planarity indicated that the trithiafulvene moiety had a planar conformation and that the S(5) atom deviated by 0.109 Å from this plane, while the cycloheptatriene moiety had a boat conformation.

In the crystal structure, a noticeable amount of overlapping was observed between two parallel-stacked trithiafulvenes as shown in Fig. 2. The interplanar distance of these rings was 3.57 Å. A three-dimensional network was also formed by intermolecular S ···· S interactions as shown in Fig. 3. The network was formed by four molecular linkages, which consisted of two types of S ···· S contacts, S(1) ···· S(4)=3.43 Å and S(2) ···· S(5)=3.57 Å, both shorter than the Van der Waals contact of 3.7 Å.

The formation of **3** is hypothesized to proceed as follows. The reaction is thought to be initiated by a nucleophilic attack of the oxygen atom of **1** on the carbonyl carbon of the benzoyl group of **2** to form the

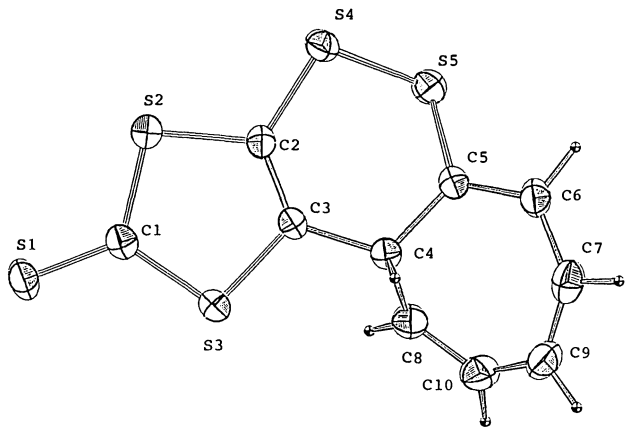

Fig. 1. ORTEP drawing of the crystal structure of **3a**.

Table 1. Fractional Atomic Coordinated (×10^4) and Equivalent Temperature Factors (Å^2). The Form of B_{eq} is $(4/3)\sum_{ij}\beta_{ij}(\boldsymbol{a}_i \cdot \boldsymbol{a}_j)$

Atom	x	y	z	B_{eq}
S1	5600(1)	−2567(1)	5584(1)	2.8
S2	4919(1)	−1568(1)	3273(1)	2.6
S3	3006(1)	−1288(1)	4568(1)	2.3
S4	3234(1)	−240(1)	1269(1)	2.4
S5	1943(1)	1569(1)	1266(1)	2.5
C1	4562(3)	−1862(4)	4535(2)	2.2
C2	3417(3)	−794(3)	2629(2)	2.0
C3	2511(3)	−671(3)	3225(2)	1.9
C4	1113(3)	−177(3)	2876(2)	1.9
C5	749(3)	616(3)	1788(2)	1.9
C6	−518(3)	693(4)	1267(3)	2.5
C7	−1591(3)	297(4)	1750(3)	2.8
C8	685(3)	917(4)	3661(3)	2.5
C9	−1633(3)	488(5)	2802(3)	3.1
C10	−587(4)	1109(5)	3637(3)	3.0

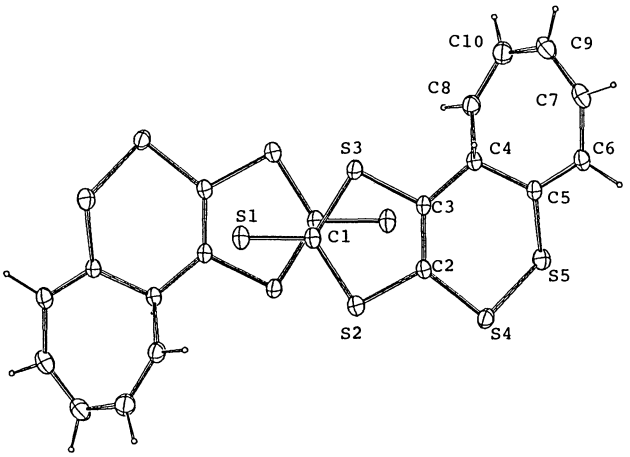

Fig. 2. The molecular overlap between two planar trithiafulvene moieties in molecules related by symmetry operations of x, y, z, and $1-x$, $-y$, $1-z$. The interplanar distance is 3.57 Å.

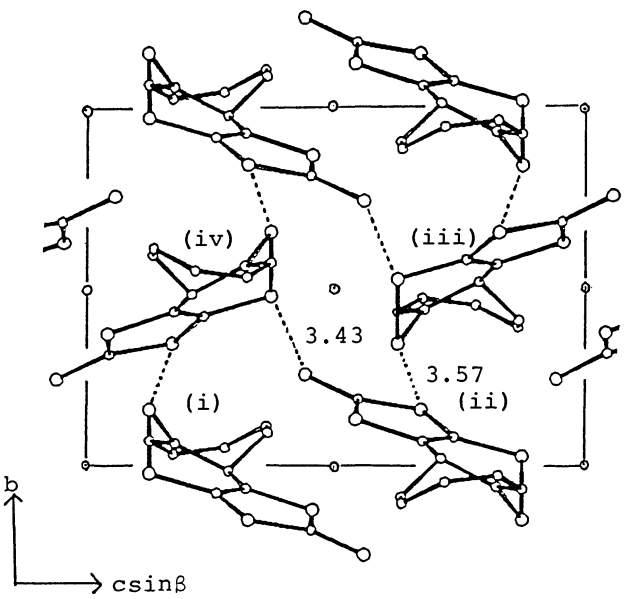

Fig. 3. The crystal structure viewed along the a axis. The network is formed by four molecular linkages of two types of S···S contacts. Symmetry operations of the molecules are (i)=x, y, z; (ii)=$1-x$, $-y$, $1-z$; (iii)=x, $1/2-y$, $1/2+z$; (iv)=$1+x$, $1/2+y$, $1/2-z$.

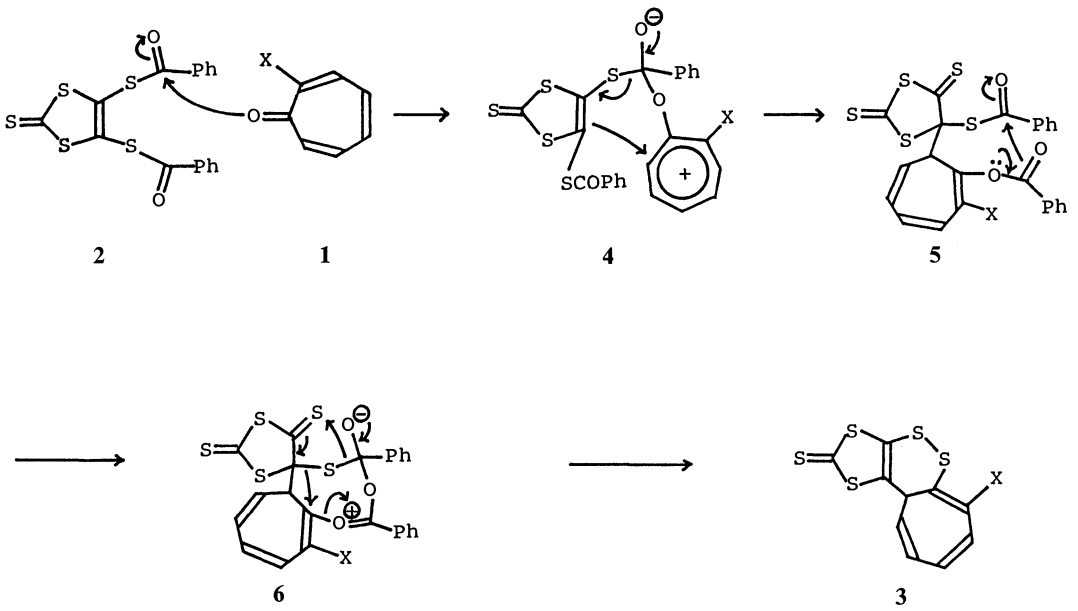

Scheme 2.

Table 2. Net Atomic Charges of Tropones (**1a**—**1f**)

X		Oxygen atom	Carbon atom of carbonyl group
H	(**1a**)	−0.3302	+0.2731
Ph	(**1b**)	−0.3234	+0.2833
C_6H_4OMe(-*p*)	(**1c**)	−0.3386	+0.2948
Me	(**1d**)	−0.3325	+0.2896
Cl	(**1e**)	−0.2981	+0.2744
CN	(**1f**)	−0.3093	+0.2811

tropylium cation intermediate **4** (Scheme 2). The following observation seems to support this hypothesis.[7] Analogous reactions using tropones bearing electron-withdrawing groups such as a chloro (**1e**) or cyano (**1f**) group failed to give products of type **3**, but resulted in quantitative recoveries of the starting materials.

The MO calculations obtained by the MNDO method showed the existence of a relatively large charge separation between the carbon and the oxygen atoms of the carbonyl groups of **1a**—**1d**, supporting an initial nucleophilic attack by the carbonyl oxygen in the reaction as described above. The failure of the reactions of tropones bearing electron-attracting substituents such as chloro (**1e**) or cyano (**1f**) groups is thought to be attributable to the small degree of negative charge at the carbonyl oxygen atoms of these tropones (Table 2).[12]

The subsequent cleavage of a C–S bond and a nucleophilic attack of a C=C double bond of the trithiafulvene part on the tropylium cation moiety gives intermediate **5**. The substitution of four sulfur atoms is thought to contribute to the promotion of the nucleophilicity of the C=C bond. An attack by the carbonyl oxygen on the carbon atom of another carbonyl group yields intermediate **6**. A C–S bond cleavage and the elimination of benzoic anhydride produces the final product **3**.

The important role of the tropylium cation moiety in the reaction pathway was shown by the following experiment. Reaction of tropone tosylhydrazone (**7**)[13] with **2** in benzene at room temperature for 3 d gave no product corresponding to **3**, but yielded tropone *N*-benzoyltosylhydrazone (**8**) in a 74% yield (Scheme 3).

The reaction is thought to proceed through a pathway analogous to that of **1** initiated by an attack of the amino group of **7** on the carbonyl group of **2** to form an intermediate (**9**), which then undergoes a C–S bond cleavage.[14]

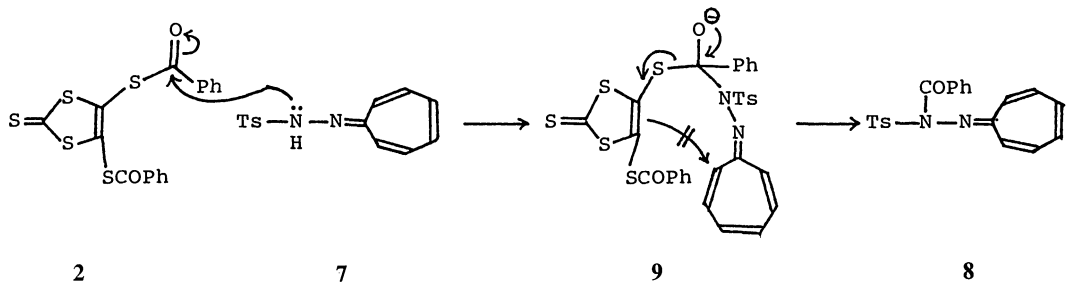

Scheme 3.

Experimental

Melting points were recorded on a Yanagimoto Micro Melting Point Apparatus and were uncorrected. The NMR spectra were measured with Hitachi R20B or Varian XL-200 spectrometers. IR, UV, and MS spectra were measured with JASCO FT/IR-5300, Hitachi 220A, and Hitachi M-2000S spectrometers, respectively. Wakogel C-200 and Wakogel B5-F were used for column and thin-layer chromatography, respectively.

Reaction of Tropone (1a) and 2. A mixture of **1a** (2.00 g, 20 mmol) and **2** (410 mg, 1 mmol) was stirred at room temperature for 3 d. Separation of the reaction mixture by column chromatography on silica gel gave crystals of **3a** (110 mg, 39% yield, with hexane), recovery of **2** (80 mg, with hexane–ethyl acetate 9 : 1), benzoic acid (78 mg, 32% yield, with hexane–ethyl acetate 4 : 1), and recovery of **1a** (1.67 g, with hexane–ethyl acetate 3 : 1). Recrystallization from benzene gave yellow plates of **3a**: Mp 147—149 °C. Found: C, 41.78; H, 2.00; S, 56.06%. Calcd for $C_{10}H_6S_5$: C, 41.93; H, 2.11; S, 55.96%. MS m/z (rel intensity) 286 (M^+, 46), 253 (41), 210 (46), 177 (82), and 146 (100). IR (KBr) 3030, 1360, 1050, 1030, 790, and 710 cm^{-1}. ^1H NMR ($CDCl_3$) δ=2.72 (dd, H_a), 5.43 (dd, H_b), 6.45 (m, H_c), and 6.62—6.84 (m, 3H, $H_{d,e,f}$). Coupling constants in Hz: J_{ab}=6.0, J_{ac}=1.0, J_{bc}=9.2, and J_{cd}=4.8. ^{13}C NMR ($CDCl_3$) δ=42.4, 122.7, 123.8, 126.7, 127.1, 130.2, and 131.7.

Reaction of 2-Phenyltropone (1b) and 2. A solution of **1b** (960 mg, 6 mmol) and **2** (410 mg, 1 mmol) in benzene (5 ml) was heated at 60 °C for 4 d. The reaction mixture was separated by column chromatography on silica gel to give crystals of **3b** (34 mg, 14% yield, with hexane–ethyl acetate 49 : 1), recovery of **2** (130 mg, with hexane–ethyl acetate 11 : 1), benzoic acid (60 mg, 25% yield, with hexane–ethyl acetate 11 : 1), and recovery of **1b** (830 mg, by hexane–ethyl acetate 9 : 1). Recrystallization from benzene gave yellow plates of **3b**: Mp 144—145 °C. High-resolution MS Found: m/z 361.9382. Calcd for $C_{16}H_{10}S_5$: m/z 361.9385. MS m/z (rel intensity) 362 (M^+, 14), 197 (50), and 165 (100). IR (KBr) 3030, 1480, 1070, 760, and 700 cm^{-1}. ^1H NMR ($CDCl_3$) δ=3.38 (d, H_a), 5.47 (dd, H_b), 6.38 (dd, H_c), 6.81 (d, H_e), 6.90 (dd, H_d), and 7.26—7.52 (m, 5H, Ph). Coupling constants in Hz: J_{ab}=6.0, J_{bc}=8.0, J_{cd}=4.8, and J_{de}=10.4. ^{13}C NMR ($CDCl_3$) δ=48.0, 123.4, 123.9, 125.7, 128.6, 129.7, 132.2, 134.0, 135.3, and 137.7.

Reaction of 2-(*p*-Methoxyphenyl)tropone (1c) with 2. A solution of **1c** (760 mg, 4 mmol) and **2** (410 mg, 1 mmol) in benzene (5 ml) was reacted at 60 °C for 5 d. The reaction mixture was separated by column chromatography on silica gel to give recovery of **2** (200 mg, with hexane–ethyl acetate 1 : 9), recovery of **1c** (680 mg, with hexane–ethyl acetate 1 : 4), and **3c** as an oil (50 mg, 26% yield, with hexane–ethyl acetate 1 : 9).

3c: High-resolution MS Found: m/z 391.9501. Calcd for $C_{17}H_{12}OS_5$: m/z 391.9492. MS m/z (rel intensity) 392 (M^+, 40), 290 (14), and 239 (100). IR (oil) 3030, 1600, 1500, 1240, 1060, 760, and 700 cm^{-1}. ^1H NMR ($CDCl_3$) δ=3.34 (d, H_a), 3.88 (s, 3H, Me), 5.48 (dd, H_b), 6.38 (dd, H_c), 6.82 (d, H_e), 6.91 (dd, H_d), and 6.96—7.40 (AA'BB', 4H, benzene ring protons). Coupling constants in Hz: J_{ab}=4.5, J_{bc}=6.6, J_{cd}=3.9, and J_{de}=8.4. ^{13}C NMR ($CDCl_3$) δ=47.7, 55.2, 113.8, 114.1, 123.0, 123.3, 125.5, 129.9, 130.0, 131.0, 132.1, and 134.1.

Reaction of 2-Methyltropone (1d) with 2. A solution of **1d** (390 mg, 3 mmol) and **2** (410 mg, 1 mmol) in benzene (5 ml) was heated at 60 °C for 6 d. The reaction mixture was separated by column chromatography on silica gel to give **3d** as an oil (41 mg, 26% yield, with hexane), recovery of **2** (190 mg, with hexane–ethyl acetate 4 : 1), and recovery of **1d** (290 mg, with hexane–ethyl acetate 7 : 3).

3d: High-resolution MS Found: m/z 299.9217. Calcd for $C_{11}H_8S_5$: m/z 299.9229. MS m/z (rel intensity) 300 (M^+, 17), 205 (39), and 110 (100). IR (oil) 3020, 2950, 1050, 760, and 700 cm^{-1}. ^1H NMR ($CDCl_3$) δ=2.08 (s, 3H, Me), 3.30 (d, H_a), 5.41 (dd, H_b), 6.26 (dd, H_c), 6.73 (dd, H_d), and 6.87 (d, H_e). Coupling constants in Hz: J_{ab}=4.2, J_{bc}=6.8, J_{cd}=3.1, and J_{de}=8.3. ^{13}C NMR ($CDCl_3$) δ=29.7, 30.3, 123.2, 123.6, 125.4, 125.5, 130.9, and 135.5.

Reaction of Tropone Tosylhydrazone (7) with 2. A solution of **7** (280 mg, 1 mmol) and **2** (200 mg, 0.5 mmol) in benzene (5 ml) was stirred at room temperature for 4 d. The reaction mixture was separated by column chromatography on silica gel to give recovery of **2** (110 mg, with hexane–ethyl acetate 4 : 1) and an oil of a mixture of **7** and **8** (330 mg, with hexane–ethyl acetate 7 : 3). The mixture was subjected to preparative thin-layer chromatography on silica gel using chloroform–hexane 2 : 1 as a developing solvent to give **8** as an oil (63 mg, 74% yield, R_f=0.16).

8: High resolution MS Found: m/z 378.1045. Calcd for $C_{21}H_{18}N_2O_3S$: m/z 378.1039. MS m/z (rel intensity) 378 (M^+, 100), 278 (41), and 245 (38). IR (oil) 3030, 2980, 1670, 1530, 1350, 1250, and 1160 cm^{-1}. ^1H NMR ($CDCl_3$) δ=2.44 (s, 3H, Me), 6.60—7.00 (m, 6H, seven-membered ring protons), and 7.28—8.00 (m, 9H, benzene-ring protons). ^{13}C NMR ($CDCl_3$) δ=21.6, 127.7, 128.5, 128.9, 129.2, 129.6, 131.8, 133.0, 134.1, 134.9, 135.0, 135.1, 135.6, 136.6, 144.7, and 173.8.

Single Crystal X-Ray Analysis of 3a. The colorless crystals of $C_{10}H_6S_5$ belonged to the monoclinic space group $P2_1/c$. The cell constants were a=10.536(2), b=8.603(1), c=12.624(5) Å, β=102.62(2)°, and V=1116.6(6) Å^3. The unit cell contained four molecules giving a calculated density of 1.70 g cm^{-3}. A total of 4799 reflections within 2θ=65° were collected on a Rigaku-AFC-5PR defractometer with a rotating anode (200 mA, 45 kV) using graphite monochromated Mo-$K\alpha$ radiation (λ=0.71069 Å) with 2θ–ω mode. The structure was solved by the direct method and refined by the block-diagonal least-squares method anisotropically for non-hydrogen atoms and isotropically for hydrogen atoms which were located by a D-Fourier map. The final R-factor was 0.069 (R_w=0.054) for 4177 unique reflections with $F_o<3\sigma(F_o)$. All calculations were carried out on an ACOS2000 computer at Tohoku University using the applied library program UNICSIII.[15] A listing of positional and thermal parameters, bond lengths and angles, and structure factors are deposited as Document No. 8948 at the Office of the Editor of Bull. Chem. Soc. Jpn.

References

1) R. Gompper and R. Guggenberger, *Tetrahedron Lett.*, **27**, 159 (1986); R. R. Schumaker, S. Rajewari, M. V. Joshi, M. P. Cava, M. A. Takassi, and R. M. Metzger, *J. Am. Chem. Soc.*, **111**, 308 (1989); T. Tsuchiya, M. Yasumoto, I. Shibuya, Y. Taguchi, K. Yonemoto, and M. Goto, *Chem. Lett.*, **1990**, 1423; Y. Tominaga, H. Norisue, C. Kamio, T. Masunami, Y. Miyashiro, and A. Hosomi, *Heterocycles*, **31**, 1 (1990).

2) G. Steimecke, H.-J. Sieler, R. Kirmse, and E. Hoyer,

Phosphorus Sulfur, 7, 49 (1979).

3) a) K. S. Varma, A. Bury, N. J. Harris, and A. E. Underhill, *Synthesis,* **1987**, 837; M. Sorm, S. Nespurek, O. Ryba, and V. Kubanek, *J. Chem. Soc., Chem. Commun.,* **1987**, 696; K. S. Varma, J. Evans, S. Edge, A. E. Underhill, G. Bojesen, and J. Becher, *ibid.,* **1989**, 257. b) M. Narita and C. U. Pittman, Jr., *Synthesis,* **1976**, 489; K. Nakasuji, M. Nakatsuka, and I. Murata, *Yuki Gosei Kagaku Kyokaishi,* **41**, 204 (1983).

4) B. R. O'Connor and N. F. Jones, *J. Org. Chem.,* **35**, 2002 (1970); R. Okazaki, F. Ishii, K. Sunagawa, and N. Inamoto, *Chem. Lett.,* **1978**, 51; F. L. Lu, M. Keshavarz-K., G. Srdanov, R. H. Jacobson, and F. Wudl, *J. Org. Chem.,* **54**, 2165 (1989).

5) A. DiGicomo and C. P. Smyth, *J. Am. Chem. Soc.,* **74**, 4411 (1952); Y. Kurita, S. Seto, T. Nozoe, and M. Kubo, *Bull. Chem. Soc. Jpn.,* **26**, 272 (1953); M. Ogasawara, T. Iijima, and M. Kimura, *Bull. Chem. Soc. Jpn.,* **45**, 3277 (1972); M. J. Barrow, O. S. Mills, and G. Filippini, *J. Chem. Soc., Chem. Commun.,* **1973**, 66; L. Lombardo and D. Wege, *Tetrahedron Lett.,* **1975**, 115.

6) T. Nozoe, T. Mukai, and T. Takase, *Sci. Repts., Tohoku Univ., I,* **39**, 164 (1956); T. Mukai, *Bull. Chem. Soc. Jpn.,* **31**, 846 (1958); C. A. Cupas, W. E. Heyd, and M.-S. Kong, *J. Am. Chem. Soc.,* **93**, 4623 (1971).

7) C. Jutz, I. Rommel, I. Lengyel, and J. Feeney, *Tetrahedron,* **22**, 1809 (1966); J. Ciabattoni and H. W. Anderson, *Tetrahedron Lett.,* **1967**, 3377; L. A. Paquette and N. Horton, *ibid.,* **1968**, 2289; G. R. Tian, S. Sugiyama, A. Mori, and H. Takeshita, *Bull. Chem. Soc. Jpn.,* **61**, 2393 (1988); R. P. Gandhi and M. P. S. Ishar, *Chem. Lett.,* **1989**, 101.

8) T. Machiguchi, T. Hoshi, J. Yoshino, and Y. Kitahara, *Tetrahedron Lett.,* **1973**, 3873; H. A. Dugger and A. S. Dreiding, *Helv. Chim. Acta,* **59**, 747 (1976); T. Machiguchi, T. Hasegawa, H. Otani, and Y. Ishii, *J. Chem. Soc., Chem. Commun.,* **1987**, 1375; T. Machiguchi, T. Hasegawa, and S. Itoh, *J. Am. Chem. Soc.,* **111**, 1920 (1989); T. Machiguchi and S. Yamabe, *Chem. Lett.,* **1990**, 1511.

9) K. Saito, H. Kojima, T. Okudaira, and K. Takahashi, *Bull. Chem. Soc. Jpn.,* **56**, 175 (1983); K. Saito and H. Kojima, *ibid.,* **58**, 1918 (1985); K. Saito, *J. Organomet. Chem.,* **338**, 265 (1988); K. Saito, T. Watanabe, and K. Takahashi, *Chem. Lett.,* **1989**, 2099; K. Ito, Y. Noro, K. Saito, and K. Takahashi, *Bull. Chem. Soc. Jpn.,* **63**, 2573 (1990).

10) All the yields were calculated on the basis of the actually consumed starting materials.

11) Irradiations of the phenyl groups of **3b** and **3c** resulted in 10 and 6% enhancements of the signals of proton H_e, respectively, but the signals of H_a showed no change. This fact showed that the phenyl groups are located close to H_e but not to H_a, suggesting the product structures to be **3**, but not **10** (Fig. 4).

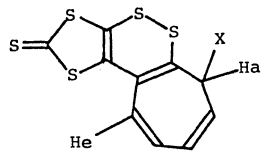

10

Fig. 4.

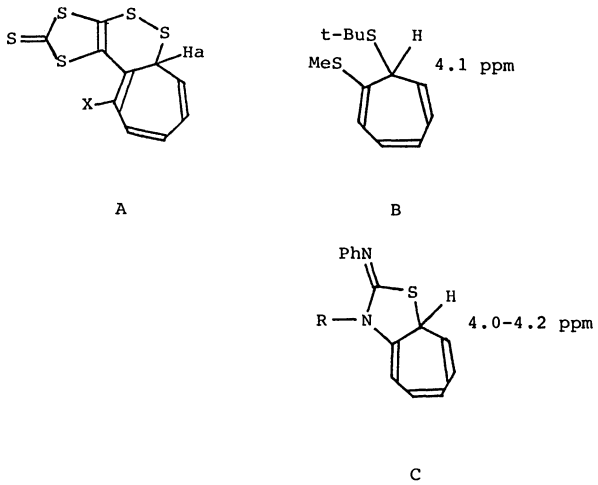

Fig. 5.

Other possible structures such as A (Fig. 5) can be rejected by the fact that the chemical shifts of H_a of A should be expected to be about δ=4.0—4.2 refering to the analogous compounds B or C in the literatures. The observed chemical shifts of H_a of **3** (δ=2.72—3.38) are obviously different from these values, supporting the structures of **3** shown in Scheme 1. Y. Yamamoto, S. Kajigaeshi, and S. Kanemasa, *Chem. Lett.,* **1977**, 85; M. Cawazza, G. Morganti, and F. Pietra, *J. Chem. Soc., Chem. Commun.,* **1978**, 945.

12) Molecular orbital calculations were carried out at the computer center of the Institute for Molecular Science using the MOPAC program (J. J. P. Stewart, *Q. C. P. E. Bull.,* **3**, 43 (1983)).

13) W. M. Jones and C. L. Ennis, *J. Am. Chem. Soc.,* **89**, 3069 (1967).

14) The subsequent nucleophilic attack by the double bond on the seven-membered ring, which was observed in intermediate **4**, did not occur. This discrepancy in the results can be explained by the difference between the reactivities of the tropilium cation moiety in **4** and the iminotropone moiety in **9** toward nucleophiles.

15) T. Sakurai and K. Kobayashi, *Sci. Rep. Inst. Phys. and Chem. (Jpn.),* **55**, 69 (1979).

The Cycloaddition of *N*,α-Diarylnitrones and Substituted *p*-Benzoquinones

Shinsaku SHIRAISHI,* Yukihiko INOUE, and Kiyoshi IMAMURA
The Institute of Industrial Science, The University of Tokyo, Roppongi 7-22-1, Minatoku, Tokyo 106
(Received February 26, 1991)

N,α-Diarylnitrones reacted with 2,5- or 2,6-dialkyl-*p*-benzoquinones at their C=C bond regioselectively to give fused isoxazolidine cycloadducts. These cycloadducts were proved to undergo retrocycloaddition. *p*-Benzoquinones having electron-withdrawing substituents did not give any cycloadduct.

p-Benzoquinone derivatives play an important role in bioorganic redox reactions and the modification reactions of *p*-benzoquinones were paid much attention in the synthetic chemistry. 1,3-Dipolar cycloaddition reaction is known as a versatile synthetic reaction because of its regioselectivity and mild reaction conditions. 1,3-Dipolar cycloaddition reaction of *p*-benzoquinones was reported with many 1,3-dipoles; nitrile ylide,[1] phenyl azide,[2] diazoalkane[3] etc., but site selectivity or regioselectivity of the reactions is still uncertain. As dipolarophile, *p*-Benzoquinones have two kinds of potential reactive sites, i.e. C=C and C=O bonds, and were considered to be good probe compounds for such investigation. In the previous papers,[4] cycloaddition reactions of substituted *p*-benzoquinones with aromatic nitrile *N*-oxides were reported and discussed.

Nitrones compose a class of typical 1,3-dipoles and their cycloaddition reactions have been widely investigated. However, very few reports on the reactions with *p*-benzoquinones have been reported. Mourad and Nour-el-Din[5] described the formation of charge transfer complex between substituted *N*,α-diarylnitrones and *p*-benzoquinones having electron-withdrawing substituents. Schultz et al. reported successful intramolecular nitrone–quinone cycloaddition, attempted intermolecular cycloaddition being unsuccessful.[6]

In this paper, we report the reactions of substituted *p*-benzoquinones with *N*,α-diarylnitrones, some of which gave cycloaddition products. This is the first example of the successful intermolecular nitrone–quinone cycloaddition.

Results and Discussion

As nitrones, *N*,α-diphenylnitrone (**1a**) and *N*,α-bis(substituted phenyl)nitrones (**1b**—**e**) were employed. The nitrones were prepared from the corresponding arenecarbaldehydes and *N*-arylhydroxylamines by a known method.

Nitrones were allowed to react with quinones in refluxing benzene, unless otherwise noted. In the reaction of **1a** with 2,5-dimethyl-*p*-benzoquinone (25DMQ), practically no color change was observed at the initial stage of the reaction, but with the progress of the reaction the color changed gradually from yellow to light orange. The progress of the reaction was followed by TLC or HPLC analyses during the reaction period and it was confirmed that the reaction gave one product, except for the decomposition of **1a** (less than 5%), along with the decrease of **1a** and 25DMQ. After two days, the product was isolated from the reaction mixture by chromatographic technique followed by recrystallization from hexane, and the product was

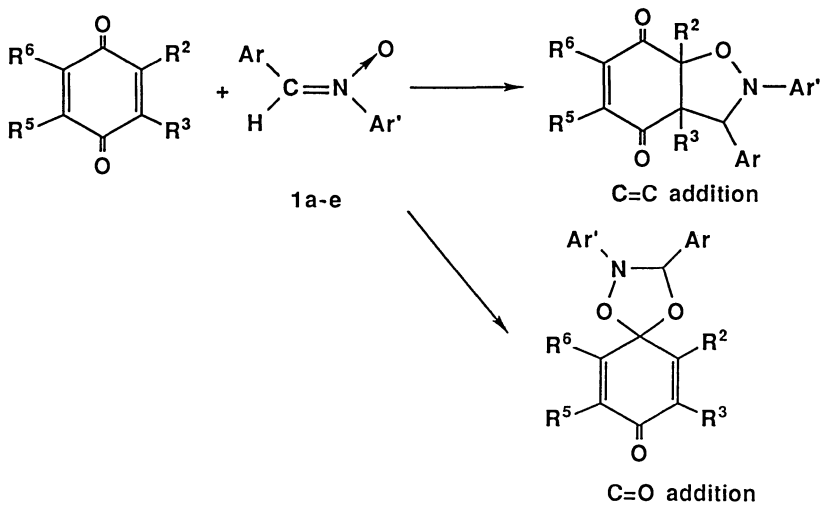

Scheme 1. Possible reaction course of the nitrone–quinone cycloaddition.

obtained as light orange powder.

The structure of the product was determined by IR, ^1H and ^{13}C NMR, mass spectra and elemental analyses. Elemental analyses and mass spectra showed that the product was 1 : 1 adduct of the nitrone and the quinone.

To determine the structure of this adduct, the first problem is the site selectivity of this addition; the addition to the C=C double bond to give a fused isoxazolidine derivative, or to C=O double bond to give spirodioxazolidine derivative (Scheme 1). ^{13}C NMR spectrum has two signals around 195 ppm which are assignable to carbonyl carbons. The IR spectrum showed a strong absorption at 1680 cm^{-1}. These facts suggest that two carbonyls arising from 25DMQ remain in the product, suggesting that the addition reaction proceeded at the C=C double bond.

^1H NMR spectrum showed two doublets at δ=3.68 and 5.00 having coupling constants J=7 Hz and integrating each one proton. This is well-consistent with the structure **2a**, 3,6-dimethyl-8,9-diphenyl-7-oxa-8-azabicyclo[4.3.0]-3-nonen-2,5-dione, and not with the regio-isomer **2a'** (Scheme 2).

Two stereoisomers are possible for the structure **2a** (Scheme 3). The coupling constant of two protons at 3- and 4-position in isoxazolidine ring was 7 Hz, suggesting the protons being in *cis*-position. The coupling constants reported for *N,α*-diarylnitrones-*N*-phenylmaleimide cycloadducts[7] were 8 Hz when the two protons were in *cis*-position and 1 Hz in *trans*. However,

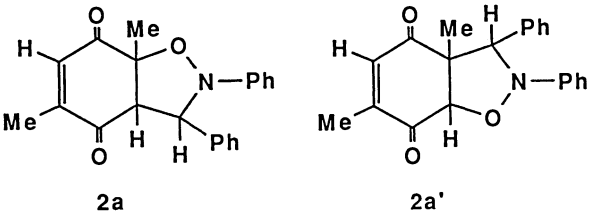

Scheme 2. Regioselectivity of the cycloaddition reaction of **1a** with 25DMQ.

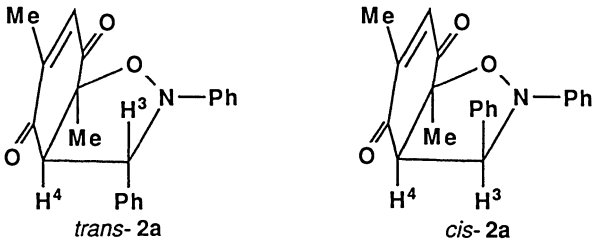

Scheme 3. Possible stereoisomer of the cycloadduct **2a**.

Table 1. The Reactions of 25DMQ with Various Nitrones (**1a—e**)

Nitrones	X	X'	Products	Yields/%
1a	H	H	**2a**	20
1b	Cl	H	**2b**	11
1c	NO_2	H	**2c**	19
1d	Me	H	**2d**	4
1e	H	Cl	**2e**	9

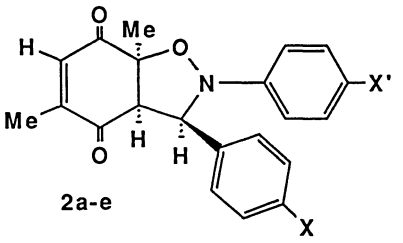

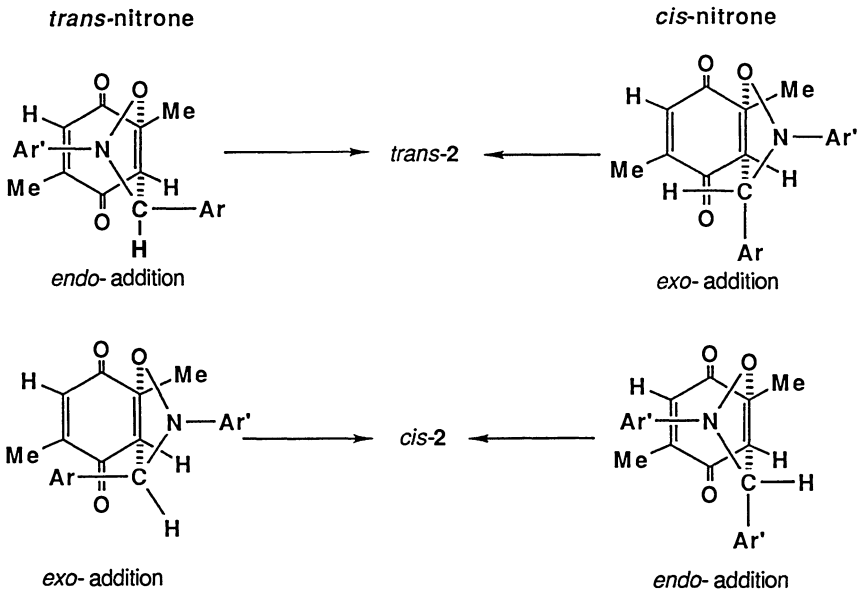

Scheme 4. Relationship of transition states of cycloaddition and the product configurations.

Table 2. Reactions of *N*,α-Diphenylnitrone (**1a**) and Substituted *p*-Benzoquinones

Nitrones	Quinones				Method[a)]	Products	Yields/%
	R^1	R^2	R^3	R^4			
1a	Me	H	Me	H	A	**2a**	20
1a	Me	Me	H	H	A	**2f**	16
1a	*t*-Bu	H	*t*-Bu	H	A	**2g**	10
1a	*t*-Bu	*t*-Bu	H	H	A,B	—	Trace
1a	H	H	H	H	A	—	0
1a	Cl	Cl	Cl	Cl	B	—	0
1a	Cl	Cl	CN	CN	B	—	0

a) Method A; in refluxing benzene. B; in refluxing 1,2-dichroloethane. Yield shows quinone conversion by HPLC analysis. (For details, see experimental section.)

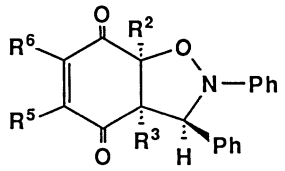

2a,f,g

various values were reported to the coupling constants of isoxazolidine ring protons,[8)] and these values are not always the same due to the changes in the conformation of isoxazolidine ring. Therefore, the structure determination by X-ray diffraction analysis was desirable, but attempts to obtain well-crystallized sample of **2a** were unsuccessful.

The reactions of 25DMQ with substituted *N*,α-diarylnitrones (**1b—e**) were summarized in Table 1. All of these reactions gave 1 : 1-C=C adducts (**2b—e**) as the sole product. The spectral pattern of the products was very similar to those of **2a**. There was no marked difference in the yield with the substitution on either benzene rings.

There are two possible reaction patterns for the formation of *cis*-adduct, *exo*-addition of the *trans*-nitrone and *endo*-addition of the *cis*-nitrone (Scheme 4). In all of these reactions, *cis*-adduct was the sole product. It is known that **1d** exists exclusively as a *trans*-form under the temperature conditions where the reactions are carried out.[9)] Therefore, the *endo*-addition of the *cis*-nitrone could be ruled out. Thus, diarylnitrones are proved to react with 2,5-dimethyl-*p*-benzoquinone at C=C site, in such an orientation as forming *cis*-adducts via *exo*-cycloaddition.

The reactions of **1a** with other *p*-benzoquinones were also examined (Table 2). The reactions of **1a** with 2,6-dimethyl-*p*-benzoquinone and with 2,5-di-*t*-butyl-*p*-benzoquinone gave corresponding adducts **2f** and **2g**, respectively. In each of these reactions, **2f** or **2g** was the only product which was recognized by chromatographic analyses. The reaction of **1a** with 2,6-di-*t*-butyl-*p*-benzoquinone gave an indication of the formation of a trace amount of an product from **1a** and quinone in HPLC analysis, but the isolation of the product was not successful.

The reaction of **1a** with unsubstituted *p*-benzoquinone gave a tarry material and attempts to isolate a definite product were unsuccessful. In the reaction of *p*-benzoquinone and benzonitrile *N*-oxide, it is known that the reaction gave isoxazoline cycloadduct and the adduct and starting materials undergo complex redox reactions.[10)] In this reaction, similar complex reactions were thought to be involved but nothing was clarified.

In the reactions of **1a** with *p*-benzoquinones having electron-withdrawing substituents, e.g. chloranil and 2,3-dichloro-5,6-dicyano-*p*-benzoquinone (DDQ), instantaneous color changes were observed when the solution of the nitrone and the quinone was mixed (yellow to red in the reaction with chloranil, and yellow to blue with DDQ) presumably due to the formations of charge-transfer complexes.[5)] HPLC analyses of the reaction mixtures showed gradual degradation of **1a** and no adduct formation.

Temperature effect on the reaction of **1a** with 25DMQ was also examined (Table 3). No significant difference was observed in the reactions at room temperature, in refluxing benzene (80 °C), and in refluxing toluene (110 °C). However, in refluxing xylene (140 °C), the reaction mixture after the removal of the solvent left black tarry material, and no cycloadduct nor any definite product could be isolated. Thermal analyses of **2a** (TG and DTA) showed thermal degradation of the compound just above the melting point (>92 °C).

The retrocycloaddition reaction was observed when

Table 3. The Reaction of 2,5-Dimethyl-*p*-benzoquinone with **1a** at Various Temperature

Solvent	Temperature/°C	Reaction time/d	Yields/%
Benzene	Room temp.	7	18
Benzene	80(reflux)	2	20
Toluene	110(reflux)	2	18
Xylene	140(reflux)	2	0

2a was placed in the cycloaddition reaction conditions. The reaction was confirmed with NMR and HPLC analyses. (see experimental section). This retroaddition was thought to be responsible to the low yields of the cycloaddition reactions. The reason of the result of Schultz et al. that *C*-phenyl-*N*-methylnitrone and 2,6-dimethyl-*p*-benzoquinone did not give any adduct[6] may be ascribed to that the nitrone is less reactive than *N*,α-diarylnitrones[9] as well as that the lack of *N*-aryl group destabilize the isoxazolidine to be labile to undergo the retroaddition reaction.

In conclusion, *N*,α-diarylnitrones cycloadded to alkyl-substituted *p*-benzoquinones at quinone C=C double bond to give fused isoxazolidine derivatives but electron-deficient quinones did not give any adduct. The isoxazolidines were found to undergo retrocycloadditions.

Experimental

Melting points were measured with a micro melting point measuring apparatus (Yazawa BY-1) and are uncorrected. The IR spectra were recorded with a JASCO IRA-1 spectrometer. The ^{1}HNMR and ^{13}CNMR spectra were measured in $CDCl_3$, unless otherwise indicated, with JEOL JMN-MH100 and GX-270 spectrometers respectively, and chemical shifts were reported in ppm from internal tetramethylsilane. Mass spectra were recorded with a Hitachi RMU-7M spectrometer. Thermal analysis (DTA and TGA) was measured with Shimadzu DT-30 apparatus.

Materials. *p*-Benzoquinone, 2,5-di-*t*-butyl-*p*-benzoquinone, 2,6-di-*t*-butyl-*p*-benzoquinone, chloranil and 2,3-dicyano-5,6-dichloro-*p*-benzoquinone(DDQ) were commercially obtained. 2,5-dimethyl-*p*-benzoquinone and 2,6-dimethyl-*p*-benzoquinone were synthesized with Jones oxidation of 2,5-xylenol and 2,6-xylenol, respectively[11] and purified by column chromatography. All of the quinones except for DDQ were recrystallized from hexane. *N*,α-Diarylnitrones (**1a**—**e**) were prepared in dry ethanol from corresponding arenecarbaldehydes and *N*-arylhydroxylamines[12] which were synthesized by the zinc mediated reduction of the corresponding nitroaryl compounds.

Reactions of *N*,α-Diphenylnitrones(1a) with 2,5-Dimethyl-*p*-benzoquinone. Method A: To 50 ml of benzene, 592 mg of **1a** (3.00 mmol) and 408 mg of 2,5-dimethyl-*p*-benzoquinone (3.00 mmol) were dissolved. The mixture was heated to reflux for 2 d. The reaction was followed by TLC analysis (Merck, Kieselgel 60 F-254, benzene as an eluent). After the reaction, solvent was evaporated under reduced pressure and the residue was subjected to column chromatography on silica gel (Wakogel C-200, Wako Chemicals Co., Ltd.) using benzene as an eluent. 2,5-Dimethyl-*p*-benzoquinone and the product were eluted in this order. After the evaporation of the solvent, 207 mg (51%) of 2,5-dimethyl-*p*-benzoquinone was recovered. The fraction of the product was concentrated under reduced pressure, triturated with hexane and recrystallized from hexane and 198 mg (20%) of 1 : 1 cycloadduct (**2a**) was obtained. The reactions with other nitrones (**1b**—**e**) or with other benzoquinones were performed with the same procedures. In all of these reaction, the 1 : 1-C=C cycloadduct was a sole product (**3b**—**g**) and no other product formation was observed in TLC analyses in each of these reactions.

Table 4. Characterization Data of Cycloadducts (**3a**—**g**)

Adducts	θ/°C		Anal./% Found	Anal./% Calcd	$\nu_{C=O}$
2a	90.5—92	C	75.63	75.66	1680
		H	5.63	5.74	
		N	4.33	4.20	
2b	110.5—111.5	C	68.80	68.57	1670
		H	5.03	4.93	
		N	3.84	3.81	
2c	140—141	C	66.77	66.66	1680
		H	4.53	4.79	
		N	7.71	7.40	
2d	91—94	C	75.92	76.06	1680
		H	5.80	6.09	
		N	4.06	4.03	
2e	164—165.5	C	68.78	68.76	1680
		H	4.88	4.67	
		N	3.79	3.81	
2f	112.5—114	C	75.71	75.66	1670,1685
		H	5.81	5.74	
		N	4.19	4.20	
2g	137.5—139.5	C	77.93	77.67	1680
		H	7.41	7.48	
		N	3.33	3.35	

Table 5. ^{1}H NMR Spectra of the Adducts (**2a**—**g**)[a]

Adducts	Chemical shifts (δ)
2a	1.59 (s, 3H), 2.00 (s, 3H), 3.68 (d, 1H, *J*=7 Hz), 5.00 (d, 1H, *J*=7 Hz), 6.62 (s, 1H,), 7.0—7.9 (m, 10H)
2b	1.56 (s, 3H), 1.98 (s, 3H), 3.62 (d. 1H, *J*=7 Hz), 4.98 (d, 1H, *J*=7 Hz), 6.62 (s, 1H,), 6.9—7.7 (m, 9H)
2c	1.73 (s, 3H), 2.06 (s, 3H), 3.78 (d, 1H, *J*=7 Hz), 5.40 (d, 1H, *J*=7 Hz) 6.88 (s,1H,), 7.0—8.7 (m, 9H)
2d	1.58 (s, 3H), 1.98 (s, 3H), 2.36 (s, 3H),[b] 3.68 (d, 1H, *J*=7 Hz), 4.98 (d, 1H, *J*=7 Hz), 6.67 (s, 1H,), 7.0—7.7 (m, 9H)
2e	1.52 (s, 3H), 1.64 (s, 3H), 4.00 (d, 1H, *J*=7 Hz), 5.00 (d, 1H, *J*=7 Hz), 6.56 (s, 1H), 6.9—7.7 (m, 9H)
2f	1.66 (s, 3H), 2.10 (s, 3H), 3.81 (d, 1H, *J*=7 Hz), 5.35 (d, 1H, *J*=7 Hz), 6.83 (s, 1H,), 7.0—8.0 (m, 10H)
2g	1.12 (s, 9H), 1.32 (s, 9H), 3.97 (d, 1H, *J*=7 Hz), 4.63 (d, 1H, *J*=7 Hz), 6.69 (s, 1H,), 6.8—7.7 (m, 10H)

a) Assignment Alkyl moieties H^{7a} H^{8} Vinyl proton Aromatic moieties

b) Signal of Substituent Methyl Group at 9-*p*-Tolyl Moiety.

The yields and characterization data for these products were summarized in Tables 1 and 2, and in Tables 4 and 5, respectively.

Method B: The reaction was carried out in refluxing 1,2-dichloroethane (80 °C) with the same concentration as Method A. The reaction progress was followed by HPLC analysis (ODS column, 85% acetonitrile as an eluent, detector (UV) wavelength 254 m, 100 mg of biphenyl as an internal stan-

dard). After 2 d, the solution was worked up in the same manner as described in method A.

Temperature Effect on the Reaction of 2a with 25DMQ. The reaction was carried out in benzene (room temperature), refluxing benzene (80 °C), toluene (110 °C), or xylene (140 °C). The other reaction conditions and the treatments after the reaction were the same as method A. The results of the reactions were summarized in Table 3.

Retrocycloaddition Reaction of 2a. Compound **2a** (100 mg) was dissolved in 50 ml of 1,2-dichloroethane, and allowed to reflux overnight. After the reaction, the reaction mixture was subjected to HPLC analysis. The chromatogram indicated that **2a** was decomposed almost completely and **1a** and 25DMQ were produced. It was found that some amount of **1a** (less than 10%) was decomposed. But the identification of the degradation product was unsuccessful. ^{1}H NMR analysis was also performed. Compound **2a** (4 mg) was dissolved in 2 ml of benzene-d_6 and heated to 80 °C for 2 d. The reaction mixture was subjected to ^{1}H NMR analysis. The spectrum showed the overlap of **1a** (confirmed with the multiplet signal at 8.5 ppm), 25DMQ (confirmed with two singlet signals at 6.1 ppm and 2.6 ppm), and **2a**. The other signals were very weak and negligible (less than 5% from the integral intensity). The integral ratio of 25DMQ : **2a** was about 3 : 1.

References

1) W. Stegmann, P. Uebelhart, and H. Heimgartner, *Helv. Chim. Acta,* **66**, 2252 (1983), and references sited therein.

2) L. Wolff and G. R. Grau, *Liebigs Ann. Chem.,* **399**, 274 (1913); F. D. Chattaway and G. D. Parke, *J. Chem. Soc.,* **127**, 1307 (1925).

3) There are many reports of the diazoalkane–quinone cycloaddition. For review, M. Regits and H. Heydt in "1,3-Dipolar Cycloaddition Chemistry," ed by A. Padwa, John Wiley & Sons, Vol. 1, Chap. 4, pp. 450—452.

4) S. Shiraishi, B. S. Holla, and K. Imamura, *Bull. Chem. Soc. Jpn.,* **56**, 3457 (1983); S. Shiraishi, T. Hayakawa, and K. Araki, *ibid.*, **57**, 1643 (1984).

5) A. L. Nour-el-Din and A. E. Mourad, *Monatsh. Chem.,* **114**, 211 (1983).

6) A. G. Schultz, W. G. McMahon, and R. K. Kullnig, *J. Org. Chem.,* **52**, 3905 (1987).

7) A. M. Nour-el-Din, A. E. Mourad, and H. Abdel-Nabi, *J. Chem. Eng. Data,* **31**, 259 (1986).

8) For example, R. Huisgen, R. Grashey, H. Hauck, and H. Seidl, *Chem. Ber.,* **101**, 2548 (1968); P. M. Wovkulich and M. R. Uskoković, *Tetrahedron,* **41**, 3455 (1985); J. Wityak, S. J. Gould, S. J. Hein, and D. A. Keszler, *J. Org. Chem.,* **52**, 2179 (1987).

9) J. J. Tufariello in "1,3-Dipolar Cycloaddition Chemistry," ed by A. Padwa, John Wiley & Sons, Vol. 2, Chap. 9.

10) Ch. Grundmann and P. Gruenanger, "The Nitrile Oxides," Springer Verlag, Berlin (1971).

11) D. Liotta, J. Arbiser, J. W. Short, and M. Saindane, *J. Org. Chem.,* **48**, 2932 (1983).

12) K. Koyano and H. Suzuki, *Bull. Chem. Soc. Jpn.,* **42**, 3306 (1969).

 © 1991 The Chemical Society of Japan Bull. Chem. Soc. Jpn., 64, 2393—2397 (1991)

Reactions of 2-Aminoazulenes with Electron-Deficient Acetylenes

Noritaka ABE
Department of Chemistry, Faculty of Science, Yamaguchi University, Yamaguchi 753
(Received February 27, 1991)

2-Aminoazulene (**1a**) reacted with dimethyl acetylenedicarboxylate (DMAD) to give dimethyl 1,2-azulenedicarboxylate, tetramethyl 2,2′-(2-amino-1,3-azulenediyl)bis[fumarate], and dimethyl 2-(4-methoxycarbonyl-2-oxo-1,2-dihydroazuleno[2,1-*b*]pyridin-10-yl)fumarate. The reaction of ethyl 2-amino-1-azulenecarboxylate (**1b**) with DMAD gave dimethyl 2-(2-amino-3-ethoxycarbonyl-1-azulenyl)fumarate and 10-ethyl 4-methyl 2-oxo-1,2-dihydroazuleno[2,1-*b*]pyridine-4,10-dicarboxylate (**8a**). The treatment of **8a** with phosphoryl chloride gave the 2-chloroazuleno[2,1-*b*]pyridine derivative. Reactions of **1a** and **1b** with methyl propiolate gave corresponding Michael adducts and the azuleno[2,1-*b*]pyridin-3(4*H*)-one derivatives. Reactions of **1a** and **1b** with dibenzoylacetylene gave 4-benzoyl-2-phenylazuleno[2,1-*b*]pyridine derivatives.

Cycloaddition of azaazulenes to acetylenic esters has received attention,[1–6] and it is known that the reactions are strongly influenced by the substituents and/or reaction conditions. In the study of carbocyclic azulene chemistry, it was discovered that azulene reacts with electron-deficient acetylenes or electron-deficient olefines to give Michael-type adducts.[7,8] Later, K. Hafner reported that azulene reacted with reactive acetylenes in aprotic solvent and gave cycloadducts via dipolar intermediates.[9,10] At present, the effects of substituents in these reactions have not been investigated. In order to determine how the substituents on the azulene ring influence the reactions, I investigated the reactions of 2-aminoazulenes with electron-deficient acetylenes. The reactions preferentially gave Michael adducts and azuleno[2,1-*b*]pyridin-2(1*H*)-ones; cycloaddition occurred only rarely.

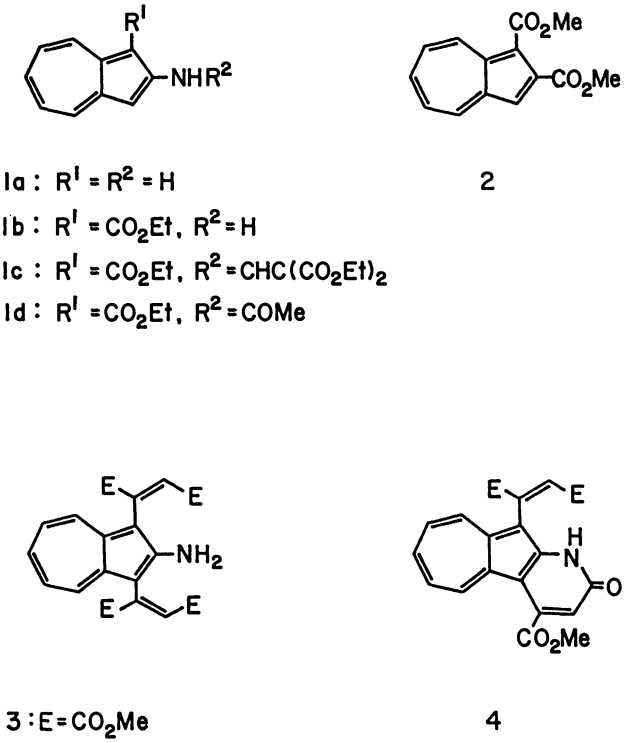

Fig. 1.

The treatment of 2-aminoazulene (**1a**) with dimethyl acetylenedicarboxylate (DMAD) in refluxing *t*-butylbenzene for 1 h gave a complex mixture. From the mixture, three compounds, dimethyl 1,2-azulenedicarboxylate[1,11,12] (**2**), tetramethyl 2,2′-(2-amino-1,3-azulendiyl)bis[fumarate] (**3**), and dimethyl 2-(4-methoxycarbonyl-2-oxo-1,2-dihydroazuleno[2,1-*b*]-pyridin-10-yl)fumarate (**4**) in 0.3, 3, and 15% yields, respectively, were isolated by column chromatography on silica gel. The structures of these compounds were determined on the basis of their spectra, especially ^{1}H NMR spectra, as well as elemental analyses. The yields of **3** and **4** were somewhat increased at room temperature by ultrasonic irradiation, but **2** was not produced. Therefore, I concluded that the formation of **2** required high temperature.

The treatment of ethyl 2-amino-1-azulenecarboxylate (**1b**) with DMAD in benzene at room temperature for 4 d gave dimethyl 2-[(1-ethoxycarbonyl-2-azulenyl)-amino]maleate (**5**) (13% yield), azulenylmaleate derivative **6a** (18% yield), azulenylfumarate derivative **7** (24% yield), and azuleno[2,1-*b*]pyridin-2(1*H*)-one derivative **8a** (35% yield). Ultrasonic irradiation facilitated the reaction which was complete within 6 h, though the yields were slightly low. When the reactions were carried out with heat, **5** was not produced. Refluxing in acetonitrile rather than benzene enhanced the yield of **6a** (61% yield).

To confirm the structure of **8a**, which had the 2-oxo, rather than 4-oxo, form, cyclizations of **6a** and **7** were attempted. Treatment of **6a** with triethylamine in refluxing acetonitrile for 1 h or the contact of **6a** with silica gel for 50 d gave **8a** in 73.5 and 81% yields, respectively. The fumarate **7** did not react under these conditions, but gave **8a** (47% yield) after treatment with 1,8-diazabicyclo[5.4.0]undec-7-ene (DBU) in refluxing xylene for 15 h.

Furthermore, for the purpose of comparison, azuleno[2,1-*b*]pyridin-4(1*H*)-one derivative **9** was synthesized. Treatment of **1b** with diethyl (ethoxy-

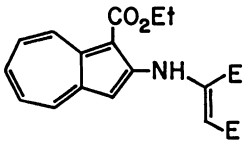

5: E = CO_2Me

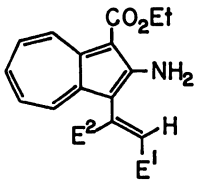

6a: $E^1 = E^2 = CO_2Me$

6b: $E^1 = CO_2Me$, $E^2 = H$

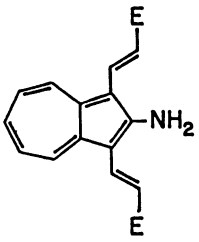

10: E = CO_2Me

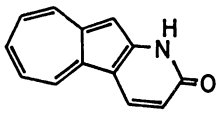

11

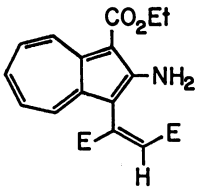

7: E = CO_2Me

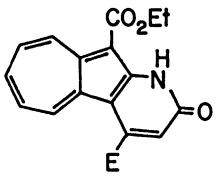

8a: E = CO_2Me

8b: E = H

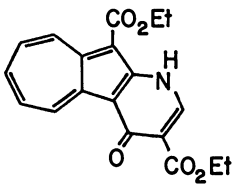

9

Fig. 2.

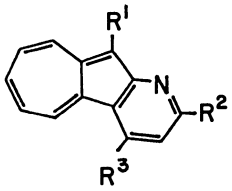

12a: R^1 = H, R^2 = Ph, R^3 = COPh

12b: R^1 = COPh C=CHCOPh, R^2 = Ph, R^3 = COPh

12c: $R^1 = CO_2Et$, R^2 = Ph, R^3 = COPh

12d: $R^1 = CO_2Et$, R^2 = Cl, $R^3 = CO_2Me$

Fig. 3.

methylene)malonate (DEEM) gave diethyl [*N*-(1-ethoxycarbonyl-2-azulenyl)aminomethylene]malonate (**1c**) in a 74% yield. Heating of **1c** in refluxing *t*-butylbenzene for 5 h gave **9** in a 95% yield. In the ^{1}H NMR spectra, the H-5 proton of **8a** resonated at δ=8.88, whereas the H-5 proton of **9** resonated at δ=10.31. These results supported my conclusion that the structure of **8a** was in the 2-oxo form. The downfield shift of the H-5 proton in **9** may be due to a shielding effect by the carbonyl group at C-4.

Reactions of **1a** and **1b** with methyl propiolate (MP) gave results similar to the reactions with DMAD. Thus, the treatment of **1a** with MP in refluxing *t*-butylbenzene in the presence of Pd–C gave **10** (7% yield) and **11** (16% yield). The treatment of **1b** with MP in refluxing *t*-butylbenzene in the presence of Pd–C gave **6b** (16%) and **8b** (14.5%). The *trans*-configurations of the vinylic protons of **10** and **6b** were confirmed by their ^{1}H NMR spectra, in which pertinent vicinal coupling constants (both J=15.9 Hz) were observed. Compound **6b** produced **8b** (11% yield) when reacted with DBU in refluxing xylene for 4 d.

When **1a** was treated with dibenzoylacetylene (DBA) in benzene with ultrasonic irradiation in the presence of Pd–C, azuleno[2,1-*b*]pyridine derivatives[13] **12a** (28.5% yield) and **12b** (53% yield) were obtained. Reaction of **1b** with DBA under similar conditions gave **12c** in a 63% yield.

All the results showed that the Michael adducts were obtained in greater yields than the cycloadducts in the reactions of 2-aminoazulenes with electron-deficient acetylenes. The resonance form **A** of the intermediates may facilitate the prototropy of the dipolar intermediates leading to the preferential formation of the Michael adducts. I believe that the amino substituent may enhance the reactivity of the C-1 position of **1a** (and the C-3 position of **1b**) allowing the reaction of **1a** (or **1b**) to occur under milder conditions than those used for azulene.[9] The presence of an electron-withdrawing group on the amino group, such as an acetylamino group, should supress the reaction. Indeed, ethyl 2-acetylaminoazulene-1-carboxylate (**1d**) reacted very lit-

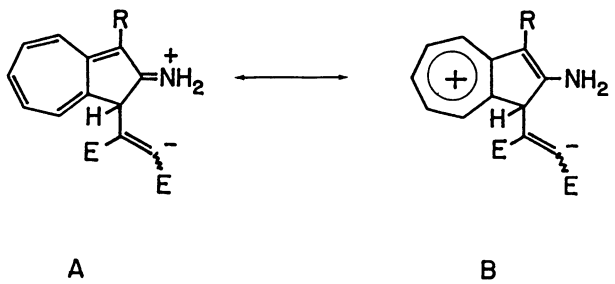

A B

Fig. 4.

tle with DMAD even under refluxing tetralin; over 95% of the starting material was recovered after 70 h.

Chlorination of **6a** with phosphoryl chloride gave the azuleno[2,1-*b*]pyridine derivative **12d** in a 54% yield. In its ^{1}H NMR spectrum, the H-10 proton resonated at δ=9.31, and this again supported the 2-oxo form of 8a. A large divergence of the vicinal spin–spin coupling constants in the seven-membered ring protons of **12d**, $\Delta J=J_{8,9}-J_{5,6}$=1.8 Hz, was observed. This indicated a bond alternation in the azulene ring, reflecting the large aromaticity of the pyridine ring.[14,15]

Experimental

Melting points were uncorrected. ^{1}H NMR spectra (250 MHz) were taken on a Hitachi R-250H spectrometer using $CDCl_3$ as a solvent (TMS as an internal standard) unless otherwise stated. IR spectra were recorded for Nujol mulls with a Hitachi 270-50 infrared spectrophotometer. Column chromatography was performed on Kieselgel 60.

Reaction of 1a with DMAD. a) A mixture of **1a**[16] (0.500 g) and DMAD (1.50 g) in dry *t*-butylbenzene (20 ml) was refluxed for 1 h. The solvent was then evaporated, and cromatography of the residue with benzene gave **2**[1,11,12] (0.003 g, 0.3% yield). Elution with benzene–chloroform (1 : 1) gave **3** (0.041 g, 23% yield) and **4** (0.249 g, 15% yield), successively.

3: Red prisms (from hexane–dichloromethane); mp 155—157 °C; ^{1}H NMR δ=3.82 (6H, s), 3.89 (6H, s), 5.91 (2H, brs), 6.11 (2H, s), 7.20—7.60 (3H, m), and 8.09 (2H, dm, J=9.8 Hz); IR 3452, 3340 (NH), 1730, and 1710 cm^{-1} (C=O). Found: C, 61.73; H, 4.94; N, 3.19%. Calcd for $C_{22}H_{21}NO_8$: C, 61.82; H, 4.95; N, 3.28%.

4: Red needles (from hexane–dichloromethane); mp 199—200 °C; ^{1}H NMR δ=3.86 (3H, s), 3.92 (3H, s), 4.09 (3H, s), 6.22 (1H, s), 6.77 (1H, s), 7.52 (2H, t, J=9.8 Hz), 7.73 (1H, t, J=9.8 Hz), 8.57 (1H, d, J=9.8 Hz), 8.77 (1H, d, J=9.8 Hz), and 10.28 (1H, brs); IR 3092 (NH), 1738, 1728, 1720, and 1648 cm^{-1} (C=O). Found: C, 63.47; H, 4.46; N, 3.26%. Calcd for $C_{21}H_{17}NO_7$: C, 63.79; H, 4.34; N, 3.54%.

b) A mixture of **1a** (0.500 g), DMAD (1.50 g), and 5% Pd–C (0.500 g) in *t*-butylbenzene (30 ml) was refluxed for 1 h. The solvent was then evaporated, and chromatography of the residue with benzene gave **2** (0.005 g, 0.6% yield). Elution with benzene–chloroform (1 : 1) gave **3** (0.103 g, 7% yield) and **4** (0.212 g, 15% yield), successively.

c) A mixture of **1a** (0.500 g), DMAD (1.50 g), and 5% Pd–C (0.500 g) in dry benzene (50 ml) was ultrasonically irradiated for 1 h. The solvent was then evaporated, and chromatography of the residue with benzene–chloroform (1 : 1) gave **3** (0.144 g, 9% yield) and **4** (0.356 g, 26% yield).

Reaction of 1b with DMAD. a) A mixture of **1b**[16] (0.215 g) and DMAD (0.430 g) in dry benzene (50 ml) was set for 4 d at room temperature. The solvent was then evaporated, and the residue was chromatographed. Elution with benzene gave **5** (0.045 g, 13% yield) and **6a** (0.064 g, 18% yield), successively. Elution with benzene–chloroform (1 : 1) gave **7** (0.085 g, 24% yield). Elution with chloroform gave **8a** (0.115 g, 35% yield).

5: Red needles (from hexane); mp 116—117; ^{1}H NMR δ=1.51 (3H, t, J=7.0 Hz), 3.80 (3H, s), 3.86 (3H, s), 5.62 (1H, s), 6.47 (1H, s), 7.36—7.60 (3H, m), 8.04 (1H, d, J=9.8 Hz), 9.22 (1H, d, J=10.4 Hz), and 11.78 (1H, s); IR 3248 (NH), 1735, 1696, and 1668 cm^{-1} (C=O). Found: C, 64.19; H, 5.38; N, 4.06%. Calcd for $C_{19}H_{19}NO_6$: C, 63.86; H, 5.36; N, 3.92%.

6a: Orange needles (from hexane); mp 96—97 °C; ^{1}H NMR δ=1.46 (3H, t, J=7.3 Hz), 3.82 (3H, s), 3.88 (3H, s), 4.44 (2H, q, J=7.3 Hz), 6.14 (1H, s), 6.90 (2H, brd), 7.28—7.46 (3H, m), 8.08—8.15 (1H, m), and 9.00 (1H, d, J=9.8 Hz); IR 3480, 3324 (NH), 1738, 1714, and 1662 cm^{-1} (C=O). Found: C, 63.45; H, 5.26; N, 3.86%. Calcd for $C_{19}H_{19}NO_6$: C, 63.86; H, 5.36; N, 3.92%.

7: Red needles (from hexane); mp 123—124 °C; ^{1}H NMR δ=1.47 (3H, t, J=7.3 Hz), 3.55 (3H, s) , 3.76 (3H, s), 4.45 (2H, q, J=7.3 Hz), 5.6—6.5 (2H, br), 7.23 (1H, t, J=9.2 Hz), 7.30 (1H, t, J=9.2 Hz), 7.39 (1H, t, J=9.2 Hz), 7.53 (1H, d, J=9.2 Hz), and 8.99 (1H, d, J=9.2 Hz); IR 3440, 3332 (NH), 1714, and 1668 cm^{-1} (C=O). Found: C, 63.71; H, 5.43; N, 3.91%. Calcd for $C_{19}H_{19}NO_6$: C, 63.86; H, 5.36; N, 3.92%.

8a: Red needles (from hexane–dichloromethane); mp 175—176 °C; ^{1}H NMR δ=1.53 (3H, t, J=7.0 Hz), 4.10 (3H, s), 4.56 (2H, q, J=7.0 Hz), 6.79 (1H, d, J=2.4 Hz), 7.68 (1H, dd, J=10.2 and 9.8 Hz), 7.76 (1H, dd, J=10.4 and 9.8 Hz), 7.87 (1H, dd, J=10.2 and 9.8 Hz), 8.88 (1H, d, J=9.8 Hz), 9.64 (1H, d, J=10.4 Hz), and 10.84 (1H, brd, J=2.4 Hz); IR 3388 (NH), 1734, 1696, and 1668 cm^{-1} (C=O). Found: C, 66.17; H, 4.84; N, 4.19%. Calcd for $C_{18}H_{15}NO_5$: C, 66.46; H, 4.65; N, 4.31%.

b) A mixture of **1b** (0.430 g), DMAD (0.860 g), and 5% Pd–C (0.500 g) in dry benzene (100 ml) was ultrasonically irradiated for 3 h at room temperature. The solvent was then evaporated, and chromatography of the residue as above gave **5** (0.067 g, 9% yield), **6a** (0.117 g, 16% yield), **7** (0.113 g, 16% yield), and **8a** (0.116 g, 18% yield).

c) A mixture of **1b** (0.430 g) and DMAD (0.86 g) in *t*-butylbenzene (30 ml) was refluxed for 3 h. The solvent was then evaporated, and chromatography of the residue as above gave **6a** (0.187 g, 26% yield), **7** (0.070 g, 9% yield), and **8a** (0.133 g, 20.5% yield).

d) A mixture of **1b** (0.500 g), DMAD (0.99 g), and 5% Pd–C (0.500 g) in *t*-butylbenzene (30 ml) was refluxed for 2 h. The residue was then evaporated, and chromatography of the residue as above gave **6a** (0.164 g, 20% yield), **7** (0.143 g, 17% yield), and **8a** (0.148 g, 20% yield).

e) A mixture of **1b** (0.580 g) and DMAD (1.15 g) in acetonitrile (50 ml) was refluxed for 6 h. The solvent was then evaporated, and chromatography of the residue as above gave **6a** (0.587 g, 61% yield), **7** (0.117 g, 12% yield), and **8a** (0.102 g, 12% yield).

Reaction of 7 with Triethylamine. A solution of **7** (0.13 g) and triethylamine (0.5 ml) in acetonitrile (10 ml) was refluxed for 1 h. The solvent was then evaporated, and the residue was chromatographed with benzene to give **8a** (0.087 g, 73.5% yield).

Cyclization of 7 on Silica Gel. A mixture of **7** (0.045 g) and silica gel (5.0 g) in chloroform (20 ml) was allowed to stand at room temperature for 50 d. The mixture was then filtered and residual silica gel was washed with chloroform. Evaporation of the combined filtrates gave **8a** (0.033 g, 81% yield).

Reaction of 6a with DBU. A mixture of **6a** (0.160 g) and DBU (0.3 ml) in dry xylene (50 ml) was refluxed for 15 h. The solvent was then evaporated, and chromatography of the residue with benzene gave **8a** (0.068 g, 47% yield).

Reaction of 1b with DEEM. A mixture of **1b** (0.250 g) and DEEM (0.750 g) in ethanol (50 ml) was refluxed for 64 h.

The solvent was then evaporated, and chromatography of the residue with benzene gave **1c** (0.424 g, 95% yield), which was recrystallized from hexane–dichloromethane to give red needles, mp 118—119 °C; ^{1}H NMR δ=1.37 (3H, t, J=7.3 Hz), 1.40 (3H, t, J=7.0 Hz), 1.52 (3H, t, J=7.0 Hz), 4.30 (2H, q, J=7.3 Hz), 4.40 (2H, q, J=7.0 Hz), 4.58 (2H, q, J=7.0 Hz), 7.12 (1H, s), 7.42 (1H, d, J=9.8 Hz), 7.52 (1H, dd, J=9.8 and 9.2 Hz), 7.60 (1H, t, J=9.8 Hz), 8.21 (1H, d, J=9.8 Hz), 8.65 (1H, d, J=14.0 Hz), 9.31 (1H, d, J=9.2 Hz), and 12.59 (1H, brd, J=14.0 Hz); IR 3260 (NH), 1698, 1680, and 1660 cm^{-1} (C=O). Found: C, 65.42; H, 6.06; N, 3.55%. Calcd for $C_{21}H_{23}NO_6$: C, 65.44; H, 6.01; N, 3.63%.

Cyclization of 1c. A solution of **1c** (0.210 g) in *t*-butylbenzene (15 ml) was refluxed for 5 d. The solvent was then evaporated, and chromatography of the residue with ethyl acetate gave **9** (0.176 g, 95% yield), which was recrystallized from hexane–dichloromethane to give orange needles, mp 185—187 °C; ^{1}H NMR δ=1.44 (3H, t, J=7.0 Hz), 1.52 (3H, t, J=7.0 Hz), 4.43 (2H, q, J=7.0 Hz), 4.55 (2H, q, J=7.0 Hz), 7.83 (1H, t, J=9.8 Hz), 7.88 (1H, dd, J=9.8 and 9.2 Hz), 7.96 (1H, t, J=9.8 Hz), 8.61 (1H, s), 9.50 (1H, d, J=9.8 Hz), 10.31 (1H, d, J=9.2 Hz), and 10.95 (1H, brs); IR 3320 (NH), 1724, 1690, and 1644 cm^{-1} (C=O). Found: C, 67.17; H, 4.99; N, 4.23%. Calcd for $C_{19}H_{17}NO_5$: C, 67.25; H, 5.05; N, 4.13%.

Reaction of 1a with MP. A mixture of **1a** (0.500 g), MP (0.880 g), and 5% Pd–C (0.500 g) in dry *t*-butylbenzene (30 ml) was refluxed for 1 h. The solvent was then evaporated, and the residue was purified by silica-gel column chromatography with benzene–chloroform (1 : 1) to give **10** (0.075 g, 7% yield). Elution with chloroform gave **11** (0.068 g, 16% yield).

10: Red-brown prisms (from hexane–dichloromethane); mp 188—190 °C; ^{1}H NMR δ=3.85 (6H, s), 5.38 (2H, brs), 6.25 (2H, d, J=15.9 Hz), 7.30—7.50 (3H, m), 8.19 (2H, d J=10.4 Hz), and 8.26 (2H, d, J=15.9 Hz); IR 3384, 3250 (NH), 1710, 1690, and 1652 cm^{-1} (C=O). Found: C, 69.16; H, 5.39; N, 4.64%. Calcd for $C_{18}H_{17}NO_4$: C, 69.44; H, 5.51; N, 4.50%.

11: Red needles (from hexane–dichloromethane); mp 280 °C (decomp); ^{1}H NMR δ (DMSO-d_6)=6.31 (1H, d, J=9.8 Hz), 7.06 (1H, s), 7.37 (1H, t, J=9.8 Hz), 7.45 (1H, dd, J=9.8 and 9.2 Hz), 7.64 (1H, t, J=9.8 Hz), 8.36 (1H, d J=9.8 Hz), 8.47 (1H, d, J=9.8 Hz), 8.62 (1H, d, J=9.2 Hz), and 12.12 (1H, brs); IR 3200 (NH) and 1642 cm^{-1} (C=O). Found: C, 79.65; H, 4.78; N, 7.18%. Calcd for $C_{13}H_9NO$: C, 79.98; H, 4.64; N, 7.17%.

Reaction of 1b with MP. A mixture of **1b** (0.500 g), MP (0.590 g), and 5% Pd–C (0.500 g) in dry *t*-butylbenzene (30 ml) was refluxed for 2 h. The solvent was then evaporated, and the residue was purified by silica-gel column chromatography with benzene to give **1b** (0.117 g, 23% yield) and **6b** (0.112 g, 16% yield), successively. Elution with chloroform gave **8b** (0.135 g, 14.5% yield).

6b: Red needles (from hexane); mp 107—108 °C; ^{1}H NMR δ=1.49 (3H, t, J=7.0 Hz), 3.84 (3H, s), 4.48 (2H, q, J=7.0 Hz), 6.22 (2H, d, J=15.9 Hz), 6.5—7.0 (2H, br), 7.35—7.58 (3H, m), 8.21 (1H, dm, J=10.4 Hz), 8.23 (1H, d, J=15.9 Hz), and 9.02 (1H, d, J=9.8 Hz); IR 3500, 3348 (NH), 1720, and 1672 cm^{-1} (C=O). Found: C, 68.50; H, 5.68; N, 4.80%. Calcd for $C_{17}H_{17}NO_4$: C, 68.21; H, 5.73; N, 4.68%.

8b: Red-violet needles (from hexane–dichloromethane); mp 209—210 °C; ^{1}H NMR δ=1.53 (3H, t, J=7.0 Hz), 4.56 (2H, q, J=7.0 Hz), 6.57 (1H, d, J=9.2 Hz), 7.65—7.90 (3H, m), 8.23 (1H, d, J=9.8 Hz), 8.59 (1H, d, J=9.2 Hz), 9.60 (1H, d, J=10.4 Hz), and 10.44 (1H, brs); IR 3392 (NH), 1682, and 1660 cm^{-1} (C=O). Found: C, 71.83; H, 4.97; N, 5.18%. Calcd for $C_{16}H_{13}NO_3$: C, 71.90; H, 4.90; N, 5.24%.

Reaction of 6b with DBU. A solution of **6b** (0.110 g) and DBU (0.1 ml) in dry xylene (20 ml) was refluxed for 4 d. The residue was then evaporated, and chromatography of the residue with chloroform gave **6b** (0.057 g, 52% yield) and **8b** (0.011 g, 11% yield), successively.

Reaction of 1a with DBA. A mixture of **1a** (0.500 g), DBA (2.454 g), and 5% Pd–C (0.500 g) in dry benzene (50 ml) was ultrasonically irradiated for 3 h. The solvent was then evaporated, and chromatography of the residue with benzene gave **12a** (0.358 g, 28.5% yield), and **12b** (1.092 g, 53% yield).

12a: Blue-green needles (from hexane–dichloromethane); mp 182—183 °C; ^{1}H NMR δ=6.92 (1H, dd, J=11.0 and 8.6 Hz), 7.01 (1H, dd, J=11.0 and 8.5 Hz), 7.25 (1H, dd, J=11.0 and 8.5 Hz), 7.42—7.68 (6H, m), 7.65 (1H, s), 7.70 (1H, s), 7.96 (2H, dd, J=7.9 and 1.8 Hz), 8.06 (1H, d, J=8.6 Hz), 8.14 (1H, d, J=11.0 Hz), and 8.19 (2H, dd, J=7.9 and 1.2 Hz); IR 1668 (C=O), 714, and 700 cm^{-1} (phenyl). Found: C, 87.21; H, 4.91; N, 3.96%. Calcd for $C_{26}H_{17}NO$: C, 86.88; H, 4.77; N, 3.90%.

12b: Yellow-brown prisms (from hexane–dichloromethane); mp 184—186 °C; ^{1}H NMR δ=7.06 (1H, dd, J=11.0 and 8.6 Hz), 7.19 (1H, dd, J=11.0 and 8.6 Hz), 7.30—7.55 (11H, m), 7.57 (1H, brd, J=6.7 Hz), 7.66 (1H, brd, J=6.7 Hz), 7.79 (1H, s), 7.95 (4H, dd, J=7.9 and 1.2 Hz), 8.07 (2H, dd, J=7.3 and 1.2 Hz), 8.18 (1H, d, J=8.6 Hz), 8.26 (2H, dd, J=7.9 and 1.2 Hz), 8.42 (1H, s), and 8.70 (1H, d, J=11.0 Hz); IR 1668, 1634 (C=O), 714, and 688 cm^{-1} (phenyl). Found: C, 85.01; H, 4.70; N, 2.42%. Calcd for $C_{42}H_{27}NO_3$: C, 84.97; H, 4.58; N, 2.36%.

Reaction of 1b with DBA. A mixture of **1b** (0.160 g), DBA (0.350 g), and 5% Pd–C (0.200 g) in dry benzene (50 ml) was urtrasonically irradiated for 4 h. The solvent was then evaporated, and chromatography of the residue with benzene–chloroform (1 : 1) gave **12c** (0.166 g, 63% yield).

12c: Brown-violet needles (from hexane); mp 176—177 °C; ^{1}H NMR δ=1.66 (3H, t, J=7.0 Hz), 4.65 (2H, q, J=7.0 Hz), 7.26 (1H, dd, J=9.8 and 8.5 Hz), 7.40—7.70 (8H, m), 7.80 (1H, s), 7.92 (2H, dd, J=7.3 and 1.2 Hz), 8.36 (2H, dd, J=7.9 and 1.5 Hz), 8.41 (1H, d, J=8.6 Hz), and 9.66 (1H, d, J=9.8 Hz); IR 1680, 1666 (C=O), 714, and 700 cm^{-1} (phenyl). Found: C, 80.70; H, 4.98; N, 3.11%. Calcd for $C_{29}H_{21}NO_3$: C, 80.71; H, 4.91; N, 3.26%.

Chlorination of 8a. A mixture of **8a** (0.100 g), phosphoryl chloride (10 ml), and a drop of pyridine was refluxed for 1 h. The mixture was poured into ice-water, neutralized with sodium hydrogen carbonate, and extracted with chloroform. The extract was dried (Na_2SO_4) and the solvent was evaporated. Chromatography of the residue with benzene gave **12d** (0.057 g, 54% yield), which was recrystallized from hexane–dichloromethane to give violet needles, mp 150—151 °C; ^{1}H NMR δ=1.55 (3H, t, J=7.0 Hz), 4.13 (3H, s), 4.59 (2H, q, J=7.0 Hz), 7.58 (1H, dd, J=10.4 and 9.2 Hz), 7.62 (1H, dd, J=11.0 and 7.9 Hz), 7.68 (1H, s), 7.80 (1H, dd, J=10.4 and 7.9 Hz), 9.31 (1H, d, J=9.2 Hz), and 9.64 (1H, d, J=11.0 Hz); IR 1728 and 1686 cm^{-1} (C=O). Found: C, 63.04; H, 4.26; N, 4.15%. Calcd for $C_{18}H_{14}ClNO_4$: C, 62.89; H, 4.10; N, 4.08%.

I am grateful to Dr. Akira Mori, Kyushu University, for the elemental analyses.

References

1) N. Abe and T. Takehiro, *Bull. Chem. Soc. Jpn.*, **61**, 1225 (1988), and references cited therein.
2) N. Abe and K. Yatabe, *Bull. Chem. Soc. Jpn.*, **64**, 1704 (1991).
3) T. Nishiwaki and N. Abe, *Heterocycles*, **15**, 547 (1981).
4) O. Meth-Cohn, C. Moore, and P. H. van Rooyen, *J. Chem. Soc., Perkin Trans. 1*, **1985**, 1793.
5) K. Hafner, *Lect. Heterocycl. Chem.*, **3**, 33 (1976).
6) K. Hafner and J. Haring, *Erdoel Kohle, Erdgas, Petrochem.*, **32**, 136 (1979).
7) W. Treibs, *Naturwissenschaften*, **47**, 156 (1960); *ibid.*, **52**, 452 (1965); *Chimia*, **24**, 440 (1970).
8) K. Hafner and K. L. Moritz, *Ann. Chem.*, **650**, 92 (1961).
9) K. Hafner, H. Diehl, and U. Süss, *Angew. Chem., Int. Ed. Engl.*, **15**, 104 (1976).
10) K. Hafner, H. J. Lindner, and W. Ude, *Angew. Chem., Int. Ed. Engl.*, **18**, 161 (1979); *ibid.*, **18**, 162 (1979).
11) W. von E. Doering and D. W. Wiely, *Tetrahedron*, **11**, 183 (1960).
12) I. Kawamoto, Y. Sugimura, N. Soma, and Y. Kishida, *Chem. Lett.*, **1972**, 931.
13) An azuleno[2,1-*b*]pyridine system was synthesized. T. Nozoe, K. Takase, T. Nakazawa, S. Sugita, and M. Saito, *Bull. Chem. Soc. Jpn.*, **47**, 1750 (1974); T. Nozoe and K. Kikuchi, *Bull. Chem. Soc. Jpn.*, **36**, 633 (1963).
14) D. J. Bertelli and P. Crewa, *Tetrahedron*, **26**, 4717 (1970).
15) T. Morita, T. Nakadate, and K. Takase, *Heterocycles*, **15**, 835 (1980).
16) T. Nozoe, S. Seto, S. Matsumura, and Y. Murase, *Bull. Chem. Soc. Jpn.*, **35**, 1179 (1962).

Synthesis of 5-Deoxy-5-phenylphosphino- and 5-Phenylphosphinyl-D-glucopyranoses

Tadashi HANAYA, Akihito AKAMATSU, Heizan KAWAMOTO, Margaret-Ann ARMOUR,† Alan M. HOGG,† and Hiroshi YAMAMOTO*

Department of Chemistry, Faculty of Science, Okayama University, Tsushima, Okayama 700
†Department of Chemistry, University of Alberta, Edmonton, Alta., T6G 2G2 Canada

(Received March 29, 1991)

(5*R* and 5*S*)-3-*O*-Acetyl-5-deoxy-1,2-*O*-isopropylidene-5-[(methoxy)phenylphosphinyl]-6-*O*-(tetrahydro-2-pyranyl)-α-D-*xylo*-hexofuranoses (**7**) were prepared from 3-*O*-acetyl-5,6-dideoxy-6-nitro-α-D-*xylo*-hex-5-enofuranose in 4 steps. Reduction of **7** with sodium dihydridobis(2-methoxyethoxy)aluminate followed by acid hydrolysis provided the title compounds, among which the 5-deoxy-5-phenylphosphino-D-glucoses are the first example of hexopyranose analogs having a phosphinidene group in place of hemiacetal ring-oxygen. These compounds were converted into 1,2,3,4,6-penta-*O*-acetates, whose structures were established by spectroscopy.

In the chemical modification of sugar compounds, various sugar analogs containing phosphorus as the ring heteroatom have been prepared.[1] As for analogs of D-glucopyranose type, 5-deoxy-5-hydroxyphosphinyl- (**1**)[2] and 5-ethylphosphinyl-D-glucopyranoses (**2**)[3] have been reported. In this paper we wish to describe the synthesis of hitherto unreported 5-deoxy-5-arylphosphino- and 5-arylphosphinyl-D-glucopyranose analogs by taking phenyl as a model functional group. Besides, the former compound becomes the first hexopyranose analog having a phosphinidene group in the hemiacetal ring.[4]

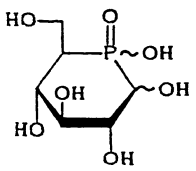

1

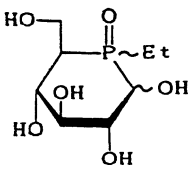

2

Results and Discusion

The addition reaction of methyl hydrogenphenylphosphinate to 3-*O*-acetyl-5,6-dideoxy-6-nitro-α-D-*xylo*-hex-5-enofuranose (**3**)[5] in the presence of triethylamine (TEA) at 25 °C gave an inseparable mixture (9:9:1:1) of two major D-"gluco" and two minor L-"ido" furanoses (**4**) in a 85% yield (Scheme 1). The assignments of the configuration of the products were made by comparison of their spectral data with those of other 5-phosphinyl compounds having similar structures;[2,6] see the Experimental section. Catalytic hydrogenation of **4** over palladium hydroxide on carbon [to convert it into 6-amino derivatives (**5**)], followed by diazotization and then hydrolysis, gave (5*R* and 5*S*)-3-*O*-acetyl-5-deoxy-1,2-*O*-isopropylidene-5-[(methoxy)-phenylphosphinyl]-α-D-*xylo*-hexofuranose (**6**). Compound **6** was converted into 6-*O*-(tetrahydro-2-pyranyl) derivatives (**7**) by treatment with dihydropyran in the presence of pyridinium *p*-toluenesulfonate (PPTS).

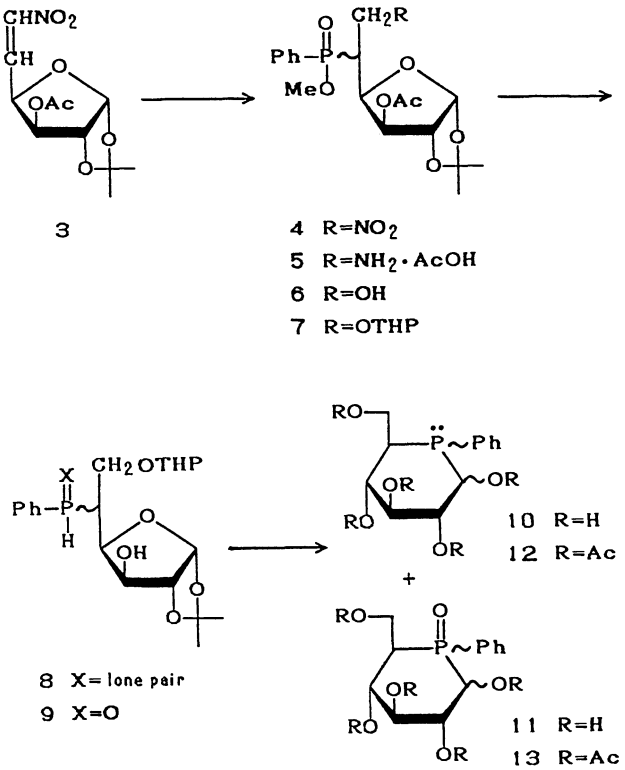

Scheme 1.

Compound **7** was then subjected to the reduction with sodium dihydridobis(2-methoxyethoxy)aluminate (SDMA), giving an unstable colorless syrup. This was found to consist exclusively of compounds having a 5-phenylphosphino structure (**8**) on the basis of the characteristic ^{31}P NMR data (δ=−53.4 and −51.5); judging from the presence of a very weak ^{31}P NMR signal (δ=30.1), only an extremely small proportion (<5%) of a 5-phenylphosphinyl compound (**9**) appeared to be present among the above reduction products. This presents a rather unexpected contrast to the fact that when the 5-[(ethyl)methoxyphosphinyl] congener of **7** was subjected to the SDMA reduction, its 5-

ethylphosphinyl derivative was exclusively obtained.[3] The reason for this difference has remained to be studied.

The phenylphosphino intermediate **8** was hydrolyzed in ethanolic 0.25 M hydrochloric acid (1 M=1 mol dm^{-3}) to effect the ring transposition, affording 5-deoxy-5-phenylphosphino-D-hexopyranose (**10**) and a minor proportion of their 5-phenylphosphinyl derivatives (**11**) as well (Scheme 1). Despite the attempted inert atmosphere during the procedure, **11** is presumably derived either from the oxidized intermediate **9** before the ring enlargement or from compound **10**; both **8** and **10** would become liable to suffer autoxidation upon prolonged heating at 90 °C.

Because of the difficulty in separation and purification, compounds **10** and **11** were converted into the corresponding per-*O*-acetyl derivatives (**12** and **13**, respectively) by the usual method for characterization. By purification in a column of silica gel, the following penta-*O*-acetyl compounds were isolated: 5-[(*R*)-phenylphosphino]-α-D-glucopyranose (**12a**, 2.0% overall yield from **7**), its β-anomer **12b** (9.9%), 5-[(*S*)-phenylphosphinyl]-α-D-glucopyranose (**13a**, 4.5%), and its β-anomer (**13b**, 5.3%). Besides these compounds, a small amount (ca. 2%) of three additional products were obtained as an inseparable mixture (ca. 1 : 1 : 1). The products were presumed to be the two remaining diastereomers of **13a,b** (namely, 5-[(*R*)-phenylphosphinyl]-α,β- isomers) and an L-idopyranose on the basis of ^{31}P NMR data, although the exact structures of these extremely minor products remained unestablished.

Structures of the final products **12a,b** and **13a,b** were established on the basis of high-resolution mass spectrometry and ^{1}H and ^{31}P NMR spectral data (see, Table 1). As large $J_{4,5}$ values (11.1—11.6 Hz) of **12a,b** and **13a,b** are characteristic coupling constants for an axial–axial conformation of H-4 and H-5, all of these compounds have D-glucopyranose configuration with $^{4}C_{1}$(D) conformation. With regard to the anomeric orientation of C-1, small $J_{1,2}$ values (2.2 and 2.8 Hz) of **12a** and **13a** indicate α-configuration, whereas large $J_{1,2}$ values (10.8 and 11.2 Hz) of **12b** and **13b** indicate β-configuration. The anti connection of H–C_1–P=O for **12b** and **13b** is confirmed by the smaller $J_{1,P}$ values (5.0 and 3.0 Hz) compared with the corresponding parameters (9.3 and 10.6 Hz) of **12a** and **13a** having this group in the gauche connections.[3] The H-2, H-4, and H-6′ signals of **13a,b** appear at a considerably downfield compared with those of **12a,b**. This can be explained by deshielding effect of the axial P=O bond at 1,3-diaxial positions, while the axial P-lone pair does not exert such an effect. The precise NMR parameters summarized in Table 1 are thought to be of value in determining the structures of other sugar analogs having similar constituents.

It should be noticed that while the precursor **7** was a ca. 9 : 1 mixture of D-gluco and L-idofuranose, the final, isolated products **12a,b** and **13a,b** all possessed D-glucopyranose configuration. This indicates that no epimerization apparently takes place at C-5 of **7** by the strongly basic reagent SDMA during the reduction to yield phosphine **8**.[7]

Although yields of some of the steps of the reaction scheme have to be improved, the present work thus demonstrates a possible way for preparation of 5-deoxy-5-arylphosphino- and 5-arylphosphinyl-D-glucopyranoses from an appropriate intermediate. Extension of this work including studies of reactivities of the phosphinidene functional group of **12a,b**, as well as biological evaluation of all products, is in progress.

Table 1. ^{1}H and ^{31}P NMR Parameters for **12a,b** and **13a,b** in $CDCl_3$

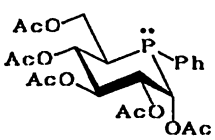

12a

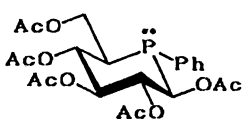

12b

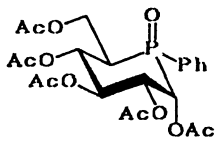

13a

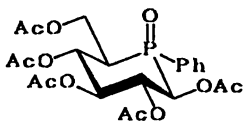

13b

Compd	Chemical shifts (δ)															
	H-1	H-2	H-3	H-4	H-5	H-6	H-6′	Ac-1,2,3,4,6[a]					Ph(*o*)	Ph(*m*)	Ph(*p*)	^{31}P
12a	5.76	5.33	5.52	5.49	3.30	4.29	3.97	1.85,	2.04,	2.02,	1.95,	1.93	7.55	7.42	7.42	−30.7
12b	5.78	5.44	5.26	5.42	2.65	4.16	3.88	1.82,	2.03,	2.01,	1.97,	1.84	7.64	7.43	7.43	−32.6
13a	5.68	5.72	5.59	5.73	3.19	4.37	4.32	1.56,	2.08,	2.06,	2.05,	1.96	7.77	7.54	7.61	27.3
13b	5.65	5.81	5.42	5.69	2.81	4.32	4.31	1.46,	2.06,	2.04,	1.98,	1.87	7.79	7.55	7.62	26.1

	Coupling constants/Hz												
	$J_{1,2}$	$J_{1,P}$	$J_{2,3}$	$J_{2,P}$	$J_{3,4}$	$J_{4,5}$	$J_{4,P}$	$J_{5,6}$	$J_{5,6'}$	$J_{5,P}$	$J_{6,P}$	$J_{6',P}$	$J_{6,6'}$
12a	2.2	9.3	10.1	3.2	9.6	11.1	3.2	4.7	4.4	3.9	13.2	9.4	11.8
12b	10.8	5.0	9.6	4.6	10.0	11.5	3.8	4.9	3.9	4.2	13.3	10.3	11.8
13a	2.8	10.6	10.5	0	9.7	11.6	1.9	7.4	6.2	5.4	11.6	14.8	11.6
13b	11.2	3.0	9.8	2.9	9.9	11.6	2.5	6.8	6.8	3.3	14.1	14.1	—

a) The assignments of acetoxyl groups may have to be interchanged.

Experimental

Melting points were determined with a Yanagimoto MP-S3 instrument and are uncorrected. All reactions were monitored by TLC (Merck silica gel 60F, 0.25 mm) with an appropriate solvent system [(A) AcOEt, (B) 1:1, (C) 2:1 AcOEt–hexane, and (D) 5:3:1 2-propanol–AcOEt–H_2O]; components were detected by spraying the plates with 20% sulfuric acid–ethanol, with subsequent heating. Column chromatography was performed by Wako C-200 silica gel. The ^1H and ^{31}P NMR spectra were measured in $CDCl_3$ with Varian VXR-500 (500 MHz for ^1H) and VXR-200 (81 MHz for ^{31}P) instrument (the SC-NMR Lab., Okayama Univ.) at 21 °C, except for compound **7** [which was measured with Hitachi R600 (60 MHz) instrument]. Chemical shifts are reported as δ values relative to tetramethylsilane (internal standard for ^1H) and 85% phosphoric acid (external standard for ^{31}P). The mass spectra were taken on an A.E.I. MS 50 ultrahigh resolution instrument and were given in terms of m/z (rel intensity) compared with the base peak.

(5*R* and 5*S*)-3-*O*-Acetyl-5,6-dideoxy-1,2-*O*-isopropylidene-5-[(*R* and *S*)-(methoxy)phenylphosphinyl]-6-nitro-α-*xylo*-hexofuranoses (4). TEA (0.10 ml, 0.72 mmol) was added dropwise at 0 °C to a mixture of **3**[5] (464 mg, 1.70 mmol) and methyl hydrogenphenylphosphinate (1.41 g, 9.04 mmol) in benzene (2 ml). The mixture was stirred for 3 h at 25 °C and then poured into saturated aq $NaHCO_3$. The resulting solution was stirred overnight and extracted three times with CH_2Cl_2. The extracts were washed with saturated aq NaCl, dried (Na_2SO_4), and evaporated in vacuo. The residue was purified in a column of silica gel with AcOEt–hexane as an eluant, giving an inseparable mixture [9:9:1:1 (two D-gluco and two L-ido isomers)] of **4** as a colorless syrup, the ratio being determined by ^1H and ^{31}P NMR: 620 mg (85%); R_f=0.28 (B); ^1H NMR (500 MHz) for two D-gluco isomers δ=1.25, 1.28*, 1.45, 1.48* (3H each, 4s, CMe_2), 1.70, 2.09* (3H, 2s, AcO-3), 3.58, 3.61* (1H, 2m, H-5, their splitting patterns uncertain because of overlapping with other proton signals), 3.60, 3.67* (3H, 2d, J_{POMe}=11.1 Hz, POMe), 4.39, 4.48* (1H, 2d, $J_{1,2}$=3.8, 3.6* Hz, H-2), 4.50, 4.59* (1H, 2ddd, $J_{4,5}$=9.7, 9.1*, $J_{4,P}$=5.7, 7.4*, $J_{3,4}$=2.8, 2.9* Hz, H-4), 4.51, 4.87* (1H, 2td, $J_{6',P}$=14.9, 15.2*, $J_{6,6'}$=14.9, 15.0*, $J_{5,6'}$=4.9, 5.4* Hz, H-6'), 4.77, 4.89* (1H, 2ddd, $J_{6,P}$=12.2, 13.7*, $J_{5,6}$=6.4, 7.0* Hz, H-6), 4.99, 5.25* (1H, 2d, H-3), 5.74, 5.78* (1H, 2d, H-1), 7.54, 7.54* [2H, m, Ph(*m*)], 7.63, 7.64* [1H, 2m, Ph(*p*)], 7.74, 7.78* [2H, 2m, Ph(*o*)], * for another diastereomer with regard to the phosphorus atom (the assignment of some of the δ values may have to be interchanged); ^{31}P NMR δ=39.1 and 38.0 (D-gluco), 39.4 and 38.6 (L-ido isomers); MS m/z 430 (M+1; 1.0), 414 (24), 354 (33), 340 (28), 312 (13), 293 (18), 265 (38), 258 (55), 211 (44), 173 (31), 155 (100). Found: m/z 430.1273. Calcd for $C_{18}H_{25}NO_9P$: M+1, 430.1267.

(5*R* and 5*S*)-3-*O*-Acetyl-5-deoxy-1,2-*O*-isopropylidene-5-[(*R* and *S*)-(methoxy)phenylphosphinyl]-α-D-*xylo*-hexofuranoses (6). Compound **4** (585 mg, 1.36 mmol) dissolved in a mixture of ethanol (3 ml) and acetic acid (0.15 ml, 2.6 mmol) was hydrogenolyzed in the presence of 20% $Pd(OH)_2$ on carbon (630 mg, 0.90 mmol) at 20 °C under atmospheric pressure of H_2. After 24 h, the catalyst was filtered off and the filtrate was evaporated in vacuo, giving 6-ammonio-hexofuranose acetate derivatives **5** as a colorless syrup: R_f=0.49 (D).

To a stirred solution of **5** in water (15 ml) was added, at 0 °C, acetic acid (0.20 ml, 3.5 mmol) and then sodium nitrite (384 mg, 3.57 mmol). After 2 h, the mixture was twice extracted with $CHCl_3$. The combined organic layers were washed with aq $NaHCO_3$ and then water, dried (Na_2SO_4), and evaporated in vacuo. The residue was separated by column chromatography (with AcOEt as an eluant), giving two fractions.[#]

The faster-eluting fraction [R_f=0.27 (A)] gave a colorless syrup which was one D-gluco isomer of **6** [but contained a minor amount (<10%) of an L-ido isomer]: 138 mg (25% from **4**): ^1H NMR (500 MHz) δ=1.30, 1.53 (3H each, 2s, CMe_2), 2.08 (3H, s, AcO-3), 2.63 (1H, dddd, $J_{5,P}$=13.9, $J_{4,5}$=10.9, $J_{5,6}$=5.1, $J_{5,6'}$=4.0 Hz, H-5), 3.60 (3H, d, J_{POMe}=11.0 Hz, POMe), 3.90 (1H, ddd, $J_{6',P}$=23.5, $J_{6,6'}$=11.9 Hz, H-6'), 3.91 (1H, ddd, $J_{6,P}$=7.0 Hz, H-6), 4.05 (1H, m, HO-6), 4.50 (1H, d, $J_{1,2}$=3.9, $J_{2,3}\approx$0 Hz, H-2), 4.77 (1H, ddd, $J_{4,P}$=5.0 Hz, $J_{3,4}$=2.8 Hz, H-4), 5.34 (1H, d, H-3), 5.85 (1H, d, H-1), 7.52 [2H, m, $J_{o,m}=J_{m,p}$=7.5, $J_{m,P}$=3.5 Hz, Ph(*m*)], 7.61 [1H, m, $J_{o,p}=J_{p,P}$=1.4 Hz, Ph(*p*)], 7.71 [2H, m, $J_{o,P}$=11.7 Hz, Ph(*o*)]; ^{31}P NMR δ=42.0.

The slower-eluting fraction [R_f=0.20 (A)] gave a colorless syrup which was mainly the other D-gluco isomer **6** [but contained a minor amount (<10%) of another L-ido isomer]: 144 mg (27% from **4**); ^1H NMR (500 MHz) δ=1.26, 1.42 (3H each, 2s, CMe_2), 1.96 (3H, s, AcO-3), 2.75 (1H, ddt, $J_{5,P}$=17.1, $J_{4,5}$=10.8, $J_{5,6}$=5.5, $J_{5,6'}$=5.4 Hz, H-5), 3.64 (3H, d, J_{POMe}=11.2 Hz, POMe), 3.68 (1H, m, HO-6), 4.04 (1H, ddd, $J_{6,6'}$=11.8, $J_{6',P}$=10.7 Hz, H-6'), 4.08 (1H, ddd, $J_{6,P}$=10.2 Hz, H-6), 4.38 (1H, ddd, $J_{4,P}$=6.0, $J_{3,4}$=2.7 Hz, H-4), 4.42 (1H, d, $J_{1,2}$=3.9, $J_{2,3}\approx$0 Hz, H-2), 5.08 (1H, d, H-3), 5.79 (1H, d, H-1), 7.53 [2H, m, Ph(*m*)], 7.61 [1H, m, Ph(*p*)], 7.74 [2H, m, Ph(*o*)]; ^{31}P NMR δ=42.0; MS m/z 401 (M+1; 1.0), 385 (16), 325 (13), 283 (21), 253 (25), 229 (54), 211 (20), 199 (37), 173 (34), 155 (100). Found: m/z 401.1353. Calcd for $C_{18}H_{26}NO_8P$: M+1, 401.1365.

(5*R* and 5*S*)-3-*O*-Acetyl-5-deoxy-1,2-*O*-isopropylidene-5-[(*R* and *S*)-(methoxy)phenylphosphinyl]-6-*O*-(tetrahydro-2-pyranyl)-α-D-*xylo*-hexofuranose (7). A solution of **6**[#] (140 mg, 0.350 mmol) and dihydropyran (0.10 ml, 1.1 mmol) in dry CH_2Cl_2 (1.5 ml) containing PPTS (50 mg, 0.20 mmol) was stirred for 10 h at 20 °C. The solution was diluted with ether, washed with half-saturated brine, dried (Na_2SO_4), and evaporated in vacuo. The residue was purified by column chromatography (with 3:1 AcOEt–hexane), giving **7** (154 mg, 90%) as a colorless syrup: R_f=0.45—0.30 (A); ^1H NMR (60 MHz) δ=1.25—1.65 [6H, m, C-(CH_2)$_3$-C-O-6], 1.28, 1.35, 1.45, 1.48 (6H, 4s, CMe_2), 1.96, 2.01, 2.06, 2.10 (3H, 4s, AcO-3), 2.45—2.85 (1H, m, H-5), 3.47, 3.50, 3.59 (3H, 3d, J_{POMe}=11.0 Hz, POMe), 3.50—4.15 (4H, m, CH_2-O-C-O-6, H_2-6), 4.25—4.65 (2H, m, H-4, CH-O-6), 4.45 (1H, d, $J_{1,2}$=4.0 Hz, H-2), 5.34 (1H, d, $J_{3,4}$=2.8 Hz, H-3), 5.80 (1H, d, H-1), 7.45—7.70, [3H, m, Ph(*m,p*)], 7.70—7.90 [2H, m, Ph(*o*)]; MS m/z 481 (M^+; 0.6), 469 (1.7), 401 (15), 385 (19), 325 (18), 283 (27), 253 (20), 229 (41), 199 (34), 173 (42), 155 (100). Found: m/z 484.1843. Calcd for $C_{23}H_{33}O_9P$: M, 483.1862.

1,2,3,4,6-Penta-*O*-acetyl-5-deoxy-5-phenylphosphino- (12) and 5-Phenylphosphinyl-α,β-D-glucopyranoses (13). To a solution of **7** (264 mg, 0.545 mmol) in dry benzene (5 ml) was added, with stirring, a solution of SDMA (3.4 M toluene

[#] Because the separation of the two fractions of **6** was rather difficult and each fraction was expected to give the same mixture of **8** and/or **9** after the SDMA reduction (Ref. 8), the combined fractions of **6** were used for the practical preparation of **7**.

solution, 0.50 ml, 1.7 mmol) in dry benzene (2 ml) in small portions at 5 °C under an argon atmosphere. The stirring was continued at this temp for 1 h. Then, water (0.5 ml) was added and the mixture was stirred for 30 min. The precipitate was centrifuged and washed with several portions of benzene. The organic layers were combined and evaporated in vacuo, giving the 5-phenylphosphino derivative **8** as a colorless syrup: R_f=0.78—0.70 (A): ^{31}P NMR δ=−53.4, −51.5; besides these strong signals, a weak signal (less than a 5% relative intensity) was observed at δ=30.1 most likely assignable to **9**.

The above syrup (mostly **8**) was immediately treated with a mixture of ethanol (5 ml) and 0.5 M hydrochloric acid (5 ml) at 90 °C for 3 h under an argon atmosphere. After cooling, the reactants were neutralized with weakly basic ion-exchange resin Amberlite IRA-45. The resin was filtered off and washed with water, and the filtrate was evaporated in vacuo to give a mixture of 5-deoxy-5-phenylphosphino- [**10**, R_f=0.74 (D), major] and 5-phenylphosphinyl-D-glucopyranoses [**11**, R_f=0.58 (D), minor] as a colorless syrup.

This was acetylated with acetic anhydride (1 ml) in dry pyridine (2 ml) for 12 h at 20 °C and then the mixture was concentrated in vacuo. The residue was separated by column chromatography with a gradient eluant of 1:1 AcOEt–hexane→AcOEt, into three fractions A—C.

Fraction A [R_f=0.56 (C)] gave a chromatographically inseparable mixture (31.3 mg) consisting of 5-[(*R*)-phenylphosphino]-α-D-glucopyranose **12a** (2.0% from **7**) and its β-isomer **12b** (9.9%). Pure compound **12b** was obtained by recrystallization of the above mixture from 1:1 AcOEt–hexane: colorless prisms, mp 148—149 °C; ^{1}H and ^{31}P NMR, see Table 1; MS *m/z* 483 (M+1; 0.8), 440 (4.1), 381 (100), 339 (27), 321 (12), 279 (32), 261 (12), 237 (23), 219 (28), 125 (22). Found: C, 54.35; H, 5.58%; *m/z* 483.1420. Calcd for $C_{22}H_{27}O_{10}P$: C, 54.77; H, 5.64%. Calcd for $C_{22}H_{28}O_{10}P$: (M+1), 483.1420.

Fraction B [R_f=0.20 (C)] gave colorless crystals (26.7 mg) which consisted of 5-[(*S*)-phenylphosphinyl]-α-D-glucopyranose **13a** (4.5% from **7**) and its β-isomer **13b** (5.3%); mp 226—228 °C (1:1 mixture, from AcOEt); ^{1}H and ^{31}P NMR, see Table 1; MS *m/z* 499 (M+1; 3.8), 456 (5.2), 397 (70), 355 (100), 337 (18), 295 (60), 253 (39), 234 (45), 159 (36), 125 (47). Found: C, 53.22; H, 5.54%; *m/z* 499.1382. Calcd for $C_{22}H_{27}O_{11}P$: C, 53.02; H, 5.46%. Calcd for $C_{22}H_{28}O_{11}P$: (M+1), 499.1369.

Fraction C [R_f=0.15—0.10 (C)] gave an inseparable mixture of products as a colorless syrup (5 mg, ca. 2% from **7**); ^{31}P NMR δ=24.5, 25.8, 26.3; for their structures, see the main text.

The present work was partially supported by Grant-in-Aids for Scientific Research No. 02740269 (to T. H.) from the Ministry of Education, Science and Culture.

References

1) H. Yamamoto and T. Hanaya, "Studies in Natural Products Chemistry," ed by T. I. Atta-ur-Rahman, Elsevier, Amsterdam (1990), Vol. 6, pp. 351—384; H. Yamamoto and S. Inokawa, *Adv. Carbohydr. Chem. Biochem.*, **42**, 135 (1984).

2) T. Richter, P. Luger, T. Hanaya, and H. Yamamoto, *Carbohydr. Res.*, **193**, 9 (1989); H. Yamamoto, T. Hanaya, H. Kawamoto, S. Inokawa, M. Yamashita, M.-A. Armour, and T. T. Nakashima, *J. Org. Chem.*, **50**, 3516 (1985).

3) H. Yamamoto, T. Hanaya, H. Kawamoto, and S. Inokawa, *J. Org. Chem.*, **53**, 4790 (1988); H. Yamamoto, K. Yamamoto, S. Inokawa, M. Yamashita, M.-A. Armour, and T. T. Nakashima, *ibid.*, **48**, 435 (1983); H. Yamamoto, H. Murata, S. Inokawa, M. Yamashita, M.-A. Armour, and T. T. Nakashima, *Carbohydr. Res.*, **133**, 45 (1984).

4) The only P-in-ring sugar analogs having a phosphinidene group prepared so far are 5-deoxy-5-ethylphosphino-3-*O*-methyl-D-xylopyranoses and their 5-phenyl congeners: T. Hanaya, N. Shigetoh, H. Yamamoto, M.-A. Armour, and A. M. Hogg, *Bull. Chem. Soc. Jpn.*, **63**, 421 (1990).

5) R. L. Whistler and R. E. Pyler, *Carbohydr. Res.*, **12**, 201 (1970).

6) H. Paulsen and W. Greve, *Chem. Ber.*, **106**, 2114 (1973).

7) When the 5-[(ethyl)methoxyphosphinyl] congener of **7** was subjected to the SDMA reduction, the 5-ethylphosphinyl derivatives corresponding to **9** were obtained accompanied by exclusive epimerization at C-5: see Ref. 3. The reason for this seeming discrepancy is still under intensive study.

8) The SDMA reduction of similar sugar analogs bearing either an [(*R*)- or [(*S*)-(alkoxy)phenylphosphinyl] group is known to accompany epimerization of the phosphorus atom to give an identical [(*R,S*)-phenylphosphinyl] derivative: T. Hanaya, N. Shigetoh, and H. Yamamoto, *Bull. Chem. Soc. Jpn.*, **61**, 2499 (1988), and references cited therein.

Reaction of Thioaldehydes with Amines

Kentaro OKUMA,* Yasuo KOMIYA, and Hiroshi OHTA
Department of Chemistry, Faculty of Science, Fukuoka University, Jonan-ku, Fukuoka 814-01
(Received May 7, 1991)

The reaction of phosphonium ylides with elemental sulfur gave thioaldehydes, which changed to the corresponding thioamides in good yields when treated with amines. When thioaldehydes containing α-hydrogens were treated with secondary amines, the corresponding enamines or reduction products were obtained.

The chemistry of thiocarbonyl compounds has been of current interest.[1] Several authors have reported the formation of thioaldehydes (**1**). Kirby and Lochead reported the generation of thioaldehydes from S-esters of sodium hydrogenthiosulfate.[1a] Generation of thioaldehydes also occurs from the Norrish cleavage of phenacyl sulfides.[1b] Recently, we also showed that the reaction of phosphonium ylides (**2**) with elemental sulfur or thiiranes gave symmetrical olefins via thiocarbonyl compounds.[2] Reactions of these relatively unstable thioaldehydes are of much interest. However, there are quite a few reports on the reaction of these thioaldehydes with amines. Okazaki has reported that the reaction of 2,4,6-tri-*t*-butylthiobenzaldehyde with primary amines afforded the corresponding imines.[3] Recently, we reported the reaction of **1** with secondary amines (**3**) afforded the corresponding thioamides (**4**) in good yields.[4] In this paper, we would like to give a detailed account on the reaction of thioaldehydes with amines.

Results and Discussion

We first tried the reaction of methoxycarbonylmethylenetriphenylphosphorane (**2a**) with sulfur in the presence of secondary amines, **3**. Treatment of **2a** with elemental sulfur and morpholine in toluene gave the corresponding thioamide (**4a**) in 75% yield. As shown in Table 1, other thioamides, **4**, were obtained in good yields. Since thioaldehyde (**1a**) could be also synthesized by the reaction of the corresponding sulfenyl chloride with triethylamine,[1a] we also carried out the reaction of **1a** starting from methyl mercaptoacetate (methyl thioglycolate) (**5a**) with morpholine. The reaction of thioaldehydes derived from thiols with N-chlorosuccinimide (NCS) with secondary amines also gave the corresponding thioamides, **4**, in good yields. Other reactions were carried out in a similar manner. However, when phenylmethanethiol (**5d**) and methanethiol (**5e**) were used as starting thiols, only the corresponding sulfenamides (**6**) were obtained. Thus, electron-withdrawing groups were required to obtain thioamides in this reaction. (Table 2)

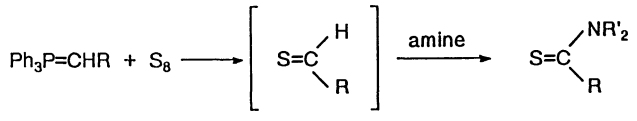

Scheme 1.

Table 1. Reaction of Thioaldehydes with Secondary Amines

Thioaldehyde 1	R	Amine 3	Thioamide (yield/%) 4	
a	COOMe	Morpholine	**4a**	75
a	COOMe	Dimethylamine	**4b**	76
a	COOMe	Piperidine	**4c**	60
a	COOMe	Pyrrolidine	**4d**	47
b	COOEt	Morpholine	**4e**	73
c	Ph	Morpholine	**4f**	56

Milligan and Swan reported that the reaction of *O*-carbamoylmethyl thiosulphate with primary and secondary amines afforded 2-amino-2-thiooxoacetoamides and disulfides. They suggested that these compounds might be formed in a complex manner from thioaldehyde intermediates.[5] As to the formation of thioamides, **4**, the following mechanism is reasonable: Thioaldehydes, **1**, were converted to the corresponding bis(dialkylamino)alkanes, **7**, (aminal) by treatment with amines in a manner similar to the reaction of amines with aldehydes. The resulting **7** further reacted with the hydrogen sulfide produced to give thioamides, **4**.

The above mechanism was confirmed by the following two reactions. When the reaction of **2c** with sulfur in the presence of morpholine was carried out at 50 °C, **7** was isolated in 70% yield instead of **4f**. Additionally,

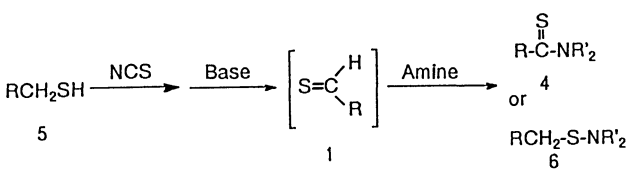

Scheme 2.

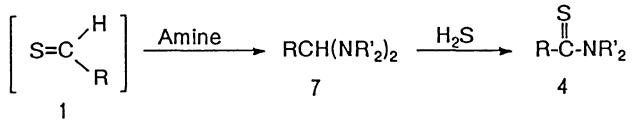

Scheme 3.

Table 2. Reaction of Thiols with NCS Followed by the Addition of Amines

Thiol 5	R	Conditions: Base	Solvent	Temperature/°C	Amine	Products (Yield/%)	
5a	COOMe	DBU	CH_2Cl_2	Reflux	Morpholine	**4a**	55
		DBU	THF	Reflux	Morpholine	**4a**	65
		BuLi	THF	0	Morpholine	**4a**	75
		DBU	CH_2Cl_2	Reflux	Dimethylamine	**4b**	65
		BuLi	THF	0	Dimethylamine	**4b**	75
5b	COOEt	BuLi	THF	0	Morpholine	**4e**	70
5c	4-$NO_2C_6H_4$-	DBU	CH_2Cl_2	Reflux	Morpholine	**4g**	91
5d	Ph	DBU	CH_2Cl_2	Reflux	Morpholine	**6a**	55
		BuLi	THF	0	Morpholine	**6a**	70
5e	H-	BuLi	THF	0	Morpholine	**6b**	70

treatment of **7** with hydrogen sulfide afforded the corresponding thioamide, **4f**, 65% yield. It is well known that thioamides were formed by the reaction of sulfur with aryl alkyl ketones (Willgerodt–Kindler reaction).[6] In this case, the primary step might be the formation of aminals, **7**, resulting from the action of the amine on the ketones, which then changed to thioamides as shown in the present reaction.

We further tried the reaction of **1a** with sulfur in the presence of primary amines. Treatment of **1a** with sulfur in the presence of isobutylamine also gave thioamides, **4h**. The resulting **4h** further reacted with isobutylamine to give *N*,*N*′-diisobutyl-2-amino-2-thiooxoacetamide (**8**) in 64% yield. However, when benzylidenetriphenylphosphorane, **2c**, was treated with elemental sulfur and isobutylamine, the observed products were benzylideneisobutylamine and triphenylphosphine sulfide. The corresponding thioamide could not be obtained. Electron-withdrawing groups on the phosphonium ylides might be necessary for thioamide synthesis.

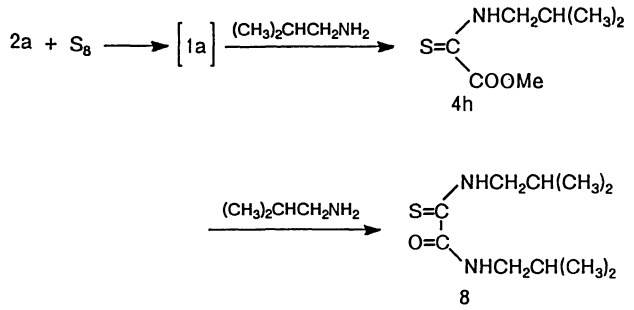

Scheme 4.

To confirm the formation of thioaldehydes, **1**, in this reaction, we tried the reaction of phosphonium ylides, **2**, with sulfur in the presence of dienes. Treatment of phosphonium ylide, **2a**, with elemental sulfur in the presence of 2,3-dimethyl-1,3-butadiene or cyclopentadiene afforded the corresponding Diels–Alder adduct, **9** or **10**, in 56% or 64% yield, respectively.

We then tried the reaction of thioaldehydes containing α-hydrogens with secondary amines. The results of these reactions were different from previous ones. First, we tried the reaction of phenethyltriphenylphosphonium bromide with elemental sulfur and secondary amines. The obtained products were the corresponding enamine (**11**) and triphenylphosphine

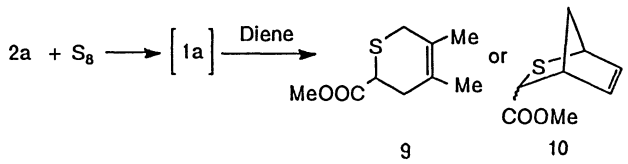

Scheme 5.

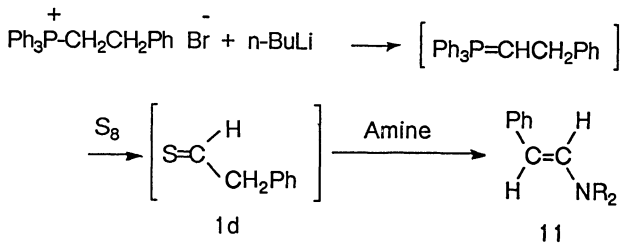

Scheme 6.

Table 3. Reaction of Thioaldehyde **1d** with Sulfur in the Presence of Secondary Amines

Compound 1	R	Amine	Conditions: Solvent	Time/h	Products (yield%) 11	
d	CH_2Ph	Morpholine	Benzene	2	**11a**	10
d	CH_2Ph	Pyrrolidine	Benzene	2	**11b**	13
d	CH_2Ph	Dimethylamine	Benzene	2	**11c**	10

Table 4. Reaction of Thioaldehyde **1e** with Sulfur in the Presence of Amines

Compound 1	R	Secondary Amine	Conditions		Compounds (yield/%) 12	
			Solvent	Time/h		
e	CH_2COOEt	Morpholine	Benzene	2	**12a**	60
e	CH_2COOEt	Dimethylamine	Benzene	2	**12b**	60
e	CH_2COOEt	Butylamine	Benzene	2	**12c**	57

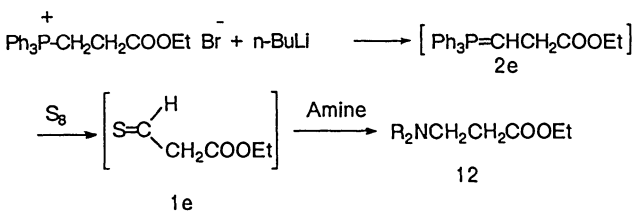

Scheme 7.

sulfide. This result suggested that these reactions would proceed through thiobenzaldehyde intermediates, which further reacted with amines to give enamines. However, the yields of enamines were very low and other unidentifiable products were obtained. Meyer and Gewald reported that enamines were easily changed to the corresponding thioamides in good yields.[7] However, we could not isolate the corresponding thioamides in the present work. The difference in the reactivity might be due to the difference in the substituents.

We then tried the reaction of other types of thioaldehydes. Treatment of 2-ethoxycarbonylethylidenetriphenylphosphoran (**2e**) with elemental sulfur and morpholine afforded ethyl 3- morpholinopropionate (**12a**) and triphenylphosphine sulfide in 60 and 82% yields, respectively. Asinger et al. reported the reaction of alkyl aryl ketones with sulfur and NH_3.[6] They suggested that these ketones were converted to the corresponding thioketones, the thiocarbonyl group of which was reduced to the methylene group by treatment of hydrogen sulfide. The present reaction might proceed in a similar manner.

Thioamide syntheses from thioaldehydes were previously reported by only one group. Fischer and coworkers reported that the reaction of thioaldehyde-metal complexes with ynamines afforded thioamides by cycloaddition followed by extrusion of metals and the addition of carbon monooxide.[8]

In summary, we found that thioaldehydes show a different reactivity upon treatment with amines depending on whether the aldehydes have α-hydrogens or not. Thioaldehydes with the α-hydrogens gave the reduction products. On the other hand, thioaldehydes without the α-hydrogens afforded thioamides in good yields.

Experimental

General. Melting points are uncorrected. ^1H NMR spectra were determined with a JEOL PMX-60, a FX-90, or a GX-400 spectrometer. Mass spectra were recorded on a JEOL GS 270 spectrometer.

Materials. Stable phosphonium ylides were prepared by a method mentioned in the literature.[9] Methyl thioglycolate, *N*-chlorosuccinimide, 4-nitrobenzyl bromide were purchased from Wako Pure Chem. Compounds **12a** and **12b** were prepared by the reaction of ethyl acrylate with the corresponding amines.[10]

Reaction of 2a with Sulfur in the Presence of Secondary Amines. To a solution of **2a** (1.67 g, 10 mmol) and morpholine (1.74 g, 20 mmol) in toluene (25 ml) was added a solution of sulfur (0.64 g, 20 mmol) in toluene (20 ml). After refluxing for 12 h, the reaction mixture was washed with water and evaporated to give yellow oily crystals. This mixture was extracted with hexane (30 ml×3). The combined extracts were evaporated to give thioamide **4a**. Other reactions were carried out in a similar manner.

4a; 0.71 g (3.7 mmol, 75%), mp 77—79 °C, ^1H NMR ($CDCl_3$) δ=3.56—3.65 (m, 2H), 3.74—3.86 (m, 4H), 3.87 (s, 3H), 4.15—4.24 (m, 2H). Precise mass for $C_7H_{11}NO_3S$: 189.0459 (calcd), 189.0492 (found).

4b; 0.44 g (3.8 mmol, 76%), ^1H NMR($CDCl_3$) δ=3.17 (s, 3H), 3.30 (s, 3H), 3.83 (s, 3H). Precise mass for $C_5H_9NO_2S$: 147.0354 (calcd), 147.0419 (found).

4c; 0.58 g (2.8 mmol, 60%), ^1H NMR ($CDCl_3$) δ=1.88—2.20 (m, 4H), 3.49—3.78 (m, 4H), 3.86 (s, 3H). Precise mass for $C_8H_{13}NO_2S$: 187.0667 (calcd), 187.0631 (found).

4d; 0.41 g (2.4 mmol, 47%), ^1H NMR ($CDCl_3$) δ=1.58—1.85 (m, 4H), 3.40—3.86 (m, 2H), 3.86 (s, 3H), 3.96—4.23 (m, 2H). Precise mass for $C_7H_{11}NO_2S$: 173.0510 (calcd), 173.0473 (found).

4e; 0.68 g (3.6 mmol, 73%), ^1H NMR ($CDCl_3$) δ=1.32 (t, 3H), 3.53—4.11 (m, 8H), 4.29 (q, 2H). Precise mass for $C_8H_3NO_3S$: 203.0616 (calcd), 203.0562 (found).

Reaction of 2c with Sulfur in the Presence of Morpholine. To a solution of benzyltriphenylphosphonium bromide (2.25 g, 5 mmol) in benzene (30 ml) was added a solution of butyllithium (4.5 ml, 10% w/v, 7 mmol) in hexane at room temperature. After stirring for 1 h, morpholine (4.35 g, 50 mmol) and sulfur (0.32 g, 10 mmol) were added and refluxed for 2 h. The resulting mixture was washed with water (20 ml×2) and evaporated to give yellow oily crystals. This mixture was extracted with hexane (30 ml×3). The combined extracts were evaporated to give *N*-thiobenzoylmorpholine **4f** (0.58 g, 2.8 mmol, 56%), mp 134—134.5 °C, (lit,[11] mp 134.5—136 °C). ^1H NMR ($CDCl_3$) δ=3.62 (br s, 4H), 3.89 (m, 2H), 4.48 (m, 2H), 7.27 (m, 5H). Anal. Calcd for $C_{11}H_{13}NOS$: C, 63.74; H, 6.32; N, 6.76%. Found: C,63.95; H, 6.67; N, 6.90%.

Preparation of 4-Nitrophenylmethanethiol, (5c). To a solution of sodium thiosulfate (4.96 g, 20 mmol) in water (50 mL) was added a solution of 4-nitrobenzyl bromide (4.32 g, 20 mmol) in ethanol (20 mL). Afer stirring for 24 h, 5 mL of concd HCl was added to this solution and refluxed for 3 h.

The resulting solution was condensed to 40 mL and extracted with dichloromethane (15 mL) for three times. The combined extract was dried over $MgSO_4$ and evaporated to give the corresponding thiol, **5c** (2.21 g, 65%), mp 56—57 °C, (lit,[132] mp 58 °C).

Reaction of Methyl Thioglycolate with *N*-Chlorosuccinimide Followed by the Addition of DBU and Elemental Sulfur. To a solution of *N*-chlorosuccinimide (0.81 g, 6.0 mmol) in 20 mL of dichloromethane was added a solution of methyl thioglycolate (0.53 g, 5.0 mmmol) in dichloromethane (10 mL). After stirring for 2 h, the resulting suspension was filtered. The yellow filtrate was added to a solution of DBU (1.17 g, 7.0 mml) and morpholine (0.52 g, 6.0 mmol) in dichloromethane (30 mL) After refluxing for 3 h, the reaction mixture was washed with water and extracted with ether (15 mL×3). The combined extracts were dried over sodium sulfate and evaporated to give a pale yellow oil. The resulting oil was chromatographed over silica gel by elution with dichloromethane–ethyl acetate to afford **4a** in 65% yield. Mp 77—79 °C. Thioamides **4b** and **4e** were also prepared in a similar manner.

Reaction of 4-Nitrophenylmethanethiol, (5c), with NCS Followed by the Addition of DBU and Morpholine. To a solution of NCS (0.67 g, 5 mmol) in dichloromethane (20 mL) was added a solution of 4-nitrophenylmethanethiol (0.68 g, 4 mmol) in dichloromethane (10 mL) at room temperature. After stirring for 2 h, the resulting suspension was filtered. The filtrate was added a solution of morpholine (0.35 g, 4 mmol) and DBU (0.76 g, 5 mmol) in dichloromethane (30 mL) and refluxed for 3 h. The reaction mixture was washed with water, dried over $MgSO_4$, and evaporated to give pale yellow crystals. Recrystallization from methanol afforded colorless crystals of thioamide, **4g** (yield 91%). Mp 193—194 °C; Anal. Calcd for $C_{11}H_{12}N_2O_3S$: C, 52.37; H, 4.79; N, 11.10%. Found: C, 52.02; H, 4.86; N, 11.07%.

Reaction of Methanesulfenyl Chloride with Morpholine. To a solution of morpholine (0.87 g, 10 mmol) in 30 ml of THF was added a solution of methanesulfenyl chloride (0.28 g, 3 mmol) in THF at −15 °C. Immediately, white crystals of morpholinium chloride were precipitated. The suspension was stirred for 3 h, washed with water, and extracted with hexane (15 mL×3). The combined extracts were dried over $MgSO_4$ and evaporated to give a pale brown oil, which was subjected to bulb-to-bulb distillation to give a pale yellow oil of methylsulfenylmorpholide (mp 40—50 °C/0.5 mmHg; lit,[13] 48—49 °C/5 mmHg, 1mmHg=133.322 Pa). *N*-benzylsulfenylmorpholine, (**6a**), was obtained in a similar manner. Mp 73—74 °C, (lit,[13]) mp 73.5—74.5 °C.

Reaction of 2c with Morpholine in the Presence of Sulfur at 50 °C (Preparation of 7). To a suspension of benzyltriphenylphosphonium chloride (1.94 g, 5 mmol) in benzene (25 mL) was added butyllithium (10% w/v, 4 mL, 6 mmol) in hexane. To this suspension, morpholine (1.74 g, 20 mmol) and sulfur (0.32 g, 10 mmol) were added portionwise at room temperature. After stirring for 1 h at 50 °C, the reaction mixture was evaporated to give pale yellow oily crystals. Recrystallization from ethanol gave colorless crystals of aminal **7** (0.71 g, 3.25 mmol), mp 100—101 °C, (lit,[14] 100—101.5 °C).

Reaction of 2c with Sulfur in the Presence of Primary Amines. To a solution of benzyltriphenylphosphonium bromide (2.25 g, 5 mmol) in benzene was added a solution of butyllithium (4.5 ml, 10% w/v, 7 mmol) at room temperature. After stirring for 1 h, butylamine (3.60 g, 50 mmol) and sulfur (0.32 g, 10 mmol) were added and refluxed for 2 h. The resulting mixture was washed with water and evaporated to give yellow oily crystals. The mixture was extracted with hexane (30 ml×3). The combined extracts were evaporated to give a yellow oil, which was distilled under reduced pressure (bulb-to-bulb distillation) to give a colorless oil of benzylidenebutylamine. Other reaction was carried out in a similar manner. Benzylidenebutylamine: 0.41g (2.6 mmol, 51%), 50—60 °C/4 mmHg, (lit,[15] 128—131 °C/25 mmHg), ^{1}H NMR ($CDCl_3$) δ=0.70—2.00 (m, 7H), 3.72—3.87 (m, 2H), 7.10—7.93 (m, 5H), 8.17 (s, 1H). Benzylideneisobutylamine; 0.56 g (3.5 mmol, 70%), 50—60 °C/4 mmHg, ^{1}H NMR ($CDCl_3$) δ=0.99 (d, $2CH_2$ J=6.8 Hz), 1.78—2.30 (m, 1H), 3.43 (d, CH_2, J=6.8 Hz), 7.20—7.72 (m, 5H), 8.06 (s, 1H).

Reaction of 2a with Sulfur in the Presence of Diene. To a solution of **2a** (1.68 g, 5.0 mmol) and 2, 3-dimethyl-1,3-butadiene (2 ml, 20 mmol) in toluene (40 ml) was added elemental sulfur (0.64 g, 20 mmol). After refluxing for 20 h, the resulting mixture was evaporated to give reddish-brown oily crystals. This mixture was extracted with methanol(30 ml×2). The combined extracts were evaporated to give a reddish-brown oil, which was chromatographed over silica gel by elution with hexane–dichloromethane (3:1) to give adduct **9** (0.52 g, 2.8 mmol, 56%).[2,16] Adduct **10** was prepared in a similar manner.

10;[2] 0.54 g (3.2 mmol, 64%), ^{1}H NMR ($CDCl_3$) (*Endo*) δ=1.66 (br s, CH_2), 3.56 (s, Me), 3.75 (br s, CH), 4.18 (br CH), 4.44 (d, CH, J=3.0 and 5.1 Hz); (*Exo*) δ=1.84 (br s, CH_2), 3.29 (s, CH), 3.54 (br, CH), 3.86 (s, Me), 4.07 (br, CH), 5.91 (dd, =CH, J=3.2 and 6.2 Hz), 6.36 (dd, =CH, J=3.2 and 4.8 Hz).

Reaction of 2a with Sulfur in the Presence of Primary Amines, To a solution of **2a** (1.67 g, 5 mmol) and isobutylamine (1.82 g, 25 mmol) in benzene (50 mL) was added a solution of sulfur (0.32 g, 10 mmol) in benzene. After refluxing for 5 h, the reaction mixture was washed with water and evaporated to give yellow oily crystals. This mixture was extracted with hexane (30 ml×3). The combined extracts were evaporated to give a yellow oil, which was distilled under reduced pressure (bulb-to-bulb distillation) to give a colorless oil of **8**.

8; 0.66 g (3.1 mmol, 61%), mp 90—100 °C/2.5 mmHg. ^{1}H NMR ($CDCl_3$) δ=0.94 (d, 2 CH_3, J=3.2 Hz), 1.01 (d, 2 CH_3 J=3.4 Hz), 1.65—2.33 (m, 2 H), 3.16 (t, CH_2, J=6.6 Hz), 3.44—3.60 (m, CH_2), 8.59 (br, NH), 10.00 (br, NH). ^{13}C NMR ($CDCl_3$) δ=20.02 (CH_3), 20.28 (CH_3), 27.39 (CH), 28.43 (CH), 48.02 (CH_2), 53.39 (CH_2), 158.71 (C=O), 186.53 (C=S). Precise mass for $C_{11}H_2N_2ON_2OS$: 216.1296 (calcd) , 216.1273 (found).

Reaction of 2d with Sulfur in the Presence of Secondary Amines (Preparation of Enamines). To a solution of phenethyltriphenylphosphonium bromide (2.24 g, 5 mmol) in the benzene was added a solution of butyllithium (4.5 ml, 10% w/v, 7 mmol) in hexane at room temperature. After stirring for 1 h, morpholine (2.18 g, 25 mmol) and sulfur (0.32 g, 10 mmol) were added and stirred for 2 h. The resulting mixture was washed with water and evaporated to give brown oily crystals. This mixture was extracted with hexane (15 mL×3). The combined extracts were evaporated to give a yellow oil, which was distilled under reduced pressure (bulb-to-bulb distillation) to give a colorless oil of **11a**.

11a; 0.095 g (0.5 mmol, 10%), mp 100—110 °C/1.0 mmHg. ^{1}H NMR ($CDCl_3$) δ=2.98 (t, 4H, J=4.63 and 5.13 Hz), 3.73 (t, 4H,J= 4.88 Hz), 5.41 (d, =CH, J=14.16 Hz), 6.59,

(d, =CH, J=14.16 Hz), 7.18 (m, 5H). ^{13}C NMR ($CDCl_3$) δ= 49.03 (CH_2), 66.36 (CH_2), 101.47 (=CH), 124.28, 124.38, 128.50, 138.74 (Ar), 139.66 (=CH). Precise mass for $C_{12}H_{15}NO$: 189.1154 (calcd), 189.1167 (found).

11b; 0.11 g (0.065 mmol, 13%), mp 140—150 °C/1.5 mmHg.[17] ^{1}H NMR ($CDCl_3$ δ=1.90 (m, 4H), 3.21 (m, 4H), 5.08 (d, =CH, J=13.92 Hz), 6.96—7.18 (m, Ar and =CH). ^{13}C NMR ($CDCl_3$) δ=25.25 (CH_2), 48.97 (CH_2, 97.62 (=CH), 122.92, 123.36, 128.50, 140.20 (Ar), 135.82 (=CH).

11c; 0.08 g (0.05 mmol, 10%), mp 90—100 °C/1.0 mmHg. ^{1}H NMR ($CDCl_3$ δ=2.77 (S, 2 CH_3), 5.17 (d, =CH), 6.76 (d, =CH), 7.20 (m, 5 H).

Reaction of 2e with Sulfur in the Presence of Amines. To a suspension of (2-ethoxycarbonylethyl)triphenylphosphonium bromide (2.22 g, 5 mmol) in benzene was added a solution of butyllithium (4.5 ml, 10% w/v, 7.0 mmol) in hexane at room temperature. After stirring for 1 h, morpholine (4.35 g, 50 mmol) and sulfur (0.32 g, 10 mmol) were added and the solution was refluxed for 2 h. The resulting mixture was washed with water and evaporated to give yellow oily crystals. This mixture was extracted with hexane(30 ml×3). The combined extracts were evaporated to give a yellow oil, which was distilled under reduced pressure (bulb-to-bulb distillation) to give a colorless oil of **12a**. Other reactions were carried out in a similar manner.

12a; 0.56 g (3.0 mmol, 60%), mp 80—90 °C/2.0 mmHg. ^{1}H NMR ($CDCl_3$) δ= 1.27 (t, CH_3), 2.32—2.72 (m, 8H), 3.57 (m, 4H), 4.14 (q, 2H). ^{13}C NMR ($CDCl_3$) δ=14.30 (CH_3), 32.29 (CH_2), 53,52 (CH_2), 54.07 (CH_2), 60.35 (CH_2), 66.96 (CH_2).

12b; 0.44 g (3.0 mmol, 60%), 100—110 °C/3.0 mmHg. ^{1}H NMR ($CDCl_3$) δ=1.26 (t, CH_2, J=7.08 Hz), 2.25 (s, 2CH_3), 2.55 (m, 4H), 4.15 (q, 2H, J=7.33 and 7.08 Hz). ^{13}H NMR ($CDCl_3$) δ=14.25 (CH_2), 33.05 (CH_2), 45.24 (2CH_3), 54.93 (CH_2), 60.35 (CH_2), 172.49 (C=O).

Ethyl 3-Butylaminopropionate (12c); 0. 50 g (2.9 mmol, 57%), mp 90—100 °C/2.5 mmHg. ^{1}H NMR ($CDCl_3$) δ= 0.69—1.58 (m, 7H), 1.25 (t, CH_3), 2.25—1.96 (m, 6H), 4.06 (q, 2H). Precise mass for $C_9H_{19}NO_2$; 173.1415 (cald), 173.1396 (found).

This work was partly supported by the Central Research Institute of Fukuoka University and a Grant-in-Aid for Scientific Research No. 02640415 from the Ministry of Education, Science and Culture. We are grateful to Dr. Haruo Matsuyama at Tokyo Metropolitan University for the high-resolution mass spectroscopic analysis.

References

1) a) G. W. Kirby and A. W. Lochead, *J. Chem. Soc., Chem. Commun.*, **1983**, 1325; b) G. W. Kirby, A. W. Lochead, G. Baldwin, and R. C. Gerald Kopez, *J. Chem. Soc., Chem. Commun.*, **1983**, 1029; *Tetrahedron*, **39**, 1487 (1983); c) E. Block and S. Ahmad, *J. Am. Chem. Soc.*, **106**, 8295 (1984); d) G. A Krafft and P. T. Meinke, *Tetrahedron Lett.*, **26**, 1947 (1985).

2) K. Okuma, Y. Tachibana, J. Sakata, T. Komiya, I. Kaneko, Y. Komiya, S. Yamamoto, and H. Ohta, *Bull. Chem. Soc. Jpn.*, **61**, 4323 (1988). K. Okuma, Y. Yamasaki, T. Komiya, Y. Komiya, Y. Kodera, and H. Ohta, *Chem. Lett.*, **1987**, 357.

3) R. Okazaki, *Nippon Kagaku Kaishi.*, **1987**, 1142.

4) K. Okuma, Y. Komiya, and H. Ohta, *Chem. Lett.*, **1988**, 1145.

5) B. Milligan and J. M. Swan, *J. Am. Chem. Soc.*, **81**, 2969 (1959)

6) F. Asinger, W. Schäfer, K. Halcour, A. Saus, and H. Triem, *Angew. Chem., Int. Ed. Engl.*, **3**, 19 (1964), and references cited therein.

7) R. Meyer and K. Gewald, *Angew. Chem., Int. Ed. Engl.*, **6**, 294 (1967).

8) H. Fischer, A. Tiriliomis, U. Gerbing, B. Huber, and G. Müller, *J. Chem. Soc., Chem. Commun.*, **1987**, 559.

9) G. Wittig and U. Schollkopf, *Chem. Ber.*, **78**,1318 (1954).; For reviews, see J. Emsley and D. Hall,"The Chemistry of Phosphorus," Harper & Row Ltd., London (1976), pp. 274—278; A. Maecker, *Org. React., N. Y.*, **14**, 270 (1965).

10) R. W. Holley and A. D. Holley, *J. Am. Chem. Soc.*, **71**, 2124 (1949).

11) F. H. McMillan and J. A. King, *J. Am. Chem. Soc.*, **70**, 4143 (1948).

12) W. J. Horn, *J. Am. Chem. Soc.*, **43**, 2603 (1921).

13) H. Minato, K. Okuma, and M. Kobayashi, *J. Org. Chem.*, **43**, 652 (1978).

14) M. Zief and J. P. Mason, *J. Am. Chem. Soc.*, **64**, 1 (1942).

15) K. N. Campbell, C. H. Helbing, M. P. Flokowski, and B. K. Campbell, *J. Am. Chem. Soc.*, **70**, 3868 (1948).

16) C. M. Bladen, I. E. G. Fergguson, G. W. Kirby, A. W. Lochead, and D. C. McDougall, *J. Chem. Soc., Chem. Commun.*, **1983**, 423.

17) H. Böhme and G. Berg, *Chem. Ber.*, **99**, 2127 (1966).

 © 1991 The Chemical Society of Japan Bull. Chem. Soc. Jpn., 64, 2407—2410 (1991)

The Reaction of (Arylthio)trimethylstannanes with 1-Aryl-1-bromoethanes: Effect of Substituent on the Process Shifting from Unimolecular to Bimolecular Substitution

Seizi KOZUKA* and Hisashi NAKAMURA
Department of Applied Chemistry, Faculty of Engineering, Osaka City University, Sugimoto 3-Chome, Sumiyoshi, Osaka 558
(Received May 8, 1991)

A kinetic study has been conducted on the reaction of (arylthio)trimethylstannanes with 1-aryl-1-bromoethanes. The reaction of the arylbromoethane bearing an electron-donating substituent was found involving unimolecular ionization of the arylbromoethane. The other reactions, however, were found to be second-order reactions. The nature of the second-order reactions was shifted from one involving unimolecular ionization as the minor process, to a clear bimolecular nucleophilic reaction, according to the electron-withdrawing nature of the substituents on the arylbromoethanes.

The mechanisms of the reactions of (arylthio)trimethylgermanes have been known to be dependent on the nature of the substrates regardless of their quite similar aspects in the products. Namely, the reaction with benzoyl chloride was found to proceed by five-coordination of the germanium atom (Eq. 1).[1] The reaction with benzyl bromides, on the other hand, involved nucleophilic attack of the sulfur atom on the benzyl moiety (Eq. 2).[2]

$$(CH_3)_3GeSC_6H_4X + YC_6H_4COCl \xrightarrow{\text{5-Co. of Ge}} (CH_3)_3GeCl + YC_6H_4CO\text{–}SC_6H_4X \quad (1)$$

$$(CH_3)_3GeSC_6H_4X + YC_6H_4CH_2Br \xrightarrow{\text{Nu. attack of S}} (CH_3)_3GeBr + YC_6H_4CO\text{–}SC_6H_4X \quad (2)$$

The difference of those two reactions in their mechanisms has been rationalized in terms of different steric requirements of the individual substrates. The benzyl moiety provides enough room to be attacked by the sulfur atom of the bulky thiogermane. On the other hand, a similar attack of the sulfur of the thiogermane on the carbon atom of benzoyl functional group would be difficult by steric hindrance. Formation of the tetrahedral addition intermediate bearing four heavy atoms, including the sulfur with bulky trimethylgermyl group, would be difficult since they require much space around the central carbon atom. Hence, the reaction proceeds by five-coordination process when forced to proceed.

In this connection, it is quite natural that the analogous thiostannane could attack not only on benzyl[3] but also on benzoyl[4] substrates (Eq. 3). The bulky trimethylstannyl group does not inhibit the nucleophilic attack of the sulfur atom because the stannyl–sulfur bond is long enough providing a room around the reaction center of the sulfur atom.[2]

$$(CH_3)_3SnSC_6H_5X + YC_6H_4COCl \text{ (or } YC_6H_4CH_2Br) \xrightarrow{\text{Nu. attack of S}} (CH_3)_3GeCl \text{ (or Br)} + YC_6H_4CO\text{–}SC_6H_4X \text{ (or } YC_6H_4CH_2\text{–}SC_6H_4X) \quad (3)$$

On the other hand, the sulfur atom in the shorter silyl-sulfur linkage could not act as a nucleophile. The bulky trimethylsilyl group nearby the nucleophile of the sulfur, disturbs the reactivity by steric hindrance. Thus, the reaction of (arylthio)trimethylsilane with a haloalkane, phenacyl bromide, was found to proceed by another process i.e., five-coordination of the silicon atom (Eq. 4)[5]

$$(CH_3)_3SiSC_6H_4X + RBr \xrightarrow{\text{5-Co. of Si}} (CH_3)_3SiBr + RSC_6H_4X \quad (4)$$
(R=PhCOCH$_2$)

Standing on these results, an increment of steric hindrance on benzyl moiety would disturb the bimolecular nucleophilic attack. The reaction of (arylthio)trimethylgermanes with 1-aryl-1-bromoethanes (1-arylethyl bromides) was examined expecting mechanism shift from bimolecular nucleophilic to five-coordination process.

Unexpected unimolecular ionization of 1-aryl-1-bromoethanes was found as the mechanism. The result was also unexpected in view of the reaction conditions used, since the reaction was carried out under typical second order reaction conditions, with nearly equal amount of diluted nucleophile. The solvent was also unusual for the process because the reactions were carried out in aprotic solvents. The unexpected mechanism was undoubtedly due to the nature of the starting arylbromoalkane. The arylbromoalkane was a secondary alkyl bromide bearing an α-phenyl group which gives much stabilized carbenium ion on ionization (Eq. 5).[6]

$$(CH_3)_3GeSC_6H_4X + YC_6H_4CH(CH_3)Br \rightarrow [YC_6H_4C^+HCH_3\ Br^-] \rightarrow (CH_3)_3GeBr + YC_6H_4CH(CH_3)\text{–}SC_6H_4X \quad (5)$$

We have now extended our study to the reaction of (arylthio)trimethylstannane with 1-aryl-1-bromoethanes. The longer stannyl–sulfur bond may provide enough space for a bimolecular nucleophilic attack of the sulfur atom on the particular haloalkane, regardless of its facile unimolecular ionization. Preliminary aspects of

the reaction have been communicated recently.[7]

Results and Discussion

Trimethyl(phenylthio)stannane (1 g) was heated with an equimolar amount of 1-bromo-1-phenylethane at 110 °C for 24 h in a sealed tube. Only phenyl 1-phenylethyl sulfide and bromotrimethylstannane were found by ^{1}H NMR analysis of the resulting mixture. The products were isolated by fractional distillation and identified (Eq. 6).

$$(CH_3)_3SnSC_6H_5 + C_6H_5CH(CH_3)Br \xrightarrow{110\,^\circ C,\ 24\ h} (CH_3)_3SnBr + C_6H_5CH(CH_3)\text{–}SC_6H_5 \quad (6)$$

Rate of the reaction was measured by ^{1}H NMR analysis observing ratio of the trimethyl signals of the starting and the product stannanes at time. There were several limitations on the choice of the kinetic conditions. Some of the target trimethyl signals of the stannanes with certain substituents, could be observed separately under any reaction conditions. While, the signals of the other stannanes usually submerged into one signal by ligand-exchange reaction in common solvents. Pseudo-first-order kinetic conditions in less polar solvent of chloroform were chosen for the present study. Under these reaction conditions, the target signals could be observed separately for all the reactions of the stannanes bearing various substituents. Polar solvents and second-order reaction conditions could not be used for the present study.

A good linear pseudo-first-order kinetic plot was obtained up to 60% completion of the reaction in chloroform with 10-fold excess of 1-aryl-1-bromoethanes. A slight upward deviation of the plot was observed above 60% completion of the reaction. The deviation might due to the acceleration of the reaction by the products. In fact, additions of the products into the reaction solutions resulted noticeable acceleration of the rates of the reactions. Accordingly, rate constants for the reactions were obtained less than 60% completion of the reactions where such acceleration was nearly negligible.

Rate dependency on the concentration of 1-bromo-1-phenylethane was observed employing different concentrations of the arylbromoethane (Table 1, Entries 1, 2, and 3). Plot of the results gave a straight line of slope 1.1. Thus, first-order dependency on the concentration of the arylbromoethane was confirmed within experimental error. The result revealed total second-order reaction, dependent on both the concentrations of trimethyl(phenylthio)stannane and 1-bromo-1-phenyl-

Table 1. Pseudo-First-Order Rate Constants for the Reactions of $(CH_3)_3SnSC_6H_4$–X (SnS) with Y–$C_6H_4CH(CH_3)Br$ (PhEBr) in Chloroform

Entry	[SnS]×10² / mol dm⁻³	X	[PhEBr]×10 / mol dm⁻³	Y	Temp / °C±0.1	k×10⁵ / s⁻¹
1	6.0	H	3.0	H	100	5.17±0.41[a]
2	6.0	H	6.0	H	100	11.8±0.7[a,b]
3	6.0	H	7.5	H	100	15.7±0.9[a]
4	6.0	H	6.0	H	90	5.82±0.44[b,c,e]
5	6.0	H	6.0	H	80	2.55±0.24[b]
6	6.0	*p*-OCH_3	6.0	H	90	7.13±0.28[c]
7	6.0	*p*-CH_3	6.0	H	90	6.71±0.24[c]
8	6.0	*p*-Cl	6.0	H	90	5.01±0.26[c]
9	6.0	*m*-Cl	6.0	H	90	4.55±0.14[c]
10	6.0	H	6.0	*p*-CH_3	90	167[d,e]
11	6.0	H	6.0	*p*-CH_3	30	1.84±0.10
12	6.0	H	6.0	*p*-CH_3	40	3.98±0.25
13	6.0	H	6.0	*p*-CH_3	50	10.6±0.6[f]
14	6.0	H	6.0	*p*-Cl	90	4.00±0.35[e]
15	6.0	H	6.0	*m*-Cl	90	0.95±0.04[e]
16	6.0	H	6.0	*p*-NO_2	90	0.75±0.02[c,g,h]
17	4.62	H	6.0	*p*-CH_3	50	11.1±0.5[f]
18	8.58	H	6.0	*p*-CH_3	50	10.1±0.6[f]
19	4.62	H	6.0	*p*-NO_2	90	0.50±0.05[g]
20	8.58	H	6.0	*p*-NO_2	90	0.99±0.03[g]
21	6.0	*p*-OCH_3	6.0	*p*-NO_2	90	1.35±0.06[h]
22	6.0	*p*-CH_3	6.0	*p*-NO_2	90	1.10±0.10[h]
23	6.0	*p*-Cl	6.0	*p*-NO_2	90	0.43±0.01[h]
24	6.0	*m*-Cl	6.0	*p*-NO_2	90	0.29±0.02[h]

a) First-order dependency on [PhEBr](slope 1.1) for the reactions X=Y=H, (Entry 1, 2, and 3). b) $\Delta H^{\neq}_{400}$=84.8 kJ mol^{-1}, $\Delta S^{\neq}_{400}$=−95.2 J K^{-1} mol^{-1}, correlation coefficient (γ)= 0.9999, (2, 4, and 5). c) Effect of X for the reactions Y=H: $\rho_{X(\sigma)}$=−0.31, γ=0.9991, (4, 6 to 9). d) Estimated value (11, 12, and 13). e) No linear plot for the effect of Y, when X=H, (4, 10, and 14 to 16). f) No dependency on [SnS] for the reaction of Y=*p*-CH_3 (13, 17, and 18). g) First-order dependency on [SnS] (slope 1.1) for the reactions: X=H, Y=*p*-NO_2 (16, 19, and 20). h) Effect of X for the reactions Y=*p*-NO_2: $\rho_{X(\sigma)}$=−1.04, γ=0.999, (16, 21 to 24).

ethane.

Rates were measured for the reactions with (substituted arylthio)trimethylstannanes with 1-bromo-1-phenylethane. A small negative ρ_x value due to the effect of the substituent (X) was thus obtained (Table 1, $\rho_{X(\sigma)}=-0.31$, Entries 4, 6 to 9), with a straight Hammett plot. The second-order kinetic behavior together with the negative Hammett plot, would suggest a bimolecular nucleophilic attack of the sulfur atom on 1-bromo-1-phenylethane. The reaction, however, seems to be not fully consisted by the mechanism. The absolute ρ_x value appeared too small. There would be another contributing process, that might be an unimolecular ionization of 1-bromo-1-phenylethane, in view of the small absolute ρ_x value. The contribution of unimolecular process was confirmed by the reaction of the arylbromoethane having electron-withdrawing substituent. The detailed results of the unimolecular reaction will be described below. The results would suggest the contribution of the unimolecular process for the reaction of the unsubstituted 1-bromo-1-phenylethane at least in some extent.

Definitely, no dependency of the rate of the reaction on the concentration of the thiostannane was observed for the reaction of 1-bromo-1-(*p*-tolyl)ethane (Table 1, Y=*p*-CH_3, Entries 13, 17, and 18). The reaction with the arylbromoethane bearing an electron-donating substituent (Y=*p*-CH_3) would involve an unimolecular ionization of the arylbromoethane as the mechanism. The reaction of another arylbromoethane having more powerful electron-donating substituent (*p*-OCH_3) would proceed by the same manner. The arylbromoethane bearing *p*-OCH_3 as the substituent, Y could not be prepared in pure form due to its instability. The substituents, X effect would not be expected for the reactions when the 1-aryl-1-bromoethanes possesses electron-donating substituents.

On the contrary, another electronic nature of the 1-aryl-1-bromoethanes, that is the arylbromoethane bearing nitro group on the aryl ring, gave clearly contrasted result in the substituent (X) effect. Appreciable negative ρ_x value was observed for the reactions of the arylbromoethane bearing nitro group as the substituent, Y (Table 1, Y=*p*-NO_2, $\rho_{X(\sigma)}=-1.04$, Entries 16, 21 to 24). Rate dependency on the concentration of the thiostannane was examined for the reaction with the arylbromoethane bearing nitro group. A clear first-order dependency was observed on the concentration of the thiostannane within experimental error (Table 1, Entries 16, 19, and 20, slope=1.1). These results would clearly suggest a bimolecular nucleophilic attack of the sulfur atom as the mechanism for the reaction of 1-bromo-1-(*p*-nitrophenyl)ethane.

The expected mechanism shift from bimolecular nucleophilic to five-coordination, has not been observed. The present study, however, revealed that the nature of the arylbromoethanes effects dramatically on the course of the reaction. The process of the reactions clearly changed from first-order unimolecular ionization to second-order bimolecular nucleophilic attack.

The substituent effect on the benzylic substrates for bimolecular nucleophilic reactions usually gives complicated Hammett plots, although negative tendency appears as a whole.[8] A similar bent plot with a negative tendency was also observed for the analogous reaction of benzyl bromides with (arylthio)trimethylgermanes.[2] A particular electronic effect was discussed by Hudson et.al., explaining the bent plot.[8] On the other hand, slightly bent upwards, but almost linear and clearly large negative Hammett plots have been observed for the unimolecular reactions of benzylic substrates.[9] The upward deviations of Hammett plots for the unimolecular reactions have been rationalized by considering minor contribution of a bimolecular process.[6,9] A bent plot can be drawn in the present study for the effect of the substituent Y. However, the acceleration due to the *p*-methyl group appeared abnormally too much in comparison with that commonly observed for bimolecular reactions of benzylic substrates. Neither σ nor σ^+ constants gave linear correlations (Entries 4, 10, and 14 to 16). The abnormal acceleration due to *p*-methyl group was rationalized, as discussed above, by considering shift of the reaction mechanism.

The shift of the process would undoubtedly be dependent on the nature of the 1-aryl-1-bromoethanes. The easier ionize arylbromoethane, especially bearing electron-donating substituent, exclusively facilitated the unimolecular pathway. The opposite nature of the substituent, on the other hand, brought in exclusive contribution of the bimolecular process, as shown in Scheme 1.

It is interesting to note here, the similarities and differences of the present reactions to those of the analogous thiogermanes with the same substrates.[6] Unimolecular ionization of the arylbromoethanes was found as the mechanism for the reaction of (arylthio)-trimethylgermanes with all the substituted arylbromoethanes. Clear bimolecular nucleophilic substitution was not observed, although minor contribution of the process could not be ruled out for the reaction with the thiogermane.[6] On the contrary, the arylbromoethanes bearing electron-withdrawing substituents (Y=*p*-NO_2) have been found exclusively to accept bimolecular nucleophilic attack of the sulfur atoms of various (arylthio)trimethylstannanes in the present study. Difference in nucleophilicity of the sulfur atoms of the thiogermanes and the thiostannanes may be a factor accounting for the difference in the mechanisms of those two reactions. On the other hand, different bond lengths between germyl–sulfur and stannyl–sulfur bonds would be the important factor controlling the mechanism, in view of the steric control of the mechanisms in analogous reactions, as discussed previously.[2] The longer stannyl–sulfur bond pushes off the bulky trimethylstan-

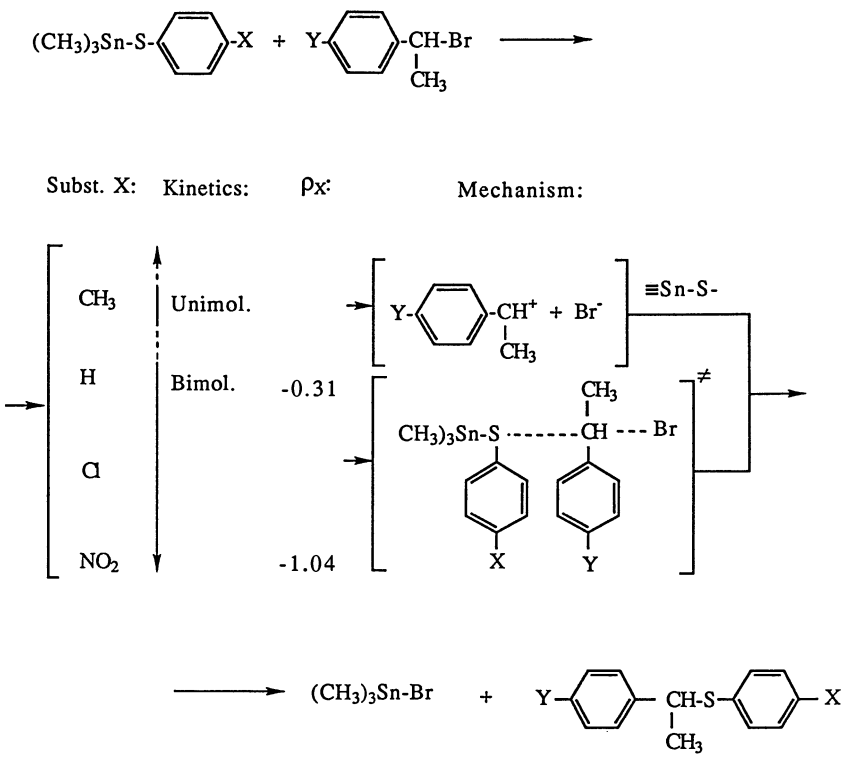

Scheme 1.

nyl group and provides a room around the sulfur allowing to act it as a nucleophile even toward a secondary carbon atom.

Experimental

Materials. (Arylthio)trimethylstannanes were prepared from bromotrimethylstannane and appropriate arenethiol as described previously.[3] Substituted 1-aryl-1-bromoethanes were prepared by reduction of the corresponding acetophenone followed by bromination.[10] Substituent (Y), yield of the arylbromoethane, and its bp were as follows: *p*-CH_3, 65%, 73 °C/mmHg (1 mmHg=133.322 Pa), *p*-Cl, 70%, 120 °C/28 mmHg, *m*-Cl, 70%, 100 °C/2 mmHg, *p*-NO_2, 76%, 120 °C/2 mmHg. Kinetic solvent, chloroform was dried over magnesium sulfate and simply distilled before use without removal of ethanol of the stabilizer.

Product Analysis. (Phenylthio)trimethylstannane (1.00 g, 3.68 mmol) was heated at 110 °C for 24 h in a sealed tube in the presence of an equimolar amount of 1-bromo-1-phenylethane. ^{1}H NMR Analysis of the resulting mixture showed signals corresponding to bromotrimethylstannane and phenyl 1-phenylethyl sulfide. The products were separated by distillation obtaining bromotrimethylstannane, bp 59 °C/26 mmHg, 50% yield, and the sulfide, bp 120 °C/1 mmHg, 52% yield. The isolated products were characterized by their physical properties and spectra.

Kinetics. The procedure was essentially the same to that reported previously.[3] Concentrations and temperature for the kinetic experiments are recorded in the Table. Addition of 2.3×10^{-2} mol dm^{-3} of either bromotrimethylstannane or phenyl 1-phenylethyl sulfide resulted ca. 5% acceleration of the reaction of trimethyl(phenylthio)stannane with 1-bromo-1-phenylethane.

References

1) S. Kozuka, S. Tamura, T. Yamazaki, S. Yamaguchi, and W. Tagaki, *Bull. Chem. Soc. Jpn.*, **58**, 3277 (1985).

2) S. Kozuka, S. Tamura, S. Ishibashi, O. Ohya, and W. Tagaki, *Bull. Chem. Soc. Jpn.*, **60**, 4061 (1987).

3) S. Kozuka and S. Ohya, *Bull. Chem. Soc. Jpn.*, **51**, 2651 (1978).

4) S. Kozuka and I. Naribayashi, *Bull. Chem. Soc. Jpn.*, **52**, 3638 (1979).

5) S. Kozuka, T. Higashino, and T. Kitamura, *Bull. Chem. Soc. Jpn.*, **54**, 1420 (1981).

6) S. Kozuka, T. Nitta, S. Tamura, and W. Tagaki, *Bull. Chem. Soc. Jpn.*, **62**, 2594 (1989).

7) S. Kozuka and H. Nakamura, *Chem. Express*, **5**, 393 (1990).

8) R. F. Hudson and G. Klopman, *J. Chem. Soc.*, **1962**, 1062.

9) H. C. Brown and Y. Okamoto, *J. Am. Chem. Soc.*, **79**, 1913 (1957).

10) M. Kuchar, B. Brunova, V. Reiholec, Z. Roubal, and O. Nemecek, *Coll. Czech. Chem. Commun.*, **41**, 633 (1976).

 © 1991 The Chemical Society of Japan Bull. Chem. Soc. Jpn., 64, 2411—2415 (1991)

The Catalysis of Maghemite and Hematite on the Aldol and the Retro-Aldol Condensation of Acetone

Haruo WATANABE* and Jun'etsu SETO
Sony Corporation Research Center, 174 Fujitsuka-cho, Hodogaya-ku, Yokohama 240
(Received December 25, 1990)

The catalytic activities of maghemite on the aldol condensation of acetone and on the retro-aldol condensation of diacetone alcohol are found to be higher than those of hematite. Further, the catalytic activity of maghemite on the formation of mesityl oxide is significantly higher than that of hematite. The active sites are considered to be surface hydroxyl groups which behave as a Brønsted base and acid points. Maghemite has more basic surface hydroxyl groups than does hematite, and far more acidic surface hydroxyl groups than does hematite they are sufficiently strong to make its average surface acidity greater than that of hematite. The basic surface hydroxyl groups of maghemite are speculated to be those which bond to the iron ions of the octahedral sites the acidic ones are those of the tetrahedral sites of the spinel lattice of the surface.

Maghemite is a ferrimagnetic inverse-spinel type iron oxide, which is widely used for magnetic recording tapes. Its surface properties have a large influence on its dispersibility in paint and, thus, on the output and noise characteristics of tape. However, there have been relatively few studies on the surface properties of maghemite, compared to these of hematite.

In previous papers,[1-3] the nature of the surface hydroxyl groups of maghemite were examined by identifying either the PZC (Point of Zero Charge) or IEP (Isoelectric Point); the heat of formation of the surface hydroxyl groups was examined through measurements of the heat of immersion, compared with that of hematite. It was clarified that the surface hydroxyl groups of maghemite are more acidic than those of hematite, and that the heat of formation of the surface hydroxyl groups is lower than that for hematite. These differences between maghemite and hematite have been attributed to differences in the bulk crystal structure. However, these properties are related to the averaged parameters of the surface hydroxyl groups; more microscopic differences between maghemite and hematite are expected.

In the present work, the specific acidity and basicity of the surface hydroxyl groups of maghemite compared with those of hematite were studied using the Brønsted acid and base points as well as their effect on the catalysis of the aldol and the retro-aldol condensations of acetone. From the view point of heterogeneous catalysts for aldol or retro-aldol condensations, reports concerning iron oxides[4] have been fewer than those for aluminum oxides[5-8] or alkali earth metal oxides.[9-14]

Experimental

Samples. The maghemite sample used in the present work was prepared from synthetic acicular α-FeOOH (geothite) by sequential dehydration, reduction, and oxidation processes. The hematite sample was prepared by a heat treatment of the above-mentioned maghemite sample in air at 550 °C. In all cases, the samples were purified as follows: first, washing with an alkali solution, then distilled water and, finally, by electrodialysis. The samples were then filtered, dried at 100 °C for 24 h in an oven, and stored in a desiccator. The samples and purification procedure are the same as those reported previously.[1] The specific surface areas of the samples were 19 $m^2 g^{-1}$ for maghemite and 16 $m^2 g^{-1}$ for hematite, measured by using the BET method of nitrogen adsorption at liquid-nitrogen temperature, assuming the cross-sectional area of a nitrogen molecule to be 16.2 $Å^2$. The surface porosity of the samples was checked by a *t*-plot; the existance of surface pores less than 30 Å in diameter was confirmed to be negligible. The surface hydroxyl groups, which could behave as catalytic active sites, had densities of 11.8 groups nm^{-2} for maghemite samples and 12.8 groups nm^{-2} for hematite samples, as determined in a previous study.[2]

Chemicals and Reactions. The acetone used in the present work was of spectral grade, dehydrated with Drierite. Diacetone alcohol (4-hydroxyl-4-methyl-2-pentanone) was obtained from Wako Pure Chem. Ind. Ltd., and purified by vacuum distillation.

One-gram samples were ultrasonically dispersed in 40.0 g of acetone or diacetone alcohol in tightly stoppered 100 ml conical flasks; these were then placed in an incubator with water thermostated to an accuracy of less than ±0.05 °C. The products were analyzed by a gas chromatograph equipped with a 3 m column of PEG-20, and a detector for flame ionization, on the supernatant of the dispersion (sampled after a constant time and filtered by a membrane filter). The reaction times of both reaction systems were 15 h for the condensation of acetone and 10 h for the decomposition of diacetone alcohol.

Results and Discussion

Aldol Condensation of Acetone. The aldol condensation of acetone to form diacetone alcohol (hereafter abbreviated to DAA) is known to be catalyzed by the Brønsted basic point of heterogeneous catalysts.[12] The following dehydration reaction of DAA to form mesityl oxide (4-methyl-3-penten-2-one (hereafter abbreviate MO)) is known to be catalyzed by the Brønsted acid.[15] A series of reactions is as follows:

$$2\,(CH_3)_2CO \underset{\text{base point}}{\rightleftarrows} (CH_3)_2(OH)C\text{–}CH_2CO\text{–}CH_3$$

$$\xrightleftharpoons[\text{acid point}]{-H_2O} (CH_3)_2C{=}CH\text{–}CO\text{–}CH_3$$

In the present work, the catalytic activity of the aldol condensation (the catalytic activity of surface Brønsted base point) was measured on the samples as the conversion of acetone to the total products of DAA plus MO.

In all of these cases, the total conversions in the present reaction systems were less than 1.5%, which is far less than the reaction equilibrium;[16] no products excluding DAA or MO (such as the trimeric condensed product[17-19]) were detected in the present reaction systems. The rate of this reaction, even when it follows second-order kinetics, could be regarded as following zero-order kinetics and can be approximated by the following integrated form of the reaction rate formula:

$$kt = x/a(a-x) \fallingdotseq x/a^2 \ (x \ll a).$$

Here, k is the reaction rate constant, a the initial concentration of the reactant (i.e. acetone), and x the concentration of products (i.e. DAA plus MO after a reaction time of t). Therefore, the conversions x at a constant t are proportional to the rates of reaction k. Figure 1 shows this total conversion per unit surface area of samples after a constant time of 15 h in an Arrhenius plot. These findings show that the catalytic activity of maghemite is slightly higher than that of hematite, and

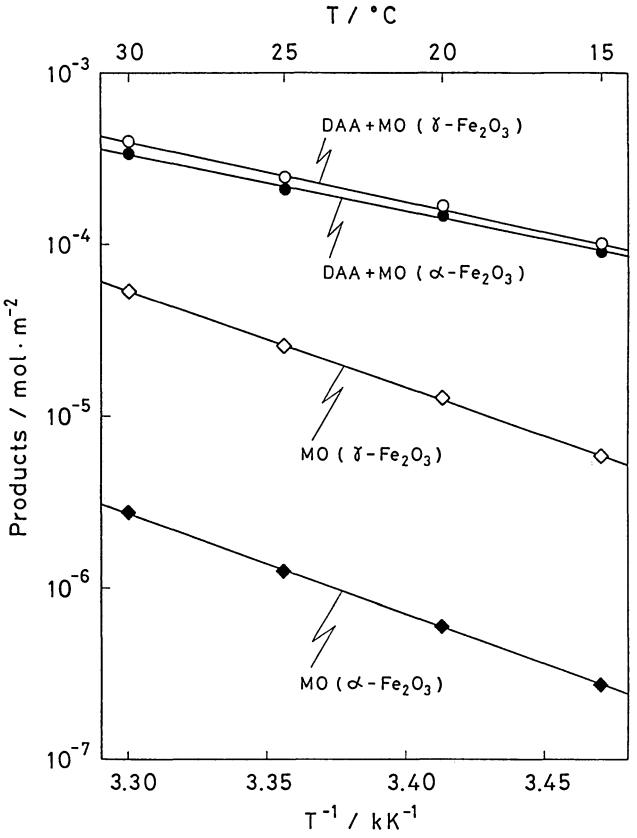

Fig. 1. Temperature dependences of the amounts of the reaction products of acetone after a reaction time of 15 h. Total amount of (DAA+MO) of maghemite (γ-Fe_2O_3): ○; total amount of (DAA+MO) of hematite (α-Fe_2O_3): ●; amount of MO of maghemite (γ-Fe_2O_3): ◇; amount of MO of hematite (α-Fe_2O_3): ◆.

that the activation energies of both samples are of the same value, 70.6±0.5 kJ mol^{-1} for maghemite and 67.3±0.5 kJ mol^{-1} for hematite, respectively. Regarding the similar values for the activation energies of this reactions, it is considered that the rate-determining step does not depend on the activity of the samples. This consideration is well supported by the work of Zhang et al.,[13] which shows that the rate-determining step for C–C bond formation is the coupling of acetone and carbanion.

Conversions to the MO per unit surface area of the samples are also shown in Fig. 1, and have a linear relationship in an Arrhenius-type plot. It is remarkable that the conversions of maghemite to MO are much higher than that of hematite. This is caused by the catalytic activities of the acidic points of the surface (surface hydroxyl groups) and are higher for maghemite compared to hematite.

Regarding the catalytic activity of maghemite, an identical magnitude of activity was confirmed for aldolization and dehydration with a commercially available maghemite sample. The sample has an acicular shape with a length of 0.2—0.4 μm and an acicular ratio of 8—10. The saturation magnetization is 73.0 emu g^{-1} and the specific surface area is 24 m^2 g^{-1}. Purification of this sample was the same as that mentioned in the experimental section.

Retro-Aldol Condensation of Diacetone Alcohol. The retro-aldol condensation of DAA, which forms acetone, is known to be catalyzed by the Brønsted basic points of heterogeneous catalysts.[9,10] The MO is also formed (as mentioned above) in the presence of the Brønsted acid points. In the present work concerning this reaction system the products, except for acetone and MO, were negligibly small. The conversion of the retroaldolisation to acetone was less than 2%, which is also far less than equilibrium;[16] the rate of this reaction was reported to follow either zero-orders[6] or first-order kinetics.[9] The rate of this reaction, even when it follows the first-order kinetics, could be regarded as following zero-order kinetics, and can be approximated by the following integrated form of the reaction rate formula:

$$kt = \ln a/(a-x) \fallingdotseq x/a \ (x \ll a).$$

Then, conversions x at a constant t are proportional to the rates of reaction k. The conversions per unit surface area to acetone after a constant reaction time of 10 h are plotted in an Arrhenius plot in Fig. 2. The catalytic activity of acetone formation for maghemite is higher than that for hematite; this tendency does not change from the viewpoint of activity per hydroxyl group on the surface, considering the surface density of the hydroxyl groups. The activation energies for this reaction are 64.0±0.5 kJ mol^{-1} for maghemite and 66.9±0.5 kJ mol^{-1} for hematite. Both values are compatible with each other, and agree with the values reported in the literature.[9]

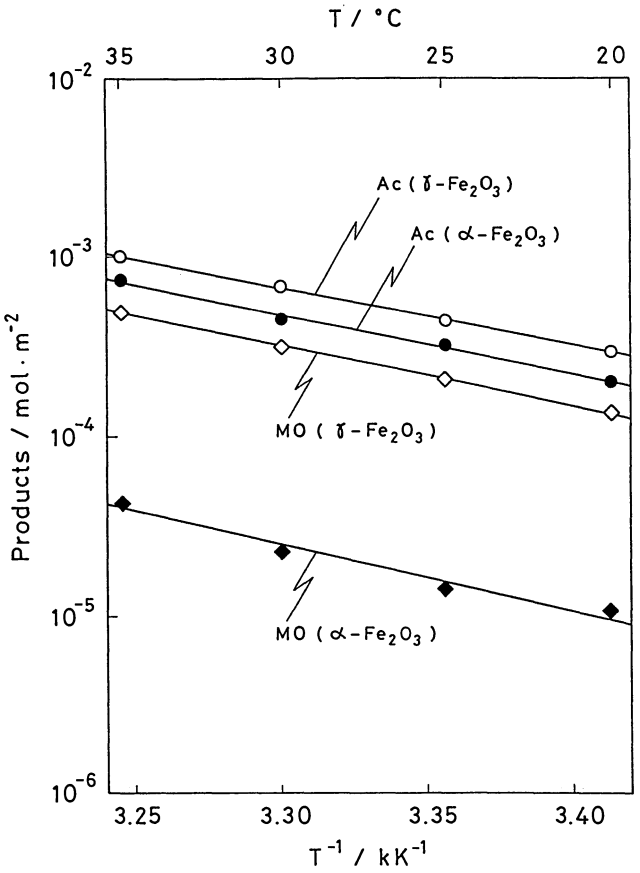

Fig. 2. Temperature dependences of the amounts of the reaction products of DAA after a reaction time of 10 h. Amount of acetone of maghemite (γ-Fe_2O_3): ○; amount of acetone of hematite (α-Fe_2O_3): ●; amount of MO of maghemite (γ-Fe_2O_3): ◇; amount of MO of hematite (α-Fe_2O_3): ◆.

Regarding the dehydration to MO, the conversion was less than 2%, which is far less than equilibrium; the rates of this reaction, reported to follow first-order kinetics,[15] could be approximated as mentioned before to be proportional to the conversions. The conversions per unit surface area of the samples after a constant reaction time of 10 h are plotted in an Arrhenius plot in Fig. 2. The catalytic activity of maghemite for the dehydration of DAA to MO has been found to be much higher than that of hematite. However, the activation energies of this reaction are almost the same (66.5±0.5 kJ mol^{-1} for maghemite and 71.9±0.5 kJ mol^{-1} for hematite), and almost equal to the value reported in the literature.[15]

Acidity and Basicity of the Surface Hydroxyl Groups. The catalysis used in the present work, originated from the acidic or basic nature of the surface hydroxyl groups, and could be explained from the view point of the Brønsted acid and base.

For acidic catalysis (that is, the dehydration reaction of DAA to MO) the catalytic activity of maghemite is higher than that of hematite. The fact that the acidity of maghemite is higher than that of hematite is well supported by the following view points. Concerning the enthalpy of formation of a bulk crystal, of which maghemite is higher than that of hematite,[20] the partial charges of the oxygen atoms of maghemite should be less than those of hematite, causing a higher acidity of maghemite than that of hematite.[21] This is well confirmed by the chemical shift of O(1s) of XPS[3,22] as well as the point of the PZC (Point of Zero Charge), of which the value for maghemite is lower than that for hematite.[1] Regarding for the dissociation and association of the proton of the surface hydroxyl groups, the equilibrium constants were determined in a previous study;[3] the chemical reactions and those values are as follows:

$$FeOH_2^+ \overset{K_{a1}^{int}}{\rightleftarrows} FeOH + H^+, \quad FeOH \overset{K_{a2}^{int}}{\rightleftarrows} FeO^- + H^+.$$

Maghemite: $pK_{a1}^{int} = 2.7$, $pK_{a2}^{int} = 8.3$

Hematite : $pK_{a1}^{int} = 3.2$, $pK_{a2}^{int} = 10.2$

The Brønsted acidity of maghemite is higher by a factor of 2 orders of magnitude than that of hematite, considering the values of pK_{a2}^{int}. According to the above-mentioned points, the results of the present work indicate that the acidic catalytic activity of maghemite is higher than that of hematite, which is reasonable in view of these acidities of the surface hydroxyl groups.

Regarding the basic catalysis (that is, the aldolization or retro-aldolization between acetone and DAA) the catalytic activity of maghemite is higher than that of hematite. This result is in contradiction to the fact that the Brønsted basicity of maghemite is lower than that of hematite, e.g. these values for PZC and the values for pK_{a1}^{int}. Concerning this point, further discussion is necessary, and the average basicity is not available. Especially the surface hydroxyl groups on maghemite are not more uniform than are those of hematite, since the crystal structure of maghemite is an inverse-spinel type which has iron ions in the tetrahedral coordination sites (the coordination number (CN) is 4) and in the octahedral coordination sites (the coordintion number (CN) is 6), whereas the crystal structure of hematite is the corundum type, which only has iron ions at the octahedral coordination sites.

Specific Acidity and Basicity of the Surface Hydroxyl Groups. Regarding the acidity or basicity of the surface hydroxyl groups as as a function of the value of PZC, Parks[23] again showed that the surface hydroxyl groups bonding to the metal ions of the tetrahedral coordination sites show a lower value of 2.4 pH units, compared with those of octahedral coordination sites. For an evaluation of PZC, maghemite can be treated as being a complex oxide comprising iron oxide in the tetrahedral coordination as well as the octahedral coordination. For the PZC of a complex oxide containing n distinct component oxides, Parks[24] also showed that

$$PZC = \sum_{i=1}^{n} f_i \, PZC_i,$$

in which PZC_i is the PZC of the component oxides (i), and f_i is the atomic fraction on the surface. On the other hand, PZC has the following relations with K_{a1}^{int} and K_{a2}^{int}:

$$PZC = 1/2\,(pK_{a1}^{int} + pK_{a2}^{int}).$$

The PZC of a complex oxide can thus be written as

$$PZC = 1/2\left(\sum_{i=1}^{n} f_i\, pK_{a1}^{int}{}_i + \sum_{i=1}^{n} f_i\, pK_{a2}^{int}{}_i\right),$$

where $K_{a1}^{int}{}_i$ and $K_{a2}^{int}{}_i$ are the K_{a1}^{int} and K_{a2}^{int} of the component oxides (i). To examine the specific basicity of the surface hydroxyl groups, the component values of $K_{a1}^{int}{}_i$ as well as those of the fraction of f_i are more important than the average value of K_{a1}^{int}. It is still difficult to evaluate or determine the values of $K_{a1}^{int}{}_i$. The $K_{a1}^{int}{}_i$ are related, as mentioned above, with the PZC_i as follows:

$$PZC_i = 1/2\,(pK_{a1}^{int}{}_i + pK_{a2}^{int}{}_i).$$

The values of PZC_i correspond with those of the $K_{a1}^{int}{}_i$. Yoon et al.[25] have proposed improvements to Parks' semiempirical equation for PZC in the following manner; for a complex oxide, when the correction of the crystal field stabilization energy of the metal ion by the hydroxide ion is not required, as in the case of Fe^{3+} ion with the tetrahedral or octahedral coordination,[26]

$$PZC = \sum_{i=1}^{n} f_i\, PZC_i$$

$$= 18.43 - 53.12 \sum_{i=1}^{n} f_i\,(v/L_s)_i - 0.5 \sum_{i=1}^{n} f_i \log((2-v)/v)_i.$$

Here, v is the bond valence, i.e., the valency of the metal ion per coordination number, and L_s ($=L+r$) is the sum of the mean M–O bond length (L) and the O–H distance (r), taken to be 1.01 Å. According to the above equation, the component values of PZC_i and those of the fraction of f_i are calculated using the parameters of Fe^{3+} ions and the Fe–O bonds, referring to crystallographic data for maghemite[27] and hematite.[28]

These numerical parameters and values are listed in Table 1. The Fe^{3+} ions of maghemite are arranged in a spinel-type crystal lattice, and are divided into 4 classes as Fe^{3+} (1), Fe^{3+} (2), Fe^{3+} (3), and Fe^{3+} (4), respectively. The Fe^{3+} ions of hematite are entirely equivalent to Fe^{3+} (5) in Table 1. These Fe^{3+} ions are arranged in a corundum-type crystal lattice.

The values of the PZC, i.e. the summation of the f_i PZC_i, according to the above equation, are higher than those values determined by measurements carried out in a previous paper,[1] i.e. 5.5 for maghemite and 6.7 for hematite. The semiempirical equations by Parks and Yoon et al., in which the constants are defined using the PZG values of the hydrated samples, show higher values than do those for the unhydrated samples, as used in the present work and the previous paper.[1] The differences between the values of the PZC for maghemite and hematite are 1.2 pH units by measurement and 1.3 pH units by using the above-mentioned calculation, and are almost the same in value. This fact well supports the validity of the application of the above equations to the present work.

The results from the above calculations can be used to understand the catalytic activities of maghemite and hematite, that the PZC_i values of octahedral sites of maghemite are higher than those of hematite. This fact indicates that the values of $pK_{a1}^{int}{}_i$ of the surface hydroxyl groups bonding to the surface iron ions of octahedral sites of maghemite (Fe^{3+} (2), (3), (4)) are higher than those of hematite (Fe^{3+} (5)). In other words, the Brønsted basicity of the surface hydroxyl groups bonding to the iron ions of the octahedral sites of maghemite is higher than that of hematite. This consideration leads to a reasonable explanation that the basic catalytic activity of the aldolization or the retro-aldolization of acetone of maghemite is higher than that of hematite.

It is also worthwhile noting from the above calculations that the value of PZC_i of the tetrahedral sites Fe^{3+} (1) of maghemite is far lower than that of the octahedral sites (Fe^{3+} (2), Fe^{3+} (3), and Fe^{3+} (4)) compared with the

Table 1. Parameters of Fe^{3+} Ions and Fe–O Bonds, and Component Values of PZC_i for Maghemite (γ-Fe_2O_3) and Hematite (α-Fe_2O_3)

	Fe^{3+} ions			Fe–O bonds				PZC_i	PZC $\sum_{i=1}^{n} f_i PZC_i$
		CN[a]	N_m[b]	v	L_s/Å	N_b[c]	f_i		
Maghemite (γ-Fe_2O_3)	Fe^{3+}(1)	4	8	3/4	1.88	32	0.286	4.53	
	Fe^{3+}(2)	6	4	1/2	2.03	24	0.214	9.45	
	Fe^{3+}(3)	6	8	1/2	2.02	48	0.429	9.42	
	Fe^{3+}(4)	6	4/3	1/2	2.13	8	0.071	9.73	
									8.05
Hematite (α-Fe_2O_3)	Fe^{3+}(5)	6	36[d]	1/2	1.99	216	1.000	9.34	
									9.34

a) CN is the coordination number. b) N_m is the number of Fe^{3+} ions per unit cell. c) N_b is the number of Fe–O bonds per unit cell. d) In the hexagonal unit cell.

value given in Parks' review,[23] in which a difference between the values of 2.4 pH units is reported. More than double the value of the difference is derived from a calculation. This also suggests that the value of $pK_{a2}^{int}{}_i$ is far lower than the average value of pK_{a2}^{int} of 8.3 for maghemite. These sites would show strong Brønsted acidity and promote the acidic catalysis of the dehydration reaction to MO.

Conclusion

(1) The catalytic activities of maghemite on the aldol condensation of acetone and the retro-aldol condensation of diacetone alcohol are higher than those of hematite.

(2) The catalytic activity of maghemite for the formation of mesityl oxide is significantly higher than that of hematite.

(3) Maghemite has the more basic surface hydroxyl groups than hematite and far more acidic surface hydroxyl groups than hematite, which are strong enough to make the average surface acidity higher than hematite.

(4) The basic surface hydroxyl groups of maghemite are bonded to the iron ions of the octahedral sites, and the acidic ones are of the tetrahedral sites of the spinel lattice of the surface.

The authors wish to thank Professor Yoshiyuki Nishiyama of the Chemical Research Institute of Non-Aqueous Solutions of Tohoku University, for useful discussions.

References

1) H. Watanabe and J. Seto, *Bull. Chem. Soc. Jpn.*, **59**, 2683 (1986).
2) H. Watanabe and J. Seto, *Bull. Chem. Soc. Jpn.*, **61**, 3067 (1988).
3) H. Watanabe and J. Seto, *Bull. Chem. Soc. Jpn.*, **63**, 2916 (1990).
4) L. Nondek and J. Malek, *Coll. Czech. Chem. Commun.*, **44**, 2384 (1979).
5) G. Zhang, H. Hattori, and K. Tanabe, *React. Kinet. Catal. Lett.*, **34**, 255 (1987).
6) L. Nondek and J. Malek, *React. Kinet. Catal. Lett.*, **14**, 381 (1980).
7) J. A. Lercher, Ch. Colombier, and H. Noller, *React. Kinet. Catal. Lett.*, **23**, 365 (1983).
8) J. M. Campelo, A. Garcia, D. Luna, and J. M. Marinas, *Can. J. Chem.*, **62**, 638 (1984).
9) Y. Fukuda, K. Tanabe, and S. Okazaki, *Nippon Kagaku Kaishi*, **1**, 513 (1972).
10) K. Tanabe and Y. Fukuda, *React. Kinet. Catal. Lett.*, **1**, 21 (1974).
11) J. Barrios, J. M. Marinas, and J. V. Sinisterra, *Bull. Soc. Chim. Belg.*, **95**, 107 (1986).
12) G. Zhang, H. Hattori, and K. Tanabe, *Appl. Catal.*, **36**, 189 (1988).
13) G. Zhang, H. Hattori, and K. Tanabe, *Appl. Catal.*, **40**, 183 (1988).
14) G. Zhang, H. Hattori, and K. Tanabe, *Bull. Chem. Soc. Jpn.*, **62**, 2070 (1989).
15) Y. K. Kim and J. D. Hatfield, *J. Chem. Eng. Data*, **30**, 149 (1985).
16) Y. M. Paushkin, I. S. Panidi, N. V. Ryabtseva, A. S. Kazanskaya, A. M. Sladkov, S. V. Meshcheryakov, O. I. Yatsko, and A. F. Lunin, *Kinet. Catal.*, **11**, 1311 (1970).
17) W. T. Reichle, *J. Catal.*, **63**, 295 (1980).
18) V. A. Bell and H. S. Gold, *J. Catal.*, **79**, 286 (1983).
19) W. T. Reichle, *J. Catal.*, **94**, 547 (1985).
20) J. M. Trautmann, *Bull. Soc. Chim. Fr.*, **1966**, 992.
21) K. Tanaka and K. Tamaru, *Bull. Chem. Soc. Jpn.*, **37**, 1862 (1964).
22) N. S. McIntyre and D. G. Zetauk, *Anal. Chem.*, **49**, 1521 (1977).
23) G. A. Parks, *Chem. Rev.*, **65**, 177 (1965).
24) G. A. Parks, *Adv. Ghem. Ser.*, **67**, 121 (1967).
25) R. H. Yoon, T. Salman, and G. Donnay, *J. Colloid Interface Sci.*, **70**, 483 (1979).
26) F. Basolo and R. G. Pearson, "Mechanisms of Inorganic Reactions," 2nd ed, John Wiley and Sons Inc., New York (1969).
27) C. Greaves, *J. Solid State Chem.*, **49**, 325 (1983).
28) R. W. G. Wyckoff, "Crystal Stracture," 2nd ed, Interscience, New York (1963).

Local Structure of Polyethylene Glycol–NaI Solid Polyelectrolyte as Studied by ^{13}C and ^{23}Na NMR

Takahiro UEDA,† Hiroshi OHKI,†† Nobuo NAKAMURA,* and Hideaki CHIHARA†††
Department of Chemistry, Faculty of Science, Osaka University, Toyonaka, Osaka 560
(Received January 24, 1991)

^{13}C CP/MAS NMR, ^{23}Na powder NMR, and ^{23}Na two dimensional nutation NMR were applied to complexes of NaI with polyethylene glycol (PEG) and tetraethylene glycol (TEG) to study the conformation of the polyethers and local structure around the Na^+. ^{13}C chemical shift data suggest strongly that the polyether chains assume the gauche conformation in the complexes. ^{23}Na NMR spectrum of TEG–NaI complex gave a broad asymmetric line; simulation of the line shape led to e^2Qq/h=590 kHz and η=0.7. No significant temperature dependence of the line shape was observed between 200 K and room temperature. For PEG–NaI complex e^2Qq/h and η were estimated to be about 320 kHz and 0.7, respectively, from the nutation spectrum. On the basis of the above results, new model structures of PEG–NaI complex were presented.

Complexes of polyethylene glycol (PEG) with inorganic salts such as NaI, NaSCN, and KSCN[1,2] exhibit ionic conductivitiy of the order of 10^{-4}—10^{-3} S cm^{-1} and are classified to solid polyelectrolytes. Among them, the complex of PEG with NaI has been extensively studied by conductivity measurements, X-ray diffraction, and various other experimental methods.[3–7] Thus, Fauteux et al.[7] have reported that the ionic conductivity exhibits an Arrhenius behavior, and that the apparent activation energy above 60 °C depends on the salt concentration of the solid electrolyte. As to the structure of PEG–NaI complex, Himba[5] performed an X-ray fiber diffraction experiment and proposed a monoclinic unit cell with cell constants of a=1.701, b=0.8, c=1.688 nm, and β=115.1° in which PEG chains were oriented along the b-axis, but the detailed molecular arrangement was not determined. Also, Chatani and Okamura[6] reported results of their X-ray experiment on the PEG–NaI complex and proposed a model structure that Na^+ and I^- ions alternate with each other to form a zigzag chain around which a helical PEG chain which possesses *tg* conformation forms an envelope.

^{13}C CP/MAS (cross polarization/magic angle sample spinning) NMR is one of the most powerful experimental tools for conformational analysis of polymer molecules in solid state and has been successfully applied to various kinds of polymers.[8–12] In the present work we applied this method to PEG–NaI and its model oligomer complex, tetraethylene glycol (TEG)–NaI, in order to study the conformation of the chain in these complexes. We also measured the ^{23}Na NMR lineshapes[13,14] to deduce some information on the coordination of ethylene oxide units to the sodium ion. This paper describes the results of these experiments and presents possible model structures for PEG and TEG complexes based on the analysis of the experimental data. We also present the results of ^1H and ^{23}Na spin-lattice relaxation time (T_1) measurements and show that, although the sodium ion transport has been believed to govern the high conductivity in PEG–NaI complex, the diffusion rate of Na^+ is very slow in the crystalline state.

Experimental

Polyethylene glycol #4000 (reagent grade: M_w=3000—3700), tetraethylene glycol and NaI (extra pure reagent grade) were purchased from Nakarai Tesque Inc. As PEG and NaI are both sensitive to the atmospheric moisture, they were dried and stored in a desiccator over P_2O_5 and $CaCl_2$. The polymer-salt complex with the molar ratio 4:1 (O:Na) was prepared by the standard method.[3] The stoichiometric mixture of NaI and the ethylene oxide unit of polymer (1:4) was dissolved in dry methanol and stirred for 24 h at room temperature. The solvent was then slowly evaporated at room temperature to dryness and the complex thus deposited as thin-film was stored in a desiccator over P_2O_5 and $CaCl_2$.

The tetraethylene glycol (TEG)–NaI complex was prepared by dissolving the mixture of TEG and NaI with the molar composition of 1:1 in tetrahydrofuran (THF), concentrated to about one-third of its original volume and then being kept at 4 °C; the deposited white polycrystals were collected and recrystallized twice from THF. The complex was dried and stored in a desiccator over P_2O_5 and $CaCl_2$.

For the ^{13}C NMR measurements each specimen was packed into the MAS sample rotor (ZrO_2) under the N_2 atmosphere and dried under vacuum at room temperature for several hours. The specimen for the ^{23}Na and ^1H measurements were sealed into an ampoule with the He heat exchange gas.

^{13}C CP/MAS and ^{23}Na spectra, and ^{23}Na spin-lattice relaxation times, T_1, were measured with the Bruker MSL-200 spectrometer. A home-built pulse NMR spectrometer operating at 17 MHz was used for ^1H relaxation time measurements. The experimental errors in the ^1H and ^{23}Na relaxation measurements were estimated to be within 5% and 10%, respectively. The temperature was controlled within ±1 K with the Bruker VT-1000 unit for the ^{23}Na relaxation measurements. It was measured to within ±0.5 K by Chromel-*p*-Constantan thermocouples for ^1H relaxation measurements.

^{13}C CP/MAS NMR experiments were done at 50 MHz with the sample spinning rate of ca. 3 kHz at room temperature.

† Present address: National Chemical Laboratory for Industry, Tsukuba, Ibaraki 305.
†† Present address: Department of Chemistry, The University of Tsukuba, Tsukuba, Ibaraki 305.
††† Present address: Japan Association for International Chemical Information, Gakkai Center Building, 2-4-16 Yayoi, Bunkyo-ku, Tokyo 113.

^{13}C chemical shifts were determined with the external standard tetramethylsilane.

^{23}Na NMR lineshapes, the spin-lattice relaxation times and 2D nutation spectra[15] for the two complexes were measured at the resonance frequency of 53 MHz. In order to derive the quadrupole coupling constant, e^2Qq/h, and the asymmetry parameter of the electric field gradient tensor, η, we prepared computer program[16] to describe the evolution of the spin system using the Liouville operator formalism[17] and used it to simulate the ^{23}Na nutation spectral data.

Results and Discussion

^{13}C CP/MAS NMR Spectra. Figure 1 shows the ^{13}C CP/MAS NMR spectrum of PEG–NaI complex and the ^{13}C dipolar decouple(DD)/MAS NMR spectrum of PEG at room temperature. The spectrum of PEG sample consists of two sharp peaks due to carbons in the crystalline part and of a broad component which comes from the noncrystalline part.[18] The fact that the intensity of the broad component is rather high indicates that the crystallinity of our PEG specimen is relatively poor.

On the other hand, the spectrum of the PEG–NaI complex gives only a single sharp peak, which shows strongly that the complexation gives rise to almost perfect crystalline material. Moreover, all the carbon atoms in the complex are equivalent and only one kind of conformation can exist with respect to the carbon bonds.

In order to examine the effect of the complexation on the conformation of the $-O-CH_2CH_2-$ chain in more detail we measured the ^{13}C CP/MAS spectrum in the TEG–NaI complex which can be regarded as a model compound for the PEG–NaI complex. The ^{13}C CP/MAS–NMR spectrum of the TEG–NaI complex together with ^{13}C high resolution NMR spectrum of the neat liquid of TEG are shown in Fig. 2.

In the case of liquid TEG the spectrum consists of three peaks with the intensity ratio of 1 : 2 : 1 in the order of decreasing field. These peaks are easily assigned as follows: The terminal carbon bonded to the hydroxyl group gives the peak at the highest field, the one next to the terminal carbon appears at the lowest field and the other four carbons give the central peak.

In contrast to pure TEG, the TEG–NaI complex gave two peaks with the intensity ratio of 1 : 3. The magnitude of the chemical shift at the highest field is the same as that of the terminal carbon in the pure TEG, suggesting strongly that the terminal OH groups of TEG do not participate in the complexation. The strong signal due to inner carbons shows an upfield shift due obviously to the complexation. The fact that the inner carbons give

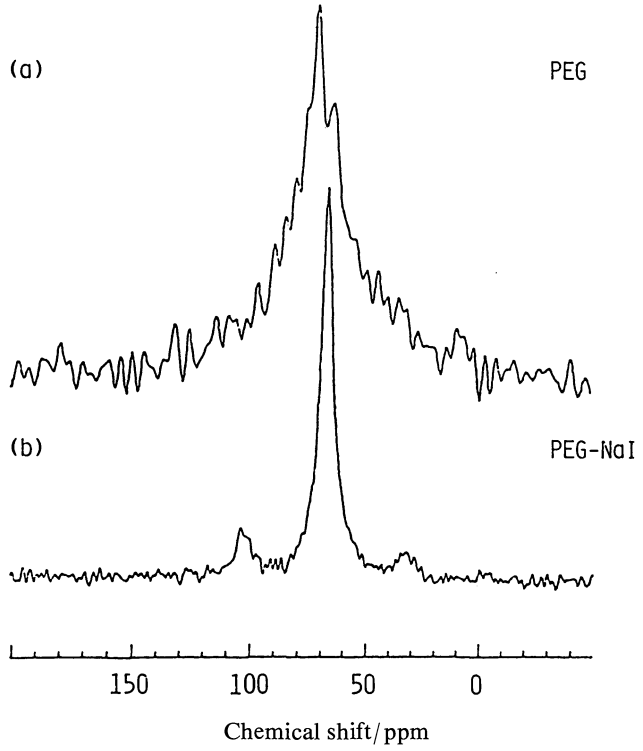

Fig. 1. ^{13}C dipolar decouple (DD)/MAS NMR spectrum of PEG (a) and ^{13}C CP/MAS NMR spectrum of PEG–NaI complex (b) at room temperature. The spinning rates for samples: (a) 3 kHz; (b) 2 kHz. The small peaks in the spectrum (b) are the spinning side bands.

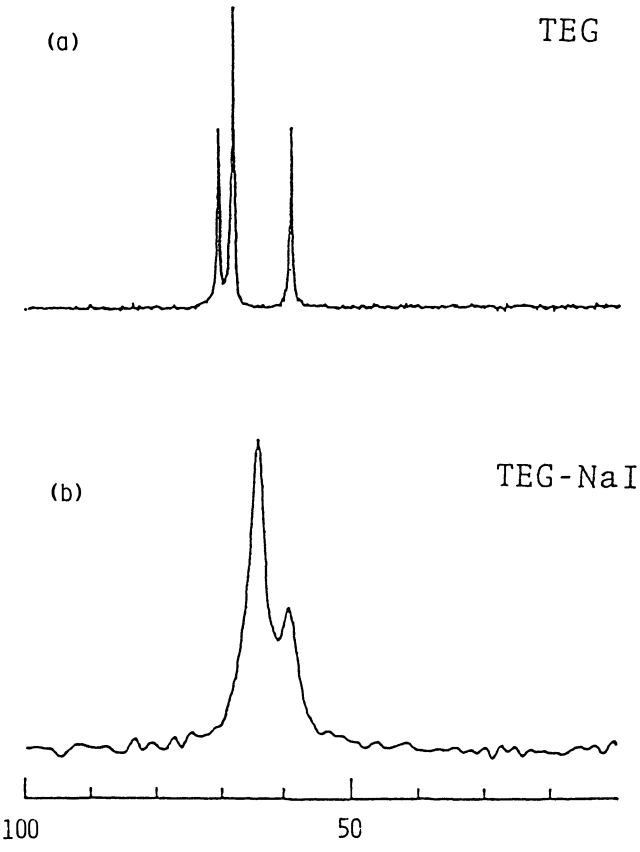

Fig. 2. ^{13}C NMR spectrum of pure TEG (neat liquid) (a) and ^{13}C CP/MAS NMR spectrum of TEG–NaI complex (b) at room temperature. The spinning rate for the TEG–NaI complex is 3.5 kHz.

Table 1. ^{13}C Chemical Shifts of TEG and PEG, and their Complexes with NaI (ppm from TMS)

Sample	I	II	III
PEG (solid)	70.6 64.0	—	—
PEG–NaI	67.2	—	—
PEG (soln)	69.6	72.0	60.6
TEG–NaI	63.7	—	58.8
TEG (liq.)	66.0	70.3	58.8

$$-O-\underset{I}{\underline{CH_2CH_2}}-O-\underset{II}{\underline{CH_2}}-\underset{III}{\underline{CH_2}}-OH$$

altogether only a single peak indicates that all the inner carbon atoms assume the same conformation. The values of the chemical shifts determined in the present ^{13}C CP/MAS-NMR experiments are listed in Table 1. A systematic work on the ^{13}C CP/MAS-NMR spectra of crown ether complexes by Saito et al.[11] showed that the *tg* conformer(–O^g–C^t–C–) gives the ^{13}C signal at about 71 ppm whereas the *gg* conformer(–O^g–C^g–C–) at about 67 ppm. Although the value of the chemical shift, 67.2 ppm, in the present NaI complex does not coincide with these values, it is lower than 69.6 ppm in the pure PEG solution which is the weighted average of the chemical shifts of the *tg* and *gg* conformations. Thus, the peak at 67.2 ppm in the NaI–PEG complex is assigned to the *gg* conformer.

^{23}Na NMR Spectra. The ^{23}Na–NMR spectrum of the TEG–NaI complex is shown in Fig. 3. This spectrum corresponds to the central transition broadened by the second order quadrupolar perturbation. We carried out the simulation for the lineshape by the usual procedure[13,14] and estimated, from comparison with the observed spectrum, the quadrupole coupling constant, e^2Qq/h, and the asymmetry parameter, η, of the electric field gradient tensor, to be 590±10 kHz and 0.7±0.1, respectively. The simulated spectrum with these parameters is given in Fig. 3 by the broken line. Fig. 4(a) shows the projection onto the F_1 axis of the ^{23}Na two dimensional nutation NMR spectrum. The spectrum indicates that all the Na^+ occupy crystallographically equivalent sites. The simulated spectrum with the above values of e^2Qq/h and η is shown by the broken line, reproducing fairly well the experimental result. The large e^2Qq/h and η suggest that the Na^+ is coordinated by the oxygens asymmetrically.

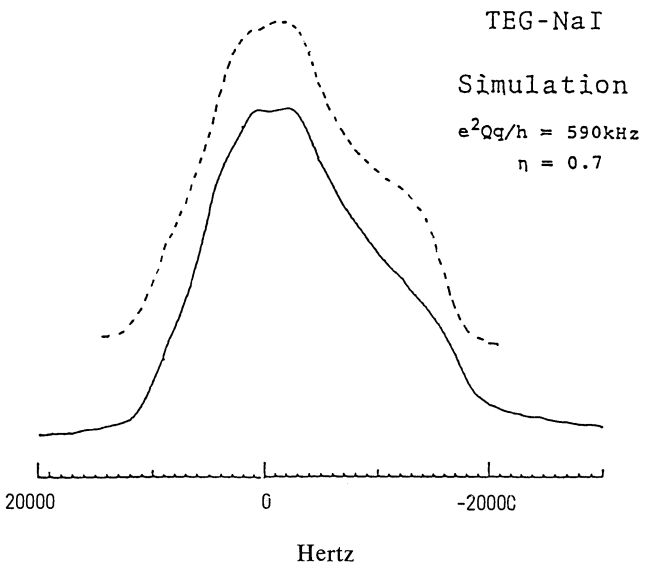

Fig. 3. ^{23}Na NMR spectrum of TEG–NaI complex (solid line) at room temperature and the simulated spectrum (broken line) with e^2Qq/h=590 kHz and η=0.7.

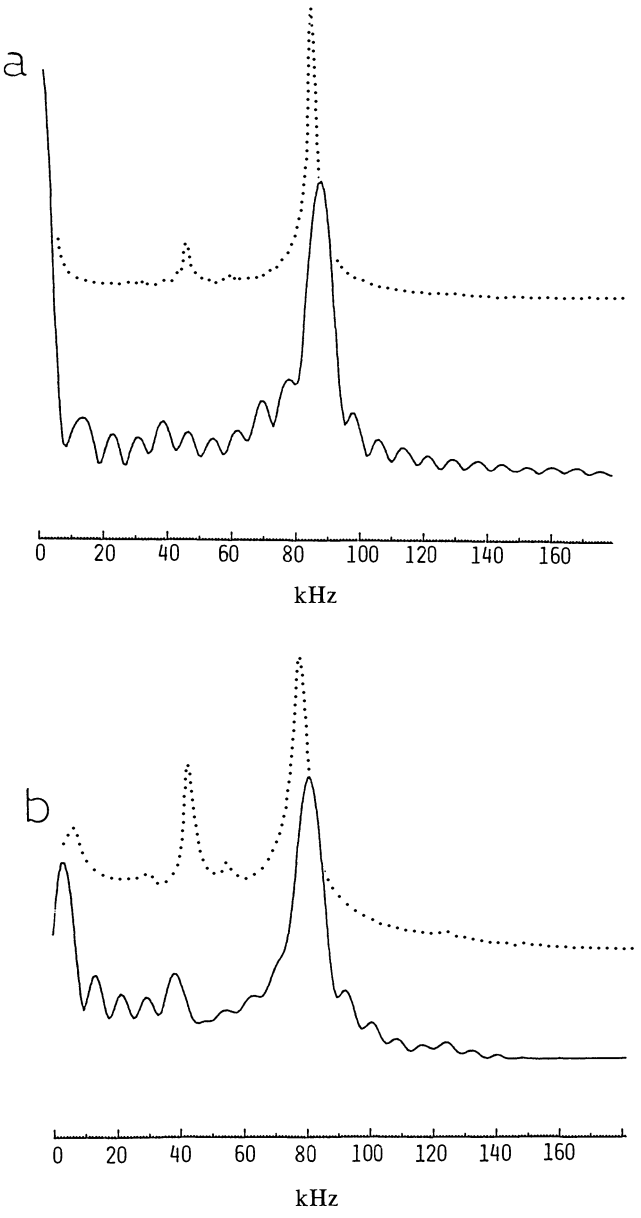

Fig. 4. ^{23}Na 2D nutation NMR spectrum of the TEG–NaI complex (a) and of the PEG–NaI complex (b), and the simulated spectrum (broken line) with e^2Qq/h =590 kHz, η=0.8 and ω_{rf}=39.3 kHz for the TEG–NaI complex and e^2Qq/h=320 kHz, η=0.7 and ω_{rf}=37.5 kHz for the PEG–NaI complex.

In the case of the PEG–NaI complex, the ^{23}Na NMR gives a relatively narrow, symmetric spectrum at room temperature as shown in Fig. 4. A similar spectrum was reported for the PEO–$NaClO_4$ (EO : Na^+=4.5 : 1) by Greenbaum.[19] These results predict a fairly small quadrupole interaction. In order to confirm this point we conducted a 2-dimensional nutation NMR experiment for ^{23}Na in the PEG–NaI complex. The information for quadrupole interaction are involved in the projection of the 2D spectrum onto the F_1 axis as is shown in Fig. 4. From the computer simulation of the nutation spectrum we estimated the quadrupole coupling constant and the asymmetry parameter of ^{23}Na to be about 320±10 kHz and about 0.7±0.1, respectively, for the PEG–NaI complex. As in the TEG–NaI complex all Na^+ occupy crystallographically equivalent sites.

Conductometric studies[20] of PEO–KSCN complex in methanol and experiments[21] on ^{23}Na NMR chemical shift in Na-containing complexes in solutions give some evidence that the cations are probably coordinated tetrahedrally by four ether oxygens. The value of the asymmetry parameter, η, which reflects the site symmetry of the Na^+ ion site, is also similar to the values for the $NaBr \cdot 2(D_2O)$ and $NaCl \cdot 2(D_2O)$ (0.7962 and 0.77, respectively).[23] In these compounds, the Na^+ ions are coordinated by four oxygens of water. Therefore, it is reasonable to consider that each Na^+ in the PEG–NaI complex is also coordinated tetrahedrally in the solid state. But the coordinated tetrahedron is appreciably distorted so as to produce a finite and highly asymmetric electric field gradient at the cation site. Assumption of the distorted tetrahedral coordination under the conditions that the *gg* conformation applies to each carbon–carbon bond and that a unit cell contains two monomer units as shown by a previous X-ray diffraction experiment[5] allows us to build some probable model structures for PEG–NaI complex. Among a few model structures which satisfy the above conditions, two of the most probable models are presented in Fig. 5. In these two model structures each EO segment assumes the *gg* conformation and all ether oxygens coordinate favorably to the cation. The model(a) looks, however, less stable than model(b) because in the former structure the distance between the protons in the $-CH_2-O-CH_2-$ segments is unreasonably short (ca. 1.4 Å) as the van der Waals distance. Therefore we adopt only the model structure(b). The characteristics of our model structure(b) for the PEG–NaI complex is compared with the previous model by Chatani and Okamura (C–O model)[5] as follows:

(1) The molar ratio (EO : Na) is 4 : 1 for our model, whereas the previous one (C–O model) is 3 : 1.

(2) Na^+ ions are arranged so as to make the EO molecule to form a zigzag chain in our model, while Na^+ and I^- ions are arranged alternately to realize a 2/1 helix in the C–O model. Although at present we cannot locate the large anions(I^-), we may presume that the coordination number with respect to the Na^+–I^- coordination is 2.

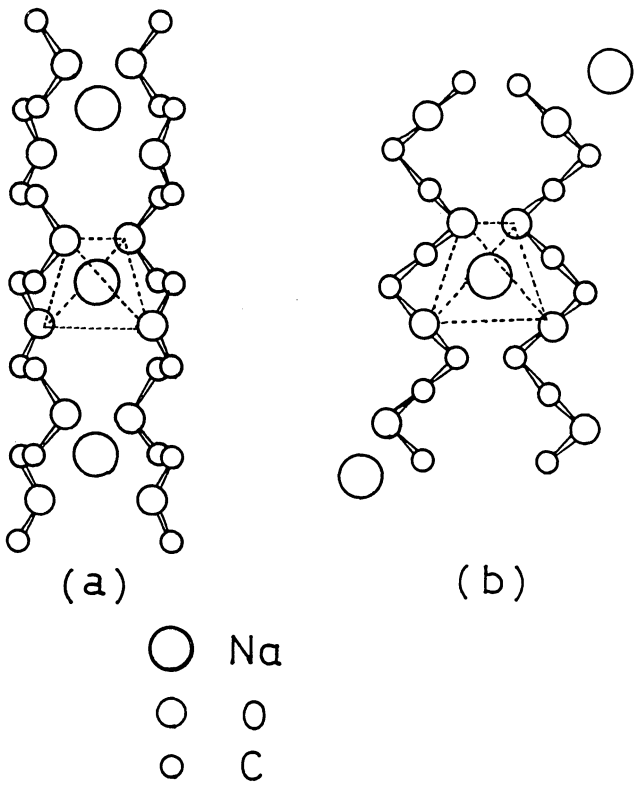

Fig. 5. The model structures of PEG–NaI complex. The conformation of the PEG chain is *gg*. The PEG chain has S-shape in the model (a) and forms helix in the model (b).

(3) The Na^+ and I^- are incorporated into a helical PEG chain that makes a fiber period of 7.98 Å with six EO units in the case of the X-ray experiment, while in our model structure Na^+ are interposed by two helical PEG chains that make the fiber period of 13.8 Å with four EO units. The polymer chain assumes a 4/3 helix and the conformation is *gg* ($-O^g-C^g-C-$) conformer.

(4) Each Na^+ ion is coordinated by four ether oxygens and the Na^+–O distance in our model structure is 2.15 Å. In the C–O model the Na^+ is coordinated by three oxygens and two I^- ions with the Na^+–O distances of 2.28, 2.48, and 2.70 Å which are longer than 2.15 Å in our model.

(5) The *gg* conformation in our model structure can interpret the ^{13}C NMR results but the C–O model which is based on the *tg* conformation predicts the ^{13}C chemical shift of about 71 ppm, conflicting with our experimental results.

A point to be interpreted is why the polymer assumes the *gg* conformation in the complex in spite of reduced stability of this conformation[22] which is obviously less stable than the *tg* or the *tt* conformation observed in other polymers. Energy consideration upon the stability of the whole system will be required.

^{1}H and ^{23}Na Relaxation Times. We measured the ^{1}H

and ^{23}Na spin-lattice relaxation times, T_1, at 17 MHz and 53 MHz, respectively, for PEG–NaI complex for the purpose of examining the possible relation between the ionic motion and the high conductivity in this material. The results are shown in Fig. 6. ^{23}Na relaxation time does not change appreciably below about 200 K; it means that lattice vibrations of only small amplitude govern the relaxation. The monotonous decrease in T_1 above about 200 K indicates that some motion which contributes to the relaxation is excited above 200 K. The slope in Fig. 6 gives the activation energy for that motion 12 kJ mol^{-1}. This value is much smaller than 81 kJ mol^{-1} obtained in the conductivity measurement.[7]

The T_1 for the proton also decreases monotonously on heating, leading to the activation energy of ca. 13 kJ mol^{-1}, which is comparable with that for ^{23}Na. The T_1 for the proton changes discontinuously at the eutectic point (321 K) of the complex.[7] Above this temperature the motion of the polymer chain is rapid compared with the Larmor frequency and its apparent activation energy is 25 kJ mol^{-1}; it is impossible to identify the motion at the present stage. These results show that in the crystalline state of the complex a motion or motions are responsible commonly for the relaxation of both ^{23}Na and ^{1}H and, because the dipolar relaxation of ^{1}H must be governed by some large amplitude motion of the CH_2 segments; this motion of CH_2 groups is ascribed to the result of motion of a polymer chain such as twisting of the ethylene groups. The relaxation of Na^+, on the other hand, is caused by small fluctuation of EFG associated with such chain motion: We could not therefore detect the diffusion nor the hopping of Na^+ by NMR at least up to the eutectic point of complex. The present relaxation measurements suggest that the rate of the Na^+ transport is very low in the crystalline state.

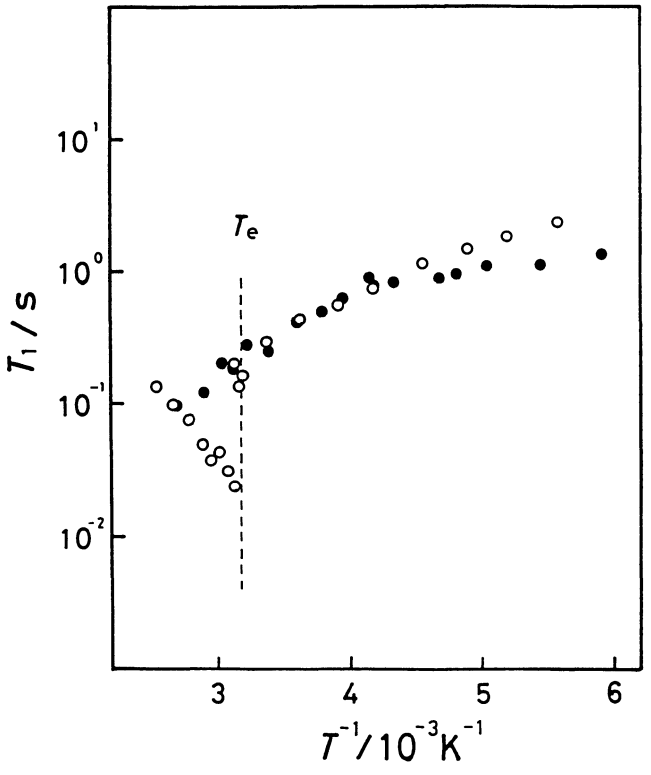

Fig. 6. Temperature dependence of ^{1}H (○) and ^{23}Na (●) spin-lattice relaxation times (T_1) in PEG–NaI complex at 17 MHz and 53 MHz, respectively. The eutectic point (T_e) is 321 K.

Conclusion

The ^{13}C CP/MAS NMR experiments on the PEG–NaI and the TEG–NaI complexes revealed that the bond conformation around each ethylene carbon atom is *gg*. This fact conflicts with model structure for the PEG–NaI complex presented recently on the basis of X-ray fiber diffraction. Quadrupole-perturbed ^{23}Na NMR spectrum together with 2D ^{23}Na nutation NMR showed that the quadrupole coupling constants and the asymmetry parameters are significantly large in both complexes, implying that distorted tetrahedral coordination of oxygens to the cation is realized. Based on the present ^{13}C and ^{23}Na NMR data we proposed a new model for the PEG complex. The results of ^{1}H and ^{23}Na relaxation time measurements indicated that the rate of transport of Na^+ is extremely low at ambient temperature.

The present work was partially supported by a Grand-in-Aid for Scientific Research No. 61430006 from the Ministry of Education, Science and Culture. We are also grateful to Asahi Chemical Industry Co., Ltd. and Mitsubishi Electric Coorporation for partial financial supports.

References

1) P.V. Wright, *Br. Polym. J.*, **7**, 319 (1975).
2) M. B. Armand, J. M. Chabagno, and M. J. Doclot, "Fast Ion Transort in Soilds," ed by Vashiha, Mundey, and Shenoy, North-Holland, New York (1979).
3) C. C Lee and P. V. Wright, *Polymer*, **23**, 681 (1982).
4) B. L. Papke, M. A. Ratner, and D. F. Shriver, *J. Phys. Chem. Solids*, **42**, 493 (1981).
5) T. Himba, *Solod State Ionics*, **9/10**, 1101 (1983).
6) Y. Chatani and S. Okamura, *Polymer*, **28**, 1815 (1987).
7) D. Fauteux, M. D. Lupien, and C. D. Robitaille, *J. Electrochem. Soc.*, **134**, 2761 (1987).
8) D. L. VanderHart, *J. Magn. Reson.*, **44**, 117 (1981).
9) D. L. VanderHart and F. Khoury, *Polymer*, **25**, 1589 (1984).
10) M. Moller, W. Gronski, H. J. Cantow, and H. Hocker, *J. Am. Chem. Soc.*, **106**, 5093 (1984).
11) R. Tabeta and H. Saito, *Bull. Chem.Soc. Jpn.*, **58**, 3215 (1985).
12) T. Ueda, S. Takeda, N. Nakamura, and H. Chihara, *Bull. Chem. Soc. Jpn.*, **64**, 1299 (1991).
13) M. H. Cohen and F. Reif, *Solid State Physics*, **5**, 312, (1957).
14) K. Narita, J. Umeda, and H. Kusumoto, *J. Chem. Phys.*, **44**, 2719 (1966).
15) H. Ohki, Thesis, Osaka University, 1990.

16) H. Ohki, N. Nakamura, and H. Chihara, to be submitted to *J. Magn. Reson.*
17) R. R. Ernst, G. Bodenhausen, and A. Workaum, "Principles of Nuclear Magnetic Resonance in One and Two Dimensions," Oxford Univ. Press, Oxford (1987).
18) T. M. Connor and A. Hartland, *J. Polym. Sci., Part A-2,* **7,** 1005 (1969).
19) S. G. Greenbaum, *Solid State Ionics,* **15**, 257 (1985).
20) K. Ono, H. Konami, and K. Murakami, *J. Phys. Chem.,* **83**, 2665 (1979).
21) C. Detellier and P. Laszlo, *Helv. Chem. Acta,* **49**, 1333 (1976).
22) J. E. Mark and P. J. Flory, *J. Am. Chem. Soc.,* **87**, 1415 (1965).
23) K. E. Haland and B. Pedersen, *J. Chem. Phys.,* **58**, 3472 (1973).

Combined Temperature-Programmed Reduction (TPR)-Temperature-Programmed Desorption (TPD) Study of Supported Platinum Catalysts

Kohki EBITANI and Hideshi HATTORI*
Department of Chemistry, Faculty of Science, Hokkaido University, Sapporo 060
(Received February 27, 1991)

Successive temperature-programmed desorption (TPD) after temperature-programmed reduction (TPR) (Combined TPR-TPD) was performed in order to characterize supported platinum catalysts (Pt/SiO_2, Pt/Al_2O_3, Pt/ZrO_2 and Pt/TiO_2) as well as to judge the validity of the apparent TPR profiles. In successive H_2-TPD runs obtained after cooling in the absence of hydrogen from 450 °C to room temperature, the hydrogen desorption peak was observed only for the Pt/TiO_2 sample, indicating that the hydrogenic species were kept on Pt/TiO_2 sample, while no hydrogenic species were retained on the other samples after TPR up to 450 °C. For both Pt/Al_2O_3 and Pt/TiO_2 samples, hydrogen spillover seemed to proceed. Hydrogen incorporation during TPR was greater for Pt/TiO_2 than for the others. This hydrogen spillover causes an overestimation of the consumed H_2/Pt value determined by the apparent TPR profile for Pt/TiO_2. For Pt/SiO_2 and Pt/ZrO_2 samples, the apparent TPR profiles were mostly due to a reduction of the supported Pt oxides. For the Pt/TiO_2 sample, the hydrogen incorporation/emission at different temperatures during TPR was investigated. To generate SMSI states, desorption of the spiltover hydrogen is suggested to play a significant role; the role of hydrogen incorporation/emission in the generation of SMSI states is also discussed.

Since Tsuchiya et al. revealed by a temperature-programmed desorption (TPD) method that four types of hydrogen adsorption occurred on platinum surfaces,[1] TPD has been frequently used to characterize the surface properties of catalysts. Temperature-programmed reduction (TPR) is a method similar to TPD, and has especially been developed to characterize supported metal catalysts.[2–4] In principle, a hydrogen-containing stream perfuses over a catalyst sample while the temperature is being raised linearly. By measuring the concentration of hydrogen in an effluent stream as a function of the temperature, the TPR profile is obtained. The direct, useful information provided by TPR profiles is the reducibility of the supported metal precursors. The preparative method, pretreatment temperature, modifications with the other metal components, and morphology were reflected in the reducibility of the metal oxides.[2,5–8]

The "reducibility" of metal oxides has usually been discussed based on the features and areas of the apparent TPR profiles. However, the apparent TPR profiles (hydrogen consumption profiles) are not completely due to a reduction of the metal cations. As suggested by Huang et al.,[9] a reduced metal is capable of adsorbing hydrogen from the gas phase, and the adsorbed hydrogen on metallic sites can desorb into the carrier gas. Also, the migration of adsorbed hydrogen on metallic sites to the support (hydrogen spillover[10,11]) and/or its reverse process (back-spillover[12]) should be taken into consideration regarding an analysis of the apparent TPR profiles. From this point of view, Huang et al. carried out successive TPR experiments while trying to remove any contribution of chemical processes other than reduction to the apparent TPR profiles for monometallic Pt/Al_2O_3, Ir/Al_2O_3, and bimetallic $Pt/Ir/Al_2O_3$. However, only repetitions of TPR runs cannot be used to distinguish hydrogenic species retained on a surface at the end of the 1st run from those formed by a low-temperature adsorption of hydrogen. We wish to report here on the combined TPR-TPD results concerning supported platinum catalysts (Pt/SiO_2, Pt/ZrO_2, Pt/Al_2O_3 Pt/TiO_2) in order to judge the validity of the apparent TPR profiles of these catalysts. Furthermore, we examined the combined TPR-TPD for Pt/TiO_2 by changing the upper temperature of the TPR measurement in order to elucidate the role of H_2 consumption/emission in the generation of the Strong Metal Support Interaction (SMSI) state, which is well known as the temperature-dependent process.[13,14]

Experimental

Catalyst Preparation and Apparatus. The supported Pt catalysts were prepared by impregnation with a H_2PtCl_6 aqueous solution. We prepared 2 wt% Pt/SiO_2 and 0.6 wt% Pt/Al_2O_3 catalysts with Fuji Davison-Type ID SiO_2 and JRC-ALO-4 (Reference catalyst of Catalysis Society of Japan), respectively. The 0.5 wt% Pt/ZrO_2 and 0.6 wt% Pt/TiO_2 catalysts were prepared with $Zr(OH)_4$ and $Ti(OH)_4$, respectively. $Zr(OH)_4$ and $Ti(OH)_4$ were obtained by the hydrolysis of $ZrOCl_2 \cdot 8H_2O$ and $TiCl_4$, respectively, with 25% aqueous ammonia followed by filtration. The obtained hydroxide gel was washed with distilled water until no Cl^- ions could be detected. These catalysts were dried at 110 °C and calcined at 400 °C. Prior to TPR experiment, each sample was calcined at 300 °C for 2 h, and then heated in Ar flow in situ at 300 °C for 2 h.

The TPR apparatus used in this study is shown in Fig. 1. A mixture of 3% H_2 in Ar was used as a reductive gas. This mixture was purified over reduced copper in order to remove any trace oxygen, followed by passing it through 13X molecular sieves to remove water. The change in the concentration of H_2 as a function of the temperature was monitored by a thermal conductivity detector (TCD), yielding the TPR pro-

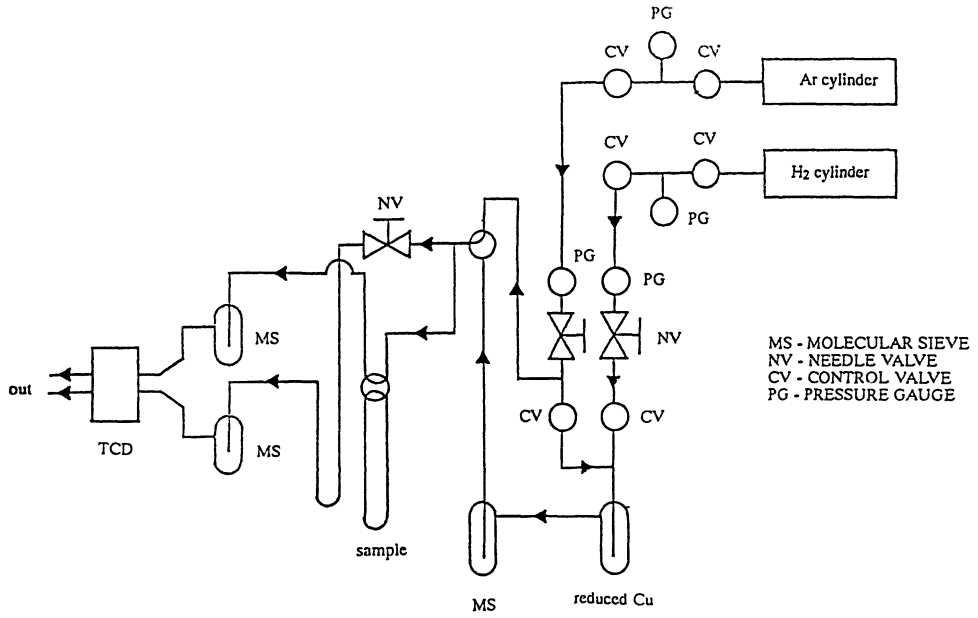

Fig. 1. Schematic diagram of the TPR apparatus.

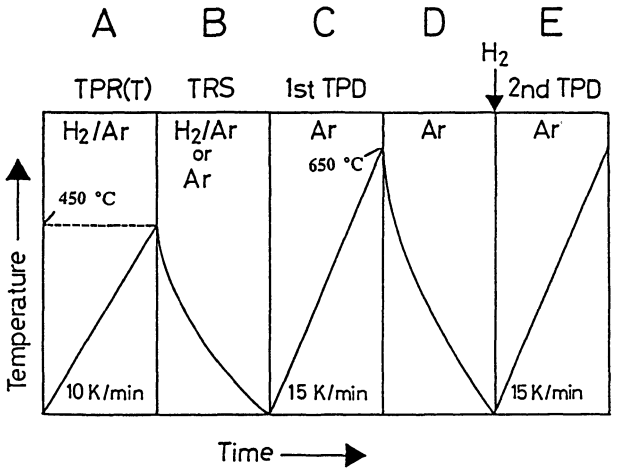

Fig. 2. Sequence of the combined TPR-TPD.
A) TPR, B) TRS (Temperature-Resolved Sorption), C) 1st TPD, D) Cooling, E) 2nd TPD.
The heating rates are indicated.
At the end of D), 23 Torr H_2 was introduced over the sample for 1 min.

file. Since water is formed during the reduction process, gas coming from the reactor was dried over 5A molecular sieves before entering the TCD.

The TPD experiment was carried out succesively after the TPR experiment in the same apparatus. As a carrier gas, pure Ar was used. The Ar gas was purified by the same procedures described in the TPR section. The heating rates for TPR and TPD were 10, and 15 $K\,min^{-1}$, respectively. The amounts of consumed hydrogen were calibrated to the amount for reducing of CuO.

Combined TPR-TPD. Although the methodology used in this work was essentially the same as that reported by Huang et al.,[9] we used pure Ar as a carrier gas for the TPD measurement instead of a H_2/Ar mixture in order to avoid any H_2 adsorption during the TPD experiment.

The procedures in this work are illustrated together with a thermoprofile in Fig. 2, and are as follows:

(1) The apparent TPR profile is obtained up to T (T is usually 450 °C).

(2) The sample is cooled to room temperature in a H_2/Ar gas stream.

(3) At room temperature, the H_2/Ar gas mixture switches into pure Ar gas. Then, without H_2 adsorption, the temperature of the sample is raised in an Ar gas stream to 650 °C. The resulting TPD profile is designated the 1st TPD profile.

(4) The sample is cooled to room temperature in an Ar gas stream.

(5) The H_2 gas (3 vol% H_2 in Ar) is then exposed to the sample at ca. 40 °C for 1 min. The temperature of the sample is raised in an Ar gas stream to 650 °C. The resulting TPD profile is designated the 2nd TPD profile.

The difference between the 1st TPD obtained after cooling in the presence of hydrogen and the 2nd TPD reveals the effect of adsorption temperature on the desorption of the hydrogenic species. In some experiments, the sample was cooled to room temperature under a pure Ar stream instead of a H_2/Ar mixed-stream in the procedure (2).

Results and Discussion

Combined TPR-TPD. Figure 3 shows the apparent TPR profiles up to 450 °C of the supported platinum catalysts. Single apparent hydrogen consumption peaks were observed for Pt/ZrO_2, Pt/Al_2O_3, and Pt/TiO_2, appearing at 225, 254, and 145 °C, respectively. These peak temperatures are in good agreement with those reported for Pt/Al_2O_3[5–7] and Pt/TiO_2.[15] On the other hand, two apparent consumption peaks at 130 and 240 °C were observed for the Pt/SiO_2 sample. The appearance of two consumption peaks was reported by Augustine and Sachtler for Pt/Al_2O_3,[16] who suggested that they are due to two-dimensional PtO_2 and three-

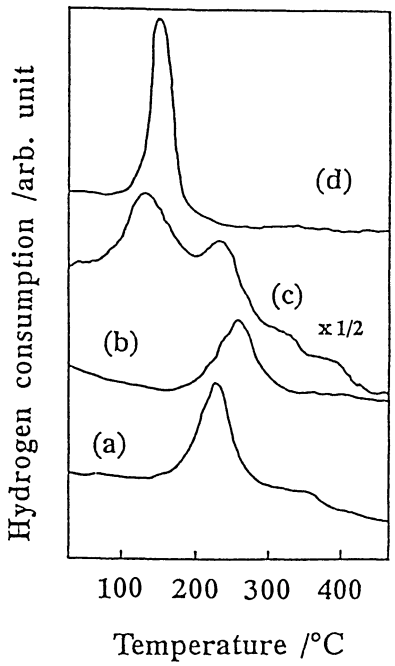

Fig. 3. The apparent TPR profiles of the supported platinum.
(a) Pt/ZrO_2, (b) Pt/Al_2O_3, (c) Pt/SiO_2, (d) Pt/TiO_2.

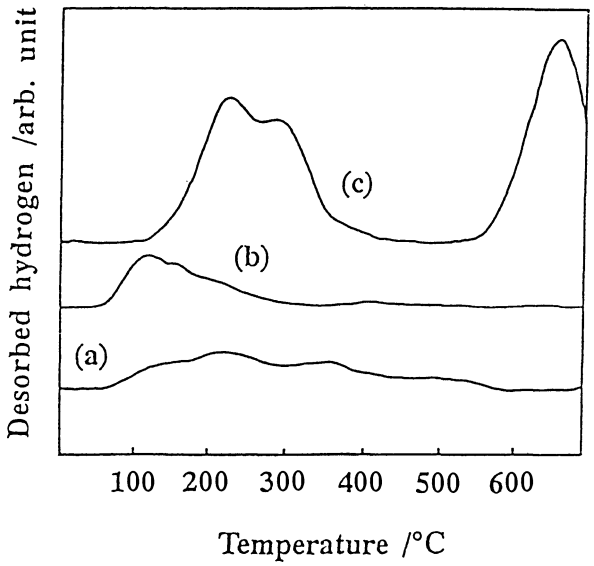

Fig. 4. The 1st TPD profiles of the supported platinum obtained after cooling in the presence of hydrogen.
(a) Pt/Al_2O_3, (b) Pt/SiO_2, (c) Pt/TiO_2.

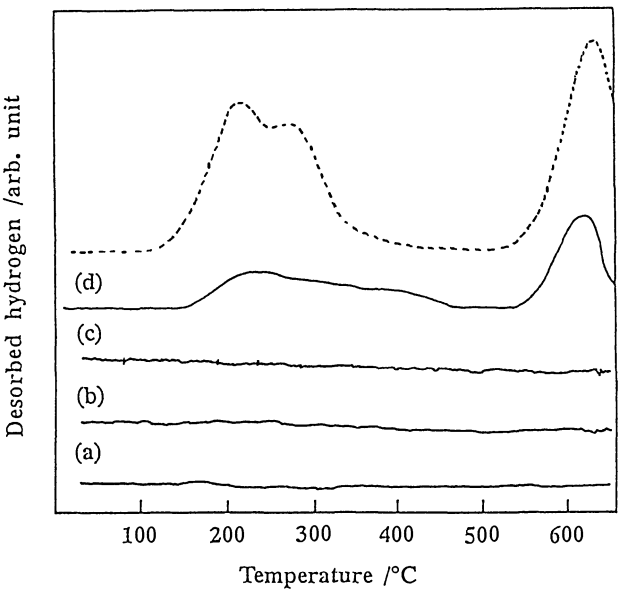

Fig. 5. The 1st TPD profiles of the supported platinum obtained after cooling in the absence of hydrogen.
(a) Pt/ZrO_2, (b) Pt/Al_2O_3, (c) Pt/SiO_2, (d) Pt/TiO_2.
Broken line; Fig. 4-(c).

dimensional platinum oxide. The apparent consumption peak temperatures are tabulated in Table 1 together with the ratio of the consumed hydrogen during the TPR experiment to the total platinum content in the sample (consumed H_2/Pt). It is clearly shown in Table 1 that the consumed H_2/Pt value for Pt/TiO_2 is larger than those for other samples.

The 1st TPD profiles obtained after cooling in the presence of hydrogen are shown in Fig. 4. These TPD profiles were measured by increasing the sensitivity of the detector. In the 1st TPD, hydrogen desorption was not observable for Pt/ZrO_2. For Pt/Al_2O_3, the desorption peaks were broad and appeared over a wide temperature range (70—600 °C). For Pt/SiO_2, the desorption peak was more clear than that for Pt/Al_2O_3, and appeared at 125 °C. In the case of Pt/TiO_2, at least three desorption peaks appeared at 215, 280, 635 °C. The amount of desorbed hydrogen from Pt/TiO_2 was larger than that for other samples. This means that a large amount of the hydrogenic species was kept over the Pt/TiO_2 sample after cooling down in the presence of hydrogen.

When a sample was cooled in the absence of hydrogen after the 1st TPD, a hydrogen desorption peak was observed only for the Pt/TiO_2 sample. However, the area of the observed TPD profile for Pt/TiO_2 was smaller than that obtained after cooling in the presence of hydrogen (Fig. 5). No desorption of hydrogen was found for Pt/Al_2O_3 or Pt/SiO_2, indicating that the

Table 1. Results for the Apparent TPR Profiles of Supported Platinums

Sample	Peak temp/°C	H_2/Pt[a)]
Pt/ZrO_2	225	1.9
Pt/SiO_2	130 340	0.5
Pt/Al_2O_3	254	1.0
Pt/TiO_2	145	3.4

a) The ratio of the consumed hydrogen determined by the apparent TPR profile up to 450 °C to the platinum.

origin of the desorbed hydrogen in 1st TPD shown in Fig. 4 occurs during cooling to low temperature in the presence of hydrogen; the surfaces of Pt/Al_2O_3 and Pt/SiO_2 were free from any adsorbed hydrogenic species at the end of the TPR measurement up to 450 °C. On the other hand, for Pt/TiO_2, the existence of desorptions in the 1st TPD obtained after cooling in the absence of hydrogen confirmed that hydrogenic species are formed over Pt/TiO_2 during the TPR measurement; these species remained at the end of TPR measurement up to 450 °C.

Judging from the appearence of a peak in the 1st TPD obtained after cooling in the absence of hydrogen and a consumed H_2/Pt value greater than 1 (Table 1), the apparent TPR profile of Pt/TiO_2 shown in Fig. 3 must be due to both a reduction of the supported platinum oxides and hydrogen incorporation over Pt/TiO_2.

Figure 6 shows the 2nd TPD profiles which were measured after hydrogen adsorption (23 Torr, 1 Torr=133.322 Pa) at ca. 40 °C for 1 min. Single desorption peaks were observed for Pt/ZrO_2, Pt/Al_2O_3, and Pt/SiO_2 at 100, 90, and 140 °C, respectively. These desorption temperatures are close to those for the hydrogen species adsorbed at platinum metallic sites.[17] For the Pt/TiO_2 sample, two desorption peaks were observed at 80 and 290 °C. No desorption peak was observed around 600 °C, which is the most prominent difference. The 2nd TPD profiles of Pt/TiO_2 and Pt/Al_2O_3 are different from the 1st TPD profiles obtained after cooling in the presence of hydrogen (Fig. 4-a,c). It should be noted that these desorption temperatures are lower than those at which hydrogen consumption occurs during the apparent TPR measurements shown in Fig. 3.

The difference between the 1st TPD obtained after cooling in the presence of hydrogen and the 2nd TPD is considered to show the effect of the H_2 adsorption temperature on the binding state of the adsorbed hydrogenic species. In other words, the hydrogenic species formed during cooling in the presence of hydrogen can be detected in the 1st TPD profile. It is well-known that the hydrogen adsorption temperature affects the hydrogen adsorption states;[9,11,18–23] high-temperature hydrogen adsorption causes a hydrogen spillover for both Pt/TiO_2[18–23] and Pt/Al_2O_3.[9,11] It is thus postulated that the difference between the 2nd and 1st TPD obtained after cooling in the presence of hydrogen is due to spiltover hydrogens. The concentration of these species for Pt/TiO_2 (Fig. 4-c) is much greater than that for Pt/Al_2O_3 (Fig. 4-a).

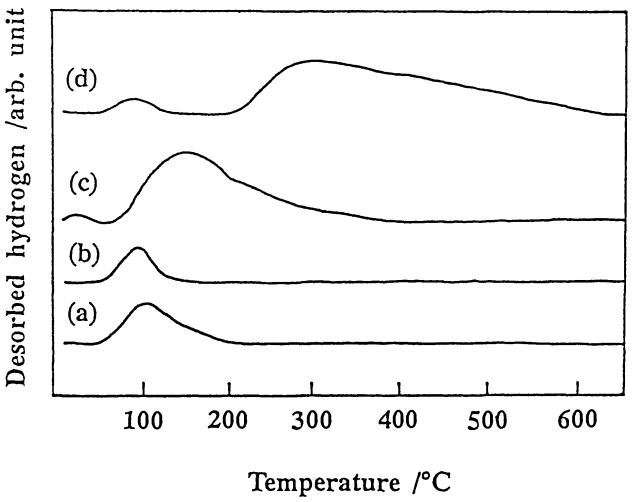

Fig. 6. The 2nd TPD profiles of the supported platinum.
(a) Pt/ZrO_2, (b) Pt/Al_2O_3, (c) Pt/SiO_2, (d) Pt/TiO_2.

The above-mentioned results clearly show that Pt/TiO_2 posesses the hydrogenic species, even at 450 °C, in the TPR measurement and that these hydrogenic species were formed by exposure to hydrogen at high temperatures via a hydrogen spillover process. The formation of these hydrogenic species on Pt/TiO_2 created by exposure to hydrogen at high temperatures causes an overestimation of the consumed H_2/Pt value if determined by the apparent TPR profile. The apparent hydrogen consumption (TPR) profile of Pt/TiO_2 contains the hydrogen adsorption (spillover) process in addition to a reduction of the supported platinum oxides. Chang et al.[24] also reported that the hydrogen consumption peak below 300 °C in the TPR profile for Pd/TiO_2 is due to hydrogen spillover to the TiO_2 support.

For Pt/SiO_2, Pt/ZrO_2, and Pt/Al_2O_3, the apparent TPR profile is mostly due to a reduction of the supported platinum oxides, since the desorption rate is faster (Fig. 6) than the adsorption rate at the temperatures at which hydrogen consumption occurs in TPR measurements (Table 1). The low consumed H_2/Pt value observed for Pt/SiO_2 might indicate the presence of unreduced platinum oxides after a TPR measurement up to 450 °C. An alternative explanation might be that Pt/SiO_2 was not completely oxidized by calcination at 400 °C.

Interaction of Hydrogen with Pt/TiO_2. It is well-known that a high-temperature reduction causes the Strong Metal-Support Interaction (SMSI) state of the supported platinum for Pt/TiO_2.[13,14] The occurrence of SMSI is believed to contain the hydrogen incorporation/emission process, which is temperature dependent.[17–22] We thus examined the effect of the upper temperature of the TPR on the 1st TPD in order to clarify the role of the hydrogen incorporation/emission process in the generation of SMSI states.

The apparent TPR profile of Pt/TiO_2 over a wide range of temperatures is shown in Fig. 7. We chose three temperatures (350, 450, 650 °C) as the upper temperature of the TPR measurement; they are indicated in Fig. 7. The 1st TPD profiles obtained after TPR measurements up to 350, 450, and 650 °C are shown in Fig. 8. These TPD profiles were obtained after cooling in the absence of hydrogen and, thus, reflect only changes in the upper temperatures of the

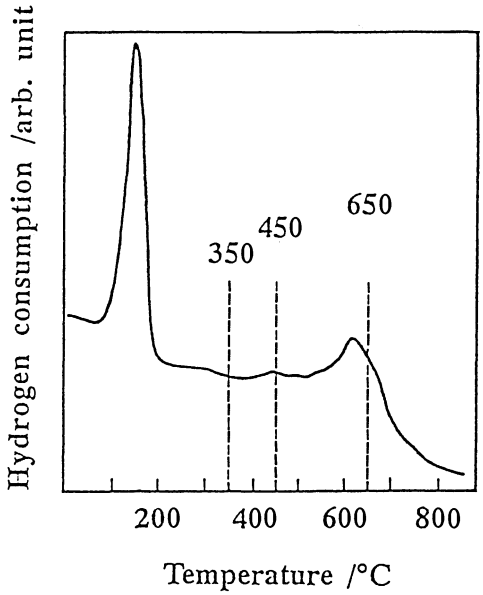

Fig. 7. The apparent TPR profile of Pt/TiO_2 up to 830 °C.

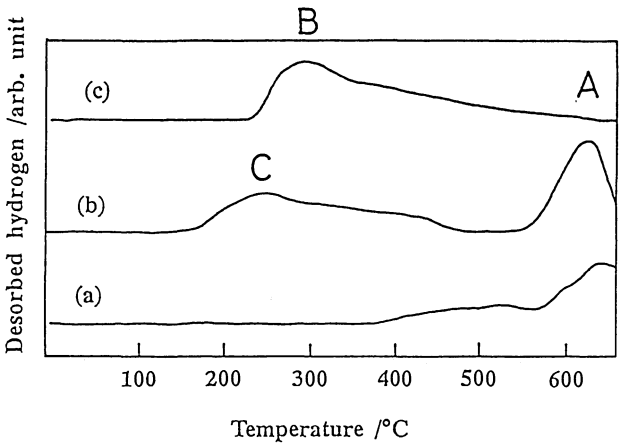

Fig. 8. The 1st TPD profiles of Pt/TiO_2 obtained after the TPR measurement up to (a) 350 °C, (b) 450 °C, (c) 650 °C, and cooling down in the absence of hydrogen.

TPR measurement. In the TPD profile obtained after a TPR measurement up to 350 °C, a single desorption peak above 600 °C was observed. Upon increasing the upper temperature of the TPR measurement to 450 °C, a new desorption peak at around 250 °C appeared in the successive TPD. Following TPR to an upper temperature of 600 °C, the desorption peak became single at 290 °C. At least three hydrogen desorptions were observed. These desorption peaks have been designated as peaks A (above 600 °C), B (around 290 °C), and C (at 250 °C), as indicated in Fig. 8.

The change in the hydrogen exposure temperature changed both the hydrogen adsorption state and the state of Pt/TiO_2. Hongli et al. studied hydrogen TPD from the Pt/TiO_2 related to the SMSI states,[12] and reported that the single desorption peak at 290 °C is a characteristic of the SMSI states. The single desorption peak B at 290 °C, obtained for a sample run up to 650 °C, suggests that a hydrogen treatment up to 650 °C creates SMSI states.

A desorption temparature of 290 °C, obtained for the SMSI state of Pt/TiO_2, is higher than those for the other supported platinum catalysts such as Pt/Al_2O_3 (90 °C), Pt/ZrO_2 (100 °C), and Pt/SiO_2 (140 °C). Raupp and Dumesic studied hydrogen adsorption on titania-deposited Ni polycrystalline, and reported that the adsorption strength of Ni toward hydrogen was enhanced by the presence of titania moieties in the vicinity of Ni metal.[25] The existence of the titania species over metal particles has recently been evidenced by a high-resolution transmittance electron microscopic investigation.[26] It is, therefore, considered that the higher desorption temperature for the SMSI state of Pt/TiO_2 is caused by the presence of titania moieties located in the vicinity of Pt particles.

As seen in Fig. 8, desorption peak A disappeared upon a hydrogen treatment up to 650 °C, indicating that the hydrogenic species producing peak A were desorbed during a TPR measurement between 450 and 650 °C. It is suggested that the desorption of hydrogenic species A plays an important role in the generation of SMSI states.

Hydrogen desorption peak A was observed in the TPD profile after a TPR measurement up to 350 °C. Huizinga and Prins[18] as well as Beck et al.[19] have attributed the hydrogenic species over Pt/TiO_2 formed by hydrogen adsorption below 220—300 °C to represent the spillover state on the TiO_2 support. We therefore consider desorption peak A as being the desorption of spiltover hydrogens on the TiO_2 support. A desorption of these spiltover hydrogens is thought to be necessary to generate SMSI states from this work.

Munuera et al.[22] and Sanz et al.[23] claimed that a further incorporation of hydrogen into the Ti^{3+} cations to form diamagnetic hydride-like species, such as $[Ti-H]^{3+}$, is necessary to generate SMSI states. If their conclusion is correct, hydrogen adsorption would have occurred between 450—650 °C. However, in this work, since hydrogen desorption occurred for the SMSI state, their suggestion is not plausible. A suggestion by Munuera and Sanz[22,23] was made in terms of the ESR result: that the number of Ti^{3+} centers decreases upon reduction at 500 °C, in spite of a continuous incorporation of H_2 into TiO_2 support which occurs under these conditions. The decrease in the Ti^{3+} number during an increase in the reduction temperature seems to be due to both spin pairing and spin–spin relaxation, as interpreted by Bonneviot and Haller.[27]

The role of hydrogen desorption in the generation of the SMSI states has been proposed.[12,18,22] Huizinga and Prins[18] as well as Kunimori et al.[20] have proposed that a dehydration of the support takes place at 500 °C in the neighborhood of the metal particles, thus produc-

ing a reduced form of $TiO_2(Ti_4O_7)$[28] in the vicinity of the Pt particles. They proposed that hydrogen is desorbed in the form of water. On the other hand, Hongli et al.[12] as well as Conesa et al.[21] suggested that any back-spillover of the hydrogen species from the support to the metal (metal-catalyzed hydrogen desorption) plays an important role in producing SMSI behavior. In this case, hydrogen is desorbed in the form of hydrogen molecules.

It was also shown in the present work that the role of the hydrogen desorption at around 450—650 °C in the generation of the SMSI states is significant. Since hydrogen was desorbed in the form of molecular hydrogen within the temperature range 450—650 °C, a desorption of spiltover hydrogens seems to be plausible, even though it is not certain whether dehydration also occurs or not. It is proposed that titania migrates with the adsorbed hydrogen onto platinum particles to create the SMSI state. On platinum particles, hydrogen-containing titanium suboxides release hydrogen atoms which recombine to form molecular hydrogen while leaving the surface.

This work was supported by a Grant-in-Aid for Scientific Research on Priority Areas from the Ministry of Education, Science and Culture.

References

1) S. Tsuchiya, Y. Amenomiya, and K. J. Cvetanovic, *J. Catal.*, **19**, 245 (1970).
2) J. W. Jenkins, B. D. McNicol, and S. D. Robertson, *CHEMTECH*, **7**, 316 (1977).
3) G. J. K. Acres, A. J. Bird, J. W. Jenkins, F. King, "Characterization of Catalysts," ed by J. M. Thomas and R. M. Lambert, John Wiley & Sons, Chichester, New York, Brisbane, Tront (1980), p. 55.
4) N. W. Hurst, S. J. Gentry, and A. Jones, B. D. McNicol, *Catal. Rev.-Sci. Eng.*, **24(2)**, 233 (1982).
5) B. H. Isaacs and E. E. Pertersen, *J. Catal.*, **77**, 43 (1982).
6) N. Wagstaff and R. Prins, *J. Catal.*, **59**, 434 (1979).
7) R. L. Mieville, *J. Catal.*, **87**, 437 (1984).
8) J. C. Vis, J. van't Blik, T. Huizinga, J. van Grondelle, and R. Prins, *J. Catal.*, **95**, 333 (1985).
9) Y.-J. Huang, J. Xue, and J. A. Schwarz, *J. Catal.*, **111**, 59 (1988).
10) "Spillover of Adsorbed Species," ed by G. M. Pajonk, S. J. Teichner, and J. E. Germain, Elsevier, Amsterdam 1983.
11) R. Kramer and M. Andre, *J. Catal.*, **58**, 287 (1979).
12) W. Hongli, T. Sheng, X. Maosong, X. Guoxing, and G. Xiexian, "Metal-Support and Metal-Additive Effects in Catalysis," ed by B. Imelik et al., Elsevier, Amsterdam (1982), p. 19.
13) S. J. Tauster, S. C. Fung, and R. L. Garten, *J. Am. Chem. Soc.*, **100**, 170 (1978); S. J. Tauster, S. C. Fung, R. T. K. Baker, and J. A. Horsley, *Science*, **221**, 1121 (1981).
14) G. L. Haller and D. E. Resasco, *Adv. Catal.*, **36**, 173 (1989).
15) B. A. Sexton, A. E. Hughes, and K. Foger, *J. Catal.*, **77**, 85 (1982).
16) S. M. Augustine and W. M. H. Sachtler, *J. Catal.*, **116**, 184 (1989).
17) J. J. F. Scholten, A. P. Pijpers, and A. M. L. Hustings, *Catal. Rev.-Sci. Eng.*, **27(1)**, 151 (1985).
18) T. Huiginga and R. Prins, *J. Phys. Chem.*, **85**, 2156 (1981).
19) D. D. Beck and J. M. White, *J. Phys. Chem.*, **88**, 2764 (1984); D. D. Beck, A. O. Bawagan, and J. M. White, *J. Phys. Chem.*, **88**, 2771 (1984).
20) K. Kunimori, S. Matsui, and T. Uchijima, *J. Catal.*, **85**, 253 (1984).
21) J. C. Conesa, P. Malet, G. Munuera, J Sanz, and J. Soria, *J. Phys. Chem.*, **88**, 2986 (1984).
22) G. Munuera, A. R. Gonzarez-Elipe, J. P. Espinos, J. C. Conesa, J Soria, and J. Sanz, *J. Phys. Chem.*, **91**, 6625 (1987).
23) J. Sanz, J. M. Rojo, P. Malet, G. Munuera, M. Blasco, J. C. Conesa, and J. Soria, *J. Phys. Chem.*, **89**, 5427 (1985).
24) T.-C. Chang, J.-J Chen, and C.-T. Yeh, *J. Catal.*, **96**, 51 (1985).
25) G. B. Raupp and J. A. Dumesic, *J. Catal.*, **95**, 587 (1985).
26) E. J. Braunschweig, A. D. Logan, A. K. Datye, and D. J. Smith, *J. Catal.*, **118**, 227 (1989).
27) L. Bonneviot and G. L. Haller, *J. Catal.*, **113**, 96 (1988).
28) R. T. K. Baker, E. B. Prestridge, and R. L. Garten, *J. Catal.*, **56**, 390 (1979).

Strong Acid Sites Created on Small-Sized Anatase

Hirotoshi NAKABAYASHI,* Noriyoshi KAKUTA,† and Akifumi UENO†
Department of Industrial Chemistry, Kochi College of Technology,
Monobe, Nankoku, Kochi 783
†Department of Materials Science, Toyohashi University of Technology,
Tempaku, Toyohashi, Aichi 441
(Received March 1, 1991)

The acid properties of anatase having different crystalline sizes were estimated by measuring the temperature-programmed desorption (TPD) of ammonia as well as the infrared spectrum of adsorbed pyridine at elevated temperature. The size-controlled anatase was prepared by hydrolysis of the titanium tetraisopropoxide dissolved in propyl alcohol using various amounts of distilled water. The acid properties of the anatase were confirmed to be strongly affected by the crystalline size. Especially, the strength of acid sites was found to remarkably increase with a decrease in the crystalline size. The specific activity and the activation energy for 1-butene isomerization on the anatase also depended on the crystalline size. The generation of strong acid sites on the surface is discussed in terms of the crystalline size.

Acid sites on metal oxides are believed to be ascribed to surface hydroxyl groups or a charge imbalance localized on the surface. Localization of deficient amounts of electrons results from a local imbalance between positive and negative charges of the constituents, and acts as a Lewis acid for catalytic reactions. Since a charge imbalance can be expected by substituting the metal ions with other metal ions possessing different charges, new acid sites could be designed on the surface of doped and/or mixed metal oxides.[1-3] A charge imbalance might emerge, however, even on single-component metal oxides comprising small-sized crystallites, since the electronic properties of tiny metal or metal oxide crystallites have been widely expected to be somewhat different from that of bulk materials.[4] These differences are partially attributed to surface imperfections of crystallographic structures in small-sized crystallites. The typical imperfections in small crystallites are metal or oxygen vacancies, which cause a local charge imbalance.

The idea that new, strong acid sites might be generated on small crystallites has been preliminary demonstrated on TiO_2 by a titration test using several kinds of color indicators.[5] This type titration test, however, sometimes provides us with an ambiguous determination of the acid strength due to a vague change in the color of indicators. The purpose of the present work was to confirm the idea using more reliable methods in measurements of the acid properties, and to understand the generation of strong acid sites in terms of crystalline size.

Experimental

Size-controlled anatase was prepared in the same manner as described elsewhere.[5] In short, 0.025 mol of titanium tetraisopropoxide (Kishida Kagaku Co., 99.9% purity) was dissolved in 50 mL of propyl alcohol, followed by hydrolysis with the desired amounts of distilled water in order to control the size of the resultant TiO_2. The obtained precipitates were dried at 383 K and then calcined at 693 K for 3 h in air. All of the powders, thus produced, were anatase and no trace of rutile was detected by X-ray diffraction measurements, since the phase transformation of anatase to rutile is reported to occur only at temperatures higher than 873 K.[6] The mean sizes of the anatase crystallites were estimated by X-ray line broadening at $2\theta=25.3°$ using the Scherrer equation; 4 kinds of TiO_2 with sizes of around 70, 100, 130, and 170 Å, respectively, were examined. BET surface areas were obtained by N_2 adsorption at 77 K.

The TPD of ammonia on the anatase was carried out using a He purge with a flow rate of 100 mL min^{-1} and a temperature rising rate of 10 K min^{-1}. The sample powder (0.2 g) was first calcined at 693 K in air, and then treated in flowing O_2 at 573 K for 1 h, followed by cooling to room temperature with evacuation. A certain amount of ammonia was iteratively injected into the carrier gas (He), which was introduced over the powder until no more adsorption of ammonia was observed. Pyridine was adsorbed on anatase at 423 K in order to avoid its physical adsorption, followed by evacuation at the desired temperatures. Infrared spectroscopy was employed at room temperature to monitor pyridine still adsorbed on TiO_2, even after evacuation at elevated temperatures.

Isomerization of 1-butene was carried out at temperatures from 413 to 493 K using a closed circulation system made of glass. The sample powder (0.5 g) was first calcined at 693 K in air, and then recalcined at 573 K for 1 h in an O_2 atmosphere, followed by evacuation at room temperature prior to the reaction. The rate constant was estimated, assuming a first-order reaction concerning 1-butene. The initial pressure of 1-butene was always set at 11.8 cmHg (15.72×10^3 Pa) in the present work.

Results

The BET surface areas and the mean crystalline sizes of TiO_2 used in this work are given in Table 1. The highest acid strengths detected by indicators are also given in Table 1. In Fig. 1 are shown the TPD spectra of ammonia on TiO_2 with sizes of about 75, 102, 125, and 162 Å respectively. Three peaks centered around 413, 523, and 663 K are observed in these spectra; the first peak is mainly ascribed to the desorption of ammo-

nia physically adsorbed over TiO_2. Assuming a log-normal distribution for the first peak, the amounts of ammonia chemisorbed were estimated by weighing the other two peaks on the chart. Since ammonia adsorbs on an acid site, the number of acid sites per g and/or m^2 of TiO_2 was calculated (see Fig. 2).

The infrared spectra of pyridine still adsorbed at 423, 523, 623, 673, and 723 K are given in Fig. 3, where the crystalline sizes of TiO_2 used were 82, 125, and 175 Å, respectively. Four absorption peaks were observed at 1610, 1575, 1490, and 1445 cm^{-1} when pyridine was adsorbed on TiO_2 at 423 K. All of the peaks observed

Table 1. BET Surface Areas and the Mean Crystalline Sizes of TiO_2 Studied in This Work.[5] Amounts of Water Employed for the Hydrolysis of $Ti(OC_3H_7)_4$ are Also Given

Sample no.	Water added	Surface area	Crystalline size	Highest Acid strength
	mL	$m^2 g^{-1}$	Å	(H_0)
TiO_2(1)	2000	130	75, 82	−3.0
TiO_2(2)	1000	120	102	−3.0—+1.5
TiO_2(3)	300	105	125	+1.5—+3.3
TiO_2(4)	50	81	162, 175	+3.3—+4.0
TiO_2(5)	Commercial	39	1500—2300	+4.8

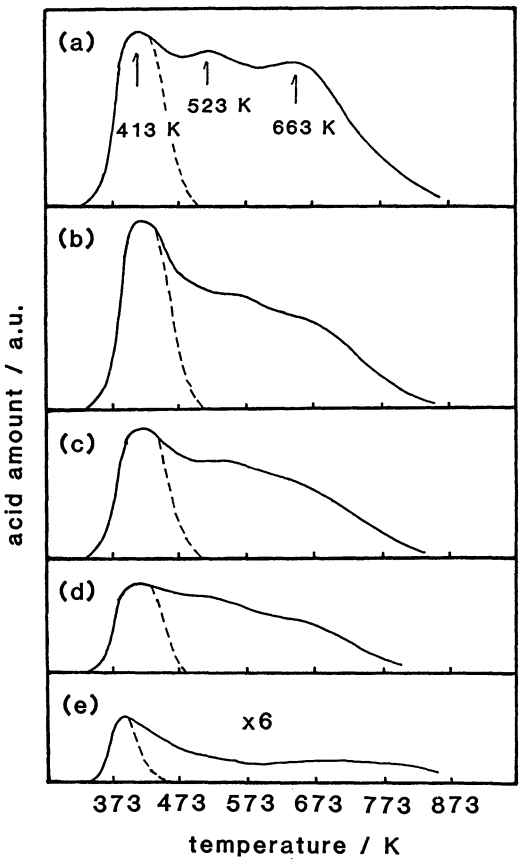

Fig. 1. TPD spectra of ammonia adsorbed on TiO_2 sized 75 Å (a), 102 Å (b), 125 Å (c), and 162 Å (d). For comparison, TPD spectrum of commercial TiO_2 sized around 2000 Å is also depicted.

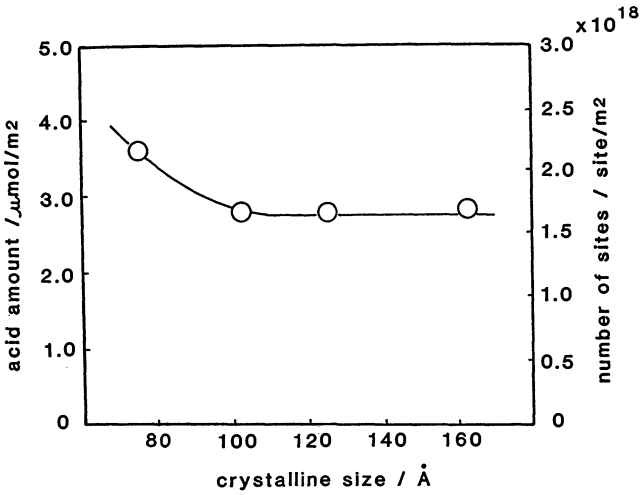

Fig. 2. Numbers of acid sites on TiO_2, given in Fig. 1, expressed in terms of "sites/g" and "sites/m^2".

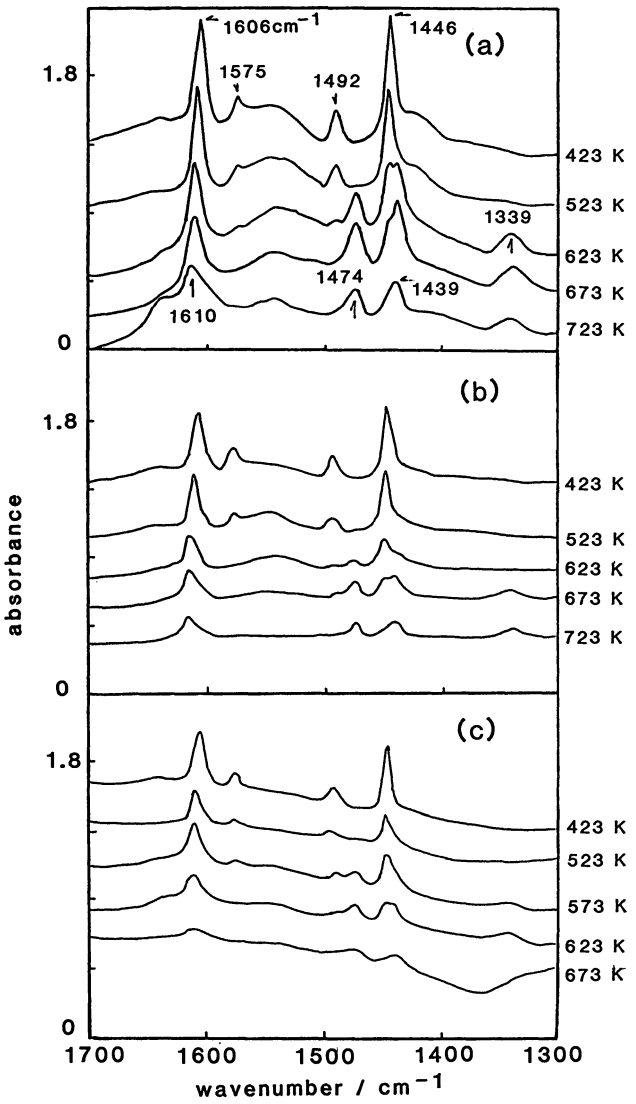

Fig. 3. Infrared spectra of pyridine still adsorbed on TiO_2 at elevated temperatures. TiO_2 studied are sized 82 Å (a), 125 Å (b), and 175 Å (c), respectively.

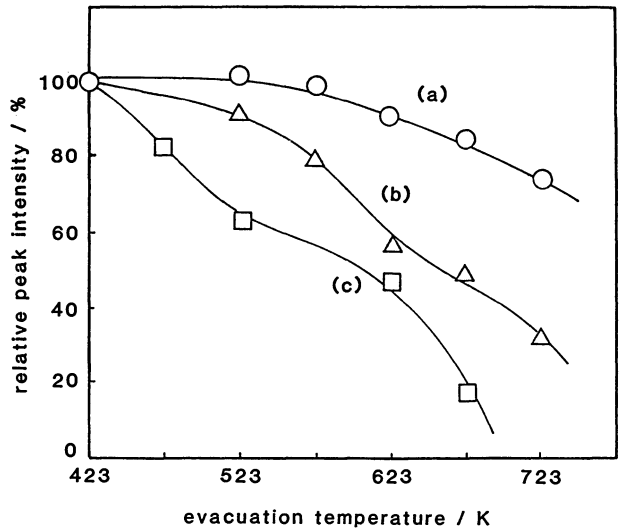

Fig. 4. Decrease in the absorption peak intensity at 1610 cm^{-1} at elevated temperatures. The peak intensities are normalized by the intensity observed after a He purge at 423 K.

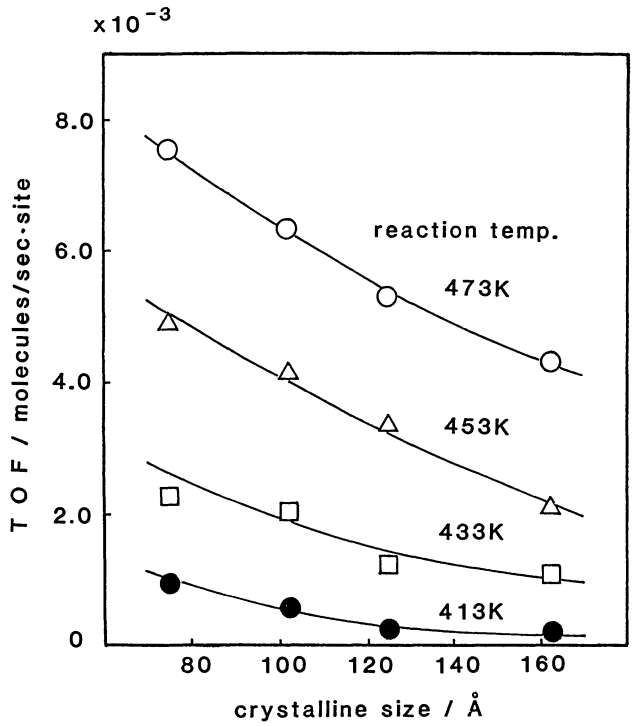

Fig. 5. Change in the turnover frequency of 1-butene isomerization on TiO_2 with the TiO_2 crystalline size.

are ascribed to pyridine adsorbed on the Lewis acid sites,[7] and still remained at temperatures higher than 623 K. Since the area of the absorption peak is proportional to the amounts of pyridine adsorbed, the changes in the peak area at 1610 cm^{-1} with the temperature were monitored for TiO_2 with the crystalline sizes mentioned above. In order to clearly show the difference in these changes, the peak areas were normalized by the peak

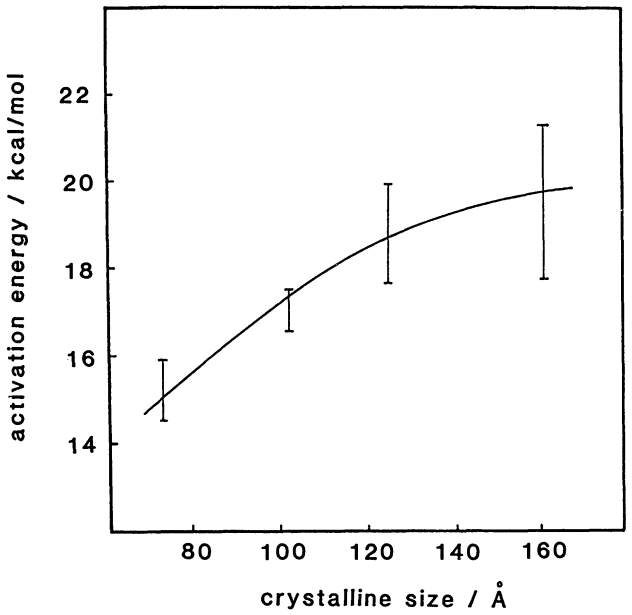

Fig. 6. Change in the activation energy for 1-butene isomerization on TiO_2 with the TiO_2 crystalline size. The activation energies were calculated from the results shown in Fig. 5.

area observed at 423 K for every sample, as shown in Fig. 4.

Since the number of acid sites on TiO_2 was known, the specific activity for 1-butene isomerization on TiO_2 could be expressed in terms of "molecules/sec/site". The obtained results are depicted in Fig. 5 against the crystalline size of TiO_2 used, allowing us to calculate the activation energy on TiO_2 (see Fig. 6).

Discussion

As is obviously shown in Table 1, the crystalline size of TiO_2 decreased as the amount of water used for hydrolysis increased. Although it was not necessarily reproducible to obtain TiO_2 with sizes smaller than 60 Å, which exhibit the highest acid strength of H_0=−5.6, crystallites with sizes of around 70—80 Å with the highest acid strength of H_0=−3.0, could be prepared using more than 2 L of water for hydrolysis. Strong acid sites over the smaller TiO_2 crystallite are also indicated by the TPD of pyridine on TiO_2 with various sizes. In Fig. 3(a) the pyridine adsorbed on TiO_2 with sizes of 82 Å, with H_0(max)=−3.0, is still considerable, even after evacuation at 723 K; on TiO_2 with sizes of around 175 Å (H_0(max)=−8.3), however, only small amounts of pyridine were detected by evacuation at 673 K, as is shown in Fig. 3(c). The fractions of pyridine still adsorbed at various temperatures (drawn in Fig. 4) were determined by monitoring the peak areas at 1610 cm^{-1} and normalizing the areas by the peak areas observed at 423 K. As can clearly be seen in Fig. 4, the fraction of pyridine remaining at elevated temperatures strongly depends on the crystalline size of the

TiO_2 employed; larger amounts of pyridine still remain on smaller TiO_2 crystallites, leading to the conclusion that strong acid sites are created on small-size TiO_2 crystallites. In addition, it would be interesting to discuss the peak shifts which occur in Fig. 3. Although the peak at 1610 cm^{-1} has been reported to shift somewhat toward long wavenumbers with evacuation at elevated temperatures,[8] other peaks observed at 1490 and 1445 cm^{-1} at 423 K were also shown to move to 1475 and 1438 cm^{-1} respectively, after evacuation at 623 K. These shifts could be recognized in all of the samples studied here (see Fig. 3). The new peaks at 1475 and 1438 cm^{-1} were never observed on TiO_2 evacuated at 623 K prior to pyridine adsorption. What happened on the adsorbed pyridine by evacuation at 623 K is yet another problem to be resolved.

The amounts of acid sites over the surface of size-controlled TiO_2 were estimated by measuring the peak areas due to chemisorbed ammonia in ammonia-TPD spectra, assuming one ammonia molecule per one acid site. Although the acid amounts on 1 g of TiO_2 increased with a decrease in the crystalline size, the acid-site density (expressed in terms of "site/m^2") was constant at 1.7×10^{18} sites/m^2 when the crystalline size was larger than 100 Å (see Fig. 2). This indicates that although new acid sites are not created on TiO_2 with sizes larger than 100 Å the acid strength of the sites is modified to be stronger as the crystalline size decreases. Over the surface of TiO_2 with sizes smaller than 100 Å the acid-site densities slightly increased with a decrease in the crystalline size, indicating the generation of new acid sites over the finely divided TiO_2 crystallites. The generation of new acid sites on TiO_2 crystallites with sizes smaller than 100 Å seems to be attributable to metal and/or oxygen ions vacancies which emerged on the surfaces of small TiO_2 crystallites, since these vacancies have been reported to be enhanced in small-size crystallites.[9] In the present work sample powders were reoxidized at 573 K prior to the TPD measurements, suggesting smaller amounts of oxygen ion vacancies on the surface of the TiO_2 used. Consequently, the new acid sites on the finely divided TiO_2 crystallites are tentatively assigned to Ti ion vacancies on the surface.

The strong acid sites over the surface of small TiO_2 crystallites can be elucidated in terms of the electronic properties, which have been widely accepted to be somewhat different from those of bulk-like materials.[4] A blue-shift in the absorption edge of UV-visible spectrum has been reported on tiny TiO_2 particles.[10] This indicates an increase in the bandgap between the conduction and valence band levels of TiO_2 semiconductors. An increase in the bandgap with crystalline size has been estimated by Brus,[11] who calculated the energy of the lowest excited states of various semiconductors. This calculation has been applied to TiO_2 particles,[12] and an increase in the bandgap of small-size TiO_2 has been assigned to an elevation of the conduction band edge. Though the change in the top of the valence band has not been mentioned in this paper, it might be natural to deduce a descent of the valence band edge to expand the bandgap of small TiO_2. A change in the valence band level results in a change in the acid strength of TiO_2 when used as a catalyst, since the positive holes formed in the valence band act as Lewis acid sites during catalysis. Consequently, the descent of the valence band edge in small-sized TiO_2 causes Lewis acid sites with higher acid strengths.

Finally, we tried to relate the acid properties of the finely-divided TiO_2 crystallites to their catalytic performance for the isomerization of 1-butene to *cis*- or *trans*-2-butenes. The product ratio of *cis*/*trans* obtained here was always within the range 1 to 2, suggesting no basic sites, such as Ti^{3+} over TiO_2; this is because the ratio observed on the basic sites has been believed to be much higher than that obtained here.[13] All of the acid sites on the present TiO_2 have been confirmed to be that of the Lewis acid, as discussed above. The isomerization (double bond migration) of 1-butene on Lewis acid sites has been considered to proceed via butenyl cations, which are produced by an elimination of H^- ions from 1-butene adsorbed on the Lewis acid sites.[14] Because the elimination step might be rate-determining regarding doble-bond migration, the catalytic performance of a site strongly depends upon the acid strength. On a stronger acid site, the elimination proceeds faster, leading to a higher turnover frequency on stronger acid sites. The turnover frequencies observed on the present TiO_2 become higher as the crystalline sizes become smaller, as shown in Fig. 5. This coincides well with the results obtained in our preliminary work that strong acid sites emerge on small-size TiO_2 crystallites. From the results shown in Fig. 5, the way in which the activation energies depend upon the size of TiO_2 crystallites is revealed (see Fig. 6).

The generation of both new and strong acid sites on the surfaces of finely-divided TiO_2 crystallites was concluded in the present work; this idea will be extended to the generation of both new and strong acid sites on binary oxides containing tiny TiO_2 crystallites.

References

1) G. L.Thomas, *Ind. Eng. Chem.*, **41**, 2564 (1949).

2) K. Tanabe, "Catalysis, Science and Technology," ed by J. R. Anderson and M. Boudart, Splinger-Verlag, Berlin-Heidelberg-New York (1981), Vol. 2, p. 231; K. Tanabe, "Solid Acids and Base," Kodansha, Tokyo, Academic Press, New York, London (1970).

3) G. Connell and J. A. Dumesic, *J. Catal.*, **102**, 216 (1986); **105**, 285 (1987).

4) J. R. Anderson, "Structure of Metallic Catalysts," Academic Press, New York (1989); M .Boudart, *Adv. Catal.*, **20**, 153 (1969).

5) K. Nishiwaki, N. Kakuta, A. Ueno, and H. Nakabayashi, *J. Catal.*, **118**, 498(1989).

6) R. D. Shannon and J. A. Pask, *J. Am. Chem. Soc.*, **77**, 391 (1965).

7) E. P. Parry, *J. Catal.*, **2**, 371 (1963).
8) M. Primet, P. Pichart, and M. Mathieu, *J. Phys. Chem.*, **75**, 1221 (1971).
9) E. Fujita, *Nihon Kinzoku Gakkaishi*, **30**, 322 (1966); N. F. Mott, *Proc. R. Soc., Ser. A*, **171**, 944 (1939); M. F.Mott, *Trans. Faraday Soc.*, **35**, 1175 (1939); **36**, 472 (1940); **43**, 429 (1947).
10) D. Dounghong, J. Ramsden, and M. Gratzel, *J. Am. Chem. Soc.*, **104**, 2977 (1982); A. Henglein, *Ber. Bunsen-Ges. Phys. Chem.*, **86**, 241 (1982); A. Nojik, F. Williams, M. T. Nenadovic, and O. I. Micic, *J. Phys. Chem.*, **89**, 397 (1985); M. Haase, H. Weller, and A. Henglein, *J. Phys. Chem.*, **92**, 482 (1988).
11) L. E. Brus, *J. Phys. Chem.*, **80**, 4403 (1984); R. Rossetti, S. Nakahara, and E. L. Brus, *J. Phys. Chem.*, **79**, 1986 (1983).
12) C. Korman, D. W. Bahnemann, and M. R. Hoffmann, *J. Phys. Chem.*, **92**, 5196 (1988).
13) Y. Fukuda, H. Hattori, and K. Tanabe, *Bull. Chem. Soc. Jpn.*, **51**, 3150 (1978); M. P. Rosynek and J. S. Fox, *J. Catal.*, **49**, 285 (1977).
14) H. P. Lrftin and E. Hermana, *Proc. Int. Congr. Catal., 3rd, Amsterdam*, **1964** (Put **1965**), No. 2, 1064.

 © 1991 The Chemical Society of Japan Bull. Chem. Soc. Jpn., 64, 2433—2437 (1991)

Intramolecular Electron Transfer and S_N2 Reactions in the Radical Anions of 1-Benzoyl-ω-haloalkane Studied by Pulse Radiolysis

Norio KIMURA* and Setsuo TAKAMUKU
The Institute of Scientific and Industrial Research, Osaka University, 8-1 Mihogaoka, Ibaraki, Osaka 567
(Received March 6, 1991)

A one-electron reduction of 1-benzoyl-ω-haloalkane (Cl, Br, I) by solvated electrons and a subsequent intramolecular reaction of the radical anions, thus formed, have been investigated by using a pulse radiolysis technique. The reaction mechanism, electron transfer (ET) or S_N2, and the rate constants were found to change as a function of the nature of the halide and the methylene chain length of the substrate. Although the order of reactivity based on leaving halogen atoms was I, Br, and Cl, the ease of the S_N2 reaction was found to be in the order Cl>Br>I. In addition, the reaction rates were also affected by the polarity of the solvent used. On the basis of these results, it is discussed how the ET–S_N2 dichotomy takes place.

Radical anions ($D^{\cdot-}$) are often used as electron-transfer (ET) reagents. They are easily generated by electrochemical and radiation-chemical reactions, as well as by the reaction of aromatic hydrocarbon with an alkali metal. The most widely investigated reaction is a reductive cleavage of a C–X bond in aliphatic halides (RX) (Eq. 1).[1–8] Mechanistic and kinetic information

$$D^{\cdot-} + RX \rightarrow D + R\cdot + X^- \quad (1)$$

is available for this reaction from electrochemical[1–3] and pulse radiolysis[4–6] studies. There is a large variation in the reaction rate, depending on the oxidation potential of the radical anion donor ($D^{\cdot-}$) and the reduction potential of the alkyl halide acceptor (RX).

On the other hand, Lund and Simonet[9] have studied an electrochemical reaction of fluorenone with alkyl halide and confirmed a C–O bond formation at an α-carbon atom of the halide. An S_N2 reaction of the fluorenone radical anion with alkyl halide was proposed in order to explain the results. This reaction mechanism was also supported by the results from pulse radiolysis.[5]

In a previous investigation concerning the intramolecular reaction in the radical anions of 1-(4-biphenylyl)-ω-haloalkane,[10] an S_N2 reaction yielding a spirocyclic radical occurred competitively to an ET reaction, leading to a terminal carbon radical. However, no such a competitive intramolecular reaction was investigated in other reaction systems.

In the present work, we investigated the one electron reduction of 1-benzoyl-ω-haloalkane ($Ph–CO–(CH_2)_n–X$ (BZ_X-n), X=Cl, Br, I; n=2, 3, 4) by solvated electrons and the subsequent intramolecular reaction of the radical anions, thus formed, by using a pulse radiolysis technique. Further, in order to obtain information concerning the reaction mechanism, the solvent effects on the reaction rates were also investigated.

Results and Discussion

Effects of Chain Length, *n*, and Leaving Halogen Atom. Hexamethylphosphoric triamide (HMPA) solutions of BZ_X-n were irradiated with an 8-ns electron pulse at room temperature. The transient absorption spectra of BZ_X-n (X=Cl, Br, I; n=3, 4) recorded at various times after the pulse are presented in Fig. 1. The spectra observed immediately after the pulse exhibit λ_{max} at 330 and 490 nm, and agree very closely with the spectrum of the radical anion of acetophenone (λ_{max}=330 and 490 nm) which was measured in this work under the same

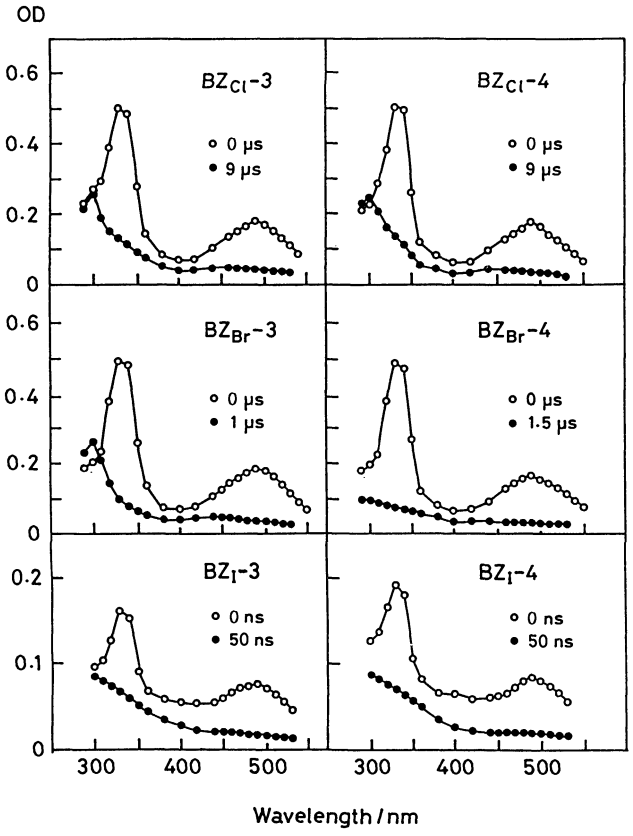

Fig. 1. Transient absorption spectra recorded at various times after the irradiation of an 8-ns electron pulse to HMPA solutions (3×10^{-3} mol dm^{-3}) containing 1-benzoyl-ω-haloalkane (BZ_X-n, X=Cl, Br, I; n=3, 4) at room temperature.

reaction conditions. The initial intensities of these bands observed from BZ_{Cl}-3, BZ_{Cl}-4, BZ_{Br}-3, and BZ_{Br}-4 are almost the same to those of the acetophenone radical anion. However, the initial intensities of the 330 and 490 nm bands observed from BZ_{I}-3 and BZ_{I}-4 are weaker than those of BZ_{Cl}-*n* and BZ_{Br}-*n*, which possess the same chain length (*n*), respectively. This can be explained by the short lifetime of the radical anion (**1** in Scheme 1), as described later. The decay of the 330 and 490 nm bands of all radical anions (**1**) followed first-order kinetics, and the rates were independent of both the solute concentration (1×10^{-2}—1×10^{-3} mol dm^{-3}) and absorption dose. These results indicate that the decay reaction of the radical anion (**1**) proceeds unimolecularly.

On the other hand, in the case of BZ_{Br}-3, the decay of the initial bands are characterized by the formation of a new band with λ_{max} at 300 nm. Further, a similar 300 nm band was also observed in the cases of BZ_{Cl}-3 and BZ_{Cl}-4. This new band coincides with that of an α-methoxybenzyl radical, PhĊH(OMe) (λ_{maxc}=300 nm), formed by a one-electron reduction of benzaldehyde dimethyl acetal. The similarity between both spectra indicates the formation of a similar species, i.e., a cyclic ether radical (**3** in Scheme 1; 2-phenyltetrahydro-2-furyl and 2-phenyltetrahydro-2-pyranyl radicals).

The rate constants (*k*, s^{-1}) measured from the decay of the 490 nm bands are summarized in Table 1, together with the yields of the alkyl phenyl ketone (**4**) by γ-irradiation. In the cases of BZ_{Cl}-2, BZ_{Br}-2, BZ_{Br}-4, BZ_{I}-3, and BZ_{I}-4, the *G*-values (1.8—2.1) of the formation of (**4**) are close to the *G*-value of the solvated electron, i.e., $G(e_s^-)$=2.3 in HMPA.[11] Therefore, in these compounds, it is clear that an intramolecular ET reaction leading to the production of a terminal carbon radical (**2**) preferentially occurs (Scheme 1).

On the other hand, in the cases of BZ_{Cl}-3, BZ_{Cl}-4, and BZ_{Br}-3, the yields of (**4**) were very low ($G<0.1$); the values are quite different from the *G*-values (2.3—2.5) of the substrate disappeared. In these compounds, a formation of the 300 nm bands assigned to a cyclic ether

Table 1. Pulse Radiolysis[a] and γ-Radiolysis[b] of BZ_X-*n* in HMPA Solution at Room Temperature

X	*n*	k/s^{-1}	G(ketone 4)[c]
Cl	2	8.3×10^6	2.0
Cl	3	2.9×10^5	<0.1 (2.3)[d]
Cl	4	2.5×10^5	<0.1 (2.5)[d]
Br	2	1.8×10^7	2.0
Br	3	3.2×10^6	<0.1 (2.4)[d]
Br	4	2.9×10^6	1.8
I	3	8.6×10^7	1.9
I	4	6.0×10^7	2.1

a) Absorption dose was 0.7 kGy/pulse. Substrate concentration: 3.0×10^{-3} mol dm^{-3}. b) Absorption dose was 2.3 kGy. Substrate concentration: 5.0×10^{-2} mol dm^{-3}. c) The 100 eV yield of alkyl phenyl ketone. d) The *G* value of the substrate disappeared.

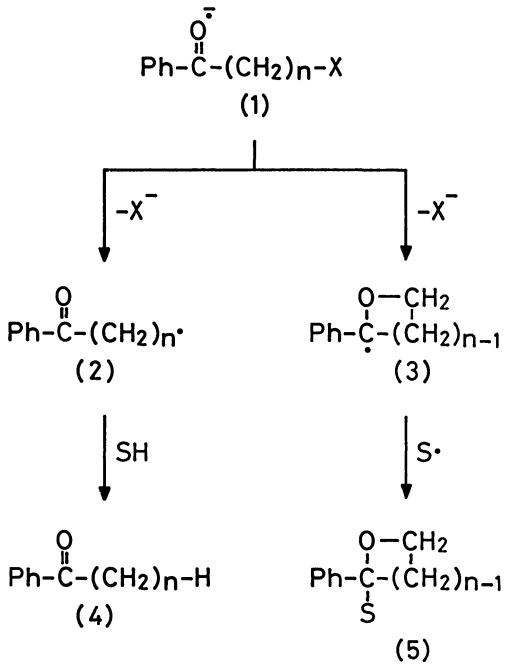

Scheme 1.

radical (**3**) was observed. Although the final products of this radical have not been confirmed, the mass spectra of the main products showed the formation of an adduct with a solvent radical (S·). These results provide clear evidence which support the idea that an intramolecular nucleophilic substitution (i.e., S_N2) is the main chemical process in these compounds.

As described previously, the reaction mechanism and the decay rate constants of the radical anion (**1**) were found to change by the nature of the halide and the methylene chain length (*n*). The decay rate constants of the radical anion (**1**) with the same chain length are in the order I > Br > Cl, which is consistent with the ease of reducing the alkyl halides.[2] On the other hand, the intramolecular S_N2 reaction occurred predominantly in BZ_{Cl}-3, BZ_{Cl}-4, and BZ_{Br}-3. Thus, the S_N2 reaction seems to require a reaction system in which an efficient release of a halide ion does not occur. Further, in the present reaction system, an important factor for an S_N2 reaction is the contribution of a cyclic structure which assists a favorable conformation for a backside attack onto a terminal carbon atom, i.e. , at least a five- or six-membered ring is required.

On the other hand, Pross and Shaik[12,13] proposed that,at the transition state in nucleophilic substitution reactions, one half of the negative charge on the nucleophile anion is transfered to the substrate, and that a negative charge is localized in the leaving group, regardless of the position of the transition state along the reaction coordinate. However, when the nucleophile or leaving group is modified, so as to make the reaction faster, the product energy level becomes lower, and the transition state occurs earlier, in accord with the

Leffler–Hammond postulate.[14,15]

According to the proposed theory, a negative charge is distributed to the carbonyl oxygen and the leaving halogen atom in equal amounts in the transition state. However, the reaction coordinate hardly progresses in the cases of BZ_I-3 and BZ_I-4, i.e., the transition state geometry (**7**) is close to that of a loose association complex (**6**) produced by an ion–dipole interaction (Eq. 2). Thus, it becomes harder to form a new bond, since the interaction of the two bonding orbitals (O···CH_2) is weak and the O–C–I angle is different from 180° in the transition state. However, in the cases of BZ_{Cl}-3, BZ_{Cl}-4, and BZ_{Br}-3, the reaction coordinate progresses to satisfy the S_N2 conditions, which allow an attack of the central carbon in the axis of the C–X bond and a partial bond formation in the transition state.

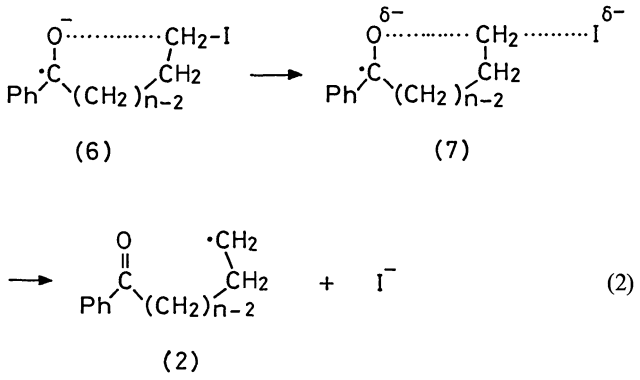

(6) (7)

(2)

On the other hand, molecular models indicate that the O–C–X angle in the six-membered-ring transition state slightly differs from 180°, while the O–C–X angle in the five-membered-ring transition state is very close to 180°. It, thus, appears that a six-membered ring is more difficult to form in the S_N2 transition state than a five-membered ring. For this reason, in the case of BZ_{Br}-4, which reacts more rapidly than does BZ_{Cl}-4, a new bond was not formed in the same manner as BZ_I-4. Further, the cyclic transition state of BZ_X-2 (X=Cl, Br) is too strained to form the S_N2 transition state, i.e., the carbonyl oxygen anion hits a terminal carbon from other direction than the axis.

The following conclusion thus emerges from these results. The ET and S_N2 reactions involve a common mechanism in which an electron is transfered from the carbonyl oxygen anion to a terminal carbon accompanied by a simultaneous fission of the C–X bond. Therefore, the S_N2 reaction is considered to be an extreme case in electron-transfer reactions accompanied by a fission of the C–X bond. That is, the S_N2 reaction selectively occurs when the conditions for the S_N2 reaction (described above) are satisfied.

Effeects of Solvent on the Reaction Rates. In order to make the reaction mechanism clear, solvent effects on the reaction rates were investigated using five different solvents such as DMA, DMF, DMSO, HMPA, and NMP (*N*-methyl-2-pyrrolidone). The transient absorption spectra observed immediately after the pulse were similar to that observed in HMPA. However, the decay rate constants of the 330 and 490 nm bands were dependent on the nature of the solvent used. A correlation of the rate constants ($\log k$) with an acceptor number (AN)[16] of the solvent was examined in the same manner as in the case of a unimolecular dissociation of the radical anions of aryl chloride[17] and chloroacetophenone isomers.[18] In these cases, good linear correlations were obtained. Plots of $\log k$ measured from BZ_X-*n* (X=Cl, Br, I; *n*=3, 4) vs. AN are shown in Fig. 2. These plots show a quite different shape, depending on the nature of the leaving halogen atom. Similar correlations were also obtained when the Reichardt–Dimroth polarity parameter, $E_T(30)$,[19] was used.

The extent of the solvation for anions is dependent on the charge density, which differs according to the ion radius and the structure.[20] Such different solvations for anions in the transition state, intermediates, or reactants causes either a retardation or acceleration of the reaction rate.

In the case of BZ_{Cl}-*n* (*n*=2—4), it is apparent that the rate constants increase with increasing AN, namely the solvent polarity. Therefore, stronger solvations are

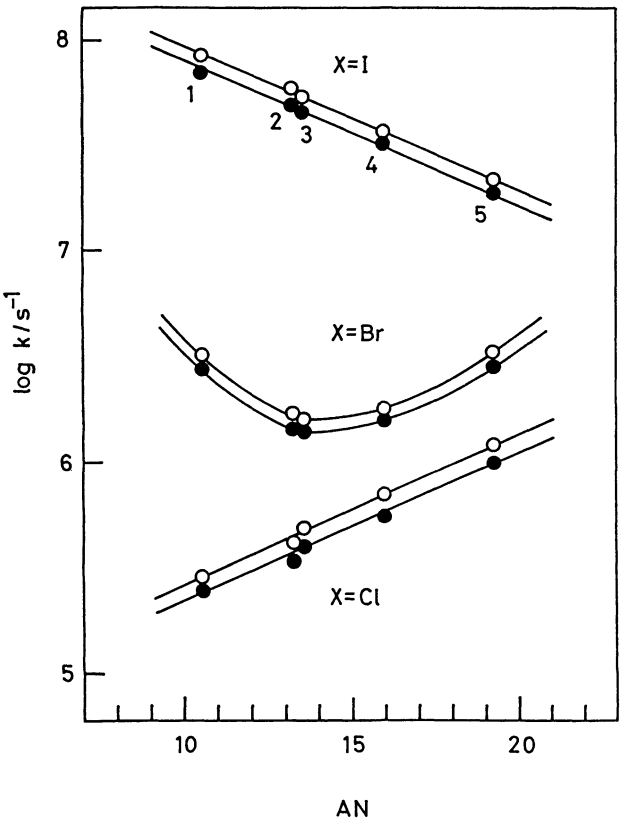

Fig. 2. Relationship between the decay rate constants ($\log k$) of the radical anions of BZx-3 (○; X=Cl, Br, I) and BZx-4 (●; X=Cl, Br, I) and acceptor number (AN) of the solvents: 1, HMPA; 2, NMP; 3, DMA; 4, DMF; 5, DMSO.

expected for the leaving chloride ion than for the ketone radical anion. Thus, an increase in the solvent polarity resulted in an increase in the rate. However, in the case of BZ_I-n (n=3, 4), the correlations are reversed. This means that the degree of solvation is higher for the ketone radical anion than for the iodide ion. Unlike these halides, U-shaped plots were obtained in the case of BZ_{Br}-n (n=2—4). Such a correlation is hardly explained at the moment, but may be the result of a difference in the solvation power for each individual anion of the solvent used.

However, plots of $\log k$ vs. the polarity parameters had the same shape for each halide, though the reaction mechanism is state in different terms (ET and S_N2) with different chain lengths (n). These results suggest that the bond-breaking process, concerted with an electron transfer which is involved in both the ET and S_N2 reactions, occurs as the rate-determining step.

These results strongly support the conclusion described in the preceding section. Accordingly, the fundamental mechanistic difference between the ET and S_N2 reactions is whether a new bond formation synchronized to the concerted electron transfer and bond-breaking processes occurs or not.

Experimental

Materials. 1-Benzoyl-2-chloroethane (BZ_{Cl}-2) from Tokyo Kasei was used without further purification. 1-Benzoyl-3-chloropropane (BZ_{Cl}-3) from Aldrich was purified by distillation under reduced pressure.

1-Benzoyl-4-chlorobutane (BZ_{Cl}-4). To a mixture of 8.0 g (0.06 mol) of $AlCl_3$ in dry benzene (100 ml) was added 7.0 g (0.05 mol) of 5-chlorovaleryl chloride at 0 °C. The mixture was stirred for 2 h at room temperature and then hydrized with ice water. The benzene layer was separated, washed with water, dried over sodium sulfate, and evaporated. The residue was recrystallized from pentane: Mp 49—50 °C (lit,[21] 50 °C) (Found: C, 67.20; H, 6.70; Cl, 18.01%).

1-Benzoyl-2-bromoethane (BZ_{Br}-2), 1-Benzoyl-3-bromopropane (BZ_{Br}-3), and 1-Benzoyl-4-bromobutane (BZ_{Br}-4). These compounds were prepared by using the previously described procedure for 3-bromopropionyl chloride, 4-bromobutyryl chloride, and 5-bromovaleryl chloride. BZ_{Br}-2: Mp 60—61 °C (lit,[22] 60 °C) (Found: C, 50.80; H, 4.30; Br, 37.56%). BZ_{Br}-3: Mp 38—39 °C (lit,[23] 38.5 °C) (Found: C, 52.62; H, 4.82; Br, 35.50%). BZ_{Br}-4: Mp 58—59 °C (lit,[21] 58.5 °C) (Found: C, 54.90; H, 5.55; Br, 32.90%).

1-Benzoyl-3-iodopropane (BZ_I-3) and 1-Benzoyl-4-iodobutane (BZ_I-4). The corresponding bromides were refluxed in methyl ethyl ketone containing 10-fold excess of KI for 10 h. The organic layer was evaporated and the residue was recrystallized from pentane. BZ_I-3: Mp 51—52 °C (Found: C, 43.95; H, 4.20; I, 46.06%). BZ_I-4: Mp 71—72 °C (lit,[21] 71.5 °C) (Found: C, 46.14; H, 4.46; I, 44.29%).

Apparatus. The samples held in Suprasil quartz cells were irradiated with an 8-ns pulse of 28 MeV electrons from a linear accelerator of Osaka University. The transient species were monitored with a pulsed Xe lamp. The monitoring light was passed through a monochrometer (Nikon G-250) after being passed through the sample cell and monitored with an R928 photomultiplier (Hamamatsu Photonics). The output of the photomultiplier was digitized bya programable transient digitizer (Tektronix 7912AD) interfaced with a microcomputer (Sharp X68000ACE), which was also used to store the data on a disc and to analyze the data.

N,N-Dimethylacetamide (DMA), *N,N*-dimethylformamide (DMF), dimethyl sulfoxide (DMSO), hexamethylphosphoric triamide (HMPA), and *N*-methyl-2-pyrrolidone (NMP) used as a solvent were distilled over CaH_2 under reduced pressure. Solutions were prepared immediately before irradiation and were degassed under high vacuum.

Product analysis was carried out by GLC (Shimazu GC-7A; using 1-m×3-mm glass column packed with 5% Silicone OV-1 on Chromosorb WAW DMCS, 60—80 mesh) and GLC-MS (JEOL JMS-DX300) after extraction by pentane from γ-irradiated HMPA solution.

The mass spectra of the main products (Yields: 60—70% based on the substrate disappeared) from BZ_{Cl}-3, BZ_{Cl}-4, and BZ_{Br}-3 showed the formation of an adduct (**5**) of a cyclic

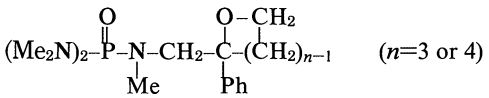

(n=3 or 4)

(**5**)

ether radical (**3**; see text) with HMPA. Results were as follows: adduct **5** (n=3); m/z 325 ($M^{+\cdot}$), 281 ($M^{+\cdot}-Me_2N$), 178 ($M^{+\cdot}-147$), 147 {[Ph–C–$(CH_2)_3$–O]$^+$}, 135 {$[(Me_2N)_2PO]^+$, major peak}, 105 $[(PhCO)^+]$, 77 (Ph^+), 58 $[(Me_2NCH_2)^+]$, 44 (Me_2N^+); adduct **5** (n=4); m/z 339 ($M^{+\cdot}$), 295 ($M^{+\cdot}-Me_2N$), 178 ($M^{+\cdot}-161$), 161 {[Ph–C–$(CH_2)_4$–O]$^+$}, 135 {$[(Me_2N)_2PO]^+$, major peak}, 105 $[(PhCO)^+]$, 77 (Ph^+), 58 $[(Me_2NCH_2)^+]$, 44 (Me_2N^+).

References

1) L. Eberson, *Acta Chem. Scand., Ser. B,* **36**, 553 (1982).
2) C. P. Andrieux, I. Gallard, J. M. Saveant, and K. B. Su, *J. Am. Chem. Soc.,* **108**, 638 (1986).
3) T. Lund and H. Lund, *Acta Chem. Scand., Ser. B,* **40**, 470 (1986).
4) B. Bockrath and L. M. Dorfman, *J. Phys. Chem.,* **77**, 2618 (1973).
5) E. Honda, M. Tokuda, H. Yoshida, and M. Ogasawara, *Bull. Chem. Soc. Jpn.,* **60**, 851 (1987).
6) J. Grimshow, J. R. Langan, and G. A. Salmon, *J. Chem. Soc., Chem. Commun.,* **1988**, 851.
7) L. Eberson, "Elelectron Transfer Reactions in Organic Chemistry," Springer-Verlag, Berlin (1987).
8) J. F. Garst, *Acc. Chem. Res.,* **4**, 400 (1971).
9) H. Lund and J. Simonet, *Bull. Soc. Chim. Fr.,* **1973**, 1843.
10) H. Kigawa, S. Takamuku, S. Toki, N. Kimura, S. Takeda, K. Tsumori, and H. Sakurai, *J. Am. Chem. Soc.,* **103**, 5176 (1981).
11) E. A. Shaede, L. M. Dorfman, J. Flynn, and D. C. Walker, *Can. J. Chem.,* **51**, 3905 (1973).
12) A. Pross and S. S. Shaik, *Tetrahedron Lett.,* **1982**, 5467.
13) A. Pross, *Adv. Phys. Org. Chem.,* **21**, 99 (1985).
14) J. E. Leffler, *Science,* **117**, 340 (1953).
15) G. S. Hammond, *J. Am. Chem. Soc.,* **77**, 334 (1955).
16) V. Gutmann, *Electrochim. Acta,* **21**, 661 (1976).

17) N. Kimura and S. Takamuku, *Radiat. Phys. Chem.*, **29**, 179 (1987).
18) N. Kimura and S. Takamuku, *Bull. Chem. Soc. Jpn.*, **59**, 3653 (1986).
19) C. Reichardt, *Angew. Chem., Int. Ed. Engl.*, **18**, 98 (1979).
20) A. J. Parker, *Chem. Rev.*, **69**, 1 (1969).
21) P. J. Wagner, M. I. Lindstron, J. H. Sedon, and D. R. Ward, *J. Am. Chem. Soc.*, **103**, 3842 (1981).
22) S. Oae, *J. Am. Chem. Soc.*, **78**, 4030 (1956).
23) R. Bird, G. Griffiths, G. S. Griffiths, and C. J. M. Stirling, *J. Chem. Soc., Perkin Trans. 2*, **1982**, 579.

Effects of Temperature and Pressure on the Charge-Transfer Complex Formation through Hydrogen Bonding and Ionization Reactions between 2,6-Dibromo-4-[(3,5-dibromo-4-hydroxyphenyl)(2-ethoxycarbonylphenyl)-methylene]-2,5-cyclohexadien-1-one and Amines

Norio NISHIMURA,* Yoshihiro OSAWA, Kohji KURAMOTO, and Kazuo SUKEMICHI
Department of Chemistry, Faculty of Science, Okayama University, Okayama 700
(Received April 8, 1991)

The effects of temperature and pressure on the formation of charge-transfer (CT) complexes between 2,6-dibromo-4-[(3,5-dibromo-4-hydroxyphenyl)(2-ethoxycarbonylphenyl)methylene]2,5-cyclohexadien-1-one (TBPE) and amines in nonpolar solvents have been studied, and the thermodynamic parameters estimated. It was found that the heat of formation (ΔH°) as well as the reaction volume (ΔV°) are largely negative, compared with those for ordinary CT complex formation. The electronic spectra in the visible region due to the outer CT complexes are well-characterized for primary and secondary amines in nonpolar solvents that have no proton-donating/-accepting nature. In other cases, the CT spectra are broad. Ionization of TBPE in polar solvents takes place as evidenced by the electronic spectrum of TBPE anion. However, ΔH° as well as ΔV° are unusually small. When Proton Sponge is used in nonpolar solvents, ion pairs are formed. In this case, ΔH° and ΔV° are largely negative as expected.

In 1954, Davis and Hetzer[1] found that when a benzene solution of 2,6-dibromo-4-[(3,5-dibromo-4-hydroxyphenyl)(2-ethoxycarbonylphenyl)methylene]2,5-cyclohexadien-1-one (TBPE) was poured to solid tribenzylamine, the yellow solution of TBPE acquired a slightly pink tinge which disappeared on heating but returned on cooling. Sakai and co-workers have shown that the thermochromic nature of the TBPE–amine systems in 1,2-dichloroethane (DCE) could be applied to the selective determination of antihistamine drugs.[2–6] They suggested that TBPE associates with amines to form a kind of charge-transfer (CT) complex through hydrogen bonding.

In a preliminary paper,[7] we have shown that the complexes formed between TBPE and triethylamine (TEA) and between TBPE and *N,N*-dimethy-2-(diphenylmethoxy)ethylamine (DHA) are of a new type of CT complex as characterized by their strong CT band in the visible region, large equilibrium constant, and large negative values of the heat of reaction and reaction volume.

In this paper, we report the thermodynamic quantities for the CT complex formation between TBPE and primary, secondary, and tertiary aliphatic amines, together with those for the ion-associate formation between TBPE and *N,N,N′,N′*-tetramethyl-1,8-naphthalenediamine (Proton Sponge, PS).

Experimental

Materials. Reagent grade potassium salt of TBPE was dissolved into an H_2O–EtOH mixture. An aqueous solution of oxalic acid was added slowly to the mixture until the blue color of the solution changed to orange red. TBPE as a free phenol, was extracted by chloroform and the solution evaporated to dryness. Recryctallization of TBPE was made by adding hexane dropwise to its chloroform solution, mp 215—217 °C (lit,[8] 210—215 °C). Reagent grade Proton Sponge was recrystallized from a cyclohexane–petroleum ether mixture. Triethylamine (TEA), dipropylamine (DPA), and propylamine (PA) were dried over potassium hydroxide and distilled under a reduced pressure. Solvents were purified in the usual manner.

Procedures. Spectra of the CT complex and the ion-associate at 0.1 MPa were recorded on a Union SM-401 spectrophotometer. The measurement temperature was regulated within ±0.1 °C by circulating thermocontrolled water. A high-pressure vessel with a water jacket for temperature control was used for spectral measurements.[9] It was set in a cell compartment of a Hitachi 100-50 double-beam spectrophotometer. Using available data, the changes of solvent density with temperature and pressure were taken into account. The equilibrium constants for the formation of the CT complex and the ion-associate were determined from the Benesi–Hildebrand (B–H) plot[10] with the base in great excess over TBPE. The enthalpy and entropy of formation were determined from the variation of the equilibrium constants with temperature according to the van't Hoff equation.

The equilibrium constant in logarithmic scale was plotted against external pressures, and the plots were fitted to the following quadratic equation by means of a computer program.

$$\ln K_p/K_0 = ap^2 + bp + c \quad (1)$$

where K_p and K_0 are the equilibrium constants at p and 0.1 MPa, respectively. The volume of reaction extrapolated at atmospheric pressure (ΔV°) was calculated by

$$bRT = -\Delta V^\circ - \Delta n\, \kappa_T RT \quad (2)$$

where κ_T denotes the isothermal compressibility of solvents, and Δn the difference in the number of molecules between products and reactants. The second term arises from the translational energy loss associated with reaction.[11]

Results

The temperature dependence of the absorption spectrum in the visible region is shown in Fig. 1. The

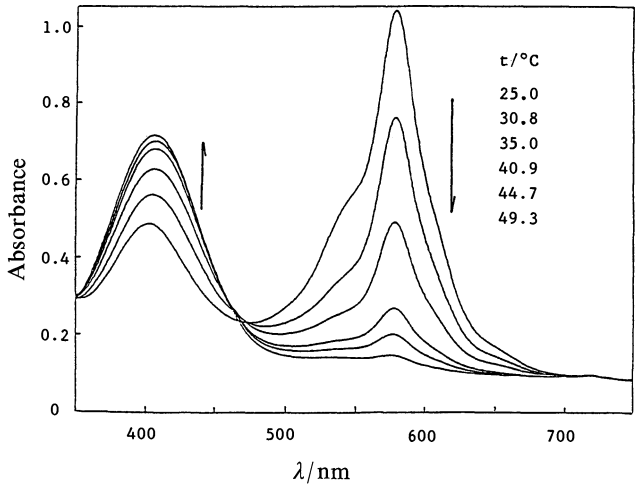

Fig. 1. Temperature dependence of the absorption spectrum in benzene; $[TBPE]_o=6.04\times10^{-5}$ mol dm^{-3}, $[PA]_o=2.08\times10^{-4}$ mol dm^{-3}.

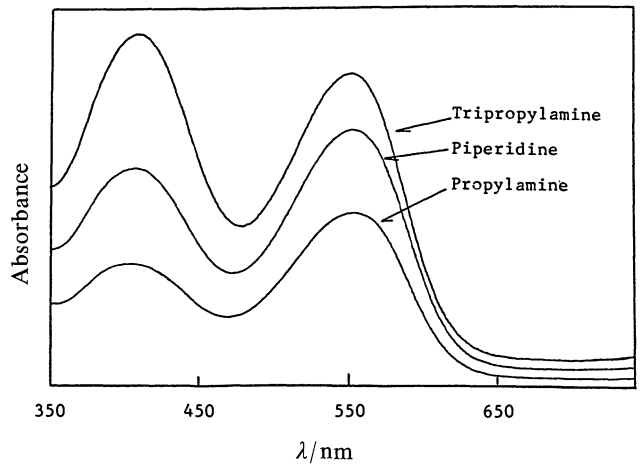

Fig. 2. Absorption bands of TBPE in 1,4-dioxane in the presence of primary, secondary, and tertiary amines.

absorption band at ca. 580 nm can be ascribed to the CT complex and the band at ca. 400 nm to TBPE. As the temperature raises, the CT band decreases, while the TBPE band increases but less rapidly and shifts toward a longer wavelength side. Thus the band at ca. 400 nm must involve some contribution of the CT complex. The B–H plots were performed using the absorbance of the CT band for this reason. The shape and the position of the CT band depend on the combination of amines and solvents. This is shown in Figs. 2 and 3. It was found that each B–H plot for the CT complex formation is linear. Representative B–H plots are shown in Fig. 4. Remarkable pressure effects on the equilibrium were observed. By the aid of Eqs. 1 and 2, the reaction volumes were estimated. The thermodynamic parameters are given in Table 1. When TBPE

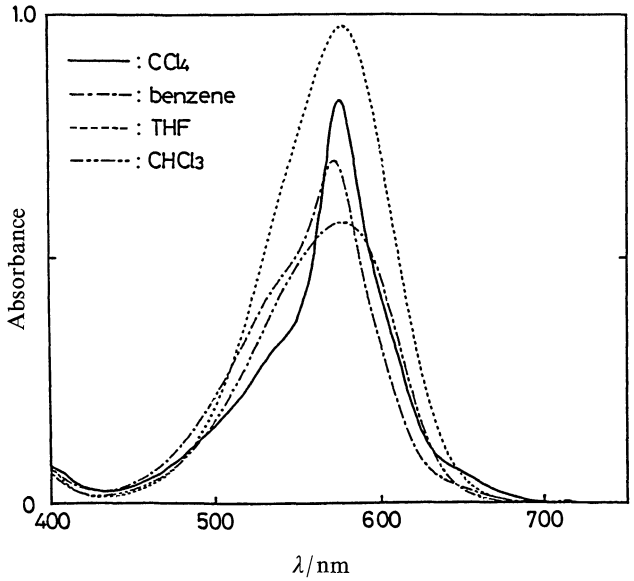

Fig. 3. Absorption bands of a mixture of propylamine and TBPE in CCl_4, benzene, $CHCl_3$, and THF.

Table 1. Thermodynamic Quantities for the Reaction

TBPE + Amines $\rightleftarrows$ CT Complex

Amine	Solvent[a]	K(25 °C)[b]	$\Delta H°$	$\Delta S°$	$\Delta V°$(30 °C)
		dm^3 mol^{-1}	kJ mol^{-1}	J K^{-1} mol^{-1}	cm^3 mol^{-1}
TEA	$CHCl_3$	26000	−58±6	−110±20	−23.2
	Toluene	26000	−64±3	−130±20	−24.9
	DX	2500	−43±3	−79±10	−22.3
DPA	CB	29000	−100±9	−250±30	−31.1
	DE	27000	−70±3	−150±9	−35.3
	DX	2300	−55±1	−120±5	−23.1
PA	Benzene	6000	−114±7	−310±20	−31.5
	CB	520	−96±7	−270±25	−31.2
	DE	1100	−68±4	−170±15	−34.8
	DX	2300	−55±1	−120±5	−31.9

a) DX: 1,4-dioxane, CB: chlorobenzene, DE: 1,2-dichloroethane. b) Interpolated values from the van't Hoff plot.

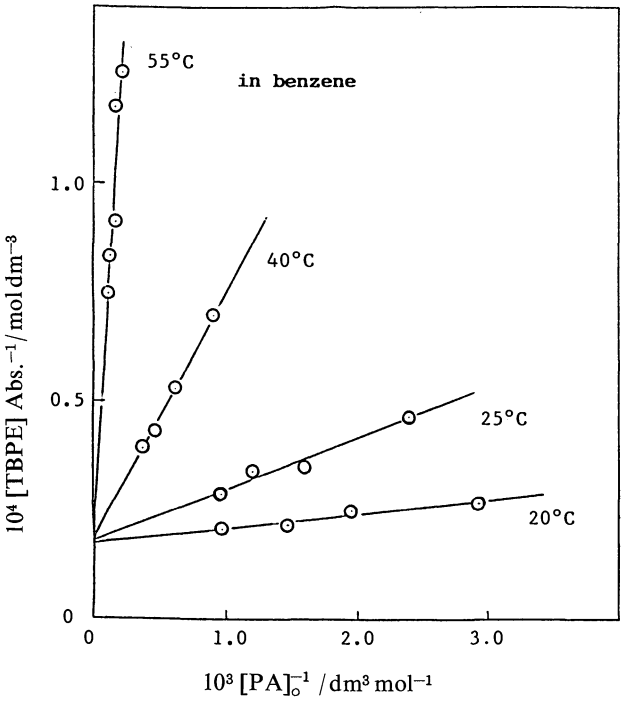

Fig. 4. B–H plots for the TBPE–PA system at various temperatures.

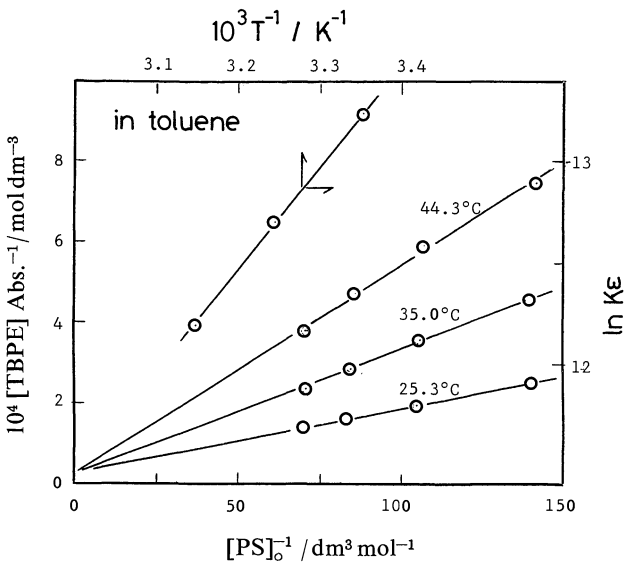

Fig. 5. B–H and van't Hoff plots for the TBPE–PS system.

was mixed with PS in nonpolar solvents, a band appeared at ca. λ_{max}=620 nm. This band can be assigned to the TBPE anion, since both the position and the spectral pattern agreed with those of the potassium salt of TBPE. Remarkable temperature and pressure dependences on the equilibrium were observed in this case, too. Figure 5 shows the B–H plot. The thermodynamic quantities for the formation of the ion-associate in some nonpolar solvents were estimated and are given in Table 2.

Table 2. Thermodynamic Quantities for the Reaction TBPE + PS $\rightleftarrows$ Ion Pair[a)]

Solvent	K(25 °C)[b)]	$\Delta H°$	$\Delta S°$	$\Delta V°$(25 °C)
	dm^3 mol^{-1}	kJ mol^{-1}	J K^{-1} mol^{-1}	cm^3 mol^{-1}
Benzene	19	−44±4	−125±15	−35.4
Toluene	22	−39±2	−105±20	−35.8
$CHCl_3$	470	−57±4	−140±40	−38.5
1-Chloro-butane	110	−46±1	−115±40	−30.7

a) Molar absorptivity estimated from the B–H plot is 36000±1500 dm^3 mol^{-1} cm^{-1}. b) Interpolated values from the van't Hoff plot.

Discussion

Charge-Transfer Complex Formation Reaction. We have reported[7)] that the tertiary amines such as TEA react with TBPE to form a new type of CT complex in nonpolar solvents, and that the system exhibits a remarkable thermochromism as well as piezochromism. We proposed that the origin of the strong CT band could be ascribed to the canonical electronic structures of the following type.

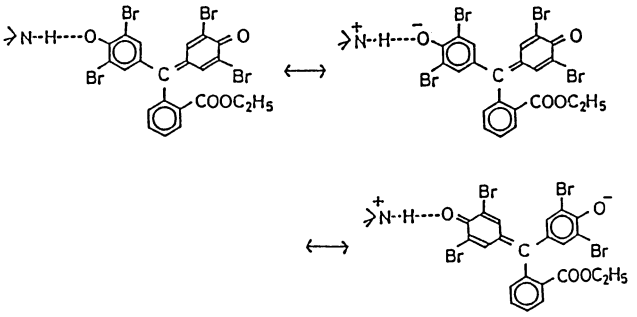

Figure 1 shows a remarkable thermochromic nature for the TBPE–propylamine system, too. From the B–H plot, the equilibrium constants were estimated. By means of the van't Hoff plot, the heat of reaction and the entropy of reaction were estimated (Table 1). The reaction volumes are between −22 and −35 cm^3 mol^{-1}. These (absolute) values are remarkably greater than those for ordinary CT complex formation (0—−15 cm^3 mol^{-1}).[12)] Therefore, due to the predominant contribution of the dative structures (vide supra), the present CT complex must be more "tight" than the ordinary one.

In 1,4-dioxane (DX) and tetrahydrofuran (THF), the spectral pattern of the CT band is very similar to each other, irrespective of primary, secondary and tertiary amines (Fig. 2). The spectral pattern of the TBPE–TEA system in benzene, chloroform, and THF is also the same as that in Fig. 2. On the other hand, when primary or secondary amines are used, the spectral pattern changes remarkably, depending on the nature of solvents (Fig. 3). With auxiliary experiments, it has

been confirmed that the CT spectrum is sharp and exhibits a "structure" (shoulder) only when TBPE and primary or secondary amines are dissolved in nonpolar solvents that have no proton donating/accepting ability.

According to our view, hydrogen bonding is playing an important role. There are some possible combinations of hydrogen bonding. In DX and THF, the hydrogen-bond formation between TBPE and these solvents will disfavor the CT complex formation. The situation will be the same for the hydrogen bonding between primary/secondary amines and DX/THF. The comparatively small values of the equilibrium constants in DX may be ascribed to this reason. Primary and secondary amines can donate as well as accept the hydrogen atom that can form hydrogen bond. In benzene and CCl_4, they will form a kind of (dynamic) cluster through hydrogen bonding. The amine cluster taking part in the formation of CT complex would give rise to its enhanced effective mass, resulting in a less mobile conformation (see type A indicated below). Hydrogen bonding of the type B is also possible.

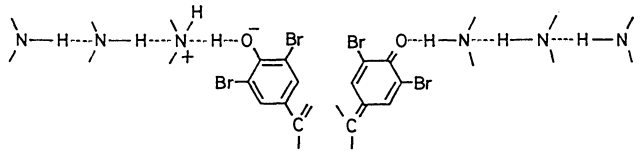

Type A Type B

It is likely that either or both of the above types of hydrogen bonding are responsible for the well-characterized CT band. Meanwhile, the formation of cluster is disfavored in DX due to the predominant hydrogen bonding between primary/secondary amines and excessively existing DX. It is evident that the cluster formation is impossible for tertiary amines in any kinds of solvents. The above idea would explain the spectral patterns in Figs. 2 and 3.

In order to obtain evidence for supporting the cluster formation, the shift of the CT band with solvent was examined. In Fig. 6, $\bar{\nu}_{max}$ is plotted against the E_T-value, a solvent polarity parameter. For the TBPE–TEA system, a fairly well correlation may be seen (line A). For the TBPE–PA system, solvents that have hydrogen-bonding ability seem to fall on the same line. Judging from the chemical shift of ^{1}H NMR of chloroform (δ=7.25 ppm vs.TMS, 60 MHz ^{1}H NMR), chloroform could, be regarded to this group of solvents. The position of diethyl ether is rather critical. On the other hand, solvents that have no hydrogen-bonding ability seem to constitute an other group (line B). The shift is less remarkable, and this is in harmony with the assumption of cluster formation, proposed in the foregoing paragraph. That is, the formation of amine cluster will disfavor the access of solvent molecules to the CT complex, resulting in the small red shift.

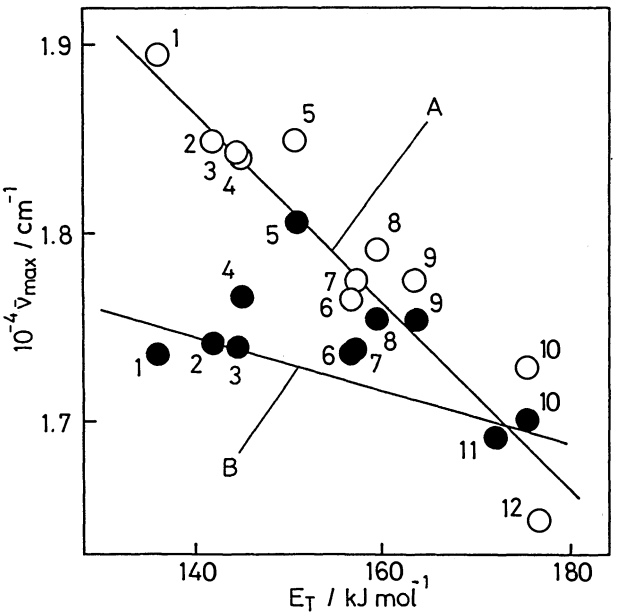

Fig. 6. Relationship between $\bar{\nu}_{max}$ (CT band) and E_T-value for the TBPE–TEA (○) and TBPE–PA (●) systems. Entry number: 1, CCl_4; 2, toluene; 3, benzene; 4, Et_2O; 5, DX; 6, THF; 7, chlorobenzene; 8, ethyl acetate; 9, $CHCl_3$; 10, DE; 11, dichloromethane; 12, acetone.

When ordinary aromatic amines of low basicity are used, the formation of CT complex was not observed in the usual conditions. Hence the equilibrium would be related to the amine basicity. The value of pK_a for TEA and PA are 11.01 and 10.71, respectively. Although the value of pK_a for DPA is not available, it would be very near to that of TEA, referring to the pK_a of diisopropylamine (10.96). Although the above pK_a-values are those in water, the equilibrium constants for the TBPE–PA system is, as a whole, smaller than those for the other two; this may be ascribed to the difference in the pK_a value. The solvent effects on the thermodynamic data in Table 1 seem to be entangled, and it is difficult to find a definite trend. Perhaps the complication could be ascribed to the intervention of various types of hydrogen-bond formations, the steric factor, and the amine basicity etc., and further study is neccesary.

Ionization Reaction. It is generally known that ionization is enhanced by temperature and pressure. The observation of considerable volume decrease has been interpreted in terms of electrostriction. The electrostriction becomes pronounced when the ion is small, the charge large and localized, and the solvent nonpolar. Typical ionization of phenols is accompanied by the volume change from −4 to −30 cm^3 mol^{-1}.[13] When TBPE alone or TBPE and small amount of aliphatic amine was dissolved in polar solvents, the formation of TBPE anion was observed. We examined the temperature dependence on the equilibrium and found that the equilibrium scarcely shifts with temperature in acetoni-

trile, acetone, and methanol. This indicates that the heat of ionization is near zero and the entropy change so small. In agreement with our observation, Sakai[2] also reported that the temperature dependence on the equilibrium between TBPE anion/quaternary ammonium ion-associates and its nonionized components in 1,2-dichloroethane is negligibly small. The effect of pressure on the equilibrium was also examined in acetone and methanol. The approximate ΔV°-value estimated by means of Eqs. 1 and 2 was 1.0 ± 1.0 cm^3 mol^{-1} in acetone and negligibly small in methanol. The above findings are unusual in view of normal ionization reactions where remarkable enthalpy, entropy, and volume decreases are observed.

A possible cause might be due to the symmetrical structure of TBPE anion; the electric charge will be delocalized over the molecule, and this might give rise to the small temperature effects. Free phenol corresponding to galvinoxyl (so-called "hydrogalvinoxyl", see below) could be regarded as a model compound for examining the above presumption. We expected that the temperature effects for the following equilibrium

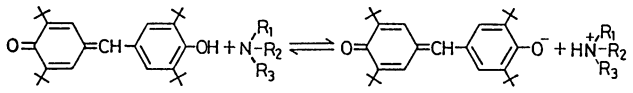

"hydrogalvinoxyl"

will be similar, since the anion has symmetrical electronic structures similar to those of TBPE anion. However, remarkable temperature dependence was observed for this system. The estimated values of the heat of formation were -29 kJ mol^{-1} in acetone and -46 kJ mol^{-1} in acetonitrile.[14] Although the reason is not clear, this temperature/pressure-insensitive nature seems peculiar to the ionization of TBPE in polar solvents.

When TBPE and PS were mixed in nonpolar solvents, the proton from TBPE was trapped by PS to form ion pairs, as evidenced by the appearance of well-characterized spectrum of TBPE anion in the vicinity of 600 nm. In contrast to the case of the CT complex, the pattern of the spectrum does not change with solvent at all. Substantial temperature and pressure effects were observed. The thermodynamic data are given in Table 2. The volumes of reaction for the formation of ion-pair are between -30 and -39 cm^3 mol^{-1} as expected in the ordinary ion-pair formation reactions. The enthalpy and entropy changes are those usually observed. Using the data in Tables 1 and 2, we tentatively plotted ΔH° against ΔS° (Fig. 7). In spite of the intervention of a various types of hydrogen bonding, it seems that the approximate linear free energy relationship[15] holds for both the CT complex and ion-pair formations. Figure 8 shows the relation between $\bar{\nu}_{max}$ and E_T-value. For solvents of smaller E_T-values, a small but clear red-shift trend may be seen, as usually observed for π–π^* transitions. In contrast, a rather blue-shift trend may be seen for solvents of larger E_T-values, indicating that the ground state of the anion is a little more stabilized than the excited state. A good correlation between $\bar{\nu}_{max}$ and E_T-values for a series of alcohols suggests a substantial role of hydrogen bonding. The comparatively small solvatochromic shift over a wide E_T range is in accord with our expectation, since the dipole moment of the ion pair in the ground state will not be so different from that in the excited state.

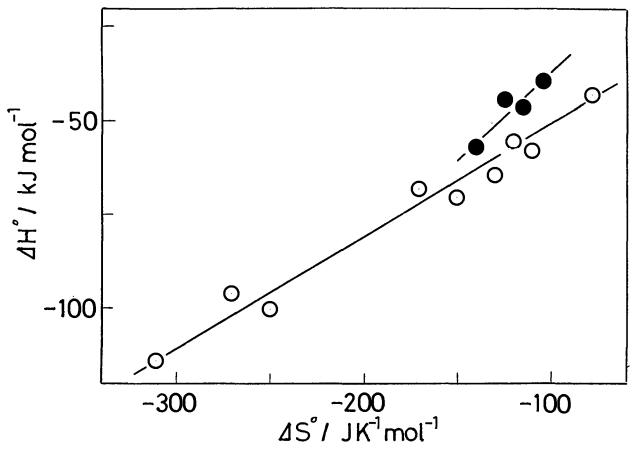

Fig. 7. Linear free energy relationship for CT complex formation (○) and ion-pair formation (●).

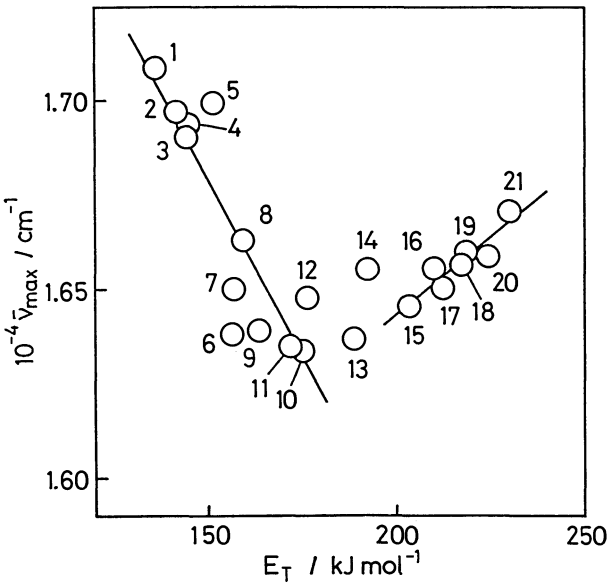

Fig. 8. Plot of $\bar{\nu}_{max}$ against E_T-value for the TBPE–PS system. Entry number: 1—12, same as in Fig. 6; 13, DMSO; 14, CH_3CN; 15, 2-propanol; 16, 1-butanol; 17, 1-propanol; 18, EtOH; 19, 2-methoxyethanol; 20, EtOH/H_2O=80/20 vol-%; 21, MeOH.

References

1) M. Davis and H. B. Hetzer, *J. Am. Chem. Soc.*, **76**,

4247 (1954).
2) T. Sakai, *J. Pharm. Sci.*, **68**, 875 (1979).
3) T. Sakai and N. Ohno, *Analyst*, **106**, 584 (1981).
4) T. Sakai and N. Ohno, *Analyst*, **107**, 634 (1982)
5) T. Sakai, *Analyst,* **107**, 640 (1982).
6) T. Sakai and N. Ohno, *Talanta*, **33**, 415 (1986).
7) N. Nishimura, K. Masaki, Jun'ichi Miyake, and T. Sakai, *Chem. Lett.*, **1988**, 1239.
8) R. Nietzki and Ed. Burckliardt, *Chem. Ber.*, **30**, 176 (1897).
9) Y. Sueishi and N. Nishimura, *Bull. Chem. Soc. Jpn.*, **56**, 2598 (1983).
10) A. H. Benesi and J. H. Hildebrand, *J. Am. Chem. Soc.*, **71**, 2703 (1949).
11) Y. Yoshimura and M. Nakahara, *J. Chem. Phys.*, **81**, 4080 (1984)
12) T. Asano and W. J. le Noble, *Chem. Rev.*, **78**, 474 (1978).
13) R. V. Eldik, T. Asano, and W. J. le Noble, *Chem. Rev.*, **89**, 549 (1989).
14) Unpublished data obtained in our laboratory.
15) J. E. Leffler and E. Grunwald, "Rates and Equilibria of Organic Reactions," John Wiley and Sons, Inc., New York (1963).

The Pitzer Formalism vis-à-vis the Mixture Rule for the Estimation of Apparent Molal Volumes of Aqueous NaCl–KCl, NaCl–KBr, and NaCl–K_2SO_4 Mixtures at 298.15 K

Prafulla MAHAPATRA, Moni Mohan BHATTACHARYYA, and Mihir SENGUPTA*
Department of Chemistry, University College of Science,
92, Acharya Prafulla Chandra Road, Calcutta 700009, India
(Received July 30, 1990)

The density data reported by Wirth for aqueous solutions of KCl, KBr, and K_2SO_4 in NaCl solutions of five different fixed concentrations at 298.15 K have been used to calculate the apparent molal volumes of the mixtures; the results have been compared with those calculated by the Pitzer formalism as also the Young and Smith's mixture rule.

Recently, attention has been drawn to the successful extension of the Pitzer formalism[1,2] by Kumar[3–5] for the calculation of volume properties of a number of mixed electrolytes in aqueous solutions. Humffray[6] has also proposed a comparatively simpler treatment by adopting the Young and Smith's "mixture rule"[7] for estimating the densities and apparent molal volumes of mixtures of electrolytes from those of the individual components, and obtained a better agreement for NaCl–KBr mixtures than from Pitzer's equations. Kumar[8a] has however observed that the good agreement obtained by Humffray is due to the fact that the variation of the densities of the mixtures happens to be linear with respect to the component densities. It is the purpose of this investigation to extend such studies to a number of other electrolyte mixtures in order to investigate further the extent of agreement between the experimental values and those calculated from the mixture rule, and the Pitzer's equations.

For this purpose, we have made use of the entire set of precise density data reported by Wirth (for the mixtures: NaCl–KCl, NaCl–KBr, and NaCl–K_2SO_4)[9] by suitable interpolation of the data, without and with proper reformulation of the empirical equations given for the representation of the mixture density, so that the latter could be represented for constant total ionic strengths within the range: 0.25 to 1 mol kg^{-1}.

Calculations and Results

Wirth's reported density data in terms of molarity have been converted to molality for meaningful comparison with the recent data, by means of the following conversion formula deduced in analogy with that for the pure components:[10]

$$\frac{\sum c_i}{\sum m_i} = d_{\mathrm{mix}} - \frac{\sum c_i M_i}{1000}. \qquad (1)$$

The experimental ϕ_v^* values for the mixtures are then calculated with the help of the following equation

$$\phi_v^* = \frac{1000(d_0 - d_{\mathrm{mix}})}{d_{\mathrm{mix}}\, d_0 \sum m_i} + \frac{\sum m_i M_i}{d_{\mathrm{mix}} \sum m_i}. \qquad (2)$$

Here d_{mix} and d_0 are the densities of the mixture and the solvent respectively, m_i is the molality and M_i the molecular weight of the ith component in the mixture.

Wirth[9] reported the density values of KCl, KBr, and K_2SO_4 in NaCl solutions of five fixed concentrations [viz., 0.04, 0.16, 0.35, 0.62, and 0.97 equiv] in which the concentration of the first electrolyte generally varied from 0.04 to 0.64 equiv except in the case of K_2SO_4. All density values of the mixtures of different electrolytes were represented by means of least square equations:[9]

$$(d_3 - d_2)/c_3 = a - b(\mu_v^{1/2} - c_2^{\circ 1/2}). \qquad (3)$$

From the experimental data as reported by Wirth in Tables 2, 3, and 4, Ref. 9, it has been possible to interpolate the experimental densities and apparent molal volumes of the different mixed electrolytes at a number of constant total ionic strengths between 1 and 0.25 mol kg^{-1}. However, such calculations with Wirth's reported equations produce only a set of three to four density values for each ionic strength, which is inadequate for the present purpose. In order to obtain more data for meaningful comparison, we have introduced the following technique. Instead of a fixed concentration of NaCl in the mixtures as reported by Wirth, the concentration of the other electrolyte is now made fixed, so as to vary the concentration of NaCl in the mixtures. All these density values are then represented in the form of equations analogous to Wirth's equation by the computerized least squares method with proper 'a' and 'b' values.

With the help of these reformulated equations it is now possible to calculate the densities or apparent molal volumes at suitable ional fractions other than those calculated directly from Wirth's reported equations. The thus calculated values of densities [or rather, the density differences ($\Delta d = d_3 - d_2$)] and apparent molal volumes, at the total ionic strengths of 1, 0.75, 0.50, and 0.25 mol kg^{-1}, are shown in columns 3 and 4 of Table 1, for the NaCl—KCl mixture only (two 1—1 type electrolytes with common anion). The consistency of the density values obtained from our reformulated equation with those calculated using Wirth's equations, has been tested and found to be excellent.

Table 1. Experimental Δd and ϕ_v^* Values (Wirth's data) together with the Corresponding Estimated ϕ_v^* Values by Young's Rule and Pitzer's Equation for NaCl–KCl Mixtures at 298.15 K

m_{NaCl}	m_{KCl}	$\Delta d \times 10^3$ / g cm^{-3}	ϕ_v^* / cm^3 mol^{-1} (Wirth)	ϕ_v^* / cm^3 mol^{-1} (Pitzer)	ϕ_v^* / cm^3 mol^{-1} (Young's rule)
			m=1.0		
1.0000	0.0000	39.189	18.47	—	—
0.9926	0.0074	39.220	18.55	18.54	18.55
0.9605	0.0395	39.362	18.93	18.86	18.88
0.8792	0.1208	39.708	19.87	19.67	19.72
0.7577	0.2423	40.269	21.23	20.89	20.97
0.6285	0.3715	40.842	22.50	22.28	22.30
0.4810	0.5190	41.675	24.15	23.73	23.82
0.3501	0.6499	42.317	25.37	25.09	25.17
0.0000	1.0000	44.451	28.78	—	—
				σ_1=0.12	σ_3=0.20
				σ_2=0.05	σ_4=0.04
			m=0.75		
0.7500	0.0000	29.716	18.22	—	—
0.7105	0.0395	29.902	18.81	18.75	18.76
0.6285	0.1215	30.269	19.98	19.84	19.89
0.5077	0.2423	30.904	21.77	21.61	21.54
0.3898	0.3602	31.528	23.41	23.08	23.16
0.2310	0.5190	32.416	25.54	25.28	25.34
0.1557	0.5943	32.824	26.47	26.33	26.37
0.0000	0.7500	33.773	28.51	—	—
				σ_1=0.12	σ_3=0.17
				σ_2=0.03	σ_4=0.03
			m=0.50		
0.5000	0.0000	20.052	17.92	—	—
0.4605	0.0395	20.255	18.78	18.71	18.73
0.3501	0.1499	20.827	21.08	20.94	21.00
0.2577	0.2423	21.344	23.05	22.83	22.90
0.1557	0.3443	21.905	25.08	24.93	24.99
0.0386	0.4614	22.588	27.45	27.37	27.40
0.0000	0.5000	22.837	28.19	—	—
				σ_1=0.08	σ_3=0.09
				σ_2=0.03	σ_4=0.02
			m=0.25		
0.2500	0.0000	10.168	17.53	—	—
0.2105	0.0395	10.390	19.18	19.12	19.18
0.1557	0.0943	10.696	21.43	21.36	21.39
0.1292	0.1208	10.851	22.54	22.45	22.48
0.0386	0.2114	11.371	26.22	26.17	26.19
0.0077	0.2423	11.558	27.46	27.45	27.45
0.0000	0.2500	11.604	27.77	—	—
				σ_1=0.04	σ_3=0.04
				σ_2=0.01	σ_4=0.01

Table 2. ϕ_v° Values of the Electrolytes and Pitzer Coefficients (Pressure Derivatives) for the Different Cation–Anion Interactions (least squares fit to Pitzer equation[5])

Cation–Anion	ϕ_v° / cm^3 mol^{-1}	$\left(\frac{\partial\beta^0}{\partial P}\right)_T \times 10^5$	$\left(\frac{\partial\beta^1}{\partial P}\right)_T \times 10^5$	$\left(\frac{\partial C^\phi}{\partial P}\right)_T \times 10^5$	σ / cm^3 mol^{-1}
Na–Cl	16.62 (16.60)[a]	2.41	−1.74	−1.31	0.00
K–Cl	26.96 (26.86)[a]	4.31	−6.42	−2.42	0.02
Na–Br	23.83 (23.37)[a]	1.69	−4.66	−0.31	0.01
K–Br	34.17 (34.04)[a]	4.33	−7.74	−2.50	0.03
Na–SO_4	11.40	5.94	15.55	−1.29	0.00
K–SO_4	32.26	−1.45	31.80	8.21	0.06

a) From Redlich-Meyer equation.

Table 3. Pitzer Mixing Parameters Obtained by Best Fit to θ_v Expression, for NaCl–KCl, NaCl–KBr, and NaCl–K_2SO_4 Mixtures at 298.15 K

I / mol kg^{-1}	$\theta_{Na^+-K^+}\times10^5$	$\theta_{Cl^--Br^-}\times10^5$	$\theta_{Cl^--SO_4^{2-}}\times10^5$
1.0	1.55	0.56	−0.06
0.75	1.54	0.44	0.81
0.50	2.00	0.25	2.56
0.25	1.71	1.01	4.85

Pitzer's Equation. The form of the Pitzer equation[11] which was used by Kumar[5] has also been utilized here. The apparent molal volume of an ith type ion in a mixture can be estimated by the following equation (which is slightly different from that of Kumar[8]):

$$\phi_{v_i}=\phi^\circ_{v_i}+\frac{z_i^2 A_v}{2b}\ln(1+bI^{1/2})+RT\sum_j B^v_{ij}m_j + \frac{BT}{|z_i|^{1/2}}\sum_j C^v_{ij}m_j^2|z_j|^{1/2}, \quad (4)$$

where

$$B^v_{ij}=B^\circ_{ij}+\frac{1}{2I}B^1_{ij}[1-(1+2I^{1/2})\exp(-2I)^{1/2}];$$

$$B^\circ_{ij}=\left(\frac{\partial\beta^{(0)}_{ij}}{\partial P}\right)_T,\ B^1_{ij}=\left(\frac{\partial\beta^{(1)}_{ij}}{\partial P}\right)_T;$$

$$C^v_{ij}=\left(\frac{\partial C^\phi_{ij}}{\partial P}\right)_T/2;\ A_v=1.8743,\ b=1.2.$$

The apparent molal volume of the Jth salt in a mixture can then be obtained by summing over the component ionic values: $\phi_{v_J}=\sum_i \nu_i\phi_{v_i}$ which in turn calculates the theoretical mean apparent molal volumes ϕ^*_v of the mixtures: $\phi^*_{v_{cal}}=(\sum_J m_J\phi_{v_J})/\sum_J m_J$.

In order to calculate the ϕ^*_v values of the different mixtures by the Pitzer formalism the values of the pure electrolyte parameters $(\partial\beta^{(0)}/\partial P)_T$, $(\partial\beta^{(1)}/\partial P)_T$, and $(\partial C^\phi/\partial P)_T$ (as also ϕ°_v) for the different cation–anion pairs such as Na–Cl, K–Cl, Na–Br, Na–SO_4, and K–SO_4 are required. The experimental ϕ_v values at different concentrations over the range 0.01—1.04 M (1 M=1 mol dm^{-3}) were directly calculated for NaCl, KCl, KBr, and K_2SO_4 from Wirth's reported pure electrolyte density values, using 10—15 data points, whereas those for NaBr and Na_2SO_4 were obtained from Isano's data[12] using five data points for each in the concentration range 0.05—4 M. The values of the pressure derivative parameters and ϕ°_v for the individual electrolytes were then calculated with the help of the Pitzer equation by the nonlinear least squares method. The calculated values for the individual electrolytes, together with the standard deviations of fit (σ) are shown in Table 2. The calculated values of ϕ^*_v at the specified ionic strengths for all the systems mentioned have been incorporated in column 5 of Table 1.

In the Pitzer equation (Eq. 4) the contributions arising out of the interactions between like charges were ignored. However, the consideration of such interactions, called the "mixing terms", gives a better representation for the data studied here. The different binary mixing terms $\theta^v[\equiv\theta_{ik}(m_Am_k\nu_i+m_Bm_i\nu_k)+\theta_{jl}(m_Am_l\nu_J+m_Bm_j\nu_l)]$ both for cation–cation and anion–anion types, are calculated from the difference between the experimental and estimated ϕ^*_v values as usual: $\theta^v=[(\phi^*_{v_{exp}}-\phi^*_{v_{cal}})(m_A+m_B)]/RT$, where m_A, m_B are the molalities of the salts whose cations as well as anions are under consideration for interaction, the ν's being the moles of ionic species produced per mole of the salts (assumed that θ^v_{ii} etc.=0). The θ_{ik} and θ_{jl} values for the NaCl–KCl, NaCl–KBr, and NaCl–K_2SO_4 mixtures considered are shown in Table 3. The extended Pitzer equation for calculating ϕ_{v_i} in a mixture with the use of the mixing terms is obtained by simply adding the term $RT\sum_k \theta_{ik}m_k$ to Eq. 4. Also included in Table 1are the various standard deviations of fit without and with the binary mixing terms for the systems studied (σ_1 and σ_2 respectively).

Mixture Rule. For the calculation of the mean apparent molal volume using Young and Smith's mixture rule,[7] the following equation has been used:

$$\phi^*_v=\frac{n_A\phi_A+n_B\phi_B}{n_A+n_B}, \quad (5)$$

where ϕ^*_v, ϕ_A, and ϕ_B are respectively the apparent molal volumes of the mixtures and the components A and B, all at the same ionic strength. The calculated values of ϕ^*_v at different ional fractions of various systems are shown in column 6 of Table 1. For the calculation of the "mixing terms", the excess volumes of mixing ΔV^{ex}_{mix} for the systems mentioned, which are related to interactions of like charged ions, were calculated by using Millero's equation:[13,14]

$$\Delta V^{ex}_{mix}/\sum_J m_J=\phi^*_{v_{exp(mix)}}-\sum_J m_J\phi'_{v_J}/\sum_J m_J,$$

where ϕ'_{v_J} indicates the $\phi_{v_{exp}}$ value of each individual electrolyte in the mixture at the ionic strength of the

Table 4. Friedman Mixing Parameters Obtained by Least Squares Fit of Eq. 6, for the Three Systems NaCl–KCl, NaCl–KBr, and NaCl–K_2SO_4 at 298.15 K

I	NaCl–KCl		NaCl–KBr		NaCl–K_2SO_4	
mol kg^{-1}	ν_0	ν_1	ν_0	ν_1	ν_0	ν_1
1.0	1.1006	−0.1711	1.2670	−0.1354	1.2007	−0.3062
0.75	1.2089	−0.0882	1.1105	−0.0791	1.0278	−0.3438
0.50	1.0011	0.0252	0.5723	−0.2406	1.4368	−0.5413
0.25	0.8618	0.0595	0.8525	0.0747	1.3815	−0.0631

mixture. The ΔV^{ex}_{mix} values thus obtained are fitted to an equation of the form:[15]

$$\Delta V^{ex}_{mix} = I^2 y_B(1-y_B)[\nu_0+\nu_1 I(1-2y_B)], \quad (6)$$

where ν_0 and ν_1 are related to the ionic interaction parameters[16] (ν_0 to θ_{MN}) and their values are shown in Table 4; (y_B=the ionic strength fraction of component B).

The ΔV^{ex}_{mix} values thus obtained are now incorporated in the ϕ^*_v values estimated from the mixture rule; thus:

$$\phi^*_{v_{cal}} = (\sum_J m_J \phi_{vJ})/\sum_J m_J + \Delta V^{ex}_{mix}/\sum_J m_J, \quad (7)$$

and the standard deviations of fit with the $\phi^*_{v_{exp}}$ values, without and with the mixing terms (σ_3 and σ_4 respectively), are also shown in Table 1 for the NaCl–KCl system mentioned.

Discussion

The ϕ°_v values for NaCl, KBr, NaBr, and KCl obtained in this study are slightly higher than those reported by Kumar for the same systems. We have also calculated the ϕ°_v values using the Redlich–Meyer equation:[17] $\phi_v = \phi^\circ_v + S_v\sqrt{c} + hc$, where S_v is the theoretical limiting slope (=1.868 $cm^3\,dm^{3/2}$ for 1—1 electrolytes at 25 °C) and 'h' is an empirical constant. The different ϕ°_v values obtained from the least squares plots of $(\phi_v - S_v\sqrt{c})$ vs. c are also included in Table 2.

The standard deviations of fit for the ϕ^*_v values of the different mixtures without using the mixing parameters (i.e., σ_1 and σ_3) (Table 1) indicate that for all the mixtures, the Pitzer approach gives better agreement with the experimental values than does the "mixture rule" at the higher two ionic strengths, while at the lower two ionic strengths the agreement is evenly balanced. For the NaCl–KBr mixtures, Humffray[6] observed better agreement using Pitzer's equation at I=1—3 m, while at I=4 m the mixture rule gave a better fit. With the addition of the "volume mixing terms" to Young's rule, as also the interaction terms θ to Pitzer equation, the estimated values of ϕ^*_v in both cases have improved considerably, as is evident from the σ_2 and σ_4 values shown in Table 1. We now find that both the "mixture rule" and the "Pitzer approach" are almost equally successful in predicting the ϕ^*_v values for the mixtures considered.

Figure 1 illustrates the variation of $\phi^{\circ,*}_v$ values of NaCl in the three binary electrolyte mixtures, with different fixed concentrations of KCl, KBr, and K_2SO_4 respectively. The different $\phi^{\circ,*}_v$ values of NaCl in the mixtures containing fixed concentration of the other electrolyte were obtained from the intercepts of various reformulated equations representing the density data. It is interesting to note that the extrapolated ϕ°_v values of pure NaCl obtained by the nonlinear least squares method for the above three types of mixtures containing KCl, KBr, or K_2SO_4 all agree excellently well with the experimental ϕ°_v value of pure NaCl solution.

Very recently Connaughton, Millero, and Pitzer[18] have summarized the Pitzer equations for the volume change on mixing any combination of the four sea salts NaCl, Na_2SO_4, $MgSO_4$, $MgCl_2$ at constant ionic strength. They find that the inclusion of mixing terms based on the differences in the interactions of ions of the same sign is of marginal value at 25 °C. At other temperatures the agreement without the mixing terms is good, but significant improvement is obtained by inclusion of some binary mixing terms. Among the three different mixtures considered by us only the NaCl–K_2SO_4 mixture resembles, as regards the charge type, one of the mixtures considered by Connaughton et al.,[18] namely NaCl–Na_2SO_4 (though the former has no common ions while the latter is a common cation mixture); our other two mixtures are of different charge types than the ones considered by the said authors. The $\theta^v_{Cl^-,SO_4^{2-}}$ value found by Millero is approximately equal to 2×10^{-6} at 25 °C. The values found by us for the same vary from -0.6×10^{-6} to 48×10^{-6} over the ionic strength range 1.0—0.25 mol kg^{-1}.

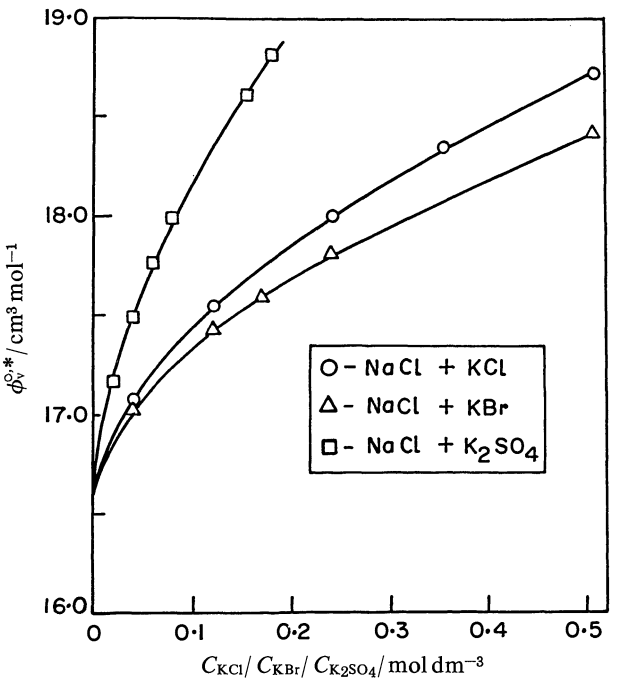

Fig. 1. Variation of $\phi^{\circ,*}_v$ values of NaCl in three binary electrolyte mixtures, with different fixed concentrations of KCl, KBr, and K_2SO_4.

The help received from Swami Satyapriyananda of the R. K. Mission V.C . College, Rahara, in the computer processing of data is thankfully acknowledged.

References

1) K. S. Pitzer, *J. Phys. Chem.*, **77**, 268 (1973).
2) K. S. Pitzer and J. J. Kim, *J. Am. Chem. Soc.*, **96**, 5701 (1974).
3) A. Kumar, G. Atkinson, and R. D. Howell, *J. Solution Chem.*, **11**, 857 (1982).
4) A. Kumar and G. Atkinson, *J. Phys. Chem.*, **87**, 5504

(1983).
5) A. Kumar, *J. Chem. Eng. Data,* **31**, 21 (1986).
6) Alan A. Humffray, *Can. J. Chem.,* **65**, 833 (1987).
7) T. F. Young and M. B. Smith, *J. Phys. Chem.,* **58**, 716 (1954).
8) a) A. Kumar, *Can. J. Chem.,* **66**, 288 (1988); b) *ibid.,* **63**, 3200 (1985).
9) H. E. Wirth, *J. Am. Chem. Soc.,* **59**, 2549 (1937).
10) H. S. Harned and B. B. Owen, "The Physical Chemistry of Electrolyte Solutions," 3rd ed, Reinhold Pub. Corp., New York (1958).
11) P. P. Saluja, K. S. Pitzer, and R. C. Phutela, *Can. J. Chem.,* **64**, 1328 (1986).
12) T. Isano, *J. Chem. Eng. Data,* **29**, 45 (1984).
13) F. J. Millero and M. I. Lampreia, *J. Solution Chem.,* **14**, 853 (1985).
14) L. M. Connaughton and F. J. Millero, *J. Solution Chem.,* **16**, 491 (1987).
15) H. L. Friedman, *J. Chem. Phys.,* **33**, 1134 (1960).
16) F. J. Millero, L. M. Connaughton, F. Vinokurova, and P. V. Chetirkin, *J. Solution Chem.,* **14**, 837 (1985).
17) O. Redlich and D. M. Meyer, *Chem. Rev.,* **64**, 221 (1964).
18) L. M. Connaughton, F. J. Millero, and K. S. Pitzer, *J. Solution Chem.,* **18**, 1007 (1989).

 © 1991 The Chemical Society of Japan Bull. Chem. Soc. Jpn., 64, 2449—2453 (1991)

X-Ray, Electrical and Catalytic Studies of the System $CoFe_2O_4$-Co_2TiO_4

Gulabshankar Ramkhelawan DUBE and Vishnu Shivram DARSHANE*
Institute of Science, 15, Madam Cama Road, Bombay 400032, India
(Received October 18, 1990)

The system $Co_{1+x}Fe_{2-2x}Ti_xO_4$ has been studied with a view to investigating the cation distribution and to correlate the catalytic behavior of spinel with electrical and structural properties. To investigate cation distribution, techniques like X-ray diffraction, electrical conductivity, and thermo emf. have been used. The catalytic evaluation was carried out in the temperature range of 473—673 K using benzyl alcohol as a probe molecule. Our results show $CoFe_2O_4$ to be better catalyst for benzyl alcohol decomposition compared to Co_2TiO_4 or pure oxides of the system.

Oxidic spinels shows interesting electrical, magnetic, and catalytic properties. In these compounds, the properties are controlled by the nature of ions, their charge, and the site distribution amongst tetrahedral and octahedral sites. Several workers[1-3] have reported solid spinel solution of ferrites by substituting ions at tetrahedral and octahedral sites.

Ferrites have been used as efficient catalysts for the decomposition of alkenes,[4,5] hydrogen peroxide,[6,7] and alcohol.[8,9]

We have studied $CoFe_2O_4$–Co_2TiO_4 with a view to investigating the cation distribution and the effect of substitution on the tetrahedral and octahederal sites with reference to catalytic behavior.

Materials and Methods

The different compositions of the system were prepared by coprecipitation techniques.[10] A. R. grade soluble chlorides viz. $CoCl_2 \cdot 6H_2O$, $TiCl_4$ (15% solution), and $FeCl_3 \cdot 6H_2O$ were used to get Co^{2+}, Fe^{3+}, and Ti^{4+} ions in solution.

An aqueous solutions containing these ions in the required molar proportion were prepared by dissolving above salts in distilled water. The corresponding hydroxides were precipitated using 10% NaOH and maintaining the pH between 9.0 and 9.5. The precipitate was heated on water bath at 360 K for 3 h. and was then oxidized by adding calculated amount of 30% H_2O_2 (100% vol) with constant stirring. The precipitate was filtered, washed and dried in vacuum cryostat at 350 K for 2 h.

To measure electrical conductivity and thermoelectric power, pellets were prepared using 2% poly(vinyl acetate) solution as binder. The pellets were heated slowly in air (275 K min^{-1}.) to remove binder and then sintered at 1173 K.

The compositions of the product were checked by chemical analysis and were found to be in agreement with the theoretical values. The particle size was determined from XRD analysis and was found to be approximately 4 μm.

X-Ray powder patterns were recorded on diffractometer (Siemens D-Crystalloflex) using Cu $K\alpha$ radiation with Ni-filter. X-Ray patterns of all the compositions indicated formation of single spinel phase. To measure the intensity, area under different $h\ k\ l$ peaks were determined and the values obtained in relation to the peak area for 311 reflection was taken as 100. To calculate relative integrated intensity, I, of given $h\ k\ l$ reflection, following formula[11] was used where notations have their usual meaning,

$$I_{h\,k\,l} = |F_{h\,k\,l}|^2 \times P \times \frac{1+\cos^2 2\theta}{\sin^2\theta\cos\theta}$$

The atomic scattering power values for various ions were taken from International Table.[12] To determine cation distribution and it's variation with compositions, the intensity ratios I_{200}/I_{400}, I_{220}/I_{440}, I_{422}/I_{400}, I_{400}/I_{422} for different possible models were calculated and compared with the observed intensity ratios.

DC resistivity measurements were carried out using LCR-Markoni bridge. The flat faces of each pellet were coated with thin layer of conducting silver paste and resistivity as well as thermo emf. measurements were carried out from room temperature to 673 K.

Each composition of the system has been investigated for its catalytic activity in the temperature range of 473—673 K. 3.0 g of the powdered catalyst was packed in a 25 cm long quartz

Table 1. Cation Distribution, Lattice Constant, Activation Energy (ΔE) and Thermoelectric Coefficient (α) of the System $Co_{1+x}Fe_{2-2x}Ti_xO_4$

Compositions (x)	Cation distribution		Lattice constant	Activation energy/eV	Thermo emf.coeff(α)
	A-site	B-site			
0.0	Fe^{3+}	$Co^{2+}Fe^{3+}_{1.0}$	8.368	0.52	−40.00
0.2	$Fe^{3+}_{0.8}Co^{2+}_{0.2}$	$Co^{2+}Fe^{3+}_{0.8}Ti^{4+}_{0.2}$	8.382	0.60	−10.00
0.4	$Fe^{3+}_{0.6}Co^{2+}_{0.4}$	$Co^{2+}Fe^{3+}_{0.6}Ti^{4+}_{0.4}$	8.395	0.68	+155.00
0.6	$Fe^{3+}_{0.4}Co^{2+}_{0.6}$	$Co^{2+}Fe^{3+}_{0.4}Ti^{4+}_{0.6}$	8.405	0.73	+198.00
0.8	$Fe^{3+}_{0.2}Co^{2+}_{0.8}$	$Co^{2+}Fe^{3+}_{0.2}Ti^{4+}_{0.8}$	8.410	0.79	+225.00
1.0	$Co^{2+}_{1.0}$	$Co^{2+}Ti^{4+}_{1.0}$	8.423	0.83	+255.00

Table 2. Comparison of Intensity Ratios for the Compound $Co_{1.6}Fe_{0.8}Ti_{0.6}O_4$

Cations at		I_{440}/I_{422}		I_{220}/I_{440}		I_{422}/I_{400}		I_{220}/I_{400}	
A-Site	B-Site	Obsd	Calcd	Obsd	Calcd	Obsd	Calcd	Obsd	Calcd
$Co^{2+}_{1.0}$	$Fe^{3+}_{0.8}Co^{2+}_{0.6}Ti^{4+}_{0.6}$		5.1		1.20		0.75		1.20
$Co^{2+}_{0.6}Fe^{3+}_{0.4}$	$Fe^{3+}_{0.4}Co^{2+}_{1.0}Ti^{4+}_{0.6}$	4.22	4.22	0.64	0.64	0.59	0.58	1.58	1.59
$Co^{2+}_{0.4}Ti^{4+}_{0.6}$	$Fe^{3+}_{0.8}Co^{2+}_{1.2}$		4.35		0.59		0.53		1.45
$Co^{2+}_{0.2}Fe^{3+}_{0.6}Ti^{4+}_{0.2}$	$Fe^{3+}_{0.2}Co^{2+}_{1.4}Ti^{4+}_{0.4}$		4.00		0.45		0.69		1.85

reactor with 10 mm internal diameter. The reactor was equipped with thermocouple to monitor the temperature of the catalyst bed. The vapours of benzyl alcohol were passed over catalyst and the products were condensed using conventional techniques and were analyzed by gas chromatography. The products were further confirmed by GCMS.

Results and Discussion

X-Ray diffractometer patterns of all the compositions showed single spinel phase. The results of X-ray analysis are given in Table 1. From table it is observed that all the compositions of the system possess cubic symmetry. The lattice constant increases linearly from $CoFe_2O_4$ to Co_2TiO_4 obeying Vegard's law. The increase in lattice constant from $CoFe_2O_4$ is due to replacement of Fe^{3+} by slight bigger Co^{2+} and Ti^{4+} ions at octahedral site.

The cation distribution between two sites in the system has been arrived at by X-ray intensity calculations. The observed and calculated intensity ratios for different models for the composition x=0.6 is given in Table 2. From table, it is observed that the model with Ti^{4+} at B-site, Co^{2+} both A- and B-sites while Fe^{3+} distributed equally between A- and B- site shows better agreement. Our results on cation distribution are in close agreement with the values reported earlier on $CoFe_2O_4$ and Co_2TiO_4.[13,14]

Electrical Properties: DC resistivity of the compounds of the system $Co_{1+x}Fe_{2-2x}Ti_xO_4$ measured as a function of temperature varied between 10^6 and 10^7 ohm-cm. The plot of $\log\rho$ vs. $10^3/T$ showed a linear nature obeying Wilsen's law.

$$\rho = \rho_o \exp(\Delta E/KT).$$

High values of resistivity indicate that elements with stable oxidation state are present at B-site.

From Table 1, it is observed that with subsequent replacement of Fe^{3+} by Co^{2+} and Ti^{4+} activation energy increases. This is due to the fact that Ti^{4+} (d^0) orbitals have much lower energy i.e. they are very stable and are much more contracted than Fe^{3+} d-orbitals. Also as concentration of Fe^{3+} ion decreases in the lattice, the mobility of charge carriers decreases resulting in the increase in the activation energy.

Thermoelectric coefficient values of the series varied between -40.00 and $+255.00\ \mu V\ K^{-1}$. The compounds with $x \leqslant 0.2$ are n-type while $0.4 \leqslant x \leqslant 1.0$ are p-type (Table 1) semiconductors. p-Type semiconductivity of cobalt rich compounds can be attributed to the formation fo Co^{2+}/Co^{3+} ion pairs but unfortunately the presence of Co^{3+} ions could not be detected from X-ray intensity calculations as the concentration may be very small.

Catalytic Studies: Decomposition of benzyl alcohol has been reported by several workers using pure metal

Table 3. Catalytic Performance Data for the Decomposition of Benzyl Alcohol

Catalyst bed temp/K	Conversion %	% Selectivity Benzaldehyde	% Selectivity Toluene
	Catalyst: $CoFe_2O_4$		
473	2.3	75.85	22.59
523	5.68	63.55	27.50
573	18.66	50.78	35.72
623	32.04	39.8	40.17
673	49.62	27.09	45.00
	Catalyst: $Co_{1.2}Fe_{1.6}Ti_{0.2}O_4$		
473	2.0	83.0	12.5
523	5.5	68.5	14.05
573	14.02	60.0	25.0
623	24.01	43.85	25.0
673	36.0	33.17	31.0
	Catalyst: $Co_{1.4}Fe_{1.2}Ti_{0.4}O_4$		
473	1.77	90.43	4.56
523	2.78	77.99	11.75
573	11.76	65.08	18.46
623	21.05	52.39	24.79
673	30.35	40.31	31.04
	Catalyst: $Co_{1.6}Fe_{0.8}Ti_{0.4}O_4$		
473	1.0	90.2	4.0
523	2.5	77.59	20.4
573	10.05	68.5	14.2
623	54.0	54.0	23.0
673	27.0	43.75	29.0
	Catalyst: $Co_{1.8}Fe_{0.4}Ti_{0.8}O_4$		
473	0.52	95.0	4.0
523	2.0	80.0	9.7
573	10.5	70.5	15.5
623	16.5	58.0	26.5
673	24.05	45.39	28.0
	Catalyst: $Co_2Ti_{1.0}O_4$		
473	0.442	97.62	2.26
523	1.83	85.47	7.52
573	8.0	72.73	13.86
623	14.0	60.99	20.83
673	22.45	47.02	26.43

oxides and various zeolites.[15–18] However literature survey indicates that not much work has been reported where spinels have been used as catalysts for the decomposition of benzyl alcohol.

Decomposition of benzyl alcohol mainly yields benzaldehyde and toluene.

$$C_6H_5CH_2OH \xrightarrow{\text{Catalyst}} C_6H_5CHO + 2H^*$$
$$C_6H_5CH_2OH + 2H^* \longrightarrow C_6H_5CH_3 + H_2O$$

Results of benzyl alcohol decomposition over various compositions of the system $Co_{1+x}Fe_{2-2x}Ti_xO_4$ are listed in Table 3. From table it is observed that conversion of benzyl alcohol on $CoFe_2O_4$ is always greater at all the temperatures compared to other catalyst compositions. The conversion of benzyl alcohol vs. temperature for the various compositions of the system is reported in Fig. 1. Further from Fig. 1 it is observed that conversion of benzyl alcohol decreases from $CoFe_2O_4$ to Co_2TiO_4. The decreases in the catalytic activity from cobalt-ferrite to cobalt titanate can be explained on the basis of cation distribution in the spinel.

$CoFe_2O_4$ being an inverse spinel, Fe^{3+} ions are present both, tetrahedral as well as octahedral site. Since Fe^{3+} can hop between +2 and +3 states, provide more active centers for the catalytic reaction. Therefore $CoFe_2O_4$ is more active. Subsequent replacement of Fe^{3+} by Co^{2+} and Ti^{4+} ions, an equivalent amount of Fe^{3+} ion is replaced by Co^{2+} at A-site while at B-site, it is substituted by Ti^{4+} ion. Thus B-site of the spinel system is occupied by the ions with stable oxidation state (Ti^{4+} and Co^{2+}) with increase in concentration of X which favors the formation of benzaldehyde, a dehydrogenation product.

With decrease in the iron(III) concentration in the spinel, toluene selectivity decreases and aldehyde selectivity increases indicating that ions at tetrahedral site are

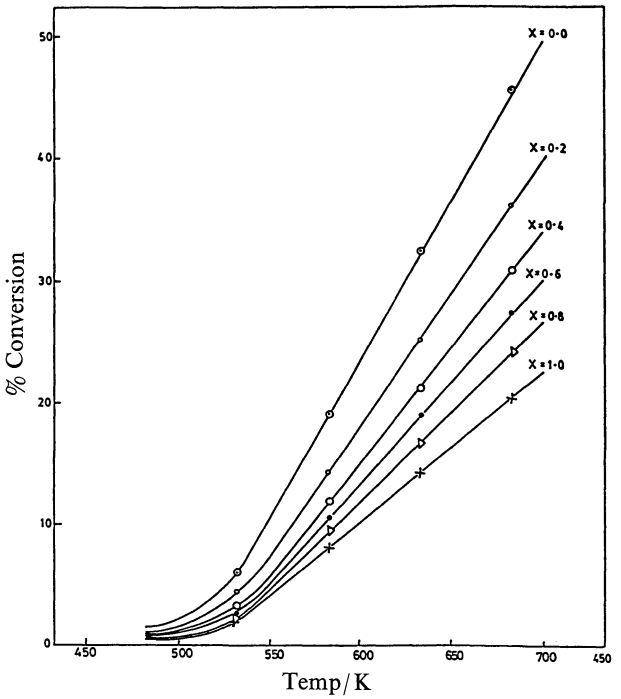

Fig. 1. Plot of % conversion of benzyl alcohol vs. temp over different compositions of the system $Co_{1+x}Fe_{2-2x}Ti_xO_4$.

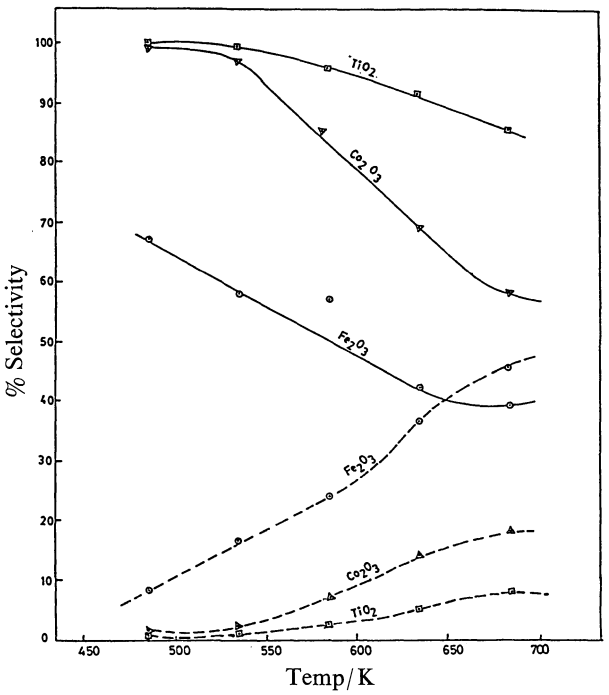

Fig. 2. Plot of aldehyde (——) and toluene (– –) selectivity of pure oxides vs. temp of the system $Co_{1+x}Fe_{2-2x}Ti_xO_4$.

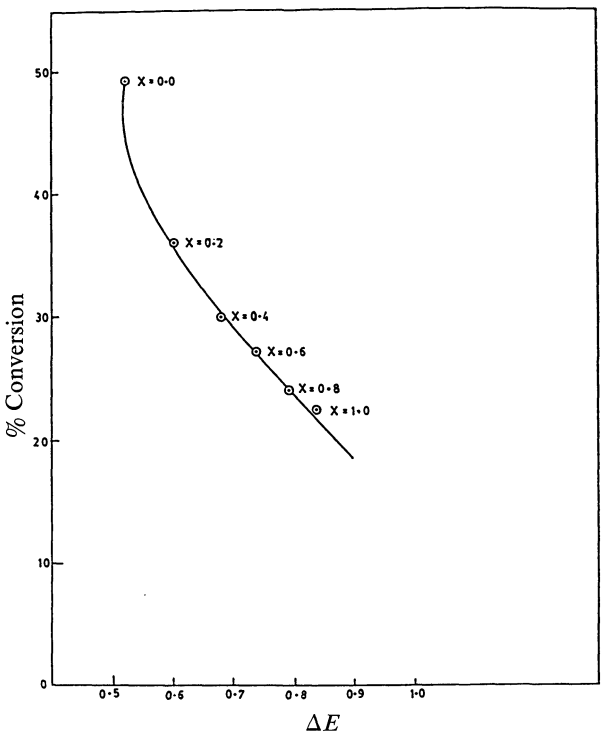

Fig. 3. Plot of % conversion vs. activation energy for the system $Co_{1+x}Fe_{2-2x}Ti_xO_4$ at 673 K.

responsible for the reduction of benzyl alcohol. Similar results have also been reported by Onchuku[19] in the investigation of decomposition of hydrogen peroxide using Cu–Ni–ferrite system.

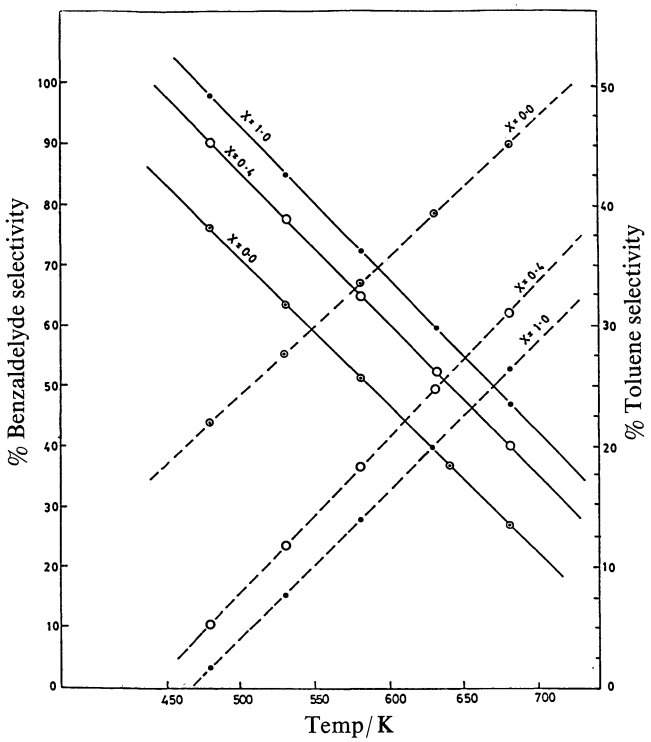

Fig. 4. Plot of % benzaldelyde and toluene selectivity over x=0.0, 0.4, and 1.0 for the system $Co_{1+x}Fe_{2-2x}Ti_xO_4$.

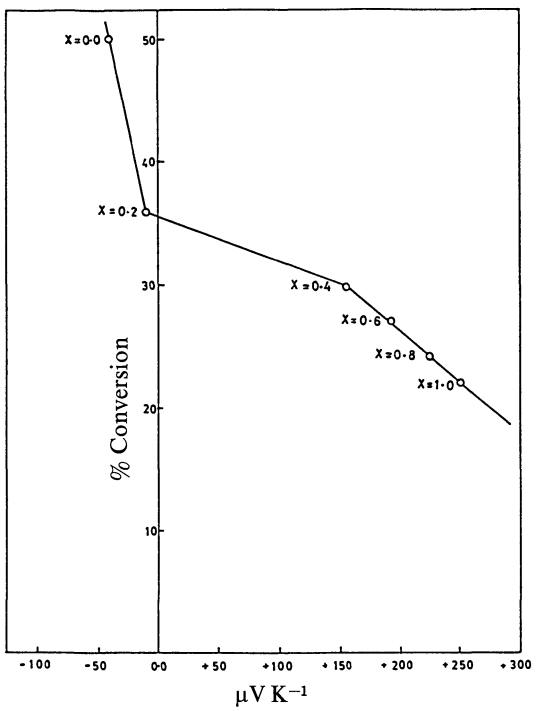

Fig. 5. Plot of % benzyl alcohol conversion vs charge carrier of the system $Co_{1+x}Fe_{2-2x}Ti_xO_4$.

The above observation is further supplemented by Fig. 2 which gives toluene selectivity over pure oxides of the system i.e. Fe_2O_3, Co_2O_3, and TiO_2. From Fig. 2 it is observed that Fe_2O_3 and Co_2O_3 yield maximum toluene while TiO_2 gives mainly benzaldehyde.

The substitution of Co^{2+} and Ti^{4+} results in the increase in the activation energy of the system from 0.52 eV ($CoFe_2O_4$) to 0.83 eV (Co_2TiO_4). Further from Fig. 3 it is noted that $CoFe_2O_4$ is the most active catalyst with the highest percentage conversion (49.62%) over any titanium containing compositions. The change in activation energy greatly influences the catalytic activity. The catalytic activity is due to transfer of electrons/holes from catalyst surface to substrate and is reversible. Hence greater the value of activation energy more will be the energy required for electronic transitions resulting in decrease in catalytic activity i.e. decrease in percentage benzyl alcohol decomposition.

From Fig. 4 it is observed that aldehyde selectivity increases and toluene selectivity decreases with increase in value of x. $CoFe_2O_4$ indicated 75.85% benzaldehyde selectivity at 473 K while at the same temperature Co_2TiO_4 showed 97.62% selectivity (Table 3).

It is well known that n-type semiconductors are always more active and selective towards dehydration of alcohols due to rapid migration of electrons while p-type semiconductors are active and selective towards dehydrogenation due to migration of holes.[20] The effect of nature of charge carriers on the catalytic activity of spinels is shown in Fig. 5. $CoFe_2O_4$ (α=40 $\mu V K^{-1}$) is most active for dehydration due to $Fe^{3+} \rightleftarrows Fe^{2+} + e^-$ hopping process (Table 3) where electrons are predominently the charge carriers. As the concentration of iron(III) decreases in the lattice ($x \geqslant 0.4$) the holes become predominent charge carriers result in decrease in overall catalytic activity.

Conclusion

Thus from X-ray intensity, electrical conductivity and thermo emf measurements the probable cation distribution of the system $Co_{1+x}Fe_{2-2x}Ti_xO_4$ is suggested as $Co_x^{2+}Fe_{1-x}^{3+}[Co_{1.0}^{2+}Fe_{1-x}^{3+}Ti_x^{4+}]\ O_4^{2-}$. Further it is observed that $CoFe_2O_4$ is most active catalyst towards benzyl alcohol decomposition while Co_2TiO_4 is most selective dehydrogenation catalyst.

References

1) Landolt-Borstein, "Magnetic Oxides and Related Compounds," Springer, Berlin (1970), Vol. 3/4b.

2) Prabha Nathwani and V. S. Darshane, *Pramana—J. Phys.*, **28**, 675 (1987).

3) A. Meenakshisundaram and V. Srinivasan, *Phys. Status Solidi A*, **69**, K15 (1973).

4) Renard, Jr. and W. H. Kehl, *J. Catal.*, **22**, 452 (1975).

5) W. Ronald Cares and Joe W. Hightower, *J. Catal.*, **39**, 36 (1975).

6) J. R. Goldstein and A. C. C. Tseung, *J. Catal.*, **32**, 452

(1974).
7) H. M. Cota, M. Chin, and F. J. Schoenweis, *Nature,* **19**, 1281 (1964).
8) P. K. Sharpe, J. C. Vickerman, and M. H. Stancy, Proce. 6th Internat. Cong. Catal., London (1976).
9) M. V. Joshi, V. G. Khanwalkar, and V. S. Darshane, "Advances in Ferrites," (1989), Vol. II, p. 1191.
10) P. M. Khopkar, J. A. Kulkarni, and V. S. Darshane, *Thermochim. Acta,* **93**, 481 (1985).
11) M. J. Burger, "Crystal Structure Analysis," John Wiley, New York (1960).
12) "International Tables for X-Ray Crystallography," Kynoch, Bermingham (1974), Vol. 4, pp. 72—98.
13) Prabha Nathwani and V. S. Darshane, *J. Phys. C, Solid State Phys.,* **21**, 3191 (1988).
14) J. K. Shrivastava, J. A. Kulkarni, S. Ramkrishnan, S. Singh, V. R. Marathe, G. Chandra, V. S. Darshane, and R. Vijayaraghavan. *J. Phys. C, Solid State Phys.,* **20**, 2139 (1987).
15) Ishinge Mayashosi, Sakal Koji, Kawai Mashutoshi, Hata Kajuo, *Bull. Chem. Soc. Jpn.,* **43**, 2186 (1970).
16) C. N. Pillai, M. Jayamani, and N. Murgesan, *J. Catal.,* **85**, 527 (1965).
17) S. Walter Trahanvoski and Brewster L. Young, *J. Chem. Soc.,* **8**, 5777 (1965).
18) Takatome and Kazushige, *Nagasaki Daigaku, Kyoikugakubu, Shizen Kagakukenkyu Hokoku,* **34**, 31 (1983).
19) A. I. Onchuku, *J. Chem. Soc., Faraday Trans. 1,* **80**, 1447 (1984).
20) O. V. Krylov, "Catalysis by Non-Metals," Academic Press, New York (1970).

Raman Phonon Spectroscopic Study of Phase Transition in *trans*-Stilbene Crystal

Subhasis CHAKRABARTI and Tridibendra Narayan MISRA*
Department of Spectroscopy, Indian Association for the Cultivation of Science, Calcutta 700032, India
(Received November 19, 1990)

Raman phonon spectroscopy in the 10—170 cm^{-1} range has been used to study phase transition in *trans*-stilbene crystal. At 77 K, eight distinct phonon modes and an internal mode are observed whereas at 300 K the spectrum shows only four phonon bands and an internal mode. The temperature dependence of spectral pattern and some phonon band width suggest that the phase transition in this crystal is quasi-continuous over a small temperature range 215—225 K. The absence of a soft mode and a strong increase of the phonon band width, when approaching the T_c from below, suggest that the phase transition is of order-disorder type. The well established disordered structure of *trans*-stilbene crystal at room temperature attains an ordered structure at low temperature at least through one, possibly two order–disorder transitions.

Raman phonon spectroscopy has been used extensively to investigate phase transition in crystals.[1—4] Phonon spectroscopy is suited for such studies particularly in organic molecular crystals due to the fact that in such crystals the intermolecular forces are 10—100 times weaker than the intramolecular forces and the internal and external motions of molecules in most cases fall in different domain of frequencies. The lattice vibrational frequencies in organic crystals generally lie below 200 cm^{-1}. In *trans*-stilbene crystal, however, some internal modes representing torsion of the phenyl ring also lie in this low frequency range and the Raman active internal modes in this spectral range has been identified by Bree and Edelson.[5] We have used this Raman phonon spectroscopic technique to study phase transition in *trans*-stilbene crystal.

trans-Stilbene is a very flexible molecule in the ground state. The crystal belongs to the monoclinic space group $P2_1/c$ with four molecules in the unit cell.[6,7] At room temperature however the structure is highly disordered, one of the two independent sites shows orientational disorder.[6] In contrast to that at 300 K, at 113 K, the second orientation of the molecule at one of the sites almost disappears and the lattice becomes more ordered.[8] No studies of phase transition in *trans*-stilbene crystal based on standard X-ray or neutron diffraction technique seem to have been reported. Extensive Raman spectroscopic study of this crystal both in external lattice modes and in internal molecular modes by Bree and Edelson[5] did not observe any phase transition in 113—4.2 K range as no significant change in relative intensities of internal modes could be detected by them. However contrary to that observed in first-order structural phase transition, no sharp change in frequency or intensity may occur in second-order phase transition. Also often it is difficult to identify slow and gradual change in Raman band intensity. The study of Bree and Edelson[5] was, however, less extensive at high temperature domain.

Temperature dependence of phonon band width has been shown to be very useful to indicate phase transition in organic crystals.[3] The band width broadening is often related to the progressive setting of disorder when temperature increases.[9,10] When the translational symmetry of the crystal breaks due to disorder, some modes of the whole Brillouin zone can become Raman active. This broadens the phonon bands of the dispersive modes. Phase transition in this crystal at high-temperature domain has recently been reported by Ghoshal et al.[11] by "Photokinematical Approach" which utilized a luminescence intensity change of a dopant as the host crystal goes through a phase transition temperature. They identified two phase transitions in this crystal.

We have undertaken a careful study of Raman phonon spectral pattern and their band widths as a function of temperature. Our studies add further credence to the luminescence technique developed by Ghoshal et al.[11] for phase transition studies and in addition provide information about the nature of phase transition.

Experimental

The compound *trans*-stilbene was obtained from M/S Aldrich Chemical Company Ltd., U.S.A. and purified by repeated crystallization from benzene followed by zone refining with 75 passes. Crystals were grown in a bridgman furnace. Both polycrystalline samples and single crystals were used to obtain the Raman spectra. Unfortunately polarized spectra could not be studied due to lack of facilities.

Raman spectra were obtained using a Spex double monochromator Model 1403 and the 5145 Å line of Spectra Physics Model 2020-5 Argon Ion Laser. Spex Datamate 1B was used for data acquisition and analysis and the band position should be accurate within 1 cm^{-1}. A Superveritemp model 10DT of Janis Research U.S.A. was used to cool the crystal from room temperature down to 77 K. Temperatures were measured and controlled by Lake Shore Model 805 temperature controller. Liquid nitrogen temperature spectrum was run with the crystal immersed in the cryogen.

Results and Discussion

Temperature Dependence of Phonon Spectra. In *trans*-stilbene crystal, the four molecules in the unit cell occupy the inversion centers. Twelve librational phonons are expected to be Raman active. The Raman phonon spectra of *trans*-stilbene crystal at a series of

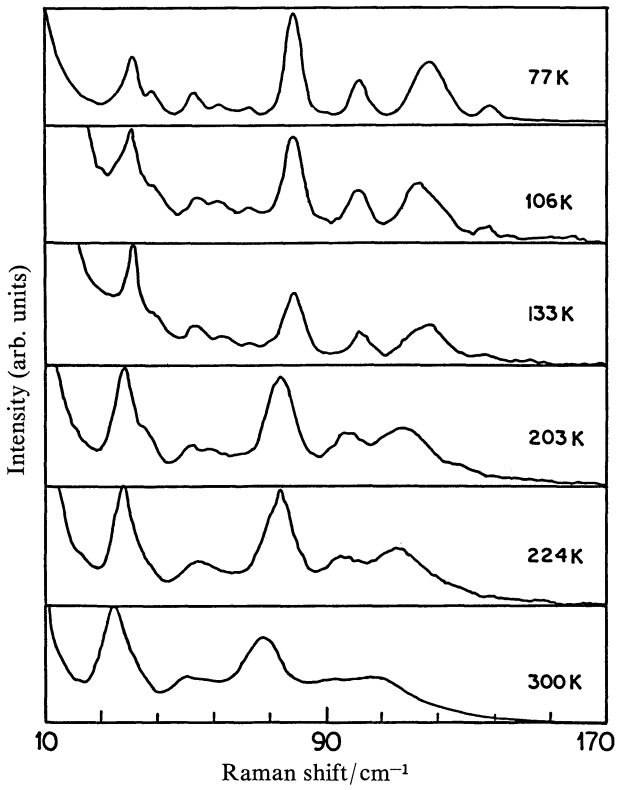

Fig. 1. Raman phonon spectra of *trans*-stilbene crystal at several temperatures. The spectral resolution is 1 cm^{-1}.

temperature are shown in Fig. 1. At 77 K, nine distinct low frequency modes at 34.4, 39.4, 52.2, 60.6, 68.2, 81.0, 99.4, 118.8, and 135.2 cm^{-1} are observed whereas at 300 K, only five broad bands at 29.4, 51.8, 71.8, 92.5, and 101.2 cm^{-1} persist. The 92.5 and 101.2 cm^{-1} bands at 300 K are very broad and are hardly resolved. Our low frequency Raman spectra at 77 K and that reported by Bree and Edelson[5] at 4.2 K can be compared and the bands can be easily correlated. Such correlation is shown in Table 1. Bree and Edelson assigned the quartet at 120.7, 123.4, 127.0, and 131.7 cm^{-1} as factor-group split components of an internal mode. We accordingly assign our 118.8 cm^{-1} band as an internal mode and the remaining eight as lattice modes.

Table 1. Correlation of Low Frequency Raman Bands (in cm^{-1}) at Two Temperatures

Bree and Edelson[5] (4.2 K)	Present work (77 K)
34.9	
40.5	34.4
46.1	39.4
58.0	52.2
64.7	60.6
68.1	
74.0	68.2
86.5	81.0
93.3	
105.3	99.4
120.7	
123.4	118.8
127.0	
131.9	
143.9	135.2

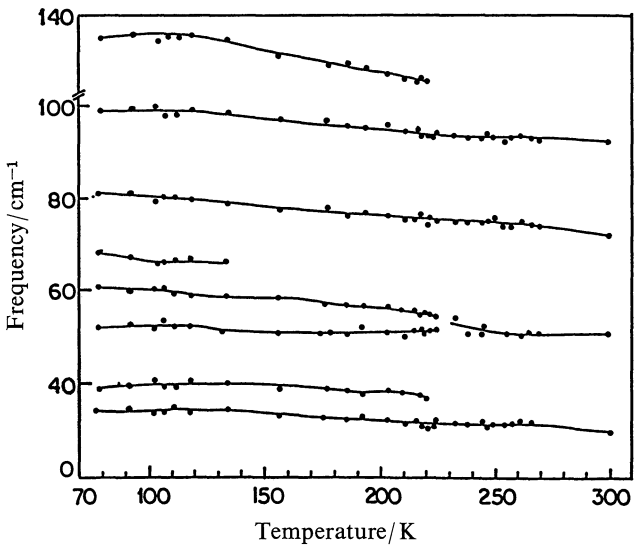

Fig. 2. Temperature dependence of Raman active lattice phonon frequencies in *trans*-stilbene crystal.

A close inspection of the spectra in Fig. 1. reveals that some distinct changes occur in a small temperature range 215—225 K. The medium intense broad phonon band of frequency 51.8 cm^{-1} observed at 300 K flattens out and splits into two bands of frequencies 51.2 and 57.2 cm^{-1} in the 215—225 K temperature range. A third component appears and becomes distinctly observable at 133 K as a phonon band of frequency 66 cm^{-1}. All these three bands intensify and shift to higher frequencies with cooling. At 220 K a third band at 124.8 cm^{-1} appears. These bands intensify and shift to higher frequencies as the temperature is lowered.

The temperature dependence of the Raman active phonon frequencies is shown in Fig. 2. As the temperature is raised, the phonon frequencies shift to lower values. The phonon band around 40 cm^{-1} shows a gradual decrease in intensity with increasing temperature and disappears after 215—225 K. Similar behavior is observed in the 135.2 cm^{-1} phonon band. The triplet structure in the 52—68 cm^{-1} region observed at low temperature fuses into a single broad band in this temperature domain. Further the intensity ratio of 29.4 and 71.8 cm^{-1} bands at 300 K and the corresponding bands at 34.4 and 81.2 cm^{-1} at 77 K are significantly different and this change occurs in the temperature domain 215—225 K.

All these results suggest that there is a continuous phase transition in *trans*-stilbene crystal spread over a small temperature range 215—225 K.

Temperature Dependence of Phonon Band Width. Temperature dependence of phonon band width indicates phase transition in organic crystals.[3] In Fig. 3 we

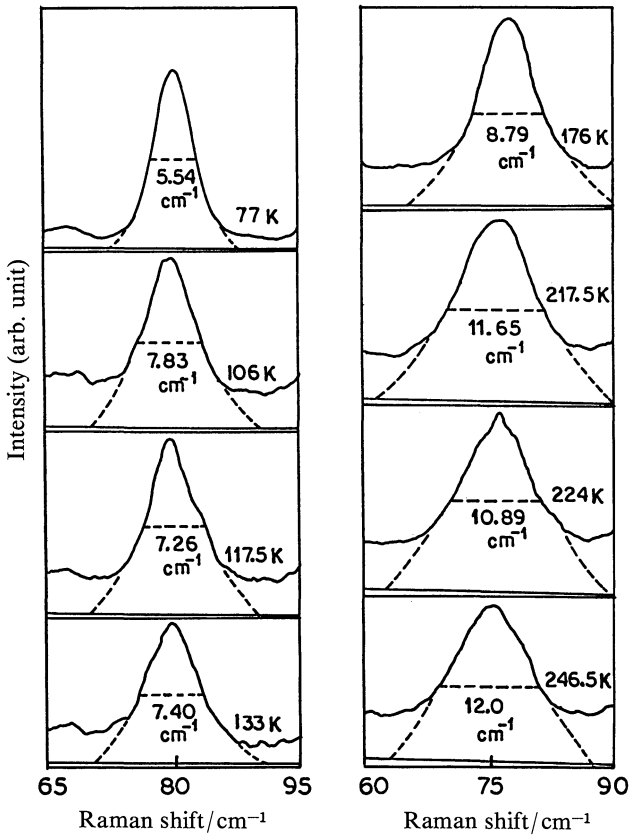

Fig. 3. Band widths (FWHM) of 81 cm^{-1} (at 77 K) band at several temperatures in extended scale. Extrapolation of the bands to the base line is shown by broken lines.

show 81 cm^{-1} (at 77 K) phonon band in extended scale at several temperatures near the transition regions and in Fig. 4. temperature dependence of band widths of 81 and 34.4 cm^{-1} (at 77 K) phonon bands are shown. The variation of width seems to be continuous or very close to be so except at two temperature domains where the continuity pattern is broken and the width shows some small but definite decrement with temperature rise. One of the break points of the curves coincides with the transition temperature region 215—225 K suggested by the temperature dependence of phonon spectral patterns. The other break point in the 105—115 K temperature region is not indicated in the spectral pattern. The change in the band width for this temperature region, however, seems to be within the error bar of the experimental Raman resolution and no definite conclusion about a phase transition at this temperature range can be drawn. The break points in the continuity pattern of the band width-temperature plot is more pronounced in 81 cm^{-1} phonon than in 34.4 cm^{-1} band. This is possibly due to the fact that the 34.4 cm^{-1} phonon band overlaps with other band at 39.4 cm^{-1} and the overlapping becomes significant at higher temperature. For the other modes, the quantitative analysis of their band widths has not been possible owing to their multiple overlapping.

Temperature Dependence of Internal Modes. We have also studied the Raman spectra of the crystal representing internal modes of *trans*-stilbene molecule at various temperatures. There is no significant change in the internal modes except that with lowering of temperature the frequencies change slightly to the higher values. However, the B_g mode at 558 cm^{-1} and the A_g mode at 869 cm^{-1} show distinct intensity reversal in a small temperature range around 110 K. This is shown in Fig. 5. This temperature domain agrees with the low temperature peak in the temperature dependence of band width plot as shown in Fig. 4. Ghoshal et al.[11] suggested a phase transition in the *trans*-stilbene crystal at this temperature from their luminescence studies. The agreements of our two approaches coupled with the photokinematical report of Ghoshal et al.[11] about a second phase transition at 110±5 K is interesting.

Nature of Phase Transitions. In first-order phase

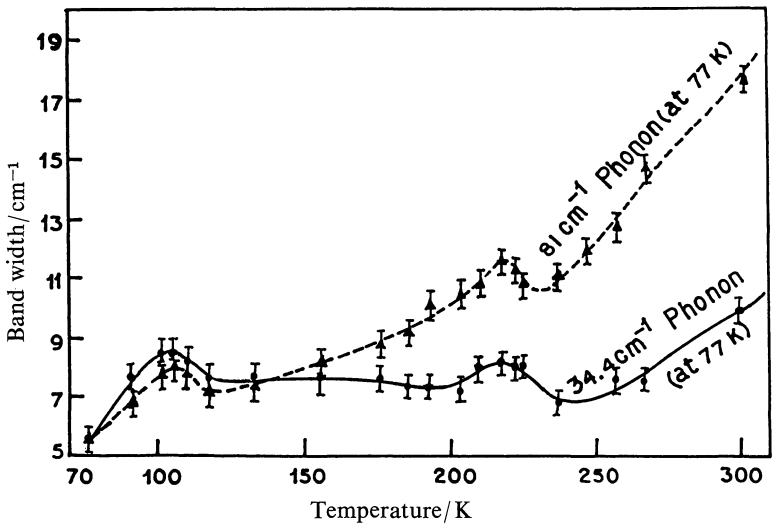

Fig. 4. Temperature dependence of band widths of Raman phonon bands of *trans*-stilbene crystal.

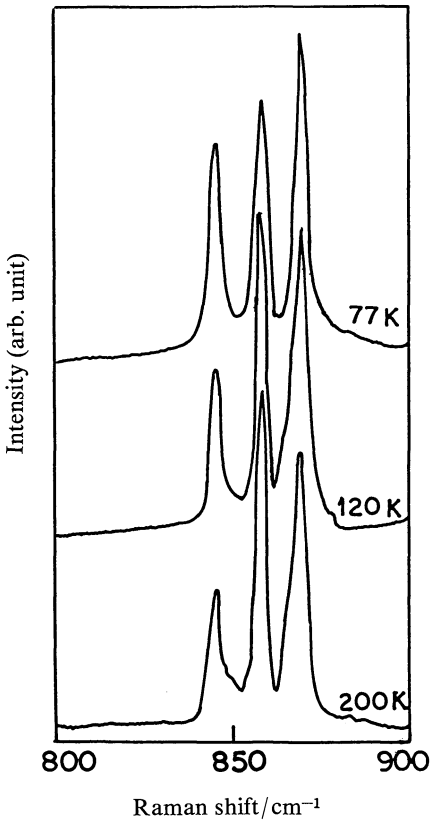

Fig. 5. Raman spectra of *trans*-stilbene crystal in 800—900 cm^{-1} region at several temperatures.

transition, the structural deformation occurs abruptly at one temperature. The second-order phase transition, on the other hand, is continuous and occurs over a temperature range. In *trans*-stilbene we find progressive evolution of phonon spectra as the critical temperature T_c (spread over a range) is approached with no sudden change. The phase transition of this crystal is quasi-continuous (pseudo-second order).

Order–disorder transition is described by a double well potential near T_c. In the phase above T_c there is large amplitude motions from one potential well to another. Below T_c, the molecules lie on the same side of the double well and oscillation occurs in an essentially quadratic well. The system then can be characterized by two characteristic frequencies, one is quasi-harmonic frequency within either side of the double well and a second frequency which describes the relaxational behavior from one well to the other.

In some cases where order–disorder phase transition is established,[12] a large enhancement of Rayleigh intensity is observed as T_c is approached from above. This has been attributed to the relaxational mode describing the jump from one side of the double well to the other. In our experimental result though such enhancement of Rayleigh intensity is not unequivocally established as the first phase transition temperature domain 215—225 K is reached. Such intensity enhancement is, however, observed as 105—115 K is approached. This is evident from Fig. 1. The second order–disorder phase transition at 105—115 K as proposed from "Photokinematical Approach" therefore, seems plausible.

X-Ray analysis shows that at room temperature, the structure of *trans*-stilbene is not highly ordered. One of the two independent sites show orientational disorder.[6] It is, therefore, expected that an ordered structure will be attained at some lower temperature. Indeed at about 113 K, the second orientation of the molecules in the lattice is hardly present.[8] It thus seems that the disordered structure of *trans*-stilbene crystal at 300 K attains the ordered structure at low temperature through at least one order–disorder transition.

Conclusion

We have used Raman phonon spectroscopy to study phase transition in *trans*-stilbene crystal. The temperature dependence of spectral pattern and phonon band width suggest that there is a quasi-continuous phase transition over a small temperature range 215—225 K. The absence of a soft mode and a strong increase of the phonon band width when approaching the T_c from below suggest that the phase transition is of order–disorder type. The disordered structure at room temperatute attains an ordered structure at low temperature through at least one, possibly two order–disorder transitions.

References

1) R. Zallen, C. H. Griffiths, M. L. Stade, H. Hayek, and O. Brafman, *Chem. Phys. Lett.*, **39**, 85 (1976).
2) B. A. Bolton and P. N. Prasad, *Chem. Phys.*, **35**, 334 (1978).
3) A. Girard, M. Sanguer, and Y. Delugeard, *Chem. Phys.*, **96**, 427 (1985).
4) Y. Ebisuzaki, L. H. Askari, and A. M. Bryan. *J. Chem. Phys.*, **87**, 6659 (1987).
5) A. Bree and M. Edelson, *Chem. Phys.*, **51**, 77 (1980).
6) C. J. Finder, M. G. Newton, and M. Allinger, *Acta Crystallogr., Sect. B,* **30**, 411 (1974).
7) J. A. Browstra, A. Schoutern, and J. Kroon, *Acta Crystallogr., Sect. C,* **40**, 428 (1984).
8) H. A. Hoekstra, P. Meertens, and A. Vos, *Acta Crystallogr., Sect. B,* **31**, 2813 (1975).
9) C. Sourisseau and G. Lucazcau, *J. Raman Spectrosc.*, **8**, 311 (1979).
10) J. L. Souvajol, *J. Raman Spectrosc.*, **13**, 270 (1982).
11) S. K. Ghoshal, S. K. Sarkar, and G. S. Kastha, *Mol. Cryst. Liq. Cryst.*, **91**, 1 (1983).
12) P. D. Laray, J. M. Lunacek, N. A. Clark, and G. B. Benedict, ln "Light Scattering Spectra in Solids," ed by G. B. Wright, Springer, New York (1969), p. 593.

Structure and Properties of $(NEt_4)[Mo^VO(\alpha,2\text{-toluenedithiolato})_2]$. Distorted Tetragonal-Pyramidal $MoOS_4$ Core

Norikazu UEYAMA, Naoto YOSHINAGA, Atsushi KAJIWARA, Akira NAKAMURA,* and Masami KUSUNOKI†
Department of Macromolecular Science, Faculty of Science, Osaka University, Toyonaka, Osaka 560
†Institute for Protein Research, Osaka University, Suita, Osaka 565
(Received November 13, 1990)

An oxomolybdenum(V) complex with two chelating ligands of alkane- and arenethiolate parts, $(NEt_4)[Mo^VO(\alpha,2\text{-toluenedithiolato})_2]$, was prepared and characterized by visible, ESR, IR, and Raman spectroscopies. Four distinct ligand-to-metal charge transfer absorption bands were observed in visible region. The complex crystallizes in the space group $P2_1$ with a=9.535(2), b=16.582(9), c=8.085(1) Å, β=90.757(4)°, V=1278.3(8) Å^3, Z=2, and d_{calcd}=1.431 g cm^{-3}. The structure was solved and refinement based on 2102 reflections converged at R=0.089 and R_w=0.100. The complex takes an apical oxo and trans bis(α,2-toluenedithiolato) structure with a distorted $MoOS_4$ core from a tetragonal-pyramidal geometry.

The molybdenum center of sulfite oxidase has been considered to be bound to a bidentate dithiolene ligand connecting pterin and phosphate groups.[1,2] Recent EXAFS and ESR results indicate that the molybdenum center has one or more thiolate ligands besides the dithiolene ligand.[3,4] A $(Mo^VO)^{3+}$ complex having an unsymmetrical chelating dithiolato ligand has become of interest because tetrapeptide, Cys–X–Y–Cys (X,Y=amino acid residues), has a possibility to serve as an unsymmetrical dithiolate to activate $(Mo^VO)^{3+}$ ion.[5]

A simple model complex, $[Mo^VO(SPh)_4]^-$,[6] has been studied in detail. Some monooxomolybdenum(V) complexes having symmetrical dithiolate chelates have been reported as the precursor model complexes for the resting species of the active site of molybdoenzyme, e.g. $(Mo^VO(SCH_2CH_2S)_2]^-$,[7] $[Mo^VO(bdt)_2]^-$ (bdt=1,2-benzenedithiolato).[8] Relation between the number of thiolate ligands and the ESR parameter in $(MoOL_{4-x}L'_x)^-$ has been established.[9—11] Monooxomolybdenum(V) complexes have been systematically studied using a tridentate chelating ligand, e.g. hydrotris(3,5-dimethyl-1-pyrazolyl)borate.[12]

Complexation of two dithiolene type ligands and two alkanethiolates to $(MoO)^{3+}$ ion in unsymmetrical dithiolate, α,2-toluenedithiolate, seems to form an appropriate model complex for the active center of sulfite oxidase.

Experimental

All procedures were performed in argon atmosphere by the Schlenk technique. All solvents were dried and distilled under argon gas before use.

$(NEt_4)[Mo^VO(SPh)_4]$ was prepared by the reported method.[6] α,2-Toluenedithiol was synthesized by standard literature methods.[13]

Synthesis of (NEt_4) $[Mo^VO(\alpha\text{-tdt})_2]$ (α-tdt=α,2-toluenedithiolato) (1). The titled complex was synthesized by the following two methods. The crystals for the X-ray analysis were obtained by the method a.

a) From $(NEt_4)[MoO(SPh)_4]$ with Ligand Exchange Method. To a DMF solution (5 ml) of 35.7 mg (0.04 mmol) of $(NEt_4)[Mo^VO(SPh)]$ was added 0.017 ml (0.09 mmol) of α,2-toluenedithiol at room temperature. The solution was stirred overnight at room temperature and concentrated in vacuo to 0.5 ml volume. Addition of 10 ml of diethyl ether gave dark blue powder. The powder was collected with filtration and washed with 5 ml of diethyl ether. Recrystallization from DMF–diethyl ether gave dark blue microcrystals in 70% yield. Found: C, 47.13; H, 5.90; N, 2.75%. Calcd for $C_{22}H_{32}NOS_4Mo$: C, 47.98; H, 5.86; N, 2.54%.

b) From $MoOCl_3(thf)_2$. To an acetonitrile solution (10 ml) of 0.05 ml (0.3 mmol) of α,2-toluenedithiol and 0.09 ml (0.6 mmol) of triethylamine was added dropwise an acetonitrile solution of $MoOCl_3(thf)_2$ (58 mg, 0.16 mmol) at 0 °C. The solution turned dark green and was allowed to stand at room temperature for 5 h, before tetraethylammonium chloride (30 mg, 0.18 mmol) in methanol (6 ml) was added. After filtration the filtrate was concentrated in vacuo to 2 ml. Addition of methanol (30 ml) to the solution gave dark purple powder. The crude product was recrystallized from acetonitrile–methanol. Yield, 53%. Found: C, 47.17; H, 5.71; N, 2.61%. Calcd for $C_{22}H_{32}NOS_4Mo$: C, 47.98; H, 5.86; N, 2.55%.

Physical Measurements. Visible spectra were recorded in a solution of **1** or in a KBr disk on a JASCO Ubest-30 spectrophotometer. Infrared spectrum was taken in 400—200 cm^{-1} region as Nujol mulls and in 1000—400 cm^{-1} region as a KBr disc on a JASCO DS-402G spectrophotometer. Raman spectrum was obtained on a JASCO R-800 spectrophotometer equipped with an HTV-R649 photomultiplier. A powder sample in a capillary was irradiated with a 632.8 nm He–Ne laser excitation line. The frequency calibration of the spectrometer was carried out with indene as a standard. Electrochemical measurements were carried out using a Yanaco P-1100 instrument in acetonitrile solution that contained 0.1 M (1 M=1 mol dm^{-3}) tetrabutylammonium perchlorate as a supporting electrolyte. $E_{1/2}$ value, determined as $(E_{p,a}+E_{p,c})/2$, was referenced to the SCE electrode at room temperature and a value uncorrected with junction potential was obtained. ESR spectra in DMF–acetonitrile (1/4, v/v) were recorded on a JEOL JES-FE1X spectrometer at room temperature and at ca. 80 K.

X-Ray Structure and Determination. Single crystals of **1** grew from acetonitrile–ethanol. The crystal was sealed in a glass capillary under argon atmosphere for the X-ray measure-

Table 1. Crystallographic Data for $(NEt_4)[Mo^VO(\alpha\text{-tdt})_2]$ (**1**)

Chemical formula	$C_{22}H_{32}NOS_4Mo$
Fw	550.706
Cryst system	Monoclinic
a/Å	9.535(2)
b/Å	16.582(9)
c/Å	8.085(2)
β/deg	90.76(4)
V/Å^3	1278.3(8)
Z	2
Space group	$P2_1$
t/°C	20
d_{calcd}/g cm^{-3}	1.431
Radiation	Mo$K\alpha$
$2\theta_{max}$/deg	55.0
Scan type	θ–2θ
No. of reflections	Measured 3032
$I>3\sigma(I)$	Used 2102
R[a]	0.089
R_w[b]	0.100

a) $R=\sum||F_o|-|F_c||/\sum|F_o|$. b) $R_w=[\sum w(|F_o|-|F_c|)^2/\sum w|F_o|^2]^{1/2}$; $w=1/\sigma^2(|F_o|)$.

ment. The space group and approximate cell dimensions of the crystal were determined from oscillation and Weissenberg photographs. X-ray measurement was performed at 20 °C on a Rigaku AFC-4 diffractometer equipped with a Rotaflex rotating anode X-ray generator. The radiation used was Mo$K\alpha$ monochromatized with graphite (0.71069 Å). No absorption correction was made, although Lorentz and polarization corrections were applied. The basic crystallographic parameters for **1** are listed in Table 1. Unit cell dimensions were refined with 25 reflections. Three standard reflections were chosen and monitored with every 100 reflections and did not show any significant change. The positions of Mo, O, and S atoms were determined by the direct method using MULTAN 80. Subsequent Fourier synthesis based on the phases of Mo, O, and S atoms revealed the positions of the remaining non-hydrogen atoms. The final refinement was carried out using full-matrix least-squares techniques with non-hydrogen atoms. The y coordinate of the molybdenum atom was fixed in the refinement. The refinement with anisotropic thermal parameters is converged at R=0.089. Atom scattering factors and dispersion corrections were taken from the International Table.[14] The absolute configurations of the structure were determined from five Bijvoet pairs of reflections with large differences in $|F_o|$.

EHMO Calculations. In order to simplify extended Hückel MO calculations using an NEC PC-98 EHMO program obtained from Kodansha Sci. Co., $[Mo^VO(SCH{=}CH\text{-}CH_2S)_2]^-$ was employed instead of $[Mo^VO(\alpha\text{-tdt})_2]^-$ as a model complex. Two geometries were examined in the above model complex to evaluate the distortion of the Mo^VOS_4 core in $[Mo^VO(\alpha\text{-tdt})_2]$. One is a C_{4v} $MoOS_4$ core using the crystallographical parameters of $[Mo^VO(SPh)_4]^-$ reported in a literature.[6] Another is an idealized C_2 structure in $[Mo^VO(SCH{=}CH\text{-}CH_2S)_2]^-$ although $[Mo^VO(\alpha\text{-tdt})_2]^-$ as determined in this work has an approximate C_2 structure in Fig. 2. Mo–O, Mo–S, S–C, C–C, and C–H bond distances used are 1.680, 2.403, 1.760, 1.540, and 1.070 Å, respectively. A value, 109.9°, was employed for both Mo–S–C–H(CH_2) and Mo–S–C–H(CH=) torsion angles. A torsion angle, 120°, was adopted for S–C(H)=C–H and S–C(H_2)–C–H. The EHMO atomic parameters for Mo(V) were taken from a literature.[15]

Results and Discussion

Crystal Structure. The complex crystallizes in the space group $P2_1$ and the unit cell contains two $[Mo^VO(\alpha\text{-tdt})_2]^-$ anions and two NEt_4^+ cations. An ORTEP view of the $[Mo^VO(\alpha\text{-tdt})_2]^-$ ion is shown in Fig. 1. Only a trans isomer was obtained by the present synthetic method.

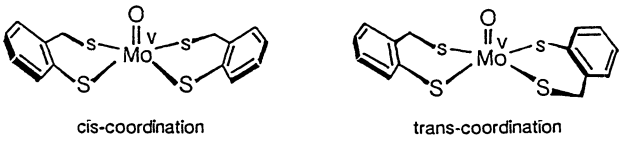

Table 2 lists the atomic coordinates of the non-hydrogen atoms and the estimated standard deviations. Selected bond distances and angles are listed in Table 3.[16] The coordination around the molybdenum atom is a distorted tetragonal-pyramidal geometry with an approximate C_2 symmetry, containing the one terminal oxo, the two alkanethiolato and the two arenethiolato ligands. The Mo=O distance is 1.688(18) Å which is in a range 1.64—1.72 Å observed for various Mo(V)=O

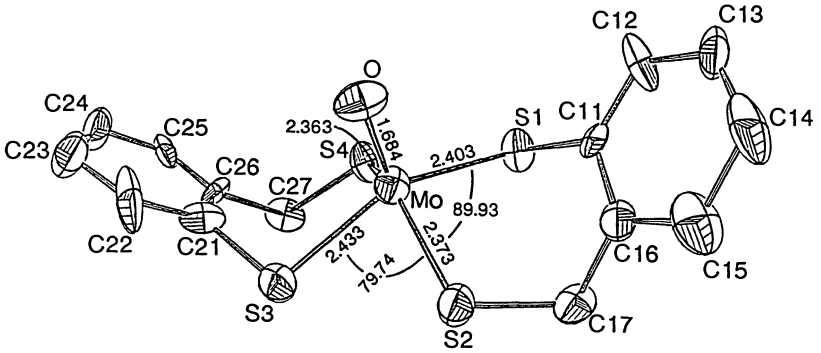

Fig. 1. ORTEP view of $(NEt_4)[Mo^VO(\alpha\text{-tdt})_2]$ (**1**) showing the atom-labeling scheme.

Table 2. Atomic Coordinates and Equivalent Isotropic Thermal Parameters for $(NEt_4)[Mo^VO(\alpha\text{-tdt})_2]$ (1)

Atom	x	y	z	B_{eqv}[a)]/Å^2
Mo	0.8719(2)	0.1620(0)	0.7103(3)	1.80(2)
S1	0.6901(7)	0.0621(4)	0.7326(8)	3.05(10)
S2	0.9214(6)	0.1159(4)	0.4400(8)	3.05(10)
S3	1.1189(7)	0.1969(5)	0.6938(8)	3.24(11)
S4	0.9104(6)	0.1144(5)	0.9830(8)	3.07(10)
O	0.7890(19)	0.2519(10)	0.7107(21)	1.95(32)
C11	0.5888(20)	0.0729(12)	0.5486(27)	2.05(33)
C12	0.4460(21)	0.0946(13)	0.5532(28)	2.96(41)
C13	0.3704(26)	0.0979(18)	0.4115(30)	3.22(49)
C14	0.4273(28)	0.0847(18)	0.2530(38)	4.08(56)
C15	0.5762(27)	0.0599(17)	0.2462(36)	2.91(53)
C16	0.6538(24)	0.0588(16)	0.3916(35)	3.18(45)
C17	0.7994(25)	0.0308(15)	0.3830(33)	3.25(42)
C21	1.1436(25)	0.2586(15)	0.8762(28)	3.33(41)
C22	1.1754(29)	0.3393(18)	0.8617(37)	4.50(56)
C23	1.1996(30)	0.3878(17)	0.9976(43)	3.91(57)
C24	1.1792(26)	0.3509(15)	1.1610(32)	3.38(49)
C25	1.1505(20)	0.2681(14)	1.1683(28)	3.39(35)
C26	1.1315(22)	0.2238(15)	1.0328(34)	3.41(42)
C27	1.0994(24)	0.1349(12)	1.0382(26)	2.85(38)
N	0.3227(19)	−0.1448(12)	0.7822(26)	3.50(36)
C31	0.1896(30)	−0.1555(17)	0.6724(41)	3.31(58)
C32	0.1589(39)	−0.0781(26)	0.5774(56)	3.81(104)
C33	0.3417(30)	−0.2281(15)	0.8744(36)	3.24(56)
C34	0.4664(29)	−0.2300(23)	1.0041(45)	4.20(66)
C35	0.4555(26)	−0.1254(18)	0.6822(34)	3.39(48)
C36	0.4911(41)	−0.1847(24)	0.5470(47)	4.87(96)
C37	0.3047(36)	−0.0772(19)	0.9075(43)	3.61(70)
C38	0.1758(37)	−0.0853(21)	1.0299(38)	4.06(68)

a) B_{eqv} is defined as the equivalent isotropic displacement parameter as $1/3[a^2a^{*2}B_{11}+b^2b^{*2}B_{22}+c^2c^{*2}B_{33}+2ab(\cos\gamma)a^*b^*B_{12}+2ac(\cos\beta)a^*c^*B_{13}+2bc(\cos\alpha)b^*c^*B_{23}]$.

Table 3. Selected Intramolecular Distances and Angles for $(NEt_4)[Mo^VO(\alpha\text{-tdt})_2]$ (1)[17]

	Bond distances	l/Å
Mo–O		1.688(18)
Mo–S(1)		2.406(7)
Mo–S(2)		2.368(7)
Mo–S(3)		2.431(7)
Mo–S(4)		2.366(7)
S(1)–C(11)		1.771(23)
S(2)–C(17)		1.881(27)
S(3)–C(21)		1.811(26)
S(4)–C(27)		1.881(24)
S(1)–S(2)		3.375(9)
S(2)–S(3)		3.075(10)
S(3)–S(4)		3.379(10)
S(4)–S(1)		3.025(9)
	Bond angles	θ/°
S(1)–Mo–O		105.34(64)
S(2)–Mo–O		112.92(64)
S(3)–Mo–O		104.53(64)
S(4)–Mo–O		110.92(64)
S(1)–Mo–S(2)		89.93(23)
S(2)–Mo–S(3)		79.74(23)
S(3)–Mo–S(4)		89.28(23)
S(4)–Mo–S(1)		78.75(23)
S(1)–Mo–S(3)		150.10(24)
S(2)–Mo–S(4)		136.15(23)

complexes. Two types of Mo–S bonds were found; longer ones (2.40(1) Å and 2.43(1) Å) for the molybdenum-arenethiolate and shorter ones (2.37(1) Å and 3.37(1) Å) for the molybdenum-alkanethiolate bonds. This trend is expected from the difference in the bond lengths between $[Mo^VO(SPh)_4]^-$ and $[Mo^VO(SCH_2CH_2S)_2]^-$.[6,7] The larger S pπ-donation of alkanethiolato ligand to $(MoO)^{3+}$ contributes to increase of the Mo–S bond order. Figure 2 shows the schematic drawing of the distortion in **1**. The two alkanethiolate Mo–S bonds give larger O–Mo–S bond angles (mean 112°) and a smaller trans S–Mo–S angle (136.2(3)°) while the two arenethiolate Mo–S bonds provide smaller O–Mo–S bond angles (mean 105°) and a larger trans S–Mo–S (150.1(3)°). The Mo^VOS_4 core

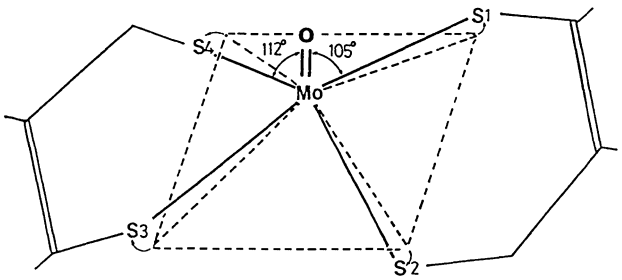

Fig. 2. Schematic drawing of the distortion of $(NEt_4)[Mo^VO(\alpha\text{-tdt})_2]$ (1).

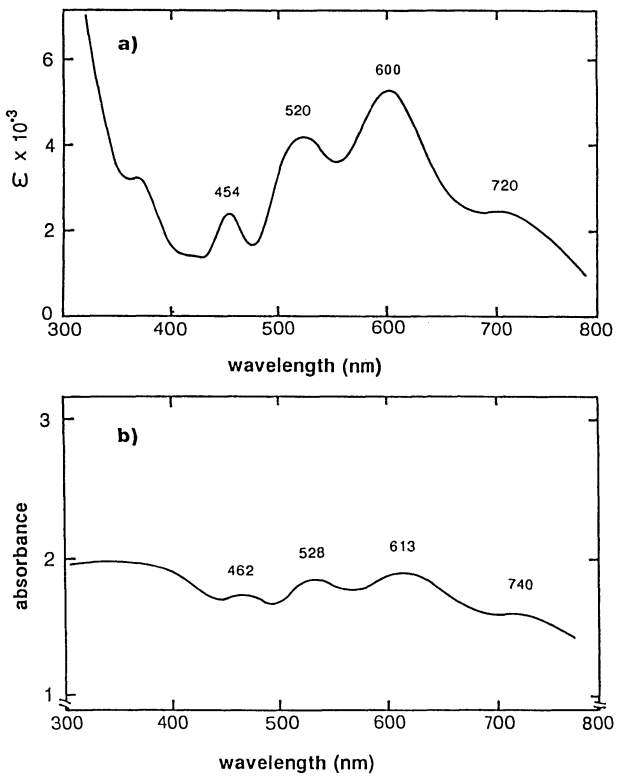

Fig. 3. Visible spectra of $(NEt_4)[Mo^VO(\alpha\text{-tdt})_2]$ (1) a) in acetonitrile solution and b) in the solid state (KBr matrix).

of $[Mo^{V}O(SPh)_4]^-$ was reported to have two O–Mo–S angles, 108.5(3)° and 111.2(3)°. Only one example for similar distortion has been reported for $[Mo^{V}O(SCH_2CH_2CH_2S)_2]^-$ which has two kinds of large trans S–Mo–S angle (149.9(1)° and small trans S–Mo–S angle (138.8(1)°).[17] The presence of two kinds of S–Mo–S bond angles is probably due to the large bite angle ca. 89° of α,2-toluenedithiolate. It is noticeable that the distortion of the $MoOS_4$ core in **1** is the largest among the known ones.

Properties of 1. Figures 3-a and 3-b shows the visible spectra of **1** in solution and in the solid KBr matrix, respectively. Four distinct absorption maxima were observed at 454 nm (ε, 2300 $mol^{-1}cm^{-1}$), 520 nm (4100), 600 nm (5200), and 720 nm (2300) in an acetonitrile solution. Four maxima at 462, 528, 613, and 740 nm were also obtained in the KBr matrix with the same ratio of the absorbance as shown in Fig. 3-b. The spectra of **1** indicate that only the trans isomer exists both in solutions and in the solid state as established by the crystallographic analysis. These intense absorption maxima (ε, 2300—5200 $mol^{-1}cm^{-1}$) could be assigned to ligand-to-metal charge-transfer (LMCT) bands. Actually, the broad absorption maxima due to LMCT in the visible region of approximate C_{4v} Mo(V)=O complexes, e.g. 602 nm (6400 $mol^{-1}cm^{-1}$ in acetonitrile) for $(NEt_4)[Mo^{V}O(SPh)_4]$, have been extensively studied by Ellis et al.[18] They have pointed out that the low energy d-d transition due to Mo(V)=O group is masked by the dominant LMCT bands. For example, only a weak absorption maximum has been reported at 670 nm with 20 $mol^{-1}cm^{-1}$ in this region for $[Mo^{V}OCl_4]^-$ in CH_2Cl_2.[19]

EHMO calculations were carried out to interpret the difference between the ideal square-pyramidal structure (four trans S–Mo–S angles are 140°) and the distorted structure (two trans S–Mo–S angles are 136° and 150°) in $[Mo^{V}O(SCH_2CH{=}CHS)_2]^-$. The distorted structure corresponds to that of **1** analyzed cystallographically. No significant difference was found in the energy levels of d-orbitals between them. This result suggests that the four distinct absorption maxima are ascribed not to d-d transition but to the ligand-to-metal charge transfer from two or more sulfur pπ orbitals to Mo(V) d_{xy} orbital as induced by the lower symmetry of α,2-toluenedithiolate. Figure 4 shows the IR and Raman spectra of **1** in solid state. The Raman and IR spectra in solid state showed a strong ν(Mo=O) mode at 940 and 938 cm^{-1}, respectively. An IR Mo=O band has been reported to appear in the same region at 929 cm^{-1} for $(NEt_4)[Mo^{V}O(SPh)_4]$.[6] The higher-wavenumber shift is ascribed to the less π-donor ability of arenethiolate ligand than alkanethiolate liagnd. Actually, the higher-wavenumber shift has been established in the case of the larger π-donor ability of the thiolate ligands in $[MoO(SR)_4]^-$ (SR=SPh, S-4-$CH_3C_6H_4$, S-4-ClC_6H_4, S-3-ClC_6H_4, S-4-FC_6H_4, S-2,6-$Cl_2C_6H_3$, and SC_6F_5).[18] Intense Raman bands at 444 and 352 cm^{-1} are tentatively assigned to ν(Mo–S). Strong IR bands observed at 385, 361, 344, and 302 cm^{-1} are associated with IR active ν(Mo–S) frequencies. The results reflect decrease in symmetry of **1**.

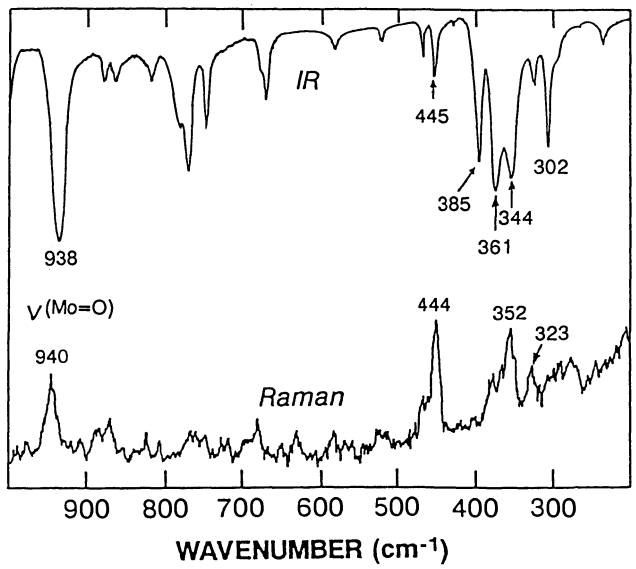

Fig. 4. IR and Raman spectra of $(NEt_4)[Mo^{V}O(\alpha\text{-}tdt)_2]$ (**1**) in solid state.

The electrochemical property of **1** was studied using cyclic voltammetry of a solution in 0.1 M $(n\text{-}Bu)_4NCl$–DMF. A reversible couple was observed at −0.73 V vs. SCE that corresponds to a one-electron reduction of the complex. An irreversible oxidation peak was given at +0.65 V due to the Mo(V)/Mo(VI) couple. The Mo(V)/Mo(IV) redox potential of **1** in DMF is expected to be higher compared with that of $(NEt_4)[Mo^{V}O(SPh)_4]$ (−0.75 V in acetonitrile) because of the larger electron donation from alkanethiolato to $(Mo^{V}O)$ ion than that of arenethiolato. The redox potential is found to become more positive by the electron-withdrawing character of the thiolate ligands as has been pointed for *p*-substituted benzenethiolate molybdenum(V) complexes by Ellis et al.[18] Therefore, **1** would be expected to exhibit a more negative redox potential due to the presence of two alkanethiolate ligands, but it shows a more positive one (−0.73 V vs. SCE in acetonitrile) than that (−0.77 V in acetonitrile) of $[Mo^{V}O(SPh)_4]^-$.[6] We examined the difference in SOMO orbital energies between the regular square-pyramidal and the distorted structures for the simple model complex, $[Mo^{V}O(SCH_2CH{=}CHS)_2]^-$, using EHMO calculations. The SOMO orbital energies for the regular structure and the distorted structure are −10.315 and −10.323 eV, respectively. The results can be explained by the ease of reduction of the distorted **1**. It is likely that this distortion induces the variation of O=Mo–S–C torsion angle accompanied with the change of π-interaction in Mo–S bond.

A DMF–CH_3CN solution (1 : 4) of **1** exhibited an axial ESR signals at room temperature and at ca. 80 K

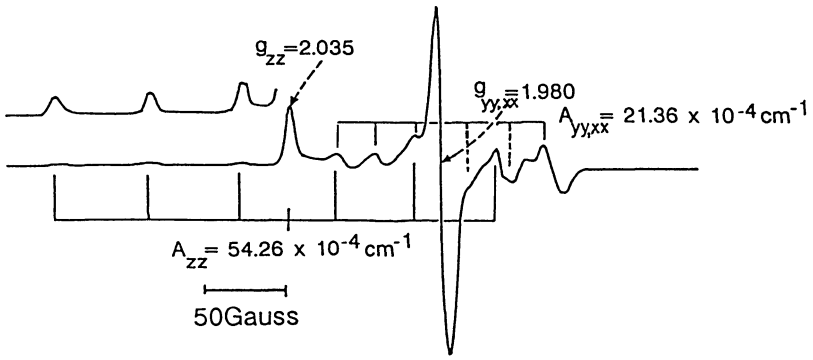

Fig. 5. ESR spectra of $(NEt_4)[Mo^VO(\alpha\text{-tdt})_2]$ (**1**) in DMF–acetonitrile freezing solution at ca. 80 K.

Table 4. ESR Parameters of $(NEt_4)[Mo^VO(\alpha\text{-tdt})_2]$ (**1**) and Various Related Mo(V) Thiolate Complexes

Complex	g_{zz}	g_{yy}	g_{xx}	A_{zz}	A_{yy}	A_{xx}	Ref
				$\times 10^4$ cm^{-1}			
$[MoO(SCH_2CH_2S)_2]^-$	2.012	1.997	1.975				11
$[MoO(bdt)_2]^-$	2.022	1.984	1.976	47.2			12
$[MoO(\alpha\text{-tdt})_2]^-$	2.035	1.980		54.3	21.3		This work
$[MoO(SPh)_4]^-$	2.017	1.979		52.3	22.3		10

Table 5. Influence of the $MoOS_4$ Core Distortion on Molybdenum(V) Ion MO Coefficients of the SOMO in $[Mo^VO(SCH_2CH{=}CHS)_2]^-$

Geometry	MO coefficients of SOMO in Mo(V) ion								
	s	p_x	p_y	p_z	$d_{x^2-y^2}$	d_{z^2}	d_{xy}	d_{xz}	d_{yz}
Regular $MoOS_4$ all O–Mo–S 110°	0.005	0.00	0.00	−0.023	−0.034	0.044	−0.937	0.00	0.00
Distorted $MoOS_4$ O–Mo–S1, O–Mo–S3=113° O–Mo–S2, O–Mo–S4=105°	0.004	0.00	0.00	−0.022	−0.049	0.044	−0.933	0.00	0.00

as shown in Fig. 5. The low-temperature ESR measurement for **1** provided g_{zz}=2.035 at ca. 80 K which is a relatively large value in the synthetic molybdenum(V) thiolate complexes. The ESR parameters are compared with those of various molybdenum(V) thiolate complexes in Table 4. The axial signals for **1** are obtained even in the distortion from a tetragonal-pyramidal to an approximate C_2 structure as revealed by the crystallographic analysis. In the various cases of monooxomolybdenum(V) complexes, g tensor has been determined to coincide with Mo=O direction, e.g. $[Mo^VOCl_4]^-$.[19] The large g_{zz} value should reflect the ligand field equatorial to the Mo=O bond axis because of spin-orbit coupling between Mo and sulfur. Furthermore, the low-energy charge-transfer transition also contributes to the observed g_{zz} value shift in addition to the above ligand field because the SOMO of Mo(V) calculated by the EHMO method shows the contribution from S $p\pi$-orbitals as described later. Therefore, the reported small value of g_{zz} for $[Mo^VO(SCH_2CH_2S)_2]^-$ is in conflict with the tendency of large electron-donating character of the alkanethiolato ligand.

Table 5 lists the MO coefficients of the SOMO in the simple model complex, $[Mo^VO(SCH_2CH{=}CHS)_2]^-$ for **1** to evaluate the influence of the distortion to the ESR signals of **1**. The EHMO calculations were carried out in two geometries which are regular and distorted. The difference between the SOMO electron densities for the two geometries by mixing p_z and d_{z^2} orbitals in the z direction is not so large that the distortion of the $MoOS_4$ core does not influence the MO electron density in SOMO contributing to the shift of the g_{zz} value. The results are coincident with a small change reported in the ESR signals between $[Mo^VOCl_4]^-$ and $[Mo^VOCl_5]^{2-}$.[19] Further study will be required to examine this trend on the ESR parameters.

We thank Professor Mikiharu Kamachi for the ESR measurement. We gratefully acknowledge partial support of this research by a Grant-in-Aid for Scientific Research on Priority Areas of "Macromolecular Com-

plexes" No63612093 from the Ministry of Education, Science and Culture.

References

1) R. C. Wahl and K. V. Rajagopalan, *J. Biol. Chem.*, **257**, 1354 (1982).
2) J. L. Johnson and K. V. Rajagopalan, *Proc. Natl. Acad. Sci. U.S.A.*, **79**, 6856 (1982).
3) S. P. Cramer, R. Wahl, and K. V. Rajagopalan, *J. Am. Chem. Soc.*, **103**, 7721 (1981).
4) R. C. Bray, *Adv. Enzymol. Relat. Areas Mol. Biol.*, **51**, 107 (1980).
5) N. Ueyama, N. Yoshinaga, A. Kajiwara, and A. Nakamura, *Chem. Lett.*, **1990**, 1781.
6) a) G. R. Hanson, A. A. Brunette, A. C. McDonell, K. S. Murray, and A. G. Wedd, *J. Am. Chem. Soc.*, **103**, 1953 (1981). b) I. W. Boyd, I. G. Dance, K. S. Murry, and A. G. Wedd, *Aust. J. Chem.*, **31**, 279 (1978).
7) S. R. Ellis, D. Collison, C. D. Garner, and W. Clegg, *J. Chem. Soc., Chem. Commun.*, **1986**, 1483.
8) S. Boyde, S. R. Ellis, C. D. Garner, and W. Clegg, *J. Chem. Soc., Chem. Commun.*, **1986**, 1541.
9) R. C. Bray, "Enzymes," 3rd ed, 1975, Vol. 12, p. 299.
10) J. T. Spence, M. Minelli, P. Kroneck, M. I. Scullane, and N. D. Chasteen, *J. Am. Chem. Soc.*, **100**, 8002 (1978).
11) M. I. Scullane, R. D. Tylor, M. Minelli, J. T. Spence, K. Yamanouchi, J. H. Enemark, and N. D. Chasteen, *Inorg. Chem.*, **18**, 3213 (1979).
12) C. G. Young, J. H. Enemark, D. Collison, and F. E. Mabbs, *Inorg. Chem.*, **26**, 2925 (1987).
13) a) E. Klingsberg and A. M. Schreiber, *J. Am. Chem. Soc.*, **84**, 2941 (1962). b) A. G. Hortmann, A. J. Aron, and A. K. Bhattacharya, *J. Org. Chem.*, **43**, 3374 (1978).
14) "International Tables for a X-Ray Crystallography," Kynoch, Birmingham, England (1974), Vol. IV, p. 99.
15) M. Kamata, K. Hirotsu, T. Higuchi, K. Tatsumi, R. Hoffmann, T. Yoshida, and S. Otsuka, *J. Am. Chem. Soc.*, **103**, 5772 (1981).
16) The table of anisotropic parameters of non-hydrogen atoms, the F_o-F_c table and the tables of bond distances and angles are deposited as Document No. 8953 at the Office of the Editor of Bull. Chem. Soc. Jpn.
17) P. T. Bishop, J. R. Dilworth, J. Hutchinson, and J. A. Zubieta, *J. Chem. Soc., Chem. Commun.*, **1982**, 1052.
18) S. R. Ellis, D. Collison, and C. D. Garner, *J. Chem. Soc., Dalton Trans.*, **1989**, 413.
19) C. D. Garner, L. H. Hill, F. E. Mabbs, D. L. McFadden, and A. T. McPhail, *J. Chem. Soc., Dalton Trans.*, **1977**, 853.

Synthesis, Crystal Structure, and Property of Novel Tetranuclear Nickel(II) Complex with Multidentate Ligand 7-[(3,5-Dichloro-2-pyridyl)azo]-8-hydroxyquinoline-5-sulfonic Acid

Hu HUANG, Fumiaki KAI,* Yoshifumi ASAI,† Masaaki HIROHATA,† and Masaaki NAKAMURA†
Department of Environmental Science, Graduate School of Natural Science and Technology, Kumamoto University, Kumamoto 860
†Department of Chemistry, Faculty of Science, Kumamoto University, Kumamoto 860
(Received January 14, 1991)

Reaction of nickel(II) perchlorate with the title ligand (Hpahqs) in aqueous solution followed by standing for about six months produces a complex having the formulation $[Ni_4(pahqs)_4(H_2O)_4]\cdot 20H_2O$. A single crystal X-ray analysis revealed that the complex contained the four nickel(II) and four ligand molecules and showed a novel structure of oxygen bridged tetranuclear nickel(II) complex. Crystal data: triclinic, space group $P\bar{1}$, a=17.884(7), b=22.071(8), c=12.819(8) Å, α=100.77(4)°, β=92.55(4)°, γ=71.46(4)°, Z=2. Except one N atom in each azo-group, all the other donor atoms in the ligand were fully used in coordination to nickel(II), forming either *N,N,O*- or *N,O*-chelate rings, simultaneously. The geometry around each of the four nickel(II) was distorted octahedron. The bond lengths of Ni–N(N atoms in *N,N,O*-terdentate moieties) were elongated compared with those of the corresponding complex, and the lengths of Ni–N(N atoms in quinoline rings) were kept almost similar values to those of the Ni(II)-8-hydroxyquinoline complex. The bond lengths of Ni–O were elongated compared with those of the nickel(II) complexes with either *N,N,O*- or *N,O*-chelate rings, resulting in the contraction of the angles of N–Ni–N or N–Ni–O. The angles of Ni–O–Ni around four nickel(II) sites were ca. 140°. The antiferromagnetic exchange interaction was operating between the four nickel(II) via bridging oxygen atoms.

The multidentate ligands of ortho-hydroxyazo system containing more than two groups of potentially chelating donor atoms have become of interest in connection with the coordination selectivity for a variety of metal ions.[1] Previously, we prepared the new multidentate ligands, 7-[(3,5-dihalo-2-pyridyl)azo]-8-hydroxyquinoline-5-sulfonic acid (abbr. as Hpahqs), and investigated their coordination behavior toward metal(II) ions in aqueous solution. As a result, Ni(II), Zn(II), and Cd(II) ions, which are classified as soft or medium acids, coordinated selectively to the *N,N,O*-terdentate moiety containing azo-group to form the 1:2 (metal:pahqs) complexes having four five-membered fused chelate rings.[2] On the contrary, VO(IV) (hard acid) bonded selectively to the only *N,O*-skeleton in hydroxyquinoline(HQ) moiety.[3]

The metal complexes of azo system ligands are difficult to isolate as a single crystal. There are only several studies for syntheses and analyses of single crystals of metal(II) complexes with ortho-hydroxyazo ligands, and, in addition, all these complexes have simple mononuclear or dinuclear structures.[4] In the present work,[5] a single crystal of Ni(II) complex with the title ligand having the peculiar composition of Ni(II):pahqs=4:4 was isolated and its structure has been characterized by X-ray crystallography. The most striking aspect of the present results was that, in this complex, except one N atom in each azo-group, all the other donor atoms in pahqs were fully used in coordination to Ni(II), and the four Ni(II) were bridged by O atoms in the HQ moieties, showing a first novel structure of tetranuclear Ni(II) complex. The difference in composition of metal to ligand of the species in solution[2] and of the present solid complex can not be explained so clear at this stage. Furthermore, it was found that an antiferromagnetic interaction was operating between the four Ni(II) via bridging oxygen atoms. These results suggest that this multidentate ligand will be expected to form various tetranuclear metal complexes via bridging oxygen atoms with other metal ions, which will be interested in structural and magnetic chemistry.[6,7]

Table 1. Crystal Data, Experimental Conditions, and Refinement Details

Chemical formula	$C_{56}H_{24}N_{16}O_{16}Cl_8S_4Ni_4\cdot 24H_2O$
Formula weight	2255.98
Crystal system	Triclinic
Space group	$P\bar{1}$
a/Å	17.884(7)
b/Å	22.071(8)
c/Å	12.819(8)
α/deg	100.77(4)
β/deg	92.55(4)
γ/deg	71.46(4)
V/Å^3	4712(4)
Z	2
D_c/g cm^{-3}	1.589
D_m/g cm^{-3}	1.587
μ(Cu $K\alpha$)/mm^{-1}	4.638
Crystal size/mm^3	0.33×0.24×0.16
Scan mode	ω–2θ
Scan range/deg	$0\leqq\theta\leqq 50$
Number of reflections measured	10224
Number of unique reflections with $[\lvert F_o\rvert \geqq 2.3\sigma(\lvert F_o\rvert)]$	8224
Number of variables	1190
Maximum residual electron density/eÅ^{-3}	0.91
R	0.105
R_w	0.145

Experimental

Synthesis of Ligand. The ligand was prepared by the method described in our previous paper.[2)]

Preparation of Crystal of $[Ni_4(pahqs)_4(H_2O)_4]\cdot 20H_2O$. To a solution of the ligand (0.205 g, 0.44 mmol) in 250 cm^3 of water was added $Ni(ClO_4)_2\cdot 6H_2O$ (0.195 g, 0.53 mmol) under stirring. The pH of the solution was adjusted to 2.81 by adding a perchloric acid (60%). The solution was stirred

Table 2. Atomic Coordinates($\times 10^4$) and Equivalent Isotropic Temperature Factors with esd Values in Parentheses

Atom	x	y	z	B_{eq}/Å$^{2a)}$	Atom	x	y	z	B_{eq}/Å$^{2a)}$
Ni(1)	663(1)	2577(1)	−2488(2)	4.51(6)			Ligand C		
Ni(2)	2202(1)	2848(1)	−206(1)	4.12(5)	C(2C)	1409(7)	4261(6)	−505(10)	3.42(39)
Ni(3)	2475(1)	1037(1)	248(1)	4.11(5)	C(3C)	1360(7)	4789(5)	−950(11)	3.67(40)
Ni(4)	1750(1)	689(1)	−2688(1)	4.24(5)	C(4C)	1923(8)	4764(6)	−1681(12)	4.30(45)
		Ligand A			C(5C)	2515(7)	4187(6)	−1932(11)	3.68(42)
C(2A)	−609(7)	3970(6)	−2251(10)	3.74(40)	C(6C)	2582(6)	3659(5)	−1453(9)	2.52(34)
C(3A)	−873(7)	4592(6)	−2422(11)	3.81(39)	C(9C)	3630(6)	2046(5)	−1298(9)	2.56(34)
C(4A)	−416(9)	4820(7)	−2965(12)	4.80(48)	C(10C)	4405(6)	1846(5)	−1752(10)	2.80(35)
C(5A)	307(8)	4422(6)	−3286(10)	3.69(41)	C(11C)	4874(6)	1229(6)	−1775(9)	2.82(36)
C(6A)	600(7)	3787(6)	−3060(10)	3.25(38)	C(12C)	4592(6)	746(5)	−1432(9)	2.41(34)
C(9A)	2176(6)	2326(5)	−3429(9)	2.42(34)	C(13C)	5019(7)	80(6)	−1546(10)	3.46(40)
C(10A)	2832(7)	2367(6)	−4003(10)	3.46(40)	C(14C)	4660(8)	−327(6)	−1222(12)	4.34(45)
C(11A)	3481(6)	1837(6)	−4242(10)	2.94(37)	C(15C)	3898(7)	−71(5)	−766(10)	2.96(36)
C(12A)	3538(6)	1219(6)	−3968(9)	2.57(35)	C(17C)	3845(6)	967(5)	−947(9)	2.33(33)
C(13A)	4204(7)	662(6)	−4135(10)	3.31(38)	C(18C)	3355(6)	1631(5)	−811(9)	2.40(33)
C(14A)	4166(7)	98(6)	−3885(10)	3.66(41)	N(1C)	2006(5)	3715(4)	−731(7)	2.56(28)
C(15A)	3462(7)	91(6)	−3392(10)	3.20(38)	N(7C)	3195(5)	3082(4)	−1674(7)	2.83(30)
C(17A)	2876(7)	1181(5)	−3447(9)	2.70(35)	N(8C)	3086(5)	2651(4)	−1230(7)	2.27(27)
C(18A)	2180(6)	1731(5)	−3199(10)	2.94(36)	N(16C)	3515(5)	556(4)	−607(7)	2.40(27)
N(1A)	132(6)	3568(5)	−2543(8)	3.30(32)	O(22C)	5999(5)	1586(4)	−2366(8)	4.47(31)
N(7A)	1369(6)	3377(4)	−3388(8)	3.03(30)	O(23C)	5984(5)	488(4)	−3125(8)	5.07(32)
N(8A)	1489(5)	2806(4)	−3193(7)	2.37(27)	O(24C)	6304(5)	750(5)	−1311(9)	5.33(35)
N(16A)	2850(5)	615(4)	−3212(7)	2.49(28)	O(25C)	2684(4)	1836(3)	−286(6)	2.73(23)
O(22A)	3988(6)	2544(5)	−5227(9)	6.14(38)	S(21C)	5881(2)	989(2)	−2201(3)	3.72(10)
O(23A)	4944(6)	1752(6)	−4420(9)	6.56(43)	Cl(19C)	581(2)	5494(2)	−606(4)	5.94(13)
O(24A)	4302(5)	1404(5)	−5963(7)	4.92(33)	Cl(20C)	3224(2)	4098(2)	−2881(4)	5.99(14)
O(25A)	1572(4)	1665(3)	−2764(5)	2.36(22)			Ligand D		
S(21A)	4246(2)	1897(2)	−5021(3)	3.85(11)	C(2D)	1612(9)	363(7)	−5119(10)	4.14(45)
Cl(19A)	−1819(2)	5059(2)	−2017(4)	6.45(14)	C(3D)	1152(9)	342(7)	−6033(10)	4.34(47)
Cl(20A)	911(2)	4693(2)	−4000(3)	5.70(13)	C(4D)	328(8)	552(6)	−5991(11)	4.13(46)
		Ligand B			C(5D)	2(7)	742(6)	−4986(11)	3.42(40)
C(2B)	3574(8)	3175(6)	1104(12)	4.14(45)	C(6D)	461(7)	708(5)	−4101(10)	2.89(36)
C(3B)	3873(7)	3400(7)	2091(13)	4.82(48)	C(9D)	418(6)	937(5)	−1327(9)	2.37(33)
C(4B)	3463(8)	3554(7)	3015(12)	4.97(49)	C(10D)	−313(7)	907(6)	−961(9)	2.99(37)
C(5B)	2724(8)	3475(7)	2955(11)	4.32(45)	C(11D)	−438(7)	1047(5)	99(11)	3.23(38)
C(6B)	2438(8)	3254(6)	1992(10)	3.74(41)	C(12D)	103(7)	1264(5)	868(10)	3.01(37)
C(9B)	717(7)	3026(5)	803(9)	2.68(35)	C(13D)	−60(7)	1501(5)	1942(10)	3.28(38)
C(10B)	120(7)	3147(6)	1582(10)	3.23(38)	C(14D)	508(8)	1710(6)	2538(10)	3.69(41)
C(11B)	−600(7)	3080(6)	1270(11)	3.53(40)	C(15D)	1251(8)	1653(6)	2059(10)	3.39(39)
C(12B)	−719(7)	2824(6)	208(11)	3.24(38)	C(17D)	835(6)	1237(5)	434(10)	2.59(34)
C(13B)	−1424(7)	2688(7)	−162(12)	4.23(46)	C(18D)	1021(6)	1034(5)	−672(9)	2.31(32)
C(14B)	−1473(8)	2459(7)	−1217(13)	4.75(50)	N(1D)	1257(6)	537(5)	−4194(7)	3.07(31)
C(15B)	−873(7)	2372(6)	−1935(12)	3.93(44)	N(7D)	108(5)	830(5)	−3094(8)	2.92(30)
C(17B)	−145(6)	2723(5)	−571(10)	2.75(35)	N(8D)	608(5)	846(4)	−2368(8)	2.54(28)
C(18B)	605(7)	2827(5)	−264(11)	3.34(39)	N(16D)	1388(5)	1424(4)	1057(7)	2.72(29)
N(1B)	2851(5)	3119(4)	1101(8)	2.77(29)	O(22D)	−1847(5)	1551(5)	935(10)	5.98(37)
N(7B)	1655(6)	3221(5)	1970(8)	3.56(33)	O(23D)	−1018(7)	588(6)	1477(11)	7.55(47)
N(8B)	1469(5)	3059(4)	998(8)	2.71(28)	O(24D)	−1527(8)	531(8)	−248(10)	10.71(65)
N(16B)	−213(5)	2500(4)	−1620(8)	2.97(30)	O(25D)	1722(4)	950(3)	−1019(6)	2.45(22)
O(22B)	−1592(7)	2782(5)	2325(10)	7.27(44)	S(21D)	−1299(2)	930(2)	591(3)	4.37(11)
O(23B)	−1955(6)	3843(5)	1937(11)	7.66(45)	Cl(19D)	1626(3)	54(2)	−7253(3)	6.26(15)
O(24B)	−1003(8)	3585(8)	3215(10)	9.96(62)	Cl(20D)	−1016(2)	1015(2)	−4850(3)	5.25(12)
O(25B)	1130(4)	2738(3)	−992(6)	2.60(22)			Oxygen atom in coordinated water		
S(21B)	−1344(2)	3336(2)	2280(3)	4.79(12)	OW(1)	187(6)	2310(5)	−3946(8)	5.29(34)
Cl(19B)	4801(3)	3488(3)	2058(4)	7.43(17)	OW(2)	2476(4)	180(4)	656(7)	3.36(25)
Cl(20B)	2168(3)	3652(3)	4105(3)	7.27(17)	OW(3)	3069(5)	1239(4)	1579(7)	4.16(30)
					OW(4)	2058(5)	−262(4)	−2522(7)	3.83(27)

a) $B_{eq}=(4/3)\sum_i\sum_j\beta_{ij}(\boldsymbol{a}_i\cdot\boldsymbol{a}_j)$, where β_{ij} is the anisotropic temperature factor, and $\boldsymbol{a}_i$ and $\boldsymbol{a}_j$ are lattice parameters.

for ca. 12 h and then allowed to stand for about six months. The violet prismatic crystals (65.4 mg, yield: 28%) were obtained. Found: C, 30.04; H, 2.81; N, 10.00%. Calcd for $C_{56}H_{24}N_{16}O_{16}Cl_8S_4Ni_4 \cdot 24H_2O$: C, 29.82; H, 2.86; N, 9.93%. Thermogravimetric analysis of the complex indicates a weight loss of 18.98% in the region 292—480 K (heating rate 3 K min^{-1}). This is in good agreement with the calculated weight loss (19.17%) for twenty-four water molecules from the complex. All the other chemicals used were of an analytical or equivalent grade and were used as received.

Physical Measurements. Infrared spectra of KBr pellets were recorded on a JASCO-A102 spectrometer. Polarograms were recorded on a Yanaco Polarographic Analyzer P-1100 in an aqueous solution. A three-electrode system comprising a dropping mercury working electrode (DME), a Pt-wire auxiliary electrode, and a saturated calomel reference electrode (SCE) was used for measurements. TG-DTA analyses were performed using Rigakudenki PTC-10A Differential Thermogravimetric Analyzer. Magnetic susceptibilities (χ_A) were measured by the Faraday method in the temperature range from 80 to 300 K. The apparatus was calibrated by the use of $[Ni(en)_3]S_2O_3$.[8] All the susceptibilities were corrected for a diamagnetism of the constituting atoms by the use of Pascal's constants.[9] The effective magnetic moments were calculated by the equation, $\mu_{eff}=2.828[(\chi_A-N_\alpha)T]^{1/2}$. In which, the temperature-independent paramagnetic contribution (N_α) was taken as 230×10^{-6}emu mol^{-1} (1 emu=$4\pi\times10^{-6}$ m^3).

Crystallographic Data Collection and Refinement of the Structure. Three dimensional X-ray diffraction data were collected on an Enraf–Nonius CAD4F-11 diffractometer with graphite monochromated Cu-$K\alpha$ radiation using an ω–2θ scan mode. The data reduction was carried out using the Enraf–Nonius structure determining package.[10] The structure was solved by direction method using MALTAN11/82 program.[11] The positional and thermal parameters of all non-hydrogen atoms were determined and refined by successive block-diagonal least-squares method using BDLS program (UNICS III).[12] The atomic scattering factors for all atoms and the anomalous dispersion corrections for non-hydrogen atoms were taken from Ref. 13. Comparatively large R value (ca. 10%) may be due to the disordered waters of crystallization in the crystal.

Details of the crystal data, intensity measurements, and refinements are given in Table 1, final atomic fractional coordinates in Table 2, and selected bond distances and angles in Table 3, respectively.

Tables of structure factors, anisotropic thermal parameters, mean square displacement tensor of atoms, coordinates of atoms, and complete bond lengths and angles are deposited as Document No. 8954 at the Office of the Editor of Bull. Chem. Soc. Jpn.

Results and Discussion

The structure consists of discrete $[Ni_4(pahqs)_4(H_2O)_4]$ molecule. The position of twenty water molecules of crystallization could not be definitely determined. The molecular and chemical structures of the complex are given in Figs. 1 and 2, respectively. The four ligands were differentiated as A, B, C, and D. The atom-numberings for the ligands and nickel(II) sites are shown in Fig. 2. The O atoms in the coordinated water molecules are represented by OW(i) (i=1—4).

Coordination Geometry around Nickel Atoms. Figure 3 shows the coordination environments of the four

Table 3. Selected Bond Distances (Å) and Angles (°) with esd Values in Parentheses

	Distance of Ni–X		
Ni(1)–N(1A)	2.103(10)	Ni(1)–N(8A)	2.004(11)
Ni(1)–N(16B)	2.030(11)	Ni(1)–OW(1)	2.081(10)
Ni(1)–O(25A)	2.127(7)	Ni(1)–O(25B)	2.188(8)
Ni(2)–N(1B)	2.099(10)	Ni(2)–N(8B)	1.960(10)
Ni(2)–N(1C)	2.067(10)	Ni(2)–N(8C)	1.986(9)
Ni(2)–O(25B)	2.188(8)	Ni(2)–O(25C)	2.107(7)
Ni(3)–N(16C)	2.067(8)	Ni(3)–N(16D)	2.093(9)
Ni(3)–OW(2)	2.054(9)	Ni(3)–OW(3)	2.023(9)
Ni(3)–O(25C)	2.147(9)	Ni(3)–O(25D)	2.083(7)
Ni(4)–N(1D)	2.101(10)	Ni(4)–N(8D)	2.008(9)
Ni(4)–N(16A)	2.054(10)	Ni(4)–OW(4)	2.042(9)
Ni(4)–O(25D)	2.107(8)	Ni(4)–O(25A)	2.096(8)
	Distance of Ni–Ni		
Ni(1)···Ni(2)	4.021(3)	Ni(2)···Ni(3)	4.020(3)
Ni(3)···Ni(4)	3.943(3)	Ni(4)···Ni(1)	3.963(3)
	Angle of X–Ni–Y		
O(25A)–Ni(1)–N(8A)	79.2(3)	N(8A)–Ni(1)–N(1A)	76.5(4)
N(16B)–Ni(1)–O(25B)	81.5(4)	O(25B)–Ni(2)–N(8B)	78.0(4)
N(8B)–Ni(2)–N(1B)	76.4(4)	N(1C)–Ni(2)–N(8C)	76.7(4)
N(8C)–Ni(2)–O(25C)	80.0(4)	O(25C)–Ni(3)–N(16C)	79.8(3)
N(16D)–Ni(3)–O(25D)	80.2(3)	O(25D)–Ni(4)–N(8D)	78.9(3)
N(8D)–Ni(4)–N(1D)	76.2(4)	N(16A)–Ni(4)–O(25A)	80.4(3)
	Angle of O–Ni–O		
O(25A)–Ni(1)–O(25B)	87.0(3)	O(25B)–Ni(2)–O(25C)	91.3(3)
O(25C)–Ni(3)–O(25D)	90.1(3)	O(25D)–Ni(4)–O(25A)	88.2(3)
	Angle of Ni–O–Ni		
Ni(1)–O(25B)–Ni(2)	141.5(4)	Ni(2)–O(25C)–Ni(3)	141.8(4)
Ni(3)–O(25D)–Ni(4)	140.5(5)	Ni(4)–O(25A)–Ni(1)	139.6(4)

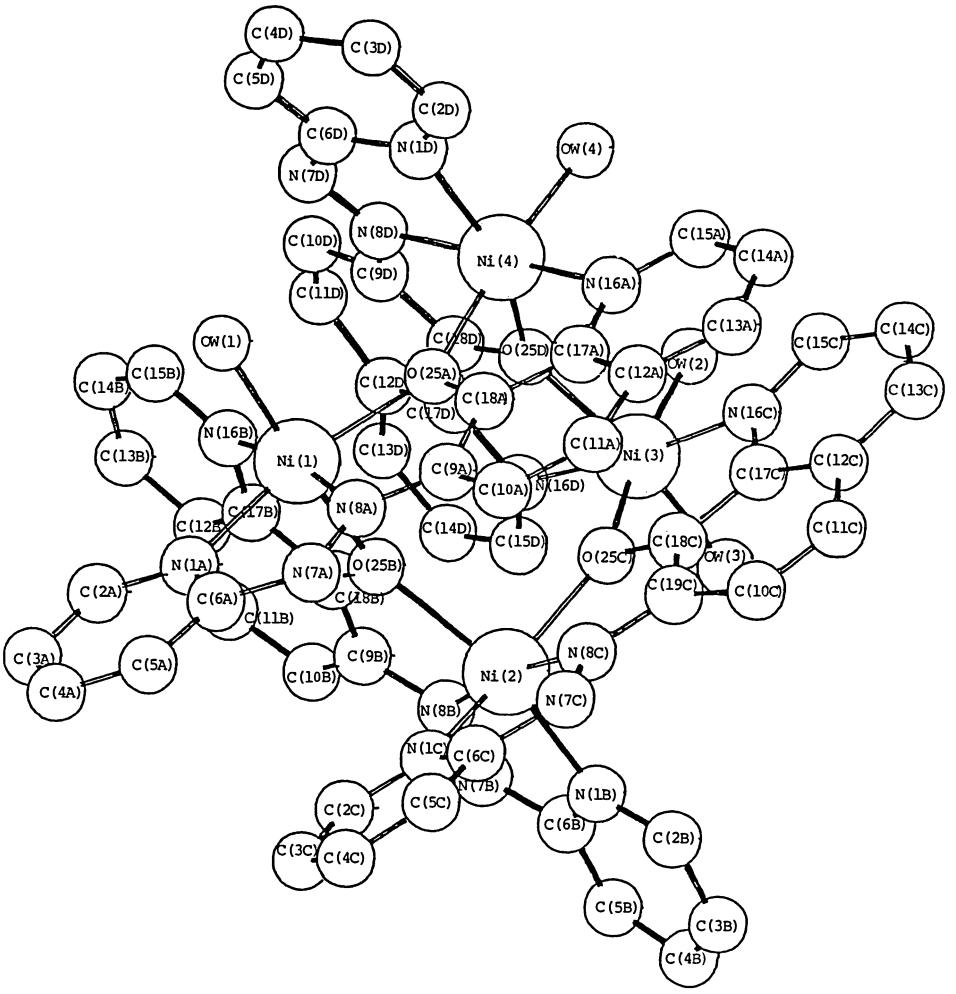

Fig. 1. Perspective view and atomic numbering for the complex. Substituent groups in aromatic rings are omitted for simplicity.

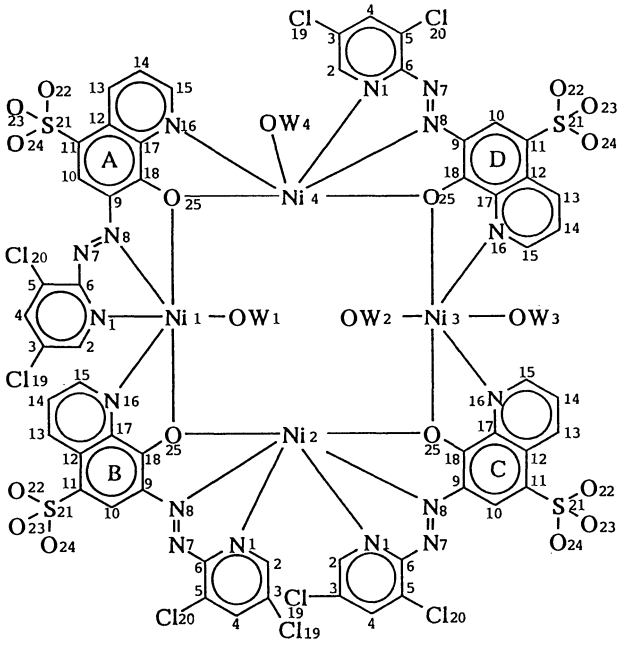

Fig. 2. Chemical structure of Ni(II) complex with pahqs. OW denotes coordinated water molecules.

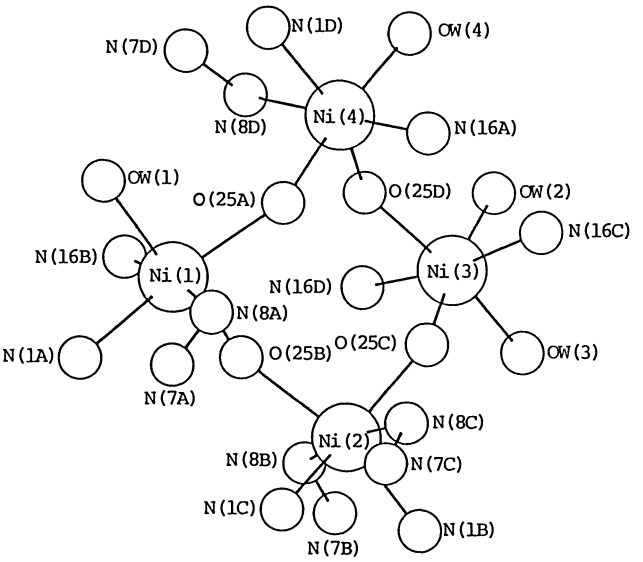

Fig. 3. Coordination environments of four Ni(II) sites.

nickel(II) sites. Each of the ligands bonded to two nickel(II) by N atom in the pyridine ring, N atom in the azo-group adjacent to the HQ moiety, O atoms of the hydroxyquinolinate and N atom in the quinoline ring to form three five-membered chelate rings (two *N,N,O*- and one *N,O*-chelate rings), where all the nickel(II) were bridged by O atom of the hydroxyquinolinate. In other words, in this complex, except one N atom in each azo-group, all the other donor atoms in pahqs were fully used in coordination to nickel(II), forming either *N,N,O*- or *N,O*-chelate rings, simultaneously. A part of the chelate ring was the same as that expected for Ni(II)-αPAN (2-(2-pyridylazo)-1-naphthol), Ni(II)-βPAN (1-(2-pyridylazo)-2-naphthol), and Ni(II)-HQ complexes in aqueous solution[2,14] and that observed for Cu(II)-βPAN and Ni(II)-HQ complexes by single crystal X-ray analyses.[4b,4c,15,16] The geometry around each of the four nickel(II) was distorted octahedron. As can be seen from Fig. 3, the complex contained three types of nickel(II) sites with respect to their coordination groups: 1) two *N,N,O*-terdentate moieties of the ligands coordinate to nickel(II) with *mer*-configuration (Ni(2) site); 2) two *N,O*-bidentate moieties of the ligands and two water molecules coordinate to nickel(II) with *cis-cis-cis* configuration (Ni(3) site); 3) one *N,N,O*-terdentate moiety and one *N,O*-bidentate moiety of the ligands and one water molecule coordinate to nickel(II) with formation of a mixed chelate system (Ni(1) and Ni(4) sites).

The bond lengths of Ni(1,2,4)-N(N atoms in pyridine rings, 2.067(10)—2.103(10) Å; N atoms in azo-groups, 1.960(10)—2.008(9)Å), and Ni(1,2,4)-O(2.107(7)—2.188(8) Å, O atoms in *N,N,O*-terdentate moietites) were slightly longer than those of Ni-N (1.93(5) Å, N atom in azo-group) , Ni-N (1.97(4) Å, N atom in thiazole ring) , Ni-O (1.98(4) Å of an analogous nickel(II) complex with thiazolylazo dye.[4a] And the angles of N-Ni-N (76.2(4)—76.7(4)°) and N-Ni-O (78.0(4)—80.0(4)°) were smaller than those of N-Ni-N (78(2)°) and N-Ni-O (80(2)°) of the analogous complex, in which a ligand also acted as *N,N,O*-terdentate one.[4a] On the other hand, the bond lengths of Ni(1,3,4)-N (N atoms in quinolinolate, 2.030(11)—2.093(9) Å) were almost similar to that of Ni-N (2.043(2)—2.082(2)°) in Ni(II)-HQ complex,[17] and Ni(1,3,4)-O (O atoms in *N,O*-bidentate moieties, 2.083(7)—2.188(8) Å) were significantly longer than those of Ni-O (2.054(1)—2.058 (1) Å) of the nickel (II) complex with HQ.[17] The average angles of N-Ni-O (80.5(3)°, *N,O*-bidentate moieties) were smaller than those of N-Ni-O (86.50(6)°[17]) of the nickel(II) complex with HQ. In any event, the bond lengths of Ni-N (N atoms in *N,N,O*-terdentate moieties) were elongated compared with those of the corresponding complex,[4a] and the bond lengths of Ni-N (N atoms in quinoline rings) were kept similar values to those of Ni(II)-HQ complex,[17] this may be associated with the electron-rich N atoms in the quinoline rings.[17] The bond lengths of Ni-O were elongated compared with those of the corresponding nickel(II) complexes with either *N,N,O*- or *N,O*-chelate rings, resulting in the contractions of the angles of N-Ni-N or N-Ni-O, since O atoms acted as bridging donor atoms between nickel(II) sites.

Properties of the Complex. The complex exhibits characteristic IR spectra due to ligand vibration modes. The most significant difference of the IR bands between the present complex and those of the pahqs itself was that the $\nu_{(N=N)}/cm^{-1}$ (1367, 1324) in the complex was shifted to lower frequencies compared with that of the free ligand ($\nu_{(N=N)}$, 1375 cm^{-1}), and was split into two bands. This may be resulted from a delocalization of the negative charge on the azo-group by the complexation with nickel(II) which lead to a reduction of the N=N bond order.[18]

The half wave potential of the azo-group in the aqueous solution of the complex (−0.405 V vs. SCE at pH=6.9) at the same pH values was markedly shifted toward the negative side compared with that of the ligand itself (−0.272 V vs. SCE at pH=6.9), showing that the very stable *N,N,O*-chelate rings of the complex were present even in the solution state.[2,19]

The variation of the magnetic susceptibility (χ_A) and effective magnetic moment (μ_{eff}) with temperature for the complex is illustrated in Fig. 4. It can be seen in this fugure that the effective magnetic moment per nickel(II) ion, μ_{eff}/Ni, was 2.95 BM at 296.3 K and gradually decreased with the lowering of temperature. This indicates that antiferromagnetic exchange interaction is operating between the four nickel(II) via bridging oxygen atoms. It is reasonable to suggest that the angles of Ni-O-Ni (ca. 140°) may lead to the antiferromagnetic interaction.[7]

Further study on the magnetic exchange mechanism among the four nickel(II) sites is continuing.

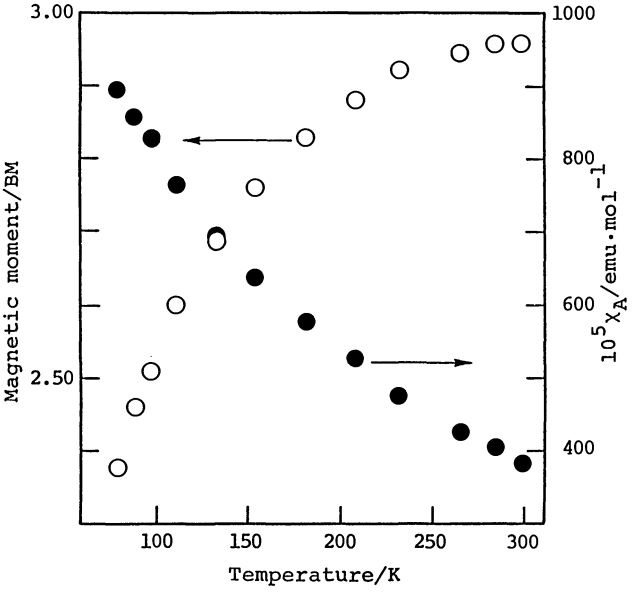

Fig. 4. Temperature dependence of magnetic moments (μ_{eff}/Ni) and magnetic susceptibilities (χ_A).

The authors are grateful to Dr. I. Ueda (Emeritus Professor of Kyushu University), Mr. N. Marubayashi and Mr. N. Setoguchi of Yoshitomi Pharmaceutical Industries Co., Ltd., and Professor T. Nohara of Kumamoto University for help in obtaining the X-ray crystallographic data. The authors also would like to express their hearty thanks to Associate Professor T. Tokii of Saga University for obtaining the magnetic data and for his helpful discussion.

References

1) a) K. Hayashi, K. Okamoto, J. Hidaka, and H. Einaga, *J. Chem. Soc., Dalton Trans.*, **1982**, 1377; b) M. Noritake, K. Okamoto, J. Hidaka, and H. Einaga, *Bull. Chem. Soc. Jpn.*, **63**, 353 (1990), and Refs. therein.

2) H. Huang, H. Chikushi, M. Nakamura, and F. Kai, *Bull. Chem. Soc. Jpn.*, **63**, 1985(1990).

3) H. Huang, Y. Asai, M. Hirohata, M. Nakamura, and F. Kai, *Nippon Kagaku Kaishi*, **1990**, 1348.

4) a) M. Kurahashi, *Bull. Chem. Soc. Jpn.*, **47**, 2067 (1974); b) G. R. Desiraju, H. R. Luss, and D. L. Smith, *J. Am. Chem. Soc.*, **100**, 6375 (1978); c) H. Wada, M. Shiro, A. Yuchi, and G. Nakagawa, *Bull. Chem. Soc. Jpn.*, **61**, 3869 (1988); d) M. Kurahashi, *Bull. Chem. Soc. Jpn.*, **49**, 3053 (1976), and Refs. therein.

5) A preliminary report: H. Huang, F. Kai, Y. Asai, M. Hirohata, and M. Nakamura, *Chem. Lett.*, **1991**, 65.

6) M. Bell, A. J. Edwards, B. F. Hoskins, E. H. Kachab, and R. Robson, *J. Am. Chem. Soc.*, **111**, 3603 (1989), and Refs. therein.

7) W. L. Gladfelter, M. W. Lynch, W. P. Schaefer, D. N. Hendrickson, and H. B. Gray, *Inorg. Chem.*, **20**, 2390 (1981), and Refs. therein.

8) N. F. Curtis, *J. Chem. Soc.*, **1961**, 3147.

9) A. Earnshow, "Introduction to the Magnetic Chemistry," Academic Press, London (1968) , p. 4.

10) B. A. Frenz, Enraf–Nonius Structure Determination Package, Version 17, Delft, 1982.

11) P. Main, S. J. Fiske, S. E. Hull, L. Lessinger, J. P. Declercq, and M. M. Woolfson, "MULTAN11/82. A System of Computer Programs for the Automatic Solution of Crystal Structures from X-ray Diffraction Data," University of New York, England and Louvain-1a-Nerve, Belgium (1982).

12) T. Sakurai and K. Kobayashi, *Rep. Inst. Phys. Chem. Res.*, **55**, 69 (1979).

13) "International Tables for X-Ray Crystallography," ed by J. A. Ibers and W. C. Hamilton, Kynoch Press, Birmingham (1974), Vol. 4.

14) C. F. Richard, R. L. Gustafson, and A. E. Martell, *J. Am. Chem. Soc.*, **81**, 1033 (1959).

15) S. Ooi, D. Carter, and Q. Fernando, *Chem. Commun.*, **1967**, 1301.

16) A. Yuchi, M. Shiro, H. Murakami, H. Wada, and G. Nakagawa, *Bull. Chem. Soc. Jpn.*, **63**, 677 (1990), and Refs. therein.

17) H. Kiriyama, Y. Yamagata, and K. Suzuki, *Acta Crystallogr., Sect. C*, **42**, 785 (1986).

18) S. Ferrer, J. Borras, C. Miratvilles, and A. Fuertes, *Inorg. Chem.*, **28**, 160 (1989).

19) a) T. Takahashi and N. Tanaka, *Nippon Kagaku Zasshi*, **91**, 339 (1970); b) G. W. Latimer, Jr., *Talanta Rev.*, **15**, 1 (1968); c) L. Holleck, J. M. Abd El Kader, and A. M. Shams El Din, *J. Electroanal. Chem.*, **20**, 287 (1969).

Association of Tris(acetylacetonato)chromium(III) with Chlorinated Phenols in the Liquid-Liquid Partition System

Shoichi KATSUTA, Hisanori IMURA,† and Nobuo SUZUKI*
Department of Chemistry, Faculty of Science, Tohoku University, Sendai 980
(Received March 5, 1991)

The liquid–liquid partition behavior of tris(acetylacetonato)chromium(III) ([Cr(acac)$_3$]) between heptane and 0.10 mol dm^{-3} aqueous sodium perchlorate solutions has been studied in the presence of a series of chlorinated phenols (HA) at 298.2 K. A large enhancement of the partition coefficient of [Cr(acac)$_3$] with HA has been observed, e.g., it rises by about 1000-fold in the presence of 0.02 mol dm^{-3} 3,5-dichlorophenol in the organic phase. This effect is ascribable to the association of [Cr(acac)$_3$] with HA in the organic phase. From a partition-equilibrium analysis, the association complexes have been identified as being [Cr(acac)$_3$]·iHA (i=1,2), and the association constants ($\beta_{ass,i}$) determined. The $\beta_{ass,i}$ value increases with an increase of the acid-dissociation constant of HA in the family of HA with the same combination of substituents at the 2,6-positions, i.e., the association is due to hydrogen bonding of the hydroxyl hydrogen atom of HA to [Cr(acac)$_3$]. A linear free-energy relationship has been found between the $\beta_{ass,i}$ values of [Cr(acac)$_3$] and those of [Co(acac)$_3$] previously reported.

The liquid–liquid partition of electrically neutral metal chelates is the most important process governing the extractability and separation efficiency of metal ions with a chelating agent in both solvent extraction and liquid chromatography. Suzuki and his coworkers have studied the partition coefficients of a large number of metal chelates, and have shown that the solvent effect on the partition coefficient can generally be interpreted in terms of regular solution theory.[1–4] In the case of acetylacetonato (2,4-pentanedionato) complexes, however, even for coordinatively saturated complexes such as tris(acetylacetonato)chromium(III) ([Cr(acac)$_3$]) and -cobalt(III) ([Co(acac)$_3$]), the effect of some solvents, such as chloroform and 1-octanol, could not be interpreted quantitatively.[3] This may be due to a specific interaction, such as hydrogen bonding between the metal acetylacetonates and the solvents. The hydrogen bonding between metal complexes and organic compounds might be very important for not only the partition behavior, but also regarding other chemical properties, such as the solubility and reactivity of metal complexes.[5] There have been a few studies concerning the interaction between metal β-diketonates and proton-donor solvents, such as chloroform and methanol.[1,5,6] However, the interaction observed in their systems was rather weak. The specific interaction between these chelates and chlorinated phenols, which are considered to be strong proton donors, has not yet been studied, except for our previous work, in which it was found that [Co(acac)$_3$] forms highly stable association complexes with chlorinated phenols in heptane.[7] Such the association with the phenols may occur for other metal chelates, such as [Cr(acac)$_3$]. It is necessary to accumulate systematic data concerning the specific interaction in order to quantitatively discuss both the nature and characteristics of the specific interaction between metal chelates and proton donors.

† Present address: Department of Chemistry, Faculty of Science, Ibaraki University, Mito 310.

In this paper, the effect of a series of chlorinated phenols on the partition of [Cr(acac)$_3$] between heptane and 0.1 mol dm^{-3} aqueous sodium perchlorate solutions was investigated in detail. The association constants of [Cr(acac)$_3$] with the phenols in heptane were determined by a partition-equilibrium analysis; they are discussed by comparing them with those of [Co(acac)$_3$].

Theoretical

The partition coefficient of [Cr(acac)$_3$] (P_0) in the absence of chlorinated phenols is defined as the ratio of the equilibrium molar concentration of the complex in the organic phase to that in the aqueous phase,

$$P_0=[[\mathrm{Cr(acac)_3}]]_{org}/[[\mathrm{Cr(acac)_3}]]_{aq}, \quad (1)$$

where the subscripts aq and org denote the aqueous and organic phases, respectively.

When [Cr(acac)$_3$] and chlorinated phenols (HA) form association complexes ([Cr(acac)$_3$]·iHA) in the organic phase, the apparent partition coefficient of [Cr(acac)$_3$] (P') in the presence of HA can be expressed as

$$P'=\frac{[[\mathrm{Cr(acac)_3}]]_{org}+\sum_{i=1}^{n}[[\mathrm{Cr(acac)_3}]\cdot i\mathrm{HA}]_{org}}{[[\mathrm{Cr(acac)_3}]]_{aq}} \quad (2)$$

$$=P_0(1+\sum_{i=1}^{n}\beta_{ass,i}[\mathrm{HA}]_{org}{}^{i}), \quad (3)$$

where $\beta_{ass,i}$ is the association constant in the organic phase corresponding to the following equilibrium:

$$[\mathrm{Cr(acac)_3}]_{org}+i\mathrm{HA}_{org}\rightleftarrows[\mathrm{Cr(acac)_3}]\cdot i\mathrm{HA}_{org},$$

$$\beta_{ass,i}=\frac{[[\mathrm{Cr(acac)_3}]\cdot i\mathrm{HA}]_{org}}{[[\mathrm{Cr(acac)_3}]]_{org}[\mathrm{HA}]_{org}{}^{i}}. \quad (4)$$

Therefore, the following equation can be derived:

$$P'/P_0=1+\sum_{i=1}^{n}\beta_{ass,i}[\mathrm{HA}]_{org}{}^{i}. \quad (5)$$

An enhancement of the partition coefficient of

[Cr(acac)3] in the presence of HA is directly related to the association constant and the equilibrium concentration of HA in the organic phase by Eq. 5.

Experimental

Reagents. [Cr(acac)3] was obtained from Dojin Chem. Lab., recrystallized from hexane, and dried in vacuo. The purity was checked by a melting-point measurement and elemental analysis: Mp, 214 °C (literature value, 216 °C[8]). Found: C, 52.36; H, 6.14%. Calcd for $C_{15}H_{21}O_6Cr$: C, 51.58; H, 6.06%. 3-Chlorophenol (3-CP), 2,3-dichlorophenol (2,3-DCP), 3,5-dichlorophenol (3,5-DCP), 2,3,5-trichlorophenol (2,3,5-TCP), 2,3,6-trichlorophenol (2,3,6-TCP), and 2,4,5-trichlorophenol (2,4,5-TCP), which were of more than 98% purity, were commercially obtained and further purified by recrystallization from hexane or vacuum sublimation. Pentachlorophenol (PCP) (Aldrich, more than 98% purity) was used as obtained. Heptane was purified by ordinary methods. Water was doubly distilled. Other reagents were of analytical reagent grade and used without further purification.

Partition Measurements. An aqueous solution of 1.0×10^{-5}—7.7×10^{-4} (1 M=1 mol dm^{-3}) [Cr(acac)3] was prepared by partitioning [Cr(acac)3] from its heptane solution to water just before use, in order to minimize the dissociation of the complex in aqueous solution. The aqueous solution of [Cr(acac)3] was mechanically shaken with pure heptane or a heptane solution of 3.5×10^{-4}—1.0×10^{-1} M chlorinated phenols for 5—60 min at 350 strokes per min in a thermostated room at 298.2±0.5 K. The two phases were separated by centrifugation at 3000 rpm. The absorbance of [Cr(acac)3] in the aqueous phase before ($A_{i,aq}$) and after (A_{aq}) shaking was measured at 331 nm with a Hitachi U-3200 or JASCO Uvidec-2 spectrophotometer. The phenols had no absorption at this wavelength and did not affect the molar absorption coefficient of [Cr(acac)3] in the aqueous phase. The partition coefficient of [Cr(acac)3] in the absence (P_0) or presence (P') of chlorinated phenols was calculated using

$$P_0 \text{ or } P' = (A_{i,aq} - A_{aq}) V_{aq} A_{aq}^{-1} V_{org}^{-1}, \quad (6)$$

where V_{aq} and V_{org} are the volumes of aqueous and organic phases, respectively; the volume ratio V_{aq}/V_{org} was chosen to be 1—4 according to the magnitude of P' so as to minimize the absorbance-measurement error of the aqueous phase. The proton concentration of the aqueous phase was adjusted to 10^{-2}—10^{-3} M with perchloric acid to suppress any dissociation of the phenols. The ionic strength was adjusted to 0.10 M with sodium perchlorate.

Results

No dissociation of [Cr(acac)3] in the partition experiment was confirmed as follows: The equilibrated aqueous phase was shaken with chloroform to remove [Cr(acac)3] completely from the aqueous phase. Chloroform has a high partition coefficient for [Cr(acac)3], 5.70×10^3.[3] No absorption due to dissociated complexes, such as $[Cr(acac)]^{2+}$, and $[Cr(acac)_2]^+$, was detected in the remaining aqueous phase. All partition equilibria of [Cr(acac)3] were found to be established within 5-min shaking.

It was confirmed that the partition coefficient of [Cr(acac)3] (P_0) in the absence of chlorinated phenols is independent of the [Cr(acac)3] concentration within the range 1.3×10^{-5}—1.3×10^{-4} in the organic phase. The average and standard deviation of the P_0 value of [Cr(acac)3] for 12 measurements were 0.370±0.018, which is in good agreement with a value from the literature, 0.351.[9]

The apparent partition coefficient of [Cr(acac)3] (P') measured in the presence of a series of chlorinated phenols (HA) is shown in Fig. 1 as plots of $\log(P'/P_0)$ against the logarithmic value of the equilibrium concentration of the phenols in the organic phase, $\log[HA]_{org}$. Here, $[HA]_{org}$ is calculated from the initial concentration in the organic phase (C_{HA}) and the partition coefficient (P_{HA}) of those phenols as follows:

$$[HA]_{org} = C_{HA}/(V_{aq} V_{org}^{-1} P_{HA}^{-1} + 1), \quad (7)$$

where the P_{HA} values were quoted from our previous study,[10] i.e., 0.534 for 3-CP, 21.5 for 2,3-DCP, 2.61 for 3,5-DCP, 89.8 for 2,3,5-TCP, 96.6 for 2,3,6-TCP, 62.9 for 2,4,5-TCP, and 980 for PCP. The $[HA]_{org}$ calculated here should be approximately equal to the equilibrium concentration of HA free from association with [Cr(acac)3], since the total concentration of [Cr(acac)3] was always made to be smaller than 3% of C_{HA}. In all of the systems, the apparent partition coefficient of

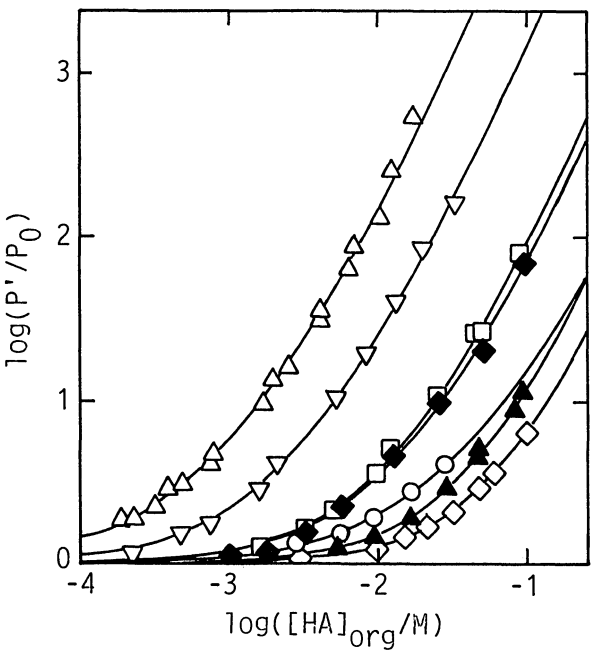

Fig. 1. Enhancement of the partition coefficient of [Cr(acac)3] as a function of the equilibrium concentration of chlorinated phenols (HA) in the organic phase. The solid lines indicate the regression curves by the nonlinear least-squares procedure based on Eq. 5.
▽, 3-CP; ▲, 2,3-PCP; △, 3,5-DCP; ◆, 2,3,5-TCP; ◇, 2,3,6-TCP; □, 2,4,5-TCP; ○, PCP.

$[Cr(acac)_3]$ rapidly increases with an increase in the phenol concentration in the organic phase. The largest effect is found in the 3,5-DCP system: the partition coefficient of $[Cr(acac)_3]$ rises by about 1000-fold in the presence of 0.02 M 3,5-DCP. This enhancement effect is remarkably different among the phenols, and increases according to the following order: 2,3,6-TCP<2,3-DCP<PCP<2,3,5-TCP≈2,4,5-TCP<3-CP<3,5-DCP.

Discussion

The enhancement of the apparent partition coefficient of $[Cr(acac)_3]$ in the presence of the chlorinated phenols can be ascribed to an association of $[Cr(acac)_3]$ with the phenols in the organic phase. According to Eq. 5, the slope of the plot of $\log(P'/P_0)$ vs. $\log[HA]_{org}$ is equal to the mean number of HA molecule associating with one molecule of $[Cr(acac)_3]$. The plots in Fig. 1 for 3-CP, 3,5-DCP, 2,3,5-DCP, and 2,4,5-TCP, which give especially great enhancement of the partition coefficient of $[Cr(acac)_3]$, are close to straight lines with a slope of 2 in the higher concentration region of the phenols. In the case of 2,3-DCP and 2,3,6-TCP, although no such limiting slope can be observed, the slopes of the plots increase to higher than unity at high concentrations of the phenols. These results mean that the maximum association number of the chlorinated phenols is two under these experimental conditions. From the plots given in Fig. 1, the association constants, $\beta_{ass,1}$ and $\beta_{ass,2}$ were computed by a nonlinear least-squares procedure (SALS program, The University of Tokyo) based on Eq. 5, and listed in Table 1. In the case of PCP, the P' measurement was only possible for a limited concentration range of PCP due to its low solubility (ca. 0.03 M in heptane); the slope of the plot is nearly unity, even at higher concentrations. In accordance with the results for other chlorinated phenols, however, the association constants were computed by assuming the formation of 1:1 and 1:2 association complexes. Hence, the $\beta_{ass,2}$ value of PCP may involve a fairly large error. The solid lines in Fig. 1 indicate regression curves by the obtained association constants; they are well fitted to the experimental plots. The largest values of the association constants are found in the 3,5-DCP system. All of these values for the chlorinated phenols are very large compared with the very few data concerning the association constants of $[Cr(acac)_3]$ with other proton donors reported so far, e.g., the $\log \beta_{ass,1}$ values with chloroform and methanol in carbon tetrachloride at 298 K are −0.52 and 0.11, respectively.[5]

Table 1. Association Constants of $[Cr(acac)_3]$ with Chlorinated Phenols (HA) in Heptane at 298.2 K

No.	HA	$\log(\beta_{ass,1}/M^{-1})$	$\log(\beta_{ass,2}/M^{-2})$
1	3-CP	3.02 (0.03)	5.13 (0.03)
2	2,3-DCP	1.63 (0.03)	2.83 (0.03)
3	3,5-DCP	3.56 (0.02)	6.04 (0.03)
4	2,3,5-TCP	2.26 (0.05)	3.72 (0.06)
5	2,3,6-TCP	1.39 (0.03)	2.49 (0.04)
6	2,4,5-TCP	2.27 (0.03)	3.87 (0.03)
7	PCP	1.97 (0.01)	2.71 (0.08)

Numerals in parentheses show the standard deviations calculated by SALS program.

The possibility of a direct coordination of the phenols to the inner sphere of $[Cr(acac)_3]$ was completely denied by the fact that the absorption band at 560 nm of $[Cr(acac)_3]$ in heptane, assigned to the d-d transition,[11] did not change in the presence of 0.05 M 3,5-DCP. If the association is caused by hydrogen bonding, the association constant is expected to correlate with the acid-dissociation constant of the chlorinated phenols.[12] Figure 2 shows the association constant of $[Cr(acac)_3]\cdot HA$ ($\log \beta_{ass,1}$) as a function of the acid-dissociation constant of the chlorinated phenols ($\log K_a = -pK_a$); the pK_a values are cited from the literature, i.e., 8.97 for 3-CP, 7.71 for 2,3-DCP, 8.25 for 3,5-DCP, 6.43 for 2,3,5-TCP, 5.80 for 2,3,6-TCP, 6.72 for 2,4,5-TCP, and 4.74 for PCP.[13] Good correlations are found for three families of phenols with the same combination of substituents at the 2,6-positions: (1) 3-CP and 3,5-DCP, (2) 2,3-DCP, 2,3,5-TCP, and 2,4,5-TCP, and (3) 2,3,6-TCP and PCP. In each family, the association constant increases with an increase in the acid-dissociation constant of the phenols; such relations indicate that the association of $[Cr(acac)_3]$ with the chlorinated phenols is due to hydrogen bonding of the hydroxyl hydrogen atom of the phenols to $[Cr(acac)_3]$. In addition, these three families lie at different regions in Fig. 2, and the

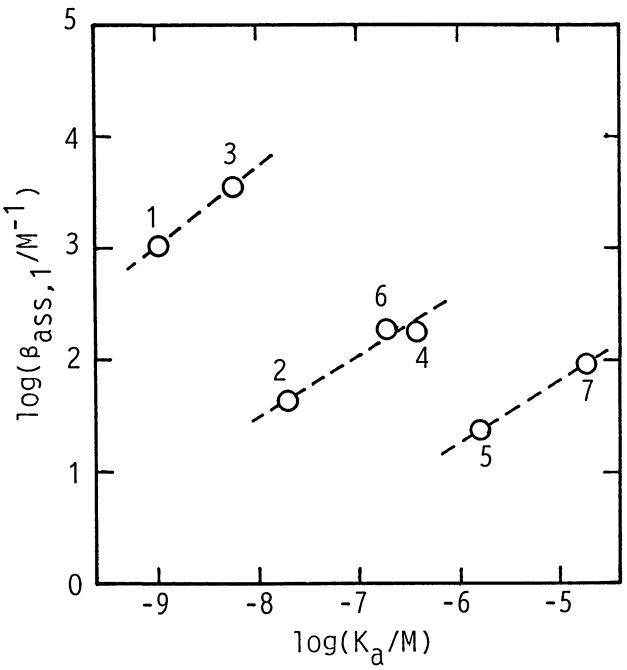

Fig. 2. Correlation between the logarithmic values of the association constant ($\beta_{ass,1}$) and the acid-dissociation constant (K_a) of chlorinated phenols. The numbers in figure correspond to those in Table 1.

association constants decrease as family(1)>family(2) >family(3). This difference among the families can be mainly interpreted in terms of the formation of an intramolecular hydrogen bond between the hydroxyl hydrogen atom and the chlorine atoms at the 2,6-positions, which should reduce the intermolecular association with [Cr(acac)3].[12] The intermolecular association may also be hindered sterically by bulky chlorine atoms at the 2,6-positions. Consequently, 3,5-DCP has the highest association ability among the investigated phenols, since this phenol has no chlorine atoms at the 2,6-positions and its acidity is relatively strong due to the electron-withdrawing nature of chlorine atoms at the 3,5-positions.

The association reaction of [Cr(acac)3] was compared with that of the same type of tris(acetylacetonato) complex, [Co(acac)3], which also forms 1 : 1 and 1 : 2 association complexes with the chlorinated phenols.[7] Figure 3 shows the correlation between the logarithmic value of the association constant of [Cr(acac)3] ($\beta_{ass,i}$(Cr)) with the chlorinated phenols and that of [Co(acac)3] ($\beta_{ass,i}$(Co)) with the corresponding phenols. The same and good linear free-energy relationships are found with respect to both $\beta_{ass,1}$ and $\beta_{ass,2}$:

$$\log(\beta_{ass,i}(\mathrm{Cr})/\mathrm{M}^{-i}) = 0.90 \log(\beta_{ass,i}(\mathrm{Co})/\mathrm{M}^{-i}) + 0.04, \quad (8)$$

with a correlation coefficient of r=0.998. This reveals that these association reactions for [Cr(acac)3] and [Co(acac)3] are the same regarding type. As shown by the slope of 0.90, the association constants of [Cr(acac)3] are always somewhat smaller than those of [Co(acac)3]. That is to say, the proton-acceptor ability of [Cr(acac)3] is a little inferior to that of [Co(acac)3]. In order to discuss the reason for this difference between [Cr(acac)3] and [Co(acac)3] in detail, further investigations concerning other metal acetylacetonates may be necessary.

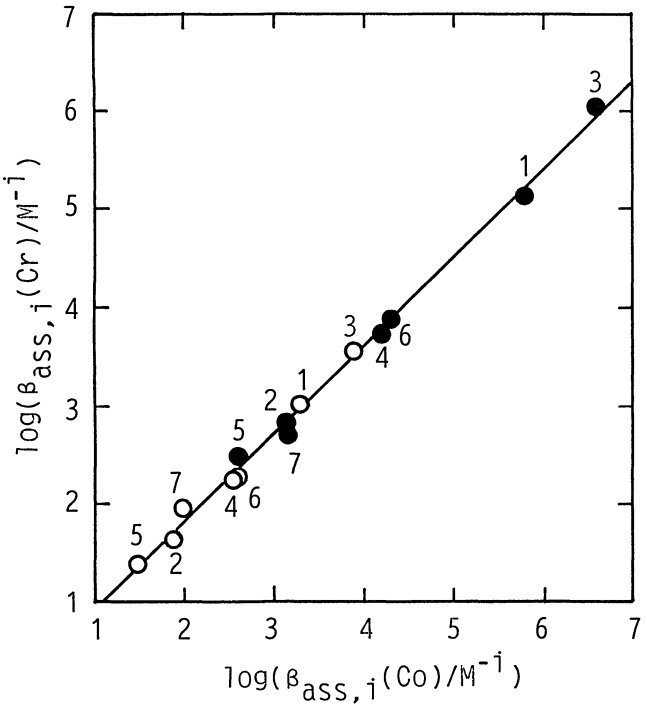

Fig. 3. Correlation between the logarithmic values of the association constants of [Cr(acac)3] ($\beta_{ass,i}$(Cr)) and [Co(acac)3] ($\beta_{ass,i}$(Co)) with chlorinated phenols in heptane. The solid line indicates the regression line by the linear least-squares procedure (Eq. 8). The numbers in figure correspond to those in Table 1. ○, i=1; ●, i=2.

The structure of the association complex may be estimated from the maximum association number of the phenols observed for both tris(acetylacetonato) complexes. The tris(acetylacetonato) complex has an octahedral configration with the ligand oxygen atoms about the central metal atom.[14] In the eight octahedral faces, two faces perpendicular to the C_3 axis of the tris-complex, each of which comprises three closely positioned oxygen atoms from three acetylacetonato ligands, are relatively open to the approach of phenols. The hydroxyl hydrogen of the phenol probably interacts with equal probability with the three oxygens on each of these two faces and, consequently, one molecule of the complex can associate with two molecules of the phenols.

In conclusion, it was found that [Cr(acac)3] forms highly stable 1 : 1 and 1 : 2 association complexes with chlorinated phenols by hydrogen bonding in heptane. This association reaction causes a great enhancement of the partition of the metal acetylacetonate between heptane and aqueous solutions in the presence of the chlorinated phenols. Many other metal chelates can probably associate with the chlorinated phenols and, from an analytical viewpoint, the addition of the chlorinated phenols can be expected to provide a great enhancement for the solvent extraction of various metal chelates or to strongly affect the retention behavior of metal chelates in liquid chromatography.

References

1) H. Imura and N. Suzuki, *J. Radioanal. Nucl. Chem.*, **88**, 63 (1985).
2) H. Imura and N. Suzuki, *Talanta*, **32**, 785 (1985).
3) H. Imura, J. Kodera, and N. Suzuki, 8th Symposium on Solution Chemistry, Kanazawa, October 1985, Abstr., p. 72.
4) N. Suzuki, S. Matsumora, and H. Imura, *Polyhedron*, **6**, 497 (1987).
5) V. M. Nekipelov and K. I. Zamaraev, *Coord. Chem. Rev.*, **61**, 185 (1985), and the references cited therein.
6) P. L. Wang, J. H. Lee, and L. P. Hwang, *J. Phys. Chem.*, **91**, 4856 (1987).
7) H. Imura, S. Katsuta, and N. Suzuki, *Polyhedron*, in press.
8) W. C. Fernelius and J. E. Blanch, *Inorg. Synth.*, **5**, 130 (1957).
9) H. Awano, H. Watarai, and N. Suzuki, *J. Inorg. Nucl. Chem.*, **41**, 124 (1979).
10) S. Katsuta, M. Sc. Thesis, Tohoku University, Sendai, 1989.

11) D. W. Barnum, *J. Inorg. Nucl. Chem.*, **21**, 221 (1961).
12) M. M. Davis, "Brønsted Acid-Base Behavior in "Inert" Organic Solvents," in "The Chemistry of Nonaqueous Solvents," ed by J. J. Lagowski , Academic Press, New York (1970), Vol. 3, Chap. 1.
13) J. Drahonovsky and Z. Vacek, *Collect. Czech. Chem. Commun.*, **36**, 3431 (1971).
14) P. K. Hon and C. E. Pfluger, *J. Coord. Chem.*, **3**, 67 (1973).

 © 1991 The Chemical Society of Japan Bull. Chem. Soc. Jpn., 64, 2475—2483 (1991)

Synthesis, Structure, and Reactions of Stable Titanacyclopentanes

Kazushi MASHIMA, Nozomu SAKAI, and Hidemasa TAKAYA*
Department of Industrial Chemistry, Faculty of Engineering, Kyoto University, Yoshida, Kyoto 606
(Received March 15, 1991)

Titanacyclic compounds of the formula $Cp^*_2Ti(CH_2CH_2C(CH_2CHR)CH_2)$ (**5a**; R=H and **5b**; R=C_6H_5, Cp^*=pentamethylcyclopentadienyl), the first stable titanacyclopentanes, have been prepared by the reaction of bis(pentamethylcyclopentadienyl)titanium–ethylene complex (**3**) with methylenecyclopropanes (**4**), and their structures were determined based on both spectroscopic data and X-ray crystallography. Complex **5b** crystallized in space group $P2_1/a$ (Z=4) with cell constants, a=21.832(3), b=8.580(1), c=14.759(2) Å, β=96.81(1)°, U=2744.9(6) Å^3 (4261 reflections, R=0.053). The reaction of **5** with carbon monoxide afforded spiro[2.4]heptan-5-ones in 98% yield. The thermal decomposition of **5** has been investigated, and possible mechanisms of the reactions have been proposed based on deuterium-labeled experiments. A novel formal reductive elimination of organic ligands giving 1-phenylspiro[2.4]hexane has been observed in the thermolysis of **5b**. A structure–reactivity relationship has been discussed.

The chemistry of metallacyclic compounds has been the subject of considerable interest since many synthetically important organic reactions mediated by transition-metal complexes proceed via metallacyclic intermediates.[1] Although numerous metallacyclic compounds have been known, only a limited number of such compounds of the first transition series elements have been isolated and characterized.[2,3] Metallacyclopentanes, when they are heated in solution or in solid state, suffer from several kinds of thermal reactions which can be classified into three modes of reactions (paths A, B, and C), as shown in Scheme 1. A simple reductive elimination produces cyclobutane (mode A), while a β-hydrogen elimination followed by a reductive elimination (mode B) gives rise to 1-butene. The third important reaction is the β-carbon–carbon bond fission (mode C) giving two moles of olefins, which is sometimes reversible; an oxidative coupling of two olefins on a metal gives back metallacyclopentanes. The product distribution varies depending on the nature of metals, ligands, and other experimental conditions. Usually, compounds of the late transition elements suffer from mode A and B reactions, while those of the early transition elements tend to decompose by paths B and C.

Bis(cyclopentadienyl)titanacyclopentane (**1**) (Cp=cyclopentadienyl) has been known to be unstable in solution, even at −30 °C, and all attempts to isolate **1** have been unsuccessful. A facile β-elimination reaction (mode B reaction) and a β-carbon–carbon bond fission (mode C reaction) giving 1-butene and ethylene, respectively, might be the major reason of its instability (Eq. 1).[3] Isolation of complex **2** (Cp^*=pentamethylcyclopentadienyl) is also very difficult because it is in equilibrium with ethylene complex **3** and free ethylene (Eq. 2). Here, a selective cleavage of the β-C–C bond is the main pathway of decomposition.[3c] We thought that if a strained olefin is used in place of ethylene, this equilibrium will be forced to shift to the left-hand side so that the strain of the olefin would be released. Such an effect would stabilize the titanacyclopentane **2**. For the purpose of carrying out detailed structure–reactivity studies on this class of compounds, we have investigated this subject. We describe here the isolation, structures, and some reactions concerning new stable titanacyclopentanes derived from **3** and methylenecyclopropanes **4**.[4]

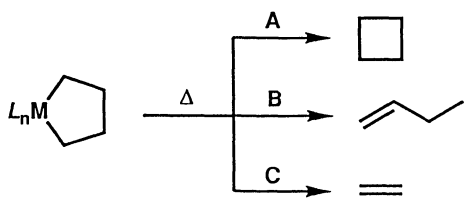

Scheme 1.

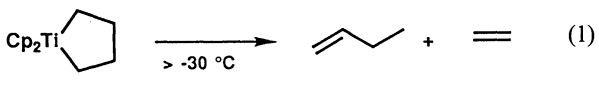

1 (1)

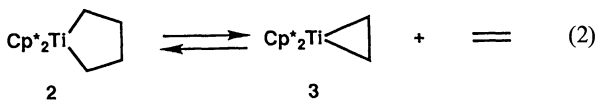

2 3 (2)

Results and Discussion

Synthesis and Characterization of Stable Titanacyclopentanes 5. Decamethyltitanocene–ethylene complex **3** has been conveniently prepared in 43% isolation yield by a reaction of $Cp^*_2TiCl_2$ and two equivalent of butyllithium under atmospheric pressure of ethylene. When a mixture of **3** and an excess amount of methylenecyclopropane (**4a**) in hexane was stirred at −10 °C for 48 h under an argon atmosphere, titanacyclopentane **5a** was obtained as orange needles in 65% yield after recrystallization of the crude product from hexane at

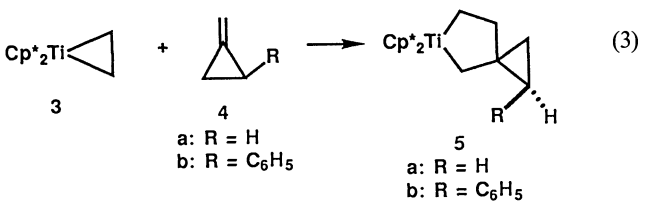

(3)

−80 °C (Eq. 3). Complex **5a** melted at 156—158 °C with decomposition, while slowly decomposing in toluene at 95 °C ($t_{1/2}$=91 min).

The structure of **5a** was supported by its spectral data. The ^{1}H NMR spectrum of **5a** in toluene-d_8 showed that each methylene proton is magnetically equivalent and exhibited no substantial change down to −90 °C; this indicates that the conformational change of the titanacyclopentane ring is rapid, even at −90 °C. Similarly, the phenyl derivative **5b** was prepared as deep-red prisms in 83% yield by treatment of **3** with 2-phenyl-1-methylenecyclopropane (**4b**) at 20 °C for 48 h. The half-life of **5b** in toluene at 95 °C is ca. 3 min. The structure of **5b** was determined by its spectral data and X-ray crystallography.

The molecular structure of **5b** is shown in Fig. 1. Selected bond distances and angles are summarized in Tables 1 and 2. Complex **5b** is monomeric and has the coordination geometry of a distorted tetrahedron defined by two pentamethylcyclopentadienyl ligands and two carbon atoms of the metallacyclopentane ring. The bond lengths of 1.513(5) Å for C(3)–C(4), 1.529(5) Å for C(3)–C(7), and 1.527(4) Å for C(6)–C(7) are comparable, which is in contrast with the fact that the stable metallacyclopentanes of the first transition elements such as Fe,[2g] Co,[2c,5] and Ni[2a,b,6] have a tendency for the bond distances of C_β—C_β' to usually be shorter than those of C_α–C_β. This relatively long C_β–C_β' bond distance in **5b** might be related to an easy cleavage of the C_β–C_β' bond of titanacyclopentanes. The five-membered ring of **5b** is fixed in a puckered form and the C(1)–C(3) bond occupies a pseudoequatorial position. The C(4)–Ti–C(6) angle is 80.6(1)°, showing that this angle is considerably distorted from the ideal value of 110° calculated for Cp_2TiH_2.[7] This deformation of

Table 1. Selected Bond Distances (Å) and Their esd's for **5b**[a]

Ti–C4	2.214(3)	Ti–C6	2.189(3)
Ti–Cp1	2.483(3)	Ti–Cp2	2.449(3)
Ti–Cp3	2.451(3)	Ti–Cp4	2.442(3)
Ti–Cp5	2.468(3)	Ti–Cp11	2.490(3)
Ti–Cp12	2.480(3)	Ti–Cp13	2.431(3)
Ti–Cp14	2.472(3)	Ti–Cp15	2.441(3)
Ti–Cp*1	2.146	Ti–Cp*2	2.150
C1–C2	1.516(5)	C1–C3	1.536(4)
C1–CB1	1.483(6)	C2–C3	1.509(5)
C3–C4	1.513(5)	C3–C7	1.529(5)
C6–C7	1.527(4)		
CB1–CB2	1.378(7)	CB1–CB6	1.384(5)
CB2–CB3	1.380(7)	CB3–CB4	1.351(6)
CB4–CB5	1.360(7)	CB5–CB6	1.395(6)
Cp1–Cp2	1.412(4)	Cp1–Cp5	1.408(4)
Cp1–Cp6	1.510(5)	Cp2–Cp3	1.409(4)
Cp2–Cp7	1.508(5)	Cp3–Cp4	1.416(4)
Cp3–Cp8	1.510(5)	Cp4–Cp5	1.404(5)
Cp4–Cp9	1.514(5)	Cp5–Cp10	1.516(5)
Cp11–Cp12	1.408(4)	Cp11–Cp15	1.417(4)
Cp11–Cp16	1.511(4)	Cp12–Cp13	1.411(4)
Cp12–Cp17	1.509(5)	Cp13–Cp14	1.422(4)
Cp13–Cp18	1.501(5)	Cp14–Cp15	1.403(4)
Cp14–Cp19	1.491(5)	Cp15–Cp20	1.502(5)

a) Cp*1 and Cp*2 are the centroids of two cyclopentadienyl rings, Cp1–Cp5 and Cp11–Cp15, respectively.

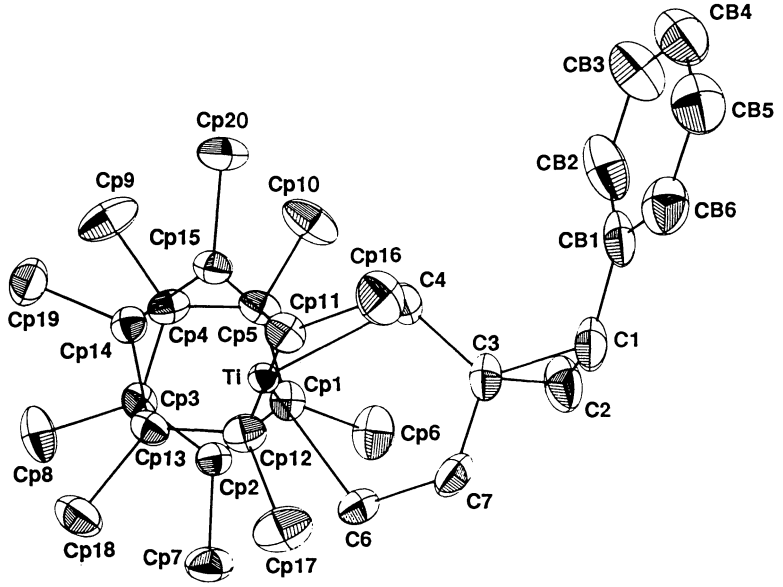

Fig. 1. ORTEP drawing of **5b** with the labeling scheme. The hydrogen atoms were omitted for clarity.

Table 2. Selected Bond Angles (degree) and Their esd's for **5b**[a]

C4–Ti–C6	80.6(1)	C4–Ti–Cp*1	106.3
C4–Ti–Cp*2	106.1	C6–Ti–Cp*1	105.9
C6–Ti–Cp*2	105.8	Cp*1–Ti–Cp*2	137.6
C2–C1–C3	59.2(2)	C2–C1–CB1	122.7(4)
C3–C1–CB1	122.9(3)	C1–C2–C3	61.1(2)
C1–C3–C2	59.7(2)	C1–C3–C4	121.3(3)
C1–C3–C7	115.2(3)	C2–C3–C4	120.0(3)
C2–C3–C7	116.3(3)	C4–C3–C7	114.0(3)
C3–C4–Ti	109.8(2)	C7–C6–Ti	107.2(2)
C3–C7–C6	109.0(3)		
C1–CB1–CB2	124.8(3)	C1–CB1–CB6	119.7(4)
CB2–CB1–CB6	115.5(4)	CB1–CB2–CB3	122.7(4)
CB2–CB3–CB4	120.7(5)	CB3–CB4–CB5	118.8(4)
CB4–CB5–CB6	120.5(4)	CB1–CB6–CB5	121.8(4)
Cp2–Cp1–Cp5	107.7(3)	Cp2–Cp1–Cp6	125.4(3)
Cp5–Cp1–Cp6	126.5(3)	Cp1–Cp2–Cp3	108.1(3)
Cp1–Cp2–Cp7	126.3(3)	Cp3–Cp2–Cp7	125.1(3)
Cp2–Cp3–Cp4	107.9(3)	Cp2–Cp3–Cp8	124.7(3)
Cp3–Cp3–Cp8	125.5(3)	Cp3–Cp4–Cp5	107.8(3)
Cp3–Cp4–Cp9	126.8(3)	Cp5–Cp4–Cp9	123.7(3)
CP1–Cp5–Cp4	108.5(3)	Cp1–Cp5–Cp10	126.9(3)
Cp4–Cp5–Cp10	123.9(3)		
Cp12–Cp11–Cp15	107.5(3)	Cp12–Cp11–Cp16	126.2(3)
Cp15–Cp11–Cp16	125.1(3)	Cp11–Cp12–Cp13	108.5(3)
Cp11–Cp12–Cp17	126.9(3)	Cp13–Cp12–Cp17	122.9(3)
Cp12–Cp13–Cp14	107.6(2)	Cp12–Cp13–Cp18	124.2(3)
Cp14–Cp13–Cp18	127.1(3)	Cp13–Cp14–Cp15	107.7(3)
Cp13–Cp14–Cp19	125.8(3)	Cp15–Cp14–Cp19	124.6(3)
Cp11–Cp15–Cp14	108.5(3)	Cp11–Cp15–Cp20	124.8(3)
Cp14–Cp15–Cp20	126.3(3)		

a) Cp*1 and Cp*2 are the centroids of two cyclopentadienyl rings, Cp1–Cp5 and Cp11–Cp15, respectively.

angle C(4)–Ti–C(6), however, is not considered to destabilize the complex very much, since the difference in the total energy of the complex was calculated to be only within 3 kcal mol^{-1} over the range 75—130°.[5]

Complex **5** can be considered to arise from a mixed-ligand complex of type **6** by oxidative coupling of the

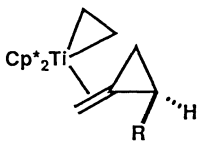

6

two ligands on titanium or by migratory insertion of the olefin into the Ti–C bond.[8] Selective formation of a related mixed-ligand complex has been proposed for a [2+2] cyclocoupling of norbornadiene and methylenecyclopropane (Eq. 4), in which a subtle balance of the coordination abilities of the two olefins is considered to be an important factor.[9] On the other hand, another possible mechanism is a direct [2+2] suprafacial reaction of the olefinic part of methylenecyclopropane and the strained Ti–C bond of **3**.[8a]

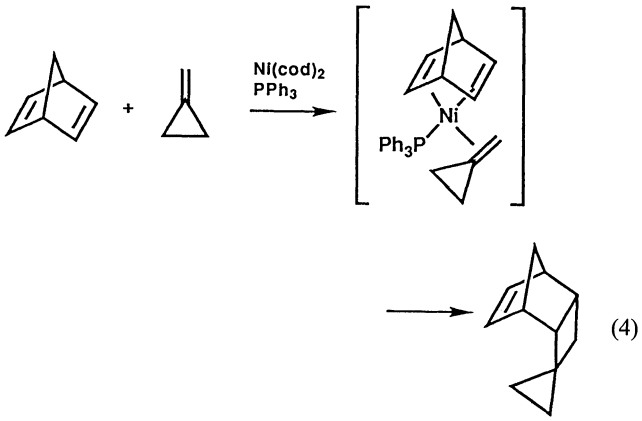

(4)

When 2,2-diphenyl-1-methylenecyclopropane (**4c**) was stirred with **3** in toluene at room temperature, no reaction took place, which can be ascribed to a steric repulsion between bulky pentamethylcyclopentadienyl ligands and two phenyl substituents of **4c**. At an elevated temperature (70 °C), however, **4c** isomerized catalytically to 1,3-butadiene derivative **7** in quantitative yield (Scheme 2). The catalytic conversion of **4c** to **7** can be viewed as proceeding by the mechanism shown in Scheme 2, which involves a cyclopropylmethyl—3-butenyl rearrangement. Titanium hydride **8** is considered to be a catalytically active species.[10,11]

The reaction of **3** with phenylallene has also been investigated; only a ligand-exchange reaction occurred to give a new titanocene–phenylallene complex **9** (Eq. 5). The structure of **9** was determined by a comparison

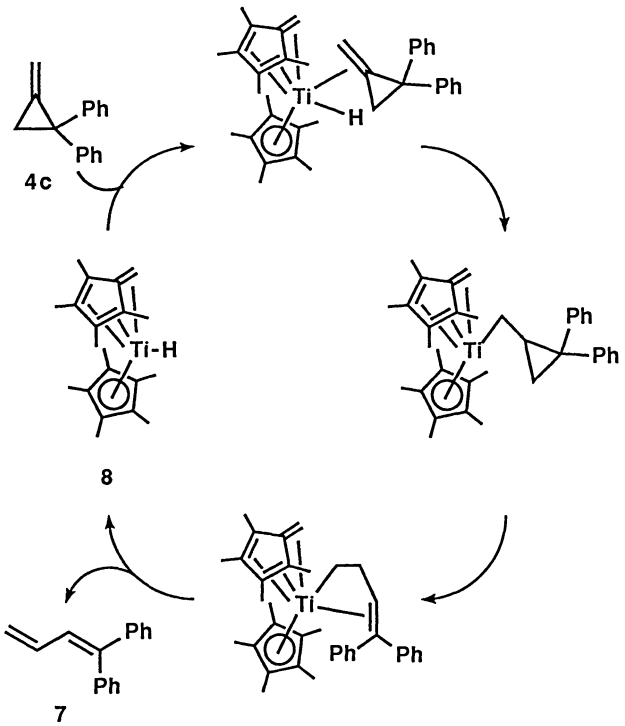

Scheme 2.

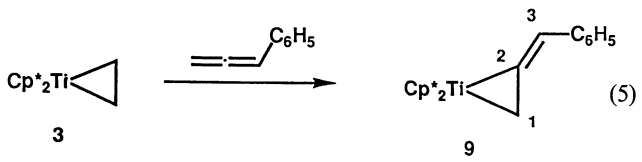

of the ^1H and ^{13}C NMR chemical shift values as well as the C–H coupling constants of **9** and those of free phenylallene.[3c,7] No stereochemical assignment has been performed, though the structure of a sterically less-hindered isomer has been tentatively presented. Phenylallene was released from **9** when it decomposed upon exposure to air.

Reactions of 5a and 5b. Complexes **5** are quite stable in dilute hydrochloric acid. However, when a benzene solution of **5a** was treated with silica gel or alumina, a smooth hydrolysis occurred to give 1-ethyl-1-methylcyclopropane (**10a**) in 96% yield (Eq. 6). A similar treatment of **5b** in benzene with silica gel afforded *r*-1-ethyl-1-methyl-*t*-2-phenylcyclopropane (**10b**) in 88% yield. Compounds **10a** and **10b** were also obtained in quantitative yields when **5a** and **5b** were treated with hydrogen (3 atm).

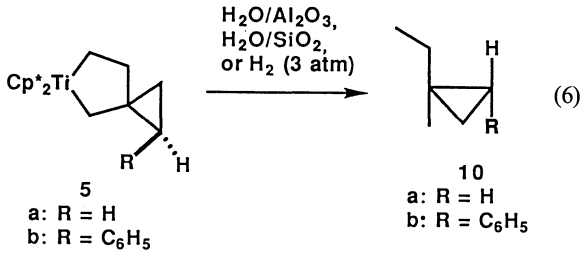

When **5a** or **5b** in hexane was exposed to three atmospheric pressure of carbon monoxide at room temperature, cyclopentanone derivative **11a** or **11b** was obtained in almost quantitative yields, respectively (Eq. 7).[12,13] This is in contrast with the reported fact that the reaction of complex $Cp^*_2\overline{TiCH_2(CH_2)_2CH_2}$ (**2**) with carbon monoxide did not give cyclopentanone, but resulted in the formation of ethylene and $Cp^*_2Ti(CO)_2$.[3c]

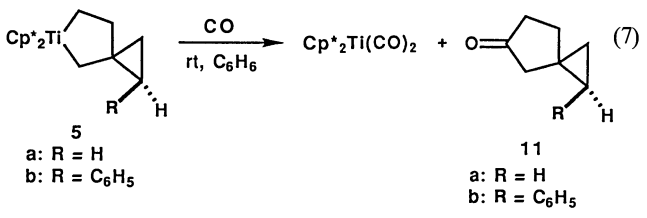

Thermal Decompositions of 5a and 5b. Thermal reactions of complexes **5** were carried out by rapidly heating a solid sample at 200 °C under reduced pressure; the resulting organic products were collected and analyzed. The results are summarized in Schemes 3 and 4. Two pathways were observed for **5a**, in which a β-carbon–carbon bond cleavage occurred predominantly to give ethylene (43%), butadiene (31%), and methylcyclopropane (19%) (Scheme 3). 1,3-Diene **12** (16%) was also obtained, which is considered to arise from a cleavage of the C(1)–C(3) bond of the spiro[2.4]heptane ring. No products arising from a simple β-hydrogen elimination were detected. In contrast, the thermolysis of complex **5b** did not undergo via the β-carbon–carbon bond fission, but gave 1,3-diene **13** in 70% yield (Scheme 4). Interestingly, the reductive elimination product, a cyclobutane derivative **14** (6%), was also obtained. To our knowledge, this is the first example of a direct reductive elimination of cycloalkanes from the metallacycles of group-4 transition metals. Recently, an oxidative decomposition of titanacyclobutanes has been reported to give cyclopropanes.[14] The remarkable differences in the reaction modes observed for **5a** and **5b** might be partly attributed to the presence of a weak benzylic carbon–carbon bond in **5b**. Another possible factor is the fact that the bulky phenyl substituent deforms the titanacyclopentane ring so that it occupies a pseudoequatorial position, which might make the β-carbon–carbon bond fission more difficult to occur. A similar structure–reactivity relationship has been discussed for the transition-metal-catalyzed valence isomerization of 1,8-bishomocubane.[15]

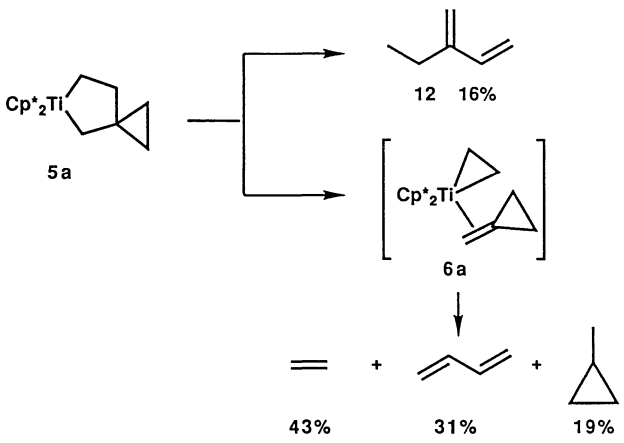

Scheme 3.

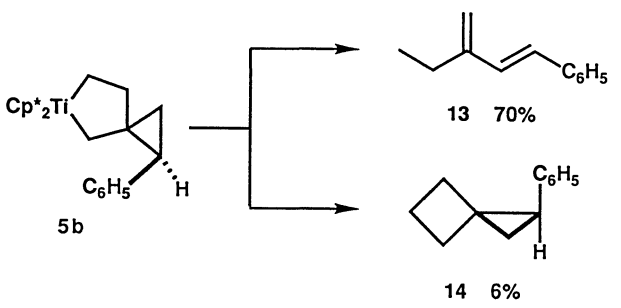

Scheme 4.

The formation mechanism of the 1,3-dienes **12** and **13** is worthy of further consideration. Three machanisms, Schemes 5—7, can be considered, a priori, whose stereochemical courses are shown for deuterium-labeled complex **15**. Mechanism A shown in Scheme 5 involves an initial rearrangement of complex **15** to **16**, followed by β-hydrogen elimination and reductive elimination. The formation of six-membered metallacycle **16** can be accounted for by a skeletal rearrangement from a cyclopropylmethyl to a 3-butenyl structure.[16] A number of examples of this type of rearrangements have so far been presented for the transition-metal-catalyzed reactions of methylenecyclopropanes.[17–21] From **16**, in which the bulky phenyl substituent occupies an equatorial position, the 1,3-diene **17** with deuterium at the terminal position will be formed by an elimination of the axial deuterium atom followed by a reductive elimination reaction.

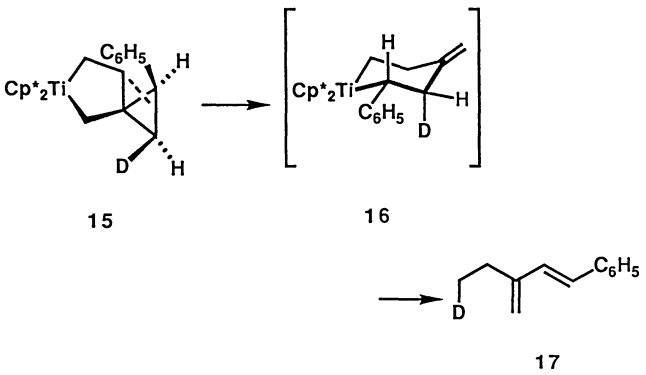

Scheme 5.

Mechanism B is illustrated in Scheme 6. This reaction is initiated by a heterolytic cleavage of the Ti–C bond, giving zwitterionic species **18**. In the next step, this eclipsed conformer **18** proceeds to a more stable gauche conformer **19** by least motion, so that the phenyl substituent at C(1) comes to the *s*-trans position. Subsequent trans hydride abstraction by titanium gives an alkyltitanium hydride species, and reductive elimination affords the 1,3-diene product **20** with deuterium at the 2-position.

Mechanism C (Scheme 7) involves a direct γ-elimination of one of the two C(2) methylene hydrogens, leading to **17**. Here, deuterium abstraction by titanium is also expected, since the Ti–D distance (4.39 Å) is shorter than that of Ti–H (4.74 Å). This mechanism can not be ruled out, even though such an elimination process seems to be unlikely in view of the long distances between Ti and these hydrogens.

In order to obtain information concerning the reaction mechanism, we studied the stereochemical course of the reaction using deuterium-labeled complex **15**. When isolated complex **15** was heated at 200 °C under vacuum, 1,3-diene **20** was obtained as the major product. Thus, the formation of **20** could be reasonably explained by mechanism B shown in Scheme 6.

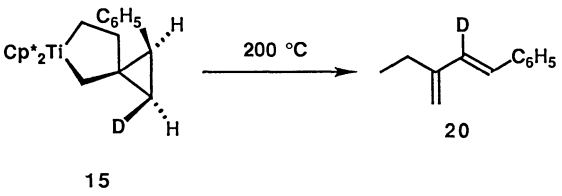

(8)

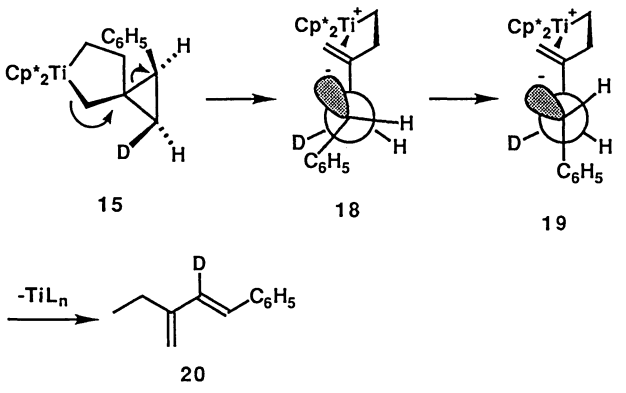

Scheme 6.

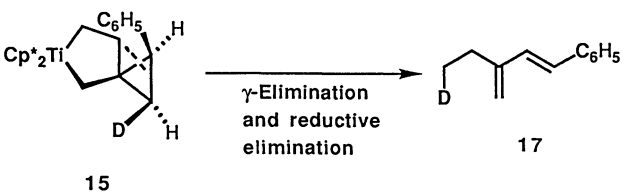

Scheme 7.

As a result, all of the three reactions (A—C illustrated in Scheme 1) are possible for titanacyclopentanes **5**, and the product distributions are highly dependent on the substituent on the metallacycles. The difference in the conformation of the five-membered ring of **5** as well as the presence of substituents in the ring may, at least in part, be a factor which controls the reaction modes.

Experimental

General. All manipulations involving air- and moisture-sensitive organometallic compounds were carried out by the use of the standard Schlenk technique under an argon atmosphere purified through a BASF-Catalyst R3-11 column. All solvents were purified by distillation under argon after drying over calcium hydride or sodium benzophenone ketyl. ^{1}H NMR spectra were recorded on a Varian EM-390 (90 MHz), a JEOL EX 270 (270 MHz), or a JEOL GX400 (400 MHz) spectrometer. ^{13}C NMR spectra were measured on a JEOL EX 270 (67.5 MHz) or a JEOL GX400 (100 MHz) spectrometer. Other spectra were recorded by the use of the following instruments: IR, Hitachi 295; low-resolution mass and high-resolution mass spectra, JEOL D300 (70 eV); gas chromatographic (GLC) analyses, Hitachi 263-30 equipped with a flame ionization detector. Elemental analyses were performed by

the Wako Pure Chemical Ind. Ltd. All melting points were measured in sealed tubes and uncorrected. Methylenecyclopropane,[22] 2-phenyl-1-methylenecyclopropane,[23] and 2,2-diphenyl-1-methylenecyclopropane[23] were prepared by the modified literature methods. Cyclobutanone was obtained from Aldrich Chem. Co.

Preparation of Decamethyltitanocene-Ethylene Complex 3. To a solution of $Cp^*_2TiCl_2$ (2.65 g, 6.8 mmol) in toluene (100 mL) was added dropwise a solution of butyllithium (15 mmol) in hexane (10 mL) at −78 °C. The reaction mixture was exposed to an atmospheric pressure of ethylene; the temperature was then allowed to rise to 20 °C. After stirring the mixture for a period of 2 days, all volatiles were removed under reduced pressure. The resulting residue was extracted with hexane (200 mL); the hexane solution was then filtered through a pad of Celite 545. The filtrate was concentrated to ca. 30 mL, and the solution was kept at −20 °C overnight to afford the ethylene complex **3** (1.01 g, 43% yield) as light-green crystals, whose NMR spectral data were superimposable with those reported.[3c]

Preparation of 5a. To a solution of decamethyltitanocene–ethylene complex **3** (0.43 g, 1.24 mmol) in hexane (50 mL) (0.43 g, 1.24 mmol) cooled at −70 °C was added methylenecyclopropane (**4a**) (2 mL, excess) by a trap-to-trap method. When the reaction mixture was slowly warmed up to −20 °C during 2 h, the light-green color changed to orange. This homogeneous solution was further stirred at −20 °C for a period of 48 h. The resulting deep-red solution was concentrated under reduced pressure; crystallization of the residue from hexane at −80 °C gave **5a** (0.32 g, 65% yield) as orange needles, mp 156—158 °C (decomp). ^{1}H NMR (400 MHz, C_6D_6) δ=0.37 (s, $2H_1$ and $2H_2$), 0.62 (s, $2H_4$), 0.63 (t, $2H_6$, $J_{6,7}$=6.8 Hz), 1.79 (t, $2H_7$), and 1.87 (s, C_5Me_5). ^{13}C NMR (100 MHz, C_6D_6) δ=12.32 ($C_5\mathit{Me}_5$, $J_{C\text{-}H}$=126 Hz), 20.48 (C_1 and C_2, 157 Hz), 25.01 (C_3), 41.59 (C_7, 123 Hz), 63.48 (125 Hz) and 65.60 (125 Hz) for C_4 and C_6, and 120.82 (C_5Me_5). IR (KBr) ν 3045 (w), 2960 (s), 2880 (s), 2800 (s), 1492 (w), 1434 (m), 1375 (s), 1314 (w), 1260 (w), 1180 (m), 1017 (m), 992 (m), 827 (w), 801 (w), 626 (w), 587 (w), 532 (w), 479 (w), 440 (w), 400 (m), and 370 (w) cm^{-1}. Mass spectrum m/z, 400 (M^+), 398 ($M^+ - 2$), 318 ($M^+ - C_6H_{10}$, base peak), 181 ($M^+ - 219$). Exact mass spectrum m/z, Calcd for $C_{26}H_{40}{}^{48}$Ti: M, 400.2609. Found: m/z 400.2584. Found: C, 77.56; H, 9.58%. Calcd for $C_{26}H_{40}$Ti: C, 77.98; H, 10.07%.

Preparation of 5b. A light-green solution of **3** (1.68 g, 4.86 mmol) and 2-phenyl-1-methylenecyclopropane (**4b**) (1.0 mL, 6.3 mmol) in hexane (50 mL) was stirred at 20 °C. After 48 h, a deep-red solution was obtained. All volatiles were removed under reduced pressure and the resulting residue was crystallized from hexane at −80 °C to give **5b** (1.92 g, 83% yield) as red plates. An analytical sample of **5b** was obtained by recrystallization from toluene at −80 °C as deep-red prisms, mp 122—124 °C (decomp). ^{1}H NMR (400 MHz, C_6D_6) δ=−0.13 (ddd, H_{6a}, $J_{6a,6b}$=11.0 Hz, $J_{6a,7b}$=5.5 Hz, and $J_{6a,7a}$=5.5 Hz), 0.09 and 0.39 (ABq, $2H_4$, $J_{4a,4b}$=11.9 Hz), 0.88 (dd, H_{2cis}, $J_{1,2cis}$=6.1 Hz and $J_{2cis,2trans}$=4.1 Hz), 0.97 (dd, H_{2trans}, $J_{1,2trans}$=8.6 Hz), 1.33 (ddd, H_{6b}, $J_{6b,7a}$=11.0 Hz, $J_{6b,7b}$=5.8 Hz), 1.53 (ddd, H_{7a}, $J_{7a,7b}$=12.3 Hz), 1.63 (dd, H_1), 1.69 (s, C_5Me_5), 1.87 (s, C_5Me_5), 2.31 (ddd, H_{7b}), 7.10—7.30 (m, C_6H_5). Stereochemical assignments of the ring methylene protons have not been performed. ^{13}C NMR (100 MHz, C_6D_6) δ= 12.08 ($C_5\mathit{Me}_5$, $J_{C\text{-}H}$=127 Hz), 12.33 ($C_5\mathit{Me}_5$, 127 Hz), 28.74 (C_2, 157 Hz), 34.17 (C_1, 154 Hz), 34.85 (C_3), 44.15 (C_7, 122 Hz), 55.36 (C_4, 125 Hz), 64.98 (C_6, 123 Hz), 120.89 (C_5Me_5), 121.02 (C_5Me_5), and aromatic carbons at 124.49, 127.49, 128.38, and 142.52. IR (KBr) ν 3045 (w), 2970 (s), 2900 (s), 2800 (s), 1640 (m), 1601 (m), 1497 (m), 1445 (m), 1378 (s), 1304 (w), 1077 (w), 1063 (w), 1019 (m), 821 (m), 774 (m), 737 (m), 697 (s), 636 (m), 401 (w) cm^{-1}. Mass spectrum m/z, 476 (M^+), 318 ($M^+ - C_{12}H_{14}$), 158 ($M^+ - Cp^*_2Ti$), 129 ($M^+ - 347$, base peak). Exact mass spectrum m/z, Calcd for $C_{32}H_{44}{}^{48}$Ti: M, 476.2921. Found: m/z 476.2900. Found: C, 80.17; H, 9.95%. Calcd for $C_{32}H_{44}$Ti: C, 80.65; H, 9.31%.

X-Ray Structure Determination of 5b. Deep-red crystals of **5b** were grown from a saturated toluene solution at −20 °C overnight. The crystals were mounted in thin-walled glass capillaries under argon and then flame-sealed. Pertinent details concerning the data collection and the final cell dimensions, which were obtained from a least-squares refinement of 2θ values of 50 independent reflections in the range of $19°<2\theta<30°$, are given in Table 3.

The 4261 unique raw intensity data were converted to values of the structure factor by corrections for Lorentz and polarization effects. Inspection of the standard three reflections ((8 0 0), (0 4 0), and (0 0 4)) measured after every 50 reflections showed no systematic variation in the intensity. A systematic absence, (h 0 l) with h=odd and (0 k 0) with k=odd, indicated the space group $P2_1/a$.

The location of the titanium atom was determined by a direct method (MULTAN-78 program).[25] A series of standard block-diagonal least-squares refinements and Fourier syntheses revealed the remaining carbon atoms as an anisotropic temperature factor. The hydrogen atoms were located both by the difference Fourier syntheses and calculations. All non-hydrogen atoms as an anisotropic and hydrogen atoms as an isotropic temperature factor were refined to $R=\sum||F_o|-|F_c||/\sum|F_o|=0.053$ and $R_w=[\sum w(|F_o|-|F_c|)^2/\sum w|F_o|^2]^{1/2}=0.056$. A weighting scheme, $1/w=\sigma_c{}^2+(0.015|F_o|)^2$, was employed. A final difference Fourier map indicated that no

Table 3. Crystal Data and Data Collection Parameters of **5b**

Formula	$C_{32}H_{44}$Ti
Fw	476.58
Crystal system	Monoclinic
Space group	$P2_1/a$
a/Å	21.832(3)
b/Å	8.580(1)
c/Å	14.759(2)
β/deg	96.81(1)
U/Å^3	2744.9(6)
Z	4
D_{calcd}/g cm^{-3}	1.154
Crystal size/mm	0.22×0.32×0.40
μ(Mo $K\alpha$)/cm^{-1}	3.42
Diffractometer	Rigaku AFC-5
Scan type	ω–2θ
Scan range/deg	1.1+0.5 tan θ
bkgd/sec	8 at each end of the scan
Scan speed/deg min^{-1}	3
Data collected	$\pm h$, k, l
$2\theta_{max}$/deg	60.0
No. of reflctns	4938
No. of unique reflctns, $\|F_o\|>3\sigma(F_o)$	4261
No. of variables	475
R	0.053
R_w	0.056

significant residual peak remained. The selected bond lengths and angles are listed in Tables 1 and 2, respectively.

Catalytic Isomerization of 2,2-Diphenyl-1-methylenecyclopropane (4c). A sealed NMR tube containig complex **3** (2.0 mg, 0.057 mmol) and 2,2-diphenyl-l-methylenecyclopropane (**4c**) (35 mg, 0.17 mmol) in toluene-d_8 (0.5 mL) was heated at 70 °C for a period of 1 h. The light-green color changed to orange. ^{1}H NMR spectrum showed that **4c** was converted to 1,1-diphenyl-1,3-butadiene (**7**),[26] which was isolated by preparative TLC (Merck silica gel 60 F_{254}). **7**: ^{1}H NMR ($CDCl_3$) δ=5.12 (dd, H_3, $J_{2,3}$=10.1 and $J_{3,4}$=1.8 Hz), 5.38 (dd, H_4, $J_{2,4}$=16.8 Hz), 6.44 (ddd, H_2, $J_{1,2}$=11.0 Hz), 6.71 (d, H_1). ^{13}C NMR ($CDCl_3$) δ=118.48 (C_4, J_{C-H}=158 Hz), 127.26 (160 Hz), 127.37 (160 Hz), 127.44 (160 Hz), 128.03 (160 Hz), 128.06 (160 Hz), 130.27 (162 Hz), 128.39 (C_3, 155 Hz), 134.85 (C_2, 156 Hz), 139.53, 141.96, 143.02. Mass spectrum m/z, 206 (M^+, base peak), 191 ($M^+ - 15$), 178 ($M^+ - 28$), 165 ($M^+ - 41$). Exact mass spectrum, m/z, Calcd for $C_{16}H_{14}$: M, 206.1095, Found: m/z 206.1076.

Reaction of 3 with Phenylallene. To a solution of **3** (140 mg, 0.405 mmol) in toluene (10 mL) was added dropwise phenylallene (304 mg, 2.62 mmol) in toluene (5 mL) at −50 °C. This solution was stirred at room temperature overnight. The color of the solution turned from light-green to red. The resulting solution was concentrated in vacuo; the residue was then dissolved in hexane (5 mL). Upon cooling the solution at −20 °C, complex **9** (90 mg, 75% purity, 38% yield) precipitated as a green powder. In spite of repeated recrystallization from hexane, no pure sample of **9** could be obtained. ^{1}H NMR (C_6D_6) δ=1.67 (s, $2C_5Me_5$), 2.60 (d, H_3, $J_{1,3}$=3.3 Hz, H_3), 5.12 (d, H_1), 7.0—7.5 (m, C_6H_5). ^{13}C NMR (C_6D_6) δ=11.60 ($C_5\mathit{Me}_5$, J_{C-H}=126 Hz), 86.54 (C_3, 147 Hz), 119.53 (C_5Me_5), 120.83 (C_1, 156 Hz), 244.15 (C_2), 124.56 (160 Hz), 126.05 (146 Hz), 128.43 (158 Hz), and 142.00 (aromatic carbons).

Oxidation of complex **9** by O_2 in C_6D_6 afforded phenylallene in quantitative yield (by ^{1}H NMR).

Hydrolysis of 5a. A solution of **5a** (24 mg, 0.06 mmol) in octane (5 mL) was treated with Al_2O_3 (0.5 g) at room temperature. The orange-red color changed immediately to pale-yellow. GLC analysis indicated that 1-methyl-1-ethylcyclopropane (**10a**) was formed in 96% yield. An authentic sample of **10a** was prepared by the Simmons–Smith[27] methylenation of 2-methyl-1-butene. ^{1}H NMR ($CDCl_3$) δ=0.22 (m, cyclopropane ring protons, 4H), 0.92 (t, CH_3CH_2, J=7.32 Hz), 1.02 (s, CH_3), 1.25 (q, $CH_3\mathit{CH}_2$). ^{13}C NMR ($CDCl_3$) δ=10.82 ($\mathit{C}H_3CH_2$, J_{C-H}=125 Hz), 12.61 (cyclopropane ring carbons, 158 Hz), 16.30 (C_1), 22.19 (CH_3, 126 Hz), 31.97 ($CH_3\mathit{C}H_2$, 124 Hz). Mass spectrum m/z, 84 (M^+), 69 ($M^+ - CH_3$, base peak).

Hydrolysis of 5b. Complex **5b** (64 mg, 0.13 mmol) in benzene (5 mL) was treated with Al_2O_3 (0.5 g) to give 1-ethyl-1-methyl-2-phenylcyclopropane (**10b**) in 88% yield (determined by ^{1}H NMR). The stereochemistry of **10b** was determined to be the *r*-1-ethyl-*t*-2-phenyl isomer by a comparison of its GLC retention time and the ^{1}H NMR spectrum with those of the authentic sample.

Preparation of (*E*)- and (*Z*)-2-Methyl-1-phenyl-1-butene. The title compounds have been reported as being a mixture of *E* and *Z* isomers.[28] These isomers were separated by preparative GLC (DIDP, 140 °C, 0.6 kg cm^{-1}). *Z*-isomer: ^{1}H NMR ($CDCl_3$) δ=1.09 (t, $CH_2\mathit{CH}_3$, J=7.63 Hz), 1.88 (s, CH_3), 2.24 (q, CH_2CH_3), 6.25 (s, -CH=), 7.18—7.31 (m, C_6H_5). ^{13}C NMR ($CDCl_3$) δ=12.74 (C_4, J_{C-H}=127 Hz), 23.43 (CH_3, 134 Hz), 25.43 (C_3, 124 Hz), 124.73 (C_1, 153 Hz), 125.72 (162 Hz), 127.93 (158 Hz), 128.39 (155 Hz), 138.48, 140.92. *E*-isomer: ^{1}H NMR ($CDCl_3$) δ=1.11 (t, CH_3CH_2, J=7.63 Hz), 1.86 (s, CH_3), 2.18 (q, $CH_3\mathit{CH}_2$), 6.26 (s, olefinic proton), 7.15—7.32 (m, C_6H_5). ^{13}C NMR ($CDCl_3$) δ=12.65 (C_4, J_{C-H} =127 Hz), 17.60 (CH_3, 127 Hz), 33.24 (C_3, 127 Hz), 123.51 (C_1, 151 Hz), 125.63 (160 Hz), 127.88 (160 Hz), 128.72 (157 Hz), 138.69, 140.70. The stereochemistry was determined on the basis of ^{13}C NMR spectrum.[29] Mass spectrum m/z, 146 (M^+), 131 ($M^+ - CH_3$, base peak).

Preparation of *r*-1-Ethyl-1-methyl-*c*-2-phenylcyclopropane and *r*-1-Ethyl-*t*-2-phenyl Isomers.[30] Both isomers of the title compound were prepared by the Simmons–Smith methylenation[27] of (*E*)- and (*Z*)-2-methyl-1-phenyl-1-butene, respectively. *c*-2-Phenyl isomer: ^{1}H NMR ($CDCl_3$) δ=0.74 (dd, H_{3t}, $J_{3t,3c}$=5.89 Hz), 0.79 (t, CH_3CH_2, J=7.48 Hz), 0.84 (dd, H_{3c}), 0.93 and 1.13 (ABX pattern, $CH_3\mathit{CH}_2$), 1.21 (s, CH_3), 1.95 (dd, H_2, $J_{2,3t}$=8.24 and $J_{2,3c}$=5.80 Hz), 7.18—7.35 (m, C_6H_5). ^{13}C NMR ($CDCl_3$) δ=10.60 (CH_3, J_{C-H}=124 Hz), 17.20 (C_3, 157 Hz), 23.89 (CH_3, 125 Hz), 24.04 (C_1), 26.52 (CH_2, 123 Hz), 30.42 (C_2, 158 Hz), 125.30 (162 Hz), 127.66 (160 Hz), 128.81 (160 Hz), and 140.02 for aromatic carbons. *t*-2-Phenyl isomer **10b**: ^{1}H NMR ($CDCl_3$) δ=0.76 (s, CH_3), 0.76—0.80 (m, H_{3t} and H_{3c}), 1.03 (m, $CH_2\mathit{CH}_3$), 1.32 and 1.53 (ABX pattern, CH_2CH_3, J=6.1 and 12.0 Hz), 1.87 (t, H_2, J=6.0 Hz), 7.17—7.30 (m, C_6H_5). ^{13}C NMR ($CDCl_3$) δ=10.93 (CH_3, J_{C-H}=125 Hz), 17.09 (CH_3, 125 Hz), 17.58 (C_3, 157 Hz), 23.91 (C_1), 28.74 (C_2, 158 Hz), 33.84 (CH_2, 123 Hz), 125.30 (160 Hz), 127.69 (160 Hz), 128.87 (160 Hz), 148.15 for aromatic carbons. The mass spectrum of the trans and cis mixture m/z, 160 (M^+), 145 ($M^+ - CH_3$), 131 ($M^+ - C_2H_5$, base peak). Exact mass spectrum m/z, Calcd for $C_{12}H_{16}$: M, 160.1252. Found: m/z 160.1252.

Reaction of 5a with H_2. After placing a solution of **5a** (32 mg, 0.081 mmol) in octane (4 mL) into a glass pressure bottle, hydrogen was introduced up to 3 atm. After 20 h at room temperature, 1-ethyl-1-methylcyclopropane (**10a**) was obtained in 86% yield (GLC). The structure was identified by a comparison of the GLC retention time and the ^{1}H NMR spectrum with those of the authentic sample.

Reaction of 5b with H_2. After placing a solution of **5b** (37 mg, 0.078 mmol) in hexane (10 mL) into a glass pressure bottle, hydrogen was introduced up to 3 atm. Then, after stirring the mixture at room temperature for 40 h, the orange-red solution turned to orange. *r*-1-Ethyl-1-methyl-*t*-2-phenylcyclopropane (**10b**) was obtained in 88% yield (GLC).

Reaction of 5a with CO. An orange solution of **5a** (131 mg, 0.327 mmol) in hexane (10 mL) was placed in a glass pressure bottle (100 mL); carbon monoxide (3 atm) was then pressured. After stirring at room temperature for 45 min, the starting complex was converted to spiro[2.4]heptan-5-one (**11a**) in 98% yield, the structure of which was confirmed by a comparison of the ^{1}H, ^{13}C, mass, and IR spectra with the reported ones.[31]

Reaction of 5b with CO. A solution of complex **5b** (99.3 mg, 0.21 mmol) in toluene (10 mL) was placed in an autoclave. Carbon monoxide was then pressured to 30 atm. After 20 min at room temperature, the decrease in the CO pressure stopped. 1-Phenylspiro[2.4]heptan-5-one (**11b**) was obtained in 98% yield (GLC) which was isolated by preparative GLC (SE-30, 220 °C) separation. **11b**: ^{1}H NMR ($CDCl_3$) δ=1.13 (d, H_2, $J_{1,2}$=7.64 Hz), 1.91 and 2.04 (ABq, H_4), 2.05 (ABX,

$2H_7$), 2.12 (t, H_1), 2.41 (t, $2H_6$, $J_{6,7}$=7.78 Hz), 7.05—7.28 (m, C_6H_5). ^{13}C NMR ($CDCl_3$) δ=16.58 (C_2, J_{C-H}=159 Hz), 27.40 (C_3), 28.61 (C_1, 158 Hz), 33.69 (132 Hz), 39.32 (131 Hz), and 42.05 (131 Hz) for C_4, C_6, and C_7, 125.92 (160 Hz), 127.73 (158 Hz), 128.15 (158 Hz), and 138.69 for aromatic carbons, 217.79 (C_5). IR (neat) ν 1747 cm^{-1} (C=O). Mass spectrum m/z, 186 (M^+), 142 ($M^+ - 44$), 129 ($M^+ - 57$), 91 ($M^+ - 95$, base peak). Exact mass spectrum m/z, Calcd for $C_{13}H_{14}O$: M, 186.1045. Found: m/z 186.1045.

Thermolysis of 5a. The isolated complex **5a** (21 mg, 0.053 mmol) was placed in a Schlenk tube and rapidly heated up to 200 °C under reduced pressure in an oil bath. The products were condensed into an NMR tube, and the tube was sealed. ^{1}H NMR and GLC analysis (Durapak) indicated that methylcyclopropane[32] (19%), butadiene (31%), 2-ethyl-1,3-butadiene **12** (16%), and ethylene (43%) were obtained. These compounds were also analyzed by GC-Mass spectroscopy.

Thermolysis of 5b. Complex **5b** (146 mg, 0.31 mmol) was heated at 200 °C under reduced pressure, and the volatile products were condensed on a liquid-nitrogen cold finger. GLC and ^{1}H NMR analysis indicated that 1-phenyl-3-ethyl-1,3-butadiene (**13**)[33] (70%) and 1-phenylspiro[2.3]hexane (**14**) (6%) were obtained. The structure of **12** was determined by a comparision of the ^{1}H NMR and GLC retention time with those of an authentic sample. **13**: ^{1}H NMR ($CDCl_3$) δ=1.18 (t, CH_2CH_3, J=7.5 Hz), 2.37 (q, CH_2CH_3), 5.09 and 5.14 (=CH_2), 6.60 (d, H_1, J=16.3 Hz), 6.84 (d, H_2), 7.21—7.45 (m, C_6H_5). ^{13}C NMR ($CDCl_3$) δ=12.68, 24.66, 115.03, 126.31, 127.24, 127.66, 128.48, 137.42, 147.64. Mass spectrum m/z, 158 (M^+), 143 ($M^+ - CH_3$), 129 ($M^+ - C_2H_5$, base peak). Exact mass spectrum m/z, Calcd for $C_{16}H_{14}$: M, 158.1095. Found: m/z 158.1089.

Preparation of Benzylidenecyclobutane. In an 80 mL Schlenk tube equipped with a magnetic stirring bar was stirred a solution of cyclobutanone (1.0 g, 14 mmol) dissolved in 20 mL of THF. This was cooled to −60 °C; then a solution of benzylmagnesium chloride (15 mmol) in THF (20 mL) was added dropwise over 0.5 h. When the addition was completed, the homogeneous solution was slowly warmed to room temperature over a period of 2 h. The reaction mixture was poured into ice-water, and the mixture was extracted with three 50-mL portions of ether. The crude alcohol was treated with 6 equiv H_2SO_4 at 70—80 °C for 2 h. The products were extracted with ether (50 mL). The ether layer was washed with aq $NaHCO_3$ and dried over sodium sulfate. Crude benzylidenecyclobutane (0.77 g, 37% yield) was obtained by short-path distillation and used without further purification. ^{1}H NMR ($CDCl_3$) δ=2.09 (m, $CH_2CH_2CH_2$), 2.87 (t, $CH_2CH_2CH_2$, J=7.8 Hz), 3.03 (t, $CH_2CH_2CH_2$, J=7.9 Hz), 6.06 (s, olefinic proton), 7.11—7.31 (m, C_6H_5).

Preparation of 1-Phenylspiro[2.3]hexane (14). A mixture of benzylidenecyclobutane (0.75 g, 5.2 mmol), diiodomethane (3.0 g, 11 mmol), and zinc–copper (2.49 g, 38 mmol) in ether (40 mL) was heated at reflux for 30 h. The solution was filtered and the solid was washed with two 30-mL portions of ether. The filtrate and washings were treated with aq. sodium hydrogencarbonate (30 mL, twice), and then with saturated aq. sodium chloride. The ether layer was dried over sodium sulfate. Short-path distillation yielded a colorless oil (0.46 g). A GLC analysis indicated that the product was contaminated with several impurities. Preparative GLC separation (DIDP column) gave a pure sample of **14**. ^{1}H NMR ($CDCl_3$) δ=0.85 (dd, H_{2trans}, $J_{1,2trans}$=8.85 Hz, $J_{2cis,2trans}$=5.49 Hz), 1.06 (dd, H_{2cis}, $J_{1,2cis}$=5.80 Hz), 1.83 (dd, H_1), 1.89—2.27 (m, cyclobutane methylene protons), 6.95—7.27 (m, C_6H_5). ^{13}C NMR ($CDCl_3$) δ=16.49 (C_5, J_{C-H}=138 Hz), 20.44 (C_2, 160 Hz), 26.38 (132 Hz) and 31.35 (135 Hz) for C_4 and C_6, 28.08 (C_1, 158 Hz), 28.54 (C_3), 124.88 (161 Hz), 126.49 (158 Hz), 127.84 (158 Hz), and 141.28 for aromatic carbons. IR (KBr) ν 3058 (m), 3020 (m), 2978 (m), 2942 (s), 2920 (s), 2848 (m), 1602 (m), 1498 (s), 1452 (m), 1204 (w), 1107 (w), 1086 (w), 1062 (w), 1037 (w), 918 (w), 833 (w), 787 (w), 761 (m), 741 (m), 702 (s) cm^{-1}. Mass spectrum m/z, 158 (M^+), 143 ($M^+ - CH_3$), 130 ($M^+ - C_2H_4$, base peak), 115 ($M^+ - C_3H_7$), 104 ($M^+ - C_4H_6$). Exact mass spectrum m/z, Calcd for $C_{12}H_{14}$: M, 158.1095. Found: m/z 158.1099.

Preparation of *cis*-3-Deuterio-2-phenyl-1-methylenecyclopropane (*cis*-4b-d_1). This compound was prepared by essentially the same method as that described in the literature.[24] Only modification is used for the preparation of *cis*-3-deuterio-1,1-dibromo-2-phenylcyclopropane with a phase-transfer catalyst system.[23a]

Thermolysis of 15. Complex **15** has been thermally decomposed as described for **5b**. 2-Deuterio-1-phenyl-3-ethyl-1,3-butadiene (**20**) was obtained. Within the limit of ^{1}H NMR detection, deuterium was only located at the C(2) position. The deuterium content of **20** was 88%.

We thank the Ministry of Education, Science and Culture, Japan, for financial supports of this work (Nos. 59740256 and 03650699).

References

1) J. P. Collman, L. S. Hegedus, J. R. Norton, and R. G. Finke, "Principles and Applications of Organotransition Metal Chemistry," University Science Books, Mill Valley, California (1987), Chap. 9.

2) For example: a) S. Takahashi, Y. Suzuki, K. Sonogashira, and N. Hagihara, *J. Chem. Soc., Chem. Commun.*, **1976**, 839. b) M. J. Doyle, J. McMeeking, and P. Binger, *J. Chem. Soc., Chem. Commun*, **1976**, 376. c) Y. Wakatsuki, K. Aoki, and H. Yamazaki, *J. Am. Chem. Soc.*, **101**, 1123 (1979). d) R. J. McKinney, T. H. Tulip, D. L. Thorn, T. S. Coolbaugh, and F. N. Tebbe, *J. Am. Chem. Soc.*, **103**, 5584 (1981). e) J. B. Lee, K. C. Ott, and R. H. Grubbs, *J. Am. Chem. Soc.*, **104**, 7491 (1982). f) P. Diversi, G. Ingrosso, and A. Lucherini, *Inorg. Synth.*, **22**, 171 (1983). g) E. Lindner, E. Schauss, W. Hiller, and R. Fawzi, *Angew. Chem., Int. Ed. Engl.*, **23**, 711 (1984). h) S. A. Cohen and J. E. Bercaw, *Organometallics*, **4**, 1006 (1985).

3) a) J. X. McDermott, M. E. Wilson, and G. M. Whitesides, *J. Am. Chem. Soc.*, **98**, 6529 (1976). b) R. H. Grubbs and A. Miyashita, *J. Chem. Soc., Chem. Commun.*, **1977**, 864. c) S. A. Cohen, P. R. Auburn, and J. E. Bercaw, *J. Am. Chem. Soc.*, **105**, 1136 (1983).

4) A part of this work has been communicated: K. Mashima and H. Takaya, *Organometallics*, **4**, 1464 (1984).

5) P. Diversi, G. Ingrosso, A. Lucherini, W. Porzio, and M. Zocchi, *Inorg. Chem.*, **19**, 3590 (1980).

6) P. Binger, M. J. Doyle, C. Krüger, and Y.-H. Tsay, *Z. Naturforsch., B: Anorg. Chem., Org. Chem.*, **34b**, 1289 (1979).

7) J. W. Lauher and R. Hoffmann, *J. Am. Chem. Soc.*, **98**, 1729 (1976).

8) a) M. L. Steigerwald and W. A. Goddard, III, *J. Am. Chem. Soc.*, **107**, 5027 (1985). b) A. Stockis and R.

Hoffmann, *J. Am. Chem. Soc.*, **102**, 2952 (1980), and the references cited therein.

9) R. Noyori, T. Ishigami, N. Hayashi, and H. Takaya, *J. Am. Chem. Soc.*, **95**, 1674 (1973).

10) M. Akita, H. Yasuda, K. Nagasuna, and A. Nakamura, *Bull. Chem. Soc. Jpn.*, **56**, 554 (1983).

11) M. Akita, H. Yasuda, and A. Nakamura, *Bull. Chem. Soc. Jpn.*, **57**, 480 (1984).

12) For compound **1**, an insertion of carbon monoxide followed by a reductive elimination reaction to give cyclopentanone has been reported.[3a)]

13) J. M. Manriquez, D. R. McAlister, R. D. Sanner, and J. E. Bercaw, *J. Am. Chem. Soc.*, **100**, 2716 (1978).

14) a) R. H. Grubbs and W. Tumas, *Science*, **243**, 907 (1989). b) M. J. Burk, W. Tumas, M. D. Ward, and D. R. Wheeler, *J. Am. Chem. Soc.*, **112**, 6133 (1990). c) M. J. Burk, D. L. Staley, and W. Tumas, *J. Chem. Soc., Chem. Commun.*, **1990**, 809.

15) R. Noyori, M. Yamakawa, and H. Takaya, *J. Am. Chem. Soc.*, **98**, 1471 (1976).

16) Anion rearrangement: D. J. Patel, C. L. Hamilton, and J. D. Roberts, *J. Am. Chem. Soc.*, **87**, 5144 (1965). Radical rearrangement: A. Effio, D. Griller, K. U. Ingold, A. L. J. Beckwith, and A. K. Serelis, *J. Am. Chem. Soc.*, **102**, 1734 (1980).

17) Transition-metal catalyzed reactions of methylenecyclopropanes in the presence of olefinic substrates give a variety of homo- and cross-coupling products,[18–21)] for which mechanisms involving similar type of rearrangements have been proposed.[18,21)]

18) a) H. Takaya, N. Hayashi, T. Ishigami, and R. Noyori, *Chem. Lett.*, **1973**, 813. b) P. Binger, A. Brinkmann, and P. Wedemann, *Chem. Ber.*, **116**, 2920 (1983).

19) a) R. Noyori, T. Odagi, and H. Takaya, *J. Am. Chem. Soc.*, **92**, 5780 (1970). b) R. Noyori, Y. Kumagai, I. Umeda, and H. Takaya. *J. Am. Chem. Soc.*, **94**, 4018 (1972). c) R. Noyori, M. Yamakawa, and H. Takaya, *Tetrahedron Lett.*, **1978**, 4823.

20) a) P. Binger, *Angew. Chem., Int. Ed. Engl.*, **11**, 309 (1972). b) P. Binger, *Synthesis*, **1973**, 427.

21) a) P. Binger, M. J. Doyle, and R. Benn, *Chem. Ber.*, **116**, 1 (1983). b) P. Binger, T. R. Martin, R. Benn, A. Rufinska, and G. Schroth, *Z. Naturforsch., B: Anorg. Chem., Org. Chem.*, **39b**, 993 (1984).

22) R. Köster, S. Arora, and P Binger, *Synthesis*, **1971**, 322.

23) a) L. Skattebøl, G. A. Abskharoun, and T. Greibrokk, *Tetrahedron Lett.*, **1973**, 1367. b) K. Kitatani, T. Hiyama, and H. Nozaki, *Bull. Chem. Soc. Jpn.*, **50**, 3288 (1977). c) S. Arora and P. Binger, *Synthesis*, **1974**, 801.

24) A. R. Pinhas, A. G. Samuelson, R. Risemberg, E. V. Arnold, J. Clardy, and B. K. Carpenter, *J. Am. Chem. Soc.*, **103**, 1668 (1981).

25) MULTAN-78 and UNICS-III program system of Computer Center of IMS.

26) U. Schöllkopf and F. Gerhart, *Angew. Chem., Int. Ed. Engl.*, **7**, 805 (1968).

27) R. S. Shank and H. Shechter, *J. Org. Chem.*, **24**, 1825 (1959).

28) a) D. Seyferth and J. Fogel, *J. Organomet. Chem.*, **6**, 205 (1966). b) C. Rüchardt and H. Trautwein, *Chem. Ber.*, **98**, 2478 (1965).

29) L. Hevesi, J. B. Nagy, A. Krief, and E. G. Derouane, *Org. Mag. Reson.*, **10**, 14 (1977).

30) W. Engel, E. Seeger, H. Teufel, and H. Machleidt, *Chem. Ber.*, **104**, 248 (1971).

31) A. Sonoda, I. Moritani, J. Miki, T. Tsuji, and S. Nishida, *Bull. Chem. Soc. Jpn.*, **45**, 1777 (1972).

32) M. F. Hawthorne, *J. Am. Chem. Soc.*, **82**, 1886 (1960).

33) J. Mulzer, U. Kühl, and G. Brüntrup, *Tetrahedron Lett.*, **1978**, 2953.

 © 1991 The Chemical Society of Japan Bull. Chem. Soc. Jpn., 64, 2484—2487 (1991) [Vol. 64, No. 8

Reversed Phase Extraction Chromatographic Separation of Germanium with Aliquat 336S from Citric Acid

Sarat Kumar SAHOO
Department of Metallurgical Engineering, Indian Institute of Technology, Bombay 400076, India
(Received October 18, 1990)

Germanium was extracted from 0.005 mol dm^{-3} citric acid at a pH between 2.5 and 6.5 on a column of silica gel coated with Aliquat 336S as the stationary phase. Germanium was then stripped with 0.5 mol dm^{-3} hydrochloric acid and determined spectrophotometrically as its complex with phenylfluorone. Germanium was separated from alkali and alkaline earths, manganese, iron, cobalt, nickel, copper, and zinc in binary mixtures by the exploitation of difference in pH for formation of citrato complexes. It was separated from antimony, bismuth, tin, gallium, indium, and thallium by taking advantage of stability of chloro and sulfato complexes. This method was applied to the determination of germanium in coal fly ash.

The solvent extraction methods for the separation of germanium with liquid anion exchangers as extractants are limited. Germanium has been separated from tin and lead with Amberlite LA-1.[1] Trioctylamine in kerosine was used for the extraction of germanium from oxalic acid.[2,3] The separation of germanium from cobalt and copper by extraction chromatography was carried out with trioctylamine.[4] However, germanium was not separated from associated elements. In continuation of our work with citric acid[5] as the complexing media, extraction chromatographic studies were extended for the separation of germanium on a column of silica gel coated with Aliquat 336S as the stationary phase. This paper describes the separation of germanium from associated elements.

Experimental

Apparatus and Reagents. Spectrophotometer GS 886C (ECIL, India) with matched corex glass cells and Orion Research Microprocessor Ionalyser 901 (Orion, USA) were used.

A stock solution of germanium (3.976 mg cm^{-3}) was prepared by fusing 0.573 g of germanium oxide (ExcelaR grade, Qualigens, India) with 0.5 g of sodium hydroxide in a platinum crucible, neutralizing the residue with hydrochloric acid and diluting to 100 cm^3 with distilled water, and standardized gravimetrically.[6] A solution containing 15 μg cm^{-3} of germanium was prepared by appropriate dilution.

Aliquat 336S (trialkylmethylammonium chloride) was obtained from Fluka and used without further purification.

The silica gel (100—200 mesh) was dried at 120 °C for 2 h, and then packed in a U-tube. A stream of dry nitrogen was passed for 3 h through a small Drechsel bottle containing 25 cm^3 of dimethyldichlorosilane, and then through U-tube containing the silica gel, to convert the surface silanol groups to silyl ether groups. The silica gel was then washed with anhydrous methanol to form methoxyl groups from the unreacted hydroxyl groups, as well as to remove hydrochloric acid from the silica gel. The treated silica gel was then dried at 100 °C. In routine work 1 cm^3 of dimethyldichlorosilane is adequate to render 10 g of silica gel hydrophobic.

A solution of 1 cm^3 of Aliquat 336S in benzene was prepared and transferred into a flask containing 4 g of the hydrophobic silica gel. The benzene was slowly removed from the suspension, in a rotary vacuum evaporator, until dry silica gel was obtained; a low vacuum was applied to remove air from the micropores and to accelerate evaporation of benzene. The silica gel coated with Aliquat 336S was then slurried with citric acid solution and poured into a column having a bed dimension of 10×0.8 cm, where 4 g of the coated silica gel was sufficient to give a bed height of 8 cm which was used for the column studies. The column is not affected with use of strong acids or alkalies as stripping agents.

General Procedure. An aliquot of solution containing 15 μg of germanium was mixed with 5 cm^3 of 0.005 mol dm^{-3} citric acid and the pH of the resulting solution was adjusted to 4.0 either with 0.005 mol dm^{-3} citric acid or sodium hydroxide. The solution was passed through the column at a flow rate of 1 cm^3 min^{-1} where germanium was extracted as its anionic citrato complex by Aliquat 336S. It was stripped with various mineral acids and alkalies. Eight 5 cm^3 fractions were collected. The amount of germanium from each fraction was determined spectrophotometrically as its complex with phenylfluorone at 530 nm.[7]

Results and Discussion

Germanium can be quantitatively extracted with 0.1 mol dm^{-3} Aliquat 336S in xylene from 0.01 mol dm^{-3} citric acid at a pH between 3.0 and 6.0 employing batch

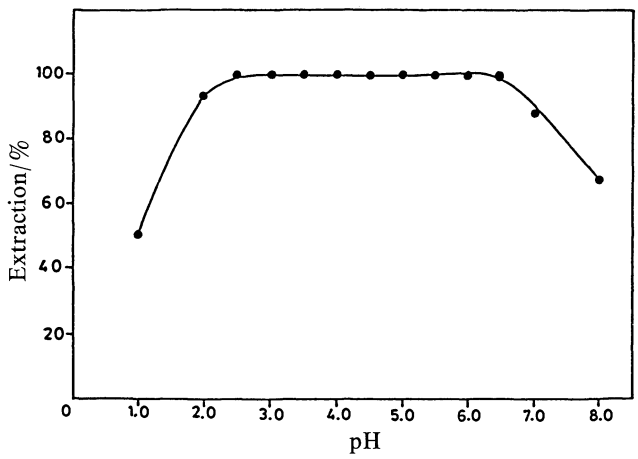

Fig. 1. Effect of pH on extraction of germanium from citric acid.

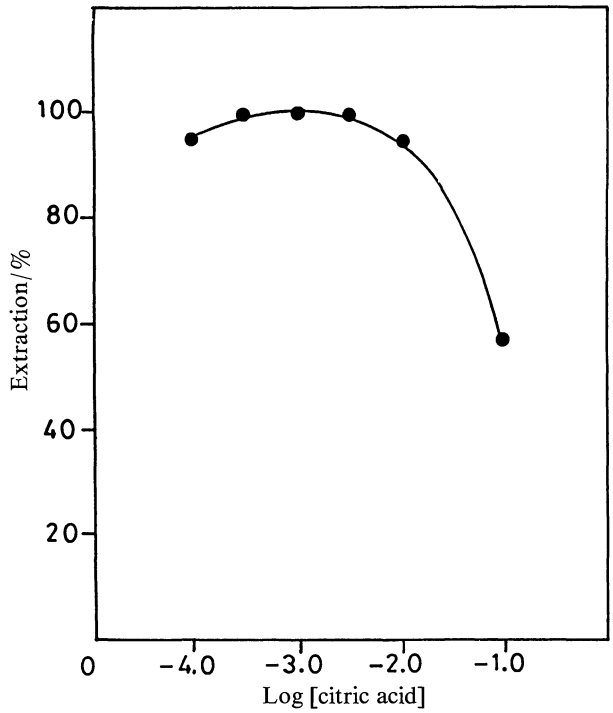

Fig. 2. Effect of citric acid concentration on extraction of germanium.

extraction.[8] However in the extraction chromatographic method, this procedure was modified. The study of extraction of germanium as a function of pH was carried out in the pH range of 1.0 to 8.0. The extraction commenced at pH 1.0 (51.4%) and was quantitative in the pH range of 2.5 to 6.5. Above pH 6.5 (96.2% extracted), the amount of germanium extracted decreased (Fig. 1). The optimum pH for the extraction of germanium used was 4.0 as it is intermediate between 2.5 to 6.0 where extraction was quantitative.

The optimum concentration of citric acid for the complete extraction of germanium was ascertained by extracting from aqueous solution containing 1×10^{-4} to 1×10^{-2} mol dm^{-3} of citric acid. The extraction was incomplete below 1×10^{-4} mol dm^{-3} (Fig. 2). Above 1×10^{-2} mol dm^{-3} citric acid concentration the extraction decreased probably due to presence of competitive equilibria between anionic citrato complex of germanium and citrate anion of Aliquat 336S.

The germanium extracted was stripped from the stationary phase with various mineral acids and alkalies. Hydrochloric acid (0.5—4 mol dm^{-3}), nitric or sulfuric acid (0.25—8 mol dm^{-3}) was capable of stripping of germanium quantitatively. Similarly, 0.25—1.0 mol dm^{-3} of sodium hydroxide or sodium carbonate was also effective for stripping of germanium. At high concentration of hydrochloric acid (>6 mol dm^{-3}) germanium forms negatively charged chloro complex which in turn was reextracted on the column. Hydrochloric acid was selected as a stripping agent considering its use in the spectrophotometric determination of germanium (Table 1).

Separation of Germanium from Other Ions. Germanium was separated from several elements in binary mixtures by utilizing the differences in their capability to form anionic complexes. Thus, since alkali and alkaline earths, manganese, iron, cobalt, nickel, zinc, cadmium, aluminium, and lead can not form anionic citrato complexes they were not extracted and hence were separated from germanium. Some metal ions forming stable complexes with citrate were strongly retained on the column but these were effectively separated from germanium by using suitable stripping agents. Since germanium forms anionic chloro complexes at higher concentration of hydrochloric acid, it was possible to separate it from scandium, titanium, zirconium, hafnium, vanadium, thorium, and palladium as they can not form such complexes and were stripped out with 6 mol dm^{-3} hydrochloric acid. Germanium, which was retained in the form of anionic chloro complex on the liquid anion exchanger, was subsequently stripped with 0.5 mol dm^{-3} hydrochloric acid. Germanium has been separated from gallium, indium, thallium, tin, antimony, and bismuth in binary mixtures by the judicious choice of stripping agents. Germanium was stripped with 3 mol dm^{-3} hydrochloric acid when other elements were reextracted as chloro complexes and later stripped with specific eluents (Table 2). In all these separations, the elements were determined spectrophotometrically by using appropriate chromogenic reagents.[9] Examples of the separation of germanium from multicomponent mixtures are given in Table 3.

Analysis of Germanium in Fly Ash. A 0.5 g of fly ash was dissolved in a mixture (10 cm^3) of aqua regia and hydrofluoric acid (1 : 1) in a Teflon container[10] and evaporated to almost dryness. The residue was dis-

Table 1. Effect of Stripping Agents. Amount of Ge Taken, 15 μg

Stripping agent	Recovery/%									
mol dm^{-3}	0.1	0.25	0.5	1.0	2.0	3.0	4.0	5.0	6.0	8.0
HCl	0.0	92.4	100.1	100.1	100.1	100.1	100.1	14.5	0.0	0.0
HNO_3	65.5	99.8	99.9	99.8	99.8	99.9	99.8	99.9	99.8	99.8
H_2SO_4	24.4	99.9	99.9	99.8	99.8	99.9	99.9	99.8	99.9	99.9
NH_4OH	48.4	53.2	58.8	66.4						
NaOH	99.9	99.9	99.8	99.9						
Na_2CO_3	74.2	100.1	100.1	100.1						

Table 2. Separation of Germanium from Other Elements in Binary Mixtures
Amount of Germanium Taken, 15 μg

Foreign ion	Added as	Amount of foreign ion added / mg	Recovery of Ge / %	Stripping agent / mol dm^{-3}
Mn^{II}	$MnSO_4 \cdot 7H_2O$	1.2	98.7	H_2O
Co^{II}	$Co(NO_3)_2 \cdot 6H_2O$	1.2	99.1	H_2O
Ni^{II}	$Ni(NO_3)_2 \cdot 6H_2O$	1.1	99.8	H_2O
Cu^{II}	$CuSO_4 \cdot 5H_2O$	1.4	99.0	H_2O
Zn^{II}	$ZnSO_4 \cdot 7H_2O$	1.0	99.6	H_2O
Cd^{II}	$3CdSO_4 \cdot 8H_2O$	0.9	99.4	H_2O
Pb^{II}	$Pb(NO_3)_2$	1.75	99.6	H_2O
Al^{III}	$Al(NO_3)_3 \cdot 9H_2O$	1.05	99.2	H_2O
Ga^{III}	$GaCl_3$	0.5	99.4	0.5 HCl[b]
In^{III}	$In_2(SO_4)_3 \cdot 5H_2O$	0.35	99.8	0.5 HCl[b]
Tl^{III}	Tl_2O_3	0.5	100.1	1.0 $HClO_4$[b]
Sn^{IV}	SnO_2	0.5	98.8	0.5 H_2SO_4[b]
Sb^{III}	$SbCl_3$	0.4	99.2	0.5 H_2SO_4[b]
Bi^{III}	$Bi(NO_3)_3 \cdot 5H_2O$	0.2	99.4	0.5 H_2SO_4[b]
Au^{III}	$AuCl_3 \cdot 2H_2O$	0.15	99.2	0.5 NaOH[b]
Sc^{III}	$Sc(NO_3)_3$	0.4	98.4	6.0 HCl[a]
Ti^{IV}	$TiCl_4$	0.25	99.2	6.0 HCl[a]
Zr^{IV}	$Zr(NO_3)_4 \cdot 5H_2O$	0.4	98.2	6.0 HCl[a]
Hf^{IV}	$Hf(SO_4)_2$	0.5	99.1	6.0 HCl[a]
V^{IV}	$VOCl_2$	0.5	99.2	6.0 HCl[a]
U^{VI}	$UO_2(NO_3)_2 \cdot 6H_2O$	1.0	98.8	0.5 HCl[b]
Th^{IV}	$Th(NO_3)_4 \cdot 4H_2O$	0.4	99.2	6.0 HCl[a]

a) Before stripping of germanium. b) After stripping of germanium.

Table 3. Separation of Germanium from Multicomponent Mixtures

Mixture No.	Element	Stripping agent / mol dm^{-3}	Amount taken / μg	Recovery / %
1.	Pb	H_2O	250.0	98.8
	Ge	3.0 HCl	15.0	99.4
	Sn	0.5 H_2SO_4	75.0	98.9
2.	Ag	H_2O	325.0	99.4
	Ge	3.0 HCl	15.0	98.9
	Au	1.0 NaOH	100.5	99.2
3.	Ge	4.0 HCl	15.0	99.8
	Fe	0.05 HCl	200.0	99.4
	Sb	5.0 HNO_3	150.0	98.7
	In	0.5 HCl	100.0	98.8
4.	Al	H_2O	150.0	99.4
	Bi	0.05 H_2SO_4	250.0	99.8
	Ge	1.0 H_2SO_4	15.0	99.8
	Tl	1.0 $HClO_4$	150.0	99.9

solved in dilute hydrochloric acid. An aliquot of solution containing germanium was passed through the column as described in General Procedure. Copper, cobalt, zinc, and cadmium were not retained and so they passed through column. Thorium was then stripped with 6 mol dm^{-3} hydrochloric acid and finally germanium with 3 mol dm^{-3} hydrochloric acid. The germanium content found was 18.8 ppm against the standard value of 19.0 ppm.

The advantages of the proposed method over solvent extraction method is that it couples the favorable features of solvent extraction and ion exchange. Multiple extractions are possible in a single column. In batch extractions, 10 cm^3 of 0.1 mol dm^{-3} Aliquat 336S is used for one extraction whereas in extraction chromatography same amount can be used for twenty extractions on a single column.

The proposed method is rapid and reasonably selective. The time required for complete separation and determination is 2 h.

I am thankful to Professor S. M. Khopkar, Depart-

ment of Chemistry for his guidance and encouragement and to Professor T. R. Rama Mohan, Department of Metallurgical Engineering for providing the necessary facilities.

References

1) G. Nakagawa, *Nippon Kagaku Zasshi,* **81**, 1255 (1960).
2) I. P. Aleksandrov, A. I. Perfil'ev, L. M. Avdosovich, and A. I. Sharkov, *Ukr. Khim. Zh.,* **40**, 980 (1974); *Anal. Abstr.,* **28**, 4B 83 (1975).
3) K. Yakabe and S. Minami, *Nippon Kagaku Kaishi,* **1981**, 969.
4) G. I. Agapkina and T. A. Bol'shova, Deposited Doc. VINITI 4777 (1981); *Chem. Abstr.,* **98**, 154414y (1983).
5) S. K. Sahoo and S. M. Khopkar, *Analyst,* **113**, 1781 (1988).
6) A. I. Vogel, "A Text Book of Quantitative Inorganic Analysis," Longmans Green, London (1964), p. 653.
7) A. I. Busev, V. G. Tiptosova, and V. M. Ivanov, "Analytical Chemistry of Rare Elements," Mir Publishers, Moscow (1981), p. 131.
8) C. P. Vibhute and S. M. Khopkar, *Bull. Chem. Soc. Jpn.,* **59**, 3229 (1986).
9) Z. Marczenko, "Spectrophotometric Determination of Elements," Ellis Horwood, Chichester (1976).
10) Y. Y. Vin and S. M. Khopkar, *Anal. Chim. Acta,* **221**, 183 (1989).

 © 1991 The Chemical Society of Japan Bull. Chem. Soc. Jpn., 64, 2488—2496 (1991) [Vol. 64, No. 8

The Design of Amino Hydroxamic Metal Chelates and Their Activity in Biological Systems. Formation Constants between 2-Amino-4-methylpentanehydroxamic Acid with Proton, Copper(II), and Iron(III) in Aqueous Solution

Enrico LEPORATI* and Gianluca NARDI
Istituto di Chimica Generale ed Inorganica, Universita' degli Studi di Parma,
Viale delle Scienze, 78, 43100-PARMA, Italy
(Received November 9, 1990)

The complex-formation equilibria and relative stability constants of species present in aqueous solution of copper(II) and iron(III) with "L-leucinehydroxamic acid" (2-amino-4-methylpentanehydroxamic acid, ahmpe) have heen determined by using potentiometric and spectrophotometric titrations in 0.5 mol dm^{-3} KCl solution at 25 °C. Their acid-base reaction stoicheiometries have heen evaluated and the protonation constants calculated from potentiometric data with the aid of the GAUSS Z and SUPERQUAD programs. The complex formation constants have heen determined by using SQUAD (absorbance data), SUPERQUAD and STBLTY (potentiometric data) programs. The ligand is bound to the metal ions through the coordination of the N atoms of the α-amino group and the deprotonated $-NHO^-$ group in copper(II)–ahmpe system. For iron(III)–ahmpe system the coordination is referred to oxygen atoms of carboxylate and hydroxamate moieties. The UV-visible studies provide important evidence for the formation of several complex species depending on the pH. The experimental curves [$\varepsilon=f(\lambda)$], deduced from refinement of absorbance data with the program SQUAD, have been split up into precisely positioned absorption bands by Gaussian analysis using a nonlinear least-squares computer program NLIN. So the solution electronic spectra have been also employed to estimate the coordination sphere and have let us to suppose a weak tetragonal coordination [$CuL_2(H_2O)_2$] and octahedral for Fe^{3+} complexes. The determination of formation constants and the coordination pattern proposed have a great interest in terms of metal chelate structures and their important role in biological systems.

Several studies have been recently carried out on hydroxamic acids and their metal complexes owing to the possible biological activity connected with these compounds. Some of these have shown to be potent inhibitors of aminopeptidase,[1–3] a zinc metallo-protease, of enzyme 5-Lipoxygenase[4,5] which is associated with a variety of diseases states as asthma and allergy. Besides several peptide–hydroxamic acids have been designed as inhibitors of human skin collagenase[6] (*Z*-Pro–Leu–Gly–NHOH), Enkephalin-Degrading Enzymes[7,8] (Tyr–Gly–Gly–Phe–Leu), Thermolysin[9] and of a Converting Enzyme of Angiotensin I[10] (L-Glu–(NHOH)–L-Pro for example). Because of the interest about peptide–hydroxamic acids, especially tripeptide such as Pro–Leu–Gly–NHOH, recent works[11,12] have pointed out the importance of thermodynamic stabilities of metal transition complexes containing peptide–hydroxamic polydentate ligands. The authors have not found a relationship with the peptide chain indicating there is no significant interaction in solution. A more recent interest in the class of hydroxamic acids has been increasing mainly due to their capabilities of binding Fe^{3+}. The so-called siderophores are iron chelates microbially produced; they can be divided in iron chelates based on hydroxamic moiety and iron chelates based on catechol group, such as Enterobactin.[13] Several tripod-like hydroxamates and dihydroxamic acids have been synthesized[14,15] and, in order to simulate the properties of natural siderophores ferrichrome,[16] tests in vivo have been carried out. In fact an adequate iron supply is necessary to the growth of bacters. Iron is an essential element for almost all living organisms and also in human body (ca. 4 g), but it is very toxic when in excess. The complex Fe^{3+}–glycinehydroxamic acid has been proposed in veterinary terapy against iron anemy and has been proved to react with Apotransferrin, an iron transport protein.[17] Besides certain macrocyclic ligands[18] containing hydroxamate moieties make the reduction potentials Fe(III)/Fe(II) highly negative but also complexes with unusually high oxidation states are stabilized. For example hydroxamic acids form high colored chelates with V(V) or V(IV); these complexes have been employed extensively as analytical reagents for the detection of this metal.[19–21] In the light of potentiometric and spectrophotometric studies some authors[22,23] have discussed the mechanism of complex formation of Fe^{3+}–glycinehydroxamic acid and Ni^{2+}–pyridoxal-glycinehydroxamic acids. Important results have been obtained about the reactive species [$Fe(OH)^{2+}$, $Fe(OH)_2^+$, Ni^{2+}, and $Ni(OH)^+$] implicated in the formation equilibria. It must be emphasized that it's important to investigate the complexing ability of hydroxamic acids not only with iron but also with Cu^{2+}, Zn^{2+}, Ni^{2+}, Mn^{2+}, Co^{2+}, and Cr^{3+}. So the inhibition of urease has been interpreted in terms of reversible binding to the active site nickel ion[24] and other complexes, once considered harmful to organisms, today are regarded necessary in animal nutrition. In continuation of our efforts, potentiometric and spectrophotometric studies have been carried out dealing with transition metal complexes of L-Leucinehydroxamate with iron(III) and copper(II).

Experimental

Reagents. The ligand ahmpe was obtained from Sigma (St. Louis, MO) and its purity was checked through potentiometric titrations. Doubly distilled and deionized water was used in all titrations prepared to have a final volume of 25 cm^3 and thermostatted at 25.0±0.1 °C, with a Paratherm electronic (Julabo) circulating constant temperature water bath. All titrations were carried out under an atmosphere of purified nitrogen. The concentration of stock solution of bivalent metal chloride [$CuCl_2 \cdot 2H_2O$] (AnalaR Products) was determined by using an electrogravimetric method, while standard stock solution for atomic absorption spectrometry has been employed determining iron [$Fe(NO_3)_3$]. The ionic strength was kept at 0.5 mol dm^{-3} with KCl (Merck). Potassium hydroxide (carbonate free) was utilized as titrating solution (0.3840 mol dm^{-3}) and standardized according to Gran's method as previously described.[25,26] Molarity of hydrochloric acid was determined with anhydrous sodium carbonate, using phenolphthalein (solution at 10%) as indicator.

Potentiometric Measurements. Potentiometric titrations were performed using a Metrohm E 636 Titroprocessor and a combined electrode 8102SC ROSS (ORION Research). Quantities of the titrant KOH were added by using a Metrohm Dosimat E 635 autoburet. All titration solutions were prepared with a final volume of 25 cm^3 and kept at constant temperature of 25±0.1 °C. The solution was shaken employing a mechanical stirrer and it was maintained in the vessel a stream of nitrogen presaturated with water vapor, by bubbling over the surface of the solution. The range of concentration of ligand in potentiometric titrations was 0.0077—0.0096 mol dm^{-3} for ahmpe-H^+ (pH range 3.20—11.24; number of titrations 6); 0.0076—0.0082 mol dm^{-3} for ahmpe-Cu^{2+} (pH range 3.02—10.67; number of titrations 6); 0.0104—0.0239 mol dm^{-3} for ahmpe-Fe^{3+} (pH range 1.77—7.58; number of titrations 10). The concentration of metal varied between 0.00164—0.00532 mol dm^{-3} for ahmpe-Cu^{2+} and 0.00153—0.00785 mol dm^{-3} for ahmpe-Fe^{3+} system using as supporting electrolyte potassium chloride (I=0.5 M) (1 M=1 mol dm^{-3}). Periodic titrations (dynamic) of hydrochloric acid were carried out with standard carbonate-free potassium hydroxide solution according to Gran's method.

Spectrophotometric Measurements. Absorption spectra in the ranges 400—820±0.3 nm for Cu^{2+}-ahmpe and 300—700±0.3 nm for Fe^{3+}-ahmpe systems were recorded on Kontron Uvikon 860 spectrophotometer to the fourth decimal place with a stepping of 2 nm. Solution containing ligand and metal ion, prepared and maintained under nitrogen with ionic strength 0.5 mol dm^{-3} (KCl), were analysed at a series of pH from 3.30 to 8.80, using 10 mm cells for Cu^{2+}-ahmpe and from 1.89 to 7.89 pH values using 1 mm cells for Fe^{3+}-ahmpe systems.

Calculations. Great accuracy has been taken in the calculation and critical evaluation of some parameters ($E^{\ominus}$, A_j, B_j, N, K_w) relative to potentiometric calibration curves, using different mathematical procedures as previously described.[27,28] An initial estimate of complex formation constants was achieved by the program GAUSS Z.[29] In this program the function $\bar{n}$ against pH let us to estimate the stoicheiometries of possible complexes in the case of binary systems. Successively the SUPERQUAD program[30] was employed to refine the formation constants which minimize the sum of squared residual between observed and calculated emf values (Eq. 1):

$$U=\sum_{i=1}^{z} w_i (E_i^{obsd} - E_i^{calcd})^2, \quad (1)$$

where z is the total number of potentiometric data and w_i is the weighting factor defined by equation (Eq. 2):

$$w_i = 1/[\sigma_{E_i}^2 + (\partial E_i/\partial v_i)^2 \sigma_{v_i}^2], \quad (2)$$

where σ_E(=0.2) and σ_v(=0.008) are respectively the error in emf and in the volume used in the refinement. Moreover STBLTY was utilized to refine formation constants (K-forms or β-forms). In this program a recent pH titration method (FICS) has been used to calculate free metal ions and free ligand concentrations from experimental data without any hypothesis about species for the system.[31,32] The calculation of stability constants then can be reduced to a linear least-square problem by using any of the mass balance equations. The subprogram NONLINEAR LS REFINE is the most commonly used refinement program in STBLTY. The final choice between different SUPERQUAD analyses was based on graphical comparisons between calculated curves and the corresponding simulated data obtained from the HALTAFALL[33] computer program. Besides a further confirmation of potentiometric data has been performed on spectrophotometric values by means of program SQUAD,[34] in which formation constants are refined on the basis of comparison between observed and calculated absorbance values. All the calculations were carried out on the CRAY Y-MP8/432 and IBM 4341/10 computers of the Consorzio per la Gestione del Centro di Calcolo Elettronico dell' Italia Nord Orientale, Casalecchio di Reno, Bologna, Italy, with financial support coming from the University of Parma. Listing of experimental data and final computations from SUPERQUAD, GAUSS Z, NBAR, and SQUAD are available on request from the authors.

Results and Discussion

Protonation Equilibria. Starting from the set of potentiometric data, first the overall protonation constants and the initial amounts (mmol) of reagents (T_L, T_H) were refined simultaneously by using SUPERQUAD. In this calculation the liquid junction potentials (A_j, B_j) have been neglected because of their littleness (pH interval 3.20—10.54) as shown in already published papers.[27,28] The variances (σ^2) in the quantities T_L and T_H of this refinement were respectively 5.2137×10^{-7} and 1.353×10^{-6} $mmol^2$. It might be pointed out (Fig. 1) the excellent agreement between observed and calculated pH values as a function of volume of added titrating solution. The trend of these curves also reflects the presence of two distinct buffering zones separated between them by a small inflection point. The first buffer zone in the pH range 6.10—8.45 corresponds to deprotonation of the oxygen atom ($\log K_2^H$=7.263); the second zone in the pH range 8.00—10.30 is due to deprotonation of α-amino group ($\log K_1^H$=9.152). Besides two titrations have been stopped at pH 7.7 (Fig. 1a) and 8.2 (Fig. 1b) because of the low solubility of ligand in aqueous solution due to its lipophilic character. The cumulative and stepwise protonation and complex formation constants of ahmpe are quoted in

Table 1. Cumulative and Stepwise Protonation Complex Formation of 2-Amino-4-methylpentanehydroxamic Acid (ahmpe) at 25 °C and I=0.5 mol dm^{-3} (KCl)

	SUPERQUAD			GAUSS Z	STBLTY (Nonlinear Ls=pM pL pH DATA)	
	H^+	Cu^{2+}	Fe^{3+}	H^+	H^+	Fe^{3+}
$\log\beta_{011}$	9.152(3)			9.152(2)	9.156(3)	
$\log\beta_{021}$	16.416(4)			16.411(2)	16.417(2)	
$\log K_2^{H}$ a)	7.263(4) b)			7.260(2)	7.261(2)	
$\log\beta_{101}$		10.626(50)				
$\log\beta_{102}$		19.202(21)	22.89(9)			22.85(3)
$\log\beta_{1-12}$		9.175(83)	15.98(3)			15.94(2)
$\log\beta_{2-12}$		20.592(19)				
$\log K_2$		8.576(38)				
$\log\beta_{111}$			16.65(2)			16.67(1)
$\log\beta_{112}$			28.50(3)			28.56(1)
$\log\beta_{122}$			32.60(1)			32.61(1)
$\log\beta_{103}$			28.00(9)			28.08(3)
$\log\beta_{2-22}$			21.48(7)			21.45(3)
$\log\beta_{113}$			35.55(5)			35.62(2)
$\log\beta_{123}$			41.93(5)			42.02(2)
$\log\beta_{2-13}$			35.40(9)			35.36(3)
z c)	230	209	430	230	230	378
U	3.43×10^{1}	1.32×10^{3}	1.19×10^{3}	8.11×10^{-3} f)	2.75×10^{2}	
χ^2 d)	2.56	7.0	8.77			
σ e)	0.3985	2.5373	1.70	3.56×10^{-5} g)	1.099	0.54/0.46/3.54
R h)					0.3%	0.3/0.2/1.7%

a) $\log K_n=\log\beta_{0n1}-\log\beta_{0n-11}$. b) $\sigma(\log K_n)=\{[\sigma^2(\log\beta_{0n1})+\sigma^2(\log\beta_{0n-11})/2]\}^{1/2}$. c) Total number of experimental data points used in the refinement. d) Observed χ^2; calculated value (6, 0.95) should be 12.6, where 6 is the number of degrees of freedom and 0.95 is the confidence coefficient in the χ^2 distribution. e) $\sigma=\sqrt{\sum_{i=1}^{z}w_i(E_i^{obsd}-E_i^{calcd})^2/(Z-m)}$ for SUPERQUAD and $\sigma=\sqrt{\sum_{i=1}^{z}w_i(pH_i^{obsd}-pH_i^{calcd})^2/(Z-m)}$ for STBLTY, where m is the number of parameters to be refined. f) $U=\sum_{i=1}^{z}(\bar{n}_i^{calcd}-\bar{n}_i^{obsd})^2$, where $\bar{n}_i$ is the observed (obsd) or calculated (calcd) average number of hydrogen ions bound to each central ligand molecule. g) $\sigma^2=\sum_{i=1}^{z}(\bar{n}_i^{calcd}-\bar{n}_i^{obsd})^2/(Z-m)$. h) $R=\sqrt{\sum_{i=1}^{z}(\bar{n}_i^{obsd}-\bar{n}_i^{calcd})^2/\sum_{i=1}^{z}(\bar{n}_i^{obsd})^2}\times100$ for GAUSS Z and $R=\sqrt{\sum_{i=1}^{z}(pH_i^{obsd}-pH_i^{calcd})^2/\sum_{i=1}^{z}(pH_i^{obsd})^2}\times100$ for STBLTY.

Table 1.

The ligand exhibits two protonation centers: The terminal hydroxamate moiety (H^1; Chart 1) and the α-amino group (H^2; Chart 1). In addition to SUPERQUAD, GAUSS Z and STBLTY programs were employed to refine protonation constants starting from the same experimental data and the results agree closely. Kurzak and collaborators[35] reported values of $\log\beta_{011}$=9.12 and $\log\beta_{021}$=16.26 at 0.1 mol dm^{-3} ($NaClO_4$) at 25 °C. Small differences with our values might be justified (especially for $\log K_2$=7.14) by the influence of the ionic strength on the protonation constants, which we obtain at I=0.5 mol dm^{-3} (KCl). It must be noticed that the presence of the α-amino group in ahmpe increases the acidity of the OH group (-NHOH) in comparison with the corresponding hydroxamic acid $CH_3CH(CH_3)$-CH_2CH_2-CONHOH [$\log K$=9.67(3)[36]]. In the same way the replacement of -NHOH moiety for the OH group lowers considerably the protonation constant of the α-amino group due to the greater electron-withdrawing effect of the -NHOH group.

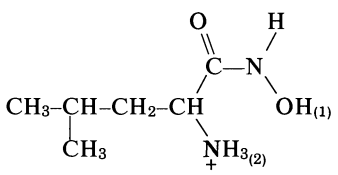

Hahmpe

Chart 1. H_2L^+ with the two removable protons (1 and 2).

Metal Complex Equilibria. Starting from several sets of potentiometric data, obtained in different ligand to metal ratios, many attempts have been carried out to obtain the best fitting chemical models applying SUPERQUAD program, whereas all the protonation constants were kept constant. The refinement included as fixed contributions (very small) the known metal hydrolysis constants[37,38] for the species $[Fe(OH)]^{2+}$, $[Fe(OH)_2]^{+}$, $[Fe_2(OH)_2]^{4+}$, and $[Fe_3(OH)_4]^{5+}$. All the overall formation constants calculated by both computer methods (SUPERQUAD and STBLTY, see Table 1) agreed closely, even though the standard deviations of the refined quantities calculated by SUPERQUAD program were slightly higher. Equilibria between Co^{2+} and Ni^{2+} ions and ahmpe cannot be studied because

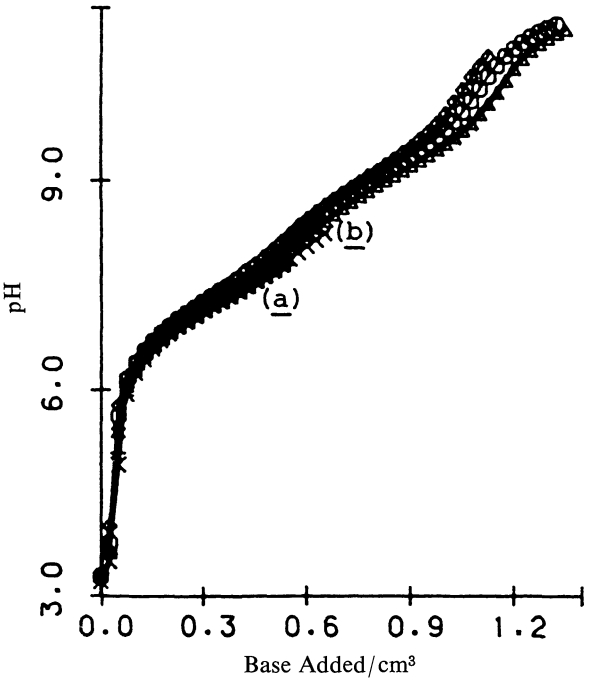

Fig. 1. Experimental and calculated (by SUPERQUAD program) titration curves of pH as a function of volume of KOH added for H^+–ahmpe system, V_o=25 cm³, C_{KOH}=0.38412 mol dm^{-3} [T_L range 0.19365—0.24025, T_H range 0.40614—0.49798]. T_L and T_H are mmol of ahmpe and hydrogen ion in the titration vessel.

precipitation occurs at already acid pH. The refinement converged satisfactorily when only species present for Cu^{2+}–ahmpe system were $[CuL]^+$, $[Cu_2(OH)L_2]^+$, $[CuL_2]$ and $[Cu(OH)L_2]^-$. The most consistent set of complexes found for Fe^{3+}–ahmpe system, together with their respective formation constants shown in Table 1, was $[FeL_2]^+$, $[FeHL]^{3+}$, $[FeH_2L_2]^{3+}$, $[FeHL_2]^{2+}$, $[Fe_2(OH)_2L_2]^{2+}$, $[Fe_2(OH)L_3]^{2+}$, $[FeH_2L_3]^{2+}$, $[FeHL_3]^+$, $[FeL_3]$, and $[Fe(OH)L_2]$. In Fig. 2 species distribution curves are reported. In the case of Cu^{2+}–ahmpe system the complexation begins at pH ca. 3.0 with the formation of $[CuL]^+$ and the dimer $[Cu_2(OH)L_2]^+$ species, which reaches its maximum concentration of 87.0% at pH 4.75. Previous authors[39,40] too have concluded that the dimer is in equilibrium with the mononuclear complex $[CuL]^+$, which is present in small quantity (maximum of 19.99% at pH 3.80). The species $[CuL_2]$ reaches a maximum concentration of 99.8% total copper at pH 7.2 (Fig. 2a)]. Typical absorption spectra for Cu^{2+}–ahmpe are plotted in Fig. 3a, in the pH range 3.75—6.32. At low pH a broad absorption spectrum is present and its maximum shifts towards visible region as the pH increases [maximum, 0.064 A at 724 nm(1); 0.154 A at 654 nm(2); 0.218 A at 644 nm(3); Fig. 3a]. The first maximum of absorbance in the range 586—724 nm occurs at pH 4.66 and λ_{max} of 644 nm and corresponding ca. to the maximum concentration of the hydrolyzed dimeric complex (see Fig. 2a). The increase in absorp-

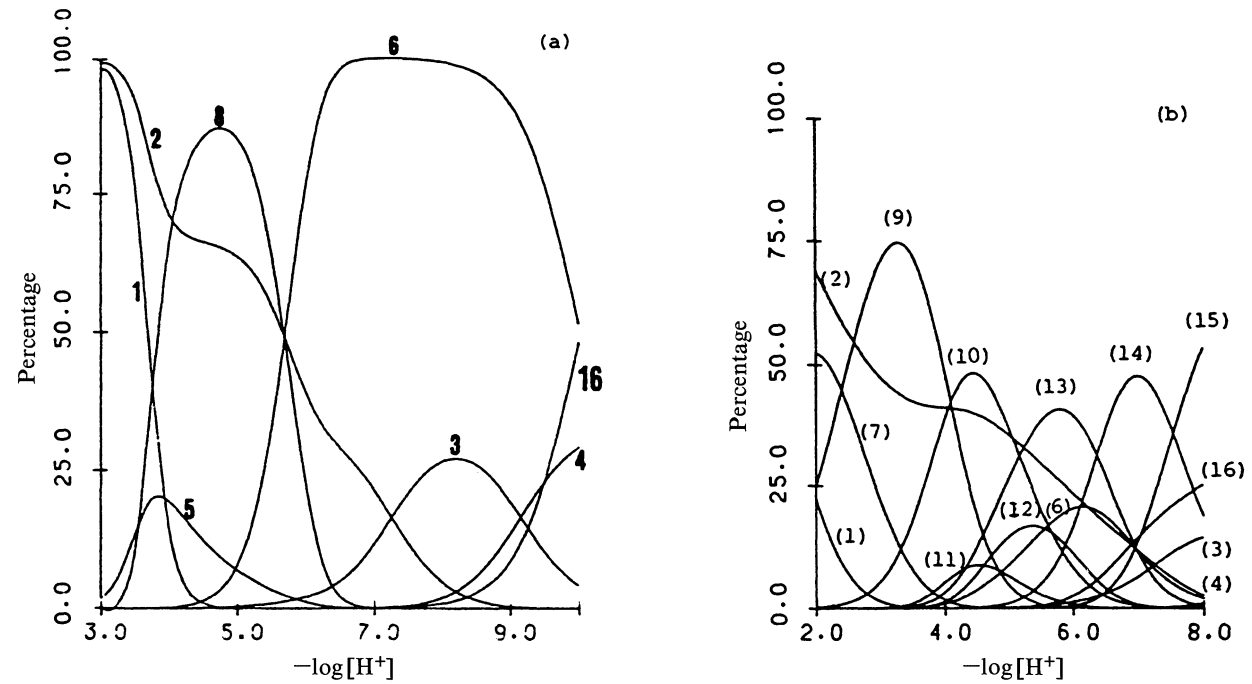

Fig. 2. Typical distribution diagrams for M^{n+}–ahmpe system. The percentage of each species has been calculated from the data of a hypothetical solution of metal ions (0.004 mol dm^{-3} for Cu^{2+} and 0.006 mol dm^{-3} for Fe^{3+}) and ahmpe (0.012 mol dm^{-3} for Cu^{2+} and 0.02 mol dm^{-3} for Fe^{3+}) by the HALTAFALL program (N. Ingri, W. Kakalowicz, L. G. Sillén, and B. Warnqvist, **14**, 1261 (1967)), and using a PLOTTER Calcomp 936. The concentrations of the species not containing metal were calculated as percentages of the total ligand, those containing metal as percentages of the total metal. (a) Cu^{2+}–ahmpe, (b) Fe^{3+}–ahmpe; (1) M^{n+}, (2) H_2L; (3) HL; (4) L; (5) CuL; (6) ML_2; (7) FeHL; (8) $Cu_2(OH)L_2$; (9) FeH_2L_2; (10) $FeHL_2$; (11) $Fe_2(OH)_2L_2$; (12) $Fe_2(OH)L_3$; (13) FeH_2L_3; (14) $FeHL_3$; (15) FeL_3; (16) M $(OH)L_2$.

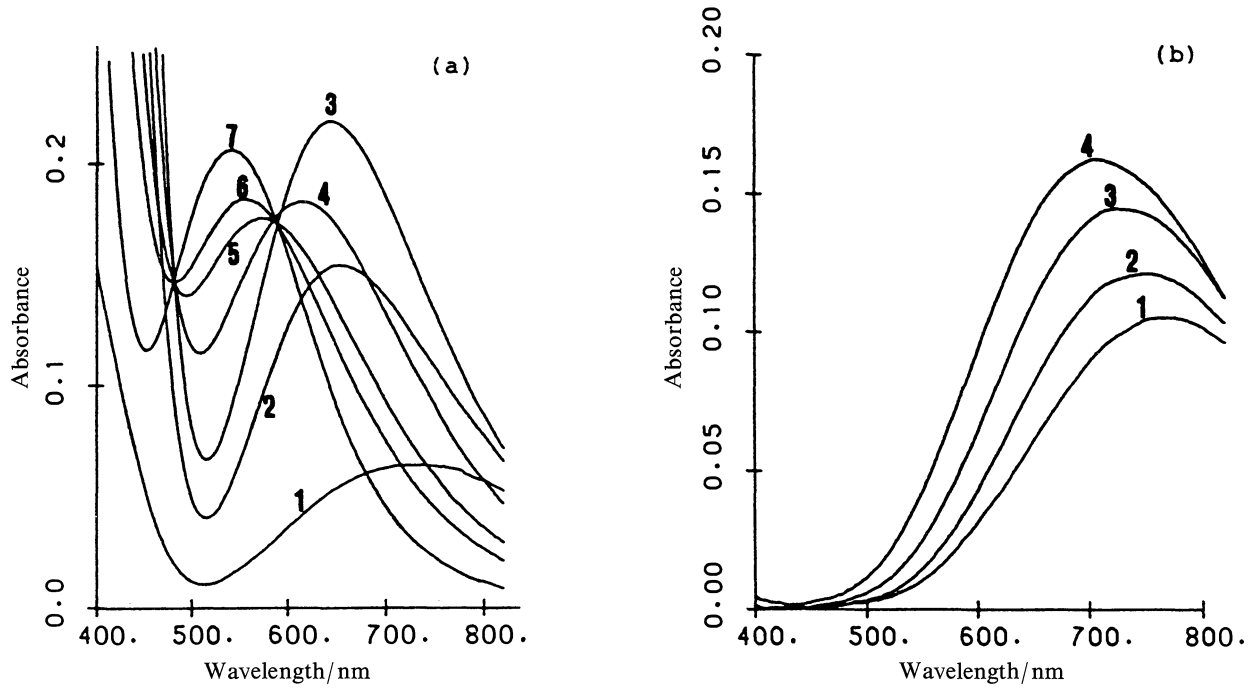

Fig. 3. Plots of experimental absorbance data versus wavelength for solutions [(a), C_L range 7.592×10^{-3}—7.726×10^{-3} mol dm^{-3}, C_M range 2.469×10^{-3}—2.513×10^{-3} mol dm^{-3}; (1), pH=3.754; (2), pH=4.052; (3), pH=4.660; (4), pH=5.483; (5), pH=5.745; (6), pH=5.875; (7), pH=6.317; (b), C_L range 7.157×10^{-3}—7.219×10^{-3} mol dm^{-3}, C_M range 4.824×10^{-3}—4.866×10^{-3} mol dm^{-3}; (1), pH=3.431; (2), pH=3.783; (3), pH=4.218; (4), pH=4.736] of Cu^{2+}–ahmpe system at 25 °C using the program VISION with the Plotter Calcomp 936.

tion (hyperchromic effect) of the broad spectrum near the IR region and the shift towards smaller wavelengths (hypsochromic effect) of the same band with increasing pH indicates greater complexation, due to the appearance of the hydrolyzed binuclear complex, $[Cu_2(OH)L_2]^+$ (intense green color). When the pH is increased further on from 4.66 to 6.32 (Fig. 3a) small hypochromic and high hypsochromic effects [maximum, 0.218 A at 644 nm(3); 0.182 A at 614 nm(4); 0.175 A at 574 nm(5); Fig. 3a] are observed (change of color from intense green to purple in acid media), while for pH >5.745 a simultaneous increase in the absorption (hyperchromic shift) and a small decrease in the wavelength (hypsochromic effect) [maximum, 0.175 A at 574 nm(5); 0.183 A at 558 nm(6); 0.205 A at 542 nm(7); Fig. 3a] occurs with the formation of the complex $[Cu(OH)L_2]^-$. The color changes from purple to reddish purple. Two distinctive isosbestic points appear at 589 and 483 nm (Fig. 3a). These correspond to an equilibrium between species $[Cu_2(OH)L_2]^+/[CuL_2]$ (each species is present for the 49.0% total copper at pH 5.7, Fig. 2a) and $[CuL_2]/[Cu(OH)L_2]^-$, respectively. It must be noticed that some solutions, several days old, containing Cu^{2+} and ahmpe ligand, both at acid and basic pH values, exhibited a different trend (Fig. 3b). They showed an azure coloring which becomes more intense as the pH increasing (hyperchromic effect), while the maximum shifts slightly towards lower wavelength (hypsochromic shift) [maximum, 0.104 A at 768 nm(1); 0.120 A at 754 nm(2); 0.144 A at 726 nm(3); 0.162 A at 706 nm(4); Fig. 3b]. In order to explain this behavior, we have supposed that the hydroxamate ligand hydrolyzes with the formation

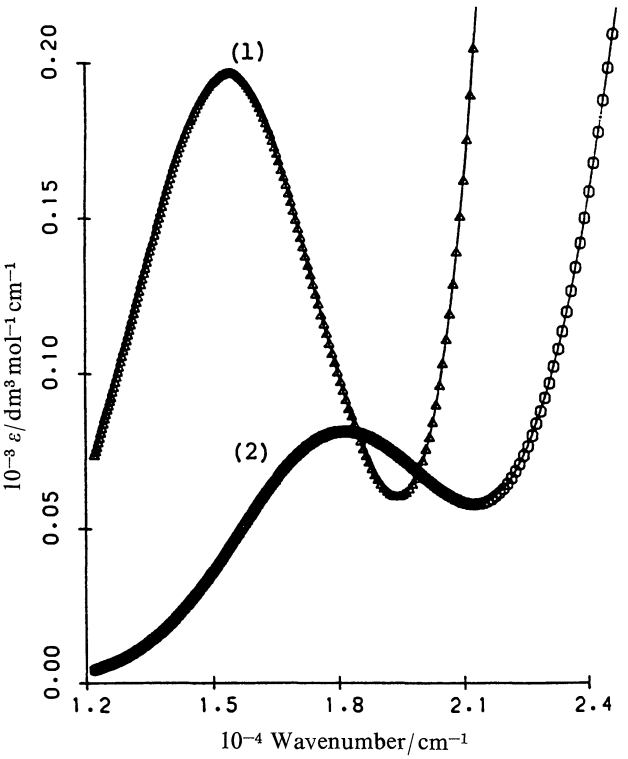

Fig. 4. Plots of molar absorption coefficients (ε) of the two complexed species of Cu^{2+}–ahmpe at 25 °C by program SQUAD: $\varepsilon_{[Cu_2(OH)L_2]^+}$ (1), $\varepsilon_{[CuL_2(H_2O)_2]}$ (2).

of the corresponding amino acid-complexes even in acid solution. In Fig. 4 we have reported molar absorption coefficients (ε) of $[Cu_2(OH)L_2]^+$ and $[CuL_2]$ obtained by use of the program SQUAD in the range 1.2×10^{-4}—2.5×10^{-4} cm^{-1}. The molar absorption coefficients were refined employing 2954 points and obtaining a standard deviation in the absorbance data of 5.9×10^{-2}. By means of the positions of the absorption maxima (Fig. 4), it's possible to check with good precision the ligand-field contribution of ligands about absorbing complexes. According to Billo,[41] the ligand-field contribution of each N (amino) is equal to 4530 cm^{-1}; we can calculate the contribution of each nitrogen of the hydroxamate groups in the $[CuL_2]$ with λ_{max}=18215 cm^{-1} corresponding to: (18215—9060)/2=4577 cm^{-1}. For the hydrolyzed dinuclear complex $[Cu_2(OH)L_2]^+$ with λ_{max}=648 nm, if we suppose coordination of one leucine-hydroxamate residue to each copper ion via the nitrogens of the α-amino and hydroxamate moieties, the global contribution of nitrogen atoms ($-NH_2$ and

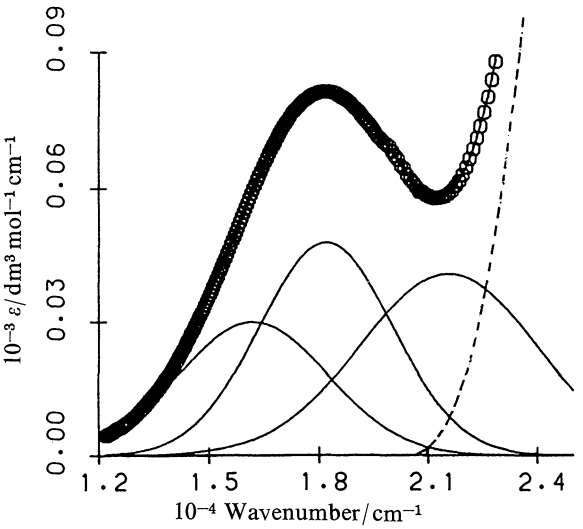

Fig. 5. Absorption spectrum of $[CuL_2(H_2O)_2]$ complex; experimental (symbol) and calculated (line) spectrum; —— components bands, --- unassigned band.

Table 2. Absorption Maxima (nm) and Isosbestic Points (nm) for $[Cu_2(OH)L_2]^+$, $[Cu(OH)L_2]^-$, and $[CuL_2(H_2O)_2]$ Complexes. Parameters (ε/$dm^3\,mol^{-1}\,cm^{-1}$, ν/cm^{-1}, $\Delta\nu$/cm^{-1}) of the Component Bands Obtained from Gaussian Analysis of the Absorption Spectrum of $[CuL_2(H_2O)_2]$ (L=leucinehydroxamate), f Values Refer to the Oscillator Strengths for the Transitions.[a]

Assignment $[CuL_2(H_2O)_2]$	ε	ν	$\Delta\nu$	f
$^2B_{1g}\longrightarrow{}^2A_{1g}$	29.908	16 199.9	4 773.0	6.5667×10^{-4}
	27.38[b]	16 647.5	3 798.7	4.7844×10^{-4}
	29.29[c]	16 797.8	4 000.1	5.3900×10^{-4}
	34.26[d]	16 800.5	4 001.2	6.3052×10^{-4}
	53.71[e]	16 800.2	4 001.1	9.886×10^{-4}
	33.58[f]	16 799.2	4 147.8	6.404×10^{-4}
	25.734[g]	16 820.4	5 119.6	6.057×10^{-4}
$^2B_{1g}\longrightarrow{}^2B_{2g}$	48.125	18 199.9	4 282.5	9.4807×10^{-4}
	61.00[b]	18 451.4	3 996.9	1.1215×10^{-3}
	54.50[c]	18 492.7	4 378.5	1.0977×10^{-3}
	48.00[d]	18 501.4	4 374.6	9.6595×10^{-4}
	80.93[e]	18 500.2	4 374.9	1.629×10^{-3}
	48.11[f]	18 824.0	4 191.8	9.272×10^{-4}
	53.571[g]	18 382.3	4 861.7	1.197×10^{-3}
$^2B_{1g}\longrightarrow{}^2E_g$	40.985	21 550.1	5 661.5	1.067×10^{-3}
	44.62[b]	21 550.9	5 663.6	1.1625×10^{-3}
	35.26[c]	20 496.3	4 707.9	7.6397×10^{-4}
	36.10[d]	20 500.1	4 705.8	7.8149×10^{-4}
	48.46[e]	20 499.2	4 706.1	1.049×10^{-3}
	29.56[f]	20 517.7	5 066.8	6.855×10^{-4}
	42.472[g]	20 490.9	5 211.2	1.017×10^{-3}

Ligand	$[Cu_2(OH)L_2]^+$	$[Cu(OH)L_2]^-$	$[CuL_2(H_2O)_2]$	Isosbestic point
adhp[e]	653 nm	496 nm	547 nm	594 nm
adhb[d]	651	508	553	595
ahpr[c]	648	518	540	593
ahmpe	648		549	589
aimahp[b]	648	450	536	591
ahbt[h]	647	538	562	602
ahmpe[g]	649		530	595

a) Relative standard deviation (%) or coefficient of variation for Cu^{2+}–ahmpe system=0.23; region of spectrum 12 195—25 000 cm^{-1}. b) Cu^{2+}–aimahp system, Ref. 45. c) Cu^{2+}–ahpr system, Ref. 43. d) Cu^{2+}–adhb system, Ref. 44. e) Cu^{2+}–adhp system, Ref. 46. f) Cu^{2+}–ahpr system, Ref. 39. g) Cu^{2+}–ahmpe system, Ref. 35. h) Cu^{2+}–ahbt system, Ref. 47.

$-NHO^-$) is 9107 cm^{-1}, so the two remaining groups would have to contribute ca. 3162 cm^{-1}. This value agrees well with the predicted contribution of OH^- or H_2O groups of 3010 cm^{-1}. The most important details arising from this work are thermodynamic conclusions, which in some case suggest the structures of the complexes present in aqueous solution. Spectral investigations of structures perceive only those aspects of the structure that are involved in electronic transitions. On the other hand, the spectrophotometric characteristics and the numerical interpretation of the most stable complexes (CuL_2 or FeH_2L_2, $FeHL_2$, and FeL_3) reflect all bond strengths, ring strains, the coordination sphere around the metal ions, and configurations. In order to interpret the $[CuL_2(H_2O)_2]$ spectrum, a careful and detailed Gaussian analysis of the experimental spectrum of $[CuL_2(H_2O)_2]$ (Fig. 5, 201 ε data points in the ν interval of 12200—25000 cm^{-1}) was performed by using the NLIN computer program.[42] This procedure is based on the nonlinear Gauss–Newton least-squares method. In these calculations the parameters of the components bands and related maxima positions were carefully determined. As previously described,[43,44] the assignments and calculated maxima positions of the components bands (Fig. 5, Table 2) allowed D_{4h} symmetry (tetragonally distorted) with four short copper–ligand bonds in one plane (xy) and two longer copper–H_2O bonds lying along the z axis above and below this plane. In this case, the B_{1g} term will be the ground state and three spin-allowed transitions from the $^2B_{1g}$ state to the other doublet states are to be expected.

$[CuL_2(H_2O)_2]$

$$\nu_1 = E(B_{1g} \rightarrow A_{1g}) = -4D_s - 5D_t$$
$$\nu_2 = E(B_{1g} \rightarrow B_{2g}) = 10D_q$$
$$\nu_3 = E(B_{1g} \rightarrow E_g) = 10D_q - 3D_s + 5D_t$$
$$D_q = \nu_2/10 = 1820.0 \text{ cm}^{-1}$$
$$D_s = 1/7[\nu_2 - \nu_1 - \nu_3] = -2792.9 \text{ cm}^{-1}$$
$$D_t = 1/35[4(\nu_3 - \nu_2) - 3\nu_1] = -1005.7 \text{ cm}^{-1}$$

In Table 2 the comparison of the spectrophotometric properties of copper(II)–ahmpe complexes ($[Cu_2(OH)L_2]^+$, $[CuL_2(H_2O)_2]$, and $[Cu(OH)L_2]^-$) with others of amino hydroxamic acids[35,39,43–47] already studied is summarized. From the results obtained, it is possible to verify an excellent agreement between the parameters of the components bands (ε, ν, f, $\Delta\nu$) for the different systems, meaning that a similar behavior (thermodynamic stability, structure, configuration, coordination sphere, etc.) takes place through the $[CuL_2(H_2O)_2]$ complex formation. In particular our results concerning this system are in good agreement with those reported earlier for copper (II)–ahmpe.[35] As regards the compositions and stability constants of the complexes, our results are in fairly good agreement with the above mentioned ones. However, the small differences observed in the parameters D_s and D_t for the different systems means that the energies for a tetragonal distortion, commonly given in terms of the radial parameters, are slightly different for $[CuL_2(H_2O)_2]$. The differences observed in the values D_q and ε could be due to various factors: changes in the metal ligand distance, while the increment in the molar absorption intensity (ε) of the components bands involves a change from centrosymmetric coordination sphere to weakly acentric molecules. Typical titration curves (observed and calculated) for Fe(III)–ahmpe mixtures are shown in Figs. 6a, b. The titration curves obtained on variation of iron and ligand concentration (Figs. 6a, b) were processed in addition to SUPERQUAD program by

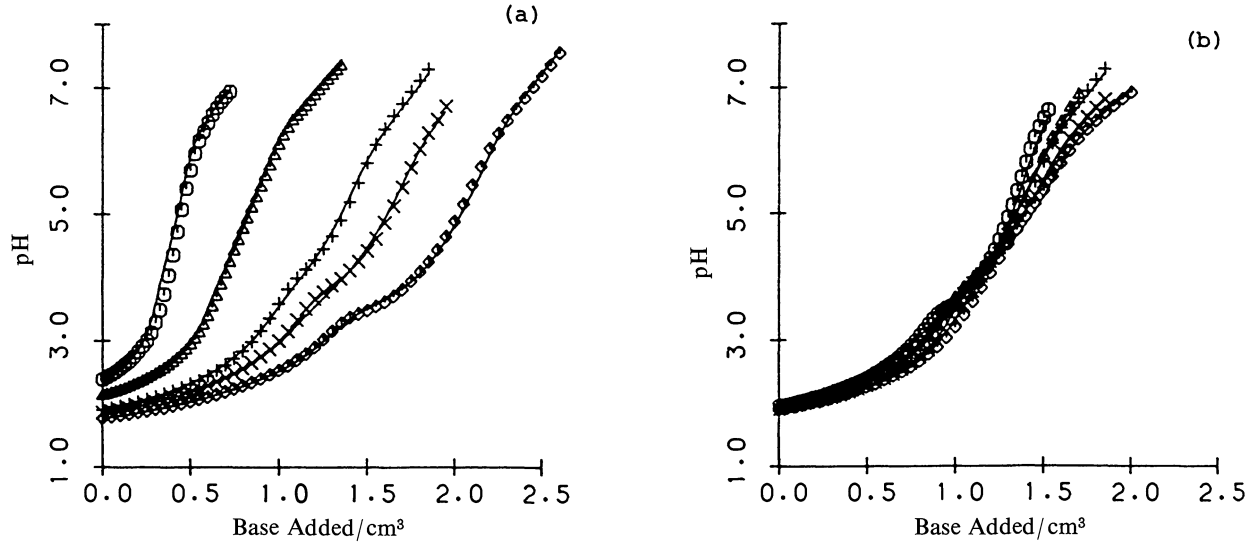

Fig. 6. Experimental and calculated (by SUPERQUAD program) titration curves of pH as a function of volume of KOH added for Fe^{3+}–ahmpe system, V_o=25 cm^3. (a), C_{KOH}=0.46364 mol dm^{-3} [T_L= 0.37732, T_M range 0.03839—0.19628, T_H range 0.81563—1.06633]; (b), C_{KOH}=0.46403 mol dm^{-3}, [T_L range 0.26070—0.59685, T_M=0.12798, T_H range 0.72466—1.39698]. T_L, T_M, and T_H are mmol of ahmpe, iron(III), and hydrogen ion in the titration vessel.

procedures in the FICS method to give $\partial C_H/\partial C_M$ or $\partial C_H/\partial C_L$ respectively, as a function of pH. Finally, the NONLINEAR LS REFINE subprogram of STBLTY[31,32,45,47,48] was applied to select and refine the existing species in the system. From numerous models, the one which yielded the best fit of the titration data (see Figs. 6a, b) is given in Table 1. Our model is only in partial agreement with those given by Brown et al.[17] and El-Ezaby and Hassan[22] for the analogous iron(III)–amino hydroxamate systems. In particular, besides other species of minor importance, the totally deprotonated species $[FeL]^{2+}$ was not found in a quite acid pH range. The relative importance of the various species in each pH range is shown by the typical distribution graph for Fe^{3+}–ahmpe (Fig. 2b). In the presence of Fe^{3+}, the species distribution curves show that complexation begins at low pH values <1.6 for $[Fe(HL)]^{3+}$ species (max. 52.4% total iron at pH 2.0) corresponding to the displacement of one proton. As the pH increases, the proton liberation data shows that complexation proceeds further and at pH 3.3 the predominant species is $[FeH_2L_2]^{3+}$ (74.7%) corresponding to the displacement of two protons. At pH 4.45, the proton displacement value rises to about 3.0 and can be attributed to the formation of the $[FeHL_2]^{2+}$ (48.3%) species when the hydroxamate moiety is about 59.8% ionized. As the pH increases further, the major species present are: $[FeH_2L_3]^{2+}$ (max. 40.9% at pH 5.85), $[FeHL_3]^{+}$ (max. 47.8% at pH 7.05), and $[FeL_3]$ (max. 53.4% at pH 8.0). In these last species three hydroxamate groups can satisfy the octahedral configuration around iron (III), but the $[FeL_3]$ complex formation can be reached only at very high free ligand concentration. Additionally, the formation of protonated, deprotonated and/or mixed hydroxo complexes can be assumed. The spectrophotometric study was carried out on a series of solutions containing ahmpe and iron ions, with concentrations and pH values selected from those employed in the potentiometric titrations. The visible spectra of the Fe^{3+}–ahmpe system as a function of pH are shown in Fig. 7. When the pH is increased from 1.784 to 3.060 [maximum, 0.605 A at 480 nm(1); 0.663 A at 480 nm(2); 0.738 A at 474 nm(3); 0.858 A at 472 nm(4); 1.059 A at 464 nm(5); Fig. 7] small hypsochromic and high hyperchromic effects are observed (intense reddish brown), indicating that complexation at this pH interval presumably gives $[FeHL]^{3+}$, $[FeH_2L_2]^{3+}$, and $[FeHL_2]^{2+}$ (Fig. 2b). A maximum at 464 nm [curve (5), Fig. 7] is reached at pH 3.060, which corresponds to the maximum in the concentration (71.0%) of the protonated complex, $[FeL_2L_2]^{3+}$.

As the pH increases further on a decrease in the wavelength and an increase in the absorption occurs with a maximum at 448 nm [curve (7), Fig. 7]. The color of the solution changes from wine red [intense reddish brown, pH 1.78 to 3.93] to orange red at pH ca. 4.5 and remains this color up to pH 8.0. Componentization of the visible spectra (300—700 nm) data deduced by refinement procedure with program SQUAD indicates at least six colored species are present between 1.784—7.900 pH values. The 13 spectra, each containing 201 absorbance values between 300 and 700 nm, could be presented as linear combinations of six "components"

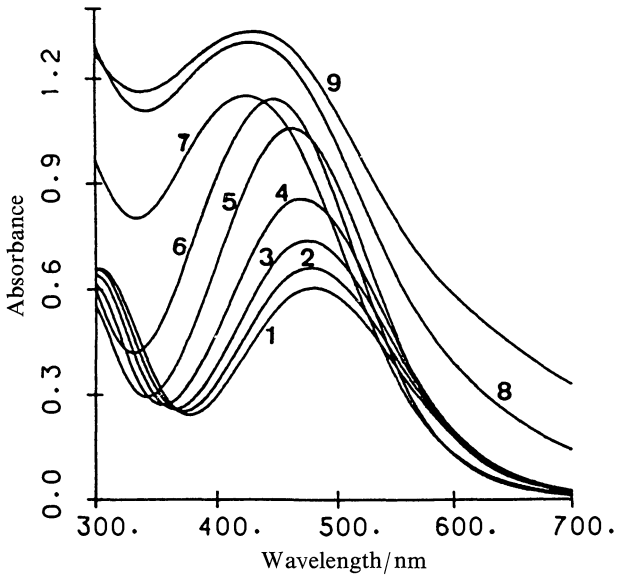

Fig. 7. Plots of experimental data versus wavelength for solutions [C_L range 1.517×10^{-2}—1.647×10^{-2} mol dm^{-3}, C_M range 5.659×10^{-3}—6.143×10^{-3} mol dm^{-3}; (1), pH=1.784; (2), pH=1.930; (3), pH=2.139; (4), pH=2.455; (5), pH=3.060; (6), pH=3.931; (7), pH=5.233; (8), pH=6.592; (9), pH=7.442] of Fe^{3+}–ahmpe system at 25 °C using the program VISION with the Plotter Calcomp 936.

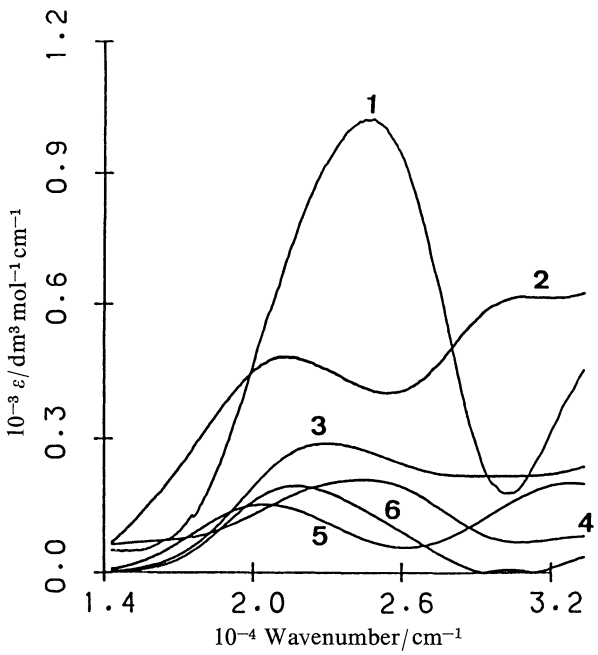

Fig. 8. Plots of molar absorption coefficients (ε) of the six complexed species of Fe^{3+}–ahmpe system: (1) $\varepsilon_{Fe_2(OH)L_3}$, (2) ε_{FeHL_3}, (3) ε_{FeHL_2}, (4) ε_{FeL_3}, (5) $\varepsilon_{FeH_2L_2}$, (6) ε_{FeHL}.

(or molar extinction coefficients, Fig. 8) spectra within standard deviation in absorbance of 0.0201. The least-squares modeling of the spectra included a very small contribution from absorption by Fe^{3+} and its hydrolyzed species (determined from the absorbance of dilute $Fe(NO_3)_3$ solutions at different pH values) in addition to major contributions from six Fe^{3+}–ahmpe complexes. Since iron(III) is a typical hard ion, we presume the coordination of O,O atoms of hydroxamate moiety of ahmpe. Accordingly, the protonated $[FeHL]^{3+}$ $[FeH_2L_2]^{3+}$, $[FeHL_2]^{2+}$, $[FeH_2L_3]^{2+}$, and $[FeHL_3]^{+}$ complexes contain the amino group in its protonated form. This assumption is supported by the spectrophotometric results (see Fig. 7) and those recorded for iron(III)–hydroxamate systems.[45,49–51]

Grateful acknowledgement is made to the Ministero della Pubblica Istruzione (Rome) and National Research Council of Italy (C.N.R.) for generous grants. I am greatly indebted to Professors P. Gans, A. Sabatini, and A. Vacca for their generous support of the program SUPERQUAD.

References

1) J. O. Baker, S. H. Wilkes, M. E. Bayliss, and J. M. Prescott, *Biochemistry,* **22**, 2098 (1983).
2) S. H. Wilkes and J. M. Prescott, *J. Biol. Chem.,* **258**, 13517 (1983).
3) M.-A. Coletti-Previero, A. Crastes de Paulet, H. Mattras, and A. Previero, *Biochem. Biophys. Res. Commun.,* **107**, 465 (1982).
4) J. B. Summers, H. Mazdijasni, J. H. Holms, J. D. Ratajczyk, R. D. Dyer, and G. W. Carter, *J. Med. Chem.,* **30**, 574 (1987).
5) E. J. Corey, J. R. Cashman, S. R. Kantner, and S. W. Wright, *J. Am. Chem. Soc.,* **106**, 1503 (1984).
6) W. M. Moore and C. A. Spilburg, *Biochem. Biophys. Res. Commun.,* **136**, 390 (1986).
7) S. Blumberg, Z. Vogel, and M. Altstein, *Life Sci.,* **28**, 301 (1981).
8) R. Boubouton, G. Waksman, J. Devin, N. C. Fournie-Zaluski, and B. P. Roques, *Life Sci.,* **35**, 1023 (1984).
9) N. Nishino and J. C. Powers, *Biochem. Biophys. Res. Commun.,* **17**, 2846 (1978).
10) R. B. Harris, P. D. M. Strong, and I. B. Wilson, *Biochem. Biophys. Res. Commun.,* **116**, 394 (1983).
11) E. Farkas and I. Kiss, *J. Chem. Soc., Dalton Trans.,* **1990**, 749.
12) C. A. Chang, V. C. Sekhar, B. S. Garg, F. S. Guziec, and T. Carrera Russo, *Inorg. Chim. Acta,* **135**, 11 (1987).
13) W. R. Harris, C. J. Carrano, S. R. Cooper, S. R. Sofen, A. E. Avdeef, J. V. Mc Ardle, and K. N. Raymond, *J. Am. Chem. Soc.,* **101**, 6097 (1979).
14) Chiu Yuen Ng, S. J. Rodgers, and K. N. Raymond, *Inorg. Chem.,* **28**, 2062 (1989).
15) D. A. Brown, R. Geraty, J. D. Glennon, and N. N. Choileain, *Inorg. Chem.,* **25**, 3792 (1986).
16) A. Shanzer, J. Libman, R. Lazar, and Y. Tor, *Pure Appl. Chem.,* **61**, 1529 (1989).
17) D. A. Brown, M. V. Chidambaram, and J. D. Glennon, *Inorg. Chem.,* **19**, 3260 (1980).
18) K. N. Raymond and T. M. Garrett, *Pure Appl. Chem.,* **60**, 1807 (1988).
19) Y. K. Agrawal and G. D. Mehd, *Int. J. Environ. Anal. Chem.,* **10**, 183 (1981).
20) D. C. Bhura and S. B. Tandon, *Anal. Chim. Acta,* **53**, 379 (1971).
21) R. M. Cassidy and D. E. Ryan, *Can. J. Chem.,* **46**, 327 (1968).
22) M. S. El-Ezaby and M. M. Hassan, *Polyhedron,* **4**, 429 (1985).
23) M. S. El-Ezaby, H. M. Marafie, and H. M. Abu-Soud, *Polyhedron,* **5**, 973 (1986).
24) N. E Dixon, R. L. Blakely, and B. Zerner, *Can. J. Biochem.,* **58**, 1323 (1980).
25) G. Gran, *Analyst (London),* **77**, 661 (1952).
26) H. S. Harris and R. S. Tobias, *Inorg. Chem.,* **8**, 2259 (1969).
27) E. Leporati, *J. Chem. Soc., Dalton Trans.,* **1985**, 1605.
28) E. Leporati, *J. Chem. Soc., Dalton Trans.,* **1986**, 199.
29) R. S. Tobias and M. Yasuda, *Inorg. Chem.,* **2**, 1307 (1963).
30) P. Gans, A. Sabatini, and A. Vacca, *J. Chem. Soc., Dalton Trans.,* **1985**, 1195.
31) B. Sarkar and T. P. A. Kruck, *Can. J. Chem.,* **51**, 3541 (1973).
32) R. Osterberg, *Acta Chem. Scand.,* **14**, 471 (1960).
33) N. Ingri, W. Kakalowicz, L. G. Sillén, and B. Warnqvist, *Talanta,* **14**, 1261 (1967).
34) D. J. Leggett and W. A. E. Mc Bryde, *Anal. Chem.,* **47**, 1065 (1975).
35) B. Kurzak, K. Kurzak, and J. Jezierska, *Inorg. Chim. Acta,* **130**, 189 (1987).
36) A. Gergely, I. Sovago, I. Nagypal, and R. Kiraly, *Inorg. Chim. Acta,* **6**, 435 (1972).
37) G. H. Khoe, P. L. Brown, R. N. Sylva, and R. G. Robins, *J. Chem. Soc., Dalton Trans.,* **1986**, 1901.
38) C. F. Baes, Jr. and R. E. Mesmer, "The Hydrolysis of Cations," Wiley Interscience, New York (1976).
39) B. Kurzak, K. Kurzak, and J. Jezierska, *Inorg. Chim. Acta,* **125**, 77 (1986).
40) E. B. Paniago and S. Carvalho, *Inorg. Chim. Acta,* **92**, 253 (1984).
41) E. J. Billo, *Inorg. Nucl. Chem. Lett.,* **10**, 613 (1974).
42) "SAS User's Guide: Statistics, Version 5," SAS Institute Inc., Cary, Nc. (1985), p. 576.
43) E. Leporati, *J. Chem. Soc., Dalton Trans.,* **1989**, 1299.
44) E. Leporati, *Inorg. Chem.,* **28**, 3752 (1989).
45) E. Leporati and G. Nardi, *Gazz. Chim. Ital.,* **121**, 147 (1991).
46) E. Leporati, *Gazz. Chim. Ital.,* **119**, 183 (1989).
47) E. Leporati, *J. Chem. Res. (S),* **1990**, 14.
48) D. J. Leggett, "Computational Methods for the Determination of Formation Constants," Plenum Press: New York and London (1987), p. 355.
49) E. Farkas, J. Szoke, T. Kiss, K. Kozlowski, and W. Bal, *J. Chem. Soc., Dalton Trans.,* **1989**, 2247.
50) J. Neilands, *Struct. Bonding (Berlin),* **1**, 59 (1966).
51) D. A. Brown, R. Mageswaran, *Inorg. Chim. Acta,* **161**, 267 (1989).

Oxidation of Sulfite and Thiosulfate by the Cobalt(III) Complex of Dipicolinate in Aqueous Medium

Mahammad Ali, Swapan K. Saha, and Pradyot Banerjee*
Department of Inorganic Chemistry, Indian Association for the Cultivation of Science, Jadavpur, Calcutta 700032, India
(Received November 15, 1990)

The oxidation of sulfite and thiosulfate by $Co(dipic)_2^-$ (where H_2dipic=2,6-pyridinedicarboxylic acid) was studied in aqueous medium. The reactions were carried out by varying reagent concentrations, pH, and ionic strength. For thiosulfate oxidation, the rate is zero order in complex and second order in thiosulfate. The reaction rates were found to increase with the acidity and the general rate law is expressed as $k_{obs}=\{k_0'+k_1'[H^+]\}[S_2O_3^{2-}]^2$ where k_0' and k_1' denote the acid independent and dependent paths respectively. The values of rate parameters are $k_0'=(2.87\pm0.20)\times10^{-8}$ mol dm^{-3} s^{-1} and $k_1'=(0.57\pm0.02)$ mol^{-2} dm^6 s^{-1} at 30 °C. A plausible mechanism is suggested by considering the formation of an intermediate active species in the rate-determining step. The sulfite oxidation was, however, first order both in complex and reagent. An inverse dependence on $[H^+]$ was obtained for this reaction indicating a higher reactivity of the anionic species in solution. The general rate law is given by $k_{obs}=2(k_1[SO_2\cdot H_2O]+k_2[HSO_3^-]+k_3[SO_3^{2-}])$ and the evaluated second-order rate constants are: $k_1=(5.60\pm0.04)\times10^{-5}$ mol^{-1} dm^3 s^{-1}, $k_2=(3.02\pm1.21)\times10^{-3}$ mol^{-1} dm^3 s^{-1} and $k_3=(4.91\pm0.05)\times10^{-2}$ mol^{-1} dm^3 s^{-1} at 60 °C. The reactivity order $SO_3^{2-}>HSO_3^->SO_2\cdot H_2O$ has been explained successfully by considering the two isomeric structures for these species in solution. An overall rate law has been derived to interpret these results over the whole range of pH. The theoretical pH rate profile calculated from the different rate parameters shows an excellent agreement with the experimental one suggesting the validity of the proposed mechanism.

Very recently, we reported the oxidation of sulfite[1] and thiosulfate[2] with a substitution inert complex, dodecatungstocobaltate(III), in aqueous acidic solution. In the oxidation of sulfite, a mixed order dependence on sulfite concentration and a variable product distribution in accordance with stoichiometry was obtained. The thiosulfate oxidation was, however, a simple second-order reaction and in both these studies an alkali metal ion catalysis was observed. But these studies were limited to a pH range 1.5—5.5, as the complex was unstable beyond this pH and the reductants were unstable at low pH. Correspondingly, reactivities of the mono- and divalent anionic forms of the sulfite were determined. In the present study we have chosen a complex, $Co(dipic)_2^-$ (where H_2dipic=2,6-pyridinedicarboxylic acid), which is stable both in acidic and alkaline media and only one reactive species exists within the experimental pH range, and it has a standard reduction potential value[3] (E°=0.747 V), little lower than the dodecatungstocobaltate(III)[2] (E°=1.00 V). The choice of the complex is also significant because $Co(dipic)_2^-$ posseses a hydrophobic π-conjugated ligand and is much more reactive with the redox centers in metalloproteins than the redox reagents having hydrophilic electron transfer surfaces.[3-6] The aim of this study is to determine and compare the reactivities of all the species of these reductants available in aqueous solution and also to obtain additional information regarding the mechanistic behavior of the complex towards the reaction.

Experimental

Materials and Reagents. The complex, ammonium salt of bis(dipicolinato)cobaltate(III), $NH_4[Co(dipic)_2]$, was prepared and standardized by the same procedure as reported earlier.[7] Analytical grade reagents were used without further purification. Solutions were prepared in double distilled water and purged with dinitrogen before reaction. The sulfite solution was prepared by dissolving an appropriate amount of sodium sulfite in double distilled water which has been purged with dinitrogen adequately. In a similar fashion thiosulfate solution was prepared and standardized iodimetrically. All solutions were prepared just prior to use. Sodium perchlorate and potassium nitrate used in this study were of analytical grade and also recrystallized thrice before use. Sodium acetate–acetic acid and sodium borate–hydrochloric acid were used as buffers to maintain the pH of the solution as required.

Kinetic Measurements. The reactions were followed in a Pye-Unicam SP8-150 UV/VIS spectrophotometer equipped with thermostated cell compartments. Temperature was controlled using a Haake F3 thermostat. The pH measurements were carried out in a Systronics digital pH meter (model 335, India). Extra precautions were taken to eliminate the loss of sulfurous acid as SO_2 and to prevent air oxidation of thiosulfate. Reactions were carried out in air-tight stoppered quartz cells.

Test for Free Radicals. Both the reactions were tested for free radical generation during the reaction. For this purpose acrylonitrile (5 ml. 20% v/v, degassed with nitrogen) was added to a deaerated reaction mixture. Appearance of a heavy white precipitate within 10 min of reaction confirmed the presence of free radicals in the reaction mixture of sulfite. No polymerization was encountered when acrylonitrile was added to the deaerated solution of complex and reagents separately.

Stoichiometry and Reaction Products. For the thiosulfate oxidation, the reaction stoichiometry was determined iodimetrically by estimating the unreacted thiosulfate in reaction mixtures of thiosulfate and complex in different ratios. The stoichiometry thus obtained is 1:1 ($[Co(dipic)_2^-]$: $[S_2O_3^{2-}]$). The reaction product was tetrathionate and confirmed by the method of Kolthoff and Belcher[8] using the reaction,

$$S_4O_6^{2-} + 3CN^- + H_2O \longrightarrow S_2O_3^{2-} + SO_4^{2-} + SCN^- + 2HCN \quad (1)$$

For the sulfite oxidation, the stoichiometry was determined spectrophotometrically by estimating the excess $[Co(dipic)_2^-]$ in a $Co(dipic)_2^-$–sulfite reaction mixture. With excess sulfite, the stoichiometry was determined by estimating excess sulfite iodimetrically. Under both conditions, a 2:1 $[(Co(dipic)_2^-]$:[S(IV)] stoichiometry was obtained. The corresponding reaction product obtained was sulfate.

Results and Discussion

Oxidation of Thiosulfate by $Co(dipic)_2^-$. The reaction between $Co(dipic)_2^-$ and thiosulfate was followed at 510 nm (ε_{max}=630 $mol^{-1}\,dm^3\,cm^{-1}$) by following the decrease in absorbance of the complex. Na_2edta (1.0×10^{-5} mol dm^{-3}) was used as the masking agent throughout the experiment to avoid any catalysis caused by the presence of foreign metal ions. A 30—35% decrease in rate was observed compared to that in the absence of EDTA. Variation of [EDTA] shows no further effect on the reaction rate. Under pseudo-first-order conditions, the plots of absorbance vs. time are all linear (80 to 90%, of total reaction) indicating a zero-order dependence of rate in complex. The corresponding k_{obs} are calculated from the slope of such plots. A plot of k_{obs} vs. $[S_2O_3^{2-}]$ gives a curvature of increasing slope in the range of $[S_2O_3^{2-}]$=0.005—0.05 mol dm^{-3} at pH 4.5, I=0.60 mol dm^{-3} ($NaClO_4$), and temperature 30 °C. But a plot of k_{obs} vs. $[S_2O_3^{2-}]^2$ is a straight line passing through the origin indicating a second-order dependence of rate on $[S_2O_3^{2-}]$ (Fig. 1). The effect of

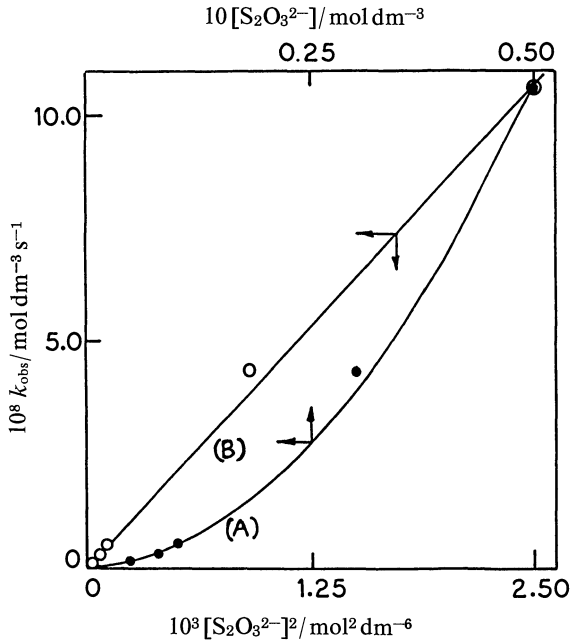

Fig. 1. Different plots showing the dependence of the observed rate on the reductant concentrations (A) k_{obs} vs. $[S_2O_3^{2-}]$, (B) k_{obs} vs. $[S_2O_3^{2-}]^2$. Conditions are; $[Co(dipic)_2^-]=4.0\times10^{-4}$ mol dm^{-3}, I=0.60 mol dm^{-3}, pH=4.5, $[EDTA]=1.0\times10^{-5}$ mol dm^{-3}, and at 30 °C.

Table 1. Dependence of Rate on pH for the Oxidation of Thiosulfate by $Co(dipic)_2^-$ at $[S_2O_3^{2-}]$=0.03 mol dm^{-3}, $[Na^+]$=0.60 mol dm^{-3}, [Complex]=4.0×10^{-4} mol dm^{-3}, [EDTA]=1.0×10^{-5} mol dm^{-3}, and at 30 °C

pH	$10^8\,k_{obs}$ / mol $dm^{-3}\,s^{-1}$
3.90	9.24 (13.2)
4.01	7.90 (11.3)
4.25	6.05 (9.60)
4.50	4.35 (6.50)
4.90	3.45 (5.30)

The parenthetical values represent the k_{obs} in the absence of EDTA added externally. $k_0'=(2.87\pm0.20)\times10^{-8}$ mol $dm^{-3}\,s^{-1}$; $k_1'=(0.57\pm0.02)$ $dm^6\,mol^{-2}\,s^{-1}$.

hydrogen ion concentration on the reaction rates was studied in the pH range 3.90—4.90 at $[S_2O_3^{2-}]$=0.03 mol dm^{-3}, I=0.60 mol dm^{-3} ($NaClO_4$) and temperature 30 °C. The reaction rates increase with the increase in $[H^+]$ and the corresponding results are given in Table 1. A plot of k_{obs} vs. $[H^+]$ gives a straight line with a positive intercept on the rate axis and follows a rate law of the type,

$$\text{rate} = k_0'[S_2O_3^{2-}]^2 + k_1'[H^+][S_2O_3^{2-}]^2 \quad (2)$$

where k_0' represents the acid independent path and k_1', the acid dependent path. The values of k_0' and k_1' are evaluated and summarized in Table 1. Considering the stoichiometry of the reaction and the above rate dependence, the mechanism of the oxidation of thiosulfate by $Co(dipic)_2^-$ may be postulated as,

$$S_2O_3^{2-} + S_2O_3^{2-} \underset{k_{0-}''}{\overset{k_0''}{\rightleftharpoons}} [S_2O_3,S_2O_3]^{4-} \quad (3)$$

$$S_2O_3^{2-} + HS_2O_3^- \underset{k_{1-}''}{\overset{k_1''}{\rightleftharpoons}} [S_2O_3,HS_2O_3]^{3-} \quad (4)$$

$$[S_2O_3,S_2O_3]^{4-} + 2\,Co(dipic)_2^- \xrightarrow{fast} S_4O_6^{2-} + 2\,Co(dipic)_2^{2-} \quad (5)$$

$$[S_2O_3,HS_2O_3]^{3-} + 2\,Co(dipic)_2^- \xrightarrow{fast} S_4O_6^{2-} + 2\,Co(dipic)_2^{2-} + H^+ \quad (6)$$

The above mechanism thus accounts for both the zero-order dependence in complex and the second-order dependence in thiosulfate. Therefore, the rate law may be given as

$$-\text{d[complex]}/dt = k_0''[HS_2O_3^-][S_2O_3^{2-}] + k_1''[S_2O_3^{2-}][S_2O_3^{2-}] \quad (7)$$

Considering the dissociation of $HS_2O_3^-$ as

$$HS_2O_3^- \underset{}{\overset{K_2'}{\rightleftharpoons}} H^+ + S_2O_3^{2-} \quad (8)$$

and $[S_2O_3^{2-}]=[S_2O_3^{2-}]+[HS_2O_3^-]$, the above rate law may be modified as

$$-\frac{\text{d[complex]}}{dt} = 2\cdot\frac{(k_0''K_2'+k_1''[H^+])}{(K_2'+[H^+])^2}\cdot K_2'[S_2O_3^{2-}]^2 \quad (9)$$

The second dissociation constant[9] of sulfurous acid is $K_2'=1.0\times10^{-2}$ mol dm^{-3}. So under the experimental conditions, $K_2' \gg [H^+]$, and the above equation may be reduced to,

$$-d[\text{complex}]/dt = k_1 = 2(k_0''+k_1''K_2'^{-1}[H^+])[S_2O_3^{2-}]^2 \quad (10)$$

The equation (10) simplifies to the observed rate law (2) with $k_0'=2\,k_0''$ and $k_1'=2\,k_1''K_2'^{-1}$.

An attempt has been made to determine the effect of ionic strength on the reaction rate. Under the conditions, $[S_2O_3^{2-}]=0.03$ mol dm^{-3}, pH=4.50, $[Co(dipic)_2^-]=4.0\times10^{-4}$ mol dm^{-3} and at 30 °C, no effect of ionic strength is observed in the range, I=0.2—1.5 mol dm^{-3} ($NaClO_4$).

It is to be noted here that no sulfur deposition was observed in the experimental pH region during the course of reaction. However, at high acid, rapid sulfur deposition occurs and this phenomenon was studied by Dinegar et al.[10] The decomposition rate of thiosulfate thus obtained (k=0.5 mol^{-2} dm^6 s^{-1}) is of the same order as to the oxidation rate (k_1'=0.57±0.02 mol^{-2} dm^6 s^{-1}) in this study. The experimental rate constants for the oxidation of thiosulfate ions by $Fe(CN)_6^{3-}$,[11] (k=0.6 mol^{-2} dm^6 s^{-1}) and $W(CN)_8^{3-}$,[12] (k=0.30 mol^{-2} dm^6 s^{-1}) are also of the same order as that in this study and favors the proposed mechanism. We have also studied the effect of cations and anions on the reaction rate for this system. Neither the charge nor the size of the cations or anions have appreciable effect on the reaction rate. A 30—35% decrease in rate in the presence of added EDTA was observed (Table 1) and may be attributed to the catalytic effect caused by the presence of trace amount of multivalent cations.

Oxidation of S(IV) by $Co(dipic)_2^-$. The stoichiometric equation for the oxidation of S(IV) by $Co(dipic)_2^-$ both in acidic and alkaline medium may be written as

$$2\,Co(dipic)_2^- + S(IV) \longrightarrow 2\,Co(dipic)_2^{2-} + SO_4^{2-} \quad (11)$$

Table 2. Dependence of Rate on the [S(IV)] for the Oxidation of Sulfite by $Co(dipic)_2^-$ at Different pH, Conditions are [Complex]=4.0×10^{-4} mol dm^{-3}, I=0.50 mol dm^{-3}, and at 60 °C

[S(IV)]		$10^3\,k_{obs}/s^{-1}$		
mol dm^{-3}	pH	2.0	4.5	8.0
0.01			0.10	1.00
0.03			0.24	2.50
0.05		0.12	0.36	4.76
0.07		0.16	0.53	5.70
0.10		0.22	0.71	8.90
0.15		0.33		

$k_1=(5.60\pm0.04)\times10^{-5}$ dm^3 mol^{-1} s^{-1}, $k_2=(3.02\pm1.21)\times10^{-3}$ dm^3 mol^{-1} s^{-1}, and $k_3=(4.91\pm0.05)\times10^{-2}$ dm^3 mol^{-1} s^{-1}; $K_1=(5.03\pm0.01)\times10^{-3}$ mol dm^{-3}, and $K_2=(4.26\pm0.10)\times10^{-7}$ mol dm^{-3}.

where S(IV) indicates all type of the reacting sulfite species (e.g. $SO_2\cdot H_2O$, HSO_3^-, and SO_3^{2-}). Sulfate was only the reaction product as confirmed by the usual tests.

The spectral change for the reaction between $Co(dipic)_2^-$ and S(IV) was noted at pH 3.0, 4.5, and 8.0 with I=0.50 mol dm^{-3} ($NaClO_4$) and at 25 °C. All the spectral scannings gave an isosbestic point near 450 nm and indicated the absence of an appreciable amount of stable intermediate formed during the course of reaction. Measurement of the reaction rate was accomplished by monitoring the decrease in optical density at 510 nm (the absorption maximum of $Co(dipic)_2^-$ species). All the experiments were carried out under pseudo-first-order conditions keeping S(IV) concentration at least tenfold in excess over $Co(dipic)_2^-$ concentration. The plots of $-\log(A_t-A_\infty)$ against time (where A_t and A_∞ have their usual significance) are all linear upto 85% of the total reaction and thus ensures a first-order dependence on complex concentration. Dependence of rate on S(IV) is first order and is shown by the linearity of the plot of k_{obs} vs. [S(IV)] at pH 2.0, 4.5, and 8.0 at I=0.50 mol dm^{-3} ($NaClO_4$) and temperature 60 °C. The corresponding data are listed in Table 2.

The effect of hydrogen ion concentration on the oxidation rate was investigated in the pH range 2.0—8.0 at a constant temperature (60 °C) and ionic strength (I=0.50 mol dm^{-3}, $NaClO_4$). The dissociation constants of sulfurous acid[12] are reported to be $K_1=1.05\times10^{-2}$ mol^{-1} dm^3 and $K_2=4.36\times10^{-7}$ mol^{-1} dm^3 at 25 °C. Therefore, all the molecular and both mono- and divalent anionic species of the reductant would be present in

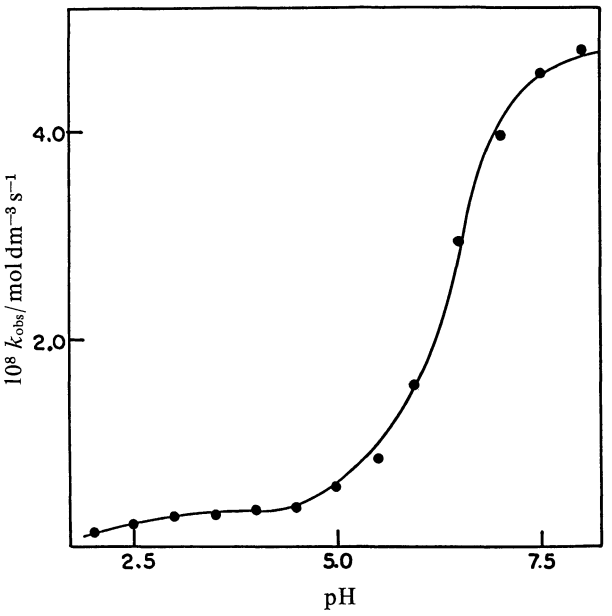

Fig. 2. Plot of k_{obs} vs. pH for the oxidation of sulfite with $Co(dipic)_2^-$ at [complex]=4.0×10^{-4} mol dm^{-3}, [S(IV)]=0.05 mol dm^{-3}, I=0.50 mol dm^{-3} ($NaClO_4$) and at 60 °C. Bold line represents the experimental graph and the theoretical values are shown by ●.

the experimental pH range. We made an attempt to find out the reactivities of individual species separately. For this purpose, we have chosen two different pH regions (i) pH 2.0—5.0, around the pK_1, where only molecular ($SO_2 \cdot H_2O$) and monovalent anionic (HSO_3^-) species are present and (ii) pH 5.5—8.0, around the pK_2, where only monovalent (HSO_3^-) and divalent (SO_3^{2-}) anionic species are only reactive. The corresponding equilibria are described later (in Eqs. 13 and 14). Under both the conditions the plot of k_{ox} vs. $[H^+]^{-1}$ gives the limiting curves of decreasing slope with non-zero intercept on the rate axis. This involves the necessity of three parameters leading to the equation of the form

$$k_{ox}=\frac{a+b[H^+]}{c+[H^+]} \tag{12}$$

where $k_{ox}=k_{obs}/2[S(IV)]$ and 2 is the stoichiometric factor. Data were fit to this equation using a non linear least-squares computer-fit program with each point weighed as k_{ox} and corresponding values of *a, b, c* under the two conditions are given as (i) a=(1.64±0.01)×10^{-5}; *b*=(5.60±0.04)×10^{-5}; *c*=(5.03±0.01)×10^{-3} and (ii) *a*=(2.09±0.04)×10^{-8}; *b*=(3.02±1.21)×10^{-3}; *c*=(4.26±0.09)×10^{-7}.

It is well-known that sulfurous acid exists as hydrated sulfur dioxide in aqueous solution but both HSO_3^- and SO_3^{-2} do exist in aqueous media. The dissociation of sulfurous acid in aqueous solution may be given as[13]

$$SO_2 \cdot H_2O \overset{K_1}{\rightleftharpoons} HSO_3^- + H^+ \tag{13}$$

$$HSO_3^- \overset{K_2}{\rightleftharpoons} SO_3^{2-} + H^+ \tag{14}$$

where K_1 and K_2 are the first and second dissociation constants of sulfurous acid. Considering the stoichiometry and above observations, the possible mechanism corresponding to the oxidation of S(IV) by $Co(dipic)_2^-$ may be proposed as

$$Co(dipic)_2^- + SO_2 \cdot H_2O \xrightarrow{k_1} SO_3^{\cdot-} + Co(dipic)_2^{2-} + 2H^+ \tag{15}$$

$$Co(dipic)_2^- + HSO_3^- \xrightarrow{k_2} SO_3^{\cdot-} + Co(dipic)_2^{2-} + H^+ \tag{16}$$

$$Co(dipic)_2^- + SO_3^{2-} \xrightarrow{k_3} SO_3^{\cdot-} + Co(dipic)_2^{2-} \tag{17}$$

$$S(V)(H\dot{S}O_3 \text{ or } SO_3^{\cdot-}) + Co(dipic)_2^- + H_2O \xrightarrow{\text{fast}} SO_4^{2-} + Co(dipic)_2^{2-} \tag{18}$$

Now considering the pH region 2.0—5.0, as in condition (i), where k_1 and k_2 paths are operative, the corresponding rate law may be given as

$$k_{obs}=2\frac{k_2K_1+k_1[H^+]}{K_1+[H^+]}[S(IV)] \tag{19}$$

$$k_{ox}=\frac{k_2K_1+k_1[H^+]}{K_1+[H^+]} \tag{20}$$

where k_{obs} is the pseudo-first-order rate constant. Similarly in the pH region 5.5—8.0, as in the condition (ii), where the HSO_3^- and SO_3^{2-} are the reactive species, the rate expression can be given as

$$k_{ox}=\frac{k_3K_2+k_2[H^+]}{K_2+[H^+]} \tag{21}$$

and both Eqs. 19 and 20 are consistent to Eq. 11 with a=K_1k_2, *b*=k_1 and *c*=K_1 in Eq. 19 and with *a*=K_2k_3, *b*=k_2 and *c*=K_2 in Eq. 20. The values of k_1, k_2, k_3, and dissociation constants K_1 and K_2 thus obtained are listed in Table 2. There is an excellent agreement between the reported values of K_1 and K_2 and those obtained from the computer-fit program for the experimental data.

Considering the reaction of all the species in the pH range 2.0—8.0, the general rate expression for the reaction between $Co(dipic)_2^-$ and S(IV) can be given as

$$k_{obs}=2\frac{k_1[H^+]^2+K_1k_2[H^+]+K_1K_2k_3}{[H^+]^2+K_1[H^+]+K_1K_2}[S(IV)] \tag{22}$$

Using the above values of k_1, k_2, and k_3 and the values of first and second dissociation constants of sulfurous acid the values of k_{obs} are calculated from the above expression at different $[H^+]$. An excellent agreement between the calculated and observed rate (Fig. 1) provides further support in favor of the proposed mechanism.

A comparison of the reactivities of the different S(IV) species obtained in solution shows the reactivity order $SO_2^{2-}>HSO_3^->SO_2 \cdot H_2O$. In fact SO_3^{2-} is 16 times more reactive than HSO_3^- and HSO_3^- is 53 times more reactive than $SO_2 \cdot H_2O$. This difference in reactivity may be explained by considering the following equilibria,[14]

$$HSO_3^- + H^+ \rightleftharpoons \underset{(A)}{H:SO_3:H} \rightleftharpoons \underset{(B)}{HO\text{–}S\text{–}OH}$$

$$SO_3^{2-} + H^+ \rightleftharpoons \underset{(C)}{H:SO_3} \rightleftharpoons \underset{(D)}{HO:SO_2}$$

In the acidic medium (pH 2.0) an appreciable amount of $SO_2 \cdot H_2O$ is believed to exist in solution. In the (A) form the lone pair is tied up with proton whereas in (B) the electron density will be withdrawn from the sulfur atom by the two OH groups. Similar phenomenon may occur for (C) and (D) also but the electron density will be more on the sulfur atom since the electrons on the sulfur atom are tied up by one proton in (C) or pulled up by one OH group in (D). For SO_3^{2-}, no such consideration occurs and thus electron density will be more available and consequently would show the highest reactivity which actually we found.

The present study provides a systematic approach to the oxidation of sulfur dioxide and thiosulfate in aqueous medium. This study constitutes a rare example where the reactivities of all the species of sulfur dioxide available in aqueous solution have been determined and compared.

The zero-order rate in complex for the thiosulfate oxidation also is one of the very few examples of thiosulfate oxidation where the rate-determining step is

the formation of some active intermediate which in turn reacts with the complex in a fast step. This study has some special importance. Generally in the oxidation reactions of thiosulfate by metal ions and complexes, a zero-order dependence on [complex] is encountered for oxidants having $E^\circ \leqslant 0.54$ V and a first-order dependence for oxidants[2,15-17] having $E^\circ \geqslant 0.80$ V. The present study, therefore, cites a unique example where zero-order rate in complex is obtained though the oxidation potential is sufficiently high ($E^\circ = 0.75$ V). Possibly π-donating character of the dipicolinate ligand makes the metal-center reluctant to electron transfer and thus follows a zero-order rate in complex. Our experimental results are comparable to the reported k_2 values with other oxidants in the presence of added EDTA. But none has reported the acid independent k_0' path which we found significant in the present study.

References

1) M. Ali, S. K. Saha, and P. Banerjee, *J. Chem. Soc., Dalton Trans.*, **1990**, 187.

2) M. Ali, S. K. Saha, and P. Banerjee, *Indian J. Chem., Sect. A*, **29**, 528 (1990).

3) N. H. Williams and J. K. Yandell, *Aust. J. Chem.*, **36**, 2377 (1983).

4) S. Wherland, W. R. Cullen, D. Dolphin, and B. R. James, "Biological Aspects of Inorganic Chemistry," Wiley, New York (1977), p. 289.

5) S. Wherland and H. B. Gray, *Proc. Natl. Acad. Sci. U.S.A.*, **73**, 2950 (1976).

6) C. Creutz and N. Sutin, *Biol. Chem.*, **247**, 6932 (1972).

7) A. R. Mauk, C. L. Coyle, E. Bordignon, and H. B. Gray, *J. Am. Chem. Soc.*, **101**, 5054 (1979).

8) I. M. Kolthoff and R. Belcher, "Volumetric Analysis," Interscience, New York (1957), Vol. 3.

9) L. G. Sillen, "Stability Constant of Metal Ion Complexes," Special Publ., The Chemical Society, London (1964), pp. 224 and 229.

10) R. H. Dinegar, R. H. Smellie, and V. K. La Mer, *J. Am. Chem. Soc.*, **73**, 2050 (1951).

11) K. E. Howlet and B. L. Wedzicha, *Inorg. Chim. Acta*, **18**, 133 (1976).

12) C. R. Dennis, J. G. Leipoldt, S. S. Basson, and G. J. Lamprecht, *Polyhedron*, **4**, 1621 (1985).

13) J. C. Bailar, H. J. Emeleus, D. Nyholm, and A. F. Trotman Dickenson, "Comprehensive Inorganic Chemistry," Pergamon Press, Oxford (1973), Vol. 2, p. 879.

14) R. E. Connick, T. M. Tam, and E. Von Denster, *Inorg. Chem.*, **21**, 103 (1982).

15) G. J. Lamprecht, J. G. Leipoldt, C. R. Dennis, and S. S. Basson, *React. Kinet. Catal. Lett.*, **13**, 269 (1980).

16) I. Balda and G. Niac, *Inorg. Chem.*, **9**, 110 (1970).

17) K. A. Muirhead, G. P. Haight, Jr., and J. K. Beattie, *J. Am. Chem. Soc.*, **94**, 3006 (1972).

Mössbauer and Infrared Spectroscopic Studies of Some Alkyl- and Arylamine Coordinated Pentacyanoferrate(II) Complexes

Ratnakar Balkrishna LANJEWAR and Amar Nath GARG*
Department of Chemistry, Nagpur University, Nagpur 440010, India
(Received December 3, 1990)

Mössbauer spectra of alkyl- and arylamine coordinated pentacyanoferrate(II) complexes, $Na_3[Fe(CN)_5L]\cdot xH_2O$ where L=$(CH_3)_3N$, $(CH_3)_2CHNH_2$, $(CH_3)_2CHCH_2NH_2$, $(CH_3)_3C-NH_2$, $C_6H_5NH_2$, $C_6H_5NHCH_3$, $C_6H_5N(CH_3)_2$, $C_6H_5NHC_2H_5$, o-$ClC_6H_4NH_2$, and p-$ClC_6H_4NH_2$ have been studied. All compounds exhibit a well-resolved quadrupole doublet. An unusually high quadrupole splitting is observed for isobutylamine coordinated complex (ΔE_Q=1.75 mm s^{-1}). Other complexes show ΔE_Q=0.67—0.86 mm s^{-1}. A correlation of δ vs. ΔE_Q suggests a positive sign of electric field gradient for isobutylamine coordinated complex and negative for all other complexes. Partial isomer shift (p.i.s.) and δ have been correlated with partial quadrupole splitting (p.q.s.). Also characteristic CN and Fe–N stretching frequencies have been correlated with δ to derive information on σ-donor and π-acceptor properties of the ligands.

Mössbauer spectroscopic studies of coordinated pentacyanoferrate(II) complexes, $[Fe(CN)_5L]^{n-}$ where L= H_2O, NH_3, CO, NO_2, SO_3^{2-}, py, NO^+, DMSO, RNH_2, R_3N etc. have been reported extensively.[1—14] In these studies main emphasis has been to know the extent of deformation in octahedral geometry and correlate isomer shift (δ) with quadrupole splitting (ΔE_Q) to predict the sign of electric field gradient (EFG). Also bonding characteristics with regard to σ-donor and π-acceptor properties of the ligands have been investigated.[8—10] In our earlier studies on mono-, di-, and trialkylamine coordinated pentacyanoferrates(II), it has been observed that though substituted alkylamines, (R_nNH_{3-n}) are primarily σ-donors but in some cases indirect π-interaction is also possible.[11] In the present studies we have synthesized some new pentacyanoferrate(II) complexes, $Na_3[Fe(CN)_5L]\cdot xH_2O$ where L=$(CH_3)_3N$, $(CH_3)_2CHNH_2$, $(CH_3)_2CHCH_2NH_2$, $(CH_3)_3C-NH_2$ $C_6H_5NHCH_3$, $C_6H_5N(CH_3)_2$, $C_6H_5NHC_2H_5$, o-ClC_6H_4-NH_2, and p-$ClC_6H_4NH_2$ and studied their Mössbauer and infrared spectra. We have also attempted to see the validity δ vs. ΔE_Q correlation in predicting the sign of EFG.

Experimental

All reagents used were AR, GR (S. Merck) or of high purity grade (Koch-Light, UK and Fluka, Switzerland). Solvents were distilled and dried before use. The complexes were prepared by slightly modified procedure described in the literature.[15,16]

Preparation of Trimethylamine, Isopropylamine, Isobutylamine, and *t*-Butylamine Coordinated Complexes: Three gram of sodium pentacyanonitrosylferrate(II) (1 mol) and 2 g of sodium acetate were dissolved in 20 ml water and mixed with ice cold solution of the respective amine (20—25 ml) in ethanol. The solution was continuously stirred and additional amount of amine was added till a negative test for pentacyanonitrosylferrate(II) was obtained. The mixture was kept in freezing mixture for 2—4 h during which the complexes separated out.

Preparation of Arylamine Coordinated Complexes: In order to prepare these complexes, sodium amminepentacyanoferrate(II), $Na_3[Fe(CN)_5NH_3]\cdot 3H_2O$ (SPF) was synthesized[16] which was used for further synthesis of arylamine coordinated complexes. Freshly prepared 3 g SPF (1 mol) was dissolved in 20 ml water, cooled and mixed with an ice cold solution of respective amine (20—25 ml). The solution was continuously stirred for 3—4 h. On addition of cold absolute ethanol

Table 1. Mössbauer Parameters and Characteristic IR Frequencies in Aminepentacyanoferrate(II) Complexes, $Na_3[Fe(CN)_5L)\cdot xH_2O$

	Complex	Isomer shift[a] δ/mm s^{-1}	Quadrupole splitting[a] ΔE_Q/mm s^{-1}	p.i.s. mm s^{-1}	p.q.s. mm s^{-1}	ν(CN) cm^{-1}	δ(Fe–CN) cm^{-1}	ν(Fe–N) cm^{-1}	δ(Fe–c) cm^{-1}
I	$Na_3[Fe(CN)_5(CH_3)_3N]\cdot H_2O$	0.27	0.78	0.06	−0.45	2025s	570s	225w	410w
II	$Na_3[Fe(CN)_5(i\text{-}PrNH_2)]\cdot H_2O$	0.24	0.76	0.03	−0.46	2060s	560m	310w	450m
III	$Na_3[Fe(CN)_5(i\text{-}BuNH_2)]\cdot 3H_2O$	−0.04	1.75	−0.25	0.04	2140s 1950s	540s	315w	410w
IV	$Na_3[Fe(CN)_5(t\text{-}BuNH_2)]\cdot H_2O$	0.23	0.86	0.02	−0.41	2060s	580m	240w	430m
V	$Na_3[Fe(CN)_5(PhNH_2)]\cdot 2H_2O$	0.28	0.74	0.07	−0.47	2040s	570s	280w	400w
VI	$Na_3[Fe(CN)_5(PhNHCH_3)]\cdot H_2O$	0.29	0.69	0.08	−0.50	2040s	570m	260w	410w
VII	$Na_3[Fe(CN)_5(PhNHC_2H_5)]\cdot 3H_2O$	0.29	0.77	0.08	−0.46	2050s	570s	220sh	410b
VIII	$Na_3[Fe(CN)_5(p\text{-}ClC_6H_4NH_2)]\cdot H_2O$	0.25	0.82	0.04	−0.43	2050s	540s	220sh	410b
IX	$Na_3[Fe(CN)_5(o\text{-}ClC_6H_4NH_2)]\cdot H_2O$	0.26	0.71	0.05	−0.48	2040s	560m	230w	430w
X	$Na_3[Fe(CN)_5(C_6H_5NMe_2)]\cdot H_2O$	0.27	0.67	0.06	−0.51	2040s	560s	240w	420m

a) Standard deviations are within ±0.03 mm s^{-1}.

complexes were precipitated. These were filtered and dried in vacuo over $CaCl_2$ in a desiccator. The complexes were characterized by the elemental analysis of C, H, N, and Fe. Number of water molecules were matched with the suggested molecular formulae (Table 1).

Mössbauer spectra were recorded on a transducer driven Mössbauer spectrometer in constant acceleration mode (Nucleonix, Hyderabad) at room temperature. A ca. 5 mCi $^{57}Co(Rh)$ source was used. The spectrometer was calibrated using natural iron foil and sodium pentacyanonitrosylferrate(II) dihydrate (SNP) was used as standard. Spectral lines were assumed to have Lorentzian line shape and the Mössbauer parameters were calculated from visual fitting. Errors were estimated from replicate spectral recording. Infrared spectra (4000—200 cm^{-1}) in KBr pellets were recorded on Perkin-Elmer-157 IR spectrophotometer.

Results and Discussion

The Mössbauer spectra of all the complexes exhibit a well-resolved quadrupole doublet at room temperature. The Mössbauer parameters of all the individual complexes are listed in Table 1. Also given in the Table 1 are characteristic infrared frequencies for ν(C≡N), δ(Fe-CN), ν(Fe-C), and ν(Fe-N). Typical Mössbauer spectra of isobutylamine and *t*-butylamine coordinated complexes are shown in Fig. 1.

If one of the cyano ligands in hexacyanoferrate(II), $[Fe(CN)_6]^{4-}$ is replaced by a neutral ligand L to give $[Fe(CN)_5L]^{3-}$, then octahedral geometry remains unaffected but the symmetry is lowered from O_h to approximately C_{4v}.[7] Even though the electronic configuration will be t_{2g}^6 but it will further split into d_{YZ}, d_{ZX}, and d_{XY} (also called e and b_2). All the complexes are expected to be diamagnetic. All amines are essentially σ-donors. The five cyano ligands have vacant π* $2p_y$, $2p_z$ orbitals

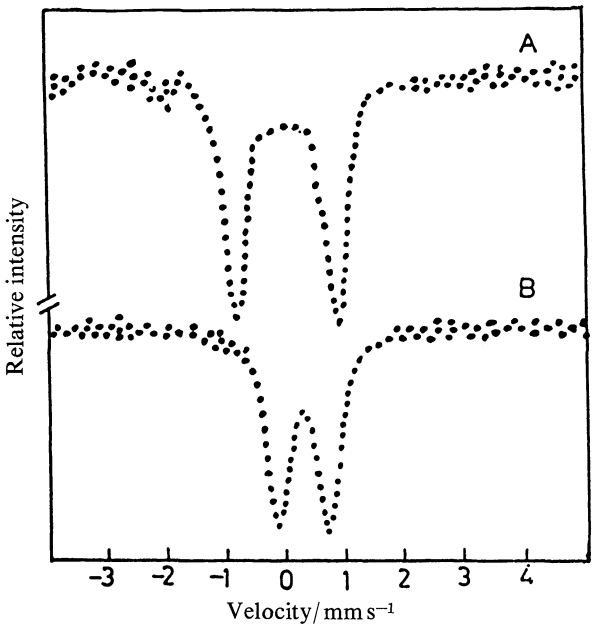

Fig. 1. Mössbauer Spectra of (A) isobutylamine and (B) *t*-butylamine coordinated pentacyanoferrate(II) complexes at room temperature.

available for back bonding, while no such orbitals are available in the case of amines. X-Ray crystal structure determination[17,18] of sodium pentacyanonitrosylferrate(II) has shown that the ligand NO^+ and *trans*-cyano are approximately colinear with central Fe atom slightly displaced in the direction of NO ligand from the plane of four pseudoequivalent CN ligands. Manoharan et al.[19] have studied several hexanitroferrates(II) and confirmed π* $2p_y$, $2p_z$-bonding ability of NO_2^- but found it to be much less than that of CN^- ligands.

(i) Mössbauer Parameters: All compounds show large quadrupole splitting (ΔE_Q) indicating quite significant distortion in octahedral geometry. Since all the six 3d-electrons form a closed shell (t_{2g}^6), no quadrupole splitting is expected due to valence electron contribution. However, due to substitution of sixth cyano with an amine ligand distortion in octahedral geometry is expected. Therefore, ΔE_Q is a direct measure of the distortion due to ligand contribution although small electronic contribution may also be expected due to further lifting of degeneracy in t_{2g} level as suggested by Manoharan and Gray[20] for sodium pentacyanonitrosylferrate(II). All ΔE_Q values fall in the range, 0.67—1.75 mm s^{-1} and can be divided into two subgroups; Gr. I with ΔE_Q=0.67—0.86 mm s^{-1} and Gr. II with ΔE_Q=1.75 mm s^{-1}. Surprisingly isobutylamine coordinated complex exhibits largest ΔE_Q=1.75 mm s^{-1} which is more than double compared to other complexes.

Isomer shift values of all the complexes are in the range −0.04—0.29 mm s^{-1} with respect to SNP as standard. These are well within the typical range for iron(II) low spin complexes.[1-3,10] For all the six aniline coordinated complexes, the isomer shift values are within 0.27±0.02 mm s^{-1} and are comparable with other alkylamine coordinated complexes. It indicates that substitution of alkyl or aryl group or even that of chloro at ortho or para position on phenyl group of aniline ligand does not have any significant effect on s-electron density at the Fe nucleus. It may be further noted that δ value for isobutylamine coordinated complex (−0.04 mm s^{-1}) is very low and it is almost equal to that for dibutylamine and butylamine coordinated complexes studied earlier in our laboratory.[11] It is known that on substitution with bulkier groups in NH_3, its basic character changes resulting in an increase in electron density and hence decrease in δ value is expected. As mentioned δ values for aniline coordinated complexes do not vary significantly indicating that change in basic character of amines may not affect the σ-donor property of the amine ligands.

As already mentioned, a strong asymmetry is generated due to the presence of sixth odd ligand L, resulting in quadrupole splitting. Earlier several workers have observed $\Delta E_Q \approx 0.80$ mm s^{-1} in amine and monoalkylamine coordinated complexes.[4-11] It is suggested that since alkyl- or arylamines are only σ bonded, d_π orbitals of iron remain distributed among five CN^- ligands only. Hence the nature of alkyl or aryl groups should not

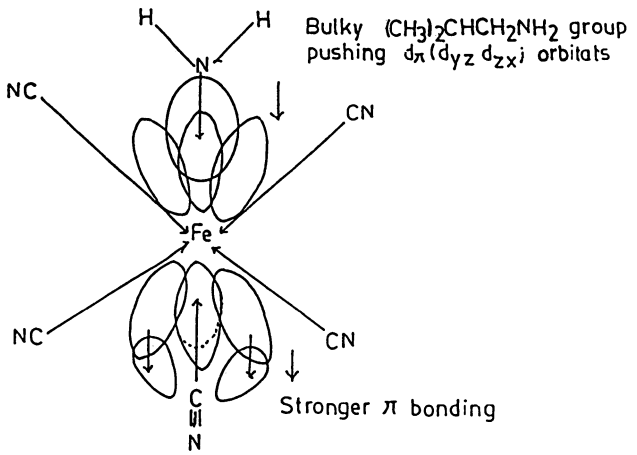

Fig. 2. Diagrammatic representation of isobutylamine ligand pushing π-orbitals (only d_{YZ} and d_{ZX}) of Fe atom which may result in increased π-bonding with trans CN ligand.

cause any significant change in ΔE_Q values. However, for isobutylamine coordinated complex an unusually high ΔE_Q=1.75 mm s^{-1} is observed. It is comparable with sodium pentacyanonitrosylferrate(II) (ΔE_Q=1.71 mm s^{-1}) where it is attributed to excessive π-bonding character of NO.[8] Therefore, in the case of isobutylamine coordinated pentacyanoferrate(II) complex also it may be possible that the central Fe atom is slightly pushed towards trans CN^- by the bulkier isobutyl group and also due to greater π-bonding ability of CN^-. This is schematically illustrated in Fig. 2.

These observations, viz. almost similar values of δ and ΔE_Q for various monoalkyl- and arylamines in these complexes are in accordance with the observation of Ballhausen and Gray.[21]

(ii) Correlation of δ and ΔE_Q: Several workers have attempted to correlate δ and ΔE_Q values and used this correlation in predicting the sign of EFG and bonding characteristics.[22–25] On plotting δ vs. ΔE_Q for all the complexes studied here a linear correlation is observed as shown in Fig. 3. ΔE_Q decreases with increasing δ for all the complexes of the type $[Fe(CN)_5(NH_2R)]^{3-}$ with various alkyl or aryl groups. This is based on the assumption that a positive sign of EFG exists for isobutylamine coordinated complex (similar to SNP) and a negative sign for all other coordinated complexes. However, this sign of EFG needs to be experimentally verified by a crystal orientation or magnetic perturbation method.

(iii) Infrared Spectra: Various vibrational modes of the complexes were assigned by comparison with those for other pentacyanoferrate(II) complexes.[5,8,13] The most important of all vibrational frequencies is the most intense C≡N stretching band which is observed in the region 2140—2040 cm^{-1}. Earlier three modes have been observed for ν(CN) of some di- and trialkylamine coordinated complexes.[11,12] In the present studies, however, we have observed only one band at ca. 2040 cm^{-1} for ν(CN) in all the pentacyanoferrate(II) complexes except for isobutylamine coordinated complex where two intense bands at 2140, 1950 cm^{-1} were observed. Both these bands are either at higher or lower by ca. 100 cm^{-1} compared to normal ν(CN) mode

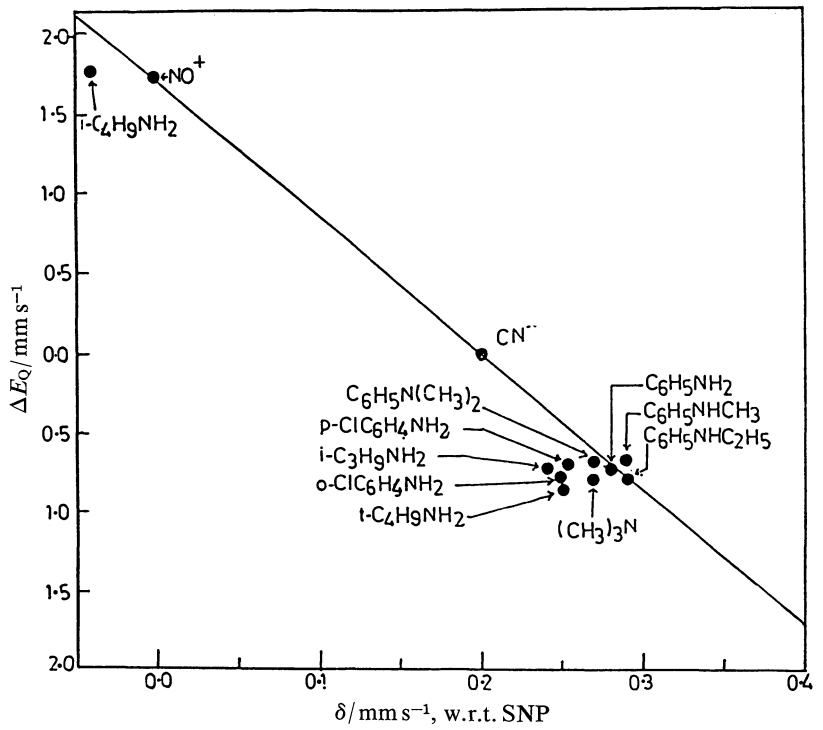

Fig. 3. Correlation of isomer shift (δ) vs. quadrupole splitting (ΔE_Q) values in alkyl- and arylamine coordinated pentacyanoferrate(II) complexes.

observed at ca. 2040 cm^{-1}. Another important characteristic mode of medium intensity is due to Fe–C≡N bending observed in the range 580—540 cm^{-1}. A very weak band observed in the range 450—400 cm^{-1} has been assigned to Fe–C stretching vibrations in acccordance with the assignments of Fluck et al.[8] Another weak band was observed in the range 315—225 cm^{-1} which may be assigned to Fe–N stretching.[8-27] A sharp medium intensity band is also observed at ca. 1600 cm^{-1} and assigned to bending mode of H_2O molecules occupying interstitial position. Interestingly for isobutylamine coordinated complexes ν(CN), δ(Fe–CN) and to some extent ν(Fe–N) are shifted by ca. 100 cm^{-1} in comparison with other complexes. This shift may be a sufficient indication of the difference in bonding characteristics of the isobutylamine coordinated complex compared with others. It may be noted that ν(Fe–C) remains almost unaffected on substitution. Rachlewicz et al.[27] have found ν(Fe–N) to be sensitive to further substitution and changes in bonding characteristics. Therefore, on the basis of ν(Fe–N) and other frequencies, we can conclude that bonding in isobutylamine coordinated complex is certainly different than other complexes.

Since σ-donor and π-acceptor properties of the ligands CN^- and RNH_2 are playing a dominant role, an attempt has been made to correlate ν(CN) and ν(Fe–N) with δ values of the respective complexes as shown in Fig. 4. In both cases straight line correlations have been observed indicating a decrease in δ value with both the stretching modes. Brar and Muzumdar[12] and Inoue et al.[13] have also correlated δ with ν(CN) in pentacyanoferrate(II) complexes. Earlier we have observed a similar trend for ν(CN) and δ(Fe–C≡N) for di- and trialkylamine coordinated complexes.[10] It has been argued that if d_π–p_π back donation from Fe to CN is reduced than Fe–C bond strength should decrease. Following the same argument Fe–N bond strength should also be affected depending on the interaction of ligand orbitals with the metal d_π orbitals. Again a clear trend dividing the ligands into two subgroups is evident. Gr. I complexes exhibiting $\Delta E_Q \approx 0.75$ mm s^{-1} show ν(CN) and ν(Fe–N) at lower frequencies. On the other hand isobutylamine coordinated complex exhibiting unusually high ΔE_Q shows the respective bands at higher frequencies. Almost similar kind of trend is observed for δ(Fe–CN) (Table 1).

(iv) Partial Isomer Shift and Quadrupole Splitting: Several attempts have been made to evaluate partial isomer shift (p.i.s) and partial quadrupole splitting (p.q.s.) values of the ligands in a series of isostructural complexes and correlating them with bonding characteristics.[28,29] These values were calculated using the equations:

$$[L]_{p.i.s.} = \delta - 0.21$$

$$[L]_{p.q.s.} = 1/2(\Delta E_Q - 1.68)$$

where δ and ΔE_Q are observed values. These are listed in Table 1. Plots of p.q.s. vs. δ and p.i.s. show straight line correlations as shown in Fig. 5. In both cases p.q.s. values increase with decreasing δ or p.i.s. values. For distorted octahedral complexes of the type $[Fe(CN)_5L]^{3-}$ it has been observed that δ values are affected depending on whether L is a better σ-donor or

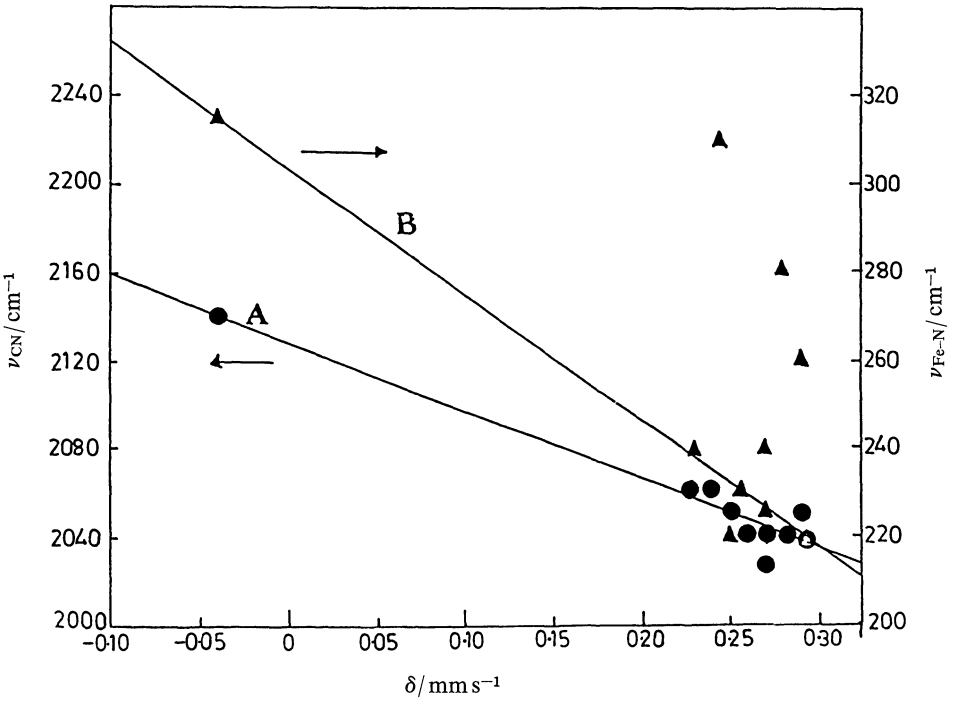

Fig. 4. Variation of isomer shift (δ) with (A) ν(C≡N) and (B) ν(Fe–N) stretching frequencies in $Na_3[Fe(CN)_5(RNH_2)] \cdot xH_2O$ complexes.

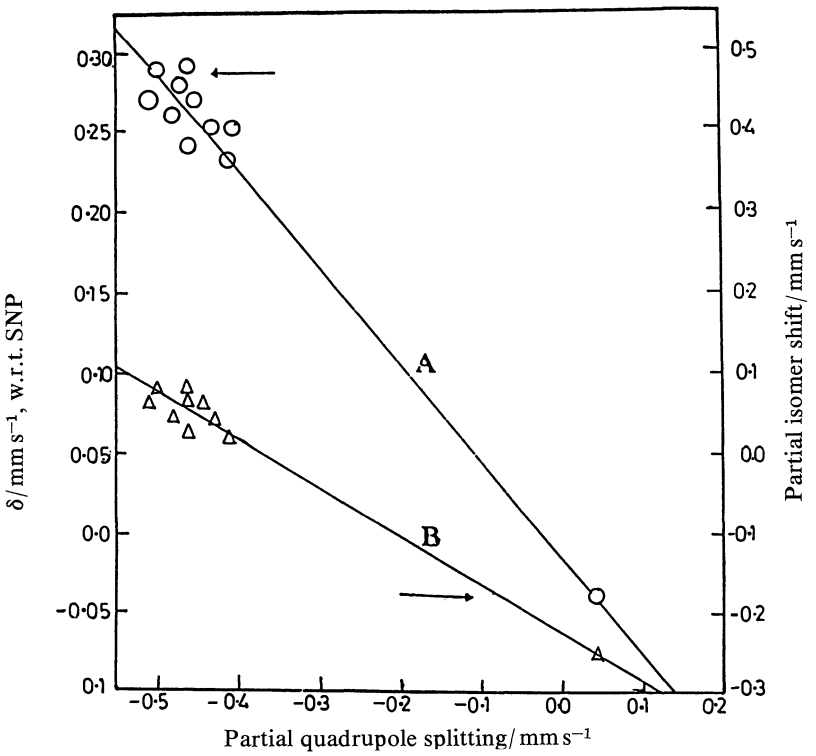

Fig. 5. Correlation of partial quadrupole splitting (p.q.s.) with (A) isomer shift (δ) and (B) partial isomer shift (p.i.s.) in $Na_3[Fe(CN)_5(RNH_2)] \cdot x\ H_2O$ complexes.

π-acceptor than and CN^- ligand.[26] In the present study where all the ligands are alkyl- or aryl-group substituted amines, their σ-donor property is affected by the substitution. It could be correlated with the change in base strength of amines as well. For example alkylamines with bulkier alkyl group are stronger bases and with arylamines are weaker bases than NH_3. However, this does not seem to affect the σ-donor property of the respective amines significantly except in the case of isobutylamine as indicated by its low values of δ and p.i.s. Presumably it is not just the σ-donor property but a combination of σ-donor and π-acceptor characteristics, both of which are operating simultaneously and can not be separated.

Conclusion

Mössbauer spectra of alkylamine and arylamine coordinated pentacyanoferrate(II) complexes exhibit a well resolved quadrupole doublet. Isobutylamine coordinated complex exhibits unusually high ΔE_Q and low δ which are comparable with sodium pentacyanonitrosylferrate(II). Correlation of δ vs. ΔE_Q gives a straight line suggesting a positive sign of EFG for isobutylamine coordinated complex. Stretching modes of CN and Fe–N also correlate well with the isomer shift data suggesting significant differences in its bonding characteristics compared with other alkyl- and arylamine coordinated complexes.

Our grateful thanks are due to Council of Scientific and Industrial Research, New Delhi for financial assistance. Thanks are also due to RSIC, Lucknow for providing C, H, N analysis and IR spectral data.

References

1) E. Fluck, W. Kerler, and W. Neuwirth, *Angew. Chem., Int. Ed. Engl.*, **2**, 277 (1963); *Z. Phys.*, **175**, 200 (1963).
2) E. Fluck, *Adv. Inorg. Chem. Radiochem.*, **6**, 433 (1964).
3) E. Fluck and P. Kuhn, *Z. Anorg. Allg. Chem.*, **350**, 263 (1967).
4) H. E. Toma, E. Giesbrecht, J. M. Malin, and E. Fluck, *Inorg. Chim. Acta*, **14**, 11 (1975).
5) J. A. Olabe and P. J. Aymonino, *J. Inorg. Nucl. Chem.*, **36**, 1221 (1974); *ibid.*, **38**, 225 (1976).
6) P. J. Aymonino, M. A. Blesa, J. A. Olabe, and E. Frank, *Z. Naturforsch., B*, **31**, 1532 (1976).
7) C. P. Monagham and J. C. Fanning, *J. Phys. Chem.*, **82**, 1045 (1978).
8) E. Fluck, H. Inoue, M. Nagao, and S. Yanagisawa, *J. Inorg. Nucl. Chem.*, **41**, 287 (1979).
9) A. N. Garg and P. N. Shukla, *Z. Naturforsch., B*, **36**, 59 (1981).
10) D. V. Parwate and A. N. Garg, *Z. Naturforsch., B*, **40**, 1495 (1985).
11) D. V. Parwate and A. N. Garg, *Polyhedron*, **5**, 999 (1986).
12) A. S. Brar adn S. K. Muzumdar, *Radiochem. Radioanal. Lett.*, **48**, 329 (1981); *Solid State Commun.*, **45**, 981 (1983).
13) H. Inoue, M. Sasagawa, E. Fluck, and T. Shirai, *Bull.*

Chem. Soc. Jpn., **56**, 3434 (1983).
14) H. E. Toma and J. A. Vanin, *Inorg. Chim. Acta Lett.*, **33**, 159 (1979).
15) G. Brauer, "Handbook of Preparative Inorganic Chemistry," Academic Press, New York (1965), Vol. 2, p. 1513.
16) D. J. Kenney, T. P. Flynn, and J. B. Gallini, *J. Inorg. Nucl. Chem.*, **20**, 75 (1961).
17) P. T. Manoharan and W. C. Hamilton, *Inorg. Chem.*, **2**, 1043 (1963).
18) F. Bottomley and P. S. White, *Acta Crystallogr., Sect. B*, **35**, 2193 (1975).
19) P. T. Manoharam, S. S. Kaliraman, V. G. Jadhao, and R. M. Singru, *Chem. Phys. Lett.*, **13**, 585 (1972).
20) P. T. Manoharan and H. B. Gray, *J. Am. Chem. Soc.*, **87**, 3340 (1965).
21) C. J. Ballhausen and H. B. Gray, *Inorg. Chem.*, **2**, 426 (1963).
22) R. W. Grant, "Mössbauer Effect Methodology," ed by I. J. Gruverman, Plenum Press, New York (1966), Vol. 2, p. 23.
23) Y. Hazony and R. C. Axtmann, *Chem. Phys. Lett.*, **8**, 571 (1971).
24) M. G. Clark, A. G. Maddock, and R. C. Platt, *J. Chem. Soc.*, **1972**, 281.
25) D. V. Parwate and A. N. Garg, *J. Radioanal. Nucl. Chem. Lett.*, **87**, 379 (1984).
26) P. G. Rasmussen and E. A. Meyers, *Polyhedron*, **3**, 183 (1984).
27) K. Rachlewicz, J. Pietrzyk, and K. Drabent, *Polyhedron*, **4**, 1777 (1985).
28) G. M. Bancroft, M. J. Mays, and B. E. Prater, *Chem. Commun.*, **1968**, 1374; *J. Chem. Soc. A*, **1970**, 956.
29) G. M. Bancroft, "Mössbauer Spectroscopy; An Introduction for Inorganic Chemists and Geochemists," McGraw Hill, London (1973), p. 94.

Regioselective Hydrogenation Using Platinum-Support Zeolite Modified by CVD-Method

Hideyuki KUNO,* Makoto SHIBAGAKI, Kyoko TAKAHASHI, Ichiro HONDA, and Hajime MATSUSHITA
Life Science Research Laboratory, Japan Tobacco Inc., 6-2 Umegaoka, Midori-ku, Yokohama, Kanagawa 227
(Received February 16, 1991)

A platinum-support zeolite coupled with a silica layer was prepared by Chemical Vapor Deposition (CVD) of tetraethoxysilane, and was investigated in order to determine the catalytic characterization in an analysis of the surface. With this catalyst system, it was demonstrated that the terminal carbon–carbon double bond is preferentially hydrogenated in the case of several unsaturated hydrocarbons. Further, it was elucidated that a highly regioselective hydrogenation of compounds which possess plural double bonds was achieved over this catalyst system. As a result, a reaction model regarding this catalyst system has been put forward.

In order to achieve highly regioselective reactions with heterogeneous catalyst systems, it is desirable to have a high efficiency in substrate-recognizing ability. In previous papers,[1,2] we have reported that the regioselective hydrogenation of unsaturated alcohols and acids proceeded efficiently by the use of a platinum–silica or platinum–alumina catalyst modified by a long carbon-chain layer. However, these catalyst systems do not have a wide range of applications, since, for instance, the reactants are restricted to aliphatic alcohols or acids. Further, it is difficult to control the degree of modification of the surfaces on the catalysts in these systems.

It was reported that, using the CVD (Chemical Vapor Deposition)-method, a finely deposited silica layer can be formed on the surface of zeolite and, further, that the diameter of micro pores in zeolite can be controlled.[3–5] It is thought that the silica layer is combined to the silanol group on the zeolite surface by covalent bonds and not combined to any part of the metal. It is also expected that the degree of modification can be controlled by using the CVD-method. Accordingly, it is considered that the reaction field constructed by the CVD-method would be effective in the application of highly regioselective reactions.

A platinum–zeolite catalyst coupled with tetraethoxysilane was prepared by the CVD-method. Hydrogenation of the unsaturated hydrocarbons was carried out over this CVD-modified catalyst; it was elucidated that the differences in the hydrogenation rates were dependent on the positions of the carbon–carbon double bond in the unsaturated hydrocarbons. Compared with the modified catalyst previously reported by us, the following advantages exist: (1) highly regioselective hydrogenation, (2) no restrictions regarding the reactants, (3) high stability under various conditions.

In this paper we report that the regioselective hydrogenation of several compounds with plural double bonds was achieved over a CVD-modified catalyst, and that the terminal double bond is preferentially hydrogenated. The characterization of the CVD-modified catalyst was also investigated.

It was also investigated whether the reactivity and selectivity of the hydrogenation are influenced by the variety of active metals and solid-supports in a CVD-modified catalyst system.

Experimental

Materials. Commercial reagents were used for the reactions without further purification.

Preparation of CVD-Modified Catalyst. Using the ion-exchange method,[6] platinum on zeolite-4A was prepared. The CVD-treatments were performed in a glass-flow reactor in flowing nitrogen gas (60 $cm^3 min^{-1}$). The platinum–zeolite-4A catalyst (4.0 g) was treated at 400 °C for 2 h, at 100 °C for 1 h with diethyl ether (5 $cm^3 h^{-1}$), at 200 °C for 3 h with tetraethoxysilane (1 $mmol h^{-1}$)), at 200 °C for 1 h, and at 300 °C for 1 h with deionized water (hydrolysis treatment of ethoxyl group). This series of treatments was repeated several times and, finally, the catalyst was treated at 200 °C for 1 h without hydrolysis treatment.[7]

Analysis of CVD-Modified Catalyst. After the ion-exchange treatment, the filtrate was subjected to Inductively Coupled Plasma (ICP) analysis in order to determine the metal loading. The CVD-modified catalysts were analyzed by X-ray photoelectron spectroscopy (XPS) to determine the composition of the surface phase.

Hydrogenation of Mixture of Two Alkenes. In a 10 cm^3 round-bottom flask, 150 mg of a CVD-modified catalyst, or 30 mg of a 1.2% platinum–zeolite-4A (control catalyst), was suspended in 5 cm^3 of hexane containing 0.1 mmol of undecane as an internal standard; 5 cm^3 of hexane containing 1-octene (0.1 mmol) and *trans*-4-octene (0.1 mmol) was added with stirring at 25 °C under a hydrogen atmosphere. The reactants and products were analyzed by gas chromatography (a capillary column DB-1 30 m). The compounds were assigned and their concentrations were determined using authentic samples and an internal standard.

Hydrogenation of Alkadienes. In a 10 cm^3 round-bottom flask, 5 cm^3 of hexane containing tetradecane (0.05 mmol) as an internal standard and diene (0.1 mmol) were stirred with 300 mg of CVD-catalyst or 60 mg of the control catalyst at 25 °C under a hydrogen atmosphere. Both the reactants and products were analyzed in a similar manner to that described above. The assignment of the products was performed using gas chromatography and GC-MS.

Results and Discusssion

Characterization of CVD-Modified Catalyst. The

CVD-treatment on the metal-supports was repeated 5 times. The surface of the platinum–zeolite-4A coupled with tetraethoxysilane by 5-cycle CVD-treatment (5cCVD-modified catalyst A) was analyzed by XPS; the results are listed in Table 1. The relative amounts of silicon and oxygen on the CVD-modified catalyst are larger than those in the non-modified catalyst. From these data, it was elucidated that the silica layer was deposited on the surface of the platinum–zeolite-4A.[8] The thickness of the silica layer on zeolite-4A is shown by the following Eq. 1, as reported by Niwa et al.:[9]

$$(\mathrm{Si/Al})_{\mathrm{xps}} = (d+t)/(d-t), \quad (1)$$

where $(\mathrm{Si/Al})_{\mathrm{xps}}$ is the ratio of Si atom to Al atom by XPS analysis, t: the thickness of silica, and d: the releasing depth of the photoelectron (ca. 50).

The value of $(\mathrm{Si/Al})_{\mathrm{xps}}$ was dependent on the Pt loading, which is shown in Fig. 1. As can be seen from the figure, a straight line is obtained. These results suggested that the silica layer was not combined with platinum particles by the CVD-treatment, and that the platinum was highly dispersed. It is reasonable to estimate the value of $(\mathrm{Si/Al})_{\mathrm{xps}}$ in the case of no Pt loading. As being ca. 1.8, and, using this in Eq. 1, the thickness of the silica in 5cCVD-modified catalyst A is estimated to be ca. 14.3 Å. On the basis of the XPS analysis, it was demonstrated that most of the catalyst surface is covered with the 5 layers of the silica except for platinum particles, and that the small holes in the silica layer were formed around these platinum particles.

Table 1. Ratio of Elemental of Surface Phase by XPS

Catalyst	Al	Si	O	Pt
Pt(1.2%)/zeolite (A)	1.00	0.98	3.02	0.08
5cCVD-A	1.00	1.44	3.79	0.07

5cCVD-A: 5cCVD-modified catalyst A.

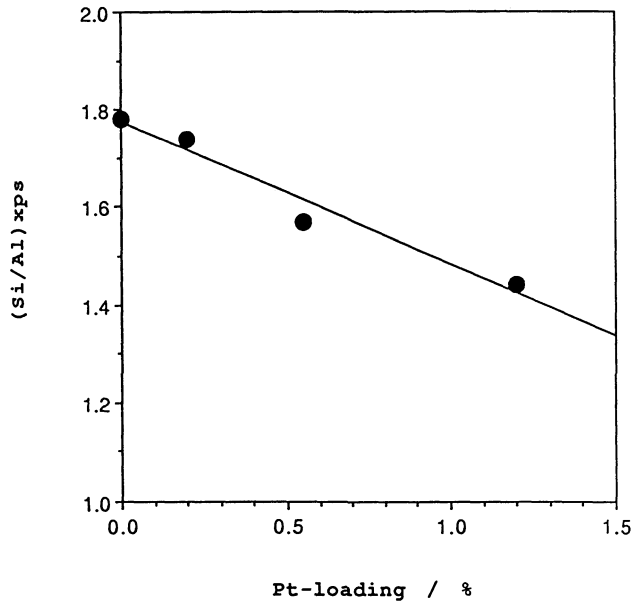

Fig. 1. Relation of Pt volume and $(\mathrm{Si/Al})_{\mathrm{xps}}$.

Competitive Hydrogenation of Two Alkenes. The hydrogenation of a mixture of 1-octene and *trans*-4-octene was carried out over the several CVD-modified catalysts. It was elucidated that R1/R2 (R1: initial rate of 1-octene, R2: initial rate of *trans*-4-octene) is dependent on the number of times of the CVD-treatment and the results are shown in Fig. 2. In the range of 0 to 5, R1/R2 increases with the number of the CVD-treatments. However, R1/R2 does not increase with more than 5 treatments. Consequently, it is considered that 5-cycle CVD treatment is the most effective to attain regioselective hydrogenation.

The hydrogenation of a mixture of 1-octene and other octenes was carried out over 5cCVD-modified catalyst A and platinum–zeolite-4A (control catalyst). As shown in Table 2, selective hydrogenation was observed by the use of 5cCVD-modified catalyst A in all cases. Compared with the hydrogenation over the control catalyst, R1/R2 was dependent on the variety of the other octene in the case of the hydrogenation over 5cCVD-modified catalyst A. In other words, the selectivity with regard to the double bond near the terminal site in the 5cCVD-modified catalyst A system is much higher in comparison with that in the control catalyst system. In the case of a mixture of 1-nonene and *trans*-4-nonene, the result was similar to those for the two-octene system.

In the case of these hydrogenations, it is considered that a catalytic active site mainly exists on the outside

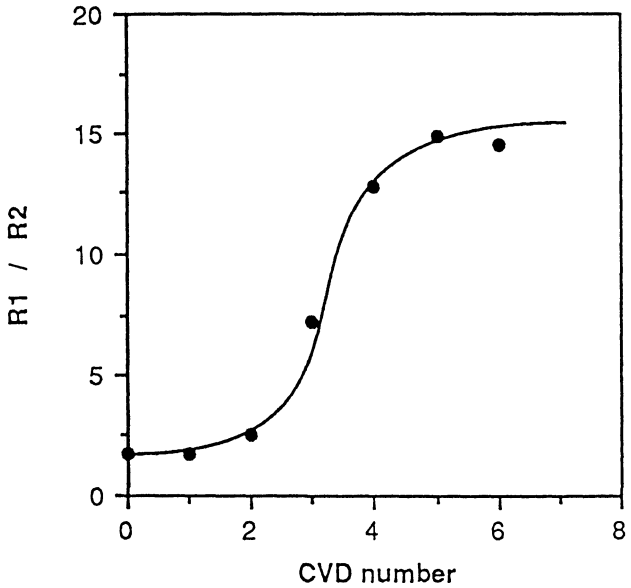

Fig. 2. Relation of R1/R2 and CVD number.
R1: Initial rate of 1-octene, R2: Initial rate of *trans*-4-octene.
Conditions: CVD-catalyst A, 150 mg; control catalyst, 30 mg; 1-octene, 0.1 mmol; *trans*-4-octene, 0.1 mmol; hexane, 10 cm^3; reaction temperature, 25 °C.

Table 2. Initial Rate of Hydrogenation for Mixture of Two Alkenes[a)]

Catalyst[b)]	Substrate		Initial rate/mol g^{-1} h^{-1}		R1/R2
	S1	S2	R1	R2	
Pt/zeolite-4A(A)	1-Octene	*trans*-4-Octene	6.56×10^{-3}	4.08×10^{-3}	1.61
5CVD-A	1-Octene	*trans*-4-Octene	4.89×10^{-4}	3.28×10^{-5}	14.90
Pt/zeolite-4A(A)	1-Nonene	*trans*-4-Nonene	7.28×10^{-3}	3.36×10^{-3}	2.17
5CVD-A	1-Nonene	*trans*-4-Nonene	4.77×10^{-4}	2.63×10^{-5}	18.14
Pt/zeolite-4A(A)	1-Octene	*trans*-3-Octene	6.38×10^{-3}	3.28×10^{-3}	1.95
5CVD-A	1-Octene	*trans*-3-Octene	5.96×10^{-4}	9.44×10^{-5}	6.31
Pt/zeolite-4A(A)	1-Octene	*trans*-2-Octene	7.10×10^{-3}	4.40×10^{-3}	1.61
5CVD-A	1-Octene	*trans*-2-Octene	5.64×10^{-4}	1.92×10^{-4}	2.94
Pt/zeolite-4A(A)	1-Octene	*cis*-2-Octene	8.24×10^{-3}	5.52×10^{-3}	1.49
5CVD-A	1-Octene	*cis*-2-Octene	7.20×10^{-4}	2.16×10^{-4}	3.33

a) Conditions: alkene, 0.1 mmol; hexane, 10 cm^3; reaction temperature, 25 °C. b) A, Pt(1.2%)/zeolite-4A (30 mg); 5CVD-A, 5cCVD-modified catalyst A (150 mg).

surface of zeolite. From the XPS data, it is suggested that the small holes are formed around the platinum particles, and the hydrogenation would be exclusively performed in these holes. Therefore regioselectivity would be caused by steric hindrance around the platinum in the holes. The carbon-carbon double bond in 1-octene can more easily approach the platinum than that in the other octenes, for instance *trans*-4-octene, because the conformation of the substrates is regulated by the silica layer on platinum–zeolite. Accordingly, the less hindered carbon–carbon double bond is easily hydrogenated in the 5cCVD-modified catalyst A system (Fig. 3).

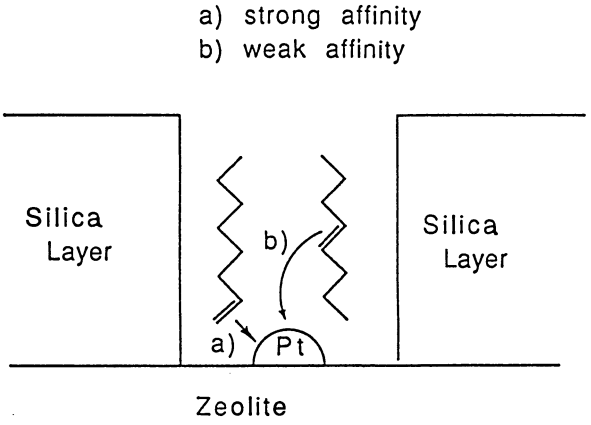

Fig. 3. Reaction Model for Hydrogenation of Octene in 5CVD-catalyst A system.

Dependence on Variety of Metals on Zeolite. In order to elucidate the dependence on the variety of metals in the CVD-modified catalyst, the hydrogenation of the mixture of 1-nonene and *trans*-4-nonene was carried out over several CVD-modified catalysts. These results are listed in Table 3. It was elucidated that the R1/R2 value in the 5cCVD-modified catalyst (5-cycle CVD-modified catalyst) system is much larger than that in the control catalyst in all cases. In the case of using platinum or rhodium-catalyst, isomerization did not occur during the reaction, but 10% of the isomers of nonene, for instance *cis-trans* isomer, were detected in the case of palladium. As the results show in Table 3, the CVD-modification (5-cycle) is effective in construction of a reaction field for the regioselective hydrogenation, regardless of the variety of metals.

Dependence on Variety of Supports. The hydrogenation of the mixture of 1-nonene and *trans*-4-nonene was carried out over a 5cCVD-modified catalyst with a variety of supports. The results are shown in Table 4. The Rl/R2 values in the 5cCVD-modified catalyst system were much larger than those in the control catalyst in the cases of zeolite-4A, zeolite-13X, and silica. However, if titania or hydrous zirconium(IV) oxide is used as a support, the R1/R2 value in the 5cCVD-modified catalyst system is similar to that in the control

Table 3. Rate of Hydrogenation for 1-Nonene and *trans*-4-Nonene with a Variety of Metals[a)]

Catalyst	Initial rate of/mol g^{-1} h^{-1}		R1/R2
	1-Nonene(R1)	*trans*-4-Nonene(R2)	
Pt/zeolite-4A(A)[b)]	7.28×10^{-3}	3.36×10^{-3}	2.17
5cCVD-modified A[c)]	4.77×10^{-4}	2.63×10^{-5}	18.14
Rh/zeolite-4A(B)[b)]	1.50×10^{-3}	8.00×10^{-4}	1.88
5cCVD-modified B[c)]	9.33×10^{-4}	4.67×10^{-5}	19.98
Pd/zeolite-4A(C)[b)]	1.36×10^{-3}	4.65×10^{-3}	2.92[d)]
5cCVD-modified C[c)]	2.67×10^{-4}	5.83×10^{-6}	45.80[d)]

a) Conditions: 1-nonene, 0.1 mmol; *trans*-4-nonene, 0.1 mmol; hexane, 10 cm^3; reaction temperature, 25 °C. b) 30 mg. c) 150 mg. d) Isomerization occurred.

Table 4. Rate of Hydrogenation for 1-Nonene and *trans*-4-Nonene with a Variety of Supports[a)]

Catalyst	Initial rate of/mol h^{-1} g^{-1}		R1/R2
	1-Nonene(R1)	*trans*-4-Nonene(R2)	
Pt/zeolite-4A(A)[b)]	7.28×10^{-3}	3.36×10^{-3}	2.17
5cCVD-modified A[c)]	4.77×10^{-4}	2.63×10^{-5}	18.14
Pt/zeolite-13X(D)[b)]	6.47×10^{-3}	1.73×10^{-3}	3.73
5cCVD-modified D[c)]	1.07×10^{-4}	4.00×10^{-6}	26.75
Pd/SiO_2(E)[b)]	1.20×10^{-2}	5.49×10^{-3}	2.19
5cCVD-modified E[c)]	2.67×10^{-3}	3.07×10^{-4}	8.70
Pt/hydrous zirconium oxide(F)[b)]	1.57×10^{-4}	1.11×10^{-4}	1.41
5CVD-midified F[c)]	2.40×10^{-5}	1.33×10^{-5}	1.80
Pt/TiO_2(G)[b)]	1.11×10^{-2}	4.23×10^{-3}	2.62
5CVD-modified G[c)]	1.06×10^{-2}	3.79×10^{-3}	2.80

a) Conditions: 1-nonene, 0.1 mmol; *trans*-4-nonene, 0.1 mmol; hexane, 10 cm^3; reaction temperature, 25 °C. b) 30 mg. c) 150 mg.

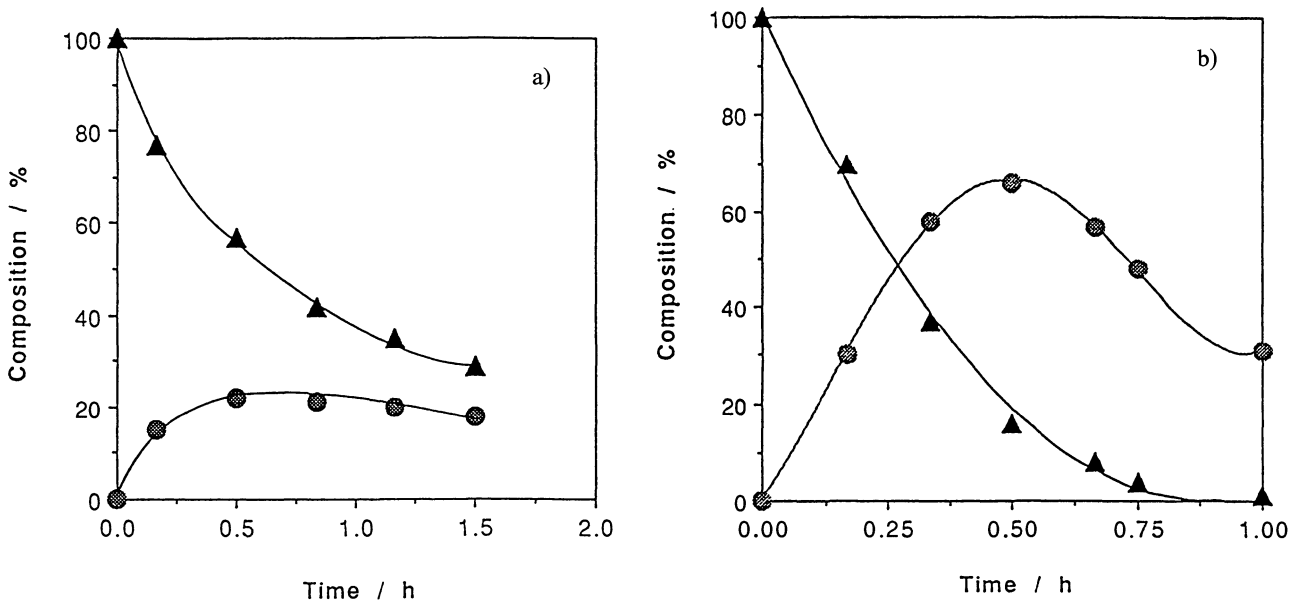

Fig. 4. Hydrogenation of 1,5-Tridecadiene. a) Control catalyst system. b) 5CVD-catalyst system.
Conditions: 5CVD-catalyst, 300 mg; control catalyst, 60 mg; 1,5-tridecadiene, 0.1 mmol; hexane, 5 cm^3; reaction temperature, 25 °C.
▲: $CH_2=CH(CH_2)_2CH=(CH_2)_6CH_3$. ●: $CH_3(CH_2)_3CH=CH(CH_2)_6CH_3$.

catalyst. It was also elucidated that the regioselectivity of the hydrogenation in the 5cCVD-modified catalyst is dependent on the variety of supports. The surface of zeolite was finely covered by a homogeneous silica layer because of the high reactivity between tetraethoxysilane and zeolite, and the reaction field was effectively constructed for the regioselective hydrogenation. On the other hand, the homogeneous silica layer was not finely constructed on titania and hydrous zirconium oxide because of the difference in ion radius between the support and silica layer. Accordingly, it is considered that zeolite is the best support as the binder of the silica layer.

Hydrogenation of Several Alkadienes. It was anticipated that the regioselective hydrogenation of a hydrocarbon possessing a number of carbon–carbon double bonds could be achieved since differences in the hydrogenation rates were found for different positions of the carbon–arbon double bond in octene and nonene. The hydrogenation of 1,5-tridecadiene was investigated over the 5cCVD-modified catalyst A and over the control catalyst. The regioselectivity for the hydrogenation of 1,5-tridecadiene was low over the control catalyst, as shown in Fig. 4a. However, when using 5cCVD-modified catalyst A, the highly regioselective hydrogenation of 1,5-tridecadiene was achieved (Fig. 4b). The hydrogenation of other alkadienes, for instance limonene, 8-cyclohexyl-1,5-octadiene, and 1,5-undecadiene, was carried out in the 5cCVD-modified catalyst A and control catalyst systems, these results are listed in Table 5. From these results, it can be seen that similar tendencies are observed in the hydrogenation of the other compounds as with 1,5-tridecadiene. Further, in the case of the hydrogenation conditions which are shown

Table 5. Regioselective Hydrogenation for Diene-Compounds Catalyzed by 5cCVD-Modified Pt/Zeolite-4A[a]

Catalyst	Substrate	Product	Max. Yield/%
Pt/zeolite-4A(A)[b]	1,5-Tridecadiene	5-Tridecene	20.8
5cCVD-A[c]	1,5-Tridecadiene	5-Tridecene	65.2
Pt/zeolite-4A(A)[b]	1,5-Undecadiene	5-Undecene	5.0
5cCVD-A[c]	1,5-Undecadiene	5-Undecene	34.8
Pt/zeolite-4A(A)[b]	Limonene	4-Isopropyl-1-methyl-1-cyclohexene	59.3
5cCVD-A[d]	Limonene	4-Isopropyl-1-methyl-1-cyclohexene	87.8
Pt/chacoal[e]	Limonene	4-Isopropyl-1-methyl-1-cyclohexene	78.9
Pt/zeolite-4A(A)[b]	8-Cyclohexyl-1,5-octadiene	1-Cyclohexyl-3-octene	2.4
5cCVD-A[c]	8-Cyclohexyl-1,5-octadiene	1-Cyclohexyl-3-octene	58.9
Pt/chacoal[e]	8-Cyclohexyl-1,5-octadiene	1-Cyclohexyl-3-octene	39.5

a) Conditions: Substrate, 0.1 mmol; hexane(solvent), 5 cm^3; reaction temperature, 25 °C.
b) 60 mg. c) 300 mg. d) 600 mg. e) 10 mg.

in Table 5, it was also elucidated that the 5cCVD-modified catalyst is superior to platinum (5%)-charcoal which is known as an effective catalyst for the regioselective hydrogenation of limonene.[10]

In conclusion, a highly regioselective hydrogenation of the carbon–carbon double bond in unsaturated compounds was achieved with a CVD-modified catalyst.

References

1) H. Kuno, K. Takahashi, M. Shibagaki, and H. Matsushita, *Bull. Chem. Soc. Jpn.*, **62**, 3779 (1989).
2) H. Kuno, K. Takahashi, M. Shibagaki, and H. Matsushita, *Bull. Chem. Soc. Jpn.*, **63**, 3320 (1990).
3) M. Niwa, H. Itoh, S. Kata, T. Hattori, and Y. Murakami, *J. Chem. Soc., Chem. Commun.*, **1982**, 819.
4) M. Niwa and Y. Murakami, *Hyomen*, **22**, 319 (1984).
5) M. Niwa, S. Kata, T. Hattori, and Y. Murakami, *J. Chem. Soc., Faraday Trans. 1*, **80**, 3135 (1984).
6) H. Arai, *Shokubai*, **19**, 365 (1977).
7) H. Itoh, S. Okamoto, and A. Furuta, *Nippon Kagaku Kaishi*, **1984**, 420.
8) Y. Teraoka, K. Kunitake, S. Shikagawa, and M. Iwamoto, *Nippon Kagaku Kaishi*, **1989**, 424.
9) M. Niwa, S. Morimoto, M. Kato, T. Hattori, and Y. Murakami, *Proc. Int. Congr. Catal., 8th*, **1984**, IV-701.
10) W. F. Newhall, *J. Org. Chem.*, **23**, 1274 (1958).

 © 1991 The Chemical Society of Japan Bull. Chem. Soc. Jpn., 64, 2513—2518 (1991)

Aerobic Epoxidation of Olefinic Compounds Catalyzed by Tris(1,3-diketonato)iron(III)

Toshihiro TAKAI,* Eiichiro HATA,† Tohru YAMADA, and Teruaki MUKAIYAMA††
Basic Research Laboratories for Organic Synthesis, Mitsui Petrochemical Industries, Ltd., Nagaura, Sodegaura-shi, Chiba 299-02
†Chemical Synthesis Laboratories, Mitsui Petrochemical Industries, Ltd., Waki, Waki-cho, Kuga-gun, Yamaguchi 740
††Department of Applied Chemistry, Faculty of Science, Science University of Tokyo, Kagurazaka, Shinjuku-ku, Tokyo 162
(Received March 30, 1991)

Tris[1,3-bis(*p*-methoxyphenyl)-1,3-propanedionato]iron(III) ($Fe(dmp)_3$) was found to be an excellent catalyst for oxygenation of a number of olefinic compounds including styrene analogues and olefinic alcohols into the corresponding epoxides in good to quantitative yields with combined use of molecular oxygen and an aldehyde at room temperature.

Iron complexes are considered to be one of the most promising catalysts for oxygenation, because iron is a relatively inexpensive and less poisonous metal compared with other transition metals.[1] Therefore much research works have been made for iron complex-catalyzed epoxidation of olefins with various oxidants, such as iron(III) porphyrins/iodosobenzene[2a] and sodium hypochlorite,[2b] or iron(III) perchlorate/α-siloxyalkyl perbenzoate.[2c] Molecular oxygen can also be used for epoxidation of olefins by employing the following catalysts; iron(III) porphyrins/O_2/H_2 on colloidal platinum,[2d] iron(III) complexes of artificial bleomycin/O_2/2-mercaptoethanol[2e] or (μ_3-oxo)triiron cluster $[Fe_3O(OCOR)_6L_3]$.[2f] In the above epoxidation reactions, however, the limitation of substrates, olefinic compounds, remained as an important problem to be solved.

Through our continued study on the aerobic epoxidation of olefins catalyzed by oxovanadium(IV) complexes[3a] or nickel(II) complexes,[3b–e] it could be pointed out that the behavior of the active oxidant generated from transition metal complexes with combined use of molecular oxygen and reductants is different from that of generally employed epoxidation reagents, such as *m*-chloroperbenzoic acid (*m*CPBA). For example, in the aerobic epoxidation of styrene (**1**) catalyzed by nickel(II) complex,[3f] styrene oxide (**2**) was obtained but in unsatisfactory yield (34%) accompanying C=C bond fission of styrene (**1**) into benzaldehyde (**3**, 31% yield), and similar results were also reported by other researchers.[2e,4] Recently, $Pr(OAc)_3$ was shown as an effective catalyst for the aerobic epoxidation of olefins in the coexistence of an aldehyde.[5] Taking the above results into account, our interests were focused on finding a suitable common transition metal catalyst which might be employed in the oxidation of a wide variety of olefinic compounds. After screening several metal complexes, it was found that tris(1,3-diketonato)-iron(III) has an excellent catalytic activity on aerobic epoxidation far better than bis(1,3-diketonato)iron(II). Of several tris(1,3-diketonato)iron(III) catalysts, tris-[1,3-bis(*p*-methoxyphenyl)-1,3-propanedionato]iron(III) ($Fe(dmp)_3$) (**11a**) was found to be the most effective catalyst for epoxidation of olefinic compounds with an atmospheric pressure of oxygen and an aldehyde at room temperature. Concerning the similar iron(III) complex, epoxidation of propylene with molecular oxygen and crotonaldehyde catalyzed by tris(acetylacetonato)iron(III) have already been reported to proceed in low conversion (<40%).[6]

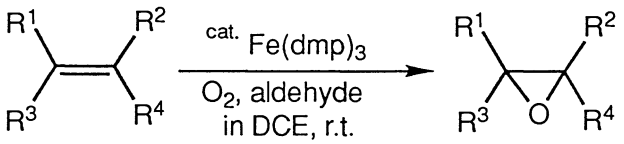

Scheme 1.

Results and Discussion

Epoxidation of Styrene Catalyzed by Various Iron Complexes. As mentioned before, styrene (**1**) is highly reactive toward oxygenation and rather difficult to obtain styrene oxide (**2**) selectively due to C=C bond cleavage of styrene (**1**) into benzaldehyde (**3**). Thus, in order to examine the effect of iron complexes for aerobic epoxidation, styrene (**1**) was taken as a model substrate and treated with combination of molecular oxygen and an aldehyde in 1,2-dichloroethane (DCE) at room temperature in the presence of a catalytic amount of bis- or tris(acetylacetonato)iron complexes (see Table 1). Of several iron(II) and iron(III) complexes, the highest yield of styrene oxide (**2**) was achieved when Fe(III)(acac)$_3$ (**6**) was employed as a catalyst (Entry 3).

Thus, various tris(1,3-diketonato)iron(III) type catalysts were prepared and their catalytic activities in aerobic epoxidation of styrene (**1**) were examined. As shown in Table 2, undesired cleavage of C=C bond was

Table 1. Epoxidation of Styrene (**1**) Catalyzed by Bis- or Tris(acetylacetonato)iron[a]

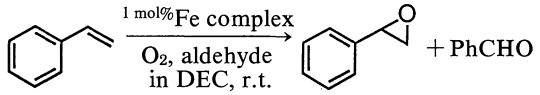

1 **2** **3**

Entry	Iron complex	Time/h	Conversion/%[b]	Yield/%[b]	
				2	**3**
1	$Fe(II)(acac)_2$ (**4a**)	8	67	44	9
2	$Fe(III)(acac)_2Cl$ (**5**)	8	66	37	10
3	$Fe(III)(acac)_3$ (**6**)	10	100	82	8

a) Reaction conditions; styrene (**1**) 3.0 mmol, 2-ethylbutyraldehyde 18.0 mmol, iron complex 0.03 mmol (1.0 mol%) in 1,2-dichloroethane (DCE) 10.0 ml, O_2 1 atm. b) Determined by GC analysis.

suppressed when 1,3-diketones having electron-donating substituents, such as 2-acetylcyclohexanone (=Hach **9b**), 3-methyl-2,4-pentanedione (=Hmac **10b**) or 1,3-bis(*p*-methoxyphenyl)-1,3-propanedione (=Hdmp **11b**) were used, and the yield of styrene oxide (**2**) was improved up to 87—89% (Entries 4—6). Meanwhile, 1,3-diketones having electron-withdrawing substituents, such as 1,1,1-trifluoro-2,4-pentanedione (=Htfa **7a**) or 1,1,1,5,5,5-hexafluoro-2,4-pentanedione (=Hhfa **8b**), were not so efficient for selective epoxidation of styrene (**1**) (Entries 2 and 3).

Several styrene analogues, such as *cis*-1-phenylpropene (**13**), *p*-chlorostyrene (**15**) or *trans*-stilbene (**17**), were also oxygenated in the above procedure by using iron(III) complexes (see Entries 2—4 in Table 3). In all cases, the corresponding epoxides, 1-phenyl-1,2-epoxy-

Table 2. Epoxidation of Styrene (**1**) Catalyzed by Various Iron(III) Complexes ($Fe(III)L_3$)[a]

Entry	Catalyst		Ligand(LH)		Time/h	Conversion/%[b]	Yield/%[b]	
							2	**3**
1	$Fe(III)(acac)_3$	(**6**)		(Hacac) (**4b**)	10	100	82	8
2	$Fe(III)(tfa)_3$	(**7a**)	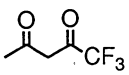	(Htfa) (**7b**)	13	99	74	12
3	$Fe(III)(hfa)_3$	(**8a**)	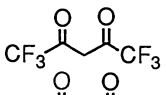	(Hhfa) (**8b**)	13	100	59	22
4	$Fe(III)(ach)_3$	(**9a**)	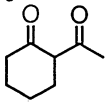	(Hach) (**9b**)	13	100	87	8
5	$Fe(III)(mac)_3$	(**10a**)		(Hmac) (**10b**)	9	100	88	12
6	$Fe(III)(dmp)_3$	(**11a**)	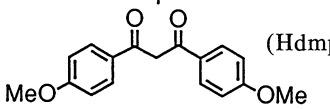	(Hdmp) (**11b**)	9	100	89	10

a) Reaction conditions; styrene (**1**) 3.0 mmol, 2-ethylbutyraldehyde 18.0 mmol, iron(III) complex 0.03 mmol (1.0 mol%) in 1,2-dichloroethane (DCE) 10.0 ml, O_2 1 atm. b) Determined by GC analysis.

Table 3. Epoxidation of Styrene Analogues[a]

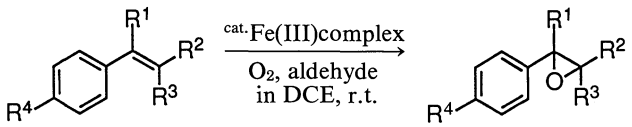

Entry	Styrene analogue					Time/h	Epoxide	Yield/%
	R^1	R^2	R^3	R^4				
1	H	H	H	H	(**1**)	9	Styrene oxide (**2**)	89[c]
2[b]	H	H	Me	H	(**13**)	14	1-Phenyl-1,2-epoxypropane (**14**)	Quant.[c,d]
3	H	H	H	Cl	(**15**)	14	2-(*p*-Chlorophenyl)oxirane (**16**)	Quant.[c]
4[b]	H	Ph	H	H	(**17**)	14	*trans*-Stilbene oxide (**18**)	99[e]

a) Reaction conditions; styrene analogues 3.0 mmol, 2-ethylbutyraldehyde 18.0 mmol, $Fe(dmp)_3$ (**11a**) 0.03 mmol (1.0 mol%) in 1,2-dichloroethane (DCE) 10.0 ml, O_2 1 atm, r.t. b) $Fe(acac)_3$ (**6**) 0.03 mmol was used. c) GC yield. d) Mixture of *cis* and *trans* isomers (11/89). e) Isolated yield.

propane (**14**), 2-(*p*-chlorophenyl)oxirane (**16**), or *trans*-stilbene oxide (**18**) were obtained in quantitative yields respectively without any undesirable over-oxidation as cleavage of C=C double bond affording aromatic aldehydes.

Epoxidation of Various Olefinic Compounds Catalyzed by Fe(dmp)$_3$ (11a). The above procedure was also successfully applied to various olefinic compounds. Aliphatic trisubstituted, 1,2-disubstituted or *exo*-terminal olefins afforded the corresponding epoxides in high to quantitative yields (see Entries 1—4 in Table 4). And in the case of cyclohexene (**23**), undesirable allylic oxidation affording 2-cyclohexen-1-ol was suppressed down to 5%. In a similar fashion, the corresponding epoxides were obtained in quantitative yields from acetates of olefinic alcohol, such as citronellyl acetate (**27**) and linalyl acetate (**29**) (Entries 5 and 6). Cholesteryl acetate (**31**) was selectively oxygenated into the corresponding β-epoxide **32** similar to the nickel(II)-catalyzed epoxidation.[3f] In the cases of geranyl acetate (**33**) and neryl acetate (**36**), double bonds at C^6–C^7 position were oxygenated preferentially over allylic double bonds, and the corresponding epoxides were obtained as mixtures of monoepoxides **34**, **37** and diepoxides **35**, **38** (Entries 8 and 9).

Epoxidation of Olefinic Alcohols Catalyzed by Fe(dmp)$_3$ (11a). Since olefinic alcohols were not efficiently oxygenated into the corresponding epoxy alcohols by using nickel(II) complexes, iron(III) complex-catalyzed epoxidation of citronellol (**39**), an olefinic alcohol, was examined. As shown in Table 5, epoxy alcohol **40** was obtained in quantitative yield without any over-oxidation of hydroxyl group by using Fe(dmp)$_3$ (**11a**) as a catalyst (Entry 1), whereas nickel(II) complex-catalyzed epoxidation of citronellol (**39**) stopped half-way and yield of epoxy alcohol **40** was moderate (Entry 2). It was assumed that nickel(II) complex was deactivated due to the undesirable coordination by hydroxyl group of olefinic alcohol, while iron(III) complexes having three 1,3-diketone ligands might not be preferable for

Table 4. Fe(dmp)$_3$ Catalyzed Epoxidation of Various Olefinic Compounds[a]

Entry	Olefin		Time/h	Epoxide		Yield/%
1	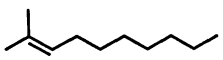	(**19**)	4	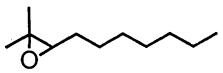	(**20**)	Quant.[b]
2	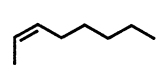	(**21**)	12	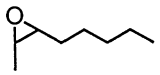	(**22**)	95[b,d]
3		(**23**)	12	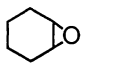	(**24**)	80[b]
4	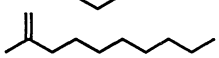	(**25**)	7	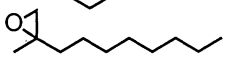	(**26**)	98[b]
5	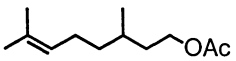	(**27**)	7	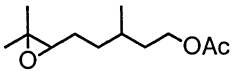	(**28**)	Quant.[b]
6	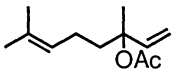	(**29**)	12	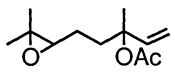	(**30**)	Quant.[c]
7	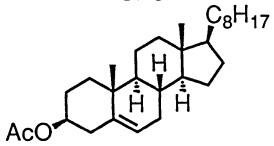	(**31**)	12	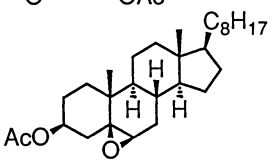	(**32**)	86[c-e]
8	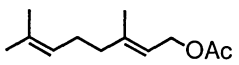	(**33**)	7	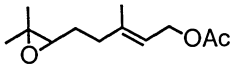	(**34**)	50[c]
				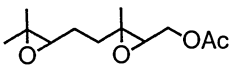	(**35**)	38[c]
9	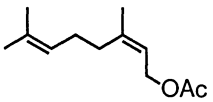	(**36**)	12	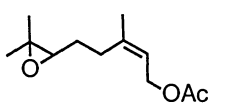	(**37**)	69[c]
				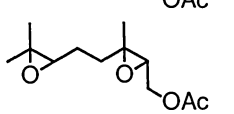	(**38**)	28[c]

a) Reaction conditions; olefin 3.0 mmol, isobutyraldehyde 9.0 mmol, Fe(dmp)$_3$ (**11a**) 0.03 mmol (1.0 mol%), 1,2-dichloroethane (DCE) 10 ml, r.t., O_2 1 atm. b) Determined by GC analysis. c) Isolated yield. d) Mixture of *cis* and *trans* isomers (65/35). e) Mixture of α and β isomers (29/71).

Table 5. Epoxidation of Citronellol (**39**)[a]

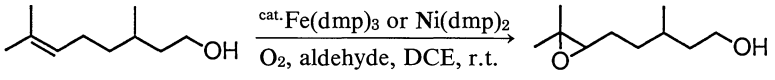

39 **40**

Entry	Catalyst		Time/h	Conversion of **39**/%	Yield of **40**/%[b]
1	$Fe(dmp)_3$	(**11a**)	4.5	100	Quant.
2	$Ni(dmp)_2$	(**12a**)	4.5	67[b]	57

a) Reaction conditions; citronellol (**39**) 3.0 mmol, isobutyraldehyde 18.0 mmol, catalyst 0.03 mmol (1.0 mol%) in 1,2-dichloroethane (DCE) 10.0 ml, O_2 1 atm. b) Isolated.

Table 6. Epoxidation of Olefinic Alcohols[a]

Entry	Olefinic alcohol	Time/h	Epoxy alcohol	Yield/%
1	Citronellol (**39**)	4.5	3,7-Dimethyl-6,7-epoxyoctan-1-ol (**40**)	Quant.[b]
2	3-Methyl-3-buten-1-ol (**41**)	14	3-Methyl-3,4-epoxybutan-1-ol (**42**)	Quant.[c]
3	*cis*-3-Hexen-1-ol (**43**)	14	3,4-Epoxyhexan-1-ol (**44**)	80[c,d]
4	*trans*-2-Hexen-1-ol (**45**)	14	*trans*-2,3-Epoxyhexan-1-ol (**46**)	67[c]

a) Reaction conditions; olefinic alcohol 3.0 mmol, isobutyraldehyde 18.0 mmol, $Fe(dmp)_3$ (**11a**) 0.03 mmol (1.0 mol%) in 1,2-dichloroethane (DCE) 10.0 ml, O_2 1 atm. b) Isolated yield. c) GC yield. d) Mixture of *cis* and *trans* isomers (1/1).

the coordination by hydroxyl function.

Further, several olefinic alcohols, such as homoallylic alcohol **41** and **43**, or allylic alcohol **45** were oxygenated into the corresponding epoxy alcohols in good to quantitative yields (see Entries 2—4 in Table 6).

Conclusion

A wide variety of epoxides were prepared by the aerobic epoxidation of olefinic compounds including styrene analogues or olefinic alcohols in good to quantitative yields by using tris(1,3-diketonato)iron(III) complex, and particularly tris[1,3-bis(*p*-methoxyphenyl-1,3-propanedionato]iron(III) ($Fe(dmp)_3$) (**11a**) was found to be the most excellent catalyst in present oxygenation.

Experimental

General: Melting points were measured on a Mettler FP62 apparatus and uncorrected.

(a) Spectrometers: IR spectra were obtained by using a JASCO Model IR-700 infrared spectrometer on KBr pellets or liquid film on KBr. ^1H NMR spectra were recorded with a JEOL Model FX-270 spectrometer using $CDCl_3$ as solvent and with tetramethylsilane as internal standard.

(b) Chromatography: GC-analysis were performed on a Shimadzu GC-15A using a glass capillary column (Shimadzu CBP-l0, 25 m), and the peak areas were obtained with a Shimadzu chromatopack CR-5A.

Preparation of 1,3-Diketones and Tris(1,3-diketonato)iron-(III) Complexes. Tris(acetylacetonato)iron(III) (**6**, $Fe(acac)_3$) were purchased from Tokyo Kasei Kogyo Co., Ltd. (TCI) Bis(acetylacetonato)iron(II) (**4a**, $Fe(acac)_2$),[7] chlorobis(acetylacetonato)iron(III) (**5**, $Fe(acac)_2Cl$),[8] tris(1,1,1-trifluoro-2,4-pentanedionato)iron(III) (**7a**, $Fe(tfa)_3$),[9] tris(1,1,1,5,5,5-hexafluoro-2,4-pentanedionato)iron(III) (**8a**, $Fe(hfa)_3$),[10] tris-(2-acetylcyclohexanonato)iron(III) (**9a**, $Fe(ach)_3$),[11] and tris(3-methyl-2,4-pentanedionato)iron(III) (**10a**, $Fe(mac)_3$)[12] were prepared according to the reported methods, respectively, and ligands were purchased from TCI Co., Ltd. (**4b, 7b, 8b,** and **9b**) and Aldrich Chemical Company, Inc. (**10b**), respectively.

1,3-Bis(*p*-methoxyphenyl)-1,3-propanedione (11a, Hdmp);[3c,13] A refluxing suspension of sodium hydride (0.39 mol) in cyclohexane (400 ml), a solution of *p*-methoxyacetophenone (0.33 mol) and ethyl *p*-methoxybenzoate (0.33 mol) in cyclohexane (200 ml) was added over 1 h, and reflux was continued for another 2 h. After cooling, reaction mixture was quenched with 1.0 mol dm^{-3} aqueous HCl, then crude product was extracted with THF–Et_2O. The organic extract was washed with brine, and dried over anhydrous sodium sulfate, then solvent was removed in vacuo. Recrystallization from hexane–ethyl acetate gave slightly colored needles (58% yield): Mp 131—138 °C; ^1H NMR ($CDCl_3$) δ=3.90 (6H, s), 6.80 (1H, s), 7.00 (4H, m), 7.95 (4H, m); IR (KBr) 2938, 2840, 1687, 1605, 1507, 1429, 1305, 1263, 1230, 1170 cm^{-1}

Tris[1,3-bis(*p*-methoxyphenyl)-1,3-propanedionato]iron-(III) (11b, Fe(dmp)$_3$); To a stirred mixture of Hdmp (30.0 mmol) in THF-MeOH (1/1, 100 ml), an aqueous solution of $FeCl_3$ (10.0 mmol, 50 ml) was added over 10 min. Precipitated reddish-brown solid was filtered and washed with MeOH and water. After drying in vacuo (90 °C/0.1 mmHg, 1 mmHg=133.322 Pa), $Fe(dmp)_3$ **11a** was yielded as reddish-purple solid. Found: C, 66.78; H, 5.18%. Calcd for $C_{45}H_{45}O_{12}Fe$: C, 64.83; H, 5.44%.

Melting Points and IR Spectra of Iron Complexes. Bis-(acetylacetonato)iron(II) (4a, Fe(acac)$_2$); Red solid; mp 169.0—169.4 °C; IR (KBr) 2918, 1571, 1562, 1525, 1376, 1270 cm^{-1}.

Chlorobis(acetylacetonato)iron(III) (5, Fe(acac)$_2$Cl); Red solid; mp 180.4—181.0 °C; IR (KBr) 2992, 2918, 1571, 1525, 1364, 1290 cm^{-1}.

Tris(1,1,1-trifluoro-2,4-pentanedionato)iron(III) (7a, Fe(tfa)$_3$); Orange solid; mp 212.4—212.8 °C; IR (KBr) 1615, 1510, 1292, 1147 cm^{-1}.

Tris(1,1,1,5,5-hexafluoro-2,4-pentanedionato)iron(III) (8a,

Fe(hfa)$_3$); Yellowish-orange solid; mp 162.0—162.6 °C; IR (KBr) 1647, 1619, 1565, 1540, 1445, 1255, 1210, 1146 cm^{-1}.

Tris(2-acetylcyclohexanonato)iron(III) (9a, Fe(ach)$_3$); Reddish-purple solid; mp 228.6—229.0 °C; IR (KBr) 2930, 2854, 1573, 1460, 1374, 1331, 1278 cm^{-1}.

Tris(3-methyl-2,4-pentanedionato)iron(III) (10a, Fe(mac)$_3$); Reddish-purple solid; mp 189.6—190.0 °C; IR (KBr) 2998, 2960, 2918, 1876, 1574, 1467, 1424, 1360, 1330, 1292 cm^{-1}.

Tris[1,3-bis(*p*-methoxyphenyl)-1,3-propanedionato]iron-(III) (11a, Fe(dmp)$_3$) Reddish-purple solid; mp 278.0—279.4 °C; IR (KBr) 2930, 2836, 1604, 1587, 1527, 1492, 1377, 1305, 1257, 1228, 1175 cm^{-1}.

Epoxidation of 1,5-Dimethyl-1-vinyl-4-hexenyl Acetate (Linalyl Acetate, 31). (see Entry 6 in Table 5). A mixture of linalyl acetate (**29**) (3.0 mmol), Fe(III)(dmp)$_3$ (**11a**) (0.03 mmol, 1.0 molo%), isobutyraldehyde (9.0 mmol) in 1,2-dichloroethane (10.0 ml) was stirred under an atmospheric pressure of oxygen at room temperature for 12 h. Reaction mixture was washed with saturated aqueous $NaHCO_3$ solution, and, after drying over anhydrous sodium sulfate, solvent was removed in vacuo. Purification of the residue by column chromatography on SiO_2 (hexane–ethyl acetate) afforded 1-(3,4-epoxy-4-methylpentyl)-1-methylallyl acetate (**30**) (639 mg, quantitative yield).

^{1}H NMR and IR Spectra of Epoxides (in Tables 3—6). Styrene Oxide (2), 1,2-Epoxycyclohexane (24). ^{1}H NMR spectra, IR spectra and retention time in GC analysis agreed with those of the authentic samples.

***cis*-1-Phenyl-1,2-epoxypropane (14);** ^{1}H NMR ($CDCl_3$) δ=1.09 (3H, d, J=5.28 Hz), 3.34 (1H, dq, J_1=5.28 Hz, J_2=4.29 Hz), 4.06 (1H, d, J=4.29 Hz), 7.3 (5H, m); IR (neat) 3028, 2996, 2994, 2928, 1496, 1451, 1259 cm^{-1}.

2-(*p*-Chlorophenyl)oxirane (16); ^{1}H NMR ($CDCl_3$) δ=2.75 (1H, m), 3.14 (1H, m), 3.83 (1H, m), 7.21 (2H, d, J=8.57 Hz) 7.32 (2H, d, J=8.57 Hz); IR (neat) 3050, 2990, 2918, 1495, 1089 cm^{-1}.

***trans*-Stilbene Oxide (18);** ^{1}H NMR ($CDCl_3$) δ=3.86 (2H, s), 7.3—7.4 (10H, m); IR (KBr) 3060, 3030, 2974, 1606, 1497, 1452 cm^{-1}.

2,3-Epoxy-2-methyldecane (20); ^{1}H NMR ($CDCl_3$) δ=0.88 (3H, t, J=6.92 Hz), 1.26 (3H, s,), 1.28 (10H, m), 1.31 (3H, s), 1.50 (2H, m), 2.71 (1H t, J=6.27 Hz); IR (neat) 2925, 2850, 1465 cm^{-1}.

***cis*-2,3-Epoxyoctane (22);** ^{1}H NMR ($CDCl_3$) δ=0.93 (3H, t, J=7.09 Hz), 1.27 (3H, d, J=5.28 Hz), 1.35—1.45 (4H, m), 1.48—1.55 (4H, m), 2.90 (1H, m), 3.06 (1H, m); IR (neat) 2958, 2928, 2856, 1466, 1381 cm^{-1}.

1,2-Epoxy-2-methyldecane (26); ^{1}H NMR ($CDCl_3$) δ=0.88 (3H, t, J= 6.80 Hz), 1.27 (3H, s), 1.29 (14H, m), 2.55 (1H, d, J=10.9 Hz), 2.57 (1H, d, J=10.9 Hz); IR (neat) 2924, 2852, 1465 cm^{-1}.

6,7-Epoxy-3,7-dimethyloctyl Acetate (28); ^{1}H NMR ($CDCl_3$) δ=0.94 (3H, d, J=6.27 Hz), 1.27 (3H, s), 1.31 (3H, s) , 1.40—1.60 (7H, m), 2.05 (3H, s) , 2.70 (1H, t, J=6.06 Hz), 4.11 (2H, m); IR (neat) 2960, 2924, 2872, 1741, 1461, 1379, 1367, 1241 cm^{-1}.

1-(3,4-Epoxy-4-methylpentyl)-1-methylallyl Acetate (30); ^{1}H NMR ($CDCl_3$) δ=1.20 (3H, d, J=6.92 Hz), 1.26 (3H, s), 1.30 (3H, s), 1.5—1.6 (4H, m), 2.00 (3H, s), 2.71 (1H, t, J=6.26 Hz), 5.15 (2H, m), 5.95 (1H, m); IR (neat) 2974, 2932, 1738, 1461, 1372, 1249 cm^{-1}.

5,6-Epoxycholesteryl Acetate (32) Mixture of α and β Isomers; ^{1}H NMR ($CDCl_3$) δ=0.60 (3H, m), 0.80—1.60 (6H, m), 1.80—2.20 (34H, m), 2.00 (3H, s), 2.90 (0.29H, d, J=2.90 Hz, H-6β), 3.10 (0.71H, d, J=2.00 Hz, H-6α), 4.70—5.00 (1H, m) IR (KBr) 2950, 1734, 1470, 1368, 1247, 1041 cm^{-1}.

***trans*-6,7-Epoxy-3,7-dimethyl-2-octenyl Acetate (34);** ^{1}H NMR ($CDCl_3$) δ=1.26 (3H, s), 1.31 (3H, s), 1.60—1.80 (5H, m), 2.05 (3H, s), 2.10—2.30 (2H, m), 2.70 (1H, t, J=6.26 Hz), 4.59 (2H, d, J=7.25 Hz), 5.40 (1H, m); IR (neat) 2960, 2926, 1740, 1454, 1380, 1234 cm^{-1}.

***cis*-2,3 : 6,7-Diepoxy-3,7-dimethyloctyl Acetate (35);** ^{1}H NMR ($CDCl_3$) δ=1.30 (6H, m), 1.50—1.80 (7H, m), 2.10 (3H, s), 2.70 (1H, m), 3.05 (1H, m), 4.05 (1H, m), 4.30 (1H, m); IR (neat) 2970, 2929, 1743, 1455, 1380, 1232 cm^{-1}.

***cis*-6,7-Epoxy-3,7-dimethyl-2-octenyl Acetate (37);** ^{1}H NMR ($CDCl_3$) δ=1.27 (3H, s), 1.31 (3H, s), 1.63 (2H, dt, J_1=7.75 Hz, J_2=6.27 Hz), 1.78 (3H, s), 2.05 (3H, s), 2.26 (2H, t, J=7.75 Hz), 2.71 (1H, t, J=6.27 Hz), 4.58 (2H, d, J=6.60 Hz), 5.41 (1H, t, J=6.60 Hz); IR (neat) 2964, 2930, 1739, 1670, 1453, 1379, 1234 cm^{-1}.

***trans*-2,3 : 6,7-Diepoxy-3,7-dimethyloctyl Acetate (38);** ^{1}H NMR ($CDCl_3$) δ=1.28 (3H, s), 1.32 (3H, s), 1.35 (3H, s), 1.60—1.80 (4H, m), 2.10 (3H, s), 2.72 (1H, m), 3.00 (1H, m), 4.09 (1H, m), 4.35 (1H, m); IR (neat) 2970, 2931, 1744, 1455, 1378, 1234 cm^{-1}.

3,7-Dimethyl-6,7-epoxyoctan-1-ol (40); ^{1}H NMR ($CDCl_3$) δ=0.93 (3H, d, J=6.26Hz), 1.27 (3H, s), 1.30 (3H, s), 1.4—1.5 (2H, m), 1.5—1.8 (5H, m), 1.90 (1H, s), 2.7 (1H, t, J=6.10 Hz), 3.7 (2H, m); IR (neat) 3420, 2960, 2932, 2872, 1463 cm^{-1}.

3-Methyl-3,4-epoxybutan-1-ol (42); ^{1}H NMR ($CDCl_3$) δ= 1.39 (3H, s), 1.80—2.00 (2H, m), 2.66 (1H, d, J=4.29 Hz), 2.83 (1H, d, J=4.29 Hz), 3.70—3.80 (2H, m), 4.70 (1H, s); IR (neat) 3450, 2980, 1420 cm^{-1}.

***cis*-3,4-Epoxyhexan-1-ol (44);** ^{1}H NMR ($CDCl_3$) δ=1.05 (3H, t, J=7.59 Hz), 1.50—1.60 (2H, m), 1.65—1.75 (1H, m), 1.85—2.00 (1H, m), 2.94 (1H, dt, J_1=6.43 Hz, J_2=4.20 Hz), 3.23 (1H, dt, J_1=7.91 Hz, J_2=4.20 Hz), 3.65 (1H, s), 3.80—3.90 (9H, m); IR (neat) 3424, 2970, 2934, 2878, 1468, 1057 cm^{-1}.

***trans*-2,3-Epoxyhexan-1-ol (46);** ^{1}H NMR ($CDCl_3$) δ= 0.96 (3H, t, J=7.26 Hz), 1.40—1.60 (4H, m), 2.29 (1H, s), 2.95 (2H, m), 3.61 (1H, m), 3.92 (1H, m); IR (neat) 3412, 2960, 2932, 2872, 1464 cm^{-1}.

References

1) K. A. Jörgensen, *Chem. Rev.*, **89**, 431 (1989).

2) a) J. T. Groves and T. E. Nemo, *J. Am. Chem. Soc.*, **105**, 5786 (1983); J. T. Groves and R. S. Myers, *ibid.*, **105**, 5791 (1983); b) E. Guilmet and B. Meunier, *Tetrahedron Lett.*, **21**, 4449 (1980); J. P. Collman, T. Kodadek, S. A. Raybuck, and B. Meunier, *Proc. Nat. Acad. Soc., U.S.A.*, **80**, 7039 (1983); S. Takagi, E. Takahashi, T. Miyamoto, and Y. Sasaki, *Chem. Lett.*, **1986**, 1275; c) R. Nagata and I. Saito, *Synlett*, **1990**, 291; d) B. Meunier, *Bull. Soc. Chim. Fr.*, **1986**, 578; e) Y. Kaku, M. Otsuka, and M. Ohno, *Chem. Lett.*, **1989**, 611; f) S. Ito, K. Inoue, and M. Matsumoto, *J. Am. Chem. Soc.*, **104**, 6450 (1982).

3) a) T. Takai, T. Yamada, and T. Mukaiyama, *Chem. Lett.*, **1990**, 1657; b) T. Mukaiyama, T. Takai, T. Yamada, and O. Rhode, *ibid.*, **1990**, 1661; c) T. Yamada, T. Takai, O. Rhode, and T. Mukaiyama, *ibid.*, **1991**, 1; d) T. Takai, T. Yamada, O. Rhode, and T. Mukaiyama, *ibid.*, **1991**, 281; e) T. Yamada, T. Takai, O. Rhode, and T. Mukaiyama, *Bull. Chem. Soc. Jpn.*, **64**, 2109 (1991); f) T. Yamada, T. Takai, O. Rhode, and T. Mukaiyama, unpublished results.

4) J. T. Groves and M. K. Stern, *J. Am. Chem. Soc.*, **110**, 8628 (1988); H. Kanai, H. Hayashi, K. Koike, M. Ohsuga, and

M. Masakatsu, 57th Annual Meeting of the Chemical Society of Japan, Fukuoka, 1988, Abstr., I. p. 349.

5) Praseodymium(III) acetate ($Pr(OAc)_3$) catalyzed aerobic epoxidation of various olefinic compounds (e.g. terpenes) in the coexistence of an aldehyde was reported. Shell International Research, JP Patent Tokkaisho 59-231077 (1984).

6) Y. Maeda, M. Ai, and S. Suzuki, *Kogyo Kagaku Zasshi,* **73**, 99 (1970).

7) J. P. Fackler, Jr., D. G. Holar, D. A. Buckingham, and J. T. Henry, *Inorg. Chem.,* **4**, 920 (1965).

8) D. M. Puri and R. C. Mehrotra, *J. Less-Common Met.,* **5**, 2 (1963).

9) T. Fujinaga, T. Kuwamoto, Y. Nakamura, and N. Matsubara, *Bunseki Kagaku,* **29**, 799 (1980).

10) K. W. Chambers, E. A. Cherniak, G. Taylor, and J. Yu, *Can. J. Chem.,* **54**, 2116 (1976).

11) G. S. Hammond and R. P. Foss, *J. Phys. Chem.,* **68**, 3739 (1964).

12) A. R. Butler, A. M. Calsy, and C. Glidwell, *J. Organomet. Chem.,* **341**, 439 (1988).

13) H. Okawa, K. Ueda, and S. Kida, *Inorg. Chem.,* **21**, 1594 (1982).

Dipeptide Side Chain-Side Chain Hydrophobic Interactions as Conformational Core for Chymotrypsin Inhibition

Hiroshi SAKAMOTO, Yasuyuki SHIMOHIGASHI,* Tomohisa OGAWA, Keiichi KAWANO,† and Motonori OHNO
Laboratory of Biochemistry, Department of Chemistry, Faculty of Science, Kyushu University, Fukuoka 812
†Department of Prosthetic Dentistry I, Faculty of Dentistry, Kyushu University, Fukuoka 812
(Received April 11, 1991)

A series of dipeptides with the sequence of H-D-Leu-L-Phe-R, where R denotes 4-phenylpiperidide, 4-phenylpiperazide, and their derivatives, have been synthesized to examine their ability to inhibit chymotrypsin. Dipeptide phenylpiperidide and phenylpiperazide inhibited chymotrypsin fairly strongly (K_i=7.5×10^{-4} M and 1.4×10^{-3} M, respectively) (1 M=1 mol dm^{-3}), while their phenyl-substituted analogs were inactive. In high resolution ^{1}H NMR measurements, it was found that the proton signals of D-Leu γ-CH and β-CH$_2$ shifted considerably to the upfield when compared with those of H-D-Leu-L-Ala-OH, suggesting that these upfield shifts are due to the magnetic anisotropy effect by the benzene ring of the Phe residue. This was confirmed by measuring NOE between D-Leu-isobutyl and L-Phe-phenyl groups. These NMR data indicate that the side chains of both D-Leu and L-Phe are in close proximity, resulting in formation of a hydrophobic complex. It was suggested that, in the inhibitory conformation of dipeptides against chymotrypsin, the phenyl group of phenylpiperidide or phenylpiperazide moiety fits the S_1 site, while the side chain-side chain hydrophobic complexing core fits the S_2 site.

The discovery of various chymotrypsin-like proteases that play crucial roles in pathological lesions has required highly specific and selective inhibitors for depressing these proteases.[1] We have recently reported that dipeptide methyl esters containing 2,3-methanophenylalanine (∇Phe),[2] H-∇Phe-L-Phe(or Leu)-OMe, inhibits chymotrypsin fairly strongly (K_i=1.6—14×10^{-4} M).[3] It was assumed that these dipeptide methyl esters construct an inhibitory conformation with a hydrophobic core between ∇Phe-phenyl and ester-methyl groups.[4,5] Such inhibitory conformation was considered to be compelled by the extremely constrained three-membered ring of ∇Phe, which restricts the ϕ and ψ angles very severely.[5,6] Similar inhibitory conformation was also found for H-D-Phe-L-Phe-OMe, which inhibited chymotrypsin strongly (K_i=9.0×10^{-5} M).[7]

In these inhibitory conformations, the hydrophobic core was assumed to fit the chymotrypsin S_2 site, while the L-Phe or L-Leu residue in the position 2 fits the S_1 site.[3,4,7] The formation of a hydrophobic core appears to be the most important structural requirement for this particular inhibition. If this formation occurs without compulsion, the molecular conformation may stabilize much more strongly. Deber and Joshua[8] reported the synthesis of a series of linear dipeptides of the type H-L-Phe-L- or -D-Xxx-OH, where Xxx represented various amino acid residues, and found the presence of an intramolecular side chain-side chain complexing for H-L-Phe-D-Xxx-OH, but not for H-L-Phe-L-Xxx-OH. In the present study, we noted this side chain-side chain interaction in aromatic dipeptides as one of possible ways to construct a hydrophobic core for chymotrypsin inhibition.

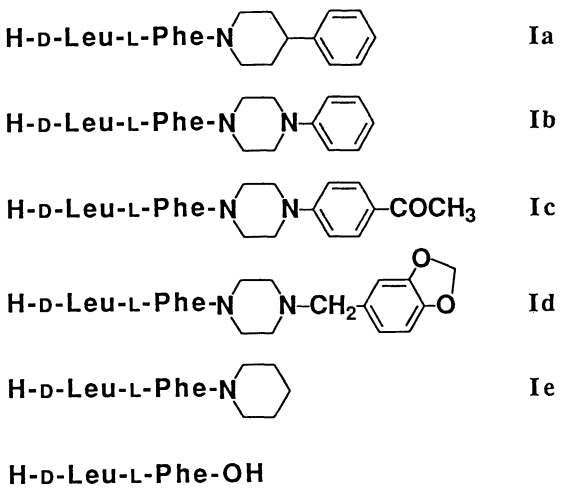

Fig. 1. Structure of dipeptide phenylpiperidide (**Ia**), phenylpiperazide (**Ib**), and their derivatives.

We have designed a series of H-D-Leu-L-Phe-R (**Ia—e**), where R denotes 4-phenylpiperidide, 4-phenylpiperazide, and their derivatives (Fig. 1). In this paper the synthesis of dipeptides and their inhibitory activity for chymotrypsin will be described together with their conformational analysis by ^{1}H NMR.

Results and Discussion

The synthetic scheme is depicted in Fig. 2. A series of Boc-L-Phe amides (**IIa—e**) were prepared by a mixed anhydride coupling method between Boc-L-Phe-OH and amines in yields of 66—95%. The resulting amides were treated with trifluoroacetic acid (TFA) to remove the Boc group, and then coupled with Boc-D-Leu-OH using 1-ethyl-3-(3-dimethylaminopropyl)carbodiimide (EDC) in the presence of 1-hydroxybenzotriazole (HOBt) (43—77% yields). The desired dipeptide amides (**Ia—e**) as hydrochlorides were obtained from Boc-D-Leu-L-Phe amides by treatment with hydrogen chloride in dioxane.

Inhibitory activity for chymotrypsin was analyzed

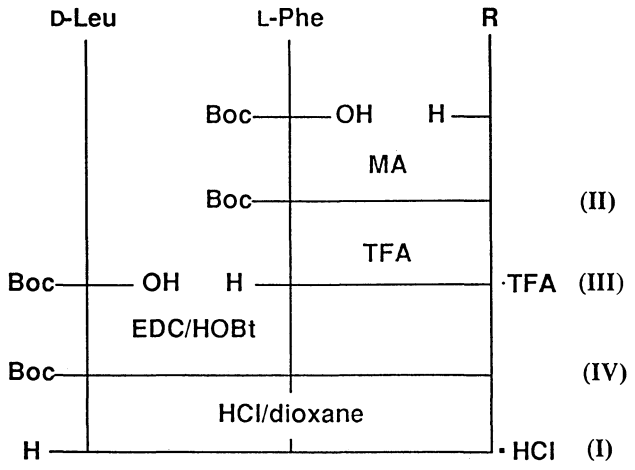

Fig. 2. Synthetic scheme of H-D-Leu-L-Phe-R.
R designates the amide derivatives of 4-phenylpiperidine, 1-phenylpiperazine, 4'-piperazinoacetophenone, 1-piperonylpiperazine, and piperidine.

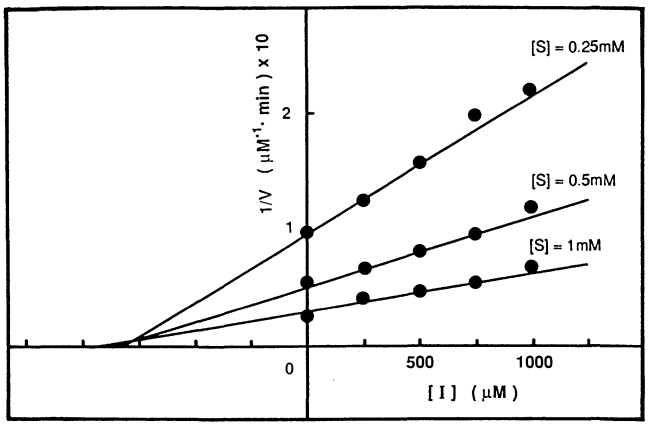

Fig. 3. Dixon plot for hydrolysis of succinyl-Ala-Ala-Pro-Phe-*p*NA by chymotrypsin in the presence of H-D-Leu-L-Phe-phenylpiperidide (**Ia**) at pH 7.8. Concentrations of the substrate are indicated in the figure.

Table 1. Inhibitory Activities of Dipeptides for Chymotrypin

Peptides	K_i/M
Ia	7.5×10^{-4}
Ib	1.4×10^{-3}
Ic	No inhibition
Id	No inhibition
Ie	No inhibition
H-D-Leu-L-Phe-OH	No inhibition
H-D-Leu-L-Ala-OH	No inhibition

using succinyl-Ala-Ala-Pro-Phe-*p*NA as a substrate,[9] because significant UV absorption due to the inhibitors at wavelengths below 250 nm made the spectroscopic monitor at 237 nm of hydrolysis of another popular substrate Ac-Tyr-OEt difficult. It was found that the dipeptide phenylpiperidide (**Ia**) and phenylpiperazide (**Ib**) inhibit chymotrypsin moderately. Analyses by Dixon plots[10] and Lineweaver-Burk plots[11] indicated the inhibition manner to be competitive. In Fig. 3 the Dixon plot of compound **Ia** is shown. The K_i values of **Ia** and **Ib** were 7.5×10^{-4} and 1.4×10^{-3} M, respectively (Table 1). It should be noted that the inhibitory potencies of these dipeptides are almost equal to those of ▽Phe-containing dipeptides.[3] This suggests that incorporation of a sterically constrained amino acid such as ▽Phe is not necessarily crucial for constructing the inhibitory conformation.

Dipeptides with phenyl-substituted piperazide (**Ic—d**) showed no inhibition. Also, H-D-Leu-L-Phe piperidide (**Ie**) did not inhibit chymotrypsin at all. These results imply that the phenyl group in the R moiety of H-D-Leu-L-Phe-R should not be substituted to elicit an inhibitory activity against chymotrypsin.

In 400-MHz ^{1}H NMR measurements, the signal assignments were carried out by the two-dimensional COSY experiment. The chemical shift values were carefully read off for comparison. When the chemical shifts of D-Leu side chain protons were compared with those of H-D-Leu-L-Ala-OH, considerable upfield shifts became prominent for all dipeptides having the D-Leu-L-Phe sequence: δ=0.13—0.38 for D-Leu β-CH_2; and δ=0.28—0.49 for D-Leu γ-CH. Even protons of δ-methyl groups showed a small upfield shift (δ=0.12—0.15). These results indicate that the side chain of D-Leu is in very close proximity to the phenyl group and undergoes the anisotropy effect of the benzene ring. Since H-D-Leu-L-Phe-OH and H-D-Leu-L-Phe piperidide (**Ie**), which has no phenyl in the *C*-terminal R

Table 2. Chemical Shifts of Leucine Side Chain Protons of Dipeptides

Dipeptide	Chemical shifts (ppm) of leucine residue					
	βCH_2		γCH		δCH_3	
H-D-Leu-L-Ala-OH	1.526	(0.000)	1.678	(0.000)	0.890	(0.000)
H-D-Leu-L-Phe-OH	1.147	(0.379)	1.299	(0.379)	0.763	(0.127)
Ia	1.275	(0.251)	1.275	(0.403)	0.764	(0.126)
	1.384	(0.142)	1.384	(0.294)	0.823	(0.067)
Ib	1.268	(0.258)	1.268	(0.410)	0.764	(0.126)
Ic	1.293	(0.233)	1.293	(0.385)	0.774	(0.166)
Id	1.184	(0.342)	1.184	(0.494)	0.741	(0.149)
Ie	1.399	(0.127)	1.399	(0.279)	0.772	(0.118)

portion, also showed such upfield shifts of D-Leu side chain (Table 2), the shielding phenyl group apparently belongs to L-Phe in the position 2.

The presence of side chain interaction between D-Leu-isobutyl and L-Phe-phenyl was confirmed by measurements of the nuclear Overhauser effect (NOE). H-{H} NOE difference spectra of H-D-Leu-L-Phe-piperidide (**Ie**) were obtained by irradiation of each selected proton signal (Fig. 4). When the proton signals of the D-Leu-β-methylene, γ-methine, and δ-methyl groups were irradiated separately, the enhancement as positive NOE was observed for the proton signals of L-Phe-phenyl in the aromatic envelope (Figs. 4B and 4C). Similar enhancement was also observed for the D-Leu β-methylene, γ-methine, and δ-methyl protons by irradiation of L-Phe-phenyl proton signals (Fig. 4D). These NOE observed indicate that the side chains of D-Leu and L-Phe in D-Leu-L-Phe dipeptides are spatially in close proximity to each other.

Deber and Joshua[8] found a similar type of side chain interactions for L-Phe-D-Xxx dipeptides. They observed distinct upfield shifts (0.2—0.7 ppm) for the signals of D-Xxx β- and γ-methylene protons in 100-MHz ^{1}H NMR. Although they suggested that these upfield shifts are due to the shielding effect of L-Phe-phenyl, no direct evidence has been presented. Since the side chain interactions were not observed for L-Phe-L-Xxx dipeptides, it seems that this side chain-side chain interaction in dipeptides is stabilized in the configurational sequences of L-D and D-L. In fact, the building study using the CPK model indicated that a tight side chain complexing is feasible for and L-D and D-L.

The hydrophobic complex formed between the side chains of the adjacent residues in D-Leu-L-Phe dipeptides appears to be too bulky to fit the S_1 hydrophobic pocket of chymotrypsin active center. Since the S_2 site of chymotrypsin is Trp-215,[12] the moiety in hydrophobic complexing seems to interact with this Trp hydrophobic site. In the case, the phenyl group of phenylpiperidide and phenylpiperazide should occupy the S_1 pocket. Inactivity of dipeptides having phenyl-substituted piperidine residues (Table 1) is due probably to their bulkiness that makes the dipeptide incapable to fit the S_1 site, while inactivity of H-D-Leu-L-Phe-OH would be explained by lack of the substituent at the *C*-terminal carboxyl group.

We have previously reported the inhibitory conformation of H-D-Phe-L-Phe-OMe,[7] in which D-Phe-phenyl and ester-methyl groups construct a hydrophobic core responsible for interaction with the chymotrypsin S_2 site. This was demonstrated by NOE experiments. As proven in the present study, it is also likely that a conformer with the side chain-side chain complex exists in the enzyme assay solution, although we could not confirm it by NOE experiments because of overlapping of the proton signals of the two phenyl groups. How-

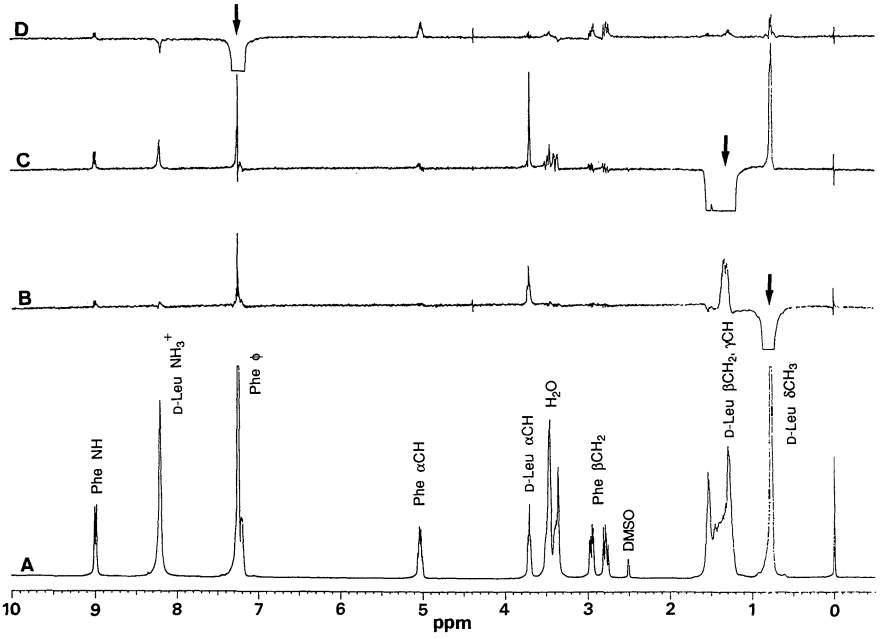

Fig. 4. 400-MHz ^{1}H NMR spectra of H-D-Leu-L-Phe-piperidide (**Ie**) hydrochloride in DMSO-d_6 at 25 °C.
A: The control spectrum acquired with irradiation in a blank region of the spectrum.
B—D: The NOE difference spectra obtained by subtraction of the control spectrum from the spectra acquired with irradiation of particular signals indicated by arrows; D-Leu δCH_3(B), D-Leu βCH_2 and γCH (C), and Phe-phenyl (D).

ever, this conformation would not cause an inhibition of chymotrypsin, since no group to interact with the S_1 site is present in this conformation. For D-Leu-L-Phe dipeptides, the presence of a conformer with the hydrophobic complex formed between D-Leu-isobutyl and *C*-terminal phenyl groups, a type of complex observed for H-D-Phe-L-Phe-OMe, is also partly feasible. However, the competitive inhibition by this conformer is unlikely due to the undetectable inhibition by dipeptides **Ic** and **Id** (Table 1). Collectively, the conformation to induce the enzyme inhibition, namely the inhibitory conformation, appears to differ between D-Leu-L-Phe and D-Phe-L-Phe dipeptides, while both dipeptide inhibitors seems to resemble each other in the size and spatial arrangement of P_1 and P_2 sites.

In ^{1}H NMR spectrum of H-D-Leu-L-Phe-phenylpiperidide (**Ia**), which is the most potent inhibitor synthesized in this study (Table 1), two sets of proton signals were observed, suggesting the presence of conformers (Table 2). These conformers would be characterized by the difference in either axial or equatorial positioning of the phenyl group on the piperidine ring. Although we could not assign these conformations, it is clear that the conformer in the major conformation (65%) constructs the intramolecular hydrophobic side chain complex as shown by obvious upfield shifts of the D-Leu-isobutyl side chain (Table 2). It is thus suspected that the intrinsic inhibitory activity of this isomer would be much stronger than that observed for the mixture of isomers.

The present study indicates that the side chain-side chain hydrophobic interaction can be constructed in dipeptides with the D-L configurational sequence, and that a hydrophobic core formed has a conformation suitable to fit the active site of chymotrypsin. The hydrophobic interaction between the dipeptide and the enzyme should result in inhibition of the enzyme catalytic action. Analyses of such an inhibitory conformation of dipeptides might lead to elucidation of the subtle structure of the chymotrypsin active center.

Experimental

Synthesis. High performance (HP)-TLC was carried out on Silica Gel G (Merck, Frankfurt) with the following systems (v/v): R_f^1, $CHCl_3$–MeOH (9 : 1), R_f^2, *n*-BuOH–AcOH–pyridine–H_2O (4 : 1 : 1 : 2). Optical rotations were measured with a Union high sensitivity polarimeter PM-71. All melting points were uncorrected.

Boc-L-Phe-amides (IIa—e): To a solution of Boc-L-Phe-OH (1.327 g, 5.0 mmol) in tetrahydrofuran was added isobutyl chloroformate (0.65 ml, 5.0 mmol) at −15 °C. After 10 min, amine (4-phenylpiperidine, 1-phenylpiperazine, 4′-piperazinoacetophenone, 1-piperonylpiperazine, or piperidine) (10 mmol) was added. The reaction mixture was stirred for 2 h at 0 °C and overnight at room temperature, and evaporated. The residue was dissolved in EtOAc and the solution was washed successively with 4% $NaHCO_3$, 5% $KHSO_4$, and water, and then dried over Na_2SO_4. Physical properties of each compound are shown in Table 3.

Table 3. Physical Properties of Synthetic Peptides

Peptides	Yield %	Mp °C	$[\alpha]_D^{20}$/° *c* 0.5, DMF	(HP)-TLC R_f
Boc-L-Phe-R (**II**)				
IIa	97	Oil	—	R_f^1=0.92
IIb	66	105—107	−19.2	0.84
IIc	93	152—155	−18.2	0.84
IId	75	Oil	—	0.76
IIe	>100	Oil	—	0.78
Boc-D-Leu-L-Phe-R (**IV**)				
IVa	52	123—125	−16.8	0.86
IVb	43	133—135	−17.2	0.84
IVc	66	139—140	−16.8	0.81
IVd	53	120—122	−17.4	0.81
IVe	77	134—136	−16.6	0.76
H-D-Leu-L-Phe-R(**I**)·HCl				
Ia	79	93—94	−16.2	R_f^2=0.81
Ib	92	213 (decomp)	−14.4	0.82
Ic	93	173 (decomp)	−15.1	0.79
Id	62	180 (decomp)	−15.6	0.67
Ie	72	88—89	−16.4	0.79

Boc-D-Leu-L-Phe-amides (IVa—e): Boc-L-Phe-amides (**IIa—e**) (2.0 mmol) were treated with TFA at 0 °C for 30 min. After evaporation and trituration with the aid of dry diethyl ether, the resulting powder (**IIIa—e**) was collected and dried. To a solution of this TFA salt and Et_3N (0.28 ml, 2.0 mmol) in DMF (10 ml) were added Boc-D-Leu-OH·H_2O (530 mg, 2.0 mmol), EDC·HCl (422 mg, 2.2 mmol), and HOBt (324 mg, 2.4 mmol) at 0 °C. The reaction mixture was treated as described above. Physical properties are shown in Table 3.

H-D-Leu-L-Phe-amide (Ia—e) Hydrochlorides: Compounds **IVa—e** (0.5 mmol) were dissolved in 4.6 M HCl in dioxane (2.2 ml, 10 mmol) at 0 °C for 2—5 h. After evaporation, the residue was crystallized from MeOH–diethyl ether. Physical properties are shown in Table 3.

Enzyme Assay. Dipeptides synthesized were tested for their inhibitory activity against bovine chymotrypsin (Worthington Biochemical Co., Freehold, New Jersey). Substrate succinyl-Ala-Ala-Pro-Phe-*p*NA was synthesized by the conventional solution method. For the kinetic analyses of interactions between dipeptides and chymotrypsin, the standard method was carried out. Briefly, substrate was dissolved in 0.1 M Tris-HCl buffer (pH 7.8) with or without inhibitors. The enzyme reaction was initiated by adding an aliquot (30 μl) of the chymotrypsin solution (final concentration, 1.3 μg ml^{-1}) to the solution of substrate and inhibitor (1470 μl). The final concentrations of the substrate and inhibitors varied as 6.25, 12.5, 25 μM and 0, 250, 500, 750, 1000 μM, respectively. The rate of hydrolysis of the substrate was determined in duplicate by the spectroscopic measurement of liberated *p*-nitroanilide at 410 nm using a Hitachi 124 spectrometer. Inhibition constants, K_i, were determined by the Dixon plot analysis[10] and summarized in Table 1.

^{1}H NMR Measurements. Samples were prepared by dissolving 10 mg of the peptide in 0.5 ml of DMSO-d_6 (99.96% *d*, Aldrich, Milwaukee, Wisconsin). All ^{1}H NMR spectra were recorded on a Bruker AM-400 spectrometer operating at 400-MHz ^{1}H frequency at 25 °C. The chemical shifts were determined using tetramethylsilane as an internal standard and the signals were assigned by the two-dimensional COSY. The

COSY spectra were obtained by using the standard method.[13] Two hundreds fifty-six FIDs were acquired with successive t_1 values. The digital resolution was 9.76 Hz/pt. The H–{H} NOE data were recorded by a gated irradiation pulse sequence. The NOE difference spectra were obtained by subtracting the control spectrum from an original NOE spectrum produced by presaturation of selected proton signal with a low decoupling power for 3 s before pulse.

References

1) J. S. Bond and P. E. Butler, *Ann. Rev. Biochem.*, **56**, 333 (1987).

2) Abbreviations: EDC, 1-ethyl-3-(3-dimethylaminopropyl)carbodiimide; HOBt, 1-hydroxybenzotriazole; NOE, nuclear Overhauser effect; ▽Phe, 2,3-methanophenylalanine, or 1-amino-2-phenylcyclopropanecarboxylic acid; *p*NA, *p*-nitroanilide; and TFA, trifluoroacetic acid.

3) T. Ogawa, H. Yoshitomi, H. Kodama, M. Waki, C. H. Stammer, and Y. Shimohigashi, *FEBS Lett.*, **250**, 227 (1989).

4) T. Ogawa, H. Kodama, K. Yoshioka, and Y. Shimohigashi, *Pept. Res.*, **3**, 35 (1990).

5) Y. Shimohigashi, C. H. Stammer, and T. Costa, "Advanced in Biotechnological Process, Synthetic Peptides in Biotechnology," ed by A. Mizrahi and A. L. van Wezl, Alan R. Liss Inc., New York (1988), Vol. 10, p. 203.

6) C. H. Stammer, "Opioid Peptides: Medicinal Chemistry. NIDA Research Monograph," ed by R. S. Rapaka, G. Barnett, and R. L. Howks, Government Printing Press, Maryland (1986), Vol. 69, p. 148.

7) Y. Shimohigashi, T. Ogawa, H. Kodama, H. Sakamoto, H. Yoshitomi, M. Waki, and M. Ohno, *Biochem. Biophys. Res. Commun.*, **166**, 1460 (1990).

8) C. M. Deber and H. Joshua, *Biopolymers*, **11**, 2493 (1972).

9) E. G. DelMar, C. Largman, J. W. Brodrick, and M. C. Geokas, *Anal. Biochem.*, **99**, 316 (1979).

10) M. Dixon, *Biochem. J.*, **55**, 170 (1953).

11) H. Lineweaver and D. Burk, *J. Am. Chem. Soc.*, **56**, 658 (1934).

12) R. A. Blevins and A. Tulinsky, *J. Biol. Chem.*, **260**, 8865 (1985).

13) W. A. Aue, E. Bartholdi, and R. R. Ernest, *J. Chem. Phys.*, **64**, 2229 (1976).

A Novel Catalyst System, Trimethylsilyl Chloride and Indium(III) Chloride, as an Efficient Catalyst in the Sulfide Synthesis

Teruaki MUKAIYAMA, Takashi OHNO, Takashi NISHIMURA, Jeong Sik HAN, and Shū KOBAYASHI
Department of Applied Chemistry, Faculty of Science, Science University of Tokyo, Kagurazaka, Shinjuku-ku, Tokyo 162
(Received April 12, 1991)

O-Trimethylsilyl monothioacetals, which are generally difficult to activate under acidic conditions due to their rapid disproportionation, smoothly react with triethylsilane in the presence of a novel catalyst system, trimethylsilyl chloride and indium(III) chloride, to afford the corresponding sulfides in good to high yields. One pot synthesis of sulfides from aldehydes is also attained in high yields by successive treatments of aldehydes with trimethylsilyl alkyl (aryl) sulfides and triethylsilane in the presence of the above catalyst system under extremely mild conditions.

Utilities of acetals are widely extended during last few decades, not only as protective groups but also as electrophiles in various coupling reactions, especially carbon–carbon bond forming reactions.[1] *O*-trimethylsilyl monothioacetals are also useful intermediates as masked carbonyl compounds, however, activations of these compounds in the reaction with some nucleophiles are generally difficult because of their readiness to disproportionate under acidic conditions, and hitherto only a few examples of the reactions of *O*-trimethylsilyl monothioacetals with nucleophiles were reported.[2]

A novel method for the preparation of sulfides from carbonyl and related compounds, reduction of *O*-trimethylsilyl monothioacetals, was prelimirarily reported in the previous communication.[3] In this paper, we would like to describe on a novel catalyst system, trimethyisilyl chloride (TMSCl) and indium(III) chloride ($InCl_3$), which effectively catalyzes the reaction of *O*-trimethylsilyl monothioacetals with triethylsilane. Further, one pot synthesis of sulfides just starting from aldehydes using trimethylsilyl alkyl(aryl) sulfide and triethylsilane in the presence of the above catalyst system is described in detail.

Synthesis of Sulfides from *O*-Trimethylsilyl Monothioacetals. An Efficient Activation of *O*-Trimethylsilyl Monothioacetals Using TMSCl and $InCl_3$ as a Catalyst. In the first place, the reaction of 1-ethylthio-1-trimethyisiloxy-3-phenylpropane (**4**) with triethylsilane was chosen as a model and several reaction conditions were examined. When a typical Lewis acid such as $TiCl_4$, $SnCl_4$, BF_3OEt_2 or $ZnCl_2$ etc. was employed, no desired product was obtained after examination of several reaction conditions such as solvent, reaction temperature, amount of promoter, etc (Table 1, Entries 1—3). In these reactions, disproportionation of **4** took place quite readily to result in the formation of dithioacetal, an undesirable by-product. Trimethylsilyl triflate (TMSOTf) or trimethylsilyl iodide (TMSI), which was reported to be an effective catalyst in the reaction of ethylthio(phenyl)trimethylsiloxymethane (**1**) or 1-ethylthio-1-trimethylsiloxycyclohexane with trimethylsilane,[4] did not work well in the case when Et_3SiH was employed as a reducing reagent (Table 1, Entries 4 and 5). These results indicated that, under these reaction conditions of employing the above mentioned Lewis acids, the reaction systems were so acidic that the disproportionation proceeded faster than the desired reduction did. Therefore, milder reaction conditions were supposed to be necessary to accomplish this reaction. We have recently developed quite efficient catalyst system, TMSCl–$SnCl_2$[5] or TrCl–$SnCl_2$,[6] in the aldol or Michael reactions of silyl enol ethers with aldehydes or α,β-unsaturated ketones. These catalysts consist of a neutral molecule and a weak Lewis acid and effectively lead to the completion of the reactions under mild conditions. Bearing in mind these catalyst sys-

Table 1. Effect of Promoter or Catalyst

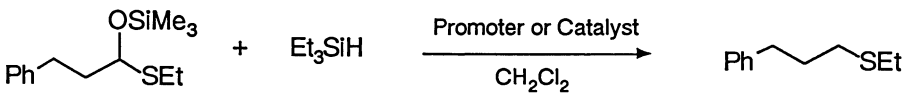

4 11

Entry	Promoter or Catalyst (mol%)	Temp/°C	Yield/%
1	$TiCl_4$ (100)	−78→0	0
2	BF_3OEt_2 (100)	−78→0	0
3	$SnCl_4$ (20)	−78→0	0
4	TMSOTf (20)	0	0
5	TMSI (20)	0	0
6	TMSCl (50)+$SnCl_2$ (20)	R.T.	0
7	TMSCl (50)+$InCl_3$ (20)	R.T.	68

Table 2. Synthesis of Sulfides from *O*-Trimethylsilyl Monothioacetals

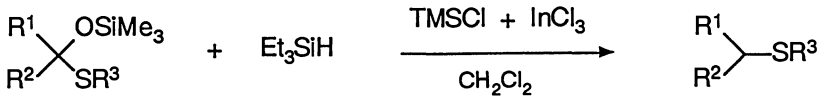

Entry	*O*-Trimethylsylilyl monothioacetal				Temp/°C	Product	Yield/%
	R^1	R^2	R^3				
1	Ph	H	Et	(1)	R.T.	**8**	83
2	Ph	H	^{i}Pr	(2)	0→R.T.	**9**	88
3	Ph	H	Ph	(3)	R.T.	**10**	77
4	$Ph(CH_2)_2$	H	Et	(4)	R.T.	**11**	68
5	$CH_3(CH_2)_7$	H	Et	(5)	R.T.	**12**	70
6	Ph	Me	Et	(6)	R.T.	**13**	97
7	$-(CH_2)_5-$		Et	(7)	0→R.T.	**14**	96

tems, we employed TMSCl–$SnCl_2$ as a catalyst in the present reaction. While **1** smoothly reacts with Et_3SiH at rt in the presence of 10 mol% each of TMSCl and $SnCl_2$ give the corresponding sulfide in 63% yield, no desired reduction product was obtained in the reaction of **4** with Et_3SiH (Table 1, Entry 6). We further searched for novel catalyst systems, and after screening several weak Lewis acids other than $SnCl_2$, $InCl_3$ was found to be very effective and the desired sulfide was obtained in 68% yield when a novel catalyst system, TMSCl–$InCl_3$, was employed (Table 1, Entry 7). It should be noted that neither TMSCl nor $InCl_3$ alone is effective in the present reaction and the reaction proceeds only when TMSCl and $InCl_3$ are combined.

Several examples of the present reaction of *O*-trimethylsilyl monothioacetals with triethylsilane are demonstrated in Table 2. In every case, the desired sulfides are obtained in good to high yields.

Concerning the structure of the novel catalyst system, we assumed the following equilibrium and the generation of the cationic species shown in Chart 1 similar to

Chart 1.

that in the case of TMSCl–$SnCl_2$ or TrCl–$SnCl_2$. The most important point is preferential activation of trimethylsiloxy group (Scheme 1, path A) to ethylthio group (path B) using TMSCl–$InCl_3$ catalyst system, which depends on stronger affinity of silicon atom toward oxygen atom than toward sulfur atom.[9] When path A and path B proceed parallelly in the case of using other Lewis acid catalysts such as $TiCl_4$, BF_3OEt_2, $SnCl_4$, etc., a dithioacetal **19** is mainly formed by the reaction of the intermediate **16** (or **17**) with ethylthiotrimethylsilane **18**, which is more reactive than Et_3SiH. It is also notable that $InCl_3$ is a quite mild Lewis acid and do not participate in the direct activation of **15**.

Thus, a novel catalyst system, TMSCl–$InCl_3$, effectively catalyzes the reaction of *O*-trimethylsilyl monothioacetals with triethylsilane. It should be noted that

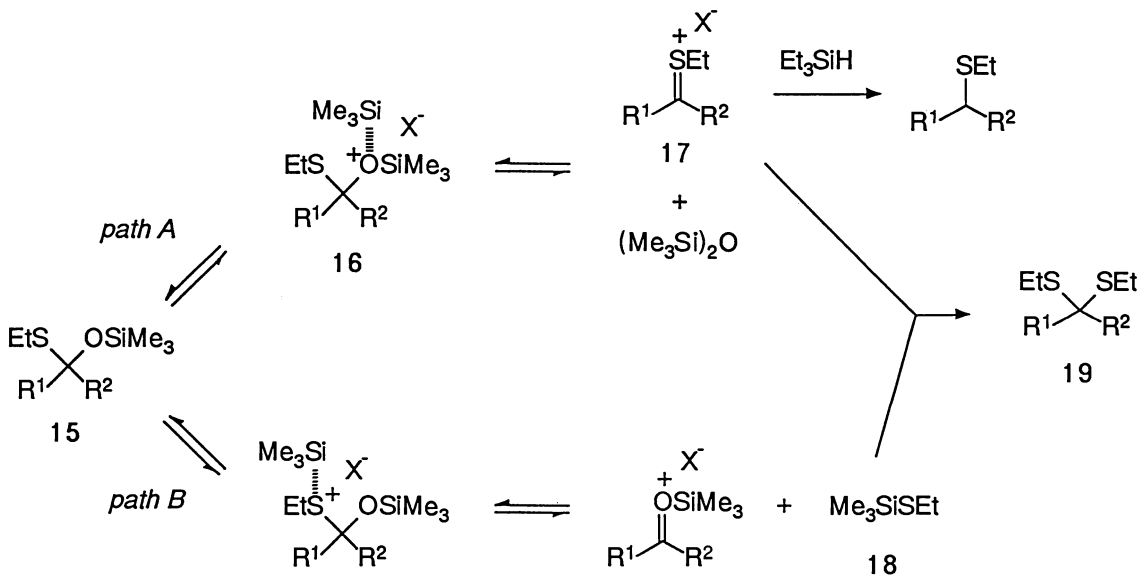

Scheme 1.

Table 3. One Pot Synthesis of Sulfides from Aldehydes

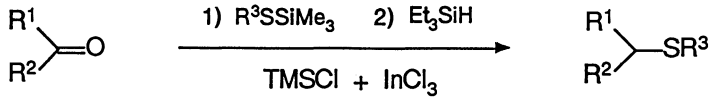

Entry	R^1	R^2	R^3	Temp/°C	Product	Yield/%
1	Ph	H	Et	−23→R.T.	**8**	87
2	Ph	H	^{i}Pr	0→R.T.	**9**	83
3	Ph	H	Ph	0→R.T.	**10**	82
4	$Ph(CH_2)_2$	H	Et	0→R.T.	**11**	81
5	$CH_3(CH_2)_7$	H	Et	R.T.	**12**	78
6	Ph	Me	Et	−78→R.T.	**13**	98
7	$-(CH_2)_5-$		Et	0→R.T.	**14**	93

the undesirable disproportionation of *O*-trimethylsilyl monothioacetal is restricted and effective activation of this mixed acetal in the reaction with Et_3SiH is realized by employing the novel catalyst system under extremely mild reaction conditions.

One-Pot Snythesis of Sulfides from Aldehydes. *O*-trimethylsilyl monothioacetals used in the first section are prepared by the reaction of aldehydes with trimethylsilyl alkyl(aryl) sulfide in the presence of a catalytic amount of TMSOTf or ZnI_2 and imidazole.[2] If this reaction is catalyzed by TMSCl–$InCl_3$, one pot synthesis of sulfides will be successfully achieved; namely aldehydes react with trimethylsilyl alkyl(aryl) sulfide under the influence of TMSCl and $InCl_3$ to generate *O*-trimethylsilyl monothioacetals in situ, which are readily reduced by Et_3SiH to afford the corresponding sulfides.

According to this hypothesis, benzaldehyde was successively treated with trimethylsilyl alkyl(aryl) sulfide and Et_3SiH in the presence of a catalytic amount of TMSCl–$InCl_3$. The reaction smoothly proceeded to give the corresponding sulfide in 87% yield. Similarly, other aldehydes and ketones can be converted to the corresponding sulfides in high yields according to the present procedure (Table 3). It is noteworthy that the yields of the sulfides by this one pot synthesis consisting of two successive reactions are improved in most cases compared with those of the reaction of *O*-trimethylsilyl monothioacetals with Et_3SiH.

Though several methods for the preparation of sulfides have been reported, one pot synthesis from aldehydes is rare.[8] The present reaction provides a convenient route to sulfides from aldehydes under extremely mild reaction conditions. Current work to develop other useful synthetic reactions employing this novel catalyst system is now in progress.

Experimental

IR spectra were recorded on Horiba FT-300 infrared spectrometer. ^1H NMR spectra were recorded on a Hitachi R-1100, R-1200, or JEOL JNR-EX270L spectrometer, and tetramethylsilane (TMS) served as internal standard. Column chromatography was performed on Silica gel 60 (Merck) or Wakogel B5F. All reactions were carried out under argon atmosphere in dried glassware.

Indium(III) chloride ($InCl_3$) was purchased from Soekawa Rika Co., Ltd., and was used without further purification. Trimethylsilyl chloride (TMSCl) was distilled before use and was stored as 0.25 M (1 M=1 mol dm^{-3}) dichloromethane solution.

O-trimethylsilyl monothioacetals **1**—**3** and **7** were prepared from the corresponding aldehydes according to the literature.[2] Similarly, other *O*-trimethylsilyl monothioacetals **4** and **5** were synthesized. In the synthesis of **6**, zinc(II) iodide (ZnI_2) was used instead of trimethylsilyl trifluoromethanesulfonate (TMSOTf).

1-Ethylthio-1-trimethylsiloxy-3-phenylpropane (4). Bp 86—89 °C (0.2 mmHg, 1 mmHg=133.322 Pa); IR (neat) 1100, 840 cm^{-1}; ^1H NMR (CCl_4) δ=0.13 (s, 9H), 1.24 (t, 3H, J=7.2 Hz), 1.82—2.25 (m, 2H), 2.29—2.89 (m,4H), 4.73 (t, 1H, J=6.0 Hz), 7.13—7.33 (m, 5H). Found: C, 62.42; H, 9.11; S, 11.67%. Calcd for $C_{14}H_{24}OSSi$: C, 62.63; H, 9.01; S, 11.94%.

1-Ethylthio-1-trimethylsiloxynonane (5). Bp 76—77 °C (0.15 mmHg); IR (neat) 2960, 1250, 1090, 870 cm^{-1}; ^1H NMR (CCl_4) δ=0.14 (s, 9H), 0.84—1.94 (m, 20H), 2.54 (q, 2H, J=6.0 Hz), 4.67 (t, 1H, J=6.0 Hz). Found: C, 60.50; H, 11.93; S, 11.38%. Calcd for $C_{14}H_{32}OSSi$: C, 60.80; H, 11.66; S, 11.59%.

1-Ethylthio-1-phenyl-1-trimethylsiloxyethane (6). Bp 73—75 °C (0.50 mmHg); IR (neat) 1140, 850 cm^{-1}; ^1H NMR (CCl_4) δ=0.25 (s, 9H), 0.99 (t, 3H, J=6.6 Hz), 1.84 (s, 3H), 2.16 (t, 2H, J=6.6 Hz), 6.80—7.30 (m, 5H). Found: C, 61.21; H, 8.88; S, 12.02%. Calcd for $C_{13}H_{22}OSSi$: C, 61.36; H, 8.71; S, 12.60%.

A Typical Procedure for the Synthesis of Sulfides from *O*-Trimethylsilyl monothioacetal. A typical procedure is described for the reaction of 1-ethylthio-1-phenyl-1-trimethylsiloxyethane (**2**) with Et_3SiH; to a suspension of $InCl_3$ (0.056 mmol) in dichloromethane (1 ml) was added 0.25 M (1 M=1 mol dm^{-3}) dichloromethane solution of TMSCl (0. 14 mmol), and the reaction mixture was stirred for 30 min at room temperature. Then **2** (0.28 mmol) in dichloromethane (1 ml) and triethylsilane (0.34 mmol) in dichloromethane (1 ml) was successively added and the reaction mixture was further stirred for 5 h at room temperature. Then aqueous sodium hydrogen carbonate was added at 0 °C and the aqueous layer was extracted with dichloromethane. The organic layer was washed with brine and dried over $MgSO_4$. After the removal of the solvents under reduced pressure, benzyl ethyl sulfide (**8**)[4] was isolated by thin layer chromatography on silica gel (83% yield). IR (neat) 2950, 1450, 700 cm^{-1}; ^1H NMR

($CDCl_3$) δ=1.22 (t, 3H, J=7.3 Hz), 2.43 (q, 2H, J=7.3 Hz), 3.71 (s, 2H), 7.21—7.38 (m, 5H).

A Typical Procedure of the One Pot Synthesis of Sulfides from Aldehydes. A typical procedure is described for the one pot synthesis of benzyl ethyl sulfide (**8**) from benzaldehyde; to a suspension of $InCl_3$ (0.071 mmol) in dichloromethane was added 0.25 M dichloromethane solution of TMSCl (0.17 mmol) and the reaction mixture was stirred for 30 min at room temperature. The reaction mixture was cooled down to −23 °C, and benzaldehyde (0.35 mmol) in dichloromethane (1 ml), ethylthiotrimethylsilane (**18**, 0.42 mmol) in dichloromethane (1 ml) and Et_3SiH (0.42 mmol) in dichloromethane (1 ml) were successively added. The mixture was further stirred for 5 h at room temperature, then aqueous sodium hydrogen carbonate was added at 0 °C and the aqueous layer was extracted with dichloromethane. The organic layer was washed with brine and dried over $MgSO_4$. After the removal of the solvents under reduced pressure, benzyl ethyl sulfide (**8**) was isolated by thin layer chromatography on silica gel (87% yield).

Other spectral data are presented below.

Benzyl 2-Propyl Sulfide (9). IR (neat) 2950, 1450, 700 cm^{-1}; ^1H NMR ($CDCl_3$) δ=1.25 (d, 6H, J=6.6 Hz), 2.72—2.84 (m, 1H), 3.74 (s, 2H), 7.19—7.34 (m, 5H). Found: C, 72.23; H, 8.65; S, 19.43%. Calcd for $C_{10}H_{14}S$: C, 72.23; H, 8.49; S, 19.28%.

Benzyl Phenyl Sulfide (10).[8] IR (neat) 1450, 700 cm^{-1}; ^1H NMR ($CDCl_3$) δ=4.10 (s, 2H), 7.15—6.31 (m, 10H).

Ethyl 3-Phenylpropyl Sulfide (11). IR (neat) 2900, 1450, 700 cm^{-1}; ^1H NMR ($CDCl_3$) δ=1.24 (t, 3H, J=7.3 Hz), 1.85—1.96 (m, 2H), 2.49—2.57 (m, 4H), 2.72 (t, 2H, J=7.7 Hz), 7.15—7.31 (m, 5H). Found: C, 72.80; H, 8.92; S, 17.70%. Calcd for $C_{11}H_{16}S$: C, 73.27; H, 8.94; S, 17.78%.

Ethyl Nonyl Sulfide (12). IR (neat) 2920 cm^{-1}; ^1H NMR (CCl_4) δ=0.70—1.82 (m, 20H), 2.14—2.65 (m, 4H). Found: C, 70.19; H, 13.01; S, 16.75%. Calcd for $C_{11}H_{24}S$: C, 70.14; H, 12.84; S, 17.02%.

Ethyl 1-Phenylethyl Sulfide (13).[9] IR (neat) 2970, 700 cm^{-1}; ^1H NMR (CCl_4) δ=1.10 (t, 3H, J=7.2 Hz), 1.48 (d, 3H, J=7.8 Hz), 2.22 (q, 2H, J=8.4 Hz), 3.86 (q, 1H, J=8.4 Hz), 7.00—7.35 (m, 5H).

Ethyl Cyclohexyl Sulfide (14).[4] IR (neat) 2930 cm^{-1}; ^1H NMR (CCl_4) δ=1.03—2.13 (m, 13H), 2.25—2.80 (m, 3H).

The present research is partially supported by Grant-in Aids for Scientific Research on Priority Areas (Multiplex Organic Systems) from Ministry of Education, Science and Culture.

References

1) T. Mukaiyama and M. Murakami, *Synthesis,* **1987**, 1043; T. Mukaiyama, K. Wariishi, M. Furuya, and S. Kobayashi, *Chem. Lett.,* **1989**, 1277.

2) M. B. Sassaman, G. K. S. Prakash, and G. A. Olah, *Synthesis,* **1990**, 104, and references cited therein.

3) T. Mukaiyama, T. Ohno, T. Nishimura, J. S. Han, and S. Kobayashi, *Chem. Lett.,* **1990**, 2239.

4) M. B. Sassaman, G. K. S. Prakash, and G. A. Olah, *Tetrahedron,* **44**, 3771 (1988).

5) N. Iwasawa and T. Mukaiyama, *Chem. Lett.,* **1987**, 463; T. Mukaiyama, K. Wariishi, Y. Saito, M. Hayashi, and S. Kobayashi, *Chem. Lett.,* **1988**, 1101.

6) T. Mukaiyama, S. Kobayashi, M. Tamura, and Y. Sagawa, *Chem. Lett.,* **1987**, 491; T. Mukaiyama, H. Sugumi, H. Uchiro, and S. Kobayashi, *Chem. Lett.,* **1988**, 1291.

7) Trityl salts are efficient activators of dithioacetals. M. Ohshima, M. Murakami, and T. Mukaiyama, *Chem. Lett.,* **1985**, 1871; **1986**, 1593.

8) R. S. Glass reported conversion of aldehydes into sulfides using a trimethyisilyl alkyl sulfide and "mixed hydride" (lithium aluminum hydride and aluminum chloride in 1 : 3.3—4.0 molar ratio). R. S. Glass, *Synth. Commun.,* **6**, 47 (1976).

9) T. Mukaiyama, T. Izawa, K. Saigo, and H. Takei, *Chem. Lett.,* **1973**, 355.

Mono-, Di-, and Tri-C-Deuteration of 1,5-Anhydro-D-glucitol

Masuo FUNABASHI* and Toshimori HASEGAWA
Chemistry Department, College of Arts and Sciences, Chiba University, Yayoi-cho, Chiba 260
(Received April 23, 1991)

Deuterium was effectively introduced into the title sugar (**1a**) at C-1, C-3, C-5, and C-6 to afford 1,5-anhydro-D-[1-$^2H_1$], -[3-^2H], -[5-^2H], -[1-$^2H_2$], -[6-$^2H_2$], and -[5,6-$^2H_3$]glucitols respectively as primary targets for a basic study of the unknown metabolism of **1a**, which had been suggested to be a candidate of metabolic indexes for insulin-dependent diabetes mellitus.

1,5-Anhydro-D-glucitol (polygalitol: **1a**) which had been known as a component of some plants such as *polygala amara,*[1] *polygala vulgaris,*[2] and *polygala tenuifolia*[3] has been first identified in human cerebrospinal fluid from diabetic uremic patients by pitkänen,[4] and confirmed later by Smith et al.[5]

Yoshioka and his co-workers,[6] on the other hand, have also confirmed the presence of a considerable amount of the sugar alcohol (average: 2.5 mg dl^{-1}) in human plasma from healthy persons of various ages and they observed a gradual recovery of **1a** in the plasma of diabetic patients receiving insulin regularly during several months, in contrast with the fact that the content of **1a** in the plasma from diabetic patients receiving no insulin remained negligibly small.

Though both physiological and metabolic meaning of this minor sugar is still uncertain, some studies concerning feeding suppression in rats,[7] transport inhibition in hamster[8] or inhibitory effects to enzymes such as hexokinase[9] and α-glucosidase[10] have been reported so far.

These phenomena prompted us to prepare both hot and cold labeled derivatives of **1a** in order to elucidate the unknown metabolism of the sugar alcohol.

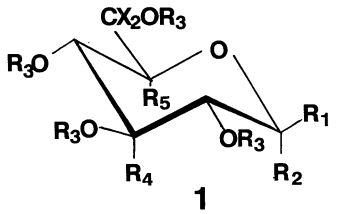

1

a) R_1=R_2=R_3=R_4=R_5=X=H
b) R_1=$OCOCH_3$, R_2=D, R_3=$COCH_3$, R_4=R_5=X=H
c) R_1=D, R_2=OH, R_3=Bn, R_4=R_5=X=H
d) R_1=H, R_2=D, R_3=Bn, R_4=R_5=X=H
e) R_1=H, R_2=D, R_3=$COCH_3$, R_4=R_5=X=H
f) R_1=R_2=R_5=X=H, R_4=D, R_3=$COCH_3$
g) R_1=R_2=R_4=X=H, R_3=$COCH_3$, R_5=D
h) R_1=R_2=D, R_3=Bn, R_4=R_5=X=H
i) R_1=R_2=D, R_3=$COCH_3$, R_4=R_5=X=H
j) R_1=R_3=R_4=R_5=X=H, R_2=D
k) R_1=R_2=R_3=R_5=X=H, R_4=D
l) R_1=R_2=R_3=R_4=X=H, R_5=D
m) R_1=R_2=D, R_3=R_4=R_5=X=H
n) R_1=R_2=R_3=R_4=R_5=H, X=D
o) R_1=R_2=R_4=R_5=H, R_3=$COCH_3$, X=D
p) R_1=R_2=R_4=H, R_3=$COCH_3$, R_5=X=D
q) R_1=R_2=R_3=R_4=H, R_5=X=D

In a previous communication,[11a] we briefly reported a synthesis of 1,5-anhydro-D-[1-$^2H_1$]glucitol (**1j**) and 1,5-anhydro-D-[1-$^2H_2$]glucitol (**1m**) as preliminary targets.

The present paper comprehensively describes mono-, di-, and tri-C-deuteration of **1a** in detail.

Results and Discussion

For the synthesis of **1a**, there are several useful methods such as direct reduction of 2,3,4,6-tetra-*O*-acetyl-α-D-glucopyranosyl bromide with lithium aluminum hydride,[12] palladium on carbon[13] or tributylstannane,[14] and reductive desulfurization[15] of phenyl 2,3,4,6-tetra-*O*-acetyl-1-thio-β-D-glucopyranoside with Raney-nickel.

From the standpoint of stereospecificity and work-up, the direct reduction of protected glucosyl halides with lithium aluminum hydride (LAH) or lithium aluminum deuteride (LAD) is our main choice and the respective syntheses are described as follows.

(1) Mono-C-deuteration

(a) (1*R*)-1,5-Anhydro-D-[1-$^2H_1$]glucitol (1j). Two different routes were achieved for the synthesis of **1j**. First, we chose, as a starting material, 1,2,3,4,6-penta-*O*-acetyl-β-D-[1-^{2}H]glucopyranose[11] (**1b**) obtained in two steps from D-gluco-1,5-lactone. The pentaacetate (**1b**) was then converted into 2,3,4,6-tetra-*O*-acetyl-α-D-[1-^{2}H]glucopyranosyl bromide, which was directly treated with excess amount of LAH to afford the desired product (**1j**) having 1*R* configuration. ^{1}H NMR of the acetate (**1e**) showed the disappearence of H_1 axial proton at δ=3.00 and the presence of H_1 equatorial proton at δ=4.15 having $J_{1,2}$=5.6 Hz. ^{13}C NMR of **1e** also revealed the signal of C_1 at δ=66.86 was missing.

Comparison of mass spectra of **1e** with that of the peracetate of **1a** clearly demonstrated the shift of one mass unit in several peaks [97 to 98, 170 to 171, 212 to 213, 273 to 274, and 333 (M^++1) to 334 (M^++1)].

Secondly, we chose 2,3,4,6-tetra-*O*-benzyl-α-D-[1-^{2}H]glucopyranosyl chloride easily obtained by treating 2,3,4,6-tetra-*O*-benzyl-α-D-[1-^{2}H]glucopyranose (**1c**) with methanesulfonyl chloride, and the resulting glucosyl chloride was reduced with an equimolar amount of LAH in dry ether to yield a syrupy (1*R*)-2,3,4,6-tetra-*O*-

benzyl-1,5-anhydro-D-[1-$^2H_1$]glucitol (**1d**) in a 58% yield. The benzyl groups of **1d** were then removed conventionally in the presence of Pd/C (10%) in acetic acid to afford the compound **1j** described above.

The second route requires multi-step reactions, and was less satisfactory as for a scale-up of preparation.

(b) 1,5-Anhydro-D-[3-^{2}H]glucitol (1k). 1,2,3,4,6-Penta-*O*-acetyl-β-D-[3-^{2}H]glucopyranose was first prepared by the reported method[16] in four steps from 1,2;5,6-di-*O*-isopropylidene-α-D-[3-^{2}H]allofuranose,[17] and next converted to the corresponding glucopyranosyl bromide, which was successively reduced with LAH in the same manner described above to give the desired compound **1k** in a total yield of 7% from D-glucose. ^{13}C NMR spectrum of the tetraacetate (**1f**) disclosed complete disappearence of C-2 signal observed at δ=73.79 in the corresponding light compound. Mass spectrum of **1f** also indicated the presence of m/z 334 (M^++1).

(c) 1,5-Anhydro-D-[5-^{2}H]glucitol (1l). 1,2,3,4,6-Penta-*O*-acetyl-β-D-[5-^{2}H]glucopyranose prepared stepwise by the known method[18] from 3-*O*-benzyl-1,2-*O*-isopropylidene-6-*O*-trityl-α-D-xylofurano-5-ulose, was first transformed into the corresponding bromide, which was then similarly treated with LAH to afford the compound (**1l**) in an overall yield of 35% from the 5-ulose. ^{13}C NMR spectrum of the tetraacetate (**1g**) showed the absence of C-5 signal at δ=76.47, and the mass spectrum also indicated the presence of m/z 334 (M^++1) peak.

(2) Di-C-deuteration

(a) 1,5-Anhydro-D-[1-$^2H_2$]glucitol (1m). Direct reduction of 2,3,4,6-tetra-*O*-benzyl-α-D-[1-^{2}H]glucopyranosyl chloride described in the case of **1c** was effected with LAD in dry ether to afford the corrresponding 2,3,4,6-tetra-*O*-benzyl-1,5-anhydro-D-[1-$^1H_2$]glucitol (**1h**) in 63% yield. Removal of benzyl groups in **1h** by means of hydrogenolysis in the presence of Pd/C (10%) gave **1m** as crystals, which was then converted to 2,3,4,6-tetra-*O*-acetyl-1,5-anhydro-D-[1-$^2H_2$]glucitol (**1i**). Double introduction of deuterium into C-1 of was unambiguously confirmed by ^{1}H NMR spectrum of **1i**, in which both H_1 axial proton at δ=3.30 and H_1 equatorial proton at δ=4.15 completely disappeared. ^{13}C NMR spectrum of **1i** disclosed the absence of C-1 signal at δ=66.86, coinciding with the result of ^{1}H NMR.

The presence of m/z 335 (M^++1) peak in the mass spectrum of **1i** clearly indicates two mass unit increase in comparison with that of the light compound.

An alternative route to **1m** was similarly achieved by reducing 2,3,4,6-tetra-*O*-acetyl-α-D-[1-^{1}H]glucopyranosyl bromide with LAD in dry ether. In terms of economy of LAD, which was excessively required in the latter case, the former seems to be better, but the latter is superior from the standpoint of short reaction steps and convenience.

(b) 1,5-Anhydro-D-[6-$^2H_2$]glucitol (1n). 1,2,3,4,6-Penta-*O*-acetyl-β-D-[6-$^2H_2$]glucopyranose,[18] prepared in three steps [(i) reduction with LAD, (ii) hydrolysis with 80% acetic acid, and (iii) acetylation with acetic anhydride/sodium acetate] from 1,2-*O*-isopropylidene-α-D-glucofuranurono-6,3-lactone, was brominated and successively reduced with LAH to afford the desired product (**1n**) in a total yield of 32%. ^{1}H and ^{13}C NMR spectra of the acetate (**1o**) showed the disappearence of H-6 multiplet at δ=4.17 and C-6 signal at δ=62.22 respectively. The octet of H-5 signal at δ=3.59 was definitely changed to doublet ($J_{4,5}$=9.9 Hz). The presence of m/z 335 (M^++1) peak in the mass spectrum of **1o** also supported the double deuteration of **1a**.

(3) Tri-C-deuteration

1,5-Anhydro-D-[5,6-$^2H_3$]glucitol (1q). 1,2-*O*-isopropylidene-α-D-[5,6-$^2H_3$]glucofuranose, obtained by stereoselective reduction[19] of 1,2-*O*-isopropylidene-α-D-xylohexofuranurono-6,3-lactone with sodium borodeuteride, was similarly converted to 2,3,4,6-tetra-*O*-acetyl-α-D-[5,6-$^2H_3$]glucopyranosyl bromide, and the bromide was immediately reduced with LAH to afford the desired compound (**1q**) in a total yield of 19% from the starting lactone. ^{13}C NMR spectrum of the peracetate (**1p**) disclosed both signals at δ=62.22 (C-6) and 76.47 (C-5) were completely disappeared, and the presence of m/z 336 (M^++1) peak in the mass spectrum of **1p** also supported the triple deuteration.

Experimental

Melting points were determined on a YAZAWA micro hotstage and were uncorrected. Solvents were evaporated off in vacuo below 40 °C. Optical rotations were measured with a JASCO DIP-140 digital polarimeter. ^{1}H and ^{13}C NMR spectra were recorded on a JEOL GX-100 spectrometer in $CDCl_3$ using TMS as internal standard. Mass spectra measured with a Hitachi M-60 mass spectrometer connected with Hitachi data processing system M-003. TLC were carried out on Merck plates (silica gel 60, 0.25 mm). Column chromatography was performed on Wakogel C-200 or C-300.

1,2,3,4,6-Penta-*O*-acetyl-β-D-[1-^{2}H]glucopyranose (1b): To a cooled solution (0 °C) of D-glucono-1,5-lactone (10 g, 0.56 mmol) in a buffer solution (130 ml) of sodium acetate–acetic acid (pH 5.7) was gradually added sodium borodeuteride (Merck 98%, 1 g, 24 mmol) for 10 min and keeping pH at below 6.0 (dropwise addition of acetic acid). The reaction solution was then treated with IR-120 (H^+) and the resin was filtered off. The filtrate was concentrated in vacuo with aid of methanol and ethanol repeatedly. The resulting amorphous residue was dried, and acetylated with acetic anhydride (100 ml) and sodium acetate (5 g). The reaction mixture was then poured into ice-water, and the precipitate was filtered, and recrystallized from ethanol, giving 9.9 g (45%). mp 131—132 °C (lit,[20] 132 °C). ^{1}H NMR: no peak due to H-1 at δ=5.73. Anal. ($C_{16}H_{22}O_{11}$) C, H.

2,3,4,6-Tetra-*O*-benzyl-α-D-[1-^{2}H]glucopyranose (1c): A solution of 2,3,4,6-tetra-*O*-benzyl-D-glucono-1,5-lactone[21] (540 mg, 1 mmol) in dry ether (40 ml) and boron trifluoride

etherate (7.5 ml) was gradually added to a suspension of lithium aluminum deuteride (Merck 98%; 490 mg, 12 mmol) in dry ether (40 ml) under ice-cooling. The reaction mixture was then heated to reflux for 2 h and cooled. Dilute hydrochloric acid (2 M, 5 ml) was carefully added to the mixture, and the precipitate was filtered off. The filtrate was washed with aqueous $NaHCO_3$ and brine. The ethereal layer was dried ($MgSO_4$), concentrated to a crystalline mass, which was recrystallized from ethanol giving 0.49 g (90%); mp 150—151 °C, $[\alpha]_D^{12}$ +14.0° (*c* 1.0, $CHCl_3$); MS (70 eV) *m/z* (rel intensity) 432 (M^+−109; 0.60), 253 (14), 181(19), 92 (100), 79 (12), 65 (13). Anal. ($C_{34}H_{36}O_6$) C, H.

(1*R*)-2,3,4,6-Tetra-*O*-benzyl-1,5-anhydro-D-[1-$^2H_1$]glucitol (1d): To a solution of **1c** (2.2 g, 4.2 mmol) in CH_2Cl_2 (20 ml) was added *s*-collidine (2 g, 16.5 mmol) and methanesulfonyl chloride (0.96 g, 8.4 mmol), and the reaction mixture was kept overnight at room temperature (16 °C). The solution was successively treated with 1 M HCl, aqueous $NaHCO_3$, and water. The organic layer was dried ($CaCl_2$), and concentrated to a syrup, which was directly treated with lithium aluminum hydride (0.5 g, 13 mmol) in dry ether (50 ml). Excess of LAH was then decomposed with ethyl acetate and water, and the precipitate was filtered off. The ethereal layer was concentrated to a pale yellow syrup, which was chromatographed on a silica gel (C-200) with benzene–ethyl acetate (10/1). Evaporation of the eluates gave a pure syrup (1.23 g, 58%), having $[\alpha]_D^{14}$ +7.5° (*c* 0.42, $CHCl_3$); ^1H NMR ($CDCl_3$) δ=7.2—7.4 (20H, aromatic), 4.46—5.00 (8H, m, CH_2Ph), 4.04 (1H, H-1, d, $J_{1,2}$=4.6 Hz), 3.37 (1H, m, H-5). No peak due to H-1 axial (δ=3.21). Anal. ($C_{34}H_{36}O_5$) C, H.

(1*R*)-1,5-Anhydro-D-[1-^{2}H]glucitol (1j): (a) 2,3,4,6-tetra-*O*-acetyl-α-D-[1-^{2}H]glucopyranosyl bromide (1.8 g), prepared by reacting **1b** (2.1 g) with 10 ml of a chilled solution of 25% HBr in acetic acid, was dissolved in dry ether (20 ml). This ethereal solution was gradually added to a stirred suspension of lithium aluminum hydride (1 g) in dry ether (30 ml) with keeping gentle reflux. Excess hydride was then decomposed with ethyl acetate and water. The precipitate was filtered and washed twice with water. The aqueous layer was then deionized with IR-l20 (H^+) and IR-45 (OH^-), and concentrated in vacuo in the presence of benzene and ethanol to a thick syrup, which gradually solidified. Recrystallization from methanol gave crystals (0.42 g, 58%); mp 143—144 °C, $[\alpha]_D^{9}$ +43.2° (*c* 0.74, H_2O) [lit,[12] nondeuterated: Mp 142—143 °C, $[\alpha]_D$ +42.3° (*c* 0.84, H_2O)]. Anal. ($C_6H_{12}O_5$) C, H.

(b) A mixture of **1d** (1.57 g) and palladium on carbon (10%, 1.5 g) in acetic acid (25 ml) was shaken at room temperature with hydrogen until absorption ceased. The catalyst was filtered and washed with water. The combined and washings were concentrated in vacuo to a syrup, which was dried in the presence of ethanol and benzene azeotropically. The solidified mass was recrystallized from methanol to give 0.25 g (52%) of crystals; mp 142—143 °C, $[\alpha]_D^{12}$ +43.0° (*c* 0.5, H_2O).

(1*R*)-2,3,4,6-Tetra-*O*-acetyl-1,5-anhydro-D-[1-$^2H_1$]glucitol (1e): A solution of **1j** (0.50 g) dissolved in acetic anhydride (6 ml) and pyridine (6 ml) was kept overnight at room temperature, and poured into ice-water containing $NaHCO_3$.

The resulting mixture was then extracted with $CHCl_3$ (30 ml), and the $CHCl_3$ layer was washed with aqueous $NaHCO_3$ and water, dried ($MgSO_4$), and concentrated to a syrupy residue, which was chromatographed on a silica gel (Wako gel C-300) with benzene–ethyl acetate (5/1) to give a crystalline mass; mp 71—72 °C, $[\alpha]_D^{12}$ +42.0° (*c* 0.87, $CHCl_3$); ^1H NMR ($CDCl_3$) δ=2.028 (9H, s, $COCH_3$), 2.034 (3H, s, $COCH_3$), 3.60 (1H, m, H-5), 4.14 (1H, dd, H-6, $J_{5,6}$=2.3, $J_{6,6}$=12.2 Hz), 4.15 (1H, d, H-1 equatorial, $J_{1,2}$=5.6 Hz), 4.19 (1H, dd, H-6′ *J*=4.6 Hz), 5.01 (1H, dd, H-2, $J_{2,3}$=9.5 Hz), 5.03 (1H, t, H-4, $J_{3,4}=J_{4,5}$=9.5 Hz), 5.20 (1H, t, H-3). Anal. ($C_{14}H_{20}O_9$) C, H.

1,5-Anhydro-D-[3-^{2}H]glucitol (1k): 1,2,3,4,6-Penta-*O*-acetyl-β-D-[3-^{2}H]glucopyranose (1.5 g), obtained by acetylation of D-[3-^{2}H]glucopyranose[16] with acetic anhydride–sodium acetate, was treated with 10 ml of 25% solution of HBr in acetic acid, and the resulting bromide was reduced with lithium aluminum hydride (0.80 g) as menthioned above. After the same work-up, the compound **1k** was obtained as crystals (0.32 g); mp 142—143 °C, $[\alpha]_D^{12}$ +42.5° (*c* 0.65, H_2O).

2,3,4,6-Tetra-*O*-acetyl-1,5-anhydro-D-[3-^{2}H]glucitol (1f): The compound **1k** (0.21 g) was acetylated in the same manner as **1j** and chromatographed on silica gel to give a solid mass (0.26 g); mp 71—73 °C, $[\alpha]_D^{12}$ +42.0° (*c* 0.52, $CHCl_3$); ^{13}C NMR ($CDCl_3$) δ=20.59—20.71 ($\underline{C}H_3$×4), 62.24 (t, C-6), 66.85 (t, C-1), 68.39 (d, C-4), 68.91 (d, C-2), 76.47 (d, C-5), 169.49—170.62 ($\underline{C}O$×4).

1,5-Anhydro-D-[5-^{2}H]glucitol (1l): 1,2,3,4,6-Penta-*O*-acetyl-β-D-[5-^{2}H]glucopyranose (1.2 g), prepared from D-[5-^{2}H]-glucopyranose,[19] was treated with 25% solution (10 ml) of HBr in acetic acid, and the resulting bromide was reduced with lithium aluminum hydride (0.6 g) to give crystals after the same work-up; yield 0.24 g, mp 142—143 °C, $[\alpha]_D^{12}$ +42.7° (*c* 0.51, H_2O).

2,3,4,6-Tetra-*O*-acetyl-1,5-anhydro-D-[5-^{2}H]glucitol (1g): The compound (0.20 g) was acetylated and chromatographed in the same conditions as **1e** to give a crystalline mass (0.24 g); mp 72—73 °C (ether–petroleum ether), $[\alpha]_D^{13}$ +42.5° (*c* 0.50, $CHCl_3$); ^1H NMR δ=2.028 (9H, s, $COCH_3$), 2.034 (3H, s, $COCH_3$), 3.30 (1H, t, H-1 axial, $J_{1,2}=J_{1,1}$=10.6 Hz), 4.13 (1H, d, H-6, $J_{2,6'}$=12.2 Hz), 4.14 (1H, dd, H-1 equatorial, $J_{1,2}$=5.6 Hz), 4.20 (1H, d, H-6′), 5.01 (1H, m, H-2), 5.03 (1H, d, H-4, $J_{3,4}$=9.5 Hz), 5.20 (1H, t, H-3, $J_{2,3}=J_{3,4}$).

2,3,4,6-Tetra-*O*-benzyl-1,5-anhydro-D-[1-$^2H_2$]glucitol (1h): 2,3,4,6-Tetra-*O*-benzyl-α-D-[1-^{2}H]glucopyranosyl chloride (2.0 g), described in the preparation of **1d**, was reduced with lithium aluminum deuteride (0.6 g) in dry ether. The excess of LAD was then decomposed in the same manner as **1c** to give a crude syrup, which was chromatographed on silica gel (Wako gel C-300). Evaporation of the corresponding fractions gave a clear syrup (1.18 g, 63%); $[\alpha]_D^{15}$ +7.0 (*c* 0.50, $CHCl_3$); ^1H NMR ($CDCl_3$) δ=3.38 (1H, m, H-5), 3.55—3.67 (5H, m, H-2, H-3, H-4, H-6 and H-6′), 4.47—4.99 (8H, m, $\underline{C}H_2Ph$), 7.2—7.4 (20H, aromatics).

1,5-Anhydro-D-[1-$^2H_2$]glucitol (1m): (a) Hydrogenolysis of **1h** (2.1 g) was carried out in the same manner as described in **1d** to give a crystalline residue (0.40 g, 60%), which was recrystallized from methanol; mp 143—144 °C, $[\alpha]_D^{13}$ +43.0° (c 1.0, H_2O).

(b) Lithium aluminum deuteride reduction of 2,3,4,6-tetra-*O*-acetyl-α-D-[1-^{2}H]glucopyranosyl bromide (2.1 g, see experiment **1j**) gave the compound **1m** (0.48 g, 57%).

2,3,4,6-Tetra-*O*-acetyl-1,5-anhydro-D-[1-$^2H_2$]glucitol (1i): Acetylation of **1m** (0.30 g) followed by chromatography and recrystallization described in the preparation of **1e** gave a crystalline compound **1i** (0.45 g) having mp 72—73 °C and $[\alpha]_D^{13}$ +43.0° (*c* 0.50, $CHCl_3$); ^{13}C NMR δ=20.59—20.71 ($\underline{C}H_3CO$), 62.22 (t, C-6), 68.47 (d, C-4), 68.99 (d, C-2), 73.74 (d, C-3), 76.47 (d, C-5), 169.5—170.6 ($\underline{C}OCH_3$).

1,5-Anhydro-D-[6-$^2H_2$]glucitol (1n): 1,2,3,4,6-Penta-*O*-acetyl-

β-D-[6-$^2H_2$]glucopyranose[18] (1.0 g) was converted to the corresponding bromide (see experiment **1j**), which was then reduced with LAH (0.30 g) to give crystals (0.72 g); mp 142—143 °C, $[\alpha]_D^{13}$ +42.8° (*c* 1.0, H_2O).

2,3,4,6-Tetra-*O*-acetyl-1,5-anhydro-D-[6-$^2H_2$]glucitol (1o): The compound **1n** (0.20 g) was acetylated and chromatographed in the same conditions as **1e** to give a clear syrup (0.26 g), which gradually crystallized; mp 71—73 °C, $[\alpha]_D^{13}$ +42.0° (*c* 0.52, $CHCl_3$); ^{13}C NMR δ=20.60—20.71 ($\underline{C}H_3CO$), 66.88 (t, C-1), 68.47 (d, C-4), 68.98 (d, C-2), 73.74 (d, C-3), 76.38 (d, C-5), 169.5—170.6 ($\underline{C}O\times4$). Anal. ($C_{16}H_{20}O_9$) C, H.

2,3,4,6-Tetra-*O*-acetyl-1,5-anhydro-D-[5,6-$^2H_2$]glucitol (1p): 1,2,3,4,6-Penta-*O*-acetyl-β-D-[5,6-$^2H_3$]glucopyranose[19] (1.56 g) was treated with 30% HBr solution (1.0 ml) in acetic acid, and the resulting bromide was reduced with LAH in the same manner as **1j** to give a syrupy residue, which was then acetylated with acetic anhydride (10 ml)/pyridine (10 ml), and chromatographed on silica gel with benzene–ethyl acetate (5/1). Evaporation of the eluates afforded a clear syrup (1.08 g), which gradually crystallized; mp 72—73 °C, $[\alpha]_D^{13}$ +42.5° (*c* 0.65, $CHCl_3$); ^{13}C NMR ($CDCl_3$) δ=20.59, 20.67 ($\underline{C}H_3CO$), 66.86 (t, C-1), 68.44 (d, C-4), 68.99 (d, C-2), 73.74 (d, C-3), 169.5—170.6 ($\underline{C}O\times4$). Anal. ($C_{14}H_{20}O_9$) C, H.

1,5-Anhydro-D-[5,6-$^2H_3$]glucitol (1q): The tetraacetate **1p** (1.00 g) was deacetylated with sodium methoxide in methanol and deionized with IR-120 (H^+). The aqueous methanol solution was then concentrated in vacuo to a syrupy residue (0.42 g), which was treated with methanol to give crystals (0.26 g); mp 142—143 °C, $[\alpha]_D^{13}$ +43.0° (*c* 0.53, H_2O). Anal. ($C_6H_{12}O_5$) C, H.

The authors are very thankful to the members of Chiba University Analytical Center for the measurements of NMR and Mass spectra as well as for elemental analyses.

References

1) R. Chodat, *Arch. Sci. Phys. Nat.*, **18**, 228 (1887); **19**, 290 (1888); **20**, 599 (1888).
2) P. Picard, *Bull. Soc. Chim. Biol.*, **9**, 692 (1927).
3) J. Shinoda, S. Sato, and D. Sato, *Ber.*, **65**, 1219 (1932).
4) E. Pitkänen, *Clin. Chim. Acta*, **48**, 159 (1973); C. Serbo, J. Palo, and E. Pitkänen, *Acta Neurol. Scand.*, **56**, 111 (1977).
5) S. L. Smith, M. Novotny, and E. L. Weber, *Clin. Chem.*, **24**, 545 (1978).
6) S. Yoshioka, S. Saitoh, T. Fujisawa, A. Fujimori, O. Taketani, and M. Funabashi, *Clin. Chem., (Winston-Salem, N. C.)*, **28**, 1283 (1982); S. Yoshioka, S. Saitoh, C. Negishi, T. Fujisawa, A. Fujimori, O. Taketani, and M. Funabashi, *ibid.*, **29**, 1396 (1983).
7) K. Tsutsui, T. Sakata, Y. Oomura, K. Arase, M. Fukushima, and Y. Hinohara, *Physiol. Behav.*, **31**, 493 (1983).
8) R. K. Crane, *Biochem. Biophys. Acta*, **45**, 477 (1960).
9) R. A. Ferrari, P. Mandelstam, and R. K. Crane, *Arch. Biochem. Biophys.*, **80**, 372 (1959).
10) J. Hartmann-Schreier and P. Schreier, *Food Chem.*, **26**, 201 (1987).
11) a) M. Funabashi and S. Yoshioka, *Chem. Lett.*, **1984**, 677, b) L. A. Berven and S. G. Withers, *Carbohydr. Res.*, **156**, 282 (1986).
12) R. K. Ness, H. G. Fletcher, Jr., and C. S. Hudson, *J. Am. Chem. Soc.*, **72**, 4547 (1950).
13) L. Zervas and C. Zioudrou, *J. Chem. Soc.*, **1956**, 214.
14) J. Auge and S. David, *Carbohydr. Res.*, **59**, 255 (1977); P. Kocienski and C. Plant, *ibid.*, **110**, 330 (1982).
15) N. K. Richtmyer, "Methods in Carbohydrate Chemistry," (1963), Vol. II, p. 194.
16) H. G. Koch and A. S. Perlin, *Carbohydr. Res.*, **15**, 403 (1970).
17) J. Leroux and A. S. Perlin, *Carbohydr. Res.*, **67**, 163 (1978); J. J. Patroni and R. V. Stick, *Aust. J. Chem.*, **32**, 2531 (1979).
18) A. S. Perlin and E. V. Rudloff, *Can. J. Chem.*, **43**, 2071 (1965); R. U. Lemieux and J. D. Stevens, *ibid.*, **44**, 249 (1966); P. A. J. Gorin, *ibid.*, **52**, 458 (1974).
19) W. Mackie and A. S. Perlin, *Can. J. Chem.*, **43**, 2921 (1965).
20) M. L. Wolfrom and A. Thompson, "Methods in Carbohydrate Chemistry," (1963), Vol. II, p. 212.
21) H. Kuzuhara and H. G. Fletcher, Jr., *J. Org. Chem.*, **32**, 2531 (1967).

Gamma Radiolysis of Flavin Mononucleotide and Flavin-Adenine Dinucleotide in Aqueous Solution

Abhijit SAHA, Parikshit Chandra MANDAL, and Sudhindra Nath BHATTACHARYYA*
Nuclear Chemistry Division, Saha Institute of Nuclear Physics, 1/AF, Bidhannagar, Calcutta 700064, India
(Received July 17, 1990)

Flavin-adenine dinucleotide (FAD) and flavin mononucleotide (FMN) were irradiated with ^{60}Co γ-ray and *G*-values for their decomposition under aerated, argon and nitrous oxide saturated conditions at pH 6.5 were determined by spectrophotometric, fluorescence and HPLC measurements. Among the water-borne radicals the hydroxyl radical (OH) was found to be responsible for causing permanent changes in FAD and FMN. The striking similarity between the difference spectra of irradiated FAD and FMN in N_2O saturated conditions shows that the OH radicals attack at the isoalloxazine moiety. A plausible mechanism for the reaction of the OH radicals with the isoalloxazine moiety has been discussed. The rate constant for the reaction of isoalloxazine moiety of FAD with OH radicals was determined to be 4.7×10^9 dm^3 mol^{-1} s^{-1} by competition kinetic studies using glucose as the reference solute. From the kinetic consideration and *G*-values it is evident that ca. 50% of the OH radicals attack at the AMP (adenosine monophosphate) portion of FAD apart from isoalloxazine moiety. The attack at the AMP portion of FAD is supported by the observed phosphate release in the irradiated FAD solution. Effect of Fe^{3+} ion on the radiolysis of FAD and FMN was also studied.

A large number of dehydrogenase enzymes which are very important in biological functions, e.g., electron transport in mitochondria, biosynthesis of pyrimidine bases, etc. contain flavin mononucleotide (FMN) and flavin-adenine dinucleotide (FAD) as their prosthetic groups. When exposed to ionizing radiation these enzymes lose their activity. But actual mechanism of inactivation of these flavoenzymes is yet to be known. To have an insight on the mechanism of radiation inactivation it is therefore necessary to study the chemical changes produced by radiation on free FMN and FAD molecules.

Winstead and Moss[1] have studied the inactivation of FAD by γ-irradiation in dilute aqueous solution both in presence and absence of air. From the spectral changes owing to varying doses absorbed they have suggested that the inactivation is due to attack by the water-borne free radicals derived from water radiolysis ($H_2O\rightsquigarrow H, OH, e_{aq}^-$)[2] at the isoalloxazine moiety of FAD.

In this paper we present our investigation on the role of the OH radicals in the decomposition of FAD and FMN in terms of *G*-values, the rate constant for the reaction of the OH radicals with isoalloxazine moiety of FAD, the possible sites of attack of OH radicals and the effect of iron(III) ion on the radiolysis of FAD and FMN in dilute aqueous solution.

Experimental

Materials. FAD and FMN were purchased from Sigma Chemical Company. Glucose, ferric ammonium sulfate, and other reagents that were used in the investigation were of 'AnalaR' grade. Triply distilled water was used to prepare the solutions. A phosphate buffer (2×10^{-2} mol dm^{-3}) was used for maintaining the pH at 6.5 of FAD and FMN solutions. Acetonitrile was of HPLC grade (Aldrich). Argon and N_2O gases of high purity were used for flushing the solutions. A ^{60}Co γ-source (dose rate=12 or 3.3 Gy min^{-1}) was used for irradiating the solutions. The dose rate was measured by Fricke dosimetry.

Analysis. The loss of flavin chromophore in FAD and FMN on γ-irradiation was estimated spectrophotometrically by measuring the absorbance of their solutions at 450 nm. The spectra of FAD and FMN were measured on a recording spectrophotometer. In the case of absorbance measurements of FAD and FMN in argon or N_2O saturated solutions a stoppered quartz spectrophotometer cell was used. The loss of FMN was also determined by measuring the loss of fluorescence intensity at 530 nm using an excitation wavelength of 450 nm.

The amount of FMN and FAD in irradiated samples was ascertained by separating them from their radiolysed products by HPLC. The HPLC separation was done by using Waters Liquid Chromatograph with an ODS-C_{18} column. A mobile phase of 1×10^{-2} mol dm^{-3} disodium hydrogenphosphate (adjusted to pH 5.5 with dilute H_3PO_4)–acetonitrile (100 : 12) was filtered, degassed, and used at a flow rate of 1.0 mL min^{-1}. The column eluents were monitored by the UV absorption at 450 nm and 210 nm using a variable wavelength detector.

Inorganic phosphate release from FAD after irradiation was measured by the method of Lowry and Lopez.[3]

Iron(II) ion concentration was measured spectrophotometrically by means of 1,10-phenanthroline reagent.[4]

Results

Figure 1a—c illustrates the effect of γ-irradiation on the spectral properties of 2.5×10^{-5} mol dm^{-3} FAD (pH 6.5) in aerated, N_2O saturated and argon saturated solutions. The spectrum after aeration of the irradiated solution has been shown in each case. It is evident that under argon saturated conditions, the absorbance decreased due to irradiation are partially restored by aeration of the irradiated samples. This suggests that some products formed radiolytically are partially oxidized to regenerate the parent molecule. Similar observations have also been obtained in the case of FMN.

Figure 1d shows that the loss of chromophore in FAD is not linear with the increase of the absorbed dose. The initial *G*-values for flavin chromophore loss in FAD have been determined from the initial slope of the

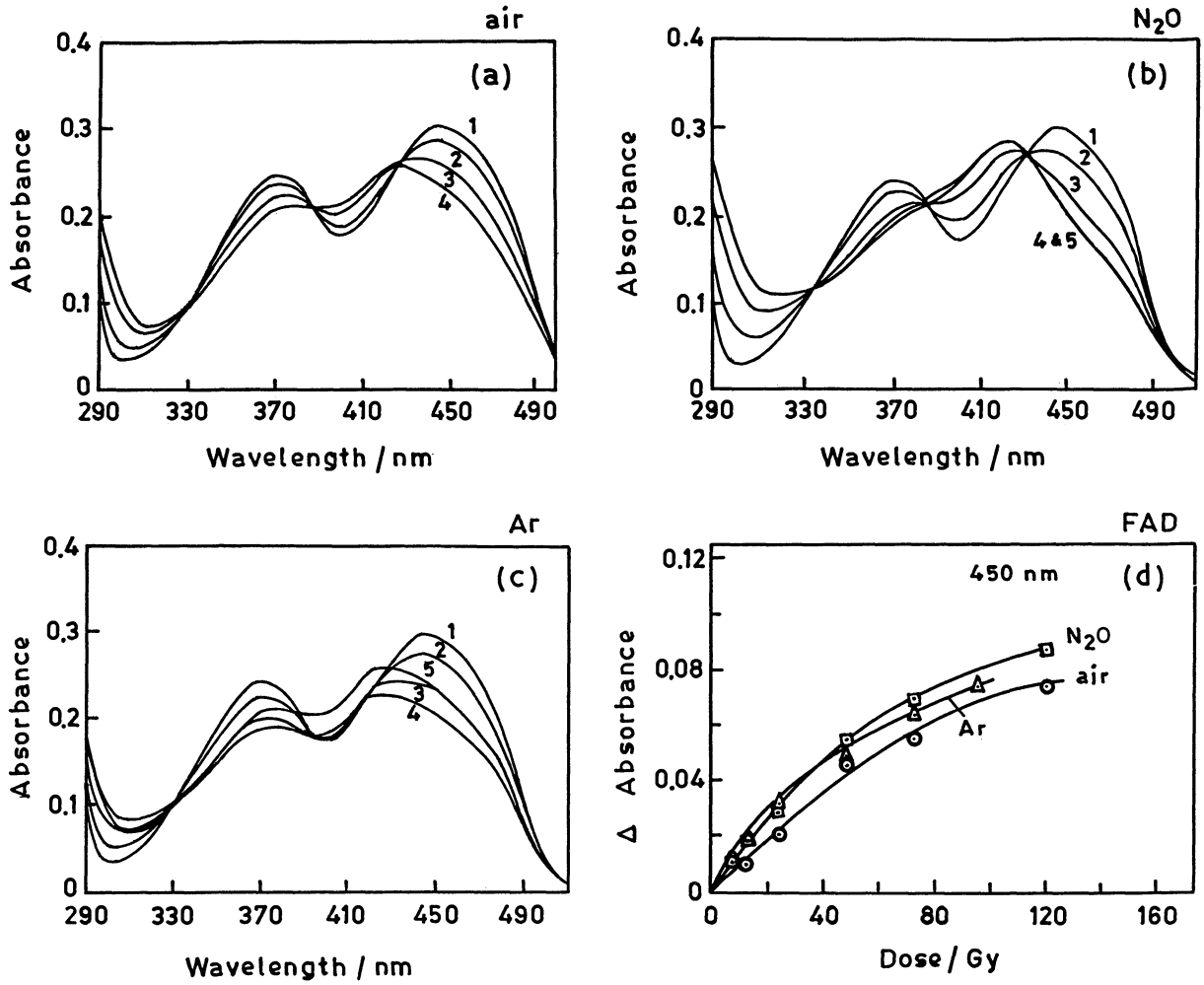

Fig. 1. Absorption spectra of FAD (2.5×10^{-5} mol dm^{-3}) in 2×10^{-2} mol dm^{-3} phosphate buffer irradiated under aerated (a), N_2O-saturated (b), and argon saturated (c), conditions. Absorbed dose: 1: 0.0 Gy; 2: 24 Gy; 3: 72 Gy; 4: 120 Gy 5: spectra obtained after aeration of the FAD solution irradiated with a dose of 120 Gy. (d) Changes of A_{450} for FAD solution with absorbed dose under aerated (⊙), N_2O-saturated (⊡), and argon saturated (△) solutions.

curves. The flavin chromophore loss in FMN was also determined in the same way. The results are presented in Table 1.

The fluorescence spectra of unirradiated and irradiated FMN solutions are shown in Fig. 2. This figure shows that on irradiation the fluorescence intensity decreased but there was no change in spectral shape of irradiated samples from the unirradiated one. The loss in fluorescence intensity was found to be linear with absorbed doses. Hence G(-FMN) values in aerated and N_2O saturated conditions were determined from the slope of the linear plot of loss of fluorescence intensity versus absorbed dose. The G(-FMN) values determined from such fluorescence measurements are in good agreement with those determined from HPLC analysis (Table 1) and from absorbance measurements. Therefore it would appear that the spectrophotometric determination of G-values from the disappearance of FMN absorbance is relatively free from significant error. In the case of FAD, although the spectral shape of the fluorescence remained same, there was increase in the fluorescence intensity at 530 nm after gamma irradiation of low doses. Hence the loss of flavin moiety in FAD on irradiation could not be determined fluorometrically. Further, the loss of FAD measured by HPLC differed markedly from that by loss of absorbances. Hence the decrease of absorbance at 450 nm gives only the extent

Table 1. G-Values for Flavin Loss under Different Conditions, [FAD]=[FMN]=2.5×10^{-5} mol dm^{-3}, pH=6.5

G-Values	Solution saturated with		
	Air	Argon	Nitrous oxide
G(-chromophore)$_{FMN}$[a]	1.23	2.1(1.20)[b]	
G(-chromophore)$_{FAD}$[a]	0.68	1.38(0.70)[b]	1.30
G(-FMN)	1.16(1.10)[c]	—	2.8(2.66)[c]
G(-FAD)	1.30	—	2.50

a) Determined spectrophotometrically. b) Measured after aeration of the radiolysed solution. c) Determined fluorometrically.

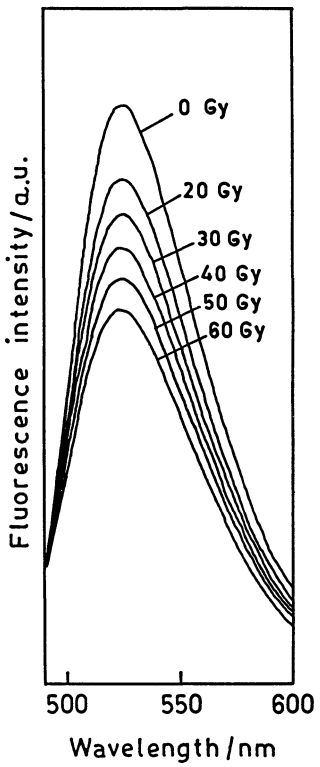

Fig. 2. Changes in the fluorescence emission of FMN (2.5×10^{-5} mol dm^{-3}) solution after γ-irradiation under aerated conditions. Excitation wavelength= 450 nm.

of modification of flavin chromophore in FAD. That is why G-values determined spectrophotometrically and by HPLC are expressed as G(-chromophore) in the former case and by G(-FAD) or G(-FMN) in the latter case.

Since some products generated on irradiation of FAD and FMN under argon are found to be reverted back by aerating the irradiated solution, the G-values in these cases could not be measured by HPLC.

The rate constant for the reaction of isoalloxazine moiety in FAD with the OH radicals has been determined by the competition kinetic technique using glucose as the reference solute. When irradiation was carried out in N_2O-saturated medium, e_{aq}^- reacts exclusively with N_2O to give a stoichiometric equivalent of OH radicals.

$$e_{aq}^- + N_2O \longrightarrow N_2 + OH + OH^-. \quad (1)$$

Therefore, when an aqueous solution of FAD and glucose is irradiated in N_2O saturated conditions, there would be a competition of FAD and glucose (GLH) for the OH radicals. The yields of chromophore loss of FAD should then follow the relationship

$$\frac{G(\text{-chromophore})_0}{G(\text{-chromophore})} = 1 + \frac{k_1}{k_2}\frac{[\text{GLH}]}{[\text{FAD}]}, \quad (2)$$

where G(-chromophore)$_0$ and G(-chromophore) are the yields of chromophore loss of FAD in the absence and

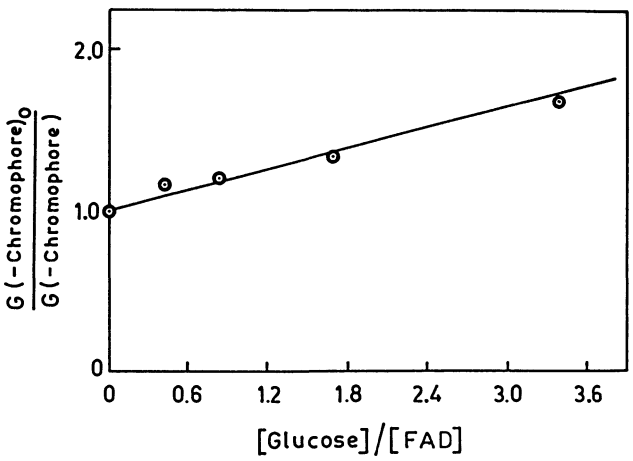

Fig. 3. Kinetic plot for the competition reactions of OH radicals between FAD and glucose. [FAD]= 2.5×10^{-5} mol dm^{-3}.

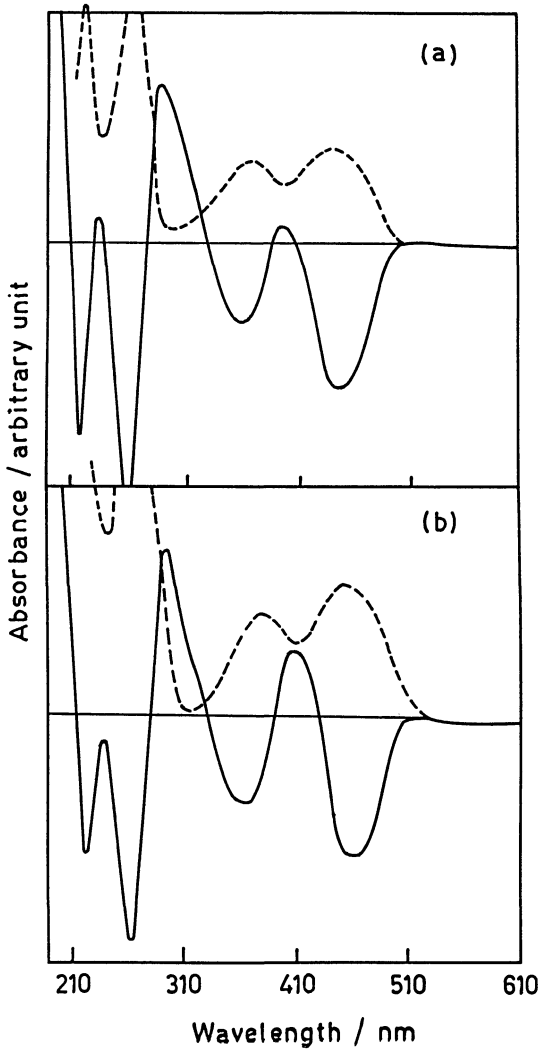

Fig. 4. Difference spectra of the products formed in FAD, (a), and FMN, (b) solutions irradiated with a dose of 120 Gy under N_2O-saturated solutions. Dashed curves are the respective absorption spectra.

presence of glucose, respectively; [GLH] and [FAD] are the molar concentrations of glucose and FAD, k_1 and k_2 being the rate constants for the reactions of OH radicals with glucose and the isoalloxazine moiety in FAD respectively. If G(-chromophore)$_0$/ G(-chromophore) is plotted against [GLH]/[FAD], a straight line with a slope of k_1/k_2 is expected. The observed results are plotted in Fig. 3. From the slope of straight line the value of k_1/k_2 could be determined. Taking the value of k_1 as 1×10^9 dm^3 mol^{-1} s^{-1},[5] the value of k_2, the rate constant for the reaction of isoalloxazine moiety in FAD with the OH radicals, has been estimated to be 4.7×10^9 dm^3 mol^{-1} s^{-1}.

The difference spectra of irradiated FAD and FMN in N_2O saturated medium are shown in Fig. 4a,b. The figure shows that in both cases there are three peaks at nearly identical wavelengths 408, 296, and 240 nm. The similarity of the product peaks obtained under the similar experimental conditions indicates that the same types of products have been formed in both cases.

As some of the flavoenzymes contain iron(III) the role of this metal ion in modification of radiosensitivity of flavins was also studied. Because of the instability of iron(III) ions in aqueous solution at pH 6.5 the study was to be carried out at pH ca. 2. The role of Fe^{3+} ions at pH ca. 2 on isoalloxazine moiety of FAD and FMN could be extrapolated to pH 6.5, since the pK value for $Fl+H^+=FlH^+$ is nearly zero[6] (where Fl represents flavin moiety). Therefore, flavin would remain in a neutral state at both pH 6.5 and ca. 2. Thus, when FAD is irradiated in the presence of iron(III) ion in argon saturated medium at pH ca. 2 the loss of flavin chromophore in FAD has been found to be the same as that obtained in absence of iron(III) ion. But the reduction yield of iron(III) ion $G(Fe^{2+})$ was found to increase with

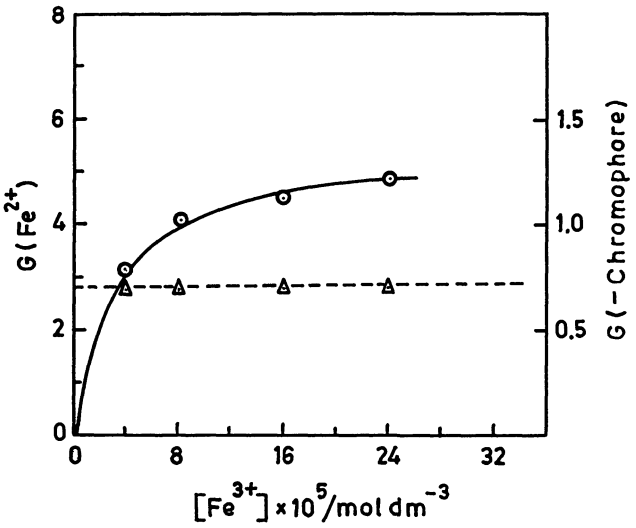

Fig. 5. Dependence of $G(Fe^{2+})$, (⊙) and G(-chromophore) in FAD, (△) on concentration of Fe^{3+} ion in the γ-radiolysis of FAD in the presence of Fe^{3+} ions at pH ca. 2 under argon saturated conditions, [FAD]=2.5×10^{-5} mol dm^{-3}.

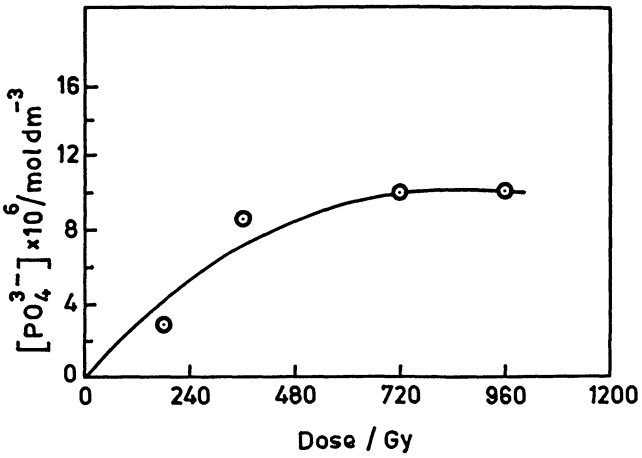

Fig. 6. Extent of phosphate release from FAD on γ-radiolysis under N_2O-saturated conditions, [FAD]= 2.5×10^{-4} mol dm^{-3}.

the increase in its concentration and reached a plateau value of ca. 4.8 at higher $[Fe^{3+}]$ as shown in Fig. 5. The reduction yield of iron(III) ion in the presence of FMN was found to be identical with that observed in the presence of FAD under similar experimental conditions.

In addition to the flavin moiety the FAD molecule also contains a phosphate-sugar linkage. It is well-known that when OH radicals react with the sugar moiety of nucleotides, inorganic phosphates are released.[7] To ascertain whether OH radicals react with FAD at sites other than the isoalloxazine ring, the amount of inorganic phosphate released in irradiated FAD was determined. Figure 6 shows the extent of phosphate release in γ-irradiated FAD in N_2O saturated medium against the absorbed dose. The initial G-value for the phosphate release was estimated to be ca. 0.23. But no detectable amount of phosphate release was observed on γ-irradiation of FMN under the similar conditions.

Discussion

In the aerated medium e_{aq}^- and H radicals are scavenged by oxygen forming the superoxide anion (O_2^-) and hydroperoxyl (HO_2) radicals as given in the Eqs. 3 and 4.

$$e_{aq}^- + O_2 \longrightarrow O_2^- \quad (3)$$

$$H + O_2 \longrightarrow HO_2 \quad (4)$$

Since the redox potential of O_2/O_2^- (E_0=−0.33 V)[8] is lower than those of Fl/Fl^- (E_0=−0.3 V),[9] the superoxide anions could reduce flavins to dihydroflavins. But these dihydroflavins would be oxidized readily by molecular oxygen by a complex mechanism[10] to give back flavins. Hence there would be no net modification of flavins due to reaction with O_2^- in aerated medium.

In N_2O saturated medium G_{OH} is twice than that in aerated medium. From Table 1, it is seen that the

chromophore loss in FAD and FMN in N_2O saturated medium are nearly twice that observed in aerated medium. This result definitely shows that OH radicals have important contribution to the modification of FAD and FMN during the irradiation by γ-rays. The flavin chromophore loss of FAD and FMN under the deaerated conditions was found to be larger than that observed under the aerated conditions (Table 1). This may be attributed to the reactions of FAD with e_{aq}^- and H radicals. Ahmad et al.[11] have shown that FAD and FMN are reduced by e_{aq}^- to form dihydroflavins, FlH_2.

$$Fl + e_{aq}^- + H^+ \longrightarrow FlH \quad (5)$$

$$2\,FlH \xrightarrow{\text{disproportionation}} Fl + FlH_2 \quad (6)$$

As stated earlier these dihydroflavins are oxidized by molecular oxygen to flavins. This explains the partial recovery of absorbances of irradiated FAD and FMN by aeration as shown in Fig. 1c. But in the case of dinitrogen monoxide saturated condition the absorption spectra of the irradiated sample remained unchanged (Fig. 1b) on aeration. Since the major damaging species in N_2O saturated medium is OH radicals, it could be inferred that OH radicals cause a permanent damage to FAD and FMN. This permanent change in absorption caused by OH radicals might be due to modification of the isoalloxazine moiety of flavins. The absorption behavior of the products formed from such reactions could be studied following the difference spectra of the products formed in the reactions. Figure 4 shows that there are three negative peaks in the difference spectra of the products with minima at those wavelengths (260, 370, and 450 nm) which correspond to the maxima in the absorption spectrum of unirradiated FAD and FMN. These negative peaks indicate the removal of ground-state absorption of FAD and FMN on radiolysis. The absorption peaks of the products have shifted to shorter wavelengths than those of starting flavins. This spectral shift may imply that OH radical reaction causes the loss of π-conjugation of isoalloxazine moiety of flavins.

From Table 1 it is evident that under aerated or N_2O saturated conditions the decomposition yield of flavins, viz. FMN is equal to half the value of G_{OH}. To account for this G-value, a disproportionation reaction of the transient intermediate formed by the reaction of OH radicals with the flavin should take place as was suggested previously.[12] Heelis et al.[13] have suggested that possible oxidation sites at the fiavin moiety are the C-8 methyl group and the extended π-conjugated system. They have shown that $SO_4^{\cdot-}$ radical causes oxidation predominantly by abstracting electron from the π-conjugated system followed by deprotonation from N-3 atom. Kishore et al.[14] have shown by pulse radiolysis studies that OH radical causes oxidation only at π-conjugated system in flavin moiety of lumichrome. To explain the chromophore loss in FAD and FMN an analogous mechanism may be shown as Schemes 1 and

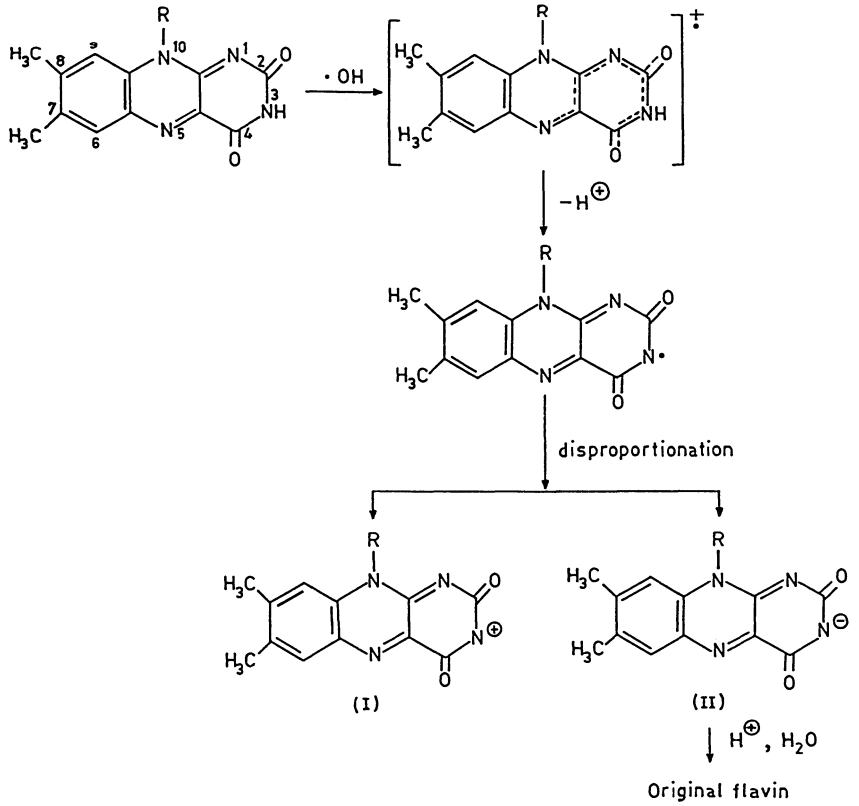

Scheme 1.

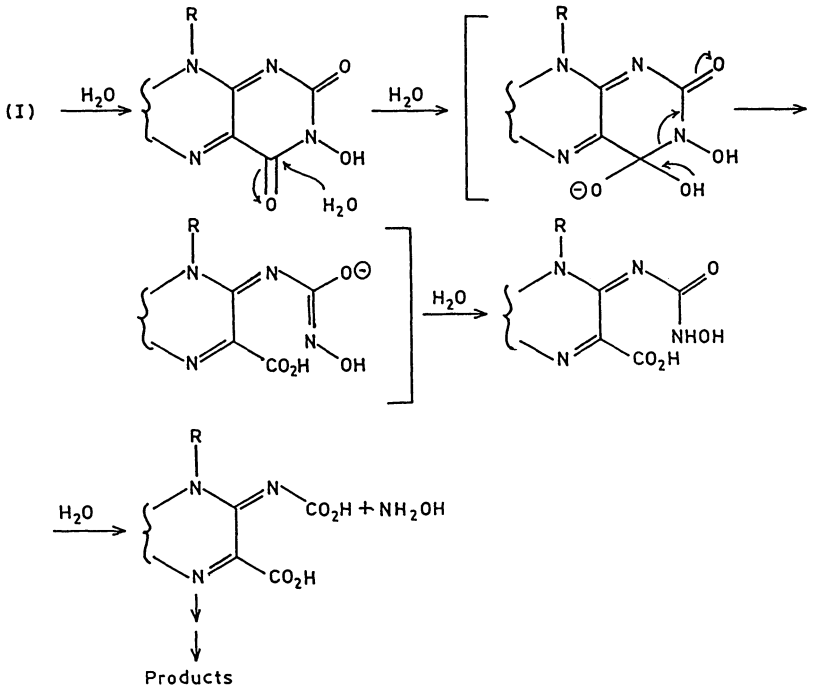

Scheme 2.

2.

But the above mechanism cannot account for the observed G(-chromophore) in FAD. Table 1 shows that under N_2O saturated conditions the G(-chromophore) for FAD is only 1.3 which is much less than the value expected from the reaction mechanism. The possible reason for this discrepancy is that apart from the isoalloxazine moiety a significant portion of the total OH radicals attacks at the AMP (adenosine monophosphate) portion of FAD. The rate constant for the reaction of OH radicals with adenosine (ca. 3.7×10^9 $dm^3\,mol^{-1}\,s^{-1}$) is comparable to that with flavin moiety of FAD and calculation shows that ca. 50% of the total OH radicals would react with the AMP moiety of FAD molecule. This is supported from the fact that in both aerated and N_2O saturated media the G(-chromophore) values in FAD are nearly half of that in FMN under identical conditions. However, when the loss of FAD was measured after separating the products by HPLC, G(-FAD) was found to be ca. 2.5, which is much higher than the value obtained from the spectrophotometric measurements. This increased degradation of FAD is due to the modification of AMP moiety in FAD. The attack of OH radicals at the AMP portion is further confirmed from the phosphate release on γ-irradiation of FAD in N_2O saturated medium, because the attack of OH radical on the AMP results in phosphate release from the molecule.

The role of Fe^{3+} in the radiolysis of FAD and FMN has also been studied. In both cases the reduction of Fe^{3+} has been observed. At pH ca. 2 under deaerated conditions, the $G(Fe^{2+})$ value in absence of FAD and FMN was 3.0 which is almost equal to the radiation chemical yield of the H atoms.[2] But in the presence of FAD or FMN the $G(Fe^{2+})$ value was found to be 4.8. This increase of the $G(Fe^{2+})$ value might be due to the reaction of Fe^{3+} with the transient intermediate formed by the reaction of OH radicals with flavins or by other reducing products formed in the reaction. It is interesting to note that the chromophore loss in FAD and FMN were not influenced by the presence of Fe^{3+} during irradiation. Hence the reduction of Fe^{3+} by the transient radical is unlikely. The only possible pathway to account for the formation of reduced iron is the reduction of Fe^{3+} by the product formed in the solvolysis of (I) (Schemes 1 and 2). Hydroxylamine or the hydroxamic acid derivative (III) could reduce two equivalents of Fe^{3+}. Thus according to the aforesaid discussion $G(Fe^{2+})$ is expected to be $G_H+2\times G$(-chromophore)$=3.0+2\times1.2=5.4$ for FMN and $G_H+2\times G$(-chromophore) $=3.0+2\times0.7=4.4$ for FAD. If a small loss of Fe^{2+} ion due to aereal oxidation during measurements is considered, then the observed results are found to be in conformity with that expected in the case of FMN. But for the case of FAD, the observed $G(Fe^{2+})$ is ca. 4.8 (Fig. 5) which is slightly higher than the expected value. It is important to mention here that the attack of OH radicals towards AMP would produce radicals which are easily reduced and oxidized in nature.[15] Thus reducing radicals might react with Fe^{3+} ions giving Fe^{2+}. As a result, the yield of Fe^{2+} could be increased without affecting G(-chromophore) of FAD molecule.

References

1) J. A. Winstead and S. A. Moss, *Radiat. Res.*, **52**, 520

(1972).
2) I. G. Draganic and Z. D. Draganic, "The Radiation Chemistry of Water," Academic Press, New York and London (1971).
3) O. H. Lowry and J. A. Lopez, *J. Biol. Chem.*, **162**, 421 (1946).
4) A. I. Vogel, "A Text Book of Quantitative Inorganic Analysis," 4th ed, E. L. B. S. and Longmans, Green and Co., Ltd., London (1985), p. 742.
5) M. Anbar and P. Neta, *Int. J. Appl. Radiat. Isot.*, **16**, 227 (1965).
6) E. J. Land and A. J. Swallow, *Biochemistry,* **8**, 2117 (1969).
7) J. F. Ward, *Int. J. Radiat. Phys. Chem.*, **3**, 239 (1971).
8) P. Wardman, *J. Phys. Chem. Ref. Data,* **18**, 1637 (1989).
9) R. F. Anderson, *Biochim. Biophys. Acta,* **722**, 158 (1983).
10) F. Muller, *Free Radical Biology and Medicine,* **3**, 215 (1987).
110 R. Ahmad and D. A. Armstrong, *Biochemistry,* **21**, 5445 (1982).
12) K. Kishore, P. N. Moorthy, and K. N. Rao, *Radiat. Eff. Lett.*, **67**, 153 (1982).
13) P. F. Heelis, B. J. Parsons, G. O. Phillips, and A. J. Swallow, *J. Phys. Chem.*, **90**, 6833 (1986).
14) K. Kishore, S. N. Guha, and P. N. Moorthy, Seminar on Radiation and Photophysical Sciences, Organised by Indian Society for Radiation and Photochemical Sciences, 1987, Abstr., p. 23.
15) J. Cadet and M. Berger, *Int. J. Radiat. Biol.*, **47**, 127 (1985).

 © 1991 The Chemical Society of Japan Bull. Chem. Soc. Jpn., 64, 2539—2543 (1991)

Inclusion Compounds of α-Truxillic Acid. X-Ray Crystal Structures of the Coordinatoclathrates with Methanol (1:2) and Dimethylacetamide (1:2)

Ingeborg CSÖREGH,* Mátyás CZUGLER,§ Alajos KÁLMÁN,† Edwin WEBER,†† and Manfred HECKER††
Department of Structural Chemistry, Arrhenius Laboratory, Stockholm University, S-106 91 Stockholm, Sweden
†Central Research Institute for Chemistry of the Hungarian Academy of Sciences, P. O. Box 17, H-1525 Budapest, Hungary
††Institut für Organische Chemie und Biochemie der Universität Bonn, Gerhard-Domagk-Strasse 1, D-5300 Bonn 1, Germany
(Received December 25, 1990)

The crystal structures of the inclusion compounds of the 2*c*,4*t*-diphenylcyclobutane-1*r*,3*t*-dicarboxylic acid (α-truxillic acid) host (**1**) with methanol [MeOH] (1:2) and with dimethylacetamide [DMA] (1:2) have been determined by single crystal X-ray diffraction. The substantial difference between the effects of the protic (MeOH) and aprotic (DMA) guests on the molecular packing is discussed. Crystal data: **1**·2MeOH: monoclinic ($P2_1/n$), a=12.528(4), b=5.589(1), c=13.715(4) Å, β=101.16(4)°, Z=2, R=0.064 for 1300 reflections; **1**·2DMA: monoclinic ($P2_1/c$), a=6.151(1), b=26.586(2), c=7.938(1) Å, β=105.32(6)°, Z=2, R=0.056 for 1488 observations. In both clathrates, half of the rigid α-truxillic acid molecule occupies the asymmetric unit together with one guest molecule. The hydrogen bonds between the trans-positioned functional groups of the host acid and the guest molecules in **1**·2MeOH give rise to infinite layers parallel with the crystallographic *ac* diagonal. In contrast, the only one-way hydrogen bond from host to guest in **1**·2DMA leads to discrete 1:2 host–guest aggregates. In this latter case, the hosts and guests are stacked separately, along the *c* axis direction.

Elucidation of new models for molecular recognition is a recent challenge for organic chemistry.[1] In this regard, inclusion compounds in general and lattice inclusions in particular will remain in good standing for a while. Recent crystal structure determinations have revealed a new brand of lattice inclusions in which the guest entities are anchored to the framework formed by the host molecules through hydrogen bonds.[2] This feature is such an eminent characteristic of the crystals that the term coordinatoclathrate has been coined for them.[2,3] Hosts that display this behavior are mainly based on rigid and symmetric dicarboxylic acids.[4] In the compounds studied earlier,[2,4–10] the number of bridging carbon atoms between the –COOH functions is even, and the two –COOH groups are oriented more or less at right angles to one another.[2] Here we report on the structures of two solid coordinatoclathrates of α-truxillic acid (2*c*,4*t*-diphenylcyclobutane-1*r*,3*t*-dicarboxylic acid, **1**), which has an odd number (3) of carbon atoms between two symmetry-related –COOH functions with diametrically opposite orientations. (The synthesis and the inclusion properties of this host have been published elsewhere.[9,10]). The methanol (MeOH) and dimethylacetamide (DMA) guests possess protic and aprotic character, respectively.

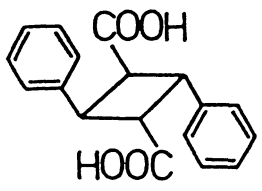

1

§ Permanent address: Central Research Institute for Chemistry of the Hungarian Academy of Sciences, P. O. Box 17, H-1525 Budapest, Hungary.

Experimental

Sample Preparation. The α-truxillic acid host was prepared as previously described.[9] Crystals of the inclusion compounds were obtained by dissolution of the host in the respective guest solvent, followed by slow solvent evaporation.

X-Ray Data Collection and Processing. The single crystals selected for X-ray measurement were sealed in glass capillaries. The intensitites were collected on a STOE/AED2 diffractometer at room temperature with graphite monochromatized Cu $K\alpha$ radiation (λ=1.5418 Å), using the 2θ–ω scan mode within the range $3<2\theta<140°$. The unit cell parameters were refined against θ values of 30 and 50 reflections for **1**·2MeOH and **1**·2DMA, respectively, within the range $27<2\theta<44°$.

The net intensities were corrected for Lorentz and polarization effects but not for absorption. Crystal data and selected experimental details are summarized in Table 1.

Structure Analysis and Refinement. Reasonable starting models of the structures were derived by direct methods, using MULTAN[11] for **1**·2MeOH and SHELXS[12] for **1**·2DMA. Only structure factors with $F>6\sigma(F)$ were included in the subsequent full-matrix least-squares refinements [SHELX[13]]. The positions of the non-hydrogen atoms were refined together with their anisotropic thermal parameters, whereas isotropic temperature factors were refined for the hydrogen atoms.

The H atoms in **1**·2MeOH, except for the methyl hydrogens of the guest, were located from a difference electron density map, and their positions were kept riding on their 'mother' atoms during the subsequent refinements. The methanol $-CH_3$ group was refined as a rigid group with free rotation

Table 1. Crystal Data and Some Selected Experimental Details (esd's, where given, are in parentheses)

Compound	**1**·2MeOH	**1**·2DMA
Formula unit	$C_{18}H_{16}O_4 \cdot 2CH_4O$	$C_{18}H_{16}O_4 \cdot 2C_4H_9ON$
Formula weight	360.41	470.56
Crystal size/mm	0.4×0.5×0.5	0.6×0.3×0.2
Unit cell dimensions		
a/Å	12.528(4)	6.151(1)
b/Å	5.589(1)	26.586(2)
c/Å	13.715(4)	7.937(1)
β/°	101.16(4)	105.32(6)
V_c/Å^3	942.2(5)	1251.8(5)
Space group	$P2_1/n$	$P2_1/c$
Z	2	2
D_c/Mg m^{-3}	1.270	1.248
$F(000)$	384	504
$\mu_{CuK\alpha}$/cm^{-1}	7.34	6.87
N of reflections measured	1724	2266
N_{obs} (unique, non-zero)	1450	1952
N_{ref} [with $I/\sigma(I)>3$]	1300	1488
$N_{variables}$	131	175
R ($=\sum\|\Delta F\|/\|\sum F_o\|$)	0.064	0.056
R_w ($=[\sum w\|\Delta F\|^2/\sum w\|F_o\|^2]^{1/2}$)	0.094	0.072
$R_{w,tot}$	0.113	0.083
Weighting: g in SHELX[a)]	0.0003	0.00008
Highest residual electron density/e Å^{-3}	0.20	0.16

a) Weights of the structure factors in SHELX[13] are estimated as w=const./$(\sigma^2(F)+g \cdot F^2)$.

around the O–C bond.

The guest in the **1**·2DMA structure shows positional disorder. The difference electron density map, calculated for the structural model containing C, O, and N atoms, remained blurred in the region of the guest molecule. It was, however, possible to construct a proper model of the disorder with the aid of molecular modelling [CHEM-X 86[14]]. This model consists of two orientations of the DMA molecule, partly overlapping each other (cf. Fig. 1b). Accordingly, the refinement was extended to two additional peaks representing the alternative positions for C(D2) and N(3) atoms, and two sets of hydrogens for the C(D4), C(D5), and C(D6) methyl carbons

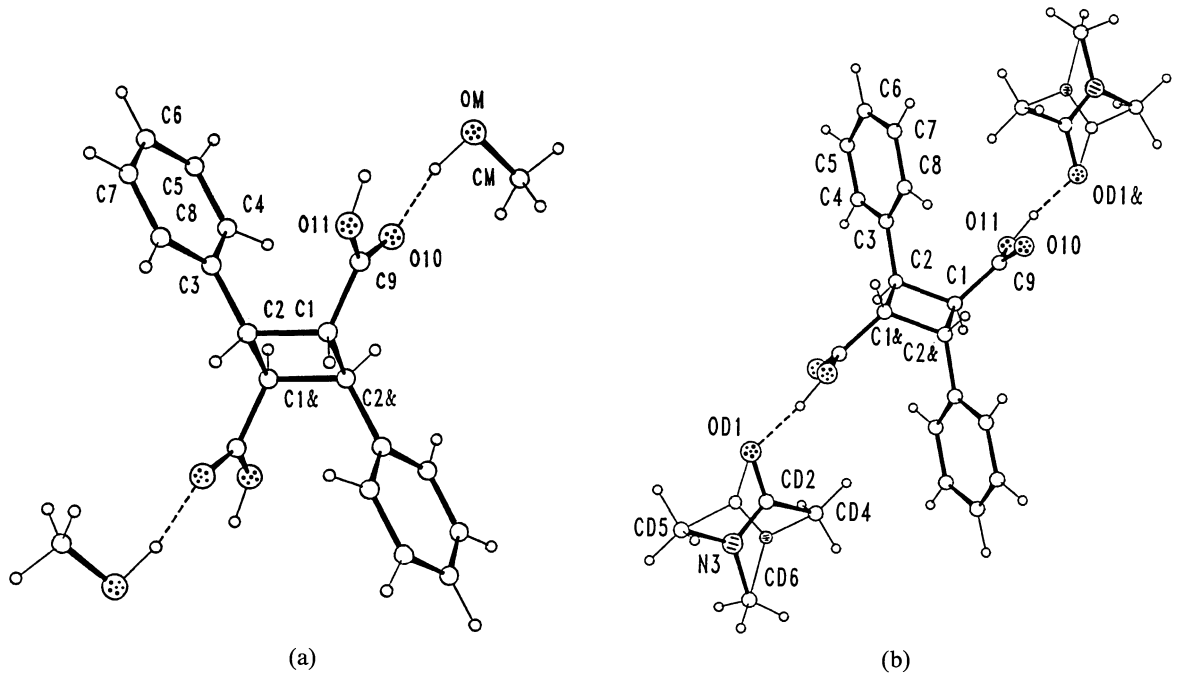

(a) (b)

Fig. 1. Perspective views of the formula units of (a) **1**·2MeOH and (b) **1**·2DMA, with atoms labeled as in the text. Solid and dashed lines represent covalent and hydrogen bonds, respectively; O atoms are dotted, N atoms are hatched. In the structure of **1**·2DMA, the guest shows rotational disorder: it assumes two orientations partly overlapping each other.

were included in the structure factor calculations. The hydrogens of the host molecule, except for three H atoms, were assumed to be at geometrically predictable positions. H(1) and H(2) of the *c*-butane ring (Fig. 1b) and the carboxylic H(11) atom were located by difference electron density calculation and were kept riding on their 'mother' atoms. The refinement of the alternative C(D2a)/C(D2b) and N(3a)/N(3b) disorder sites yielded site occupancies of 0.47/0.53, respectively.

Some strong low-θ reflections (26 for **1**·2MeOH and 30 for **1**·2DMA), with considerably higher F_c than F_o, probably due to extinction effects, were excluded from the last refinements, where the final residual indices (R and R_w in Table 1) were reached.

Results and Discussion

Figure 1 shows perspective views of the formula units of the present two inclusion compounds of α-truxillic acid (**1**). The final atomic positional parameters are given in Table 2. Hydrogen bond geometries are listed in Table 3. The helical chain of hydrogen bonds in **1**·2MeOH is illustrated in Fig. 2, whereas the crystal packings are depicted in Figs. 3 and 4.[15]

Molecular Structures. In the two inclusion compounds the geometry of α-truxillic acid (**1**), possessing C_i molecular symmetry, is similar within experimental error (Fig. 1). The cyclobutane ring is planar with somewhat strained bond lenghts and bond angles: C(1)–C(2)=1.581(3) and 1.571(4), C(1)–C(2)&=1.551(1) and 1.539(4) Å, ∠C(1)–C(2)–C(1)&=89.4(2) and 89.8(2), ∠C(2)–C(1)–C(2)&=90.6(2) and 90.7(2)° in **1**·2MeOH and **1**·2DMA, respectively (&=1−x, 1−y, 1−z for **1**·2MeOH and −x, 1−y, 1−z for **1**·2DMA). The C(2)–C(1)–C(9)–C(11) torsion angles[16] [84.2(3) and 82.5(3)°] indicate similar orientations of the carboxyl functions. Even the rotational angles of the phenyl rings about the C(2)–C(3) bond differ by only 14°. The dihedral angles between the least-squares (LS) planes[17] of the cyclobutane and the phenyl rings are 76.9(1) and 82.8(1)°, whereas the COO(H) groups are inclined through 66.8(2) and 63.9(2)° away from the attached phenyl substituents in **1**·2MeOH and **1**·2DMA, respectively.

Two distinct models (termed hereinafter *A* and *B*) can be used to describe the disorder of the DMA with respect to the rotation axis through the oxygen and one of the *N*-methyl carbon [C(D6)] atoms. Thus, the C(4D)/C(5D) atomic pair occupies alternatively the same positions with about 50% probability, whereas C(D2) and N(3) have two disorder sites (Fig. 1b). The

Table 2. Fractional Atomic Coordinates and Equivalent Isotropic[a] or Isotropic Temperture Factors of the Non-Hydrogen Atoms and of the Hydrogens, Involved in the Hydrogen Bonds, in Compounds **1**·2MeOH and **1**·2DMA, Respectively (esd's, where given, are in parentheses)

Atom	x/a	y/b	z/c	U_{eq}[a]/U (Å²)
1·2MeOH				
C(1)	0.9995(2)	0.3401(5)	0.5468(2)	0.040(1)
C(2)	0.9431(2)	0.4133(4)	0.4377(2)	0.041(1)
C(3)	0.8208(2)	0.4079(4)	0.4108(2)	0.043(1)
C(4)	0.7564(2)	0.5765(5)	0.4458(2)	0.054(1)
C(5)	0.6433(2)	0.5671(6)	0.4193(3)	0.063(1)
C(6)	0.5940(2)	0.3840(6)	0.3590(3)	0.064(1)
C(7)	0.6562(3)	0.2150(6)	0.3249(2)	0.061(1)
C(8)	0.7691(2)	0.2253(5)	0.3503(2)	0.053(1)
C(9)	0.9230(2)	0.2831(5)	0.6144(2)	0.044(1)
O(10)	0.8934(2)	0.4242(4)	0.6704(2)	0.063(1)
O(11)	0.8884(2)	0.0586(4)	0.6049(2)	0.057(1)
O(M)	0.7874(2)	0.4872(5)	0.8252(2)	0.085(1)
C(M)	0.8704(3)	0.6231(9)	0.8801(3)	0.097(2)
H(11)	0.8325	0.0237	0.6409	0.08(1)
H(OM)	0.8193	0.4605	0.7562	0.17(2)
1·2DMA				
C(1)	−0.0974(4)	0.5346(1)	0.4663(4)	0.049(1)
C(2)	0.0393(4)	0.5092(1)	0.6408(4)	0.049(1)
C(3)	0.2353(4)	0.5370(1)	0.7597(4)	0.048(1)
C(4)	0.2359(5)	0.5474(1)	0.9309(4)	0.054(1)
C(5)	0.4193(5)	0.5710(1)	1.0435(4)	0.064(1)
C(6)	0.6024(5)	0.5851(1)	0.9840(4)	0.064(2)
C(7)	0.6030(5)	0.5760(1)	0.8129(4)	0.060(1)
C(8)	0.4210(5)	0.5516(1)	0.7016(4)	0.054(1)
C(9)	−0.0249(5)	0.5863(1)	0.4273(4)	0.053(1)
O(10)	0.0977(4)	0.5951(1)	0.3354(3)	0.070(1)
O(11)	−0.1096(4)	0.6216(1)	0.5089(3)	0.077(1)
O(D1)	0.0038(5)	0.2847(1)	0.5230(4)	0.104(2)
C(D2a)	−0.2032(23)	0.2731(5)	0.4417(14)	0.077(5)
C(D2b)	−0.1143(15)	0.2470(4)	0.4747(11)	0.070(3)
N(3a)	−0.2456(17)	0.2238(4)	0.4242(11)	0.078(4)
N(3b)	−0.3314(14)	0.2551(4)	0.3959(10)	0.078(3)
C(D4)	−0.4044(7)	0.3079(2)	0.3653(6)	0.111(2)
C(D5)	−0.0479(7)	0.1911(2)	0.5003(7)	0.101(2)
C(D6)	−0.4787(7)	0.2097(2)	0.3259(7)	0.128(3)
H(11)	−0.0301	0.6541	0.4883	0.086(4)

a) $U_{ij}=1/3\sum_i\sum_j U_{ij}\alpha_i^*\alpha_j^*\boldsymbol{a}_i\cdot\boldsymbol{a}_j$.

Table 3. Bond Lengths and Bond Angles in Possible Hydrogen Bonds in Compounds **1**·2MeOH and **1**·2DMA (esd's, where given,[a] are in parentheses)

Atoms involved	Symmetry	Distances/Å			Angle/°
		O···O	O–H	H···O	∠O–H···O
1·2MeOH					
O(11)–H(11)···O(M)	1.5−x, −0.5+y, 1.5−z	2.596(3)	0.95	1.67	164
O(M)–H(OM)···O(10)	x, y, z,	2.737(3)	1.11	1.65	167
1·2DMA					
O(11)–H(11)···O(D1)	−x, 1−y, 1−z	2.605(3)	1.03	1.64	154

a) The position of the hydrogens involved in hydrogen bonds are taken from difference electron density maps and are not refined.

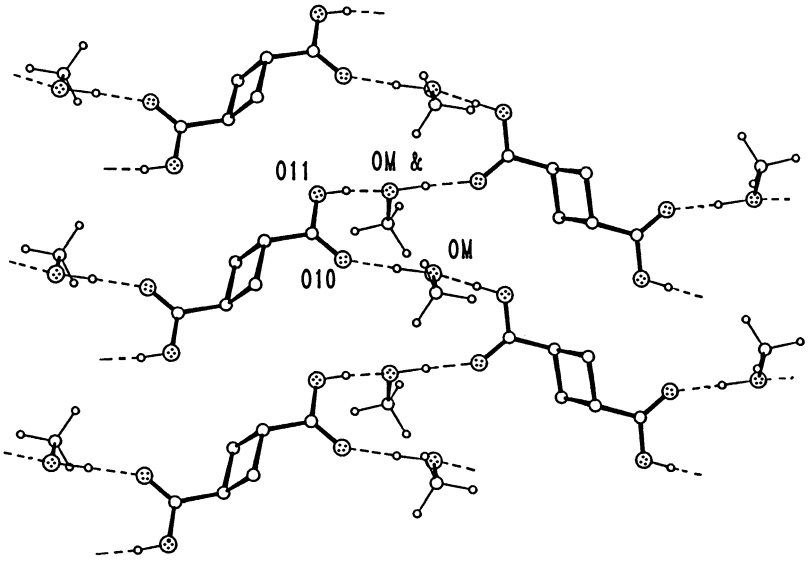

Fig. 2. Diagram of the hydrogen bond network in the crystal structure of **1**·2MeOH. The phenyl substituents and the hydrogens of the host, except H(11), which is involved in H-bonding, are omitted for clarity. Solid and dashed lines represent covalent and hydrogen bonds, respectively.

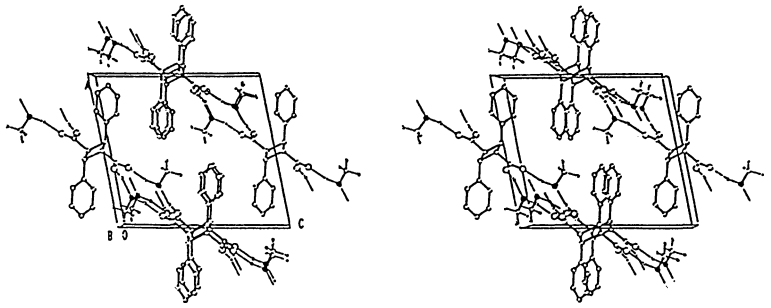

Fig. 3. Stereo packing illustration of the **1**·2MeOH crystal structure. The O atoms of the guest are in bold. The hydrogens of the host, not invloved in hydrogen bonds, are omitted for clarity.

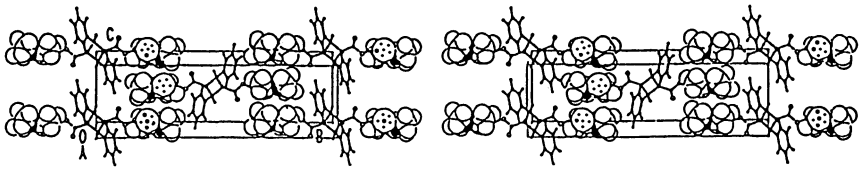

Fig. 4. Stereo packing diagram of the **1**·2DMA crystal structure. The host molecule is shown in ball-and-stick style, the guest molecule is drawn as space filling models with only one disorder site for each C(2D) and N(3). The N and O atoms of the guest are indicated by black filling and dotting, respectively.

non-hydrogen atoms of the DMA molecule are coplanar within 0.040 and 0.072 Å in *A* and *B*, respectively.

Packing Relations and Host-Guest Interactions. The protic MeOH and aprotic DMA arrange the host entities in substantially different ways (Figs. 3 and 4).

In **1**·2MeOH the hydrogen bonding between the host acid and the alcoholic guests results in infinite helices (Fig. 2), similar to those found in the alcoholic inclusions of the related 3,3-diphenyl-*cis*-cyclopropane-1,2-dicarboxylic acid.[9,10,18] Nevertheless, due to the intramolecular hydrogen bond between the *cis*-positioned –COOH groups, the cyclopropane host behaves externally as monofunctional, forming inclusions usually with 1 : 1 stoichiometry. As a consequence, the H-

bonded helices in the EtOH[18] and *t*-BuOH inclusions[9,10] of the *cis*-cyclopropanedicarboxylic acid host are endless in one dimension, and are held together by weaker Van der Waals' forces.

In contrast, the *trans*-truxillic acid (**1**) is a bifunctional host, forming inclusions usually with 1 : 2 host–guest stoichiometry. In its MeOH inclusion the alcoholic guests, helically arranged around the screw axes at 1/4, *y*, 1/4 and 3/4, *y*, 3/4, connect both ends of the hosts via strong OH···O bonds. The divalent host entities, located either at *a*/2 or *c*/2 are linked together by the hydrogen-bonded helices (cf. Fig. 4) into infinite layers. These two-dimensional, infinite 'supramolecules' are then held together by Van der Waals' forces between the hydrophobic phenyl rings.

In **1**·2DMA (Fig. 4) the one-way hydrogen bond interaction between host and guests gives rise to discrete host–guest aggregates. The single OH···O hydrogen bond, from the donor at each end of **1** to the carbonyl group of the DMA molecule, fixes the DMA·**1**·DMA aggregates along the *b* axis. The twofold screw axes translate these aggregates and the two apolar DMA units fit exactly between two other DMA molecules separated by the short [7.937(1)Å] *c* axis. It seems probable that the bulky, closely packed DMA molecules assume alternatively either disorder form *A* or *B* in order to avoid formation of short, (<2.4 Å) unfavorable H···H intermolecular contacts. The infinite columns of the apolar DMA guests completely isolate the host molecules. This particular mode of packing suggests possibilities for future applications in topochemical reactivity[19] and for the development of other crystalline materials properties.[20]

The authors are indebted to Professor P. Kierkegaard (Stockholm University) for his continuous support and encouragement. M. C. is grateful to the Swedish Institute for a research grant, No. 4149-1, and together with I. C. also thanks the Swedish Natural Scientific Research Council (NFR) for financial support. E. W. is grateful to the Deutsche Forschungsgemeinschaft (SFB 334) and to the Fonds der Chemischen Industrie for financial support.

References

1) W. Saenger and F. Vögtle, "Book of Abstracts, VI. International Symposium on Molecular Recognition and Inclusion," TIB Verlag, Berlin (1990).

2) E. Weber, I. Csöregh, B. Stensland, and M. Czugler, *J. Am. Chem. Soc.*, **104**, 3297 (1984).

3) a) E. Weber and H.-P. Josel, *J. Inclusion Phenom.*, **1**, 79 (1983); b) E. Weber and M. Czugler, "Molecular Inclusion and Molecular Recognition-Clathartes II," (Topics in Current Chemistry, Vol. 149), ed by E. Weber, Springer Verlag, Berlin-Heidelberg-New York (1988).

4) E. Weber, *J. Mol. Graphics*, **7**, 12 (1989).

5) I. Csöregh, A. Sjögren, M. Czugler, M. Cserzö, and E. Weber, *J. Chem. Soc., Perkin Trans. 2*, **1986**, 507.

6) E. Weber, I. Csöregh, J. Ahrendt, S. Finge, and M. Czugler, *J. Org. Chem.*, **53**, 5831 (1988).

7) I. Csöregh, M. Czugler, and E. Weber, "Molecular Structure, Chemical Reactivity and Biological Activity," ed by J. J. Stezowski, Publ. by the International Union of Crystallography, Oxford University Press, Oxford (1988), pp. 390—395.

8) I. Csöregh, M. Czugler, E. Weber, and J. Ahrendt, *J. Inclusion Phenom., Mol. Recogn. Chem.*, **8**, 275 (1990).

9) E. Weber, M. Hecker, I. Csöregh, and M. Czugler, *J. Am. Chem. Soc.*, **111**, 7866 (1989).

10) E. Weber, M. Hecker, I. Csöregh, and M. Czugler, *Mol. Cryst. Liq. Cryst.*, **187**, 165 (1990).

11) P. Main, S. J. Fiske, S.E. Hull, L. Lessinger, G. Germain, J-P. Declerq, and M. M. Woolfson, MULTAN 80, A System of Computer Programs for the Automatic Solution of Crystal Structures from X-ray Diffraction Data, University of York, England (1980).

12) G. M. Sheldrick, SHELXS 84, Program for Crystal Structure Solution, University of Göttingen, Germany, personal communication.

13) G. M. Sheldrick, SHELX 76, Program for Crystal Structure Determination. Univ. of Cambridge, England (1976).

14) CHEM-X, developed and distributed by Chemical Design Ltd. Oxford, England (1986).

15) The list of intramolecular bond lengths and bond angles involving the non-hydrogen atoms (Tables 4 and 5), coordinates of the hydrogens (Table 6), bond distances and bond angles involving the hydrogen atoms (Table 7), anisotropic vibrational parameters of the non-hydrogen atoms (Table 8) as well as the observed and calculated structure factors are depositied as Document No. 9113 at the Editor of the Office of the Bull. Chem. Soc. Jpn.

16) a) W. Klyne and W. Prelog, *Experientia*, **16**, 521 (1960); b) R. H. Stanford, Jr. and J. Waser, *Acta Crystallogr., Sect. A*, **28**, 213 (1972).

17) M. Nardelli, A. Musatti, P. Domiano, and G. Andreetti, *Ric. Sci.*, **15**, 807 (1965).

18) I. Csöregh and E. Weber, unpublished results.

19) G. R. Desiraju, "Crystal Engineering—The Design of Organic Solids," (Materials Science Monographs, Vol. 54), Elsevier, Amsterdam (1989).

20) E. Weber, "Book of Abstracts, New Materials 90," Japan, Osaka (1990).

Conductivity of Manganese(II) Sulfate in Aqueous Solution at Various Temperatures

Eiji KUBOTA,* Satoru TAKIZAWA, Wataru KASHIWAGI, and Masatoki YOKOI
Department of Chemistry, Faculty of Science, Shinshu University, Asahi, Matsumoto 390
(Received October 31, 1990)

Synopsis. The molar conductivity of manganese(II) sulfate, $MnSO_4$, in aqueous solution was measured in a temperature range of 10—45 °C. The acquired data were analyzed by the Quint–Viallard equation, and the resulting ion association constant, K_A, was used in the Bjerrum equation to determine the contact ion size, R_B. The limiting ionic molar conductivity λ_0 (1/2 Mn^{2+}) for the manganese ion at 15, 25, 35, and 45 °C are 40.8, 53.1, 65.2, and 79.8 S cm^2 mol^{-1}, respectively. The resulting thermodynamic properties for the ion association reaction are: $\Delta G^\circ_{298}=-13.5$ kJ mol^{-1}, $\Delta H^\circ=7.91$ kJ mol^{-1}, and $\Delta S^\circ_{298}=74.1$ J K^{-1} mol^{-1}.

Though the conductivity of manganese(II) sulfate in aqueous solutions at 25 °C has been the subject of extensive works,[1–4] its molar conductivity in aqueous solutions at other temperatures has never been studied. We previously measured the molar conductivity of iron(II) sulfate at various temperatures.[5] In this paper, the measurement was extended to manganese(II) sulfate in a temperature range of 10—45 °C. The temperature dependence of the ionic molar conductivity of divalent metal ions in aqueous solution is discussed in terms of the ion size.

Experimental

Reagent grade $MnSO_4$ was repeatedly recrystallized and purified in the usual manner. Preparation and purification of $MnSO_4$ were conducted under nitrogen atmosphere. Conductivity water was prepared by distilling water three times, and then allowed to pass very slowly through a mixed bed ion-exchange resin shortly before use.

All the measurements were made under nitrogen atmosphere. Conductivities were measured at a frequency of 1 kHz with a linear type bridge[6] in a temperature range of 10—45 °C, with the temperature controlled to ±0.005 °C. The conductivity cell was equipped with a platinized platinum electrode, and the cell constant was 0.99877±0.00001 cm^{-1} at 25 °C. No detectable change in the cell constant was observed over the temperature range of 10—45 °C.

On starting each run, nitrogen gas was passed gently through the conductivity water in the cell for about 20 min, and the conductivity of water was measured equilibrium value, which was less than 1.1×10^{-7} S cm^{-1}. The concentration of the sample solution was determined gravimetrically by the weight buret technique. A stock solution was poured from the weight buret into the cell without opening the cell to prevent contamination from CO_2 in the air. About 30 min was required for the reading of resistance to reach an equilibrium value. The measured resistance exhibited little drift with time after the thermal equilibration.

Results and Discussion

The molar conductivities, Λ, measured as a function, of concentration, c, in the temperature range 10—45 °C are given in Table 1. Using the successive approximation method, the conductivity data were analyzed in terms of the Quint–Viallard equation, Eq. 1.[17]

Table 1. Conductivity Data for Aqueous $MnSO_4$ Solution at Various Temperatures[a]

10 °C		15 °C		20 °C		25 °C	
10^4c	Λ	10^4c	Λ	10^4c	Λ	10^4c	Λ
7.0245	77.189	9.9630	84.416	4.3636	103.12	3.7170	116.95
10.002	74.397	15.637	79.725	9.4219	95.633	9.7315	106.40
11.567	73.156	19.093	77.487	17.459	88.221	17.162	98.560
23.943	66.246	29.092	72.507	31.619	80.205	30.909	89.536
31.665	63.342	33.679	70.708	45.109	75.135	40.123	85.348
48.021	58.830	46.776	66.569	60.210	70.901	52.789	80.863
60.123	56.313	51.372	65.365	81.108	66.422	71.573	75.803
						86.157	72.671

30 °C		35 °C		40 °C		45 °C	
10^4c	Λ	10^4c	Λ	10^4c	Λ	10^4c	Λ
8.4681	119.31	9.0125	130.17	9.6862	140.79	17.345	140.63
13.212	112.70	13.601	123.23	13.205	134.90	25.751	131.40
21.098	105.02	25.084	111.81	23.561	122.95	37.398	122.43
31.631	97.942	36.495	104.42	34.236	114.81	49.623	115.49
43.809	92.071	45.501	99.995	46.347	108.10	58.981	111.29
63.146	85.354	57.643	95.208	57.671	103.22	67.376	108.00
82.418	80.382	65.987	92.456	69.131	99.162	75.368	105.24
		80.963	88.269			86.572	101.83

a) c/mol dm^{-3}; $\Lambda(1/2MnSO_4)$/S cm^2 mol^{-1}, molar conductivity.

$$\Lambda = \gamma[\Lambda_0 - Sc^{1/2}\gamma^{1/2} + Ec\gamma \log c\gamma + J_1 c\gamma - J_2 c^{3/2}\gamma^{3/2}]. \quad (1)$$

Here

$$K_A = (1-\gamma)/c\gamma^2 f_\pm^2, \quad (2)$$

$$-\log f_\pm = Ac^{1/2}\gamma^{1/2}/(1+B\mathring{a}c^{1/2}\gamma^{1/2}), \quad (3)$$

where c is the concentration, γ the degree of dissociation, K_A the ion association constant, $f_\pm$ the mean ionic activity coefficient given by the Deby-Hückel theory,[8] and $\mathring{a}$ the ion size parameter. The coefficients S, E, J, A, and B contain solvent properties, and J_1 and J_2 are functions of the ion size parameter $\mathring{a}_{J2}$.

In the analysis, the ion size parameters appearing in the J_1 and $f_\pm$ terms were fixed at the Bjerrum's distance, q. The best-fit $\mathring{a}_{J2}$ values for J_2 were calculated by minimizing the value of $\sigma\Lambda$ defined by

$$\sigma\Lambda = [\Sigma(\Lambda_{calcd} - \Lambda_{obsd})^2/(N-3)]^{1/2}, \quad (4)$$

Table 2. Conductivity Parameters for Aqueous $MnSO_4$ Solution at Various Temperatures[a]

t/ °C	Λ_0	$\mathring{a}_{J2}$	K_A	$\sigma\Lambda$	R_B
10	91.6±0.1	11.7±0.1	234±1	0.02	4.0
15	104.6±0.1	11.8±0.1	249±2	0.02	4.0
20	118.3±0.1	11.8±0.1	259±1	0.02	4.0
25	133.1±0.1	11.8±0.1	277±1	0.04	3.9
30	147.6±0.1	11.8±0.1	291±1	0.03	3.9
35	163.2±0.1	11.8±0.1	307±1	0.03	3.9
40	179.3±0.1	11.8±0.1	324±1	0.03	3.9
45	196.1±0.2	11.9±0.1	337±2	0.04	3.8

a) $\Lambda_0(1/2MnSO_4)$/S cm^2 mol^{-1}, limiting molar conductivity. $\mathring{a}_{J2}$/Å, ion size parameter for J_2 term. K_A/dm^3 mol^{-1}, ion association constant. $\sigma\Lambda$/%, relative standard deviation in Λ. R_B/Å, contact ion size for the Bjerrum's equation.

where N is the number of experimental points.[9] The results are given in Table 2.

When a conductivity equation containing the $c^{3/2}$ term as in Eq. 1 is applied, the fitting of the data is generally better.[5,9] If an ion association is represented by the Bjerrum's equation, Eq. 5, the contact ion size, R_B(Å), can be calculated from the K_A value given by Eq. 2;[5,10]

$$K_A(calcd) = \frac{4\pi N}{1000}\int_{R_B}^{q} r^2 \exp(e^2/r\,DkT)dr. \quad (5)$$

The results for R_B are also given in Table 2.

As can be seen in Table 2, Λ_0 and K_A tend to increase with raising temperature. This is also the case for other sulfates of divalent transition metal ions ($FeSO_4$,[5] $CoSO_4$,[3] $NiSO_4$,[3] and $ZnSO_4$[3]). Among these sulfates, $MnSO_4$ exhibits the smallest Λ_0 value and the largest K_A value while $ZnSO_4$ exhibits the greatest Λ_0 value and the smallest K_A value.

The limiting ionic molar conductivity, $\lambda_o(1/2\ Mn^{2+})$ =53.1 S cm^2 mol^{-1}, for Mn^{2+} at 25 °C is in good agreement with the literature value: 53.1 S cm^2 mol^{-1} by Broadwater and Evans[11] and 53.2 S cm^2 mol^{-1} by Hallada and Atkinson,[12] with the value $\lambda_0(1/2\ SO_4^{2-})$= 80.0 S cm^2 mol^{-1}.[8] Althogh the ion size parameter $\mathring{a}_{J2}$ is relatively large, reflecting the nature of the adjustable parameter, R_B has a reasonable value (the sum of the ionic crystal radii is ≈3.4 Å[13]).

The λ_0's for the Mn^{2+} ion at a series of temperatures are given in Table 3 together with those for other divalent ions; these were calculated using the Λ_0 values for $CaSO_4$[3] and the λ_0 values for the Ca^{2+} ion at 15, 35, and 45 °C.[8] As is evident in Table 3, the limiting molar conductivities for a series of divalent transition metal ions show a similar increase with a rise in the temperature. The value of λ_0^{2+} generally increases from Mn^{2+}

Table 3. Limiting Ionic Conductivity of Several Divalent Ions in Aqueous Solution at Various Temperatures

t/°C	$\lambda_0(1/2M^{2+})$[a]					
	SO_4^{2-}	Mn^{2+}[b]	Fe^{2+}[c]	Co^{2+}[d]	Ni^{2+}[d]	Zn^{2+}[d]
15	63.8	40.8	41.2	41.1	41.6	41.7
25	80.0[e]	53.1	53.8	52.8	53.5	54.3
35	98.0	65.2	69.1	65.1	65.9	67.1
45	116.3	79.8	—	80.1	80.6	82.2
R_c[g]	2.58[f]	0.97	0.92	0.89	0.83	0.88
$r(M^{2+}-OH_2)$[h]		2.20	2.12	2.08	2.04	2.08

a) $\lambda_0(1/2M^{2+})$/S cm^2 mol^{-1}, limiting ionic molar conductivity. b) This work. c) Ref. 5. d) Ref. 3. e) Ref. 8. f) Ref. 14. g) R_c/Å, crystal ionic radius (as octahedron).[13] h) $r(M^{2+}-OH_2)$/Å, distance of $M^{2+}-OH_2$.[15]

Table 4. Thermodynamic Parameters for Ion Association in Aqueous Solution

Reaction	$K_{A(298)}$	$\Delta G^\circ_{(298)}$	ΔH°	$\Delta S^\circ_{(298)}$
	dm^3 mol^{-1}	kJ mol^{-1}	kJ mol^{-1}	J K^{-1} mol^{-1}
$Mn^{2+}\cdot SO_4^{2-}$,[a]	277	−13.5 ±0.1	7.91±0.03	74.1±0.3
$Fe^{2+}\cdot SO_4^{2-}$,[b]	247	−13.7 ±0.1	9.72±0.05	78.5±0.4
$Co^{2+}\cdot SO_4^{2-}$,[c]	178	−12.80±0.04	5.00±0.30	59.8±1.2
$Ni^{2+}\cdot SO_4^{2-}$,[c]	187	−12.97±0.04	5.18±0.16	60.9±0.6
$Zn^{2+}\cdot SO_4^{2-}$,[c]	165	−12.65±0.04	8.65±0.34	71.4±1.3

a) This work. b) Ref. 5. c) Ref. 3.

to Zn^{2+} except for Fe^{2+} at 35 °C. In particular, this trend is conspicuous at elevated temperatures of 35 and 45 °C.

From Mn^{2+} to Ni^{2+}, the order of the λ_0^{2+} value is opposite to those of the crystal ionic radii and the size of the first hydration sphere revealed by X-ray diffraction on the aqueous solutions.[15] This may suggest that the ionic mobility is inversely proportional to the crystal ionic radii of divalent transition metal ions and of the hydrated ion size.

The $\log K_A - 1/T$ plot to obtain ΔH^0 or ΔS^0 exhibits a good linearity. The resulting thermodynamic constants for the ion association reaction are given in Table 4 together with those of other sulfates. It is seen that the parameters for $Mn^{2+} \cdot SO_4^{2-}$ are similar in magnitude to those for the sulfate ion pairs compared.

The authors wish to thank the staffs of the Shinshu University Nagoya University, and the University of Tokyo Computation Centers for the use of the computers.

References

1) V. M. M. Lobo, "Electrolyte Solution Literature Data on Thermodynamic and Transport Properties," Coimbra, Portugal, Vol. I (1984); Vol. II (1981), pp. 744.
2) B. B. Owen and R. W. Gurry, *J. Am. Chem. Soc.*, **60**, 3074 (1938).
3) S. Katayama, *Bull. Chem. Soc. Jpn.*, **46**, 109 (1973); *J. Solution Chem.*, **5**, 241 (1976).
4) A. D. Phethybridge and S. S. Taba, *Faraday Discuss. Chem. Soc.*, **64**, 274 (1977).
5) E. Kubota, Y. Mochizuki, and M. Yokoi, *Bull. Chem. Soc. Jpn.*, **61**, 3723 (1988).
6) Conductivity bridge: Model 360-S by Fusou Seisakusho, Ltd. Standard resistor: esi, Ltd., within ±0.01%/°C.
7) J. Quint and A. Viallard, *J. Solution Chem.*, **7**, 135, 525, 533 (1977).
8) R. A. Robinson and R. H. Stokes, "Electrolyte Solutions," Butterworth, London (1965), pp. 229, 457, 463.
9) E. Kubota and M. Yokoi, *Bull. Chem. Soc. Jpn.*, **49**, 674 (1976); *ibid.*, **50**, 1422 (1977).
10) J. C. Justice, *J. Chem. Phys. Physicochem. Biol.*, **65**, 353 (1968); E. Renard and J. C. Justice, *J. Solution Chem.*, **3**, 633 (1974).
11) T. R. Broadwater and F. Evans, *J. Solution Chem.*, **3**, 57, (1974).
12) C. J. Hallada and G. Atkinson, *J. Am. Chem. Soc.*, **83**, 3759 (1961).
13) R. D. Shannon, *Acta Crystallogr., Sect. A*, **32**, 751 (1976).
14) E. D. B. Jenkins and K. P. Thakur, *J. Chem. Educ.*, **6**, 576, (1979).
15) H. Ohtaki, *Rev. Inorg. Chem.*, **4**, 103 (1982); H. Ohtaki, T. Yamaguchi, and M. Maeda, *Bull. Chem. Soc. Jpn.*, **49**, 701, (1976).

The Excited-State Dipole Moment of Nitrobenzene Estimated from Solvent Spectral Frequency Shifts

Takehiro ABE
College of General Education, Tohoku University, Kawauchi, Aoba-ku, Sendai 980
(Received March 20, 1991)

Synopsis. The excited-state dipole moment of nitrobenzene has been estimated to be 33.7×10^{-30} C m from solvent spectral frequency shifts. This value agrees well with that ($(31.7\pm3.3)\times10^{-30}$ C m) determined from an electrooptical absorption measurement.

Many theories[1] have previously been proposed regarding solvent spectral frequency shifts of organic molecules. On the basis of some of these, dipole moments and/or polarizabilities have been estimated for the excited states of organic molecules. As mentioned in a previous paper,[2] comparisons of the excited-state dipole moments and/or polarizabilities estimated from the solvent spectral shifts with those determined from electrooptical measurements are necessary, in part, to justify the theoretical expressions for the solvent spectral frequency shifts. Among the theoretical expressions, those expressions that give excited-state dipole moment and polarizability values that are comparable to those of electrooptical measurements will survive. Recently, Sinha and Yates[3] have reported the excited-state dipole moment of nitrobenzene from an electrooptical measurement. Nitrobenzene is one of the typical molecules used for the study of the solvent spectral frequency shifts, because the shifts of nitrobenzene are large. This paper, therefore, applies Abe's improved equation[2,4] to data for nitrobenzene in order to examine the accuracy of this equation by comparing an excited-state dipole moment estimated from the solvent spectral shifts with that obtained from the electrooptical measurement.

Results and Discussion

In a previous paper,[2] Abe's improved expression for the solvent spectral frequency shift of a neutral solute molecule in solution is given by

$$A\times(p_{00}^{A}\cos\theta)p_{ii}^{A}+B\times(p_{ii}^{A})^2+C\times\alpha_{ii}^{A}=\sigma_{0i}^{\circ}-\sigma_{0i}+D, \quad (1)$$

where

$$E=\frac{(d^{S}/M_{r}^{S})^{2/3}}{(r_{A}+r_{S})^4}\times\frac{\pi}{hc}\left(\frac{4\pi L}{3}\right)^{2/3}, \quad (2)$$

$$A=E\times\frac{2(p_{00}^{S})^2}{3(4\pi\varepsilon_0)^2kT}, \quad (3)$$

$$B=E\times\frac{\alpha_{00}^{S}}{4\pi\varepsilon_0}, \quad (4)$$

$$C=E\times\left\{\frac{(p_{00}^{S})^2}{4\pi\varepsilon_0}+\frac{3}{2}\times\frac{I_0^{S}I_0^{A}\alpha_{00}^{S}}{I_0^{S}+I_0^{A}}\right\}, \quad (5)$$

and

$$D=E\times\left[\frac{2(p_{00}^{S})^2(p_{00}^{A})^2}{3(4\pi\varepsilon_0)^2kT}+\frac{1}{4\pi\varepsilon_0}\times\{(p_{00}^{S})^2\alpha_{00}^{A}+\alpha_{00}^{S}(p_{00}^{A})^2\}+\frac{3}{2}\times\frac{I_0^{S}I_0^{A}\alpha_{00}^{S}\alpha_{00}^{A}}{I_0^{S}+I_0^{A}}\right]. \quad (6)$$

Here σ_{0i}° and σ_{0i} are the wave numbers of a transition from the ground state to the ith-excited state of a molecule in the vapor state and in solution, respectively. The A and S superscripts/subscripts denote the solute and solvent molecules, respectively. The subscripts 00 and ii denote the ground and ith-excited states, respectively. The dipole moment and polarizability are denoted by p and α, respectively. The angle between p_{00}^{A} and p_{ii}^{A} is denoted by θ. The symbol c is the speed of light in a vacuum, h is Planck's constant, L is Avogadro's constant, ε_0 is the permittivity of a vacuum, M_r is the relative molecular mass, d is the density, and I_0 is the ionization potential of the ground state. In applying Eq. 1, the method of detailed calculations was the same as that used in Ref 2.

Macovei[5] has investigated in detail the effects of a solvent on the absorption maximum of the 41820 cm^{-1} band[6] of nitrobenzene in the vapor phase. Data for 13 solvents from his spectral data involving 26 solvents were chosen for this study. Data for protic solvents and for solvents lacking information regarding ionization potentials were excluded. Moreover, data for the solvents 1,2-dichloroethane, acetonitrile, and 1,4-dioxane were excluded. 1,2-Dichloroethane is a mixture of rotational isomers having different dipole moments. The aceonitrile molecule has a large dipole moment (3.92 D, where 1 D=3.333×10^{-30} C m). In Abe's theory,[4] the solvent molecule is assumed to have a small enough dipole moment that it is not tightly oriented with nitrobenzene (4.21 D). According to Marcus,[7] 1,4-dioxane has a dipole moment of 0.45 D. Which of 0 and 0.45 D should be used as the dipole moment of dioxane is not clear. Therefore, the datum for 1,4-dioxane was excluded. In applying Eq. 1, the temperature was assumed to be 20 °C. Data used for nitrobenzene were r_A=0.344 nm, $\alpha_{00}^{A}=126.29\times10^{-25}$ cm^3, I_0^{A}=9.88 eV, and $\cos\theta=1$.[3] The values of p_{ii}^{A} and α_{ii}^{A} estimated by means of Calculation 1 in Ref. 2 are 10.1 D and 397×10^{-25} cm^3, respectively. Even if a value of -1 was used for $\cos\theta$, the same excited-state values (i.e., $p_{ii}^{A}=-10.1$ D and $\alpha_{ii}^{A}=397\times10^{-25}$ cm^3) were still obtained. This supports the assumption that p_{00}^{A} and p_{ii}^{A} are collinear. By using the p_{ii}^{A} and α_{ii}^{A} values so estimated, one can calculate the frequencies. The correlation between the experimental frequencies ($\sigma_{0i,\,obsd}$) and the calculated ones ($\sigma_{0i,\,calcd}$) is shown in Fig. 1. On the whole, the correlation is good.

The present estimation of p_{ii}^{A}=10.1 D closely agrees with the experimental values of (9.5 ± 1)[3] and (9 ± 2)[8] D

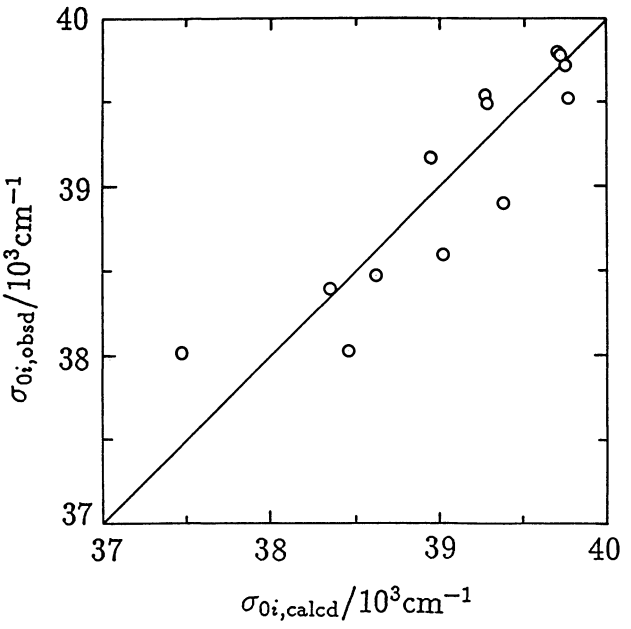

Fig. 1. A plot of $\sigma_{0i,obsd}$ vs. $\sigma_{0i,calcd}$.

determined from the electrooptical measurements. Several values for the excited-state dipole moment of nitrobenzene have hitherto been estimated from the solvent spectral frequency shifts: by applying McRae's equation,[9] Macovei[5] obtained $p_{ii}^{A}=7.19$ D. Using the simple equation based on the Onsager model,[10] Suppan and Ledger[11,12] obtained $p_{ii}^{A}=6.3$ D. Modifying the equation proposed by Amos and Burrows,[13] Millefiori et al.[14] obtained a good result of $p_{ii}^{A}-p_{00}^{A}=4.37$ D. By applying McRae's equation, Prabhumirashi obtained $p_{ii}^{A}=5.84$ D[15] and 7.99 D.[16] A comparable result for nitrobenzene, as determined by the electrooptical measurements and the present analysis, shows that Fq. 1 can be applied for estimating the excited-state dipole moment of a polar solute molecule, as already described in Ref. 2.

References

1) For example, see Ref. 2.
2) T. Abe and I. Iweibo, *Bull. Chem. Soc. Jpn.*, **58**, 3415 (1985).
3) H. K. Sinha and K. Yates, *J. Chem. Phys.*, **93**, 7085 (1990).
4) T. Abe, *Bull. Chem. Soc. Jpn.*, **54**, 327 (1981).
5) V. Macovei, *Rev. Roum. Chim.*, **21**, 1137 (1976).
6) W. M. Schubert, H. Steadly, and J. M. Craven, *J. Am. Chem. Soc.*, **82**, 1353 (1960).
7) Y. Marcus, "Ion Solvation," John Wiley and Sons, Chichester (1985), p. 139.
8) H. Labhart and G. Wagniere, *Helv. Chim. Acta*, **46**, 1314 (1963).
9) E. G. McRae, *J. Phys. Chem.*, **61**, 562 (1957).
10) L. Onsager, *J. Am. Chem. Soc.*, **58**, 1486 (1936).
11) M. B. Ledger and P. Suppan, *Spectrochim. Acta, Part A*, **23**, 641 (1967).
12) P. Suppan, *J. Chem. Soc., Part A*, **1968**, 3125.
13) A. T. Amos and B. L. Burrows, *Adv. Quant. Chem.*, **7**, 289 (1973).
14) S. Millefiori, F. Zuccarello, and G. Buemi *J. Chem. Soc., Perkin Trans. 2*, **1978**, 849.
15) L. S. Prabhumirashi, *Spectrochim. Acta, Part A*, **39**, 91 (1983).
16) L. S. Prabhu Mirashi and S. S. Kunte, *Spectrochim. Acta, Part A*, **45**, 1147 (1989).

Synthesis and Crystal Structure of Seven-Coordinate (*trans*-1,2-Cyclohexanediamine-*N,N,N',N'*-tetraacetato)aquavanadate(III)

Mamoru SHIMOI, Shigeru MIYAMOTO, and Hiroshi OGINO*
Department of Chemistry, Faculty of Science, Tohoku University, Aoba-ku, Sendai 980
(Received January 25, 1991)

Synopsis. Potassium, sodium, and ammonium salts of $[V(cydta)(H_2O)]^-$ complexes were prepared, where cydta denotes *trans*-1,2-cyclohexanediamine-*N,N,N',N'*-tetraacetate. Crystal structure analysis of $Na[V(cydta)(H_2O)]\cdot 5H_2O$ revealed that the vanadium(III) atom adopts a capped trigonal-prism structure, a cydta acting as a sexidentate ligand and an aqua ligand occupying the capping position.

Usually vanadium(III) forms complexes with coordination number six.[1] However, we have recently shown that vanadium(III) forms seven-coordinate complexes with edta and hedtra,[2] the geometries of which are capped-trigonal prisms.[3-5] Our current work investigates whether vanadium(III) adopts the same structure with other edta-type aminopolycarboxylates. Here we report the synthesis and crystal structure of a cydta complex of vanadium(III). In contrast to the well known pentagonal bipyramidal structures of iron(III)-EDTA complexes,[6-8] the iron(III)–CyDTA complex adopts a capped trigonal prismatic structure.[9] This suggests that vanadium(III)–CyDTA might also adopt a capped trigonal prismatic structure. This hypothesis is experimentally confirmed. The structures of capped trigonal-prism complexes with edta-like ligands are compared.

Experimental

General Procedure. The complexes were prepared under a nitrogen atmosphere. A column (10 mmϕ) of Dowex 50W-X8 (50—100 mesh) was used for exchanging cation in vanadium(III)–CyDTA complex.

Synthesis of $K[V(cydta)(H_2O)]\cdot 2H_2O$ (1a). To a suspension of 7.29 g (20 mmol) of H_4cydta in 50 cm^3 of water was added 2.76 g (20 mmol) of potassium carbonate. The addition of VCl_3 (3.15 g, 20 mmol) to the solution results in a dark green gel. Upon addition of 4.00 g of potassium hydrogencarbonate (40 mmol), the gel dissolved and the color of the solution turned to brown. The solution volume was reduced to 20 cm^3 by evaporation, and the pale brown precipitate was collected by filtration and washed with water and ethanol successively. Yield 6.67 g (69%). Found: C, 34.56; H, 4.86; N, 5.77%. Calcd for $C_{14}H_{24}KN_2O_{11}V$: C, 34.57; H, 4.97; N, 5.76%.

Syntheses of $Na[V(cydta)(H_2O)]\cdot 5H_2O$ (1b) and $NH_4[V(cydta)(H_2O)]\cdot 4H_2O$ (1c). An aqueous solution (5 cm^3) of **1a** (1.0 g, 2.0 mmol) was passed through a column packed with 3.8 cm^3 of Na-type cation exchange resin. Brown plate crystals suitable for X-ray diffraction work were obtained by standing the aqueous solution in a methanol vapor. Found: C, 32.74; H, 5.53; N, 4.90%. Calcd for $C_{14}H_{30}N_2NaO_{14}V$: C, 32.07; H, 5.77; N, 5.34%.[10]

1c was obtained by almost the same procedure as the sodium salt. Found: C, 33.57; H, 6.11; N, 8.00%. Calcd for $C_{14}H_{32}N_3O_{13}V$: C, 33.54; H, 6.43; N, 8.38%.

X-Ray Crystal Structure Determination of 1b. General procedures for data collection and analysis are the same as those described in the previous paper.[5] Crystal data are listed in Table 1. As one of the sites of water of crystallization was found to be partially occupied, the occupancy factor was also refined to give the value 0.25. Anisotropic temperature factors were applied for the non-hydrogen atoms except for the partially occupied oxygen atom. The coordinates of hydrogen atoms attached to carbon atoms were calculated and fixed.

Table 1. Crystal Data for $Na[V(cydta)(H_2O)]\cdot 5H_2O$

Formula	$C_{14}H_{30}N_2NaO_{14}V$
Fw	524.39
Crystal system	Orthorhombic
Space group	*Pbca*(No. 61)
a/Å	13.806(2)
b/Å	22.799(3)
c/Å	13.472(2)
U/Å^3	4240(1)
Z	8
d_{calcd}/g cm^{-3}	1.60
d_{measd}/g cm^{-3}	1.59
μ(Mo $K\alpha$)/cm^{-1}	5.94
Cryst size/mm	0.4×0.3×0.4
Temp/°C	20
2θ range/deg	3—60
Scan mode	ω–2θ
ω-scan width/deg	1.0+0.35 tan θ
No. of unique data	6856
No. of data used with $\lvert F_o\rvert>3\sigma(F_o)$	3057
R[a]	0.078
R_w[b]	0.090

a) $R=\sum\lvert\lvert F_o\rvert-\lvert F_c\rvert\rvert/\sum\lvert F_o\rvert$ b) $R_w=[\sum w(\lvert F_o\rvert-\lvert F_c\rvert)^2/\sum w\lvert F_o\rvert^2]^{1/2}$; $w=[\sigma^2(\lvert F_o\rvert)+aF_o^2]^{-1}$, where a is 0.0015.

Results and Discussion

Bond lengths and angles around the vanadium atom were listed in Table 2.[11] An ORTEP drawing of the $[V(cydta)(H_2O)]^-$ anion is shown in Fig. 1. Cydta acts as a sexidentate ligand and a water molecule occupies the seventh coordination site, thus the geometry is a monocapped twisted trigonal-prism which resembles $[V(hedtra)(H_2O)]$[3] and $[V(edta)(H_2O)]^-$.[4,5] The N(1)–O(1)–O(3) and N(2)–O(5)–O(7) planes are almost parallel, the dihedral angle between the planes being 4.1°. The complex has an approximate 2-fold axis through the vanadium–aqua bond, although it has some tendency to form a 4:3 piano stool structure[12] like edta complexes: planarity of N(1)–N(2)–O(7)–O(1) (deviations from the least-squares plane are 0.15, −0.17, −0.11, and 0.17 Å) is much better than N(1)–N(2)–O(5)–O(3) (0.33, −0.26, −0.28, and 0.27 Å) and the former plane is parallel to O(3)–O(5)–O(W), the dihedral angle between the planes being 3.0°. The cyclohexane ring takes the chair form as expected.

Table 3 compares the torsion angles[13] of edta and

Table 2. Interatomic Distances and Angles for Na[V(cydta)(H_2O)]·5H_2O (**1b**)

Bond length	l/Å	Bond length	l/Å
V–N(1)	2.244 (5)	V–N(2)	2.240 (5)
V–O(1)	2.085 (4)	V–O(3)	2.045 (5)
V–O(5)	2.050 (4)	V–O(7)	2.043 (5)
V–O(W1)	2.083 (5)		
Bond angle	**ϕ/deg**	**Bond angle**	**ϕ/deg**
O(1)–V–O(W1)	73.5 (2)	O(3)–V–O(W1)	87.0 (2)
O(5)–V–O(W1)	78.3 (2)	O(7)–V–O(W1)	90.9 (2)
O(W1)–V–N(1)	134.1 (2)	O(W1)–V–N(2)	149.2 (2)
O(1)–V–O(3)	107.1 (2)	O(5)–V–O(7)	92.2 (2)
O(1)–V–O(7)	79.6 (2)	O(3)–V–O(5)	79.9 (2)
O(1)–V–N(1)	72.3 (2)	O(3)–V–N(1)	74.9 (2)
O(5)–V–N(2)	74.0 (2)	O(7)–V–N(2)	77.0 (2)
O(1)–V–O(5)	150.4 (2)	O(3)–V–O(7)	172.0 (2)
O(1)–V–N(2)	130.1 (2)	O(3)–V–N(2)	101.1 (2)
O(5)–V–N(1)	136.3 (2)	O(7)–V–N(1)	111.8 (2)
N(1)–V–N(2)	76.5 (2)		

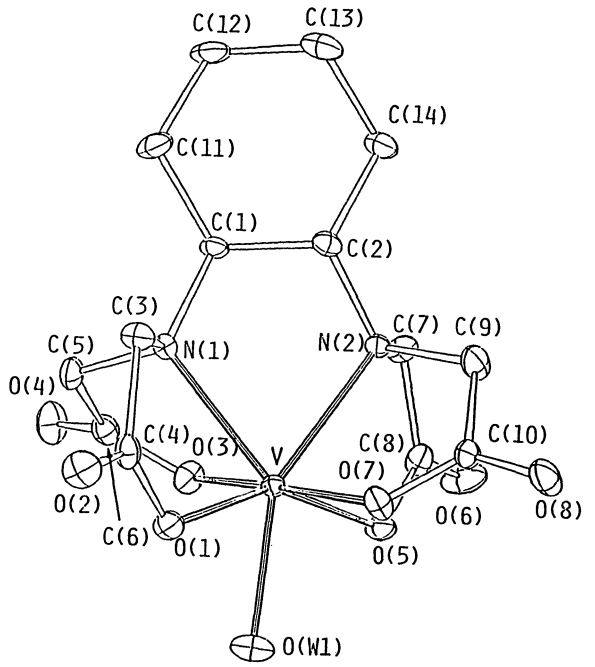

Fig. 1. ORTEP diagram of the [V(cydta)(H_2O)]$^-$ anion in Na[V(cydta)(H_2O)]·5H_2O. Hydrogen atoms are omitted for clarity.

edta-related complexes with capped trigonal prism structures. The range of angles is quite wide but all are less than 27°. In pentagonal bipyramidal structures such as [Fe(edta)(H_2O)]$^-$, the corresponding angles are more than 45°.[6-8] A capped trigonal-prism structure is also reported for [Fe(cydta)(H_2O)]$^-$,[9] but the torsion angles for [Fe(cydta)(H_2O)]$^-$ are much larger than those for [V(cydta)(H_2O)]$^-$. The average bond lengths between metal and donor atoms are 2.127 and 2.113 Å for the iron and vanadium complexes, respectively. This difference is slightly larger than that of Shannon's ionic radii ($r_{Fe^{3+}}$=0.0645 Å vs. $r_{V^{3+}}$=0.0640 Å).[14]

The sodium ion is six-coordinate with crystal water molecules and carboxylato oxygen atoms with Na–O bond lengths in the range 2.331 (6)—2.727 (5) Å. The sodium ions and water molecules form a hydrophilic sheet along the [020] plane, and the complex anions are layered between them. The partially occupied water molecule is not connected to any of the surrounding atoms via hydrogen bonding.

Table 3. Comparison of Torsion Angles of Capped Trigonal-Prismatic Seven-Coordinate Complexes with edta and Related Ligands

Complex	θ_1/deg	θ_2/deg	θ_3/deg
[V(hedtra)(H_2O)][a]	16.25 (6)	11.10 (7)	14.80 (7)
Na[V(edta)(H_2O)]·3H_2O[b]	14.79 (8)	3.49 (8)	21.09 (8)
NH_4[V(edta)(H_2O)]·2.5H_2O[b]	12.2 (1)	2.1 (1)	18.2 (1)
	9.7 (1)	4.2 (1)	18.2 (1)
Na[V(cydta)(H_2O)]·5H_2O[c]	20.0 (2)	13.0 (2)	22.3 (2)
Ca[Fe(cydta)(H_2O)]·8H_2O[d]	26.9 (2)	26.3 (2)	23.4 (2)

a) Ref. 3. b) Ref. 5. c) This work. d) Ref. 9.

Thus, the cydta complex of vanadium(III) also forms a capped trigonal-prismatic seven-coordinate complex as do the edta and hedtra complexes. Although the geometry is more symmetrical than the edta complex, it shows some tendency towards a 4:3 piano stool structure similarly to the edta complex.

References

1) L. V. Boas and J. C. Pessoa, "Comprehensive Coordination Chemistry," ed by G. Wilkinson, Pergamon, Oxford (1987), Vol. 3, pp. 453—583.

2) Abbreviations used in this paper: cydta, *trans*-1,2-cyclohexanediamine-*N,N,N',N'*-tetraacetate; edta, ethylenediamine-*N,N,N',N'*-tetraacetate; hedtra, *N'*-(2-hydroxyethyl)-ethylenediamine-*N,N,N'*-triacetate.

3) H. Ogino, M. Shimoi, and Y. Saito, *Inorg. Chem.*, **28**, 3596 (1989).

4) M. Shimoi, Y. Saito, and H. Ogino, *Chem. Lett.*, **1989**, 1675.

5) M. Shimoi, Y. Saito, and H. Ogino, submitted to *Bull. Chem. Soc. Jpn.*

6) M. D. Lind, M. J. Hamor, T. A. Hamor, and J. L. Hoard, *Inorg. Chem.*, **3**, 34, (1964).

7) X. Solans, M. F. Altaba, and J. Garcia-Oricain, *Acta Crystallogr., Sect. C*, **40**, 635 (1984).

8) X. Solans, M. Font-Altaba, and J. Garcia-Oricain, *Acta Crystallogr., Sect. C*, **41**, 525 (1985).

9) G. H. Cohen and J. L. Hoard, *J. Am. Chem. Soc.*, **88**, 3228 (1966).

10) As shown later, the fifth crystal water molecule is easy to effloresce and the analytical values are in better agreement with the calculated ones for [V(cydta)(H_2O)]·4.25H_2O ($C_{14}H_{28.5}O_{13.25}N_2NaV$): C, 32.91; H, 5.62; N, 5.48%.

11) Final atomic parameters, some additional bond lengths and angles, crystal packing diagram, and F_o-F_c tables are deposited as Document No. 8950 at the Office of the Editor of Bull. Chem. Soc. Jpn.

12) E. B. Dreyer, C. T. Lam, and S. J. Lippard, *Inorg. Chem.*, **18**, 1904 (1979).

13) Torsion angles θ_1, θ_2, and θ_3 are defined as the dihedral angles N(1)–CE1–CE2–N(2), O(1)–CE1–CE2–O(7), and O(3)–CE1–CE2–O(5), where CE1 and CE2 are the centers of gravity of the triangles N(1)–O(1)–O(3) and N(2)–O(5)–O(7). See Ref. 5.

14) R. D. Shannon and C. T. Prewitt, *Acta Crystallogr., Sect. B*, **25**, 925 (1969); R. D. Shannon, *Acta Crystallogr., Sect. A*, **32**, 751 (1976).

Circular Dichroism Spectrum of C_i-*trans*(O)-[Co(C(*S*)-edma-d_1)$_2$]$^+$ Containing Chiral Methylene Formed by Stereospecific Deuteration

Tomoharu AMA,* Takaji YASUI, and Jinsai HIDAKA†
Department of Chemistry, Faculty of Science, Kochi University, Akebono-cho, Kochi 780
†Department of Chemistry, University of Tsukuba, Tsukuba, Ibaraki 305
(Received March 25, 1991)

Synopsis. C_i-*trans*(O)-[Co(C(*S*)-edma-d_1)$_2$]$^+$ was prepared by way of the stereospecific deuteration of the facially coordinated edma (ethylenediamine-*N*-acetate) in $(-)^{CD}_{543}$-C_2-*trans*(O)-[Co(edma)$_2$]$^+$. The vicinal CD spectrum due to the C(*S*)-edma-d_1 in the C_i-*trans*(O) complex was investigated in connection with the D→H exchange in the ligands, suggesting a two-step mechanism.

Ethylenediamine-*N*-acetate (edma=$NH_2CH_2CH_2$-$NHCH_2COO^-$) coordinates to cobalt(III) to form various geometrical and optical isomers.[1–5] Of these isomers, the one in which edma coordinated facially to cobalt(III) has been remarked because of the characteristic reactivity of the coordinated edma. In the course of our studies on stereochemistry of Co(III) complexes with edma and its derivatives, it was found that one of the methylene protons in the glycinate moiety (G-ring) of the facially coordinated edma is stereospecifically deuterated in a basic D_2O solution to form an asymmetric center; $NH_2CH_2CH_2NHC^*HDCOO^-$.[2] This note is concerned with the preparation of optically active edma (C(*S*)-edma-d_1) due to the stereospecific deuteration of $(-)^{CD}_{543}$-C_2-*trans*(O)-[Co(edma)$_2$]$^+$,[6] and the preparation and CD spectrum of C_i-*trans*(O)-[Co(C(*S*)-edma-d_1)$_2$]$^+$[6] which has only the vicinal CD contribution arising from the asymmetric carbon atoms, -C*HD-, of the ligands.

Experimental

Preparation of Complexes. $(-)^{CD}_{543}$-C_2-*trans*(O)-[Co(edma)$_2$]Cl and C_i-*trans*(O)-[Co(edma)$_2$](ClO$_4$): These complexes were prepared according to the method described in the previous paper[2] and the absolute configuration of $(-)^{CD}_{543}$-C_2-*trans*(O)-[Co(edma)$_2$]Cl has been determined as $\Delta\Delta\Delta$(N_R, N_R).[2]

***C_i*-trans(O)-[Co(C(*S*)-edma-d_1)$_2$](ClO$_4$):** A buffer solution (pH 10.30) was prepared by adding a few drops of 2 mol dm^{-3} DCl–D_2O to a solution containing 1.0 g of Na_2CO_3 in 20 cm^3 of D_2O. About 1.0 g of $(-)^{CD}_{543}$-C_2-*trans*(O) isomer was dissolved into the buffer solution (20 cm^3), and the solution was kept at 40.0 °C for ca. 25 min in order to deuterate one of the two protons in the methylene of G-ring in the facially coordinated edma.[2] The deuteration of the G-ring $-CH_2-$ was confirmed by means of ^{1}H NMR measurements (Fig. 2). The solution was acidified to pH 6 with 2 mol dm^{-3} HCl to stop the reaction. Zinc powder (2 g) was added to the solution to reduce the central cobalt(III) to cobalt(II), and then the mixture was stirred for 5 min at room temperature (about 20 °C). After the excess of zinc was filtered off, lead dioxide (7 g) was added to the solution adjusted to pH 6. The mixture was stirred for 15 min at room temperature to reconstitute the cobalt(III) complex with the deuterated edma. After the reactant solution had been filtered, the filtrate was poured onto a column of SP-Sephadex (Na^+ form, 5.0 cm×60 cm) and then the adsorbed band was eluted with a 0.2 mol dm^{-3} NaCl aqueous solution. Three bands: brown (by-product), red, and another red (other geometrical isomers of deuterated [Co(edma)$_2$]$^+$), were eluted in this order.[1,2] After the earlier red band containing the deuterated C_2-*trans*(O) and C_i-*trans*(O) isomers was eluted out, two drops of 1 mol dm^{-3} acetic acid solution was added to the eluate and then the eluate was concentrated to ca. 50 cm^3 in a rotary evaporator under reduced pressure at 35 °C. Addition of about 1 cm^3 of saturated $NaClO_4$ solution to the concentrated solution gave the crude C_i-*trans*(O) isomer as fine yellowish orange crystals. The ClO_4^- salt of C_i-*trans*(O) is less soluble than that of C_2-*trans*(O) isomer. The crystals were quickly filtered and washed with a few milliliters of cold water. Recrystallization was carried out from a small amount of warm water by addition of five drops of saturated $NaClO_4$ solution. Found: C, 24.42; H, 4.61; N, 14.05%. Calcd for C_i-*trans*(O)-[Co(C(*S*)-edma-d_1)$_2$](ClO$_4$) (F.W.=394.65): C, 24.35; H (1.008×18/F.W.), 4.60; N, 14.20%.[8]

Measurements. The absorption and CD spectra were measured by a JASCO UVIDEC 670-type spectrophotometer and JASCO J-22 and J-600 spectropolarimeters, respectively. The ^{1}H NMR spectra were recorded on a Hitachi R-90H Fourier Transform NMR spectrometer, using TSP [3-(trimethylsilyl)propionic-2,2,3,3-d_4 acid sodium salt] as an internal standard.

Results and Discussion

The two geometrical isomers in this report, C_2-*trans*(O)-[Co(edma)$_2$]$^+$ and C_i-*trans*(O)-[Co(edma)$_2$]$^+$ are illustrated in Fig. 1. The ^{1}H NMR spectrum of the starting complex, $(-)^{CD}_{543}$-C_2-*trans*(O)-[Co(edma)$_2$]$^+$, right after dissolving in basic D_2O solution shows an AB quartet signal (at δ=ca. 3—4) due to the methylene protons of G-ring (Fig. 2(a)). The two higher-field and two lower-field peaks of this AB quartet have been assigned to the inside methylene proton (H_a in Fig. 3(a)) and the outside one (H_b in Fig. 3(a)), respectively.[2] Moreover, it has been known that one of the G-ring methylene protons in $(-)^{CD}_{543}$-C_2-*trans*(O)-[Co(edma)$_2$]$^+$ is stereospecifically deuterated in a basic D_2O solution, namely, the outside proton (H_b) is deuterated faster than the inside one (H_a).[2] In fact, the lower-field peaks (H_b) disappeared and the higher-field ones (H_a) turned out to the singlet one, twenty-five minutes after dissolving in the solution (Fig. 2(b)). This spectral behavior indi-

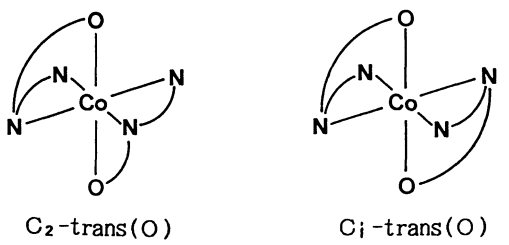

Fig. 1. Two geometrical isomers, C_2-*trans*(O)- and C_i-*trans*(O)-[Co(edma)$_2$]$^+$.

cates that one of the G-ring methylene protons in $(-)^{CD}_{543}$-C_2-*trans*(O)-[Co(edma)$_2$]$^+$ was deuterated to form asymmetric centers, –C*HD–. Here, it is to be noted that the G-ring methylene carbons are regulated to C(*S*) configuration, because both the secondary nitrogen atoms of the facially coordinated ligands in $(-)^{CD}_{543}$-C_2-*trans*(O)-[Co(edma)$_2$]$^+$ take N(*R*) configuration (Fig. 3(b)). $(-)^{CD}_{543}$-C_2-*trans*(O)-[Co(C(*S*)-edma-d_1)$_2$]$^+$ thus obtained was converted into C_i-*trans*(O)-[Co(C(*S*)-edma-d_1)$_2$]$^+$ (Fig. 3(c)) as described in experimental section.

The absorption and CD spectra in the d-d transition band region of $(-)^{CD}_{543}$-C_2-*trans*(O)-[Co(C(*S*)-edma-d_1)$_2$]$^+$ and the converted complex are shown in Fig. 4. The absorption spectral pattern of the latter differs significantly from that of the former and then, coincides with that of the C_i-*trans*(O)-[Co(edma)$_2$]$^+$,[2] suggesting that the converted complex takes a C_i-*trans*(O) geometry. When the formation of this C_i-*trans*(O) complex proceeded with retention of the configuration of C(*S*)-edma-d_1, the secondary nitrogen atoms of the coordinated ligands should take N(*R*) configuration for C(*S*)edma-d_1 having inside proton and N(*S*) configuration for C(*S*)-edma-d_1 having outside proton, as shown in Fig. 3(c). This is confirmed from the comparison with ^{1}H NMR spectra (Figs. 5(a) and (b)) of C_i-*trans*(O)-[Co(edma)$_2$]$^+$ and the converted C_i-*trans*(O) complex, in line with the assignment of $(-)^{CD}_{543}$-C_2-*trans*(O)-[Co(edma)$_2$]$^+$ and the deuterated one. Namely, two singlet peaks (at δ=ca. 4.1 and ca. 3.3) due to two G-ring –C*HD– are observed for the spectrum of the converted C_i-*trans*(O) complex (Fig. 5(b)), and the signal peak at δ=ca. 4.1 is assigned to the outside proton and the peak at δ=ca. 3.3 to the inside one. Thus, the converted C_i-

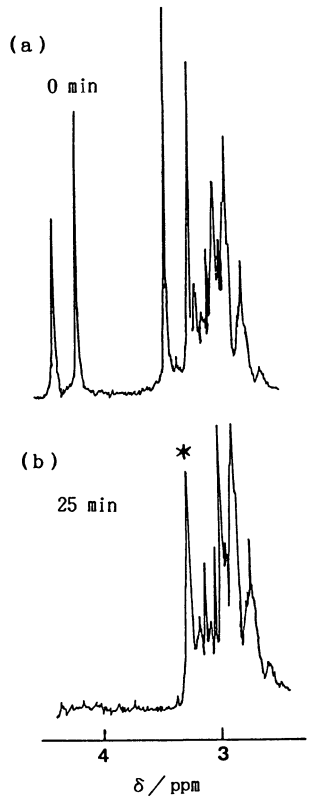

Fig. 2. ^{1}H NMR spectral change with time of $(-)^{CD}_{543}$-C_2-*trans*(O)-[Co(edma)$_2$]$^+$ in basic D_2O solution. Asterisked peak: G-ring –C*HD–.

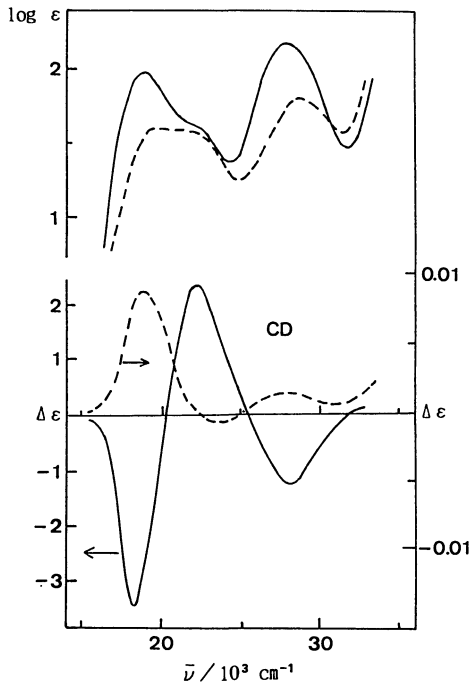

Fig. 4. Absorption and CD spectra of C_i-*trans*(O)-[Co(C(*S*)-edma-d_1)$_2$]$^+$ (——) and $(-)^{CD}_{543}$-C_2-*trans*(O)-[Co(C(*S*)-edma-d_1)$_2$]$^+$ (——).

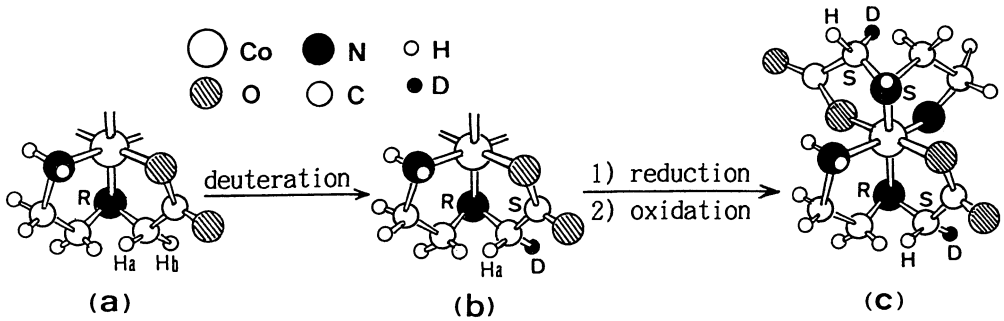

Fig. 3. Stereoselective deuteration on the G-ring –CH_2– of the facially coordinated edma. (a): Undeuterated edma; (b) stereospecifically deuterated edma; and (c): C_i-*trans*(O)-[Co(C(*S*)-edma-d_1)$_2$]$^+$ converted from $(-)^{CD}_{543}$-C_2-*trans*(O)-[Co(C(*S*)-edma-d_1)$_2$]$^+$.

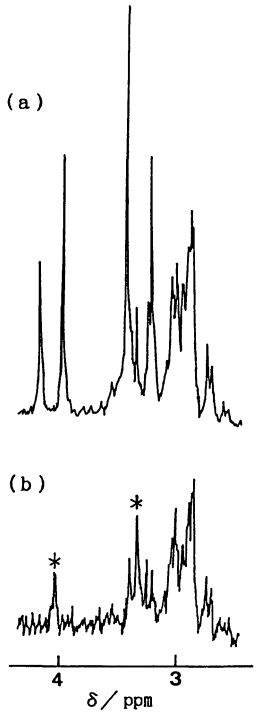

Fig. 5. ^{1}H NMR spectra of C_i-*trans*(O)-[Co(edma)$_2$]$^+$. (a) Undeuterated complex and (b) deuterated complex. Asterisked peaks: G-ring –C*HD–.

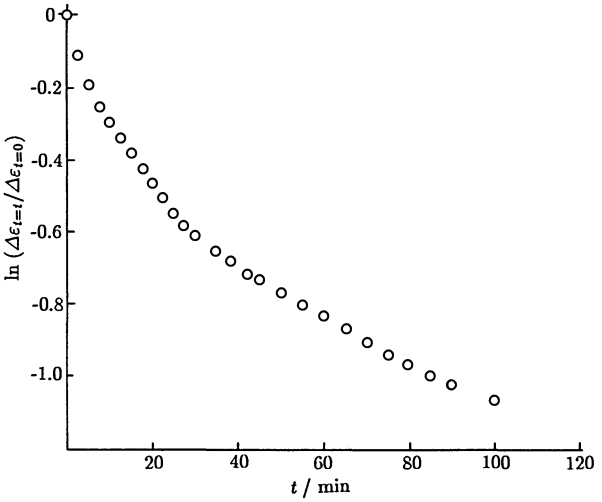

Fig. 6. The time-course change of CD intensity for C_i-*trans*(O)-[Co(C(*S*)-edma-d_1)$_2$]$^+$ which was kept in a buffered aqueous solution (pH 10.33) at 40.1 °C.

trans(O) complex is assigned to C_i-*trans*(O)-[Co(C(*S*)-edma-d_1)$_2$]$^+$.

In the d-d transition band region, C_i-*trans*(O)-[Co(C(*S*)-edma-d_1)$_2$]$^+$ shows extremely weak CD bands ($\Delta\varepsilon$: +0.0084 at 19000 cm^{-1} and +0.0018 at 27500 cm^{-1}) whose sign pattern differs obviously from that of $(-)^{CD}_{543}$-C_2-*trans*(O)-[Co(C(*S*)-edma-d_1)$_2$]$^+$ (Fig. 4). This reflects that the optical activity of the C_i-*trans*(O) complex arises only from the asymmetric carbon atoms, –C*HD–, of the ligands, while that of the $(-)^{CD}_{543}$-C_2-*trans*(O) complex is contributed from the configuration *Δ* of complex and asymmetric nitrogen atoms, N(*R*)N(*R*), besides that from –C*HD– of the ligands. In general, the vicinal CD contribution arising from the asymmetric carbon atom of coordinated ligand is very weak in intensity compared with the CD contribution from the configurational chirality, for example, [Co(L-ala)(NH$_3$)$_4$]$^{2+}$ shows weak CD bands ($\Delta\varepsilon$: ca. −0.02, +0.07, and −0.22 at 18300, 19500, and 20200 cm^{-1}, respectively) in the d-d transition region.[7] In the corresponding region, C_i-*trans*(O)-[Co(C(*S*)-edma-d_1)$_2$]$^+$ shows much weaker CD intensity than [Co(L-ala)(NH$_3$)$_4$]$^{2+}$ (Fig. 4). This may be ascribed to the difference between the substituents on the methylene carbon of the ligands, namely, –C*H(CH$_3$)– and –C*HD–.

C_i-*trans*(O)-[Co(C(*S*)-edma-d_1)$_2$]$^+$ loses its optical activity by D→H exchange of the ligands in an aqueous solution and the CD change with time at 525 nm is shown in Fig. 6. The exchange seems to proceed with two steps and the two $t_{1/2}$ values are roughly estimated from the figure as 8.8 and 130 min. Taking into consideration that the outside proton (H$_b$) exchanges more easily than the inside one (H$_a$) in the deuteration,[2] it is probable that the earlier step results from the exchange of outside D with H on C(*S*)-edma-d_1 having N(*R*) configuration and the later step from the exchange of inside D on C(*S*)-edma-d_1 having N(*S*) configuration. The ratio of the exchange rates of the outer and inner D is about 15.

References

1) T. Yasui, H. Kawaguchi, and T. Ama, *Chem. Lett.*, **1983**, 1277.
2) T. Ama, H. Kawaguchi, T. Yasui, K. Matsumoto, and S. Ooi, *Bull. Chem. Soc. Jpn.*, **58**, 2561 (1985).
3) T. Ama, R. Niiyama, H. Kawaguchi, and T. Yasui, *Bull. Chem. Soc. Jpn.*, **60**, 119 (1987).
4) T. Yasui, T. Shikiji, N. Koine, T. Ama, and H. Kawaguchi, *Bull. Chem. Soc. Jpn.*, **60**, 595 (1987).
5) H. Kawaguchi, H. Fukaki, T. Ama, T. Yasui, K. Okamoto, and J. Hidaka, *Bull. Chem. Soc. Jpn.*, **61**, 2359 (1988).
6) The prefixes C_2 and C_i denote that the *trans*(O) complex ion has a C_2 axis or inversion center.
7) T. Yasui, J. Hidaka, and Y. Shimura, *Bull. Chem. Soc. Jpn.*, **39**, 2417 (1966).
8) A TCD cell-type C,H,N-Analyzer which was normalized to natural H was used for the present elemental analysis. Accordingly, atomic weight of D in the analyzed gas can be regarded to 1.01 as within the experimental error. However, weighing the sample, the atomic weight of D should be regarded to 2.01.

Preparation and X-Ray Crystal Structure of *trans*-Dinitro(1,4,7,10-tetraazacycloheptadecane)cobalt(III) Tetrafluoroborate, *trans*-[$Co(NO_2)_2(N_410)$]BF_4

Masanobu TSUCHIMOTO, Masakazu KITA, and Junnosuke FUJITA,*
Department of Chemistry, Faculty of Science, Nagoya University,
Chikusa-ku, Nagoya 464-01
(Received March 28, 1991)

Synopsis. A new tetraaza-macrocyclic complex involving a ten-membered chelate ring, *trans*-[$Co(NO_2)_2(N_410)$]BF_4 (N_410=1,4,7,10-tetraazacycloheptadecane) was prepared and the structure was determined by the X-ray diffraction method. The ten-membered chelate ring takes a distorted boat–chair–boat form with the N–Co–N bite angle of 105.4(1)°.

In previous papers,[1–3] we reported the preparation and characterization of 1,4,7,10-tetraazacyclotetradecane (N_47), -pentadecane (N_48), and -hexadecane (N_49) complexes of Co(III), which involve a seven-, eight-, and nine-membered chelate ring, respectively. In this note, we report the preparation and crystal structure of a new *trans*-dinitrocobalt(III) complex with 1,4,7,10-tetraazacycloheptadecane (N_410) which involves a ten-membered chelate ring.

Experimental

1,4,7,10-Tetrakis(*p*-tolylsulfonyl)-1,4,7,10-tetraazacycloheptadecane (1) and 1,4,7,10-Tetraazacycloheptadecane Trihydrobromide (2). **1** was prepared by a method similar to those for analogous cyclotetradecane, -pentadecane, and -hexadecane.[4] ^{13}C NMR ($CDCl_3$, TMS) δ=21.5(C–Ts–), 25.3, 27.2, 28.0(C–C–C), 48.7, 49.9, 50.2, 50.7(N–C–C), 127.3, 127.4, 129.6, 129.8, 135.1, 135.2, 143.3, 143.6(phenyl). **1** was detosylated by refluxing in a mixture of 47% hydrobromic acid and acetic acid for 2 d to give **2**, which was recrystallized from water and ethanol. Found: C, 32.08; H, 6.89; N, 11.41%. Calcd for $C_{13}H_{33}N_4Br_3$: C, 32.19; H, 6.86; N, 11.55%. ^{13}C NMR (D_2O, dioxane(δ=67.4)) δ=24.9, 26.7(C–C–C), 44.3, 45.3, 46.8, 47.6(N–C–C).

***trans*-[$Co(NO_2)_2(N_410)$]BF_4.** This complex was prepared by oxidizing an aqueous solution containing $CoCl_2\cdot 6H_2O$, $NaNO_2$ and N_410 with air according to a method similar to those for the corresponding N_48 and N_49 complexes.[1] Found: C, 32.67; H, 6.35; N, 17.72%. Calcd for $C_{13}H_{30}N_6O_4Br_4Co$: C, 32.52; H, 6.30; N, 17.50%. ^{13}C NMR (DMSO-d_6, TMS) δ=22.0, 26.1, 27.2(C–C–C), 49.8, 52.4, 54.3, 56.5(N–C–C). Electronic spectra {in CH_3CN, $\tilde{\nu}/10^3$ cm^{-1} ($\log(\varepsilon/mol^{-1}\,dm^3\,cm^{-1})$)}: 21.5(2.53), 28.2(3.59), 38.7(4.36).

^{13}C NMR spectra were obtained on a Hitachi R-90HS spectrometer, and electronic spectra on a Hitachi U-3400 spectrophotometer.

Crystal Structure Determination. Crystals of *trans*-[$Co(NO_2)_2(N_410)$]BF_4 were grown by slow evaporation of an aqueous solution of the complex. An orange crystal of approximate dimensions 0.83×0.43×0.63 mm^3 was used for the measurement.

Crystal Data: *trans*-[$Co(NO_2)_2(C_{13}H_{30}N_4)$]$BF_4$, MW=480.2, monoclinic, $P2_1/n$, a=11.982(1), b=19.340(2), c=9.698(1) Å, β=113.63(1)°, V=2059.0(4) Å^3, Z=4, D_c=1.549 g cm^{-3}, D_m=1.55 g cm^{-3}, μ(Mo$K\alpha$)=8.955 cm^{-1}. Diffraction data were collected on a Rigaku AFC-5R diffractometer with graphite monochromatized Mo$K\alpha$ radiation (λ=0.71069 Å). The ω–2θ scan technique was employed with the scan rate 4/° min^{-1} and the scan range 1.2+0.5tanθ/°. Within the range $2\theta<60°$, 6124 independent reflections were measured. No absorption correction was applied.

Table 1. Positional Parameters (×10^4; ×10^5 for Co) and Equivalent Isotropic Temperature Factors[8]

Atom	x	y	z	B_{eq}/Å^2
Co	26722(3)	15241(2)	42579(4)	2.6
F(1)	8167(5)	1180(2)	3606(4)	9.6
F(2)	8627(14)	1262(4)	6012(7)	26.6
F(3)	7423(5)	2032(3)	4541(7)	12.6
F(4)	9200(6)	2004(6)	5050(9)	18.3
O(1)	1305(2)	1980(2)	1320(3)	5.0
O(2)	266(2)	1929(2)	2627(3)	5.4
O(3)	4260(2)	510(1)	6024(3)	4.7
O(4)	4845(2)	1518(2)	6853(3)	5.5
N(1)	1947(2)	554(1)	3849(3)	3.4
N(2)	1757(2)	1617(2)	5497(3)	3.9
N(3)	3254(2)	2445(1)	4937(3)	3.5
N(4)	3676(2)	1604(1)	3035(3)	3.0
N(5)	1255(2)	1864(1)	2537(3)	3.6
N(6)	4098(2)	1139(1)	5920(3)	3.3
C(1)	1285(4)	444(2)	4865(5)	5.0
C(2)	1712(4)	937(3)	6168(5)	5.1
C(3)	2188(4)	2232(3)	6492(5)	5.4
C(4)	2438(4)	2782(2)	5551(5)	4.9
C(5)	3527(3)	2806(2)	3767(5)	4.3
C(6)	4286(3)	2306(2)	3333(4)	4.1
C(7)	4569(3)	1044(2)	3124(4)	3.6
C(8)	4832(4)	963(2)	1722(5)	4.9
C(9)	3777(4)	722(3)	290(5)	5.6
C(10)	3337(5)	−24(3)	291(6)	6.4
C(11)	2672(4)	−188(2)	1307(5)	5.3
C(12)	1674(3)	318(2)	1157(4)	4.4
C(13)	1143(3)	283(2)	2326(4)	4.3
B	8255(5)	1564(3)	4824(6)	5.5

The calculations were carried out on a HITAC M-680H computer at the Computer Center of Institute for Molecular Science with the program system UNICS III.[5] The structure was solved by the heavy-atom method using 4831 unique reflections with $|F_o|>3\sigma(|F_o|)$. The function $\sum w(|F_o|-|F_c|)^2$ was minimized by block-diagonal least-squares with anisotropic thermal parameters for non-hydrogen atoms and isotropic for hydrogen atoms. Complex neutral-atom scattering factors were used.[6] The positions of all hydrogen atoms were identified in the difference synthesis. Final R and R_w were 0.057 and 0.061, respectively. The atomic parameters of non-hydogen atoms are listed in Table 1.[7]

Results and Discussion

The $[Co(NO_2)_2(N_410)]^+$ complex shows three signals for C–C–C and four signals for N–C–C groups in the ^{13}C NMR spectrum and can be assigned as the *trans*-isomer with either C_2 or C_s symmetry.[1] In the elec-

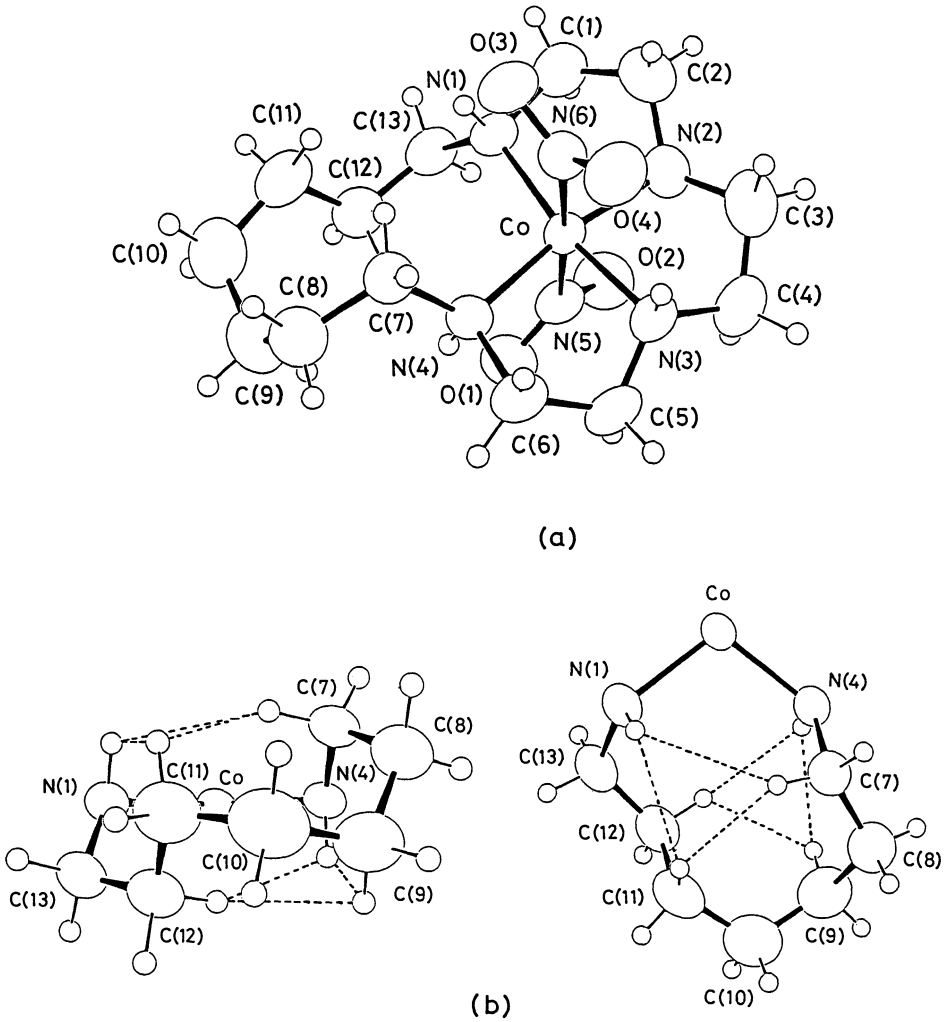

Fig. 1. ORTEP drawings[9] of (a) *trans*-$[Co(NO_2)_2(N_410)]^+$ and (b) views of the ten-membered chelate ring.

Table 2. Selected Intra- and Intermolecular Distances and Bond Angles

Distance (l/Å)				Bond angles (ϕ/°)			
Co–N(1)	2.040(3)	N(3)–C(4)	1.483(6)	N(1)–Co–N(2)	84.4(1)	C(4)–N(3)–C(5)	119.1(3)
Co–N(2)	1.933(4)	N(3)–C(5)	1.477(6)	N(1)–Co–N(3)	169.5(1)	Co–N(4)–C(6)	108.4(2)
Co–N(3)	1.930(3)	N(4)–C(6)	1.513(5)	N(1)–Co–N(4)	105.4(1)	Co–N(4)–C(7)	119.5(2)
Co–N(4)	2.005(3)	N(4)–C(7)	1.501(5)	N(1)–Co–N(5)	89.3(1)	C(6)–N(4)–C(7)	111.0(3)
Co–N(5)	1.957(2)	C(1)–C(2)	1.500(7)	N(1)–Co–N(6)	88.5(1)	Co–N(5)–O(1)	121.5(2)
Co–N(6)	1.965(2)	C(3)–C(4)	1.508(7)	N(2)–Co–N(3)	85.4(1)	Co–N(5)–O(2)	120.4(3)
O(1)–N(5)	1.227(5)	C(5)–C(6)	1.499(6)	N(2)–Co–N(4)	170.0(1)	O(1)–N(5)–O(2)	118.0(3)
O(2)–N(5)	1.229(4)	C(7)–C(8)	1.522(7)	N(2)–Co–N(5)	89.1(1)	Co–N(6)–O(3)	119.9(2)
O(3)–N(6)	1.231(4)	C(8)–C(9)	1.529(6)	N(2)–Co–N(6)	92.8(1)	Co–N(6)–O(4)	121.1(2)
O(4)–N(6)	1.228(4)	C(9)–C(10)	1.536(8)	N(3)–Co–N(4)	84.8(1)	O(3)–N(6)–O(4)	119.0(3)
N(1)–C(1)	1.507(7)	C(10)–C(11)	1.529(9)	N(3)–Co–N(5)	93.0(1)	N(1)–C(1)–C(2)	111.7(4)
N(1)–C(13)	1.497(4)	C(11)–C(12)	1.506(7)	N(3)–Co–N(6)	89.6(1)	N(2)–C(2)–C(1)	104.8(4)
N(2)–C(2)	1.478(6)	C(12)–C(13)	1.508(7)	N(4)–Co–N(5)	89.5(1)	N(2)–C(3)–C(4)	105.8(4)
N(2)–C(3)	1.486(6)			N(4)–Co–N(6)	89.1(1)	N(3)–C(4)–C(3)	104.8(3)
				N(5)–Co–N(6)	176.9(1)	N(3)–C(5)–C(6)	104.9(3)
O(1)···N(4)	2.753(3)	O(1)···HN(4)	2.10(3)	Co–N(1)–C(1)	107.3(2)	N(4)–C(6)–C(5)	109.4(3)
O(2)···N(2)	2.705(4)	O(2)···HN(2)	2.05(4)	Co–N(1)–C(13)	124.7(2)	N(4)–C(7)–C(8)	114.8(3)
O(3)···N(1)	2.730(3)	O(2)···HN(2)	2.05(3)	C(1)–N(1)–C(13)	107.3(3)	C(7)–C(8)–C(9)	116.8(4)
O(4)···N(3)	2.733(4)	O(4)···HN(3)	2.02(3)	Co–N(2)–C(2)	108.7(3)	C(8)–C(9)–C(10)	116.5(4)
F(4)···N(2)	3.012(8)	F(4)···HN(2)	2.21(5)	Co–N(2)–C(3)	110.0(3)	C(9)–C(10)–C(11)	117.6(5)
				C(2)–N(2)–C(3)	119.4(3)	C(10)–C(11)–C(12)	113.6(4)
HN(1)···HC(7)	2.46(7)	HN(1)···HC(11)	2.34(8)	Co–N(3)–C(4)	109.6(2)	C(11)–C(12)–C(13)	117.1(4)
HN(4)···HC(9)	2.22(6)	HN(4)···HC(12)	2.11(5)	Co–N(3)–C(5)	109.6(2)	N(1)–C(13)–C(12)	115.3(3)
HC(7)···HC(11)	2.08(6)	HC(9)···HC(12)	2.15(7)				

tronic spectrum, the complex gives two strong charge-transfer bands at 28200 and 38700 cm^{-1}. The positions and intensities of these bands are similar to those for *trans*-$[Co(NO_2)_2(N_4x)]^+$(x=7, 8, 9).[1] The *cis*-$[Co(NO_2)_2(N_4x)]^+$(x=5, 6, 7) isomers show both of them at higher energy, ca. 30000 and 40000 cm^{-1}.[1] The *trans*-isomer of the present complex was confirmed by the X-ray structure determination described below.

A perspective view of the complex cation is shown in Fig. 1(a). Table 2 lists the selected bond distances and angles together with the short interatomic distances. The complex is a *trans*-dinitro isomer. The four chiral amino nitrogen atoms have an RSSR(SRRS) configuration. The same chiralities of the four nitrogen atoms have been found for analogous N_4x complexes, *trans*-$[NiCl_2(N_47)]$,[10] $[Cu(N_47)]^{2+}$,[11] *trans*-$[CoCl_2(N_48)]^+$,[2] and *trans*-$[NiCl_2(N_49)]$.[10] The two NO_2^- ions coordinate to the Co(III) through the nitrogen atom and are oriented toward the nitrogen atoms of the macrocycle to form short O ··· HN hydrogen bondings (2.02—2.10 Å). The Co–NO_2 bond lengths (1.957(2) and 1.965(2) Å) are a little longer than those found in *trans*-dinitro Co(III) complexes, such as *trans*-$[Co(NO_2)_2(NH_2CH_2CH_2NH_2)_2]^+$ (av. 1.938(2) Å)[12] and *trans*-$[Co(NO_2)_2(NH_2CH_2CH_2CH_2CH_2NH_2)_2]^+$ (av. 1.934(4) Å).[13] The lengthening of the Co–NO_2 bonds may be attributed to the steric repulsion between the NO_2^- ion and the methylene protons as observed short O ··· HC distances (2.45(4)—2.70(4) Å). The bond distances of Co–N(1)(2.040(3) Å) and Co–N(4)(2.005(3) Å) for the ten-membered chelate ring are longer by ca. 0.09 Å than those of Co–N(2)(1.933(4) Å) and Co–N(3) (1.930(3) Å). The N(1)–Co–N(4) bite angle of the ten-membered chelate ring is 105.4(1)°, while those of three five-membered chelate rings are 84.4(1), 85.4(1), and 84.8(1)°. The same elongation of the Co–N bond and widening of the N–Co–N bite angle have been observed for the eight-membered chelate ring in *trans*-$[CoCl_2(N_48)]^+$.[2] The fairly large distortion from the regular octahedron is attributable to the strain arising from the planar arrangement of three five-membered chelate rings and the repulsion among hydrogen atoms of the medium-sized ten-membered chelate ring. The five membered chelate rings involving N(1)–C(1)–C(2)–N(2) and N(3)–C(5)–C(6)–N(4) moieties take a distorted envelope conformation, and that involving a N(2)–C(3)–C(4)–N(3) moiety forms a gauche conformation. The conformation of the ten-membered chelate ring is assigned as a distorted boat–chair–boat (BCB) form as shown in Fig. 1(b). A similar BCB form has been found in 1,6-*cis*-diaminocyclodecane-dihydrochloride.[14] All the bond angles around the nitrogen and carbon atoms of the ten-membered chelate ring are larger than the tetrahedral angle, in particular the Co–N–C angles are large, 124.7(2)° and 119.5(2)°. Trans-annular hydrogen–hydrogen interactions are also observed among the sets of HN(1), HC(7) and HC(11), and of HN(4), HC(9) and HC(12), which are depicted as dashed lines in Fig. 1(b).

The present work was partially supported by the Grant-in-Aid for Scientific Research No. 02740301 from the Ministry of Education, Science and Culture. The authors wish to thank the Institute for Molecular Science for the use of X-ray and computation facilities.

References

1) M. Tsuchimoto, M. Kita, M. Nonoyama, and J. Fujita, *Bull. Chem. Soc. Jpn.*, **63**, 227 (1990).
2) M. Tsuchimoto, H. Takazawa, M. Kita, M. Nonoyama, S. Ohba, Y. Saito, and J. Fujita, *Bull. Chem. Soc. Jpn.*, **63**, 785 (1990).
3) M. Tsuchimoto, M. Kita, and J. Fujita, *Bull. Chem. Soc. Jpn.*, **63**, 3410 (1990).
4) M. Sugimoto, M. Nonoyama, T. Ito, and J. Fujita, *Inorg. Chem.*, **22**, 950 (1983).
5) T. Sakurai and K. Kobayashi, *Rikagaku Kenkyusho Houkoku*, **55**, 69 (1979).
6) "International Tables for X-Ray Crystallography," Kynoch Press, Birmingham (1974), Vol. IV.
7) Lists of observed and calculated structure factors, the anisotropic temperature factors for non-hydrogen atoms, the atomic parameters of hydogen atoms, bond lengths and angles involving hydrogen atoms, and torsion angles in the chelate rings, are deposited as Document No. 8952 at the Office of the Editor of Bull. Chem. Soc. Jpn.
8) $B_{eq}=4/3\{\sum_i\sum_j B_{ij}\boldsymbol{a}_i\boldsymbol{a}_j\}$.
9) C. K. Johnson, ORTEPII, Report ORNL-5138, Oak Ridge National Laboratory, Tennessee (1976).
10) M. Sugimoto, J. Fujita, H. Ito, K. Toriumi, and T. Ito, *Inorg. Chem.*, **22**, 955 (1983).
11) A. Bianchi, L. Bologni, P. Dapporto, M. Micheloni, and P. Paoletti, *Inorg. Chem.*, **23**, 1201 (1984).
12) O. Bortin, *Acta Chem. Scand., Ser. A*, **30**, 657 (1976).
13) M. Shimoi, Y. Fujinawa, H. Ogino, K. Kanamori, and K. Kawai, *Bull. Chem. Soc. Jpn.*, **61**, 3496 (1988).
14) J. D. Dunitz and K. Venkatesan, *Helv. Chim. Acta*, **44**, 2033 (1961).

A Fusarubin Isomer[1)]

Yasuhiro TANOUE,* Akira TERADA,*,† and Yasuo UMEZU†
Department of Food Science and Technology, Shimonoseki University of Fisheries,
Nagatahonmachi, Shimonoseki, Yamaguchi 759-65
†Department of Chemistry, Kyushu Institute of Technology, Tobata, Kitakyushu, Fukuoka 804
(Received November 11, 1990)

Synopsis. An isomer of fusarubin, 2-acetonyl-5,8-dihydroxy-7-hydroxymethyl-3-methoxy-1,4-naphthoquinone, was prepared from 2-hydroxymethyl-7-(2-hydroxypropyl)-1,4,5,6,8-pentamethoxynaphthalene.

Several new antibiotics, such as fusarubin (**1**),[2a)] erythrostominone,[2b)] javanicin,[2c)] bostrycin,[2d)] purpuromycin,[3)] and fredericamycin A,[4)] contain a 2-methoxynaphthazarin moiety; for the antibiotics above, that moiety is 5,8-dihydroxy-2-methoxy-1,4-naphthoquinone. We have already prepared two intermediates of them, **2** and **3**, as shown in Chart 1.[5)]

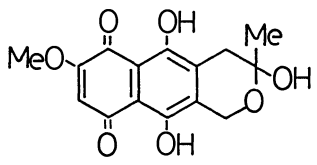

1

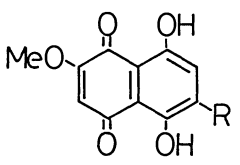

2: R=CHO
3: R=CH_2OH

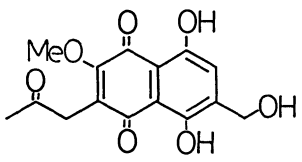

4

Chart 1.

As a part of our study of synthetic naphthoquinone derivatives, synthesis of fusarubin isomer (**4**) was attempted from 2-hydroxymethyl-7-(2-hydroxypropyl)-1,4,5,6,8-pentamethoxynaphthalene (**5**).

Results and Discussion

To specifically oxidize the 2-hydroxypropyl group of **5**,[6)] selective protection of the hydroxymethyl group in **5** was needed. Treatment of **5** with bulky pivaloyl chloride gave the monoester **6** in 46% yield as the major product, along with the diester **7** (10% yield). Oxidation of the secondary hydroxyl group in **6** with chromium(VI) oxide-pyridine(1/2)[7)] produced the ketone **8** (88% yield), which was reacted with sodium methoxide in methyl alcohol to give the alcohol **9** (91% yield) (Scheme 1).

Two-step demethylations[8)] of pentamethoxynaphthalene **9** were carried out by reaction with cerium(IV) ammonium nitrate (CAN) followed by reaction with aluminum chloride. Oxidative demethylation of **9** with CAN gave two quinones. One of them was presumed to be 3,5,8-trimethoxynaphthoquinone (**10**) (48% yield). Previously, in NMR studies of 1,4-naphthoquinone, it

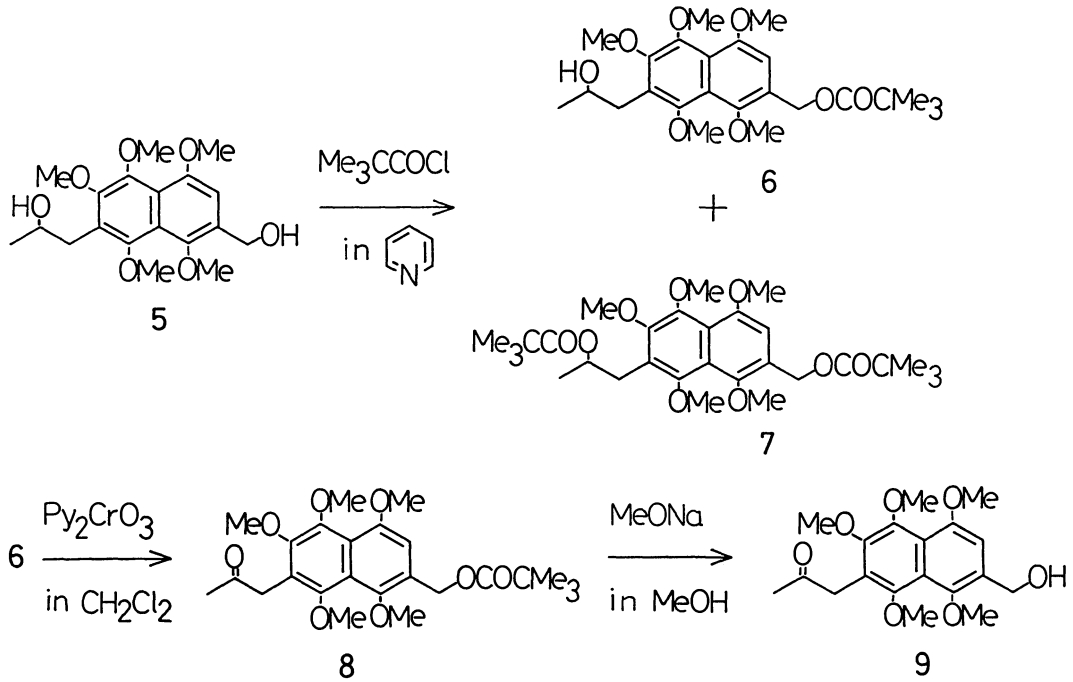

Scheme 1.

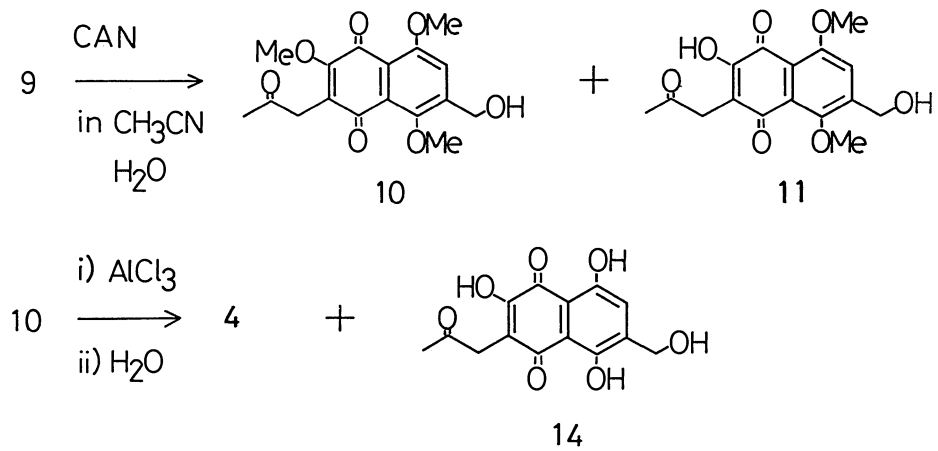

Scheme 2.

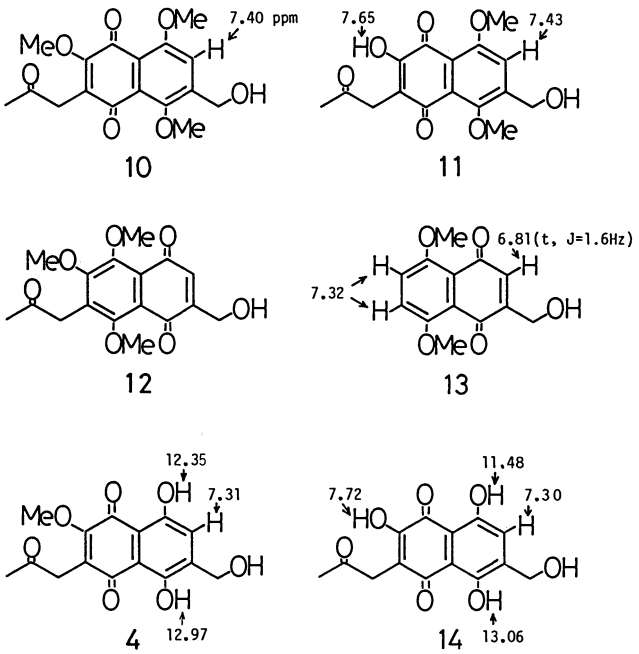

Chart 2.

was shown that the signals attributable to the quinone ring proton were always observed further upfield than the signals of the benzene ring protons and were located at δ=6—7.[9] If the structure of our product was **12**, the quinone ring proton should be observed as a triplet around δ=6.8 (the quinone proton signal of 2-hydroxymethyl-5,8-dimethoxy-1,4-naphthoquinone (**13**) was reported to be at δ=6.81).[10] However, our main product showed a singlet signal at δ=7.40, and it was confirmed that this proton was a benzene ring proton. The major product was therefore shown to be **10**. The minor product was similarly determined to be 5,8-dimethoxynaphthoquinone (**11**) (14% yield).

The second demethylation of **10** with aluminum chloride in dichloromethane gave 2-acetonyl-5,8-dihydroxy-7-hydroxymethyl-3-methoxy-1,4-naphthoquinone (**4**) (46% yield). This is a fusarubin isomer. 2-Acetonyl-3,5,8-trihydroxy-7-hydroxymethyl-1,4-naphthoquinone (**14**) was also produced in the reaction in 14% yield (Scheme 2). Their ^{1}H NMR spectra were assigned as shown in Chart 2.

Experimental

Melting points were determined with a Yanagimoto micro-melting point apparatus and were uncorrected. ^{1}H and ^{13}C NMR spectra were taken on a JEOL JNM-60 in $CDCl_3$ solutions unless otherwise specified, using Me_4Si and $CDCl_3$ as internal standards, respectively. Mass spectra and IR spectra were obtained with a JEOL DX-300 spectrometer, and a Hitachi 260-30 spectrometer, respectively. Column chromatography was carried out on silica gel (Wakogel C-200) eluting with chloroform.

The Reaction of 5 with Pivaloyl Chloride. To a solution of **5** (72 mg, 0.197 mmol) in dried pyridine (2 ml) was added pivaloyl chloride (28 mg, 0.236 mmol) at 0 °C. The reaction mixture was kept in a refrigerator (5 °C) overnight, then quenched with ice water and extracted with chloroform. The chloroform solution was washed sequentially with dil. HCl, aqueous $NaHCO_3$, and brine, then dried over Na_2SO_4 and concentrated. The residue was purified by silica-gel chromatography to give two oily products in the following order: 2-pivaloyloxymethyl-7-[2-(pivaloyloxy)propyl]-1,4,5,6,8-pentamethoxynaphthalene (**7**) (11 mg, 10% yield), 2-(2-hydroxypropyl)-7-pivaloyloxymethyl-1,3,4,5,8-pentamethoxynaphthalene (**6**) (41 mg, 46% yield).

6: IR (neat) 1730 (C=O), 1618, 1600, 1360, 1150, and 1050 cm^{-1}; ^{1}H NMR δ=1.25 (s, 9H, 3×CH_3), 1.30 (m, 4H, CH_3, OH), 3.05 (m, 2H, -C<u>H</u>$_2$CH(OH)-), 3.76 (s, 6H, 2×OCH_3), 3.85, 3.96, 4.00 (each s, 3H, OCH_3), 3.90 (m, 1H, CH), 5.33 (s, 2H, -C<u>H</u>$_2$OCOC$(CH_3)_3$-), and 6.79 (s, 1H, ArH); MS *m/z* 450 (M^+), 403, 349, 333, 289, and 57. HRMS, Found: *m/z* 450.2234. Calcd for $C_{24}H_{34}O_8$: M, 450.2253.

7: IR (neat) 1730 (C=O), 1600, 1360, 1150, and 1050 cm^{-1}; ^{1}H NMR δ=1.10 (s, 9H, 3×CH_3), 1.24 (d, *J*=6.0 Hz, 3H, CH_3), 1.25 (s, 9H, 3×CH_3), 3.07 (m, 2H, -C<u>H</u>$_2$CH(OCOC$(CH_3)_3$)-), 3.75 (s, 6H, 2×OCH_3), 3.82 (s, 3H, OCH_3), 3.88 (m, 1H, CH), 3.95, 4.00 (each s, 3H, OCH_3), 5.33 (s, 2H, -C<u>H</u>$_2$OCOC$(CH_3)_3$-), 6.77 (s, 1H, ArH); MS *m/z* 534 (M^+), 450, 392, 289, and 57. HRMS, Found: *m/z* 534.2884. Calcd for $C_{29}H_{42}O_9$: M, 534.2829.

2-Acetonyl-7-pivaloyloxymethyl-1,3,4,5,8-pentamethoxynaphthalene (8). Anhydrous chromium (VI) oxide (65 mg, 0.65 mmol) was added to a mixture of dried dichloromethane (5 ml) and pyridine (0.11 mml, 1.3 mmol) and stirred for 15 min. The alcohol **6** (49 mg, 0.11 mmol) in dried dichloromethane (2 ml) was added to the solution, stirred at room temperature for 30 min, and filtered. The filtrate was worked

up as usual and the residue was chromatographed on silica gel to give **8** (43 mg, 88% yield) as an oil. IR (neat) 1725 (ester, ketone C=O), 1600, 1355, 1150, and 1050 cm^{-1}; ^1H NMR δ=1.26 (s, 9H, 3×CH_3), 2.27 (s, 3H, $COCH_3$), 3.71 (s, 2H, $-CH_2CO-$), 3.76, 3.84 (each s, 3H, OCH_3), 3.94 (s, 6H, 2× OCH_3), 3.97 (s, 3H, OCH_3), 5.34 (s, 2H, $-CH_2OCOC(CH_3)_3-$), and 6.80 (s, 1H, ArH); MS *m/z* 448 (M^+), 433, 405, 347, 289, and 57. HRMS, Found: *m/z* 448.2115. Calcd for $C_{24}H_{32}O_8$: M, 448.2107.

2-Acetonyl-7-hydroxymethyl-1,3,4,5,8-pentamethoxynaphthalene (9). Sodium methoxide (117 mg, 2.15 mmol) was added to a solution of **8** (194 mg, 0.43 mmol) in methyl alcohol (3 ml) and stirred overnight at room temperature in the dark. The solvent was removed under reduced pressure and the residue was decomposed by the addition of water, and extracted with chloroform. Column chromatography on silica gel gave **9** (143 mg, 91% yield) as an oil. IR (neat) 3450 (broad, OH), 1720 (C=O), 1600, 1360, and 1050 cm^{-1}; ^1H NMR: δ=1.88 (broad, 1H, OH), 2.26 (s, 3H, $COCH_3$), 3.70, 3.76, 3.84, 3.94, 3.99 (each s, 3H, OCH_3), 3.88 (s, 2H, $-CH_2CO-$), 4.86 (s, 2H, $-CH_2OH$), and 6.86 (s, 1H, ArH); ^{13}C NMR δ=29.53 ($CO\underline{C}H_3$), 39.85 ($\underline{C}H_2CO$), 56.57 (CH_2OH), 60.92 (2C, OMe), 61.56, 62.34, and 62.68 (OMe), 106.63 (C-6), 121.20, 122.47, 123.26 (C-2), 129.66 (C-7), 144.92, 146.23, 149.36, 149.81, and 152.59 (C-OMe), and 183.15 (C=O); MS *m/z* 364 (M^+), 334, 301, 259, and 115; HRMS, Found: *m/z* 364.1513. Calcd for $C_{19}H_{24}O_7$: M, 364.1522.

Oxidative Demethylation of 9 with CAN. A solution of CAN (1.72 g, 3.25 mmol) in water (3 ml) was added dropwise to a solution of **9** (457 mg, 1.3 mmol) in acetonitrile (5 ml) and stirred at room temperature for 30 min. The reaction mixture was diluted with water and extracted with chloroform. The usual work-up and chromatographic purification (silica gel) gave two products: 2-acetonyl-7-hydroxymethyl-3,5,8-trimethoxy-1,4-naphthoquinone (**10**) (195 mg, 48% yield) and 2-acetonyl-3-hydroxy-7-hydroxymethyl-5,8-dimethoxy-1,4-naphthoquinone (**11**) (58 mg, 14% yield).

10: Orange crystals (hexane–ethanol (10:1)); mp 130—131 °C; IR (KBr) 1705 (ketone C=O), 1655, 1630 (each quinone C=O), 1580, 1215, and 1030 cm^{-1}; ^1H NMR δ=2.29 (s, 3H, $COCH_3$), 2.50 (broad, 1H, OH), 3.68 (s, 2H, $-CH_2CO-$), 3.76, 3.98, 4.08 (each s, 3H, OCH_3), 4.79 (s, 2H, $-CH_2OH$), and 7.40 (s, 1H, ArH); ^{13}C NMR δ=30.18 (CH_3), 38.41 ($\underline{C}H_2COCH_3$), 56.70 (CH_2OH), 60.18, 61.04, and 61.78 (OMe), 116.99 (C-6), 119.05, 124.60, 126.31 (C-2), 145.17 (C-7), 150.60, 156.43, and 158.49 (C-OMe), 179.93 (C-4), 184.32 (C-1), and 204.73 (C=O); MS *m/z* 334 (M^+), 319, 291, 277, and 231. HRMS, Found: *m/z* 334.1065. Calcd for M, 334.1053. Found: C, 60.80; H, 5.39%. Calcd for $C_{17}H_{18}O_7$: C, 61.07; H, 5.43%.

11: Orange crystals (hexane–ethanol(3:1)); mp 186.5—187.5 °C; IR (KBr) 3420, 3200 (each OH), 1695 (ketone C=O), 1660, 1640 (each quinone C=O), 1360, 1220, 1085, and 1040 cm^{-1}; ^1H NMR δ=2.30 (s, 4H, $COCH_3$, $-CH_2O\underline{H}$), 3.69 (s, 2H, $-CH_2CO-$), 3.79, 4.04 (each s, 3H, OCH_3), 4.85 (d, *J*=5.0 Hz, 2H, $-C\underline{H}_2OH$), 7.44 (s, 1H, ArH), and 7.65 (s, 1H, ArOH); ^{13}C NMR (DMSO-d_6) δ=29.38 (CH_3), 37.84 ($\underline{C}H_2COCH_3$), 56.36 (CH_2OH), 57.90 and 60.93 (OMe), 116.60 (3C: C-2, C-6), 124.14, 147.46 (C-7), 149.80, 155.06, and 156.08 (C-OH, 2× C-OMe), 178.72 (C-4), 183.29 (C-1), and 203.99 (C=O); MS *m/z* 320 (M^+), 305, 278, 260, 245, and 217. Found: C, 59.80; H, 5.11%. Calcd for $C_{16}H_{16}O_7$: C, 60.00; H, 5.03%.

Demethylation of 10 with Aluminum Chloride. Aluminum chloride (730 mg, 5.5 mmol) was added to a solution of **10** (183 mg, 0.55 mmol) in dichloromethane (5 ml) cooled in an ice bath. After stirring at room temperature for 2 h, the reaction mixture was decomposed by the addition of 5 wt% aqueous oxalic acid (100 ml) and extracted with chloroform. The usual work-up and chromatographic purification (silica gel) gave two products, a fusarubin isomer **4** (77 mg, 46% yield) and 2-acetonyl-3,5,8-trihydroxy-7-hydroxymethyl-1,4-naphthoquinone (**14**) (22 mg, 14% yield).

4: Red-brown crystals (hexane–ethanol); mp 173.5—174.5 °C; IR (KBr) 3430 (broad, OH), 1710 (ketone C=O), 1605 (quinone C=O), 1420, 1270, 1170, and 1080 cm^{-1}; ^1H NMR δ=2.31 (s, 3H, $COCH_3$), 3.75 (s, 2H, $-CH_2CO-$), 4.18 (s, 3H, OCH_3), 4.78 (s, 2H, $-C\underline{H}_2OH$), 7.31 (s, 1H, ArH), 12.35 (s, 1H, C-5-OH), and 12.97 (s, 1H, C-8-OH); ^{13}C NMR (DMSO-d_6) δ=29.84 (CH_3), 57.50 (CH_2OH), 61.56 (OMe), 109.74, 110.20, 124.54 (C-6), 128.88 (C-2), 145.92 (C-7), 156.26, 158.72, 159.58 (C-OMe, 2×C-OH), 180.15 (C-4), 185.41 (C-1), and 203.81 (C=O); MS, *m/z* 306 (M^+), 264, 249, 246, and 203. HRMS, Found: *m/z* 306.0761. Calcd for M, 306.0740. Found: C, 58.62; H, 4.83%. Calcd for $C_{15}H_{14}O_7$: C, 58.82; H, 4.61%.

14: Red crystals (ligroin–benzene–ethanol (10:1:1)); mp 218 °C (decomp); IR (KBr) 3420, 3230 (each OH), 1700 (ketone C=O), 1610 (quinone C=O), 1560, 1420, 1310, 1180, and 1090 cm^{-1}; ^1H NMR δ=2.31 (s, 3H, $COCH_3$), 3.74 (s, 2H, $-CH_2CO-$), 4.80 (s, 2H, $C\underline{H}_2OH$), 7.30 (s, 1H, ArH), 7.72 (s, 1H, C-3-OH), 11.48 (s, 1H, C-5-OH), and 13.06 (s, 1H, C-8-OH); ^{13}C NMR (DMSO-d_6) δ=29.61 (CH_3), 37.38 ($\underline{C}H_2COCH_3$), 57.61 (CH_2OH), 109.34, 109.51, 118.37 (C-2), 122.71 (C-6), 145.92 (C-7), 153.40, 156.94, and 157.80 (C-OH), 181.69 (C-4), 187.98 (C-1), and 203.87 (C=O); MS *m/z* 292 (M^+), 250, 232, and 43. HRMS, Found: *m/z* 292.0563. Calcd for M, 292.0582. Found: C, 57.69; H, 4.61%. Calcd for $C_{14}H_{12}O_7$: C, 57.54; H, 4.14%.

References

1) Paper XI, on Synthesis of Naphthoquinone Derivatives. Paper X, Y. Tanoue and A. Terada, *Bull. Chem. Soc. Jpn.*, **64**, 2295 (1991).

2) R. H. Thomson, "Naturally Occurring Quinones," 2nd ed, Academic Press, London (1971), a) p. 291, b) p.297, c) p. 287, and d) p. 476.

3) C. Coronelli, H. Pagani, M. R. Bardone, and G. C. Lancini, *J. Antibiot.*, **27**, 161 (1974).

4) R. C. Pandey, M. W. Toussaint, R. M. Stroshane, C. C. Kalita, A. A. Asgalos, A. L. Garretson, T. T. Wei, K. M. Byrne, R. F. Geoghegan, Jr., and R. J. White, *J. Antibiot.*, **34**, 1389 (1981); D. J. W. Pickle, K. M. Byrne, R. C. Pandey, and R. J. White, *ibid.*, **34**, 1402 (1981); R. Misra, R. C. Pandey, and J. V. Silverton, *J. Am. Chem. Soc.*, **104**, 4478 (1982); T. R. Kelly, N. Ohashi, R. J. Armstrong-Chong, and S. H. Bell, *J. Am. Chem. Soc.*, **108**, 7100 (1986).

5) Y. Tanoue, A. Terada, T. Tsuboi, T. Hayashida, and O. Tsuge, *Bull. Chem. Soc. Jpn.*, **60**, 2927 (1987).

6) Y. Tanoue and A. Terada, *Bull. Chem. Soc. Jpn.*, **64**, 2295 (1991).

7) J. C. Collins and W. W. Hess, *Org. Synth.*, **52**, 5 (1972).

8) Y. Tanoue and A. Terada, *Bull. Chem. Soc. Jpn.*, **61**, 2039 (1988); K. Nomura, K. Okazaki, K. Hori, and E. Yoshii, *J. Am. Chem. Soc.*, **109**, 3402 (1987). Yoshii et al. have succeeded in a total synthesis of (±) granaticin by a two-step *O*-demethylation reaction using CAN and $AlCl_3$–Et_2S.

9) R. E. Moore and P. J. Scheuer, *J. Org. Chem.*, **31**, 3272 (1966).

10) Y. Tanoue, Ph. D. Thesis, Kyushu University, Fukuoka, Japan, 1989, p. 57.

Synthesis of Urushiols with Pentadecatrienyl Side Chain, Two Constituents of the Sap of a Lac Tree, *Rhus Vernicifera*

Tetsuo MIYAKOSHI,* Hidenori KOBUCHI, Noriyasu NIIMURA, and Yoshiro YOSHIHIRO
Department of Industrial Chemistry, Meiji University, Higashimita, Tama-ku, Kawasaki-shi 214
(Received January 17, 1991)

Synopsis. Two phenolic lipids, 3-[(8*Z*,11*Z*)-8,11,14- and 3-[(8*Z*,11*E*,13*E*)-8,11,13-pentadecatrienyl]catechol, which are the major constituents of the sap from a Japanese or Chinese lac tree, *Rhus vernicifera*, have been synthesized via the Wittig reaction of ylides derived from 3,6- and 3,5-heptadienylphosphonium salts with 3-(8-oxooctyl)catechol diacetate.

The fluid sap exuded from several kinds of Japanese or Chinese lac trees, *Rhus vernicifera*, dries into a tough and brilliant film and has been used as a naturally occurring coating material for thousands of years in the Orient.[1] It is a latex composed of urushiols (60%), water (30%), plant gum (7%), water-insoluble glycoproteins (2%), and copper glycoproteins (ca. 0.1%).[2–5] The structures of urushiols have been determined to be catechols substituted at position 3 of the aromatic ring with a C_{15}-alkyl or alkenyl side chain.[5] The urushiols with an unsaturated side chain, **1** and **2**, are important contributors to the industrially useful polymerization properties of these natural products.[1,6] The presence of **1** in *poison ivy* and the sap from Japanese laquer was reported by Dawson et al.[7] and Hashimoto et al.[8] In a previous paper we reported the synthesis of 3-[(8*Z*,11*Z*)-8,11,14- and (8*Z*,11*E*,13*E*)-8,11,13-pentadecatrienyl]-veratrole by a Wittig reaction between 3-(8-oxooctyl)-veratrole and the ylide derived from [(*Z*)-3,6- (**3**) and [(3*E*,5*E*)-3,5-heptadienyl]triphenylphosphonium iodide (**4**).[9] In this paper we describe an efficient synthesis of **1** and **2**.

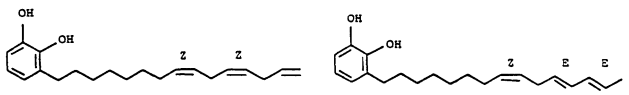

1 **2**

Results and Discussion

Protection of hydroxyl groups of catechol as methyl ethers is now widely used and the protected form is very stable under various basic conditions.[9] However, deprotection cannot be carried out in acid-sensitive molecules such as urushiols having a pentadecatrienyl side chain.[10] Acetylation is also not exempted from some of these disadvantages. Urushiol was synthesized by a stepwise procedure based on repeated protection and deprotection of the hydroxyl group of catechol in good yields.[11]

The synthetic pathways to compounds **1** and **2** are illustrated in Scheme. For the synthesis of 3-(8-oxooctyl)catechol diacetate (**9**), veratrole was subjected to alkylation[12] with 1,8-dibromooctane (84%), demethylation[13] with boron tribromide (92%), and acetylation with acetic anhydride (76%) to give the bromide **7**. This was converted to the iodide **8** (88%) and oxidized with DMSO–$NaHCO_3$ to afford **9** (71%).

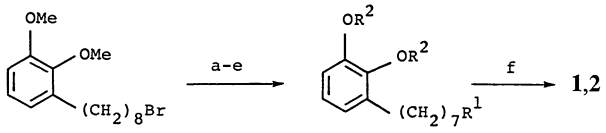

5 **6—11**

6 $R^1=CH_2Br$, $R^2=H$
7 $R^1=CH_2Br$, $R^2=Ac$
8 $R^1=CH_2I$, $R^2=Ac$
9 $R^1=CHO$, $R^2=Ac$
10 $R^1=CH{=}CHCH_2CH{=}CHCH_2CH{=}CH_2$, $R^2=Ac$
11 $R^1=CH{=}CHCH_2CH{=}CHCH{=}CHCH_3$, $R^2=Ac$

Scheme. Reagents: a, BBr_3, CH_2Cl_2; b, Ac_2O, C_5H_5N; c, NaI, Me_2CO; d, DMSO, $NaHCO_3$; e, BuLi, C_6H_6, **3** or **4**; f, $LiAlH_4$: *t*-BuOH=3 : 1, THF.

First, the Wittig reaction between **9** and the ylide derived from **3** gave 8,11,14-pentadecatrienyl compounds (45%). The main product **10** was isolated by HPLC. In the infrared spectrum of **10**, intense absorption bands of a monosubstituted olefin were observed at 910 and 990 cm^{-1}, without the characteristic *trans*-double bond absorption at 970 cm^{-1}. The stereochemistry of **10** was confirmed by a 270 MHz ^1H NMR spectrum with extensive decoupling experiments. Furtheremore, the stereochemistry of the olefin formed by the Wittig reaction was determined to be *cis* from the diagnostic shift of the allylic methylene carbon (δ=27.2 $\underline{C}H_2C{=}C$), which is to appear at δ=33—35 if the bond was *trans*.[14,15] The ^{13}C NMR spectrum also demonstrated the 8-*cis*-configuration exhibiting the 8- and 9-olefinic carbon atoms at δ=130.4 and 126.9. The 10- and 13-carbon atoms of **10** occurred at δ=25.6 and 31.5 in the ^{13}C NMR spectrum. These values are typical of such a long-chain dienyl and trienyl compounds.[16–18] Although these reaction conditions were known to result in a *cis*-stereoselective Wittig olefination,[18] the crude product contained 8% of (8*E*)-isomer, as demonstrated by GLC and HPLC.

3-[(8*Z*,11*E*,13*E*)-8,11,13-Pentadecatrienyl]catechol diacetate **11** was synthesized in a similar way from **9** and **4** in 40% yield. The resulting product **11** had an infrared absorption band at 985 cm^{-1} due to disubstituted *trans,trans*- conjugated double bonds. The (8*Z*,11*E*,13*E*)-olefinic configuration was confirmed by ^1H–^1H, ^1H–^{13}C COSY and a J-resolved NMR experiment. The (8*E*)-isomer could not be detected in this reaction product.

When **10** was treated with $LiAlH_4$ in tetrahydrofuran (THF) at room temperature, partial hydrogenation of the double bonds took place. The protecting groups of **10** were removed by treatment with $LiAlH_4$–*t*-butyl alcohol (1 : 3) in THF at −50 °C to give urushiol **1** (61%). The structure of the synthetic **1** was identified

by comparison of IR, ^{1}H NMR and EI-MS spectra with those of the reported data.[5]

3-[(8*Z*,11*E*,13*E*)-8,11,13-Pentadecatrienyl]catechol (**2**) was synthesized from **11** in the same reductive procedure. The structure was identified by comparing the IR and ^{1}H NMR spectra with the reported data.[5]

In conclusion, we have succeeded in the synthesis of urushiols **1** and **2** via the Wittig reaction of ylides derived from the heptadienylphosphonium salts **3** and **4** with di-*O*-acetyl-protected aldehyde **9**, respectively. This synthetic method may be applicable to the preparation of such long-chain polyene-substituted phenols as other urushiol analogues and cardanols.[6]

Experimental

All ^{1}H NMR spectra were taken in chloroform-*d* or carbon tetrachloride with tetramethylsilane as internal standard on a Varian EM 390 spectrometer (90 MHz) and JEOL GSX 270 spectrometer (270 MHz). All ^{13}C NMR spectra were recorded on a JEOL GSX 270 spectrometer operated at 67.9 MHz. Low resolution mass spectra were taken on a JEOL DX-300 mass spectrometer. The spectra were run at 70 eV or with an emission current of 100 μA. High-performance liquid chromatograph (HPLC) was performed on a Gilson liquid chromatography with GPC (TSK gel, G1000H$_8$ 60×2.2 cm×2, eluent: chloroform, flow rate, 4.0 ml min^{-1} and silica gel (Develosil 10 mm×25 cm, 5 μm, eluent: hexane–ethyl acetate=96:4, flow rate, 1.5 ml min^{-1}).

(3*Z*)-3,6-Heptadienyltriphenylphosphonium Iodide (3). To a solution of (*Z*)-7-iodo-1,4-heptadiene (4.0 g, 18 mmol), triphenylphosphine (7.08 g, 27 mmol) in 50 ml of acetonitrile was added under stirring for 24 h at 90 °C. After 18 h the solution was filtered. The solid was washed with THF, and dried to give **3**,[9] 7.67 g (88%).

3-(8-Bromooctyl)veratrol (5). Butyllithium 66.2 ml (1.5 M in hexane, 99.3 mmol, 1 M=1 mol dm^{-3}) was added to a stirred solution of veratrole (41.1 g, 0.298 mol) in 1300 ml of dry THF at 0 °C under nitrogen atmosphere. After stirring for 2 h at room temperature, a solution of 1,8-dibromooctane (27.0 g, 99.3 mmol) in 50 ml of dry THF was added and the mixture was refluxed for 5 h. A saturated NH_4Cl solution was added to the mixture at room temperature. The mixture was poured into a saturated NH_4Cl solution and extracted with ethyl acetate. The ethyl acetate solution was washed with brine, dried (K_2CO_3), and concentrated in vacuo to give crude products. The remaining veratrole was taken off under reduced pressure (5 Torr, 1 Torr=133.322 Pa) at 70 °C. The residual oil was chromatographed over silica gel eluting with hexane to remove 1,8-dibromooctane then with benzene to give **12**,[9] 27.5 g (84% yield).

3-(8-Bromooctyl)catechol (6). To a stirred solution of boron tribromide (25.0 g, 99.6 mmol) in 50 ml of dichloromethane was added dropwise a solution of **5** (23.1 g, 70.2 mmol) in 150 ml of dichloromethane for 30 min at 0 °C. The mixture was allowed to warm up slowly to room temperature over 12 h. The mixture was treated with water, and the dichloromethane layer was treated with brine, dried ($MgSO_4$), and concentrated in vacuo. The residual oil was chromatographed (benzene–ethyl acetate=1:1 as eluent) to give **6** as an oil (19.4 g, 92%). R_f=0.58 (benzene–ethyl acetate=1:1); IR (neat): 3500, 1600, 1500, 780, 730, 640 cm^{-1}; ^{1}H NMR (90 MHz, CCl_4) δ=1.1—2.0 (m, 12H, CH_2), 2.53 (t, *J*=7 Hz, 2H, CH_2Ar), 3.33 (t, *J*=7 Hz, 2H, CH_2Br), 5.22 (br. s, 2H, OH, D_2O exchangeable), 6.62 (br. s, 3H, ArH); EI-MS *m/z* (rel intensity, %) 302 (M^+, 12), 300 (M^+, 12), 180 (21), 179 (25), 136 (7), 124 (89), 123 (100).

3-(8-Bromooctyl)catechol Diacetate (7). A solution of **6** (16.8 g, 55.8 mmol), acetic anhydride (17.1 g, 0.168 mol), and pyridine (0.89 g, 11.3 mmol) was stirred at 100 °C for 4 h, added to water, and extracted with ethyl acetate. The extract was washed with dil aq HCl and then neutralized with dil aq NaOH. The extract was dried (K_2CO_3) and concentrated in vacuo. The residue was chromatographed to afford **7** (16.3 g, 76%) as an oil. R_f=0.37 (benzene–ethyl acetate=9:1); IR (neat) 1780, 1600, 1500, 1220 cm^{-1}; ^{1}H NMR (90 MHz, CCl_4) δ=1.1—2.0 (m, 12H, CH_2), 2.27 (s, 3H, CH_3CO), 2.31 (s, 3H, CH_3CO), 2.51 (t, *J*=7 Hz, 2H, CH_2Ar), 3.33 (t, *J*=7 Hz, 2H, CH_2Br), 7.04 (m, 3H, ArH); EI-MS *m/z* (rel intensity, %) 386 (M^+, 3), 384 (M^+, 3), 302 (99), 300 (100), 124 (54), 123 (75).

3-(8-Iodooctyl)catechol Diacetate (8). After a mixture of **7** (5.26 g, 13.7 mmol) and NaI (3.07 g, 20.5 mmol) in 50 ml of acetone was stirred at 60 °C for 3 h, the resulting mixture was poured into a saturated sodium chloride solution and the product was extracted with ethyl acetate. The extract was washed with $Na_2S_2O_3$, dried over $MgSO_4$, and concentrated in vacuo. Purification of the crude oil by column chromatography on silica gel (benzene–ethyl acetate=98:2 as eluent) afforded **8** (5.21 g, 88%) as an oil. R_f=0.40 (benzene–ethyl acetate=98;2); IR (neat) 1780, 1600, 1500, 1220 cm^{-1}; ^{1}H NMR (90 MHz, CCl_4) δ=1.1—2.0 (m, 12H, CH_2), 2.27 (s, 3H, CH_3CO), 2.31 (s, 3H, CH_3CO), 2.51 (t, *J*=7 Hz, 2H, CH_2Ar), 3.05 (t, *J*=7 Hz, 2H, CH_2I), 6.92 (m, 3H, ArH); EI-MS *m/z* (rel intensity, %) 432 (M^+, 3), 390 (15), 348 (60), 263 (4), 222 (4), 207 (8), 123 (100).

3-(8-Oxooctyl)catechol Diacetate (9). A mixture of **8** (18.5 g, 42.8 mmol), 200 ml of DMSO, $NaHCO_3$ (7.1 g, 84.5 mmol), and 200 ml of benzene was stirred at 90 °C for 4 h under nitrogen atmosphere. Then the mixture was poured into water and extracted with benzene. The combined extracts were dried over $MgSO_4$, filtered, and evaporated. Column chromatography (gradient elution, benzene–eth l acetate=9:1—3:1) gave **9** as a colorless oil (9.7g, 71% yield). R_f=0.33 (benzen–ethyl acetate=9:1); IR (neat) 2720, 1780, 1730, 1600, 1500, 1220 cm^{-1}; ^{1}H NMR (90 MHz, CCl_4) δ=1.1—1.8 (m, 10H, CH_2), 2.27 (s, 3H, CH_3CO), 2.31 (s, 3H, CH_3CO), 2.35 (t, *J*=7 Hz, 2H, CH_2CO), 2.50 (t. *J*=7 Hz, 2H, CH_2Ar), 6.97 (m, 3H, Ar), 9.63 (br. s, 1H, CHO); EI-MS *m/z* (rel intensity, %) 320 (M^+, 2), 278 (14), 236 (100), 218 (9), 124 (31), 123 (44). Found: C, 67.31; H, 7.58%. Calcd for $C_{18}H_{24}O_5$: C, 67.48; H, 7.55%.

3-[(8*Z*,11*Z*)-8,11,14-Pentadecatrienyl]catechol Diacetate (10). To a suspension of **3** (2.31 g, 4.8 mmol) in 80 ml of dry benzene was added butyllithium (3.3 ml, 1.5 M in hexane, 4.8 mmol) at 20 °C under nitrogen and the resulting reddish solution was stirred for 1 h. The upper layer of the phosphorane solution was taken up by a syringe and added to a stirred solution of **9** (1.02 g, 3.18 mmol) in 10 ml of dry benzene over 0.5 h at 25 °C. Stirring was continued for 3 h at 25 °C. The mixture was poured into a saturated aqueous ammonium chloride solution, extracted with benzene, and dried over $MgSO_4$. The solvent was distilled under reduced pressure and the residue was extracted with hexane. Concentration of the hexane solution under reduced pressure gave a crude product. The crude product was chromatographed over silica gel with benzene–ethyl acetate (9:1) as eluent and GPC with chloroform as eluent. The residue was purified by HPLC to give **10** (0.524 g, 42%) as an oil. R_f=0.48 (benzene–ethyl acetate=9:1); IR (neat) 3020, 2920, 1770, 1600, 1465, 1370, 1260, 1205, 1160, 1010, 995, 910, 780, 720 cm^{-1}; ^{1}H NMR (270 MHz, $CDCl_3$) δ=1.13—1.75 (m, 10H, 2,3,4,5,6-CH_2), 2.03 (m, 2H, 7-CH_2), 2.27 (s, 3H, CH_3COO), 2.31 (s, 3H, CH_3COO), 2.50 (t, *J*=7 Hz, 2H, CH_2Ar), 2.82 (m, 4H, C=CCH_2C=CCH_2C=C), 4.80—5.09 (m, 2H, 15-C=CH, $J_{cis\text{-}14,15}$=10.0, $J_{gem\text{-}15,15}$=1.7, $J_{trans\text{-}14,15}$=17.0, $J_{13,15}$=1.6 Hz), 5.27 (m, 4H, 8,9,11,12-C=CH), 5.74—5.89 (m, 1H, 14-C=CH, $J_{trans\text{-}14,15}$=17.0, $J_{cis\text{-}14,15}$=10.0, $J_{13,14}$=6.1 Hz), 6.78—7.25 (m, 3H, ArH), ^{13}C NMR ($CDCl_3$) δ=20.3 (CH_3CO), 20.9 (CH_3CO), 25.6 (C-10), 27.2 (C-7), 31.5

(C-13), 114.6 (C-15), 120.8 (ArC-6), 126.2 (ArC-4), 126.9 (C-9), 127.2 (ArC-5), 127.8 (C-11), 129.4 (C-12), 130.4 (C-8), 136.6 (ArC-3), 136.8 (C-14), 140.5 (ArC-2), 142.4 (ArC-1), 168.2 (C=O), 168.3 (C=O); EI-MS m/z (rel intensity, %) 398 (M^+, 5), 355 (12), 136 (27), 124 (26), 123 (100); Found: C, 75.21; H, 8.55%. Calcd for $C_{25}H_{34}O_4$: C, 75.34; H, 8.60%. The spectral data of (8*E*)-isomer are as follows: IR (neat) 3020, 2920, 1770, 1600, 1465, 1370, 1260, 1205, 1160, 1010, 995, 970, 910, 780, 720 cm^{-1}, EI-MS m/z (rel intensity, %) 398 (M^+, 4), 355 (11), 136 (20), 123 (100).

3-[(8*Z*,11*E*,13*E*)-8,11,13-Pentadecatrienyl]catechol Diacetate (11). Compound **9** and **4** were allowed to react in a similar manner to that described in the preparation of **10** to give **11** as an oil (40%). R_f=0.43 (benzene–ethyl acetate=9 : 1); IR (neat) 3015, 2926, 1770, 1615, 1591, 1469, 1370, 1258, 1210, 1170, 1213, 1013, 985, 909, 789, 725 cm^{-1}; ^1H NMR (270 MHz, $CDCl_3$) δ=1.33 (m, 6H, 3,4,5-CH_2), 1.57 (m, 4H, 2,6-CH_2), 1.73 (d, J=7 Hz, 3H, CH_3C=C), 2.03 (m, 2H, 7-CH_2), 2.29 (s, 3H, CH_3COO), 2.33 (s, 3H, CH_3COO), 2.51 (t, J=8 Hz, 2H, CH_2Ar), 2.82 (m, 2H, C=CCH_2C=C), 5.31—5.45 (m, 2H, 8,9-C=CH), 5.45-5.66 (m, 2H, 11,14-C=CH), 5.90—6.10 (m, 2H, 12,13-C=CH), 7.03 (m, 1H, ArH), 7.09—7.21 (m, 2H, Ar). The accurate chemical shifts and coupling constants were determined by the decoupling experiments: 8-CH: 5.43, 9-CH: 5.37, 11-CH: 5.51, 12,13-CH: 6.01, 14-CH: 5.58; $J_{7,8}$=6.2, $J_{8,9}$=11.0, $J_{11,12}$=$J_{13,14}$=14.4, $J_{10,11}$=$J_{14,15}$=6.5 Hz. ^{13}C NMR ($CDCl_3$) δ=18.0 (C-15), 20.3 (CH_3CO), 20.9 (CH_3CO), 27.1 (C-7), 29.1, 29.2, 29.4, 29.5, 29.7 (C-2-6), 30.0 (C-1), 30.2 (C-10), 120.8 (ArC-6), 126.2 (ArC-4), 126.3 (C-9), 127.1 (C-8), 127.2 (ArC-5), 129.8 (C-14), 129.4 (C-12), 130.8 (C-11), 131.5 (C-13), 136.6 (ArC-3), 140.5 (ArC-2), 142.4 (ArC-1), 168.2 (C=O), 168.3 (C=O); EI-MS m/z (rel intensity, %) 398 (M^+, 57), 355 (55), 313 (24), 285 (10), 135 (45), 124 (56) ,123 (100), Found: C, 75.38; H, 8.49%. Calcd for $C_{25}H_{34}O_4$: C, 75.34; H, 8.60%.

3-[(8*Z*,11*Z*)-8,11,14-Pentadecatrienyl]catechol (1). To a solution of $LiAlH_4$ (68 mg, 1.8 mmol) in 5 ml of dry THF was added *tert*-butyl alcohol (400 mg, 5.4 mmol) in dry THF (5 ml) at 0 °C and the mixture was stirred for 10 min. To the resulting mixture, a solution of **10** (78 mg, 0.2 mmol) in 5 ml of dry THF was added at −50 °C, and the mixture was stirred for 50 min. Methanol (1 ml) was added to the mixture at −50 °C. After warming to room temperature, the mixture was poured into an aq saturated NH_4Cl solution and the product was extracted with ethyl acetate. The organic layer was dried over Na_2SO_4 and concentrated in vacuo below 25 °C. The residue was chromatographed over silica gel (benzene–ethyl acetate=9 : 1 as eluent) and by HPLC (silica gel Si 60, 5 μm, 10 mm×25 cm eluting with hexane–ethyl acetate=94 : 6, 1.5 ml min^{-1}) to give **1** (39 mg, 61%) as an oil. R_f=0.34 (benzene–ethyl acetate=9 : 1); IR (neat) 3450, 3030, 2920, 1600, 1500, 1475, 1360, 1275, 990, 910, 720 cm^{-1}; ^1H NMR (270 MHz, $CDCl_3$) δ=1.13—1.75 (m, 10H, 2,3,4,5,6-CH_2), 2.03 (m, 2H, 7-CH_2), 2.55 (t, J= 7Hz, 2H, CH_2Ar), 2.82 (m, 4H, C=CCH_2C=CCH_2C=C), 4.80—5.09 (m, 2H, 15-C=CH, $J_{cis\text{-}14,15}$=10.0, $J_{gem\text{-}15,15}$=1.7, $J_{cis\text{-}14,15}$=17.0, $J_{13,15}$=1.6 Hz), 5.1—5.3 (m, 2H, OH, D_2O exchangeable), 5.27—5.49 (m, 4H, 8,9,11,12-C=CH), 5.74—5.89 (m, 1H, 14-C=CH, $J_{trans\text{-}14,15}$ =17.0 Hz), 6.60 (s, 3H, ArH); EI-MS m/z (rel intensity, %) 314 (M^+, 5), 179 (25), 136 (21), 124 (27), 123 (100). Retention time of **1** on GLC (10.40 min; OV-1, 0.32 mm×25 m, programed from 200 to 280 °C at 5 °C min^{-1}).

3-[(8*Z*,11*E*,13*E*)-8,11,13-Pentadecatrienyl]catechol (2). This was prepared from **11** and $LiAlH_4$–*t*-BuOH in THF in a similar manner to that described in the preparation of **1**. **2**: Yield; 65% oil; R_f=0.39 (benzene-ethyl acetate=9 : 1); IR (neat) 3480, 3030, 2940, 2860, 1625, 1600, 1475, 1375, 1270, 1230, 1178, 985, 825, 770, 730 cm^{-1}; ^1H NMR (270 MHz, $CDCl_3$) δ=1.31 (m, 8H, 3,4,5,6-CH_2), 1.57 (m, 2H, 2-CH_2), 2.03 (m, 2H, 7-CH_2), 2.59 (t, J=8 Hz, 2H, CH_2Ar), 2.81 (m, 2H, C=CCH_2C=C), 5.31—5.45 (m, 3H, 8,9-CH_2), 5.45—5.66 (m, 2H, 11,14-C=CH), 5.7 (br. s, 2H, OH, D_2O exchangeable), 5.92—6.09 (m, 2H, 12,13-C=CH), 6.69 (s, 3H, ArH); The accurate chemical shifts and coupling constants were determined by decoupling experiments: 8-CH: 5.43, 9-CH: 5.37, 11-CH: 5.53, 12, 13-CH: 6.02, 14-CH: 5.58; $J_{8,9}$=10.4, $J_{9,10}$=$J_{7,8}$=6.5, $J_{10,11}$=$J_{14,15}$=7.0, $J_{13,14}$=$J_{11,12}$=14.4 Hz; ^{13}C NMR ($CDCl_3$) δ=19.0 (C-15), 27.1 (C-7), 29.1, 29.2, 29.4, 29.5, 29.6 (C-2-6), 29.8 (C-1), 30.3 (C-10), 112.0 (ArC-6), 120.0 (ArC-4), 122.0 (ArC-5), 127.0 (C-9), 127.2 (C-8), 129.4 (C-14), 129.9 (C-12), 130.4 (C-11), 130.7 (C-13), 131.5 (ArC-3), 142.0 (ArC-2), 143.1 (ArC-1); EI-MS m/z (rel intensity, %) 314 (M^+, 9), 179 (5), 136 (11), 124 (27), 113 (100). Compound **2** was identified by comparison of the retention times on GLC (10.25 min; OV-1, 0.32 mm×25 m, programed from 200 °C to 280 °C at 5 °C min^{-1}) and HPLC (11.35 min; silica gel, 10 mm×25 cm, 5 μm, hexane–ethyl acetate=96 : 4, 1.5 ml min^{-1}) with those of the natural sample and by GC-MS analysis.

The present work was partially supported by a Grant-in-Aid for Scientific Reserch No. 62550678 from the Ministry of Education, Science and Culture. The authors are grateful to Dr. Ju Kumanotani and Dr. Ryuichi Oshima for invaluable discussion.

References

1) J. Kumanotani, in "Polymer Application of Renewable Resource Materials," ed by C. E. Carraher and L. H. Sperling, Plenum Press, New York (1983), pp. 225—248.
2) R. Majima, *Ber. Dtsch. Chem. Ges. B,* **55**, 172 (1922).
3) S. V. Sunthanker and C. R. Dawson, *J. Am. Chem. Soc.,* **76**, 5070 (1954).
4) Y. Yamauchi, R. Oshima, and J. Kumanotani, *J. Chromatogr.,* **243**, 71 (1982).
5) Y. Du, R. Oshima, and J. Kumanotani, *J. Chromatogr.,* **284**, 463 (1984).
6) J. H. P. Tyman, *Chem. Soc. Rev.,* **8**, 499 (1979).
7) W. F. Symes and C. R. Dawson, *J. Am. Chem. Soc.,* **76**, 2959 (1954).
8) O. Hashimoto and K. Minami, *Mokuzai Gakkaishi,* **25**, 789 (1979).
9) T. Miyakoshi and H. Kobuchi, *Nippon Kagaku Kaishi,* **1990**, 1271.
10) T. Miyakoshi, T. Saito, and Y. Du, *Yukagaku,* **39**, 56 (1990).
11) T. Miyakoshi, N. Niimura, and H. Kobuchi, 56th National Meeting of the Chemical Society of Japan, Tokyo, April 1988, Abstr., 3XIB36.
12) H. Halim, H. D. Locksley, and J. J. Memon, *J. Chem. Soc., Perkin Trans. 1,* **1980**, 2331.
13) J. H. P. Tyman, *Chem. Ind.,* **1974**, 526.
14) J. W. de Haan and L. J. M. de Ven, *Org. Mag. Reson.,* **5**, 147 (1979).
15) R. M. Silverstein, G. C. Bassler, and T. C. Morrill, in "Spectrometric Identification of Organic Compounds," John Wiley & Sons, New York (1981), p. 249.
16) M. V. Sargent and S. Wangchareontrakul, *J. Chem. Soc., Perkin Trans. 1,* **1989**, 1171.
17) C. P. Gorst-Allman, P. S. Steyn, T. Heyl, M. J. Wells, and D. M. C. Fourie, *South. Afr. J. Chem.,* **40**, 82 (1987).
18) M. V. Sargent, S. Wangchareontrakul, and A. Jefferson, *J. Chem. Soc., Perkin Trans. 1,* **1989**, 431.
19) I. Gosney and A. G. Rowley, in "Organophosphorus Reagent in Organic Synthesis," ed by J. I. G. Cadogan, Academic Press, London (1979), Chap. 2.

Diastereoselective Synthesis of 2,3-*anti*-5-Benzyloxy-2,4-dimethyl-1,3-pentanediols via Cyclic Hydroboration

Yasushi YOKOYAMA,* Yuji TERADA, and Hideyuki KAWASHIMA
Department of Materials Science, Faculty of Engineering, Yokohama National University, Tokiwadai, Hodogaya-ku, Yokohama 240
(Received February 7, 1991)

Synopsis. The treatment of (2*E*,4*S*)- and (2*Z*,4*S*)-1-benzyloxy-5-ethenyloxy-2,4-dimethyl-2-pentene with borane both with and without a catalytic amount of $Rh(Ph_3P)_3Cl$ gave 2,3-*anti*-3,4-*anti*-(2*R*,3*R*,4*S*)- and 2,3-*anti*-3,4-*syn*-(2*R*,3*R*,4*R*)-5-benzyloxy-2,4-dimethyl-1,3-pentanediols, respectively, with fair to good diastereoselectivity.

The enantioselective preparation of polypropionate antibiotics, particularly macrolides, has attracted the strong attention of a large number of synthetic organic chemists.[1] As the synthon of polypropionates, 2,4-dimethyl-1,3,5-pentanetriol derivatives **1a—d** and the related compounds are very useful, and have been used in the synthesis of biologically important natural compounds.[2–4] An excellent review concerning these compounds has already appeared.[5]

We have recently reported an allylic 1,3-strain-controlled cyclic hydroboration, used to produce acyclic compounds possessing a 1,2-*anti*-2-methyl-1,4-diol unit.[6] In this article we would like to report on the diastereoselective construction of 2,3-*anti*-2,4-dimethyl-1,3,5-pentanetriol derivatives via the cyclic hydroboration method.

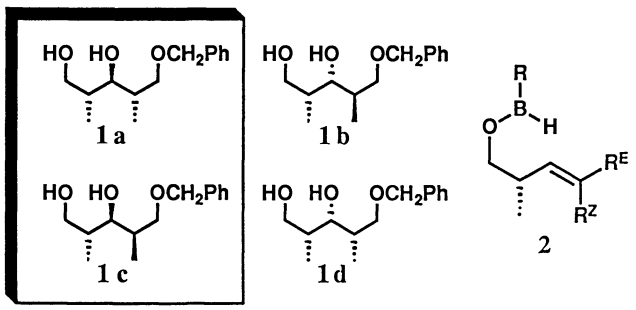

Our target molecules to prepare were **1a** and **1c**. Since species **2** was known not to afford intramolecular hydroboration products (because of its low reactivity toward olefins[7]), we had to find a new reaction system. We chose ethenyl ethers as the intramolecular borane carrier. The advantage of using ethenyl ethers is that this C_2 unit is known to fall off as an ethene molecule during the intramolecular hydroboration reaction;[8] therefore, no ether cleavage reaction, (which is sometimes difficult[9]) was necessary for a further chemical transformation (Scheme 1).

Ethenyl ethers **3E** and **3Z** were prepared from the corresponding optically active alcohols, **4E** and **4Z**, respectively, with almost complete control of the double-bond geometry (>98 : <2)[6b] without any loss of chirality.[2]

The reaction of *E* isomer **3E** with borane in THF at

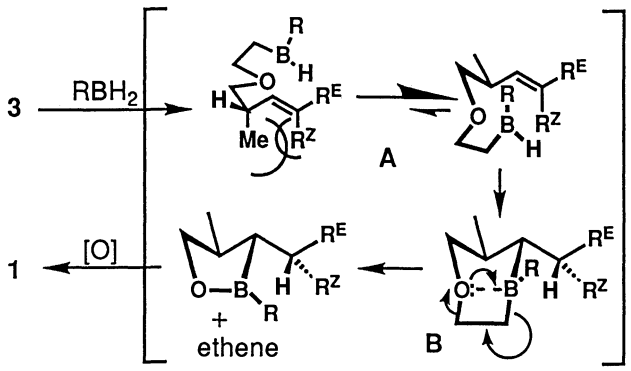

Scheme 1.

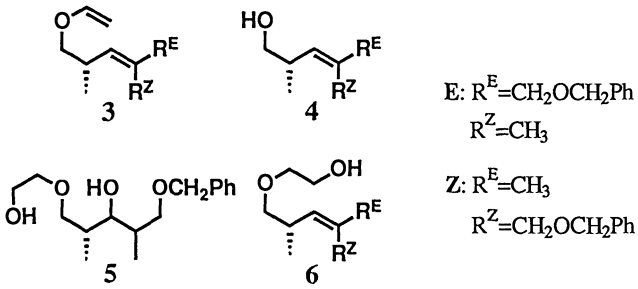

−70 °C to room temperature, followed by an alkaline hydrogen peroxide treatment, gave an inseparable mixture of two triol monobenzyl ethers (**1a** and **1b**, 56%), together with 2-hydroxyethyl ether **5** (15%). The diastereomeric ratio, **1a**/**1b**, was determined to be 80/20 by comparing the ^1H NMR data with that described in the literature.[2,3] In a low-Lewis-basic solvent, CH_2Cl_2, which might accelerate ethene extrusion by avoiding solvent coordination to the boron atom of cyclic intermediate **B** in Scheme 1, no hydroxyethyl ether **5** was detected, though a smaller amount of a mixture of diols (75/25, 36%) was obtained with homoallylic ether **6E** (10%).

It was found that (1,1,2-trimethylpropyl)borane (thexylborane) is not effective in this reaction. The steric bulkiness interfered not only a stereoselective reaction, but even cyclic hydroboration, itself.

Similar results were obtained for ethenyl ether **3Z** (Table 1).

The diastereoselectivity of this reaction was lower than that of 1,4-dienes.[6] Although Harada et al. observed that boranes reacted with the electron-rich, sterically-uncongested ethenyloxy moiety faster than with the trisubstituted double bond,[8] the low reactivity of **A** in Scheme 1 might have allowed a reversely diaster-

Table 1. Cyclic Hydroboration of Ethenyl Ethers **3E** and **3Z**

Substrate	Borane	Solvent	Time/h[a]	**1** Yield/% (*anti*/*syn*)		**5** Yield/%	**6** Yield/%
3E	BH_3	THF	16.5	56	(80/20)	15	0
3E	BH_3	Ether	12.5	60	(75/25)	9	0
3E	BH_3	CH_2Cl_2	20	36	(75/25)	0	10
3E	$ThexBH_2$[b]	THF	14(5)	33	(50/50)	7	25
3Z	BH_3	THF	15	77	(70/30)	17	4
3Z	BH_3	Ether	18	71	(70/30)	8	0
3Z	BH_3	CH_2Cl_2	20.5	53	(70/30)	0	0
3Z	$ThexBH_2$[b]	THF	15(3.5)	44	(75/25)	42	6

a) Reaction time at room temperature. Additional refluxing time before quenching, if done, is in the parenthesis. b) $ThexBH_2$ stands for (1,1,2-trimethylpropyl)borane.

Table 2. Cyclic Hydroboration of Ethenyl Ethers **3E** and **3Z** with Borane in THF in the Presence of $Rh(PPh_3)_3Cl$

Substrate	Rh(I)/mol%	Time/h	**1** Yield/% (*anti*/*syn*)		**5** Yield/%	**6** Yield/%
3E	2.1	18	53	(60/40)	22	0
3Z	4.6	17.5	53	(90/10)	0	10

eoselective *intermolecular* hydroboration of a borane species toward the trisubstituted double bond of **A** to give isomers **1b** or **1d**.

In 1985 Männig and Nöth reported that hydroboration reactions using 1,3,2-benzodioxaborole (catecholborane) were greatly accelerated by a catalytic amount of $Rh(PPh_3)_3Cl$.[10] Recently, further developments and applications of this reaction have been reported.[11–14] Pt-catalyzed hydrosilylation, closely related to Rh-catalyzed hydroboration, was also reported by Tamao et al.[15] Since the intramolecular hydroboration of intermediate **A** in Scheme 1 was not very fast at −78 °C, it would be accelerated by the Rh(I) catalyst. While hoping to improve the *anti*/*syn* selectivity of the diols, we next carried out a reaction (borane, THF, −78 °C to room temperature) with 2—5 mol% of $Rh(PPh_3)_3Cl$. The results are given in Table 2.

Although ethenyl ether **3E** gave a 60/40 mixture of diols **1a** and **1b** in 53%, **3Z** gave a mixture of **1c**/**1d** with a 90/10 ratio in 53% yield. A similar observation, that the selectivity of the Pt-catalyzed hydrosilylation reaction of (*Z*)-olefin was better than that of (*E*)-olefin, has been reported by Tamao et al. According to them, the hydrosilylation-oxidation reaction of **3E** gives **1a** in a 3.5/1 ratio, while **3Z** gives **1c** in >10/1.[15]

Experimental

The IR spectra were measured using a JASCO A-202 IR spectrometer. The ^1H NMR spectra were recorded with a JEOL JNM-FX-90Q or JEOL JNM-PMX-60 spectrometer in $CDCl_3$, unless otherwise noted. The low- and high-resolution mass spectra were taken with a JEOL JMS D-300 mass spectrometer. All reactions were carried out in dry solvents under a nitrogen atmosphere.

(2*E*,4*R*)-1-Benzyloxy-2,4-dimethyl-5-ethenyloxy-2-pentene (3E). To a mixture of mercury(II) acetate (287 mg, 0.90 mmol, 1.53 equiv) and ethenyl ethyl ether (2 ml) at room temperature was added a solution of (2*R*,3*E*)-5-benzyloxy-2,4-dimethyl-3-penten-1-ol (**4E**) (130 mg, 0.59 mmol) in 3.5 ml ethenyl ethyl ether; the resulting mixture was refluxed for 17.5 h. During that period, another 5 ml of ethenyl ethyl ether was added. At the end of the reaction, 5 ml of ether and 6 ml of 5% aqueous potassium hydroxide solution were successively added. Extraction with ether followed by the usual work up and purification with silica gel flash column chromatography (hexane–ethyl acetate, 95:5) gave 131 mg (90%) of ethenyl ether (**3E**). ^1H NMR (CCl_4, 60 MHz) δ=1.03 (3H, d, J=7.0 Hz), 1.69 (3H, s), 2.8 (1H, m), 3.47 (2H, d, J=6.3 Hz), 3.80 (2H, s), 3.88 (1H, dd, J=6.7, 2.0 Hz), 4.31 (1H, dd, J=14.2, 2.0 Hz), 4.39 (2H, s), 5.21 (1H, d, J=9.2 Hz), 6.39 (1H, dd, J=14.2, 6.7 Hz), 7.23 (5H, s); IR (neat) 1630 (sh), 1610, 1200, 700 cm^{-1}; MS *m*/*z* (rel intensity) 246 (M^+; 0.1), 138 (M^+-PhCH_2OH; 100). Found: *m*/*z* 138.1052. Calcd for $C_9H_{14}O$ ($M-PhCH_2OH$): 138.1045.

(2*Z*,4*R*)-1-Benzyloxy-2,4-dimethyl-5-ethenyloxy-2-pentene (3Z). Essentially the same procedure described above using mercury(II) acetate (450 mg, 1.41 mmol, 1.19 equiv), ethenyl ethyl ether (9 ml), and (2*R*,3*Z*)-5-benzyloxy-2,4-dimethyl-3-penten-1-ol (**4Z**) (262 mg, 1.19 mmol) gave 283 mg (97%) of ethenyl ether (**3Z**). ^1H NMR (CCl_4, 60 MHz) δ=0.94 (3H, d, J=7.0 Hz), 1.80 (3H, s), 2.8 (1H, m), 3.46 (2H, d, J=6.3 Hz), 3.93 (1H, dd, J=7.0, 2.0 Hz), 4.01 (2H, s), 4.34 (1H, dd, J=14.1, 2.0 Hz), 4.44 (2H, s), 5.18 (1H, d, J=9.2 Hz), 6.37 (1H, dd, J=14.1, 7.0 Hz), 7.29 (5H, s); IR (neat) 1630 (sh), 1607, 1200, 700 cm^{-1}; MS *m*/*z* (rel intensity) 246 (M^+; 0.1), 138 (M^+-PhCH_2OH; 100). Found: *m*/*z* 138.1046. Calcd for $C_9H_{14}O$ ($M-PhCH_2OH$): 138.1045.

Typical Procedure of Cyclic Hydroboration. Ethenyl ether **3Z** (112 mg, 0.454 mmol) was dissolved in ether (5 ml); the solution was then cooled to −74 °C, to which was added (dropwise over a period of 2 h) a mixture of a 2.0 mol dm^{-3} ethereal solution of borane–dimethyl sulfide complex (1/1) (0.25 ml, 0.5 mmol, 1.1 equiv) and ether (5 ml). After the addition was completed, the cooling bath was removed, and the reaction mixture was stirred for 18 h at room temperature. To it was added 1 ml water, 1 ml 1 mol dm^{-3} aq sodium hydroxide, and 0.3 ml 35% aq hydrogen peroxide successively; the mixture was then stirred at 60 °C for 2 h. Extraction with ethyl acetate followed by the usual work up and silica-gel flash column chromatography (hexane–ethyl acetate, 70:30 to 50:50) gave a mixture of **1c** and **1d** (61 mg, 0.258 mmol, 57%), **1d** (15 mg, 0.063 mmol, 14%), and 2-hydroxyethyl ether **5** (11

Table 3. Selected ^{1}H NMR Data of Diol **1d**[a)]

In C_6D_6			
Data from Ref. 2	0.55 (3H, d, J=6.9 Hz)	0.93 (3H, d, J=6.9 Hz)	4.22 (2H, s)
Our data	1.03 (3H, d, J=7.4 Hz)	1.11 (3H, d, J=7.1 Hz)	4.26 (2H, s)
In $CDCl_3$			
Data from Ref. 3	1.01 (3H, d, J=7.0 Hz)	1.05 (3H, d, J=7.0 Hz)	4.50 (2H, s)
Our data	1.00 (3H, d, J=6.8 Hz)	1.05 (3H, d, J=6.8 Hz)	4.49 (2H, s)

a) Given in δ (ppm) downfield from tetramethylsilane as an internal standard.

mg, 0.037 mmol, 8%). The **1c**/**1d** ratio of the diol mixture was analyzed by ^{1}H NMR to be 90/10.

Typical Procedure of Cyclic Hydroboration with Rh(PPh$_3$)$_3$Cl. Ethenyl ether **3E** (133 mg, 0.538 mmol) was dissolved in THF (6 ml), and the solution was cooled to −74 °C. To it was added (dropwise over a period of 2 h) a mixture of a 2.0 mol dm^{-3} ethereal solution of borane–dimethyl sulfide complex (1/1) (0.30 ml, 0.6 mmol, 1.1 equiv) and THF (6 ml). To this was added (at that temperature) a solution of Rh(PPh$_3$)$_3$Cl (11 mg, 0.011 mmol, 2.1 mol%) in THF (4 ml). After the addition was completed, the cooling bath was removed, and the reaction mixture was stirred for 18 h at room temperature. To it was added 1 ml water, 1 ml 1 mol dm^{-3} aq sodium hydroxide, and 0.6 ml 35% aq hydrogen peroxide, successively; the mixture was then stirred at 60 °C for 2 h. Extraction with ethyl acetate followed by the usual work up and silica-gel flash column chromatography (hexane–ethyl acetate, 70 : 30 to 50 : 50) gave a mixture of **1a** and **1b** (68 mg, 0.285 mmol, 53%) and 2-hydroxyethyl ether **5** (33 mg, 0.116 mmol, 22%). The **1a**/**1b** ratio was analyzed by ^{1}H NMR to be 60/40.

Assignment of the Product Stereochemistry. The product ratio was determined by ^{1}H NMR. Namely, the chemical shift values of two doublet methyls were compared with the values reported in the Refs. 2 and 3; the ratio was calculated from the integration values. It should be noted that the chemical shift values of the diol **1d** in C_6D_6 reported by Nagaoka and Kishi in Ref. 2 are not in good accordance with those of ours. However, ours were identical with the data of **1d** in $CDCl_3$ reported by Oikawa et al. in Ref. 3. The chemical shift data of **1d** are listed in Table 3.

Methyl (*R*)-3-hydroxy-2-methylpropanoate was kindly provided by Kanegafuchi Chemical Industries, Co., and is greatly acknowledged.

References

1) a) I. Paterson and M. M. Mansuri, *Tetrahedron,* **41**, 3569 (1985); b) R. K. Boeckmann, Jr. and S. W. Goldstein, "The Total Synthesis of Macrocyclic Lactones," in "The Total Synthesis of Natural Products," ed by J. ApSimon, John Wiley & Sons, New York (1988), Vol. 7, pp. 1—139.

2) H. Nagaoka and Y. Kishi, *Tetrahedron,* **37**, 3873 (1981).

3) Y. Oikawa, T. Nishi, H. Itaka, and O. Yonemitsu, *Tetrahedron Lett.,* **24**, 1987 (1983).

4) D. V. Patel, F. VanMiddlesworth, J. Donaubauer, P. Gannett, and C. J. Sih, *J. Am. Chem. Soc.,* **108**, 4603 (1986).

5) R. W. Hoffmann, *Angew. Chem., Int. Ed. Engl.,* **26**, 489 (1987).

6) a) Y. Yokoyama, H. Kawashima, and H. Masaki, *Chem. Lett.,* **1989**, 453; b) Y. Yokoyama, H. Kawashima, M. Kohno, Y. Ogawa, and S. Uchida, *Tetrahedron Lett.,* **32**, 1479 (1991).

7) C. H. Heathcock, E. T. Jarvi, and T. Rosen, *Tetrahedron Lett.,* **25**, 243 (1984).

8) T. Harada, Y. Matsuda, J. Uchimura, and A. Oku, *J. Chem. Soc., Chem. Commun.,* **1989**, 1429.

9) M. V. Bhatt and S. U. Kulkarni, *Synthesis,* **1983**, 249.

10) D. Männig and H. Nöth, *Angew. Chem., Int. Ed. Engl.,* **24**, 878 (1985).

11) a) D. A. Evans, G. C. Fu, and A. H. Hoveyda, *J. Am. Chem. Soc.,* **110**, 6917 (1988); b) D. A. Evans and G. C. Fu, *J. Org. Chem.,* **55**, 2280 (1990).

12) K. Burgess and M. J. Ohlmeyer, *Tetrahedron Lett.,* **30**, 395 (1989).

13) T. Hayashi, Y. Matsumoto, and Y. Ito, *J. Am. Chem. Soc.,* **111**, 3426 (1989).

14) M. Sato, N. Miyaura, and A. Suzuki, *Tetrahedron Lett.,* **31**, 231 (1990).

15) K. Tamao, T. Nakajima, R. Sumiya, H. Arai, N. Higuchi, and Y. Ito, *J. Am. Chem. Soc.,* **108**, 6090 (1986).

Halogenation Using Quaternary Ammonium Polyhalides. XXXI[1] Halogenation of Thiophene Derivatives with Benzyltrimethylammonium Polyhalides

Tsuyoshi OKAMOTO, Takaaki KAKINAMI, Hiroshi FUJIMOTO, and Shoji KAJIGAESHI,*,†
Department of Chemical and Biological Engineering, Ube Technical College, Tokiwadai, Ube 755
†Department of Industrial Chemistry, Faculty of Engineering, Yamaguchi University, Tokiwadai, Ube 755
(Received February 27, 1991)

Synopsis. The reactions of thiophene derivatives with benzyltrimethylammonium tetrachloroiodate, benzyltrimethylammonium tribromide, and benzyltrimethylammonium dichloroiodate in acetic acid or in acetic acid–zinc chloride under mild conditions gave chloro-, bromo-, and iodo-substituted thiophene derivatives, respectively, in satisfactory yields.

Since thiophene derivatives (**1**) are sensitive toward the electrophilic substitution reactions, the halogenation of **1** generally gives a mixture of mono-, di-, and other polysubstituted halogenation products. For example, direct chlorination of thiophene (**1a**) with chlorine gave a mixture of 2-chloro-, 2,5-dichloro-, 2,3,4-trichloro-, 2,3,5-trichloro-, and 2,3,4,5-tetrachlorothiophene.[2] Bromination of **1a** with an equimolar amount of bromine gave 2-bromothiophene accompanying 2,5-dibromo- and a smaller amount of tribromothiophene as by-products.[3] Only 2-iodo- and 2,5-diiodothiophene can be synthesized by direct iodination of **1a** with iodine in the presence of mercury(II) oxide,[4] and other iodothiophenes can be prepared indirectly by the reaction of acetoxymercurio derivative with iodine.[5] Direct halogenation of 2-methylthiophene (**1b**) with chlorine[6] and bromine,[7] also gave the mixtures, respectively. By the iodination of **1b** with iodine–mercury(II) oxide, 5-iodo derivative is obtained,[8] and other iodo derivatives have been synthesized by indirect methods.

We have recently shown that benzyltrimethylammonium polyhalides such as benzyltrimethylammonium tetrachloroiodate (BTMA ICl_4),[9] benzyltrimethylammonium tribromide (BTMA Br_3),[10] and benzyltrimethylammonium dichloroiodate (BTMA ICl_2)[11] are useful aromatic chlorinating, brominating, and iodinating agents. In this paper we wish to report on the direct selective halogenation of aromatic heterocyclic compounds, especially **1**, with BTMA ICl_4, BTMA Br_3, and BTMA ICl_2.

Results and Discussion

The reaction of **1** with BTMA ICl_4 in acetic acid gave chloro-substituted thiophene derivatives (**2**). The reaction of **1** with BTMA Br_3 or BTMA ICl_2 in acetic acid in the presence of zinc chloride gave bromo- (**3**) or iodo-substituted thiophene derivatives (**4**), respectively. The results are summarized in Table 1.

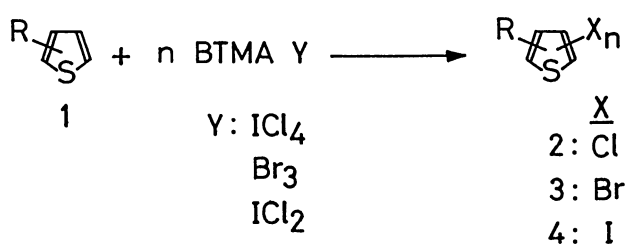

As shown in the Table 1, these reactions usually proceeded stoichiometrically. However, in many cases, the reaction of **1** with BTMA ICl_4 gave a mixture of several chloro-substituted thiophene derivatives **2**, which could not be separated from each other.

In the cases of bromination and iodination, used zinc chloride may form complexes with BTMA Br_3 and BTMA ICl_2, producing such active species as $[PhCH_2(CH_3)_3N]^+[ZnCl_2Br_2]^{2-}Br^+$ and $[PhCH_2(CH_3)_3N]^+[ZnCl_4]^{2-}I^+$, respectively.[27]

We believe that the procedure for the direct halogenation of **1** using benzyltrimethylammonium polyhalides (stable solid reagents) is more useful and effective than that using molecular chlorine, bromine, or iodine, because of ease, simplicity and generality. As a limitation to the procedure, attempts at the monochlorination of **1** using an equimolar amount of BTMA ICl_4 were unsuccessful due to contamination of the polychlorinated products.

Experimental

3-Methyl-2,4,5-trichlorothiophene (2c-3); Typical Procedure for the Chlorination: BTMA ICl_4 (6.50 g, 15.5 mmol) was added to a solution of 3-methylthiophene (**1c**) (0.49 g, 5 mmol) in acetic acid (50 ml); the mixture was stirred at 70 °C for 24 h. During this time, the color of the solution turned black, and a yellow precipitate was deposited. After the solution was cooled to room temperature, the yellow precipitate (BTMA ICl_2) was filtered off. The filtrate was concentrated in vacuo and the obtained residue was treated with 5% $NaHSO_3$ (10 ml) and with 5% $NaHCO_3$ (10 ml), and then extracted with dichloromethane (50 ml×3). The black organic layer was separated and dried over $MgSO_4$. Then, a trace amount of acetic acid and black impurities in the solution were removed by column chromatography on alumina. The eluent was concentrated in vacuo to give a colorless oil **2c-3**; yield 0.64g (63%); bp 219 °C/760 mmHg (lit,[20] bp 115—116 °C/23 mmHg, 1 mmHg=133.322 Pa).

3,5,3′,5′-Tetrachloro-2,2′-dithienyl (2f-4): Mp 120—121 °C; ^1H NMR ($CDCl_3$) δ=6.77 (2H, s, 4- and 4′-H). Found: C, 31.42; H, 0.72%. Calcd for $C_8H_2S_2Cl_4$: C, 31.60; H, 0.66%.

2,5-Dibromothiophene (3a-2); Typical Procedure for the Bromination: BTMA Br_3 (3.90 g, 10 mmol) and $ZnCl_2$ (ca. 1 g) were added to a solution of thiophene (**1a**) (0.42 g, 5 mmol) in acetic acid (30 ml); the mixture was then stirred at room temperature for 2 h until the disappearance of the orange color of the reagent. Aqueous $NaHSO_3$ (5%, 10 ml) was added to the mixture; this mixture was extracted with hexane (50 ml×3). The organic layer was dried over $MgSO_4$, and passed through a short alumina-column. The eluent was concentrated in vacuo to give **3a-2** as a colorless oil; yield 0.65 g

Table 1. Halogenation of Thiophene Derivatives **1** with Benzyltrimethylammonium Polyhalides in AcOH

Substrate 1		Molar ratio Reagent/1	Reaction conditions[a] Temp/°C	Time/h	Product[b] 2,3,4		Yield[c] %	Mp(°C) or Bp(°C/mmHg) Found	Reported
	1a	2.0	70	49	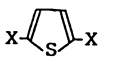	—[d]		—	—
			rt	2		**3a**—**2**	54	217—218/760	68/2[12]
			rt	22		**4a**—**2**	41	42—43	41[13]
			70	24	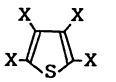	**2a**—**4**	33	225.5/760	233.4/760[14]
		4.1	70	5		**3a**—**4**	72	106—107	117[15]
			70	21		**4a**—**4**	39	202—204	199—200[16]
	1b	1.0	rt	4	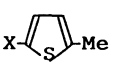	—[d]		—	—
			rt	27		—[e]		—	—
			rt	4		**4b**—**1**	42	oil	88.8—89/14[17]
			70	23	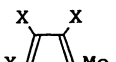	—[d]		—	—
		3.1	rt	15		**3b**—**3**	55	81.5—82.5	91[7]
			70	24		—[f]		—	—
	1c	2.0	rt	24	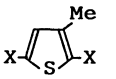	**2c**—**2**	81	185.3/760	65/11[18]
			rt	15		**3c**—**2**	97	226—227/760	226—230/760[19]
			rt	4		**4c**—**2**	92	238—240/760	120—121/2.5[20]
			70	24	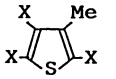	**2c**—**3**	63	219/760	115—116/23[21]
		3.1	rt	15		**3c**—**3**	72	27—28.5	33[19]
			rt	15		**4c**—**3**	94	73—74	75-76[20]
	1d	2.1	70	24	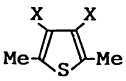	—[d]		—	—
			rt	20		**3d**—**2**	50	223—224/760	44—45[22]
			rt	28		**4d**—**2**	98	80.5—81.5	83[19]
	1e	1.0	rt	22	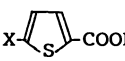	—[d]		—	—
			rt	17		**3e**—**1**	86	174—175/760	113—114/6[23]
			70	19		—[f]		—	—
			70	24	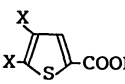	—[d]		—	—
		3.1	70	25		**3e**—**2**	55	48—49	—
			70	24		**4e**—**2**	77	96—97	—
	1f	2.1	rt	24	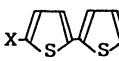	—[d]		—	—
			rt	27		**3f**—**2**	99	145—146	146—147[24]
			rt	15		**4f**—**2**	60	163—165	167—168[25]
			70	24	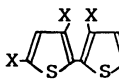	**2f**—**4**	48	120—121	—
		4.1	70	26		**3f**—**4**	95	132—133	139—140[26]
			70	19		—[f]		—	—

a) In the cases of both bromination and iodination, $ZnCl_2$ was used as catalyst. b) Known products were characterized by comparing their ^1HNMR spectra and bp or mp with those of authentic samples or reported data. c) Yield of isolated product. d) Mixture of several chloro-substituted products. e) Mixtrue of several bromo-substituted products. f) Mixture of several iodo-substituted products.

(54%); bp 217—218 °C/760 mmHg (lit,[12] bp 68 °C/2 mmHg).

Ethyl 4,5-Dibromo-2-thiophenecarboxylate (3e-2): Mp 55 °C; ^1HNMR ($CDCl_3$) δ=1.47 (3H, t, J=7 Hz, $CH_2C\underline{H}_3$), 4.17 (2H, q, J=7 Hz, $C\underline{H}_2CH_3$), and 7.64 (1H, s, 3-H). Found: C, 26.50; H, 1.81%. Calcd for $C_7H_6O_2SBr_2$: C, 26.78; H, 1.93%.

2,5-Diiodo-3-methylthiophene (4c-2); Typical Procedure for the Iodination: BTMA ICl_2 (3.65 g, 10 mmol) and $ZnCl_2$ (ca. 1.5 g) were added to a solution of **1c** (0.49 g, 5 mmol) in acetic acid (30 ml); the mixture was stirred at room temperature for 4 h. During this time, a color of the solution turned black. Aqueous $NaHSO_3$ (5%, 10 ml) was added to the mixture; this mixture was extracted with hexane (50 ml×3). The organic layer was dried over $MgSO_4$, and then passed through a short alumina-column in order to remove any trace amount of acetic acid or black impurities. The eluent was concentrated in vacuo to give a colorless oil **4c-2**; yield 1.61 g (92%); bp 238—240 °C/760 mmHg (lit,[20] bp 120—121 °C/2.5 mmHg).

Ethyl 4,5-Diiodo-2-thiophenecarboxylate (4e-2): Mp 77 °C; ^1HNMR ($CDCl_3$) δ=1.33 (3H, t, J=7 Hz, $CH_2C\underline{H}_3$), 4.30 (2H, q, J=7 Hz, $C\underline{H}_2CH_3$), and 7.48 (1H, s, 3-H). Found: C, 20.58; H, 1.45%. Calcd for $C_7H_6O_2SI_2$: C, 20.61; H, 1.48%.

References

1) Part XXX; S. Kajigaeshi, M. Moriwaki, S. Fujisaki, and T. Kakinami, *Chem. Express,* **6**, 185 (1991).

2) F. F. Blicke, "Halothiophenes" in "Heterocyclic Compounds," ed by R. C. Elderfield, John Wiley & Sons, New York (1959), Vol. 1, Chap. 5, p. 221.

3) F. F. Blicke and J. H. Burckhalter, *J. Am. Chem. Soc.,* **64**, 477 (1942).

4) W. Minnis, *Org. Synth.,* Coll. Vol. II, 357 (1950).

5) W. Steinkopf, H. F. Schmitt, and H. Fiedler, *Justus Liebigs Ann. Chem.,* **527**, 237 (1937).

6) St. Opolski, *Anz. Akad. Wiss. Krakow,* **1904**, 730; *Chem. Zentralbl.,* **76**, I, 1255 (1905).

7) W. Steinkopf, *Justus Liebigs Ann. Chem.,* **513**, 281 (1934).

8) A. Vlastelitza, *J. Russ. Phys. Chem. Soc.*, **46**, 790 (1914); *Chem. Abstr.*, **9**, 1750 (1915).
9) a) S. Kajigaeshi, Y. Shinmasu, S. Fujisaki, and T. Kakinami, *Chem. Lett.*, **1989**, 415; b) S. Kajigaeshi, Y. Ueda, S. Fujisaki, and T. Kakinami, *Bull. Chem. Soc. Jpn.*, **62**, 2096 (1989); c) S. Kajigaeshi, Y. Shinmasu, S. Fujisaki, and T. Kakinami, *Bull. Chem. Soc. Jpn.*, **63**, 941 (1990); d) S. Kajigaeshi, Y. Shinmasu, S. Fujisaki, and T. Kakinami, *Chem. Express*, **5**, 141 (1990).
10) S. Kajigaeshi and T. Kakinami, *Yuki Gosei Kagaku Kyokai Shi*, **46**, 986 (1988), and references cited therein.
11) S. Kajigaeshi and T. Kakinami, *Yuki Gosei Kagaku Kyokai Shi*, **48**, 1062 (1990), and references cited therein.
12) G. H. Jeffery, R. Parker, and A. I. Vogel, *J. Chem. Soc.*, **1961**, 570.
13) W. Minnis, *Org. Synth.*, Coll. Vol. II, 357 (1943).
14) H. L. Coonradt, H. D. Hartough, and G. C. Johnson, *J. Am. Chem. Soc.*, **70**, 2564 (1948).
15) R. Keswani and H. Freiser, *J. Am. Chem. Soc.*, **71**, 218 (1949).
16) I. J. Rinkes, *Recl. Trav. Chim. Pays-Bas*, **55**, 991 (1936); *Chem. Abstr.*, **31**, 1802 (1937).
17) W. Steinkopf and W. Hanske, *Justus Liebigs Ann. Chem.*, **527**, 264 (1937).
18) E. Campaigne and W. M. Lesuer, *J. Am. Chem. Soc.*, **71**, 333 (1949).
19) W. Steinkopf and H. Jacob, *Justus Liebigs Ann. Chem.*, **515**, 273 (1935).
20) W. Steinkopf and W. Hanske, *Justus Liebigs Ann. Chem.*, **532**, 236 (1937).
21) W. Steinkopf and W. Köhler, *Justus Liebigs Ann. Chem.*, **532**, 250 (1937).
22) J. L. Melles and H. J. Backer, *Recl. Trav. Chim. Pays-Bas*, **72**, 314 (1953); *Chem. Abstr.*, **48**, 2635 (1954).
23) E. Imoto, Y. Otsuji, and T. Hirai, *Nippon Kagaku Zasshi*, **77**, 804 (1956); *Chem. Abstr.*, **52**, 9066 (1958).
24) H. Wynberg and A. Bantjes, *J. Org. Chem.*, **24**, 1421 (1959).
25) D. Brown, J. C. Craig, N. H. Dyson, and J. W. Westley, *J. Chem. Soc. C*, **1966**, 89.
26) W. Steinkopf, H. J. V. Petersdorff, and R. Gording, *Justus Liebigs Ann. Chem.*, **527**, 272 (1937).
27) S. Kajigaeshi, T. Kakinami, M. Moriwaki, T. Tanaka, S. Fujisaki, and T. Okamoto, *Bull. Chem. Soc. Jpn.*, **62**, 439 (1989).

Synthesis and Properties of Gramicidin S Analogs Consisting of Eight Amino Acid Residues

Makoto TAMAKI* and Sadatoshi AKABORI
Department of Chemistry, Faculty of Science, Toho University,
Miyama, Funabashi-shi, Chiba 274
(Received March 20, 1991)

Synopsis. Three cyclic octapeptides (des-Val$^{1,1'}$-gramicidin S, des-Leu$^{3,3'}$-gramicidin S and des-Val^{1},Leu$^{3'}$-gramicidin S), showed no antibiotic activity. Although their CD spectra resembled each other, they differed from that of gramicidin S. These results indicate that the removal of two of the Val and/or Leu residues at positions 1, 1', 3, and 3' of gramicidin S greately affects both the antibiotic activity and conformation.

Gramicidin S (GS)[1] is an antibiotic cyclodecapeptide, cyclo(-Val-Orn-Leu-D-Phe-Pro-)$_2$,[2] with a rigid β-pleated sheet conformation.[3] In order to investigate the contribution of the ring size to both the antibiotic activity and conformation, many GS analogs with a variety of ring sizes have been synthesized.[4–6] Recently, in synthetic studies of several cyclododeca- and cyclotetradecapeptides related to GS and gratisin (GR), we have reported that the primary structure of GS with ten residues is not always necessary for exhibiting strong activity, and that the CD spectra of these synthetic peptides mainly reflect the amino acid sequence around their β-turn part (-D-Phe-Pro-).[7–9] However, we have not yet evaluated the structure-activity correlation of its analogs with a smaller ring size than that of GS.

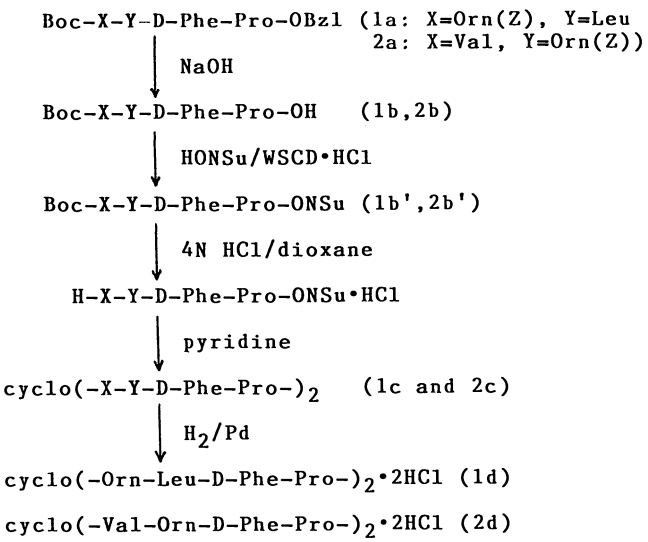

Fig. 1. Synthetic scheme of des-Val$^{1,1'}$- and des-Leu$^{3,3'}$-GS.

In this paper we describe the syntheses, antibiotic activity, and CD spectra of three cyclooctapeptides (cyclo(-Orn-Leu-D-Phe-Pro-)$_2$ (des-Val$^{1,1'}$-GS, **1d**), cyclo(-Val-Orn-D-Phe-Pro-)$_2$ (des-Leu$^{3,3'}$-GS, **2d**), and cyclo(-Orn-Leu-D-Phe-Pro-Val-Orn-D-Phe-Pro-) (des-Val^{1},Leu$^{3'}$-GS, **3d**)) which lack two residues of the Val or Leu residues at positions 1, 1', 3, and 3' of GS. We also discuss the contribution of the ring size to both the antibiotic activity and conformation.

The synthetic routes of these analogs are shown in Figs. 1 and 2. These methods are similar to those described in previous papers of this series.[7,10] In the syntheses of des-Val$^{1,1'}$- and des-Leu$^{3,3'}$-GS, cyclizations of H-Orn(*Z*)-Leu-D-Phe-Pro-ONSu (**1b'**) and H-Val-Orn(*Z*)-D-Phe-Pro-ONSu (**2b'**) were carried out in pyr-

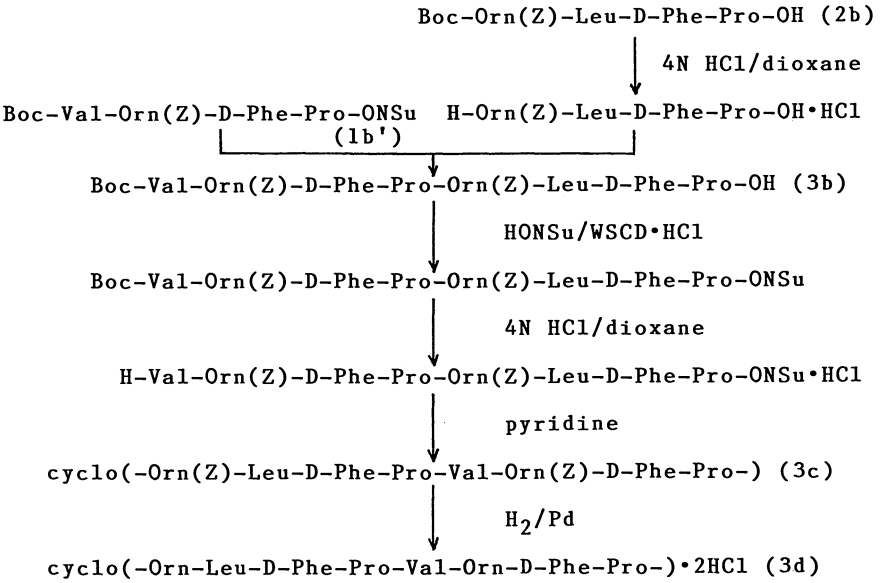

Fig. 2. Synthetic scheme of des-Val^{1}, Leu$^{3'}$-GS.

idine at 25 °C for 1 d. The final concentration of the active esters was 3 mM (1 M=1 mol dm^{-3}). High-performance liquid chromatography (HPLC) profiles of the crude cyclic products are shown in Fig. 3. The molecular weight of each cyclic product isolated by semipreparative HPLC was determined by FAB mass spectrometry. The cyclic products from the tetrapeptide active esters have widely different molecular weights. Compound **1b'** produced the cyclic dimer (30%), trimer (4%), and tetramer (0.5%); Compound **2b'** produced the cyclic dimer (35%), trimer (6%), and tetramer (0.5%). These active esters, however, did not produce a cyclic monomer. The numbers in parentheses are the yields of each cyclic product calculated from **1b** and **2b**. Recently, regarding the cyclization of H-Val-Orn(*Z*)-Leu-D-Phe-Pro-ONSu and H-Tyr(Bzl)-Val-Orn(*Z*)-Leu-D-Phe-Pro-ONSu containing the D-Phe-Pro sequence at the C-terminal, we reported that the former yields exclusively the cyclic dimer, while the latter produces the cyclic monomer and dimer.[10] The present results indicate that the lengths of these active esters greatly affect their mode of cyclization.

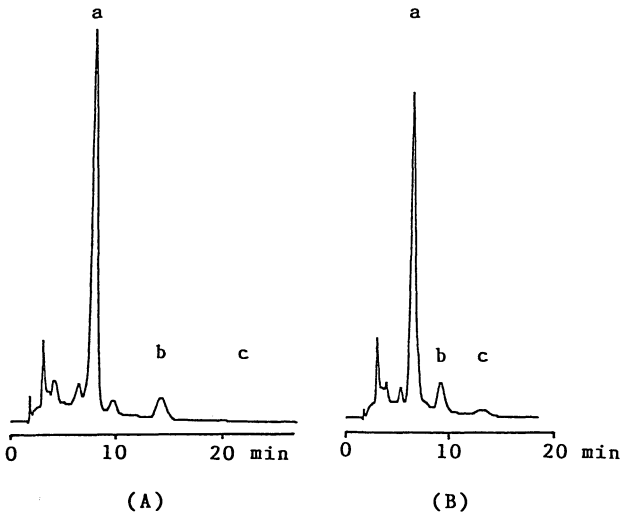

Fig. 3. HPLC profiles[a] of products in cyclization of H-Orn(Z)-Leu-D-Phe-Pro-ONSu (A) and H-Val-Orn(Z)-D-Phe-Pro-ONSu (B).
(a: cyclic dimer, b: cyclic trimer, c: cyclic tetramer)
a) Elution solvent used in these HPLC analysis was MeOH-H_2O (6 : 1).

The yields, physical properties and analytical data of intermediary products and GS analogs are summarized in Tables 1 and 2.

Des-Val$^{1,1'}$-GS, des-Leu$^{3,3'}$-GS and des-Val^{1}, Leu$^{3'}$-GS showed no antibiotic activity against all of the microorganisms tested. We also found that cyclo(-Orn-D-Phe-Pro-)$_2$ shows no activity.[11] On the other hand, we have reported that some cyclododecapeptides related to GR with various seqeunces at the β-turn part show strong activity,[7,8] and that several cyclotetradecapeptides related to GS possess 1/4—1/8 activity of GS.[9] These results indicate that removing either two or four of the Val and/or Leu residues at positions 1, 1', 3, and 3' from GS results in a loss of activity, while the addition of two or four amino acid residues to GS makes it feasible to take a suitable conformation for exhibiting antibiotic activity.

The CD spectra of these synthetic peptides and GS in an aqueous solution are shown in Fig. 4. These CD

Table 1. Yields and Analytical Data of Intermediary Products of GS Analogs

	Yield	Mp	$[\alpha]_D^{25}$/°		Elemental analysis/%						
	%	°C	(*c* 1, DMF)			C	H	N		C	H	N
1a.	60[a]	89—92	−35.4	$C_{45}H_{59}O_9N_5 \cdot 0.5H_2O$	Found:	65.79	7.34	8.70	Calcd:	65.67	7.35	8.51
1b.	92	94—96	−40.7	$C_{38}H_{53}O_9N_5 \cdot 0.5H_2O$	Found:	62.59	7.70	9.02	Calcd:	62.28	7.43	9.35
1c.	30	120—126	−6.7[b]	$C_{66}H_{86}O_{12}N_{10} \cdot H_2O$	Found:	64.18	7.24	11.13	Calcd:	64.47	7.21	11.39
2a.	67[a]	72—75	−21.7	$C_{44}H_{57}O_9N_5 \cdot 0.5H_2O$	Found:	65.27	7.20	8.82	Calcd:	65.33	7.23	8.66
2b.	97	73—78	−27.3	$C_{37}H_{51}O_9N_5$	Found:	62.25	7.28	9.38	Calcd:	62.61	7.24	9.87
2c.	35	131—137	+8.7[b]	$C_{64}H_{82}O_{12}N_{10} \cdot 1.5H_2O$	Found:	63.12	6.97	11.65	Calcd:	63.51	7.08	11.57
3b.	87	116—122	−36.0	$C_{70}H_{94}O_{15}N_{10} \cdot 1.5H_2O$	Found:	62.74	7.22	10.42	Calcd:	62.62	7.28	10.43
3c.	64	120—125	−0.3[b]	$C_{65}H_{84}O_{12}N_{10} \cdot 2H_2O$	Found:	63.37	7.03	11.49	Calcd:	63.29	7.19	11.36

a) The yields of **1a** and **2a** were calculated on the basis of the amount of Pro-OBzl · HCl as a starting material.
b) *c* 0.5.

Table 2. Yields and Analytical Data of GS Analogs

1d.	Yield, 80%; mp, 232—235 °C; $[\alpha]_D^{25}$−97.1° (*c* 0.5, EtOH); MS(FAB) *m/z* 944 (MH^+). Amino acid analysis: Orn, 1.96; Leu, 2.07; Phe, 1.97; Pro, 2.00. Found: C, 55.82; H, 7.60; N, 12.96%. Calcd for $C_{50}H_{74}O_8N_{10} \cdot 2HCl \cdot 3.5\ H_2O$: C, 55.65; H, 7.75; N, 12.98%.
2d.	Yield, 80%; mp, 251—254 °C; $[\alpha]_D^{25}$−42.2° (*c* 0.5, EtOH); MS(FAB); *m/z* 915 (MH^+). Amino acid analysis: Val, 2.09; Orn, 2.03; Phe, 1.95; Pro, 1.92. Found: C, 53.31; H, 7.29; N, 12.80%. Calcd for $C_{48}H_{70}O_8N_{10} \cdot 2HCl \cdot 5H_2O$: C, 53.47; H, 7.67; N, 12.99 %.
3d.	Yield, 90%; mp, 226—230 °C; $[\alpha]_D^{25}$−108.8° (*c* 0.5, EtOH); MS(FAB) *m/z* 929 (MH^+). Amino acid analysis: Val, 1.05; Orn, 2.00; Leu, 1.07; Phe, 1.90; Pro, 1.99. Found: C, 54.30; H, 7.41; N, 12.89 %. Calcd for $C_{49}H_{72}O_8N_{10} \cdot 2HCl \cdot 4.5H_2O$: C, 54.34; H, 7.72; N, 12.93%.

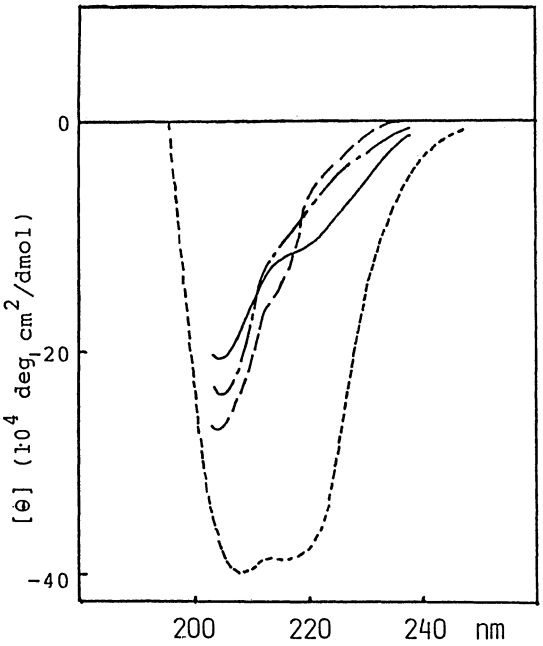

Fig. 4. CD spectra of GS and its analogs in aqueous solution.
des-Val$^{1,1'}$-GS, ——; des-Leu$^{3,3'}$-GS, ——; des-Val^{1}, Leu$^{3'}$-GS, — - —; GS, ------.

spectra resemble each other; although a trough is observed at 204 nm and a shoulder near 217 nm, their CD patterns differ from that of GS, even though these peptides possess the D-Phe–Pro seqeunce. We recently reported that the CD spectra of cyclo(–Val–Orn–Leu–D-Phe–Pro–Tyr–)$_2$ and cyclo(–Val–Orn–Leu–Leu–D-Phe–Pro–Leu–)$_2$ having the D-Phe–Pro sequence are similar to that of GS.[7,9] On the other hand, the CD spectrum of cyclo(–Orn–D-Phe–Pro–)$_2$ resembles those of the synthetic cyclooctapeptides, rather than GS; a trough was observed near 200 nm and a shoulder near 220 nm.[12] Kopple et al. reported from NMR studies that this cyclohexapeptide possesses a β-turn caused by a D-Phe–Pro seqeunce as GS.[13] Further, the same β-turn was also found in cyclo(–Ala–Gly–D-Phe–Pro–)$_2$, which possesses the Ala–Gly sequence in place of the Orn–Leu or Val–Orn sequence of the cyclooctapeptides synthesized in our studies.[14] These facts suggest that the synthetic cyclooctapeptides have a β-turn similar to that of GS, and that the difference between these synthetic cyclooctapeptides and GS in CD spectra may result from removing two of Val and / or Leu residue from GS, in other words, a distinction of the ring size.

Experimental

All melting points are uncorrected. The CD spectra were measured by a JASCO J-500 spectropolarimeter at a concentration of 1.5—2.0×10^{-4} M. The molecular weights of these synthetic peptides were determined by FAB mass spectrometry using a JEOL JMS-D-300 mass spectrometer. Amino acid analyses were carried out using a Hitachi 835 amino acid analyzer after hydrolysis in 6 M HCl at 110 °C for 24 h. HPLC analysis was carried out using an 800 series (JASCO). A Finepak SIL C18 column (10 μm, 250×4.6 mm I.D., or 250×6.7 mm I.D., JASCO) was used: flow rate, 1 ml min^{-1}; solvent, MeOH–H_2O (6:1) or MeOH-5%–$NaClO_4$ (4:1); monitoring wavelength, 220 nm.

Microbiological Assays. The microorganisms employed were *Staphylococcus aureus* ATCC 6538, *Streptomyces pyogenes* N.Y.5, *Corynebacterium diphtheriae* P.W.8, *Micrococcus pyogenes* ATCC 10240, *Bacillus subtilis* ATCC 6633, *Escherichia coli* NIHJ-JC2, and *Proteus vulgaris* OX 19. The minimum concentration of compounds necessary to completely inhibit the growth of these microorganisms was determined by an agar dilution method with 10^6 organisms per milliliter.

We thank Professor Ichiro Muramatsu, Rikkyo University, for helpful discussion. We also thank the staff of the Research Laboratories of Toyo Jozo Co. for elemental analyses, microbiological assays, and measurement of FAB mass spectra.

References

1) A. R. Battersby and L. C. Craig, *J. Am. Chem. Soc.*, **73**, 1887 (1951).
2) The abbreviations used in this paper are those recommended by IUPAC-IBU: *Eur. J. Biochem.*, **138**, 9 (1984). Additional abbreviations: HONSu, *N*-hydroxysuccinimide; WSCD·HCl, 1-ethyl-3-(3-dimethylaminopropyl)carbodiimide hydrochloride.
3) D. C. Hodgkin and B. M. Oughton, *Biochem. J.*, **65**, 752 (1957).
4) N. Izumiya, T. Kato, H. Aoyagi, M. Waki, and N. Kondo, "Synthetic Aspects of Biologically Active Cyclicpeptide-Gramicidin S and Tyrocidines," Kodansha, Tokyo, Halsted Press, New York (1979), pp. 49—70.
5) M. Waki and N. Izumiya, *Bull. Chem. Soc. Jpn.*, **40**, 1687 (1967).
6) S. Matsuura, M. Waki, T. Kato, and N. Izumiya, *Bull. Chem. Soc. Jpn.*, **46**, 977 (1973).
7) M. Tamaki, *Bull. Chem. Soc. Jpn.*, **57**, 3210 (1984).
8) M. Tamaki, M. Takimoto, and I. Muramatsu, *Bull. Chem. Soc. Jpn.*, **60**, 2101 (1987).
9) M. Tamaki, M. Takimoto, and I. Muramatsu, *Bull. Chem. Soc. Jpn.*, **61**, 3925 (1988).
10) M. Tamaki, M. Takimoto, M. Hayashi, and I. Muramatsu, *Bull. Chem. Soc. Jpn.*, **62**, 594 (1989).
11) Cyclo(–Orn–D-Phe–Pro–)$_2$ was synthesized by Kopple et al.,[13] but its antibiotic activity has not been reported yet. We synthesized this peptide according to the similar method described in the synthesis of **3d**, and measured the antibiotic activity of this peptide.
12) C. A. Bush, S. K. Sarkar, and K. D. Kopple, *Biochemistry*, **17**, 4951 (1978).
13) K. D. Kopple, A. Co, T. J. Schauper, and C. S. Wilcox, *J. Am. Chem. Soc.*, **95**, 6090 (1973).
14) E. Blout, *Biopolymers*, **20**, 1901 (1981).

Crystal Structure of the Gold(III) Complex, Trichloro(dibenzyl sulfide)gold(III)

Kazuhiro TAKAHASHI
Department of Chemistry, Faculty of Science, Shimane University,
Nishikawatsu-cho, Matsue 690
(Received February 21, 1991)

Synopsis. The structure of the title complex has been determined. The crystal is orthorhombic, with the space group *Pnma*, Z=4, a=13.331 (2), b=16.130 (3), and c=7.6949 (9) Å. The complex has a square-planar coordination geometry. The Au and the 3Cl1S donor atoms are located on a crystallographic mirror plane. The length of the Au–Cl bond trans to the Au–S bond is slightly longer than those of the other two Au–Cl bonds.

Ever since two complexes consisting of halogen, gold, and dibenzyl sulfide (DBS) were first isolated in 1905,[1] many investigations for gold(I), gold(III), and mixed-valence gold(I)-gold(III) complexes of DBS have been undertaken in the fields of coordination chemistry and physical chemistry.[2–5] However, exact X-ray crystal structure analyses of these complexes, except for gold(I) complexes,[5] were not carried out until quite recently.

The author and collaborators have studied the DBS–gold complexes with interests in the coordination structures and a correlation between structures and physical properties. We have so far reported the structures of [$AuBr_3$(DBS)] and *catena*-[AuCl(DBS)]-[$AuCl_3$(DBS)],[6,7] and the optical properties of DBS–gold complexes.[8] In this study, the structure of the title complex, [$AuCl_3$(DBS)], has been determined by a single crystal X-ray diffraction method in order to reveal details of the coordination structure. Its structural features are compared with those of related gold(III) complexes, mainly focusing on the coordination structure and the trans influence of DBS. Further characterization has been carried out in terms of the electronic spectra.

Experimental

[$AuCl_3$(DBS)] was prepared according to the Ray and Sen's procedure,[2] using $HAuCl_4 \cdot 4H_2O$ as a metal source instead of $AuCl_3$. A yellow prismatic crystal was obtained by recrystallization from a benzene–toluene (95/5 v/v) solution at ca. 5 °C (Found: C, 32.70; H, 2.73%). The electronic spectra were recorded on a Shimadzu MPS-2000 spectrophotometer (280—800 nm). The intensity data were collected at 295±1 K, by use of an Enraf–Nonius CAD4 automated four-circle X-ray diffractometer (graphite monochromated Mo K_α radiation, λ=0.71073 Å). All the computations were carried out on a DEC MicroVAXII, using the programs in CAD4 Structure Determination Package (SDP, 4th ed). The unit cell parameters were determined from 25 reflections with $22<2\theta<31$ °.

Crystal Data: $C_{14}H_{14}SCl_3Au$; M=517.7; orthorhombic; *Pnma*; a=13.331(2), b=16.130(3), and c=7.6949(9) Å; V=1654.6(8) Å^3; D_m=2.1 (by floatation), D_c=2.08 g cm^{-3}; Z=4; μ=94.7 cm^{-1}; crystal size=0.30×0.25×0.28 mm^3.

A total of 2191 reflections were collected (scan type: ω–2θ; scan range: $2 \leqq 2\theta \leqq 55°$; scan width: $\Delta\omega$= (0.8+0.35 tan θ)°; ω scan rates: 2.75° min^{-1} for a preliminary scan, variable (1.18—2.75° min^{-1}, depending on intensity) for the final scan). The intensities of five standard reflections monitored at 90 min intervals showed good stability during data collection. The intensity data were corrected for the Lorentz-polarization effects, and for the absorption based on Ψ scans of the nine reflections ($80<\chi<88°$).[9] The structure was solved by the direct method (MULTAN in SDP) using 1314 independent reflections with $I>3\sigma(I)$, and was then refined by the full-matrix least-squares procedure. Anisotropic thermal parameters were adopted for non-hydrogen atoms. Hydrogen atoms were not included in the structure calculations. The final R values were $R=\sum||F_o|-|F_c||/\sum|F_o|=0.0319$ and $R_w=[\sum w(|F_o|-|F_c|)^2/\sum w|F_o|^2]^{1/2}=0.0435$, where the weighting scheme is $w=1/\sigma^2(|F_o|)=4|F_o|^2/\{\sigma(I)^2+(0.04|F_o|^2)^2\}$.

Results and Discussion

The final atomic coordinates are given in Table 1.[#] Figure 1 shows the molecular structure of [$AuCl_3$(DBS)]. The complex has a square-planar coordination geometry ordinarily observed in mononuclear four-coordinated Au(III) complexes. The Au and the four donor atoms form a perfectly planar coordination sphere since these atoms lie on the crystallographic mirror plane. The four bond angles subtended at the Au (86—92°) are slightly deviated from the ideal angle of 90°. These slight deviations are suggestive of very weak steric constraints of the bulky ligand, DBS. The lengths of three Au–Cl coordination bonds (2.27—2.29 Å) fall within the range observed for $[AuCl_4]^-$ (2.27—2.30 Å),[4,10] and for Au(III) complexes with 3Cl1L donor atom set (2.27—2.35 Å, L=P of triphenylphosphine,[11] and L=S of thianthrene[12]).

Table 1. Fractional Coordinates (×10^4) and Isotropic Thermal Parameters with Their Estimated Standard Deviations in Parentheses

Atom	x	y	z	B_{eq}/Å^2 [a]
Au	2915.4(3)	2500	3738.1(3)	3.572(7)
Cl(1)	4019(3)	2500	5988(4)	6.71(9)
Cl(2)	1597(3)	2500	5640(5)	6.89(8)
Cl(3)	1841(2)	2500	1447(4)	6.48(8)
S	4298(2)	2500	1927(3)	3.80(5)
C(1)	4100(7)	3367(5)	436(7)	4.7(2)
C(2)	4137(6)	4171(5)	1417(7)	4.3(1)
C(3)	5037(7)	4479(5)	2045(4)	5.1(2)
C(4)	5056(8)	5246(6)	2890(5)	5.6(2)
C(5)	4202(8)	5701(6)	3097(8)	6.1(2)
C(6)	3275(8)	5394(6)	2552(15)	6.8(2)
C(7)	3228(7)	4608(7)	1670(11)	5.6(2)

a) $B_{eq}=4/3\sum_i\sum_j\beta_{ij}\boldsymbol{a}_i\boldsymbol{a}_j$.

[#] Lists of structure factors, anisotropic thermal parameters, bond distances and angles, and the results of least-squares plane calculations are deposited as Document No. 8951 at the Office of the Editor of Bull. Chem. Soc. Jpn.

The Au–S bond length (2.310(3) Å) falls within the range observed for sulfur-coordinated square-planar Au(III) complexes (2.28—2.36 Å).[12,13] The molecular structure of [$AuCl_3$(DBS)] resembles the tribromo complex, [$AuBr_3$(DBS)].[6] The lengths of the three Au–Cl bonds are shorter than those of the corresponding Au–Br bonds in [$AuBr_3$(DBS)] (2.41—2.43 Å). A difference between Au–Cl and Au–Br distances (average 0.14 Å) is expected from a difference in the effective ionic radius between Cl^- (1.67 Å) and Br^- (1.82 Å), and also from that in the covalent radius between Cl (0.99 Å) and Br (1.14 Å).[14] Figure 2 shows the crystal structure of [$AuCl_3$(DBS)]. A significant intermolecular contact smaller than 3.5 Å is observed only between the phenyl rings of adjacent molecules (C(4)–C(4)' (symmetry code: $1-x,1-y,1-z$), 3.347(6) Å). The crystals of [$AuCl_3$(DBS)] and of [$AuBr_3$(DBS)] (triclinic) are not isomorphous. No close contact among chlorides less than the sum of the van der Waals radii is observed in the present crystal, in contrast to the close Br–Br contact (3.46 Å) observed in the [$AuBr_3$(DBS)] crystal.[6] The shortest Cl–Cl distance is 4.203(5) Å of the Cl(1)–Cl (3)″ ($1/2+x$, $1/2-y$ or $y,1/2-z$).

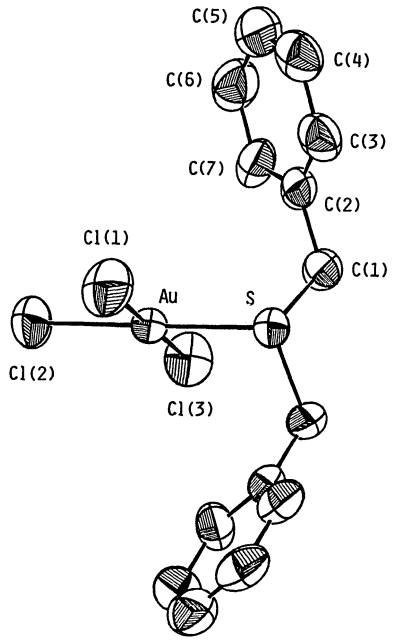

Fig. 1. ORTEP drawing of the [$AuCl_3$(DBS)] molecule with atom numbering scheme (thermal ellipsoids are drawn at 50% probability level). Selected interatomic distances (l/Å) and angles (ϕ/°) around the coordination sphere of the gold(III) ion are: Au–Cl(1) 2.272(3), Au–Cl(2) 2.287(4), Au–Cl(3) 2.272(3), Au–S 2.310(3) Å; Cl(1)–Au–Cl(2) 90.6(1), Cl(1)–Au–Cl(3) 178.8(1), Cl(1)–Au–S 86.7(2), Cl(2)–Au–Cl(3) 90.7(1), Cl(2)–Au–S 177.4(1), Cl(3)–Au–S 92.0(1)°.

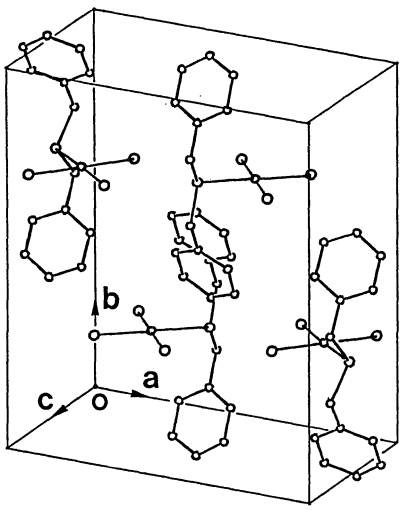

Fig. 2. Perspective view of the molecular arrangement in the unit cell.

In the molecules of square-planar trihalogeno(phosphine)gold(III) complexes, [$AuCl_3(PPh_3)$],[11] and [$AuBr_3\{P(C_2H_5)_3\}$],[15] the Au–halogen bond trans to the Au–P bond is appreciably longer than the other two Au–halogen bonds. This lengthening is attributed to the electrostatic trans influence of phosphines.[11,15,16] A similar pattern is observed in the [$AuCl_3$(DBS)] molecule, i.e., the Au–Cl(2) bond (2.287(4) Å) trans to the Au–S is longer than the other two Au–Cl bonds (both 2.272(3) Å). It should be noted here that no such distinct lengthening is observed in the [$AuBr_3$(DBS)] molecule,[6] and that a difference in the length between the Au–Cl(2) bond and the other two Au–Cl bonds (0.01—0.02 Å, evaluated by considering their standard deviations) is smaller than those of the phosphine complexes (0.05—0.09 Å).[11,15] These facts indicate that the trans influence of DBS is very weak compared with the phosphine ligands in square-planar trihalogenogold(III) complexes. Taking into account the fact that the Au–S bond of the present complex is shorter than that in [$AuBr_3$(DBS)] (2.349(3) Å), the relative strength of the trans influence of ligands seem to be in the order, $Cl^- < Br^- \approx$ DBS, for the trihalogeno(DBS)gold(III) complexes.

The electronic spectra of [$AuCl_3$(DBS)] in $CHCl_3$ and Nujol mull are shown in Fig. 3. The solution and solid spectra show a single broad absorption band, with the absorption maxima at 29600 (ε=4860 $mol^{-1}\,dm^3\,cm^{-1}$)

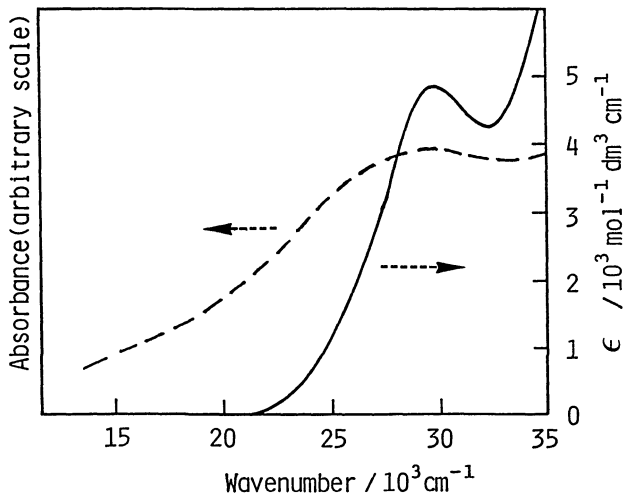

Fig. 3. Electronic spectra of [$AuCl_3$(DBS)].
———: $CHCl_3$ solution (5×10^{-4} mol dm^{-3}),
— — —: Nujol mull.

and 29400 cm^{-1}, respectively. This intense and broad band is attributable to a charge transfer interaction between Au^{3+} and ligands.[17] The d–d bands are presumably hidden in this intense band.

The X-ray experiment was carried out in the Electrotechnical Laboratory (ETL). The author is grateful to Dr. Hiroshi Tanino (ETL), Assoc. Professor Masahiro Mikuriya, Mr. Toshinori Fujii (Kwansei Gakuin Univ.), Dr. Makoto Handa, and Professor Kuninobu Kasuga (Shimane Univ.), for their kind and helpful supports.

References

1) F. Herrmann, *Ber.*, **38**, 2813 (1905).
2) P. C. Ray and D. C. Sen, *J. Indian Chem. Soc.*, **7**, 67 (1930).
3) For example: F. H. Brain, C. S. Gibson, J. A. J. Jarvis, R. F. Phillips, H. M. Powell, and A. Tyabji, *J. Chem. Soc.*, **1952**, 3686; T. P. A. Viegers, J. M. Trooster, P. Bouten, and T. P. Rit, *J. Chem. Soc., Dalton Trans.*, **1977**, 2074; L. V. Interrante and F. P. Bundy, *J. Inorg. Nucl. Chem.*, **39**, 1333 (1977); C. Janiak and R. Hoffmann, *Inorg. Chem.*, **28**, 2743 (1989).
4) H.-N Adams and J. Strähle, *Z. Anorg. Allg. Chem.*, **485**, 65 (1982).
5) J. Strähle, W. Hiller, and W. Conzelmann, *Z. Naturforsch., B,* **39**, 538 (1984).
6) K. Takahashi and K. Kato, *Bull. Chem. Soc. Jpn.*, **61**, 991 (1988).
7) K. Takahashi and H. Tanino, *Chem. Lett.*, **1988**, 641.
8) H. Tanino, K. Takahashi, M. Tajima, M. Kato, and T. Yao, *Phys. Rev. B,* **38**, 8327 (1988); K. Takahashi and H. Tanino, *KEK Photon Factory Activity Report,* **4**, 176 (1987).
9) A. C. T. North, D. C. Phillips, and F. S. Mathews, *Acta Crystallogr., Sect. A,* **24**, 351 (1968).
10) P. F. Theobald and H. Omrani, *Acta Crystallogr., Sect. B,* **36**, 2932 (1980); H. Kiriyama, N. Matsushita, and Y. Yamagata, *ibid., Sect. C,* **42**, 277 (1986); W. Willing, S. Ruangsuttinarupap, U. Müller, and K. Dehnicke, *ibid., Sect. C,* **42**, 1263 (1986).
11) G. Bandori, D. A. Clemente, G. Marangoni, and L. Cattalini, *J. Chem. Soc., Dalton Trans.*, **1973**, 886.
12) N. W. Alcock, K. P. Ang, K. F. Mok, and S. F. Tan, *Acta Crystallogr., Sect. B,* **34**, 3364 (1978).
13) P. T. Beurskens, H. J. A. Blaauw, J. A. Cras, and J. J. Steggerda, *Inorg. Chem.*, **7**, 805 (1968); P. T. Beurskens, J. A. Cras, and J. G. M. van der Linden, *ibid.*, **9**, 475 (1970).
14) J. E. Huheey, "Inorganic Chemistry," 3rd ed, Harper & Row, New York (1983), Chap. 6.
15) D. S. Eggleston, D. F. Chodosh, D. T. Hill, and G. R. Girard, *Acta Crystallogr., Sect. C,* **40**, 1357 (1984).
16) J. E. Huheey, "Inorganic Chemistry," 3rd ed, Harper & Row, New York (1983), Chap. 11.
17) Y. Murakami and I. Sakata, "Chelate Kagaku," ed by K. Ueno, Nankōdō, Tokyo (1976), Vol. 1, Chap. 2, pp. 207—209.

A New Calix[6]arene-Based Uranophile with Phosphonate Groups as Ligands

Takeshi NAGASAKI, Takashi ARIMURA, and Seiji SHINKAI*
Department of Organic Synthesis, Faculty of Engineering, Kyushu University, Fukuoka 812
(Received March 1, 1991)

Synopsis. A new calix[6]arene-based uranophile which has six phosphonomethyl groups on the upper rim was synthesized. This compound forms a 1 : 1 complex with uranyl ion (UO_2^{2+}). The stability constant was estimated to be $10^{17.5}$ M^{-1},# which is satisfactorily comparable with those for calix[6]arene-based uranophiles bearing OH or COOH groups on the lower rim.

The selective extraction of uranium from sea water has been of much concern for chemists because of its importance in relation to energy problems. In order to design such a ligand that can selectively extract uranyl ion (UO_2^{2+}), one faces a difficult problem, namely, the ligand must strictly discriminate between UO_2^{2+} and other metal ions which are present in great excess in sea water. A possible unique solution for this difficult problem is to use a cyclic ligand suitably structured to perform the UO_2^{2+} binding. As UO_2^{2+} complexes adopt either a pseudoplanar pentacoordinate or hexacoordinate structure,[1] a macrocyclic ligand with a nearly coplanar arrangement of either five or six donating groups would serve as a specific ligand for UO_2^{2+} (i.e., as a uranophile). This sort of approaches has been reported by a few research groups.[2-5] We recently found that pentasodium 31,32,33,34,35-pentahydroxycalix[5]arene-5,11,17,23,29-pentasulfonate (**1**$_5$) and hexasodium 37,38,39,40,41,42-hexahydroxycalix[6]arene-5,11,17,23,29,35-hexasulfonate (**1**$_6$) have remarkably high stability constants (K_{uranyl}=$10^{18.7-19.2}$ M^{-1}) and selectivity factors (K_{uranyl}/K_{M^+}=10^{10-17}) in water.[6,7] In particular, the "super-uranophile" nature of the calix[6]arene derivatives is of great significance from a practical viewpoint because they can be synthesized from commercially-available calix[6]arene-37,38,39,40,41,42-hexol in good yields.[8,9] The remarkably high selectivity is attributed to the rigid skeleton of calix[5]arene and calix[6]arene which can provide the pre-organized penta- and hexacoordination geometry for the binding of UO_2^{2+} but cannot accommodate a square-planar or tetrahedral coordination geometry appropriate for other metal cations.[6,7,10,11] We here synthesized 37,38,39,40,41,42-hexamethoxy-5,11,17,23,29,35-hexakis(phosphonomethyl)calix[6]arene (**2**) and estimated the stability constant for the complex formation with UO_2^{2+}.

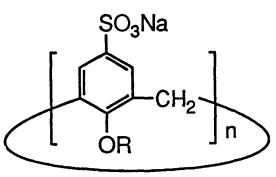

1$_n$
R=H or CH_2COOH

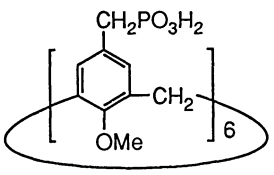

2

1 M=1 mol dm^{-3}.

Results and Discussion

pH Dependence. It is known that both calix[*n*]arenepolyols and their *O*-carboxymethyl derivatives (**1**$_n$: R=CH_2COOH) are poorly soluble in water.[10,12] To determine the stability constant, the moderate solubility in water is required. To satisfy this requirement we previously introduced sulfonate groups into the *p*-positions to the hydroxyl groups on the lower rim. On the other hand, compound **2** showed sufficient solubility in water.

We first estimated pK_a values of **2** and sodium methoxybenzylphosphonate (**3**). The titration curve for **2** is illustrated in Fig. 1. The pK_a values for **2** were estimated to be 2.91 and 8.86 and those for **3** to be 2.16 and 7.71. The result indicates that the phosphonate group in **2** show the pK_a values higher by 0.75—1.15 pK units than that in **3**. A Henderson-Hasselbach plot (pH=pK_a−n·log [(1−α)/α] where n becomes greater than unity when the dissociation groups interact with each other) for the second acid dissociation of the phosphonate groups in **2** gave n=1.5 whereas that for the second acid dissociation of the phosphonate group in **3** gave n=1.0. The results establish that the pK_a values for **2** are raised because of the intramolecular interactions among the phosphonate groups.

Addition of **2** to uranyl dinitrate ($UO_2(NO_3)_2$) solution at 25 °C increased the UV and visible absorption band over a wide wavelength range (225—600 nm) owing to the competitive association of **2** with UO_2^{2+} (the spectrum is similar to Fig. 1 in Ref. 7). The spectral change after mixing was relatively slow: it usually took 4 to 5 h to reach the equilibrium spectrum. On the other hand, addition of acyclic **3** (used as a

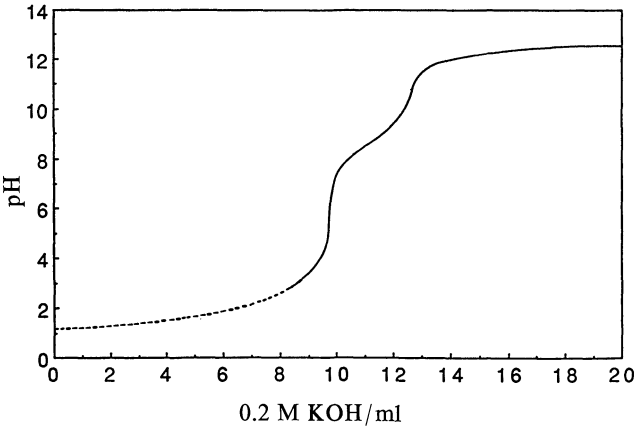

Fig. 1. Potentiometric titration of **2** by an autotitrator: 25±0.5 °C, μ=0.10 with KCl, [**2**]=5.00×10^{-3} M (in 20 ml of 7.00×10^{-2} M HCl). Below pH 2.8, the solution was not clear because of the precipitation of **2** (shown by a dotted line).

reference compound: [3]=6·[2]) to uranyl dinitrate solution did not increase the absorption band. The difference shows that the efficient UO_2^{2+} binding to **2** is based on the ring structure of calix[6]arenehexol.

In Fig. 2, we plotted the absorbance at 449 nm (a shoulder of the spectrum: A_{449}) against pH. It is seen from Fig. 2 that the A_{449} for **2** sharply increases at pH 8—9, forms a plateau at pH 11.4—11.8, and decreases above pH 12. The increase at pH 8—9 is ascribed to the dissociation of the phosphonate groups whereas the decrease above pH 12 is ascribed to the competitive association of UO_2^{2+} with OH^- present in great excess at this pH range. In fact, the precipitation of the hydroxide complex was observed pH 12.5. Judging from the pK_a values determined above, the "active" ligands for the UO_2^{2+}-binding are dianionic phosphonate groups (i .e., $-CH_2P(=O)O_2^{2-}$). Careful examination of Fig. 2 reveals, however, that at around pH 8.86 (average pK_a of **2**) the complex formation scarcely takes place. In other words, the plot of A_{449} versus pH (Fig. 2) shifts to higher pH region than the titration curve (Fig. 1). The discrepancy suggests that the half-dissociated **2** bearing three $-CH_2P(=O)O_2^{2-}$ and three $-CH_2P(=O)O_2H^-$ cannot yet serve as the "active" ligand. We consider that the coordination ability of the $-CH_2P(=O)O_2^{2-}$ groups is suppressed by the intramolecular hydrogen-bonding interaction with the $-CH_2P(=O)O_2H^-$ groups.

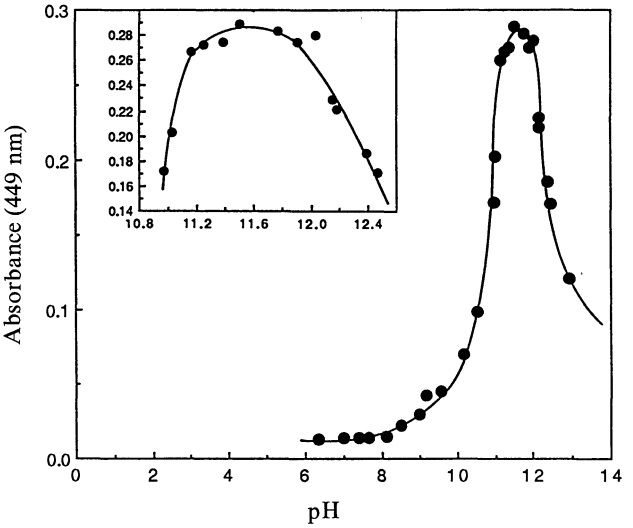

Fig. 2. pH dependence for the formation of the UO_2·**2** complex: $[UO_2(NO_3)_2]$=[**2**]=0.33 mM, μ=0.1 with KCl, 25 °C.

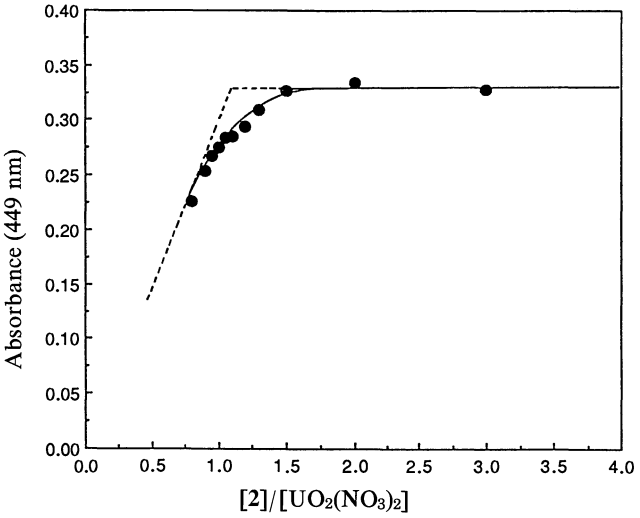

Fig. 3. Molar ratio plot for UO_2·**2** complex: $[UO_2(NO_3)_2]$=0.29 mM (constant), pH 11.5 with KOH, μ=0.1 with KCl, 25 °C.

Stoichiometry and Stability Constants. As a prelude to estimate the stability constant, we determined the stoichiometry of the UO_2·**2** complex. In Fig. 3, the A_{449} was plotted against [**2**]/$[UO_2^{2+}]$. A break-point appeared at [**2**]/$[UO_2^{2+}]$=1.0, supporting the formation of a 1: complex. From the A_{449} value at the plateau one can estimate the ε_{449} to be 1170 $M^{-1}cm^{-1}$ for the UO_2·**2** complex, which is comparable with those (about 1400 $M^{-1}cm^{-1}$) for the UO_2·**1** complexes.[7]

UO_2^{2+} is known to form a stable carbonate complex, $[UO_2(CO_3)_3]^{4-}$ and the stability constant ($K_{carbonate}$=$[UO_2(CO_3)_3^{4-}]/[UO_2^{2+}][CO_3^{2-}]^3$) is estimated to be $10^{12.5}$ M^{-3} at 25 °C and pH 10.4.[13] When **2** is added to the uranyl tricarbonate solution, the competitive displacement of carbonates by **2** takes place and reaches an equilibrium after a few hours. This process is expressed by Eq. 1. One can thus estimate the displacement equilibrium constant (K_e) from the spectral change. Finally, the stability constant for UO_2^{2+} (K_{uranyl}=$[UO_2$·**2**$]/[UO_2^{2+}]$[**2**] can be determined by Eq. 2.[14]

$$[UO_2(CO_3)]^{4-} + 2 \overset{K_e}{\rightleftarrows} UO_2\cdot 2 + 3CO_3^{2-} \quad (1)$$

$$K_{uranyl} = K_e \cdot K_{carbonate} \quad (2)$$

At pH 10.4 (where 91.4% of the phosphonomethyl groups exist as $-CH_2P(=O)O_2^{2+}$. This pH is not the optimum condition for the formation of the UO_2·**2** complex: see Fig. 2) the K_{uranyl} was estimated to be $10^{16.3}$ M^{-1}. This value is smaller by about three orders of magnitude than those for **1**$_5$ and **1**$_6$[7] (Table 1). Assuming that the $K_{carbonate}$ is scarcely affected at pH 10.3—11.6, we can calculate the K_{uranyl} at pH 11.5 (where 98.3% of the phosphonomethyl groups exist as $-CH_2P(=O)O_2^{2-}$. This pH is the optimum condition for the formation of the UO_2·**2** complex) to be $10^{17.5}$ M^{-1}. This value is smaller only by 1.2—1.7 pK units than those for the UO_2·**1** complexes.[7]

In conclusion, the present study demonstrated that the phosphate group serves as an excellent ligand for the complexation with UO_2^{2+}. We are currently devoting our research efforts toword the synthesis of calix[6]arene-based uranophiles bearing phosphonate groups

Table 1. Stability Constants (K_{uranyl}) for Calixarene-Based Uranophiles[a]

Calixarene	pH	log K_{uranyl}
1$_5$ (R=H)	10.4	18.9±0.6[b]
1$_6$ (R=H)	10.4	19.2±0.1[b]
1$_6$ (R=CH_2COOH)	10.4	18.7±0.1[b]
2	10.4	16.3±0.3
2	11.5	17.5±0.2

a) 25 °C, μ=0.1 with KCl, 0.01 M carbonate buffer. b) Cited from Ref. 7.

on the lower rim.

Experimental

Materials. The synthesis of **2** was independently reported (as communications) by Almi et al.[15] and by us.[16]

37,38,39,40,41,42-Hexamethoxy-5,11,17,23,29,35-hexakis-(*O,O*-diethylphosphonomethyl)calix[6]arene (4). 37,38,39,40,41,42-Hexamethoxy-5,11,17,23,29,35-hexakis(chloromethyl)-calix[6]arene (910 mg; 0.90 mmol) was refluxed in triethyl phosphite (27 g; 160 mmol) for 14 h. After cooling, unreacted triethyl phosphite was distilled under reduced pressure. The residue was dissolved in chloroform and subjected to column chromatography (stationary phase, silica gel; mobile phase, chloroform–methanol (10 : 1 v/v)). The concentration of the eluent gave **4** in 96% yield; mp 149—151 °C; IR (neat) $\nu_{P=O}$ 1245 cm^{-1}, ν_{P-O-C} 960 and 1055 cm^{-1}; ^1H NMR ($CDCl_3$) δ=1.21 (6H, t, C–CH_3), 2.75 (2H, d(J_{PH}=21 Hz), $ArCH_2P$), 3.43 (3H, s, OCH_3), 3.89 (2H, s, $ArCH_2Ar$), 3.94 (4H, dq(J_{PH}=7.3 Hz, J_{HH}=7.3 Hz), $POCH_2C$), 6.79 (2H, s, ArH). Found: C, 55.90; H, 7.60%. Calcd for $(C_{13}H_{19}O_4P)_6 \cdot 3H_2O$: C, 55.91; H, 7.22%.

37,38,39,40,41,42-Hexamethoxy-5,11,17,23,29,35-hexakis-(phosphonomethyl)calix[6]arene (2). Compound **4** (810 mg; 0.50 mmol) was refluxed in dioxane (10 ml)-concd HCl (10 ml) mixed solvent for 12 h. After cooling, the solution was evaporated to dryness under reduced pressure and the residue was recrystallized from ethanol–ether: Colorless powder, mp >300 °C, yield 82%; IR (nujol) ν_{OH} 3600 cm^{-1}, $\nu_{P=O}$ 1240 cm^{-1}, ν_{P-O-C} 1005 cm^{-1}; ^1H NMR (CD_3OD) δ=2.85 (2H, m, $ArCH_2P$), 3.01 (3H, s, OCH_3), 3.93 (2H, s, $ArCH_2Ar$), 6.91 (2H, s, ArH). Found: C, 48.23; H, 5.33%. Calcd for $(C_9H_{11}O_4P)_6 \cdot 3H_2O$: C, 48.44; H, 5.22%.

Determination of the Stability Constants. The stability constants for UO_2^{2+} were evaluated by a displacement method[17] at 25 °C. The details of the method were described previously.[7]

Potentiometric Titration. Potentiometric titration of **2** and **3** ([**2**]=5.00×10^{-3} M and [**3**]=2.00×10^{-2} M in 20 ml of 7.00×10^{-2} M HCl) was carried out at 25±0.5 °C by using an auto-titrator (Kyoto Electronics, Model APB-117). The details of the measurement conditions are described in a caption to Fig. 1.

References

1) R. Graziani and E. Forselline, *J. Chem. Soc., Dalton Trans.*, **1972**, 2059, references cited therein.

2) A. H. Alberts and D. J. Cram, *J. Am. Chem. Soc.*, **99**, 3880 (1977).

3) I. Tabushi, Y. Kobuke, K. Ando, M. Kishimoto, and E. Ohara, *J. Am. Chem. Soc.*, **102**, 5948 (1980).

4) I. Tabushi, Y. Kobuke, and A. Yoshizawa, *J. Am. Chem. Soc.*, **106**, 2481 (1984).

5) Y. Kobuke, I. Tabushi, K. Oh, and T. Aoki, *J. Org. Chem.*, **53**, 5933 (1988).

6) S. Shinkai, H. Koreishi, K. Ueda, and O. Manabe, *J. Chem. Soc., Chem. Commun.*, **1986**, 233.

7) S. Shinkai, H. Koreishi, K. Ueda, T. Arimura, and O. Manabe, *J. Am. Chem. Soc.*, **109**, 6371 (1987).

8) C. D. Gutsche, *Acc. Chem. Res.*, **16**, 161 (1983).

9) C. D. Gutsche, "Calixarenes," Royal Society of Chemistry, Cambridge (1989).

10) S. Shinkai, Y. Shirahama, H. Satoh, O. Manabe, T. Arimura, K. Fujimoto, and T. Matsuda, *J. Chem. Soc., Perkin Trans. 2*, **1989**, 1167.

11) For a comprehensive review for UO_2^{2+} complexes see I. Tabushi and Y. Kobuke, *Nippon Kaisui Gakkaisi*, **36**, 205 (1982).

12) A. Arduini, A. Pochini, S. Riverberi, and R. Ungaro, *J. Chem. Soc., Chem. Commun.*, **1984**, 981.

13) Ref. 4 and related papers cited therein.

14) At pH 11.5 the K_{uranyl} value was constant (log K_{uranyl}= 17.5±0.2) over the carbonate concentration range 0.004—0.02 M. This indicates that the displacement proceeds according to Eq. 1.

15) M. Almi, A. Arduini, A. Casnati, A. Pochini, and R. Ungaro, *Tetrahedron Lett.*, **45**, 2177 (1989).

16) T. Arimura, T. Nagasaki, S. Shinkai, and T. Matsuda, *J. Org. Chem.*, **54**, 3766 (1989).

17) K. Ueno, "Chelate Kagaku," Nankodo, Tokyo (1971), Chap. 4.

The Formation of Two New Ring-Enlargement Products in the Lead Tetraacetate Oxidation of *l*-2(10)-Pinene[1)]

Yoshiharu MATSUBARA, YUAN Youzhu,† CHENG Zhi,†
Shin-ichi TAKEKUMA,* and Hiroshi YAMAMOTO*,††
Department of Applied Chemistry, Faculty of Science and Engineering, Kinki University, Kowakae, Higashi-Osaka 577
†Department of Chemical Engineering, Nanjing Forestry University, Nanjing, China
††Department of Chemistry, Okayama University, Okayama 700
(Received March 6, 1991)

Synopsis. The oxidation of *l*-2(10)-pinene with lead tetraacetate in glacial acetic acid at 60 °C afforded, besides fifteen known other products, (1*S*,6*S*)-7,7-dimethylbicyclo [4.1.1]octan-3-one (**2**) and (1*R*,6*S*)-2-one isomer (**3**), whose structures were established on the basis of their spectroscopic data. A possible reaction pathway for the formation of these new compounds **2** and **3** involving novel ring-enlargement is described.

One of us (Y. M.) and his co-worker[2)] have studied the lead tetraacetate oxidation of *l*-2(10)-pinene (**1**) by employing trilead tetraoxide in a mixture of acetic acid and acetic anhydride at 60 °C. Hydrolysis of the oily reactant with aqueous potassium hydroxide afforded six major products [mirtenol (**4**), 1-*p*-menthene-7,8-diol (**5**), *trans*- and *cis*-1(7),8-*p*-menthadien-2-ol (**6**,**7**), *trans*- and *cis*-1(7)-*p*-menthene-2,8-diol (**8**,**9**)] and nine minor products [*trans*-pino-carveol (**10**), α-terpineol (**11**), *n*-borneol (**12**), 1(7),4(8)-*p*-menthadien-2-ol (**13**), periryl alcohol (**14**), *p*-cymen-7-ol (**15**), carvacrol (**16**), 1,4(8)-*p*-menthadien-7-ol (**17**), 1,4(8)-*p*-menthadien-9-ol (**18**)]. All of the major products can easily be converted into periryl alcohol which is useful as flavor. Meanwhile, the lead tetraacetate oxidation was performed on other terpene hydrocarbons such as camphene[3)] and longifolene[4)] that have a terminal methylene group between a quaternary carbon and tertiary carbon. The oxidation was found to give ring-enlargement products (*R*-homocamphenilone and longi-homocamphenilone) in good yields.

If the terminal methylene group of *l*-2(10)-pinene (**1**) undergoes a similar ring-enlargement reaction, the corresponding products are expected to become highly important synthetic intermediates for preparation of β- and γ-thujaplicins.[5)] We wish to report herein our detailed reinvestigation on the oxidation of **1** with lead tetraacetate, which enabled us to isolate two unique ring-enlargement compounds.

When the trilead tetraoxide oxidation of *l*-2(10)-pinene (**1**) was carried out in glacial acetic acid alone at 60 °C for 2.5 h and then the reaction mixture was hydrolyzed, we found that two minor compounds (**2** and **3**) were produced beside the fifteen, already identified compounds[2)] **4**—**18** on the evidence of GLC and GC-MS analyses. Yields of these products based on GLC analysis are summarized in Table 1. Compounds **2** and **3** were purified by silica-gel column chromatography, followed by removal of alcoholic compounds by employing phthalic anhydride,[6)] and finally by the use of preparative GLC.

Compound **2** was a colorless oil, and its EI-MS showed the molecular ion peak at *m*/*z* 152. The molecular formula of **2** was found to be $C_{10}H_{16}O$ by HR-MS. The IR spectrum showed the presence of a carbonyl group (1697 cm^{-1}) and methylene group(s) (1470 and 1454 cm^{-1}) in compound **2**. The ^1H NMR spectrum of **2** exhibited two methyl proton signals at δ=0.75 and 1.28, but no signals due to terminal methylene protons. The complex signals at δ=1.75—2.90 in the spectrum were studied by examining the cross peaks of the 2D ^1H NMR (H–H COSY) and 2D ^{13}C NMR (C–H COSY) spectra, as well as by proton–proton decoupling experiments. The assignment of each proton signal was made as follows. First, the interrelations between carbon and proton signals were established by the analysis of the C–H COSY spectrum, thus disclosing that compound **2** consisted of one carbonyl group, one quaternary carbon, two methine groups, and four methylene groups (A, B, C, and D), besides the two methyl groups. Then, one of the methine protons (δ=2.06) was shown to have vicinal couplings with four protons of two methylene groups A (δ=1.79, 2.552) and B (δ=2.42, 2.61). Another methine proton (δ=2.20) had vicinal couplings with four protons of two methylene groups A and C (δ=1.82, 1.84). The latter methylene protons (C) were further coupled with two protons of another methylene group D (δ=2.550, 2.82). Therefore, combination of these NMR spectral data and the mode of the formation pathways (see later) has led to the structure, 7,7-dimethylbicyclo[4.1.1]octan-3-one, for compound **2**. The precise δ and *J* values of all proton signals, which have been confirmed by a computer-assisted simulation analysis, are shown in the Experimental section.

Table 1. Yield/% of the Oxidation Products from **1** with Trilead Tetraacetate[a)]

Product	Yield/%	Product	Yield/%
2	3	**11**	4
3	0.1	**12**	1
4	14	**13**	3
5	25	**14**	9
6	5	**15**	0.3
7	0.2	**16**	0.2
8	15	**17**	0.2
9	0.5	**18**	2
10	11	Others	6

a) Yields (based on GLC analysis) represent the result of several runs of the same experiment.

Compound **3** was also a colorless oil, whose EI-MS showed the molecular ion peak at *m*/*z* 152. The molecular formula of **3** was identical with **2** ($C_{10}H_{16}O$, by HR-MS). The IR spectrum of **3** similarly showed the pres-

ence of a carbonyl (1687 cm^{-1}) and methylene groups (1469, 1455 cm^{-1}). The analysis of ^1H and ^{13}C NMR spectra (including their 2D NMR) of compound **3** was carefully made in a manner similar to the case of **2**. It was noted that the methine proton signal at lower field (δ=2.68) showed vicinal couplings only with two, methylene protons (δ=1.96, 2.46) besides a long-range coupling with another methine proton (δ=2.25); this indicated the position of the carbonyl group adjacent to the former methine group. As a result, the isomeric structure, 7,7-dimethylbicyclo[4.1.1]octan-2-one, is assigned to **3**. The δ and J values of all signals for compound **3** are shown in the Experimental section.

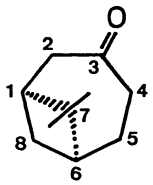

2

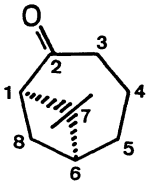

3

The most likely pathways for the formation of compounds **2** and **3** from **1** are illustrated in Scheme 1. The initial lead intermediate **19** is presumed to undergo a heterolytic cleavage accompanied by two, competitive 1,2-anionotropic shifts (path 'a' and 'b' in **20**).[7] The relative yield between **2** and **3** suggests a predominant migration of the tertiary carbon (C_1) (path 'a') compared with that of the secondary carbon (C_3) (path 'b') of intermediate **20**. Because no inversion of the configuration of the bridge-head carbon (C_1) in **20** is considered to take place, the absolute configuration of compounds **2** and **3** are assigned to be (1*S*,6*S*) and (1*R*,6*S*), respectively, as shown in the formulas.[8]

Experimental

Commercially available *l*-2(10)-pinene (**1**) was washed with dilute aq Na_2CO_3, then with water, and dried (Na_2SO_4). This was distilled through a spinning band precision distillation column under a reduced pressure to provide freshly distilled **1**: Bp 70—75 °C/111 mmHg (1 mmHg=133.322 Pa), n_D^{25}=1.4715, d_4^{25}=0.8722, $[\alpha]_D^{25}$=−18.6° (neat) [lit,[9] $[\alpha]_D$=−22.1° (neat) for (1*S*,5*S*) form].

Column chromatography was performed with Wako C-300 silica-gel. Preparative GLC was carried out with a Yanaco G1800 gas liquid chromatograph system equipped with a TCD (thermal conductivity detector) and PEG 20M steel column (ϕ 3 mm×5 m). GLC analysis was conducted with a Yanaco G2800 gas liquid chromatograph system equipped with a HFID (hydrogen flame ionization detector) and PEG 20M glass capillary column (ϕ 0.28 mm×20 m, column temp. 60—180 °C/2 °C min^{-1}). Optical rotations were measured with a JASCO DIP-140 spectrophotometer. IR spectra were taken on a JASCO IR-A-202 Grating spectrometer. Mass spectra were taken on a JEOL JMS-HX100 (with a JEOL JMA-DA5000 mass data system) high-resolution instrument and are given in terms of m/z (rel intensity) compared with the base peak. NMR spectra were recorded in $CDCl_3$ with a JEOL GX-500 (500 MHz for ^1H and 125 MHz for ^{13}C) at 27 °C. The assigments of all signals were made by employing a first-order analysis with the aid of decoupling, H–H COSY and C–H COSY techniques, and the parameters were confirmed by a computer-assisted simulation analysis.

Oxidation of *l*-2(10)-Pinene (1) with Lead Tetraacetate. A solution of **1** (136 g, 1.0 mol) in glacial acetic acid (1.8 l) was stirred at 60±2 °C. Trilead tetraoxide (690 g, 1.0 mol) was slowly added to the above solution during a period of 90 min and the stirring was continued for further 1 h. The reactant was carefully neutralized with aq Na_2CO_3. The precipitated solid of $PbCO_3$ was removed by filtration and the filtrate was extracted with hexane (3×1 l). The combined extracts were washed with water, dried (Na_2SO_4), and evaporated in vacuo to give an almost colorless oil (145.9 g): n_D^{25}=1.4676, d_4^{25}=1.0012, $[\alpha]_D^{22}$=−47.1° (neat), EV (ester value)=324. Hydroly-

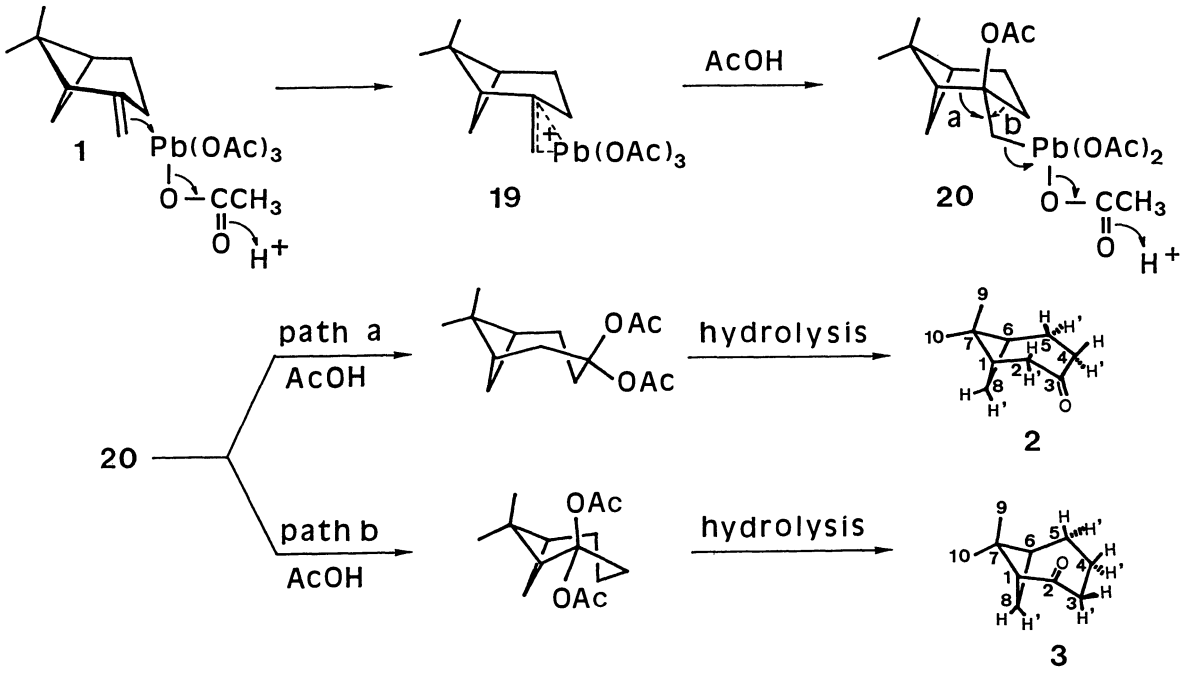

Scheme 1. Possible reaction pathways for the formation of **2** and **3**.

sis of the reactant oil was performed by following a general method,[2] affording hydrolytic products (107.9 g). Their structures were confirmed by comparing the GLC and GC-MS data with those of the authentic samples **4**—**18**.[2] The yields of these compounds based on GLC analysis are summarized in Table 1. The new minor products **2** and **3** were carefully separated by silica-gel column chromatography, followed by removal of alcoholic compounds by employing phthalic anhydride,[6] and then preparative GLC.

(1*S*,6*S*)-7,7-Dimethylbicyclo[4.1.1]octan-3-one (2): A colorless oil; n_D^{25}=1.4810; d_4^{25}=0.9818; $[\alpha]_D^{25}$=−57° (*c* 0.11, $CHCl_3$); IR (neat) 1697 (C=O), 1470, 1454 cm^{-1} (CH_2); EI-MS *m/z* 152 (M^+; 25.1%), 137 (3.9), 111 (51.4), 95 (8.0), 93 (8.1), 83 (89.0), 69 (97.8), 55 (100), 41 (49.3); ^1H NMR δ=0.75 (Me-9), 1.28 (Me-10), 1.79 (H-8′), 1.82 (H-5), 1.84 (H-5′), 2.06 (H-1), 2.20 (H-6), 2.42 (H-2), 2.550 (H-4), 2.552 (H-8), 2.61 (H-2′), 2.82 (H-4′), $J_{1,2}$=3.5, $J_{1,2'}$=4.3, $J_{1,6}$=4.0, $J_{1,8}$=8.0, $J_{1,8'}$=1.5, $J_{2,2'}$=−17.0, $J_{2',4}\approx J_{2',8}\approx$1.5, $J_{4,4'}$=−13.5, $J_{4,5}\approx$2, $J_{4,5}\approx$6.5, $J_{4',5}$=12, $J_{4',5'}$=7.5, $J_{4',6}\approx$0.5, $J_{5,5'}$=−14.5, $J_{5,6}\approx$5.5, $J_{5',6}\approx$3, $J_{6,8}$=8.0, $J_{6,8'}\approx$1, $J_{8,8'}$=−12.0 Hz; ^{13}C NMR δ=19.95 (C-9), 23.40 (C-5), 24.59 (C-8), 30.42 (C-10), 38.51 (C-1), 40.07 (C-7), 41.87 (C-6), 41.90 (C-4), 45.30 (C-2), 214.62 (C-3). Found: *m/z* 152.1185. Calcd for $C_{10}H_{16}O$: M, 152.1168.

(1*R*,6*S*)-7,7-Dimethylbicyclo[4.1.1]octan-2-one (3): A colorless oil; n_D^{25}=1.4831; $[\alpha]_D^{22}$=+50° (*c* 0.24, $CHCl_3$); IR (neat) 1687 (C=O), 1469, 1455 cm^{-1} (CH_2); EI-MS *m/z* 152 (M^+; 14.3%), 137 (7.1), 123 (4.3), 110 (22.4), 98 (20.7), 83 (100), 82 (94.3), 67 (42.1), 55 (38.6), 41 (29.3); ^1H NMR δ=1.01 (Me-9), 1.35 (Me-10), 1.90 (H-4), 1.93 (H-5), 1.96 (H-8′), 2.02 (H-5′), 2.03 (H-4′), 2.25 (H-6), 2.46 (H-8), 2.52 (H-3′), 2.68 (H-1), 2.84 (H-3), $J_{1,3}\approx$0.5, $J_{1,6}$=4.3, $J_{1,8}$=7.5, $J_{1,8}\approx$1, $J_{3,3'}$=−16.5, $J_{3,4}$=4.0, $J_{3,4'}$=7.5, $J_{3',4}$=10.0, $J_{3',4'}$=4.5, $J_{4,4'}\approx$−12, $J_{4,5}\approx$2, $J_{4,5'}\approx$7, $J_{4',5}\approx$4, $J_{4',5}\approx$4, $J_{5,5'}\approx$−12, $J_{5,6}\approx$5.5, $J_{5',6}\approx$2.5, $J_{6,8}$=8.0, $J_{6,8'}\approx$1.5, $J_{8,8'}$=−12.5 Hz; ^{13}C NMR δ=20.30 (C-5), 21.51 (C-9), 23.38 (C-8), 26.34 (C-4), 31.00 (C-10), 40.13 (C-7), 42.06 (C-3), 42.71 (C-6), 60.38 (C-1), 214.92 (C-2). Found: *m/z* 152.1191. Calcd for $C_{10}H_{16}O$: M, 152.1168.

References

1) A part of the results were presented at the 1989 International Chemical Congress of Pacific Basin Societies, Honolulu, December 1989, Abstr., No. ORGN 754.

2) Y. Matsubara, *Nippon Kagaku Kaishi,* **75**, 804 (1954); *ibid.,* **75**, 894 (1954); K. Yokoi and Y. Matsubara, *ibid.,* **1979**, 641.

3) Y. Matsubara, *Nippon Kagaku Kaishi,* **75**, 1088 (1954); *ibid.,* **75**, 1092 (1954); *ibid.,* **76**, 726 (1956); *ibid.,* **76**, 736 (1956).

4) M. Kasano and Y. Matsubara, *Yukagaku,* **27**, 309 (1978).

5) Studies on a convenient synthesis of β- and γ-thujaplicins from compounds **2** and **3** will be reported elsewhere.

6) B. Helferich and O. Lecher, *Ber.,* **54**, 932 (1921); L. V. Auwers and F. Dersch, *J. Prakt. Chem.,* **124**, 228 (1930); F. Tiemann and P. Krüger, *Ber.,* **29**, 902 (1896); R. H. Pickard, W. O. Littlebury, and J. Kenyon, *J. Chem. Soc.,* **91**, 1978, 2059 (1907); R. H. Pickard and W. O. Littlebury, *ibid.,* **101**, 113 (1912); K. Stephan, *J. Prakt. Chem.,* **60**, 248 (1899); *ibid.,* **62**, 523 (1890); W. Hückel, *Justus Liebigs Ann. Chem.,* **477**, 121, 136 (1930).

7) An analogous oxidative 1,2-shift has been observed in the oxidation of cyclohexene with lead tetraacetate to afford ring-contracted cyclopentanecarbaldehyde : K. B. Wiberg and S. D. Nielsen, *J. Org. Chem.,* **26**, 3353 (1964).

8) Optimization of the yields of compounds **2** and **3** from **1** by the present method or by the use of other methods is currently under intensive investigation.

9) M. de Botlon, *Compt. Rend.,* **179**, 501 (1924): Bp 52—52.5 °C/13 mmHg, n_D^{15}=1.4795, d_4^{19}=0.868.

Stepwise Reduction of Acetals to the Corresponding Hydrocarbons. A Mild and Effective Transformation via Carbinyl Bromides

Takeshi ORIYAMA,* Yuichi ICHIMURA, and Gen KOGA
Department of Chemistry, Faculty of Science, Ibaraki University, Bunkyo, Mito 310
(Received March 15, 1991)

Synopsis. Stepwise reduction of two alkoxyl groups in acetal was effected by the action of triethylsilane along with acetyl bromide and $SnBr_2$ and then of tributyltin hydride (or lithium aluminium hydride) providing methyl or methylene compounds in good yields under very mild conditions.

The dealkoxylation of aldehyde- or ketone-acetals to the corresponding methyl or methylene compounds is one of the reactions of potential usefulness in organic synthesis. Although a methodology similar to this transformation via dithioacetals has been well-established,[1] dealkoxylative reduction of dialkyl acetals usually leads to the mono-dealkoxylated products[2] which are sluggish to further reduction.[3]

Now we wish to report a mild and convenient procedure to effect stepwise reduction of two alkoxyl groups in acetals to give the corresponding methyl or methylene compounds.

Our previous investigation[4] on the halogenative reduction of acetals to corresponding carbinyl halides with triethylsilane promoted by SnX_2/AcX[5] suggested that the subsequent reduction of thus obtained halides to alkanes would provide a two-step conversion of acetals to alkanes, which would constitute a mild and convenient alternative to Wolff-Kizhner[6] or Clemmensen reduction[7] of the parent carbonyl compounds.

In the first place, we undertook to examine the reduction of 1-naphthaldehyde dimethyl acetal to 1-methylnaphthalene. First reduction of acetal to 1-bromomethylnaphthalene was carried out according to the procedure described in the previous paper.[4] Subsequent reduction of the bromide to 1-methylnaphthalene was effected by tributyltin hydride in benzene. The two-step conversion either with or without the purification of the intermediate, 1-bromomethylnaphthalene, invariably afforded 1-methylnaphthalene in 85% overall yield. A one-pot operation with an intermediary manipulation for solvent exchange has proved to be satisfactory enough with a minimal loss of yield (77% overall). While the tin hydride reduction for the second step is most mild and effective, less selective lithium aluminium hydride may also be employed as an alternative reagent of choice in cases where the radical reduction is hampered by undesirable side reactions.

The reaction was conducted with various acetals under the optimum conditions and the results are summarized in Table 1. Higher yields were obtained in the cases of aromatic aldehyde acetals (Entries 1—7). Ketone acetals also gave the corresponding methylene compounds in good yields (Entries 9—14). In the case of aliphatic ketone acetals, a small amount of olefin (9—25%) was obtained as a by-product (Entries 12, 13, and 14). The reaction was also effective to ethylene acetal to result in the corresponding hydrocarbon (Entries 3 and 11).

Table 1. Stepwise Reduction of Acetals to the Corresponding Hydrocarbons[a]

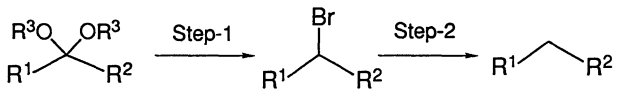

OR^3, OR^3=OMe, OMe
$O(CH_2)_2O$

Method A: Step-1, $Et_3SiH/SnBr_2$–AcBr/CH_2Cl_2; Step-2, *n*-Bu_3SnH/AIBN/benzene
Method B: Step-1, $Et_3SiH/SnBr_2$–AcBr/CH_2Cl_2; Step-2, $LiAlH_4$/THF

Entry	Acetal	Method	Step-1		Step-2		Yield[b]/%
1	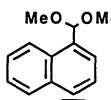	A	0 °C,	1.5 h	Reflux,	0.5 h	85
2		B	0 °C,	1 h	R.T.,	2.5 h	84
3	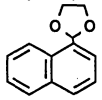	A	R.T.,	4 h	Reflux,	0.75 h	72
4	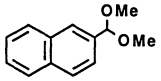	A	0 °C,	3.5 h	Reflux,	0.75 h	85
5		B	0 °C,	3.5 h	R.T.,	2.5 h	86
6	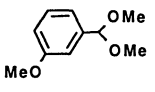	A	R.T.,	2.5 h	Reflux,	0.5 h	90
7		B	R.T.,	2.5 h	R.T.,	2.5 h	92

Table 1. (Continued)

Entry	Acetal	Method	Step-1		Step-2		Yield[b]/%
8	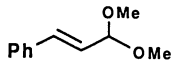	B	0 °C,	5 h	R.T.,	3.5 h	92
9	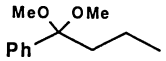	A	0 °C,	2 h	Reflux,	0.5 h	79
10		B	0 °C,	2.5 h	R.T.,	15 h	82
11	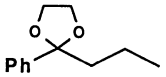	A	R.T.,	2 h	Reflux,	0.5 h	77
12	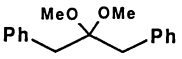	A[c]	R.T.,	24 h	Reflux,	0.5 h	55[d]
13	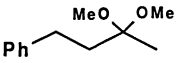	A	R.T.,	4 h	Relux,	0.5 h	60[e]
14	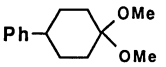	A	R.T.,	24 h	Reflux,	0.5 h	67[f]

a) All the products gave satisfactory ^{1}H NMR and IR spectra. b) Isolated yield from acetal. c) $Sn(OTf)_2$ was used in place of $SnBr_2$. d) 1.3-Diphenylpropene was obtained in 9% yield. e) 1-Phenyl-2-butene was obtained in 25% yieid. f) 4-Phenylcyclohexene was obtained in 14% yield.

Experimental

Followings are the typical procedures for the reduction of 1-naphthaldehyde dimethyl acetal.

Method A: To a suspension of tin(II) bromide (6.9 mg, 0.02 mmol) and 1-naphthaldehyde dimethyl acetal (135 mg, 0.67 mmol) in dichloromethane (2 ml) were added triethylsilane (107 mg, 0.92 mmol) in dichloromethane (1.5 ml) and acetyl bromide (187 mg, 1.52 mmol) in dichloromethane (1.5 ml), successively at ice-bath temperature under argon atmosphere. The mixture was stirred for 1.5 h at this temperature and quenched with a phosphate buffer (pH 7). The organic materials were extracted with dichloromethane, dried over Na_2SO_4, and evaporated to leave the crude 1-bromomethylnaphthalene as an oil. The crude bromide was dissolved into benzene (3 ml) and *n*-Bu_3SnH (304 mg, 1.04 mmol) and a catalytic amount of azobisisobutyronitrile was added to it. After the mixture was refluxed for 30 min, the solvent was evaporated and 1-methylnaphthalene (80.7 mg, 85%) was isolated from the residue by thin layer chromatography over silica gel.

Method B: First step reduction was the same as that of Method A. To a suspension of $LiAlH_4$ (36.2 mg, 0.95 mmol) in THF (1 ml) was added a THF (4 ml) solution of the crude bromide from 1-naphthaldehyde dimethyl acetal (128 mg, 0.63 mmol). The mixture was stirred for 2.5 h. The reaction was quenched with a phosphate buffer (pH 7), and the precipitates were removed by Celite filtration. The organic materials were extracted with Et_2O and dried over $MgSO_4$. Filtration and concentration in vacuo gave an oily residue which was purified by thin layer chromatography over silica gel to afford 1-methylnaphthalene (74.9 mg, 84% from acetal).

One-Pot Operation: After completion of first-step reduction of acetals, solvents and volatile materials were removed from reaction flask using water-jet aspirator. The resultant residue was dissolved into benzene and subjected to the second-step reduction as described in the method A procedure.

The present work was partially supported by a Grant-in-Aid for Scientific Research No. 02854053 from the Ministry of Education, Science and Culture.

References

1) For reviews, see: G. R. Pettit and E. E. van Tamelen, *Org. React.*, **12**, 356 (1962); H. Hauptmann and W. F. Walter, *Chem. Rev.*, **62**, 347 (1962).

2) T. Tsunoda, M. Suzuki, and R. Noyori, *Tetrahedron Lett.*, **1979**, 4679, and references cited therein.

3) For reduction of dialkyl ethers to alkanes, see: T. Morita, Y. Okamoto, and H. Sakurai, *Synthesis*, **1981**, 32; R. O. Hutchins and K. Learn, *J. Org. Chem.*, **47**, 4380 (1982).

4) T. Oriyama, K. Iwanami, K. Tsukamoto, Y. Ichimura, and G. Koga, *Bull. Chem. Soc. Jpn.*, **64**, 1410 (1991).

5) T. Oriyama, K. Iwanami, Y. Miyauchi, and G. Koga, *Bull. Chem. Soc. Jpn.*, **63**, 3716 (1990).

6) For a review, see: D. Todd, *Org. React.*, **4**, 378 (1948).

7) For a review, see: E. L. Martin, *Org. React.*, **1**, 155 (1942).

The Oxidation of *p*-Substituted Phenols Using a *t*-Butyl Hydroperoxide–Heteropolyacid System

Masao SHIMIZU,* Hideo ORITA, Takashi HAYAKAWA, Yoshihito WATANABE, and Katsuomi TAKEHIRA*
National Chemical Laboratory for Industry, Tsukuba Research Center, Tsukuba, Ibaraki 305
(Received March 13, 1991)

Synopsis. The oxidation of *p*-substituted phenols with *t*-BuOOH in the presence of heteropolyacids was carried out. 4-*t*-Butylperoxy-2,5-cyclohexadien-1-ones were obtained in good yields by the oxidation of 2,4,6-trialkylsubstituted phenols in this oxidation system.

Heteropolyacids are useful catalysts for the oxidation of hydrocarbons since they possess both oxidizing ability and acid catalyst center.[1] Hydrogen peroxide oxidation of various organic substrates has been done by use of heteropolyacid as catalyst[2] since aqueous hydrogen peroxide is inexpensive, environmentally clean, and easy to handle. Meanwhile, it is well-known that *t*-butyl hydroperoxide is also a convenient oxidizing agent, especially for highly selective oxygenation of olefins and acetylenes.[3] However, there have been few reports on the oxidation with *t*-butyl hydroperoxide catalyzed by heteropolyacids. It was reported that secondary alcohols were selectively oxidized to ketones using a *t*-BuOOH–hexadecylpyridinium molybdophosphate system.[4]

We previously reported that 2,6-di-*t*-butyl-4-hydroperoxy-4-methyl-2,5-cyclohexadien-1-one was determined as an intermediate in the oxidation of 2,6-di-*t*-butyl-4-methylphenol to 2,6-di-*t*-butyl-*p*-benzoquinone with a H_2O_2–heteropolyacid system.[5] Here, we report the oxidation of several *p*-substituted phenols with a *t*-BuOOH–heteropolyacid system.

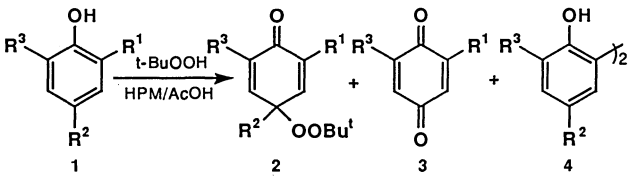

HPM=$H_3PMo_{12}O_{40}\cdot nH_2O$

Results and Discussion

When 2,6-di-*t*-butyl-4-methylphenol (**1a**) was stirred with 80% *t*-butyl hydroperoxide in the presence of 12-molybdophosphoric acid at 30 °C in acetic acid for 5 h, 2,6-di-*t*-butyl-4-*t*-butylperoxy-4-methyl-2,5-cyclohexadien-1-one (**2a**) was obtained in 44% yield. This product is analogous to the compound obtained in the oxidation of **1a** with the H_2O_2–heteropolyacid system.[5] 2,6-Di-*t*-butyl-*p*-benzoquinone (**3a**) was also obtained in 9% yield as a by-product. The oxidations of **1a** with *t*-butyl hydroperoxide were carried out using other heteropolyacid as catalyst (Table 1). Molybdic compounds showed higher catalytic activities than tungstic ones. Although carboxylic acids such as acetic and propionic acids were employed as a solvent to afford **2a** in good yields, the oxidation did not proceed efficiently in alcohols such as methanol and ethanol; this tendency is similar to that obtained with the H_2O_2–heteropolyacid system.[5]

Table 1. Oxidation of **1a** Using *t*-BuOOH–Heteropolyacid[a]

Catalyst	Conv./%	Yield/%	
		2a	**3a**
$H_3PMo_{12}O_{40}\cdot nH_2O$	99.0	47.9	8.6
$H_3PW_{12}O_{40}\cdot nH_2O$	46.7	26.2	0.8
$H_4SiMo_{12}O_{40}\cdot nH_2O$	99.9	41.6	9.3
$H_4SiW_{12}O_{40}\cdot nH_2O$	58.1	27.4	3.3
H_2MoO_4	17.1	14.1	—
None	17.5	17.1	—

a) Reaction conditions: **1a**, 2 mmol; *t*-BuOOH (80%), 1 ml; catalyst, 100 mg; AcOH, 10 ml; 30 °C, 5 h.

Table 2. Oxidation of Phenols Using *t*-BuOOH–Heteropolyacid[a]

	R^1	R^2	R^3	Yield/%		
				2	**3**	**4**
a	*t*-Bu	Me	*t*-Bu	61.6	12.7	—
b	Me	Me	Me	31.4	—	—
c	*t*-Bu	Me	Me	33.5	11.5	—
d	H	*t*-Bu	*t*-Bu	—	—	26.3
e	H	Me	*t*-Bu	—	—	3.9
f	*t*-Bu	$AcOCH_2$	*t*-Bu	—	64.9	—
g	*t*-Bu	MeO	*t*-Bu	—	91.2	—

a) Reaction conditions: phenol, 2 mmol; *t*-BuOOH (80%), 1 ml; $H_3PMo_{12}O_{40}\cdot nH_2O$, 100 mg; AcOH, 10 ml; 30 °C, 3 h.

When 2,4,6-trialkylsubstituted phenols were oxidized with the *t*-BuOOH–heteropolyacid system, peroxides were obtained as main products (Table 2). However, the quinone (**3a**) became as a main product when the phenols which have more eliminative substituents than methyl group on the para positions, such as **1f** and **1g**, were treated with *t*-butyl hydroperoxide. In the reactions of 2,4-disubstituted phenols, no peroxide formed but dimerized products at the ortho position of the phenol rings were obtained.

From the above results, the oxidation mechanism is considered as follows. When the 6-unsubstituted phenols were oxidized in the *t*-BuOOH–heteropolyacid system, the corresponding dimers were formed. This result suggests that the oxidations proceed by way of phenoxyl radical intermediates. Although two 6-unsubstituted phenols couple each other at the ortho position of the phenol rings to afford dimers, 2,4,6-trisubstituted phenols are difficult to dimerize due to

sterical hindrance. The radicals generated from the 2,4,6-trisubstituted phenols react with *t*-butyl hydroperoxide at the para position of the phenyl rings to afford the peroxides. *p*-Benzoquinones were formed by decomposition of the peroxides. A similar reaction mechanism from the peroxide to the *p*-benzoquinone under acidic conditions was reported.[6] As previously reported,[5] a 4-hydroperoxy-2,5-cyclohexadien-1-one was obtained as a main product from 2,6-di-*t*-butyl-4-methylphenol with H_2O_2–heteropolyacid oxidation system. It seems that the first step of the phenol oxidation with the H_2O_2–heteropolyacid system is similar to that with the present system.

Consequently, 4-*t*-butylperoxy-2,5-cyclohexadien-1-ones were obtained in good yield by the oxidation of 2,4,6-trialkylsubstituted phenols with the *t*-BuOOH–heteropolyacid system. Cobalt(II) salts have usually been used as catalyst for synthesis of the peroxide. This is one of rare examples of peroxide synthesis with other metal species than cobalt as catalyst.[7]

Experimental

Melting points were determined on a Yanagimoto micro-melting apparatus. ^{1}H NMR spectra were recorded on a Hitachi R-40 High Resolution NMR Spectrometer (90 MHz). IR spectra were recorded on a JASCO FT/IR-7000 Fourier Transfer Infrared Spectrometer. Gas chromatograph analyses were performed on a Shimadzu GC-7A gas chromatograph using a Thermon 3000 column. *t*-Butyl hydroperoxide (about 80% solution in di-*t*-butyl peroxide, Merck-Schuchardt) was used without further purification.

General Procedure for the Oxidation of a Phenol Using a *t*-BuOOH–Heteropolyacid System. *t*-Butyl hydroperoxide (2 ml) was added dropwise to a solution of a phenol (2 mmol) and a catalyst (100 mg) in acetic acid (10 ml). The reaction mixture was stirred at 30 °C under nitrogen atmosphere. Water was added to the solution and products were extracted with dichloromethane three times. The organic layer was washed with water and dried over anhydrous magnesium sulfate. Yields of the products were determined by an internal standard technique using the GC method for **2a**, and by isolation for the others.

2,6-Di-*t*-butyl-4-*t*-butylperoxy-4-methyl-2,5-cyclohexadien-1-one (2a). The crude product was chromatographed on silica gel using benzene–hexane (1 : 3) mixture as eluent. The product was recrystallized from hexane; mp 84—85 °C (lit,[6] mp 85.5—86.5 °C). ^{1}H NMR ($CDCl_3$) δ=1.15 (s, 9H), 1.22 (s, 18H), 1.30 (s, 3H), 6.55 (s, 2H); IR (KBr) 1665, 1644, 1364, 1247, 1199, 1162, 1058, 884, 872 cm^{-1}.

4-*t*-Butylperoxy-2,4,6-trimethyl-2,5-cyclohexadien-1-one (2b). The crude product was chromatographed on silica gel using dichloromethane as eluent. Bp 28 °C (1.33 Pa); ^{1}H NMR ($CDCl_3$) δ=1.17 (s, 9H), 1.33 (s, 3H), 1.86 (s, 6H), 6.57 (s, 2H); IR ($CHCl_3$) 1680, 1640, 1450, 1365, 1065, 909 cm^{-1}. Found: C, 69.96; H, 9.11%. Calcd for $C_{13}H_{20}O_3$: C, 69.64; H, 8.93%.

2-*t*-Butyl-4-*t*-butylperoxy-4,6-dimethyl-2,5-cyclohexadien-1-one (2c). The crude product was chromatographed on silica gel using benzene as eluent. Bp 35 °C (1.33 Pa); ^{1}H NMR ($CDCl_3$) δ=1.17 (s, 9H), 1.22 (s, 9H), 1.32 (s, 3H), 1.83 (s, 3H), 6.60 (m, 2H); IR ($CHCl_3$) 1644, 1458, 1360, 1065, 903 cm^{-1}. Found: C, 72.78; H, 10.04%. Calcd for $C_{16}H_{26}O_3$: C, 72.18; H, 9.77%.

3,3′,5,5′-Tetra-*t*-butyl-2,2′-biphenyldiol (4d). The crude product was chromatographed on silica gel using benzene as eluent. The product was recrystallized from methanol; mp 193—194 °C (lit,[8] mp 200—201 °C). ^{1}H NMR ($CDCl_3$) δ=1.29 (s, 18H), 1.44 (s, 18H), 5.17 (s, 2H), 7.10 (d, 2H, *J*=2.5 Hz), 7.40 (d, 2H, *J*=2.5 Hz); IR (KBr) 3528, 1479, 1437, 1363, 1334, 1284, 1238, 1203, 1170, 1096, 882, 816 cm^{-1}.

3,3′-Di-*t*-butyl-5,5′-dimethyl-2,2′-biphenyldiol (4e). The crude product was chromatographed on silica gel using benzene as eluent. This compound was obtained as glass.[9] ^{1}H NMR ($CDCl_3$) δ=1.42 (s, 18H), 2.27 (s, 6H), 5.11 (s, 2H), 6.90 (br s, 2H), 7.15 (br s, 2H); IR ($CHCl_3$) 3536, 1435, 1394, 1365, 1328, 1276, 1172, 1096, 870 cm^{-1}.

References

1) For example, review: M. Ootake, *Yuki Gosei Kagaku Kyokai Shi,* **39**, 385 (1981).

2) Y. Ishii and M. Ogawa, *Yuki Gosei Kagaku Kyokai Shi,* **47**, 889 (1989); M. Shimizu, H. Orita, T. Hayakawa, and K. Takehira, *Tetrahedron Lett.,* **30**, 471 (1989).

3) A. Pfenninger, *Synthesis,* **1986**, 89; K. B. Sharpless and T. R. Verhoeven, *Aldrichimica Acta,* **12**, 63 (1979).

4) K. Yamawaki, T. Yoshida, H. Nishihara, Y. Ishii, and M. Ogawa, *Synth. Commun.,* **16**, 537 (1986).

5) M. Shimizu, H. Orita, T. Hayakawa, Y. Watanabe, and K. Takehira, *Bull. Chem. Soc. Jpn.,* **63**, 1835 (1990).

6) W. H. Starnes, Jr., *J. Org. Chem.,* **31**, 3164 (1966).

7) J. Muzart, *J. Chem. Res. (S),* **1990**, 96.

8) E. C. Horswill and K. U. Ingold, *Can. J. Chem.,* **44**, 269 (1966).

9) W. W. Kaeding, *J. Org. Chem.,* **28**, 1063 (1963); D. R. Armstrong, C. Cameron, D. C. Nonhebel, and P. G. Perkins, *J. Chem. Soc., Perkin Trans. 2,* **1983**, 589.

Triethylborane Induced Selective 1,4-Reduction of α,β-Unsaturated Carbonyl Compounds with Triphenyltin Hydride or Tributyltin Hydride

Kyoko NOZAKI, Koichiro OSHIMA,* and Kiitiro UTIMOTO*
Department of Industrial Chemistry, Faculty of Engineering, Kyoto University, Sakyo-ku, Kyoto 606
(Received April 5, 1991)

Synopsis. Reduction of α,β-unsaturated ketones and esters with triphenyltin hydride or tributyltin hydride in the presence of triethylborane has been studied. Whereas the reaction of α,β-unsaturated ketones ($R^1CH=CHCOR^2$) with triphenyltin hydride provided the corresponding saturated ketones ($R^1CH_2CH_2COR^2$), treatment of α,β-unsaturated ester (PhCH=CHCOOMe or $CH_3CH=CHCOO$-n-C_6H_{13}) afforded an adduct ($PhCH_2CH(SnPh_3)COOMe$ or $CH_3CH(SnPh_3)CH_2COO$-n-C_6H_{13}).

1,4-Selective reduction of α,β-unsaturated carbonyl compounds has been achieved by triphenyltin hydride in refluxing toluene.[1] Recently we have reported that triethylborane induced a facile addition of triphenyltin hydride to an acetylenic bond to give alkenylstannane effectively.[2] The reaction proceeded at low temperature compared with the conventional method which uses azobisisobutyronitrile or peroxide as a radical initiator. Taking this advantage, we applied our method to the title reaction and found that selective reduction of α,β-unsaturated carbonyl compounds to saturated carbonyl compounds proceeded efficiently by treatment with triphenyltin hydride or tributyltin hydride in benzene at 25 °C.

Treatment of a benzene solution of 2-cyclododecenone **1** and Ph_3SnH with Et_3B at 25 °C for 6 h

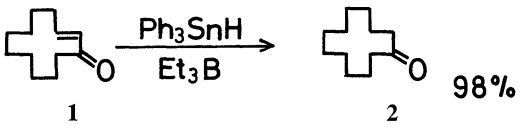

1 **2**

Scheme 1.

provided cyclododecanone **2** in 98% yield (Scheme 1). The other representative results are shown in Table 1.

The reduction of β-ionone (**3**) provided α,β-unsaturated ketone **4** in 88% yield selectively and no 1,6-reduction product was observed in the reaction mixture (Entry 7 in Table 1). α,β-Unsaturated aldehyde was converted into saturated aldehyde in good yield which was exemplified by the reduction of citral (**5**) (Entry 8 in Table 1). Over-reduction of 3,7-dimethyl-6-octenal (**6**) into alcohol (3,7-dimethyl-6-octen-1-ol) was not observed because of the mildness of the reaction conditions.[3] An alkynone such as 3-octyn-2-one was reduced to 2-octanone in 50% yield with 4 equivalents of Ph_3SnH.

The use of less than 2 equivalents of triphenyltin hydride resulted in an incompletion of the reduction. However, the amount of triethylborane could be reduced to catalytic amount without decrease of the

Table 1. 1,4-Reduction of α,β-Unsaturated Ketones with Ph_3SnH[a]

Entry	Unsaturated ketone	Reaction time/h	Product	Yield/%
1	3-Dodecen-2-one	12	2-Dodecanone	86
2	2-Dodecen-4-one	12	4-Dodecanone	85
3	2-Cyclohexenone	3	Cyclohexanone	74[b]
4	4-Methyl-2-cyclohexenone	3	4-Methylcyclohexanone	98[b]
5	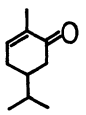	5	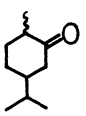	84
6	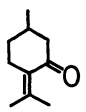	7	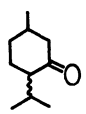	80
7	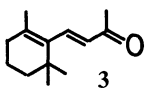 **3**	12	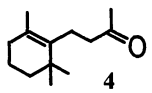 **4**	88
8	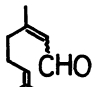 **5**	12	**6**	80
9	n-$C_4H_9C{\equiv}CCO$-n-C_6H_{13}	12	n-$C_4H_9CH_2CH_2CO$-n-C_6H_{13}	50[c]

a) Triethylborane (2.2 mol), triphenyltin hydride (2.2 mol), and α,β-unsaturated ketones (1.0 mol) were empolyed. b) GLPC yields. c) Triphenyltin hydride (4.0 mol) was employed.

yield of saturated ketones. For instance, an addition of catalytic amount of triethylborane (0.1 mmol) to a solution of 2-cyclohexenone (1.0 mmol) and triphenyltin hydride (2.2 mmol) provided cyclohexanone in 77% yield after stirring for 3 h at 25 °C. Tributyltin hydride could be used instead of triphenyltin hydride and the reaction of 2-cyclododecenone with tributyltin hydride in the presence of triethylborane gave cyclododecanone in 98% yield after 7 h at 25 °C.

We are tempted to assume following reaction mechanism: (1) Triphenyltin hydride or tributyltin hydride adds to α,β-unsaturated ketones ($R^1CH=CHCOR^2$) in 1,4-fashion to give $R^1CH_2CH=CR^2$ ($OSnR_3$) (R=Ph or *n*-Bu) and (2) subsequent hydrogenolysis with second triphenyltin hydride or tributyltin hydride to provide saturated ketones and $R_3Sn-SnR_3$ (R=Ph or *n*-Bu).

Treatment of α,β-unsaturated ester with triphenyltin hydride in the presence of triethylborane gave β-triphenylstannyl or α-triphenylstannyl carboxylic ester (**7** or **8**) in contrast to the reaction of α,β-unsaturated ketones (Scheme 2). Triphenylstannyl radical attacked β-carbon of hexyl crotonate to give a carbon radical $Ph_3SnCH(Me)\dot{C}HCOO$-*n*-C_6H_{13} which abstracted hydrogen from Ph_3SnH to form the product. In contrast, triphenylstannyl radical attacked α-carbon of methyl cinnamate to provide a carbon radical $Ph\dot{C}HCH(SnPh_3)COOMe$ because phenyl group stabilizes an adjacent carbon radical more effectively than carboalkoxy group.[5] The reaction of tributyltin hydride in place of triphenyltin hydride with α,β-unsaturated ester was sluggish and resulted in an incompletion.[6-8] Treatment of PhCH=CHCOOMe with tributyltin hydride in the presence of triethylborane provided $PhCH_2CH(Sn$-*n*-$Bu_3)COOMe$ in 50% yield along with recovered starting material (10%) and saturated ester, $PhCH_2CH_2COOMe$ (10%). The reaction of $CH_3CH=CHCOO$-*n*-C_6H_{13} with tributyltin hydride gave β-tributylstannylated ester, $CH_3CH(Sn$-*n*-$Bu_3)CH_2COO$-*n*-C_6H_{13} in 15% yield along with starting ester (47%).

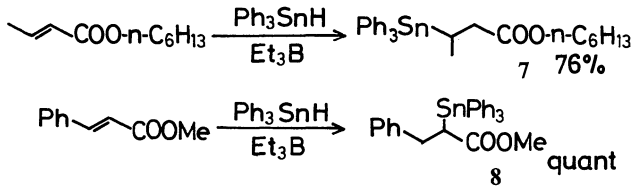

Scheme 2.

In conclusion, the coexistence of triethylborane facilitate the reduction of α,β-unsaturated ketones into saturated ketones with triphenyltin hydride or tributyltin hydride. The reduction proceeded under mild conditions (25 °C) compared with the conventional methods which require high reaction temperature (100—150 °C).

Experimental

Analytical gas chromatography (GLPC) was performed with a Shimadzu gas chromatograph, Model GC-8A using thermal conductivity detector and helium as carrier gas. ^1H NMR and ^{13}C NMR spectra were taken on a Varian XL-200 spectrometer, $CDCl_3$ was used as solvent and chemical shifts were given in δ with tetramethylsilane as an internal standard. IR spectra were determined on a JASCO IR-810 spectrometer. The elemental analyses were carried out at the Elemental Analysis Center of Kyoto University.

General Procedure for the Reduction of α,β-Unsaturated Ketones with Triphenyltin Hydride. The reduction of 2-cyclododecenone is representative. A hexane solution of triethylborane[4] (1.0 M, 1 M=1 mol dm^{-3}, 2.2 ml, 2.2 mmol) was added to a solution of 2-cyclododecenone (0.18 g, 1.0 mmol) and triphenyltin hydride (0.77 g, 2.2 mmol) in benzene (10 ml) at 25 °C under argon atmosphere. After stirring for 6 h at 25 °C, the reaction mixture was concentrated and the residue was submitted to silica-gel column chromatography using hexane–ethyl acetate (10 : 1) as an eluant to give cyclododecanone (0.18 g) in 98% yield

Reduction of 2-Cyclohexenone with Triphenyltin Hydride. A hexane solution of triethylborane (1.0 M, 2.2 ml, 2.2 mmol) was added to a solution of 2-cyclohexenone (96 mg, 1.0 mmol) and triphenyltin hydride (0.77 g, 2.2 mmol) in benzene (10 ml) at 25 °C under argon atmosphere. After stirring for 3 h at 25 °C, nonane (90 mg, 0.85 mmol) was added to the resulting mixture. The yield of cyclohexanone was determined by GLPC (OV-1 2% on Chromosorb W AW DMCS 60—80 mesh, 2 m, 65 °C, cyclohexanone: t_r=2.54 min, nonane: t_r=3.35 min).

The Reaction of α,β-Unsaturated Ester with Triphenyltin Hydride. The reaction of hexyl crotonate with triphenyltin hydride is a typical example. A hexane solution of triethylborane (1.0 M, 2.2 ml, 2.2 mmol) was added to a solution of hexyl crotonate (0.17 g, 1.0 mmol) and triphenyltin hydride (0.77 g, 2.2 mmol) in benzene (10 ml) at 25 °C under argon atmosphere. The reaction mixture was stirred for 3 h at 25 °C and concentrated in vacuo. The residual oil was submitted to silica-gel column chromatography to give hexyl 3-triphenylstannylbutanoate (**7**, 0.39 g) in 76% yield as a colorless oil: IR (neat) 3062, 2954, 2926, 2856, 1725, 1481, 1459, 1428, 1351, 1294, 1190, 1147, 1074, 909, 727, 698 cm^{-1}; ^1H NMR ($CDCl_3$) δ=0.87 (t, *J*=6.6 Hz, 3H), 1.05—1.70 (m, 8H), 1.42 (d, *J*=7.4 Hz, 3H), 2.32 (m, 1H), 2.67 (dd, *J*=12.0, 7.0 Hz, 1H), 2.73 (dd, *J*=16.0, 7.0 Hz, 1H), 3.88 (t, *J*=6.7 Hz, 2H), 7.35—7.56 (m, 9H), 7.56—7.83 (m, 6H); ^{13}C NMR ($CDCl_3$) δ=13.99, 18.27, 19.04, 22.50, 25.50, 28.43, 31.38, 39.97, 64.68, 128.4, 128.7, 137.3, 138.8, 173.9. Found: C, 64.79; H, 6.70%. Calcd for $C_{28}H_{34}O_2Sn$: C; 64.52; H, 6.57%.

Methyl 3-Phenyl-2-triphenylstannylpropanoate (8): Mp 94.5—95.5 °C; IR (KBr) 3055, 2948, 1720, 1425, 1303, 1202, 1145, 1078, 1040, 995, 830, 765, 740, 720, 698 cm^{-1}; ^1H NMR ($CDCl_3$) δ=3.03 (dd, *J*=13.8, 4.7 Hz, 1H), 3.27 (s, 3H), 3.31 (dd, *J*=9.8, 4.7 Hz, 1H), 3.49 (dd, *J*=13.8, 9.8 Hz, 1H), 7.05—7.70 (m, 20H); ^{13}C NMR ($CDCl_3$) δ=34.15, 36.33, 50.85, 126.2, 128.4, 128.6, 129.4, 136.7, 137.1, 137.4, 141.6. Found: C, 65.25; H, 5.16%. Calcd for $C_{28}H_{26}O_2Sn$: C, 65.53; H, 5.11%.

Reduction of Methyl Cinnamate with Tributyltin Hydride. A hexane solution of triethylborane (1.0 M, 2.2 ml, 2.2 mmol) was added to a solution of methyl cinnamate (0.16 g, 1.0 mmol) and tributyltin hydride (0.64 g, 2.2 mmol) in benzene (10 ml) at 25 °C under argon atmosphere. After stirring for 15 h at 25 °C, the resulting mixture was concentrated in vacuo. The residual oil was submitted to silica-gel column chromatography using hexane–ethyl acetate (10 : 1) as an eluant to give methyl 3-phenyl-2-tributylstannylpropanoate (0.23 g, 50%) and methyl 3-phenylpropanoate (16 mg, 10%) along with recovered methyl cinnamate (16 mg, 10%). Following the literature,[8] a solution of 3-phenyl-2-tributylstannylpropanoate (0.23 g, 0.5 mmol) and benzoic acid (0.12 g, 1.0 mmol) was heated at reflux for 3 h to give methyl 3-phenylpropanoate (65 mg, 80%).

Reduction of Hexyl Crotonate with Tributyltin Hydride. A hexane solution of triethylborane (1.0 M, 2.2 ml, 2.2 mmol)

was added to a solution of hexyl crotonate (0.17 g, 1.0 mmol) and tributyltin hydride (0.64 g, 2.2 mmol) in benzene (10 ml) at 25 °C under argon atmosphere. After stirring for 15 h at 25 °C, the resulting mixture was concentrated. The residual oil was submitted to silica-gel column chromatography to give hexyl 3-tributylstannylbutanoate (68 mg, 15% yield) along with recovered hexyl crotonate (80 mg, 47%). Hexyl 3-tributylstannylbutanoate: Bp 110—120 °C (2 Torr, 1 Torr=133.322 Pa, bath temp); IR (neat) 2954, 2924, 2854, 1732, 1459, 1377, 1288, 1185, 1134, 1072 cm^{-1}; ^1H NMR ($CDCl_3$) δ=0.77—0.91 (m, 18H), 1.16—1.65 (m, 24H), 2.41—2.50 (m, 2H), 4.05 (t, J=6.8 Hz, 2H); ^{13}C NMR ($CDCl_3$) δ=8.33, 13.69, 13.98, 14.95, 18.68, 22.52, 25.60, 27.54, 28.63, 29.23, 31.42, 40.37, 64.43, 174.3. Found: C, 57.14; H, 10.27%. Calcd for $C_{22}H_{46}O_2Sn$: C, 57.28; H, 10.05%.

References

1) E. Yoshii, T. Koizumi, H. Ikeshima, K. Ozaki, and I. Hayashi, *Chem. Pharm. Bull. Jpn.*, **23**, 2496 (1975); H. R. Wolf and M. P. Zink, *Helv. Chim. Acta*, **56**, 1062 (1973); N. Pereyre and J. Valade, *C. R. Acad. Sci.*, **260**, 581 (1965); *idem., Bull. Soc. Chim. Fr.*, **1967**, 1928; U. Pommerenk, H. Sengewein, and P. Welzel, *Tetrahedron Lett.*, **1972**, 3415. Recently palladium catalyzed selective hydrogenation with *n*-Bu_3SnH have been reported. E. Keinan and P. A. Gleize, *Tetrahedron Lett.*, **23**, 477 (1982); I. Ojima, T. Kogure, and Y. Nagai, *ibid.*, **1972**, 5035; Y. T. Xian, P. Four, F. Guibe, and G. Balavoine, *Nouv. J. Chim.*, **8**, 611 (1984); P. Four and F. Guibe, *Tetrahedron Lett.*, **23**, 1825 (1982).

2) K. Nozaki, K. Oshima, and K. Utimoto, *Tetrahedron*, **45**, 923 (1989).

3) Reduction of carbonyl compounds with Ph_3SnH or *n*-Bu_3SnH has been reported. H. G. Kuivila and O. F. Beumel, Jr., *J. Am. Chem. Soc.*, **83**, 1246 (1961); N. Y. M. Fung, P. de Mayo, J. H. Schauble, and A. C. Weedon, *J. Org. Chem.*, **43**, 3977 (1978); E. J. Enholm and G. Prasad, *Tetrahedron Lett.*, **30**, 4939 (1989).

4) We thank Toso Akzo Co. for a gift of a hexane solution of triethylborane.

5) A. Luedtke, K. Meng, and J. W. Timberlake, *Tetrahedron Lett.*, **28**, 4255 (1987).

6) M. Pereyre, G. Colin, and J. Valade, *Tetrahedron Lett.*, **1967**, 4805.

7) M. Pereyre, G. Colin, and J. Valade, *Bull. Soc. Chim. Fr.*, **1968**, 3358.

8) A. Rahm and M. Pereyre, *J. Organomet. Chem.*, **88**, 79 (1975).

Acid-Induced Dimerization Reactions of *N*-(Diphenylphosphinyl)-2-propenimines Leading to Pyridine Derivatives

Hidetaka KAKIUCHI, Tomoshige KOBAYASHI,* and Hiroshi KATO*
Department of Chemistry, Faculty of Science, Shinshu University, Asahi, Matsumoto 390
(Received April 6, 1991)

Synopsis. Treatment of *N*-(diphenylphosphinyl)-3-aryl-1-phenyl-2-propenimines with *p*-toluenesulfonic acid in heated xylene provided 4-aryl-2,6-diphenylpyridines and 4-aryl-3-arylmethyl-2,6-diphenylpyridines via an unprecedented dimerization reaction of the 2-propenimine.

Previously, we described on the reactions of the *N*-phosphinyl-1-azaallyl anions, generated from the corresponding *N*-phosphinyl imine and enamine, with α,β-unsaturated carbonyl compounds[1] or aromatic aldehydes[2] to afford pyridine derivatives. We also reported on the synthesis of *N*-(diphenylphosphinyl)-1,3-diphenyl-2-propenimine (**1a**) and its chemical behavior under basic conditions.[2] In contrast to simple *N*-phosphinyl imines,[3] little is known on the chemical properties of the *N*-phosphinyl-2-propenimines which are supposed to be rather electron-deficient 1-azadienes, except for the aza-Diels–Alder reaction under high pressure.[4] In this note, we describe on the acid-induced reaction of the *N*-phosphinyl-2-propenimines **1a—d** giving pyridine derivatives.

Results and Discussion

The imine **1a** was treated with a catalytic amount of anhydrous *p*-toluenesulfonic acid in refluxing xylene to give 2,4,6-triphenylpyridine (**2a**) and 3-benzyl-2,4,6-triphenylpyridine (**3a**). Similar reactions with the imines **1b** and **1c** provided 3-aryl-2,6-diphenylpyridines (**2b** and **2c**) and 4-aryl-3-arylmethyl-2,6-diphenylpyridines (**3b** and **3c**). In these reactions, the presence

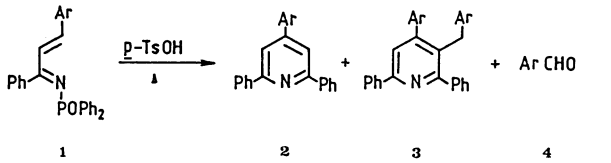

1 2 3 4

Fig. 1.

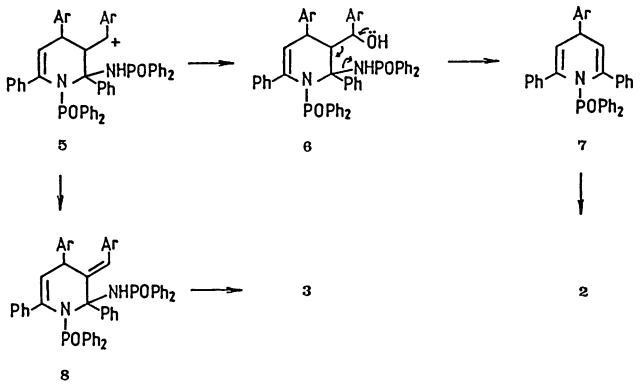

Fig. 2.

Table 1. Yields of the Products by the Acid-Induced Reaction of the 2-Propenimines **1a—d**

Imine	Ar	Yield/%			
		2	(mp; °C)[a]	3	4
1a	C_6H_5	30	(140—141)	20	GLC[b]
1b	*p*-MeC_6H_4	30	(124—125)	25	GLC[b]
1c	*p*-$MeOC_6H_4$	28	(103—104)	20	GLC[b]
1d	*p*-$Me_2NC_6H_4$	27	(133—134)	0	16[c]

a) Undepressed on admixture with authentic specimens.[2] b) Detected by GLC analyses. c) Isolated as the corresponding 2,4-dinitrophenylhydrazone.

of aromatic aldehydes **4a—c** originating from the 3-aryl substituents of the imines **1a—c** was observed by GLC analysis. The reaction with the *p*-dimethylamino derivative **1d** afforded the pyridine **2d** and *p*-(dimethylamino)benzaldehyde (**4d**), identified as the corresponding 2,4-dinitrophenylhydrazone, but the (arylmethyl)pyridine **3d** was not isolated. The yields of the products are summarized in Table 1.

Some control experiments were conducted to clarify the mechanistic aspect of the present reaction. The use of an acid is essential for the present transformation, because the imine **1a** was quantitatively recovered when heated in xylene in the absence of *p*-toluenesulfonic acid. In the presence of water, the reaction of **1a** with *p*-toluenesulfonic acid gave the pyridine **2a** and the 1,3-diphenyl-2-propenone in 26 and 34% yield, respectively, and the benzylpyridne **3a** was not obtained. Thus, the present transformation can be best explained by the mechanism as shown in Fig. 2. The initial step would be an acid-catalyzed dimerization of the imine **1** giving an intermediate **5**, which would react with a trace amount of water to afford **6**. Elimination of the aldehydes **4** and diphenylphosphinic amide from **6** leads to the pyridines **2** via the dihydropyridines **7**. On the other hand, the formation of the (arylmethyl)pyridines **3** can be ascribed to a sequence of deprotonation, elimination of the phosphorus moieties, and isomerization. Although the reason why the (arylmethyl)pyridine **3d** was not formed in the reaction of **1d** is ambiguous, the *p*-dimethylamino group may stabilize the cationic intermediate **5** and facilitate its reaction with water prior to its deprotonation.

Although two examples of dimerization reactions of 2-propenimines giving pyridines and pyrimidines have been reported,[5,6] the reaction described above seems to be an unprecedented type of dimerization reaction of the 2-propenimines.

Experimental[7]

***N*-(Diphenylphosphinyl)-3-(*p*-methylphenyl)-1-phenyl-2-propenimine (1b):** 60%; mp 139—140 °C (Et_2O); IR (KBr)

1612 (C=N), 1190 (P=O) cm^{-1}; ^1H NMR ($CDCl_3$) δ=2.20 (3H, s), 6.90 (1H, d, J=16.2 Hz), 7.10—7.50 (13H, m), 7.64—7.80 (2H, m), 7.82—8.20 (4H, m), 8.29 (1H, dd, J=16.2, 1.1 Hz); ^{13}C NMR ($CDCl_3$) δ=20.5, 127.5—145.0, 180.2 (d, J_{P-C}=8.5 Hz); ^{31}P NMR ($CDCl_3$) δ=18.8; MS m/z (rel intensity) 421 (M^+, 31), 220 (100). Found: C, 79.72; H, 5.84; N, 3.21%. Calcd for $C_{28}H_{24}NOP$: C, 79.79; H, 5.74; N, 3.32%.

***N*-(Diphenylphosphinyl)-3-(*p*-methoxylphenyl)-1-phenyl-2-propenimine (1c):** 69%; mp 140—141 °C (Et_2O); IR (KBr) 1614 (C=N), 1190 (P=O) cm^{-1}; ^1H NMR ($CDCl_3$) δ=3.81 (3H, s), 6.76—7.08 (3H, m), 7.24—7.58 (11H, m), 7.64—7.80 (2H, m), 7.82—8.10 (4H, m), 8.12 (1H, dd, J=16.0, 1.0 Hz); ^{13}C NMR ($CDCl_3$) δ=54.9, 114.0—148.5, 180.4 (d, J_{P-C}=8.6 Hz); ^{31}P NMR ($CDCl_3$) δ=18.6; MS m/z (rel intensity) 437 (M^+, 19), 249 (100, M^+-POPh_2), 201 (85). Found: C, 76.73; H, 5.40; N, 3.21%. Calcd for $C_{28}H_{24}NO_2P$: C, 76.87; H, 5.53; N, 3.20%.

***N*-(Diphenylphosphinyl)-3-[*p*-(dimethylamino)phenyl]-1-phenyl-2-propenimine (1d):** 61%; mp 186—187 °C (benzene); IR (KBr) 1629 (C=N), 1181 (P=O) cm^{-1}; ^1H NMR ($CDCl_3$) δ=2.88 (6H, s), 6.56 (2H, d, J=8.6 Hz), 6.88 (1H, d, J=15.2 Hz), 7.10—7.48 (11H, m), 7.56—7.73 (2H, m), 7.74—8.18 (5H, m); ^{13}C NMR ($CDCl_3$) δ=39.8, 111.7—151.8, 181.1 (d, J_{P-C} =8.5 Hz); ^{31}P NMR ($CDCl_3$) δ=18.2; MS m/z (rel intensity) 450 (M^+, 19), 249 (100, M^+-POPh_2), 201 (46). Found: C, 76.97; H, 6.12; N, 6.02%. Calcd for $C_{29}H_{27}N_2OP$: C, 77.31; H, 6.04; N, 6.22%.

Acid-Induced Reaction of the 2-Propenimines 1a—d. Hydrated *p*-toluenesulfonic acid (9 mg, 0.05 mmol) was added in xylene (20ml) and water was removed by azeotropic distillation. To the resultant solution was added the imine **1** (0.5 mmol) and the mixture was refluxed for 48 h under nitrogen. The presence of aromatic aldehydes **4a—c** was detected by GLC analysis on 10%-SE30 (90 °C) and 10%-Carbowax (130 °C) columns. The solution was washed with aq $NaHCO_3$ and dried over $MgSO_4$. After removal of the solvent in vacuo, the residue was separated on TLC (silica gel, benzene) to give 4-aryl-2,6-diphenylpyridines **2a—d** and 4-aryl-3-arylmethyl-2,6-diphenylpyridines **3a—c**. In the reaction with **1d**, *p*-(dimethylamino)benzaldehyde **4d** was isolated as the 2,4-dinitrophenylhydrazone. The yields of the products are summarized in Table 1.

3-Benzyl-2,4,6-triphenylpyridine (3a): Mp 142—143 °C (pentane) (lit,[8] 137—138 °C); IR (KBr) 1582, 1536 cm^{-1}; ^1H NMR ($CDCl_3$) δ=4.08 (2H, s), 6.48—6.72 (2H, m), 6.90—7.09 (3H, m), 7.12—7.60 (13H, m), 7.62 (1H, s), 8.02—8.18 (2H, m); MS m/z (rel intensity) 397 (M^+, 100). Found: C, 90.62; H, 6.00; N, 3.35%. Calcd for $C_{30}H_{23}N$: C, 90.64; H, 5.83; N, 3.52%.

4-(*p*-Methylphenyl)-3-[(*p*-methylphenyl)methyl]-2,6-diphenylpyridine (3b): Mp 157—158 °C (pentane); IR (KBr) 1580, 1512 cm^{-1}; ^1H NMR ($CDCl_3$) δ=2.21 (3H, s), 2.34 (3H, s), 4.03 (2H, s), 6.55 (2H, d, J=8.1 Hz), 6.90 (2H, d, J=8.1 Hz), 7.13—7.57 (12H, m), 7.61 (1H, s), 7.96—8.20 (2H, m); ^{13}C NMR ($CDCl_3$) δ=21.0, 21.2 34.6, 120.8—152.4, 154.5, 160.4; MS m/z (rel intensity) 425 (M^+, 70), 424 (100), 334 (6), 105 (4). Found: C, 89.97; H, 6.46; N, 3.25%. Calcd for $C_{32}H_{27}N$: C, 90.31.; H, 6.39; N, 3.29%.

4-(*p*-Methoxyphenyl)-3-[(*p*-methoxyphenyl)methyl]-2,6-diphenylpyridine (3c): Mp 168—169 °C (pentane); IR (KBr) 1601, 1512 cm^{-1}; ^1H NMR ($CDCl_3$) δ=3.70 (3H, s), 3.80 (3H, s), 4.01 (2H, s), 6.58 (4H, s), 6.87 (2H, d, J=8.9 Hz), 7.17 (2H, d, J=8.9 Hz), 7.18—7.56 (8H, m), 7.61 (1H, s), 8.02—8.16 (2H, m); ^{13}C NMR ($CDCl_3$) δ=34.3, 55.2, 113.6—157.8, 159.4, 160.4; MS m/z (rel intensity) 457 (M^+, 31), 455 (100), 121 (16). Found: C, 83.92; H, 6.07; N, 3.27%. Calcd for $C_{32}H_{27}NO_2$: C, 84.00; H, 5.95; N, 3.06%.

***p*-(Dimethylamino)benzaldehyde 2,4-Dinitrophenylhydrazone:**[9] Mp and mixed mp 230 °C (decomp); IR (KBr) 3287, 1620, 1603, 1507, 1425, 1141, 1125 cm^{-1}.

Acid-Induced Reaction of the Imine 1a in the Presence of Water. Water (36 mg, 2 mmol) was added to a solution of the imine **1a** (203 mg, 0.5 mmol) and *p*-toluenesulfonic acid (10 mg, 0.05 mmol) in xylene (5 ml) and the mixture was refluxed for 22 h. After removal of the solvent, the residue was separated on TLC (silica gel, benzene) to give 2,4,6-triphenylpyridine **2a** (20 mg, 26%) and 1,3-diphenyl-2-propenone identified as the 2,4-dinitrophenylhydrazone[9] (66 mg, 34%): Mp and mixed mp 248 °C.

References

1) T. Kobayashi, H. Kawate, H. Kakiuchi, and H. Kato, *Bull. Chem. Soc. Jpn.*, **63**, 1937 (1990).

2) T. Kobayashi, H. Kakiuchi, and H. Kato, *Bull. Chem. Soc. Jpn.*, **64**, 392 (1991).

3) For the reactions of simple *N*-phosphinyl imines, see the references cited in Refs. 1 and 2.

4) D. L. Boger and A. M. Kasper, *J. Am. Chem. Soc.*, **111**, 1517 (1989); D. L. Boger, W. L. Corbett, T. T. Curran, and A. M. Kasper, *J. Am. Chem. Soc.*, **113**, 1713 (1991).

5) A. R. Forrester, M. Gill, and R. H. Thomson, *J. Chem. Soc., Perkin Trans. 1*, **1979**, 616.

6) M. Nitta and Y. Iino, *Bull. Chem. Soc. Jpn.*, **59**, 2365 (1986).

7) The *N*-phosphinyl-2-propenimines **1b—d** were prepared by a similar procedure previously described for **1a** in Ref. 2. Spectra of the pyridines **2a—d**, and general conditions and instruments used in this work have been described in Ref. 1. The ^{31}P NMR spectra were taken by use of 85%-H_3PO_4 as an external standard.

8) The pyridine **3a** was unambiguously identified by comparison of the spectral properties with the reported data on **3a** which has been prepared by an authentic procedure: G. W. Fischer, *J. Prakt. Chem.*, **327**, 983 (1985).

9) G. D. Johnson, *J. Am. Chem. Soc.*, **75**, 2720 (1953).

Synthesis of Dimethyl 1,2-Cycloalkanedicarboxylates by Electrochemical Cyclization of Dimethyl α,α′-Dibromoalkanedioates Using a Copper Anode

Masao TOKUDA,* Atsushi HAYASHI, and Hiroshi SUGINOME*
Department of Chemical Process Engineering, Faculty of Engineering, Hokkaido University, Sapporo 060
(Received April 6, 1991)

Synopsis. The electrochemical cyclization of dimethyl α,α′-dibromoalkanedioates by making use of a platinum cathode and a copper anode in the presence of sodium iodide gave three- to six-membered dimethyl 1,2-cycloalkanedicarboxylates in good yields.

The electrochemical reductive cyclization of 1,3-dihalides has been proved to be useful for the preparation of cyclopropanes, bicyclobutanes, or spiropentanes.[1,2] The electroreductive cyclization of 1,4-dihalides has also been reported to give cyclobutane rings.[1] The preparation of higher-membered cycloalkanes by the electrochemical reduction of α,ω-dihalides, however, was not successful until we found that the electroreductive cyclization of α,ω-dibromides carrying alkoxycarbonyl groups at their terminal carbons afforded three- to seven-membered cycloalkanes.[3] We have also reported that ten-, twelve-, or fourteen-membered (*E,E*)- and (*Z,Z*)-1,5-cycloalkadienes can be prepared by the electroreductive cyclization of allylic α,ω-dibromides.[4] The preparation of substituted cyclopentanes by similar electroreductive cyclization has recently been reported.[5]

In this paper we report on the results concerning the electrochemical cyclization of α,ω-dibromides carrying alkoxycarbonyl groups at their terminal carbons. The use of a copper metal as an anode in a one-compartment cell was found to be of importance in this cyclization although the cyclization itself proceeds via reductive pathways. By using a copper anode instead of a platinum anode, much higher yields of three- to six-membered cycloalkanes could be obtained. The present work was carried out as part of our efforts to find effective carbon-carbon bond forming reactions by making use of reactive metal anodes.[6—9]

Results and Discussion

We previously reported that the electrochemical reduction of methallyl bromide gave 2,5-dimethyl-1,5-hexadiene in quantitative yield when electrolysis was carried out in the presence of one molar equivalent of sodium iodide while using a copper anode.[6] We found that this electrolysis using a reactive metal anode is also effective for the electrochemical cyclization of dimethyl α,α′-dibromoalkanedioates. The results of electrochemical cyclization of dimethyl 2,6-dibromoheptanedioate (**1c**) under various conditions are summarized in Table 1. Thus, the electrolysis of **1c** using a copper anode instead of a platinum anode gave cyclization product **2c** in 67% yield, while cyclization using a platinum anode gave only 48% yield of **2c**. We found that the addition of two molar equivalents of sodium iodide in this cyclization enhanced the yield to 85%.

Table 1. Electrochemical Cyclization of Dimethyl 2,6-Dibromoheptanedioate (**1c**) under Various Conditions[a]

Entry	Cathode	Anode	Additive	Product (**2c**)	
				Yield/%[b]	trans : cis
1	Pt	Pt	—	48	73 : 27
2	Pt	Pt	2 equiv NaI	24	56 : 44
3	Pt	Cu[c]	—	67	75 : 25
4	Pt	Cu[d]	2 equiv NaI	85	65 : 35
5	Pt	Cu–Pt[e]	—	71	72 : 28
6	Pt	Cu–Pt[e]	2 equiv NaI	47	72 : 28

a) Carried out according to the procedure described in the Experimental Section. b) GLC yield. c) A copper anode dissolved: 2.6 mol/mol of **1c**. d) A copper anode dissolved: 3.6 mol/mol of **1c**. e) A copper-modified platinum anode was used. The cathode and anode were alternated at 10-min intervals (0.5 Faraday/mol of **1c**). In total, an electricity of 5 Faradays per mol of **1c** was passed.

Copper equivalent to 2.6—3.6 mol per mol of **1c** was found to be dissolved into the electrolytic solution during the electrolysis using a copper anode (Table 1, Entries 3 and 4). This loss of the copper anode can be appreciably reduced by the following new procedure using a copper-modified platinum anode. This method requires only 0.64 molar equivalent of copper dissolution for the modification of the platinum anode. Furthermore, the modified copper can be recycled between the cathode and anode by alternating their polarities at constant intervals during the electrolysis. The electrolysis of **1c** by using a platinum cathode and a copper-modified platinum anode, and by alternating the polarities at 0.5 Faraday intervals gave **2c** in 71% yield along with 20% of dimethyl heptanedioate (Entry 5).

The electrolysis of dimethyl α,α′-dibromoalkanedioates (**1a—d**) using a platinum cathode and a copper anode in the presence of two molar equivalents of sodium iodide gave the corresponding dimethyl 1,2-cycloalkanedicarboxylates (**2a—d**) (Scheme 1). Table 2 summarizes the yields and isomer ratios of the cyclization products. Dimethyl esters of 1,2-cyclopropane-, cyclopentane-, and cyclohexanedicarboxylates (**2a**, **2c**, and **2d**) were obtained in isolated yields more than 70%. The formation of the four-membered ring was found to be less efficient.

The role of the sodium iodide would be to act as a nucleophile in transforming the starting α-bromo esters into the corresponding iodides, which are more reactive than the starting bromides. It has, in fact, been proved that 33% of the carbon–bromine bonds of **1d** are converted into carbon–iodine bonds when **1d** is stirred for

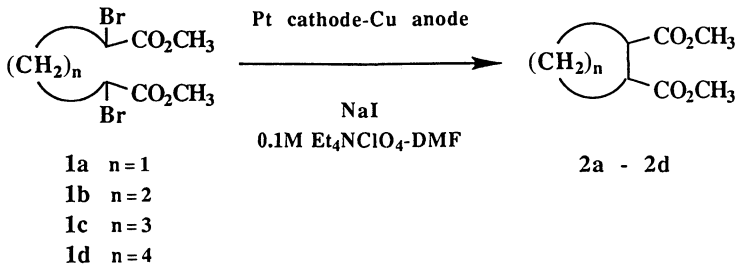

1a n=1
1b n=2
1c n=3
1d n=4

2a - 2d

Scheme 1.

Table 2. Electrochemical Cyclization of Dimethyl α,α'-Dibromoalkanedioates[a]

Dibromide	n	Product	Yield[b] %	trans : cis
1a	1	**2a**	75 (83)	70 : 30
1a[c]	1	**2a**	— (65)	63 : 37
1b	2	**2b**	30 (58)	70 : 30
1c	3	**2c**	71 (85)	65 : 35
1c[c]	3	**2c**	60 (71)	72 : 28
1d	4	**2d**	77 (86)	36 : 64

a) Carried out according to the procedure described in the Experimental Section. b) Isolated yields. GLC yields are shown in the parentheses. c) Electrolysis was carried out using a platinum cathode and a copper-modified platinum anode; the cathode and anode were alternated at 10-min intervals (0.5 Faraday/mol of **1a**—**d**).

30 min at room temperature in the presence of two molar equivalents of sodium iodide.

In the electrochemical cyclization of **1d**, small amounts of dimethyl octanedioate, dimethyl 2-bromooctanedioate, and dimethyl 2-iodooctanedioate were obtained as by-products along with the major product **2d**. This result indicates that the formation of the observed cycloalkanes (**2**) involves a stabilized carbanion generated by a two-electron reduction of one of the carbon–bromine or the carbon–iodine bonds of the starting dihalides (**1**), followed by an intramolecular nucleophilic displacement of the halogen atom.

It is likely that some organocopper species formed by the electrochemical reaction of organic halides with the copper anode[10] are precursors in the present cyclization or that the copper anode participates in the reaction by anodic dissolution,[9] which effectively captures the halide ions generated by the electrochemical reduction of **1**.

Experimental

N,N-Dimethylforamide (DMF) was dried over molecular sieve 4A and distilled over phosphorus pentaoxide under reduced pressure. Spectral measurements and quantitative GLC analyses were carried out using our standard methods.[4]

Preparation of Dibromo Diesters (1a—d). Starting dimethyl α,α'-dibromoalkanedioates (**1a—d**) were prepared in 70—90% yield from the corresponding alkanedioic acids by the method of Vogel[11] and Shreiner.[12] **1a**: Bp 110—113 °C (0.9 mmHg, 1 mmHg=133.322 Pa); **1b**: Mp 75—77 °C; **1c**: Bp 132—135 °C (0.7 mmHg); **1d**: Bp 149 °C (0.6 mmHg).

General Procedure for Electrolysis. A one-compartment cell (32 mm dia.) was used for the electrolysis.[4] A mixture of dibromides **1a—d** (1.5 mmol) and sodium iodide (3 mmol) in 30 ml of DMF solution containing 0.1 M (1 M=1 mol dm^{-3}) tetrabutylammonium perchlorate (TBAP) was electrolyzed under a nitrogen atmosphere at a constant current of 1 A dm^{-2} using a platinum cathode and a copper anode (0.3×0.4 dm^2). The electricity passed was 5 Faradays per mol of the dibromide.

The copper-modified platinum electrode was easily prepared by the electrolysis of a DMF solution containing 0.1 M TBAP using a platinum cathode and a copper anode. When an electricity of 1 Faraday per mol of the dibromide was passed through the solution, 0.64 molar equivalent of copper were dissolved from the copper anode.

The usual work-up of the electrolyzed solution gave a product mixture which was subjected to preparative TLC (silica gel; benzene–diethyl ether 4 : 1) to give pure products.

Dimethy *trans*-1,2-Cyclopropanedicarboxylate (*trans*-2a): n_D^{25} 1.4438 (lit,[13] n_D^{26} 1.4523); IR (neat) 1736, 1170, 1020 cm^{-1}; ^{1}H NMR ($CDCl_3$) δ=1.45 (m, 2H, J=5.9, 7.3, and 8.8 Hz), 2.18 (m, 2H, J=5.9 and 8.8 Hz), 3.71 (s, 6H); mass spectrum m/z 158 (M^+, 2), 157 (19), 127 (100), 126 (55), 99 (58), 98 (82), 59 (65), 39 (46). Anal. Calcd for $C_7H_{10}O_4$: M, 158.0579. Found: m/z 158.0561.

Dimethyl *cis*-1,2-Cyclopropanedicarboxylate (*cis*-2a): n_D^{25} 1.4455 (lit,[13] n_D^{27} 1.4434); IR (neat) 1735, 1173, 1020 cm^{-1}; ^{1}H NMR ($CDCl_3$) δ=1.26 (dt, 1H, J=4.8 and 8.4 Hz), 1.69 (dt, 1H, J=4.8 and 6.6 Hz), 2.07 (dd, 2H, J=6.6 and 8.4 Hz), 3.70 (s, 6H); mass spectrum m/z 158 (M^+, 1), 157 (3), 127 (100), 126 (16), 99 (33), 98 (28), 59 (22), 39 (13). Anal. Calcd for $C_7H_{10}O_4$: M, 158.0579. Found: m/z 158.0592.

Dimethyl *trans*-1,2-Cyclobutanedicarboxylate (*trans*-2b): n_D^{25} 1.4422 (lit,[13] n_D^{25} 1.4430); IR (neat) 1735, 1170 cm^{-1}; ^{1}H NMR ($CDCl_3$) δ=2.18 (m, 4H), 3.42 (m, 2H), 3.69 (s, 6H); mass spectrum m/z 172 (M^+, 3), 171 (9), 141 (55), 140 (43), 113 (77), 81 (51), 71 (49), 59 (100), 53 (68). Anal. Calcd for $C_8H_{12}O_4$: M, 172.0736. Found: m/z 172.0725.

Dimethyl *cis*-1,2-Cyclobutanedicarboxylate (*cis*-2b): n_D^{25} 1.4445 (lit,[13] n_D^{27} 1.4453); IR (neat) 1737, 1174 cm^{-1}; ^{1}H NMR ($CDCl_3$) δ=2.27 (m, 4H), 3.41 (m, 2H), 3.68 (s, 6H); mass spectrum m/z 141 (50), 140 (26), 113 (100), 81 (62), 71 (40), 59 (47), 55 (71), 53 (69).

Dimethyl *trans*-1,2-Cyclopentanedicarboxylate (*trans*-2c): n_D^{25} 1.4501 (lit,[13] n_D^{25} 1.4482); IR (neat) 1736, 1200, 1174 cm^{-1}; ^{1}H NMR ($CDCl_3$) δ=1.7—1.9 (m, 4H), 2.0—2.15 (m, 2H), 3.13 (m, 2H, J=2.2, 6.2, and 7.7 Hz), 3.70 (s, 6H); mass spectrum m/z 186 (M^+, 1), 155 (40), 154 (31), 126 (76), 113 (29), 95 (54), 67 (100). Anal. Calcd for $C_9H_{14}O_4$: M, 186.0892. Found: m/z 186.0894. ^{1}H NMR spectrum of ***trans*-2c** was identical to that reported previously.[14]

Dimethyl *cis*-1,2-Cyclopentanedicarboxylate (*cis*-2c): n_D^{25} 1.4530 (lit,[13] n_D^{27} 1.4512); IR (neat) 1735, 1195, 1170 cm^{-1}; ^{1}H NMR ($CDCl_3$) δ=1.8—2.1 (m, 6H), 3.05 (m, 2H, J=2.2, 5.1, and 7.3 Hz), 3.66 (s, 6H); mass spectrum m/z 186 (M^+, 0.4), 155 (46), 154 (32), 126 (48), 113 (45), 95 (41), 67 (100). Anal. Calcd for $C_9H_{14}O_4$: M, 186.0892. Found: m/z

186.0886. ^{1}H NMR spectrum of ***cis*-2c** was identical to that reported previously.[14,15]

Dimethyl *trans*-1,2-Cyclohexanedicarboxylate (*trans*-2d): n_D^{25} 1.4512 (lit,[13] n_D^{25} 1.4518); IR (neat) 1735, 1194, 1170, 1044 cm^{-1}; ^{1}H NMR ($CDCl_3$) δ=1.32 (m, 4H), 1.79 (m, 2H), 2.06 (m, 2H), 2.62 (m, 2H, J=3.0 and 11.4 Hz), 3.67 (s, 6H); mass spectrum m/z 200 (M^+, 0.3), 169 (30), 168 (36), 140 (51), 109 (36), 108 (26), 81 (100). Anal. Calcd for $C_{10}H_{16}O_4$: M, 200.1049. Found: m/z 200.1040.

Dimethyl *cis*-1,2-Cyclohexanedicarboxylate (*cis*-2d): n_D^{25} 1.4559 (lit,[13] n_D^{25} 1.4578); IR (neat) 1734, 1173, 1131, 1038 cm^{-1}; ^{1}H NMR ($CDCl_3$) δ=1.46 (m, 4H), 1.77 (m, 2H), 1.95—2.1 (m, 2H), 2.83 (m, 2H, J=4.0 and 8.8 Hz), 3.68 (s, 6H); mass spectrum m/z 200 (M^+, 0.9), 169 (29), 168 (31), 140 (72), 109 (29), 108 (48), 81 (100), 80 (48). Anal. Calcd for $C_{10}H_{16}O_4$: M, 200.1049. Found: m/z 200.1020. ^{1}H NMR spectrum of ***cis*-2d** was identical to that reported previously.[15]

This work was supported by a Grant-in-Aid for Scientific Research on Priority Areas No. 01607001 from the Ministry of Education, Science and Culture.

References

1) M. R. Rifi, *Org. Synth.*, Coll. Vol. 6, 153 (1988), and references cited therein; K. B. Wiberg and G. A. Epling, *Tetrahedron Lett.*, **1974**, 1119.

2) G. Gerdil, *Helv. Chim. Acta,* **53**, 2100 (1970); A. J. Fry and W. E. Britton *J. Org. Chem.*, **38**, 4016 (1973); Azizullah and J. Grimshaw, *J. Chem. Soc., Perkin Trans. 1,* **1973**, 425; T. Adachi, T. Iwasaki, M. Miyoshi, and I. Inoue, *J. Chem. Soc., Chem. Commun.*, **1977**, 248; M. Mitani, Y. Yamamoto, and K. Koyama, *ibid.*, **1983**, 1446.

3) S. Satoh, M. Itoh, and M. Tokuda, *J. Chem. Soc., Chem. Commun.*, **1978**, 481.

4) M. Tokuda, K. Satoh, and H. Suginome, *Bull. Chem. Soc. Jpn.*, **60**, 2429 (1987).

5) M. Mitani, H. Takeuchi, and K. Koyama, *Chem. Lett.*, **1986**, 2125.

6) M. Tokuda, K. Endate, and H. Suginome, *Chem. Lett.*, **1988**, 945.

7) M. Tokuda, M. Uchida, Y. Katoh, and H. Suginome, *Chem. Lett.*, **1990**, 461.

8) M. Tokuda, S. Satoh, Y. Katoh, and H. Suginome, "Electroorganic Synthesis-Festschrift in Honor of Manuel M. Baizer," ed by R. D. Little and N. Weinberg, Marcel Dekker, New York (1991), pp. 83—90.

9) For review, see: J. Chaussard, J-C. Folest, J-Y. Nedelec, J. Perichon, S. Sibille, and M. Troupel, *Synthesis,* **1990**, 369.

10) D. G. Tuck, *Pure Appl. Chem.*, **51**, 2005 (1979).

11) A. I. Vogel, *J. Chem. Soc.*, **1948**, 644.

12) R. L. Shreiner and R. E. Damschroder, *J. Am. Chem. Soc.*, **60**, 894 (1938).

13) D. S. Seigler and J. L. Bloomfield, *J. Org. Chem.*, **38**, 1375 (1973).

14) D. Wilkening and B. P. Mundy, *Synth. Commun.*, **14**, 227 (1984).

15) D. E. James and J. K. Stille, *J. Am. Chem. Soc.*, **98**, 1810 (1976).

Palladium Catalyzed Stereoselective Hydrodehalogenation of Alkenyl Halides with Tributyltin Hydride

Masahiko TANIGUCHI, Yoshihiro TAKEYAMA, Keigo FUGAMI,
Koichiro OSHIMA,* and Kiitiro UTIMOTO*
Department of Industrial Chemistry, Faculty of Engineering, Kyoto University, Yoshida, Sakyo-ku, Kyoto 606
(Received April 10, 1991)

Synopsis. The reduction of alkenyl halides with tributyltin hydride in the presence of a catalytic amount of tetrakis(triphenylphosphine)palladium has been studied. Alkenyl iodides reacted easily with tributyltin hydride at 25 °C to give the corresponding hydrocarbons stereoselectively. However, the reaction of alkenyl bromides were sluggish at 25 °C and needed heating at 75 °C to complete.

Triethylborane-induced hydrodehalogenation of alkeny halides with tributyltin hydride proceeded non-stereoselectively. For instance, the reduction of (*E*)-1-deuterio-1-iodo-1-dodecene (**1**) or (*Z*)-1-deuterio-1-iodo-1-dodecene with Et_3B–*n*-Bu_3SnH gave a similar isomeric mixture of (*Z*)-1-deuterio-1-dodecene (**2**) and (*E*)-isomer **3** (**2**:**3**=39:61, Scheme 1).[1] Here we report that the reduction of alkenyl iodides with tributyltin hydride in the presence of palladium catalyst proceeds effectively to give the corresponding alkenes with high stereoselectivity.[2]

A number of alkenyl iodides and bromides were reduced with *n*-Bu_3SnH in the presence of $Pd(PPh_3)_4$ catalyst and the results are summarized in Table 1. Whereas (*E*)-1-iodo-1-dodecene reacted easily with *n*-Bu_3SnH at 25 °C to give 1-dodecene in 92% yield after 3 h, (*E*)-1-bromo-1-dodecene was recovered unchanged after treatment with *n*-Bu_3SnH-$Pd(PPh_3)_4$ at 25 °C for 5 h. Heating a benzene solution of (*E*)-1-bromo-1-dodecene, *n*-Bu_3SnH, and $Pd(PPh_3)_4$ at 75 °C for 5 h gave 1-dodecene in 37% yield. The reduction of alkenyl iodides essentially proceeded stereoselectively except for the case of (*E*)-1-deuterio-1-iodo-1-dodecene (**1**). Treatment of **1** (1.0 mmol) with *n*-Bu_3SnH (1.3 mmol) in the presence of $Pd(PPh_3)_4$ (2 mol%) catalyst gave a mixture of (*Z*)-1-deuterio-1-dodecene (**2**) and (*E*)-isomer **3** (**2**:**3**=79:21) in 93% yield. The contamination of (*Z*)-isomer **2** by (*E*)-isomer **3** was attributed to the successive isomerization of (*Z*)-isomer **2**, which was a primary product, by the action of excess *n*-Bu_3SnH under the reaction conditions. In fact, a partial isomerization was observed upon treatment of (*Z*)-1-deuterio-1-dodecene (**2**) with a catalytic amount of *n*-Bu_3SnH and $Pd(PPh_3)_4$. Stirring a benzene solution of **2** (1.0 mmol), *n*-Bu_3SnH (0.2 mmol), and $Pd(PPh_3)_4$ (2 mol%) at 25 °C for 2 h gave a mixture of (*Z*)- and (*E*)-1-deuterio-1-dodecene (**2**:**3**=73:27). The contamination of (*Z*)-isomer **2** by (*E*)-isomer **3** was suppressed by slow addition of an equimolar amount of *n*-Bu_3SnH (1.0 mmol per 1.0 mmol of **1**) to a benzene solution of **1** and Pd catalyst with syringe drive over 1 h (Scheme 2).

As well as (*E*)-1-iodo-1-dodecene, trisubstituted alkenyl iodide such as (*E*)-1-iodo-1-trimethylsilyl-1-dodecene and (*E*)-6-iodo-6-dodecene were easily reduced with *n*-Bu_3SnH–$Pd(PPh_3)_4$ system (Entries 4, 6, 8, and 9 in Table 1). However, (*Z*)-alkenyl iodides such as (*Z*)-1-iodo-1-dodecene and (*Z*)-6-iodo-6-dodecene reacted more slowly than the corresponding (*E*)-iodides because of its steric hindrance. The reaction of (*Z*)-1-iodo-1-dodecene or (*Z*)-6-iodo-6-dodecene took 5 h at 25 °C or 75 °C to complete (Entries 2 or 7 in Table 1).

The method was successfully applied to the reduction of aryl iodides[3] as shown below (Scheme 3). The reduction of 1-iodonaphthalene with *n*-Bu_3SnH in the presence of Pd catalyst proceeded easily at 25 °C. In contrast, the reaction of 1-bromonaphthalene was sluggish at 25 °C. Heating a benzene solution of 1-bromonaphthalene at 75 °C for 5 h gave naphthalene in 72% yield along with recovered 1-bromonaphthalene (11%). Treatment of 1-iodo-2-(3-methyl-3-butenyl)-benzene (**4**) with *n*-Bu_3SnH–$Pd(PPh_3)_4$ gave (3-methyl-3-butenyl)benzene (**5**) in 73% yield. The result showed sharp contrast to the radical reduction of **4** with Et_3B–*n*-Bu_3SnH system. The latter system gave a mixture of 1,1-dimethylindan (18%), 2-methyl-1,2,3,4-tetrahydronaphthalene (33%) and **5** (6%).[1]

We assume the following reaction mechanism: (1)

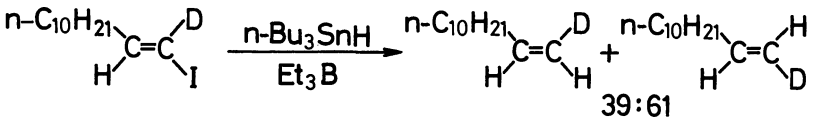

1 **2** **3**

Scheme 1.

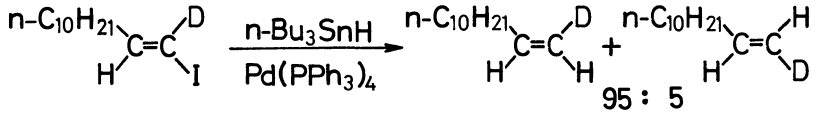

1 **2** **3**

Scheme 2.

Table 1. Reduction of Alkenyl Halides with n-Bu_3SnH–$Pd(PPh_3)_4$

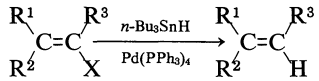

Entry	Alkenyl halide	Reaction condition		Product yield/% (Z:E)
		Temp/°C	Time/h	
1	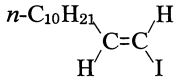	25	3	92
2	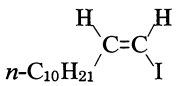	25	5	82
3	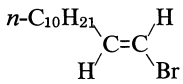	75	5	37
4	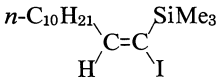	25	3	67 (95:5)
5	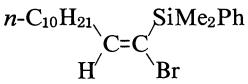	75	5	35 (5:95)
6	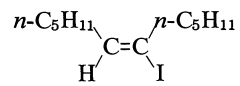	25	1	89 (94:6)
7	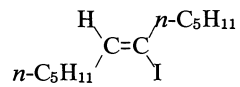	75	5	90 (0:100)
8	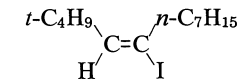	25	3	71 (100:0)
9	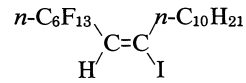	25	3	97 (100:0)
10	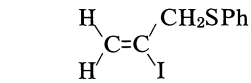	25	1	82

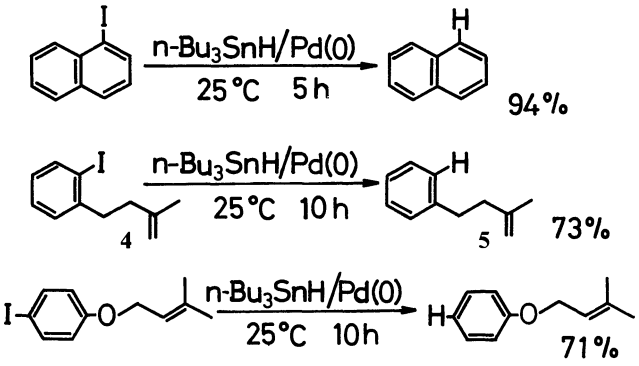

Scheme 3.

Oxidative addition of alkenyl iodides to palladium, (2) reaction of the resulting alkenylpalladium iodides with tributyltin hydride to provide alkenylpalladium hydrides,[4] and (3) reductive elimination from the palladium compounds to give the corresponding alkenes and regenerate the palladium(0) complex.

Experimental

Distillation of the products was performed by use of Kugelrohr (Büchi) and boiling points are indicated by an air-bath temperature without correction. ^{1}HNMR and ^{13}CNMR spectra were taken on a Varian XL-200 spectrometer and $CDCl_3$ was used as solvent unless otherwise noted. Chemical shifts are given in δ with tetramethylsilane as an internal standard. IR spectra were determined on a JASCO IR-810 spectrometer. The analyses were carried out at the Elemental Analysis Center of Kyoto University. Purification of products was performed by silica-gel (Wakogel C-100) column chromatography.

Preparation of Alkenyl Iodides. (*E*)-1-Iodo-1-dodecene and (*E*)-1-bromo-1-dodecene were prepared following the reported procedure.[5] (*E*)-1-Deuterio-1-iodo-1-dodecene was prepared by hydroalumination of 1-deuterio-1-dodecyne with i-Bu_2AlH followed by iodination.[1] (*E*)-1-Iodo-1-trimethylsilyl-1-dodecene and (*E*)-1-bromo-1-dimethylphenylsilyl-1-dodecene were prepared according to the literature.[6] (*E*)-6-Iodo-6-dodecene and (*Z*)-6-iodo-6-dodecene were prepared from 6-dodecyne following the reported procedure for the preparation of (*E*)-3-iodo-3-hexene[7] and (*Z*)-3-iodo-3-

hexene.[8] Hydroalumination of 2,2-dimethyl-3-undecyne with *i*-Bu_2AlH followed by iodination gave a mixture of (*E*)-2,2-dimethyl-4-iodo-3-undecene and (*E*)-2,2-dimethyl-3-iodo-3-undecene (2:1). The former was purified by preparative glpc (OV-1 2% on Chromosorb W 60—80 mesh, 2 m, 150 °C, t_r=6.72 min ((*E*)-2,2-dimethyl-4-iodo-3-undecene) and t_r=8.64 min ((*E*)-2,2-dimethyl-3-iodo-3-undecene). (*E*)-1,1,1,2,2,3,3,4,4,5,5,6,6-Tridecafluoro-8-iodo-7-octadecene was prepared by the reaction of 1-dodecyne with *n*-$C_6F_{13}I$ in the presence of triethylborane.[9]

(*E*)-6-Iodo-6-dodecene: Bp 60—65 °C (bath temp, 1 Torr, 1 Torr=133.322 Pa); IR (neat) 2954, 2924, 2854, 1729, 1630, 1466, 1459, 1379, 1269, 1195, 1136, 1108, 727 cm^{-1}; ^1H NMR ($CDCl_3$) δ=0.89 (t, *J*=6.7 Hz, 3H), 0.90 (t, *J*=6.5 Hz, 3H), 1.20—1.69 (m, 12H), 2.02 (td, *J*=7.3, 7.2 Hz, 2H), 2.36 (t, *J*=7.3 Hz, 2H), 6.18 (t, *J*=7.6 Hz, 1H); ^{13}C NMR ($CDCl_3$) δ=14.01, 22.45, 22.52, 28.80, 28.87, 30.55, 30.84, 31.28, 38.37, 103.6, 141.4. Found: C, 48.85; H, 8.06%. Calcd for $C_{12}H_{23}I$: C, 48.99; H, 7.88%.

(*Z*)-6-Iodo-6-dodecene: Bp 60—65 °C (bath temp, 1 Torr); IR (neat) 2954, 2924, 2854, 1729, 1643, 1465, 1459, 1429, 1378, 1274, 1134, 726 cm^{-1}; ^1H NMR ($CDCl_3$) δ=0.90 (t, *J*=6.8 Hz, 6H), 1.20—1.69 (m, 12H), 2.10 (td, *J*=6.8, 6.7 Hz, 2H), 2.45 (t, *J*=7.6 Hz, 2H), 5.46 (t, *J*=6.7 Hz, 1H); ^{13}C NMR ($CDCl_3$) δ=14.04, 22.42, 22.55, 28.10, 29.03, 30.37, 31.35, 36.35, 45.09, 109.8, 134.8. Found: C, 48.88; H, 8.00%. Calcd for $C_{12}H_{23}I$: C, 48.99; H, 7.88%.

(*E*)-2,2-Dimethyl-4-iodo-3-undecene: Bp 75—80 °C (bath temp, 1 Torr); IR (neat) 2954, 2924, 2854, 1730, 1618, 1465, 1365, 1243, 1202, 1114 cm^{-1}; ^1H NMR ($CDCl_3$) δ=0.89 (t, *J*=7.0 Hz, 3H), 1.12 (s, 9H), 1.25—1.45 (m, 8H), 1.50—1.70 (m, 2H), 2.44 (t, *J*=7.6 Hz, 2H), 6.24 (s, 1H); ^{13}C NMR ($CDCl_3$) δ=14.10, 22.64, 23.74, 29.17, 30.32, 30.93, 31.78, 36.84, 40.52, 106.3, 150.7. Found: C, 50.84; H, 8.35%. Calcd for $C_{13}H_{25}I$: C, 50.66; H, 8.17%.

(*E*)-1,1,1,2,2,3,3,4,4,5,5,6,6-Tridecafluoro-8-iodo-7-octadecene: Bp 105—110 °C (bath temp, 1 Torr); IR (neat) 2926, 2854, 1636, 1466, 1365, 1240, 1204, 1146, 1067 cm^{-1}; ^1H NMR ($CDCl_3$) δ=0.88 (t, *J*=5.8 Hz, 3H), 1.15—1.40 (m, 14H), 1.40—1.70 (m, 2H), 2.63 (t, *J*=7.3 Hz, 2H), 6.32 (t, *J*=14.4 Hz, 1H); ^{13}C NMR ($CDCl_3$) δ=14.05, 22.71, 28.47, 29.34, 29.48, 29.59, 30.10, 31.94, 41.18, 123.1 (t, *J*=6.5 Hz), 126.5 (t, *J*=24.0 Hz). Found: C, 35.45; H, 3.87%. Calcd for $C_{18}H_{22}F_{13}I$: C, 35.31; H, 3.62%.

2-Iodo-3-phenylthio-1-propene. 3-Bromo-2-iodo-1-propene[10] (2.47 g, 10 mmol) was added to a methanol solution of sodium benzenethiolate, generated from benzenethiol (1.1 g, 10 mmol) and sodium (0.23 g, 10 mg-atom) in methanol under argon atmosphere. After stirring for 1.5 h, the resulting mixture was poured into water. Extractive workup followed by silica-gel column chromatography gave the title compound (1.5 g) in 65% yield: Bp 103—108 °C (bath temp, 1 Torr); IR (neat) 3056, 2954, 2924, 1728, 1619, 1609, 1583, 1480, 1439, 1400, 1273, 1226, 1191, 1088, 1025, 900, 737, 688 cm^{-1}; ^1H NMR ($CDCl_3$) δ=3.83 (s, 2H), 5.73 (bs, 1H), 6.57 (bs, 1H), 7.3—7.5 (m, 5H); ^{13}C NMR ($CDCl_3$) δ=48.96, 105.8, 127.0, 127.7, 128.9, 130.7, 134.6. Found: C, 39.01; H, 3.10%. Calcd for C_9H_9IS: C, 39.15; H, 3.29%.

General Procedure for the Reduction of Alkenyl Iodides and Aryl Iodides. The reduction of (*E*)-1-iodo-1-dodecene was representative. Tributyltin hydride (0.38 g, 1.3 mmol) was added dropwise by syringe drive over 20 min to a solution of (*E*)-1-iodo-1-dodecene (0.29 g, 1.0 mmol) and $Pd(PPh_3)_4$ (23 mg, 2 mol%) at 25 °C under argon atmosphere. After completion of the addition, stirring was continued for another 1 h. The resulting mixture was poured into water and extracted with ethyl acetate (20 ml×3). Combined organic layers were dried over Na_2SO_4 and concentrated in vacuo to give a colorless oil which was submitted to silica-gel column chromatography using hexane as eluant to give 1-dodecene (0.15 g) in 92% yield. In the case of the reduction of (*Z*)-iodoalkenes, an addition of benzene solution of *n*-Bu_3SnH was achieved over 2 h by syringe drive.

Isomerization of (*Z*)-1-Deuterio-1-dodecene. Tributyltin hydride (58 mg, 0.2 mmol) was added to a solution of (*Z*)-1-deuterio-1-dodecene (**2**, 0.17 g, 1.0 mmol) and $Pd(PPh_3)_4$ (23 mg, 2 mol%) at 25 °C under argon atmosphere. After stirring for 2 h, the reaction mixture was poured into water and extracted with ethyl acetate. The examination of the crude product by ^1H NMR showed that (*Z*)-isomer **2** was partially isomerized into (*E*)-isomer **3** (**2**:**3**=73:27).

(*Z*)-2,2-Dimethyl-3-undecene: Bp 88—90 °C (bath temp, 13 Torr); IR (neat) 2954, 2922, 1729, 1466, 1363, 1273 cm^{-1}; ^1H NMR ($CDCl_3$) δ=0.88 (t, *J*=6.7 Hz, 3H), 1.10 (s, 9H), 1.20—1.48 (m,10H), 2.11—2.21 (dt, *J*=7.0, 7.0 Hz, 2H), 5.15 (dt, *J*=12.0, 7.0 Hz, 1H), 5.31 (d, *J*=12.0 Hz, 1H); ^{13}C NMR ($CDCl_3$) δ=14.12, 22.67, 28.37, 29.26, 29.37, 30.32, 31.16, 31.86, 33.07, 129.1, 139.5. Found: C, 85.61; H, 14.54%. Calcd for $C_{13}H_{26}$: C, 85.63; H, 14.37%.

(*Z*)-1,1,1,2,2,3,3,4,4,5,5,6,6-Tridecafluoro-7-octadecene: Bp 85—90 °C (bath temp, 1 Torr); IR (neat) 2926, 2856, 1729, 1664, 1466, 1364, 1240, 1203, 1146, 1121, 1102, 1067, 842, 810, 766, 743, 733, 718, 703 cm^{-1}; ^1H NMR ($CDCl_3$) δ=0.88 (t, *J*=6.2 Hz, 3H), 1.20—1.60 (m, 16H), 2.20—2.46 (m, 2H), 5.38—5.68 (m, 1H), 6.05—6.28 (m, 1H); ^{13}C NMR ($CDCl_3$) δ=14.08, 22.69, 28.57, 29.05, 29.13, 29.34, 29.53, 31.90, 115.9 (t, *J*=23.4 Hz), 145.7 (t, *J*=5.9 Hz). Found: C, 44.74; H, 4.66%. Calcd for $C_{18}H_{23}F_{13}$: C, 44.45; H, 4.77%.

References

1) K. Miura, Y. Ichinose, K. Nozaki, K. Fugami, K. Oshima, and K. Utimoto, *Bull. Chem. Soc. Jpn.*, **62**, 143 (1989).

2) Reduction of alkenyl iodides with *i*-PrMgCl in the presence of a catalytic amount of $MnCl_2$ has been reported. G. Cahiez, D. Bernard, and J. F. Normant, *J. Organomet. Chem.*, **113**, 107 (1976).

3) There are a number of methods for the reduction of aryl halides using transition metals. $NiCl_2$-Zn-H_2O: J. Yamashita, Y. Inoue, T. Kondo, and H. Hashimoto, *Bull. Chem. Soc. Jpn.*, **58**, 2709 (1985). Pd/C-Et_3N^+H HCO_2^-: N. A. Cortese and R. F. Heck, *J. Org. Chem.*, **42**, 3491 (1977). $Pd(PPh_3)_4$-NaOMe: A. Zask and P. Helquist, *ibid.*, **43**, 1619 (1978). $Fe(CO)_5$: S. J. Nelson, G. Detre, and M. Tanabe, *Tetrahedron Lett.*, **1973**, 447.

4) W. J. Scott, G. T. Crisp, and J. K. Stille, *J. Am. Chem. Soc.*, **106**, 4630 (1984); V. P. Baillargeon and J. K. Stille, *ibid.*, **105**, 7175 (1983).

5) G. Zweifel and C. C. Whitney, *J. Am. Chem. Soc.*, **89**, 2753 (1967).

6) J. J. Eisch and G. A. Damasevitz, *J. Org. Chem.*, **41**, 2214 (1976); K. Uchida, K. Utimoto, and H. Nozaki, *ibid.*, **41**, 2215 (1976).

7) G. Zweifel and R. B. Steele, *J. Am. Chem. Soc.*, **89**, 2754 (1967).

8) G. Zweifel and R. B. Steele, *J. Am. Chem. Soc.*, **89**, 5085 (1967).

9) Y. Takeyama, Y. Ichinose, K. Oshima, and K. Utimoto, *Tetrahedron Lett.*, **30**, 3159 (1989).

10) S. Hara, H. Dojo, S. Takinami, and A. Suzuki, *Tetrahedron Lett.*, **24**, 731 (1983).

Selective Halofluorination Reaction Mediated by Hexafluoropropene-Diethylamine Complex and *N*-Haloimides

Makoto SHIMIZU, Masaya OKAMURA, and Tamotsu FUJISAWA*
Department of Chemistry for Materials, Mie University, Tsu, Mie 514
(Received April 15, 1991)

Synopsis. Olefins were halofluorinated with hexafluoropropene–diethylamine and *N*-haloimides in a highly regio- and stereoselective manner.

Growing interests in organofluorine chemistry prompt us to develop new methodologies for the introduction of a fluorine atom into molecules in highly selective ways.[1] For the introduction of a fluorine atom into molecules, halofluorination of olefins is one of the most straightforward ways.[2] However, there still remain several important problems associated mainly with selectivities of the reaction, the tedious experimental procedures, and the need for the use of special reaction vessels. A non-trivial problem often accompanies halofluorinations, which concerns the use of hydrogen fluoride-a readily available and inexpensive fluoride ion source but the handling holds certain problems,[2a] and in situ generation of a limited amount of hydrogen fluoride in the reaction medium appears to circumvent some of the problems associated with the conventional halofluorination reactions.

We have now found that the use of hexafluoropropene–diethylamine complex (HFP–DA)[3] and *N*-haloimides enables us to carry out halofluorination reactions quite readily with high regio-and stereoselectivities in an ordinary glassware vessel (Scheme 1). Initial survey of the hydrogen fluoride sources involves the use of acid fluorides (CH_3COF or CH_3SO_2F)–water or metal fluorides (CsF, KF, CoF_2, CoF_3, SbF_3 or SbF_5)–water, which resulted in utter failure. However, the combined use of HFP–DA complex and water revealed a ready accessibility of a limited amount of hydrogen fluoride,

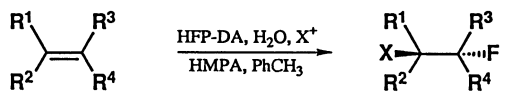

Scheme 1.

Table 1. Halofluorination of 1-Dodecene[a]

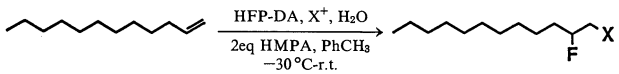

Entry	X^+ source (equiv)	H_2O (equiv)	Yield[b]/%
1	DBH (1.5)[c]	1.5	41
2	DBH (1.5)	1.5	51
3	DBH (1.7)	1.7	58
4	DBH (2.5)	2.5	64
5	DBH (2.5)	0	17
6	DCH (1.7)	1.7	44
7	NIS (1.7)	1.7	61
8	NIS (2.5)	2.5	78

a) The reaction was carried out at −30 °C—room temp for 24 h. b) Isolated yield. c) In 1,4-dioxane.

and the halofluorination of 1- dodecene was successfully performed (see Table 1).

As shown in Table 1, the best result was obtained when the reaction was carried out with HFP–DA (2.0 equiv), *N*-iodosuccinimide (NIS, 2.0—2.5 equiv) or 1,3-dibromo-5,5-dimethylhydantoin (DBH, 2,0—2.5 equiv), H_2O (2.5 equiv) and hexamethylphosphoric triamide (HMPA, 2.0 equiv) in toluene at −30 °C to room temperature, whereas the reaction with 1,3-dichloro-5,5- dimethylhydantoin (DCH) met with moderate success presumably due to the less stable nature of the bridged halonium ion intermediate relative to its iodo or bromo counterpart (see Entries 3, 6, and 7). Under the optimum reaction conditions found for 1 - dodecene a variety of olefins were converted into the corresponding halofluorides in good to excellent yields, and Table 2 shows the results.

Aromatic, aliphatic, and alicyclic olefins all underwent halofluorination with high regio- and stereoselectivities, where iodofluorination in general showed better yield than the bromo analogue. The fluorine atom was always introduced into the more substituted carbons and the trans orientation of fluorine to the other halogen was usually observed. In particular bromofluorination of (*Z*)-1-phenyl-1-propene is noteworthy; (1*R**, 2*R**)-bromofluoride **2** was formed predominantly in the present case (Entry 15), showing a distinct contrast to the methods reported previously[2l] in which (1*R**, 2*S**)-isomer **1** is obtained as a sole product. Close examination of the present halofluorination reveals that the reaction proceeds most probably via generation of a limited amount of hydrogen fluoride from HFP–DA complex and H_2O followed by formation of XF species with NIS or DBH as the following equation shows.

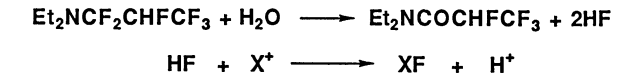

Application of the present halofluorination reaction to the synthesis of a biologically interesting molecule was readily performed via iodofluorination followed by reduction with *n*-Bu_3SnH in good overall yield. Scheme 2 shows the preparation of a fluorine analogue

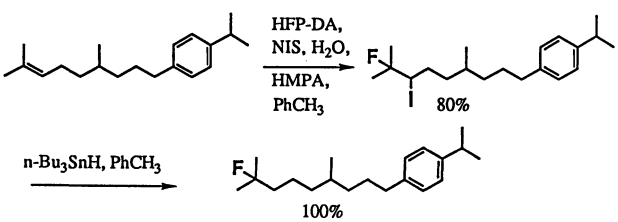

Scheme 2.

Table 2. Halofluorination of Olefins

Entry	Olefin	X^+ source	Product	Yield[a]/%
9		DBH	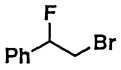	44
10		NIS	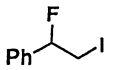	45
11		DBH	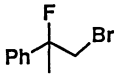	70
12		NIS	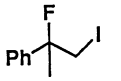	87
13	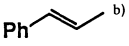 [b]		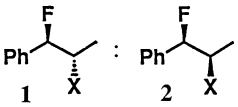 1 2	
		DBH	X=Br (94:6)	63
14		NIS	X=I (100:0)	93
15	[c]	DBH	X=Br (17:83)	46
16		NIS	X=I (27:73)	38
17	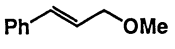	DBH	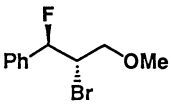	78
18	[d]	DBH	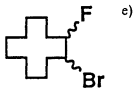 [e]	46
19		NIS	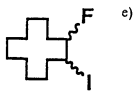 [e]	88
20		NIS	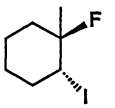	70

a) Isolated yield. b) $E:Z=99:1$. c) $E:Z=10:90$. d) A 1:1 mixture of (*E*)- and (*Z*)-isomers. e) A 1:1 mixture of *cis*- and *trans*-isomers.

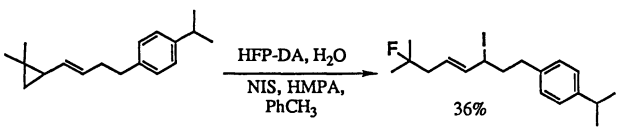

Scheme 3.

of a juvenile hormone MV-678.[4]

Halofluorination reaction exercised in the present study provides a ready procedure for the introduction of fluorine into olefins with high regio- and stereoselectivities under mild conditions using a normal glassware apparatus. With slight modification of the substrate[5] the present halofluorination is further applicable to the synthesis of homologous fluorides, as Scheme 3 illustrates.

Experimental

Infrared spectra of neat liquid film samples (unless otherwise noted) were determined on a JASCO IR-810 spectrometer. ^{1}H NMR spectra were taken on a JEOL JNM-RMX60si spectrometer using tetramethylsilane as an internal standard. ^{19}F NMR spectra were recorded on a Hitachi R-24F spectrometer using $CFCl_3$ as an internal standard. Mass spectra were taken on a Shimadzu QP 1000 spectrometer. Preparative TLC plates were prepared with Merck Kiesel Gel PF_{254}. Column chromatography was carried out with silica gel (Wakogel C-300).

General Procedure for the Halofluorination of Olefins: The following is a typical experimental procedure. In an ordinary glassware vessel to NIS (562 mg, 2.5 mmol) were added toluene (1.5 ml), HFP–DA (0.87 ml, 2.5 mmol), HMPA (0.35 ml, 2.0 mmol), and H_2O (45 ml, 2.5 mmol) successively at −30 °C, and the mixture was stirred at that temperature for 15 min. A solution of 1-dodecene (169 mg, 1.0 mmol) in toluene (1.5 ml) was added and the reaction mixture was allowed to stand at room temperature for 24 h. The normal workup followed by purification by silica-gel column chromatography gave 2-fluoro-1-iodododecane (245 mg, 78%) as a colorless oil. The spectroscopic properties were identical with the reported data.[2d] IR (neat) 2940, 2860, 1470, 1420, 1380, 1195, 995, 800, 730, and 640 cm^{-1}; ^{1}H NMR (CCl_4) δ=0.68—2.20 (21H, m),3.22 (2H, dd, J=6.0, 18.0 Hz), 4.43

(1H, dm, J=48.0 Hz); ^{19}F NMR (CCl_4) δ=−173.0 (m).

1-Bromo-2-fluorododecane:[2d] IR (neat) 2940, 2860, 1475, 1430, 1385, 1020, 830, 730, 695, and 685 cm^{-1}; ^{1}H NMR (CCl_4) δ=0.67—2.10 (21H, m), 3.40 (2H, dd, J=6.0, 18.0 Hz), 4.53(1H, dm, J=48.0 Hz); ^{19}F NMR (CCl_4) δ=−180.0 (m).

2-Bromo-1-fluoro-1-phenylethane:[2i]. IR (neat) 3050, 3020, 2950, 2910, 1450, 1400, 1200, 1170, 1050, 955, 760, 740, 690, and 590 cm^{-1}; ^{1}H NMR (CCl_4) δ=3.65 (2H, dd, J=6.0, 21.0 Hz, a signal at δ=3.37 appears as multiplet), 5.50 (1H, dt, J=6.0, 46.0 Hz), 7.30 (5H, s); ^{19}F NMR (CCl_4) δ=−178.0 (m).

1-Fluoro-2-iodo-1-phenylethane:[2i] IR (neat) 3050, 3020, 2950, 2910, 1450, 1400, 1200, 1170, 1050, 955, 760, 740, 690, and 570 cm^{-1}; ^{1}H NMR (CCl_4) δ=3.40 (2H, dd, J=6.0, 18.0 Hz, a signal at δ=3.27 appears as multiplet), 5.47 (1H, dt, J=6.0, 46.0 Hz), 7.26 (5H, s); ^{19}F NMR (CCl_4) δ=−170.0 (m).

1-Bromo-2-fluoro-2-phenylpropane:[2g] IR (neat) 3060, 3030, 2990, 2930, 1500, 1450, 1380, 1295, 1220, 1180, 1060, 1050, 770, 700, and 595 cm^{-1}; ^{1}H NMR (CCl_4) δ=1.78 (3H, d, J=22.0 Hz), 3.53 (2H, d, J=22.0 Hz, a signal at δ=3.40 appears as doublet, J=2.0 Hz), 7.28 (5H, s); ^{19}F NMR (CCl_4) δ=−151.0 (tq, J=19.0, 19.0 Hz).

1-Iodo-2-fluoro-2-phenylpropane:[2i] IR (neat) 3060, 3020, 2980, 2925, 1450, 1380, 1290, 1200, 1170, 1070, 1050, 1030, 760, 750, and 580 cm^{-1}; ^{1}H NMR (CCl_4) δ=1.82 (3H, d, J=22.0 Hz), 3.50 (2H, d, J=20.0 Hz), 7.33 (5H, s); ^{19}F NMR (CCl_4) δ=−145.0 (tq, J=19.0, 19.0 Hz).

(1*R, 2*S**)-2-Bromo-1-fluoro-1-phenylpropane:**[2l] IR (neat) 3070, 3030, 2980, 2930, 1455, 1380, 1200, 1020, 970, 760, 700, 665, and 580 cm^{-1}; ^{1}H NMR (CCl_4) δ=1.72 (2H, d, J=7.0 Hz), 3.83—4.67 (1H, m), 5.43 (1H, dd, J=6.0, 46.0 Hz), 7.30 (5H, s); ^{19}F NMR (CCl_4) δ=−182.0 (dd, δ=19.0, 47.0 Hz).

(1*R, 2*R**)-2-Bromo-1-fluoro-1-phenylpropane:**[2l] IR (neat) 3070, 3000, 2920, 2850, 1450, 1000, 600, and 540 cm^{-1}; ^{1}H NMR (CCl_4) δ=1.55 (2H, d, J=7.0 Hz), 3.73—4.67 (1H, m), 5.30 (1H, dd, J=6.0, 46.0 Hz), 7.30 (5H, s); ^{19}F NMR (CCl_4) δ=−176.0 (dd, J=19.0, 47.0 Hz).

(1*R, 2*S**)-1-Fluor-2-iodo-1-phenylpropane:**[2l] IR (neat) 3060, 3030, 2970, 2920, 1500, 1450, 1380, 1160, 1150, 1060, 1010, 960, 760, and 700 cm^{-1}; ^{1}H NMR (CCl_4) δ=1.92 (2H, d, J=7.0 Hz), 3.93—4.77 (1H, m), 5.50 (1H, dd, J=6.0, 47.0 Hz), 7.30 (5H, s); ^{19}F NMR (CCl_4) δ=−176.0 (dd, J=19.0, 47.0 Hz).

(1*R, 2*R**)-1-Fluoro-2-iodo-1-pheylpropane:**[2l] IR (neat) 3060, 3020, 2970, 2910, 1500, 1450, and 760 cm^{-1}; ^{1}H NMR (CCl_4) δ=1.83 (2H, d, J=7.0 Hz), 3.87—4.72 (1H, m), 5.22(1H, dd, J=6.0, 46.0 Hz), 7.32 (5H, s); ^{19}F NMR (CCl_4)δ=−169.0 (dd, J=19.0, 47.0 Hz).

(1*R, 2*S**)-2-Bromo-1-fluoro-3-methoxy-1-phenylpropane:**[2l] IR (neat) 3050, 3020, 2980, 2920, 2810, 1460, 1190, 1120, 1010, 960, 760, 700, 590, and 530 cm^{-1}; ^{1}H NMR (CCl_4) δ=3.33 (3H, s), 4.07—4.57 (1H, m), 5.56 (1H, dd, J=6.0, 46.0 Hz), 7.27 (5H, s); ^{19}F NMR (CCl_4) δ=−178.0 (dd, J=18.0, 46.0 Hz) MS m/z (rel intensity in %) 227 (M^+−19, 3), 226 (M^+−20, 3), 184 (24), 182 (27), 166 (12), 147 (23), 135 (94), 115 (60), 109 (100).

1-Bromo-2-fluorocyclododecane:[2g] IR (neat) 2950, 2850, 1470, 1440, and 1000 cm^{-1}; ^{1}H NMR (CCl_4) δ=1.07—2.40 (20H, m), 3.83—5.30 (2H, m); ^{19}F NMR (CCl_4) δ=−183 (m), −186 (m).

2-Fluoro-1-iodocyclododecane:[2g] IR (neat) 3060, 3045, 2980, 2825, 1460, 1210, 1085, 960, 760, and 700, cm^{-1}; ^{1}H NMR (CCl_4)δ=1.07—2.30 (20H, m), 3.63—4.97 (2H, m); ^{19}F NMR (CCl_4) δ=−173 (m), 179 (m).

(1*R, 2*R**)-1-Fluoro-2-iodo-1-methylcyclohexane:**[2h] ^{1}H NMR (CCl_4) 1.20—2.60 (8H, m), 1.52 (3H, d, J=22.0 Hz), 4.10—4.53 (1H, m); ^{19}F NMR (CCl_4) δ=−140.0 (m).

2-Fluoro-9-(*p*-isopropylphenyl)-2,6-dimethylnonane: IR (neat) 3020, 2950, 2850, 2820, 1510, 1460, 1370, 1250, 880, 840, and 760 cm^{-1}; ^{1}H NMR (CCl_4) δ=0.33—2.00 (25H, m), 2.30—3.10 (4H, m), 7.00 (4H, s); ^{19}F NMR (CCl_4) δ=−141 (m); MS m/z (rel intensity in %) 273 (M^+−19, 3), 272(20), 201 (2), 187 (9), 159 (13), 147 (15), 146 (100), 145 (11), 133 (59), 132 (35), 131 (50).

References

1) See for example, M. Hudlichky, *Org. React.*, **35**, 513 (1988); J. T. Welch, *Tetrahedron*, **43**, 3123(1987); C. J. Wang, *Org. React.*, **34**, 319 (1985).

2) a) C. M. Sharts and W. A. Sheppard, *Org.React.*, **21**, 125 (1974), and earlier references cited therein; b) G. A. Olah, J. T. Welch, Y. D. Yashwant, D. Vanker, M. Nojima, J. Kerekles, and J. A. Olah, *J. Org. Chem.*, **44**, 3872 (1979); c) G. Boche and U. Fahremann, *Chem. Ber.*, **114**, 4005 (1981); d) S. Rozen and M. Brand, *J. Org. Chem.*, **50**, 3342 (1985); e) G. E. Hearsley, I. M. Janes, S. R. Stark, and B. L. Robinson, *Tetrahedron Lett.*, **26**, 1811 (1985); f) G. Haufe, G. Alvernhe, and A. Laurent, *Tetrahedron Lett.*, **27**, 4449 (1986); g) G. Alvernhe, A. Laurent, and G. Haufe, *Synthesis*, **1987**,562; h) R. D. Evans and J. H. Schauble, *ibid.*, **1987**, 551; i) A. Gregorcic and M. Zupan, *Bull. Chem. Soc. Jpn.*, **60**, 3083 (1987); j) D. Y. Chi, D. O. Kiesenwetter, and J. A. Kazenellenborgen, *J. Fluorine Chem.*, **31**, 99 (1986); k) T. Ando, D. G. Cork, M. Fujita, T. Kimura, and T. Tatsuno, *Chem. Lett.*, **1988**, 1877; l) M. Shimizu, Y. Nakahara, and H. Yoshioka, *J. Chem. Soc., Chem. Commun.*, **1989**, 1881; m) F. Camps, E. Chamorro, V. Gasol, and A. Guerrero, *J. Org. Chem.*,**54**, 4294 (1989); n) J. Ichihara, K. Funabiki, and T. Hanafusa, *Tetrahedron Lett.*, **31**, 3167 (1990); o) H. Suga, T. Hamatani, Y. Guggisberg, and M. Schlosser, *Tetrahedron*, **46**, 4255 (1990); p) M. Kuroboshi and T. Hiyama, *Synlett*, **1991**, 185.

3) A. Takaoka, H. Iwakiri, and N. Ishikawa, *Bull. Chem. Soc. Jpn.*, **52**, 3377 (1979). HFP–DA is commercially available from Tokyo Kasei Co.

4) Cf. *Chem. Eng. News*, **1982**, 27.

5) S. Kanemoto, M. Shimizu, and H. Yoshioka, *Bull. Chem. Soc. Jpn.*, **62**, 2024 (1989).

Oxidative Cleavage of Chalcones by Electrochemically Generated Superoxide Ion ($O_2^{\cdot-}$)

Manorama SINGH, Krishna Nand SINGH, and Ram Achal MISRA*
Department of Chemistry, Faculty of Science, Banaras Hindu University, Varanasi 221005, India
(Received November 26, 1990)

Synopsis. Various chalcones were efficiently cleaved to carboxylic acid(s), in considerably high yield by the reaction with electrochemically generated superoxide ion ($O_2^{\cdot-}$) at mercury cathode and molecular oxygen.

Superoxide ion ($O_2^{\cdot-}$), which is an anion radical and one of the activated oxygen species, plays important roles in biological systems[1-11] and provides impetus to organic chemists to study its chemical reactivity from synthetic considerations.[12-15] It has been recognized that superoxide ion, depending upon the nature of organic substrate, can act as a base, nucleophile, ligand, radical, or an oxidant.[14-22] The electrochemical generation of $O_2^{\cdot-}$ in aprotic medium, in presence of tetraalkylammonium salt by reducing molecular oxygen, is known since 1965[23] and remains a method of choice for preparing and using in situ generated superoxide ion more satisfactorily than using KO_2–crown ether.[24]

The chemistry of superoxide ion with a wide range of simple organic compounds is very little known and needs further investigations. Recently, we have reported the superoxide-initiated oxidation of some secondary alcohols,[25] primary alcohols,[26] and fragmentation of some tosylhydrazones of carbonyl compounds using electrochemically generated superoxide ion.[27] Reactions of electrogenerated $O_2^{\cdot-}$ with chalcones have not been studied so far. A survey of literature reveals that there exists only one report in which Rosenthal and Frimer[28] have studied the reaction of chalcones with KO_2 in 18-crown-6-ether. The reaction of chalcones with electrogenerated superoxide ion has been reinvestigated from following reasons:

a) The best available sample of KO_2 is only 95% pure and is always contaminated with free bases and other impurities.

b) The KO_2 in reaction medium easily results in other activated oxygen species such as hydroxyl ($OH^{\cdot}$) and peroxyl ($OOH^{\cdot}$) radicals thereby delimiting the interpretation of results.

c) The electrogeneration of superoxide ion affords a stable and pure solution of the species in aprotic medium and gives opportunity for in situ reactions with chalcones.

Experimental

Instruments. Melting points were measured with a Buchii melting point apparatus and are uncorrected. IR spectra were recorded on a Perkin–Elmer 783 grating spectrophotometer. ^{1}H NMR spectra were measured at 90 MHz with

Table 1. Reaction of Electrochemically Generated Superoxide Ion with Chalcones (1—7); Mercury Pool: Cathode, Platinum Disc: Anode. Temp: 25—30 °C

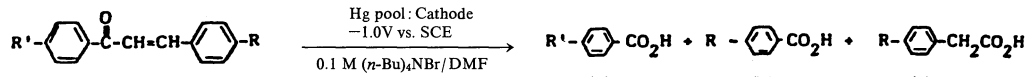

(a) (b) (c)

Entry	Chalcone (1—7; 0.5 g)	Current/mA		Electricity passed	Reaction time	Product (Yield/%)		
		Initial	Final	Coulomb[a]	h	a	b	c
1	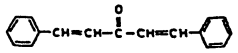	100	10	610	10	$C_6H_5CO_2H$ (95)		
2	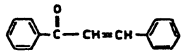	95	05	686	13	$C_6H_5CO_2H$ (75)	$C_6H_5CO_2H$	$C_6H_5CH_2CO_2H$ (5)
3	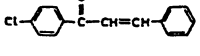	100	20	590	18	$ClC_6H_4CO_2H$ (54)	$C_6H_5CO_2H$ (20)	$C_6H_5CH_2CO_2H$ (7)
4	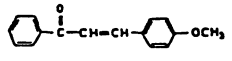	120	10	600	15	$C_6H_5CO_2H$ (65)	$MeOC_6H_4CO_2H$ (14)	$MeOC_6H_4CH_2CO_2H$ (8)
5	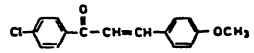	75	10	525	10	$ClC_6H_4CO_2H$ (60)	$C_6H_5CO_2H$ (15)	$MeOC_6H_4CH_2CO_2H$ (6)
6	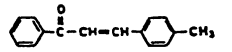	100	15	643	12	$C_6H_5CO_2H$ (64)	$MeC_6H_4CO_2H$ (10)	$MeC_6H_4CH_2CO_2H$ (3)
7	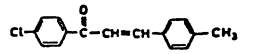	95	15	566	12	$ClC_6H_4CO_2H$ (62)	$C_6H_5CO_2H$ (15)	$MeC_6H_4CH_2CO_2H$ (5)

a) Measured using copper coulometer.

JEOL FT-NMR spectrometer FX-90 Q, chemical shifts are expressed as δ/ppm, downfield from the internal tetramethylsilane reference. Carbon and hydrogen were analyzed using Perkin–Elmer model 240 C elemental analyzer. GLC was carried out on a Shimadzu Gas Chromatograph, GC-9A in conjuction with Shimadzu C-R 6A chromatopac. Cyclic voltammograms were recorded with an X–Y (t) recorder (Servogor type 733). All measurements were carried out at 25 °C by a three electrode system consisting of a counter (stationary platinum disc: 22 mm in diameter), a platinum rod test electrode, 0.1 M (1 M=1 mol dm^{-3}) TBAP (tetrabutylammonium perchlorate) in DMSO (spectroscopic grade) served as supporting electrolyte. The scan rate of the potential was 200 mV s^{-1}.

Chalcones (**1**—**7**; Table 1) were prepared according to the reported method[29] and were characterized by their physico-chemical and spectral studies. These were subjected to the reaction with electrochemically in situ generated superoxide ion. After electrolysis and work-up, all the products isolated were fully characterized by their physico-chemical and spectroscopic data.

Oxidative Cleavage of Chalcones. Typical Procedure for 4-Methoxychalcone (4): Apparatus. Wenking Potentioscan POS 73 (Bank-Electronik, Germany) is used for constant potential macro electrolysis. The electrochemical cell consists of a double walled glass cell (volume 150 ml) in which a medium porosity glass frit separates the anodic and cathodic chambers. The mercury pool (23.76 cm^2) and platinum foil (3.78 cm^2) served as an anode and a cathode respectively. Saturated Calomel Electrode (SCE) served as a reference electrode.

Electrolysis. A solution of tetrabutylammonium bromide (3.22 g; 0.1 M) in DMF (100 ml) was used as supporting electrolyte. The cathodic chamber containing 50 ml of the electrolyte was purged with nitrogen for 15 min. The electrolytic solution was pre-electrolyzed at −1.9 V vs. SCE until the background current drops to about 2 mA. Now 2 ml of cyclohexene was added to anolyte for absorption of liberated bromine. Catholyte was saturated with oxygen for 30 min. Chalcone (**4**; 0.5 g; 2.1×10^{-4} M) was added to the cathodic chamber and reaction was carried out at constant potential of −1.0 V vs. SCE until the loss of starting material as checked by TLC and current falls appreciably (Table 1).

Work-Up. Upon completion of electrolysis, catholyte was taken in 100 ml of cold water and to it was added 25 ml of saturated solution of $NaHCO_3$. The above mixture was extracted with ether (20 ml×3), dried (Na_2SO_4), filtered and evaporated to yield unreacted chalcone. Now the aqueous layer was acidified with dil aq HCl and extracted with ether (25 ml×4), dried (Na_2SO_4), filtered and solvent was removed to yield mixture of acids. These acids were separated by column chromatography on 70—230 mesh silica gel (Merck Kieselgel 60 Art. No. 7734) using benzene–MeOH–AcOH (05:04:01) as eluent. Yields were established (after their esterification) by GLC. Products were identified by their physico-chemical and spectral data.

Results and Discussion

During present investigation chalcones (**1**—**7**) are made to react with in situ electrochemically generated superoxide ion at −1.0 V vs. SCE in the atmosphere of molecular oxygen in DMF solution. The chalcones under this reducing conditions, owing to the mediation of O_2^-/O_2 are oxidatively cleaved to carboxylic acids (Table 1).

Cyclic Voltammetry. The cyclic voltammogram of superoxide ion formation is shown by dotted line (----) and the CV of oxygen reduction in the presence of chalcone (**2**) by solid line (——) (Fig. 1).

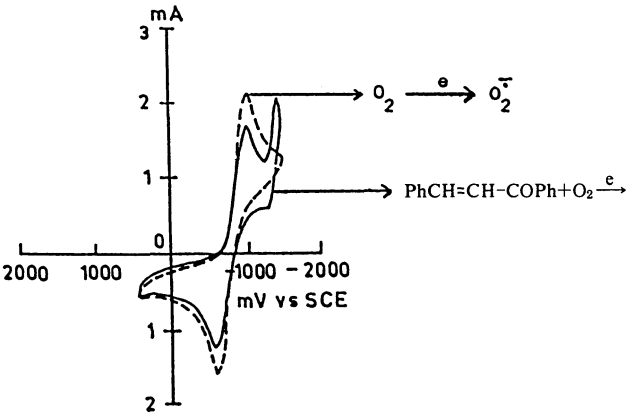

Fig. 1. Cyclic voltammogram for oxygen reduction (----) and in the presence of chalcone (**2**) (——). Solvent: DMSO+0.1 M TBAP; T: 20 °C. Scan rate: 200 mV s^{-1} at Pt.

Examination of Fig. 1 reveals that molecular oxygen is reduced at −0.9 V to O_2^-, this species is reoxidized in the reverse sweep of potential at −0.60 V. The value of 0.30 V as ΔE_p shows that the electrode process is quasi-reversible.[30] In the CV of superoxide ion in presence of substrate, in addition to CV peak of O_2^- (−0.9 V) another peak at −1.45 V is observed, attributable to a possible reduction of substrate. The O_2^- oxidation peak at −0.60 V does not disappear as is observed in the CV of superoxide ion reaction with primary alcohols,[26] but its disappearance in the case of tosylhydrazones[27] probably indicates that superoxide ion is destroyed in a fast follow up chemical reaction between the superoxide ion and the substrate. The cathodic peak current (ipc) in absence of chalcone is 2.15 mA and in presence of chalcone is 1.65 mA (decrease 0.5 mA). Similarly the anodic peak current (ipa) in absence and presence of

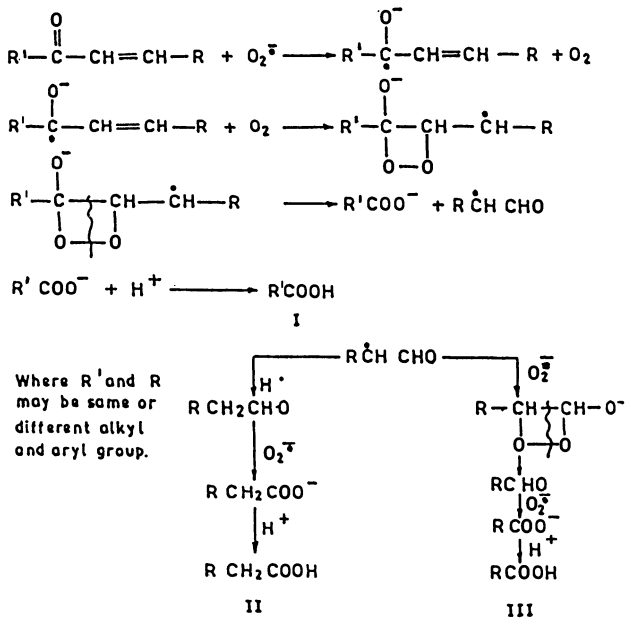

Scheme 1.

chalcone is 1.6 mA and 1.25 mA respectively (decrease 0.35 mA). Thus the decrease in current ratio is 1.42 (Fig.1).

On the basis of product isolation and CV studies the following mechanism is proposed for the oxidative cleavage of chalcones (Scheme 1).

Thus, superoxide ion reacts with chalcone forming radical anion of the substrate, which reacts with surrounding molecular oxygen to form unstable adduct and is readily cleaved to carboxylate anion ($RCOO^-$) and aldehyde radical ($R\dot{C}HCHO$). The latter, with a sequence of steps involving O_2^- affords the products.

The authors (M.S. and K.N.S.) thank the CSIR, New Delhi for the award of Senior Research Fellowships and (R.A.M.) to Alexander Von Humboldt Foundation, Germany, for the gift of a Wenking Potentioscan POS 73.

References

1) G. A. Hamilton, "Chemical Models and Mechanisms for Oxygenases in Molecular Mechanisms of Oxygen Activation," ed by O. Hayaishi, Academic Press, New York (1975), p. 405.
2) J. M. McCord and I. Fridovich, *J. Biol. Chem.*, **244**, 6049 (1969).
3) I. Fridovich, *Acc. Chem. Res.*, **5**, 321 (1972).
4) J. A. Fee and J. S. Valentine, "Superoxide and Superoxide Dismutase," ed by A. M. Michelson, J. M. McCord, and I. Fridovich, Academic Press, New York (1977), pp. 19—60.
5) J. M. McCord, *Science*, **185**, 529 (1974).
6) D. W. Martin, Jr., "Structure and Function of a Protein Hemoglobin," in "Harper's Review of Biochemistry," 19th ed, Maruzen Asian Edition, Tokyo (1983).
7) A. L. Lehninger, "Biochemistry," 2nd ed, Kalyani Publishers, Ludhiana, New Delhi (1982), Chap. 18.
8) N. Ahmed, *Biochem. Educ.*, **15**, 58 (1987).
9) I. Fridovich, *Acc. Chem. Res.*, **15**, 200 (1982).
10) I. Fridovich, *Adv. Enzymol.*, **41**, 35 (1974).
11) J. M. McCord, *Adv. Free Radical Biol. Med.*, **2**, 325 (1986).
12) M. M. Baizer, *Tetrahedron*, **40**, 935 (1984).
13) S. Torii, *Synthesis*, **1986**, 873.
14) D. T. Sawyer and J. S. Valentine, *Acc. Chem. Res.*, **14**, 393 (1981).
15) E. Lee. Ruff, *Chem. Soc. Rev.*, **6**, 195 (1977).
16) D. T. Sawyer and M. J. Gibian, *Tetrahedron*, **35**, 1471 (1979).
17) P. M. Allen, U. Hess, C. S. Foote, and M. M. Baizer, *Synth. Commun.*, **12**, 123 (1982).
18) W. T. Monte, M. M. Baizer, and R. D. Little, *J. Org. Chem.*, **48**, 803 (1983).
19) M. Sugawara, M. M. Baizer, W. T. Monte, R. D. Little, and W. Hess, *Acta Chem. Scand., Ser. B*, **37**, 509 (1983).
20) H. Inoue, T. Nagano, and M. Hirobe, *Tetrahedron Lett.*, **25**, 317 (1984).
21) M. Sugawara and M. M. Baizer, *J. Org. Chem.*, **48**, 4931 (1983).
22) E. J. Nanni, Jr., M. D. Stallings, and D. T. Sawyer, *J. Am. Chem. Soc.*, **102**, 4481 (1980).
23) D. L. Maricle and W. G. Hodgson, *Anal. Chem.*, **37**, 1562 (1965).
24) J. S. Valentine, A. R. Miksztal, and D. T. Sawyer, *Methods Enzymol.*, **105**, 71 (1984).
25) M. Singh and R. A. Misra, *Synthesis*, **1989**, 403.
26) M. Singh, K. N. Singh, S. Dwivedi, and R. A. Misra, *Synthesis*, **1991**, 291.
27) M. Singh, S. C. Mishra, and R. A. Misra, *Bull. Chem. Soc. Jpn.*, **63**, 1233 (1990).
28) I. Rosenthal and A. Frimer, *Tetrahedron Lett.*, **32**, 2805 (1976).
29) B. S. Furniss, A. J. Hannaford, V. Rogers, P. W. G. Smith, and A. R. Tatchell, "Vogel's Textbook of Practical Organic Chemistry," 4th ed, ELBS and Longman, London (1978), pp. 795—796.
30) C. K. Mann and K. K. Barnes, "Electrochemical Reactions in Nonaqueous Systems," Marcel Dekker, Inc., New York (1970), p. 9.

EXAFS Investigation of Pentasil-Structured Gallium-Containing Metallosilicates

Kiyomi OKABE, Nobuyuki MATSUBAYASHI,* Kazuhiro SAYAMA, Hironori ARAKAWA, and Akio NISHIJIMA
Surface Chemistry Division, National Chemical Laboratory for Industry, Tsukuba, Ibaraki 305
(Received January 28, 1991)

Synopsis. Pentasil-structured bimetallosilicates were prepared by adding Ga and Fe (or Sr) salts simultaneously during the hydrothermal synthesis of a pentasil silicate, and local structures around Ga were directly elucidated by means of EXAFS for the first time. It was found that Fe and Ga independently substituted the silicate framework, and that the local structure around Sr was the same as that in Sr^{2+}-exchanged gallosilicate.

It was reported that tectosilicate frameworks are substituted by such elements as B, Be, Al, Fe, Ga, Ge, Cr, P, and Mg.[1] Among these elements, B, Al, Fe, and Ga are most frequently used for preparing metallosilicate catalysts, since the acidity of the catalysts can be altered by the substitution. Pentasil metallosilicates, thus prepared, have a unique channel structure, and the framework metals are atomically dispersed. These characteristics provide long catalytic life as well as high activity in the conversion of methanol to hydrocarbons.[2] Selectivity is often improved by additives during the hydrothermal synthesis of the silicates.[3] However, interaction between the second metal and the metal in the framework of the silicates is not well-characterized at the present time. It is of great importance to elucidate the interaction, since the interaction may give rise to a change in electronic states of the active sites, improving the catalytic property. The purpose of the present investigation is to clarify the micro-structure around Ga in Ga-containing bimetallosilicates and to show the intermetallic interaction between Ga and the second metal by means of EXAFS. In the present investigation, Fe and Sr were chosen as the second metals, since (a) the former is typical of an isomorphous substitutional element and the latter is non-substitutional, as mentioned above, and (b) both are catalytically important additives and a large amount of data has been accumulated on their ability to modify the acidity of catalysts.[4]

Experimental

Colloidal silica, gallic nitrate (and/or iron(III) nitrate), tetrapropylammonium bromide (TPABr), sodium hydroxide, and distilled water were mixed together to form a metallosilicate (M-silicate; M=Ga, Fe) gel having the following composition; SiO_2/Ga_2O_3 (and/or Fe_2O_3)=200, SiO_2/TPABr=10, SiO_2/OH=10. The gel was crystallized by autoclaving at 433 K. Some of the crystalline metallosilicates were treated with 0.1 mol dm^{-3} aqueous solutions of $SrCl_2$ or $Ga(NO_3)_3$ at 373 K after calcination at 773 K, and the Na^+ of the pentasil silicates was replaced by Sr^{2+} or Ga^{3+}. Sr-containing gallosilicate was prepared by adding strontium acetate (Sr/Ga=10) during the hydrothermal synthesis of gallosilicate. The K-edge EXAFS spectra of Ga, Sr, and Fe were measured at the Photon Factory (BL-10B and BL-7C) of the National Laboratory for High Energy Physics. In Fourier transforms of the EXAFS data, the phase shifts due to an absorbing atom and backscattering atoms were corrected using parameters calculated by Teo and Lee[5] for M–O (M=Ga, Sr, Fe). Furthermore, the distances were corrected using the results for standard samples (Ga_2O_3, SrO, and Fe_2O_3).

Results and Discussion

Figure 1 shows the Fourier transforms of Ga K-edge EXAFS of (a) Ga_2O_3 and (b—e) gallosilicates at the various stages of the hydrothermal reaction. The profile of the gel mixture at an initial stage (b) was quite different from that of Ga_2O_3 (a). The peaks at 1.9 and 3.2 Å of Ga_2O_3 are assigned to Ga–O and Ga–O–Ga, respectively. The latter peak was not found in the spectra of the gallosilicates (b—e). The profiles of the silicates were almost unchanged during the hydrothermal reaction. The peaks at 3.1 and 3.5 Å may correspond to Ga–O–Si distances, as assigned previously.[6] The fact that the second neighboring atoms on Ga are

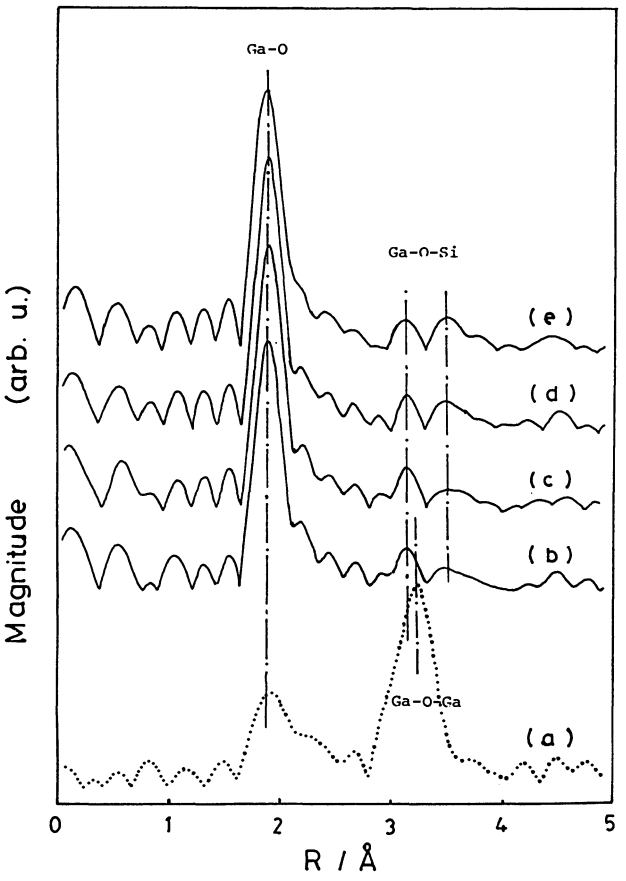

Fig. 1. Fourier transforms of Ga K-edge EXAFS with phase-shift correction of (a) Ga_2O_3, and gallosilicates after hydrothermal reaction of (b) 0 h, (c) 2 h, (d) 2.5 h, and (e) 6 h.

not Ga but Si indicates that Ga is highly dispersed in the silicate, even at the very beginning of the hydrothermal reaction. The atomic isolation of the metal in the silica matrix is different from the previous case of ferrisilicate, where FeO(OH) was formed in the starting gel.[6] The identical peak positions in the EXAFS profiles between the amorphous and crystalline phases strongly suggest that the micro-structure around Ga was formed in a very early stage of the hydrothermal reaction without the formation of an oxide or hydroxide of Ga, and that the local environment around Ga was almost unchanged throughout the hydrothermal reaction.

However, the relative intensity of the peaks at 3.5 Å increased and that at 3.1 Å decreased slightly with hydrothermal reaction time, as illustrated in Fig. 2. The change in XRD intensity at a spacing d(501) of the silicates (△) indicates that the silicate bulk was crystallized during a short period of time after a hydrothermal reaction time of 2 h. These results suggest that the peaks at 3.1 Å correspond to the Ga–O–Si distance in an amorphous silicate and the ones at 3.5 Å to that of the pentasil structure, and that the regularity of the micro-structure around Ga in the pentasil framework increased with time.

Figure 3 shows the Fourier transforms of Ga K-edge EXAFS of (a) Ga_2O_3, (b) Ga^{3+}-exchanged Fe-silicate, (c) Fe, Ga-bimetallosilicate, (d) Sr-containing Ga-silicate, and (e) pentasil structured Sr^{2+}-exchanged Ga-silicate.

The peak positions of (b) are different from those of Ga_2O_3 (a) or Ga-silicate (Fig. 1), implying that most of the Ga of (b) was in the form of counter cations to acid sites caused by the framework Fe. The peak at 3.0 Å of the silicate corresponds to the distance to the second neighboring atoms on Ga. The dissimilarity of the profiles suggests that the peak may correspond to the Ga^{3+}–O–Fe distance, since a peak of the same distance

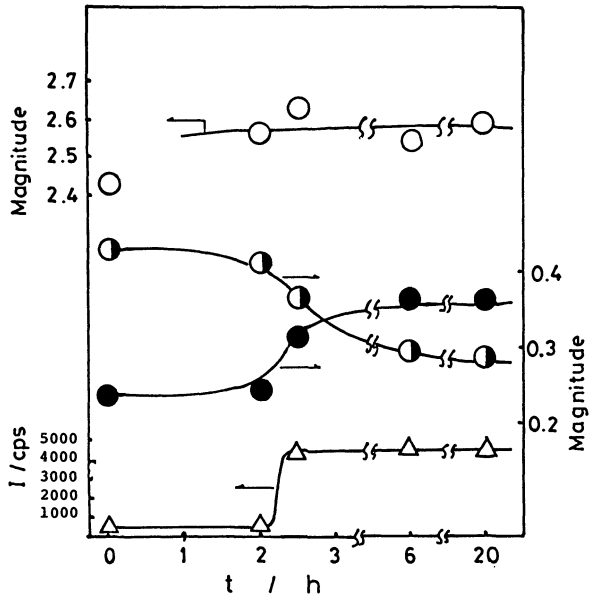

Fig. 2. Changes in peak intensities at 1.9 Å (○), 3.1Å (◑) and 3.5 Å (●) of Fig. 1, and in XRD peak intensities at 2θ=23.2° (△) with hydrothermal reaction time.

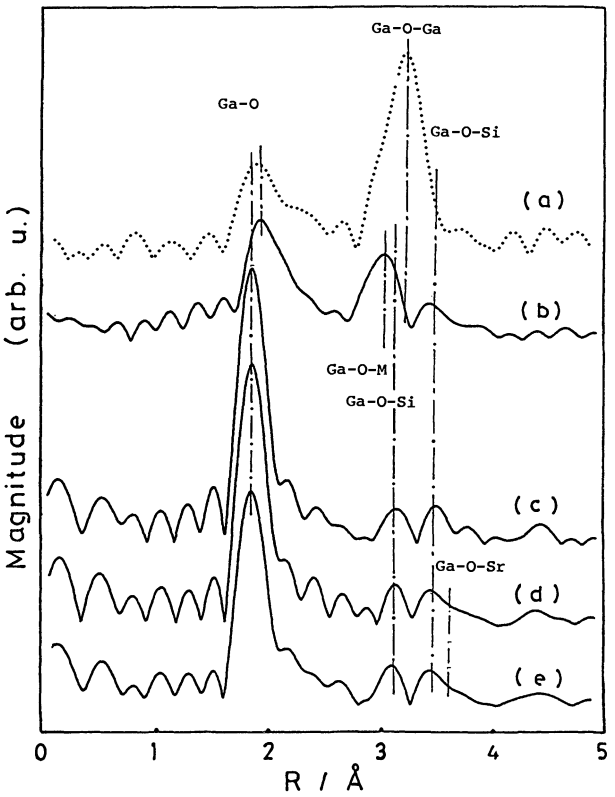

Fig. 3. Fourier transforms of Ga K-edge EXAFS, with phase-shift correction, of (a) Ga_2O_3, (b) Ga^{3+}-exchanged ferrisilicate, (c) Fe,Ga-bimetallosilicate, (d) Sr-containing gallosilicate, and (e) Sr^{2+}-exchanged gallosilicate.

was also found in the Fourier transform of Fe K-edge EXAFS of Ga^{3+}-exchanged Fe-silicate. A weaker peak was found at 3.45 Å in profile (b) in Fig. 3. The relative peak intensity depends on many factors, the atomic weight of the adjacent atoms being one of them. By simply assuming that the atomic weight corresponding to the peak at 3.45 Å is about half that of the peak at 3.0 Å and that the other factors are the same between these two peaks, the weak peak can be explained in terms of the Ga–O–M distance. Si may be the most appropriate candidate for the M element, since the relative atomic weight ratio of Si/Fe is 0.5 and the distance derived from the peak position is similar to the Ga–O–Si distance in crystalline gallosilicate, as mentioned above. Thus, the peaks at 3.0 and 3.45 Å may be assigned to the Ga^{3+}–O–Fe and Ga^{3+}–O–Si distances, respectively.

The Ga–O distance in (c) is 1.9 Å, and is shorter than that in (b) by 0.1 Å. The profile of (c) in the range of 3.0—3.5 Å is also different from that of (b), and exactly the same as that of Ga-silicate. The peaks at 3.1 and 3.5 Å of Ga-silicate were both assigned to Ga–O–Si, as described above. The fact that no other peaks of Ga–O–M (M=Ga, Fe) are found in (c) suggests that Ga and Fe are atomically and independently dispersed in the silicate crystals without mutual interaction.

The profile of (d) is the same as (e), indicating that the local structures around Ga are similar to each other. The profiles are also similar to that of Ga-silicate (Fig.

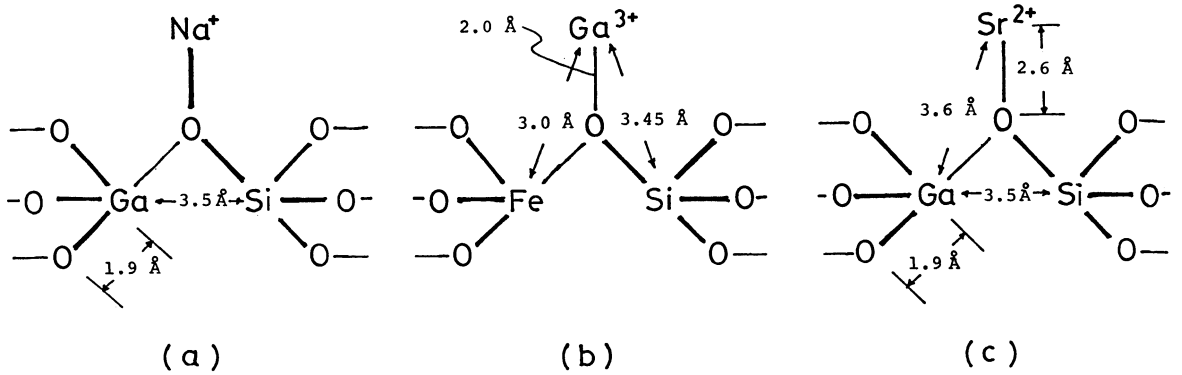

Fig. 5. Intermetallic distances determined by EXAFS of (a) gallosilicate, (b) Ga^{3+}-exchanged ferrisilicate, and (c) pentasil-structured Sr-containing gallosilicate.

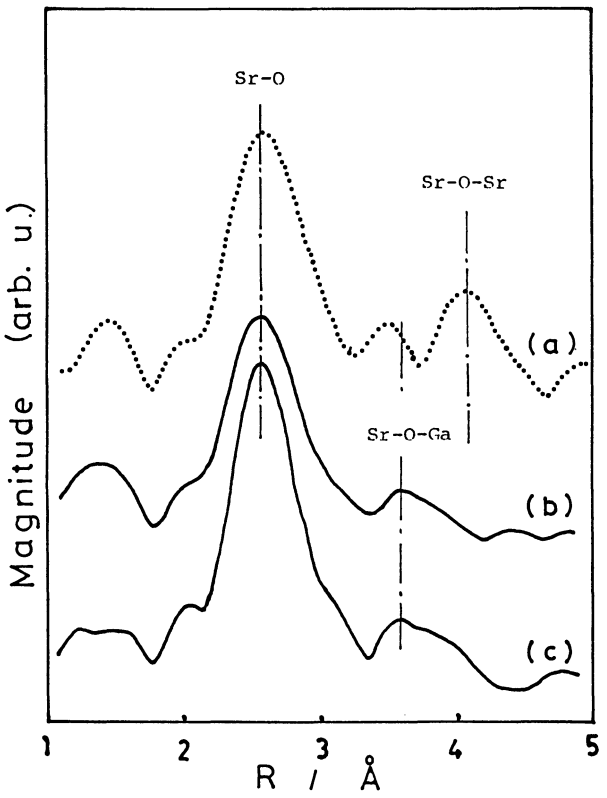

Fig. 4. Fourier transforms of Sr K-edge EXAFS, with phase-shift correction, of (a) SrO, (b) Sr-containing gallosilicate, and (c) Sr^{2+}-exchanged gallosilicate.

1), except for the peak broadening at 3.5—3.6 Å. It is well known that framework Ga gives rise to an acid site, and that Sr of (e) is in the form of an extra-framework cation attached to this site. Therefore, the broadening of the peak suggests that it actually consists of two peaks, Ga–O–Si (3.5 Å) and Ga–O–Sr^{2+} (3.6 Å). The latter peak was also found in the Fourier transforms of Sr K-edge EXAFS of Sr^{2+}-exchanged Ga-silicate and Sr-containing Ga-silicate, as depicted in Fig. 4. The similarity between the profiles of Sr^{2+}-exchanged Ga-silicate and Sr-containing Ga-silicate implies that most of Sr in the latter are not contained in the silica matrix, but are in extra-framework ion-exchanging sites.

In conclusion, intermetallic distances of pentasil-structured bimetallosilicates were directly and precisely determined by means of EXAFS, providing the following information on interactions between the metals:

(1) The micro-structure around Ga of gallosilicate was formed in a very early stage of the hydrothermal reaction, before bulk crystallization, without the formation of an oxide or hydroxide of Ga.

(2) In the crystallization of Fe, Ga-bimetallosilicate, no interactions between Fe and Ga were found structurally, and the silicate framework was substituted by either metal independently.

(3) The micro-structure around Sr in Sr-containing gallosilicate was similar to that of Sr^{2+}-exchanged silicate, and Sr was in an extra-framework ion-exchanging site.

It is believed that precise control of the interactions between metals in metallosilicates is prerequisite for improving the catalytic property. To accomplish this control, a large amount of data on interactions must be accumulated. We have found EXAFS to be a very powerful tool for clarifying the interaction from a structural point of view at the atomic level. More detailed structural data will be produced with further investigations by EXAFS.

References

1) R. M. Barrer, "Hydrothermal Chemistry of Zeolites," Academic Press, London (1982), p. 251.

2) T. Inui, O. Yamase, K. Fukuda, A. Itoh, J. Tarumoto, N. Morinaga, T. Hagiwara, and Y. Takegami, 8th International Congress on Catalysts, Berlin, 1984, Vol. 3, p. 569.

3) H. Okado, H. Shoji, K. Kawamura, Y. Shiomi, K. Fujisawa, H. Hagiwara, and H. Takaya, *Nippon Kagakukaishi,* **1987**, 962.

4) H. Hagiwara, K. Kawamura, S. Ikai, F. Mizuno, and H. Okado, "Progress in C_1 Chemistry in Japan," Kodansha, Tokyo (1989), p. 331.

5) B. K. Teo and P. A. Lee, *J. Am. Chem. Soc.,* **101**, 2815 (1979).

6) K. Okabe, N. Matsubayashi, H. Shimada, H. Hagiwara, and A. Nishijima, *Chem. Lett.,* **1990**, 955.

Synthesis of *N*-Methylaniline and *N,N*-Dimethylaniline with Methanol over Alumina Catalyst

Hiromi MATSUHASHI* and Kazushi ARATA
Department of Science, Hokkaido University of Education, Hachiman-cho, Hakodate 040
(Received January 28, 1991)

Synopsis. Alumina catalysts prepared by different methods were used for the synthesis of *N*-methylaniline and *N,N*-dimethylaniline from aniline and methanol. Al_2O_3 catalysts prepared from isopropoxide and nitrate showed high activity and JRC-ALO-1 and JRC-ALO-3 supplied by the Catalysis Society of Japan showed low activity. The highest selectivity for *N,N*-dimethylaniline was 82.8% with 90.1% aniline conversion. The catalytic activity of Al_2O_3 was not poisoned by pyridine and CO_2.

N-Alkylation of aniline with methanol was catalyzed by solid acid and base catalysts. Silica gel and ZSM-5 zeolites were applied for this reaction,[1,2] but catalytic activities of these catalysts were not high. In the case of acid catalysts, the activity for this reaction might be suppressed by the adsorption of aniline since aniline, itself, has a strong basic characteristic. It therefore seems that the use of a strong acid catalyst is not suitable for this reaction. Takemiya et al. reported aniline alkylation with methanol over solid base catalysts: MgO[3] and $NaOH/Al_2O_3$.[4] The products consisted exclusively of *N*-methylaniline. Alumina is one of the best catalysts for this reaction.[5] In this study, we report that Al_2O_3 catalysts prepared from isopropoxide and nitrate showed high activity for the *N*-methylation of aniline. We anticipate that Al_2O_3 has an acid-base bifunctional characteristic.

Four kinds of Al_2O_3 were used in this study.

Al_2O_3-1. Aluminum hydroxide was obtained by hydrolyzing $Al[OCH(CH_3)_2]_3$ (Wako Pure Chemicals, Guaranteed Reagent) dissolved in dried ethanol with distilled water. Water and ethanol were evaporated. Then, $Al(OH)_3$ was suspended in distilled water again and boiled for 1 h. Excess water was evaporated.

Al_2O_3-2. Aqueous ammonium was added to an aqueous solution of $Al(NO_3)_3 \cdot 9H_2O$ (Wako Pure Chemicals, Guaranteed Reagent) to precipitate $Al(OH)_3$. The final pH of the suspension was 7—8. The precipitate was washed with distilled water, dried, and heated at 773 K in air.

Al_2O_3-3 and Al_2O_3-4 were JRC-ALO-1 and JRC-ALO-3, supplied by the Catalysis Society of Japan as reference catalysts. MgO was prepared by boiling commercial high-purity MgO (Merck) in water, followed by drying and a thermal treatment at 773 K in a He stream. ZrO_2 was obtained by hydrolyzing $ZrO(NO_3)_2 \cdot 8H_2O$ (Wako Pure Chemicals, Guaranteed Reagent) with aqueous ammonia, washing, drying, and a thermal treatment at 773 K in air. Li^+/Al_2O_3 and Na^+/Al_2O_3 were prepared by an impregnation method. Al_2O_3-1 was suspended in aqueous Li^+ or Na^+ carbonate; the water was evaporated to dryness over a hot plate. The content of alkali ions was 10 mol%.

All catalysts were heated in glass reaction tubes at 773 K for 3 h in a He stream before reaction. The catalytic reaction experiments were carried out with a conventional flow microreactor. After the catalyst (0.2 g) was heat-treated in a reactor in the He stream (20 cm^3 min^{-1}), a vaporized mixture of methanol and aniline (mole ratio=5) was passed through the catalyst bed at a feed rate of 4.09 $cm^3 h^{-1}$. The partial pressure of methanol and aniline was 5.15×10^4 Pa and 1.03×10^4 Pa respectively. The product stream was cooled and condensed at a reservoir attached under the reactor. The liquid product was sampled every 30 min and analyzed by using a G.L.C. column (2 m×3 mm o.d.), packed with SE-30. The products were identified by GC-MS. The conversion is explained as being proportions of *N*-methylaniline and *N,N*-dimethylaniline based on aniline.

The conversion and composition of the products between 60 and 90 min at 623 K are summarized in Table 1. In all cases, even though the catalytic activity

Table 1. *N*-Methylation of Aniline over Various Catalysts at 623 K

Catalyst	Conversion	Selectivity/%	
	%	*N*-Methylaniline	*N,N*-Dimethylaniline
Al_2O_3-1	32.1	78.2	21.8
Al_2O_3-1[a]	66.1	60.4	39.6
Al_2O_3-1[a,b]	81.2	39.0	61.0
Al_2O_3-1[a,c]	90.1	17.2	82.8
Al_2O_3-2	30.5	70.1	29.9
Al_2O_3-3	21.7	69.6	30.4
Al_2O_3-4	17.5	83.3	13.7
ZrO_2	Trace	Trace	
Li^+/Al_2O_3	4.7	100	—
Na^+/Al_2O_3	0.8	100	—
MgO	Trace	Trace	

a) Reaction temperature: 673 K. b,c) Methanol/Aniline (mole ratio): b) 10, c) 15.

decreased rapidly during the initial period of the reactions, the catalysts showed almost constant activity after 60 min. Among the tested catalysts, the Al_2O_3 catalysts showed higher activity than did the other acid or base catalysts. In particular, Al_2O_3-1 and Al_2O_3-2 gave 32.1% and 30.5% methylated products, respectively. The selectivity for *N,N*-dimethylaniline was high when the flow rate of the He carrier was low. Table 1 also suggests that higher reaction temperatures and large ratios of methanol to aniline lead to a higher selectivity for *N,N*-dimethylaniline. In this study, the highest selectivity for *N,N*-dimethylaniline was 82.8%, with a 90.1% conversion. No liquid product was obtained when the reaction temperature was 723 K or higher. The activity of MgO, a typical solid base, was very low under the present conditions. ZrO_2, which is known to hold basic sites together with acidic ones on the surface,[6,7] also showed low activity.

Pyridine, CO_2, and H_2O were adsorbed on the Al_2O_3 surface for characterizing the active site. The supplement of the reactant mixture was stopped after a reaction for 120 min, and the adsorbant was introduced into the reaction system. The amount of pyridine or H_2O introduced was 0.5 cm^3 (as liquid); CO_2 was fed for 30 min. The results are shown in Table 2. The addition of pyridine and CO_2 had no (or less) effect on the catalytic activity, suggesting that the reaction did not occur at strong acid sites which were poisoned by pyridine. It was expected that the reaction proceeded on the basic site of Al_2O_3. Because the activity became slightly decreased by the adsorption of CO_2, Li^+/Al_2O_3 and Na^+/Al_2O_3 were applied for the reaction. The basicity of Al_2O_3-1 was enhanced[4] by doping of Li^+ and Na^+. However, as is shown in Table 1, both of these catalysts showed much less activity. It was therefore clear that this reaction did not occur only at the basic sites.

Table 2. Effect of Adsorption of Pyridine, CO_2, and H_2O

Addition	Conversion ratio (after/before)
Pyridine, 0.5 ml	1.0
CO_2, 30 min	0.95
H_2O, 0.5 ml	0.48

Adsorbants were added after the reaction for 2 h.
Reaction condition, see Text.

As is shown in above, the catalytic activity was affected by the doping of Na^+. Since Al_2O_3-3 and -4 contain 0.03% and 0.3% Na_2O, respectively, the reason for the low activity of Al_2O_3-3 and -4 was estimated to be that a small amount of Na^+ was contained as an impurity.

The effect of the addition of H_2O was, however, larger than that of pyridine or CO_2, and the activity was decreased to half before the addition.

Since water molecules poison both acidic and basic sites and the activity of Al_2O_3 or *N*-methylation of aniline, acid-catalyzed dehydration was very high, and even though the catalyst did not have a strong acid character, it could be presumed that the Al_2O_3 catalyst might act as a bifunctional catalyst in this reaction.

References

1) C. M. Naccache and Y. B. Taarit, *J. Catal.*, **22**, 171 (1971).
2) P. Y. Chen, M. C. Chen, H. Y. Chu, N. S. Chang, and T. K. Chuang, "Proc. 7th Intern. Zeolite Conf.," Kodansha, Tokyo (1986), p. 739.
3) N. Takamiya, Y. Koinuma, K. Ando, and S. Murai, *Nippon Kagaku Kaishi*, **1979**, 1453.
4) N. Takamiya, H. Yamabe, K. Ando, and S. Murai, *Nippon Kagaku Kaishi*, **1980**, 1316.
5) T. H. Evans and A. N. Bourns, *Can. J. Tech.*, **29**, 1 (1951).
6) T. Yamaguchi, Y. Nakano, and K. Tanabe, *Bull. Chem. Soc. Jpn.*, **51**, 2482 (1978).
7) Y. Nakano, T. Iizuka, H. Hattori, and K. Tanabe, *J. Catal.*, **57**, 1 (1979).

Sedimentation Potential Measurements and Partial Molar Volumes of Univalent Ions in Water-Acetone Mixtures

Fumio KAWAIZUMI,* Hiromitsu HIRAKAWA,† Eiji KUBOTA,†† and Hiroyasu NOMURA†††
Institute for Molecular Science, Myodaiji, Okazaki 444
†Department of Electrical Engineering, Faculty of Engineering, Kagoshima University, Korimoto, Kagoshima 891
††Department of Chemistry, Faculty of Science, Shinshu University, Matsumoto 390
†††Department of Chemical Engineering, School of Engineering, Nagoya University, Chikusa-ku, Nagoya 464-01
(Received March 11, 1991)

Synopsis. Sedimentation potentials and electrical conductivities were measured for NaCl, NaBr, sodium tetraphenylborate Na[BPh4], and tetraphenylphosphonium chloride [Ph4P]Cl in water–acetone systems (up to 50 wt% of acetone). Using the data obtained and the reported values of partial molar volumes V_2^∞, the ionic division of V_2^∞ was carried out. The values of V_2^∞ (Na^+) evaluated for NaCl, NaBr, and Na[BPh4] were self-consistent and they work as references for ionic division of V_2^∞ (MX).

As a continuation of our series of work on the division of the partial molar volume of an electrolyte V_2^∞ (MX) to the cationic and anionic parts,[1–4] we have measured the sedimentation potentials for NaCl, NaBr, Na[BPh4], [Ph4P]Cl, and [Ph4P]Br dissolved in water–acetone mixtures up to 50 wt% of acetone.

We reported earlier[5] that in water–acetone system, the V_2^∞'s of NaCl, KCl, CsCl, NaBr, KBr, and [Ph4P]Cl vary only slightly with solvent composition, while for the salt Na[BPh4], rather abrupt increase in V_2^∞ appears in solvents containing 10 to 30 wt% of acetone. Main purpose of this work is to see whether this increase of V_2^∞ (Na[BPh4]) is attributable to the ion Na^+ or the ion $[BPh_4]^-$.

For the ionic division of V_2^∞ of an electrolyte MX, data of transport number of the electrolyte MX are needed. Thus, conductivities of the sample salts have also been measured.

Experimental

Samples. Commercially available highest grade Na[BPh4] (Dojin Co., Ltd. or Fluka) was used without further purification. The [Ph4P]Cl and [Ph4P]Br used were the products of Fluka or Merck. The solvent acetone was purified for conductivity measurements by refluxing the guaranteed grade sample with molecular sieves but no purification was done for acetone for sedimentation potential measurements.

Sedimentation Potentials. The sedimentation potentials were measured at Kagoshima University. The experimental set-up was principally the same as before,[1] but in the course of this work some modifications were given on the sample cell and the measuring procedures. First, we prepared a new sample cell which is wholly made of teflon, while so far[1–4] part of the cell was made of acrylic resin. The platinum electrodes in the sample cell were directly connected to the outer electric circuit through a coaxial connector. Second, in our previous work[1–4] the electrodynamic vibrator was vibrated at frequency 100 Hz but in this work the frequency was 150 Hz for NaCl, NaBr, and [Ph4P]Cl, and 1000 Hz for Na[BPh4] and [Ph4P]Br. By adopting higher frequencies, we can reduce the effects of the so-call $1/f$ noise and the interference by the commercial AC of 60 Hz. The theory[6] predicts that even at frequency 1000 Hz no relaxation due to the electrophoretic effect of the ionic cloud appears in solutions with solute concentration less than 10^{-3} mol dm^{-3}.

In our sedimentation potential measurements, the amount of acceleration applied externally by the electrodynamic vibrator is expressed as $\omega^2 x$, where ω is the angular frequency and x is the amplitude of oscillation produced in solution. Thus far we have evaluated the magnitude of acceleration by measuring the amplitude x with stroboscope and microscope. We confirmed that change of the frequency from 100 to 150 Hz accompanies the corresponding decrease of the amplitude, the acceleration remaining constant. At frequency 1000 Hz, we monitored the degree of acceleration by an accelerometer, for the amplitude of vibration is too small to observe by microscope. The accelerometer (IMV Co., Ltd.) consists of a piezoelectric acceleration pick-up (IH-02) and a digital charge vibrometer (VM-1970). The acceleration applied to the cell was 7.0 G. Combined use of higher vibration frequencies and aceceleration meter permitted us to reduce the number of run needed to have the reliable sedimentation potential values in solutions.

Sedimentation potentials should be proportional to the externally applied acceleration. As is shown in Fig. 1, excellent linear relations passing through the origin hold for solutions of NaBr dissolved in water and in the solvent containing 30 wt% of acetone. In our apparatus, the vibration at frequency 100 Hz and amplitude 0.062 cm produces the acceleration 17.7 G. Extrapolation of the linear relations of Fig. 1 to the state of 17.7 G gives the identical values obtained at 100 Hz and amplitude 0.062 cm. The sedimentation potentials in aqueous solutions of Na[BPh4] and [Ph4P]Br at 7.0 G also

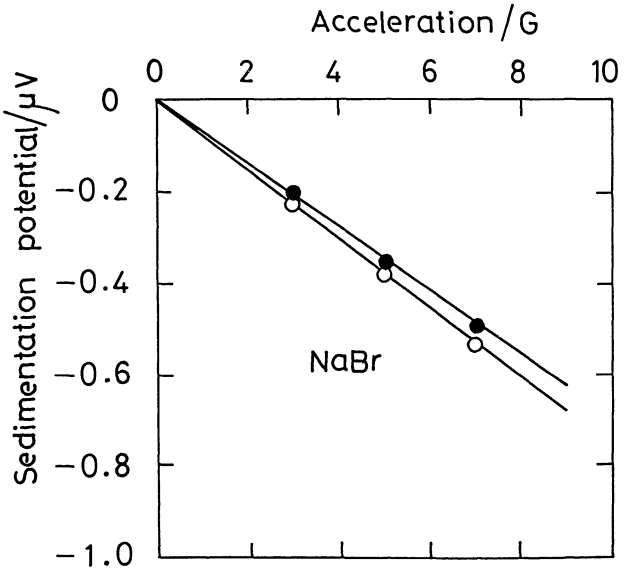

Fig. 1. Relation between the applied acceleration and the sedimentation potentials produced in solutions of NaBr dissolved in water (—○—) and 30 wt% of acetone (—●—).

correspond excellently to the values obtained at 100 Hz and amplitude 0.062 cm.

Electric Conductivities. The conductivities were measured at Shinshu University. The specific conductivities of the conductivity water and acetone were 1.3×10^{-7} and 0.9×10^{-8} S cm^2, respectively. A linear-type bridge and platinum black electrodes (cell constant 0.12305 cm^2) were used for the measurement. The sample solutions were in the ranges 10^{-4}—10^{-3} mol dm^{-3}, and the concentrations were changed in the cell by measuring the weight.

Results and Discussion

Electric Conductivities and Transport Numbers. We used the Fuoss–Onsager equation[7] to analyze the conductivity data:

$$\Lambda=\Lambda^{\infty}-S\,c^{1/2}+Ec\log c+Jc \qquad (1)$$

where c is the solute concentration in mol dm^{-3} and the coefficients S, E, and J are the parameters given by the

Table 1. Limiting Molar Conductivities of the Salts NaCl, NaBr, [Ph$_4$P]Cl, [Ph$_4$P]Br, and Na[BPh$_4$] in Water–Acetone at 25 °C

[Acetone]	Λ^{∞}/S cm^2 mol^{-1}				
wt%	NaCl	NaBr	[Ph$_4$P]Cl	[Ph$_4$P]Br	Na[BPh$_4$]
0	126.6	128.1	96.63	98.2	69.9
	126.45[a]	128.24[a]	96.76[b]		69.94[c]
10	102.5	104.0	76.2	77.7	59.2
20	86.1	87.5	65.0	66.5	52.1
30	76.1	77.5	58.5	60.1	48.0
40	71.4	72.8	55.0	56.4	46.3
50	68.9	70.3	54.0	56.0	46.5

a) R. A. Robinson and R. H. Stokes, "Electrolyte Solutions," 2nd ed, Butterworths. London (1970). p. 463. b) Ref. 9. c) J. K. Skinner and R. M. Fuoss, *J. Phys. Chem.*, **68**, 1882 (1964).

Table 2. Observed Sedimentation Potentials E, Cation Transport Numbers t_+, Partial Molar Volumes V_2^{∞}, and Ionic Partial Molar Volumes V_+^{∞} and V_-^{∞} for NaCl, NaBr, [Ph$_4$P]Cl, [Ph$_4$P]Br, and Na[BPh$_4$] in Water–Acetone at 25 °C

[Acetone]	ρ	E[a]	t_+[b]	V_2^{∞}[c]	V_+^{∞}	V_-^{∞}
wt%	g cm^{-3}	μV		cm^3 mol^{-1}	cm^3 mol^{-1}	cm^3 mol^{-1}
			NaCl			
0	0.9970	+0.08	0.396	16.7	−3.56	20.26
10	0.9833	+0.10	0.417	16.7	−3.19	19.89
20	0.9694	+0.13	0.425	16.8	−3.47	20.27
30	0.9638	+0.12	0.430	16.6	−3.40	20.00
40	0.9360	+0.16	0.438	16.3	−4.15	20.45
50	0.9160	+0.18	0.444	16.7	−4.28	20.98
			NaBr			
0	0.9970	−1.32	0.391	23.4	−4.03	27.43
10	0.9833	−1.27	0.411	23.1	−3.67	26.77
20	0.9694	−1.22	0.418	23.8	−3.76	27.56
30	0.9638	−1.20	0.421	23.7	−4.20	27.90
40	0.9360	−1.17	0.430	23.5	−4.40	27.90
50	0.9160	−1.19	0.444	23.8	−3.82	27.62
			[Ph$_4$P]Cl			
0	0.9970	−0.58	0.211	312.2	299.37	12.83
10	0.9832	−0.56	0.217	314.3	301.84	12.46
20	0.9694	−0.52	0.238	314.7	303.81	10.89
30	0.9639	−0.51	0.261	311.2	303.90	7.30
40	0.9360	−0.48	0.273	310.0	305.00	5.00
50	0.9160	−0.42	0.294	309.2	307.21	1.99
			[Ph$_4$P]Br			
0	0.9970	−0.71	0.207	318.9	288.51	30.39
10	0.9833	−0.72	0.212	320.7	291.37	29.33
20	0.9694	−0.70	0.233	321.7	294.21	27.50
30	0.9639	−0.73	0.255	318.3	296.31	21.99
40	0.9360	−0.72	0.266	317.2	297.62	19.58
50	0.9160	−0.72	0.284	316.3	300.92	15.38
			Na[BPh$_4$]			
0	0.9970	+0.21	0.716	277.2	−4.19	281.39
10	0.9833	+0.20	0.721	279.3	−4.00	283.30
20	0.9694	+0.24	0.702	294.6	−3.68	298.28
30	0.9638	+0.21	0.681	300.1	−3.50	303.60
40	0.9360	+0.21	0.676	299.9	−5.78	305.68
50	0.9160	+0.08	0.658	300.1	−3.56	303.66

a) For NaCl, NaBr, and [Ph$_4$P]Cl, values at 17.7 G. For [Ph$_4$P]Br and Na[BPh$_4$], values at 7.0 G. b) Calculated from the electrical conductivities given in Table 1. c) For [Ph$_4$P]Br, see the text.

theory.[7] Data anaylsis showed that in any case investigated ion association is negligible. The limiting molar conductivities determined are summarized in Table 1. We then estimated the ionic molar conductivities based on the assumption that Λ^∞ ($[Ph_4P]^+$)=Λ^∞ ($[BPh_4]^-$). We have two ways of estimation:

$$\Lambda^\infty([Ph_4P]^+)=\Lambda^\infty([BPh_4]^-)$$
$$=(1/2)\{\Lambda^\infty(Na[BPh_4])+\Lambda^\infty([Ph_4P]Cl)-\Lambda^\infty(NaCl)\}$$
$$=(1/2)\{\Lambda^\infty(Na[BPh_4])+\Lambda^\infty([Ph_4P]Br)-\Lambda^\infty(NaBr)\}.$$

Both estimations lead to practically identical ionic molar conductivities. The worst is the system with 50 wt% of acetone for which the differences amount to three in the first decimal place. Transport numbers for each electrolyte were calculated using the ionic molar conductivities thus estimated. Our transport number for the ion Na^+ 0.418 for NaBr in 20 wt% of acetone is in fair agreement with the literature value 0.425.[8]

Sedimentation Potentials. The limiting sedimentation potentials[1] are given in Table 2 along with the numerical values of the solvent density used in the calculation.

Division of Partial Molar Volume into V_2^∞ into V_+^∞ and V_-^∞. The relation between the sedimentation potential E and the ionic partial molar volumes V_+^∞ and V_-^∞ is expressed as follows:[4]

$$E=(ad/F)\cdot[(t_+/z_+)\cdot(m_+-V_+^\infty\rho) - (t_-/z_-)\cdot(m_--V_-^\infty\rho)], \quad (2)$$

where the symbols are the same as in our previous work.[4] We have divided the partial molar volumes V_2^∞ (MX) of a salt MX into two ionic parts V_+^∞ (M^+) and V_-^∞ (X^-) by combining Eq. 2 and the additivity rule that V_2^∞ (MX)=V_+^∞(M^+) + V_-^∞(X^-). The V_2^∞ (MX) values are available,[5] except for V_2^∞ ([Ph4P]Br), which were estimated from V_2^∞ ([Ph4P]Cl), V_2^∞ (NaCl), and V_2^∞ (NaBr).

Ionic partial molar volumes obtained are included in Table 2. The values of V_+^∞ (Na^+) calculated from V_2^∞'s of NaCl, NaBr, and Na[BPh4] agree each other within experimental errors over the whole solvent composition investigated. On the contrary, the V_-^∞ (Br^-) values calculated from V_2^∞ (NaBr) and V_2^∞ ([Ph4P]Br) differ considerably in solvents containing more than 30 wt% of acetone. As for the ion $[Ph_4P]^+$, the values from ([Ph4P]Cl) are always larger than those from the V_2^∞ ([Ph4P]Br) by 6—11 $cm^3\,mol^{-1}$. For the ion Cl^-, differences in the values of V_-^∞ (Cl^-) from V_2^∞ (NaCl) and V_2^∞ ([Ph4P]Cl) become progressively larger with the amount of acetone in the solvent. The reason for these inconsistent results for the salt [Ph4P]X (X=Cl or Br) is unclear for us at present. According to Perie, Perie, and Chemla,[9] the ion $[Ph_4P]^+$ decomposes at the cathode, although they mentioned nothing about the degree of decomposition. Taking into account all factors we have taken the values of V_+^∞ (Na^+) averaged over those calculated from V_2^∞ (NaCl), V_2^∞ (NaBr), and V_2^∞ (Na[BPh4]) as references for ionic division of V_2^∞ (MX). The values of V_+^∞ (Na^+) are: −3.9, −3.6, −3.6, −3.7, −4.3 (averaged over NaCl and NaBr), and −3.9 $cm^3\,mol^{-1}$ at 0, 10, 20, 30, 40, and 50 wt % of acetone, respectively.

Dielectric constant of water–acetone mixture decreases with wt% of acetone. In spite of the decrease in the dielectric constant, the ionic partial molar volumes of the simple univalent ions Na^+, Cl^-, and Br^-, hence, the V_2^∞ (NaCl) and V_2^∞ (NaBr) remain practically constant. Also the ion $[Ph_4P]^+$ shows the behavior independent of the solvent composition. Through ionic division of V_2^∞, it has become clear that the abrupt increase of V_2^∞ (Na[BPh4]) in the solvent composition ranges 20—30 wt % of acetone as reported earlier[5] is due to the ion $[BPh_4]^-$ and not to the ion Na^+.

Part of this work was reported in the Fourth Asia Pacific Physics Conference held in Seoul in August in 1990. This work was supported by Grant-in-Aid for Scientific Research on Priority Area of "Molecular Approaches to Non-equilibrium Processes in Solutions" No. 02245101 from the Ministry of Education, Science and Culture.

References

1) H. Hirakawa, *J. Phys. Chem.*, **91**, 3452 (1987).
2) H. Hirakawa, H. Nomura, and F. Kawaizumi, *Bull. Chem. Soc. Jpn.*, **61**, 3315 (1988).
3) H. Hirakawa, H. Nomura, and F. Kawaizumi, *J. Phys. Chem.*, **93**, 3784 (1989).
4) H. Hirakawa, H. Nomura, and F. Kawaizumi, *Bull. Chem. Soc. Jpn.*, **62**, 1781 (1989).
5) F. Kawaizumi, F. Nakao, and H. Nomura, *J. Chem. Eng. Data*, **33**, 204 (1988).
6) P. Debye, *J. Chem. Phys.*, **1**, 13 (1933).
7) R. M. Fuoss, *J. Am. Chem. Soc.*, **81**, 2659 (1959).
8) C. Treiner, A. Le Besnerais, and C. Micheletti, in "Thermodynamic Behavior of Electrolytes in Mixed Solvents. II," ed by W. F. Furter, American Chemical Society, Washington, D. C. (1979).
9) M. Perie, J. Perie, and M. Chemla, *J. Solution Chem.*, **17**, 203 (1988).

Thermodynamic Study of Brij 35 in Aquo-Polyethylene Glycol Solvents

Leena KOSHY and Animesh Kumar RAKSHIT*
Department of Chemistry, Faculty of Science, M. S. University of Baroda, Baroda 390002, India
(Received September 25, 1990)

Synopsis. The critical micelle concentrations of Brij 35 in aquo PEG 200 solutions were determined by the iodine solubilization method at five different temperatures at various PEG percents. The thermodynamic quantities of micellization as well as the free energies of micellization at infinite dilution were computed and rationalized.

As a part of our interest on the thermodynamics of micellization of nonionic surfactant, Brij 35, in aqueous solution in the presence of various solutes, it was decided to study the effect of polyethylene glycol 200 (PEG 200) on the micellization process of this surfactant in water. Effect of sucrose[1] was studied earlier. PEG 200 is an oligomer and its effect on micellization of Brij 35 was expected to be more chemical than electrochemical in nature. We choose PEG 200 because a literature survey did not show any study with this oligomer. This paper deals with PEG 200 at concentration of 2 to 10% w/v. Due to the importance of nonionic surfactants in industry, e.g., detergency,[2] in the formation of microemulsion[3] which may be useful in tertiary oil recovery and so on, the importance of detailed knowledge of thermodynamics of micellization of nonionic surfactants in presence of other components has become topical. Though there are reasonably large number of studies of the nonionic surfactant Triton X100,[4,5] we have not found detailed systematic study of Brij 35 in literature. Therefore a systematic thermodynamic study of the effect of PEG 200 on the micellization of Brij 35 is reported here.

PEG 200 (Merck, India) was used without any further treatment. Brij 35 (BDH, England) was also used as received. Its chemical formula is $C_mH_{2m+1}(OCH_2CH_2)_nOH$ where m=12 and n=23 with molar mass 1198. Iodine (Sarabhai, India) was sublimed before use and water was doubly distilled from $KMnO_4$. The iodine solubilization method[1,6] was used for determining critical micelle concentration (cmc). The experimental procedure adopted was explained in an earlier publication.[1] There was always a possibility of PEG interacting with iodine and thereby affecting the result. Hence direct surface tension determination by the Wilhelmy plate method was done for a few systems in absence of iodine to determine the critical micelle concentration. The results were comparable with each other as can be seen from Table 1.

Table 1. Critical Micelle Concentration, cmc (μmol dm^{-3}) of Brij 35 in Various Aquo–PEG Solutions at Different Temperatures

Solvent (% PEG 200)	cmc at				
	30 °C	35 °C	40 °C	45 °C	50 °C
0.0	46	43	40	37	34
2.0	31	33(33)[a]	35	37(36)[a]	39
4.0	27	30	33	36	38
6.0	26	29(29)[a]	33	36	38
8.0	25	28	30	35	37
10.0	23	25	28	30	35

a) By direct surface tension determination by Wilhelmy plate method in absence of iodine.

In Table 1 the cmc in water as well as in 2,4,6,8, and 10% PEG 200–water solution at the experimental temperatures of 30,35,40,45, and 50 °C are reported. The maximum error in these values was estimated to be 1.0 μmol from at least three separate measurements and then the standard deviation of the mean was computed. In Fig. 1 we plot the variation of cmc (mole fraction scale) as a function of concentration of PEG at different temperatures. It seems that the effect of increase in temperature and that of increase in PEG amount is similar. It is well known that increase in temperature effects the three dimensional water matrix by breaking it. It seems that the addition of PEG has similar effect. When PEG is added to water, by virtue of its very presence, it breaks the water matrix and then interacts with water to form a different three dimensional structure. The variation of cmc seems to be dependent on the water structure to a very large extent and not to be so much on the water–PEG matrix. Formation of structured solvent should probably have increased the

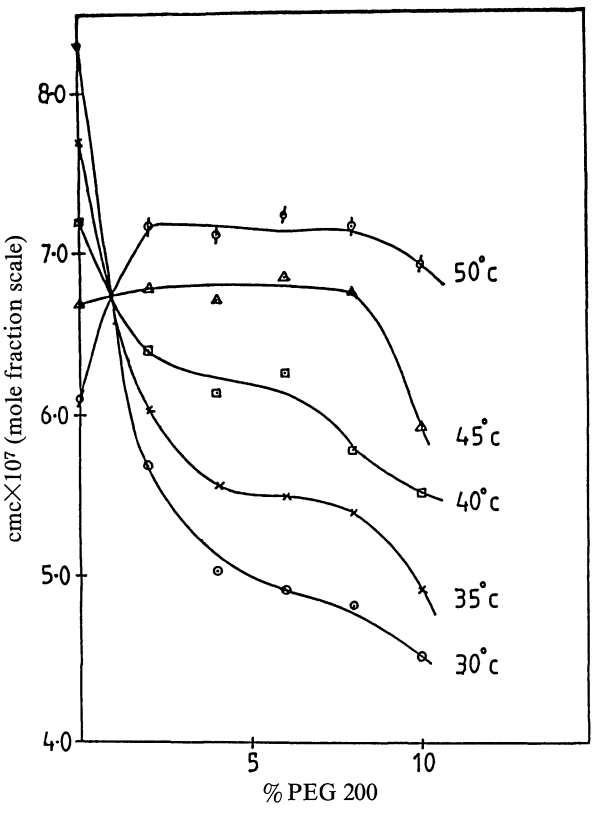

Fig. 1. Plot of cmc vs. % PEG 200 in aquo–PEG 200 solutions at various temperatures.

Table 2. Free Energy, Enthalpy, and Entropy of Micellization of Brij 35 in Aquo–PEG 200 Solutions

Solvent (% PEG)	ΔG_m/kJ mol^{-1}					ΔH_m/kJ mol^{-1}					ΔS_m/J mol^{-1} K^{-1}				
	30 °C	35 °C	40 °C	45 °C	50 °C	30 °C	35 °C	40 °C	45 °C	50 °C	30 °C	35 °C	40 °C	45 °C	50 °C
0.0	35.3	35.9	36.7	37.5	38.3	11.4	11.8	12.2	12.6	13.0	154	155	156	157	159
2.0	36.2	36.7	37.1	37.5	38.0	−8.8	−9.1	−9.4	−9.7	−10.1	90.4	89.3	88.4	87.4	86.5
4.0	36.5	36.9	37.2	37.6	38.0	−13.3	−13.7	−14.2	−14.6	−15.1	76.7	75.2	73.6	72.1	71.0
6.0	36.6	36.9	37.2	37.5	38.0	−14.9	−15.5	−15.9	−16.5	−17.0	71.5	69.6	67.7	66.2	64.9
8.0	36.6	36.9	37.4	37.6	38.0	−15.3	−15.8	−16.3	−16.8	−17.3	70.5	68.8	67.3	65.2	63.9
10.0	36.8	37.2	37.5	37.9	38.1	−15.9	−16.4	−16.9	−17.5	−18.0	69.1	67.4	65.7	64.2	62.0

cmc. Now in Table 1 we find that there is increase in the cmc values at 50 °C with the addition of PEG (2%). That is why we believe that the water–PEG structure has also some effect on cmc values. Two opposing effects are present in the system. These are (1) water structure break down and (2) water–PEG structured matrix formation. The cmc values depend on the effect of these two factors on micelle formation. The quantitative effect of each of these factors is difficult to estimate at this moment. From Fig. 1 it is observed that at about 1% PEG all cmc-concentration of PEG isotherms intersect. This fact indicates that probably at this concentration of PEG the processes of micellization of Brij 35 at all temperatures are similar.

In Table 2 the thermodynamic quantities calculated for these systems are given. The free energy, enthalpy, and entropy of micellization were computed by using the following well known relations

$$\Delta G_m = RT \ln(\text{cmc}),$$
$$\Delta H_m = -RT^2 \, \mathrm{d} \ln(\text{cmc})/\mathrm{d}T,$$
$$\Delta S_m = (\Delta H_m - \Delta G_m)/T,$$

where cmc was taken in mole fraction scale. The transfer process here means the formation of the micelle in the corresponding solvent from solvated free monomer surfactant whose mole fraction was unity. To calculate ΔH_m, ln(cmc) was plotted against T and a linear plot was obtained. The slope of the line was taken as $\mathrm{d} \ln(\text{cmc})/\mathrm{d}T$. This value was found to be positive for all PEG containing systems. Therefore the micellization process was exothermic for all of them. Only for pure aqueous solution the micellization was endothermic in nature. The maximum error in ΔG_m was estimated to be ±0.3%. The error in ΔH_m was ±3.0% which was determined from the standard deviation of the slope of ln(cmc)–T plot by regression analysis. The error in ΔS_m values was ±1.0%.

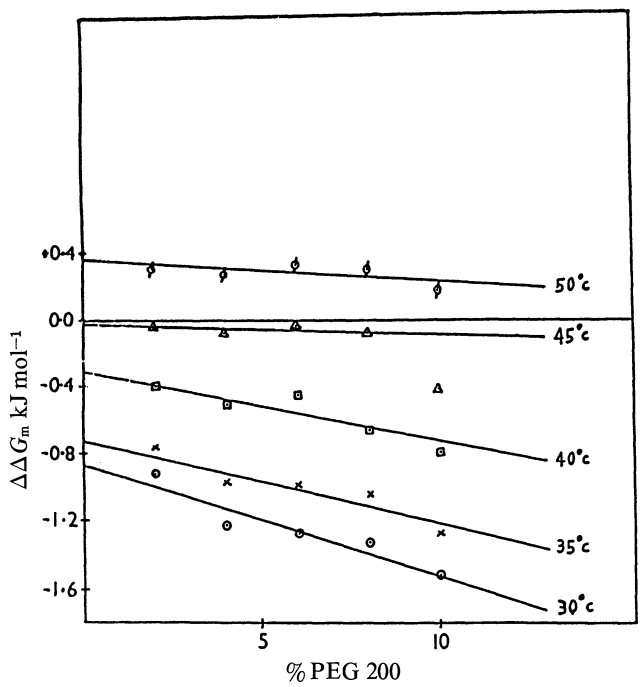

Fig. 2. Plot of $\Delta\Delta G_m$ vs. % PEG 200 at various temperatures.

From Table 2 we find that the ΔS_m is of the order of 70 J mol^{-1} K^{-1}. This type of high entropy change is generally associated with phase changes. Hence it can be assumed that the micelle behaves as a new phase here. It has also been suggested[7] that the positive values of ΔS_m can be attributed to the increase in entropy due to water structure breakdown on micellization as well as due to release of water molecules associated with hydrocarbon chains[8,9] which overshadows the decrease in entropy due to micelle formation. Shaw[10] suggests that it might be due to the freedom of movement of the hydrocarbon chain in the core of the micelle.

It is possible to calculate $\Delta\Delta G_m$ for these systems. This quantity is the free energy of transfer of micelle from pure aqueous environment to PEG containing solution environment plus the medium effect i.e. the free energy of transfer of free monomer surfactant from water to the particular solvent. Pure solvent at atmospheric pressure was taken as the standard state. In Fig. 2 such $\Delta\Delta G_m$ is plotted against % PEG at all temperatures. It is observed that at the highest temperature of study i.e. at 50 °C these processes of transfer together is nonspontaneous one whereas at 45 °C the transfer free energy change is around zero. At other temperatures of 30, 35, and the 40 °C the Brij 35, in monomeric form and also as micelle, prefers the PEG containing solvent rather than the aqueous one (for example at 2% PEG Δcmc in comparison with aqueous solution at 30 °C is 15 units whereas at 50 °C it is −5 units, Table 1). Also

Table 3. $\Delta\Delta G_m$ and $\Delta G_m^{s,0}$ in Aquo–PEG Solvent Systems

Temperature/°C	$\lim_{c\to 0} \Delta\Delta G_m$	$\Delta G_m^{s,0}$
	kJ mol^{-1}	kJ mol^{-1}
30	−0.87	−36.2
35	−0.73	−36.6
40	−0.32	−37.0
45	−0.03	−37.5
50	0.36	−37.9

this linear plot can be extrapolated to $c=0$ where c is the concentration of PEG. On can then write

$$\lim_{c\to 0} \Delta\Delta G_m = \Delta G_m^{s,0} - \Delta G_m^{w}$$

where s is solvent, w is water and 0 indicates that the solvent is infinitely diluted in terms of PEG. This quantity signifies whether the micelle prefers an infinitely dilute PEG containing aqueous environment to a purely aqueous surrounding or not.

The data so calculated for $\Delta G_m^{s,0}$ range between -36.2 to -37.9 kJ mol^{-1} at between 30 and 50 °C respectively which are quite similar to that in a sucrose system[1] suggesting similar effect by these two solutes on overall water matrix.

LK thanks the authorities of this university for providing a teaching assistantship.

References

1) B. G. Sharma and A. K. Rakshit, *J. Colloid Interface Sci.*, **129**, 139 (1989).
2) W. von Rybinski and M. J. Schwuger, in "Nonionic Surfactants Physical Chemistry," ed by M. J. Schick, Marcel Dekker Inc., New York (1987), Surfactant Science Series, Vol. 23.
3) J. T. G. Overbeek, P. L. de Bruyn, and F. Verhoeckx, in "Surfactants," ed by Th. F. Tadros, Academic Press, London (1984).
4) L. Panda and G. B. Behera, *J. Indian Chem. Soc.*, **62**, 44 (1985).
5) A. B. Mandal, S. Ray, A. M. Biswas, and S. P. Moulik, *J. Phys. Chem.*, **84**, 856 (1980).
6) S. Ross and J. P. Olivier, *J. Phys. Chem.*, **63**, 1671 (1959).
7) K. Meguro, M. Ueno, and K. Esumi, in "Nonionic Surfactants Physical Chemistry," ed by M. J. Schick, Marcel Dekker Inc., New York (1987), Surfactant Science Series, Vol. 23.
8) H. S. Frank and M. W. Evans, *J. Chem. Phys.*, **13**, 507 (1945).
9) J. Marrignau, P. Basserau, and P. Delard, *J. Phys. Chem.*, **90**, 645 (1986).
10) D. J. Shaw, "Introduction to Colloid and Surface Chemistry," Butterworths, London (1978).

Spectrophotometric Detection for Flow Injection Analysis of Tertiary Alkylamines in Terms of the Intermolecular Charge-Transfer Interaction with Iodine

Bunji Uno,* Kiho Nakajima, and Satoshi Kawai
Gifu Pharmaceutical University, Mitahora-higashi, Gifu 502
(Received February 25, 1991)

Synopsis. Spectroscopic studies of the intermolecular charge-transfer interaction with iodine have been extended in order to develop a new spectrophotometric detection method for flow injection analysis (FIA). Tertiary alkylamines, as a model compound of spectroscopically inactive species, have been determined with high detection sensitivity by FIA using the present detection method.

Although both spectrophotometric and electrochemical detectors are generally used for flow injection analysis (FIA) or high-performance liquid chromatography (HPLC), it is necessary for compounds inactive to both detectors to be derivatized to active species.[1,2] Some compounds are, however, allowed to be derivatized by a few methods with experimental difficulties.[2,3] It is therefore very significant and important to develop a direct detection method for spectroscopically inactive species without derivatization. On the other hand, the intermolecular charge-transfer (CT) process of organic molecules has been investigated in various fields of chemistry, physics, and biophysics. However, analytical applications using this CT interaction have been quite limited in number. In this paper we have addressed ourselves to the development of a new spectrophotometric detection method for flow systems in terms of intermolecular CT spectra with iodine, adopting an FIA method in order to avoid problems concerning chromatographic separation. The present technique has been examined by the determination of tertiary alkylamines as a model compound possessing no bands in the ultraviolet—visible region, and being extremely difficult to be derivatized to spectroscopically active species.

Experimental

Spectral Measurements. Iodine molecular complexes with alkylamines were studied in heptane and dichloromethane. Their spectral measurements were performed using 1 or 10 cm matched quartz cells equipped with stoppers, regulated to 25 °C by circulating constant temperature water throughout the cell compartment by the use of a Taiyo thermoleader (Model EZL-80).

Flow Injection System. The FIA apparatus is shown schematically in Fig. 1; it comprises Shimadzu LC-6AD and LC-3A HPLC pumps to provide a flow of the dichloromethane carrier and to deliver a dichloromethane solution of iodine; a Rheodyne 7125 injector with a 20-μl loop is used to introduce the analyte. A Gasukuro Kogyo low-dead-volume mixing tee was used to mix the mobile phase carrying the analyte with the iodine solution. A Shimadzu SPD-6A spectrophotometric detector was set at 290 nm. These instruments were connected using a stainless-steel pipe with an inner diameter 0.3 mm (Fig. 1).

Chemicals and Solvents. The samples employed here were triethylamine, tripropylamine, and tributylamine, which were commercially available from Nacalai Tesque, Inc., and were purified by repeated distillation under reduced pressure. Solvents used for spectroscopic observations were heptane and dichloromethane of spectrograde purity, dried over CaH_2 and then carefully rectified. Dichloromethane of special guaranty grade was used as an FIA carrier without any further treatment. The carriers available for the present detection scheme were solvents inactive to iodine, that is, having no electron-donating character such as saturated hydrocarbons or alkyl chlorides. If heptane was used as a carrier, we failed to pump quantitatively throughout the apparatus because of its low viscosity.

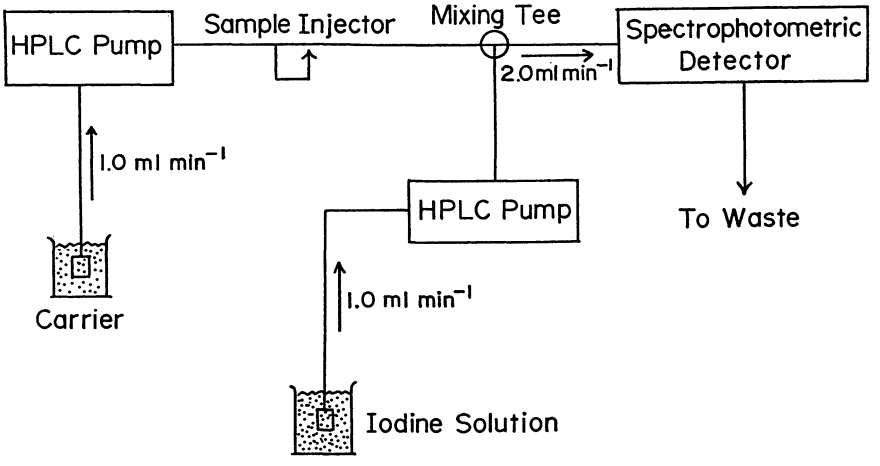

Fig. 1. Schematic diagram of the flow injection apparatus.

Results and Discussion

Formation of the Iodine Complexes with Tertiary Alkylamines. The intermolecular n-σ type CT interaction of alkylamines with strongly electron-accepting iodine has been both theoretically and experimentally investigated in detail.[4-6] The spectral measurements and their analyses gave constants (K) of the iodine CT complex formations of triethylamine, tripropylamine and tributylamine in heptane at 25 °C as 4840, 807 and 1370 mol^{-1} dm, respectively, by the use of Kubota's and Benesi-Hildebrand's equations;[7-9] this value for triethylamine was in fair agreement with that determined by Nagakura.[5] A theoretical analysis using the above equations has made it possible to evaluate the absorption maximum (λ_{max}) and its molecular extinction coefficient (ε_{max}) of the intermolecular CT bands for tertiary alkylamines-iodine-heptane system as ca. 280 nm and 2.5×10^4, respectively. The CT spectra were also recorded in dichloromethane with the addition of alkylamines to an iodine solution, showing an isosbestic point resulting from the 1 : 1 complex formation. Since the concentration ratio of alkylamines to iodine was unsuitable for the above equations, accurate K values in dichloromethane could not be evaluated. However, the absorbance of the CT spectra observed is linearly dependent on the donor concentration, indicating that the CT complexes are considered to form quantitatively in dichloromethane in view of the large K values in heptane.[10] The apparent λ_{max} and ε_{max} of the CT transition were evaluated in dichloromethane as 288 nm and 1.54×10^4 for triethylamine, 291 nm and 1.10×10^4 for tripropylamine, and 291 nm and 1.93×10^4 for tributylamine, respectively. Therefore, these bands seem to be applicable to the determination of tertiary alkylamines with a spectrophotometric detector.

The amines are no sooner added to the iodine solution than the solution apparently changes color, indicating that the CT complexes are formed promptly. The temperature dependence on the K values of the iodine CT complexes were investigated;[5,7] it is thus concluded that the lower is the temperature the easier is formation, since the change in enthalpy is negative for complex formation. However, the 10^{-4} mol dm^{-3} level of iodine was sufficient to quantitatively form CT complexes with the amines under 10^{-5} mol dm^{-3} at room temperature, owing to their large K values.

FIA Determination of Tertiary Alkylamines. Optimum FIA conditions were established as follows on the basis of a series of preliminary investigations. A mode of post-injection was adopted to the present FIA determination, since direct injection to the carrier containing iodine did not give the expected increase in the FIA response. The FIA peak height was practically independent of the period from mixing to detection, indicating that the formation rate of the CT complexes is very fast. A commercial mixing tee without further improvement is capable of mixing the carrier with the iodine solution. The pumps were operated at a flow rate of 1.0 ml min^{-1}, which was adequate to obtain a sharp peak. With regard to the concentration of iodine, the 10^{-4} mol dm^{-3} level is sufficient for a quantitative formation of the CT complexes, as mentioned above. The use of a solution of more than 10^{-3} mol dm^{-3} gave an unstable base line. Detection at 290 nm was selected in consideration of the λ_{max} of the CT

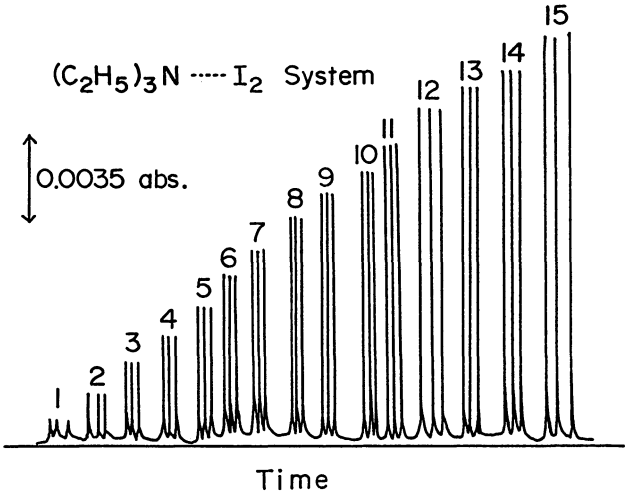

Fig. 2. Flow injection response of triethylamine. The time required for an appearance of the peak is 1.5 min after injection of a sample. Conditions: flow rate of carrier, 1.0 ml min^{-1}; flow rate of iodine solution, 1.0 ml min^{-1}; sample injection, 20 μl; detection wavelength, 290 nm. Concentration of iodine solution is 1.13×10^{-4} mol dm^{-3}. Concentrations of triethylamine are (1) 0.67, (2) 1.34, (3) 2.01, (4) 2.68, (5) 3.35, (6) 4.02, (7) 4.69, (8) 5.36, (9) 6.03, (10) 6.70, (11) 7.37, (12) 8.04, (13) 8.71, (14) 9.38, and (15) 10.1×10^{-6} mol dm^{-3}.

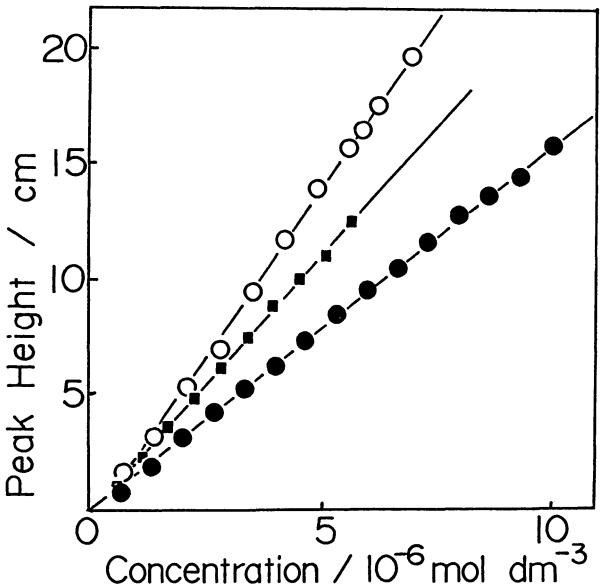

Fig. 3. Concentration (C) dependence of FIA peak height (PH) for triethylamine (●), tripropylamine (■), and tributylamine (○). The regression equations are PH=1.57C−0.137 (sample number (n)=15, standard deviation (s)=0.103, regression coefficient (r)=0.9995) for triethylamine, PH=2.24C−0.320 (n=10, s=0.103, r=0.9997) for tripropylamine, and PH=2.89C+0.867 (n=11, s=0.319, r=0.9988) for tributylamine.

Table 1. Detection Limit for Tertiary Alkylamines by the Present FIA method

Compounds	Detection limit[a]		
	mol dm^{-3}	10^{-9} g	10^{-12} mol
Triethylamine	6.71×10^{-7}	1.36	13.4
Tripropylamine	5.70×10^{-7}	1.63	11.4
Tributylamine	7.11×10^{-7}	2.63	14.2

a) The detection limit was examined with a 20-μl injection.

spectra for iodine-tertiary alkylamines-dichloromethane systems.

A typical response of FIA for the determination of triethylamine is shown in Fig. 2. The FIA response was very good for all of the samples, and the peak height was linearly dependent on the sample concentration (Fig. 3). The detection limit collected in Table 1 was determined as the lower linear range of the calibration lines, since an unavoidable background signal appears with sample injection to an FIA apparatus equipped with a spectrophotometric detector set at high sensitivity. Therefore, good linearity was obtained down to the detection limit determined here, as shown in Fig. 3. It may be allowed to detect more sensitively by adopting the present method to HPLC analysis. However, the detection limit obtained is far superior to the 4×10^{-5} mol dm^{-3} of triethylamine determined by the use of the derivatization method to chemiluminescence based on the oxidation of tertiary amines by benzoyl peroxide.[3] The other methods concerning the derivatization of tertiary amines permit the detection of these analytes at only 2—10×10^{-6} g.[2] Recently, Danielson et al. reported a generation of the chemiluminescent metal complexes of aliphatic amines with tris(2,2′-bipyridine)ruthenium(III).[11] This method can be considered to be very superior and efficient for the determination of aliphatic amines with respect to the detection limits, permitting the limit of these analytes at the 0.04—2×10^{-9} g level. However, the chemiluminescent method upon reaction with tris(2,2′-bipyridine)-ruthenium(III) seems to require the high technique in terms of treating unstable reagents and the construction of a spectroscopic cell to detect the emission of the short lifetime chemiluminescence. Therefore, our CT interaction method can be regarded being both profitable and useful as a simple determination of aliphatic amines in many respects.

As a conclusion, we may safely say that intermolecular CT interactions are applicable for the detection of tertiary alkylamines by FIA with a spectrophotometric detector. The present method appears to be very promising as a HPLC postcolumn detector. Further, since iodine forms CT complexes with many organic substances as a strong σ-electron acceptor, particularly with those having nonbonding electrons,[4-8] this detection scheme might well be adopted for the determination of these compounds possessing no good chromophore.

References

1) N. D. Danielson, M. A. Targove, and B. E. Miller, *J. Chromatogr. Sci.*, **26**, 362 (1988).
2) M. Pesez and J. Bartos, "Colorimetric and Fluorimetric Analysis of Organic Compounds and Drugs," Marcel Dekker, New York (1974), p. 161.
3) J. L. Burguera and A. Townsherd, *Talanta,* **26**, 795 (1979).
4) R. S. Mulliken and W. B. Person, "Molecular Complexes," Wiley Interscience, New York (1969).
5) S. Nagakura, *J. Am. Chem. Soc.*, **80**, 520 (1958).
6) I. Jano, *Theor. Chim. Acta,* **71**, 305 (1987).
7) T. Kubota, *J. Am. Chem. Soc.*, **87**, 458 (1965).
8) B. Uno, N. Kaida, K. Kano, and T. Kubota, *Spectrochim. Acta, Part A,* **45**, 937 (1989).
9) H. A. Benesi and J. H. Hildebrand, *J. Am. Chem. Soc.*, **71**, 2703 (1949).
10) A. Kuboyama, "Kagaku Zoukan 48; Charge Transfer Complexes," ed by S. Tazuke, H. Tsubomura, J. Tokura, and R. Mikawa, Kagaku Dojin, Kyoto (1971), p. 83.
11) J. B. Noffsinger and N. D. Danielson, *Anal. Chem.*, **59**, 865 (1987); M. A. Targova and N. D. Danielson, *J. Chromatogr. Sic.*, **28**, 505 (1990); J. B. Noffsinger and N. D. Danielson, *J. Chromatogr.*, **387**, 520 (1987).

Extraction-Spectrophotometric Determination of Vanadium(V) with Pyrocatechol and N^1-Hydroxy-N^1,N^2-diphenylbenzamidine

Chandresh AGRAWAL,* Khageshwar Singh PATEL, and Rajendra Kumar MISHRA
Department of Chemistry, Ravishankar University, Raipur 492010, M. P., India
(Received April 12, 1990)

Synopsis. A sensitive procedure for spectrophotometric determination of V(V) with pyrocatechol and N^1-hydroxy-N^1,N^2-diphenylbenzamidine (HDPBA) is described. The value of molar extinction coefficient (ε) of the colored complex in chloroform is 5.60×10^5 dm^3 mol^{-1} cm^{-1} at λ_{max} 410 nm. The optimization of analytical variables, effect of diverse ions and application of the method to environmental samples have been investigated.

Vanadium is reported toxic to human being, animal, and plants .[1-3] Therefore, many sensitive spectrophotometric methods (e.g. xanthene derivative,[4,5] 3,5-dinitrocatechol with brilliant green[6] and rhodamine B,[7] phenylethylenediantipyrinylmethane,[8] diphenylcarbazide,[9] *N*-(*o*-sulphonic benzoyl)-*N*-pyridine (*N*-(2-pyridyl)-2-sulphobenzamide)[10] and hexadecyltrimethyl ammonium[11]) for determination of V(V) in a variety of complex materials are claimed. Most of these methods suffer from interelemental interferences. In the present investigation, another type of new, selective and sensitive method for the spectrophotometric determination of V(V) with pyrocatechol and N^1-hydroxy-N^1,N^2-diphenylbenzamidine is described. The sensitivity of the present method is comparable to other reported methods whereas the selectivity is seen to be superior.

Experimental

Apparatus. A Varian DMS-100 UV-vis spectrophotometer (double beam) matched with 1 cm quartz cells was used for the absorbance measurements. A Systronic pH meter model-335 was employed for measuring the pH values.

Reagents. All chemicals used were of analytical grade. A standard V(V) stock solution (100 μg V/cm^3) was prepared by dissolving the weighed amount of ammonium metavanadate in double distilled water and standardized as in literature.[12] N^1-hydroxyamidine were prepared as described in literature.[12] A pH 6.0 buffer was prepared by dissolving the appropriate amount of sodium hydroxide–potassium hydrogen phosfate.[13] A 0.4% w/v (0.036 mol dm^{-3}) pyrocatechol in water and 0.4% w/v (0.0138 mol dm^{-3}) N^1-hydrory-N^1,N^2-diphenylbenzamidine solution in ethanol was employed.

Procedure. An aliquot of the solution containing upto 1.0 μg V(V) is taken in a 50 cm^3 beaker and heated with 2.0 cm^3 pyrocatechol and 5.0 cm^3 ethanolic solution of N^1-hydroxyamidine. The pH of the solution is adjusted to 6.0 with sodium hydroxide–potassium hydrogen phosfate buffer (1.0 cm^3) in the 10 cm^3 total solution. The solution is heated over boiling water bath till volume of the solution is reduced to nearly half. Then the cold solution is transferred to a 100 cm^3 separatory funnel by maintaining total aqueous volume to 8.0±2.0 cm^3 with distilled water. The aqueous solution is shaken with 8.0 cm^3 chloroform and the organic phase is separated. The aqueous phase is further washed with 1×2 cm^3 fresh chloroform. All the extract is dried over anhydrous sodium sulfate (2 g) in a 25 cm^3 beaker. All the extract after drying is transferred to 10 cm^3 volumetric flask and filled upto the mark with chloroform. The spectra of the complex formed is scanned against the reagent blank.

Table 1. Spectral Characteristics of Different Species Formed with V(V)+Pyrocatechol or V(V)+Pyrocatechol+HDPBA

Analytical characteristics	Solvent	λ_{max} / nm	ε / dm^3 mol^{-1} cm^{-1}
V(V)+Pyrocatechol (9.0×10^{-3} mol dm^{-3})	Water	420	4650
V(V)+Pyrocatechol (1.6×10^{-1} mol dm^{-3})	Water	590	7600
V(V)+Pyrocatechol (9.0×10^{-3} mol dm^{-3}) (upon heating)+ HDPBA in Chloroform	Chloroform	410	15000
V(V)+Pyrocatechol+ 1 ml ethanol (upon heating) +HDPBA in Chloroform	Chloroform	410	18000
V(V)+Pyrocatechol+ HDPBA in ethanol (at room temperature)	Water–ethanol	410	17500
V(V)+Pyrocatechol+ HDPBA in ethanol (upon heating)	Water–ethanol	390	1.37×10^5
V(V)+Pyrocatechol+ HDPBA in ethanol (upon heating)	Chloroform	410	5.6×10^5

Results and Discussion

Spectral characteristics of the colored complexes formed with V(V)+pyrocatechol, V(V)+N^1-hydroxyamidine, and V(V)+pyrocatechol+N^1-hydroxyamidine at different analytical conditions are summarized in Table 1.

Absorption Spectra. The absorption spectra of the colored complex formed among V(V)+pyrocatechol +HDPBA against the reagent blank in chloroform and that of the reagent blank against chloroform are shown in Fig. 1. The absorption maximum of the colored complex formed, lie at 410 nm. At this region, the reagent blank shows some absorption, hence all the measurements were made against the reagent blank.

Effect of Variables on Formation of the Colored Complex: The effect of pH of the aqueous solution before heating is studied. The optimum pH range is found to be 5.5—6.5. A 40—70% (v/v) ethanol concentration is adequate for maximum color development. Removal of excess of ethanol is necessary in order to prevent miscibility of the aqueous and organic phase. At least 0.005 and 0.007 mol dm^{-3} of pyrocatechol and HDPBA is needed for maximum and constant color development and addition of more pyrocatechol and HDPBA upto 0.01 and 0.017 mol dm^{-3}, respectively cause no adverse effect on the color development of the complex. A heating time of at least 8 min (over boiling water bath) is required for the maximum color development of complex formed in aqueous ethanol solution and prolonged heating upto 15 min cause no adverse effect.

Effect of Variables on the Extraction of the Colored Complex: The colored complex formed among V(V)+pyrocatechol+N^1-hydroxyamidine is quantitatively extractable into chloroform, carbon tetrachloride, benzene, and toluene. Of these, toluene gives the most sensitive color reaction (ε=11.0×10^5 dm^3 mol^{-1} cm^{-1}, λ_{max} 420 nm) but after 5 min the organic phase becomes hazy probably due to low solubility of N^1-hydroxyamidine. Hence, chloroform (5.60×10^5 dm^3 mol^{-1} cm^{-1}, λ_{max} 410 nm) has been chosen for the extraction of the complex in the present investigation.

The variation of the temperature of the aqueous phase from 15—40 °C cause no change in the absorbance of the extract. The color of the extract is stable for at least 1 h at room temperature (22±2 °C). The volume ratio of the organic to the aqueous phase from 5 : 2 to 1 : 2 do not affect the color intensity of the extract. A shaking time of 2 min is sufficient for maximum extraction.

The optimum concentration range on the basis of Beer's law is found to be 0—1.0 μg V(V)/10 cm^3 in chloroform with a correlation coefficient of 0.98. The molar absorptivity of the colored complex and the limit for detection of the metal are 5.60×10^5 dm^3 mol^{-1} cm^{-1} and 0.1 μg dm^{-3} (more than the absorbance value of the blank and twice of standard deviation of the blank for 10 replicate measurements) at λ_{max} 410 nm, respectively. The relative standard deviation of 10 replicate measurements at level of 0.4 μg V/10 cm^3 in chloroform is found to be ±2% and the confidence limit at 95% probability is (5.60±0.05)×10^5 dm^3 mol^{-1} cm^{-1}.

Percentage Extraction. A 10 and 20 μg standard solution of V(V) is taken and color is developed as in the

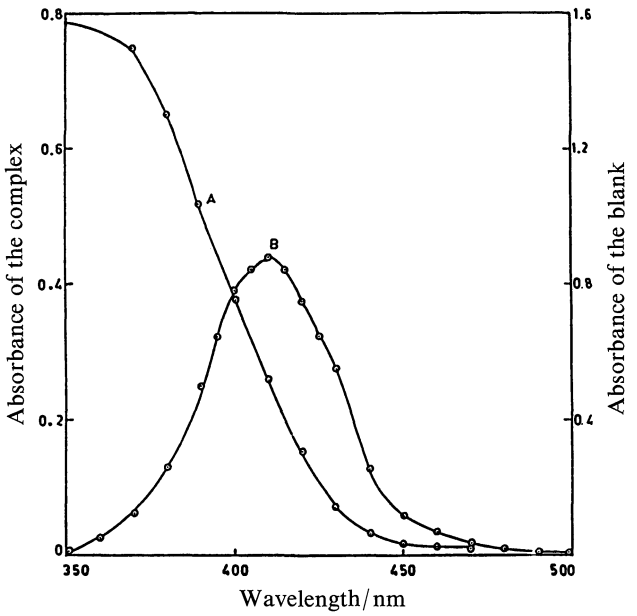

Fig. 1. Absorption spectra of the solvated complex formed by heating V(V) with HDPBA and pyrocatechol as in the procedure.
$C_{pyrocatechol}$=9.0×10^{-3} mol dm^{-3},
C_{HDPBA}=1.4×10^{-2} mol dm^{-3},
pH=6.0±0.2,
(A) Reagent blank.
(B) Vanadium(V) colored complex.
$C_{V(V)}$=7.8×10^{-7} mol dm^{-3}.

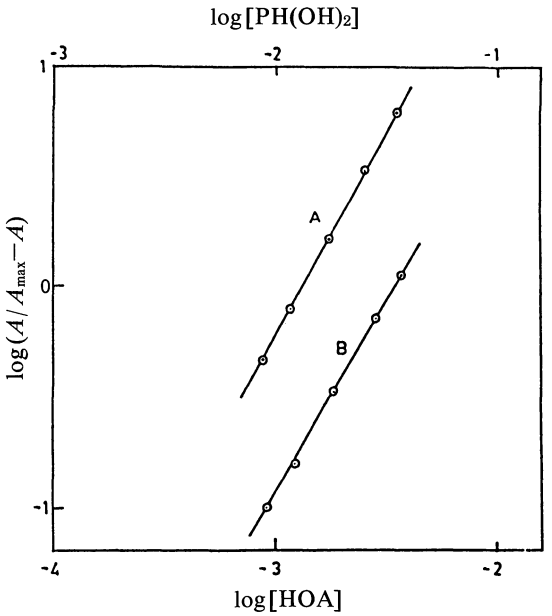

Fig. 2. Determination of ratio of the metal to the reagent in the colored complex.
$C_{V(V)}$=9.8×10^{-7} mol dm^{-3}, in the aqueous solution
pH=6.0±0.2,
(A) $\log A/(A_{max}-A)$ versus log[pyrocatechol]
C_{HDPBA}=1.4×10^{-2} mol dm^{-3},
(B) $\log A/(A_{max}-A)$ versus log[HDPBA]
$C_{pyrocatechol}$=9.0×10^{-3} mol dm^{-3}.

Table 2. Determination of Vanadium(V) in Environmental Samples

Sample	V(V) found by PAR method[a]	V(V) found by this method[a]	Rel. std. dev. of this method
	ppb	ppb	±%
Puri, Orissa, India	26	27	1.8
Jam Nagar, Gujrat, India	9	10	2.2
Adwani Oerlikon, Urla, Raipur	77	79	1.7
Singhania Steel, Urla, Raipur	100	102	1.6
Swastik Wires, Urla, Raipur	68	71	1.8
Allied Steel, Tatibandh, Raipur	34	36	1.9
Super Steel, Sarona, Raipur	49	52	2.0
Blast Furnace, Bhilai (M.P.)	14	16	2.1
Total Waste Water, Bhilai Steel Plant, Bhilai (M.P.)	4	3.5	2.3
Cement dust, CCI, Mandhar (MP)	790	795	1.8
Coal dust, CCI, Mandhar (MP)	1610	1659	1.6

a) Average of five determinations.

procedure. The colored complex is extracted, the extract is evaporated, digested with acids and determined by 4-(2-pyridylazo)resorcinol as in the literature.[15] The percentage extraction is found to be 98±0.2% in a single extraction.

Stoichiometry of Extraction. The ratio of the metal to pyrocatechol or HDPBA was determined by plotting $\log A/(A_{max}-A)$ versus log molar concentration of pyrocatechol or HDPBA in the organic solution. The slope for pyrocatechol and HDPBA curves are found to be 1.98 and 1.86, respectively, close to integer 2, suggesting the involvement of vanadium : pyrocatechol : HDPBA in 1 : 2 : 2 ratio in the formation of chloroform extractable colored complex. V(V) is reduced to V(IV),[14] by means of pyrocatechol to react further with 2 moles each of pyrocatechol and N^1-hydroxyamidine. The probable reaction mechanism can be written as:

$$VO^{2+} + 2\ PyO_2^{2-} + 2\ HDPBA + n\ EtOH + 2H^+ \rightleftarrows [V(PyO_2)_2]\cdot 2\ HDPBA\cdot n\ EtOH + 2H_2O$$

The complex so formed is extractable into chloroform

$$[V(PyO_2)_2]\cdot 2\ HDPBA\cdot n\ EtOH + 2H_2O \rightleftarrows [V(PyO_2)_2]\cdot 2\ HDPBA\cdot n\ EtOH_o + 2H_2O$$

Where o, PyO_2^{2-}, and HDPBA denote the organic phase, pyrocatechol anion, and N^1-hydroxy-N^1,N^2-diphenylbenzamidine, respectively.

Effect of Diverse Ions: The effect of the diverse ions on the determination of 0.4 μg V(V) was studied as in procedure. No diverse ions were found to interfere in the spectrophotometric determination of the metal. Their tolerance limit are summarized in parenthesis in μgs:
Cu(II) (200), Ag(I) (150), Ba(II) (100), Cd(II) (40), Hg(II) (50), Al(III) (200), La(III) (100), Pb(II) (40), Zr(IV) (200), As(V) (75), Sb(V) (50), Nb(V) (50), Cr(III) (125), W(VI) (50), Fe(III) (50), Co(II) (100), Ni(II) (100), Os(VIII) (25), U(VI) (150), EDTA (400), F^- (150), $C_2O_4^{2-}$ (50), NO_3^- (50), PO_4^{3-} (400).

Application. The validity of this method is tested to environmental samples e.g. cement dust, coal dust, sea water, and industrial waste water. The solid sample is digested with aqua regia and concentrated hydrochloric acid and the dried residue is dissolved in water. In case of 4-(2-pyridylazo)resorcinol method, the metal is prior separated by extraction with N^1-hydroxy-N^1,N^2-diphenylbenzamidine from 6 mol dm^{-3} CH_3COOH as described in the literature.[12] The extract is evaporated, digested by acids treatment, dissolved in water and determined spectrophotometrically by 4-(2-pyridylazo)resorcinol.[15] The metal content analysed by these two procedures are comparable (Table 2).

References

1) F. W. Oehme, "Toxicity of Heavy Metals in the Environment," Marcel Dekker Inc., New York (1979), Part 2.
2) R. J. Hickey, E. P. Schoff, and R. C. Chelland, *Arch. Environ. Health,* **15**, 728 (1967).
3) N. I. Sax, "Dangerous Properties of Industrial Materials," 6th ed, Von Nostrand Reinhold Company, New York (1984).
4) I. Mori, Y. Fujita, K. Fujita, T. Tanaka, Y. Nakahashi, and A. Yoshil, *Anal. Lett.,* **20**, 747 (1987).
5) I. Mori, Y. Fujita, K. Fujita, Y. Koshiyama, and T. Tanaka, *Bull. Chem. Soc. Jpn.,* **59**, 3997 (1987).
6) Z. Marczenko and R. Lobinski, *Talanta,* **35**, 1001 (1988).
7) R. Lobinski and Z. Marczenko, *Anal. Sci.,* **4**, 629 (1988).
8) P. Li and J. Pan, *Lihuna Jianyan Huaxue Fence,* **24**, 159 (1988).
9) Y. Jin, *Fenxi Shiyanshi,* **6**, 57 (1987).
10) B. K. Sharma, S. P. Mathur, and V. Iyer, *J. Inst. Chem. (India),* **54**, 189 (1982).
11) M. Jarosz and Z. Marczenko, *Analyst,* **109**, 35 (1984).
12) K. Satyanarayana and R. K. Mishra, *Anal. Chem.,* **46**, 1609 (1974).
13) N. A. Lange, "Handbook of Chemistry," 10th ed, McGraw Hill Inc., New York (1967), p. 972.
14) V. Patrovsky, *Collect. Czech. Chem. Commun.,* **31**, 3392 (1966).
15) O. Budevsky and L. Johnova, *Talanta,* **12**, 291 (1965).

Reforming of Ethanol —Dehydrogenation to Ethyl Acetate and Steam Reforming to Acetic Acid over Copper-Based Catalysts—

Nobuhiro IWASA* and Nobutsune TAKEZAWA*
Department of Chemical Process Engineering, Hokkaido University, Sapporo 060
(Received February 12, 1991)

The title reactions, $2CH_3CH_2OH \rightarrow CH_3COOC_2H_5+2H_2$ and $CH_3CH_2OH+H_2O \rightarrow CH_3COOH+2H_2$, were carried out over copper-based catalysts (Cu, Cu/SiO_2, Cu/ZrO_2, Cu/Al_2O_3, Cu/MgO, and Cu/ZnO). The selectivities to ethyl acetate and acetic acid markedly depended upon the supports used. Acetaldehyde was formed by the dehydrogenation of ethanol and transformed to either ethyl acetate or acetic acid through steps in which a nucleophilic addition of ethanol (or ethoxide ions) or water (or hydroxide ions) to acetaldehyde occurred. The rates of the transformation steps to ethyl acetate and acetic acid were appreciably affected by the kinds of supports used. The transformation steps proceeded slowly, compared with the dehydrogenation step.

Although alcohols are rapidly dehydrogenated to aldehydes or ketones over copper-based catalysts,[1] the dehydrogenation of higher alcohols is poorly selective. The aldehydes and ketones formed partly undergo an aldol condensation and/or transformation to esters.[2,3] In the dehydrogenation of methanol, methyl formate is produced in high selectivity over copper-based catalysts.[4-6] We have shown that this reaction proceeds consecutively through the dehydrogenation of methanol to formaldehyde and the reaction between the formaldehyde and methanol (or methoxide ions).[7] When water was present along with methanol, steam reforming of methanol ($CH_3OH+H_2O \rightarrow CO_2+3H_2$) occurs selectively.[8,9] The formaldehyde produced reacted rapidly with water to form carbon dioxide and hydrogen via surface formate or formic acid.[10]

Although Kawamoto et al. previously studied the dehydrogenation of various higher alcohols over unsupported copper,[2,3] their experiments were conducted within a restricted range of operating conditions. Regarding the steam reforming of higher alcohols over copper-based catalysts, no paper has been published according to our knowledge.

In the present study, the title reactions were carried out over various copper-based catalysts under a wider range of operating conditions, and differences in the mechanisms of the reactions involving methanol and ethanol were elucidated.

Experimental

The catalysts used in the present experiments were unsupported Cu, Cu/SiO_2 (0.5—90 wt% Cu), Cu/ZrO_2 (0.5—30 wt% Cu). $CuAl_2O_3$ (6.3 and 30 wt% Cu), Cu/MgO (6.2 and 30 wt% Cu), and Cu/ZnO (30 wt% Cu). Support-free Cu was prepared by the decomposition of copper(II) nitrate at 773 K in air for 3 h. The supported catalysts were prepared by impregnation of metal oxides with a solution of copper(II) nitrate and calcined at 773 K in air for 3 h. Prior to the reaction, the catalysts, thus prepared, were reduced in a hydrogen stream of 12 cm^3 min^{-1} at 523 K for 18 h. Experiments were carried out in a manner similar to those in a previous study.[7] A conventional flow reactor was used; the concentrations of the reactants and the products in the effluent were determined by gas chromatography. The selectivities to carbon-containing products were evaluated on the carbon basis.

The valence states of copper were determined by diffuse reflectance UV-vis spectroscopy. The amount of metallic copper exposed on the surface was determined by a reaction with dinitrogen monoxide.[11]

Results and Discussion

Dehydrogenation of Ethanol. 1) Reaction Pathway to Ethyl Acetate: The dehydrogenation of ethanol occurred above 380—420 K, giving acetaldehyde, ethyl acetate and C_4-species (butyraldehyde, 1-butanol, and methyl ethyl ketone). The selectivities to these products depended upon the reaction conditions and the catalysts used. Figure 1 shows the mole fraction of the products against space time over 30 wt% Cu/SiO_2. Both ethyl acetate and butyraldehyde increase with space time. Acetaldehyde increases with an increase in space time,

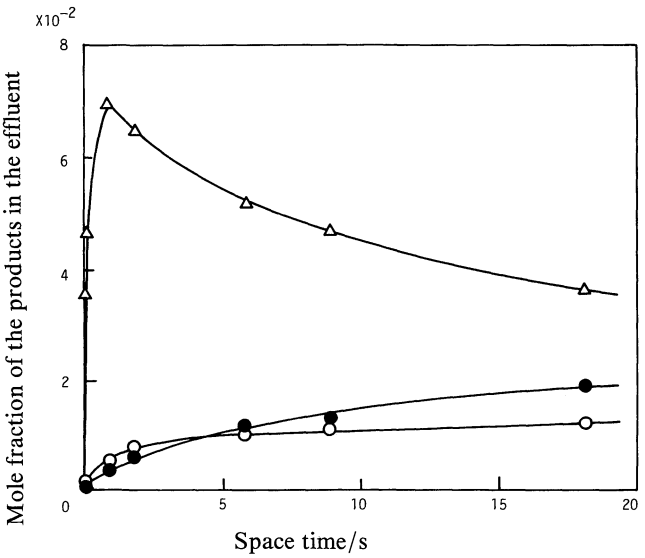

Fig. 1. Mole fraction of the products in the effluent against space time in dehydrogenation of C_2H_5OH over 30 wt% Cu/SiO_2. Temperature: 493 K. Inlet partial pressure $P^0_{C_2H_5OH}$: 20.5 kPa. (△) CH_3CHO, (●) $CH_3COOC_2H_5$, (○) C_3H_7CHO.

passes through a maximum and then decreases. These results strongly suggest that ethyl acetate and butyraldehyde are formed via acetaldehyde. The values of a parameter, $K=P_{CH_3CHO}P_{H_2}/P_{C_2H_5OH}$, which was estimated from the partial pressures of acetaldehyde, hydrogen and ethanol in the effluent, were found to be close to that of the equilibrium constant, K_p,[12,13] of the dehydrogenation of ethanol $C_2H_5OH \rightarrow CH_3CHO+H_2$ at 493 K. Hence, under the reaction conditions the formation of acetaldehyde was much more rapid than those of ethyl acetate and butyraldehyde.

Figure 2 illustrates the selectivity for ethyl acetate formation against conversion of ethanol over 30 wt% Cu/SiO_2 at different temperatures. The selectivity increases considerably with an increase in the conversion of ethanol. At 493 K and an ethanol conversion of 76%, a 56% selectivity was attained. At a given conversion of ethanol, the selectivity increases appreciably with a decrease in the temperature.

To examine the pathway to ethyl acetate, reactions involving acetaldehyde were carried out. In Figs. 3(I) and (II), the mole fraction of various carbon-containing products in the effluent is plotted against time at 433 K. When only acetaldehyde was fed over 30 wt% Cu/SiO_2, crotonaldehyde was exclusively produced. No ethyl acetate was detected in the effluent. However, upon switching acetaldehyde to ethanol, ethyl acetate was

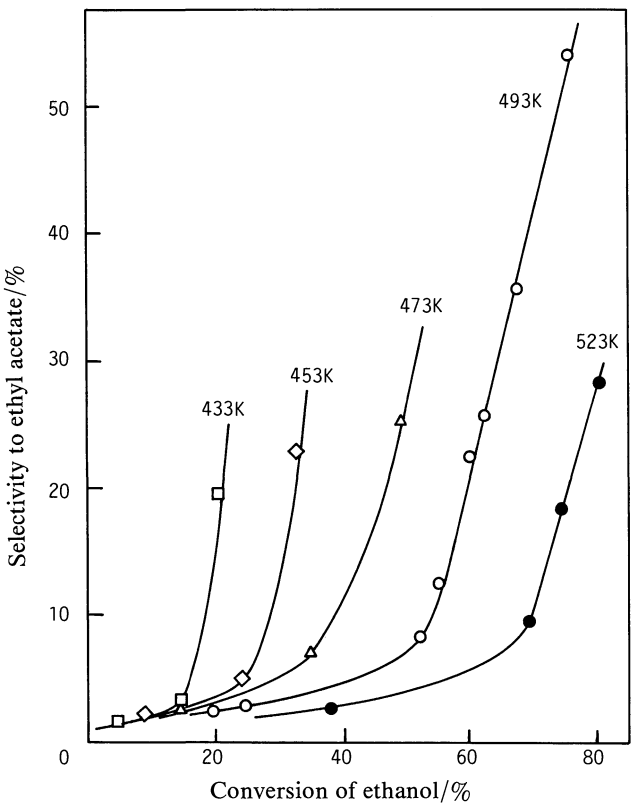

Fig. 2. Selectivity to ethyl acetate against conversion of ethanol over 30 wt% Cu/SiO_2. Inlet partial pressure $P^0_{C_2H_5OH}$: 20.5 kPa.

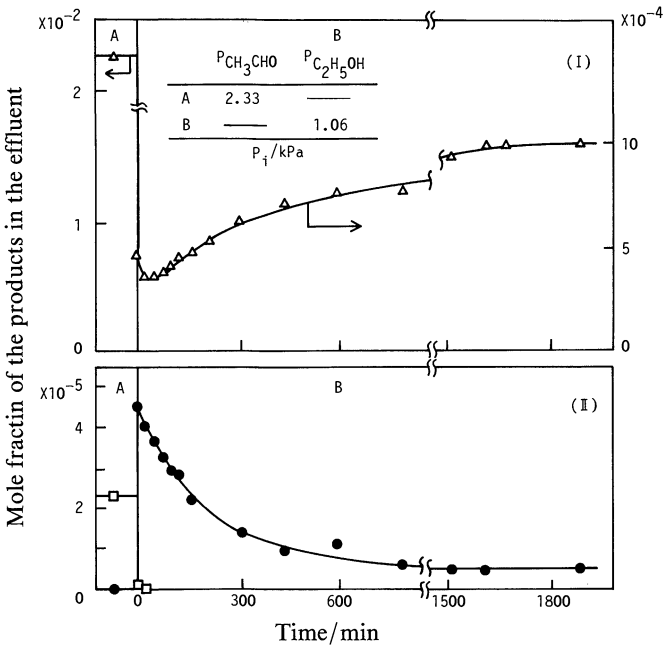

Fig. 3. Carbon-containing products formed in the reactions involving CH_3CHO over 30 wt% Cu/SiO_2: (A) in the absence of C_2H_5OH, (B) in the presence of C_2H_5OH. Temperature: 433 K. (△) CH_3CHO, (●) $CH_3COOC_2H_5$, (□) $CH_3CH=CHCHO$.

formed rapidly, and decreased to a steady value. Crotonaldehyde diminished rapidly. Acetaldehyde in the effluent initially decreased, but then increased with time as the dehydrogenation of ethanol proceeded. When ethanol was fed over the acetaldehyde-free catalyst, ethyl acetate was formed together with acetaldehyde. Since these products increased with time in a monotonic manner, reaching steady values, it was strongly suggested that ester formation occurred appreciably in the presence of adsorbed acetaldehyde. Since methanol was dehydrogenated to methyl formate via reaction between formaldehyde and methanol (or methoxide),[7] we concluded that the acetaldehyde formed by the dehydrogenation of ethanol was subjected to a nucleophilic addition of ethanol (or ethoxide) and transformed to ethyl acetate.

2) Effect of the Supports upon the Reaction: Table 1 lists the selectivity to the carbon-containng products and the product ratio, (C_4/Ester), of C_4-species to ethyl acetate at an ethanol conversion of 50% over various copper-based catalysts. These parameters are greatly affected by the kinds of supports. Cu/ZrO_2 and Cu/ZnO are highly selective for ethyl acetate formation. The C_4-species and diethyl ether are produced appreciably over Cu/Al_2O_3. However, when KOH (1 wt% K) was doped on Cu/Al_2O_3 (not listed in Table 1), the product ratio decreased from 4.3 to 0.4, and the formation of diethyl ether was completely suppressed. These results strongly suggested that C_4-species such as butyraldehyde, methyl ethyl ketone and 1-butanol were

Table 1. Dehydrogenation of Ethanol — Selectivity to Carbon-Containing Products and Product Ratio (C_4/Ester) at 493 K and $P^0_{C_2H_5OH}$=20.5 kPa —

Catalyst[a]	Selectivity[b]/%					C_4/Ester[d]
	Acetaldehyde	Acetone	Diethyl ether	C_4-species[c]	Ethyl acetate	
Cu/Al_2O_3	54.1	Trace	19.3	21.6	5.0	4.3
Cu/SiO_2	77.9	0.4	0.3	13.9	7.5	1.9
Cu/MgO	74.2	4.0	0	8.0	13.8	0.6
Cu/ZrO_2	57.3	0.5	0	14.6	27.6	0.5
Cu/ZnO	67.3	0.7	0	3.9	28.1	0.1
Cu[e]	70.6	1.7	0	7.4	20.3	0.4

a) Supported Cu catalyst: 30 wt% Cu. b) Selectivity to carbon-containing products at ethanol conversion of 50%. c) Including butyraldehyde, methyl ethyl ketone, and 1-butanol. d) Ratio of mole fraction of C_4-species to ethyl acetate in the effluent at ethanol conversion of 50%. e) Obtained at ethanol conversion of 45%.

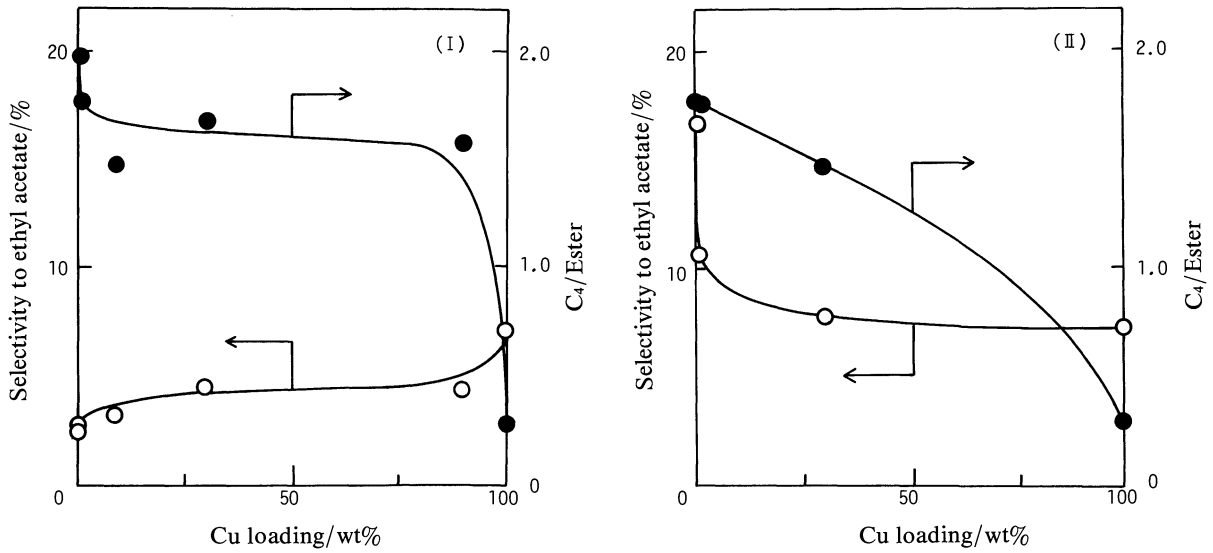

Fig. 4. Selectivity to ethyl acetate and product ratio C_4/Ester obtained at C_2H_5OH conversion of 35%: over Cu/SiO_2, (II) over Cu/ZrO_2. Temperature: 493 K. Inlet partial pressure $P^0_{C_2H_5OH}$: 20.5 kPa.

produced by acid-catalyzed reactions.

Figures 4(I) and (II) illustrate the selectivity to ethyl acetate and the product ratio obtained at an ethanol conversion of 35% over Cu/SiO_2 and Cu/ZrO_2 with various copper loadings. These parameters depend upon the copper loading as well as the kinds of supports. Over Cu/SiO_2, the selectivity for ethyl acetate formation gradually decreases with a decrease in copper loading. On the other hand, the product ratio increases considerably when the copper loading changes from 100 wt% to 90 wt% Cu. This ratio gradually increases with decreasing loading from 90 wt% to 1 wt% Cu; at 0.5 wt% Cu increases considerably. At low copper loadings an appreciable amount of diethyl ether was detected in the effluent. This again suggested that the formation of C_4-species was enhanced in the presence of an acid. Over Cu/ZrO_2 ester formation slowly increases slowly with a decrease in copper loading to 1 wt% Cu. At 0.5 wt% Cu the selectivity to ester increases to a great extent. The product ratio increases with decreases in copper loading.

3) Active Site: When the catalyst was previously reduced to metallic copper, the dehydrogenation of ethanol took place rapidly. No reactions occurred over unreduced catalysts or the supports. The catalysts used for the reaction gave a typical color due to metallic copper. The UV/VIS spectra of the catalysts only exhibited the absorption edge at 560 nm ascribed to metallic copper.[14] This strongly suggested that the dehydrogenation occurred over the metalic copper surface.

Table 2 illustrates the results for the reaction between ethanol and adsorbed acetaldehyde over Cu/SiO_2, Cu/ZrO_2, SiO_2, and ZrO_2. The ethyl acetate formation over 30 wt% Cu/ZrO_2 is about 30 times as fast as that over 30 wt% Cu/SiO_2. The selectivity to this species is 70% over Cu/ZrO_2, whereas that over Cu/SiO_2 is 18%. Over SiO_2 and ZrO_2 supports, no reactions occurred with ethanol alone. However, when acetaldehyde was preadsorbed over the supports, ethyl acetate was produced. Over ZrO_2, ester formation is highly selective and rapid. This reaction proceeds at a rate comparable to that obtained over 30 wt% Cu/ZrO_2. On the other hand,

Table 2. Ethyl Acetate Formation from Adsorbed Acetaldehyde and Ethanol at 433 K

Catalyst[a]	Ethyl acetate formation[b]	
	Rate/cm^3 min^{-1} g-cat^{-1}	Selectivity/%
Cu/ZrO_2	8.4×10^{-2}	70
Cu/SiO_2	0.29×10^{-2}	18
ZrO_2	8.3×10^{-2}	100
SiO_2	0.03×10^{-2}	0.18

a) Cu/ZrO_2, Cu/SiO_2: 30 wt% Cu. b) Obtained at $P^0_{C_2H_5OH}$=1.3 kPa. Acetaldehyde was preadsorbed at P_{CH_3CHO}=2.0 kPa and at 433 K.

over SiO_2 ethyl acetate is produced sluggishly. The selectivity to this species is extremely low compared with that over ZrO_2. The rate of ethyl acetate formation over SiO_2 alone is one-tenth that over 30 wt% Cu/SiO_2. These results strongly suggests that over Cu/SiO_2 this step proceeded practically over copper surface, whereas over Cu/ZrO_2 the support played a role in the formation of ethyl acetate.

Steam Reforming of Ethanol. 1) Reaction Pathway to Acetic Acid: When the mixture of ethanol and water was fed over copper-based catalysts, acetic acid was formed together with products of the dehydrogenation of ethanol. The formation of ethyl acetate and the C_4-species was appreciably retarded by the presence of water. In Fig. 5, the mole fraction of the ethyl acetate and the C_4-species in the effluent is plotted against space time over 30 wt% Cu/SiO_2. Acetaldehyde increases with an increase in space time, and then decreases through a maximum. By contrast, both acetic acid and ethyl acetate increase steadily with increasing space time, suggesting that both of these species are produced through parallel pathways via acetaldehyde. The selectivity to acetic acid increased with an increase in the conversion level of ethanol. At an ethanol conversion of 88%, the selectivity was found to be 43%. At high conversion levels, the dehydrogenation of ethanol to acetaldehyde was found to be practically in equilibrium, suggesting that this step proceeded rapidly, compared with the step for acetic acid formation.

When the mixture of acetaldehyde and water was fed over 30 wt% Cu/SiO_2, acetic acid was formed at a rate comparable to that in the steam reforming of ethanol.

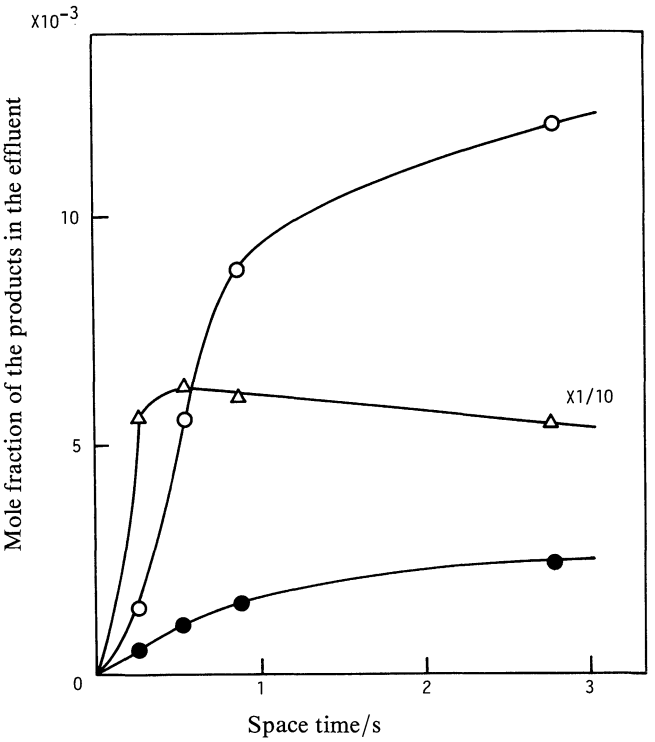

Fig. 5. Mole fraction of carbon-containing products against space time in steam reforming of C_2H_5OH over 30 wt% Cu/SiO_2. Temperature: 523 K. Inlet partial pressure: $P^0_{C_2H_5OH}$: 10.1 kPa, $P^0_{H_2O}$: 20.2 kPa. (○) CH_3COOH, (●) $CH_3COOC_2H_5$, (△) CH_3CHO.

No ethyl acetate was detected in the effluent. These findings were quite similar to those in the reaction between formaldehyde and water.[10] This suggested that adsorbed acetaldehyde underwent a nucleophilic addition of water (or hydroxide ions), giving acetic acid.

Table 3 summarizes the selectivity to the carbon-containing products in the steam reforming over various copper-based catalysts (30 wt% Cu) at an ethanol conversion of 80%. The selectivity to acetic acid is greatly affected by the kinds of supports. Over Cu/ZnO, the selectivity was attained to 38% at this conversion level.

Difference in the Mechanisms of Reforming of Ethanol and Methanol. Reforming of methanol has been studied over various copper-based catalysts.[4-11,15] In

Table 3. Steam Reforming of Ethanol — Selectivity to Carbon-Containing Products at 523 K, $P^0_{C_2H_5OH}$=10.1 kPa and $P^0_{H_2O}$=20.2 kPa —

Catalyst[a]	Selectivity[b]/%					
	Acetaldehyde	Acetone	Diethyl ether	Acetic acid	C_4-species[c]	Ethyl acetate
Cu/Al_2O_3	55.1	0.2	7.0	5.7	16.1	15.9
Cu/SiO_2	53.9	0.3	Trace	24.5	5.9	15.4
Cu/ZrO_2	56.2	4.7	0	0	8.5	30.7
Cu/ZnO	36.4	8.6	0	38.0	0	17.0
Cu[d]	88.0	0.7	0	5.2	0	6.1

a) Supported Cu catalyst: 30 wt% Cu. b) Selectivity to carbon-containing products at ethanol conversion of 80%. c) Including butyraldehyde, and 1-butanol. d) Obtained at ethanol conversion of 64%.

the absence of water, methyl formate and hydrogen were produced, whereas in the presence of water carbon dioxide and hydrogen were produced. These reactions were highly selective. Formaldehyde was produced in the course of the reactions and subsequently transformed to the final products through a reaction with methanol (or methoxide) or water (or hydroxide ions).[7,10] The dehydrogenation to formaldehyde was concluded to be rate-determining in the reforming of methanol.[4-10]

In the reforming of ethanol, ethyl acetate and acetic acid were produced, respectively, in the absence and presence of water. These reactions proceeded in a similar way to those of methanol. The dehydrogenation step to acetaldehyde occurred much more rapidly than the steps to ethyl acetate and acetic acid. The steps to ethyl acetate and acetic acid were strongly affected by the kinds of supports, compared with that to acetaldehyde. Hence, the selectivities for the reforming of ethanol were considerably lower than those for the reforming of methanol and were strongly affected by the kinds of supports. By contrast, since the dehydrogenation step was rate-determining in the reforming of methanol, the effect of the support upon the reaction was not as appreciable as that upon the reforming of ethanol.

References

1) For example, G. C. Bond, "Catalysis by Metals," Academic Press, London (1962).
2) K. Kawamoto and Y. Nishimura, *Bull. Chem. Soc. Jpn.*, **44**, 819 (1971).
3) K. Kawamoto, Y. Nishimura, and T. Hiraki, *Bull. Chem. Soc. Jpn.*, **41**, 932 (1968).
4) E. Miyazaki and I. Yasumori, *Bull. Chem. Soc. Jpn.*, **40**, 2012 (1967).
5) A. Igarashi, S. Fujiwara, and Y. Ogino, *Nippon Kagaku Kaishi*, **1978**, 935.
6) T. Sodesawa, M. Nagacho, A. Onodera, and F. Nozaki, *J. Catal.*, **102**, 460 (1986).
7) K. Takahashi, N. Takezawa, and H. Kobayashi, *Chem. Lett.*, **1983**, 1061.
8) A. Sugier and O. Bloch, *Proc. Congr. Catal., 4th, Moscow*, ed by B. A. Kazanskii, Akademiai, Taido. Budapest (1971), p. 238.
9) H. Kobayashi, N. Takezawa, and C. Minochi, *Chem. Lett.*, **1976**, 1347.
10) K. Takahashi, H. Kobayashi, and N. Takezawa, *Chem. Lett.*, **1985**, 759.
11) J. J. F. Scholten and J. A. Konvalinka, *Trans. Faraday Soc.*, **65**, 465 (1969).
12) K. S. Pitzer and W. Weltner, *J. Am. Chem. Soc.*, **71**, 2842 (1949).
13) S. Yada and Y. Mihara, *Kagaku Kogaku*, **25**, 518 (1961).
14) M. Shimokawabe, N. Takezawa, and H. Kobayashi, *Appl. Catal.*, **2**, 363 (1982).
15) H. Kobayashi, N. Takezawa, and C. Minochi, *J. Catal.*, **69**, 487 (1981).
16) H. Hayashi, N. Nishi, Y. Watanabe, and T. Ozaki, *J. Catal.*, **69**, 44 (1981).
17) Yokota, Abe, and Okabe, Preprint of the 60th Catalysis Soiety Meeting, Fukuoka, 1987, 4B 25.

Efficient Selective Reduction of Aromatic Nitro Compounds Affording Aromatic Amines under CO/H_2O Conditions Catalyzed by Amine-Added Rhodium-Carbonyl Complexes

Kotohiro NOMURA,* Masaru ISHINO, and Motoo HAZAMA
Organic Synthesis Research Laboratory, Sumitomo Chemical Co., Ltd.,
10-1, Tsukahara 2-Chome, Takatsuki-shi, Osaka 569
(Received April 5, 1991)

Remarkably high catalytic activities for the reduction of aromatic nitro compounds affording aromatic amines using CO (1 atm) and water at room temperature were exhibited by using amine-added rhodium carbonyl complexes ($Rh(CO)_2(acac)$, $Rh_4(CO)_{12}$, and $Rh_6(CO)_{16}$) in 2-methoxyethanol or diglyme (diethylene glycol dimethyl ether) containing a 5 equiv NaOH aqueous solution. The reduction proceeded not only with high catalytic activities, but also with remarkably high nitro-group selectivities, as exhibited in the case of 1-nitroanthraquinone affording 1-aminoanthraquinone, without any other unsaturated groups, such as C=O, being reduced. The T. O. F. (turnovers/time) of 1776 mol-cat^{-1} h^{-1} (296 g-atom Rh^{-1} h^{-1}) was attained for the reduction of *p*-nitroanisole yielding *p*-anisidine using $Rh_6(CO)_{16}$-1,8-bis(dimethylamino)-naphthalene catalyst.

Water-Gas-Shift Reaction (WGSR) has drawn considerable attention from the viewpoint of industrial utilization of carbon monoxide; it is now commercially used as a pure hydrogen source.[1] Many studies have, therefore, already been made concerning this subject

$$H_2O + CO \rightarrow CO_2 + H_2 \quad (1)$$

using both homogeneous and heterogeneous catalysts.[2]

As one of its applications related to WGSR, organic synthesis under CO/H_2O conditions using a homogeneous transition metal complex catalysts, such as hydrogenation, reduction, hydroformylation, hydromethylation, or hydrocarbonylation, are very intriguing subjects,[2] especially the selective reduction of unsaturated compounds has been paid particular attention.[3]

The reduction of aromatic nitro compounds affording aromatic amines using carbon monoxide and water with homogeneous catalysts is an also very attractive subject, and many studies have already been made.[2,3] Alper found that the reduction proceeded under atmospheric

$$ArNO_2 + 3CO + H_2O \rightarrow ArNH_2 + 3CO_2 \quad (2)$$

pressure of CO and room temperature by using $Ru_3(CO)_{12}$ in a benzene–2-methoxyethanol–5 equiv NaOH aqueous solution in the presence of a phase-transfer catalyst ($PhCH_2N(C_2H_5)_3^+Cl^-$)[3a], Kaneda also reported that amine-, diamine-added $Rh_6(CO)_{16}$ showed catalytic activities for the reduction of $PhNO_2$ in 2-ethoxyethanol–H_2O solution at 80 °C,[3b] and Alessio exhibited that $Rh_6(CO)_{16}$–phenanthrolines, especially 3,4,7,8-tetramethyl-1,10-phenanthroline, in ethanol was also effective for this reduction.[3d,e] However, catalytic reduction under mild reaction conditions with high activity has not yet been reported (T. O. F. of 6 g-atom-Ru^{-1} h^{-1} was reported in Ref. 3a).

In the present papers, we describe that amine-, diamine-added rhodium carbonyl complexes shows remarkably high catalytic activities as well as high nitro group selectivities for the reduction of aromatic nitro compounds under extremely mild reaction conditions of room temperature and of 1 atm of CO in 2-methoxyethanol or diglyme containing a 5 equiv NaOH aq solution.[4]

Experimental

General Procedure. All manipulations were carried out under a nitrogen atmosphere, or in vacuo. Water and 2-methoxyethanol, diglyme (diethylene glycol dimethyl ether) and nitrobenzene (Nakarai Tesque Co., Ltd.) were distilled and stored in a Schlenck-type tube under a nitrogen atmosphere. Other aromatic nitro compounds were used as reagent grade (Nakarai Tesque Co., Ltd. or Tokyo Kasei Co., Ltd.). $Rh_4(CO)_{12}$, $Rh(CO)_2(acac)$, and $Rh_6(CO)_{16}$ were also used as reagent grade (N.E. Chem. Cat. Co., Ltd.).

Reduction of Aromatic Nitro Compounds under CO/H_2O. The reaction was typically carried out as follows: a solution with $Rh_6(CO)_{16}$ (0.001 mmol) in 2-methoxyethanol (15 ml) under a nitrogen atmosphere in a Schlenck-type tube was stirred magnetically and the required amount of amine added. Then, the addition of a 5 equiv-NaOH aq solution (5 ml) and aromatic nitro compounds (5 mmol) into the reaction mixture was followed by the introduction of CO (1 atm). The mixture, equipped with CO gas bag, was allowed to react at room temperature (25 °C) for the prescribed time. The reaction product was then determined by GLC using an internal standard, and was identified using GLC by co-injection with an authentic sample (column OV-225, 3 m) and GC-MS (QP-1000, Shimadzu Co., Ltd.).[5,6]

The reduction of 1-nitroanthraquinone (Tokyo Kasei Co., Ltd.) was performed similarly. A certain excess amount of water was added into the reaction medium after the reaction; a red precipitate which was obtained by filteration was dried and redissolved in *N*,*N*-dimethylformamide and was determined by GLC (column OV-210 1 m) using an internal standard.

Results and Discussion

1. Reduction of Nitrobenzene Using CO and Water Catalyzed by Amine-Added $Rh(CO)_2(acac)$ Complexes. The results for the reduction of $PhNO_2$ catalyzed by various amine-added $Rh(CO)_2(acac)$ complexes in a 2-methoxyethanol–5 equiv NaOH aqueous solution under 1 atm of CO and room temperature (25 °C) for 3 h are summarized in Table 1. The reduction proceeded at remarkable rates with the use of a NaOH aqueous solution; a corresponding amount of aniline was obtained as the reaction product (Table 1).[5,6]

It should be noted that the rate markedly increased upon the addition of a small amount of amines; especially, 9,10-diaminophenanthrene and *o*-phenylenediamine were effective for this reaction. As revealed from this table, the catalytic activities shown here (ex. 57 g-atom-Rh^{-1} h^{-1} for $Rh(CO)_2(acac)$–9,10-diaminophenanthrene cat.) are much higher than those previously reported (ex. 6 g-atom-Ru^{-1} h^{-1} from Ref. 3a, it is the highest value so far reported).

Table 2 shows a time-course plot for this reaction using a $Rh(CO)_2(acac)$-9,10-diaminophenanthrene catalyst. It was revealed that the reaction proceeded at a significant rate during the initial stage (72 turnovers for 1 h), but that the rate decreased gradually, because of, perhaps, changes in the NaOH base concentrations (Na_2CO_3 was accompanied, accumlated from NaOH and CO_2 in the reaction mixture) as mentioned below.

The results for the reduction of nitrobenzene under various NaOH concentration conditions are shown in Table 3. The 5 equiv NaOH aqueous solution used was thought to play an important role in this reaction to proceed with a significant rate. 2-methoxyethanol was also favorable as a solvent.

2. Selective Catalytic Reduction of Aromatic Nitro Compounds Using Amine-Added $Rh_4(CO)_{12}$ Complexes.

2-1. Reduction of Aromatic Nitro Compounds Using 9,10-Diaminophenanthrene-Added $Rh_4(CO)_{12}$ Complex. As shown in Table 4, the reaction rate for the reduction of nitrobenzene using a $Rh_4(CO)_{12}$ complex also remarkably increased upon the addition of 9,10-diaminophenanthrene (from 108 to 225 turnovers with a diamine/Rh molar ratio varying from 0 to 2.25, respectively). Turnovers of 610 mol-cat^{-1} (153 g-atom-Rh^{-1}), for 3 h were obtained at low $Rh_4(CO)_{12}$ concentration.

The results for the reduction of various substituted nitrobenzenes using the $Rh_4(CO)_{12}$–9,10-diaminophenanthrene catalyst system for 90 min. are summarized in

Table 1. The Reduction of Nitrobenzene Catalyzed by Amine-Added $Rh(CO)_2(acac)$ Complexes — The Effect of Amine Additives —

Amine	Molar ratio[a]	Turnovers[d]
None[b]	—	<1
None	—	37
$H_2N(CH_2)_2NH_2$	1.5	52
$Me_2N(CH_2)_2NMe_2$	1.5	68
o-Phenylenediamine	1.5	155
2,3-Diaminonaphthalene	1.5	99
9,10-Diaminophenanthrene	1.5	122
9,10-Diaminophenanthrene	1.5	172[c]
1,8-Diaminonaphthalene	1.5	68
Pyridine	3.0	61
NEt_3	3.0	66

Reaction conditions: 2-methoxyethanol/5 equiv NaOH aq=15/5 (ml), $Rh(CO)_2(acac)$ 0.02 mmol, $PhNO_2$ 5 mmol, 25 °C, CO 1 atm, 3 h. a) Molar ratio of amine/Rh. b) H_2O (5 ml) was used instead of 5 equiv NaOH aq solution. c) $Rh(CO)_2(acac)$ 0.01 mmol. d) Turnovers= amount of aromatic amine produced (mmol)/amount of catalyst (mmol).

Table 2. Time-Course for Reduction of Nitrobenzene Catalyzed by $Rh(CO)_2(acac)$–9,10-Diaminophenanthrene Catalyst under CO/H_2O Conditions

Time/h	Aniline formed/mmol	Turnovers
1	1.44	72
3	2.44	122
6	3.62	181
10	4.34	217

Reaction conditions: $Rh(CO)_2(acac)$/9,10-diaminophenanthrene (0.02/0.03 mmol), 2-methoxyethanol/5 equiv NaOH aq=15/5 (ml), $PhNO_2$ 5 mmol, CO 1 atm, 25 °C.

Table 3. 9,10-Diaminophenanthrene-Added $Rh(CO)_2(acac)$ Catalyzed Reduction of Nitrobenzene under CO/H_2O Conditions

Solvent (ml)	NaOH aq Base conditions (ml)	Turnovers
2-Methoxyethanol (15)	1.5 equiv NaOH aq (5)	64
2-Methoxyethanol (15)	3 equiv NaOH aq (5)	94
2-Methoxyethanol (15)	5 equiv NaOH aq (2.5)	78
2-Methoxyethanol (15)	5 equiv NaOH aq (5)	122
2-Methoxyethanol (8)	5 equiv NaOH aq (5)	79
2-Propanol (15)	5 equiv NaOH aq (5)	69

Reaction conditions: $Rh(CO)_2(acac)$/9,10-diaminophenanthrene=0.02/0.03 (mmol), $PhNO_2$ 5 mmol, CO 1 atm, 25 °C, 3 h.

Table 4. Reduction of Nitrobenzene Catalyzed by 9,10-Diaminophenanthrene-Added $Rh_4(CO)_{12}$ Complex under CO/H_2O

Molar ratio[a]	Turnovers/mol-cat^{-1}
0	108
1.09	200
2.25	225
1.50	610[b]

Reaction conditions: $Rh_4(CO)_{12}$ 0.02 mmol, 2-Methoxyethanol/5 equiv NaOH aq=15/5 (ml), $PhNO_2$ 5 mmol, CO 1 atm, r.t. (25 °C), 3 h. a) Molar ratio of 9,10-diaminophenanthrene/Rh. b) $Rh_4(CO)_{12}$ 0.005 mmol.

Table 5. It should be noted that these reductions proceeded not only with significant rates but also with high nitro-group selectivities. The order *p*-NH_2 (>250)>*o*-NH_2 (233)>*p*-Cl (218)>*o*-Cl (190)>*p*-Me (178), *p*-OMe (175)>H (158) was obtained for this reaction, which is somewhat different from that previously obtained using $Rh_4(CO)_{12}$–dppe (dppe: $Ph_2P(CH_2)_2PPh_2$) catayst system (*p*-NH_2 (>250)>*o*-Cl (210)>*o*-NH_2 (190)>*p*-Cl (158)>*p*-OMe (140), *p*-Me (128)>H (110 turnovers, mol-cat^{-1} for 90 min)) under the same reaction conditions,[4a] although the high nitro-group selectivities were almost the same as those obtained using Rh–dppe catalyst system.[7] Further, the reduction of aromatic nitro compounds came to completing upon further stirring; *p*-nitrobenzonitrile was converted to afford *p*-aminobenzonitrile almost exclusively without the C=N bond being reduced (Table 6).

2-2. Reduction of 1-Nitroanthraquinone Affording 1-Aminoanthraquinone Catalyzed by Amine-Added $Rh_4(CO)_{12}$ Complexes under CO/H_2O Conditions. Importantly, it was also found that 1-nitroanthraquinone was completely reduced to produce 1-aminoantharquinone (10 h, >99.9% yield, >250 turnovers) using the above-mentioned $Rh_4(CO)_{12}$–diamine catalyst without any other unsaturated groups, such as C=O, being reduced (Table 6). Aminoanthraquinone has been one of the most important key materials used as dyes and their intermediates; although it has been commercially produced by either a stoichiometric or catalytic reduction of nitroanthraquinone or by sulfonating before amination, there are still some problems. We believe that the above-mentioned fact is very important from both industrial and synthetic viewpoints; it may be commercially used in the future as a process for the production of amines by a selective catalytic reduction of aromatic nitro compounds after much further development of this subject.

The results for the reduction of 1-nitroanthraquinone with various amine-added $Rh_4(CO)_{12}$ are summarized in in Table 7. The reduction rate increased upon the addition of only a small amount of amines, especially NEt_3 and 4-dimethylamino) pyridine.[7] The important fact was also found that the effective amines were different between the reduction of $PhNO_2$ using amine-added $Rh(CO)_2(acac)$ and that of 1-nitroanthraquinone

Table 5. Selective Reduction of Aromatic Nitro Compounds Using CO and Water with $Rh_4(CO)_{12}$–9,10-Diaminophenanthrene Catalyst

Reactant	Product	Turnovers/mol-cat^{-1}
Nitrobenzene	Aniline	158
o-Chloronitrobenzene	*o*-Chloroaniline	190
o-Nitroaniline	*o*-Phenylenediamine	233
p-Nitroaniline	*p*-Phenylenediamine	>250[a]
p-Nitroanisole	*p*-Anisidine	175
p-Nitrotoluene	*p*-Toluidine	178
p-Chloronitrobenzene	*p*-Chloroaniline	218

Reaction conditions: $Rh_4(CO)_{12}$/9,10-diaminophenanthrene=0.02/0.12 (mmol), 2-methoxyethanol/5 equiv NaOH aq=15/5 (ml), aromatic nitro compounds 5 mmol, CO 1 atm, r.t. (25°C), 3 h. a) >99% yield.

Table 6. Reduction of Aromatic Nitro Compounds under CO/H_2O Conditions

Reactant	Product	Yield/%
Nitrobenzene	Aniline	>99
o-Chloronitrobenzene	*o*-Chloroaniline	>99
p-Nitrobenzonitrile	*p*-Aminobenzonitrile	>99
1-Nitroanthraquinone	1-Aminoanthraquinone	>99

Reaction conditions: $Rh_4(CO)_{12}$/9,10-diaminophenanthrene=0.02/0.12 (mmol), 2-methoxyethanol/5 equiv NaOH aq=15/5 (ml), aromatic nitro compounds 5 mmol, CO 1 atm, r.t. (25°C), 10 h.

Table 7. Reduction of 1-Nitroanthraquinone Affording Added $Rh_4(CO)_{12}$ Complexes

Amine	Molar ratio[a]	Turnovers/mol-cat^{-1}
None	—	373
9,10-Diaminophenanthrene	1.5	419
NEt_3	3.0	554
4-(Dimethylamino)pyridine	3.0	529
1-Aminoanthraquinone	3.0	469

Reaction conditions: Diglyme (diethylene glycol dimethyl ether)/5 equiv NaOH aq=30/10 (ml), 1-nitroanthraquinone 10.7 mmol, $Rh_4(CO)_{12}$ 0.01 mmol, CO 1 atm, r.t. (25°C), 3 h. a) Molar ratio of amine/Rh.

Table 8. Catalytic Reduction of Nitrobenzene under CO/H_2O or under H_2 Conditions

Catalyst	Conditions	Temp/°C	Time/h	Turnovers[a)]
$Rh(CO)_2(acac)$–9,10-Diaminophenanthrene	CO/H_2O	r.t.	3	122
	H_2	r.t.	3	16
5%-Pd/C	H_2	r.t.	24	Trace
	H_2	50	3	134

Reaction conditions: a) undr CO/H_2O; $Rh(CO)_2(acac)$/diamine=0.02/0.03 (mmol), 2-methoxyethanol/5 equiv aq=15/5 (ml), nitrobenzene 5 mmol, CO 1 atm. b) under H_2; the same reaction conditions except that 5 equiv NaOH aq was not added. a) g-atom catalyst metal^{-1}.

Table 9. Efficient Catalytic Reduction of Aromatic Nitro Compounds Affording Corresponding Amines Using Amine-Added $Rh_6(CO)_{16}$ Complexes under CO/H_2O Conditions

Amine	Molar ratio[a)]	Reactant	Turnovers mol-cat^{-1} (g-atom-Rh^{-1}
$Me_2N(CH_2)_4NMe_2$	1	*p*-Nitrotoluene	1050 (175)
o-Phenylenediamine	1	*p*-Nitrotoluene	738 (123)
$PhCH_2NMe_2$	3	*p*-Nitrotoluene	1218 (203)
N^nBu_3	3	*p*-Nitrotoluene	1008 (168)
1,8-Bis(dimethylamino)naphthalene	1.5	*p*-Nitroanisole	1776 (296)
2-Pyridinol	3	*p*-Nitroanisole	1764 (294)
$PhCH_2NMe_2$	3	*p*-Nitroanisole	1350 (225)
N^nBu_3	3	*p*-Nitroanisole	1416 (236)
None	—	Nitrobenzene	486 (81)[b)]

Reaction conditions: $Rh_6(CO)_{16}$ 0.001 (mmol), 2-methoxyethanol/5 equiv NaOH aq=15/5 (ml), nitro compounds 5 mmol, CO 1 atm, r.t. (25°C), 1 h. a) Amount of amine or diamine (mmol)/amount of catalyst metal (mmol). b) $Rh_6(CO)_{16}$ 0.001 mmol, 5 h.

using amine-added $Rh_4(CO)_{12}$.

3. Catalytic Reduction of Nitrobenzene under CO/H_2O or H_2 Conditions Catalyzed by 9,10-Diaminophenanthrene-Added $Rh(CO)_2(acac)$ Complex. Particular attention should be paid to Table 8 regarding the different reaction rates obtained for the reduction of nitrobenzene under CO/H_2O and under H_2 conditions. Hydrogen gas was not formed after the reaction mixture under these CO/H_2O conditions;[8)] clearly indicating that reduction under CO/H_2O using this catalyst system did not proceed by the reaction of aromatic nitro compounds and the hydrogen gas that was formed by the Water-Gas-Shift-Reaction. This suggests that a different reaction mechanism can be considered for this reduction under CO/H_2O.[9)]

4. Efficient Catalytic Reduction of Aromatic Nitro Compounds Affording Amines Using Amine-Added $Rh_6(CO)_{16}$ Catalyst Systems under CO/H_2O Conditions. The results show the effects of various amine additives on the reductions of *p*-nitroanisole and *p*-nitrotoluene with $Rh_6(CO)_{16}$ in a 2-methoxyethanol–5 equiv-NaOH aqueous solution under 1 atm of CO at room temperature (25°C) for 1 h (summarized in Table 9).

It should be noted that the rate remarkably increased upon the addition of a very small amount of amines, especially *N*,*N*-dimethylbenzylamine, *N*,*N*,*N*′,*N*′-tetramethyl-1,4-diaminobutane, and tributylamine for the reduction of *p*-nitrotoluene and 1,8-bis(dimethylamino)naphthalene, 2-pyridinol, and tributylamine for the reduction of *p*-nitroanisole. It should be noted that the effective amines are different between these two compounds. The catalytic activity (T. O. F.) of 1776 mol-cat^{-1} h^{-1} (296 g-atom-Rh^{-1} h^{-1}) was attained for the reduction of *p*-nitroanisole, even under these extremely mild reaction conditions. The catalytic activities shown in Table 9 are, as far as we know, much higher than those previously reported.[3)]

The factors affecting these reduction rates and mechanistic studies are now under investigation.

Summary

In conclusion, this paper can be summarized as follows:

(i) Remarkably high catalytic activities for the reduction of aromatic nitro compounds to yield aromatic amines were exhibited by using amine-added rhodium carbonyl complexes under extremely mild reaction conditions: room temperature and atmospheric pressure of carbon monoxide in the presence of a sodium hydroxide aqueous solution.

(ii) The reduction proceeded not only with high catalytic activities, but also with remarkably high nitro-group selectivities, as exhibited in the case of 1-nitroanthraquinone affording 1-aminoanthraquinone and so on.

(iii) Taking into account the above results, a different reaction mechanism will be considered for the selective reduction of aromatic nitro compounds using amine-added rhodium carbonyl complexes under CO/H_2O conditions; this subject is now under investigation.

The authors would like to express grateful acknowledgement to Dr. Gohfu Suzukamo (Organic Synthesis Research Laboratory, Sumitomo Chemical Co., Ltd.) for his helpful discussions and continuous encouragement throughout this research. We also acknowledge Professor Yasukazu Saito (The University of Tokyo) for his helpful comments.

References

1) For example (Review), R. M. Laine and E. J. Crawford, *J. Mol. Catal.*, **44**, 357 (1988); P. C. Ford and A. Rokicki, *Adv. Organomet. Chem.*, **28**, 139 (1988).

2) For example (Review), P. Escaffre, A. Thorez, and P. Kalck, *J. Mol. Catal.*, **33**, 87 (1985); Y. Sugi, *Shokubai*, **25**, 464 (1983).

3) For example, a) H. Alper and S. Amaratunga, *Tetrahedron Lett.*, **21**, 2603 (1980); b) K. Kaneda, M. Hiraki, T. Imanaka, and S. Teranishi, *J. Mol. Catal.*, **12**, 385 (1981); c) R. C. Ryan, G. M. Wilemon, M. P. Dalsanto, and C. U. Pittman, Jr., *ibid.*, **5**, 319 (1979); d) E. Alessio, G. Zassinovich, and G. Mestroni, *ibid.*, **18**, 113 (1983); e) E. Alessio, F. Vinzi, and G. Mestroni, *ibid.*, **22**, 327 (1984); f) K. Januszkiewicz and H. Alper, *ibid.*, **19**, 139 (1983); g) K. E. Hashem, J. F. Petrignani, and H. Alper, *ibid.*, **26**, 285 (1984); h) M. Miura, M. Shinohara, and M. Nomura, *ibid.*, **45**, 151 (1988).

4) We recently have discovered new catalyst systems for selective reduction of aromatic nitro compounds under the mild reaction conditions of room temperature (25 °C) and CO atmosphere: a) K. Nomura, M. Ishino, and M. Hazama, *J. Mol. Catal.*, **65**, L5 (1991); b) *idem., ibid.*, **66**, L1 (1991); c) *idem., ibid.*, **66**, L11 (1991); d) *idem., ibid.*, **66**, L19 (1991).

5) During and after the reaction, sodium carbonate was accompanied which was generated from the reaction of sodium hydroxide and CO_2.

6) The reaction products were only corresponding amines and no other products were observed on this reaction, except that trace amount of other deoxygenated products (azobenzene, azoxybenzene) were sometimes observed on GLC scale in the reduction of nitrobenzene.

7) The rate also increased at higher reaction temperature, or higher CO pressure; K. Nomura, unpublished results.

8) The important fact was also found that a trace amount of dihydrogen (ca. 0.026 mmol) from the reaction mixture was detected after the reduction of $PhNO_2$ (ca. 5 mmol) using $Rh_4(CO)_{12}$ (0.02 mmol) in 2-methoxyethanol (15 ml)–5 equiv NaOH aq solution (5 ml) under CO (1 atm) at 25 °C for 4 h. This result, that the reduction proceeded without by-producing dihydrogen that was formed by Water-Gas-Shift-Reaction, is very important from the industrial viewpoints, and also indicates the above-mentioned assumption.

9) We believe that an original reaction pathway, such as via metal-nitrene intermediate, should be considered for this selective reduction under CO/H_2O conditions; mechanistic studies are now being carried out. For example, R. A. Sheldon, "Chemicals from Synthesis Gas," D. Reidel Publishing Co., Ltd., Dordrecht, Netherland (1981), p. 181; T. Ikariya, *Shokubai*, **5**, 271 (1989).

 © 1991 The Chemical Society of Japan Bull. Chem. Soc. Jpn., 64, 2629—2634 (1991)

Syntheses and Crystal Structures of Seven-Coordinate (Ethylenediamine-*N*,*N*,*N*′,*N*′-tetraacetato)aquavanadate(III) Complexes

Mamoru SHIMOI, Yoko SAITO, and Hiroshi OGINO*
Department of Chemistry, Faculty of Science, Tohoku University, Aoba-ku, Sendai 980
(Received December 25, 1990)

$K[V(edta)(H_2O)]\cdot 2H_2O$ (**1a**) was prepared by the reaction of VCl_3 with K_4edta. The compound was converted to its sodium and ammonium salts by use of a cation exchange resin. Crystal structure analyses of $Na[V(edta)(H_2O)]\cdot 3H_2O$ (**1b**) and $NH_4[V(edta)(H_2O)]\cdot 2.5H_2O$ (**1c**) revealed that in both compounds the vanadium atom adopts a capped trigonal-prismatic structures with a hexadentate ethylenediaminetetraacetato ligand and an aqua ligand. Crystal data are as follows: **1b**: Monoclinic, $P2_1/a$, a=17.831 (3), b=8.408 (1), c=11.595 (2) Å, β=109.39 (1)°, Z=4, R=0.045 for 6321 reflections; **1c**: Monoclinic, Aa, a=8.552 (1), b=59.948 (6), c=7.226 (1) Å, β=114.95 (1)°, Z=8, R=0.050 for 6087 reflections.

The coordination chemistry of vanadium(III) is attracting attention in connection with its biological importance in tunichromes[1] and vanadium-containing nitrogenase.[2] Vanadium(III) usually forms complexes with coordination number six,[3] but its chemistry has been poorly investigated.

In the course of our research in electron transfer reactions, we found that the kinetics of the electron transfer reactions between $[V^{III}(hedra)(H_2O)]$[4] and halogenopentaamminecobalt(III) complexes obey the zeroth-order rate law when excess V(III) is used.[5] To elucidate the mechanism of this reaction, we analyzed the crystal structures of the reactant $[V^{III}(hedra)(H_2O)]\cdot 2H_2O$ and the final product $K[V^{IV}O(hedra)]\cdot H_2O$. To our surprise, V(III) adopts a capped trigonal-prismatic seven-coordinate structure: The coordinated hedtra ligand is hexadentate and one water molecule occupies the seventh coordination position of vanadium(III).[6] This prompted us to study the structures of vanadium(III) complexes containing edta-related aminopolycarboxylate ligands. Some preliminary results for $Na[V(edta)(H_2O)]\cdot 3H_2O$ have already been reported.[7,8] It was apparent that the edta complex also forms a capped trigonal-prismatic seven-coodinate structure. The geometry of $[V(edta)(H_2O)]^-$ is quite deformed: The coordination sphere was shown to lack an approximate two-fold axis along the V–H_2O bond in contrast to the $[V(hedtra)(H_2O)]$ complex. Many edta complexes with an aqua ligand have also been reported to adopt seven coordination as capped trigonal prisms or pentagonal bipyramids. However, they usually have an exact or approximate two-fold axis along the M–H_2O bond. Furthermore, coordination structures of some seven-coordinate edta complex anions depend on the nature of cation. Thus $[Mg(edta)(H_2O)]^{2-}$ adopts a capped trigonal prismatic structure in the sodium salt,[9] while in the magnesium salt it is pentagonal bipyramidal.[10] The iron(III)–edta complex forms six-coordinate structure in the lithium[11] and guanidinium salts,[12] and pentagonal bipyramidal seven-coodinate structure in many other salts.[13–18] Therefore it would be important to elucidate whether the large deformation observed in the coordination sphere of the $[V(edta)(H_2O)]^-$ anion is intrinsic to a single ion or is due to steric hindrance related to ion packing. In this paper, the crystal structure of the ammonium salt of vanadium(III)–edta complex is analyzed and compared it with those of $[V^{III}(hedtra)(H_2O)]\cdot 2H_2O$[6] and $Na[V(edta)(H_2O)]\cdot 3H_2O$.

Experimental

General Procedure. The complexes were prepared and handled under a nitrogen or argon atmosphere. A column (10 mmϕ) of Dowex 50W-X8(50—100 mesh) was used for exchanging cations in the vanadium(III)–edta complex.

Synthesis of $K[V(edta)(H_2O)]\cdot 2H_2O$ (1a). H_4edta (11.69 g, 40 mmol) was added to 100 cm^3 of water and neutralized with 11.20 g (80 mmol) of potassium carbonate. To the solution was added 6.30 g (40 mmol) of VCl_3 and the solution was stirred for 15 min. Evaporation of the solvent using a rotary evaporator followed by addition of ethanol gave pale brown flocculent crystals, which were collected by filtration and washed with ethanol and ether, successively. Yield 15.5 g (90%). Found: C, 27.55; H, 4.36; N, 6.61%. Calcd for $C_{10}H_{18}KN_2O_{11}V$: C, 27.78; H, 4.20; N, 6.48%.

Synthesis of $Na[V(edta)(H_2O)]\cdot 3H_2O$ (1b). An aqueous solution (6 cm^3) containing 1.0 g (2.3 mmol) of $K[V(edta)(H_2O)]\cdot 2H_2O$ was passed through a column packed with 2.5 cm^3 of Na-type cation exchange resin. The sodium salt was obtained as pale purple crystals almost quantitatively by evaporation of the eluate using a rotary evaporator followed by addition of ethanol. Found: C, 28.43; H, 4.44; N, 6.18%. Calcd for $C_{10}H_2ON_2NaO_{12}V$: C, 27.66; H, 4.64; N, 6.45%. Parallel-piped crystals suitable for X-ray diffractometry were obtained by standing a saturated aqueous solution in a desiccator over phosphorus pentoxide under an argon atmosphere.

Synthesis of $NH_4[V(edta)(H_2O)]\cdot 2.5H_2O$ (1c). The title compound was prepared by the same procedure as the preparation of **1b**, using a requisite amount of NH_4-type cation exchange resin instead of the Na-type one. Yield 88%. Found: C, 28.45; H, 5.78; N, 9.94%. Calcd for $C_{10}H_{23}N_3O_{11.5}V$: C, 28.58; H, 5.52; N, 10.00%. Columnar crystals suitable for X-ray diffractometry were also obtained by the same procedure as for the sodium salt.

X-Ray Crystal Structure Determination of 1b and 1c. Diffraction data were collected on a Rigaku AFC-6A four-

Table 1. Crystal Data for $Na[V(edta)(H_2O)]\cdot 3H_2O$ (**1b**) and $NH_4[V(edta)(H_2O)]\cdot 2.5H_2O$ (**1c**)

	1b	**1c**
Formula	$C_{10}H_{20}N_2NaO_{12}V$	$C_{10}H_{23}N_3O_{11.5}V$
Fw	534.20	430.25
Crystal system	Monoclinic	Monoclinic
Space group	$P2_1/a$	Aa
a/Å	17.831(3)	8.552(1)
b/Å	8.408(1)	59.948(6)
c/Å	11.595(2)	7.226(1)
β/deg	109.39(1)	114.95(1)
U/Å^3	1639.8(5)	3358.9(8)
Z	4	8
d_{calcd}/g cm^{-3}	1.76	1.70
d_{measd}/g cm^{-3}	1.74	1.69
μ/cm^{-1}	7.44	6.99
Cryst size/mm	0.5×0.3×0.3	0.40×0.12×0.26
Temp/°C	20	20
2θ range/deg	3—65	3—70
Scan mode	ω–2θ	ω
ω-Scan width/deg	1.1+0.35 tan θ	1.2
No. of unique data	6321	7484
No. of data used with $\lvert F_o\rvert>3\sigma(F_o)$	4216	6087
No. of parameters refined	284	565
R[a)]	0.045	0.050
R_w[b)]	0.085	0.062

a) $R=\Sigma\|\lvert F_o\rvert-\lvert F_c\rvert\|/\Sigma\lvert F_o\rvert$. b) $R_w=[\Sigma w(\lvert F_o\rvert-\lvert F_c\rvert)^2/\Sigma w\lvert F_o\rvert^2]^{1/2}$; $w=[\sigma^2(\lvert F_o\rvert)+aF_o^2]^{-1}$, where a is 0.015 for **1a** and 0.003 for **1c**.

circle diffractometer with graphite-monochromated Mo$K\alpha$ radiation (λ=0.71073 Å). Crystallographic and experimental data for the complexes are listed in Table 1. The reflection data were corrected for Lorentz and polarization factors. No correction was applied for absorption or extinction. All the structures were solved by the conventional heavy-atom method and the parameters were refined by the block-diagonal least-squares method. Anisotropic tempeprature factors were applied for the non-hydrogen atoms. Positions of hydrogen atoms, except for those of water molecules, were deduced from difference Fourier syntheses and refined with isotropic temperature factors. Two hydrogen atom positions for **1b** were fixed at the calculated coordinates. There is ambiguity in the identification of nitrogen atoms of ammonium ions, and oxygen atoms of water of crystallization for **1c**. The atoms with maximum number of hydrogen bonds were assigned as the ammonium nitrogen atoms. This assignment gave a reasonable arrangement of anions and cations in the crystal. The inverse chirality for **1c** gave a larger R value (0.052). Atomic scattering factors for non-hydrogen atoms and hydrogen atoms were taken from Refs. 19 and 20, respectively. The calculations were performed on a Nippon Electric Co. ACOS-2000 computer at the Computer Center of Tohoku University using the Universal Computation Program System UNICS III.[21]

Results and Discussion

Syntheses and Properties of the Vanadium(III) Complexes. The complex was prepared by direct reaction of the potassium salt of edta with vanadium(III) chloride. This method is more convenient than the reduction of the $[VO(edta)]^{2-}$ complex using sodium amalgam.[22] The complexes are reasonably air-stable in

Table 2. Final Atomic Coordinates (×10^4) and Equivalent Isotropic Temperature Factors for $Na[V(edta)(H_2O)]\cdot 3H_2O$ (**1b**)

Atom	x	y	z	B_{eq}/Å^2[a)]
V	8416.7(2)	8079.8(5)	3011.8(4)	1.2
O(1)	7260(1)	8782(2)	2083(2)	1.9
O(2)	6088(1)	8195(3)	703(2)	2.5
O(3)	8569(1)	7391(3)	4793(2)	2.1
O(4)	8002(1)	6407(4)	6077(2)	2.8
O(5)	9606(1)	8567(2)	3842(2)	1.7
O(6)	10813(1)	7523(3)	4689(2)	2.8
O(7)	8575(1)	9057(2)	1520(2)	1.9
O(8)	9377(1)	9168(3)	413(2)	2.2
O(W1)	8344(1)	10351(3)	3649(2)	2.1
N(1)	7633(1)	5976(3)	2861(2)	1.5
N(2)	9050(1)	6139(3)	2422(2)	1.3
C(1)	8081(2)	4482(3)	2911(3)	1.7
C(2)	8575(2)	4645(3)	2085(2)	1.8
C(3)	6947(2)	6074(3)	1722(2)	1.7
C(4)	6732(1)	7798(3)	1466(2)	1.6
C(5)	7352(2)	6057(4)	3931(2)	1.9
C(6)	8020(2)	6639(4)	5036(2)	1.8
C(7)	9759(2)	5852(3)	3506(3)	1.9
C(8)	10103(2)	7430(3)	4070(2)	1.7
C(9)	9304(2)	6737(3)	1407(3)	1.8
C(10)	9075(2)	8455(3)	1085(2)	1.5
Na	−88.9(7)	1769(1)	841(1)	1.9
O(W2)	229(2)	1308(4)	2976(2)	4.4
O(W3)	802(2)	3823(3)	1596(2)	3.6
O(W4)	2477(2)	3314(4)	737(3)	3.9

a) The equivalent isotropic temperature factors for non-hydrogen atoms were computed using the following expression: $B_{eq}=4/3(B_{11}a^2+B_{22}b^2+B_{33}c^2+B_{13}ac\cos\beta)$. B_{ij} is defined by: $\exp[-(h^2B_{11}+k^2B_{22}+l^2B_{33}+2hkB_{12}+2hlB_{13}+2klB_{23})]$.

the solid state, though prolonged exposure of aqueous solutions to air results in oxidation to vanadium(IV) complexes. The crystals of $Na[V(edta)(H_2O)]\cdot 3H_2O$ and $NH_4[V(edta)H_2O)]\cdot 2.5H_2O$ exhibit dichroism and look purple or grayish green depending on the direction.

Structures of $Na[V(edta)(H_2O)]\cdot 3H_2O$ (1b) and $NH_4[V(edta)(H_2O)]\cdot 2.5H_2O$ (1c). Final atomic coordinates and equivalent isotropic temperature factors for $Na[V(edta)(H_2O)]\cdot 3H_2O$ (**1b**) and $NH_4[V(edta)(H_2O)]\cdot 2.5H_2O$ (**1c**) are listed in Tables 2 and 3, respectively. Bond lengths and angles for **1b** and **1c** are given in Table 4.[23] ORTEP drawings of the $[V(edta)(H_2O)]^-$ ions are shown in Fig. 1. Crystals of the ammonium salt are composed of two crystallographically independent complex anions, but the structures of both complexes are almost the same and are also quite similar to that of the sodium salt.

In the complexes, edta acts as a hexadentate ligand forming a twisted trigonal prism, and one water molecule is also coordinated to the vanadium atom in a capping position. Thus the geometry around the vanadium atom is a capped trigonal-prism. The structure of

Table 3. Final Atomic Coordinates ($\times 10^4$ for x and z and $\times 10^5$ for y) and Equivalent Isotropic Temperature Factors for $NH_4[V(edta)(H_2O)]\cdot 2.5H_2O$ (**1c**)

Atom	x	y	z	B_{eq}/Å^{2} [a]	Atom	x	y	z	B_{eq}/Å^{2} [a]
V(1)	5000	44756(1)	5000	1.4	O(24)	−636(5)	35116(6)	708(5)	3.5
V(2)	2821.3(7)	30243(1)	3912.4(9)	1.3	O(25)	4272(3)	30166(4)	2277(4)	2.1
O(11)	6613(4)	46245(4)	7741(4)	2.3	O(26)	6711(4)	31044(6)	2055(5)	3.4
O(12)	7350(4)	46535(5)	11069(4)	2.8	O(27)	4300(4)	27623(4)	5478(5)	2.6
O(13)	6383(4)	42456(4)	4206(4)	2.3	O(28)	6878(4)	26248(5)	7511(5)	2.9
O(14)	8458(5)	39900(6)	5245(5)	3.4	O(2W1)	1322(4)	28052(4)	1626(4)	2.1
O(15)	3555(3)	44819(5)	1921(4)	2.2	N(21)	2093(3)	32824(4)	5573(4)	1.6
O(16)	1102(5)	43968(6)	−738(5)	3.5	N(22)	5355(3)	31898(4)	5993(4)	1.6
O(17)	3520(3)	47379(4)	5085(5)	2.5	C(21)	3373(4)	34668(5)	6228(5)	1.9
O(18)	953(4)	48737(5)	4550(6)	2.9	C(22)	5157(4)	33711(6)	7293(5)	2.0
O(1W1)	6493(3)	46942(4)	4204(4)	2.0	C(23)	1906(5)	31755(6)	7324(5)	2.1
N(11)	5738(3)	42172(4)	7397(4)	1.6	C(24)	1127(4)	29484(6)	6644(5)	1.9
N(12)	2468(4)	43084(4)	4538(4)	1.7	C(25)	400(4)	33720(6)	4104(5)	2.0
C(11)	4445(4)	40333(5)	6756(5)	1.9	C(26)	387(4)	33838(5)	2014(5)	2.1
C(12)	2665(4)	41308(6)	6046(6)	2.0	C(27)	5999(5)	32890(6)	4549(6)	2.4
C(13)	5907(5)	43233(6)	9321(5)	2.1	C(28)	5693(4)	31254(6)	2846(5)	2.0
C(14)	6703(4)	45512(5)	9432(5)	1.9	C(29)	6571(5)	30155(6)	7261(6)	2.4
C(15)	7417(4)	41294(6)	7619(5)	2.1	C(210)	5895(5)	27839(5)	6701(5)	1.9
C(16)	7424(5)	41163(6)	5522(6)	2.1	N(3)	8144(5)	26196(6)	2009(6)	2.7
C(17)	1841(5)	42127(6)	2467(5)	2.3	N(4)	9675(5)	48789(6)	7769(6)	2.7
C(18)	2135(4)	43770(6)	1061(5)	2.1	O(W1)	4549(5)	25879(6)	874(6)	3.4
C(19)	1249(5)	44827(6)	4592(7)	2.6	O(W2)	3922(8)	37540(9)	1964(8)	5.1
C(110)	1944(4)	47179(5)	4722(5)	1.9	O(W3)	817(6)	37128(9)	8271(7)	5.1
O(21)	1208(4)	28753(4)	5035(4)	2.4	O(W4)	7019(6)	37895(8)	1380(7)	4.7
O(22)	478(4)	28448(5)	7626(4)	2.7	O(W5)	3276(5)	49129(6)	235(6)	3.4
O(23)	1448(4)	32534(4)	1740(4)	2.2					

a) The equivalent isotropic temperature factors for non-hydrogen atoms were computed using the following expression: $B_{eq}=4/3(B_{11}a^2+B_{22}b^2+B_{33}c^2+B_{13}ac\cos\beta)$. B_{ij} is defined by: $\exp[-(h^2B_{11}+k^2B_{22}+l^2B_{33}+2hkB_{12}+2hlB_{13}+2klB_{23})]$.

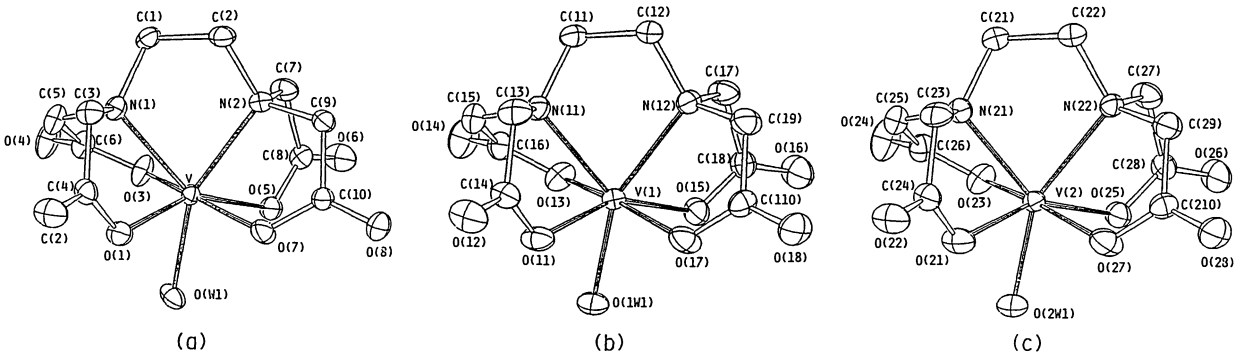

Fig. 1. Molecular structures of $[V(edta)(H_2O)]^-$ with atomic numbering scheme. Hydrogen atoms are omitted for clarity. (a) $Na[V(edta)(H_2O)]\cdot 3H_2O$ (**1b**), (b) complex 1 of $NH_4[V(edta)(H_2O)]\cdot 2.5H_2O$ (**1c**), and (c) complex 2 of **1c**.

$[V(edta)(H_2O)]^-$ is quite similar to that of $[V(hedtra)(H_2O)]\cdot 2H_2O$ (**2**).[6] The averaged V–O(carboxylato) bond lengths are 2.052 (23) Å for **1b** and 2.051 (16) for **1c**, these values being almost equal to that in **2** (2.048(13) Å).[6] However, the bond lengths in $[V(edta)(H_2O)]^-$ range more widely than those in $[V(hedtra)(H_2O)]$. This difference is reflected in the difference of configurations of both complexes. Figure 2 shows the projections of coordination spheres for $[V(edta)(H_2O)]^-$ and $[V(hedtra)(H_2O)]$ along the axis passing through the centers of gravity, CE1 and CE2, of the N(*n*1)–O(*n*1)–O(*n*3) and N(*n*2)–O(*n*5)–O(*n*7) triangular faces, where *n* is zero for **1b** and **2**, respectively, and is the first digit of atomic numbering, 1 or 2, for **1c**. In each complex these triangles are almost parallel to each other (dihedral angles between the planes are 4.90 for **1b**, 3.28 and 3.11 for **1c**, and 2.20° for **2**, respectively), but they are twisted with respect to each other. As parameters for the degree of twist between the two trianglular surfaces, we can define the twist angles as θ_1: N(*n*1)–CE1–CE2–N(*n*2), θ_2: O(*n*1)–CE1–CE2–O(*n*5), and θ_3: O(*n*3)–CE1–CE2–O(*n*7). These angles are also given in Fig. 2. Although $[V(hedtra)(H_2O)]$ has an approximate C_2 axis along the V–H_2O bond, $[V(edta)(H_2O)]^-$ has no such symmetry. On the other hand, the O(*n*1), O(*n*7), N(*n*1), and N(*n*2) atoms for $[V(edta)(H_2O)]^-$ are almost coplanar; they deviate from the least-squares plane by only −0.028, +0.026, +0.029, and −0.027 Å for **1b**, +0.013, −0.012, −0.013, and +0.013 Å for the complex 1 of **1c**, and +0.12, −0.12, −0.12, and +0.12 Å for the complex 2 of **1c**, respectively. These planes are almost parallel to the O(*n*3)–O(*n*5)–O(*n*W) plane. The dihedral angles between the planes are 4.96° for **1b** and 4.93° for complexes 1 and 2 of **1c**, respectively. Thus the geometry of $[V(edta)(H_2O)]^-$ may also be described as a 4:3 piano stool[24] or tetragonal base-trigonal base.[25] It is of interest to note that the edta ligand, which has higher symmetry than the hedtra ligand, adopts a coordination structure of lower symmetry than the latter ligand. In the previous communication we mentioned that this low symmetry for $[V(edta)(H_2O)]^-$ is peculiar among the various seven coordinate structures with edta and aqua ligands. Table 5 shows the twist angles, θ_1, θ_2, and θ_3, of the capped trigonal-prismatic complexes with edta-like ligands. All complexes except for $[V(edta)(H_2O)]^-$ have an approximate or crystallographic two-fold axis along the M–H_2O bond as is shown by the equivalence of θ_2 with θ_3. The lack of symmetry in $[V(edta)(H_2O)]^-$ is also reflected in the large difference in the angles, O(*n*1)–N(*n*1)–O(*n*3) and O(*n*5)–N(*n*2)–O(*n*7): 84.1 (1) vs. 62.31 (7)° for **1b**, 81.9(1) vs. 62.2(1) and 81.7(1) vs. 61.5(2) for **1c**. The corresponding angles for **2** are much less different: 75.41 (6) vs. 70.67 (6)°.

Figure 3 shows the packing diagram of $Na[V(edta)(H_2O)]\cdot 3H_2O$. Two O(8) atoms of neighboring anions bridge two sodium ions around the center of symmetry (Na···Na=3.628 (3) Å), and the sodium ions are coordinated tetrahedrally with crystal water molecules (O(W2) and O(W3)) and two O(8) atoms, with bond distances ranging from 2.312(3) to 2.381 (3) Å. In

Table 4. Interatomic Distances and Angles for $Na[V(edta)(H_2O)]\cdot 3H_2O$ (**1b**) and $NH_4[V(edta)(H_2O)]\cdot 2.5H_2O$ (**1c**)

Bond length	*l*/Å		
	1b	**1c**	
	n=0	*n*=1	*n*=2
V(*n*)–N(*n*1)	2.225(2)	2.208(3)	2.203(3)
V(*n*)–N(*n*2)	2.218(3)	2.279(3)	2.278(2)
V(*n*)–O(*n*1)	2.071(2)	2.078(2)	2.075(4)
V(*n*)–O(*n*3)	2.074(2)	2.050(3)	2.043(2)
V(*n*)–O(*n*5)	2.058(2)	2.039(2)	2.043(3)
V(*n*)–O(*n*7)	2.017(2)	2.036(3)	2.034(2)
V(*n*)–O(*n*W1)	2.067(2)	2.073(3)	2.076(2)
C(*n*4)–O(*n*1)	1.279(3)	1.271(5)	1.271(5)
C(*n*4)–O(*n*2)	1.241(3)	1.237(4)	1.237(6)
C(*n*6)–O(*n*3)	1.273(4)	1.258(4)	1.275(5)
C(*n*6)–O(*n*4)	1.235(4)	1.243(6)	1.244(4)
C(*n*8)–O(*n*5)	1.271(3)	1.273(4)	1.285(4)
C(*n*8)–O(*n*6)	1.233(3)	1.231(4)	1.233(6)
C(*n*10)–O(*n*7)	1.267(4)	1.265(5)	1.281(4)
C(*n*10)–O(*n*8)	1.239(4)	1.232(5)	1.242(4)
N(*n*1)–C(*n*1)	1.480(3)	1.490(4)	1.486(4)
N(*n*1)–C(*n*3)	1.474(3)	1.479(5)	1.486(5)
N(*n*1)–C(*n*5)	1.486(4)	1.473(5)	1.488(4)
N(*n*2)–C(*n*2)	1.493(3)	1.481(5)	1.492(5)
N(*n*2)–C(*n*7)	1.476(3)	1.476(4)	1.494(6)
N(*n*2)–C(*n*9)	1.483(4)	1.488(5)	1.486(4)
C(*n*1)–C(*n*2)	1.508(5)	1.505(5)	1.502(5)
C(*n*3)–C(*n*4)	1.504(4)	1.513(5)	1.504(5)
C(*n*5)–C(*n*6)	1.512(3)	1.520(6)	1.507(6)
C(*n*7)–C(*n*8)	1.516(4)	1.510(6)	1.507(6)
C(*n*9)–C(*n*10)	1.514(4)	1.518(5)	1.493(5)
Bond angle	*φ*/deg		
O(*n*1)–V(*n*)–O(*n*W1)	75.65(8)	75.74(10)	75.47(12)
O(*n*3)–V(*n*)–O(*n*W1)	84.56(9)	81.50(12)	81.49(9)
O(*n*5)–V(*n*)–O(*n*W1)	80.00(8)	81.17(11)	81.23(12)
O(*n*7)–V(*n*)–O(*n*W1)	88.47(9)	89.06(12)	89.11(9)
O(*n*W1)–V(*n*)–N(*n*1)	130.56(9)	130.94(11)	130.99(10)
O(*n*W1)–V(*n*)–N(*n*2)	152.72(8)	153.59(11)	153.73(9)
O(*n*1)–V(*n*)–O(*n*3)	112.09(8)	109.05(11)	109.16(12)
O(*n*1)–V(*n*)–O(*n*7)	80.61(8)	79.09(10)	79.06(12)
O(*n*3)–V(*n*)–O(*n*5)	79.39(8)	82.10(11)	82.15(12)
O(*n*5)–V(*n*)–O(*n*7)	84.50(8)	85.43(10)	85.27(12)
O(*n*1)–V(*n*)–N(*n*1)	72.21(8)	72.45(9)	72.66(13)
O(*n*3)–V(*n*)–N(*n*1)	74.21(8)	74.93(11)	75.12(10)
O(*n*5)–V(*n*)–N(*n*2)	74.90(8)	75.36(10)	75.58(11)
O(*n*7)–V(*n*)–N(*n*2)	78.75(9)	77.27(11)	76.95(9)
N(*n*1)–V(*n*)–N(*n*2)	76.21(8)	75.29(10)	75.13(10)
V(*n*)–N(*n*1)–C(*n*1)	110.8(2)	110.2(2)	110.9(2)
V(*n*)–N(*n*1)–C(*n*3)	109.8(2)	108.5(2)	108.5(2)
V(*n*)–N(*n*1)–C(*n*5)	105.9(2)	106.2(2)	106.2(2)
V(*n*)–N(*n*2)–C(*n*2)	113.4(2)	113.7(2)	113.8(2)
V(*n*)–N(*n*2)–C(*n*7)	103.7(1)	103.6(2)	103.9(2)
V(*n*)–N(*n*2)–C(*n*9)	108.4(2)	108.7(2)	108.9(2)
V(*n*)–O(*n*1)–C(*n*4)	121.8(2)	121.0(2)	120.7(3)
V(*n*)–O(*n*3)–C(*n*6)	120.2(2)	120.7(3)	120.6(3)
V(*n*)–O(*n*5)–C(*n*8)	119.1(2)	122.6(2)	121.8(3)
V(*n*)–O(*n*7)–C(*n*10)	119.8(2)	122.8(2)	122.5(2)

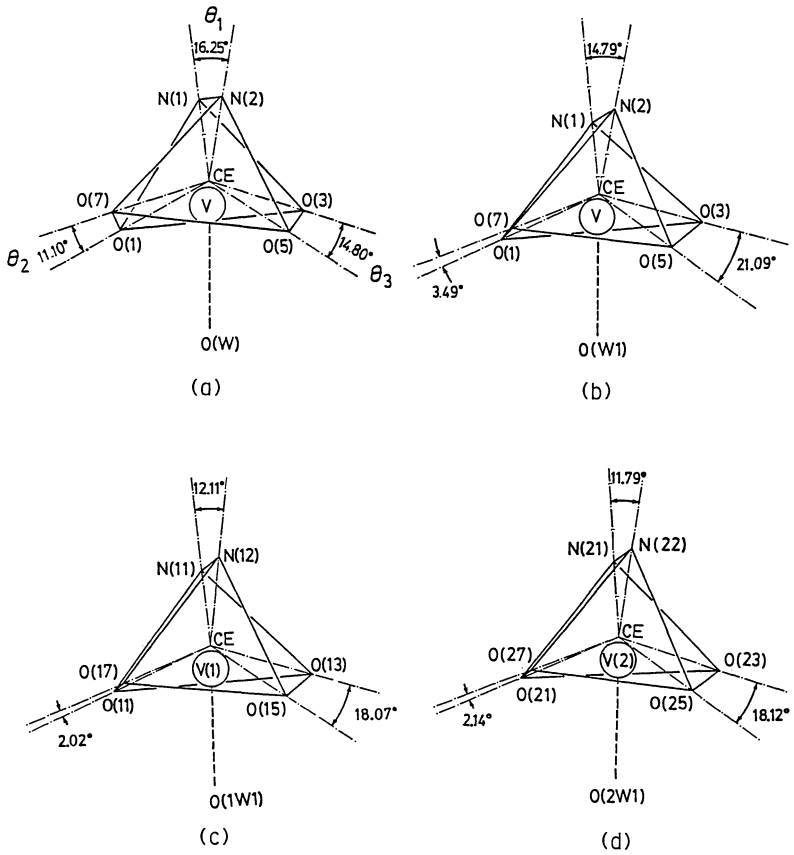

Fig. 2. Projections of the coordination spheres for (a) $[V(hedtra)(H_2O)]$, (b) $[V(edta)(H_2O)]^-$ of the sodium salt, (c) and (d) $[V(edta)(H_2O)]^-$ of the ammonium salt, along the axis passing through the centers of gravity (CE) of the trianguler faces. Twist angles between the triangular faces, θ_1, θ_2, and θ_3, are also depicted.

Table 5. Comparison of Twist Angles, θ_1, θ_2, and θ_3,[a] of Capped Trigonal-Prismatic Seven-Coordinate Complexes with Edta-Like Ligands

Complex	θ_1/deg	θ_2/deg	θ_3/deg
$[V(hedtra)(H_2O)]$[b]	16.25	11.10	14.80
$Na[V(edta)(H_2O)]\cdot 3H_2O$[c]	14.79	3.49	21.09
$NH_4[V(edtra)(H_2O)]\cdot 2.5H_2O$[c]	12.11	2.02	18.07
	11.79	2.14	18.12
$Na_2[Mg(edta)(H_2O)]\cdot 5H_2O$[d]	8.67	8.32	8.32
$MnH_2[Mn(edta)(H_2O)]_2\cdot 10H_2O$[e]	27.21	23.98	26.03
$[Os(edta)(H_2O)]\cdot H_2O$[f]	22.25	18.36	12.30
$Ca[Fe(cydta)(H_2O)]\cdot 8H_2O$[g]	26.86	26.26	23.44

a) See text and Fig. 2(a). b) Ref. 6. c) This work. d) Ref. 26. e) Ref. 27. f) Ref. 28. g) Ref. 29.

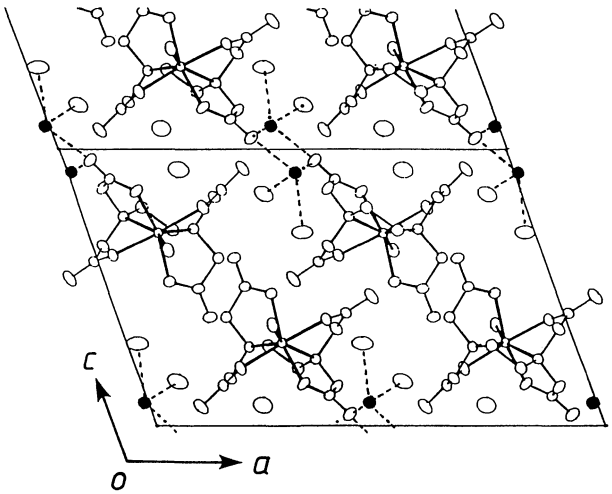

Fig. 3. Cell projection for $Na[V(edta)(H_2O)]\cdot 3H_2O$ (**1b**) along *b*. Sodium ions are depicted by solid elipsoids. Coordination bonds between sodium and oxygen atoms are shown with dotted lines.

the ammonium salt (Fig. 4), the cations are hydrogen-bonded to O(*n*8) atoms: N(3)···O(28^{i})=2.961 (4), N(4)···O(18^{ii})=2.958 (7) Å, where i and ii denote the symmetry operations x, y, $1+z$, and $1+x$, y, z, respectively. However, these hydrogen bonds are weak compared to the other hydrogen bonds found between the ammonium cations and water molecules (the hydrogen bond distances range from 2.822 (5) to 2.898 (5) Å). Thus the distortion of the complex anions found in the sodium and ammonium salts may be due to the interaction between

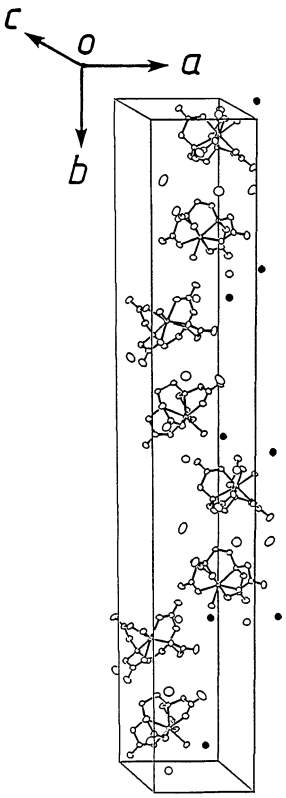

Fig. 4. Perspective of the unit cell for $NH_4[V(edta)(H_2O)]\cdot 2.5H_2O$ (**1c**). Ammonium nitrogen atoms are depicted by solid elipsoids.

the O(*n*8) atom and the cation; rather, the large deformation may be intrinsic to the $[V(edta)(H_2O)]^-$ anion and due to the d^2 configuration of vanadium(III) ion. For $[V(hedtra)(H_2O)]$, this distortion may be compensated by the rather weak bond between vanadium and the hydroxyethyl group.

The capped trigonal-prismatic structure of $[V^{III}(edta)(H_2O)]^-$ is in contrast to the pentagonal-bipyramidal structure of $[Fe^{III}(edta)(H_2O)]^-$,[13-18] although the ionic radii of Fe(III) and V(III) are almost the same ($r_{Fe^{3+}}$=0.645 vs. $r_{V^{3+}}$=0.640 Å).[30] This may be due to the difference of electronic configurations between iron(III) and vanadium(III): d^5 and d^2, respectively.

References

1) E. M. Oltz, R. C. Bruening, M. J. Smith, K. Kustin, and K. Nakanishi, *J. Am. Chem. Soc.*, **110**, 6162 (1988).

2) B. J. Hales, E. E. Case, J. E. Morningster, M. F. Dzeda, and L. A. Mauterer, *Biochemistry*, **25**, 7251 (1986); J. M. Arber, B. R. Dobson, R. R. Eady, P. Stevens, S. S. Hasnain, C. D. Garner, and B. E. Smith, *Nature*, **325**, 372 (1987).

3) L. V. Boas and J. C. Pessoa, "Comprehensive Coordination Chemistry," ed by G. Wilkinson, Pergamon, Oxford(1987), Vol. 3, pp. 453—583.

4) Abbreviations used in this paper: hedtra, *N'*-(2-hydroxyethyl)ethylenediamine-*N,N,N'*-triacetate; edta, ethylenediamine-*N,N,N',N'*-tetraacetate.

5) H. Ogino, M. Shimura, N. Yamamoto, and N. Okubo, *Inorg. Chem.*, **27**, 172 (1988).

6) H. Ogino, M. Shimoi, and Y. Saito, *Inorg. Chem.*, **28**, 3596 (1989).

7) M. Shimoi, Y. Saito, and H. Ogino, *Chem. Lett.*, **1989**, 1675.

8) Bond distances and angles reported in Ref 7 are somewhat revised in this paper.

9) J. J. Stezowski, R. Countryman, and J. L. Hoard, *Inorg. Chem.*, **12**, 1749 (1973).

10) E. Passer, J. G. White, and K. L. Cheng, *Inorg. Chim. Acta*, **24**, 17 (977).

11) N. V. Novozhilova, T. N. Polynova, M. A. Porai-Koshits, N. J. Pechuvova, L. I. Martynenko, and A. Khadi, *Zh. Strukt. Khim.*, **14**, 745 (1973).

12) Ya. M. Nesterova, T. N. Polynova, and M. A. Porai-Koshits, *Koord. Khim.*, **1**, 966 (1975).

13) M. D. Lind, M. J. Hamor, T. A. Hamor, and J. L. Hoard, *Inorg. Chem.*, **3**, 34, (1964).

14) X. Solans, M. Font-Altaba, and J. Garcia-Oricain, *Acta Crystallogr., Sect. C*, **40**, 635 (1984).

15) X. Solans, M. Font-Altaba, and J. Garcia-Oricain, *Acta Crystallogr., Sect. C*, **41**, 525 (1985).

16) X. Solans, M. Font-Altaba, and J. Garcia-Oricain, *Acta Crystallogr., Sect. C*, **41**, 572 (1985).

17) J. M. Lopetz-Alcala, M. C. Puerta-Vizcaino, F. Gonzalez-Vilchez, E. N. Duesler, and R. E. Tapscott, *Acta Crystallogr., Sect. C*, **40**, 939 (1984).

18) N. V. Novozhilova, T. N. Polynova, and M. A. Porai-Koshits, *Zh. Strukt. Khim.*, **16**, 865 (1975).

19) "International Tables for X-Ray Crystallography," Kynoch Press, Birmingham, U. K. (1974), Vol. 4, pp. 92, 150.

20) R. F. Stewart, E. R. Davidson, and W. T. Simpson, *J. Chem. Phys.*, **42**, 3175 (1965).

21) T. Sakurai and K. Kobayashi, *Rikagaku Kenkyusho Hokoku*, **55**, 69 (1979).

22) G. Schwarzenbach and J. Sandera, *Helv. Chim. Acta*, **36**, 1089 (1953).

23) Some additional bond lengths and angles, the positional and the thermal parameters of hydrogen atoms, the final anisotropic thermal parameters, and F_o—F_c tables are deposited as Document No. 8955 at the Office of the Editor of The Bull. Chem. Soc. Jpn.

24) E. B. Dreyer, C. T. Lam, and S. J. Lippard, *Inorg. Chem.*, **18**, 1904 (1979).

25) E. L. Muetterties and C. M. Wright, *Quart. Rev.*, **21**, 109 (1967).

26) J. J. Stezowski, R. Countryman, and J. L. Hoard, *Inorg. Chem.*, **12**, 1749 (1973).

27) S. Richards, B. Pedersen, J. V. Silverton, and J. L. Hoard, *Inorg. Chem.*, **3**, 27 (1964).

28) M. Saito, T. Uehiro, F. Edina, T. Iwamoto, A. Ouchi, and Y. Yoshinio, *Chem. Lett.*, **1979**, 997; M. Saito, Ph.D. Dissertation, Tokyo University, Tokyo, Japan, 1979.

29) G. H. Cohen and J. L. Hoard, *J. Am. Chem. Soc.*, **88**, 3228 (1966).

30) R. D. Shannon and C. T. Prewitt, *Acta Crystallogr., Sect. B*, **25**, 925 (1969); R. D. Shannon, *Acta Crystallogr., Sect. A*, **32**, 751 (1976).

 © 1991 The Chemical Society of Japan Bull. Chem. Soc. Jpn., 64, 2635—2643 (1991)

Preparation and Characterization of *N,N*-Bridged and/or *S,S*-Bridged Sexidentate-N_2,O_2,S_2 Cobalt(III) Complexes. Crystal Structure of {(3*S*, 8*S*)-2,2,9,9-Tetramethyl-1,10-dithia-4,7-diazacyclotetradecane-3,8-dicarboxylato}cobalt(III) Bromide

Ken-ichi Okamoto,* Norio Fushimi, Takumi Konno, and Jinsai Hidaka
Department of Chemistry, University of Tsukuba, Tsukuba, Ibaraki 305
(Received March 27, 1991)

Four kinds of cobalt(III) complexes with *N,N*-bridged, *S,S*-bridged, or *N,N*- and *S,S*-bridged (cyclo type) sexidentate-N_2,O_2,S_2 ligand containing two D-penicillaminate moieties were newly synthesized. Of these complexes, the crystal structure of the title complex was determined by the X-ray diffraction method. The crystal was orthorhombic, space group $P2_12_12_1$, a=16.935(5), b=23.506(7), c=13.057(6) Å, V=5198(3) Å^3, Z=8, and the final R value was 0.0685. The ligand coordinates to the cobalt atom as the *N,N*- and *S,S*-bridged sexidentate-N_2,O_2,S_2. The absolute configurations of the nitrogen and sulfur donor atoms are *S*(N),*S*(N) and *R*(S),*R*(S) respectively. The *N,N*-bridged five-membered ring is the gauche form with the δ conformation and the *S,S*-bridged seven-membered ring is the twist-chair form with the λ conformation. The other three complexes were characterized by their electronic absorption, ^{13}C NMR, and circular dichroism (CD) spectra. The *N,N*- and/or *S,S*-bridged complexes showed the characteristic absorption and CD spectral behavior in the region of 16—24×10^3 cm^{-1}.

Cobalt(III) complexes with an *N,N*- or *S,S*-bridged sexidentate-N_2,O_2,S_2 thioether type ligand containing two *S*-methyl-L-cysteinate (L-smc) or L-cysteinate (L-cys) moieties have been investigated for the stereochemical and spectrochemical interests.[1,2] For example, the cobalt(III) complexes with *S,S'*-ethylenebis(L-cysteinate), *S,S'*-trimethylenebis(L-cysteinate), *N,N'*-ethylenebis(*S*-methyl-L-cysteinate), and *N,N'*-trimethylenebis(*S*-methyl-L-cysteinate) exhibited an extreme trans(O) selectivity concerning the formation of the geometrical isomers, where the expectant isomers are trans(O) and trans(N) for the *S,S*-bridged complexes, and trans(O) and trans(S) for the *N,N*-bridged ones.[1,2] This stereochemical characteristic seems to reveal that the cobalt(III) complexes with an *N,N*- and *S,S*-bridged (cyclo type) sexidentate-N_2,O_2,S_2 ligand are possibly formed.

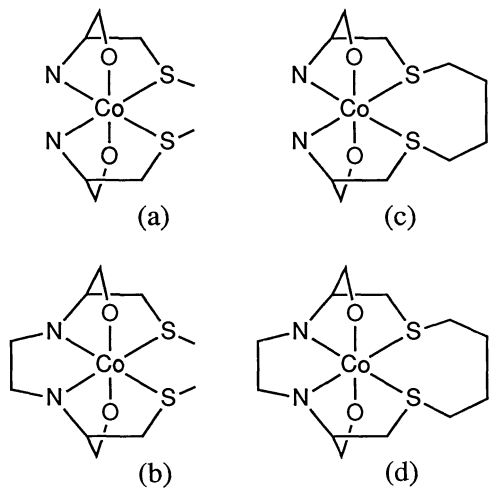

Fig. 1. Structure of (a) *trans*-(O)-[Co(D-smp)$_2$]$^+$, (b) *trans*-(O)-[Co(*N,N*-ebsmp)]$^+$, (*N,N*-bridged complex), (c) *trans*-(O)-[Co(*S,S*-tmbp)]$^+$, (*S,S*-bridged one), and (d) [Co(cyc-etmbp)]$^+$ (cyclo type one).[3]

The cyclo type complex is of interest not only in preparative work, but also in spectrochemistry. In the present work, D-penicillaminate (D-pen), which has the same framework as L-cysteinate, was used as the two terminals of the sexidentate-N_2,O_2,S_2 ligand. The trans(O) cobalt(III) complexes with the *N,N*-bridged, *S,S*-bridged, or cyclo type ligand[3] were synthesized by the alkylation reaction of the thiolato complex[4] containing two D-penicillaminate moieties with dimethyl sulfate, 1,2-dibromoethane, or 1,4-dibromobutane (Fig. 1). This paper reports the isolation of the four kinds of cobalt(III) complexes with the sexidentate-N_2,O_2,S_2 ligand, and their stereochemical and spectrochemical behavior. Of these complexes, the crystal structure of the cyclo type complex, [Co(*cyc*-etmbp)]$^+$ (Fig. 1), was determined by X-ray diffraction method.

Experimental

Materials. All reagents were purchased from the Wako Pure Chemical Ind. Co., Ltd., or Tokyo Chemical Ind. Co., Ltd. in Japan. All chemicals were of reagent grade and were used without further purification.

Preparation of Ligands. 1) *N,N'*-Ethylenebis(D-penicillamine): *N,N*-H$_4$ebp. This ligand was prepared by a procedure similar to that used for *N,N'*-ethylenebis(*S*-benzyl-L-cysteine).[5] The reaction solution was adjusted to pH 5 with hydrochloric acid and allowed to stand at 0 °C for 2 h. The deposited precipitate was collected by filtration, washed with deaerated cold water and methanol, and then dried in a vacuum desiccator. Found: C, 42.50; H, 7.31; N, 8.15%. Calcd for $H_4ebp\cdot 3/4H_2O=C_{12}H_{24}N_2O_4S_2\cdot 3/4H_2O$: C, 42.65; H, 7.60; N, 8.29%. ^{1}H NMR[100 MHz; solvent D_2O; standard DSS δ=2.99 (2H, S, CH), 2.65 (4H, broad, CH_2), 1.47 (6H, s, CH_3), 1.35 (6H, s, CH_3)]. ^{13}C NMR δ: see Table 4.

Preparation of Complexes. 2) *trans*(O)-Bis(*S*-methyl-D-penicillaminato)cobalt(III) Perchlorate: *trans*(O)-[Co(D-smp)$_2$]ClO$_4$. This complex was prepared by the procedure described in the literature,[4] and obtained as the perchlorate salt

by using a column of QAE-Sephadex A-25 (ClO_4^- form, 3 cm×35 cm). Found: C, 28.60; H, 5.37; N, 5.52%. Calcd for $[Co(D\text{-}smp)_2]ClO_4\cdot 3/2H_2O = C_{12}H_{24}N_2O_4S_2CoClO_4\cdot 3/2H_2O$: C, 28.27; H, 5.34; N, 5.49%.

3) *trans*(O)-*N*,*N*′-Ethylenebis(*S*-methyl-D-penicillaminato)cobalt(III) Hexafluorophosphate: *trans*(O)-[Co(*N*,*N*-ebsmp)]PF_6. To a solution containing 1 g of $[Co(NH_3)_6]Cl_3$[6] in 30 cm^3 of hot water (ca. 60 °C) were added 2 g of *N*,*N*′-ethylenebis(D-penicillamine) described in (1) and 0.5 g of activated charcoal. The mixture was stirred at 60 °C for 15 min, cooled to room temperature, and then filtered to remove insoluble materials. From the absorption spectral measurements and the column chromatographic behavior, it was found that the reaction mixture contained only *trans*(O)-[Co(*N*,*N*-ebp)]$^-$.[3] To the filtrate was added ca. 10 cm^3 of a 2.0 mol dm^{-3} aqueous solution of $NaClO_4$. This solution was concentrated to a small volume with a rotary evaporator and the deposited NaCl was filtered off. To the filtrate was added an appropriate amount of acetone and it was kept in a refrigerator for 6 h. The resulting brown precipitate was collected by filtration, washed with acetone, and then dried in a vacuum desiccator. Found: C, 29.81; H, 5.48; N, 5.82%. Calcd for $Na[Co(N,N\text{-ebp})]\cdot 3H_2O\cdot 1/2NaCl = C_{12}H_{20}N_2O_4S_2CoNa\cdot 3H_2O\cdot 1/2NaCl$: C, 29.68; H, 5.40; N, 5.77 %.

About 10 cm^3 of dimethyl sulfate was added to the reaction solution containing *trans*(O)-[Co(*N*,*N*-ebp)]$^-$ and the mixture was stirred for a few minutes. After being allowed to stand at room temperature overnight, the solution separated into two layers. The upper reddish layer was poured onto a column of SP-Sephadex C-25 (Na^+ form, 4.5 cm×45 cm). After sweeping the column with water, the adsorbed band was eluted with a 0.02 mol dm^{-3} aqueous solution of Na_2SO_4. Only deep red band was eluted and fractionated. From the absorption spectral measurements, it was found that each eluate contained only *trans*(O)-[Co(*N*,*N*-ebsmp)]$^+$. The eluates were combined and concentrated to a small volume with a rotary evaporator. The deposited Na_2SO_4 was filtered off. To the filtrate was added an appropriate amount of saturated NH_4PF_6 aqueous solution. The solution was concentrated to a small volume again and kept in a refrigerator overnight. The resulting deep red crystals were collected by filtration, washed with ethanol and ether, and then dried in a vacuum desiccator. Found: C, 28.38; H, 5.26; N, 4.77 %. Calcd for $[Co(N,N\text{-ebsmp})]PF_6\cdot 2H_2O = C_{14}H_{26}N_2O_4S_2PF_6Co\cdot 2H_2O$: C, 28.48; H, 5.12; N, 4.74 %.

4) *trans*(O)-*S*,*S*′-Tetramethylenebis(D-penicillaminato)cobalt(III) Perchlorate: *trans*(O)-[Co(*S*,*S*-tmbp)]ClO_4. *trans*(O)-[Co(D-pen)$_2$]$^-$ was prepared by the same procedure as that used for *trans*(O)-[Co(*N*,*N*-ebp)]$^-$ described in (3), using D-penicillamine (2 g) instead of *N*,*N*-H_4ebp. The greenish brown filtrate was concentrated to a small volume with a rotary evaporator, and to this was added to 10 cm^3 of 1,4-dibromobutane in 50 cm^3 of dimethyl sulfoxide. After being allowed to stand at room temperature for 1 d, unreacted 1,4-dibromobutane and dimethyl sulfoxide were extracted into diethyl ether. The leaving deep purple solution was poured onto a column of SP-Sephadex C-25 (Na^+ form, 4.5 cm×45 cm). After sweeping the column with water, the adsorbed band was eluted with a 0.05 mol dm^{-3} aqueous solution of NaCl. The five bands, dark red, reddish purple, purple, dark purple, and purple, were eluted in this order. The faster moving dark red band was transferred to another column of SP-Sephadex C-25 (Na^+ form, 4 cm×90 cm) and eluted with a 0.05 mol dm^{-3} aqueous solution of NaCl, because the other four bands were decomposed or disappeared during elution. The dark red band was separated into the three bands, dark red, reddish purple, and purple, in this order. From the absorption and ^{13}C NMR spectral measurements, it was found that the faster moving band contained the desired complex but the other two eluates were by-products whose sulfur atoms were not spanned by tetramethylene bridge. Then, the first moving dark red band was concentrated to a small volume with a rotary evaporator. The deposited NaCl was filtered off. The filtrate was passed through a column of QAE-Sephadex A-25 (ClO_4^- form, 3 cm×35 cm) eluting with water. After the eluate had been concentrated again, an appropriate amount of ethanol was added to it. The resulting red precipitate was collected by filtration, washed with ethanol and ether, and then dried in a vacuum desiccator. Found: C, 31.46; H, 5.61; N, 5.06%. Calcd for $[Co(S,S\text{-tmbp})]ClO_4\cdot 3/2H_2O = C_{14}H_{26}N_2O_4S_2CoClO_4\cdot 3/2H_2O$: C, 31.38; H, 5.45; N, 5.22%.

5) *trans*(O)-*S*,*S*′-Ethylenebis(D-penicillaminato)cobalt(III) Chloride: *trans*(O)-[Co(*S*,*S*-ebp)]Cl. This complex was prepared and chromatographed by a procedure similar to that used in (4), using 1,2-dibromoethane instead of 1,4-dibromobutane. The only purple band was eluted. From the absorption spectral measurements, it was found that the eluate contained only *trans*(O)-[Co(*S*,*S*-ebp)]$^+$. The eluate was concentrated to a small volume with a rotary evaporator. The deposited NaCl was filtered off. The filtrate was poured onto a column of Sephadex G-10 (3 cm×70 cm) eluting with water. After the eluate had been concentrated to a small volume again, an appropriate amount of ethanol was added to it. The solution was kept in a refrigerator for 5 h. The resulting purple crystals were collected by filtration, washed with ethanol and ether, and then dried in a vacuum desiccator. Found: C, 32.97; H, 5.53; N, 6.42 %. Calcd for $[Co(S,S\text{-ebp})]Cl\cdot H_2O = C_{12}H_{22}N_2S_2O_4ClCo\cdot H_2O$: C, 33.15; H, 5.56; N, 6.44 %.

6) {(3*S*,8*S*)-2,2,9,9-tetramethyl-1,10-dithia-4,7-diazacyclotetradecane-3,8-dicarboxylato}cobalt(III) Nitrate: [Co(*cyc*-etmbp)]NO_3. To a solution containing 1.5 g of *trans*(O)-$Na[Co(N,N\text{-ebp})]\cdot 3H_2O\cdot 1/2NaCl$ (described in (3)) in 30 cm^3 of dimethyl sulfoxide was added about 10 cm^3 of 1,4-dibromobutane. After being allowed to stand at room temperature for 18 h, the reaction mixture turned to deep red. Dimethyl sulfoxide and unreacted 1,4-dibromobutane were extracted into diethyl ether. The leaving dark red oil was poured onto a column of SP-Sephadex C-25 (Na^+ form, 4 cm×65 cm). After sweeping the column with water, the adsorbed band was eluted with a 0.05 mol dm^{-3} aqueous solution of NaCl. Two bands, orange red and red, were eluted in this order. Since the faster moving band seemed to contain two isomers, it was transferred to another column of SP-Sephadex C-25 (Na^+ form, 4.5 cm×45 cm). By developing the band with a 0.05 mol dm^{-3} aqueous solution of NaCl, two bands, orange red and red, were eluted in this order. From the absorption and CD spectral measurements, it was found that the orange red band contained the desired complex and the two red bands were by-products whose sulfur atoms were not spanned by tetramethylene bridge. The faster moving band was concentrated to a small volume with a rotary evaporator. The deposited NaCl was filtered off. The filtrate was passed through a column of QAE-Sephadex A-25 (NO_3^- form,

Table 1. Final Atomic Coordinates and Equivalent Isotropic Thermal Parameters ($Å^2$) for the Non-H Atoms

Atom	*x*	*y*	*z*	B_{eq}[a)]
Co(A)	0.9417(1)	0.0649(0)	0.9180(1)	2.09(4)
S(1A)	1.0689(1)	0.0637(1)	0.9620(2)	2.64(8)
S(2A)	0.9548(1)	0.0596(1)	0.7484(2)	2.67(8)
O(1A)	0.9370(4)	−0.0157(2)	0.9255(5)	3.23(27)
O(2A)	0.9461(7)	−0.0851(3)	1.0411(6)	6.33(46)
O(3A)	0.9442(3)	0.1455(2)	0.9149(4)	2.40(22)
O(4A)	0.8740(4)	0.2182(3)	0.8530(5)	3.62(29)
N(1A)	0.9184(4)	0.0614(3)	1.0618(5)	2.61(28)
N(2A)	0.8291(4)	0.0749(3)	0.8935(5)	2.63(29)
C(1A)	0.9495(7)	−0.0348(4)	1.0190(8)	3.80(44)
C(2A)	0.9671(6)	0.0116(4)	1.0971(7)	3.45(41)
C(3A)	1.0556(7)	0.0288(4)	1.0912(7)	3.61(42)
C(4A)	1.1109(8)	−0.0214(5)	1.1063(10)	5.48(59)
C(5A)	1.0761(7)	0.0755(5)	1.1697(7)	4.05(47)
C(6A)	0.8843(5)	0.1672(4)	0.8655(7)	2.63(34)
C(7A)	0.8299(5)	0.1224(4)	0.8194(6)	2.63(34)
C(8A)	0.8636(5)	0.1006(4)	0.7146(7)	2.93(37)
C(9A)	0.8063(6)	0.0574(5)	0.6651(7)	4.08(46)
C(10A)	0.8786(7)	0.1515(4)	0.6439(8)	4.10(48)
C(11A)	0.8313(5)	0.0521(4)	1.0742(7)	3.25(40)
C(12A)	0.7926(5)	0.0895(4)	0.9929(7)	3.19(38)
C(13A)	1.1217(7)	0.0144(4)	0.8761(8)	4.05(47)
C(14A)	1.1622(6)	0.0467(5)	0.7930(8)	4.12(47)
C(15A)	1.1128(6)	0.0621(5)	0.6984(8)	4.41(50)
C(16A)	1.0394(5)	0.1018(4)	0.7121(7)	3.56(43)
Co(B)	0.2211(1)	0.2733(0)	0.7672(1)	1.98(4)
S(1B)	0.1319(1)	0.3100(1)	0.8733(2)	2.48(8)
S(2B)	0.2556(1)	0.1988(1)	0.8607(2)	2.24(7)
O(1B)	0.1417(4)	0.2303(3)	0.7009(5)	2.99(26)
O(2B)	0.0319(4)	0.2425(3)	0.6068(7)	4.91(37)
O(3B)	0.3006(3)	0.3194(2)	0.8270(4)	2.36(22)
O(4B)	0.4312(4)	0.3281(3)	0.8310(6)	1.61(26)
N(1B)	0.1916(4)	0.3310(3)	0.6689(5)	2.42(27)
N(2B)	0.3048(4)	0.2504(3)	0.6749(5)	2.35(27)
C(1B)	0.0890(6)	0.2619(4)	0.6572(8)	3.36(41)
C(2B)	0.1047(5)	0.3256(4)	0.6703(7)	3.01(37)
C(3B)	0.0729(5)	0.3454(4)	0.7723(7)	3.14(38)
C(4B)	−0.0170(6)	0.3342(6)	0.7866(10)	4.85(55)
C(5B)	0.0922(7)	0.4104(4)	0.7877(9)	4.44(49)
C(6B)	0.3734(5)	0.3024(3)	0.8055(6)	2.52(33)
C(7B)	0.3743(5)	0.2477(4)	0.7461(7)	2.78(35)
C(8B)	0.3621(5)	0.1963(4)	0.8171(7)	2.69(34)
C(9B)	0.3684(6)	0.1391(4)	0.7596(9)	3.64(42)
C(10B)	0.4189(5)	0.1963(5)	0.9056(8)	3.64(43)
C(11B)	0.2289(6)	0.3150(4)	0.5709(7)	3.55(42)
C(12B)	0.3121(6)	0.2951(4)	0.5957(7)	3.35(40)
C(13B)	0.0755(6)	0.2511(4)	0.9238(7)	3.59(42)
C(14B)	0.1044(6)	0.2372(4)	1.0347(7)	3.66(43)
C(15B)	0.1768(6)	0.1995(4)	1.0440(7)	3.42(41)
C(16B)	0.2550(5)	0.2181(4)	0.9965(6)	3.01(37)
Br(1)	0.7132(1)	−0.0431(0)	0.8618(1)	3.90(4)
Br(2)	0.1983(1)	−0.0624(1)	0.5274(1)	5.76(6)
O(W1)	0.2972(6)	0.1006(4)	0.2735(8)	7.0(5)
O(W2)	0.7779(8)	0.3400(5)	0.4714(8)	8.9(7)
O(W3)	0.1880(6)	0.0717(5)	0.4265(9)	7.9(6)
O(W4)	0.9712(7)	0.0671(5)	0.4374(12)	10.7(9)
O(W5)	0.0619(10)	0.1626(6)	0.4382(10)	13.1(11)
O(W6)	0.2947(6)	0.2156(5)	0.2979(9)	7.7(6)
O(W7)	0.1076(8)	0.4206(5)	0.1358(11)	10.4(8)
O(W8)	0.9380(8)	0.3166(5)	0.4856(12)	11.6(9)
O(W9)	0.1075(12)	0.3532(5)	0.2944(12)	13.2(11)
O(W10)	0.4832(10)	0.0387(8)	−0.0341(25)	22.8(19)
O(W11)	0.1343(10)	0.2397(6)	0.3084(14)	12.5(11)

$B_{eq}=(8\pi^2/3)\sum_i\sum_j U_{ij}a_i^*a_j^*\boldsymbol{a}_i\cdot\boldsymbol{a}_j$.

Table 2. Bond Distances (Å) and Angles(°)

Co(A)–S(1A)	2.230(2)	Co(B)–S(1B)	2.223(2)
Co(A)–S(2A)	2.229(2)	Co(B)–S(2B)	2.214(2)
Co(A)–O(1A)	1.899(6)	Co(B)–O(1B)	1.892(6)
Co(A)–O(3A)	1.895(5)	Co(B)–O(3B)	1.896(6)
Co(A)–N(1A)	1.919(7)	Co(B)–N(1B)	1.933(7)
Co(A)–N(2A)	1.948(7)	Co(B)–N(2B)	1.937(7)
S(1A)–C(3A)	1.890(10)	S(1B)–C(3B)	1.852(10)
S(1A)–C(13A)	1.844(11)	S(1B)–C(13B)	1.807(10)
S(2A)–C(8A)	1.874(9)	S(2B)–C(8B)	1.892(8)
S(2A)–C(16A)	1.806(10)	S(2B)–C(16B)	1.830(9)
O(1A)–C(1A)	1.318(12)	O(1B)–C(1B)	1.294(11)
O(2A)–C(1A)	1.218(11)	O(2B)–C(1B)	1.254(12)
O(3A)–C(6A)	1.306(10)	O(3B)–C(6B)	1.324(10)
O(4A)–C(6A)	1.224(10)	O(4B)–C(6B)	1.198(11)
N(1A)–C(2A)	1.505(12)	N(1B)–C(2B)	1.477(11)
N(1A)–C(11A)	1.501(12)	N(1B)–C(11B)	1.476(12)
N(2A)–C(7A)	1.478(11)	N(2B)–C(7B)	1.502(11)
N(2A)–C(12A)	1.478(11)	N(2B)–C(12B)	1.478(11)
C(1A)–C(2A)	1.523(13)	C(1B)–C(2B)	1.530(13)
C(2A)–C(3A)	1.553(15)	C(2B)–C(3B)	1.510(13)
C(3A)–C(4A)	1.519(16)	C(3B)–C(4B)	1.556(13)
C(3A)–C(5A)	1.541(14)	C(3B)–C(5B)	1.575(14)
C(6A)–C(7A)	1.522(12)	C(6B)–C(7B)	1.502(12)
C(7A)–C(8A)	1.568(12)	C(7B)–C(8B)	1.536(12)
C(8A)–C(9A)	1.546(14)	C(8B)–C(9B)	1.545(12)
C(8A)–C(10A)	1.534(14)	C(8B)–C(10B)	1.504(13)
C(11A)–C(12A)	1.526(13)	C(11B)–C(12B)	1.521(14)
C(13A)–C(14A)	1.493(15)	C(13B)–C(14B)	1.563(14)
C(14A)–C(15A)	1.535(15)	C(14B)–C(15B)	1.518(14)
C(15A)–C(16A)	1.565(15)	C(15B)–C(16B)	1.525(13)
S(1A)–Co(A)–S(2A)	99.1(1)	S(1B)–Co(B)–S(2B)	98.2(1)
S(1A)–Co(A)–O(1A)	90.8(2)	S(1B)–Co(B)–O(1B)	90.6(2)
S(2A)–Co(A)–O(1A)	90.0(2)	S(2B)–Co(B)–O(1B)	91.0(2)
S(1A)–Co(A)–O(3A)	89.8(2)	S(1B)–Co(B)–O(3B)	90.3(2)
S(2A)–Co(A)–O(3A)	91.9(2)	S(2B)–Co(B)–O(3B)	92.1(2)
O(1A)–Co(A)–O(3A)	178.0(3)	O(1B)–Co(B)–O(3B)	176.7(3)
S(1A)–Co(A)–N(1A)	86.9(2)	S(1B)–Co(B)–N(1B)	88.1(2)
S(2A)–Co(A)–N(1A)	171.6(2)	S(2B)–Co(B)–N(1B)	171.7(2)
O(1A)–Co(A)–N(1A)	84.1(3)	O(1B)–Co(B)–N(1B)	83.5(3)
O(3A)–Co(A)–N(1A)	94.0(3)	O(3B)–Co(B)–N(1B)	93.3(3)
S(1A)–Co(A)–N(2A)	171.8(2)	S(1B)–Co(B)–N(2B)	173.0(2)
S(2A)–Co(A)–N(2A)	86.6(2)	S(2B)–Co(B)–N(2B)	86.0(2)
O(1A)–Co(A)–N(2A)	95.0(3)	O(1B)–Co(B)–N(2B)	95.0(3)
O(3A)–Co(A)–N(2A)	84.2(3)	O(3B)–Co(B)–N(2B)	84.0(3)
N(1A)–Co(A)–N(2A)	88.0(3)	N(1B)–Co(B)–N(2B)	88.3(3)
Co(A)–S(1A)–C(3A)	96.9(4)	Co(B)–S(1B)–C(3B)	95.6(3)
Co(A)–S(1A)–C(13A)	108.7(4)	Co(B)–S(1B)–C(13B)	106.8(3)
C(3A)–S(1A)–C(13A)	109.1(4)	C(3B)–S(1B)–C(13B)	108.5(4)
Co(A)–S(2A)–C(8A)	97.1(3)	Co(B)–S(2B)–C(8B)	96.3(3)
Co(A)–S(2A)–C(16A)	108.0(3)	Co(B)–S(2B)–C(16B)	109.7(3)
C(8A)–S(2A)–C(16A)	108.0(4)	C(8B)–S(2B)–C(16B)	107.7(4)
Co(A)–O(1A)–C(1A)	112.4(5)	Co(B)–O(1B)–C(1B)	112.6(6)
Co(A)–O(3A)–C(6A)	112.5(5)	Co(B)–O(3B)–C(6B)	113.7(5)
Co(A)–N(1A)–C(2A)	102.8(5)	Co(B)–N(1B)–C(2B)	100.9(5)
Co(A)–N(1A)–C(11A)	108.3(5)	Co(B)–N(1B)–C(11B)	106.6(5)
C(2A)–N(1A)–C(11A)	113.1(7)	C(2B)–N(1B)–C(11B)	114.5(7)
Co(A)–N(2A)–C(7A)	100.9(5)	Co(B)–N(2B)–C(7B)	101.5(5)
Co(A)–N(2A)–C(12A)	107.0(5)	Co(B)–N(2B)–C(12B)	107.4(5)
C(7A)–N(2A)–C(12A)	113.8(7)	C(7B)–N(2B)–C(12B)	113.4(7)
O(1A)–C(1A)–O(2A)	122.9(9)	O(1B)–C(1B)–O(2B)	123.7(9)
O(1A)–C(1A)–C(2A)	114.1(7)	O(1B)–C(1B)–C(2B)	113.1(8)
O(2A)–C(1A)–C(2A)	123.0(9)	O(2B)–C(1B)–C(2B)	123.1(9)
N(1A)–C(2A)–C(1A)	104.1(7)	N(1B)–C(2B)–C(1B)	104.9(7)
N(1A)–C(2A)–C(3A)	108.1(7)	N(1B)–C(2B)–C(3B)	109.9(7)
C(1A)–C(2A)–C(3A)	110.0(8)	C(1B)–C(2B)–C(3B)	109.8(8)

Table 2. (Continued)

S(1A)–C(3A)–C(2A)	105.8(6)	S(1B)–C(3B)–C(2B)	107.3(6)
S(1A)–C(3A)–C(4A)	112.3(8)	S(1B)–C(3B)–C(4B)	111.6(7)
C(2A)–C(3A)–C(4A)	112.7(8)	C(2B)–C(3B)–C(4B)	113.8(8)
S(1A)–C(3A)–C(5A)	104.9(6)	S(1B)–C(3B)–C(5B)	103.4(7)
C(2A)–C(3A)–C(5A)	111.7(8)	C(2B)–C(3B)–C(5B)	109.8(8)
C(4A)–C(3A)–C(5A)	109.1(9)	C(4B)–C(3B)–C(5B)	110.6(9)
O(3A)–C(6A)–O(4A)	124.0(8)	O(3B)–C(6B)–O(4B)	123.4(8)
O(3A)–C(6A)–C(7A)	113.4(7)	O(3B)–C(6B)–C(7B)	112.1(7)
O(4A)–C(6A)–C(7A)	122.6(8)	O(4B)–C(6B)–C(7B)	124.6(8)
N(2A)–C(7A)–C(6A)	105.6(6)	N(2B)–C(7B)–C(6B)	106.0(7)
N(2A)–C(7A)–C(8A)	109.1(7)	N(2B)–C(7B)–C(8B)	107.6(6)
C(6A)–C(7A)–C(8A)	110.6(7)	C(6B)–C(7B)–C(8B)	111.1(7)
S(2A)–C(8A)–C(7A)	105.2(6)	S(2B)–C(8B)–C(7B)	106.6(5)
S(2A)–C(8A)–C(9A)	106.2(6)	S(2B)–C(8B)–C(9B)	103.8(6)
C(7A)–C(8A)–C(9A)	110.6(7)	C(7B)–C(8B)–C(9B)	112.5(8)
S(2A)–C(8A)–C(10A)	114.0(7)	S(2B)–C(8B)–C(10B)	112.2(6)
C(7A)–C(8A)–C(10A)	109.3(7)	C(7B)–C(8B)–C(10B)	112.2(7)
C(9A)–C(8A)–C(10A)	111.4(8)	C(9B)–C(8B)–C(10B)	109.2(8)
N(1A)–C(11A)–C(12A)	105.3(7)	N(1B)–C(11B)–C(12B)	106.9(7)
N(2A)–C(12A)–C(11A)	107.3(7)	N(2B)–C(12B)–C(11B)	106.9(8)
S(1A)–C(13A)–C(14A)	110.2(7)	S(1B)–C(13B)–C(14B)	109.4(7)
C(13A)–C(14A)–C(15A)	117.0(9)	C(13B)–C(14B)-C(15B)	116.7(8)
C(14A)–C(15A)–C(16A)	118.8(9)	C(14B)–C(15B)–C(16B)	120.1(8)
S(2A)–C(16A)–C(15A)	109.4(7)	S(2B)–C(16B)–C(15B)	109.2(6)

3 cm×35 cm) eluting with water. The eluate was concentrated to a small volume again and kept in a refrigerator for 6 h. The resulting dark red crystals were collected by filtration, washed with ethanol and ether, and then dried in a vacuum desiccator. Found: C, 36.63; H, 5.96; N, 7.97%. [Co(*cyc*-etmbp)]NO_3·3/2H_2O=$C_{16}H_{28}N_3O_7S_2Co$·3/2H_2O: C, 36.64; H, 5.95; N, 7.97%.

The nitrate salt of the complex was dissolved with the appropriate amount of water and it was passed through a column of QAE-Sephadex A-25 (Br^- form) eluting with water. The eluate was concentrated to a small volume and kept in a refrigerator. The resulting crystals, [Co(*cyc*-etmbp)]Br·5.5H_2O, were suitable for X-ray structure analysis and could be collected by filtration.

Measurements. The electronic absorption spectra were recorded with a JASCO UVIDEC-610C or UVIDEC-505 spectrophotometer, and the CD spectra with a JASCO J-20 or J-600 spectropolarimeter. All the measurements were carried out in aqueous solutions at room temperature. The ^1H and ^{13}C NMR spectra were recorded with a JEOL JNM-FX-100 or -FX-90Q NMR spectrometer in a deuterium oxide (D_2O) or acetonitrile-d_3 (CD_3CN) solvent at the probe temperature. Sodium 2,2-dimethyl-2-silapentane-5-sulfonate (DSS) or tetramethylsilane (TMS) was employed as the internal reference.

Crystallography. X-Ray Data Collection. Unit cell parameters and intensity data for the single orange-red crystal (ca. 0.55×0.55×0.35 mm^3) were measured on an Enraf Nonius CAD4 diffractometer with graphite-monochromated Mo $K\alpha$ radiation (λ 0.71069 Å, 50 kV and 26 mA). Unit cell parameters were determined by least-squares refinement from 25 reflections with $20°<2\theta<24°$. Crystal data: [$CoC_{16}H_{28}N_2O_4S_2$]Br·5.5H_2O, M=614.47, orthorhombic, space group $P2_12_12_1$, a=16.935(5), b=23.506(7), c=13.057(6) Å, U=5198(3) $Å^3$, Z=8, D_C=1.57 g cm^{-3}, $F(000)$=2536, μ=23.2 cm^{-1}, and room temperature.

The intensity data were collected by the ω–2θ scan mode up to $2<2\theta<56°$ ($0\leqq h\leqq 23$, $0\leqq k\leqq 33$, $0\leqq l\leqq 18$) with scan width $(0.8+0.350\tan\theta)°$ and scan rate varied from 1 to 5° min^{-1} (on ω). The intensities were corrected for Lorentz and polarization, and not for absorption. A total of 5929 independent reflections with $|F_o|>3\sigma(|F_o|)$ of the measured 8286 reflection were considered as "observed" and used for structure determination.

Determination of Crystal Structure. The cobalt and four coordinated atoms were located by the direct methods of the crystallographic program package SDP/VAN.[7] The remaining non-hydrogen atoms were found by conventional difference Fourier techniques to give a trial structure. The structure was refined by the full-matrix least-squares technique using SHELX76[8] on the FACOM M780/20 computer at the Computer Center of the University of Tsukuba. Anisotropic temperature factors were applied to all non-hydrogen atoms. Hydrogen atoms were fixed by geometrical constrains (C–H=0.95 Å) and isotropic thermal parameters (U=0.05 $Å^2$). The water hydrogen atoms were not included in the calculation. The final refinement gave R=0.0685 and R_w=0.0708 with the weighting scheme $w=1.5254/\{\sigma^2(F_o)+0.002334F_o^2\}$. The final difference Fourier synthesis indicated no significant peaks larger than 1.0 eA^{-3}. Atomic positional parameters are given in Table 1 and selected bond distances and angles within the cations are summarized in Table 2.[9]

Results and Discussion

Crystal Structure of [Co(*cyc*-etmbp)]$^+$. A perspective drawing of the typical complex cation (A species) is shown in Fig. 2, together with its atomic numbering scheme. There are two crystallographically independent complex cations in an asymmetric unit, through their shapes and sizes remarkably resemble each other. In the both complex cations, the cobalt atom is octahedrally surrounded by two cis N, two trans O, and two cis S atoms, that is, the ligand coordinates to cobalt

atom as a sexidentate to take the trans(O) configuration. Two D-penicillaminate moieties are spanned by ethylene and tetramethylene to form the *N,N*-bridged five-membered and *S,S*-bridged seven-membered rings. As the result of bridging, the complex cations acquire two kinds of additionally optically active sources with regard to the chiral configuration of nitrogen donor atom (*R*(N) and *S*(N)) and sulfur donor one (*R*(S) and *S*(S)). The absolute configurations of these donor atoms and the chelate ring conformations in the complex cations can be confirmed on the basis of the asymmetric carbon atoms, *S*(C), in the two D-penicillaminate moieties.[10] Both of the chiral nitrogen donor atoms take selectively the *S*(N) configuration and the *N,N*-bridged five-membered ring has a gauche form with a δ conformation (Fig. 3(b)). Further, the two sulfur donor atoms take the *R*(S) configuration and the *S,S*-bridged seven-membered ring has a twist-chair form with a λ conformation (Fig. 3(a)), which is quite similar to those of the *N;N*-bridged seven-membered ring in *cis*-$[Co(NO_2)_2(tmd)_2]^+$ (tmd=1,4-butanediamine).[11]

The bond distances and angles are similar to those for the cobalt(III) complexes with thioether or thiolate ligands containing the cys, pen, or their derivatives (Table 3).[1,10,12-14] Especially, [Co(*cyc*-etmbp)]$^+$ shows quite similar bond distances and angles to *trans*(O)-[Co(*N,N*-ebsmc)]$^+$, except for the Co–S and S–C distances. The Co–S (2.214—2.230(2) Å; av. 2.224 Å) and S–C (1.852—1.892(10) Å; av. 1.877 Å) distances of the cyc-etmbp complex coincide with those of the *S,S*-bridged complex, $(+)^{CD}_{560}$-[Co{(2*R*,9*S*)-2,9-diamino-3,3,8,8-tetramethyl-4,7-dithia-1,10-decanedioato}]$^+$ (Co–S: 2.199(7) and 2.221(8) Å; S–C: 1.89(2) and 1.91(2) Å),[13] but differ from those of *trans*(O)-[Co(*N,N*-ebsmc)]$^+$ (Co–S: av. 2.261(4) Å; S–C; av. 1.843(14) Å)[1,3] and *trans*(S)-[Co(L-smc)$_2$]$^+$ (Co–S: 2.270(2) and 2.273(2) Å; S–C: 1.835(10) and 1.838(10) Å).[3,12] It is noteworthy that the bond angles of S–Co–S (98.2(1) and 99.1(1)°) are larger than those of N–Co–N of the *N,N*-bridged chelate rings, *cis*-$[Co(NO_2)_2(tmd)_2]^+$ (92.0—93.4(1)°; av. 92.4°).[11]

Characterization. The absorption and CD spectra of the present [Co(sexidentate-N_2,O_2,S_2)]$^+$ type complexes are shown in Figs. 4 and 5, and their data are summarized in Table 3. For the thioether type complexes such as [Co(L-smc)$_2$]$^+$, [Co(D-smp)$_2$]$^+$, and [Co(L-met)$_2$]$^+$, it has been known that the cis(S) isomer exhibits the intense broad absorption band at ca. 34×10^3 cm^{-1} and the trans(S) isomer the intense sharp one at ca. 28×10^3 cm^{-1}, arising from the sulfur-to-metal charge-transfer (SMCT) transition.[1,2,4,15] Taking these facts into consideration,

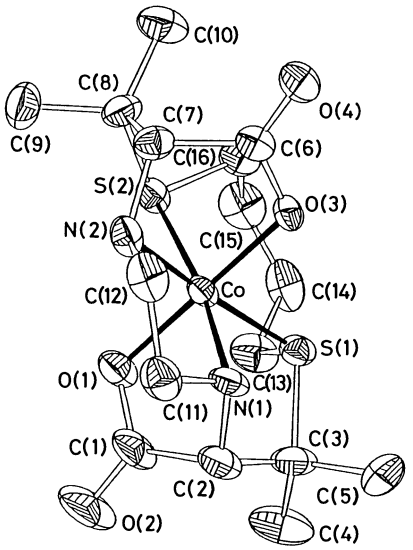

Fig. 2. A perspective drawing of [Co(*cyc*-etmbp)]$^+$ (A species) cation (50% probability thermal ellipsoids). The hydrogen atoms are omitted for clarity.

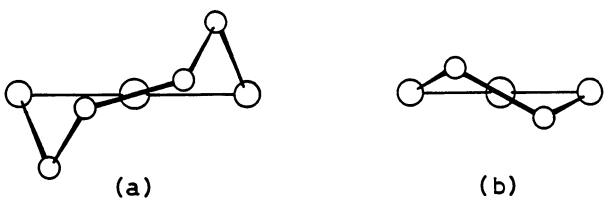

Fig. 3. Conformation of *S,S*-bridged seven-membered ring (a) and *N,N*-bridged five-membered ring (b) in [Co(*cyc*-etmbp)]$^+$.

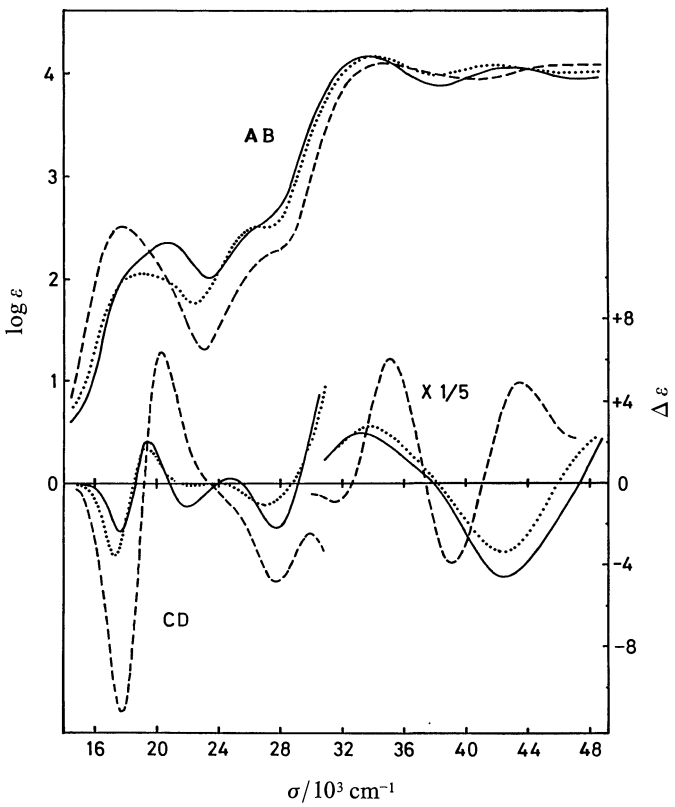

Fig. 4. Absorption and CD spectra of *trans*-(O)-[Co(*N,N*-ebsmp)]$^+$ (——), *trans*-(O)-[Co(*S,S*-ebp)]$^+$ (-----), and *trans*-(O)-[Co(D-smp)$_2$]$^+$ (·····).

Table 3. Absorption and CD Spectral Data of [Co(sexidentate-N_2,O_2,S_2)] Type Complexes

Complex ion	Absorption $\sigma/10^3$ cm^{-1} ($\log \varepsilon$/mol^{-1} dm^3 cm^{-1})	CD $\sigma/10^3$ cm^{-1} ($\Delta\varepsilon$/mol^{-1} dm^3 cm^{-1})
[Co(*cyc*-etmbp)]$^+$	18.87 (1.86)	18.73 (+3.40)
	21.83 (1.99)	22.03 (−2.82)
	33.11 (4.18)	25.08 (+0.53)
	43.5 (4.07 sh)[a]	27.69 (−0.90)
		32.55 (+26.1)
		42.74 (−38.3)
trans(O)-[Co(*S,S*-tmbp)]$^+$	18.79 (1.82)	18.19 (+1.92)
	20.92 (1.85)	21.85 (−0.06)
	33.22 (4.13)	23.90 (+0.37)
	42.55 (4.10)	26.10 (−0.24)
		31.91 (+18.6)
		42.12 (−31.1)
trans-(O)-[Co(*S,S*-ebp)]$^+$	17.86 (2.52)	17.70 (−11.4)
	27.4 (2.25 sh)	20.28 (+6.48)
	34.97 (4.11)	27.78 (−4.81)
	47.62 (4.09)	31.55 (−4.05)
		35.21 (+30.6)
		39.22 (−19.0)
		43.48 (+24.8)
trans(O)-[Co(*S,S*-ebc)]$^+$[b]	17.61 (2.48)	17.76 (+10.3)
	27.9 (2.27 sh)	20.45 (−6.59)
	35.21 (4.06)	27.93 (+6.80)
		32.00 (+6.90)
		35.71 (−29.3)
		40.32 (+21.3)
trans(O)-[Co(*N,N*-ebsmp)]$^+$	18.5 (2.13 sh)	17.70 (−2.29)
	20.83 (2.35)	19.60 (+2.05)
	26.7 (2.52 sh)	22.08 (−1.07)
	33.78 (4.16)	24.81 (+0.26)
	43.10 (4.05)	27.70 (−2.15)
		33.33 (+12.2)
		42.74 (−23.1)
trans(O)-[Co(*N,N*-ebsmc)]$^+$[c]	18.5 (2.13 sh)	17.33 (+2.82)
	20.83 (2.35)	19.27 (−2.68)
	26.7 (2.52 sh)	21.93 (+1.38)
	33.78 (4.16)	24.57 (−0.17)
	43.10 (4.05)	27.47 (+2.64)
		33.67 (−10.8)
		43.48 (+19.2)
trans(O)-[Co(D-smp)$_2$]$^+$[d]	19.20 (1.99)	17.40 (−3.61)
	26.47 (2.46)	19.40 (+1.71)
	34.27 (4.00)	22.27 (−0.12)
		26.86 (−1.07)
		33.87 (+14.6)
		42.33 (−19.1)

a) sh denotes a shoulder. b) Ref. 2. c) Ref. 1 d) Ref. 4.

all the present complexes, which exhibit the intense broad SMCT band at ca. 34×10^3 cm^{-1}, are assigned to take the cis(S) configuration, that is, the trans(O) or trans(N) isomer. Of the present three complexes except for the cyc-etmbp complex, the *N,N*-ebsmp complex is assignable to *trans*(O)-[Co(*N,N*-ebsmp)]$^+$ (Fig. 1), because the two cis nitrogen donor atoms are spanned by ethylene to form the five-membered ring. This assignment is supported by the fact that the *N,N*-ebsmp complex exhibits quite similar absorption and CD spectral patterns to *trans*(O)-[Co(*N,N*-ebsmc)]$^+$ over the whole region (Fig. 4 and Table 3), which has a quite similar framework to the *N,N*-ebsmp complex and its configuration has been determined by the X-ray structure analysis.[1] The absorption and CD spectral patterns of the *S,S*-tmbp complex, which was prepared by the reaction of *trans*(O)-[Co(D-pen)$_2$]$^-$ with 1,4-dibromobutane, coincides well with those of [Co(*cyc*-etmbp)]$^+$ over the whole region (Fig. 5 and Table 3). Accordingly, the *S,S*-tmbp complex is probably assigned to *trans*(O)-[Co(*S,S*-tmbp)]$^+$ (Fig. 1). The *S,S*-ebp complex, which was prepared by a similar reaction to the *S,S*-tmbp complex using *trans*(O)-[Co(D-pen)$_2$]$^-$ and 1,2-dibromoethane, exhibits quite similar absorption spectrum

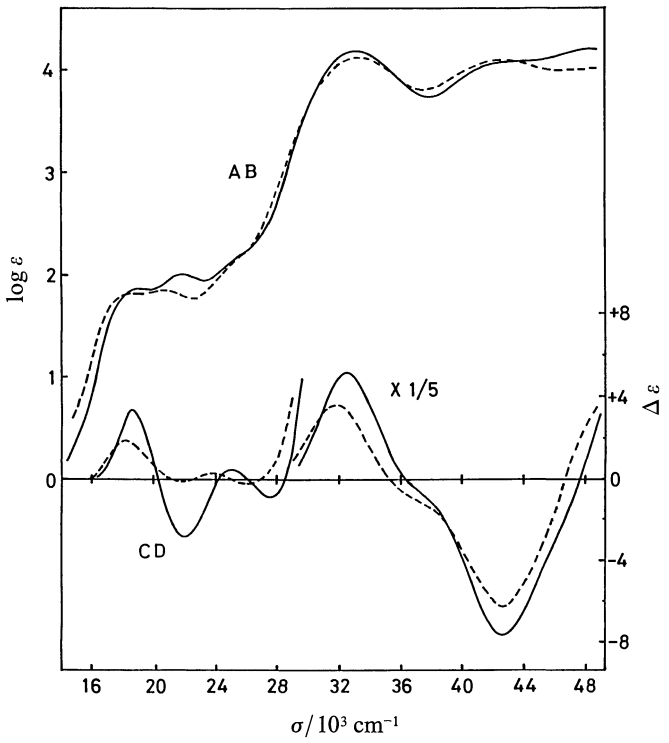

Fig. 5. Absorption and CD spectra of [Co(*cyc*-etmbp)]$^+$ (——) and *trans*-(O)-[Co(*S*,*S*-tmbp)]$^+$ (-----).

and CD pattern to those of *trans*(O)-[Co(*S*,*S*-ebc)]$^+$ over the whole region (Table 3).[2] These similarities suggest that the *S*,*S*-ebp complex takes a trans(O) configuration, *trans*(O)-[Co(*S*,*S*-ebp)]$^+$. These assignments based on their absorption and CD spectra are supported by their ^{13}C NMR spectral measurements.

The ^{13}C NMR chemical shift data for the four cobalt(III) complexes and *S*,*S*-H$_4$ebp are summarized in Table 4. Each signal was assigned on the basis of the insensitive nuclei enhanced by polarization transfer (INEPT) method and of the comparison with the chemical shift data for the related complexes.[1,2] [Co(*cyc*-etmbp)]$^+$ exhibits the eight resonance lines for the sixteen carbon atoms, indicating a C_2 symmetry of the complex. This reveals that the *cyc*-etmbp complex in solution retains the same conformation as in crystal. *trans*(O)-[Co(*S*,*S*-tmbp)]$^+$ exhibits a similar ^{13}C NMR spectral behavior to the *cyc*-etmbp complex, except that the resonance line (δ=75.47) due to the methine carbon atom appears significantly higher field than that (δ=81.42) of [Co(*cyc*-etmbp)]$^+$ whose two nitrogen donor atoms were spanned by ethylene. This suggests that the *S*,*S*-bridged seven-membered ring of the *S*,*S*-tmbp complex takes the twist-chair form with the λ conformation as in the *cyc*-etmbp complex. The ^{13}C NMR spectrum of *trans*(O)-[Co(*S*,*S*-ebp)]$^+$ exhibits six resonance lines due to the twelve carbon atoms, suggesting that the complex also has a C_2 symmetry, that is, the *S*,*S*-bridged five-membered ring takes a gauche form with a λ conformation and the chiral sulfur donor atoms takes the *S*(S), *S*(S) configuration. These regulations are probably ascribed to the rigid framework of the two D-terdentate terminal moieties.

In contrast with the three *S*,*S*-bridged complexes, the ^{13}C NMR spectrum of *trans*(O)-[Co(*N*,*N*-ebsmp)]$^+$ exhibits three resonance lines for each carbon atom of the two D-terdentate terminal moieties and of the *N*,*N*-bridged five-membered ring (Table 4). This suggests that the *N*,*N*-ebsmp complex is a mixture of the isomers (*R*(S),*R*(S), *R*(S),*S*(S) and/or *S*(S),*S*(S)) with regard to the chiral sulfur donor atoms. The *R*(S),*S*(S) isomer of *trans*(O)-[Co(*N*,*N*-ebsmp)]$^+$ being a C_1 symmetry is expected to show two sets of the resonance lines for each carbon atom, while one set of resonance lines is expected for the *R*(S),*R*(S) or *S*(S),*S*(S) isomer because of a C_2 symmetry of the complex cation. Accordingly, the *N*,*N*-ebsmp complex is assumed to be a mixture of either the *R*(S),*R*(S) and *R*(S),*S*(S) isomers or the *S*(S),*S*(S) and *R*(S),*S*(S) ones. *trans*(O)-[Co(*N*,*N*-ebsmc)]$^+$, which has the same framework as the present *N*,*N*-ebsmp complex, consists of the two isomers, *S*(S),*S*(S) and *R*(S),*S*(S), in crystal, although the *N*,*N*-ebsmc complex was proportionated to three isomers, *R*(S),*R*(S), *R*(S),*S*(S), and *S*(S),*S*(S), in solution.[1] Taking the structure of the *N*,*N*-ebsmc complex in crystal into consideration, it is probable that *trans*(O)-[Co(*N*,*N*-ebsmp)]$^+$ consists of the *R*(S),*R*(S) and *R*(S),*S*(S) isomers even in solution.

In the region of 16—24×10^3 cm^{-1}, the present trans(O) complexes with the *N*,*N*-bridged, *S*,*S*-bridged, or cyclo type sexidentate-N$_2$,O$_2$,S$_2$ ligand show the characteristic absorption spectral behavior in connection with the bridging type of the ligands. In comparison with the

Table 4. ^{13}C NMR Chemical Shifts[a]

Compound	COO	N–CH	S–C	N–CH$_2$	S–CH$_2$–CH$_2$	CH$_3$(pen)	S–CH$_3$
N,*N*-H$_4$ebp	183.87	80.88	50.98	46.54		37.38 32.29	
trans(O)-[Co(*N*,*N*-ebp)]$^+$	185.33	82.13	50.54	54.77		35.43 33.91	
trans(O)-[Co(*S*,*S*-ebp)]$^+$	182.51	74.11	61.05		38.30	29.58 26.22	
trans(O)-[Co(*S*,*S*-tmbp)]$^+$	182.71	75.47	58.08		36.84 30.77	30.77 24.38	
[Co(*cyc*-etmbp)]$^+$[b]	181.65	81.42	60.24	55.80	36.84 30.61	30.88 24.97	
trans(O)-[Co(*N*,*N*-ebsmp)]$^+$[b]	177.26	79.42	57.05	54.28		28.93 24.11	15.33
	176.23	78.88	56.88	54.01		28.50 23.67	15.01
	176.07	78.66	55.69			28.28 22.43	

a) ppm from DSS in D_2O. b) ppm from TMS in CD_3CN.

broad absorption band of *trans*(O)-[Co(D-smp)$_2$]$^+$ in this region, *trans*(O)-[Co(*S,S*-ebp)]$^+$ intensifies markedly the lower energy absorption component of the corresponding band, while *trans*(O)-[Co(*N,N*-ebsmp)]$^+$ intensifies the higher energy component (Fig. 4 and Table 3). On the other hand, *trans*(O)-[Co(*S,S*-tmbp)]$^+$ shows a similar absorption spectral pattern to [Co(*cyc*-etmbp)]$^+$, and furthermore, their intensities are similar to that of *trans*(O)-[Co(D-smp)$_2$]$^+$ (Figs. 4 and 5, and Table 3). These facts suggest that the strain due to the *S,S*-bridging contributes more dominantly to the absorption spectral behavior in the d-d transition region than that due to the *N,N*-bridging.

The CD spectral behavior of *trans*(O)-[Co(*S,S*-ebp)]$^+$ differs significantly from that of *trans*(O)-[Co(D-smp)$_2$]$^+$. This is attributed to the difference in steric regulation between the chiral sulfur donor atoms in the complexes. The CD contribution due to the chiral sulfur donor atoms in *trans*(O)-[Co(D-smp)$_2$]$^+$ is probably canceled, because the D-smp complex is a mixture of three isomers (*R*(S),*R*(S), *R*(S),*S*(S), and *S*(S),*S*(S)).[4] While, the *S,S*-bridged five-membered ring of *trans*(O)-[Co(*S,S*-ebp)]$^+$ takes a gauche form with the λ conformation, and accordingly, the two sulfur donor atoms are regulated to the *S*(S),*S*(S) configuration. In contrast with the *S,S*-ebp complex, *trans*(O)-[Co(*N,N*-ebsmp)]$^+$ shows a similar CD spectral pattern to *trans*(O)-[Co(D-smp)$_2$]$^+$ over the whole region (Fig. 4 and Table 3).[4] This similarity suggests that the *N,N*-ebsmp complex consists of two isomers, *R*(S),*R*(S) and *R*(S),*S*(S), in solution as mentioned above. Here, it takes notice that the *N,N*-bridged five-membered ring of the *N,N*-ebsmp complex takes a gauche form with the δ conformation, that is, *S*(N),*S*(N) with regard to the bridged nitrogen donor atoms. However, the contribution to the CD spectral pattern will be minor in this case, because the chiral sulfur donor atoms contribute to the CD spectral pattern much larger than the chiral nitrogen atoms do.[16,17] The similar consideration is applicable to the similarity in CD spectral behavior between [Co(*cyc*-etmbp)]$^+$ and *trans*(O)-[Co(*S,S*-tmbp)]$^+$ over the whole region (Fig. 5 and Table 3). Namely, each of the chiral sulfur donor atoms of both complexes are fixed to the *R*(S) configuration because of the twist chair form with the λ conformation of the *S,S*-bridged seven-membered ring.

References

1) K. Okamoto, T. Isago, M. Ohmasa, and J. Hidaka, *Bull. Chem. Soc. Jpn.*, **55**, 1077 (1982).

2) T. Konno, K. Okamoto, and J. Hidaka, *Bull. Chem. Soc. Jpn.*, **56**, 2631 (1983).

3) Abbreviation used in this paper: D- or L-pen=D- or L-penicillaminate, D-smp=*S*-methyl-D-penicillaminate, L-smc=*S*-methyl-L-cysteinate, *N,N*-ebsmp=*N,N'*-ethylenebis(*S*-methyl-D-penicillaminate), *N,N*-ebsmc=*N,N'*-ethylenebis(*S*-methyl-L-cysteinate), *N,N*-ebp=*N,N'*-ethylenebis(D-penicillaminate), *S,S*-ebp=*S,S'*-ethylenebis(D-penicillaminate), *S,S*-ebc=*S,S'*-ethylenebis(L-cysteinate), *S,S*-tmbp=*S,S'*-tetramethylenebis(*S*-methyl-D-penicillaminate), *cyc*-etmbp=*N,N'*-ethylene-*S,S'*-tetramethylenebis(*S*-methyl-D-penicillaminate) or (3*S*,8*S*)-2,2,9,9-tetramethyl-1,10-dithia-4,7-diazacyclotetradecane-3,8-dicarboxylate.

4) K. Wakayama, K. Okamoto, H. Einaga, and J. Hidaka, *Bull. Chem. Soc. Jpn.*, **56**, 165 (1983).

5) P. Blondeau, C. Berse, and D. Gravel, *Can. J. Chem.*, **45**, 49 (1967).

6) J. Bierrum and J. P. McReynols, *Inorg. Synth.*, **2**, 216 (1946).

7) B. A. Frens, "The Enraf-Nonius CAD4 SDP—A Real-time System for Concurrent X-Ray Data Collection and Crystal Structure Determination," in Computing in Crystallography, ed by H. Schenk, R. O. Hazekamp, H. van Koningsveld, and C. G. Bassi, Delft University Press, Delft, Holland (1987), pp. 64—71.

8) G. M. Sheldrick, SHELX76. Program for Crystal Structure Determination, University of Cambridge, England (1976).

9) Lists of structure factors, anisotropic thermal parameters for non-hydrogen atoms and positional parameters for hydrogen atoms are deposited as Document No. 8957 at the Office of the Editior of Bull. Chem. Soc. Jpn.

10) K. Okamoto, K. Wakayama, H. Einaga, M. Ohmasa, and J. Hidaka, *Bull. Chem. Soc. Jpn.*, **55**, 3473 (1982).

11) M. Shimoi, Y. Fujinawa, H. Ogino, K. Kanamori, and K. Kawai, *Bull. Chem. Soc. Jpn.*, **61**, 3491 (1988).

12) P. de Meester and D. J. Hodgson, *J. Chem. Soc., Dalton Trans.*, **1976**, 618.

13) M. Kanesaka, K. Okamoto, M. Nomoto, and J. Hidaka, *Bull. Chem. Soc. Jpn.*, **57**, 3111 (1984).

14) K. Okamoto, H. Umehara, M. Nomoto, H. Einaga, and J. Hidaka, *Bull. Chem. Soc. Jpn.*, **60**, 1709 (1987).

15) J. Hidaka, S. Yamada, and Y. Shimura, *Chem. Lett.*, **1974**, 1487.

16) C. W. Van Saun and B. E. Douglas, *Inorg. Chem.*, **8**, 1145 (1969); R. D. Gillard, *Spectrochim. Acta*, **20**, 1431 (1964).

17) K. Yamanari, J. Hidaka, and Y. Shimura, *Bull. Chem. Soc. Jpn.*, **50**, 2451 (1977), and references therein.

Stereoselectivity in Diastereomeric Tetrahedral Metal(II) Complexes of Chiral Salicylideneamines: Crystal Structure and Molecular Mechanics Calculation of Bis[*N*-(*l*-menthyl)salicylideneaminato]cobalt(II)

Hiroshi SAKIYAMA,* Hisashi ŌKAWA,* Naohide MATSUMOTO, and Sigeo KIDA†
Department of Chemistry, Faculty of Science, Kyushu University, Hakozaki, Higashiku, Fukuoka 812
(Received April 11, 1991)

Stereoselectivity of bis[*N*-(*l*-menthyl)salicylideneaminato]cobalt(II) [Co(sal-ment)$_2$] has been studied by single crystal X-ray analysis and molecular mechanics calculations. The X-ray analysis has revealed a nearly tetrahedral surrounding (dihedral angle of 82.5°) and *Δ* configuration about the metal ion. Molecular mechanics calculations were made based on MM2 program, assuming a tetrahedral surrounding about the metal ion and fixing the four donor atoms and six atoms adjacent to the donor atoms at the positions as determined by the single crystal X-ray analysis. The most stable structure obtained from the MM2 calculation coincides well with that from the crystal structure analysis. Together with the X-ray structural results for [Cu(sal-ment)$_2$] and bis[*N*-[(*R*)-1-phenylethyl]salicylideneaminato]cobalt(II) [Co(sal-Rmb)$_2$] studied in this study and for related [Zn(sal-Rmb)$_2$] and [Cu(sal-Rmb)$_2$] studied previously, the factors responsible for the stereoselectivities of those bis(salicylideneaminato)metal(II) complexes have been discussed.

Studies of enantiomeric and diastereomeric metal complexes have been stimulated by the interests to elucidate the correlation between circular dichroism induced in the visible region and the absolute configuration about the metal ion and to explore the factors responsible for the stereoselective behavior found for those complexes.[1] Tetrahedral or pseudo-tetrahedral bis-chelate complexes of the general type [M(A–B)$_2$] are enantiomeric and can in principle exist in two absolute configurations, *Δ* and *Λ*[2] (see Fig. 1). The resolution of the enantiomers has been hardly attained with a very few exceptions[3] because of the lability of tetrahedral complexes. The stereoselectivities of diastereomeric tetrahedral or pseudo-tetrahedral complexes of bidentate salicylideneamines or related Schiff bases have been investigated by ^{1}H NMR[2,4–8] and circular dichroism[8,9] spectroscopies and single crystal X-ray structural analysis.[9,10] It is generally accepted that interligand non-covalent interactions plays an important role in the predominant formation of one of the diastereomers.[11] A direct evidence for the operation of such interligand noncovalent interactions was obtained for tetrahedral bis[*N*-[(*R*)-1-phenylethyl]salicylideneaminato]zinc(II) [Zn(sal-Rmb)$_2$][9] where the chiral *N*-substituent of one ligand is in a close contact with the adjacent chelate ring of the other ligand, affording *Δ* configuration about the zinc(II) ion. In bis[*N*-[(*R*)-1-phenylethyl]salicylideneaminato]copper(II) [Cu(sal-Rmb)$_2$][10] the preferred configuration about the copper is pseudo-tetrahedral and of *Δ*. In this complex an interligand interaction occurs between the hydrogen attached to the asymmetric carbon in the *N*-substituent and the phenolic oxygen of the adjacent chelate ring. As seen in the above examples, the factors contributing to the stereoselectivity of diastereomeric tetrahedral complexes of salicylideneamines are not straightforward.

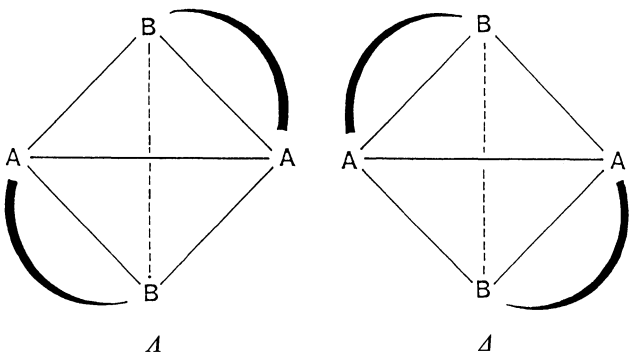

Fig. 1. Two absolute configurations (*Δ* and *Λ*) for tetrahedral complexes.

In this study the stereoselectivity of bis[*N*-(*l*-menthyl)salicylideneaminato]cobalt(II) [Co(sal-ment)$_2$] has been studied by single-crystal X-ray method and molecular mechanics calculations by MM2 program. Further, we have examined the crystal structures of bis[*N*-(*l*-menthyl)salicylideneaminato]copper(II) [Cu(sal-ment)$_2$] and bis[*N*-[(*R*)-1-phenylethyl]salicylideneaminato]cobalt(II) [Co(sal-Ramb)$_2$] and found that the former is isomorphous to [Co(sal-ment)$_2$] and the latter to [Zn(sal-Rmb)$_2$].[9] From the inspection of both the X-ray analytical results for those complexes and the molecular mechanics calculations for [Co(sal-ment)$_2$] it is aimed to elucidate the main factors responsible for stereoselectivities of the tetrahedral or pseudo-tetrahedral complexes of salicylideneamines.

Experimental

Preparations. [Co(sal-ment)$_2$] and [Cu(sal-ment)$_2$] were prepared by the literature methods.[8]

[Co(sal-Rmb)$_2$]. An ethanolic solution of (*R*)-1-phenylethylamine purchased from Tokyokasei Chemical Co. (0.48 g, 4 mmol) and salicylaldehyde (0.48 g, 4 mmol) was refluxed for 2 h. To this were added powdered NaHCO$_3$

† Present address: Kumamoto Institute of Technology, Ikeda 4-22-1, Kumamoto 860

Table 1. Crystal Data for [Co(sal-ment)$_2$]

Formula	$CoO_2N_2C_{34}H_{48}$
F.W.	575.70
Crystal system	Trigonal
Space group	$P3_1$
a/Å	8.971(3)
c/Å	34.01(1)
Volume/Å	2370(2)
Z	3
D_x/g cm^{-3}	1.21
R/%	7.65
R_w/%	8.27
Observed reflection $\|F_o\|>3\sigma(\|F_o\|)$	2167

(0.34 g, 4 mmol) and cobalt(II) acetate tetrahydrate (0.49 g, 2 mmol), and the mixture was stirred at 60 °C for 2 h and allowed to stand overnight at ambient temperature. The resulted red crystals were recrystallized from ethanol.

Found: C, 70.84; H, 5.51; N, 5.54%. Calcd for $C_{30}H_{28}CoN_2O_2$: C, 71.00; H, 5.52; N, 5.56%.

Single-Crystal X-Ray Analyses. Single crystals of [Co(sal-ment)$_2$] were grown by the slow crystallization from a chloroform–ethanol (3 : 1 in volume) mixture, and a crystal with approximate dimensions of 0.4×0.4×0.2 mm was used for the study. Intensities and lattice parameters were obtained on a Rigaku AFC-5 automated four-circle diffractometer, using graphite-monochromated Mo $K\alpha$ radiation (λ=0.71073 Å) at 20±1 °C. Lattice parameters and their estimated standard deviations were obtained from a least-squares fit to 25 2θ values in the range 15°<2θ<30°. For the intensity data collections, the ω–2θ scan mode was used at a scan rate of 6° min^{-1}. The octant measured was $+h$, $+k$, $+l$. Three standard reflections were monitored every 100 reflections and their intensities showed a good stability. The intensity data were corrected for Lorentz-polarization effects but not for absorption. The crystal data of [Co(sal-ment)$_2$] are summarized in Table 1.

The structures were solved by the heavy-atom method and refined by the block-diagonal least-squares method. Atomic scattering factors were taken from Ref. 12. Hydrogen atoms were included in their calculated positions and held fixed. All the calculations were carried out on a FACOM M-780 computer in the Computer Center of Kyushu University by the use of local version of the UNICS-III and ORTEP programs.[13,14] The final positional parameters for [Co(sal-ment)$_2$] are given in Table 2. The F_o–F_c tables, thermal parameters, H-atom parameters, and full bond distances and angles are deposited as Document No. 8958 at the Office of the Editor of Bull. Chem. Soc. Jpn.

[Cu(sal-ment)$_2$] was found to be isomorphous to [Co(sal-ment)$_2$]: Formula=$CuO_2N_2C_{34}H_{48}$, F.W.=580.31, trigonal, space group=$P3_1$, a=8.874(3), c=34.645(9) Å, V=2365(2) Å^3, Z=3, D_x=1.22 g cm^{-3}.

[Co(sal-Rmb)$_2$] was also found to be isostructural with [Zn(sal-Rmb)$_2$]: Formula=$Co_2O_4N_4C_{60}H_{54}$, F.W.=1012.98, space group=$P2_12_12_1$, orthorhombic, a=17.771(3), b=29.681(9), c=9.892(6) Å, V=5218(3) Å^3, Z=4, D_x=1.28 g cm^{-3}.

Molecular Mechanics Calculations. The molecular mechanics calculations were carried out by the use of the MM2 program.[15] The most stable structure of [Co(sal-ment)$_2$] was obtained by the procedures as described as follows. As the first step the complex was divided into two parts, the *l*-menthyl part and the rest, and their most stable structures were calculated for imaginal "*l*-menthylmethane" (1-isopropyl-2,4-dimethylcyclohexane) and tetrahedral bis(salicylideneaminato)cobalt(II) [Co(sal-ment)$_2$], respectively. As the second step the initial steric energy of [Co(sal-ment)$_2$] was calculated for both Δ and Λ forms every 30° by rotating the *l*-menthyl groups with respect to the N–C(menthyl) bond, while maintaining the most stable structures of the constituents obtained in the first step. Finally, the conformer with the lowest steric energy was used in the energy minimization to obtain the most stable structure of the whole complex molecule. Since the parameters of sp^2 nitrogen atom and cobalt atom are lacking, the parameters of sp^2 carbon atom were used for the sp^2 nitrogen and the four donor atoms and the six atoms attached to the donor atoms were fixed at the positions determined from the crystal structure analysis. In other words, the cobalt atom was not included in the energy minimization. The MM2 calculational data are deposited as supplementary materials (Table S5—S10).

Table 2. Atomic Parameters of [Co(sal-ment)$_2$]

Atom	x	y	z	B_{eq}/Å^2
Co	0.4101(2)	0.4099(2)	−0.0172(1)	2.74(6)
O1	0.397(1)	0.225(1)	0.0138(3)	3.1(3)
O2	0.228(1)	0.398(1)	−0.0482(3)	3.9(4)
N1	0.608(2)	0.442(2)	−0.0495(3)	3.0(4)
N2	0.437(1)	0.608(1)	0.0163(3)	2.6(4)
C1	0.532(2)	0.209(2)	0.0222(4)	2.9(5)
C2	0.534(2)	0.131(2)	0.0573(4)	3.7(5)
C3	0.675(3)	0.116(2)	0.0666(5)	5.6(8)
C4	0.816(2)	0.170(2)	0.0411(5)	5.6(7)
C5	0.818(2)	0.255(2)	0.0079(4)	3.7(5)
C6	0.679(2)	0.275(2)	−0.0017(4)	3.4(5)
C7	0.702(2)	0.374(2)	−0.0384(4)	3.1(5)
C8	0.663(2)	0.545(2)	−0.0868(4)	3.3(5)
C9	0.712(2)	0.725(2)	−0.0750(5)	4.0(5)
C10	0.773(2)	0.849(2)	−0.1109(4)	4.5(6)
C11	0.814(3)	1.031(2)	−0.0991(6)	6.0(8)
C12	0.628(2)	0.772(2)	−0.1418(4)	4.3(6)
C13	0.582(2)	0.593(2)	−0.1531(4)	4.3(6)
C14	0.515(2)	0.472(2)	−0.1176(4)	3.9(6)
C15	0.445(3)	0.282(2)	−0.1263(4)	5.1(8)
C16	0.571(3)	0.245(3)	−0.1469(6)	6.8(10)
C17	0.274(2)	0.206(3)	−0.1476(5)	5.9(8)
C18	0.216(2)	0.532(2)	−0.0570(4)	3.2(5)
C19	0.131(2)	0.534(2)	−0.0928(4)	3.9(6)
C20	0.115(2)	0.675(2)	−0.1018(4)	4.3(6)
C21	0.170(2)	0.810(2)	−0.0790(5)	4.8(7)
C22	0.255(2)	0.819(2)	−0.0425(6)	5.2(6)
C23	0.279(2)	0.680(2)	−0.0307(4)	3.2(5)
C24	0.375(2)	0.702(2)	0.0051(4)	3.4(5)
C25	0.543(2)	0.663(2)	0.0524(5)	4.4(7)
C26	0.727(2)	0.717(2)	0.0425(4)	3.4(5)
C27	0.848(2)	0.770(2)	0.0763(5)	5.0(6)
C28	1.027(2)	0.813(3)	0.0634(5)	6.1(7)
C29	0.776(3)	0.631(2)	0.1078(6)	6.1(8)
C30	0.593(2)	0.582(2)	0.1185(4)	5.2(8)
C31	0.470(2)	0.513(2)	0.0810(3)	2.8(5)
C32	0.282(2)	0.449(2)	0.0902(5)	4.6(6)
C33	0.246(3)	0.571(3)	0.1171(5)	5.6(8)
C34	0.207(2)	0.279(2)	0.1130(5)	5.4(7)

Results and Discussion

Crystal Structures of [Co(sal-ment)$_2$] and [Cu(sal-ment)$_2$]. These complexes are isomorphous (see Table 1). The crystal structure of the cobalt complex is described here. Its perspective view is given in Fig. 2, together with the numbering system. Relevant bond lengths and angles are listed in Table 3.

The deprotonated form of the Schiff base functions as a bidentate ligand to form a nearly tetrahedral surrounding about the cobalt ion. The dihedral angle between the plane defined by Co, N(1), and O(1) and the plane defined by Co, N(2), and O(2) is 82.5°. We analyzed the molecular structure by taking into account the established configuration of the *l*-menthyl group and found the dextral disposition of two ligands along the C_2 axis, i.e. *Δ* configuration.

The cyclohexane ring of the *l*-menthyl group assumes a chair form and the salicylideneamine moiety is equatorially bonded to the cyclohexane ring. The conformation with respect to the N(1)–C(8) bond is such that the hydrogen attached to C(8) is eclipsed to the hydrogen attached to C(7). This conformation must be the most preferred one. In any other conformations a large interligand steric repulsions is expected between the azomethine hydrogen and *l*-menthyl group.

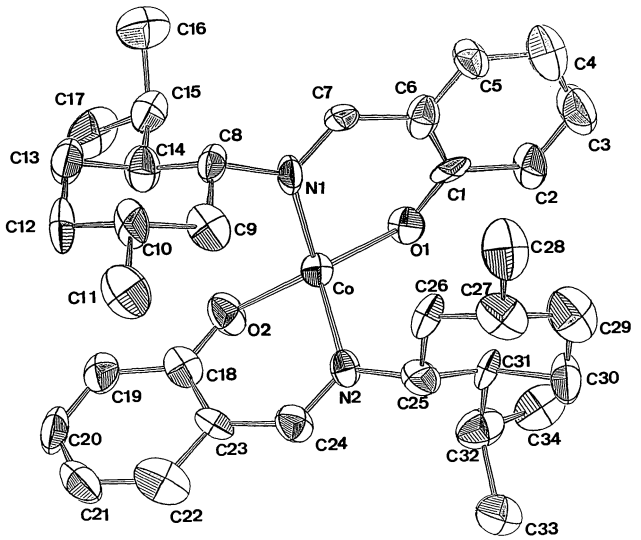

Fig. 2. ORTEP view of [Co(sal-ment)$_2$] with numbering system.

Table 3. Relevant Bond Distances and Angles of [Co(sal-ment)$_2$]

Bond distances (Å)	
Co-O1	1.91(1)
Co-O2	1.90(1)
Co–N1	1.98(1)
Co–N2	2.02(1)
Bond angles (deg)	
O1–Co–O2	125.0(3)
O1–Co-N1	95.5(5)
O1-Co–N2	112.3(4)
O2–Co–N1	112.5(4)
O2–Co–N2	94.9(5)
N1–Co–N2	118.6(4)
Distances between non-bonded atoms (Å)	
O1–C31	3.26(2)
O2–C14	3.31(2)

In the crystal the C(14) of the *l*-menthyl group is in a close proximity of the phenolic oxygen O(2) of the adjacent chelate ring with the interatomic distance of 3.31(2) Å. Similarly the C(31)–O(1) interatomic distance is 3.26(2) Å. Even taking the C–H–O angles into consideration, those short distances suggest the presence of the hydrogen bonding between these atoms.

[Co(sal-Rmb)$_2$]. The X-ray study has shown that the crystal of this complex is isomorphous to that of [Zn(sal-Rmb)$_2$]. This zinc complex assumes a nearly tetrahedral environment about the metal ion and the absolute configuration is *Λ*. The detailed structure of this complex has been reported in our recent paper.[9]

Molecular Mechanics Results. *l*-Menthylmethane. This molecule assumes a chair structure.[16] In our calculations only the rotation of the isopropyl group with respect to C(cyclohexane)–C(isopropyl) bond was considered. The result indicates that the isopropyl group is subjected to a severe steric effect from the adjacent methyl group. The most preferred conformation is such that the isopropyl hydrogen (–C<u>H</u>(CH$_3$)$_2$) is eclipsed to the adjacent methyl group and the two methyl groups of the isopropyl moiety are thrust away to the opposite side.

[Co(sal-ment)$_2$]. The most stable structure of [Co(sal-ment)$_2$] obtained by molecular mechanics calculations is shown in Fig. 3. This structure is essentially the same as the molecular structure determined by the single crystal X-ray method (see Fig. 2). The bond distances and bond angles determined by the two methods agree within 0.1 Å and 4°, respectively, except for those of the aromatic part.

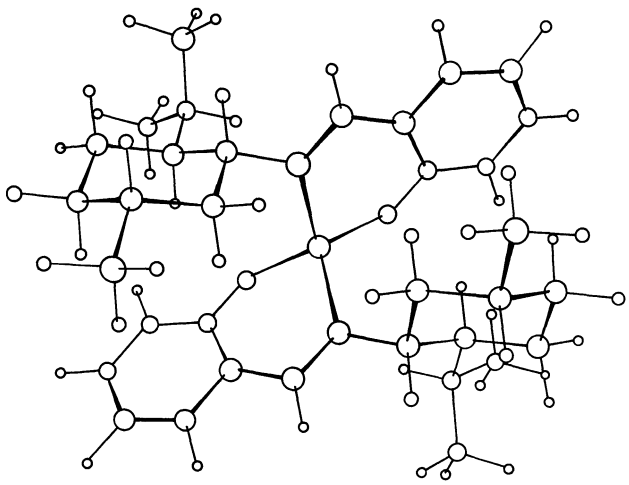

Fig. 3. The most stable structure of [Co(sal-ment)$_2$] obtained by the molecular mechanics calculation.

The ligand moiety in the complex molecule retains the most stable structure of free (sal-ment)$^-$, in which the conformation about the N–C(menthyl) bond is such that the hydrogen on the asymmetric carbon attached to the nitrilo nitrogen is eclipsed to the azomethine carbon so as to reduce the steric repulsion between the *l*-menthyl group and the aromatic part. A large rotational barrier about the N–C(menthyl) bond is probably the cause to retain this conformation even in the complex molecule. The *Λ* form is possible if the *l*-menthyl group is rotated by ca. 180° about the N–C(menthyl) bond from the most stable conformation of the free ligand, but this form is unfavorable because of a steric repulsion between the aromatic ring and *l*-menthyl group.

Factors Responsible for Stereoselectivity. Though the structurally well-characterized, tetrahedral or pseudo-tetrahedral complexes of salicylideneamines with a chiral N-substituent are still limited, their stereochemistries are significantly diversed, depending upon the nature of the central metal ion and the Schiff base ligand. In this study we have aimed to deduce dominant factors responsible for the stereochemistry in each complex. Four factors can be considered here: (A) the preferred configuration of the central metal ion, (B) the preferred conformation of salicylideneamines mainly due to the intraligand steric repulsion, (C) an interligand steric repulsion between ligands, and (D) an interligand noncovalent attracting interaction.

The preferred configurations for four-coordinate cobalt(II) and zinc(II) ions are tetrahedral whereas that for copper(II) ion is planar.[17,18] The most stable structures of (sal-ment)$^-$ and (sal-Rmb)$^-$ are such that the N-substituent and the aromatic part are disposed as far as possible because of the steric repulsion. With respect to the rotational barrier due to the steric repulsion, (sal-Rmb)$^-$ is more flexible than (sal-ment)$^-$.

(1) [M(sal-ment)$_2$] (M=Co, Cu). The tetrahedral surrounding has been proved for both complexes. Because of the interligand steric repulsion tetrahedral configuration is preferable rather than square planar configuration. This configuration is also preferable to cobalt(II) but not to copper(II). The ligand moiety retains the most stable conformation in the complexes because of the rotational barrier due to the intraligand steric repulsion. If two (sal-ment)$^-$ ligands maintaining the most stable conformation were disposed planarly about a metal ion, a severe interligand steric hinderance would occur. Thus, such a steric effect is the cause for the tetrahedral distortion of the copper complex. The stereoselectivity to afford *Δ* configuration about the central metal may also be attributed to an interligand steric repulsion between the two chiral ligands.

(2) [Cu(sal-Rmb)$_2$]. In this complex the dihedral angle around the metal ion is rather small (39.5°).[10] This is because the steric requirement of the copper(II) to prefer a planar configuration is larger than the intraligand steric repulsion in each ligands. The ligand conformation is significantly altered from the most stable free-ligand conformation so as to reduce the interligand steric repulsion. It is also obvious that the hydrogen bonding between the asymmetric carbon and the phenolic oxygen of the neighboring chelate ring is cotributing to the stabilization. The difference of the steric hindrance between the methyl group and the phenyl group gives rise to the stereoselectivity to afford the *Δ* configuration.

(3) [M(sal-ment)$_2$] (M=Co, Cu). (3) [M(sal-Rmb)$_2$ (M=Co, Zn). Both the cobalt(II) and zinc(II) complexes assume a tetradedral structure which is preferable to both metal ions. Since this configuration causes little interligand steric hindrance, the ligand retains essentially its most stable form of the free ligand. The stereoselectivity of those complexes to afford *Λ* configuration about the metal ion should be attributed to the intramolecular interligand interaction between the N-substituent and the chelate ring of another ligand of the complex.

References

1) For example: J. H. Dunlop and R. D. Gillard, *Adv. Inorg. Chem. Radiochem.*, **9**, 185 (1966); R. D. Gillard, *Prog. Inorg. Chem.*, **7**, 215 (1966); A. M. Sargeson, *Transition Met. Chem., N. Y.*, **3**, 303 (1966); R. D. Gillard and H. M. Irving, *Chem. Rev.*, **65**, 603 (1965).

2) R. E. Ernst, M. J. O'conner, and R. H. Holm, *J. Am. Chem. Soc.*, **89**, 6104 (1967).

3) For example: Hein and Regler, *Naturwissenshaften*, **23**, 320 (1935); W. H. Mills and R. A. Gott, *J. Chem. Soc.*, **1926**, 3121.

4) R. H. Holm, A. Chakravorty, and G. O. Durek, *J. Am. Chem. Soc.*, **86**, 379 (1964).

5) M. J. O'Conner, R. E. Ernst, J. E. Schoenborn, and R. H. Holm, *J. Am. Chem. Soc.*, **90**, 1744 (1968).

6) M. J. O'Connor, R. E. Ernst, and R. H. Holm, *J. Am. Chem. Soc.*, **90**, 4561 (1968).

7) R. E. Ernst, M. J. O'Conner, and R. H. Holm, *J. Am. Chem. Soc.*, **90**, 5735 (1968).

8) H. Ōkawa, M. Nakamura, and S. Kida, *Inorg. Chim. Acta*, **120**, 185 (1986).

9) H. Sakiyama, H. Ōkawa, N. Matsumoto, and S. Kida, *J. Chem. Soc., Dalton Trans.*, **1990**, 2935.

10) T. Kawamoto, A. Takeuchi, H. Kuma, and Y. Kushi, 39th Symposium on Coordination Chemistry of Japan, Mito, 1989.

11) H. Ōkawa, *Coord. Chem. Rev.*, **92**, 1 (1988).

12) "International Tables for X-Ray Crystallography," Kynoch Press, Birmingham (1974), Vol. 4.

13) T. Sakurai and K. Kobayashi, *Rikagaku Kenkyusho Houkoku*, **55**, 69 (1979).

14) S. Kawano, *Rep. Comput. Cent., Kyushu Univ.*, **13**, 39 (1980).

15) N. L. Allinger and Y. H. Yuh, *QCPE*, **12**, 395 (1980).

16) E. I. Eliel, N. L. Allinger, S. J. Angyal, and G. A. Morrison, "Conformational Analysis," John Willey & Sons, New York (1965).

17) S. Yamada, *Coord. Chem. Rev.*, **1**, 415 (1966).

18) L. Sacconi, *Coord. Chem. Rev.*, **1**, 126 (1966); *ibid.*, **1**, 192 (1966).

Reactions of Leuco Bindschedler's Green with Some *p*-Benzoquinones in Acetone

Yoshihiro OSAWA, Norio NISHIMURA,* and Shunzo YAMAMOTO
Department of Chemistry, Faculty of Science, Okayama University,
Tsushima, Okayama 700
(Received September 10, 1990)

The rate of reaction between Leuco Bindschedler's Green (BGH) and some *p*-benzoquinone derivatives (Q's) in acetone was followed spectrophotometrically by means of the stopped-flow technique. The reaction was found to proceed reversibly. The rate data and the activation parameters for the forward and backward reactions were estimated. The rates were susceptible to the oxidation–reduction potentials of the Q's. The absorption spectra observed at low temperatures indicated that three kinds of intermediates were involved. Radicals formed during the reaction were detected by the ESR method. The results have been discussed in relation to those previously obtained for systems involving Leuco Crystal Violet (LCV) and Leuco Malachite Green (LMG).

Hydride-transfer reactions have been an attractive research subject together with proton-transfer reactions in vivo as well as in vitro. In hydride-transfer reactions, *N*-benzyl-1,4-dihydronicotinamide (BNAH) and related compounds have been regarded as model compounds of dihydronicotinamide coenzymes. Westheimer and co-workers[1,2] suggested that the oxidation–reduction reactions involved direct hydride transfers, and this idea was believed for a long time. However, Steffens and Chipman[3] suggested first that the so-called hydride-transfer reactions involved an intermediate with the character of a charge-transfer (CT) complex. Ohno and Kito,[4] and Fukuzumi and Tanaka[5] demonstrated that a CT complex as an intermediate is really involved in such reaction systems. The oxidations of 9,10-dihydro-10-methylacridine and its derivatives to the corresponding acridinium ions by π-acceptors were investigated by Colter and co-workers.[6,7] They obtained spectroscopic and kinetic evidence for CT complexing between the reactants. The involvement of quantum-mechanical tunneling in the "hydride-transfer" reaction between LCV and chloranil (CA) was advocated by Isaacs and co-workers.[8,9] We have observed the formation of CT complexes in the same system and in the LMG/CA system.[10,11] Thus, the one-step hydride-transfer mechanism is debatable. It was found in this work that the hydrogen atom on the nitrogen in BGH is abstracted in the form of a hydride ion much more easily than the hydrogen atom on the central carbon atom in LCV and LMG. We were interested in knowing how situations would change if LCV and LMG were replaced by BGH. In a preliminary study,[12] we briefly reported the reaction of BGH with tetracyanoethylene and found the reaction proceeded reversibly. The present paper reports an investigation of the reactions of BGH with a series of *p*-benzoquinones.

Experimental

Materials. Reagent-grade BGH manufactured by Dojin Chemicals Ltd. was used as received, since this compound is very difficult to purify in the usual manner; mp 119—120.5 °C. Reagent-grade tetrachloro-*p*-benzoquinone (chloranil, CA), 2,6-dichloro-*p*-benzoquinone (2,6-DCQ), 2,5-dichloro-*p*-benzoquinone (2,5-DCQ), 2,3-dichloro-5,6-dicyano-*p*-benzoquinone (DDQ), *p*-benzoquinone (BQ), and tetramethyl-*p*-benzoquinone (TMQ) were purchased from Tokyo Kasei Kogyo and recrystalized twice from benzene. $BGH^{+\cdot}$ perchlorate (Würster's Blue) was prepared according to the method of Michaelis and Granick;[13] dark purple, mp 147—148 °C. Reagent-grade solvents were dried on Molecular Sieves 4A-1/16, and distilled before use.

Kinetic Measurements. When the acetone solution of BGH was mixed with that of benzoquinones, a characteristic band due to Bindschedler's Green cations (BG^+) appeared at λ_{max}=725 nm. All the runs were performed with excess quinone concentrations, i.e., $[BGH]_0$: $(4—5)\times10^{-5}$ mol dm^{-3}, and $[Quinones]_0$: $(0.5—8)\times10^{-3}$ mol dm^{-3}. Separately-prepared reactant solutions were deaerated by nitrogen gas bubbling and were charged in drive syringes which were thermostatically regulated within ±0.1 °C. The mixing was performed within 1 ms by means of nitrogen gas pressure. After mixing, the change in the absorbance at 725 nm was monitored by using a Unisoku USP-519 spectrophotometer. The runs were repeated 10 to 30 times and curve smoothing was performed by means of an attached computer.

Electronic Spectra at Low Temperatures. A specially designed cryostat with optical windows was set in a Union SM-401 spectrophotometer, and spectra in the visible region at various low temperatures were recorded. In order to prevent the deposition of dew on the windows, dry nitrogen gas was blown onto the windows during the measurements.

ESR Measurements. Reactant solutions of BGH and Q were introduced separately into an H-shaped tube with a side tube (i.d. 1 mm) for ESR measurements. After the solutions were degassed by freezing and thawing under vacuum, the solutions were mixed and transferred into the side tube. A JEOL JES-FE3XG spectrometer equipped with a 100 kHz field modulator and a TE 011 cavity was used for ESR measurements. The temperature in the cavity was controlled by a JEOL variable temperature regulator.

Results

A representative spectrum in the initial stage of reaction between BGH and CA is shown in Fig. 1. The absorption band at λ_{max}=725 nm can be attributed to

Table 1. Apparent First-Order Rate Constants for the Reaction between BGH and *p*-Benzoquinones at Various Temperatures in Acetone

Temp	$[CA]_0$	k_{obsd}	$[2,6\text{-DCQ}]_0$	k_{obsd}	$[2,5\text{-DCQ}]_0$	k_{obsd}
°C	mmol dm^{-3}	s^{-1}	mmol dm^{-3}	s^{-1}	mmol dm^{-3}	s^{-1}
13.5	0.554	9.26				
	1.107	12.0				
	1.660	14.5				
	2.214	17.3				
18.5[b]	0.550	9.99	2.22	0.419	2.26	0.0667
	1.099	12.9	4.05	0.627	4.00	0.0739
	1.648	15.7	6.02	0.870	6.34	0.0931
	2.197	18.6	7.91	1.000	7.91	0.109
25.0	0.508	10.6	2.23	0.569	2.49	0.092
	1.107	14.0	3.95	0.815	3.93	0.103
	1.525	16.7	5.99	1.14	6.02	0.127
	2.033	19.3	8.22	1.42	8.28	0.157
32.0	0.503	11.6	2.17	0.712	2.46	0.134
	1.001	15.2	4.08	1.10	3.89	0.169
	1.509	18.0	5.99	1.42	5.96	0.196
	2.012	21.2	7.55	1.67	8.19	0.222
40.0	0.497	12.9	2.15	0.963	2.24	0.203
	0.994	16.3	4.04	1.51	3.95	0.244
	1.491	19.8	5.9	1.91	5.91	0.293
	1.988	23.2	7.46	2.25	7.90	0.346
50.0			2.10	1.21	2.19	0.267
			3.83	1.84	3.87	0.324
			5.70	2.50	5.78	0.393
			7.48	2.93	7.73	0.482

a) 17.5°C for 2,6-DCQ, and 18.0°C for 2,5-DCQ.

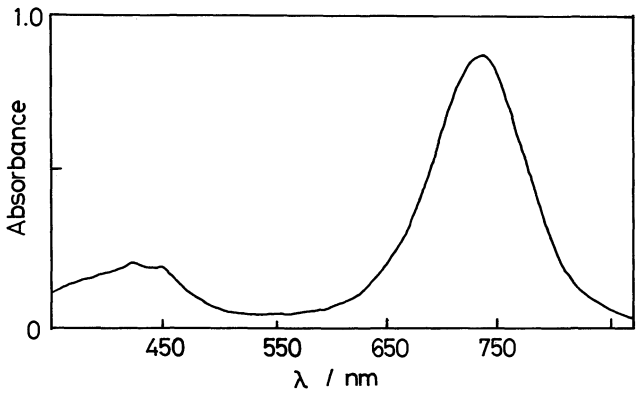

Fig. 1. Electronic spectrum of the BGH/CA system in excess of CA after the initial stage of reaction in acetone at 25°C.

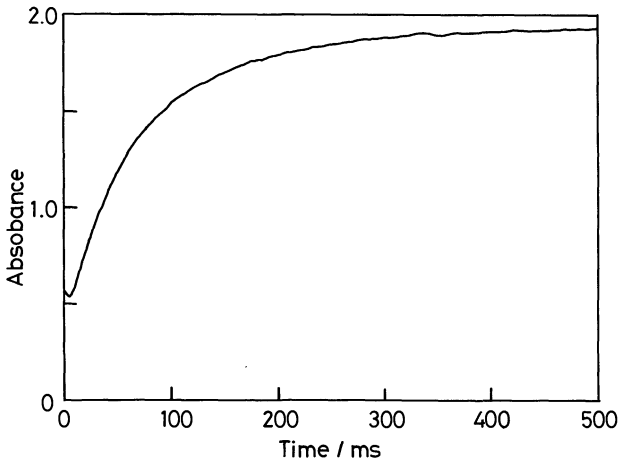

Fig. 2. Initial rise of absorbance at 725 nm as a function of time (20 cycles) in the reaction of BGH (6.92×10^{-5} mol dm^{-3}) with CA (1.53×10^{-3} mol dm^{-3}) at 25°C.

BG^+, and the peculiarly-shaped absorption band in the vicinity of 450 nm is due to semiquinone anion radicals.[10,14] A time-dependent curve in the initial stage of the absorbance at 725 nm after averaging the repeated runs is shown in Fig. 2. After a pseudo-equilibrium had been attained in this time scale, the absorbance at 725 nm increased gradually when the observation time scale was changed by a factor of 10^3. By setting an appropriate time region in the initial stage, the curve was analyzed by the Damping Gauses–Newton method combined with the aid of an attached computer program. The estimated rate data (k_{obsd}) are given in Table 1.

In Fig. 3, the apparent first-order rate constants for the BGH/CA system at various temperatures are plotted as a function of initial CA concentrations. This figure shows that the rate is first-order with respect to CA at each temperature and that the reaction involves a reverse process. The same type of plots were obtained for other quinones.

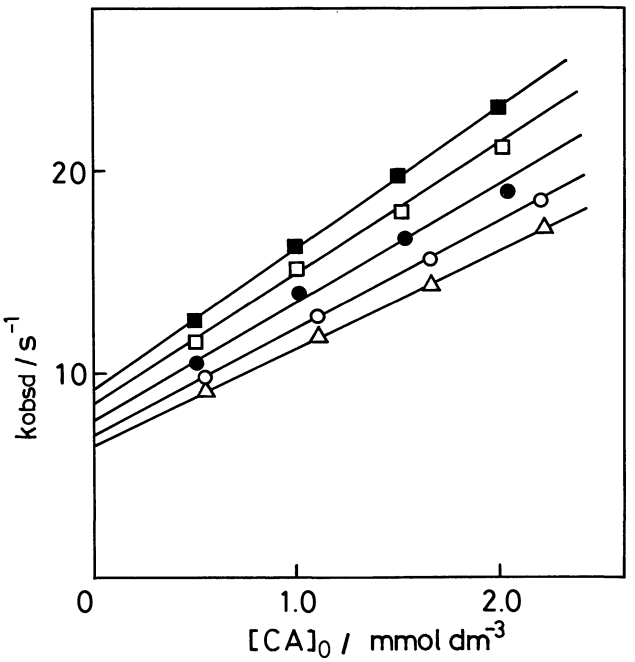

Fig. 3. Plots of k_{obsd} against the initial concentration of CA at temperatures (°C): 13.5 (Δ), 18.5 (○), 25.0 (●), 32.0 (□), and 40.0 (■).

In Fig. 4, the electronic spectra for the BGH/CA system in an EPA solution at various temperatures are shown. For comparison, the change in the electronic spectrum of a mixture of *N*-methyldiphenylamine (MDA) and CA in EPA is shown in Fig. 5. It is noted that the pattern of the spectrum in Fig. 4 and its temperature dependence are very different from those in Fig. 5. The pattern and the band position of the spectrum in Fig. 5 are rather similar to those of the LCV/CA and LMG/CA systems.[10,11]

For the BGH/CA and BGH/DDQ systems, ESR spectra assignable to the corresponding semiquinone anion radicals were observed at room temperature. For both the BGH/2,5-DCQ and BGH/2,6-DCQ systems, a very broad signal appeared at 25 °C. However, when the temperature was lowered below −45 °C, the signal pattern changed to an expected 1 : 2 : 1 triplet.

Discussion

Rate Equations and Reaction Mechanism. From the above results, the rate of BG^+ formation in the initial stage, under the condition $[BGH]_o \ll [Quinones]_o$, can be given by:

$$d[BG^+]/dt = k_{obsd}([BG^+]_e - [BG^+]) \quad (1)$$

where $[BG^+]$ and $[BG^+]_e$ denote the concentrations of BG^+ at time t and at the pseudo-equilibrium, respectively. Fukuzumi and co-workers[15] studied a hydride-transfer reaction between BNAH and the Q's. They found that a CT complex was first formed between BNAH and Q as evidenced by the appearance of a CT complex spectrum

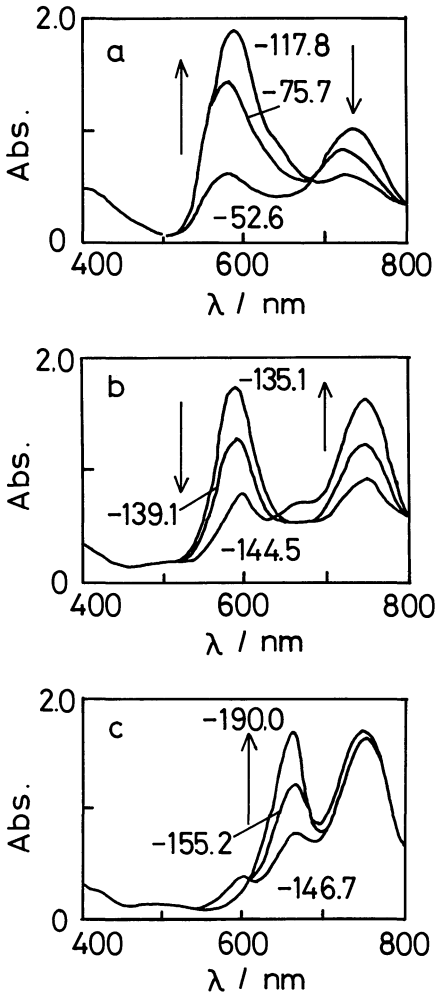

Fig. 4a—c. Spectral change as a function of temperature for the BGH/CA system in EPA. Arrows show the direction of decreasing temperature, and numerical values in the figure denote measurement temperatures in °C; $[BGH]_o$, $[CA]_o \approx 10^{-5}$ mol dm^{-3}.

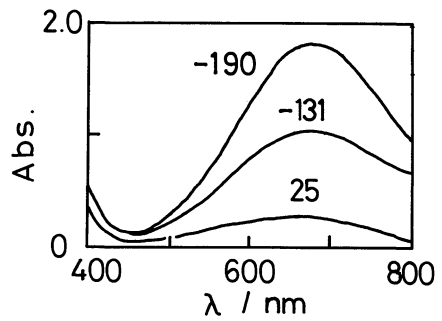

Fig. 5. Temperature dependence of a CT band that appeared in the CA/MDA system. Numerical values in the figure denote measurement temperatures in °C.

in the visible region at room temperature. They proposed that, the CT complex was in rapid equilibrium with the radical ion pair ($BNAH^{+\cdot}Q^{-\cdot}$). Thereafter, irreversible proton transfer takes place to form the radical pair

(BNA$^{\cdot}$ QH$^{\cdot}$). Subsequently, electron transfer yielding BNA^+ and QH^- takes place.

If we accept their proposed mechanism as a whole and take into account the reverse reaction and the gradual increase in BG^+ after the pseudo-equilibrium is reached, a plausible reaction mechanism in harmony with the above empirical equation may be as follows:

$$BGH + Q \underset{}{\overset{K_1}{\rightleftharpoons}} CTC \overset{K_2}{\rightleftharpoons} (BGH^{+\cdot}\ Q^{-\cdot}) \underset{k_b}{\overset{k_f}{\rightleftharpoons}} (BG^{\cdot}\ QH^{\cdot}) \overset{K_3}{\rightleftharpoons} (BG^+\ QH^-)$$

$$(BG^+\ QH^-) + Q \longrightarrow BG^+ + Q^{-\cdot} + QH^{\cdot}$$

$$2QH^{\cdot} \longrightarrow \text{Dimerization},$$

where Q denotes benzoquinones, and parentheses denote cages. Hydride-transfer reactions usually show large kinetic isotope effects (k_H/k_D).[3,6,8,10] Therefore, if the rate-determining step involves a proton transfer and the other steps are in rapid equilibrium in the initial stage, k_{obsd} can be given by:

$$k_{obsd} = k_b/K_3 + K_1K_2k_f[Q]_o \quad (2)$$

From the plots of k_{obsd} against the initial concentration of quinones (Fig. 3), the values of $K_1K_2k_f$ and k_b/K_3 were estimated and are given in Table 2. The activation parameters are given in Table 3. The overall pseudo-equilibrium constant K is given by:

$$K = K_1K_2(k_f/k_b)K_3 \quad (3)$$

By utilizing the kinetic data, K can be calculated. For example, K at 25 °C for the BGH/CA system is 713 dm^3 mol^{-1}. Under the condition $[BGH]_o \ll [CA]_o$, K is given by:

$$K = [BG^+\ QH^-]_e/[BGH]_e[CA] = \frac{A_e/\varepsilon}{([BGH]_o - A_e/\varepsilon)[CA]_o} \quad (4)$$

where A_e denotes the absorbance at 725 nm after the pseudo-equilibrium has been attained, and ε the molar absorptivity at this wavelength. Unfortunately, the ε-value is not known. However, if we assume ε as

Table 2. Rate Data for the Forward and Backward Reactions between BGH and *p*-Benzoquinones in Acetone (probable errors in parentheses)

			$K_1K_2k_f$ / dm^3 mol^{-1} s^{-1}			
T/°C	13.5	18.5[a]	25.0	32.0	40.0	50.0
CA	4810(50)	5210(20)	5670(180)	6280(140)	6920(20)	
2,6-DCQ		105(6)	143(4)	177(5)	240(9)	324(14)
2,5-DCQ		7.56(0.56)	11.4(0.6)	14.9(1.2)	25.3(0.3)	38.8(1.3)
DDQ			1.46(0.20)×10^6			
			k_b/K_3 / s^{-1}			
CA	6.61(0.07)	7.14(0.03)	7.95(0.25)	8.60(0.20)	9.45(0.03)	
2,6-DCQ		0.200 (0.031)	0.257 (0.018)	0.350 (0.027)	0.484 (0.044)	0.574 (0.071)
2,5-DCQ		0.0469 (0.0030)	0.0605 (0.0031)	0.104 (0.007)	0.145 (0.002)	0.177 (0.007)
DDQ			284(13)			

a) 17.5 °C for 2,6-DCQ, 18.0 °C for 2,5-DCQ.

Table 3. Activation Parameters for Reactions between BGH and *p*-Benzoquinones

System	Solvent	Forward		Backward	
		E_a / kJ mol^{-1}	$\Delta S^{\neq}_{298K}$ / J K^{-1} mol^{-1}	E_a / kJ mol^{-1}	$\Delta S^{\neq}_{298K}$ / J K^{-1} mol^{-1}
BGH/CA	Acetone	10.2±0.1	−147±1	10.1±0.2	−202±1
BGH/2,6-DCQ	Acetone	27.1±0.4	−121±1	26.6±1.3	−175±4
BGH/2,5-DCQ	Acetone	40.2±1.1	−99±4	34.6±2.6	−160±8
LCV/CA[a]	$CHCl_3$	30.1±0.8	−148±3		
	CH_3CN	43.1	−135		
LMG/CA[b]	CH_3CN	86.0±0.8	−55±3		

a) Data cited from Ref. 10. b) Data cited from Ref. 11.

74000 $dm^3\ mol^{-1}\ cm^{-1}$, and use the A_e-values obtained for various initial CA concentrations, the average K-value was found to agree well with the one obtained from the kinetic data.

When we compare the kinetic data for the BGH/CA system with those for the LCV/CA and LMG/CA systems, we can notice two distinctive points: the rate is faster in the order of 10^3—10^5 and the activation energy is remarkably smaller (Table 3) than those for the LCV/CA and LMG/CA systems. Secondly, the reaction involves a reversible process in the rate-determining step. Moreover, the electronic spectra which appeared in the visible region are remarkably different from those observed in the LCV/CA and LMG/CA systems.

Substituent Effects. The values of $K_1K_2k_f$ as well as k_b/K_3 decrease in the order DDQ≫CA>2,6-DCQ>2,5-DCQ≫BQ, TMQ (Table 2). In the hydride-transfer reaction of BNAH with the Q's, Fukuzumi et al.[15] found that the rate varies significantly with the redox potentials $E°(Q/Q^{-\cdot})$. In our case, if one-electron transfer takes place prior to the hydrogen transfer (or successive proton and electron transfer), the rate of the forward reaction will also be correlated to $E°(Q/Q^{-\cdot})$. In Fig. 6, the $K_1K_2k_f$ values in logarithmic scale are plotted as a function of $E°$. Since there are no available data for $E°$ in acetone, we used the values of $E°$ in acetonitrile.[16] It can be seen that the plot of $\log K_1K_2k_f$ vs. $E°$ is approximately parallel to that of the BNAH/Q system. This fact suggests that the mechanisms for both systems are similar. It was found that the linear free energy relationship holds well for both the forward and backward reactions, suggesting that these reactions proceed by the single interaction mechanism.[17] However, it is hard to explain the remarkably large negative values of $\Delta S^{\neq}$ for the backward process. We propose the following reason: according to the absolute rate theory, the rate constant is given by:

$$k = (e\,\kappa k_B T/h)e^{\Delta S^{\neq}/R}\cdot e^{-Ea/RT} \quad (5)$$

where κ denotes the transmission coefficient. We usually calculate $\Delta S^{\neq}$ on the assumption of $\kappa=1$. However, if the formation of (BG· QH·) takes place via a triplet transition state, the value of κ must be much smaller than unity due to intersystem crossing. In this case, the assumption of $\kappa=1$ gives rise to an apparent small $\Delta S^{\neq}$ value. The activation energies for the forward and backward processes are similar (Table 3). This means that the heat of reaction is nearly equal to zero. As ion-pair formation reactions from neutral species are generally exothermic, this is another curious point. At present, the cause is not obvious.

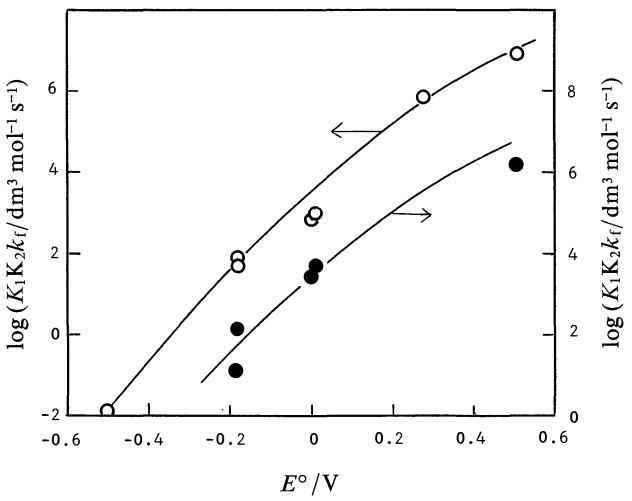

Fig. 6. Correlation between $\log(K_1K_2k_f)$ and the redox potential of p-benzoquinones $E°$; ●: this work, ○: data cited from Ref. 15.

Electronic Spectra at Low Temperatures. The electronic spectra of a mixture of BGH and CA in EPA solution were taken at low temperatures (Fig. 4a—c). In the figure, the band due to the semiquinone radical (Fig. 1) is obscure. This was found to be caused by an instrumental problem, not by the absence of the radical. It is notable that these spectral changes, as shown in Fig. 4, have not been reported so far for similar hydride-transfer systems. Due to experimental limitations, we were forced to start the spectral measurements after the pseudo-equilibrium had been attained. At −52.6 °C, we can see two distinct bands at λ_{max}=730 nm (referred to as band A) and at λ_{max}=590 nm (band B). Since λ_{max} for BG^+ is known to be 725 nm at room temperature, it is obvious that BG^+ is responsible for the band A. A small red shift upon cooling may be due to solvent effects. As the temperature was lowered, the intensity of the band B increased at the expense of the band A (Fig. 4a). This provides direct evidence of the reverse process. At lower temperatures, new bands appeared at λ_{max}=750 nm (band C) and λ_{max}=660 nm (band D) (Fig. 4b, c).

It is very difficult to assign these spectra unambiguously. From the viewpoint of the canonical electronic structures of BG·, it would not be responsible for any of the bands in Fig. 4. On the other hand, the electronic structures of the moiety $BGH^{+\cdot}$ can be described as follows:

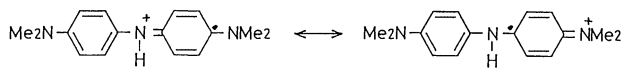

Therefore, it is likely that one of these bands may be assigned to $BGH^{+\cdot}$. Foster and Thomson[18] observed the electronic spectrum of the cation radicals of *N,N,N',N'*-tetramethyl-*p*-phenylenediamine (TMPD) in the vicinity of 600 nm. Nakayama and Suzuki[19] examined the temperature dependence of the spectra of Würster's cation radicals including $TMPD^{+\cdot}$, and found that at lower temperatures the absorption band of their dimers appears on the longer wavelength side. If these situations are taken into account, the band B could be assigned to $BGH^{+\cdot}$ and the band D to its dimer.

In order to confirm this, $BGH^{+\cdot}ClO_4^-$ was prepared and dissolved in ethanol-rich EPA. The solution was cooled rapidly to −188.5 °C. We observed two distinct bands (λ_{max} at 660 and 750 nm). As the temperature was increased (−155 °C), the intensity of the band at λ_{max}= 660 nm decreased, and at the same time, a shoulder appeared in the vicinity of 600 nm. Above −100 °C, the band at 660 nm and the shoulder disappeared and only the band on the longer wavelength side assignable to BG^+ survived; the process of BG^+ formation from $BGH^{+\cdot}$ is not clear. It is noted that in this system the formation of a CT complex is impossible. Accordingly, the band D observed in the BGH/CA system could be assigned to the dimer of $BGH^{+\cdot}$, and the shoulder to $BGH^{+\cdot}$. Temperature dependence of the intensity of the band B relative to D, and the band positions are somewhat different from those for the BGH/CA system in usual EPA. This is probably due to solvent effects.

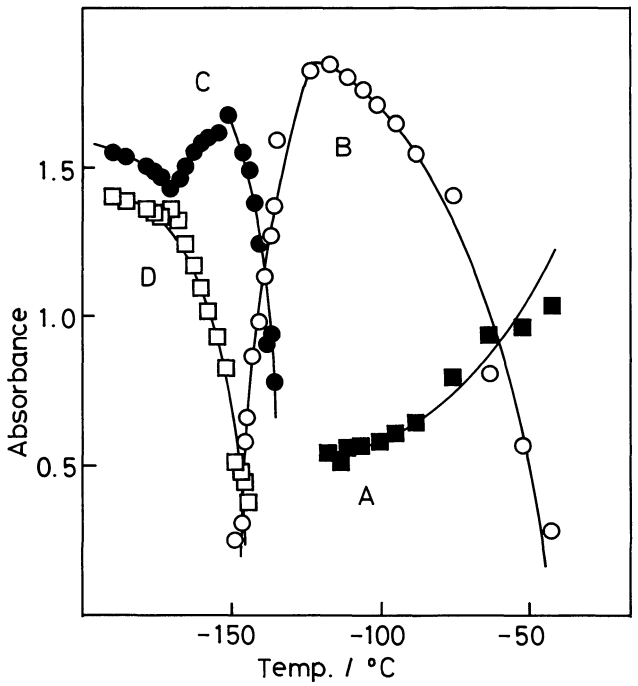

Fig. 7. The change in absorbances at λ_{max}/nm: 730 (band A), 590 (band B), 750 (band C), and 660 (band D) as a function of temperature.

It is recognized that the absorption band due to outer CT complexes between CA and aromatic amines appears in the range of 500—800 nm. For example, the λ_{max}-values are 616 nm for *N*,*N*-dimethylaniline, 660 nm for MDA (Fig. 5), 680 nm for LCV,[10] 670 nm for LMG,[11] and 800 nm for TMPD.[18] In the light of these situations, we can expect the formation of an outer CT complex in the present system, too. Judging from the temperature dependence of the band C, this band could be assigned to an outer CT complex if the assignments of the bands, A, B, and D are correct.

Temperature dependence of the intensities of the above bands is shown in Fig. 7. It was confirmed that the spectral change with temperature took place reversibly. Similar absorption bands and the temperature dependence of their intensities were observed for the BGH/2,5-DCQ system, too. Using the data in Fig. 7, together with the Arrhenius parameters (Table 2), and assuming dimer formation, we constructed an approximate energy diagram as shown in Fig. 8. The heat of formation of the dimer agrees with those reported for similar systems (ca. 35 kJ mol^{-1}).[19] The energy levels of usual outer CT complexes are known to be at most 20 kJ mol^{-1} lower than that of the reactants, while the energy level of the proposed CT complex in this study is too low. Therefore, a different character of CT complex seems to be formed in our system. Indeed, the band C is well-characterized (Fig. 4), while the outer CT band is generally very broad (Fig. 5). Recently, we

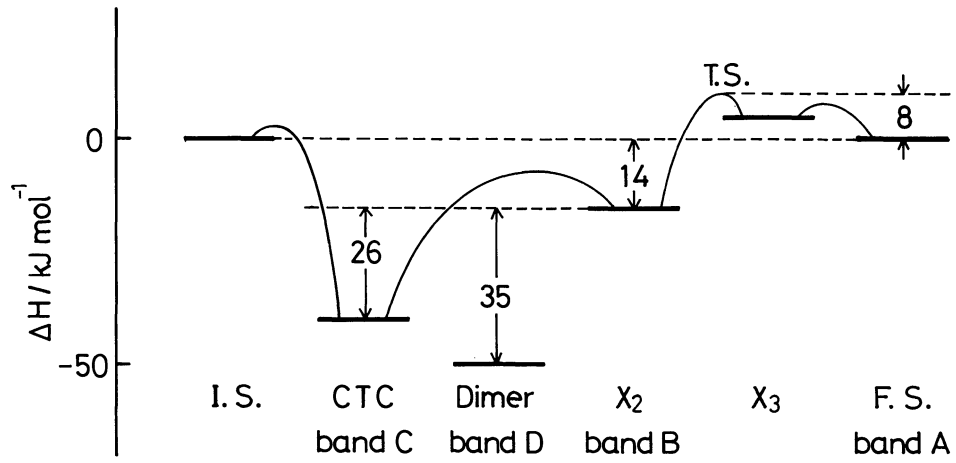

Fig. 8. Approximate energy diagram for the reaction between BGH and CA. X_2 denotes ($BGH^{+\cdot}$ $Q^{-\cdot}$) and X_3 denotes ($BG^{\cdot}QH^{\cdot}$).

reported that a CT complex was formed between TBPE* and aliphatic amines through hydrogen bonding.[20] This CT complex exhibited a well-characterized absorption at ca. λ_{max}=550 nm. It has been accepted that hydrogen bonding involves a CT character.[21,22] Because of the large electronegative nature of nitrogen atom, the formation of such a type of CT complex is likely. In this CT complex, electron transfer will take place easily through hydrogen bonding followed by the forward and backward H-atom (or proton + electron) oscillations. The heat of hydrogen bond formation may be ca. 20 kJ mol^{-1}. If this value is taken into account for the formation of the above type of CT complex, the energy diagram in Fig. 8 may not be so surprising. The well-characterized structure of band C suggests that this CT complex is "tight".

ESR Spectra. For the BGH/CA system, a singlet ESR spectrum with g=2.0058 was obtained in acetone at 25 °C. This can be assigned to the corresponding semiquinone anion radical ($Q^{-\cdot}$).[10] This radical is comparatively stable, but it decays according to the strict first-order kinetics with $k_{decay}=1.29\times10^{-4}$ s^{-1} (25 °C). For the BGH/DDQ system, a quintet ESR spectrum with intensity ratios of 1 : 2 : 3 : 2 : 1 was obtained. The signal is assignable to the corresponding semiquinone anion radicals.[23] Spin trapping is known to be a powerful method for detecting unstable neutral radicals. 2-Methyl-2-nitrosopropane (MNP) is known as a radical trap. In order to obtain further information for radicals occurring in our systems, we added MNP to the BGH/DDQ system. Figure 9a is the resulting ESR signal. We can easily see that the signal is composed of three kinds of radical species. A quintet near the center is obviously due to the semi-quinone. A triplet with a hyperfine coupling constant (hfcc) of 1.56 mT and g=2.0057 can be ascribed to a spin adduct.

Lai and Colter[23] reported that *N*-methyl-acridanyl radical was trapped by MNP in the oxidation reaction of *N*-methylacridan by 2,3-dicyano-1,4-benzoquinone. Since our system is similar to theirs, the trapped radical may be BG$^{\cdot}$ rather than QH$^{\cdot}$.

The remaining wavy signal spreading over a wide range of the magnetic field (>3 mT) is very weak, but shows a remarkably small hfcc. The g-value was estimated to be about 2.003. The authentic ESR signal of $BGH^{+\cdot}$ obtained by dissolving $BGH^{+\cdot}$ perchlorate in acetone at 25 °C is shown in Fig. 9b. The g-value was calculated to be 2.0030. If these situations and the proposed mechanism are taken into account, the wavy weak signal could be attributed to $BGH^{+\cdot}$. Kolodny and Bowers[24] reported that when acetonitrile solutions of *p*-phenylenediamine (PPD) and DDQ were mixed in a flow system, superimposed ESR signals attributable to $PPD^{+\cdot}$ and $DDQ^{-\cdot}$ were obtained. They found that the intensity of the $PPD^{+\cdot}$ signal was much weaker and decayed rapidly. Although the reason is not clear, the weak signal in our case is in line with their observation.

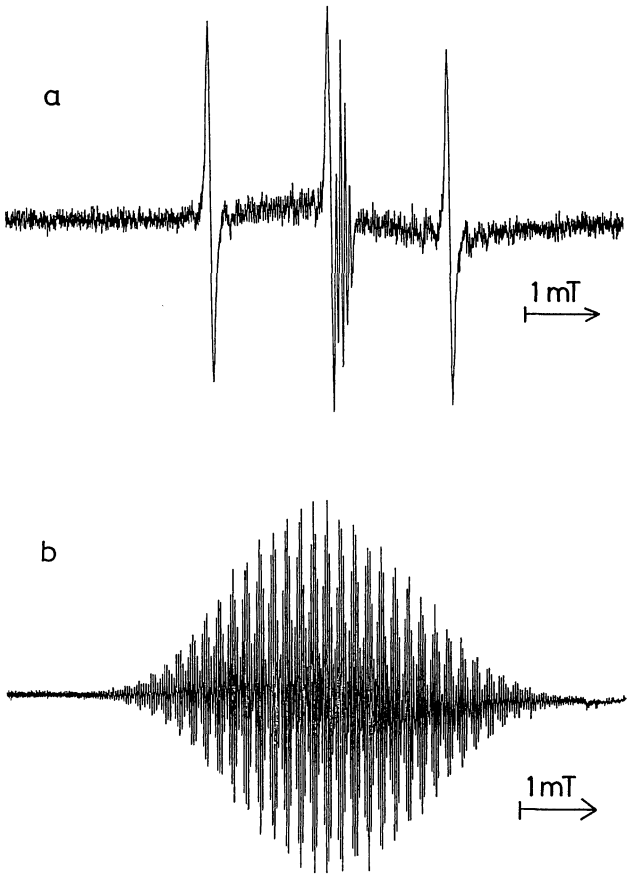

Fig. 9. (a) ESR spectra for the BGH/DDQ system in the presence of MNP in acetonitrile, $[BGH]_o$=1.08, $[DDQ]_o$=0.27, $[MNP]_o$=12.9 mmol dm^{-3}. (b) ESR signal of $BGH^{+\cdot}$.

The above findings, together with the spectrophotometric observations, provide direct evidence for the existence of the intermediates, assumed to be formed during the stepwise pathway for the present reaction systems.

* 2,6-Dibromo-4-[3,5-dibromo-4-hydroxyphenyl)(2-ethoxycarbonylphenyl)methylene]-2,5-cyclohexadien-1-one.

References

1) D. Mauzerall and F. H. Westheimer, *J. Am. Chem. Soc.*, **77**, 2261 (1955).
2) R. H. Abeles, R. F. Hutton, and F. H. Westheimer, *J. Am. Chem. Soc.*, **79**, 712 (1957).
3) J. J. Steffens and D. M. Chipman, *J. Am. Chem. Soc.*, **93**, 6694 (1971).
4) A. Ohno and N. Kito, *Chem. Lett.*, **1972**, 369.
5) S. Fukuzumi and T. Tanaka, *Chem. Lett.*, **1982**, 1513.
6) A. K. Colter, G. Saito, and F. J. Sharom, *Can. J. Chem.*, **55**, 2740 (1977).
7) A. K. Colter, P. Plank, J. P. Bergsma, R. Lahti, A. A. Quesnel, and A. G. Parsons, *Can. J. Chem.*, **62**, 1780 (1984).
8) N. S. Isaacs, K. Javaid, and E. Rannala, *Nature*, **268**, 372 (1977).

9) N. S. Isaacs, K. Javaid, and E. Rannala, *J. Chem. Soc., Perkin Trans. 2,* **1978**, 709.
10) N. Nishimura and T. Motoyama, *Bull. Chem. Soc. Jpn.,* **57**, 1 (1984); **58**, 1013 (1985).
11) N. Nishimura and T. Motoyama, *Bull. Chem. Soc. Jpn.,* **58**, 3639 (1985).
12) N. Nishimura, H. Ninomiya, and Y. Osawa, *Chem. Express,* **5**, 945 (1990).
13) L. Michaelis and S. Granick, *J. Am. Chem. Soc.,* **65**, 1747 (1943).
14) Y. Shirota, K. Kawai, N. Yamamoto, K. Tada, T. Shida, H. Mikawa, and H. Tsubomura, *Bull. Chem. Soc. Jpn.,* **45**, 2683 (1972).
15) S. Fukuzumi, N. Nishizawa, and T. Tanaka, *J. Org. Chem.,* **49**, 3571 (1984).
16) D. H. Evans, "Encyclopedia of Electrochemistry of the Elements. Organic Section," ed by A. J. Bard, Marcel Dekker, N. Y. (1978), Vol. XII.
17) J. E. Leffler and E. Grunwald, "Rates and Equilibria of Organic Reactions", John Wiley and Sons, New York (1963).
18) R. Foster and T. J. Thomson, *Trans. Faraday Soc.,* **58**, 860 (1962).
19) S. Nakayama and K. Suzuki, *Bull. Chem. Soc. Jpn.,* **46**, 3694 (1973).
20) N. Nishimura, K. Masaki, J. Miyake, and T. Sakai, *Chem. Lett.,* **1988**, 1239.
21) H. Tsubomura, *J. Chem. Phys.,* **24**, 927 (1956).
22) S. Nagakura and M. Gouterman, *J. Chem. Phys.,* **26**, 881 (1957).
23) C. C. Lai and A. K. Colter, *J. Chem. Soc., Chem. Commun.,* **1980**, 1115.
24) N. H. Kolodny and K. W. Bowers, *J. Am. Chem. Soc.,* **94**, 1113 (1972).

Preparation of Optically Active [1-(Methoxycarbonyl)ethyl]cobaloximes Coordinated with Various Axial Ligands and Their Photoracemization. Remarkable Steric Effect of Axial Ligand on the Co-C Bond Homolysis[1)]

Yoshiaki OHGO,* Hideki WADA, Chiyako OHTERA, Makoto IKARASHI, Shoe BABA, and Seiji TAKEUCHI
Niigata College of Pharmacy, Kamishin'ei-cho, Niigata 950-21
(Received November 28, 1990)

Optically active [1-(methoxycarbonyl)ethyl]cobaloximes coordinated with various axial bases were prepared and their photoracemization rates were measured in a solution state. It was found that although the electronic effect of the axial ligand was negligible on the rate of photochemical Co–C bond homolysis, the steric bulkines accelerated the rate remarkably. These results had a similar tendency to those observed in a previously reported reaction wtih 1-cyanoethyl cobaloximes, though the degree of rate enhancement due to the steric bulkiness of the axial ligand was extremely enlarged. The reason is also discussed.

Extensive investigations concerning the reactions of alkyl cobalt complexes have been carried out by spectrophotometric methods using achiral complexes. However, these methods include inherent possibilities for underestimating the rate of Co–C bond homolysis (k_1) (Eq. 1), when accompanied by a rapid backward reaction (recombination of alkyl radical and Co(II) species).

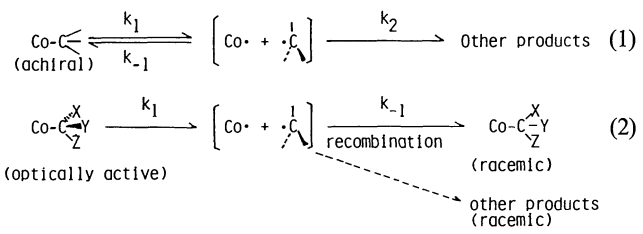

On the other hand, a chiroptical measurement using optically active alkylmetal complexes provides a more simple and precise evaluation of the forward rate (k_1). Since the alkyl radicals formed by bond homolysis are either planar or a rapidly inverting pyramid, the recombination of these species with Co(II) and other subsequent reactions (such as radical coupling and beta-elimination) should give substantially racemic or achiral products (Eq. 2). Thus, the Co–C bond homolysis rate constant of alkyl cobalt complexes (k_1) can be directly evaluated from the optical rotational change. We have shown that optically active alkylcobalt complexes are useful for the elucidation of both solution-state[2-4)] and solid-state[5-13)] reactions involving cobalt–carbon bond formation and cleavage, especially for the case of a system accompanied by an extremely rapid backward reaction.

In a previous paper[2a)] we reported on the photoracemization of 1-cyanoethyl cobaloxime complexes. Here, we wish to describe the preparation of new optically active [1-(methoxycarbonyl)ethyl]bis(dimethylglyoximato)cobalt(III) complexes which have chirality at the carbon bound directly to the cobalt atom; we also describe the effect of the axial ligand on the rate of photochemical Co–C bond homolysis.

Results and Discussion

Preparation of Optically Active [1-(Methoxycarbonyl)ethyl]cobaloxime Complexes. Bis(dimethylglyoximato)[(*S*)-1-(methoxycarbonyl)ethyl][(*S*)-1-phenylethylamine]cobalt(III), (***S,S***)-**1**, was prepared according to almost the same procedure as that described in a previous paper in which the preparation of the enantiomer, (***R,R***)-**1**, was reported.[2b)] Five recrystallizations gave a constant optical rotation ($[\alpha]_{589}$ −205.6, $[\alpha]_{578}$ −226.7, $[\alpha]_{546}$ −253.3(*c* 0.180, chloroform)). 4-Substituted pyridine complexes of bis(dimethylglyoximato)[(*S*)-1-(methoxycarbonyl)ethyl]cobalt(III) were easily prepared by a ligand exchange of (*S*)-1-phenylethylamine [(*S*)-1-PEA] with the corresponding pyridine derivatives in methanol in the presence of dilute hydrochloric acid. Tributylphosphine, ethyldiphenylphosphine, and diethylphenylphosphine complexes of bis(dimethylglyoximato)[(*R*)-1-(methoxycarbonyl)ethyl]cobalt(III) were also prepared by an axial ligand exchange of (***R,R***)-**1** with the corresponding phosphines in methanol in the presence of dilute hydrochloric acid. The newly prepared complexes were characterized by IR, NMR, and elemental analyses (see experimental part); the structures are shown in Fig. 1. Triphenylphosphine and tricyclohexylphosphine-coordinated complexes can not be isolated in their pure form, probably due to partial ligand dissociation. These complexes were, accordingly, prepared in situ by an addition of the corresponding axial ligand to a solution of aqua complex:

$$(CH_3CHCOOCH_3)Co(Hdmg)_2(H_2O)+B \longrightarrow (CH_3CHCOOCH_3)Co(Hdmg)_2B+H_2O.$$

The addition of 50-fold free phosphine was found to be sufficient to complete the ligand-exchange reaction, even in the case of the most bulky tricyclohexylphosphine (Fig. 2). The (*RS*)-1-phenylethylamine-coordinated complex was also prepared in situ by the addition of

(*RS*)-1-phenylethylamine to a solution of the aqua complex. The structures of the substrates prepared in situ are also shown (bracketed) in Fig. 1.

Photoracemization. The optical rotation of a chloroform solution of optically active 1-(methoxycarbonyl)ethyl cobaloxime complexes which were coordinated with various axial ligands(shown in Fig. 1) gradually decreased due to Co–C bond homolysis upon visible-light irradiation. Kinetic studies were performed by measuring the decrease in the optical rotation of a 3.79×10^{-3} mol dm^{-3} chloroform solution of each complex (containing a 100-fold excess of a corresponding ligand, which is sufficient to prevent ligand dissociation) under either a nitrogen or argon atmosphere at room temperature (23±2 °C). The first-order rate plots ($\ln\alpha$ vs. time) exhibited excellent linearity and yielded the photoracemization rate constants (summarized in Table 1). In the cases of triphenylphosphine and tricyclohexylphosphine-coordinated complexes, racemization occurred even in the dark. The rates were therefore corrected for the corresponding thermal racemization under the same conditions. The reaction rate of a series of amine-coordinated complexes remained almost unaltered, in spite of the rather wide range of pK_a change. On the other hand, the rate in a series of phosphine-coordinated complexes (Entry 6—10) changed remarkably, and although the order was independent of the pK_a value of the axial ligand, the rates increased with increasing cone angle.[14a,b] A similar tendency was previously observed in the photoracemization of a series of 1-cyanoethyl cobaloximes; this tendency was remarkably enlarged in the present series (Fig. 3). The acute dihedral angle (θ) between the planes of the two dimethylglyoximato groups, the displacement (d) of the Co atom toward the axial ligand from the mean plane (composed of four nitrogen atoms in the equatorial ligand), and the Co–P bond length of a series of 1-cyanoethyl cobaloximes[2a,10,11] have been shown to increase with an increase in the cone angle of the phosphine ligand, in order to avoid repulsion due to the short contacts between the substituent of phosphine ligand and dimethylglyoxime

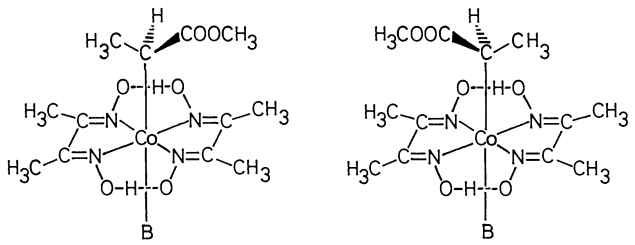

(*S*) (*R*)

Fig. 1. Structures of Chiral Alkyl Cobaloximes

(*S*,*S*)-**1**	B=(*S*)-1-PEA	[(*R*)-**1**	B=(*RS*)-1-PEA]
(*S*)-**2**	B=pyridine	(*R*)-**5**	B=aqua
(*S*)-**3**	B=4-CN-pyridine	(*R*)-**6**	B=Bu_3P
(*S*)-**4**	B=4-Me-pyridine	(*R*)-**7**	B=Et_2PhP
		(*R*)-**8**	B=$EtPh_2P$
		[(*R*)-**9**	B=Ph_3P]
		[(*R*)-**10**	B=(*c*-$C_6H_{11})_3$P]

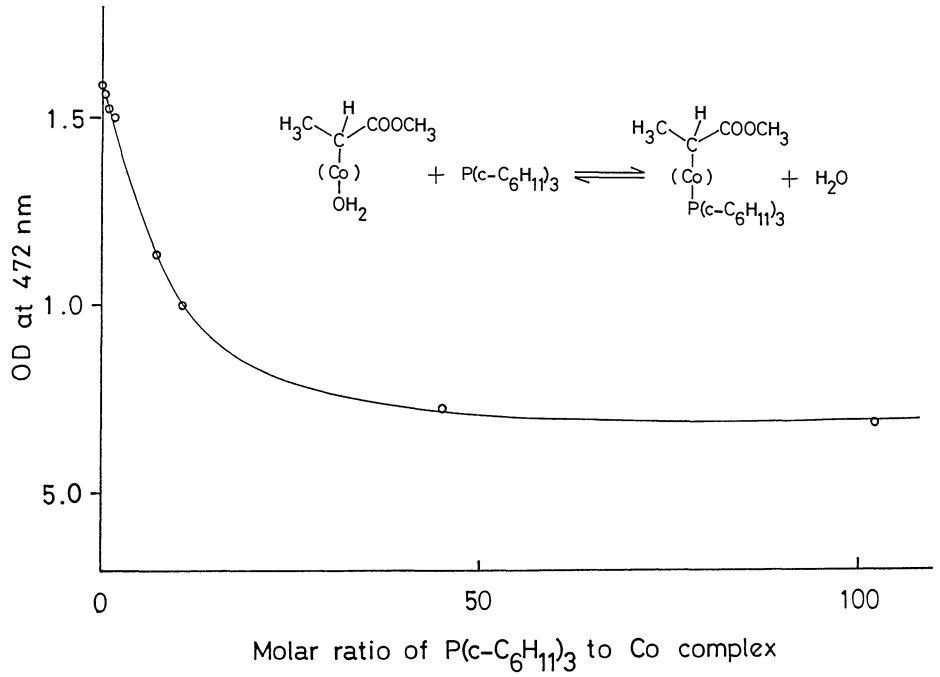

Fig. 2. Absorbance change at 472 nm with added tricyclohexylphosphine to aqua[(*R*)-1-(methoxycarbonyl)ethyl]cobaloxime in cyclohexanone.

Table 1. Photoracemization Rate Constants of Optically Active 1-(Methoxycarbonyl)ethyl Cobaloximes in a Chloroform Solution

Entry	Complex	Rate constant (κ) 10^{-5} s^{-1}	Axial base (B)	pK_a[e]	Cone angle deg
1	(*S*)-**3**	8.9	4-CN-py	1.86	
2	(*S*)-**2**	9.2	Pyridine	5.19 5.25	
3	(*S*)-**4**	8.7	4-Me-py	6.03	
4	(*R*)-**1**	9.9	1-PEA[a]	a)	
5	(*R*)-**5**	8.1	Aqua		
6	(*R*)-**6**	6.4	Bu_3P	8.43	127[b]
7	(*R*)-**7**	7.3	Et_2PhP	6.25	136[c]
8	(*R*)-**8**	8.9	$EtPh_2P$	4.91	140[b]
9	(*R*)-**9**	14.4(15.5)[d]	Ph_3P	2.73	159[b]
10	(*R*)-**10**	38(62)[d]	$(c\text{-}C_6H_{11})_3P$	9.70	173[b]

a) 1-PEA: 1-Phenylethylamine; the pK_a of 1-phenylethylamine was not reported, but is expected to be about 9—10 from those of $PhCH_2NH_2$ (9.35) and $PhC(Me)_2NH_2$ (10.27). b) Experimental cone angle (see Ref. 14b). c) Tolman's cone angle (see Ref. 14a). d) The rate constants are corrected for the thermal racemization at 23°C under the same conditions: the rate constants in parenthesis are net observed values in which the contribution from the thermal racemization is involved. e) See Ref. 19 for those of pyridine derivative, and Ref. 20 for phosphines.

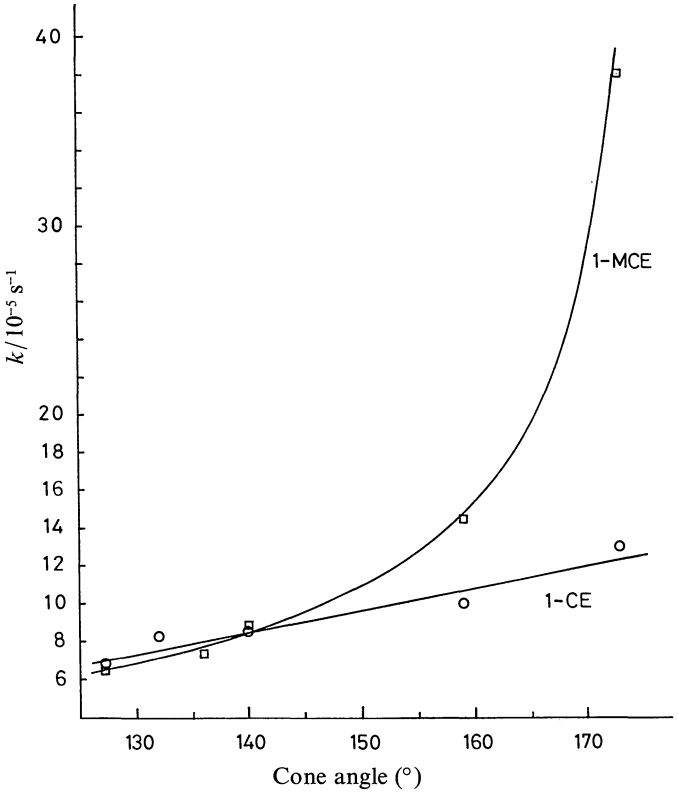

Fig. 3. The correlation between racemization rates of 1-(methoxycarbonyl)ethyl cobaloximes (1-MCE) and the cone angles of the coordinated phosphines, in comparison with that of 1-cyanoethyl cobaloximes (1-CE).

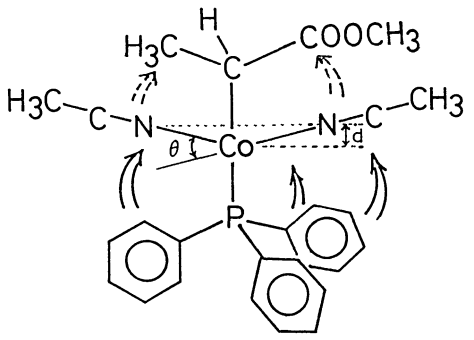

Fig. 4. Repulsive interaction in the phosphine-coordinated cobaloximes.

moiety. Although we do not have X-ray crystallographic data for a series of 1-(methoxycarbonyl)ethyl cobaloximes, a similar situation may be expected to occur for the series as well (Fig. 4). Since the Co–C bond lengths in 1-(methoxycarbonyl)ethyl cobaloximes[12,13,17] are not so much lengthened, compared with those in 1-cyanoethyl derivatives,[2a,7,15,16] and the bond lengths are almost unaltered with a change in the axial phosphine ligand,[2a,10,11] a steric repulsion between the larger alkyl (1-(methoxycarbonyl)ethyl) and the in-plane dimethylglyoximato ligand are much more serious than that between 1-cyanoethyl group and the in-plane ligands. Consequently, the Co–C bonds in 1-(methoxycarbonyl)ethyl cobaloximes are more highly strained than those in 1-cyanoethyl cobaloximes with increasing bulkiness of the axial ligand, being more susceptible to photochemical Co–C bond homolysis. In conclusion, it follows that the electronic effect of the axial ligand is negligible and that the steric effect is overwhelmingly dominant in determining the rate of photochemical Co–C bond homolysis in the solution state: the steric bulkiness of both the axial base and the axial alkyl group accelerates the rate (k_1) both remarkably and cooperatively.

Experimental

The IR spectra were recorded on a JASCO A-3 spectrometer. The NMR spectra were obtained on a JEOL FX-200 spectrometer, using TMS as the internal standard. The optical rotations were measured on a Perkin–Elmer 241 polarimeter.

Photoracemization. All of the operations, except for photoreactions, were carried out in the dark. Each sample (3.79 mmol dm^{-3}) and 100-fold excess of the corresponding axial ligand were dissolved in degassed chloroform under an Ar atmosphere. In the cases of Entries 5, 9 and 10, 3.79 mmol dm^{-3} of (*R*)-aqua[1-(methoxycarbonyl)ethyl]cobaloxime and 100 fold of (*RS*)-1-phenylethylamine, triphenylphosphine or tricyclohexylphosphine were dissolved in degassed chloroform under an Ar atmosphere. Each solution was transferred to a glass (Pyrex) cell in order to measure the optical rotation. The cell was placed at a distance of ca.3.0 m from the light source [four 40 W fluorecent lamps "white" (Matsushita Electric Ind. Co.)], at that distance, the flux density was 0.009 mW cm^{-2}. The optical rotation, which gradually decreased upon irradiation, was measured at regular time intervals.

Materials. Bis(dimethylglyoximato)[(*S*)-1-(methoxycarbonyl)ethyl][(*S*)-1-phenylethylamine]cobalt(III) [(*S,S*)-1] was prepared by almost the same procedure as the enantiomer, except for using (*S*)-1-phenylethylamine (Aldrich, $[\alpha]_D$ −39) as the axial ligand. Five recrystallizations from methanol–water gave a constant optical rotation: $[\alpha]_{589}$ −205.6, $[\alpha]_{578}$ −226.7, $[\alpha]_{546}$ −253.3 (*c* 0.180, chloroform). Found: C, 48.40; H, 6.46; N, 13.93%. Calcd for $C_{20}H_{32}N_5O_6Co$: C, 48.29; H, 6.48; N, 14.08%.

Bis(dimethylglyoximato)[(*S*)-1-(methoxycarbonyl)ethyl](pyridine)cobalt(III). To a methanol (10 cm^3) solution of 1 g of **(*S,S*)-1** was added 2 cm^3 of 2 mol dm^{-3} hydrochloric acid and 0.32 cm^3 of pyridine with stirring. After standing for 15—20 min at room temperature, the reaction mixture was extracted with dichloromethane and washed with water. The dichloromethane layer was dried over anhydrous sodium sulfate, and concentrated in vacuo to give 0.72 g of a crude product (79%). The crude product (0.4 g) was recrystallized from methanol (4.5 cm^3) and water (5.5 cm^3) to give leaflets (0.32 g), $[\alpha]_{589}$ −172.2, $[\alpha]_{578}$ −189.3, $[\alpha]_{546}$ −227.8 (*c* 0.170, chloroform). The IR and NMR spectra were identical with those of the (*R*)-isomer.

(4-Cyanopyridine)bis(dimethylglyoximato)[(*S*)-1-(methoxycarbonyl)ethyl]cobalt(III). To a methanol (10 cm^3) solution of 1 g of **(*S,S*)-1** was added 2 cm^3 of 2 mol dm^{-3} hydrochloric acid and 0.48 g of 4-cyanopyridine with stirring. After 5 min small amounts of crystals were deposited. After 20 min the reaction mixture was extracted with dichloromethane and washed with water. The dichloromethane layer was dried over anhydrous sodium sulfate and concentrated in vacuo to give 0.76 g (79%). The crude product (0.4 g) was recrystallized from methanol (7 cm^3) and water (9 cm^3) to give dark-red crystals (0.31 g). ^{1}H NMR ($CDCl_3$) δ=0.375 (d, 3H, $C\underline{H}_3CH(Co)COOCH_3$), 2.199 and 2.216 ($CH_3$ of dmgH, in the same region the signal of $CH_3C\underline{H}(Co)COOCH_3$ is overlapped), 3.487 (s, 3H, $COOCH_3$), 7.54 (d, 2H, cyanopyridine), 8.76 (d, 2H, cyanopyridine). $[\alpha]_{589}$ −150.6, $[\alpha]_{578}$ −165.9, $[\alpha]_{546}$ −194.5 (*c* 0.132, chloroform). Found: C, 45.08; H, 5.22; N, 17.46%. Calcd for $C_{18}H_{25}N_6O_6Co$: C, 45.01; H, 5.25; N, 17.50%.

Bis(dimethylglyoximato)[(*S*)-1-(methoxycarbonyl)ethyl](4-methylpyridine)cobalt(III). To a methanol (10 cm^3) solution of 1 g of **(*S,S*)-1** was added 2 cm^3 of 2 mol dm^{-3} hydrochloric acid and 0.36 cm^3 of 4-methylpyridine with stirring. After 7 min the crystals began to deposit (0.2 g). After standing for about 20 min at room temperature the reaction mixture was extracted with dichloromethane and washed with water. The dichloromethane layer was dried over anhydrous sodium sulfate, and concentrated in vacuo to give 0.7 g of a crude product. The combined yield was 0.9 g (95%). The crude product (0.4 g) was recrystallized from methanol (18 cm^3) and water (22 cm^3) to give plates (0.28 g). ^{1}H NMR ($CDCl_3$) δ=0.404 (d, 3H, $C\underline{H}_3CH(Co)COOCH_3$), 2.190 and 2.207 ($CH_3$ of dmgH, and in the same region the signal of $CH_3C\underline{H}(Co)COOCH_3$ is overlapped), 2.317 (s, 3H, CH_3 of 4-methylpyridine), 3.484 (s, 3H, $COOCH_3$), 7.06 (d, 2H, arom-H of 4-methylpyridine), 8.32 (d, 2H, arom-H of 4-methylpyridine). $[\alpha]_{589}$ −152.9, $[\alpha]_{578}$ −171.2, $[\alpha]_{546}$ −211.8 (*c* 0.170, chloroform). Found: C, 45.58; H, 5.93; N, 14.63%. Calcd for $C_{18}H_{28}N_5O_6Co$: C, 46.06; H, 6.01; N, 14.92%.

(Tributylphosphine)bis(dimethylglyoximato)[(*R*)-1-(methoxycarbonyl)ethyl]cobalt(III). To a methanol (13 cm^3) solution of 1 g of **(*R,R*)-1** ($[\alpha]_{578}$ +223.0, *c* 0.145, chloroform) was added 1.5 cm^3 of 2 mol dm^{-3} hydrochloric acid and 0.5 cm^3 of tributylphosphine with stirring. The reaction was monitored by TLC. After completion of a ligand exchange, 9 cm^3 of water was added to the reaction mixture. The solution was left standing overnight in a refrigerator. Crude crystals (0.43 g) were deposited. Another crop of crystals (0.11 g) was obtained from the filtrate. The combined yield was 0.54 g (46%). The crude product was recrystallized twice from methanol–water (2/1) to give light-yellow crystals. ^{1}H NMR ($CDCl_3$) δ=0.560 (t, 3H, $C\underline{H}_3CH(Co)COOCH_3$), 0.884 (t, 9H, 3×$CH_3$ of Bu_3P), 1.1—1.4 (m, 18H, methylene of Bu_3P), 1.649 (s, 2H, 2×OH of dmgH). $[\alpha]_{589}$ +143.1, $[\alpha]_{578}$ +156.6, $[\alpha]_{546}$ +207.1 (*c* 0.139, chloroform). Found: C, 49.62; H, 8.75; N, 9.66%. Calcd for $C_{24}H_{48}N_4O_6PCo$: C, 49.82; H, 8.36; N, 9.68%.

(Ethyldiphenylphosphine)bis(dimethylglyoximato)[(*R*)-1-(methoxycarbonyl)ethyl]cobalt(III). To a methanol (19 cm^3) solution of 2 g of **(*R,R*)-1** ($[\alpha]_{578}$ +212.6, *c* 0.180, chloroform) was added 3 cm^3 of 2 mol dm^{-3} hydrochloric acid and 0.9 cm^3 of ethyldiphenylphosphine with stirring. The reaction was monitored by TLC. After completion of a ligand exchange, water (14.5 cm^3) was added to the reaction mixture. The solution was left standing overnight in a refrigerator. Crude crystals (1.92 g, 81% yield) deposited, which was recrystallized twice from methanol–water (10/8—10/9) to give dark-red crystals. ^{1}H NMR ($CDCl_3$) δ=0.502 (t, 3H, $C\underline{H}_3CH(Co)COOCH_3$), 0.805 (quint, methyl of $EtPh_2P$), 1.947, 1.962, 1.972, 1.986 (12H, methyl of dmgH), 2.094 (quint, 1H, $CH_3C\underline{H}(Co)COOCH_3$), 2.31 (m, 2H, methylene of $EtPh_2P$), 3.405 (s, 3H, $COOCH_3$), 7.38 (m, 10H, Ph). $[\alpha]_{589}$ +153.4, $[\alpha]_{578}$ +167.5, $[\alpha]_{546}$ +218.9 (*c* 0.121, chloroform). Found: C, 52.84; H, 6.32; N, 9.49%. Calcd for $C_{26}H_{36}N_4O_6PCo$: C, 52.89; H, 6.15; N, 9.49%.

(Diethylphenylphosphine)bis(dimethylglyoximato)[(*R*)-1-(methoxycarbonyl)ethyl]cobalt(III). To a methanol (15 cm^3) solution of 1.6 g of **(*R,R*)-1** ($[\alpha]_{578}$ +212.6, *c* 0.180, chloroform) was added 3 cm^3 of 2 mol dm^{-3} hydrochloric acid and 0.701 cm^3 of diethylphenylphosphine with stirring. The reaction was monitored by TLC. After completion of a ligand exchange, water (4 cm^3) was added to the reaction mixture. The solution

was left standing overnight in a refrigerator. Crystals (0.48 g) deposited. ^{1}H NMR ($CDCl_3$) δ=0.556 (t, 3H, $C\underline{H}_3CH(Co)COOCH_3$), 0.935 (quint, 6H, $(C\underline{H}_3CH_2)_2P$), 1.947, 1.962, 1.972, 1.986 (12H, CH_3 of dmgH), 1.9—2.2 (m, signals of $(CH_3C\underline{H}_2)_2PhP$ and $CH_3C\underline{H}(Co)COOCH_3$ were overlapped in this region), 3.418 (s, 3H, $COOCH_3$), 7.04 (m, 2H, arom), 7.36 (m, 3H, arom). $[\alpha]_{589}$ +168.0, $[\alpha]_{578}$ +184.1, $[\alpha]_{546}$ +247.3 (*c* 0.260, chloroform). Found: C, 48.52; H, 6.95; N, 10.31%. Calcd for $C_{22}H_{36}N_4O_6PCo$: C, 48.71; H, 6.69; N, 10.33%. Another crop of crystals (0.63 g) was obtained from the filtrate. The combined yield was 1.11 g (64%).

This work was partly supported by a Grant-in-Aid for Scientific Research from the Ministry of Education, Science and Culture.

References

1) Preparation and Reaction of Optically Active Organotransition Metal Complexes. III. For the preceding report of this series, II, see Ref. 2a.

2) a) S. Baba, Y. Ohgo, and S. Takeuchi, *Bull. Chem. Soc. Jpn.*, **60**, 3967 (1987); b) Y. Ohgo, S. Takeuchi, Y. Natori, J. Yoshimura, Y. Ohashi, and Y. Sasada, *ibid.*, **54**, 3095 (1981).

3) Y. Ohgo and S. Takeuchi, *Chem. Lett.*, **1985**, 407.

4) Y. Ohgo, K. Orisaku, E. Hasegawa, and S. Takeuchi, *Chem. Lett.*, **1986**, 27.

5) Y. Ohgo and S. Takeuchi, *J. Chem. Soc., Chem. Commun.*, **1985**, 21.

6) Y. Ohashi, K. Yanagi, T. Kurihara, Y. Sasada, and Y. Ohgo, *J. Am. Chem. Soc.*, **103**, 5805 (1981).

7) Y. Ohashi, K. Yanagi, T. Kurihara, Y. Sasada, and Y. Ohgo, *J. Am. Chem. Soc.*, **104**, 6353 (1982).

8) Y. Ohashi, A. Uchida, Y. Sasada, and Y. Ohgo, *Acta Crystallogr., Sect. B*, **39**, 54 (1983).

9) T. Kurihara, Y. Ohashi, Y. Sasada, and Y. Ohgo, *Acta Crystallogr., Sect. B*, **39**, 243 (1983).

10) T. Kurihara, A. Uchida, Y. Ohashi, Y. Sasada, Y. Ohgo, and S. Baba, *Acta Crystallogr., Sect. B*, **39**, 431 (1983).

11) Y. Tomotake, A. Uchida, Y. Ohashi, Y. Sasada, Y. Ohgo, and S. Baba, *Acta Crystallogr., Sect. C*, **40**, 1684 (1984).

12) T. Kurihara, A. Uchida, Y. Ohashi, Y. Sasada, and Y. Ohgo, *J. Am. Chem. Soc.*, **106**, 5718 (1984).

13) T. Kurihara, A. Uchida, Y. Ohashi, Y. Sasada, and Y. Ohgo, *Acta Crystallogr., Sect. B*, **40**, 478 (1984).

14) a) C. A. Tolmann, *Chem. Rev.*, **77**, 313 (1977); b) W. C. Trogler and L. G. Marzilli, *Inorg. Chem.*, **14**, 2942 (1975).

15) Y. Ohashi, Y. Sasada, S. Takeuchi, and Y. Ohgo, *Bull. Chem. Soc. Jpn.*, **53**, 627 (1980).

16) Y. Ohashi, Y. Sasada, S. Takeuchi, and Y. Ohgo, *Bull. Chem. Soc. Jpn.*, **53**, 1501 (1980).

17) Y. Ohashi and Y. Sasada, *Bull. Chem. Soc. Jpn.*, **50**, 2863 (1977).

18) C. Gianotti and B. Septe, *J. Organomet. Chem.*, **52**, C36 (1973); C. Gianotti and C. Fontaine, *ibid.*, **52**, C41 (1973); C. Gianotti, C. Fontaine, and B. Septe, *ibid.*, **71**, 107 (1974).

19) A. Fischer, W. J. Galloway, and J. Vaugham, *J. Chem. Soc.*, **1964**, 3591.

20) G. M. Kosolapoff and L. Maier, "Organic Phosphorus Compounds," Wiley-Interscience, New York (1972), Vol. 1, pp. 124—168.

 © 1991 The Chemical Society of Japan Bull. Chem. Soc. Jpn., 64, 2661—2667 (1991)

Selective Formation of α-Cleavage Cycloadduct of Oxirane with Heterocumulene Promoted by High-Coordinated Trialkyltin Complexes

Katsunori YANO, Nobuyoshi AMISHIRO, Akio BABA,* and Haruo MATSUDA
Department of Applied Chemistry, Faculty of Engineering, Osaka University,
2-1 Yamada-Oka, Suita, Osaka 565
(Received March 14, 1991)

In the reaction of monosubstituted oxiranes and heterocumulenes, trialkyltin iodides coordinated by phosphine oxides effectively catalyzed the formation of heterocycles via cleavage at the substituted site in the oxirane ring, while other types of organotin complexes or noncomplexed organotin iodides promoted selective cleavage at the opposite site. A mechanistic investigation demonstrated that the coordination of phosphine oxide promotes the reverse reaction of the oxirane-ring cleavage leading to the predominant formation of α-cleavage cycloadducts.

Although the cycloaddition of monosubstituted oxiranes with heterocumulenes has been a useful method for the synthesis of five-membered heterocycles,[1-6] most reactions were reported to proceed via the cleavage of oxiranes at their nonsubstituted site (β-cleavage).[7,8] The change of the regioselectivity of oxirane-ring cleavage from β-cleavage to α-cleavage (cleavage at the substituted site) is a simple and useful tool to increase the scope of cycloaddition of oxiranes with heterocumulenes. Although many regioselective cleavages were reported in the reaction of oxiranes with nucleophiles, the effective change in cycloaddition reactions with nucleophiles has rarely been reported.[9,10] We recently reported that tetraphenylstibonium iodide was a versatile catalyst for the selective α-cleavage cycloaddition of general monosubstituted oxiranes.[11] However, the activity of this catalyst is highly dependent on the substrates used; for example, 1,2-epoxy-3-chloropropane and sulfur-containing heterocumulenes were not reactive at all. On the other hand, although some organotin halide complexes were briefly reported to catalyze β-cleavage cycloaddition, their activity and structures vary in accordance with the combination of tin halides with ligands.[12-19] These results and the high affinity of tin for sulfur compounds[20-24] prompted us to investigate a selective α-cleavage cycloaddition of oxiranes to heterocumulenes including isothiocyanates by means of complexation of organotin iodides.[25]

In this paper, we wish to report the regio-controlled cycloaddition of monosubstituted oxiranes with heterocumulenes such as isocyanates, carbodiimides and isothiocyanates. The direction of oxirane-ring cleavage is strongly dependent on the complexation mode. Trialkyltin iodides coordinated by phosphine oxides promoted α-cleavage cycloaddition, yielding 3,4-disubstituted five-membered heterocycles. On the other hand, the complex of Bu_2SnI_2 and noncomplexed organotin iodide resulted in a selective β-cleavage cycloaddition. A plausible reaction path is explainable in terms of an equilibrium in the oxirane cleavage step. The effect of complexation was demonstrated by using an intermediary adduct, while no such adduct could be detected in the Ph_4SbI catalyst system though a similar reaction path has been proposed.[26]

Results and Discussion

Cycloaddition with Isocyanates and Carbodiimides. Table 1 lists the results of cycloadditions of monosubstituted oxiranes with carbodiimides or isocyanates, noncomplexed Bu_3SnI catalyzed the selective β-cleavage addition (Entry 1). For α-cleavage addition, the addition of bases was indispensable, and the complexes

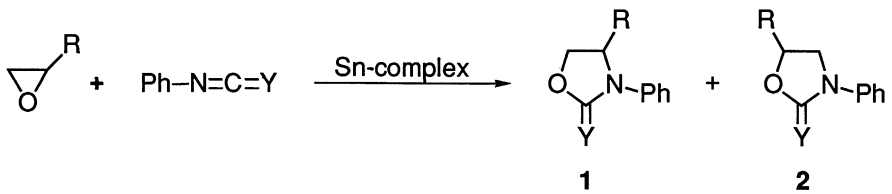

1 (α-cleavage) **2** (β-cleavage)

	Y	R		Y	R
a	N-Ph	Me	**f**	N-Bu^n	Et
b	N-Ph	Et	**g**	O	Me
c	N-Ph	Ph	**h**	O	Et
d	N-Ph	CH_2OPh	**i**	O	*n*-Hex
e	N-Ph	CH_2Cl	**j**	O	Ph

Scheme 1.

Table 1. Cycloaddition of Monosubstituted Oxirane with Carbodiimide and Isocyanate

Entry	R	Y	Sn	Base (ratio)[a]	Time/h	Yield/%	1/2
1	Et	*N*-Ph	*n*-Bu_3SnI	—	12	82	0/100
2	Et	*N*-Ph	*n*-Bu_3SnI	*n*-Bu_3PO (1/1)	9	88	71/29
3	Et	*N*-Ph	*n*-Bu_3SnI	Et_3N (1/1)	4	79	31/69
4	Et	*N*-Ph	*n*-Bu_3SnI	*n*-Bu_3P (1/1)	5	83	55/45
5	Et	*N*-Ph	*n*-Bu_2SnI_2	*n*-Bu_3P (1/1)	1	100	41/59
6	Et	*N*-Ph	*n*-Bu_2SnI_2	Ph_3P (1/1)	1	92	0/100
7	Et	*N*-Ph	*n*-Bu_3SnCl	*n*-Bu_3PO (1/1)	36	16	0/100
8	Et	*N*-Ph	*n*-Bu_3SnI	*n*-Bu_3PO (10/1)	14	100	82/18
9	Et	*N*-Ph	*n*-Bu_3SnI	HMPA (50/1)[c]	36	61	91/9
10	Et	*N*-Ph	Me_3SnI	HMPA (50/1)[c]	10	97	89/11
11	Me	*N*-Ph	*n*-Bu_3SnI[b]	*n*-Bu_3PO (1/1)	1.5	73	82/18
12	Ph	*N*-Ph	Me_3SnI	HMPA (1/1)	23	75	94/6
13	CH_2OPh	*N*-Ph	*n*-Bu_3SnI	HMPA (50/1)[c]	29	66	73/27
14	CH_2Cl	*N*-Ph	*n*-Bu_3SnI[b]	*n*-Bu_3PO (1/1)	3	70	55/45
15	Et	*N*-Bu^n	*n*-Bu_3SnI[b]	*n*-Bu_3PO (1/1)	24	57	65/35
16	Et	O	*n*-Bu_3SnI	HMPA (50/1)[c]	2	93	24/76
17	Et	O	*n*-Bu_3SnI[b]	*n*-Bu_3PO (1/1)	1	97	62/38
18	Me	O	*n*-Bu_3SnI[b]	*n*-Bu_3PO (1/1)	1	93	46/54
19	*n*-Hex	O	*n*-Bu_3SnI[b]	*n*-Bu_3PO (1/1)	1	99	66/34
20	Ph	O	*n*-Bu_3SnI	HMPA (50/1)[c]	2	81	90/10

Sn-complex/NCY/oxirane=0.2/2/20 mmol, 50°C. a) Base/Sn ratio. b) 2 mmol. c) Sn/HMPA/NCY/oxirane=0.2/10/2/4 mmol.

investigated were the combination of tributyltin iodide and phosphine oxides such as tributylphosphine oxide and hexamethylphosphoric triamide (HMPA). These complexes predominantly gave 3,4-disubstituted oxazolidines **1** which have been obtained in small amounts by the action of conventional catalysts such as Lewis bases (triethylamine[27] and sodium ethoxide[10]), -acids ($AlCl_3$[10] and LiCl[28]) and tetraalkylammonium halides.[29,30] Moreover, the use of excess amounts of phosphine oxides gave a higher selectivity of **1** (91%), although a longer reaction time was required (Entry 9). This problem was overcome by the use of Me_3SnI (which is more active due to its high acidity) instead of Bu_3SnI (89% selectivity, Entry 10). However, the α-cleavage ability enhanced by the addition of bases, could not be explained in terms of Lewis acidity since a stronger Lewis acid, noncomplexed Bu_3SnI, is considered to cleave an oxirane ring more easily at the substituted site.[10] The formation of **1** in the case of (chloromethyl)oxirane (Entry 14) is particularly noteworthy since even the versatile catalyst Ph_4SbI could not produce it at all.

The above results strongly suggest that the complexation mode and the stability of the resulting complexes are responsible for the regio-control of oxazolidine formation. It was reported that phosphine oxides coordinate to tributyltin iodide to form five-coordinated complexes, while they form six-coordinated complexes with dibutyltin diiodide.[31-34] It is interesting that the former showed the opposite regioselectivity of the latter. The stability of the complexes also seems to be important for α-cleavage cycloaddition, since if the complexes dissociate to the original tributyltin iodide and ligands, the resulting free tributyltin iodide would promote the β-cleavage of oxiranes. Tributylphosphine oxide and HMPA are superior to either tributylphospine or triethylamine due to the higher coordination ability toward tin atoms.[35] Moreover, excess amounts of phosphine oxides disturb the dissociation of complexes, although the interaction between oxiranes and tin complexes would be weakened to reduce reactivity.

The addition of isocyanates to oxiranes was less selective than carbodiimides and suffered from the requirement of an equimolar amount of tributyltin iodide (Entries 17—19). Isocyanates perhaps were so active that catalytic control could not be enhanced.

Cycloaddition of Oxirane with Isothiocyanate. The lower electrophilicity and high affinity for tin atoms prompted us to use isothiocyanates instead of carbodiimides in the cycloaddition reactions. Results are shown in Table 2. The catalyst, an Me_3SnI–HMPA system, effected a regioselective cycloaddition to give 4-substituted 2-imino-1,3-oxathiolane **3** and 3,4-disubstituted 1,3-oxazolidine-2-thione **4**. This result was very interesting since other organotin halide complexes gave β-cleavage cycloadducts, as previously reported.[7] Moreover, a large excess of HMPA was not required as was the case with the carbodiimides.

The fact that no consumption of **3** was observed under

Table 2. Catalytic Cycloaddition of Monosubstituted Oxiranes with Isothiocyanates

Entry	R	R′	Time/h	**3** (%)	**4** (%)	**5** (%)
1	Me	Ph	5	78	14	7
2	Et	Ph	10	56	19	5
3	Ph	Ph	5	59	18	Trace
4	Et	Me	30	16	0	51

Me_3SnI/HMPA/oxirane/NCS=0.2/0.6/10/2 mmol.

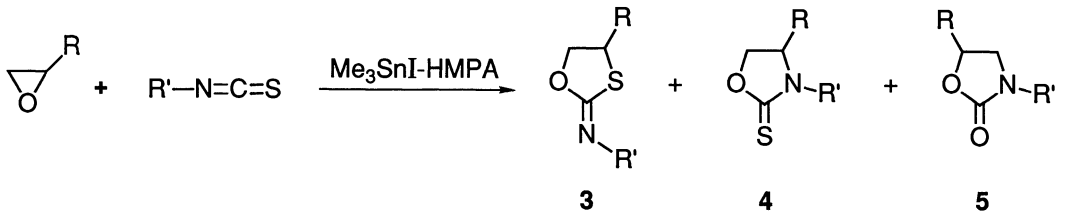

	R	R'
a	Me	Ph
b	Et	Ph
c	Ph	Ph
d	Et	Me

Scheme 2.

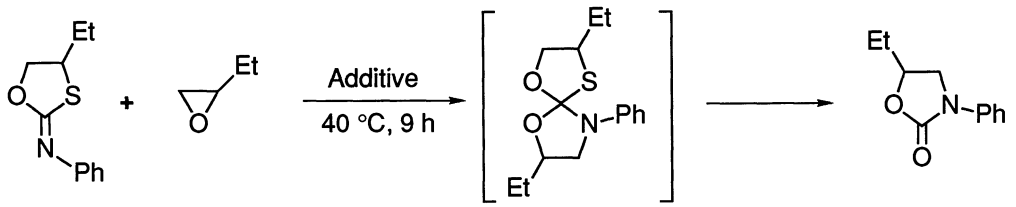

Me_3SnI	17 %
Me_3SnI-HMPA (1/3)	0
$AlCl_3$ (0.3 h)	86

Scheme 3.

the same conditions as those used for the cycloaddition showed that there was no rearrangement of **3** to **4**.

In this type of cycloaddition, a desulfurization has often been reported,[7] which is assumed to be caused by the addition of oxirane to **3**, producing oxazolidinones **5** as depicted in Scheme 3. Consequently, the 3,5-disubstituted oxazolidinones **5** would probably not be produced via a β-cleavage of the oxirane ring. This type of rearrangement was confirmed as follows. Strong Lewis acids such as $AlCl_3$ readily caused this transformation in an 86% yield, while no oxazolidinone formation was promoted by the Me_3SnI complex. This result may be ascribed to the low acidity of Me_3SnI coordinated by HMPA. Although methyl isothiocyanate gave **5** in a 51% yield, this side reaction was observed only minimally with the addition of phenyl isothiocyanate.

Reaction Mechanism. The reaction path way to 3,4- and 3,5-disubstituted five-membered heterocycles is illustrated in Scheme 4 and is exemplified by the addition of methyloxirane to diphenylcarbodiimide.

The first step, cleavage of the oxirane ring, appears to be a key step for regio-control of this addition. The cleavage of methyloxirane by trimethyltin iodide (Me_3SnI) in the presence of $Bu_3P{=}O$ proceeded readily at room temperature. However, the identification of the resulting adducts and the ratio of **6** and **7** could not be determined by NMR, though the predominant formation of **7** was indicated. This result suggested that the predominant formation of the α-cleavage adduct was not due to the selective α-cleavage of oxiranes at the first step. On the other hand, in the absence of $Bu_3P{=}O$, the addition of Me_3SnI to methyloxirane was exothermic and resulted in the quantitative formation of a distillable trimethyltin 2-iodopropoxide, and the resulting propoxide was added to diphenylcarbodiimide, forming **2a** quantitatively when reacted at 50 °C for 1 h. This selective formation of **2a** indicates that methyloxirane would be cleaved at the β-site to give **7**. On the other hand, surprisingly, in the presence of $Bu_3P{=}O$, this propoxide **7** gave **1a** in a 40% yield together with **2a** (60%) as shown in Scheme 5. This result seemed to suppose the transformation of the 3,5-disubstituted product by the complex $Bu_3P{=}O$ and Me_3SnI, but this idea was proved false by the fact that no consumption of **2a** by the complex was observed even under far more drastic conditions (80 °C, 3 h). A similar result was observed in the reaction with benzoyl chloride (Scheme 5).

Next, the transformation of 2-iodoisopropoxide **7** to 2-iodoisopropoxide **6** will be considered. The isolation of **6** from the mixture of **7** and $Bu_3P{=}O$ was attempted. The distillation of the adduct, however, was failed, and methyloxirane was regenerated in a 78% yield. The methyloxirane was thought to be generated from **7** by the

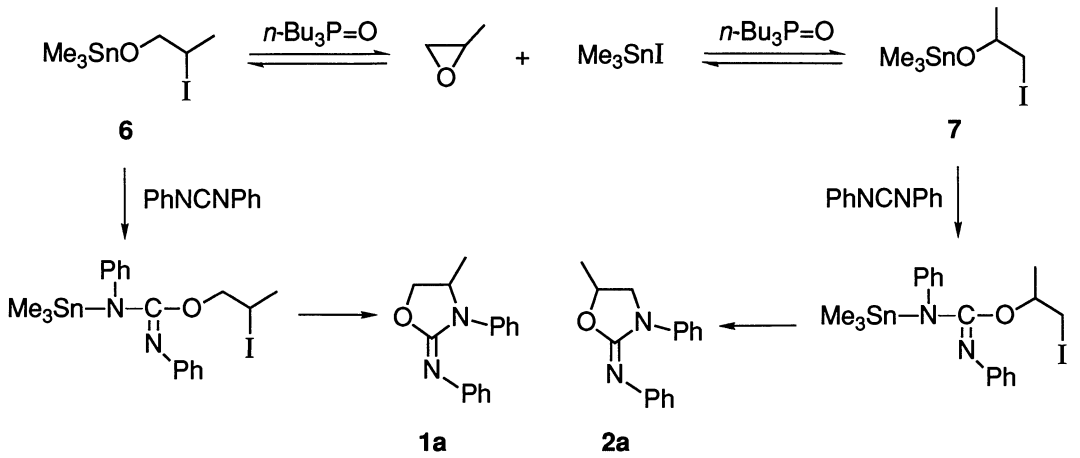

Scheme 4.

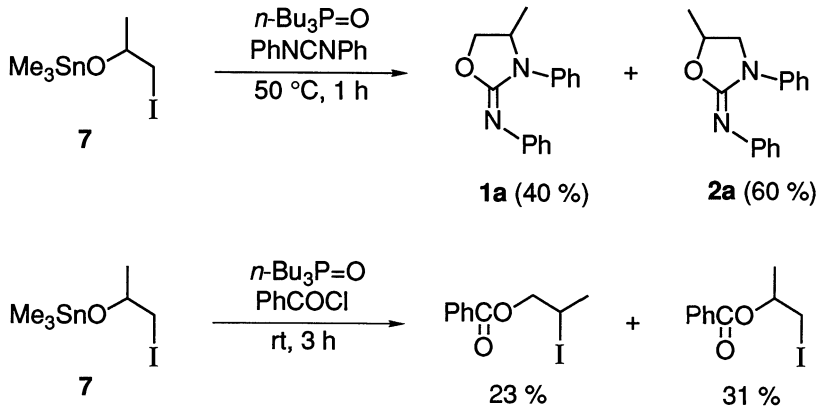

Scheme 5.

action of $Bu_3P{=}O$ during distillation. This result strongly suggested that facile equilibrium between **7** and the starting substrates was promoted by $Bu_3P{=}O$. Moreover, although the oxirane ring is subject to cleavage at the β-site even in the presence of $Bu_3P{=}O$, the participation of **6** is apparently plausible from the results shown in Scheme 5 in spite of the lack of visual evidence such as NMR spectra.

On the basis of the above results, the reaction mechanism for the predominant formation of 3,4-disubstituted cycloadducts can be explainable in terms of the equilibrium of the addition of oxirane and Me_3SnI as shown in Scheme 4. At first, the cleavage of oxirane results in the formation of **6** and **7**. Diphenylcarbodiimide adds electrophilically to both tin iodoalkoxides, where the alkoxide **6** would preferentially react because of the higher reactivity of a primary alkoxide over a secondary one (**7**). The addition is followed by the cyclization into 3,4-disubstituted oxazolidine **1a**. In the presence of $Bu_3P{=}O$, a facile transformation of **7** to **6** leads to the predominant formation of **1a**. The coordination of bases accelerates the addition of heterocumulenes to tin ω-haloalkoxides as already reported.[7,16,36-39] On the other hand, an isocyanate, a higher reactive heterocumulene, can readily react even with the secondary alkoxide **7**, and the selective formation of 3,4-disubstituted oxazolidinones is difficult. The lower electrophilicity of isothiocyanate, of course, results in a selective α-cleavage cycloaddition.

Conclusion

The complexes of organotin iodides with Lewis bases controlled the regiospecific addition of monosubstituted oxirane to heterocumulenes. The coordination of appropriate bases has some notable potentials: Activation of the addition, specification of the regioselectivity, and limitation of side reactions.

Experimental

Apparatus and Materials. Melting points are uncorrected. IR spectra were recorded on a Hitachi 260-30 spectrophotometer. ^1H NMR and ^{13}C NMR spectra were measured on a Hitachi R-90H or a JEOL JNM-GSX-400 spectrometer. Mass spectra were obtained with a JEOL JMS-DS303

spectrometer. Microanalyses were recorded on a JEOL JMS-DX303 spectrometer (data software processing, JMS-DA 5000). Analytical GLC was performed on a Shimadzu GC-8A using a 2 m×3 mm glass column packed with Silicone OV-1 on Uniport HP (5%, 60—80 mesh). Short-path distillations of products were carried out in a Kugelrohr apparatus.

All oxiranes were freshly distilled from CaH_2. All Lewis bases were purified by general procedures. Isothiocyanates and PhNCO were obtained from commercial sources and used without further purification. PhNCNPh,[40] BuNCNPh,[41] and organotin iodides[42,43] were prepared according to the described methods.

Reaction of Oxirane with Carbodiimide. Diphenylcarbodiimide (2 mmol) was added to a solution of Me_3SnI (2 mmol) and Bu_3PO (2 mmol) in ethyloxirane (20 mmol) under dry nitrogen. The mixture was stirred at 50 °C until the infrared absorption of N=C=N (2150 cm^{-1}) disappeared, and the yields of **1b** (82%) and **2b** (18%) were determined by GLC. The products were isolated by column chromatography on silica gel, giving **1b** (eluted by chloroform; 399 mg, 75%) and **2b** (eluted by benzene; 69 mg, 13%).

4-Methyl-3-phenyl-2-phenylimino-1,3-oxazolidine (1a):[11] Mp 89 °C; IR (KBr) 1680 cm^{-1} (C=N).

5-Methyl-3-phenyl-2-phenylimino-1,3-oxazolidine (2a):[44] Mp 72—73 °C; IR (KBr) 1670 cm^{-1} (C=N); ^1H NMR ($CDCl_3$) δ=1.45 (3H, d, J=6.0 Hz), 3.55 (1H, dd, J=7.0 and 8.0 Hz), 4.05 (1H, t, J=8.0 Hz), 4.50—4.90 (1H, m), and 6.90—7.80 (10H, m); MS m/z 252 (M^+).

4-Ethyl-3-phenyl-2-phenylimino-1,3-oxazolidine (1b): Bp 200 °C/0.01 mmHg (1 mmHg=133.322 Pa); IR 1680 cm^{-1} (C=N); ^1H NMR ($CDCl_3$) δ=0.92 (3H, t, J=6.9 Hz), 1.40—1.97 (2H, m), 3.90—4.58 (3H, m), and 6.57—7.97 (10H, m); ^{13}C NMR ($CDCl_3$) δ=8.41 (q), 24.51 (t), 58.42 (d), 68.60 (t), 122.14 (d), 122.45 (d), 123.30 (d), 124.15 (d), 128.36 (d), 128.85 (d), 138.31 (s), 146.72 (s), and 147.45 (s); MS m/z 266 (M^+). Found: C, 76.53; H, 6.87; N, 10.50%. Calcd for $C_{17}H_{18}ON_2$: C, 76.67; H, 6.81; N, 10.52%.

5-Ethyl-3-phenyl-2-phenylimino-1,3-oxazolidine (2b): Bp 170 °C/0.01 mmHg; IR 1680 cm^{-1} (C=N); ^1H NMR ($CDCl_3$) δ=0.97 (3H, t, J=6.8 Hz), 1.35—1.95 (2H, m), 3.52 (1H, dd, J=6.8 and 8.1 Hz), 3.92 (1H, t, J=8.1 Hz), 4.15—4.70 (1H, m), and 6.60—8.23 (10H, m); ^{13}C NMR ($CDCl_3$) δ=8.78 (q), 27.44 (t), 50.74 (t), 76.16 (d), 119.34 (d), 122.82 (d), 123.30 (d), 124.03 (d), 129.03 (d), 139.34 (d), 140.44 (s), 148.05 (s), and 148.79 (s); MS m/z 266 (M^+). Found: C, 76.75; H, 6.72; N, 10.51%. Calcd for $C_{17}H_{18}ON_2$: C, 76.67; H, 6.81; N, 10.52%.

3,4-Diphenyl-2-phenylimino-1,3-oxazolidine (1c):[11] Mp 122 °C; IR (KBr) 1680 cm^{-1} (C=N).

3,5-Diphenyl-2-phenylimino-1,3-oxazolidine (2c):[11] Mp 111—113 °C; IR (KBr) 1680 cm^{-1} (C=N).

4-Phenoxymethyl-3-phenyl-2-phenylimino-1,3-oxazolidine (1d): Mp 77—79 °C; IR (KBr) 1675 cm^{-1} (C=N); ^1H NMR ($CDCl_3$) δ=3.83—4.27 (2H, m), 4.27—4.86 (3H, m), and 6.32—7.85 (15H, m); ^{13}C NMR ($CDCl_3$) δ=56.86 (d), 66.16 (t), 67.44 (t), 114.49 (d), 121.50 (d), 122.11 (d), 122.32 (d), 123.24 (d), 124.46 (d), 128.36 (d), 129.03 (d), 129.46 (d), 138.12 (s), 147.17 (s), 149.74 (s), and 157.97 (s); MS m/z 344 (M^+). Found: C, 76.59; H, 5.71; N, 8.29%. Calcd for $C_{22}H_{20}O_2N_2$: C, 76.72; H, 5.85; N, 8.31%.

5-Phenoxymethyl-3-phenyl-2-phenylimino-1,3-oxazolidine (2d): Mp 105—106 °C; IR (KBr) 1690 cm^{-1} (C=N); ^1H NMR ($CDCl_3$) δ=3.70—4.01 (4H, m), 4.48—4.81 (1H, m), and 6.64—8.10 (15H, m); ^{13}C NMR ($CDCl_3$) δ=48.52 (t), 67.92 (t), 72.79 (d), 114.81 (d), 118.83 (d), 121.70 (d), 122.43 (d), 122.98 (d), 123.41 (d), 128.53 (d), 128.83 (d), 129.63 (d), 139.69 (s), 147.19 (s), 148.19 (s), and 158.16 (s); MS m/z 344 (M^+). Found: C, 76.68; H, 5.70; N, 8.08%. Calcd for $C_{22}H_{20}O_2N_2$: C, 76.72; H, 5.85; N, 8.31%.

4-Chloromethyl-3-phenyl-2-phenylimino-1,3-oxazolidine (1e): Due to its thermal instability **1e** was purified by column chromatography: IR 1680 cm^{-1} (C=N); ^1H NMR ($CDCl_3$) δ=3.50—3.82 (2H, m), 4.28—4.77 (3H, m), and 6.58—7.80 (10H, m); ^{13}C NMR ($CDCl_3$) δ=42.93 (t), 58.17 (d), 67.32 (t), 122.51 (d), 123.18 (d), 124.95 (d), 128.42 (d), 129.15 (d), 137.45 (s), 146.90 (s), and 149.40 (s); MS m/z 286 (M^+). Found: C, 66.94; H, 5.22; N, 9.71; Cl, 12.58%. Calcd for $C_{16}H_{15}ON_2Cl$: C, 67.01; H, 5.27; N, 9.77; Cl, 12.36%.

5-Chloromethyl-3-phenyl-2-phenylimino-1,3-oxazolidine (2e): Mp 86—88 °C; IR (KBr) 1690 cm^{-1} (C=N); ^1H NMR ($CDCl_3$) δ=3.75 (2H, d, J=5.8 Hz), 3.90—4.35 (2H, m), 4.70—5.00 (1H, m), and 6.90—7.90 (10H, m); ^{13}C NMR ($CDCl_3$) δ=44.51 (t), 49.26 (t), 73.26 (d), 122.22 (d), 122.51 (d), 123.39 (d), 124.22 (d), 128.43 (d), 128.91 (d), 138.26 (s), 147.61 (s), and 150.15 (s); MS m/z 286 (M^+). Found: C, 66.77; H, 5.25; N, 9.80; Cl, 12.63%. Calcd for $C_{16}H_{15}ON_2Cl$: C, 67.01; H, 5.27; N, 9.77; Cl, 12.36%.

2-Butylimino-4-ethyl-3-phenyl-1,3-oxazolidine (1f): Mp 190 °C/0.01 mmHg; IR 1675 cm^{-1} (C=N); ^1H NMR ($CDCl_3$) δ=0.80—1.03 (6H, m), 1.26—1.86 (6H, m), 3.27 (2H, t, J=6.5 Hz), 3.99—4.46 (3H, m), and 6.94—7.72 (5H, m); ^{13}C NMR ($CDCl_3$) δ=7.77 (q), 13.54 (q), 20.15 (t), 23.66 (t), 33.51 (t), 45.86 (t), 57.29 (d), 67.11 (t), 120.16 (d), 121.96 (d), 127.97 (d), 138.85 (s), and 149.67 (s); MS m/z 246 (M^+). Found: C, 72.95; H, 9.05; N, 11.36%. Calcd for $C_{15}H_{12}ON_2$: C, 73.13; H, 9.00; N, 11.37%.

2-Butylimino-5-ethyl-3-phenyl-1,3-oxazolidine (2f): Bp 120 °C/0.01 mmHg; IR 1670 cm^{-1} (C=N); ^1H NMR ($CDCl_3$) δ=0.88—1.19 (6H, m), 1.23—1.95 (6H, m), 3.31 (2H, t, J=6.7 Hz), 3.51 (1H, dd, J=8.2 and 6.9 Hz), 3.94 (1H, t, J=8.0 Hz), 4.32—4.61 (1H, m), and 6.89—7.73 (5H, m); ^{13}C NMR ($CDCl_3$) δ=8.84 (q), 13.93 (q), 20.85 (t), 27.50 (t), 33.90 (t), 46.37 (t), 50.89 (t), 75.28 (d), 117.60 (d), 121.38 (d), 128.33 (d), 140.44 (s), and 149.19 (s); MS m/z 246 (M^+). Found: C, 73.48; H, 8.95; N, 11.32%. Calcd for $C_{15}H_{12}ON_2$: C, 73.13; H, 9.00; N, 11.37%.

Reaction of Oxirane with Isocyanate. As a typical procedure, phenyl isocyanate (2 mmol) was added dropwise to a solution of Bu_3SnI (2 mmol) and Bu_3PO (2 mmol) in methyloxirane (20 mmol) for 1 h with stirring at 50 °C under dry nitrogen. Following addition, the formation and the yields of two products, α-cleavage cycloadduct **1g** (43%) and β-cleavage cycloadduct **2g** (50%), were monitored by GLC. The excess oxirane was removed in vacuo, and the mixture was subjected to isolation by column chromatography on silica gel, giving viscous **1g** (eluted by chloroform; 135 mg, 38%) and crystalline **2g** (eluted by benzene; 152 mg, 43%).

4-Methyl-3-phenyl-1,3-oxazolidin-2-one (1g):[11] Mp 51 °C; IR (KBr) 1740 cm^{-1} (C=O).

5-Methyl-3-phenyl-1,3-oxazolidin-2-one (2g):[5] Mp 81 °C; IR (KBr) 1740 cm^{-1} (C=O); ^1H NMR ($CDCl_3$) δ=1.52 (3H, d, J=6.0 Hz), 3.60 (1H, t, J=7.5 Hz), 4.10 (1H, t, J=8.0 Hz), 4.62—4.96 (1H, m), and 7.00—7.60 (5H, m); MS m/z 177 (M^+).

The following compounds were obtained in a similar manner.

4-Ethyl-3-phenyl-1,3-oxazolidin-2-one (1h):[11] Bp 120 °C/

0.1 mmHg; IR 1750 cm^{-1} (C=O).

5-Ethyl-3-phenyl-1,3-oxazolidin-2-one (2h):[7] Bp 124 °C/1.5 mmHg; IR 1750 cm^{-1} (C=O).

4-Hexyl-3-phenyl-1,3-oxazolidin-2-one (1i): Bp 170 °C/0.01 mmHg; IR 1750 cm^{-1} (C=O); ^1H NMR ($CDCl_3$) δ=0.68—1.97 (13H, m), 4.02—4.21 (1H, m), 4.21—4.65 (2H, m), and 6.88—7.79 (5H, m); MS m/z 247 (M^+). Found: C, 72.66; H, 8.66; N, 5.71%. Calcd for $C_{15}H_{21}NO_2$: C, 72.84; H, 8.56; N, 5.67%.

5-Hexyl-3-phenyl-1,3-oxazolidin-2-one (2i): Mp 63 °C; IR 1750 cm^{-1} (C=O); ^1H NMR ($CDCl_3$) δ=0.41—2.37 (13H, m), 3.65 (1H, t, J=8.1 Hz), 4.07 (1H, t, J=8.1 Hz), 4.46—5.00 (1H, m), and 6.52—7.87 (5H, m); MS m/z 247 (M^+). Found: C, 72.89; H, 8.52; N, 5.61%. Calcd for $C_{15}H_{21}NO_2$: C, 72.84; H, 8.56; N, 5.67%.

3,4-Phenyl-1,3-oxazolidin-2-one (1j):[11] Mp 79 °C; IR 1750 cm^{-1} (C=O).

3,5-Phenyl-1,3-oxazolidin-2-one (2j):[11] Mp 130 °C; IR 1740 cm^{-1} (C=O).

Reaction of Oxirane with Isothiocyanate. PhNCS (2 mmol) was added to a solution of Me_3SnI (0.2 mmol), HMPA (0.6 mmol) and ethyloxirane (10 mmol) under dry nitrogen. The mixture was stirred at 40 °C (5 h) until the infrared absorption of N=C=S disappeared, and the yields of the products, **3a** (78%), **4a** (14%) and **5a** (=**2a**) (7%) were monitored by GLC. The products, **3a** (271 mg, 70%), **4a** (46 mg, 12%) and **5a** (21 mg 6%) were subjected to isolation by TLC, and identified as follows.

4-Methyl-2-phenylimino-1,3-oxathiolane (3a): Oil; IR 1650 cm^{-1} (C=N); ^1H NMR ($CDCl_3$) δ=1.38 (3H, d, J=6.4 Hz), 3.74—4.09 (2H, m), 4.36—4.51 (1H, m), and 6.68—7.46 (5H, m); ^{13}C NMR ($CDCl_3$) δ=18.81 (q), 43.05 (d), 75.52 (t), 120.98 (d), 123.88 (d), 128.76 (d), 148.88 (s), and 168.67 (s); MS m/z 193 (M^+). HRMS. Found: m/z 193.0559. Calcd for $C_{10}H_{11}ONS$: M, 193.0562.

4-Methyl-3-phenyl-1,3-oxazolidine-2-thione (4a): Oil; IR 1180 cm^{-1} (C=S); ^1H NMR ($CDCl_3$) δ=1.28 (3H, d, J=6.4 Hz), 4.23 (1H, t, J=8.2 Hz), 4.45—4.58 (1H, m), 4.83 (1H, t, J=8.7 Hz), and 7.36—7.50 (5H, m); ^{13}C NMR ($CDCl_3$) δ=18.29 (q), 58.65 (d), 73.38 (t), 127.01 (d), 128.32 (d), 129.46 (d), 137.04 (s), and 187.76 (s); MS m/z 193 (M^+). HRMS. Found: m/z 193.0573. Calcd for $C_{10}H_{11}ONS$: M, 193.0562.

4-Ethyl-2-phenylimino-1,3-oxathiolane (3b): Isolated by column chromatography eluted by benzene and purified by distillation. Bp 104—106 °C/0.01 mmHg; IR 1650 cm^{-1} (C=N); ^1H NMR ($CDCl_3$) δ=0.93 (3H, t, J=7.3 Hz), 1.55—2.00 (2H, m), 3.60—3.95 (1H, m), 4.10 (1H, dd, J=9.2 and 5.9 Hz), 4.44 (1H, dd, J=9.2 and 5.9 Hz), and 6.85—7.33 (5H, m); ^{13}C NMR ($CDCl_3$) δ=12.20 (q), 27.07 (t), 50.49 (d), 73.97 (t), 121.20 (d), 124.06 (d), 128.94 (d), 149.13 (s), and 163.24 (s); MS m/z 207 (M^+). HRMS. Found: m/z 207.0707. Calcd for $C_{11}H_{13}ONS$: M, 207.0719.

4-Ethyl-3-phenyl-1,3-oxazolidine-2-thione (4b): Isolated and purified in a similar manner as above. Bp 84—85 °C/0.01 mmHg; IR 1180 cm^{-1} (C=S); ^1H NMR ($CDCl_3$) δ=0.79 (3H, t, J=7.4 Hz), 1.40—1.70 (2H, m), 4.17—4.45 (2H, m), 4.57—4.71 (1H, m), and 7.20—7.54 (5H, m); ^{13}C NMR ($CDCl_3$) δ=8.14 (q), 24.85 (t), 63.48 (d), 71.19 (t), 126.68 (d), 128.03 (d), 129.19 (d), 137.11 (s), and 187.54 (s); MS m/z 207 (M^+). HRMS. Found: m/z 207.0720. Calcd for $C_{11}H_{13}ONS$: M, 207.0719.

4-Phenyl-2-phenylimino-1,3-oxathiolane-2-imine (3c): Mp 85—86 °C; IR (KBr) 1680 cm^{-1} (C=N); ^1H NMR ($CDCl_3$) δ=4.40 (1H, dd, J=7.8 and 8.8 Hz), 4.71 (1H, dd, J=6.3 and 8.8 Hz), 4.97 (1H, t, J=6.8 Hz), and 6.70—7.35 (10H, m); ^{13}C NMR ($CDCl_3$) δ=52.08 (d), 75.55 (t), 121.17 (d), 124.25 (d), 127.36 (d), 128.64 (d), 129.00 (d), 136.38 (s), and 148.88 (s); MS m/z 255 (M^+). HRMS. Found: m/z 255.0708. Calcd for $C_{15}H_{13}ONS$: M, 255.0719.

3,4-Diphenyl-1,3-oxazolidine-2-thione (4c): Mp 106—107 °C; IR (KBr) 1180 cm^{-1} (C=S); ^1H NMR ($CDCl_3$) δ=4.51 (1H, dd, J=6.8 and 9.0 Hz), 5.00 (1H, t, J=9.0 Hz), 5.41 (1H, dd, J=6.8 and 9.0 Hz), and 7.07—7.30 (5H, m); ^{13}C NMR ($CDCl_3$) δ=67.04 (d), 74.12 (t), 126.26 (d), 126.99 (d), 128.88 (d), 129.09 (d), 136.75 (s), 137.36 (s), and 187.57 (s); MS m/z 255 (M^+). HRMS. Found: m/z 255.0723. Calcd for $C_{15}H_{13}ONS$: M, 255.0719.

4-Ethyl-2-Methylimino-1,3-oxathiolane (3d): Bp 78 °C/2 mmHg; IR 1650 cm^{-1} (C=N); ^1H NMR ($CDCl_3$) δ=1.05 (3H, t, J=7.5 Hz), 1.62—1.90 (2H, m), 3.05 (3H, s), 3.51—3.78 (1H, m), 3.89—4.20 (1H, m), and 4.40 (1H, dd, J=9.5 and 6.8 Hz); ^{13}C NMR ($CDCl_3$) δ=12.08 (q), 27.08 (t), 50.19 (d), 65.59 (q), 73.09 (t), and 162.67 (s); MS m/z 145 (M^+); HRMS. Found: m/z 145.0558. Calcd for $C_6H_{11}ONS$: M, 145.0562.

5-Ethyl-3-methyl-1,3-oxazolidin-2-one (5d): Bp 70 °C/2 mmHg; IR 1750 cm^{-1} (C=O); ^1H NMR ($CDCl_3$) δ=0.99 (3H, t, J=7.3 Hz), 1.50—1.88 (2H, m), 2.90 (3H, s), 3.16 (1H, dd, J=7.1 and 8.5 Hz), 3.61 (1H, t, J=8.5 Hz), and 4.27—4.51 (1H, m); ^{13}C NMR ($CDCl_3$) δ=8.64 (q), 27.82 (t), 30.83 (q), 51.69 (t), 74.28 (d), and 158.22 (s); MS m/z 129 (M^+).HRMS. Found: m/z 129.0804. Calcd for $C_6H_{11}O_2N$: M, 129.0790.

Reaction of Methyloxirane with Me_3SnI. The mixture of Me_3SnI (10 mmol) and methyloxirane (4 ml) was stirred for 1 h at room temperature under dry nitrogen. The excess oxirane was removed in vacuo, and **7** was isolated by distillation (bp 53 °C/0.1 mmHg; 2.13 *g*, 61%). ^1H NMR ($CDCl_3$) δ=0.47 (9H, s), 1.27 (3H, d, J=6.0 Hz), 3.18 (2H, d, J=5.3 Hz), 3.60—3.98 (1H, m); ^{13}C NMR ($CDCl_3$) δ=−2.44 (q), 21.22 (q), 51.59 (t), 69.21 (d).

Transformation of 3b to 5b (=2b). **3b** (1 mmol) was added to a solution of $AlCl_3$ (0.1 mmol) and ethyloxirane (5 mmol), and the mixture was stirred at 40 °C under dry nitrogen (0.3 h). The formation and the yield of **5b** (86%) was determined by GLC. **5b** (292 mg, 77%) was isolated by silica gel column treatment (eluted by benzene). The spectrum data of **5b** were the same as those of **2b**.

This study was financially supported by a Grant-in-Aid for Scientific Research No. 02650609 from the Ministry of Education, Science and Culture, and Nagase Science and Technology Foundation.

References

1) C. H. Behrens and K. B. Sharpless, *Aldrichimica Acta,* **16**, 67 (1983).

2) A. S. Rao, S. K. Paknikar, and J. G. Kirtane, *Tetrahedron,* **39**, 2323 (1983).

3) J. G. Smith, *Synthesis,* **1984**, 629.

4) H. Ulrich, "Cycloaddition Reaction of Heterocumulenes," Academic Press, New York (1967).

5) M. E. Dyen and D. Swern, *Chem. Rev.,* **67**, 197 (1967).

6) S. Ozaki, *Chem. Rev.,* **72**, 457 (1972).

7) I. Shibata, A. Baba, H. Iwasaki, and H. Matsuda, *J. Org.*

Chem., **51**, 2177 (1986).
8) A. Baba, I. Shibata, and H. Matsuda, *Synthesis*, **1985**, 1144.
9) J. E. Herweh, T. A. Foglia, and D. J. Swern, *J. Org. Chem.*, **33**, 4031 (1968).
10) D. Braun and J. Weinert, *Ann. Chem.*, **1979**, 200.
11) M. Fujiwara, A. Baba, and H. Matsuda, *J. Heterocycl. Chem.*, **25**, 1351 (1988).
12) D. W. Allen, D. J. Derbyshire, J. S. Brooks, and P J. Smith, *J. Organomet. Chem.*, **251**, 45 (1983).
13) D. W. Allen, D. J. Derbyshire, and I. W. Nowell, *J. Organomet. Chem.*, **260**, 263 (1984).
14) O. A. Reutov, V. S. Petrosyan, N. S. Yashina, and E. I. Gefel, *J. Organomet. Chem.*, **341**, C31 (1988).
15) M. Nardelli, C. Pelizzi, and G. Pelizzi, *J. Organomet. Chem.*, **112**, 263 (1976).
16) A. Baba, H. Kashiwagi, and H. Matsuda, *Organometallics*, **6**, 137 (1987).
17) A. K. Sawyer, "Organotin Compounds," Marcel Dekker, New York (1971), Vol. 1, p. 81.
18) T. F. Bolles and R. S. Drago, *J. Am. Chem. Soc.*, **88**, 5730 (1966).
19) A. Baba, H. Meishou, and H. Matsuda, *Makromol. Chem., Rapid Commun.*, **5**, 655 (1984).
20) S. Sakai, Y. Asai, Y. Kiyohara, K. Itoh, and Y. Ishii, *Organomet. Chem. Synth.*, **1**, 45 (1970).
21) S. Sakai, Y. Kobayashi, and Y. Ishii, *Chem. Commun.*, **1970**, 235.
22) S. Sakai, Y. Fujimura, and Y. Ishii, *J. Organomet. Chem.*, **50**, 113 (1973).
23) S. Sakai, Y. Kiyohara, K. Itoh, and Y. Ishii, *J. Org. Chem.*, **35**, 2347 (1970).
24) S. Sakai, H. Miini, and Y. Ishii, *J. Organomet. Chem.*, **72**, 103 (1974).
25) Ricci reported the selective α-cleavage of monosubstituted oxiranes by Me_3SnI to give the corresponding tin β-iodoalkoxides. (M. Piorenza, A. Ricci, M. T. Daniele, *Synthesis*, **1983**, 640.) However, our attempt to effect an α-cleavage cycloaddition using this iodoalkoxide was unsuccessful.
26) M. Fujiwara, A. Baba, and H. Matsuda, *Bull. Chem. Soc. Jpn.*, **63**, 1069 (1990).
27) K. Gulbins and K. Hamann, *Angew. Chem.*, **79**, 705 (1958).
28) K. Gulbins, G. Benzing, K. Maysenholden, and K. Hamann, *Chem. Ber.*, **93**, 1975 (1960).
29) G. P. Seperanza and W. J. Peppel, *J. Org. Chem.*, **23**, 1922 (1958).
30) J. E. Herweh, T. A. Foglia, and D. Swern, *J. Org. Chem.*, **33**, 4029 (1968).
31) Y. Farhangi and D. P. Graddon, *J. Organomet. Chem.*, **87**, 67 (1975).
32) A. K. Sawyer, "Organotin Compounds," Marcel Dekker: New York (1971), Vol. 1, p. 125.
33) R. Hulme, *J. Chem. Soc.*, **1963**, 1524.
34) I. R. Beattie and G. P. McQuillan, *J. Chem. Soc.*, **1963**, 1519.
35) L. A. Aslanov, W. M. Attiya, V. M. Ionov, A. B. Permin, and V. S. Petrosyan, *J. Struct. Chem. (Engl. Transl.)*, **18**, 884 (1977).
36) A. Baba, I. Shibata, M. Fujiwara, and H. Matsuda, *Tetrahedron Lett.*, **26**, 5167 (1985).
37) A. Baba, H. Kishiki, I. Shibata, and H. Matsuda, *Organometallics*, **4**, 1329 (1985).
38) A. Baba, I. Shibata, H. Kashiwagi, and H. Matsuda, *Bull. Chem. Soc. Jpn.*, **59**, 341 (1986).
39) I. Shibata, A. Baba, and H. Matsuda, *Bull. Chem. Soc. Jpn.*, **59**, 4000 (1986).
40) J. J. Monagle, *J. Org. Chem.*, **27**, 3851 (1962).
41) C. Palomo and R. Mestres, *Synthesis*, **1981**, 373.
42) W. J. Jones, D. P. Evans, and D. C. Griffith, *J. Chem. Soc.*, **1935**, 39.
43) S. Matsuda and H. Matsuda, *Bull. Chem. Soc. Jpn.*, **35**, 208 (1962).
44) K. Gulbims and K. Hamann, *Chem. Ber.*, **94**, 3287 (1961).

Benzo[*b*]cyclohepta[*e*][1,4]thiazines and Their Diazine Analogues. III.[1] π-Electronic Structures of 5*H*, 11*H*$^+$-Cyclohepta[*b*]quinoxalinium Ions and Their O- and S-Analogues

Teruo KURIHARA,* Kimio SHINDO,* Sumio ISHIKAWA, and Tetsuo NOZOE†
Department of Chemistry, Faculty of Science, Josai University,
Sakado, Saitama 350-02
† Tokyo Research Laboratories, Kao Corporation, 1-3 Bunka,
Sumidaku, Tokyo 131
(Received March 20, 1991)

π-Electronic structures of 5*H*,11*H*$^+$-cyclohepta[*b*]quinoxalinium ions and their O- and S-analogues were elucidated by means of ^{1}H and ^{13}C NMR spectra, electronic spectra, and theoretical calculations. Consequently, it was shown that these compounds had very stable aromatic characters with positive resonance energies and that the 6π-tropylium-6π-benzonoid form plays an important role for the π-conjugation structure.

On of the authors (T.N.) and his co-workers[2] reported more than thirty years ago that the reaction of 2-chloro- and 2-methoxytropone (**1a,b**) with *o*-phenylenediamine (**2a**) gave 5*H*-cyclohepta[*b*]quinoxaline (**3a**), which they named "benzo[*b*]tropazine".

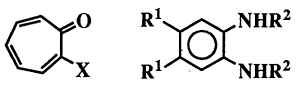

1 a X=Cl, b X=OMe

2	R^1	R^2
a	H	H
b	Me	H
c	H	Me

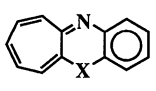

3 a X=NH, b X=NMe, c X=O, d X=S

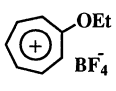

4

In 1971, Fukunaga[3a] reported that the reaction of ethoxytropylium tetrafluoroborate (**4**) with **2a** and its dimethyl derivative (**2b**) gave greenish-black crystals of **5a** and **5b**, which upon basification produced free compounds **6a** and **6b** that reverted to **5a,b** quantitatively

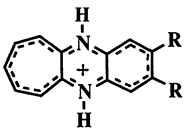

5 a R=H, b R=Me

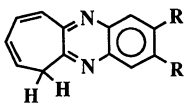

6 a R=H, b R=Me

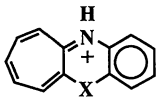

7 a X=NH, b X=NMe, c X=O, d X=S

upon acidification. He proposed that the structure of **6** was the quinoxaline form (namely an isomer of **3a**), and that the salt **5** existed as a resonance-stabilized, peripheral anti-Hückel 16π-electron system based on the evidence of detailed NMR studies of **3a** and its related compounds.[3b] He also suspected that our colorless compound[2] reported as "purified" benzotropazine should have been a dimer of his 6*H*-cyclohepta[*b*]quinoxaline **6a**, but he did not study the structure of the dimer any further. On the other hand, according to our study, benzo[*b*]cyclohept[*e*][1,4]oxazine **3c** and its S-analogue **3d**[5,6] gave the red-colored cations **7c** and **7d**, respectively, under acidic conditions. Later, we also confirmed[1] that compound **3a** existed as a tautomeric form **6a**, and on acidification **6a** was converted into a dark-green salt **7a** which showed intense long-wavelength absorption bands at 500—800 nm; no such bands were observed in the spectra of **7c** and **7d** in acid.

From the standpoint of synthetic and theoretical interest, we recently started the re-investigation of the electronic structures and reactivities of various troponoids and azulenoid compounds. In a previous paper, we reported[7] that the fundamental skeleton of the tropones possessing a unique heptagonal structure may be predicted to be aromatic with positive resonance energies[8] conforming to Gimarc's topological charge stabilization rule (TCS rule).[9] We also found that naturally occurring tropolones nicely fit the theory that conformity to the TCS rule provides a stable molecular system.

In order to clarify the π-electronic structures of the neutral species **3a**—**d** and their cationic species **7a**—**d**, we now wish to describe here a detailed study of their NMR spectra, electronic spectra, and theoretical considerations. Resonance energies, circuits resonance energies, and ring currents of these compounds were also estimated by the use of Aihara's method.[8] The HMO theory is assumed to be in its simplest form. Streitwieser evaluated the heteroatom parameters for the amine nitrogen, the imine nitrogen, the ether oxygen, and the ketone oxygen.[10] In this paper, we adopted these values with some other heteroatom parameters.[11,12]

Results and Discussion

NMR Spectra. The ^{1}H NMR spectra of **3b** and its O- and S-analogues were compared with the spectra of some related compounds such as aromatic amines **2a,c** and **8a,b**, 1*H*-2,3-dihydrocycloheptapyrazines **9a,b** and their thiazine analogue **9c**, and their cations **10a**—**c**,[13] *N*-methylated cations **11a,b**[13] and **12a**—**c**,[1,6,14] quinoxaline (**13**) and phenazine (**14**).

The average chemical shift (δ_{av}) values of protons on the seven-membered and benzene rings and the differences ($\Delta\delta_{av}$) of the average chemical shift values be-

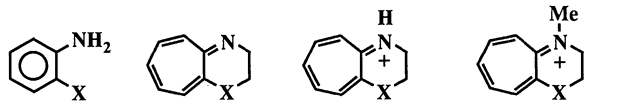

8a X=OH **b** X=SH

9a X=NH **b** X=NMe **c** X=S

10a X=NH **b** X=NMe **c** X=S

11a X=NMe **b** X=S

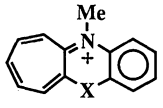

12a X=NMe **b** X=O **c** X=S

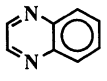

13

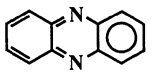

14

tween the neutral species and the corresponding cationic species are listed in Table 1.

Noting the differences of the average chemical shifts of the rings between solvents, the signals in CD_3CN shifted slightly to a lower field compared with those in $CDCl_3$, but this difference was smaller than 0.1 ppm. Under acidic conditions, the chemical shifts moved with the acid concentration, but this change in 20% CF_3COOD nearly agreed with those in CF_3COOD, and its difference as compared with that of the BF_4^- salt in CD_3CN was smaller than 0.1 ppm, suggesting that there were no problems in discussing $\Delta\delta_{av}$.[15]

In order to clarify the relationship between the NMR chemical shifts and π-electron distributions, the π-electron densities of **3a**—**d** and the related compounds were calculated by the MNDO method.[16] There is a quantitative relationship between NMR chemical shifts and electron distributions in aromatic molecules, as reported by many authors.[17] The suggested equations for protons (1) and for carbons (2) seem to have gathered the most support, where the $\Delta\delta$ values are the chemical shift changes and ρ_π is the change in charge.

$$\Delta\delta_H = 10.7\,\rho_\pi \quad (1)$$

$$\Delta\delta_C = 160\,\rho_\pi \quad (2)$$

The $\Delta\delta_{av}$ values of aromatic diamines **2a**—**c** were shown to be larger than those of **8a,b**. The relative values were related to the basicity of these amines.[18] In the NMR spectra of 1*H*-2,3-dihydrocyclohepta[*b*]-pyrazines (**9a,b**)[13] and their S-analogue **9c**,[13] the δ_{av} values of the protons on the seven-membered ring became slightly smaller compared with those of the benzene ring of the aromatic amines **2a**—**c** and **8a,b**. The $\Delta\delta_{av}$ value of **9c** was slightly larger than those of diamines **9a,b** which have higher basicity. The $\Delta\delta_{av}$ values of *N,N'*-dimethyl (**11a**)[13] and *N*-methyl cation (**11b**)[13] are nearly equal to those of the cationic species **10a** and **10c**. The π-electron densities of compounds **9**—**11** are shown in Fig. 1.

The π-electron distributions of the troponeimine part of **9** and **11** were similar to each other, whereas the π-electron densities on the nitrogen atom at position 1 of **10** were more negative than those of **9** and **11**. The sum of the π-electron densities of the seven-membered ring carbons of the cationic species were smaller than those of the neutral species. Though the δ_{av} values of the benzene ring of free compound **6a** were similar to those of quinoxaline **13** and phenazine **14**, these values were demonstrated to be shifted to a lower magnetic field compared with those of *N*-methyldiazine **3b** and its O-(**3c**) and S-analogues (**3d**). These results suggested that, as the π-conjugated system of **6a** differed from those of

Table 1. ^{1}H NMR of Cyclohepta[*b*]quinoxalines and Their O- and S-Analogues and Their Related Compounds

Compd	Protons	δ_{av}		$\Delta\delta_{av}$	Compd	Protons	δ_{av}		$\Delta\delta_{av}$
		Neutral (1)	Acidic (2)	(2)—(1)			Neutra (1)	Acidic (2)	(2)—(1)
2a	H_{3-6}	6.54[a]	7.28[c]	0.74	**3c**	H_{1-4}	6.61[a]	6.80[a,s]	0.10
2b	$H_{3,6}$	6.37[a]	7.23[c]	0.86		H_{6-10}	5.83	7.14	1.31
2c	$H_{3,6}$	6.70[b]	7.75[d]	1.05	**12b**	H_{1-4}	6.61[g]	6.97[a,s]	0.36
8a	H_{3-6}	6.60[e]	7.15[f]	0.55		H_{6-10}	5.83[g]	7.36	1.53
8b	H_{3-6}	6.90[a]	7.40[c]	0.50	**3d**	H_{1-4}	6.96[a]	6.95[a,s]	−0.01
13	$H_{2,3}$	8.86[a]	9.31[c]	0.45		H_{6-10}	6.22	7.13	0.91
	H_{5-8}	7.97	8.31	0.34	**12c**	H_{1-4}	6.96[g]	7.31	0.35
14	H_{1-4}	8.06[e]	8.45[f]	0.39		H_{6-10}	6.22[g]	7.68	1.46
9a	H_{5-9}	6.32[b]	7.33[c]	1.01	**6a**	H_{1-4}	7.96[b]		
9b	H_{5-9}	6.35[b]	7.32[c]	0.97		H_{7-10}	6.62		
11a	H_{5-9}	6.35[g]	7.23[a]	0.88	**7a**	H_{1-4}		6.32	
9c	H_{5-9}	6.45[b]	7.61[c]	1.16		H_{6-10}		6.13	
10c	H_{5-9}	6.45[g]	7.55[a]	1.10	**6b**	H_{1-4}	7.36[b]		
3b	H_{1-4}	6.47[a]	6.57[a,s]	0.10		H_{7-10}	6.33		
	H_{6-10}	5.33	6.38	1.05	**5b**	H_{1-4}		5.94[a,s]	
12a	H_{1-4}	6.47[g]	6.81[a,s]	0.34		H_{6-10}		6.00	
	H_{6-10}	5.33[g]	6.71	1.38					

Solvent: a) CD_3CN. b) $CDCl_3$. c) CD_3CN+CF_3COOD. d) $CDCl_3$+CF_3COOD (6:1). e) CD_3CN+$CDCl_3$ (1:1). f) CD_3CN+$CDCl_3$+CF_3COOD (2:2:1). g) Value for the neutral species of the parent compounds. s) The BF_4^- or SO_3F^- salt.

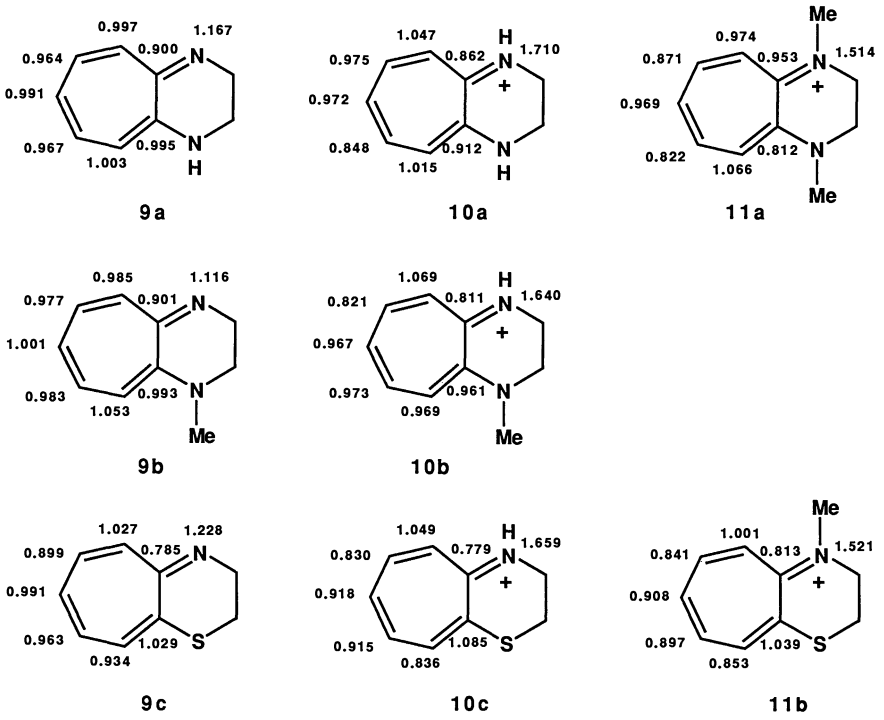

Fig. 1. π-Electron densities of **9**, **10**, and **11** by the MNDO method.

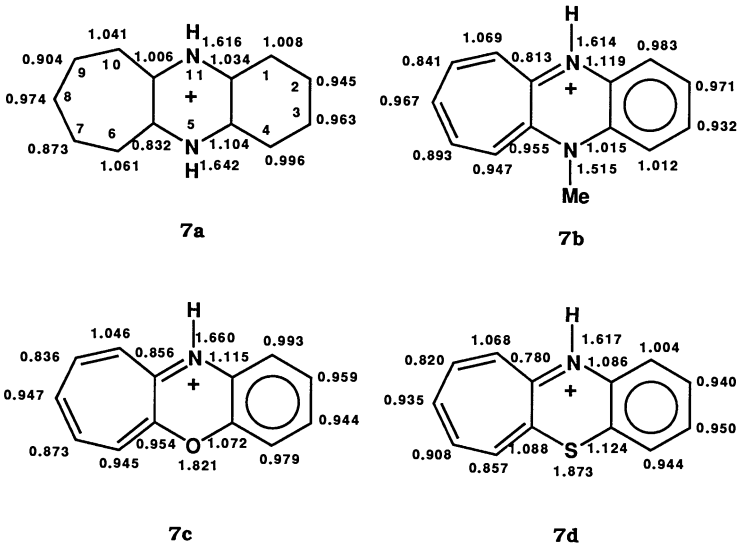

Fig. 2. π-Electron densities of **7** by the MNDO method.

3b—**d**, compound **6a** be removed from discussion of the π-electronic systems of **3a**—**d** and **7a**—**d**. The δ_{av} values of the protons on the benzene and seven-membered rings of $5H,11H^{+}$-cyclohepta[*b*]quinoxalinium ion (**7a**) appeared upfield by 0.5—0.6 and 1.0 ppm, respectively, compared with those of the O-(**7c**) and S-analogues (**7d**). The latter values were approximately proportional to differences in their π-electron density (Fig. 2). Although it was not possible to interpret their chemical shift changes in terms of the change in charge, the π-electron density of **7a** was larger than those of **7c** and **7d**. The $\Delta\delta_{av}$ between **7a** and **7c** or **7d** were calculated to be 0.36 ppm from Eq. 1. The δ_{av} values of **3b** and **7b** were smaller than those of **3c,d** and **7c,d**.

The $\Delta\delta_{av}$ values of the protons on the benzene ring of **3b**—**d** were much smaller than those of the aromatic amines **2a**—**c**, whereas the $\Delta\delta_{av}$ values of the seven-membered protons of **3b**—**d** were larger than those of **2a**—**c** and were similar to those of dihydropyrazines **9a,b**. In the NMR spectra of **3b**—**d**, the signals of the protons

on the benzene ring shifted slightly to a lower field, whereas the signals of the seven-membered ring protons shifted largely to a lower field under acidic conditions. The π-electron densities of **6a,3**, and **12** are shown in Fig. 3. The correlation coefficients between the calculated $\Delta\delta_H$ values and the observed $\Delta\delta_{av}$ values of the seven-membered rings in the N-, O-, and S-analogues were 0.92, 0.99, and 0.97, respectively.

The δ_{av} and $\Delta\delta_{av}$ values of the ^{13}C chemical shifts of **3b—d**, **7a—d**, and **12a** are listed in Table 2, where the $\Delta\delta_{av}$

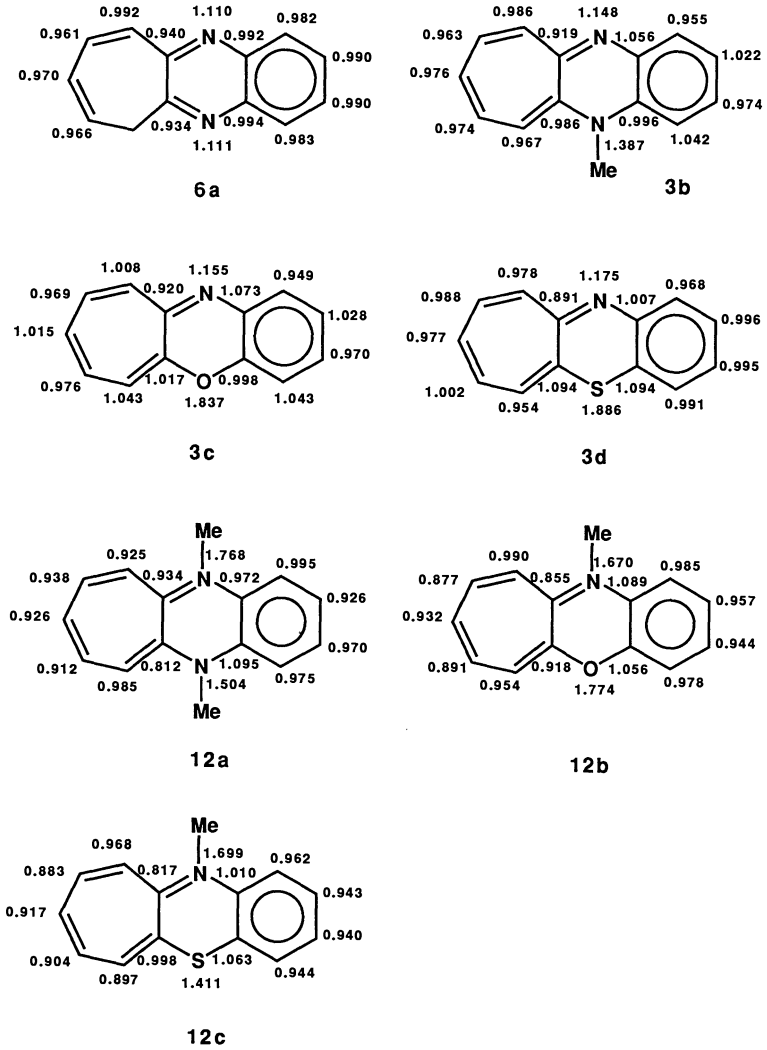

Fig. 3. π-Electron densities of **6**, **3**, and **12** by the MNDO method.

Table 2. ^{13}C NMR of Cyclohepta[*b*]quinoxalines and Their O- and S-Analogues (100 MHz in CD_3CN)

	δ_{av} Benzene ring (1)	δ_{av} Seven-membered ring (2)	$\Delta\delta_{av}$ (2)—(1)	$\Delta\delta_C^{calcd}$
7a	125.8	141.5	15.7	8.4
7b	126.7	141.6	14.9	12.6
12a	126.4	141.9	15.5	11.2
7c	127.8	144.5	16.7	14.1
7d	127.5	144.7	17.2	13.8
3b	129.1	136.8	7.7	6.6
3c	130.0	138.8	8.8	2.8
3d	129.0	138.8	9.8	4.2

$\Delta\delta_C^{calcd}$ values were calculated from Eq. 2.

values were the differences between the δ_{av} of the seven-membered and benzene ring carbons. The $\Delta\delta_{av}$ of **7a,b** and **12a** were similar in magnitude to their O- and S-analogues. The cationic species had larger $\Delta\delta_{av}$ values than the neutral species.

From the above-cited NMR spectral data, the heteroatoms of **3b—d** and related compounds were closely related to the seven-membered ring rather than the benzene ring. The cationic species had the smallest values for π-electron densities compared with their neutral species. The change in charge seemed to be one of the reasons for its lower field shifts.

Resonance Energies and Circuit Currents. Resonance energies, circuit resonance energies, and circuit currents of **3**, **7**, and **12** were calculated by Aihara's graph theory of aromaticity.[8] Geometrically unidentical π-electron circuits are shown and numbered in Fig. 4. The results are listed in Table 3. Compounds **3**, **7**, and **12** could be regarded as aromatics with positive resonance energies. The cationic species possessed larger resonance energies than the neutral species. From the calculated circuit resonance energies of each ring, the circuit resonance energies of r_1 and r_3 showed positive values, while the values of r_2, r_4, r_5, and r_6 were very small or negative. Consequently, compounds **3a,b** and **7a,b** were stabilized as the 6π-tropylium-6π-benzenoid form similar to the O- and S-analogues, but not as a 16π-peripheral system as was suggested by Fukunaga.[3]

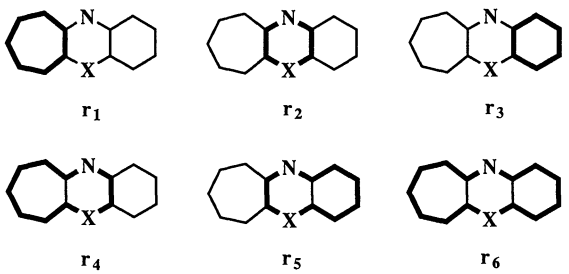

Fig. 4. Geometrically unidentical π-electron circuits.

The calculated circuit currents are also shown in units of I_0 in Table 3. The plus and minus signs in the Table indicate diatropism and paratropism, respectively. Large diatropism was predicted to arise from r_1 and r_3, while large paratropism was predicted to arise from r_4 and r_6. As for compound **3b**, the diatropism effect due to the 6π-tropylium structure (i.e., structure r_1: $0.997I_0$) and the 6π-benzenoid part (i.e., structure r_3: $0.881I_0$) was the main contributor to the magnetic effect, although a small contribution came from the diatropism effect of the heterocyclic part (i.e., structure r_2: $0.094I_0$, r_5: $0.175I_0$) and the paratropism effect due to the peripheral 16π-structure (i.e., structure r_6: $-0.155I_0$). Such a tendency was also found for the O- and S-analogues. Thus, theoretical considerations suggested that the 6π-tropylium-6π-benzenoid form played a crucial role in the stabilization of 5*H*,11*H*$^+$-cyclohepta[*b*]quinoxalinium ions and their O- and S-analogues, and the downfield shifts of the seven-membered ring protons were due to its large diatropism.

Electronic Spectra of 3 and 7. In the electronic spectra of **7a—d**, the bands in the visible region showed large red shifts with increased intensities compared with those of the corresponding neutral species **3a—d**, as mentioned previously.[1,4,6] Compounds **3b** and **3c** showed four electronic absorption bands in the long wavelength region (500—800 nm). It is interesting to note that the cationic species, **7a**, **7b**, and the free *N*-methyl compound **3b**, had almost the same deep green color and very similar absorption bands. For example, **7b** showed long wavelength absorption bands at 564, 616, 670, and 752 nm (log ε 3.01, 2.91, 2.83, and 2.34). On the other hand, compounds without a benzene ring, such as **9a—c**, **10a—c**, and **11a,b**, did not show these absorption bands in the same region.[13] These absorption bands were thus closely related to the π-electronic structure of the benzene ring.

We have also calculated the electronic transition of these compounds by the CNDO/S-CI method.[19] The coefficient distribution of the three highest occupied and the three lowest unoccupied π orbitals are shown in Fig.

Table 3. Resonance Energies, Circuit Resonance Energies, and Circuit Currents of Title Compounds

	Resonance energies and circuit resonance energies (in β units)							Circuit currents (in benzene, I_0 units)					
	RE	r_1	r_2	r_3	r_4	r_5	r_6	r_1	r_2	r_3	r_4	r_5	r_6
3c	0.310	0.118	0.011	0.198	−0.019	0.005	−0.015	1.037	0.051	0.893	−0.488	0.084	−0.802
3d	0.256	0.113	0.019	0.196	−0.014	0.009	−0.020	0.993	0.085	0.880	−0.610	0.157	−1.043
3a	0.299	0.116	0.017	0.197	−0.024	0.008	−0.020	1.023	0.078	0.886	−0.610	0.136	−1.023
3b	0.291	0.113	0.021	0.196	−0.026	0.010	−0.022	0.997	0.094	0.881	−0.676	0.175	−1.155
7c	0.446	0.175	−0.002	0.216	−0.006	−0.001	−0.004	1.544	−0.007	0.970	−0.151	−0.018	−0.230
12b	0.420	0.173	−0.001	0.215	−0.007	−0.001	−0.005	1.527	−0.005	0.967	−0.168	−0.014	−0.258
7d	0.426	0.168	0.001	0.213	−0.008	−0.000	−0.006	1.478	0.004	0.958	−0.201	−0.003	−0.313
12c	0.420	0.166	0.002	0.212	−0.009	0.000	−0.007	1.463	0.008	0.954	−0.222	0.004	−0.349
7a	0.446	0.175	−0.002	0.216	−0.006	−0.001	−0.004	1.544	−0.007	0.970	−0.151	−0.018	−0.230
7b	0.421	0.168	0.001	0.213	−0.009	−0.000	−0.007	1.476	0.003	0.957	−0.221	−0.004	−0.343
12b	0.434	0.172	−0.000	0.214	−0.007	−0.001	−0.006	1.511	−0.002	0.963	−0.187	−0.010	−0.289

RE: Resonance energy (in β units).

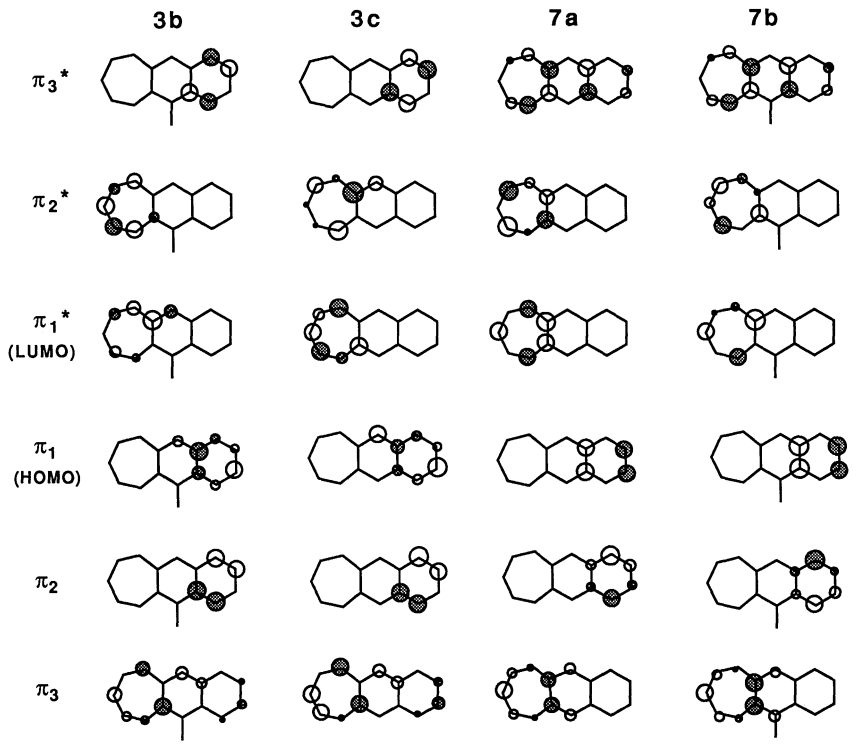

Fig. 5. Topology of the frontier orbitals of **3b**, **c** and **7a**, **b** (CNDO/S-CI calculations). Sizes of circles are roughly proportional to the coefficient values.

Table 4. Electronic Transitions (eV) in the Long Wavelength Region of Compounds **3b**, **7a**, and **7b**

3b			7a			7b		
E[a)]	f	Nature	E[a)]	f	Nature	E[a)]	f	Nature
2.36	0.001	$\pi_1 \rightarrow \pi_3^*$	2.02	0.004	$\pi_1 \rightarrow \pi_2^*$	2.05	0.037	$\pi_1 \rightarrow \pi_1^*$
2.58	0.298	$\pi_1 \rightarrow \pi_1^*$	2.12	0.050	$\pi_1 \rightarrow \pi_1^*$	2.26	0.006	$\pi_1 \rightarrow \pi_2^*$
3.09	0.007	$\pi_1 \rightarrow \pi_2^*$	2.36	0.015	$\pi_2 \rightarrow \pi_2^*$	2.35	0.009	$\pi_2 \rightarrow \pi_1^*$
3.32	0.045	$\pi_3 \rightarrow \pi_2^*$	2.42	0.000	$\pi_2 \rightarrow \pi_1^*$	2.44	0.000	$\pi_1 \rightarrow \pi_5^*$
3.41	0.029	$\pi_2 \rightarrow \pi_1^*$	2.51	0.011	$\pi_2 \rightarrow \pi_2^*$	2.54	0.004	$\pi_3 \rightarrow \pi_2^*$
3.53	0.056	$\pi_1 \rightarrow \pi_4^*$	2.65	0.001	$\pi_3 \rightarrow \pi_2^*$	2.55	0.000	$\pi_2 \rightarrow \pi_2^*$
3.59	0.036	$\pi_4 \rightarrow \pi_1^*$	2.70	0.009	$\pi_3 \rightarrow \pi_1^*$	2.65	0.022	$\pi_3 \rightarrow \pi_1^*$
3.85	0.197	$\pi_1 \rightarrow \pi_5^*$	3.49	0.000	$\pi_1 \rightarrow \pi_3^*$	3.49	0.004	$\pi_1 \rightarrow \pi_4^*$
4.05	0.193	$\pi_2 \rightarrow \pi_2^*$	3.87	0.067	$\pi_2 \rightarrow \pi_6^*$	3.82	1.170	$\pi_4 \rightarrow \pi_2^*$

a) E (eV) is the energy of the transitions; f (dimensionless) is the oscillator strength.

5. They were similar to each other. Therefore, the calculated electronic transitions were predicted to have very similar absorption bands. The electronic transitions calculated for **3b**, **7a**, and **7b** are collected in Table 4. The free *N*-methyl compound **3d** showed two $\pi \rightarrow \pi^*$ electronic transitions at 2.58 and 3.09 eV, corresponding to $\pi_1 \rightarrow \pi_1^*$ and $\pi_1 \rightarrow \pi_2^*$, whereas its cation **7b** showed corresponding transitions at 2.05 and 2.26 eV, respectively.

From the coefficient distribution as shown in Fig. 5, these bands could be attributed to an intramolecular charge-transfer transition from the benzene ring part to the seven-membered ring part. CNDO/S calculations satisfactorily reproduced the red shift observed in the long wavelength region of the neutral spcies and their cationic species **7a**—**d**.

Molecular Geometries. The geometry optimizations of **3**, **6**, **7**, and **9**—**12** were carried out with optimization of all geometrical parameters with no assumptions whatsoever. In **3b**—**d** and related compounds, the C–C bonds of the benzene ring were 1.40—1.43 Å, the formular double bonds of the seven-membered ring were 1.35—1.39 Å, the C–C single bonds were 1.40—1.47 Å, except for the C-5a–C-10a bonds which were 1.45—1.49 Å. The C-10a–N-11 bonds were 1.31—1.37 Å, the C-11a–N-11 bonds were 1.40—1.44 Å. In the oxazines,

the C–O bonds were 1.35—1.38 Å.

In the thiazines, the C–S bonds were 1.68—1.70 Å. CNDO/S calculations adopted these optimized values.

Concluding Remarks

Fukunaga[3b] compared the NMR and electronic spectra of compounds **6a—b**, **15**, and **16** with the reference compounds **5a,b**.

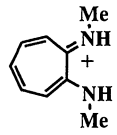

15

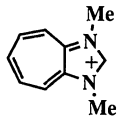

16

The ^{1}H NMR spectra of **5a—b** indicated large upfield shifts of the ring-proton signals compared with those of the benzene ring of **6** and the seven-membered ring protons of **15** by 1.2—1.9 ppm. Such a large upfield shift arose from the paramagnetic ring current effect. He believed that **5a,b** existed as a resonance-stabilized, peripheral 4nπ-electron system. We assumed three models (I—III) for the π-electronic structures of **7a—d**.

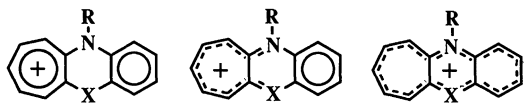

I II III

From the above-cited spectral data and theoretical calculations, we propose that the heteroatoms of **7a—d** are closely related to the seven-membered ring rather than the benzene ring. The positive charge is delocalized over the seven-membered ring (Type I). This suggests that contributions of the 10π-2-aminotroponiminium structure (Type II) and 16π-peripheral conjugation structure (Type III) are negligible. The electronic structures of **7a—d** can not be elucidated solely by II, because the electronic spectra of **10** and **11** do not show absorption bands in the long wavelength region. In view of these absorption bands that can be attributed to an intramolecular charge-transfer transition, the π-conjugation system of 5*H*,11*H*$^+$-cyclohepta[*b*]quinoxalinium ions and their O- and S-analogues are shown by the contribution of I. Therefore, we conclude that the title compounds are stabilized as a 6π-tropylium–6π-benzenoid system (I) and the appearance of their color is due to the intramolecular charge-transfer transition.

Experimental

General. NMR spectra were re-measured as CD_3CN and $CDCl_3$ solutions on JEOL JNM PS100 (100 MHz), GX 270 (270 MHz) and GX 400 (400 MHz) spectrometers with TMS as the internal standard. The UV-vis spectra were recorded with Shimadzu UV-202 or Hitachi 557 spectrometers.

Materials. Aromatic amines were purchased from Wako Pure Chemicals Ind. Benzo[*b*]cyclohepta[*e*][1,4]thiazines and the related compounds were prepared according to the reported methods.[1,4,6,13]

***o*-Phenylenediamine (2a):** ^{1}H NMR (CD_3CN) δ=6.54 (4H, s, ar-H) and 3.60 (4H, br, NH_2); (20% CF_3COOD–CD_3CN) δ=7.28 (4H, ar-H).

4,5-Dimethyl-*o*-phenylenediamine (2b): ^{1}H NMR (CD_3CN) δ=2.04 (6H, s, CH_3), 3.40 (4H, br, NH_2), and 6.37 (2H, s, ar-H); (20% CF_3COOD–CD_3CN) δ=2.27 (6H, s, CH_3) and 7.23 (2H, s, ar-H).

***N,N'*-Dimethyl-*o*-phenylenediamine (2c):** ^{1}H NMR ($CDCl_3$) δ=2.82 (6H, s, CH_3), 3.15 (2H, br, NH), and 6.70 (4H, s, ar-H); (10% CF_3COOD-$CDCl_3$) δ=3.40 (6H, s, CH_3) and 7.75 (4H, s, ar-H).

5-Methyl-5*H*-cyclohepta[*b*]quinoxaline (3b): ^{1}H NMR (400 MHz) (CD_3CN) δ=2.64 (3H, s, CH_3), 4.46 (1H, d, *J*=10 Hz, H-6), 5.21 (1H, t, *J*=10.7 Hz, H-8), 5.39 (1H, d, *J*=12 Hz, H-10), 5.80 (2H, m, H-7,9), 6.23 (1H, d, *J*=8 Hz, H-4), 6.47 (1H, d, *J*=8 Hz, H-1), 6.52 (1H, t, *J*=8 Hz, H-2), and 6.67 (1H, t, *J*=8 Hz, H-3); ^{13}C NMR (100 MHz) (CD_3CN) δ=34.8 (CH_3), 109.8 (C-6), 114.0 (C-4), 123.6 (C-8), 123.8 (C-2), 126.6 (C-1), 127.9 (C-3), 134.0 (C-10), 138.0 (C-7 or 9), 138.1 (C-9 or 7), 140.8 (C-4a), 141.3 (C-11a), 151.3 (C-5a), and 163.8 (C-10a).

Benzo[*b*]cyclohept[*e*][1,4]oxazine (3c): ^{1}H NMR (270 MHz) ($CDCl_3$) δ=5.37 (1H, d, *J*=9.5 Hz, H-6), 5.75 (1H, dd, *J*=10.5 and 8 Hz, H-8), 5.94 (1H, t, *J*=10.5 and 9.5 Hz, H-7), 5.97 (1H, d, *J*=12 Hz, H-10), 6.11 (1H, dd, *J*=12 and 8 Hz, H-9), 6.35 (1H, d, *J*=7.9 Hz, H-4), and 6.69 (3H, m, H-1,2,3); ^{13}C NMR (67.8 MHz) (CD_3CN) δ=114.1 (C-6), 115.1 (C-4), 125.5 (C-1), 126.6 (C-2), 128.2 (C-3), 129.2 (C-8), 134.7 (C-7 or 9), 136.8 (C-4a), 137.0 (C-10), 137.3 (C-9 or 7), 147.9 (C-11a), 158.1 (C-5a), and 161.2 (C-10a).

Benzo[*b*]cyclohept[*e*][1,4]thiazine (3d): ^{1}H NMR (400 MHz) (CD_3CN) δ=6.10 (1H, d, *J*=8 Hz, H-6), 6.13 (1H, d, *J*=12 Hz, H-10), 6.19 (1H, ddt, *J*=11, 7, and 1 Hz, H-8), 6.31 (1H, ddt, *J*=11, 8, and 1 Hz, H-7), 6.37 (1H, ddd, *J*=12, 7, and 1 Hz, H-9), 6.85 (1H, dd, *J*=7 and 1.5 Hz, H-4), 6.95 (1H, td, *J*=7 and 1.8 Hz, H-3), 7.00 (1H, dd, *J*=7 and 1.8 Hz, H-1), and 7.04 (1H, ddd, *J*=7 and 1.5 Hz, H-2); ^{13}C NMR (100 MHz) (CD_3CN) δ=126.6 (C-4), 127.6 (C-3), 128.2 (C-4a), 128.3 (C-1), 128.6 (C-2), 130.0 (C-10), 132.6 (C-8), 134.5 (C-6), 134.6 (C-11a), 134.7 (C-9), 135.3 (C-7), 144.4 (C-5a), and 160.3 (C-10a).

2,3-Dimethyl-5*H*,11*H*$^+$-cyclohepta[*b*]quinoxalinium Tetrafluoroborate (5b): ^{1}H NMR (270 MHz) (CD_3CN) δ=1.90 (6H, s, CH3), 5.55 (2H, d, *J*=11.0 Hz, H-10), 5.92 (1H, t, *J*=9.3 Hz, H-8), 5.94 (2H, s, H-1,4), and 6.50 (2H, dd, *J*=11.0 and 9.3 Hz, H-7,9).

2,3-Dimethyl-6*H*-cyclohepta[*b*]quinoxaline (6b): ^{1}H NMR (270 MHz) ($CDCl_3$) δ=2.48 (6H, s, CH3), 3.55 (2H, d, *J*=6.6 Hz, H-6,6), 6.06 (1H, dt, *J*=10.0 and 6.6 Hz, H-7), 6.25 (1H, dd, *J*=10.0 and 5.5 Hz, H-8), 6.77 (1H, dd, *J*=12.1 and 5.5 Hz, H-9), and 7.24 (1H, d, *J*=12.1 Hz, H-10).

5*H*,11*H*$^+$-Cyclohepta[*b*]quinoxalinium Tetrafluoroborate (7a): ^{1}H NMR (400 MHz) (CD_3CN) δ=5.65 (2H, d, *J*=11 Hz, H-6,11), 6.04 (1H, t, *J*=9.5 Hz, H-8), 6.11 (2H, m, H-1,4), 6.52 (2H, m, H-2,3), 6.60 (2H, dd, *J*=11 and 9.5 Hz, H-7,9), and 7.83 (2H, br, NH); ^{13}C NMR (100 MHz) (CD_3CN) δ=116.9 (C-1,4), 124.0 (C-6,10), 128.2 (C-2,3), 131.4 (C-8), 132.2 (C-4a,11a), 147.9 (C-7,9), and 157.7 (C-5a, 10a).

11*H*$^+$-5-Methylcyclohepta[*b*]quinoxalinium Tetrafluorobo-

rate (7b): ^{1}H NMR (400 MHz) (CD_3CN) δ=2.85 (3H, s, CH_3), 5.88 (1H, d, *J*=11 Hz, H-6 or 10), 5.93 (1H, d, *J*=11 Hz, H-10 or 6), 6.26 (1H, t, *J*=9.5 Hz, H-8), 6.39 (1H, dd, *J*=7.5 and 1.5 Hz, H-1 or 4), 6.43 (1H, d, *J*=8 Hz, H-4 or 1), 6.69 (1H, td, *J*=7.5 and 1.5 Hz, H-2 or 3), 6.77 (1H, td, *J*=7.5 and 1.5 Hz, H-3 or 2), 6.90 (1H, ddd, *J*=11, 9.5, and 1.5 Hz, H-7 or 9), 6.93 (1H, ddd, *J*=11, 9.5, and 1.5 Hz, H-9 or 7), and 8.48 (1H, br, NH); ^{13}C NMR (100 MHz) (CD_3CN) δ=37.0 (CH_3), 117.5 (C-1 or 4), 117.6 (C-4 or 1), 123.9 (C-6 or 10), 125.1 (C-10 or 6), 127.6 (C-2 or 3), 128.8 (C-3 or 2), 131.3 (C-8), 132.1 (C-4a), 136.7 (C-11a), 147.5 (C-7 or 9), 148.2 (C-9 or 7), 156.0 (C-5a), and 159.0 (C-10a).

11*H*$^+$-Benzo[*b*]cyclohept[*e*][1,4]oxazinium Tetrafluoroborate (7c): ^{1}H NMR (400 NHz) (CD_3CN) δ=6.67 (1H, dd, *J*=8 and 1.5 Hz, H-1 or 4), 6.70 (1H, dd, *J*=7.5 and 1.5 Hz, H-4 or 1), 6.85 (1H, d, *J*=11.5 Hz, H-6 or 10), 6.89 (1H, td, *J*=7.5 and 1.5 Hz, H-2 or 3), 6.92 (1H, dd, *J*=10.3 and 1 Hz, H-10 or 6), 6.95 (1H, td, *J*=8 and 1.5 Hz, H-3 or 2), 7.09 (1H, ddd, *J*=10.3, 9, and 1Hz, H-8), 7.34 (1H, td, *J*=10.3 and 1.5 Hz, H-7 or 9), 7.49 (1H, dd, *J*=11.5, 9, and 1 Hz, H-9), and 9.40 (1H, br, NH); ^{13}C NMR (100 MHz) (CD_3CN) δ=117.4 (C-1 or 4), 118.5 (C-4 or 1), 126.4 (C-11a), 128.0 (C-2 or 3), 129.8 (C-6 or 10), 130.0 (C-10 or 6), 131.1 (C-3 or 2), 138.2 (C-8), 145.1 (C-7 or 9), 145.6 (C-4a), 149.0 (C-9 or 7), 157.6 (C-10a), and 161.5 (C-5a).

11*H*$^+$-Benzo[*b*]cyclohepta[*e*][1,4]thiazinium Tetrafluoroborate (7d): ^{1}H NMR (400 MHz) (CD_3CN) δ=6.76 (1H, d, *J*=11.5 Hz, H-6 or 10), 6.82 (2H, m, H-1,4), 7.07 (3H, m, H-2,3,8), 7.18 (1H, d, *J*=9 Hz, H-10 or 6), 7.22 (1H, td, *J*=9 and 1.5 Hz, H-7 or 9), 7.41 (1H, ddd, *J*=11.5, 9, and 1.5 Hz, H-9 or 7), and 9.55 (1H, br, NH); ^{13}C NMR (100 MHz) (CD_3CN) δ=120.4 (C-4), 121.2 (C-4a), 127.6 (C-1), 129.4 (C-6), 130.6 (C-2 or 3), 130.9 (C-3 or 2), 134.4 (C-11a), 140.5 (C-10), 142.2 (C-8 or 9), 144.2 (C-9 or 8), 145.7 (C-5a), 148.1 (C-7), and 162.9 (C-10a).

***o*-Aminophenol (8a):** ^{1}H NMR (50% $CDCl_3$-CD_3CN) δ=6.60 (s, ar-H); (1:2:2, CF_3COOD-$CDCl_3$-CD_3CN) δ=6.75—7.45 (m, ar-H).

2-Aminobenzenethiol (8b): ^{1}H NMR (CD_3CN) δ=4.0 (3H, br, NH and SH) and 6.50—7.40 (4H, m, ar-H); (20% CF_3COOD-CD_3CN) δ=7.20—7.70 (m, ar-H).

2,3-Dihydro-1*H*-cyclohepta[*b*]pyrazine (9a): ^{1}H NMR (270 MHz) (CD_3CN) δ=3.40 (4H, s, CH_2), 6.00 (1H, t, *J*=9.3 Hz, H-7), 6.15 (2H, d, *J*=11.5 Hz, H-5,9), and 6.46 (2H, dd, *J*=11.5 and 9.3 Hz, H-6,8); (20% CF_3COOD-CD_3CN) δ=3.59 (4H, s, CH_2), 7.13 (1H, t, *J*=10 Hz, H-7), 7.26 (2H, d, *J*=11 Hz, H-5,9), and 7.51 (2H, dd, *J*=11 and 10 Hz, H-6,8).

2,3-Dihydro-1-methyl-1*H*-cyclohepta[*b*]pyrazine (9b): ^{1}H NMR (270 MHz) (20% CF_3COOD+CD_3CN) δ=3.35 (3H, s, CH_3), 3.68 (2H, t, *J*=5.0 Hz, CH_2), 3.78 (2H, t, *J*=5.0 Hz, CH_2), 7.08 (1H, t, *J*=9.3 Hz, H-7), 7.21 (2H, d, *J*=11.0 Hz, H-5,9), 7.50 (1H, dd, *J*=11.0 and 9.3 Hz, H-8), and 7.58 (1H, dd, *J*=11.0 and 9.3 Hz, H-6).

5,11-Dimethyl-5*H*-cyclohepta[*b*]quinoxalinium Tetrafluoroborate (12a): ^{1}H NMR (400 MHz) (CD_3CN) δ=3.08 (6H, s, CH_3), 6.27 (2H, d, *J*=12 Hz, H-6,10), 6.56 (1H, t, *J*=9.5 Hz, H-8), 6.70 (2H, m, H-1,4), 6.93 (2H, m, H-2,3), and 7.22 (2H, dd, *J*=12 and 9.5 Hz, H-7,9); ^{13}C NMR (100 MHz) (CD_3CN) δ=37.6 (CH_3), 118.0 (C-1,4), 124.7 (C-6,10), 128.0 (C-2,3), 131.5 (C-8), 133.2 (C-4a, 11a), 147.9 (C-7,9), and 158.3 (C-5a, 10a).

We wish to thank Professor Jun-ichi Aihara (Shizuoka Univ.) for helpul discussions on the resonance energy and ring currents. We are gratefull to Dr. Tadamichi Fukunaga (E. I. du Pont de Nemours and Co.) for sending unpublished NMR and other experimental data[3b] and to Professor Hiroshi Yamamoto (Okayama Univ.) for some advice. We also wish to thank Dr. Hiroshi Naganawa (Inst. Bio-org. Chem., Shinagawa) for the NMR measurements.

References

1) Part II: K. Shindo, S. Ishikawa, and T. Nozoe, *Bull. Chem. Soc. Jpn.*, **62**, 1158 (1989).

2) T. Nozoe, T. Kitahara, K. Takase, and M. Sasaki, *Proc. Jan. Acad.*, **32**, 349 (1956); we were unable to determine the position of this H-atom of **3a**, because an appropriate instrument, such as NMR, was not available at that time.

3) a) T. Fukunaga, presented at the 23rd IUPAC Congress, Boston, 1971, Abstr., p. 103; b) private communication to T. Nozoe (1971)., **15** (X=CF_3COO^-): ^{1}H NMR (CF_3COOH) δ=7.34 (H-3,7), 7.35 (H-5), and 7.81 (H-4,6), and δ_{av} 7.53; **5a** (X=BF_3^-): ^{1}H NMR (CD_3CN) δ=5.68 (H-6,10), 6.05 (H-8), 6.12 (H-1,4), 6.52 (H-2,3), and 6.62 (H-7,9); λ_{max} (EtOH) 236, 290, 313, 345, 440sh, 465, 490, 573, and 623 nm (log ε 4.31, 4.61, 4.05, 3.99, 4.03, 4.16, 4.04, 3.06, 3.09, and 2.96); **5b** (X=Cl^-): ^{1}H NMR (CD_3CN) δ=5.56 (H-6,10), 5.95 (H-8), 5.81 (H-1,4), and 6.51 (H-7,9); **16** (X=I^-): λ_{max} (CH_3CN) 254, 350sh, 365, 470, and 490 nm (log ε 4.59, 4.05, 4.23, 3.37, and 3.73).

4) T. Nozoe, H. Okai, and T. Someya, *Bull. Chem. Soc. Jpn.*, **51**, 2185 (1983); T. Nozoe and T. Someya, *ibid.*, **51**, 3316 (1978); T. Someya, H. Okai, H. Wakabayashi, and T. Nozoe, *ibid.*, **56**, 2756 (1983); T. Nozoe, H. Okai, H. Wakabayashi, and S. Ishikawa, *Chem. Lett.*, **1984**, 1145.

5) T. Nozoe, T. Asao, and K. Takahashi, *Bull. Chem. Soc. Jpn.*, **34**, 146 (1961); *ibid.*, **39**, 1980 (1960).

6) K. Shindo, S. Ishikawa, and T. Nozoe, *Bull. Chem. Soc. Jpn.*, **85**, 165 (1985).

7) T. Kurihara, S. Ishikawa, T. Nozoe, and J. Aihara, *Bull. Chem. Soc. Jpn.*, **63**, 2531 (1990).

8) J. Aihara, *J. Am. Chem. Soc.*, **98**, 2750 (1976); J. Aihara, *Bull. Chem. Soc. Jpn.*, **51**, 3540 (1978); J. Aihara, *J. Am. Chem. Soc.*, **101**, 5913 (1979); J. Aihara and T. Horikawa, *Bull. Chem. Soc. Jpn.*, **56**, 1853 (1983).

9) B. M. Gimarc, *J. Am. Chem. Soc.*, **105**, 1979 (1983); B. M. Gimarc and J. J. Ott, *ibid.*, **108**, 4298 (1986); J. J. Ott and B. M. Gimarc, *ibid.*, **108**, 4303 (1986).

10) A. Streitwieser, Jr., "Molecular Orbital Theory for Organic Chemists," Wiley, New York (1961).

11) B. A. Hess, Jr. and L. J. Schaad, *J. Am. Chem. Soc.*, **95**, 3907 (1973).

12) B. Pullman and A. Pullman, *Rev. Mod. Phys.*, **32**, 428 (1960).

13) T. Nozoe, S. Ishikawa, and K. Shindo, *Heterocycles*, **28**, 733 (1989).

14) Y. Yamashita, K. Hagiya, G. Saito, and T. Mukai, *Bull. Chem. Soc. Jpn.*, **61**, 271 (1988).

15) For example, the δ_{av} values of protons on the benzene and seven-membered rings of oxazine **3c** in CD_3CN are 6.61 and 5.83 ppm, whereas these values are 6.72 and 5.83 ppm in $CDCl_3$, respectively. The corresponding values for thiazine **3d** are 6.96 and 6.22 ppm in CD_3CN, whereas these values are 6.95 and 6.17 ppm in $CDCl_3$, respectively. The δ_{av} values of protons on the benzene and seven-membered rings of diazine **3b** in CD_3CN

are 6.47 and 5.33 ppm, whereas these values are 6.49 and 5.46 ppm in $CDCl_3$, respectively.

16) J. J. P. Stewart and F. J. Seiler, *QCPE* Program No. 549.

17) D. G. Farnum, *Adv. Phys. Org. Chem.*, **11**, 123 (1975); G. J. Martin, M. L. Martin, and S. Odiot, *Org. Magn. Reson.*, **7**, 2 (1975); S. Flizar, G. Cardinal, and M-T. Beraldin, *J. Am. Chem. Soc.*, **102**, 5287 (1982); H. Baumann and H. Olsen, *Hev. Chim. Acta*, **61**, 2202 (1978); B. Eliasson, D. Johnels, I. Sethson, U. Edlund, and K. Mullen, *J. Chem. Soc., Perkin Trans. 2*, **1990**, 897.

18) Y. Kawazoe and M. Ohnishi, *Chem. Pharm. Bull.*, **11**, 243 (1963).

19) H. H. Jáffe, *QCPE* Program No. 315 (1975).

 © 1991 The Chemical Society of Japan Bull. Chem. Soc. Jpn., 64, 2677—2680 (1991)

Molecular Orbital Approach to Antioxidant Mechanisms of Phenols by an Ab Initio Study

Kazunori TANAKA, Shogo SAKAI,† Shogo TOMIYAMA, Tomihiro NISHIYAMA, and Fukiko YAMADA*
Department of Applied Chemistry, Faculty of Engineering, Kansai University,
Yamatecho, Suita, Osaka 564
(Received February 4, 1991)

An ab initio molecular orbital theory has been applied to a study of the hydrogen abstractions of phenolic antioxidants in the chain process of autoxidation. The optimum structures of phenols, of peroxides, and of those compounds in the transition states were obtained with a Hartree–Fock/STO-3G basis set. From the values of enthalpy (ΔH) and activation energy (E_a) obtained, it was found that the rates of the reaction of peroxyl radical with phenolic antioxidant were faster than those with organic substrate in the propagation, and that the effect of the aromatic ring of the antioxidants not only stabilized a product state but also decreased an energy level in the transition state. The para-substituent effect that an electron-releasing substituent increased the antioxidant activity, whereas an electron-withdrawing one decreased it, was recognized. The relationship between ΔH and E_a values followed the Evans–Polanyi rule. The transition states in the hydrogen abstractions with lower E_a values prefer reactant-like structures, whereas those with higher E_a values prefer product-like ones.

Antioxidants have commonly been used to prevent deterioration due to the autoxidation of organic substrates. Autoxidations at various temperatures have been well characterized as radical chain reactions. Such antioxidants as phenol and aromatic amine derivatives react as chain-breaking inhibitors of the peroxyl radical:[1)]

$$ROO\cdot + ArOH \rightarrow ROOH + ArO\cdot, \quad (a)$$

where ROO· denotes the peroxyl radical and ArOH represents antioxidant phenols. Another possible reaction is the direct attack on the alkyl radical:

$$R\cdot + ArOH \rightarrow RH + ArO\cdot \quad (b)$$

In the absence of the antioxidant, the following propagation reactions proceed:

$$R\cdot + {}^3O_2 \rightarrow ROO\cdot \quad (c)$$
$$ROO\cdot + RH \rightarrow ROOH + R\cdot, \quad (d)$$

where RH is the organic substrate. It is assumed that reaction (c) proceeds with zero activation energy.[1)] The main reactions can be represented by reactions (a) and (d) and thus, reaction (a) occurs easily in comparison with reaction (d). The radical ArO· from the antioxidant is less reactive and consequently it is difficult for a new chain reaction to become initiated (e), as was first reported by Bolland and Ten Have.[2)]

$$ArO\cdot + RH \rightarrow ArOH + R\cdot \quad (e)$$

The ArO· radical would be expected to act as the ideal radical to capture other ROO· radicals. Namely, the reactivity of ArO· is attributed to its resonance structure to fulfill the ideal conditions.

† Present address: Osaka Sangyo University, Daito-shi, Osaka 574.

In 1988, Scott described in his review[3)] that electron-releasing groups in the aromatic ring increase antioxidant activity, whereas electron-attracting groups decrease it, and substituents delocalizing the electron in the aryloxyl or arylaminyl radicals increase the antioxidant activity. These facts can be rationalized on the basis of the transition state involved in hydrogen abstraction by alkylperoxyl radical. There is both partial separation of charge between the alkylperoxyl and the aromatic ring and partial delocalization of the electron in the π-bond system. Consequently, substituents which release electrons or delocalize the unpaired electron decrease the transition state energy.

In this paper, further examinations of the reactivities of elementary reactions in autoxidations in the absence or presence of the antioxidants are described on the following model reactions:

Reaction between R· and triplet oxygen

$$C_6H_5\cdot + {}^3O_2 \rightarrow C_6H_5OO\cdot \quad (1)$$

Reaction between R· and an antioxidant

$$C_6H_5\cdot + ArOH \rightarrow C_6H_6 + ArO\cdot \quad (2)$$

Propagation reaction

$$CH_4 + \cdot OOH \rightarrow CH_3\cdot + HOOH \quad (3)$$
$$C_6H_6 + \cdot OOH \rightarrow C_6H_5\cdot + HOOH \quad (4)$$

Chain-breaking reaction

$$HOH + \cdot OOH \rightarrow HO\cdot + HOOH \quad (5)$$
$$ArOH + \cdot OOH \rightarrow ArO\cdot + HOOH \quad (6)$$

Reaction between methoxyl or phenoxyl radical and a substrate

$$CH_3O\cdot + CH_4 \rightarrow CH_3OH + CH_3\cdot \quad (7)$$
$$ArO\cdot + CH_4 \rightarrow ArOH + CH_3\cdot \quad (8)$$

Subsequently, the para-substituent effects of phenol antioxidants in the hydrogen abstraction by ROO· radicals are investigated in detail.

Structure I depicts the hydrogen abstraction in the transition state and the various substituents, R and X, are shown below.

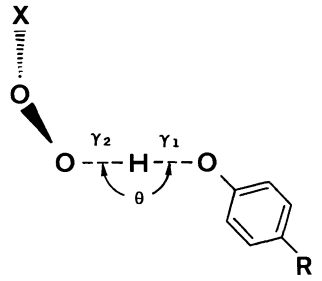

Structure I

Eq.[a]	R	X	Eq.	R	X
6	H	H	14	H	CH_3
9	CH_3	H	15	CH_3	CH_3
10	OCH_3	H	16	OCH_3	CH_3
11	NH_2	H	17	NH_2	CH_3
12	F	H	18	Cl	CH_3
13	Cl	H			

a) R-C_6H_4OH+·OOX→R-C_6H_4O·+HOOX.

Experimental

Determination of Antioxidant Activity. Measurements of oxygen-absorption rates were performed with an isobaric gas-absorption apparatus under a closed-flow system (2.0±0.1 L oxygen h^{-1}) provided with an electrolyser using 50 cm^3 of tetralin containing an antioxidant (0.001 mol dm^{-3}) and azobis(isobutyronitrile) as the initiator (0.01 mol dm^{-3}). The oxidation temperature was kept at 60±0.1 °C and oxygen absorption was periodically measured in a constant-pressure closed system. The induction period (IP) was determined in the usual way.[4]

Computation

Ab initio molecular orbital calculations were carried out for the reactions, Eqs. 1—18, corresponding to the elementary reactions, (a)—(e), with the GAUSSIAN 80 programs.[5] Geometries for all the structures were optimized at the HF level with the STO-3G basis set[6] by using the energy gradient method.[7] The energies and structures of the transition states were also calculated in the same way mentioned above, but the aromatic ring involved in reactions 4, 6, and 8—18, was only fixed with that of optimized phenol geometry. Concerning reactions 3, 5, and 7, these values were calculated with the HF/3-21G basis set.[8,9] Thus, the electronic correlation energies in these three reactions were computed by means of Møller-Plesset (MP) pertubation up to the third order.[10] The ΔH and E_a values were obtained from the total energies for the optimum structures of both systems and the energy of the transition state (E_{ts}), as follows:

$$\Delta H(\text{kJ mol}^{-1}) = -2625.460[E_{total}(\text{reactants}) - E_{total}(\text{products})]$$

$$E_a(\text{kJ mol}^{-1}) = -2625.460[E_{total}(\text{reactants}) - E_{ts}]$$

$$1 \text{ A.U.} = 2625.460 \text{ kJ mol}^{-1}$$

The activation parameters obtained are shown in Tables 1—4.

Results and Discussion

The Initial Channel of the Chain-Breaking Inhibition. Table 1 shows the calculated ΔH values of Eqs. 1 and 2, along with the energy profiles of both exothermic reactions. The difference between the ΔH values in Eqs. 1 and 2 is 33.48 kJ mol^{-1}. Therefore, the C_6H_5OO· radical is stable in comparison with the product of Eq. 2. In Eq. 1, the direct interaction between the radical and triplet oxygen having the feature of a biradical proceeds with no barriers, whereas the reaction of Eq. 2 reaches the product state through the transition state.

In the autoxidation of organic substrates, an alkyl radical is formed by addition of an initiator such as azobis(isobutyronitrile) and is further transformed into the ROO· radical after interaction with triplet oxygen (Eq. c). Bolland and ten Have[2] determined the initial rates of the autoxidations under several conditions: The variations of antioxidants or substrates, concentration, and oxygen pressure. Thus, they concluded that antioxidants react with ROO· radicals and not with R· radicals. This conclusion agrees with the results of our calculations supporting the idea that the initial channel of the chain-breaking inhibition by antioxidants is the

Table 1. Activation Parameters for Eqs. 1 and 2

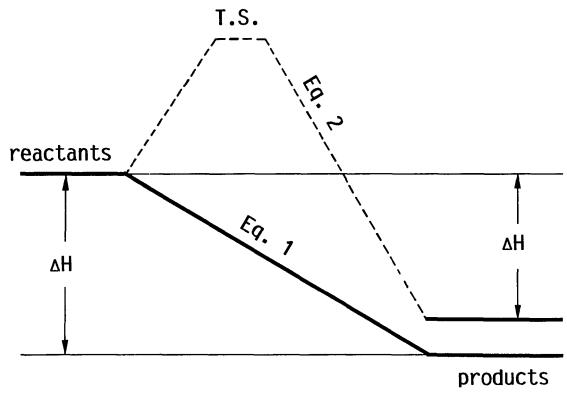

Eq.	ΔH/kJ mol^{-1}	
	HF/STO-3G	HF/3-21G
1	−161.34	—
2	−127.86	−54.06

reaction with the ROO· radical.

Reactivity of the HOO· Radical. Concerning Eq. 3 in Table 2, the values of ΔH and E_a at the MP3/3-21G level are 119.62 and 130.88 kJ mol^{-1}, and in Eq. 5 these values are 69.50 and 97.86 kJ mol^{-1}, respectively. The differences in the ΔH and E_a values between Eqs. 3 and 5 are 50.12 and 33.02 kJ mol^{-1}, respectively. The rate of hydrogen abstraction from the O–H bond was much faster than that from the C–H bond. In other words, the methyl radical is unstable compared with the hydroxyl radical and Eq. 3 has the feature of reversible reaction.

Subsequently, the influence of an aromatic ring was considered at the STO-3G level (see Table 2). The differences in the ΔH and E_a values between Eqs. 3 and 4 are 97.36 and 67.66 kJ mol^{-1}, respectively, while those between Eqs. 5 and 6 are 79.88 and 43.68 kJ mol^{-1}, respectively. Consequently, by introducing an aromatic ring to the reaction system, their reactivities are increased. The E_a value of Eq. 4, which is the model of the propagation reaction (d), was exceedingly large in comparison with that of Eq. 6 which is the model of the chain-breaking reaction (a).

From these results, it was confirmed that the rate of the chain-breaking reaction was much faster than the propagation reaction and that the aromatic ring in the antioxidant molecules tends to decrease the activation energy of the chain-breaking reaction and to stabilize the energy of the phenoxyl radical produced after the hydrogen abstraction.

Table 2. Activation Parameters for Reaction Models, Eqs. 3—8

Eq.	Basis set//geometry	ΔH/kJ mol^{-1}	E_a/kJ mol^{-1}
3	HF/STO-3G//STO-3G	231.25	237.99
	HF/3-21G//3-21G	136.15	166.31
	MP2/3-21G//3-21G	115.02	123.72
	MP3/3-21G//3-21G	119.62	130.88
4	HF/STO-3G//STO-3G	133.89	170.33
5	HF/STO-3G//STO-3G	85.90	139.70
	HF/3-21G//3-21G	61.30	129.96
	MP2/3-21G//3-21G	83.64	92.93
	MP3/3-21G//3-21G	69.50	97.86
6	HF/STO-3G//STO-3G	6.02	96.02
7	HF/STO-3G//STO-3G	187.28	199.03
	HF/3-21G//3-21G	105.73	143.01
	MP2/3-21G//3-21G	72.09	79.96
	MP3/3-21G//3-21G	83.14	93.68
8	HF/STO-3G//STO-3G	225.22	211.04

Reactivity of the Phenoxyl Radical. It is known that one molecule of simple phenol captures two molecules of ROO· radicals; one is captured by the hydrogen abstraction of the phenolic OH group, and the other by the coupling reaction with the 4-oxo-2,5-cyclohexadienyl radical produced from the phenoxyl radical by the rearrangement of the π-electron (see reactions a and f).[1]

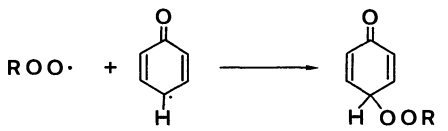

(f)

The data from Eqs. 7 and 8 in Table 2 indicate the closeness of both energy levels of the transition and product states, and the E_a values of Eq. 8 is larger than that of Eq. 7 at the STO-3G level. Both Eqs. 7 and 8 are the model system of the reaction (e). It was noted that the system returns readily from the transition state to the reaction state. From these results, it can be concluded that the reaction between the phenoxyl radical and a substrate cannot proceed readily, whereas the 4-oxo-2,5-cyclohexadienyl radical reacts with the peroxyl radical smoothly to terminate chain reactions.

Substituent Effect of Phenolic Antioxidant. The calculated ΔH and E_a values in the cases of Eq. 6 and Eqs. 9—18, of the reactions of *p*-substituted phenols with two kinds of peroxyl radicals (see Structure I, X=H and CH_3), are shown in Table 3. By using the values in Eqs. 6 (R=H) and 14(R=H), the $\Delta(\Delta H)$ and ΔE_a were evaluated. An approximately linear relationship between both values is shown in Fig. 1. The slope value (α), $\Delta E_a/\Delta(\Delta H)$, is 0.395 except for the value in Eq. 17. This fact indicates that the hydrogen abstraction in the chain-breaking reaction follows the Polanyi–Evans rule.[11]

Table 3. *p*-Substituent Effects of Phenols with Activities as Antioxidants

Eq.	X	R	ΔH/kJ mol^{-1}	E_a/kJ mol^{-1}	n[a]	IP/min[b]	IP/min[c]	IP/min[d]
6	H	H	6.02	96.02	2.1			
9	H	CH_3	5.48	95.44	2.5			
10	H	OCH_3	19.46	100.71	2.0			
11	H	NH_2	11.05	96.69				
12	H	F	10.29	96.44				
13	H	Cl	10.75	97.03	1.7			
14	CH_3	H	3.60	93.35		75	60	23
15	CH_3	CH_3	3.05	92.80		210	165	121
16	CH_3	OCH_3	17.03	97.99				
17	CH_3	NH_2	8.58	92.01		2340	1470	551
18	CH_3	Cl	8.33	94.18		45		

a) The n value was obtained by the induction period method in Ref. 12 (cumene was used as the substrate). b) The data in Ref. 13 (cracked gasoline). c) The data in Ref. 14 (Pennsylvania gasoline). d) This work (tetralin).

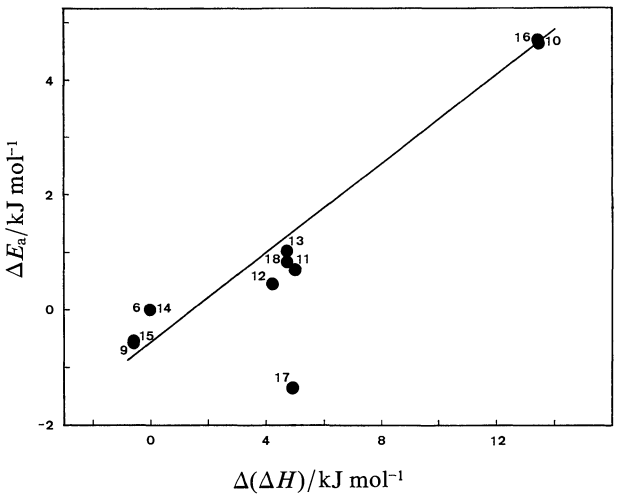

Fig. 1. Plot of ΔE_a vs. $\Delta(\Delta H)$ values.

Ingold et al.[12] reported on the stoichiometric coefficient, n, for substituted phenols using cumene as a substrate at 65 °C by the induction period method. The n values in Table 3, change inversely with the ΔH and E_a values except for those in Eq. 10. This indicates that the electron-releasing substituent in phenol decreases the ΔH and E_a values and increases the antioxidant activity, whereas the electron-attracting substituent increases both values and decreases the activity. The relationship between the E_a and induction period (IP) values indicates an antioxidant activity, by the uses of two kinds of gasolines[13,14] and tetralin as substrates, and confirms the result mentioned above, as can be seen in Table 3.

Geometry of the Transition State. The geometry of the molecular model of the hydrogen abstraction in the transition state was defined by both distance and angle parameters, as shown in Table 4. These values indicate linear binding between the hydrogen atom of the OH substituent of the phenol and the oxygen atom of the peroxyl radical. Figure 2 shows the relation between the E_a and r_1 values, except for Eqs. 10, 11, 16, and 17, in the cases of the substituents OCH_3 and NH_2. The E_a values increase with increasing r_1 values. It was, therefore, thought that the structures of the transition states in the reactions which have lower E_a values are reactant-like, whereas those which have higher values are product-like. This result agrees with the postulation by Hammond.[15]

Table 4. Structural Parameters of the Transition States[a]

Eq.	r_1/Å	r_2/Å	θ/deg.
6	1.220	1.156	180.5
9	1.219	1.157	180.7
10	1.221	1.156	180.6
11	1.215	1.160	180.1
12	1.222	1.155	180.2
13	1.227	1.151	180.2
14	1.220	1.156	180.3
15	1.219	1.157	180.4
16	1.221	1.158	180.4
17	1.200	1.178	180.1
18	1.227	1.151	180.3

a) See Structure I.

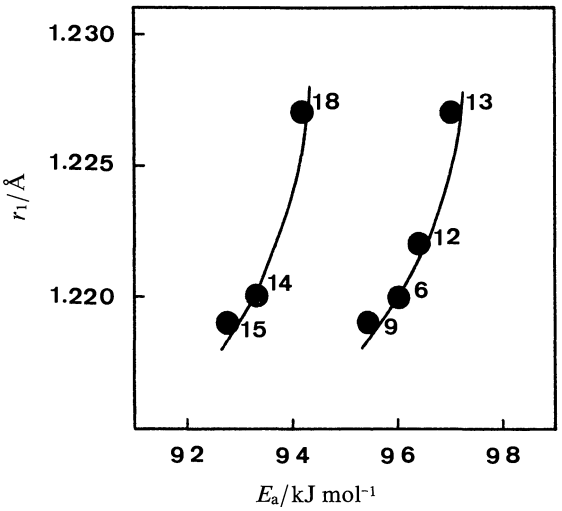

Fig. 2. Plot of r_1 vs. E_a values.

References

1) a) N. Uri, "Autoxidation and Antioxidant," ed by W. O. Lundberg, John Wiley & Sons, New York(1961), Vol. I, Chap. 4. b) G. Scott, "Atmospheric Oxidation and Antioxidant," Elsevier, Amsterdam(1965), Chap. 4.

2) J. L. Bolland and P. Ten Have, *Discuss. Faraday Soc.*, **2**, 252 (1947); *Trans. Faraday Soc.*, **43**, 201 (1947).

3) G. Scott, *Bull. Chem. Soc. Jpn.*, **61**, 165 (1988).

4) F. Yamada, T. Nishiyama, M. Yamamoto, and K. Tanaka, *Bull. Chem. Soc. Jpn.*, **62**, 3603 (1989).

5) J. S. Binkley, R. A. Whiteside, R. Krishnan, R. Seeger, D. J. DeFrees, H. B. Schlegel, S. Topiol, L. R. Kahn, and J. A. Pople, GAUSSIAN 80, Carnegie Mellon University, Pitttsburg, PA (1980).

6) W. J. Hehre, R. F. Stewart, and J. A. Pople, *J. Chem. Phys.*, **51**, 2657 (1969).

7) A. Komornicki, K. Ishida, K. Morokuma, R. Ditchfield, and M. Conrad, *Chem. Phys. Lett.*, **45**, 595 (1977).

8) J. S. Binkley, J. A. Pople, and W. J. Hehre, *J. Am. Chem. Soc.*, **102**, 939 (1980).

9) M. S. Gordon, J. S. Binkley, J. A. Pople, W. J. Pietro, and W. J. Hehre, *J. Am. Chem. Soc.*, **104**, 2797 (1982).

10) MP2: J. S. Binkley and J. A. Pople, *Int. J. Quantum Chem., Symp.*, **9**, 229 (1975); MP3: J. A. Pople, J. S. Binkley, and R. Seeger, *ibid.*, **10**, 1 (1976).

11) M. G. Evans and M. Polanyi, *Trans. Faraday Soc.*, **31**, 875 (1935).

12) E. C. Horswill, J. A. Howard, and K. D. Ingold, *Can. J. Chem.*, **44**, 985 (1966).

13) G. Egloff, J. C. Morrell, C. D. Lowry, and C. G. Dryer, *Ind. Eng. Chem.*, **24**, 1375 (1932).

14) J. C. Morrell and C. G. Dryer, *Ind. Eng. Chem.*, **25**, 804 (1933).

15) G. S. Hammond, *J. Am. Chem. Soc.*, **77**, 334 (1955).

Hydration of Propene over Proton- and Metal Ion-Exchanged Zeolite Catalysts at Atmospheric Pressure

Hiroshi MORI,† Noritaka MIZUNO, Toshihiro SHIROUZU,†† Shuichi KAGAWA,†† and Masakazu IWAMOTO*
Catalysis Research Center, Hokkaido University,
Sapporo 060
† Department of Industrial Chemistry, Miyakonojo National
College of Technology, Miyakonojo 885
†† Department of Industrial Chemistry, Faculty of Engineering,
Nagasaki University, Nagasaki 852
(Received March 1, 1991)

The gas-phase hydration of propene over proton-exchanged or metal ion-exchanged zeolites with various Si/Al ratios and structures (such as ZSM-5, mordenite, ferrierite, and Y-type) has been studied. It was found that the catalytic activity of proton-exchanged zeolites for the conversion of propene to 2-propanol did not depend on their framework structure, but showed a volcano-shaped dependence on the Al content, as was observed in the hydration of ethene. On the basis of temperature-programmed desorption experiments of NH_3 adsorbed on the zeolites, it was confirmed that the activity is controlled by the acidity of the catalysts. The catalytic activity of metal ion-exchanged Y zeolites increased with an increase in the electronegativity of the metal ion.

Hydration of lower olefins over proton-exchanged zeolites has been investigated at atmospheric and high pressures in the gas[1-5] and liquid[6] phases. Although efforts have been made to clarify the factors controlling the activity for hydration, they have been ambiguous because the conditions are complex and the activity of the catalyst depends on several factors.

We have previously reported that in the hydration of ethene over proton-exchanged zeolites at atmospheric pressure the catalytic activity of the zeolites is independent on the framework structure, showing a volcano-shaped dependence on the Al content or a SiO_2/Al_2O_3 molar ratio; a linear correlation between the activity and the number of acid sites on the zeolite was observed.[1] Further, it was suggested that the Brønsted acid site is the active site, since the temperature dependency of the activity is similar to that of a number of Brønsted acid sites. Eguchi et al.[4] as well as Kikuchi et al.[5] have, indeed, reported high catalytic activities of zeolites for the reaction. The former group has also claimed that no correlation was observed between the catalytic activity of zeolites for the hydration of propene and the number of acidic sites.[4] These results are not consistent with the correlation concerning the activity of zeolites for ethene hydration with the acid amount reported by the present group[1,3] and by Kikuchi et al.[5] This may be due to the high partial pressure of water vapor in their experiment, caused by a decrease in the number of acidic sites, owing to too much water being observed on mordenite by Kikuchi et al.[7]

In this work, therefore, catalytic hydration of propene was carried out over various zeolites including metal ion-exchanged Y zeolites in a simpler system, at both a low partial pressure of water vapor and at atmospheric pressure. We investigated how the activity for the hydration of lower olefins can be recognized by the amounts of acidic sites and tried to make the effects of the metal ion clearer on the basis of such recognition. This paper clarifies the primary factors controlling the activity for the hydration of propene over proton-exchanged and metal ion-exchanged zeolite catalysts, and summarizes catalytic hydration over zeolites together with the previously reported results for ethene, 2-methylpropene, and 1-butene. It may be important to reveal the primary factors controlling the activity for hydration in order to design zeolite catalysts, since ion-exchange resins have disadvantages in that they decrease in catalytic activity with time and display thermal instability; alternative effective catalysts have been desired, although they are used preferentially as solid catalysts for the hydration of lower olefins.

Experimental

The parent zeolites (ZSM-5 (denoted as MFI), ferrierite (FER), and ultrastable Y-type (Y-12 and 40)) were supplied by Tosoh Corporation. Mordenite (MOR-15) and Y-type (Y-5.6) corresponding to JRC-Z-HM-15 and JRC-Z-HY-5.6, respectively, were obtained from the Catalysis Society of Japan. The number in the sample name represents the SiO_2/Al_2O_3 molar ratio in the zeolite framework, which was confirmed by ^{29}Si MASNMR (Brucker PC-250, 49.66 MHz). Proton-exchanged zeolites were prepared by the calcination (723 K, 2 h) of NH_4^+-exchanged zeolites which were supplied or prepared by three repetitions of an ion exchange of the parent Na^+-exchanged zeolites with a 2 wt% aqueous NH_4NO_3 solution at room temperature overnight. Metal ion-exchanged Y zeolites were prepared as follows: 10 g of proton-exchanged ultrastable Y zeolite (SiO_2/Al_2O_3=12.3) was ion-exchanged in 500 cm^3 of an aqueous solution of metal nitrates or chlorides with 10 mmol cm^{-3}.# The obtained solid was then

#As shown in Table 2, the exchange level of Co^{2+} or Ni^{2+} was very low, indicating that the ion exchange of Co^{2+} or Ni^{2+} with H^+ is more difficult than those of the other metal ions. Similar phenomena have been reported for the ion exchange of Co^{2+} or Ni^{2+} with Na^+ in various zeolites (W. Romanowski and J. M. Jablonski, "Catalysis on Zeolites," ed by D. Kallo and K. M. Minachev, Akademiai Kiado, Budapest (1988), p. 277).

dried in air at 393 K. The ion exchange levels were determined by using atomic absorption spectroscopy after the samples were dissolved in a HF solution.

The catalytic reaction was carried out in a continuous flow reactor at atmospheric pressure using 1 g of catalysts. The reactants and products were analyzed by gas chromatography connected directly to the reaction apparatus. The flow rates of propene and water vapor were 2.6 and 5.2 $cm^3\ min^{-1}$, or 5.2 and 10.4 $cm^3\ min^{-1}$, respectively. The total flow rate was 30 $cm^3\ min^{-1}$ (N_2 balance).

Results and Discussion

Catalytic Activities of Various Proton-Exchanged Zeolites. An approximately steady formation of 2-propanol was attained within 1 h, and the conversion of propene into 2-propanol changed little with the reaction time. 2-Propanol was the main product during the steady state of all experiments; small amounts of acetone, acetaldehyde, methanol, ethyl methyl ketone, 1-propanol, and 1,5-hexadiene were observed as by-products above 413 K. Hereafter, the conversion to 2-propanol per gram of the catalyst was used as a measure of the catalytic activity. The catalytic activities of various proton-exchanged zeolites for the hydration of propene are summarized in Table 1. All of the proton-exchanged zeolites used were active for a 2-propanol synthesis. The temperature dependence of the activities of HFER-16 is shown in Fig. 1 as an example. At first, the activity increased with an increase in the reaction temperature. The reason for the decline in activities at higher temperature involves a reduction in the equilibrium conversion, indicated by the broken line in Fig. 1. The maximum yield of 2-propanol was achieved at 383—403 K. The best yield (2.2%) was obtained at 383 K upon the HFER-16 zeolite.

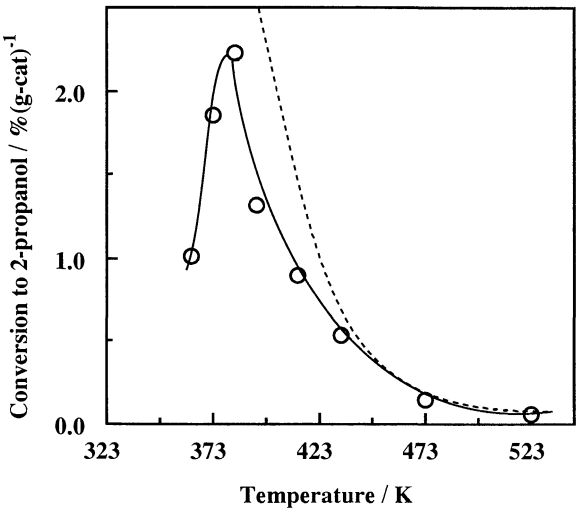

Fig. 1. Temperature dependence of the catalytic activity of HFER-16 for the hydration of propene. Reaction conditions were the same as those in Table 1. The broken line corresponds to the equilibrium conversion.

Figure 2a shows the effect of the Al content on the conversion of propene. Here, conversions at 393 K are plotted, since conversions above 403 K were too close to the equilibrium conversions to compare the activities. A similar tendency was observed when conversions at 373 K were plotted against the Al constents. The optimum SiO_2/Al_2O_3 molar ratio for 2-propanol formation is about 15—16, as shown in Fig. 2a. This value is in agreement with those reported by Fajula et al.[6] as well as ours[3] for the catalytic hydration of 1-butene in an aqueous solution and a gas phase, respectively. It should be noted that the activities of the HY zeolites with

Table 1. Properties of Proton-Exchanged Zeolites Used and Their Catalytic Activities for Hydration of Propene[a]

Catalyst	SiO_2[b] / Al_2O_3	Pore[c] diameter / nm	H^+[b,d] / %	Temp/K and amount of β-NH_3 desorption[b,e]		% Conversion of C_3H_6 into 2-propanol Reaction temp/K				
				mmol g^{-1}		373	383	393	403	413
HY-5.6	5.6	0.74	72	729	0.57	0.10	—	0.16	0.37	0.94
HY-12	12.2	0.74	—	—	—	0.08	—	1.16	1.27	0.92
HY-40	40	0.74	—	—	—	0.96	—	1.39	1.26	—
HMOR-15	14.9	0.67×0.70	99	876	1.20	0.50	—	1.78	—	0.91
HFER-12	12.3	0.43×0.55	99	823	1.02	0.36	0.43	0.70	—	0.58
HFER-16	16.3	0.43×0.55	94	853	1.14	1.85	2.22	1.32	—	0.90
HMFI-23[f]	23.3	0.54×0.56	99	686[g]	0.28[g]	—	0.99	0.76	—	0.76
Equil.conv.[h]/%						5.09	3.40	2.29	1.57	1.10

a) Reaction conditions: C_3H_6, 2.6 $cm^3\ min^{-1}$; H_2O, 5.2 $cm^3\ min^{-1}$; N_2, 22.2 $cm^3\ min^{-1}$; catalyst=1.0 g; pressure=1 atm. b) Cited from Ref. 8. c) Cited from G. T. Kokotairo, "Proceedings of the NATO Advanced Study Institute on Zeolites: Sciences and Technology," ed by F. R. Ribeiro, A. E. Rodrigues, L. D. Rollmann, and C. Naccache, Martinus Nijhoff Publishers, Hague (1984), p. 83. The value indicated correspond to the diameter of larger pores if the zeolite has pores with different size. d) Exchange level of H^+. e) Obtained from profiles of temperature programmed desorption of ammonia. The amount and its peak temperature of β-NH_3, which well reflect the number of acid sites and its strength, respectively, as was described previously,[8] were shown. f) Prepared with HNO_3 solution. g) These values are uncertain owing to overlap of α- and β-NH_3 peaks. h) Equilibrium conversion (%).

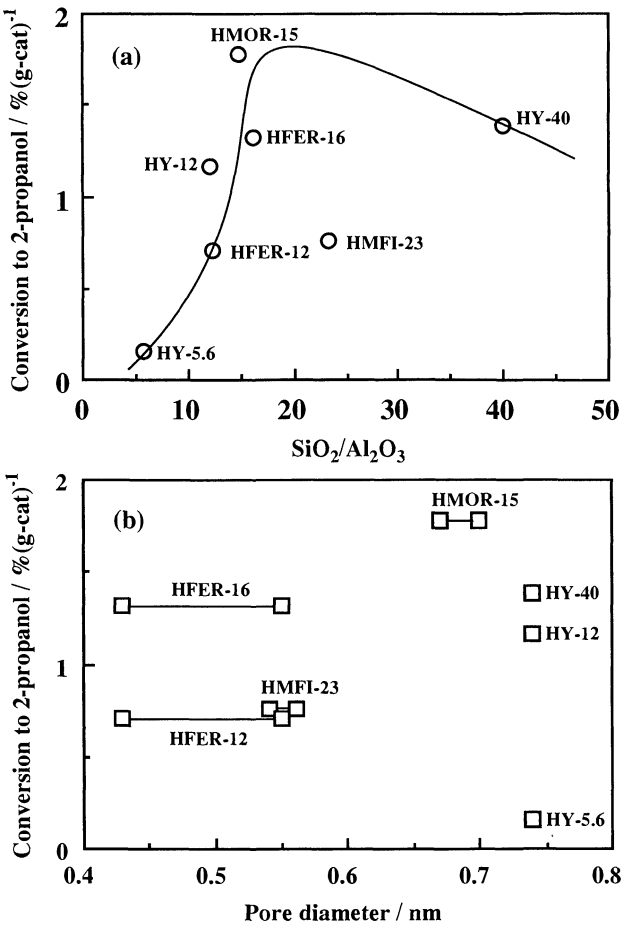

Fig. 2. Effect of Al content (SiO_2/Al_2O_3) (a) and framework (b) of zeolites on the conversion of propene to 2-propanol at 393 K. Reaction conditions were the same as those in Table 1.

various Al contents were much different from one another, as is shown in Fig. 2b. These figures indicate that the activity of the zeolites for the hydration of propene is dependent on their Al contents, not on their framework structure or pore diameter.

Taking into consideration that the hydration of olefins is an acid-catalyzed reaction, a more fruitful approach would be to compare the activity of the zeolites with the number or strength of their acid sites. The correlation between the number of acid sites of proton-exchanged zeolites and the relative catalytic activity for the hydration of propene is depicted in Fig. 3b. The conversion to 2-propanol increased with an increase in the number of acid sites, which is represented in Table 1 by the amount of desorbed β-NH_3. This correlation is in good agreement with those observed in the hydration of ethene[1] (Fig. 3a), 2-methylpropene[3] (Fig. 3c), and 1-butene[3] (Fig. 3d). Although the number and strength of the acid sites on HMFI-23 zeolite have also been measured by the t.p.d method (Table 1), the results for HMFI-23 are not plotted in the figures, since it has been reported that the β-peak temperature is close to the α-peak temperature and that separation is very difficult and ambiguous.

Next, the correlation between the acid strength and the catalytic activity is discussed. As shown in Table 1, the peak temperature of β-NH_3 varied with the zeolites, generally indicating a change in the acid strength of protons, though it has been pointed out that the peak temperature of NH_3 desorption does not always correspond to the true acid strength, but varies with the experimental conditions as well as the amount of NH_3 adsorbed.[9] Fair correlations between the activities for the hydration of propene and the peak temperature of β-NH_3 have been recognized, while a poor correlation was observed in the hydration of ethene; no conclusion was obtained with 2-methylpropene or 1-butene because of the very few plots obtained. No appearance of universality among the correlations suggests that the acid strength is not the primary factor in the hydration of olefins. It follows from Fig. 3 that the acid sites with an acid strength above a certain level would all be effective for the reaction, and that the more important factor for the hydration reaction would be the number of acid sites, compared to the acid strength. This idea is supported by a report that the acidic sites giving a β-peak well correspond to the active sites on proton-exchanged ferrierite in the hydration of ethene.[5]

Propene hydration in this work was carried out at a lower partial pressure of water vapor than those used by Eguchi et al.[4] as well as by Kikuchi et al.[5] If one takes into account that the water vapor decreases the number of strong acid sites (probably due to a decrease in the acid strength[7] or the fact that the adsorption of water inhibits the chemisorption of propene on the acidic site) the higher activity of mordenite over those reported by Eguchi et al.[4] as well as by Kikuchi et al.[5] can be readily understood; further, the hydrophobic properties of the zeolites would not much affect the present conclusion. If hydration is carried out at a higher partial pressure of water vapor, it is probable that the maximum activity is obtained at a higher SiO_2/Al_2O_3 ratio than that given in Fig. 2a, since the hydrophobic properties[10] and strong acid sites[6] of catalysts would be necessary.

Unfortunately, it was very difficult to directly compare the reactivities of olefins over the zeolites, since the equilibrium conversion and the most reactive temperature of each olefin or the most active catalyst for each olefin could not be specified.

Catalytic Activities of Metal Ion-Exchanged Zeolites. It has been reported that the activity for the hydration of ethene was increased by a metal ion exchange,[11] and it may be important to clarify the effect of metal ions on the basis of the recognition of the number of acidic sites as a primary factor which controls the activity under the present experimental conditions. The catalytic activities of metal ion-exchanged zeolites were therefore investigated on an ultrastable Y zeolite (HY-12). The change in the conversion with time was similar to that of

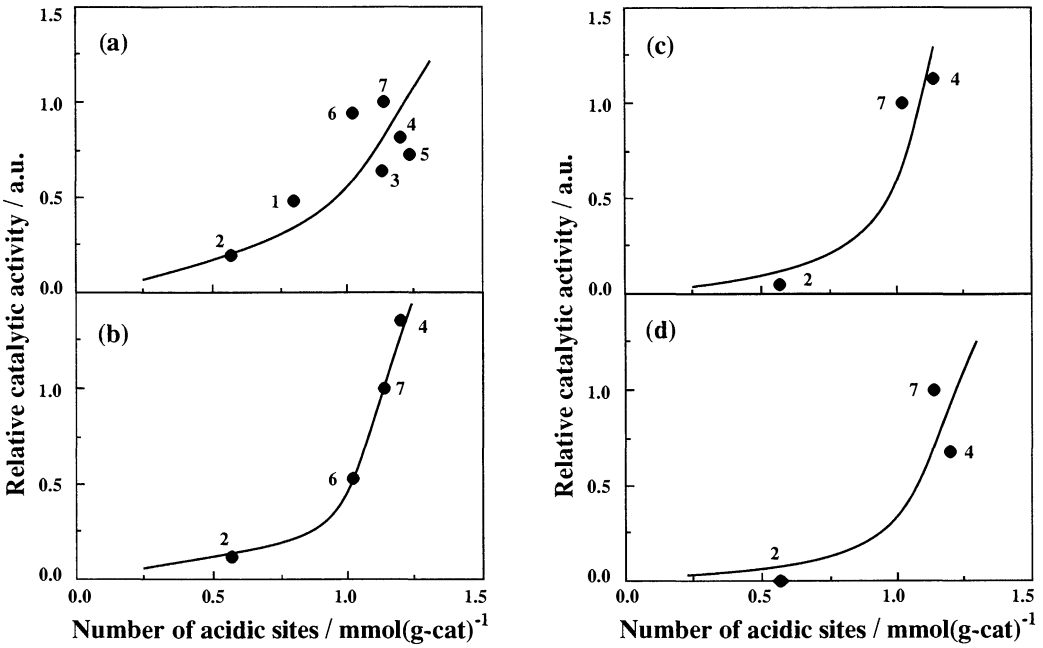

Fig. 3. Correlations between the number of acid sites of proton-exchanged zeolites and the relative catalytic activities for the hydration of ethene (a), propene (b), 2-methylpropene (c), and 1-butene (d). The catalytic activities for the hydration of ethene, 2-methylpropene, and 1-butene are cited from Refs. 1, 3, and 3, respectively. The catalytic activity of HFER-16 was taken as unity. The notations of 1, 2, 3, 4, 5, 6, and 7 in Figs. (a)—(d) correspond to the catalysts of HY-4.8, HY-5.6, HMOR-10, HMOR-15, HMOR-20, HFER-12, and HFER-16, respectively.

Table 2. Conversion of Propene to 2-Propanol over Metal Ion-Exchanged Zeolites at 393 K[a)]

Catalyst	Exchange level/%	Conversion/%
HY-12		0.08
Fe^{3+}Y-12	50.9	0.92
Cr^{3+}Y-12	88.4	0.60
Zn^{2+}Y-12	52.2	0.30
Co^{2+}Y-12	21.7	0.27
Ni^{2+}Y-12	17.5	0.17
Cu^{2+}Y-12	43.0	0.61
Equi. conv./%[b)]		4.44

a) Reaction conditions: C_3H_6, 5.2 cm^3 min^{-1}; H_2O, 10.4 cm^3 min^{-1}; N_2, 11.8 cm^3 min^{-1}; O_2, 2.6 cm^3 min^{-1}; catalyst=1.0 g; pressure=1 atm. b) See Table 1.

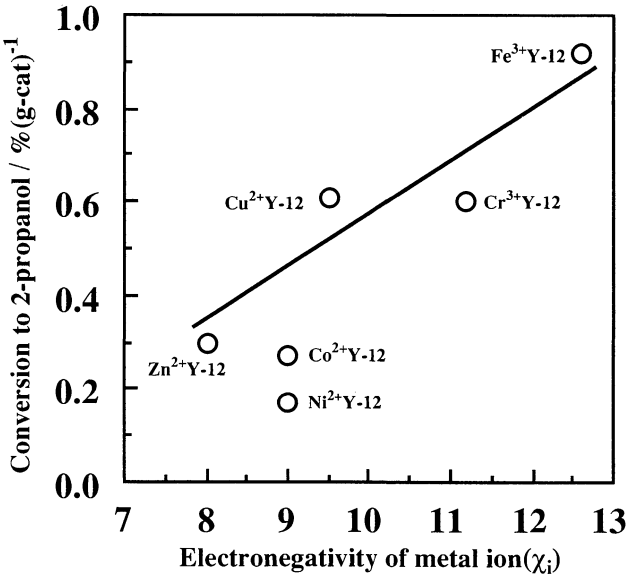

Fig. 4. Correlation between catalytic activities of metal ion-exchanged zeolites and the electronegativities of metal ions (χ_i). χ_i reported by Tanaka et al. (Ref. 12) was used. Reaction conditions were the same as those in Table 2.

the proton-type. The rates and selectivities were little changed by the addition of oxygen to the reactant gas. The results are summarized in Table 2. The conversion was increased by the exchange of transition metal ions at 393 K, but was very low (less than one quarter of equilibrium conversion).

Figure 4 shows the correlation between the conversion to 2-propanol and the electronegativity of metal ions.[13)] The conversion on Fe^{3+}, Cr^{3+}, Zn^{2+} and Cu^{2+} were in the range of 0.28—0.49 mmol g^{-1} while those on Co^{2+} (0.18 mmol g^{-1}) and Ni^{2+} (0.15 mmol g^{-1}) were much lower. A fair correlation was observed and the conversion increased with an increase in the electronegativity. The deviation of the conversions on Co^{2+}Y-12 and Ni^{2+}Y-12 to a lower extent from a linear line is probably due to the lower amounts of metal ions (or lower ion exchange levels) than those of the others. As

discussed in the previous section, the number of active centers is one of the factors which control the activity for the hydration of propene. The linear dependence in Fig. 4 shows that not only the number of acidic sites, but also the electronegativity of metal ions, controls the activity. The role of electronegativity in hydration can be explained as follows. Metal ions with a higher electronegativity would show a greater ability to coordinate olefin and/or water molecules, as has been reported for an A-type zeolite by Tanabe at al.[11] This ability may result in the higher catalytic activity.

Thus, all findings in the present work lead to the conclusion that the hydration of propene over proton-exchanged zeolites proceeds on a Brønsted acid site, and that the catalytic activity of zeolites is not influenced by the framework structure, but shows a volcano-shaped dependence on the Al content. Further, the activity of the Y-type zeolite was increased by a transition metal ion exchange.

References

1) M. Iwamoto, M. Tajima, and S. Kagawa, *J. Chem. Soc., Chem. Commun.*, **1985**, 228; *J. Catal.*, **101**, 195 (1986).

2) M. Nakano, K. Sekizawa, S. Fujii, and Y. Tsutsumi, *Nippon Kagaku Kaishi*, **1986**, 535.

3) M. Iwamoto, H. Mori, M. Tajima, and S. Kagawa, "Proceedings of the International Symposium on Acid-Base Catalysis," ed by K. Tanabe, H. Hattori, T. Yamaguchi, and T. Tanaka, Kodansha, Tokyo (1986), p. 453.

4) K. Eguchi, T. Tokiai, and H. Arai, *Appl. Catal.*, **34**, 275 (1987).

5) E. Kikuchi, T. Matsuda, K. Shimomura, K. Kawahara, and Y. Morita, "New Developments in Zeolite Science and Technology," ed by Y. Murakami, A. Iijima, and J. W. Ward, Kodansha, Tokyo (1986), p. 771.

6) F. Fajula, R. Ibarra, F. Figueras, and C. Gueguen, *J. Catal.*, **89**, 60 (1984).

7) E. Kikuchi, K. Shimomura, K. Kawahara, and Y. Morita, 1st Meeting of Zeolite, Zeolite Research Soc. Jpn., Tokyo, 1985, Abstr., A19.

8) M. Iwamoto, M. Tajima, and S. Kagawa, *J. Chem. Soc., Chem. Commun.*, **1986**, 598.

9) M. Niwa, M. Iwamoto, and K. Segawa, *Bull. Chem. Soc. Jpn.*, **59**, 3735 (1986).

10) S. Namba, N. Hosomura, and T. Yashima, *J. Catal.*, **72**, 16 (1981).

11) K. Tanabe and M. Nitta, *Bull. Jpn. Pet. Inst.*, **14**, 47 (1972).

12) K. Tanaka and A. Ozaki, *J. Catal.*, **8**, 1 (1967).

Entropy Change Associated with the Charge Transfer Reation of Various Quinones in Aprotic Solvents

Kenji KOMAGUCHI, Yasuhiro HATSUSEGAWA, Akira KITANI, and Kazuo SASAKI*
Department of Applied Chemistry, Hiroshima University, Kagamiyama, Higashi-Hiroshima 724
(Received March 18, 1991)

Temperature dependence of the cathodic reduction potentials of various *p*-benzoquinone derivatives have been determined in five aprotic solvents, benzonitrile, acetonitrile, propylene carbonate, *N*,*N*-dimethylformamide, and dimethyl sulfoxide. As for the first electron transfer reactions, the free energy of transfer between any two of solvents has been found to be less than 1.0 kcal mol^{-1}, which is much smaller than the solvation enthalpy of ordinary anions. As a result, the transfer entropy is compensated almost perfectly by the transfer enthalpy. The compensation effect also appears in the transfer energies of the second electron transfer reaction though not perfect.

In the previous paper,[1] we have stated that the free energy of transfer of quinone/quinone anion radical systems in several aprotic solvents is negligibly small. This statement was derived from the experimental fact that the first electrode potential ($E_1°$) of various quinones determined in a solvent M, aligns on a straight line of unit slope when they are plotted against those determined in another solvent N.

The fact is expressed as the following equation,

$$E_1°(\mathrm{i,M}) = E_1°(\mathrm{i,N}) + \mathrm{const.} \quad (1)$$

where i expresses individual substrate and M and N specify two different solvents. Eq. 1 is of course an empirical equation and $E°$ values are apparent ones. Formally speaking, however, the equation should also hold for the absolute potentials though their numerical values are unknown.

$$E_1°(\mathrm{i,M})_{abs} = E_1°(\mathrm{i,N})_{abs} + K \quad (2)$$

Our conclusion was that K appearing in Eq. 2 is very small and is within the experimental uncertainty. In this paper, we will add a quantitative base for the above conclusion by analyzing the entropy change in the redox reaction of various quinone derivatives.

The entropy change associated with the electrode reactions of aromatic compounds has been studied extensively by Svaan and Parker[2] and more recently by Jaworsky[3,4] and also by Nagaoka et al.[5] Entropy change of various quinone derivatives in the gas phase electron attachment is discussed by Heinis et al.[6]

Experimental

A nonisothermal cell arrangement[2,3] was used for determining the temperature coefficient of electrode potentials. In one compartment of the cell, the temperature of which was varied in the range of 10—50 °C at a step of 10 °C, a set of test electrodes were placed. The other compartment, in which a reference electrode was placed, was kept at a fixed temperature (25±0.1 °C) and the temperature gradient was set up over the length of a liquid bridge connecting the two compartments. Potential sweep technique (sweep rate : 0.1 V s^{-1}) was employed for the potential determination at various temperatures. The potential values were determined as the mean of cathodic peak potential and its anodic counterpart. Test solutions contained 0.1 mol dm^{-3} Et_4NClO_4 and 5×10^{-3} mol dm^{-3} of a given substrate. The working electrode was a Pt wire (0.5 mm in diameter and 0.5 cm in length) and the counter electrodes was a Pt plate. The reference electrodes used were low-chloride calomel electrodes whose potentials are dependent on the perchlorate concentration.[7] These electrodes were prepared individually for each solvent system using the respective solvent.

Since all solvents studied are hygroscopic in nature and moistening of the test solution affected strongly the measurement, a special caution was necessary for avoiding the moistening. All the solvents used were dehydrated with CaH_2 or molecular sieves overnight and distilled just before use. Water content was checked by gas chromatography to be less than the limit of detection (8×10^{-4} mol dm^{-3}). The measurements carried out in the course of ascending temperature were repeated in the reverse course of descending temperature so as to confirm the agreement of the two values. The temperature coefficient thus determined has an uncertainty of ±0.02 mV K^{-1}.

Results and Discussion

The temperature coefficients of electrode potentials as well as derived values of entropy change for both the first and second electron transfer reactions of 13 quinones in 5 aprotic solvents are compiled in Table 1. Jaworski's data[4] are also listed for reference. It is evident that our data are always smaller than his by a factor of 2 to 4. We cannont understand why such big differences appeared. Thermal diffusion of silver ion, which was used by him as the potential reference, might be the source of the discrepancy. Enthalpy data were calculated by assuming zero free energy change for the reaction of *p*-benzoquinone **1** in every solvent studied.[8]

Before discussing the nature of the present data, it will be worthwhile to check the reliability of our measurements. Svaan and Parker,[2] who studied the problem with various types of compounds, reported that $\Delta S_1°$ values of dinitrobenzenes ranged from −5.05 (1,4-dinitrobenzene, $T\Delta S_1° = -1.50$ kcal mol^{-1}; 1 cal=4.184 J) to −9.41 e.u. (2,5-dimethyl-1,3-dinitrobenzene, $T\Delta S_1° = -2.80$ kcal mol^{-1}). Our values for various

Table 1. Temperature Coefficients of Reduction Potentials of Various Quinones

Compd[a]	Solvent[b]	dE_1/dT	dE_2/dT	$-T\Delta S_1°$	ΔH_1[c]	$-T\Delta S_2°$	ΔH_2
		(mV K^{-1})		(kcal mol^{-1})			
1	BN	0.82	2.21	5.6	−5.6	15.2	−0.1
	AN	0.62	3.13	4.3	−4.3	21.5	−0.9
		(1.5±0.2)[d]					
	PC	0.44	1.28	3.0	−3.0	8.80	2.0
		(1.4±0.1)[d]					
	DMF	0.38	1.01	2.6	−2.6	6.94	14.8
	DMSO	0.42	1.58	2.9	−2.9	10.9	10.3
		(1.6±0.3)[c]					
2	BN	0.71	3.36	4.9	−12.2	23.1	−12.1
	AN	0.23	1.47	1.6	−9.1	10.1	−1.1
	PC	0.26	2.03	1.8	−9.6	14.0	−7.2
	DMF	0.24	1.62	1.6	−9.4	11.1	3.2
	DMSO	0.11	1.45	0.78	−8.09	9.96	3.0
3	BN	0.48	2.44	3.3	−15.0	16.8	−9.2
	AN	0.18	1.39	1.2	−13.4	9.55	−3.32
	PC	−0.05	1.96	−0.4	−11.7	13.5	−9.1
	DMF	−0.09	1.09	−0.6	−11.7	7.49	1.15
	DMSO	−0.03	1.22	−0.2	−11.2	8.38	−0.86
4	BN	0.18	1.42	1.2	−25.1	9.77	−13.2
	AN	−0.05	1.15	−0.4	−23.2	7.90	−12.6
	PC	−0.17	1.39	−1.2	−21.7	9.55	−15.0
	DMF	−1.42	1.05	−9.76	−13.5	7.21	−10.5
5	BN	0.69	1.87	4.7	−2.3	12.9	6.1
	AN	0.67	2.02	4.6	−2.6	13.9	5.2
	PC	0.78	0.87	5.4	−3.5	6.0	7.3
	DMF	0.29	1.28	2.0	−0.2	8.80	25.1
	DMSO	0.40	1.52	2.7	−0.9	10.4	12.1
6	BN	0.69	3.69	4.7	−0.2	25.4	−4.0
	AN	0.60	4.62	4.1	−7.8	31.8	−13.1
	DMF	0.28	0.96	2.0	1.6	6.6	15.0
	DMSO	0.43	1.66	2.9	0.8	11.4	13.1
7	BN	0.86	3.66	5.9	−0.9	24.8	−6.2
	AN	0.53	2.11	3.7	0.6	14.5	4.4
		(1.1±0.2)[d]					
	PC	0.78	1.60	5.4	−1.2	11.0	2.5
		(1.1±0.1)[d]					
	DMF	0.45	1.29	3.1	0.9	8.86	14.2
	DMSO	0.18	1.22	1.2	3.0	8.38	14.7
		(1.2±0.1)[d]					
8	BN	0.58	2.51	4.0	−5.3	17.3	−2.7
	AN	0.28	1.65	2.0	−3.7	11.3	2.8
	PC	0.14	2.96	0.95	−2.7	20.3	−10.9
	DMF	0.28	1.28	1.9	−4.0	8.80	8.5
	DMSO	0.24	1.26	1.7	−3.6	8.66	7.4
9	BN	0.73	3.90	5.0	2.0	26.8	−5.1
	AN	0.83	2.07	5.7	0.7	14.2	7.6
	PC	0.70	1.80	4.8	1.5	12.4	4.7
	DMF	0.41	1.29	2.8	3.4	8.86	16.7
	DMSO	0.24	1.32	1.6	4.4	9.07	15.6
10	BN	0.87	2.33	6.0	4.7	16.0	8.2
	AN	0.41	1.92	2.8	7.1	13.2	9.3
		(1.0±0.1)[d]					
	PC	0.34	2.58	2.3	7.6	17.7	−0.2
		(1.0±0.1)[d]					
	DMF	0.24	1.15	1.7	7.9	7.90	18.7
	DMSO	0.51	1.50	3.5	6.0	10.3	15.8
		(1.1±0.2)[d]					
11	BN	0.85	1.96	5.9	5.7	13.5	10.4
	AN	0.51	1.71	3.5	7.1	11.7	12.7
	PC	0.37	2.43	2.6	8.0	16.7	1.4
	DMF	0.21	2.27	1.5	8.6	15.6	11.5
	DMSO	0.35	1.19	2.4	7.8	8.18	18.4

Table 1. (Continued)

Compd[a]	Solvent[b]	dE_1/dT	dE_2/dT	$-T\Delta S_1°$	ΔH_1[c]	$-T\Delta S_2°$	ΔH_2
		(mV K^{-1})		(kcal mol^{-1})			
12	BN	0.65	2.09	4.5	8.2	14.4	10.6
	AN	0.32	1.61	2.2	9.8	11.1	13.1
	PC	0.47	1.63	3.2	8.7	11.2	8.5
	DMF	−0.34	0.87	−2.3	14.0	6.0	21.3
	DMSO	0.53	1.14	3.7	8.5	7.83	18.8
13	BN	0.51	1.76	3.5	12.6	12.1	13.9
	AN	0.35	1.45	2.4	13.2	9.96	15.4
	DMF	0.19	0.86	1.3	15.3	5.9	22.7

a) Compounds. **1**: 1,4-benzoquinone (BQ), **2**: 2,5-dichloro BQ, **3**: tetrachloro-BQ, **4**: 2,3-dicyano-5,6-dichloro-BQ, **5**: Me-BQ, **6**: 2,5-diMe-BQ, **7**: 1,4-naphthoquinone (NQ), **8**: 2,3-dichloro-NQ, **9**: 2-Me-NQ, **10**: 9,10-anthraquinone (AQ), **11**: 2-Me-AQ, **12**: 1-amino-AQ, **13**: 1,4-diamino-AQ. b) Solvents, BN: Benzonitrile, AN: Acetonitrile, PC: Propylene carbonate, DMF: *N*,*N*-dimethylforamide, DMSO: Dimethyl sulfoxide. c) Enthalpy data were calculated by assuming tentatively the free energy change associated with the firsr electron transfer reactions of para benzoquinone to be always zero.[8] d) Values in the parenthesis were cited from Jaworski.[3]

quinones are very close to those of dinitrobenzenes. On the other hand, Jaworski's values are very large and almost near our $\Delta S_2°$ vlaues.

The entropy change associated with the charge transfer reaction is mostly determined from the potential difference in a nonisothermal cell. It should be noted that such a measurement unavoidably involves irreversible entropy production intrinsic to the transport phenomena, heat flow and Soret effect.[9] Fortunately, de Bethune[10] showed that, if the potential determining electrode reactions are regarded as reversible, the irreversible entropy productions can be ignored and the standard entropy change can be safely determined. Actually, however, it is also true that many organic compounds do not behave reversibly at electrodes. Quinones are no exception. This is particularly true for the second electron transfer reaction between anion radicals and their dianions as has been described in the previous paper. Accordingly, our attention will mainly be focused on the first electron transfer reactions.

As are seen in Table 1, the variation of $-T\Delta S_1°$ of each individual substrate makes it rather complicated to find some systematic correlation with their molecular characteristics. A notable thing appearing in this table is that there are some compounds which have a positive entropy value. The entropy change for gaseous electron attachment reaction of various quinones have been reported by Heinis et al.[6] According to them, the values are all negative irrespective of the nature of substituents. It is interesting to note that the positive values in Table 1 always appear in the reaction of chlorinated compounds.[11] We have mentioned[1] that there is a significant contrast between the solvation behavior of chlorinated and nonchlorinated compounds. Heinis et al. also noticed a similar substituent effect of Cl in the correlation between electron affinity and electrode potential.[6] To the extension that the solvent is considered as a dielectric continuum, the entropy change should have a negative value. Since the reaction

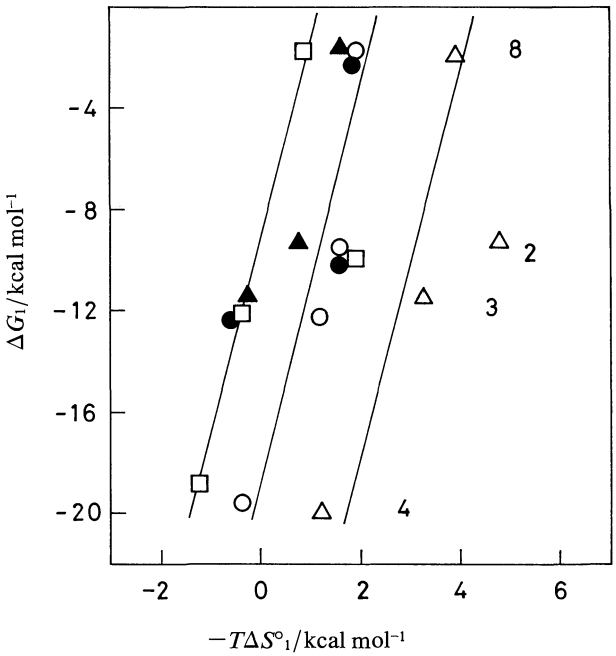

Fig. 1. Entropy change in the first electron transfer reaction of chlorinated compounds. ΔG_1's are relative values referred to 1,4-benzoquinone. Numerical figures indicate compound number given on the margin of Table 1. Symbols specify solvents used. △: BN, □: PC, ○: AN, ●: DMF, ▲: DMSO.

entropy reflects the difference in the structure ordering around the product and reactant, a positive entropy change will indicate that the degree of order is higher with the neutral reactant molecule than that of the charged product. This point is worthy of a more detailed analysis in future studies. Regarding this, there is another point to be noted, though qualitative, that variation of $T\Delta S_1°$ of chlorinated compounds in a given solvent seems to be discriminated from other nonchlorinated compounds. As is seen in Fig. 1, $-T\Delta S_1°$ of chlorinated compounds in a given solvent (solvent is

specified by different symbols), increases with decreasing number of chlorine (or cyano group) substitution; **4>3>2>8**. In addition, if we ignore the point for **4** in DMF, which has an anomalously large positive value and is omitted from the figure, $T\Delta S_1°$ seems to be roughly proportional to ΔG_1.[8] On the other hand, no such simple correlation seems to exist in nonchlorinated compounds. Qualitatively, irrespective of the nature of substrates, $-T\Delta S_1°$ in DMF (●) and DMSO (▲) exhibit smaller values than those in other solvents, particularly in BN (△). Regarding this, it will be worth noting the work of Hupp and Weaver,[12] who studied the entropy change in the redox system of some coordinated transition metal compounds. They showed that, in accordance with the simple Born equation, the reaction entropy changes linearly with the reciprocal of ionic radius. In the present case, however, no such a simple correlation was observed and the entropy change seems to be insensitive to the size of substrate studied.[13] The

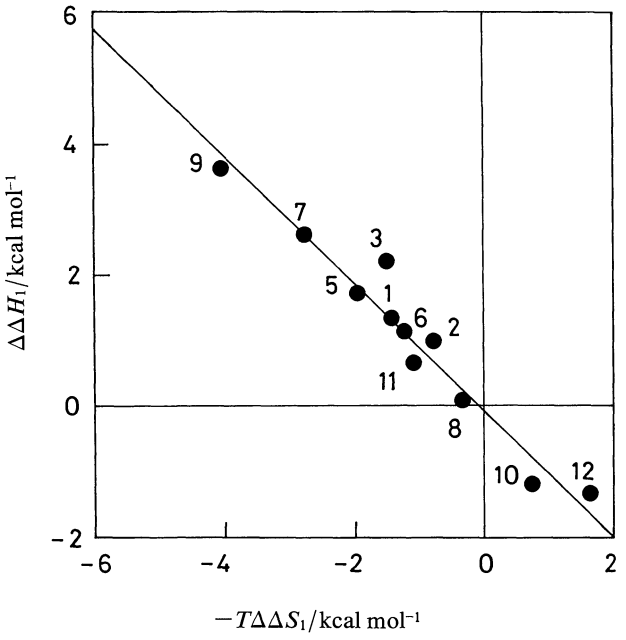

Fig. 2. Correlation between two transfer energies of the first electron transfer reaction transferred from AN to DMSO.

different size dependence appeared in transition metals and quinone systems may be attributed to the difference in the surrounding conditions of charge in molecule. In case of metal complexes, the charge of the central metal ion is separated by ligands from the surrounding solvent molecules and the polarizing force will be directly affected by the size of ligands. On the other hand, in the case of quinone anion radical, most of the negative charge is localized on carbonyl oxygen and the charge density at oxygen will be independent of the size of aromatic ring. The solvation at carbonyl oxygen mainly contributes to entropy change and relatively small size effect would be expected for quinone systems. The spherical symmetry of the metal complexes and planer structure of the quinones should also be accounted for.

Although individual values of $T\Delta S_1°$ vary in a rather complicated fashion, we can find a very simple rule for the transfer entropies, i.e., the difference in two different solvents. A typical example is shown in Fig. 2, where the transfer entropy, $-T\Delta\Delta S_1°$ from AN to DMSO is plotted against the corresponding transfer enthalpy, $\Delta\Delta H_1$.[8] One can readily see that a compensation effect exists between two energies, $T\Delta\Delta S_1°$ and $\Delta\Delta H_1$, for the transfer process concerned. More or less similar correlations were found for every combination of two solvents. Since the compensation between $T\Delta\Delta S_1°$ and $\Delta\Delta H_1$ arises when the free energy of transfer is almost null, the results obtained here provide a strong support to our previous conclusion.

The compensation effect can be analyzed in a little more detail. Table 2, which lists the least square parameters in the following equation, was prepared for this purpose.

$$T\Delta\Delta S_1° = a\Delta\Delta H_1 + b$$

Generally speaking, when the compensation is perfect and the potential of the reference electrode is invariable throughout the different solvents studied, the slope "a" should be unity and the intersect "b" must be zero. If, on the other hand, the transfer free energy is not zero but is a constant, b will have a finite value. Of course, the potential of the reference electrode cannot be regarded to be invariable because the perchlorate activity will vary slightly from solvent to solvent. According to Parker,[14]

Table 2. Parameters Appearing in the Compensation Equation,[8] $T\Delta\Delta S_1° = a\Delta\Delta H_1 + b$

Solvent couple from	Solvent couple to	a/kcal mol^{-1}	b/kcal mol^{-1}	Correlation coefficient
AN	BN	0.94±0.09	0.54±0.15	0.954
PC	BN	0.83±0.10	0.72±0.23	0.943
DMF	BN	0.86±0.06	1.01±0.23	0.980
DMSO	BN	0.82±0.12	1.01±0.31	0.913
PC	AN	0.86±0.06	0.06±0.07	0.980
DMF	AN	0.95±0.05	0.14±0.15	0.988
DMSO	AN	0.99±0.08	0.07±0.14	0.973
DMF	PC	1.01±0.02	0.19±0.07	0.998
DMSO	PC	0.97±0.07	0.01±0.14	0.981
DMSO	DMF	0.91±0.08	−0.16±0.10	0.969

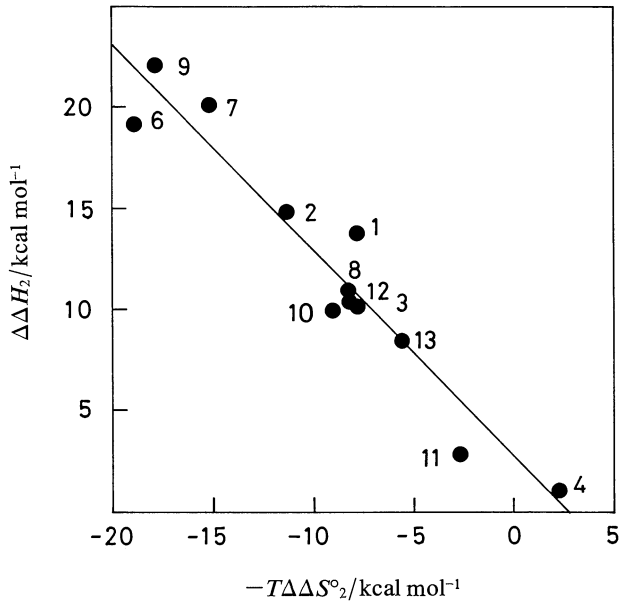

Fig. 3. Correlation between two transfer energies of the second electron transfer reaction transferred from BN to DMF.

the activity coefficient of perchlorate anion changes from −0.3 in DMSO to −0.4 in DMF. The resultant variation of the electrode potential is less than 1 mV(0.02 kcal mol^{-1}). The largest value of b in Table 2 is 1.01±0.3 kcal mol^{-1} for the transfer process from DMSO to BN. It should be noted in the first place that an enthalpy change of 1.0 kcal mol^{-1} is much smaller than the solvation enthalpy of typical anions (65 to 115 kcal mol^{-1} for I^- to F^-)[15] and is still of the order of the experimental uncertainty, which is estimated to be less than 0.3 kcal mol^{-1}.

It is interesting to note that, however, the b values seem to vary rather systematically according to the order of solvation energies observed previously for the second electrode potential, ($E_2°$): DMSO-DMF>PC>AN>BN. Final conclusions on this matter can thus be summarized as follows.

1. The free energy of transfer of the quinone/quinone anion radical system among several aprotic solvents studied here does not exceed 1.01±0.3 kcal mol^{-1} and is almost negligible.

2. There is a possibility that a very small solvent effect yet exists, however, within the limit of 1.0 kcal mol^{-1}.

A similar compensation effect can also be found in the second electron transfer reactions as is shown in Fig. 3. Except for the solvent combination of PC and DMF, we can find a fairly good linear correlation between $\Delta\Delta H_2$ and $T\Delta\Delta S_2°$ suggesting that the two transfer energies, $T\Delta\Delta S_2°$ and $\Delta\Delta H_2$, are largely though not perfectly compensating each other. As for the second electron transfer reactions, scattering of data is enhanced and it seems difficult to draw meaningful correlations.

The authors are grateful to Mr. Yasushi Ohsaki, Mr. Masahiro Ohura, and Mr. Tomoyuki Kashimura for their preliminary work of this research.

References

1) K. Sasaki, T. Kashimura, M. Ohura, and Y. Ohsaki, *J. Electrochem. Soc.*, **137**, 2438 (1990).

2) M. Svaan and A. J. Parker, *Acta Chem. Scand., Ser. B,* a) **35**, 559 (1981). b) **36**, 351, 357, 365 (1982), c) **38**, 751, 759, 767 (1984).

3) J. S. Jaworski, *Electrochim. Acta,* **31**, 85 (1986).

4) J. S. Jaworski, *J. Electroanal. Chem.*, **219**, 209 (1987).

5) T. Nagaoka, T. Yoshino, and S. Okazaki, *J. Electroanal. Chem.*, **242**, 323 (1988).

6) T. Heinis, S. Chowdhury, S. L. Scott, and P. Kebarle, *J. Am. Chem. Soc.*, **110**, 400 (1989).

7) O. Bravo and R. T. Iwamoto, *J. Electroanal. Chem.*, **23**, 419 (1969).

8) It should be noted that the entropy values here discussing are the absolute ones while those of ΔG and ΔH are relative values determined on the arbitrary assumption : ΔG_1 for the reaction of *p*-benzoquinone is always zero irrespective of solvent. As a result, ΔH values in Table 1 involve a constant difference from the absolute values. The assumption, however, does not contain any drawback since we are discussing the difference of two ΔH values ($\Delta\Delta H$).

9) I. Prigogine, "Thermodynamics of Irreversible Processes," 3rd ed, Interscience Publishers, New York (1967) ; S. R. De Groot, "Thermodynamics of Irreversible Processes," North Holland Publishing Company, Amsterdam (1952).

10) A. J. de Bethune, T. S. Licht, and N. Swendman, *J. Electrochem. Soc.*, **106**, 616 (1959).

11) There is a possibility that chloride ion is detached from the quinoid ring as a follow up reaction to the electron transfer. This will act to increase the negative entropy value, however.

12) J. T. Hupp and M. J. Weaver, *Inorg. Chem.*, **23**, 3639 (1984).

13) Estimated radius varies from 4.1 to 5.7 Å for unsubstituted benzoquinone to 9,10-anthraquinone, while corresponding variation in the entropy change ($-T\Delta S_1$) are from 5.62 to 5.97 in BN, 4.27 to 2.80 in AN, and so on (see Table 1).

14) A. J. Parker, *Chem. Rev.*, **69**, 1 (1969).

15) J. O'M Bockris, A. K. N. Reddy, "Modern Electrochemistry," Plenum Press, New York (1970), Chap. 2.

 © 1991 The Chemical Society of Japan Bull. Chem. Soc. Jpn., 64, 2691—2694 (1991)

Mixed Adsorbed Film and Micelles of Sodium Taurocholate and Sodium Taurodeoxycholate

Atsunori WADA, Norihiro MATUBAYASI,* and Kinsi MOTOMURA†
Faculty of Fisheries, Nagasaki University, 1-14 bunkyoumachi, Nagasaki 852
† Department of Chemistry, Faculty of Science, Kyushu University 33, Fukuoka 812
(Received April 8, 1991)

The surface tension of an aqueous mixture of sodium taurocholate (NaTC) and sodium taurodeoxycholate (NaTDC) in the presence of 0.1 mol kg^{-1} sodium chloride was measured as a function of the total concentration and composition of the bile salts at 25 °C. The result, processed by a thermodynamic treatment based on excess thermodynamic quantities, showed that NaTC and NaTDC are freely miscible in an adsorbed film, while mixing in a limited composition region of the micelle.

The sterol nucleus constitutes a hydrophobic group of a variety of surfactants having a biological origin. In our previous papers we have shown the strong lateral attractive force of the sterol nucleus and how it mixes with a hydrocarbon chain in a mixed adsorbed film.[1-3] Sodium taurocholate (NaTC) and sodium taurodeoxycholate (NaTDC) are typical surfactants which have the sterol nucleus as a hydrophobic group, and in which the hydrophobic property is changed accounting to the number of hydroxyl groups. For NaTDC, dihydoxy bile salt, the characteristic behavior (such as their small aggregation number and unusual shapes of the micelle) have been shown.[4-6] For NaTC, trihydoxy bile salt, the critical formation of a micelle has been questioned because of its broad critical concentration region.[4-8]

In order to understand the properties of bile salts better, such as micelle formation and lateral interaction arising from the difference in the number of hydroxyl groups, we have chosen an NaTC–NaTDC mixed system in an aqueous solution with 0.1 mol kg^{-1} sodium chloride added. This mixed system is suitable for differentiating between trihydoxy and dihydoxy bile salts, since NaTC and NaTDC have chemically the same structure, except for their 7 position. We have measured the surface tension of the aqueous mixtures as a function of the concentration and composition of bile salts at 25 °C. It has been shown that the thermodynamic properties of synthetic surfactants in micelles are quite similar to that in an adsorbed film.[9-11] A thermodynamic treatment seems to be applicable to the NaTC–NaTDC system, although the micelle structure of the bile salts is very different from that of synthetic surfactants. Special interest is put on the relation of the compositions between the bulk, the adsorbed film, and the micelle. We hope to demonstrate some of the characteristics of the lateral interaction of bile salts in the micelle and the adsorbed film using thermodynamic analysis.

Materials and Method

Sodium taurocholate (NaTC) and sodium taurodeoxycholate (NaTDC) were purchased from Sigma Chem. Co. and used without purification. As shown in the result section, the measured surface tension vs. concentration curves for NaTDC and their mixtures show no minimum around their critical micell concentration (cmc). Aqueous solutions of bile salts were prepared with a 0.1 mol kg^{-1} sodium chloride solution. Sodium chloride was used as received, and water was twice distilled from an alkaline permanganate solution. The surface tension was measured by a drop volume technique, described elsewhere.[12] The drop was permitted to stand for 15 min in order to confirm the adsorption equilibrium.

Result

Mixed Adsorbed Film of NaTC and NaTDC. In order to analyze the mixed adsorbed film of NaTC and NaTDC, we measured the surface tension of aqueous solutions of the mixture as a function of the total concentration of bile salts (m_t) in a molality scale defined by

$$m_t = m_1 + m_2. \tag{1}$$

The composition of the bile salts (X_2^W) was defined as

$$X_2^W = m_2/m_t \tag{2}$$

at constant pressure and temperature, 25 °C.[13] Here, subscripts 1 and 2 refer to NaTC and NaTDC, respectively, and superscript W refer the aqueous phase. The results are shown in Fig. 1. The surface tension decreases steeply with increasing total concentration, representing the high surface activity of bile salts.

In the solution measured, the ith salts completely dissociated into $\nu_{i,k}$ k-ions. Then, the variation of the surface tension (γ) at constant temperature and pressure is given as[9-14]

$$d\gamma = -\sum_k \sum_i \nu_{i,k} \Gamma_k^H d\mu_k, \tag{3}$$

where Γ_k^H and μ_k refer to the surface densities and chemical potential of the kth ions. Subscript i counts for NaTC, NaTDC, and NaCl, respectively, and k counts for taurocholate anion (TC), taurodeoxycholate anion (TDC), Cl^-, and Na^+, respectively. In the present system all ions behave almost ideally up to the cmc,[6] the chemical potential of ion k is thus given as

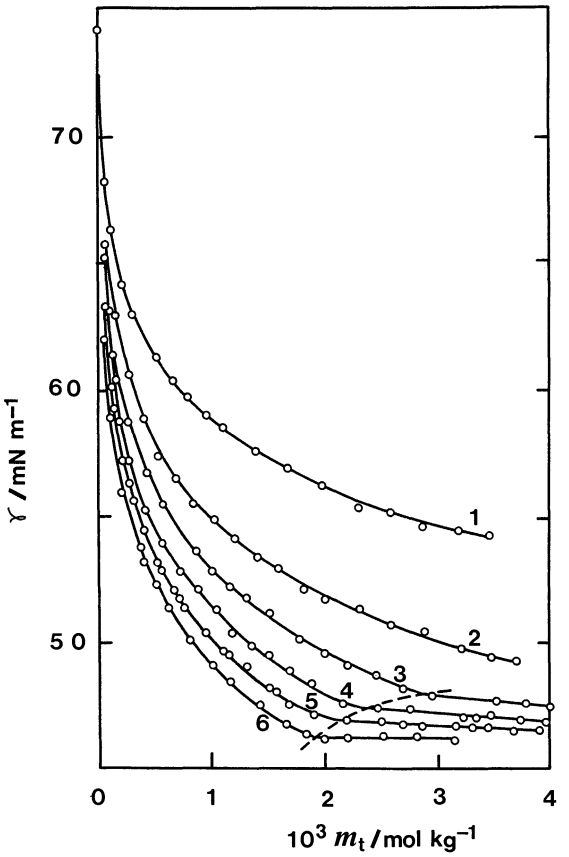

Fig. 1. Surface tension vs. concentration curves of NaTC–NaTDC mixed system in 0.1 mol kg^{-1} sodium chloride aqueous solution at constant composition: (1) X_2^W=0.0; (2) 0.2; (3) 0.4; (4) 0.6; (5) 0.8; (6) 1.0. The dotted line connects the cmc.

$$\mu_k = \mu_k^\circ(T,p) + RT\ln\sum_i \nu_{i,k}\, m_i. \tag{4}$$

Rearranging of Eq. 3 using Eqs. 1, 2, and 4 leads to

$$d\gamma = -RT\left(\frac{\Gamma_t^H}{m_t} + \frac{\Gamma_t^H}{m_t+m_3} + \frac{\Gamma_{Cl}^H}{m_t+m_3}\right) dm_t - RT\left(\frac{\Gamma_2^H}{X_2^W} - \frac{\Gamma_1^H}{X_1^W}\right) dX_2^W, \tag{5}$$

where subscript 3 refers the added NaCl and Γ_t^H refers to the total interfacial density defined as

$$\Gamma_t^H = \Gamma_1^H + \Gamma_2^H. \tag{6}$$

Taking into account the fact that Γ_{Cl}^H is smaller than Γ_t^H as well as the high concentration of NaCl, the third term within the first brackets in Eq. 5 is negligible compared to the other terms. Then, the Γ_t^H and the composition of the adsorbed film (X_2^H) are evaluated, respectively, using the relations

$$\Gamma_t^H = -\frac{m_t(m_t+m_3)}{RT(2m_t+m_3)}\left(\frac{\partial\gamma}{\partial m_t}\right)_{T,p,X_2^W}, \tag{7}$$

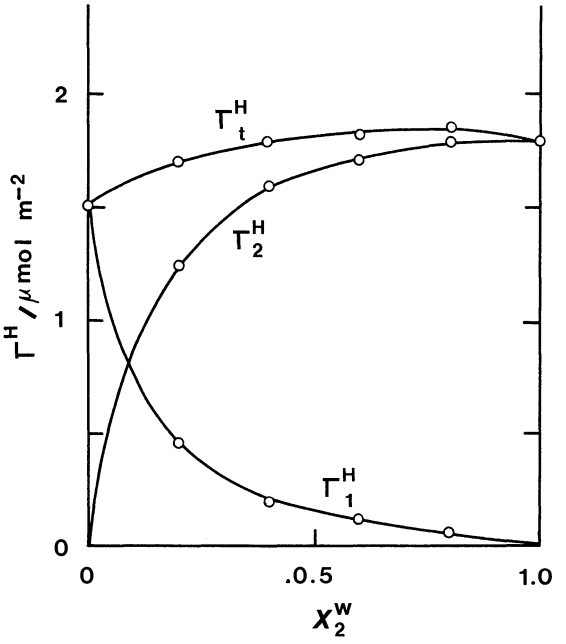

Fig. 2. Surface density vs. composition curves at constant total concentration of 1.0×10^{-3} mol kg^{-1}.

$$X_2^H = X_2^W - (X_1^W X_2^W/RT\Gamma_t^H)(\partial\gamma/\partial X_2^W)_{T,p,m_t}, \tag{8}$$

and

$$X_2^H = X_2^W - [1/m_t + 1/(m_t+m_3)]X_1^W X_2^W \times (\partial m_t/\partial X_2^W)_{T,p,\gamma}. \tag{9}$$

The adsorption isotherms for both bile salts rise sharply at low concentrations and almost reach a plateau over a total concentration of about 0.5×10^{-3} mol kg^{-1}. In Fig. 2, the evaluated total surface density is plotted against the bulk composition at a total concentration of 1×10^{-3} mol kg^{-1}. Here, the total surface density shows increases in going from pure TC and a plateau in going to pure TDC over an X_2^W of about 0.4. Applying Eqs. 8 and 9 for graphs of m_t vs. X_2^W at constant γ and γ vs. X_2^W at constant m_t (obtained from the Fig. 1), the values of the composition in a mixed adsorbed film were calculated and plotted against the bulk composition at a constant surface tension value of 55 mN m^{-1} (Fig. 3). It can be seen that the composition in the adsorbed film lies close to TDC compared with that of a bulk solution. Using this value, the surface densities of TC and TDC are also plotted in Fig. 2. The surface density of TC drops steeply, while that of TDC increases rapidly with increasing X_2^W. These results agree well with previous work in that the adsorbed mixed film is enriched by the component which shows a stronger cohesive interaction in the film.[2,3,12,13]

The interaction in the mixed film can easily be seen in a plot of the mean area per molecule (A) (A=1/$N_A\Gamma_t^H$, where N_A is the Avogadro's number) against the com-

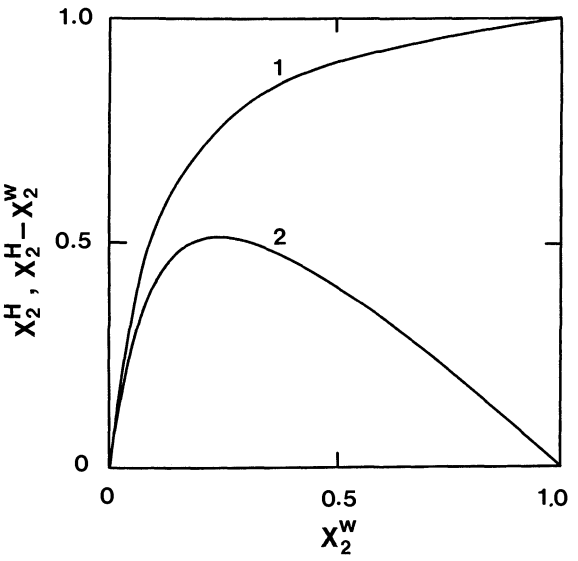

Fig. 3. Relation between compositions in the adsorbed film and aqueous solution in equilibrium at constant surface tension of 55 mN m^{-1}: (1) X_2^H vs. X_2^W; (2) $X_2^H - X_2^W$ vs. X_2^W.

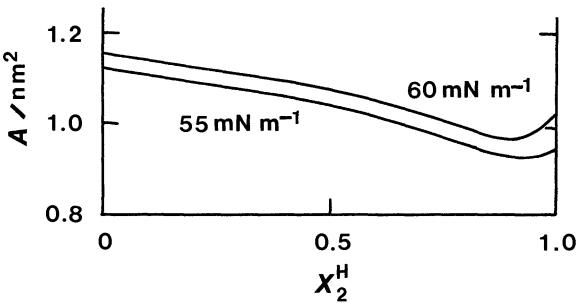

Fig. 4. Mean area occupied per molecule vs. composition in the adsorbed film curves at constant surface tension values.

position of the mixed film, as shown in Fig. 4. In the TC-rich region the mean area shows almost ideal mixing, while a slight attractive interaction in the TDC-rich region can be seen.

Mixed Micelle of NaTC and NaTDC. In order to obtain the cmc of a mixture of NaTC and NaTDC, the surface tension of the aqueous mixtures was measured at a high total concentration under a fixed NaCl concentration of 0.1 mol kg^{-1} at 25 °C. For NaTDC the slope of the plot changes markedly at 1.89×10^{-3} mol kg^{-1}. Above this concentration the surface tension remains constant, giving evidence that the aggregation number is sufficiently large to determine the cmc by surface tension measurements. The value of the cmc agrees well with the interpolated value from emf measurements in several added NaCl concentrations reported by Ryu et al.[6] For NaTC the surface tension gradually decreases with m_t over the entire concentration range measured. For mixtures, there are sharp breaks

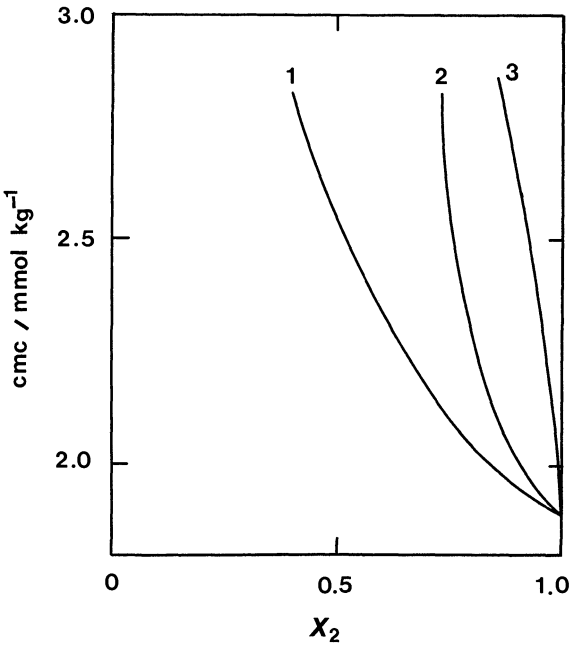

Fig. 5. Critical micelle concentration vs. composition curves. (1) cmc vs. X_2^W; (2) cmc vs. X_2^M; (3) cmc vs. $X_2^{H,cmc}$.

in the plots, except for X_2^W=0.2. However, the changes of the slopes at the break points become less sharp in going to pure TC, and at concentrations above the break point the surface tension gradually decreases with increasing concentration. We can assume that the aggregations which can be designated as micellization occur at these break points, since the curve connecting these break points is monotonous. The cmc's, thus obtained, are plotted against X_2^W in Fig. 5. It is important to note that the cmc depends strongly on the bulk composition and is difficult to extrapolate to the pure NaTC axis, indicating that a pure NaTC micelle can not be formed in a moderate concentration region.

By a thermodynamic treatment based on the excess thermodynamic quantities, similar to those used for the adsorbed film, the Gibbs–Duhem equation of the mixed micelle is given as[15]

$$\sum_k \sum_i \nu_{i,k} N_k^M d\mu_k = 0. \quad (10)$$

Denoting the composition of a mixed micelle by X_2^M ($X_2^M = N_1 + N_2$, where N is the number of k-ions in a mixed micelle) and using Eqs. 4 and 10 yields

$$X_2^M = X_2^W - X_1^W X_2^W [1/\text{cmc} + 1/(\text{cmc} + m_3)] \times (\partial \text{cmc}/\partial X_2^W)_{T,p}, \quad (11)$$

where assumptions that the condition of electroneutrality holds for a micelle, the solution can be treated ideally, and N_{Cl^-}/N_t smaller than unity are achieved.[15] Applying this relation to the curve in Fig. 5, the composition of a micelle at the cmc is shown as cmc vs.

X_2^M plots in Fig. 5. The composition in an adsorbed mixed film at cmc is calculated by the following equation[11] (and plotted in Fig. 5):

$$X_2^{H,cmc} = X_2^M - (X_1^W X_2^W / RT\Gamma_t^{H,cmc})(\partial\gamma^{cmc}/\partial X_2^W)_{T,p}. \quad (12)$$

If the aggregation numbers of bile salts are as small as dimers or trimers, a thermodynamic treatment for micelles based on excess thermodynamic quantities is not applicable. The experimental result is that the surface tension vs. concentration curve of pure NaTDC gives constant values after cmc. This confirms an aggregation number which is sufficiently large for a thermodynamic treatment. Furthermore, the evaluated values of the composition in the adsorbed film at the cmc's using Eq. 12 agree well with the values obtained from Eq. 7. These results demonstrate that micelles composed of bile salts can be adequately treated by the thermodynamic treatment employed here, although the treatment assumes a hypothetical dividing surface in the micelle.

Discussion

TC and TDC have the same chemical structure, except for a hydroxyl group in the TC 7 position of the cholanic acid residue. The number of hydroxyl groups results in the difference in their aggregation behavior. It has been shown that TDC forms a micelle while TC does not in a moderate concentration region.[4-6] This behavior is clearly shown in the cmc vs. X_2^W graph shown in Fig. 5. For mixtures, the cmc's were observed above about X_2^W=0.2. Even at such a low composition of TDC in solution the calculated composition in the mixed micelles shows a value of nearly 0.8; the cmc vs. X_2^M curve shows an almost vertical change at that composition, indicating a solubility limit of TC in the TDC micelle.

For synthetic surfactants it has been shown that the molecular interaction in a micelle is quite similar to that in an adsorbed film.[11] For bile salts we can also assume that the molecular interaction in micelles is basically the same as that in the adsorbed film, even though the size and structure of bile salt micelles are unlike that of synthetic surfactants.[15] In the adsorbed film TC and TDC shows a slight attractive interaction, as shown in the A vs. X_2^H relations. This result indicates that TC and TDC will attract each other and mix freely in their micelles. However, there is a significant difference in the compositions of the adsorbed film and micelle. A deviation of the compositions from that of a bulk solution is a useful indication of the geometrical packing factor in the micelle, since the interactions between monomeric bile salts in a bulk solution are negligible. In studies of a series of alkyl ammonium salt mixtures,[11,17,18] differences have been clearly shown among compositions of the solution, the adsorbed film, and the micelle arising from the chemical structure of the surfactants and the micelle. For the decylammonium bromide–decylammonium chloride (DeAC) system,[17] in which the difference is their counter ions, both salts mix ideally and the X_2^W, $X_2^{H,cmc}$, and X_2^M have almost the same values, even though they differ significantly due to differences in their cmc's and in the surface tension values at the cmc of pure salts. For the dodecylammonium chloride (DAC)–DeAC system,[11] the $X_2^{H,cmc}$ and X_2^M lie close to TDC and $X_2^{H,cmc}$ is slightly larger than the X_2^M, indicating that the stronger cohesive interaction is weakened at the curved interface. On the other hand, the cone-shaped dodecyltrimethylammonium chloride (DTAC) aggregates into a micelle rather than into an adsored film. For the DeAC–DTAC system,[18] X_2^M shows a remarkably larger value than does $X_2^{H,cmc}$.

Together with these findings, the relation among the compositions of the NaTC–NaTDC system indicates that the structure of the bile salt micelle is very different from that of the plane interface; the stronger cohesive force of NaTDC is weakened appreciably in the micelle due to the geometry of the mixed micelle.

References

1) N. Matubayasi and K. Motomura, *Langmuir,* **2**, 777 (1986).
2) N. Matubayasi, R. Matsunaga, and K. Motomura, *Langmuir,* **5**, 1048 (1989).
3) N. Matubayasi, R. Matsumoto, and K. Motomura, *Langmuir,* **6**, 822 (1990).
4) J. P. Kratohvil, *Adv. Colloid Interface Sci.,* **26**, 131 (1986).
5) J. P. Kratohvil, W. P. Hsu, and D. I. Kwok, *Langmuir,* **2**, 256 (1986).
6) K. Ryu, J. M. Lowery, D. F. Evans, and E. L. Cussler, *J. Phys. Chem.,* **87**, 5015 (1983).
7) P. Schurtenberger, N. Mazer, and W. Kanzlg, *J. Phys. Chem.,* **87**, 308 (1983).
8) S. M. Mayerhoffer and L. B. McGown, *Langmuir,* **6**, 187 (1990).
9) K. Motomura, S. Iwanaga, M. Yamanaka, M. Aratono, and R. Matuura, *J. Colloid Interface Sci.,* **86**, 151 (1982).
10) M. Yamanaka, H. Iyota, M. Aratono, K. Motomura, and R. Matuura, *J. Colloid Interface Sci.,* **94**, 451 (1983).
11) K. Motomura, H. Matsukiyo, and M. Aratono, *ACS Symp. Ser.,* **311**, 163 (1986).
12) K. Motomura, S. Iwanaga, Y. Hayami, S. Uryu, and R. Matuura, *J. Colloid Interface Sci.,* **80**, 32 (1981).
13) M. Aratono, S. Uryu, Y. Hayami, Motomura, and R. Matuura, *J. Colloid Interface Sci.,* **93**, 162 (1983).
14) K. Motomura, M. Aratono, N. Matubayasi, and R. Matuura, *J. Colloid Interface Sci.,* **67**, 247 (1978).
15) K. Motomura, M. Yamanaka, and M. Aratono, *Colloid Polym. Sci.,* **262**, 948 (1984).
16) N. A. Mazer, M. C. Carey, P. F. Kwasnik, and G. B. Benedek, *Biochemistry,* **18**, 3064 (1979).
17) H. Matsuki, N. Ando, M. Aratono, and K. Motomura, *Bull. Chem. Soc. Jpn.,* **62**, 2507 (1989).
18) N. Ikeda, E. Shiota, M. Aratono, and K. Motomura, *Bull. Chem. Soc. Jpn.,* **62**, 410 (1989).

 © 1991 The Chemical Society of Japan Bull. Chem. Soc. Jpn., 64, 2695—2699 (1991)

Solvatochromic Shift of Aromatic Ketyl Anions due to Hydrogen Bonding

Tsuneki ICHIKAWA,* Ken-ichi UEDA, and Hiroshi YOSHIDA
Faculty of Engineering, Hokkaido University, Sapporo 060
(Received April 20, 1991)

The electronic spectra of fluorenone radical anions generated by γ-irradiation at 77 K in glassy matrices of ethanol and ethanol–2-methyltetrahydrofuran mixtures have been measured for elucidating the mechanism of the spectral change due to solvation of the radical anions by alcohols. Three kinds of the radical anions are generated in the mixed solvent: the radical anions without hydrogen bond ($\varepsilon = 1.05\times10^4$ dm^3 mol^{-1} cm^{-1} at λ_{max}=568 nm), with one ethanol molecule ($\varepsilon = 0.67\times10^4$ dm^3 mol^{-1} cm^{-1} at λ_{max}=529 nm) and two ethanol molecules ($\varepsilon = 0.37\times10^4$ dm^3 mol^{-1} cm^{-1} at λ_{max}=448 nm) hydrogen-bonded through the π electron on the carbonyl oxygen. The spectral shift and the decrease of the molar extinction coefficient of aromatic ketyl radical anions are explained as due to the stabilization of a carbonyl antibonding π orbital by hydrogen bonding.

One of the powerful methods for studying solvation dynamics is the pulse radiolysis technique. In this method solute molecules are first generated by irradiation of a solution with a pulsed ionizing radiation, and the spectral change of the solute due to solvation are detected using a fast optical detection system.[1] However the technique is not always suitable for studying the solvation structure, because the spectral resolution of the detection system is not necessarily high enough for discriminating the solutes with different solvation structures.

The solvation dynamics of benzophenone radical anions in alcohols have been extensively studied by using the pulse radiolysis technique,[2-6] since solvation of the radical anions entails exceptionally large spectral shift. In these studies the spectral shift was attributed to electrostatic effects induced by the reorientation of solvent dipoles. On the other hand, Shida et al. attributed the spectral shift to hydrogen bonding between the anion radical and alcohol. They measured absorption spectra of benzophenone radical anions in γ-irradiated matrices at 77 K, and found the absorption maximum at 630 nm in ethanol matrix but at 800 nm in aprotic matrices.[7,8] Hoshino et al. measured transient absorption spectra of several aromatic ketyl radical anions in alcohols and found a gradual blue shift of the absorption maxima except for the fluorenone radical anion.[9] They claimed that the spectral shift was not due to hydrogen bonding but to reorientation of solvent dipoles. They considered that the neutral aromatic ketones had already been hydrogen-bonded to alcohols.[10] However, it was suggested later that the hydrogen bond could be formed through the out-of-plane π electron of the radical anion.[11,12] We recently studied in detail the solvation of benzophenone radical anion in γ-irradiated ethanol–2-methyltetrahydrofuran mixtures at cryogenic temperatures and concluded that the spectral shift is due to hydrogen bonding between the radical anion and ethanol.[13] The out-of-plane π electron localized mainly on the carbonyl oxygen is invoked for the bond. The preexisting in-plane hydrogen bond between the neutral aromatic ketone and alcohol is considered not to affect the absorption spectrum due to π–π transitions.

Although the molecular structure of fluorenone is similar to that of benzophenone, Hoshino et al. failed to detect the spectral shift of the former radical anion by solvation. On the other hand, Shida et al. observed the solvent dependency of the absorption spectrum and proposed that the hydrogen bonding with one and two alcohol molecules is responsible for the apparently complex spectra of the fluorenone radical anion in alcoholic matrices.[11,12,14]

In the present study the electronic spectra of the fluorenone radical anion in γ-irradiated ethanol–2-methyltetrahydrofuran mixtures have been measured at 77 K to elucidate the nature of the solvation process. A molecular orbital explanation is given for the spectra change of aromatic ketyl radical anions due to the formation of hydrogen bond.

Experimental

Ethanol (Wako Pure Chemical Co.; >99.5%) was used without further purification. 2-Methyltetrahydrofuran (MTHF) was used after purification with usual procedures.[3] The volume fractions of ethanol in the ethanol–MTHF mixture were 0, 0.25, 0.5, and 1 at 293 K. The solutions containing 0.04 mol dm^{-3} of fluorenone were degassed by several freeze-pump-thaw cycles and then sealed in high-purity quartz cells with an optical path length of 0.2 cm. The samples were then immersed in liquid nitrogen to produce crack-free glass matrices.

The samples were irradiated at 77 K with ^{60}Co γ-rays to a dose of 2.2 kGy to generate the fluorenone radical anion by the following reactions,

$$S\wwwwwr S^+ + e^-,\quad e^- + Fl \longrightarrow Fl^-,$$

where S and Fl denote the solvent and fluorenone molecules, respectively. The absorption spectra were measured at 77 K on a Shimadzu MPS-5000 spectrophotometer equipped with a cryostat for optical measurements. The concentration of the radical anion was calculated from the absorbed dose using the yields of 2.35 and 2.55 scavengeable electrons per 100 eV absorbed by ethanol and MTHF, respectively.[8] The yield for the mixed matrices was assumed to be proportional to the composition of the solvent molecules.

Results

Figure 1 shows the absorption spectra of fluorenone radical anion in neat MTHF, neat ethanol, and in the equivolume mixture of MTHF and ethanol. The radical anion in neat MTHF showed an absorption maximum at 568 nm with the molar extinction coefficient of 1.05×10^4 dm^3 mol^{-1} cm^{-1}. In neat ethanol, the absorption maximum was shifted to 448 nm. The hatched part of the spectrum in Fig. 1 is due to the neutral fluorenone ketyl radical generated by proton transfer to the radical anion.[8,14] The yield of the ketyl radical was estimated to be 16% of the electron yield. After the correction for the conversion into the neutral radical, the extinction coefficient of the radical anion in ethanol was determined to be 0.37×10^4 dm^3 mol^{-1} cm^{-1}. The radical anion in the mixed matrix showed a new peak in addition to the peaks corresponding to those in neat MTHF and ethanol. The appearance of the three peaks clearly indicates that the radical anion exists in three forms, i.e., without and with one and two ethanol molecules hydrogen-bonded to the radical anion.

The absorption spectrum of the radical anion with one hydrogen-bonded ethanol molecule was obtained by substracting the spectra for neat MTHF and ethanol from the spectrum for the mixed matrix. The absorption of the overlapping neutral ketyl radical was corrected by assuming that the ratio of the radical against the radical anion with two hydrogen-bonded ethanols is independent of the composition of the mixed solvent. Fig. 2 shows the normalized spectra of the three components, $I_0(\lambda)$, $I_1(\lambda)$, and $I_2(\lambda)$, corresponding to the fluorenone radical anion with zero, one, and two

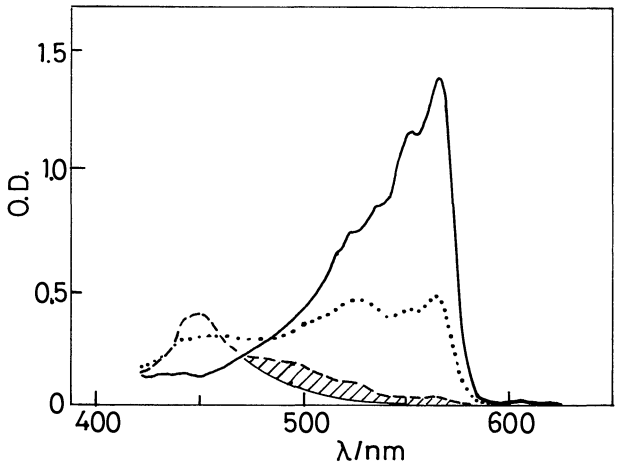

Fig. 1. Absorption spectra of fluorenone radical anions in glassy matrices of (—) neat MTHF, (---) neat ethanol, and (···) 1:1 mixture of MTHF and ethanol.

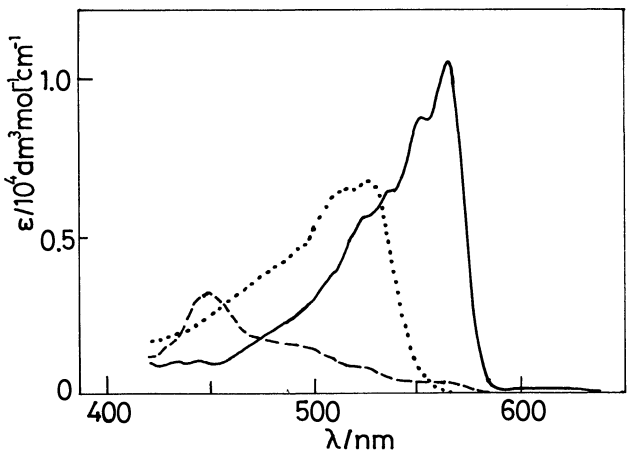

Fig. 2. Spectral components of the absorption spectra of fluorenone radical anions in ethanol–MTHF mixed matrices.

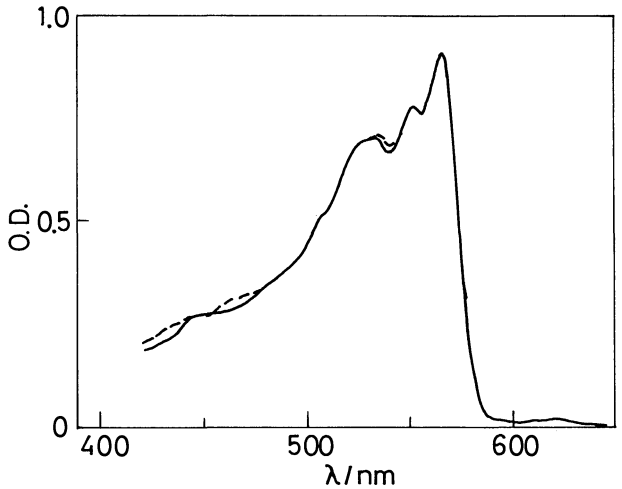

Fig. 3. Comparison of the (—) observed and (---) calculated spectra of fluorenone radical anions in 25% ethanol matrix.

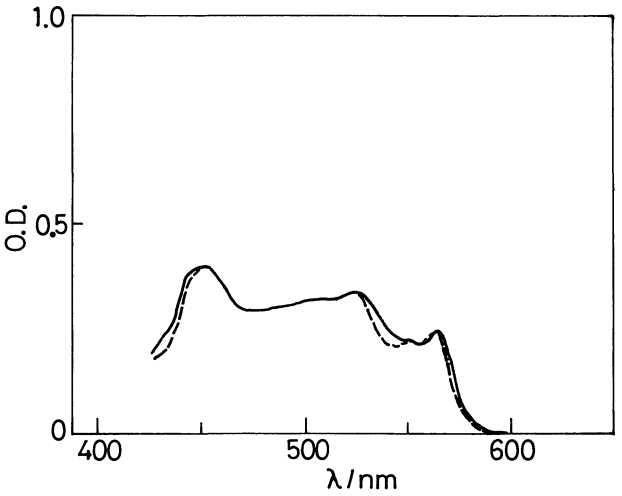

Fig. 4. Comparison of the (—) observed and (---) calculated spectra of fluorenone radical anions in 75% ethanol matrix.

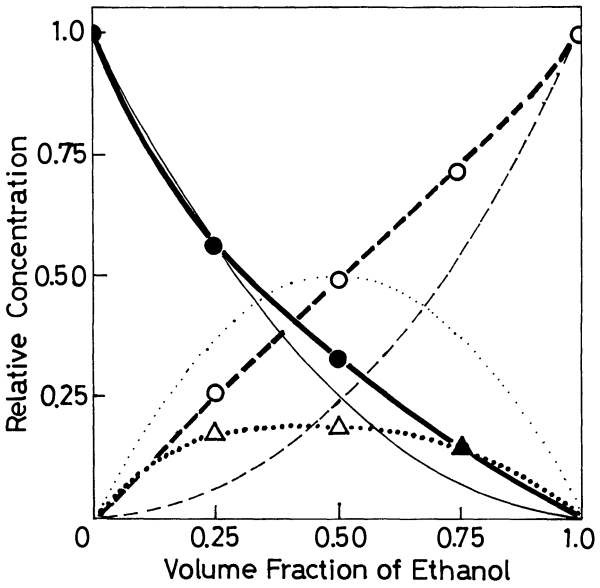

Fig. 5. Dependence of ethanol concentration on the relative concentration of three types of fluorenone radical anions in ethanol–MTHF mixed matrix: the radical anion (●, —) without ethanol, (△, ···) with one, and (○, ---) two hydrogen-bonded ethanol molecules. Thinner curves show the relative concentrations calculated under the assumption of random spatial distribution of ethanol (see Eq. 2 in the text).

hydrogen-bonded ethanol molecules, respectively. The absorption spectrum, $S(\lambda)$, for the mixed matrix of volume fraction x of ethanol is expressed as a sum of the three spectral components,

$$S(\lambda)=[W_0(x)I_0(\lambda)+W_1(x)I_1(\lambda)+W_2(x)I_2(\lambda)]C(x), \quad (1)$$

where $W_i(x)$ is the mole fraction of the three types of the radical anion with respect to the total radical anions, and $C(x)$ is the yield of the scavengeable electrons. Figs. 3 and 4 compare the observed and calculated spectra for the mixed matrices of x=0.25 and 0.75, respectively. The value of $W_i(x)$ was determined by best-fitting the calculated spectrum with the observed one. The fair agreement of the spectra indicates that only three types of the radical anion exist in the mixed matrices. The mole fractions determined from the observed spectra are shown in Fig. 5.

Discussion

Since the observed absorption spectra of the fluorenone radical anion in the mixed matrices of ethanol and MTHF can be reconstructed from the three components, the solvation process for the fluorenone radical anion is considered to be essentially the same as that for benzophenone and other aromatic ketyl radical anions; the radical anion is viewed as hydrogen-bonded with one and two ethanol molecules through the out-of-plane π electron on the carbonyl oxygen.

If there is no specific interaction between the neutral fluorenone and ethanol, and if the ethanol molecules are randomly distributed around fluorenone, the probability that a fluorenone radical anion finds an ethanol molecule at the site for hydrogen bonding is given by x. The probability of the hydrogen bond formation is then given by

$$W_0(x)=(1-x)^2,\ W_1(x)=2x(1-x),\ W_2(x)=x^2. \quad (2)$$

The shapes of $W_i(x)$ in Eq. 2 are also shown with thinner curves in Fig. 5. Although $W_0(x)$ is close to the observed curve, $W_1(x)$ is much higher while $W_2(x)$ is lower than the observed $W_i(x)$. This suggests that a considerable part of the radical anion with one hydrogen-bonded ethanol molecule is converted into the radical anion with two hydrogen-bonded ethanol molecules. A candidate for the second hydrogen bond might be an in-plane ethanol molecule which has been hydrogen-bonded to neutral fluorenone.

Now the reason why Hoshino et al. failed to detect the spectral shift of the fluorenone radical anion is clear. The absorption of the radical anion with one hydrogen-bonded alcohol molecule is very weak due to the first conversion of the radical anion into that with two hydrogen-bonded alcohol molecules. The absorption of the latter radical anion is also weak due to the small extinction coefficient. The low spectral resolution in their pulse radiolysis study allowed them to detect only the wavelength-independent decrease of the absorption band of the radical anion without hydrogen bond.

The characteristic features of the spectral change of aromatic ketone radical anions due to formation of the new hydrogen bond are the blue shift and the decrease in the molar extinction coefficients. These features can be qualitatively understood by a simple molecular orbital consideration. Shida et al. made molecular orbital calculations on the radical anions of aromatic ketones and found that the excess charge is located mainly on the carbonyl group in the ground state and on the aromatic group in the excited states.[8] They also assigned the visible absorption bands to intramolecular charge transfer bands. The ground and the excited states of the radical anion are therefore given by a linear combination of two structures; one is ψ_a with an excess negative charge on the carbonyl group (carbonyl antibonding π orbital) and the energy E_a, and the other is ψ_b with a negative charge on the benzene rings and the energy E_b. Neglecting the overlap integral between ψ_b and ψ_b, the transition energy $h\nu$ and the transition moment μ_{EG} for the charge transfer band are approximately given by

$$h\nu \simeq (E_b-E_a)[1+4H_{ab}^2/(E_b-E_a)^2]^{1/2}, \quad (3)$$
$$\mu_{EG} \simeq -H_{ab}(\mu_{aa}-\mu_{bb})/h\nu-[(E_b-E_a)/h\nu]\mu_{ab}, \quad (4)$$

where H_{ab} is the resonance integral between ψ_a and ψ_b, and μ_{jk} is a transition or an electric moment. The absolute value of μ_{ab} is much smaller than that of $\mu_{aa}-\mu_{bb}$. The value of (E_b-E_a) is close to $h\nu$. Therefore, the

transition moment, square root of the transition probability, linearly decreases with increasing transition wavelength. The decrease in the transition probability arises from the decrease in the mixing of the ψ_a and ψ_b states due to the incease in the energy gap, $E_b - E_a$.

Due to the negative charge on the carbonyl oxygen, the radical anion in the ground state easily forms a hydrogen bond, which stabilizes the ψ_a and hence the ground states. Since the contribution of the ψ_a state is very low in the excited state, the excited state is not stabilized by hydrogen-bonding. The formation of the hydrogen bond therefore causes a blue shift of the absorption spectrum and the decrease in the transition probability. Since the transition probability is proportional to the product of the transition wavelength and the molar extinction coefficient, formation of the hydrogen bond also causes a decrease in the extinction coefficient. Figure 6 shows the relation between the wavelength at the absorption maximum, λ_{max}, and the extinction coefficient at λ_{max} for the fluorenone and the benzophenone radical anions. The extinction coefficient decreases with decreasing λ_{max}, which supports the validity of the above consideration. The extinction coefficient would increase with decreasing λ_{max}, if the transition probability were not decreased by formation of the hydrogen bond.

Provided the energy of the excited state is scarcely influenced by the formation of the hydrogen bond, the stabilization energy by hydrogen bonding is approximately the same as the energy of the spectral shift. The values of the stabilization energy are −0.22 and −0.20 eV for the first and the second hydrogen bonding to the benzophenone radical anion, respectively. For the fluorenone radical anion, the values are −0.16 and −0.42 eV, respectively. The large stabilization energy of −0.42 eV suggests that the formation of the second hydrogen bond is accelerated by the first hydrogen bond. The relative concentration of the fluorenone radical anion with one hydrogen-bonded ethanol is thus lower than the statistical one.

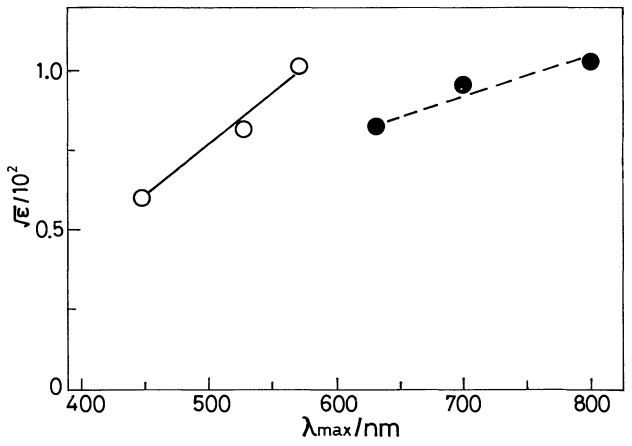

Fig. 6. Plot of the square root of molar extinction coefficients of (○) fluorenone and (●) benzophenone radical anions versus the wavelength at absorption maxima.

Very recently Murai et al. made a pulse radiolysis study on the spectral shift of benzophenone and fluorenone radical anions in MTHF due to ionic association with sodium cations.[15] They found stepwise shifts of the absorption spectra: 800 nm→720 nm→630 nm for the benzophenone radical anion and 570 nm→530 nm→450 nm for the fluorenone radical anion. The spectral shift is quite similar to that due to hydrogen bonding. They attributed the spectral shift to stepwise association of the ions: free ketyl anions→ketyl anion-sodium cation ion pairs→higher ion aggregates (dimer of the ion pair or the ketyl anion coordinating two sodium cations). The fair agreement of the absorption spectra between the higher ion aggregates and the radical anions with two hydrogen-bonded ethanol molecules strongly suggests that the higher ion aggregate corresponds to the radical anion coordinating two sodium cations instead of two alcohol molecules. The reaction rate for the formation of the higher ion aggregate was approximately the same as that for the ion pair formation, which also suggests that the higher ion aggregate corresponds to the ketyl anion coordinating two sodium cations. The reaction would be much slower if the aggregate were formed by a second-order reaction with the ion pairs. Luckhurst and Orgel measured ESR spectra of chemically-prepared fluorenone radical anions in the mixed solvent of *N,N*-dimethylformamide and methanol or ethanol.[16] They attributed the spectral shift by the alcohols to the formation of hydrogen bond between the fluorenone radical anion and the alcohol molecule. The ESR spectrum of the radical anion in pure alcohol was very similar to the spectrum of the radical anion coordinating a divalent metal cation,[17] this suggests that the electronic structure of the aromatic ketyl radical anion with two hydrogen-bonded alcohol molecules is very similar to that coordinating two monovalent cations or one divalent cation.

This work was supported by a Grant-in-Aid for Developmental Scientific Research No. 01540353 from the Japanese Ministry of Education, Science and Culture.

References

1) M. A. Lewis and C. D. Jonah, *J. Phys. Chem.*, **90**, 5378 (1986), and the references therein.

2) M. Hoshino, S. Arai, and M. Imamura, *J. Phys. Chem.*, **78**, 1473 (1974).

3) M. Ogasawara, H. Yoshida, S. Karolczak, Cz. Stadovski, and J. Kroh, *Red. Phys. Chem.*, **23**, 711 (1984).

4) R. K. Huddleston and J. R. Miller, *Radiat. Phys. Chem.*, **17**, 383 (1981).

5) J. L. Marignier and B. Hickel, *Chem. Phys. Lett.*, **86**, 95 (1982).

6) J. L. Marignier and B. Hickel, *J. Phys. Chem.*, **88**, 5375 (1984).

7) T. Shida and W. J. Hamill, *J. Am. Chem. Soc.*, **88**, 3683 (1966).
8) T. Shida, S. Iwata, and M. Imamura, *J. Phys. Chem.*, **78**, 741 (1974).
9) M. Hoshino, S. Arai, M. Imamura, and A. Namiki, *Chem. Phys. Lett.*, **26**, 82 (1974).
10) R. S. Becker, *J. Mol. Spectrosc.*, **3**, 1 (1959).
11) T. Shida and H. Kubodera, Symposium on Molecular Structures, Tokyo, 1979, Abstr., p. 364.
12) T. Shida and H. Kubodera, VIth International Symposium on Solute–Solvent Interactions, Osaka, 1982, Abstr., p. 185.
13) T. Ichikawa, Y. Ishikawa, and H. Yoshida, *J. Phys. Chem.*, **92**, 508 (1988).
14) T. Shida, "Electronic Absorption Spectra of Radical Ions," Physical Science Data, Elsvier, Amsterdam (1988), Vol. 34, p. 15, 299.
15) H. Murai, K. Kotani, M. Ogasawara, and H. Yoshida, *Nippon Kagaku Kaishi*, **1989**, 1319.
16) G. R. Luckhurst and L. E. Orgel, *Mol. Phys.*, **8**, 117 (1964).
17) N. Hirota "Radical Ions," ed by E. T. Kaiser and L. Kevan, Interscience Publishers, New York (1968), p. 43.

Thermal Decomposition of Ammonium Amidotriphosphate $(NH_4)_4P_3O_9NH_2 \cdot H_2O$

Atsushi TAKENAKA,* Junichi OOE, Itaru MOTOOKA,† and Hiroyuki NARIAI†
Department of Industrial Chemistry, Yonago National College of Technology, 4448, Hikona-cho, Yonago, Tottori 683
† Department of Chemistry, Faculty of General Education, Kobe University, Tsurukabuto, Nada-ku, Kobe 657
(Received March 13, 1991)

Ammonium amidotriphosphate $(NH_4)_4P_3O_9NH_2 \cdot H_2O$ was heated at 5 K min^{-1} up to 100, 145, 180, and 240 °C in four different atmospheres : in a stream of dry air, humid air, ammonia, and dry hydrogen chloride. The products were analyzed by HPLC-FIA, X-ray diffractometry, and IR spectrophotometry. A new phase of ammonium *cyclo*-triphosphate was observed at lower temperatures, except for in the ammonia atmosphere. Oligophosphates (chain length=4—12) were more abundant in samples heated to 145 and 180 °C in hydrogen chloride. The *cyclo*-tri- and oligophosphates were most probably formed via a zwitterion form. When heated to 240 °C, the samples were changed to ammonium polyphosphates. Elemental analyses for the sample heated to 240 °C in dry air showed that the ammonium polyphosphates formed contained some phosphorus–nitrogen bonds. Isothermal experiments at 180 °C in dry air indicated that the new phase of ammonium *cyclo*-triphosphate was converted completely to ammonium polyphosphates.

Inorganic phosphates with phosphorus–nitrogen bonds are potential candidates as a new class of fertilizer. They attracted our attention also as flame-proofing materials, and probably in view of this several reports have been published regarding their thermal decomposition.[1-11] Especially, amidophosphates have been studied by many workers.[2-11]

Amidotriphosphate ion has such a structure that the terminal oxygen atom of triphosphate ion is replaced with an amino group. It is well known that amidotriphosphates are prepared by ammonolyses of *cyclo*-triphosphate in aqueous solutions.[12-14] Quimby and Flautt,[12] and Feldmann and Thilo[13] also reported that amidotriphophate ions cyclized again to *cyclo*-triphosphate ions in acidic solutions. We have been interested in whether the cyclization also takes place or not in solid state. Whether phosphorus–nitrogen phosphates are produced or not in such a solid-state reaction is also of interest.

In general, thermal decomposition of inorganic phosphates depends on temperature and time of heating, cooling of the melts, and atmosphere of heating.[15]

We studied the thermal decomposition of some inorganic phosphates with regard to the effect of atmosphere, especially of humidity.[16,17] As an extension thermal decomposition of ammonium amidotriphosphate $(NH_4)_4P_3O_9NH_2 \cdot H_2O$ was studied in the present work in four different atmospheres: dry air, humid air (relative humidity 90% at 25 °C), ammonia, and dry HCl. The products were analyzed by HPLC-FIA, X-ray diffractometry, and IR spectrophotometry as in the preceding work.[16,17]

Experimental

Preparation of Ammonium Amidotriphosphate $(NH_4)_4P_3O_9NH_2 \cdot H_2O$. Ammonium amidotriphosphate was prepared by ammonolysis of ammonium *cyclo*-triphosphate.[13] The latter was obtained according to Ref. 18, but the X-ray diffraction data were different from those in Ref. 18. The present data are listed in Table 1. Analyses of the new ammonium *cyclo*-triphosphate clarified that it was an anhydrous form and was pure. After allowing the sample to stand for about six months below room temperature, the X-ray diffraction lines changed to those reported in Ref. 18 while several of the original lines remained. The *cyclo*-triphosphate ions were not decomposed. The ammonium *cyclo*-triphosphate thus formed was heated again at 5 K min^{-1} to 300 °C in a stream of ammonia. Its *cyclo*-triphosphate ions were not decomposed and the X-ray diffraction data agreed completely with those of the new ammonium *cyclo*-triphosphate. These indicate that the new phase of ammonium *cyclo*-triphosphate, in line with the data in Table 1, is its high-temperature phase.

HPLC-FIA data for several $(NH_4)_4P_3O_9NH_2 \cdot H_2O$ samples thus prepared showed that more than 95.0% of the phosphorus atoms exist as amidotriphosphate ions. Found: P, 26.93; $N(NH_4^+)$, 16.02; $N(NH_2^-)$, 3.89%. Calcd for $(NH_4)_4P_3O_9NH_2 \cdot$

Table 1. X-Ray Diffraction Data for a New Phase of Ammonium *cyclo*-Triphosphate $(NH_4)_3P_3O_9$

d/Å	Intensity[a]	d/Å	Intensity
8.66	M	3.11	S
6.37	W	3.05	VW
6.23	S	2.99	VW
5.94	M	2.90	M
5.75	VS	2.87	M
5.40	M	2.85	W
4.72	W	2.68	W
4.35	W	2.59	VW
4.15	W	2.50	VW
3.91	W	2.47	VW
3.86	W	2.43	VW
3.67	W	2.38	VW
3.64	W	2.35	VW
3.49	M	2.30	VW
3.40	M	2.27	W
3.25	W		

a) VS: very strong, S: strong, M: medium, W: weak, VW: very weak.

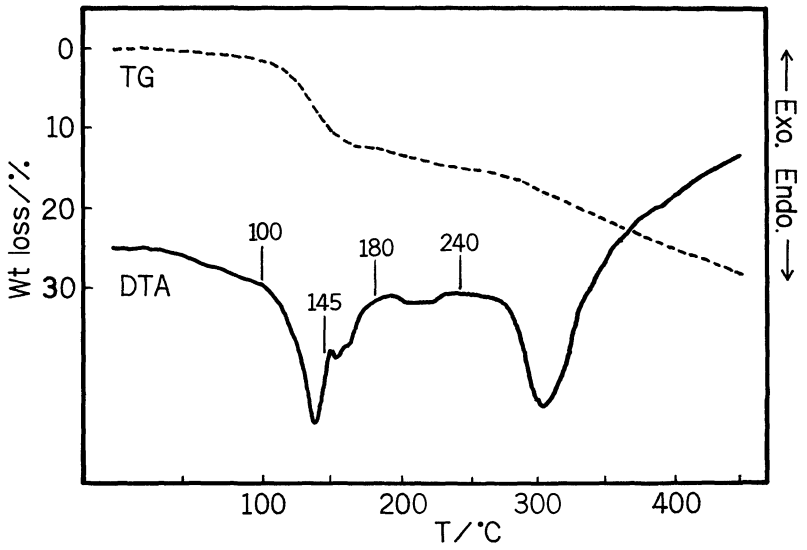

Fig. 1. Thermal analytical curve for $(NH_4)_4P_3O_9NH_2 \cdot H_2O$ in stationary air. Heating rate: 5 K min^{-1}

H_2O: P, 27.07; $N(NH_4^+)$, 16.33; $N(NH_2^-)$, 4.08%. The ammonium amidotriphosphate sample used throughout thermal decomposition experiments was pure.

Thermal Decomposition. Thermal decomposition experiments were carried out in a cylindrical electric furnace, by means of dynamic heating methods (heating rate: 5 K min^{-1}) or isothermal methods. The effect of atmosphere on the decomposition was examined by the use of a stream of dry air (50 cm^3 min^{-1}) and humid air (50 cm^3 min^{-1}). The former was obtained by passing air through molecular sieves, and the latter with a humidity generator give 90% of relative humidity at 25 °C.[17] A stream of ammonia (purity: 99.9%) was also used by introducing it directly from a cylinder. Hydrogen chloride was prepared by adding concentrated sulfuric acid to ammonium chloride, then dried with concentrated sulfuric acid. Before heating, the cylindrical furnace was purged with these gases of about twice its volume.

Analyses. Total nitrogen was determined by the Kjeldahl method. Nitrogen present as ammonium ions, $N(NH_4^+)$, was determined by an ammonia-distillation method without decomposition by use of concentrated sulfuric acid. Nitrogen present as amino or imino groups, $N(NH_2^-)$, was calculated by subtracting the $N(NH_4^+)$ from the total nitrogen.[13] Thermal analyses (TG-DTA) were carried out in stationary air at a heating rate of 5 K min^{-1}. The composition of phosphates was determined by an HPLC-FIA method. A 10 mg portion of a sample was dissolved in 2 cm^3 of a 0.1 mol dm^{-3} sodium hydroxide aqueous solution to prevent the cyclization of amidotriphosphate ions to *cyclo*-triphosphate ions, that readily occurs in acidic solutions.[12-14] The solution was diluted to 500 cm^3 with distilled water, and was immediately analyzed with an HPLC-FIA system. Total phosphorus was determined colorimetrically with the HPLC-FIA system.[16] IR spectra were recorded on a JASCO IR spectrophotometer IR-700 by a KBr disc method. Other procedures were essentially the same as those described previously.[16,17]

Results and Discussion

Thermal Decomposition in Stationary Air. Figure 1 shows a result of thermal analyses (TG-DTA) in stationary air. Four endothermic peaks are seen at about 140, 155, 210, and 300 °C. The peak at 300 °C reflects the melting of sample.

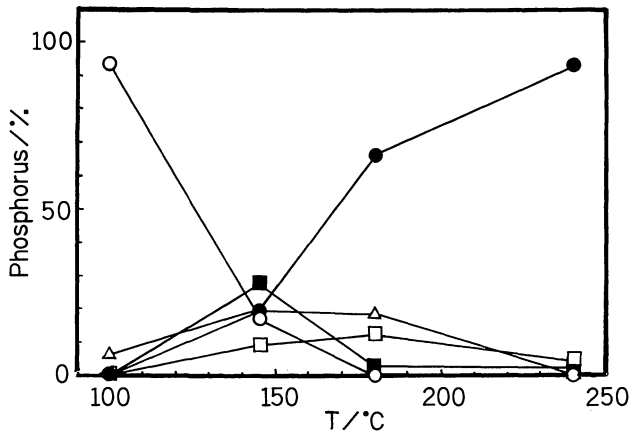

Fig. 2. Changes in amounts of phosphates in the products decomposed at 5 K min^{-1} in stationary air. ○: amidotri-, ●: poly-, □: mono-, di-, and tri-, ■: oligo- (chain length=4—11), △: *cyclo*-tri-.

Figure 2 depicts the percentage of phosphorus atoms existing as amidotri-, mono- to tri-, oligo- (chain length n=4—11), poly-, and *cyclo*-triphosphates in the products obtained by heating to the temperatures indicated on the DTA curve in Fig. 1. Peaks not assignable to these phosphate ions were occasionally detected on the HPLC-FIA chromatograms. In view of the short retention time, they are probably short-chain phosphate ions with one or several phosphorus–nitrogen bonds, and are denoted as "other" phosphates in Table 2. Since these amount to only less than ca. 4% as phosphorus atoms, they are neglected in Fig. 2.

Release of the water of crystallization from $(NH_4)_4P_3O_9NH_2 \cdot H_2O$ would give 5.25% of weight loss. The weight loss at 145 °C was significantly larger, ca. 12.1%. Therefore, the endothermic peak at about 140 °C may reflect elimination of ammonia as well as the water of crystallization.

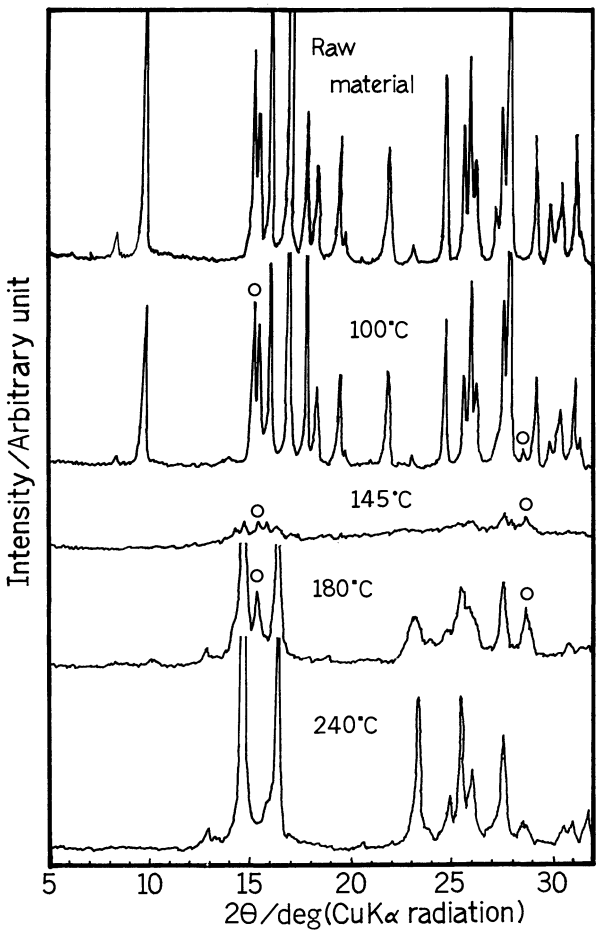

Fig. 3. X-Ray diffraction patterns of the samples decomposed in stationary air. Heating rate: 5 K min^{-1}. O: the lines were attributable to the ammonium *cyclo*-triphosphate indicated in Table 1.

The X-ray diffraction pattern of the sample heated to 180 °C showed the lines for ammonium polyphosphate (I-form)[19] and those for ammonium *cyclo*-triphosphate given in Table 1 (Fig. 3). The lines at 15.4 and 28.8° (2θ) are attributable to the *cyclo*-triphosphate. The sample heated to 240 °C was mostly ammonium polyphosphate as judged from Figs. 2 and 3. The weight loss on the TG curve at 240 °C was ca. 15.4%, which is close to that calculated according to the following equation (15.18%):

$$(NH_4)_4P_3O_9NH_2 \cdot H_2O \rightarrow 3(NH_4)PO_3 + 2NH_3 + H_2O$$

The weight loss at temperatures above 240 °C might be due to the release of ammonia, water, or phosphorus pentoxide from the sample.

Effect of Atmosphere on the Thermal Decomposition. Samples of ammonium amidotriphosphate were heated at 5 K min^{-1} to 100, 145, 180, and 240 °C, in streams of four different gases. Table 2 shows the composition of phosphates of the products. At 100 and 145 °C in dry air, dehydration of $(NH_4)_4P_3O_9NH_2 \cdot H_2O$ induced rapid decomposition of the amidotriphosphate ions. As water vapor suppresses the dehydration and consequently the decomposition of amidotriphosphate ions, the latter reaction is expected to proceed slowly in a humid atmosphere. Indeed at 100 and 145 °C, there remain markedly more amidotriphosphate ions undecomposed when heated in humid air than in dry air. Amidotriphosphate ions were stable up to 180 °C in a stream of ammonia; this implies that amidotriphosphates also were cleaved by elimination of ammonia.

It was reported that amidotriphosphate ions cyclized again to *cyclo*-triphosphate ions in acidic solutions.[12-14] As seen in Table 2, the products occasionally contained *cyclo*-triphosphates. Such samples exhibited necessari-

Table 2. Effect of the Atmosphere on the Phosphates Composition in the Products Obtained by Heating of $(NH_4)_4P_3O_9NH_2 \cdot H_2O$

T/°C	Atmosphere	Composition/P%					
		Amidotri-	Mono-, di-, and tri-	Oligo-[a]	Poly-	*cyclo*-Tri-	Other[b]
100	Dry air	88.9	—	0.7	1.6	8.8	—
	Humid air	95.6	—	—	—	4.4	—
	NH_3	100.0	—	—	—	—	—
	Dry HCl	51.3	5.4	7.5	3.3	32.6	—
145	Dry air	17.4	7.1	25.0	31.7	13.6	5.2
	Humid air	67.7	4.9	7.8	5.3	12.3	2.0
	NH_3	79.7	6.1	12.4	—	—	1.9
	Dry HCl	3.4	34.1	44.2	2.3	15.9	—
180	Dry air	3.0	8.3	3.2	63.1	21.8	0.6
	Humid air	—	20.6	4.7	52.6	22.2	—
	NH_3	70.7	8.3	5.9	15.2	—	—
	Dry HCl	—	36.9	60.6	2.5	—	—
240	Dry air	—	2.9	0.8	96.4	—	—
	Humid air	—	12.8	5.1	82.2	—	—
	NH_3	—	4.8	—	95.2	—	—

a) Chain length from 4 to 12. b) See text.

ly two diffraction lines at 15.4 and 28.8° (2θ), which agreed with those listed in Table 1. Quimby and Flautt,[12] and Feldmann and Thilo[13] described that a zwitterion was formed as an intermediate in the course of the cyclization of amidotriphosphate ion. Table 2 shows that *cyclo*-triphosphate ions exist most abundantly in samples heated to 100 °C in hydrogen chloride. This is probably due to the formation and subsequent cyclization of the zwitterion expressed by the following equations:

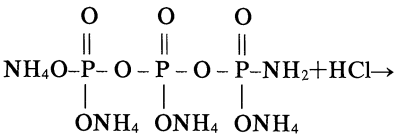

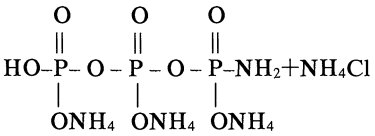

(1)

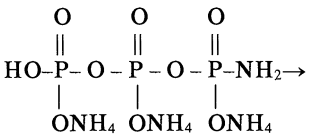

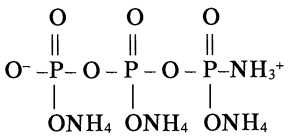

(2)

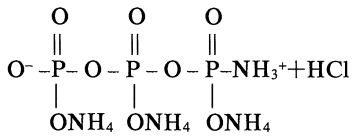

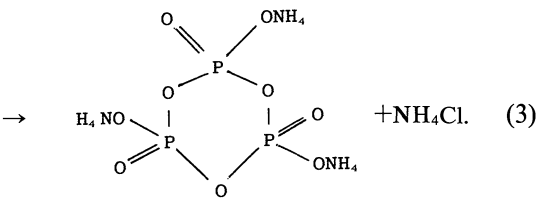

(3)

Oligophosphates (n=4—12) were formed more in samples heated to 145 and 180 °C in dry HCl than in the other atmospheres. Sato et al. reported that polyphosphates were produced by condensation of the zwitterions resulting from a reaction of amidophosphates with hydrogen chloride.[20,21] Therefore, the oligophosphates may also be formed by condensation of the zwitterions indicated on the right-hand side of Eq. 2. The zwitterions must be also resulted from a reaction of amidotriphosphate ions with water. Sato et al. suggested the occurrence of such a reaction.[20,21]

The IR spectrum of $(NH_4)_4P_3O_9NH_2 \cdot H_2O$ showed a large peak of ammonium ions at 1400—1500 cm^{-1}[22] and a small peak of amino groups at 1630 cm^{-1}.[23] The sample heated to 100 °C in HCl showed a peak at 1400—1500 cm^{-1}, and a faint peak at 1670 cm^{-1}. The shift from 1630 to 1670 cm^{-1} might be due to the formation of hydrogen bonds. Although Corbridge and Lowe reported that the zwitterions of amidophosphates all exhibited absorption at 1618—1615 cm^{-1} and at 1470—1468 cm^{-1},[22] we were unable to identify the zwitterions of the amidotriphosphates by the IR spectra.

Hydrogen chloride and water are expected to act as hydrolytic agents at higher temperatures. As a result of hydrolysis of the amidotriphosphates, mono- to triphosphates were indeed formed more in samples heated to 145 and 180 °C in HCl and in those heated to 180 and 240 °C in humid air (Table 2). Table 2 shows that there were no *cyclo*-triphosphates in samples heated in ammonia, which may indicate that the zwitterions are not formed in the presence of ammonia molecules.

The products heated to 240 °C entirely consisted of polyphosphate ions, and showed an X-ray diffraction pattern of I-form of ammonium polyphosphate.[19] The sample heated to 240 °C in dry air was analyzed: P, 31.17; N(NH_4^+), 12.86; N(NH_2^-), 0.69%. The result reveals the presence of some phosphorus–nitrogen bonds in the ammonium polyphosphate.

Isothermal Decomposition in a Stream of Dry Air. Ammonium amidotriphosphate $(NH_4)_4P_3O_9NH_2 \cdot H_2O$ thermally produced a new phase of ammonium *cyclo*-triphosphate. The *cyclo*-triphosphate disappeared at higher temperatures. In order to investigate the process in more detail, isothermal runs were carried out in a stream of dry air. The essential features of the results obtained are displayed in Figs. 4 and 5. Mono- to triphosphates were hardly observed (less than 1%) in

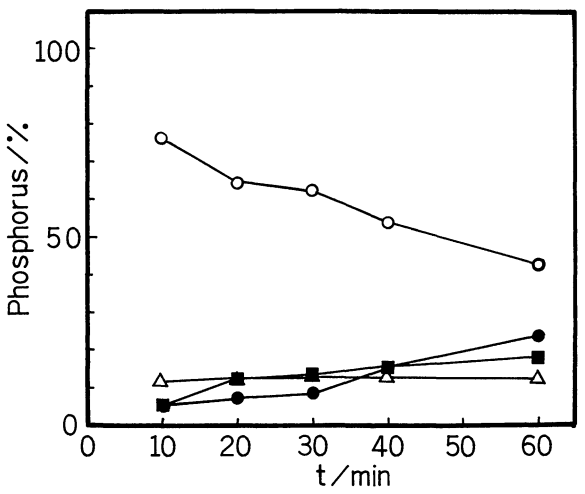

Fig. 4. Changes in the amounts of phosphates in products decomposed at 100°C in a stream of dry air. ○: amidotri-, ●: poly-, ■: oligo- (chain length= 4—12), △: *cyclo*-tri-.

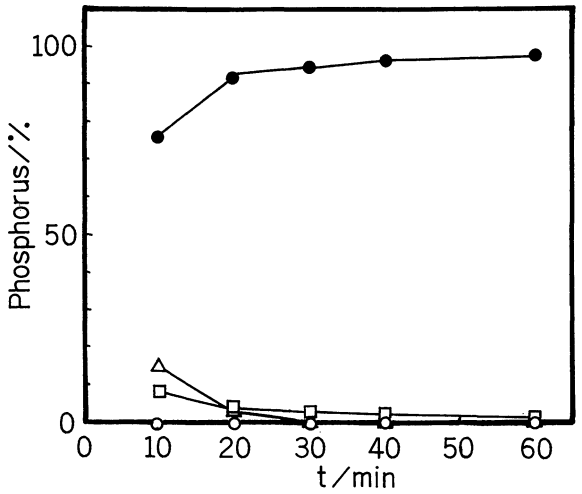

Fig. 5. Changes in the amounts of phosphates in products decomposed at 180°C in a stream of dry air. ○: amidotri-, ●: poly-, □: mono-, di-, and tri-, △: *cyclo*-tri-.

samples heated at 100 °C. Tetra- and pentaphosphates were the only species among oligophosphates in samples heated at 180 °C. However, since their total quantity was less than 1.6%, they are neglected in Fig. 5. The chromatograms of samples heated at 100 and 180 °C both showed no peaks of "other" phosphates.

At 100 °C the amount of *cyclo*-triphosphate ions did not change with reaction time, and that of oligophosphates was also constant after 20 min (Fig. 4). These ions were probably formed via the zwitterions. *cyclo*-Triphosphate ions were detected clearly at 10 min at 180 °C (Fig. 5). They decreased with the passage of time to disappear completely in 30 min. X-Ray diffraction analyses gave the same results. Therefore, at higher temperatures, the *cyclo*-triphosphates were converted to ammonium polyphosphates (I-form).

The present work was partially supported by a Grand-in-Aid for Scientific Research No. 03750588 from the Ministry of Education, Science and Culture.

References

1) R. Klement and G. Biberacher, *Z. Anorg. Allg. Chem.*, **285**, 74 (1956).
2) M. Goehring and J. Sambeth, *Chem. Ber.*, **90**, 232 (1957).
3) R. Klement and H. Bar, *Z. Anorg. Allg. Chem.*, **300**, 221, (1959).
4) C. Shimasaki, Y. Oono, F. Takai, M. Shoji, and M. Yoshizawa, *Nippon Kagaku Zasshi*, **1982**, 376.
5) M. Watanabe, T. Inagaki, and S. Sato, *Bull. Chem. Soc. Jpn.*, **56**, 458 (1983).
6) M. Watanabe, T. Inagaki, Y. Morii, and T. Yamada, *Sekko To Sekkai*, **184**, 111 (1983).
7) M. Watanabe, Y. Morii, and S. Sato, *Bull. Chem. Soc. Jpn.*, **57**, 2087 (1984).
8) M. Watanabe, Y. Morii, and S. Sato, *Bull. Chem. Soc. Jpn.*, **57**, 2914 (1984).
9) C. Shimasaki, S. Ookawa, and R. Ishizaka, *Bull. Chem. Soc. Jpn.*, **58**, 592 (1985).
10) S. Sato and M. Watanabe. *Bull. Chem. Soc. Jpn.*, **58**, 3513 (1985).
11) C. Shimasaki, H. Suzuki, and H. Toda, *Bull. Chem. Soc. Jpn.*, **60**, 3050 (1987).
12) O. T. Quimby and T. J. Flautt, *Z. Anorg. Allg. Chem.*, **296**, 220 (1958).
13) W. Feldmann and E. Thilo, *Z. Anorg. Allg. Chem.*, **328**, 113 (1964).
14) W. Feldmann, *Z. Chem.*, **5**, 26 (1965).
15) e. g., T. Umegaki, "Inorganic Phosphate Materials," ed by T. Kanazawa, Kodansha, Tokyo (1989), Chap. 9.
16) A. Takenaka, I. Motooka, and H. Nariai, *Bull. Chem. Soc. Jpn.*, **60**, 4299 (1987).
17) A. Takenaka, T. Hieda, K. Kimura, I. Motooka, and H. Nariai, *Bull. Chem. Soc. Jpn.*, **63**, 964 (1990).
18) R. V. Coates and G. D. Woodard, *J. Chem. Soc.*, **1964**, 1780.
19) C. Y. Shen, N. E. Stahlheber, and D. R. Dyroff, *J. Am. Chem. Soc.*, **91**, 62 (1969).
20) S. Sato, T. Takayanagi, and M. Watanabe, *Bull. Chem. Soc. Jpn.*, **60**, 1303 (1987).
21) S. Sato, T. Takayanagi, and M. Watanabe, *Bull. Chem. Soc. Jpn.*, **60**, 3941 (1987).
22) D. E. C. Corbridge and E. J. Lowe, *J. Chem. Soc.*, **1954**, 493.
23) E. Steger, *Z. Elektrochem.*, **61**, 1004 (1957).

 © 1991 The Chemical Society of Japan Bull. Chem. Soc. Jpn., 64, 2705—2709 (1991)

Association of Cycloalkanes with Cyclodextrins in Aqueous Medium

Tomonori OSAJIMA, Toshio DEGUCHI, and Isao SANEMASA*
Department of Chemistry, Faculty of Science, Kumamoto University, Kurokami 2-39-1,Kumamoto 860
(Received April 15, 1991)

The complex formation of α-, β-, and γ-cyclodextrins (CyDs, hosts) with five cycloalkanes (guests), cyclo(pentane, hexane, heptane, octane, and decane), has been studied in aqueous media at 25 °C by making use of the volatilization rate of guest molecules from the aqueous into gas phase. In the excess of the host, α-CyD forms both 1 : 1 and 2 : 1 (host : guest) complexes, while β- and γ-CyDs form 1 : 1 complexes with an exception that β-CyD forms a 2 : 1 complex with cylodecane. The 2 : 1 complex formation constants of α-CyD with cyclo(hexane, heptane, octane, and decane), particularly with cyclooctane, are extremely large compared with their 1 : 1 formation constants. The host–guest spatial fitting models are proposed.

We studied host–guest associations using α-, β-, and γ-cyclodextrins (CyDs) as hosts and C_5—C_9 normal alkanes as guests.[1] The results are summarized as follows.

With an increase in the chain length of alkane, both 1 : 1 and 2 : 1 (host–guest) formation constants for three CyDs increase; in the case of α-CyD, the 1 : 1 formation constant is saturated at C_8. The cross section diameter of an alkane molecule being close to that of α-CyD cavity (5 Å), the guest molecule is assumed to be included in α-CyD along the fully extended alkyl chain. Relatively large formation constants of β-CyD indicate that the cavity diameter of β-CyD (6.9 Å) is sufficiently large to allow a conformational change of the guest alkyl chain so that the guest molecule contacts favorable with the cavity wall. In view of the large cavity diameter (8.5 Å), γ-CyD might form much weaker complexes with alkanes. Contrary to this expectation, however, the formation constants with shorter-chain alkanes are comparable to α-CyD complexations and those with longer-chain alkanes are comparable to β-CyD complexations. In order to rationalize these observations, we made two hypotheses: (1) a flexible conformation of alkyl chain to get contact as widely as possible with the γ-CyD cavity wall and (2) γ-CyD accepts a guest molecule without releasing water molecules originally present in the cavity.

In the present work, cycloalkanes of C_5 to C_8 and C_{10} have been used as guests. These guest molecules, compared to normal alkanes, are more bulky and more rigid. The cavity of α-CyD is too small to include even a cyclopentane molecule as a whole, while, if the guest takes a suitable puckered ring conformation, β-, and γ-CyDs can accept a cycloalkane molecule of fairly large ring. The object of this study is to elucidate the relationship between the guest size and the stability of CyD complexes.

In analytical chemistry, CyDs have been recently used to modify the partition of hydrophobic solutes between organic and aqueous phase.[2] In the field of organic syntheses, water-insoluble CyD derivatives are used in organic solvents.[3] Since cycloalkanes are of common choise as organic solvents, the knowledge of their associations with CyDs is required. There are, nevertheless, few data available concerning the host–guest systems. Cyclohexane–α-, and –β-CyD systems have been so far studied by solubility measurements.[4] The method used in this work to determine the association constant is the same as that employed in our previous works.[1,5]

Experimental

Deionized distilled water was used throughout the experiments. An appropriate amount of α-, β-, and γ-CyDs of guaranteed grade (Nacalai Chemical Co.), dried over phosphorus pentoxide under vacuum, was weighed and dissolved in water to prepare CyD stock solutions of desired concentrations. Five guest substances were used as received; cyclopentane (Nacalai Chemical Co., 98%), cyclohexane (Wako Pure Chemical Co., 99.5%), cycloheptane (Tokyo Kasei Kogyo Co., 98%), cyclooctane (Nacalai Chemical Co., 99%), and cyclodecane (Aldrich, the purity is not specified).

The same device described in the previous paper,[1] was used to prepare aqueous solutions saturated with cycloalkane and to vaporize the guest with a nitrogen gas stream. Depending on the volatility of the guest, the N_2 gas flow rate was adjusted constant at 20 (cyclopentane) to 100 $cm^3\ min^{-1}$ (cyclodecane). As was described previously,[1] the vaporized guest was collected with Tenax GC resin, determined by gas chromatography, and the ammount of guest vaporized during a definite time, ΔQ_ϕ, was calculated.

The concentration of cycloalkane in the saturated aqueous solution was not determined in this work; the data were taken from the literature.[6] The concentrations of hosts and guests employed in the present study are given in Table 1.

Results and Discussion

Association Constants. The 1 : 1 and 2 : 1 (host : guest) association constants, K_1 and K_2, were estimated using an equation derived in the previous paper:[5]

$$\ln(C_\phi - Q_\phi V^{-1}) = -kt/(1+K_1C_{CyD}+K_1K_2C^2_{CyD}) + \ln C_\phi = -k't + \ln C_\phi, \quad (1)$$

where C_{CyD} and C_ϕ refer to the total concentration of host and that of guest, respectively, Q_ϕ is the sum of ΔQ_ϕ from time 0 to t, V is the volume of the aqueous solution,

k is the rate constant for transfer of guest molecules from the aqueous to gas phase, and

$$k'=k/(1+K_1C_{CyD}+K_1K_2C^2_{CyD}). \quad (2)$$

Rearrangement of Eq. 2 yields

$$1/k'=K_1K_2C^2_{CyD}/k+K_1C_{CyD}/k+1/k. \quad (3)$$

The plots according to Eq. 1 for all the cycloalkane–CyD systems examined in this work gave straight lines over the whole aeration time, during which ca. 50 to 70% of the guest molecules present initially in the sample solutions were purged. The slopes of the resulting straight lines, k' (and k), were evaluated by the least-squares method. Typical $1/k'$ vs. C_{CyD} plots are shown in Figs. 1 through 3. The plots exhibit upward curvatures for α-CyD complexations with the cycloalkanes studied here and for the β-CyD–cyclodecane system, indicating the formation of both 1 : 1 and 2 : 1 (host–guest) complexes. The plots for the other host–guest systems are linear, supporting the formation of 1 : 1 complexes. The K_1 and K_2 values were determined by the curve-fitting method and are summarized in Table 1.

Wishnia and Lappi reported K_1 of 4.2×10^2 M^{-1} (1 M=1 mol dm^{-3}) and K of 5.3×10^3 M^{-1} at 25 °C for cyclohexane–α- and β-CyDs, respectively.[4] The cavity of α-CyD is too small to include completely any cycloalkane molecule studied in this work; even cyclopentane has a diameter of ca. 6 Å. In this view, the literature K_1 value of cyclohexane seems too large. Matsui and Mochida studied associations of various alcohols with α- and β-CyDs.[7] Their 1 : 1 association constants of cyclopentanol, cyclohexanol, cycloheptan-

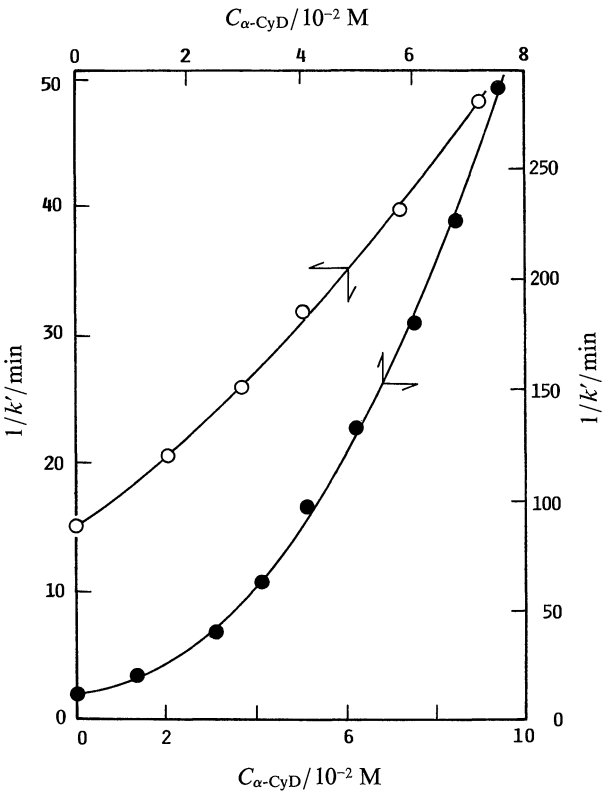

Fig. 1. Plots of $1/k'$ vs. $C_{\alpha\text{-CyD}}$. Cyclopentane (○), cyclohexane (●).

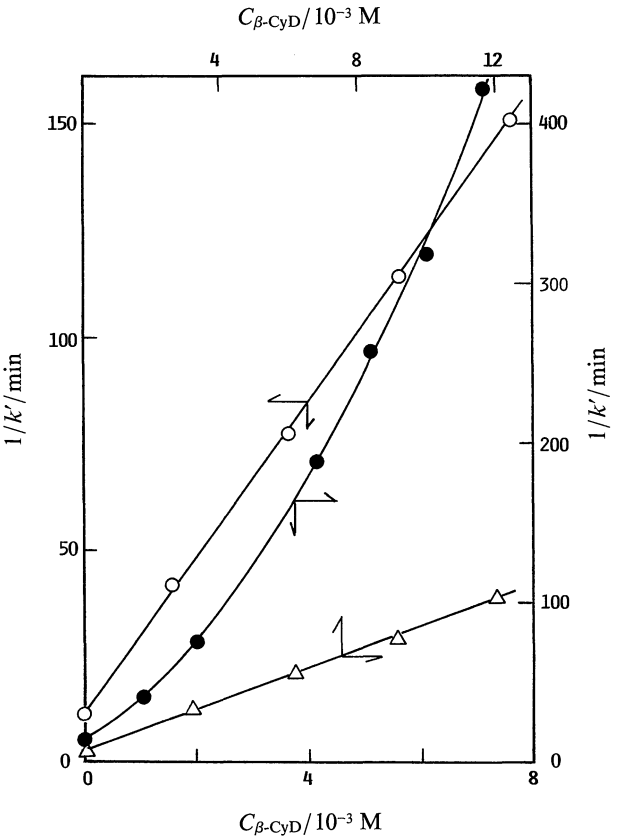

Fig. 2. Plots of $1/k'$ vs. $C_{\beta\text{-CyD}}$. Cycloheptane (△), cyclooctane (○), cyclodecane (●).

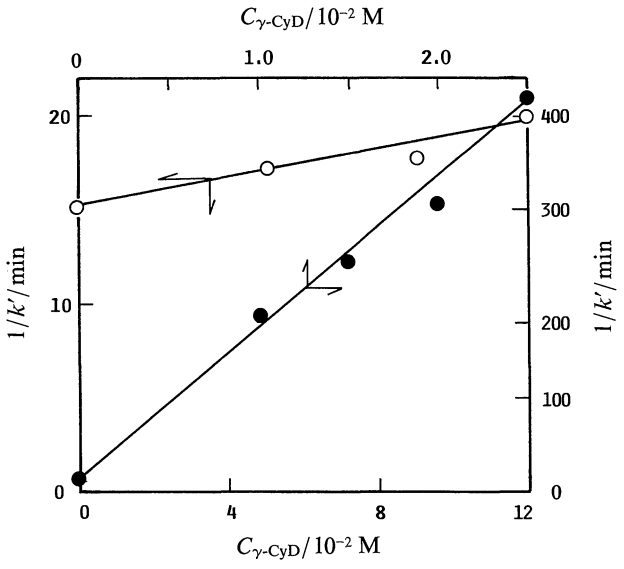

Fig. 3. Plots of $1/k'$ vs. $C_{\gamma\text{-CyD}}$. Cyclopentane (○), cyclodecane (●).

Table 1. Concentrations of Host and Guest and the Association Constants, K_1 (1:1) and K_2 (2:1) of (Host:Guest) Complexes at 25°C

	C_{CyD}[a]	Formation constant	
		K_1	K_2[b]
	10^{-2} M	M^{-1}	M^{-1}
Cyclopentane: C_ϕ[c]=2.80×10^{-5} M			
α-CyD	2.01 —9.01	18±1	4±2
β-CyD	0.405—1.41	90±20	—
γ-CyD	5.01 —12.0	3±1	—
Cyclohexane: C_ϕ[c]=4.13×10^{-5} M			
α-CyD	1.05 —7.51	9±3	(6.0±2.0)×10^2
β-CyD	0.623—1.41	156±8	—
γ-CyD	4.01 —9.90	11±3	—
Cycloheptane: C_ϕ[c]=3.86×10^{-5} M			
α-CyD	0.502—4.01	20±8	(9.0±5.0)×10^2
β-CyD	0.310—1.20	(7.4±0.3)×10^2	—
γ-CyD	2.50 —7.49	16±2	—
Cyclooctane: C_ϕ[c]=3.54×10^{-5} M			
α-CyD	0.506—2.00	0.6±0.2	(7.0±2.0)×10^4
β-CyD	0.154—0.758	(1.7±0.1)×10^3	—
γ-CyD	1.01 —5.01	70±20	—
Cyclodecane: C_ϕ[c]=3.54×10^{-5} M			
α-CyD	0.514—2.51	(1.8±0.4)×10^2	(3.1±0.8)×10^2
β-CyD	0.102—0.717	(1.62±0.07)×10^3	(2.1±0.3)×10^2
γ-CyD	1.01 —2.50	(1.1±0.1)×10^3	—

a)Total concentration of cyclodextrin. b) Dash sign indicates that K_2 was not evaluated, because $1/k'$ vs. C_{CyD} plots gave a nearly straight line. c) Initial concentration of guest after being mixed with CyD aqueous solution.

ol, and cyclooctanol are 45.7, 64.6, 79.4, and 178 M^{-1} with α-CyD, 120, 501, 1700, and 2000 M^{-1} with β-CyD, respectively. The literature values of cycloalkanols are considerably larger than the present cycloalkane–α-CyD data, but well comparable to the cycloalkane–β-CyD data. The hydroxyl group of alcohols has a potential ability to bind through hydrogen bonding with primary or secondary OH groups on the rims of CyD molecule or with glycosidic oxygens that constitute the cavity.

Association Model. It is difficult to explain our extraordinarily large K_1 value observed for the cyclodecane–α-CyD system. A plausible explanation is that the high flexibility of the large ring allows the molecule to take such a conformation that a part of the ring, which can be inserted more deeply into the α-CyD cavity, is formed more easily. While the K_1 values of cyclohexane, cycloheptane, and cyclooctane are small, their K_2 values are extremely large. Cromwell et al. suggested that if K_2 is larger than K_1, the cross-section of secondary hydroxyl group sides of two CyDs are situated parallel to each other in a suitable distance to form hydrogen bond.[8] Taking cyclohexane as an example, the 2 : 1 (host : guest) association model is depicted in Fig. 4(A). Two α-CyDs, including in their cavities a part of the cycloalkane ring, (–CH_2–CH_2–), attach to the guest molecule from the oposite side. The magnitude of K_2 depends on the distance between the two CyDs to cooperate with each other to form hydrogen bonds; the distance may be too short for cyclopentane and may be a little long for cyclodecane (the K_2 of cyclodecane is larger than its K_1, but smaller than the K_2 of cyclooctane, cycloheptane, or cyclohexane). It is noteworthy that

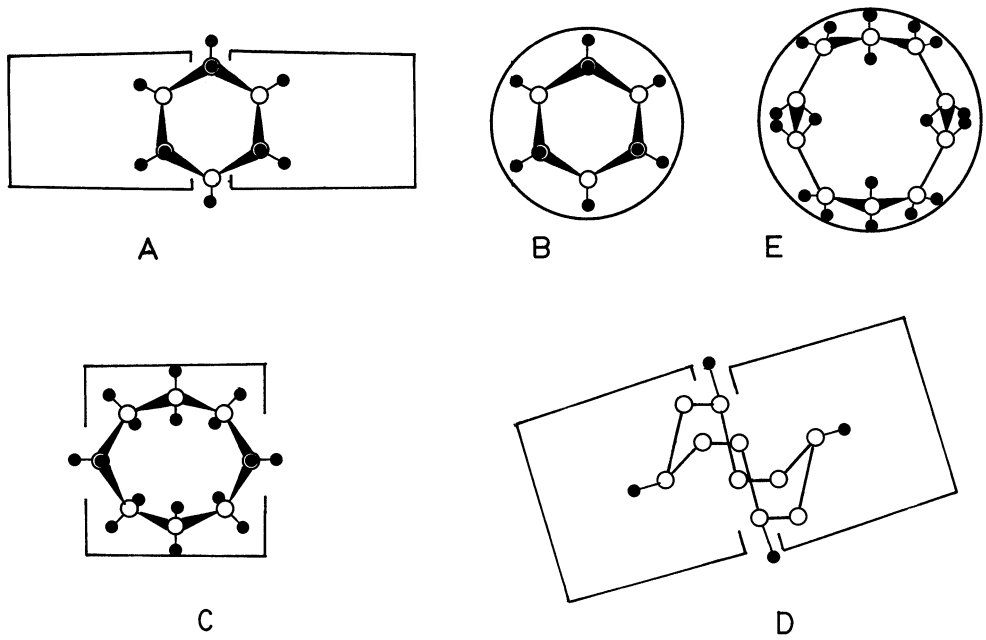

Fig. 4. Inclusion model. A: α-Cyclohexane; B: β-cyclohexane (cross section); C: β-cyclooctane; D: β-cyclodecane; E: γ-cyclodecane (cross section).

the K_2 of cyclooctane is larger by about two orders of magnitude than that of C_6, C_7, or C_{10} cycloalkane; the distance between the two α-CyDs sandwiching a cyclooctane molecule may be most suitable among the cycloalkanes studied to form hydrogen bonds.

Wishnia and Lappi presented a model of association of chair cyclohexane, which has a diameter of 7.0 Å and a thickness of 4.7 Å, with β-CyD.[4] Their model is shown in Fig. 4(B); the guest is best fitted by its periphery with the inner wall of the host cavity. This association mode, however, cannot be applied to the guests of ring size larger than cyclohexane. For these guests, we speculate that the guest enters the host cavity with the ring-planes of both host and guest perpendicular to each other. The association model considered to be reasonable for cyclooctane is shown in Fig. 4(C). The oblate ellipsoid of this guest has a diameter of 7.3 and 8 Å. The diameter of 7.3 Å is a little larger than that of β-CyD cavity employed in this study, but the cavity size itself is still uncertain; ranging from 4.5 to 6.0 Å (α-CyD), from 6.0 to 8.0 Å (β-CyD), and from 8.0 to 10.0 Å (γ-CyD).[9] Cyclodecane has a diameter of 7.6 (the minor axis) and 8.3 Å (the major axis), that is a little larger than the corresponding value of cyclooctane. Cyclodecane can also enter fully the β-CyD cavity, if we employ the larger cavity size, along the longer axis of the guest molecule. It is noteworthy that cyclodecane forms a 2:1 complex. This observation cannot be explained by a simple consideration that the length of the longer axis of cyclodecane exceeds the cavity depth (the cavity is 7 Å deep irrespectively of the type of CyD), because this is also the case for cyclooctane. We speculate, therefore, that the diameter of the shorter axis of cyclodecane is a littile larger than that of β-CyD so that a complete inclusion by the host is inhibited. The 2:1 (β-CyD : cyclodecane) association model is depicted in Fig. 4(D).

The cavity diameter of γ-CyD is sufficiently large to accept any cycloalkane studied in this work. If we adopt 8.5 Å for the host diameter, a cyclodecane molecule is snugly fitted in the host cavity with the ring-planes of both host and guest parallel to each other, as illustrated in Fig. 4(E).

The Volume of Guest and the Association Constant. In preceding studies on associations of CyDs with polynuclear aromatic hydrocarbons,[10] halogenated benzenes,[11] normal alkanes,[1] we pointed out that there is a linear relationship between the total surface area of guest and log K_1. In the case of cycloalkane, the volume of a guest molecule is a better parameter to judge the host–guest fitness, because the part inside the ring of the guest molecule does not take part in the contact with the host cavity wall. Taking the molar volume of cycloalkane from the literature,[12] the plots are shown in Fig. 5. There is no linear relationship for α-CyD, indicating that a cycloalkane molecule is not included as a whole in this host cavity. For β- and γ-CyDs, on the other hand, good linear relationships are observed. In the case of β-CyD, the inclusion is saturated at cyclooctane. The volume inside the host cavity is 150 (α), 270 (β), and 400 Å^3 (γ).[8] In this view, the saturation phenomenon should occur at cyclodecane. Cyclodecane, however, due to the steric hindrance, does not seem to be fully included in the cavity of β-CyD; this is a reasonable explanation why the cylodecane–β-CyD system forms a 2:1 complex. In Fig. 5 are also plotted association constants of cycloalkanol–β-CyD systems taken from the literature,[7] against the molar volume of cycloalkane on the assumption that β-CyD includes only the ring part of a cycloalkanol molecule. It is noteworthy that the plot is almost paralell to that of the cycloalkane –β-CyD system. A slight stabilization observed for cycloalkanols is probably due to their hydrogen bonding with the periphery of β-CyD.

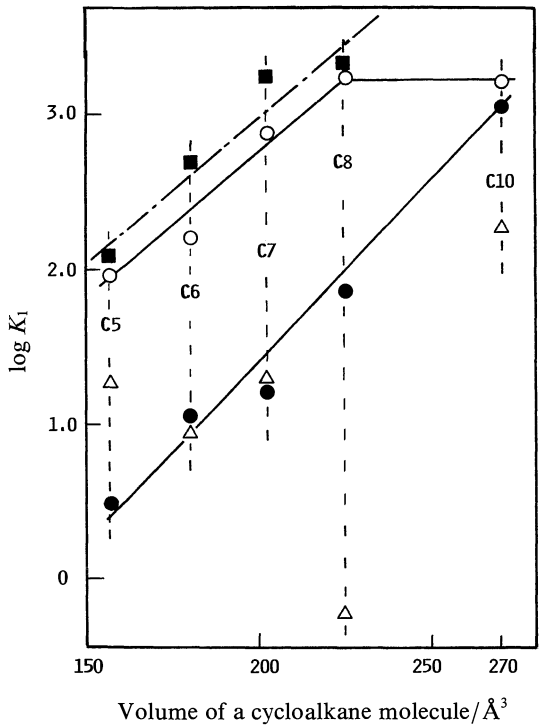

Fig. 5. Dependence of association constant on the volume of a cycloalkane molecule. Cycloalkane–α-CyD (△), –β-CyD (○), –γ-CyD (●), Cycloalkanol–β-CyD (■) (Ref. 7).

Normal and Cycloalkanes. It is interesting to note that, in the complex formation with γ-CyD, the K of a cycloalkane is almost comparable to that of a normal alkane of the same carbon number. This supports one of the hypotheses proposed in our preceding paper.[1] Namely, an alkyl chain takes a herix-coil conformation in the cavity of γ-CyD to get contact as widely as possible with the cavity wall; the cross section of the helix-coil conformation resembles a cycloalkane molecule., With the present study, we reject another hypothesis that takes into account the presence of water in the host cavity. As

for β-CyD, the space inside the cavity is not so large as to allow for an alkyl chain to take a cycloalkane-like arrangement.

References

1) I. Sanemasa, T. Osajima, and T. Deguchi, *Bull. Chem. Soc. Jpn.*, **63**, 2814 (1990).
2) K. Matsunaga, M. Imanaka, T. Ishida, and T. Oda, *Anal. Chem.*, **56**, 1980 (1984); L. A. Blyshak, T. M. Rossi, G. Patonay, and I. M. Warner, *ibid.*, **60**, 2127 (1988).
3) M. Komiyama, H. Yamamoto, and H. Hirai, *Chem. Lett.*, **1984**, 1081.
4) A. Wishnia and S. J. Lappi, *J. Mol. Biol.*, **82**, 77 (1974).
5) I. Sanemasa and Y. Akamine, *Bull. Chem. Soc. Jpn.*, **60**, 2059 (1987).
6) A. S. Kertes, "IUPAC Solubility Data Series," ed by D. G. Shaw, Pergamon, Oxford (1989), Vols. 37 and 38.
7) Y. Matsui and K. Mochida, *Bull. Chem. Soc. Jpn.*, **52**, 2808 (1979).
8) W. C. Cromwell, K. Byström, and M. R. Eftink, *J. Phys. Chem.*, **89**, 326 (1985).
9) G. Nelson, G. Patonay, and I. M. Warner, *Anal. Chem.*, **60**, 274 (1988).
10) I. Sanemasa, T. Takuma, and T. Deguchi, *Bull. Chem. Soc. Jpn.*, **62**, 3098 (1989).
11) T. Takuma, T. Deguchi, and I. Sanemasa, *Bull. Chem. Soc. Jpn.*, **63**, 1246 (1990); *ibid.*, **64**, 480 (1991).
12) C. McAuliffe, *J. Phys. Chem.*, **70**, 1267 (1966).

Surface and Subsurface Fluorometry under Normal Incidence Conditions

Xing-Zheng Wu, Takehiko Kitamori, Norio Teramae,† and Tsuguo Sawada*
Department of Industrial Chemistry, Faculty of Engineering, The University of Tokyo,
7-3-1 Hongo, Bunkyo-ku, Tokyo 113
† Department of Applied Chemistry, Faculty of Engineering, Nagoya University,
Hurouchou 1, Chigusaku, Nagoya 464
(Received April 20, 1991)

Laser induced fluorescence spectroscopy under normal incidence conditions has been applied to a thick film sample, and identification of surface and subsurface fluorescent components was demonstrated. A model film sample adsorbing different fluorescent compounds on its two sides was prepared. Fluorescence spectra from the surface and subsurface regions were separately obtained for observation angles larger and smaller than the critical angle, and it was shown that the same information as the conventional attenuated total reflection method can be obtained with the normal incidence conditions, which is anticipated by the reciprocal principle. Dependence of fluorescence intensity on observation angle agreed well with theoretical calculation results based on the reciprocal principle, which supports the methodology propriety.

Fluorescence spectroscopy has been applied to spectrochemical surface measurement and characterization of various materials, such as organic solids,[1] surface dynamics of biomolecules,[2] and adsorption behavior of proteins at a solid/liquid interface.[3-6] However, in these works, the attenuated total reflection (ATR) conditions has been used to obtain surface fluorescence, in which an excitation beam is incident on the prism/sample interface at an angle larger than the critical angle and fluorescence is measured from the normal direction to the prism. Recently, we have verified that laser induced fluorescence spectroscopy under normal incidence conditions can be used to determine the monolayer level concentration depth profile of an ultrathin film sample,[7,8] by the method based on the reciprocal theory.[9] From an instrumentational viewpoint, normal incidence excitation can obtain the fluorescence angular distribution without changing the irradiation area, and the excitation beam can be easily scanned. These merits are more suitable than the conventional ATR configuration for the local analyses, future dynamic measurements, and three dimensional analyses.[7-9] Therefore, this method is expected to be developed for various applications.

In this paper, we apply this method to surface and subsurface analysis of a thick film sample. According to the reciprocal theory, this fluorescence method using the normal incidence excitation configuration can obtain the same information as with the conventional ATR configuration. Two kinds of fluorescent dyes are adsorbed on different sides of the model film sample surface, and we demonstrate that fluorescence spectra from a dye distributed in the surface and subsurface regions of the film can be detected separately by changing observation angles. Moreover, the measured dependence of the fluorescence intensity on observation angle is compared with theoretical calculation results which are obtained according to the reciprocal principle.

Theoretical Background

Figure 1 shows a schematic illustration of laser induced fluorescence spectroscopy under normal incidence conditions based on the reciprocal principle. Fluorescence intensity $F(\theta)$ determined at the observation angle θ in the prism side can be expressed as the convolution of the concentration depth profile $C(z)$ of a fluorophore and a transmission function $T(\theta, z)$:[7,10]

$$F(\theta) = k\int_0^t C(z)T(\theta, z)\mathrm{d}z, \quad (1)$$

where t is the film thickness, k is a constant. In the case where the sample is an ultrathin film sample, $T(\theta, z)$ can be obtained by the theoretical analysis of the multiple reflection of fluorescence electromagnetic waves between prism/film and film/air interfaces.[9] On the other hand, in the case when the sample is a bulk or a thick film sample, $T(\theta, z)$ can be obtained by considering the

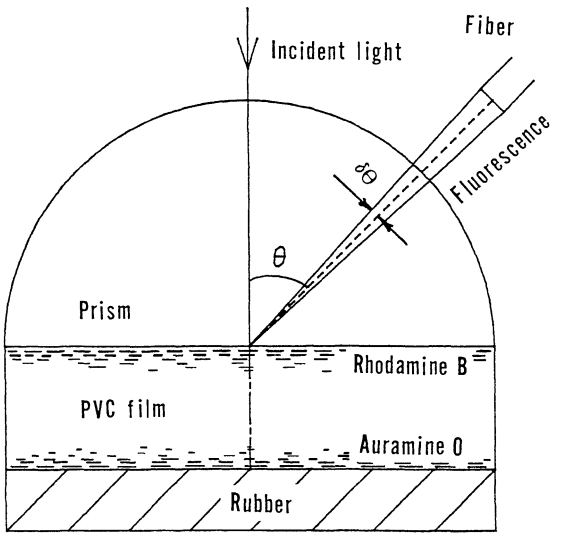

Fig. 1. Schematic illustration of central part of the experimental set up and the model film sample.

reflection and refraction effects of fluorescence occurring at the prism/sample interface. Snell's law and basic electromagnetic theory state that light incident from the prism to the prism/sample interface at an angle larger or smaller than the critical angle θ_c will create an evanescent wave or a transmitted wave in the sample, respectively. The transmitted wave propagates through the whole sample and its intensity is homogeneous over the whole sample. On the other hand, the evanescent wave exists only in the surface region of the sample with a depth on the order of the excitation light wavelength from the prism/film interface, and its intensity decreases exponentially with the distance z. According to the reciprocal theory, fluorescence observed in the prism side at $\theta>\theta_c$ and $\theta<\theta_c$ are an evanescent component and a propagating component, respectively.[11-13] Moreover, the reciprocal theory predicts that the evanescent fluorescence component observed must be from a surface region with a depth on the order of the fluorescence wavelength from the prism/film interface, and the propagating fluorescence component observed is from the whole sample including the surface and subsurface regions. The transmission factors $T(\theta, z)$ of the evanescent and propagating fluorescence components are given by the Fresnel transmission factor $T_f(\theta)$ and the attenuation factor $\exp(-2z/dp)$ as Eq. 2a, and the square of the Fresnel transmission factor $T_f(\theta)$ as Eq. 2b, respectively.[10-13]

$$T(\theta, z)=|T_f(\theta)|^2\exp(-2z/dp), \qquad \theta>\theta_c \tag{2a}$$

$$T(\theta, z)=|T_f(\theta)|^2. \qquad \theta<\theta_c \tag{2b}$$

In Eq. 2a, dp is the penetration depth of the fluorescence which can be obtained from the fluorescence wavelength λ and the refractive indices of prism (n_p) and film (n_f),

$$dp=\lambda/2\pi n_p[\sin^2\theta-(n_f/n_p)^2]^{1/2}. \tag{3}$$

The Fresnel transmission factor $T_f(\theta)$ and the critical angle θ_c can be obtained from n_p and n_f.[11-13] The fluorescence intensity $F(\theta)$ of the evanescent and propagating components can be expressed as follows by substituting Eqs. 2a and 2b into Eq. 1,

$$F(\theta)=k|T_f(\theta)|^2\int_0^t C(z)\exp(-2z/dp)\mathrm{d}z, \qquad \theta>\theta_c \tag{4a}$$

$$F(\theta)=k\int_0^t C(z)|T_f(\theta)|^2\mathrm{d}z=K|T_f(\theta)|^2, \qquad \theta<\theta_c \tag{4b}$$

where the constants K in Eq. 4b can be expressed as Eq. 5,

$$K=k\int_0^t C(z)\mathrm{d}z. \tag{5}$$

Therefore, using the normal incidence excitation configuration shown as Fig. 1, surface and subsurface fluorescence information can be obtained separately at $\theta>\theta_c$ and $\theta<\theta_c$, respectively. This is demonstrated in the following experiement.

Experimental

The experimental set up has been described elsewhere in detail.[7] Figure 1 shows the central part of the set up and the model film sample. An Ar^+ ion laser provided the excitation light (output power, 10 mW), the wavelength of which was selected as 457.9 nm because both the fluorescence compounds Rhodamine B and Auramine O in model film sample can be excited by this laser line. The maximum absorption wavelengths of plasticized poly(vinyl chloride) (PVC) film samples adsorbing Rhodamine B and Auramine O were determined to be about 550 and 440 nm, respectively, by a spectrophotometer and their maximum fluorescence wavelengths were determined to be about 575 and 500 nm, respectively, by a spectrofluorometer. The excitation light was focused on the focal plane of a hemicylindrical prism (n_p, 1.88) which was mounted on the two rotating stages. In order to ensure the model sample made direct contact with the prism, a piece of rubber was used and pressure was applied to the rubber. The side with adsorbed Rhodamine B was in direct contact with the prism. A step index type optical fiber bundle was used to collect the fluorescence. Its diameter was 0.11 cm and the numerical aperture was 0.57. One end of the fiber bundle was fixed at the focal plane of the prism. The other end was coupled with a monochromator. A photomultiplier (Hamamatsu R928) was used as a detector.

The model sample was prepared by an adsorption of fluorescent dyes onto a PVC film (n_f, 1.53) obtained from Okamoto Industry Corporation. The preparation procedure was based on the method proposed by Kaneko et al.[14] in which 1 ml 1×10^{-4} mol dm^{-3} Rhodamine B solution was dropped onto the PVC film sheet (thickness, 0.20 mm). The droplet of Rhodamine B solution remained on the PVC film sheet due to surface tension and the dye molecules diffused into the PVC film, adsorbing in it. After 20 min, the droplet was removed and the PVC film sheet was rinsed with water twice. In the same way, 1 ml 1×10^{-4} mol dm^{-3} Auramine O (with 1×10^{-2} mol dm^{-3} NaOH) solution was dropped onto the other side of PVC film sheet and dye were adsorbed.

Fluorescence microscopic measurements of a cross section of a PVC film sample immersed in 1×10^{-4} mol dm^{-3} Rhodamine B solution for 20 min indicated that the adsorbed fluorescent dye distributed from the surface to a depth of about 40 μm in the PVC film. Similar results were also obtained by the photoacoustic depth profiling method.[15]

Results and Discussion

It has been stated that fluorescence measured at $\theta>\theta_c$ is surface fluorescence which comes from the surface regions with a depth on the order of the fluorescence wavelength from the prism/sample interface, and fluorescence measured at $\theta<\theta_c$ is from the whole sample, including the surface and subsurface regions. The fiber bundle has a finite size, it collects fluorescence from a finite range of observation angles, from $\theta-\delta\theta$ to $\theta+\delta\theta$ as shown in Fig. 1. Therefore the surface fluorescence is

obtained practically at $\theta>\theta_c+\delta\theta$. For the prism/PVC film interface, the calculated θ_c from n_p and n_f is 54.5 °C, and $\delta\theta$ is calculated to be 1.5 °C from the fiber diameter (1.1 mm) and the distance (2.14 cm) between the illumination point and fiber bundle. Therefore, in our experiments, surface fluorescence should be obtained at $\theta>56$ °C.

The fluorescence spectra of the model sample was determined at different observation angles under normal incidence conditions, and two kinds of fluorescence spectra were obtained. They are shown in Fig. 2. The fluorescence spectrum obtained at an observation angle=50 °C ($<\theta_c$) is shown by the the solid line, where two peaks appear at about 575 and 500 nm, respectively. They correspond to the fluorescence of Rhodamine B and Auramine O, respectively. The fluorescence spectrum obtained at observation angle=60 °C ($>\theta_c+\delta\theta$) is shown by the dashed line, where only one peak at about 575 nm corresponding to the fluorescence of Rhodamine B is observed. The chain line is the blank fluorescence spectrum, i.e., the fluorescence spectrum of PVC film without adsorption of fluorescent dye.

As shown in Fig. 1, the side of the PVC film surface adsorbing Rhodamine B is in direct contact with the prism, therefore in the prism/film interface region only Rhodamine B is present. On the other hand, apparently Auramine O distributes in the region away from the interface of the prism/film. Therefore, the results of Fig. 2 demonstrate that surface and subsurface fluorescence information can be obtained by changing the observation angle using the normal incidence excitation configuration, which is anticipated in the theoretical section. Although the reciprocity in the angular distribution of fluorescence has been pointed out,[9,11-13] this work is the first spectroscopical demonstration that surface and subsurface information can be separately obtained by the normal incidence excitation configuration.

Figure 3-A shows the theoretical and measured dependence of fluorescence intensity on the observation angle for $\theta<\theta_c$. The theoretical results were obtained from Eq. 4b, and are represented by a solid line. The measured data were obtained at fluorescence wavelength=575 nm, and are shown by circles. The measured fluorescence intensities agree well with the calculated ones. Figure 3-B shows the theoretical and measured dependence of fluorescence intensity on observation angle for $\theta>\theta_c$. The theoretical and measured fluorescence intensities are represented by a solid line and circles, respectively. The measured fluorescence intensities were obtained at fluorescence wavelength=575 nm. The theoretical results were obtained from Eq. 4a assuming $C(z)$ is a constant. As stated above, at $\theta>\theta_c$, the measured fluorescence is from the surface region with a depth on the order of the

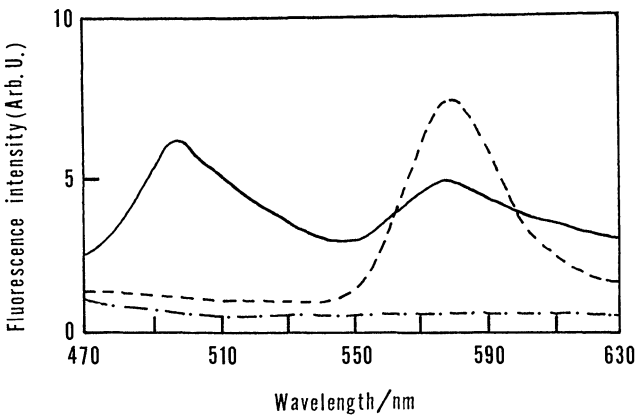

Fig. 2. Fluorescence spectra of the model film sample under normal incidence conditions at different observation angles. The solid and dashed lines represent the fluorescence spectra obtained at 50° and 60°, respectively. The blank fluorescence spectrum is represented by the chain line.

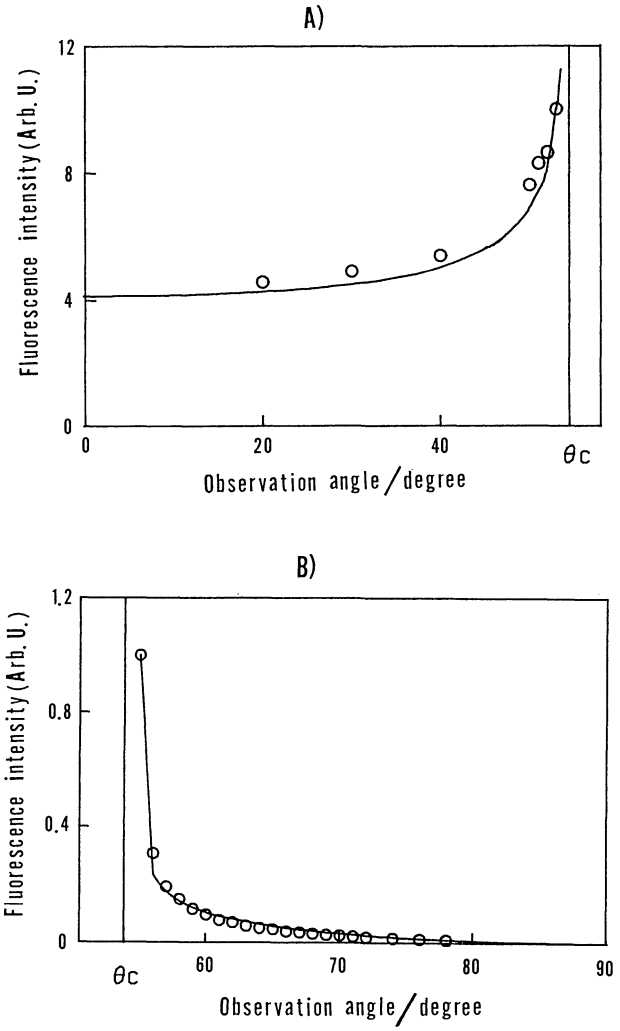

Fig. 3. Theoretical and determined dependence of fluorescence intensity on the observation angles. A: the observation angle is smaller than the critical angle. B: the observation angle is larger than the critical angle.

fluorescence wavelength from the prism/film interface, while adsorbed Rhodamine B is distributed from the surface to a depth of about 40 μm. Therefore the concentration distribution $C(z)$ of Rhodamine B from the surface to a depth on the order of the fluorescence wavelength can be considered as a constant. The results of Fig. 3 indicate that the dependence of fluorescence intensity on observation angle can be quantitatively described by Eqs. 4a and 4b, which confirms propriety of this method, obtained on the basis of the reciprocal principle.[10-13]

In our previous reports, the validity of laser induced fluorescence spectroscopy under normal incidence conditions to an ultrathin film sample was proved.[7,8] In the present work, it was demonstrated that this fluorescence method can also be applied to a bulk or a thick film sample. As a result, the surface fluorescence of these samples can be distinguished from the subsurface fluorescence by this method. The present method provides the possibility to determine the surface fluorescence and subsurface fluorescence simultaneously with two detectors.

References

1) H. Masuhara, S. Tazuke, N. Tamai, and I. Yamazaki, *J. Phys. Chem.*, **90**, 5830 (1986).
2) N. L. Thompson, T. P. Burghardt, and D. Axelrod, *Biophys. J.*, **33**, 435 (1981).
3) V. Hlady and J. D. Andrade, *Colloids Surfaces*, **32**, 359 (1988).
4) V. Hlady, D. R. Reinecke, and J. D. Andrade, *J. Colloid Interface Sci.*, **111**, 555 (1986).
5) V. Hlady, C. Golander, and J. D. Andrade, *Colloids Surfaces*, **25**, 185 (1987).
6) K. C. Hartner, J. W. Carr, and J. M. Harris, *Appl. Spectrosc.*, **43**, 81 (1989).
7) X-Z. Wu, T. Kitamori, N. Teramae, and T. Sawada, *Bull. Chem. Soc. Jpn.*, **64**, 755 (1991).
8) X-Z. Wu, T. Kitamori, and T. Sawada, *Bull. Chem. Soc. Jpn.*, **64**, 1757 (1991).
9) P. A. Suci and W. M. Reichert, *Appl. Spectrosc.*, **42**, 120 (1988).
10) P. A. Suci and W. M. Reichert, *Langmuir*, **4**, 131 (1988).
11) W. M. Reichert, P. A. Suci, J. T. Ives, and J. D. Andrade, *Appl. Spectrosc.*, **41**, 503 (1987).
12) C. K. Carniglia and L. Mandel, *J. Opt. Soc. Am.*, **62**, 479 (1972).
13) El-Hang Lee, R. E. Benner, J. B. Fenn, and R. K. Chang, *Appl. Opt.*, **18**, 862 (1979).
14) E. Kaneko, H. Tanno, and T. Yotsuyanagi, *Mikrochim. Acta*, **111**, 333 (1988).
15) A. Harata and T. Sawada, *J. Appl. Phys.*, **65**, 959 (1989).

Enantioselective Extraction of Di-*O*-benzoyltartrate Anion by Ion-Pair Extractant Having Binaphthyl-Unit

Akira OHKI,* Ryo MIYASHITA, Kensuke NAKA, and Shigeru MAEDA
Department of Applied Chemistry, Faculty of Engineering, Kagoshima University, 1-21-40, Korimoto, Kagoshima 890
(Received April 22, 1991)

A lipophilic diphosphonium salt **1** having binaphtyl-type axial chirality was developed as a novel ion-pair extractant. By use of (*R*)-**1**, (−)-di-*O*-benzoyltartrate ((−)-DBT) was extracted more effectively than (+)-DBT. The enantioselectivity ($\alpha = D_{(-)}/D_{(+)}$; D: distribution ratio) was 1.3—1.4. When monophosphonium-type extractants (**2** and **3**) having structures similar to that of **1** were used, the enantioselectivity was heavily lowered. Equilibrium studies revealed that the extraction occurs *via* formation of a 1 : 1 ion-pair complex between **1** and DBT at pH 7.5—8.0. The effects of pH, ionic strength, and temperature on the extractability and the enantioselectivity were investigated. The enantioselectivity decreased with lowering pH, and was higher at lower temperatures. The optical purity of DBT in the aqueous phase was gradually enhanced by multistage extraction. From an NMR analysis of the **1**·DBT complex, the resonances of methylene-protons adjacent to phosphonium in the more extractable complexes ((*R*)-**1**·(−)-DBT and (*S*)-**1**·(+)-DBT) shifted to a higher field compared to those of the less extractable complexes ((*R*)-**1**·(+)-DBT and (*S*)-**1**·(−)-DBT).

Resolution of enantiomers has been discussed mainly in crystallization systems and in chromatography systems. In the field of solvent extraction, optical resolution (chirality recognition) has so far been scarcely studied, except for the works with Cram's chiral crown ethers.[1-6]

Crown ethers interact only with cationic species such as amino acids and amines. To extract anionic species, the use of ion-pair extraction is essential. However, in the framework of ion-pair extraction there are few reports on the chirality recognition.[7,8] Ion-pair complexes are generally outer sphere complexes between cations and anions; these ions frequently combine with each other through mediation by several water molecules within the complexes. Therefore, it is generally believed that the specificity is not appreciably expected in ion-pair formation itself, whereas a selectivity could be attained via i) a difference in the solubility to aqueous phase, ii) that to organic phase, iii) acid-base reaction, and iv) complex formation in aqueous media. However, two enantiomers in ion-pair extraction systems would behave quite similarly regarding the factors i)—iv).

In order to separate enantiomers by ion-pair extraction, a specificity should exist in the ion-pair formation itself; a difference in the steric hindrance between the enantiomers can result in a specificity when they form ion-pair complexes with chiral ion-pair extractants. However, such a difference hardly reflects the difference in distribution ratios of each enantiomer. This may be a main reason for the scarcity of reports on the chirality recognition in ion-pair extractions.

Recently, we studied ion-pair extractions of organic anions from the viewpoint of molecular recognition.[9-16] In a previous communication,[17] we briefly reported a new type of ion-pair extractant having an axial chirality (binaphthyl unit), which exhibited the ability of chirality recognition in the ion-pair extraction of an organic dicarboxylate anion, di-*O*-benzoyltartrate (DBT). This demonstrates a possibility of chirality recognition by proper design of the extractant molecule. However, the extractant reported has a low lipophilicity and hence is not of practical use as an anion-exchange extractant.

In the present study, we synthesized a chiral extractant of high lipophilicity, (*R*)-(−)- or (*S*)-(+)-1,1′-binaphthyl-2,2′-diylbis[(*p*-octylbenzyl)diphenylphosphonium] dibromide (abbreviated as (*R*)-**1** or (*S*)-**1**; Fig. 1). By using this as an ion-pair extractant (anion-exchange extractant), we examined factors affecting the chirality recognition and extractability. Further, the ion-pair complexes of optical isomer were investigated by NMR. The potential of optical resolution by use of the chiral ion-pair extractant is discussed.

In the field of chromatography, it is known that optical resolution of ionic enantiomers in aqueous media is considerably difficult. Ion-pair extraction is the basis of ion-pair chromatography, and thus, the study of chiral ion-pair extraction is important from such a point of view, as well.

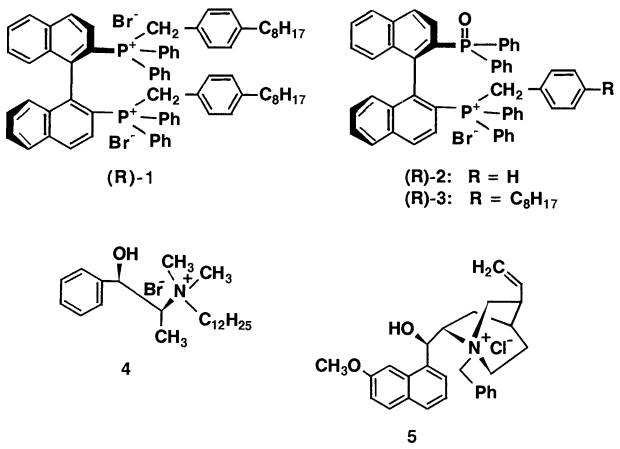

Fig. 1. Ion-pair extractants having chirality.

Experimental

Synthesis of (*R*)-1. *p*-Octylbenzyl bromide was obtained from *p*-octylbenzonic acid via methylation, $LiAlH_4$-reduction, and bromination by phosphorus tribromide. The bromide (4.5 g, 16 mmol), (*R*)-(+)-2,2′-bis(diphenylphosphino)-1,1′-binaphthyl ((*R*)-BINAP; 2.0 g, 3.2 mmol), and *N*,*N*-dimethylformamide (DMF, 10 mL) were charged in a grass tube, which was then sealed along with a stirring magnet under vacuum after several freeze-pump-thaw cycles. The sealed tube was heated at 130 °C for 3 h with internal stirring. After removal of DMF and unreacted *p*-octylbenzyl bromide from the reaction mixture by evaporation with a rotary pump, white crude crystals were obtained. The crystals were purified by column chromatography on silica gel. The column with the crude product was washed with 1,2-dichloroethane and the product was eluted with ethanol. Colorless crystals were obtained. Yield (3.1 g, 81%), mp 214—216 °C. Found: C, 74.58; H, 6.50%. Calcd for $C_{74}H_{78}P_2Br_2$: C, 74.74; H, 6.61%. $[\alpha]_D^{25}$ −142°, $[\alpha]_{546}^{25}$ −186°, $[\alpha]_{435}^{25}$ −487° (*c* 1.0, ethanol). ^1H NMR ($CDCl_3$) δ=0.87 (6H, t; CH_3), 1.15—1.5 (24H, br; CCH_2C), 2.42 (4H, t; CH_2Ph), 4.72 and 4.75 (2H, two d, $J_{PCH}\approx J_{HCH}\approx$12 Hz; $PhCH_2P$), 5.26 and 5.29 (2H, two d, $J_{PCH}\approx J_{HCH}\approx$12 Hz; $PhCH_2P$), and 6.6—8.3 (40H, m; aromatic). ^{31}P NMR ($CDCl_3$) δ^P (from H_3PO_4)=20.9 (s). (*S*)-**1** was similarly prepared from (*S*)-BINAP (Yield; 2.9 g, 76%). Its physicochemical properties were identical with those of the enantiomer except in the sign of rotation. Found: C, 74.48; H, 6.71%.

Synthesis of (*R*)-2. (*R*)-BINAP (2.0 g, 3.2 mmol), benzyl bromide (0.55 g, 3.2 mmol), and DMF (18 mL) were charged in a grass tube and treated in a manner similar to that for (*R*)-**1** synthesis (130 °C, 20 h). Then, 1.1 g of hydrogen peroxide solution (30%) was added to the reaction mixture, and this was heated at 100 °C for 3 h. Yield (1.4 g, 54%), mp 175—179 °C. Found: C, 75.53; H, 4.95%. Calcd for $C_{51}H_{39}OP_2Br$: C, 75.65; H, 4.85%. $[\alpha]_D^{25}$ −49° (*c* 1.0, ethanol). ^1H NMR ($CDCl_3$) δ=3.81 and 3.84 (1H, two d, $J_{PCH}\approx J_{HCH}\approx$12 Hz; $PhCH_2P$), 5.52 and 5.57 (1H, two d, $J_{PCH}\approx J_{HCH}\approx$12 Hz; $PhCH_2P$), and 6.4—8.0 (36H, m; aromatic). (*R*)-**3** was similarly prepared from (*R*)-BINAP and *p*-octylbenzyl bromide. The product was identified by elemental analysis and ^1H NMR.

Reagents. (−)-*N*-Dodecyl-*N*-methylephedrinium bromide (**4**) and (−)-*N*-benzylquininium chloride (**5**) were purchased from Merck and used after recrystallization. Other chemicals were of reagent grade and used without further purification.

Extraction Procedure. An aqueous solution containing the chiral anion (DBT) was shaken with an organic solution containing an extractant in a stoppered centrifuge tube for 3 h in a thermostated bath (±0.1 °C). As extracting solvent, a mixture of 1,2-dichloroethane and carbon tetrachloride (1 : 1) was mainly used. After a phase-separation procedure was rapidly carried out, the concentration of the anion in the aqueous phase was determined by HPLC with a Shimadzu LC-6A liquid chromatograph equipped with a UV detector SPD-6A (275 nm). A column packed with octadecylsilyl (ODS) silica (150 mm×4.6 mm, Wakosil 5C18-200) was used. The eluent was a mixed solution (water–methanol 3 : 2) containing 2 mM (1 M=1 mol dm^{-3}) Na_2HPO_4–KH_2PO_4 buffer. Enantioselectivity (α), the ratio between the distribution ratios of both enantiomers, was obtained as an average of more than three runs.

Multistage Extraction. An aqueous solution (10 mL) containing 5 mM racemic DBT, 15 mM NaBr, and 0.1 M Na_2HPO_4–KH_2PO_4 buffer (pH 7.5) was shaken with an organic solution (1,2-dichloroethane, 10 mL) containing 10 mM (*R*)-**1** for 3 h at 2 °C. After phase separation, the concentration of DBT in the aqueous phase was determined, and the optical rotation of the solution was measured by a polarimeter (JASCO DIP-370 with Hg lamp (435 nm); 10 cm cell) (first-step extraction).

A 9.6 mL aliquot of the aqueous phase after the extraction was taken up, in which 0.1 mL of 0.5 M NaBr solution was added. The resulting solution was shaken with 4 mL of the fresh organic solution containing 10 mM (*R*)-**1** in a similar manner. After phase separation, the concentration and the optical rotation were measured (second-step extraction). Then, 9.2 mL of the aqueous phase after the second-step extraction was taken up, and the solution was treated in a similar manner, except that 0.05 mL of 0.5 M NaBr solution was added (third-step extraction).

In the case of (*S*)-**1** extractant, the extraction procedure was similarly carried out except that 9.4 mL of the aqueous phase was used in the second-step extraction and 9.0 mL, the third-step extraction.

NMR Analysis of Ion-Pair Complex. An aqueous solution (20 mL) containing 50 mM (−)- or (+)-DBT and 0.5 M Na_2HPO_4–KH_2PO_4 buffer (pH 7.5) was shaken with a 1,2-dichloroethane solution (20 mL) containing 5 mM (*R*)- or (*S*)-**1** for 2 h at room temperature. The organic phase was separated. After removal of the solvent by evaporation, the ion-pair complex was obtained (yield: 93%). A portion of it was dissolved in $CDCl_3$ and analyzed by NMR with a JEOL JNM-GSX 400 instrument.

Results and Discussion

Extraction of Enantiomeric DBT. Table 1 summarizes the extraction of enantiomeric DBT by use of various extractants having chirality. When (*R*)-**1** was used, which is a dicationic diphosphonium salt having an axially chiral unit (binaphtyl unit), (−)-DBT was more effectively extracted than (+)-DBT. In contrast, (+)-DBT was more efficiently extracted than (−)-DBT by use of (*S*)-**1** as extractant. Thus, "enantioselective" extraction took place by use of **1** as an ion-pair extractant. The enantioselectivity α was 1.36. When the extraction using (*R*)-**1** was performed at 20 °C, the enantioselectivity was lower than 1.36. When pure 1,2-dichloroethane was used as extracting solvent instead of the mixture solvent (1,2-dichloroethane+carbon tetrachloride) under otherwise identical conditions, the enantioselectivity somewhat decreased.

Compounds **2** and **3** have structures similar to that of **1** but are monocationic phosphonium salts (Fig. 1). When they were used as extractants, the enantioselectivity was considerably lower. Compounds **4** and **5** are commercial phase-transfer catalysts having asymmetric carbons. These did not exhibit chirality recognition as ion-pair extractants.

In the extraction of mandelate by (*R*)-**1**, the (−)-isomer was somewhat more extracted than the (+)-isomer

Table 1. Extraction of Enantiomeric DBT by Chiral Extractant[a]

Extractant	Buffer mM	pH	[NaBr] mM	Temp °C	(+) or (−)[b]	Distribution ratio[c] D_A	D_B	$\alpha=D_A/D_B$
(*R*)-**1**	5	7.5	0.4	2	(−)	0.400	0.294	1.36
(*S*)-**1**	5	7.5	0.4	2	(+)	0.392	0.290	1.35
(*R*)-**1**	2	7.0	0.3	2	(−)	1.10	0.818	1.34
(*R*)-**1**	2	7.0	0	20	(−)	1.08	0.911	1.18
(*R*)-**2**	2	7.0	0	20	(−)	1.93	1.84	1.05
(*R*)-**3**	2	7.0	0	20	−	3.68		d)
4	2	7.0	0	20	−	1.58		d)
5[e]	2	6.1	0	20	−	0.74		d)

a) The aqueous phase initially contained 0.1 mM DBT, NaBr, and Na_2HPO_4–KH_2PO_4 buffer, while the organic phase (1,2-dichloroethane+carbon tetrachloride, 1:1) contained 0.2 mM extractant. b) More extractable enantiomeric DBT. c) D_A and D_B denote the distribution ratios of more and less extractable enantiomeric DBTs, respectively. d) The α value could not be evaluated ($\alpha<1.02$). e) 5 mM of the extractant was added.

(α=1.1). However, in the extraction of dansyl-amino acids such as dansyl-phenylalanine and dansyl-serine by **1** and **3**, the enantioselective extraction was hardly attained under relevant conditions.

Extraction Equilibrium. The extraction of DBT by **1** was investigated in detail. We assume that extraction of the dianion (DBT) by the dicationic extractant (**1**) involves the formation of a 1:1 ion-pair complex between **1** and DBT. The reaction and the extraction constant (K_{ex}) are defined as follows:

$$(Q{\cdot}Br_2)_o + (A^{2-})_w \rightleftharpoons (Q{\cdot}A)_o + 2(Br^-)_w, \quad (1)$$

and

$$K_{ex} = [Q{\cdot}A]_o[Br^-]_w^2/[Q{\cdot}Br_2]_o[A^{2-}]_w, \quad (2)$$

where Q^{2+} and A^{2-} denote **1** and DBT, respectively, and subscripts w and o denote the aqueous and organic phases, respectively. Eq. 2 is converted into a logarithmic form:

$$\log [Q{\cdot}A]_o/[Q{\cdot}Br_2]_o[A^{2-}]_w = \log K_{ex} - 2\log [Br^-]_w. \quad (3)$$

The $Q{\cdot}Br_2$ and the complex, Q·A, are highly lipophilic and do not appreciably dissolve in the aqueous phase. The distribution ratio of $Q{\cdot}Br_2$ was larger than 100 in 1,2-dichloroethane/water system. Thus, the values of $\log [Q{\cdot}A]_o/[Q{\cdot}Br_2]_o[A^{2-}]_w$ and $\log [Br^-]_w$ in Eq. 3 can be easily obtained experimentally.

Figure 2 shows the plots of $\log [Q{\cdot}A]_o/[Q{\cdot}Br_2]_o[A^{2-}]_w$ against $\log [Br^-]_w$ in the extraction of DBT by (*R*)-**1** at pH 7.5 and 8.0. The plot is a straight line with a slope of 2. This indicates that the extraction reaction (1) occurs via the formation of a 1:1 ion-pair complex between **1** and DBT under the relevant pH conditions. The ratio, K_{ex} ((−)-DBT)/K_{ex}((+)-DBT)=1.47, was obtained at pH 7.5.

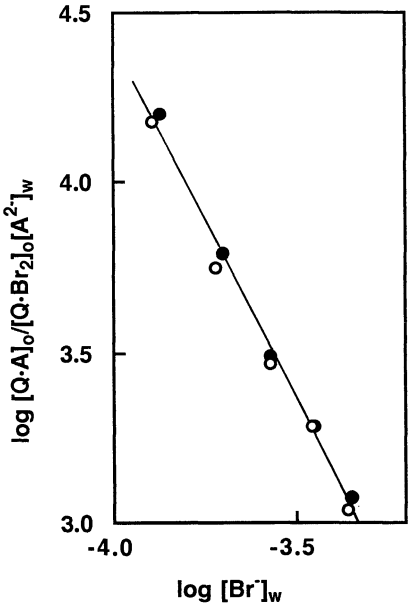

Fig. 2. Extraction of (−)-DBT by (*R*)-**1** at pH 7.5 (●) and at pH 8.0 (○). The aqueous phase initially contained 0.1 mM (−)-DBT, 0—0.4 mM NaBr, and 5 mM Na_2HPO_4–KH_2PO_4 buffer, while the organic phase (1,2-dichloroethane+carbon tetrachloride, 1:1) contained 0.2 mM (*R*)-**1** (2°C).

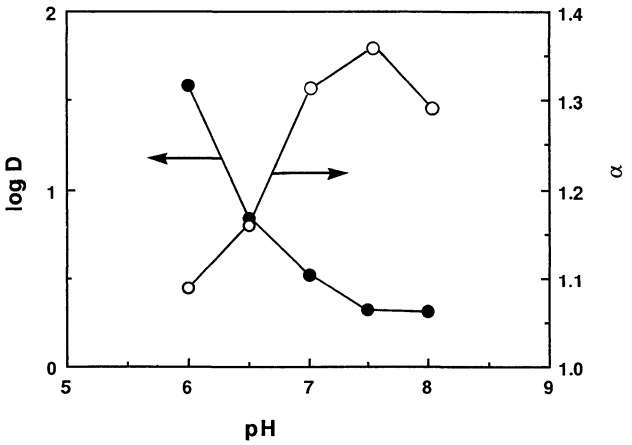

Fig. 3. Effect of pH on the extractability of (−)-DBT and the enantioselectivity (α). Conditions were the same as those in Fig. 2 except that pH was varied (NaBr: 0 mM).

Effect of pH and Ionic Strength. Figure 3 shows the plot of log D (D: distribution ratio of DBT) against pH in the aqueous phase. The extractability of DBT was decreased with increasing pH in the range 6.0—7.5, and is almost constant at pH above 7.5. This suggests that by lowering pH, the protonated DBT is involved to a higher degree in the extraction reaction ($Q^{2+}\cdot Br^-\cdot AH^-$ complex is extracted) and thus the extractability is raised. As mentioned above, the 1 : 1 ion-pair complex ($Q^{2+}\cdot A^{2-}$) is only extracted via Eq. 1 at pH above 7.5.

The enantioselectivity was enhanced with an increase in pH (Fig. 3). A two-point ion-pair formation within the complex between **1** and DBT may play an important role in the enantioselectivity, as will be discussed later.

Figure 4 depicts the effect of ionic strength in the aqueous phase. The extractability is nearly independent of the ionic strength, while the enantioselectivity decreases slightly, as the ionic strength increases.

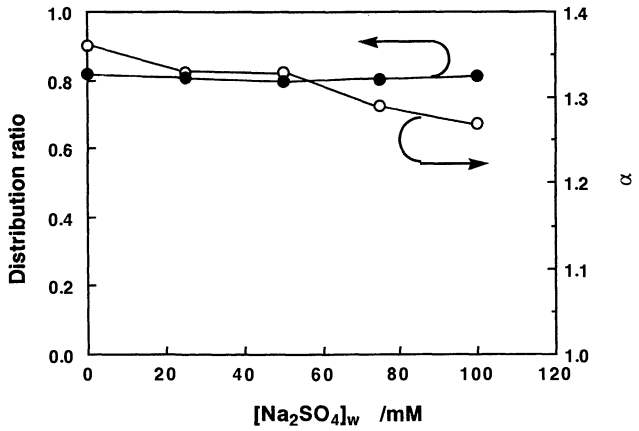

Fig. 4. Effect of ionic strength on the extractability of (−)-DBT and the enantioselectivity (α). Conditions were the same as those in Fig. 2 except that a prescribed amount of Na_2SO_4 was added and 2 mM buffer was used (pH: 7.5; NaBr: 0.2 mM).

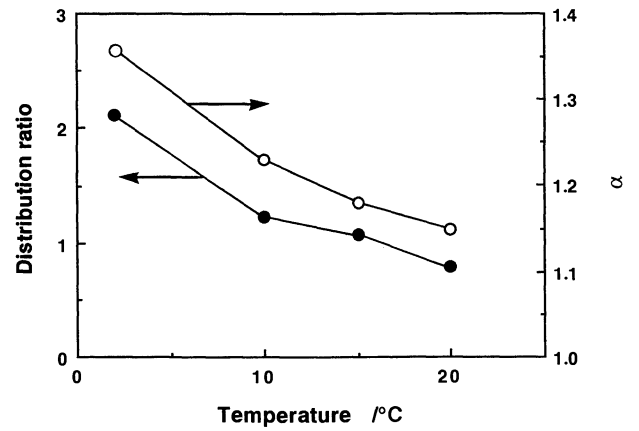

Fig. 5. Effect of temperature on the extractability of (−)-DBT and the enantioselectivity (α). Conditions were the same as those in Fig. 2 except that the temperature was varied (NaBr: 0 mM; pH: 7.5).

Effect of Temperature. The effect of temperature is given in Fig. 5. Both the extractability and the enantioselectivity decrease with an increase in the temperature. The chirality recognition of **1** may come from a difference between the steric hindraces of binaphtyl unit for both enantiomers. As the temperature is lowered, the rigidity of binaphtyl unit increases, resulting in the enantioselectivity enhancement. A similar situation was reported in the studies of Cram's crown ether.[3]

Multistage Extraction. Table 2 summarizes the results of multistage extraction. In each extraction step, the conditions were adjusted to give the % extraction of roughly 50%. As the extraction step went up in the case of (*R*)-**1** extractant, the optical purity of (+)-DBT in the aqueous phase was gradually enhanced; however, the concentration of DBT in the aqueous phase was inevitably decreased. Conversely, when (*S*)-**1** was used, the optical purity of (−)-DBT was increased. The conditions of multistage extraction in the cases of (*R*)-**1** and (*S*)-**1** were somewhat different from each other. Therefore, as seen in Table 2, the optical purities obtained in both cases were a little different.

The enantioselectivity (α) calculated from the optical purity in the first step was 1.42, which is comparable to the values obtained from the separate-mode extraction experiments ((+)- and (−)-DBTs were separately extracted) shown in Table 1 etc. Table 2 shows that the optical purity is improved as the extraction step is repeated. By designing a sophisticated device such as a counter-current extraction system, complete resolution of racemic DBT could be attained.

NMR Analysis of Ion-Pair Complex. Table 3 summarizes the chemical shifts of ^1H and ^{31}P within the ion-pair complex, **1**·DBT, in $CDCl_3$. The chemical shifts of the two methylene-protons adjacent to the phosphonium phosphorus atom in **1** (H^a and H^b) are different from each other. Free rotation of the methylene-carbon is limited because of a steric hindrance around the phosphorus atom. A similar situation was observed in the case of the methylene-protons within **2**

Table 2. Multistage Extraction[a)]

Extractant **1**	Extraction step	$[DBT]_w$[b)] mM	O.R.[c)] °	O.P.[d)] %
(*R*)	1	2.42	+0.027	9.2
	2	1.40	+0.030	18
	3	0.555	+0.024	36
(*S*)	1	2.39	−0.027	9.3
	2	1.33	−0.029	18
	3	0.522	−0.022	34

a) Extraction conditions are described in text. b) The concentration of DBT remained in the aqueous phase after each extraction step. c) Optical rotation of the aqueous phase (λ=435 nm). d) Optical purity of DBT in the aqueous phase.

Table 3. Chemical Shifts of H and P within the Ion-Pair Complex **1**·DBT in $CDCl_3$[a]

Complex[b]	**1**[c]			DBT
	H^a	H^b	P	H^c
(*R*)·Br_2	5.27	4.73	20.9	—
(*S*)·Br_2	5.29	4.75	20.9	—
(*R*)·(−)	5.05	4.41	21.1	5.87
(*R*)·(+)	5.15	4.56	21.1	5.89
(*S*)·(−)	5.14	4.58	21.1	5.88
(*S*)·(+)	5.07	4.40	21.1	5.88

a) $\delta(^1H)$ from tetramethylsilane; $\delta(^{31}P)$ from H_3PO_4. b) For example, (*R*)·(−) denotes the complex between (*R*)-**1** and (−)-DBT. c) For H^a and H^b, the top of apparent triplet peak (two doublet peaks are overlapped) is indicated.

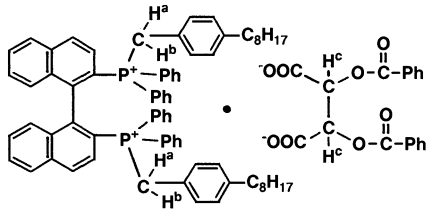

1-DBT ion-pair complex

and **3** (see experimental section).

The couple of the ion-pair complexes enantiomeric to each other, (*R*)·(−)-(*S*)·(+) couple and (*R*)·(+)-(*S*)·(−) couple, naturally exhibited almost the same chemical shifts for the methylene-protons (H^a and H^b); e.g., (*R*)·(−) denotes the complex between (*R*)-**1** and (−)-DBT. However, the chemical shifts for the former couple ((*R*)·(−) and (*S*)·(+)) were shifted to higher field by 40—70 Hz compared to those in the latter couple ((*R*)·(+) and (*S*)·(−)).

As previously described, the extractabilities of (*R*)·(−) and (*S*)·(+) were higher than those of (*R*)·(+) and (*S*)·(−) (Table 1). It is considered that the extractability is enhanced when the ion-pair is more tightly formed. In this case, the electron-withdrawing property of phosphonium decreases, so that the methylene-protons (H^a and H^b) are shifted to higher field.

The chemical shifts of phosphonium phosphorus atom itself and the methine-proton in DBT are nearly common among the four optical isomers (Table 3).

Chirality Recognition in Ion-Pair Extraction. It is found that the enantioselective extraction of DBT is possible by use of **1** as ion-pair extractant. To our knowledge, there has been only one report dealing with the chirality recognition of ionic species in ion-pair extraction system.[7] An enantioselective extraction of mandelate anion is studied, in which a chiral ammonium salt, a derivative of α-methylbenzylamine, is used as extractant. So far, ion-pair extractants having axial chirality have not been studied.

The concept of "three-point interaction" has often been used to explain the mechanism of chirality recognition in chromatographic studies.[18] This concept is applicable to the present system of ion-pair extraction. There is a three-point interaction between **1** and DBT, two ion-pair interactions and one steric interaction (or π–π interaction) of aromatic rings.

When the monocationic extractants **2** and ***3*** were used, the enantioselectivity was heavily decreased (Table 1). These extractants cannot perform such a three-point interaction. Moreover, as shown in Fig. 3, the enantioselectivity was decreased with lowering pH in the aqueous phase. As the pH is lowered, the involvement of protonated DBT to the extraction reaction rises. Thus, the three-point interaction hardly works between **1** and DBT. Consequently, the three-point interaction can be favorably at work, only when the extraction reaction involves both the dicationic **1** and dianionic DBT, leading to high chirality recognition.

The chiral ion-pair extractant **1** possesses a high chirality recognition ability and a high extraction ability resulting from its high lipophilicity. The chirality recognition by ion-pair extraction may open a new realm of optical resolution for ionic species in aqueous media.

The authors wish to express their thanks to Professor M. Takagi of Kyushu University for his helpful suggestions and discussions.

References

1) E. P. Kyba, K. Koga, L. R. Soura, M. G. Siegel, and D. J. Cram, *J. Am. Chem. Soc.*, **95**, 2692 (1973).
2) J. M. Timko, R. C. Helgeson, and D. J. Cram, *J. Am. Chem. Soc.*, **100**, 2828 (1978).
3) E. P. Kyba, J. M. Timko, L. J. Kaplan, F. de Jong, G. W. Gokel, and D. J. Cram, *J. Am. Chem. Soc.*, **100**, 4555 (1978).
4) S. C. Peacock, L. A. Domeier, F. C. A. Gaeta, R. C. Helgeson, J. M. Timko, and D. J. Cram, *J. Am. Chem. Soc.*, **100**, 8190 (1978).
5) D. S. Lingenfelter, R. C. Helgeson, and D. J. Cram, *J. Org. Chem.*, **46**, 393 (1981).
6) T. Yamaguchi, K. Nishimura, T. Shinbo, and M. Sugiura, *Chem. Lett.*, **1985**, 1549.
7) S. J. Romano, K. H. Wells, H. L. Rothbart, and W. Rieman, III, *Talanta*, **16**, 581 (1969).
8) J. M. Lehn, A. Moradpour, and J. P. Behr, *J. Am. Chem. Soc.*, **97**, 2532 (1975).
9) X-L. Xiao, A. Ohki, H. Nakamura, and M. Takagi, *Anal. Sci.*, **1**, 135 (1985).
10) A. Ohki, X-L. Xiao, K. Tsukada, S. Maeda, and M. Takagi, *Anal. Sci.*, **4**, 143 (1988).
11) A. Ohki, M. Yamura, S. Kumamoto, S. Maeda, T. Takeshita, and M. Takagi, *Chem. Lett.*, **1989**, 95.
12) A. Ohki, S. Takenaka, K. Tsukada, S. Maeda, and M. Takagi, *Anal. Sci.*, **6**, 283 (1990).
13) A. Ohki, M. Yamura, Y. Sumiyoshi, M. Takagi, and S. Maeda, *Anal. Sci.*, **6**, 291 (1990).
14) A. Ohki, M. Yamura, M. Takagi, and S. Maeda, *Anal. Sci.*, **6**, 585 (1990).
15) A. Ohki, H. Dohmitsu, and S. Maeda, *Bull. Chem. Soc.*,

Jpn., **64**, 476 (1991).
16) A. Ohki, K. Tsukada, S. Maeda, and M. Takagi, *Mikrochim. Acta,* in press.
17) A. Ohki, R. Miyashita, M. Takagi, T. Takeshita, and S. Maeda, *Chem. Lett.*, **1989**, 1551.
18) S. G. Allenmark, "Chromatographic Enantioseparation," E. Horwood Ltd., Chichester (1988), Chap. 5.

Formation and Properties of Ferroelectric Liquid Crystalline Compound Containing -C(O)-S-O- Linkage

Kohki TAKATOH* and Masanori SAKAMOTO
Chemical Lab., Toshiba R&D Center, Komukai Toshiba-cho, Saiwai-ku Kawasaki 210
(Received February 7, 1991)

During our investigations of the synthesis of ferroelectric liquid crystal compounds containing a fluorenone nucleus, the formation of a novel compound having a -C(O)-S-O- linkage was discovered as a by-product when a derivative of fluorenone carboxylic acid was treated with thionyl chloride and a phenol. This compound also exhibited ferroelectric liquid crystal properties. Compounds with a -C(O)-S-O- linkage have been little reported; this is the first report concerning a liquid crystalline compound with this type linkage. The thermal stability of the mesophase is reduced upon changing from the -C(O)-O- linkage to the -C(O)-S-O- linkage. The synthesis and properties of this compound are discussed in detail.

The authors previously reported the properties of ferroelectric liquid crystals containing fluorene and fluorenone structures.[2,3] During the synthesis of some fluorenone compounds **1**, small amounts of by-products (compounds **2**) appeared during

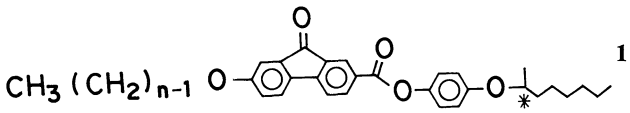

1

the esterification step. After isolation and purification, compound **2** (n=10) was found to show a liquid crystal phase over a wide range of temperatures under a polarized microscope. For a novel molecular structure of liquid crystalline material and a new reaction, the molecular structure was identified and the properties as a ferroelectric liquid crystal were investigated.

Experimental

Measurements. Measurements of transition temperature and observations of the microscopic texture of the mesophases were carried out using an Olympus polarizing microscope in conjunction with a Mettler FP82 heating stage, a FP80 control unit and a Seikohdenshi differential scanning calorimeter (model DSC 200). ^{1}H NMR spectra were measured using a JEOL JNM-GSX-270 NMR spectrometer for a solution in $CDCl_3$, with tetramethylsilane used as the internal standard. The IR spectra were recorded on a KBr disc with a JASCO Report-100 infrared spectrometer. The purity of each sample was checked by HPLC JASCO TWINCLE and element analysis.

The Synthesis and Purification of Compound 1 (n=10) and Compound 2. 7-Decyloxy-9-oxo-2-fluorenecarboxylic acid (3.00 g, 7.89 mmol) in 35 ml of thionyl chloride was warmed at 70 °C for 2 h. After evaporating the thionyl chloride, 25 ml of dry pyridine was added. Then 4-((*S*)-1-methylheptyloxy)-phenol (2.21 g, 9.95 mmol) in 10 ml of dry pyridine solution was added and the mixture was warmed at 80 °C for 3 h. It was then poured into ice water. After acidification, the precipitate was collected and purified by column chromatography. By recrystallizing the first fraction product from petroleum ether and an ethanol solution, 1.02 g (1.75 mmol, 22%) of yellowish needles were obtained. By recrystallizing the second fraction product from petroleum ether and toluene, 0.84 g (1.29 mmol, 16%) of yellowish needles were obtained.

The molecular structures of these compounds were confirmed using ^{1}H NMR, IR, UV-spectra, and elemental analyses.

Results and Discussion

Formation. The formation of this by-product (compound **2**) has only been confirmed in a few cases. However, in the case of the synthesis of compound **1** (n=10), for example, a good amount of compound **2** (n=10) was obtained. The authors discuss this particular case here and give a detailed description of the conditions in the experimental section.

Molecular Structure. The molecular structure of compound **2** (n=10) was determined by the ^{1}H NMR, IR, UV-spectra, as well as elemental analysis. All of the data are consistent with the molecular structure **2** (n=10), shown below.

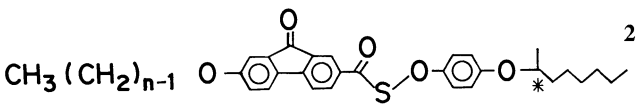

2

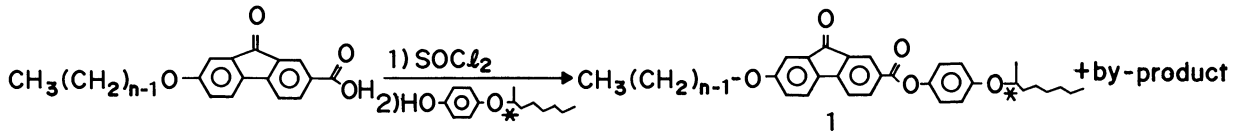

1

(n=10 22% 16%)

Scheme 1.

Table 1. NMR Spectra of Compound **1** and Compound **2**

Assignment	Chemical shift δ_H/ppm		Pattern (Integral)
	Compound **1**	Compound **2**	
$-(CH_2)_8CH_3$ and $-C(CH_3)(CH_2)_5CH_3$	1.84—0.86	1.86—0.85	m (35H)
R-CH_2-O-fluorenone	4.03	4.01	t (2H)
Ar-O-CH(Me)R	4.29—4.36	4.32—4.21	m (1H)
-OArO-H-2, 3, 5, and 6	6.95—6.89 7.14—7.08	7.14—6.99	m (4H)
Fluorenone H-3	7.05 J_{5-6}=8.1 Hz J_{6-8}=2.7 Hz	6.81 J_{5-6}=8.1 Hz J_{6-8}=2.7 Hz	dd (1H)
Fluorenone H-1	7.26	7.21	d (1H)
Fluorenone H-4 or H-5	7.51	7.45	d (1H)
Fluorenone H-4 or H-5	7.54	7.47	d (1H)
Fluorenone H-6	8.31 J_{3-4}=8.1 Hz J_{1-3}=2.7 Hz	8.26 J_{3-4}=8.1 Hz J_{1-3}=2.7 Hz	dd (1H)
Fluorenone H-8	8.40	8.33	d (1H)

Table 2. IR and UV-Spectra and Elemental Analysis of Compound **1** and Compound **2**

Compound **1**	IR/cm^{-1} (KBr)	2930, 2860, 1740 (CO), 1720 (CO), 1600, 1510, 1470, 1300, 1270, 1240, 1200, 1090
	λ_{max}/nm (CH_2Cl_2)	435, 339, 325, 283, 252, 231
Compound **2**	IR/cm^{-1} (KBr)	2930, 2860, 1740 (CO), 1720 (CO), 1610, 1490, 1470, 1300, 1260, 1200, 1100
	λ_{max}/nm (CH_2Cl_2)	439, 340, 326, 283, 231
	Elemental analysis/%	C 74.28 (73.99)
	(Calcd for $C_{38}H_{48}O_5S$)	H 7.96 (7.84)
		S 5.44 (5.20)

The ^{1}H NMR spectra of compound **1** (n=10) and **2** (n=10) are shown in Table 1. The assignment of each peak was carried out by a comparison with the data for other fluorenone derivatives.[2,3] The chemical shifts and splitting patterns of compounds **1** (n=10) and **2** (n=10) were almost identical.

IR, UV-spectra, and elemental analyses of compound **1** (n=10) and **2** (n=10) are shown in Table 2. The IR spectrum of compound **2** (n=10) is very similar to that of compound **1** (n=10), except that a strong characteristic peak at 1260 cm^{-1} appears and the peak at 1510 cm^{-1} of compound **1** (n=10) disappears. The UV-spectra of the two fluorenone derivatives are essentially the same in the region above 260 nm. These spectral properties imply that the main structures comprising compound **1** (n=10), such as the fluorenone moiety as well as the phenyl and alkyl groups, remain in compound **2** (n=10).

Compound **2** (n=10) was purified by triple recrystallization, and elemental analysis was carried out at each stage. All of the analytical results were coincident within experimental error with the calculated values for the formula $C_{38}H_{48}O_5S$.

Judging from all of these results, compound **2** (n=10) was determined to have chemical formula of **2** (n=10).

One possible structure which could explain these data is one with the -C(O)-O-S- linkage. Nevertheless, there seems to be no possibility to form this structure, considering the reaction mechanism.

Compounds containing the -C(O)-S-O- linkage structure have been little reported. The author has found those compounds mentioned in only 10 papers among the literature published since 1962.

For example, Haas et al.[4] reported on the formation of $FC(O)SOC(O)CF_3$ by a reaction of fluorocarbonylsulfenic acid chloride (FC(O)SCl) and silver trifluoroacetate ($F_3CC(O)OAg$). Schuphan and Casida[5] showed the formation of $(R)_2NC(O)SOCH_2CCl{=}CH_2$ through a [2,3]sigmatropic rearrangement of *S*-(3-chloroallyl) thiocarbamate sulfoxide ($(R)_2NC(O)S(O)CH_2CCl{=}CH_2$).

Moon and Oh,[6] Islam and Kwart,[7] and U. Hildebrand et al.[8] reported the formation of a compound containing the -C(O)-S-O- linkage by the reaction of acylsulfenyl chloride derivatives with appropriate alcohol derivatives.

There has been no report concerning a compound with the -C(O)-S-O- linkage, which is formed through a reaction of alcohols or phenols with products formed from carboxylic acids and thionyl chloride.

Phase Transition Behavior. The phase transition behavior of compound **2** was observed using a polarized microscope in conjunction with a heating stage and differential scanning calorimeter.

The phase transition behavior of compound **2** (n=10) is shown below, along with that of compound **1** (n=10) for a comparison.

$$\text{Cr} \xrightarrow{93\,^\circ\text{C}} \text{S}_{c^*} \xrightarrow{102\,^\circ\text{C}} \text{ISO} \quad \text{compound } \mathbf{2}\ (n=10)$$

$$\text{Cr} \xrightarrow{81\,^\circ\text{C}} \text{S}_{c^*} \xrightarrow{118\,^\circ\text{C}} \text{S}_A \xrightarrow{127\,^\circ\text{C}} \text{ISO} \quad \text{compound } \mathbf{1}\ (n=10)$$

Compound **2** (n=10) shows no tendency to decompose when heated to 200 °C in air. A phase determination was possible, since it showed the broken fan texture characteristic of the smectic C phase under a polarized microscope. Miscibility tests were carried out with liquid crystalline materials of which the phase transition behavior was already known. The material exhibits a direct transition from isotropic liquid into the chiral smectic C phase. It has a higher melting point and a lower isotropic liquid–liquid crystal transition temperature than does compound **1** (n=10).

The decrease in the mesophase thermal stability (the transition temperature from the liquid crystal phase to the isotropic liquid phase) of compound **2** (n=10), compared with compound **1** (n=10), can be attributed to the fact that the change from the –C(O)–O– linkage to the –C(O)–S–O– linkage increases the molecular width, decreases the linearity of the molecule and increases the flexibility of the linkage. Especially, the disappearance of the smectic A phase in the case of compound **2** (n=10) means a decrease in the lateral attractive intermolecular interaction, due to the factors mentioned above.

After purification by triple recrystallization and checking the purity using elemental analysis and HPLC each time, the sample was sufficiently pure; however, the isotropic and chiral smectic C phases coexisted in equilibrium over several degrees. The authors experienced this phenomenon in liquid crystalline materials which have a direct transition from an isotropic liquid to the smectic C phase.[3)]

Tilt Angle and Spontaneous Polarization. The temperature dependence of the tilt angle and spontaneous polarization for the compound were measured. These measurements were carried out by a previously reported method.[3)] Liquid crystal cells having a 1×1 cm^2 electrode area were used. Alignment was achieved by coating the glass surfaces with polyimide and buffing the surface in one direction. The cell spacing was 2.0 μm, which was obtained using fiber spacers. In Fig. 1, the temperature dependence of the tilt angle for compounds **1** (n=10) and **2** (n=10) are shown.

The tilt angle of compound **1** (n=10) gradually increases with decreasing temperature, a characteristic of a second-order transition. On the other hand, the tilt angle of compound **2** (n=10) increases abruptly to 29 degrees just below the transition from an isotropic liquid to the chiral smectic C phase; no significant change was observed. These are characteristic of a first-order transition.

The temperature dependence of spontaneous polarization of compounds **1** (n=10) and **2** (n=10) are shown in Fig. 2.

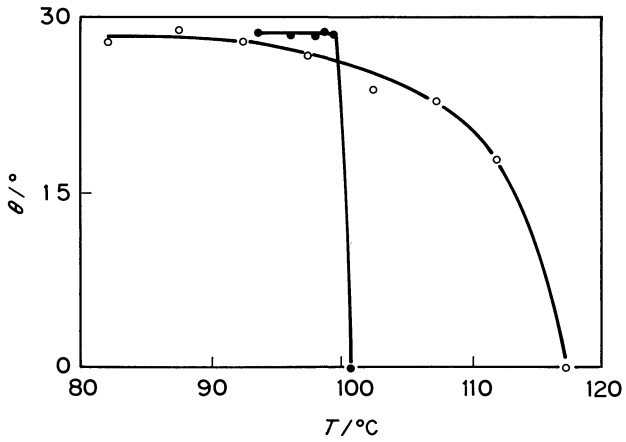

Fig. 1. Tilt angle (θ) temperature dependences of compound (**1**) and compound (**2**). ○ and ● denote compound (**1**) and compound (**2**), respectively.

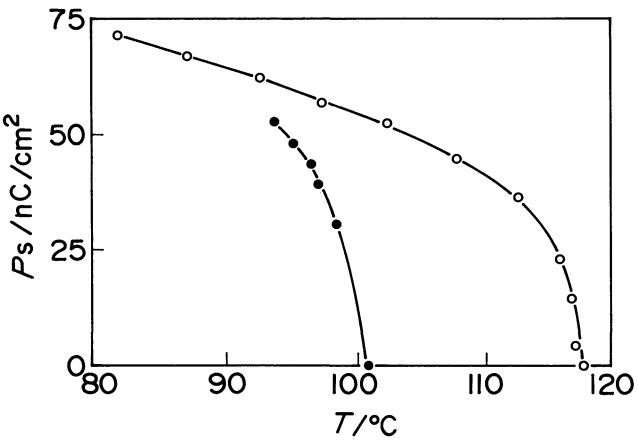

Fig. 2. Spontaneous polarizations (Ps) temperature dependences of compound (**1**) and compound (**2**). ○ and ● denote compound (**1**) and compound (**2**), respectively.

Over the entire temperature range, compound **2** (n=10) shows a lower spontaneous polarization than does compound **1** (n=10). Just below the transition temperature, ths slope of compound **2** (n=10) is steeper than that of compound **1** (n=10) for the ISO-S_{c^*} type first-order transition. However, spontaneous polarization gradually increases with decreasing temperature, in spite of the first-order transition. This could be ascribed to the fact that, in the case of compound **2** (n=10), the transition between the isotropic liquid phase and the chiral smectic C phase is ambiguous and both phases coexist until about 95 °C. From these results, it can be said that the change from the –C(O)–O– linkage to the –C(O)–S–O– linkage does not greatly influence the magnitudes of the tilt angle and spontaneous polarization.

References

1) A part of the results in this paper was presented in the 56th Annual Meeting of the Chemical Society of Japan, 1989, Abstr., 4B IIB 10 138 and the International Liquid Crystal Conference, 1990, Abstr., FER 46P.

2) K. Takatoh, K. Sunohara, and M. Sakamoto, *Mol. Cryst. Liq. Cryst.*, **164**, 167 (1988).

3) K. Takatoh and M. Sakamoto, *Mol. Cryst. Liq. Cryst.*, **182B**, 339 (1990).

4) A. Haas, J. Helmbrecht, W. Klug, B. Koch, H. Reinke, and J. Sommerhoff, *J. Fluorine Chem.*, **3**, 383 (1973).

5) I. Schuphan and J. E. Casida, *Tetrahedron Lett.*, **1979**, 841.

6) S. S. Moon and D. Y. Oh, *Taehan Hwahkhoe Chi*, **27**(2), 157 (1983).

7) N. B. Islam and H. Kwart, *J. Chem. Eng. Data.*, **30**, 507 (1985).

8) U. Hildebrand, J. Huebner, and H. Budzikiewicz, *Tetrahedron*, **42**, 5969 (1986).

Dye-Sensitized Oxygenation and Dimerization of 4-Methoxystyrene through Electron Transfer

Masanobu KOJIMA,* Yasunao KURIYAMA,† Hirochika SAKURAGI,*,† and Katsumi TOKUMARU†
Faculty of Liberal Arts, Shinshu University, Asahi 3-1-1, Matsumoto 390
†Department of Chemistry, University of Tsukuba, Tsukuba, Ibaraki 305
(Received March 22, 1991)

Photoreactions of 4-methoxystyrene (**1**) sensitized with dyes such as Acriflavine, Rhodamine 6G, and Methylene Blue in methanol under oxygen afforded 4-methoxybenzaldehyde, its dimethyl acetal, and 2-methoxy-2-(4-methoxyphenyl)ethanol as oxidation products together with the corresponding dimers, *cis*- and *trans*-cyclobutanes in a ratio of cis/trans ca. 5/95. On the basis of quenching studies of fluorescence and T–T absorption of the dyes, the oxygenation and dimerization are proposed to proceed through an electron transfer from **1** to excited singlet dyes but not to involve generation of singlet oxygen.

Dye-sensitized oxygenation of olefins has been investigated and in most cases singlet oxygen has been proposed as an oxygenating intermediate;[1] however, some oxygenations have recently been proposed to take place through an electron transfer from olefins to excited dyes to give olefin radical cations followed by their reactions.[2,3] This paper now reports, based on quenching studies of fluorescence and T–T absorption of the sensitizers, that the dye-sensitized oxygenation of 4-methoxystyrene (**1**) in methanol proceeds in the singlet state through the cation radical of **1** to afford oxidation products together with dimerization products, and that singlet oxygen usually resulting from sensitization with dye triplets plays no role in this reaction.

Experimental

^{1}H NMR and ^{13}C NMR spectra were recorded on a JEOL FX-90Q spectrometer. Fluorescence spectra were obtained on a Hitachi F-4000 fluorescence spectrophotometer. Fluorescence lifetimes were measured using a single photon counting apparatus, Horiba NAES 1100.

Materials. Acriflavine, Methylene Blue (Nakalai Tesque), Eosin Y, Rose Bengal (Wako), and Rhodamine 6G (Tokyo Kasei) were used without further purification in dye-sensitized oxygenation and dimerization reactions of **1**. The dyes were purified by recrystallization from ethanol/benzene for measurements of fluorescence spectra and lifetimes, and for laser flash photolyses.

4-Methoxystyrene (**1**),[4] *cis*- (**2**),[5] and *trans*-1,2-bis(4-methoxyphenyl)cyclobutane (**3**)[5] were prepared as described previously.

4-Methoxybenzaldehyde dimethyl acetal (**5**)[6] was prepared from 4-methoxybenzaldehyde (**4**) by refluxing with methyl orthoformate in the presence of a catalytic amount of ammonium chloride in methanol; bp 102 °C/5 Torr (1 Torr=133.322 Pa); ^{13}C NMR ($CDCl_3$) δ=159.7 (s), 130.5 (s), 127.8 (d), 113.5 (d), 103.1 (d), 55.0 (q), 52.4 (q); ^{1}H NMR ($CDCl_3$) δ=7.40—6.81 (q, 4H, aromatic H), 5.33 (s, 1H, CH), 3.75 (s, 3H, OCH_3), 3.28 (s, 6H, OCH_3). Calcd for $C_{10}H_{14}O_3$: C, 65.92; H, 7.74%. Found: C, 66.05; H, 7.56%.

(4-Methoxyphenyl)oxirane (**7**)[7,8] was prepared from 4-methoxybenzaldehyde with dimethyloxosulfonium methylide;[9] yield 18%, bp 80 °C/2 Torr (lit,[7] bp 76 °C/0.037 Torr).

2-Methoxy-2-(4-methoxyphenyl)ethanol (**6**)[10] was prepared by stirring the oxirane, **7**, in methanol with a few drops of conc. HCl for 17 h; yield 55%, bp 140 °C/3 Torr (lit,[10] bp 137—139 °C/5.5 Torr); ^{13}C NMR ($CDCl_3$) δ=159.5 (s), 130.5 (s), 128.1 (d), 114.0 (d), 84.3 (d), 67.2 (t), 56.5 (q), 55.2 (q); ^{1}H NMR ($CDCl_3$) δ=7.28—6.84 (q, 4H, aromatic H), 4.34—4.18 (m, 1H, CH), 3.78 (s, 3H, OCH_3), 3.78—3.59 (m, 2H, CH_2), 3.30 (s, 3H, OCH_3), 2.86 (broad, 1H, OH).

Irradiation of 4-Methoxystyrene with Dye under Oxygen. 4-Methoxystyrene (**1**, 0.6 M, M=mol dm^{-3}) was irradiated in the presence of dyes (2—3×10^{-3} M) in methanol under oxygen in a uranium glass tube ($\geqslant$340 nm) with a 400-W high-pressure mercury lamp (Riko UVL-400HA) through a filter solution [K_2CrO_4 0.27 g and Na_2CO_3 1 g in 1 dm^3 of H_2O (optical path length, 1 cm)]. The yields of products were determined with a Shimadzu GC-8A gas chromatograph equipped with a flame ionization detector.

Quantum Yields. Quantum yields for the formation of *trans*-1,2-bis(4-methoxyphenyl)cyclobutane (**3**) and 4-methoxy benzaldehyde (**4**) were determined by using potassium tris(oxalato)ferrate(III) actinometry.[11] Irradiation was performed with 436-nm light from a 400-W high-pressure mercury lamp through a cut filter (Shibata Harzlas FS, $\geqslant$400 nm) and a filter solution [$CuSO_4 \cdot 5H_2O$ in H_2O (4.4 g dm^{-3})+2.7 M NH_4OH]. The solutions were quantitatively analyzed on the gas chromatograph and a JASCO 800 series high-performance liquid chromatograph.

Laser Flash Photolyses. Laser flash photolyses were performed with 460-nm laser pulses (Coumarin 47, 10-ns fwhm) from a XeCl (308 nm) excimer laser(Lambda Physik EMG-101)-pumped dye laser (Lambda Physik FL-3002) and with a pulsed xenon arc (Wacom KXL-151, 150 W) as a monitoring light source. The monitoring light coming from a monochromator (JASCO CT-25C) was amplified by a photomultiplier (Hamamatsu Photonics R928) and stored in a storage scope (Iwatsu TS-8123), and the signals were transferred to a personal computer (NEC PC-9801VX21) and accumulated for 3—5 times to be averaged. The system was computer-controlled and the decay curves were analyzed by this computer system. Sample solutions containing Acriflavine (5.0×10^{-4} M) and **1** (0—4.8×10^{-2} M) were deaerated by bubbling with nitrogen for 30 min.

Redox Potentials. Redox potentials were measured by cyclic voltammetry with a potentiostat-galvanostat (Nikko Keisoku NPGS-501) and a function generator (Nikko Keisoku

NFG-3). The measurements were carried out in acetonitrile using a three-electrode cyclic voltammetric cell. A platinum disk and a platinum wire were used as the working and counter electrodes, respectively, and the reference electrode was a Ag/AgCl or an SCE. Tetraethylammonium perchlorate (0.1 M) was used as a supporting electrolyte.

Results and Discussion

Dye-Sensitized Oxygenation and Dimerization of 4-Methoxystyrene. Acriflavine (AF), Rhodamine 6G (R6G), Methylene Blue (MB), Eosin Y (EY), and Rose Bengal (RB) were used as sensitizer. Although these sensitizers exhibit fairly different absorption spectra in the visible region, they have an intense band with a molar extinction coefficient of $\approx 10^5$ at the absorption maximum (Table 1).

Irradiation of a methanol solution of **1** (0.6 M) in the presence of AF (2×10^{-3} M) under oxygen with visible light (>400 nm) gave *cis*- (**2**) and *trans*-1,2-bis(4-methoxyphenyl)cyclobutane (**3**), the corresponding cyclobutane dimers (yield 19% based on **1** consumed at 31% conversion, with an isomer ratio of **2**/**3**=3/97), 4-methoxybenzaldehyde (**4**, 23%), its dimethyl acetal (**5**, 15%), and 2-methoxy-2-(4-methoxyphenyl)ethanol (**6**, 8%), as shown in Scheme 1.

Table 1. Absorption Spectrum Data for Dyes in Methanol

Dye	λ_{max}/nm	ε_{max}	ε_{436}
AF	461	67100	35600
R6G	527	108000	1960
MB	653	96200	730
EY	523	96300	1730
RB	557	110000	2000

The dimers, **2** and **3** (10% at 8% conversion), were also formed under nitrogen together with polymers on AF sensitization in methanol. In this case, however, AF was bleached completely during irradiation.

The photooxygenation and photodimerization of **1** proceeded similarly on sensitization with R6G, MB, RB, and EY to afford, with lower efficiencies, the same products as those from the AF sensitization (Table 2). The isomer ratio **2**/**3** (=3/97—7/93) under oxygen is independent of the dye employed except MB (12/88), and **3** was produced somewhat selectively compared to the reaction under nitrogen (**2**/**3**=23/77—11/89).

In control experiments, aldehyde **4** and (4-methoxyphenyl)oxirane (**7**) were methoxylated in methanol in the presence of a catalytic amount of benzoic or hydrochloric acid to give **5** and **6**,[10] respectively. These results indicate that **5** and **6** are the secondary products derived from the oxygenation products **4** and **7**, respectively, under the reaction conditions.[14]

Effects of Singlet Oxygen Quenchers and Solvents on Photooxidation of 4-Methoxystyrene. Oxygenation of olefins gives generally carbonyl compounds and epoxides in various pathways. 4-Methoxybenzaldehyde, **4**, might be afforded by a reaction of **1** with singlet oxygen possibly generated from dye sensitization.[12] Also, *N*-vinylcalbazole has been reported to dimerize in the

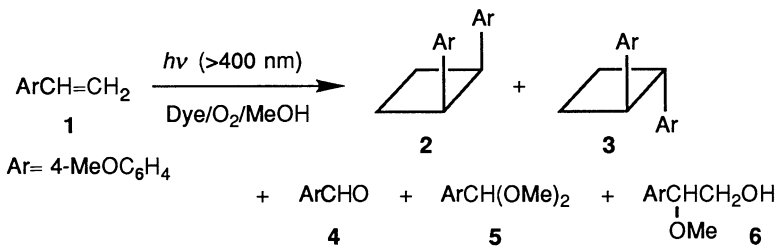

Scheme 1.

Table 2. Dye-Sensitized Oxygenation and Dimerization of **1** in Methanol

Dye	O_2/N_2[a]	Conv./%	Yield of products[b]/%				Isomer ratio
			(2+3)	4	5	6	2/3
AF	O	31	19	23	15	8	3/97
	N	8	10	—	—	—	23/77
R6G	O	10	14	34	—	1	7/93
	N	7	14	—	—	—	11/89
MB	O	4	22	28	—	—	12/88
	N	3	31	—	—	—	15/85
EY	O	17	6	35	2	4	7/93
	N	11	6	—	—	—	14/86
RB	O	18	5	10	—	8	7/93
	N	11	3	—	—	—	12/88

a) O: Under oxygen, N: under nitrogen. b) Yields of products based on **1** consumed.

Table 3. AF-Sensitized Oxygenation and Dimerization of **1** in Methanol in the Presence of TME and Dabco[a]

Additive	Concn./M	Conv./%	Yield of products[b]/%			
			(2+3)	**4**	**5**	**6**
TME	0	28	13	22	15	3
	0.2	26	14	12	20	4
	0.6	25	14	8	21	4
Dabco	0.01	11	10	3	Trace	Trace
	0.05	7	6	9	Trace	Trace
	0.1	5	5	9	Trace	Trace

a) [**1**]=0.6 M, [AF]=2×10^{-3} M. b) Yields based on **1** consumed.

Table 4. Quantum Yields for Formation of Dimer **3** (ϕ_3) and Aldehyde **4** (ϕ_4) on Dye-Sensitized Irradiation of **1**[a]

Dye	ϕ_3	ϕ_4
AF	0.013±0.002	0.58±0.03
R6G	0.067±0.003	0.28±0.03
EY	$(2.1\pm0.2)\times10^{-4}$	0.067±0.002
RB	$(3.4\pm1.0)\times10^{-4}$	0.025±0.001

a) Irradiated with 436-nm light in oxygen-saturated methanol.

presence of singlet oxygen.[13]

On AF-sensitized irradiation under oxygen the conversion of **1** was scarcely changed (within 3%) even in the presence of 2,3-dimethyl-2-butene (TME, 0.2 or 0.6 M in methanol) as an efficient singlet oxygen trap; the product distribution was similar to that in the absence of TME (Table 3). This observation indicates that singlet oxygen plays no role in the AF-sensitized oxygenation of **1**.

As shown in Table 3, 1,4-diazabicyclo[2.2.2]octane (Dabco) quenched more efficiently the AF-sensitized oxygenation of **1** than the dimerization of **1**. Although Dabco is an effective singlet oxygen quencher, it also inhibits autoxidation[14] and quenches radical cations of organic substrates as an electron donor;[15] in fact, Dabco has a much lower oxidation potential (0.68 V vs. SCE) than **1** (1.31 V). These results together with the above observation that TME exerts no effects on the efficiency of reaction and the distribution of products suggest that Dabco quenches the reaction not only as a radical inhibitor but also an electron donor, but not as a singlet oxygen quencher; the oxygenation proceeds through electron transfer and autoxidation, but not through singlet oxygen oxidation.

In an acetonitrile–methanol (4:1 by volume) mixed solvent the conversion of **1** was analogous to that in methanol, but the yield of dimers was higher (33%) than in methanol. The use of Freon 113–methanol (4:1) decreased both of the conversion of **1** and the yield (8%) of dimers. These results show that the efficiency of dimerization of **1** is affected by the polarity of solvents but is not correlated with the reported lifetime of singlet oxygen.[16,17]

Quantum Yields for Oxygenation and Dimerization. The quantum yields for formation of dimer **3** and aldehyde **4** were determined by irradiating methanol solutions of **1** (0.6 M) and dyes (ca. 5×10^{-3} M) at 436 nm under bubbling with oxygen, and are summarized in Table 4. At first glance the product distributions mentioned above seem to be inconsistent with these results; however, the discrepancy might be explained by photolability of **4** under oxygen. The high ϕ_4 values may be attributed to efficient formation of **4** through radical chain reactions as described below. It is noticeable that the AF- and R6G-sensitized reactions proceed with much higher efficiencies compared to those with EY and RB as sensitizer. According to Rehm–Weller's equation (Eq. 1),[18] the changes of Gibbs' free energy (ΔG) associated with the electron transfer from ground-state **1** to excited singlet AF and R6G are estimated to be exothermic in acetonitrile ($\Delta G=-3.9$ kcal mol^{-1} for AF and -2.4 kcal mol^{-1} for R6G), while those to excited singlet EY and RB are largely endothermic. The calculated ΔG values are listed in Table 5, where E_{ox}^{D} and E_{red}^{A} are the oxidation potential of a donor and the reduction potential of an acceptor, respectively, and E^* is the singlet or triplet excitation energy of the donor (or the acceptor). The efficiencies of the dye-sensitized reactions are consistent with the calculated ΔG values. AF is most effective among the sensitizers employed to give the dimers (**2** and **3**) and the oxidation products (**4**—**6**).

$$\Delta G = E_{ox}^{D} - E_{red}^{A} - E^* - 0.06 \text{ eV} \quad (1)$$

Quenching of Dye Fluorescence by 4-Methoxystyrene and Oxygen. The fluorescence lifetime of AF (τ_f=5.34 ns in MeCN under argon) was quenched at nearly and completely diffusion-controlled rate constants by **1** and oxygen, respectively, as shown in Tables 5 and 6. However, the concentration of **1** (0.6 M) used in the present reaction was much higher than that of oxygen (8.1×10^{-3} M). Therefore, it is reasonable to consider that the excited singlet state of AF interacts with ground-state **1** to generate the cation radical of **1** and the anion radical of AF, but does not practically interact with oxygen. The estimation of the quenching rate, $k_q[Q]$, shows that **1** quenches the excited singlet AF at the rate of 2.5×10^{9} s^{-1} (Table 6), which is larger by a factor of ca. 20 than that for oxygen ($k_q[O_2]=1.1\times10^{8}$ s^{-1}). This shows that 90% of the AF excited singlets interact with **1**, and under these conditions the quantum yield for AF triplet formation is estimated to be less than 0.06, even if oxygen quenching led to a complete formation of the AF triplets. Thus, singlet oxygen could not be efficiently generated in the present system.

Contrary to the cases of AF, R6G, and MB, fluorescence quenching by **1** was much less efficient for EY and RB; the rate constants (k_q) are 4.0×10^{8} and

Table 5. Kinetic Parameters for Fluorescence Quenching of Dyes by **1** and Calculation of Free-Energy Changes (ΔG) Associated with Electron Transfer from **1** to the Excited Singlet Dyes

Dye	ϕ_{isc}[a]	τ_f[b]	$k_q\tau_f$	k_q	E_{red}[c]	E_s[d]	ΔG[e]
		ns	M^{-1}	$10^8\ M^{-1}\ s^{-1}$	V	kcal mol^{-1}	kcal mol^{-1}
AF	0.53[f]	4.61	26.7	58	−1.06	59.2	−3.9
R6G	0.002[g]	4.16	7.6	18	−0.83	52.4	−2.4
MB	0.52[h]	0.75	13.9	185	−0.32	42.7	−4.4
EY	0.44[f]	4.44	1.8	4.0	−1.19	52.8	+5.5
RB	0.76[i]	2.68	1.0	3.7	−1.15	50.5	+6.9

a) Quantum yields for intersystem crossing of dyes. b) Fluorescence lifetimes of dyes in aerated MeCN. c) Reduction potentials of dyes vs. Ag/AgCl in MeCN. d) Singlet excitation energies of dyes estimated from the absorption and fluorescence spectra. e) Calculated using 1.40 V (vs. Ag/AgCl in MeCN) as the oxidation potential of **1**. f) K. Kikuchi, M. Ozaki, H. Kokubun, M. Kikuchi, and Y. Usui, *J. Photochem.*, **16**, 19 (1981). g) V. E. Korobov, V. V. Shubin, and A. K. Chibisov, *Chem. Phys. Lett.*, **45**, 498 (1977). h) M. Koizumi and Y. Usui, *Mol. Photochem.*, **4**, 57 (1972). i) K. Gollnick and G. O. Schenck, *Pure Appl. Chem.*, **9**, 507 (1964).

Table 6. Rate Constants for Quenching of Fluorescence Lifetime of AF by **1** and Oxygen[a]

Quencher	$k_q/10^9\ M^{-1}\ s^{-1}$[b]	$k_q[Q]/10^9\ s^{-1}$[c]
1	4.1	2.5
O_2	14	0.11

a) $[AF]=5\times10^{-5}$ M. b) The lifetime of the excited singlet AF is 5.34 ns in MeCN under argon. c) [Q]= 0.6 M for **1** and 0.0081 M for oxygen.

$3.7\times10^8\ M^{-1}\ s^{-1}$ for EY and RB, respectively. This might be due to the positive ΔG values (Table 5).

Laser Flash Photolysis. On laser flash photolysis of AF (5×10^{-5} M) with 460-nm pulses in deaerated acetonitrile a transient absorption spectrum was obtained in the region of 300—800 nm (λ_{max} 550 and 650 nm), the lifetime being 4.6 μs as monitored at 550 nm (Fig. 1). This spectrum can be attributed to AF triplets.[19] The initial intensity (ΔOD) and lifetime of the absorption decreased with increasing concentration of **1** added ($1.6—4.8\times10^{-2}$ M). A Stern–Volmer plot of $\Delta OD_0/\Delta OD$ ($=\phi_{isc}^0/\phi_{isc}$) against [**1**] gives a good linear relationship (Eq. 2); the slope ($=k_q\tau_f$) is 47.2 M^{-1} (Fig. 2), where ΔOD_0 and ΔOD are the initial optical densities at 550 nm, and ϕ_{isc}^0 and ϕ_{isc} are the quantum yields for intersystem crossing, in the absence and presence of **1**, respectively. The reduced formation of AF triplet with **1** can be attributed to the quenching of the excited singlet AF by **1**. By using τ_f=5.34 ns, k_q is estimated to be $8.8\times10^9\ M^{-1}\ s^{-1}$, which is in agreement with the rate constants obtained from quenching of the fluorescence spectrum and lifetime of AF by **1**, 5.8×10^9 and $4.1\times10^9\ M^{-1}\ s^{-1}$, respectively.

$$\Delta OD_0/\Delta OD = \phi_{isc}^0/\phi_{isc} = 1 + k_q\tau_f[\mathbf{1}] \quad (2)$$

The decay rate of T–T absorption of AF was accelerated on addition of **1**; however, the quenching rate constant was as small as ca. $10^6\ M^{-1}\ s^{-1}$. The ΔG value for electron transfer from the ground-state **1** to the excited triplet AF is largely endothermic. Therefore, it is reasonably concluded that olefin **1** interacts efficiently with the excited singlet state of AF, but much less efficiently with its excited triplet state.

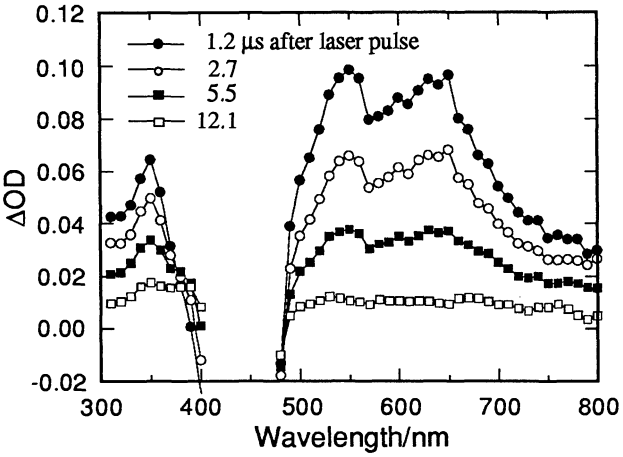

Fig. 1. T–T Absorption spectra of AF in acetonitrile.

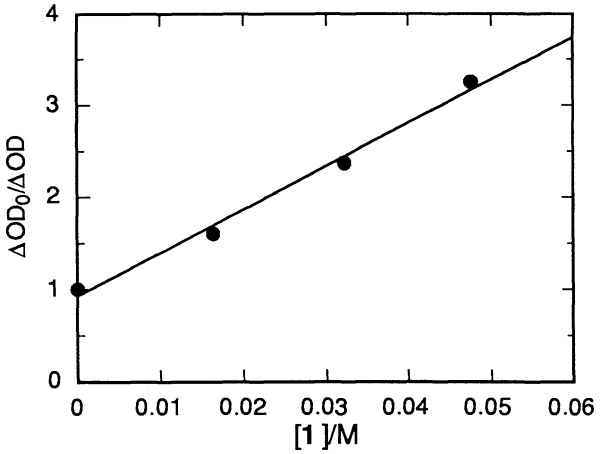

Fig. 2. Quenching of T–T absorption of AF by **1**.

Mechanism. We reported previously that the photodimerization of **1** to give **2** and **3** with a ratio of **2**/**3**=3/97 under oxygen in acetonitrile proceeds through the cation radical of **1** generated on excitation of the

contact charge transfer paor (UV absorption: 320—370 nm) between **1** and molecular oxygen.[5] Moreover, Yamamoto et al. have also reported that the photodimerization of **1** in the presence of 1,4-dicyanobenzene proceeds through the same intermediate.[20] A similar dominant formation of **3** over **2** in the present dye-sensitized cases indicates the intermediacy of $\mathbf{1}^{+\cdot}$ as the key intermediate.

The fluorescence quenching and laser flash photolyses together with the energetic considerations show that the excited singlet state of the dyes undergoes electron transfer with **1**. Also, the aforementioned AF-sensitized reactions of **1** in the presence of TME or Dabco rule out the possibilities of dimerization of **1** catalyzed by singlet oxygen and of electron transfer from **1** to singlet oxygen to generate superoxide anion, though *N*-vinylcalbazole has been reported to dimerize in the presence of singlet oxygen.[12]

As shown in Scheme 2, an electron transfer from the ground-state **1** to the excited singlet dye generates the radical ion pair of $\mathbf{1}^{+\cdot}$ and $Dye^{-\cdot}$ The monomer cation radical ($\mathbf{1}^{+\cdot}$) reacts with another neutral **1** to afford the dimer cation radical of **1** (**8**), which finally collapses to the trans cyclobutane dimer **3** with high selectivity, or reacts with methanol to give a neutral radical (**9**), initiating autoxidation of **1** to afford the aldehyde, **4**, and the oxirane, **7**, through chain processes similar to those reported already.[14,21] The cation radical $\mathbf{1}^{+\cdot}$ would react with oxygen species ($O_2^{-\cdot}$ or O_2) or methanol to generate radical intermediates (**10** and **11**[22]), which also would be able to initiate autoxidation of **1**. The back electron transfer process from $Dye^{-\cdot}$ to $\mathbf{1}^{+\cdot}$ to produce the excited triplet of **1** ($^3\mathbf{1}^*$, $E_T \approx 60$ kcal mol^{-1})[23] is safely ruled out, based on the consideration of the free energy change in the process [$\Delta G = E(\text{Dye}/\text{Dye}^{-\cdot}) - E(\mathbf{1}^{+\cdot}/\mathbf{1}) \approx -57$ kcal mol^{-1} (for AF)].

The free-energy change [$\Delta G = E(\text{Dye}/\text{Dye}^{-\cdot}) - E(O_2/O_2^{-\cdot})$] for the secondary electron-transfer process from the anion radical of dyes to molecular oxygen would be an important factor for reproducing neutral dyes [Process (4) in Scheme 2].[24] It has been reported that the electron transfer from the anion radical of MB ($MB^{-\cdot}$) to O_2 is endothermic;[3] actually, in the present reaction MB was rapidly bleached under oxygen compared to AF.

Another factor affecting the reaction efficiency seems to be the singlet lifetime of the dye employed, but the quantum yield of intersystem crossing (ϕ_{isc} in Table 5) is not such a factor; actually, AF, the most effective sensitizer, has the longest fluorescence lifetime, but its ϕ_{isc} is much larger than ϕ_{isc} of R6G.

Conclusion

By use of high concentrations of the olefin, the dye singlets are almost quenched by the olefin under oxygen atmosphere. Under these conditions the yield of the dye triplets are nearly negligible, and therefore singlet oxygen plays no role in oxidation of the olefin. The oxygenation of the olefin proceeds in methanol mainly through electron-transfer induced autoxidation to give the carbonyl and oxirane compounds (and/or their methanol adduct) together with the dimerization products.

References

1) H. H. Wasserman and R. W. Murray, "Singlet Oxygen," Academic Press, New York (1979).
2) R. A. Carruthers, R. A. Crellin, and A. J. Ledwith, *J. Chem. Soc., Chem. Commun.*, **1969**, 252.
3) L. E. Manring, J. Eriksen, and C. S. Foote, *J. Am. Chem. Soc.*, **102**, 4245 (1980).
4) R. H. Wiley and N. R. Smith, *Org. Synth.*, Coll. Vol. 4, 731 (1963).

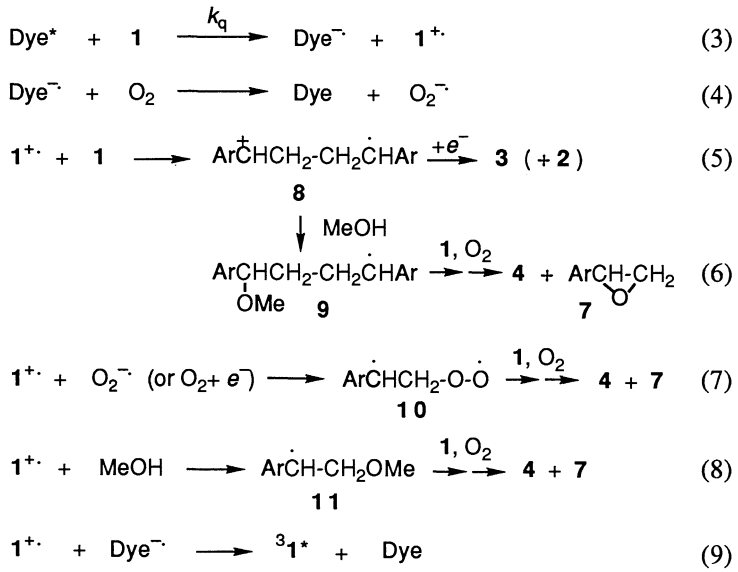

Scheme 2.

5) a) M. Kojima, H. Sakuragi, and K. Tokumaru, *Tetrahedron Lett.*, **22**, 2889 (1981); b) M. Kojima, H. Sakuragi, and K. Tokumaru, *Bull. Chem. Soc. Jpn.*, **62**, 3863 (1989); c) K. Onodera, G. Furusawa, M. Kojima, M. Tsuchiya, S. Aihara, R. Akaba, H. Sakuragi, and K. Tokumaru, *Tetrahedron*, **41**, 2215 (1985).

6) E. Fischer and G. Giebe, *Ber.*, **30**, 3053 (1897).

7) A. P. Borsetti and D. R. Crist, *J. Heterocycl. Chem.*, **12**, 1287 (1975).

8) A. C. Knipe, *J. Chem. Soc., Perkin Trans. 2*, **1973**, 589.

9) E. J. Corey and M. Chaykovsky, *Org. Synth.*, Coll. Vol. **5**, 755 (1973).

10) F. G. Baddar, *J. Am. Chem. Soc.*, **76**, 1161 (1954).

11) S. L. Murov, "Handbook of Photochemistry," Marcel Dekker, New York (1973), p. 111.

12) Rio and Berthelot reported a very slow photooxygenation of styrenes with or without an electron-donating group on the aromatic ring; G. Rio and J. Bertholet, *Bull. Soc. Chim. Fr.*, **1969**, 3609.

13) S. Nishimoto and T. Kagiya, *Chem. Lett.*, **1978**, 973.

14) T. Kanno, M. Hisaoka, H. Sakuragi, and K. Tokumaru, *Bull. Chem. Soc. Jpn.*, **54**, 2330 (1981).

15) Dabco quenches the excited singlet states of aromatic compounds with a charge-transfer mechanism; R. H. Young and R. L. Martin, *J. Am. Chem. Soc.*, **94**, 5183 (1972).

16) H. Sakuragi, G. Furusawa, K. Ueno, and K. Tokumaru, *Chem. Lett.*, **1981**, 1213.

17) D. R. Kearns, in "Singlet Oxygen," ed by H. H. Wasserman and R. W. Murray, Academic Press, New York (1979), p. 115.

18) D. Rehm and A. Weller, *Isr. J. Chem.*, **8**, 259 (1970).

19) K. Kikuchi, "Triplet–Triplet Absorption Spectra," Bunshin, Tokyo (1989), p. 50.

20) M. Yamamoto, T. Asanuma, and Y. Nishijima, *J. Chem. Soc., Chem. Commun.*, **1975**, 53.

21) F. R. Mayo, *Acc. Chem. Res.*, **1**, 193 (1968), and references cited therein.

22) J. Eriksen and C. S. Foote, *J. Am. Chem. Soc.*, **102**, 6083 (1980).

23) S. L. Murov, "Handbook of Photochemistry," Marcel Dekker, New York (1973), p. 20.

24) The reduction potential of oxygen was −0.85 V vs. Ag/AgCl in acetonitrile.

A New Reduction of Some Carboxylic Esters with Sodium Borohydride and Zinc Chloride in the Presence of a Tertiary Amine

Tomio YAMAKAWA,* Mitsuo MASAKI,† and Hiroyuki NOHIRA
Department of Applied Chemistry, Faculty of Engineering,
Saitama University, Shimo-ohkubo, Urawa 338
† Research Laboratories, Nippon Chemiphar Co.,Ltd.,
Hikokawato, Misato, Saitama 341
(Received April 2, 1991)

In the presence of a tertiary amine, sodium borohydride ($NaBH_4$) combined with zinc chloride ($ZnCl_2$) showed powerful reducing properties and carboxylic esters were smoothly reduced to their corresponding alcohols which were not obtained by reduction with $NaBH_4$ and $ZnCl_2$ alone. Tetrahydrofuran (THF) was an efficient solvent, and the effective molar ratio of the reducing agents, $NaBH_4$: $ZnCl_2$: tertiary amine, was 2 : 1 : 1. In particular, aminobenzoates such as anthranilic esters, were reduced to aminobenzyl alcohols with high yields without the addition of a tertiary amine. Further, it was also found that this combination reduced nitro, cyano, and amido groups to their corresponding amino groups.

It is known that $NaBH_4$ does not usually reduce carboxylic esters. However, several reports have suggested the possibility of $NaBH_4$ reduction of ester groups. The esters were reported to be reduced by using a large excess (20 equiv) of $NaBH_4$ in methanol,[1] and esters having complex-forming neighboring functional groups, such as oxo[2] or hydroxy esters[3] can be reduced. Soai et al. reported an efficient reducing system with $NaBH_4$–*t*-butyl alcohol–methanol for esters,[4] and Kitsuki and Fujikura reported the reduction with $NaBH_4$–2-(2-ethoxyethoxy)ethanol–xylene.[5]

On the other hand, Kollonitsch et al. reported briefly that carboxylic esters are reduced with $NaBH_4$ in the presence of a metal halide such as lithium, magnesium or calcium halide.[6] Further, Brown et al. reported the utility of aluminium chloride ($AlCl_3$) as a metal halide to be used in combination with $NaBH_4$.[7]

In this paper, a new reduction system, a combination of $NaBH_4$ and $ZnCl_2$ in the presence of a tertiary amine, by which carboxylic esters can be reduced smoothly to their corresponding alcohols with high yields, is reported.

Results and Discussion

Methyl benzoate was reduced successfully with 2.0 equiv of $NaBH_4$ and 1.0 equiv of $ZnCl_2$ in the presence of 1.0 equiv of *N,N*-dimethylaniline in THF under reflux conditions to produce an 82% isolated yield of benzyl alcohol as shown in Scheme 1. Triethylamine was similarly proved to be a very effective tertiary amine. Only 8% yield of benzyl alcohol was obtained in the absence of the tertiary amine. *N,N*-Dimethylaniline was preferable as a tertiary amine to triethylamine, because the latter formed a complex with BH_3 in the reaction mixture, which led to difficulty in separation and purification of the product.

Reduction of benzoates with bromo, alkylthio, nitro, and hydroxy moieties was carried out under the same conditions. The results are shown in Table 1.

A bromo or benzylthio group on the benzene ring had little or no influence on the reduction of the ester function. Reduction of methyl 4-nitrobenzoate gave 4-nitrobenzyl alcohol in a rather low yield probably owing to the competitive reduction of the nitro group. In the case of methyl 4-hydroxybenzoate, *p*-cresol was obtained in a 52% isolated yield possibly owing to further reduction of the 4-hydroxybenzyl alcohol initially produced. Similar reduction was reported by Brewster et al. in which 4-methoxybenzyl alcohol was reduced to 4-methylanisole with $LiAlH_4$–$AlCl_3$.[8]

As shown in Table 2, various other esters could also be reduced to their corresponding alcohols with satisfactory isolated yields. However, the reduction of ethyl

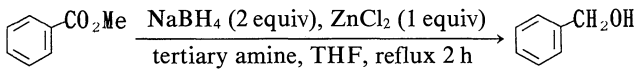

	Yield
tertiary amine: *N,N*-dimethylaniline	82%
: triethylamine	80%
: none	8%

Scheme 1.

Table 1. Reduction of Substituted Benzoate Derivatives[a]

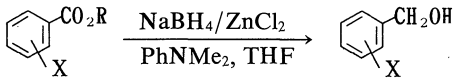

X	R	Yield/%
2-Br	Me	89
2-SCH_2Ph	Et	98
4-NO_2	Me	56
4-OH	Me	52[b]

a) A mixture of a substituted benzoate (1.0 mmol), $NaBH_4$ (2.0 mmol), $ZnCl_2$ (1.0 mmol), and *N,N*-dimethylaniline (1.0 mmol) was refluxed in THF for 2 h and all products isolated gave satisfactory ^1H NMR spectra. b) *p*-Cresol was obtained.

Table 2. Reduction of Aromatic and Aliphatic Esters[a]

$$RCO_2R^1 \xrightarrow[PhNMe_2,\ THF]{NaBH_4/ZnCl_2} RCH_2OH$$

Ester	Alcohol	Yield/%
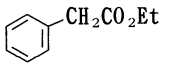	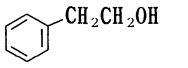	85
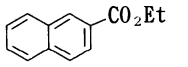	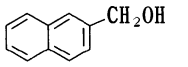	79
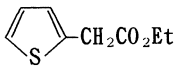	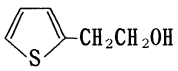	82
$CH_3(CH_2)_{16}CO_2Me$	$CH_3(CH_2)_{16}CH_2OH$	99
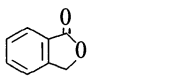	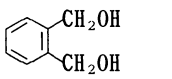	79
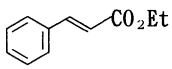	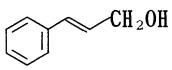	46

a) A mixture of an ester (1.0 mmol), $NaBH_4$ (2.0 mmol), $ZnCl_2$ (1.0 mmol), and *N,N*-dimethylaniline (1.0 mmol) was refluxed in THF for 2 h, and all products isolated gave satisfactory ^1H NMR spectra.

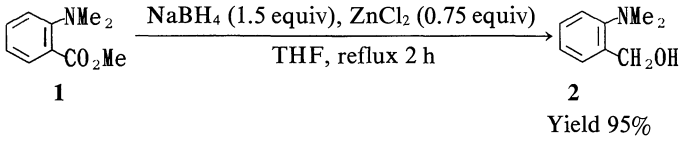

1 2

Yield 95%

Scheme 2.

cinnamate gave a 46% yield of cinnamyl alcohol together with the double bond-reduced product.

Our reaction conditions were applied to reduction of a few esters with tertiary amino groups, and the reduction was expected to proceed smoothly in the absence of the tertiary amine. Thus, methyl *N,N*-dimethylanthranilate (**1**) could be reduced with 1.5 equiv of $NaBH_4$ and 0.75 equiv of $ZnCl_2$ without the addition of *N,N*-dimethylaniline to give 2-dimethylaminobenzyl alcohol (**2**) as shown in Scheme 2.

Furthermore, the reductions of other aminobenzoates with this reducing system were investigated. These results are summarized in Table 3.

Dialkylamino benzoates were reduced to their corresponding benzyl alcohols with high yields, but the yields were somewhat low in the cases of *N*-unsubstituted or *N*-monoalkyl-substituted derivatives.

Various metal halides were investigated in place of $ZnCl_2$ in the reduction of methyl *N,N*-dimethylanthranilate (**1**). The yield of 2-dimethylaminobenzyl alcohol (**2**) was determined by gas chromatographic (GC) analysis. The results are summarized in Table 4. Lithium and magnesium halide did not enhance the reducing ability of $NaBH_4$, in spite of Kollonitsch's

Table 3. Reduction of Aminobenzoate Derivatives[a]

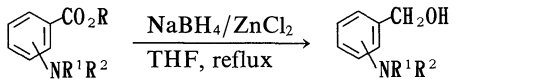

NR^1R^2	R	Yield/%
2-NHMe	Me	81
2-NH_2	Me	79
2-NEt_2[b]	Et	96
3-NMe_2	Me	96

a) A mixture of an aminobenzoate (1.0 mmol), $NaBH_4$ (2.0 mmol), and $ZnCl_2$ (1.0 mmol) was refluxed in THF for 2 h and the structure of all products isolated was determined by ^1H NMR and elemental analyses (C, H, N±0.3). b) This compound was reduced with 1.5 mmol of $NaBH_4$ and 0.75 mmol of $ZnCl_2$.

Table 4. Reduction of **1** with $NaBH_4$ and Metal Halide[a]

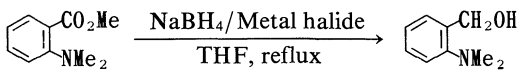

1 **2**

Metal halide	mmol[b]	Yield[c]/%
$ZnCl_2$	0.75	95
LiCl	1.5	0
LiBr	1.5	0
$CaCl_2$	0.75	14
$MgCl_2$	0.75	0
$FeCl_2$	0.75	44
$ZnBr_2$	0.75	11
$BF_3{\cdot}OEt_2$	0.5	41
$SnCl_4$	0.5	10
$AlCl_3$	0.5	85[d]

a) A mixture of **1** (1.0 mmol), $NaBH_4$ (1.5 mmol), and an appropriate metal halide was refluxed in THF for 2 h. b) An equimolar amount of an additive required for metal borohydride was used, except for $SnCl_4$. c) Established by GC analysis with benzyl alcohol as an internal standard. d) The reduction was carried out at 25°C for 24 h.

report mentioned above. However, $AlCl_3$ showed a good effect as reported by Brown et al.,[7] and the reduction proceeded at room temperature but was accompanied by the formation of some decomposition products possibly owing to the strong Lewis acidity of $AlCl_3$.

Solvent effects were investigated in the reduction of methyl *N,N*-dimethylanthranilate (**1**) with $NaBH_4$ and $ZnCl_2$ under refluxing for 2 h. As shown in Table 5, no reduction product was obtained in ethers such as diethyl ether, diisopropyl ether (IPE), and dioxane, but the reduction product was obtained in a low yield in dimethyl ether of diethylene glycol (diglyme). The reduction in ethanol produced only a small amount of ester-exchanged product without the reduction product. THF was the most suitable solvent for this reduction possibly owing to the solubility of the reagents.

The mechanism of the present reduction might be

Table 5. Reduction of **1** with $NaBH_4$ and $ZnCl_2$ in Various Solvents[a]

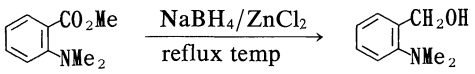

1 **2**

Solvent	Yield[b]/%
THF	95
Ether	0
IPE	0
Dioxane	0
Diglyme[c]	22
EtOH	0[d]

a) A mixture of **1** (1.0 mmol), $NaBH_4$ (1.5 mmol), and $ZnCl_2$ (0.75 mmol) was refluxed in each solvent for 2 h. b) Established by GC analysis with benzyl alcohol as an internal standard. c) The reaction was carried out at 25°C for 24 h. d) A small amount of ester-exchanged product was detected.

Table 6. Reduction with Varying Molar Ratios of $NaBH_4$ and $ZnCl_2$[a]

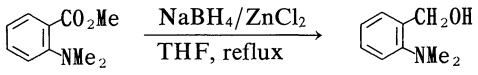

1 **2**

$ZnCl_2$	Yield[b]/%	
mmol	1 h	2 h
0	0	0
0.5	49	63
0.75	100	100
1.5	93	92

a) 1.5 mmol of $NaBH_4$ to 1.0 mmol of **1** was used. b) Established by GC analysis with benzyl alcohol as an internal standard.

explained by the initial formation of $Zn(BH_4)_2$ followed by the reduction of esters with $Zn(BH_4)_2$ which is activated by a tertiary amine. In order to clarify this, the reduction was studied by varying the molar ratio of $NaBH_4$ and $ZnCl_2$ as shown in Table 6.

When the molar ratio of $NaBH_4$ and $ZnCl_2$ was 2:1, the corresponding 2-dimethylaminobenzyl alcohol (**2**) was produced quantitatively after 1 h. Use of less $ZnCl_2$ served to slow down the rate of the reaction, while use of more $ZnCl_2$ gave a small amount of decomposition product after 1 h owing to the Lewis acidity of $ZnCl_2$, and no appreciable increase of reduction product was observed even after a prolonged reaction time. These results also suggested the formation of $Zn(BH_4)_2$. The formation of $Zn(BH_4)_2$ from $NaBH_4$ and $ZnCl_2$ has been reported by Gensler et al.[9]

Furthermore, the optimum molar ratio of $NaBH_4$ to **1** was proved to be 1.5:1, while the reduction with an equimolar amount of $NaBH_4$ to **1** afforded ca. an 80% yield of **2** after 4 h. The curve of reaction yield showed

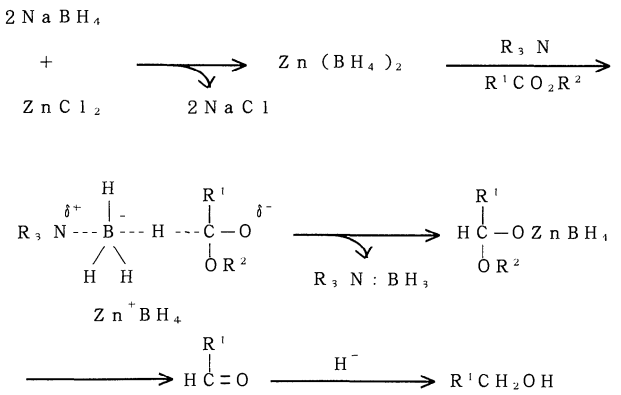

Scheme 3.

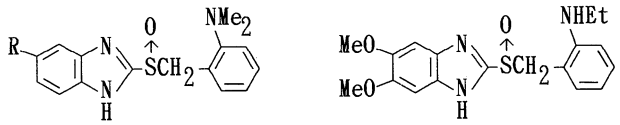

NC-1300 : R=H
NC-1300-B : R=OMe

S-3337

Scheme 4.

that the reaction would be completed only after a prolonged reaction time. These results revealed that only one hydride on $NaBH_4$ was effective for the reduction of an ester group to an aldehyde. A possible mechanism is shown in Scheme 3.

This reduction technique using $NaBH_4$–$ZnCl_2$–tertiary amine seems very useful because of the possibility of industrial applications in place of reductions with $LiAlH_4$ which is flammable and expensive. For example, the reduction of anthranilates is necessary for producing 2-aminobenzyl alcohols which are key intermediates of new H^+/K^+-ATPase inhibitors[10] as shown in Scheme 4. The reduction of anthranilate has been performed successfully only by using $LiAlH_4$.[11]

Further, the applicability of this reduction system to the reduction of other functional groups, such as amide, nitro, and cyano groups, was studied. The results are shown in Table 7. *N,N*-Dimethylbenzamide and 4-methylbenzonitrile were reduced to the corresponding benzylamine in good yields. However, the yield of the product in the reduction of 2-dimethylaminonitrobenzene without a tertiary amine was relatively low; the addition of *N,N*-dimethylaniline increased the yield. It seemed that the electron-withdrawing nitro group in the molecule decreased the basicity of the tertiary amino group.

Experimental

Nuclear magnetic resonance (NMR) spectra were recorded on a JEOL JNM-FX90Q NMR spectrometer with

Table 7. Reduction of Other Functional Groups[a)]

Starting material	Amine	Product	Yield/%
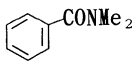	$PhNMe_2$	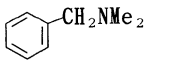	84
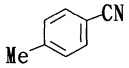	$PhNMe_2$	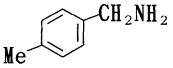	79
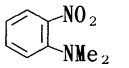	NONE	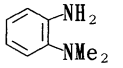	40
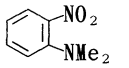	$PhNMe_2$	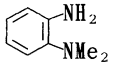	85

a) A mixture of a substrate (1.0 mmol), $NaBH_4$ (2.0 mmol), and $ZnCl_2$ (1.0 mmol) in the presence or absence of *N,N*-dimethylaniline (1.0 mmol) was refluxed in THF for 2 h, and the structure of all products isolated was determined by ^1H NMR and elemental analysis (C, H, N±0.3).

tetramethylsilane as the internal standard. GC analyses were performed on a 1.0 m column of 1% SE-30 on a JEOL JGC-20K gas chromatograph, operating at 30—200 °C. Elemental analyses (C,H,N) were performed on a Heraus C,H,N-Rapid instrument.

Materials. Sodium borohydride and metal halides (lithium chloride, lithium bromide, calcium chloride, magnesium chloride, iron(III) chloride, zinc chloride, zinc bromide, boron trifluoride–diethylether (1/1), tin(IV) chloride, and aluminum chloride) were commercially available. Tetrahydrofuran was purified through aluminum oxide. Commercial diglyme was distilled over calcium hydride and then redistilled under reduced pressure from a small quantity of lithium aluminum hydride. Other etheric solvents, such as diethyl ether, diisopropyl ether, and dioxane, were purified by standard methods followed by a distillation from lithium aluminum hydride. Commercial ethanol (95%) was utilized without further purification. *N,N*-Dimethylaniline, triethylamine, methyl benzoate, methyl 4-nitrobenzoate, methyl 4-hydroxybenzoate, ethyl phenylacetate, ethyl 2-thiopheneacetate, methyl stearate, phthalide, ethyl cinnamate, methyl *N,N*-dimethylanthranilate (**1**), methyl *N*-methylanthranilate, methyl anthranilate, *N,N*-dimethylbenzamide, and 4-methybenzonitrile were commercially available. Ethyl *N,N*-diethylanthranilate was prepared by ethylation of ethyl anthranilate with diethyl sulfate. Ethyl 2-benzylthiobenzoate was prepared by esterification of 2-mercaptobenzoic acid followed by alkylation with benzyl bromide. Methyl 3-dimethylaminobenzoate, ethyl 2-naphthalenecarboxylate, and methyl 2-bromobenzoate were prepared by esterification of the corresponding carboxylic acids. *N,N*-Dimethyl-2-nitroaniline was prepared by the standard method.[12)]

Reduction of Methyl Benzoate. A mixture of methyl benzoate (13.6 g, 100 mmol), $NaBH_4$ (7.60 g, 200 mmol), $ZnCl_2$ (13.6 g, 100 mmol), and *N,N*-dimethylaniline (12.1 g, 100 mmol) was refluxed with stirring in THF (200 ml) for 2 h. The reaction mixture was cooled with ice-cold water, and 10% NH_4Cl solution and chloroform were added. The organic layer was separated, washed with water and saturated NaCl solution, and dried over anhydrous Na_2SO_4. The solvent was evaporated and distilled to give 8.86 g (82% yield) of benzyl alcohol as a colorless oil. Reduction of substituted benzoates and other aromatic and aliphatic esters was carried out by a similar procedure. The results are summarized in Tables 1 and 2.

Reduction of Methyl *N,N*-Dimethylanthranilate (1). A mixture of **1** (1.79 g, 10.0 mmol), $NaBH_4$ (570 mg, 15.0 mmol), and $ZnCl_2$ (1.02 g, 7.5 mmol) was refluxed in THF (50 ml) for 2 h. The reaction mixture was cooled with ice-cold water, and 10% NH_4Cl solution and chloroform were added. The organic layer was separated, washed with water and saturated NaCl solution, and dried over Na_2SO_4. The solvent was evaporated and the residue was purified on a silica-gel column (chloroform) to produce 1.43 g (95% yield) of 2-dimethylaminobenzyl alcohol (**2**) as a colorless oil. ^1H NMR ($CDCl_3$) δ=2.68 (s, 6H), 4.78 (s, 2H), 6.9—7.3 (m, 4H). Other aminobenzoate derivatives were reduced by a procedure similar to that described for **1**. The results are summarized in Table 3.

General Procedure for the Study on the Effect of Metal Halides. A mixture of **1** (1.0 mmol), $NaBH_4$ (1.5 mmol), and an appropriate metal halide (0.5—1.5 mmol) was refluxed with stirring in THF (5 ml) for 2 h. The yield of 2-dimethylaminobenzyl alcohol (**2**) was determined by GC analysis with benzyl alcohol as an internal standard. The results are summarized in Table 4.

General Procedure for the Study of Solvent Effects. A mixture of **1** (1.0 mmol), $NaBH_4$ (1.5 mmol), and $ZnCl_2$ (0.75 mmol) in a solvent (5 ml) was refluxed with stirring for 2 h. The yield of **2** was determined by GC analysis with benzyl alcohol as an internal standard. The results are summarized in Table 5.

General Procedure for the Study of the Effect of the Molar Ratio of $NaBH_4$ and $ZnCl_2$. A mixture of **1** (1.0 mmol), $NaBH_4$ (1.5 mmol), and $ZnCl_2$ (0, 0.5, 0.75, 1.5 mmol) in THF (5 ml) was refluxed with stirring for 2 h. The yield of **2** was determined by GC analysis with benzyl alcohol as an internal standard. The results are shown in Table 6.

General Procedure for the Reduction of Other Functional Groups. A mixture of an amide, nitro or cyano compound (1.0 mmol), $NaBH_4$ (2.0 mmol), and $ZnCl_2$ (1.0 mmol) in the presence or absence of *N,N*-dimethylaniline (1.0 mmol) in THF (5 ml) was refluxed with stirring for 2 h. The reaction was quenched with 20% NH_4Cl solution and the reaction mixture was extracted with $CHCl_3$. The organic layer was washed with saturated NaCl, dried over anhydrous Na_2SO_4, and the solvent was evaporated in vacuo. The residue was purified on a silica-gel column (ether–hexane) to give the corresponding reduced compound. The yields are summarized in Table 7.

References

1) M. S. Brown and H. Rapoport, *J. Org. Chem.*, **28**, 3261 (1963).

2) V. Boekelheide and R. J. Windgassen, Jr., *J. Am. Chem. Soc.*, **81**, 1456 (1959).

3) J. E. G. Barnett and P. W. Kent, *J. Chem. Soc.*, **1963**, 2743.

4) K. Soai, H. Oyamada, and A. Ookawa, *Synth. Commun.*, **12**, 463 (1982).

5) T. Kitsuki and Y. Fujikura, 34th Symposium on the Chemistry of Aromatic Chemicals, Terpenes and Essential Oil, Takamatsu, Japan, Oct. 1990, Abstr., p. 104.

6) J. Kollonitsch, O. Fuchs, and V. Gabor, *Nature*

(London), **175**, 346 (1955).

7) H. C. Brown, E. J. Mead, and B. C. Subba Rao, *J. Am. Chem. Soc.,* **77**, 6209 (1955); H. C. Brown and B. C. Subba Rao, *ibid.,* **78**, 2582 (1956).

8) J. H. Brewster, H. O. Bayer, and S. F. Osman, *J. Org. Chem.,* **29**, 110 (1964).

9) W. J. Gensler, F. Johnson, and A. D. B. Sloan, *J. Am. Chem. Soc.,* **82**, 6074 (1960).

10) S. Okabe, E. Higaki, T. Higuchi, M. Sato, and K. Hara, *J. Pharmacol. Jpn.,* **40**, 239 (1986); S. Okabe, Y. Akimoto, S. Yamasaki, and H. Nagai, *Dig. Dis. Sci.,* **33**, 1425 (1988); G. W. Adelstein, C. H. Yen, R. A. Haack, S. Yu, G. Gullikson, D. V. Price, C. Anglin, D. L. Decktor, H. Tsai, and R. H. Keith, *J. Med. Chem.,* **31**, 1215 (1988); A. W. Herling, M. Bickel, H.-J. Lang, K. Weidmann, M. Rösner, H. Metzger, R. Rippel, H. Nimmesgern, and K.-H. Scheunemann, *Pharmacology,* **36**, 289 (1988).

11) M. Lora-Tamayo, R. Madronero, and G. G. Munoz, *Chem. Ber.,* **94**, 208 (1961).

12) H. F. Hodson and G. F. Smith, *J. Chem. Soc.,* **1957**, 3544.

13) T. W. Campbell, *J. Am. Chem. Soc.,* **71**, 740 (1949).

 © 1991 The Chemical Society of Japan Bull. Chem. Soc. Jpn., 64, 2735—2738 (1991)

Syntheses and Reactions of Metal Organics. XVI. Synthesis and Hydrolysis of Dimethoxysilanediyl Bis(polyfluoroalkanoate)

Norio YOSHINO,* Shin-ichi TOMINAGA, and Hidefumi HIRAI
Department of Industrial Chemistry, Faculty of Engineering, Science University of Tokyo, Kagurazaka, Shinjuku-ku, Tokyo 162
(Received April 18, 1991)

Four new silicon compounds, dimethoxysilanediyl bis(5*H*-octafluoropentanoate), $(CH_3O)_2Si[OCO(CF_2)_4H]_2$, dimethoxysilanediyl bis(7*H*-dodecafluoroheptanoate), $(CH_3O)_2Si[OCO(CF_2)_6H]_2$, dimethoxysilanediyl bis(9*H*-hexadecafluorononanoate), $(CH_3O)_2Si[OCO(CF_2)_8H]_2$, and dimethoxysilanediyl bis(pentadecafluorooctanoate), $(CH_3O)_2Si[OCO(CF_2)_6CF_3]_2$, were prepared by the reaction of dichlorodimethoxysilane with sodium salts of fluoro-substituted carboxylic acid. The ^1H NMR, ^{13}C NMR, and ^{19}F NMR and IR spectral data of these silicon compounds were obtained. In the course of a study of the stability of the silicon compounds against hydrolysis by using ^1H NMR spectral measurements, it was found that the ease of hydrolysis of the SiOCOR and the $SiOCH_3$ moieties was exactly same.

Metal alkoxides have been the subject of extensive research owing to their potential as precursor materials for several applications, such as new ceramics, adhesives, and coupling agents, which are molecular bridges between the interface of an inorganic filler and an organic polymer. Many alkyl or aryl orthosilicates and their halogenated derivatives have been prepared[1] and the reactivities of these orthosilicates towards various types of electron donors such as amides and amines have been reported.[2]

In recent years, dramatic developments have been made in the utilization of organofluoro compounds, resulting in new high-performance materials. However, only a few research reports concerning fluoro-substituted alkoxides of metals have appeared in the literature.[3-7] In previous papers we reported on the syntheses of fluoroalkyl and fluoroaryl titanates[8] as well as the syntheses of fluoroalkyl silicates.[9] Although these alkoxides were expected to be stable against moisture, since many of the compounds having the fluorinated carbon structure possess water repellency, all of the products were very sensitive to water and were easy to decompose.

In our last paper, we reported the results of the syntheses and characterizations of new titanium compounds having three fluoro-substituted alkanoyloxyl groups and one butoxyl group.[10] An application for the surface modification against calcium carbonate was also reported. These compounds were found to be an effective substance for a new-type coupling agent, which increases the affinity between organofluoro polymers and some inorganic substances.

In this paper, the results of the syntheses and characterizations of new silicon compounds having two fluoro-substituted alkanoyloxyl groups and two methoxyl groups per molecule are reported.

The stability of these products against hydrolysis is also discussed.

Experimental

Special precautions were adopted to avoid any hydrolysis of the starting materials and products, and all experiments were carried out under an atmosphere of purified nitrogen to preclude oxygen and moisture.

Materials. Silicon tetrachloride (bp 57.5—58.0 °C) was obtained from Kanto Chemical Co., Inc. and purified by distillation. Dichlorodimethoxysilane (bp 100—102 °C) was prepared by the reaction of silicon tetrachloride with methanol; Found: Si, 17.3; Cl, 44.1; OCH_3, 38.3%, Calcd for $C_2H_6Cl_2O_2Si$: Si, 17.4; Cl, 44.0; OCH_3, 38.5%. 5*H*-Octafluoropentanoic acid (bp 40—42 °C/120 Pa), 7*H*-dodecafluoroheptanoic acid (bp 60—61 °C/106 Pa), 9*H*-hexadecafluorononanoic acid (bp 92—93 °C/53 Pa) and perfluorooctanoic acid (bp 89—90 °C/4000 Pa) were received as gifts[11] from Daikin Industries, Ltd. and purified by distillation. The purity of these acids was checked by the use of ^{19}F NMR spectra and gas chromatography (GLC), and no impurities were detected. Sodium salts of these acids were synthesized by the reaction of fluoro-substituted carboxylic acid with excess sodium hydrogencarbonate in tetrahydrofuran (THF). The solvents used were purified by the usual method.

Measurements and Instruments. The FT-IR spectra were measured in a liquid film or by a KBr method with a JEOL JIR-5300 spectrophotometer. Each spectrum was recorded at a resolution of 4 cm^{-1} with a total of 30 scans. Pulsed Fourier Transform 100-MHz ^1H NMR and 25-MHz ^{13}C NMR spectra were run in THF-d_8 with TMS as an internal standard using a JEOL JNR-PX-100 spectrometer at room temperature: ^1H NMR spectra (pulse repetition time, 5 s; number of accumulations, 20) and ^{13}C NMR spectra (pulse repetition time, 2.0 s; number of accumulations, 40000). The FT mode 90-MHz ^{19}F NMR spectra were recorded at 27 °C on a JEOL JNM-FX-90Q in THF with fluorobenzene (−113.6 ppm[12] from $CFCl_3$ in $CDCl_3$) as an external standard: pulse repetition time, 0.5 s; number of accumulation, 20. The assignments of the ^{19}F NMR spectra were referred to in the data book.[12] Gas chromatography was performed with a Hitachi 063 (PEG-6000 supported Chromosorb A NAW 30/60 mesh 5 m packed column, TCD) or Hitachi G-3000 gas chromatograph (OV-1 25 m Fused capillary column, FID) and these intensities were

measured with a Hitachi 834 chromato processor or a Hitachi D-2500 chromato integrator.

Analytical Methods. Silicon was determined gravimetrically as silicon dioxide after the hydrolysis of silicon compounds by adding aqueous ammonia and burned in a quartz crucible. Chlorine was quantified by the Mohr method. Methoxyl groups were measured quantitatively as methanol by GLC after the hydrolysis of the products by adding a sodium hydroxide solution. The contents of the fluorinated alkanoyloxyl group having hydrogen at the end of the chain were estimated indirectly from the intensities against methoxyl protons by ^{1}H NMR spectra.

Syntheses of Dimethoxysilanediyl Bis(polyfluoroalkanoate). Synthesis of Dimethoxysilanediyl Bis(5*H*-octafluoropentanoate), $Si(OCH_3)_2[OCO(CF_2)_4H]_2$: Sodium 5*H*-octafluoropentanoate (6.18 g (23.1 mmol)) was added to a stirred solution of dichlorodimethoxysilane (1.69 g (10.5 mmol)) in 80 ml 1,1,2-trichloro-1,2,2-trifluoroethane at room temperature in a two-necked 200-ml flask connected with a reflux condenser and a three-way stop cock. The heterogeneous mixture was refluxed with stirring for 15 h. Completion of the reaction was checked by adding a silver nitrate solution to a portion of the clear upper solution. Sodium chloride produced and excess sodium 5*H*-octafluoropentanoate were removed by filtration. A transparent, slightly yellow, liquid was obtained after removing the solvent under reduced pressure (yield 5.08 g, 83.5%): IR 2965, 2855, 1782, 1462, 1402, 1340, 1270, 1198, 1162, 1080, 1049, 955, 928, 905, 855, 805, 775, 742, and 708 cm^{-1}; ^{1}H NMR δ=3.64(CH_3, s(singlet), 4.31H), 3.68(CH_3, s, 0.46H), 3.78(CH_3, s, 0.98H), 3.95(CH_3, s, 0.25H), and 5.98(CF_2H, t(t)(triplet(triplet)), J=51.6 (5.0) Hz, 2.0H); ^{13}C NMR δ=52.3(f, s), 52.5(f, s), 53.6(f, s), 55.1(f, s), 109.2(a, t(t), J=253.5(30.8) Hz), 109.3(b, t(m(multiplet)), J=265.6 Hz), 110.3(c, t(m), J=266.7 Hz), 111.6(d, t(t), J=266.7(31.5) Hz), 157.3(e, t, J=30.0 Hz), and 159.5(e, t, J=29.3 Hz) for $(HC^aF_2C^bF_2C^cF_2C^dF_2C^eOO)_2Si(OC^fH_3)_2$; ^{19}F NMR δ=−25.4 (a, d(doublet), J=51.3 Hz, 4F), −17.3(b, s, 4F), −12.3(c, s, 4F), and −6.6(d, s, 4F) for $(HCF_2^aCF_2^bCF_2^cCF_2^dCOO)_2Si(OCH_3)_2$. Found: Si, 5.00; CH_3O, 10.8; $H(CF_2)_4COO$, 49.9 %. Calcd for $C_{12}H_8F_{16}O_6Si$: Si, 4.84; CH_3O, 10.7; $H(CF_2)_4COO$, 50.0 %.

Synthesis of Dimethoxysilanediyl Bis(7*H*-dodecafluoroheptanoate), $Si(OCH_3)_2[OCO(CF_2)_6H]_2$, Dimethoxysilanediyl Bis(9*H*-hexadecafluorononanoate), $Si(OCH_3)_2[OCO(CF_2)_8H]_2$, and Dimethoxysilanediyl Bis(pentadecafluorooctanoate), $Si(OCH_3)_2[OCO(CF_2)_6CF_3]_2$: The procedures and purification techniques were almost the same as those for the preparation of dimethoxysilanediyl bis(5*H*-octafluoropentanoate).

Dimethoxysilanediyl bis(7*H*-dodecafluoroheptanoate) was a slightly brown liquid (yield 81.9%): IR 2970, 2870, 1786, 1465, 1408, 1348, 1300, 1195, 1135, 1080, 1060, 940, 865, 835, 800, 775, 728, and 673 cm^{-1}; ^{1}H NMR δ=3.64(CH_3, s, 4.93H), 3.67(CH_3, s, 0.31H), 3.78(CH_3, s, 0.65H), 3.95(CH_3, s, 0.11H), and 6.0(CF_2H, t(t), J=51.6(5.0) Hz, 2.0H); ^{13}C NMR=52.3(h, s), 52.5(h, s), 53.6(h, s), 55.1(h, s), 109.3(a, t(t), J=253.5(31.5) Hz), 110.8—113.1 (b—f), 156.8(g, t, J=30.0 Hz), 156.1(g, t, J=31.5 Hz), 156.8(g, t, J=30.0 Hz), and 159.3(g, t, J=29.3 Hz) for $(HC^aF_2C^bF_2C^cF_2C^dF_2C^eF_2C^fF_2C^gOO)_2Si(OC^hH_3)_2$; ^{19}F NMR δ=−25.4 (a, d, J=51.3 Hz, 4F), −17.3(b, s, 4F), −11.1(c, s, 4F), −10.4(d, s, 4F), −9.2(e, s, 4F), and −6.2(f, s, 4F) for $(HCF_2^aCF_2^bCF_2^cCF_2^dCF_2^eCF_2^fCOO)_2Si(OCH_3)_2$. Found: Si, 3.52; CH_3O, 7.78; $H(CF_2)_6COO$, 62.6 %. Calcd for $C_{16}H_8F_{24}O_6Si$: Si, 3.60; CH_3O, 7.95; $H(CF_2)_6COO$, 62.8 %.

Dimethoxysilanediyl bis(9*H*-hexadecafluorononanoate) was a slightly brown liquid (yield 70.5%): IR 2966, 2863, 1790, 1464, 1402, 1354, 1323, 1211, 1147, 1063, 997, 953, 854, 806, 769, 730, and 665 cm^{-1}; ^{1}H NMR δ=3.68(CH_3, s, 3.88H), 3.78(CH_3, s, 1.90H), 3.97(CH_3, s, 0.22H), and 5.9(CF_2H, t(t), J=51.1(5.0) Hz, 2.0H); ^{13}C NMR δ=52.4(j, s), 53.3(j, s), 54.8(j, s), 108.0(a, t(t), J=255.0(32.2) Hz), 108.3—112.5 (b—h), 155.5(i, t, J=30.8 Hz), and 156.4(i, t, J=30.8 Hz) for $(HC^aF_2C^bF_2C^cF_2C^dF_2C^eF_2C^fF_2C^gF_2C^hF_2C^iOO)_2Si(OC^jH_3)_2$; ^{19}F NMR δ=−24.2(a, d, J=51.3 Hz, 4F), −16.4(b, s, 4F), −10.3(c, s, 4F), −8.7(d—g, br(broad), 16F), and −5.4(h, s, 4F) for $(HCF_2^aCF_2^bCF_2^cCF_2^dCF_2^eCF_2^fCF_2^gCF_2^hCOO)_2Si(OCH_3)_2$. Found: Si, 3.15; CH_3O, 6.30; $H(CF_2)_8COO$, 70.2%. Calcd for $C_{20}H_8F_{32}O_6Si$: Si, 3.07; CH_3O, 6.33; $H(CF_2)_8COO$, 70.4%.

Dimethoxysilanediyl bis(pentadecafluorooctanoate) was a slightly brown liquid (yield 82.8%): IR 2952, 2849, 1780, 1480, 1440, 1402, 1330, 1240, 1202, 1148, 1100, 1080, 1018, 883, 838, 820, 812, 803, 778, 745, 735, 720, 698, and 660 cm^{-1}; ^{1}H NMR δ=3.64(CH_3, s, 1.65H), 3.67(CH_3, s, 3.05H), 3.79(CH_3, s, 0.14H), and 3.96(CH_3, s, 1.16H); ^{13}C NMR δ=52.4(i, s), 52.5(i, s), 52.7(i, s), 53.0(i, s), 111.6—118.7(a—g), and 156.8(h, t, J=30.8 Hz) for $(C^aF_3C^bF_2C^cF_2C^dF_2C^eF_2C^fF_2C^gF_2C^hOO)_2Si(OC^iH_3)_2$; ^{19}F NMR δ=−13.9(b, s, 4F), −11.3 (c, s, 4F), −10.4(d, s, 4F), −9.2(e and f, br, 8F), −2.0(g, s, 4F), and 31.0 (a, t, J=12.2 Hz, 6F) for $(CF_3^aCF_2^bCF_2^cCF_2^dCF_2^eCF_2^fCF_2^gCOO)_2Si(OCH_3)_2$. Found: Si, 2.95; CH_3O, 6.85%. Calcd for $C_{18}H_6F_{30}O_6Si$: Si, 2.87; CH_3O, 6.77 %.

Results and Discussion

The reaction of the synthesis of dimethoxysilanediyl bis(polyfluoroalkanoate) was heterogeneous in every cases, the same as the preparation of titanium butoxide tris(polyfluoroalkanoate).[10] However, the time to complete the reaction was comparably shorter than that of the titanium butoxide tris(polyfluoroalkanoate) synthesis, even in the reaction with the sodium fluoro-substituted alkanoate having a longer chain.

The NMR spectra of dimethoxysilanediyl bis(5*H*-ctafluoropentanoate), $Si(OCH_3)_2[OCO(CF_2)_4H]_2$, are shown in Figs. 1—3. In the ^{1}H NMR spectrum, three small signal peaks (δ=3.68(0.46H), 3.78(0.98H), and 3.95(0.25H)) were detected along with the main signal peak which originated from methyl protons at δ=3.64(4.31H). This fact shows that a part of the silicon compound was disproportionated to methoxysilanetriyl tris(5*H*-octafluoropentanoate), trimethoxysilyl 5*H*-octafluoropentanoate and tetramethoxysilane. The same observations were detected two kinds of carbons ($\underline{C}H_3$– and –$\underline{C}OO$–) in the ^{13}C NMR spectrum. On the other hand, the effect of the disproportionation on the chemical shift against the $\underline{H}CF_2$– proton signal was very slight and only a broadening was observed in the ^{1}H NMR spectrum. The effect of the disproportionation on the chemical shift of the ^{19}F NMR spectrum was not observed. The ^{13}C NMR spectrum was relatively complicated especially for the –$\underline{C}F_2$– signals (see Fig. 2). The resonance peaks of a carbon atom were coupled magnetically with the geminal and vicinal fluorine atoms.

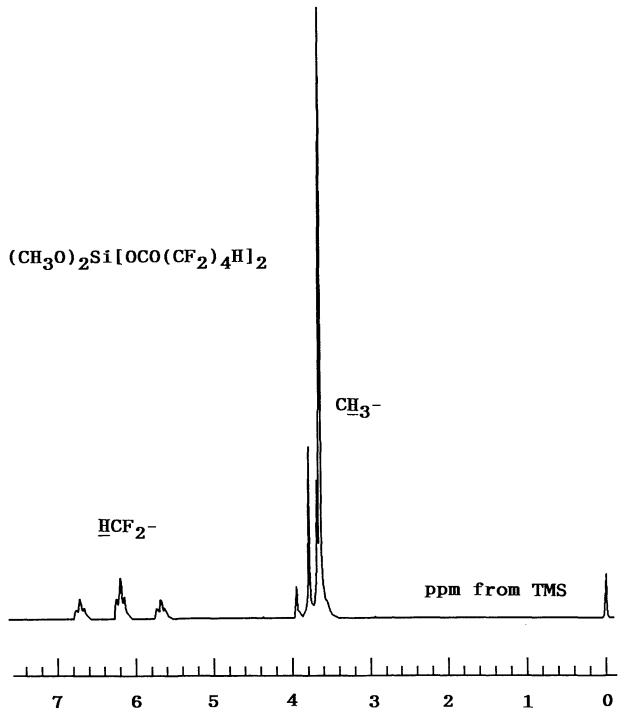

Fig. 1. Pulsed fourier transform 100 MHz ^{1}H NMR spectrum of $(CH_3O)_2Si[OCO(CF_2)_4H]_2$ in THF-d_8.

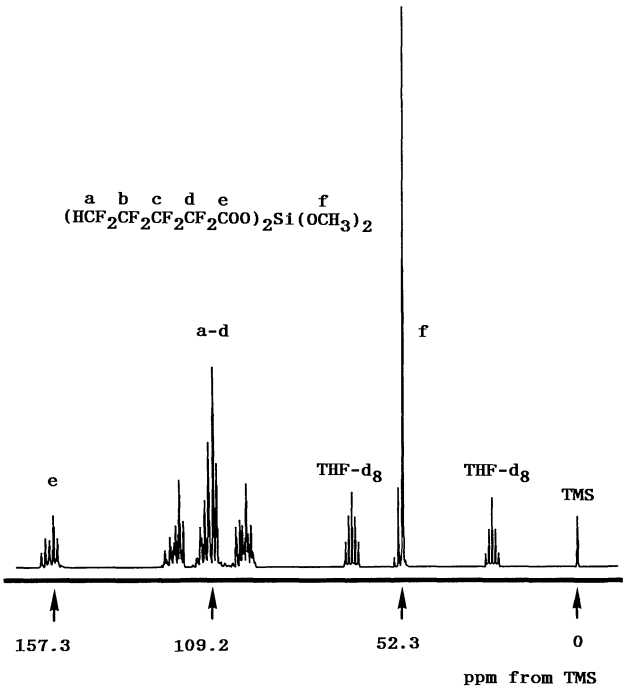

Fig. 2. Pulsed fourier transform 25 MHz ^{13}C NMR spectrum of $(CH_3O)_2Si[OCO(CF_2)_4H]_2$ in THF-d_8.

A group of stronger intensity peaks from the terminal HCF_2– (triplet(triplet)) was observed at 109.2 ppm from TMS in THF-d_8, and the other $-CF_2-$ peaks were weaker.

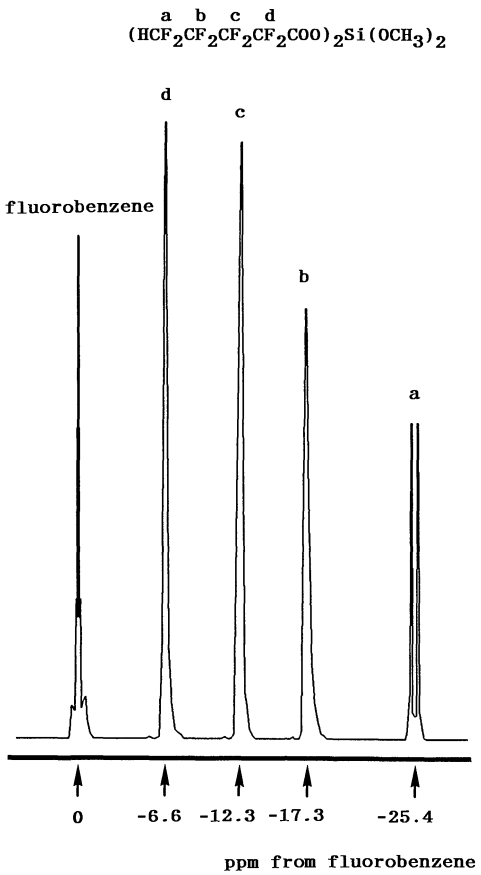

Fig. 3. Pulsed fourier transform 90 MHz ^{19}F NMR spectrum of $(CH_3O)_2Si[OCO(CF_2)_4H]_2$ in THF.

In the case of the ^{13}C NMR spectra, it is well known that for fluorinated carbon atoms, the peak intensities of a carbon bonded to a hydrogen atom, such as HCF_2–, H_2CF–, or –HCF–, are stronger than those of a carbon bonded only to fluorine atoms, such as CF_3– or $-CF_2-$. In the ^{13}C NMR spectra, it was very difficult to make assignments against $-CF_2-$ of almost all the silicon compounds prepared. Only for the simplest one, dimethoxysilanediyl bis(5*H*-octafluoropentanoate), were we able to make an assignment.

These silicon compounds possessed a structure essentially similar to that of the titanate-type coupling agents having fluorocarbon chains.[10] In the titanate-type coupling agents, the TiOCOR moiety was stable in water, although the TiOR' was only moderately stable against water. Therefore, the stability of the silicon compounds to hydrolysis was investigated. From the ^{1}H NMR spectrum of the reaction mixture of dimethoxysilanediyl bis(7*H*-dodecafluoroheptanoate) and water (molar ratio 10:1) in THF-d_8 (internal standard TMS), the intensity ratio of the produced acid COOH (13.9 ppm) and the produced methanol OH (4.0 ppm) was precisely 1:1. This means that the ease of hydrolysis of the SiOCOR and the $SiOCH_3$ moieties was exactly same. The same observation was obtained from

the other prepared silicon compounds.

Moreover, the instabilities to hydrolysis of these silicon compounds were proved as follows. In a 100-ml beaker, 1 g of dimethoxysilanediyl bis(7*H*-dodecafluoroheptanoate) in 50 cm^3 methanol was stirred exposed to the atmosphere at room temperature for 24 h. A white precipitate formed. A white powder was obtained after filtration, washing with 1,1,2-trichloro-1,2,2-trifluoroethane and vacuum drying. The FT-IR spectrum of this powder was the same as that of silica gel. The same observation was obtained from the other silicon compounds.

In conclusion, these dimethoxysilanediyl bis(polyfluoroalkanoate)s were very sensitive to water and decomposed easily, although they had the fluorinated carbon structure which exhibits the property of water repellency.

The present work was partially supported by a Grant-in-Aid for Scientific Research No.62550618 from the Ministry of Education, Science and Culture, to which the authors are grateful.

References

1) a) W. Gerrard and A. H. Woodhead, *J. Chem. Soc.*, **1961**, 519; b) D. C. Bradley, R. C. Mehrotra, and W. Wardlaw, *J. Chem. Soc.*, **1952**, 5020; c) L. Sheng-Lich and W. Hsiuchin, *J. Chin. Chem. Soc.*, **13**, 188 (1966); *Chem. Abstr.*, **68**, 2947 (1968); d) W. Rothe, Ger. Patent 1298972 (1969); *Chem. Abstr.*, **71**, 90804 (1969); e) M. Wojnowska and W. Wojnowski, *Rocz. Chem.*, **44**, 1019 (1970); *Chem. Abstr.*, **73**, 130577 (1970); f) F. Augst and F. Sufraga, Ger. Offen Patent 2033373 (1971); *Chem. Abstr.*, **74**, 125839 (1971); g) A. P. Kreshkov and D. A. Karteev, *Zh. Obsch. Khim.*, **27**, 2715 (1957); h) J. Goubeau and H. Behr, *Z. Anorg. Allg. Chem.*, **272**, 2 (1953); i) W. Airey and G. M. Sheldrick, *J. Inorg. Nucl. Chem.*, **32**, 1827 (1970).

2) a) N. Yoshino and T. Yoshino, *Kogyo Kagaku Zasshi*, **74**, 1404 (1971); b) N. Yoshino and T. Yoshino, *Syn. React. Inorg. Metal-Org. Chem.*, **4(3)**, 263 (1974).

3) D. C. Bradley, M. E. Redwood, and C. J. Willis, *Proc. Chem. Soc.*, **1964**, 416.

4) M. E. Redwood and C. J. Willis, *Can. J. Chem.*, **43**, 1893 (1965).

5) P. N. Kapoor and R. C. Mehrotra, *Chem. Ind.*, **1966**, 1034.

6) P. N. Kapoor, R. N. Kapoor, and R. C. Mehrotra, *Chem. Ind.*, **1968**, 1314.

7) K. S. Mazdiyashi, B. J. Schaper, and L. M. Brown, *Inorg. Chem.*, **10**, 889 (1971).

8) N. Yoshino, J. Tomita, and H. Hirai, *Bull. Chem. Soc. Jpn.*, **62**, 2208 (1989).

9) N. Yoshino, H. Terajima, and H. Hirai, *Synth. React. Inorg. Met.-Org. Chem.*, **20(6)**, 729 (1990).

10) N. Yoshino, Y. Shiraishi, and H. Hirai, *Bull. Chem. Soc. Jpn.*, **64**, 1648 (1991).

11) a) M. Joyce, U.S. Patent 2559628 (1951); b) D. R. Bear, *Ind. Eng. Chem.*, **51**, 829 (1959).

12) K. Kushida and A. Watanabe, "Proton and Fluorine Nuclear Magnetic Resonance Spectral Data 1988 Edition," ed by Varian Instruments Ltd. and Japan Halon Co., Ltd., Tokyo, Japan.

Asymmetric Michael Addition of the *N*-Alkylidene Derivative of an α-Amino Ester to Methyl (*E*)-3-[(3*R*,7a*S*)-2-Phenylperhydropyrrolo[1,2-*c*]imidazol-3-yl]propenoate

Hidetoshi YAMAMOTO,† Shuji KANEMASA,* and Eiji WADA
Institute of Advanced Material Study, Kyushu University, Kasugakoen, Kasuga 816
† Department of Molecular Science and Technology, Interdisciplinary Graduate School of Engineering Sciences, Kyushu University, Kasugakoen, Kasuga 816
(Received April 25, 1991)

The exclusively diastereoselective asymmetric Michael addition of the lithiated methyl *N*-(2,2-dimethylpropylidene)glycinate to methyl (*E*)-3-[(3*R*,7a*S*)-2-phenylperhydropyrrolo[1,2-*c*]imidazol-3-yl]propenoate is described. The synperiplanar conformer of the acceptor propenoate participated in the reaction where the *re*-face of the acceptor molecule was attacked by the *re*(β)-face of the lithiated intermediate.

It has been reported that *N*-alkylidene-substituted α-amino esters can be lithiated with a variety of lithiating reagents including lithium bromide/triethylamine or lithium bromide/1,8-diazabicyclo[5.4.0]undec-7-ene (DBU) to generate reactive nucleophiles, *N*-lithiated azomethine ylides or lithium enolates.[1] The lithiated intermediates of *N*-alkylidene-substituted α-amino esters so generated undergo stereoselective cycloaddition to α,β-unsaturated carbonyl compounds leading to 2-pyrrolidinecarboxylates. It is now accepted that the chelation as well as the frontier orbital interaction operating in the transition state is responsible for the observed high selectivities.[1] When the *N*-alkylidene-substituted α-amino esters are derived from bulky aldehydes or ketones, such as 2,2-dimethylpropanal or 2-bornanone, the lithiated intermediates generated from them undergo Michael addition to α,β-unsaturated carbonyl compounds, instead of dipolar cycloaddition, again in a highly stereoselective fashion.[1c,2]

Dipolar cycloaddition reaction of *N*-alkylidene-substituted α-amino esters has been developed to the asymmetric version by utilizing the α,β-unsaturated carbonyl compounds bearing a gem-diamino type chiral controller at the β-position[3a,b,d] or utilizing the *N*-alkylidene-substituted α-amino ester derived from an optically pure alcohol.[3c] On the other hand, the *N*-bornanylidene-substituted α-amino esters[4] or the *N*-pinanylidene-substituted α-amino esters[5] were found to function as excellent Michael donors in the asymmetric Michael reaction. However, no application has been so far reported on the asymmetric Michael addition using a chiral α,β-unsaturated carbonyl compound and achiral *N*-alkylidene-substituted α-amino esters. In this report, we present the exclusively diastereoselective asymmetric Michael addition of the lithium derivative of an *N*-alkylideneglycine methyl ester to a chiral α,β-unsaturated ester, methyl (*E*)-3-[(3*R*,7a*S*)-2-phenylperhydropyrrolo[1,2-*c*]imidazol-3-yl]propenoate.[6]

Results and Discussion

Treatment of methyl *N*-(2,2-dimethylpropylidene)-glycinate (**1**) with lithium bromide (2 equiv) and DBU (1.2 equiv) gave the lithiated *N*-alkylideneglycinate **2**, which was allowed to react with methyl (*E*)-3-[(3*R*,7a*S*)-2-phenylperhydropyrrolo[1,2-*c*]imidazol-3-yl]propenoate (**3**) in tetrahydrofuran (THF) at −78 °C for 6.5 h to produce the Michael adduct **4** in 98% yield as the sole product (confirmed by ^{1}H NMR of the crude product, Scheme 1).[7] The Michael adducts produced from lithiated *N*-alkylideneglycinates bear a remaining acidic hydrogen adjacent to the imine nitrogen (α-position of the *N*-alkyl group) and the ready epimerization usually occurs at this position under basic conditions.[2] However, no sign of occurrence of epimerization was detected in this reaction. Presumably this is because the

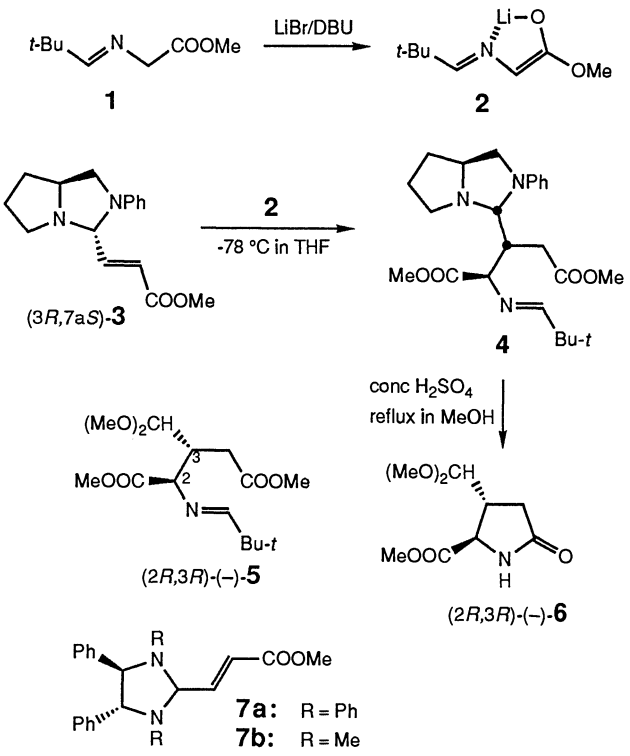

Scheme 1.

deprotonation at the α-position of the *N*-alkyl group was sterically hindered by the bulky chiral controller substituent just as previously observed in the case of bornanimines.[4] When the reaction was carried out at room temperature, formation of two side products resulted (1 h, 6% and 5% by ^{1}H NMR). One of the side products was temporarily assigned as the epimer with respect to the position adjacent to the imine nitrogen because its ratio increased with the prolonged reaction time (57 h at room temperature, 18% and 5% by ^{1}H NMR).[8] The other product produced in 5% yield in the reaction at room temperature may be the diastereomer of **4** resulting from the different diastereoselection. As a result, the diastereoselectivity in the reaction at room temperature was calculated to be 95 : 5.

Although α,β-unsaturated esters **7a,b** bearing a C_2-symmetric imidazolidine chiral controller at the β-position[3d] were applied to carry through the same purpose, they were found to be much less reactive than **3**. Thus, no addition product was obtained under various reaction conditions (both at −78 °C and at room temperature). Even when the lithium derivative of *N*-alkylidene-substituted glycine methyl ester **2** was irreversibly generated from **1** and lithium diisopropylamide (LDA), no formation of the Michael adduct was observed. Such unsuccess of reaction is certainly due to the steric hindrance around the β-position of **7a,b** as well as the decreased reactivity of the lithiated intermediate of methyl *N*-(2,2-dimethylpropylidene)glycinate (**1**) compared with that of the lithiated intermediate of methyl *N*-benzylideneglycinate.[2] However, such difference of reactivities, especially that of **7b**, was much more than our anticipation.

High susceptibility of the Michael adduct **4** to hydrosis at the C=N linkage let us abandon the attempt of purification by column chromatography.[9] Therefore, **4** was converted without further purification to (2*R*,3*R*)-(−)-**6** by refluxing in MeOH in the presence of concentrated sulfuric acid.[10] The processes involved in this conversion are acetal exchange to dimethyl acetal (2*R*,3*R*)-(−)-**5**, hydrolysis of the C=N moiety, and cyclization. Assignment of the absolute configurations of (2*R*,3*R*)-**5** and (2*R*,3*R*)-**6** will be discussed below.

The authentic sample of the racemate of (2*R*,3*R*)-**5**, *rac*-**5**, was prepared in quantitative yield from a similar reaction of methyl (*E*)-4,4-dimethoxy-2-butenoate (**8**) with **2** (−78 °C, 3 h)(Scheme 2). Treatment of *rac*-**5** so prepared with hydroxylamine hydrochloride in methanol at room temperature gave *rac*-**6** in quantitative yield. Structure of *rac*-**6** was confirmed by spectral data and analytical data.

According to the transition state[3b] proposed for the diastereoselective cycloaddition of the lithiated methyl *N*-benzylideneglycinate to (3*R*,7a*S*)-**3**, the *re*(β)-face of the synperiplanar conformer of (3*R*,7a*S*)-**3** should be attacked by the *re*-face of **2**. Therefore, it was expected that the Michael addition of **2** to (3*R*,7a*S*)-**3** would produce dimethyl (2*R*,3*R*)-*N*-(2,2-dimethylpropylidene)-3-[(3*R*,7a*S*)-2-phenylperhydropyrrolo[1,2-*c*]-imidazol-3-yl]glutamate (**4**), and hence further (2*R*,3*R*)-**5** and (2*R*,3*R*)-**6**.

On the other hand, it has been reported that the *N*-bornanylideneglycinates derived from natural (1*R*)-(+)-2-bornanone react, after lithiation, with α,β-unsaturated esters to give 2-substituted glycinates with the unnatural configuration, the 2*R*-configuration, through the chelated transition state **TS-A** (Scheme 3).[4b] Therefore, the Michael addition of the lithiated intermediate of bornanimine **9** would be successfully applied to prepare the authentic sample of (2*R*,3*R*)-**6**. Thus, the reaction of **8** with **9** was performed under the conditions of reversible lithiation (−78 °C, butyllithium/*t*-butyl alcohol in THF, 1 h) to produce **10** as the sole product.

The Michael adduct **10** was converted to methyl ester **11** by treatment with methanol in the presence of concentrated sulfuric acid, and then the 2-bornanylidene chiral controller of **11** was removed off by heating it with hydroxylamine hydrochloride in methanol to give cyclized product **6**. The sign of its optical rotation ($[\alpha]_D^{24}$ =−40.8° (*c* 0.51, $CHCl_3$)) was found to be the same as that of (2*R*,3*R*)-(−)-**6**, indicating the (2*R*,3*R*)-absolute configuration of **4**.

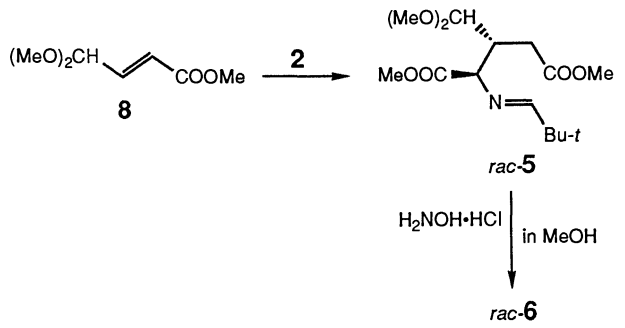

Scheme 2.

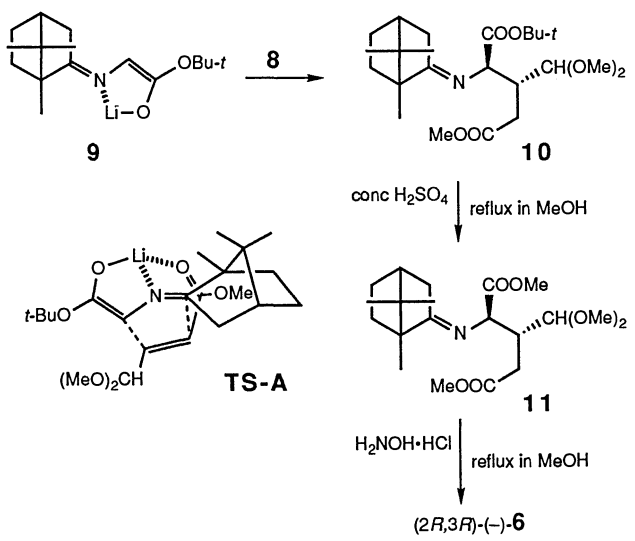

Scheme 3.

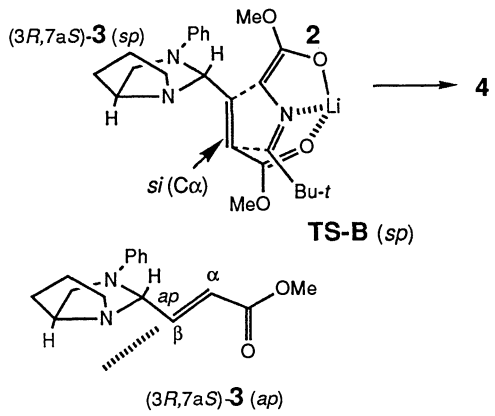

Fig. 1. Proposed transition state for the asymmetric Michael addition of *N*-lithiated azomethine ylide **2** to (3*R*,7a*S*)-**3**.

As previously discussed,[3a,b] the attack of a 1,3-dipole to the α,β-unsaturated ester moiety of (3*R*,7a*S*)-**3** took place from the direction opposite to the bulky *N*-phenyl substituent. Since the Michael adduct **4** was assigned to have (2*R*,3*R*)-configuration in the present work, it is clear that the synperiplanar conformation of (3*R*,7a*S*)-**3** was exclusively involved in the transition state. The transition state **TS-B**(*sp*) is the case (Fig. 1). The participation of the less stable synperiplanar conformation was previously observed in the dipolar cycloaddition of *N*-metalated azomethine ylides with the α,β-unsaturated esters bearing a gem-diamino type chiral controller at the β-position.[3a,b,d] In the transition state involving the thermodynamically more favored antiperiplanar conformer (3*R*,7a*S*)-**3** (*ap*), some more steric hindrance may be caused between the framework of the (3*R*,7a*S*)-2-phenylperhydropyrrolo[1,2-*c*]-imidazol-3-yl chiral controller and the methoxy group of **2** along the hashed line directing from the α-carbon to the β-carbon of **3**.

In conclusion, the lithium derivative of *N*-(2,2-dimethylpropylidene)glycine methyl ester underwent exclusively diastereoselective asymmetric Michael addition to methyl (*E*)-3-[(3*R*,7a*S*)-2-phenylperhydropyrrolo[1,2-*c*]imidazol-3-yl]propenoate. The synperiplanar conformer of the acceptor molecule participated in the reaction in which the *re*-face of the acceptor molecule was attacked by the *re*(β)-face of the lithiated intermediate of the *N*-alkylidene-substituted α-amino ester.

Experimental

General. Melting points were recorded on a Yanagimoto melting point apparatus and are uncorrected. IR spectra were taken with JASCO IRA-1 and A-702 spectrometers. ^{1}H and ^{13}C NMR spectra were recorded with Hitachi R-40 (^{1}H NMR; 90 MHz) and GSX-270 (270 MHz for ^{1}H NMR and 67.94 MHz for ^{13}C NMR) instruments. Chemical shifts are reported in parts per million downfield (δ) from internal tetramethylsilane. Mass spectra and high resolution mass spectra (HRMS) were recorded with a JEOL-01SG-2 spectrometer operating at an ionization energy of 70 eV. Elemental analyses were performed with a Hitachi 026 CHN analyzer. Optical rotations were recorded with a Horiba SEPA-200 polarimeter. For preparative column chromatography, Wakogel C-200, Wako C-300, and Merck Silica gel 60 were employed. Flash chromatography was performed with an Eyera EF-10 apparatus on a 20×180 mm column packed with 0.04—0.063 mm silica gel 60.

Materials. Methyl *N*-(2,2-dimethylpropylidene)glycinate (**1**),[2] methyl (*E*)-3-[(3*R*,7a*S*)-2-phenylperhydropyrrolo[1,2-*c*]imidazol-3-yl]propenoate (**3**),[3b] methyl (*E*)-4,4-dimethoxy-2-butenoate (**8**),[3b] and *t*-butyl (1*R*,4*R*)-*N*-(2-bornylidene)glycinate[4b] were prepared according to the reported procedures.

Michael Addition of 2 to (3*R*,7a*S*)-3 Leading to 4. To a solution of LiBr (0.521 g, 6 mmol) in dry THF (8 ml) were added, at −78 °C under nitrogen, a solution of **1** (0.474 g, 3 mmol) in THF (4 ml), DBU (0.548 g, 3.6 mmol), and a solution of (3*R*,7a*S*)-**3** (0.545 g, 2 mmol) in THF (4 ml) in that order. The mixture was stirred at −78 °C for 6.5 h. Saturated aqueous NH_4Cl (20 ml) was added to the mixture which was then extracted with Et_2O (30 ml×3). The combined extracts were dried ($MgSO_4$) and then evaporated in vacuo to give dimethyl (2*R*,3*R*)-*N*-(2,2-dimethylpropylidene)-3-[(3*R*,7a*S*)-2-phenylperhydropyrrolo[1,2-*c*]imidazo-3-yl]-glutamate (**4**, 0.841 g, 98%) as pale yellow oil. This compound **4** was so liable to hydrolysis that its purification by column chromatography was unsuccessful. Only ^{1}H and ^{13}C NMR spectra were recorded. Pale yellow liquid; ^{1}H NMR ($CDCl_3$) δ=1.10 (9H, s, *t*-Bu), 1.69—1.84 (3H, m, H-6′ and one of H-7′), 2.04—2.18 (1H, m, the other of H-7′), 2.35 (1H, dd, J_{gem}=10.3 and J_{4-3}=8.1 Hz, one of H-4), 2.44 (1H, dd, J_{gem}=10.3 and J_{4-3}=5.1 Hz, the other of H-4), 2.43—2.52 (1H, m, one of H-5′), 2.84 (1H, t, J_{gem}=$J_{1'-7a}$=8.8 Hz, one of H-1′), 3.05—3.12 (1H, m, the other of H-5′), 3.18 (1H, dddd, J_{3-4}=8.1, 5.1, J_{3-2}=7.7, and $J_{3-3'}$=4.8 Hz, H-3), 3.33 (3H, s, COOMe), 3.53 (1H, dd, J_{gem}=8.8 and $J_{1'-7a}$=7.3 Hz, the other of H-1′), 3.70 (3H, s, COOMe), 3.91 (1H, m, H-7a′), 3.99 (1H, d, J_{2-3}=7.7 Hz, H-2), 4.67 (1H, d, $J_{3'-3}$=4.8 Hz, H-3′), 6.65—6.74 and 7.16—7.27 (5H, m, Ph), and 7.62 (1H, d, *J*=0.7 Hz, CH=N); ^{13}C NMR ($CDCl_3$) δ=24.54 (C-6′), 26.71 (*t*-Bu), 29.85, 32.35 (C-3 and C-7′), 36.73 (*t*-Bu), 43.81 (C-4), 50.93 (C-5′), 51.75 (C-1′), 54.70, 55.06 (2×COOMe), 62.19 (C-7a′), 72.74 (C-2), 82.33 (C-3′), 112.87, 116.73, 128.94, 147.17 (each Ph), 171.92, 173.01 (each COOMe), and 176.84 (C=N).

Conversion of the Michael Adduct 4 to (2*R*,3*R*)-(−)-6. To a solution of **4** (0.128 g, 0.3 mmol) in MeOH (5 ml) was added concentrated H_2SO_4(0.1 ml). The mixture was refluxed for 7.5 h and then poured into saturated aqueous NaCl(2 ml). After neutralized with solid Na_2CO_3, the mixture was concentrated to dryness under a reduced pressure. The residual solid was triturated with CH_2Cl_2 (50 ml) and the inorganic substances were filtered off. The filtrate was evaporated under a reduced pressure to give a deep red oil (0.096 g). This oil was chromatographed on silica gel (EtOAc) to give methyl (2*R*,3*R*)-(−)-3-(dimethoxymethyl)-5-oxo-2-pyrrolidinecarboxylate [(2*R*,3*R*)-(−)-**6**] (0.048 g, 75%): Pale yellow liquid; $[\alpha]_D^{24}$=−41.3 (*c* 0.53, $CHCl_3$); IR (neat) 3200, 2890, 1664, 1416, 1352, 1184, 1048, and 900 cm^{-1}; ^{1}H NMR ($CDCl_3$) δ=2.34 (1H, dd, J_{gem}=17.6 and J_{4-3}=4.8 Hz, one of H-

4), 2.48 (1H, dd, J_{gem}=17.6 and J_{4-3}=9.5 Hz, the other of H-4), 2.85 (1H, dddd, J_{3-4}=9.5, 4.8, J_{3-2}=6.2, and J_{3-CH}=2.9 Hz, H-3), 3.40 (6H, s, 2×OMe), 3.79 (3H, s, COOMe), 4.20 (1H, d, J_{CH-3} =2.9 Hz, 3-CH), 4.35(1H, d, J_{2-3}=6.2 Hz, H-2), and 7.12 (1H, br s, NH); ^{13}C NMR ($CDCl_3$) δ=30.88 (C-3), 40.55 (C-4), 52.74 (COOMe), 54.15, 54.66 (2×OMe), 56.80 (C-2), 104.75 (3-CH), 172.41 (C-5), and 177.39 (COOMe); MS (20 eV) *m/z* (rel intensity, %) 217 (M^+, 0.2), 186 (18), 185 (54), 170 (10), 158 (25), and 75 (base peak). Found: C, 49.86; H, 6.91; N, 6.59%. Calcd for $C_9H_{15}NO_5$: C, 49.76; H, 6.96; N, 6.45%.

Michael Addition of 2 to 8 Leading to *rac*-5 and Further to *rac*-6. To a solution of LiBr (0.49 g, 5.62 mmol) in dry THF (4 ml) were added, at −78 °C under nitrogen, a solution of **1** (0.59 g, 3.75 mmol) in THF (2 ml), DBU (0.684 g, 4.5 mmol, in THF (2 ml), and **8** (0.4 g, 2.5 mmol, in THF (2 ml)) in that order. After stirring at −78 °C for 3 h, the mixture was treated with saturated aqueous NH_4Cl (10 ml), and then extracted with Et_2O (30 ml×3). The combined extracts were dried ($MgSO_4$) and evaporated in vacuo to give a pale yellow oil of *rac*-**5** (0.807 g) [^{1}H NMR ($CDCl_3$) δ=1.07 (9H, s, *t*-Bu), 2.42 (1H, dd, J_{gem}=16.5 and J_{4-3}=6.6 Hz, one of H-4), 2.55 (1H, dd, J_{gem}=16.5 and J_{4-3}=5.5 Hz, the other of H-4), 3.01 (1H, m, H-3), 3.31, 3.32 (each 3H, each s, MeO), 3.66, 3.71 (each 3H, each s, COOMe), 3.97 (1H, d, J_{2-3}=5.9 Hz, H-2), 4.22 (1H, d, J_{CH-3} =7.0 Hz, 3-CH), and 7.55 (1H, s, CH=N)]. To a solution of this crude product *rac*-**5** (0.32 g, 1 mmol) in MeOH (5 ml) was added NH_2OH·HCl (0.14 g, 2 mmol). The mixture was stirred at room temperature for 1 h and was then evaporated in vacuo. The residual colorless oil was triturated with CH_2Cl_2 (50 ml) and the colorless solid precipitated was filtered off. The filtrate was evaporated in vacuo. The residual oil (0.285 g) was chromatographed on silica gel (EtOAc–EtOH, 5:1 v/v) to give methyl *rac*-3-(dimethoxymethyl)-5-oxo-2-pyrrolidinecarboxylate (*rac*-**6**, 0.216 g, 99% based on **8**): Colorless solid; mp 80.5—81.0 °C.

Michael Addition of the Lithiated *t*-Butyl (1*R*,4*R*)-*N*-(2-Bornanylidene)glycinate with 8 Leading to 10. To a solution of **9** (0.398 g, 1.5 mmol) in dry THF (5 ml) were added, at −78 °C under nitrogen, *n*-BuLi (1.59 M in hexane, 0.94 ml, 1.8 mmol), *t*-BuOH (0.133 g, 1.8 mmol, in THF (2.5 ml)), and **8** (0.202 g, 1.26 mmol, in THF (2.5 ml)) in that order. After stirring at −78 °C for 24 h, the mixture was treated with saturated aqueous NH_4Cl (10 ml) and then extracted with Et_2O (30 ml×3). The combined extracts were dried ($MgSO_4$) and evaporated in vacuo. The residue (0.584 g) was chromatographed on silica gel (hexane–EtOAc, 6:1 v/v) to yield 1-*t*-butyl methyl (2*R*,3*R*)-*N*-[(1*R*,4*R*)-2-bornanylidene]-3-(dimethoxymethyl)glutamate **10** (0.376 g, 70%): Colorless liquid; $[\alpha]_D^{23.5}$=+69.28° (*c* 1.6, $CHCl_3$); IR (neat) 2919, 1716, 1672, 1428, 1360, 1240, 1144, 1064, and 840 cm^{-1}; ^{1}H NMR ($CDCl_3$) δ=0.80, 0.92, 0.95 (each 3H, each s, 3×Me), 1.14—1.35 (2H, m, 2-bornanylidene), 1.43 (9H, s, *t*-Bu), 1.63—1.72 (1H, m, 2-bornanylidene), 1.80—1.95 (3H, m, 2-bornanylidene), 2.32—2.42 (1H, m, 2-bornanylidene), 2.51 (2H, d, J_{4-3}=5.9 Hz, H-4), 3.03 (1H, dq, J_{3-CH}=7.0 and J_{3-2}=J_{3-4}=5.9 Hz, H-3), 3.32, 3.33 (each 3H, each s, 2×OMe), 3.65 (3H, s, COOMe), 4.07 (1H, d, J_{2-3}=5.9 Hz, H-2), and 4.28 (1H, d, J_{CH-3}=7.0 Hz, 3-CH); MS (75 eV) *m/z* (rel intensity, %) 425 (M^+, 10), 411 (14), 410 (54), 355 (12), 354 (57), 352 (14), 338 (33), 337 (20), 336 (16), 324 (32), 308 (12), 294 (12), 265 (28), 264 (18), 250 (13), 209 (39), 208 (10), 89 (10), and 75 (base peak). Found: C, 64.92; H, 9.02; N, 3.22%. Calcd for $C_{23}H_{39}NO_6$: C, 64.91; H, 9.23; N, 3.29%.

Conversion of 10 to 11. Concentrated H_2SO_4 (0.75 ml) was added at 0 °C to a solution of **10** (0.463 g, 1.1 mmol) in MeOH (15 ml). After stirring at 0 °C for 0.5 h and refluxing for 24 h, the mixture was poured into CH_2Cl_2–ice water (60 ml/10 ml). After neutralized with solid $NaHCO_3$ to pH 7, the mixture was extracted with CH_2Cl_2 (30 ml×3). The combined extracts were dried ($MgSO_4$) and evaporated in vacuo. The residual oil (0.419 g) was chromatographed on silica gel (hexane–EtOAc, 4:1 v/v) to give dimethyl (2*R*,3*R*)-*N*-[(1*R*,4*R*)-2-bornanylidene]-3-(dimethoxymethyl)glutamate (**11**, 0.233 g, 56%): Colorless liquid; $[\alpha]_D^{22}$ =+70.13° (*c* 1.21, $CHCl_3$); ^{1}H NMR ($CDCl_3$) δ=0.76, 0.92, 0.96 (each 3H, each s, Me), 1.15—1.33 (2H, m, 2-bornanylidene), 1.64—1.73 (1H, m, 2-bornanylidene), 1.77—1.93 (3H, m, 2-bornanylidene), 2.30—2.39 (1H, m, 2-bornanylidene), 2.52 (1H, dd, J_{gem}=16.1 and J_{4-3}=6.6 Hz, one of H-4), 2.56 (1H, dd, J_{gem}=16.1 and J_{4-3}=5.5 Hz, the other of H-4), 3.05 (1H, m, H-3), 4.20 (1H, J_{2-3}=5.5 Hz, H-2), and 4.27 (1H, d, J_{CH-3}=7.3 Hz, 3-CH); ^{13}C NMR ($CDCl_3$) δ=11.39 (C-10′), 19.02 (C-8′), 19.40 (C-9′), 27.52 (C-5′), 31.22 (C-6′), 32.24 (C-3), 36.10, 40.65, 43.84 (C-3′, C-4, and C-4′), 47.47 (C-7′), 51.46, 51.83 (COOMe), 53.63 (C-1′), 54.22, 54.35 (each OMe), 63.38 (C-2), 105.04 (3-CH), 171.84, 173.51 (each COOMe), and 186.76 (C-2′); MS (75 eV) *m/z* (rel intensity, %) 383 (M^+, 10), 369 (20), 368 (base peak), 352 (28), 351 (24), 308 (33), 223 (54), 222 (20), and 75 (64). Found: C, 62.89; H, 8.36; N, 3.89%. Calcd for $C_{20}H_{33}NO_6$: C, 62.64; H, 8.67; N, 3.65%.

Conversion of 11 to (2*R*,3*R*)-(−)-6. To a solution of **11** (0.229 g, 0.6 mmol) in MeOH (20 ml) was added NH_2OH·HCl (0.166 g, 2.39 mmol). After refluxing for 24 h, another portion of NH_2OH·HCl (0.166 g, 2.39 mmol) was added and the mixture was refluxed for additional 24 h. The mixture was condensed to dryness in vacuo and the residual oil was triturated with CH_2Cl_2 (100 ml). The solid precipitated was filtered off and the filtrate was evaporated in vacuo. The residue (0.218 g) was chromatographed on silica gel (EtOAc–EtOH, 10:3 v/v) to give (2*R*,3*R*)-(−)-**6** (0.049 g, 38%). $[\alpha]_D^{24}$ =−40.8° (*c* 0.51, $CHCl_3$).

References

1) a) O. Tsuge, S. Kanemasa, and M. Yoshioka, *J. Org. Chem.*, **53**, 1384 (1988); b) D. A. Barr, R. Grigg, H. Q. N. Gunaratne, J. Kemp, P. McMeekin, and V. Sridharan, *Tetrahedron*, **44**, 557 (1988); c) S. Kanemasa, M. Yoshioka, and O. Tsuge, *Bull. Chem. Soc. Jpn.*, **62**, 869 (1989); c) S. Kanemasa, M. Yoshioka, and O. Tsuge, *ibid.*, **62**, 2196 (1989); d) D. A. Barr, R. Grigg, and V. Sridharan, *Tetrahedron Lett.*, **30**, 4727 (1989); e) S. Kanemasa, O. Uchida, E. Wada, and O. Tsuge, *Chem. Lett.*, **1990**, 105.

2) S. Kanemasa, O. Uchida, and E. Wada, *J. Org. Chem.*, **55**, 4411 (1990).

3) a) S. Kanemasa and H. Yamamoto, *Tetrahedron Lett.*, **31**, 3633 (1990); b) S. Kanemasa, H. Yamamoto, E. Wada, T. Sakurai, and K. Urushido, *Bull. Chem. Soc. Jpn.*, **63**, 2857 (1990); c) D.A. Barr, M. J. Dorrity, R. Grigg, J. F. Malone, J. Montgomery, S. Rajviroongit, and P. Stevenson, *Tetrahedron Lett.*, **31**, 6569 (1990); d) S. Kanemasa, T. Hayashi, J. Tanaka, H. Yamamoto, and T. Sakurai, *J. Org. Chem.*, **56**, 4473 (1991).

4) a) S. Kanemasa, A. Tatsukawa, E. Wada, and O. Tsuge, *Chem. Lett.*, **1989**, 1301; b) S. Kanemasa, A. Tatsukawa, and E. Wada, *J. Org. Chem.*, **56**, 2875 (1991).

5) A. E. Achqar, M. Boumzebra, M.-L. Roumestant, and

P. Viallefont, *Tetrahedron,* **44**, 5319 (1988).

6) Michael reaction of this acceptor molecule to Grignard reagents was previously reported (M. Asami and T. Mukaiyama, *Chem. Lett.,* **1979**, 569.

7) The crude mixture showed only one imine proton at δ=7.62 (^{1}H NMR).

8) Formation of three products was observed in the reaction at room temperature (**4**: δ=4.67 (H-3′), 7.62 (CH=N); side product **A**: 4.61 (H-3′), 7.65 (CH=N); side product **B**: 4.72 (H-3′), 7.69 (CH=N)). At −78 °C for 6.5 h, **4** was the only product. At −78 °C for 48 h, **4** was accompanied by a trace amount (less than 1%) of **A**. At room temperature for 1 h, **4**:**A**:**B** was 89:6:5 (by ^{1}H NMR). At room temperature for 57 h, **4**:**A**:**B** was 77:18:5 (by ^{1}H NMR).

9) Chromatographic purification of **4** through silica gel column resulted in the partial decomposition by hydrolysis of the C=N moiety.

10) Similar conversion of the perhydropyrrolo[1,2-*c*]imidazole chiral controller to a dimethoxymethyl group was reported in our previous papers (See Ref. 3b).

Catalytic Functions of Artificial Enzyme Composed of Simple Vitamin B_{12} Model and Synthetic Bilayer Membrane†

Yukito MURAKAMI,* Yoshio HISAEDA, Xi-Ming SONG, Sheng-Di FAN, and Teruhisa OHNO
Department of Organic Synthesis, Faculty of Engineering, Kyushu University,
Hakozaki, Higashi-ku, Fukuoka 812
(Received April 30, 1991)

An artificial enzyme was constructed with a combination of the single-walled vesicle of *N*,*N*-dihexadecyl-N^{α}-[6-(trimethylammonio)hexanoyl]-L-alaninamide bromide ($N^{+}C_5Ala2C_{16}$) and a simple vitamin B_{12} model; (11-hydroxyimino-4,10-dipropyl-5,9-diazatrideca-4,9-dien-3-one oximato)cobalt, [Co(C_2C_3)(DO)(DOH)pn], or [*N*-(2-hydroxyiminocyclohexylidene)-*N'*-(cyclohexyliden-2-one oximato)-1,3-diaminopropane]cobalt, [Co(ch)(DO)(DOH)pn]. Carbon-skeleton rearrangement reactions of alkyl ligands bound to the cobalt complex were markedly favored in the single-walled vesicle, relative to the reactions in methanol and benzene, under anaerobic photolysis conditions at ordinary temperatures. The cobalt complex incorporated into the intramembrane domain is subjected to significant repression of its molecular motion and to desolvation as confirmed by fluorescence and fluorescence polarization measurements. The 1,2-migration of cyano and carboxylic ester groups involved in the alkyl ligands is plausibly enhanced by such effects.

It is well known that metal ions play important roles as essential trace elements in biological systems. Metallocoenzymes involved in holoenzymes exhibit efficient catalyses only under specific micro-environments provided by the corresponding apoproteins. Vitamin B_{12}-dependent enzymes catalyze various isomerization reactions as formally given by Eq. 1.[1] The catalysis includes four carbon-skeleton rearrangements of reversible nature as follows;[2,3] methylmalonyl-SCoA⇌succinyl-SCoA, isobutyryl-SCoA⇌butyryl-SCoA, β-methylaspartate⇌glutamate, and methylitaconate⇌α-methyleneglutarate, as shown by Eqs. 2—5, respectively.

(1)

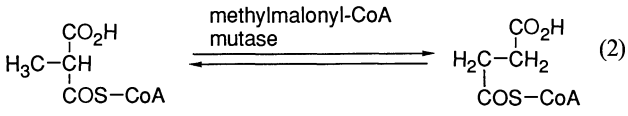

(2)

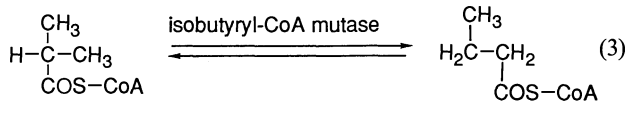

(3)

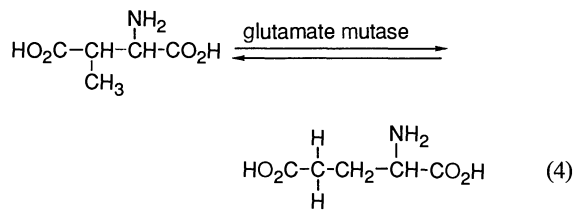

(4)

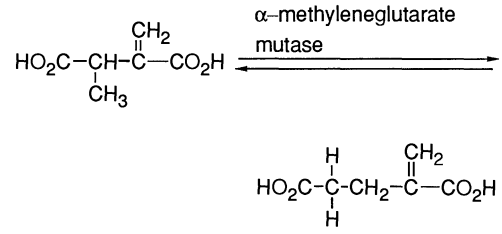

(5)

The naturally occurring apoproteins, which provide relevant reaction sites for vitamin B_{12}, are considered to play crucial roles in the molecular rearrangements.[4,5] In this regard, we have been interested in the catalytic activity of vitamin B_{12} in hydrophobic micro-environments to simulate the catalytic functions of the holoenzymes concerned. We have succeeded in constructing holoenzyme models,[6-8] as composed of a synthetic bilayer membrane and a hydrophobic vitamin B_{12} which has ester groups in place of the peripheral amide moieties of the naturally occurring vitamin B_{12}.[9-16] This finding prompted us to develop simple model complexes which are capable of catalyzing the carbon-skeleton rearrangements in similar bilayer membranes. We adopted Costa-type complexes with some modifications of the original one, [Co^{III}\{(C_2C_3)-

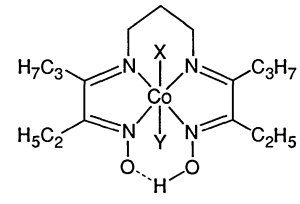

[Co^{III}\{(C_2C_3)(DO)(DOH)pn\}I_2] (**1**): X = Y = I

[Co^{III}\{(C_2C_3)(DO)(DOH)pn\}\{$CH_2C(CO_2C_2H_5)_2CH_3$\}Br] (**2**):
X = $CH_2C(CO_2C_2H_5)_2CH_3$, Y = Br

[Co^{III}\{(C_2C_3)(DO)(DOH)pn\}\{$CH_2C(CO_2C_2H_5)(CN)CH_3$\}Br] (**3**):
X = $CH_2C(CO_2C_2H_5)(CN)CH_3$, Y = Br

† Contribution No. 941 from this Department. Preliminary communication; see Ref. 31.

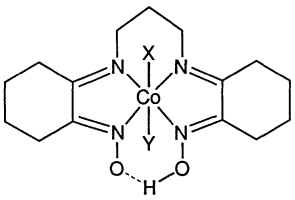

$[Co^{III}\{(ch)(DO)(DOH)pn\}Br_2]$ (**4**): X = Y = Br

$[Co^{III}\{(ch)(DO)(DOH)pn\}I_2]$ (**5**): X = Y = I

$[Co^{III}\{(ch)(DO)(DOH)pn\}\{CH_2C(CO_2C_2H_5)_2CH_3\}Br]$ (**6**):
X = $CH_2C(CO_2C_2H_5)_2CH_3$, Y = Br

(DO)(DOH)pn}(XY)] and $\{Co^{III}\{(ch)(DO)(DOH)pn\}$-(XY)] (refer to **1**—**6**), since these complexes show redox behavior analogous to that of vitamin B_{12} with respect to the nuclear cobalt.[17-19] A single-walled bilayer membrane composed of a synthetic peptide lipid is quite effective as an apoprotein model.[20-23] On these grounds, we report here the carbon-skeleton rearrangements of alkyl ligands coordinated to the vitamin B_{12} model complexes in the $N^+C_5Ala2C_{16}$ vesicle.

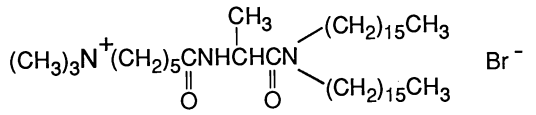

$N^+C_5Ala2C_{16}$

Experimental

General Analyses and Measurements. Elemental analyses were performed at the Microanalysis Center of Kyushu University. IR spectra were taken on a JASCO IR-810 infrared spectrophotometer, while electronic absorption spectra were recorded on a Hitachi 220A or a Hitachi 340 spectrophotometer. ^1H NMR spectra were taken on a Hitachi R-24B, a Bruker AC-250P, and a Bruker AMX-500 spectrometer installed at the Advanced Instrumental Analysis Center of Kyushu University. Assignments of NMR signals for the cobalt complexes were performed by means of the 2D-NMR technique (H–H COSY). Fluorescence spectra were obtained with a Hitachi 650-60 spectrophotometer, and fluorescence polarization measurements were performed with a Union Giken FS-501A fluorescence polarization spectrophotometer equipped with a Union Giken System-77 computer; emission at 530 nm was monitored upon excitation at 340 nm with a slit width of 3.5 nm for both excitation and emission sides. Fluorescence polarization (*P*) was calculated according to a previous method.[24,25] GLC analyses were carried out on a Shimadzu GC-9A apparatus equipped with a Shimadzu C-R3A-FFC chromatopac for data processing.

Materials. Diiodo(11-hydroxyimino-4,10-dipropyl-5,9-diazatrideca-4,9-dien-3-one oximato)cobalt(III), $[Co^{III}\{(C_2C_3)(DO)(DOH)pn\}I_2]$ (**1**), and its alkylated complexes (**2** and **3**), were prepared by methods identical with those reported previously.[26] *N*,*N*-Bis(2-hydroxyiminocyclohexylidene)propane-1,3-diamine, $(ch)(DOH)_2pn$, and its cobalt complexes with various axial ligands (**4**, **5**, and **6**) were prepared by referring to reported procedures[18,27-29] along with some modifications as shown in Scheme 1. An artificial lipid, *N*,*N*-dihexadecyl-N^{α}-[6-(trimethylammonio)hexanoyl]-L-alaninamide bromide ($N^+C_5Ala2C_{16}$), was prepared after a reported procedure.[20,21] Preparation of a fluorescent probe, *N*-[5-(dimethylamino)-1-naphthylsulfonyl]-2-(4-imidazolyl)-ethylamine (dansylhistamine), was described elsewhere.[14] Alkyl

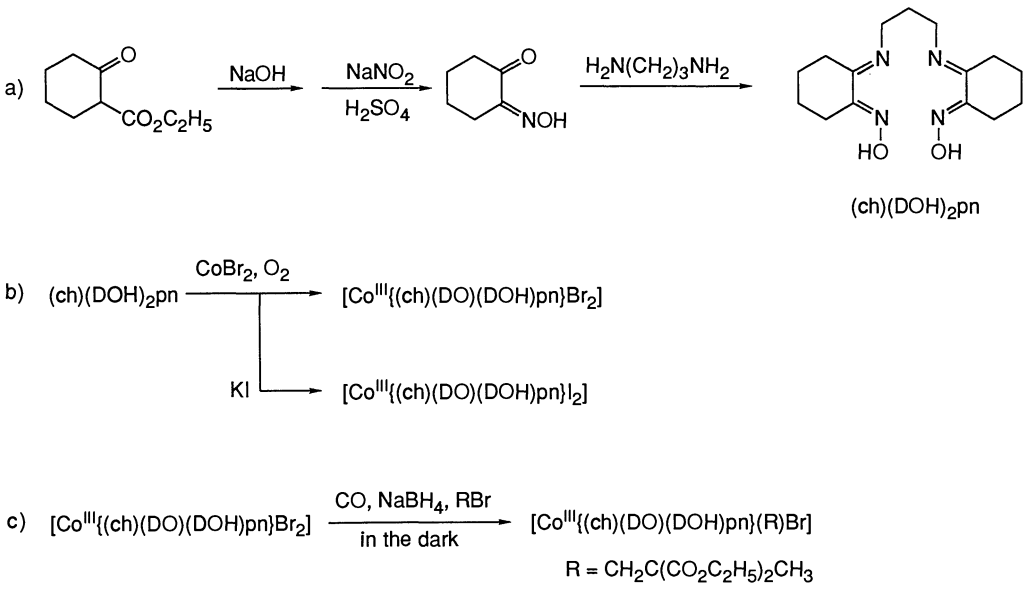

Scheme 1.

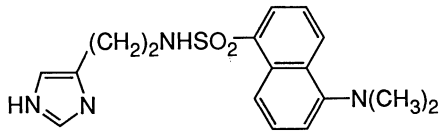

dansylhistamine

halides, diethyl 2-bromomethyl-2-methylmalonate and ethyl 3-bromo-2-cyano-2-methylpropanoate, and authentic samples of the corresponding products such as diethyl 2,2-dimethylmalonate (**A**), diethyl 2-methylsuccinate (**B**), ethyl 2-cyano-2-methylpropanoate (**C**), ethyl 3-cyanobutyrate (**D**), and ethyl 3-cyano-2-methylpropanoate (**E**) were prepared according to literature methods[13] and confirmed to be sufficiently pure by ^{1}H NMR and GLC.

***N*,*N*′-Bis(2-hydroxyiminocyclohexylidene)propane-1,3-diamine, (ch)(DOH)$_2$pn.** This ligand was synthesized by the condensation of 1,2-cyclohexanedione monooxime (15.8 g, 0.12 mol), which was prepared from ethyl 2-oxocyclohexanecarboxylate and sodium nitrite,[30] with 1,3-diaminopropane (5.20 g, 0.07 mol): Yield 12.5 g (71.0%), mp 50—51 °C; IR (KBr) 3300 (OH), 1640 (C=N), 970 (N–O) cm^{-1}; 60 MHz ^{1}H NMR ($CDCl_3$, TMS) δ=1.75 (8H, m, $ONCCH_2C\underline{H_2}C\underline{H_2}$-$CH_2$), 2.10 (2H, m, $NCH_2C\underline{H_2}CH_2N$), 2.55 (4H, t, J=6.1 Hz, $ONCCH_2CH_2CH_2C\underline{H_2}$), 2.92 (4H, t, J=6.1 Hz, $ONCC\underline{H_2}$-$CH_2CH_2CH_2$), 4.91 (4H, t, J=4.5 Hz, $NC\underline{H_2}CH_2C\underline{H_2}N$), 7.20 (2H, br s, OH). Found: C, 59.51; H, 8.24; N, 19.28%. Calcd for $C_{15}H_{24}N_4O_2$: C, 59.62; H, 8.27; N, 19.17%.

Dibromo[*N*-(2-hydroxyiminocyclohexylidene)-*N*′-(cyclohexyliden-2-one oximato)-1,3-diaminopropane]cobalt(III), [Co^{III}{(ch)(DO)(DOH)pn}Br$_2$] (4). An acetone solution (5 mL) of (ch)(DOH)$_2$pn (1.46 g, 5.0×10^{-3} mol) was added dropwise to an aqueous solution (150 ml) of cobalt dibromide hexahydrate (2.0 g, 6.0×10^{-3} mol) while air was bubbled through the latter aqueous solution. After the reaction mixture was stirred for 4 h, precipitates were recovered by filtration and washed with water. The resulting cobalt complex was recrystallized from acetone–water (1:1 v/v) to afford green needles: yield 1.66 g (65%), mp 251—252 °C; IR (KBr) 720 (Co–N) cm^{-1}; 500 MHz ^{1}H NMR ($CDCl_3$, TMS) δ=1.86 (4H, m, $ONCCH_2C\underline{H_2}CH_2CH_2$), 1.90 (4H, m, $ONCCH_2CH_2C\underline{H_2}CH_2$), 2.59 (2H, m, $NCH_2C\underline{H_2}CH_2N$), 3.01 (4H, t, J=6.16 Hz, $ONCCH_2CH_2CH_2C\underline{H_2}$), 3.21 (4H, t, J=6.46 Hz, $ONCC\underline{H_2}CH_2CH_2CH_2$), 4.07 (4H, t, J=4.52 Hz, $NC\underline{H_2}CH_2C\underline{H_2}N$), 19.0 (1H, s, OH). Found: C, 35.36; H, 4.54; N, 10.92%. Calcd for $C_{15}H_{23}Br_2CoN_4O_2$: C, 35.32; H, 4.54; N, 10.99%.

Diiodo[*N*-(2-hydroxyiminocyclohexylidene)-*N*′-(cyclohexyliden-2-one oximato)-1,3-diaminopropane]cobalt(III), [Co^{III}{(ch)(DO)(DOH)pn}I$_2$] (5). This complex was prepared in the presence of a large excess of potassium iodide by the method employed for the preparation of **4**. The crude product was purified by column chromatography on silica gel (Wakogel C-100) with benzene–acetone (4:1 v/v) as eluant to give dark green powder: Yield 61%, mp 262—263 °C; λ_{max} (CH_2Cl_2) 340 (ϵ 1.15×10^4), 462 nm (6.27×10^3); IR (KBr) 720 (Co–N) cm^{-1}; 500 MHz ^{1}H NMR ($CDCl_3$, TMS) δ=1.83 (4H, m, $ONCCH_2C\underline{H_2}CH_2CH_2$), 1.85 (4H, m, $ONCCH_2CH_2$-$C\underline{H_2}CH_2$), 2.63 (2H, br s, $NCH_2C\underline{H_2}CH_2N$), 2.94 (4H, t, J=6.09 Hz, $ONCCH_2CH_2CH_2C\underline{H_2}$), 3.18 (4H, t, J=6.45 Hz, $ONCC\underline{H_2}CH_2CH_2CH_2$), 4.10 (4H, br s, $NC\underline{H_2}CH_2C\underline{H_2}N$), 19.0 (1H, s, OH). Found: C, 29.94; H, 3.93; N, 9.50%. Calcd for $C_{15}H_{23}I_2CoN_4O_2$: C, 29.82; H, 3.85; N, 9.28%.

Bromo{2,2-bis(ethoxycarbonyl)propyl}[*N*-(2-hydroxyiminocyclohexylidene)-*N*′-(cyclohexyliden-2-one oximato)-1,3-diaminopropane]cobalt(III), [Co^{III}{(ch)(DO)(DOH)pn}-{$CH_2C(CO_2C_2H_5)_2CH_3$}Br] (6). A methanol solution (300 mL) containg **4** (400 mg, 7.8×10^{-4} mol) and diethyl 2-bromomethyl-2-methylmalonate (800 mg, 3.0×10^{-3} mol) was stirred while carbon monoxide was introduced into it until saturation was attained. After being stirred for 1 h, the solution turned pale yellow, indicating formation of the Co^{II} complex. Sodium tetrahydroborate in methanol was added dropwise to the resulting solution until the solution turned deep blue under carbon monoxide atmosphere. The solution changed its color to reddish orange, after it was refluxed for 4 h in the dark. The solution was evaporated to dryness, a solid material insoluble in dichloromethane (15 mL) was removed by filtration, and then the dichloromethane solution was concentrated to ca. 3 mL. Hexane (50 mL) was added to the resulting solution, and precipitates were recovered by filtration and purified by gel-filtration chromatography on a column of Sephadex LH-20 with methanol as eluant to give reddish brown powder: Yield 262 mg (55%); IR (KBr) 1725 (C=O) cm^{-1}; λ_{max} (CH_3OH) 475 nm. Found: C, 46.03; H, 6.23; N, 8.91%. Calcd for $C_{24}H_{38}BrCoN_4O_6\cdot1/2H_2O$: C, 46.02; H, 6.28; N, 8.94%.

Equilibrium Measurements for Incorporation of Vitamin B$_{12}$ Model Complexes into Single-Compartment Vesicles. A dichloromethane solution (1 mL) containing $N^+C_5Ala2C_{16}$ (1.0×10^{-5} mol) and a cobalt complex (2.0×10^{-7} mol), [Co^{III}-{(C_2C_3)(DO)(DOH)pn}I$_2$] or [Co^{III}{(ch)(DO)(DOH)pn}I$_2$], was evaporated in vacuo to remove the solvent completely, and an aqueous potassium iodide solution (1 mL, 5.0×10^{-4} mol dm^{-3}) was added to the residue. The resulting mixture was sonicated for 30 s with a probe-type sonicator at 30 W to give a clear solution. An extent of incorporation of the cobalt complex into the single-walled vesicle was examined by gel-filtration chromatography on a column of Sephadex G-50 with an aqueous potassium iodide solution (5.0×10^{-4} mol dm^{-3}) as eluant. The bound complex was eluted first in the column void volume, and the free complex was followed as the second fraction with a retention time close to the bed volume. An amount of the incorporated complex was determined by electronic spectroscopy. As for complexes with the cobalt–carbon bond, [Co^{III}{(C_2C_3)(DO)(DOH)pn}{$CH_2C(CO_2C_2H_5)_2$-CH_3}Br] and [Co^{III}{(ch)(DO)(DOH)pn}{$CH_2C(CO_2C_2H_5)_2$-CH_3}Br], a methanol solution (10 μL) of each complex was injected into the vesicular solution which was prepared in a manner as stated above, so that any cleavage of the cobalt–carbon bond caused by sonication was avoided.

Photolysis and Product Analyses. $N^+C_5Ala2C_{16}$ (5.0×10^{-5} mol) was dispersed in aqueous potassium bromide (10 mL, 5.0×10^{-4} mol dm^{-3}) by Vortex mixing, and the dispersion sample was then sonicated for 2 min with a probe-type sonicator at 30 W to give a clear solution of single-walled vesicles. A methanol solution (10 μL) of the alkylated complex (5.0×10^{-7} mol), [Co^{III}{(C_2C_3)(DO)(DOH)pn}RBr] or [Co^{III}{(ch)(DO)(DOH)pn}RBr], was added to the vesicular solution. Then, the resulting solution was irradiated with a 500 W tungsten lamp at a distance of 30 cm and at an appropriate temperature. After the alkylated complex was

completely decomposed as confirmed by electronic spectroscopy, the products were extracted with dichloromethane (10 mL×3) and analyzed by GLC. Reaction products were identified by coinjection of the corresponding authentic samples into columns of Silicone DC-550 (Shimadzu Co.) and Silicone SE-30 (Gasukuro Kogyo Inc.) as described previously in detail.[8] A capillary column of Polyethylene Glycol-20M (Gasukuro Kogyo) was used for identification of isomers having similar structures. Each product separated by preparative GLC on Silicone DC-550 was identified by means of ^{1}H NMR spectroscopy. As for reactions in methanol and benzene, a reaction mixture was evaporated to dryness in vacuo before dichloromethane was added. Total yields listed in Tables 1—3 are less than 100% owing to losses during extraction and evaporation treatments in vacuo. However, we confirmed that no other by-productus were obtained.

Results and Discussion

Incorporation of Vitamin B_{12} Model Complexes into Single-Compartment Vesicles. Complexes **1**, **2**, **5**, and **6** were incorporated into the $N^+C_5Ala2C_{16}$ vesicle to the extents of 82—90, 55—60, 16—20, and 54—56% of their total amounts in molar fraction, respectively.[31] The amounts of the complexes incorporated into the vesicle were little affected by temperature change in the range of 5—50 °C. The extents of solubility of these complexes in water were found as follows: **1**, 1.1×10^{-4} mol dm^{-3}; **2**, 2.0×10^{-4} mol dm^{-3}; **5**, 3.1×10^{-4} mol dm^{-3}; **6**, 8.1×10^{-4} mol dm^{-3}. We have already found that the extent of incorporation of hydrophobic vitamin B_{12} derivatives into the $N^+C_5Ala2C_{16}$ vesicle is primarily controlled by the hydrophobicity of the complexes.[8] In other words, the incorporation of those complexes into the vesicle becomes increasingly favored as those become less soluble in aqueous media. However, the solubility parameter alone can not provide a reasonable explanation for the incorporation behavior of the present complexes. The incorporation behavior seems to depend on various factors, such as size, dipolar property, and hydrophobicity of the complex, which give out different modes of interactions with the membrane.

Table 1. Product Analyses for Photolysis of **2** in Various Media[a]

Medium[b]	Temp[c]/°C	Yield[d]/%		B/A[e]
		A	B	
CH_3OH	20.0	74—77	8—11	0.13
C_6H_6	20.0	76—80	5—9	0.09
$N^+C_5Ala2C_{16}$ vesicle	5.0	41—44	46—50	1.13
	20.0	48—51	39—42	0.82
	50.0	54—59	31—33	0.57

a) A solution containing **2** (5.0×10^{-5} mol dm^{-3}) was irradiated with a 500 W tungsten lamp at a distance of 30 cm for 4 h. b) $N^+C_5Ala2C_{16}$ (5.0×10^{-3} mol dm^{-3}) in aqueous potassium bromide (5.0×10^{-4} mol dm^{-3}). c) Accuracy, ±0.1 °C. d) Products were analyzed by GLC. e) Ratio of the rearrangement product.

Product Analyses for Photolysis of Alkylated Complexes in Various Media. The cobalt–carbon bond involved in alkylated complexes **2** and **6** was cleaved in the vesicular solution upon irradiation with visible light as reported previously.[31] Likewise, **3** underwent the photolytic cleavage. After the alkylated complex was completely decomposed as confirmed by electronic spectroscopy, the products were analyzed by GLC. Product analyses for the photolysis of alkylated complexes **2** and **3** in various media are summarized in Tables 1 and 2. We identified the products, which were obtained by the photolysis reaction of complex **2**, as diethyl 2,2-dimethylmalonate (**A**, the simple hydrogenated product without rearrangement) and diethyl 2-methylsuccinate (**B**, the rearrangement product) (refer to Eq. 6). As for complex **3**, ethyl 2-cyano-2-methylpropanoate (**C**, the simple hydrogenated product), ethyl 3-cyanobutyrate (**D**, the ester-migrated product), and ethyl 3-cyano-2-methylpropanoate (**E**, the cyano-migrated product) were confirmed to be obtained (refer to Eq. 7).

The following findings are based on the product analyses. (i) The major products are the unrearranged ones in benzene and methanol, but the rearrangement products are largely obtained in the vesicular solution. Consequently, the carbon-skeleton rearrangement is

Table 2. Product Analyses for Photolysis of **3** in Various Media[a]

Medium[b]	Temp[c]/°C	Yield[d]/%			(D+E)/C[e]
		C	D	E	
CH_3OH	5.0	80—85	0	0	0
	20.0	80—85	0	0	0
	50.0	80—85	0	0	0
C_6H_6	5.0	80—85	0	0	0
	20.0	80—85	0	0	0
	50.0	80—85	0	0	0
$N^+C_5Ala2C_{16}$ vesicle	5.0	42—45	21—24	14—16	0.86
	20.0	47—50	19—22	12—15	0.70
	50.0	52—56	16—20	10—14	0.56

a) A solution containing **3** (5.0×10^{-5} mol dm^{-3}) was irradiated with a 500 W tungsten lamp at a distance of 30 cm for 4 h. b) $N^+C_5Ala2C_{16}$ (5.0×10^{-3} mol dm^{-3}) in aqueous potassium bromide (5.0×10^{-4} mol dm^{-3}). c) Accuracy, ±0.1 °C. d) Products were analyzed by GLC. e) Ratio of the rearrangement products.

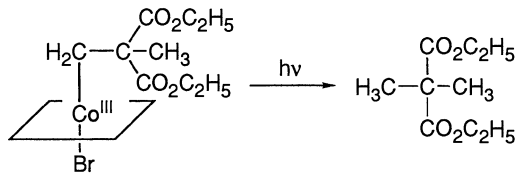

2 or 6 A

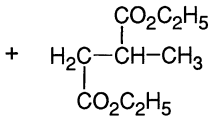

B (6)

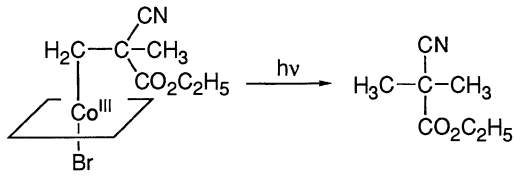

3 C

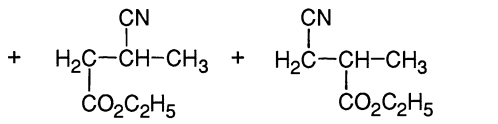

D E (7)

much enhanced in the vesicle relative to the reaction in homogeneous solutions. (ii) The product ratio **B**/**A** for complex **2** in the vesicular solution is quite large as compared with the one for the corresponding hydrophobic vitamin B_{12} (**B**/**A**=0.12).[8] The photolysis must cause the homolytic cleavage of the cobalt–carbon bond in the initial stage.[32] The radical mechanism was assigned to the carbon-skeleton rearrangement of hydrophobic vitamin B_{12} derivatives which do not hold an anionic ligand trans to the substituted alkyl moiety. However, the ester group migrates more readily via formation of an anionic intermediate relative to the reaction via formation of a radical intermediate even in the vesicle.[33] Therefore, the bromide ion coordinated to the cobalt atom at the axial site seems to take a role in inducing the heterolytic cleavage of the cobalt–carbon bond involved in the model complex so that an anionic intermediate is produced, as caused by one-electron transfer immediately after the homolytic cobalt–carbon cleavage. (iii) The product ratios of the rearranged ones, **B**/**A** and (**D**+**E**)/**C**, increase in the vesicle along with temperature decrease as shown in Tables 1 and 2. Since the single-walled $N^+C_5Ala2C_{16}$ vesicle was found to show a broad phase transition from the gel to the liquid-crystalline state at 20±5 °C by differential scanning calorimetry,[21] the synthetic bilayer membrane favors formation of the rearrangement product in the gel state. A similar result was obtained for complex **6** bearing cyclohexane moieties in the ligand portion, as is apparent from the data in Table 3.

Table 3. Product Analyses for Photolysis of **6** in Various Media[a]

Medium[b]	Temp[c]/°C	Yield[d]/%		B/A[e]
		A	B	
CH_3OH	20.0	75—79	7—9	0.10
C_6H_6	20.0	81—87	0—3	0.02
$N^+C_5Ala2C_{16}$ vesicle	5.0	49—54	31—35	0.64
	20.0	59—63	21—25	0.38
	50.0	76—80	5—9	0.09

a) A solution containing **6** (5.0×10^{-5} mol dm^{-3}) was irradiated with a 500 W tungsten lamp at a distance of 30 cm for 4 h. b) $N^+C_5Ala2C_{16}$ (5.0×10^{-3} mol dm^{-3}) in aqueous potassium bromide (5.0×10^{-4} mol dm^{-3}). c) Accuracy, ±0.1 °C. d) Products were analyzed by GLC. e) Ratio of the rearrangement product.

Microenvironment around Vitamin B_{12} Model Complexes in Single-Compartment Vesicle. In order to understand microenvironmental properties experienced by the vitamin B_{12} model complexes in the vesicle, the cobalt complex coordinated at the axial site with dansylhistamine as a fluorescent probe was adopted. The axial ligation constants (K) for [Co^{III}\{(C_2C_3)(DO)(DOH)pn\}Br_2] and [Co^{III}\{(ch)(DO)(DOH)pn\}I_2] with dansylhistamine were determined by electronic spectroscopy after a reported procedure:[9] log K=5.2 and 5.0 in methanol, and 5.3 and 5.2 in benzene, respectively. These data indicate that the metal complexes are largely coordinated with dansylhistamine under the present experimental conditions. The microscopic polarity experienced by the dansyl moiety bound to the vitamin B_{12} model complex is reflected in its fluorescence maximum.[34] In order to obtain the reference data, the fluorescence maxima of dansylhistamine coordinated to the vitamin B_{12} model complexes were measured in various mixtures of water and dioxane as shown in Fig. 1. The fluorescence maximum is shifted to lower wavelength as the solvent polarity decreases. It is clear that the single-walled vesicle of $N^+C_5Ala2C_{16}$ provides a microenvironment for the dansyl moiety that is equivalent to a medium polarity between those of methanol and ethanol. These values are comparable to that obtained for a hydrophobic vitamin B_{12}.[8] The result leads us to conclude that an axial ligand bound to the complex is significantly desolvated in the vesicle.

The microscopic viscosity experienced by the dansyl moiety bound to the vitamin B_{12} model was examined by means of fluorescence polarization (P) measurements. P values for the dansylhistamine-coordinated vitamin B_{12} models in methanol and benzene are 0.004—0.005 and 0.009—0.02, respectively, in the temperature

range 5—50 °C. On the other hand, the identical complexes gave large *P* values in the vesicular solution as shown in Fig. 2. This apparently indicates that the molecular motion of the guest molecules in the vesicle is markedly suppressed.[35] Thus, the microenvironmental effect provided by the vesicle is quite different from those given by simple organic solvents which solubilize the vitamin B_{12} models homogeneously.

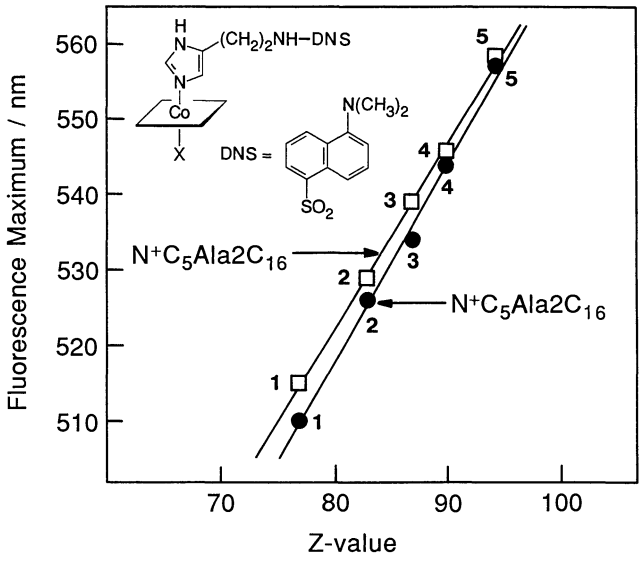

Fig. 1. Medium effect on fluorescence of dansylhistamine (1.0×10^{-5} mol dm^{-3}) coordinated to [Co^{III}{(ch)(DO)(DOH)pn}I] (□, X=I; 1.0×10^{-5} mol dm^{-3}) and [Co^{III}{(C_2C_3)(DO)pn}Br] (●, X=Br; 1.0×10^{-5} mol dm^{-3}), both complexes being incorporated into the $N^+C_5Ala2C_{16}$ (5.0×10^{-3} mol dm^{-3}) vesicle in phosphate–borate buffer (0.05 mol dm^{-3}; pH 9.2) at 20.0±0.1°C. Reference data obtained in water-dioxane at the following ratios (v/v): 1, 1:9; 2, 3:7; 3, 1:1; 4, 7:3; 5, 1:0. The Z-value refers to Kosower's parameter.

The present study demonstrates that a vitamin B_{12}-dependent artificial holoenzyme can be prepared by utilizing a synthetic bilayer membrane and a simple vitamin B_{12} model complex. It is clear that the carbon-skeleton rearrangement of an alkyl ligand coordinated to the simple vitamin B_{12} model takes place much favorably in the vesicular phase. This 1,2-migration must arise from both repression of molecular motion and desolvation effects operating on the alkylated complex in the vesicle, in a manner as observed by utilizing a hydrophobic vitamin B_{12}.[8]

The present work was supported by a Grant-in-Aid for Scientific Research on Priority Area No. 01649513 from the Ministry of Education, Science and Culture.

References

1) B. T. Golding and D. N. Rao, "Adenosylcobalamin-dependent Enzymic Reaction," in "Enzyme Mechanisms," ed by M. I. Page and A. Williams, The Royal Society of Chemistry, London (1987), pp. 404—428.

2) J. M. Pratt, "Coordination Chemistry of the B_{12} Dependent Isomerase Reactions," in "B_{12}," ed by D. Dolphin, John Wiley, New York (1982), Vol. 1, pp. 325—392.

3) J. Rétey, *Angew. Chem., Int. Ed. Engl.*, **29**, 355 (1990); G. Brendelberger, J. Rétey, D. M. Ashworth, K. Reynolds, F. Willenbrock, and J. A. Robinson, *Angew. Chem., Int. Ed. Engl.*, **27**, 1089 (1988).

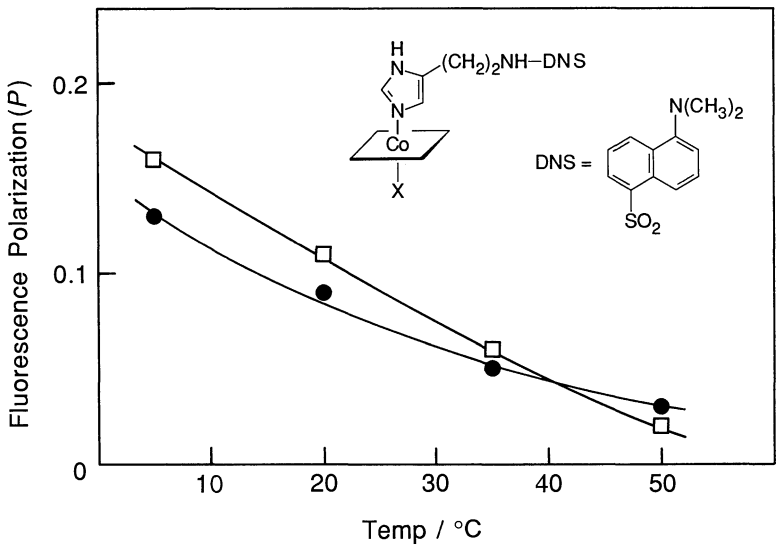

Fig. 2. Temperature effect on fluorescence polarization (*P*) of dansylhistamine (1.0×10^{-5} mol dm^{-3}) coordinated to [Co^{III}{(ch)(DO)(DOH)pn}I] (□, X=I; 1.0×10^{-5} mol dm^{-3}) and [Co^{III}{(C_2C_3)(DO)(DOH)pn}Br] (●, X=Br; 1.0×10^{-5} mol dm^{-3}), both complexes being incorporated into the $N^+C_5Ala2C_{16}$ (5.0×10^{-3} mol dm^{-3}) vesicle in phosphate–borate buffer (0.05 mol dm^{-3}; pH 9.2).

4) J. M. Pratt, *Chem. Soc. Rev.*, **14**, 161 (1985).
5) R. G. Finke, D. A. Schiraldi, and B. J. Mayer, *Coord. Chem. Rev.*, **54**, 1 (1984).
6) Y. Murakami, Y. Hisaeda, T. Ohno, and Y. Matsuda, *Chem. Lett.*, **1988**, 621.
7) Y. Murakami, Y. Hisaeda, and T. Ohno, *J. Chem. Soc., Chem. Commun.*, **1988**, 856.
8) Y. Murakami, Y. Hisaeda, and T. Ohno, *J. Chem. Soc., Perkin Trans. 2*, **1991**, 405.
9) Y. Murakami, Y. Hisaeda, and A. Kajihara, *Bull. Chem. Soc. Jpn.*, **56**, 3642 (1983).
10) Y. Murakami, Y. Hisaeda, A. Kajihara, and T. Ohno, *Bull. Chem. Soc. Jpn.*, **57**, 405 (1984).
11) Y. Murakami, Y. Hisaeda, and T. Ohno, *Bull. Chem. Soc. Jpn.*, **57**, 2091 (1984).
12) Y. Murakami and Y. Hisaeda, *Bull. Chem. Soc. Jpn.*, **58**, 2652 (1985).
13) Y. Murakami, Y. Hisaeda, T. Ozaki, T. Tashiro T. Ohno, Y. Tani, and Y. Matsuda, *Bull. Chem. Soc. Jpn.*, **60**, 311 (1987).
14) Y. Murakami, Y. Hisaeda, J. Kikuchi, T. Ohno, M. Suzuki, Y. Matsuda, and T. Matsuura, *J. Chem. Soc., Perkin Trans. 2*, **1988**, 1237.
15) Y. Murakami, Y. Hisaeda, and T. Ohno, *J. Coord. Chem.*, **21**, 13 (1990).
16) Y. Murakami, Y. Hisaeda, and T. Ohno, *Bioorg. Chem.*, **18**, 49 (1990).
17) G. Costa, *Coord. Chem. Rev.*, **8**, 63 (1972).
18) C. M. Elliott, H. Hershenhart, R. G. Finke, and B. L. Smith, *J. Am. Chem. Soc.*, **103**, 5558 (1981).
19) Y. Murakami, Y. Hisaeda, S.-D. Fan, and Y. Matsuda, *Bull. Chem. Soc. Jpn.*, **62**, 2219 (1989).
20) Y. Murakami, A. Nakano, and H. Ikeda, *J. Org. Chem.*, **47**, 3137 (1982).
21) Y. Murakami, A. Nakano, A. Yoshimatsu, K. Uchitomi, and Y. Matsuda, *J. Am. Chem. Soc.*, **106**, 3613 (1984).
22) Y. Murakami, J. Kikuchi, T. Takaki, K. Uchimura, and A. Nakano, *J. Am. Chem. Soc.*, **107**, 2161 (1985).
23) Y. Murakami, A. Nakano, and K. Akiyoshi, *Bull. Chem. Soc. Jpn.*, **55**, 3004 (1982).
24) Y. Murakami, J. Kikuchi, M. Suzuki, and T. Takaki, *Chem. Lett.*, **1984**, 2139.
25) Y. Murakami, J. Kikuchi, K. Nishida, and A. Nakano, *Bull. Chem. Soc. Jpn.*, **57**, 1371 (1984).
26) Y. Murakami, Y. Hisaeda, S.-D. Fan, and Y. Matsuda, *Bull. Chem. Soc. Jpn.*, **62**, 2219 (1989).
27) G. Costa, G. Mestroni, and E. de Savorgnani, *Inorg. Chim. Acta*, **3**, 323 (1969).
28) G. Costa, G. Mestroni, G. Pellizer, G. Tauzher, and T. Licari, *Inorg. Nucl. Chem. Lett.*, **5**, 515 (1969).
29) G. Costa, G. Mestroni, and G. Tauzher, *J. Chem. Soc., Dalton Trans.*, **1972**, 450.
30) A. F. Ferris, *J. Org. Chem.*, **24**, 1726 (1959).
31) Y. Murakami, Y. Hisaeda, X.-M. Song, and S.-D. Fan, *Chem. Lett.*, **1989**, 877.
32) Y. Murakami, Y. Hisaeda, T. Ozaki, and T. Ohno, *Chem. Lett.*, **1985**, 1711.
33) Y. Murakami, Y. Hisaeda, T. Ozaki, T. Ohno, S.-D. Fan, and Y. Matsuda, *Chem. Lett.*, **1988**, 839.
34) C. J. Seliskar and L. Brand, *J. Am. Chem. Soc.*, **93**, 5414 (1971).
35) G. Weber, *Adv. Protein Chem.*, **8**, 415 (1953).

Flash Photolytic Generation of a Dithio Carbocation from 1,3-Dithiolane Derivatives and Its Reaction with Nucleophiles[1)]

Tadashi OKUYAMA,* Naoki HAGA, Shin-ya TAKANE, Kenji UENO, and Takayuki FUENO
Faculty of Engineering Science, Osaka University, Toyonaka, Osaka 560
(Received May 15, 1991)

2-Phenyl-1,3-dithiolanylium ion is generated as a transient intermediate by flash photolysis of aqueous ethanol and acetonitrile solutions of 2-methoxy and other dithiolane derivatives with a xenon lamp. Decay of the absorption (342 nm) of the cation generated from the 2-methoxy derivative follows pseudo-first-order kinetics. Rate constants were measured for the reaction of the cation with various nucleophiles. Decay curves for the cations generated from 2-arylthio and 2-sulfonyl derivatives are steep and show second-order kinetic character owing to the recombination of the cation with the counter anions (thiolate and sulfinate).

Sulfur-stabilized carbocations are intermediates for acid-catalyzed reactions of ortho thioesters and thioacetals and their stability and reactivity have attracted considerable interest in relation to those of oxygen analogs.[2)] Dithio carbocations are stable enough to be isolated as salts.[3-7)] Chemistry of the isolated salts has been examined.[2,8)]

Ogura[9)] found that 1-(methylthio)alkyl aryl sulfones are easily hydrolyzed by photoirradiation of the aqueous solution. Thio carbocations are assumed as intermediates for this photosolvolysis.

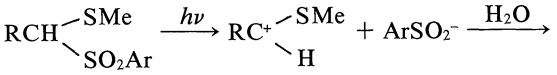

$$RCH(SMe)(SO_2Ar) \xrightarrow{h\nu} RC^+(SMe)(H) + ArSO_2^- \xrightarrow{H_2O} RCHO + MeSH + ArSO_2H \quad (1)$$

This report suggested us that thio carbocations can be photochemically generated from appropriate precursors. This may provide us good means for examination of rapid reactions of the cations in ground state by using a flash-photolytic technique. We thus considered that, if a nucleofugal group of the precursor sould be a main chromophore for the photolysis, the excited nucleofuge could be efficiently released to leave a ground-state carbocation. For such precursors for dithio carbocations, we have first chosen 2-(*p*-tolylsulfonyl)-1,3-dithiolanes, **1a** and **1b**.

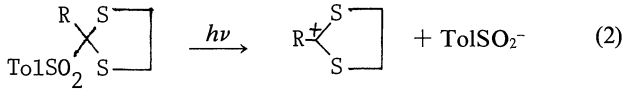

1a, R=H
1b, R=Ph
Tol=*p*-$CH_3C_6H_4$

Irradiation of alcoholic solutions of the sulfone derivatives **1** with a low-pressure Hg lamp gave 2-alkoxy derivatives in high yields. Flash photolysis of aqueous solutions of **1** showed formation of the dithiolanylium ion **2**. However, because of high nucleophilicity of the accompanying sulfinate ion, kinetics of decay of the cation **2** was complicated. A 2-arylthio derivative also behaved similarly.

A 2-alkoxy derivative **3b** was later found to give the carbocation **2b** on irradiation in spite of the non-light-absorbing nucleofugal group.[1,10)]

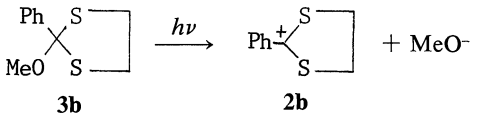

3b **2b**

Triarylcarbenium ions can be generated by photolysis of various precursors with a nucleofuge such as cyanide,[11,12)] hydroxide,[11,13-16)] acetate,[17,18)] and phenoxide ion.[17,18)] Nonabsorbing nucleofuges can be liberated by photolysis of suitable precursors. McClelland and co-workers[14,17-19)] have extensively studied reactivities of these carbocations by flash photolysis. Reaction of 2-phenyl-1,3-dithiolan-2-ylium ion **2b** generated from **3b** with some nucleophiles is a main subject in the present paper but photolysis of other precursors **1** is also presented.

Results and Discussion

Photolysis was carried out with a xenon lamp usually in 1:1 (v/v) ethanol–water and 1:1 (v/v) acetonitrile–water solutions. On flash irradiation of **3b**, the spectrum with a maximum absorption at 342 nm develops instantaneously and disappears slowly. The spectra of the transient intermediate were recorded with

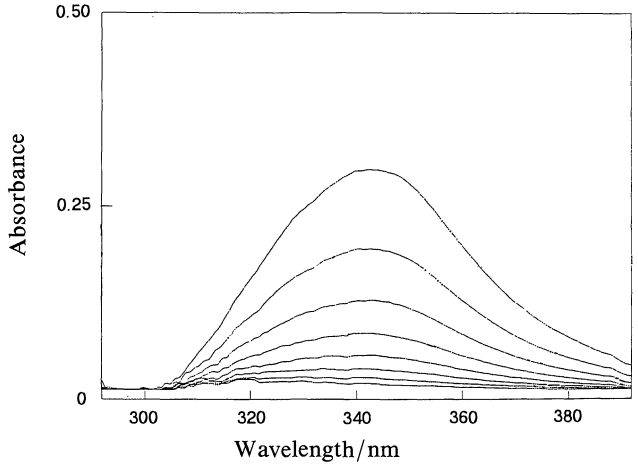

Fig. 1. Transient spectra observed on photolysis of **3b** in 1:1 (v/v) EtOH–H_2O at [HCl]=10^{-3} M. The time interval of the spectra was 120 ms.

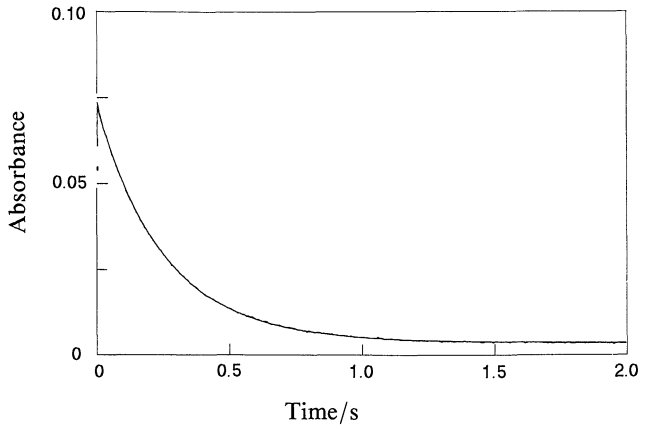

Fig. 2. A trace of the absorption at 342 nm on photolysis of **3b** in 1:1 (v/v) EtOH–H_2O at [HCl]=10^{-3} M. A theoretical pseudo-first-order curve is also drawn.

Table 1. Observed Rate Constants for Decay of **2b** in Aqueous Solutions[a)]

[HCl]/M	k_{obsd}/s^{-1}	
	1:1 EtOH–H_2O	1:1 MeCN–H_2O
0	3.98	0.62
10^{-6}	3.75	0.57
10^{-5}	3.92	0.53
10^{-4}	3.78	0.53
10^{-3}	3.72	
Average	3.83	0.56

a) Measured at 25°C and an ionic strength of 0.10 (KCl).

an MCPD detector in time intervals of order of milliseconds as shown in Fig. 1. The absorption maximum agrees with that observed for the cation **2b** in strong acid.[4)] Time-dependent absorbance changes at 342 nm follow a pseudo-first-order ceday curve as shown in Fig. 2. Bubbling of the solution with oxygen or argon did not affect the transient absorption spectrum or decay curve. The decay was not influenced by addition of acid but accelerated with added nucleophiles as will be presented below. From these observations the transient is identified as the free dithiolanylium ion **2b**. Further support for this intermediate was obtained by photosolvolysis that **3b** undergoes upon stationary irradiation with a low-pressure Hg lamp.[10)]

From a decay curve like that shown in Fig. 2, pseudo-first order rate constants k_{obsd} were obtained by the nonlinear least-squares curve fitting. In aqueous solutions, k_{obsd} is not affected with acid (Table 1). This decay of **2b** must be due to reaction with nucleophilic solvent. The k_{solv} in aqueous ethanol and acetonitrile solutions are 3.83 and 0.56 s^{-1}, respectively. Formation of a thioester was confirmed as a final product by stationary photolysis.[10)]

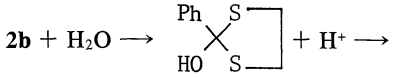

$$PhCOSCH_2CH_2SH + H^+ \quad (4)$$

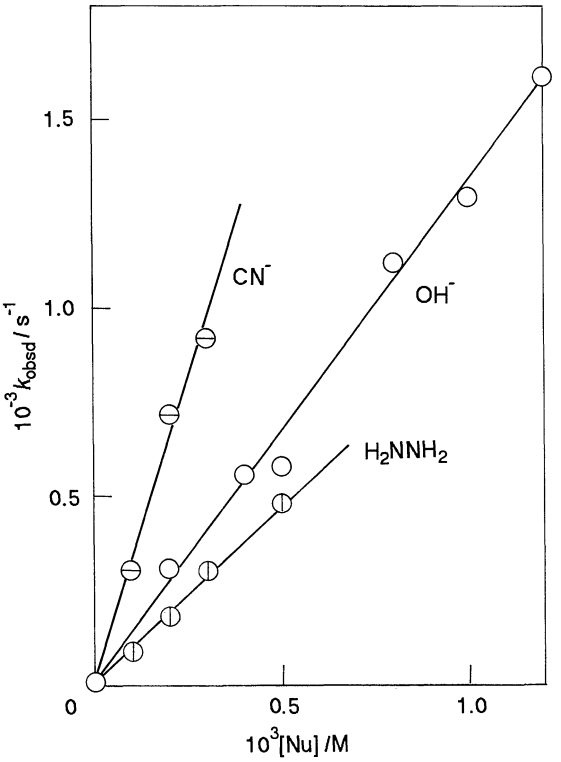

Fig. 3. Plots of k_{obsd} against concentrations of added nucleophiles for OH^- (○), CN^- (⊖), and hydrazine (◑). Data for the latter two were taken in the presence of NaOH at [OH^-]=10^{-4} M.

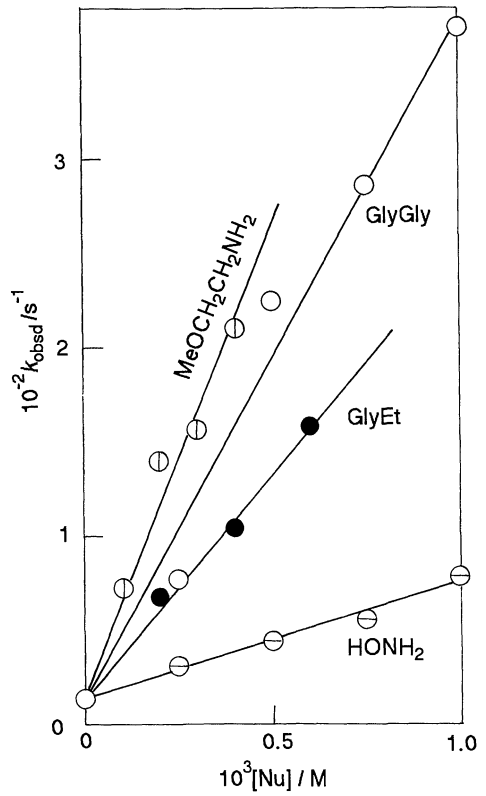

Fig. 4. Plots of k_{obsd} vs. concentrations of nucleophiles for 2-methoxyethylamine (◑), glycylglycine (○), ethyl glycinate (●), and hydroxylamine (⊖). Rates were measured at [OH^-]=10^{-4} M.

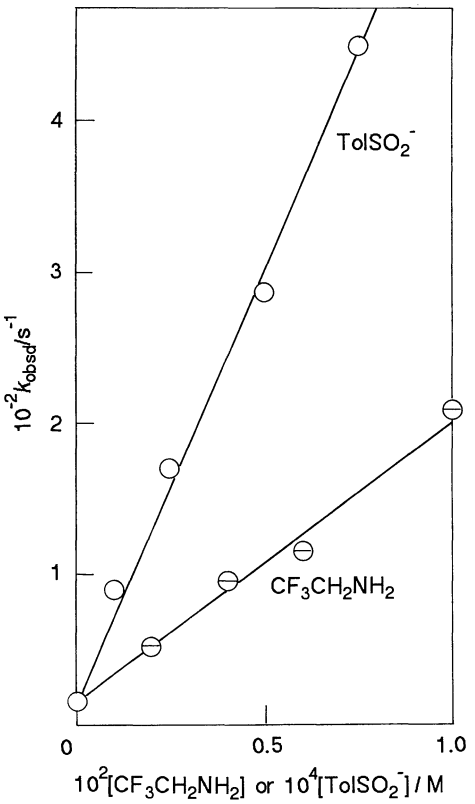

Fig. 5. Plots of k_{obsd} vs. concentrations of nucleophiles for *p*-toluenesulfinate (○) and 2,2,2-trifluoroethylamine (⊖). Rates were measured at $[OH^-]=10^{-4}$ M.

Addition of sodium hydroxide greatly increases the decay rate as is seen in Fig. 3. The k_{obsd} increases linearly with $[OH^-]$. Contamination of carbon dioxide retards the reaction at $[OH^-] < 10^{-4}$M (M=mol dm^{-3}). Other nucleophiles also accelerate the decay of the cation **2b**, following Eq. 5 (Figs. 3-5). The primary reaction involved is the addition of the nucleophile to **2b** (Eq. 6).

$$k_{obsd} = k_0 + k_{Nu}[Nu] \quad (5)$$

$$\mathbf{2b} + Nu^- \xrightarrow{k_{Nu}} \text{Ph(S)(Nu)S} \quad (6)$$

The nucleophilic reactions were mostly examined in the presence of hydroxide ion at $[OH^-]=10^{-4}$ M to avoid formation of the conjugate acid of the nucleophile but contamination of CO_2 was not completely precluded. The rate constants obtained are summarized in Table 2.

Reaction of *p*-toluenesulfinate was also carried out in acidic aqueous acetonitrile solutions. The apparent second-order rate constants k_2, where $k_{obsd}=k_0+k_2[TolSO_2H]_t$, change sigmoidally with pH in the range 1—4 as shown in Fig. 6. This shows that only the sulfinate ion is a nucleophile but conjugate acid is unreactive. Since the fraction of the conjugate base is given by $K_a/(K_a+[H^+])$, the observed k_2 can be expressed

Table 2. Rate Constants for the Nucleophilic Reactions of **2b** in 1:1 (v/v) Aqueous Ethanol

Nucleophile	pK_a[a]	N_+[b]	k_{Nu}/M^{-1} s^{-1}
H_2O/EtOH	(−1.7)	0.73	3.83[c]
OH^-	15.7	4.75	1.3×10^6
$(CF_3)_2CHO^-$	9.3		2.4×10^6
$CF_3CH_2NH_2$	5.7	3.45	1.8×10^4
$EtOCOCH_2NH_2$	7.75	4.40	2.4×10^5
$^-OCOCH_2NHCOCH_2NH_2$	8.13	4.69	3.6×10^5
$MeOCH_2CH_2NH_2$	9.20	5.07	4.6×10^5
$HONH_2$	5.97	5.05	6.4×10^4
H_2NNH_2	8.10	6.01	9.3×10^5
CN^-	9.40	4.12	3.2×10^6
$TolSO_2^-$	1.99		5.8×10^6
p-$ClC_6H_4S^-$	6.14[d]	9.10[e]	4.5×10^8[f]

a) pK_a of the conjugate acid. Taken from "Handbook of Biochemistry," ed by H. A. Sober, CRC Press, Cleveland, Ohio (1968). b) Nucleophilicity parameter.[22] c) In s^{-1}. d) Taken from P. DeMaria, A. Fini, and F. M. Hall, *J. Chem. Soc., Perkin Trans. 2,* **1973**, 1969. e) A value for benzenethiolate. f) Evaluated in 1:1 (v/v) MeCN–H_2O.

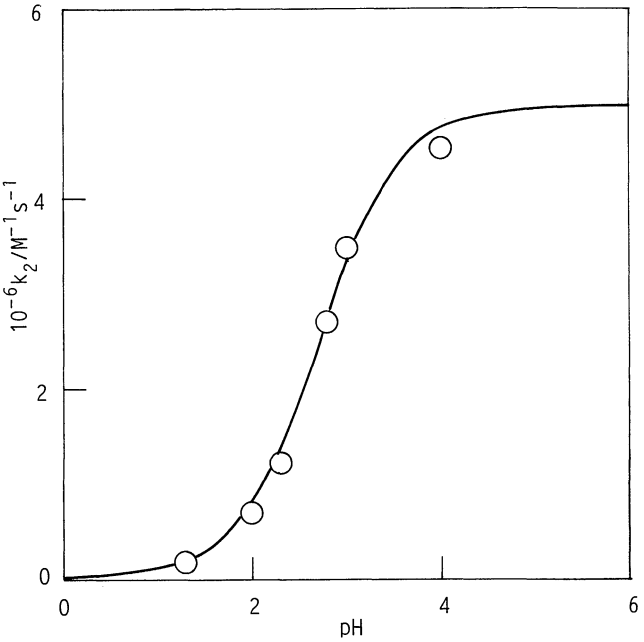

Fig. 6. Plots of apparent second-order rate constants against pH for the reaction of **2b** with *p*-toluenesulfinate in 1:1 (v/v) MeCN–H_2O. Acidity was controlled with HCl. The solid curve is a sigmoid with pK_a=2.7, k_{min}=0, and $k_{max}=5\times10^6$ M^{-1} s^{-1}.

by Eq. 7 The theoretical curve in Fig. 6 is drawn with pK_a=2.7 obtained spectrophotometrically for the sulfinic acid and limiting k_2 at lower and higher pH being 0 and 5.0×10^6 M^{-1} s^{-1}(k_{Nu}). The k_{Nu} agrees reasonably well with that obtained in an alkaline aqueous ethanol solution.

$$k_2 = k_{Nu}K_a/(K_a + [H^+]) \quad (7)$$

Reaction of *p*-chlorobnzenethiol was examined in acidic aqueous acetonitrile solutions. The observed

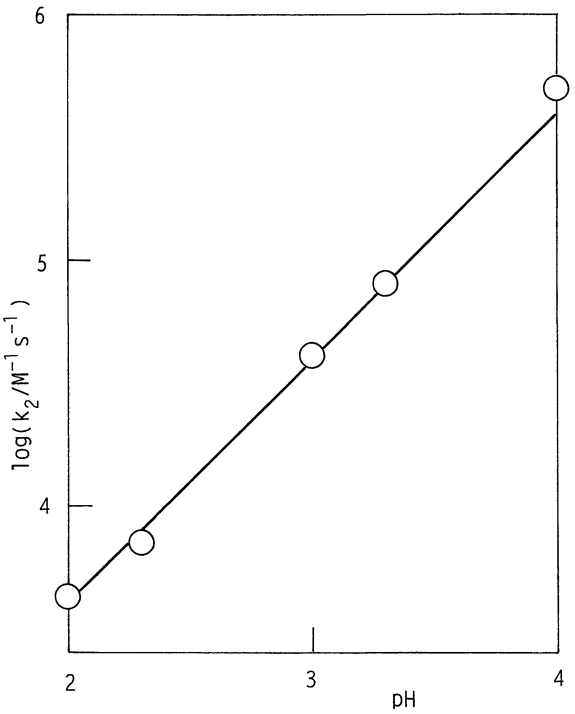

Fig. 7. Logarithmic plots of apparent second-order rate constants against pH for the reaction of **2b** with *p*-chlorobenzenethiol in 1:1 (v/v) MeCN–H_2O. Acidity was controlled with HCl.

second-order rate constants k_2 are dependent on acid concentration (Fig. 7). In this case, both the neutral thiol ArSH and thiolate ArS^- can be good nucleophiles, and the k_2 should obey Eq. 8.

$$k_2 = (k_{ArS^-}K_a + k_{ArSH}[H^+])/(K_a + [H^+]) \quad (8)$$

In the pH region where $[H^+] \gg K_a$, Eq. 8 is reduced to Eq. 9 or 10.

$$k_2 = k_{ArS^-}K_a/[H^+] + k_{ArSH} \quad (9)$$

$$\log k_2 = -\log[H^+] + \log(k_{ArS^-}K_a + k_{ArSH}[H^+]) \quad (10)$$

The logarithmic plots of k_2 against pH ($-\log[H^+]$) fall on a straight line of a unit slope as is seen in Fig. 7. That is, $k_{ArSH}[H^+]$ is negligibly small at $[H^+] = 10^{-4}$—10^{-2} M as compared with $k_{ArS^-}K_a$ in Eq. 10. The reactive species of the thiol reaction is thiolate ion ArS^- even in the acidic media where most of the thiol is present in a conjugate acid form ArSH ($[H^+] \gg K_a$). The k_{ArS^-} for the thiolate ion was evaluated to be 4.5×10^8 M^{-1} s^{-1} using pK_a=7.06 for *p*-chlorobenzenethiol in 49:51 (v/v) ethanol–water solution.[20]

Flash photolysis of aqueous solutions of 2-(*p*-chlorophenylthio)-2-phenyl-1,3-dithiolane (**1c**) and the 2-sulfonyl derivative **1b** showed also formation of the cation **2b**. However, the decay curves of **2b** monitored at 342 nm in this photolysis are different from that observed with **3b** and do not follow psedo-first-order kinetics. The decay of **2b** generated from **1c** fitted the second-order kinetics while the decay observed with **1b** was usually a mixed first- and second-order reaction. These observations must be due to the recombination of **2b** with the accompanying counter anions in a free form. Both of the thiolate and sulfinate ions are very effective nucleophiles and recombination reaction can be a main reaction (in the thiolate case) or an appreciable one (in the sulfinate case) even at very low concentrations in the order of 10^{-6} M as generated by photolysis.

The unsubstituted dithiolanylium ion **2a** (λ_{max}=333 nm) can be generated from the sulfonyl precursor **1a**. The decay curve was also that of mixed first- and second-order reaction. Similar photolysis of 2-methoxy-1,3-dithiolane was also examined but no appreciable cation formation was observed, probably owing to the low efficiency of light absorption.

Photochemical bond cleavage can occur even if the chromophore of the molecule is not directly bonded to the atom involved in the bond breaking. The excess energy of the electronically excited molecule may be transferred to the vibrational states and cleavage of a weaker bond may lead to heterolysis in the present case. All the physical and chemical events in excited states take place in solution within a time scale of nanoseconds and the reactions we observed here are those of photochemical reaction intermediates in the ground state. The main chromophore of the present reaction must be the phenyl group. Although the C–S bondings have a weak absorption around 250 nm, they cannot be

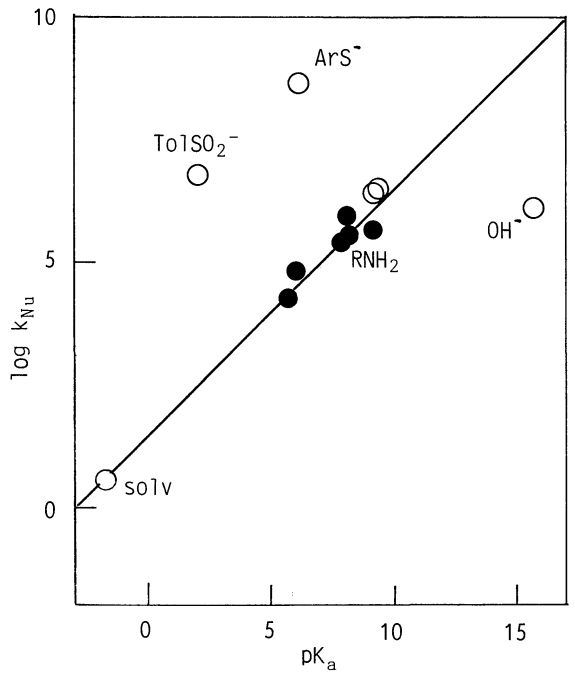

Fig. 8. Correlation of the rate constants with pK_a for the nucleophilic reactions of **2b**. A point for k_{solv} is placed at pK_a of H_3O^+.

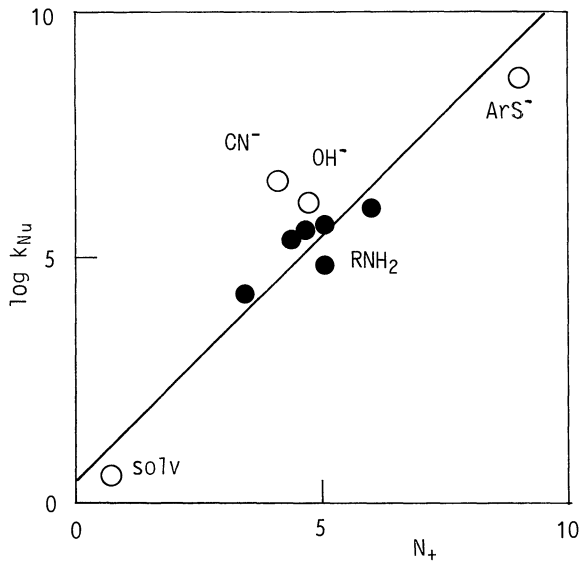

Fig. 9. Correlation of the rate constants with N_+ for the nucleophilic reactions of **2b**. The k_{solv} is plotted against N_+ of H_2O.

satisfactory light absorbers. The unsubstituted dithiolanylium ion **2a** cannot be generated by photolysis of the 2-methoxy derivative.

Rate constants for the nucleophilic reactions of **2b** are correlated with pK_a of the conjugate acid of nucleophiles in aqueous solution (Fig. 8). Although the points for the thiolate and sulfinate ions derivate greatly upward, the points for amines closely fall on the line of a slope β=0.5. The "α-effect" amines,[21] hydroxylamine or hydrazine, do not show appreciable deviations, indicating lack of enhanced reactivity. The thiolate and sulfinate deviations are additional examples of enhanced nucleophilicity of these sulfur nucleophiles.

The k_{Nu} are logarithmically plotted against Ritchie's N_+ nucleophilicity parameters[22] in Fig. 9. Although considerable scatterings are evident, the points fall in the vicinity of a line of a unit slope. The slope of a similar correlation for a less stable triphenylmethylium ion (pK_R=−6.63) was found to be much smaller than unity.[17] The reactivity of the cation **2b** (pK_R=2.5)[2] seems to be in the range of category of the simple Ritchie relationship of a unit slope which was found for reactions of stable carbocations (pK_R>1) with nucleophiles.[22]

Experimental

Materials. Hydroxylamine hydrochloride, hydrazine hydrochloride, potassium cyanide, and potassium chloride were obtained from Wako Pure Chemical. Glycylglycine, ethyl glycinate, and 2,2,2-trifluoroethylamine hydrochloride were from Sigma Chemical. 2-Methoxyethylamine, 1,1,1,3,3,3-hexafluoro-2-propanol, and *p*-chlorobenzenethiol obtained from Aldrich were distilled. Sodium *p*-toluenesulfinate (Wako) was dried at 130 °C for 6 h. Ethanol and acetonitrile were distilled from activated magnesium and calcium hydride, respectively.

A carbon dioxide-free solution of sodium hydroxide was prepared by dissolving metallic sodium in dry ethanol and dilution with freshly boiled water and titrated with a standard hydrochloric acid.

2-Methoxy-2-phenyl-1,3-dithiolane (**3b**) was prepared from the dithiolanylium perchlorate as described previously.[4,10]

2-(*p*-Tolylsulfonyl)-1,3-dithiolane (1a). To a solution of 1,3-dithiolan-2-ylium perchlorate, prepared from 1,2-bis(1,3-dithiolan-2-ylthio)ethane (5.6 mmol),[4] in acetonitrile (30 cm³) was added dry sodium *p*-toluenesulfinate (11.4 mmol) and stirred for 3 h at room temperature. After removal of most of the solvent in vacuo, the residues were dissolved in chloroform, washed with aqueous potassium carbonate, and dried over $MgSO_4$. Removal of the chloroform gave crude solids. Recrystallizations from benzene afforded **1a** in 17% yield. Mp 142—143 °C. Anal. Calcd for $C_{10}H_{12}O_2S_3$: C, 46.12; H, 4.65; S, 36.94%. Found: C, 46.04; H, 4.56; S, 36.48%. ^{1}H NMR ($CDCl_3$) δ=2.45 (s, 3H), 3.40 (s, 4H), 5.35 (s, 1H), 7.23—8.0 (m, 4H). UV (heptane): λ_{max}=226 nm (ε 12000).

2-Phenyl-2-(*p*-tolylsulfonyl)-1,3-dithiolane (1b). Reaction of 2-phenyl-1,3-dithiolan-2-ylium perchlorate obtained from benzoyl chloride and 1,2-ethanedithiol[4] with sodium *p*-toluenesulfinate in the same way as **1a** gave crystalline **1b** in 35% yield (based on benzoyl chloride). Mp 131—132 °C (benzene–ethanol). Anal Calcd for $C_{16}H_{16}O_2S_3$: C, 57.11; H, 4.79; S, 28.59%. Found: C, 56.94; H, 4.73; S, 28.12%. ^{1}H NMR ($CDCl_3$) δ=2.36 (s, 3H), 3.28—3.75 (m, 4H), 6.29—7.50 (m, 9H). UV (heptane): λ_{sh} 250 nm (ε 10000).

2-(*p*-Chlorophenylthio)-2-phenyl-1,3-dithiolane (1c). To a solution of the dithiolanylium perchlorate, prepared from 25 mmol of benzoyl chloride and 1,2-ethanedithiol,[4] in acetonitrile (30 cm³) was added an acetonitrile solution of *p*-chlorobenzenethiol (25 mmol) and excess triethylamine under stirring. After standing for 4 h at room temperature, the solvent was mostly removed by vacuum evaporation. The residues were dissolved in ether, washed with sodium bicarbonate, and dried over $MgSO_4$. The remaining solids after removal of the ether were recrystallized from benzene–hexane to give white plates in an overall yield of ca. 30%. Mp 106—107 °C. Anal. Calcd for $C_{15}H_{13}ClS_3$: C, 55.45; H, 4.03; S, 29.60%. Found: C, 55.27; H, 4.03; S, 29.03%. ^{1}H NMR ($CDCl_3$) δ=3.53 (m, 4H), 7.1—7.5 (m, 9H).

Flash Photolysis. A flash-photolytic apparatus Union RA-412 equipped with a xenon flash lamp (half-height width, ca. 10 s) was used for photolysis. A tungsten lamp was employed with a Pyrex filter for a source of detection light (stationary). Data were fed to and processed with a Union RA-401 processor linked through a photomultiplier or an MCPD (multichannel photodiode array) detector. Rate constants are obtained by nonlinenar least-squares curve fittings (the damping Gauss–Newton method) of the decay curves.

Reactions were carried out in 1:1 (v/v) ethanol–water or 1:1 (v/v) acetonitrile–water usually at an ionic strength of 0.10 maintained with KCl and at 25 °C kept constant with circulating water. The initial substrate concentration was usually 5×10^{-4} M and a stock solution in ethanol or acetonitrile was prepared by weighing. Solutions of nucleophiles were also prepared by weighing. A necessary amount of the substrate stock solution was added with a microsyringe to the reaction solution in a cuvette immediately before photolysis.

We thank Professor S. Otsuka for use of a data processor Union RA-401. This work was in part supported by Grant-in-Aid for Scientific Research from the Ministry of Education, Science and Culture.

References

1) Presented in part in the First International Conference on Heteroatom Chemistry, Kobe, July 19—24, 1987, Abstr., p. 300.

2) T. Okuyama, *Rev. Heteroatom Chem.*, **1**, 46 (1988).

3) R. A. Olofson, S. W. Walinsky, J. P. Marino, and J. L. Jernow, *J. Am. Chem. Soc.*, **90**, 6554 (1968). E. J. Corey and S. W. Walinsky, *ibid.*, **94**, 8932 (1972).

4) T. Okuyama, *Tetrahedron Lett.*, **23**, 2665 (1982). T. Okuyama, W. Fujiwara, and T. Fueno, *Bull. Chem. Soc. Jpn.*, **59**, 453 (1986).

5) J. Klaveness and K. Undheim, *Acta Chem. Scand., Ser. B*, **37**, 687 (1983). J. Klaveness, F. Rise, and K. Undheim, *ibid.*, **40**, 398 (1986).

6) L. Hevesi, S. Desauvage, B. Georges, G. Evrard, P. Blanpain, A. Michel, S. Harkema, and G. J. van Hummel, *J. Am. Chem. Soc.*, **106**, 3784 (1984).

7) I. Stahl, *Chem. Ber.*, **118**, 1785 (1985).

8) T. Okuyama, W. Fujiwara, and T. Fueno, *J. Am. Chem. Soc.*, **106**, 657 (1984).

9) K. Ogura, *Pure Appl. Chem.*, **59**, 1033 (1988).

10) T. Okuyama, N. Haga, and T. Fueno, *Bull. Chem. Soc. Jpn.*, **63**, 3056 (1990).

11) E. O. Holms, Jr., *J. Phys. Chem.*, **70**, 1037 (1966).

12) M. L. Herz, *J. Am. Chem. Soc.*, **97**, 6777 (1975).

13) M. Irie, *J. Am. Chem. Soc.*, **105**, 2078 (1983).

14) R. A. McClelland, N. Babait, and S. Steenken, *J. Am. Chem. Soc.*, **111**, 2929 (1989).

15) R. E. Minto and P. K. Das, *J. Am. Chem. Soc.*, **111**, 8858 (1989).

16) T. Okuyama, K. Ueno, Y. Morishima, M. Kamachi, and T. Fueno, *Chem. Lett.*, **1990**, 1129.

17) R. A. McClelland, N. Banait, and S. Steenken, *J. Am. Chem. Soc.*, **108**, 7023 (1986).

18) R. A. McClelland, V. M. Kanagasabapathy, N. S. Banait, and S. Steenken, *J. Am. Chem. Soc.*, **111**, 3966 (1989).

19) R. A. McClelland, V. M. Kanagasabapathy, N. S. Banait, and S. Steeken, *J. Am. Chem. Soc.*, **113**, 1009 (1991).

20) G. Schwarzenbach and H. Egli, *Helv. Chim. Acta*, **17**, 1176 (1934). G. Schwazenbach and E. Rudin, *ibid.*, **22**, 360 (1939).

21) S. Hoz and E. Buncel, *Isr. J. Chem.*, **26**, 313 (1985).

22) C. D. Ritchie, *J. Am. Chem. Soc.*, **97**, 1170 (1975); *Can. J. Chem.*, **64**, 2239 (1986).

 © 1991 The Chemical Society of Japan Bull. Chem. Soc. Jpn., 64, 2757—2761 (1991)

Photochemistry of 2*H*-Azirine—Formation of Nitrile Ylide Evidenced by Laser Flash Photolysis and Pulse Radiolysis—

Ikuo NAITO,* Hideaki MORIHARA, Akito ISHIDA,† Setsuo TAKAMUKU,†
Kazuaki ISOMURA,†† and Hiroshi TANIGUCHI††
Department of Photography, Kyushu Sangyo University, Matsugadai,
Higashi-ku, Fukuoka 813
† The Institute of Scientific and Industrial Research, Osaka University,
Mihogaoka, Ibaraki, Osaka 567
†† Faculty of Engineering, Kyushu University, Hakozaki,
Higashi-ku, Fukuoka 812
(Received January 14, 1991)

Laser flash photolysis of 3-(4-biphenylyl)-2*H*-azirine (AZ) was carried out in cyclohexane for the direct detection of a nitrile ylide (NY). Two kinds of transient species, triplet AZ (T_1) and NY, have been measured. Decay rates of these species were determined to be 6.7×10^5 s^{-1} (T_1) and 8×10 s^{-1} (NY). The rate constants for the reactions of NY toward acetone and acrylonitrile were determined to be 2.5×10^3 dm^3 mol^{-1} s^{-1} and 2.3×10^6 dm^3 mol^{-1} s^{-1}, respectively. These results were supported by the results of pulse radiolysis of AZ in benzene and stational irradiations of AZ.

Nitrile ylide (NY) is an important reaction intermediate for the synthesis of heterocyclic compounds. This species is one of a group of 1,3-dipoles and is highly reactive toward a wide variety of dipolarophiles such as olefins, ketones, and esters. Various dehydrohalogenation reactions of imidoyl chloride deviatives to yield this species have initially been investigated by Husgen.[1] Padwa[2] and Schmid[3] have independently shown that 2*H*-azirine undergoes facile ring opening on photoirradiation to give NY which reacts with olefins to give 3,4-dihydropyrrole (Eq. 1).

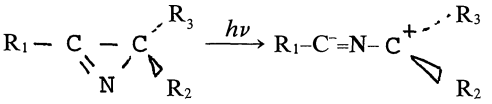

(2*H*—Azirine) (Nitrile Ylide)

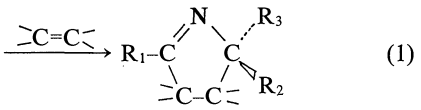

(2*H*-Pyrrole) (1)

The NY thus formed was originally detected by the photoirradiation of arylazirine in a rigid matrix at 77 K by Schmid and coworkers.[4] However, the reaction dynamics of NY were not clarified because of the experimental limitations of stational photoirradiation at low temperature.

Recently, NY produced by the addition reaction of carbenes with nitriles was studied throughly by using a laser flash technique.[5] Scaiano and co-workers reported that the reaction rate constants of the intermediate, which was produced by the addition reaction of 1-naphtylcarbene and acetonitrile with acrylonitrile and diethylfumalate were similar to the values obtained for the 1,3-dipolar addition of NY.[6]

Currently the laser flash photolysis of 2*H*-azirine is the most powerful method to study the charactristics and reactivities of NY. Padwa and co-workers carried out the laser flash photolysis of 2,2- and 2,3-diphenyl-2*H*-azirine.[7] They reported the absorption spectra of NY and the existence of a new complex in the 1,3-dipolar addition reaction. Unfortunately, the profiles of the 2*H*-azirine photoreactions have not been clarified.

Biphenyl compounds are activated by 308 nm irradiation. The transient species formed to excite is expected to be stabilized by the large chromophor and also to be assigned easily. In this study, we carried out the 308 nm laser flash photolysis and a pulse radiolysis of a 2*H*-azirine derivatives substituted at the 3-position with a biphenyl group, 3-(4-biphenylyl)-2*H*-azirine (AZ, R_1=4-biphenylyl, R_2=R_3=H), to elucidate the reaction mechanism for the formation of NY. The stational photoirradiation of AZ was also carried out in order to obtain further experimental support of the mechanism.

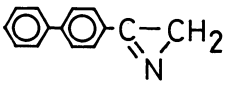

[3-(4-Biphenylyl)-2*H*-azirine, AZ]

Results and Discussion

1. Transient Species. Laser flash photolysis of AZ was carried out in argon-saturated cyclohexane ([AZ]=1.0×10^{-3} mol dm^{-3}). Figure 1 shows the transient absorption spectra recored at various times after the flash and decay traces monitored at 410 nm. The traces indicate the presence of two kinds of transient species with different lifetimes which are indicated as **A** (short-lived) and **B** (long-lived) in Fig. 1 (Eq. 2) in the laser flash photolysis of 2,2-diphenyl-3-methyl-2*H*-azirine reported by Padwa and co-workers.[7] The decay

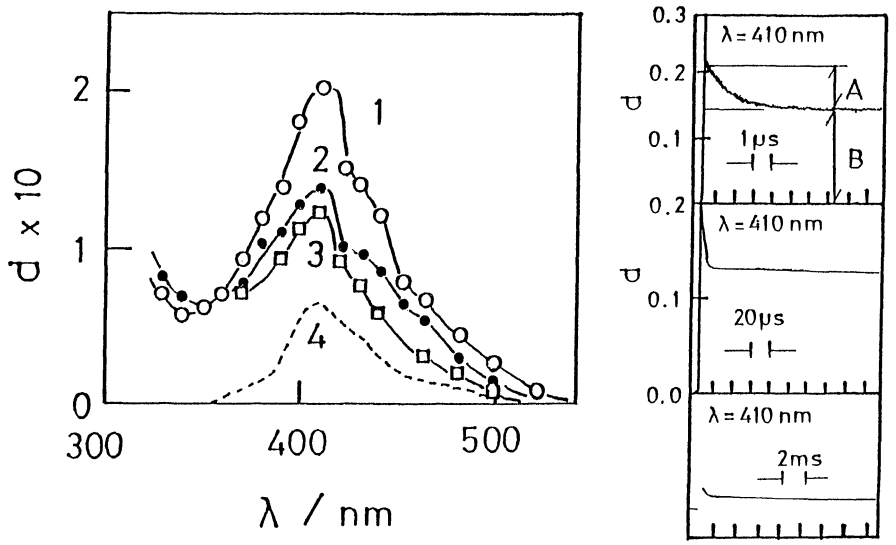

Fig. 1. Transient absorption spectra and the decay traces. Recorded at 0.1 (1), 6 (2), and 160 μs (3) after the flash. Dotted line shows the difference spectrum (1—2). [AZ]=1.0×10^{-3} mol dm^{-3} in cyclohexane.

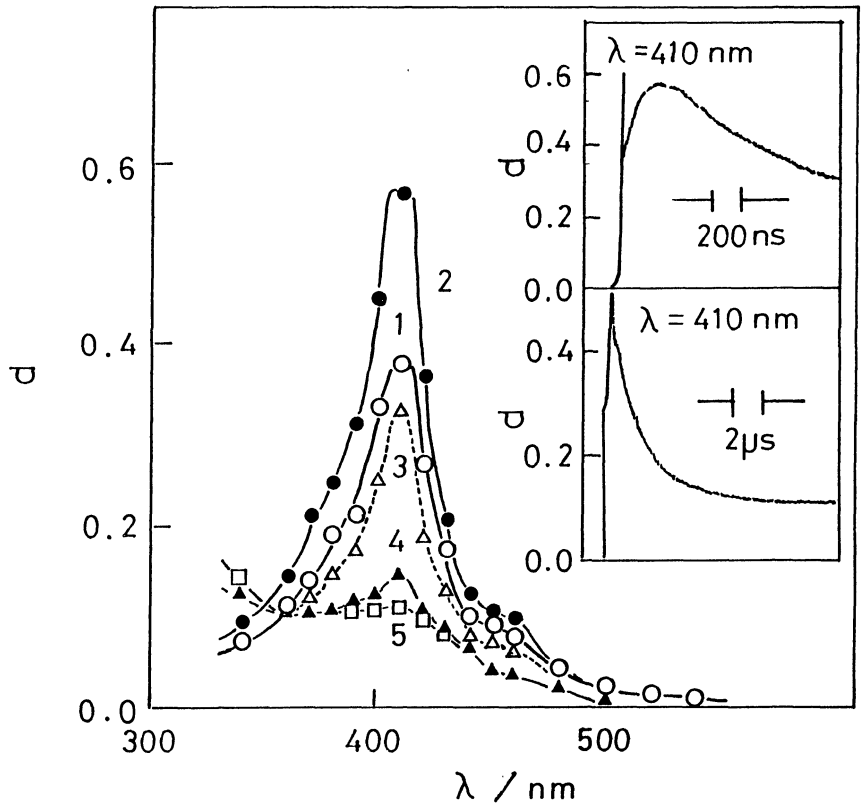

Fig. 2. Transient absorption spectra and digitizer traces measured in the laser flash photolysis of AZ in the presence of acetone. Recorded at 0.1 (1), 0.35 (2), 1.64 (3), and 6 μs (4) after the flash. [AZ]=1.0×10^{-3} mol dm^{-3}, [Acetone]=0.5 mol dm^{-3} in cyclohexane.

of these species follows first-order kinetics and the rate constants for **A** and **B** are 6.7×10^5 s^{-1} and 8×10 s^{-1}, respectively. The absorption spectrum of **A** is exhibited by the difference spectrum as shown by a dotted line in Fig. 1 and is similar to that of **B** (spectra 2 and 3). Both have an absorption maximum around 410 nm. In the presence of oxygen, **A** was quenched whereas **B** was not affected. Thus, it was obvious that **A** was not a precursor of **B** and they were produced simultaneously.

$$\text{AZ} \xrightarrow[\text{Ar-saturated cyclohexane}]{h\nu} \text{Short-lived Species (A)} + \text{Long-lived Species (B)} \quad (2)$$

2. Effect of Acetone. The laser flash photolysis of AZ was also carried out in the presence of acetone as a triplet sensitizer in cyclohexane. The result are shown in Figs. 2 and 3. Since triplet acetone does not absorb light with wavelengths longer than λ=320 nm,[8] the signals measured are due to the transient species of AZ or the reaction intermediates. The rise of the transient species with a λ_{max} at 410 nm was observed at acetone concentrations higher than 0.2 mol dm^{-3}. The yield of **A** increased with increasing acetone concentration (Fig. 3a). On the other hand, the decay rate of **A** (k=7.3×10^5 s^{-1}) was independent of the acetone concentration and was identical to the value obtained by the direct photolysis of AZ. The decay rate of **B** increased with increasing acetone concentration. Based on the linear plots in Fig. 3b, the rate constant for the reaction between **B** and acetone was calculated to be 2.5×10^3 dm^3 mol^{-1} s^{-1}. Since NY reacts with acetone to give 3-oxazoline,[9] species **B** was believed to be NY (Eq. 3).

$$\text{B} + \text{acetone} \longrightarrow \text{Adducts (3-Oxazoline ?)} \quad (3)$$

3. Effect of Acrylonitrile. NY was reported to react with an electron-deficient olefin such as acrylonitrile (AN).[10] The laser flash photolysis of AZ was, therefore, carried out in the presence of AN and oxygen. The initial absorbance of **B** was not affected by the AN. The decay rate of **B** increased with increasing AN concentration, as shown in Fig. 4. The rate constant was determined to be 2.3×10^6 dm^3 mol^{-1} s^{-1}. The stational irradiation of AZ in the presence of AN gave 5-(4-biphenylyl)-3-cyano-3,4-dihydro-2*H*-pyrrole quantitatively. As a result, it was concluded that **B** can be assigned to NY.

4. Pulse Radiolysis of AZ. Pulse radiolysis in bensene is an excellent method to give the triplet state of the solute.[11] The pulse radiolysis of AZ was carried out in benzene to study triplet AZ and its reactivity ([AZ]=1.0×10^{-2} mol dm^{-3}). The transient species measured immediately after the pulse had a λ_{max} around 415 nm. This band decayed exponentially to zero with a decay rate constant of 6.7×10^5 s^{-1} which was consistent with that of species **A** in the direct photolysis reaction. This species was quenched by oxygen; k=6×10^9 dm^3 mol^{-1} s^{-1}.[12] From these results, **A** was concluded to be triplet AZ, although there were a few possibilities that other species, e. g. a radical anion, were formed by the electron pulse.

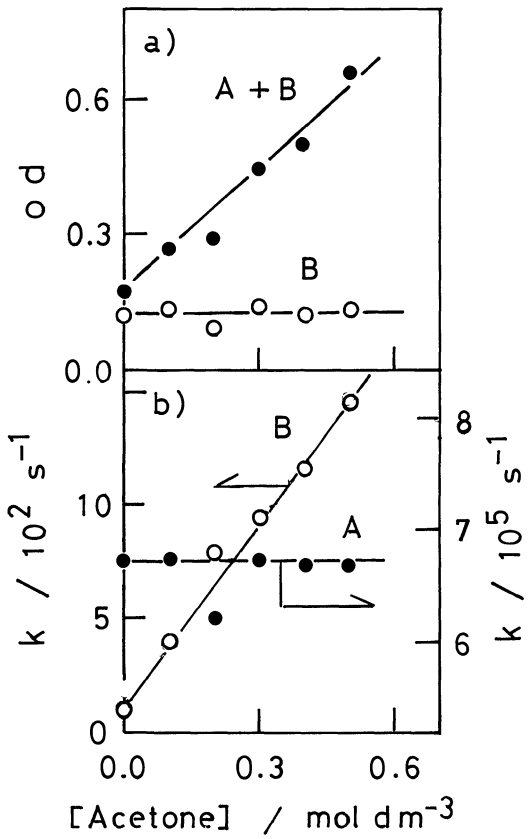

Fig. 3. Effect of acetone on the transient species absorbance (a) and decay rate (b) of the short-lived species (**A**) and the long-lived species (**B**).

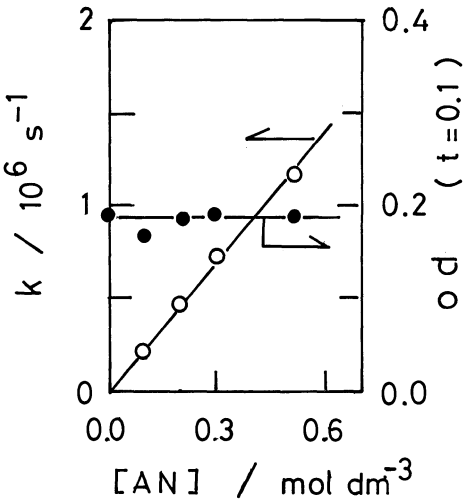

Fig. 4. Effect of AN on the long-lived species [decay rate and absorbance at 0.1 μs after the flash]. The laser flash photolyses were carried out in the presence of oxygen in cyclohexane.

In order to confirm the formation of triplet AZ, the pulse radiolysis of AZ was carried out in the presence of benzophenone (BP) ([AZ]=1.0×10^{-3} mol dm^{-3}, [BP]=2.0×10^{-2} mol dm^{-3} in benzene). Figure 5 shows the time-resolved absorption spectra obtained in this reaction. Immediately after the pulse, an absorption band with a λ_{max} at 530 nm, which was assigned to triplet BP,[13] was measured. The 530 nm band according to pseudo first-order kinetics (3.3×10^{6} s^{-1}) with the simultaneous formation of a 420 nm band. The spectra measured at 460 ns after the pulse (spectrum 5 in Fig. 4), is similar to A. The rate of the latter band formation (4×10^{6} s^{-1}) agrees well with that of the decay of the 530 nm band. Therefore, it was concluded that species A was the triplet state of AZ and was formed by energy transfer from triplet BP (Eq. 4). An ε_{max} value of triplet AZ was estimated to be 3.8×10^{5} dm^{2} mol^{-1} by means of the ε_{max} value of triplet BP.[13]

$$^{3}BP^{*} + AZ \longrightarrow BP + {}^{3}AZ^{*} \quad (4)$$

5. Stational Photoirradiation. In order to obtain information on the reaction products, the stational photoirradiation of AZ was carried out in cyclohexane. A dimer, 4,5-di(4-biphenylyl)-1,3-diazabicyclo[3,1,0]-hex-3-ene (**C**) was obtained in a good yield (83%, Eq. 5). In the presence of AN (0.5 mol), 5-(4-biphenylyl)-3-cyano-3,4-dihydro-2*H*-pyrrole (**D**) was formed almost quantitatively (89%) along with an AN-polymer (Eq. 6). These compounds were produced by the 1,3-dipolar addition of NY with AZ or AN as reported by Padwa and co-workers.[10]

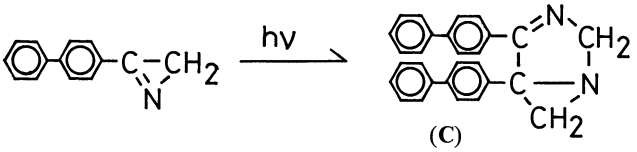

+ Other Products (5)

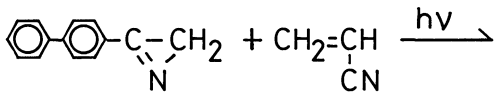

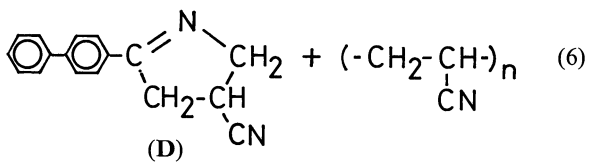

(6)

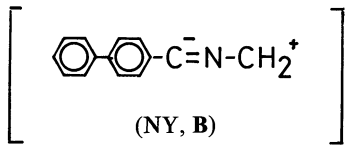

Upon irradiation with 360 nm light in the presence of BP, an adduct such as 3-oxazidine was not obtained and AZ was mainly recovered. BP was activated to the triplet state by the irradiation. The triplet state of AZ must then have been produced by energy transfer from triplet BP, as shown in Eq. 4. Triplet AZ was unreactive and was deactivated to the ground state.

6. Reaction Mechanism. In the laser flash photolysis of AZ, two kinds of transient species, triplet AZ and NY, were detected. It seemed that the excited singlet state

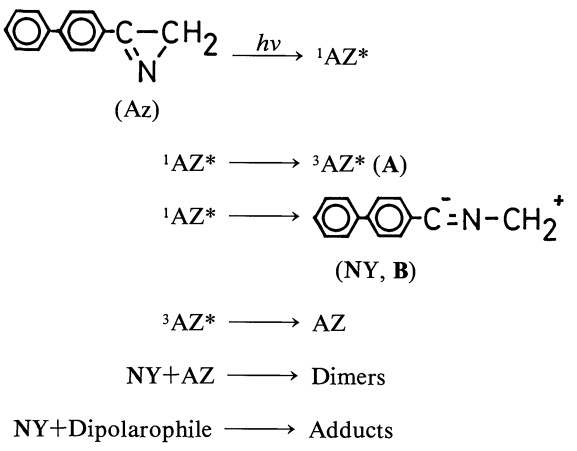

$^{1}AZ^{*} \longrightarrow {}^{3}AZ^{*}$ (**A**)

$^{3}AZ^{*} \longrightarrow AZ$

NY+AZ ⟶ Dimers

NY+Dipolarophile ⟶ Adducts

Scheme 1.

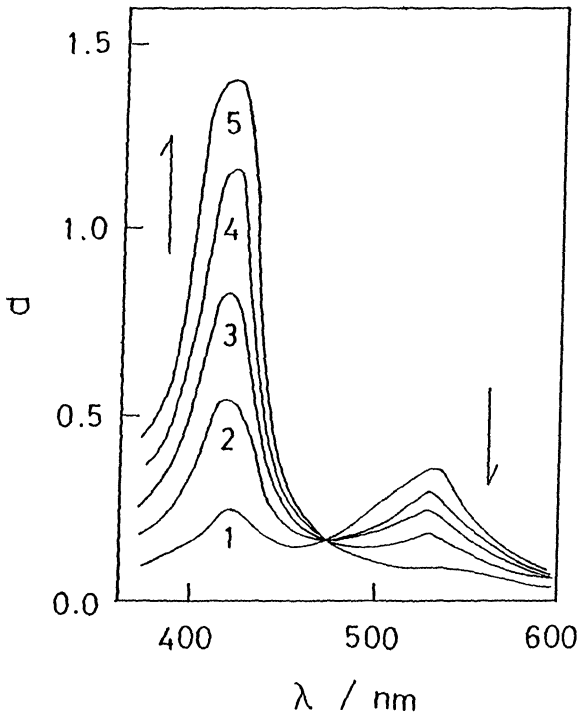

Fig. 5. Time-resolved absorption spectra measured in the pulse radiolysis of AZ in the presence of BP in benzene. Recorded at 10 (1), 50 (2), 100 (3), 200 (4), and 460 ns (5) after the pulse. [AZ]=1.0×10^{-3} mol dm^{-3}, [BP]=2.0×10^{-2} mol dm^{-3} in benzene.

decayed very rapidly to triplet AZ and/or NY. The quenching rate constant of oxygen toward triplet AZ (6×10^9 dm^3 mol^{-1} s^{-1}) also supported the above assigment of the transient species. Since the stational photoirradiation of AZ in the presence of BP didn't give any adducts, the structure of triplet AZ was the closed form and decayed to the ground state. NY was assigned by the reactions with acetone and AN. NY was relatively stable in the absence of the dipolarphile, with a decay rate of 8×10 s^{-1}. It seemed that the rate was the value of the dimer (**C**) formation. The present results support the following mechanism (Scheme 1).

Experimental

AZ was synthesized from 4-vinylbiphenyl by way of 4-(1-azidoethyl)-biphenyl as reported by Hortmann and coworkers.[14] AZ was purified by column chromatography (Florisil) and several recrystallizations from hexane. The yield of AZ for starting olefin was 80.8%. Pale yellow crystals; mp 73.5—74.2 °C; *m*/*z* 193 (M^+); Elementary analysis, Found: C, 86.87; H, 5.74; N, 7.21%; Calcd for $C_{14}H_{11}N$: C, 87.01; H, 5.84; N, 7.15%. ^{1}H NMR ($CDCl_3$, TMS) δ=1.81 (s, 2H) and 7—8 (m, biphenyl); IR (KBr) $\nu_{C=N}$=1742 cm^{-1}, δ_{CH_2}=1442 cm^{-1}, and ν_{C-N}=986 cm^{-1}; UV (cyclohexane) λ_{max}=268.8 nm (1.99×10^5 dm^2 mol^{-1}).

Spectroscopic grade benzene, cyclohexane, and acetone were used without further purification.

Benzophenone (BP) was purified by two recrystallizations from ethanol.

Acrylonitrile (AN) was washed three times with a 5% NaOH aqueous solution, then three times with distilled water. After drying on sodium carbonate, the monomer was distilled twice under a N_2 stream.

Apparatus. The laser flash photolyses were carried out with the aid of a Lambda Phisik EMG 501 lamp with Xe and Cl_2 gases. This apparatus generates a λ=308 nm light pulse (pulse width: 15 ns, ca. 0.1 J).

The pulse radiolyses were carried out with the aid of the L-band electron beam linear accelator at Osaka University (pulse width: 8 ns, ca. 1 kGy).[15]

Stational Photoirradiations. The photoirradiations were carried out by using a 300 W high-pressure Hg lamp and a pyrex filter (thickness: 2 mm). Since AZ absorbs light of wavelengths shorter than 340 nm, an excitation wavelength of 313 nm was used. AZ (0.300 g) was irradiated in cyclohexane (0.5 dm^3) at room temperature for two hours. After several recrystallizations of the products from hexane, 0.249 g 4,5-di(4-biphenylyl)-1,3-diazabicyclo-[3.1.0]hex-3-ene (**C**) was obtained (yield: 83%). White crystals; mp 214—215.2 °C; *m*/*z*=386 (M^+); Elementary analysis, Found: C, 86.78; H, 5.77; N, 7.11%. Calcd for $C_{28}H_{22}N_2$: C, 87.01; H, 5.84; N, 7.15%. ^{1}H NMR ($CDCl_3$, TMS) δ=2.05 (s, $-CH_2-$N), 3.04 (s, N$-CH_2-$N=), and 7.3—8.0 (m, biphenyl); IR (KBr) $\nu_{C=N}$=612 cm^{-1} and ν_{C-N}=1332 cm^{-1}.

AZ (0.135 g) was irradiated with 0.50 mol of AN at 4 °C for three hours in cyclohexane (0.5 dm^3). The products were the adduct, 5-(4-biphenylyl)-3-cyano-3,4-dihydro-2*H*-pyrrole (0.154 g, **D**) and polyacrylonitrile (0.84 g). The adduct was isolated from the polymer by reprecipitations. White crystals; mp 170.2—170.6 °C; *m*/*z*=246 (M^+); Elementary analysis, Found: C, 82.89; H, 5.80; N, 11.21%. Calcd for $C_{17}H_{14}N_2$: C, 82.90; H, 5.73; N, 11.37%. ^{1}H NMR ($CDCl_3$, TMS) δ=2.05 (m, -CHCN-), 3.43 (dd, $-C-CH_2-$), 4.43 (dd, $-N-CH_2-$), and 7.3—8.0 (m, biphenyl); IR (KBr) ν_{CN}=2240 cm^{-1}, $\nu_{C=N}$=1618 cm^{-1}, δ_{CH_2}=1450, 1428 cm^{-1}, and ν_{C-N}=1364 cm^{-1}.

The irradiation of AZ (0.097 g) was carried out in the presence of BP (1.92 g) in cyclohexane (0.1 dm^{-3}) by using a 500 W Xe lamp and an interference filter (λ_{max}=360 nm, T_{max}=21%, $\Delta_{1/2}$=10 nm) for 20 h. AZ was mainly recovered and a small amount of diphenylmethanol was also obtained.

References

1) R. Huisgen, *Proc. Chem. Soc. London,* **1961**, 357; R. Huisgen, *Angew. Chem. Res.,* **75**, 604, 702, 704 (1963).

2) A. Padwa. *Acc. Chem. Res.,* **9**, 371 (1976); A. Padwa, *Chem. Rev.,* **77**, 37 (1977).

3) H. Giezendanner, M. Märky, B. Jackson, H-J. Hansen, and H. Schmid, *Helv. Chim. Acta,* **55**, 745 (1972); P. Claus, T. Dopper, N. Georgarakis, H. Giezendanner, P. Gilgen, H. Heimgarther, B. Jackson, M. Märky, N. S. Narasimhan, H. J. Rosenkranz, A. Wunderli, H-J. Hansen, and H. Schmid, *Pure Appl. Chem.,* **33**, 339 (1973).

4) W. Sieber, P. Gilgen, S. Chalopka, H-J. Hansen, and H. Schmid, *Helv. Chim. Acta,* **56**, 745 (1973); A. Orahovats, H. Heimgartner, and H. Schmid, *Helv. Chim. Acta,* **58**, 2662 (1975).

5) P. B. Grasse, B-E. Brauer, J. J. Zupancic, K. J. Kaufmann, and G. B. Schuster, *J. Am. Chem. Soc.,* **105**, 6833 (1985).

6) D. Griller, C. R. Montgomery, J. C. Scaiano, M. S. Platz, and L. Handel, *J. Am. Chem. Soc.,* **104**, 6813 (1982); R. L. Barcus, L. M. Hadel, L. J. Johnston, M. S. Platz, T. G. Savino, and J. C. Scaiano, *J. Am. Chem. Soc.,* **108**, 3928 (1986).

7) A. Padwa, R. J. Rosenthal, W. Dent, P. Filho, N. J. Turro, D. A. Hrovat, and I. R. Gould, *J. Org. Chem.,* **49**, 3174 (1984).

8) I. Naito and W. Schnabel, *Bull. Chem. Soc. Jpn.,* **57**, 771 (1984).

9) P. Claus, P. Gilgen, H-J. Hansen, H. Heimgartner, B. Jackson, and H. Schmid, *Helv. Chim. Acta,* **57**, 2173 (1973).

10) A. Padwa, M. Dharan, J. Smolanoff, and S. I. Wetmore, *J. Am. Chem. Soc.,* **95**, 1945 (1973); A. Padwa and S. I. Wetmore, *J. Am. Chem. Soc.,* **96**, 2414 (1974).

11) A. J. G. Barwise, A. A. Gorman, and M. A. J. Rodgers, *Chem. Phys. Lett.,* **38**, 313 (1976).

12) The rate constant was calculated by means of the saturated oxygen concentration in cyclohexane reported ($[O_2]=2.3\times10^{-3}$ mol dm^{-3}). S. L. Murov, "Handbook of Photochemistry," Marcel Dekker Inc., New York (1973), p. 89. $[O_2]$ in an air-saturated solution is estimated to be 4.8×10^{-4} mol dm^{-3}.

13) R. Bensasson and E. J. Land, *Trans. Faraday Soc.,* **67**, 1904 (1971).

14) A. G. Hortmann, D. A. Robertson, and B. K. Gillard, *J. Org. Chem.,* **37**, 322 (1972).

15) S. Takamuku, H. Kigawa, H. Suematsu, S. Toki, K. Tsumori, and H. Sakurai, *J. Phys. Chem.,* **86**, 1861 (1982).

The Synthesis of Hyptol and Its C-15 Epimer from (+)-Dehydroabietic Acid

Takashi MATSUMOTO,* Hiromitsu TERAO, Makoto WADA,† and Sachihiko IMAI††
Department of Applied Material Science, Faculty of Integrated Arts and Sciences, University of Tokushima, Minamijosanjima, Tokushima 770
† Department of Chemistry, College of General Education, University of Tokushima, Minamijosanjima, Tokushima 770
†† Suzugamine Women's College, Inokuchi, Nishi-ku, Hiroshima 733
(Received March 27, 1991)

In order to elucidate the absolute configuration of C-15 in natural hyptol, methyl (15*S*)-12,16-dihydroxy-8,11,13-abietatrien-18-oate and its (15*R*)-epimer were transformed into (15*S*)-12,16-epoxy-11,14-dihydroxy-8,11,13-abietatrien-7-one (**1a**) and its (15*R*)-epimer (**1b**), respectively. The synthetic **1a** was identical to natural hyptol. Thus, the stereochemistry of C-15 in the natural compound was conclusively assigned as *S*-configuration.

Hyptol, a rare abietane-type diterpene possessing a dihydrofuran moiety, has been isolated from the roots of *Hyptis fructicosa* (Labiatae) by Monache et al.[1] On the basis of chemical and spectroscopic studies, they deduced the structure of hyptol to be 12,16-epoxy-11,14-dihydroxy-8,11,13-abietatrien-7-one (**1**). However, the absolute configuration of the C-15 position in the natural compound remained unsolved. In order to elucidate the unknown stereochemistry at the C-15 position, we have attempted the syntheses of (15*S*)-12,16-epoxy-11,14-dihydroxy-8,11,13-abietatrien-7-one (**1a**) and its (15*R*)-epimer (**1b**). For this purpose, methyl (15*S*)-12,16-dihydroxy-8,11,13-abietatrien-18-oate (**2a**)[2] and its (15*R*)-epimer (**2b**)[2] were chosen as convenient relay intermediates, because these compounds have recently been synthesized in our laboratory starting from (+)-dehydroabietic acid.

To introduce an oxygen function at the C-11 position, the (15*S*)-12,16-dihydroxy compound (**2a**) was refluxed with benzoyl peroxide in chloroform to give a mixture of methyl 11-benzoyloxy-12,16-dihydroxy-8,11,13-abietatrien-18-oate (**3a**) and its 12-benzoyloxy-11,16-dihydroxy isomer (**4a**) (ca. 1:1 ratio) in a 36% yield. The mixture of **3a** and **4a** was further transformed into a dihydrobenzofuran compound (**5a**: 70% yield) by a series of reactions: mesylation with methanesulfonyl chloride in pyridine, refluxing with sodium iodide in ethyl methyl ketone, and treatment with aqueous sodium hydroxide in refluxing methanol. Reduction of **5a** with lithium aluminum hydride in ether followed by mesylation of the resulting alcohol (**6a**) with methanesulfonyl chloride in pyridine afforded a mesylate (**7a**). This was treated with sodium iodide and zinc powder in *N*,*N*-dimethylformamide at 120—125 °C to give a 4,4-dimethyl compound (**8a**) in a 56% yield from **5a**. Oxidation of **8a** with Fremy's salt and potassium dihydrogenphosphate in aqueous *N*,*N*-dimethylformamide afforded a para-quinone (**9a**) in an 80% yield. This was submitted to reductive acetylation with zinc powder and acetic anhydride in pyridine to give a diacetate (**10a**: 94% yield), which was further oxidized with chromium trioxide in acetic acid to give a ketone (**11a**: 72% yield). Hydrolysis of **11a** with dilute hydrochloric acid in refluxing ethanol afforded the desired (15*S*)-hyptol (**1a**: 98% yield), the physical and spectral data of which were identical to those of natural hyptol.

For direct comparison with **1a**, the synthesis of (15*R*)-hyptol (**1b**) was also carried out in the same manner as that described for the preparation of **1a**. Oxidation of the (15*R*)-12,16-dihydroxy compound[2] (**2b**) with benzoyl peroxide in refluxing chloroform produced a mixture of methyl 11-benzoyloxy-12,16-dihydroxy-8,11,13-abietatrien-18-oate (**3b**) and its 12-benzoyloxy-11,16-dihydroxy isomer (**4b**) (ca. 1:1 ratio, 38% yield). This mixture was converted into a dihydrobenzofuran compound (**5b**), which was further transformed into a para-quinone (**9b**) via an alcohol (**6b**), a mesylate (**7b**), and a 4,4-dimethyl compound (**8b**). Reductive

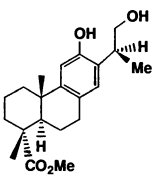

2a

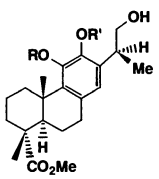

3a R=Bz, R'=H
4a R=H, R'=Bz

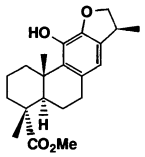

5a

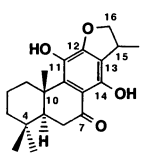

1

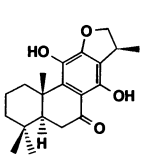

1a

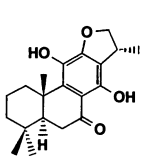

1b

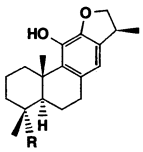

6a R=CH2OH
7a R=CH2OMs
8a R=Me

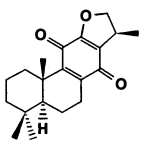

9a

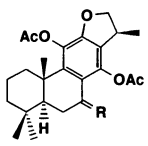

10a R=H2
11a R=O

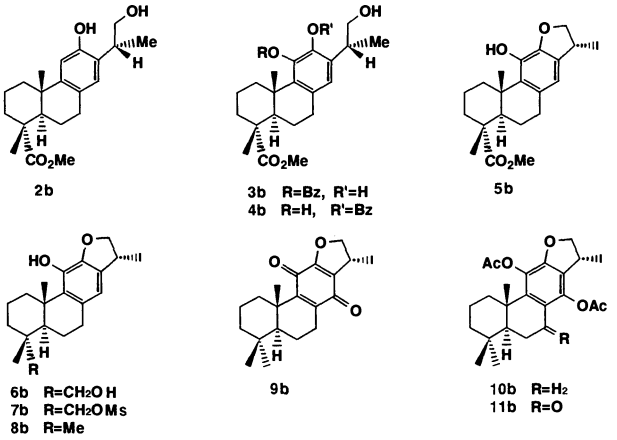

acetylation of **9b** followed by oxidation of the resulting diacetate (**10b**) afforded a ketone (**11b**). This was hydrolyzed with dilute hydrochloric acid in refluxing ethanol to give (15*R*)-hyptol (**1b**). The physical and spectral data of the synthetic **1b** were not identical to those of natural hyprol.

From the present study, the stereochemistry of the C-15 position in natural hyptol was conclusively assigned as *S*-configuration.

Experimental

All melting points are uncorrected. The IR spectra and optical rotations were measured in chloroform, and the ^{1}H NMR spectra in deuteriochloroform at 90 MHz with tetramethylsilane as an internal standard, unless otherwise stated; s: singlet, bs: broad singlet, d: doublet, bd: broad doublet, dd: double doublet, t: triplet, m: multiplet. The column chromatography was performed using Merck silica gel (0.063 mm).

Oxidation of Methyl (15*S*)-12,16-Dihydroxy-8,11,13-abietatrien-18-oate (2a) and Its (15*R*)-Epimer (2b) with Benzoyl Peroxide. a): A solution of **2a**[2] (1.852 g) and benzoyl peroxide (1.944 g) in chloroform (21 ml) was gently refluxed for 3.5 h. After the addition of ether (30 ml) acetic acid (14 ml), and aqueous potassium iodide (20%, 60 ml), the mixture was stirred at room temperature for 2 h and then washed successively with water, aqueous sodium thiosulfate, aqueous sodium hydrogencarbonate, and brine. The dried solution was evaporated in vacuo. The residue was chromatographed on silica gel (25 g), using ether–benzene (5:95) as an eluent, to give a mixture of methyl 11-benzoyloxy-12,16-dihydroxy-8,11,13-abietatrien-18-oate (**3a**) and its 12-benzoyloxy-11,16-dihydroxy isomer (**4a**) (902 mg: 36.1% yield). IR 3575, 3300, 1737 sh, and 1723 cm^{-1}. ^{1}H NMR of **3a** (60 MHz) δ=1.19 and 1.28 (each 3H and s, 4-CH_3 and 10-CH_3), 3.64 (3H, s, -CO_2CH_3), 6.63 (1H, s, 14-H), and 7.3—7.7 (3H, m) and 8.18 (2H, bd, J=7 Hz) (-C_6H_5). ^{1}H NMR of **4a** (60 MHz) δ=1.24 and 1.30 (each 3H and s, 4-CH_3 and 10-CH_3), 3.64 (3H, s, -CO_2CH_3), 6.50 (1H, s, 14-H), and 7.3—7.7 (3H, m) and 8.18 (2H, bd, J=7 Hz) (-C_6H_5). Found: C, 72.37; H, 7.08%. Calcd for $C_{28}H_{34}O_6$: C, 72.08; H, 7.35%.

b): A solution of **2b**[2] (2.532 g) and benzoyl peroxide (2.657 g) in chloroform (28 ml) was gently refluxed for 3.5 h. After the work-up as described in a), the crude product was chromatographed on silica gel (25 g), using ether–benzene (5:95) as an eluent, to give a mixture of methyl 11-benzoyloxy-12,16-dihydroxy-8,11,13-abietatrien-18-oate (**3b**) and its 12-benzoyloxy-11,16-dihydroxy isomer (**4b**) (1.310 g: 38.4% yield). IR 3575, 3435, 1735 sh, and 1720 cm^{-1}. ^{1}H NMR of **3b** δ=1.21 and 1.30 (each 3H and s, 4-CH_3 and 10-CH_3), 3.63 (3H, s, -CO_2CH_3), 6.64 (1H, s, 14-H), and 7.4—7.7 (3H, m) and 8.18 (2H, dd, J=8 and 2 Hz) (-C_6H_5). ^{1}H NMR of **4b** δ=1.26 and 1.33 (each 3H and s, 4-CH_3 and 10-CH_3), 3.65 (3H, s, -CO_2CH_3), 6.53 (1H, s, 14-H), and 7.4—7.7 (3H, m) and 8.18 (2H, dd, J=8 and 2 Hz) (-C_6H_5). Found: C, 72.22; H, 7.57%. Calcd for $C_{28}H_{34}O_6$: C, 72.08; H, 7.35%.

Methyl (15*S*)-12,16-Epoxy-11-hydroxy-8,11,13-abietatrien-18-oate (5a) and Its (15*R*)-Epimer (5b). a): Methanesulfonyl chloride (0.19 ml) was added to a stirred solution of a mixture of **3a** and **4a** (ca. 1:1 ratio, 955 mg) in pyridine (2.0 ml) at 0—5 °C. The mixture was stirred at this temperature for 30 min and then at room temperature for 3 h, then poured into ice-dilute hydrochloric acid and extracted with ether. The ether extract was washed successively with aqueous sodium hydrogencarbonate and brine, dried, and evaporated in vacuo to give a mixture of mesylates (1.111 g).

A stirred mixture of the above crude mesylates (1.111 g) and sodium iodide (612 mg) in ethyl methyl ketone (22 ml) was refluxed for 4 h. The mixture was cooled, diluted with ether, and washed successively with water, aqueous sodium thiosulfate, and brine. The dried solution was evaporated in vacuo to give a mixture of iodides (1.160 g).

A mixture of the above crude iodides (1.160 g) and aqueous sodium hydroxide (20%, 2.9 ml) in methanol (14 ml) was refluxed for 1 h. After removal of the methanol in vacuo, the residue was acidified with dilute hydrochloric acid and extracted with ether. The ether extract was washed with aqueous sodium hydrogencarbonate and brine, dried, and evaporated in vacuo. The residue was chromatographed on silica gel (25 g), using hexane–benzene (3:7) as an eluent, to give **5a** (478 mg: 69.5% yield), mp 155.5—157 °C (from hexane), $[\alpha]_D$+65.9 ° (c 0.41), IR 3560, 3375, and 1720 cm^{-1}; ^{1}H NMR δ=1.25 and 1.32 (each 3H and s, 4-CH_3 and 10-CH_3), 1.27 (3H, d, J=7 Hz, 15-CH_3) 3.66 (3H, s, -CO_2CH_3), 4.03 (1H, t, J=8 Hz) and 4.68 (1H, t, J=8 Hz) (15-CH_2O-), 4.87 (1H, s, 11-OH), and 6.40 (1H, s, 14-H). Found: C, 73.49; H, 8.38%. Calcd for $C_{21}H_{28}O_4$: C, 73.22; H, 8.19%.

b): A solution of a mixture of **3b** and **4b** (ca. 1:1 ratio, 1.120 g) in pyridine (4.0 ml) was mesylated with methanesulfonyl chloride (0.23 ml) as described in a). The crude mesylates (1.295 g) were treated with sodium iodide (713 mg) in refluxing ethyl methyl ketone (25 ml) to give a mixture of iodides (1.286 g). This was further refluxed with aqueous sodium hydroxide (20%, 3.2 ml) in methanol (16 ml) for 1 h. The crude product was chromatographed on silica gel (25 g), using hexane–benzene (3:7) as an eluent, to give **5b** (520 mg, 60.7% yield), mp 167.5—169 °C (from hexane), $[\alpha]_D$+33.0 ° (c 0.58), IR 3560, 3375, and 1718 cm^{-1}; ^{1}H NMR δ=1.25 and 1.32 (each 3H and s, 4-CH_3 and 10-CH_3), 1.27 (3H, d, J=7 Hz, 15-CH_3), 3.66 (3H, s, -CO_2CH_3), 4.04 (1H, dd, J=8 and 7 Hz) and 4.68 (1H, t, J=8 Hz) (15-CH_2O-), 4.87 (1H, s, 11-OH), and 6.42 (1H, s, 14-H). Found: C, 73.04; H, 8.45%. Calcd for $C_{21}H_{28}O_4$: C, 73.22; H, 8.19%.

(15*S*)-12,16-Epoxy-8,11,13-abietatriene-11,18-diol (6a) and Its (15*R*)-Epimer (6b). a): A mixture of **5a** (794 mg) and lithium aluminum hydride (149 mg) in dry ether (7.0 ml) was stirred at room temperature for 1 h. The mixture was poured into ice-dilute hydrochloric acid and extracted with ether. The ether extract was washed with brine, dried, and evaporated in vacuo to give a crude **6a** (740 mg). This was recrystallized from acetone–hexane, mp 159—160.5 °C, $[\alpha]_D$+78.9 ° (*c* 1.47), IR 3630, 3565, and 3450 cm^{-1}; ^{1}H NMR (60 MHz) δ=0.89 (3H, s, 4-CH_3), 1.27 (3H, d, *J*=7 Hz, 15-CH_3), 1.39 (3H, s, 10-CH_3), 3.16 (1H, d, *J*=11 Hz) and 3.50 (1H, d, *J*=11 Hz) (-C$\underline{H_2}$OH), 4.01 (1H, t, *J*=8 Hz) and 4.67 (1H, t, *J*=8 Hz) (15-CH_2O-), 5.12 (1H, bs, 11-OH), and 6.40 (1H, s, 14-H). Found: C, 75.92; H, 9.21%. Calcd for $C_{20}H_{28}O_3$: C, 75.91; H, 8.92%.

b): A mixture of **5b** (1.006 g) and lithium aluminum hydride (189 mg) in dry ether (15 ml) was stirred at room temperature for 1 h. The mixture was treated as described in a) to give a crude **6b** (1.001 g). This was recrystallized from acetone–hexane, mp 183.5—185.5 °C, $[\alpha]_D$+66.7 ° (*c* 2.03), IR 3625, 3565, and 3450 cm^{-1}; ^{1}H NMR (60 MHz) δ=0.88 (3H, s, 4-CH_3), 1.28 (3H, d, *J*=7 Hz, 15-CH_3), 1.39 (3H, s, 10-CH_3), 3.16 (1H, d, *J*=10 Hz) and 3.50 (1H, d, *J*=10 Hz) (-C$\underline{H_2}$OH), 4.04 (1H, t, *J*=8 Hz) and 4.65 (1H, t, *J*=8 Hz) (15-CH_2O-), 5.20 (1H, s, 11-OH), and 6.43 (1H, s, 14-H). Found: C, 76.08; H, 9.14%. Calcd for $C_{20}H_{28}O_3$: C, 75.91; H, 8.92%.

(15*S*)-12,16-Epoxy-8,11,13-abietatrien-11-ol (8a) and Its (15*R*)-Epimer (8b). a): A mixture of the crude **6a** (730 mg) and methanesulfonyl chloride (0.26 ml) in pyridine (7.0 ml) was stirred at 0—5 °C for 30 min and then at room temperature for 2.5 h. The mixture was poured into ice-dilute hydrochloric acid and extracted with ether. The ether extract was washed with aqueous sodium hydrogencarbonate and brine, dried, and evaporated in vacuo to give a crude mesylate (**7a**) (1.025 g), ^{1}H NMR (60 MHz) δ=0.98 (3H, s, 4-CH_3), 1.30 (3H, d, *J*=7 Hz, 15-CH_3), 1.40 (3H, s, 10-CH_3), 3.01 (3H, s, -$CH_2OSO_2C\underline{H_3}$), 3.75 (1H, d, *J*=9 Hz) and 4.10 (1H, d, *J*=9 Hz) (-C$\underline{H_2}$OMs), 4.02 (1H, t, *J*=8 Hz) and 4.67 (1H, t, *J*=8 Hz) (15-CH_2O-), and 6.42 (1H, s, 14-H).

A stirred mixture of the above crude **7a** (1.010 g), sodium iodide (1.95 g), and zinc powder (1.68 g) in *N*,*N*-dimethylformamide (24 ml) was heated at 120—125 °C for 10 h. The mixture was cooled, diluted with ether, and then filtered. The filtrate was washed successively with aqueous sodium thiosulfate and brine, dried, and evaporated in vacuo. The residue was chromatographed on silica gel (30 g), using hexane–benzene (3:2) as an eluent, to give **8a** (389 mg: 56.2% yield from **5a**). IR 3575 cm^{-1}, $[\alpha]_D$+76.3 ° (*c* 0.93); ^{1}H NMR (60 MHz) δ=0.95 (6H, s, -$\underset{|}{C}(CH_3)_2$), 1.28 (3H, d, *J*=7 Hz, 15-CH_3), 1.35 (3H, s, 10-CH_3), 4.01 (1H, t, *J*=8.5 Hz) and 4.65 (1H, t, *J*=8.5 Hz) (15-CH_2O-), 4.91 (1H, s, 11-OH), and 6.40 (1H, s, 14-H). Found: C, 79.75; H, 9.58%. Calcd for $C_{20}H_{28}O_2$: C, 79.95; H, 9.39%.

b): A solution of the crude **6b** (1.050 g) in pyridine (10 ml) was treated with methanesulfonyl chloride (0.37 ml) as described in a) to give a crude mesylate (**7b**) (1.239 g). ^{1}H NMR (60 MHz) δ=0.99 (3H, s, 4-CH_3), 1.29 (3H, d, *J*=7 Hz, 15-CH_3), 1.38 (3H, s, 10-CH_3), 3.01 (3H, s, -$CH_2OSO_2C\underline{H_3}$), 3.72 (1H, d, *J*=9 Hz) and 4.08 (1H, d, *J*=9Hz) (-C$\underline{H_2}$OMs), 4.03 (1H, dd, *J*=9 and 6 Hz) and 4.68 (1H, t, *J*=9 Hz) (15-CH_2O-), 5.02 (1H, s, 11-OH), and 6.42 (1H, s, 14-H).

A stirred mixture of the above crude **7b** (1.239 g), sodium iodide (2.36 g), and zinc powder (2.05 g) in *N*,*N*-dimethylformamide (20 ml) was heated at 120—125 °C for 10 h. After the work-up as described in a), the crude product was chromatographed on silica gel (30 g), using hexane–benzene (3:2) as an eluent, to give **8b** (469 mg: 53.4% yield from **5b**). IR 3565 cm^{-1}; ^{1}H NMR (60 MHz) δ=0.93 (6H, s, -$\underset{|}{C}(CH_3)_2$), 1.27 (3H, d, *J*=7 Hz, 15-CH_3), 1.33 (3H, s, 10-CH_3), 4.00 (1H, dd, *J*=8 and 7 Hz) and 4.63 (1H, t, *J*=8 Hz) (15-CH_2O-), 4.96 (1H, s, 11-OH), and 6.40 (1H, s, 14-H). Found: C, 79.82; H, 9.63%. Calcd for $C_{20}H_{28}O_2$: C, 79.95; H, 9.39%.

(15*S*)-12,16-Epoxy-8,12-abietadiene-11,14-dione (9a) and Its (15*R*)-Epimer (9b). a): A stirred solution of **8a** (33.2 mg) in *N*,*N*-dimethylformamide (4.0 ml) was protected from light with aluminum foil. After the addition of a solution of Fremy's salt (potassium nitrosodisulfonate) (149 mg) and potassium dihydrogenphosphate (58 mg) in water (6.0 ml), the mixture was stirred at room temperature under a stream of nitrogen for 2 h. The mixture was then extracted with ether. The ether extract was washed with brine, dried, and evaporated in vacuo. The residue was chromatographed on silica gel (5 g), using hexane–chloroform (1:1) as an eluent, to give recovered **8a** (3.8 mg: 11.4% yield). Further elution afforded **9a** (28.0 mg: 80.2% yield), mp 143.5—144.5 °C (from methanol), $[\alpha]_D$+11.6 ° (*c* 1.73), IR 1670, 1650, and 1640 cm^{-1}; ^{1}H NMR δ=0.88 and 0.91 (each 3H and s, -$\underset{|}{C}(CH_3)_2$), 1.25 (3H, s, 10-CH_3), 1.28 (3H, d, *J*=7 Hz, 15-CH_3), 3.50 (1H, m, 15-H), and 4.18 (1H, dd, *J*=9 and 6 Hz) and 4.71 (1H, t, *J*=9 Hz) (15-CH_2O-). Found: C, 76.08; H, 8.52%. Calcd for $C_{20}H_{26}O_3$: C, 76.40; H, 8.34%.

b): A stirred solution of **8b**(180.0 mg) in *N*,*N*-dimethylformamide (21.6 ml) was protected from light with aluminum foil. After the addition of a solution of Fremy's salt (804 mg) and potassium dihydrogenphosphate (310 mg) in water (32.4 ml), the mixture was stirred at room temperature under a stream of nitrogen for 2 h. After the work-up as described in a), the crude product was chromatographed on silica gel (15 g), using hexane–chloroform (1:1) as an eluent, to give recovered **8b** (14.9 mg: 8.3% yield) and **9b** (155.7 mg: 82.6% yield), mp 154—155 °C (from methanol), $[\alpha]_D$+128 ° (*c* 0.85), IR 1670, 1650, and 1640 cm^{-1}; ^{1}H NMR δ=0.89 and 0.92 (each 3H and s, -$\underset{|}{C}(CH_3)_2$), 1.25 (3H, s, 10-CH_3), 1.30 (3H, d, *J*=7 Hz, 15-CH_3), 3.50 (1H, m, 15-H), and 4.18 (1H, dd, *J*=9 and 6 Hz) and 4.72 (1H, t, *J*=9 Hz) (15-CH_2O-). Found: C, 76.33; H, 8.54%. Calcd for $C_{20}H_{26}O_3$: C, 76.40; H, 8.34%.

(15*S*)-11,14-Diacetoxy-12,16-epoxy-8,11,13-abietatriene (10a) and Its (15*R*)-Epimer (10b). a): A mixture of **9a** (73.4 mg), acetic anhydride (0.5 ml), and zinc powder (50 mg) in pyridine (1.0 ml) was stirred at 0—5 °C for 10 min and then at room temperature for 2.5 h. The mixture was poured into ice-dilute hydrochloric acid and extracted with ether. The ether extract was washed successively with aqueous sodium hydrogencarbonate and brine, dried, and evaporated in vacuo. The residue was chromatographed on silica gel (10 g), using ether–benzene (1:99) as an eluent, to give **10a** (88.0 mg: 94.1% yield), mp 161—162 °C (from hexane), $[\alpha]_D$+47.2 ° (*c* 1.63), IR 1758 cm^{-1}; ^{1}H NMR δ=0.88 and 0.91 (each 3H and s, -$\underset{|}{C}(CH_3)_2$), 1.23 (3H, s, 10-CH_3), 1.23 (3H, d, *J*=7 Hz, 15-CH_3), 2.27 (6H, s, 2-$OCOCH_3$), 3.52 (1H, m, 15-H), and 4.08 (1H, dd, *J*=9 and 6 Hz) and 4.63 (1H, t, *J*=9 Hz)

(15-CH_2O-). Found: C, 72.20; H, 8.26%. Calcd for $C_{24}H_{32}O_5$: C, 71.97; H, 8.05%.

b): A mixture of **9b** (53.0 mg), acetic anhydride (0.3 ml), and zinc powder (30 mg) in pyridine (0.5 ml) was stirred at 0—5 °C for 10 min and then at room temperature for 2.5 h. After the work-up as described in a), the crude product was recrystallized from hexane to give **10b** (48.2 mg: 71.4% yield), mp 168—170 °C, $[\alpha]_D$+87.5 ° (*c* 0.96), IR 1760 cm^{-1}; ^1H NMR δ=0.89 and 0.91 (each 3H and s, $-C(CH_3)_2$), 1.20 (3H, d, *J*=7 Hz, 15-CH_3), 1.23 (3H, s, 10-CH_3), 2.27 (6H, s, 2-$OCOCH_3$), 3.51 (1H, m, 15-H), and 4.08 (1H, dd, *J*=9 and 6 Hz) and 4.62 (1H, t, *J*=9 Hz) (15-CH_2O-). Found: C, 72.08; H, 8.17%. Calcd for $C_{24}H_{32}O_5$: C, 71.97; H, 8.05%. The mother liquor of recrystallization was evaporated in vacuo. The residue was chromatographed on silica gel (5 g), using ether–benzene (1:99) as an eluent, to give additional **10b** (16.5 mg: 24.4% yield).

(15*S*)-11,14-Diacetoxy-12,16-epoxy-8,11,13-abietatrien-7-one (11a) and Its (15*R*)-Epimer (11b). a): A mixture of **10a** (72.3 mg) and chromium trioxide (54.1 mg) in acetic acid (0.7 ml) was stirred at 0—5 °C for 5 min and then at room temperature for 1 h. The mixture was diluted with water and extracted with ether. The ether extract was washed successively with water, aqueous sodium hydrogencarbonate, and brine, dried, and evaporated in vacuo. The residue was chromatographed on silica gel (10 g), using ether–benzene (1:99) as an eluent, to give **11a** (53.8 mg: 71.9% yield), $[\alpha]_D$+63.2 ° (*c* 0.87) (natural hyptol diacetate, $[\alpha]_D$+63.8 ° (*c* 0.24)[3]), IR 1765 and 1670 cm^{-1}; ^1H NMR δ=0.92 and 0.94 (each 3H and s, $-C(CH_3)_2$), 1.32 (3H, d, *J*=7 Hz, 15-CH_3), 1.33 (3H, s, 10-CH_3), 2.30 and 2.36 (each 3H and s, 2-$OCOCH_3$), 3.60 (1H, m, 15-H), and 4.19 (1H, dd, *J*=9 and 6 Hz) and 4.73 (1H, t, *J*=9 Hz) (15-CH_2O-). Found: C, 69.77; H, 7.48%. Calcd for $C_{24}H_{30}O_6$: C, 69.54; H, 7.30%.

b): A mixture of **10b** (120.1 mg) and chromium trioxide (90 mg) in acetic acid (1.2 ml) was stirred at 0—5 °C for 5 min and then at room temperature for 1 h. After the work-up as described in a), the crude product was chromatographed on silica gel (10 g), using ehter-benzene (5:95) as an eluent, to give **11b** (91.9 mg: 72.4% yield), mp 178—179 °C (from hexane), $[\alpha]_D$+119 ° (*c* 2.39), IR 1765 and 1670 cm^{-1}; ^1H NMR δ=0.91 and 0.94 (each 3H and s, $-C(CH_3)_2$), 1.27 (3H, d, *J*=6 Hz, 15-CH_3), 1.30 (3H, s, 10-CH_3), 2.29 and 2.35 (each 3H and s, 2-$OCOCH_3$), 3.57 (1H, m, 15-H), and 4.21 (1H, dd, *J*=9 and 6 Hz) and 4.72 (1H, t, *J*=9 Hz) (15-CH_2O-). Found: C, 69.50; H, 7.40%. Calcd for $C_{24}H_{30}O_6$: C, 69.54; H, 7.30%.

(15*S*)-12,16-Epoxy-11,14-dihydroxy-8,11,13-abietatrien-7-one (Hyptol) (1a) and Its (15*R*)-Epimer (1b). a): A mixture of **11a** (19.1 mg) and dilute hydrochloric acid (15%, 0.2 ml) in ethanol (1.0 ml) was refluxed for 24 h. After removal of the ethanol in vacuo, the residue was extracted with ether. The ether extract was washed with brine, dried, and evaporated in vacuo. The residue was chromatographed on silica gel (5 g), using hexane–chloroform (1:2) as an eluent, to give **1a** (14.9 mg: 98.0% yield), mp 200—203 °C (from hexane), $[\alpha]_D$+52.5 ° (*c* 0.20), IR 3570, 3325, and 1620 cm^{-1}; ^1H NMR δ=0.95 (6H, s, $-C(CH_3)_2$), 1.36 (3H, s, 10-CH_3), 1.39 (3H, d, *J*=7 Hz, 15-CH_3), 3.68 (1H, m, 15-H), 4.26 (1H, dd, *J*=9 and 6 Hz) and 4.77 (1H, t, *J*=9 Hz) (15-CH_2O-), 4.63 (1H, s, 11-OH), and 13.39 (1H, s, 14-OH). Found: C, 72.81; H, 7.76%. Calcd for $C_{20}H_{26}O_4$: C, 72.70; H, 7.93%. The physical and spectral data of the synthetic **1a** were identical to those of natural hyptol, mp 202—203 °C,[1] $[\alpha]_D$+56 °;[1] ^1H NMR[3] δ=0.95 (6H, s, $-C(CH_3)_2$), 1.36 (3H, s, 10-CH_3), 1.39 (3H, d, *J*=7 Hz, 15-CH_3), 3.68 (1H, m, 15-H), 4.26 (1H, dd, *J*=9 and 6 Hz) and 4.77 (1H, t, *J*=9 Hz) (15-CH_2O-), 4.62 (1H, s, 11-OH), and 13.39 (1H, s, 14-OH).

b): A mixture of **11b** (52.6 mg) and dilute hydrochloric acid (15%, 0.3 ml) in ethanol (2.0 ml) was refluxed for 23 h. After the work-up as described in a), the crude product was chromatographed on silica gel (5 g), using hexane–chloroform (1:2) as an eluent, to give **1b** (30.0 mg: 71.6% yield), mp 210—211 °C (from hexane), $[\alpha]_D$+127 ° (*c* 0.46), IR 3575, 3350, and 1620 cm^{-1}; ^1H NMR δ=0.95 (6H, s, $-C(CH_3)_2$), 1.34 (3H, s, 10-CH_3), 1.38 (3H, d, *J*=6 Hz, 15-CH_3), 3.70 (1H, m, 15-H), 4.25 (1H, dd, *J*=9 and 6 Hz) and 4.79 (1H, t, *J*=9 Hz) (15-CH_2O-), 4.63 (1H, s, 11-OH), and 13.39 (1H, s, 14-OH). Found: C, 72.57; H, 8.14%. Calcd for $C_{20}H_{26}O_4$: C, 72.70; H, 7.93%.

The authors are grateful to Professor F. D. Monache, Universita Cattolica S. Cuore, for kindly supplying the samples and spectral date of natural hyptol and its diacetate.

References

1) F. D. Monache, F. Marletti, G. Marini-Bettolo, J. F. D. Mello, and I. L. D'Albuquerque, *Gazz. Chim. Ital.*, **107**, 319 (1977).

2) T. Matsumoto, S. Imai, and N. Hayashi, *Bull. Chem. Soc. Jpn.*, **61**, 2405 (1988).

3) Optical rotation and ^1H NMR spectrum were measured in our laboratory.

 © 1991 The Chemical Society of Japan Bull. Chem. Soc. Jpn., 64, 2766—2771 (1991) [Vol. 64, No. 9

Substituent Effect in *o*-Nitroperbenzoic Acid Oxidation of *m*- and *p*-Substituted Acetophenones

Katsuo TOKEN,* Kenji HIRANO, Tai YOKOYAMA, and Katsumi GOTO
Department of Chemistry, Faculty of Science, Toyama University,
Gofuku, Toyama 930
(Received March 29, 1991)

The Baeyer–Villiger reaction of *m*- and *p*-substituted acetophenones (substituents: H, *p*-MeO, *p*-*t*-Bu, *p*-*i*-Pr, *p*-Et, *p*-Me, *p*-Cl, *p*-Br, *m*-MeO, *m*-Me, *m*-Cl) with *o*-nitroperbenzoic acid was studied in chloroform at 30 °C. The rate constants for the general acid catalysis were measured at several concentrations of *o*-nitrobenzoic acid which acted as an acid catalyst. The uncatalyzed and acid-catalyzed rate constants obtained afforded ρ values of −2.16 and −4.11 with σ, respectively. The results indicated that the rate-determining step is the migration of the phenyl group in the peroxy acid-carbonyl adduct for all the substituents studied, whether the reaction is acid-catalyzed or not, and that the acid catalyst intervenes only in the formation of the acid-ketone adduct in the initial state and not in the migration step. The variation of the leaving group abilities required the variation of the substituent constants applied, whereas the acid intervention in the addition step was reflected only in the variation of the ρ value, not in the substituent constants to be applied. The smaller resonance demand for *o*-nitroperbenzoic acid indicated that the structure of the transition state in the migration step was looser and that the position of the transition state was earlier than those for *m*-chloroperbenzoic acid.

It is generally accepted that the Baeyer–Villiger reaction[1a-d] is subject to general acid catalysis and the rate-determining step is the migration in the peroxy acid-carbonyl adduct[2] as depicted in Scheme 1, although

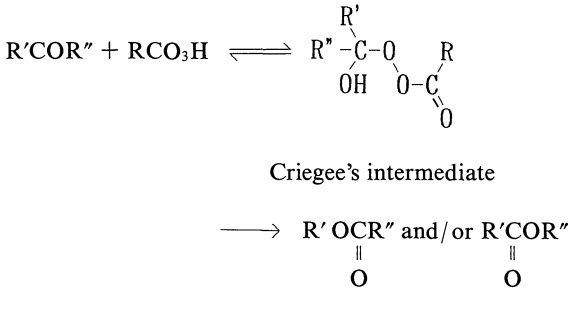

Scheme 1.

there is a possibility that the addition step is rate-determing if the migrating group has a strong electron-releasing moiety.[3] The substituent effect on the Baeyer–Villiger reaction has been studied by many investigators, although reliable data are few because of small numbers of data sets with large experimental errors. Most studies have been done either under conditions where an uncatalyzed "spontaneous" process prevails or under conditions where an acid-catalyzed process prevails. The uncatalyzed reaction of *p*-substituted acetophenones with *m*-chloroperbenzoic acid in chloroform has afforded a ρ value of −1.36 with σ^+,[4] while the acid-catalyzed reactions of *m*- and *p*-substituted acetophenones with trifluoroperacetic acid in the presence of trifluoroacetic acid in ethylene chloride and in acetonitrile have afforded ρ values of −1.10 and −1.45 with σ, respectively.[2] This implies that the substituent constant employed as well as the magnitude of the reaction constant obtained vary with the peroxy acid employed and with the reaction conditions employed, although both reaction systems seem to accompany the other suppressed process to some extent. As to the above acid-catalyzed reaction, the measurements of UV spectra have clearly indicated the presence of a complex of trifluoroacetic acid with acetophenone in ethylene chloride,[2] implying the intervention of the catalyst in the addition step, but no evidence was obtained about whether the migration step is also acid-catalyzed. If the migration step proceeds by a concerted mechanism between the migrating group and the leaving group, the variation of the leaving group abilities is expected to cause some variations in the parameters. Comparisons between the parameters for both processes may give information about whether the catalyst operates in the migration step or not. A similar line of argument is applicable to the addition step. Thus, a correct interpretation of the difference between the parameters is only possible by eliminating the differences in experimental conditions except for the catalyst. With the above goals in mind, we studied the reaction of *o*-nitroperbenzoic acid with *m*- and *p*-substituted acetophenones in chloroform under conditions where both the uncatalyzed and the acid-catalyzed processes proceeded simultaneously.

Results and Discussion

Determination of the Kinetic Law. In order to obtain the kinetic law, an equimolar (5×10^{-2} M) (1 M= 1 mol dm^{-3}) reaction of *p*-methylacetophenone with *o*-nitroperbenzoic acid in chloroform at 30 °C was carried out as a typical example. It was followed by iodometric titration of the residual peroxy acid. Even when the reaction was allowed to start without the acid catalyst, the reaction did not follow any definite kinetic law due to autocatalysis. However, when a certain amount of *o*-nitrobenzoic acid, e.g., 1.5×10^{-2} M, was initially present in the above chloroform solution, the reaction proceeded with an adequate rate and the initial reaction rate strictly

obeyed first-order kinetics (corr coeff: more than 0.999) with respect to the ketone or the peroxy acid concentration to ca. 30% completion of the reaction, although the reaction conditions did not satisfy those of pseudo-first-order kinetics:

$$v = k_{obs}[K], \quad (1)$$

where [K] is the ketone concentration.[5] The influence of the product ester on the reaction rate was not observed at least to 20% completion of the reaction.[6] Equation 1 was followed over the initial ketone concentrations from 2×10^{-2} M to 1.5×10^{-1} M with the invariable observed rate constant so far as the initial concentrations of the other two reactants remained unaltered. To elucidate the apparent simplicity of the kinetics in spite of a lack of pseudo-first-order conditions, it was necessary to examine the relationships between the observed rate constant and the concentration of the other two reactants. The observed rate constant was proportional to the initial peroxy acid concentration over a range of 2.5×10^{-2} to 7.5×10^{-2} M, with the initial concentration of the ketone and the acid kept at 5×10^{-2} and 1.5×10^{-2} M, respectively:

$$k_{obs} = k'_{obs}[PA]_0, \quad (2)$$

where $[PA]_0$ is the initial peroxy acid concentration and k'_{obs} is a constant that depends on the initial acid concentration. With increasing concentrations of the initial acid catalyst over a range of 7.5×10^{-4} to 2.4×10^{-2} M, the value of $k_{obs}/[PA]_0$ linearly increased as shown in Fig. 1, and was expressed as Eq. 3:

$$k_{obs}/[PA]_0 = k_0 + k_{HA}[HA]_0, \quad (3)$$

where $[HA]_0$ is the initial acid concentration, and k_0 and k_{HA} are the rate constants for the uncatalyzed and the acid-catalyzed processes, respectively. The values of these constants were evaluated from the intercept and slope, respectively, by plotting $k_{obs}/[PA]_0$ against $[HA]_0$. The reproducibility of the k_{obs} value was within ±2% on repeated runs, and was considered to be sufficient to calculate k_0 and k_{HA} values. The values obtained are summarized in Table 1. Hammett plots for k_0 and k_{HA} are shown in Figs. 2 and 3, giving ρ values of −2.16 (corr coeff: 0.995) and −4.11 (corr coeff: 0.992) with σ, respectively. Data for m-MeO, p-Cl, and p-Br, which considerably deviated upward from the correlation lines, were not employed for these calculations. Examination of the product(s) by gas chromatography and ^{1}H NMR indicated that the product ester was derived from the exclusive migration of the phenyl group, i.e., p-substituted phenyl acetate in p-methoxy-, p-methyl-, p-chloro-, and unsubstituted acetophenones. Another product anticipated from the methyl migration was not detected at all.

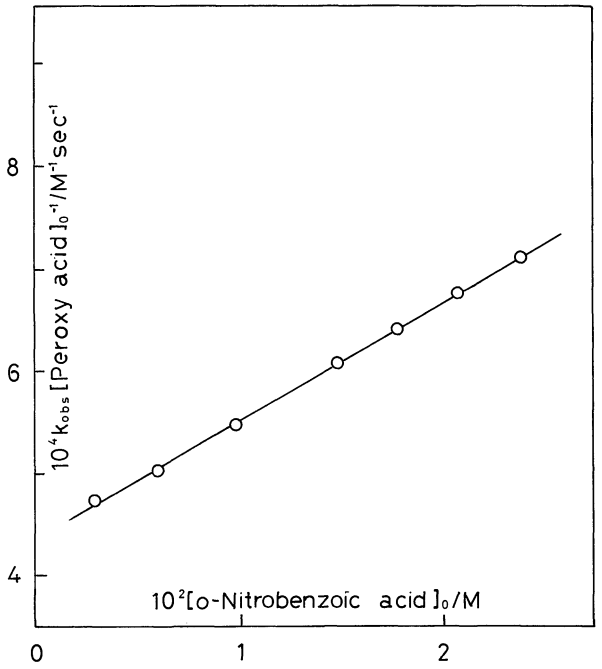

Fig. 1. The plot of $k_{obs}/[PA]_0$ against $[HA]_0$ for p-methylacetophenone.

Table 1. k_0 and k_{HA} Values for o-Nitroperbenzoic Acid Oxidation of m- and p-Substituted Acetophenones in Chloroform at 30°C

Substituent	$10^4 k_0/M^{-1} s^{-1}$	$10^3 k_{HA}/M^{-2} s^{-1}$
H	1.79±0.02	1.99±0.02
p-MeO	7.19±0.08	26.1±0.3
p-t-Bu	4.84±0.02	13.8±0.1
p-i-Pr	4.73±0.02	14.5±0.1
p-Et	4.69±0.01	13.4±0.03
p-Me	4.34±0.05	11.4±0.1
p-Cl	1.10±0.01	0.752±0.003
p-Br	1.05±0.01	0.654±0.004
m-MeO	2.91±0.04	4.43±0.06
m-Me	3.16±0.01	6.92±0.02
m-Cl	0.311±0.001	0.0723±0.0002

Rate-Determining Step and Dependence of Substituent Constant on the Leaving Group. The ρ values obtained in the two plots (see Figs. 2 and 3) were negative, indicating that the migration step played a decisive role for the overall energy of the reaction and therefore was rate-determining for both the uncatalyzed (k_0 process) and the acid-catalyzed (k_{HA} process) processes. With reference to Palmer and Fry's work[4] on the ^{14}C-kinetic isotope effect and substituent effect on m-chloroperbenzoic acid oxidation of a series of p-substituted acetophenones-1′-^{14}C in chloroform, Ogata and Sawaki[3] pointed out that strong electron-releasing substituents such as p-MeO changed the rate-determining step from the migration step to the addition step on the grounds that the p-MeO showed no kinetic isotope effect and a downward deviation by ca. 0.5 log unit[7] in Hammett

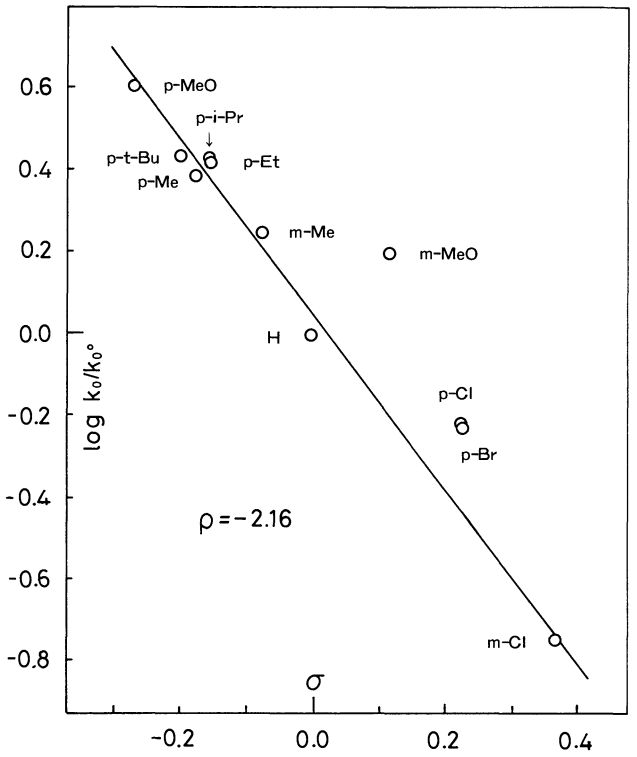

Fig. 2. Hammett plot for the k_0 process.

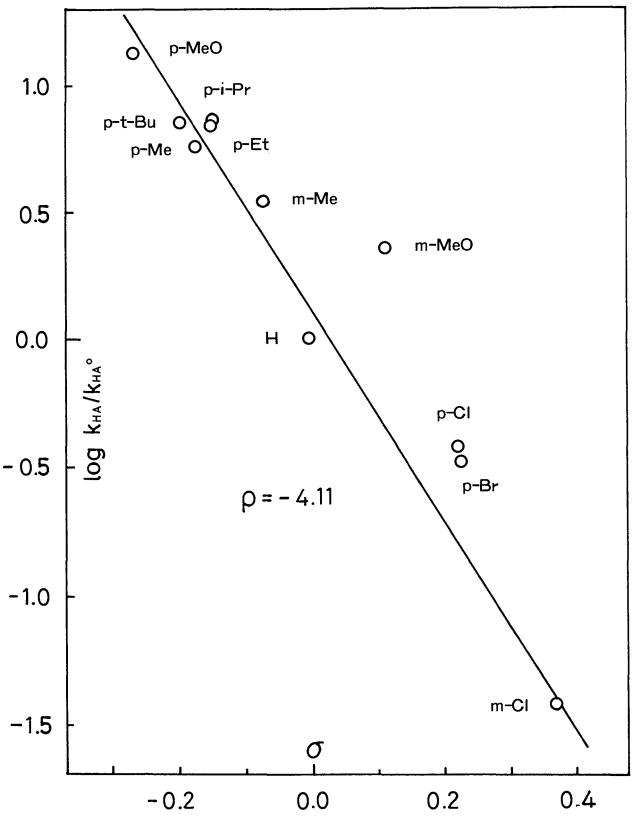

Fig. 3. Hammett plot for the k_{HA} process.

plots with σ^+. The substituent on the peroxy acid may have had little effect on the addition step, because the attack of the peroxy acid on the carbonyl carbon of the acetophenone occurs at its terminal oxygen conjugatively insulated from the rest of the peroxy acid. The substituent on the phenyl group of the acetophenone should have a normal effect expected from the ordinary carbonyl addition reactions in this step. On the other hand, in the migration step, the benzoyloxyl group, which originates from part of the peroxy acid, acts as a leaving group. A substituent on the group is expected to influence the reaction, as is described below. The substituent effect due to the migrating phenyl group should largely depend on the degree of the participation of the migrating phenyl on the migration-terminus oxygen. The degree of the phenyl participation, in turn, depends on the ability of the leaving group to depart from the oxygen, as long as the migration proceeds synchronously. As a whole, the difference in the substituent effects observed between the case for *m*-chloroperbenzoic acid and that for *o*-nitroperbenzoic acid is exclusively attributable to the difference in the leaving abilities of the benzoyloxyl groups between the peroxy acids in the migration step, and is not ascribed to the difference in the substituent effects between the peroxy acids in the addition step, since the electrophiles employed were the same for both reaction systems. If the leaving group ability is closely related to the acidity of the carboxylic acid from which the leaving group is derived, the leaving ability of the *m*-chlorobenzoyloxyl group is lower than that of the *o*-nitrobenzoyloxyl group. A better leaving group decreases the energy of the transition state more in the migration step. The rate-determining step in our case was the migration step for all the substituents studied, including the *p*-MeO group. The case for *m*-chloroperbenzoic acid should have been in the same category as that for *o*-nitroperbenzoic acid, since, in the former case, the reaction required more energy of the transition state in the migration step and therefore later transition state[8] and stronger π-interaction between the migrating phenyl π-system and the migration-terminus oxygen than those for *o*-nitroperbenzoic acid. Since the reported rate constants to which the Brown $\rho^+\sigma^+$ equation was applied were of second order (first order in ketone and first order in peroxy acid), it seemed to imply that the reaction had been carried out under the condition $k_0 \gg k_{HA}[HA]$ for *m*-chloroperbenzoic acid. Even if the rate constants observed corresponded to the k_0 values, it was still better to apply the data set to the Yukawa–Tsuno equation than the Brown $\rho^+\sigma^+$ equation used by Palmer and Fry,[4] and by Ogata and Sawaki.[3] The former equation gave a ρ value of -1.62 and a corr coeff of 0.993 when an r value of 0.54 was adopted.[9] Thus, the variation of the leaving group abilities required the variation of the substituent constants applied. The variation of the resonance demand suggested that the structure of the transition

state in the migration step was tighter for *m*-chloroperbenzoic acid than for *o*-nitroperbenzoic acid and therefore the position of the transition state was relatively late for the former, and vice versa. This was in good agreement with theoretical predictions for the transition-state geometry of the Baeyer–Villiger reaction.[10]

Acid Catalysis in the k_{HA} Process. The k_0 process gave a ρ value of -2.16 with σ as a result of opposite substituent effects between the addition step and the migration step. In the k_{HA} process, a ρ value of -4.11 was obtained with σ. The magnitude of the $|\rho|$ value for the k_{HA} process was almost twice as large as that for the k_0 process. This large difference in magnitude could be rationalized by examining the influence of the acid intervention on the individual steps in the k_{HA} process. If the acid catalyst acts only on the carbonyl or acyloxy oxygen of the leaving group in the migration step, the leaving group departs much more easily from the rest of the Criegee's intermediate. The better leaving group induced by the acid catalyst would thus decrease the energy of the transition state more in this step, promoting the earlier transition state and making it more reactant-like,[8] viz., more Criegee's intermediate-like. The substituent effect on the migration step would therefore decrease due to the less effective participation of the phenyl group on the migration-terminus oxygen in the k_{HA} process than that in the k_0 process. Thus, the overall substituent effect on the k_{HA} process was expected to become much smaller in magnitude than that on the k_0 process. The relative magnitude of the observed ρ values, however, showd the reverse, which indicated that the contribution of the acid catalyst to the migration step of the k_{HA} process should have been negligibly small or ruled out. On the other hand, if the acid catalyst operates only on the carbonyl group of the acetophenone in the initial state, the polarization of the carbonyl group is enhanced even by weak hydrogen bonding,[11] making the ketone more reactive to the nucleophile. It has been shown that acid-catalyzed carbonyl addition reactions are relatively insensitive to the substituent effect.[2,12] The acid-catalyzed addition step in this reaction would therefore be facilitated with a smaller contribution of the substituent effect. Consequently, the overall substituent effect would be mainly governed by the substituent effect on the migration step. A larger $|\rho|$ value was expected in the k_{HA} process than in the k_0 process. This was in good accordance with the relative magnitude of the $|\rho|$ values obtained in both processes. Since the substituent effect on the migration step was nearly the same for the k_0 process and the k_{HA} process in this case, the difference (1.95) in the observed ρ values between the two processes should refer to the intervention of the acid catalyst in the addition step of the k_{HA} process. The last possibility is that the acid catalyzes both the addition step and the migration step successively. As discussed above separately, the intervention of the acid catalyst decreases the substituent effect on each step. Neither of the influences of the decreases in the individual steps on the ρ value is therefore predominant, and the decrease in the rate-determining migration step would probably be a little larger than that in the addition step. The ρ value in the k_{HA} process was therefore expected to become one between the ρ values for the two extreme cases mentioned above, and to be comparable to that in the k_0 process. As for the trifluoroperacetic acid oxidation of *m*- and *p*-substituted acetophenones in the presence of trifluoroacetic acid,[2] the acid-catalyzed process seemed to predominte ($k_0 \ll k_{HA}[HA]$). The low nucleophilicity and the low basicity of the leaving group were coincident with the applicability of the σ value. Although the ρ value for the k_0 process was not available for trifluoroperacetic acid, the fact that the magnitude of the ρ value for trifluoroperacetic acid was ca. a third of that for *o*-nitroperbenzoic acid in the k_{HA} process seemed to imply the acid intervention in the migration step as well as in the addition step.

Similarity Between the k_0 Process and the k_{HA} Process. In Fig. 4 the logarithmic rates for the k_{HA} process are plotted against those for the k_0 process, giving a linear correlation with a corr coeff of 0.999 including *m*-MeO, *p*-Cl, and *p*-Br which deviated upward from the lines of Hammett plots (Figs. 2 and 3). This indicated that these two processes proceeded essentially by the same mechanism, although there was pre-equilibrium for the formation of the acid-ketone adduct in the k_{HA} process.

Abnormality for Some Substituents. *m*-Methoxyacetophenone deviated upward from the Hammett lines (Figs. 2 and 3) by ca. 0.4 and 0.7 log unit for the k_0 process and for the k_{HA} process, respectively, while *p*-methoxyacetophenone showed normal behavior on the lines. The basicity of the substituent, *p*-MeO, is decreased due to its conjugation with the carbonyl of the

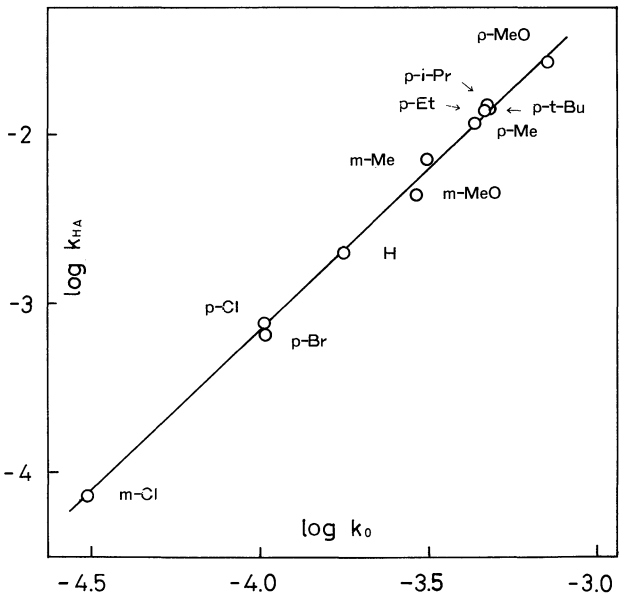

Fig. 4. Linear free energy relationship of k_{HA} vs. k_0.

ketone, whereas *m*-MeO is conjugatively insulated from the carbonyl. It is conceivable that *m*-MeO maintains its basicity enough to form a hydrogen bond with the solvent (specific solvation effect) in the initial state, making the substituent more electron-attractive and therefore making the ketone more reactive in the addition step. Similar enhancement has been observed for *m*-MeO by Friess and Soloway[13] in the reaction of *m*- and *p*-substituted acetophenones with perbenzoic acid in chloroform. The substituents *p*-Cl and *p*-Br also showed upward deviations from the Hammett lines by ca. 0.23—0.24 and 0.34—0.38 log unit for the k_0 process and for the k_{HA} process, respectively. These deviations are a little too large to be regarded as experimental errors. Considering that *m*-Cl behaved well, it might be conceivable that a free radical path (homolytic fission of the -O-O- bond in the Criegee's intermediate)[14] for *p*-Cl and *p*-Br was accompanied in the migration step. The radical reaction may have been accelerated by *p*-halophenyl participation on the migration-terminus oxygen.

Experimental

The boiling points are uncorrected. ^{1}H NMR spectra were obtained on a JEOL JNM-MH 60 spectrometer in δ values relative to the internal TMS. Gas chromatographic analyses were carried out on a Hitachi K 53 with a 30-m golay column of apiezon L high vacuum grease and FID.

***o*-Nitroperbenzoic Acid.** The title compound was prepared by the reaction of *o*-nitrobenzoic acid with 90% hydrogen peroxide in methanesulfonic acid, according to the procedure described by Silbert et al.[15] Further treatment was necessary for its use in the kinetic experiments. The compound obtained was dissolved in purified chloroform at room temperature, washed with distilled water four times in order to remove a trace of methanesulfonic acid, and then dried over anhydrous sodium sulfate for a few minutes. After the sodium sulfate was removed by filtration, the filtrate was concentrated under reduced pressure at 30 °C until a certain amount of the compound had precipitated. This precipitate was redissolved at a temperature not above 40—45 °C within ten minutes. After filtration, the solution was cooled to −20 °C to give light yellow needles. The amount of active oxygen was estimated to be 100±1% by iodometric titration. The compound was kept in a refrigerator.

***p*-Substituted Acetophenones.** *p*-Methyl-, *p*-chloro-, and *p*-bromoacetophenones were prepared by Friedel–Crafts reactions following the usual procedure in carbon disulfide.[16] *p*-Methoxy-, *p*-*t*-butyl-, *p*-isopropyl-, and *p*-ethylacetophenones were prepared by the Perrier modification[17] of the Friedel–Crafts reaction in carbon tetrachloride. The compounds were purified through the recrystallization of their semicarbazones except for *p*-methoxyacetophenones, followed by repeated distillations of regenerated ketones using concd HCl. *p*-Methoxyacetophenone was purified by fractional recrystallization, followed by distillation. Commercially-obtained acetophenone was purified by repeated distillations. The compounds thus obtained were all pure according to gas chromatography. Substituents and boiling points for these compounds were as follows: *p*-MeO, 142.0—142.5 °C/18 mmHg (lit,[18] 139 °C/15 mmHg) (1 mmHg=133.32 Pa); *p*-*t*-Bu, 140—140.5 °C/18 mmHg (lit,[17] 137—138 °C/16 mmHg); *p*-*i*-Pr, 123.0—123.5/14.5 mmHg (lit,[19] 115 °C/10 mmHg); *p*-Et, 127 °C/22 mmHg (lit,[17] 116—117 °C/13 mmHg); *p*-Me, 105 °C/18.5 mmHg (lit,[18] 93.5 °C/7 mmHg); *p*-Cl, 118 °C/20 mmHg (lit,[18] 99.0 °C/7 mmHg); *p*-Br, 133.5—134.0 °C/19.5 mmHg (lit,[18] 117.0 °C/7 mmHg); H, 84.5—85.0 °C/17 mmHg (lit,[18] 88.5 °C/16 mmHg).

***m*-Substituted Acetophenones.** *m*-Methoxy-, *m*-methyl-, and *m*-chloroacetophenones were prepared by the usual procedures from *m*-hydroxyacetophenone, *m*-methylbenzoic acid and *m*-aminoacetophenone, respectively, and were purified by the same manner as described in the preparation of the *p*-substituted acetophenones. The compounds obtained were all pure according to gas chromatography. Substituents and boiling points for these compounds were as follows: *m*-MeO, 132 °C/20 mmHg (lit,[20] 125—126 °C/12 mmHg); *m*-Me, 109 °C/22 mmHg (lit,[21] 65—71 °C/0.2 mmHg); *m*-Cl, 110.5—111.5 °C/17 mmHg (lit,[22] 80 °C/2.5 mmHg).

Solvent. Chloroform used for the kinetics as a solvent was purified by washing with concd sulfuric acid as described in the literature[23] just prior to use.

Product Analyses. The reaction products were analyzed by use of ^{1}H NMR and gas chromatography. The analytical procedures in the case of acetophenone described below were also applied to the other cases of *p*-methoxy-, *p*-methyl-, and *p*-chloroacetophenones. At the end of a kinetic run, the residual solution was examined by ^{1}H NMR, which showed no signal (δ=3.94) for the methyl group of the methyl ester but showed a signal (δ=2.28) for that of the acetate and a signal (δ=2.62) for that of the unreacted ketone. Blank tests proved that the detection of the methyl ester was possible when the molar ratio of methyl ester to acetate was higher than 3/100. Another portion of the residual solution was washed successively with cold 5% potassium iodide aq once, with cold 3% sodium thiosulfate aq twice, with cold 6% sodium hydrogencarbonate aq three times, and finally with cold water twice. After the solution was dried on a small amount of sodium sulfate, the solvent was evaporated under reduced pressure. Gas chromatographic analysis of the liquid residue showed the complete absence of the methyl ester. Blank tests proved that neither the methyl ester nor the acetate was hydrolyzed throughout the above treatment, and that the detection of the methyl ester was possible when the molar ratio of methyl ester to acetate was higher than 1/100, except for *p*-chloroacetophenone where the retention times were the same for the unreacted ketone and the methyl ester. As for the other ketones listed above, the results obtained were similar to those of acetophenone.

Kinetic Measurements. The reaction rates were determined by iodometry of unreacted peroxy acid using the usual ampule technique. In a 100-ml glass-stoppered flask ca. 5×10^{-3} moles of ketone and ca. 1.5×10^{-3} moles of *o*-nitrobenzoic acid were weighed accurately and were dissolved in 50-ml of chloroform. In another 100-ml glass-stoppered flask ca. 5×10^{-3} moles of *o*-nitroperbenzoic acid were weighed accurately and were likewise dissolved in 50-ml of chloroform. After the flasks and the contents were cooled to 0—5 °C in an ice-bath, the *o*-nitroperbenzoic acid solution was added to the solution of the ketone and the acid. The combined solution was swirled quickly and 7—8-ml samples of the solution were sealed in

twelve ampules for each kinetic run. They were immersed into a bath thermostated at 30.00±0.02 °C at the same time. The ampules were withdrawn at adequate intervals and quenched with ice. A 5-ml portion of the solution was pipetted out and transferred into 30-ml of a 2.5% aqueous solution of potassium iodide to which 10-ml of 1 equiv HCl solution had been added immediately before pipetting. The iodine thus liberated was titrated with a 0.1 equiv $Na_2S_2O_3$ solution. All kinetic measurements satisfied the first-order kinetic equation with a correlation coefficient $R>0.999$ to ca. 30% completion of the reaction.

The authors are grateful to Professor Kiyoyasu Kawai of Toyama University for his encouragement during this work.

References

1) a) C. H. Hassall, *Org. React. (N. Y.)*, **9**, 74 (1957). b) P. A. S. Smith, "Molecular Rearrangements," ed by P. de Mayo, Interscience, New York, N. Y. (1963), Vol. I, p. 579. c) R. Criegee, *Justus Liebigs Ann. Chem.*, **560**, 127 (1948). d) W. von E. Doering and E. Dorfman, *J. Am. Chem. Soc.*, **75**, 5595 (1953).

2) M. F. Hawthorne and W. D. Emmons, *J. Am. Chem. Soc.*, **80**, 6398 (1958), and the references cited therein.

3) Y. Ogata and Y. Sawaki, *J. Org. Chem.*, **37**, 2953 (1972).

4) B. W. Palmer and A. Fry, *J. Am. Chem. Soc.*, **92**, 2580 (1970). Recalculation based on the reported data gave a ρ^+ value of −1.37 (corr coeff: 0.987) with σ^+.

5) The empirical Eq. 1 can be paraphrased by

$$v = k_{obs}[PA], \quad (1')$$

where [PA] is the peroxy acid concentration. We can not distinguish Eq. 1 from Eq. 1′ in practice, because the behavior of the ketone and the peroxy acid is the same in terms of the stoichiometry.

6) When the reaction was allowed to start with the same initial concentration ratio of each reactant as the composition ratio at 20% completion of the reaction excluding product ester, the reaction-rate constant observed was still the same as the rate constant at the standard conditions employed in this study.

7) Ogata and Sawaki also regarded *p*-CN as an improper substituent because of a possibility of methyl migration for *p*-cyanoacetophenone. Thus, they used three substituents, i.e., H, *p*-Me, and *p*-Cl among five substituents reported by Palmer and Fry to correlate with σ^+. The downward deviation by ca. 0.5 log unit for the *p*-MeO is that from the correlation line.

8) G. S. Hammond, *J. Am. Chem. Soc.*, **77**, 334 (1955).

9) We included here *p*-CN and *p*-MeO to calculate the correlation line by use of the equation $\log k/k_0=\rho[\sigma+r(\sigma^+-\sigma)]$ for a wider coverage (the notation k_0 in this equation means the rate constant for the unsubstituted compound). There is no distinct evidence for the methyl migration in the case of *p*-cyanoacetophenone.

10) V. A. Stoute, M. A. Winnik, and I. G. Csizmadia, *J. Am. Chem. Soc.*, **96**, 6388 (1974).

11) W. P. Jencks, "Mechanism and Catalysis of Simple Carbonyl Group Reactions," in "Progress in Physical Organic Chemistry," ed by S. G. Cohen, A. Streitwieser, Jr., and R. T. Taft, Interscience Publishers, Inc., New York (1964), Vol. 2, p. 63.

12) B. M. Anderson and W. P. Jencks, *J. Am. Chem. Soc.*, **82**, 1773 (1960).

13) S. L. Friess and A. H. Soloway, *J. Am. Chem. Soc.*, **73**, 3968 (1951).

14) J. C. Robertson and A. Swelin, *Tetrahedron Lett.*, **1967**, 2871.

15) L. S. Silbert, E. Siegel, and D. Swern, *J. Org. Chem.*, **27**, 1336 (1962).

16) R. Adams and C. R. Noller, *Org. Synth.*, Coll. Vol. I, 2nd ed, 109 (1956).

17) D. T. Mowry, M. Renoll, and W. F. Huber, *J. Am. Chem. Soc.*, **68**, 1105 (1946).

18) C. R. Noller and R. Adams, *J. Am. Chem. Soc.*, **46**, 1889 (1924).

19) G. Baddeley, G. Holt, and W. Pickles, *J. Chem. Soc.*, **1952**, 4162.

20) K. v. Auwers, *Justus Liebigs Ann. Chem.*, **408**, 212 (1915).

21) W. F. Forbes, W. A. Mueller, A. S. Ralph, and J. F. Templeton, *Can. J. Chem.*, **35**, 1049 (1957).

22) N. J. Leonard and S. N. Boyed, Jr., *J. Org. Chem.*, **11**, 405 (1946).

23) J. A. Reddick and E. E. Toops, Jr., "Organic Solvent," in "Technique of Organic Chemistry," 2nd ed, ed by A. Weissberger, Interscience Publishers, Inc., New York (1955), Vol. VII, p. 411.

Photochemical Reactions of Vinyl-, Styryl-, and Benzyl-Substituted Digermanes

Kunio MOCHIDA,* Haruhiko KIKKAWA, and Yasuhiro NAKADAIRA†
Department of Chemistry, Faculty of Science, Gakushuin University,
1-5-1 Mejiro, Tokyo 171
† The University of Electro-Communications, 1-5-1 Chofugaoka,
Chofu, Tokyo 182
(Received April 16, 1991)

Photochemical reactions of vinyl-, styryl-, and benzyl-substituted digermanes were investigated by chemical trapping experiments. Photolysis of vinylpentamethyldigermane afforded 1-trimethyl-2-(pentamethyldigermyl)-ethane as a major product, and styrylpentamethyldigermanes gave mainly styryltrimethylgermane. On the other hand, photolysis of benzyl-substituted digermanes (benzylpentamethyldigermane and 1,2-dibenzyltetramethyldigermane) gave hydrogermanes and hydrodigermanes as main products, respectively. These products were derived from germyl radicals generated by photoinduced homolysis of the germanium–germanium bond. In carbon tetrachloride (CCl_4), these germyl radicals were converted to the corresponding chlorogermanes by abstraction of a chlorine atom. Germylene species were also to be evolved from such photolyses.

Recently, the photochemistry of organosilicon compounds having σ(Si–Si)–π(C–C) conjugated systems has been investigated extensively. However, the photochemical behavior of germanium analogues is particularly intriguing from the view of group 14 element chemistry.[1] Previously, we reported the generation of germyl radicals on photolysis of phenyl-substituted digermanes.[2,3] We herein describe the photoreactions of σ(Ge–Ge)–π(C–C) conjugated vinyl- and styryl-substituted digermanes, and benzyl-substituted digermanes as a further extension of our studies.

The photolyses of vinyldisilanes have been reported to induce 1,3-silyl migration to give the corresponding silaethenes as highly reactive intermediates, which were proved by trapping experiments with methanol (Eq. 1).[4]

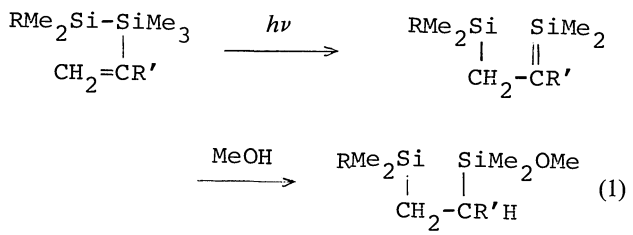

(1)

Similarly, styryldisilanes undergo 1,2-silyl migration to give the corresponding silacyclopropanes as reactive intermediates, which were also evidenced by trapping experiments (Eq. 2).[5]

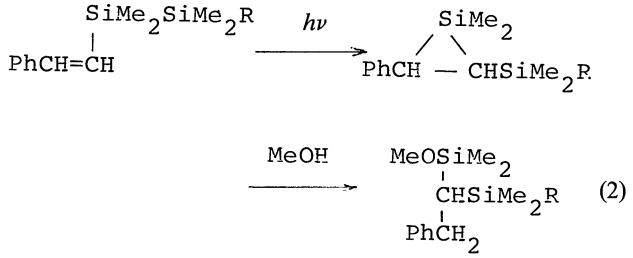

(2)

On the other hand, the irradiation of benzyldisilanes gives a pair of organosilyl radicals by homolysis of the silicon-silicon σ bond (Eq. 3).[6]

$$PhCH_2Me_2Si\text{–}SiMe_3 \xrightarrow{h\nu} PhCH_2Me_2Si\cdot + \cdot SiMe_3 \quad (3)$$

The purpose of the studies described here is to clarify the photochemical behavior of digermanes and to compare their reactivities with thoes of the analogous vinyl-, styryl-, and benzyl-substituted disilanes.

Results and Discussion

Photochemical Reactions of Vinylpentamethyldigermane. Vinylpentamethyldigermane, CH_2=$CHMe_2Ge$-$GeMe_3$ (**1**) in cyclohexane (ca. 0.2 M, 1 M=1 mol dm^{-3}) was irradiated with a 110 W low-pressure Hg arc lamp (a spiral type) at room temperature under argon for 10 h. In addition to a large excess of an unidentified high-boiling product, 1-trimethylgermyl-2-(pentamethyldigermyl)ethane ($Me_3GeCH_2CH_2Ge_2Me_5$, 8% yield) was obtained as a main product together with trace amounts of trimethylgermane (Me_3GeH), vinyldimethylgermane (CH_2=$CHGeMe_2H$), pentamethyldigermane (Me_5Ge_2H), vinyltrimethylgermane (CH_2=$CHGeMe_3$), hexamethyldigermane (Me_6Ge_2), and 1,2-bis(pentamethyldigermyl)ethane ($Me_5Ge_2CH_2$-$CH_2Ge_2Me_5$). Along with hydrogermanes (Me_3GeH and CH_2=$CHMe_2GeH$), formation of digermane (Me_6-Ge_2) indicated the intermediacy of germyl radicals. Since organogermyl radicals abstract a chlorine atom from CCl_4 effectively and rapidly to trap these germyl radical intermediates,[7] the photolysis of compound **1** was carried out in cyclohexane containing CCl_4. As expected, the corresponding chlorogermanes (CH_2=CH-Me_2GeCl and Me_3GeCl) and hexachloroethane were obtained along with (2-chloroethyl)pentamethyldigermane ($ClCH_2CH_2Ge_2Me_5$), pentamethylchlorodigermane (Me_5Ge_2Cl), and CH_2=$CHGeMe_3$. The forma-

tion of Me_5Ge_2H also implied that digermyl radicals and vinyl radicals were generated by homolysis of the carbon–germanium bond along with the germanium–germanium bond. This was further substantiated by the formation of Me_5Ge_2Cl from the photolysis of **1** in the presence of CCl_4. The expected $CH_2=CH_2$ and $CH_2=CHCl$ were not detected with and without CCl_4, respectively, due to their high degree of volatility. The formation of $ClCH_2CH_2Ge_2Me_5$ could be explained as follows. Addition of a chlorine radical generated by photolysis of CCl_4 to gave the 1-(pentamethyldigermyl)-2-chloroethyl radical ($ClCH_2\dot{C}HGe_2Me_5$), followed by abstraction a hydrogen atom from solvents to produce $ClCH_2CH_2Ge_2Me_5$.

A trace amount of dimethyldichlorogermane (Me_2GeCl_2) was detected in the photolysate. The formation of Me_2GeCl_2 may be accounted for by thermal decomposition of (trichloromethyl)dimethylchlorogermane (CCl_3Me_2GeCl), which is produced by insertion of photochemically generated dimethylgermylene into the C–Cl bond of CCl_4,[8] or chlorine abstraction from CCl_4 stepwise by dimethylgermylene as shown in the silicon cases.[9]

The material balance and yields of the chlorogermanes were poor.

Radical Pair Processes (Main Path).

$$(CH_2=CH)Me_2Ge\text{–}GeMe_3 \xrightarrow{h\nu} \begin{cases} \xrightarrow{CCl_4} (CH_2=CH)Me_2GeCl + Me_3GeCl \\ \xrightarrow{CCl_4} CH_2=CHCl + ClMe_2GeGeMe_3 \end{cases} \quad (4)$$

On the other hand, the presence of $CH_2=CHGeMe_3$ in the photolysate implied that dimethylgermylene was generated on the photolysis of **1** under a variety of irradiation conditions. This was supported by the following trapping experiments. In cyclohexane containing a large excess of 2,3-dimethyl-1,3-butadiene as a germylene trapping agent,[10] the photolysis of **1** gave 1,1-dimethylgermacyclopent-3-ene (3% yield).

Germylene Formation Process (Minor Path).

$$(CH_2=CH)Me_2Ge\text{–}GeMe_3 \xrightarrow{h\nu} CH_2=CHGeMe_3 + [:GeMe_2] \quad (5)$$

$$[:GeMe_2] + \text{ 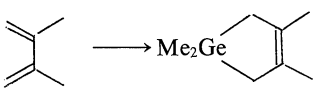 } \longrightarrow Me_2Ge \quad (6)$$

In the photolysis of vinyldisilanes, 1,2-disilylethenes were formed as important intermediates.[4] The germanium–carbon double-bonded species (germenes) are known to react quite effectively with methanol to give the corresponding methoxygermanes.[11] Hence, to confirm the formation of germenes, the photolysis of **1** was examined in cyclohexane containing a large excess of methanol. As a result, no methoxygermanes were detected in the photolysate. Thus, this meant that no germanium–carbon double-bonded species (germenes) were formed as reactive intermediates in the photolysis of vinyl-substituted digermanes (**1**).

These photochemical results are summarized in Table 1.

Photochemical Reactions of Styrylpentamethyldigermane. Styrylpentamethyldigermane ($PhCH=CHMe_2GeGeMe_3$) (**2**) in cyclohexane (ca. 0.1 M) was similarly irradiated with a 110 W low-pressure Hg arc lamp at room temperature under argon for 6 h. Together with a large amount of unidentified polymeric compounds containing germanium atoms, styryltrimethylgermane ($PhCH=CHGeMe_3$, 15% yield) as a major product and trace amounts of Me_3GeH and Me_5Ge_2H were obtained. The presence of $PhCH=CHGeMe_3$ in the photolysate implied the generation of dimethylgermylene under these reaction conditions. To trap this dimethylgermylene, the photolysis of **2** in cyclohexane solution containing a large excess of 2,3-dimethyl-1,3-butadiene[10] was carried out. As expected, 1,1-dimethylgermacyclopent-3-ene (5% yield) was produced. These trapping results suggested that 2,3-dimethyl-1,3-butadiene did not effectively trap photoinduced dimethylgermylene.[12] Dimethylgermylene may have similarly arisen from a simple extrusion process as observed in the vinyldigermane.

$$PhCH=CHGeMe_2GeMe_3 \xrightarrow{h\nu} PhCH=CHGeMe_3 + [:GeMe_2] \quad (7)$$

Formation of trace amounts of hydrogermanes (Me_3GeH and Me_5Ge_2H) indicated the intermediate involvement of germyl radicals. This was confirmed by the formation of the corresponding chlorogermanes ($PhCH=CHMe_2GeCl$ and Me_3GeCl) in the presence of CCl_4.[7] Me_5Ge_2Cl and $PhCH=CHCl$ were also detected in the photolysate. These chlorides indicated the presence of digermyl radicals and styryl radicals, which were generated by homolysis of the germanium–carbon bond. Under these conditions, neither digermanes nor hydrogermanes were detected in the photolysate.

Interestingly, in the photolysis of **2**, a small amount of styrylheptamethyltrigermane ($PhCH=CHMe_2GeMe_2GeGeMe_3$) was detected. This implied that dimethylgermylene is able to insert into a germanium–germanium bond under these reaction conditions.[3]

In the photolysis of styryldisilanes, silacyclopropanes have been reported to be key reactive species.[5] Germacyclopropanes were effectively trapped with methanol to give 1,1-digermyl-2-phenylethanes.[13] Therefore, to examine the possibility of germacyclopropanes as reactive intermediates, the photolysis of **2** in cyclohexane with methanol was carried out. However,

Table 1. Photoproducts and Yields from the Photolysis of the Vinyl-, Styryl-, and Benzyl-Substituted Digermanes **1**—**4** in Cyclohexane

Dimetal	Trapping agent	Photoproducts[a] (yield/%)
$CH_2=CHGe_2Me_5$ **1**	None	Me_3GeH (20), $Me_3GeCH_2CH_2Ge_2Me_5$ (8), $Me_5Ge_2CH_2CH_2Ge_2Me_5$ (1), $(c\text{-}C_6H_{11})_2$ (1)
	CCl_4	$CH_2=CHMe_2GeCl$ (9), Me_5Ge_2Cl (13), $ClCH_2CH_2Ge_2Me_5$ (60), C_2Cl_6 (61), Me_3GeCl (trace), $CH_2=CHGeMe_3$ (trace)
	MeOH	$Me_3GeCH_2CH_2Ge_2Me_5$ (2), $Me_5Ge_2CH_2CH_2Ge_2Me_5$ (1)
	Diene	Me_3GeH (6), (3)
$PhCH=CHGe_2Me_5$ **2**	None	$PhCH=CHGeMe_3$ (15), $(c\text{-}C_6H_{11})_2$ (8)
	CCl_4	Me_5Ge_2Cl (51), $PhCH=CHGeMe_3$ (3), C_2Cl_6 (54)
	Diene	$PhCH=CHGeMe_3$ (25), 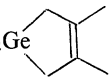 (5)
$PhCH_2Ge_2Me_5$ **3**	None	Me_3GeH (12), Me_5Ge_2H (5), $(PhCH_2Me_2Ge)_2O$ (1), Me_8Ge_3 (2), $PhCH_2Ge_3Me_7$ (1), $(PhCH_2)_2$ (5)
	CCl_4	$PhCH_2Me_2GeCl$ (21), Me_5Ge_2Cl (29), C_2Cl_6 (50)
	MeOH	$(PhCH_2Me_2Ge)_2O$ (1), $(PhCH_2)_2$ (11)
	Diene	Me_5Ge_2H (1), 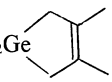 (3)
$(PhCH_2Me_2Ge)_2$ **4**	None	$PhCH_2Me_2GeH$ (7), $(PhCH_2)_2GeMe_2$ (2), $PhCH_2Me_2GeMe_2GeH$ (7), $(PhCH_2)_2$ (7)
	CCl_4	$PhCH_2Me_2GeCl$ (39), $PhCH_2Me_2GeMe_2GeCl$ (23), C_2Cl_6 (45)
	MeOH	$PhCH_2Me_2GeMe_2GeH$ (10), $(PhCH_2)_2$ (10)
	Diene	$(PhCH_2)_2GeMe_2$ (1), $PhCh_2Me_2GeMe_2GeH$ (1), $(PhCH_2)_2$ (3)

a) Ttace amounts of other products were obtained.

no methoxy-substituted compounds were detected in the photolysate. Thus, this result strongly indicated either no formation of germacyclopropanes as reactive intermediates in the photochemical reaction of **2** or that the life time of the germacyclopropane was too fast to be trapped chemically under these conditions.

The results of these photochemical reactions of **2** are also included in Table 1.

Photochemical Reactions of Benzyl-Substituted Digermanes. Benzylpentamethyldigermane ($PhCH_2Me_2GeGeMe_3$) (**3**) and 1,2-dibenzyltetramethyldigermane ($PhCH_2Me_2GeGeMe_2CH_2Ph$) (**4**) in cyclohexane (each 0.1 M) were irradiated with a 110 W low-pressure Hg arc lamp at room temperature under argon for 3—4 h. Many photoproducts were formed in low yields. Among with a large amount of polymeric materials, photolysis of **3** in cyclohexane gave Me_3GeH (12% yield), Me_5Ge_2H (5% yield), and bibenzyl (5% yield) as major products and trace amounts of benzyldimethylgermane ($PhCH_2Me_2GeH$), benzyltrimethylgermane ($PhCH_2GeMe_3$), Me_6Ge_2, dibenzyldigermanoxane ($(PhCH_2Me_2Ge)_2O$), bis(pentamethyldigermyl)oxide ($(Me_5Ge_2)_2O$), octamethyltrigermane (Me_8Ge_3), and 1-benzylheptamethyltrigermane ($PhCH_2Me_7Ge_3$) were also detected. On the other hand, photolysis of **4** in cyclohexane afforded $PhCH_2Me_2GeH$ (7% yield), dibenzyldimethylgermane ($(PhCH_2)_2GeMe_2$) (2% yield), $PhCH_2Me_2GeGeMe_2H$ (7% yield), and $(PhCH_2)_2$ (7% yield).

The origin of the oxygen atom involved in the digermanoxanes is not certain at this stage. In spite of efforts to minimize moisture and air, the digermanoxanes were still obtained in appreciable amounts.

Along with hydrogermanes (Me_3GeH and $PhCH_2GeMe_2H$ for **3** and $PhCH_2GeMe_2H$ for **4**, respectively), formation of digermanes (Me_6Ge_2 for **3** and $(PhCH_2Me_2Ge)_2$ for **4**, respectively) indicated intermediary germyl radicals. To trap such germyl radical intermediates as the corresponding chlorides, the photolyses of **3** and **4** were carried out in cyclohexane containing CCl_4.[8] The corresponding chlorogermanes were obtained and neither digermanes nor hydrogermanes were detected as shown in Table 1. The formation of benzyldimethylchlorogermane ($PhCH_2Me_2GeCl$) and Me_5Ge_2Cl for **3**, and benzyltetramethyldigermyl chloride ($PhCH_2Me_2GeMe_2GeCl$) for **4**, also implied that homolysis of the germanium-carbon bond of benzyl-substituted digermanes **3** and **4** occured along with the homolysis of the germanium-germanium bond.

Radical Pair Processes (Main Path).

$$PhCH_2\text{–}Me_2Ge\text{–}GeMe_2R \xrightarrow{h\nu} \begin{cases} \xrightarrow{CCl_4} PhCH_2Me_2GeCl + RMe_2GeCl \\ \xrightarrow{CCl_4} PhCH_2Cl + ClMe_2GeGeMe_2R \end{cases} \quad (8)$$

R=Me, $PhCH_2$

On the other hand, the formation of $PhCH_2GeMe_3$ for **3** and $(PhCH_2)_2GeMe_2$ for **4**, respectively, with and without CCl_4 implied that dimethylgermylene was generated under a variety of irradiation conditions. 1,1-Dimethylgermacyclopent-3-ene (3% yield and trace amounts for **3** and **4**, respectively) was formed in the photolysis of **3** and **4** in cyclohexane with a large excess of 2,3-dimethyl-1,3-butadiene.[10]

Germylene Formation Process (Minor Path).

$$PhCH_2Me_2GeGeMe_2R \xrightarrow{h\nu} PhCH_2GeMe_2R + [:GeMe_2] \quad (9)$$
$$R=Me,\ PhCH_2$$

The photochemical behavior of benzyl-substituted digermanes was similar to that of the silicon analogues. However, no formation of silylenes has been reported so far.[6]

The photochemical results of benzyl-substituted digermanes (**3** and **4**) are also summarized in Table 1.

Mechanism of Photochemical Reactions of Vinyl-, Styryl-, and Benzyl-Substituted Digermanes. The results obtained from the analysis of the photoproducts were best rationalized on basis of a pair of radicals generated from the photoinduced homolysis of the germaium–germanium and germanium–carbon bonds (Eqs. 4 and 8) as a main path, and of simple extrusion of dimethylgermylene (Eqs. 5, 7, and 9) as a minor path.

Photolysis of digermanes **1**—**4** caused germanium–germanium and germanium–carbon bond cleavage to yield the corresponding pairs of radicals. In CCl_4 the photogenerated germyl-centered radicals and carbon-centered radicals abstracted a chlorine atom effectively to give the corresponding chlorides.[8,14] Thus, in contrast to the silicon analogues, both germyl radicals and carbon radicals appeared to act as reactive intermediates in these photoreactions.

In addition to the homolysis, the extrusion of dimethylgermylene to yield the corresponding monogermanes also occured. Dimethylgermylene arising from a simple extrusion process was also a reactive intermediate independent of the homolytic process.

Thus, the photoproducts isolated here were rationalized to arise from either the radical pair generated from photoinduced homolytic fission of the germanium–germanium and germanium–carbon bonds or extrusion of dimethylgermylene from the starting digermanes. We obtained no evidence for the formation of a germanium–carbon double-bonded species (germene) or germacyclopropane derived from 1,3- and 1,2-germyl migration. On irradiation, however, the silicon analogues underwent 1,3- and/or 1-2-silyl migration to give the corresponding silicon–carbon double-bonded species (silene) and/or silacyclopropane; these could be rationalized also to have arisen by way of the radical pair generated from the photoinduced homolysis of the silicon–silicon bond.

These differences in the photoreactions between the two 14 group metal compounds may be attributed to the difference in the energy of the bond cleaved, namely, germanium–germanium and germanium–carbon bonds are weaker than those of the corresponding silicon–silicon and silicon–carbon bonds. The difference in the thermodynamic stability of germyl and silyl radicals may also contribute to prefential formation of radical products in the photolysis of the digermanes. The strong radical nature of the reaction intermediates may suffer some deterioration of product yields and the material balance of the photolysis.

Experimental

^1H NMR spectra were recorded on a JEOL GX270 using tetramethylsilane as the internal standard. GC-MS spectra were obtained with a JEOL JMS-DX 303 mass spectrometer, and only major peaks are shown. Infrared spectra were recorded on a Shimadzu FT IR 4200 spectrometer. UV and visible spectra were recorded on a JASCO Ubest 50 spectrometer. Gas chromatography was performed on a Shimadzu GC-6A and 8A with 2 m 20% SE30 and 1 m 20% Apiezon L columns.

Materials. 2,3-Dimethyl-1,3-butadiene, CCl_4, and MeOH were commerically available and distilled prior to use. $CH_2=CHMe_2Ge-GeMe_3$,[15] Me_3GeH,[16] $CH_2=CHGeMe_3$,[17] Me_5Ge_2Cl,[15] 1,1-dimethylgermacyclopent-3-ene,[18] Me_5Ge_2H,[19] $PhCH_2Me_2GeCl$,[20] Me_8Ge_3,[21] Me_6Ge_2,[22] and Me_2GeCl_2[16] were prepared as described in the cited references.

Solvent. Cyclohexane was distilled from benzophenone/sodium under argon.

Preparation of Styrylpentamethyldigermane ($PhCH=CHGe_2Me_5$). Styrylmagnesium bromide was prepared from 4.8 g (26 mmol) of styryl bromide and 0.63 g (26 mmol) of magnesium in 40 ml of THF. To this Grignard reagent, 3.4 g (13 mmol) of pentamethylchlorodigermane dissolved in 40 ml of THF was added and refluxed gently for 4 h. After hydrolysis with water, reaction mixtures were extracted with ether, and the organic layer was dried over anhydrous sodium sulfate. After the solvent was removed, fractional distillation gave styrylpentamethyldigermane (3.6 g, 85% yield), bp 119—131 °C/31 mmHg (1 mmHg=133.322 Pa). Pure digermane was isolated by preparative GLC (SE30 20% 2 m column). ^1H NMR (CCl_4) δ=0.25 (s, 9H), 0.35 (s, 6H), 6.65 (m, 2H), and 7.22 (m, 5H); MS (70 eV) *m/z* 324 (6), 207 (100), 119 (26), and 105 (48); UV (in cyclohexane) λ_{max} 266.3 nm (ε 19000); IR (neat) 795m 825, 1665, 1703, 2930, and 2980 cm^{-1}. Found: C, 48.50; H, 6.56%. Calcd for $C_{13}H_{22}Ge_2$: C, 48.27; H, 6.86%.

Preparation of Benzylpentamethyldigermane ($PhCH_2Ge_2Me_5$). Benzylmagnesium chloride was prepared from 2.5 g (20 mmol) of benzyl chloride and 0.5 g (21 mmol) of magnesium in dry ether (30 ml). To this Grignard reagent, 2.0 g (7.8 mmol) of pentamethylchlorodigermane dissolved in dry ether (30 ml) was added. The reaction mixture was stirred with refluxing for 1 h. After hydrolysis with dilute HCl, the reaction mixture was extracted with ether and the organic layer was washed with water. The organic layer was dried over calcium chloride. After removal of the solvent,

fractional distillation gave benzylpentamethyldigermane (1.8 g, 75% yield). The digermane was purified by preparative GLC. ^{1}H NMR (CCl_4) δ=0.17 (s, 15H), 2.27 (s, 2H), and 6.89—6.97 (m, 5H); MS (70 eV) *m/z* 312 (9), 221 (52), 119 (100), and 91 (60); UV (in cyclohexane) λ_{max} 288.8 (ε 12500); IR (neat) 690, 744, 1490, 1595, 2900, 2960, and 3070 cm^{-1}. Found: C, 46.42; H, 7.36%. Calcd for $C_{12}H_{22}Ge_2$: C, 46.27; H, 7.12%.

Preparation of 1,2-Dibenzyltetramethyldigermane ((Ph-$CH_2Me_2Ge)_2$). Dibenzyltetramethyldigermane was prepared from lithium metal (0.21 g, 30 mmol) and benzyldimethylchlorogermane (6.8 g, 30 mmol) in THF (15 nl). The reaction mixture was gently refluxed for 8 h. After completion of this reaction, the reaction mixture was hydrolyzed with diute HCl and extracted with ether. The organic layer was washed with water and dried over sodium sulfate. After removal of the solvent, fractional distillation gave digermane (1.8 g, 31% yield), bp 129—138 °C/3 mmHg. The digermane was purified by preparative GLC. ^{1}H NMR (CCl_4) δ=0.10 (s, 12H), 2.17 (s, 4H), and 6.67—6.90 (m, 10H); MS (70 eV) *m/z* 373 (1), 297 (34), 195 (34), and 91 (100); UV (in cyclohexane) λ_{max} 238.4 nm (ε 14000); IR (neat) 695, 746, 790, 1490, 1605, 2920, 2970, and 3030 cm^{-1}. Found: C, 55.80; H, 7.90%. Calcd for $C_{18}H_{26}Ge_2$: C, 55.78; H, 6.76%.

Identification of the Photoproducts. These compounds were separated by preparative GLC and the structures were assigned by comparing the NMR and GC data of similar compounds reported.

1-Trimethyl-2-(pentamethyldigermyl)ethane: MS (70 eV) *m/z* 366 (15), 323 (25), 247 (20), 221 (95), 207 (14), 119 (100), 104 (7), and 89 (18); ^{1}H NMR ($CDCl_3$) δ=0.10 (s, 9H), 0.17 (s, 6H), 0.22 (s, 9H), 0.64—0.73 (m, 2H), and 0.70—0.90 (m, 2H).

Chloroethylpentamethyldigermane: MS (70 eV) *m/z* 288; ^{1}H NMR ($CDCl_3$) δ=0.26 (s, 6H), 0.27 (s, 9H), 1.23—1.29 (m, 2H), and 2.60—2.66 (m, 2H).

Trace amounts of photoproducts were very carefully identified by comparing the GC data of similar compounds reported.

Vinyldimethylchlorogermane: MS (70 eV) *m/z* 166 (100), 129 (78), 94 (31), and 59 (9).

Vinyldimethylgermane: MS (70 eV) *m/z* 131 (100), 113 (5), 105 (40), 97 (8), 89 (10), and 70 (8).

Bis(pentamethyldigermyl)ethane: MS (70 eV) *m/z* 470 (6), 425 (9), 323 (19), 221 (100), 206 (19), 119 (97), and 89 (9).

Styryltrimethylgermane: MS (70 eV) *m/z* 222 (9), 207 (100), 191 (14), 151 (10), 117 (10), 105 (73), 89 (23), 77 (5).

1-Styrylheptamethyltrigermane: MS (70 eV) *m/z* 428 (1), 413 (8), 325 (36), 293 (12), 221 (64), 207 (40), 119 (100), 105 (16), and 89 (12).

Benzyldimethyldigermanoxane: MS (70 eV) *m/z* 402 (6), 387 (6), 285 (100), 219 (6), 194 (15), and 119 (19).

1-Benzyltetramethylchlorodigermane: MS (70 eV) *m/z* 332 (9), 297 (9), 241 (59), 195 (86), 119 (6), 195 (100).

Dibenzyldimethylgermane: MS (70 eV) *m/z* 286 (6), 195 (100), 165 (9), and 91 (90).

1-Benzyl-1,1,2,2-tetramethyldigermane: MS (70 eV) *m/z* 283 (8), 207 (82), 195 (40), 165 (38), 119 (100), 105 (20), and 91 (80).

Photochemical Reactions of Vinyl-, Styryl-, and Benzyl-Substituted Digermanes. A typical photochemical experiment was as follows: The digermane (ca. 200 mg) was dissolved in dry cyclohexane (6 ml) in a quartz tube. The tube was degassed under vacuum and the atmosphere was replaced with argon. The sample was irradiated with a 110 W low-pressure Hg arc lamp (Sen Tokushu Kogen Co. Ltd.) at room temperature. After irradiation, the photoproducts were identified by comparing the retention times and GC-MS with those of authentic samples.

This research was supported in part by Grant-in-Aid for Scientific Research on Priority Nos. 0164518, 02231227, and 02640387 from the Ministry of Education, Science and Culture.

References

1) R. West, "Comprehensive Organometallic Chemistry," ed by G. Wilkinson, F. G. A. Stone, and E. W. Abel, Pergamon Press, New York (1982), Vol. 2, Chap. 9.4; M. Ishikawa, *Pure Appl. Chem.*, **50**, 11 (1978); M. Ishikawa and M. Kumada, *Adv. Organomet. Chem.*, **19**, 51 (1981); H. Sakurai, *J. Organomet. Chem.*, **200**, 261 (1980); H. Sakurai, Y. Nakadaira, and H. Tobita, *Kagaku no Ryoiki*, **33**, 879, 973 (1979).

2) K. Mochida, M. Wakasa, Y. Nakadaira, Y. Sakaguchi, and H. Hayashi, *Organometallics*, **7**, 1869 (1988).

3) K. Mochida, H. Kikkawa, and Y. Nakadaira, *Chem. Lett.*, **1988**, 1089; *idem., J. Organomet. Chem.*, **412**, 9 (1991).

4) H. Sakurai, Y. Kamiyama, and Y. Nakadaira, *J. Am. Chem. Soc.*, **98**, 7424 (1976); M. Ishikawa, T. Fuchigami, and M. Kumada, *J. Organomet. Chem.*, **117**, C58 (1976); **149**, 37 (1978); P. Boudjouk and L. H. Sommer, *J. Chem. Soc., Chem. Commun.*, **1973**, 54; R. D. Bush, C. M. Gollino, C. M. Homer, and L. H. Sommer, *J. Organomet. Chem.*, **80**, 37 (1974).

5) R. L. Lambert, Jr. and D. Seyferth, *J. Am. Chem. Soc.*, **94**, 9246 (1972); D. Seyferth, C. K. Hess, and D. C. Annavelli, *J. Organomet. Chem.*, **80**, 37 (1973); D. Seyferth, D. P. Duncan, and S. C. Vicks, *ibid.*, **125**, C5 (1977); D. Seyferth, S. C. Vick, M. L. Shannon, T. F. Olin, and D. P. Duncan, *ibid.*, **56**, C7 (1977).

6) M. Kira, H. Sakurai, and H. Yoshida, *J. Am. Chem. Soc.*, **107**, 7767 (1985).

7) H. Sakurai, K. Mochida, A. Hosomi, and F. Mita, *J. Organomet. Chem.*, **38**, 275 (1972).

8) W. P. Neumann and M. Schriever, *Tetrahedron Lett.*, **1980**, 3273.

9) R. Nakano, K. Oka, T. Dohmaru, Y. Nagata, and T. Fukumoto, *J. Chem. Soc., Chem. Commun.*, **1985**, 766.

10) M. Schriever and W. P. Neumann, *J. Am. Chem. Soc.*, **105**, 897 (1983).

11) J. Barrau, J. Escudie, and J. Satgé, *Chem. Rev.*, **90**, 283 (1990).

12) For example: K. Mochida, I. Yoneda, and M. Wakasa, *J. Organomet. Chem.*, **339**, 53 (1990).

13) For example: W. Ando and T. Tsumuraya, *Organometallics*, **7**, 1882 (1988).

14) M. L. Poustma, "Free Radicals," ed by J. K. Kochi, John Wiley & Sons, New York (1973), Vol. 2, Chap. 16.

15) K. Yamamoto and M. Kumada, *J. Organomet. Chem.*, **35**, 297 (1972).

16) A. E. Finholt, *Nucl. Sci. Abstr.*, **6**, 617 (1957).

17) A. N. Egorochkin, N. S. Vyazankin, and S. Ya. Khorshev, *Izv. Akad. Nauk SSSR, Ser. Khim.*, **1971**, 2074.

18) P. Mazerolles and G. Manuel, *Bull. Chim. Soc. Fr.*, **1**, 167 (1973).

19) D. P. Paaquin, R. J. O'Conner, and M. A. Ring, *J.*

Organomet. Chem., **80**, 341 (1974).
20) K. Mochida, M. Kira, and H. Sakurai, *Chem. Lett.*, **1981**, 645.
21) O. M. Nefdof and S. P. Kolesnokov, *Izv. Akad. Nauk SSSR*, **4**, 773 (1964).
22) M. P. Brown and G. W. A. Fowles, *J. Am. Chem. Soc.*, **80**, 2811 (1958).

Synthetic Photochemistry. LVII.[1] Facile Photochemical Construction of Hexahydro-*as*-indacene Skeleton, a Carbon Framework of Ikarugamycin, from High-Pressure Diels-Alder Adducts of Tropones-Cyclopentenone

Zhi-Hong Li, Akira Mori,† Nobuo Kato,† and Hitoshi Takeshita*,†
Graduate School of Engineering Sciences, 39, Kyushu University,
Kasuga-koen, Kasuga, Fukuoka 816
† Institute of Advanced Material Study, 86, Kyushu University,
Kasuga-koen, Kasuga, Fukuoka 816
(Received April 30, 1991)

The high-pressure Diels–Alder reaction of tropones with 2-cyclopenten-1-one afforded isomeric mixtures of adducts. Upon UV irradiation, these adducts isomerized to hexahydro-*as*-indacene, via [1,3] acyl migration, and tetracyclo[7.3.0.0^{3,7}.0^{6,8}]undecene derivatives through a ketene intermediate via a di-π-methane rearrangement. The former tricyclic system corresponds to the carbon skeleton of ikarugamycin. An "*exo* [6+4] adduct" of tropone and 1,4-cyclopentadien-1-ol, an enol form of 2-cyclopentenone, was obtained as a by-product.

Tropones, electron-deficient cyclic trienones, are known to form Diels–Alder adducts with various electron-deficient dienophiles such as maleic anhydride,[2] *N*-phenylmaleimide,[3] and acrylonitrile.[4] Application of a high-pressure technique made even less-reactive dienophiles feasible; recently we examined the reaction of tropones with *p*-benzoquinones.[5] This prompted us to investigate further cycloaddition with an enone such as 2-cyclopenten-1-one, which afforded no product under 1 bar (1 bar=10^5 Pa.).

Since the photoisomerization of dihydrohomobarrelenones to dihydroindenones is well-known,[6] Diels–Alder adducts from a cyclic enone and tropone were expected to form tricyclic analogs.

In this paper, we report high-pressure Diels–Alder reactions between tropones and 2-cyclopenten-1-one and the subsequent photoconversion to a tricyclic compound, which has a framework similar to the decahydro-*as*-indacene subunit (**A**) of ikarugamycin.[7]

Results and Discussion

Cycloaddition Reaction. When a toluene solution of tropone (**1**) and 2-cyclopenten-1-one (**2**) was heated at 100 °C for 10 h under 10 kbar, four 1:1-adducts (**3**—**6**) were obtained. The dihydrohomobarrelenone framework for **3**, **4**, and **5** was evident from NMR spectra; e.g., the ^{1}H NMR spectrum of **3** showed the signal of the doublet of doublets at δ=7.12 (J=11.0, 8.4 Hz), ascribable to the β-proton of the α,β-unsaturated ketone. The stereochemistry of the methine protons H-2 and H-6 was determined to be exo by the value ($J_{1,2}$=0 Hz) of the coupling constant. The position of the carbonyl group was found to be at C-3 by analysis of the 2D COSY spectrum, where H-6 showed a correlation with H-12. Therefore, **3** was shown to be tricyclo[5.3.2.0^{2,6}]dodeca-9,11-diene-3,8-dione.

The second product, **4**, was determined to be an *exo* [4+2] adduct from the magnitudes ($J_{1,2}$=5.5 Hz and $J_{6,7}$=8.1 Hz) of the coupling constants of H-1 at δ=3.77 and H-7 at δ=3.71. The third product **5** was another *endo* [4+2] adduct as shown by the coupling constant ($J_{6,7}$=0 Hz), and the position of the carbonyl group was determined to be on C-3.

The spectral data of the remaining product, **6**, was quite different from those of the [4+2] adducts (**3**—**5**); showing no signal lower than δ=6.1 eliminated a [4+2]

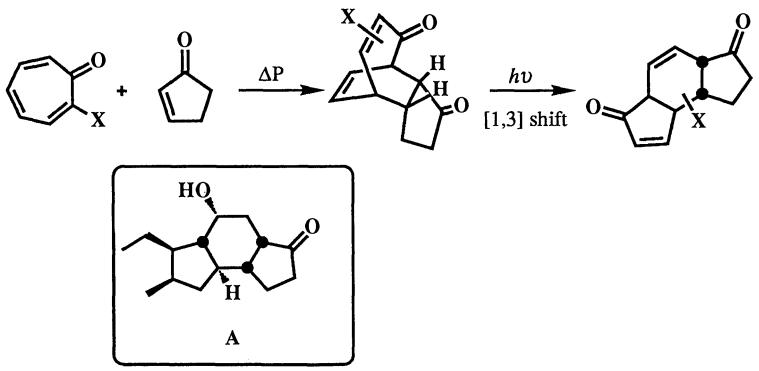

Scheme 1.

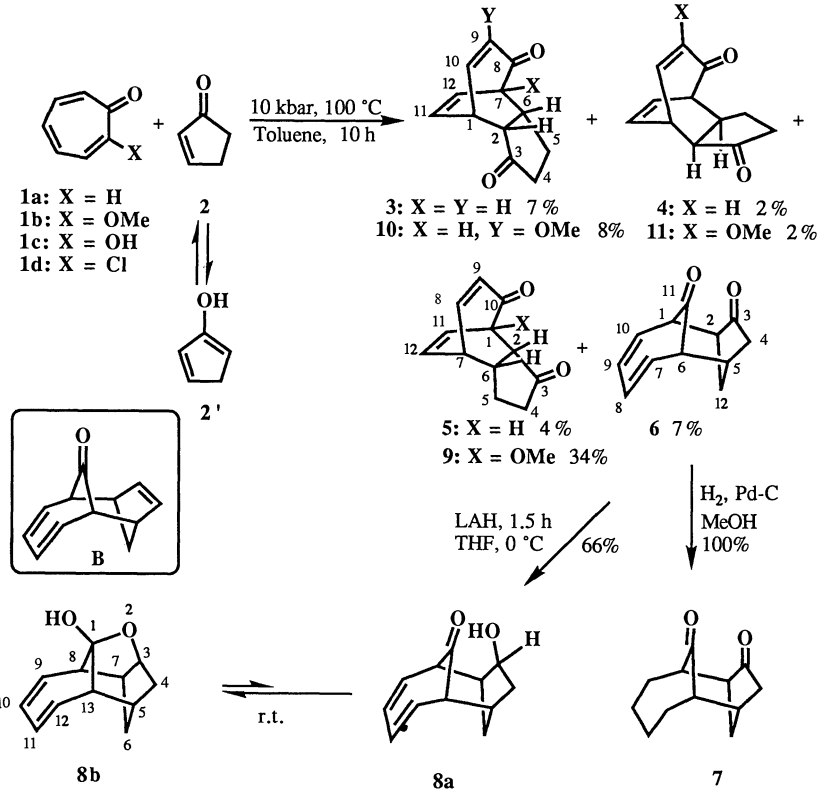

Scheme 2.

structure. In addition, the ^{1}H NMR spectrum of **6** exhibited four olefinic protons, which also eliminated an [8+2] structure. Its IR spectrum showed two carbonyl absorptions at 1736 and 1713 cm^{-1}; the latter is similar to the absorption (1715 cm^{-1}) of the [6+4] adduct (**B**) between **1a** and cyclopentadiene.[8] The UV spectrum of **6** also resembled that of **B**. These observations are consistent with those of tricyclo[4.4.1.1^{2,5}]dodeca-7,9-diene-3,11-dione, which can be derived from **1a** and 1,4-cyclopentadien-1-ol, an enol form of **2**. One of the two sets of methylene proton pairs [δ=1.84 (dt, J=13.0, 4.8 Hz) and 2.66 (dd, J=13.0, 4.0 Hz), and 2.37 (dd, J=19.1, 4.0 Hz) and 2.58 (dd, J=19.1, 7.1 Hz)] revealed a large *gem*-spin coupling constant which indicated the presence of a CO–CH$_2$ group.

In order to determine the stereochemistry, **6** was hydrogenated to a tetrahydro derivative (**7**). However, the signals of the methylene protons overlapped each other in the ^{1}H NMR spectrum. This indicated that the methylene protons at δ=1.84 and 2.26 and the diene part of **6** are in proximity. Furthermore, upon lithium aluminum hydride (LAH) reduction, **6** gave a dihydro derivative, which showed broad signals, indicating an equilibration between the ketol form (**8a**) and the hemiacetal form (**8b**) at room temperature. Thus, **6** was shown to be an *exo*-adduct. We also observed a temperature-dependent equilibrium, i.e., a 14:86 mixture of **8a** and **8b** at 0 °C, while only **8b** was detected at -50 °C. The ^{1}H NMR spectral coupling sequence of **8b** was analyzed by means of decoupled NMR experiments at 0 °C. Two allylic protons signals (H-7 and H-12) appeared at δ=2.94 (dd, J=6.6, 4.0 Hz) and 2.70 (dd, J=7.7, 3.0 Hz), which were coupled with olefinic protons at δ=5.59 (H-8, dd, J=11.7, 7.3 Hz) and 5.61 (H-11, dd, J=11.7, 6.6 Hz), respectively. The absence of spin coupling of these two allylic protons with H-2 at δ=4.59 (m), the proton on the etheral carbon, led us to the conclusion that the structure of **8b** was 2-oxatetracyclo[6.5.0^{3,7}.0^{5,13}]trideca-9,11-dien-1-ol.

The reason why the five-membered carbonyl group was predominantly reduced was speculated as follows: since a five-membered ring has a larger bond-angle strain than a seven-membered ring, the change from an sp^2 carbon to an sp^3 carbon of the five-membered carbonyl group would be accelerated to release the strain.[9] Alternatively, the preferential reduction of the five-membered cabonyl group was explained by the Cieplak stereoelectronic effect,[10] since the five-membered carbonyl group had a C–H bond antiperiplanar to the incipient σ* orbital.

Similar explanations would apply to the predominant acetal formation with the confronted hydroxyl group in **8** since the seven-membered carbonyl group in a fused system was more hindered than a monocyclic moiety.

The reaction between 2-methoxytropone (**1b**) and **2** under 10 kbar gave three products (**9**—**11**). The

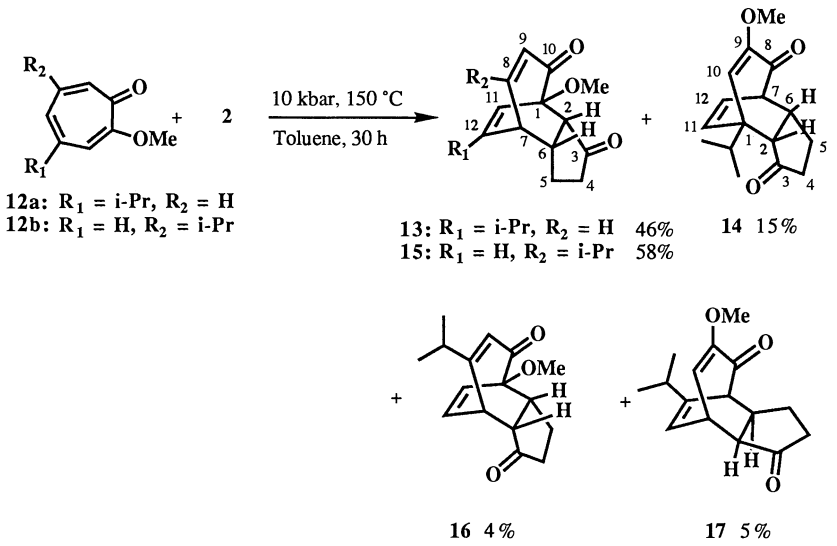

Scheme 3.

structures were determined by the ^{1}H NMR spectral comparison with those of the [4+2] adducts (**3**—**5**). In this case, no [6+4] adduct was detected. Attempted reactions between tropolone (**1c**) and 2-chlorotropone (**1d**) with **2** were unsuccessful; from **1d**, only a resinous material was obtained, and from **1c**, no product other than the starting material was recovered in 80% yield.

Furthermore, reactions between 4-isopropyl- and 6-isopropyl-2-methoxytropones (**12a** and **12b**) and **2** afforded two adducts (**13** and **14**) from **12a** and three adducts (**15**—**17**) from **12b**, respectively.

The ^{1}H NMR spectrum of the main product **13** from **12a** showed the typical doublet of doublets of a [4+2] adduct at δ=7.11 (J=11.0, 8.4 Hz) and a doublet at δ=3.00 (J=9.2 Hz). Since the latter was assigned to the α-methine proton of the carbonyl group, **13** was deduced to be an *endo* [4+2] adduct. The position of the carbonyl group was deduced from the structure of the photorearrangement product as will be discussed later.

One of the olefinic protons of **14** appeared as a singlet at δ=5.77 and two remaining protons coupled with each other, whose coupling constant (J=8.4 Hz) implied that a methoxyl group was located at C-9 of the bridge and an isopropyl group was at the bridgehead, C-1. Since the α-methine proton of the carbonyl group appeared as a doublet (J=8.8 Hz) at δ=2.90, **14** was another *endo* [4+2] adduct.

From the ^{1}H NMR spectrum, the main product **15** from **12b** was deduced to have an isopropyl group at C-8 from the coupling constants of the olefinic protons, two of which coupled with each other (J=9.2 Hz). Since the bridgehead proton H-7 appeared as a doublet (J=7.3 Hz), being coupled with the olefinic proton at C-12, **15** was an *endo* [4+2] adduct. However, the position of the carbonyl group was not unambiguously determined at this stage.

The patterns of three olefinic protons of **16** were similar to those of **15**, indicating a similar type of reaction. Since the signal of H-2 at δ=2.73 was a doublet, which meant $J_{1,2}$=0 Hz, **16** was an *endo* [4+2] adduct. Therefore, **16** was a regioisomer of **15**.

The positions of the methoxyl and isopropyl groups of **17** were deduced by the observation of only two olefinic proton signals in the ^{1}H NMR spectrum. The bridgehead proton, H-1, appeared as a doublet of doublets of doublets (J=9.2, 7.3, 5.5 Hz), which meant that H-1 coupled with the methine proton, H-2, with a coupling constant of 5.5 Hz. Therefore, **17** was an *exo* [4+2] adduct. Since the splitting pattern of H-2, a doublet of doublets, indicated two adjacent protons, the position of the carbonyl group was at C-3.

Thus, tropones reacted with **2** mostly as a 4π-cycloaddend. The regioselectivity of **1b** was parallel to those previously reported.[11] It is quite interesting that **2** behaved as a 4π-component in the reaction with **1a**.[12]

Photochemical Reaction. Upon UV-light irradiation by means of a 400-W high-pressure mercury lamp through a quartz filter in deuteriochloroform ($CDCl_3$), **3** gave a single product, **18**, in 60% yield while no reaction occurred upon irradiation through a Pyrex filter with or without benzophenone, a triplet sensitizer. The ^{1}H NMR spectrum of **18** showed four olefinic protons, in which the signals at δ=7.59 (dd, J=5.6, 2.6 Hz) and 6.19 (dd, J=5.6, 2.4 Hz) indicated the generation of a cyclopentenone moiety. The sequential alignment of four methine protons was determined by the values of the coupling constants. Since the doublet signal (J=7.2 Hz) at δ=2.56 was assigned to be an H-3a proton at the terminal position of the alignment, this indicated the structure of **18** was *cis-transoid-cis*-2,3,3a,5a,8a,8b-hexahydro-*as*-indacene-1,6-dione.

The irradiation of **9** in $CDCl_3$ through a Pyrex filter

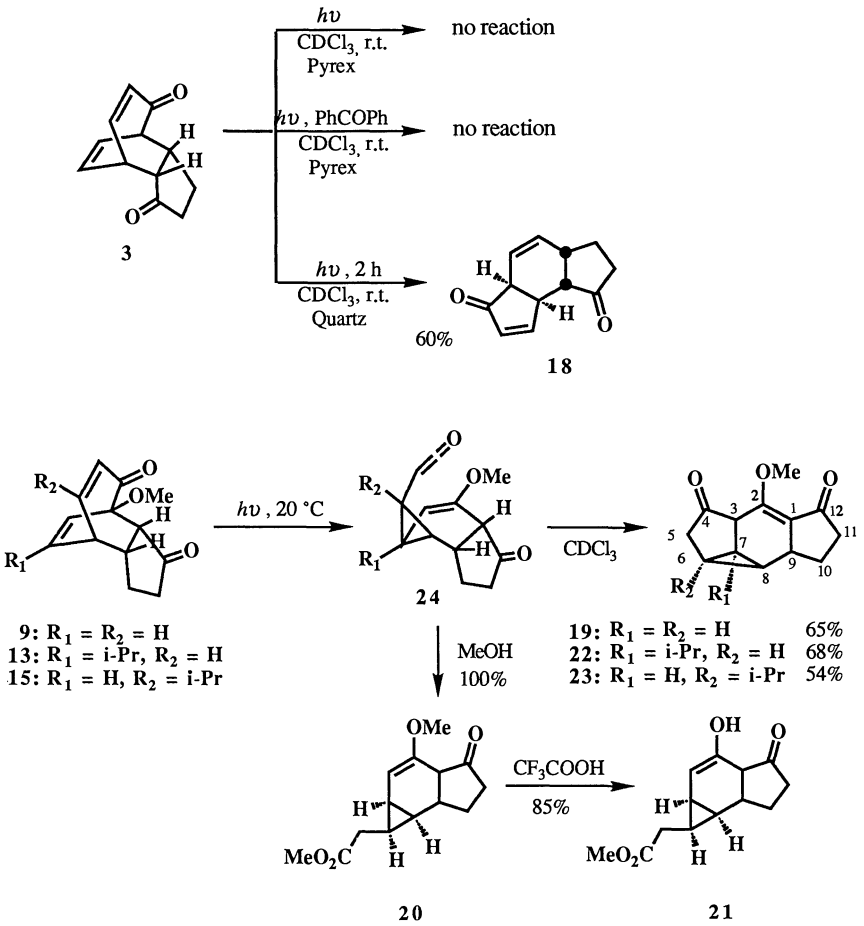

Scheme 4.

gave a single product **19**, whose ^{13}C NMR spectrum showed two carbonyl groups at δ=201.8 and 212.8 and two olefinic carbons at δ=114.2 and 160.7, assignable to a vinyl ether. Since no C=C double bonds were observed, **19** was a tetracyclic enedione. A pair of methylene protons at δ=2.03 and 2.78 was assigned to be H-5α and H-5β since the proton at δ=2.78 coupled with H-3 at δ=3.74. Therefore, the double bond was located between C-1 and C-2. Furthermore, H-3 coupled with H-7 at δ=2.00, which further split to a doublet of doublets (J=8.1 and 7.7 Hz) to indicate the presence of a cyclopropane ring. Therefore, **19** was 2-methoxytetracyclo[7.3.0.0^{3,7}.0^{6,8}]undec-1-ene-4,12-dione.

When **9** was irradiated in methanol, a methyl ester, **20**, was obtained. The olefinic proton appeared at δ=4.64 as a doublet (J=4.0 Hz), which coupled with one of three cyclopropane ring protons at δ=1.57 (td, J=8.4 and 4.0 Hz). The coupling constants among protons on the cyclopropane ring showed *cis*-geometry.

Photoproduct **20** gave a demethylated product, **21**, in 85% yield in trifluoroacetic acid.

Similarly, irradiations of **13** and **15** gave tetracyclic derivatives **22** and **23**, respectively. Their ^1H and ^{13}C NMR spectra as well as UV data were similar to those of **19**. Therefore, the positions of the carbonyl groups in the five-membered rings of **13**, **15**, and **16** were determined as shown.

A substituent at the bridgehead affected the photoisomerization course of the [4+2] cycloadducts. Photoreactions of **9**, **13**, and **15**, all of which have a methoxyl group at the bridgehead position, gave tetracyclic derivatives, whereas photoreaction of **3** gave the tricyclic compound **18**. The formation of tetracyclic derivatives was due to the electron-releasing nature of the methoxyl group at the bridgehead.

The formation of a methyl ester, **20**, constitued an intermediacy of a ketene, **24**. In $CDCl_3$, **24** was trapped as **23** via an intramolecular path.

In the photoreaction of **3**, no product formed from either direct irradiation in a Pyrex tube or sensitized irradiation with benzophenone in a Pyrex tube. These data clearly indicate that **3** isomerized to **18** via a π, π^* singlet state, a [1,3] acyl shift. The predominant [1,3] acyl migrations of **3** were similar to those of the dihydrohomobarrelenones[6] and benzohomobarrelenone.[13]

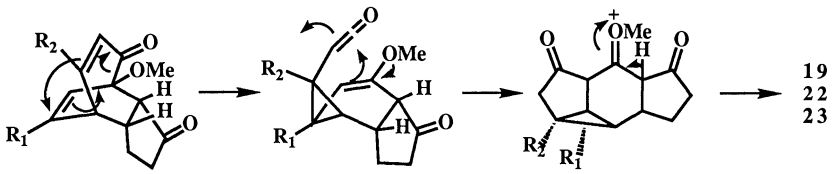

9: $R_1 = R_2 = H$
13: R_1 = i-Pr, $R_2 = H$
15: $R_1 = H$, R_2 = i-Pr

24

Scheme 5.

Experimental

Elemental analyses were performed by Miss S. Hirashima and Miss T. Mizoguchi, of Institute of Advanced Material Study, Kyushu University. NMR spectra were measured by JEOL FX 100 Model, JEOL GSX 270 H Model, and GSX-500 Model spectrometers in a $CDCl_3$ solution (unless otherwise specified); chemical shifts were expressed in the unit δ. Mass spectra were measured with a JEOL O1SG-2 spectrometer. IR spectra were taken as KBr disks or as a liquid film inserted between NaCl plates using a JASCO IR-A 102 spectrometer. UV spectra were measured by a Hitachi U-3200 spectrophotometer. HPLC separation was performed on a Waters Type 510 system with a UV-detecter and a Microporasil column.

Cycloaddition Reaction of 1a and 2. A toluene solution (4 cm³) of **1a** (424 mg) and **2** (640 mg) was heated at 100 °C for 10 h under 10000 bar. The solvent was removed under reduced pressure and the residue was purified by SiO_2 column chromatography and HPLC (AcOEt:hexane=1:1) to give 53 mg (7%) of **3**, 14 mg (2%) of **4**, 27 mg (4%) of **5**, and 55 mg (7%) of **6**.

3: Colorless crystals, mp 73—74 °C; ^{1}H NMR δ=1.6—1.8 (1H, m), 2.2—2.4 (2H, m), 2.94 (1H, br d, J=10.3 Hz), 3.0—3.1 (1H, m), 3.49 (1H, dm, J=7.3 Hz), 3.67 (1H, ddd, J=8.4, 7.3, 1.8 Hz), 5.77 (1H, ddd, J=11.0, 1.8, 0.7 Hz), 6.14 (1H, ddm, J=8.4, 7.3 Hz), 6.47 (1H, dd, J=8.4, 7.3 Hz), and 7.12 (1H, dd, J=11.0, 8.4 Hz); ^{13}C NMR δ=27.0, 36.8, 37.9, 39.8, 53.7, 59.3, 127.0, 130.4, 138.0, 151.9, 196.3, and 217.0; IR (KBr) 3048, 2956, 1726, 1656, 1626, 1387, 1269, 1248, 1178, 801, and 706 cm^{-1}; UV (MeOH) 224 (ε 5200) and 242 nm (3900 sh); MS m/z (%) 188 (M$^+$, 40), 160 (68), 131 (58), 118 (61), 104 (76), 103 (51), 78 (74), 77 (41), 56 (41), 55 (50), 51 (75), 39 (87), 28 (100), and 26 (89).

Found: m/z 188.0835 (M$^+$). Calcd for $C_{12}H_{12}O_2$: M, 188.0836.

4: A colorless oil; ^{1}H NMR δ=1.5—1.7 (1H, m), 2.1—2.3 (2H, m), 2.45 (1H, dddd, J=19.1, 11.4, 9.9, 1.5 Hz), 2.86 (1H, ddd, J=11.4, 5.5, 0.7 Hz), 3.10 (1H, ddd, J=11.4, 8.4, 8.1 Hz), 3.71 (1H, ddm, J=8.4, 8.1 Hz), 3.77 (1H, dddm, J=8.4, 8.1, 5.5 Hz), 5.79 (1H, ddd, J=11.0, 1.8, 1.1 Hz), 6.22 (1H, ddd, J=8.4, 7.3, 0.7 Hz), 6.56 (1H, ddd, J=8.1, 7.3, 0.7 Hz), and 7.04 (1H, dd, J=11.0, 8.4 Hz); ^{13}C NMR δ=24.2, 37.7, 38.0, 40.1, 53.8, 58.0, 129.3, 131.2, 137.5, 153.0, 197.4, and 218.0; IR (oil) 3046, 2950, 1738, 1701, 1659, 1628, 1387, 1326, 1240, 1170, 1015, 809, 711, and 675 cm^{-1}; UV (MeOH) 223 nm (ε 3400); MS m/z (%) 188 (M$^+$, 52), 160 (87), 132 (40), 131 (87), 118 (44), 117 (55), 104 (100), 103 (47), 91 (47), 78 (8), 77 (60), 51 (68), 39 (59), 28 (53), and 26 (78).

Found: m/z 188.0835 (M$^+$). Calcd for $C_{12}H_{12}O_2$: M, 188.0836.

5: A colorless oil; ^{1}H NMR δ=1.50 (1H, m), 2.2—2.5 (3H, m), 2.75 (1H, d, J=10.7 Hz), 3.21 (1H, br t, J=8.6 Hz), 3.28 (1H, br t, J=8.4 Hz), 3.84 (1H, dm, J=8.1 Hz), 5.73 (1H, ddd, J=11.1, 2.1, 1.6 Hz), 6.12 (1H, ddm, J=8.1, 7.2 Hz), 6.50 (1H, ddm, J=8.4, 7.2 Hz), and 7.15 (1H, dd, J=11.1, 8.4 Hz); ^{13}C NMR δ=26.9, 40.2, 41.6, 42.6, 47.9, 54.1, 127.8, 129.7, 137.5, 152.8, 195.3, and 215.9; IR (oil) 3046, 2960, 1737, 1668, 1629, 1391, 1265, 1116, 797, and 705 cm^{-1}; UV (MeOH) 229 nm (ε 5200); MS m/z (%) 188 (M$^+$, 100), 164 (57), 131 (63), 117 (28), 104 (34), 91 (44), 78 (39), 55 (42), 39 (42), and 27 (33).

Found: m/z 188.0836 (M$^+$). Calcd for $C_{12}H_{12}O_2$: M, 188.0836.

6: Colorless crystals, mp 163—164 °C; ^{1}H NMR δ=1.84 (1H, dt, J=13.0, 4.8 Hz), 2.37 (1H, dd, J=19.1, 4.0 Hz), 2.58 (1H, dd, J=19.1, 7.1 Hz), 2.66 (1H, dd, J=13.0, 4.0 Hz), 2.8—2.9 (1H, m), 3.23 (1H, dt, J=7.5, 4.0 Hz), 3.32 (1H, dt, J=7.5, 4.0 Hz), 5.60 (1H, dd, J=11.5, 7.5 Hz), 5.73 (1H, ddd, J=11.5, 7.5, 4.8 Hz), and 6.0—6.05 (2H, m); ^{13}C NMR δ=26.7, 40.1, 47.2, 54.8, 57.6, 59.6, 125.1, 126.5, 127.1, 127.7, 207.0, and 215.4; IR (KBr) 3038, 2956, 1736, 1713, 1397, 1195, 1161, 1021, 862, and 709 cm^{-1}; UV (MeOH) 213 (ε 3100), 222 (2600, sh), 262 (3200), 269 (3100), and 300 nm (260, sh); MS m/z (%) 188 (M$^+$, 100), 129 (24), 117 (44), 91 (32), 81 (30), 69 (58), 55 (22), 43 (20), 41 (38), 39 (27), 28 (99), and 26 (23).

Found: C, 76.71; H, 6.43%. Calcd for $C_{12}H_{12}O_2$: C, 76.57; H, 6.43%.

Catalytic Hydrogenation of 6. A MeOH solution (5 cm³) of **6** (40 mg) was stirred under H_2 atmosphere for 30 min in the presence of Pd/C (10 mg). The catalyst was filtered and the solvent was removed under reduced pressure. The residue was chromatographed on a SiO_2 column (AcOEt:hexane=1:1) to give 40.9 mg (100%) of **7**.

7: A colorless oil; ^{1}H NMR δ=1.6—1.7 (4H, m), 1.75—2.0 (5H, m), 2.07 (1H, dd, J=19.1, 3.6 Hz), 2.23 (1H, ddd, J=19.1, 6.6, 0.7 Hz), 2.54 (1H, m), 2.65 (1H, m), and 2.7—2.8 (3H, m); ^{13}C NMR δ=26.6, 26.8, 27.7, 28.0, 28.3, 38.2, 44.2, 53.1, 53.4, 55.1, 212.3, and 216.7; IR (oil) 2930, 2866, 1741, 1707, 1478, 1453, 1405, 1208, 1154, 1100, 1017, and 983 cm^{-1}; MS m/z (%) 192 (M$^+$, 100), 164 (31), 119 (23), 93 (28), 81 (23), 80 (28), 79 (38), 67 (34), 41 (29), 39 (26), and 26 (23).

Found: m/z 192.1150 (M$^+$). Calcd for $C_{12}H_{16}O_2$: M, 192.1151.

Lithium Aluminum Hydride Reduction of 6. A dry THF solution (3 cm³) of **6** (30 mg) was stirred with LAH (1.7 mg) at 0 °C for 1.5 h. A small portion of sat. NaCl solution was then added. The THF solution was concentrated and the residue was chromatographed on PTLC (20 cm×10 cm,

AcOEt:hexane=1:1) to give 20 mg (66%) of **8**.

8: Colorless crystals, mp 103—103.5 °C; ^{1}H NMR at −50 °C, δ=1.25 (1H, ddd, J=12.5, 6.6, 3.3 Hz), 1.53 (1H, dt, J=12.1, 4.7 Hz), 2.02 (1H, dd, J=12.5, 2.9 Hz), 2.10 (1H, dd, J=12.1, 2.9 Hz), 2.45 (1H, br s), 2.70 (1H, dd, J=7.7, 3.0 Hz), 2.81 (1H, dd, J=6.6, 5.5 Hz), 2.94 (1H, dd, J=6.6, 4.0 Hz), 4.59 (1H, m), 5.36 (1H, br s), 5.59 (1H, dd, J=11.7, 7.3 Hz), 5.61 (1H, dd, J=11.7, 6.6 Hz), 5.90 (1H, dd, J=11.7, 7.0 Hz), and 6.03 (1H, dd, J=11.7, 7.3 Hz); ^{13}C NMR δ=30.4, 44.0, 44.2, 44.6, 50.7, 55.7, 78.1, 99.6, 126.2, 128.2, 128.8, and 130.6; IR (KBr) 3318, 3010, 2942, 1373, 1268, 1158, 1057, 981, 972, 961, 850, and 700 cm^{-1}; MS m/z (%) 190 (M^+, 100), 145 (40), 130 (86), 129 (46), 128 (53), 124 (44), 117 (55), 107 (65), 105 (59), 91 (83), 79 (99), 78 (49), 77 (63), 67 (44), and 39 (61).

Found: C, 75.77; H, 7.37% and m/z 190.0994 (M^+). Calcd for $C_{12}H_{14}O_2$: C, 75.76; H, 7.42% and 190.0993 (M).

Cycloaddition Reaction of 1b and 2. A toluene solution (2 cm^3) of **1b** (136 mg) and **2** (160 mg) was heated at 120 °C for 12 h under 10000 bar. The solvent was removed under reduced pressure and the residue was purified by SiO_2 column chromatography and HPLC (AcOEt:hexane=1:1) to give 74 mg (34%) of **9**, 18 mg (8%) of **10**, and 5 mg (2%) of **11**.

9: A colorless oil; ^{1}H NMR δ=1.6—1.7 (1H, m), 2.1—2.5 (3H, m), 3.02 (1H, d, J=9.5 Hz), 3.05—3.15 (1H, m), 3.36 (1H, ddd, J=8.4, 7.3, 1.1 Hz), 3.64 (3H, s), 5.78 (1H, dd, J=11.0, 0.7 Hz), 6.11 (1H, dd, J=9.2, 0.7 Hz), 6.59 (1H, dd, J=9.2, 7.3 Hz), and 7.10 (1H, dd, J=11.0, 8.4 Hz); ^{13}C NMR δ=27.0, 40.1, 40.7, 43.2, 50.5, 54.3, 88.5, 128.2, 131.6, 134.9, 151.9, 193.7, and 212.8; IR (oil) 3030, 2944, 1743, 1677, 1638, 1380, 1211, 1153, 1110, 987, 697, and 681 cm^{-1}; MS m/z (%) 218 (M^+, 70), 189 (22), 161 (25), 147 (95), 121 (43), 108 (100), 91 (45), 78 (40), 65 (61), 56 (39), 51 (33), 44 (39), 40 (76), and 27 (54).

Found: C, 71.23; H, 6.43% and m/z 218.0941 (M^+). Calcd for $C_{13}H_{12}O_3$: C, 71.54; H, 6.47% and 218.0942 (M).

10: Colorless crystals, mp 87—89 °C; ^{1}H NMR δ=1.65—1.8 (1H, m), 2.2—2.4 (3H, m), 2.89 (1H, dm, J=10.3 Hz), 3.0—3.1 (1H, m), 3.55 (3H, s), 3.65 (1H, dm, J=7.3 Hz), 3.72 (1H, ddm, J=9.5, 7.3 Hz), 6.11 (1H, d, J=9.5 Hz), 6.12 (1H, dd, J=8.4, 7.3 Hz), and 6.54 (1H, ddd, J=8.4, 7.3, 1.1 Hz); ^{13}C NMR δ=26.8, 35.2, 36.6, 39.6, 54.3, 54.9, 58.4, 118.7, 126.5, 139.4, 151.4, 192.0, and 217.4; IR (KBr) 3058, 2950, 1736, 1672, 1631, 1615, 1372, 1228, 1128, 1098, 835, 820, and 772 cm^{-1}; UV (MeOH) 232 (ε 2600) and 278 nm (2300); MS m/z (%) 218 (M^+, 100), 164 (28), 147 (24), 131 (28), 108 (56), 91 (49), 78 (29), 65 (26), 39 (31), and 26 (24).

Found: m/z 218.0942 (M^+). Calcd for $C_{13}H_{14}O_3$: M, 218.0942.

11: Colorless crystals, mp 104—105 °C; ^{1}H NMR δ=1.5—1.65 (1H, m), 2.1—2.25 (2H, m), 2.3—2.5 (1H, m), 2.77 (1H, ddd, J=11.7, 5.5, 1.1 Hz), 3.0—3.15 (1H, m), 3.50 (3H, s), 3.79 (1H, dddd, J=9.2, 7.3, 5.5, 1.1 Hz), 3.87 (1H, dd, J=7.3, 6.6 Hz), 5.99 (1H, d, J=9.2 Hz), 6.20 (1H, dd, J=8.4, 7.3 Hz), and 6.64 (1H, dd, J=8.4, 7.3 Hz); ^{13}C NMR δ=24.1, 34.7, 37.8, 40.1, 52.9, 55.1, 56.6, 118.3, 128.5, 139.1, 152.3, 192.8, and 218.2; IR (KBr) 3044, 2924, 1736, 1672, 1616, 1372, 1225, 1118, 824, and 764 cm^{-1}; UV (MeOH) 226 (ε 2400) and 280 nm (3100); MS m/z (%) 218 (M^+, 100), 175 (20), 174 (35), 131 (31), 130 (46), 105 (22), 91 (40), and 78 (25).

Found: C, 71.49; H, 6.76%. Calcd for $C_{13}H_{14}O_3$: C, 71.54; H, 6.47%.

Cycloaddition Reaction of 1c and 2. A toluene solution (2 cm^3) of **1c** (143 mg) and **2** (160 mg) was heated at 100 °C for 10 h under 10000 bar. The solvent was removed under reduced pressure to leave a polymerized material.

Cycloaddition Reaction of 1d and 2. A toluene solution (2 cm^3) of **1d** (122 mg) and **2** (160 mg) was heated at 120 °C for 12 h under 10000 bar. The solvent was removed under reduced pressure and 98 mg (80%) of **1d** was recovered after SiO_2 chromatography (AcOEt:hexane=1:1).

Cycloaddition Reaction of 12a and 2. A toluene solution (4 cm^3) of **12a** (360 mg) and **2** (320 mg) was heated at 120 °C for 50 h under 10000 bar. The solvent was removed under reduced pressure and the residue was purified by SiO_2 column chromatography and HPLC (AcOEt:hexane=1:2) to give 180 mg (46%) of **13**, 60 mg (15%) of **14**, and 87 mg (24%) of **12a**.

13: A colorless oil; ^{1}H NMR δ=1.05 (3H, d, J=7.3 Hz), 1.08 (3H, d, J=7.3 Hz), 1.5—1.6 (1H, m), 2.0—2.4 (4H, m), 3.00 (1H, d, J=9.2 Hz), 3.07 (1H, m), 3.15 (1H, d, J=8.4 Hz), 3.65 (3H, s), 5.62 (1H, s), 5.77 (1H, d, J=11.0 Hz), and 7.11 (1H, dd, J=11.0, 8.4 Hz); ^{13}C NMR δ=20.0, 20.7, 26.5, 34.9, 40.2, 40.4, 46.5, 49.8, 54.3, 88.0, 121.1, 128.6, 151.7, 154.8, 194.1, and 213.1; IR (oil) 2960, 2872, 1744, 1678, 1604, 1463, 1410, 1384, 1229, 1209, 1159, 1107, and 978 cm^{-1}; UV (MeOH) 228 (ε 5600), 281 (2200), 302 (1500), and 313 nm (1200); MS m/z (%) 261 (M^+ +1, 8), 260 (M^+, 39), 218 (23), 217 (100), 189 (8), 151 (15), and 83 (6).

Found: m/z 260.1412 (M^+). Calcd for $C_{16}H_{20}O_3$: M, 260.1412.

14: A colorless oil; ^{1}H NMR δ=1.07 (3H, d, J=6.6 Hz), 1.18 (3H, d, J=6.6 Hz), 1.8—1.9 (1H, m), 2.2—2.25 (3H, m), 2.58 (1H, sept, J=6.6 Hz), 2.90 (1H, d, J=8.8 Hz), 3.03 (1H, ddm, J=8.8, 7.4 Hz), 3.54 (1H, d, J=7.3 Hz), 3.58 (3H, s), 5.77 (1H, s), 6.14 (1H, ddd, J=8.4, 7.3, 0.7 Hz), and 6.35 (1H, d, J=8.4 Hz); ^{13}C NMR δ=17.5, 18.4, 28.1, 31.4, 38.4, 40.6, 49.2, 53.6, 54.9, 58.7, 119.0, 124.9, 143.6, 150.2, 191.8, and 216.7; IR (oil) 3008, 2962, 2876, 1734, 1689, 1635, 1613, 1462, 1373, 1243, 1208, 1153, 1125, and 754 cm^{-1}; UV (MeOH) 228 (ε 2500) and 278 nm (2500); MS m/z (%) 261 (M^++1, 19), 260 (M^+, 100), 232 (34), 217 (49), 204 (19), 189 (20), 178 (49), 161 (20), 150 (40), 137 (19), and 135 (40).

Found: m/z 260.1411 (M^+). Calcd for $C_{16}H_{20}O_3$: M, 260.1412.

Cycloaddition Reaction of 12b and 2. A toluene solution (2 cm^3) of **12b** (180 mg) and **2** (160 mg) was heated at 150 °C for 12 h under 10000 bar. The solvent was removed under reduced pressure and the residue was purified by SiO_2 column chromatography and HPLC (AcOEt:hexane=1:2) to give 153 mg (58%) of **15**, 11 mg (4%) of **16**, 13 mg (5%) of **17**, and 22 mg (12%) of **12b**.

15: A colorless oil; ^{1}H NMR δ=1.13 (3H, d, J=7.0 Hz), 1.14 (3H, d, J=7.0 Hz), 2.2—2.4 (4H, m), 2.52 (1H, sept, J=7.0 Hz), 2.9—3.0 (2H, m), 3.22 (1H, d, J=7.3 Hz), 3.63 (3H, s), 5.55 (1H, d, J=1.1 Hz), 6.10 (1H, d, J=9.2 Hz), and 6.51 (1H, dd, J=9.2, 7.3 Hz); ^{13}C NMR δ=20.1, 20.2, 27.6, 37.0, 40.1, 41.4, 47.2, 50.8, 54.1, 87.9, 121.0, 132.3, 134.0, 172.9, 194.1, and 213.1; IR (oil) 2960, 1743, 1669, 1463, 1411, 1385, 1211, 1167, 1113, and 663 cm^{-1}; UV (MeOH) 230 (ε 5900), 258 (3500), and 310 nm (700); MS m/z (%) 261 (M^++1, 21), 260 (M^+, 100), 217 (31), and 137 (14).

Found: m/z 260.1412 (M^+). Calcd for $C_{16}H_{20}O_3$: M, 260.1412.

16: A colorless oil; ^{1}H NMR δ=1.13 (6H, d, J=6.6 Hz), 2.1—2.4 (4H, m), 2.52 (1H, sept, J=6.6 Hz), 2.73 (1H, dm, J=10.6 Hz), 3.14 (1H, dddd, J=10.6, 8.4, 7.0, 1.5 Hz), 3.57 (3H,

s), 3.59 (1H, dm, J=7.0 Hz), 5.63 (1H, t, J=1.5 Hz), 6.11 (1H, ddd, J=9.2, 1.5, 0.7 Hz), and 6.31 (1H, dd, J=9.2, 7.0 Hz); ^{13}C NMR δ=20.0, 20.2, 22.8, 37.1, 38.9, 41.1, 41.5, 53.0, 53.4, 89.0, 122.2, 131.8, 134.0, 172.4, 195.6, and 216.5; IR (oil) 2962, 2874, 1741, 1669, 1629, 1463, 1408, 1385, 1173, 1113, and 665 cm^{-1}; UV (MeOH) 228 (ε 5500), 259 (3400, sh), and 270 nm (2500, sh); MS m/z (%) 260 (M^+, 100), 217 (85), 204 (30), 203 (25), 189 (55), 173 (26), 161 (52), 108 (27), 91 (32), 77 (25), 41 (29), and 26 (30).

Found: m/z 260.1414 (M^+). Calcd for $C_{16}H_{20}O_3$: M, 260.1412.

17: Colorless crystals, mp 96—98 °C; ^{1}H NMR δ=1.01 (6H, d, J=6.2 Hz), 1.6—1.65 (1H, m), 2.1—2.25 (2H, m), 2.3—2.4 (2H, m), 2.75 (1H, dd, J=11.3, 5.5 Hz), 3.00 (1H, ddt, J=11.3, 8.8, 6.2 Hz), 3.50 (3H, s), 3.72 (1H, ddd, J=9.2, 7.3, 5.5 Hz), 3.82 (1H, dd, J=6.2, 1.5 Hz), 6.02 (1H, d, J=9.2 Hz), and 6.18 (1H, dd, J=7.3, 1.5 Hz); ^{13}C NMR δ=20.7, 20.8, 24.0, 33.8, 34.5, 38.5, 40.1, 53.5, 55.0, 60.2, 119.3, 128.4, 147.8, 152.1, 193.5, and 218.6; IR (KBr) 3052, 2956, 2870, 1738, 1670, 1653, 1614, 1449, 1379, 1246, 1232, 1132, 999, and 881 cm^{-1}; UV (MeOH) 251 (ε 3300) and 277 nm (2400); MS m/z (%) 261 (M^++1, 18), 260 (M^+, 100), 232 (11), 217 (14), 178 (11), 164 (30), and 150 (41).

Found: m/z 260.1412 (M^+). Calcd for $C_{16}H_{20}O_3$: M, 260.1412.

Irradiation of 3. a) A $CDCl_3$ solution (1 cm^3) of **3** (40 mg) was purged with N_2 gas in a Pyrex NMR tube and the solution was irradiated by a 400-W high-pressure mercury lamp for 2 h at room temperature. The solvent was removed under reduced pressure and 38 mg (98%) of **3** was recovered.

b) A $CDCl_3$ solution (1 cm^3) of **3** (32 mg) and benzophenone (31 mg) was purged with N_2 gas in a Pyrex NMR tube and the solution was irradiated by a 400-W high-pressure mercury lamp for 3 h at room temperature. The solvent was removed under reduced pressure and 27 mg (84%) of **3** was recovered after SiO_2 chromatography (AcOEt:hexane=1:1).

c) A $CDCl_3$ solution (1 cm^3) of **3** (25 mg) was purged with N_2 gas in a quartz NMR tube and the solution was irradiated by a 400-W high-pressure mercury lamp for 2 h at room temperature. The solvent was removed under reduced pressure and the residue was chromatographed on PTLC (20 cm×10 cm, AcOEt:hexane=1:2) to give 15 mg (60%) of **18**.

18: A colorless oil; ^{1}H NMR δ=1.94 (1H, dd, J=12.7, 9.1 Hz), 2.07 (1H, dddd, J=12.7, 11.5, 9.1, 6.4 Hz), 2.16 (1H, ddd, J=19.1, 11.5, 9.1 Hz), 2.28 (1H, dd, J=19.1, 9.1 Hz), 2.56 (1H, br d, J=7.2 Hz), 2.81 (1H, br s, $h_{1/2}$=16 Hz), 2.98 (1H, ddd, J=8.3, 4.8, 2.4 Hz), 3.74 (1H, ddd, J=7.2, 4.8, 2.6 Hz), 5.57 (1H, d, J=9.9 Hz), 5.77 (1H, ddd, J=9.9, 4.4, 2.4 Hz), 6.19 (1H, dd, J=5.6, 2.4 Hz), and 7.59 (1H, dd, J=5.6, 2.6 Hz); ^{13}C NMR δ=26.6, 33.0, 34.0, 39.1, 44.4, 50.2, 126.9, 129.9, 133.7, 166.2, 206.9, and 216.9; MS m/z (%) 188 (M^+, 76), 164 (65), 160 (100), 146 (40), 131 (40), 118 (80), 117 (48), 104 (62), and 91 (94).

Found: m/z 188.0834 (M^+). Calcd for $C_{12}H_{12}O_2$: M, 188.0836.

Irradiation of 9. a) A $CDCl_3$ solution (1 cm^3) of **9** (100 mg) was purged with N_2 gas in a Pyrex NMR tube and the solution was irradiated by a 400-W high-pressure mercury lamp for 120 min at 20 °C. The solvent was removed under reduced pressure and the residue was purified by PTLC (20 cm×10 cm, AcOEt:hexane=1:1) to give 65 mg (65%) of **19**.

19: Colorless crystals, mp 104—104.5 °C; ^{1}H NMR δ=1.30 (1H, td, J=7.7, 1.7 Hz), 1.7—1.8 (2H, m), 2.00 (1H, ddd, J=8.1, 7.7, 6.4 Hz), 2.03 (1H, d, J=20.3 Hz), 2.31 (1H, dd, J=12.2, 5.0 Hz), 2.33 (1H, dd, J=9.0, 2.8 Hz), 2.35—2.45 (2H, m), 2.78 (1H, ddd, J=20.3, 6.5, 2.4 Hz), 3.74 (1H, dd, J=6.4, 2.4 Hz), and 4.04 (3H, s); ^{13}C NMR δ=15.6, 19.4, 21.5, 30.2, 33.8, 37.3, 39.1, 48.4, 59.8, 114.2, 160.7, 201.8, and 212.8; IR (KBr) 2950, 1735, 1708, 1613, 1409, 1291, 1194, and 756 cm^{-1}; UV (MeOH) 282 (ε 9400), 302 (6300), and 310 nm (5500); MS m/z (%) 218 (M^+, 100), 190 (34), 175 (48), 158 (43), 147 (27), 116 (36), 109 (84), 91 (40), 77 (31), 44 (25), 41 (31), 39 (30), and 28 (32).

Found: C, 71.81; H, 6.48% and m/z 218.0944 (M^+). Calcd for $C_{13}H_{14}O_3$: C, 71.54; H, 6.47% and 218.0942 (M).

b) A MeOH solution (1 cm^3) of **9** (60 mg) was purged with N_2 gas in a Pyrex NMR tube and the solution was irradiated by a 400-W high-pressure mercury lamp for 40 min at room temperature. The solvent was removed under reduced pressure and the residue was purified by means of PTLC (20 cm×10 cm, AcOEt:hexane=1:1) to give 64.2 mg (100%) of **20** and 4 mg of **9**.

20: A colorless oil; ^{1}H NMR δ=0.99 (1H, td, J=8.4, 2.6 Hz), 1.32 (1H, tt, J=8.4, 7.3 Hz), 1.57 (1H, td, J=8.4, 4.0 Hz), 1.9—2.5 (6H, m), 2.52 (1H, d, J=7.7 Hz), 2.60 (1H, m), 3.59 (3H, s), 3.69 (3H, s), and 4.64 (1H, d, J=4.0 Hz); ^{13}C NMR δ=15.0, 16.2, 19.7, 29.0, 29.3, 33.6, 35.7, 51.7, 52.3, 54.8, 90.1, 153.9, 173.9, and 215.9; IR (oil) 3000, 2950, 1733, 1660, 1438, 1377, 1353, 1313, 1270, 1208, 1173, 1129, 1038, 1009, and 810 cm^{-1}; MS m/z (%) 251 (M^++1, 8), 250 (M^+, 37), 163 (49), 149 (23), 121 (100), and 91 (19).

Found: C, 66.90; H, 7.04% and m/z 250.1199 (M^+). Calcd for $C_{14}H_{18}O_4$: C, 67.18; H, 7.25% and 250.1204 (M).

Demethylation of 20 with CF_3COOH. A $CDCl_3$ solution (1 cm^3) of **20** (25 mg) and CF_3COOH (1 drop) was kept in an NMR tube overnight at room temperature. The solvent was removed under reduced pressure and the residue was chromatographed on a SiO_2 column (AcOEt:hexane=1:1) to give 20 mg (85%) of **21**.

21: Colorless crystals, mp 87—88 °C; ^{1}H NMR δ=1.09 (1H, br t, J=8.4 Hz), 1.3—1.35 (2H, m), 1.68 (1H, m), 2.0—2.1 (3H, m), 2.3—2.65 (5H, m), and 3.17 (3H, s); ^{13}C NMR δ=12.2, 14.6, 16.5, 23.4, 29.4, 31.4, 32.3, 37.5, 51.8, 112.0, 168.1, 173.3, and 207.0; IR (KBr) 3244, 2950, 2836, 1735, 1687, 1631, 1439, 1315, 1199, 1170, 1107, 1007, 841, and 753 cm^{-1}; UV (MeOH) 222 nm (ε 8400); MS m/z (%) 236 (M^+, 22), 205 (19), 186 (21), 177 (27), 163 (100), 162 (47), 161 (25), 158 (30), 149 (40), 123 (58), 121 (35), 109 (26), 91 (28), 82 (19), and 77 (26).

Found: C, 66.23; H, 6.82%. Calcd for $C_{13}H_{16}O_4$: C, 66.08; H, 6.83%.

Irradiation of 13. A $CDCl_3$ solution (1 cm^3) of **13** (50 mg) was purged with N_2 gas in a Pyrex NMR tube and the solution was irradiated by a 400-W high-pressure mercury lamp for 2 h at room temperature. The solvent was removed under reduced pressure and the residue was chromatographed by PTLC (20 cm×10 cm, AcOEt:hexane=1:1) to give 34 mg (68%) of **22**.

22: A colorless oil; ^{1}H NMR δ=0.87 (3H, d, J=6.6 Hz), 0.99 (3H, d, J=6.6 Hz), 1.10 (1H, br d, J=8.1 Hz), 1.5—1.8 (3H, m), 2.12 (1H, d, J=20.5 Hz), 2.3—2.5 (4H, m), 2.80 (1H, ddd, J=20.5, 6.2, 2.2 Hz), 3.52 (1H, s), and 4.06 (3H, s); ^{13}C NMR δ=20.2 (2C) 20.6 (2C), 27.0, 30.5, 33.0, 34.4, 38.7, 39.3, 51.5, 59.4, 114.5, 161.7, 201.7, and 212.5; IR (oil) 2956, 2870, 1741, 1700, 1604, 1462, 1410, 1386, 1305, 1196, 1169, 1147, 1005, 841, and 621 cm^{-1}; UV (MeOH) 282 (ε 7300), 302 (4500), and 311 nm (3600); MS m/z (%) 261 (M^++1, 17), 260 (M^+, 100), 232

(7), 218 (31), 189 (13), and 151 (57).

Found: m/z 260.1412 (M^+). Calcd for $C_{16}H_{20}O_3$: M, 260.1412.

Irradiation of 15. A $CDCl_3$ solution (1 cm^3) of **15** (100 mg) was purged with N_2 gas in a Pyrex NMR tube and the solution was irradiated by a 400-W high-pressure mercury lamp for 110 min at room temperature. The solvent was removed under reduced pressure and the residue was purified by SiO_2 chromatography and HPLC (AcOEt:hexane=1:1) to give 38 mg (54%) of **23** and 30 mg (30%) of **15**.

23: A colorless oil; ^1H NMR δ=0.95 (3H, d, J=6.6 Hz), 1.01 (3H, d, J=6.6 Hz), 1.11 (1H, d, J=8.8 Hz), 1.39 (1H, sept, J=6.6 Hz), 1.74 (1H, m), 1.75 (1H, dd, J=8.8, 6.6 Hz), 1.99 (1H, d, J=20.1 Hz), 2.38 (4H, m), 2.63 (1H, d, J=20.1 Hz), 3.75 (1H, d, J=6.6 Hz), and 4.02 (3H, s); ^{13}C NMR δ=19.5, 19.9, 24.8 (2C), 27.7, 30.5, 33.5, 34.0, 34.6, 39.0, 39.1, 49.6, 58.9, 114.1, 161.1, 201.8, and 211.9; IR (oil) 2956, 2872, 1742, 1702, 1611, 1462, 1416, 1387, 1366, 1199, 1167, 1147, 1004, and 842 cm^{-1}; UV (MeOH) 282 (ε 6200), 302 (4500), and 311 nm (3600); MS m/z (%) 261 (M^++1, 19), 260 (M^+, 93), 232 (46), 217 (47), 201 (19), 200 (100), 189 (20), 185 (32), 164 (28), 85 (32), and 83 (51).

Found: m/z 260.1413 (M^+). Calcd for $C_{16}H_{20}O_3$: M, 160.1412.

References

1) Part LVI. A. Mori, Y. Nukii, A. Endo, and H. Takeshita, *Bull. Chem. Soc. Jpn.*, **64**, 208 (1991).

2) S. Ito, H. Takeshita, Y. Shoji, Y. Toyooka, and T. Nozoe, *Tetrahedron Lett.*, **1968**, 3215; S. Ito, A. Mori, Y. Shoji, and H. Takeshita, *ibid.*, **1972**, 2685.

3) J. Meinwald, S. L. Emerman, N. C. Yang, and G. Büchi, *J. Am. Chem. Soc.*, **77**, 4401 (1955).

4) S. Ito, H. Takeshita, and Y. Shoji, *Tetrahedron Lett.*, **1969**, 1815.

5) A. Mori, Z.-H. Li, H. Nakashima, and H. Takeshita, *Bull. Chem. Soc. Jpn.*, **63**, 1636 (1990).

6) T. Sasaki, K. Kanematsu, and K. Hayakawa, *J. Chem. Soc., Perkin Trans. 1*, **1972**, 1951.

7) R. K. Boeckman, Jr., C. H. Weidner, R. B. Perni, and J. J. Napier, *J. Am. Chem. Soc.*, **111**, 8036 (1989); L. A. Paquette, D. Macdonald, L. G. Anderson, and J. Wright, *J. Am. Chem. Soc.*, **111**, 8037 (1989); L. A. Paquette, J. L. Romine, and H.-S. Lin, *Tetrahedron Lett.*, **28**, 31 (1987).

8) R. C. Cookson, B. V. Drake, J. Hudec, and A. Morrison, *J. Chem. Soc., Chem. Commun.*, **1966**, 15; S. Ito, Y. Fujise, T. Okuda, and Y. Inoue, *Bull. Chem. Soc. Jpn.*, **39**, 1351 (1966).

9) E. L. Eliel, "Stereochemistry of Carbon Compounds," Kogakusha, Tokyo, Chap. 9, pp. 204—246.

10) A. S. Cieplak, B. D. Tait, and C. R. Johnson, *J. Am. Chem. Soc.*, **111**, 8447 (1989); A. S. Cieplak, *ibid.*, **103**, 4540 (1981).

11) T. Uyehara, S. Miyakoshi, and Y. Kitahara, *Bull. Chem. Soc. Jpn.*, **52**, 2023 (1979).

12) Related examples have been reported; M. Petrzilka and J. I. Grayson, *Synthesis*, **1981**, 753.

13) A. S. Kende, Z. Goldschmidt, and P. T. Izzo, *J. Am. Chem. Soc.*, **91**, 6858 (1969).

H-Aggregate of a Long-Chain Crystal Violet Dye in Langmuir-Blodgett Films[1)]

Akio MIYATA,* Yutaka UNUMA, and Yoshiyuki HIGASHIGAKI
Tokyo Research Laboratories, Sharp Corporation, Kashiwa, Chiba 277
(Received February 22, 1991)

The molecular orientation and aggregate formation in Crystal Violet (CV) dye monomolecular layers have been investigated by means of polarized reflection and absorption spectral measurements at an incident angle of 60°. A relatively sharp absorption band at 2.04 eV and a broad band around 2.23 eV assignable to the J-dimer and the H-dimer, respectively, were observed in the optical measurement geometry with polarized light either parallel(p) or perpendicular(s) to the incident plane. A sharp band at 2.61 eV, assigned to the H-aggregate (tetramer), was detected by p-polarized spectral measurement, but not s-polarized measurement. The J- and H-dimers have horizontal transition moments and the H-aggregate has a vertical transition moment. The H-aggregate peak shifted from 2.53 eV (10 mN m^{-1}) to 2.61 eV (40 mN m^{-1}) with increasing surface pressure. This is due to an increase in the slip angle between the transition dipole moments and their center-to-center lines because the chromophoric planes become to be gradually oriented normal to the water surface. The behavior of these aggregates is interpreted in terms of the extended dipole model.

Dye aggregates can easily be obtained in well-ordered layer structures using the Langumir–Blodgett (LB) method. Merocyanine,[2)] cyanine,[3)] and squarylium[4)] dyes form J- and H-aggregates and this has attracted much attention on account of their optical and electrical functions as photosensitizers. It is desirable to control the orientation and aggregation of the chromophores in layered structures with functions such as energy and electron transfer. Sugi et al. reported that J-aggregates in the merocyanine LB films show a high photoelectric conversion efficiency.[2)] In order to attain higher efficiency, several photoelectrical LB heterojunctions have been prepared.[5)] For example, the electrical and photoelectrical characteristics of organic p-n junction diodes consisting of an n-type Crystal Violet (CV) dye and a p-type merocyanine dye have been studied in comparison with homogeneous merocyanine LB films. Nakahara et al. reported that energy transfer occurred from the merocyanine J-aggregates to the CV dye in hetero-type LB films.[6)]

It is necessary to control the orientation and structure of dye aggregate in the monolayers for developing functional organic thin films with high quality and good structure. The molecular orientations in monolayers on water are determined by cohesive forces of chromophores, by hydrophobic interactions between long alkyl chains, and by adsorptive interactions between chromophores and the water surface. Möbius et al. reported that the orientation of chromophores and aggregates, i.e., dimer, J- and H-aggregates can be investigated by measurements of reflection spectra with linearly polarized light.[7-9)] The transition moments for a porphyrin, a cyanine dye, and an azo dye are oriented within the monolayer plane, with the exception of an azo dye H-aggregate which is oriented normal to the monolayer plane. In this paper we report the optical properties of the CV dye aggregates in the monolayer on water at various surface pressures and the LB films. The configuration of the dye aggregates are discussed in terms of Kuhn's extended dipole model.[10)]

Experimental

Materials. The Crystal Violet dye with a long alkyl chain was purchased from Nippon Kankoh-Shikiso Kenkyusho Co. and was used without further purificaiton. The chemical structure is shown in Fig. 1. Chloroform of spectroscopic grade was used for spreading the monolayers.

Procedures. The subphase was water containing $NaHCO_3$ at pH 6.7—6.8 and at 20—21 °C. Monolayers were spread on the subphase from a 4×10^{-4} M (1 M=1 mol dm^{-3}) chloroform solution of the dye. The measurements of surface pressure-area (π–A) isotherms and preparations of monolayers for absorption spectra were carried out by means of a conventional Langmuir trough (Joyce Loebl Ltd., model IV) equipped with a Wilhelmy balance. The absorption spectra of monolayers at incident angles of 0° and 60° were measured using a multichannel spectrophotometer (Otsuka Electronics Co., model MCPD-200) as illustrated in Fig. 2. The incident plane was perpendicular to the direction of compression. For absorption spectra measurements, the photodetector was positioned to detect only the beam reflected from the mirror and not that from the water surface. After spreading the solution, the monolayer was compressed to a predetermined surface pressure and maintained there for 5 min before starting spectral measurements. The substrates for visible

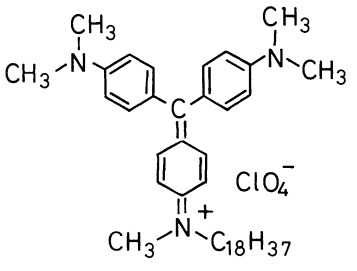

Fig. 1. Chemical structure of the Crystal Violet dye.

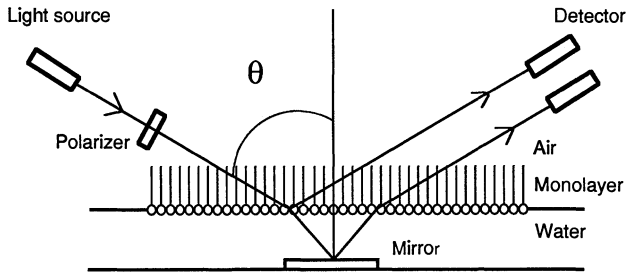

Fig. 2. Schematic diagram of polarized reflection and absorption measurements at an incident angle of 60°.

spectroscopic measurements were made fully hydrophilic by immersion in a 0.5 M KOH–ethanol solution. The monomolecular film was deposited onto a hydrophilic glass substrate by the vertical lifting method.

Results and Discussion

π–A Isotherm. Figure 3 shows a π–A isotherm for the monolayer of CV dye at the air–water interface. The CV dye gives a stable monolayer upto 50 mN m^{-1}. Various conformations of this dye can arise from free rotations of the phenylene rings and amino groups. The chromophore dimensions are about 13Å×14Å×5Å, and a planar close packed arrangement of the molecules on the water surface gives an area of about 120 Å^2 per molecule. The limiting area obtained by extrapolation of the linear portion in the π–A curve to π=0 is 50 Å^2 molecule^{-1}. This area is much too small to be consistent with the molecule lying flat on the water. Judging from this molecular area, the orientation of the chromophoric plane corresponds to lying horizontal on the water surface at 0—5 mN m^{-1}, and the molecules gradually overlap as the pressure increases and produces an upright structure at high surface pressures. For the mixed monolayer of the CV dye and cadmium arachidate, the π–A isotherms clearly gave two-step phase transitions from the expanded to condensed monolayers.[11] The marked two-step phase transitions are probably due to molecular reorientations, which did not depend on mixing ratios, but only on the change of surface pressures. It is possible that similar reorientation occurs in a neat dye monolayer.

Absorption Spectroscopy for Monolayer on Water. Figure 4 shows the normal incident absorption spectra at various surface pressures. An absorption band was observed at 2.04 eV at low surface pressures (0—5 mN m^{-1}). This 2.04 eV band is red-shifted from the monomer band (2.10 eV) in chloroform. The dye within the monolayer does not exist as isolated molecules but as a linear aggregate. The intensity of the 2.04 eV peak decreased with an increase in surface pressures from 10 to 40 mN m^{-1}, while that of the 2.24 eV peak increased. The 2.24 eV band is blue-shifted from the monomer band and assigned to an H-dimer. Its configuration is of a face-to-face structure consisting of two molecules

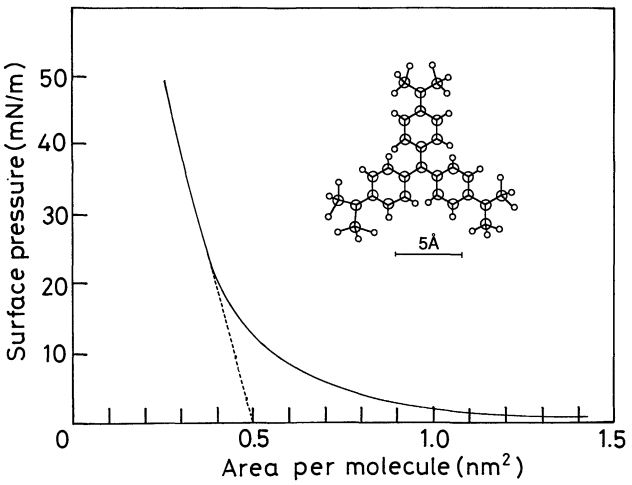

Fig. 3. Surface pressure-area isotherm for the monolayer of the CV dye.

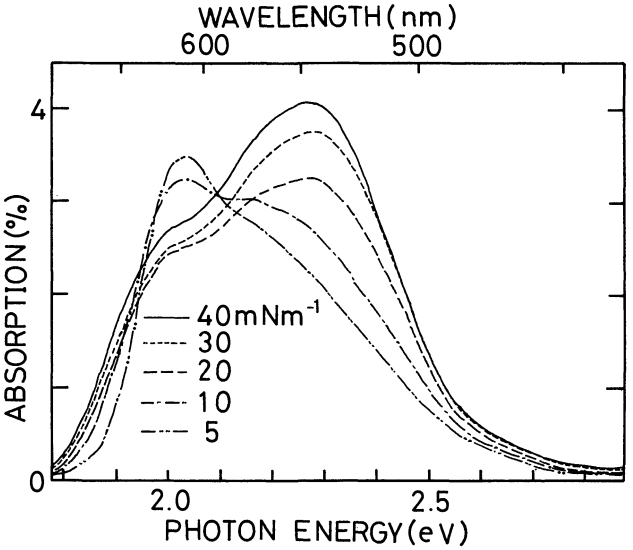

Fig. 4. Absorption spectra under normal incidence for the monolayer on water at various surface pressures.

oriented parallel to the water surface.

The molecular orientation and arrangement were further studied by measuring the polarized absorption spectra with an incident angle of 60°. The broad band around 2.23 eV was observed with polarized light either parallel(p) or perpendicular(s) to the incident plane as shown in Figure 5(a) and (b). On the contrary, the isotropic and sharp absorption band at 2.61 eV, which can be assigned to an H-aggregate, was observed in the p-polarized spectra between 20 and 40 mN m^{-1}, but not in the s-polarized spectra. Figure 6 shows the H-aggregate band detected with p-polarized light after substraction of H-dimer absorption spectra. The peak shifted from 2.53 eV at 10 mN m^{-1} to 2.61 eV at 40 mN m^{-1}. This blue-shift is due to an increase in the slip angle between the transition dipole moments and their center-to-center

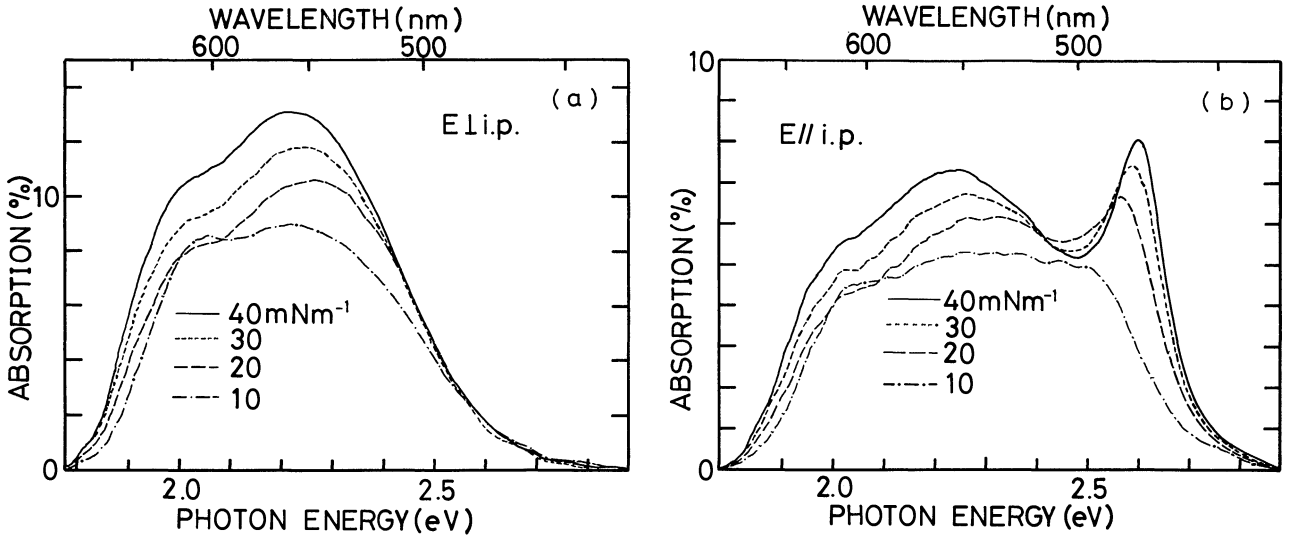

Fig. 5. Polarized absorption spectra for the monolayer on water at various surface pressures.; (a) perpendicular and (b) parallel to incident plane with polarized light of 60° incident angle.

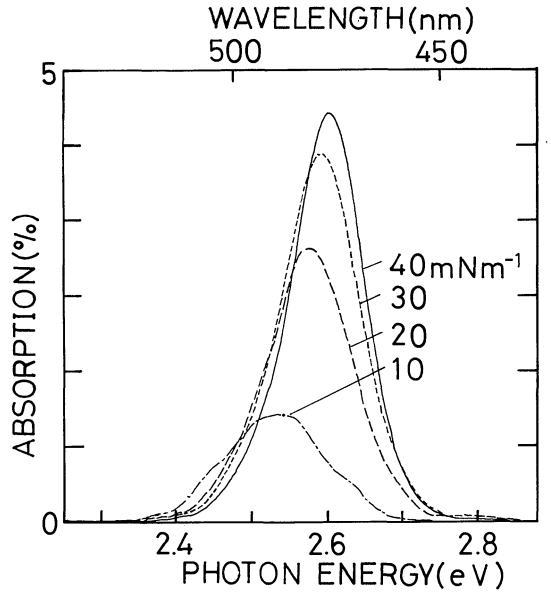

Fig. 6. Parallel polarized absorption spectra for H-aggregate band at various surface pressures.

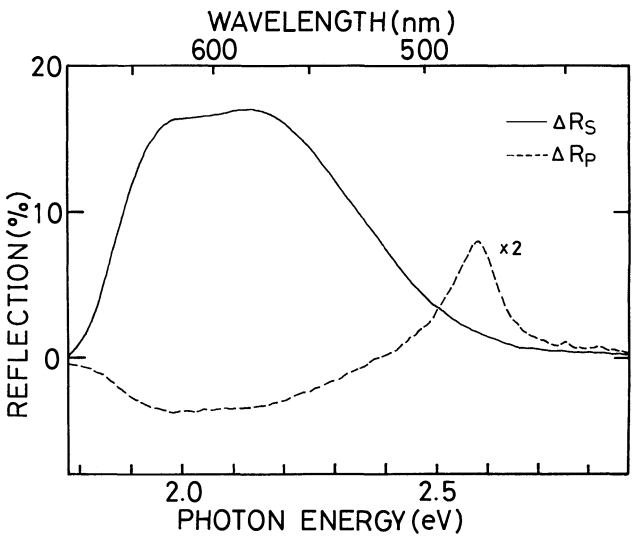

Fig. 7. Perpendicular and parallel polarized reflection spectra for the monolayer on water with 60° incident angle at a surfacce pressure of 40 mN m^{-1}.

lines with increasing surface pressures.

Reflection Spectroscopy. In order to confirm whether the chromophore lies flat or edge-on, reflection spectra were measured with an incident angle of 60°. Figure 7 shows the polarized reflection spectra of the monolayer on water at 40 mN m^{-1}. According to the Möbius' theory,[9] when the transition moment of the dye molecule lies within the surface water, s-polarized reflection (ΔR_s) with an incident angle of 60° should always be positive, and p-polarized reflection (ΔR_p) should be negative. If the transition moment is oriented normal to the water surface, ΔR_s is positive and ΔR_p cannot be observed. In the ΔR_s spectra (Fig. 7), a broad band around 2.15 eV, which is likely assigned to the H-dimer, is positive, while a sharp band assigned to the H-aggregate is almost absent. In the ΔR_p spectra, the broad H-dimer band is negative, while the H-aggregate band at 2.59 eV is positive. This result therefore supports our view that the transition moment for the H-dimer is oriented parallel to the surface plane, while that for the H-aggregate lies normal to the water surface.

Absorption Spectroscopy for Monomolecular Films on Substrate. Polarized absorption spectra were measured in order to examine whether the H-aggregates form in the LB film. The monomolecular LB film was

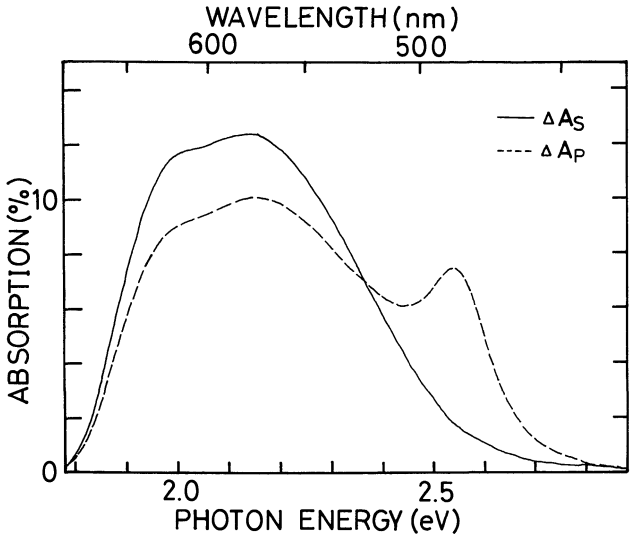

Fig. 8. Absorption spectra of perpendicular and parallel polarized light with an incident angle of 45° for the LB film at a deposition pressure of 40 mN m^{-1}.

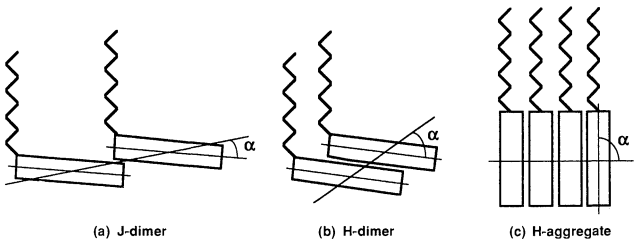

Fig. 9. Model of molecular configurations.

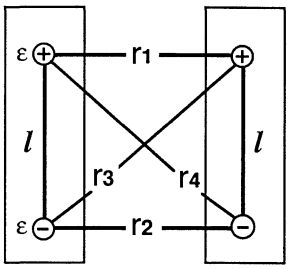

Fig. 10. An arrangement of two extended dipoles of charge ε and length l for calculation of the energy shift $\Delta E'$.

deposited at a surface pressure of 40 mN m^{-1} and a dipping speed of 6 mm min^{-1} under the same conditions for forming H-aggregate in monolayer on water. Figure 8 shows typical polarized absorption spectra of the LB film. The polarized absorption spectra of the LB film is similar to those of the monolayer on water. The H-aggregate band was observed at 2.55 eV. The red-shift from 2.61 eV (monolayer on water) to 2.55 eV indicates that the LB is in a more disordered state than the monolayer on water, and some fluctuations of the chromophores occurred during deposition process.

The Molecular Configuration Model. Figure 9 shows the models for molecular configuration to account for the present observations. Because the charged amino groups linked with three phenyl rings are anchored to the water surface, the dyes tend to assume a flat orientation at low surface pressures (0—5 mN m^{-1}). In view of the red-shifted absorption from the monomer band, dyes form a linear aggregate structure in model **a**. α is the slip angle between the transition dipole moments and their center-to-center lines. In this case the slip angle is small. At intermediate surface pressures (10—30 mN m^{-1}) the chromophores lie flat on the water surface or have an orientation with a relatively small angle between the chromophoric plane and the water surface. The dye molecule slips on the top of another adjacent molecule during film compression. The chromophoric planes are oriented parallel to each other and the dyes have a tace-to-face structure in model **b**. At high surface pressures (20—40 mN m^{-1}) the chromophoric planes are forced into an edge-on position and stack next to each other. In this case α is close to a right angle. The H-aggregate is indicated in model **c**. The appearance of this stacking structure is due to the strong dye–dye interaction between chromophoric planes with an edge-on position.

The Extended Dipole Model. Kuhn and associates proposed an extended dipole model to account for molecular arrangements in the blue- and red-shifted aggregates.[10] The interaction integrals between dye molecules in the aggregation are given by varying a series of parameters, i.e., the number of aggregate molecules, the dipole length, the slip angle α and the distance between the centers of dipoles. In Fig. 10, the molecules are replaced by extended dipoles of length l between two charges $+\varepsilon$ and $-\varepsilon$. The energy shift ($\Delta E'$) of two molecules is obtained by

$$\Delta E' = \frac{2\varepsilon^2}{D}\left(\frac{1}{r_1}+\frac{1}{r_2}-\frac{1}{r_3}-\frac{1}{r_4}\right),$$

where D is the dielectric constant of the medium (D=2.5 for hydrocarbons) and r_i is the distance between two charges. The charge ε and the length l are assumed to be related to the transition moment μ by $\mu=\varepsilon\times l$.

Thus, the transition energy ΔE_{agg} of a dye aggregate is represented with the excitation energy of the dye monomer, ΔE_m, and the interaction integral $\Delta E'$ approximated by

$$\Delta E_{agg} = \Delta E_m \pm \Delta E'.$$

In the case of an aggregate containing n molecules, the intensity of the dipole–dipole interaction between ith and jth molecules is expressed as follows:

$$\Delta E' = \frac{2\varepsilon^2}{D} \sum_{i \neq j}^{n} \left(\frac{1}{|r_i^+ - r_j^+|} + \frac{1}{|r_i^- - r_j^-|} - \frac{1}{|r_i^+ - r_j^-|} - \frac{1}{|r_i^- - r_j^+|} \right),$$

where $|r_i^+ - r_j^+|$ and $|r_i^- - r_j^-|$ are the distance between positive charges and both negative charges of ith and jth molecule, respectively. $|r_i^+ - r_j^-|$ and $|r_i^- - r_j^+|$ are the distance between opposite charges of ith and jth molecule.

The transition dipole moment μ used in our calculation is indicated in the inset of Fig. 11. The positive charge of nitrogen N_1 of the octadecylmethylamino group is assumed as $+\varepsilon$ and each of negative charges of N_2 and N_3 atom as $-0.5\,\varepsilon$. The dipole length is l=8.4 Å. The values of $\Delta E'$ can be calculated by the dipole length and also by estimating the distance between the adjacent transition moments to be about 5 Å, which corresponds to the molecular model and the transition moment μ=9.98 Debye from the chroloform solution spectrum. In correspondence to the face-to-face arrangement, the blue-shift value of the H-aggregate band is considered to be most significant. The calculated values $\Delta E'$ for various arrangements are indicated in Fig. 11. The observed shift −0.06 eV of the J-dimer was fitted to the calculated value $\Delta E'$ of −0.05 eV with n=2 and a minimum slip angle α of 26°. For the observed value between 0.12 and 0.14 eV for the H-dimer, it was calculated to be 0.12 and 0.14 eV with n=2 and slip angles between 72° and 90°. The broadness of the H-dimer band is probably due to containing the coexistence of several kinds of dimers with various slip angles. For the red shift value of 0.43 eV (10 mN m^{-1}) and 0.51 eV (40 mN m^{-1}) of the H-aggregate, it was calculated to be 0.43 eV (α=72°) and 0.49 eV (α=90°) with n=4.

In conclusion, it was found that an H-aggregate assignable to a tetramer of CV dye forms in a close-packed monomolecular layer at high surface pressures. Since the H-aggregate band is present in the p-polarized spectra and absent in the normal incident and s-polarized spectra, its chromophoric planes must be oriented normal to the monolayer. The results of polarized absorption spectral measurements indicated that a well-ordered arrangement of H-aggregate was indeed present in the monolayer on water rather than in the LB film. The H-aggregates having a vertical transition moment observed here are of much significance as optical information storage media that work with a linearly polarized light at an oblique incidence.

The authors are grateful to Dr. David Heard of Sharp Corporation and Professor Akihiko Yamagishi of College of Arts and Sciences, University of Tokyo for valuable discussions.

This work was performed under the management of the FED (the R & D Association for Future Electron Devices) as a part of the R & D of Basic Technology for Future Industries supported by NEDO (New Energy and Industrial Technology Development Organization).

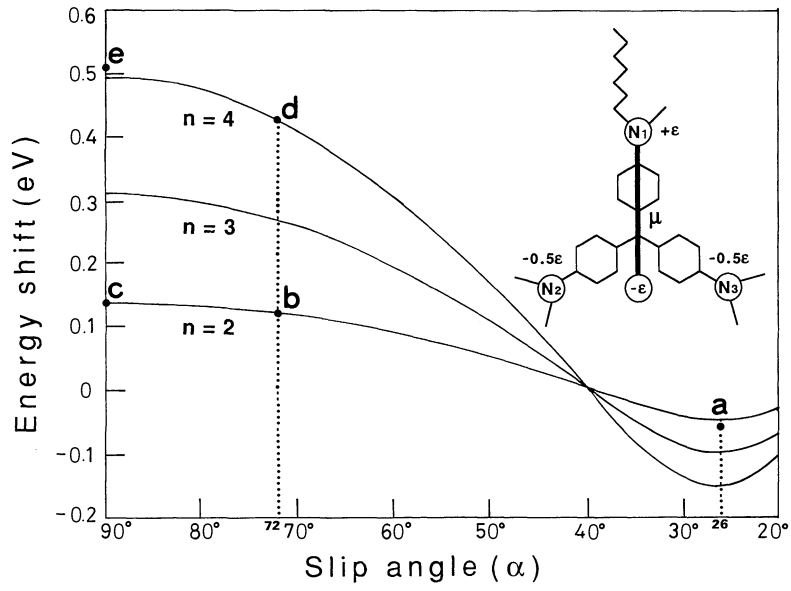

Fig. 11. The calculated energy shifts $\Delta E'$ are indicated; n is the number of molecules, the transition dipole moment μ (9.98 Debye) is charge ε and length l=8.4 Å; point a (−0.06 eV), 26° J-dimer; point b (0.12 eV), 72° H-dimer; point c (0.14 eV), 90° H-dimer; point d (0.43 eV), 72° H-aggregate (10 mN m^{-1}); point e (0.51 eV). 90° H-aggregate (40 mN m^{-1}).

References

1) Partially reported in the 37th National Meeting of the Physical Society of Japan, Nagoya, March 1987, Abstr., 27a-LB-5.

2) M. Saito, M. Sugi, and S. Iizima, *Thin Solid Films,* **100**, 117 (1983).

3) H. Bucher and H. Kuhn, *Chem. Phys. Lett.,* **6**, 183 (1970).

4) M. Furuki, S. Kim, L. S. Pu, H. Nakahara, and K. Fukuda, *Nippon Kagaku Zasshi,* **1990**, 1121.

5) M. Sugi, M. Saito, T. Fukui, and S. Iizuma, *Thin Solid Films,* **132**, 69 (1985).

6) H. Nakahara, K. Fukuda, D. Möbius, and H. Kuhn, *J. Phys. Chem.,* **90**, 6144 (1986).

7) M. Orrit, D. Möbius, H. Gruniger, and H. Meyer, *Thin Solid Films,* **132**, 41 (1985).

8) M. Orrit, D. Möbius, U. Lemann, and H. Meyer, *J. Chem. Phys.,* **85**, 4966 (1986).

9) D. Möbius and H. Gruniger, *Bioelectrochem. Bioenerg.,* **12**, 375 (1984).

10) V. Czikkely, H. D. Föresterling, and H. Kuhn, *Chem. Phys. Lett.,* **6**, 11 (1970); **6**, 207 (1970).

11) Y. Tomioka, S. Imazeki, S. Suga, and S. Yasui, The 1st Special Meeting on Colloids and Surface Chemistry, Tokyo, June 1985, Abstr., No. 1-02.

Theoretical Studies on the Potential Energy Surfaces of SO_2: Electronic States for Photodissociation from the $\tilde{C}^1B_2$ State

Kenshu KAMIYA*,† and Hiroyuki MATSUI
Department of Reaction Chemistry, The University of Tokyo, Hongo, Bunkyo-ku, Tokyo 113
(Received March 14, 1991)

The potential energy surfaces of electronically excited states of SO_2 have been investigated with ab initio molecular orbital method: Especially, the two-dimensional potential energy surface for the $\tilde{C}^1B_2$ ($2^1A'$) state as a function of both the bond angle and bond distance has been carefully analyzed, including the spin-orbit interaction. Energetically, $2^3A'$ (1^3A_1 in C_{2v}) was found to be the most probable state which concerns the reaction mechanism for the photodissociation pathway from the $\tilde{C}$ state (SO_2 ($\tilde{C}^1B_2$) $\rightarrow$ $SO(^3\Sigma^-)+O(^3P)$); however, other pathway may also be possible to go over the avoided crossing on a singlet potential surface.

Sulfur dioxide (SO_2) is well known as an important species concerning atmospheric chemistry and numerous studies have been carried out. Despite its importance, theoretical studies on SO_2, except for the ground state structure and properties, are relatively limited, especially regarding the structures of the potential energy surfaces in excited states.[1-5]

SO_2 is known to photodissociate under ultraviolet radiation at wavelengths shorter than about 220 nm;[6,7] and recent experimental studies using mainly the 193 nm line of an ArF laser have focused on its dissociation dynamics:[8-13] the photodissociation reaction has been recognized to be a predissociation from the $\tilde{C}^1B_2$ state producing the ground state product $SO(X^3\Sigma^-)$ and $O(^3P)$. The excited product ($SO(a^1\Delta)+O(^3P)$) has not been observed, even though it is energetically possible. Freedman et al.[8] first observed the time-of-flight spectrum of the dissociation product. Subsequently, the spectrum of the product SO has been measured by Kawasaki et al.[10] as well as by Felder et al.,[13] and the SO molecule has been found to be vibrationally excited with a maximum peak at $v=2$. Kanamori et al.[11] also observed a similar structure for both the vibrational and rotational distributions using a tunable diode laser. They also observed the spin polarization effect of the SO product, from which they concluded that most of the reaction proceeded via a triplet state. Moreover, they observed a minor peak of $SO(X^3\Sigma^-)$ at $v=5$, for which they suggested the mechanism via a singlet state. Ebata et al.[12] observed the rovibrational dependence of the predissociation rate and supported the mechanism via a triplet state.

In the present study we investigated the potential energy surfaces of SO_2 in excited states with ab initio CI method to clarify some aspects concerning SO_2 photochemistry, especially the possible photodissociation reaction pathways from the excited $\tilde{C}$ state and to the responsible electronic states for the reaction.

† Present address: School of Pharmaceutical Sciences, Kitasato University, Shirokane, Minato-ku, Tokyo 108.

Method

Potential energies were calculated using the configuration interaction (CI) method. Except for some preliminary search using the STO-3G basis set, the double zeta basis set augmented with polarization d-functions (DZP) were adopted for most of the calculations: the Dunning [4s, 2p][14] contraction of Huzinaga's (9s, 5p)[15] primitive set with a d-type function (exponent $\alpha=0.85$) was placed on oxygen, and the [6s, 4p][16] contraction of Huzinaga's (11s, 7p)[17] primitive set with a d-type function ($\alpha=0.6$) on sulfur. We also tried the extended basis set augmented with diffuse orbitals (DZP+d) in order to check the importance of Rydberg states. The molecular orbital sets used to construct CI expansion were calculated for the electronic ground state within the approximation of the restricted Hartree–Fock (RHF) theory and the improved virtual orbital (IVO)[18] technique. In order to refine the virtual orbitals using IVO, an electron was removed from the highest occupied $8a_1$ ($13a'$ in C_s structure) orbital to make a hole. For several calculations along the dissociation path of SO_2, the natural orbitals based on the unrestricted Hartree–Fock theory (UHFNO) were also used.

Two types of CI calculations were tried at the experimental equilibrium structure of the ground state.

1) V-SDTQ CI (valence- single, double, triple, and quadruple CI) with the DZP Basis Set: We considered all configurations up to 4 electron excitation from the ground-state configuration in the active space comprising of 10 valence orbitals (1s and 2sp orbitals of S and 1s and 2s of O were fixed as the core) with 14 electrons. The differences in energy spacing with the valence full CI, which included 6-electron excitation, were small. The numbers of configurations were between 729 and 1059 in C_{2v} symmetry.

2) MRSD CI (multi references single and double CI) with the Extended DZP+d Basis Set: s-, p-, and d-types of diffuse orbitals were placed on an S atom, and their exponents were optimized separately using RHF calculations for several Rydberg states. All of the virtual orbitals (except for several with extremely high energies) were considered to generate excitation configurations. For each spin and spatial symmetry in the C_{2v} point group, several tens of configurations were used as references; these were selected by considering preliminary small CI calculations. After perturbation selection with a 50 μhartree threshold in all of the single and double excitations from reference configurations, the dimensions of the matrices actually diagonalized were within

Table 1. The Vertical Excitation Energies at the Experimental Equilibrium Geometry of the Ground State of SO_2. The Energies in Unit of eV are Relative to 1^1A_1 State

State	MRSD CI (DZP+d)	V-SDTQ CI (DZP)	CI[a]	LDF[b]
Singlet:				
1^1A_1	0.00	0.00	0.00	0.0
1^1B_1	4.34	4.67	3.70	3.9
1^1A_2	4.47	5.00	4.77	5.0
1^1B_2	6.75	6.82	6.93	5.9
2^1A_1	9.08	8.98		
2^1B_1	8.84	8.73		
3^1A_1	9.56	9.66		
2^1A_2	9.10	8.77		
Triplet:				
1^3B_1	3.74	3.67	2.52	3.2
1^3B_2	4.23	4.60	2.54	4.8
1^3A_2	4.45	4.86		
1^3A_1	7.81	7.82	4.21	4.6
2^3B_2	8.87	9.28		
2^3B_1	8.37	8.37		
2^3A_1	10.22	9.07		
2^3A_2	9.08	8.55		

a) Single excitation CI within 6 valence orbitals using 4-31G basis set (Ref. 3). b) The local density functional calculation (Ref. 1).

the range from 3000 to 15000.

The second MRSD CI calculations were mainly intended to test the reliability of more tractable V-SDTQ CI calculations. After a comparison of the two types of calculations (Table 1), we found that the order in energy of the important low-lying states was identical in these two types of calculations, although the differences of the energy levels were several tenths of an eV. Despite the differences in energy, the results with V-SDTQ CI were used in this study for qualitative discussions concerning the reaction mechanism. In the MRSD CI calculations, Rydberg states did not appear in the region less than 10 eV, indicating a minor importance of such states in photochemical events concerning the $\tilde{C}$ state. Thus, most of the calculations were carried out with V-SDTQ CI using the DZP basis set without diffuse orbitals.

Results

1. The Equilibrium Structures and Energies. The optimum structures for the ground state $\tilde{X}^1A_1$ and the singlet excited state $\tilde{C}^1B_2(2^1A')$ were searched for using the V-SDTQ CI calculation. The excited $\tilde{C}$ state has been known to have an asymmetric structure.[19] The bond distance and angle for the ground state for the optimized structure in this calculation are R=2.775 Bohr (1.468 Å) and θ=122 degrees, respectively; they roughly agree with experimentally determined values, R=2.706 (1.432 Å) and θ=119.5.[20] Those for the $\tilde{C}$ state are R_1=2.869 Bohr (1.518 Å), R_2=3.467 Bohr (1.835 Å) and θ=108.3 degrees (experimental values are: R_1=2.818 (1.491 Å), R_2=3.097 (1.639 Å) and θ=103.75[19]). The adiabatic excitation energy, $\tilde{C}^1A'\leftarrow\tilde{X}^1A_1$, without a zero-point energy correction was calculated to be 5.00 eV, while the experimental value with zero-point energy is 5.28 eV.[19]

2. Angular Dependence of the Potential Energy. Figure 2 shows the potential energy surfaces of each electronic state as functions of the bond angle calculated in this study. Qualitatively, the shapes of the potential curves and the features of crossings are in good agreement with other theoretical results (SCF[4] or the local density functional theory[1]) although small discrepancies have been found, which may be partly due to differences in the geometries. We will discuss the features on each electronic state separately.

^{1}A′ States ($^1A_1$, $^1B_2$). The electronic configuration of the ground state is (see Fig. 1)

$\tilde{X}^1A_1$:……$(2b_1)^2(5b_2)^2(1a_2)^2(8a_1)^2$.

$\tilde{C}^1B_2(1a_2\rightarrow 3b_1)$ is the second singlet A′ state when its geometry is close to the equilibrium structure of the ground state. The state which is usually denoted 2^1A_1 shows a minimum at the angular region 40—60 degrees, and comprises the electronic state $(5b_2)^2\rightarrow(3b_1)^2$, which has 6 electrons in out-of-plane π orbitals. The corresponding state of O_3 is known to have a ring structure(D_{3h}). This state rapidly increases in energy as the angle becomes larger, and then crosses with $\tilde{X}^1A_1$. We did not attempt more detailed calculations for the coupling of the two states ($\tilde{X}^1A_1$ and 2^1A_1). At nearly 70 degrees, the state (2^1A_1), which no longer has the ring state character, crosses with 1^1B_2. Above 120 degrees the energy of 2^1A_1, whose dominant configuration is now $8a_1\rightarrow 9a_1$, decreases as the angle increases; the state crosses again with 1^1B_2 at nearly 145 degrees, and correlates adiabatically to $^1\Pi_u$ at 180 degrees, degenerating with 1^1B_1 state.

There seems to be no large contamination of the 1^1A_1 and 1^1B_2 states. In the equilibrium structure, 1^1A_1 has 6 electrons in the in-plane π orbitals (n orbitals) and 4 electrons in the out-of-plane π orbitals. This electronic configuration might be expected to correlate to a Δ state when in a linear structure as the in-plane and out-of-plane π orbitals degenerate, as reported for the O_3 molecule. In fact, the ground state correlates to the $^1\Sigma_g^+$ state when in a linear structure. We will discuss the electronic states later. The 1^1B_2 state degenerates with 2^1A_2 and correlates to $^1\Delta$.

^{1,3}A″ (B_1, A_2) State. The shapes of the potential curves are almost parallel to the corresponding singlet and triplet states, and the triplet states are slightly lower in energy than the singlets. For both spin states, the potential surfaces of the first B_1 ($8a_1\rightarrow 3b_1$) and the first A_2 ($5b_2\rightarrow 3b_1$) closely approach; the minimum of the former is at ca. 125 degrees, and that for the latter is at ca. 100 degrees, consequently giving a conical crossing between them. The $^1B_1$ and $^3B_1$ states degenerate when in a linear structure with 2^1A_1 and 1^3A_1, respectively, and correlate to Π_u states.

^{3}A′ State ($^3A_1$, $^3B_2$). Similarly to the case of A″, the

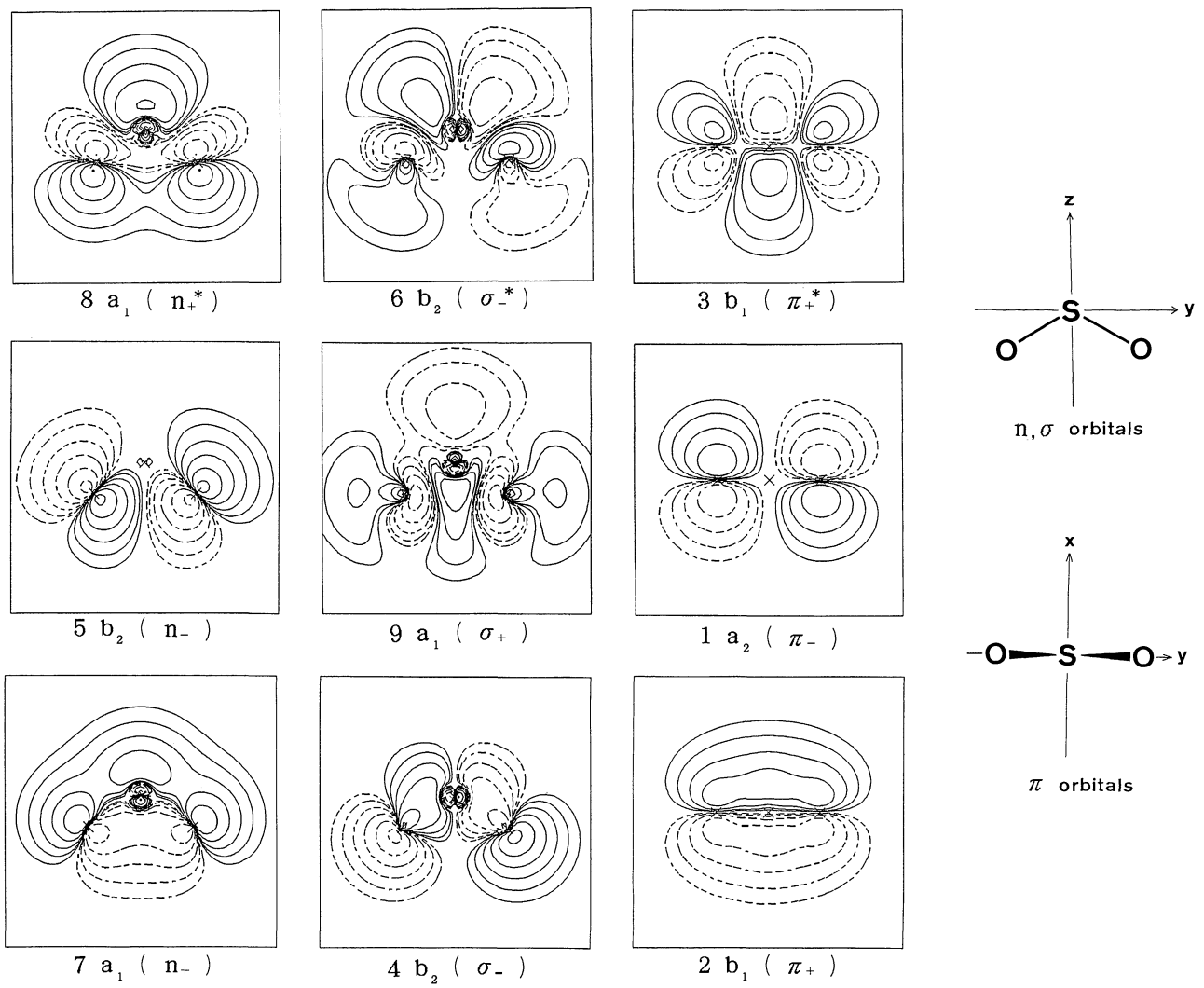

Fig. 1. The typical valence orbitals calculated with RHF/DZP for the ground state at the experimental equilibrium structure. Contour maps are drawn at the intersections with YZ- and XY-planes for n, σ, and π orbitals, respectively.

potential curves of the lower electronic states (1^3A_1 and 1^3B_2) have similar shapes as those of the corresponding singlet states (2^1A_1 and 1^1B_2). At nearly 150 degrees 1^3A_1 and 1^3B_2 cross, just as for the singlet states. 1^3A_1 correlates to $^3\Pi_u$, and degenerates with 1^3B_1.

3. Electronic States at Linear Structure. As shown in Fig. 2, the ground and low-lying excited states have energy minima with the bond angles of 90—130 degrees, except for 1^3A_1 and 2^1A_1, which are both Renner-Teller coupling pairs with 1^3B_1 and 1^1B_1, respectively. In order to resolve spectroscopic problems and photochemical processes, it is important to investigate the electronic states in a linear structure.

As described above, the electronic ground state 1^1A_1 correlates to $^1\Sigma_g^+$ in a linear structure, not $^1\Delta_g$, a degenerate state, which is reported to be the case for O_3.[21] It is 2^1A_1 that degenerates with 1^1B_1 and correlates to the $^1\Pi_u$ state. The reason why the ground state does not degenerate when in a linear structure is that the highest occupied $8a_1$ orbital (a π orbital in the molecular plane (n_+*)) couples with the $9a_1$ orbital and adiabatically correlates to σ_g^+ of a linear molecule.

Table 2 shows the energies for linear structures of O_3 and SO_2 in several electronic states, calculated with the open-shell restricted Hartree–Fock approximation. Two electrons occupying three orbitals (π_u and σ_g^+, noted above) make six independent electronic states corresponding to three electronic configurations: $(\pi_u)^2$, $(\pi_u)^1(\sigma_g)^1$, $(\sigma_g)^2$. ($^1\Delta_g$, $^3\Sigma_g^-$, $^1\Sigma_g^+$ states are from $(\pi_u)^2$, $^1\Pi_u$, $^3\Pi_u$ from $(\pi_u)^1(\sigma_g)^1$, and another $^1\Sigma_g^+$ from $(\sigma_g)^2$.) For both SO_2 and O_3, the orders in energies of the three states within $(\pi_u)^2$ and the two states within $(\pi_u)^1(\sigma_g)^1$ obey Hund's rule. The energies of the three configurations, however, were reverse in order for SO_2 and O_3 with the DZP basis set. This may reflect the difference in the order of the two orbitals, σ_g and π_u, for SO_2 and O_3. The

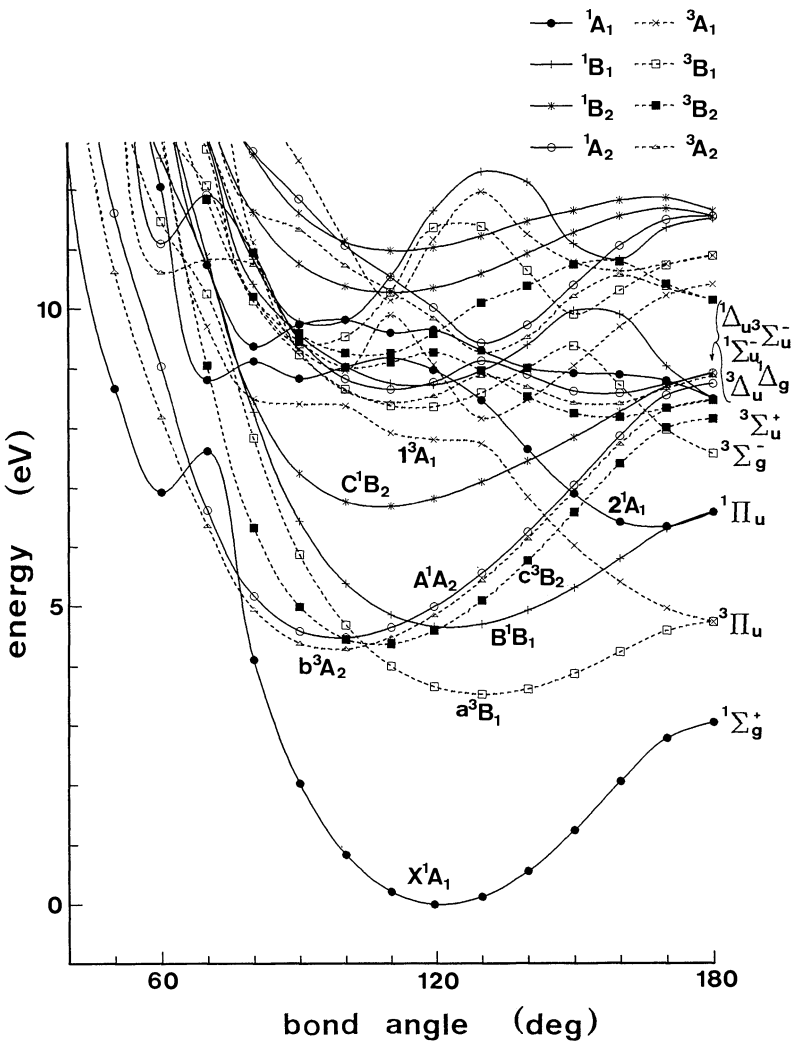

Fig. 2. The potential energies of the low lying states of SO_2 as a function of bond angle at R=2.706 Bohr (experimental equilibrium S–O distance for the ground state).

Table 2. The Energies of the Lower Electronic States of O_3 and SO_2 at Liner ($D_{\infty h}$) Structures with Experimental Bond Distances (R=2.415 Bohr (O_3), 2.7063 Bohr (SO_2)) Calculated with RHF, Units are in Hartree

State	O_3		SO_2		
	STO-3G	DZP	STO-3G	DZP	CI (DZP)
$(\pi_u)^2$					
$^3\Sigma_g^-$	−221.25460	−224.25073	−540.45524	−546.94084	−547.00815
$^1\Delta_g$	−221.21436	−224.21070	−540.42021	−546.90707	−546.97463
$^1\Sigma_g^+$	−221.17491	−224.17337	−540.38547	−546.87446	—
$(\pi_u)^1(\sigma_g)^1$					
$^3\Pi_u$	−221.04974	−224.08786	−540.40869	−547.03197	−547.11253
$^1\Pi_u$	−220.98886	−224.02859	−540.34796	−546.94870	−547.04467
$(\sigma_g)^2$					
$^1\Sigma_g^+$	−220.77410	−223.86546	−540.29289	−547.05265	−547.17483

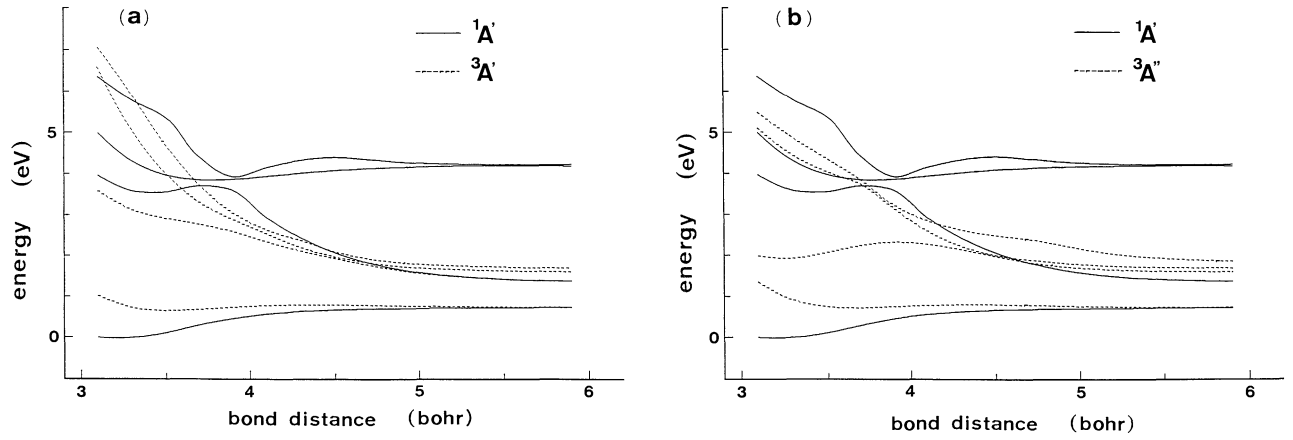

Fig. 3. The potential energy curves along the path $SO_2 \rightarrow SO + O$ as a function of the dissociative bond distance. The other bond distance and bond angle are fixed. (a) $^1A'$–$^3A'$, (b) $^1A'$–$^3A''$. (STO-3G, V-SDTQ CI).

effect of basis sets was important for calculating the order of the states in SO_2. The results with STO-3G showed a reverse order from those with DZP, while the two basis sets gave the same results for O_3.

A mechanism based on a Renner–Teller coupling of $^1A_1$ and $^1B_1$ into $^1\Delta_g$ for the ground state has been postulated[22] in order to interpret the UV absorption of SO_2 in the range from 340 to 250 nm. However the present calculation shows that the state from the Renner–Teller coupling of 2^1A_1 and 1^1B_1 is $^1\Pi_u(\sigma_g^+ \rightarrow \pi_u)$, and not the ground state, $^1A_1$.

We also checked the energy changes of each state with an asymmetric deformation. Calculations were performed while constraining one SO bond to be fixed, with the bond angle at 180 degrees. While most of the states were unstable and/or dissociative under such an asymmetric deformation, the potential curve of the ground state and the lowest triplet state, $^3\Pi_u$, showed a minimum at the point where the two SO bond distances were the same. The $^3\Pi_u$ was the only state which was lower in energy when in a $D_{\infty h}$ structure than the dissociation energy of the ground states. The $^3\Pi_u$ caused a Renner–Teller splitting under a deformation of the bond angle (as noted above), and the upper state of the pair, $^3A_1$, showed a minimum when in the $D_{\infty h}$ structure. The corresponding singlet Renner–Teller state, $^1\Pi_u$, was higher in energy than the dissociation limit of the ground state, and the upper state $^1A_1$ at $D_{\infty h}$ structure was unstable regarding both a deformation of the bond angle and the bond distance.

4. Potential Energies along the Dissociation $SO_2 \rightarrow SO + O$. In order to discuss the qualitative features of the potential energy surfaces along its dissociation path, some results of preliminary calculations using the STO-3G, V-SDTQ CI based on UHF natural orbitals are shown in Fig. 3. The UHF orbitals can approximately connect the electronic states continuously to the dissociation limit. Note that the calculated energies using STO-3G are less reliable than those using DZP basis sets. All of the degrees of freedom of the molecule were fixed to the experimental equilibrium structure of the $\tilde{C}$ state, except for the dissociative SO bond length, which was varied over a wide range. The lowest four states for each symmetry of $^1A'$, $^3A'$, and $^3A''$ are shown in this figure in order to demonstrate the relationship between the $\tilde{C}$ state and the

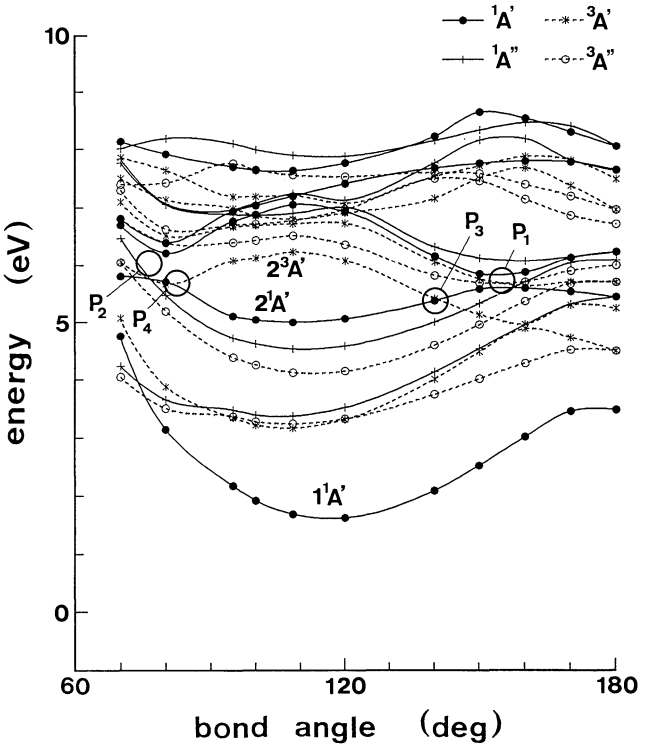

Fig. 4. The potential energies of the low lying states of SO_2 as a function of bond angle at (R_1, R_2)=(2.869 Bohr, 3.467 Bohr) (calculated equilibrium S–O distances for the $\tilde{C}$ state). Zero of energy is for the equilibrium of the ground state. Symbols P_1—P_4 are the crossing points between the $\tilde{C}$ state and $3^1A'$ or $2^3A'$ states.

other triplet states. As shown in the figures, the second $^1A'$ state (corresponds to the $\tilde{C}$ state) correlates to the excited state of products $SO(^1\Sigma^-)+O(^1D)$. The state encounters crossings and/or avoided crossings with another state which correlates to the excited-state product or with the repulsive state which correlates to the ground-state product. It should be noted that a similar structure to that of the singlet surfaces is found in the O_3 system.[23] The $\tilde{C}$ state crosses with several triplet states: 2-4$^3A'$ and 3,4$^3A''$. Although the crossing between $2^1A'$ and $2^3A'$ is not shown in the figure, the crossing appeared in more sophisticated calculations using the DZP basis set.

5. Potential Energy Surface of the Photodissociation from the $\tilde{C}$ State. As noted above, the potential energy surface of the $\tilde{C}^1B_2$ state crosses with another repulsive singlet state and with several triplet states as one of the bond distances is changed. It also crosses with the $^1A_1$ and $^3A_1$ states as the bond angle is changed. In order to examine the features of the potential energy surface crossings, we calculated the potential surfaces as a function of two parameters (one SO bond length (R) and the bond angle (θ)) with the other SO bond length fixed to 2.869 Bohr (the calculated equilibrium bond distance of the shorter SO bond of the $\tilde{C}$ state). Such constraint seems adequate for a qualitative description of the reaction system, since the bond distance of the dissociation product, $SO(^3\Sigma^-)$, calculated to be 2.909 Bohr, was not much different from that of the shorter SO bond of the equilibrium structure of the $\tilde{C}$ state.

Figure 4 shows the cross section of the potential surfaces at R=3.467 Bohr, the calculated equilibrium distance of the longer SO bond of the $\tilde{C}^1A'$ state. Although we do not show any detailed assignments for the uppper states, one can recognize the manifold of the electronic states above 6 eV from the equilibrium of the ground state. The potential curves of the $\tilde{C}^1A'$ and $3^1A'$ states (1^1B_2 and 2^1A_1 in C_{2v} structure, respectively) cross at two points (P_1 and P_2), as shown in the figure. Although the crossing should be avoided, since the two states belong to the same symmetry A' in the C_s point group, the coupling of the states was found to be weak. At crossing point P_1, which is placed at a larger bond angle and lower in energy, the dominant configurations of $2^1A'(\tilde{C}$ state) and $3^1A'$ are $\pi_-\rightarrow\pi_+^*$ and $n_+^*\rightarrow\sigma_+$, respectively. As the bond distance (R) becomes larger, the two states become strongly mixed to give a larger separation. The state which corresponds to $n_+^*\rightarrow\sigma_+$ degenerates with $1^1A''$ (1^1B_1 in C_{2v}) when in a linear

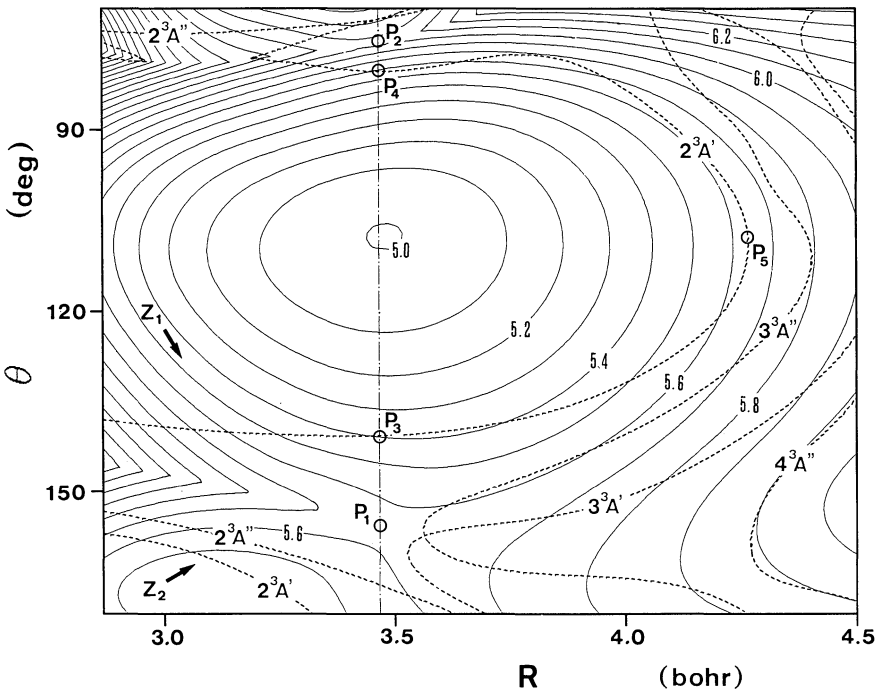

Fig. 5. The potential energy of the $\tilde{C}(2^1A')$ state as a function of the bond angle θ and one of the bond distances R with another bond distance being fixed to 2.869 Bohr. The contour energies are in eV (relative energy from the calculated ground state at equilibrium). The dashed curves are crossing seams with the triplet states ($2^3A'$, $3^3A'$, $2^3A''$, $3^3A''$, and $4^3A''$). Symbols P_3, P_4, and P_5 are the points on the crossing seams between $2^1A'$ and $2^3A'$ where magnitude of the transition probabilities were estimated (see text). The dash-dot line corresponds to the position of the cross section shown in Fig. 4. The arrows Z_1 and Z_2 are shown to indicate the approximate direction of view for (1) and (2) of Fig. 6, respectively.

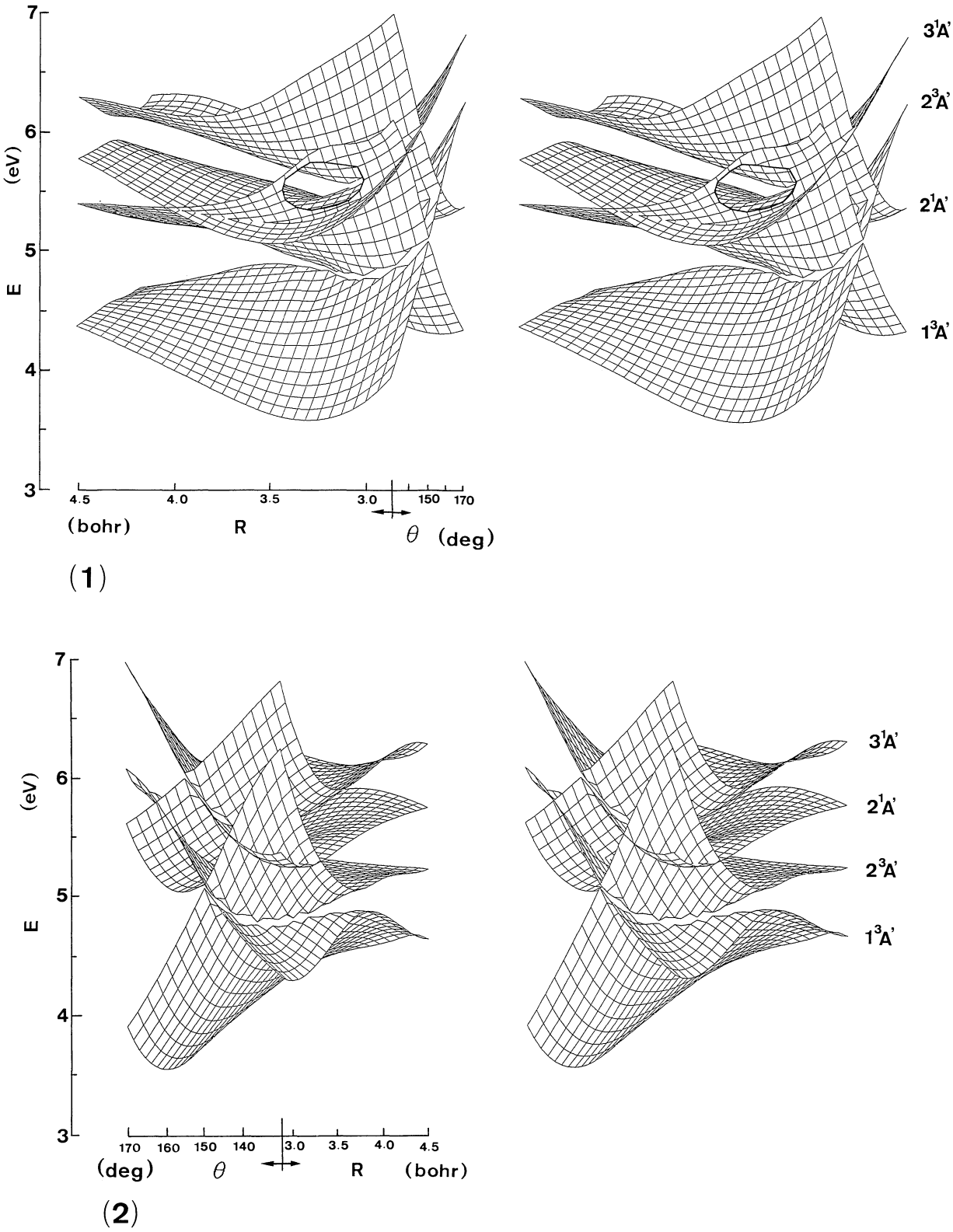

Fig. 6. Stereoscopic view of the potential energy surfaces at the region of crossing or avoided crossing including $2^1A'$ ($\tilde{C}$), $3^1A'$, $1^3A'$, and $2^3A'$ states. The potential surfaces within rectangular region (θ=130—170 degree and R=2.875—4.500 Bohr) are shown, and each approximate directions of view for (1) and (2) are shown in Fig. 5 by the arrows Z_1 and Z_2, respectively. A part of the $2^3A'$ surface in (1) is cut off to show the saddle point on the $2^1A'$ surface.

structure, giving $^1\Pi$, which correlates to the ground state of the product at infinite R.

Figure 4 also shows the crossing points between the $\tilde{C}$ state and $2^3A'(1^3A_1$ in $C_{2v})$: P_3 and P_4. They are slightly lower in energy than those between the $\tilde{C}$ state and $3^1A'$. This reflects that $2^3A'$ is lower in energy than $3^1A'$, originating from a difference in the exchange interaction of each spin state.

Figure 5 shows a potential map of the $\tilde{C}$ state as a function of R and θ. It is drawn adiabatically along the second root of CI for the $^1A'$ states. The dashed curves in the figure indicate the seams of the crossing between the $\tilde{C}$ state and other triplet states; P_3, P_4 (already shown in Fig. 4) and P_5 are the representative points on the crossing between the $\tilde{C}$ state and $2^3A'$ (discussed later). At θ=150—160 degrees, there exists a saddle due to the avoided crossing with the $3^1A'$ state. Also shown in the figure are the several triplet states crossing with the $\tilde{C}$ state surface at regions which are lower in energy than the singlet saddle point. Of these triplets, $2^3A'$ (1^3A_1 in C_{2v}), whose crossing is the lowest, is the only state to correlate to the ground-state product. Note that both the saddle point on the singlet surface and the minimum point on the crossing seam with $2^3A'$ are placed at a region of larger angle θ that the minimum of the potential.

Figure 6 shows schemata of the potential energy surfaces as functions of R and θ at the avoided crossing region of $2^1A'$ and $3^1A'$ (upper two surfaces in the figure), which is mentioned above. Although the energy spacing of the avoided crossing between the two states is not accurate, the avoided crossing region corresponds to that of the saddle point of the $^1A'$ surface. The saddle on the singlet surface is the lowest point on the crossing seam and corresponds to the possible transition point of the dissociation reaction from the $\tilde{C}$ state to the ground-state product if the reaction proceeds on a singlet adiabatic potential surface. The $2^3A'$ and $1^3A'$ states are also shown in the figure (lower two surfaces) in order to show the features of the crossings and the minimum crossing point of the $2^3A'$ and $\tilde{C}$ states. The two triplet states show crossing or avoided crossing features similar to those of the singlets, originating from the same dominant configurations, except for the spin states. The $2^3A'$ (1^3A_1 in C_{2v}) state crosses with $\tilde{C}^3B_2$ in C_{2v} symmetry and correlates to the lowest triplet state, $^3\Pi_u$, which has a minimum when in a linear structure. Although the crossing should be avoided with asymmetric deformation, both of the triplet states correlate to the ground-state product when R is infinity.

Discussion on the Reaction Pathways of the Photodissociation from the $\tilde{C}$ State

One of the experimental findings concerning the UV photodissociation on O_3 is that the excitation of the antisymmetric stretching mode enhances the reaction from the $\tilde{C}$ state.[24] SO_2 has also been reported to show a similar trend, that the excitation of the antisymmetric mode is important rather than the bending mode.[25] Because of the difference in the equilibrium structures of the ground state and the $\tilde{C}$ state, the electronically excited SO_2 is also vibrationally excited. The molecule is also expected to experience considerable vibrations within its longer lifetime than the rotational period before its predissociation.[9]

Based on our calculated results, we can discuss the highest energy point (transition state) along the minimum-energy path from the minimum of the $\tilde{C}$ state to the product ground state. If we assume that the reaction proceeds on a singlet adiabatic surface (called the singlet mechanism), the transition state should be a saddle on the barrier arising from the avoided crossing between $\tilde{C}$ state and $3^1A'$ (2^1A_1 in C_{2v}, $1^1\Pi_u$ in $D_{\infty h}$). In contrast, if the reaction is allowed one singlet-triplet transition (namely, the triplet mechanism), the most probable transition state (the lowest in energy and not requiring further crossing to reach ground state product) is the minimum point on the crossing seam between the $\tilde{C}$ states and the $2^3A'$ (1^3A_1 in C_{2v}, $1^3\Pi_u$ in $D_{\infty h}$) state. As described above, the triplet transition point was lower in energy: thus, the triplet mechanism may be advantageous from an energetical point of view. However, both transition points are placed at the larger bond-angle side of the minimum of the $\tilde{C}$ state. Thid seems to contradict the experimental result that the bending vibration is not important. However, the following comments and discussions may be possible, especially regarding the triplet mechanism.

The photon energy of the ArF laser (193 nm, 6.42 eV) is about 1.1 eV higher than the minimum energy of the $\tilde{C}$ state. According to our results, for the singlet mechanism the saddle point region is the only exit to the dissociation product with a threshold energy of 1.1 eV, meaning that bending motion is necessary for the reaction. For the triplet mechanism, however, the singlet–triplet crossing seams are located over a wide region on the surfaces, which is energetically accessible, including the larger bond distance side of the minimum of the $\tilde{C}$ state. Moreover, the crossing seam runs nearly parallel to the equipotential curves of the singlet surface, meaning that the energy change along the seam is not very drastic. That is, the singlet–triplet transition may not be so concentrated only near the minimum transition point.

It may be possible to roughly estimate the transition probabilities from the potential and the wave function. We estimated the matrix elements for a singlet–triplet spin orbit interaction in the following semiempirical way. In the usual spin orbit coupling Hamiltonian, the second term (spin-other-orbit-interaction) was neglected:

$$H_{so}=\frac{\alpha^2}{2}\sum_i\sum_A\frac{Z_A}{r_{iA}^3}(\boldsymbol{l}_{iA}\cdot\boldsymbol{s}_i)-\frac{\alpha^2}{2}\sum_{i,j}\left(\frac{\boldsymbol{r}_{ij}}{r_{ij}^3}\times\boldsymbol{p}_i\right)\cdot(\boldsymbol{s}_i+2\boldsymbol{s}_j). \quad (1)$$

Further, the multi-center integrals in the first term were neglected, and the effective nuclear charges (Z_A) were

Table 3. The Amount of the Transition Probability F between $2^1A'$ ($\tilde{C}$ State) and $2^3A'$ at the Point near the Crossing Seam between the States. One of the SO Bond is Fixed at 2.869 au

	Geometry (R/au	θ/deg)	Energy[a]/au	$\|G\|/10^{-4}$ au	$V^2/10^{-8}$ au	F[b]
P_3:	(3.467	140.0)	0.01472	3.812	6.1898	1
P_4:	(3.467	80.0)	0.02556	8.314	5.4402	0.40
P_5:	(4.250	108.3)	0.02274	3.362	9.9128	1.85

a) Mean values of the single and the triplet, relative to the minimum of $\tilde{C}(2^1A')$. b) Relative value to the point P_3.

treated as being adjustable parameters and were determined so as to fit the fine structures of the atomic spectrum. We adopted values of $Z_{sulfur}=13.698$ and $Z_{oxygen}=5.304$ using the results of SCF calculations for S and O atoms. If we consider that the velocity component which is perpendicular to the singlet-triplet crossing, determines the transition, the Landau–Zener transition probability can be expressed as follows:

$$\chi(\boldsymbol{p},\boldsymbol{q})=1-\exp(-\zeta), \tag{2}$$

where

$$\zeta=\frac{2\pi V(\boldsymbol{q})^2}{\hbar v|\boldsymbol{G}(\boldsymbol{q})|}.$$

Here, $V(\boldsymbol{q})$ denotes the absolute value of the elecronic singlet–triplet coupling, $|\langle S|H_{el}|T\rangle|$, and $\boldsymbol{G}(\boldsymbol{q})$ denotes the difference in the gradients of the singlet and triplet,

$$\boldsymbol{G}(\boldsymbol{q})=\frac{d}{d\boldsymbol{q}}({}^1E(\boldsymbol{q})-{}^3E(\boldsymbol{q})).$$

Further, v represents the velocity component perpendicular to the crossing seam

$$v=\frac{\boldsymbol{p}\cdot\boldsymbol{G}(\boldsymbol{q})}{m|\boldsymbol{G}(\boldsymbol{q})|}.$$

Here, we define $F(\boldsymbol{q})$ as being a factor which is not dependent on velocity,

$$F(\boldsymbol{q})=\frac{V(\boldsymbol{q})^2}{|\boldsymbol{G}(\boldsymbol{q})|}. \tag{3}$$

$F(\boldsymbol{q})$ can be considered to be a simple index which shows the reference value of the amount of the transition probability.

The F value was calculated at the points P_3, P_4, and P_5 on the two-dimensional potential surface of Fig. 5. P_3 and P_4 are the points where the normal of the seam corresponds to the bending (larger and smaller side of the minimum, respectively), and P_5 the point where the normal corresponds to antisymmetric stretching. As shown in Table 3, F at P_5 was 1.8-times larger than at P_3. It is thus possible that point P_5 is more important than point P_3, although the energy of the former is 8 m hartree (0.22 eV) higher than the latter.

It is apparent, however, the present calculation does not have sufficient quality to discuss further either the energetics or the quality of the wave functions, as one can find after a comparison with the larger CI calculations given in Table 1. Ebata et al.[12] observed the threshold energy of the predissociation to be about 0.35 eV higher than E_0 of the $\tilde{C}$ state; the zero point energy is about 0.1 eV. The calculated energies of points P_3 and P_5 are 0.40 and 0.62 eV higher than the minimum of the $\tilde{C}$ state, respectively. Considering that the structures of the crossing points are not fully optimized, the discussion given above is only qualitatively meaningful.

The effect of the other bond length, which was frozen at the fixed value throughout this study, may also be significant. Although the bond distances of the shorter bond of the molecule in the $\tilde{C}$ state is similar to that of the product, SO, it may be possible that the shorter bond of SO_2 is also vibrationally excited by 193 nm excitation; such an effect can be important in producing a vibrationally excited product, SO, as was observed in some experiments.

Another mechanism may be possible to interpret the minor importance of the bending mode. The bending vibration may cause multiple crossing of the seams while antisymmetric stretching motion is directly connected to dissociative motion. There is no potential structure to enhance the dissociation after the singlet–triplet transition with bending motion, since the $^3\Pi_u$ state is a bound state and has a minimum when in a linear structure.

There exist some experimental evidence that most of the reaction proceeds via a triplet state.[9-12] We have shown the advantage of the triplet mechanism regarding energy, although it is not conclusive because of difficulties in comparing the two different mechanisms.

Kanamori et al.[11] observed two types of product SO fragments; the major one, which had vibrational quantum numbers $v=1$ and $v=2$, showed a spin polarization effect; the minor one, which was in $v=5$, did not. They suggested that this result is a combination of two mechanisms: the major is via a triplet and the minor via a singlet; the possibility of the two pathways, which we suggest here, may correspond to those of Kanamori's results.

Conlcusion

The excited state potential energy surface of SO_2 was calculated using the CI method. The angular dependence of the energy level of each state was presented, showing a qualitatively similar structure as that in previous theoretical calculations.

The structure of the potential energy surfaces and their crossing with the $\tilde{C}$ state were examined in order to obtain insight into the UV photodissociation mechanism and to identify the responsible electronic states for the reaction. It was found that several triplet states did cross with the $\tilde{C}$ state in an energetically accessible region. The most probable state was $2^3A'$ (1^3A_1 in C_{2v}, $^3\Pi_u$ in $D_{\infty h}$), which became the upper state of the Renner–Teller coupling pair when in a nearly linear structure, and had an equilibrium structure with a $D_{\infty h}$ symmetry. The reaction path on the singlet adiabatic surface was also energetically possible through the avoided crossing between the $\tilde{C}$ state and other singlet excited state (2^1A_1 in C_{2v}, $1^1\Pi_u$ in $D_{\infty h}$), but energetically less favorable than the triplet mechanism.

However, the results suggested by the present work should be accepted only qualitatively. We could not give any conclusive discussion concerning the two kind of possible pathways, the singlet and the triplet mechanisms. More quantitative and sophisticated calculations are necessary for any further discussion.

The authors gratefully acknowledge to Professor K. Morokuma (Institute for Molecular Science) and Professor E. R. Davidson (Indiana University) for thier guidance and helpful discussions. All the numerical calculations were carried out at the Computer Center of Institute for Molecular Science using the program MELD.[26]

References

1) R. O. Jones, *J. Chem. Phys.*, **82**, 325 (1985).
2) I. H. Hillier and V. R. Saunders, *Mol. Phys.*, **22**, 193 (1971).
3) G. L. Bendazzoli and P. Palmieri, *Int. J. Quantum Chem.*, **9**, 537 (1975).
4) R. J. Zellmer, Master's Thesis, Department of Chemistry, The Ohio State University, Columbus, Ohio (1981).
5) P. Phillips and E. R. Davidson, *J. Comput. Chem.*, **4**, 337 (1983).
6) H. Okabe, *J. Am. Chem. Soc.*, **93**, 7095 (1971).
7) M. H. Hui and S. A. Rice, *Chem. Phys. Lett.*, **17**, 474 (1972).
8) A. Freedman, S. C. Yang, and R. Bersohn, *J. Chem. Phys.*, **70**, 5313 (1979).
9) M. Kawasaki, K. Kasatani, H. Sato, H. Shinohara, and N. Nishi, *Chem. Phys.*, **73**, 377 (1982).
10) M. Kawasaki and H. Sato, *Chem. Phys. Lett.*, **139**, 585 (1987).
11) H. Kanamori, J. E. Butler, K. Kawaguchi, C. Yamada, and E. Hirota, *J. Chem. Phys.*, **83**, 611 (1985).
12) T. Ebata, O. Nakazawa, and M. Ito, *Chem. Phys. Lett.*, **143**, 31 (1988).
13) P. Felder, C. S. Effenhauser, B. M. Haas, and J. R. Huber, *Chem. Phys. Lett.*, **148**, 417 (1988).
14) T. H. Dunning, Jr., *J. Chem. Phys.*, **53**, 2823 (1970).
15) S. Huzinaga, *J. Chem. Phys.*, **42**, 1293 (1965).
16) H. F. Schaefer, III, "Methods of Electronic Structure Theory," Plenum, New York (1977).
17) S. Huzinaga, *J. Chem. Phys.*, **53**, 451 (1970).
18) W. J. Hunt and W. A. Goddard, III, *Chem. Phys. Lett.*, **3**, 414 (1969).
19) J. C. D. Brand, P. H. Chiu, A. R. Hoy, and H. D. Bist, *J. Mol. Spectrosc.*, **60**, 43 (1976); A. R. Hoy and J. C. D. Brand, *Mol. Phys.*, **36**, 1409 (1978).
20) G. Herzberg, "Electronic Spectra and Electronic Structure of Polyatomic Molecules," Van Nostrand, Princeton (1969).
21) P. J. Hay, T. H. Dunning, Jr., and W. A. Goddard, III, *J. Chem. Phys.*, **62**, 3912 (1975); **67**, 2290 (1977).
22) L. E. Brus and J. R. McDonald, *J. Chem. Phys.*, **61**, 97 (1974).
23) P. J. Hay, R. T. Pack, R. B. Walker, and E. J. Heller, *J. Phys. Chem.*, **86**, 862 (1982).
24) D. Imre, J. L. Kinsey, A. Sinha, and J. Krenos, *J. Phys. Chem.*, **86**, 5027 (1982).
25) R. Vasudev and W. M. McClain, *J. Mol. Spectrosc.*, **89**, 125 (1981).
26) MELD: E. R. Davidson, L. E. McMurchie, S. T. Elbert, S. R. Langhoff, D. Rawlings, and D. Feller (Quantum Chemistry Group, University of Washington), IMS Computer Center, Library Program No. 030.

Molecular Structures of Trichlorovinyl(*p*-tolyl)nickel(II) Complex, and Its Thermal and Photo Isomerization Products

Jie CHEN, Yasushi KAI,* Nobutami KASAI, Masanori WADA,*,† and Makoto KUMAZOE
Department of Applied Chemistry, Faculty of Engineering, Osaka University, Suita, Osaka 565
† Department of Materials Science, Faculty of Engineering, Tottori University, Koyama, Tottori 680
(Received April 19, 1991)

The molecular structure of the trichlorovinyl(*p*-tolyl)nickel(II) complex (*trans*-[Ni(CCl=CCl$_2$)(C$_6$H$_4$Me-4)-(PMe$_3$)$_2$] (**1**)), its thermal isomerization product (*trans*-[NiCl{C(C$_6$H$_4$Me-4)=CCl$_2$}(PMe$_3$)$_2$] (**2**)) and one of its photolysis products (*trans*-[NiCl{CCl=CCl(C$_6$H$_4$Me-4)}(PMe$_3$)$_2$] (**3**)) have been determined by an X-ray diffraction method. Crystal data: **1**; triclinic, space group $P\bar{1}$, a=8.768(1), b=9.347(1), c=13.029(2) Å, α=103.79(2), β=96.23(2), γ=86.90(3)°, V=1030.4(3) Å^3, Z=2, D_c=1.393 g cm^{-3}, **2**; orthorhombic, space group $P2_12_12_1$, a=13.884(2), b=14.505(3), c=10.272(2) Å, V=2068.6(6) Å^3, Z=4, D_c=1.388 g cm^{-3}, **3**; triclinic, space group $P\bar{1}$, a=11.628(4), b=8.975(3), c=10.437(4) Å, α=102.91(3), β=99.45(3), γ=89.91(4)°, V=1046.6(7) Å^3, Z=2, D_c=1.377 g cm^{-3}. Molecules **2** and **3** were found to contain *p*-tolyl group on the α-carbon and β-carbon atoms of the vinyl ligand, respectively. Intersting structural deformations were found in **1**.

Reductive elimination and oxidative addition are unit reactions used to obtain new substances through either the fission or formation of bonds using organometallic complexes as catalysts.[1] The combined use of these reactions has been applied in the various fields of organic synthesis. One of the practical applications of these reactions is the formation of a monoorganometal complex from a diorganometal type. The thermolysis of a newly synthesized trichlorovinyl(aryl)nickel(II) complex (**1Y**), *trans*-[Ni(CCl=CCl$_2$)(C$_6$H$_4$Y)(PMe$_3$)$_2$] (Y=OMe-2, Me-2, NMe$_2$-4, Me-4, Me-3, or Cl-4), resulted in the formation of isomeric monoorganonickel(II) complexes.[2]

Three molecular structures (**2A**, **2B**, and **2C**) are possible for the thermal isomerization product of the trichlorovinyl(aryl)nickel(II) complex (**1Y**). A plausible reductive elimination of the trichlorovinyl and aryl groups, followed by an oxidative addition onto the nickel atom, may produce all of three possible isomers (Path I in Scheme 1). An α-chloro elimination of the tri-

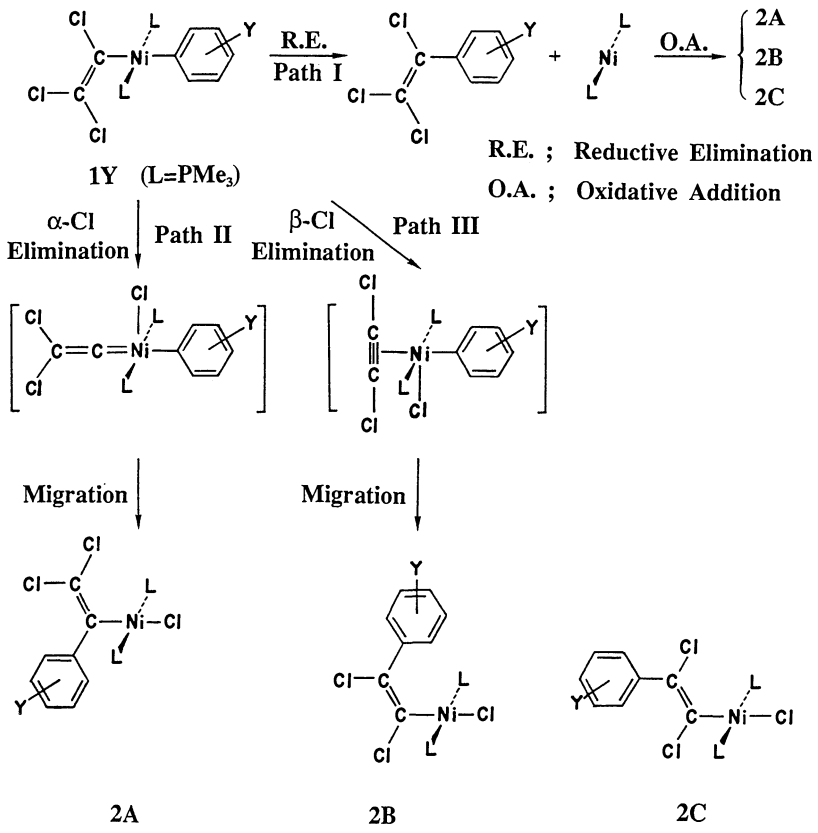

Scheme 1.

chlorovinyl ligand followed by its coordination onto a nickel atom may give a vinylidene(chloro)(aryl)nickel intermediate (Path II). The migration of the aryl ligand onto the α-carbon atom of the vinylidene ligand may give an isomer, **2A**. β-Chloro elimination in a similar manner may give an acetylene(chloro)(aryl)nickel intermediate (Path III). The migration of the aryl ligand onto the acetylene carbon atom may give an isomer, **2B**. Isomer **2C** cannot be expected through α- or β-chloro elimination pathways. In order to obtain exact structural information concerning thermal isomerization in this system, X-ray crystal structure analyses of trichlorovinyl(*p*-tolyl)nickel(II) complex, *trans*-[Ni(CCl=CCl_2)(C_6H_4Me-4)(PMe_3)$_2$] (**1**) and its thermal isomerization product, *trans*-[NiCl{C(C_6H_4Me-4)=CCl_2}(PMe_3)$_2$] (**2**) have been carried out.

The photolysis of **1Y** (Y=Me-4, Cl-4) has been studied in order to obtain little-known photochemical properties concenrning square-planar organonickel(II) complexes.[3] Two isomers were obtained in a mixture by irradiation, one of which was identical to the thermolysis product of **1Y**. The molecular structure of another Photolysis product of **1Y**, *trans*-[NiCl{CCl=CCl(C_6H_4-Me-4)}(PMe_3)$_2$] (**3**), was also determined in order to compare the stuctural characteristics with **1** and **2**.

Experimental

Crystal Data. Complexes **1**, **2**, and **3** were prepared by a procedure described previously.[2] Single crystals were obtained by recrystallization from ethanol. Crystals of **1**, **2**, and **3** are pale-yellow, brown, and dark-brown in color with regular prismatic shapes, respectively. Preliminary oscillation and Weissenberg photographs taken with Cu $K\alpha$ radiation showed that crystals **1** and **3** are triclinic, whereas **2** is orthorhombic. Unit-cell parameters were determined at room temperature by a least-squares fit of the 2θ values of 25 strong, higher-angle reflections for three complexes observed on a four-circle diffractometer. Crystal data are summarized in Table 1.

Collection and Reduction of Intensity Data. The integrated intensities were measured on a Rigaku four-circle diffractometer with graphite monochromatized Mo $K\alpha$ (λ=0.71069 Å) radiation. The θ–2θ scan technique was used at a 2θ scan rate of 4° min^{-1} with a scan width of $\Delta 2\theta$=(2.0+0.70 tan θ)°. The background intensities were measured for 7.5 s at both ends of each scan. Three standard reflections were measured after every 61 reflections in order to monitor the radiation damage and any change in the crystal orientation. No significant intensity decay of the standard reflections was observed for all crystals studied. The number of reflection intensities collected up to 2θ=55° for **1** ($\sin\theta_{max}/\lambda$=0.650), 2θ=60° for **2** ($\sin\theta_{max}/\lambda$=0.704), and 2θ=55° for **3** were 4327, 3387, and 4792, among which the observed reflections [$|F_o|>3\sigma(F_o)$] were 3482, 2745, and 3276, respectively. Although the usual Lorentz and polarization effects were

Table 1. Crystallographic and Experimental Data of *trans*-[Ni(CCl=Cl_2)(C_6H_4Me-4)(PMe_3)$_2$] **1**, and Its Isomerization Products **2** and **3**

Compound	1	2	3
Formula	$C_{15}H_{25}Cl_3P_2Ni$	$C_{15}H_{25}Cl_3P_2Ni$	$C_{15}H_{25}Cl_3P_2Ni$
Formula weight	432.4	432.4	432.4
System	Triclinic	Orthorhombic	Triclinic
Space group	$P\bar{1}$	$P2_12_12_1$	$P\bar{1}$
a/Å	8.768(1)	13.884(2)	11.628(4)
b/Å	9.347(1)	14.505(3)	8.975(3)
c/Å	13.029(2)	10.272(2)	10.437(4)
α/°	103.79(2)		102.91(3)
β/°	96.23(2)		99.45(3)
γ/°	86.90(3)		89.91(4)
V/Å^3	1030.4(3)	2068.6(6)	1046.6(7)
Z	2	4	2
D_c/g cm^{-3}	1.393	1.388	1.377
F(000)/e	448	896	448
μ(Mo $K\alpha$)/cm^{-1}	14.9	14.8	14.7
Temperature/°C	20	20	20
Crystal size/mm	0.3×0.25×0.25	0.3×0.3×0.3	0.25×0.3×0.3
Crystal color	Pale yellow	Brown	Dark brown
Crystal shape	Prismatic	Prismaic	Prismatic
2θ range/deg	4<2θ<55	4<2θ<60	4<2θ<55
Reflections measured	4327	3387	4792
Reflections observed	3482	2745	3276
No. of variables	291	291	291
GOF[a]	1.014	1.002	1.028
R[b]	0.064	0.043	0.062
R_w[c]	0.094	0.062	0.084

a) $\Sigma w(|F_o|-|F_c|)^2/(n-m)$, where n and m are the number of reflections used and variables refined, respectively. b) $R=\Sigma||F_o|-|F_c||/\Sigma|F_o|$. c) $R_w=[\Sigma w(|F_o|-|F_c|)^2/\Sigma w|F_o|^2]^{1/2}$, $w=[\sigma^2(F_o)+g(F_o)^2]^{-1}$, and g=0.003 for all the complexes.

Table 2. Final Atomic Parameters together with Their Estimated Standard Deviations in Parentheses

Atom	x	y	z	B_{eq}
(a) *trans*-[Ni(CCl=CCl_2)(C_6H_4Me-4)(PMe_3)$_2$] (**1**)				
Ni	0.34958 (8)	0.05648 (7)	0.27470 (5)	3.4
Cl (1)	0.2101 (3)	0.2456 (2)	0.4821 (2)	6.0
Cl (2)	0.1270 (3)	0.2858 (2)	0.1619 (2)	5.7
Cl (3)	0.0116 (2)	0.4485 (2)	0.3606 (2)	5.8
P (1)	0.5432 (2)	0.2030 (2)	0.3088 (2)	4.5
P (2)	0.1684 (2)	−0.1037 (2)	0.2423 (2)	4.0
C (1)	0.2151 (8)	0.2122 (7)	0.3375 (6)	5.3
C (2)	0.1287 (8)	0.3029 (7)	0.2998 (6)	5.6
C (11)	0.5026 (10)	0.4025 (8)	0.3362 (9)	8.2
C (12)	0.6592 (9)	0.1813 (9)	0.4279 (6)	6.5
C (13)	0.6821 (9)	0.1801 (10)	0.2111 (7)	7.2
C (21)	0.0159 (9)	−0.0692 (10)	0.3325 (8)	7.2
C (22)	0.0626 (10)	−0.1139 (10)	0.1134 (6)	7.6
C (23)	0.2189 (9)	−0.2967 (7)	0.2387 (7)	6.4
C (31)	0.4863 (6)	−0.0992 (6)	0.2144 (4)	3.7
C (32)	0.4981 (7)	−0.1395 (7)	0.1040 (5)	4.4
C (33)	0.5897 (8)	−0.2557 (7)	0.0559 (5)	5.0
C (34)	0.6748 (7)	−0.3426 (7)	0.1158 (5)	4.8
C (35)	0.6679 (7)	−0.3053 (6)	0.2253 (5)	4.3
C (36)	0.5752 (7)	−0.1856 (6)	0.2714 (4)	3.9
C (37)	0.7728 (10)	−0.4730 (8)	0.0632 (7)	6.8
(b) *trans*-[NiCl{C(C_6H_4Me-4)=CCl_2}(PMe_3)$_2$] (**2**)				
Ni	0.19639 (5)	0.22907 (4)	0.03421 (6)	3.0
Cl (1)	0.22991 (13)	0.16763 (10)	0.22607 (14)	4.8
Cl (2)	−0.00759 (11)	0.29723 (14)	−0.0592 (3)	6.6
Cl (3)	0.05694 (14)	0.37699 (12)	−0.3000 (2)	6.2
P (1)	0.18605 (11)	0.09064 (8)	−0.05234 (13)	3.7
P (2)	0.20653 (13)	0.36621 (9)	0.12747 (14)	4.2
C (1)	0.1773 (4)	0.2834 (3)	−0.1333 (5)	3.4
C (2)	0.0908 (5)	0.3129 (4)	−0.1648 (6)	4.2
C (11)	0.1323 (6)	0.0742 (5)	−0.2133 (7)	5.5
C (12)	0.3056 (7)	0.0420 (5)	−0.0688 (10)	7.2
C (13)	0.1207 (8)	0.0075 (5)	0.0417 (8)	7.7
C (21)	0.1889 (8)	0.4700 (4)	0.0299 (8)	7.0
C (22)	0.1217 (7)	0.3804 (6)	0.2610 (8)	7.2
C (23)	0.3244 (7)	0.3864 (5)	0.2023 (8)	6.5
C (31)	0.2606 (4)	0.2922 (3)	−0.2214 (5)	3.2
C (32)	0.2548 (5)	0.2686 (4)	−0.3543 (5)	4.1
C (33)	0.3354 (5)	0.2763 (4)	−0.4339 (5)	4.3
C (34)	0.4227 (5)	0.3082 (4)	−0.3891 (6)	4.3
C (35)	0.4292 (5)	0.3288 (5)	−0.2539 (6)	4.5
C (36)	0.3498 (4)	0.3199 (5)	−0.1748 (6)	4.2
C (37)	0.5088 (6)	0.3208 (6)	−0.4763 (7)	6.6
(c) *trans*-[NiCl{CCl=CCl(C_6H_4Me-4)}(PMe_3)$_2$] (**3**)				
Ni	0.21246 (6)	0.16008 (8)	0.43907 (7)	3.7
Cl (1)	0.0090 (2)	0.3138 (3)	0.3315 (3)	6.6
Cl (2)	0.2702 (2)	0.0354 (3)	0.5957 (2)	6.7
Cl (3)	0.1103 (2)	0.4105 (2)	0.1084 (2)	6.3
P (1)	0.2847 (2)	0.3744 (2)	0.5794 (2)	4.4
P (2)	0.1544 (2)	−0.0603 (2)	0.3005 (2)	5.1
C (1)	0.1532 (5)	0.2658 (6)	0.3104 (6)	4.1
C (2)	0.1959 (5)	0.3095 (6)	0.2131 (6)	4.1
C (11)	0.2685 (7)	0.5536 (8)	0.5265 (7)	6.1
C (12)	0.2297 (7)	0.4133 (8)	0.7338 (7)	6.1
C (13)	0.4425 (6)	0.3679 (10)	0.6305 (9)	7.2
C (21)	0.0911 (8)	−0.0635 (10)	0.1308 (9)	8.2
C (22)	0.2761 (7)	−0.1869 (9)	0.2813 (10)	7.0
C (23)	0.0524 (7)	−0.1682 (8)	0.3597 (9)	8.4
C (31)	0.3147 (5)	0.2749 (6)	0.1810 (6)	4.2
C (32)	0.3550 (8)	0.3193 (10)	0.0752 (7)	6.6
C (33)	0.4659 (8)	0.2820 (11)	0.0461 (8)	7.6
C (34)	0.5399 (6)	0.1982 (8)	0.1173 (7)	5.6
C (35)	0.5008 (6)	0.1590 (8)	0.2229 (7)	5.1
C (36)	0.3914 (5)	0.1960 (7)	0.2537 (6)	4.7
C (37)	0.6577 (8)	0.1535 (11)	0.0825 (9)	8.3

corrected for the intensity data, no absorption correction was applied.

Determination and Refinement of the Structure. The three structures were all solved using the heavy-atom method. Successive Fourier syntheses phased by the nickel atoms found in Patterson maps clearly revealed the remaining nonhydrogen atoms. The structures were refined anisotropically by a full-matrix least-squares method (XRAY SYSTEM),[4] the function minimized being $\sum w(\Delta F)^2$. All of the hydrogen atoms were located on difference Fourier maps and were included in the refinement with isotropic temperature factors. The applied weighting function was $w=[\sigma_{cs}^2(F_o)+0.003\,(F_o)^2]^{-1}$, where σ_{cs} is the standard deviation estimated from the counting statistics. The final discrepancy factors, R (R_w), are 0.064 (0.094) for **1**, 0.043 (0.062) for **2**, and 0.062 (0.084) for **3**, respectively. The refinement parameters are summarized in Table 1.

The atomic scattering factors were taken from the International Tables for X-Ray Crystallography.[5] The final atomic coordinates of complexes (**1**, **2**, and **3**) together with the equivalent isotropic temperature factors (B_{eq}[6]) for nonhydrogen atoms are listed in Table 2.[#] All of the computations were processed on an ACOS 850 computer at the Research Center for Protein Engineering, Institute for Protein Research, Osaka University.

Results and Discussion

Molecular and Crystal Structures. The molecular structures of complexes **1**, **2**, and **3** are shown in Figs. 1—3 by ORTEP drawings,[7] together with the atomic numberings. X-Ray structure analyses of complexes **1**, **2**, and **3** revealed that the thermolysis of complex **1** resulted in isomerization product **2A** (Scheme 1) through a displacement between the *p*-tolyl and *α*-chloro; photolysis gave **2B** through a displacement between the *p*-tolyl and *β*-chloro in the vinyl group. Postulated complex **2C** was not identified in the thermolysis and photolysis of **1Y**.

[#] Tables of anisotropic temperature factors, coordinates of hydrogen atoms, and observed and calculated structure factors are kept as Document No. 8959 at the Office of the Editor of Bull. Chem. Soc. Jpn.

Coordination Geometry of Nickel Atom: Selected structural parameters around the nickel atoms in complexes **1**, **2**, and **3** are given in Table 3. The first structural feature observed commonly in these molecules is that the nickel atom takes a square-planar coordination with either two phosphine ligands and two carbon ligands or one carbon and one chlorine ligand at *trans*-positions; this is similar to those in a series of *trans*-[Ni(aryl)$_2$(PR$_3$)$_2$] and *trans*-[Ni(C$_6$Cl$_5$)(PMe$_3$)$_2${C-(OMe)Me}BF$_4$ complexes.[8-10] In the complexes **1**, **2**, and **3**, five atoms defining the coordination plane of the nickel atom are nearly coplanar. The deviations from a mean plane defined by the inner co-coordination sphere, NiC$_2$P$_2$ or NiCClP$_2$, are: Ni, 0.025; P(1), −0.020; P(2), −0.020; C(1), 0.007; and C(31), 0.009 Å for **1**, Ni, 0.027; P(1), 0.037; P(2), 0.031; C(1), −0.050; and Cl(1),

Table 3. Coordination Geometries of Nickel Atoms in *trans*-[Ni(CCl=CCl$_2$)(C$_6$H$_4$Me-4)(PMe$_3$)$_2$] **1** and Its Isomerization Products **2** and **3**

	1	**2**	**3**
P(1)–Ni–P(2)	175.6(1)°	178.2(1)°	175.5(1)°
P(1)–Ni–C(1)	91.6(2)	90.2(2)	91.5(2)
P(1)–Ni–C(31)	88.0(2)	—	—
P(1)–Ni–Cl(1)	—	90.3(1)	—
P(1)–Ni–Cl(2)	—	—	89.0(1)
P(2)–Ni–C(1)	92.1(2)	91.6(2)	90.9(2)
P(2)–Ni–C(31)	88.3(2)	—	—
P(2)–Ni–Cl(1)	—	87.9(1)	—
P(2)–Ni–Cl(2)	—	—	88.9(1)
C(1)–Ni–C(31)	178.9(3)	—	—
C(1)–Ni–Cl(1)	—	175.8(2)	—
C(1)–Ni–Cl(2)	—	—	175.9(2)
θ[a] (*Ni, Vinyl*)	88.2°	82.5°	88.7°
θ (*Ni, Tolyl*)	86.5	78.8	86.2
θ (*Vinyl, Tolyl*)	2.3	43.0	2.5

a) θ: Dihedral angle between the least-squares planes (*Ni, Vinyl, Tolyl*) composed of; *Ni*: Ni, P(1), P(2), C(1), and C(31) or Cl(1) or Cl(2). *Vinyl*: C(1), C(2), Cl(1), Cl(2), and Cl(3) in **1**. C(1), C(2), Cl(2), Cl(3), and C(31) in **2**. C(1), C(2), Cl(1), Cl(3), and C(31) in **3**. *Tolyl*: C(31)–C(36).

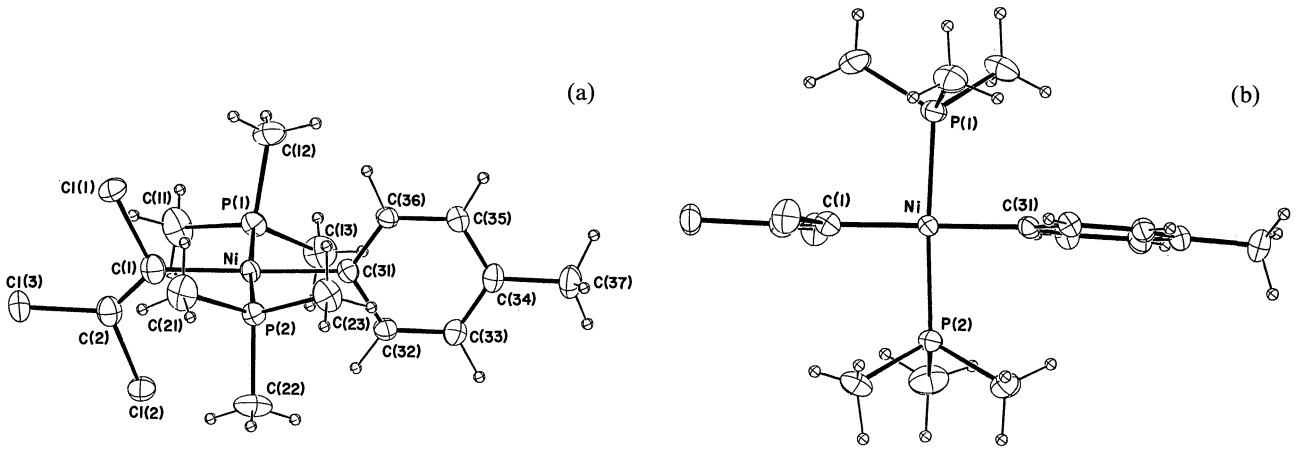

Fig. 1. Molecular structure of [Ni(CCl=Cl$_2$)(C$_6$H$_4$Me-4)(PMe$_3$)$_2$] (**1**) according to an ORTEP drawing with thermal ellipsoids at a 20% probability level; (a) top view, and (b) side view.

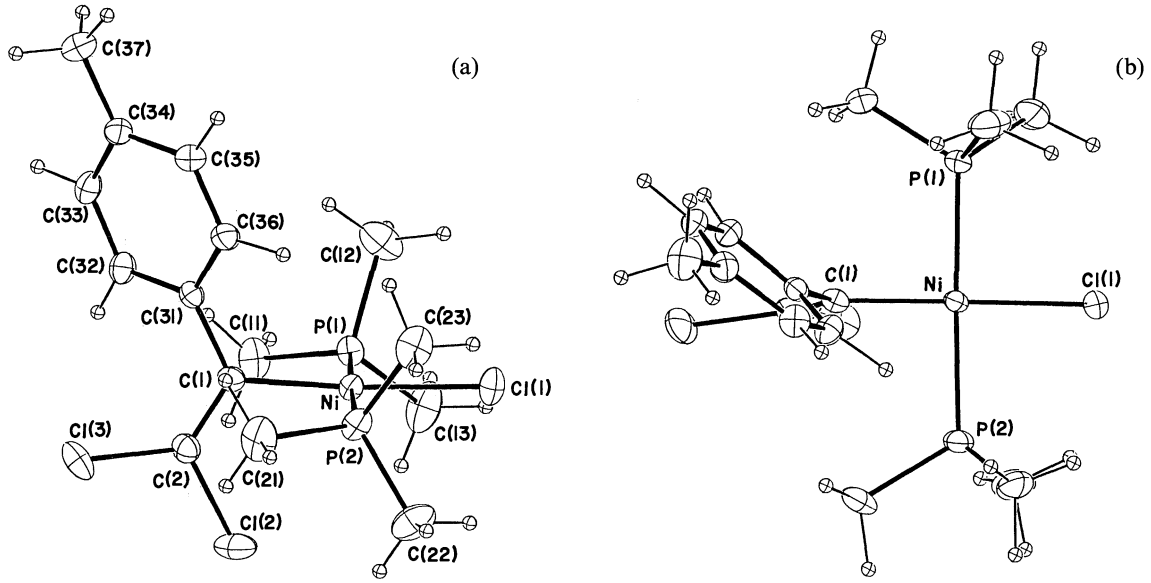

Fig. 2. Molecular structure of [NiCl{C(C$_6$H$_4$Me-4)=CCl$_2$}(PMe$_3$)$_2$] (**2**) according to an ORTEP drawing with thermal ellipsoids at a 20% probability level; (a) top view, and (b) side view.

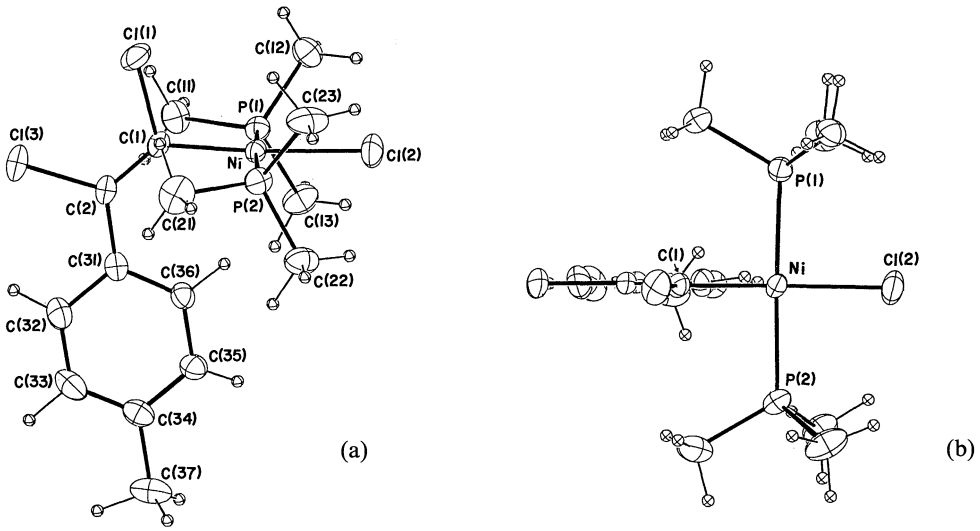

Fig. 3. Molecular structure of [NiCl{CCl=CCl(C$_6$H$_4$Me-4)}(PMe$_3$)$_2$] (**3**) according to an ORTEP drawing with thermal ellipsoids at a 20% probability level; (a) top view, and (b) side view.

−0.044 Å for **2**, Ni, 0.009; P(1), −0.091; P(2), −0.043; C(1), 0.107; and Cl(2), 0.049 Å for **3**, respectively. It is noteworthy that the P(1)–Ni–P(2) bond angles are 175.6(1)° and 175.5(1)° in complexes **1** and **3**, which show angular deviations of 4.4° and 4.5° from exact *trans* coordination; the bond angle in **2** [178.2(1)°] takes a value near to 180°. The bond angles C(1)–Ni–C(31) [178.9(3)°], C(1)–Ni–Cl(1) [175.8(2)°] and C(1)–Ni–Cl(2) [175.9(2)°] also deviate from the expected 180°, probably due to steric effects between the C or Cl and P atoms [mean C(1)···P 2.943 Å, 2.942 Å, 2.914 Å, and C(31)···P 2.850 Å, Cl(1)···P 3.100 Å, Cl(2)···P 3.088 Å for complexes **1**, **2**, and **3**, respectively]. The second feature is that the vinyl planes are approximately perpendicular to the Ni-coordination planes; the corresponding dihedral angles (θ) are 88.2° and 88.7° in complexes **1** and **3**, while that in complex **2** [82.5°] is slightly smaller. The *p*-tolyl plane in complexes **1** and **3** are also approximately perpendicular to the nickel coordination planes; the corresponding dihedral angles are 86.5° and 86.2°, respectively. The vinyl and *p*-tolyl planes in complex **2** are not coplanar with each other (dihedral angle; 43.0°) because of a nonbonded repulsion between the Cl(3) and H(32) atoms [Cl(3)···H(32); 2.82(6) Å, Cl(3)···C(32); 3.213(6) Å].

Conformation of Phosphine Ligand: Table 4 shows

Table 4. Coordination Geometries of Phosphine Ligands in *trans*-[Ni(CCl=CCl$_2$)(C$_6$H$_4$Me-4)(PMe$_3$)$_2$] **1** and Its Isomerization Products **2** and **3**

	1	**2**	**3**
ϕ[C(1)–Ni–P(1)–C(11)]	−19.1°	−17.9°	−2.0°
ϕ[C(1)–Ni–P(1)–C(12)]	98.7	102.4	120.8
ϕ[C(1)–Ni–P(1)–C(13)]	217.6	220.1	238.1
ϕ[C(1)–Ni–P(2)–C(21)]	−28.7	3.1	5.0
ϕ[C(1)–Ni–P(2)–C(22)]	89.4	125.2	124.1
ϕ[C(1)–Ni–P(2)–C(23)]	209.0	242.6	240.2
C(1)····C(11)	3.167 Å	3.204 Å	3.158 Å
C(1)····C(21)	3.219	3.188	3.139
C(31)····C(13)	3.213	—	—
C(31)····C(23)	3.148	—	—
Cl(n)[a]····C(12)	—	3.688	3.440
Cl(n)[a]····C(13)	—	3.359	3.431
Cl(n)[a]····C(22)	—	3.451	3.450
Cl(n)[a]····C(23)	—	3.443	3.514

ϕ: Torsional angle around Ni–P bonds. a) n=1 in **2**, 2 in **3**.

Table 5. Selected Structural Parameters in *trans*-[Ni(CCl=CCl$_2$)(C$_6$H$_4$Me-4)(PMe$_3$)$_2$] **1** and Its Isomerization Products **2** and **3**

	1	**2**	**3**
Ni–P(1)	2.180(2) Å	2.201(2) Å	2.212(2) Å
Ni–P(2)	2.180(2)	2.212(2)	2.205(2)
Ni–C(1)	1.907(5)	1.911(5)	1.855(6)
Ni–C(31)	1.908(5)	—	—
Ni–Cl(1)	—	2.212(2)	—
Ni–Cl(2)	—	—	2.198(2)
C(1)–C(2)	1.258(10)	1.315(8)	1.333(8)
C(1)–Cl(1)	1.840(7)	—	1.767(6)
C(1)–C(31)	—	1.474(7)	—
C(2)–Cl(2)	1.763(7)	1.759(7)	—
C(2)–Cl(3)	1.746(7)	1.736(6)	1.758(6)
C(2)–C(31)	—	—	1.490(8)
α_1	132.5(6)°	118.8(4)°	134.1(5)°
α_2	116.3(4)	118.7(4)	107.8(3)
α_3	111.2(6)	122.5(5)	118.1(4)

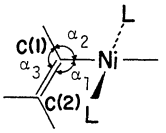

the coordination geometries of the trimethylphosphine ligands in complexes **1**, **2**, and **3**. The ϕ's shows the torsional angles around the Ni–P bonds (taking the clockwise rotation as their positive direction). The ϕ's for the Ni–P(1) and Ni–P(2) bonds are −19.1°, −17.9°, −2.0°, and −28.7°, 3.1°, 5.0°, respectively. These values indicate that the first phosphine ligand [P(1), C(11), C(12), and C(13)] in complex **1** takes a similar conformation as that in complex **2**, while the second phosphine [P(2), C(21), C(22), and C(23)] in complex **2** has the similar conformation as that in complex **3**. In complex **1**, the two phosphine ligands are mutually related by nickel atom as an approximate center of symmetry. On the other hand, in complexes **2** and **3**, the phosphine ligands are related by an approximate mirror symmetry defined by a plane passing through the C(1), Ni, Cl(1) or Cl(2) atoms, which is normal to the coordination plane. The nonbonded intramolecular atomic distances between the C(1), C(31), or Cl(1), Cl(2) and nearby methyl groups in phosphine ligands are much shorter than the sum of Pauling's van der Waals radii [3.7 Å for C···C contact, and 3.8 Å for Cl···C]. Therefore, the conformations of these phosphine ligands are delicately modified by balancing the nonbonded atomic repulsions between the bulky methyl groups and the neighboring ligands.

Bonding Structure of Vinyl and *p*-Tolyl Ligands: Table 5 summarizes the selected structural parameters to describe the bonding geometries of the vinyl and *p*-tolyl ligands to the nickel atom. Almost the same Ni–P distances for the two phosphorus atoms of each molecule are observed [2.180(2) and 2.180(2) Å] for **1**, [2.201(2) and 2.212(2) Å] for **2**, and [2.212(2) and 2.205 Å] for **3**; the distances for three compounds, however, are slightly different from each other. The bond distance between the nickel and C(31) atoms in complex **1** [1.908(5) Å] has similar value as those between the nickel and vinyl α-carbon [C(1)], 1.907(5), 1.911(5), and 1.855(6) Å for complexes **1**, **2**, and **3**, respectively. These Ni–C distances are comparable with those reported in many organonickel complexes including C(sp^2)–Ni bonds.[11-14]

A remarkable structural feature is the unique structural deformations found in the vinyl ligand in complex **1**. First, the C(1)–C(2) bond distance of 1.258(10) Å is significantly shorter than the standard value for the C=C distance of 1.337 Å, while the corresponding distance in complex **2** [1.315(8) Å] and in complex **3** [1.337(8) Å] are equal to the standard C=C distance. Second, the C(1)–Cl(1) bond distance [1.840(7) Å] in complex **1** is longer than the C–Cl standard distance [1.72 Å in CH$_2$=CHCl, 1.767 Å in CH$_3$Cl or CH$_2$Cl$_2$], whereas the C(2)–Cl distances in **1**, **2**, and **3** complexes are in the range from 1.736 to 1.763 Å. A similar structural behavior has been observed for the vinyl ligand in [Ni(CCl=CCl$_2$)$_2$(PMe$_2$Ph)$_2$].[15] Third, the Ni–C(1)–C(2) bond angles (α_1) in complex **1** [132.5(6)°] and in complex **3** [134.1(5)°] are much larger than α_2 [**1**: 116.3(4), **3**: 107.8(3)°] and α_3 [**1**: 111.2(6), **3**: 118.1(4)°], while no angular deformation was found around the α-carbon atom of the vinyl ligand in complex **2**. The molecular structure of **1** shows an interesting trend toward linearity of the trichlorovinyl group.

Crystal Structure: No intermolecular distance shorter than the normal van der Waals contacts is found in the crystal structures of **1**, **2**, and **3**.

References

1) J. P. Collman and L. S. Hegedus, "Principles and Applications of Organotransition Metal Chemistry," University Science Books, Mill Valley, California (1980), P. W.

Joly, "Comprehensive Organometallic Chemisry," Pergamon Press, Oxford (1982), Vol. 8, p. 713.

2) M. Wada, K. Nishiwaki, and M. Kumazoe, *J. Chem. Soc., Chem. Commun.*, **1984**, 980.

3) M. Wada, M. Kumazoe, Y. Matsuhiro, and T. Erabi, *Chem. Lett.*, **1986**, 1959.

4) J. M. Stewart, The X-Ray System (XRAY-76), Report TR-446, Computer Science Center, University of Maryland, College Park, Maryland (1976).

5) "International Table for X-Ray Crystallography," Kynoch Press, Birmingham (1974), Vol. IV.

6) W. C. Hamilton, *Acta Crystallogr.*, **12**, 609 (1959).

7) C. K. Johnson, "ORTEP-II, Report ORNL-5138," Oak Ridge National Laboratory, Tennessee (1974).

8) D. Xu, Y. Kai, K. Miki, N. Kasai, K. Nishikawa, and M. Wada, *Bull. Chem. Soc. Jpn.*, **57**, 1459 (1984).

9) D. Xu, K. Miki. Y. Kai, N. Kasai, and M. Wada, *J. Organomet. Chem.*, **287**, 265 (1985).

10) J. M. Coronas, G. Muller, M. Rocamora, C. Miravitlles, and X. Solans, *J. Chem. Soc., Dalton Trans.*, **1985**, 2333.

11) K. Miki, H. Taniguchi, Y. Kai, N. Kasai, K. Nishiwaki, and M. Wada, *J. Chem. Soc., Chem Commun.*, **1982**, 1178.

12) W. K. Dean, R. S. Charles, and D. G. van Derveer, *Inorg. Chem.*, **16**, 3328 (1977).

13) G. Huthner, O. Orama, and V. Bejenke, *Chem. Ber.*, **109**, 2533 (1976).

14) R. A. Bell, M. H. Chisholm, and G. G. Christoph, *J. Am. Chem. Soc.*, **98**, 6046 (1976).

15) J. Carvajal, G. Muller, J. Sales, X. Solans, and C. Miravitlles, *Organometallics*, **3**, 996 (1984).

 © 1991 The Chemical Society of Japan Bull. Chem. Soc. Jpn., 64, 2809—2813 (1991)

Synthesis, Structure, and NMR Spectra of $[Cu_2(phen)_2(\mu\text{-}(C_6H_5)_2PCH_2P(C_6H_5)_2)_2](PF_6)_2$ and Its Derivatives

Susumu KITAGAWA,* Hideki MARUYAMA, Shigetoshi WADA, Megumu MUNAKATA, Masaki NAKAMURA, and Hideki MASUDA†

Department of Chemistry, Kinki University, Higashi-Osaka 577

† Institute for Molecular Science, Okazaki 444

(Received February 8, 1991)

The bis(diphenylphosphino)methane(dppm) compounds of copper(I), $[Cu_2(\mu\text{-dppm})_2(biL)_2](PF_6)_2$ (biL=1,10-phenanthroline and its derivatives), have been synthesized and characterized by ^1H and ^{31}P NMR spectroscopy and X-ray crystallography. The molecules are found to contain a $[Cu_2(dppm)_2]^{2+}$ framework with the two copper atoms bridged by two dppm ligands to give eight-membered $Cu_2P_4C_2$ rings. This framework shows a staggered conformation subject to the coordination of additional ligands, biL. The coordination ^1H and ^{31}P shifts of the dppm are well-correlated with the basicity of the nitrogen donor atom of biL, sensitive to variations in the copper-ligand binding as well as their metal-to-ligand charge-transfer band. Crystallographic data of $[Cu_2(dppm)_2(phen)_2]$ are as follows. monoclinic space group $P2_1/c$, a=11.515(2) Å, b=27.922(4) Å, c=12.493(2) Å, β=107.68(1)°, U=3827(1) Å^3, and Z=2.

Bis(diphenylphosphino)methane (dppm) has served to afford an eight-membered ring dimer, $M_2P_4C_2$ of $M_2(\mu\text{-dppm})_2$. This stable framework adopts the three conformations shown below. The group IB metal monocation (Cu^+, Ag^+, and Au^+) gives this framework with an eclipsed (a) and (c), and a staggered (b) conformation; type (a) is found in $[Cu_2(\mu\text{-dppm})_2L_n]$ (L=CH_3CN (n=4),[1] S_2ct (n=2)[2]) and $[Ag_2(\mu\text{-dppm})_2(NO_3)_2]$;[3] type (b) is found in $[Au_2(\mu\text{-dppm})_2Cl_2]$.[4] These metal ions require additional monodentate or bidentate ligands, since each metal ion in the $M_2(dppm)_2$ framework is coordinatively unsaturated. The additional ligand not only influences the geometry around a metal ion, but also the structure of the framework including the conformation of $M_2(dppm)_2$. There are sparse literature data concerning investigations of the structure and properties of the $Cu_2(dppm)_2$ framework in relation to the additional ligand. In the present work, 1,10-phenanthroline (phen) and its derivatives were used as an additional ligand (biL), from which copper(I) complexes of $[Cu_2(\mu\text{-dppm})_2(biL)_2]^{2+}$ were synthesized. Their geometrical and electronic structures have been characterized by NMR spectroscopy and X-ray crystallography.

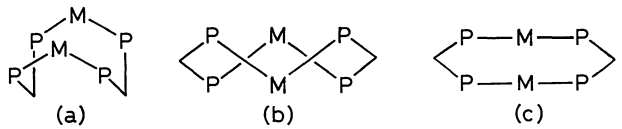

Experimental

Materials. $[Cu(CH_3CN)_4]PF_6$ was synthesized according to a method described in the literature.[5] Bis(diphenylphosphino)methane (dppm), 1,10-phenanthroline (phen) and its derivatives were obtained from Aldrich Co.

All operations were carried out under dry and purified argon by using the standard Schlenk or vacuum-line technique.

Preparation of $[Cu_2(\mu\text{-dppm})_2(phen)_2](PF_6)_2$. A 10 cm^3 acetone solution of phen (0.180 g, 1.0 mmol) and dppm (0.384 g, 1.0 mmol) was added to $[Cu(CH_3CN)_4]PF_6$ (0.373 g, 1.0 mmol), and the mixture stirred for 1 h. The resultant pale-yellow clear solution was transferred into a glass tube (7 mm inner diameter). The pale-yellow crystals were obtained after standing for 24 h at room temperature. Although most of the crystals were not suitable for X-ray crystallographic measurements, a few crystals were used.

Other phen derivatives, $[Cu_2(\mu\text{-dppm})_2(phen)_2](PF_6)_2$, were also prepared in a similar way.

Physical Measurements. The electronic absorption spectra were obtained with a Hitachi 200-10 spectrophotometer for an acetone solution in 1-cm quartz cells.

The ^1H NMR spectra were obtained on a JEOL FX200 NMR spectrometer operating in the Fourier-transform mode (16 K data points transform of 2500 Hz spectral width after 200—500 puleses) at 23 °C. ^{31}P NMR spectra were measured at 23 °C without ^1H irradiation. Between 20—50 K transients were accumulated using a 18.0 μs pulse (90°): 16 K data points were collected over a band width of 4 kHz. H_3PO_4 (85%) was used as an external standarad.

Crystallography. Crystal Data. $C_{80}H_{72}Cu_2N_4O_2F_{12}P_6$, monoclinic, space group $P2_1/c$, a=11.515(2), b=27.922(4), c=12.493(2) Å, β=107.68(1)°, U=3827(1) Å^3, Z=2, D_c=1.442 g cm^{-3}, $F(000)$=1704, λ(Mo$K\alpha$)=0.71069 Å, μ=7.56 cm^{-1}, T=23 °C.

X-Ray Data Collection. A single crystal (0.5×0.4×0.4 mm) of the compound was glued on top of a glass fiber and then studied on a Rigaku AFC5R automatic diffractometer. Unit-cell constants and an orientation matrix for data collection, obtained from a least squares refinement using the setting angles of 25 carefully centered reflections over the range $20° < 2\theta < 32°$, corresponded to a monoclinic cell.

The space group $P2_1/c$ was chosen on the basis of the observed systematic absences ($h0l$: $l=2n$; $0k0$: $k=2n$) and a successful determination of the structure.

Solution and Refinement of the Structure of $[Cu_2(\mu\text{-dppm})_2(phen)_2](PF_6)_2\cdot 2(CH_3)_2CO$. A total of 5121 reflections having $I>3\sigma(I)$ were used. The structure was solved by a direct method,[6] and refined by full-matrix least-squares calculations with anisotropic thermal parameters, including

Table 1. Fractional Coordinates for $[Cu_2(phen)_2(\mu\text{-dppm})_2](PF_6)_2 \cdot 2(CH_3)_2CO$

Atom	x	y	z	Atom	x	x	z
Cu	0.9214(1)	0.07139(4)	0.4019(1)	C(15)	0.462(1)	0.0702(5)	0.199(1)
P(1)	1.0954(2)	0.04290(8)	0.3727(2)	C(16)	0.446(1)	0.0314(5)	0.129(1)
P(2)	0.7711(2)	0.03822(8)	0.4551(2)	C(17)	0.525(1)	−0.0066(5)	0.1572(9)
P(3)	0.3412(3)	0.1606(1)	0.8639(3)	C(18)	0.621(1)	−0.0064(3)	0.2566(8)
F(1)	0.2007(8)	0.1668(4)	0.830(1)	C(19)	0.7146(8)	0.0753(3)	0.5508(7)
F(2)	0.331(1)	0.1157(5)	0.929(1)	C(20)	0.783(1)	0.1138(4)	0.6051(9)
F(3)	0.4773(9)	0.1541(6)	0.893(1)	C(21)	0.741(1)	0.1406(4)	0.678(1)
F(4)	0.343(1)	0.2051(5)	0.801(1)	C(22)	0.631(1)	0.1305(4)	0.696(1)
F(5)	0.357(1)	0.1865(8)	0.972(1)	C(23)	0.564(1)	0.0927(4)	0.643(1)
F(6)	0.316(1)	0.1304(5)	0.757(1)	C(24)	0.604(1)	0.0641(4)	0.5702(9)
O(1)	0.731(1)	0.2395(4)	0.838(1)	C(25)	1.2261(8)	0.0221(3)	0.4909(8)
N(1)	0.8390(6)	0.1066(2)	0.2477(6)	C(26)	0.7637(9)	0.0903(3)	0.1523(8)
N(2)	0.9845(7)	0.1428(3)	0.4457(6)	C(27)	0.727(1)	0.1176(4)	0.0540(8)
C(1)	1.0776(9)	−0.0018(3)	0.2650(8)	C(28)	0.770(1)	0.1633(4)	0.0537(9)
C(2)	0.973(1)	−0.0276(4)	0.231(1)	C(29)	0.851(1)	0.1823(4)	0.1524(8)
C(3)	0.958(1)	−0.0639(4)	0.147(1)	C(30)	0.902(1)	0.2284(4)	0.159(1)
C(4)	1.050(2)	−0.0712(6)	0.100(1)	C(31)	0.978(1)	0.2477(3)	0.257(1)
C(5)	1.151(1)	−0.0446(5)	0.132(1)	C(32)	1.008(1)	0.2171(3)	0.356(1)
C(6)	1.169(1)	−0.0102(4)	0.2141(9)	C(33)	1.087(1)	0.2326(3)	0.459(1)
C(7)	1.1641(8)	0.0920(4)	0.3199(8)	C(34)	1.115(1)	0.2038(5)	0.551(1)
C(8)	1.245(1)	0.1233(4)	0.392(1)	C(35)	1.058(1)	0.1594(3)	0.5400(8)
C(9)	1.288(1)	0.1635(4)	0.352(1)	C(36)	0.9583(8)	0.1713(3)	0.3532(8)
C(10)	1.248(1)	0.1744(4)	0.239(1)	C(37)	0.8787(8)	0.1517(3)	0.2486(7)
C(11)	1.167(1)	0.1456(4)	0.167(1)	C(38)	0.643(1)	0.2650(5)	0.812(1)
C(12)	1.124(1)	0.1045(3)	0.2068(9)	C(39)	0.611(2)	0.290(1)	0.900(2)
C(13)	0.6357(8)	0.0336(3)	0.3287(7)	C(40)	0.566(2)	0.2699(8)	0.702(2)
C(14)	0.555(1)	0.0718(4)	0.2986(9)				

isotropic H atoms located by a difference Fourier synthesis. Finally, a two-cycle refinement led to a convergence at $R=\sum[||F_o|-|F_c||]/\sum|F_o|=0.082$, $R_w=[\sum w(|F_o|-|F_c|)^2/\sum w|F_o|^2]^{1/2}=0.127$, $w=4F_o^2/\sigma^2(F_o^2)$, $\Delta e=0.79$ Å^{-3}, and the largest shift estimated standard deviation at the final cycle (0.13). The atomic parameters of non-hydrogen atoms are given in Table 1.[7]

Results and Discussion

Description of Molecular Structure. The crystal structure comprises of dimeric complex molecules $[(phen)Cu(\mu\text{-dppm})_2Cu(phen)]^{2+}$ (**1**); a perspective view of the inner skeleton is given in Fig. 1. The important bond lengths and angles are summarized in Table 2. This cation has an inversion center. The two copper atoms are doubly bridged by two dppm ligands to form an eight-membered $Cu_2P_4C_2$ ring. Each copper atom displays a four-coordinate form having P_2N_2 donors. The dihedral angle between the (N(1)–Cu–N(2)) and (P(1)–Cu–P(2)) planes is 84.5°, indicating a slightly distorted tetrahedral geometry around the copper atom.

In each copper moiety, all of the distances between the copper and donor atoms are different: both Cu–N(1) and Cu–N(2) are longer by 0.065—0.087 Å than the usual distaces (2.049(9) Å for $[Cu(phen)_2]ClO_4$),[8] and the gap in the two Cu–N distances is 0.022 Å. Similarly, the two Cu–P distances, 2.286(3) and 2.234(3) Å, are also different (0.052 Å), falling within the usual range for copper–dppm compounds so far synthesized: 2.296(8) Å in $[Cu_4(dppm)_4(CS_3)_2]$,[9] 2.22 Å in $[(CuI)_2(dppm)]_2$,[10]

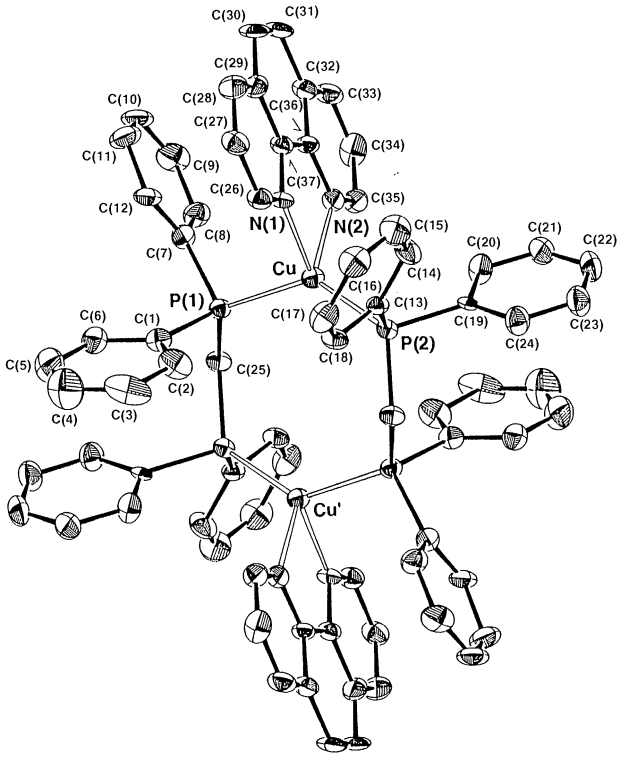

Fig. 1. View of $[Cu_2(\mu\text{-dppm})_2(phen)_2]^{2+}$ with the atomic numbering scheme. Only half the atoms are labeled, the others are related by a center of inversion at the midpoint of the Cu···Cu′ vector.

Table 2. Selected Bond Distances (Å) and Angles (degree) for $[Cu_2(phen)_2(\mu\text{-dppm})_2](PF_6)_2\cdot 2(CH_3)_2CO$

Cu–P(1)	2.286(3)	Cu–P(2)	2.234(3)
Cu–N(1)	2.114(7)	Cu–N(2)	2.136(8)
P(1)–C(1)	1.801(9)	P(1)–C(7)	1.80(1)
P(1)–C(25)	1.854(9)	P(2)–C(13)	1.856(9)
P(2)–C(19)	1.843(9)	P(2)–C(25′)	1.811(9)
N(1)–C(26)	1.32(1)	N(1)–C(37)	1.34(1)
N(2)–C(35)	1.31(1)	N(2)–C(36)	1.36(1)
O(1)–C(38)	1.20(1)	C(38)–C(39)	1.44(2)
C(38)–C(40)	1.40(2)		
P(1)–Cu–P(2)	134.34(9)	P(1)–Cu–N(1)	100.9(2)
P(1)–Cu–N(2)	96.8(2)	P(2)–Cu–N(1)	106.9(2)
P(2)–Cu–N(2)	123.0(2)	N(1)–Cu–N(2)	79.8(3)
Cu–P(1)–C(1)	117.0(3)	Cu–P(1)–C(7)	107.3(3)
Cu–P(1)–C(25)	121.4(3)	C(1)–P(1)–C(7)	102.5(5)
C(1)–P(1)–C(25)	105.0(4)	C(7)–P(1)–C(25)	100.9(4)
Cu–P(2)–C(13)	107.6(3)	Cu–P(2)–C(19)	114.7(3)
Cu–P(2)–C(25′)	124.6(3)	C(13)–P(2)–C(19)	102.7(4)
C(13)–P(2)–C(25′)	99.7(4)	C(19)–P(2)–C(25′)	104.5(4)
Cu–N(1)–C(26)	130.6(6)	Cu–N(1)–C(37)	111.8(6)
Cu–N(2)–C(35)	129.6(7)	Cu–N(2)–C(36)	111.0(6)
P(1)–C(25)–P(2′)	120.5(5)	O(1)–C(38)–C(39)	118(2)
O(1)–C(38)–C(40)	124(2)	C(39)–C(38)–C(40)	118(2)

and 2.231(3) Å in $[Cu_3(OH)(dppm)_3](BF_4)_2$.[11]

The angle of N(1)–Cu–N(2), 79.8(3)°, is close to that of $[Cu(phen)_2]ClO_4$ (81.4(3)°)[8] and $[Cu(dppe)(phen)]PF_6$ (80.7(3)°),[12] where dppe is 1,2-bis(diphenylphosphino)-ethane. On the other hand, a P(1)–Cu–P(2) angle of 134.34(9)°C in **1** is quite large. $[Cu(dppe)(phen)]PF_6$ displays an P–Cu–P angle of 91.3(1)°. Generally, the P–Cu–P angles in monomeric copper(I) compounds of dppe fall within 88—110°.[12,13] This smaller angle is not necessarily due to restraint by chelate coordination of dppe, since monodentate phosphines also give similar values:[14] P–Cu–P=109.3°, 115.9(1)°, and 125.4(1)° for $[Cu(Pph_3)_4]ClO_4$, $[Cu(Pph_3)_2(py)_2]ClO_4$, and $[Cu(Pph_3)_2(bpy)]ClO_4$, respectively. On the other hand the large P–Cu–P angle of 134.34(9)° is not simply ascribed to a restriction by the bridged form of dppm, since $[Cu(\mu\text{-dppm})(CH_3CN)_2]_2(ClO_4)_2$ (119.9(1)°)[1] and $[Cu(S_2ct)(\mu\text{-dppm})]_2$ (114.2°)[2] have normal P–Cu–P angles. Among the various $M_2(dppm)_2$ (M=Cu, Ag, and Au) frameworks, as illustrated in the inserted figures (a), (b), and (c), the staggered conformation (b) tends to open the P–M–P angle rather than the eclipsed one (non-planar type, (a)). The P–Ag–P angle of 138.3(1)° in eclipsed $[Ag_2(dppm)_2(NO_3)_2]$[3] is smaller than that of 155.9(1)° in staggered $[Au_2(dppm)_2Cl_2]$.[4] Hence, the P–Cu–P angle is greatly associated with the conformation of the $M_2(dppm)_2$ framework. Complex **1**, indeed, has a rare staggered framework, while both $[Cu(\mu\text{-dppm})(CH_3CN)_2]_2(ClO_4)_2$[1] and $[Cu(S_2ct)(\mu\text{-dppm})]_2$[2] show an eclipsed framework.

In spite of the significant degree in the opening of the P–Cu–P angle in **1**, the Cu···Cu separation of **1** is 4.742(2) Å, much greater than that of $[Cu_2(dppm)_2(CH_3CN)_2]^{2+}$ (**2**) (3.757(3) Å) and $[Cu_2(dppm)_2(S_2ct)_2]$ (**3**) (3.426(3) Å). This is because a conformation occurs in order to avoid close contact between the two coordinated bulky phen ligands, resulting in a large separation of the copper pair. Hence, each copper(I) moiety in **1** seems to be monomer-like, more than in **2** and **3**.

NMR Chemical Shifts and Metal-Ligand Binding. $[Cu(\mu\text{-dppm})(biL)]_2(PF_6)_2$ gave well-resolved ^1H NMR signals of coordinated biL and dppm, of which chemical shifts are listed in Table 3. For all of the complexes given in Table 3, large coordination shifts ($\delta_{coord}=\delta_{complex}-\delta_{metal\text{-}free}$) were obtained. In the case of phen derivative, for instance, the δ_{coord} of 2,9-H, phenyl-H, and CH_2 protons are −0.59, −0.32, and 1.11, respectively. These are clearly illustrated in Fig. 2. An inspection of Table 3 shows that δ_{coord} (2,9-H) of the dimers is much greater than that in monomeric $[Cu(dppe)(phen)]^+$. This large upfield shift can be accounted for by an anisotropic magnetic effect (ring current effect) of the coordinated dppm. Figure 1 reveals that one of the four phenyl groups of a dppm sits over the nearest-neighbor phen plane in a face-to-face fashion: the phenyl ring of C(7)–C(8)–C(9)–C(10)–C(11)–C(12) and the phen plane of N(1), N(2), and C(26)—C(35). The dihedral angle between the two

Table 3. Observed ^1H[a] and ^{31}P[b] NMR Shifts and Absorption Bands of $[Cu_2(dppm)_2(biL)_2](PF_6)_2$

biL	pK_a[c]	2-H(CH_3) 9-H(CH_3)	4-H(CH_3) 7-H(CH_3)	5-H(CH_3) 6-H	3-H(CH_3) 8-H(CH_3)	CH_2[d]	^{31}P[e]	λ_{max}[f]
5-Clphen	4.07	9.64(9.20)	8.77(8.74)		7.96(7.90)	4.07	−5.86	362
		8.64(9.13)	8.56(8.45)	8.17(8.14)	7.88(7.78)			(5230)
Phen	4.93	8.61(9.12)	8.56(8.44)	7.94(7.97)	7.84(7.74)	4.05	−5.97	355
								(4900)
5-Mephen	5.27	8.53(9.11)	8.64(8.55)	2.73(2.66)	7.85(7.76)	4.03	−6.03	364
		8.53(9.04)	8.46(8.32)	7.77(7.77)	7.81(7.68)			(5200)
4,7-Me_2phen	5.95	8.47(8.94)	2.84(2.86)	8.15(8.16)	7.70(7.56)	3.88	−6.36	370
								(5100)
3,4,7,8-Me_4phen	—	8.21(8.84)	2.76(2.71)	8.20(8.16)	2.49(2.54)	—	—	—
$[Cu(dppe)(phen)]PF_6$		9.10(9.12)	8.90(8.44)	8.34(7.97)	8.08(7.74)	2.92(2.15)		

a) Acetone solution at 23°C. Shifts in ppm referenced against $(CH_3)_4Si$. Chemical shifts of metal-free biL are shown in parenthesis. b) Shifts in ppm referenced against 85% H_3PO_4. c) Ref. 18. d) Metal-free ligand, 2.94 ppm. e) Metal-free ligand, −22.9 ppm. f) Absorption maximum in nm. Molar extinction coefficients (M^{-1} cm^{-1}) are shown in parenthesis.

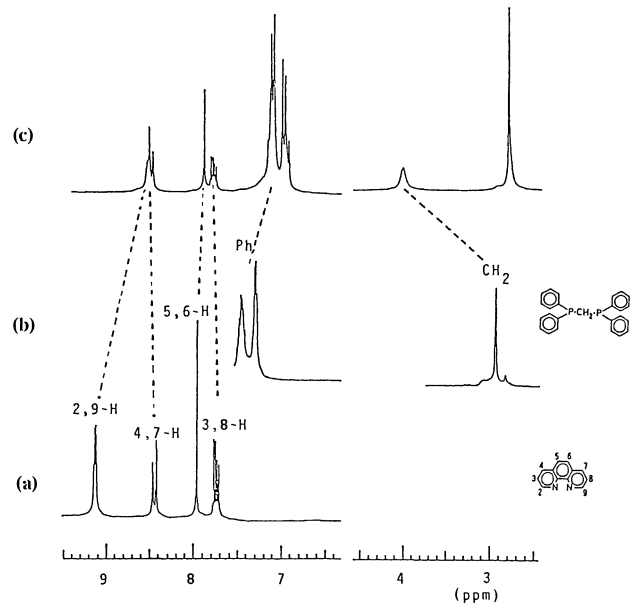

Fig. 2. ^{1}H NMR spectra at 23° of metal-free phen (a), dppm (b), and $[Cu_2(\mu\text{-dppm})_2(phen)_2]^{2+}$ (c) in acetone-d_6.

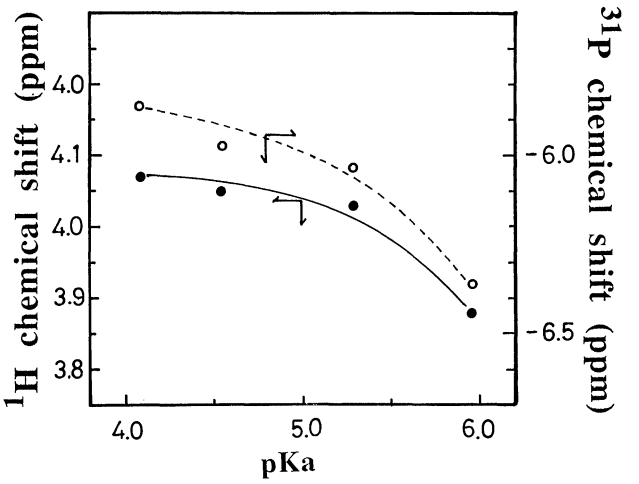

Fig. 3. Plots of the observed ^{1}H and ^{31}P NMR chemical shifts of coordinated dppm vs. pK_a of biL in $[Cu_2(\mu\text{-dppm})_2(biL)_2](PF_6)_2$. The plotted data are listed in Table 3.

mean planes of the phenyl group and phen is 19.02°, indicating that protons on both planes experience an up-field shift. The distance between the nearest-neighbor atoms on the two plane is ca. 3.4 Å, sufficiently close to cause ring a current shift. Accordingly, the phenyl protons also undergo a ring current effect due to the phen ring. This intramolecular magnetic interaction is characteristic of the dimeric structure of $[Cu(\mu\text{-dppm})(phen)]_2^{2+}$.

The molecular structure shown in Fig. 1 also indicates a magnetic inequivalence of 2- and 9-H of phen (similarly 3- to 8-H) concerning the ring current effect of a phenyl group. However, their signals are not separated. This reveals that a low-energy fluxional process is present in solution because of the flexibility of the $Cu_2C_2P_4$ framework. The phenyl ring moves around above a phen plane, depending on the ring motion, as illustrated below.

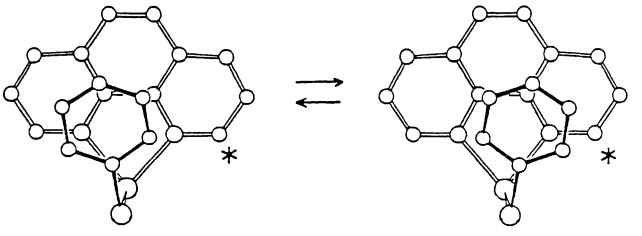

All of the biL derivatives of $[Cu(\mu\text{-dppm})(biL)]_2^{2+}$ also provided specific large shifts of these proton signals in question. Hence, all of the complexes studied here afford the dimeric form, even in solution, as well as in the solid state.

The ^{31}P spectra showed a single signal, which is ascribed to $[Cu_2(\mu\text{-dppm})_2(biL)_2]^{2+}$. The observed ^{31}P chemical shifts are plotted against the pK_a values of biL, together with the ^{1}H chemical shifts of the CH_2 of dppm (Fig. 3). Figure 3 indicates that since biL has a higher basicity, this causes up-field shifts of both the ^{1}H and ^{31}P NMR signals. It has been demonstrated[14,15] that the higher is the basicity of biL the stronger is the copper–biL bonding. The upfield ^{1}H and ^{31}P shifts indicate that Cu–P bonding is weakened. Thus, the relationship shown in Fig. 3 well demonstrates the competition between Cu–P and Cu–N bonding. Consequently, the Cu–P bonding tends to be weak when the Cu–biL bonding becomes strong.

The electronic absorption spectra of these solutions also give information concerning copper–ligand binding. A strong absorption band is observed for each solution in the region 360—370 nm, as shown in Table 3. There is no band in the case of binary systems, such as Cu/dppm and Cu/biL (biL=phen derivatives). The latter system affords a metal-to-ligand charge transfer (MLCT) band in the region greater than 400 nm.[15-17] On this basis, the band in Table 3 has been assigned to the metal-to-ligand charge-transfer bands between Cu and biL in ternary complexes. For instance, the band for $[Cu_2(\mu\text{-dppm})_2(phen)_2]^{2+}$ appears at 355 nm, while $[Cu(phen)_2]^+$ provides a band at 440 nm.[17] This remarkable blue shift (by 85 nm) shows that Cu–phen bonding is weaker in $[Cu_2(\mu\text{-dppm})_2(phen)_2]^{2+}$ than in $[Cu(phen)_2]^+$. This is consistent with the fact that the Cu–N bond distance in **1** is greater than that in $[Cu(phen)_2]^+$,[8] as mentioned above. This trend has been found for all of the complexes studied here.

We thank Mr. H. Shimono and K. Izumi for experimental assistance. This work was supported in part by

a Grant-in-Aid for Scientific Research No. 02640488 from the Ministry of Education, Science and Culture.

References

1) J. Diez, M. P. Gamasa, J. Gimeno, A. Tripicchio, and M. T. Camellini, *J. Chem. Soc., Dalton Trans.*, **1987**, 1275.

2) A. M. Lanfredi, F. Ugozzoli, A. Camus, and N. Marsich, *Inorg. Chim. Acta*, **99**, 111 (1985).

3) D. M. Ho and R. Bau, *Inorg. Chem.*, **22**, 4079 (1983).

4) H. Schmidbauer, A. Wohlleben, U. Schubert, A. Frank, and G. Huttner, *Chem. Ber.*, **110**, 2751 (1977).

5) D. F. Shriver, "Inorganic Syntheses," John-Wiley, New York (1979), Vol. 19, pp. 90—92.

6) a) MITHRIL—an integrated direct methods computer program. C. J. Gilmore, *J. Appl. Crystallogr.*, **17**, 42 (1984). b) DIRDIF—Direct methods for difference structures—an automatic procedure for phase extension and refinement of difference structure factors. P. T. Beurskens, Technical Report 1984/1, ed by Crystallography Laboratory, Toernooiveld, 6525 Nijmegen, Netherlands.

7) Table of a full listing of crystallographic data, coordinates of hydrogen atoms, bond distances and angles, anisotropic thermal parameters of non-hydrogen atoms, and observed and calculated structure factors are deposited as Document No. 8956 at the Office of the Editor of Bull. Chem. Soc. Jpn.

8) P. C. Healy, L. M. Engelhardt, V. A. Patrick, and A. H. White, *J. Chem. Soc., Dalton Trans.*, **1985**, 2541.

9) A. M. M. Lanfredi, A. Tripicchio, A. Camus, and N. Marsich, *J. Chem. Soc., Chem. Commun.*, **1983**, 1126.

10) M. Marsick, G. Nardin, and L. Randaccio, *J. Am. Chem. Soc.*, **95**, 4053 (1983).

11) D. M. Ho and R. Bau, *Inorg. Chem.*, **22**, 4073 (1983).

12) M. Munakata, S. Kitagawa, H. Maruyama, and H. Masuda, unpublished work.

13) P. Lenoi, M. Pasquali, and C. A. Ghilardi, *J. Chem. Soc., Chem. Commun.*, **1983**, 240.

14) L. M. Engelhardt, C. Pakawatchai, and A. H. White, *J. Chem. Soc., Dalton Trans.*, **1985**, 125.

15) B. R. James and R. J. P. Williams, *J. Chem. Soc.*, **1961**, 2007.

16) S. Kitagawa, M. Munakata, and N. Miyaji, *Bull. Chem. Soc. Jpn.*, **56**, 2258 (1983).

17) M. Munakata and S. Kitagawa, "Copper Coordination Chemistry: Biochemical and Inorganic Perspectives," ed by K. D. Karlin and J. Zubieta, Adenine Press, New York (1983), pp. 473—495.

18) A. E. Martell and R. M. Smith, "Crystal Stability Constants," Plenum Press, New York (1974), Vol. 1.

Co-Intercalation of Tetrahydrofuran and Propylene Carbonate with Alkali Metals in β-ZrNCl Layer Structured Crystal

Masao OHASHI,* Koji UYEOKA, Shoji YAMANAKA, and Makoto HATTORI†
Department of Applied Chemistry, Faculty of Engineering, Hiroshima University, Higashi-Hiroshima 724
(Received April 6, 1991)

Alkali metal intercalation compounds of β-ZrNCl were prepared by both chemical and electrochemical processes in tetrahydrofuran (THF) and propylene carbonate (PC), used as solvents. Among the six combinations of alkali metals (Li, Na, and K) with THF and PC, only the Na–THF system did not form a co-intercalation phase. In the other systems, the solvent molecules co-intercalated with alkali metals in mono- and double layer arrangements between the chloride layers of β-ZrNCl, the structures of which were estimated from one-dimensional electron distribution maps along the direction normal to the basal plane. The electrochemical characteristics of β-ZrNCl, used as the cathode of a lithium battery, were greatly influenced by the electrolyte solvent used. The co-intercalation mechanisms are discussed in terms of the energetics of the solvation of alkali metal ions with polar molecules and an expansion of the β-ZrNCl interlayers.

Lithium intercalations in layer-structured crystals have been extensively studied, since such crystals are promising candidates for the electrodes of secondary lithium batteries and electrochromic display (ECD) devices.[1,2] It is well-known that intercalated lithium atoms are ionized in interlayer spaces, and are often solvated with the polar organic solvents used in the preparation,[3]

$$[L] + x\mathrm{Li} + y(\mathrm{Solv}) \rightarrow \mathrm{Li}_x^+(\mathrm{Solv})_y[L]^{x-},$$

where [L] stands for layer-structured crystals such as transition metal dichalcogenides, iron chloride oxide, and graphite; Solv represents solvent molecules. Solvent molecules co-intercalated with lithium expand the basal spacing of the host layers. The degree of this expansion depends on the type of arrangement as well as the size of the molecules. Such an expansion of the interlayer spacing is considered to seriously influence the reversibility of lithium cells, since it may cause a mechanical disintegration of the electrode.[4]

β-ZrNCl is a layer-structured crystal. Each layer comprises a zirconium nitride double layer sandwiched between two close-packed chlorine layers. Such layered sequences (Cl–Zr–N–N–Zr–Cl) are stacked with each other by van der Waals interactions.[5] In a series of previous papers[6,7] we showed that β-ZrNCl is an interesting layered host for lithium intercalation, and could be used as a cathode material for the lithium battery and electrochromic devices, although the electrochemical characteristics of the electrodes are not yet satisfactory for practical use.[8] We also showed that β-ZrNCl readily forms co-intercalation phases with a variety of solvents such as THF, PC, acetonitrile, formamide, *N*,*N*-dimethylformamide, dimethyl sulfoxide, and pyridine.[7] It was considered that the formation of co-intercalation phases would have a bad influence on the performance of batteries.[9] A better understanding concerning the formation mechanism of the co-intercalation phases is indispensable for developing secondary batteries with high performance.

In this study we attempted to elucidate the formation mechanism of the co-intercalation phases of β-ZrNCl with THF and PC. The co-intercalation phases are prepared by both chemical and electrochemical processes by changing combinations of the alkali metals and solvents. The mechanisms are discussed in terms of the energetics of the solvation of alkali ions with the polar molecules and the expansion of the interlayer spacing of β-ZrNCl.

Experimental

Materials. β-ZrNCl was prepared by a reaction of ZrH_2 with ammonium chloride in a stream of dry ammonia according to a method reported elsewhere.[10] Highly crystalline β-ZrNCl was prepared by a chemical transport method;[10,11] it was then ground and sieved through a 200 mesh screen.

THF was purified by refluxing with benzophenone and sodium followed by distillation, and then stored with a molecular sieve (4A). Three kinds of 0.1 M alkali dihydronaphthylide solutions (A–Naph, A=Li, Na, and K; 1 M=1 mol dm^{-3}) were prepared by dissolving equimolar amounts of naphthalene and the respective alkali metals into THF. After 20 h, each solution was filtered through a sintered glass filter in order to remove any insoluble impurities. PC was vacuum distilled and then dried with a molecular sieve (4A). The butyllithium (BuLi) used was a 15 wt% solution from Katayama Chemical. Anhydrous alkali perchlorates were dried by evacuation at 393 K for 12 h.

Chemical Intercalation. Lithium intercalation was carried out by reactions with BuLi and Li–Naph. In the case of the former reaction, only a lithium intercalated sample was obtained,[8] which was then soaked in THF and PC in order to convert it to the respective co-intercalation phases. Varying amounts (or volumes) of Li–Naph were added to β-ZrNCl. After being allowed to stand for 24 h at room temperatures, the lithiated samples were separated by filtration in an Ar-filled glove box (Vacuum Atmosphere Co.). Sodium and potassium intercalated samples were prepared by reactions with

† Present address: Yonago National College of Technology, Hikona-cho, Yonago, Tottori 683.

Na- and K-Naph in a similar manner.

Electrochemical Intercalation. The β-ZrNCl powder sample was pressed onto a stainless-steel mesh of about 8 mm in diameter. Electrochemical cells were constructed by using the pressed sample as the cathode, an alkali metal foil as the anode and a glass filter separator soaked with 1 M Li and Na perchlorate solutions in THF and PC. A $KClO_4$/PC saturated solution was also used for the K/β-ZrNCl cell. The cells were galvanometrically discharged at a rate of 0.2 mA cm^{-2}, and the electrodes were taken out at different stages of discharge to measure the change in the basal spacing of β-ZrNCl.

Analyses. The X-ray powder diffraction (XRD) patterns of all the intercalated samples were measured under an argon atmosphere in a cylindrical cover having thin polyethylene windows by using nickel-filtered Cu $K\alpha$ radiation. The amounts of co-intercalated THF were determined from the weight loss before and after evacuation at 453 K. The amounts of alkali metals intercalated were determined by flame analysis after extraction by a procedure reported elsewhere.[8]

Results

Chemical Intercalation. The basal spacings (d) and some interlayer compositions of the chemical intercalation products are listed in Table 1. The lithium intercalate with a composition of $Li_{0.16}ZrNCl$ and a basal spacing of 0.93 nm was obtained by a reaction with a BuLi solution in hexane.[8] The nonpolar hexane molecules did not co-intercalate with lithium and, thus, the basal spacing is almost unchanged from that of the initial β-ZrNCl (d=0.92 nm). However, when the lithiated sample was dispersed in THF and PC, the basal spacing increased to 1.49 and 2.22 nm, respectively, although β-ZrNCl without lithium did not swell in these solvents. Li-Naph is a stronger reducing agent than BuLi[12] and, as shown in the table, larger amount of lithium can be intercalated by using an appropriate amount of Li-Naph. The amount of lithium intercalated increases with the amount of Li-Naph used.[9] Single-basal-spacing phases were obtained at x=0.18 and 0.20 (x in Li_xZrNCl), the amount of THF co-intercalated (y) being determined to be 0.25 and 0.35, respectively. Although the other products were mixtures of two or three phases with different basal spacing, the spacing appears to vary in the following order with increasing x:

$$0.92 \rightarrow 1.45 \rightarrow 1.85 \rightarrow 2.00 \rightarrow 1.08\ \text{nm}$$
$$\beta\text{-ZrNCl} \quad x=0.18 \quad x=0.20 \quad x=0.5 \quad x>1.0$$

It is interesting to note that the spacing increases up to 2.00 nm with the amount of lithium intercalated and then collapses to 1.08 nm when the amount of lithium (x) exceeds about 1.0.

In reactions with Na-Naph, no co-intercalation phases were obtained; a sample with a small amount of Na showed a basal spacing of 0.99 nm. As the amount of intercalated Na increases, the 0.99 nm phase changes to a 1.08 nm phase. A sample $Na_{0.40}ZrNCl$ with a basal spacing of 0.99 nm swelled in PC and the spacing increased to 2.06 nm, though it did not form any co-intercalation phase with THF.

In the interlayer spaces between the chloride layers of β-ZrNCl, there are 1/2 octahedrally co-ordinated sites and one tetrahderally co-ordinated vacant site on the ZrNCl formula basis. The stoichiometry shown in Table 1 indicates the formation of intercalation phases with $x>0.5$ (x in A_xZrNCl; A=Li and Na); this suggests that alkali metals occupy the tetrahedral as well as the octahedral vacant sites.

K-Naph forms co-intercalation phases with basal spacings of 1.47 and 1.30 nm. If a much larger amount of K-Naph was used, the layer structured phase disappeared and the formation of KCl was observed by XRD analysis. After washing out the KCl with water, the residue was calcined at 1273 K in a vacuum. The resulting compound was found to be ZrN. This finding suggests that K-Naph is a stronger reducing agent than Li- and Na-Naph, so that β-ZrNCl is reduced to ZrN by the following equation:

$$\beta\text{-ZrNCl} + \text{K-Naph} \rightarrow \text{ZrN} + \text{KCl} + \text{Naph}.$$

Electrochemical Intercalation. The discharge curves of alkali/β-ZrNCl cells with THF and PC as electrolyte

Table 1. Basal Spacings and Interlayer Compositions of the Chemical Intercalation Products of β-ZrNCl

Reagents	Basal spacing (d) d/nm	Stoichiometry/ ZrNCl
(β-ZrNCl	0.92)	
BuLi	0.93	0.16Li
+THF[a]	1.49	0.16Li+yTHF
+$LiClO_4$/PC[a]	2.22	0.16Li+0.64PC
Li-Naph[b]		
1.0	1.49	0.18Li+0.28THF
1.2	1.49, 1.85	0.19Li+yTHF
1.5	1.85	0.20Li+0.35THF
2.0	1.85, 1.08	0.40Li+yTHF
10.0	2.00, 1.85, 1.08	0.85Li+yTHF
18.0	1.08, 2.00	1.20Li+yTHF
Na-Naph[b]		
0.90	0.99	0.40Na
+PC[c]	2.06	0.40Na+yPC
1.0	0.99, 1.06	0.48Na
1.5	1.06	0.75Na
K-Naph[b]		
0.25	1.47	0.20K+0.30THF
0.75	1.30	xK+yTHF
5	—[d]	

a) The lithiated samples by BuLi were immersed in THF or a $LiClO_4$/PC solution. b) Molar ratios of alkali-Naph/ ZrNCl are given. c) The $Na_{0.40}ZrNCl$ sample was immersed in PC. d) Only the formation of KCl was observed by XRD analysis.

solvents are shown in Figs. 1 and 2, respectively. The discharges were stopped at different stages of current flow (Q) on separate samples, and the basal spacings of the β-ZrNCl cathodes were measured by an XRD analysis. The spacings listed in Table 2 are coincident with those of the samples obtained by the chemical intercalations up to the same intercalation level. It should be noted that in a battery system with Na–THF, no intercalation of THF occurred, even during the electrochemical process, as found in the chemical intercalation.

In a previous paper[8] it was revealed that in a battery of Li|$LiClO_4$/PC|β-ZrNCl, lithium could not intercalate over the stage of $x \approx 0.16$. The current discharged over this stage was used for the decomposition of PC, rather than for Li intercalation; the discharge curve showed a plateau at about 1.0 V vs. Li/Li^+. Similar decompositions accompanied by plateaus in the discharge curves were observed for Na- and K–PC systems (Fig. 2). All of the β-ZrNCl cathodes taken out at a discharge level of $x=0.10$ had very large basal spacings of 2.00—2.22 nm, indicating that PC could co-intercalate with these three kinds of alkali metals in β-ZrNCl.

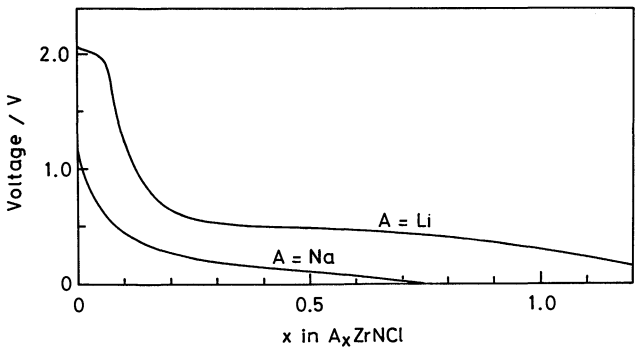

Fig. 1. Discharge curves for A|$AClO_4$/THF|β-ZrNCl cells (A=Li and Na) at a current density of 0.2 mA cm^{-2}.

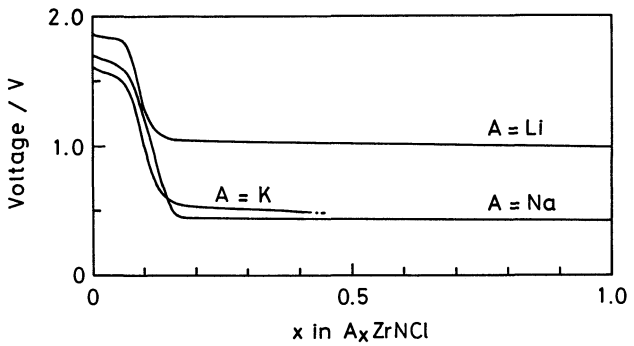

Fig. 2. Discharge curves for A|$AClO_4$/PC|β-ZrNCl cells (A=Li, Na, and K) at a current density of 0.2 mA cm^{-2}.

Interlayer Molecular Arrangements. Most of the co-intercalation phases are highly crystalline and basal reflections up to 12 orders were measured in each XRD pattern. One-dimensional electron-density distribution maps along a direction perpendicular to the basal plane were synthesized on the basis of the corrected reflection intensities on the following three samples; $Li_{0.18}(THF)_{0.28}ZrNCl$ (d=1.49 nm), $Li_{0.20}(THF)_{0.35}ZrNCl$ (d=1.85 nm), and $Li_{0.16}(PC)_{0.64}ZrNCl$ (d=2.22 nm). The presence of a mirror plane was assumed, and the signs of the structural factors were determined on the basis of the β-ZrNCl host structure expanded along the c-axis. The synthesized electron distribution maps are shown in Figs. 3 and 4. The R factors were calculated to be within the range 0.18 to 0.23. The distributions of the figures clearly show that the co-intercalated molecules are located in the Cl···Cl interlayer spaces. In the co-intercalation phase with a smaller basal spacing of 1.49 nm, the THF molecules are oriented with the molecular planes almost perpendicular to the β-ZrNCl layers and in a monolayer arrangement; in the co-intercalation phases with basal spacings of about 2.0 nm, however, the THF and PC molecules are arranged in double layers. It is very likely that the lithium ions seem to be solvated by these molecules through the oxygen atoms.

Discussion

We have examined the intercalations of three kinds of alkali metals coupled with two kinds of solvents for each metal and found that the co-intercalation behaviors are very different, depending on the combinations. In electrochemical intercalations in systems with PC, intercalation compounds $A_x(PC)_yZrNCl$ with $x>0.16$

Table 2. Basal Spacings of the Electrochemical Intercalation Products of β-ZrNCl Separated at Different Stages of Discharge

Anode	Electrolyte	Amount discharged (Q) Q/e/ZrNCl	Basal spacing (d) d/nm
Li	1M $LiClO_4$/THF	0.18	1.49
		0.20	1.85
		1.20	2.00
Na	1M $NaClO_4$/THF	0.40	0.99
K	$KClO_4$ (Satd.)/PC	0.10	2.18
Li	1M $LiClO_4$/PC	0.10	2.22
Na	1M $NaClO_4$/PC	0.10	2.00

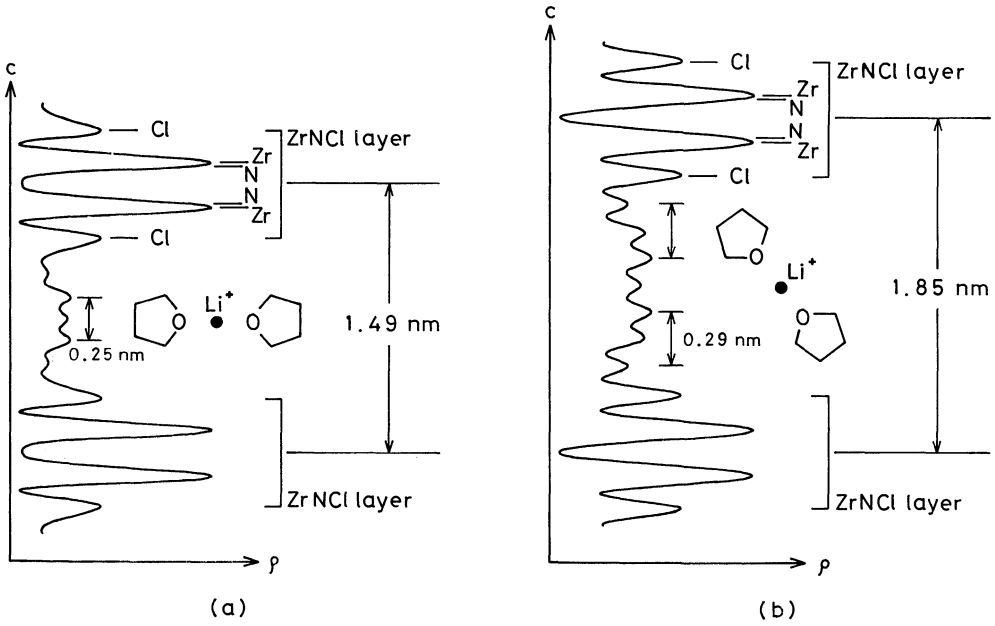

Fig. 3. One-demensional electron-density maps along the direction normal to the β-ZrNCl layers together with the estimated intrlayer molecular arrangements: (a) $Li_{0.18}(THF)_{0.28}ZrNCl$, (b) $Li_{0.20}(THF)_{0.35}ZrNCl$.

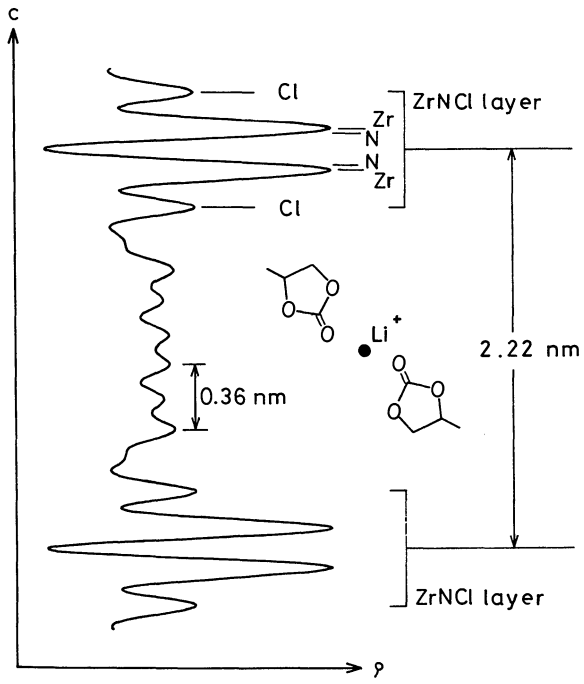

Fig. 4. One-dimensional electron-density map along the direction normal to the ZrNCl layers and the interlayer moleculer arrangement of $Li_{0.16}(PC)_{0.64}ZrNCl$.

were not formed; the current discharged over this point was used for the decomposition of PC rather than for a further intercalation of alkali metals. On the other hand, in electrochemical systems with THF, almost all of the current discharged was used for alkali metal intercalations without being accompanied by a decomposition of THF. In a previous study[8] concerning the characteristics of a $Li|LiClO_4/PC|\beta$-ZrNCl cell, it was expected that the presence of co-intercalated PC molecules in the interlayer spaces might prevent any further intercalation of Li into the interlayer spaces. However, from the comparison of the two electrochemical systems with PC and THF, it is evident that alkali metals can intercalate into the interlayer spaces of β-ZrNCl, even if the spaces are occupied by co-intercalated molecules. An electrochemical system containing PC seems to be rather a special case, in which the surface of the alkali intercalated β-ZrNCl catalyzes the decomposition of PC at relatively high voltages vs. Li^+/Li as seen in Fig. 2. In the case of the Na–THF–ZrNCl system, the intercalation compound Na_xZrNCl did not form any co-intercalation phase. Nevertheless, the cell $Na|NaClO_4/THF|\beta$-ZrNCl experienced a partial polarization for the discharge at the rate same as that used in the cell $Li|LiClO_4/THF|\beta$-ZrNCl, and showed low discharge voltages (Fig. 1). This finding also supports the above conclusion that the co-intercalated molecules do not necessarily hinder the diffusion of alkali metals into the interlayer spaces.

Among the combinations of three kinds of alkali metals (Li, Na, and K) with two kinds of polar solvents (THF and PC), only the Na–THF system does not form co-intercalation phases. In addition, in the Li–THF system, if a larger amount of Li was intercalated, the co-intercalation phase collapsed, releasing solvated THF molecules out of the interlayer spaces. The formation of co-intercalation or collapsed phases seems to be interpreted in terms of the energetics of the solvation of

alkali ions with the polar molecules and an expansion of the interlayer spacing as follows:

In the course of intercalation, work must be done by the solvent molecules to make room in the interlayer spaces. The driving force for the intercalation is mainly due to dipole-cation interactions similar to those involved in the solvation of cations in an electrolyte solution. The co-intercalation occurs if such interactions between the polar solvent molecules and the ionized alkali metals in the interlayer spaces are sufficiently strong to compensate for the energy required for expanding the interlayers. The solvation energy or the work of ion dipole interaction ($W_{I\text{-}D}$) is given by the following equation:[13]

$$W_{I\text{-}D} = \frac{Nnz_ie}{(r_i+r_s)^2}\mu_s,$$

where N is Avogadro's number, n is the co-ordination number of the solvent, z_ie is the ionic charge, r_i and r_s are the ionic radius of alkali metals and the radius of the polar solvent, respectively, and μ_s is the dipole moment of solvent molecules. The finding that PC molecules can form co-intercalation phases with all kinds of alkali-intercalated ZrNCl can be interpreted in terms of its exceptionally large dipole moment (μ_s=4.94 D; D=3.3356×10^{-30} C m). THF has a much smaller dipole moment (μ_s=1.75 D), and the systems have a smaller $W_{I\text{-}D}$ than that of the corresponding PC systems. The $W_{I\text{-}D}$ decreases with an increase in the radius of interlayer cations. In THF-containing systems, although the $W_{I\text{-}D}$ decreases in the order Li>Na>K containing systems, only the Na intercalated β-ZrNCl does not form the co-intercalation phase. This suggests that the $W_{I\text{-}D}$ of the Na–THF system would not be large enough to overcome the energy required for the THF molecules to intercalate. The $W_{I\text{-}D}$ in the K–THF system is much smaller than that of Na–THF. However, the K ions are co-intercalated with THF molecules in β-ZrNCl. This can be explained by the large ionic size of K^+ as follows: the cation radius of K^+ is larger than that of Na^+ and the interlayer spacing supported by the K ions is correspondingly larger. Therefore, only a smaller amount of energy would be required for the THF molecules to expand the interlayer spaces in the K–THF system; the K ions can be regarded as acting as pillars.

The degree of interlayer space expansion due to co-intercalation would also be determined energetically. During the early stages of intercalation, the number of co-intercalated THF molecules increases with an increase in the number of intercalated lithium ions. During this procedure, even a small increase in the number of lithium ions causes a large change in the way the intercalated THF molecules are arranged, consequently, resulting in different expansions of the interlayer spacing (Fig. 3). However, if a much larger amount of lithium is intercalated, the electrostatic interactions between the negatively ionized layers and the lithium cations may exceed the solvation energy in the Li–THF system; even if lithium ions are present between the layers, the THF molecules are released out of the interlayer spaces.

This study was partly defrayed by the Grant-in-aid for Scientific Research on Priority Area of the Ministry of Education, Science and Culture.

References

1) M. S. Whittingham, *Prog. Solid State Chem.*, **12**, 41 (1981).
2) "Intercalation Chemistry," ed by M. S. Whittingham and J. Jacobson, Academic Press Inc., New York (1982).
3) R. Schollhorn, *Angew. Chem., Int. Ed. Engl.*, **19**, 983 (1980).
4) T. Yamamoto, S. Kikkawa, and M. Koizumi, *J. Electrochem. Soc.*, **131**, 1343 (1984).
5) R. Juza and H. Friedrichsen, *Z. Anorg. Allg. Chem.*, **332**, 173 (1964).
6) S. Yamanaka, M. Ohashi, M. Sumihara, and M. Hattori, *Chem. Lett.*, **1984**, 1403.
7) M. Ohashi, S. Yamanaka, M. Sumihara, and M. Hattori, *J. Inclusion Phenom.*, **2**, 289 (1984).
8) M. Ohashi, T. Shigeta, S. Yamanaka, and M. Hattori, *J. Electrochem. Soc.*, **136**, 1086 (1989).
9) M. Ohashi, K. Uyeoka, S. Yamanaka, and M. Hattori, *Chem. Lett.*, **1990**, 93.
10) M. Ohashi, S. Yamanaka, M. Sumihara, and M. Hattori, *J. Solid State Chem.*, **75**, 99 (1988).
11) M. Ohashi, S. Yamanaka, and M. Hattori, *J. Sold State Chem.*, **77**, 342 (1988).
12) D. M. Murphy and P. A. Christian, *Science*, **205**, 651 (1979).
13) J. O'M. Bockris and A. K. N. Reddy, "Modern Electrochemistry," Plenum Press, New York (1979), Vol. 1, p. 45.

 © 1991 The Chemical Society of Japan Bull. Chem. Soc. Jpn., 64, 2819—2828 (1991)

Five- and Six-Coordinated Nitrosyl Iron(II) Complexes of Tetrakis (*p*-substituted phenyl)porphyrins. Substituent Effects on the EPR Parameters and the NO Stretching Frequencies

Tetsuhiko YOSHIMURA
The Environmental Science Institute of Hyogo Prefecture,
Yukihira-cho, Suma-ku, Kobe 654
(Received May 13, 1991)

Five- and six-coordinated nitrosyl iron(II) complexes of a series of tetrakis(*p*-substituted phenyl)porphyrins have been prepared. Their EPR and IR spectra have been measured and analyzed in order to elucidate the cis-effect of substituents on the axial nitrosyl ligand. As the first redox potentials of the free base porphyrins in the complexes became positive, the NO stretching frequencies increased in both five-coordinated and six-coordinated nitrosyl(porphyrinato)iron(II) complexes with a nitrogenous base at an axial site trans to the NO group. The positive shift of the redox potentials led to an increase in the EPR *g* values and hyperfine coupling constants at room temperature and at 77 K for the five-coordinated complexes, while it led to a decrease in *g* values and to a slight increase in hyperfine coupling constants for the six-coordinated complexes. These results are rationalized by invoking that, as the electron-withdrawing power of porphyrin peripheral substituents is enhanced, the iron-to-NO bond in both the five- and six-coordinated complexes is weakened and the iron-to-nitrogenous base bond in the six-coordinated complexes is strengthened. The difference in the cis- and trans-effects on the EPR parameters and NO stretching frequencies is also discussed.

The electronic properties of the heme at active centers of various hemoproteins and the biological functions of these proteins are markedly influenced by the electronic states of the equatorial porphyrinato and axial ligands. The porphyrin peripheral substituents and axial ligands serve as intermediaries of the electronic and steric interactions between the heme group(s) in hemoprotein and amino acid residues surrounding the heme group. From this point of view, the cis and trans effects on various properties of metalloporphyrins have been extensively investigated.[1-5]

Nitrogen monoxide (nitric oxide) is formed as an intermediate in the biological denitrification process[6] and is the most probable candidate for an endothelium-derived relaxing factor.[7] Further, nitrogen monoxide has been known as a biological ligand of nitrite reductases[8] and guanylate cyclase.[9] Thus, an increasing interest is placed on the physiological significance of nitrogen monoxide.

Because the nitrogen monoxide molecule has an unpaired electron and is coordinated as sixth ligand to the heme iron in hemoproteins, it has so far been employed as a useful electronic probe for elucidating the heme environments and the heme group.[10-13] For understanding the properties of these nitrosylhemoproteins, studies on a model complex, nitrosyl(porphyrinato)iron(II), under various conditions have yielded useful information.[14-20] In a preceding paper, we reported EPR, IR, magnetic circular dichroism (MCD), and electronic absorption spectral studies on the five-coordinated nitrosyl(porphyrinato)iron(II) complex and its six-coordinated complexes with N-, O-, and S-donor ligands under various conditions.[20] These studies on the model nitrosyl(porphyrinato)iron(II) complexes have dealt almost exclusively with elucidating the effects on the properties of an axial ligand trans to a nitrosyl group, because the identification of the axial ligand(s) is critical for hemoproteins. However, differences among the natural hemes (e. g., hemes a, b, and c) in porphyrin peripheral substituents have been demonstrated to cause pronounced changes in the spectral properties of hemoproteins.[1] In an attempt to elucidate a cis-effect on the axial nitrosyl ligand, we investigated the EPR and IR spectra of five- and six-coordinated nitrosyl iron(II) complexes of a series of tetrakis(*p*-substituted phenyl)porphyrins. The studies yielded more systematic information for the cis-effect than the electronic absorption and MCD studies.[21]

Experimental

Materials and Methods. Para-substituted tetraphenylporphyrins, H_2(*p*-X)tpp, where X=NMe_2, OCH_3, F, CO_2CH_3, and NO_2, were purchased from Midcentury Chemicals and their iron(III) chlorides were synthesized as described previously.[22] Fe(tpp)Cl and Fe[(F_5)tpp]Cl [where (F_5)tpp is the dianion of tetrakis(pentafluorophenyl)porphyrin] were purchased from Aldrich Chemical Co. In the synthesis of Fe[(*p*-NO_2)tpp]Cl, the compound was not obtained in a spectroscopically pure form as described previously.[3c] Hence a crude material was prepared as follows. After H_2(*p*-NO_2)tpp and $FeCl_2$ were refluxed in DMF, H_2O and CH_2Cl_2 were added, the CH_2Cl_2 layer was washed three times with water, dried over Na_2SO_4, and then the solvent was evaporated. The solid was redissolved in CH_2Cl_2 and heptane was added. The crude product thus obtained was dried in vacuo and used as an iron(III) complex of (*p*-NO_2)tpp for Sample Preparation.

1-Methylimidazole (*N*-MeIm) and pyridine (Py) were stored over KOH and distilled under an N_2 atmosphere. Nitrogen monoxide (99.5% minimum) purchased from Seitetsu Kagaku Co. was passed through a KOH column to remove higher nitrogen oxides. Gaseous ^{15}NO was generated by the reaction of $Na^{15}NO_2$ (99.2% enrichment, Amersham) with an ascorbic acid aqueous solution and was passed through a cold trap (about −90 °C) and a KOH column. All other chemicals were

of the highest available grade and were used without further purification.

EPR measurements at X-band frequency were carried out on a JES-ME-3X or a JES-RE-2X spectrometer with 100-kHz field modulation at room temperature (ca. 23 °C) and at 77 K. For accurate measurements of the EPR parameters, the microwave frequencies were measured with a digital frequency counter (Advantest, Model TR-5211A), and the magnetic field was calibrated with an NMR field meter (Echo Electronics, EMF 2000A).

The IR absorption spectra of chloroform or 1-methylimidazole solutions of the complexes were measured in a region 1550—1750 cm^{-1}, using CaF_2 windows with pathlength of 0.1 mm. They were recorded on a JASCO A-302 apparatus attached with a DP-A300 data processor for data accumulation and manipulation. In the IR spectrum of the complex with (p-CO_2CH_3)tpp, since the bands of the CO bond at the side chain and the NO bond partially overlapped, the frequencies of the NO band were determined from the difference spectrum of Fe(P)(NO) minus Fe(P)Cl with the same concentration.

Sample Preparation. Nitrosyl(porphyrinato)iron(II) complexes were prepared by a modified method of Kon and Kataoka.[14b,c] The reaction with NO was carried out in a Thunberg-type tube with a side arm on a vacuum line. Five-coordinated complexes were prepared as follows. Pyridine–toluene (1:1, v/v) solution of Fe(P)Cl (P=porphyrin dianion) was degassed by three successive freeze-pump-thaw cycles. Then the solution was equilibrated with NO gas; a tube containing the solution was shaken gently for about 1 h until the solution changed from dark brown to red; the solution was freed of excess NO, pyridine, and solvent in vacuo. The solid thus obtained was dissolved in degassed toluene and the solvent was evaporated. This dissolution–evaporation cycle was repeated and then the product was dried in vacuo for a week in order to completely remove the pyridine ligand. In EPR sample preparations, the product was again dissolved in degassed toluene; the solution was transferred into an EPR tube and sealed on a vacuum line. In IR sample preparations, it was dissolved in chloroform; the solution was transferred into an IR cell under an N_2 atmosphere.

The six-coordinated complexes as EPR or IR samples were prepared by the following methods. (a)EPR samples were prepared by reductive nitrosylation of iron(III) porphyrins with NO. The solution containing Fe(P)Cl and nitrogenous base in toluene was carefully degassed by freeze-pump-thaw cycles. Then the solution was equilibrated with NO gas at a pressure slightly below 1 atm, followed by standing for 1—2 h, transferred into an EPR tube, and sealed. (b)IR samples were prepared by dissolving the five-coordinated nitrosyl iron(II) complexes, obtained by the above-mentioned method, into 1-methylimidazole. The solution was transferred into an IR cell under an N_2 atmosphere.

The concentrations of Fe(P)(NO), N-MeIm, and Py in EPR samples were 2—3 mM, ca. 4 M, and ca. 4 M, respectively (1 M=1 mol dm^{-3}); those of Fe(P)(NO) in IR samples were 5—7 mM.

Results

EPR Spectra of Five-Coordinated Nitrosyl(porphyrinato)iron(II) Complexes. The EPR spectra of five-coordinated nitrosyl(porphyrinato)iron(II) complexes in toluene exhibited a well-resolved triplet for ^{14}NO complexes or a doublet for ^{15}NO complexes (Fig. 1), originated from an ^{14}N (I=1) or ^{15}N (I=1/2) of the NO ligand, respectively. Table 1 lists the g values (g_{iso}) at the central position of the triplet or doublet and the average hyperfine coupling constants (A_{iso}) in the second-derivative curve, together with the first redox potentials of free base porphyrin.

EPR spectral results of five-coordinated Fe(P)(NO) complexes at low temperatures have been utilized in elucidating the stereochemistry of the heme environment for nitrosylhemoproteins such as the NO adducts of

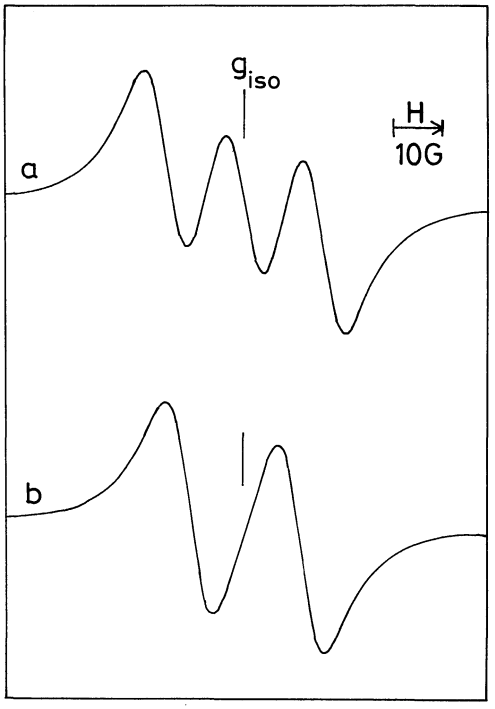

Fig. 1. EPR spectra of (a) Fe(tpp)(^{14}NO) and (b) Fe(tpp)(^{15}NO) in toluene at room temperature. Instrument settings: modulation frequency and amplitude, 100 kHz and 2G; microwave frequency and power, (a) 9.4419 GHz, (b) 9.4481 GHz and 5 mW.

Table 1. EPR Parameters of Five-Coordinated Nitrosyl(porphyrinato)iron(II) Complexes in Toluene at Room Temperature

Porphyrinato ligand	$E_{1/2}(I)^{a)}$/V	g_{iso}	A_{iso}
^{14}NO (p-NMe_2)tpp	−1.660	2.0506	16.45
(p-OCH_3)tpp	−1.593	2.0504	16.49
(p-H)tpp	−1.557	2.0507	16.45
(p-F)tpp	−1.520	2.0508	16.42
(p-CO_2CH_3)tpp	−1.435	2.0513	16.55
(F_5)tpp	−1.205	2.0555	16.81
^{15}NO (p-H)tpp	−1.557	2.0506	23.05
(F_5)tpp	−1.205	2.0555	24.31

a) First redox potential of free base porphyrin. Ref. 31.

hemoglobins in the presence of inositol hexaphosphate (IHP)[23] or sodium dodecyl sulfate,[14a] those of mutant hemoglobin M,[24] and those of cytochrome c',[13] which contain five-coordinated nitrosylheme. Five-coordinated Fe(P)(NO) complexes in nondonor solvents at low temperatures exhibit characteristic EPR spectra with an intense triplet in the g_3 (or g_z) absorption.[14c,15,20a,l]

The EPR spectra of Fe(tpp)(^{14}NO) and Fe(tpp)(^{15}NO) in glassy toluene at 77 K (Fig. 2) indicate the existence of three g values (g_1, g_2, and g_3). The higher field part of the g_2 absorption is hidden in the intense g_3, absorption. The g_1, g_2, and g_3 absorptions split into a triplet for ^{14}NO complexes or a doublet for ^{15}NO complexes. Thus, the g_2' absorption in Fig. 2 can be identified as a lowest field line of the triplet or doublet of the g_2 absorption. The absorption between g_1 and g_2 which is called an unidentified $g_?$ absorption[20m] is probably related to the coordinated NO group because it splits into a triplet or a doublet depending on the nuclear spin of the NO nitrogen. The EPR spectra of six-coordinated complexes at low temperatures also have such a $g_?$ absorption (vide infra). These $g_?$ absorptions most probably arise from another species.[10,20b,25,26] It is known that the intensity of these absorptions depends on the nature of the porphyrinato ligand, medium or solvent, temperature, and other factors.[10,14c,20b,20l,25-27] Because of the presence of small amounts of another species, there is not a good agreement between the experimental and simulated EPR spectra of nitrosylheme.

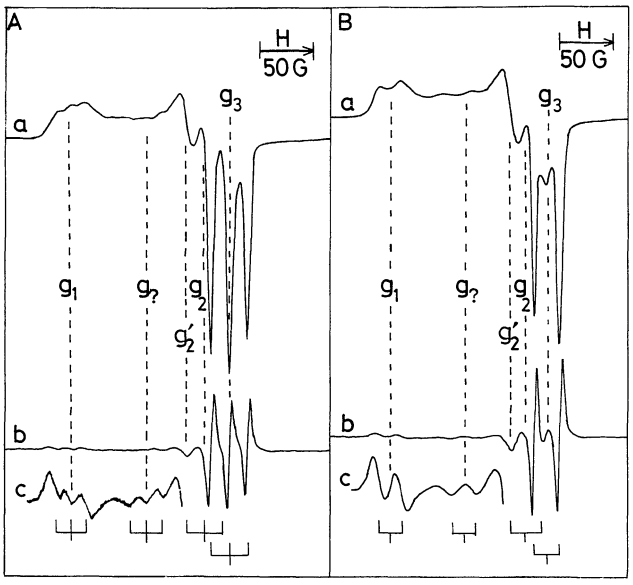

Fig. 2. EPR spectra of (A) Fe(tpp)(^{14}NO) and (B) Fe(tpp)(^{15}NO) in frozen toluene glass at 77 K; (a) first- and (b, c) second-derivative display, where (c) is the expansion of the ordinate of (b). Instrument settings: modulation frequency and amplitude, 100 kHz and 2 G; microwave frequency and power, (A) 9.1811 GHz, (B) 9.1871 GHz and 10 mW.

Table 2 lists the EPR parameters of five-coordinated nitrosyl(porphyrinato)iron(II) complexes at 77 K. The g_3 value was determined from the central line position of triplet or the center of doublet in the first-derivative display, while the g_1, g_2, g_2', and $g_?$ values were determined from those in the second derivative because of the poor resolution in the first derivative. Similarly, the A_3 value was obtained as an average of intervals in the first derivative, while the A_1, A_2, and $A_?$ values were obtained from those in the second derivative. However, the A_2 value for ^{14}NO complexes can not be determined because the two lines at the higher field side of the g_2 absorption were hidden into the g_3 absorption. Thus, the A_2 values of Fe(tpp)(NO) and Fe[(F_5)tpp](NO) were estimated from the equation $A_2(^{14}NO)=A_2(^{15}NO)-[A_3(^{14}NO)/A_3(^{15}NO)]$.

EPR Spectra of Six-Coordinated Nitrosyl(porphyrinato)iron(II) Complxes. Figure 3 shows the first- and second-derivative spectra of the Fe[(F_5)tpp](^{14}NO) complex with *N*-MeIm in toluene at room temperature; the spectra of the complexes with ^{15}NO and with the other porphyrinato ligands were virtually identical with Fig. 3 in the line shape. The first-derivative curve was slightly asymmetric and its second-derivative curve indicated overlapping of two components. These spectral features resemble those of the nitrosyl iron(II) complex of protoporphyrin IX dimethyl ester (Fe(ppixdme)(NO)) with *N*-MeIm.[20b] In contrast with the *N*-MeIm complexes, the Py complexes exhibited EPR spectra with a well-resolved triplet for ^{14}NO complexes, being similar to those of the five-coordinated complexes.

Table 2. EPR Parameters of Five-Coordinated Nitrosyl(porphyrinato)iron(II) Complexes in Toluene at 77 K

Porphyrinato ligand	$E_{2/1}$(I)[a]	g values					Hyperfine coupling const.			
	V	g_1	$g_?$	g_2'	g_2	g_3	A_1/G	$A_?$/G	A_2/G	A_3/G
^{14}NO (*p*-NMe_2)tpp	−1.660	2.104	2.060	2.035		2.0100	15.0			16.6
(*p*-OCH_3)tpp	−1.593	2.104	2.060	2.035		2.0101	15.0	15.0		16.6
(*p*-H)tpp	−1.557	2.107	2.060	2.035	2.024	2.0100	14.5	15.5	19.3	16.7
(*p*-F)tpp	−1.520	2.107	2.059	2.035		2.0102	15.0	15.6		16.9
(*p*-CO_2CH_3)tpp	−1.435	2.106	2.059	2.034		2.0103	14.7	15.9		17.0
(F_5)tpp	−1.205	2.108	2.063	2.040	2.028	2.0109	15.0	16.0	20.2	17.2
^{15}NO (*p*-H)tpp	−1.557	2.107	2.060	2.032	2.024	2.0102	20.5	21.5	26.8	23.2
(F_5)tpp	−1.205	2.108	2.061	2.037	2.028	2.0108	21.0	22.6	27.8	23.7

a) See footnote a of Table 1.

The g values at the zero-crossing in the first-derivative spectra of N-MeIm complexes and those at the central peak of the triplet in the second derivative spectra of Py complexes at room temperature are listed in Table 3, together with the first redox potentials of free base porphyrin.

The nitrosyl derivatives of many hemoproteins at low temperatures exhibited EPR spectra similar to those of six-coordinated nitrosyl(porhyrinato)iron(II) complexes with a nitrogenous base. These results have been utilized in identifying the fifth heme ligand of which the most probable candidate is an imidazolyl group of the histidine residue.[10-12] The EPR spectra of six-coordinated nitrosyl(porphyrinato)iron(II) complexes with nitrogenous bases at low temperatures exhibit a line shape characteristic of randomly oriented systems with a rhombic symmetry and its central g_2 (or g_z) absorption has mostly nine hyperfine lines or a triplet of triplets, originating from the hyperfine interaction of an unpaired electron of the NO ligand with two axial ^{14}N nuclei.[14,15,20]

The EPR spectra of Fe[(F_5)tpp](NO) complexes with N-MeIm (Fig. 4) and with Py (Fig. 5) in glassy toluene at 77 K exhibited distinct three g_1, g_2, and g_3 absorptions and an additional g_{II-1} absorption. The g_{II-1} absorption which was called the $g_?$ absorption[10] has been observed in the EPR spectra of various nitrosylhemoproteins and their model complexes.[10,11,15,20] This absorption was interpreted as a part of signal originating from another species (II), which is different in the structure of Fe–N–O unit from the dominant species (I) showing g_1, g_2, and g_3 absorptions.[20b,25,26] Another part of the g_{II} absorption which is hidden into the g_2 and g_3 absorptions could be resolved in the spectrum at a Q-band frequency.[20b] As shown in the second derivative, the g_2 absorption was highly resolved into a triplet of triplets for ^{14}NO

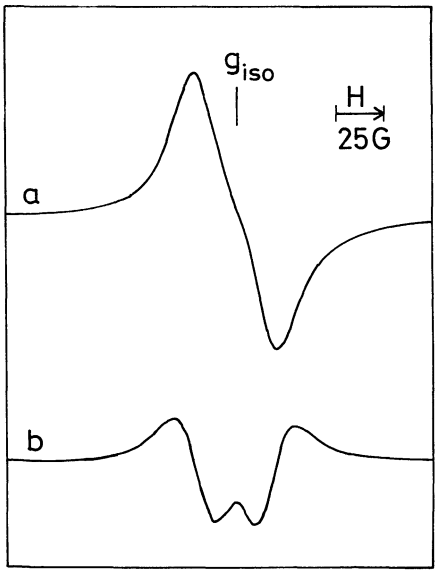

Fig. 3. EPR spectra of Fe[(F_5)tpp](^{14}NO)(N-MeIm) in toluene at room temperature; (a) first- and (b) second-derivative display. Instrument settings are similar to those in Fig. 1.

Table 3. EPR Parameters of Six-Coordinated Nitrosyl(porphyrinato)iron(II) Complexes with 1-Methylimidazole and Pyridine in Toluene at Room Temperature

Porphyrinato ligand	$E_{1/2}$(I)[a]	g_{iso}	
	V	N-MeIm	Py
(p-NMe_2)tpp	−1.660	2.021	2.0445
(p-OCH_3)tpp	−1.593	2.019	2.0366
(p-H)tpp	−1.557	2.017	2.0349
(p-F)tpp	−1.520	2.017	2.0328
(p-CO_2CH_3)tpp	−1.435	2.016	2.0316
(p-NO_2)tpp	−1.340	2.015	2.0299
(F_5)tpp	−1.205	2.014	2.0263

a) See footnote a of Table 1.

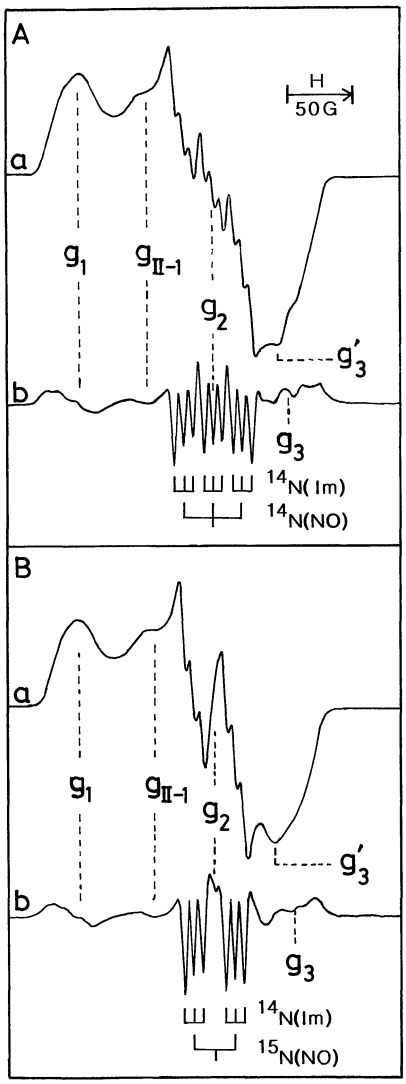

Fig. 4. EPR spectra of (A) Fe[(F_5)tpp](^{14}NO)(N-MeIm) and Fe[(F_5)tpp](^{15}NO)(N-MeIm) in frozen toluene glass at 77 K; (a) first- and (b) second-derivative display. Instrument settings are similar to those in Fig. 2.

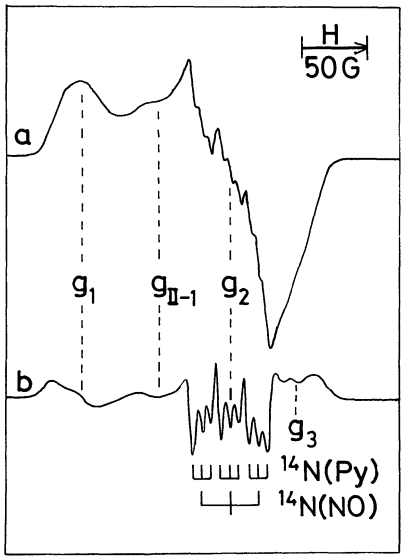

Fig. 5. EPR spectra of Fe[(F_5)tpp](^{14}NO)(Py) in frozen toluene glass at 77 K; (a) first- and (b) second-derivative display. Instrument settings are similar to those in Fig. 1.

complexes and a doublet of triplets for ^{15}NO complexes, while the g_1 and g_3 absorptions were poorly resolved into four lines for ^{14}NO complexes and three lines for ^{15}NO complexes. Thus, although the line shapes of g_1, g_2, and g_3 absorptions were affected by the isotopic substitution, the determination of hyperfine coupling constants in the g_1 and g_3 absorptions was not possible because of the poor resolution and complicated patterns. It has been demonstrated that the lack of resolved hyperfine splittings in the in-plane g_1 and g_3 absorptions results from both the inhomogeneous broadening based on unresolved hyperfine interaction with pyrrole nitrogens and the poor resolution derived from weak hyperfine interaction with two axial nitrogens.[10] Although nitrosyl cytochrome P-450 contains a six-coordinated nitrosyl iron(II) complex, the resolved hyperfine structure derived from an NO nitrogen has been detected on the in-plane absorptions because the axial site trans to NO is occupied by a thiolate sulfur (I=0).[28,29]

Tables 4 and 5 list the EPR parameters of six-coordinated nitrosyl(porphyrinato)iron(II) complexes with 1-methylimidazole and pyridine at 77 K, respectively, together with the first redox potential of free base porphyrins. The g_2 value was determined from the central line position of nine hyperfine lines for ^{14}NO

Table 4. EPR Parameters of Six-Coordinated Nitrosyl(porphyrinato)iron(II) Complexes with 1-Methylimidazole in Toluene at 77 K

Porphyrinato ligand	$E_{2/1}$(I)[a]	g values					Hyperfine coupling const.	
	V	g_1	g_{II-1}	g_2	g_3	g_3'	A_2/G	a_2/G
^{14}NO (p-NMe_2)tpp	−1.660	2.073	2.035	2.0041	1.968	1.974	22.1	6.90
(p-OCH_3)tpp	−1.593	2.072	2.035	2.0038	1.968	1.973	22.1	6.88
(p-H)tpp	−1.557	2.072	2.036	2.0036	1.968	1.974	22.3	7.00
(p-F)tpp	−1.520	2.072	2.035	2.0035	1.966	1.972	22.6	7.03
(p-CO_2CH_3)tpp	−1.435	2.072	2.034	2.0033	1.965	1.972	22.5	7.01
(p-NO_2)tpp	−1.340	2.070	2.033	2.0032	1.965	1.972	22.9	7.12
(F_5)tpp	−1.205	2.067	2.034	2.0027	1.964	1.973	22.8	7.10
^{15}NO (p-H)tpp	−1.660	2.072	2.033	2.0040	1.968	1.975	30.7	6.92
(p-OCH_3)tpp	−1.593	2.072	2.033	2.0039	1.969	1.975	30.6	7.00
(p-H)tpp	−1.557	2.072	2.032	2.0038	1.968	1.975	30.9	7.03
(F_5)tpp	−1.205	2.068	2.032	2.0027	1.965	1.975	31.7	7.10

a) See footnote a of Table 1.

Table 5. EPR Parameters of Six-Coordinated Nitrosyl(porphyrinato)iron(II) Complexes with Pyridine in Toluene at 77 K

Porphyrinato ligand	$E_{2/1}$(I)[a]	g values				Hyperfine coupling const.	
	V	g_1	g_{II-1}	g_2	g_3	A_2/G	a_2/G
^{14}NO (p-NMe_2)tpp	−1.660	2.079	2.041	2.0046	1.977	22.0	6.50
(p-OCH_3)tpp	−1.593	2.078	2.041	2.0043	1.978	21.9	6.50
(p-H)tpp	−1.557	2.078	2.039	2.0042	1.977	21.9	6.58
(p-F)tpp	−1.520	2.079	2.038	2.0041	1.975	22.1	6.66
(p-CO_2CH_3)tpp	−1.435	2.077	2.040	2.0040	1.972	22.1	6.67
(p-NO_2)tpp	−1.340	2.076	2.039	2.0039	1.971	22.0	6.67
(F_5)tpp	−1.205	2.075	2.039	2.0038	1.971	22.1	6.73

a) See footnote a of Table 1.

Table 6. NO Stretching Frequencies of Five-Coordinated Nitrosyl(porphyrinato)iron(II) Complexes and the Six-Coordinated Complexes with 1-Methylimidazole at Room Temperature in cm^{-1}

Porphyrinato ligand	$E_{1/2}(I)$[a]	Five-coordinates[b]	Six-coordinates[c]
(*p*-H)tpp	−1.557	1678	1625
(*p*-CO_2CH_3)tpp	−1.435	1687	1636
(F_5)tpp	−1.205	1703	1650

a) See footnote a of Table 1. b) Solvent; chloroform. c) Solvent; 1-methylimidazole.

complexes or the center of six hyperfine lines for ^{15}NO complexes in the second derivative. The g_3 value was also determined from the center of the g_3 absorption in the second derivative. On the other hand, the g_1 and g_3' values were determined from the extreme position of corresponding absorptions in the first derivative. Because the g_3 absorption overlapped significantly with that of g_2 appearing to be a slight hump or a shoulder, the second-derivative center may be preferable, for the determination of *g*-value, to the extreme position of the first derivative. The hyperfine coupling constants A_2 and a_2 correspond to hyperfine splittings due to the nitrogen nucleus of the NO ligand and the trans axial nitrogenous base, respectively. Both values were obtained from averaged intervals in the second derivative.

NO Stretching Frequencies. It has been demonstrated that the NO stretching frequencies in the IR spectra for five-coordinated Fe(ppixdme)(NO) and the six-coordinated complexes are comparable to those for NO-hemoglobin A in the presence of IHP and in the absence of IHP, respectively, and the binding of IHP to the protein results in cleavage of the proximal histidine to iron bonds in two of four subunits.[16] The NO stretching frequencies of the complexes vary linearly with the solvent polarity[20g] and the basicity of the axial ligand trans to NO.[20h] Thus, the NO stretching frequencies in the IR spectra of nitrosylhemoproteins and those model complexes are a useful measure of the iron-to-NO bond strength and the polarity of heme environments.

Table 6 lists the NO stretching frequencies of three nitrosyl(porphyrinato)iron(II) complexes in chloroform and in 1-methylimidazole. The IR spectra of the complexes in 1-methylimidazole showed a single NO band assigned to that of six-coordinated complexes, though those in neat liquid bases such as pyridine derivatives sometimes show both NO bands of five- and six-coordinated complexes which coexist at equilibrium.[20g] The NO stretching frequencies of five- and six-coordinated complexes with tpp agreed closely with those in KBr pellets (1670 and 1625 cm^{-1})[17] and were slightly higher than those with ppixdme (1675 and 1618 cm^{-1}, respectively).[20g]

Discussion

Introduction of electron-withdrawing or -donating groups at the periphery of a porphyrin results in the shift to positive or negative side, respectively, of the redox potentials of the porphyrin and the corresponding metalloporphyrins.[1,4,30,31] In what follows, the first redox potentials of the free base porphyrin [$E_{1/2}(I)$][31] are used as a measure of the electron-withdrawing or -donating power of the porphyrin peripheral substituents.

Alben and Caughey investigated the cis-effect of porphyrin peripheral substituents on the axial carbonyl ligand in carbonyl(2,4-substituted deuteroporphyrin IX dimethyl esterato)iron(II) complexes with pyridine.[32] They demonstrated that the CO stretching frequency increases with an increase in electron-withdrawing character of the 2,4-substituents. Similarly, the NO stretching frequencies of both five- and six-coordinated complexes in Table 6 markedly and linearly increase as the electron-withdrawing power of the substituents becomes greater. This cis-effect can be explained as follows, in the same manner as that on carbonyl complexes. An increse in the electron-withdrawing power of the porphyrin periphery results in weakening in iron-to-NO π back bonding, followed by a decrease in the electron density of iron d_π and NO π^* orbitals. Consequently, the decreased antibonding character of the NO bond induces the observed increase in the NO stretching frequencies. It is reasonable to predict that this weakening or lengthening of the iron-to-NO bond decreases the displacement of iron from the porphyrin plane toward the NO group, as is generally found in the molecular structure of nitrosyl(porphyrinato)iron(II) complexes.[17]

The changes ($\Delta\nu$) in these stretching frequencies per unit volt in the redox potential of free base porphyrins were estimated by a least-squares method from the linear relation of the NO stretching frequencies in Table 6 and the CO stretching frequencies of carbonyl(2,4-substituted deuteroporphyrin IX dimethyl esterato)iron(II) complexes[32] to $E_{1/2}(I)$ values.[31] The $\Delta\nu$ values thus obtained were 71 cm^{-1} in the five-coordinated NO complexes, 70 cm^{-1} in the six-coordinated NO complexes, and 31 cm^{-1} in the CO complexes. The $\Delta\nu$ values for the NO complexes are about twice that for the CO complexes, suggesting that the π back-bonding of the iron-to-NO ligand is more sensitive to the substitution at porphyrin peripheral side chains than that of the iron-to-

CO ligand.

On the basis of the interpretations for NO stretching frequencies of nitrosyl iron(II) porphyrin complexes, the EPR spectral results of the five- and six-coordinated complexes are analyzed as follows.

Five-Coordinated Complexes. Figures 6 and 7 illustrate the $E_{1/2}$(I) dependence of g_{iso} and A_{iso} values at room temperature and g_3 (or g_z) values at 77 K of five-coordinated nitrosyl(porphyrinato)iron(II) complexes. These g and A_{iso} values increase as $E_{1/2}$(I) becomes positive. (Other g values in Table 2 also exhibit similar tendencies).

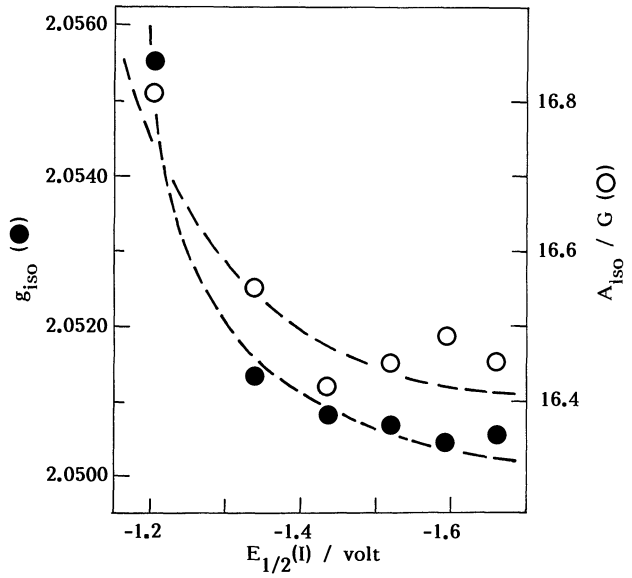

Fig. 6. Relationship between the g_{iso} values of five-coordinated Fe[(p-X)tpp](NO) complexes at room temperature and the $E_{1/2}$(I) values of (p-X)tpp. The trend in the data is indicated by the dashed lines.

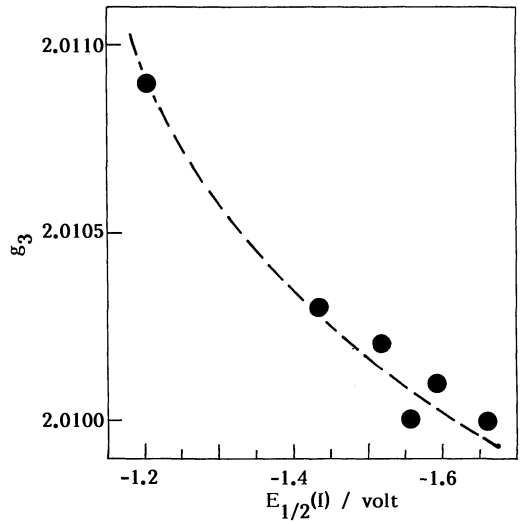

Fig. 7. Relationship between the g_3 values of five-coordinated Fe[(p-X)tpp](NO) complexes at 77 K and the $E_{1/2}$(I) values of (p-X)tpp. The trend in the data is indicated by the dashed line.

The spin density on the nitrogen of NO was estimated to be 2—3% from three hyperfine coupling constants at 77 K according to the method of McNeil et al.[33] Thus, the unpaired electron of an NO group can considerably delocalize to an iron d orbital through the d_{z^2} orbital; the spin-orbit coupling between the iron d orbitals is responsible for the deviation of the g value from a free spin value.[14b,15,34-36]

When the electron density on the iron d_π and NO π^* orbitals decreases with increasing electron-withdrawing character of peripheral substituents as described above, the unpaired electron on d_{z^2} orbital can shift toward the NO nitrogen. This slight increase of the spin density on the NO nitrogen can cause an increase in the hyperfine coupling constants, A_{iso} (Table 1 and Fig. 6) and A_3 (Table 2).

The decrease of the unpaired electron density in the d_{z^2} orbital would be accompanied by a stabilization of the d_{z^2} orbital. The consequent decrease in the separation between the d_{z^2} and d_{xy} levels leads to further spin-orbit coupling,[35] as reflected by an increase in the g values (Figs. 6 and 7).

Six-Coordinated Complexes. Figures 8 and 9 illustrate the $E_{1/2}$(I) dependence of the g_{iso} (at room temperature) and g_2 (at 77 K) values of six-coordinated

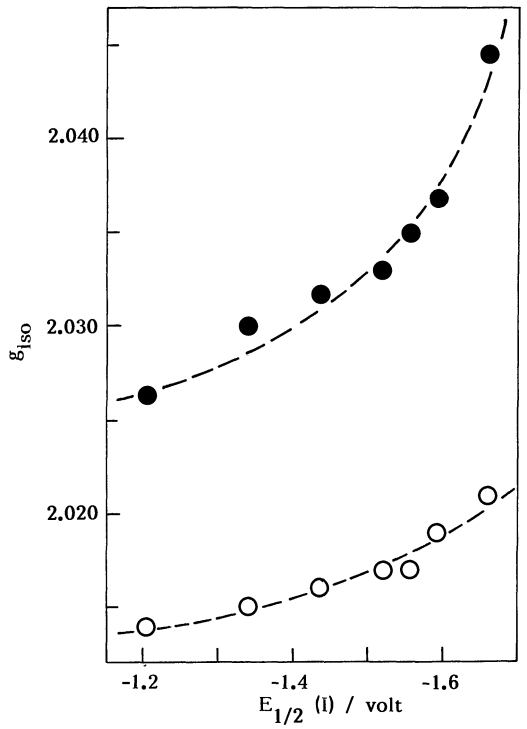

Fig. 8. Relationship between the g_{iso} values of six-coordinated Fe[(p-X)tpp](NO)(Base) complexes at room temperature and the $E_{1/2}$(I) values of (p-X)tpp. Base: ●, pyridine; ○, 1-methylimidazole. The trend in the data is indicated by the dashed lines.

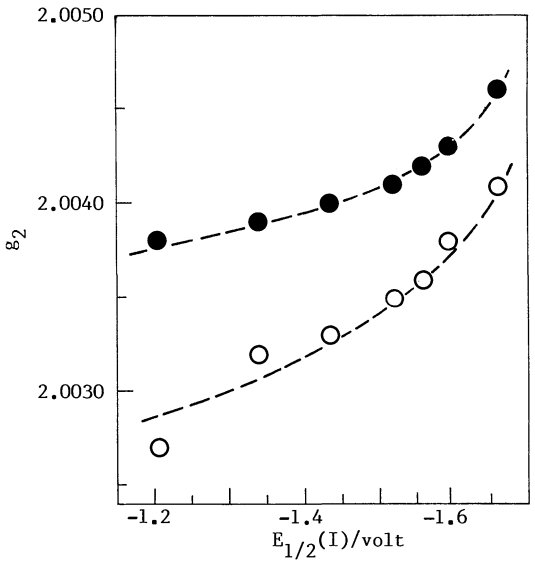

Fig. 9. Relationship between the g_2 values of six-coordinated Fe[(*p*-X)tpp](NO)(Base) complexes at 77 K and the $E_{1/2}$(I) values of (*p*-X)tpp. Base: ●, pyridine; ○, 1-methylimidazole. The trend in the data is indicated by the dashed lines.

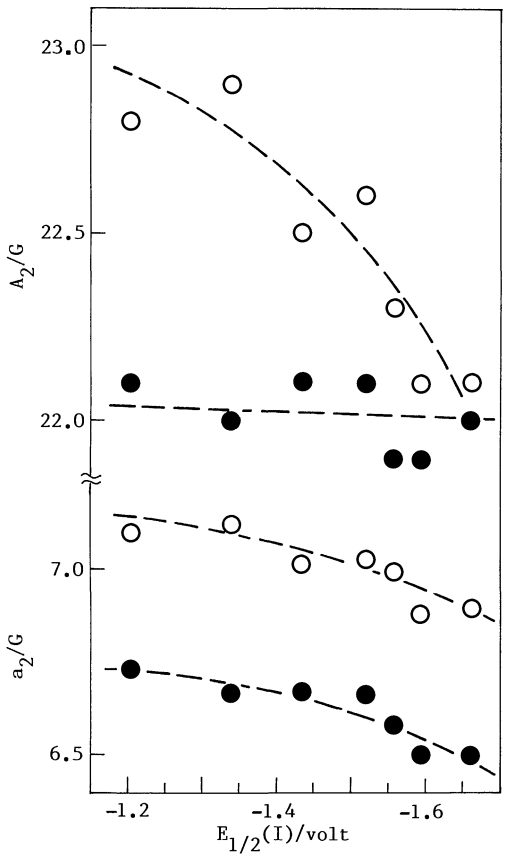

Fig. 10. Relationship between the A_2 and a_2 values of six-coordinated Fe[(*p*-X)tpp](NO)(Base) complexes at 77 K and the $E_{1/2}$(I) values of (*p*-X)tpp. Base: ●, pyridine; ○, 1-methylimidazole. The trend in the data is indicated by the dashed lines.

nitrosyl(porphyrinato)iron(II) complexes with 1-methylimidazole and pyridine. (Other g values in Table 4 also exhibit similar tendencies). As $E_{1/2}$(I) becomes positive, these g values decrease in the complexes with 1-methylimidazole and pyridine, and at the same time, both the g_{iso} value at room temperature and the $(g_1+g_2+g_3)/3$ values at 77 K approach the free spin value. As shown in Fig. 10, the hyperfine coupling constants, A_2 and a_2, increase with a shift of the $E_{1/2}$(I) to the positive side, though the A_2 values of the complexes with pyridine lie within 22.0±0.1 G. Thus, the dependencies of these EPR parameters on $E_{1/2}$(I) for the six-coordinated nitrosyl complexes are in contrast to those for the five-coordinated complexes.

In the six-coordinated nitrosyl complexes as well as the five-coordinated complexes, an enhancement in the electron-withdrawing power of porphyrin peripheral substituents results in a decrease in the electron density on the iron d_π and NO π^* orbitals and the concomitant shift of unpaired electron population on d_{z^2} orbital toward the NO nitrogen. The increase in the unpaired electron population at the NO nitrogen leads to an increase in hyperfine coupling constants. An axial position trans to NO group in the six-coordinated complexes is occupied by 1-methylimidazole or pyridine, which is primarily a σ-donor ligand.[20h,j] Therefore, the above-mentioned decrease in the electron density on iron(II) can be compensated by electron donation from the nitrogenous bases through the d_{z^2} orbital. This donation results in destabilizing the d_{z^2} orbital, which can induce the observed decrease in the g_{iso} (at room temperature) and $(g_1+g_2+g_3)/3$ (at 77 K) values toward the free spin value.

The g_{iso} (at room temperature) and g_2 values (at 77 K) for Fe[(F_5)tpp](NO) complex with 1-methylimidazole are very close to those for the Fe(ppixdme)(NO) complex with imidazolate, which is formed by deprotonation of imidazole and has greater σ-donor ability than the imidazole.[20j] This suggests that the 1-methylimidazole ligand with no dissociable proton in the former complex profoundly donates the σ electron toward iron(II) in a manner similar to the imidazolate in the latter complex.

Consequently, as the electron-withdrawing power of the substituents becomes greater, the Fe–N(nitrogenous base) bond can be strengthened (or shortened) in the six-coordinated complexes, accompanying an increase in NO stretching frequencies as described above. This is inconsistent with the result obtained by the X-ray structural and IR spectral study for six-coordinated nitrosyl(tetraphenylporphyrinato)iron(II) complexes with nitrogenous base that the Fe–N(nitrogenous base) bond lengths decrease with a decrease in the NO stretching frequencies.[17d] Further, when the trans axial ligand in the six-coordinated nitrosyl(porphyrinato)-iron(II) complexes is successively substituted, the g

values increased with an increase in the NO stretching frequencies.[20g] On the other hand, when the side chains of porphyrin periphery in the complexes are also successively substituted, the g values increased with a decrease in the NO stretching frequencies. Such reverse relations between the EPR g values and NO stretching frequencies present a striking contrast between the cis- and trans-effects. This inconsistency or contrast would arise from the fact that the cis-effect on the axial nitrosyl ligand in nitrosyl(porphyrinato)iron(II) complexes is transferred primarily through the porphyrin π and iron d_π orbitals, while the trans-effect is transferred primarily through the iron d_{z^2} orbital.

These findings provide a clue to evaluate the extent of contribution of the cis- and trans-effects to the EPR and IR parmeters in nitrosylhemoproteins and would improve the availability of a nitrosyl ligand as an electronic probe for clarifying the electronic structure and the stereochemistry around the heme.

References

1) W. S. Caughey, "Inorganic Biochemistry," ed by G. L. Eichhorn, Elsevier Scientific, Amsterdam (1973), Vol. 2, pp. 797—831.

2) J. W. Buchler, W. Kokisch, and P. D. Smith, *Struct. Bonding,* **34**, 79 (1978). J. W. Buchler, "The Porphyrins," ed by D. Dolphin, Academic Press, New York (1978), Vol. I, pp. 389—483.

3) a)F. A. Walker, I. A. Barry, V. L. Balke, G. McDermott, M. Z. Wu, and P. F. Linde, *Adv. Chem. Ser.,* **201**, 377 (1982). b)F. A. Walker, D. Reis, and V. L. Balke, *J. Am. Chem. Soc.,* **106**, 6888 (1984). c)V. L. Balke, F. A. Walker, and J. T. West, *J. Am. Chem. Soc.,* **107**, 1226 (1985).

4) K. M. Kadish, "Iron Porphyrins," ed by A. B. P. Lever and H. B. Gray, Addison-Wesley, Reading, MA (1983), Part II, pp. 161—249. K. M. Kadish, *Prog. Inorg. Chem.,* **34**, 435 (1986).

5) C. E. Castro, "The Porphyrins," ed by D. Dolphin, Academic Press, New York (1978), Vol. V, pp. 1—27.

6) C. C. Delwiche, *Ann. Rev. Microbiol.,* **30**, 241 (1976).

7) R. M. J. Palmer, A. G. Ferrige, and S. Moncada, *Nature (London),* **327**, 524 (1987).

8) a)M. K. Johnson, A. Thomson, T. A. Walsh, D. Barber, and C. Greenwood, *Biochem. J.,* **189**, 285 (1980). b)C. D. Cox, Jr., W. J. Payne, and D. V. Dervartanian, *Biochim. Biophys. Acta,* **253**, 290 (1971). c)J. C. Sadana, B. M. Khan, I. V. Fry, and R. Cammack, *Biochem. Cell Biol.,* **64**, 394 (1986). d)L. J. Young, and L. M. Siegel, *Biochemistry,* **27**, 2790 (1988).

9) a)P. A. Craven and F. R. DeRubertis, *Biochim. Biophys. Acta,* **745**, 310 (1983). b)L. J. Ignarro, R. E. Byrns, G. M. Buga, K. S. Wood, and G. Chudhuri, *J. Pharmacol. Exp. Ther.,* **244**, 181 (1988).

10) T. Yonetani, H. Yamamoto, J. E. Erman, J. S. Leigh, and G. H. Reed, *J. Biol. Chem.,* **247**, 2447 (1972).

11) L. C. Dickinson and M. C. R. Symons, *Chem. Soc. Rev.,* **12**, 387 (1983).

12) G. Palmer, "Iron Porphyrins," ed by A. B. P. Lever and H. B. Gray, Addison-Wesley, Reading, MA (1983), Part II, pp. 43—88.

13) T. Yoshimura, S. Suzuki, A. Nakahara, H. Iwasaki, M. Masuko, and T. Matsubara, *Biochemistry,* **25**, 2436 (1986).

14) a)H. Kon, *J. Biol. Chem.,* **243**, 4350 (1968). b) H. Kon and N. Kataoka, *Biochemistry,* **8**, 4757 (1969). c)H. Kon, *Biochim. Biophys. Acta,* **379**, 103 (1975).

15) B. B. Wayland and L. W. Olson, *J. Am. Chem. Soc.,* **96**, 6037 (1974).

16) J. C. Maxwell and W. S. Caughey, *Biochemistry,* **15**, 388 (1976).

17) a)W. R. Scheidt and M. Gouterman, "Iron Porphyrins," ed by A. B. P. Lever and H. B. Gray, Addison-Wesley, Reading, MA (1983), Part I, pp. 89—139. b)W. R. Scheidt and M. E. Frisse, *J. Am. Chem. Soc.,* **97**, 17 (1975). c)W. R. Scheidt and P. L. Piciulo, *J. Am. Chem. Soc.,* **98**, 1913 (1976). d)W. R. Scheidt, A. C. Brinegar, and E. B. Ferro, *J. Am. Chem. Soc.,* **99**, 8032 (1977).

18) D. W. Feng and M. D. Ryan, *Inorg. Chem.,* **26**, 2480 (1987).

19) X. H. Mu and K. M. Kadish, *Inorg. Chem.,* **29**, 1031 (1990).

20) a)T. Yoshimura, *Bull. Chem. Soc. Jpn.,* **51**, 1237 (1978). b)T. Yoshimura, T. Ozaki, Y. Shintani, and H. Watanabe, *Arch. Biochem. Biophys.,* **193**, 301 (1979). c)T. Yoshimura, *Inorg. Chim. Acta,* **46**, 69 (1980). d)T. Yoshimura, *Inorg. Chim. Acta,* **57**, 99 (1982). e)T. Yoshimura, *Arch. Biochem. Biophys.,* **216**, 625 (1982). f)T. Yoshimura, *J. Inorg. Biochem.,* **18**, 263 (1983). g)T. Yoshimura, *Arch. Biochem. Biophys.,* **220**, 167 (1983). h)T. Yoshimura, *Bull. Chem. Soc. Jpn.,* **56**, 2527 (1983). i)T. Yoshimura, *Inorg. Chim. Acta.,* **83**, 17 (1984). j)T. Yoshimura and T. Ozaki, *Arch. Biochem. Biophys.,* **229**, 126 (1984). k)T. Yoshimura, *Inorg. Chem.,* **25**, 688 (1986). l)T. Yoshimura, *Inorg. Chim. Acta,* **125**, L27 (1986). m)T. Yoshimura, *Bull. Chem. Soc. Jpn.,* **60**, 1375 (1987). n)S. Suzuki, T. Yoshimura, A. Nakahara, H. Iwasaki, S. Shidara, and T. Matsubara, *Inorg. Chem.,* **26**, 1006 (1987).

21) T. Yoshimura, *Bull. Chem. Soc. Jpn.,* **63**, 3689 (1990).

22) A. O. Adler, F. R. Longo, F. Kampas, and J. Kim, *J. Inorg. Nucl. Chem.,* **32**, 2443 (1970).

23) H. Rein, O. Ristau, and W. Scheler, *FEBS Lett.,* **24**, 24 (1972).

24) K. Nagai, H. Hori, H. Morimoto, A. Hayashi, and F. Taketa, *Biochemistry,* **18**, 1304 (1979).

25) R. H. Morse and S. I. Chan, *J. Biol. Chem.,* **255**, 7876 (1980).

26) H. Hori, M. Ikeda-Saito, and T. Yoneetani, *J. Biol. Chem.,* **256**, 7849 (1981).

27) a)M. Christahl, and K. Gersonde, *Biophys. Struct. Mech.,* **8**, 271 (1982). b)M. Christahl, H. Twilfer, and K. Gersonde, *Biophys. Struct. Mech.,* **9**, 61 (1982).

28) D. H. O'Keefe, R. E. Ebel, and J. A. Peterson, *J. Biol. Chem.,* **253**, 3509 (1978).

29) M. Tsubaki, A. Hiwatashi, Y. Ichikawa, and H. Hori, *Biochemistry,* **26**, 4527 (1987).

30) J. E. Falk, "Porphyrins and Metalloporphyrins," Elsevier, Amsterdam (1964).

31) P. Worthington, P. Hambright, R. F. X. Williams, J. Reid, C. Burnham, A. Shamin, J. Turay, D. M. Bell, and R. Kirkland, *J. Inorg. Biochem.,* **12**, 281 (1980).

32) J. O. Alben and W. S. Caughey, *Biochemistry,* **7**, 175 (1968).

33) D. A. C. McNeil, J. B. Raynor, and M. C. R. Symons, *J. Chem. Soc.,* **1965**, 410.

34) R. Hoffman, M. M. L. Chen, M. Elian, A. R. Rossi, and

D. M. P. Mingos, *Inorg. Chem.*, **13**, 2666 (1974).
35) T. Nowlin, S. Subramanian, and K. Cohn, *Inorg. Chem.*, **11**, 2907 (1972).
36) G. H. Loew, "Iron Porphyrins," ed by A. B. P. Lever and H. B. Gray, Addison-Wesley, Reading, MA (1983), Part I, pp. 1—87.

Studies of Zone Melting. VII. Distribution Coefficients of the *p*-Nitrophenol-Naphthalene Eutectic System

Hidemoto NOJIMA
Department of Industrial Chemistry, School of Science and Technology, Meiji University, Higashimita, Tama-ku, Kawasaki 214
(Received March 29, 1991)

Synopsis. In a zone-melting experiment the effective and equilibrium distribution coefficients of *p*-nitrophenol in naphthalene have been determined by a method based on a determination of the solute concentration in the terminal one zone length after a single zone pass. The effective distribution coefficient (K_e) is determined by

$$K_e=\frac{2}{Z^*+1}\left\{1-\frac{1}{Z^*-1}\left(\frac{C_s^*}{C_0}-1\right)\right\},$$

where C_0 is the initial solute concentration; C_s^* is the solute concentration described above and $Z^*=L/l-1/2$; L and l denote the specimen and zone lengths, respectively. Further, the equilibrium distribution coefficient (K_o) is obtained as

$$K_o=\frac{2(Z^*-B)}{Z^{*2}-1}.$$

The constant (B) is related to the equation $C_s^*/C_0=-AV+B$, where V is the zone travel rate and A is also a constant. The obtained values of K_e and K_o agree with those determined by a method reported previously by the author.

In zone-melting experiments an effective distribution coefficient is generally determined from either the slope or the intercept of a straight line expressing the relationship between the solute concentration and the distance from the starting end of the zone. In many systems, however, a disagreement between the values obtained from the two procedures described above is found for some reason.[1] In addition, for a eutectic system, it is difficult to exactly determine the effective distribution coefficient; it has a comparatively small value compared to that of a mixed crystal system as well as an equilibrium distribution coefficient. In a previous paper[2] the author reported on a method for determining the effective distribution coefficient of a eutectic mixture by a zone-melting process. Even upon using this method, however, disagreement between the two values described above was inevitable.

In the present work the effective distribution coefficient of *p*-nitrophenol in a naphthalene forming eutectic system was determined by a new method. The obtained result agrees with that determined from the slope of the linear equation reported previously.[2] Also, the equilibrium distribution coefficient derived from the above-mentioned result agrees with the value obtained by the previous method.[2]

Theoretical

Determination of the Effective Distribution Coefficient. Consider a rod-shaped specimen with a length L and a constant cross section comprising a uniform eutectic binary mixture;the solute distribution profile after a single zone pass for such a specimen is shown by Fig. 1,[2] from which it is obvious (from the standpoint of material balance) that areas S_1 and S_2 are the same. The line $\overline{C_1C_2}$ is expressed by Eq. 1,[2]

$$C_s=C_0\left(K_e+K_e\frac{x}{l}\right), \tag{1}$$

where C_0 is the initial uniform concentration of the solute; C_s is the solute concentration at a distance x from the top of the specimen after a single zone pass; l is the zone length and K_e is the effective distribution coefficient. Equation 1 is valid for all but the last one zone length. From the conservation of material and refering to Fig. 1,

$$(Z'-1)C_0-\int_0^{Z'-1}C_0(K_e+K_eZ)\mathrm{d}Z=C_s^*-C_0. \tag{2}$$

In Eq. 2, x/l is replaced by Z, i.e. $Z\equiv x/l$; $Z'\equiv L/l$ and C_s^* is the solute concentration in the terminal one zone length after a single zone pass. The effective distribution coefficient is obtained from Eq. 2 as

$$K_e=\frac{2}{Z^*+1}\left\{1-\frac{1}{Z^*-1}\left(\frac{C_s^*}{C_0}-1\right)\right\}. \tag{3}$$

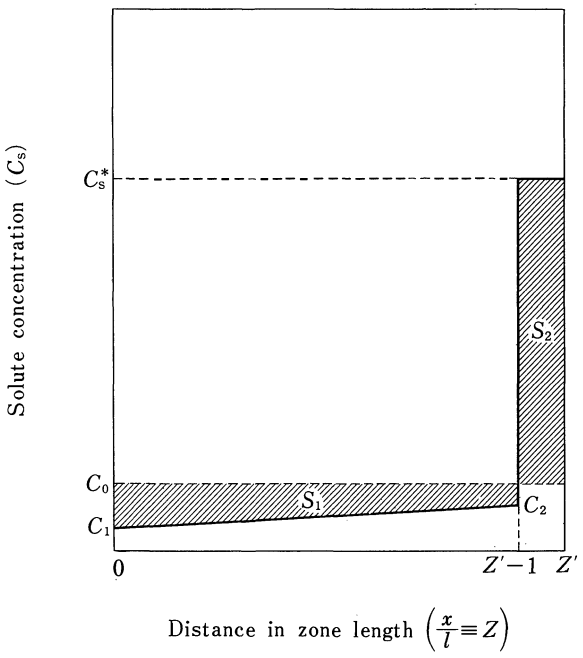

Fig. 1. Schematic diagram representing the material balance after a single zone pass for a eutectic mixture.

Since the solute concentration is determined experimentally as the average value in one zone length, Z' in Eq. 2 can be replaced by $Z^*=L/l-1/2$ in Eq. 3.

Determination of the Equilibrium Distribution Coefficient. In order to find the equilibrium distribution coefficient (K_o) on the basis of Eq. 3, it is necessary for K_e to be expressed as a function of the zone travel rate or freezing rate (V). It is well known for many systems that the relationship among K_e, K_o and V can be expressed by the following Burton–Prim–Slichter's equation:[3]

$$\ln\left(\frac{1}{K_e}-1\right)=\ln\left(\frac{1}{K_o}-1\right)-\frac{\delta}{D}V, \tag{4}$$

where D and δ are the diffusion coefficient of the solute and the diffusion layer thichness, respectively. Equation 4 is rewritten as

$$\frac{(1-K_o)K_e}{(1-K_e)K_o}=\exp\left(\frac{\delta}{D}V\right). \tag{5}$$

The conditions that $K_o \ll 1$ and $K_e \ll 1$ are valid for a eutectic system.[2] Equation 5 can thus be rewritten as

$$\frac{K_e}{K_o}=\exp\left(\frac{\delta}{D}V\right), \tag{6}$$

which, if $\delta V \ll D$, reduces to[#]

$$K_e=K_o+aV, \tag{7}$$

where $a \equiv K_o\delta/D$. From Eqs. 3 and 7, the following equation is obtained:

$$\frac{C_s^*}{C_0}=-AV+B, \tag{8}$$

where

$$A=\frac{a(Z^{*2}-1)}{2} \tag{9}$$

and

$$B=-\frac{K_o(Z^{*2}-1)}{2}+Z^*. \tag{10}$$

Constants A and B are the slope and intercept of Eq. 8 respectively, expressing the dependence of C_s^*/C_0 on the zone travel rate (V). The equilibrium distribution coefficient (K_o) can be given from Eq. 10 as

$$K_o=\frac{2(Z^*-B)}{Z^{*2}-1}. \tag{11}$$

Experimental

Materials. Commercial p-nitrophenol was purified by zone refining for 50 passes and commercial naphthalene was purified by one recrystallization from a benzene solution. Two naphthalene mixtures containing 0.5 and 1.0 wt% of p-nitrophenol were charged in a 30 cm long in Pyrex tubes with an inner diameter of 0.7 cm and outer diameter of 0.9 cm. The tubes were then sealed off under a dry nitrogen atmosphere of about 0.9 atm.

Procedures. The zone-melting experiments were carried out under the following conditions: zone travel rates of 2.47, 2.96, 5.43, 9.21, and 12.80 mm h^{-1}; 1 zone pass; a zone length of 3 cm and a zone temperature of 90±1 °C. The samples after a zone pass were cut into ten fractions, each 3 cm long and equal to the zone length. The samples from each fraction were dissolved in ethanol; color was then developed by adding a small amount of aqueous sodium hydroxide solution. The concentration of p-nitrophenol was determined spectrophotometrically by using a Hitachi 100-01 spectrophotometer at a wavelength of 400 nm.

Results and Discussion

Determination of the Effective Distribution Coefficient. As an example, the distribution of p-nitrophenol along a sample initially containing 1.0 wt% of this compound after a single zone pass at 2.96 mm h^{-1} is shown in Fig. 2; it represents the same profile as in Fig. 1, except that the ordinate is indicated by C_s/C_0 instead of C_s. The effective distribution coefficient was obtained by substituting the observed value of C_s^*/C_0 into Eq. 3. The relationship between the effective distribution coefficient and zone travel rate is shown in Fig. 3, together with the values obtained by a previously reported method,[2] i.e. values from the slope of Eq. 1. The values obtained by these two methods agreed with

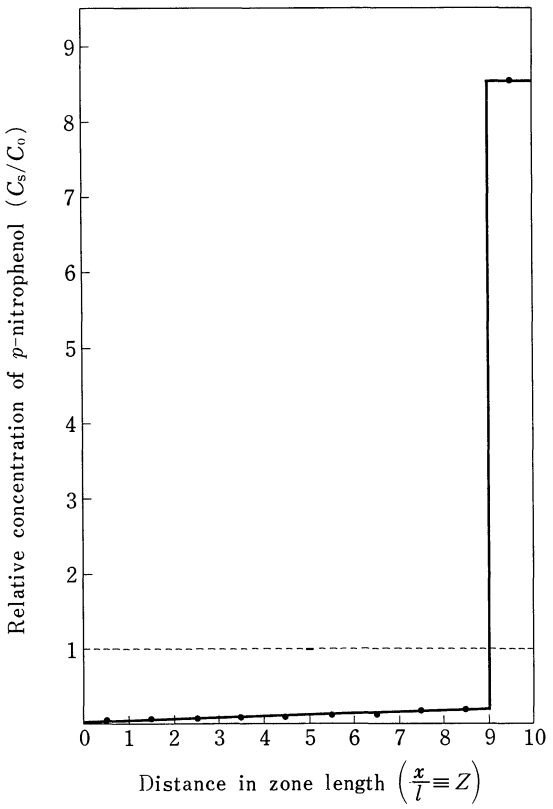

Fig. 2. Distribution of p-nitrophenol after a single zone pass at 2.96 mm h^{-1}; 1.0 wt% of p-nitrophenol.

[#] $\exp(x)=1+x+\frac{x^2}{2!}+\cdots\cdots$, $x \equiv \delta V/D$ and the squares and higher power of x can be neglected for the present case.

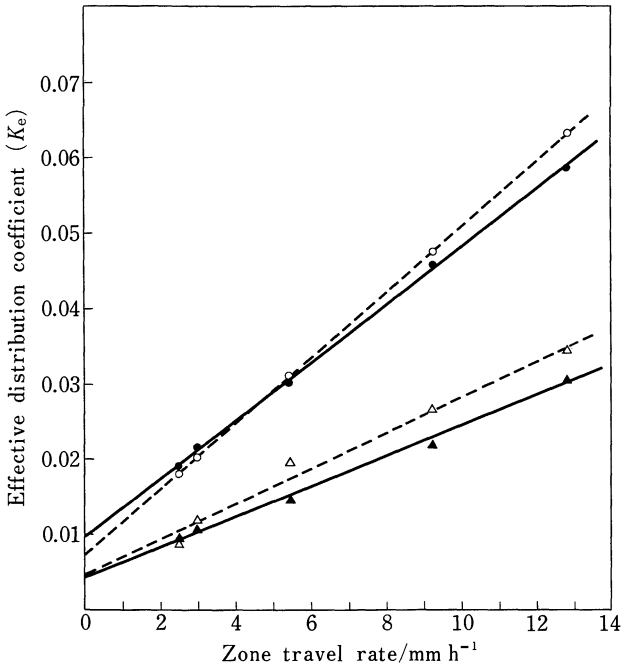

Fig. 3. Relationship between the effective distribution coefficient and the zone travel rate. ●: values for 1.0 wt% of *p*-nitrophenol determined by Eq. 3. ○: values for 1.0 wt% of *p*-nitrophenol determined from the slope of Eq. 1. ▲: values for 0.5 wt% of *p*-nitrophenol determined by Eq. 3. △: values for 0.5 wt% of *p*-nitrophenol determined from the slope of Eq. 1.

Table 1. Equilibrium Distribution Coefficients Determined by Three Methods

Methods employed	Equilibrium distribution coefficient, 0.5 wt% of *p*-nitrophenol	Equilibrium distribution coefficient, 1.0 wt% of *p*-nitrophenol
From Eqs. 8 and 11	4.26×10^{-3}	7.39×10^{-3}
From the intercepts of solid lines in Fig 3	4.23×10^{-3}	9.73×10^{-3}
From the intercepts of dotted lines in Fig. 3	4.51×10^{-3}	7.46×10^{-3}

each other, as is shown in Fig. 3; it is thus obvious that Eq. 7 is valid for this experiment.

Determination of the Equilibrium Distribution Coefficient. It is evident that Eq. 8 is valid for this experiment, as is shown in Fig. 4. By substituting the values of the intercepts of the straight lines in Fig. 4 into Eq. 11, the equilibrium distribution coefficients were evaluated. The obtained values are shown in Table 1 together with those obtained from the intercepts of the straight lines in Fig. 3, as described in a previous paper;[2] these values agree with each other.

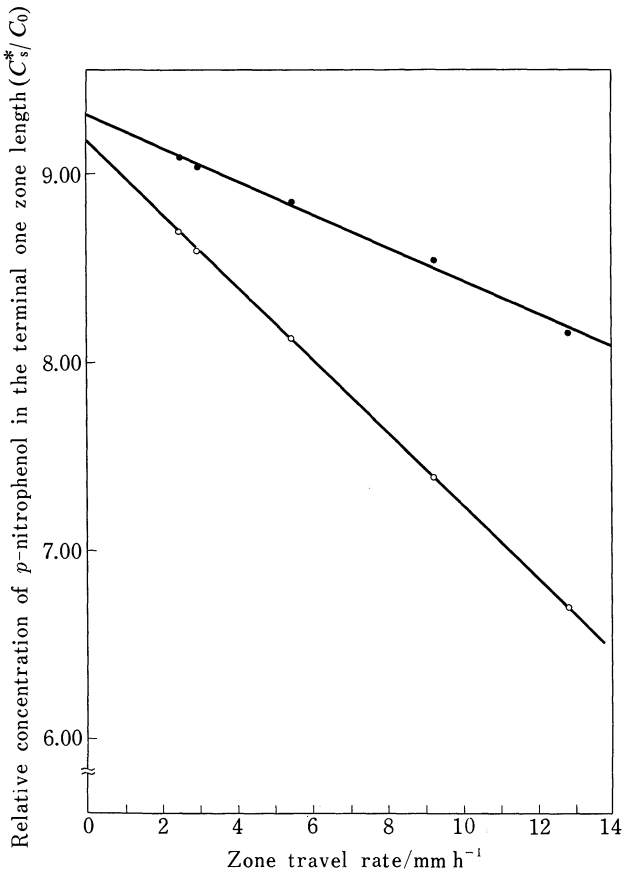

Fig. 4. Relationship between the relative concentration of *p*-nitrophenol in the terminal one zone length and the zone travel rate. ○: 1.0 wt% of *p*-nitrophenol. ●: 0.5 wt% of *p*-nitrophenol.

Conclusion

The effective distribution coefficient of *p*-nitrophenol in naphthalene could be determined by the present method, which agrees with that determined from the slope of Eq. 1. Also, the equilibrium distribution coefficient agrees with the value obtained by a previously reported method.[2] In the present method, both the effective and equilibrium distribution coefficients are determined from the solute concentration in the terminal one zone length, in which the enrichment of the solute is so large that the concentration can be accurately determined even for a specimen with a low solute concentration, in contrast with conventional methods.

The author wishes to thank the Institute of Science and Technology Meiji University for financial support.

References

1) W. R. Wilcox, "Fractional Solidification," ed by M. Zief and W. R. Wilcox, Marcel Dekker, New York (1967), Vol. 1, p. 90.
2) H. Nojima, *Nippon Kagaku Kaishi,* **1985**, 145.
3) J. A. Burton, R. C. Prim, and W. P. Slichter, *J. Chem. Phys.*, **21**, 1987 (1953).

Dielectric Properties of Poly(methylphenylsilylene) under Humidity in the Kilohertz Range[1)]

Hiroshi AWANO,* Takayoshi IWAI,† and Hiroji OHIGASHI
Department of Materials Science and Engineering, Yamagata University, Jonan, Yonezawa 992
† Consumer Products Engineering Laboratory, Toshiba Corporation, Shinsugita-cho, Isogo-ku, Yokohama 235
(Received April 11, 1991)

Synopsis. The capacitance and dielectric loss tangent of poly(methylphenylsilylene) thin films were measured under various humidities over the frequency range 0.1—1000 kHz. In the high-humidity range, both the quantities increase with decreasing frequency. The existence of an anomalously low-frequency relaxation (lower than 0.1 kHz) is suggested in which the adsorbed water molecules are involved.

Although the electrical properties of organopolysilanes have become of great interest,[2)] few studies have been carried out on the dielectric properties. In the present work, thin films of poly(methylphenylsilylene) (PMPS) were prepared and their dielectric properties measured under various humidities. An anomalous relaxation of the adsorbed water molecules has been found.

PMPS was prepared by condensation polymerization of dichloromethylphenylsilane based on the Wurtz–Fittig reaction, and purified by reprecipitation from toluene with hexane. A toluene solution of the precipitate was washed several times. Gel permeation chromatography in THF resulted in $\overline{M}_n=9.07\times10^3$ and $\overline{M}_w/\overline{M}_n=1.75$ (reduced to polystyrene). The specimen used had a sandwich structure with a gas-permeating upper electrode. A PMPS thin film with a thickness of 2—3 μm was formed by casting on a glass substrate having a couple of Cr–Au thin-film lower electrodes with a thickness of ca. 100 nm. A gas-permeating Au thin film with a thickness of 30—40 nm was formed on the PMPS film by dc sputtering. Both the capacitance and dielectric loss tangent of the film were measured with a Yokogawa Hewlett-Packard 4192A LF impedance analyzer. The relative humidity was controlled using a Shin-ei SRH-1M humidity generator. Each measurement was carried out after the specimen had been kept standing under the desired temperature and humidity for at least 20 min.

Figure 1 shows the humidity dependence of the capacitance of PMPS at 25 °C. The humidity dependence varies remarkably with the frequency. When the humidity is increased from 10 to 90%, the capacitance doubles at 1 kHz, but it increases by a maximum of 2% at 100 kHz. Moreover, the hysteresis observed at low frequencies is not ignorable, suggesting that the adsorption and desorption of water molecules are somewhat slow. Figure 2 shows the humidity dependences of both the capacitance and the loss tangent of PMPS at 10 kHz. The extent to which these quantities vary with the relative humidity becomes greater as the temperature is raised.

In order to discuss the mechanism through which these dielectric properties vary with the humidity, it may be

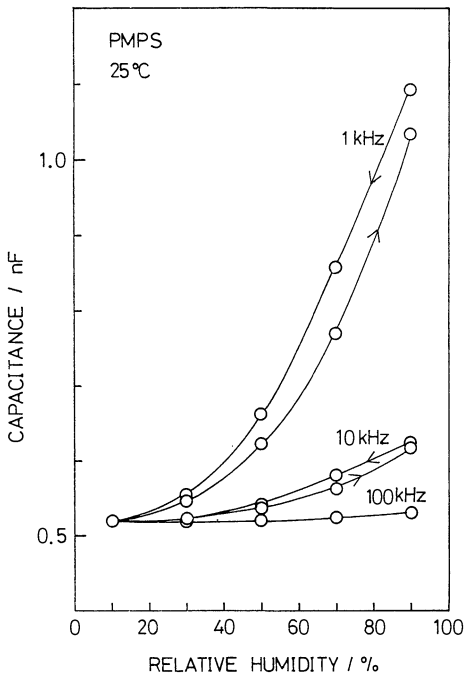

Fig. 1. Humidity dependence of the capacitance of a PMPS film at 25 °C.

convenient to use the absolute humidity or water vapor pressure rather than the relative humidity. Figure 3 shows plots of the capacitance and loss tangent against the logarithm of the water vapor pressure. Thus, as shown in the figure, all of the curves have almost the same shape, and the curves shift to the right with increasing temperature. If we regard these curves as being some kind of adsorption isotherm, the equilibrium constants of adsorption at 10 and 25 °C are greater by factors of 1.9 and 3.7, respectively, than at 40 °C. From these data, the enthalpy change of the adsorption of water has been estimated to be -32 kJ mol^{-1}. This value is near to the energy of hydrogen bonding of water ca. 40 kJ mol^{-1} (per water molecule).[3)] This suggests that the adsorption of water on a PMPS surface might involve the formation of small clusters, each of which comprises several water molecules.

Figure 4 shows the frequency dependence of both the capacitance and the loss tangent of PMPS at 25 °C in the humidity range 10 to 70%. Neither of the quantities vary with the frequency at low humidities, indicating that no relaxation exists in the kilohertz range, since the PMPS is in a glass state. At high humidities, on the

other hand, both the capacitance and loss tangent significantly increase with decreasing frequency, indicating the existence of relaxation in the lower frequency range.

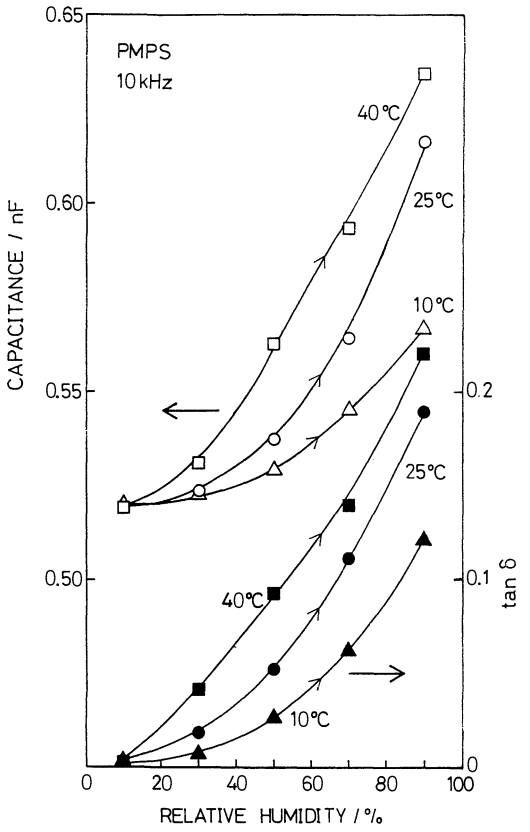

Fig. 2. Humidity dependence of both the capacitance and the dielectric loss tangent of a PMPS film at 10 kHz.

Relaxation in a range lower than kilohertz seems quite anomalous. It seems to be difficult to explain this phenomenon in terms of the usual state of water molecules. For example:

(a) Regarding ice, the relaxation time of Ice I has been reported to be about 0.2 ms.[4]

(b) Regarding the hydration of biopolymers, the rotational correlation time of water in hydrated collagen, from NMR studies, is 10^{-7} s at 25 °C.[5] From dielectric measurements, the fraction of water molecules is strongly bound to collagen with residence times on the order of 10^{-6} s.[6]

(c) In contrast to PMPS, polyimide has a capacitance that is almost invariant in the kilohertz range and a loss tangent that increases with increasing frequency above 10^5 Hz. The latter tendency becomes important as the humidity is increased.[7] This suggests that the relaxation time of the water molecules adsorbed on the polyimide is far shorter than 10^{-5} s.

Thus, a relaxation time of adsorbed water longer than 10^{-2} s is so anomalous. We can thus attribute such a long-term relaxation to hydrogen bonding between adsorbed water and the terminal hydroxyl groups of PMPS: the formation of hydrogen bonding would induce a large polarization in the glassy polymer, which can be related to long-term relaxation. The induction of polarization might involve sigma-conjugation in the silicon backbone of PMPS. We have obtained the following experimental result: the dielectric properties are almost independent of how many times the toluene solution containing PMPS has been washed with water after the synthesis of PMPS. The above result suggests that the contribution of some hydrophilic or ionic impurities to the dielectric properties must be minor. The long-range relaxation under humidity can therefore

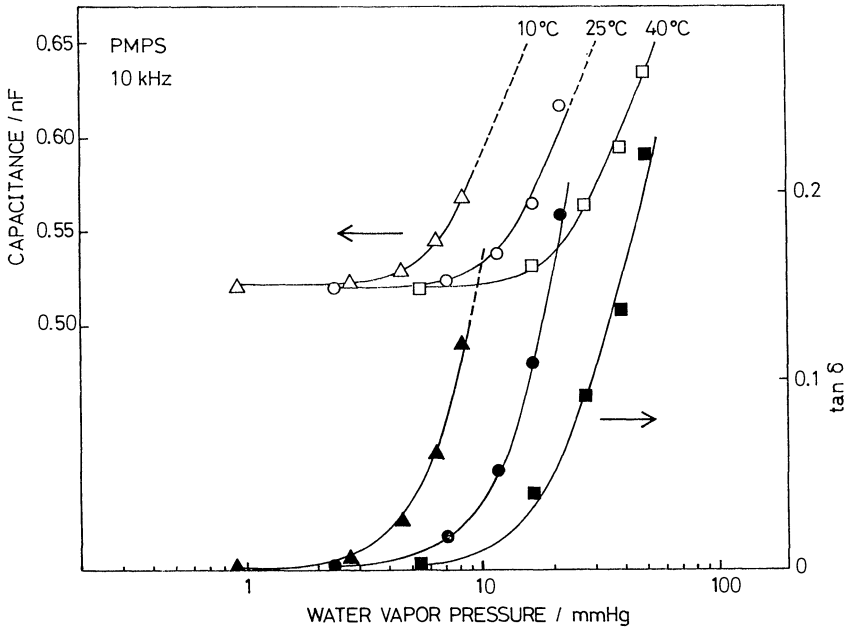

Fig. 3. Plots of the capacitance and the dielectric loss tangent of a PMPS film against the logarithm of water vapor pressure.

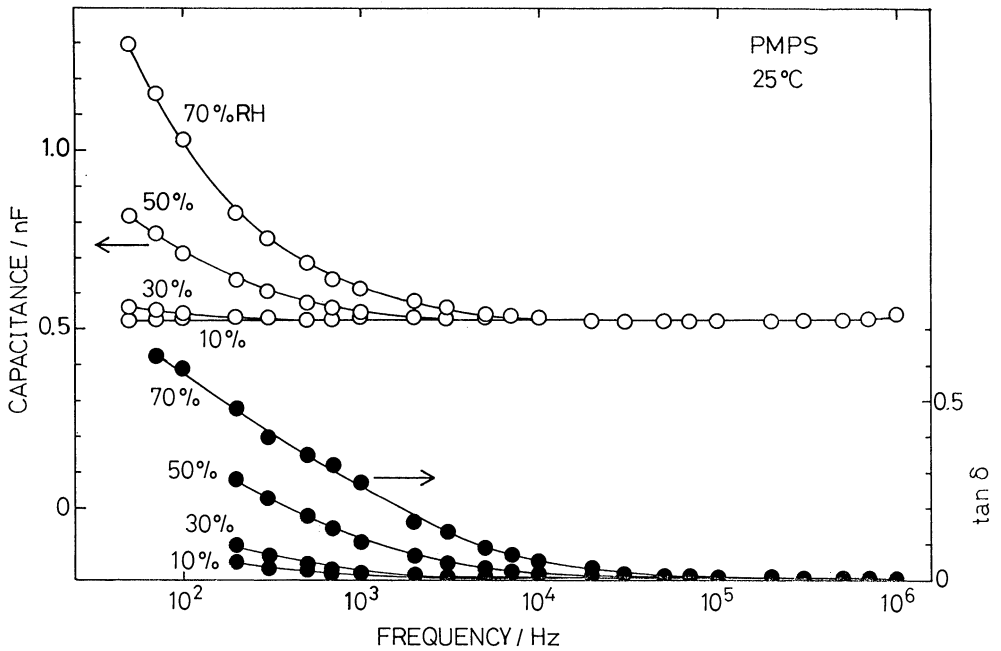

Fig. 4. Frequency dependence of both the capacitance and the dielectric loss tangent of a PMPS film at 25°C.

be attributed to hydrogen bonding between water and the terminal hydroxyl groups of PMPS, rather than to hydrophilic or ionic impurities.

The authors are grateful to Professor K. Ono of Tohoku University for valuable discussions.

References

1) Partially presented at the 39th Polymer Symposium of the Society of Polymer Science, Japan, Nagoya, October 1990.

2) As a review paper, R. D. Miller and J. Michl, *Chem. Rev.*, **89**, 1359 (1989).

3) L. Pauling, "The Nature of the Chemical Bond," Cornell University Press, Ithaca (1960), Chap. 12.

4) G. J. Wilson, R. K. Chan, D. W. Davidson, and E. Whalley, *J. Chem. Phys.*, **43**, 2384 (1965).

5) C. Migchelson and H. J. C. Berendsen, *J. Chem. Phys.*, **59**, 296 (1973).

6) J. R. Grigera, F. Vericat, K. Hallenga, and H. J. C. Berendsen, *Biopolymers*, **18**, 35 (1979).

7) T. Iwai, unpublished work.

Copper(II)-Rare Earth(III) (Ln=La, Gd, Lu) Binuclear Complexes of Bis[2-(3-carboxysalicylidene)aminoethyl]amine: Characterization and Specific Binding of Amino Alcohols

Masatomi SAKAMOTO,* Masayuki HASHIMURA, Kimihiro MATSUKI, Kunihiko TAJIMA,† Kazuhiko ISHIZU,† and Hisashi ŌKAWA††

Department of Industrial Chemistry, Faculty of Engineering, Ehime University, Bunkyo-cho, Matsuyama 790

† Department of Chemistry, Faculty of Science, Ehime University, Bunkyo-cho, Matsuyama 790

†† Department of Chemistry, Faculty of Science, Kyushu University, Hakozaki, Higashi-ku, Fukuoka 812

(Received March 7, 1991)

Synopsis. Heterometal complexes, $[CuLn(fsadien)(NO_3)(H_2O)_n]\cdot(H_2O)_{5-n}$ (Ln=La, Gd, or Lu), have been synthesized and characterized, where H_4fsadien denotes bis[2-(3-carboxysalicylidene)aminoethyl]amine. Based on electronic absorption and CD spectra, it was suggested that amino alcohols were specifically bound to the Cu(II)-Ln(III) heterometal center, through the nitrogen to the copper(II) ion and through the oxygen to the rare earth(III) ion.

Recently we have reported that the copper(II)–rare earth(III) and cobalt(II)–rare earth(III) heterometal complexes of *N*,*N*′-bis(3-carboxysalicylidene)ethylenediamine (H_4fsaen, Fig. 1a)[1,2] show a unique "selective solvations" associated with copper or rare earth ion, depending upon the the nature of the solvent. That is, in pyridine the solvation occurs at the copper site, whereas in dimethyl sulfoxide or *N*,*N*-dimethylformamide the solvation occurs exclusively at the rare earth site. This selective solvation has been extended to specific binding of amino alcohols on the copper(II)–rare earth(III) or the cobalt(II)–rare earth(III) heterometal center.[2,3]

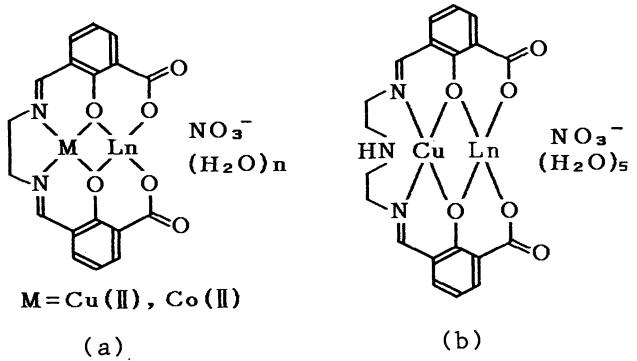

Fig. 1. Chemical structures of copper(II)- or cobalt(II)–rare earth(III) complexes of H_4fsaen (a) and copper(II)–rare earth(III) complexes of H_4fsadien (b).

In this work we have synthesized and characterized copper(II)–rare earth(III) complexes of bis[2-(3-carboxysalicylidene)aminoethyl]amine (H_4fsadien, Fig. 1b), in which copper(II) and rare earth(III) ions are bound at the inside coordination site (N_3O_2-site) and the outside coordination site (O_4-site), respectively. The specific binding of amino alcohols on the Cu(II)–Ln(III) center has been investigated on the basis of electronic absorption and CD spectra.

Experimental

Syntheses. 3-Formylsalicylic acid was prepared after the method of Duff and Bills.[4] Mononuclear copper(II) complex, $[Cu(H_2\ fsadien)]\cdot H_2O$ was synthesized according to the method reported by Casellato et al.[5]

Binuclear Complexes, $[CuLn(fsadien)(NO_3)(H_2O)_n]\cdot(H_2O)_{5-n}$(Ln=La, Gd, or Lu): A methanol solution (10 cm³) of lithium hydroxide monohydrate (2 mmol) was added to a suspension of the mononuclear copper(II) complex, $[Cu(H_2\ fsadien)]\cdot H_2O$ (1 mmol), in methanol (50 cm³). Further addition of methanol (240 cm³) and heating gave a clear solution. To the resulting solution was added a methanol solution (5 cm³) of a rare earth(III) nitrate hydrate (1 mmol), and the mixture was refluxed under stirring for 3 h. After the solution was concentrated to 50 cm³ under reduced pressure, resulted greenish crystals were collected on a glass filter, washed with methanol and then diethyl ether, and dried in the open air. the yield was about 60 %.

Analytical results are given in Table 1.

Measurements. Elemental analyses of carbon, hydrogen, and nitrogen were obtained at the Advanced Instrumentation Center for Chemical Analysis of Ehime University. Metal contents were determined by the EDTA titration of mixed nitrates, which were prepared by dissolving the ignition residue

Table 1. Elemental Analyses of Complexes

Complex	Found/% (Calcd/%)				
	C	H	N	Cu	Ln
$CuLa(fsadien)(NO_3)(H_2O)_5$	31.90 (32.03)	3.17 (3.63)	7.49 (7.47)	8.45 (8.47)	18.38 (18.52)
$CuGd(fsadien)(NO_3)(H_2O)_5$	31.29 (31.27)	3.22 (3.54)	7.38 (7.29)	8.28 (8.27)	21.30 (20.47)
$CuLu(fsadien)(NO_3)(H_2O)_5$	29.88 (30.46)	3.20 (3.45)	7.30 (7,10)	8.66 (8.06)	23.31 (22.19)

(mixed oxides) of the complex in HNO_3. Infrared spectra were measured with a JASCO IR-G Spectrometer on KBr disks, nujol mulls, or hexachlorobutadiene mulls. Absorption and reflectance spectra were obtained with a Hewlett-Packard 8452A Spectrophotometer and an Otsuka Electronics MCPD 1000 Spectrophotometer, respectively. The CD spectra were recorded on a JASCO J-20 Automatic Recording Spectropolarimeter.

Results and Discussion

Infrared spectra of the Cu(II)–Ln(III) complexes are similar to each other. The ν (C=O) vibration (ca. 1670 cm^{-1}) and ν (O–H) vibration (3000—2000 cm^{-1}) of the chelated carboxyl groups are observed for H_4fsadien and [Cu(H_2fsadien)]·H_2O, but those bands disappear on the Cu(II)–Ln(III) complex formation. Instead, the Cu(II)–Ln(III) complexes show the carboxylate vibration at 1535—1550 cm^{-1}. These observations suggest the incorporation of a rare earth(III) ion at the O_4-site. The vibrations due to the nitrate ion are observed as split bands at ca. 1430 and 1380 cm^{-1}, suggesting the bidentate coordination of the nitrate ion.[6] The ν (O–H) vibration of the water molecules appears as a broad band at 3300—3400 cm^{-1} when measured on nujol mulls or hexachlorobutadiene mulls. It is presumed that the water molecules coordinate to the rare earth ion to afford a coordination number larger than six.

Reflectance spectra are shown in Fig. 2. The spectrum of [Cu(H_2fsadien)]·H_2O exhibits a band maximum at ca. 14.3×10^3 cm^{-1} and a shoulder at ca. 17.5×10^3 cm^{-1}, suggesting a trigonal-bipyramidal surrounding about the copper(II) ion[7] with the three nitrogen atoms of the diethylenetriamine moiety and the two phenolic oxygen atoms. On the other hand, the Cu(II)–La(III), Cu(II)–Gd(III), and Cu(II)–Lu(III) complexes show an unresolved broad band at ca. 17.1×10^3, ca. 16.7×10^3, and ca. 16.5×10^3 cm^{-1}, respectively, suggesting no coordination of the central nitrogen of the lateral bridge to the copper(II) to give a square planar configuration around the copper. The model considerations support that the coordination of central nitrogen of the lateral bridge to the copper is difficult when the two carboxylate groups coordinate to a rare earth ion.

The interaction of substrates on the heteronuclear center has been studied spectroscopically by adding various substrates to a DMF solution of the Cu(II)–La(III) complex. Typical absorption spectra are given in Fig. 3 and the numerical data are summarized in Table 2.

In general, the axial coordination of a substrate to planar copper(II) results in a red shift of the d–d band

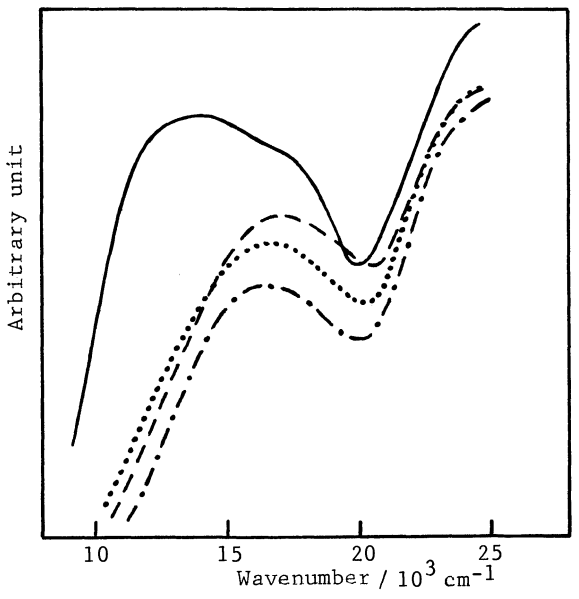

Fig. 2. Electronic spectra in solid state. (——): [Cu(H_2fsadien)]·H_2O; (———): [CuLa(fsadien)(NO_3)(H_2O)$_n$]·(H_2O)$_{5-n}$; (·····): [CuGd(fsadien)(NO_3)(H_2O)$_n$]·(H_2O)$_{5-n}$; (—·—): [CuLu(fsadien)(NO_3)(H_2O)$_n$]·(H_2O)$_{5-n}$.

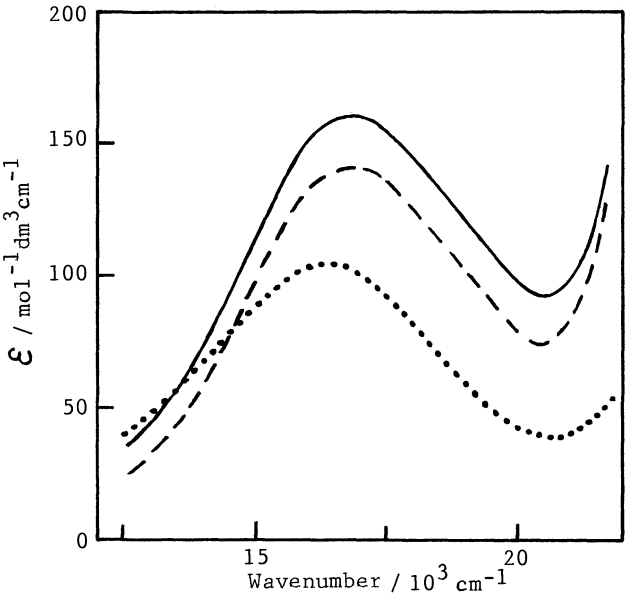

Fig. 3. Absorption spectra in DMF. Concentration of the Cu(II)–La(III) binuclear complex is 5×10^{-3} mol dm^{-3}. (——): with no substrate; (———): with 1,2-ethanediol (1 mol dm^{-3}); (·····): with 2-aminoethanol (1 mol dm^{-3}).

Table 2. The d–d Band Absorption Maxima of Cu(II)–La(III) Binuclear Complex in DMF Solution of Various Substrates[a]

Substrate	$\nu_{max}/10^3$ cm^{-1}
No substrate	16.72
Methanol[b]	16.72
Ethanol[b]	16.72
1,2-Ethanediol[c]	16.72
2-Aminoethanol[c]	16.29
3-Amino-1-propanol[c]	16.29
1-Aminopropane[c]	16.08

a) Concentration of the Cu(II)–La(III) complex is 5×10^{-3} mol dm^{-3}. b) Concentration is 5 mol dm^{-3}. c) Concentration is 1 mol dm^{-3}.

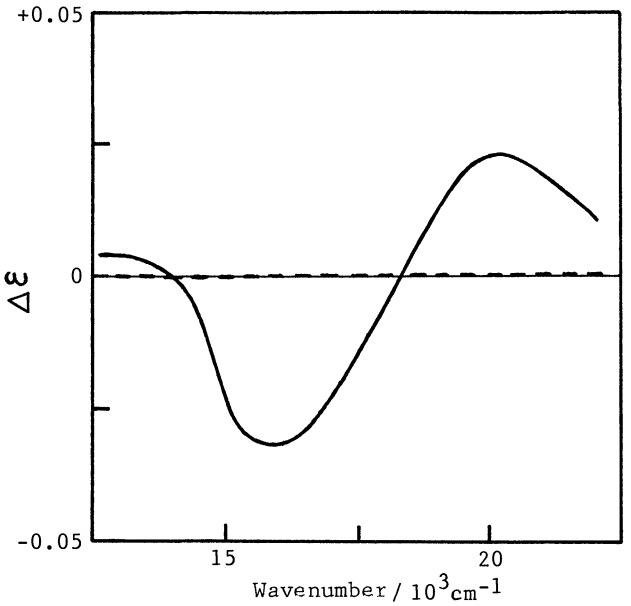

Fig. 4. The CD spectra in DMF. Concentration of the Cu(II)–La(III) binuclear complex is 5×10^{-3} mol dm^{-3}. (——): with (*R*)-(−)-1-amino-2-propanol (1 mol dm^{-3}); (———): with (*S*)-(+)-1,2-propanediol (1 mol dm^{-3}).

maximum. This is indeed the case when 1-aminopropane is added to a DMF solution of the Cu(II)–La(III) complex. A similar red shift of the d–d band was observed when 2-aminoethanol or 3-amino-1-propanol was added as the substrate. On the other hand, such a spectral change was not seen when alcohols (methanol, ethanol, or 1,2-ethanediol) were added as substrates. Obviously amines coordinate to the axial site of the copper(II) center whereas alcohols do not.

It is unclear from the above results if alcohols are bound at the lanthanum(III) center or not, but our CD spectral investigations using a chiral amino alcohol as the substrate has revealed the ligating interaction of alcohols with the lanthanum(III) center. Figure 4 shows the CD spectrum of the Cu(II)–La(III) complex when (*R*)-(−)-1-amino-2-propanol was added as the substrate. The significant circular dichroism induced at the d–d band of the copper(II) clearly demonstrates that the free rotation of the amino alcohol is hindered with respect to the Cu–N bond owing to the following reasons; (i)the hydroxyl group of the amino alcohol may be directly bound to the lanthanum(III) ion or (ii)the hydroxyl group may be involved in hydrogen bonding with DMF or H_2O molecules coordinated to the lanthanum(III) ion discussed previously.[2] Such a CD activity was not observed in the visible region when (*S*)-(+)-1,2-propanediol was added as the substrate (see Fig. 4). This is quite understandable since the chiral diol is captured on the lanthanum(III) center probably as a bidentate ligand. Thus, the present work is another illustration of specific binding of amino alcohols on d–f heterodinuclear center.

References

1) M. Sakamoto, M. Takagi, T. Ishimori, and H. Ōkawa, *Bull. Chem. Soc. Jpn.*, **61**, 1613 (1988).

2) Y. Aratake, H. Okawa, E. Asato, H. Sakiyama, M. Kodera, S. Kida, and M. Sakamoto, *J. Chem. Soc., Dalton Trans.*, **1990**, 2941.

3) M. Sakamoto, T. Ishimori, and H. Ōkawa, *Bull. Chem. Soc. Jpn.*, **61**, 3319 (1988).

4) J. C. Duff and E. J. Bills, *J. Chem. Soc.*, **1932**, 1987.

5) U. Casellato, D. Fregona, S. Sitran, S. Tamburini, and P. A. Vigato, *Inorg. Chim. Acta*, **95**, 309 (1984).

6) K. Nakamoto, "Infrared and Raman Spectra of Inorganic and Coordination Compounds," 4th ed, John Wiley & Sons, New York (1986), pp. 254—257.

7) M. Ciampolini and N. Nardi, *Inorg. Chem.*, **5**, 41 (1966); M. Ciampolini, *Struct. Bonding (Berlin)*, **6**, 52 (1969); G. Albertin, E. Bordignon, and A. A. Orio, *Inorg. Chem.*, **14**, 1411(1975); M. Duggan, N. Ray, B. Hathaway, G. Tomlinson, P. Brint, andK. Pelin, *J. Chem. Soc., Dalton Trans.*, **1980**, 1342; A. W. Addison, H. M. J. Hendriks, J. Reedijk, and L. K. Thompson, *Inorg. Chem.*, **20**, 103 (1981); K. D. Karlin, J. C. Hayes, S. Juen, J. P. Hutchinson, and J. Zubieta, *Inorg. Chem.*, **21**, 4106 (1982).

A Pd(II)-Cu(II) Catalyst for the Kjeldahl Analysis of Nitrogen in Pyridines

Shigero OISHI* and Hiroshi KOMATSUZAKI
Department of Chemistry, School of Hygienic Sciences, Kitasato University,
Kitasato, Sagamihara, Kanagawa 228
(Received April 1, 1991)

Synopsis. A serious drawback of the Kjeldahl analysis of organic nitrogen, that pyridine derivatives were difficult to degrade to ammonia, was overcome by use of a Pd(II)–Cu(II) catalyst. Three hours of digestion at approximately 320 °C using the catalyst were found to be sufficient for quantitative liberation of ammonia from pyridines.

Nitrogen determination with the Kjeldahl method does not require expensive devices nor specialized techniques, and is precise and accurate.[1] Nevertheless, it has been almost ignored as a means of organic elemental analysis. One reason for this may be because of difficult degradation of pyridine derivatives to ammonia. Mixtures of mercury and selenium were used as catalysts for the degradation.[2-6] These required a long digestion period and were not widely used because of environmental concerns. Recently, the use of hydrogen peroxide as an oxidizing reagent was reported to greatly shorten the digestion period.[6-8] However, it does not seem easy nor safe to handle 50% hydrogen peroxide at high temperatures.

By analogy to the high reactivity of palladium(II) in organometallic chemistry such as the metallation of a phenyl ring,[9] we expected that Pd(II) could provide a means to break down an inert pyridine nucleus.

Experimental

Reagents. Amidosulfuric acid of standard grade for volumetric analysis, acetanilide of standard grade for elemental analysis, and other inorganic reagents of superior grade were purchased from Wako Pure Chemical Ind. 4,4′-Dimethyl-2,2′-bipyridine and other reagent grade organic materials were purchased from Aldrich Chemical Co. and Tokyo Kasei Kogyo Co., respectively. All chemicals were used as received.

Procedure. A standard procedure for a general micro-Kjeldahl method[1] was followed with some modifications. A 10—11 mg portion of sample was weighed into a digestion flask using a small glass boat. Five hundred milligrams of potassium sulfate, catalyst, and 2 ml of concentrated sulfuric acid were added to the flask. The digestion using an electric furnace (Model ME-6, Shibata Co.) was carried out with gentle refluxing of sulfuric acid at approximately 320 °C. After 6 min of distillation of ammonia from the alkalinized mixture into 5 ml of 2% aqueous boric acid containing Methyl Red-Bromocresol Green indicator, the green solution obtained was titrated with 0.01 mol dm^{-3} aqueous amidosulfuric acid to a blue color, which was the same color as a blank run.

Results and Discussion

Figure 1 shows the dependence of nitrogen content found in 4,4′-dimethyl-2,2′-bipyridine upon the degradation time in the case of 2 mg of $PdCl_2$ as a catalyst. Diverse results at 4 h of digestion seemed to depend on the sample position on the furnace; efficiencies of heating were slightly different from place to place among six locations for digestion flasks. Six hours of digestion assured a good reproducibility, but were too long considering the period needed for preparation, distillation, and titration; 3 h may be a practical time. We tried to use a second catalyst to activate palladium to shorten the period of digestion.

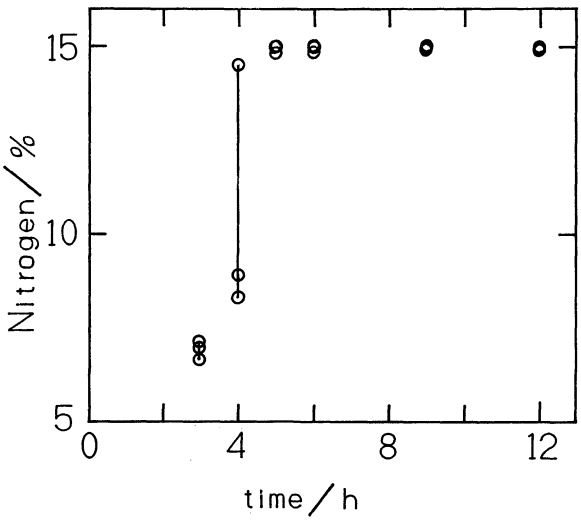

Fig. 1. Dependence of nitrogen content found for 4,4′-dimethyl-2,2′-bipyridine on the digestion time using 2 mg of $PdCl_2$ as a catalyst.

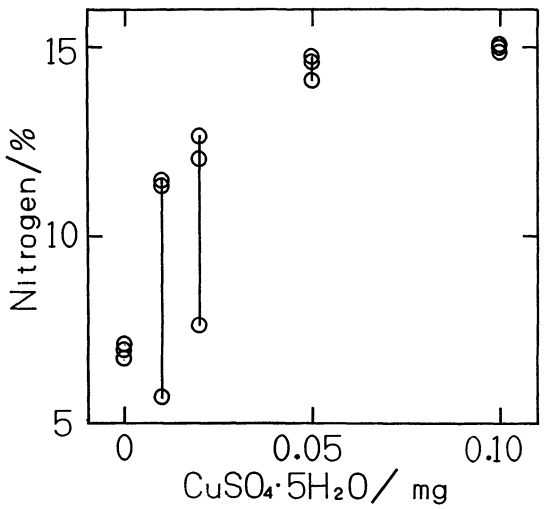

Fig. 2. Nitrogen content found for 4,4′-dimethyl-2,2′-bipyridine by digestion with 2 mg of $PdCl_2$ for 3 h using various amounts of $CuSO_4 \cdot 5H_2O$.

In the Wacker process, Pd(0), formed by the reaction of Pd(II) with ethylene to produce acetaldehyde, is oxidized to Pd(II) by oxygen with the mediation of a Cu(I)–Cu(II) redox pair.[10] By analogy to this, the effects of $CuSO_4 \cdot 5H_2O$ were examined by digesting for 3 h using 2 mg of $PdCl_2$. A very small amount of Cu(II) was found to be effective as shown in Fig. 2.

Figure 3 shows the dependence of nitrogen content found at 3 h of digestion in the presence of 30 mg of $CuSO_4 \cdot 5H_2O$ upon the amount of $PdCl_2$. Even when a large amount of $CuSO_4 \cdot 5H_2O$ was used, a quantity of $PdCl_2$ larger than 1.5 mg was found to be necessary to attain complete liberation of ammonia.

As shown in Fig. 4, the 3 h digestion time could not be shortened even by using both 2 mg of $PdCl_2$ and 30 mg of $CuSO_4 \cdot 5H_2O$.

Several pyridine derivatives, tris(2,2′-bipyridine)iron-(II) diperchlorate, and tris(2,2′-bipyridine)ruthenium(II) diperchlorate were analyzed for nitrogen under the conditions optimized above, namely, 3 h of digestion using 500 mg of K_2SO_4, 2 ml of H_2SO_4, and 30 mg of the Pd–Cu catalyst prepared previously by mixing 2 parts by weight of $PdCl_2$ with 30 parts by weight of $CuSO_4 \cdot 5H_2O$ using an agate mortar. In these experiments, three positions on the furnace were used for samples and the other three were used for reference acetanilide. Two flasks for blank runs were heated during the distillation of ammonia from the sample and reference. For reference acetanilide, we obtained 98.84±0.26% of ammonia, with a 95% confidence limit in 32 experiments, using the Pd–Cu catalyst. The difference from 100% was due to losses by manipulation. Values in Table 1 have been corrected for these losses by using values obtained in the reference runs which were carried out simultaneously. The effect of the Pd–Cu catalyst can be seen as significant. In the absence of the catalyst, no ammonia was liberated from pyridine ring. Interestingly, this appeared even in the cases of nicotinamide and cinchonine, where half of the nitrogen content could be detected, corresponding to the nitrogen of the carbamoyl group and the quinuclidine structure, respectively. In the presence of the catalyst, however, a quantitative amount of ammonia was generated, idicating complete degradation of the pyridine ring.

Although $[Ru(bpy)_3]^{2+}$ appeared to degrade by the appearance of digestion, no nitrogen was detected. The fact that the digestion of ammonium sulfate as a substrate in the presence of $RuCl_3 \cdot H_2O$ gave no ammonia in the distillate indicated that oxidation of ammonia to some volatile species was catalyzed by Ru. Platinum was also

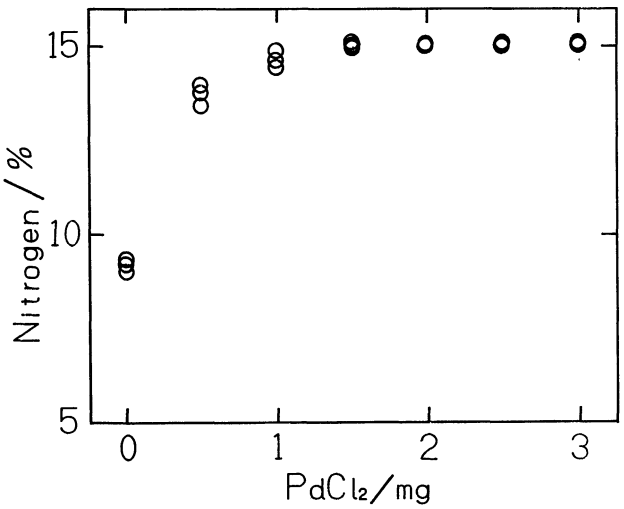

Fig. 3. Nitrogen content found for 4,4′-dimethyl-2,2′-bipyridine by digestion with 30 mg of $CuSO_4 \cdot 5H_2O$ for 3 h using various amounts of $PdCl_2$.

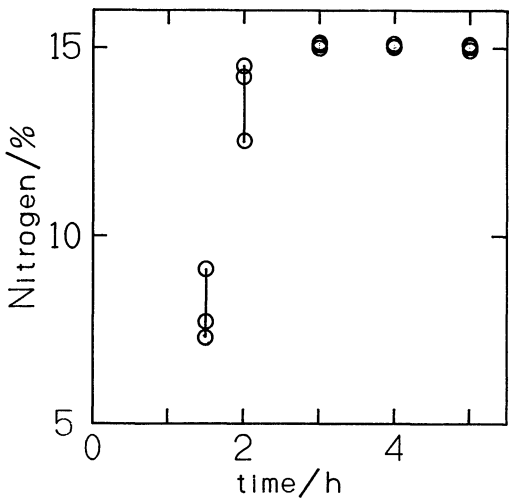

Fig. 4. Dependence of nitrogen content found for 4,4′-dimethyl-2,2′-bipyridine on the digestion time using 2 mg of $PdCl_2$ and 30 mg of $CuSO_4 \cdot 5H_2O$.

Table 1. Kjeldahl Analysis of Nitrogen in Pyridines with and without Use of the Pd–Cu Catalyst

Pyridine derivative	Formula	Nitrogen content/%		
		Calcd	Found	
			without	with
4,4′-Dimethyl-2,2′-bipyridine	$C_{12}H_{12}N_2$	15.20	0.80	15.16
2,2′-Bipyridine (bpy)	$C_{10}H_8N_2$	17.94	0.89	17.97
Acridine	$C_{13}H_9N$	7.82	0.67	7.86
Nicotinamide	$C_6H_6N_2O$	22.94	11.83	22.96
Cinchonine	$C_{19}H_{22}N_2O$	9.52	4.58	9.51
$Fe(bpy)_3(ClO_4)_2$	$FeC_{30}H_{24}N_6Cl_2O_8$	11.62	3.45	11.65
$Ru(bpy)_3(ClO_4)_2$	$RuC_{30}H_{24}N_6Cl_2O_8$	10.94	0.06	0

found to have this catalytic effect. Palladium selectively attacked a pyridine ring to liberate ammonia and did not oxidize ammonia further.

The authors thank Professor Shozo Masuda, Tokyo Science University, for valuable discussions and suggestions.

References

1) G. Ingram, "Method of Organic Elemental Microanalysis," Chapman Hall, London (1962), pp. 144—160.
2) R. B. Bradstreet, "The Kjeldahl Method for Organic Nitrogen," Academic Press, New York (1965), pp. 121—125.
3) Reviews published every two years by T. S. Ma et al. in *Anal. Chem.*, i. e., T. S. Ma, *Anal. Chem.*, **62**, 78R(1990); T. S. Ma, *Anal. Chem.*, **60**, 175R(1988); T. S. Ma and C. Y. Wang, *Anal. Chem.*, **58**, 144R(1986), etc.
4) R. L. Shirley and W. W. Becker, *Ind. Eng. Chem., Anal. Ed.*, **17**, 437(1945).
5) C. O. Willets, M. R. Coe, and C. L. Ogg, *J. Assoc. Off. Agric. Chem.*, **32**, 118(1949).
6) K. L. Watkins, T. L. Veum, and G. F. Krause, *J. Assoc. Off. Anal. Chem.*, **70**, 410(1987).
7) C. H. Hach, S. V. Brayton, and A. B. Kopelove, *J. Agric. Food Chem.*, **33**, 1117(1985).
8) C. C. Hach, B. K. Bowden, A. B. Kopelove, and S. V. Brayton, *J. Assoc. Off. Anal. Chem.*, **70**, 783(1987).
9) See, for example, P. M. Maitlis, P. Espinet, and M. J. H. Russell, "Comprehensive Organometallic Chemistry," Pergamon Press, Oxford(1982), Vol. 6, pp. 279—349.
10) J. Tsuji, *Synthesis*, **1984**, 369.

Thermal Decomposition of Barium Amidotriphosphate $Ba_2P_3O_9NH_2 \cdot 3.5H_2O$

Atsushi TAKENAKA,* Hiromu YAMASAKI, Itaru MOTOOKA,† and Hiroyuki NARIAI†
Department of Industrial Chemistry, Yonago National College of Technology,
4448, Hikona-cho, Yonago, Tottori 683
† Department of Chemistry, Faculty of General Education, Kobe University,
Tsurukabuto, Nada-ku, Kobe 657
(Received April 15, 1991)

Synopsis. Barium amidotriphosphate ($Ba_2P_3O_9NH_2 \cdot 3.5H_2O$) was heated at 5 K min^{-1} in streams of dried air, humid air, and dried hydrogen chloride. *cyclo*-Triphosphates were not observed in any products, unlike in the pyrolysis of $(NH_4)_4P_3O_9NH_2 \cdot H_2O$. Water vapor or hydrogen chloride hydrolyzed phosphorus–nitrogen and phosphorus–oxygen bonds of the products.

As a new type of fertilizer and as flame-proofing materials, interest has been focused on inorganic phosphates with phosphorus–nitrogen bonds.[1] Of all the phosphorus–nitrogen phosphates, amidotriphosphates are known to be formed by ammonolyses of *cyclo*-triphosphates in aqueous solution.[2-4]

In the preceding work, we studied the thermal decomposition of ammonium amidotriphosphate $(NH_4)_4P_3O_9NH_2 \cdot H_2O$.[5] The amidotriphosphate cyclized again to form a kind of ammonium *cyclo*-triphosphate.

Although the thermal products of inorganic phosphates partially depend on their constituent cation,[6] it was not clear whether amidotriphosphates other than $(NH_4)_4P_3O_9NH_2 \cdot H_2O$ were thermally changed to *cyclo*-triphosphates or not. As barium amidotriphosphate ($Ba_2P_3O_9NH_2 \cdot 3.5H_2O$) could be obtained easily from $(NH_4)_4P_3O_9NH_2 \cdot H_2O$, we have studied the thermal decomposition of $Ba_2P_3O_9NH_2 \cdot 3.5H_2O$ in the present work, especially with interest in the formation of *cyclo*-triphosphates. Since hydrogen chloride acted as an accelerating agent for the cyclization of $(NH_4)_4P_3O_9NH_2 \cdot H_2O$,[5] $Ba_2P_3O_9NH_2 \cdot 3.5H_2O$ was also heated in a stream of dried hydrogen chloride as well as streams of dried air and humid air.

Experimental

Eight mmol (2.617 g) of ammonium amidotriphosphate ($(NH_4)_4P_3O_9NH_2 \cdot H_2O$)[3] was dissolved in 30 cm^3 of distilled water. This solution was mixed with 7 cm^3 of a 0.5 mol dm^{-3} barium chloride aqueous solution. The precipitate was removed by filtration. A 25-cm^3 portion of the barium chloride solution was added to the filtrate. The product was filtered off and washed sequentially with water, acetone, and ether, and then air-dried. The product was characterized by HPLC-FIA and by determinations of nitrogen,[5] barium,[7] and phosphorus.[8] Ammonium nitrogen[5] was not detected in the product. Found: P, 15.17; Ba, 43.78; N, 2.24%. Calcd for $Ba_2P_3O_9NH_2 \cdot 3.5H_2O$: P, 15.73; Ba, 46.50; N, 2.37%. Fifteen mg of the product was dissolved in 20 cm^3 of a 0.1 mol dm^{-3} aqueous tetrasodium ethylenediaminetetraacetate solution. As soon as it was diluted to 500 cm^3 with distilled water, the solution was analyzed with an HPLC-FIA system.

About 13 mg of the product was placed in a platinum pan. Thermal analyses (TG-DTA) were carried out at 5 K min^{-1} in stationary air and in a stream of dried air at 50 cm^3 min^{-1}. The dried air used was prepared by the passage of air through molecular sieves.[5]

A 0.1-g portion of the product was heated in a cylindrical electric furnace at the same rate of 5 K min^{-1} as that used in TG-DTA. A stream of humid air (relative humidity 90% at 25 °C) at 50 cm^3 min^{-1} and a stream of dried hydrogen chloride were prepared as reported in Ref. 5. Before heating, the electric furnace was purged with a volume of these gases about twice the volume of the furnace. As soon as the sample reached the required temperature, it was taken out and cooled to room temperature in a desiccator, and immediately analyzed by HPLC-FIA, X-ray diffractometry, and IR spectrophotometry. HPLC-FIA was performed as mentioned above. X-Ray diffraction patterns were obtained by the use of nickel-filtered Cu $K\alpha$ radiation. IR spectra were measured with a KBr disc method.

Results and Discussion

Thermal Decomposition in Stationary Air. Figure 1 shows thermal analysis (TG-DTA) measured in stationary air and the DTA measured in a stream of dried air at 50 cm^3 min^{-1}. The endothermic peaks at 60 °C and at 90 °C in stationary air overlapped to appear as one peak at about 70 °C in a stream of dried atmosphere, which implied that the endothermic peaks were caused by the elimination of bound water (the water of crystallization).

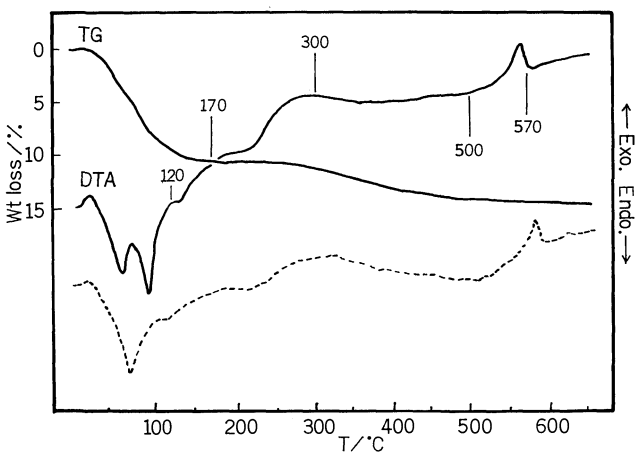

Fig. 1. Thermal analyses of $Ba_2P_3O_9NH_2 \cdot 3.5H_2O$ measured at a heating rate of 5 K min^{-1}. Solid line (—): TG and DTA measured in stationary air, dashed line (---): DTA measured in a stream of dried air.

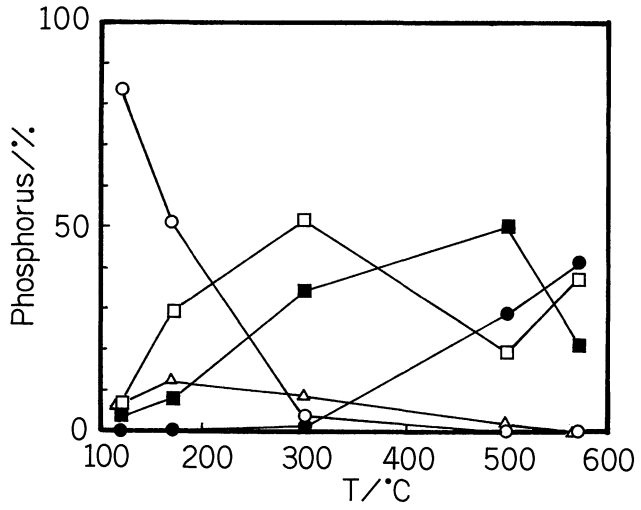

Fig. 2. Changes in amounts of phosphates in the samples heated at 5 K min^{-1} in stationary air. ○: amidotri-, ●: poly-, □: mono-, di-, and tri-, ■: oligo- (chain length=4—11), △: other (the phosphates were thought to have short or middle chain structures with one or several phosphorus-nitrogen bonds).

Figure 2 presents the percentage of phosphorus atoms present as amidotri-, from mono- to tri-, oligo- (chain length=4—12), and polyphosphates in the products obtained by heating to the temperatures indicated on the DTA curve of Fig. 1. Several peaks other than those of the above phosphate ions appeared before the peak of octaphosphate on the HPLC-FIA chromatograms. On the basis of their retention times, they were thought to be short or middle chain phosphates with one or several phosphorus–nitrogen bonds. They are also plotted in a group in Fig. 2 and expressed as "other".

Figure 3 shows the X-ray diffraction patterns of the products. The sample heated to 570 °C contained a crystalline material. The sample mainly consisted of poly- and triphosphates. Its X-ray diffraction data did not agree with any data of barium polyphosphates reported on the JCPDS cards. Therefore, perhaps, the crystalline material might have been a kind of triphosphate.

Figure 4 shows that absorptions at 1475 and at 1428 cm^{-1} appeared on the IR spectrum of the sample heated to 170 °C. Corbridge and Lowe suggested that two absorptions near 1400 cm^{-1} could be ascribed to the ammonium ion.[9] Therefore, the product heated to

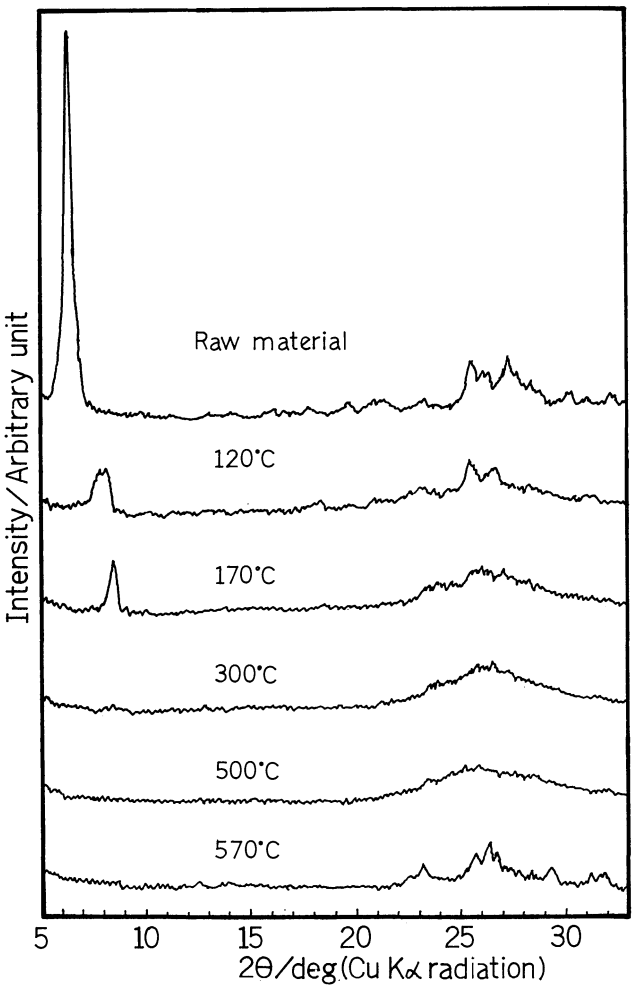

Fig. 3. X-Ray diffraction patterns of the samples heated at 5 K min^{-1} in stationary air.

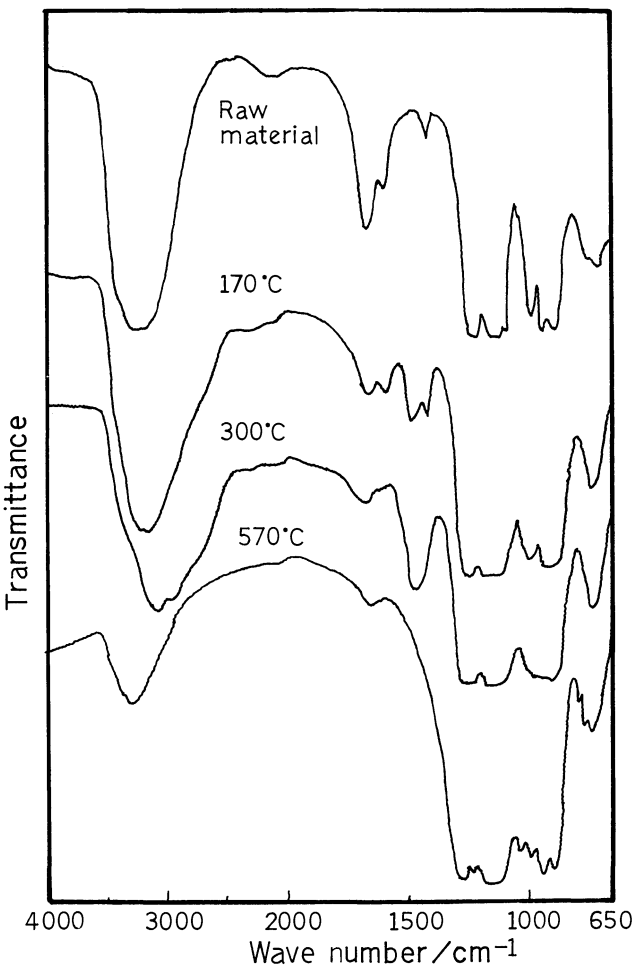

Fig. 4. IR spectra of $Ba_2P_3O_9NH_2 \cdot 3.5H_2O$ and the samples heated at 5 K min^{-1} to 170, 300, and 570 °C in stationary air.

Table 1. Effect of the Atmosphere on the Phosphates Composition in the Products Obtained by Heating of $Ba_2P_3O_9NH_2 \cdot 3.5H_2O$

T/°C	Atmosphere	Composition/P%				
		amidotri-	mono-, di-, and tri-	oligo-[a]	poly-	other[b]
120	Dried air	69.7	9.9	6.2	6.3	8.0
	Humid air	72.3	10.1	5.0	7.3	5.4
	Dried HCl	—	78.9	12.4	8.6	—
170	Dried air	44.0	23.8	13.8	4.5	14.0
	Humid air	40.8	31.5	10.8	4.5	12.3
	Dried HCl	—	88.5	5.1	6.4	—
300	Dried air	6.4	38.7	29.1	4.7	21.0
	Humid air	—	55.1	36.8	4.0	4.1
500	Dried air	—	24.5	47.2	17.7	10.6
	Humid air	—	18.6	52.1	25.3	4.0
570	Dried air	—	19.5	38.6	36.3	5.6
	Humid air	—	37.5	24.9	35.2	2.4

a) The chain length was from four to twelve. b) These anions were thought to have short or middle chain structures with one or several phosphorus-nitrogen bonds.

170 °C contained ammonium ions, which must have been formed from amino groups. The spectrum of $Ba_2P_3O_9NH_2 \cdot 3.5H_2O$ showed a small absorption at 1602 cm^{-1}. The absorption probably arose from amino groups.[9,10] It disappeared in the IR spectrum of the sample heated to 300 °C, which agreed with the result that amidotriphosphate ions were almost cleaved below 300 °C (Fig. 2).

Effect of Atmosphere on the Thermal Decomposition. The samples were heated at 5 K min^{-1} to the respective temperatures in three different atmospheres. Table 1 shows the percentage of phosphorus atoms present as the respective phosphates in the thermal products. *cyclo*-Triphosphates were observed in the thermal decomposition of ammonium amidotriphosphate ($(NH_4)_4P_3O_9NH_2 \cdot H_2O$), as reported in the preceding paper.[5] Hydrogen chloride accelerated the cyclization of the amidotriphosphate to the *cyclo*-triphosphate at lower temperatures. However, in the present work, *cyclo*-triphosphate ions could not be detected in any products. It might be attributed to the lack of formation of zwitterions reported in Ref. 5.

Table 1 shows that the above-mentioned "other" phosphates were not present and mono-, di-, and triphosphates were abundant in the samples heated in dried hydrogen chloride, which revealed that the hydrogen chloride did not act as an accelerating agent for the cyclization, but as a hydrolyzing agent for the phosphorus–nitrogen and the phosphorus–oxygen bonds. Water vapor in the atmosphere also hydrolyzed the phosphorus–nitrogen and the phosphorus–oxygen bonds present in the products.

The present work was partially supported by a Grand-in-Aid for Scientific Research No. 03750588 from the Ministry of Education, Science and Culture.

References

1) e.g., D. A. Palgrave, "Supplement to Mellor's Comprehensive Treatise on Inorganic and Theoretical Chemistry," Longman Green, London (1971), Vol. 8 P, Section 28; E. Kobayashi, *Phosphorus Lett.*, **5**, 3 (1988).
2) O. T. Quimby and T. J. Flautt, *Z. Anorg. Allg. Chem.*, **296**, 220 (1958).
3) W. Feldmann and E. Thilo, *Z. Anorg. Allg. Chem.*, **328**, 113 (1964).
4) W.Feldmann, *Z. Chem.*, **5**, 26 (1965).
5) A. Takenaka, J. Ooe, I. Motooka, and H. Nariai, *Bull. Chem. Soc. Jpn.*, **64**, 2700 (1991).
6) e.g., T. Umegaki, "Inorganic Phosphate Materials," ed by T. Kanazawa, Kodansha, Tokyo (1989), Chap. 9.
7) K. Ueno, "Kireto-Tekitei Ho," Nankodo, Tokyo (1965), Chap. 6.
8) A. Takenaka, I. Motooka, and H. Nariai, *Bull. Chem. Soc. Jpn.*, **62**, 2819 (1989).
9) D. E. C. Corbridge and E. J. Lowe, *J. Chem. Soc.*, **1954** 493.
10) E. Steger, *Z. Elektrochem.*, **61**, 1004 (1957).

Theoretical Estimation of the Entropies of Solvation of Univalent Ions

Takehiro ABE
College of General Education, Tohoku University, Kawauchi, Aoba-ku, Sendai 980
(Received April 18, 1991)

Synopsis. A simple theoretical expression for the entropies of solvation of univalent ions has been derived by using a modified Born equation and has been successfully applied to several ions in water and to the typical ions Rb^+ and Cl^- in various solvents.

Abraham and Liszi[1,2] have succeeded in calculating the entropies of solvation of univalent ions in nonaqueous solvents, using a one-layer solvation model in which an ion is surrounded by a local solvent layer, immersed in the bulk solvent. They obtained excellent agreement between the calculated and observed entropy changes. However, their model contains parameters such as the thickness of the local solvent layer and the variation of the dielectric constant with temperature. An attempt has been made, therefore, to present a simple expression which contains no adjustable parameters and roughly reproduces experimental ionic solvation entropies. Recently, Abe[3] presented the following equation for the free energy of solvation of an ion of charge Ze (where Z is the formal charge and e the charge of a proton) embedded in a continuous dielectric medium of solvent:

$$\Delta G^\circ_{\mathrm{Abe}}=\frac{e^2LZ^2}{2a}\times\left(\frac{1}{\ln\varepsilon_r}-\frac{1}{\varepsilon_r\ln\varepsilon_r}-1\right), \qquad (1)$$

where ΔG° is the increase of the standard molar Gibbs function, L the Avogadro constant, ε_r the bulk relative permittivity of the solvent, and a the radius of a spherical cavity in whose center the ion is placed. Equation 1 was derived by considering a distance-dependent relative permittivity of the solvent on the assumption that only the electrostatic free energy is predominant in the case of monoatomic and small ions. The equation reproduced experimental free energies of ions better than the Born equation[4] did.[3] Ehrenson[5] showed that the solvent parameter $\{1/\ln\varepsilon_r-1/(\varepsilon_r\ln\varepsilon_r)-1\}$ in Eq. 1 was the best in the inverse exponential radial dielectric function family of the modified Born equations for the correlation of the free energies of solvation. Moreover, Abe[6] showed that Eq. 1 can be successfully applied to the estimation of the solubilities of sparingly soluble lanthanoid iodates in dimethyl sulfoxide (DMSO)–water. Accordingly, in this paper, Eq. 1 has been applied in order to obtain a simple expression for the solvation entropies of ions. The results of calculations have been compared to those calculated by using the Born equation.

Theoretical Calculations and Discussion

On the assumptions that only the electrostatic contribution is dominant and that a does not depend on the temperature T(K), one can easily derive the following increase of standard molar entropy from Eq. 1 according to $\Delta S^\circ=-(\partial\Delta G^\circ/\partial T)_p$ (where the suffix p denotes constant pressure):

$$\Delta S^\circ_{\mathrm{Abe}}=\frac{e^2LZ^2}{2a}\times\frac{(\varepsilon_r-\ln\varepsilon_r-1)}{\varepsilon_r^2(\ln\varepsilon_r)^2}\times\frac{\mathrm{d}\varepsilon_r}{\mathrm{d}T}, \qquad (2)$$

where $e^2L/2=69.5$ nm kJ mol^{-1} (=16.6 nm kcal mol^{-1}, where 1 cal=4.184 J). On the other hand, ΔS° is easily given similarly from the Born equation by

$$\Delta S^\circ_{\mathrm{Born}}=\frac{e^2LZ^2}{2a}\times\frac{1}{\varepsilon_r^2}\times\frac{\mathrm{d}\varepsilon_r}{\mathrm{d}T}. \qquad (3)$$

Equations 2 and 3 do not contain adjustable parameters and are much simpler than the equation given by Abraham and Liszi.[1] In the present study, Eqs. 2 and 3 were applied to 10 univalent ions in water and to the typical ions Rb^+ and Cl^- in various solvents. The results of calculations were compared with experimental values[1] ($\Delta S^\circ_{\mathrm{obsd}}$) for the 12 ions, as shown in Figs. 1, 2, and 3. In applying Eqs. 2 and 3, all the values for a, ε_r, and $\mathrm{d}\varepsilon_r/\mathrm{d}T$ were taken from Ref. 7 except for the ε_r value of ammonia, for which 16.9[8] (25 °C) was adopted.

All the figures show that Eq. 2 reproduces the $\Delta S^\circ_{\mathrm{obsd}}$ values much better than does Eq. 3 and that Eq. 3 overestimates the ΔS° values as a whole. The experimental values for ΔS° have also been tabulated by Criss

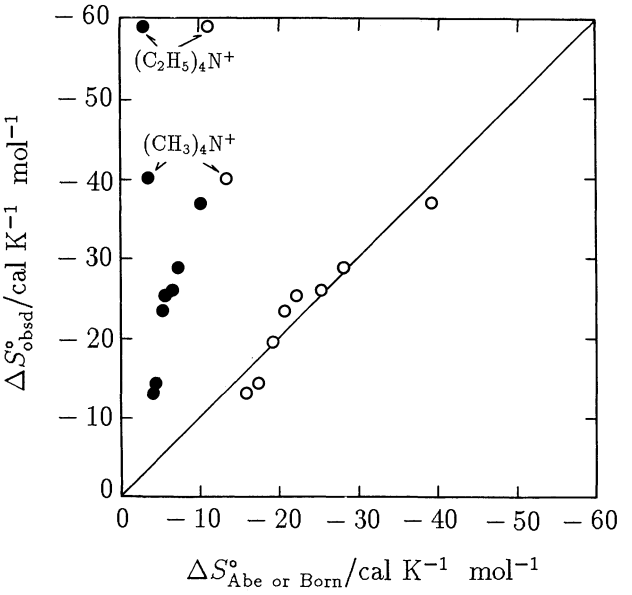

Fig. 1. Plots of observed entropies of solvation of 10 univalent ions (Na^+, K^+, Rb^+, Cs^+, $(CH_3)_4N^+$, $(C_2H_5)_4N^+$, Cl^-, Br^-, I^-, and ClO_4^-) in water (298 K) vs. $\Delta S^\circ_{\mathrm{Abe}}$ (○) and $\Delta S^\circ_{\mathrm{Born}}$ (●).

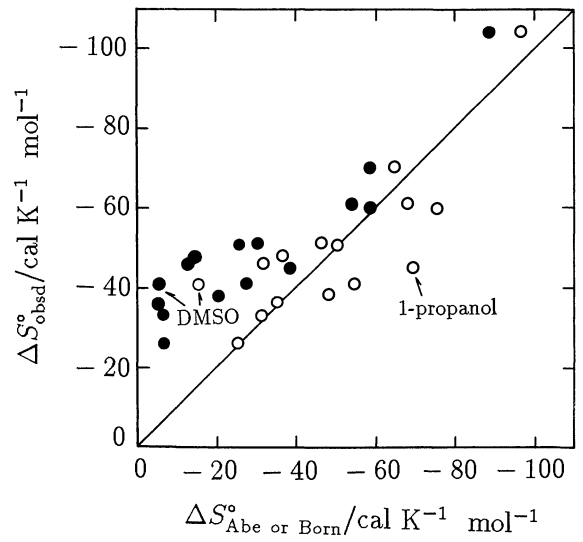

Fig. 2. Plots of observed entropies of solvation of Rb^+ in various solvents (298 K) vs. ΔS°_{Abe} (○) and ΔS°_{Born} (●).

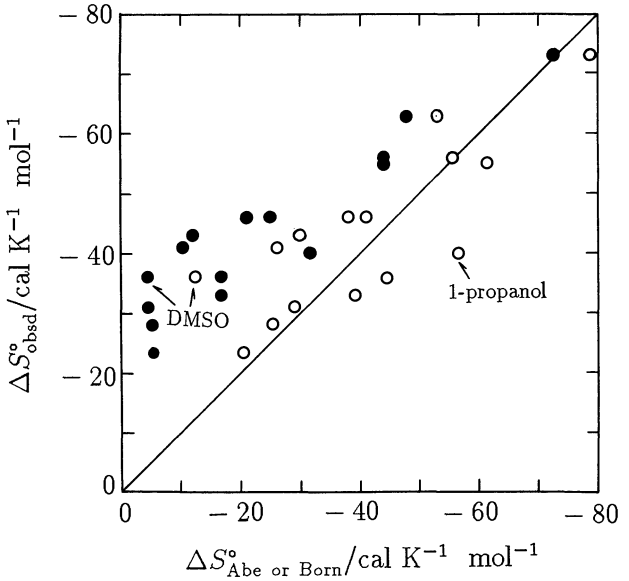

Fig. 3. Plots of observed entropies of solvation of Cl^- in various solvents (298 K) vs. ΔS°_{Abe} (○) and ΔS°_{Born} (●).

and Salomon.[9] Comparison of the values reported by Abraham and Liszi[1] and by Criss and Salomon led to the suggestion that errors in experimintal entropies of solvation are at least several calories K^{-1} mol^{-1}. It was, therefore, not surprising that there was only poor agreemont between the calculated and observed values. Abraham and Liszi[1,2] have combined the calculated electrostatic-entropy value with a nonelectrostatic contribution as the total entropy of solvation. According to them, the nonelectrostatic entropy values are quite small for solvents other than water. As shown in Figs. 1—3, however, Eq. 2, which was derived by considering only the electrostatic-entropic contribution, gave roughly the corresponding experimental values except for the cations $(CH_3)_4N^+$ and $(C_2H_5)_4N^+$ (Fig. 1). From this result, the nonelectrostatic-entropic contribution may be neglected in the case of atomic and small molecular ions. In the case of the large ions $(CH_3)_4N^+$ and $(C_2H_5)_4N^+$, the nonelectrostatic-entropic contribution may not be ignored, since the methyl and ethyl groups obviously interact nonelectrostatically with the water molecules. In Figs. 2 and 3, the plots for the DMSO solvent deviated quite a bit from the lines. Cations are strongly solvated in DMSO, whose molecule has a negative charge localized on an oxygen atom.[10] For this reason, the value of $|\Delta S^\circ_{obsd}|$ for Rb^+ in DMSO is probably larger than that of $|\Delta S^\circ_{Abe}|$ which is due only to the electrostatic-entropic contribuiton. On the other hand, anions are poorly solvated in DMSO.[10] However, this fact cannot account for the large deviation of the plot for Cl^- in DMSO from the line. The deviation suggests a special interaction between Cl^- and DMSO. This special interaction seems to be the interaction between Cl^- and a hydrogen atom of the DMSO molecule, because methylsulfinylmethanide is simply genetated from DMSO[11] and DMSO is a very weak acid.[12] For hydrogen-bonded solvents, Abraham and Liszi[1] found substantial differences between the calculated and observed ΔS° values. In Figs. 2 and 3, however, only the Eq. 2 plot of 1-propanol deviated greatly from the lines. Thus, Eq. 2 may be applied to the approximate estimation of the entropies of solvation of small univalent ions.

References

1) M. H. Abraham and J. Liszi, *J. Chem. Soc., Faraday Trans. 1*, **74**, 2858 (1978).
2) M. H. Abraham and J. Liszi, *J. Chem. Soc., Faraday Trans. 1*, **76**, 1219 (1980).
3) T. Abe, *J. Phys. Chem.*, **90**, 713 (1986).
4) M. Born, *Z. Phys.*, **1**, 45 (1920).
5) S. Ehrenson, *J. Phys. Chem.*, **91**, 1868 (1987).
6) T. Abe, *Bull. Chem. Soc. Jpn.*, **60**, 3787 (1987).
7) Y. Marcus, "Ion Solvation," John Wiley & Sons, New York (1985), pp. 46—47, 136.
8) "CRC Handbook of Chemistry and Physics," 61st ed, ed by R. C. Weast, CRC, Boca Raton (1980—1981), p. E-55.
9) C. M. Criss and M. Salomon, "Thermodynamic Measurements," in "Physical Chemistry of Organic Solvent Systems," ed by A. K. Covington and T. Dickinson, Plenum, London and New York (1973), Chap. 2, p. 261.
10) A. J. Parker, *Q. Rev., Chem. Soc.*, **16**, 163 (1962).
11) E. J. Corey and M. Chaykovsky, *J. Am. Chem. Soc.*, **84**, 866 (1962).
12) K. Bowden, *Chem. Rev.*, **66**, 119 (1966).

Redox Properties for Pentacoordinated Manganese(III) Complexes with Bis(salicylideneamino)alkanes

Masaaki NAKAMURA,* Yuri MIYANAKA, Yasuhiro OHMURA, Satoko SEKINE, Hu HUANG,† and Fumiaki KAI†
Department of Chemistry, Faculty of Science, Kumamoto University, Kumamoto 860
† Department of Environmental Science, Graduate School of Natural Science and Technology, Kumamoto University, Kumamoto 860
(Received May 7, 1991)

Synopsis. The oxidation potentials of Mn(III/IV) for pentacoordinated chloromanganese(III) complexes with bis(salicylideneamino)alkanes shifted cathodically in the presence of excess chloride ions in their solution. The formation of dichloromanganese(IV) complexes with Schiff bases was spectrophotometrically detected by addition of chloride and hydrogen ions to acetonitrile solutions of the corresponding chloromanganese(III) complexes under aerobic conditions.

The chemistry of manganese(III) and (IV) complexes has been of interest in relation to the catalytic activity of manganese enzymes, such as the oxygen evolution process of photosystem II.[1-3] Previously, Matsushita et al. described a unique synthetic method for manganese(IV) complexes, in which dichloromanganese(IV) complexes with tetradentate or bidentate Schiff bases were prepared by treating the corresponding chloromanganese(III) complexes with hydrochloric acid.[4,5] We have also prepared a tetrachlorodimanganese(IV) complex with an octadentate binucleating Schiff base from the corresponding dichlorodimanganese(III) complex by applying the same synthetic method.[6] This is of interest because hydrochloric acid is not able to oxidize manganese(III) to (IV) as an oxidizing agent.

In this study, the electrochemical properties of pentacoordinated manganese(III) complexes with tetradentate Schiff base, 1,2-bis(salicylideneamino)ethane (H_2salen) and 1,3-bis(salicylideneamino)propane (H_2saltn), were investigated; the role of hydrochloric acid is discussed here.

Experimental

Syntheses. All of the pentacoordinated manganese(III) complexes were prepared in an identical manner, employing a modified method from the literature.[7-9] This may be illustrated for Mn(saltn)Cl.

Mn(saltn)Cl: 1,3-Propanediamine (10 mmol) and salicylaldehyde (20 mmol) were dissolved in ethanol (30 cm^3) and then refluxed for 3 h. Manganese(II) chloride tetrahydrate (10 mmol) was added to the reaction mixture; it was then refluxed for 1 h under aerobic conditions. The obtained dark-green solution was filtered and the filtrate was allowed to stand over night. Dark-green fine crystals were deposited; they were then filtered off, washed with ethanol, and dried in vacuo. The yield was ca. 55%. Found: C, 54.38; H, 5.21; N, 6.65%. Calcd for $C_{17}H_{16}N_2O_2MnCl\cdot C_2H_5OH$: C, 54.75, H, 5.32, N, 6.72%.

[Mn(saltn)H_2O]ClO_4: Found: C, 44.87; H, 4.08; N, 6.13%. Calcd for $C_{17}H_{18}N_2O_7MnCl$: C, 45.10; H, 4.00; N, 6.19%.

Mn(salen)Cl: Found: C, 48.81; H, 4.60; N, 7.14%. Calcd for $C_{16}H_{14}N_2O_2MnCl\cdot 2H_2O$: C, 48.93; H, 4.62; N, 7.13%.

[Mn(salen)H_2O]ClO_4: Found: C, 43.63; H, 3.69; N, 6.36%. Calcd for $C_{16}H_{16}N_2O_7MnCl$: C, 43.81; H, 3.68; N, 6.39%.

Measurements. The electronic spectra were obtained using a Hitachi 220A or U3210 recording spectrophotometer. The electric conductivities were determined by a Horiba Conductivity Meter (Model DS-14). Polarograms were recorded on a Yanagimoto Polarographic Analyzer (Model P-1100) by the use of a three-electrode cell equipped with glassy carbon as a working electrode, a platinum coil as a auxiliary electrode, and a saturated calomel electrode (SCE) as a reference electrode. In practice, all of the potentials were normalized by using ferrocene as an internal standard.

Results and Discussion

In methanol solutions, all of the perchlorate and chloro complexes, [Mn(SB)H_2O]ClO_4 and Mn(SB)Cl (where SB is $salen^{2-}$ or $saltn^{2-}$) showed almost identical spectral features, indicating the formation of a solvated complex, such as $[Mn(SB)(CH_3OH)_2]^+$. This result is supported by their molar conductivities in methanol at 25 °C (Table 1), whose values are consistent with a 1:1 electrolyte.[10] When tetrabutylammonium chloride (TBACl) was added to the methanol solutions up to a molar ratio of [TBACl]/[complex]=200, the electronic spectra of the complexes were little affected and the specific conductivity was linearly increased with an increase in the concentration of TABCl. It is concluded that monocationic complexes can exist in a methanol solution even with excess chloride ions.

On the other hand, molar conductivity data for the chloro complexes demonstrate essentially nonelectrolyte in acetonitrile (Table 1).[10] Each of the observed spectra of the four complexes in acetonitrile and of the two chloro complexes in dichloromethane can be interpreted as being the spectrum of a pentacoordinated manganese(III) complex.[8,9,11] From optical measurements, the perchlorate complexes are changed to the corresponding chloro complexes by the addition of excess TBACl in acetonitrile, respectively. The absorption spectra of Mn(saltn)Cl and [Mn(saltn)H_2O]ClO_4 are shown in Fig. 1 as an example. A plot of the specific conductivity of the perchlorate complex vs. [TBACl]/[complex] in acetonitrile is almost constant within the TBACl concentration range below 1 in molar ratio. The above-mentioned results suggest that an apical ligand substitution occurs in the presence of the chloride ion as follow:

$$[Mn(SB)H_2O]^+ + ClO_4^- + TBA^+ + Cl^- \longrightarrow Mn(SB)Cl + H_2O + TBA^+ + ClO_4^-.$$

Each of the four manganese(III) complexes exihibits

Table 1. Molar Conductivities and Electrochemical Data for Manganese(III) Complexes

Complex	Solvent	Λ_M[a]	TBAX[b]	E_{pc}	E_{pa}	ΔE_p	$E'_{1/2}$[c]	$E_{1/2}$
		S cm^2 mol^{-1}		V	V	mV	V	V
Mn(salen)Cl	CH_3OH	0.70×10^2	ClO_4	−0.635	−0.560	75	−0.598	−0.590
								0.770
			Cl	−0.649	−0.575	74	−0.612	−0.610
								0.653
	CH_3CN	2.69	ClO_4	−0.668	−0.583	85	−0.626	−0.645
				0.423	0.651	228	0.537	0.643
			Cl	−0.728	−0.560	168	−0.644	−0.699
				0.223	0.313	90	0.268	0.264
	CH_2Cl_2		ClO_4	−0.701	−0.595	106	−0.648	−0.651
								0.571
			Cl	−0.741	−0.659	82	−0.700	−0.729
								0.291
$[Mn(salen)H_2O]ClO_4$	CH_3OH	1.08×10^2	ClO_4	−0.645	−0.570	75	−0.608	−0.600
								0.740
			Cl	−0.652	−0.574	78	−0.613	−0.601
								0.746
	CH_3CN	1.55×10^2	ClO_4	−0.606	−0.540	66	−0.573	−0.574
								1.083
			Cl	−0.755	−0.522	233	−0.639	−0.731
				0.219	0.322	103	0.271	0.268
Mn(saltn)Cl	CH_3OH	1.00×10^2	ClO_4	−0.570	−0.490	80	−0.530	−0.522
								0.780
			Cl	−0.575	−0.495	80	−0.535	−0.535
	CH_3CN	3.10	ClO_4	−0.558	−0.463	95	−0.511	−0.503
								0.467
			Cl	−0.640	−0.450	190	−0.545	−0.575
								0.285
	CH_2Cl_2		ClO_4	−0.573	−0.488	85	−0.531	−0.528
								0.597
			Cl	−0.635	−0.550	85	−0.592	−0.595
								0.245
$[Mn(saltn)H_2O]ClO_4$	CH_3OH	1.02×10^2	ClO_4	−0.565	−0.485	80	−0.525	−0.512
								0.740
			Cl	−0.565	−0.485	80	−0.525	−0.524
	CH_3CN	1.21×10^2	ClO_4	−0.459	−0.394	65	−0.427	−0.429
								1.074
			Cl	−0.617	−0.455	162	−0.536	−0.575
								0.295

a) Measured at 25°C. The concentration of the complexes was 5.0×10^{-4} mol dm^{-3}. b)TBAX means tetrabutylammonium salts used as a supporting electrolyte. c) $E'_{1/2}=(E_{pc}+E_{pa})/2$.

two redox waves attributable to the manganese center, since the ligands do not show any redox waves at these potential region (Table 1). The oxidation potentials observed are dependent on the charge of the manganese(III) complexes in solution. Namely, the monocationic complexes show irreversible oxidation waves at 0.74—0.78 V in methanol and 1.1 V in acetonitrile. The neutral chloro complexes, however, are oxidized at 0.47—0.64 V in acetonitrile and dichloromethane. When excess chloride ions exist in the solution, the oxidation potentials of the chloro complexes shift negatively to 0.26—0.30 V (Table 1). Furthermore, in the case of the acetonitrile solutions of Mn(salen)Cl and $[Mn(salen)H_2O]ClO_4$, a cathodic peak is detected in the reverse scan by the addition of excess chloride ions, in which the peak-to-peak separation (ΔE_p) is 90—103 mV and the peak ratio (i_{pc}/i_{pa}) is almost equal to unity. Under the same experimental conditions, the normally reversible one-electron oxidation of ferrocene displays rather large ΔE_p values of ca. 60 mV. Accordingly, we have tentatively assigned the oxidation waves to an irreversible one-electron transfer process for Mn(III/IV).

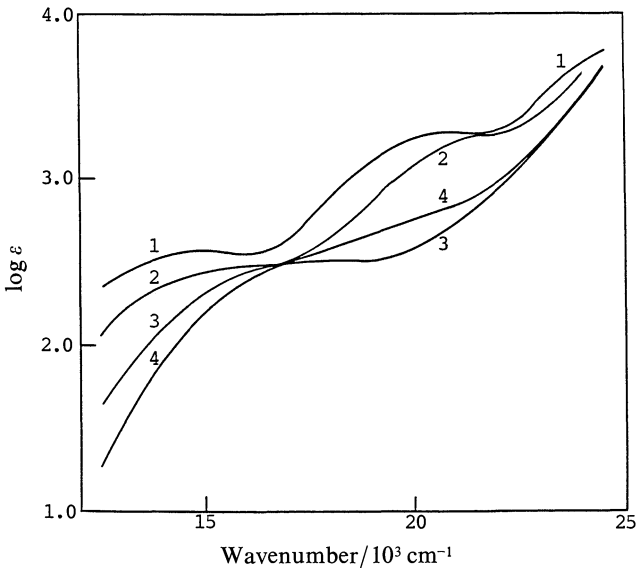

Fig. 1. Electronic spectra of Mn(saltn)Cl in dichloromethane (1), in acetonitrile (2), in methanol (3) and $[Mn(saltn)H_2O]ClO_4$ in acetonitrile (4).

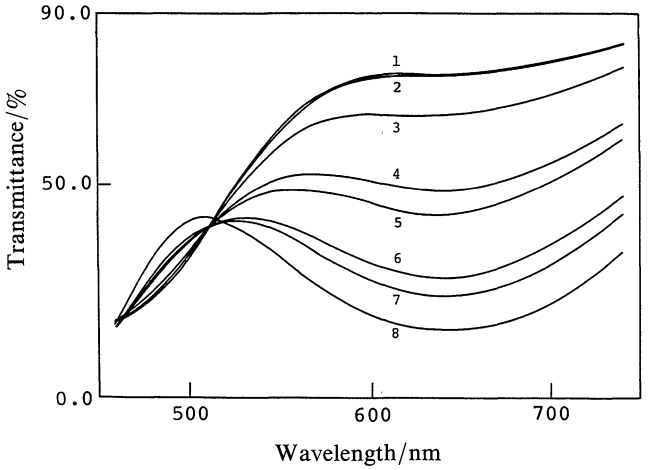

Fig. 2. Spectral changes on addition of perchloric acid to an acetonitrile solution of 5.0×10^{-4} mol dm^{-3} Mn(saltn)Cl in different molar ratios. 1: $[HClO_4]$/[complex]=0.00, 2: 0.02, 3: 0.10, 4: 0.30, 5: 0.40, 6: 0.80, 7: 1.00, 8: 2.00.

It is noted that those oxidation potentials (0.26—0.30 V) appear at a more negative region than does the reduction potential of Mn(IV/III) (0.36 V) for the dichloromanganese(IV) complex with 1,2-bis(salicylideneamino)-1-phenylethane.[6] This significant cathodic shift of the potentials is interpreted as meaning that the manganese(IV) state formed electrochemically is stabilized by a further participation of chloride ions to the manganese(IV) coordination sphere. However, only an addition of excess chloride ions to the manganese(III) complex solution is not sufficient to obtain the manganese(IV) complex.

When perchloric acid was added to the acetonitrile solution of the chloro complexes, Mn(salen)Cl and Mn(saltn)Cl, a new absorption band appeared around 640 nm. Figure 2 shows the spectral changes of Mn(saltn)Cl as an example. This band can be assigned to the CT band of the Cl^- to Mn(IV).[4] Accordingly, this spectral change suggests the formation of dichloromanganese(IV) complexes. The intensity of the CT band is increased with an increase in the concentrations of chloride and hydrogen ions. However, rapid decolorization occurs upon adding these excess ions, indicating a decomposition of the complexes. The most intense absorption band was obtained with an acetonitrile solution containing TBACl and perchloric acid at a molar ratio of [complex]:[TBACl]:$[HClO_4]$=1:3:2, in which [complex]=5.0×10^{-4} mol dm^{-3}. The yield of $Mn(salen)Cl_2$ under the above-mentioned conditions is about 42%, which is determined spectrophotometrically based on literature data for its CT band.[4]

The CT band was observed by using sulfuric acid instead of perchloric acid as a hydrogen ion source, but was not detected by using acetic acid, whose dissociation constant in acetonitrile is $10^{-22.3}$.[12] Furthermore, the presence of oxygen is necessary for the above reaction, since the CT band can not be obtained under anaerobic conditions. In a methanol solution, only the decomposition of the complexes is observed for any concentration ratios of TBACl and $HClO_4$ under aerobic conditions. These results imply that the dichloromanganese(IV) complex is formed by the addition of chloride and hydrogen ions to a solution containing the corresponding pentacoordinated chloromanganese(III) complexes under aerobic conditions.

References

1) G. D. Lawrence and D. T. Sawyer, *Coord. Chem. Rev.*, **27**, 173 (1978).
2) G. Renger, *Angew. Chem., Int. Ed. Engl.*, **26**, 643 (1987).
3) J. E. Penner-Hahn, R. M. Fronko, V. L. Pecoraro, C. F. Yocum, S. D. Betts, and N. R. Bowlby, *J. Am. Chem. Soc.*, **112**, 2549 (1990).
4) T. Matsushita, H. Kono, and T. Shono, *Bull. Chem. Soc. Jpn.*, **54**, 2646 (1981).
5) M. Fujiwara, T. Matsushita, and T. Shono, *Polyhedron*, **4**, 1895 (1985).
6) M. Nakamura, S. Shimokawa, Y. Miyanaka, H. Huang, and F. Kai, *Bull. Chem. Soc. Jpn.*, **64**, 1692 (1991).
7) C. P. Prabhakaran and C. C. Patel, *J. Inorg. Nucl. Chem.*, **36**, 3316 (1974).
8) L. J. Boucher, *J. Inorg. Nucl. Chem.*, **36**, 531 (1974).
9) F. M. Achmawy, C. A. McAuliffe, R. V. D. Parish, and J. Tames, *J. Chem. Soc., Dalton Trans.*, **1985**, 1391.
10) W. J. Geary, *Coord. Chem. Rev.*, **7**, 81 (1971).
11) L. J. Boucher and D. R. Herrington, *Inorg. Chem.*, **13**, 1105 (1974).
12) "Kagaku Binran II," ed by Chem. Soc. Jpn., Maruzen, Tokyo (1984), p. 343.

Glucose-Sensing Electrode Based on Carbon Paste Containing Ferrocene and Polyethylene Glycol-Modified Enzyme

Fumio MIZUTANI,* Soichi YABUKI, Atsushi OKUDA,† and Tatsuo KATSURA
Research Institute for Polymers and Textiles, 1-1-4 Higashi, Tsukuba, Ibaraki 305
† Hokkaido Industrial Research Institute, Kita 19, Nishi 11, Sapporo 060
(Received May 13, 1991)

Synopsis. An amperometric glucose-sensing electrode is constructed by the use of a carbon paste containing 1,1′-dimethylferrocene and a polyethylene glycol-modified glucose oxidase. The polymer-modified enzyme is soluble in organic solvents (e. g., hexane) as well as in water, and exhibits a much higher activity than native enzyme does on the surface of a hydrophobic carbon paste eletrode. The higher enzyme activity results in an enhanced electrode response: the current response to glucose on the modified enzyme-based electrode is several times as large as that obtained on a native enzyme-based electrode.

Much effort has been directed to devise an amperometric enzyme electrode for measuring glucose by combining immobilized glucose oxidase (GOD) with an immobilized electroactive species which mediates an electron transfer between the enzyme and the electrode.[1-3] Recently, a novel method for constructing such a mediated glucose-sensing electrode has been developed: a GOD/mediator-containing carbon paste electrode (CPE) has been prepared by doping the carbon paste with the enzyme and a mediator.[4-6] The GOD/mediator-doped CPE is of particular interest, since it can easily be prepared; it also has a close proximity of the enzymatic, mediating and sensing sites, thus providing a rapid current response to glucose. However, hydrophilic GOD molecules are not expected to exhibit high activity in a hydrophobic carbon paste matrix.

Inada et al.[7-9] have reported that enzymes (e.g., catalase and peroxidase) modified with polyethylene glycol (PEG) dissolve in various organic solvents as well as in water. Further, the PEG-modified enzymes have been reported to show catalytic activities, even in organic solvents. Such a PEG-modified enzyme would exhibit a higher activity than the native enzyme in the carbon paste matrix.

We have prepared a glucose-sensing CPE by the use of 1,1′-dimethylferrocene and a PEG-modified GOD. The effect of the modification of GOD on the electrode response is reported in the present paper.

Experimental

GOD (E.C. 1.1.3.4, from *Aspergillus* sp., Grade II) and peroxidase (E.C. 1.11.1.7, from horseradish, Grade I-C) were purchased from Toyobo. α-(4,6-Dichloro-1,3,5-triazin-2-yl)-ω-methoxypoly(oxyethylene) (activated PEG; molecular weight, 5×10^3)[10] was obtained from Sigma, and 1,1′-dimethylferrocene, from Aldrich. The other reagents used were of analytical-reagent grade. Deionized, doubly-distilled water was used throughout.

The GOD, as received (native GOD, 14 mg), and the activated PEG (140 mg) were added into 2 ml of 0.1 mol dm^{-3} borate–KOH buffer (pH 10); this GOD/PEG mixture was then incubated at 37 °C for 2 h, after which the reaction was stopped by adding acetic acid into the solution to make its pH 6. Unattached PEG was removed in an ultrafiltration cell (Millipore) using a PTTK membrane (Millipore; cut off molecular weight, 3×10^4) and 0.05 mol dm^{-3} $(NH_4)HCO_3$ as a dialyzing solution. Finally, a light-yellow-colored powder of PEG-modified GOD (22 mg) was obtained by lyophilization.

The molecular weight of the PEG-modified GOD was estimated by sodium dodecyl sulfate (SDS)–polyacrylamide (4—20%) gel electrophoresis; the molecular marker proteins were myoglobin (1.7×10^4), carbonic anhydrase (3.0×10^4), ovalbumin (4.5×10^4), bovine serum albumin (6.6×10^4), β-galactosidase (1.2×10^5) and myosin (2.0×10^5). The content of FAD (flavin-adenine dinucleotide) in the modified GOD was estimated by measuring the visible absorption of an aqueous solution of the modified enzyme (at 450 nm). The enzyme activities of the modified and native enzymes in solutions and on CPE's were measured by using the *o*-dianisidine/peroxidase-color-producing system.[11]

Two kinds of glucose-sensing CPE's, CPE I and II, were prepared by using the PEG-modified GOD and the native GOD, respectively. The modified or native GOD, 1,1′-dimethylferrocene and carbon paste (BAS CP-O), 10:10:80 by weight, were thoroughly mixed together. A portion of the mixture was placed in a hole (3.2 mm diameter, 4 mm deep) at the end of an electrode body (BAS 11-2010). CPE I or II thus prepared, an Ag/AgCl electrode and a platinum wire served as working, reference and auxiliary electrodes, respectively. The test solution used was a 0.1 mol dm^{-3} potassium acetate buffer solution (20 ml, pH 5, 25 °C). The solution was stirred with a magnetic bar. Oxygen was expelled from the solution by bubbling argon. CPE I and II were stored in the acetate buffer solution at 0 °C when not in use.

Results and Discussion

Figure 1 shows the result of the SDS-polyacrylamide gel electrophoresis. The native GOD gave a single band on the gel at a molecular weight of ca. 7×10^4. This value agrees fairly well with the molecular weight of the subunit in GOD, 7.5×10^4; the native GOD (molecular weight, 1.5×10^5) consists of two identical subunits. On the other hand, the modified GOD gave a broad electrophoretic pattern, indicating that the molecular weight of the subunit increased to be more than 1×10^5 upon attaching activated PEG onto the GOD molecule. The PEG-modified GOD was soluble in organic solvents as well as in aqueous media. For example, the modified enzyme (1 mg) was instantaneously dissolved in hexane (1 ml).

The acetate buffer solution containing the native GOD (5 mg ml^{-1}) and that containing the modified GOD

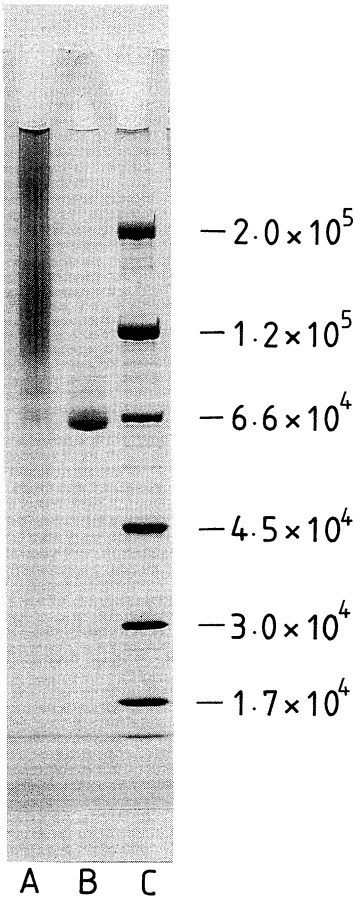

Fig. 1. Electrophoretic patterns of the modified GOD (A), native GOD (B), and marker proteins (C).

(5 mg ml^{-1}) showed optical densities of 0.52 and 0.28, respectively, at 450 nm: the content of FAD in the modified GOD is about a half that in native GOD. When native GOD was incubated in a borate–KOH buffer in the absence of activated PEG, the release of FAD from GOD molecules was not observed. It is therefore indicated that the modified GOD consists of native GOD and the modifier in a weight ratio of ca. 1:1.

The activity of modified GOD in an acetate buffer solution at 25 °C was determined to be 15 U mg^{-1}, whereas that of native GOD under the same conditions was 105 U mg^{-1}. This indicates that the enzyme activity is considerably reduced during the modification process. When the modified GOD was doped into carbon paste, on the other hand, it exhibited a mcuh higher activity than native enzyme. The GOD activities on the surfaces of CPE-I and II were ca. 0.1 and 0.02 U cm^{-2}, respectively. The higher activity of modified GOD in the carbon paste matrix may be attributable to its enhanced effinity for the hydrophobic matrix, which can be proven by the high solubility of the modified enzyme in organic solvents such as hexane.

The increase in the GOD activity in the carbon paste by a modification of the enzyme with PEG resulted in an enhanced response for glucose on CPE I, as compared to

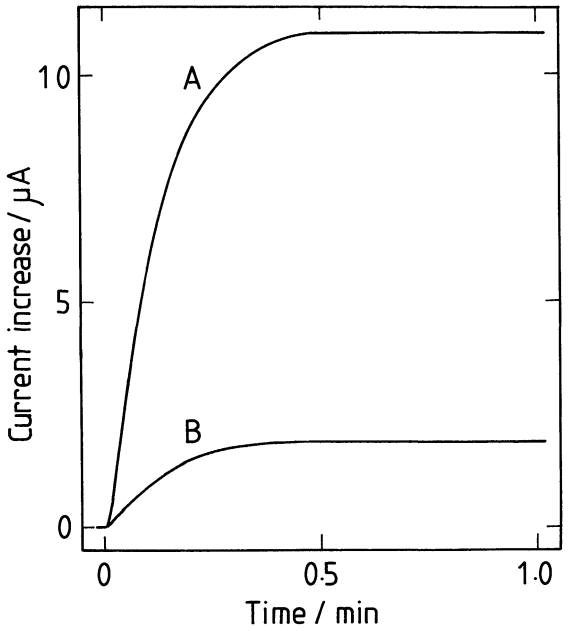

Fig. 2. Response/time curves on CPE I (A) and II (B) for 25 mmol dm^{-3} glucose.

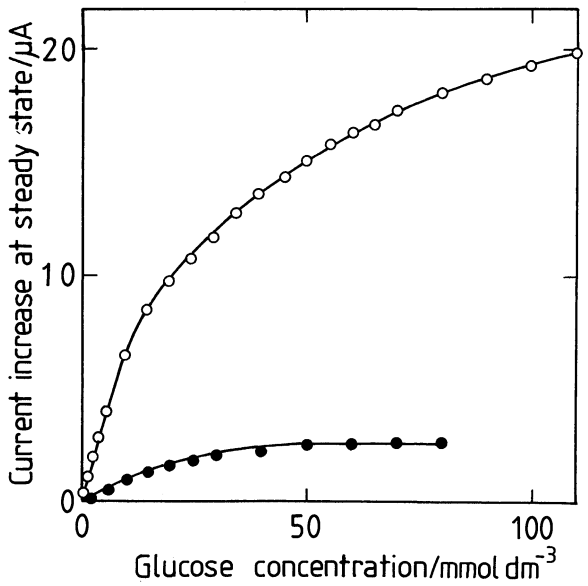

Fig. 3. Relationships between current increase and glucose concentration on CPE I (—○—) and II (—●—).

the case of CPE II. Curves A and B in Fig. 2 show the electrode responses to glucose (25 mmol dm^{-3}) on CPE I and II, respectively. The electrode potential, 0.4 V vs. Ag/AgCl, was sufficient for the oxidation of 1,1′-dimethylferrocene to produce ferricinium ion, and for obtaining ferrocene-mediated current responses to glucose.[4,12] The glucose response on CPE I was about five times as large as that on CPE II.

Figure 3 shows the calibration curves of CPE I and II. CPE I gave a linear current response up to 10 mmol dm^{-3} of glucose, and a siginificant increase in the

response with an increase in the glucose concentration within the range 10—100 mmol dm^{-3}. The detection limit of CPE I was 0.1 mmol dm^{-3} (S/N=5). On the other hand, the detection limit of CPE II was 0.5 mmol dm^{-3} (S/N=5); the electrode response reached a plateau when the glucose concentration was higher than 50 mmol dm^{-3}. These results indicate that the modification of GOD with PEG is effective for widening the dynamic range of the glucose-sensing electrode.

The effect of storage (in the acetate buffer at 0 °C) of CPE I and II was then examined. On each electrode, the response to glucose (25 mmol dm^{-3}) gradually decreased during storage and became ca. 80% of the initial value after 10 d; the long-term stability was, unfortunately, not improved by a modification of enzyme. The decrease in the electrode response was considered to be caused by a leaching of the (modified or native) enzyme out of the carbon paste matrix, since the solution used for storing CPE I or II showed significant GOD activity. Another kind of modification method, to introduce hydrophobic groups onto the surface of GOD molecule, would be required for obtaining enzyme/carbon paste systems with high stability. On the other hand, our preliminary experiments demonstrate that the coating on the surface of CPE I (and that of CPE II) with an anionic polymer (AQ-29D, Eastman)[4] is effective for preventing the enzyme from leaking out of the carbon paste, as well as for diminishing electrochemical interference with such anionic species as ascorbate.

References

1) M. F. Cardosi and A. P. F. Turner, "Biosensors: Fundamentals and Applications," ed by A. P. F. Turner, I. Karube, and G. S. Wilson, Oxford University Press, Oxford (1987), p. 257.

2) F. Mizutani and M. Asai, "Bioinstrumentation," ed by D. L. Wise, Butterworths, Boston (1990), p. 317.

3) S. P. Hendry, I. J. Higgins, and J. V. Bannister, *J. Biotechnol.*, **15**, 227 (1990).

4) L. Gorton, H. I. Karan, P. D. Hale, T. Inagaki, Y. Okamoto, and T. A. Skotheim, *Anal. Chim. Acta,* **228**, 23 (1990).

5) J. Wang, L.-H. Wu, Z. Lu, R. Li, and J. Sanchez, *Anal. Chim. Acta,* **228**, 251 (1990).

6) A. Amine, J.-M. Kauffmann, and G. J. Patriarche, *Talanta,* **38**, 107 (1991).

7) Y. Inada, H. Nishikawa, K. Takahashi, T. Yoshimoto, R. A. Sada, and Y. Saito, *Biochem. Biophys. Res. Commun.*, **122**, 845 (1984).

8) K. Takahashi, A. Ajima, T. Yoshimoto, and Y. Inada, *Biochem. Biophys. Res. Commun.*, **125**, 761 (1984).

9) K. Takahashi, A. Ajima, T. Yoshimoto, M. Okada, A. Matsushima, Y. Tamura, and Y. Inada, *J. Org. Chem.*, **50**, 3414 (1985).

10) A. Abuchowski, T. van Es, N. C. Placzuk, and F. F. Davis, *J. Biol. Chem.*, **256**, 3578 (1977).

11) H. U. Bergmeyer, K. Gawehn, and M. Grassl, "Methods in Enzymatic Analysis," ed by H. U. Bergmeyer, Verlag Chemie/Academic Press, New York and London (1974), Vol. 1, p. 457.

12) A. E. G. Cass, G. Davis, G. D. Francis, H. A. O. Hill, W. J. Aston, I. J. Higgins, E. V. Protokin, L. D. L. Scott, and A. P. F. Turner, *Anal. Chem.*, **56**, 667 (1984).

Photoinduced Cyclization of 2-Acetonyl-3-alkoxy-1,4-naphthoquinones: Formation of 2-Alkyl-Substituted 4-Methyl-naphtho[2,3-*d*]-1,3-dioxepin-6,11-diones

Katsuhiko NAKAGAWA
Department of Industrial Chemistry, Niihama National College of Technology, Niihama, Ehime 792
(Received December 25, 1990)

Synopsis. Irradiation of 2-acetonyl-3-alkoxy-1,4-naphthoquinones in benzene gave 2-alkyl-substituted 4-methyl-naphtho[2,3-*d*]-1,3-dioxepin-6,11-dione and 2-acetonyl-3-hydroxy-1,4-naphthoquinone via intramolecular hydrogen-abstraction reaction. Irradiation of quinones in methanol, however, gave the latter product exclusively.

Photochemical reaction of 2-alkoxy-1,4-naphthoquinones usually leads to the formation of quinone dimers[1] and oxetanols[2] in high yields, via intramolecular hydrogen abstraction from the 2′-position of the side chain. This reaction is similar to the Norrish type II photoreaction of aromatic ketones.[3] Recently, we developed the convenient synthesis of 2-acetonyl-3-alkoxy-1,4-naphthoquinones (**2**) by the photochemical reaction of 2-alkoxy-1,4-naphthoquinones (**1**) with 2-methoxy-1-propene.[4] Interestingly, the photochemical reaction of **2** is quite different from those of 2-alkoxy-1,4-naphthoquinones with regard to the mechanistic points.[5] In this paper, the details of the novel photo-induced cyclization of **2** is described.

Results and Discussion

When a solution of 2-acetonyl-3-alkoxy-1,4-naphthoquinones (**2**) in benzene (0.0028 mol dm^{-3}) were irradiated with a high-pressure mercury arc lamp (300 W) through Pyrex filter for 15 min, the heterocyclic 1,4-naphthoquinones **3** as a major products, accompanying with 2-acetonyl-3-hydroxy-1,4-naphthoquinone (**4**), were obtained and the results are summarized in Table 1. The structures of **3** were assigned on the basis of their spectroscopic and elemental analyses, and that of **4** was confirmed by comparison with the authentic sample.[6] The yields of the cyclized products **3** increased in the order of **2a**<**2b**<**2c**, reflecting the γ C–H bond strength.[7] In order to confirm the existence of the hydroquinones derived from **2**, **3**, and **4**, the following two experiments were done. After irradiation of **2c** in benzene for 15 min, the reaction mixture was treated with acetic anhydride and pyridine to give a mixture of diacetate **7c**

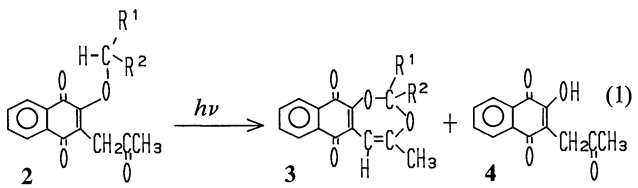

a: R^1=R^2=H, **b**: R^1=H, R^2=CH_3, **c**: R^1=R^2=CH_3

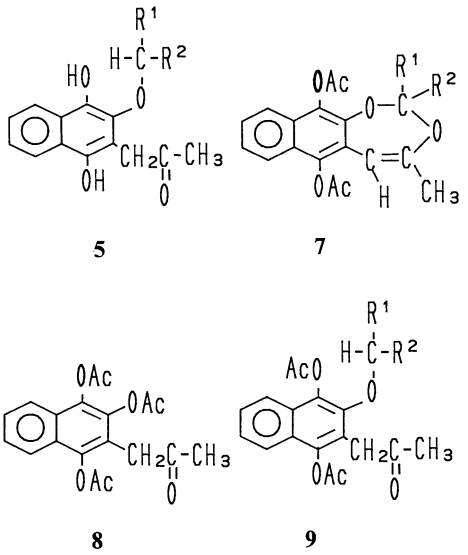

a: R^1=R^2=H, **b**: R^1=H, R^2=CH_3, **c**: R^1=R^2=CH_3

Reduction Products and Reductive Acetylation Products

Table 1. Photochemical Reaction of 2-Acetonyl-3-alkoxy-1,4-naphthoquinone **2**

Quinone R^1	Quinone R^2		Conv.[a] %	Solvent	Isolated yields/%[b] **3**	Isolated yields/%[b] **4**
H	H	**2a**	60	Ph–H	28	16
CH_3	H	**2b**	85	Ph–H	38	16
CH_3	CH_3	**2c**	87	Ph–H	77	11
H	H	**2a**	90	MeOH	—	41
CH_3	H	**2b**	99	MeOH	—	50
CH_3	CH_3	**2c**	81	MeOH	—	70

a) Conversion of **2**. b) Isolated yields were based on the consumed amounts of **2**. Irradiation time, 15 min; [**2**]=2.75×10^{-3} mol dm^{-3}.

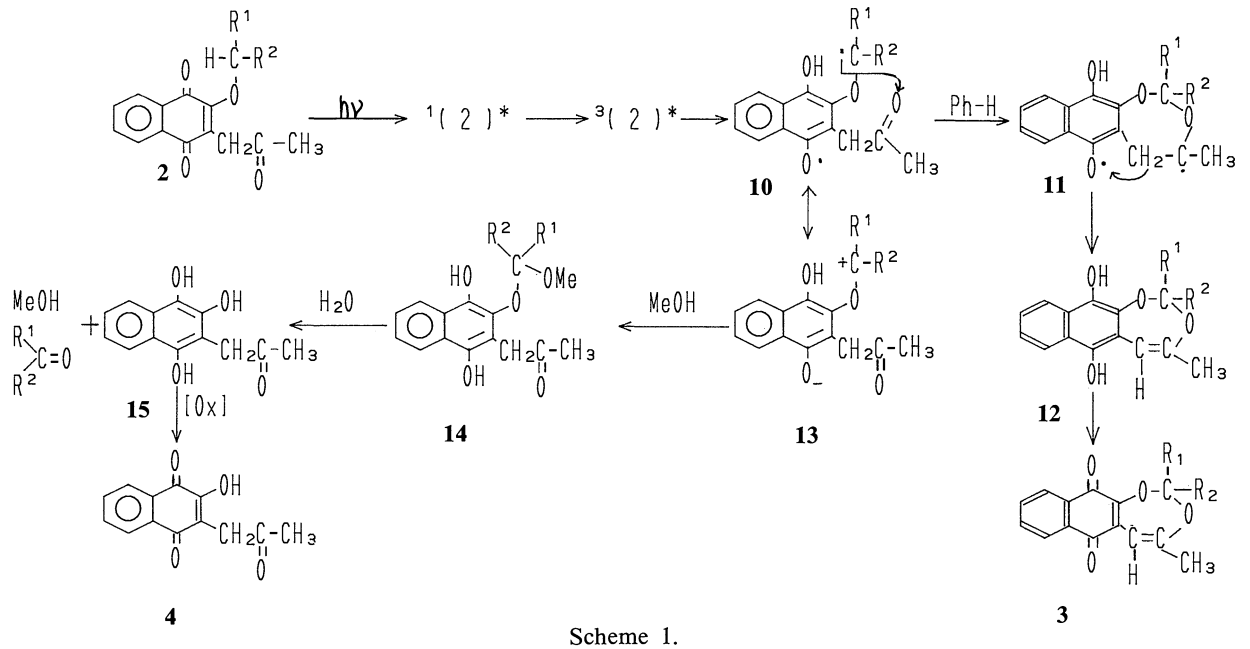

Scheme 1.

(37%) and **9c** (20%), and triacetate **8** (5%) at 90% conversion. The structures of these acetates were confirmed by comparison with the authentic samples synthesized by the reductive acetylation of the corresponding quinones (**2c**, **3c**, and **4**).[8] (Experiment 1) These results indicate that hydroquinones derived from **2**, **3**, and **4** are initial photoproducts, but they are oxidized to the corresponding quinones during work-up procedure involving chromatography over silica gel. In addition, after irradiation of **2c** in benzene-d_6 for 5 min (40% conversion), the 400 MHz ^{1}H NMR spectrum of the reaction mixture revealed the peaks assignable to the hydroquinone **5c** at δ=0.97 (d, J=6.11 Hz, 6H), 1.75 (s, 3H), 3.58 (s, 2H), and 3.74 (sept, J=6.41 Hz, 1H) which were in agreement with those of the hydroquinone **5c** obtained by the reduction of **2c** with dithionite, in addition to the peaks due to **3c** and **4**. The peaks due to **5c** disappeared after adding chloranil to the reaction mixture (Experiment 2). This novel photoinduced cyclization of **2** was sensitized by xanthone and quenched by anthracene, indicating that the reaction occurred from the triplet excited state of **2**. From these results, a plausible mechanism for the formation of **3** is given in Scheme 1. Photocylization may begin with intramolecular γ-H-abstraction by the ^{3}(n, π^*) of **2** to give biradical **10**, which intramoleculary attacks the carbonyl oxygen in the oxoalkyl side chain and cyclizes to **11**.

Intramolecular disproportionation of the biradical **11** produces hydroquinone **12**, which is oxidized by the unreacted **2** or air, to give **3**.

On the other hand, irradiation of **2a**—**c** in methanol gave preferentially **4** (41—70% yield) as shown in Table 1. In the case of the reaction of **2c** the alkoxyl group lost in the course of the photochemical reaction in methanol was detected as acetone by gas chromatography, ^{1}H NMR, and ^{13}C NMR. The yield of acetone increased with increasing irradiation time. From these results, a plausible mechanism for the formation of **4** is given in Scheme 1. The photoinduced C–O bond cleavage may begin with intramolecular γ-H-abstraction as well as the formation of **3**. In methanol the biradical **10** is stabilized by an adjacent heteroatom[9] such as oxygen to produce a zwitterionic intermediate **13**, which reacts with methanol to give the acetal **14**. Hydrolysis of **14** produces ketone (R^1R^2C=O), methanol, and hydroquinone **15**, which is oxidized by the unreacted **2** or air to give **4**.

Experimental

Apparatus. Melting points were measured on Yanagimoto micro-melting points apparatus and are uncorrected. Infrared spectra were taken on a JASCO FT-IR 5000 spectrometer. ^{1}H NMR spectra were recorded on a JEOL GX-400 (400 MHz), a JEOL GX-270 (270 MHz) and a JEOL FX-90Q (90 MHz) spectrometer with use of tetramethylsilane as an internal standard and the chemical shifts are expressed in δ values. UV spectra were taken by using a JASCO Ubest-35 spectrometer. Elemental analyses were performed at the Advanced Instrumentation Center for Chemical Analysis, Ehime University. Mass spectra were recorded on a Hitachi M-2000 spectrometer. GC analyses were performed on a Hitachi Model 163, using a 3 mm i.d., ×2 m stainless steel column packed with 10% SE-30 on celite 545 AW. Preparative separations were performed by column chromatography over silica gel (Wakogel C-200). UV irradiations were carried out in a Pyrex vessel (Fuji glass) under a nitrogen atmosphere with a Fuji glass 300W high-pressure mercury arc lamp.

Materials. 2-Acetonyl-3-alkoxy-1,4-naphthoquinones **2** were prepared by the photochemical reaction of 2-alkoxy-1,4-naphthoquinones with 2-methoxy-1-propene in benzene.[4]

General Procedure for the Photochemical Reaction of 2-Acetonyl-3-alkoxy-1,4-naphthoquinones 2. A degassed solution of 2-acetonyl-3-alkoxy-1,4-naphthoquinones **2** (0.5 mmol) in 180 cm^3 of benzene or methanol in a Pyrex vessel, using a 300 W high-pressure mercury lamp from inside. The progress of the reaction was followed by thin-layer chromatography (TLC), NMR, or GC. After removal of solvent, the residual oil was separated by chromatography on

silica gel with dichloromethane-hexane as an eluant. Final purification was usually accomplished by preparative TLC and recrystallization.

Physical Properties of Photoproducts. 4-Methylnaphtho-[2,3-*d*]-1,3-dioxepin-6,11-dione (3a): Mp 197—198°C; ^{1}H NMR (270 MHz, $CDCl_3$) δ=2.13 (3H, s), 5.51 (2H, s), 6.00 (1H, s), 7.53—7.76 (2H, m), 7.83—8.13 (2H, m); ^{13}C NMR (22.5 MHz, $CDCl_3$) δ=22.38 (q), 93.78 (t), 95.14 (d), 124.23 (s), 126.29 (d), 126.72 (d), 131.11 (s), 131.59 (s), 133.71 (d), 155.70 (s), 165.18 (s), 178.18 (s, C=O), 183.76 (s, C=O); IR (KBr) 1660, 1650, 1625, 1595, 1260 cm^{-1}; MS (20 eV), *m/z* 242 (M^+); UV (λ_{max}, nm (log ε), CH_2Cl_2) 248 (4.30), 280 (4.27), 337 (3.54), 442 (3.30); Found: C, 69.40; H, 4.10%. Calcd for $C_{14}H_{10}O_4$: C, 69.42; H, 4.16%.

2,4-Dimethylnaphtho[2,3-*d*]-1,3-dioxepin-6,11-dione (3b): Mp 188—190°C; ^{1}H NMR (270 MHz, $CDCl_3$), δ=1.79 (3H, d, *J*=7.1 Hz), 2.09 (3H, s), 5.29 (1H, q, *J*=7.1 Hz), 5.94 (1H, s), 7.67—7.70 (2H, m), 8.07—8.10 (2H, m); ^{13}C NMR (22.5 MHz, $CDCl_3$) δ=20.81 (q), 22.60 (q), 94.81 (d), 101.15 (d), 124.66 (s), 126.34 (d), 126.66 (d), 131.76 (s), 133.71 (d), 154.55 (s), 163.45 (s), 170.63 (s, C=O), 183.93 (s, C=O); IR (KBr) 1676, 1659, 1638, 1597, 1576 cm^{-1}; MS (20 eV), *m/z* 256 (M^+); UV (λ_{max}, nm (log ε), CH_2Cl_2) 278 (4.31), 452 (3.50); Found: C, 70.42; H, 4.70%. Calcd for $C_{15}H_{12}O_4$: C, 70.31; H, 4.72%.

2,2-Dimethylnaphtho[2,3-*d*]-1,3-dioxepin-6,11-dione (3c): Mp 90—91°C; ^{1}H NMR (270 MHz, $CDCl_3$), δ=1.64 (6H, s), 2.11 (3H, s), 6.04 (1H, s), 7.55—7.75 (2H, m), 7.95—8.15 (2H, m); ^{13}C NMR (22.5 MHz, $CDCl_3$) δ=23.68 (q), 25.74 (q), 95.51 (d), 104.56 (s), 126.23 (d), 126.61 (d), 131.76 (s), 133.49 (d), 133.60 (d), 150.66 (s), 160.31 (s), 179.16 (s, C=O), 183.98 (s, C=O); IR (KBr) 1650, 1620, 1590, and 1260 cm^{-1}; MS (20 eV), *m/z* 270 (M^+); UV (λ_{max}, nm (log ε), CH_2Cl_2) 273 (4.44), 446 (3.62); Found: C, 71.15; H, 5.18%. Calcd for $C_{16}H_{14}O_4$: C, 71.10; H, 5.22%.

Reductive Acetylation of the Quinones. Quinones (0.1 mmol), an excess amount of zinc powder (200 mg), and sodium acetate (30 mg) were added to acetic anhydride (3 cm^3). Then, the mixture was refluxed for 30 min. After the yellow color due to the quinone disappeared completely, the reaction mixture was hydrolyzed and neutralized with sodium carbonate. The acetate was extracted with dichloromethane from the reaction mixture and purified further by p-TLC.

Physical Properties of the Diacetate. 6,11-Diacetoxy-4-methylnaphtho[2,3-*d*]-1,3-dioxepin (7a): Mp 169—170°C; ^{1}H NMR (270 MHz, $CDCl_3$) δ=2.05 (3H, s), 2.43 (3H, s), 2.46 (3H, s), 5.43 (2H, s), 7.25—7.50 (2H, m), 7.55—7.85 (2H, m); IR (KBr) 1760, 1655, 1603, 1185, 1082 cm^{-1}; MS (20 eV), *m/z* 328 (M^+).

6,11-Diacetoxy-2,4-dimethylnaphtho[2,3-*d*]-1,3-dioxepin (7b): Mp 158—160°C; ^{1}H NMR (90 MHz, $CDCl_3$) δ=1.63 (3H, d, *J*=5.1 Hz), 2.05 (3H, s), 2.43 (3H, s), 2.49 (3H, s), 5.38 (1H, q, *J*=5.1 Hz), 5.49 (1H, s), 7.28—7.50 (2H, m), 7.55—7.90 (2H, m); IR (KBr) 1756, 1647, 1605, 1183, 1087 cm^{-1}; MS (20 eV), *m/z* 342 (M^+).

6,11-Diacetoxy-2,2,4-trimethylnaphtho[2,3-*d*]-1,3-dioxepin (7c): Mp 205—206°C; ^{1}H NMR (90 MHz, $CDCl_3$) δ=1.58 (6H, s), 2.03 (3H, s), 2.48 (3H, s), 5.50 (1H, s), 7.24—7.51 (2H, m), 7.53—7.80 (2H, m); IR (KBr) 1760, 1655, 1603, 1185, 1086 cm^{-1}; MS (20 eV), *m/z* 356 (M^+).

2-Acetonyl-1,4-diacetoxy-3-methoxynaphthalene (9a): Mp 118—120°C; ^{1}H NMR (90 MHz, $CDCl_3$) δ=1.97 (3H, s), 2.43 (3H, s), 2.47 (3H, s), 3.75 (2H, s), 3.88 (3H, s), 7.30—7.57 (2H, m), 7.60—7.90 (2H, m); IR (KBr) 1760, 1715, 1603, 1210, 1178 cm^{-1}; MS (20 eV), *m/z* 328 (M^+).

2-Acetonyl-1,4-diacetoxy-3-ethoxynaphthalene (9b): Mp 98—100°C; ^{1}H NMR (90 MHz, $CDCl_3$) δ=1.37 (3H, t, *J*=7.0 Hz), 2.11 (3H, s), 2.43 (3H, s), 2.45 (3H, s), 3.74 (2H, s), 4.08 (2H, q, *J*=7.0 Hz), 7.30—7.58 (2H, m), 7.60—7.88 (2H, m); IR (KBr) 1763, 1718, 1606, 1206, 1181 cm^{-1}; MS (20 eV), *m/z* 344 (M^+).

2-Acetonyl-1,4-diacetoxy-3-isopropoxynaphthalene (9c): Oil; ^{1}H NMR (90 MHz, $CDCl_3$) δ=1.28 (6H, d, *J*=6.1 Hz), 2.06 (3H, s), 2.40 (3H, s), 2.42 (3H, s), 3.74 (2H, s), 4.44 (1H, sept, *J*=6.1 Hz), 7.30—7.55 (2H, m), 7.57—7.82 (2H, m); IR (KBr) 1774, 1709, 1603, 1178 cm^{-1}; MS (20 eV), *m/z* 358 (M^+).

2-Acetonyl-1,3,4-triacetoxynaphthalene (8): Mp 165—167°C; ^{1}H NMR (90 MHz, $CDCl_3$) δ=2.06 (3H, s), 2.34 (3H, s), 2.44 (3H, s), 2.47 (3H, s), 3.60 (2H, s), 7.30—7.90 (4H, m); IR (KBr) 1779, 1726, 1606, 1178 cm^{-1}; MS (20 eV), *m/z* 358 (M^+).

Reduction of 2-Acetonyl-3-isopropoxy-1,4-naphthoquinone 2c: A degassed solution of **2c** (0.1 mmol) in ether (5 cm^3) was added to a degassed solution of sodium hydrosulfite (0.23 mmol) in water (4 cm^3) and stirred vigorously under a nitrogen. The solution became pale yellow in 30 min. The reaction mixture was poured into a separatory funnel. After removing the aqueous layer, the etheral solution was washed with saturated brine and dried over anhydrous sodium sulfate. The filtrate was evaporated under reduced pressure to give the hydroquinone **5c** with a small amount of **2c** which was produced by the oxidation of **5c** in the usual work up. From ^{1}H NMR spectrum of the reaction mixture in benzene-d_6, the presence of **2c** was confirmed by direct comparison with ^{1}H NMR spectrum of an anthentic sample in benzene-d_6 and the structure of **5c** was determined by the follow ^{1}H NMR spectral deta: Isopropoxy substituent at δ=0.97 (d, *J*=6.1 Hz, 6H, -OCH($\underline{CH_3}$)$_2$), and 3.74 (sept, *J*=6.4 Hz, 1H, -O$\underline{CH}$-(CH$_3$)$_2$) and acetonyl substituent at δ=1.75 (s, 3H, -$\underline{CH_2}$-COCH$_3$), and 3.58 (s, 2H, -CH$_2$CO$\underline{CH_3}$), and aromatic hydrogen at δ=7.18—7.38 (m, 2H), and 8.25—8.45 (m, 2H).

In this investigation I am particularly indebted to Professor K. Maruyama of Kyoto University for his valuable suggestions and encouragement and to Dr. A. Osuka of Kyoto University for his helpful discussions. Helps given by Dr. H. Uno at Advanced Instrumentation Center for Chemical Analysis, Ehime University is greatly appreciated.

References

1) J. V. Ellis and J. E. Jones, *J. Org. Chem.*, **40**, 485 (1975).
2) O. E. Edwards and P-T. Ho, *Can. J. Chem.*, **56**, 733 (1978).
3) P. J. Wagner, M. A. Meador, B. P. Giri, and J. C. Scaiano, *J. Am. Chem. Soc.*, **107**, 1087 (1985).
4) K. Maruyama and S. Tai, *Chem. Lett.*, **1985**, 681.
5) K. Maruyama, A. Osuka, K. Nakagawa, T. Jinsenji, and K. Tabuchi, *Chem. Lett.*, **1988**, 1505.
6) R. Hout and P. Brassard, *Can. J. Chem.*, **52**, 88 (1974).
7) "Rearrangements in Ground and Excited States," ed by P. de Mayo, Academic Press, New York (1980), Vol. 3, p. 407.
8) A. Osuka, *J. Org. Chem.*, **47**, 3131 (1982).
9) N. P. Gritsan and N. M. Bazhin, *Izv. Akad. Nauk SSSR, Ser. Khim.*, **1980**, 1275.

Conversion of (+)-8,11,13-Abietatriene into (15*R*)-16-Hydroxyferruginol and Its (15*S*)-Epimer

Takashi MATSUMOTO,* Hiromitsu TERAO, and Sachihiko IMAI†
Department of Applied Material Science, Faculty of Integrated Arts and Sciences,
University of Tokushima, Minamijosanjima, Tokushima 770
† Suzugamine Women's College, Inokuchi, Nishi-ku, Hiroshima 733
(Received April 15, 1991)

Synopsis. (+)-8,11,13-Abietatriene was converted into (15*R*)-16-hydroxyferruginol (**1a**) and its (15*S*)-epimer (**1b**) by the introduction of hydroxyl groups at the C-12 and C-16 positions.

16-Hydroxyferruginol has been isolated from the seed of *Thujopsis dolabrata* Sieb. et Zucc. var *dolabrata* by Hasegawa and Hirose.[1] In a previous paper,[2] we reported the total syntheses of (15*R*)-16-hydroxyferruginol (**1a**) and its (15*S*)-epimer (**1b**), and determined the absolute configuration of the C-15 position in the natural compound to be the *R*-configuration. These C-15 epimeric 16-hydroxyferruginols (**1a** and **1b**) are also useful intermediates for the syntheses of highly-oxygenated abietane-type diterpenes possessing an asymmetric center at the C-15 position such as (15*R*)-coleon C (**2a**),[3,4] (15*S*)-coleon C (**2b**),[3,4] lycoxanthol (**3**),[5,6] nellionol,[7] hyptol,[8] and so on. As an extension of our previous work, we describe here the syntheses of **1a** and **1b**, starting from natural (+)-8,11,13-abietatriene (**4**) as an optically-active relay compound.

Dehydrogenation of **4** with 2,3-dichloro-5,6-dicyano-1,4-benzoquinone (DDQ) in refluxing 1,4-dioxane afforded the corresponding isopropenyl compound (**5**) which was immediately submitted to hydroboration–oxidation and the resulting C-15 epimeric mixture of 8,11,13-abietatrien-16-ols (**6**: 33% yield from **4**) was further converted into 4-nitrobenzoates (**7**: 93% yield) by heating with 4-nitrobenzoyl chloride in pyridine. The Friedel-Crafts acylation of **7** with acetyl chloride and anhydrous aluminium chloride in nitrobenzene afforded a C-15 epimeric mixture (*ca.* 1:1 ratio) of 12-acetyl compounds (**8a,b**) in a 63% yield. This mixture of **8a,b** was carefully separated by repeated column chromatography and recrystallization to give pure crystalline (15*R*)-12-acetyl-16-(4-nitrobenzoyloxy)-8,11,13-abietatriene (**8a**), mp 139—142 °C, and its (15*S*)-epimer (**8b**), mp 166—167 °C. The Baeyer–Villiger oxidations of **8a** and **8b** with *m*-chloroperbenzoic acid and *p*-toluenesulfonic acid in refluxing 1,2-dichloroethane, followed by reductions of the resulting acetates, **9a** (59% yield) and **9b** (70% yield), with lithium aluminium hydride in dry ether afforded the desired **1a** (90% yield) and **1b** (97% yield), respectively. The physical and spectral data of the synthetic **1a** and **1b** were identical with those of authentic (15*R*)-16-hydroxyferruginol and its (15*S*)-epimer,[2] respectively.

Experimental

All melting points are uncorrected. The IR spectra and optical rotations were measured in chloroform. The column chromatography was performed using Merck silica gel (0.063 mm).

16-(4-Nitrobenzoyloxy)-8,11,13-abietatriene (7). A mixture of (+)-8,11,13-abietatriene (**4**) (26.00 g) and 2,3-dichloro-5,6-dicyano-1,4-benzoquinone (96%: 26.20 g) in 1,4-dioxane (260 ml) was refluxed for 4 h. The mixture was passed through an alumina (Merck Act. II-III, 220 g) column and the column was washed with benzene (800 ml). The eluate was evaporated in vacuo to give a crude 8,11,13,15-abietatetraene

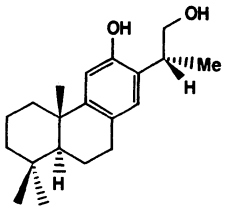

1a

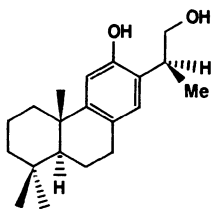

1b

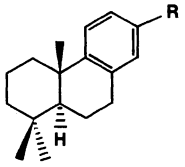

4 R=CHMe2
5 R=C(Me)=CH2

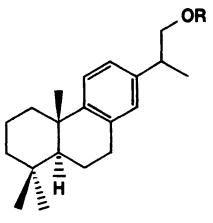

6 R=H
7 R=COC6H4NO2(p)

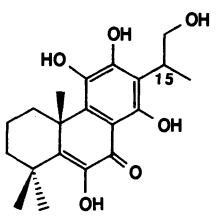

2a 15R
2b 15S

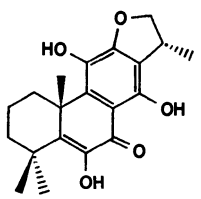

3

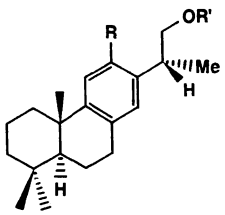

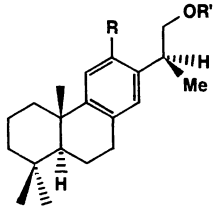

8a R=Ac, R'=COC6H4NO2(p) **8b**
9a R=OAc, R'=COC6H4NO2(p) **9b**

(**5**) (23.358 g), ^{1}H NMR (60 MHz, CCl_4) δ=0.93 (6H, s, $-C(CH_3)_2$), 1.14 (3H, s, 10-CH_3), 2.07 (3H, bs, 15-CH_3), 4.87 (1H, bs) and 5.17 (1H, bs) ($-C(CH_3)=CH_2$).

A solution of tetrahydrofuran–borane (1/1) addition compound (1 mol dm^{-3}: 43.5 ml) was added to a stirred solution of the crude **5** (23.358 g) in dry tetrahydrofuran (200 ml) at −15 to −10 °C for 30 min under a stream of nitrogen. After the mixture was stirred at 0—5 °C for 3 h, the following compounds were added successively: aqueous tetrahydrofuran (50%: 15.5 ml), aqueous sodium hydroxide (12%: 15.5 ml), and hydrogen peroxide (30%: 15.5 ml) at −15 to −5 °C. The mixture was stirred at −5—0 °C for 30 min and then at room temperature for 1.5 h, diluted with brine, and extracted with ether. The ether extract was washed with brine, dried over sodium sulfate, and evaporated in vacuo. The residue was chromatographed on silica gel (0.063—0.200 mm, 250 g), using benzene as an eluent, to give mainly recovered **4** (11.91 g). Further elution with benzene afforded a mixture of the C-15 epimeric 8,11,13-abietatrien-16-ols (**6**) (9.116 g: 33.1% yield from **4**), IR 3580 and 3425 cm^{-1}, ^{1}H NMR (60 MHz, CCl_4) δ=0.95 (6H, s, $-C(CH_3)_2$), 1.15 (3H, s, 10-CH_3), 1.18 (3H, d, J=7 Hz, 15-CH_3), 3.45 (2H, d, J=7 Hz, $-CH_2OH$), 6.72 (1H, bs, 14-H), 6.80 (1H, bd, J=8 Hz, 12-H), and 7.05 (1H, d, J=8 Hz, 11-H).

A mixture of compound **6** (2.755 g) and 4-nitrobenzoyl chloride (2.678 g) in pyridine (14 ml) was heated at 80—85 °C for 2.5 h. After the usual work-up, the crude product was recrystallized from hexane to give a C-15 epimeric mixture of **7** (1.936 g: 46.2% yield), mp 97—98 °C, IR 1720 cm^{-1}. Found: C, 74.48; H. 7.84; N, 2.94%. Calcd for $C_{27}H_{33}O_4N$: C, 74.45; H, 7.64; N, 3.22%. The mother liquor of recrystallization was evaporated in vacuo. The residue was chromatographed on silica gel (20 g), using hexane–benzene (1:1) as an eluent, to give additional **7** (1.956 g: 46.7% yield).

(15R)-12-Acetyl-16-(4-nitrobenzoyloxy)-8,11,13-abietatriene (8a) and Its (15*S*)-Epimer (8b). Anhydrous aluminium chloride (2.370 g) was added at 0—5 °C to a stirred solution of **7** (1.936 g) and acetyl chloride (1.30 ml) in nitrobenzene (12 ml). The mixture was stirred at this temperature for 30 min and then at room temperature for 1.5 h, then poured into ice-dilute hydrochloric acid and extracted with ether. The ether extract was washed with aqueous sodium hydrogencarbonate and brine, dried, and evaporated in vacuo. The residue was chromatographed on silica gel (100 g), using hexane–benzene (3:7) as an eluent, to give a mixture (ca. 1:1 ratio) of **8a** and **8b** (1.331 g: 62.7% yield). This mixture was separated into pure **8a** and **8b** by repeated column chromatography and recrystallization.

8a: Mp 139—142 °C (from acetone–hexane), $[\alpha]_D$+42.7° (*c* 1.34), IR 1722 and 1675 cm^{-1}; ^{1}H NMR (90 MHz, CCl_4) δ=0.93 (6H, s, $-C(CH_3)_2$), 1.18 (3H, s, 10-CH_3), 1.32 (3H, d, J=7 Hz, 15-CH_3), 2.50 (3H, s, $-COCH_3$), 3.97 (1H, m, 15-H), 4.36 (2H, d, J=7 Hz, 15-CH_2O–), 7.00 (1H, s, 14-H), 7.43 (1H, s, 11-H), 8.07 (2H, d, J=10 Hz) and 8.21 (2H, d, J=10 Hz) ($-C_6H_4NO_2$). Found: C, 72.74; H, 7.60; N, 2.65%. Calcd for $C_{29}H_{35}O_5N$: C, 72.93; H, 7.39; N, 2.93%.

8b: Mp 166—167 °C (from acetone–hexane), $[\alpha]_D$+35.0° (*c* 2.86), IR 1725 and 1680 cm^{-1}; ^{1}H NMR (90 MHz, CCl_4) δ=0.93 (3H, s) and 0.95 (3H, s) ($-C(CH_3)_2$), 1.18 (3H, s, 10-CH_3), 1.30 (3H, d, J=7 Hz, 15-CH_3), 2.49 (3H, s, $-COCH_3$), 3.97 (1H, m, 15-H), 4.40 (2H, d, J=7 Hz, 15-CH_2O–), 7.00 (1H, s, 14-H), 7.43 (1H, s, 11-H), 8.08 (2H, d, J=10 Hz) and 8.22 (2H, d, J=10 Hz) ($-C_6H_4NO_2$). Found: C, 72.70; H, 7.61; N, 2.79%. Calcd for $C_{29}H_{35}O_5N$: C, 72.93; H, 7.39; N, 2.93%.

(15*R*)-12-Acetoxy-16-(4-nitrobenzoyloxy)-8,11,13-abietatriene (9a) and Its (15*S*)-Epimer (9b). a): A mixture of **8a** (110.0 mg), *m*-chloroperbenzoic acid (80%: 99.4 mg), and *p*-toluenesulfonic acid (10.0 mg) in 1,2-dichloroethane (1.5 ml) was refluxed for 3 h. The mixture was cooled, diluted with ether, and the ether solution was washed successively with aqueous potassium iodide, aqueous sodium thiosulfate, aqueous sodium hydrogencarbonate, and brine. The dried solution was evaporated in vacuo. The residue was chromatographed on silica gel (5 g), using benzene as an eluent, to give **9a** (67.4 mg: 59.3% yield) which was recrystallized from methanol, mp 110—113 °C, $[\alpha]_D$+67.4° (*c* 1.41), IR 1758 and 1725 cm^{-1}. Found: C, 70.26; H, 7.33; N, 2.54%. Calcd for $C_{29}H_{35}O_6N$: C, 70.56; H, 7.15; N, 2.84%.

b): A mixture of **8b** (358.0 mg), *m*-chloroperbenzoic acid (80%: 324.0 mg), and *p*-toluenesulfonic acid (20.0 mg) in 1,2-dichloroethane (3.5 ml) was treated as described in a). The crude product was chromatographed on silica gel (15 g), using benzene as an eluent, to give **9b** (259.6 mg: 70.2% yield) which was recrystallized from acetone–methanol, mp 114—116 °C, $[\alpha]_D$+11.8° (*c* 2.64), IR 1755 and 1725 cm^{-1}. Found: C, 70.70; H, 7.35; N, 2.65%. Calcd for $C_{29}H_{35}O_6N$: C, 70.56; H, 7.15; N, 2.84%.

(15*R*)-16-Hydroxyferruginol (1a) and Its (15*S*)-Epimer (1b). a): A mixture of **9a** (51.0 mg) and lithium aluminium hydride (20.0 mg) in dry ether (1.5 ml) was stirred at room temperature for 1.5 h. The mixture was poured into ice-dilute hydrochloric acid and extracted with ether. The ether extract was washed with brine, dried, and evaporated in vacuo. The residue was chromatographed on silica gel (5 g), using ether–benzene (8:92) as an eluent, to give **1a** (28.1 mg: 90.1% yield) which was recrystallized from acetone–hexane, mp 138—139 °C, $[\alpha]_D$+64.9° (*c* 0.96), IR 3600 and 3325 cm^{-1}, ^{1}H NMR (90 MHz, $CDCl_3$) δ=0.89 (3H, s), and 0.91 (3H, s), ($-C(CH_3)_2$), 1.13 (3H, s, 10-CH_3), 1.24 (3H, d, J=7 Hz, 15-CH_3), 3.15 (1H, m, 15-H), 3.64 (1H, dd, J=10 and 7.5 Hz) and 3.88 (1H, dd, J=10 and 4 Hz) (15-CH_2OH), and 6.72 (2H, s, 11-H and 14-H). Found: C, 79.31; H, 10.28%. Calcd for $C_{20}H_{30}O_2$: C, 79.42; H, 10.00%.

b): A mixture of **9b** (179.9 mg) and lithium aluminium hydride (70.0 mg) in dry ether (4.0 ml) was treated as described in a). The crude product was chromatographed on silica gel (5 g), using ether-benzene (8:92) as an eluent, to give **1b** (107.0 mg: 97.1% yield) which was recrystallized from acetone–hexane, mp 179—180 °C, $[\alpha]_D$+ 46.0° (*c* 1.37), IR (KBr) 3550 and 3270 cm^{-1}, ^{1}H NMR (90 MHz, $CDCl_3$) δ=0.91 (6H, s, $-C(CH_3)_2$), 1.16 (3H, s, 10-CH_3), 1.26 (3H, d, J=7 Hz, 15-CH_3), 3.15 (1H, m, 15-H), 3.64 (1H, dd, J=10 and 7 Hz) and 3.88 (1H, dd, J=10 and 4 Hz) (15-CH_2OH), and 6.74 (2H, s, 11-H and 14-H). Found: C, 79.28; H, 10.23%. Calcd for $C_{20}H_{30}O_2$: C, 79.42; H, 10.00%.

References

1) S. Hasegawa and Y. Hirose, *Phytochemistry,* **21**, 643 (1982).

2) T. Matsumoto, S. Imai, S. Miuchi, and H. Sugibayashi, *Bull. Chem. Soc. Jpn.,* **58**, 340 (1985).

3) P. Ruedi, J. M. Schmid, and C. H. Eugster, *Helv. Chim. Acta,* **65**, 2181 (1982).

4) T. Matsumoto, S. Imai, and T. Yoshinari, *Bull. Chem. Soc. Jpn.,* **60**, 2435 (1987).

5) R. H. Burnell, L. Mo, and M. Moinas, *Phytochemistry,* **11**, 2815 (1972).

6) T. Matsumoto, S. Imai, and T. Yoshinari, *Bull. Chem. Soc. Jpn.,* **60**, 3639 (1987).

7) T. Matsumoto, S. Imai, and T. Yoshinari, *Bull. Chem. Soc. Jpn.,* **58**, 1165 (1985).

8) F. D. Monache, F. Marletti, G. Marini-Bettolo, J. F. Mellow, and I. L. D'Albuquerque, *Gazz. Chim. Ital.,* **107**, 319 (1977).

A Convenient Preparation of Ketones by the Oxidation of Secondary Alcohols with Chromium(VI) Trioxide in Aprotic Solvent in the Presence of "Wet"-Aluminum Oxide

Masao HIRANO, Sonoko NAGASAWA, and Takashi MORIMOTO*
Department of Applied Chemistry, Faculty of Technology, Tokyo University of Agriculture and Technology, Koganei, Tokyo 184
(Received April 22, 1991)

Synopsis. The oxidation of aliphatic and alicyclic secondary alcohols with chromium(VI) trioxide in the presence of "wet"-aluminum oxide in hexane gave the corresponding ketones in excellent yields under mild conditions.

Recently, supported reagents, consisting of a large number of combinations of agents and such inorganic solid materials as silica gel, aluminum oxide (hereafter referred as alumina), graphite, polymers, zeolites, and clay minerals, etc., have been given considerable attention because of their improved selectivity and reactivity as well as manipulative simplicity. Thus, supported reagents have been recommended for many catalytic and stoichiometric processes, including oxidation, reduction, substitution, elimination, rearrangement, hydrogenation, polymerization, etc., and especially for organic syntheses.[1,2]

In recent communications, we have reported facile and convenient oxidations of alcohols with sodium bromite ($NaBrO_2$),[3] chromium(VI) trioxide,[4] and "Oxone",[5,6] and a novel Baeyer–Villiger-type lactonization of alicyclic ketones with Oxone[7] in aprotic solvents in the presence of commercial chromatographic alumina. The oxidizing milieu of these processes are intimately analogous to a supported reagent system, but the reaction can be immediately started only by mixing alumina, a solvent, and an oxidant with a substrate without the preparation of a supported reagent. In this article, we wish to describe some observations on the facile oxidation of various aliphatic and alicyclic secondary alcohols with chromium(VI) trioxide in aprotic solvents in the presence of "wet"-alumina, since the reaction offers a convenient and selective synthesis of ketones under neutral and mild conditions.

Results and Discussion

The reaction was carried out by mixing finely-ground chromium(VI) trioxide, an alcohol, and an aprotic solvent in the presence or absence of alumina and by magnetic stirring of the heterogeneous mixture under an inert atmosphere in order to avoid autoxidation. It should be noted that efficient stirring was indispensable throughout a given period to ensure a smooth reaction and to attain a reproducible result (±5%<). A small amount of the supernatant was withdrawn at intervals and analyzed by GLC in order to follow the progress of the reaction. After a given reaction period, filtration of an insoluble material and washing of the residue with ether, followed by evaporation of the combined solvent in vacuo, left a ketone.

In the absence or presence of commercial "dry"-alumina, the reaction was rather slow. Indeed, in the oxidation of 4-methylcyclohexanol (**1**) in hexane at room temperature for 15 h ([CrO_3]/[**1**]=1.5; mole ratio), almost all or a considerable amount of **1** (98 or 71%, respectively; by GLC) was recovered, resulting only in the poor formation of 4-methylcyclohexanone (**2**) (trace or 12%, respectively). In addition, the extensive formation of an unknown by-product (16%; GLC selectivity) was observed in the latter case. On the other hand, when the reaction was conducted in the presence of "wet"-alumina (see the Experimental section), 95% of **1** was consumed under the same conditions as above, resulting in the selective formation of **2**. In view of the reactivity of CrO_3 and selectivity of the ketone, "wet"-alumina was clearly proven to play a decisive role in the oxidation. The atomic absorption analyses showed that no detectable amount of a chromium species was involved in the solvent at any time during the reaction, indicating clearly that the reaction occurred exclusively on the alumina surface. The mechanistic details of the present system are regrettably still obscure, although there have been some suggestions of a probable functional role of a support[8] and water adsorbed on a support surface.[9]

The oxidation was also performed in various aprotic solvents (carbon tetrachloride, chloroform, dichloromethane, benzene, and ethyl acetate). In carbon tetrachloride, chromium(VI) trioxide exhibited comparable reactivity to that in hexane, and similar selectivity of a ketone was observed. However, the reaction was rather slow in the other solvents. For example, when cyclododecanol (**3**) was oxidized with a CrO_3-"wet"-alumina system at 303 K for 15 h ([CrO_3]/[**3**]=1.5), the conversions of **3** were 98, 94, 15, 49, 58, and 58% in hexane, carbon tetrachloride, chloroform, dichloromethane, benzene, and ethyl acetate, respectively. Using acetone and 1,4-dioxane as a solvent should be avoided; it was proved that contact of a mixture of chromium(VI) trioxide and "wet"-alumina with these solvents caused immediate ignition. Thus, hexane was our solvent of choice based on the experimentally determined reasonable reactivity of chromium(VI) trioxide in the solvent as well as its low cost and toxicity as compared with chlorinated hydrocarbons, which are frequently used in conventional oxidations with chromium(VI)-based reagents;[10] additionally, its high volatility leads to a facile product isolation.

The oxidation of a variety of alicyclic and aliphatic secondary alcohols with chromium(VI) trioxide was examined in hexane. The alcohols underwent smooth oxidation under mild conditions in the presence of "wet"-alumina. Reaction conditions were chosen on the basis

Table 1. Oxidation of Aliphatic and Alicyclic Secondary Alcohols with Chromium(VI) Trioxide in Hexane in the Presence of "Wet"-Alumina[a)]

Entry No.	Alcohols	$[CrO_3]/[Alcohol]$	Temp	Ketones[b)]
		Mole ratio	K	%
1	2-Hexanol	1.5	313	95
2	2-Heptanol	1.5	313	91
3	2-Octanol	1.5	313	97
4	2-Decanol	1.5	313	99
5	Cyclopentanol	2.0	313	91
6	Cyclohexanol	2.0	313	97
7	Cycloheptanol	1.5	313	90
8	Cyclooctanol	1.5	313	93
9	Cyclododecanol (**3**)	1.5	303	96
10	2-Methylcyclohexanol	2.0	323	90
11	3-Methylcyclohexanol	1.5	323	89
12	4-Methylcyclohexanol (**1**)	1.5	323	87
13	2-Ethylcyclohexanol (**4**)	1.5	323	89
14	4-Ethylcyclohexanol	1.5	323	87
15	2-*t*-Butylcyclohexanol	1.5	313	95
16	4-*t*-Butylcyclohexanol	1.5	313	92
17	2-Cyclohexylcyclohexanol	2.0	313	89
18	4-Cyclohexylcyclohexanol	2.0	313	98
19	2,6-Dimethylcyclohexanol	1.5	323	92

a) Under argon for 15 h; 0.5 g of alcohol, 10 cm^3 of hexane, and 2.4 g of "wet"-alumina were used in every run.
b) Isolated yield.

of reactivity of the alcohols and selectivity of the ketones. When equimolar with an alcohol or a slightly larger amount of CrO_3 was used, the ketones were contaminated with the parent alcohols in some cases; e.g., upon oxidation of 2-ethylcyclohexanol (**4**) at 323 K for 15 h ($[CrO_3]/[\mathbf{4}]=1.2$), 21% of **4** was unreacted, whereas **4** was completely consumed under the conditions of Entry 13 in Table 1. Consequently, the oxidations were carried out by using 1.5—2.0 moles of chromium(VI) trioxide per mole of an alcohol in order to complete the reaction. The results are summarized in Table 1. The influence of carbon-chain length of 2-alkanols (Entries 1—4), ring size of simple cycloalkanols (Entries 5—9), and bulkiness or position of an alkyl substituent on the cyclohexane ring (Entries 10—19) was investigated; interestingly, however, there was no appreciable difference in the yield of the ketones. Thus, the CrO_3–"wet"-alumina system was proven to be applicable to a wide variety of secondary alcohols.

Oxidation of 1-alkanols, hexanol (**5a**), heptanol (**5b**), and octanol (**5c**), was also examined, giving a mixture of the corresponding aldehydes (**6a—c**) and the esters (**7a—c**). The selectivity of **6** and **7** was found to be dependent on the concentration of chromium(VI) trioxide.

$$\underset{\mathbf{5}}{3\,RCH_2OH} \longrightarrow \underset{\mathbf{6}}{RCHO} + \underset{\mathbf{7}}{RCOOCH_2R}$$

For instance, the oxidation of hexanol at room temperature for 15 h ($[CrO_3]/[\mathbf{5a}]=1.2$, 2.0, and 3.0) gave 42, 45, and 43% of **6a** and 11, 19, and 53% of **7a**, respectively (by GLC); in the former two cases, 36 and 9% of **5a** was recovered, respectively. The oxidation of **5b,c** at room temperature for 15 h ($[CrO_3]/[\mathbf{5}]=3.0$) gave **6b,c** in 47 and 61% yields, and **7b,c** in 48 and 33% yields, respectively. It was found that there was no remarkable difference in the reactivity of 1-alkanols and the 2-analogs. For example, the conversions of **5a** and 2-hexanol, and **5c** and 2-octanol were 98, 100, 98, and 100%, respectively, at 323 K for 15 h ($[CrO_3]/[Alcohol]=1.5$).

It was of considerable interest to extend the scope of the reaction to a chemoselective oxidation of the hydroxy group in a multifunctional substrate. Thus, the oxidation of the allylic alcohols was investigated. The oxidation of geraniol and its *cis*-isomer, nerol, at room temperature for 15 h ($[CrO_3]/[Alcohol]=3.0$) gave the corresponding aldehydes in 73 and 74% isolated yields, respectively. It is worth noting that the oxidation proceeded without an appreciable loss of the double bond stereochemistry. However, we felt that the results were not adequate enough to deserve a term of "synthetically useful tool" for the allylic oxidation. In addition, oxidation of cinnamyl alcohol was complicated by concurrent double bond cleavage, giving cinnamaldehyde and benzaldehyde both in only moderate yields. Accordingly, a further study is now being undertaken to determine favorable conditions for the chemoselective oxidation of various multifunctional alcohols.

Summing up, oxidation of aliphatic and alicyclic secondary alcohols by means of a combination of chromium(VI) trioxide and "wet"-alumina in hexane gave the corresponding ketones in excellent to almost-quantitative yields. It should be emphasized that the present reaction is fairly clean, and is performable not only instantly, but readily without suffering from the formation of the intractably tarry precipitate of a reduced chromium salt, which allows easy removal of the salt and also easy isolation of a ketone from the reaction mixture as exemplified by the procedures using alumina-

supported chromium(VI) reagents. Thus, this system can be added to a list of efficient and mild oxidants, owing to its easy accessibility, manipulative simplicity, and versatility.

Experimental

^{1}H NMR spectra were measured with a JEOL PMX-60 model spectrometer for solutions in deuteriochloroform or carbon tetrachloride. IR spectra were recorded for thin films or KBr disks on a JASCO A-100 spectrophotometer. GLC was performed on a Shimadzu GC-6A instrument with a 2 m column packed with 5% PEG-20M on Chromosorb GAW-DMCS, with temperature programming. Atomic absorption analyses were carried out on a Hitachi 170-30 model apparatus.

Starting Materials. Commercial chromium(VI) trioxide was dried in vacuo and finely ground. All of the alcohols were also commercially available and were purified by distillation or recrystallization just before use. Solvents were rigorously dried and distilled. "Wet"-alumina was prepared by adding distilled water (2 g) to commercial chromatographic super-dried alumina (ICN BIOMEDICALS, Super I; 10 g) in portions, followed by vigorous shaking of the mixture for a few minutes until a free-flowing powder was obtained.

General Oxidation Procedures. The following procedures are representative. To a heterogeneous mixture of "wet"-alumina (2.4 g) and hexane (10 cm^3) in a round-bottomed flask was added chromium(VI) trioxide (1.5 moles of an alcohol) in portions with magnetic stirring; the stirring was continued for 10 min and 2-hexanol (0.5 g) was then added in a portion. After flushing with dry argon, the flask was sealed with a glass stopper or a silicon-rubber septum, through which the supernatant was withdrawn by a microsyringe in the course of the reaction. After magnetic stirring at 313 K for 15 h, the whole reaction mixture was transferred onto a Pyrex Buchner funnel with a fritted glass disk, and the residue was thoroughly washed with dry ether. Removing the combined solvent by rotary evaporation in vacuo left 2-hexanone, which had adequate purity (nearly 100% by GLC).

All ketones thus obtained were identified by a comparison of the NMR and IR spectra and GLC retention times with those of authentic samples.

The partial financial support for the present research from Nippon Silica Industrial Co., Ltd. and Daicel Chemical Industries, Ltd. is gratefully acknowledged.

References

1) An outline of the reactions with supported reagents, including alumina-supported reagents (Part V in the following book and Ref. 2) has been reviewed in "Preparative Chemistry Using Supported Reagents," ed by P. Laszlo, Academic Press, San Diego (1987).

2) A. McKillop and D. W. Young, *Synthesis,* **1979**, 401 and 481; G. H. Posner, *Angew. Chem., Int. Ed. Engl.,* **17**, 487 (1978), and references therein.

3) T. Morimoto, M. Hirano, Y. Aikawa, and X. Zhang, *J. Chem. Soc., Perkin Trans. 2,* **1988**, 2423.

4) M. Hirano, H. Kuroda, and T. Morimoto, *Bull. Chem. Soc. Jpn.,* **63**, 2433 (1990).

5) M. Hirano, M. Oose, and T. Morimoto, *Bull. Chem. Soc. Jpn.,* **64**, 1046 (1991).

6) "Oxone", a commercial trademark of a peroxomonosulfate compound, is a stable ternary composite of $KHSO_5$, $KHSO_4$, and K_2SO_4 in a 2:1:1 molar ratio, which is available from Aldrich Chemical Co., Inc.

7) M. Hirano, M. Oose, and T. Morimoto, *Chem. Lett.,* **1991**, 331.

8) S. L. Regan and C. Koteel, *J. Am. Chem. Soc.,* **99**, 3837 (1977); A. A. Jazzaa, J. H. Clark, and M. Robertson, *Chem. Lett.,* **1982**, 405.

9) E. Keinan and Y. Mazur, *J. Org. Chem.,* **43**, 1020 (1978).

10) Oxidation with chromium(VI)-based reagents or chromium(VI) complexes was briefly summarized in the following reviews: "Shin-Jikken Kagaku Kouza," Vol. 15, I-1, p. 105; K. B. Wiberg, "Oxidation in Organic Chemistry," ed by K. B. Wiberg, Academic Press, New York (1965), Part A, p. 69; M. Hudlicky, "Oxidation in Organic Chemistry," Am. Chem. Soc., Washington, DC (1990); F. Freeman, "Organic Syntheses by Oxidation with Metal Compounds," ed by W. J. Mijs and C. R. H. I. de Jonge, Plenum Press, New York (1986), p. 41; H. O. House, "Modern Synthetic Reactions," W. A. Benjamin, Inc., California (1972), p. 257.

11) S. J. Flatt, G. W. J. Fleet, and B. J. Taylor, *Synthesis,* **1979**, 815; Y.-S. Cheng, W.-L. Liu, and S. Chen., *ibid.,* **1980**, 223.

Further Chemical Studies on Anisatin, a Neurotoxic Sesquiterpenoid Having a β-Lactone

Haruki NIWA,* Itaru TSUKADA, Masanori NISIWAKI, and Kiyoyuki YAMADA
Department of Chemistry, Faculty of Science, Nagoya University, Chikusa, Nagoya 464
(Received April 30, 1991)

Synopsis. By a series of chemical reactions, anisatin was efficiently converted into the key intermediate employed in the synthesis of anisatin.

Anisatin (**1**) is a convulsant sesquiterpenoid isolated from the seeds of Japanese star anise (*Illicium anisatum* L.; shikimi in Japanese).[1,2] The structure of anisatin (**1**) was based on extensive chemical and spectroscopic studies.[2] The unique structure particularly characterized by a novel spiro β-lactone has made anisatin (**1**) a challenging synthetic target. Recently we have achieved the first total synthesis of anisatin (**1**) in the stereocontrolled manner.[3] In the course of synthetic studies of anisatin (**1**), we further investigated the reactivity of the uniquely arranged functional groups in anisatin (**1**) and the derivatives.[4] Described herein is the successful transformation of anisatin (**1**) into lactone **2**, the key intermediate employed in our recent synthesis of anisatin (**1**).[3]

First, we converted anisatin (**1**) into noranisatin acetonide (**4**). Thus, reaction of anisatin (**1**) with 2-methoxypropene in the presence of (+)-10-camphorsulfonic acid in *N,N*-dimethylformamide furnished anisatin acetonide (**3**) in 91% yield. Subsequent oxidation of **3** with $KMnO_4$ in AcOH–H_2O provided noranisatin acetonide (**4**) in 89% yield.

Next, we performed reduction of **4** with $LiAlH_4$ under various conditions and the results are summarized in Table 1. Reduction of **4** in tetrahydrofuran (THF) at reflux temperature yielded pentol **5** and acetal **6** in 30% and 25% yield, respectively. Reduction of **4** in THF at 0°C gave carboxylic acid **7** in 29% yield (isolated and characterized as methyl ester **8**). On reduction of **4** in ether at reflux temperature, **5** and **6** were obtained in 44% and 32% yield, respectively, together with a small amount of hemiacetal **9**[5] (13%). When reduction of **4** was performed in ether at −20°C, **9** was obtained as the major product (60%) along with lactone **10** (21%) and **7** (10%).

Oxidation of **9** wtih I_2–$CaCO_3$ in H_2O–MeOH furnished **10** in 78% yield. Finally, reaction of **10** with 2-methoxypropene in the presence of (+)-10-camphorsulfonic acid in benzene afforded rearranged lactone **2** in 90% yield. Spectral and chiroptical properties of **2** [$[\alpha]_D^{21}$ +14.5° (*c* 0.444, $CHCl_3$)] derived from natural anisatin (**1**) were identical with those of **2** [$[\alpha]_D^{21}$ +14.8° (*c* 0.446, $CHCl_3$)] synthesized from (*R*)-(+)-pulegone.[3]

Table 1. Reduction of **4** with $LiAlH_4$

Entry	Solvent	Temperature	Product[a]/%				
			5	**6**	**7**	**9**	**10**
1	THF	Reflux	30	25			
2	THF	0°C			29[b]		
3	Ether	Reflux	44	32		13	
4	Ether	−20°C			10	60	21

a) Isolated yield. b) Yield refers to the derived methyl ester **8**.

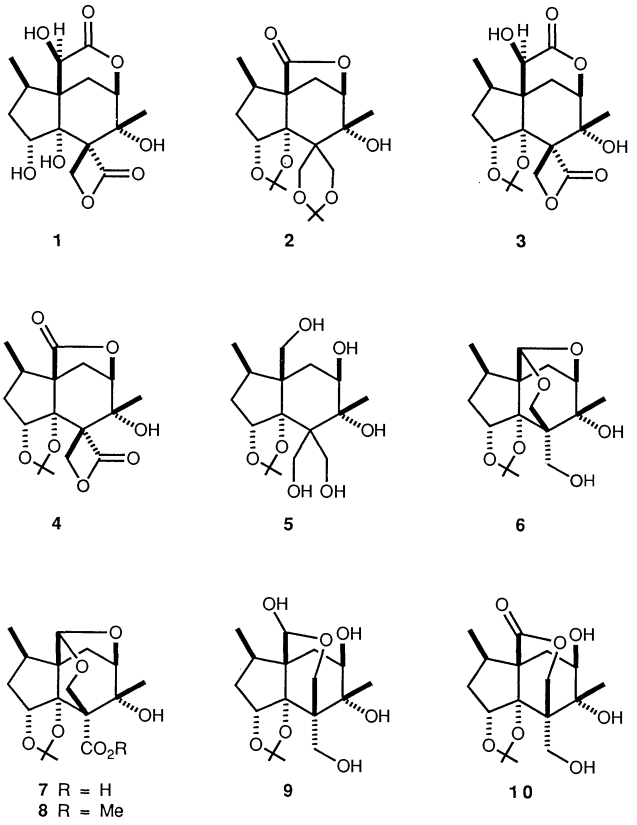

Experimental

Melting points are uncorrected. Optical rotations were measured on a JASCO DIP-181 polarimeter. Infrared (IR) spectra were obtained on a JASCO Model IR-810 spectrophotometer. Proton nuclear magnetic resonance (^1H NMR) spectra were recorded on a JEOL JNM-C675 (270 MHz) spectrometer in $CDCl_3$ using tetramethylsilane (TMS) as an internal standard. Chemical shifts are expressed in parts per million (ppm) downfield from TMS (δ=0.0) and coupling constants in Hz. The low-resolution (CIMS and EIMS) and high-resolution (HRCIMS and HREIMS) mass spectra were recorded on a JEOL JMS-LG2000 instrument using methane as the reagent gas for CIMS. Fuji-Davison silica gel BW-820MH was used for column chromatography. Merck precoated silica gel 60 F_{254} plates, 0.25 mm thickness, were used for analytical thin-layer chromatography. Benzene was distilled from Na under nitrogen. Tetrahydrofuran (THF) and ether were distilled from Na-benzophenone ketyl under

nitrogen. *N,N*-Dimethylformamide and pyridine were distilled from CaH_2 under nitrogen. Unless otherwise stated, organic solutions obtained by extractive workup were washed with saturated brine, dried over anhydrous Na_2SO_4, and concentrated under reduced pressure by a rotary evaporator.

Anisatin Acetonide (3). To a solution of anisatin (**1**) (515 mg, 1.6 mmol) in *N,N*-dimethylformamide (8 ml) were added 2-methoxypropene (0.22 ml, 2.4 ml) and (+)-10-camphorsulfonic acid (19 mg, 0.080 mmol). The reaction mixture was stirred at room temperature for 1.5 h. Pyridine (ca. 0.1 ml) was added for quenching the reaction and the mixture was concentrated in vacuo. The residue was purified by column chromatography on silica gel [30 g, benzene–acetone (5:1)] to give **3** (527 mg, 91%) as colorless needles; mp 206—208 °C (benzene); $[\alpha]_D^{23}$ +6.6° (*c* 0.14, $CHCl_3$); IR ($CHCl_3$) 3500, 3420, 1830, 1735, 1370, and 1100 cm^{-1}; ^1H NMR ($CDCl_3$, 270 MHz) δ=1.03 (3H, d, *J*=6.6 Hz), 1.54 (3H, s), 1.56 (3H, s), 1.75 (3H, s), 1.87 (1H, ddd, *J*=14.5, 8.2, 1.0 Hz), 2.02 (1H, dd, *J*=14.8, 3.6 Hz), 2.29 (1H, ddd, *J*=14.5, 11.9, 8.6 Hz), 2.44—2.53 (1H, m), 2.57 (1H, dd, *J*=14.8, 2.3 Hz), 3.26 (1H, s, –OH), 4.03 (1H, d, *J*=6.6 Hz), 4.12 (1H, br s), 4.33 (1H, dd, *J*=3.6, 2.3 Hz), 4.52 (1H, d, *J*=6.6 Hz), 4.90 (1H, dd, *J*=8.6, 1.0 Hz), and 5.44 (1H, d, *J*=1.0 Hz, –OH); CIMS *m/z* (rel intensity) 369 [$(M+H)^+$, 90], 353 (67), 339 (30), 323 (39), and 311 (100). Calcd for $C_{18}H_{24}O_8$: C, 58.69; H, 6.57%. Found: C, 58.51; H, 6.54%.

Noranisatin Acetonide (4). To a solution of **3** (1.1 g, 3.0 mmol) in acetic acid (25 ml) was added a solution of $KMnO_4$ (1.0 g, 6.6 mmol) in H_2O (25 ml). The reaction mixture was stirred at room temperature for 4 h. The reaction was quenched by the addition of saturated $Na_2S_2O_3$ solution (5 ml) and the mixture was extracted with ethyl acetate (3×5 ml). The combined organic layers were washed with saturated NaCl solution (50 ml), dried, and concentrated under reduced pressure. The residue was purified by column chromatography on silica gel [50 g, hexane–ether (6:1→4:1)] to give **4** (0.90 g, 89%) as colorless needles; mp 125.5—126.5 °C (benzene–hexane); $[\alpha]_D^{18}$ +55° (*c* 0.16, $CHCl_3$); IR ($CHCl_3$) 3480, 1830, 1775, 1385, 1375, and 1140 cm^{-1}; ^1H NMR ($CDCl_3$, 270 MHz) δ=1.09 (3H, d, *J*=6.6 Hz), 1.51 (3H, s), 1.54 (3H, s), 1.59 (3H, s), 2.02 (1H, dd, *J*=13.5, 5.9 Hz), 2.29—2.52 (3H, m), 2.75 (1H, d, *J*=12.5 Hz), 3.99 (1H, d, *J*=7.1 Hz), 4.27 (1H, br s, –OH), 4.28 (1H, d, *J*=7.1 Hz), 4.38 (1H, d, *J*=5.9 Hz), and 4.89 (1H, d, *J*=7.1 Hz); EIMS *m/z* (rel intensity) 338 (M^+, 10), 323 (100), 281 (15), and 263 (31). Calcd for $C_{17}H_{22}O_7$: C, 60.35; H, 6.55%. Found: C, 59.99; H, 6.51%.

$LiAlH_4$ Reduction of Noranisatin Acetonide (4) (Table 1).

(a) Reduction in THF at Reflux Temperature (Entry 1). To a solution of **4** (19 mg, 0.056 mmol) in THF (1 ml) was added a 1M (1M=1 mol dm^{-3}) solution of $LiAlH_4$ in THF (0.12 ml, 0.12 mmol). The reaction mixture was heated under reflux for 2 h. After the reaction mixture was cooled to room temperature, NaF (104 mg, 2.48 mmol) was added and the mixture was vigorously stirred for a while. To the ice-cooled mixture was added dropwise 10% H_2O–THF (1.5 ml). The mixture was stirred for 30 min at room temperature and filtered through a pad of Celite. The filter cake was washed thoroughly with THF. The combined organic solutions were concentrated under reduced pressure. The residue was subjected to column chromatography on silica gel [4 g, benzene–acetone (4:1→1:10→0:1)] to give pentol **5** (5.7 mg, 30%) and acetal **6** (4.1 mg, 25%) as a colorless oil, respectively.

5: $[\alpha]_D^{21}$ +1.2° (*c* 0.50, $CHCl_3$); IR ($CHCl_3$) 3450, 1390, 1150, and 1050 cm^{-1}; ^1H NMR ($CDCl_3$, 270 MHz) δ=1.02 (3H, d, *J*=6.6 Hz), 1.21 (3H, s), 1.50—1.60 (1H, m), 1.62 (3H, s), 1.68 (3H, s), 1.78 (1H, dd, *J*=14.0, 8.0 Hz), 2.08 (1H, dd, *J*=14.8, 4.0 Hz), 2.20—2.38 (1H, m), 2.49 (1H, ddd, *J*=14.0, 10.8, 8.0 Hz), 3.57—3.65 (1H, m, –OH), 3.63 (1H, d, *J*=14.0 Hz), 3.69 (1H, dd, *J*=4.0, 2.0 Hz), 3.88 (1H, d, *J*=12.0 Hz), 3.90—4.00 (1H, m, –OH), 4.18 (1H, d, *J*=13.0 Hz), 4.60—4.98 (2H, m), 4.83 (1H, d, *J*=14.0 Hz), 5.23 (1H, br s, –OH), and 5.25 (1H, d, *J*=8.0 Hz); EIMS *m/z* (rel intensity) 328 [$(M-H_2O)^+$, 43], 310 (38), 292 (21), and 55 (100). HREIMS. Found: *m/z* 310.1776. Calcd for $C_{17}H_{26}O_5$: $M-2\times H_2O$, 310.1780.

6: $[\alpha]_D^{21}$ −31.2° (*c* 0.511, $CHCl_3$); IR ($CHCl_3$) 3500, 1385, 1160, and 1035 cm^{-1}; ^1H NMR ($CDCl_3$, 270 MHz) δ=1.01 (3H, d, *J*=6.9 Hz), 1.27 (3H, s), 1.52 (3H, s), 1.56 (3H, s), 1.80 (1H, ddd, *J*=14.8, 12.8, 8.4 Hz), 1.89 (1H, dd, *J*=12.4, 5.0 Hz), 1.96 (1H, ddd, *J*=14.8, 8.4, 2.0 Hz), 2.28 (1H, d, *J*=12.4 Hz), 2.35—2.46 (1H, m), 2.46—2.55 (1H, m, –OH), 3.48 (1H, dd, *J*=12.9, 10.9 Hz), 3.64 (1H, br s, –OH), 3.82 (1H, d, *J*=5.0 Hz), 3.87 (1H, d, *J*=11.4 Hz), 4.10—4.16 (1H, m), 4.14 (1H, d, *J*=11.4 Hz), 4.98 (1H, dd, *J*=8.4, 2.0 Hz), and 5.31 (1H, s); EIMS *m/z* (rel intensity) 326 (M^+, 0.5), 311 (20), 308 (18), and 265 (100). HREIMS. Found: *m/z* 326.1709. Calcd for $C_{17}H_{26}O_6$: M, 326.1729.

(b) Reduction in THF at 0 °C (Entry 2). Reduction of **4** (19 mg, 0.056 mmol) with $LiAlH_4$ (0.12 mmol) was performed in THF at 0 °C for 20 min. After workup as described above, the crude product containing acid **7** was treated with ethereal CH_2N_2 and subjected to column chromatography on silica gel [3 g, benzene–acetone (10:1→5:1→1:1)] to give methyl ester **8** (5.5 mg, 29%) as a colorless oil: $[\alpha]_D^{21}$ −27.3° (*c* 0.134, $CHCl_3$); IR ($CHCl_3$) 3500, 1715, 1435, 1380, 1240, and 1140 cm^{-1}; ^1H NMR ($CDCl_3$, 270 MHz) δ=1.00 (3H, d, *J*=6.9 Hz), 1.24 (3H, s), 1.45 (3H, s), 1.48 (3H, s), 1.79 (1H, dd, *J*=11.8, 5.0 Hz), 1.82—1.92 (2H, m), 2.34—2.50 (1H, m), 2.56 (1H, d, *J*=11.8 Hz), 3.79 (3H, s), 3.90 (1H, d, *J*=5.0 Hz), 3.99 (1H, d, *J*=11.2 Hz), 4.45 (1H, d, *J*=11.2 Hz), 4.68 (1H, s, –OH), 5.09 (1H, dd, *J*=8.1, 1.0 Hz), and 5.29 (3H, s); EIMS *m/z* (rel intensity) 354 (M^+, 62), 339 (100), 311 (71), and 295 (63). HREIMS. Found: *m/z* 354.1675. Calcd for $C_{18}H_{26}O_7$: M, 354.1678.

(c) Reduction in Ether at Reflux Temperature (Entry 3). To a vigorously stirred suspension of $LiAlH_4$ (31 mg, 0.82 mmol) in ether (0.5 ml) was added dropwise a solution of **4** (16 mg, 0.047 mmol) in ether (1.5 ml). The reaction mixture was heated under reflux for 3 h. After workup as described above, the crude product was subjected to column chromatography on silica gel [2 g, benzene–acetone (4:1→3:1)] to give **5** (7.2 mg, 44%), **6** (5.1 mg, 32%), and hemiacetal **9**[5] (2.2 mg, 13%) as a colorless oil, respectively.

9: IR ($CHCl_3$) 3600, 3450, 1480, 1385, 1085, and 1010 cm^{-1}; ^1H NMR ($CDCl_3$, 270 MHz; signals for the major diastereomer) δ=1.02 (3H, d, *J*=6.9 Hz), 1.28 (3H, s), 1.56 (3H, s), 1.60 (3H, s), 1.88 (1H, ddd, *J*=15.8, 12.2, 8.2 Hz), 2.02 (1H, ddd, *J*=15.8, 8.5, 2.0 Hz), 2.08 (1H, dd, *J*=15.2, 4.9 Hz), 2.24 (1H, d, *J*=15.2 Hz), 2.20—2.35 (1H, m), 2.50—2.80 (1H, m, –OH), 3.52—3.70 (3H, m; 2H, m on addition of D_2O), 3.80 (1H, d, *J*=13.2 Hz), 3.93 (1H, d, *J*=13.2 Hz), 4.33 (1H, d, *J*=13.2 Hz), 4.58 (1H, br s), 4.65—4.80 (1H, m, –OH), 4.89 (1H, br s, –OH), and 5.13 (1H, dd, *J*=8.2, 2.0 Hz); EIMS *m/z* (rel intensity) 344 (M^+, 2), 326 (15), 311 (22), and 255 (100). HREIMS. Found: *m/z* 326.1733. Calcd for $C_{17}H_{26}O_6$: $M-H_2O$, 326.1730.

(d) Reduction in Ether at −20 °C (Entry 4). Reduction of **4** (43 mg, 0.13 mmol) with $LiAlH_4$ (1.3 mmol) was performed in ether at −20 °C for 3 h. After workup as described above, the crude product was subjected to column chromatography on silica gel [5 g, benzene–acetone (10:1→6:1→4:1)] to give **7** (4.3 mg, 10%; characterized as **8**), **9** (26 mg, 60%), and lactone **10** (9.1 mg, 21%) as a colorless oil, respectively.

10: $[\alpha]_D^{21}$ −85.4° (*c* 0.856, MeOH); IR ($CHCl_3$) 3600, 3460, 1735, 1455, 1385, and 1040 cm^{-1}; ^1H NMR ($CDCl_3$, 270 MHz) δ=1.21 (3H, d, *J*=6.9 Hz), 1.30 (3H, s), 1.56 (3H, s), 1.63 (3H, s), 1.60—1.70 (1H, m), 1.90 (1H, dd, *J*=14.5, 6.2 Hz), 2.20 (1H, dd, *J*=11.6, 2.7 Hz), 2.28 (1H, dd, *J*=11.6, 2.7 Hz), 2.41 (1H, dq, *J*=6.2, 6.9 Hz), 2.82—2.95 (1H, m, –OH), 3.48—3.60 (1H,

m), 3.76 (1H, dd, J=2.7, 2.7 Hz), 4.33 (1H, d, J=13.2 Hz), 4.43 (1H, d, J=11.9 Hz), 4.63 (1H, d, J=11.9 Hz), 4.78 (1H, br s, -OH), and 4.98 (1H, d, J=7.9 Hz); EIMS m/z (rel intensity) 342 (M^+, 60), 327 (81), 324 (40), 298 (46), and 294 (100). HREIMS. Found: m/z 342.1661. Calcd for $C_{17}H_{26}O_7$: M, 342.1678.

Oxidation of Hemiacetal 9 to Lactone 10. A mixture of **9** (27 mg, 0.079 mmol), I_2 (209 mg, 0.83 mmol), and $CaCO_3$ (252 mg, 2.52 mmol) in 50% H_2O–MeOH (2 ml) was stirred at 50 °C for 3 d in the dark. After cooling, the reaction mixture was filtered through a pad of Celite. The filter cake was washed thoroughly with MeOH. The filtrate and washings were combined and the solution was concentrated under reduced pressure. The residue was dilute with H_2O (5 ml) and extracted with EtOAc (4×5 ml). The combined organic layers were washed with saturated $Na_2S_2O_3$ solution and saturated NaCl solution, dried, and concentrated under reduced pressure. The crude product was purified by column chromatography on silica gel [1 g, benzene–acetone (8:1→4:1→1:1)] to give **10** (21 mg, 78%) along with the recovered **9** (2.8 mg, 10%).

Conversion of Lactone 10 into Lactone 2. A mixture of **10** (45 mg, 0.13 mmol), 2-methoxypropene (15 mg, 0.21 mmol), and (+)-10-camphorsulfonic acid (3 mg, 0.013 mmol) in benzene (3.5 ml) was stirred at room temperature for 2 h. The reaction was quenched by the addition of 2 drops of pyridine and the mixture was concentrated under reduced pressure. The residue was subjected to column chromatography on silica gel [2 g, benzene–acetone (20:1→1:1)] to give **2** (45 mg, 90%) as an amorphous solid: $[\alpha]_D^{21}$ +14.5° (c 0.444, $CHCl_3$) [synthetic **2**,[3] $[\alpha]_D^{21}$ +14.8° (c 0.446, $CHCl_3$)]; IR ($CHCl_3$) 3500, 1770, 1450, and 1380 cm^{-1}; ^1H NMR ($CDCl_3$, 270 MHz) δ=1.03 (3H, d, J=6.6 Hz), 1.32 (3H, s), 1.33 (3H, s), 1.52 (3H, s), 1.53 (3H, s), 1.56 (3H, s), 1.91 (1H, dd, J=12.8, 5.0 Hz), 2.22 (1H, dd, J=12.5, 5.3 Hz), 2.28 (1H, dd, J=12.8, 6.2 Hz), 2.32—2.47 (1H, m), 2.58 (1H, d, J=12.5 Hz), 3.25 (1H, br s, -OH), 3.55 (1H, d, J=13.2 Hz), 3.99 (1H, d, J=13.2 Hz), 3.98 (2H, s), 4.23 (1H, d, J=5.3 Hz), and 5.28 (1H, d, J=6.2 Hz); EIMS m/z (rel intensity) 382 (M^+, 1), 367 (100), 324 (87), 306 (41), and 279 (84). HRCIMS. Found: m/z 383.2069. Calcd for $C_{20}H_{31}O_7$: M+H, 383.2070.

References

1) J. F. Lane, W. T. Koch, N. S. Leeds, and G. Gorin, *J. Am. Chem. Soc.*, **74**, 3211 (1952).

2) K. Yamada, S. Takada, S. Nakamura, and Y. Hirata, *Tetrahedron*, **24**, 199 (1968).

3) H. Niwa, M. Nisiwaki, I. Tsukada, T. Ishigaki, S. Ito, K. Wakamatsu, T. Mori, M. Ikagawa, and K. Yamada, *J. Am. Chem. Soc.*, **112**, 9001 (1990).

4) Previous chemical studies: Ref. 2; see also, K. Yamada, S. Takada, and Y. Hirata, *Tetrahedron*, **24**, 1255 (1968).

5) This material was an 8:1 mixture concerning the hydroxyl group in the hemiacetal moiety.

Infrared Spectra and Intramolecular Hydrogen Bonding of 4-(Haloacetylamino)diphenylamines

Hiroko SUEZAWA,* Minoru HIROTA, Yoshiki HAMADA,† Isao TAKEUCHI,† and Takae KAWABE†
Deparment of Synthetic Chemistry, Division of Materials Science and Chemical Engineering, Faculty of Engineering, Yokohama National University, Hodogaya-ku, Yokohama 240
† Faculty of Pharmacy, Meiji University, Tempaku-ku, Nagoya 468
(Received April 30, 1991)

Synopsis. Infrared NH stretching absorptions and ^{1}H NMR chemical shifts of a series of 4-(haloacetylamino)diphenylamines were reported. The halogen atoms in haloacetamido groups are shown to participate in the intramolecular NH···X hydrogen bond. The hydrogen bond tends to be strengthened in the increasing order of atomic number of the acceptor halogen atoms.

The conformations of the molecules of pharmaceutical interest are often perturbed by intramolecular hydrogen bonding. Thus the hydrogen bonding sometimes affects the biological activity. Previously the authors had determined conformations of a series of substituted salicylanilides by infrared spectroscopy and found a correlation between the preference to the hydrogen-bonded conformation and the antibacterial activities.[1] In this connection, intramolecular hydrogen bonding of a series of 4-(haloacetylamino)diphenylamines were characterized by infrared and NMR spectroscopy in search for the structure-activity correlation.

Results and Discussion

The infrared NH and C=O absorptions, as well as the chemical shifts of NH protons, are given in Table 1. Parent 4-(acetylamino)diphenylamine has two NH stretching absorptions at 3448 and 3430 cm^{-1}. These bands were assigned to the amide and diphenylamine NH groups, respectively, by comparing to the NH absorptions of several reference compounds.[2,3] ^{1}H NMR spectra in chloroform-*d* also showed to NH signals. The one at the higher field appears at around 5.5 ppm and assigned to the NH group in diphenylamine structure. The assignment was certified by showing that the signal shifts down-field when a nitro group was introduced at the ortho position.[4] The signal at the lower field (appearing at 7.25 ppm in the spectrum of 4-acetyldiphenylamine) was assigned to the NH group of secondary amide.

The low frequency shift of the amide NH stretching absorption was observed when a halogen substituent was introduced on the acetyl group, which suggests the presence of intramolecular hydrogen bonding. Formation of the five-membered hydrogen bonded chelate ring can be expected to cause a low frequency shift of the NH band to a varying degree dependent on the hydrogen accepting ability of halogen atom (X). Hydrogen bond including fluorine atom as a hydrogen acceptor is generally weak, resulting the least low

Table 1. Infrared Spectra (in CCl_4) and ^{1}H NMR Spectra (in $CDCl_3$) of 4′-Substituted 4-(Haloacetylamino)diphenylamines $RC_6H_4NH(d)C_6H_4NHH(a)COCH_2X$

Substituent		Infrared spectra (cm^{-1})			^{1} NMR (δ/ppm)			MIC (μg ml^{-1})[c]	
R	X	NH(*d*)	NH(*a*)	C=O	NH(*d*)	NH(*a*)	CH_2	S. aureus	M. gypseum
H	H	3430	3448	1703	5.36	7.25	—	>100	>10
H	F	3431[a]		1697	5.69	7.86	4.920	>100	>10
F	F	3431[a]		1697	5.59	7.82	4.917	>100	>10
Cl	F	3432[a]		1703	5.60	7.84	4.926	>100	>10
F	Cl	3429	3411	1691	5.59	8.14	4.182	>100	>10
CH_3	Cl	3434	3412	1689	5.50 (5.27)[b]	8.12 (11.09)	4.164 (4.433)	>100	10
CH_3O	Cl	3434	3413	1691	5.50	8.11	4.176	>100	10
C_2H_5O	Cl	3433	3412	1690	5.39	8.10	4.176	—	—
H	Br	3434	3404	1686	5.50	8.03	4.008	>100	1
F	Br	3432	3403	1686	5.50	8.02	4.024	10	1
Cl	Br	3434	3402	1689	5.58	8.03	4.013	10	1
CH_3	Br	3433	3404	1685	5.59 (5.86)[b]	8.03 (11.09)	4.018 (4.356)	10	1
C_2H_5O	I	3433	3396	1691	5.50	7.66	3.833	10	1

a) The two NH bands merge into a slightly asymmetric band having a nearly twice intensity. b) The chemical shifts in pyridine solutions. c) Minimum inhibitory concentration (Ref. 7).

Table 2. Hydrogen Bond Shifts in The N–H···X Hydrogen Bonds

X	F	Cl	Br	I
$\Delta\nu/cm^{-1}$	17	36	45	52
$\Delta\delta$/ppm	0.59	0.87	0.78	0.41

frequency shift of amide NH band. Hydrogen bond shift ($\Delta\nu_{NH}$) increases in the increasing order of atomic number; i.e., F<Cl<Br<I (Table 2), which suggests the major contribution of polarizability effect. In other words, the $\Delta\nu$ is controlled by the strength of the N–H bond, which comes from the contribution of charge-transfer resonance structure (**2b**). The secondary amide moiety of the intramoecularly hydrogen-bonded conformer is enforced to take a trans geometry as depicted by **1**. The trans conformer usually absorbs in the frequency region higher than 3640 cm^{-1} (3480—3440 cm^{-1}) in contrast to the cis absorption in the lower frequency region (3435—3395 cm^{-1}).[5] Thus the NH absorption at 3448 cm^{-1} of 4-(acetylamino)diphenylamine showed the fact that it takes a trans conformation preferably. The carbonyl stretching absorptions at relatively high frequencies supported the trans-conformation in the *o*-haloacetyl derivatives.[6]

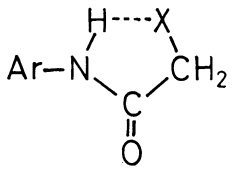

(1)

(Formula of the hydrogen-bonded conformation **1**)

N–H :X
(**2a**)

N:⁻ H–X⁺
(**2b**)

The ^1H NMR spectra also support the intramolecularly hydrogen-bonded conformation (**1**), showing considerable low field shifts of amide NH signals. The hydrogen bond shift ($\Delta\delta$) increases in the following order of halogen substituent: I<F<Br<Cl. The sequence of $\Delta\delta$ is quite different from that of infrared $\Delta\nu$. The hydrogen bond shifts ($\Delta\delta$) of NH proton chemical shifts should be controlled by the electron density plus charge displacement effects, which can be evaluated by the second and the first terms of Buckingham's equation ($\sigma_E=-2\times10^{-12}E_z+10^{-18}E^2$). Thus the electronegativity effect might affect the chemical shift considerably in addition to the delocalization effect. As a result of two opposite effects the NH protons of chloroacetanilides resonate at the lowest fields. In short, the two hydrogen bond shifts $\Delta\nu$ and $\Delta\delta$, some from different origins.

The strength of hydrogen bonding can be more properly evaluated by using the infrared hydrogen bond shift ($\Delta\nu$) as a measure. Since antibacterial activity can be governed by the nature of halogen atoms as is the case of hydrogen bonding, we could not conclude very definitely, but the general tendency that the strength of intramolecular hydrogen bond is in line with the inverse of minimal inhibitory concentration[7] was observed. Thus the possible contribution of the intramolecular hydrogen bonding to the activity was suggested by this research.

The authors thank Dr. Kazuhisa Sakakibara, Yokahama National University, for his valuable discussion throughout this work. This work was supported in part by the Grant-in-Aid for Scientific Research on Priority Areas No. 01648001 from the Ministry of Education, Science and Culture.

References

1) H. Endo, M. Hirota, Y. Ito, I. Takeuchi, and Y. Hamada, *Bull. Chem. Soc. Jpn.*, **55**, 1564 (1982).

2) a) M. Kasai, M. Hirota, Y. Hamada, and H. Matsuoka, *Tetrahedron*, **29**, 267 (1973). b) M. Hirota, K. Shinozuka, and Y. Hamada, *Bull. Chem. Soc. Jpn.*, **47**, 2696 (1974).

3) Assignment of the amide NH band was based on the fact that acetanilide absorbs at 3448 and 1703 cm^{-1} in carbon tetrachloride solution.

4) L. J. Bellamy, "The Infra-Red Spectra of Complex Molecules," Chapman and Hall, London (1975), Vol. 1, p. 233.

5) p. 240 of Ref. 4.

6) 4,4′-Dichloro-2-nitrodiphenylamine absorbs at 3357 cm^{-1} in the NH region. The absorption frequency is considerably lower than the normal NH frequencies for *o*-unsubstituted diphenylamines (3432 cm^{-1} for 4,4′-dichlorodiphenylamine).

7) Y. Hamada and H. Matsuoka, *Yakugaku Zasshi*, **96**, 447 (1976).

An Efficient Preparation of 3,3′-Methylenebisazulenes[1)]

Yoshiharu MATSUBARA, Masanori MORITA,† Shin-ichi TAKEKUMA,* Zhendong ZHAO, Hiroshi YAMAMOTO,*,†† and Tetsuo NOZOE†††

Department of Applied Chemistry, Faculty of Science and Engineering, Kinki University, Kowakae, Higashi-Osaka 577

† Kinki University Co-Operative Laboratories Center, Kowakae, Higashi-Osaka 577

†† Department of Chemistry, Okayama University, Okayama 700

††† Tokyo Research Laboratories, Takasago Corporation, Kamata, Ohta-ku, Tokyo 144

(Received May 1, 1991)

Synopsis. Various 3,3′-methylenebisazulenes were prepared in high yields upon treatment of 1-substituted azulenes with a solution of 0.1—0.2 wt% paraformaldehyde in glacial acetic acid at 25 °C for 1 h. Thus, 1-methyl-, 1-isopropyl-, 1,5-diisopropylazulene, guaiazulene, and methyl 2-hydroxy-1-azulenecarboxylate readily provided the corresponding 3,3′-methylenebisazulenes, respectively. Acetic acid which had been refluxed with 5 wt% $KMnO_4$ for 2 h and then distilled according to a purification method was found to contain 0.1—0.2 wt% formaldehyde and exert the same 3,3′-methylenebisazulene formation. 3,3′-Dideuteriomethylenebis(guaiazulene) was obtained by employing the similar distillate from acetic acid-d_4.

For the past several years, we have undertaken a systematic investigation on autoxidation of various azulenes in detail.[2)] We found that naturally originating 3,3′-methylenebis(guaiazulene) (**9**)[3)] and synthetic 3,3′-methylenebis(1,5-diisopropylazulene) (**8**), for example, gave various kinds of azulenylbenzofulvenes by autoxidation.[4,5)] Oxidation of **9** with peracetic acid has also been conducted recently, and a wide variety of azulenylbenzofulvenes and their precursors were isolated.[6)] Our interest in the physicochemical properties and biological activity of azulenylbenzofulvenes in general necessitated establishing an efficient preparative method of various 3,3′-methylenebisazulenes which in turn are expected to serve as effective intermediates for synthesis of the desired fulvenes. We wish to describe herein our results.

We employed the following 1-substituted azulenes as model substrates: 1-methylazulene (**1**), 1-isopropylazulene (**2**), 1,5-diisopropylazulene (**3**), guaiazulene (**4**), and methyl 2-hydroxy-1-azulenecarboxylate (**5**). When these compounds were treated, at 25 °C for 1 h, with a freshly prepared glacial acetic acid solution containing 0.1—0.2 wt% paraformaldehyde, we found that the corresponding 3,3′-methylenebisazulenes **6**,[7)] **7**,[8)] **8**,[5)] **9**,[9)] and **10** were best obtained (see Chart 1). Structure of the previously unknown product **10** was established on the basis of spectroscopic data (see the Experimental section). Compounds **6**—**9** had been obtained either during an attempted preparation of 3-hydroxymethylazulene derivatives or by autoxidation of the monomeric azulenes; in all cases the yields were moderate to low.

During this investigation we attempted to purify acetic acid by refluxing with 5 wt% potassium permanganate for 2 h, followed by distillation according to a standard procedure.[10)] On dissolving azulenes **1**—**5** in the above acetic acid distillate and allowing to stand at 25 °C for 1 h, we obtained 3,3′-methylenebisazulenes **6**—**10** in almost the same yields as in the case of using the paraformaldehyde solution. The analysis of the acetic acid distillate by the use of GLC and GC-MS spectrometry as well as chemical reaction with *p*-toluenesulfonohydrazide[11)] revealed that it contained 0.1—0.2 wt% formaldehyde.[12)] Commercially unavailable formaldehyde-d_2 (0.1—0.2 wt%) can therefore be prepared by the above distillation procedure with acetic acid-d_4. 3,3′-Dideuteriomethylenebis(guaiazulene) (**11**) was thus efficiently prepared in 95% yield by the present method.

The most plausible reaction pathways for the formation of formaldehyde liberated from acetic acid by the purification method[10)] and of 3,3′-methylenebisazulenes

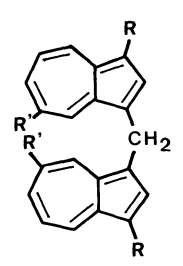

6*: R=Me, R'=H (Y=96%)

7*: R=i-Pr, R'=H (Y=97%)

8*: R=R'=i-Pr (Y=96%)

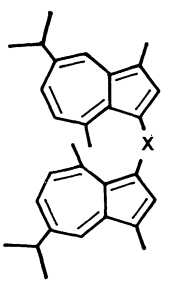

9*: X=CH_2 (Y=95%)

11: X=CD_2 (Y=95%)

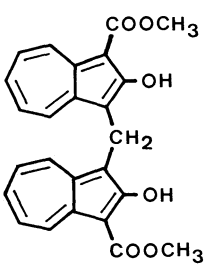

10: (Y=100%)

Chart 1. Structures and yields/% of 3,3′-methylenebisazulenes **6**—**11**.
*Previously known compound.

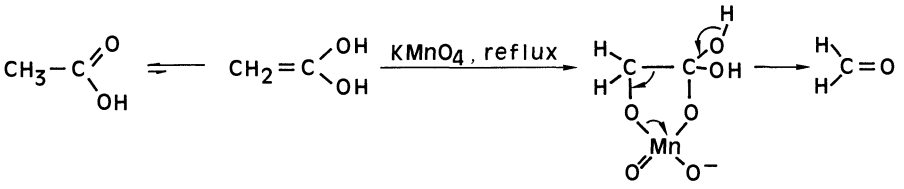

Scheme 1. A possible reaction pathway for the formation of formaldehyde present in the acetic acid distillate.

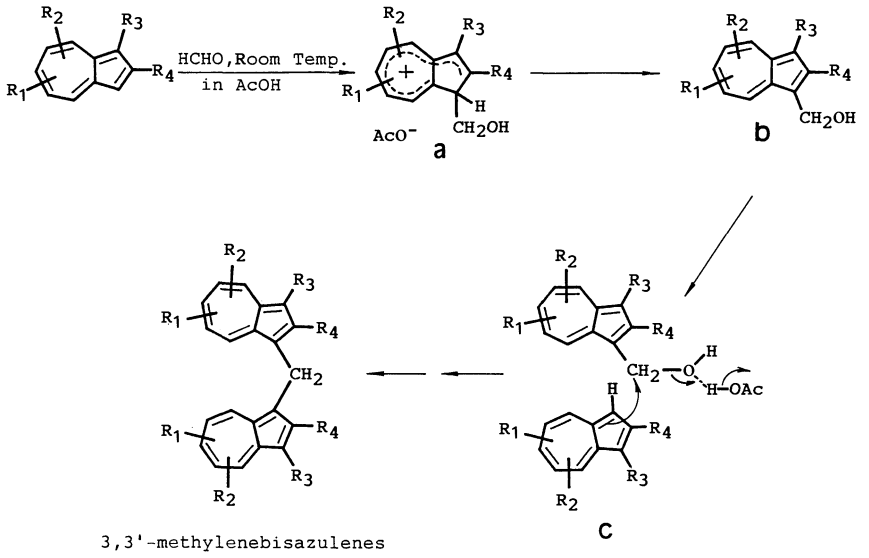

Scheme 2. A possible reaction pathway for the formation of 3,3′-methylenebisazulenes **6**—**10** from azulenes **1**-**5** and formaldehyde in acetic acid.

6—**10** from azulenes **1**—**5** are illustrated in Schemes 1 and 2, respectively. Extension of the present method to azulene itself and some other substrates is under intensive investigation.

Experimental

Melting points were determined with a Yanagimoto MP-S3 instrument and are uncorrected. GLC analysis of the acetic acid distillate was conducted with a YANACO G2800 gas liquid chromatograph system equipped with a HFID (hydrogen flame ionization detector) and a PEG 20M glass-capillary column (ϕ 0.28 mm×20 m, column temp 40—180 °C/2 °C-min^{-1}).

The UV and IR spectra were taken on a Hitachi 323 spectrophotometer and a JASCO IR-A-202 Grating spectrometer, respectively. Mass spectra were taken on a JEOL JMS-HX100 (with a JEOL JMA-DA5000 mass data system) high-resolution instrument and are given in terms of m/z (rel intensity) compared with the base peak. The ^{1}H NMR spectra were recorded in $CDCl_3$ with a JEOL FX-200 (200 MHz) cryospectrometer at 27 °C. The assignments of all singals were made by employing a first-order analysis with the aid of decoupling technique and were confirmed by a computer-assisted simulation analysis.

Preparation of 3,3′-Methylenebisazulenes (6—11). To a solution of paraformaldehyde (0.1—0.2 wt%) in acetic acid (12 ml) was added 100 mg each of 1-methylazulene (**1**), 1-isopropylazulene (**2**), 1,5-diisopropylazulene (**3**), guaiazulene (**4**), and methyl 2-hydroxy-1-azulenecarboxylate (**5**).[13] The mixture was stirred at 25 °C for 1 h under nitrogen. The precipitated 3,3′-methylenebisazulenes **6**—**10** were filtered off, washed carefully with water, and dried in a vacuum desiccator, affording pure products **6**—**10** (70—80% yields). Each of the filtrates was carefully neutralized with aq Na_2CO_3 and extracted with ether (3×30 ml). The extract was washed with water, dried (Na_2SO_4), and evaporated in vacuo, giving additional pure 3,3′-methylenebisazulenes **6**—**10** (20—25% yields). Compounds **6**—**10** were also obtained from **1**—**5** in almost the same yields by the treatment with acetic acid distillate (see later).

Previously Known Compounds: Compounds **6** (96% yield),[7] **7** (97%),[8] **8** (96%),[5] and **9** (95%)[9] were identified either by comparison of their melting points, UV-vis, ^{1}H NMR, and EI MS spectral data with those of authentic 3,3′-methylenebisazulenes.

Dimethyl 3,3′-Methylenebis(2-hydroxy-1-azulenecarboxylate) (10): Reddish orange prisms; 103 mg (100%); mp>300 °C; IR (KBr) 3650—3250 (OH) and 1640 cm^{-1} (C=O); ^{1}H NMR δ=4.03 (6H, s, $COOCH_3$-1,1′), 4.53 (2H, s, CH_2-3), 7.37 (2H, dddd, J=11.0, 10.0, 2.0, 0.3 Hz, H-5,5′), 7.37 (2H, dddd, J=11.0, 9.0, 2.0, 0.5 Hz, H-7,7′), 7.46 (2H, dddd, J=10.0, 9.0, 2.0, 1.5 Hz, H-6,6′), 8.64 (2H, ddd, J=11.0, 1.5, 0.5 Hz, H-4,4′), 8.84 (2H, ddd, J=11.0, 2.0, 0.3 Hz, H-8,8′), and 11.10

(2H, s, OH-2,2′); EI MS *m/z* 416 (M^+; 47%), 384 (5), 352 (100), 323 (23), 307 (6), 296 (7), 268 (7), 239 (22), 215 (34), 202 (7), 183 (52), 176 (34), 170 (30), 156 (5), 142 (5), 127 (5), 119 (18), 114 (7), and 106 (4). Found: *m/z* 416.1243. Calcd for $C_{25}H_{20}O_6$: M, 416.1260.

3,3-Dideuteriomethylenebis(guaiazulene) (11). This was prepared from **4** upon treatment, at 25 °C for 1 h, with the distillate obtained from acetic acid-d_4 (see below): Dark blue prisms; 98 mg (95%); mp 186 °C; ^{1}H NMR δ=1.34 (12H, d, *J*=7.0 Hz, *i*-Pr-7,7′), 2.52 (6H, s, Me-1,1′), 2.92 (6H, s, Me-4,4′), 3.00 (2H, sept, *J*=7.0 Hz, Me_2CH-7,7′), 6.77 (2H, d, *J*=11.0 Hz, H-5,5′), 7.08 (2H, s, H-2,2′), 7.22 (2H, dd, *J*=11.0, 2.0 Hz, H-6,6′), and 8.03 (2H, d, *J*=2.0 Hz, H-8,8′); EI MS *m/z* 410 (M^+; 52%), 395 (11), 367 (3), 212 (38), 205 (10), 198 (100), 183 (27), and 167 (5). Found: *m/z* 410.2940. Calcd for $C_{31}H_{34}D_2$: M, 410.2943.

Preparation of Acetic Acid Distillate. The acetic acid distillate was obtained according to the general distillation procedures of acetic acid.[10] Namely, acetic acid (1.0 kg) was refluxed with 5 wt% potassium permanganate (50 g) for 2 h and then fractionally distilled (bp 117—118 °C). Similarly, acetic acid-d_4 (100 g) was refluxed with 5 wt% potassium permanganate (5 g) for 2 h and distilled (bp 114—115 °C).

We are grateful to Professor Masafumi Yasunami (Tohoku University) for a generous gift of 1-methyl-, 1-isopropyl-, and 1,5-diisopropylazulene and to Konan Kako Co. (Osaka) for guaiazulene.

References

1) A part of the results were presented at Japan Kokai Tokkyo Koho, Y. Matsubara and S. Takekuma, JP 8860946 A2, JP 6360946 (1988); *Chem. Abstr.*, **109**, 92354p (1988).

2) S. Takekuma, Y. Matsubara, H. Yamamoto, and T. Nozoe, *Bull. Chem. Soc. Jpn.*, **61**, 475 (1988), and references cited therein.

3) M. K. W. Li and P. J. Scheuer, *Tetrahedron Lett.*, **25**, 587 (1984).

4) Y. Matsubara, S. Takekuma, K. Ibata, H. Yamamoto, and T. Nozoe, *Nippon Kagaku Kaishi,* **1987**, 1555.

5) S. Takekuma, Y. Matsubara, S. Matsui, H. Yamamoto, and T. Nozoe, *Nippon Kagaku Kaishi,* **1988**, 923.

6) S. Matsui, Y. Matsubara, S. Takekuma, H. Yamamoto, and T. Nozoe, *Nippon Kagaku Kaishi,* **1989**, 838.

7) K. Hafner and W. Senf, *Justus Liebigs Ann. Chem.*, **656**, 34 (1962); S. Takekuma, Y. Matsubara, H. Yamamoto, and T. Nozoe, *Bull. Chem. Soc. Jpn.*, **60**, 3721 (1987).

8) Y. Matsubara, S. Matsui, S. Takekuma, H. Yamamoto, and T. Nozoe, *Yukagaku,* **38**, 471 (1989).

9) W. Treibs, *Chem. Ber.*, **90**, 761 (1957); Y. Matsubara, S. Takekuma, K. Yokoi, H. Yamamoto, and T. Nozoe, *Bull. Chem. Soc. Jpn.*, **60**, 1415 (1987).

10) J. A. Riddick and E. E. Toops, Jr., "Organic Solvents," 2nd ed, Interscience, New York (1955), pp. 390—392.

11) Hydrazone **A** was obtained by the reaction of the acetic acid distillate with *p*-toluenesulfonohydrazide according to the procedures of Blankley et al. for preparation of glyoxylic acid *p*-toluenesulfonohydrazone: C. J. Blankley, F. J. Sauter, and H. O. House, *Org. Synth.*, Coll. Vol. V, 258 (1973). Hydrazone **A**: EI MS *m/z* 198 (M^+, 100%). Found: *m/z* 198.0444. Calcd for $C_8H_{10}O_2N_2S$: M, 198.0462.

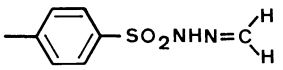

A

12) To our knowledge, this is the first report to find out the presence and concentration of formaldehyde in the distillate. Therefore care must be taken in the use of this purification method, particularly when the acetic acid distillate is employed for a formaldehyde-sensitive substrate.

13) T. Nozoe, S. Seto, K. Takase, S. Matsumura, and T. Nakazawa, *Nippon Kagaku Kaishi,* **1965**, 346.

Apparent Molal Volumes of Urea and Its Derivatives in Aqueous Alkali Chloride Solutions

Toshio OGAWA,* Kiyoshi MIZUTANI, Yukimi ANDO,† and Motoo YASUDA
Department of Chemistry, College of General Education, Nagoya University, Chikusa-ku, Nagoya 464-01
(Received March 22, 1991)

The apparent molal volumes (ϕ_v) at 25 °C have been measured for the following urea derivatives in aqueous alkali chloride solutions (from density measurements) using a digital densimeter: urea, methylurea, ethylurea, 1,1-dimethylurea, 1,3-dimethylurea, 1,1-diethylurea, and 1,3-diethylurea. The limiting values (ϕ_v°) were obtained by a linear extrapolation using the least-squares method. A notable feature of the transfer volumes found in this study was that hydrophobic urea derivatives, such as dimethylureas and diethylureas, had negative values for transfer from water to lithium chloride solutions. For the remainder, however, all transfer volumes were positive.

In a previous paper,[1] we reported on the apparent molal volumes of urea derivatives measured in several water–methanol mixtures. Due to abnormalities of the water–methanol mixtures regarding their properties, such as viscosity–composition and ultrasonic velocity–composition relationships, each plot of ϕ_v° vs. X_2, mole fraction of methanol, showed a minimum at a lower methanol concentration where the solvent is more structured than the water itself, except for unsubstituted urea which had no minimum.

The volumes of transfer from water to a more structured solvent for the more hydrophobic urea were more negative. On the other hand, the reverse order was observed for those from water to methanol, a less structured solvent than water.

Though the properties of the lithium ion are somewhat different from those of the other alkali ions, volume data measured in aqueous lithium salt solutions have been rather few. We have felt that it would be very interesting to know, particularly, the interactions between lithium ions and a hydrophobic solute. We thus determined the apparent molal volumes of urea and its derivatives in an H_2O–MCl mixed solvent (M=Li, Na, and K) from density measurements. Since the limiting values (ϕ_v°) are determined mainly by the respective intrinsic volume of the solute and the solute–solvent interactions, they can provide useful clues regarding solute–solvent interactions. In the present work the densities were measured at 25 °C for the urea (alkylurea)–alkali chloride–water ternary system at various concentrations. The alkali chloride was thought of as being a co-solvent; in other words, an aqueous alkali chloride solution was considered to be a "solvent". We used 0.5, 1, and 2 molal solutions for each of three chlorides as solvents in this study. For the 1 and 2 molal solutions, the adiabatic compressibilities of the "solvent" were determined in order to find the relationship between the adiabatic compressibility of the "solvent" and the apparent molal volume of the urea obtained in it.

† Present address: 292 Sunouchi-kou, Saijo, Ehime 793.

Experimental

The alkali chlorides used in this study were of guaranteed reagent grade from Wako Chemical Industries, Ltd., and were used without any further purification, except for lithium chloride which was used after drying for several hours at ca. 150 °C. As for urea and its alkyl derivatives, the same reagents were employed as in the previous study, some of them being recrystallized from a suitable solvent.[1]

All urea derivative solutions were prepared by weight in the concentration range 0.1—1.0 mol kg^{-1} (the number of moles of urea derivative per kg of the mixed solvent whenever the mixed solvents were used), except for the more hydrophobic urea derivatives; these urea derivatives measurements were carried out below 0.5 mol kg^{-1}, as mentioned below. The density and ultrasonic velocity measurements have been described previously.[2] The temperature control of the thermostated bath system for the densimeter was better than ±0.005 °C

Results

The apparent molal volumes of the urea derivatives were obtained by using

$$\phi_v = \frac{M}{d} + \frac{1000\,(d_o - d)}{m d_o\, d}, \quad (1)$$

where M is the molecular weight of the urea; m, its molal concentration; and d_o and d, the densities of the solvent and the solution, respectively. The data were fitted to the equation

$$\phi_v = \phi_v^\circ + S_v m, \quad (2)$$

where ϕ_v° is the infinite-dilution apparent molal volume and S_v is the experimental slope. Although the apparent molal volumes of nonelectrolytes in dilute solutions, below 1.0 mol kg^{-1} are commonly expressed as in Eq. 2, those for the more hydrophobic urea derivatives studied in alkali chloride solutions deviate from Eq. 2, even at such low concentrations as ca. 0.5 mol kg^{-1}. The limiting apparent molal volumes of 1,3-dimethylurea (1,3-DMU) and 1,3-diethylurea (1,3-DEU) were thus calculated using data for a concentration range of ca. 0.1—0.5 mol kg^{-1}. This is discussed later.

Table 1. Limiting Apparent Molal Volumes in Aqueous Alkali Chloride Solutions

Solvent	ϕ_v° / cm^3 mol^{-1}						
	U	UM	1,1-DMU	1,3-DMU	EU	1,1-DEU	1,3-DEU
H_2O	44.24	62.40	78.53	80.32	79.26	111.63	113.74
0.5m LiCl	44.52	62.46	78.55	80.27	79.29	111.92	113.66
1.0m LiCl	44.80	62.63	78.46	80.16	79.36	111.67	113.47
2.0m LiCl	45.14	62.64	78.45	80.00	79.28	111.19	112.96
0.5m NaCl	44.63	62.62	78.83	80.45	79.52	112.09	113.86
1.0m NaCl	45.08	62.90	78.86	80.59	79.80	112.31	114.02
2.0m NaCl	45.44	63.10	79.08	80.75	80.06	112.47	114.13
0.5m KCl	44.63	62.59	78.77	80.43	79.52	112.16	113.95
1.0m KCl	45.00	62.93	78.91	80.55	79.79	112.54	114.08
2.0m KCl	45.37	63.13	79.16	80.72	80.00	112.64	114.17

Table 2. Adiabatic Compressibilities of Aqueous Alkali Halide Solutions

Solution	β_s / $10^{-4}\times$bar^{-1}
H_2O	4.477
1m LiCl	4.075
2m LiCl	3.750
1m NaCl	3.979
2m NaCl	3.588
1m KCl	4.015
2m KCl	3.660

Table 1 shows the limiting values (ϕ_v°) caluculated by a linear extrapolation (Eq. 2) using the least-squares method. In this Table, U, MU, 1,1-DMU, EU, 1,1-DEU denote urea, methylurea, 1,1-dimethylurea, ethylurea, and 1,1-diethylurea, respectively. In aqueous sodium and potassium chloride solutions the values of ϕ_v° of all urea and its derivatives studied here are larger than those measured in pure water, as can be seen from Table 1. On the other hand, in aqueous lithium chloride solutions some urea derivatives have negative transfer volumes. These are well known to be hydrophobic in nature.

The adiabatic compressibilities, β_S (bar^{-1}), of the "solvent" were calculated in order to determine the correlation with ϕ_v° using Eq. 3, where u is the velocity of sound (m s^{-1}) in the solvent. The density is expressed in g cm^{-3}.

$$\beta_s=\frac{1000}{d_o\, u^2}. \tag{3}$$

The obtained values are given in Table 2; this subject will be further discussed later.

Discussion

The transfer volumes for the studied urea derivatives show that they increase in the following order:

$$Li^+ < K^+ \approx Na^+.$$

Until now, we have reported the transfer volumes of some amino acids[3] and polyalcohols[4] from water to aqueous alkali chloride solutions. The order of increasing transfer volume for these solutes was

$$Li^+ < K^+ < Na^+.$$

In the case of urea derivatives, there are no strong interactions, such as in the case of amino acids, with both the cations and anions in a mixed solvent; the absolute magnitudes of the transfer volumes are thus very small compared with those for amino acids. The lithium ion has the smallest value in each sequence; the sequence for the amino acids has been discussed by us previously.[3] While all transfer volumes were positive regarding hydrophilic solutes, such as amino acids and polyalcohols, those of the more hydrophobic urea derivatives to aqueous LiCl solutions have a negative sign.

The apparent molal volumes of tetrabuthylammonium bromide have been measured by Desrosiers and Desnoyers in aqueous solutions of NaF, NaCl, NaAc, and NH_4Ac at 25 °C[5]. Since Bu_4NBr is dilute, but not the added electrolyte, they corrected the volume data for long-range coulombic forces in order to obtain more specific noncoulombic interactions between the solute and the mixed solvent. The observed transfer volumes from water to the electrolyte solutions, corrected for the Debye-Hückel interactions, were all negative at low concentrations. The same had been observed for the sign of the transfer volume of hydrophobic nonelectrolytes, such as argon and methane,[6] from water to aqueous electrolyte solutions. They thus concluded that the noncoulombic interactions between hydrophobic and hydrophilic ions resulted in negative contributions to the volumes. In this study, since the urea derivatives were used as solute nonelectrolytes, no long-range coulombic interactions existed between the solute and alkali chloride in the "solvent"; thus, no corrections for the Debye-Hückel interactions were necessary. As mentioned above, the more hydrophobic urea derivatives have negative transfer volumes only from water to an aqueous LiCl solution; this is in contrast to the most hydrophobic solutes, for example Bu_4NBr and argon, which have negative transfer volumes from water to

aqueous NaCl and KCl solutions. Thus, the transfer volumes from water to electrolyte solutions corrected for the Debye–Hückel interactions may be used as a measure of the hydrophobicity of the solute.

The reason for the deviation in the ϕ_v data for 1,3-DMU and 1,3-DEU from Eq. 2 at low concentrations, (mentioned above) may be explained by the hydrophobicity of these solutes. In an aqueous alkali chloride solution a considerable number of water molecules are firmly combined to the alkali cations and chloride anions, so that it is likely that the concentration of the solute urea derivative virtually increases and an interaction between them (the so-called hydrophobic interaction) may result at an appreciably low solute concentration. As a result, Eq. 2 can be fitted to the data only below ca. 0.5 mol kg^{-1}. In this connection, it was reported by Wen and Saito that plots of ϕ_v *vs.* c for hydrophobic solutes, such as tetrapropylammonium and tetrabutylammonium bromides, go through a minimum at around 1 mol kg^{-1} at 15, 25, and 35 °C and then turn upward.[7] They considered this phenomenon to be related to a strong structual influence of large tetraalkylammonium salts upon water, and described by the "formation of a clathrate-like structure". Further, the such terms as the iceberg effect,[8] increase of ice-likeness,[9] and tightening of hydrogen bonds of water molecules[10] have been used to describe the structual influence.

The apparent molal volumes of urea were determined in several nonaqueous solvents as functions of the temperature by Hamilton and Stokes.[11]. They pointed out that one noteworthy feature was the large variation in the limiting apparent molal volumes with a solvent, from 37 cm^3 mol^{-1} in methanol to 45 cm^3 mol^{-1} in formamide, the latter figure being close to the molar volume of solid urea. They found that of such properties as the cohesive energy density, the dielectric constant, the molar volume and the compressibility of the solvent, which might be expected to bear some relation to ϕ_v° the last one had the only clear correlation: ϕ_v° increases as the compressibility of the solvent decreases. Since the compressibility may be regarded as being a measure of the void space in the liquid, they argued that this means that the solute molecule does not have to create a hole for itself that has the full dimentions demanded by its intrinsic size. In this connection it may be interesting to see the relation between the compressibility coefficient of the solvent shown in Table 2 and ϕ_v° of urea measured in it. In this type aqueous electrolyte "solvent", the same rule mentioned by Hamilton and Stokes has held well; ϕ_v° increases as the compressibility of the solvent decreases. This, however, does not apply to such large and hydrophobic urea derivatives as 1,3-DMU and 1,3-DEU.

As reported by us, the assumption regarding the independent solvation of both sides of the urea derivatives produced a good approximation of the molal volumes in water–methanol mixtures in the same way as in pure water and methanol.[1] An inspection of Table 1 shows that this assumption also holds to a good approximation to the apparent molal volumes in aqueous alkali chloride solutions.

In conclusion, the lithium ion shows a special behavior towards a hydrophobic solute. In order to clarify this, however, more data, especially for hydrophobic solutes in aqueous lithium salt solutions, are necessary.

References

1) K. Mizutani and M. Yasuda, *Bull. Chem. Soc. Jpn.*, **61**, 3301 (1988).
2) T. Ogawa, M. Yasuda, and K. Mizutani, *Bull. Chem. Soc. Jpn.*, **57**, 662 (1984).
3) T. Ogawa, M. Yasuda, and K. Mizutani, *Bull. Chem. Soc. Jpn.*, **57**, 2064 (1984).
4) M. Yasuda and K. Mizutani, The 11th Symposium on Solution Chemistry of Japan, Yokohama, December 1988, Abstr., No. 1A17.
5) N. Desrosiers and J. E. Desnoyers, *Can. J. Chem.*, **53**, 3206 (1975).
6) E. W. Tiepel and K. E. Gubbins, *J. Phys. Chem.*, **76**, 3044 (1972).
7) W. Y. Wen and S. Saito, *J. Phys. Chem.*, **68**, 2639 (1964).
8) H. S. Frank and M. W. Evans, *J. Chem. Phys.*, **13**, 507 (1945).
9) H. S. Frank and W. Y. Wen, *Discuss. Faraday Soc.*, **24**, 133 (1957).
10) R. M. Diamond, *J. Phys. Chem.*, **67**, 2513 (1963).
11) D. Hamilton and R. H. Stokes, *J. Solution Chem.*, **1**, 213 (1972).

Mercury(6^3P_1)- and Cadmium(5^3P_1)-Photosensitized Decompositions of Tetramethyltin

Shunzo YAMAMOTO,* Satomi INOUE, Yoshimi SUEISHI, and Norio NISHIMURA
Department of Chemistry, Faculty of Science, Okayama University, 3-1-1 Tsushima-naka, Okayama 700
(Received April 19, 1991)

The mercury(6^3P_1)-photosensitized decomposition of tetramethyltin (TMT) has been studied at 120 and 250 °C and at pressures from 10 to 20000 Pa. The gaseous products detected were ethane, methane, and hydrogen. The yields of these products increased linearly with increasing reaction time and light intensity. From the effects of O_2, NO, and H_2 on the yield of ethane, the major primary reactions of the mercury-photosensitized decomposition of TMT were concluded to be processes with an Sn–C bond cleavage. The quantum yields of these products were independent of the TMT pressure at higher pressures than 200 Pa at 120 °C. The quantum yield of ethane was also independent of the TMT pressure, while that of methane increased upon increasing the pressure at 250 °C. The cadmium (5^3P_1)-photosensitized decomposition of TMT has been studied at 280 °C. The detected products were the same as those from the mercury-photosensitized decomposition, although the yield of hydrogen was very small. The pressure dependence of the yields of ethane and methane in the cadmium-photosensitized decomposition was very similar to those in the mercury-photosensitized decomposition of TMT at 250 °C.

Organometallic compounds have been widely used for the development of microelectronic devices. There have been many quantitative studies of the thermal and photochemical decompositions of organometallic compounds in the gas phase. The major primary products of the thermal[1,2] and photochemical[3,4] decompositions of tetramethyltin (TMT) have been reported to be methane and ethane, indicating that the primary process in these decompositions is an Sn–C bond cleavage.

The mercury-photosensitized decomposition of TMT, which apparently has not been studied before, is interesting for a comparison with the mercury-photosensitized decompositions of tetramethyl compounds of other group-14 elements(neopentane (NP),[5,6] tetramethylsilane (TMS),[7,8] and tetramethylgermane (TMG)[9]) which have been quantitatively studied, and also for a comparison with the thermal decomposition and the direct photolysis of TMT. The primary processes in the mercury-photosensitized decompositions of NP, TMS, and TMG have been reported to be C–H bond cleavage; this is clearly different from that in the thermal decomposition and the direct photolysis of TMT.

The present study was undertaken in order to investigate the mercury- and cadmium-photosensitized decompositions of TMT.

Experimental

The mercury-photosensitized reaction of TMT was carried out at 120 and 250 °C in a conventional cylindrical quartz vessel (5 cm long and 4 cm in diameter) fitted with plane quartz windows at each end. Mercury vapor of constant pressure (vapor pressure at room temperature) and volume was admitted into the reaction vessel with various amounts of TMT. In this way the concentration of mercury in the vessel was kept constant irrespective of the TMT pressure and the reaction temperature ($[Hg]=9.3\times10^{-7}$ mol dm^{-3}). A low-pressure mercury lamp (Toshiba Electric Co., germicidal lamp) made of a quartz tube was used. The 184.9 nm resonance line was filtered out by a Vicor filter. The light intensity absorbed by mercury atoms at 253.7 nm was determined by means of *cis*-2-butene actinometry[10] ($I_{abs}=4.5\times10^{-9}$mol s^{-1}).

The cadmium-photosensitized reaction of TMT was carried out at 280 °C in the cylindrical quartz vessel mentioned above. A few small piecies of cadmium metal were placed within the vessel before various amounts of TMT were admitted. A home-made spiral cadmium discharge lamp (filled with about 2700 Pa Ar) made of Pyrex was used. This lamp emits only the resonance line at 326.1 nm. The absorbed light intensity at 326.1 nm was determined by *cis*-2-butene actinometry[11] ($I_{abs}=1.23\times10^{-8}$ mol s^{-1}).

Product analysis was carried out by fractionation at −196 and −89 °C, and measurements by gas buret and gas chromatography. The first portion, noncondensable at −196 °C was collected using a Toepler pump. This portion consisted of hydrogen and methane, and was analyzed by combustion over copper (II) oxide at 280 °C. Noncondensable products at −196 °C from a TMT-O_2 system were analyzed by means of gas chromatography, using a 2 m column of molecular sieve (5A) at 25 °C. The second portion, which was not condensable at −89 °C, was analyzed by means of gas chromatography, using a 6-m column of VZ-7 (Gasukuro Kogyo Co., Ltd.) at 0 °C and a 2-m column of Gasukuro-pack 55 (Gasukuro Kogyo Co., Ltd.) at 180 °C. The third portion, which was condensable at −89 °C contained a large amount of TMT; it was not analyzed.

TMT (Kanto Chemical Co., Ltd.) was dried over a molecular sieve 4A and purified by trap-to-trap distillation. *cis*-2-Butene (Nihon Tokushu Gasu K. K., pure grade), O_2, NO, N_2O, and H_2 (these inorganic gases are comercially available and all pure grade) were used as supplied.

Results

The Hg($^3P_1$)-Photosensitized Decomposition. The thermal decomposition and direct photolysis were found to be negligible under the conditions for the mercury-photosensitized reaction. The gaseous products detected in the mercury-photosensitized reaction were ethane, methane, and hydrogen. The yields of these

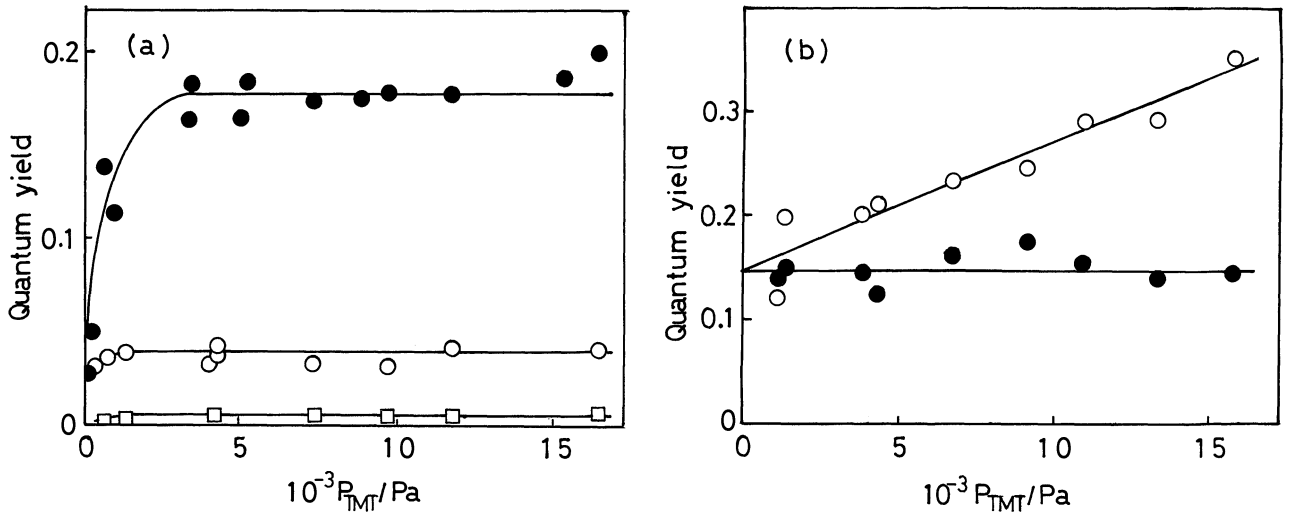

Fig. 1. Pressure dependence of the quamtum yields of ethane (●), methane (○), and hydrogen (□) in the mercury-photosensitized reaction of TMT at 120 °C (a) and 250 °C (b).

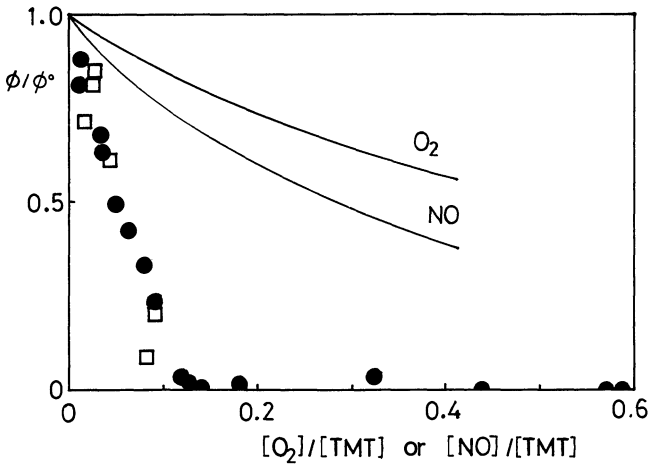

Fig. 2. Quantum yield of ethane in the mercury-photosensitized reaction of TMT at 120 °C in the presence of O_2 (●) and NO (□).

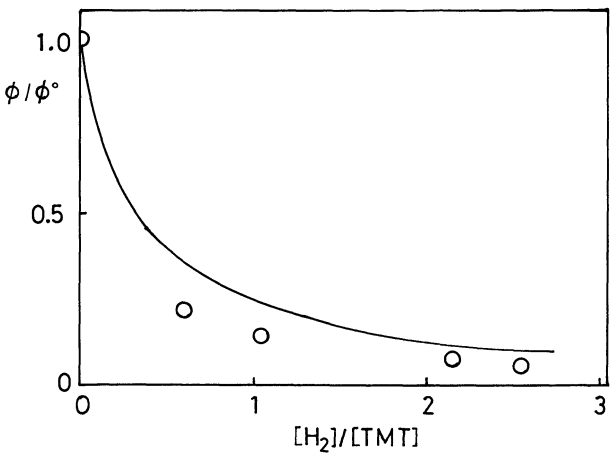

Fig. 3. Quantum yield of ethane in the mercury-photosensitized reaction of TMT at 120 °C in the presence of H_2.

products increased linearly with increasing reaction time and light intensity, showing they were primary products.

The quantum yields of these products are shown in Fig. 1 as a function of the TMT pressure (since the yield of hydrogen was very small at 250 °C, that is not shown in Fig. 1(b)). The quantum yields of all products are constant at higher pressures than 2000 Pa and decrease with decreasing TMT pressure in the low-pressure region at 120 °C (Fig. 1(a)). The quantum yield of ethane is also constant, while that of methane increases with increasing TMT pressure at 250 °C (Fig. 1(b)).

Figure 2 shows the effect of added O_2 and NO on the yield of ethane, while Fig. 3 shows the effect of added H_2 on the yield of ethane. The yield of ethane decreases with increasing the ratios of O_2 TMT, NO/TMT, and H_2/TMT.

The quenching cross section for TMT was obtained

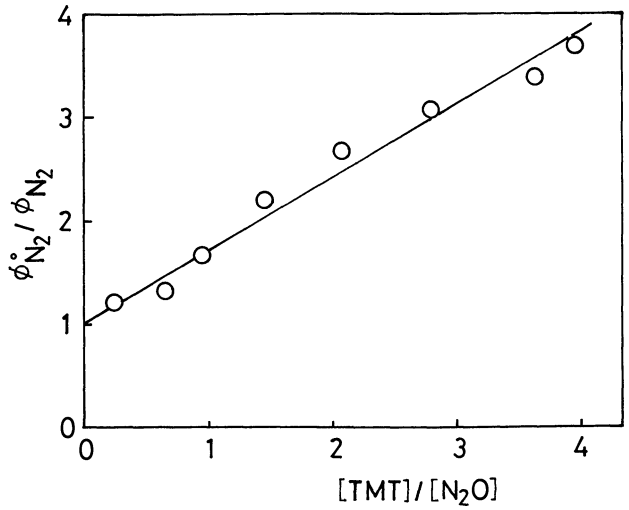

Fig. 4. Competitive quenching plot for TMT and N_2O.

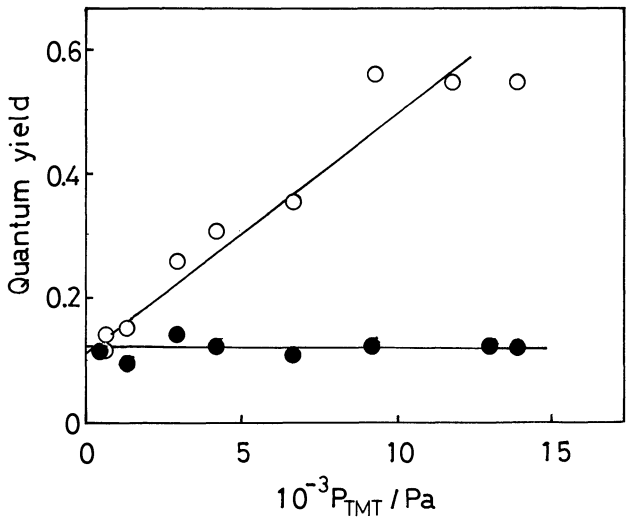

Fig. 5. Pressure dependence of the quantum yields of ethane (●) and methane (○) in the cadmium-photosensitized reaction of TMT at 280 °C.

from the competitive rates of the mercury-photosensitized reactions of TMT and N_2O. The yields of nitrogen from N_2O are expressed by

$$\frac{\phi^{\circ}_{N_2}}{\phi_{N_2}} = 1 + \beta\frac{[TMT]}{[N_2O]}, \quad (1)$$

where $\phi^{\circ}_{N_2}$ and ϕ_{N_2} are the yields of nitrogen in both the absence and presence of TMT. A β-value of 0.70 was obtained from the straight line in Fig. 4 by a least-squares method. The quenching cross section ($\sigma_Q = k_Q(8RT/\pi\mu)^{-1/2}$; k_Q is the quenching rate constant and μ is the reduced mass) for TMT can be calculated using

$$\frac{\sigma_Q(TMT)}{\sigma_Q(N_2O)} = \beta\left(\frac{1+M_{Hg}/M_{N_2O}}{1+M_{Hg}/M_{TMT}}\right)^{1/2}, \quad (2)$$

where $\sigma_Q(N_2O)$ is the cross section for N_2O; we used the value of 56.5×10^{-16} cm^2.[12] A value of 63.7×10^{-16} cm^2 for TMT was obtained. This value is considerably larger than those for NP (4.4×10^{-16} cm^2) and TMS (15.7×10^{-16} cm^2).[7]

The Cd($^3P_1$)-Photosensitized Decomposition. Primary products were the same as those from the mercury-photosensitized decomposition, with the production of ethane and methane again being linear with the reaction time. Hydrogen was a very minor product. The methane/ethane ratio of the cadmium-photosensitized decomposition was appreciably larger than that of the mercury-photosensitized decomposition at 120 °C and comparable to that at 250 °C. As Fig. 5 shows, the yield of ethane was constant and that of methane increased with increasing the TMT pressure. The effect of added H_2 on the yield of ethane was very similar to that observed in mercury-photosensitized decomposition.

Discussion

From the facts that the major products in the mercury-photosensitized reaction of TMT were ethane and methane (while hydrogen was the minor product), and that O_2 and NO in quantities of about 15% completely suppressed ethane formation (Fig. 2), the following simple sequence is indicated as being the major initial reactions:

$$Hg^* + TMT \rightarrow Hg + CH_3 + (CH_3)_3Sn, \quad (3)$$

$$CH_3 + CH_3 \rightarrow C_2H_6, \quad (4)$$

$$CH_3 + TMT \rightarrow CH_4 + CH_2Sn(CH_3)_3. \quad (5)$$

Contrary to the effect of O_2 on ethane formation,methane formation was not completely suppressed by the addition of O_2 in quantities of about 2 of O_2/TMT. The following molecular formation of methane may contribute:

$$Hg^* + TMT \rightarrow CH_4 + CH_2{=}Sn(CH_3)_2. \quad (6)$$

The primary molecular formation of methane was proposed in the direct photolysis of TMT at 185 nm.[3] Minor reactions for hydrogen formation are

$$Hg^* + TMT \rightarrow Hg + H + CH_2Sn(CH_3)_3, \quad (7)$$

and

$$H + TMT \rightarrow H_2 + CH_2Sn(CH_3)_3. \quad (8)$$

In the mercury-photosensitized rections of NP, TMS, and TMG,reactions corresponding to Reactions (7) and (8) are the major initial reactions; C–M bond cleavage (M is a central atom) as Reaction (3) was not observed.

As described above, the addition of O_2 and NO to the photosensitization system suppressed the formation of ethane (Fig. 2). As Fig. 2 shows, the yield of ethane decreases with increasing the ratios of O_2/TMT and NO/TMT. The solid lines show the relative yields calculated using the following relative quenching efficiencies for TMT, O_2, and NO:

$$k_Q(TMT)/k_Q(O_2) = 0.56$$

and

$$k_Q(TMT)/k_Q(NO) = 0.30.$$

These were obtained from the following cross sections for TMT, O_2, and NO: $\sigma_Q(TMT)=63.7\times10^{-16}$ cm^2, $\sigma_Q(O_2)=62.5\times10^{-16}$ cm^2,[12] and $\sigma_Q(NO)=111\times^{-16}$ cm^2.[12] The decreases in the yields of ethane observed in the presence of O_2 and NO are steeper than those expected by the competitive quenching of the triplet mercury atoms by TMT and O_2 or NO. This shows that O_2 and NO have an additional effect (as radical scavengers) on the formation of ethane.

The primary process in the mercury-photosensitized decompositions of NP and TMG is known to be C–H bond cleavage. It has been pointed out, however, that at high light intensities and low substrate pressures, methane is found as one of the major products, and that

atom crackings occur under these conditions.[7,9] To examine the possibility of atom cracking in the present reaction, we examined the effect of hydrogen addition to the system. If atom cracking (shown by Reactions (9) and (10)) contributes to the formation of the methyl radical, one would expect that the yield of ethane continuously increases with increasing ratio of H_2/TMT, because of the large efficiency of the formation of hydrogen atoms for H_2-triplet mercury atom system:[12]

$$H + CH_2Sn(CH_3)_3 \rightarrow TMT^* \quad (9)$$

and

$$TMT^* \rightarrow CH_3 + Sn(CH_3)_3. \quad (10)$$

As shown in Fig. 3, however, the yield of ethane decreases with increasing the ratio of H_2/ TMT. The solid line shows the relative quantum yield calculated using the following relative quenching efficiencies for H_2 and TMT ($k_Q(H_2)/k_Q(TMT)=2.90$; obtained from $\sigma_Q(H_2)=27\times10^{-16}$ cm^2 [12] and $\sigma_Q(TMT)=63.7\times10^{-16}$ cm^2). The decrease in the quantum yield can be roughly explained by a competitive quenching of the triplet mercuty by H_2 and TMT. Therefore, atom cracking can be ruled out.

The following reactions are considered to explain the pressure dependence of the yields of ethane and methane:

$$Hg^* \longrightarrow Hg + h\nu \quad k_0 \quad (11)$$

$$Hg^* + TMT \xrightarrow{\alpha_1} Hg + CH_3 + (CH_3)_3Sn \quad (3)$$

$$Hg^* + TMT \xrightarrow{\alpha_2} Hg + CH_4 + CH_2{=}Sn(CH_3)_2 \quad k_Q \quad (6)$$

$$Hg^* + TMT \xrightarrow{1-\alpha_1-\alpha_2} Hg + TMT \quad (12)$$

$$CH_3 + CH_3 \longrightarrow C_2H_6 \quad k_1 \quad (4)$$

$$CH_3 + TMT \longrightarrow CH_4 + CH_2Sn(CH_3)_3 \quad k_2 \quad (5)$$

$$CH_2Sn(CH_3)_3 \longrightarrow CH_3 + CH_2{=}Sn(CH_3)_2 \quad k_3 \quad (13)$$

Radicals → recombination reactions. (14)

From the above mechanism, the following relationship can be derived by neglecting the contribution of CH_3 and $CH_2Sn(CH_3)_3$ radicals to Reactions (14):

$$\phi(C_2H_6)=\frac{1}{2}\alpha_1 \quad (15)$$

$$\phi(CH_4)=\alpha_2+\alpha_1\frac{k_2[TMT]}{k_1[CH_3]_{ss}} \quad (16)$$

$$\frac{\phi(CH_4)}{\phi(C_2H_6)}=\frac{2\alpha_2}{\alpha_1}+\frac{2k_2}{k_1[CH_3]_{ss}}[TMT]. \quad (17)$$

Since Reaction (5) requires an activation energy, as shown by Borrell and Platt,[3] the contribution of this reaction increases with increasing temperature. If this reaction can be neglected at 120 °C, $\phi(CH_4)$ equals to α_2. Therefore, at this temperature the quantum yields of ethane and methane are independent of the pressure of TMT. This is in agreement with the experimental results shown in Fig. 1(a) (decrease in yields with decreasing TMT pressure at low pressures seem to be due to incomplete quenchlng of excited mercury atoms). At higher temperature (250 °C), however, Reaction (5) can not be neglected, and the yield of methane may depend on TMT pressure. The steady-state concentration of methyl radical can be expressed as

$$[CH_3]_{ss}=\left(\frac{\alpha_1 I_0}{2k_1}\right)^{1/2}; \quad (18)$$

this can be regarded as being independent of TMT pressure. Figure 6 shows the ratio of the yield of methane to that of ethane obtained at 120 °C and 250 °C as a function of the pressure of TMT. The ratio increases at 250 °C linearly with increasing the pressure of TMT; this is in agreement with the expectaion from Eq. 17. The slopes and intercepts of the lines in Fig. 6 are listed in Table 1.

The main products from the cadmium-photosensitized reaction of TMT were ethane and methane. The pressure dependences of the yields of these products are similar to those in the mercury-photosensitized reaction at 250 °C. The effect of H_2 on the yield of ethane is also very similar to that in the mercury-photosensitized reaction. These findings show that the reaction mechanism for the cadmium-photosensitized reaction of TMT is similar to that for the mercury-photosensitized reaction. The ratio of the yield of methane to that of ethane is shown as a function of the TMT pressure in Fig. 6. The ratio again increases linearly with increasing TMT pressure. The slope and intercept of the line for the cadmium-photosensitization are also listed in Table 1.

The values of α_2/α_1 obtained from the intercepts are listed in Table 1. The value of α_2/α_1 for the mercury-photosensitized reaction at 250 °C is very similar to that for the cadmium-photosensitized reaction. It is sensitive to temperature, and is large at high temperatures.

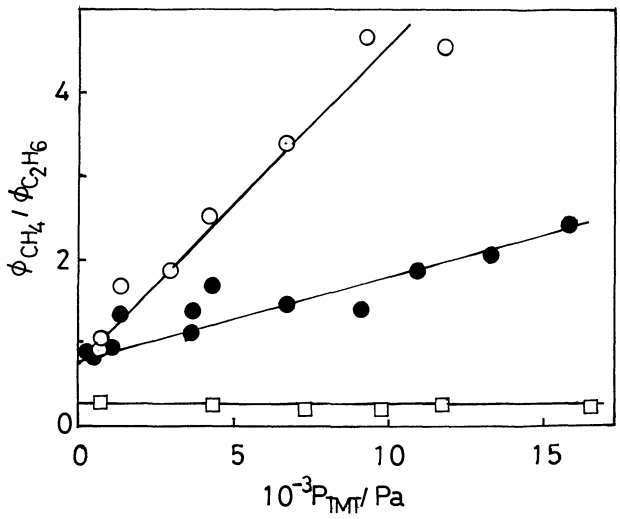

Fig. 6. Plots of $\Phi_{CH_4}/\Phi_{C_2H_6}$ against the TMT pressure for the mercury-photosensitized reaction at 120 °C (□) and 250 °C (●) and the cadmium-photosensitized reaction at 280 °C (○).

Table 1. Comparison of Various Constants for Mercury- and Cadmium-Photosensitized Reactions

	Hg		Cd
	120 °C	250 °C	280 °C
Intercept	0.12	0.89	0.80
10^5 slope/ Pa^{-1}	0	9.0	43
α_2/α_1	0.10	0.45	0.40
10^{-10} k_1/ 1 mol^{-1} s^{-1}	2.5	2.5	2.5
10^{-4} k_2/ 1 mol^{-1} s^{-1}	0.34	4.6	7.0
10^9 $[CH_3]_{ss}$/ mol l^{-1}		9.5	2.8

This shows that the ratio of the molecular formation of methane (Reaction (6)) to the formation of methyl radical (Reaction (3)) increases with increasing temperature. This molecular process for the formation of methane is known to occur in a direct photolysis of TMT vapor at 185 nm.[3] Since we have no information, however, on the temperature dependence of this process, further discussion of the temperature dependence of the α_2/α_1 seems not to be justified.

The value of the slope seems to depend on the temperature and kind of sensitizer. The k_1- and k_2-values included in the slope can be obtained from the literatures:

$$k_1/\,1\ mol^{-1}\ s^{-1} = (2.5 \pm 0.2) \times 10^{10}$$ [13]

and

$$k_2/\,1\ mol^{-1}\ s^{-1} = 1.2 \times 10^8 \exp(-4100/T).$$ [3]

These values are also listed in Table 1. The steady-state concentrations of CH_3 can be estimated from the values of the slope and those of k_1 and k_2 and are listed in Table 1. The value of $[CH_3]_{ss}$ obtained for the mercury-photosensitized reaction at 250 °C is larger than that for the cadmium-photosensitized reaction. This tendency is not apparently in agreement with the fact that the rate of the ethane formation in the mercury-photosensitized reaction of TMT is smaller than that in the cadmium-photosensitized reaction of TMT (the values of 6.7×10^{-10} and 15.7×10^{-10} mol s^{-1} for the mercury- and cadmium photosensitized reactions were obtained from the time dependences of the yield of ethane). This discrepancy may result from the difference in the volume of reaction zone, based on the differences in the cross sections of the beams of exciting light and the absorption coefficients of mercury and cadmium: that is, the mercury-photosensitized reaction occurs locally near the front window of the cell because of the large absorption coefficient of mercury (the ratio of the volumes of reaction zone ($V_{Hg}/V_{Cd} = 1/26$) is consistent with the values of $[CH_3]_{ss}$ and the apparent rate of ethane formation in the mercury- and cadmium-photosensitized reactions).

Contrary to the mercury-photosensitized decompositions of NP, TMS, and TMG, the main initial reactions of the mercury- and cadmium-photosensitized decomposition of TMT are processes with a cleavage of an Sn–C bond (the formation of CH_3 and the molecular formation of methane). In this respect, the present reactions are very similar to the direct photolysis of TMT as well as the cadmium-photosensitized reaction of acetaldehyde, which was reported to proceed through the formation of an excited complex between the Cd* and an aldehyde molecule, or after an energy transfer from Cd* to an aldehyde molecule.[14] The triplet energy of TMT is not yet known, but is probably lower than those of NP and TMS, because the absorption band of TMT shifts to a longer wavelength than do those of NP and TMS.[15] Since the quenching cross section of triplet mercury atom for TMT is larger than those for NP and TMS, as described above, the triplet energy transfer from Hg ($^3P_1$)(and Cd($^3P_1$)) to TMT to produce a triplet state of the TMT molecules seems to occur. This is the reasoning used to explain that the mechanism for TMT is different from those for NP, TMS, and TMG, and that it is rather similar to those of the cadmium-photosensitized reactions of aldehydes.

The present work was partially supported by a Grant-in-Aid for Scientific Research No. 63540342 from the Ministry of Education, Science and Culture.

References

1) R. P. Johnson and S. J. W. Price, *Can. J. Chem.*, **50**, 50 (1972).
2) A. C. Baldwin, K. E. Lewis, and D. M. Golden, *Int. J. Chem. Kinet.*, **11**, 529 (1979).
3) P. Borrell and A. E. Platt, *Trans. Faraday Soc.*, **66**, 2286 (1970).
4) M. Kawasaki, H. Sato, H. Shinohara, and N. Nishi, *Laser Chem.*, **7**, 109 (1987).
5) R. J. Norstron, O. P. Strausz, and H. E. Gunning, *Can. J. Chem.*, **42**, 2140 (1964).
6) E. Furimsky and K. J. Laidler, *Can. J. Chem.*, **50**, 1115, 1120, 1129 (1972).
7) M. A. Nay, G. N. C. Woodall, O. P. Strausz, and H. E. Gunning, *J. Am. Chem. Soc.*, **87**, 179 (1965).
8) P. Potzinger, B. Reimann, and R. S. Roy, *Ber. Bunsen-Ges. Phys. Chem.*, **85**, 1119 (1981).
9) J. Duval and Y. Rousseau, *Can. J. Chem.*, **51**, 3062 (1973).
10) R. B. Cundall and T. F. Palmer, *Trans. Faraday Soc.*, **56**, 1211 (1960).
11) S. Tsunashima and S. Sato, *Bull. Chem. Soc. Jpn.*, **41**, 284 (1968).
12) R. J. Cvetanovic, *Prog. React. Kinet.*, **2**, 39 (1964).
13) M. J. Pilling, J. A. Robertson, and G. J. Rogers, *Int. J. Chem. Kinet.*, **8**, 883 (1976).
14) K. Yamamoto, S. Tsunashima, and S. Sato, *Bull. Chem. Soc. Jpn.*, **46**, 3677 (1973).
15) H. W. Thompson and J. W. Linnett, *Proc. R. Soc. London, Ser. A*, **156**, 108 (1936).

Structural Study of Triazole Antifungals. II.[1] Crystal and Molecular Structures of the Two Diastereoisomers (4*R**,5*R**)- and (4*S**,5*R**)-5-(2,4-Difluorophenyl)-4-methyl-5-[(1*H*-1,2,4-triazol-1-yl)methyl]-3-[4-(trifluoromethyl)benzoyl]oxazolidine

Tadashi HATA,* Youji FURUKAWA, Toshiyuki KONOSU,† and Sadao OIDA†
Analytical and Metabolic Research Laboratories, Sankyo Co., Ltd.,
1-2-58 Hiromachi, Shinagawa-ku, Tokyo 140
†Medicinal Chemistry Research Laboratories, Sankyo Co., Ltd.,
1-2-58 Hiromachi, Shinagawa-ku, Tokyo 140
(Received April 30, 1991)

The title compounds were designed and synthesized as potential inhibitors of cytochrome P-450 14α-demethylase. The antifungal activity of (4*R**,5*R**)-isomer is markedly higher than that of (4*S**,5*R**)-isomer. The crystal structures of the two diastereoisomers were determined by X-ray diffraction technique. The final *R* indices of (4*R**,5*R**)- and (4*S**,5*R**)-isomers were 0.063 and 0.070 for 2840 and 2365 reflections, respectively. The different configuration at the 4-position in the oxazolidine ring causes the differences in the ring conformation and in some torsion angles. The three-dimensional structures of the two diastereoisomers are consequently different. Among the diastereoisomers and enantiomers, the (4*R*,5*R*)-enantiomer is superimposable on lanosterol, which is a substrate of cytochrome P-450 14α-demethylase, suggesting that the 4β-methyl group plays an important role in the antifungal activity.

Compounds containing the imidazole ring or the 1,2,4-triazole ring are known to be active as antifungal agents. These compounds have been shown to inhibit biosysthesis of the cell membrane in fungi. An important step in this biosynthesis is cytochrome P-450-mediated 14α-demethylation of lanosterol to give, after several steps, ergosterol, which is an essential molecule for the formation of fungal membranes.[2] Imidazole and triazole antifungals inhibit this enzyme by a mechanism in which the heterocyclic nitrogen atom (N-3 of imidazole and N-4 of triazole) binds to the heme iron atom located in the binding site of the enzyme.[3]

In a program aimed at seeking an active agent against fungal infections, new triazolylmethyloxazolidine derivatives were designed and synthesized as potential inhibitors against fungal cytochrome P-450 14α-demethylase.[4] Among them, (4*R**,5*R**)-5-(2,4-difluorophenyl)-4-methyl-5-[(1*H*-1,2,4-triazol-1-yl)methyl]-3-[4-(trifluoromethyl)benzoyl]oxazolidine shows the excellent antifungal activity. On the other hand, the (4*S**,5*R**)-diastereoisomer exhibits significantly less activity. This paper reports the results of structural studies of the two diastereoisomers using X-ray crystallographic analysis and a structural comparison with lanosterol.

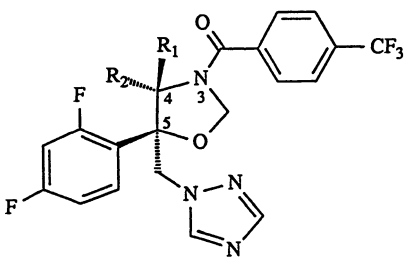

(4*R**,5*R**)-isomer: R_1=CH_3, R_2=H
(4*S**,5*R**)-isomer: R_1=H, R_2=CH_3

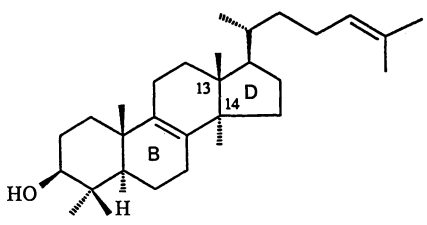

lanosterol

Experimental

(4*R,5*R**)-Isomer.** Colorless plates were grown by slow evaporation of a benzen–hexane solution at room temperature. Diffraction experiments were performed with a crystal, 0.1×0.3×0.8 mm, on a Rigaku AFC-5 diffractometer, using the monochromated Cu $K\alpha$ radiation. The crystal data are as follows: $C_{21}H_{17}N_4O_2F_5$, F.W.=452.4, triclinic, space group $P\bar{1}$, a=14.076(3), b=10.715(2), c=7.017(3) Å, α=95.12(3), β=96.29(4), γ=101.86(2)°, V=1022.7(4) Å^3, Z=2, D_c=1.47 g cm^{-3}, μ(Cu$K\alpha$)=11.4 cm^{-1}. The ω–2θ scanning mode was employed up to 2θ=128°. A total of 3523 reflections were measured, of which 2843 unique reflections with $F \geqslant 3\sigma(F)$ were used for the analysis. Three references measured every 200 reflections showed no significant variation in intensity. Correction was made for Lorentz and polarization factors, but not absorption. The structure was solved by the direct methods using MULTAN 78,[5] and refined by the block-diagonal least-squares technique with anisotropic thermal parameters. Hydrogen atoms were located on a difference Fourier synthesis and refined isotropically. A difference Fourier map revealed two positions of trifluoromethyl F atoms: both positions were included with population parameters of 0.7 and 0.3. Three low-angle reflections seemed to be affected by secondary extinction and were excluded from the data set. The final refinement converged at R=0.063 and R_w=0.062. The weighting scheme applied was $w=1/\sigma(F)$. Atomic scattering factors were taken from Ref. 6. Calculations were carried out with the DIRECT-SEARCH program system.[7] The final fractional coordinates and equivalent iso-

Table 1. Fractional Atomic Coordinates and Equivalent Isotropic Parameters for Non-H Atoms, with esd's in Parentheses

Atom	x	y	z	B_{eq}/Å^2	Atom	x	y	z	B_{eq}/Å^2
(4*R**,5*R**)-Isomer					(4*S**,5*R**)-Isomer				
O(1)	0.1428(2)	0.6487(2)	0.5607(3)	4.26(8)	O(1)	0.2529(2)	0.2192(5)	0.2027(1)	4.0(5)
C(2)	0.2297(3)	0.6174(4)	0.6460(6)	5.0(1)	C(2)	0.2983(3)	0.2544(8)	0.2785(2)	5.3(2)
N(3)	0.2904(2)	0.6215(3)	0.4943(4)	4.21(9)	N(3)	0.2870(2)	0.4853(6)	0.2902(2)	4.4(1)
C(4)	0.2706(3)	0.7189(3)	0.3723(5)	3.9(1)	C(4)	0.2514(2)	0.5979(7)	0.2193(2)	4.0(1)
C(5)	0.1637(3)	0.7231(3)	0.4043(5)	3.8(1)	C(5)	0.2049(2)	0.4062(7)	0.1706(2)	3.6(1)
C(6)	0.0876(3)	0.6564(3)	0.2361(5)	4.4(1)	C(6)	0.1993(2)	0.4209(7)	0.0929(2)	4.1(1)
N(7)	0.0999(2)	0.5271(3)	0.1719(4)	4.07(9)	N(7)	0.1688(2)	0.2256(6)	0.0503(2)	3.8(1)
N(8)	0.1546(2)	0.5093(3)	0.0301(5)	5.1(1)	N(8)	0.0912(2)	0.1732(7)	0.0220(2)	4.8(1)
C(9)	0.1521(3)	0.3850(4)	0.0244(6)	5.3(1)	C(9)	0.0900(3)	−0.0100(8)	−0.0126(2)	4.7(2)
N(10)	0.1003(3)	0.3240(3)	0.1495(5)	5.8(1)	N(10)	0.1603(2)	−0.0806(7)	−0.0093(2)	4.9(1)
C(11)	0.0685(3)	0.4171(4)	0.2401(6)	5.5(1)	C(11)	0.2078(2)	0.0726(8)	0.0311(2)	4.6(2)
C(12)	0.3460(2)	0.5365(3)	0.4413(5)	4.1(1)	C(12)	0.2986(3)	0.5839(9)	0.3534(3)	5.7(2)
O(13)	0.3819(2)	0.5414(2)	0.2910(4)	5.24(9)	O(13)	0.2796(3)	0.7767(6)	0.3552(2)	8.8(2)
C(14)	0.3621(2)	0.4414(3)	0.5769(5)	3.9(1)	C(14)	0.3365(3)	0.4602(9)	0.4239(3)	5.9(2)
C(15)	0.3632(3)	0.3174(4)	0.4944(6)	4.9(1)	C(15)	0.4041(5)	0.348(2)	0.4376(4)	9.1(3)
C(16)	0.3819(3)	0.2259(4)	0.6102(6)	5.2(1)	C(16)	0.4410(5)	0.243(2)	0.5057(4)	10.3(4)
C(17)	0.4006(3)	0.2557(3)	0.8066(5)	4.6(1)	C(17)	0.4068(4)	0.250(1)	0.5571(3)	8.6(3)
C(18)	0.4008(3)	0.3786(4)	0.8913(5)	4.6(1)	C(18)	0.3476(7)	0.377(2)	0.5434(4)	11.9(5)
C(19)	0.3813(3)	0.4694(3)	0.7731(5)	4.4(1)	C(19)	0.3093(6)	0.480(2)	0.4763(4)	10.1(4)
C(20)	0.4230(4)	0.1587(4)	0.9346(7)	6.6(2)	C(20)	0.4427(6)	0.113(2)	0.6268(3)	15.5(5)
F(21)	0.4362(4)	0.0568(3)	0.8435(6)	9.1(2)	F(21)	0.4858(6)	−0.020(1)	0.6277(3)	28.7(6)
F(22)	0.3469(4)	0.1248(4)	1.0383(7)	10.4(2)	F(22)	0.3998(4)	0.107(2)	0.6606(3)	29.4(6)
F(23)	0.4951(3)	0.2012(4)	1.0662(6)	9.8(2)	F(23)	0.4933(4)	0.238(1)	0.6751(3)	21.8(4)
C(24)	0.1478(3)	0.8595(3)	0.4588(5)	3.9(1)	C(24)	0.1248(2)	0.3803(7)	0.1754(2)	3.6(1)
C(25)	0.1513(3)	0.9469(3)	0.3293(5)	4.4(1)	C(25)	0.0677(2)	0.5403(8)	0.1483(2)	4.4(1)
C(26)	0.1382(3)	1.0712(3)	0.3710(6)	5.0(1)	C(26)	−0.0057(3)	0.5257(9)	0.1492(3)	5.3(2)
C(27)	0.1227(3)	1.1023(4)	0.5536(6)	5.3(1)	C(27)	−0.0213(3)	0.343(1)	0.1792(3)	5.8(2)
C(28)	0.1186(3)	1.0225(4)	0.6948(6)	5.5(1)	C(28)	0.0307(3)	0.1766(9)	0.2065(3)	5.6(2)
C(29)	0.1311(3)	0.8977(4)	0.6421(5)	4.7(1)	C(29)	0.1040(3)	0.1975(8)	0.2039(2)	4.6(2)
F(30)	0.1697(2)	0.9152(2)	0.1471(3)	6.00(8)	F(30)	0.0851(2)	0.7224(4)	0.1197(2)	5.7(5)
F(31)	0.1096(2)	1.2248(2)	0.6011(4)	7.6(1)	F(31)	−0.0937(2)	0.3225(6)	0.1817(2)	8.3(1)
C(32)	0.3472(3)	0.8445(4)	0.4351(7)	6.1(1)	C(32)	0.3132(3)	0.6992(8)	0.1976(3)	5.2(2)
F(21′)	0.429(1)	0.180(1)	1.106(1)	11.9(6)	C(15′)	0.384(2)	0.556(5)	0.482(1)	8(1)
F(22′)	0.511(1)	0.136(2)	0.915(2)	20(1)	C(16′)	0.423(2)	0.430(7)	0.546(1)	10(1)
F(23′)	0.358(1)	0.0442(9)	0.890(2)	13.9(6)	C(18′)	0.348(2)	0.128(5)	0.499(1)	9(1)
					C(19′)	0.311(2)	0.241(4)	0.434(1)	7(1)

tropic thermal parameters[8] are given in Tablel 1.[9]

(4*S,5*R**)-Isomer.** Recrystallization from a benzene–ether solution gave colorless plates. The crystal used has approximate dimensions of 0.2×0.4×0.6 mm; the unit cell constants area a=18.513(3), b=6.122(2), c=19.805(1) Å, β=113.13(4)°, V=2064(2) Å^3, D_c=1.46 g cm^{-3} in space group $P2_1/a$ (Z=4), μ(Cu $K\alpha$)=11.3 cm^{-1}. Of 3432 reflections measured, 2367 were independently observed at level $F \geqslant 3\sigma(F)$. Data reduction and structure determination were carried out using the methods and procedures described for (4*R**,5*R**)-isomer. The ortho- and meta-position atoms of the trifluoromethylbenzoyl group are disordered in two orientations with weights of 0.8 and 0.2. Two low-angle reflections affected by secondary extinction were left out of the refinement. With unit weights, final residuals were R=0.070 and R_w=0.063.

Results and Discussion

The atom labelling and thermal ellipsoids are shown in Fig. 1. Bond lengths and angles are given in Table 2. Some bond lengths and angles in the two diastereoisomers, particularly in the oxazolidine rings, are significantly different from each other.

The oxazolidine ring of the (4*R**,5*R**)-isomer takes the half-chair conformation, as in the (4*S**,5*R**)-isomer. However in the (4*R**,5*R**)-isomer, the C(2) and N(3) atoms of the oxazolidine ring are displaced form the plane descried by the remaining atoms, O(1), C(4), and C(5) by −0.21(1) Å and 0.25(1) Å, while in the (4*S**,5*R**)-isomer the C(4) and C(5) atoms lie out of the plane containing the other ring atoms by 0.33(2) Å and −0.22(2) Å, respectively. This discrepancy in the ring puckering might be accounted for by the difference of the configuration at the C(4) atom in the oxazolidine ring.

Remarkable differences of some torsion angles are recognized between the two molecules, as shown in Table 3. The C(32) methyl group and the triazolylmethyl group are *trans* in the (4*R**,5*R**)-isomer, contrary to the *cis* configuration in the (4*S**,5*R**)-isomer, resulting in the C(32)–C(4)–C(5)–C(6) torsion angles of 137.2(3)° in the former and −28.1(6)° in the latter. The triazole ring of the (4*R**,5*R**)-isomer is located above the oxazolidine ring with a C(4)–C(5)–C(6)–N(7) torsion angle of 49.4(4)°. The (4*S**,5*R**)-isomer can not take

Table 2. Bond Distances (l/Å) and Angles (θ/°)

	(4*R**,5*R**)-Isomer	(4*S**,5*R**)-Isomer		(4*R**,5*R**)-Isomer	(4*S**,5*R**)-Isomer
O(1)–C(2)	1.417(5)	1.419(5)	C(4)–C(5)–C(24)	114.1(3)	110.8(4)
O(1)–C(5)	1.435(4)	1.436(5)	C(6)–C(5)–C(24)	109.2(3)	113.0(3)
C(2)–N(3)	1.434(5)	1.461(6)	C(5)–C(6)–N(7)	112.4(3)	113.7(4)
N(3)–C(4)	1.459(5)	1.466(5)	C(6)–N(7)–N(8)	120.3(3)	122.9(4)
N(3)–C(12)	1.370(5)	1.330(6)	C(6)–N(7)–C(11)	129.6(3)	128.4(4)
C(4)–C(5)	1.554(5)	1.549(5)	N(8)–N(7)–C(11)	110.0(3)	108.7(3)
C(4)–C(32)	1.536(5)	1.504(8)	N(7)–N(8)–C(9)	101.6(3)	102.5(4)
C(5)–C(6)	1.519(5)	1.503(7)	N(8)–C(9)–N(10)	115.5(4)	115.5(4)
C(5)–C(24)	1.545(5)	1.530(7)	C(9)–N(10)–C(11)	102.3(3)	101.7(4)
C(6)–N(7)	1.469(5)	1.444(5)	N(7)–C(11)–N(10)	110.6(4)	111.6(4)
N(7)–N(8)	1.346(5)	1.360(5)	N(3)–C(12)–O(13)	120.7(3)	121.2(4)
N(7)–C(11)	1.322(5)	1.326(6)	N(3)–C(12)–C(14)	117.1(3)	119.5(5)
N(8)–C(9)	1.322(5)	1.309(6)	O(13)–C(12)–C(14)	122.2(3)	119.3(5)
C(9)–N(10)	1.333(6)	1.349(7)	C(12)–C(14)–C(15)	116.9(3)	119.9(6)
N(10)–C(11)	1.316(6)	1.320(6)	C(12)–C(14)–C(19)	124.2(3)	119.9(6)
C(12)–O(13)	1.218(5)	1.236(7)	C(15)–C(14)–C(19)	118.8(3)	119.7(6)
C(12)–C(14)	1.489(5)	1.499(7)	C(14)–C(15)–C(16)	120.2(3)	119.0(8)
C(14)–C(15)	1.404(5)	1.36(1)	C(15)–C(16)–C(17)	120.1(4)	119.8(8)
C(14)–C(19)	1.368(5)	1.32(1)	C(16)–C(17)–C(18)	120.6(4)	117.4(7)
C(15)–C(16)	1.376(6)	1.41(1)	C(16)–C(17)–C(20)	121.0(4)	118.8(7)
C(16)–C(17)	1.370(5)	1.39(3)	C(18)–C(17)–C(20)	118.4(3)	123.8(8)
C(17)–C(18)	1.395(5)	1.28(1)	C(17)–C(18)–C(19)	118.6(3)	123(1)
C(17)–C(20)	1.492(6)	1.53(1)	C(14)–C(19)–C(18)	121.7(3)	120(1)
C(18)–C(19)	1.384(6)	1.39(1)	C(17)–C(20)–F(21)	113.6(4)	117.6(8)
C(20)–F(21)	1.273(6)	1.14(2)	C(17)–C(20)–F(22)	109.0(4)	111.2(9)
C(20)–F(22)	1.367(7)	1.23(1)	C(17)–C(20)–F(23)	114.3(4)	105.9(9)
C(20)–F(23)	1.272(6)	1.29(1)	F(21)–C(20)–F(22)	107.9(4)	125(1)
C(24)–C(25)	1.359(5)	1.386(6)	F(21)–C(20)–F(23)	108.8(5)	96.5(8)
C(24)–C(29)	1.375(5)	1.374(7)	F(22)–C(20)–F(23)	102.5(4)	92.8(8)
C(25)–C(26)	1.393(5)	1.370(7)	C(5)–C(24)–C(25)	121.6(3)	120.8(4)
C(25)–F(30)	1.359(4)	1.345(6)	C(5)–C(24)–C(29)	120.9(3)	123.0(4)
C(26)–C(27)	1.348(6)	1.348(8)	C(25)–C(24)–C(29)	117.5(3)	116.1(4)
C(27)–C(28)	1.363(6)	1.361(7)	C(24)–C(25)–C(26)	124.0(4)	124.0(5)
C(27)–F(31)	1.380(5)	1.367(7)	C(24)–C(25)–F(30)	120.0(3)	118.5(4)
C(28)–C(29)	1.407(6)	1.385(8)	C(26)–C(25)–F(30)	116.0(3)	117.5(4)
C(14)–C(15′)		1.29(3)	C(25)–C(26)–C(27)	115.3(4)	116.4(5)
C(14)–C(19′)		1.46(3)	C(26)–C(27)–C(28)	125.4(4)	123.8(5)
C(15′)–C(16′)		1.42(4)	C(26)–C(27)–F(31)	117.2(4)	118.4(5)
C(16′)–C(17)		1.18(4)	C(28)–C(27)–F(31)	117.5(4)	117.8(5)
C(17)–C(18′)		1.44(3)	C(27)–C(28)–C(29)	116.3(4)	117.8(5)
C(18′)–C(19′)		1.39(3)	C(24)–C(29)–C(28)	121.5(4)	121.9(4)
C(20)–F(21′)	1.20(1)		C(12)–C(14)–C(15′)		121(1)
C(20)–F(22′)	1.33(2)		C(12)–C(14)–C(19′)		121.9(9)
C(20)–F(23′)	1.36(1)		C(15′)–C(14)–C(19′)		116(2)
			C(14)–C(15′)–C(16′)		119(3)
C(2)–O(1)–C(5)	109.9(3)	110.8(3)	C(15′)–C(16′)–C(17)		126(3)
O(1)–C(2)–N(3)	104.0(3)	104.6(3)	C(16′)–C(17)–C(18′)		120(2)
C(2)–N(3)–C(4)	109.2(3)	110.0(3)	C(16′)–C(17)–C(20)		129(1)
C(2)–N(3)–C(12)	128.4(3)	127.4(4)	C(18′)–C(17)–C(20)		111(1)
C(4)–N(3)–C(12)	121.5(3)	122.3(4)	C(17)–C(18′)–C(19′)		116(3)
N(3)–C(4)–C(5)	101.4(3)	99.8(3)	C(14)–C(19′)–C(18′)		121(2)
N(3)–C(4)–C(32)	109.5(3)	111.2(3)	C(17)–C(20)–F(21′)	120.8(7)	
C(5)–C(4)–C(32)	115.8(3)	115.7(4)	C(17)–C(20)–F(22′)	110.4(9)	
O(1)–C(5)–C(4)	105.8(3)	103.4(3)	C(17)–C(20)–F(23′)	112.1(7)	
O(1)–C(5)–C(6)	104.7(3)	106.5(4)	F(21′)–C(20)–F(22′)	101(1)	
O(1)–C(5)–C(24)	108.5(3)	109.6(3)	F(21′)–C(20)–F(23′)	104.2(9)	
C(4)–C(5)–C(6)	113.8(3)	113.0(4)	F(22′)–C(20)–F(23′)	107(1)	

such a conformation because of the upward *cis* methyl group attached to C(4) atom.

In order to avoid the repulsion between the O(13) atom and C(32) methyl group attached to the 4-position in the oxazolidine ring, the torsion angle of C(12)–N(3)–C(4)–C(5) to take the value of 143.6(3)° in the (4*R**,5*R**)-isomer, while it is −145.3(4)° in the (4*S**,5*R**)-isomer. Consequently, the directions of the two phenyl groups in these molecules differ from each other, as shown in Fig. 1. It may be concluded that the

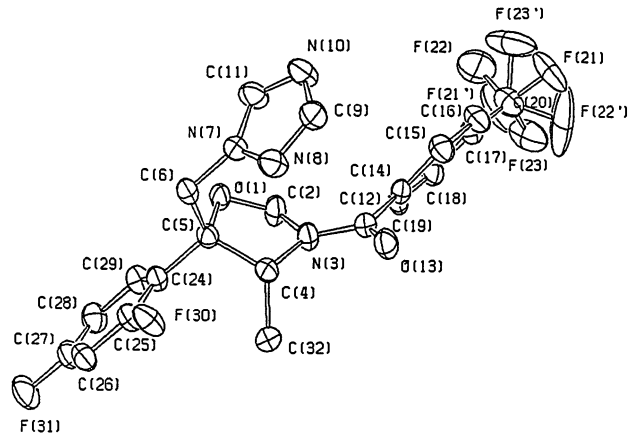

(a)

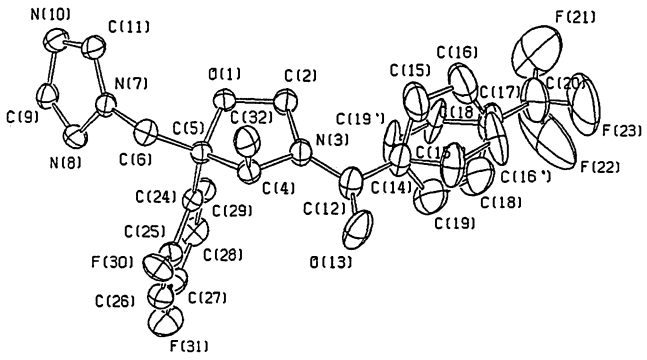

(b)

Fig. 1. ORTEP plots of the two diastereoisomers with thermal ellipsoids at the 30% probability level. (a) (4*R**,5*R**)-isomer. (b) (4*S**,5*R**)-isomer.

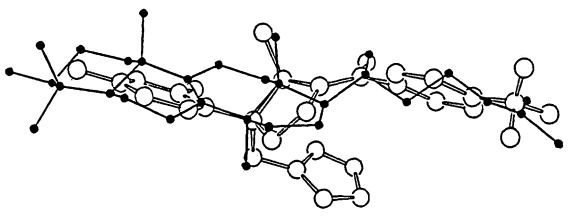

Fig. 2. Comparison of (4*R*,5*R*)-enantiomer (large open circles) and lanosterol (small closed circles).

different configurations at the 4-position in the oxazolidine rings make the two diastereoisomers adopt the different overall structures.

Antifungal azole derivatives interfere with the microsomal P-450-dependent 14α-demethylation of lanosterol, resulting in the accumulation of 14α-methyl sterols and a decreased availability of ergosterol.[10] Oxazolidine derivatives with a (4*R**,5*R**)-configuration show markedly enhanced activities, while (4*S**,5*R**)-diastereomers possess significantly decreased activities. Of the enantiomeric pair, the activity of (4*R*,5*R*)-enantiomer is far more potent than that of (4*S*,5*S*)-enantiomer.[4] Thus, we presumed that only (4*R*,5*R*)-enantiomer, among the diastereoisomers and enantiomers, has a favorable framework to fit in the active site of the enzyme, and using it we carried out a structural comparison with lanosterol. The lanosterol model was built by use of the typical bond lengths and angles and minimized by the force-field calculation of the MM2′ program.[11]

Table 3. Selected Torsion Angles (τ/°)

	(4*R**,5*R**)-Isomer	(4*S**,5*R**)-Isomer
C(5)–O(1)–C(2)–N(3)	−25.1(4)	−9.3(5)
C(2)–O(1)–C(5)–C(4)	9.2(4)	27.1(5)
O(1)–C(2)–N(3)–C(4)	32.5(4)	−13.8(5)
C(2)–N(3)–C(4)–C(5)	−26.0(4)	28.8(5)
N(3)–C(4)–C(5)–O(1)	10.0(4)	−32.8(4)
C(12)–N(3)–C(4)–C(5)	143.6(3)	−145.3(4)
C(4)–N(3)–C(12)–C(14)	179.7(3)	−178.9(4)
N(3)–C(4)–C(5)–C(6)	−104.4(3)	−147.5(3)
N(3)–C(4)–C(5)–C(24)	129.3(3)	84.6(4)
C(32)–C(4)–C(5)–O(1)	−108.4(3)	86.6(4)
C(32)–C(4)–C(5)–C(6)	137.2(3)	−28.1(6)
C(4)–C(5)–C(6)–N(7)	49.4(4)	169.4(3)
C(4)–C(5)–C(24)–C(25)	69.8(5)	66.3(5)
C(5)–C(6)–N(7)–N(8)	−92.1(4)	77.0(5)

Computer graphics showed how (4*R*,5*R*)-enantiomer can be superposed on lanosterol (Fig. 2). The 5β-difluorophenyl group and the oxazolidine ring could be regarded as the B and D rings of lanosterol, and the 4β-methyl group and the methylene carbon atom of the 5α-triazolylmethyl group as the 13β-methyl and 14α-methyl group of lanosterol, respectively. The *N*-trifluoromethylbenzoyl group might correspond to the 17-alkyl side chain of lanosterol. The 4β-methyl group is expected to play an important role in antifungal potency, since a 4-demethyloxazolidine analogue exhibits an intermediate activity between (4*R**,5*R**)- and (4*S**,5*R**)-diastereoisomers.[4]

References

1) Part I: T. Hata, H. Hanzawa, T. Konosu, and S. Oida, *Anal. Sci.*, **6**, 789 (1990).

2) Y. Aoyama, Y. Yoshida, and R. Sato, *J. Biol. Chem.*, **259**, 1661 (1984).

3) P. Gadher, E. I. Mercer, B. C. Baldwin, and T. E. Wiggins, *Pestic. Biochem. Physiol.*, **19**, 1 (1983).

4) T. Konosu, Y. Tajima, N. Takeda, T. Miyaoka, M. Kasahara, H. Yasuda, and S. Oida, *Chem. Pharm. Bull.*, **38**, 2476 (1990).

5) P. Main, S. E. Hull, L. Lessinger, G. Germain, J.-P. Declercq, and M. M. Woolfson, "MULTAN 78. A System of Computer Programs for the Automatic Solution of Crystal Structures from X-Ray Diffraction Data," Univs. of York,

England and Louvain, Belgium (1978).
6) "International Tables for X-Ray Crystallography," Kynoh Press, Birmingham (1974), Vol. IV.
7) Y. Koyama and K. Okada, *Acta Crystallogr., Sect. A,* **31**, S18 (1975).
8) W. C. Hamilton, *Acta Crystallogr.,* **18**, 502 (1965).
9) Lists of structure factors, anisotropic thermal parameters, and atomic parameters for hydrogen atoms have been deposited as Document No. 8961 at the Office of the Editor of Bull. Chem. Soc. Jpn.
10) H. Van den Bossche, G. Willemsens, W. Cools, W. F. J. Lauwers, and L. Le Jeune, *Chem.-Biol. Interact.,* **21**, 59 (1978).
11) C. Jaime and E. Ōsawa, *Tetrahedron,* **39**, 2769 (1983).

Miscibility of 2-(Octylsulfinyl)ethanol and Decylammonium Chloride in the Adsorbed Film and Micelle

Koji ABE,* Hidetsugu MATSUKIYO, Norihiro IKEDA, Makoto ARATONO, and Kinsi MOTOMURA
Department of Chemistry, Faculty of Science, Kyushu University 33, Fukuoka 812
(Received May 13, 1991)

The surface tension of the aqueous solution of 2-(octylsulfinyl)ethanol (OSE) and decylammonium chloride (DeAC) mixture was measured as a function of total molality and composition of surfactants at 298.15 K under atmospheric pressure. The total surface density and compositions in the adsorbed film and micelle of the mixture were evaluated by applying thermodynamic relations to experimental results. It was found that the phase diagrams obtained for the adsorption and micelle formation of the mixture are different in shape from those of 2-(decylsulfinyl)ethanol (DeSE)–OSE and dodecylammonium chloride (DAC)–DeAC mixtures which are assumed to mix ideally in the adsorbed film and micelle. Such a nonideal behavior was attributed to the attractive interaction between OSE and DeAC molecules. Further, the interaction is concluded to be more attractive in the micelle than in the adsorbed film.

In previous papers, the surface adsorption and micelle formation of nonionic–nonionic[1–3] and cationic–cationic[4–7] surfactant mixtures have been investigated by applying the thermodynamic relations derived on the basis of excess thermodynamic quantities to measured surface tension. It has been demonstrated that the relation among the compositions of surfactants in the bulk phase, adsorbed film, and micelle provides important information about their miscibility.

There were many reports that nonionic and ionic surfactants mix nonideally in adsorbed films and micelles.[8–17] However most of them relied on the analysis using the regular solution approximation which is considered not to be appropriate to describe the mixed adsorbed films and micelles.[4,7,15,16,18]

Now it is necessary to apply our thermodynamic treatment to nonionic–ionic mixed surfactant systems. In the present study, we choose the mixture of 2-(octylsulfinyl)ethanol (OSE) and decylammonium chloride (DeAC), because we have already investigated (i) the mixed adsorbed film of OSE and DeAC[19] in a dilute concentration range and (ii) the surface adsorption and micelle formation of mixed surfactant systems which contain either OSE or DeAC as one constituent.[1–6]

Experimental

2-(Octylsulfinyl)ethanol and decylammonium chloride were synthesized and purified by the methods described previously.[2,20,21] Water was triply distilled from dilute alkaline permanganate solution.

The equilibrium surface tension was measured by the drop volume technique at 298.15 K under atmospheric pressure.[22] Surface tension values were reproducible within 0.05 mN m^{-1}.

Results and Discussion

In order to investigate the miscibility of nonionic and ionic surfactants in the adsorbed film and micelle, it is appropriate to employ the total molality $\hat{m}$ of surfactants and the mole fraction $\hat{X}_2$ of surfactant 2 in the total surfactant introduced previously[7,18] as the experimental variables. In the case of the present system, $\hat{m}$ and $\hat{X}_2$ are related to the molality m_i of surfactant i as follows:

$$\hat{m} = m_1 + 2m_2 \quad (1)$$

and

$$\hat{X}_2 = 2m_2/\hat{m}, \quad (2)$$

where the subscripts 1 and 2 express OSE and DeAC, respectively.

The surface tension γ was measured as a function of $\hat{m}$ and $\hat{X}_2$ at 298.15 K under atmospheric pressure. The γ vs. $\hat{m}$ curve obtained at constant $\hat{X}_2$ is shown in Fig. 1. It is found that the curve has a distinct break point where the micelle formation begins. The concentration of this point is referred to as the critical micelle concentration (cmc). Another break point is seen on the curve at a relatively low concentration; this point was proved to result from the phase transformation between the gaseous and expanded states of adsorbed film.[19] The γ vs. $\hat{X}_2$ curves at constant $\hat{m}$ depicted by replotting Fig. 1 are shown together with the surface tension at the cmc

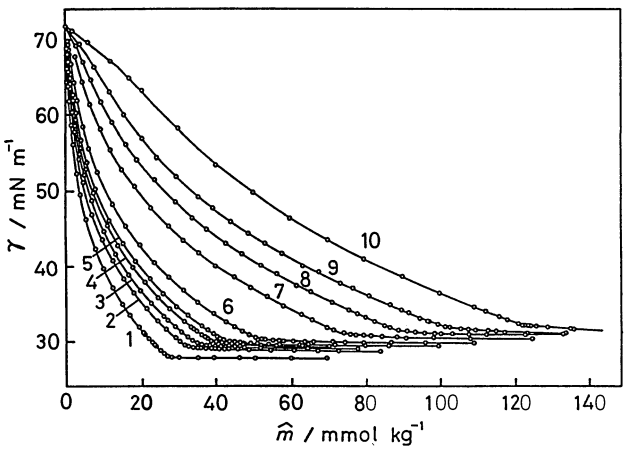

Fig. 1. Surface tension vs. total molality curves at constant composition: (1) $\hat{X}_2$=0; (2) 0.349; (3) 0.443; (4) 0.550; (5) 0.613; (6) 0.725; (7) 0.889; (8) 0.941; (9) 0.972; (10) 1.

γ^C vs. $\hat{X}_2$ curve in Fig 2. Both the γ and γ^C values increase as the composition of DeAC increases. But the curves are quite different in shape from each other; the γ^C vs. $\hat{X}_2$ curve is concave downward at a small composition and concave upward at a large composition, while the γ vs. $\hat{X}_2$ curve is concave upward over the whole range of composition. In Fig. 3, the $\hat{m}$ at constant γ and the cmc $\hat{C}$ are plotted against $\hat{X}_2$. The $\hat{m}$ and $\hat{C}$ values increase with increasing $\hat{X}_2$ and the dependence of $\hat{C}$ on $\hat{X}_2$ resembles that of $\hat{m}$.

Now let us derive the thermodynamic formulae to apply to the nonionic–uni-univalent ionic surfactant system. Adopting the two dividing planes defined so as to make the surface excess numbers of moles of water and air zero simultaneously and assuming an ideal solution, the total differential of surface tension at constant temperature and pressure is written in the form[7]

$$d\gamma = -(RT\hat{\Gamma}^{H}/\hat{m})d\hat{m} + (RT\hat{\Gamma}^{H}/\hat{X}_1\hat{X}_2)(\hat{X}_2 - \hat{X}_2^{H})d\hat{X}_2, \quad (3)$$

where $\hat{\Gamma}^{H}$ and $\hat{X}_2^{H}$ are the total surface density and composition of DeAC in the adsorbed film defined by

$$\hat{\Gamma}^{H} = \Gamma_1^{H} + \Gamma_{2+}^{H} + \Gamma_{2-}^{H} \quad (4)$$

and

$$\hat{X}_2^{H} = (\Gamma_{2+}^{H} + \Gamma_{2-}^{H})/\hat{\Gamma}^{H}, \quad (5)$$

respectively. Here Γ_1^{H}, Γ_{2+}^{H}, and Γ_{2-}^{H} are the surface excess numbers of moles of OSE, decylammonium ion, and chloride ion, respectively. Since the condition of electroneutrality holds, Γ_{2+}^{H} is equal to Γ_{2-}^{H}.

Miscibility in the Adsorbed Film at a Concentration below the cmc. First, let us examine the state of

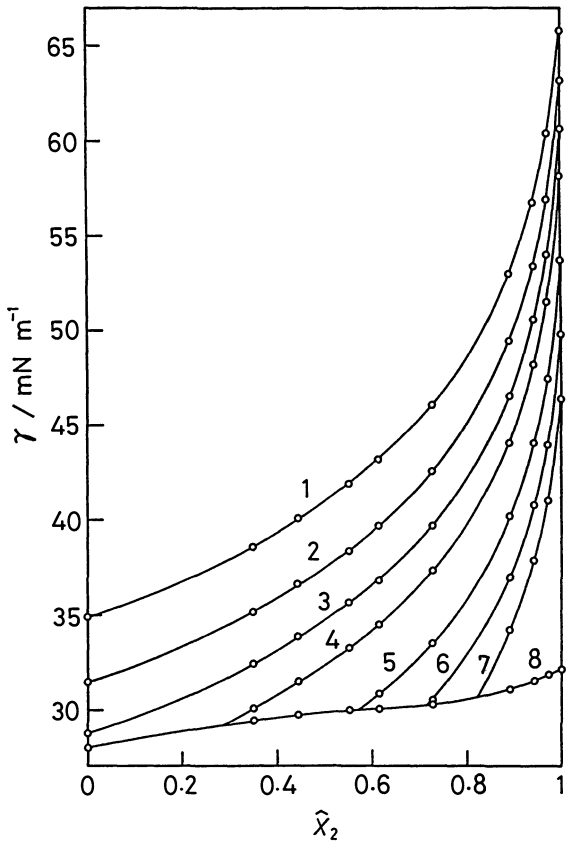

Fig. 2. Surface tension vs. composition curves at constant total molality: (1) $\hat{m}$=15 mmol kg^{-1}; (2) 20; (3) 25; (4) 30; (5) 40; (6) 50; (7) 60; (8) γ^C vs. $\hat{X}_2$.

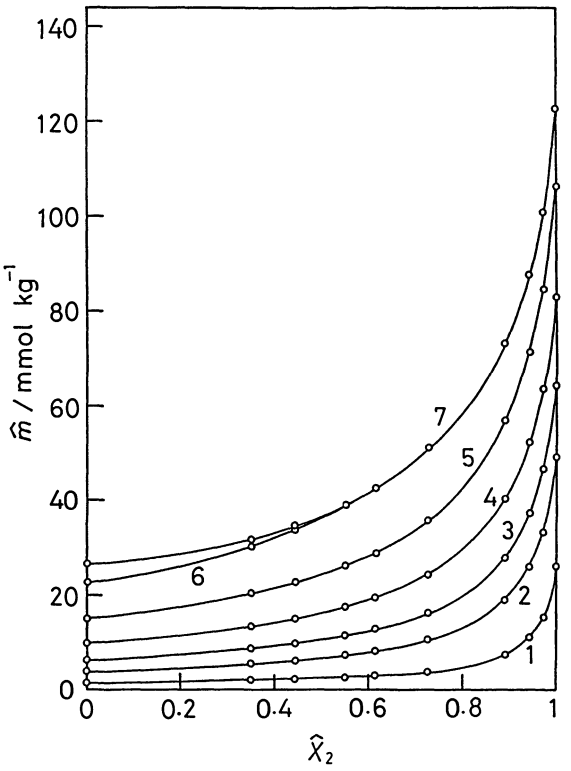

Fig. 3. Total molality vs. composition curves at constant surface tension: (1) γ=60 mN m^{-1}; (2) 50; (3) 45; (4) 40; (5) 35; (6) 30; (7) $\hat{C}$ vs. $\hat{X}_2$.

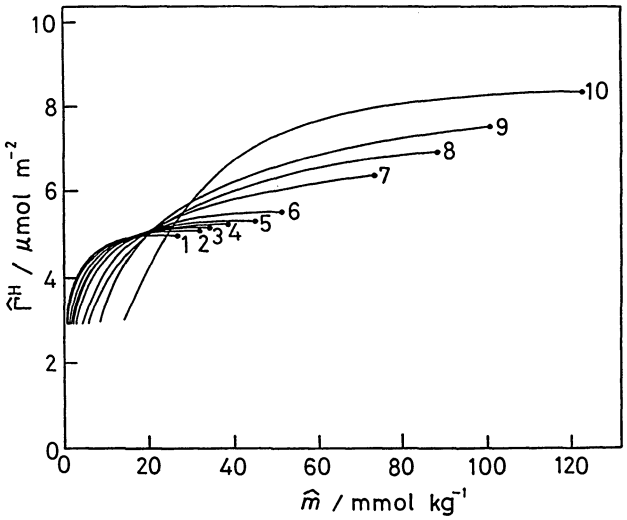

Fig. 4. Total surface density vs. total molality curves at constant composition: (1) $\hat{X}_2$=0; (2) 0.349; (3) 0.443; (4) 0.550; (5) 0.613; (6) 0.725; (7) 0.889; (8) 0.941; (9) 0.972; (10) 1; (●) total surface density at the cmc $\hat{\Gamma}^{H,C}$.

adsorbed film in terms of the total surface density $\hat{\Gamma}^{H}$. The value of $\hat{\Gamma}^{H}$ is calculated by applying the equation

$$\hat{\Gamma}^{H} = -(\hat{m}/RT)(\partial\gamma/\partial\hat{m})_{T,p,\hat{X}_2} \quad (6)$$

to the γ vs. $\hat{m}$ curve illustrated in Fig. 1; the value is plotted against $\hat{m}$ at constant $\hat{X}_2$ in Fig. 4. It is seen that the $\hat{\Gamma}^{H}$ value increases with increasing $\hat{m}$ and approaches to a saturated value at a concentration near the cmc. It is also seen that the $\hat{\Gamma}^{H}$ vs. $\hat{m}$ curve changes its shape from that of OSE to that of DeAC.

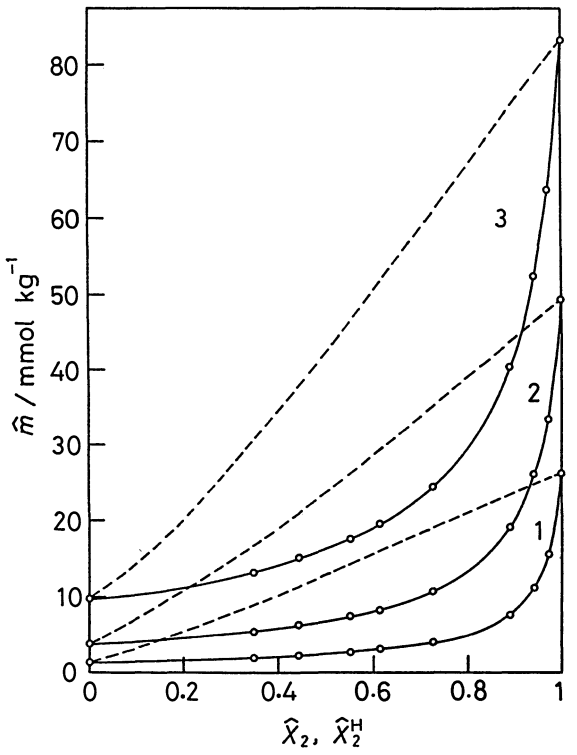

Fig. 5. Total molality vs. composition curves at constant surface tension: (1) γ=60 mN m^{-1}; (2) 50; (3) 40; (——) $\hat{X}_2$; (– – –) $\hat{X}_2^H$.

In order to clarify the miscibility of OSE and DeAC in the adsorbed film, it is useful to examine the composition in the adsorbed film. The value of $\hat{X}_2^H$ at a given γ is estimated by applying the following equation derived from Eq. 3 to the $\hat{m}$ vs. $\hat{X}_2$ curve shown in Fig. 3:

$$\hat{X}_2^H = \hat{X}_2 - (\hat{X}_1\hat{X}_2/\hat{m})(\partial\hat{m}/\partial\hat{X}_2)_{T,p,\gamma}. \quad (7)$$

The evaluated values are presented in the form of $\hat{m}$ vs. $\hat{X}_2^H$ curves at γ=60, 50, and 40 mN m^{-1} together with the corresponding $\hat{m}$ vs. $\hat{X}_2$ curves in Fig. 5. This diagram tells us that OSE and DeAC molecules are miscible with each other over the whole composition range at water/air interface and that the adsorbed film is richer in more surface active OSE molecules. Furthermore, the diagram may be said to take the shape of a distorted cigar when compared with those of 2-(decylsulfinyl)ethanol (DeSE)–OSE and dodecylammonium chloride (DAC)–DeAC systems[2,4] drawn in Fig. 6. Taking into account that the $\hat{m}$ vs. $\hat{X}_2^H$ curve deviates negatively from the straight line connecting the $\hat{m}$ values of pure OSE and DeAC, we may conclude that the OSE and DeAC molecules mix nonideally with each other in the adsorbed film.

Miscibility in the Micelle and Adsorbed Film at the cmc. Next let us proceed to see how OSE and DeAC molecules mix in the micellar state. The composition of surfactant in the micelle is defined by

$$\hat{X}_2^M = (N_{2+}^M + N_{2-}^M)/(N_1^M + N_{2+}^M + N_{2-}^M), \quad (8)$$

where N_i^M is the excess number of moles of i-species per micelle particle with reference to the dividing surface which makes the excess number of moles of water zero. Since the total molality of monomeric surfactant is

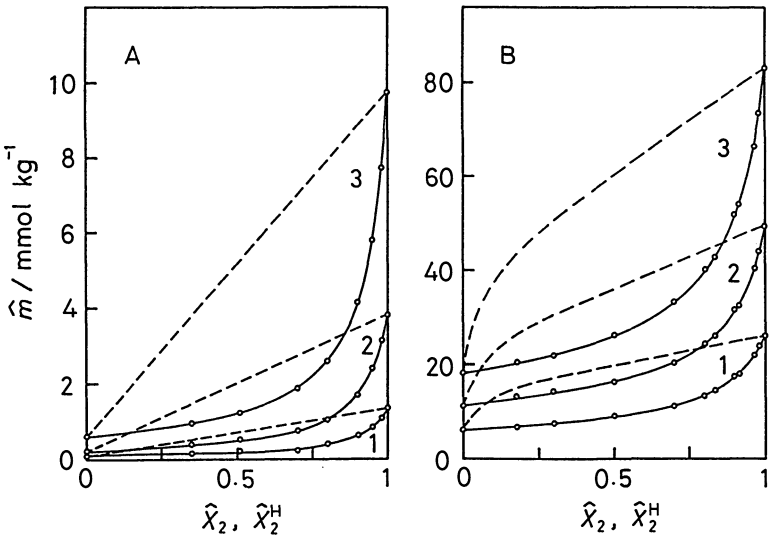

Fig. 6. Total molality vs. composition curves at constant surface tension: (A) DeSE–OSE system; (B) DAC–DeAC system; (1) γ=60 mN m^{-1}; (2) 50; (3) 40; (——) $\hat{X}_2$; (– – –) $\hat{X}_2^H$.

assumed to be equal to $\hat{C}$ in a limited concentration range near the cmc, the following relation holds at constant T and p:[7,18]

$$(RT/\hat{C})\mathrm{d}\hat{C}=(RT/\hat{X}_1\hat{X}_2)(\hat{X}_2-\hat{X}_2^{\mathrm{M}})\mathrm{d}\hat{X}_2. \quad (9)$$

Then the value of $\hat{X}_2^{\mathrm{M}}$ is immediately evaluated from the dependence of $\hat{C}$ on $\hat{X}_2$:

$$\hat{X}_2^{\mathrm{M}}=\hat{X}_2-(\hat{X}_1\hat{X}_2/\hat{C})(\partial\hat{C}/\partial\hat{X}_2)_{T,p}. \quad (10)$$

Figure 7 shows the plot of $\hat{C}$ against $\hat{X}_2^{\mathrm{M}}$ together with that of $\hat{C}$ vs. $\hat{X}_2$ curve of OSE–DeAC system deviates negatively from the straight line joining the $\hat{C}$ values of pure OSE and DeAC, although those of DeSE–OSE and DAC–DeAC systems given in Fig. 8 deviate positively. This finding indicates that OSE and DeAC molecules mix nonideally in the micelle as well as in the adsorbed film. These nonideal behavior is attributable to the attractive interaction between OSE and DeAC molecules.

On the other hand, the γ^{C} value is plotted against $\hat{X}_2$ and $\hat{X}_2^{\mathrm{M}}$ in Fig. 9. This diagram conveys some information concerning the γ vs. $\hat{m}$ curve above the cmc:[2-5] the curve of mixture is expected to increase slightly at a concentration range above the cmc. Taking into consideration that the γ values of pure OSE and DeAC decrease slightly at a concentration above the cmc, the above expectation does not contradict the results shown in Fig. 1.

Now, it is useful to inquire the relation between the compositions of micelle and adsorbed film at the cmc.

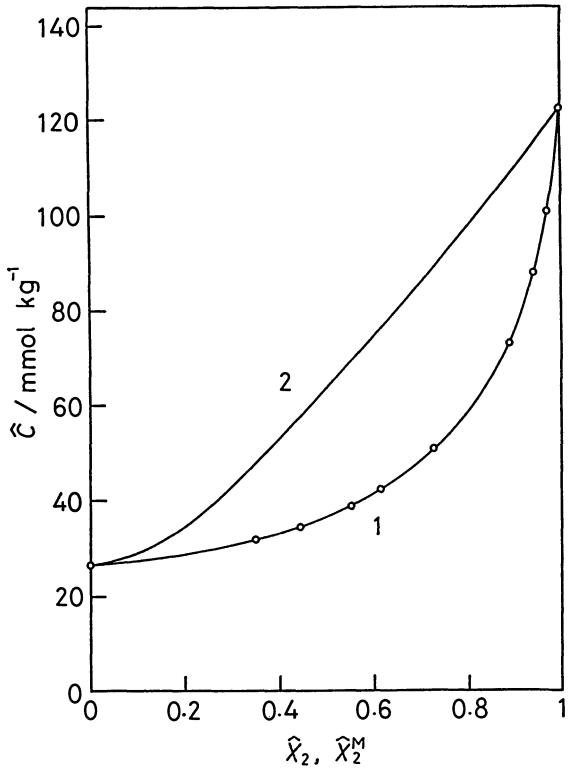

Fig. 7. Critical micelle concentration vs. composition curves: (1) $\hat{C}$ vs. $\hat{X}_2$; (2) $\hat{C}$ vs. $\hat{X}_2^{\mathrm{M}}$.

Since $\hat{m}$ is assumed to be equal to $\hat{C}$ at the cmc, Eq. 3 is rewritten as

$$\mathrm{d}\gamma^{\mathrm{C}}=-(RT\hat{\Gamma}^{\mathrm{H,C}}/\hat{C})\mathrm{d}\hat{C}+(RT\hat{\Gamma}^{\mathrm{H,C}}/\hat{X}_1\hat{X}_2)(\hat{X}_2-\hat{X}_2^{\mathrm{H,C}})\mathrm{d}\hat{X}_2, \quad (11)$$

where $\hat{\Gamma}^{\mathrm{H,C}}$ and $\hat{X}_2^{\mathrm{H,C}}$ are the total surface density and composition of adsorbed film at the cmc, respectively. Combination of Eqs. 9 and 11 leads to the equation

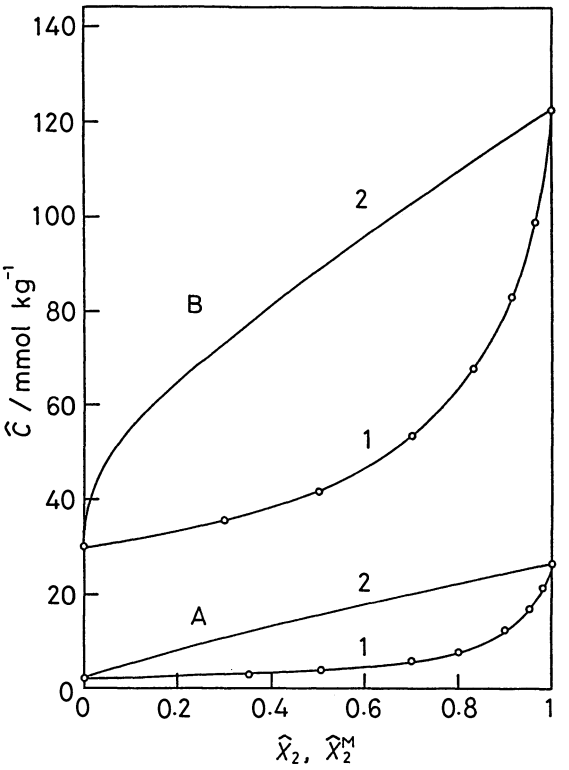

Fig. 8. Critical micelle concentration vs. composition curves: (A) DeSE–OSE system; (B) DAC–DeAC system; (1) $\hat{C}$ vs. $\hat{X}_2$; (2) $\hat{C}$ vs. $\hat{X}_2^{\mathrm{M}}$.

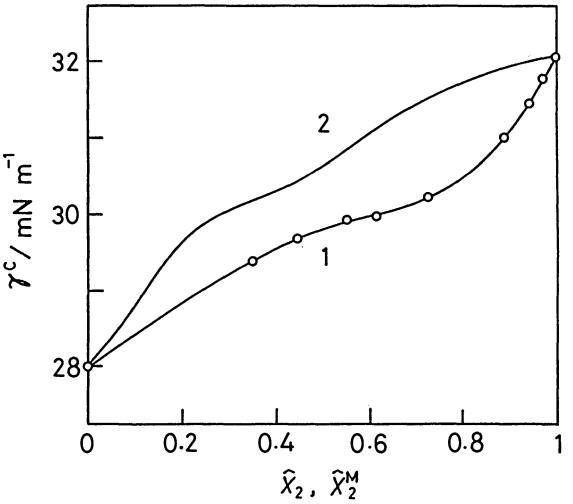

Fig. 9. Surface tension at the cmc vs. composition curves: (1) γ^{C} vs. $\hat{X}_2$; (2) γ^{C} vs. $\hat{X}_2^{\mathrm{M}}$.

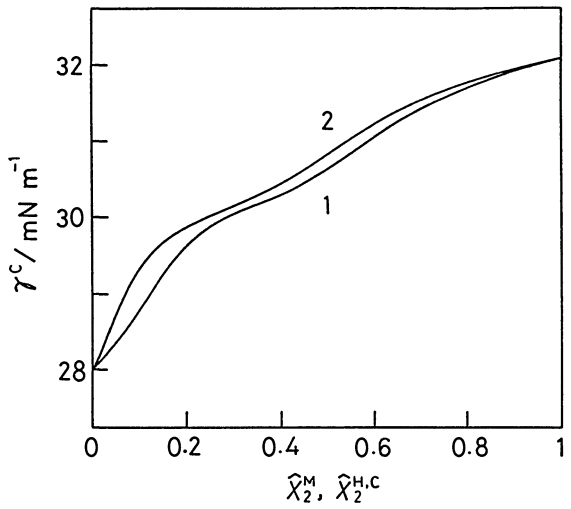

Fig. 10. Surface tension at the cmc vs. composition curves: (1) γ^C vs. $\hat{X}_2^M$; (2) γ^C vs. $\hat{X}_2^{H,C}$.

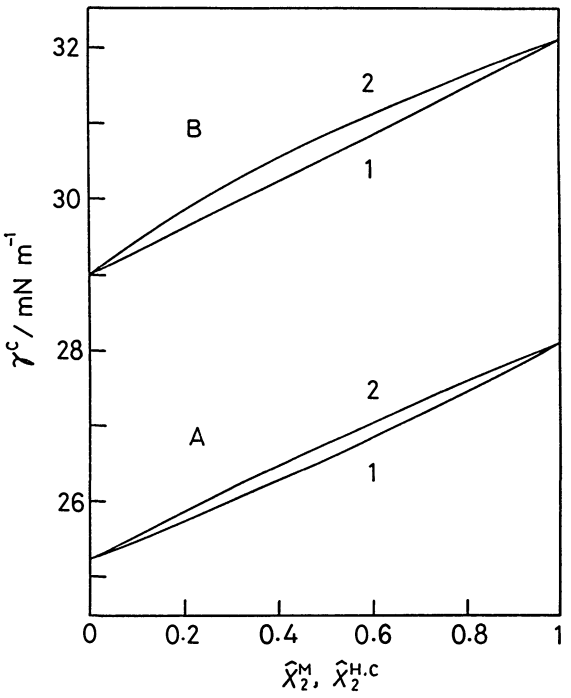

Fig. 11. Surface tension at the cmc vs. composition curves: (A) DeSE–OSE system; (B) DAC–DeAC system; (1) γ^C vs. $\hat{X}_2^M$; (2) γ^C vs. $\hat{X}_2^{H,C}$.

$$\hat{X}_2^{H,C} = \hat{X}_2^M - (\hat{X}_1\hat{X}_2/RT\hat{\Gamma}^{H,C})(\partial\gamma^C/\partial\hat{X}_2)_{T,p}. \quad (12)$$

Applying Eq. 12 to the γ^C vs. $\hat{X}_2$ curve illustrated in Fig. 2 and making use of the $\hat{\Gamma}^{H,C}$ value estimated by the extrapolation of $\hat{\Gamma}^H$ vs. $\hat{m}$ curve to the cmc in Fig. 4, we can evaluate the value of $\hat{X}_2^{H,C}$. The results are shown in Fig. 10. It is seen that the diagram has a deformed shape compared with those of the DeSE–OSE and DAC–DeAC systems given in Fig. 11. This is closely associated with the nonideal mixing of OSE and DeAC molecules in the adsorbed film and micelle. Furthermore, the γ^C vs. $\hat{X}_2^{H,C}$ curve is found to deviate more positively than the γ^C vs. $\hat{X}_2^M$ curve. Therefore, we may conclude that the interaction between OSE and DeAC molecules are more attractive in the micelle than in the adsorbed film.

It is probable from the thermodynamic viewpoint that nonionic and cationic surfactants form a negative azeotrope in the adsorbed film and micelle if their γ vs. $\hat{m}$ curves are close to each other over the whole concentration range. This will be realized for the mixture of OSE and DAC.[23]

References

1) H. Iyota and K. Motomura, *Bull. Chem. Soc. Jpn.*, **62**, 1446 (1989).
2) M. Aratono, T. Kanda, and K. Motomura, *Langmuir*, **6**, 843 (1990).
3) H. Matsuki, T. Kanda, M. Aratono, and K. Motomura, *Bull. Chem. Soc. Jpn.*, **63**, 2159 (1990).
4) K. Motomura, H. Matsukiyo, and M. Aratono, *ACS Symp. Ser.*, **311**, 163 (1986).
5) N. Ikeda, E. Shiota, M. Aratono, and K. Motomura, *Bull. Chem. Soc. Jpn.*, **62**, 410 (1989).
6) H. Matsuki, N. Ando, M. Aratono, and K. Motomura, *Bull. Chem. Soc. Jpn.*, **62**, 2507 (1989).
7) K. Motomura, N. Ando, H. Matsuki, and M. Aratono, *J. Colloid Interface Sci.*, **139**, 188 (1990).
8) C.-P. Kurzendorfer, M.-J. Schwuger, and H. Lange, *Ber. Bunsen-Ges. Phys. Chem.*, **82**, 962 (1978).
9) N. Funasaki and S. Hada, *J. Phys. Chem.*, **83**, 2471 (1979).
10) B. T. Ingram, *Colloid Polym. Sci.*, **258**, 192 (1980).
11) D. N. Rubingh, "Mixed Micelle Solution," in "Solution Chemistry of Surfactant," ed by K. L. Mittal, Plenum, New York (1979), Vol. 1, p. 337.
12) M. Abe, N. Tsubaki, and K. Ogino, *J. Colloid Interface Sci.*, **107**, 503 (1985).
13) I. W. Osborne-Lee and R. S. Schechter, *ACS Symp. Ser.*, **311**, 30 (1986).
14) P. M. Holland, *ACS Symp. Ser.*, **311**, 102 (1986).
15) P. M. Holland, *Adv. Colloid Interface Sci.*, **26**, 111 (1986).
16) J. F. Rathman and J. F. Scamehorn, *Langmuir*, **2**, 354 (1986).
17) M. J. Rosen and Z. H. Zhu, *J. Colloid Interface Sci.*, **133**, 473 (1989).
18) K. Motomura, M. Yamanaka, and M. Aratono, *Colloid Polym. Sci.*, **262**, 948 (1984).
19) S. Uryu, M. Aratono, M. Yamanaka, K. Motomura, and R. Matuura, *Bull. Chem. Soc. Jpn.*, **57**, 967 (1984).
20) K. Motomura, S. Iwanaga, S. Uryu, H. Matsukiyo, M. Yamanaka, and R. Matuura, *Colloids Surf.*, **9**, 19 (1984).
21) M. Aratono, S. Uryu, Y. Hayami, K. Motomura, and R. Matuura, *J. Colloid Interface Sci.*, **93**, 162 (1983).
22) K. Motomura, S. Iwanaga, Y. Hayami, S. Uryu, and R. Matuura, *J. Colloid Interface Sci.*, **80**, 32 (1981).
23) K. Motomura, T. Kanda, K. Abe, N. Ikeda, and M. Aratono, unpublished data.

Investigation of Ion and Solvent Transport Accompanying Redox Reactions of Polyvinylferrocene Films Using an in situ Electrochemical Quartz Crystal Microbalance Technique

Masaya MIZUNUMA,† Takeo OHSAKA,*,†† Hirohisa MIYAMOTO, and Noboru OYAMA*
Department of Applied Chemistry, Faculty of Technology, Tokyo University of Agriculture and Technology, 2-24-16 Naka-machi, Koganei, Tokyo 184
(Received May 14, 1991)

The in situ electrochemical quartz crystal microbalance (in situ EQCM) technique has been applied to study ion and solvent transport accompanying the redox reaction of polyvinylferrocene (PVF) film coated on quartz crystal electrodes in aqueous and acetonitrile media. The dependence of apparent formal potentials $(E^{f}_{poly})_{app}$ of the F_c°/F_c^{+} redox couple (F_c° and F_c^{+} represent the reduced and oxidized sites, respectively, in the PVF film) upon the concentration of supporting electrolyte has been also examined in comparison with those of solution-phase ferrocene derivatives. The PVF film is ideally permselective to ClO_4^- anion in both aqueous and acetonitrile media. The PVF oxidation (or reduction of polyvinylferricenium ion) in aqueous media is accompanied by the ingress (or egress) of one ClO_4^- ion per redox site and some solvent (ca. one H_2O per redox site). In $LiClO_4$ acetonitrile media, during the oxidation process ClO_4^- ion with some solvent inserts into the film and the reverse phenomenon occurs during the reduction process. The results demonstrate that a combination of the in situ EQCM measurement and the measurement of the dependence of $(E^{f}_{poly})_{app}$ on the concentration of supporting electrolyte makes possible to elucidate quantitatively the ion and/or solvent transport process across the polymer film/solution interface during the redox reaction.

Charge transport in electroactive polymer films, which are coated on electrode surfaces and are well-swollen with solvent/electrolyte, has been a subject of much interest in recent years from the viewpoint of the fundamental studies on the mechanism and kinetics of charge (electron and/or ion) transport as well as the potential applications (such as electrocatalysis, optical/electronic devices, sensors and energy storage) based on their interesting properties (e.g., electron transfer catalysis, ion permselectivity, redox conductivity and electrochromic property).[1] We have also been interested in this problem and have continued to conduct the kinetic and thermodynamic study of the homogeneous charge-transport process within polymer coatings for various types of redox polymer-coated electrode systems mainly using normal pulse voltammetry, potential-step chronoamperometry (chronocoulometry), AC impedance method and hydrodynamic voltammetry based on rotating disk electrodes.[2] A fruitful information about the charge transport has been obtained.[2] However, the role of electroinactive species (e.g., solvent and counter ions) in charge-transport processes can not be directly deduced using these electrochemical techniques.

The in situ electrochemical quartz crystal microbalance technique (in situ EQCM technique), which is based on the quartz crystal microbalance used in conjunction with electrochemistry, has recently received great attention as a highly useful technique capable of quantitatively measuring small mass changes (typically of the order of 10^{-9}—10^{-6} g) of electrode surfaces which occur as a result of electrochemical processes.[3] For some electroactive polymeric films (e.g., electropolymerized polymers and polymer complexes), mass changes, which occur upon electrochemical oxidation and reduction due to insertion and expulsion, respectively, of counter ions, coions and/or solvent into and out of the film phase, have been elucidated quantitatively using the in situ EQCM technique.[3,4]

In this paper, we report on the in situ EQCM responses for the redox reaction of polyvinylferrocene (PVF) film in aqueous and acetonitrile media, together with the comparison with the data reported by other workers for PVF films.[4b,c,h–j] The variation of apparent formal potential for the F_c°/F_c^{+} redox couple in the PVF film with the concentration of supporting electrolyte will be also examined in order to gain an additional insight into the mechanism of ion and solvent transport in PVF films. An analysis of apparent formal potential shifts of electroactive polymers as a function of the electrolyte concentration enables a quantitative estimation of concomitant changes in ion populations during their redox reactions.[4i,5]

Experimental

The electrochemical quartz crystal microbalance instrumentation and the experimental procedures are essentially similar to those employed in previous studies.[4a,d,e] The experiments reported here were run on a 5 MHz AT-cut quartz crystal (diameter: 13 mm, Toyo Kurafuto Ltd.) which are driven at their resonant frequency by a feedback osillator. Each side of the crystals was coated with Au (ca. 300 nm) by vaccum deposition, using Cr (ca. 2 nm) as an adhesion layer. One side of the crystal was further coated with PVF film (thickness is typically 150 nm) and used as the working electrode. A Pt wire and a sodium chloride saturated calomel electrode

† Present address: Materials & Electronic Devices Laboratory, Mitsubishi Electric Corp., Amagasaki, Hyogo 661.
†† Present address: Department of Electronic Chemistry, Graduate School at Nagatsuta, Tokyo Institute of Technology, 4259 Nagatsuta, Midori-ku, Yokohama 227.

(SSCE) were used as the counter and reference electrodes, respectively. The keyhole electrode design used is similar to that described in Ref. 6, with the piezoelectrically and electrochemically active areas being 63.6 and 47.8 mm^2,respectively. The crystal was affixed to the side of the cell via Teflon O-rings (Fig. 1). The mass change (Δm in $g\,cm^{-2}$) at the electrode surface could be estimated from the frequency change observed (Δf in Hz) according to Sauerbrey's equation;[7] $\Delta f = -C_f \Delta m$, with the proportionality constant C_f of 5.67×10^7 $Hz\,cm^2\,g^{-1}$. The resonant frequency was measured using a Hewlett Packard 5334B frequency counter. EQCM data were obtained with the use of a computer-controlled apparatus.[4a]

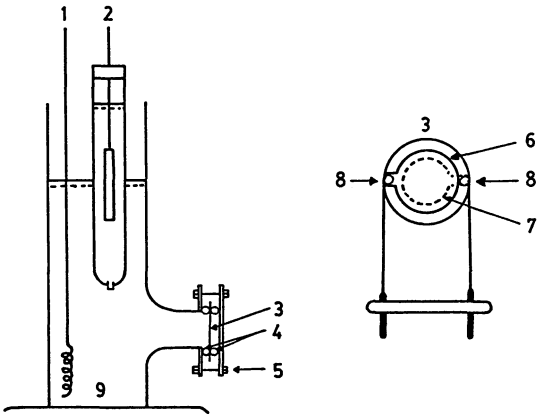

Fig. 1. A schematic depiction of the electrolyte cell and quartz crystal electrode used for in situ EQCM measurements. (1) counter electrode (Pt wire), (2) reference electrode, (3) quartz crystal (working electrode), (4) O-ring, (5) screw bolt/cap, (6) front electrode, (7) back electrode, (8) spring clip with attached lead, (9) glass cell.

The apparent formal potentials of the Fc^0/Fc^+ couple in the PVF film and the solution-phase ferrocenes in various concentrations of supporting electrolytes were obtained by cyclic voltammetry using basal-plane pyrolytic graphite (BPG, Union Carbide Co.) as a working electrode material. The reference and counter electrodes are the same as those employed in in situ EQCM experiments. The BPG disk electrodes (0.19 cm^2) were prepared and mounted into a glass tube with a heat-shrinkable polyolefin tube.

Polyvinylferrocene (PVF) was prepared according to Ref. 8. Adherent coatings of PVF were produced by transferring aliquots of a 0.1 wt% CH_2Cl_2 solution of PVF to the surface of a quartz crystal electrode and then evaporating the solvent at room temperature. The activity coefficients of ions were calculated according to the Debye–Hückel approximation.[9] All chemicals used were of reagent grade. Experiments were performed at room temperature (25±2 °C). All potentials were measured and were quoted with respect to the SSCE.

Results and Discussion

in situ EQCM Behavior of PVF Film in Aqueous Media. Figure 2 shows the typical results of in situ EQCM experiment on a PVF film-coated quartz crystal electrode in 0.26 M (1 M=1 mol dm^{-3}) $NaClO_4$ aqueous

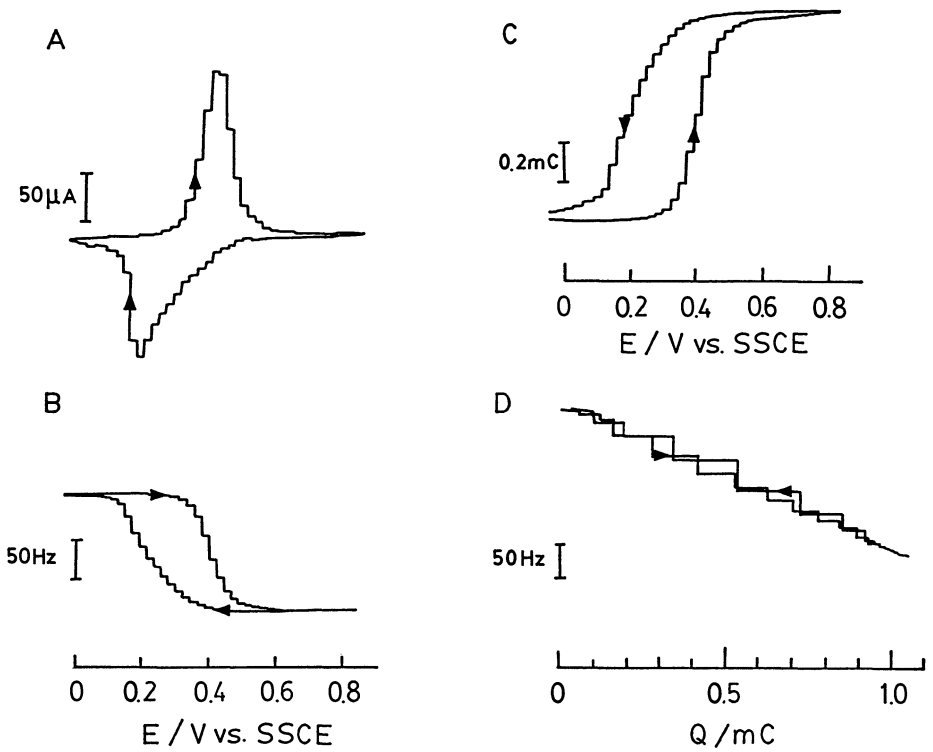

Fig. 2. (A) Current-potential, (B) frequency-potential, (C) charge-potential and (D)frequency-charge curves for a PVF film-coated quartz crystal electrode in 0.26 M $NaClO_4$ aqueous solution (pH 3.0). Amount of PVF coated on electrode: 17.3 $\mu g\,cm^{-2}$. Potential scan rate: 20 $mV\,s^{-1}$.

solution (pH 3.0). At first sight, we can see that the frequency change decreases during the oxidation process (i.e., the mass of the PVF film-coated electrode increases), while it increases during the reduction process (i.e., the mass decreases). In this case, the oscillator frequency completely returns to its initial value after the potential scan, indicating that the mass change of the PVF film accompanying its redox reaction is completely reversible on the time scale of the potential scan used (ca. 30—50 s). The half frequency change and half charge change potentials (denoted by $E_{1/2,f}$ and $E_{1/2,q}$, respectively, in this paper), at which the total frequency and charge changes, respectively, are half complete, may be used as measures of the ability of these quantities to respond to the applied potential program. At a scan rate of 20 m V s^{-1}, $E_{1/2,f}$ and $E_{1/2,q}$ are almost the same values of ca. 0.20 and 0.40 V for the negative and positive scans, respectively. This fact demonstrates that the mass transport process and electron transfer process occur simultaneously at the scan rate used, because the frequency change can be linearly correlated to the mass change according to the Sauerbrey's equation. From Fig. 2D, it is obvious that the frequency change vs. charge plots are almost linear for both anodic and cathodic processes and the slopes for both processes are almost the same (1.48×10^5 Hz C^{-1}). The increase in mass per mole of redox sites of PVF film, i.e., the molar mass equivalent (M_{eq}), could be determined to be 119 g mol^{-1} using the slopes of the Δf vs. Q plots. The physical significance of the M_{eq} obtained will be mentioned below.

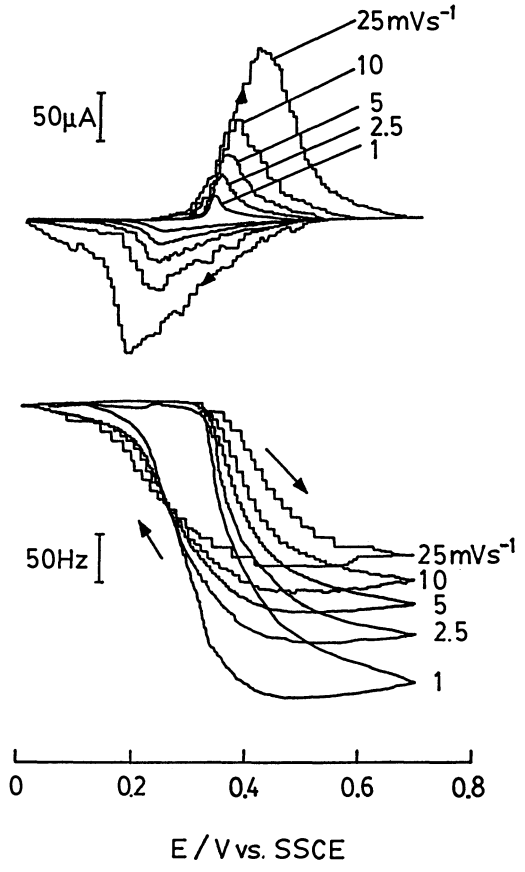

Fig. 3. Typical cyclic voltammetric and frequency-potential curves for a PVF film-coated quartz crystal electrode in 0.2 M $NaClO_4$ aqueous solution (pH 3.0) at various potential scan rates. Amount of PVF coated on electrode: 17.3 μg cm^{-2}.

Figure 3 shows typical cyclic voltammetric and frequency-potential curves for the PVF film-coated quartz crystal electrode in 0.2 M $NaClO_4$ aqueous solution (pH 3.0) at various potential scan rates of 1 to 25 m V s^{-1}. The frequency change response accompanying the redox reaction is essentially the same as that mentioned above (Fig. 2). In addition, we can see that the difference in frequency change between the oxidized and reduced states is larger at slower potential scan rate. This is qualitatively understood by considering that the number (Γ) of the redox sites in the film oxidized (or reduced) during a given potential scanning is proportional to the amount (Q) of charge passed during the period and that the oxidation (or reduction) process will require, for charge neutrality, concurrent ingress (or egress) of anion into (or out of) the film matrix. The measured values of Q, Γ, and Δf at various scan rates are summarized in Table 1, together with the calculated ones of Δm and M_{eq}. Γ and Δm increases, as expected, with decreasing potential scan rate. However, the M_{eq} values are almost constant ((123±4) g mol^{-1}). If ClO_4^- anion were the only mobile species to be transferred, the resultant value would be 99.5 g mol^{-1}. Thus, the fact that the M_{eq} obtained is larger than 99.5 g mol^{-1} may suggest the PVF oxidation (or PVF^+ reduction) is accompanied by the ingress (or egress) of one ClO_4^- ion per redox site and some solvent (ca. one H_2O per redox site), being in a qualitative agreement with the results previously reported for PVF films.[4b,h,i]

Dependence of Apparent Formal Potential on Electrolyte Concentration. When the PVF film is ideally permselective to ClO_4^- anion, the apparent formal potential ($(E^f_{poly,H_2O})_{app}$) of the F_c°/F_c^+ redox couple (F_c° and F_c^+ represent the reduced and oxidized sites, respectively, in the PVF film) in aqueous solutions could be expected to obey the following equation.

Table 1. in situ EQCM Data of PVF Film in Aqueous $NaClO_4$ Media[a)]

v[b)]	Q	$10^8\cdot\Gamma$	$-\Delta f$	$10^6\cdot\Delta m$	M_{eq}
mV s^{-1}	mC	mol cm^{-2}	Hz	g cm^{-2}	g mol^{-1}
1	1.83	3.97	286	5.03	126
2.5	1.51	3.28	235	4.13	126
5	1.36	2.95	207	3.64	123
10	1.19	2.58	181	3.18	123
25	1.06	2.30	155	2.73	119

a) Concentration of $NaClO_4$: 0.2 M. Thickness of PVF film in dry state: 150 nm. Electrochemically active area: 47.8 mm^2. See the text for the definitions of Q, Γ, Δf, Δm, and M_{eq}. b) Potential scan rate.

$$(E^{f}_{poly,H_2O})_{app} = E^{\circ}_{poly,H_2O} + E_j - \frac{RT}{F}\ln\frac{f^{F_c^{\circ}}_{poly,H_2O}}{f^{F_c^{+}}_{poly,H_2O}} - \frac{RT}{F}\ln a_{(ClO_4^-)_{soln,H_2O}}, \quad (1)$$

where $(E^{f}_{poly,H_2O})_{app}$ (vs. SSCE) was taken as the average of the anodic and cathodic peak potentials of the cyclic voltammograms for the F_c°/F_c^{+} couple obtained at the PVF film-coated BPG electrode in $NaClO_4$ aqueous solutions (0.02—2.0 M), E°_{poly,H_2O} is the standard potential of the F_c°/F_c^{+} couple in the aqueous solutions used here, E_j denotes the liquid junction potential at SSCE (aq) : $NaClO_4$ (0.02—2.0 M, aq), $f^{F_c^{+}}_{poly,H_2O}$ and $f^{F_c^{\circ}}_{poly,H_2O}$ are the activity coefficients of the F_c^{+} and F_c° redox sites, respectively and $a_{(ClO_4^-)_{soln,H_2O}}$ is the activity of ClO_4^- ion in $NaClO_4$ aqueous solutions. The last term on the right-hand side of Eq. 1 represents "Donnan potential" present at the PVF film/solution interface. On the other hand, the apparent formal potential ($(E^{f}_{soln,H_2O})_{app}$) for the monomeric ferrocene derivative (i.e., ferrocenylmethyl(trimethylammonium), F_c–N^+) dissolved in the same aqueous solutions can be written as follows:

$$(E^{f}_{soln,H_2O})_{app} = E^{\circ}_{soln,H_2O} + E_j - \frac{RT}{F}\ln\frac{f^{F_c\text{-}N^+}_{soln,H_2O}}{f^{F_c\text{-}N^{2+}}_{soln,H_2O}}, \quad (2)$$

where $(E^{f}_{soln,H_2O})_{app}$ was measured with respect to the SSCE, E°_{soln,H_2O} is the standard potential of the F_c–N^+/F_c–N^{2+} couple, and $f^{F_c\text{-}N^{2+}}_{soln,H_2O}$ and $f^{F_c\text{-}N^+}_{soln,H_2O}$ are the activity coefficients of F_c–N^+ and F_c–N^{2+}, respectively.

As can be seen from Fig. 4, the polts of $(E^{f}_{poly,H_2O})_{app}$ vs. $\log a_{(ClO_4^-)_{soln,H_2O}}$ and $(E^{f}_{soln,H_2O})_{app}$ vs. $\log a_{(ClO_4^-)_{soln,H_2O}}$ are linear in the examined range of $a_{(ClO_4^-)_{soln,H_2O}}$ with slopes of −62 and −5 mV per decade in ClO_4^- activity, respectively. Thus, the difference ($\Delta(E^{f}_{H_2O})_{app}$) between $(E^{f}_{poly,H_2O})_{app}$ and $(E^{f}_{soln,H_2O})_{app}$ can be expressed by

$$\Delta(E^{f}_{H_2O})_{app} = (E^{\circ}_{poly,H_2O} - E^{\circ}_{soln,H_2O}) - \left(\frac{RT}{F}\ln\frac{f^{F_c^{\circ}}_{poly,H_2O}}{f^{F_c^{+}}_{poly,H_2O}} - \frac{RT}{F}\ln\frac{f^{F_c\text{-}N^+}_{soln,H_2O}}{f^{F_c\text{-}N^{2+}}_{soln,H_2O}}\right) - \frac{RT}{F}\ln a_{(ClO_4^-)_{soln,H_2O}}. \quad (3)$$

This enables us to evaluate the dependence of the formal potential difference on the electrolyte activity without knowing the dependence of E_j on the electrolyte activity under the condition that the second term on the right-hand side of Eq. 3 can be assumed as a constant in the examined range of $a_{(ClO_4^-)_{soln,H_2O}}$.[11] Based on its definition, the term $(E^{\circ}_{poly,H_2O} - E^{\circ}_{soln,H_2O})$ is independent of $a_{(ClO_4^-)_{soln,H_2O}}$. If the above condition is fulfilled, the slope of $\Delta(E^{f}_{H_2O})_{app}$ vs. $\log a_{(ClO_4^-)_{soln,H_2O}}$ plot can be expected to be −59 mV per decade in ClO_4^- activity at 25 °C. The actually obtained value is −57 mV per decade. This fact strongly suggests the permselective movement of ClO_4^- anions to the PVF film in order to maintain electroneutrality in agreement with the above-mentioned in situ EQCM results. There is no evidence for cation population changes during the redox reaction under the experimental conditions employed in this study.

According to the results obtained, the following reaction mechanism can be postulated for the PVF film reaction:

$$(F_c^{\circ}, nH_2O)_{poly} + (ClO_4^-)_{soln} + m(H_2O)_{soln} \rightleftarrows (F_c^{+}\cdot ClO_4^-, (n+m)H_2O)_{poly} + e^-, \quad (4)$$

where the subscripts refer to the polymer film (poly) or supporting electrolyte solution (soln). Note that the values of the coefficients m and n are not necessarily integers, as pointed out recently.[10] The ion and solvent transport that accompanies the redox reaction of PVF film coated on the electrode is depicted schematically in Fig. 5.

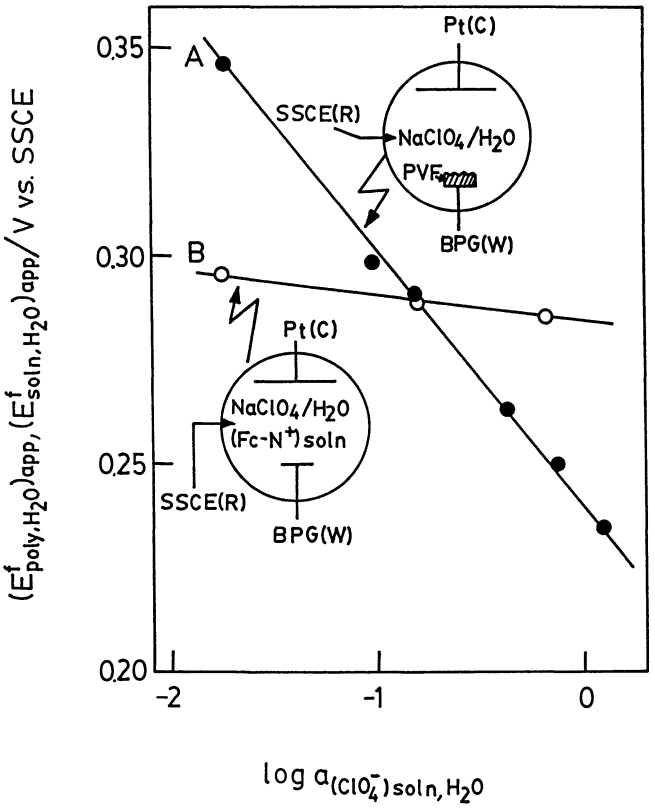

Fig. 4. Apparent formal potentials of (A) the F_c°/F_c^{+} couple in the PVF film and (B) the solution-phase F_c-N^+/F_c-N^{2+} couple as a function of the activity of the $NaClO_4$ supporting electrolyte. Amount of PVF coated on BPG electrode: 21.5 μg cm^{-2}. Concentration of F_c-N^+ in solution: 1 mM. The insets schematically represent the three-electrode systems employed to examine the dependence of $(E^{f}_{poly,H_2O})_{app}$ and $(E^{f}_{soln,H_2O})_{app}$ upon $\log a_{(ClO_4^-)_{soln,H_2O}}$.
W: working electrode, R: reference electrode, C: counter electrode.

in situ EQCM Behavior of PVF Film and Dependence of Formal Potential on Electrolyte Concentration in Acetonitrile Media. Figure 6 shows in situ EQCM data obtained on potential cycling (at 10 mV s^{-1}) of the

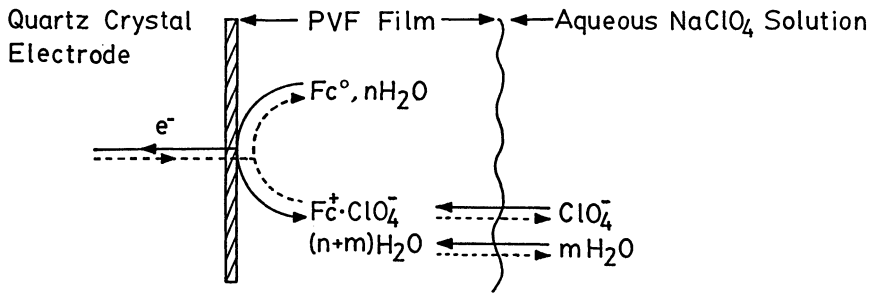

Fig. 5. Schematic representation of the ion and solvent transport that accompanies the redox reaction of the PVF film on the electrode in aqueous $NaClO_4$ solutions. F_c^+ and F_c° represent the oxidized and reduced sites, respectively, in the PVF film.
(——): oxidation process, (– – –): reduction process.

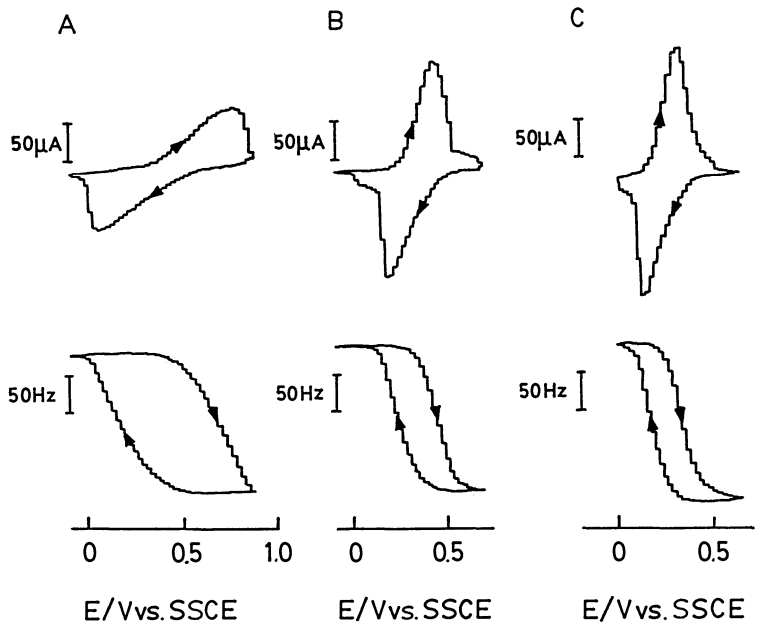

Fig. 6. Cyclic voltammetric and frequency-potential curves for a PVF film-coated quartz crystal electrode in acetonitrile solutions containing various concentrations of $LiClO_4$. Amount of PVF coated on electrode: 21.5 $\mu g\,cm^{-2}$. Concentration of $LiClO_4$ in acetonitrile electrolyte solutions: (A) 0.02, (B) 0.20, and (C) 2.0 M. Potential scan rate: 10 $mV\,s^{-1}$.

Table 2. in situ EQCM Data of PVF Film in Acetonitrile $LiClO_4$ Media[a)]

$C^{b)}$	$v^{c)}$	Q	$10^8 \cdot \Gamma$	$-\Delta f$	$10^6 \cdot \Delta m$	M_{eq}
M	$mV\,s^{-1}$	mC	$mol\,cm^{-2}$	Hz	$g\,cm^{-2}$	$g\,mol^{-1}$
0.02	20	1.29	2.80	176	3.09	110
	10	1.28	2.78	168	2.96	106
0.20	20	1.41	3.06	184	3.24	106
	10	1.45	3.15	192	3.37	107
0.63	20	1.44	3.12	187	3.29	105
	10	1.42	3.08	183	3.22	105
1.20	20	1.44	3.12	200	3.52	113

a) Thickness of PVF film in dry state: 150 nm. Electrochemically active area: 47.8 mm^2. See the text for the definitions of Q, Γ, Δf, Δm, and M_{eq}. b) Concentration of $LiClO_4$. c) Potential scan rate.

PVF film in acetonitrile solutions containing various concentrations of $LiClO_4$. The frequency change (and so the mass change) of the film-coated electrode accompanying its redox reaction seems reversible, regardless of the concentration of $LiClO_4$. Note that the large potential difference between the anodic and cathodic peak potentials of voltammogram A, compared with those of voltammograms B and C, may originate from the significant iR drop effect due to the low concentration of the supporting electrolyte used. It was also found that for a given concentration of $LiClO_4$ $E_{1/2,f}$ and $E_{1/2,q}$ coincide within 5 mV. The mass transport process and electron transfer process are thus thought to occur simultaneously.

Table 2 contains the quantitative results concerning the charge transport, estimated from the data such as those shown in Fig. 6. The values of molar mass equivalent M_{eq} are almost the same ((109±4) g mol^{-1}), regardless of the concentration of $LiClO_4$ supporting electrolyte. However, these values are essentially larger than that (99.5 g mol^{-1}) expected when ClO_4^- is the only mobile species to be transferred. As in the case of the above-mentioned $H_2O/NaClO_4$ system, the dependence of the formal potential on the activity of ClO_4^- in acetonitrile (AN) solutions was also examined. The results are shown in Fig. 7. Here, the apparent formal potentials ($(E^f_{poly,AN})_{app}$ and $(E^f_{soln,AN})_{app}$) for the Fc°/Fc^+ couple in the PVF film and the solution-phase ferrocene/ferricinium couple in acetonitrile solutions can be represented by the Nernstian expression:

$$(E^f_{poly,AN})_{app} = E^\circ_{poly,AN} + E_j' - \frac{RT}{F}\ln\frac{f^{Fc^\circ}_{poly,AN}}{f^{Fc^+}_{poly,AN}} - \frac{RT}{F}\ln a_{(ClO_4^-)_{soln,AN}}, \quad (5)$$

$$(E^f_{soln,AN})_{app} = E^\circ_{soln,AN} + E_j' - \frac{RT}{F}\ln\frac{f^{Fc^\circ}_{soln,AN}}{f^{Fc^+}_{soln,AN}}, \quad (6)$$

where $(E^f_{poly,AN})_{app}$ and $(E^f_{soln,AN})_{app}$ were measured with respect to the SSCE, E_j' is the liquid junction potential between SSCE (aq) and $LiClO_4$ (0.02—1.0 M, AN), and the other terms correspond to those of the acetonitrile solution system in place of the aqueous solution system (Eqs. 1 and 2). The plot of $(E^f_{poly,AN})_{app}$ (or $(E^f_{soln,AN})_{app}$) vs. $\log a_{(ClO_4^-)_{soln,AN}}$ gave the straight line with slope of −136 (or −78) mV per decade in ClO_4^- activity in the examined range of $a_{(ClO_4^-)_{soln,AN}}$ (see Fig. 7). Thus, one can obtain the linear relation between $\Delta(E^f_{AN})_{app}$ ($=(E^f_{poly,AN})_{app}-(E^f_{soln,AN})_{app}$) and $a_{(ClO_4^-)_{soln,AN}}$. In this case, the slope of $\Delta(E^f_{AN})_{app}$ vs. $\log a_{(ClO_4^-)_{soln,AN}}$ plot is −58 mV per decade in $a_{(ClO_4^-)_{soln,AN}}$ which almost coincides with that (−59 mV per decade) expected for the case where the PVF film is ideally permselective to ClO_4^- anion and the dependences of the activity coefficient terms for the polymer film and solution-phase systems i.e.,

$$\frac{RT}{F}\ln\frac{f^{Fc^\circ}_{poly,AN}}{f^{Fc^+}_{poly,AN}} \quad \text{and} \quad \frac{RT}{F}\ln\frac{f^{Fc^\circ}_{soln,AN}}{f^{Fc^+}_{soln,AN}}$$

upon the activity of ClO_4^- are the same.

A probable reaction scheme, by which the in situ EQCM and potentiometric data obtained may be reasonably explained, is as follows:

$$(Fc^\circ, n'S)_{poly} + (ClO_4^-)_{soln} + m'(S)_{soln} \rightleftarrows (Fc^+\cdot ClO_4^-, (n'+m')S)_{poly} + e^-, \quad (7)$$

where S represents the solvent (CH_3CN), the coefficients m' and n' are not necessarily integers as in Eq. 4.[10] The mechanism of the ion and solvent transport accompanying the redox reaction of the PVF film in acetonitrile media may be depicted schematically in the same manner as in Fig. 5. To our knowledge, this is a first report concerning the in situ EQCM behavior of PVF film in nonaqueous media.

In conclusion, the present study strongly demonstrates that a combination of the in situ EQCM measurement and the measurement of the dependence of $(E^f_{poly})_{app}$ on the electrolyte concentration allows us to elucidate quantitatively the ion and/or solvent transport process across the polymer film/solution interface accompanying the redox reaction of thin films on electrode surfaces.

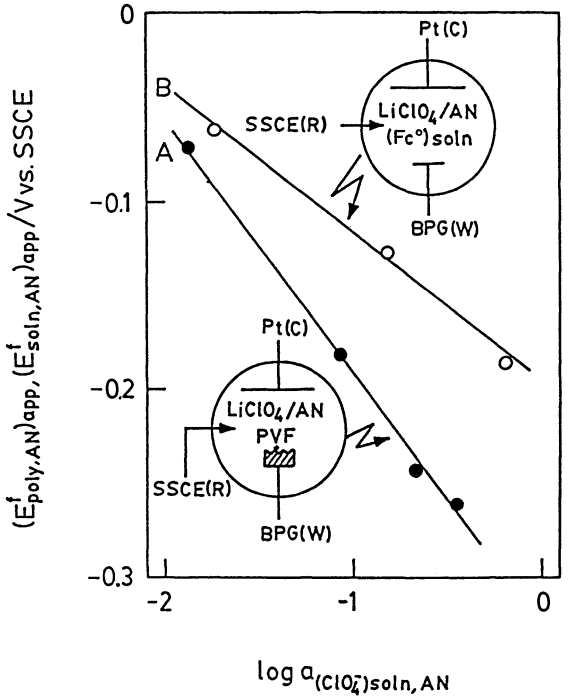

Fig. 7. Apparent formal potentials of (A) the Fc°/Fc^+ couple in the PVF film and (B) the solution-phase Fc°/Fc^+ couple as a function of the activity of the $LiClO_4$ supporting electrolyte. Amount of PVF coated on BPG electrode: 21.5 μg cm^{-2}. Concentration of ferrocene (Fc°) in solution: 1 mM. The insets schematically represent the three-electrode systems employed to examine the dependence of $(E^f_{poly,AN})_{app}$ and $(E^f_{soln,AN})_{app}$ upon $\log a_{(ClO_4^-)_{soln,AN}}$.
W: working electrode, R: reference electrode, C: counter electrode.

This work was partially supported by a Grant-in-Aid for Scientific Research Nos. 02805096 and 01470064 from the Ministry of Education, Science and Culture.

References

1) For review; a) R. W. Murray, "Electroanalytical Chemistry," ed by A. J. Bard, Marcel Dekker, New York (1984), Vol. 13, p. 191. b) A. R. Hillman, "Electrochemical Science and Technology," ed by R. G. Linford, Elsevier Applied Science, Amsterdam (1987), p. 103. c) M. Kaneko and Wöhrle, "Advances in Polymer Science 84," Springer-Verlag, Berlin (1988), p 141. d) N. Oyama and T. Ohsaka, "Molecular Design of Electrode Surfaces," ed by R. W. Murray, John Wiely, in press.

2) a) N. Oyama, T. Ohsaka, M. Kaneko, and H. Matsuda, *J. Am. Chem. Soc.*, **105**, 6003 (1983). b) N. Oyama, T. Ohsaka, and T. Ushirogouchi, *J. Phys. Chem.*, **88**, 5274 (1984). c) T. Ohsaka, T. Okajima, and N. Oyama, *J. Electroanal. Chem.*, **215**, 191 (1986). d) N. Oyama, T. Ohsaka, H. Yamamoto, and M. Kaneko, *J. Phys. Chem.*, **90**, 3850 (1986). e) T. Ohsaka, H. Yamamoto, and N. Oyama, *J. Phys. Chem.*, **91**, 3775 (1987).

3) a) M. R. Deakin and D. A. Buttry, *Anal. Chem.*, **61**, 1147A (1989). b) D. A. Buttry, "Application of the Quartz Crystal Microbalance to Electrochemistry, Analytical Chemistry," ed by A. J. Bard, Marcel Dekker, New York (1991), Vol. 17, p. 1.

4) a) N. Oyama, N. Yamamoto, O. Hatozaki, and T. Ohsaka, *Jpn. J. Appl. Phys.*, **29**, L818 (1990). b) P. T. Varineau and D. A. Buttry, *J. Phys.*, **91**, 1292 (1987). c) M. D. Ward, *J. Phys. Chem.*, **92**, 2049 (1988). d) A. J. Kelly, T. Ohsaka, N. Oyama, R. J. Forster, and J. G. Vos, *J. Electroanal. Chem.*, **287**, 185 (1990). e) H. Daifuku, T. Kawagoe, N. Yamamoto, T. Ohsaka, and N. Oyama, *J. Electroanal. Chem.*, **274**, 313 (1989). f) W. H. Smyrl and K. Naoi, *AIChE Symp. Ser.*, **86**, 71 (1990). g) N. Yamamoto, T. Ohsaka, T. Terashima, and N. Oyama, *J. Electroanal. Chem.*, **296**, 463 (1990). h) S. Bruckenstein, C. P. Wilde, M. Shay, A. R. Hillman, and D. C. Loveday, *J. Electroanal. Chem.*, **258**, 457 (1989). i) A. R. Hillman, D. C. Loveday, and S. Bruckenstein, *J. Electroanal. Chem.*, **274**, 157 (1989). j) M. D. Ward, *J. Electroanal. Chem.*, **236**, 139 (1987).

5) a) R. Naegeli, J. Redepenning, and F. C. Anson, *J. Phys. Chem.*, **90**, 6227 (1986). b) J. Redepenning and F. C. Anson, *J. Phys. Chem.*, **91**, 4549 (1987). c) A. Fitch, *J. Electroanal. Chem.*, **284**, 237 (1990).

6) S. Bruckenstein and M. Shay, *Electrochim. Acta*, **30**, 1295 (1985).

7) G. Sauerbrey, *Z. Phys.*, **155**, 206 (1959).

8) T. W. Smith, J. E. Kuder, and D. Wychik, *J. Polym. Sci., Polym. Chem. Ed.*, **14**, 2433 (1976).

9) a) R. A. Robinson and R. H. Stokes, "Electrolyte Solutions," 2nd ed, Butterworth, London (1970). b) H. S. Harned and B. B. Owen, "The Physical Chemistry of Electrolytic Solutions," 3rd ed, ACS Monograph Series, No. 137, Reinhold, New York (1957).

10) S. Bruckenstein and A. R. Hillman, *J. Phys. Chem.*, **92**, 4837 (1988).

11) The F_c°/F_c^{+} couple in the PVF film and the $F_c\text{-}N^{+}/F_c\text{-}N^{2+}$ couple are similar in their molecular structures. It is, if possible, preferable that the charges on the oxidized and reduced forms of the PVF film are the same as those of the solution-phase ferrocene compound (as in the case of the acetonitrile solution system). However, the solubility of the reduced form of ferrocene (F_c°) in the aqueous solutions used was too low to conduct usual electrochemical experiments, so that the water-soluble ferrocene derivative (i.e., $F_c\text{-}N^{+}$) was employed in this study.

Fragmentation of Energy-Selected Fluorobenzene Ion

Toshihide NISHIMURA,* Gerry G. MEISELS,† and Yoshio NIWA††
Upjohn Pharmaceuticals Limited, Tsukuba Research Laboratories, 23 Wadai, Tsukuba, Ibaraki 300-42
†Office of the Provost, University of South Florida, Tampa FL 33620, U.S.A.
††National Chemical Laboratories for Industry, Yatabe, Tsukuba, Ibaraki 305
(Received May 15, 1991)

Dissociation of the fluorobenzene ion has been studied using threshold photoelectron–photoion coincidence (TPEPICO) mass spectrometry. The detailed breakdown curves were measured over internal energies from 0 to 9 eV. Asymmetric flight time distributions due to metastable dissociation were observed for the formations of $C_6H_5^+$ and $C_4H_3F^+$, and their absolute decay rate constants were derived from their flight time distributions. The information-theoretical approach has been employed for the analysis of kinetic energy release distribution (KERD). The results of surprisal analysis demonstrated that experimental KERDs are in good agreement with the predictions based on the statistical theory of mass spectra (QET). The heat of formation of $C_4H_3F^{\cdot+}$ has been estimated to be 222±2 kcal mol^{-1}.

The quasi-equilibrium theory (QET)[1,2] on the unimolecular dissociation of gaseous ions assumes that (1) initial vibronic excitation by ionization is converted rapidly to vibrational energy of the ground electronic state of the molecular ion, that (2) all internal modes are accessible at a given total energy and vibrational energy redistribution within an energized molecular ion is much faster than dissociation (RRKM theory);[3,4]

$$k_d \ll k_{IC} \text{ and } k_{rdt}. \tag{1}$$

Here, k_d, k_{IC}, and k_{rdt} are respectively the rate constants of dissociation, internal conversion and redistribution of initial internal energy. Furthermore, QET requires (3) an equilibrium between the molecular ion M^+ and the transition state $T^{+\neq}$:

$$M^+ \underset{k_{-1}}{\overset{k_1}{\rightleftarrows}} T^{+\neq} \xrightarrow{k_d} \text{fragment ion} + \text{neutrals} \tag{2a}$$

and

$$k_1 \text{ and } k_{-1} \gg k_d. \tag{2b}$$

These assumptions result in the following QET expression of decay rate constant:[1]

$$k(E) = \sigma \int_0^{E_i - E_a} \rho^{\neq}(E)\, dE/h\, \rho(E_i), \tag{3}$$

where $\rho(E_i)$ is the state density of the molecular ion with internal energy of E_i, $\rho^{\neq}(E)$ that of the transition state for the dissociation process with the activation energy E_a and σ the degeneracy of reaction pathways.

Energized diatomic and triatomic molecules often relax by state-specific dissociation and/or radiative transition (fluorescence, etc.).[5–7] When the molecular ion is sufficiently large, radiative transition usually does not compete with internal conversion because of its high density of states. Therefore, a large molecular ion characterized by a large phase space should satisfy these hypothesis[1–3] which the quasi-equilibrium theory assumes.

Molecular ions containing a fluorine atom were frequently reported to dissociate nonstatistically, which include CF_4^+ and $C_2F_6^+$.[5,6] In the case of CF_4^+ fluorescent transition plays an important role prior to dissociation.[5] Here we have studied dissociation of the fluorobenzene by using threshold photoelectron–photoion coincidence (TPEPICO) mass spectrometry[8,9] since this molecule is an example of large molecular size and also contains a heteroatom fluorine. Time-dependent breakdown curves[10,11] have also been derived from absolute decay rate constants obtained experimentally and the information-theoretical approach[12] has been employed to study energy disposal in fragmentation.

Experimental

Our TPEPICO mass spectrometer has been described in detail previously.[13,14] It was used under the double-field source and space focusing condition.[15–17] A typical field strength in an ionization region was 20.0 V cm^{-1}, and the corresponding energy resolution for threshold photoelectrons was about 21 meV (FWHM) for the Ar $^2P_{3/2}$ state. The TOF mass resolution ($T/2\Delta T$) was about 50 amu (FWHM) for thermal ions.

Breakdown curves were constructed from relative ion abundances obtained from TOF peak areas. Overlapped ion peaks were deconvoluted assuming that a TOF mass peak is Gaussian. Because the m/z 95 ion was not fully separated from those of the m/z 96 ion under the ion extraction field of 20 V cm^{-1}, their relative abundances were evaluated from deconvolution results of those TOF peaks measured under the 34 V cm^{-1} field strength corresponding to the mass resolution of about 70 amu (FWHM). Ion loss due to initial kinetic energy was not taken into account for construction of breakdown curves.

Fluorobenzene was commercially obtained from Aldrich with a stated purity of 99% and was used without further purification. Both HeI photoionization and 70 eV electron-impact ionization mass spectra measured by an Extranuclear 324-9 quadrupole mass spectrometer and a Kratos AEI MS-50 DA, respectively, showed no significant impurity. All experiments were carried out at a source pressure of 3×10^{-5} Torr (1 Torr=133.322 Pa) and at room temperature.

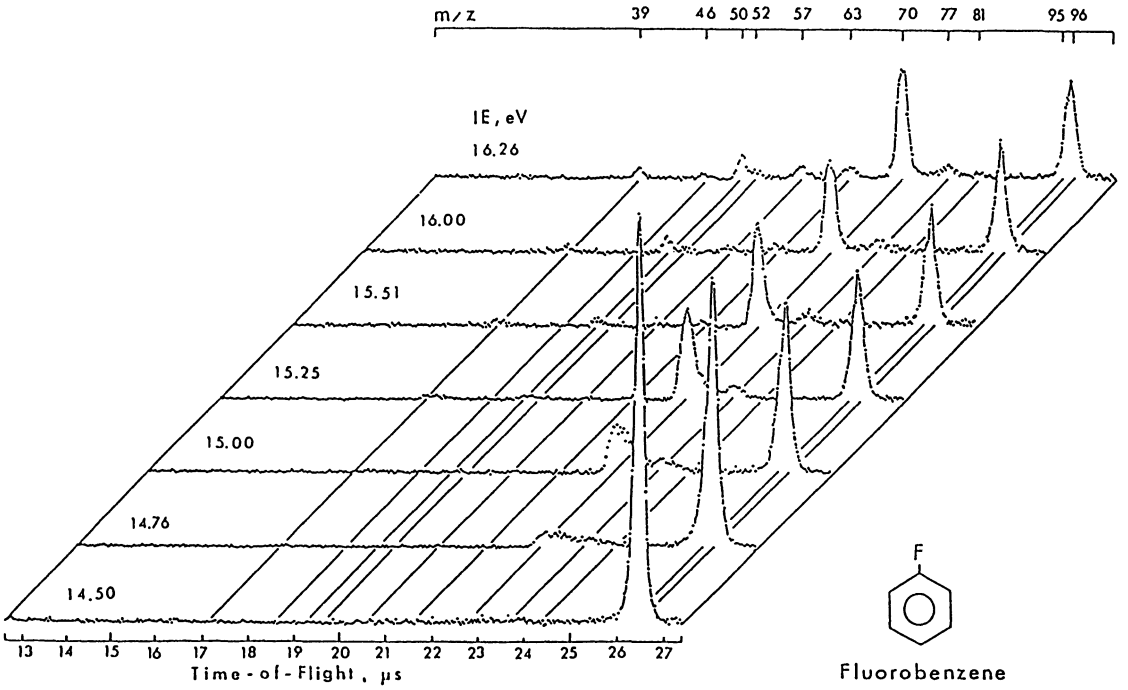

Fig. 1. Typical coincidence TOF mass spectra at several photon energies.

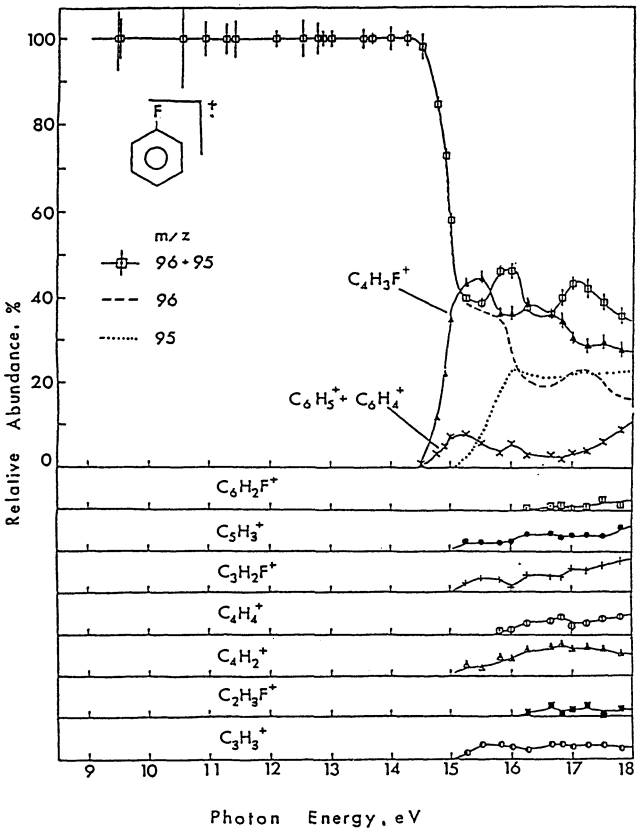

Fig. 2. The experimental breakdown curves of the fluorobenzene ion measured under an ion extraction field of 20 V cm^{-1}. The breakdown curve of $C_6H_4F^+$ was estimated from deconvolution of overlapped peaks of m/z 96 and 95 measured under the 34-V cm^{-1} extraction field, assuming the individual peaks are Gaussian.

Results and Discussion

Breakdown Curves and Fragmentation Pathways. Major products ions are $C_6H_5F^+$ (m/z 96), $C_6H_4F^+$ (m/z 95), $C_5H_2F^+$ (m/z 81), $C_6H_5^+$ (m/z 77), $C_6H_4^+$ (m/z 76), $C_4H_3F^+$ (m/z 70), $C_5H_3^+$ (m/z 63), $C_3H_2F^+$ (m/z 57), $C_4H_4^+$ (m/z 52), $C_4H_2^+$ (m/z 50), $C_2H_3F^+$ (m/z 46), and $C_3H_3^+$ (m/z 39). Fig. 1 shows typical coincidence TOF mass spectra measured at several photon energies, and the experimental breakdown curves are presented in Fig. 2. Fragmentation pathways elucidated from

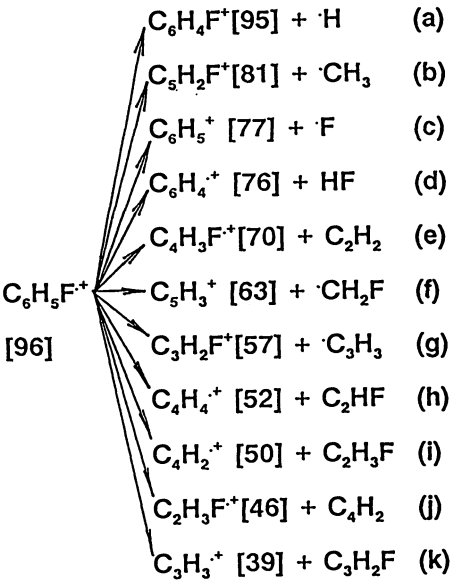

Fig. 3. Major fragmentation pathways of the fluorobenzene ion.

appearance potentials are summarized in Fig. 3. Appearance potentials obtained from breakdown curves are listed in Table 1. Among these dissociations abundant processes are (1) the C_2H_2-loss (Reaction e), (2) the hydrogen-loss (Reaction a) and (3) the fluorine elimination (Reaction c) from the molecular ion.

Table 1. Appearance Potentials (eV) for the Fragmentation Processes of Fluorobenzene Ion

m/z	Fragmentation process	Literature	This work
95	$C_6H_4F^+ + {}^\cdot H$	14.1[a]	
81	$C_5H_2F^+ + {}^\cdot CH_3$		16.13±0.13
77	$C_6H_5^+ + {}^\cdot F$	14.5±0.1[b]	13.10±0.05[e]
76	$C_6H_4^{\cdot+} + HF$	15.37±0.1[c]	
70	$C_4H_3F^{\cdot+} + C_2H_2$	14.73[d]	13.14±0.05[e]
63	$C_5H_3^+ + {}^\cdot CH_2F$		15.13±0.13
57	$C_3H_2F^+ + {}^\cdot C_3H_3$	15.77±0.1[c]	15.13±0.13
52	$C_4H_4^{\cdot+} + C_2HF$	17.00±0.1[c]	15.90±0.09
50	$C_4H_2^{\cdot+} + C_2H_3F$		15.13±0.13
46	$C_2H_3F^{\cdot+} + C_4H_2$		16.13±0.13
39	$C_3H_3^+ + {}^\cdot C_3H_2F$	14.27±0.1[c]	15.13±0.13

a) Ref. 28. b) Refs. 29 and 30. c) Ref. 31. d) Ref. 32. e) These values were adiabatic appearance potentials obtained by QET calculations (see text).

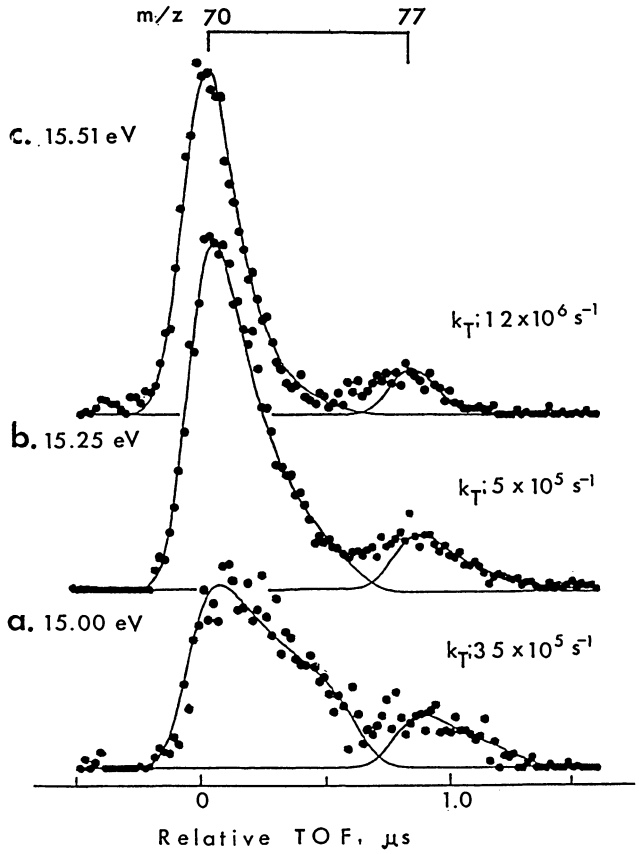

Fig. 4. The flight time distributions of m/z 70 and 77 ions (closed circles) observed at several photon energies under an ion extraction field of 34 V cm^{-1}. The solid curves are the distributions convoluted by the indicated decay rate constants.

Absolute Decay Rate Constants and Time-Dependent Breakdown Curves. A. Metastable Fragmentation. Asymmetric flight time distributions due to metastable dissociation[18] were observed for the C_2H_2- and F-eliminations from the parent ion which are formations of $C_6H_5^+$ and $C_4H_3F^+$ (Fig. 4). Total decay rate constants k_T were obtained directly from their asymmetric TOF distributions: Flight time distributions resulting from metastable fragmentation which occurs in both the first and second ion extraction fields were calculated numerically. The rate constant and initial ion kinetic energy were then adjusted until the calculated TOF distribution agrees with experiment. Experimental TOF distributions for both $C_6H_5^+$ and $C_4H_3F^+$ ions were found to be well fitted by using a single and same

Table 2. The Total Decay Rate Constants Observed for the Formations of $C_6H_5^+$ and $C_4H_3F^+$

Ionization energy (eV)	Total decay rate (×10^6 s^{-1})	
	$C_6H_5^+$	$C_4H_3F^+$
14.76	0.3±0.2	0.2±0.1
14.90	0.5±0.2	0.5±0.2
15.00	0.6±0.1	0.6±0.1
15.25	1.6±0.2	1.6±0.2
15.50	4±1	4±1

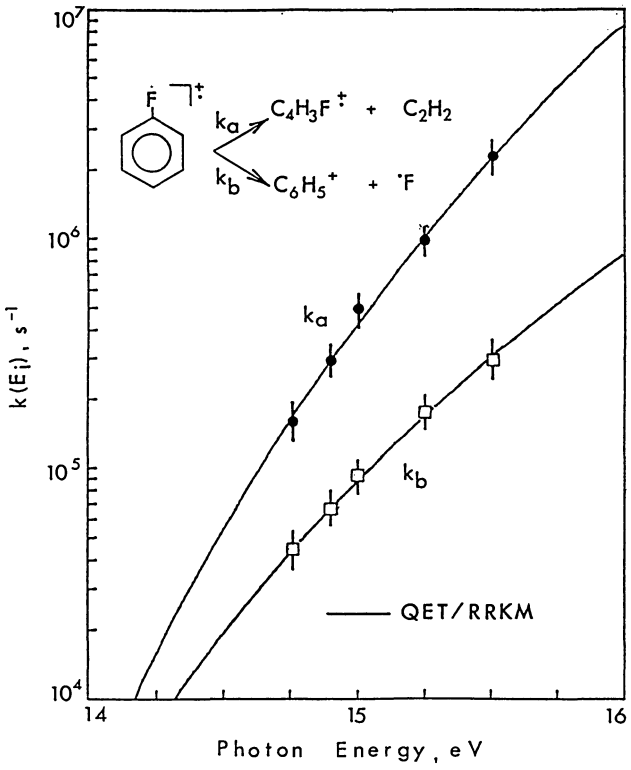

Fig. 5. Metastable decay rate constants for the formations of $C_4H_3F^+$ and $C_6H_5^+$ as a function of photon energy. Circles are the experimental decay rate constants. Solid curves are those obtained by QET calculations with the best fits to the experimental data.

rate constant (Table 2). Thus the same total rate observed suggests a competing dissociation mechanism for the fluorine and C_2H_2 loss channels. Individual rate constants for these reactions were therefore obtained from relative abundances in the breakdown diagram.

Individual decay rate constants are plotted against photon energy in Fig. 5 in comparison with those calculated by QET (the solid curves). In the QET calculation the vibrational frequencies of fluorobenzene ion were taken to be the same as those of the neutral molecule and the vibrational frequencies of the transition state were derived by multiplying those of the ion (excluding a reaction mode) by a factor F reflecting tightness ($F>1$) or looseness ($F<1$) of the transition state.[19] The frequencies and parameters used are listed in Table 3. The density of vibrational states were calculated using the Whitten–Rabinovitch approximation.[20] The activation energy E_a and factor F were used as adjustable parameters until the best fit to experiment is obtained.

Adiabatic appearance potentials were evaluated to be

Table 3. The Vibrational Frequencies Used in the QET Calculations.[a,b] The Number n in (n) Denotes the Degeneracy of Vibrational Frequency

3100	3090	3070	3050	3040	1600(2)
1500	1460	1330(2)	1220	1160(2)	1070
1020	1010	1000	970	900	820
810	750	690	610	520	500
410	400	240			

a) Ref. 33. b) For the formation of $C_4H_3F^+$, $C_6H_5^+$, and $C_6H_4F^+$ their reaction coordinates were assumed to be the ring breathing mode (1160 cm^{-1}) (F=0.9), the C–F stretching mode (1220 cm^{-1}) (F=1.1) and the C–H stretching mode (3040 cm^{-1}) (F=0.78), respectively.

respectively 13.10±0.05 eV and 13.14±0.05 eV for the formations of $C_6H_5^+$ and $C_4H_3F^+$, using the relation

$$AP_{adb} = IP + E_a, \quad (4)$$

Herein, the ionization potential IP of the fluorobenzene molecule was taken to be 9.11 eV from the literature.[27] Using these values the heat of formations $\Delta H_f(C_6H_5^+)$ and $\Delta H_f(C_4H_3F^+)$ were evaluated to be 257±2 and 222±2 kcal mol^{-1}. The heat of formation obtained in this work for the phenyl cation can be compared with the value ΔH_{f298}° ($C_6H_5^+$) of about 272 kcal mol^{-1} (1140 kJ mol^{-1}) suggested in Ref. 34 after rough correction of kinetic shift (50 kJ mol^{-1}).

B. Kinetic Shift. The experimental breakdown curves of the parent ion measured under the different field strengths of ion extraction (E_s=20 and 34 V cm^{-1}) shifted by ca. 0.1 eV. This shift results from difference in the reaction time equal to a time spending during acceleration in a TOF mass spectrometer, which are calculated to be 3.4 and 2.6 μs, respectively. The breakdown curves for these reaction times were reconstructed from the individual rate constants, and are presented in Fig. 6. In the figure a shift, about 75 meV, of crossover point between the breakdown curves of the parent ion and $C_4H_3F^+$ was consistent with experiment. The calculated breakdown curves are fairly in good agreement with the TPEPICO breakdown curves.

Such a kinetic shift leads to heat of formations higher than those derived from adiabatic potentials, and can be ascribed to a large phase space volume of the molecular ion brought about by (1) a large number of internal modes or a high density of states $\rho(E)$ and (2) a high activation energy E_a. A large phase space volume corresponds to a long lifetime of a fragmenting ion which is the average time until a given phase point crosses over the critical surface to dissociation. Our observations

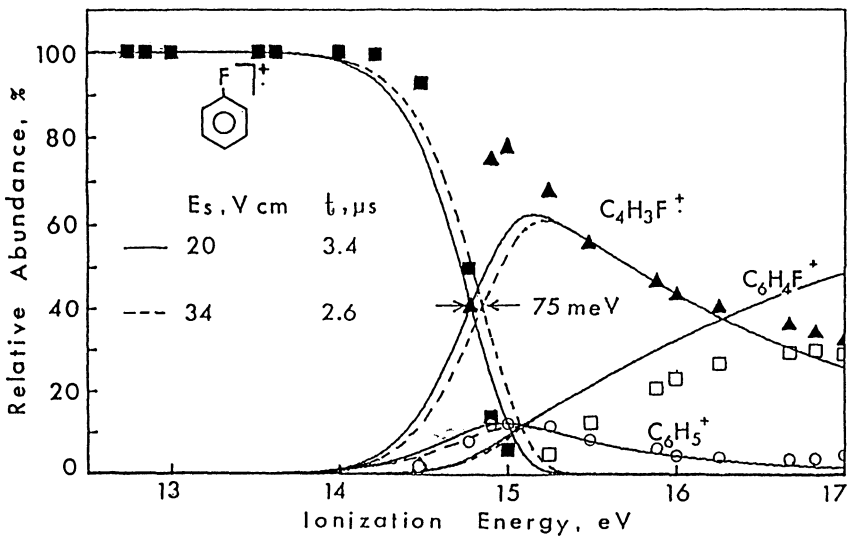

Fig. 6. The breakdown curves for the reaction times 3.4 and 2.6 μs corresponding to the extraction fields of 20 and 34 V cm^{-1}, respectively. Symbols are the corrected breakdown curves for the 20-V cm field.

are thus consistent with the prediction by QET.

Information-Theoretical Analysis of Energy Disposal in Fragmentation. A. Kinetic Energy Release Distribution (KERD). Kinetic energy release distributions for the formation of $C_4H_3F^+$ ions (m/z 70) were extracted from their flight time distributions using a linear regression method. The approach utilized here has been described previously, which follows those used by Powis et al.[21] and Baer et al.[22]

A typical deconvolution result is presented in Fig. 7. Here we used the minimum energy E_o=5.0 meV, the room temperature T=300 K and the nine discrete kinetic energy releases: $Q=(2n-1)^2 E_o$ (i=1 to 9). The experimental flight distribution $F(t)$ was convoluted by a series of calculated distributions $F(t; Q_i)$:

$$F(t)=\sum_i W(i)\, F(t; Q_i). \tag{5}$$

The KERD $P(Q_i)$ can be obtained from the coefficients $W(i)$ which give the best fit to experiment $F(t)$:

$$P(Q_i)=[W(i)/\sum_i W(i)]/[4(2n-1)E_o]. \tag{6}$$

A KERD extracted from these regression coefficients is plotted as a step graph in Fig. 8 together with the QET prediction. The QET kinetic energy release distribution $P(Q; E_i)$ to be compared to TPEPICO experiments is given to be

$$P(Q; E_i)\,dQ=\rho^{\neq}(E_i-E_a-Q)\,dQ/\,W^{\neq}(E_i-E_a). \tag{7}$$

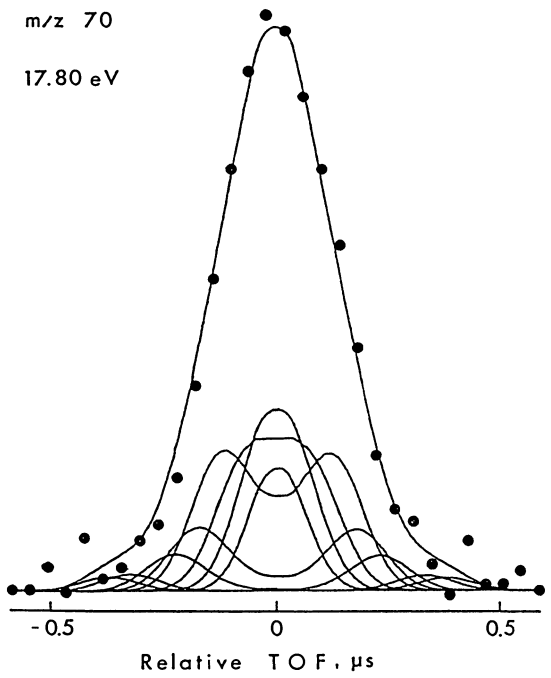

Fig. 7. An example of TOF distributions of the m/z 70 ion and a deconvolution result by the multiple linear regression method. The solid curves are the flight time distributions simulated for a series of the nine discrete kinetic energy releases and their sum to be compared with experiment.

Herein, $\rho^{\neq}(E_i-E_a-Q)$ is the state density of the transition state at internal energy of E_i-E_a-Q, and $W^{\neq}(E_i-E_a)$ is the state sum of the activated complex with excess energy E_i-E_a.

The average KERs are then obtained by

$$\langle Q\rangle_{E_i}=\int_0^{E_i-E_a} Q\, P(Q; E_i)\, dQ, \tag{8}$$

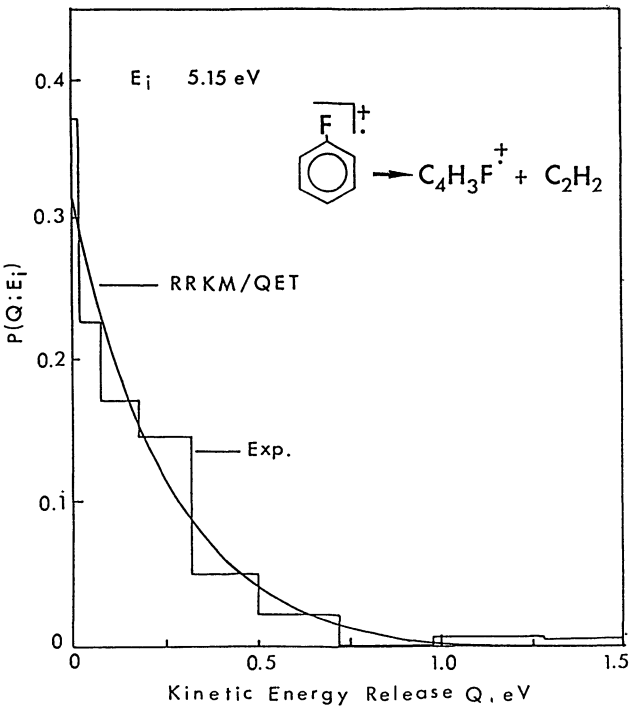

Fig. 8. A KERD for the formation of $C_4H_3F^+$ extracted from its flight time distribution is presented together with the QET prediction.

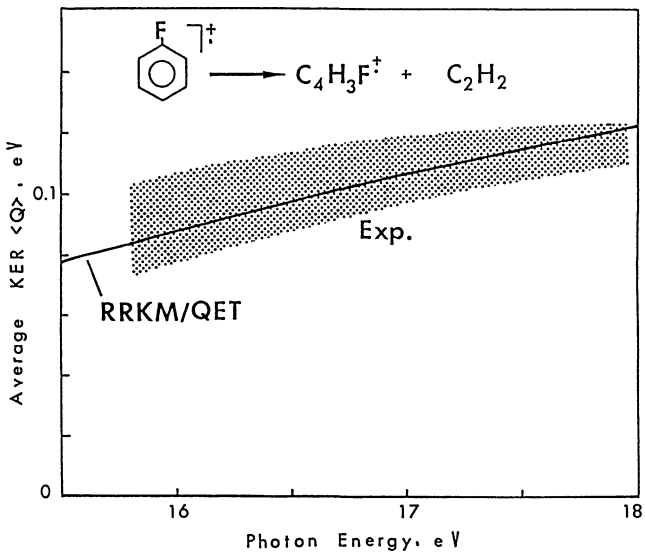

Fig. 9. Average KERs $\langle Q\rangle$ observed for the formation of $C_4H_3F^+$ (shaded area). The solid curve is the average KERs calculated by QET.

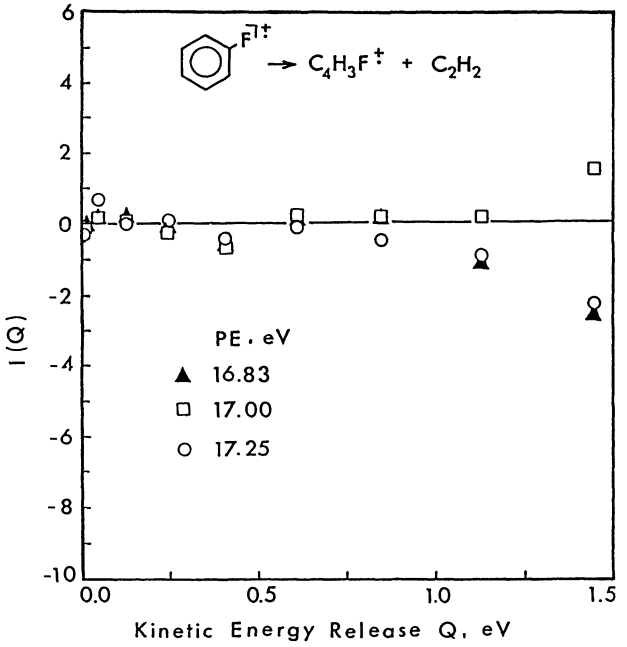

Fig. 10. Surprisal plots of KERDs observed for the $C_4H_3F^+$ formation.

and are presented in Fig. 9. Thus as seen in the figures the experimental KERDs and KERs seem to be in good agreement with the statistical expectations.

B. Surprisal Plot. Levine and Bernstein[25,26] have recently developed the thermodynamic approach to collision processes in order to bridge the gap between the equilibrium and disequilibrium on the basis of information theory. The authors[24] introduced the concept of the "surprisal" to measure how an experimental result differs from a prediction. If $P^\circ(Q)$ is the prior distribution with a kinetic energy release Q, the surprisal $I(Q)$ of an experimental distribution $P(Q)$ is defined as

$$I(Q) = -\ln[P(Q)/P^\circ(Q)]. \quad (9)$$

Here we used the QET kinetic energy release distribution as the prior distribution. The surprisal plots (Fig. 10) showed almost zero less than 0.5 eV and strongly suggest that the observed KERDs are consistent with those predicted by the statistical rate theory of mass spectra. Scattered data points over 0.5 eV corresponding to the tail of a TOF distribution are obviously due to experimental errors.

As a conclusion, whereas this molecule contains a heteroatom fluorine, statistical dissociation thus observed indicates that internal conversion controls fragmentation of the fluorobenzene ion because of its high state density.

We thank the USA Department of Energy for support of this work under Contract No. DE-AC02-76-ER02567 and the Regional Facility in Mass Spectrometry at the University of Nebraska.

References

1) H. M. Rosenstock, M. B. Wallenstein, A. L. Wharhaftig, and H. Eyring, *Proc. Natl. Acad. Sci. U.S.A.*, **38**, 667 (1952).
2) W. Frost, "Theory of Unimolecular Reactions," Academic Press, New York (1973).
3) D. L. Bunker, "Theory of Elementary Gas Reaction, Rates," Pergamon, Oxford (1967).
4) A. A. Marcus, *J. Chem. Phys.*, **20**, 359 (1952).
5) I. G. Simm, C. J. Danby, J. H. D. Eland, and P. I. Mansell, *J. Chem. Soc., Faraday Trans. 2*, **72**, 426 (1976).
6) M. G. Inghram, G. R. Hanson, and R. Stockbauer, *Int. J. Mass Spectrom. Ion Phys.*, **33**, 253 (1980).
7) T. Nishimura, G. G. Meisels, and Y. Niwa, *J. Chem. Phys.*, **91**, 4009 (1989).
8) J. H. D. Eland, "Photoelectron Spectroscopy," Butterworths, London (1974), p. 180.
9) T. Baer, in "Gas Phase Ion Chemistry," ed by M. T. Bowers, Academic Press, New York (1979), Vol. I, Chap. 5.
10) J. Dannacher, H. M. Rosenstock, R. Buff, A. C. Parr, R. L. Stockbauer, R. Bombach, and J.-P. Stadelmann, *Chem. Phys.*, **75**, 23 (1983).
11) R. Bombach, J. Dannacher, and J.-P. Stadelmann, *J. Am. Chem. Soc.*, **105**, 4205 (1983).
12) R. B. Bernstein, "Chemical Dynamics via Molecular Beam and Laser Techniques," Clarendon Press, Oxford (1982), Chap. 9.
13) C. F. Batten, J. A. Taylor, B. P. Tsai, and G. G. Meisels, *J. Chem. Phys.*, **69**, 2547 (1978).
14) C. F. Batten, J. A. Taylor, and G. G. Meisels, *J. Chem. Phys.*, **65**, 3316 (1976).
15) W. C. Wiely and I. H. McLaren, *Rev. Sci. Inst.*, **26**, 1150 (1955).
16) J. L. Franklin, P. M. Hierl, and D. A. Whan, *J. Chem. Phys.*, **47**, 3148 (1967).
17) T. Nishimura, P. R. Das, and G. G. Meisels, *J. Chem. Phys.*, **84**, 6190 (1986).
18) A. S. Werner and T. Baer, *J. Chem. Phys.*, **62**, 2900 (1975).
19) R. Bombach, J. Dannacher, and J.-P. Stadelmann, *Int. J. Mass Spectrom. Ion Proc.*, **58**, 217 (1984).
20) G. Z. Whitten and B. S. Rabinovitch, *J. Chem. Phys.*, **38**, 2466 (1963).
21) I. Powis, P. I. Munsell, and C. J. Danby, *Int. J. Mass Spectrom. Ion Phys.*, **32**, 15 (1979).
22) D. M. Mintz and T. Baer, *J. Chem. Phys.*, **65**, 2407 (1976).
23) M. L. Vestal, in "Fundamental Processes in Radiation Chemistry," ed by P. Ausloos, Interscience, New York (1968), Chap. 2.
24) R. D. Levine and R. B. Bernstein, "Molecular Reaction Dynamics," Clarendon Press, Oxford (1974).
25) I. Powis, *J. Chem. Soc., Faraday Trans. 2*, **75**, 1294 (1979).
26) C. Lifshitz, *Int. J. Mass Spectrom. Ion Phys.* **43**, 179 (1982).
27) T. P. Devies and J. W. Rabalais, *J. Electron Spectrosc. Relat. Phenm.*, **1**, 355 (1972/73).
28) A. N. H. Yeo and D. H. Williams, *Chem. Commun.*, **1970**, 886.
29) J. R. Majer and C. R. Patrick, *Trans. Faraday Soc.*, **58**, 17 (1962).
30) J. R. Majer and C. R. Patrick, *Adv. Mass Spectrom.*, **2**,

555 (1963).
31) J. Momigny, *Bull. Soc. R. Sci. Liége,* **28**, 251 (1959).
32) I. Howe and D. H. Williams, *J. Am. Chem. Soc.,* **91**, 7137 (1969).
33) L. M. Sverdlov, M. A. Kovner, and E. P. Krainov, "Vibrational Spectra of Polyatomic Molecules," John Wiely & Sons, New York (1974), p. 448.
34) H. M. Rosenstock, K. Draxl, B. W. Steiner, and J. H. Herron, *J. Phys. Chem. Ref. Data,* **6**, Supplement 1 (1977), p. I-146.

 © 1991 The Chemical Society of Japan Bull. Chem. Soc. Jpn., 64, 2901—2907 (1991)

Time-Resolved Resonance Raman Investigation of Cytochrome Oxidase Catalysis: Observation of a New Oxygen-Isotope Sensitive Raman Band

Takashi OGURA, Satoshi TAKAHASHI, Kyoko SHINZAWA-ITOH,† Shinya YOSHIKAWA,† and Teizo KITAGAWA*

Institute for Molecular Science, Okazaki National Research Institutes/The Graduate University for Advanced Studies, Myodaiji, Okazaki 444

†Department of Life Science, Faculty of Science, Himeji Institute of Technology, 1479-1 Kanaji, Kamigoricho, Akogun, Hyogo, 678-12

(Received May 24, 1991)

The reduction of dioxygen by cytochrome oxidase has been investigated, in the time interval between 0.1 and 5.4 ms after initiation of the reaction, by using time-resolved resonance Raman spectroscopy combined with the Artificial Cardiovascular System [Ogura et al., *Biochemistry,* **28**, 8022 (1989)]. At 0.5 ms we observed a new oxygen-isotope sensitive Raman band at 356 cm^{-1} for $^{16}O_2$, which shifted down to 341 cm^{-1} for $^{18}O_2$. The temporal behavior of this band was found to be very close to that of another oxygen-isotope sensitive band at 788 cm^{-1} which had been assigned previously to the Fe(IV)=O stretching mode of the ferryloxo intermediate [Ogura et al., *J. Biol. Chem.,* **265**, 14721(1990)]. However, the fact that the 788 cm^{-1} band shifts to a higher frequency (802 cm^{-1}) in ^2H_2O, taken together with the present detection of two oxygen-isotope sensitive bands, prompts us to suggest an alternative assignment; namely, that these bands arise from the O^-–O^- (788 cm^{-1}) and Fe(III)–O^- (356 cm^{-1}) stretching modes of the Fe(III)–O^-–O^-–H intermediate. This conclusion forces a reconsideration of the currently accepted view of cytochrome oxidase catalysis.

Cytochrome oxidase is the terminal enzyme in the respiratory chain of aerobic organisms.[1,2] This enzyme is a membrane protein containing two heme A groups (Fe_a and Fe_{a3}) and two copper ions (Cu_A and Cu_B) as redox active metal centers and couples the dioxygen reduction reaction with proton translocation across the membrane. The electrochemical potential across the membrane thus generated is ultimately used to synthesize ATP. A functional unit containing the Fe_a and Cu_A ions serves as an electron transfer protein from cytochrome *c* to another functional unit containing the Fe_{a3}–Cu_B binuclear dioxygen reducing site. The Fe_{a3} and Cu_B ions are in close proximity so that they could be antiferromagnetically coupled in the oxidized state, while the Fe_a and Cu_A ions are separated and EPR active.

The reaction intermediates of this enzyme have been studied mainly with visible absorption[3–6] and EPR[7] spectroscopies. Recently, time-resolved resonance Raman spectroscopy added decisive structural information on the primary oxygenated derivative of the enzyme.[8–10] As to subsequent intermediates, a Raman band assignable to the Fe(IV)=O stretching mode of the ferryloxo heme was reported by ourselves and others.[11–13] On the basis of these results, a unified view of the catalytic cycle of cytochrome oxidase was proposed.[14] However, since the observation of the Fe(IV)=O stretching Raman band is crucial to this interpretation, if its assignment were not correct, the interpretation would lack experimental basis. In this paper we present new experimental results that are incompatible with the current interpretation of the resonance Raman spectra of the Fe(IV)=O intermediate and suggest an alternative assignment of this oxygen-isotope sensitive Raman band.

Material and Method

Cytochrome oxidase was isolated from fresh bovine hearts according to the method described elsewhere.[15] The sample solution contained cytochrome oxidase (100 μM in terms of aa_3 unit), horse heart cytochrome *c* (Sigma, 16.6 μM) and sodium ascorbate (Wako Chemicals, 50 mM) in 50 mM sodium phosphate buffer, pH 7.2. At relatively high salt concentration the cytochrome *c*-cytochrome oxidase complex formation is negligible. In order to continuously generate reaction intermediates in a flow-cell over the long time period (ca. 10 h) required for data accumulation, the "Artificial Cardiovascular System"[16] was used so as to limit the amount of enzyme needed. The quartz flow cell (cross section, 0.6×0.6 mm^2) was used in this experiment and the flow rate was held constant as 40 ml min^{-1}. Accordingly, the previously described dual-beam flow apparatus[17] was attached to the flow-cell in order to change the delay time (Δt_d) of the probe beam from the pump beam. The sample temperature in the flow-cell was maintained at 5 °C. The concentration of oxygen incorporated into the solution by the "Lung" was approximately 150 μM.

An argon ion laser (Spectra Physics, 164)-pumped dye laser (Spectra Physics, 375), employing Rhodamine 6G, was used to provide the pump beam. The output at 590 nm (100 mW), focused with a cylindrical lens to a 100 μm wide slit image, was used to photolyze carbonmonoxide from the CO-bound, fully-reduced enzyme. Photodissociation initiates the reaction of the enzyme with O_2, in the presence of O_2, but simply produces the deoxy state in the absence of O_2. Under these conditions, about 95% of the CO was photolyzed from the CO-bound enzyme, as judged from the intensity of the Fe(II)–CO stretching band. The probe beam was provided by a dye laser (Spectra Physics 375B), using stilbene 420, which was excited by another Ar^+ ion laser (Spectra Physics, 2045). The output at 423 nm (10 mW) was focused to a spot (20 μm in diameter) at various distances on the downstream side of the pump

beam. Under these conditions a given molecule is exposed to the pump and probe beams for 54 and 11 μs, respectively. The $^{16}O_2$ derivative, $^{18}O_2$ derivative and the deoxy state were measured in turn at every 5 min for the identical enzyme under identical illumination geometry. Therefore their difference spectra were very accurate. Each spectrum presented is a sum of six to nine of the individual (5 min) spectra.

The scattered light was dispersed with a double monochromator (Spex 1404) and detected with an intensified photodiode array (PAR 1421Q). Pixel-to-pixel variation of sensitivity of the photodiode array was corrected with white light; the observed Raman spectrum was divided by the spectrum of the white light. Raman shifts were calibrated with alcohol observed under the same flowing conditions and the accuracy of the peak frequency was ±2 and ±4 cm^{-1} for strong and weak Raman bands, respectively.

For a large molecule like cytochrome oxidase (M_r=200 000), the lowest frequency where any Raman band could be identified for the flowing sample was 600 cm^{-1} because of increased Rayleigh scattering, even when an optical filter (short cut filter) for removing it was placed before the monochromator. In order to lower this limit frequency, a special optical filter (referred to as a spatial filter) was designed and placed between the sample and the monochromator. This device is composed of a microscope objective lens, a rectangular slit, and a collection lens which is F-matched to the monochromator used. Although details of the device and its capability will be described separately,[18] we note here that the use of this device enabled us to measure the Raman spectrum until as low as 250 cm^{-1}.

Results

Figure 1 depicts time-resolved resonance Raman spectra of cytochrome oxidase in ^2H_2O for Δt_d=0.1 ms. Figs. 1A and 1B were observed for $^{16}O_2$ and $^{18}O_2$, respectively, and Fig. 1C shows their difference (A minus B). In both Figs. 1A and 1B porphyrin in-plane vibrational modes are seen at 750 (ν_{16}), 684 (ν_7), and 342 cm^{-1} (ν_8). Although the difference between the two spectra is small, a clear derivative-like curve is seen in Fig. 1C, indicating a frequency shift due to the oxygen isotope; a Raman band at 571 cm^{-1} for $^{16}O_2$ shifts down to 544 cm^{-1} for $^{18}O_2$. One can assign this Raman band to the Fe(II)–O_2 stretching vibration (ν_{Fe-O_2}) of the primary oxygen compound, compound A.[5] Since the intensity of the Raman band due to the heme-bound oxygen was fairly weak compared with those of porphyrin bands, hereafter we will present resonance Raman spectra of reaction intermediates as difference spectra ($^{16}O_2$ minus $^{18}O_2$).

Figures 2 and 3 display the time-resolved resonance Raman difference spectra of cytochrome oxidase in H_2O and ^2H_2O, respectively. The delay time was varied from 0.1 to 5.4 ms and is specified at the right side of each spectrum. The Raman band at 573 cm^{-1} for $^{16}O_2$ in Fig. 2A (Δt_d=0.1 ms) shows a downshift to 544 cm^{-1} for $^{18}O_2$, which well reproduced the previous observations.[8–10] This band exhibited no frequency shift in ^2H_2O within the experimental uncertainty (Fig. 3A), in agreement with the recent results by Han et al.[13]

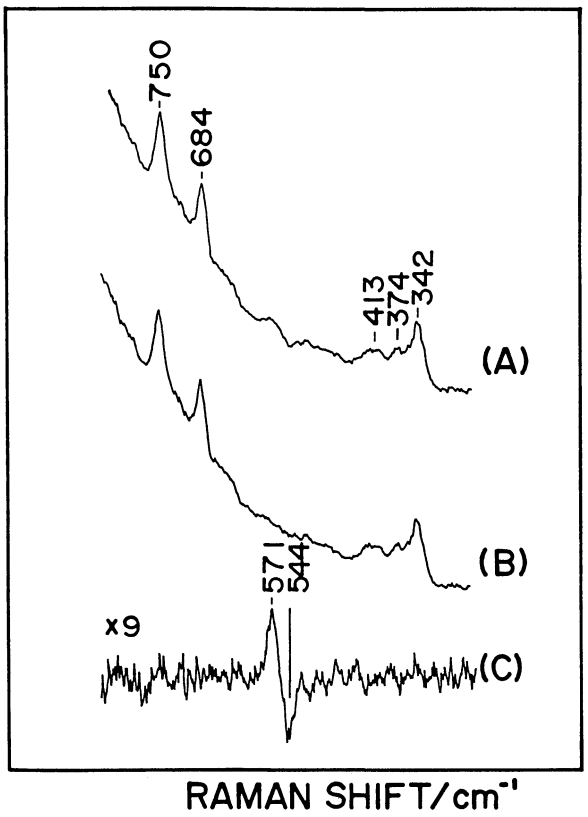

Fig. 1. Time-resolved resonance Raman spectra of cytochrome oxidase in ^2H_2O for Δt_d=0.1 ms. Spectra A and B were observed with $^{16}O_2$ and $^{18}O_2$, respectively, and trace C denotes the difference spectrum, A minus B. Accumulation time was 300 s.

In Fig. 2C, at Δt_d=0.5 ms, two new oxygen-isotope sensitive bands appeared at 788 and 356 cm^{-1} and the 573/544 cm^{-1} band apparently became weaker. The band for $^{16}O_2$ at 788 cm^{-1} exhibited a downshift to 749 cm^{-1} for $^{18}O_2$. Although it is not clear whether the 788 cm^{-1} band is actually composed of two bands or if the apparent doublet results from noise, the latter alternative appears more likely since in ^2H_2O this Raman band appeared as a singlet at 802 cm^{-1} for $^{16}O_2$ and at 766 cm^{-1} for $^{18}O_2$ as shown in Fig. 3B. The apparent upshift of the 788 cm^{-1} band is in agreement with the report by Han et al.[13] but not with that by Varotsis and Babcock.[12] This will be discussed later.

Development of the spatial filter in this study enabled us to detect another oxygen-isotope sensitive band at 356 cm^{-1} for $^{16}O_2$ which shifts to 342 cm^{-1} for $^{18}O_2$, as seen in Fig. 2C; i.e., the true positions of the 356 and 342 cm^{-1} bands might be slightly lower and higher, respectively, because those numbers were derived from the difference spectrum. This band first appears at Δt_d=0.4 ms (Fig. 2B) and persists until Δt_d=3.2 ms. In ^2H_2O the corresponding Raman band appeared at 358 and 343 cm^{-1} for $^{16}O_2$ and $^{18}O_2$, respectively. Thus, the vibrational frequency of the new band is insensitive to deuterium exchange within the experimental

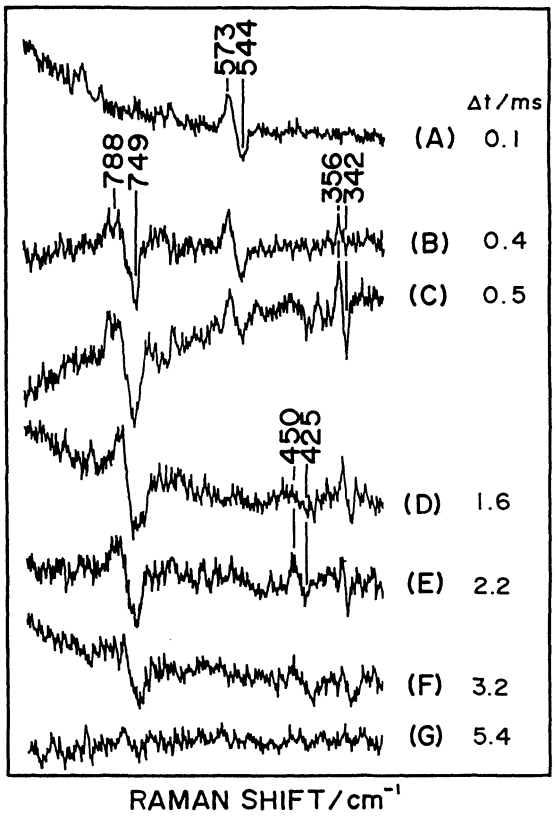

Fig. 2. Time-resolved Raman difference spectra of cytochrome oxidase in H_2O obtained by subtracting the $^{18}O_2$ spectrum from the corresponding $^{16}O_2$ spectrum. Δt_d values are specified at right side of each spectrum. The ordinate is arbitrarily scaled.

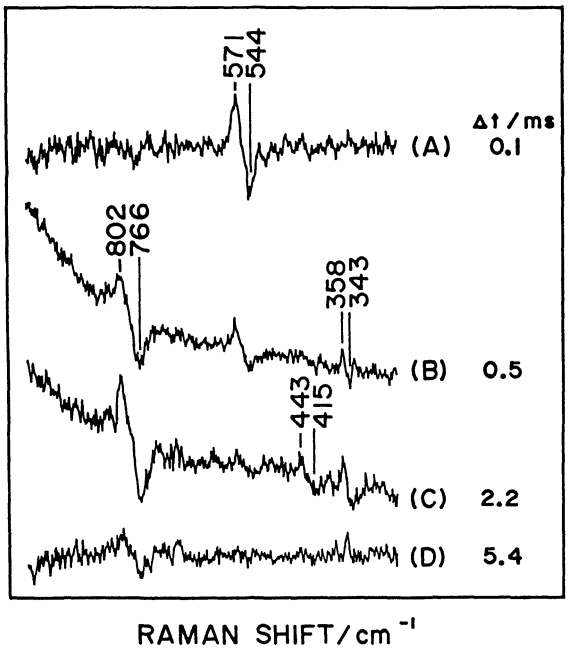

Fig. 3. Time-resolved Raman difference spectra of cytochrome oxidase in ^2H_2O obtained by subtracting the $^{18}O_2$ spectrum from the corresponding $^{16}O_2$ spectrum. Δt_d values are specified at right side of each spectrum. The ordinate is arbitrarily scaled.

uncertainty.

At Δt_d=1.6 ms the Fe(II)-O_2 stretching band at 573/544 cm^{-1} has disappeared while the other two oxygen-isotope sensitive bands remain. At Δt_d=2.2 ms (Fig. 2E) yet another oxygen-isotope sensitive Raman band is observed at 450 cm^{-1} for $^{16}O_2$, which experiences a downshift to 425 cm^{-1} for $^{18}O_2$. In ^2H_2O this Raman band appeared at 443 cm^{-1} for $^{16}O_2$ and at 415 cm^{-1} for $^{18}O_2$. This observation is consistent with the report by Han et al.[13] A simple diatomic approximation of the Fe-OH stretching mode, which is assumed to occur at 450 cm^{-1},[13] predicts a frequency shift of 19 cm^{-1} for Fe-^{18}OH and 10 cm^{-1} for Fe-O^{2}H. Accordingly, the 450 cm^{-1} band is assigned to the Fe(III)-OH stretching vibration in agreement with the reassignment by Han et al.[13] Finally, in Fig. 2G (with Δt_d=5.4 ms) no oxygen-isotope sensitive Raman band is observed, indicating that the Fe_{a3} center does not possess an oxygen ligand derived from O_2. If the Fe_{a3} had a ligand such as OH^- or H_2O group in the so-called "pulsed form",[1] the ligand

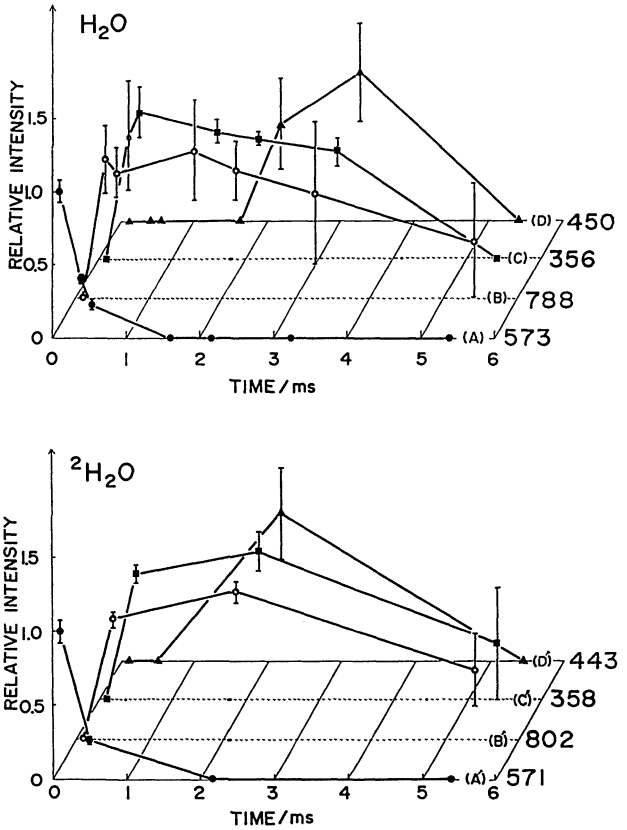

Fig. 4. Time-dependence of relatvie intensity of selected Raman bands at 573 (A, ●), 788 (B, ○), 356 (C, ■), and 450 cm^{-1} (D, ▲) for the H_2O solution and those at 571 (A′, ●), 802 (B′, ○), 358 (C′, ■) and 443 cm^{-1} (D′, ▲) in ^2H_2O solution. The trough-to-peak height of each spectrum was divided by the intensity of the porphyrin ν_7 band at 684 cm^{-1} of the original spectrum. In the plot, the highest value for individual bands is normalized to unity. Experimental uncertainty for the abscissa is smaller than the diameter of the circles.

must be exchanged with bulk water.

The peak height intensities in the difference spectra shown in Figs. 2 and 3 were evaluated with regard to the intensity of the ν_7 band (684 cm^{-1} in Fig. 1) in the corresponding raw spectra of intermediates. The relative intensities are plotted against Δt_d in Fig. 4, where the upper (A—D) and lower figures (A′—D′) present the data for the H_2O and ^2H_2O solutions, respectively. For individual curves the maximum value is normalized to unity. Plots using the ν_{16} band at 750 cm^{-1} as an intensity standard gave similar curves for all the bands (not shown). Although these two porphyrin bands experience slight intensity alterations for different Δt_d, the changes were sufficiently small that they still could serve as effective intensity standards. As expected, the 571 cm^{-1} band of the primary compound quickly loses its intensity ($t_{1/2}$<400 μs). The 788 and 356 cm^{-1} bands simultaneously increase in intensity, with a concomitant decrease in intensity of the 573 cm^{-1} band. Note that the temporal behavior of the 788 and 356 cm^{-1} bands seem to proceed parallel with respect to Δt_d throughout the entire range of Δt_d (between 0.1 and 5.4 ms). The 450 cm^{-1} band arises at Δt_d=2.2 ms and has disappeared at Δt_d=5.4 ms. These features are also retained in ^2H_2O, although the number of experimental points is smaller for ^2H_2O. It is noted that the decay of the 802 (B′) and 358 cm^{-1} (C′) bands observed for the ^2H_2O solution seem somewhat slower than those of the 788 (B) and 356 cm^{-1} (C) bands of the H_2O solution, indicating that this process involves protonation to oxygen and/or couples with the proton translocation.

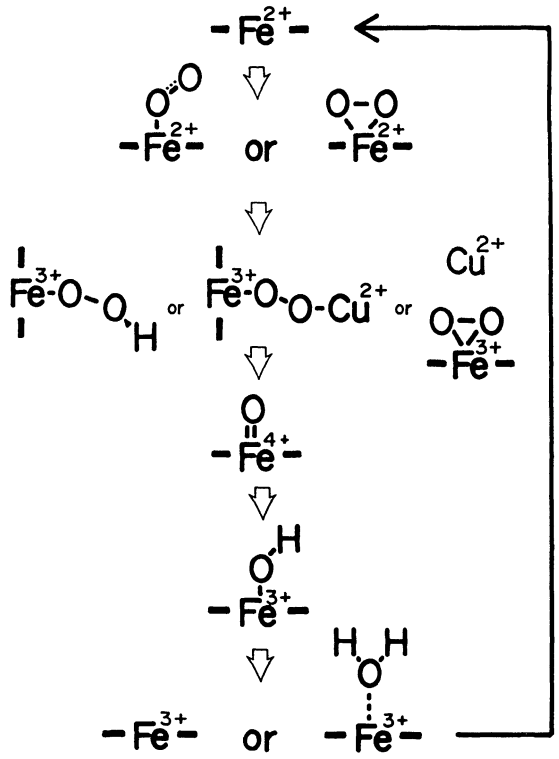

Scheme 1. Possible reaction intermediates.

Discussion

Assignment of the 788 and 356 cm^{-1} Raman Bands. The mechanism of oxygen reduction reaction by cytochrome oxidase has not been fully understood mainly due to the lack of decisive structural information of the reaction intermediates. Scheme 1 illustrates possible reaction intermediates involved at the Fe_{a3} site where the oxidation and ligation states of Cu_B are not included except for two cases. Resonance Raman spectroscopy is particularly well suited to determine which intermediates are actually involved, since their iron–oxygen and oxygen–oxygen stretching frequencies are expected to be distinct. For the primary intermediate (Δt_d=0.1 ms), the end-on structure for the dioxygen bound form is established from the Fe(II)–O_2 stretching frequency.[8–10] This frequency and the size of the $^{18}O_2$ isotopic shift are remarkably close to those of oxymyoglobin (569 cm^{-1})[19] and oxyhemoglobin (567[20] and 572[21] cm^{-1}), for which the X-ray crystallographic analysis has been completed.

In our previous study we assigned the Raman band at 788 cm^{-1} (748 cm^{-1} for $^{18}O_2$) to the Fe(IV)=O stretching vibration of the ferryloxo heme of the next intermediate, mainly based on the frequency value and its shift upon $^{16}O/^{18}O$ isotopic substitution.[11] Similar observations have recently been reported by two other groups,[12,13] although there was a discrepancy about the deuteration effect on this band; Varotsis and Babcock[12] reported that the 790 cm^{-1} band in H_2O exhibited no freqeuency shift in ^2H_2O, while Han et al.[13] reported that the 786 cm^{-1} band in H_2O shifted up to 801 cm^{-1} in ^2H_2O. The present result agrees with the latter observation; the 788 cm^{-1} band exhibiting a clear upshift to 802 cm^{-1} in ^2H_2O [at Δt_d=0.5 and 2.2 ms (Fig. 3)].

All groups assigned this band to the Fe(IV)=O stretching mode. In order to explain its upshift in ^2H_2O, Han et al.[13] assumed that the Fe(IV)=O oxygen is hydrogen bonded in H_2O but not in ^2H_2O. This assumption is based on the fact that the Fe(IV)=O stretching Raman band of compound II of horseradish peroxidase is shifted to a higher frequency at alkaline pH where the participating histidyl imidazole residue is deprotonated and the hydrogen bond ceases to exist.[22,23] However, the validity of that interpretation is questionable inasmuch as the pK_a of a hydrogen-bond donor residue should not be largely different between H_2O and ^2H_2O. If the hydrogen bond were disrupted in ^2H_2O while the pK_a value of the donor residue remained unaltered, we would have to postulate a large structural change of the protein between the H_2O and ^2H_2O solutions. Judging from the spectral similarity and kinetic behavior of the enzymes in H_2O and ^2H_2O, shown in Figs. 2—4, there is no evidence for such a large structural difference between the two solutions.

Moreover, the detection of another oxygen-isotope sensitive band (at 356 cm^{-1} in Figs. 2B—2D) reported here argues against the previous assignment for the

following reasons. The kinetic behavior of the 788 and 356 cm^{-1} bands in H_2O strongly suggest that these two bands arise from an identical intermediate. The same conclusion can be attained from the 802 and 358 cm^{-1} bands in ^2H_2O. In the case of an Fe(IV)=O heme, we expect only one oxygen-isotope sensitive Raman band; that is, the Fe(IV)=O stretching mode. While it may be argued that the Fe(IV)=O bending mode is also oxygen-isotope sensitive, this mode belongs to the E species of the C_{4v} point group appropriate to the Fe(IV)=O heme, and is expected to be infrared active but resonance Raman inactive. Consequently, it is quite unlikely that the 788 cm^{-1} band arises from an Fe(IV)=O heme moiety.

We suggest here that the 788 and 356 cm^{-1} bands are most appropriately assigned to the O^-–O^- and Fe(III)–O^- stretching modes of an Fe(III)–O^-–O^-–H fragment. The reasons for this assignment are as follows; 1) A simple diatomic approximation for Fe(III)–O_2H (and also for Fe(III)–$O_2{}^2H$) predicts a downshift of 12—13 cm^{-1} for ^{18}O substitution, which is close to the observed values (14—15 cm^{-1}), but a negligible downshift for its O-deuteration (3 cm^{-1}). 2) If the Fe(III)–O stretching force constant of the Fe(III)–O_2H complex is the same as that of Fe(III)–OH whose stretching frequency is located at 450 cm^{-1}, the diatomic approximation for the Fe(III)–O_2H bond predicts its stretching frequency at 355 cm^{-1}. This is satisfactorily close to the new Raman band observed in the present study. 3) The O–O stretching frequency of $^2H_2O_2$ is higher than that of H_2O_2 (by 4 cm^{-1}).[24] 4) In the case of oxyhemerythrin, for which the Fe–O–OH structure has been proposed, the O–O stretching mode is observed at 845 cm^{-1} and shifts to a higher frequency (by 4 cm^{-1}) in ^2H_2O.[25] 5) The observed ^{18}O isotopic frequency shift for the 788 cm^{-1} band (−40 cm^{-1}) is reasonably consistent with its assignment to the O–O stretching mode; using even the simple harmonic oscillator approximation, the expected shift is −45 cm^{-1} for the O–O stretching and −35 cm^{-1} for the Fe(IV)=O stretching mode.

Although the magnitude of the shift in ^2H_2O (+14 cm^{-1}) is appreciably larger than in the case of hemerythrin, it is not unreasonable because the upshift is caused by vibrational coupling between the O–O stretching and O–^2H bending modes.[24] If the frequency difference between the O–^2H bending and O–O stretching modes of the Fe(III)–O–O–H heme of cytochrome oxidase is much smaller than that of oxyhemerythrin, a larger upshift would be expected. In fact, for a porphyrin iron(III)–hydroxy compound, the Fe(III)–^{16}OH stretching Raman band at 541 cm^{-1} was observed to shift up by 13 cm^{-1} to 554 cm^{-1} upon its deuteration as a result of its interaction with the O–^2H bending mode.[26] Taking all these facts into consideration, it is most reasonable at the present stage to assign the 788 and 356 cm^{-1} bands to the O^-–O^- and Fe(III)–O^- stretching modes of the Fe(III)–O–O–H complex formed soon after the Fe–O_2 complex. A reaction mechanism involving the hydroperoxo intermediate instead of a μ-peroxo intermediate is compatible with the suggestion[27] from the infrared study of cyanide binding to this enzyme.

Alternatively the 356 cm^{-1} band could be assigned to the Fe(III)–O–OH bending mode. The Fe(III)–O–O bending mode is reported for oxyphthalocyanine iron-(II)[28] at 289 cm^{-1} but for all other oxy-iron porphyrins and oxy-hemeproteins the Fe(II)–O–O bending Raman band has not been identified. Such a band has not been observed for the primary intermediate of cytochrome oxidase shown in Fig. 2 (Δt_d=0.1 ms). The Fe–C–O bending Raman band for the CO-bound hemeproteins is usually much weaker than the Fe–CO stretching Raman band.[29,30] In contrast, the 356 cm^{-1} band of the intermediate in question has greater intensity than the Fe(II)–O_2 stretching mode. Consequently, the assignment of the 356 cm^{-1} band to the Fe(III)–O–O bending mode does not seem likely. However, definitive assignment of the 788 and 356 cm^{-1} bands will require experiments using $^{16}O^{18}O$ which will soon be undertaken in this laboratory.

On the basis of the present assignment, the 790 cm^{-1} Raman band reported by Varotsis and Babcock,[12] which showed no frequency shift upon deuteration, might be assigned to the Fe(IV)=O stretching mode of the ferryloxo complex. Since the peak power of the laser used by Varotsis and Babcock is higher by a factor of 10^5 than those used by the two other groups, it is certainly possible that the O–O bond of the Fe(III)–O–O–H complex suffered photocleavage and the Fe(IV)=O heme was generated. In fact, the O–O bond of Fe(II)–O–O–Fe(II) porphyrin complex is very photolabile even at low temperature and the photoreaction yields the Fe(IV)=O porphyrin.[31] If this is the case, the 790 cm^{-1} band should be regarded as an artifact and should not be assigned to a physiologically relevant intermediate, although this observation served as a basis for a unified view of the reaction scheme.[14]

Hydroperoxy and Ferryloxo Intermediates. The 788 and 356 cm^{-1} bands which apparently arise from a hydroperoxy intermediate, persisted (at 5 °C) at least up to 3.2 ms after initiation of the reaction (see Figs. 4B and 4C). The half-life is approximately 2.5 ms at 5 °C. The rate constant for the rate limiting step in the oxidation reaction of fully-reduced cytochrome oxidase with O_2, obtained from flash photolysis absorption studies, is ca. 1000 s^{-1} ($t_{1/2}$=700 μs) at 25 °C,[32] which is in good agreement with the value obtained in this study provided one takes into consideration the fact that the rate constant approximately doubles on every 10 °C temperature increase; $t_{1/2}$=700 μs at 25 °C should correspond to $t_{1/2}$=2.8 ms at 5 °C.

In Fig. 4 the hydroperoxy intermediate seems to be directly converted to the iron(III) hydroxide intermediate. However, this observation does not necessarily demand it. Involvement of a one electron reduced ferryloxo intermediate[7,33] in the process is possible,

although we could not clearly detect the Fe(IV)=O stretching Raman band, probably because of its short lifetime and/or weak enhancement of that intermediate. Different resonance Raman enhancement factors for two species may occur when the absorption maxima of the two are different. If the excitation wavelength of 423 nm in this study is accidentally much closer to the hydroperoxy intermediate rather than to that of ferryl-oxo intermediate, Raman bands of the hydroperoxy intermediate could dominate the resonance Raman spectra. Although the hydroperoxy-iron porphyrin[34] is generally much more reactive than the ferryloxo one, a shorter lifetime of the ferryloxo intermediate, compared with that of the hydroperoxy intermediate, is not unexpected, as was suggested by Oliveberg et al.[35]

It is useful to estimate the potential relative population of the ferryloxo intermediate during the cytochrome oxidase turnover. In order to gain an insight into this, we carried out a simple calculation for a chain reaction (A→B→C→D→E) in which each intermediate decays with rate constants of k_A, k_B, k_C, and k_D s^{-1}, respectively. The A, B, C, D, and E intermediates correspond to the Fe(II)-O_2, Fe(III)-O-O-H, Fe(IV)=O, Fe(III)-OH and the last Fe(III) species, respectively. As noted above, the final Fe(III) species might be a Fe(III)-OH compound but, if so, its axial ligand is exchangeable with bulk water. In this case, k_D represents the exchange rate. At time, t, after initiation of the reaction, the fractional population of each species can be represented by the following equations;

$$[A] = \exp(-k_A t),$$

$$[B] = k_A[\exp(-k_A t)/(k_B - k_A) + \exp(-k_B t)/(k_A - k_B)],$$

$$[C] = k_A k_B\{\exp(-k_A t)/[(k_B - k_A)(k_C - k_A)] + \exp(-k_B t)/[(k_A - k_B)(k_C - k_B)] + \exp(-k_C t)/[(k_A - k_C)(k_B - k_C)],$$

$$[D] = k_A k_B k_C\{\exp(-k_A t)/[(k_B - k_A)(k_C - k_A)(k_D - k_A)] + \exp(-k_B t)/[(k_A - k_B)(k_C - k_B)(k_D - k_B)] + \exp(-k_C t)/[(k_A - k_C)(k_B - k_C)(k_D - k_C)] + \exp(-k_D t)/[(k_A - k_D)(k_B - k_D)(k_C - k_D)],$$

$$[E] = 1 - ([A] + [B] + [C] + [D]).$$

Since the present experimental data are not sufficient for an accurate determination of rate constants, we tentatively used the following values for the rate constants; k_A=3000, k_B=250, k_C=1400, and k_D=1000. The calculated curves for the fractional population vs. time are depicted in Fig. 5. The curves satisfactorily reproduce the decay of the 571 cm^{-1} band, the rise and decay of the 788 and 356 cm^{-1} bands and the rise and decay of the 450 cm^{-1} band. We note that the mixmum population of the 450 cm^{-1} species takes place at t=3.5 ms. If k_C were smaller than k_B (for example, k_C=200), the increase in D [the Fe(III)-OH species] became noticeably slower and did not reproduce the observed curves. Consequently, it is likely that the population of the ferryloxo intermediate during turnover cannot be very large. Direct reduction of the hydroperoxy intermediate to Fe(III)-OH without forming a higher energy intermediate, that is, the Fe(IV)=O heme, is also possible for the cytochrome oxidase active site where two reductive equivalents are readily available through Fe_a and Cu_A as has been suggested by Yoshikawa and Caughey.[27] It is quite interesting to point out that if our assignment is correct, the decay rate of the hydroperoxy intermediate is close to the rate of proton release.[35]

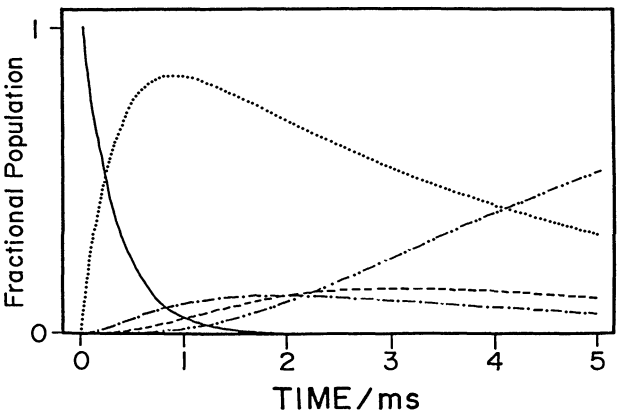

Fig. 5. Fractional population of the Fe(II)-O_2 (——), Fe(III) -O-O-H (·····), Fe(IV) =O (—·—), Fe(III) -OH (——), and the last Fe(III) compound (—··—). See text about the method of calculations, It is assumed that [Fe(II)-O_2] at time =0 is unity.

Previously Han et al.[36] reported the Fe(III)-OH stretching Raman band at 477 cm^{-1} for a compound produced under photoreduction of the resting enzyme in the presence of hexacyanoferrate(III). This compound, if correctly assigned, would be different from the Fe(III)-OH intermediate generated in the catalytic cycle. The present conclusion is consistent with another report by Han et al.[13] The iron-oxygen stretching frequency of the Fe(III)-OH compound of cytochrome oxidase is appreciably lower than those of aquametmyoglobin (490 cm^{-1}) and aquamethemoglobin (495 cm^{-1}).[37] In contrast, the iron-oxygen stretching frequency of the Fe(II)-O_2 complex of cytochrome oxidase (571 cm^{-1}) is noticeably close to those of oxymyoglobin (569 cm^{-1}) and oxyhemoglobin (567—572 cm^{-1}).[20,21] Based on these observations, it may be concluded that the distinguishing features of the cytochrome oxidase active site environment are most clearly reflected by their effects on the Fe(III)-OH stretching frequency.

The authors thank Dr. T. Egawa of IMS for his help in calculation of fractional population of intermediates and Professor Jim Kincaid of Marquett University for reading this manuscript. This study was partly supported by Grant-in-Aid for Encouragement of Young Scientists of the Ministry of Education, Science and Culture, to T. O. (02740250) and also Grant-in-Aid for Priority Areas (Bioinorganic Chemistry) to T. K. (03241105).

References

1) M. Wikstrom, K. Krab, and M. Saraste, in "Cytochrome Oxidase-A Synthesis," Academic Press, London (1981).
2) S. I. Chan and P. M. Li, *Biochemistry,* **29**, 1 (1990).
3) M. Wikstrom, *Proc. Natl. Acad. Sci. U.S.A.,* **78**, 4051 (1981).
4) Y. Orii, *Ann. N. Y. Acad. Sci.,* **550**, 105 (1988).
5) B. Chance, C. Saronio, and J. S. Leigh, Jr., *J. Biol. Chem.,* **250**, 9226 (1975).
6) G. M. Clore, L. E. Andreasson, B. Karlsson, R. Aasa, and B. G. Malmstrom, *Biochem. J.,* **185**, 139 (1980).
7) S. N. Witt and S. I. Chan, *J. Biol. Chem.,* **262**, 1446 (1987).
8) T. Ogura, S. Takahashi, K. Shinzawa-Itoh, S. Yoshikawa, and T. Kitagawa, *J. Am. Chem. Soc.,* **112**, 5630 (1990).
9) S. Han, Y. Ching, and D. L. Rousseau, *Proc. Natl. Acad. Sci. U.S.A.,* **87**, 2491 (1990).
10) C. Varotsis, W. H. Woodruff, and G. T. Babcock, *J. Am. Chem. Soc.,* **112**, 1297 (1990).
11) T. Ogura, S. Takahashi, K. Shinzawa-Itoh, S. Yoshikawa, and T. Kitagawa, *J. Biol. Chem.,* **265**, 14721 (1990).
12) C. Varotsis and G. T. Babcock, *Biochemistry,* **29**, 7357 (1990).
13) S. Han, C. Ching, and D. L. Rousseau, *Nature (London),* **348**, 89 (1990).
14) M. Wikstrom and G. T. Babcock, *Nature (London),* **348**, 16 (1990).
15) S. Yoshikawa, M. G. Choc, M. C. O' Toole, and W. S. Caughey, *J. Biol. Chem.,* **252**, 5498 (1977).
16) T. Ogura, S. Yoshikawa, and T. Kitagawa, *Biochemistry,* **28**, 8022 (1989).
17) T. Ogura, A. Maeda, M. Nakagawa, and T. Kitagawa, in "Primary Processes in Photobiology," ed by T. Kobayashi, Springer Proceedings in Physics, Vol. 20, pp. 233—241 (1987).
18) T. Ogura and T. Kitagawa, to be published.
19) H. E. Van Wart and J. Zimmer, *J. Biol. Chem.,* **260**, 8372 (1985).
20) H. Brunner, *Naturwissenshaften,* **61**, 129 (1974).
21) K. Nagai, T. Kitagawa, and H. Morimoto, *J. Mol. Biol.,* **136**, 271 (1980).
22) J. Terner, A. J. Sitter, and C. M. Reczek, *Biochim. Biophys. Acta,* **828**, 73 (1985).
23) S. Hashimoto, Y. Tatsuno, and T. Kitagawa, *Proc. Natl. Acad. Sci. U.S.A.,* **83**, 2417 (1986).
24) P. A. Giguere and T. K. K. Srinivasan, *J. Raman Spectrosc.,* **2**, 125 (1974).
25) A. K. Shiemke, T. M. Loehr, and J. Sanders-Loehr, *J. Am. Chem. Soc.,* **106**, 4951 (1984).
26) R. A. Reed, K. R. Rodgers, K. Kushmeider, T. G. Spiro, and Y. O. Su, *Inorg. Chem.,* **29**, 2881 (1990).
27) S. Yoshikawa and W. S. Caughey, *J. Biol. Chem.,* **265**, 7945 (1990).
28) K. Bajdor, H. Oshio, and K. Nakamoto, *J. Am. Chem. Soc.,* **106**, 7293 (1984).
29) N. T. Yu, E. A. Kerr, B. Ward, and C. K. Chang, *Biochemistry,* **22**, 4534 (1983).
30) M. Nagai, Y. Yoneyama, and T. Kitagawa, *Biochemistry,* **30**, 6495 (1991).
31) Y. Mizutani, S. Hashimoto, Y. Tatsuno, and T. Kitagawa, *J. Am. Chem. Soc.,* **112**, 6809 (1990).
32) Y. Orii, *Chem. Scr.,* **28A**, 63 (1988).
33) C. Kumar, A. Naqui, L. Powers, Y. Ching, and B. Chance, *J. Biol. Chem.,* **263**, 7159 (1988).
34) K. Tajima, M. Shigematsu, J. Jinno, K. Ishizu, and H. Ohya-Nishiguchi, *J. Chem. Soc., Chem. Commun.,* **1990**, 143.
35) M. Oliveberg, S. Hallen, and T. Nilsson, *Biochemistry,* **30**, 436 (1991).
36) S. Han, C. Ching, and D. L. Rousseau, *J. Biol. Chem.,* **264**, 6604 (1989).
37) S. A. Asher and T. M. Schuster, *Biochemistry,* **18**, 5377 (1979).

Chemical Analysis of Thortveitite from Oro, Mineyama-cho, Naka-gun, Kyoto Prefecture, Japan

Kazuhisa MORIYASU and Yasuharu NISHIKAWA*
Department of Chemistry, Faculty of Science and Technology, Kinki University, 3-4-1, Kowakae, Higashiosaka, Osaka, 577
(Received March 2, 1991)

The geochemically interesting rare mineral, thortveitite, from Oro, Kyoto Prefecture was studied. Major constituents, scandium, yttrium, and lanthanoids, niobium, tantalum, aluminum, titanium, iron, calcium, and manganese were determined. The chemical analysis of the mineral assemblage gave Sc_2O_3 18.20, Y_2O_3 0.72, Σ Ln_2O_3 1.70, FeO 0.97, MnO 0.54, Nb_2O_5 trace, Ta_2O_5 9.96, Al_2O_3 3.02, CaO 1.72, TiO_2 0.83, SiO_2 58.31, and H_2O 4.20; total 100.17%. This sample contained tantalite 11.47, anorthite 8.37, rutile 0.83, and quartz 37.91% in addition to thortveitite 37.40%. Scandium–tantalum substitution is suggested to occur similarly to yttrium–niobium substitution in earth acid minerals.

Thortveitite, a sorosilicate mineral which has scandium and yttrium-group rare earths as its major constituents, mainly occurs in the pegmatite layer of Norway and Madagascar.[1] The crystallographic and physical properties of thortveitite are as follows: monoclinic system; space group: $C2/m$; hardness on Mohs' scale: 6—7; specific gravity: 3.58.[2]

The distribution pattern of lanthanoid elements in thortveitite, by Goldschmidt and Thomassen,[3] has been reported to be extremely specific and selective (Goldschmidts' classification: thortveitite type), with a remarkably high content of ytterbium. Other constituents of this geochemically and mineralochemically very rare mineral type are alvite and yttrotitanite.

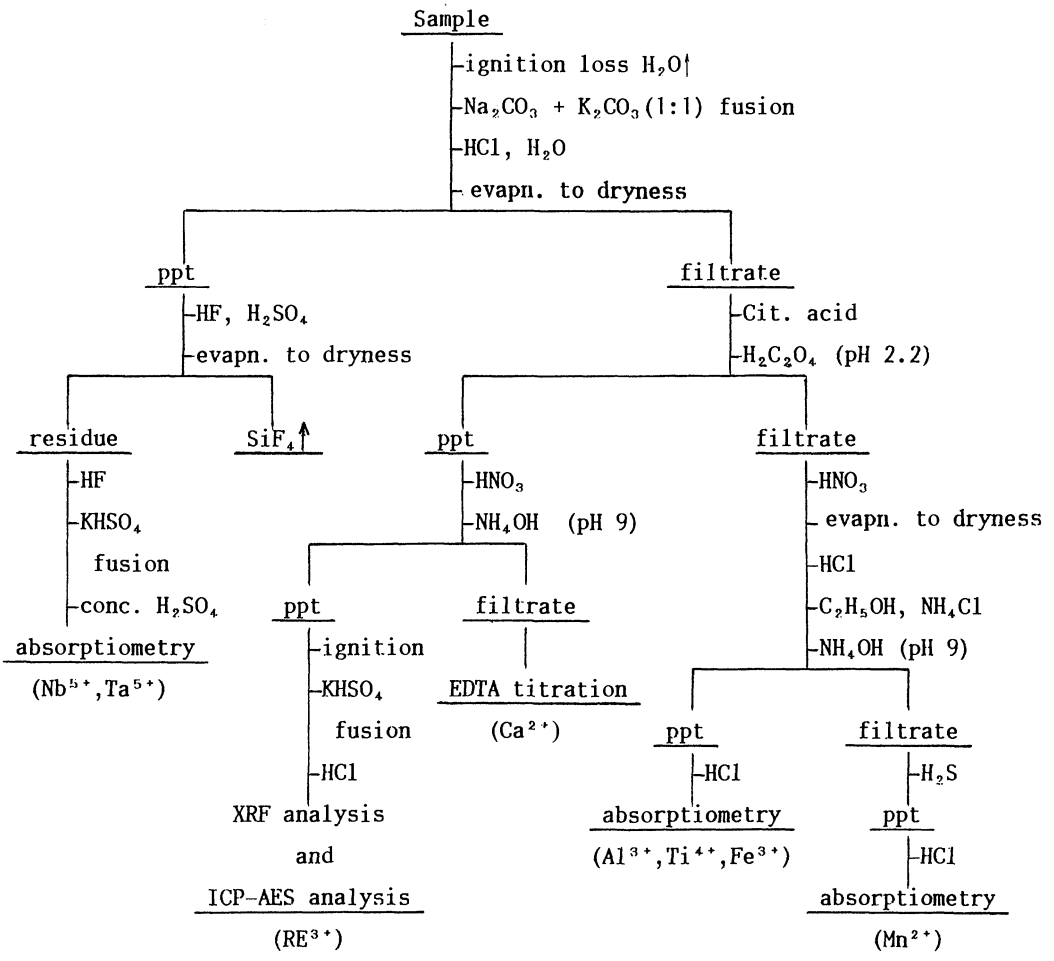

Scheme 1. Chemical analysis of thortveitite.

In Japan, thortveitite was first collected from the Shiroishi pegmatite zone at Kobe, Omiya-cho, Naka-gun, Kyoto Prefecture, analyzed and identified by Sakurai et al.[4] In Oro, Mineyama-cho, Naka-gun, Kyoto Prefecture, granites containing pegmatite are widely distributed, and some rare element minerals such as fergusonite, zircon (yamaguchilite) and yttrofluorite have been found.[5-7] There are two ore bodies, both of which consist of graphic, feldspar, and quartz zones.[8] The feldspar zone of the ore body A contained bastnaesite, zircon, and small amounts of ilmenite, monazite, and xenotime. The feldspar zone of the ore body B had biotite and magnetite containing fergusonite, zircon, and allanite.

The thortveitite examined here was collected from the ore body A of Oro and its identity was confirmed by Yamada et al. in 1980.[8] Emission spectrochemical analysis of thortveitite from the Shiroishi pegmatite zone at Kobe has been performed in detail by Nagashima et al.[4] and the detailed distribution of lanthanoid elements in the mineral has been reported. The present paper describes the results of chemical analysis, X-ray fluorescence analysis, and ICP analysis of lanthanoids in thortveitite from the ore body A, Oro, Mineyama-cho, Naka-gun, Kyoto Prefecture.

Experimental

In order to clarify the content of thortveitite as [$(Sc,Y,Ln)_2Si_2O_7$; Ln=lanthanoids] and the contents of other minerals found together with it in the ore body A, a total chemical analysis of the thortveitite sample was performed. The analytical procedure of the mineral sample is shown in Scheme 1. A portion (0.1086 g) of the powdered sample was taken in a platinum crucible, and fused with the fusing mixture $Na_2CO_3+K_2CO_3$. The melt was treated with hydrochloric acid and water. The insoluble matter was obtained by filtration, converted to oxides by ignition and weighed as the sum of silicic anhydride and earth acid metal oxides ($Nb_2O_5+Ta_2O_5$). The oxides were treated with hydrofluoric acid and sulfuric acid to remove SiO_2 as SiF_4. After the earth acid metal oxides had been fused with potassium hydrogensulfate, the melt was treated with concentrated sulfuric acid, and niobium(V), and tantalum(V) were determined by hydrogen peroxide-absorptiometry.[9] Ten milliliters of 1 mol dm^{-3} oxalic acid was added to the filtrate, and rare earth ions and calcium ion were precipitated as oxalates at pH 2.2. The precipitates were treated with 10 cm^3 of concentrated nitric acid and heated until the oxalic acid was completely decomposed. To separate calcium ion from lanthanoid ions, the pH of the solution was adjusted to 9.0 with aqueous ammonia and the lanthanoid ions were precipitated as hydroxides. Calcium ion was determined by the EDTA titration method. Lanthanoid hydroxides were converted to the oxides and fused with potassium hydrogensulfate, and, then, the trivalent ions were collected with hydroxyiminodiacetic acid (HIDA)–chelating resin. Scandium(III), and yttrium(III), and ytterbium(III) ions on the HIDA–chelating resin were determined by X-ray fluorometry (XRF analysis) as described in previous papers.[10,11] The trace amounts of other rare earth ions were determined by the ICP-AES method.[12] Aluminum, iron, and titanium ions were determined by 2-methyl-8-quinolinol[13] and 8-quinolinol[14] absorptiometry, and manganese ion was measured by potassium permanganate absorptiometry.[15]

Analytical Results and Discussion

(1) Total Analysis of Thortveitite: The results are summarized in Table 1. With the generally accepted composition of thortveitite, $(Sc,Y,Ln)_2Si_2O_7$, the four components of thortveitite amount to Sc_2O_3 18.20%, Y_2O_3 0.72%, ΣLn_2O_3 (Ln_2O_3 0.94%+Yb_2O_3 0.76%) and SiO_2 16.78% of the total oxide. The overall content of thortveitite in this mineral sample was, then, 37.40%.

The remainder of the constituents was assigned to several minerals expected to be present in the ore body A: FeO 0.97, MnO 0.54, Nb_2O_5 trace, Ta_2O_5 9.96% →tantalite [(Fe,Mn) $(Nb,Ta)_2O_6$: 11.47%]; Al_2O_3 3.02, CaO≒1.72, SiO_2 3.63%→anorthite [$CaAl_2Si_2O_8$: 8.37%]; TiO_2 0.83%→rutile [TiO_2: 0.83%]; quartz [SiO_2: 37.91%].

The present thortveitite sample was found to be a mixture of tantalite, anorthite, rutile, and quartz. It has been reported that the zirconium content in thortveitite often varies considerably (0.1—5% ZrO_2), and the HfO_2/ZrO_2 ratio is usually high (0.5—0.02).[4,16,17] However, no detectable amounts of zirconium and hafnium were present in the present sample.

(2) Distribution of Scandium, Yttrium, and Lanthanoid Elements: The content of each rare earth element was analyzed by XRF and ICP methods. The results are listed in Table 2 with the contents of other elements in thortveitite under the assumption that the present thortveitite has the composition of $(Sc,Y,Ln)_2Si_2O_7$.

Scandium in thortveitite from the ore body A, Oro,

Table 1. Analytical Results of Thortveitite from Oro, Mineyama-cho, Naka-gun, Kyoto Prefecture (Sample taken 0.10859 g)

	Content/%	Mineral assemblage
Sc_2O_3	18.20	
Y_2O_3	0.72	Thortveitite (sorosilicate)
Yb_2O_3	0.76	$(Sc, Y, Ln)_2Si_2O_7$
Ln_2O_3 (Excluding Yb)	0.94	37.40%
FeO	0.97	
MnO	0.54	Tantalite
Nb_2O_5	Trace	(Fe, Mn) $(Nb, Ta)_2O_6$
Ta_2O_5	9.96	11.47%
Al_2O_3	3.02	Anorthite (tectosilicate)
CaO	≒1.72	$CaAl_2Si_2O_8$ 8.37%
TiO_2	0.83	Rutile TiO_2 0.83%
SiO_2	58.31	Quartz SiO_2 37.91%
H_2O	4.20	
Total	100.17	

Table 2. Analytical Results of Thortveitite (Sc, Y, Ln)$_2$Si$_2$O$_7$ (Ln: Lanthanoids)

	Weight/mg	Content/%
Sc_2O_3	19.76	48.66
Y_2O_3	0.78	1.92
La_2O_3	0.01	0.02
Ce_2O_3	0.03	0.07
Pr_2O_3	0.06	0.15
Nd_2O_3	0.06	0.15
Sm_2O_3	0.05	0.12
Eu_2O_3	Trace	Trace
Gd_2O_3	0.06	0.15
Tb_2O_3	0.04	0.10
Dy_2O_3	0.16	0.39
Ho_2O_3	0.05	0.12
Er_2O_3	0.17	0.42
Tm_2O_3	0.08	0.20
Yb_2O_3	0.82	2.02
Lu_2O_3	0.27	0.66
SiO_2	18.21	44.84
Total	40.61	100.00

(La—Tb)$_2$O$_3$ 0.76%; [(La—Tb)$_2$O$_3$/Ln$_2$O$_3$=16.6%]
(Dy—Lu)$_2$O$_3$ 3.82%; [(Dy—Ln)$_2$O$_3$/Ln$_2$O$_3$=83.4%]

Table 3. Comparison of Analytical Results of Various Thortveitite Samples

	(1)	(2)	(3)	(4)
Sc_2O_3	43.63%	48.65%	37.36%	48.66%
Y_2O_3	9.22	0.75		1.92
$(HRE)_2O_3$			10.44	3.82
$(LRE)_2O_3$			1.65	0.76
SiO_2	47.15	50.60	50.55	44.84
Total	100.00	100.00	100.00	100.00

HRE: Heavy rarte earth
LRE: Light rare earth

(1) J. Schetelig: *Videnskapsselsk.-Skr.*, **1922**, No. 151.
(2) C. Boulanger, G. Urbain: *Compt. Rend.*, **174**, 1442 (1922).
(3) K. Kinoshita: "Kobutsu Shigen Jiten," Nippon Kobutsu Shumi no Kai, Kyoto (1965), p. 122.
(4) This work.

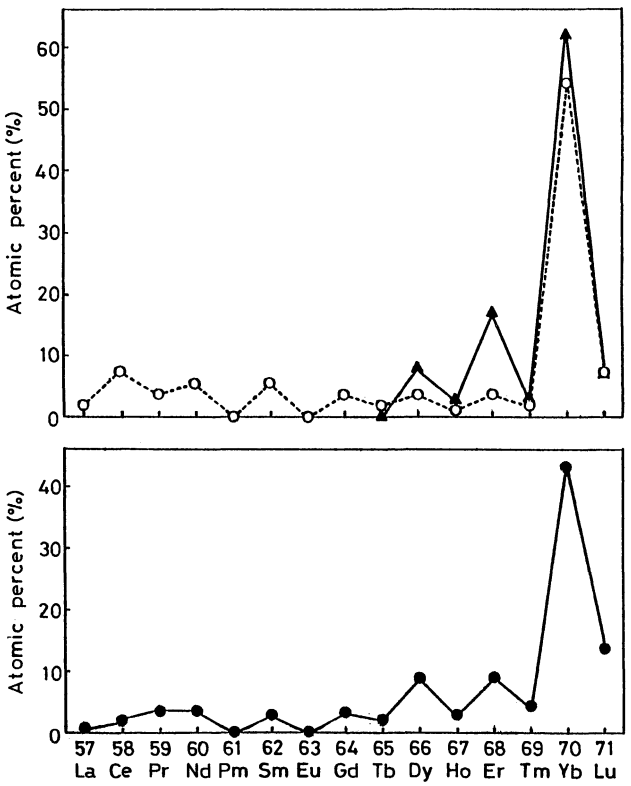

Fig. 1. Distribution of lanthanoid series elements.
---○---: Goldschmidt and Thomassen's thortveitite type (recalculated);
—▲—: Thortveitite from Kobe, Omiya-cho;
—●—: Thortveitite from Oro, Mineyama-cho (This work).

Mineyama-cho, was present in a notable amount; 48.66% as Sc_2O_3. Yttrium-group rare earths (Dy—Lu) were over 80% of the total lanthanoids.

The distribution pattern of lanthanoid elements in the thortveitite is illustrated in Fig. 1. Their amounts were compared with those of Goldschmidt.[3] and Sakurai et al.[4] for thortveitite. Although the aboundance of cerium (Z=58) and praseodymium (Z=59) are reversed, the present results on the distribution of lanthanoid elements generally conform to Oddo-Harkins' law. The ytterbium content is slightly less than that found in other studies. The abundance of an odd-numbered lutetium (Z=71) is found to be higher than those of the neighboring even-numbered dysprosium (Z=66) and erbium (Z=68). According to the Clarke number of these elements, there should be less lutetium than dysprosium and erbium.[18] But the present result may indicate that the mutual camouflage-substitution of the same valent metals in minerals is a more important factor. The camouflage-substitutions of these elements in minerals have been reported and attributed to the similarity in the ionic radius.[19] As the ionic radius of lutetium (0.99 Å) is close to that of ytterbium (1.00 Å) and scandium (0.83 Å), lutetium seems to be more selectively concentrated than other elements in thortveitite in which Yb and Sc are principal constituents.

The amount of yttrium in the present thortveitite is small, but as no detailed analytical data are available for yttrium and individual lanthanoids on thortveitite,[20–22] simple comparison of these elements with other thortveitite is difficult. The sum of yttrium oxide and heavy rare earth oxides in this thortveitite is less than that for other reported thortveitite samples as shown in Table 3.

As described in section (1), the authors have assumed that the thortveitite sample from the ore body A contains about 11% tantalite in which tantalum is more aboundant than niobium. In general, earth acid minerals such as fergusonite and columbite are constituted of large quantities of niobium and always contain yttrium as a sub-component.[5,23,24] However, the thortveitite sample analyzed in this work contains a large amount of

scandium and a little yttrium. Generally, tantalum (ionic radius: 0.64 Å) seems to be present in minerals with scandium, and niobium (0.64 Å) with yttrium. Scandium has a smaller ionic radius (0.83 Å) than yttrium (0.95 Å) and has a strong affinity for tantalum. It has been reported that Ta_2O_5 easily forms solid solutions with 2—4 mol% of Sc_2O_3 at high temperature,[25] and the crystal structure is stabilized by replacement of some Ta^{5+} by Sc^{3+}.

Financial support from the Ministry of Education, Science and Culture (Grant-in-Aid for Co-operative Research A 02303005), and Kinki University is gratefully acknowleged.

References

1) Y. Shibata, "Muki Kagaku Zensho IX-1," Maruzen Co., Tokyo (1948), p. 68.
2) W. J. Cruickshank, H. Lynton, and G. A. Barclay, *Acta Crystallogr.*, **15**, 491 (1962).
3) V. M. Goldschmidt and L. Thomassen, *Videnskapsselsk. Skr.*, [*Kl.*] *1*: *Mat.-Naturvidensk. Kl.*, No.5 (1924).
4) K. Sakurai, K. Nagashima, and A. Kato, *Bull. Chem. Soc. Jpn.*, **35**, 1776 (1962).
5) J. Takubo, *Nippon Kagaku Kaishi,* **59**, 1121 (1938).
6) T. Ogawa, *Warera no Kobutsu,* **10**, 428 (1941).
7) O. Nagashima and K. Nagashima, "Nippon Kigenso Kobutsu," Nippon Kobutsu Shumi no Kai, Kyoto (1960), p. 386.
8) S. Yamada, A. Okamoto, M. Takada, T. Fujiwara, and M. Takemura, *Chigaku Kenkyu,* **31**, 205 (1980).
9) F. C. Palilla, N. Adler, and C. F. Hiskey, *Anal. Chem.,* **25**, 926 (1953).
10) K. Moriyasu, H. Mizuta, and Y. Nishikawa, *Bunseki Kagaku,* **39**, 475 (1990).
11) K. Moriyasu, H. Mizuta, and Y. Nishikawa, *Bunseki Kagaku,* **40**, 175 (1991).
12) O. Fujino, K. Araki, Y. Kometani, M. Sugiyama, and M. Matsui, *Bunseki Kagaku,* **34**, 386 (1985).
13) K. Motojima, *Bull. Chem. Soc. Jpn.,* **29**, 455 (1956).
14) K. Motojima, *Bull. Chem. Soc. Jpn.,* **29**, 458 (1956).
15) "Muki Oyo-hishoku Bunseki 3," Kyoritsu Shuppan Co., Tokyo (1974), p. 286.
16) G. von Hevesy and V. Thal Jantzen, *Z. Anorg. Chem.,* **136**, 387 (1924).
17) M. Fleischer, *U. S. Geol. Surv., Bull.,* No. 1021 (1955).
18) "Kagaku Binran, Kiso-hen I," Maruzen Co., Tokyo (1966), p. 37.
19) O. Nagashima and K. Nagashima, "Nippon Kigenso Kobutsu," Nippon Kobutsu Shumi no Kai, Kyoto (1960), p. 15.
20) J. Schetelig, *Viedenskapsselsk.-Skr.,* **1922**, No. 1.
21) C. Boulanger and G. Urbain, *C. R.,* **174**, 1442 (1922).
22) K. Kinoshita, "Kobutsu Shigen Jiten," Nippon Kobutsu Shumi no Kai, Kyoto (1965), p. 122.
23) K. Kimura and H. Hamaguchi, *Nipoon Kagaku Kaishi,* **59**, 1124 (1938).
24) K. Kimura and K. Nagashima, *Nippon Kagaku Kaishi,* **72**, 53 (1951).
25) N. C. Stephenson and R. S. Roth, *J. Solid State Chem.,* **3**, 145 (1971).

Thermal Behavior of Alkaline-Earth Metal *cyclo*-Tetraphosphates

Hiroyuki NARIAI,* Itaru MOTOOKA, Yukio KANAJI,† and Mitsutomo TSUHAKO††
Department of Chemistry, Faculty of General Education, Kobe University, Tsurukabuto, Nada-ku, Kobe 657
†Department of Industrial Chemistry, Faculty of Engineering, Kobe University, Rokkodai-cho, Nada-ku, Kobe 657
††Kobe Women's College of Pharmacy, Kitamachi, Motoyama, Higashinada-ku, Kobe 658
(Received March 22, 1991)

The effect of water vapor on the thermal behavior of alkaline-earth metal *cyclo*-tetraphosphates, $M_2P_4O_{12}\cdot nH_2O$ (n=7.0, 3.5, 5.5, and 4.0 for M=Mg, Ca, Sr, and Ba, respectively) (P_{4m}) was examined using DTA-TG, X-ray diffraction analysis, isothermal heating in an electric furnace, and HPLC-FIA. The calcination reaction of each P_{4m} proceeded via ring opening of P_{4m} with elimination of water of crystallization, followed by condensation of soluble oligophosphates (P_{oligo}) to insoluble polyphosphates ($P_{high\ poly}$). The rates of these reactions were faster for Mg_2P_{4m} than for other metal *cyclo*-phosphates. The decomposition of P_{4m} was appreciably faster in humid air than in dry air, because of the availability of water for hydrolysis and for breaking the P–O–P linkage. However, the effect of water vapor from the atmosphere was not conspicuous, since the atmosphere contains enough water (theor. 20 mg L^{-1}) for the hydrolysis of P_{4m}. The products of calcination of $Ba_2P_{4m}\cdot 4H_2O$ were hardly influenced by water vapor from the atmosphere, because the water of crystallization was not easily released in the Ba system compared with the other metal salts.

As is well known, phosphates hydrolyze or condense on heating to yield different types of phosphates.[1–19] Most of the previous works dealt with linear phosphates. In recent papers,[20–23] we reported that water vapor remarkably affected the dehydration and condensation of various phosphates, and that the thermal behavior of *cyclo*-phosphates were significantly influenced by water vapor in the atmosphere, as well as by the rate and temperature range of heating, etc. In this study, the thermal dehydration and condensation reactions of alkaline-earth metal *cyclo*-tetraphosphates were investigated by means of DTA-TG, X-ray diffraction analysis, isothermal heating in an electric furnace, and high-performance liquid chromatography-flow injection analysis (HPLC-FIA).

Experimental

Chemicals. Guaranteed reagents of $Mg(NO_3)_2\cdot 6H_2O$, $Ca(NO_3)_2\cdot 4H_2O$, $Sr(NO_3)_2$, $Ba(NO_3)_2$, NaCl, NaOH, Na_2S, and P_2O_5 from Wako Chemical Industries, Ltd. were used. Unless otherwise stated, other chemicals were of guaranteed grade and were used without further purification.

Preparation Methods. Sodium *cyclo*-tetraphosphate tetrahydrate ($Na_4P_{4m}\cdot 4H_2O$) was prepared by methods given in the literature.[1]

Alkaline-earth metal *cyclo*-tetraphosphates, $M_2P_{4m}\cdot nH_2O$ (n=7.0, 3.5, 5.5, and 4.0 for M=Mg, Ca, Sr, and Ba, respectively) were prepared by the method similar to those described in the literatures.[8,20] Fifteen mmol of each metal nitrate was dissolved in 150 cm^3 of water, and this solution was mixed with 100 cm^3 (7.5 mmol) of a 0.075 mol dm^{-3} sodium *cyclo*-tetraphosphate aqueous solution. The precipitate was filtered off, washed with cold water, and air-dried.

Measurements. The sample solution for HPLC-FIA was prepared as follows. A 15-mg portion of a phosphate sample was dissolved in 20 cm^3 of a 0.1 mol dm^{-3} EDTA·2Na solution, and the solution was diluted to 100 cm^3 with distilled water. A 100-μL aliquot of this solution was used for HPLC-FIA. Unless otherwise noted, the analytical procedures and apparatus were essentially the same as those used in previous work.[20,21,24]

Results and Discussion

Thermal Decomposition by DTA-TG. $Ba_2P_4O_{12}\cdot 4H_2O$ $Ba_2P_{4m}\cdot 4H_2O$: Figure 1 shows the DTA-TG curves for $Ba_2P_4O_{12}\cdot 4H_2O$ at atmospheric pressure. Two endothermic peaks at 127 and 193 °C and two exothermic peaks at 222 and 487 °C were observed. A gradual lowering of the TG curve took place over a temperature range of 200 to 500 °C. A remarkable change in the DTA and TG curves was not observed above 500 °C. To clarify the reactions occurring near the endo- and exothermic peaks, the calcination products after the peaks were removed from the DTA-TG apparatus, cooled in a silica-gel desiccator, and subjected to further analysis. Figures 2 and 3 show the X-ray diffraction patterns and the liquid chromatograms of products, respectively, heated at several tempera-

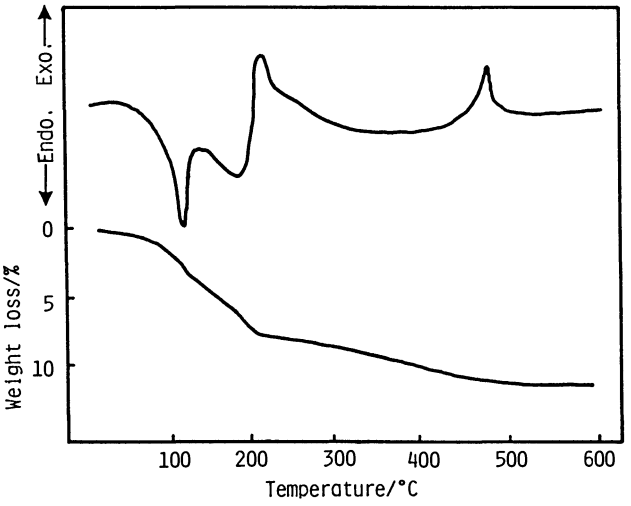

Fig. 1. DTA-TG curves for $Ba_2P_4O_{12}\cdot 4.0H_2O$.

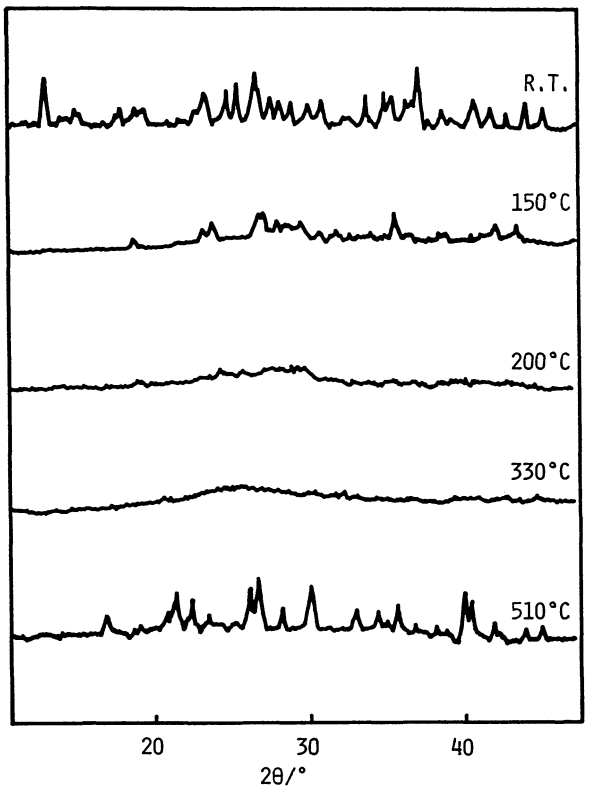

Fig. 2. X-Ray diffraction patterns of products by heating.
Sample: $Ba_2P_4O_{12}\cdot 4.0H_2O$. R. T., room temperature.

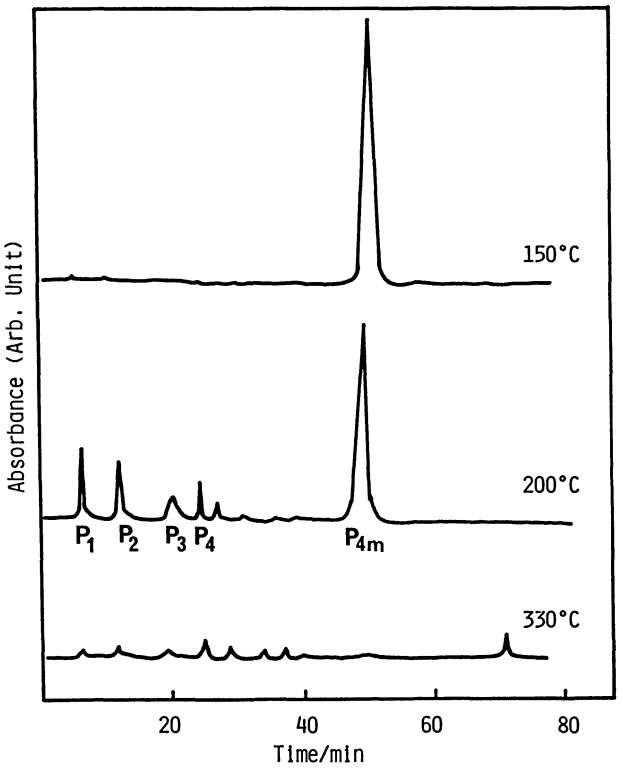

Fig. 3. Liquid chromatograms of products by heating.
Sample: $Ba_2P_4O_{12}\cdot 4.0H_2O$.

tures. In Fig. 2, the peak intensity of the anhydrous phase at 150 °C was gradually decreased with raising temperature and the product heated at 200 °C gave the X-ray difraction pattern of an amorphous phase. In view of the HPLC data at 150 °C, the P_{4m} ring structure was reserved. Therefore, the endothermic peak at 127 °C was assumed to reflect partial dehydration of the water of crystallization. The X-ray diffraction patterns of the products at a temperature range 193—330 °C were similar to that of an amorphous solid phase, as seen in Fig. 2. The HPLC trace shown in Fig. 3 suggests that decomposition of the P_{4m} ring to oligophosphates (P_{oligo}) such as ortho- (P_1), pyro- (P_2), tri- (P_3), and tetraphosphate (P_4) and the condensation of P_{oligo} to soluble polyphosphates (P_{poly}, P_5—P_{20}) occurred in the amorphous solid phase. No peak was seen in HPLC trace for product heated at 510 °C, because an insoluble polyphosphate ($P_{high\ poly}$) newly formed at this temperature. The thermal product at 510 °C showed an X-ray diffraction pattern characteristic of $Ba(PO_3)_2$. It seems that crystal growth was too slow to give one particular X-ray diffraction pattern, since under dynamic conditions the consecutive transformations of phosphates did not reach their equilibrium state, so that the X-ray diffraction pattern reflected an amorphous phase.

$Sr_2P_4O_{12}\cdot 5.5H_2O$ $Sr_2P_{4m}\cdot 5.5H_2O$: Figure 4 shows the DTA-TG curves for $Sr_2P_4O_{12}\cdot 5.5H_2O$ at atmospheric pressure. Two large endothermic peaks at about 120 and 160 °C accompanied by a weight loss are apparently due to elimination of the water of crystallization. A gradual lowering of the TG curve is noted over a temperature range of 200—400 °C. The calcinated samples were prepared in a similar manner to the barium salt and subjected to further analysis. The results of HPLC and X-ray diffraction analysis are

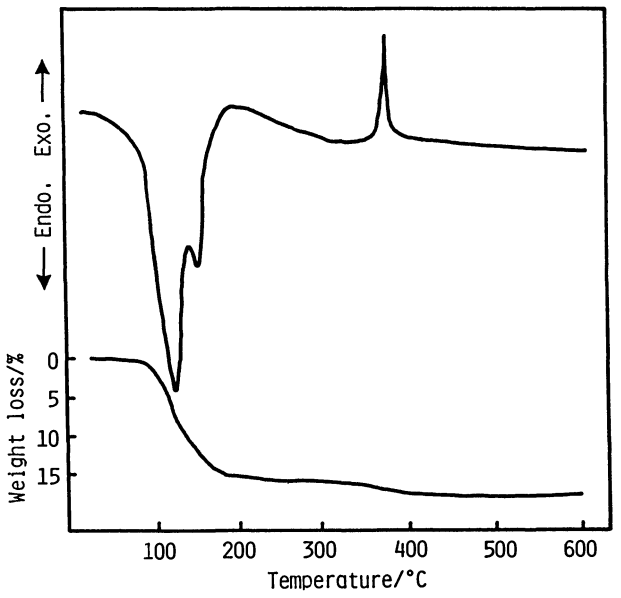

Fig. 4. DTA-TG curves for $Sr_2P_4O_{12}\cdot 5.5H_2O$.

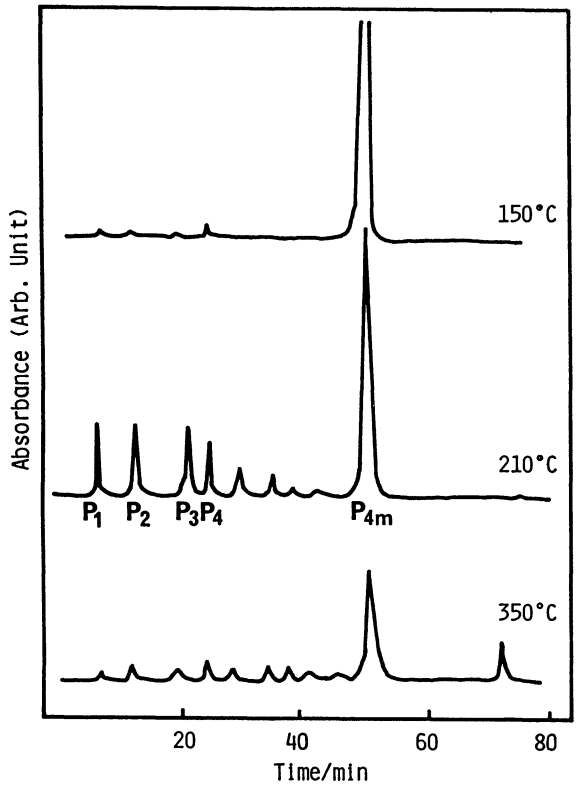

Fig. 5. Liquid chromatograms of products by heating.
Sample: $Sr_2P_4O_{12} \cdot 5.5H_2O$.

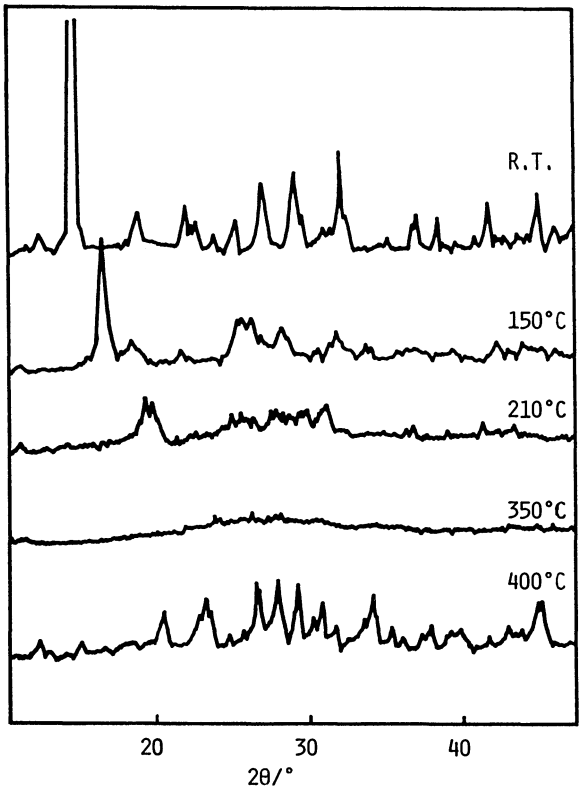

Fig. 6. X-Ray diffraction patterns of products by heating.
Sample: $Sr_2P_4O_{12} \cdot 5.5H_2O$.

shown in Figs. 5 and 6. According to the HPLC trace at 150 °C shown in Fig. 5, more than 90% of P_{4m} remained at this temperature, and the decomposition of P_{4m} to P_{oligo} was less than 10%. As seen in Fig. 6, the X-ray diffraction lines of the thermal products at temperatures from 210 to 350 °C gradually decreased by a rise in temperature and finally changed to an amorphous phase. HPLC results indicate that the decomposition of P_{4m} and the condensation of P_{oligo} to P_{poly} took place continuously. The sample heated at 400 °C did not

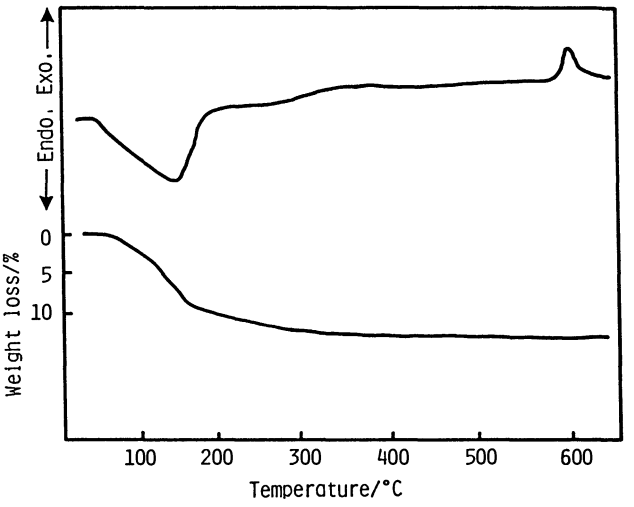

Fig. 7. DTA-TG curves for $Ca_2P_4O_{12} \cdot 3.5H_2O$.

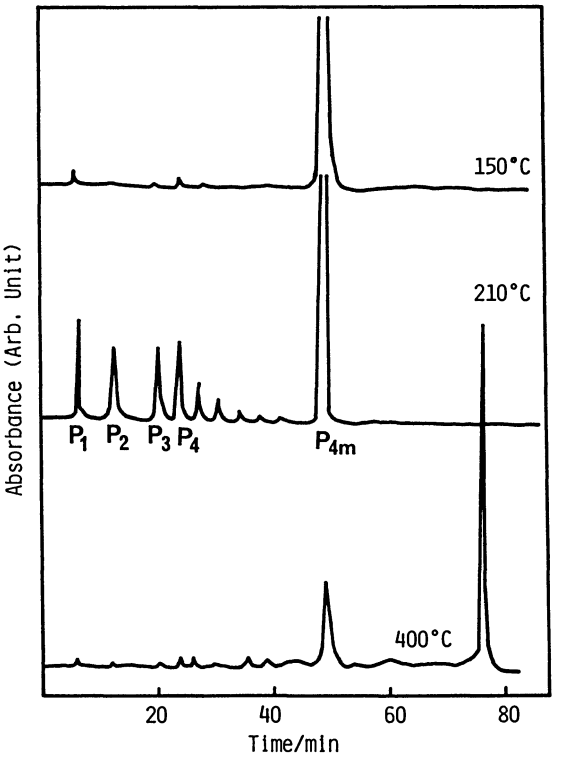

Fig. 8. Liquid chromatograms of products by heating.
Sample: $Ca_2P_4O_{12} \cdot 3.5H_2O$.

dissolve by the EDTA treatment. It seems that insoluble polyphosphates ($P_{high\ poly}$) were newly formed through dehydration and condensation reactions. The thermal product at 400 °C showed a characteristic X-ray diffraction pattern in agreement with that of $Sr(PO_3)_2$. Accordingly, the exothermic peak at 390 °C should reflect the crystallization of $Sr(PO_3)_2$.

$Ca_2P_4O_{12}\cdot 3.5H_2O$ $Ca_2P_{4m}\cdot 3.5H_2O$: Figure 7 shows the DTA-TG curves for $Ca_2P_4O_{12}\cdot 3.5H_2O$ at atmospheric pressure. The samples were prepared as described above and subjected to further analysis. The results are shown in Figs. 8 and 9. The large endothermic peak at 150 °C accompanying a weight loss may be due mainly to the release of the water of crystallization. The TG curve was gradually lowered over a temperature range of 150—350 °C. According to the HPLC data at 150 °C shown in Fig. 8, P_{4m} remained almost in an anhydride state. At 210 °C, a significant amount of P_{4m} decomposed to P_{oligo} and further condensed to P_{poly}. The sample heated at 650 °C did not dissolve by the EDTA treatment. It seems that large amounts of insoluble polyphosphates ($P_{high\ poly}$) were formed through the dehydration and condensation reactions. The X-ray diffraction patterns of products heated at 650 °C (Fig. 9) agreed with that of $Ca(PO_3)_2$. Therefore, the exothermic peak at 589 °C reflects the crystallization of $Ca(PO_3)_2$.

$Mg_2P_4O_{12}\cdot 7.0H_2O$ $Mg_2P_{4m}\cdot 7.0H_2O$: Figure 10 shows the DTA-TG curves for $Mg_2P_4O_{12}\cdot 7.0H_2O$ at atmospheric pressure. Two large endothermic peaks at 95 and 155 °C accompanying a weight loss seemed to be mainly caused by elimination of the water of crystallization. A gradual lowering of the TG curve took place over a temperature range of 200—450 °C. According to the HPLC result at 230 °C shown in Fig. 11, large

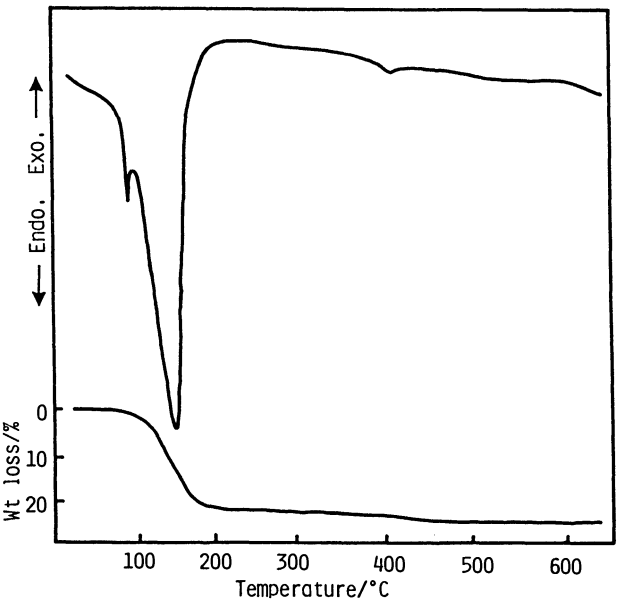

Fig. 10. DTA-TG curves for $Mg_2P_4O_{12}\cdot 7.0H_2O$.

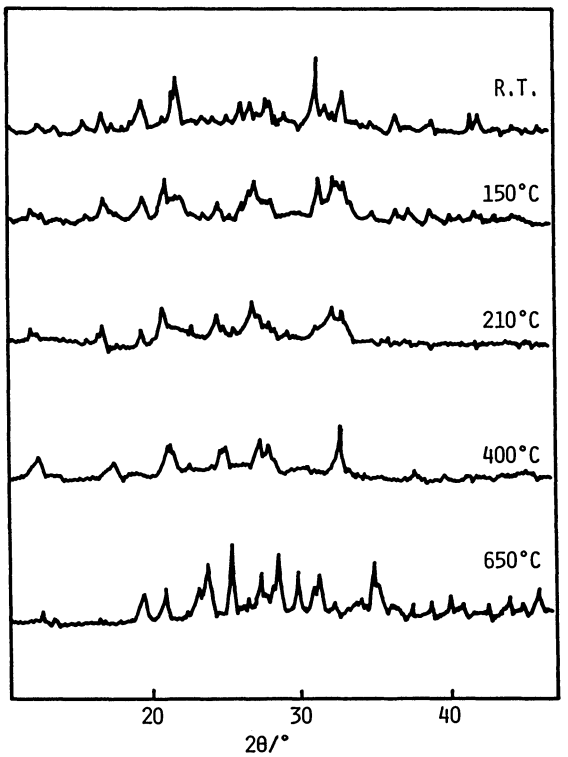

Fig. 9. X-Ray diffraction patterns of products by heating.
Sample: $Ca_2P_4O_{12}\cdot 3.5H_2O$.

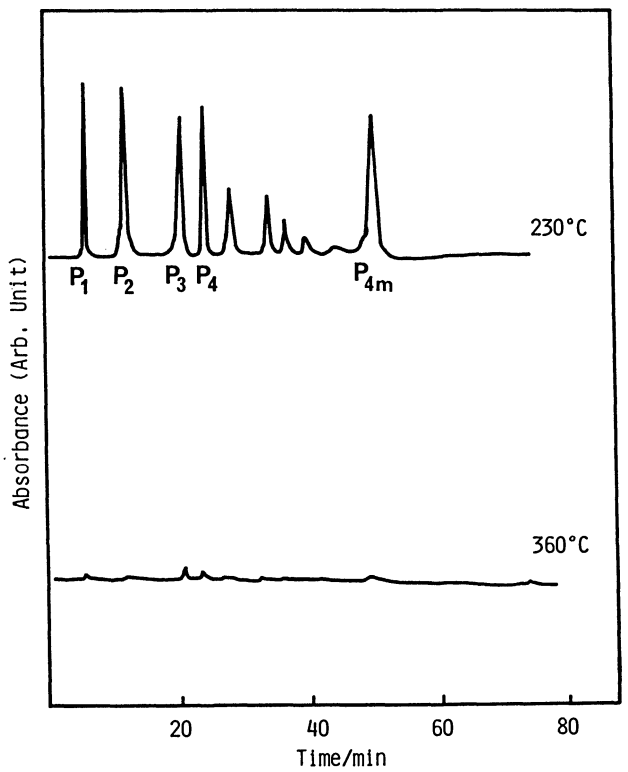

Fig. 11. Liquid chromatograms of products by heating.
Sample: $Mg_2P_4O_{12}\cdot 7.0H_2O$.

amounts of P_{4m} already decomposed to P_{oligo}. It is obvious that around this temperature the dehydration and decomposition of P_{4m} and the condensation of decomposed products of P_{4m} to P_{poly} are taking place during calcination. It is a characteristic feature of the Mg system that decomposition of P_{4m} proceeded faster than other three systems at a similar temperature. At 360 °C, no definite peaks were observed in HPLC. Therefore, it is clear that a large amount of polyphosphates ($P_{high\ poly}$) was formed through the dehydration and condensation, because the product heated at this temperature did not dissolve by the EDTA treatment. As seen in Fig. 12, the thermal products heated at 360 °C newly exhibited definite diffraction lines and they gradually increased with a rise in temperature. The X-ray diffraction lines coincided in position with those of $Mg(PO_3)_2$.

Isothermal Change. In view of the above-mentioned results, the thermal transformation of alkaline-earth metal *cyclo*-tetraphosphates, $M_2P_4O_{12}\cdot nH_2O$ (n=7.0, 3.5, 5.5, and 4.0 for M=Mg, Ca, Sr, and Ba, respectively), proceeded via dehydration, decomposition, and condensation. These reactions took place continuously, and did not reach equilibrium instantly. To examine the influence of water vapor on the thermal decomposition of $M_2P_4O_{12}\cdot nH_2O$, their isothermal decompositions were carried out in dry and humid air at various temperatures. Each $M_2P_4O_{12}\cdot nH_2O$ was heated at 200 °C for 30 min. The relationships between the amounts of various phosphates formed and the amounts of water vapor are shown in Figs. 13 through 16. P% denotes the percentage of phosphorus atoms present in these phosphate anions. The influence of the amount of water vapor on the products was not remarkable in a 20—110 mg L^{-1} range of water vapor. It is probable that there is enough water (theor. 20 mg L^{-1}) in the atmosphere for the hydrolysis of P_{4m}. However, a characteristic change was noted between the dry and the humid air. In dry air, the hydrolysis of P_{4m} was

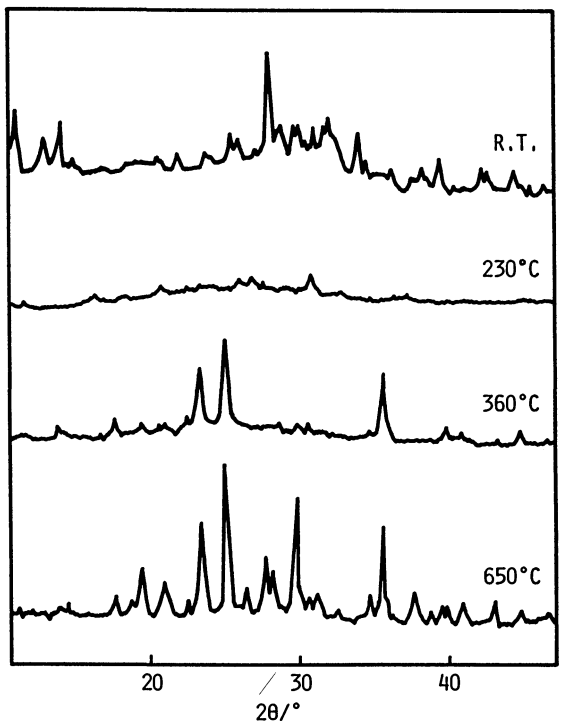

Fig. 12. X-Ray diffraction patterns of products by heating.
Sample: $Mg_2P_4O_{12}\cdot 7.0H_2O$.

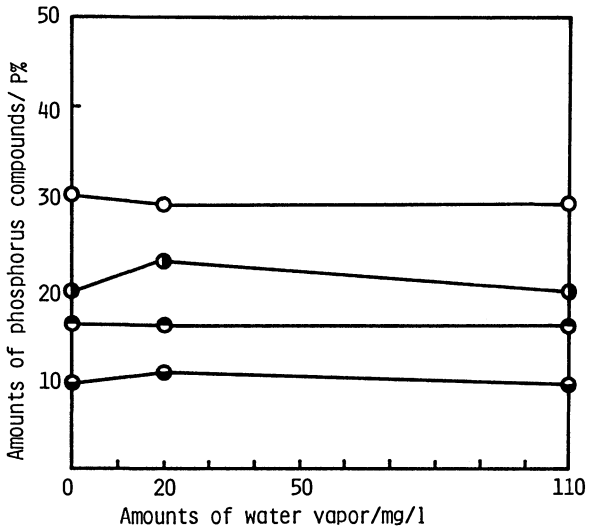

Fig. 13. Relationships between the amounts of phosphates and water vapor for the sample heated at 200 °C for 30 min.
Sample: $Ba_2P_4O_{12}\cdot 4.0H_2O$. ○: P_{4m}, ◒: P_1, ◑: P_2, ◓: P_3.
P % denotes the percentage of phosphorus atoms present in these phosphate anions.

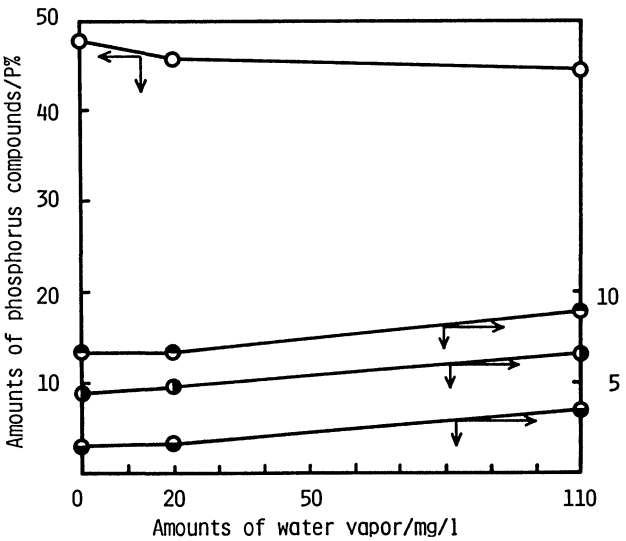

Fig. 14. Relationships between the amounts of phosphates and water vapor for the sample heated at 200 °C for 30 min.
Sample: $Sr_2P_4O_{12}\cdot 5.5H_2O$. ○: P_{4m}, ◒: P_1, ◑: P_2, ◓: P_3.

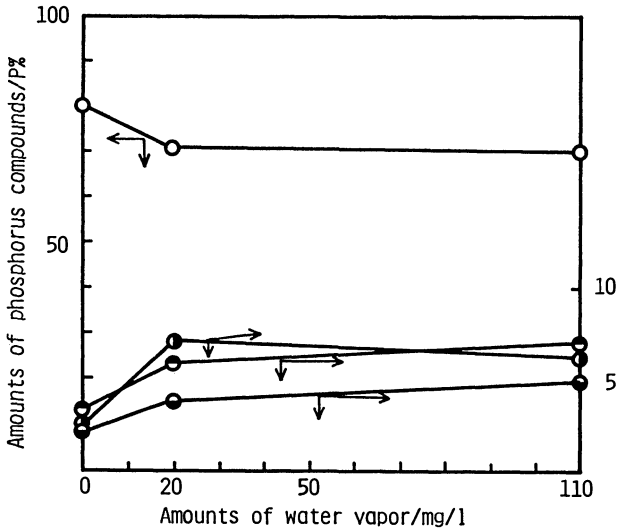

Fig. 15. Relationships between the amounts of phosphates and water vapor for the sample heated at 200 °C for 30 min.
Sample: $Ca_2P_4O_{12}\cdot 3.5\ H_2O$. ○: P_{4m}, ◒: P_1, ◑: P_2, ◓: P_3.

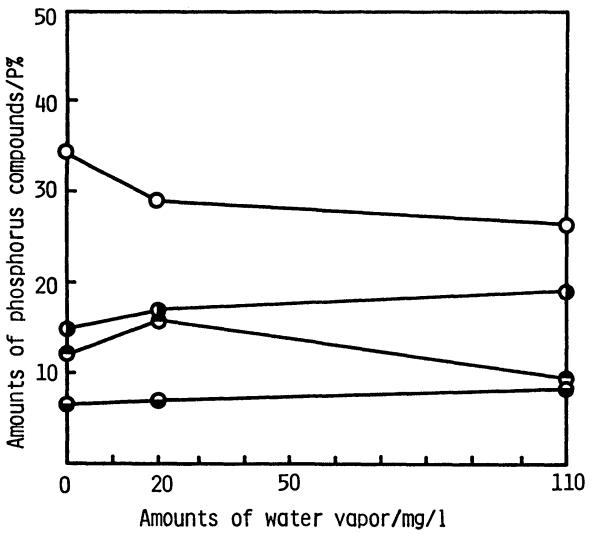

Fig. 16. Relationships between the amounts of phosphates and water vapor for the sample heated at 200 °C for 30 min.
Sample: $Mg_2P_4O_{12}\cdot 7.0H_2O$. ○: P_{4m}, ◒: P_1, ◑: P_2, ◓: P_3.

depressed, since there was not enough water necessary for hydrolysis and for breaking the P–O–P linkage. In the Ba system shown in Fig. 1, release of the water of crystallization took place at a higher temperature than in other three systems, so that the effect of water from the atmosphere was hardly discernible. According to the present results, the thermal decomposition and condensation processes may be formulated as follows:

$$M_2P_4O_{12}\cdot nH_2O \longrightarrow M_2P_4O_{12} \quad (1)$$
(M: Ba, Sr, Ca, Mg)

$$M_2P_4O_{12} \longrightarrow P_{oligo} \quad (2)$$
$$P_{oligo} \longrightarrow P_{poly} \quad (3)$$
$$P_{poly} \longrightarrow P_{high\ poly} \quad (4)$$

The thermal reactions in the first stage proceed continuously according to Processes (1) and (2), followed by Processes (3) and (4) simultaneously. The decomposition of $M_2P_4O_{12}\cdot nH_2O$ to P_{oligo} proceeds faster in humid air than in dry air. In this work, pure anhydrides could not be obtained by heating or freeze-drying of the hydrates of *cyclo*-tetraphosphates.

The authors wish to thank Mr. Seiji Fukami for his helpful work.

References

1) R. N. Bell, L. F. Audrieth, and O. F. Hill, *Ind. Eng. Chem.*, **44**, 568 (1952).
2) J. R. Van Wazer and E. Karl-Kroupa, *J. Am. Chem. Soc.*, **78**, 1772 (1956).
3) J. F. McCullough, J. R. Van Wazer, and E. J. Griffith, *J. Am. Chem. Soc.*, **78**, 4528 (1956).
4) R. P. Langguth, R. K. Osterheld, and E. Karl-Kroupa, *J. Phys. Chem.*, **60**, 1335 (1956).
5) E. Thilo and I. Grunze, *Z. Anorg. Allg. Chem.*, **290**, 209 (1957).
6) E. Thilo, *Adv. Inorg. Chem. Radiochem.*, **4**, 1 (1962).
7) E. Thilo and U. Schülke, *Z. Anorg. Allg. Chem.*, **341**, 293 (1965).
8) U. Schülke, *Z. Anorg. Allg. Chem.*, **360**, 231 (1968).
9) M. Watanabe, S. Sato, and H. Saito, *Bull. Chem. Soc. Jpn.*, **48**, 896 (1975).
10) A. V. Lavrov, T. A. Bykanova, and N. N. Chudinova, *Izv. Akad. Nauk SSSR, Neorg. Mater.*, **13**, 334 (1977).
11) A. Boudjada and A. Durif, *J. Appl. Crystallogr.*, **12**, 609 (1979).
12) M. Watanabe, M. Matsuura, and T. Yamada, *Bull. Chem. Soc. Jpn.*, **54**, 738 (1981).
13) E. V. Lazarevski, *Izv. Akad. Nauk SSSR, Neorg. Mater.*, **18** 1550 (1982).
14) E. D. Dzyuba, V. V. Pechkovskii, G. I. Salonets, V. I. Kovalishina, N. A. Ivkovich, and A. V. Chubarov, *Russ. J. Inorg. Chem.*, **27**, 1095 (1982).
15) M. Trojan and D. Brandova, *Thermochim. Acta*, **88**, 415 (1985).
16) D. Brandova, *Thermochim. Acta*, **92**, 49 (1985).
17) D. Brandova and M. Trojan, *J. Therm. Anal.*, **30**, 159 (1985).
18) M. Trojan, D. Brandova, and Z. Solc, *Thermochim. Acta*, **110**, 343 (1987).
19) M. Watanabe, K. Murata, and M. Maeda, *Bull. Chem. Soc. Jpn.*, **61**, 3877 (1988).
20) H. Nariai, I. Motooka, Y. Kanaji, and M. Tsuhako, *Bull. Chem. Soc. Jpn.*, **60**, 1337 (1987).
21) H. Nariai, I. Motooka, and M. Tsuhako, *Bull. Chem. Soc. Jpn.*, **61**, 2811 (1988).
22) A. Takenaka, I. Motooka, and H. Nariai, *Bull. Chem. Soc. Jpn.*, **62**, 2819 (1989).
23) A. Takenaka, H. Kobayashi, K. Tsuchie, I. Motooka, and H. Nariai, *Bull. Chem. Soc. Jpn.*, **62**, 3808 (1989).
24) G. Kura, *Bull. Chem. Soc. Jpn.*, **56**, 3769 (1983).

The Synthesis and Thermal Reorganization of Lithium Heptasodium *cyclo*-Octaphosphate

Makoto WATANABE,* Tomohiko HONDA, and Shinsaku FURUTA
Department of Industrial Chemistry, Chubu University, Matsumoto-cho, Kasugai, Aichi 487
(Received March 25, 1991)

Lithium heptasodium *cyclo*-octaphosphate hexahydrate, $LiNa_7P_8O_{24} \cdot 6H_2O$, has been prepared by heating lead *cyclo*-tetraphosphate tetrahydrate at 340 °C for 20 min, dissolving the thermal product in a 3% aqueous solution of tetrasodium ethylenediaminetetraacetate, and then crystallizing by the addition of lithium chloride and methanol to the solution. When the *cyclo*-octaphosphate was heated above 180 °C, it decomposed to produce phosphates with chain lenghts shorter and longer than that of the *cyclo*-octaphosphate. The thermally produced phosphates were reorganized to sodium *cyclo*-triphosphate and a small amount of insoluble polyphosphates by heating at about 300 to 350 °C. The phosphates melted at about 620 °C.

Among the many kinds of polyphosphates, di-, tri-, tetra-, penta-, *cyclo*-tri-, *cyclo*-tetra, *cyclo*-penta, *cyclo*-hexa-, *cyclo*-octa, and long-chain polyphosphates have been prepared and isolated. Polyphosphates have been used for agricultural treatment, detergents, food additives, chemical manufacturing, the ceramics industry, etc.[1—3] A dry process has usually been used for the preparation of oligo- and polyphosphates. The dry process is not favorable for the preparation of unstable polyphosphates and other techniques have been developed for making phosphates.[4] Although the synthesis of *cyclo*-octaphosphate has been reported by Schülke,[5] it has been found by the present authors that the method does not give the highest yield for the preparation of *cyclo*-octaphosphate. A modified process to make *cyclo*-octaphosphate and a thermal reorganization of the *cyclo*-phosphate were studied in the present work.

Experimental

Preparation of *cyclo*-Octaphosphate. Sodium *cyclo*-tetraphosphate tetrahydrate was made by hydrolyzing α-P_2O_5 in water cooled with ice to below 15 °C, and then adding sodium chloride to the solution. This method was modified from the original, which was proposed by Bell et al.[6] Lead *cyclo*-tetraphosphate tetrahydrate was prepared by dissolving the sodium *cyclo*-tetraphosphate in water and adding an aqueous lead nitride solution to the *cyclo*-phosphate solution. According to Schülke, sodium *cyclo*-octaphosphate hexahydrate can be obtained by heating the lead *cyclo*-tetraphosphate at 150 °C for 2 h, at 300 to 350 °C for less than 30 min, dissolving the thermal product in water together with sodium sulfide, and then adding ethanol into the resulting solution. The present authors found that the thermal product obtained with the heating process by Schülke contained only about 20 P% of *cyclo*-octaphosphate and that it was necessary to study the effects of heating temperature, heating time, and atmospheric moisture on the phosphate composition of the thermal product. It was also required to improve the wet process in order to purify the *cyclo*-octaphosphate from the thermal product.

Chemical Analysis. An atomic-absorption analysis was used for the determination of sodium and lithium ions in a sample solution by using a Shimadzu atomic-absorption spectrophotometer (AA-680). Phosphorus was determined by the Molybdenum Blue method. The water of crystallization was determined by the heating loss.

High-Performance Liquid Chromatography (HPLC). An HPLC technique was employed for the separation and determination of the phosphate species in a sample solution.[7] Aqueous 0.24, 0.40, and 0.60 mol dm^{-3} solutions of potassium chloride were used as eluents at a flow rate of 1 cm^3 min^{-1}.

^{31}P NMR Measurement. ^{31}P NMR spectrum of an aqueous phosphate solution was taken by a JNM-GX270 instrument. Phosphoric acid (85%) was used as a reference with downfield positive shifts.

X-Ray Diffractometry (XRD). An X-ray diffraction diagram of a powder sample was measured with nickel-filtered Cu $K\alpha$ radiation by using a Rigaku X-ray diffractometer (RAD-1B).

Thermogravimetry (TG) and Differential Thermal Analysis (DTA). TG-DTA measurements were carried out in air using a Rigaku TG-DTA apparatus with a heating rate of 5 °C min^{-1}.

Table 1. Composition of Polyphosphates in the Thermal Products Heated at 300, 340, 360, 400, and 460 °C for 20 min

Heating temp/°C	Phosphates/P%			
	Lowpoly[a]	*cyclo*-Tetra	*cyclo*-Octa	Highpoly[b]
300	17.8	7.1	73.6	1.5
340	14.5	—	79.8	9.3
360	11.6	—	81.6	6.9
400	10.4	—	84.5	5.1
460	14.9	—	24.2	60.9

a) Polyphosphates with chain lengths shorter than that of pentaphosphate. b) Polyphosphates with chain lengths longer than that of tetraphosphate.

Results and Discussion

Heating Temperature, Heating Time, and Humidity. Lead *cyclo*-tetraphosphate tetrahydrate was heated at a temperature between 300 and 460 °C for 20 min in dry air. The dry air was prepared by passing air through glass tubes containing silica gel and phosphorus pentaoxide. The phosphate composition of the thermal product is listed in Table 1. The results show that a suitable temperature range for the formation of lead *cyclo*-octaphosphate lies between 340 and 400 °C, and that the *cyclo*-octaphosphate content is about 80 P%.

Table 2. Composition of Polyphosphates in the Thermal Products Heated at 340 °C

Heating time/min	Phosphates/P%			
	Lowpoly[a)]	*cyclo*-Tetra	*cyclo*-Octa	Highpoly[b)]
5	39.7	36.4	23.3	0.7
10	14.5	0.2	80.9	4.5
20	10.5	—	79.8	9.3
30	9.6	—	77.7	12.7

a) Polyphosphates with chain lengths shorter than that of pentaphosphate. b) Polyphosphates with chain lenghts longer than that of tetraphosphate.

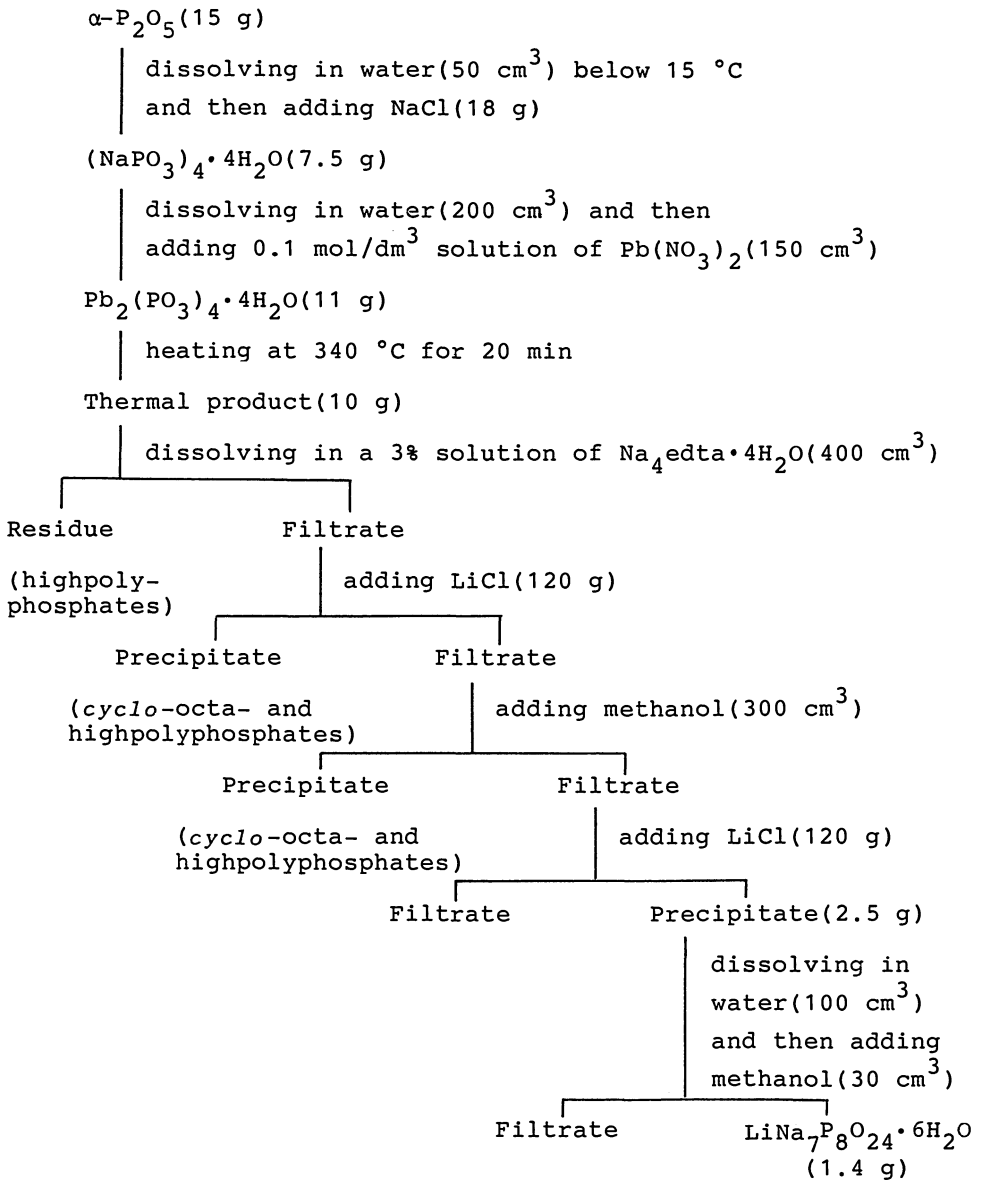

Fig. 1. Synthetic process of *cyclo*-octaphosphate.

At a lower temperature, the content of polyphosphates with shorter chain lengths increased. The content of polyphosphates with longer chain lengths increased at a higher temperature. Schülke described in his paper that the lead *cyclo*-tetraphosphate was preheated at 150 °C for 2 h, but there was not any need to heat the lead *cyclo*-tetraphosphate at that temperature. The dependence on the heating time for the phosphate composition of the thermal product at 340 °C is shown in Table 2. A heating time of 10 to 20 min seemed to be appropriate. In the case of preparation in air without drying, the content of highpolyphosphates increased at temperatures between 300 and 460 °C.

Purification of the *cyclo*-Octaphosphate. According to Schülke, the thermal product produced by heating the lead *cyclo*-tetraphosphate at between 300 and 350 °C dissolved in water. The thermal product obtained by heating the lead *cyclo*-tetraphosphate at 340 °C in this study dissolved only slightly in water and was soluble in an aqueous solution of ethylenediaminetetraacetate. The thermal product (10 g) was dissolved in 400 cm^3 of an aqueous 3% tetrasodium ethylenediaminetetraacetate tetrahydrate($Na_4edta \cdot 4H_2O$) solution, and a residue (highpolyphosphates) was filtered off. Lithium chloride (120 g) was added to the filtrate and a white precipitate (*cyclo*-octa- and highpolyphosphates) was removed by filtration. Methanol (300 cm^3) was added to the filtrate and a precipitate was filtered off. Lithium chloride (120 g) was put in the filtrate, resulting in a white precipitate (2.5 g), which was then dissolved in 100 cm^3 of water; methanol (30 cm^3) was added to the solution. About 1.4 g of a white precipitate was filtered off, washed with methanol, and dried in an air bath at 50 °C. This process is shown in Fig. 1. Found: P, 28.7; Na, 18.1; Li, 0.6; H_2O, 11.5%. Calcd for $LiNa_7P_8O_{24} \cdot 6H_2O$: P, 27.3; Na, 17.7; Li, 0.8; H_2O, 11.9%. The ^{31}P NMR spectrum of the product showed only one peak due to a middle PO_4 group at −21.5 ppm. This result indicates that the product is cyclic phosphate. The HPLC peaks of the product and several known phosphates (ortho-, di-, tri-, *cyclo*-tri-, *cyclo*-tetra-, and *cyclo*-hexaphosphates) are shown in Fig. 2. The position of the HPLC peak of the product was in accord with that of *cyclo*-octaphosphate, as shown in another paper.[8] According to these results, it was concluded that the product was lithium heptasodium *cyclo*-octaphosphate hexahydrate, $LiNa_7P_8O_{24} \cdot 6H_2O$. X-Ray diffraction data of the product are presented in Table 3, together with those of lithium *cyclo*-octaphosphate hexahydrate (JCPDS card, No. 28-0577). The *cyclo*-octaphosphate was stable at room temperature (15 to 30 °C) and had low solubility to water (about 1.9 at 20 °C).

Table 3. X-Ray Diffraction Data of *cyclo*-Octaphosphates

$LiNa_7P_8O_{24} \cdot 6H_2O$ (this study)		$(LiPO_3)_8 \cdot 6H_2O$ (JCPDS 28-0577)	
d(Å)	I/I_0	d(Å)	I/I_0
8.450	44	9.259	75
8.261	36	8.403	75
5.427	45	7.692	25
5.310	74	6.993	100
5.211	28	5.291	100
4.833	30	4.902	25
4.444	23	4.505	100
4.211	85	3.546	25
4.122	26	3.484	25
3.917	40	3.425	75
3.847	35	3.289	50
3.821	25	3.185	25
3.511	41	3.115	50
3.385	25		
3.240	67		
3.204	63		
2.983	48		
2.932	77		
2.855	35		
2.843	57		
2.804	43		
2.769	100		
2.710	79		
2.665	33		
2.455	37		
1.645	26		

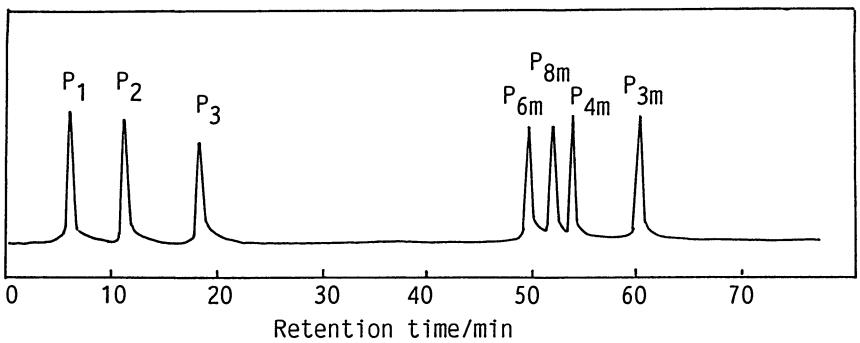

Fig. 2. HPLC profiles of polyphosphates.
P_1: Orthophosphate, P_2: diphosphate, P_3: triphosphate, P_{3m}: *cyclo*-triphosphate, P_{4m}: *cyclo*-tetraphosphate, P_{6m}: *cyclo*-hexaphosphate, P_{8m}: *cyclo*-octaphosphate (product obtained in this study).

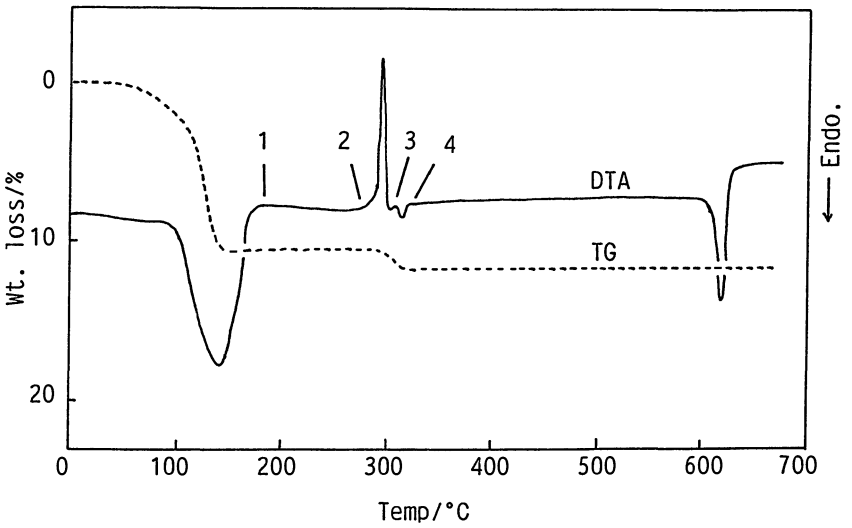

Fig. 3. TG and DTA curves of $LiNa_7P_8O_{24}\cdot 6H_2O$.

Table 4. Composition of the Thermal Products

Thermal product	Temp/°C	Wt. loss/%	XRD	Phosphates/P%						
				Ortho	Di	Tri	*cyclo*-Tri	*cyclo*-Hexa	*cyclo*-Octa	Higher
1	180	10.2	AM[a)]	1.4	3.9	4.1	—	4.4	60.0	26.2
2	270	10.4	AM	1.0	2.1	2.6	12.4	3.8	30.7	47.4
3	310	10.4	$(NaPO_3)_3$	2.7	10.1	3.6	62.5	—	10.4	10.7
4	340	11.5	$(NaPO_3)_3$	0.4	1.0	0.8	93.3	—	2.5	2.0

a) AM stands for amorphous substance.

TG and DTA Measurements. TG and DTA curves of lithium heptasodium *cyclo*-octaphosphate hexahydrate are shown in Fig. 3. The thermal products (as numbered in Fig. 3) were removed from a furnace and subjected to further analysis in order to study thermal reactions within the temperature ranges. The chemical compositions of the thermal products are listed in Table 4. The first large endotherm accompanying a large weight loss seemed to be due to an elimination of the water of crystallization. The result in Table 4 shows that the decomposition of the *cyclo*-octaphosphate to phosphates with chain lengths longer and shorter than that of *cyclo*-octaphosphate occurs at the same time. The following thermal reactions can be written for the endothermic process:

$$(MPO_3)_8\cdot 8H_2O \longrightarrow (MPO_3)_8\cdot(8-x)H_2O \quad (0<x\leqslant 8) \tag{1}$$

$$(MPO_3)_8 + H_2O \longrightarrow M_8H_2P_8O_{25} \quad \text{(octaphosphate)} \tag{2}$$

$$(MPO_3)_8 + 2H_2O \longrightarrow \begin{cases} MH_2PO_4 + M_7H_2P_7O_{22} \quad \text{(ortho- and heptaphosphates)} & (3) \\ M_2H_2P_2O_7 + M_6H_2P_6O_{19} \quad \text{(di- and hexaphosphates)} & (4) \\ M_3H_2P_3O_{10} + M_5H_2P_5O_{16} \quad \text{(tri- and pentaphosphates)} & (5) \\ 2M_4H_2P_4O_{13} \quad \text{(tetraphosphate)} & (6) \end{cases}$$

$$(MPO_3)_8 \longrightarrow 4/3(MPO_3)_6 \quad \text{(}cyclo\text{-hexaphosphate)} \tag{7}$$

$$n(MPO_3)_8 \longrightarrow 8(MPO_3)_n. \quad \text{(highpolyphosphates)} \tag{8}$$

Here, M stands for sodium and/or lithium. Since the content of highpolyphosphates with chain lengths longer than that of octaphosphate was high at this step, thermal reaction 8 seemed to be preferencial. According to the successive heatings to 270 °C, the content of the highpolyphosphates increased even more. Reaction 8 was also considered to be preferable to the other degradations through heating. Thermal products 1 and 2 were X-ray diffractometrically amorphous. After a large exothermic change at about 300 °C, the *cyclo*-triphosphate content increased. The following reorganization can be responsible for the change:

$$(MPO_3)_n \longrightarrow n/3(MPO_3)_3. \tag{9}$$

A small endothermic peak accompanying a small amount of weight loss was observed at about 330 °C. Thermal product 4 gave 93.3 P% of *cyclo*-triphosphate content and all other phosphate contents decreased through the heating. Therefore, reaction 9 progressed at this step, along with a small heating loss which may have been caused by the following condensation of the phosphates with hydrogen to *cyclo*-triphosphate:

$$M_nH_2P_nO_{3n+1} \longrightarrow n/3(MPO_3)_3 + H_2O. \tag{10}$$

Thermal products 3 and 4 gave an X-ray diffraction diagram of sodium *cyclo*-triphosphate in accord with the phosphate composition given in Table 4. Since no other X-ray diffraction peaks were observed, phosphates containing lithium may be amorphous.

References

1) J. R. Van Wazer, "Phosphorus and Its Compounds," Interscience Publishers Inc., New York (1961), Vol. II.
2) D. E. C. Corbridge, "Phosphorus," Elsevier, Amsterdam-Oxford-New York (1980).
3) T. Kanazawa, "Inorganic Phosphate Materials," Elsevier, Amsterdam-Oxford-New York-Tokyo (1989).
4) M. Watanabe, *Phosphorus Lett.*, **1989**, 3.
5) U. Schülke, *Z. Anorg. Allg. Chem.*, **360**, 231 (1968).
6) R. N. Bell, L. F. Audrieth, and O. F. Hill, *Ind. Eng. Chem.*, **44**, 568 (1952).
7) N. Yoza, Y. Sagara, H. Morioka, T. Handa, H. Hirano, Y. Baba, and S. Ohashi, *J. Flow Injection Anal.*, **3**, 37 (1986).
8) G. Kura, T. Hiraki, F. Takashiro, and H. Waki, presented at the 6th Symposium of Inorganic Phosphorus Chemistry, Hiroshima (Japan), October 1987.

Preparation and Crystal Structure of a New Barium Niobium Sulfide, $Ba_9Nb_4S_{21}$

Masanobu SAEKI* and Mitsuko ONODA
National Institute for Research in Inorganic Materials, 1-1, Namiki, Tsukuba, Ibaraki 305
(Received April 11, 1991)

A new barium niobium sulfide, $Ba_9Nb_4S_{21}$, was prepared by the reaction of CS_2 with a mixture of $BaCO_3$ and Nb_2O_5. Powder X-ray diffraction peaks and electron diffraction spots for the compound were indexable on the basis of a hexagonal cell with lattice parameters of a=6.9743(6) and c=21.599(2) Å. Refinement based on powder X-ray diffraction data suggested that the crystal structure belongs to the same series with those of $Ba_{16.5}Nb_9S_{42}$ and Ba_2NbS_5 reported by Swinnea et al.[1,2]

Three compounds, $BaNbS_3$, $Ba_{16.5}Nb_9S_{42}$, and Ba_2NbS_5 have been reported in the Ba–Nb–S system. $BaNbS_3$ is isostructural with $BaNiO_3$. According to Donohue,[3] this compound has a composition of $BaNb_{0.8}S_3$ with niobium vacancies, and the Nb atom has a formal charge of +5.

The existence of $Ba_{16.5}Nb_9S_{42}$ and Ba_2NbS_5 was reported by Swinnea.[1,2] The structures of these compounds will be described later in this paper.

In the Ba–Ta–S system, six compounds are reported as listed in Table 1. (In what follows these compounds are designated **a**, **b**, **c**, **d**, **e**, and **f**, for brevity). In the Ba–Nb–S system, types **b**, **d**, and **e** ($BaNbS_3$, $Ba_{16.5}Nb_9S_{42}$, and Ba_2NbS_5) have been found so far but types **a**, **c**, and **f** have not been reported yet. From the analogy of the chemical properties of tantalum and niobium, it is suggested that there is a possibility for the existence of those types of compounds in the Ba–Nb–S system. For this reason, the preparation of new barium niobium sulfides were attempted with the result that types **a** and **f** existed but type **c** was not found. This paper aims to report the preparation and crystal structure of type **f**, $Ba_9Nb_4S_{21}$, which has been unknown until now. The compound of type **a**, the structure of which has not yet been determined, will be described elsewhere.

Experimental

Preparation. The starting materials, $BaCO_3$ (purity 99%) and Nb_2O_5 (99.9%), were mixed in a ratio of Ba/(Ba+Nb)= 0.703. The mixture was placed in a furnace and kept at 750 °C for 3 d in an atmosphere of CS_2 carried by N_2 gas. After cooling to room temperature, the specimen was sealed in an evacuated silica tube with sulfur (1.4 wt%) and kept at 900 °C for 18 h. It was quenched in water.

Chemical Analysis. Chemical analysis was performed for Ba and Nb. The details are as follows. To determine Nb and Ba contents, about 1 g of the specimen was dissolved in 0.8 equiv HCl. Hydrogen sulfide gas was evolved as the specimen dissolved. Ba was dissolved in the solution while Nb remained as solid. The resulting precipitate consisting of the Nb-compound was separated from the solution by filtration, and was then ignited in air at 1000 °C to produce Nb_2O_5. The Nb content was obtained from the weight of Nb_2O_5.

The Ba ion in the solution was precipitated as $BaSO_4$ by adding 1 equiv H_2SO_4. The $BaSO_4$ was separated from the solution and weighed to obtain the Ba content.

The sulfur content was determined from the weight of the specimen and analytical values of Ba and Nb.

Diffraction Data. Powder X-ray diffraction data were collected with a step-scan procedure on a Rigaku RAD-2B-type diffractometer using counter-side monochromatized Cu $K\alpha$ radiation. Measurements were performed from 2θ=5° to 100° with an interval of 0.02°. It took 35 seconds to measure one point. Electron diffraction patterns were taken for crushed particles using a 100 kV electron microscope (Hitachi 500-type).

Density. The density of specimen was obtained by measuring buoyancy in carbon tetrachloride. About 0.5 g of the specimen with fine particles was placed in a bottle, the volume of which was about 2 ml, and the weight of which was 1.5 g.

Table 1. Compounds in the Ba–Ta–S System

Type	**a**	**b**	**c**	**d**	**e**	**f**
Formula	$BaTa_2S_5$	$BaTaS_3$	$Ba_3Ta_2S_8$	$Ba_{16.5}Ta_9S_{39}$	Ba_2TaS_5	$Ba_9Ta_4S_{20}$
Crystal system	H	H	M	R	H	H
Lattice const. (Å)	a= 3.33 c=25.2	a=6.85 c=5.74	a=12.6 b= 6.85 c=11.9 β=108.9°	a= 6.88 c=41.8 (Hexagonal axis)	a= 6.93 c=49.4	a= 6.96 c=21.6
Electric property	Me	S	I	I	I	I
Ref.	4	3,5	6	7	8	9

H: Hexagonal, M: Monoclinic, R: Rhombohedral, Me: Metallic, S: Semiconductor, I: Insulator.

The bottle and the specimen in carbon tetrachloride were kept at reduced pressure to remove the bubbles attached on the specimen and on the surface of the bottle. The buoyancy was obtained by measuring weights in air and in carbon tetrachloride at 25±0.1 °C.

Results

The specimen obtained was of a pure single phase, and the powder X-ray diffraction pattern did not correspond to any known barium niobium sulfides. But the diffraction pattern was very close to that of type **f** in the Ba–Ta–S system, ($Ba_9Ta_4S_{20}$), with different peak intensities. This suggests that the type **f** compound also exists in the Ba–Nb–S system.

The spots of the electron diffraction patterns were indexed on the basis of a hexagonal cell.[10] The lattice parameters were calculated from the distances between two appropriate spots, resulting in a=7 Å and c=22 Å.

In the powder X ray diffraction patterns,[10] all the peaks that were detected were indexable on the basis of a hexagonal cell with lattice parameters a=6.9743(6) and c=21.599(2) Å. These values are in excellent agreement with those from the electron diffraction.

Table 2. Chemical Composition

Element	Ba/wt%	Nb/wt%	S/wt%
Experimental	54.1, 54.6, 54.6, 54.7, 54.7	15.7, 15.7, 15.8, 15.8, 15.5	
Average	54.5	15.7	29.8
Calcd for $Ba_9Nb_4S_{21}$	54.2	16.3	29.5

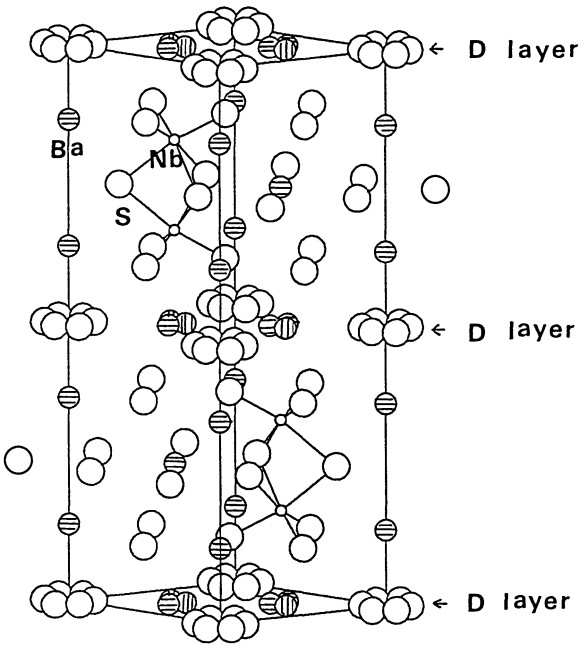

Fig. 1. Crystal structure of $Ba_9Nb_4S_{21}$.
(Niobium atoms are indicated by the small circles, barium atoms by hatched circles, and sulfur atoms by large circles.)

The results of chemical analysis of the compound are presented in Table 2. They agree with the calculated values of $Ba_9Nb_4S_{21}$ within experimental error. From the results, the compound is represented as $Ba_9Nb_4S_{21}$.

Observed densities were 4.25, 4.26 and 4.26 (g cm^{-3}), compared with the calculated one (4.16 g cm^{-3}, Z=1, V=910 Å). The specimen is an insulator, brown black in color, and generates H_2S gas by the reaction with water.

Discussion

We attempted to determine the crystal strucrure of the product ($Ba_9Nb_4S_{21}$) by refinement based on the powder X-ray diffraction pattern, which was similar to those of types **d** ($Ba_{16.5}Nb_9S_{42}$) and **e** (Ba_2NbS_5). This suggests that these three compounds belong to the same structure series.

The structures of types **d** and **e** reported by Swinnea and coworkers[1,2] are based on the stacking of BaS_3 layers in the sequence DABABDBCBCDCACA for type **d** ($Ba_{16.5}Nb_9S_{42}$) and CBDBABDBCBCDCACDCB for type **e** (Ba_2NbS_5), where the A, B, and C layers are hexagonal BaS_3 layers with Ba at (0,0,z), (2/3,1/3,z), and (1/3,2/3,z), respectively, and the D layer is a Ba-rich disordered layer in which Ba and S sites are partly occupied. The Nb atoms occupy interstices between A and B, B and C, and C and A layers, but there is no Nb atom between D and A, D, and B, and D and C layers. The structures are described in space group $R\bar{3}m$ for **d** ($Ba_{16.5}Nb_9S_{42}$) and $P6_3/mmc$ for **e** (Ba_2NbS_5).

It is assumed that the structure of $Ba_9Nb_4S_{21}$ belongs to the same series with types **d** and **e**. The structure, therefore, should have the same rule with those in stacking sequence. In addition, from the unit cell value in the c direction, it is found that 8 layers are contained in a unit cell. The chemical composition reveals that two of them are the D-layers. This information leads us to a single possible structure for $Ba_9Nb_4S_{21}$ shown in Fig. 1.

The structure refinement of the compound was attempted using a total pattern fit program RIETAN[11] based on the Rietveld method.[12] The refinement was performed for the powder X-ray diffraction pattern of $Ba_9Nb_4S_{21}$ based on the structure model given in Fig. 1, and performed for regions from d=4.4 to d=1.0 Å with 9 positional parameters, one overall temperature factor and one scaling factor. The diffraction peaks with d-values larger than 4.4 Å were ignored because it was impossible to obtain accurate intensities experimentally. The calculated pattern without the correction for the preferred orientation was in agreement with that observed (R_{wp}=16.0%, R_p=12.5%, R_I=9.1%, R_F=7.3%). See Ref. 13 for the definitions of the reliability factors R_{wp}, R_p, R_I, and R_F. Tables 3 and 4 give final values of the structure parameters and the interatomic distances.

Table 3. Crystal Data and Atomic Parameters for $Ba_9Nb_4S_{21}$

Crystal data (Hexagonal, space group $P6_3/mmc$ (No. 194)) a=6.9743(6) Å, c=21.599(2) Å, V=910 Å^3, Z=1 (According to the formula $Ba_9Nb_4S_{21}$)

Atomic parameters

Atom	Occupation	x	y	z
Nb	1.0	1/3	2/3	0.1686(8)
Ba(1)	1.0	0	0	0.1363(6)
Ba(2)	1.0	1/3	2/3	3/4
Ba(3)	0.25	0.367(2)	2x	−0.0070(6)
S(1)	1.0	0.494(3)	2x	0.120(1)
S(2)	1.0	0.159(4)	2x	1/4
S(3)	0.25	0.078(5)	2x	0.002(8)

B(Nb)=B(Ba)=B(S)=3.4(2) Å^2.

Table 4. Selected Interatomic Distances (Å) in $Ba_9Nb_4S_{21}$[a)]

Nb–S1	3×2.21(4)	S1–Nb	3×2.21(4)
–S2	3×2.75(4)	–Ba1	6×3.51(4)
Ba1–S1	6×3.51(4)	–Ba2	6×3.49(4)
–S2	3×3.12(3)	–Ba3	[1]×3.02(4)
–S3	[3]×3.08(18)	–Ba3	[2]×3.39(4)
–S3	[3]×3.10(18)	–Ba3	[1]×3.07(4)
Ba2–S1	6×3.51(4)	–Ba3	[2]×3.46(4)
–S2	6×3.49(3)		

a) Distances between Ba3 and S3 are omitted because their sites are statistically occupied.

The diffraction profile observed was compared with the calculated one.[10] The intensities calculated on the atomic parameter were compared with the integrated intensities obtained from the pattern.[10]

The structure is based on the stacking of the D- and BaS_3-layers with a sequence DABADACA. Ba and S atoms are distributed statistically at the respective sites in the D-layer. The Nb atoms occupy interstices between A and B, B and C, and C and A layers, but there is no Nb atom between D and A, D and B, and D and C layers. The structure is described in the space group $P6_3/mmc$ (No. 194) with the atomic positions given in Table 3.

$Ba_9Ta_4S_{20}$,[9] the structure of which has not yet been reported, is probably isostructural with this compound. (The refinement with the same structure model on the powder X-ray diffraction pattern of $Ba_9Ta_4S_{20}$ gave R_{wp}=12.7%, R_p=9.6%, R_I=10.8%, and R_F=6.6%).

The sulfur content in type **f** has different values in the Ba–Nb–S and Ba–Ta–S system, i.e., $Ba_9Nb_4S_{21}$ and $Ba_9Nb_4S_{20}$. They probably contain an identical amount of sulfur. The difference came from the experimental error.

From the results described above, it is concluded that there exists a previously unreported barium niobium sulfide, the chemical composition of which is $Ba_9Nb_4S_{21}$, and the refinement on the powder X-ray diffraction pattern supported the structure which belongs to the same series with the other compounds in the Ba–Nb–S system.

The authors wish to thank Dr. F. Izumi of our institute for giving us permission to use his computer program.

References

1) I. S. Swinnea, H. Steinfink, L. E. Rendon-Diazmiron, and M. Comezdaza, *J. Solid State Chem.*, **46**, 367 (1983).
2) I. S. Swinnea, H. Steinfink, L. E. Rendon-Diazmiron, and L. Banos-Lopez, *J. Solid State Chem.*, **56**, 249 (1985).
3) P. C. Donohue and J. F. Weiher, *J. Solid State Chem.*, **10**, 142 (1974).
4) M. Saeki, H. Nozaki, and M. Onoda, *Mater. Res. Bull.*, **24**, 851 (1989).
5) R. A. Gardner, M. Vlasse, and A. Wold, *Inorg. Chem.*, **8**, 2784 (1969).
6) M. Onoda and M. Saeki, *Mater. Res. Bull.*, **24**, 625 (1989).
7) M. Saeki and M. Onoda, *Mater. Res. Bull.*, **24**, 1491 (1989).
8) M. Saeki and M. Onoda, *Mater. Res. Bull.*, **25**, 723 (1990).
9) M. Saeki and M. Onoda, *Mater. Res. Bull.*, **24**, 41 (1989).
10) Electron diffraction patterns, powder X-ray diffraction profile, and d-spacing and intensities have been deposited as Documeny No. 8960 at the Office of the Editor of Bull. Chem. Soc. Jpn.
11) F. Izumi, *J. Crystallogr. Soc. Jpn.*, **27**, 23 (1985) (in Japanese).
12) H. M. Rietveld, *J. Appl. Crystallogr*, **2**, 65 (1969).
13) M. Saeki, Y. Yajima, and M. Onoda, *J. Solid State Chem.*, **92**, 286 (1991).

A Hydrogen Insertion Compound of Molybdenum Oxide Hydrate, $H_{0.12-0.22}MoO_3 \cdot H_2O$, and Its Formation Process from Hydrogen Molybdenum Bronze, H_xMoO_3

Kazuo EDA* and Noriyuki SOTANI
College of Liberal Arts, Kobe University, Tsurukabuto, Nada, Kobe 657
(Received April 19, 1991)

Based on XRD and chemical analysis results, the hydrogen insertion compound of molybdenum oxide hydrate (H-hydrate) was suggested to be a genotypic compound of yellow molybdenum trioxide monohydrate, $MoO_3 \cdot H_2O$. H-hydrate was obtained in a hot HCl solution and in hot water from hydrogen molybdenum bronze, H_xMoO_3. The hydrogen bronze with $x \leqslant 0.24$ and the molybdenum species formed in the solution played a role in the formation of H-hydrate. In this process, a temporary dissolution of Mo^{5+} was observed at the beginning of the formation.

Many molybdenum oxide hydrates or a similar class of materials have been known.[1] In a previous study[2] we reported on the formation of a compound identical with or similar to $Mo_8O_{15}(OH)_{16}$[3,4] by treating a hydrogen molybdenum bronze, H_xMoO_3 ($0.23<x<0.40$), with aqueous HCl at 353 K. We regarded it as a hydrogen insertion compound of molybdenum oxide hydrate (H-hydrate), or a hydrate of a hydrogen insertion of molybdenum oxide, which could be expressed as $H_{0.15}MoO_3 \cdot 0.88H_2O$. However, we could not decide whether the compound was identical with $Mo_8O_{15}(OH)_{16}$ or not. $Mo_8O_{15}(OH)_{16}$ was discovered by Glemser and Lutz.[3] These authors obtained it by heating a mixture of yellow $MoO_3 \cdot 2H_2O$ and Mo without air at 383 K. In a series of studies they also obtained $Mo_4O_{10}(OH)_2$ and $Mo_2O_4(OH)_2$ by reducing MoO_3 with Zn/HCl or $SnCl_2$ and by heating a mixture of MoO_3, Mo, and H_2O without air at 383 K.[3] (Although these compounds are formulated as fixed compositions for convenience, they are nonstoichiometric compounds with a rather wide range of homogeneity.) With respect to $Mo_4O_{10}(OH)_2$ and $Mo_2O_4(OH)_2$, they introduced the concept of genotypic compounds of MoO_3, due to the close resemblance of their X-ray diffraction (XRD) patterns to that of the starting material (MoO_3). They also obtained other members, $Mo_5O_7(OH)_8$ and $Mo_5O_5(OH)_{10}$, and finally confirmed four phases of this series.[5,6] These four phases were studied in more detail by Birtill and Dickens.[7] They have been known as hydrogen insertion compounds of MoO_3, H_xMoO_3: Type I blue orthorhombic ($0.23<x<0.4$), Type II blue monoclinic ($0.85<x<1.04$), Type III red monoclinic ($1.55<x<1.72$), and Type IV green monoclinic ($x=2.0$). On the other hand, $Mo_8O_{15}(OH)_{16}$ has been only reexamined by Rode and Lysanova[8] since Glemser and Lutz. According to TG-DTA and XRD results of yellow $MoO_3 \cdot 2H_2O$ by Sotani et al.,[9] the dihydrate decomposes to yellow monohydrate by releasing H_2O at the preparation temperature of $Mo_8O_{15}(OH)_{16}$ by Glemser and Lutz (383 K). This fact indicates that, though Glemser and Lutz used yellow dihydrate as a starting material, the true starting material of $Mo_8O_{15}(OH)_{16}$ was yellow monohydrate. (They believed that the hydration water of the dihydrate was completely released at 383 K and considered that the true starting material was MoO_3.) Moreover, Crouch-Baker and Dickens, recently, reported hydrogen insertion compounds of yellow hydrates of MoO_3, $H_1MoO_3 \cdot 2H_2O$ and $H_1MoO_3 \cdot H_2O$, obtained from yellow dihydrate and yellow monohydrate by catalytic hydrogenation (hydrogen spillover), and $H_xMoO_3 \cdot H_2O$ from $MoO_3 \cdot 2H_2O$ by reduction with acidified $SnCl_2$.[10] It is suggested that there is an intimate relation among the H-hydrates, $Mo_8O_{15}(OH)_{16}$, yellow monohydrate, $H_xMoO_3 \cdot H_2O$ and $H_1MoO_3 \cdot H_2O$; it is therefore important to discuss the relation.

In the present work, to obtain a single phase of H-hydrate, we explored its formation process, and succeeded in obtaining the single phase. The mechanism of H-hydrate formation was discussed. Based on XRD and chemical analysis results, the relation among H-hydrate, $Mo_8O_{15}(OH)_{16}$, $MoO_3 \cdot H_2O$, $H_xMoO_3 \cdot H_2O$ and $H_1MoO_3 \cdot H_2O$ was discussed briefly.

Experimental

Starting Materials. Three kinds of starting materials were used. The starting material with a maximum hydrogen content ($x=0.5$), called ST[1], was prepared by treating 30 g of MoO_3 with 6 g of Zn in 180 ml of a 2 M (1M=1 mol dm^{-3}) HCl solution. ST[1] was a mixture of Type I and Type II hydrogen molybdenum bronzes by an XRD method. The starting material with a medium hydrogen content ($x=0.3$), called ST[2], was prepared by introducing 4 g of Zn. This was Type I. A starting material with a minimum hydrogen content ($x=0.15$), called ST[3], was prepared by introducing 2 g of Zn and was a mixture of Type I and MoO_3.

Investigation of H-Hydrate Formation Process and Characterization of the Specimens. The formation process of H-hydrate from the three starting materials at 343, 353, and 363 K was followed by investigating the specimens treated for a fixed time (1, 2, 4, 7, and 14 days long). Because Type I is soluble in alkaline solutions, we chose three kinds of treating solutions: a 1 M HCl acid solution (non oxidative), a 1 M

HNO_3 acid solution (oxidative) and distilled water. Then, 3 g of the starting material was treated by 150 ml of each treating solution. After treatment the specimens were cooled to room temperature, filtrated, washed with water and vacuum-dried for one day. They were then investigated by using an XRD method and by chemical analysis. The XRD measurement was carried out using a Rigakudenki RINT 1200M diffractometer with Cu K_α radiation. The x values (i.e., hydrogen content) of the specimens were determined by Choain and Marion's method.[11] According to XRD results, most of the specimens were a mixture of the starting materials and/or H-hydrate. Because Type I, Type II, and H-hydrate completely turned to MoO_3 at 673 K in air, the x value was evaluated from the specimen weight at 673 K (Thermogravimetry). Molybdenum species dissolved in the treating solutions from the specimens were investigated by UV-visible spectroscopy.

With respect to 1 M HNO_3 treatments, all specimens were oxidized to MoO_3.

Results and Discussion

H-Hydrate. In this study, we obtained many resulting specimens which did not contain MoO_3 or H_xMoO_3. These specimens showed the XRD peaks of H-hydrate described in our previous study,[2] and were referred to as H-hydrate specimens. They were blue in color and had the composition $H_{0.14-0.22}MoO_3 \cdot 0.94—1.04H_2O$. The specimens did not release hydration water below 373 K and their compositions did not change upon a further vacuum drying. Upon standing in an air atmosphere for a long time, the x value gradually decreased; for example by standing for one year the specimens with $H_{0.21}$ and $H_{0.14}$ turned to those with $H_{0.16}$ and $H_{0.12}$, respectively. The XRD patterns of several freshly prepared specimens are shown in Fig. 1. These patterns are similar to each other, except for the pattern of the specimen with x=0.14. There are minor differences concerning the peaks at 16.9, 25.0, and 33.1°, which disappear when the peaks at 22.9 and 23.5° become broad. An inspection of Fig. 1 is likely to indicate that the disappearance of the peaks depends on the x value, but there was no change in their XRD patterns with a decrease in the x value upon standing in an air atmosphere.

The specimens show almost the same XRD pattern, although they were prepared under various conditions and their compositions cover a rather wide range ($H_{0.12-0.22}MoO_3 \cdot y\ H_2O$, y=about 1). The disappearance of the XRD peaks at 16.9, 25.0, and 33.1° does not depend on the x values and water content of the specimens, but are accompanied by a broadening of the peaks at 22.9 and 23.5°. We presume that the disappearance is related to distortion in the crystal lattice of the specimens. The x values in Fig. 1 can be regarded as being those during the formation of H-hydrate. The seeming dependence of the XRD pattern on the x value, which is observed in Fig. 1, may indicate that the x value during the formation affects the distortion. According to the Raman results,[12] there were no significant differences between the specimens with x=0.21 and x=0.14 in Fig. 1. Therefore, we believe that all H-hydrate specimens are of the same species; that is, they consist of a single phase of a nonstoichiometric compound with a rather wide range of homogeneity. We suggest that the XRD pattern with peaks at 16.9, 25.0, and 33.1° is typical of H-hydrate. Accurate d-spacings are shown in Table 1. Although we have tried to index them using an indexing program for powder XRD pattern,[13]

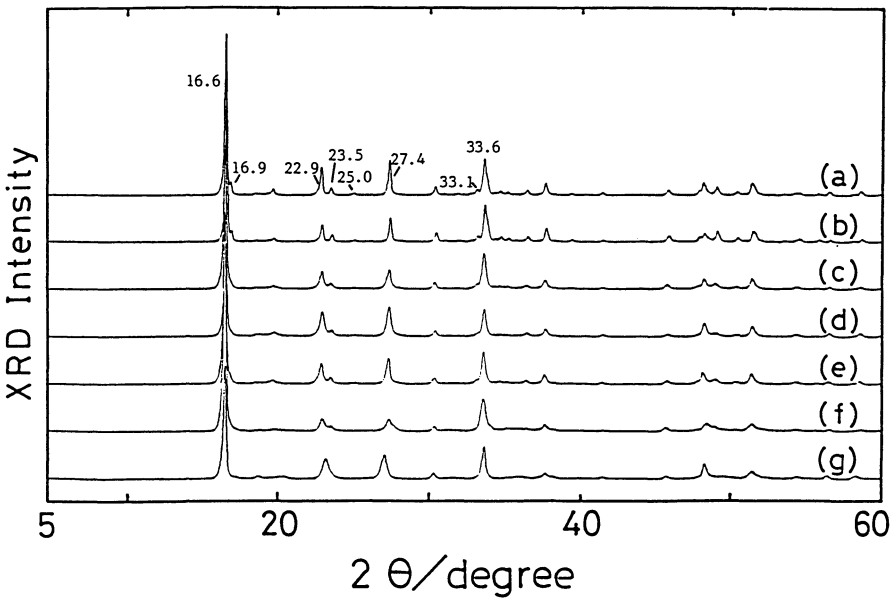

Fig. 1. Powder XRD patterns of the specimens; (a) $H_{0.22}MoO_3 \cdot 0.97H_2O$, (b) $H_{0.21}MoO_3 \cdot 1.01H_2O$, (c) $H_{0.20}MoO_3 \cdot 1.02H_2O$, (d) $H_{0.19}MoO_3 \cdot 1.02H_2O$, (e) $H_{0.18}MoO_3 \cdot 1.03H_2O$, (f) $H_{0.17}MoO_3 \cdot 1.01H_2O$, and (g) $H_{0.14}MoO_3 \cdot 0.99H_2O$.

we have not yet obtained suitable results, because the XRD pattern is too complicated.

Figure 2 shows a comparison among the XRD patterns of H-hydrate, $Mo_8O_{15}(OH)_{16}$,[3] yellow $MoO_3 \cdot H_2O$ (JCPDS 28-0666), $H_xMoO_3 \cdot H_2O$ (JCPDS 38-0066) and $H_1MoO_3 \cdot H_2O$ (JCPDS 38-0064). The XRD pattern of H-hydrate is similar to that of $Mo_8O_{15}(OH)_{16}$, except for several small peaks. According to Glemser and Lutz,[3] $Mo_8O_{15}(OH)_{16}$ was also expressed by the composition $MoO_{2.88-2.90} \cdot H_2O$. Because the composition of H-hydrate can be rewritten as $MoO_{2.89-2.94} \cdot 1.04—1.16H_2O$, H-hydrate and $Mo_8O_{15}(OH)_{16}$ are comparable to each other. On the basis of their XRD patterns and compositions, H-hydrate is identical with $Mo_8O_{15}(OH)_{16}$. The XRD pattern of $MoO_3 \cdot H_2O$ shows two strong diffraction peaks at about 16.5 and 33.0°, which are attributed to the (020) and (040) planes. This hydrate has a layer structure, and the *d*-spacing of

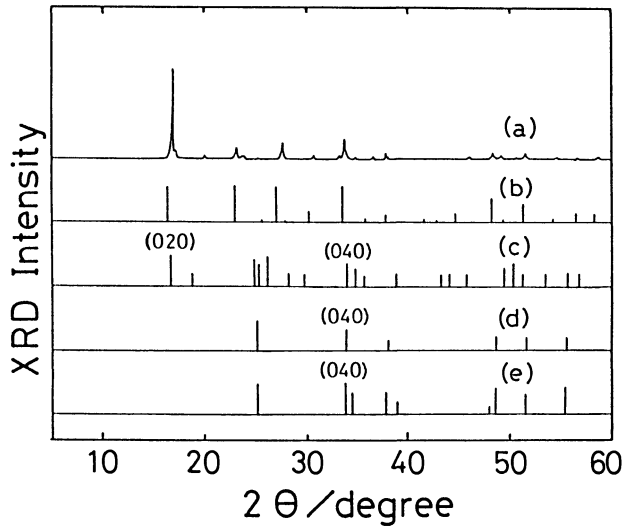

Fig. 2. Powder XRD patterns of H-hydrate (a), $Mo_8O_{15}(OH)_{16}$ (b), yellow $MoO_3 \cdot H_2O$ (c), $H_xMoO_3 \cdot H_2O$ (d), and $H_1MoO_3 \cdot H_2O$ (e).

Table 1. *d*-Spacings of H-Hydrate

2θ	*d*	I/I_1	2θ	*d*	I/I_1
16.590	5.339	100	35.104	2.554	2
16.900	5.242	8	36.436	2.464	2
17.880	4.957	1	37.672	2.386	5
18.578	4.772	1	39.360	2.287	1
19.374	4.578	1	41.468	2.1758	1
19.742	4.493	2	45.874	1.9765	2
22.896	3.881	6	47.884	1.8981	2
23.530	3.778	3	48.232	1.8852	3
25.016	3.557	1	49.028	1.8565	4
27.376	3.255	7	50.400	1.8091	2
30.382	2.940	3	51.380	1.7769	5
30.928	2.889	1	51.844	1.7621	1
31.846	2.808	1	53.300	1.7173	1
33.106	2.704	3	54.352	1.6865	2
33.580	2.667	19	55.636	1.6506	1
33.738	2.654	9	56.428	1.6293	1
34.260	2.615	2	57.946	1.5902	1
34.640	2.587	2	58.834	1.5756	2

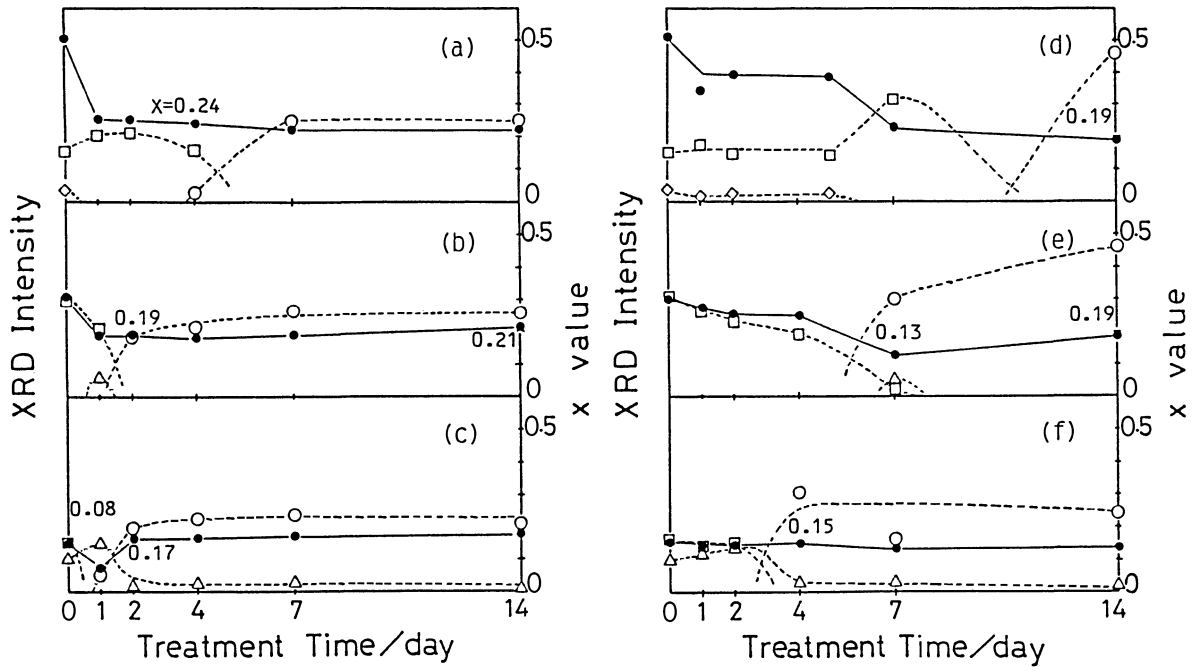

Fig. 3. Formation process of H-hydrate at 353 K by the HCl treatment from ST[1] (a), ST[2] (b), and ST[3] (c), and by the water treatment from ST[1] (d), ST[2] (e), and ST[3] (f), respectively. (□), (◇), (△), and (○) are the relative XRD intensity of the peak at 25.3° of Type I to the intensity of the peak at 28.4° of Si which was mixed with the specimens as an internal standard, that of the peak at 24.2° of Type II, that of the peak at 25.7° of MoO_3 and that of the peak at 16.6° of H-Hydrate, respectively. (●) is the *x* value of the specimen.

the (020) plane corresponds to its interlayer spacing. The XRD patterns of $H_xMoO_3 \cdot H_2O$ and $H_1MoO_3 \cdot H_2O$ also show a strong peak at about 33.0°, which is ascribed to the (040) plane. This indicates that $H_xMoO_3 \cdot H_2O$ and $H_1MoO_3 \cdot H_2O$ retain the Mo–O framework of $MoO_3 \cdot H_2O$. The two strong peaks are observed in the patterns of H-hydrate and $Mo_8O_{15}(OH)_{16}$. This fact indicates a resemblance in Mo–O framework among H-hydrate, $Mo_8O_{15}(OH)_{16}$, and yellow monohydrate. Because the starting material of $Mo_8O_{15}(OH)_{16}$ is yellow monohydrate, we suggest that $Mo_8O_{15}(OH)_{16}$, i.e., H-hydrate, is a genotypic compound of yellow monohydrate. We, thus, express H-hydrate as $H_{0.12-0.22}MoO_3 \cdot H_2O$.

The Formation Process. Figure 3 shows the formation process of H-hydrate from the three starting materials at 353 K. In the case of an HCl treatment, H-hydrate appears after 4 days of treatment for ST[1], 2 days for ST[2], and 1 day for ST[3]. In the case of a water treatment, H-hydrate formation is also observed. There is basically no difference between the results for an HCl treatment and that for a water treatment, except that H-hydrate is formed much more slowly in water than in an HCl solution. The formation of H-hydrate took place little more rapidly at 363 K, and slightly more slowly at 343 K than at 353 K. In several cases, MoO_3 temporarily appeared, or temporarily increased, just before H-hydrate appeared. This appearance or increase of MoO_3 was accompanied by a decrease in the x value. In the case of an HCl treatment at 353 K for ST[1], H-hydrate was formed without the appearance of MoO_3. In all cases, H-hydrate was formed as Type I disappeared. The formation took place when the x value of the solid phase was in the range $x \leqslant 0.24$ and Type II was not contained.

The formation of H-hydrate, followed by the disappearance of Type I, indicates that H-hydrate is formed from Type I. The maximum limit value (x=0.24) corresponds to the reduction degree [$MoO_{2.88}$]. This reduction degree is identical with that of $Mo_8O_{15}(OH)_{16}$,[3] i.e., that of H-hydrate. The temporary appearance, or temporary increase, of MoO_3 seems to be correlated with the formation of H-hydrate. However, as mentioned above, in the case of an HCl treatment of ST[1] at 353 K, formation took place without the appearance of MoO_3. To investigate whether the appearance or increase of MoO_3 is correlated with the formation, we paid much attention to specimens which contained both H-hydrate and Type I, i.e., which revealed a H-hydrate forming stage. It was then recognized that the specimens at this stage contained MoO_3 when $x<0.23$. Therefore, the appearance, or increase, of MoO_3 is not correlated with the formation of H-hydrate. It has been known that H_xMoO_3 in the range $x<0.23$ exists as a mixture of Type I and MoO_3.[7] As mentioned above, a temporary decrease in the x value was also observed just before H-hydrate formation. The temporary appearance, or temporary increase, of MoO_3 arises from a temporary decrease in the x value to less than 0.23. The temporary decrease in the x value indicates that Mo^{5+} was temporarily dissolved into the treating solution. We presume that this dissolution of Mo^{5+} takes place when the Mo–O framework based on the MoO_3 structure (H_xMoO_3) is reformed to that based on the $MoO_3 \cdot H_2O$ structure (H-hydrate).

For an HCl treatment, the supernatant solution was orange in color before H-hydrate formation took place; the color became faint as the formation proceeded. For water treatment, however, the supernatant was deep dark blue before formation, and finally the color turned to faint greenish blue. Figure 4 shows the UV-visible spectra of the supernatant solutions for ST[3]. Spectra (a) and (b) were obtained from orange (for 1 day HCl treatment at 353 K) and colorless (for 4 days HCl treatment at 353 K) supernatant solutions, respectively, while spectra (c) and (d) were obtained from deep dark blue (for 1 day water treatment at 353 K) and faint greenish blue (for 4 days water treatment at 353 K) solutions, respectively. Spectrum (a) shows a strong band below 350 nm and two weak bands at 380 and 480 nm. Spectrum (c) shows a strong band below 350 nm

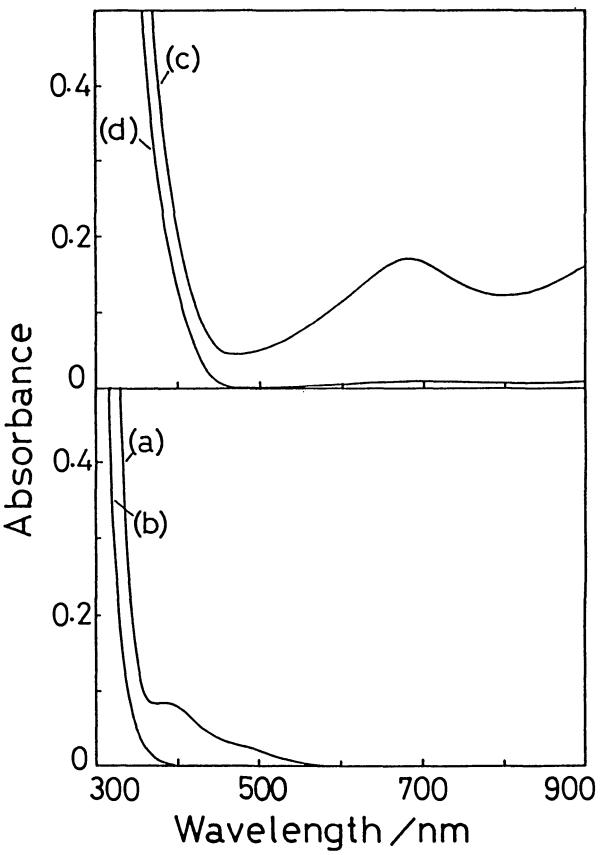

Fig. 4. Extinction spectra of supernatant solutions for HCl and water treatments of ST[3] at 353 K. The (a) and (b) spectra were obtained from the solutions for 1 day and 4 days HCl treatments, respectively, while (c) and (d), for 1 day and 4 days water treatments, respectively.

and two medium bands at 680 nm and above 900 nm. These observed bands arise from molybdenum species dissolved in the treating solutions from H_xMoO_3. The strong band below 350 nm, observed in both spectra (a) and (c), is attributed to molybdenum species consisting of Mo^{6+}. The bands at 380 and 480 nm are ascribed to mixed-valence (Mo^{6+} and Mo^{5+}) molybdenum species with a small degree of condensation, such as a dimer,[14] while the bands at 680 nm and above 900 nm are ascribed to mixed-valence molybdenum species with a large degree of condensation, which are known as isopoly-blue. The following information can be obtained from Fig. 4: (i) As the formation of H-hydrate proceeds, the amount of mixed-valence species apparently decreases. (ii) The forms of mixed-valence species depend on the treating solution; no mixed-valence molybdenum species common to both treating solutions has been observed.

This information suggests that the mixed-valence molybdenum species in the treating solution plays a role in the formation of H-hydrate. However, H-hydrate is not formed only by condensation of the molybdenum species in solution. If H-hydrate is formed only by condensation, any common mixed-valence molybdenum species with an extremely large degree of condensation should be observed in both HCl and water treating solutions during formation. As mentioned above, H-hydrate formation also depended on the x value of the solid phase (When $x \leqslant 0.24$, the formation of H-hydrate was observed). Thus, both the (mixed-valence) molybdenum species in the treating solution and H_xMoO_3, $x \leqslant 0.24$ correlate strongly with the formation of H-hydrate. There is still a question as to why these different species in an HCl solution and in water lead to the same product (H-hydrate). This question can be answered by considering that these species may also comprise of the same constituent unit, i.e., Mo–O octahedra, as H-hydrate (monohydrate of MoO_3), MoO_3, and H_xMoO_3. Mo^{5+} seems to be necessary for molybdenum species to react with the solid phase and to form H-hydrate. We conclude that H-hydrate is formed as follows:

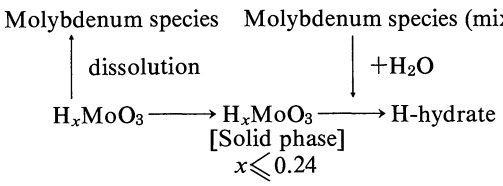

References

1) "Gmelin Handbook, Mo," Vol. B3a, 1987.
2) K. Eda and N. Sotani, *Bull. Chem. Soc. Jpn.*, **62**, 4039 (1989).
3) O. Glemser and G. Lutz, *Z. Anorg. Allg. Chem.*, **264**, 17 (1951).
4) O. Glemser, *Nachr. Akad. Wiss. Göttingen, Math. Phys.*, **1955**, 121.
5) O. Glemser, U. Hauschild, and G. Lutz, *Z. Anorg. Allg. Chem.*, **269**, 93 (1952).
6) O. Glemser, G. Lutz, and G. Meyer, *Z. Anorg. Allg. Chem.*, **285**, 173 (1956).
7) J. J Birtill and P. G. Dickens, *Mater. Res. Bull.*, **13**, 311 (1978).
8) E. Ya. Rode and G. V. Lysanova, *Dokl. Akad. Nauk SSSR*, **145**, 573 (1962).
9) N. Sotani, Y. Saito, M. Oita, and M. Hasegawa, *Nippon Kagaku Kaishi*, **1974**, 673.
10) S. Crouch-Baker and P.G. Dickens, *Mater. Res. Bull.*, **19**, 1457 (1984).
11) C. Choain and F. Marion, *Bull. Soc. Chim. Fr.*, **1963**, 212.
12) The specimens showed the same bands at 200, 260, 375, 640, 805, 890, 930, and 940 cm^{-1}. Degradation by laser irradiation did not take place.
13) J. W. Visser, *J. Appl. Crystallogr.*, **2**, 89 (1969), and references therein.
14) M. T. Pope, "Heteropoly and Isopoly Oxometalates," Springer-Verlag, Berlin, Heidelberg, New York, Tokyo (1983), Chap. 3, p. 48.

Structure and Homogeneous Chemical Equilibria of Lithium β-Diketonates in Dimethyl Sulfoxide

Yoshinori ARAKI,† Akio IWASE, Setsuko KUDO,* Toshishige M. SUZUKI, and Toshiro YOKOYAMA
Department of Chemistry, Faculty of Science, Yamagata University, Kojirakawa-machi, Yamagata 990
† Traffic Control Materials Laboratory, Yamagata 3M Ltd., Ohaza Osanagi, Higashine 999-37
(Received April 20, 1991)

The structure and the homogeneous chemical equilibria of lithium β-diketonates (LiL), viz., Li(dbm), Li(bzac), and Li(acac), in dimethyl sulfoxide (DMSO) were studied by means of ^{13}C NMR, IR spectral measurements, and rotating disk voltammetry, where dbm^-, $bzac^-$, and $acac^-$ indicate the enolate anions of dibenzoylmethane, benzoylacetone, and acetylacetone, respectively. It was found by the ^{13}C NMR and IR spectral measurements that LiL existed mainly as Li(uni-L) in DMSO, where uni- means that the ligand coordinates to the metal as unidentate. Since it is known that LiL dissociates slightly into ions in DMSO, LiL is involved in the following homogeneous chemical equilibrium:

$$\text{Li(uni-L)} \rightleftharpoons \text{Li}^+ + \text{L}^-$$

Furthermore, the apparent dissociation constant ($\log K_{app}$) of LiL was obtained by rotating disk voltammetry in DMSO containing 0.1 mol dm^{-3} tetrabutylammonium perchlorate (TBAP), i.e., Li(dbm): −3.0±0.1, Li(bzac): −2.7±0.1, and Li(acac): −2.0±0.1, respectively. It was noted that the homogeneous chemical equilibria shifted more to the right in 0.1 mol dm^{-3} TBAP–DMSO than in DMSO alone. The behavior can be explained mainly in terms of the interaction between the π-electron system of Li(uni-L) and the cations of TBAP.

In previous papers,[1–5] the homogeneous chemical equilibria of ten bis(β-diketonato)nickel(II) complexes in DMSO were investigated by means of conductivity, electronic spectral measurements, cryoscopy, polarography, and cyclic voltammetry. For instance, it was found polarographically that three complexes, viz., $Ni(dbm)_2$,[2] $Ni(bzac)_2$,[1] and $Ni(acac)_2$,[5] were involved in the following homogeneous chemical equilibria:

(a) $Ni(dbm)_2$ and $Ni(bzac)_2$

$$\text{Ni(bi-L)}_2 \rightleftharpoons \text{Ni(bi-L)(uni-L)} \rightleftharpoons \text{Ni(bi-L)}^+ + \text{L}^- \rightleftharpoons \text{Ni(uni-L)}^+$$

(b) $Ni(acac)_2$

$$\text{Polymeric species} \rightleftharpoons \text{NiL}_2 \rightleftharpoons \text{Ni(bi-L)}^+ + \text{L}^- \rightleftharpoons \text{Ni(uni-L)}^+$$

where bi- means that the ligand coordinates to the metal as bidentate and L^- indicates the enolate anion of the β-diketone. Because the polarographic measurements in the previous research were based on the reduction of the metal base of the complexes, they do not provide detailed information on the ligands.

The present paper deals with the structure and the homogeneous chemical equilibria of Li(dbm), Li(bzac), and Li(acac) in DMSO by use of ^{13}C NMR and IR spectral measurements, and in 0.1 mol dm^{-3} TBAP–DMSO by means of rotating disk voltammetry based on the oxidation of the ligand base. Since LiL is a simple compound, it was expected that this research would provide more direct information regarding the bond between the metal and the ligand, and more quantitative information with respect to homogeneous chemical equilibria for metal β-diketonates in DMSO.

Experimental

Reagents. Lithium dibenzoylmethanate [Li(dbm)] was prepared as follows: To 5 mmol of Aldrich Chemicals' dibenzoylmethane (98%) in 50 mL of methanol was added 5 mmol of Nakarai Chemicals' lithium hydroxide monohydrate (99%) in 150 mL of methanol. The resulting solution was evaporated and a small amount of diethyl ether was added to the concentrated solution. The solution was permitted to stand for a minimum of 2 h in an ice bath and then was filtered. The salt was recrystallized once with methanol–diethyl ether. Then, the salt was dried in vacuo at 105±5 °C for ca. 6 h. The yield of the salt was 30.5%. Found: C, 77.74; H, 5.01%. Calcd for $C_{15}H_{11}O_2Li$: C, 78.26; H, 4.82%. Lithium benzoylacetonate [Li(bzac)] and lithium acetylacetonate [Li(acac)] were synthesized by the same method as Li(dbm). Found: C, 71.11; H, 5.66%. Calcd for $C_{10}H_9O_2Li$: C, 71.43; H, 5.41%. Found: C, 55.74; H, 6.44%. Calcd for $C_5H_7O_2Li$: C, 56.62; H, 6.67%.

Tetrabutylammonium dibenzoylmethanate [*n*-Bu_4N(dbm)], tetrabutylammonium benzoylacetonate [*n*-Bu_4N(bzac)], and tetrabutylammonium acetylacetonate [*n*-Bu_4N(acac)] were obtained according to the method described by Buchta et al.[6] Found: C, 79.50; H, 10.10; N, 2.67%. Calcd for $C_{31}H_{47}O_2N$: 79.93; H, 10.19; N, 3.01%. Found: C, 76.92; H, 11.32; N, 3.00%. Calcd for $C_{26}H_{45}O_2N$: C, 77.35; H, 11.26; N, 3.47%. Found: C, 73.87; H, 13.01; N, 3.95%. Calcd for $C_{21}H_{43}O_2N$: C, 73.82; H, 12.71; N, 4.10%. These salts were stored in the dark under nitrogen.

The dimethyl sulfoxide and TBAP used in rotating disk voltammetry were the same as described previously.[7]

Apparatus and Procedures. ^{13}C NMR spectra were obtained with a Varian VXR-300 spectrometer at room temperature. Test solutions were prepared as 0.4 mol dm^{-3} LiL in methanol-d_4 (CD_3OD) and dimethyl-d_6 sulfoxide (DMSO-d_6). Chemical shifts were reported in ppm units, relative to internal tetramethylsilane.

IR spectra were recorded on a Hitachi 270-50 infrared spectrophotometer. Samples were prepared as 1% LiL dispersion in KBr pellets and 10 mmol dm^{-3} solutions in DMSO. The solutions were measured with a calcium fluoride cell of 0.5 mm optical length at room temperature.

Rotating disk voltammograms were obtained with a Nikko Keisoku DPGS-1 dual potentiogalvanostat, a Nikko Keisoku NFG-3 function generator, and a Watanabe WX 4421 X-Y plotter. A disk electrode was rotated by means of a Nikko Keisoku SC-4 motor speed controller and a Nikko Keisoku RRDE-1 rotating ring-disk electrode apparatus. Current–potential curves were measured with a three-electrode system at 25.0±0.2 °C. A platinum rotating disk electrode (surface area: 0.071 cm^2) was used as a working electrode, with a platinum wire as a counter electrode and an aqueous saturated calomel electrode (SCE) as a reference electrode. The rotation speed of the disk electrode ranged from 51 to 890 rad s^{-1}. Voltammograms were recorded at 20 mV s^{-1} scan rate. All test solutions were deaerated for ca. 30 min with nitrogen gas before measurements. As a supporting electrolyte, 0.1 mol dm^{-3} TBAP was used.

Results and Discussion

1. In DMSO. ^{13}C NMR Spectra: The data for the ^{13}C NMR chemical shift of LiL are summarized in Table 1. Each resonance was a singlet, except methylene carbon of Li(bzac) and Li(acac), measured in CD_3OD. Only one carbonyl carbon resonance was obtainted for Li(dbm) and Li(acac), while Li(bzac) gave two carbonyl carbon resonances, due to $-CH_3$ and –Ph substituents at ^{1}C and ^{3}C positions, which were assigned from the chemical shifts of acetone and acetophenone.[8] The Table shows that the carbonyl and methylene carbon resonances indicate drastic upfield shifts in DMSO-d_6, in comparison with the resonances in CD_3OD.

The differences between the chemical shifts in the two solvents used are also presented in Table 1, where

$$d_i = C_i(\text{in } CD_3OD) - C_i(\text{in DMSO-}d_6)\ (i=1\text{—}3) \quad (1)$$

The d_1 and d_3 values suggest that the structure of LiL in DMSO-d_6 is different from that in CD_3OD.

Raban et al. reported that Li(acac) existed almost completely in the chelated form in CD_3OD.[9] As described in section 2 of the present paper, Li(dbm) and Li(bzac) are more stable than Li(acac); therefore, they also tend to exist in the chelated form in CD_3OD. On the other hand, since LiL is strongly solvated in DMSO-d_6, it may be expected that the lithium-oxygen bond will tend to break in DMSO-d_6.

Shibata et al. studied ^{13}C NMR chemical shifts of various β-diketones in DMSO-d_6 and chloroform-d.[8] According to that paper, carbonyl carbon resonances indicated drastic upfield shifts in DMSO-d_6, in comparison with the resonances in chloroform-d, i.e., d=2.7—5.5 ppm. The results led to the conclusion that DMSO-d_6 broke the intramolecular hydrogen bond of the β-diketone and that the upfield shift was caused by the contribution of the free carbonyl carbon which was not influenced by the intramolecular hydrogen bond.

In addition, ^{13}C NMR chemical shifts of the carbonyl carbon for n-Bu_4NL were obtained in DMSO-d_6, viz., n-Bu_4N(dbm) showed 180.5 ppm and n-Bu_4N(bzac) indicated 190.9 and 179.8 ppm at ^{1}C and ^{3}C positions.[10] These findings suggest that the structure of LiL is analogous to that of n-Bu_4NL in DMSO-d_6. However, dissociation of Li(dbm) is negligible in DMSO-d_6 under the conditions used in this study, as discussed below.

The present research demonstrates that LiL does not take the chelated form in DMSO-d_6 (Scheme 1) because the behavior of LiL is very similar to that of the β-diketones reported by Shibata et al., and the carbonyl carbon resonances for LiL appear at the similar positions of those for n-Bu_4NL in DMSO-d_6. Therefore, it is found that the upfield shifts of LiL in DMSO-d_6 are

Table 1. ^{13}C NMR Chemical Shifts of LiL in CD_3OD and DMSO-d_6

Compound	Solvent	Chemical shift of carbonyl carbon/ppm				Chemical shift of methylene carbon/ppm	
		C_1	d_1[a]	C_3	d_3[b]	C_2	d_2[c]
Li(dbm)	CD_3OD	187.4				95.3	
	DMSO-d_6	182.5	4.9			91.1	4.2
Li(bzac)	CD_3OD	192.6		186.2		97.1[d]	
	DMSO-d_6	189.3	3.3	180.3	5.9	94.1	3.0
Li(acac)	CD_3OD	191.3				99.3[d]	
	DMSO-d_6	186.8	4.5			97.4	1.9

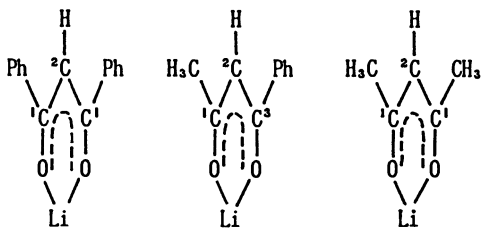

Li(dbm) Li(bzac) Li(acac)

in CD_3OD

a) d_1=C_1(in CD_3OD)−C_1(in DMSO-d_6)

b) d_3=C_3(in CD_3OD)−C_3(in DMSO-d_6)

c) d_2=C_2(in CD_3OD)−C_2(in DMSO-d_6)

d) Triplet

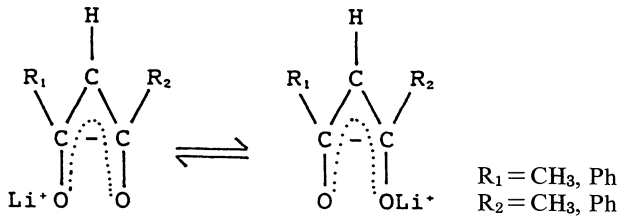

Scheme 1.

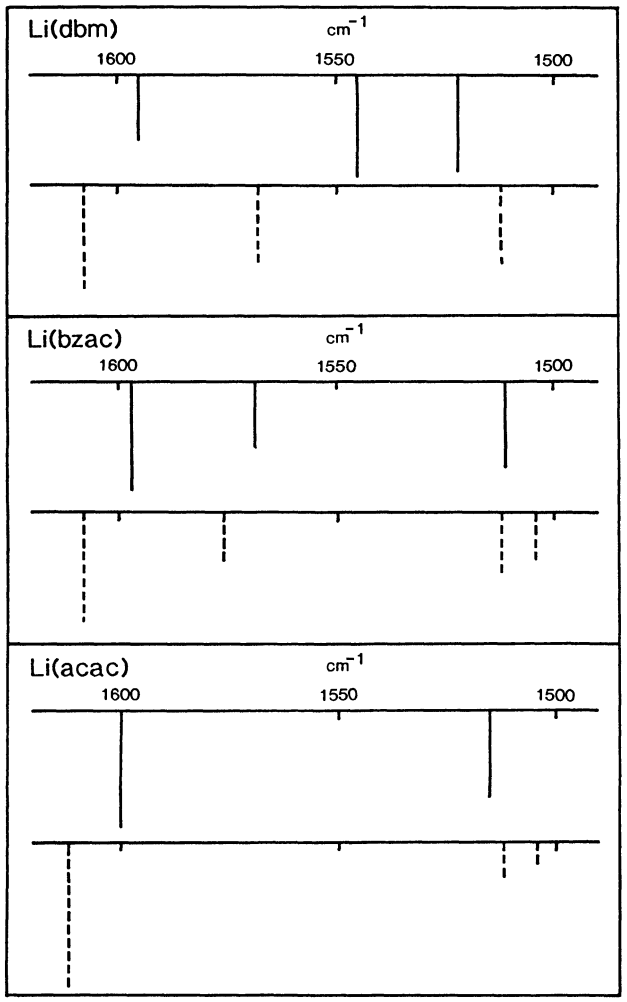

Fig. 1. IR spectra of LiL in the solid state (solid line) and in DMSO (broken line).

caused by the contribution of the free carbonyl carbon. As shown in Scheme 1, the two species contribute to the upfield shifts; however, it was not possible to separate the two species, and it was also impossible to differentiate between the free carbonyl carbon and the other within the NMR time scale. The mixture of the two species is represented as Li(uni-L) below.

IR Spectra: IR spectra of LiL in the solid state and in DMSO are diagrammed in Fig. 1. Each characteristic band of ν(C⋯O)[11,12] of Li(dbm), Li(bzac), and Li(acac) appears at 1595, 1597, and 1600 cm^{-1} in the solid state and at 1608, 1608, and 1612 cm^{-1} in DMSO, respectively. In addition, ν(C⋯O) of n-Bu_4N(dbm) was 1611 cm^{-1} in the solid state and 1612 cm^{-1} in DMSO. These findings suggest that the structure of Li(dbm) in DMSO is similar to that of n-Bu_4N(dbm). However, the degree of dissociation for Li(dbm) in DMSO is very minimal, as described below. Although it is thought that the shifts of ν(C⋯O) in DMSO are caused by the solvent effect, it is more plausible that LiL takes the unidentate structure because of the conclusion in the ^{13}C NMR study.

Chemical Equilibria: Arnett et al. reported that the dissociation constant ($\log K_D$) of Li(dbm) was -5.86 ± 0.01 in DMSO.[13] By using this datum, it is possible to calculate the degrees of dissociation for the prepared concentration in the ^{13}C NMR and IR spectral measurements. Thus, the calculated degree of dissociation is 0.2% for 0.4 mol dm^{-3} in the ^{13}C NMR study, while it is 1.2% for 10 mmol dm^{-3} in the IR study. Since these degrees of dissociation are very minimal, the dissociated species in Scheme 2, i.e., Li^+ and L^-, are negligible for the both measurements. Therefore, the main species in DMSO is Li(uni-L), and the fact is consistent with the result in ^{13}C NMR and IR studies.

2. In TBAP-DMSO. Rotating Disk Voltammetry: Typical rotating disk voltammograms of LiL and n-Bu_4NL are shown in Fig. 2. In general, a limiting current is shown by the Levich equation[14] under convective-diffusion controlled conditions, as follows:

$$i_L = 0.620nFAD^{2/3}\omega^{1/2}\nu^{-1/6}C \quad (2)$$

where i_L is the limiting current, n is the number of

$$\text{Li(uni-L)} \underset{}{\overset{K_D}{\rightleftharpoons}} \text{Li}^+ + \text{L}^-$$

Scheme 2.

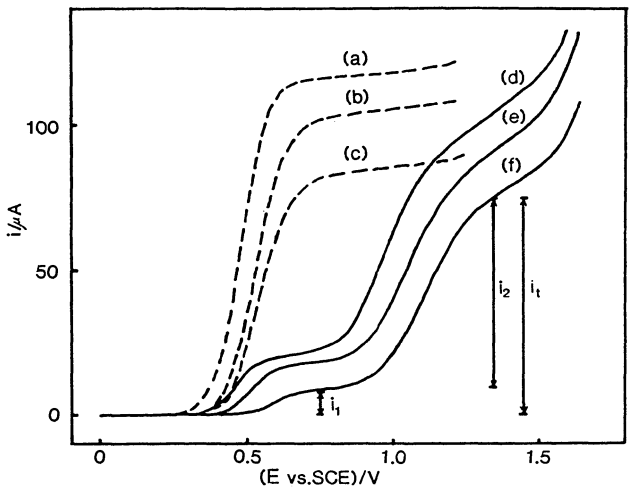

Fig. 2. Rotating disk voltammograms of 2 mmol dm^{-3} (a) n-Bu_4N(acac), (b) n-Bu_4N(bzac), (c) n-Bu_4N(dbm), (d) Li(acac), (e) Li(bzac), and (f) Li(dbm) at 775 rad s^{-1} rotation speed in 0.1 mol dm^{-3} TBAP-DMSO.

transferred electrons, F is the Faraday constant, A is the surface area of the disk electrode, D is the diffusion coefficient, ω is the rotation speed of the disk electrode, ν is the kinematic viscosity, and C is the bulk concentration. The limiting currents for LiL (i_l) and for n-Bu_4NL in Fig. 2, are proportional to the square root of ω. The plots of i_l at a constant rotation speed vs. C for LiL give a straight line in the concentration range from 1 to 10 mmol dm^{-3}.

VandenBorn et al. reported that n-Bu_4N(dbm) existed as the enolate anion in DMSO containing 0.1 mol dm^{-3} tetraethylammonium perchlorate and that controlled potential coulometry gave the n value of 0.98±0.03.[15] Therefore, the observed limiting current for n-Bu_4NL in Fig. 2 is consistent with a one-electron oxidation process; and i_l for LiL also corresponds to a totally one-electron oxidation process.

The first wave (i_1) in Fig. 2 contains a kinetic current due to a preceding chemical reaction. Figure 3 shows the correlation between i_1/i_2 and ω. As seen in Fig. 3, i_1/i_2 decreases as ω increases and it remains constant above 670 rad s^{-1}. Consequently, i_1 contains no kinetic current under the latter conditions.

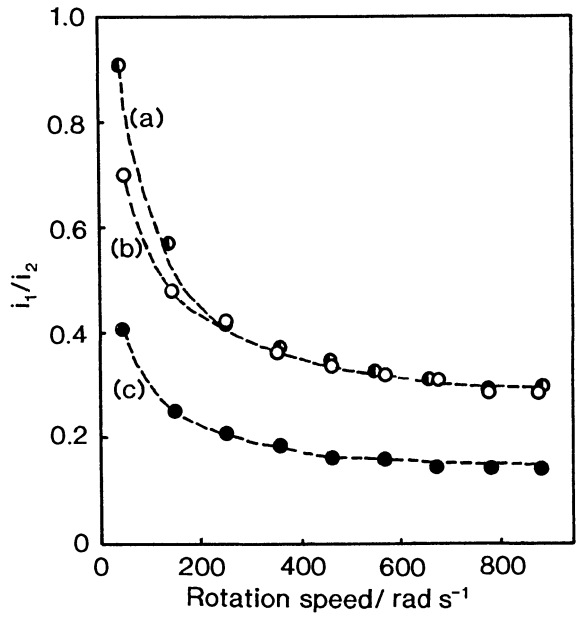

Fig. 3. Plots of i_1/i_2 vs. rotation speed for rotating disk voltammograms of 2 mmol dm^{-3} (a) Li(acac), (b) Li(bzac), and (c) Li(dbm) in 0.1 mol dm^{-3} TBAP-DMSO.

The rotating disk voltammetric data on the oxidation of LiL and n-Bu_4NL at ω=775 rad s^{-1} are summarized in Table 2. The half-wave potential and slope of i_1 for Li(bzac) and Li(acac) are almost equal to those for n-Bu_4N(bzac) and n-Bu_4N(acac) with errors of ±0.01 V and ±5 mV, respectively. While the half-wave potential of i_1 for Li(dbm) is a little different from that for n-Bu_4N(dbm), the first wave for Li(dbm) indicated the following findings:

(a) The first wave involved the kinetic current resulting from the preceding chemical reaction below ω=670 rad s^{-1}, as mentioned above.

(b) When a small amount of lithium perchlorate was added to the solution, i_1 decreased and i_2 increased under the conditions of ω=775 rad s^{-1}.

These experimental findings suggest that the first wave should be assigned to the oxidation of the enolate anion arising from the dissociative reaction; the second wave corresponds to the oxidation of Li(uni-L), on the basis of the results described in section 1 (Scheme 3).

The diffusion coefficient (D) of the enolate anion of n-Bu_4NL is calculated from the slope of the plots of limiting current vs. the square root of ω in terms of Eq. 2. The data are also presented in Table 2. The datum for n-Bu_4N(dbm) agrees with that reported VandenBorn et al.[15]

It is possible to determine the concentration of L^- (Scheme 3) in 0.1 mol dm^{-3} TBAP-DMSO in terms of Eq. 3,[14]

$$1/i_L = 1/i_K + 1/0.620nFAD^{2/3}\omega^{1/2}\nu^{-1/6}C \quad (3)$$

where i_K represents the current in the absence of any

$$\text{Li(uni-L)} \overset{K_{app}}{\rightleftharpoons} \text{Li}^+ + \text{L}^-$$
$$\downarrow -e \qquad\qquad \downarrow -e$$
2nd wave 1st wave

Scheme 3.

Table 2. Rotating Disk Voltammetric Data on the Oxidation of 2 mmol dm^{-3} LiL and n-Bu_4NL at 775 rad s^{-1} Rotation Speed in 0.1 mol dm^{-3} TBAP-DMSO

Compound	($E_{1/2}$ vs. SCE)/V	Slope/mV	$i_j^{a)}$/μA	$i_t^{a)}$/μA	D/cm^2 s^{-1}
Li(dbm)	0.60	93	8.2		
	1.10	147	59.5	67.7	
Li(bzac)	0.51	95	16.6		
	1.04	147	60.3	76.9	
Li(acac)	0.46	93	19.6		
	0.97	147	67.6	87.2	
n-Bu_4N(dbm)	0.54	104		80.4	2.3×10^{-6}
n-Bu_4N(bzac)	0.53	103		101	3.3×10^{-6}
n-Bu_4N(acac)	0.48	96		114	3.8×10^{-6}

a) The meanings of i_j and i_t are shown in Fig. 2, where j=1—2.

Table 3. Apparent Dissociation Constant (log K_{app}) of LiL at Different Concentration in 0.1 mol dm^{-3} TBAP–DMSO

Compound	C/mmol dm^{-3}	log K_{app}
Li(dbm)	1.0	—[a]
	2.0	−2.9
	5.0	−3.1
Li(bzac)	1.0	−2.7
	2.0	−2.7
	5.0	−2.6
Li(acac)	1.0	−2.0
	2.0	−2.1
	5.0	—[a]

a) It was impossible to obtain these data because of a lack of fit for the plots.

mass transfer effects. The plots of $1/i_L$ for the first wave vs. $1/\omega^{1/2}$ showed straight lines at 0.6, 0.7, and 0.8 V vs. SCE. From the slope of the line, the concentration of L^-, i.e., C, was calculated by using the D for n-Bu_4NL in Table 2 and $\nu = 0.01828$ cm^2 s^{-1}. Then, the apparent dissociation constant (log K_{app}) of LiL in 0.1 mol dm^{-3} TBAP–DMSO was obtained, as shown in Table 3.

The values decrease in the following order: Li(acac)>Li(bzac)>Li(dbm). This order agrees with that of the dissociation constants (log K_d) of β-diketones, measured in the aqueous 75 vol% dioxane, namely Hacac>Hbzac>Hdbm, which are −12.70, −12.85, and −13.75, respectively.[16] The log K_{app} of Li(dbm) is −3.0±0.1 in 0.1 mol dm^{-3} TBAP–DMSO; however, the log K_D of Li(dbm) is −5.86±0.01 in DMSO.[13] It was found that the homogeneous chemical equilibrium (Scheme 2) for Li(dbm) shifted more to the right in 0.1 mol dm^{-3} TBAP–DMSO than in DMSO alone.

The TBAP effect on the homogeneous chemical equilibrium for Li(dbm) can be considered first from the standpoint of the ionic strength of the solution. Libuś et al. reported conductometric and spectrophotometric results of copper(II) trifluoroacetate [$Cu(CF_3COO)_2$] in DMSO.[17] That paper indicated that the association constant of $CuCF_3COO^+$ in DMSO derived from the spectrophotometric results, after making activity corrections, agreed with that derived from conductometric data. If the dissociation constant of Li(dbm), after making activity corrections, is defined as K_I, the following equation is set up:

$$\log K_I = \log K_D - \log Y_{Li} - \log Y_{dbm} \quad (4)$$

where Y_{Li} and Y_{dbm} are the activity coefficients of Li^+ and dbm^-, respectively. Thus, log $K_I \approx -5.6$ is obtained by using log $K_D = -5.86$[13] and log $Y_{Li} = \log Y_{dbm} = -0.12$[18] at I (ionic strength)=0.1 in 0.1 mol dm^{-3} TBAP–DMSO. However, the log $K_I \approx -5.6$ is still different from the log $K_{app} = -3.0 \pm 0.1$.

It was described in a previous paper[19] that the dissociation of bis(benzoyltrifluoroacetonato)nickel(II), bis(2-furoyltrifluoroacetonato)nickel(II), and bis(2-thenoyltrifluoroacetonato)nickel(II) complexes in DMSO was enhanced by the presence of one of the supporting electrolytes and that it was considered that such promotion of the dissociation was caused by an interaction between the π-electron system of the complex and the cations of the electrolyte. Although it is impossible to discuss the difference between the log $K_{app} = -3.0 \pm 0.1$ and the log $K_D = -5.86 \pm 0.01$ quantitatively, the difference can be explained mainly in terms of the interaction between the π-electron system of Li(uni-dbm) and the cations of TBAP. It is thought that a similar interaction also takes place in the case of Li(bzac) and Li(acac).

The authors wish to acknowledge the useful suggestions of Professor Yuzo Nishida of Yamagata University in the field of ^{13}C NMR and IR spectroscopy.

References

1) S. Kudo, A. Iwase, I. Mogi, and N. Tanaka, *Bull. Chem. Soc. Jpn.*, **55**, 1416 (1982).
2) S. Kudo, A. Iwase, and N. Tanaka, *Nippon Kagaku Kaishi*, **1983**, 1418.
3) S. Kudo, A. Iwase, and N. Tanaka, *Nippon Kagaku Kaishi*, **1983**, 1539.
4) S. Kudo and A. Iwase, *Nippon Kagaku Kaishi*, **1984**, 1341.
5) S. Kudo and A. Iwase, *Nippon Kagaku Kaishi*, **1985**, 263.
6) R. C. Buchta and D. H. Evans, *Anal. Chem.*, **40**, 2181 (1968).
7) S. Kudo, A. Iwase, and N. Tanaka, *Bull. Chem. Soc. Jpn.*, **54**, 207 (1981).
8) C. Shibata, T. Takeuchi, M. Yamazaki, and J. Niwa, *Nippon Kagaku Kaishi*, **1978**, 836.
9) M. Raban, E. A. Noe, and G. Yamamoto, *J. Am. Chem. Soc.*, **99**, 6527 (1977).
10) The carbonyl carbon resonance for n-Bu_4N(acac) did not appear in this experiment.
11) R. C. Mehrotra, R. Bohra, and D. P. Gaur, "Metal β-Diketonates and Allied Derivatives," Academic Press, New York (1978), p. 109.
12) Y. Fukuda and K. Sone, *J. Inorg. Nucl. Chem.*, **37**, 455 (1975).
13) E. M. Arnett, V. DePalma, S. Maroldo, and L. S. Small, *Pure Appl. Chem.*, **51**, 131 (1979).
14) A. J. Bard and L. R. Faulkner, "Electrochemical Methods," Wiley, New York (1980), pp. 288—293.
15) H. W. VandenBorn and D. H. Evans, *J. Am. Chem. Soc.*, **96**, 4296 (1974).
16) L. G. Van Uitert, C. G. Haas, W. C. Fernelius, and B. E. Douglas, *J. Am. Chem. Soc.*, **75**, 455 (1953).
17) W. Libuś, D. Puchalska, and R. Pastewski, *Electrochim. Acta*, **25**, 1591 (1980).
18) A. Ringbom, "Complexation in Analytical Chemistry," Interscience Publ., New York (1963), p. 24.
19) S. Kudo and A. Iwase, *Bull. Chem. Soc. Jpn.*, **59**, 1857 (1986).

Isomerization and Racemization of the Tris(4,4′-dimethyl-2,2′-bipyridine *N,N′*-dioxide)chromium(III) Complex

Hideaki KANNO,* Junko YAMAMOTO, Satoshi MURAHASHI, Shunji UTSUNO, and Junnosuke FUJITA†

Department of Chemistry, Faculty of Science, Shizuoka University, Oya, Shizuoka 422

†Department of Chemistry, Faculty of Science, Nagoya University, Chikusa-ku, Nagoya 464-01

(Received May 1, 1991)

A new chromium(III) complex, $[Cr(4,4'\text{-}Me_2bpdo)_3]^{3+}$ (4,4′-Me_2bpdo=4,4′-dimethyl-2,2′-bipyridine *N,N′*-dioxide) was prepared and resolved into a pair of enantiomers by an SP-Sephadex column chromatographic method using an achiral eluting agent Na_2SO_4. Both perchlorate and nitrate of the complex were found to crystallize in the *lel*$_2$·*ob*($\Delta(\lambda\lambda\delta)$, $\Lambda(\delta\delta\lambda)$) form. Upon dissolution in water, the complexes isomerized to the *lel*$_3$($\Delta(\lambda\lambda\lambda)$, $\Lambda(\delta\delta\delta)$) form with a rapid change in absorption spectra, and then racemized ($\Delta \rightleftarrows \Lambda$) slowly. The rate constants at 35.0 °C were 4.39×10^{-3} s^{-1} for the isomerization and 3.46×10^{-5} s^{-1} for the racemization. These inversion reactions including conformational change ($\delta \rightleftarrows \lambda$) and configurational change ($\Delta \rightleftarrows \Lambda$) are supposed to proceed by intramolecular mechanisms. The rates of isomerization and racemizatioin of the 4,4′-Me_2bpdo complex are ca. two and ten times slower than those of $[Cr(bpdo)_3]^{3+}$ (bpdo=2,2′-bipyridine *N,N′*-dioxide), respectively.

The skew seven-membered chelate ring of 2,2′-bipyridine *N,N′*-dioxide (bpdo) in metal complexes has been confirmed by X-ray analyses of $[La(bpdo)_4](ClO_4)_3$[1] and $[UO_2(NO_3)_2(bpdo)]$.[2] The skew conformation of bpdo can exist in a pair of enantiomers, δ and λ as shown in Fig. 1. Hence a tris(bpdo) complex has four possible racemic pairs of diastereomers, *lel*$_3$($\Delta(\lambda\lambda\lambda)$, $\Lambda(\delta\delta\delta)$), *lel*$_2$·*ob*($\Delta(\lambda\lambda\delta)$, $\Lambda(\delta\delta\lambda)$), *lel*·*ob*$_2$($\Delta(\lambda\delta\delta)$, $\Lambda(\delta\lambda\lambda)$), and *ob*$_3$($\Delta(\delta\delta\delta)$, $\Lambda(\lambda\lambda\lambda)$). Bertini et al.[3] reported that the dominant isomers of $[M(bpdo)_3](PF_6)_2$ ($M=Co^{2+}, Ni^{2+}$) in acetonitrile will be either the *lel*$_3$ or *ob*$_3$ one from ^{1}H NMR studies. They also suggested that a rapid inversion of the bpdo chelate ring ($\delta \rightleftarrows \lambda$) seems unlikely because of the anticipated high barrier to interconversion of chelating bulky bpdo.

In a previous paper,[4] we reported that both racemic and optically active $[Cr(bpdo)_3](ClO_4)_3\cdot 2H_2O$[5] crystallize in the *lel*$_2$·*ob* form, but isomerize to the *lel*$_3$ one upon dissolution in water with a rapid change in absorption spectra, and then racemize ($\Delta \rightleftarrows \Lambda$) slowly. Similar isomerization and racemization were found to occur in $[Cr(acac)(bpdo)_2](ClO_4)_2\cdot H_2O$ (acac=acetylacetonate ion).[6] The complex forms the *lel*$_2$ isomer in the solid state and the *lel*·*ob* one in an aqueous solution. These facts indicate that the bpdo chelate ring is flexible and changes its conformation ($\delta \rightleftarrows \lambda$) easily. On the other hand, its conformation can be fixed when methyl groups are introduced in the 3- and 3′-positions. Thus, $[Cr(rac\text{-}3,3'\text{-}Me_2bpdo)_3]^{3+}$ (*rac*-3,3′-Me_2bpdo=racemic 3,3′-dimethyl-2,2′-bipyridine *N,N′*-dioxide) yields three of four possible isomers, *lel*$_3$, *lel*$_2$·*ob*, and *lel*·*ob*$_2$ in the formation ratio of 4, 1, and 1, respectively.[7]

In the present paper, we have studied the stereoisomerism of a new related complex, $[Cr(4,4'\text{-}Me_2bpdo)_3]^{3+}$ (4,4′-Me_2bpdo = 4,4′-dimethyl-2,2′-bipyridine *N,N′*-dioxide). The complex also crystallizes in the *lel*$_2$·*ob* isomer, isomerizes to the *lel*$_3$ one in water, and racemizes. However, these reactions are fairly slow compared with those of $[Cr(bpdo)_3]^{3+}$. The difference in rate between two complexes are discussed.

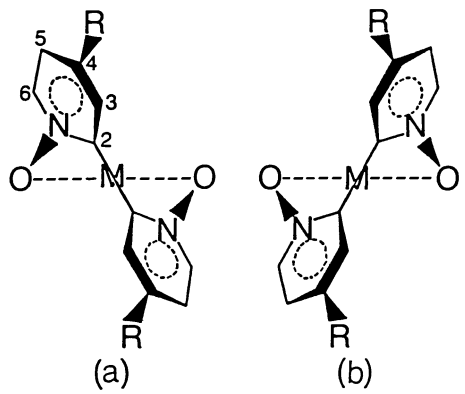

Fig. 1. Chiral conformations of bpdo (R=H) and 4,4′-Me_2bpdo ($R=CH_3$). (a) δ- and (b) λ-skew form.

Experimental

Preparation of 4,4′-Dimethyl-2,2′-bipyridine *N,N′*-Dioxide (4,4′-Me_2bpdo). An acetic acid solution (150 cm^3) of 4,4′-dimethyl-2,2′-bipyridine (25 g; Tokyo Kasei Co.) was mixed with 30% aqueous hydrogen peroxide (100 cm^3). The solution was refluxed for 4 h, then mixed with another 80 cm^3 of 30% aqueous hydrogen peroxide and refluxed for 3 h. The resulting solution was evaporated under reduced pressure to give a pale yellow oil. The residue was mixed with water (ca. 100 cm^3) and the mixture was evaporated again. This procedure was repeated twice to remove acetic acid contained in the residue. To the oily residue, 100 cm^3 of acetone was added to give pale yellow crystals. The crystals were collected by filtration, washed with acetone, and air-dried. Recrystallization from a mixture of methanol and acetone (1 : 3) gave white needles. Yield: 21 g (72%). Found: C, 66.45; H, 5.64; N, 12.76%. Calcd for $C_{12}H_{12}N_2O_2$: C, 66.65; H, 5.59; N, 12.95%.

IR (nujol mull) 1258, 1239 (ν_{N-O}), and 839 cm^{-1} (δ_{N-O}). ^{13}C NMR (D_2O, TMS) δ=20.5 (CH_3), 129.5 and 129.9 (C_3 and C_5), 139.5 (C_6), 141.7 (C_2), 144.4 (C_4) (see Fig. 1). ^1H NMR (D_2O, TSP) δ=2.49 (s, 6H, CH_3). The ^{13}C NMR spectrum was assigned from a comparison with those of the related compounds.[8]

Preparation and Resolution of Complexes. $[Cr(bpdo)_3](NO_3)_3\cdot 2H_2O$: The complex was prepared according to the literature method.[9] Recrystallization from a mixture of methanol and diethyl ether (2:1) gave green crystals. The complex is very soluble in water. Yield: 80%. Found: C, 43.06; H, 3.41; N, 14.85%. Calcd for $C_{30}N_{28}N_9O_{17}Cr$: C, 42.97; H, 3.37; N, 15.03%.

Resolution of $[Cr(bpdo)_3]^{3+}$: The resolution of $[Cr(bpdo)_3](ClO_4)_3$ with $(+)_{589}$-$Ag_3[Co(L\text{-}cysu)_3]$ (L-cysu=L-cysteinesulfinato(2−)-*S,N*)[10] was reported previously.[11] The nitrate was resolved in a similar manner using $(+)_{589}$-$K_3[Co(L\text{-}cysu)_3]$.[10] The resolving agent (1.9 g, 2.6 mmol) was dissolved in an aqueous solution (20 cm^3) of $[Cr(bpdo)_3](NO_3)_3\cdot 2H_2O$ (4.2 g, 5.1 mmol). The solution was cooled in an ice-bath to give yellowish green crystals, which were collected by filtration, washed with 50% ethanol and then ethanol, and air-dried. The diastereomeric salt (2.0 g) was dissolved in ice cold water (30 cm^3) and immediately $NaClO_4$ (1.0 g) was added to the solution with stirring to yield green crystals. They were collected by filtration, washed thoroughly with a 1 mol dm^{-3} $NaClO_4$ solution to remove the resolving agent, then with a small amount of cold water, finally with ethanol, and dried over P_4O_{10}. Yield: 1.6 g. The complex showed a negative rotation at 589 nm in water but rapidly lost its activity.[4,11] Found: C, 37.83; H, 2.93; N, 9.11%. Calcd for $(-)_{589}$-$[Cr(bpdo)_3](ClO_4)_3\cdot 2H_2O$=$C_{30}H_{28}N_6O_{20}Cl_3Cr$: C, 37.89; H, 2.97; N, 8.84%.

$[Cr(4,4'\text{-}Me_2bpdo)_3](ClO_4)_3\cdot 2H_2O$: An aqueous solution (50 cm^3) containing $Cr(NO_3)_3\cdot 9H_2O$ (2.0 g, 5 mmol) and 4,4′-Me_2bpdo (3.5 g, 16 mmol) was warmed at 80 °C for 2 h and then cooled to room temperature. Sodium perchlorate (3 g) was added to the resulting solution to yield green crystals, which were collected by filtration, washed with ice cold water, recrystallized from hot water, and dried over P_4O_{10}. Yield: 4 g (80%). Found: C, 41.98; H, 3.77; N, 8.21%. Calcd for $C_{36}H_{40}N_6O_{20}Cl_3Cr$: C, 41.77; H, 3.90; N, 8.12%.

$[Cr(4,4'\text{-}Me_2bpdo)_3](NO_3)_3\cdot 2H_2O$: The complex was prepared by a method similar to that for $[Cr(bpdo)_3](NO_3)_3\cdot 2H_2O$.[9] A methanol solution (50 cm^3) containing $Cr(NO_3)_3\cdot 9H_2O$ (2.0 g, 5 mmol) and 4,4′-Me_2bpdo (3.5 g, 16 mmol) was refluxed for 4 h, cooled to room temperature, and mixed with 40 cm^3 of diethyl ether. On standing the mixture in a refrigerator for 24 h, green needles were formed, collected by filtration, washed with acetone, and dried over P_4O_{10}. The complex was recrystallized from a mixture of methanol and diethyl ether (2:1). The nitrate is much more soluble in water than the perchlorate. Yield: 3.6 g (85%). Found: C, 46.93; H, 4.26; N, 13.62%. Calcd for $C_{36}H_{40}N_9O_{17}Cr$: C, 46.86; H, 4.37; N, 13.66%.

Resolution of $[Cr(4,4'\text{-}Me_2bpdo)_3]^{3+}$: The resolution of $[Cr(4,4'\text{-}Me_2bpdo)_3]^{3+}$ was achieved by SP-Sephadex column chromatography. All the procedures were carried out in a cold room (at ca. 5 °C) because of racemization of the complex in water at ordinary temperature. An aqueous solution of the perchlorate or nitrate (0.2 g) of the complex was applied on a column (ϕ 2.2×130 cm) of SP-Sephadex C-25. By elution with a 0.3 mol dm^{-3} Na_2SO_4 solution, the column gave two completely separate bands. The faster moving band contained the $(+)_{589}$-isomer. Each eluate of the bands was collected and mixed with $NaClO_4$ to give green crystals. They were collected by filtration, washed with a small amount of ice cold water and then ethanol, and dried over P_4O_{10}. Found for the $(-)_{589}$-isomer: C, 40.52; H, 3.94; N, 7.83%. Found for the $(+)_{589}$-isomer: C, 40.44; H, 4.03; N, 7.76%. Calcd for $[Cr(4,4'\text{-}Me_2bpdo)_3](ClO_4)_3\cdot 4H_2O$=$C_{36}H_{44}N_6O_{22}Cl_3Cr$: C, 40.37; H, 4.14; N, 7.85%. Resolution of the complex by elution with a 0.3 mol dm^{-3} $Na_2[Sb_2\{(+)_{589}\text{-tartrate}\}_2]$ solution was unsuccessful to give only one band. Very small negative and positive rotations were observed at 589 nm only for the front and rear fractions of the band, respectively. In contrast to the elution with Na_2SO_4, the $(-)_{589}$-isomer was eluted faster.

Kinetic Measurements. Isomerization of the Complexes: In aqueous solutions, both perchlorate and nitrate of $[Cr(4,4'\text{-}Me_2bpdo)_3]^{3+}$ show a rapid change in absorption spectra. The change in absorbance at 620 nm was followed using a JASCO UVIDEC-320 spectrophotometer in the temperature range of 20.0—40.0 °C (±0.1 °C). The pH and ionic strength (I=0.1) of solutions were adjusted with aqueous solutions of NaCl and HCl. The complex concentrations were in the range of 8.2—12 mmol dm^{-3} for the nitrate and 2.0—2.3 mmol dm^{-3} for the perchlorate which is hardly soluble in water. In each kinetic run, the rate of change obeyed the first-order kinetic law. The observed rate constant (k_{obsd}) is expressed as $k_{obsd}=-\ln[(A_t-A_\infty)/(A_0-A_\infty)]/t$, where A's are absorbances at the time denoted by suffixes.

The rate for isomerization of the chloride and perchlorate of $[Cr(bpdo)_3]^{3+}$ in water has been reported in our previous paper.[4] In this work, the kinetic measurements for isomerization of $[Cr(bpdo)_3](NO_3)_3\cdot 2H_2O$ were carried out by a method described above in the temperature and the complex concentration ranges of 22.0—35.0 °C and 7.0—12 mmol dm^{-3}, respectively. The rate for the nitrate agreed with those for the chloride and perchlorate.

Racemization of the Complex: The decrease in optical rotation at 589 nm of $[Cr(4,4'\text{-}Me_2bpdo)_3]^{3+}$ in water was followed using a Union PM-101 digital polarimeter. The temperatures and the complex concentrations were in the range of 40.0—55.0 °C (±0.1 °C) and 1.1—2.9 mmol dm^{-3}, respectively. The complex lost the activity in two steps with different rates, the first rapid and the subsequent slow steps (vide post). In the latter step, the rate of decrease obeyed the first-order kinetic law and the observed rate constant (k_{obsd}) is also expressed by the above equation, where A's are degrees of optical rotation.

Other Measurements. Absorption and circular dichroism (CD) spectra were recorded on a Shimadzu UV-3100 spectrophotometer and a JASCO J-500 spectropolarimeter, respectively, using a cell jacket to maintain the temperature constant. ^{13}C and ^1H NMR and IR spectra were recorded on a JEOL JNM-PFT60 and a VARIAN EM-390 spectrometer, and a JASCO IR REPORT-100 spectrophotometer, respectively.

Results and Discussion

Preparation and Properties of the Complex. White crystalline 4,4′-Me_2bpdo was obtained by a method similar to that for bpdo[12] from 4,4′-dimethyl-2,2′-bipyridine and hydrogen peroxide. The $[Cr(4,4'\text{-}Me_2bpdo)_3]^{3+}$ complex was prepared by a method similar to that for $[Cr(bpdo)_3]^{3+}$[9,11,13] from $Cr(NO_3)_3\cdot 9H_2O$ and the ligand. As shown later, both perchlorate

and nitrate of the complex crystallized in the *lel*$_2$·*ob* isomer. This isomer isomerized fairly rapidly to the *lel*$_3$ form upon dissolution in water. The complex was completely resolved into a pair of enantiomers by SP-Sephadex column chromatography carried out at 5 °C using an achiral eluting reagent, an aqueous Na_2SO_4 solution. The same chromatography at 20 °C was unsuccessful to give only one band on the column because of racemization of the complex. The $[Cr(bpdo)_3]^{3+}$ complex racemizes too fast to be resolved by a column chromatographic method.[4,11]

The achievement in resolution using Na_2SO_4 indicates that the enantiomers of the complex are discriminated by chiral SP-Sephadex resin composed of D-glucose.[14] On the contrary, elution with $Na_2[Sb_2\{(+)_{589}\text{-tartrate}\}_2]$, which is known as an effective eluting reagent for chromatographic resolution of metal complexes,[14,15] resulted in very poor resolution. The $(-)_{589}$-isomer was eluted faster in the chromatography with this chiral eluent, while the $(+)_{589}$-isomer was eluted faster with Na_2SO_4. That is to say, opposed effects were observed between the discrimination by the resin and that by $[Sb_2\{(+)_{589}\text{-tartrate}\}_2]^{2-}$. A similar behavior in chromatographic resolution was observed for the complexes, $[Cr(acac)(bpy)(bpdo \text{ and } 3,3'\text{-}Me_2bpdo)]^{2+}$ (bpy=2,2'-bipyridine).[16]

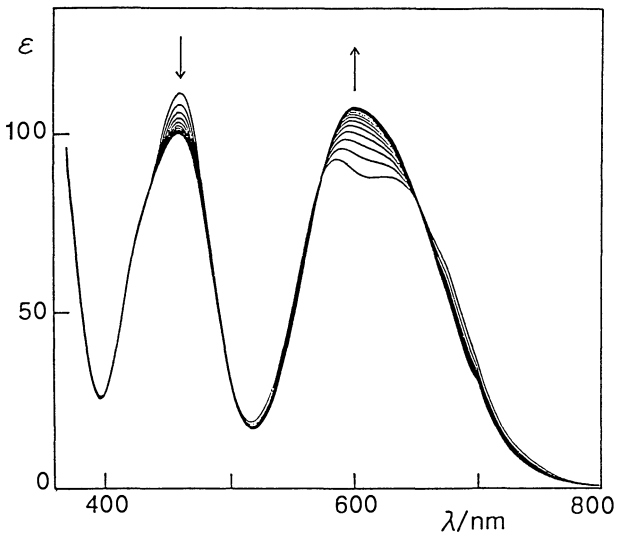

Fig. 2. Absorption spectral change with time of $[Cr(4,4'\text{-}Me_2bpdo)_3](NO_3)_3 \cdot 2H_2O$ in water at 25.0 °C. Spectra were recorded at 1—156 min after dissolution in water at regular time intervals (5 min). Trends of the spectral change are shown by arrows.

Figure 2 shows the absorption spectra of racemic $[Cr(4,4'\text{-}Me_2bpdo)_3]X_3$ ($X=NO_3^-$, ClO_4^-) in water which change rapidly with isosbestic points at 653, 575, and 437 nm. The optically active isomer behaves in the same way. Since the complex is stable in water as confirmed by column chromatography of the reaction product, the spectral change is attributable to the isomerization between two isomers of the complex. The spectrum immediately after dissolution in water closely resembles that of the *lel*$_2$·*ob* isomer of $[Cr\{(R \text{ or } S)\text{-}3,3'\text{-}Me_2bpdo\}_3]^{3+}$, while the final spectrum resembles that of the *lel*$_3$ isomer of the same complex.[7] Thus it is concluded that the nitrate and perchlorate of $[Cr(4,4'\text{-}Me_2bpdo)_3]^{3+}$ crystallize in the *lel*$_2$·*ob* isomer, but isomerize to the *lel*$_3$ one in water, and the complex exists in an equilibrium, *lel*$_2$·*ob* $\rightleftarrows$ *lel*$_3$ with a great preference for the latter (vide post). The same isomerization from *lel*$_2$·*ob* to *lel*$_3$ was observed for $[Cr(bpdo)_3]^{3+}$,[4] of which the spectral change was faster than that of $[Cr(4,4'\text{-}Me_2bpdo)_3]^{3+}$. Figure 3 shows the structures by Dreiding molecular models of the *lel*$_3$ and *lel*$_2$·*ob* isomers of $[Cr(4,4'\text{-}Me_2bpdo)_3]^{3+}$. The complex has a crowded structure, but the isomerization between the *lel*$_3$ and *lel*$_2$·*ob* isomers, a conformational inversion of one che-

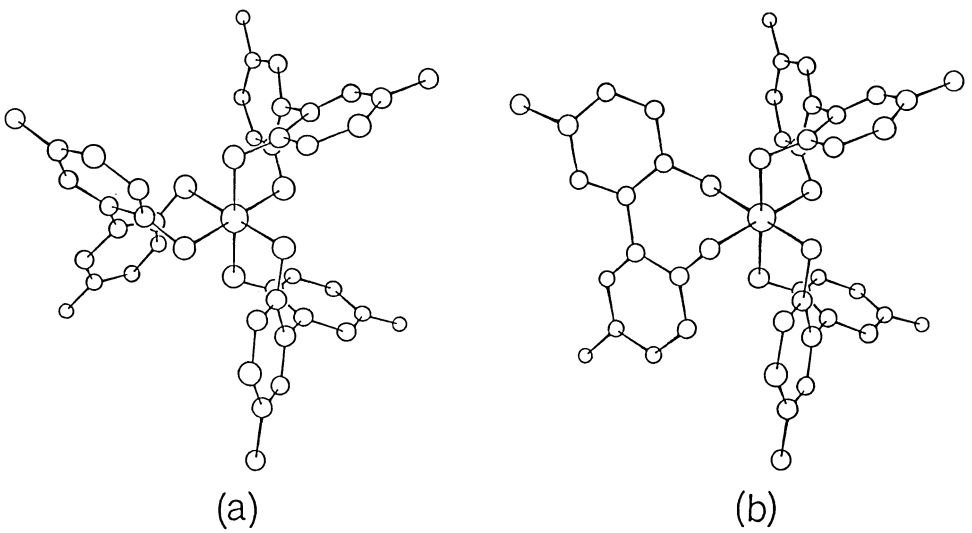

Fig. 3. Schematic drawing of the two conformational isomers of Δ-$[Cr(4,4'\text{-}Me_2bpdo)_3]^{3+}$; (a) $\Delta(\lambda\lambda\lambda)(lel_3)$, (b) $\Delta(\lambda\lambda\delta)(lel_2 \cdot ob)$.

late ring, seems to occur easily. However, the inversion is much slower than those of diamine chelate rings in [Fe(CN)4(1,2- or 1,3-diamine)]$^-$ (10^4—10^8 s^{-1} at 25 °C), the kinetics of which were studied by ^{1}H NMR spectroscopy.[17]

The two absorption bands in Fig. 2 correspond to the two d-d transitions of Cr(III), $^4T_{2g}\leftarrow{}^4A_{2g}$ and $^4T_{1g}\leftarrow{}^4A_{2g}$. The *lel*$_2$ · *ob* isomer has lower symmetry (C_2) than the *lel*$_3$ isomer (D_3) and shows the split band due to the first spin-allowed transition around 600 nm. The splitting disappears and the band becomes single and sharp with passage of time. Figure 4 shows the absorption spectra

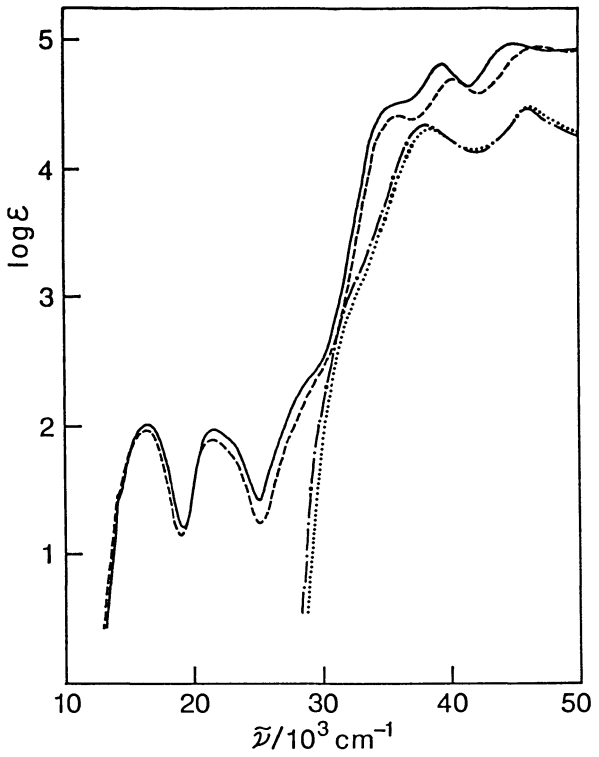

Fig. 4. Absorption spectra of [Cr(4,4'-Me2bpdo)3]3+ (——), [Cr(bpdo)3]3+ (——), 4,4'-Me2bpdo (— · —), and bpdo (·····) in water. The spectra were recorded after an equilibrium of *lel*$_2$ · *ob* ⇄ *lel*$_3$ had been reached.

Table 1. Absorption Spectral Data in Water[a]

Compound	$\tilde{\nu}$ / 10^3 cm^{-1} (log ε)
bpdo[b]	38.55 (4.32), 46.08 (4.48)
4,4'-Me2bpdo	38.20 (4.35), 46.04 (4.47)
[Cr(bpdo)3]3+ [b]	14.3 (1.5)sh, 16.41 (1.97), 21.39 (1.90), 22.7 (1.8)sh, 30.3 (2.5)sh, 35.96 (4.40), 40.26 (4.69), 46.73 (4.94)
[Cr(4,4'-Me2bpdo)3]3+	14.3 (1.5)sh, 16.56 (2.01), 21.72 (1.98), 22.7 (1.9)sh, 29.4 (2.4)sh, 36.4 (4.5)sh, 39.39 (4.81), 45.23 (4.97)

a) The data for the complexes are those for an equilibrium mixture of *lel*$_3$ and *lel*$_2$ · *ob* isomers. b) This work. sh: Shoulder.

of [Cr(4,4'-Me2bpdo)3]3+ and [Cr(bpdo)3]3+ in water at 25 °C after an equilibrium was reached between the two isomers. The spectra of free 4,4'-Me2bpdo and bpdo ligands are also given in Fig. 4. The spectral data are listed in Table 1. The spectra of these two complexes are very similar over the whole region. The first d-d band of the 4,4'-Me2bpdo complex (16560 cm^{-1}) is at higher energy by 150 cm^{-1} than that of the bpdo complex (16410 cm^{-1}). Whyman et al.[18] reported that the ligand field strength (10 Dq) of [Cr(4-Rpyo)6]3+ (4-Rpyo=4-substituted pyridine *N*-oxide) increases in the order of R=Cl<H<CH_3<CH_3O, and the Dq value increases with an increase in electron-releasing ability of the substituent at the 4-position of pyridine. The 10 Dq value of [Cr(4-CH_3pyo)6]3+ (16000 cm^{-1}) is larger by 130 cm^{-1} than that of [Cr(pyo)6]3+ (15870 cm^{-1}).[18] The shift of the band of [Cr(4,4'-Me2bpdo)3]3+ to higher energy from that of [Cr(bpdo)3]3+ is attributable to the same electron-releasing effect of two 4-methyl groups on bpdo. The [Cr(4,4'-(MeO)2bpdo)3]3+ (4,4'-(MeO)2bpdo=4,4'-dimethoxy-2,2'-bipyridine *N,N'*-dioxide) complex shows the first d-d band at 16720 cm^{-1} higher in energy by 160 cm^{-1} than that of the 4,4'-Me2bpdo complex.[19]

Figure 5 shows that (−)$_{589}$-[Cr(4,4'-Me2bpdo)3]-(ClO_4)3 · 4H_2O in aqueous solution loses optical activity in two steps with different rates. In the first rapid step (A), the decrease in activity accompanied the change of absorption spectra shown in Fig. 2, while no change of the spectra was observed in the subsequent slow step (B). Figure 6 shows the CD spectral change of the same (−)$_{589}$-isomer. In the first rapid step (Fig. 6(A)), the spectra change with isodichroic points at 596 and 510 nm, while in the second slow step (Fig. 6(B)), the spectra simply decrease the magnitude. These results support the previous conclusion that the first rapid step

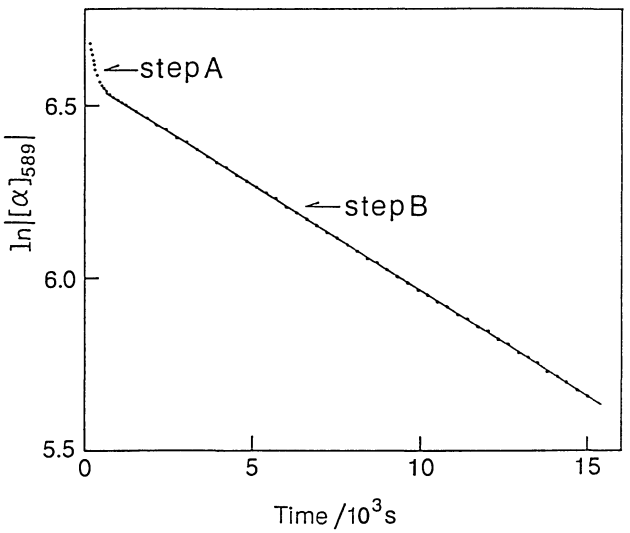

Fig. 5. Decrease in optical rotation with time of (−)$_{589}$-[Cr(4,4'-Me2bpdo)3](ClO_4)3 · 4H_2O in water at 40.0 °C. [Complex]=1.09 mmol dm^{-3}; *I*=0.1.

involves the isomerization of the *lel*$_2$·*ob* to *lel*$_3$ isomers, and the second slow step the racemization of the complex. The CD pattern of the $(-)_{589}$-isomer in the slow step (B) resembles that of $\Delta(\lambda\lambda\lambda)$-*lel*$_3$-[Cr{(*R*)-3,3'-Me$_2$bpdo}$_3$]$^{3+}$,[7] and the complex can be assigned to the Δ configuration. Thus it is concluded that $(-)_{589}$-[Cr(4,4'-Me$_2$bpdo)$_3$](ClO$_4$)$_3$·4H$_2$O crystallizes in the $\Delta(\lambda\lambda\delta)$ (*lel*$_2$·*ob*) isomer, but upon dissolution in water it isomerizes rapidly to the $\Delta(\lambda\lambda\lambda)$ (*lel*$_3$) isomer and then racemizes slowly, $\Delta(\lambda\lambda\lambda)$ (*lel*$_3$) $\rightleftarrows$ $\Lambda(\delta\delta\delta)$ (*lel*$_3$).

Kinetics of Isomerization and Racemization of [Cr(4,4'-Me$_2$bpdo)$_3$]$^{3+}$. The isomerization of [Cr(4,4'-Me$_2$bpdo)$_3$] (NO$_3$)$_3$·2H$_2$O in water, *lel*$_2$·*ob* $\rightleftarrows$ *lel*$_3$, was followed by monitoring the change in absorbance at 620 nm under the conditions described in Experimental part. The rate of spectral change obeyed the first-order kinetic law and the observed rate constant (k_{obsd}) was obtained from the slope of log ($A_\infty - A_t$) vs. time, where A's are absorbances at the time denoted by suffixes. The values of k_{obsd} are listed in Table 2, and the activation parameters in Table 3. The values for [Cr(bpdo)$_3$](NO$_3$)$_3$·2H$_2$O studied in this work are also given in the tables for comparison. The data of the nitrate of bpdo complex agreed well with those of the chloride and perchlorate reported previously.[4] The rates of both 4,4'-Me$_2$bpdo and bpdo complexes were independent of concentrations of H$^+$ and the free ligand, indicating an intramolecular reaction. The small nega-

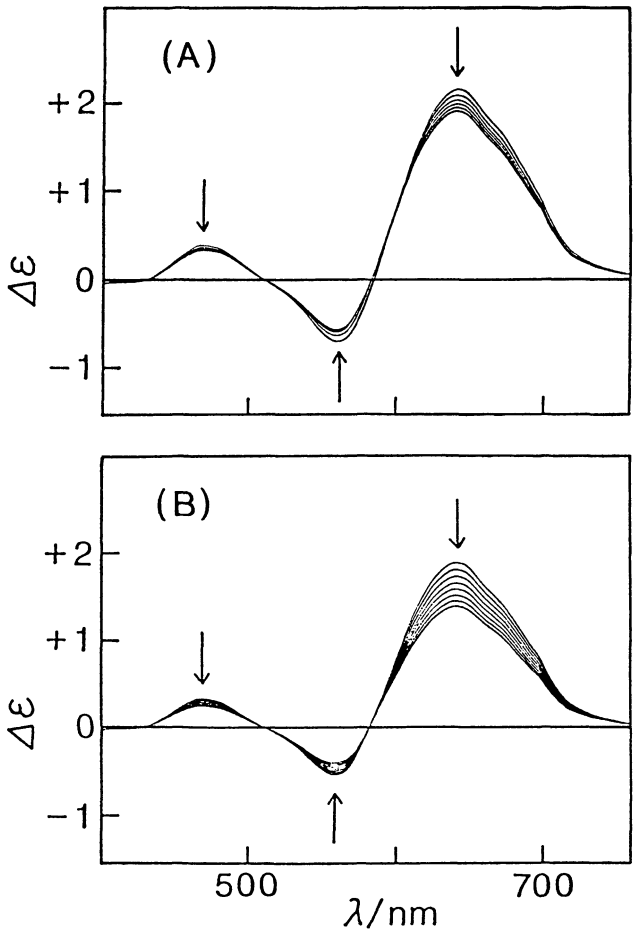

Fig. 6. CD spectral change with time of $(-)_{589}$-[Cr(4,4'-Me$_2$bpdo)$_3$](ClO$_4$)$_3$·4H$_2$O in water at 35.0 °C. Trends of the spectral change are shown by arrows. Reaction time (min): (A): 5, 10, 20, 30, 40, 50; (B): 60, 80, 100, 120, 140, 160, 180, 200 after dissolution in water.

Table 2. Rate Constants for the Isomerization of [Cr(L)$_3$](NO$_3$)$_3$ in Water (I=0.1)

t/°C	k_{obsd}/10^{-3} s^{-1}	t/°C	k_{obsd}/10^{-3} s^{-1}
	L=bpdo		
22.0	2.14±0.01[a]	30.0[b]	5.33±0.05
24.0	2.75±0.02	30.0[c]	5.36±0.04
30.0	5.35±0.04	35.0	8.69±0.08
	L=4,4'-Me$_2$bpdo		
20.0	0.755±0.002	30.0[e]	2.55±0.02
20.0[d]	0.753±0.003	35.0	4.39±0.03
25.0	1.39±0.01	35.0[b]	4.42±0.02
25.0[b]	1.38±0.01	35.0[d]	4.41±0.03
30.0	2.52±0.01	35.0[e]	4.38±0.04
30.0[b]	2.53±0.01	35.0[c,e]	4.39±0.03
30.0[c]	2.52±0.02	40.0	7.69±0.04
30.0[d]	2.53±0.02	40.0[b]	7.63±0.06

a) Errors are standard deviations estimated by least squares. b) In 0.1 mol dm^{-3} HCl. c) In 0.05 mol dm^{-3} free ligand (bpdo or 4,4'-Me$_2$bpdo). d) For the perchlorate of the complex. e) For the $(-)_{589}$-isomer.

Table 4. Rate Constants for the Racemization of $(-)_{589}$-[Cr(4,4'-Me$_2$bpdo)$_3$]$^{3+}$ in Water (I=0.1)

t/°C	k_{obsd}/10^{-5} s^{-1}	t/°C	k_{obsd}/10^{-5} s^{-1}
35.0	3.46±0.03	45.0[a]	10.0±0.02
40.0	6.09±0.02	45.0[b]	10.2±0.02
40.0[a]	6.12±0.01	45.0[b,c]	10.1±0.01
40.0[b]	6.09±0.02	50.0	17.8±0.02
40.0[c]	6.10±0.01	50.0[a]	17.6±0.03
45.0	10.2 ±0.01	55.0	29.5±0.02

a) In 0.1 mol dm^{-3} HCl. b) In 0.05 mol dm^{-3} 4,4'-Me$_2$bpdo. c) For the $(+)_{589}$-isomer.

Table 3. Isomerization Rate Constants at 35.0 °C and Activation Parameters for Complexes in Water

Complex	k_{obsd}	$\Delta H^{\ddagger}$	$\Delta S^{\ddagger}$	$\Delta G^{\ddagger}_{308.2}$
	10^{-3} s^{-1}	kJ mol^{-1}	J K^{-1} mol^{-1}	kJ mol^{-1}
[Cr(4,4'-Me$_2$bpdo)$_3$]$^{3+}$	4.39	86.0±0.3	−11.3±0.8	89.5±0.5
[Cr(bpdo)$_3$]$^{3+}$[a]	8.69	78.9±1.8	−28.4±5.9	87.7±3.6
[Cr(acac)(bpdo)$_2$]$^{2+}$[b]	12.2[c]	74.9	−38.5	86.8

a) This work. b) From Ref. 6. c) At 34.6 °C.

Table 5. Racemization Rate Constants at 35.0 °C and Activation Parameters for Complexes in Water

Complex	k_{obsd}	$\Delta H^{\ddagger}$	$\Delta S^{\ddagger}$	$\Delta G^{\ddagger}_{308.2}$
	$10^{-5}\,s^{-1}$	$kJ\,mol^{-1}$	$J\,K^{-1}\,mol^{-1}$	$kJ\,mol^{-1}$
$[Cr(4,4'\text{-}Me_2bpdo)_3]^{3+}$	3.46	87.5±0.6	−46.8±2.0	102±1
$[Cr(bpdo)_3]^{3+}$ a)	32.0	76.5	−64.0	96.2
$[Cr(acac)(bpdo)_2]^{2+}$ b)	47.6	82.4	−41.7	95.3

a) From Ref. 4. b) From Ref. 6.

tive values for the activation entropy would also indicate that the reactions proceed by an intramolecular mechanism. The activation enthalpy of 4,4'-Me_2bpdo complex is a little larger than that of the bpdo complex, and the complex isomerizes about two times slower than does the bpdo complex. The effect of two 4-methyl substituents is not clear on the conformational inversion of the 4,4'-Me_2bpdo chelate ring. The rate of racemization of the 4,4'-Me_2bpdo complex is also reduced by a factor of 10 compared with that of the bpdo complex as stated below.

Racemization of $[Cr(4,4'\text{-}Me_2bpdo)_3]^{3+}$ in water was studied by monitoring the change in optical rotation at 589 nm under the conditions described in Experimental part. The rate in step (B) in Fig. 5 obeyed the first-order kinetic law and the rate constant (k_{obsd}) was obtained from the slope of $\log|\alpha_t|$ vs. time, where α is degrees of optical rotation. The k_{obsd} values are given in Table 4, and the activation parameters in Table 5 together with those of the bpdo complexes. The rate was independent of concentrations of H^+ and the free ligand. The kinetic parameters for the 4,4'-Me_2bpdo and bpdo complexes in Table 5 are similar to those for the racemization of such complexes as $[Cr(bpy)_3]^{3+}$ or $[Cr(1,10\text{-phenanthroline})_3]^{3+}$, for which the reactions are suggested to proceed via an intramolecular twist mechanism.[20] The present dioxide complexes are supposed to racemize by such a mechanism, but the details remain unknown.

As Table 5 shows, the racemization of $[Cr(4,4'\text{-}Me_2bpdo)_3]^{3+}$ is about ten times as slow as that of $[Cr(bpdo)_3]^{3+}$. If it is assumed that these racemizations proceed by an intramolecular twist mechanism, the reactions involve both configurational ($\Delta \rightleftarrows \Lambda$) and conformational ($\delta \rightleftarrows \lambda$) inversions of three chelate rings in the complex. Studies with molecular models suggest that introduction of two methyl groups at the 4,4'-positions of bpdo scarcely exerts a steric effect on these inversions. As stated previously, the electron-releasing methyl groups on bpdo would increase the electron density of oxygen donor atoms and strengthen the Cr–O bonds to stabilize the complex. The rates of $[Cr(4,4'\text{-}Me_2bpdo)_3]^{3+}$ slower than those of $[Cr(bpdo)_3]^{3+}$ are supposed to result from such an electronic effect of the methyl substituent.

References

1) A. R. Al-Karaghouli, R. O. Day, and J. S. Wood, *Inorg. Chem.*, **17**, 3702 (1978).

2) N. W. Alcock and M. M. Roberts, *Acta Crystallogr., Sect. C*, **43**, 476 (1987).

3) I. Bertini, D. Gatteschi, and L. J. Wilson, *Inorg. Chim. Acta*, **4**, 629 (1970).

4) H. Kanno and J. Fujita, *Bull. Chem. Soc. Jpn.*, **60**, 589 (1987).

5) Elemantal analysis for racemic $[Cr(bpdo)_3](ClO_4)_3 \cdot 2H_2O$ was reinvestigated in this work, since there was somewhat ambiguity in our previous analytical result because of the complex being explosive (Ref. 11). Found: C, 37.86; H, 2.89; N, 8.88%. Calcd for $C_{30}H_{28}N_6O_{20}Cl_3Cr$: C, 37.89; H, 2.97; N, 8.84%.

6) H. Kanno, T. Shimotori, S. Utsuno, and J. Fujita, *Chem Lett.*, **1983**, 939; H. Kanno, S. Utsuno, and J. Fujita, *Bull. Chem. Soc. Jpn.*, **57**, 3443 (1984).

7) H. Kanno, K. Kashiwabara, and J. Fujita, *Bull. Chem. Soc. Jpn.*, **52**, 1408 (1979).

8) A. Marker, A. J. Canty, and R. T. C. Brownlee, *Aust. J. Chem.*, **31**, 1255 (1978); S. A. Sojka, *J. Org. Chem.*, **44**, 307 (1979).

9) S. K. Madan and W. E. Bull, *J. Inorg. Nucl. Chem.*, **26**, 2211 (1964).

10) L. S. Dollimore and R. D. Gillard, *J. Chem. Soc., Dalton Trans.*, **1973**, 933.

11) H. Kanno, K. Kashiwabara, and J. Fujita, *Bull. Chem. Soc. Jpn.*, **52**, 761 (1979).

12) I. Murase, *Nippon Kagaku Zasshi*, **77**, 682 (1956).

13) P. G. Simpson, A. Vinciguerra, and J. V. Quagliano, *Inorg. Chem.*, **2**, 282 (1963).

14) Y. Yoshikawa and K. Yamasaki, *Coord. Chem. Rev.*, **28**, 205 (1979).

15) H. Yoneda, *J. Liq. Chromatogr.*, **2**, 1157 (1979); H. Yoneda, *J. Chromatogr.*, **313**, 59 (1984).

16) H. Kanno, S. Utsuno, and J. Fujita, *Bull. Chem. Soc. Jpn.*, **59**, 1293 (1986).

17) Y. Kuroda, N. Tanaka, M. Goto, and T. Sakai, *Inorg. Chem.*, **28**, 997 (1989); Y. Kuroda, M. Goto, and T. Sakai, *Bull. Chem. Soc. Jpn.*, **62**, 3437 (1989).

18) R. Whyman, W. E. Hatfield, and J. S. Paschal, *Inorg. Chim. Acta*, **1**, 113 (1967).

19) H. Kanno, J. Yamamoto, S. Utsuno, and J. Fujita, unpublished work.

20) N. A. P. Kane-Maguire and S. A. Edwards, *J. Inorg. Nucl. Chem.*, **38**, 1037 (1976); G. A. Lawrance and D. R. Stranks, *Inorg. Chem.*, **16**, 929 (1977); G. A. Lawrance and S. Suvachittanont, *Inorg. Chim. Acta*, **32**, L13 (1979).

Preparation and Characterization of Cobalt(III), Nickel(II), and Copper(I) Complexes Containing 5,8-Diphenyl-5,8-diphospha-2,11-dithiadodecane (L), $CH_3SCH_2CH_2P(C_6H_5)CH_2CH_2P(C_6H_5)CH_2CH_2SCH_3$, and Molecular Structure of $[Ni(rac(P)\text{-}L)_2](BF_4)_2$

Tetsuji KITAGAWA, Masakazu KITA, Kazuo KASHIWABARA, and Junnosuke FUJITA*
Department of Chemistry, Faculty of Science, Nagoya University, Chikusa-ku, Nagoya 464-01
(Received May 29, 1991)

Δ-RR,Λ-SS-$[Co(acac)_2(rac(P)\text{-}L)]^+$ and $[Co(acac)_2(meso(P)\text{-}L)]^+$ were obtained by reaction of $[Co(acac)_3]$ (acac=2,4-pentanedionate ion) with 5,8-diphenyl-5,8-diphospha-2,11-dithiadodecane (L) in 1:1 molar ratio in dichloromethane in the presence of active charcoal, no *Δ-SS,Λ-RR* isomer of the *rac(P)*-L complex being formed. Five-coordinate $[Ni(rac(P)\text{-}L)_2]^{2+}$ and $[Ni(meso(P)\text{-}L)_2]^{2+}$ were yielded by reaction of Ni(II) and L in 1:2 molar ratio in methanol, and the molecular structure of less soluble $[Ni(rac(P)\text{-}L)_2](BF_4)_2$ was determined by X-ray analysis. Crystal data: monoclinic, space group $P2_1/n$, a=17.136(3), b=20.134(5), c=14.106(3) Å, β=93.30(2)°, V=4859(2) Å^3, Z=4, R=0.089 for 8001 reflections. The Ni atom is surrounded square pyramidally by four P atoms in the basal plane and one S atom at the apical position with distances of the Ni–P: 2.214(2)—2.234(2) Å and the Ni–S: 2.603(2) Å. Both $[Ni(rac(P)\text{-}L)_2]^{2+}$ and $[Ni(meso(P)\text{-}L)_2]^{2+}$ in CH_2Cl_2 solutions exchange four $-SCH_3$ groups at the apical positin on the NMR time scale. White $[Cu(rac(P)\text{-}L)]BF_4$ was precipitated selectively by reaction of $Cu(BF_4)_2\cdot 6H_2O$ and L in 1:1 molar ratio in ethanol.

In our previous papers, we have reported the preparation and stereochemistry of octahedral cobalt(III) complexes with linear quadridentate phosphine ligands of the PNNP[1–4] and NPPN[5–7] types for donor atoms. The ligand of the latter type has two chiral phosphorus donor atoms and forms various stereoisomers depending on the chirality. This paper reports the preparation and characterization of cobalt(III), nickel(II), and copper(I) complexes of 5,8-diphenyl-5,8-diphospha-2,11-dithiadodecane, $CH_3SCH_2CH_2P(C_6H_5)CH_2CH_2P(C_6H_5)CH_2CH_2SCH_3$ (L), together with the X-ray crystal structure of $[Ni(rac(P)\text{-}L)_2](BF_4)_2$. The ligand is also a linear quadridentate ligand with two chiral phosphorus and two sulfur donor atoms. However, ligand L was found to act as a bidentate in Co(III), a bidentate and a terdentate in Ni(II), and a quadridentate in Cu(I) complexes.

To our knowledge, only two papers have appeared for metal complexes of the SPPS-type ligand. Issleib and Gans[8] prepared $[MX(NH_3)(SCH_2CH_2PHCH_2CH_2PHCH_2CH_2S)]$ (M=Co, X=Br; M=Rh, X=Cl) and $[M\{SCH(R)CH_2PHCH_2CH_2PHCH_2CH(R)S\}]$ (M=Ni, Pd, Pt; R=H, CH_3). However, detailed stereochemistry for Co(III) and Rh(III) complexes was not reported. Schmelzer and Schwarzenbach[9] reported the X-ray crystal structures of *rac(P)*- and *meso(P)*-isomers of $[Ni(SCH_2CH_2P(C_6H_5)CH_2CH_2CH_2P(C_6H_5)CH_2CH_2S)]$, but experimental details and chemical properties were not described.

Experimental

The phosphine ligand was handled under an atmosphere of nitrogen until it formed metal complexes. All solvents used for the preparation of the ligand and complexes were made oxygen-free by bubbling nitrogen for 20 min immediately before use. Absorption and ^1H and ^{13}C NMR spectra were recorded on a Hitachi U3400 and a R-90H spectrometer, respectively.

Preparation of 5,8-Diphenyl-5,8-diphospha-2,11-dithiadodecane (L). A 15% hexane solution of butyl lithium (53 cm^3, 0.086 mol) was added dropwise with stirring to a dry tetrahydrofuran solution (600 cm^3) of 1,2-bis(phenylphosphino)ethane[10] (8.3 g, 0.034 mol). The solution changed from red to orange in color and gave yellow precipitate of $C_6H_5P(Li)CH_2CH_2P(Li)C_6H_5$. The precipitate was dissolved by warming at 50 °C. To the solution was added 2-chloroethyl methyl sulfide (7.5 g, 0.067 mol). The mixture was stirred at 50 °C for 5 h, and cooled to room temperature. Water (800 cm^3) was added to the solution dropwise with stirring. The ethereal layer was separated, dried over $MgSO_4$ (5 g) overnight, filtered, and the filtrate was evaporated to leave an oily product. This was used for the preparation of metal complexes without further purification. Yield: 13.2 g (98%).

Preparation of Metal Complexes. $[Co(acac)_2(meso(P)\text{-}L)]SbF_6$ (A-I) and *Δ-RR,Λ-SS*-$[Co(acac)_2(rac(P)\text{-}L)]SbF_6$ (A-II). A mixture of $[Co(acac)_3]$[11] (0.19 g, 0.53 mmol), L (0.21 g, 0.53 mmol) and active charcoal (0.03 g) in dichloromethane (20 cm^3) was stirred for 10 h. Active charcoal was filtered off, and the filtrate was evaporated to dryness under reduced pressure. The residue was dissolved in a mixture of water and methanol (2:1, 50 cm^3), and the solution was applied on a column (ϕ3 cm×120 cm) of SP-Sephadex C-25. By elution with a 0.1 mol dm^{-3} NaCl aqueous solution two large dark-red bands (**A-I** and **A-II** in the order of elution) and several small bands appeared. Each eluate of the two large bands was shaken with chloroform to extract the complex. The extract was evaporated to dryness and the residue was dissolved in water. On addition of excess $NaSbF_6$ the solution yielded orange brown crystals, which were collected by filtration and recrystallized from a hot mixture of water and methanol (1:1). Yield: 93 mg (19%) for **A-I** and 99 mg (21%) for **A-II**. Found for **A-I**: C, 40.61; H, 4.83%. Found for **A-II**: C, 40.89; H, 4.81%. Calcd for $[Co(acac)_2L]SbF_6=C_{30}H_{42}O_4S_2P_2SbF_6Co$: C, 40.61; H, 4.77%. The complexes are soluble in methanol, ethanol, chloroform, and acetone, and

slightly soluble in water and diethyl ether.

[Ni(*rac*(*P*)-L)$_2$](BF$_4$)$_2$ (B-I) and [Ni(*meso*(*P*)-L)$_2$](BF$_4$)$_2$ (B-II). Ni(BF$_4$)$_2$·6H$_2$O (0.54 g, 1.6 mmol) and L (1.2 g, 3.1 mmol) were mixed in methanol (15 cm^3) with stirring at room temperature, and then the mixture was cooled at 0 °C. After 30 min a red-brown precipitate (**B-I**) which appeared was collected by filtration and recrystallized from hot methanol. Yield: 0.43 g (27%). The filtrate was allowed to stand to evaporate slowly, yielding red-brown crystals (**B-II**). They were recrystallized from hot methanol. Yield: 0.23 g (15%). Found for **B-I**: C, 47.03; H, 5.56%. Found for **B-II**: C, 47.15; H, 5.64%. Calcd for [Ni(L)$_2$](BF$_4$)$_2$=C$_{40}$H$_{56}$P$_4$S$_4$B$_2$F$_8$Ni: C, 47.04; H, 5.53%. The complexes are soluble in chloroform and methanol, and insoluble in water and diethyl ether.

Table 1. Positional Parameters (×10^4) and Equivalent Isotropic Temperature Factors of [Ni(*rac*(*P*)-L)$_2$](BF$_4$)$_2$

Atom	x	y	z	B_{eq}/Å^2
Ni	3950.1(4)	2137.0(3)	3941.1(4)	2.4
S1	5069 (2)	3213 (1)	247 (2)	6.8
S2	5431 (2)	3324 (2)	7571 (2)	7.1
S3	870 (1)	3671 (1)	3555 (2)	7.1
S4	4604 (1)	1234 (1)	5043 (1)	3.8
P1	4945 (1)	2124 (1)	2991 (1)	3.1
P2	4513 (1)	3050 (1)	4552 (1)	3.1
P3	2802 (1)	2348 (1)	4552 (1)	2.8
P4	3361 (1)	1275 (1)	3239 (1)	2.9
F1	1522 (6)	2974 (4)	968 (10)	12.0
F2	2681 (5)	3318 (5)	1525 (6)	9.8
F3	1737 (9)	4045 (5)	1107 (19)	17.0
F4	2351 (8)	3453 (8)	28 (6)	13.4
F5	−3028 (13)	4863 (8)	3088 (18)	17.5
F6	−3350 (16)	4998 (9)	2002 (15)	17.8
F7	−2408 (17)	4246 (10)	2081 (34)	25.3
F8	−3312 (17)	3829 (9)	2771 (20)	19.2
C1	4669 (13)	3969 (7)	661 (12)	10.4
C2	5389 (4)	2821 (4)	1338 (6)	5.2
C3	4709 (4)	2605 (4)	1908 (5)	4.7
C4	5390 (3)	1367 (3)	2589 (4)	3.4
C5	5209 (4)	1120 (4)	1684 (5)	4.5
C6	5567 (5)	531 (4)	1399 (6)	5.7
C7	6070 (5)	198 (4)	1985 (7)	5.8
C8	6257 (4)	440 (4)	2863 (7)	5.9
C9	5915 (4)	1010 (4)	3190 (5)	4.3
C10	5777 (4)	2532 (4)	3655 (5)	4.4
C11	5475 (4)	3180 (4)	4027 (6)	4.9
C12	4060 (4)	3851 (3)	4302 (4)	3.5
C13	4057 (4)	4365 (4)	4963 (6)	4.8
C14	3777 (5)	4985 (4)	4707 (8)	5.9
C15	3485 (5)	5097 (4)	3808 (7)	5.6
C16	3447 (5)	4594 (4)	3130 (6)	5.6
C17	3733 (4)	3973 (4)	3406 (5)	4.7
C18	4692 (4)	3002 (3)	5856 (5)	4.2
C19	5424 (4)	3323 (5)	6283 (6)	5.5
C20	4873 (9)	4058 (8)	7755 (7)	8.7
C21	−99 (6)	3510 (7)	3875 (8)	7.7
C22	1350 (4)	2969 (4)	4139 (5)	4.4
C23	2180 (3)	2914 (4)	3809 (4)	3.9
C24	2754 (3)	2660 (3)	5757 (4)	3.4
C25	2847 (4)	2225 (4)	6498 (5)	4.8
C26	2871 (6)	2477 (7)	7426 (5)	6.9
C27	2788 (6)	3119 (6)	7615 (6)	6.9
C28	2692 (5)	3569 (6)	6866 (8)	7.0
C29	2675 (4)	3342 (4)	5931 (5)	4.7
C30	2267 (3)	1563 (3)	4545 (4)	3.3
C31	2356 (3)	1212 (3)	3604 (5)	4.0
C32	3242 (3)	1185 (3)	1953 (4)	3.5
C33	3431 (4)	589 (4)	1498 (5)	4.9
C34	3294 (5)	539 (5)	523 (6)	6.2
C35	2994 (5)	1075 (5)	−2 (6)	6.2
C36	2821 (5)	1644 (5)	451 (5)	6.0
C37	2947 (4)	1715 (4)	1433 (5)	4.4
C38	3831 (4)	503 (3)	3684 (5)	4.0
C39	3996 (4)	512 (3)	4732 (5)	4.0
C40	4676 (6)	1170 (5)	6310 (5)	6.1
B1	2077 (6)	3460 (5)	903 (7)	5.8
B2	−3181 (10)	4424 (9)	2460 (9)	9.2

[Cu(*rac*(*P*)-L)]BF$_4$. Mixing of Cu(BF$_4$)$_2$·6H$_2$O (0.13 g, 0.53 mmol) and L (0.21 g, 0.53 mmol) in methanol (10 cm^3) with stirring resulted in immediate formation of a white precipitate. It was collected by filtration and washed with water. Yield: 0.09 g (31%). Found: C, 44.03; H,5.16%. Calcd for [Cu(L)]BF$_4$=C$_{20}$H$_{28}$P$_2$S$_2$BF$_4$Cu: C, 44.10; H, 5.18%. The complex is soluble in chloroform, but insoluble in water, methanol, and diethyl ether.

X-Ray Analysis. A reddish brown crystal of [Ni(*rac*(*P*)-L)$_2$](BF$_4$)$_2$with approximate dimensions, 0.30×0.28×0.25 mm^3 was used for the data collection. Crystal data: monoclinic, $P2_1/n$, a=17.136(3), b=20.134(5), c=14.106(3) Å, β=93.30(2)°, V=4859(2) Å^3, D_X=1.40, D_m=1.39 g cm^{-3}, Z=4, and μ(Mo $K\alpha$)=7.53 cm^{-1}. Diffraction data were collected on a Rigaku AFC-5R diffractometer with graphite Mo $K\alpha$ radiation (λ=0.71069 Å). Within the range $2\theta<60°$, 8001 independent reflections with $|F_o|>3\sigma(|F_o|)$ were obtained. Absorption corrections were made by using the DABEX program.[12] The calculations were carried out on a HITAC M-680H computer at the Computer Center of the Institute for Molecular Science with the program system UNICS III.[12]. The structure was solved by the usual heavy-atom method; the position of Ni was deduced by means of the Patterson synthesis, and all the non-hydrogen atoms were located by the subsequent Fourier synthesis. The positions of 16 among 56 hydrogen atoms were identified in the subsequent difference-Fourier maps. The structure was refined by block-diagonal least squares methods with anisotropic thermal parameters for non-hydrogen atoms and isotropic for hydrogen atoms. The function minimized was $\sum w||F_o|-|F_c||^2$. Final R was 0.089 for 8001 observed unique reflections, and the atomic parameters of non-hydrogen atoms are listed in Table 1. Complete lists of observed and calculated structure factors, hydrogen atomic parameters, and anisotropic thermal parameters for non-hydrogen atoms are deposited as Document No. 8964 at the Office of the Editor of Bull. Chem. Soc. Jpn.

Results and Discussion

Cobalt(III) Complexes. Two isomers (**A-I** and **A-II**) of [Co(acac)$_2$(L)]$^+$ were obtained by reaction of [Co(acac)$_3$] with L in dichloromethane in the presence of active charcoal. The two isomers show absorption spectra very similar to each other, and give the first d-d band at 21300 (**A-I**) and 21200 cm^{-1} (**A-II**) (Fig. 1). These band positions are similar to those of [Co(acac)$_2$-{(C$_6$H$_5$)$_2$PCH$_2$CH$_2$P(C$_6$H$_5$)$_2$}]$^+$ (20200 cm^{-1})[13] and [Co(acac)$_2${(CH$_3$)$_2$PCH$_2$CH$_2$P(CH$_3$)$_2$}]$^+$ (23400 cm^{-1}),[14] indicating the coordination of two phosphorus atoms of L in these isomers. For [Co(acac)$_2$L)]$^+$, there are three

possible isomers, *Λ-RR,Λ-SS*- and *Λ-RR,Λ-SS*-[Co(acac)$_2$(*rac*(*P*)-L)]$^+$ and [Co(acac)$_2$(*meso*(*P*)-L)]$^+$. The *rac*(*P*)- and *meso*(*P*)-L complexes have C_2 and C_1 symmetries, respectively. In the ^{1}H NMR spectra isomer **A-I** exhibits six singlets for the methyl group (δ=0.96, 1.94, 2.03, 2.06, 2.16, 2.17, in $CDCl_3$) and two singlets for the methine group (δ=4.74, 5.51). Thus isomer **A-I** was assigned to the *meso*(*P*)-L complex. For isomer **A-II**, three singlet methyl signals (δ=1.04, 2.06, 2.12) and one singlet methine signal (δ=4.93) are observed, and the isomer can be assigned to the *rac*(*P*)-L complex. The assignment of either the *Λ-RR,Λ-SS* or *Λ-RR,Λ-SS* isomer was made on the basis of the chemical shift of methine proton of acac. Molecular models show that the phenyl groups of L in the *Λ-RR, Λ-SS* isomer are located over the acac chelate rings, while those in the *Λ-RR,Λ-SS* isomer are disposed away from the acac chelate rings. The methine protons of isomer **A-II** resonate at a remarkably high field (δ=4.93) compared with that (δ=5.51) of [Co(acac)$_3$]. The high field shift is attributable to the shielding effect of the phenyl group located over the acac chelate ring as has been often observed for related complexes.[3,6,7,13–15]

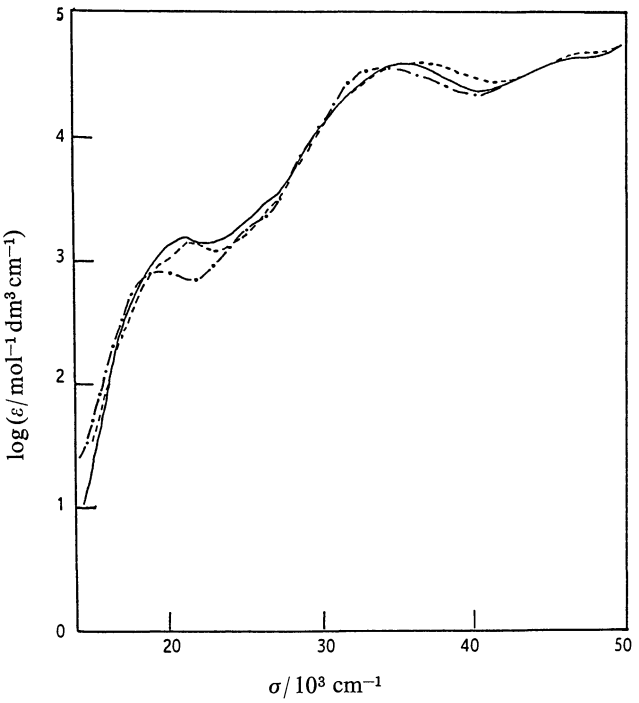

Fig. 1. Electronic spectra of [Co(acac)$_2$(X)]SbF$_6$ in CH_3CN solution; X=*rac*(*P*)-L (——), X=*meso*(*P*)-L (– – –), and [Co(acac)$_2${(C$_6$H$_5$)$_2$PCH$_2$CH$_2$P(C$_6$H$_5$)$_2$}]PF$_6$ (— · —) in ethanol.

Thus **A-II** was assigned to the *Λ-RR,Λ-SS*-L isomer. Two methine proton signals with a large chemical shift difference in the *meso*(*P*)-L complex (**A-I**) are consistent with molecular model considerations.

The formation of the other *Λ-RR,Λ-SS* isomer of the *rac*(*P*)-L complex was not observed. In this isomer the $-CH_2CH_2SCH_3$ group is disposed over the acac chelate ring, and the structure is supposed to be less stable than that of the *Λ-RR,Λ-SS* isomer with the phenyl group over the acac chelate ring. No acac complex containing quadridentate L, [Co(acac)(L)]$^{2+}$ was formed under the experimental conditions, in contrast to $NH_2(CH_2)_2P(C_6H_5)(CH_2)_nP(C_6H_5)(CH_2)_2NH_2$ (=NPPN, n=2[5,6], 3[6]) which formed only quadridentate ligand complexes, [Co(acac)(NPPN)]$^{2+}$ by similar reactions. The coordination ability of the $-SCH_3$ group would be weaker than that of acac toward Co(III).

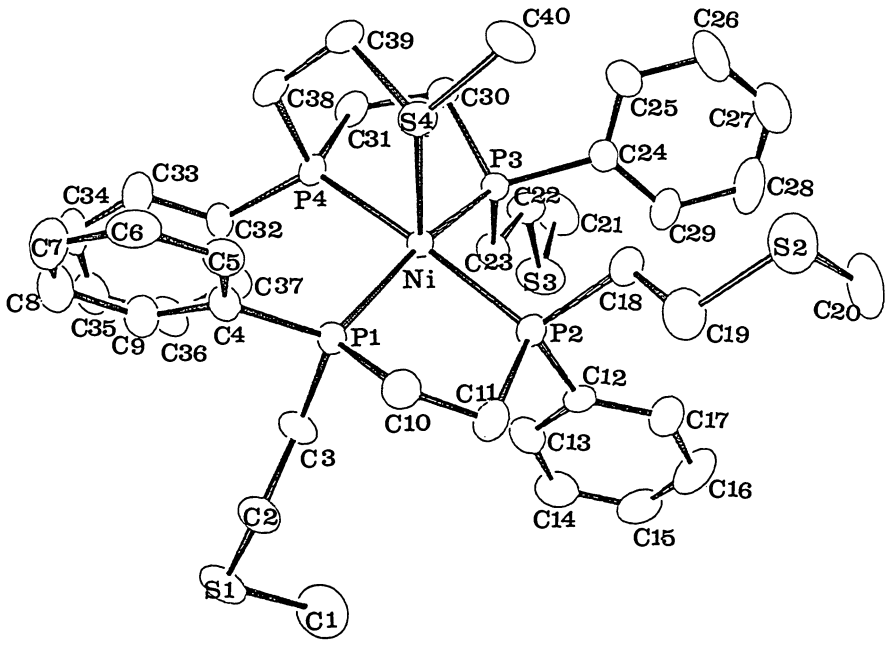

Fig. 2. A perspective view of [Ni(*rac*(*P*)-L)$_2$]$^{2+}$.

Nickel(II) Complexes. Two isomers (**B-I** and **B-II**) of $[Ni(L)_2](BF_4)_2$ were obtained by fractional crystallization from a methanol solution containing $Ni(BF_4)_2 \cdot 6H_2O$ and L in 1 : 2 molar ratio. The structure of the less soluble isomer (**B-I**) was determined by an X-ray diffraction method. A perspective view of the complex cation is shown in Fig. 2. The selected bond distances and angles are given in Table 2. The complex is a racemate consisting of $[Ni(RR(P)\text{-}L)_2]^{2+}$ and $[Ni(SS(P)\text{-}L)_2]^{2+}$. The chirality of the coordinating sulfur atom is *S* for the *RR*(*P*)-L and *R* for the *SS*(*P*)-L complexes. The Ni(II) ion forms a slightly distorted square pyramid with four phosphorus atoms in the basal plane and the sulfur atom at the apical position. The average Ni–P distance of 2.226(2) Å is very similar to those reported for square pyramidal diphosphine–Ni(II) complexes, $[NiBr(HQ)(H_2Q)] \cdot H_2O$ (av. 2.227(2) Å, H_2Q=$HO_2CCH_2P(C_6H_5)(CH_2)_2P(C_6H_5)CH_2CO_2H$, Br^- at the apical position)[16] and [NiI(depe)$_2$]I (av. 2.224(5) Å, depe =$(C_2H_5)_2P(CH_2)_2P(C_2H_5)_2$, I^- at the apical position).[17] The Ni–S distance (2.603(2) Å) is longer than those found in both square planar (2.22 Å) and octahedral (2.43 Å) Ni(II) complexes.[18] It is known that the apical Ni-ligand bond distance in a square pyramidal complex is, in general, fairly long compared with those in the basal plane.[19] For example, the apical Ni–S bond distance in the square pyramidal [NiI_2{bis(*o*-methylthiophenyl)phenylphosphine}] complex is 2.789(10) Å, while that at the basal position is 2.189(9) Å.[20]

The deviations from the mean plane formed by four phosphorus atoms are −0.111(2), 0.126(2), 0.113(2), and −0.143(2) Å for P(1), P(2), P(3), and P(4), respectively, 0.204(1) Å for the Ni(II) and 2.753(2) Å for the S atom. The two P–P chelate rings take a nearly δ gauche conformation in $[Ni(RR(P)\text{-}L)_2]^{2+}$, while the P–S chelate ring forms a λ gauche one. The dihedral angles are 45.1(5)° for P(1)–C(10)–C(11)–P(2), 41.9(4)° for P(3)–C(30)–C(31)–P(4), and 54.7(5)° for S(4)–C(38)–C(39)–P(4). Four skeletal atoms of each uncoordinated P–C–C–S group are almost in a plane (dihedral angles: 5.7(7), 7.8(7), 13.5(5)°).

The ^1H and ^{13}C NMR spectra of $[Ni(rac(P)\text{-}L)_2]^{2+}$ in CD_2Cl_2 at 30 °C show a singlet signal at δ=2.16 and 16.8, respectively, for the $-SCH_3$ groups. These results indicate that the coordinating $-SCH_3$ group in the solid state dissociates or exchanges rapidly with free $-SCH_3$ groups on the NMR time scale in solution. In Fig. 3 is compared the absorption spectrum in CH_2Cl_2 solution with the reflection spectrum in the solid state. These spectra are very similar in pattern, and the band around 25000 cm^{-1} is the one characteristic of a square pyrami-

Table 2. Bond Distances (l/Å) and Angles (ϕ/°) of $[Ni(rac(P)\text{-}L)_2](BF_4)_2$

Ni–S(4)	2.603(2)	Ni–P(1)	2.228(2)	C(21)–S(3)–C(22)	98.5(5)	Ni–S(4)–C(39)	101.1(2)
Ni–P(2)	2.227(2)	Ni–P(3)	2.233(2)	Ni–S(4)–C(40)	130.5(3)	C(39)–S(4)–C(40)	100.9(4)
Ni–P(4)	2.214(2)	S(1)–C(1)	1.782(16)	Ni–P(1)–C(3)	110.8(3)	Ni–P(1)–C(4)	123.3(2)
S(1)–C(2)	1.787(8)	S(2)–C(19)	1.816(8)	Ni–P(1)–C(10)	106.5(2)	C(3)–P(1)–C(4)	105.0(3)
S(2)–C(20)	1.786(16)	S(3)–C(21)	1.776(11)	C(3)–P(1)–C(10)	108.3(3)	C(4)–P(1)–C(10)	101.9(3)
S(3)–C(22)	1.809(8)	S(4)–C(39)	1.826(6)	Ni–P(2)–C(11)	109.6(2)	Ni–P(2)–C(12)	119.1(2)
P(1)–C(3)	1.835(7)	P(1)–C(4)	1.810(6)	Ni–P(2)–C(18)	112.6(2)	C(11)–P(2)–C(12)	100.2(3)
P(1)–C(10)	1.852(7)	P(2)–C(11)	1.863(7)	C(11)–P(2)–C(18)	107.7(3)	C(12)–P(2)–C(18)	106.5(3)
P(2)–C(12)	1.815(6)	P(2)–C(18)	1.849(7)	Ni–P(3)–C(23)	113.0(2)	Ni–P(3)–C(24)	120.9(2)
P(3)–C(23)	1.845(7)	P(3)–C(24)	1.819(6)	Ni–P(3)–C(30)	105.0(3)	C(23)–P(3)–C(24)	105.2(3)
P(3)–C(30)	1.827(6)	P(4)–C(31)	1.829(6)	C(23)–P(3)–C(30)	105.0(3)	C(24)–P(3)–C(30)	104.7(3)
P(4)–C(32)	1.823(6)	P(4)–C(38)	1.843(6)	Ni–P(4)–C(31)	109.9(2)	Ni–P(4)–C(32)	123.0(2)
C(2)–C(3)	1.516(11)	C(4)–C(5)	1.389(9)	Ni–P(4)–C(38)	109.2(2)	C(31)–P(4)–C(32)	102.7(3)
C(4)–C(9)	1.399(9)	C(5)–C(6)	1.405(12)	C(31)–P(4)–C(38)	104.3(3)	C(32)–P(4)–C(38)	106.1(3)
C(6)–C(7)	1.339(12)	C(7)–C(8)	1.352(14)	S(1)–C(2)–C(3)	112.1(5)	P(1)–C(3)–C(2)	117.0(5)
C(8)–C(9)	1.380(11)	C(10)–C(11)	1.510(11)	P(1)–C(4)–C(5)	120.9(5)	P(1)–C(4)–C(9)	120.7(5)
C(12)–C(13)	1.393(10)	C(12)–C(17)	1.375(9)	C(4)–C(5)–C(6)	119.1(7)	C(5)–C(6)–C(7)	121.6(8)
C(13)–C(14)	1.379(11)	C(14)–C(15)	1.355(14)	C(6)–C(7)–C(8)	119.6(8)	C(7)–C(8)–C(9)	121.6(8)
C(15)–C(16)	1.391(13)	C(16)–C(17)	1.390(12)	C(4)–C(9)–C(8)	119.7(7)	P(1)–C(10)–C(11)	106.8(5)
C(18)–C(19)	1.507(11)	C(22)–C(23)	1.526(9)	P(2)–C(11)–C(10)	110.3(5)	P(2)–C(12)–C(13)	123.2(5)
C(24)–C(25)	1.366(9)	C(24)–C(29)	1.402(10)	P(2)–C(12)–C(17)	119.0(5)	C(12)–C(13)–C(14)	120.8(7)
C(25)–C(26)	1.402(11)	C(26)–C(27)	1.330(18)	C(13)–C(14)–C(15)	119.9(8)	C(14)–C(15)–C(16)	121.6(8)
C(27)–C(28)	1.395(15)	C(28)–C(29)	1.395(14)	C(15)–C(16)–C(17)	117.3(8)	C(12)–C(17)–C(16)	122.5(7)
C(30)–C(31)	1.520(9)	C(32)–C(33)	1.408(10)	P(2)–C(18)–C(19)	117.5(5)	S(2)–C(19)–C(18)	111.0(6)
C(32)–C(37)	1.376(9)	C(33)–C(34)	1.385(12)	S(3)–C(22)–C(23)	109.0(5)	P(3)–C(23)–C(22)	112.9(5)
C(34)–C(35)	1.390(14)	C(35)–C(36)	1.354(14)	P(3)–C(24)–C(25)	119.0(5)	P(3)–C(24)–C(29)	120.8(5)
C(36)–C(37)	1.397(10)	C(38)–C(39)	1.489(10)	C(24)–C(25)–C(26)	118.7(8)	C(25)–C(26)–C(27)	122.7(9)
				C(26)–C(27)–C(28)	119.4(9)	C(24)–C(29)–C(28)	119.4(8)
S(4)–Ni–P(1)	91.89(6)	S(4)–Ni–P(2)	100.57(6)	P(3)–C(30)–C(31)	109.3(4)	P(4)–C(31)–C(30)	110.9(4)
S(4)–Ni–P(3)	105.11(6)	S(4)–Ni–P(4)	83.61(6)	P(4)–C(32)–C(33)	121.5(5)	P(4)–C(32)–C(37)	118.1(5)
P(1)–Ni–P(2)	84.99(6)	P(1)–Ni–P(3)	162.86(6)	C(32)–C(33)–C(34)	118.9(7)	C(33)–C(34)–C(35)	120.7(9)
P(1)–Ni–P(4)	93.87(6)	P(2)–Ni–P(3)	93.77(6)	C(34)–C(35)–C(36)	119.3(8)	C(35)–C(36)–C(37)	122.0(8)
P(2)–Ni–P(4)	175.69(6)	P(3)–Ni–P(4)	86.10(6)	C(32)–C(37)–C(36)	118.7(7)	P(4)–C(38)–C(39)	112.5(4)
C(1)–S(1)–C(2)	101.5(6)	C(19)–S(2)–C(20)	100.0(5)	S(4)–C(39)–C(38)	108.8(4)		

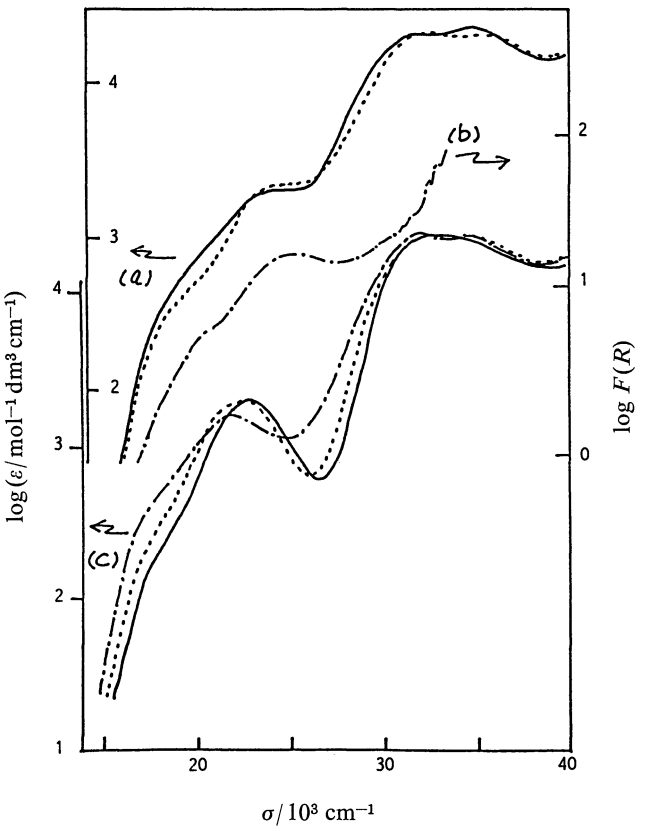

Fig. 3. Electronic spectra of Ni(II) complexes: (a) [Ni(*rac*(*P*)-L)$_2$](BF$_4$)$_2$ in CH_2Cl_2 (——), [Ni(*meso*(*P*)-L)$_2$](BF$_4$)$_2$ in CH_2Cl_2 (– – –), (b) [Ni(*rac*(*P*)-L)$_2$](BF$_4$)$_2$ in the solid state (—·—), (c) [Ni(*rac*(*P*)-L)$_2$](BF$_4$)$_2$ in CH_2Cl_2 in the presence of LiCl (——), LiBr (– – –), and KI (—·—).

dal Ni(II) complex with C_{4v} symmetry.[21] Thus it is concluded that the complex in CH_2Cl_2 solution retains the square pyramidal structure with P_4S donor atoms, but the coordinating $-SCH_3$ group exchanges with free $-SCH_3$ groups on the NMR time scale. The ligand field bands (20000—25000 cm^{-1}) of [Ni(*rac*(*P*)-L)$_2$]$^{2+}$ in CH_2Cl_2 are shifted to lower energy in the presence of excess halide ions (X^-) as shown in Fig. 3(c). The peak positions are shifted in accordance with the spectrochemical series, 29000 cm^{-1} (LiCl), 22700 cm^{-1} (LiBr), and 22000 cm^{-1} (KI). A similar spectral change was reported for square pyramidal [NiX{*o*-C_6H_4(As(CH$_3$)$_2$}$_2$]$^+$.[21] Thus [Ni(*rac*(*P*)-L)$_2$]$^{2+}$ in CH_2Cl_2 in the presence of excess halide ions would form square pyramidal [NiX(*rac*(*P*)-L)$_2$]$^+$ in which the $-SCH_3$ group is replaced by the X^- ion.

To assign the more soluble isomer **B-II**, the L ligand in this isomer was liberated from the Ni(II) ion in CH_2Cl_2 by mixing with an excess aqueous KCN solution. The [Co(acac)$_2$(L)]$^+$ complex prepared with this ligand was only the *meso*(*P*)-L complex **A-I**. Thus isomer **B-II** was assigned to [Ni(*meso*(*P*)-L)$_2$]$^{2+}$. For the arrangement of chiral phosphorus atoms in [Ni(*meso*(*P*)-L)$_2$]$^{2+}$, there are two possible isomers, *trans-RS* and *trans-RR,SS*. The ^{1}H and ^{13}C NMR spectra of isomer **B-II** in CD_2Cl_2 indicate the isomer to be a single species, but the structure could not be assigned. The absorption spectrum of isomer **B-II** in CH_2Cl_2 is very similar to that of **B-I** (Fig. 3(a)), and behaves in a similar manner to isomer **B-I** when added excess halide ions. The NMR spectra in CD_2Cl_2 show only one kind of $-SCH_3$ signal. These results indicate that isomer **B-II** is also a square pyramidal complex with the $-SCH_3$ group at the apical position, and the $-SCH_3$ group exchanges with free $-SCH_3$ groups on the NMR time scale in solution. The [Ni(*rac*(*P*)-L)(*meso*(*P*)-L)]$^{2+}$ isomer was not obtained under the experimental conditions.

Copper(I) Complex. White air-stable [Cu(L)]BF$_4$ was immediately precipitated by reaction of L and Cu(BF$_4$)$_2$·6H$_2$O in methanol. The molar conductivity of 150 S cm^2 mol^{-1} in acetonitrile shows a 1:1 electrolyte for this complex.[22] The complex exhibits a singlet $-SCH_3$ signal in the ^{1}H (δ=2.16) and ^{13}C (δ=19.1) NMR spectra in CD_2Cl_2, indicating a single species. The assignment of L, *rac*(*P*) or *meso*(*P*) in the complex was made by the same method as for [Ni(*meso*(*P*)-L)$_2$]$^{2+}$. The L ligand obtained from the copper complex gave only [Co(acac)$_2$(*rac*(*P*)-L)]$^+$. Thus the copper complex is assigned as [Cu(*rac*(*P*)-L)]$^+$, and the coordination geometry should be tetrahedral. Molecular models show that *rac*(*P*)-L can coordinate to a metal ion tetrahedrally as a quadridentate ligand without strain, while one of the two $-SCH_3$ groups of *meso*(*P*)-L can not bind to the metal ion in a tetrahedral complex. The *meso*(*P*)-L complex would remain in the reaction mixture, but was not isolated in this study. The reduction mechanism of Cu(II) to Cu(I) is not clear. In general, phosphines tend to form stable complexes with Cu(I), and only a few complexes with Cu(II) are reported.[23]

We wish to thank the Institute for Molecular Science (Okazaki) for the use of X-ray and computation facilities.

References

1) M. Atoh, K. Kashiwabara, and J. Fujita, *Bull. Chem. Soc. Jpn.*, **58**, 2793 (1985).
2) M. Atoh, K. Kashiwabara, and J. Fujita, *Bull. Chem. Soc. Jpn.*, **58**, 3492 (1985).
3) M. Atoh, K. Kashiwabara, and J. Fujita, *Bull. Chem. Soc. Jpn.*, **59**, 1001 (1986).
4) M. Jung, M. Atoh, K. Kashiwabara, and J. Fujita, *Bull. Chem. Soc. Jpn.*, **61**, 3503 (1988).
5) M. Atoh, H. Sugiura, Y. Seki, K. Kashiwabara, and J. Fujita, *Bull. Chem. Soc. Jpn.*, **60**, 1699 (1987).
6) M. Jung, M. Atoh, K. Kashiwabara, and J. Fujita, *Bull. Chem. Soc. Jpn.*, **63**, 2051 (1990).
7) K. Kashiwabara, M. Jung, and J. Fujita, *Bull. Chem. Soc. Jpn.*, **64**, 2372 (1991).
8) K. Issleib and W. Gans, *Z. Anorg. Allg. Chem.*, **491**, 163 (1982).

9) R. Schmelzer and D. Schwarzenbach, *Cryst. Struct. Commun.*, **10**, 1317 (1981).
10) K. Issleib and H. Weichmann, *Chem. Ber.*, **101**, 2197 (1968).
11) "Inorg. Synth.," Vol. V, p.188.
12) T. Sakurai and K. Kobayashi, *Rikagaku Kenkyusho Hokoku*, **55**, 69 (1979).
13) K. Kashiwabara, I. Kinoshita, T. Ito, and J. Fujita, *Bull. Chem. Soc. Jpn.*, **54**, 725 (1981).
14) K. Kashiwabara, K. Katoh, T. Ohishi, and J. Fujita, *Bull. Chem. Soc. Jpn.*, **55**, 149 (1982).
15) a) T. Ohishi, K. Kashiwabara, and J. Fujita, *Bull. Chem. Soc. Jpn.*, **56**, 1553 (1983). b) K. Katoh, H. Sugiura, K. Kashiwabara, and J. Fujita, *ibid.*, **57**, 3580 (1984). c) M. Takata, K. Kashiwabara, H. Ito, T. Ito, and J. Fujita, *ibid.*, **58**, 2247 (1985).
16) J. Podlahova, B. Kratochvil, and V. Langer, *Inorg. Chem.*, **20**, 2160 (1981).
17) E. C. Alyea and D. W. Meek, *Inorg. Chem.*, **11**, 1029 (1972).
18) S. G. Murray and F. R. Hartly, *Chem. Rev.*, **81**, 365 (1981).
19) a) L. Sacconi, F. Mani, and A. Bencini, "Comprehensive Coordination Chemistry," ed by G. Wilkinson, R. D. Gillard, and J. A. McCleverty, Pergamon Press, Oxford (1987), Vol. 5, Chap. 50, pp. 128—129. b) L. Sacconi, *Coord. Chem. Rev.*, **8**, 351 (1971).
20) D. W. Meek and J. A. Ibers, *Inorg. Chem.*, **11**, 1029 (1972).
21) J. R. Preer and H. B. Gray, *J. Am. Chem. Soc.*, **92**, 7306 (1970).
22) W. J. Geary, *Coord. Chem. Rev.*, **7**, 81 (1971).
23) a) B. J. Hathaway, "Comprehensive Coordination Chemistry," ed by G. Wilkinson, R. D. Gillard, and J. A. McCleverty, Pergamon Press, Oxford (1987), Vol. 5, Chap. 53, p. 735. b) C. A. McAuliffe and W. Leavason,"Phosphine, Arsine, and Stibine Complexes of the Transition Elements," Elesevier, Amsterdam (1979).

A Novel and Efficient Method for the Preparation of α-Hydroxyimino Carbonyl Compounds from α,β-Unsaturated Carbonyl Compounds with Butyl Nitrite and Phenylsilane Catalyzed by a Cobalt(II) Complex

Koji KATO* and Teruaki MUKAIYAMA†
Basic Research Laboratories for Organic Synthesis, Mitsui Petrochemical Industries, Ltd., Nagaura, Sodegaura, Chiba 299-02
†Department of Applied Chemistry, Faculty of Science, Science University of Tokyo, Kagurazaka, Shinjuku-ku, Tokyo 162
(Received March 22, 1991)

Various α,β-unsaturated carbonyl compounds, such as α,β-unsaturated esters, α,β-unsaturated ketones, α,β-unsaturated nitriles, and α,β-unsaturated amides, were directly converted to the corresponding α-hydroxyimino carbonyl compounds in high yields on treatment with butyl nitrite and phenylsilane in the presence of a catalytic amount of *N,N'*-bis(2-ethoxycarbonyl-3-oxobutylidene)ethylenediaminatocobalt(II) complex under mild conditions.

The introduction of a nitrogen atom into organic compounds is one of the most important reactions in organic synthesis, and several methods using various amines, nitrogen monoxide, azide, etc. with transition-metal complexes as a catalyst have been extensively investigated.[1] For example, concerning the introduction of a nitrogen atom into olefinic compounds, K. B. Sharpless and co-workers reported a method for the preparation of *cis*-2-aminocyclohexanol from cyclohexene with chloramine T (TsNClNa) catalyzed by osmium tetraoxide in *t*-butyl alcohol, followed by the reduction with sodium in liquid ammonia.[2] A method for the addition of *N*-chloro amines to olefins by using a redox catalyst, such as Cu(I)/Cu(II) or Fe(II)/Fe(III), was also presented.[3] We recently reported the α-nitrosation of α,β-unsaturated amides yielding the corresponding 2-nitroso amides with nitrogen monoxide and triethylsilane in the presence of a catalytic amount of *N,N'*-bis(2-ethoxycarbonyl-3-oxobutylidene)ethylenediaminatocobalt(II) (Co(eobe)) at room temperature.[4] However, the above-mentioned reaction is limited to α,β-unsaturated amides, and no practical methods for the direct introduction of a nitrogen atom at the α-position of α,β-unsaturated esters and α,β-unsaturated ketones catalyzed by transition-metal complexes have been reported at all.

We have considered the possibility of the employment of alkyl nitrites, which are commercially available reagents and are employed in various reactions, to introduce a nitrogen atom into organic compounds. For example, oximes of α-keto esters were prepared by the reaction of saturated esters with alkyl nitrite by a metal alkoxide.[5] Recently, the titanium chloride-promoted reaction of ketene alkyl silyl acetals with isopentyl nitrite affording oximes of α-keto esters was reported.[6]

In a previous communication,[7] we reported the α-oximation of various α,β-unsaturated esters with butyl nitrite and a silane affording the 2-hydroxyimino esters, the useful intermediates,[8] catalyzed by Co(eobe) under mild conditions. For example, when butyl crotonate (**1a**) was treated with butyl nitrite (**2**) and phenylsilane ($PhSiH_3$) in tetrahydrofuran (THF) in the presence of 10 mol% of Co(eobe) at room temperature, the corresponding oxime, butyl 2-(hydroxyimino)butyrate (**3a**), was obtained in an 89% yield (Scheme 1).

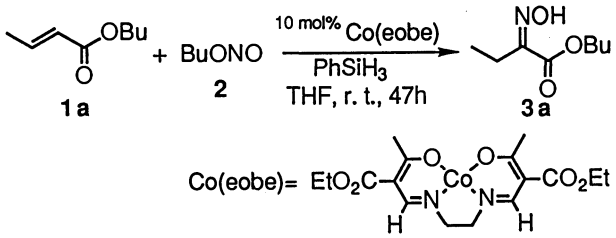

Scheme 1.

Here, we would like to discuss in detail the α-oximation of various α,β-unsaturated carbonyl compounds, such as α,β-unsaturated esters, α,β-unsaturated ketones, α,β-unsaturated nitriles, and α,β-unsaturated amides with butyl nitrite and a silane using a cobalt(II) complex as a catalyst.

Results and Discussion

α-Oximation of Butyl Crotonate (1a) with Butyl Nitrite (2). First, the reaction of butyl crotonate (**1a**) with butyl nitrite (**2**) and triethylsilane (Et_3SiH) in the presence of 10 mol% of Co(eobe) in 1,2-dichloroethane (DCE) was attempted at room temperature. It was found that butyl crotonate (**1a**) was consumed after 62 h, and butyl 2-(hydroxyimino)butyrate (**3a**) was obtained in a 28% yield (Entry 1 in Table 1). The effect of solvents on the yield of the oxime compound was studied by taking the reaction of butyl crotonate (**1a**) with butyl nitrite (**2**) and Et_3SiH catalyzed by Co(eobe) as a model. As shown in Table 1, a change in the

Table 1. α-Oximation of Butyl Crotonate (**1a**) in Various Solvents[a]

Entry	Solvent	Conversion[b]/%	Yield[c]/%
1	DCE	—	28
2	Benzene	85	39
3	AcOEt	100	55
4	THF	100	79

a) Reaction conditions; butyl crotonate (**1a**) 0.5 mmol, butyl nitrite (**2**) 1.5 mmol, Co(eobe) 0.05 mmol, Et_3SiH 1.5 mmol, solvent 2.5 ml, room temperature, under argon atmosphere. b) Determined by GC analysis. c) Isolated yield.

Table 2. α-Oximation of Butyl Crotonate (**1a**) Catalyzed by Various Cobalt(II) Complexes[a]

Entry	Co(II) complex	Conversion[b]/%	Yield[c]/%
1	Co(eobe)	100	79
2	Co(acacen)[d]	5	4
3	$Co(acac)_2$[e]	10	2
4	$Co(ecbo)_2$[f]	51	5

a) Reaction conditions; butyl crotonate (**1a**) 0.5 mmol, butyl nitrite (**2**) 1.5 mmol, Co(II) complex 0.05 mmol, Et_3SiH 1.5 mmol, THF 2.5 ml, room temperature, under argon atmosphere. b) Determined by GC analysis. c) Isolated yield. d) *N,N'*-Bis(1-methyl-3-oxobutylidene)ethylenediaminatocobalt(II). e) Bis(acetylacetonato)cobalt(II). f) Bis(2-ethoxycarbonyl-3-oxobutanalato)cobalt(II).

reaction medium from DCE to more polar solvents, such as ethyl acetate (EtOAc) and THF, improved the yield of oxime **3a**, especially in the case of THF, where oxime **3a** was obtained in a 79% yield (Entry 4).

Next, several cobalt(II) complexes were screened in the α-oximation of butyl crotonate (**1a**) in THF (See Table 2), and it was shown that Co(eobe) was the most effective catalyst for the present α-oximation of butyl crotonate (**1a**) (Entry 1). The catalytic activity of *N,N'*-bis(1-methyl-3-oxobutylidene)ethylenediaminatocobalt (II) (Co(acacen)) was very low (Entry 2), and in the cases of cobalt(II) complexes having 1,3-diketone-type ligands, the yields of oxime **3a** were low and reduction of **1a** to butyl butyrate with Et_3SiH proceeded exclusively (Entries 3 and 4).

Considering that a silane would be another important factor in the present reaction, the effect of various kinds of silanes on the α-oximation was examined by taking the reaction of butyl crotonate (**1a**) with butyl nitrite (**2**) in THF catalyzed by Co(eobe) as a model (See Table 3). Consequently, the yield of oxime **3a** increased in accordance with the reduction capability of the silane, and oxime **3a** was obtained in an 89% yield when $PhSiH_3$ was used (Entry 4). The influences of the amounts of butyl nitrite (**2**) and silane were also checked, and the oxime **3a** was produced in a 79% yield by using nearly one equivalent of $PhSiH_3$ to **1a** (Entry 5). On the other hand, the amount of butyl nitrite (**2**) influenced the reaction rate; that is, when one and a half equivalents of **2** to **1a** were used, the conversion of **1a** was reduced to 64% (Entry 6). This suggested that the step involving butyl nitrite (**2**) seemed to be the rate-determining step in the present reaction.

α-Oximation of Various α,β-Unsaturated Carbonyl Compounds with Butyl Nitrite and $PhSiH_3$ Catalyzed by Co(eobe). The above procedure was successfully applied to the α-oximation of various α,β-unsaturated carbonyl compounds such as α,β-unsaturated esters, α,β-unsaturated ketones, α,β-unsaturated nitriles, and α,β-unsaturated amides (See Table 4). First, the reactions of various α,β-unsaturated esters (**1b—i**) with butyl nitrite (**2**) and $PhSiH_3$ in the presence of 10 mol% of Co(eobe) in THF at room temperature were examined. As a result, acrylic esters (**1b** and **c**) and β-monosubstituted α,β-unsaturated esters (**1d—f**) were converted to the corresponding oximes (**3b—f**) in high yields (Entries 1—5). It was noted that the α-oximation of *p*-tolyl crotonate (**1g**) gave *p*-tolyl 2-(hydroxyimino)butyrate (**3g**) in a 78% yield accompanied without the decomposition of the *p*-tolyl ester moiety which was frequently observed when saturated esters were treated with alkyl nitrite in alcohol under basic conditions according to the conventional procedure[5] (Entry 6). The α-oximation of a functionalized α,β-unsaturated ester such as diethyl fumarate (**1h**) took place readily and the corresponding oxime **3h** was obtained in an 89% yield (Entry 7). In the case of a β,β-disubstituted α,β-unsaturated ester, such as benzyl 3-methylcrotonate (**1i**) hindered at the β-position, no reaction took place at all and the starting material was recovered (Entry 8).

Next, the α-oximation of α,β-unsaturated ketones

Table 3. α-Oximation of Butyl Crotonate (**1a**) with Various Silanes and Butyl Nitrite (**2**)[a]

Entry	Silane	Amount of silane[b]	Amount of **2**[b]	Conversion[c]/%	Time/h	Yield[d]/%
1	Et_3SiH	3.0	3.0	100	62	79
2	Et_2SiH_2	3.0	3.0	100	47	84
3	Ph_2SiH_2	3.0	3.0	100	47	88
4	$PhSiH_3$	3.0	3.0	100	47	89
5	$PhSiH_3$	1.1	3.0	100	48	79
6	$PhSiH_3$	3.0	1.5	64	85	61

a) Reaction conditions; butyl crotonate (**1a**) 0.5 mmol, Co(eobe) 0.05 mmol, THF 2.5 ml, room temperature, under argon atmosphere. b) Equivalent per **1a**. c) Determined by GC analysis. d) Isolated yield.

Table 4. α-Oximation of Various α,β-Unsaturated Carbonyl Compounds

Entry	Substrate		Time/h	Product		Yield[b]/%
1	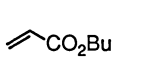	**1b**	41	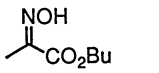	**3b**	98
2	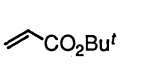	**1c**	48	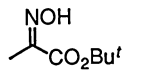	**3c**	82
3	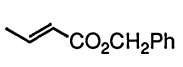	**1d**	41	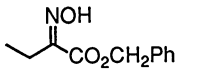	**3d**	91
4	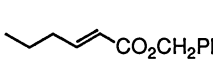	**1e**	48	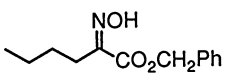	**3e**	84
5	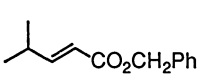	**1f**	48	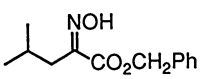	**3f**	96
6	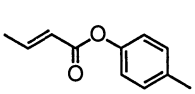	**1g**	21	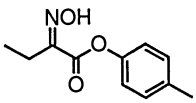	**3g**	78
7	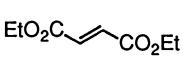	**1h**	21	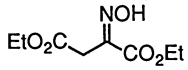	**3h**	89
8[c]	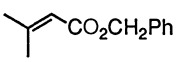	**1i**	41	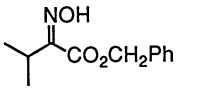	**3i**	0
9	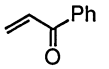	**4a**	19	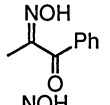	**5a**	93
10	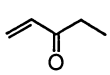	**4b**	19	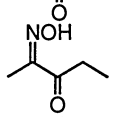	**5b**	89
11	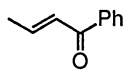	**4c**	48	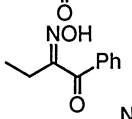	**5c**	95
12	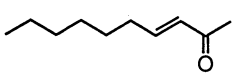	**4d**	19	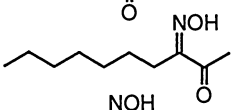	**5d**	70
13[c]	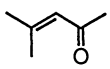	**4e**	15	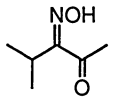	**5e**	67
14		**6a**	21	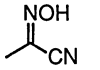	**7a**	82
15	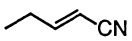	**6b**	37	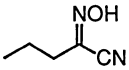	**7b**	70
16	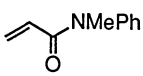	**8a**	48	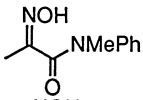	**9a**	78
17	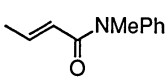	**8b**	60	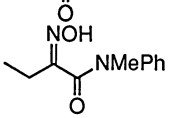	**9b**	80

a) Reaction conditions; substrate 0.5 mmol, Co(eobe) 0.05 mmol, butyl nitrite (**2**) 1.5 mmol, $PhSiH_3$ 1.5 mmol, THF 2.5 ml, room temperature, under argon atmosphere. b) Isolated yield. c) Butyl nitrite (**2**) 3.0 mmol and $PhSiH_3$ 3.0 mmol were used at 60 °C.

under the above-mentioned conditions was investigated. It was found that vinyl ketones (**4a** and **b**) and β-monosubstituted α,β-unsaturated ketones (**4c** and **d**) also reacted with butyl nitrite (**2**) and $PhSiH_3$ to afford the monooximes (**5a**—**d**) of 1,2-diketones in high yields (Entries 9—12). The present method was effective for the selective preparation of monooximes of unsymmetrical 1,2-diketones, whereas the control of the chemoselectivity was difficult in the reaction of 1,2-diketones with hydroxylamine[9] or the α-oximation of saturated

ketones having hydrogen atoms at both α-positions with alkyl nitrite under acidic conditions.[10] In the cases of α,β-unsaturated ketones, it should be pointed out that when a β,β-disubstituted α,β-unsaturated ketone such as mesityl oxide (**4e**) was treated with butyl nitrite (**2**) and $PhSiH_3$ in the presence of a catalytic amount of Co(eobe) at 60 °C, the corresponding oxime **5e** was obtained in a 67% yield, while in the case of benzyl 3-methylcrotonate (**1i**), no reaction took place at all under the same conditions (Entry 13).

The present procedure could also be applied to the α-oximation of α,β-unsaturated nitriles and α,β-unsaturated amides; for example, acrylonitrile (**6a**) and 2-pentenenitrile (**6b**) were converted to the corresponding oximes **7a** and **7b** in 82% and 70% yields, respectively (Entries 14 and 15), and acrylamide **8a** and crotonamide **8b**, respectively, afforded the 2-hydroxyimino amides **9a** and **9b** in good yields (Entries 16 and 17).

Even though the pathway of the present α-oximation has not yet been made clear, it can be assumed that the intermediate **A** shown in Scheme 2 is initially generated from α,β-unsaturated carbonyl compounds, Co(eobe), and a silane. The successive reaction of this intermediate **A** with butyl nitrite affords the corresponding oximes. This explanation is supported by the result that when acrylamide **8a** was treated with Et_3SiH and Co(eobe) in the absence of butyl nitrite (**2**), propionamide **10** (a reduced product) and a coupling product **11** of acrylamide were produced instead of the oxime as shown in Scheme 3. The difference in the reactivity

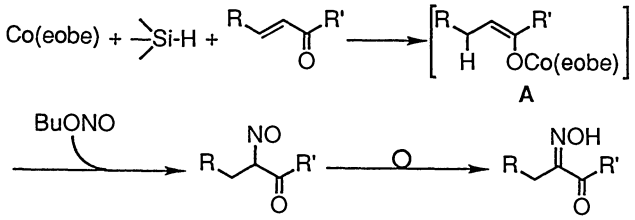

Scheme 2.

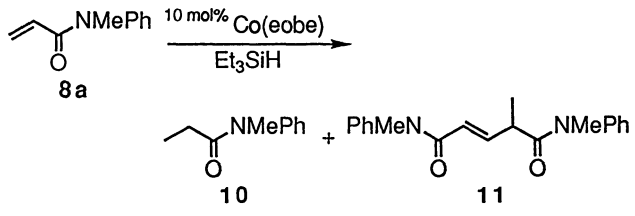

Scheme 3.

between β,β-disubstituted α,β-unsaturated ester **1i** and ketone **4e** suggests that a nucleophilic attack of the bulky active species, such as a cobalt hydride, on the β-position of α,β-unsaturated carbonyl compounds occurs first to generate the intermediate **A**.

It is concluded that butyl nitrite is an effective reagent for the α-oximation of α,β-unsaturated carbonyl compounds, such as α,β-unsaturated esters, α,β-unsaturated ketones, α,β-unsaturated nitriles, and α,β-unsaturated amides, in the presence of a silane and a catalytic amount of Co(eobe) to afford the corresponding oximes. The catalyst, Co(eobe), has the highest activity for α-oximation, and the combined use of phenylsilane in tetrahydrofuran improves the yield of the α-oximation of α,β-unsaturated carbonyl compounds. The present procedure thus provides a novel and useful method for the preparation of α-hydroxyimino carbonyl compounds directly from α,β-unsaturated carbonyl compounds under mild conditions.

Experimental

General: Melting points were measured on a Mettler FP62 apparatus and are uncorrected.

(a) Spectrometers: IR spectra were obtained by using a JASCO Model IR-700 infrared spectrometer on KBr pellets or liquid film on NaCl. ^1H NMR spectra were recorded with a JEOL Model FX270 spectrometer using $CDCl_3$ as the solvent and tetramethylsilane as an internal standard.

(b) Chromatography: Column chromatography was conducted using silica gel (Daiso gel IR-60). Preparative TLC was carried out on silica gel (E. Merck, 13895). GC-analyses were performed on a Shimadzu GC-15A chromatograph using a column packed with PEG 20M(20%) supporting Chromosorb W (3 mm×2 m), and the peak areas were obtained with a Shimadzu chromatopack CR-5A.

(c) Solvents and Reagents: 1,2-Dichloroethane and tetrahydrofuran were HPLC-grade and stored over molecular sieves. Toluene, benzene, and ethyl acetate were purified by distillation and stored over molecular sieves. Butyl nitrite (**2**) was purchased from TCI Co., Ltd. and stored in a cooled room after purification by distillation under reduced pressure. Triethylsilane, diethylsilane, diphenylsilane, and phenylsilane were purchased from Shin-Etsu Chemicals Co. and used without further purification.

(d) α,β-Unsaturated Carbonyl Compounds: Butyl acrylate (**1b**), *t*-butyl acrylate (**1c**), butyl crotonate (**1a**), *p*-tolyl crotonate (**1g**), and diethyl fumarate (**1h**) were purchased from TCI Co., Ltd. and purified by distillation. The other α,β-unsaturated esters were prepared from the corresponding acid chlorides and benzyl alcohol. Ethyl vinyl ketone (**4b**), 1-phenyl-2-buten-1-one (**4c**), 3-decen-2-one (**4d**), and mesityl oxide (**4e**) were purchased from Aldrich Chemical Company, Inc. or TCI Co., Ltd. and purified by distillation. 1-Phenyl-2-propen-1-one (**4a**) was prepared according to the reported method.[11] Acrylonitrile (**6a**) and 2-pentenenitrile (**6b**) were purchased from TCI Co., Ltd. and purified by distillation. *N*-Methylacrylanilide (**8a**) and *N*-methylcrotonanilide (**8b**) were prepared from the corresponding acid chlorides and *N*-methylaniline.

Preparation of Cobalt(II) Complexes. Bis(acetylacetonato)cobalt(II) ($Co(acac)_2$) was purchased from TCI Co., Ltd. and dried under reduced pressure (1 mmHg, 1 mmHg= 133.322 Pa) at 70 °C. *N,N'*-Bis(1-methyl-3-oxobutylidene)-ethylenediaminatocobalt(II) (Co(acacen))[12] and bis(2-ethoxycarbonyl-3-oxobutanalato)cobalt (II) ($Co(ecbo)_2$)[13] were prepared according to the reported methods, respectively. *N,N'*-Bis(2-ethoxycarbonyl-3-oxobutylidene)ethylenediaminato-

cobalt(II) (Co(eobe)) was prepared by a modified procedure of Kida's method:[14] An aqueous solution of sodium hydroxide (23.2 mmol, 11.6 ml) was added at 50 °C under an argon atmosphere to a solution of *N,N'*-bis(2-ethoxycarbonyl-3-oxobutylidene)ethylenediamine[15] (3.95 g, 11.6 mmol) in *N,N*-dimethylformamide (100 ml). After stirring for 0.5 h at 50 °C, a solution of cobalt(II) chloride hexahydrate (2.76 g, 11.6 mmol) in water (20 ml) was added, and the mixture was stirred for 0.5 h at 50 °C. After cooling at 0 °C, the orange precipitates were collected by filtration, washed with water (50 ml), and dried in vacuo at room temperature for 16 h. They were recrystallized from toluene to afford pure Co(eobe) (3.04 g, 66% yield). Mp 287—289 °C; IR(KBr) 1695 and 1585 cm^{-1} Found: C, 48.55; H, 5.71; N, 7.02%. Calcd for $C_{16}H_{22}N_2O_6Co$: C, 48.37; H, 5.58; N, 7.05%.

α-Oximation of Butyl Crotonate (1a) (*A Typical Procedure*, see Entry 4 in Table 3). Phenylsilane (162 mg, 1.5 mmol) and butyl nitrite (**2**) (159 mg, 1.5 mmol) were successively added to a solution of butyl crotonate (**1a**) (79 mg, 0.5 mmol) and Co(eobe) (20 mg, 0.05 mmol) in THF (2.5 ml). After stirring for 47 h at room temperature under an argon atmosphere, MeOH (1.5 ml) and concentrated HCl (3 drops) were added to the reaction mixture. After stirring for 30 min, water (20 ml) was added to the reaction mixture, which was then neutralized with a saturated aqueous $NaHCO_3$ solution. Organic materials were extracted with dichloromethane and the organic layer was washed with brine and dried over anhydrous magnesium sulfate. After evaporation of the solvent and purification by silica gel TLC (hexane–EtOAc, 3:1), butyl 2-(hydroxyimino)butyrate (**3a**)[16] was obtained (77 mg, 89% yield). ^1H NMR ($CDCl_3$) δ=0.95 (3H, t, *J*=7 Hz), 1.13 (3H, t, *J*=7 Hz), 1.43 (2H, sextet, *J*=7 Hz), 1.72 (2H, quintet, *J*=7 Hz), 2.64 (2H, q, *J*=7 Hz), and 4.26 (2H, t, *J*=7 Hz); IR ($CHCl_3$) 3278, 2962, and 1726 cm^{-1}.

Analytical Data of the Oximes (in Table 4). Butyl 2-(Hydroxyimino)propionate (3b): Mp 51—53 °C; ^1H NMR ($CDCl_3$) δ=0.95 (3H, t, *J*=7 Hz), 1.41 (2H, sextet, *J*=7 Hz), 1.70 (2H, quintet, *J*=7 Hz), and 4.23 (2H, t, *J*=7 Hz); IR ($CHCl_3$) 3284 and 1721 cm^{-1}. Found: C, 52.43; H, 8.26; N, 8.48%. Calcd for $C_7H_{13}NO_3$: C, 52.82; H, 8.23; N, 8.80%.

***t*-Butyl 2-(Hydroxyimino)propionate (3c):**[17] Mp 63—66 °C; ^1H NMR ($CDCl_3$) δ=1.53 (9H, s) and 2.06 (3H, s); IR ($CHCl_3$) 3280 and 1716 cm^{-1}. Found: C, 52.80; H, 8.14; N, 8.77%. Calcd for $C_7H_{13}NO_3$: C, 52.82; H, 8.23; N, 8.80%.

Benzyl 2-(Hydroxyimino)butyrate (3d): Mp 60—63 °C; ^1H NMR ($CDCl_3$) δ=1.08 (3H, t, *J*=7 Hz), 2.59 (2H, q, *J*=7 Hz), 5.25 (2H, s), and 7.37 (5H, m); IR ($CHCl_3$) 3280 and 1722 cm^{-1} Found: C, 64.02; H, 6.12; N, 6.45%. Calcd for $C_{11}H_{13}NO_3$: C, 63.76; H, 6.32; N, 6.76%.

Benzyl 2-(Hydroxyimino)hexanoate (3e): Mp 75—78 °C; ^1H NMR ($CDCl_3$) δ=0.89 (3H, t, *J*=7 Hz), 1.33 (2H, sextet, *J*=7 Hz), 1.50 (2H, quintet, *J*=7 Hz), 2.59 (2H, t, *J*=7 Hz), 5.25 (2H, s), and 7.33 (5H, m); IR ($CHCl_3$) 3278 and 1722 cm^{-1}. Found: C, 65.84; H, 7.25; N, 6.05%. Calcd for $C_{13}H_{17}NO_3$: C, 66.36; H, 7.28; N, 5.95%.

Benzyl 2-Hydroxyimino-4-methylpentanoate (3f): Mp 84—86 °C; ^1H NMR ($CDCl_3$) δ=0.89 (6H, d, *J*=7 Hz), 2.05 (2H, septet, *J*=7 Hz), 2.51 (2H, d, *J*=7 Hz), 5.27 (2H, s), and 7.35 (5H, m); IR ($CHCl_3$) 3286 and 1722 cm^{-1}. Found: C, 66.06; H, 7.45; N, 6.10%. Calcd for $C_{13}H_{17}NO_3$: C, 66.36; H, 7.28; N, 5.95%.

***p*-Tolyl 2-(Hydroxyimino)butyrate (3g):** Mp 118—121 °C; ^1H NMR ($CDCl_3$) δ=1.16 (3H, t, *J*=7 Hz), 2.34 (3H, s), 2.70 (2H, q, *J*=7 Hz), 7.03 (2H, AB. d, *J*=6 Hz), and 7.19 (2H, AB. d, *J*=6 Hz); IR ($CHCl_3$) 3292 and 1738 cm^{-1}. Found: C, 63.33; H, 6.52; N, 6.80%. Calcd for $C_{11}H_{13}NO_3$: C, 63.76; H, 6.32; N, 6.76%.

Diethyl 2-(Hydroxyimino)succinate (3h):[18] ^1H NMR ($CDCl_3$) δ=1.25 (3H, t, *J*=7 Hz), 1.33 (3H, t, *J*=7 Hz), 3.69 (2H, s), 4.18 (2H, q, *J*=7 Hz), and 4.32 (2H, q, *J*=7 Hz); IR ($CHCl_3$) 3150 and 1730 cm^{-1}.

2-Hydroxyimino-1-phenyl-1-propanone (5a): Mp 110—111 °C (lit,[10] mp 112—113 °C); ^1H NMR ($CDCl_3$) δ=2.18 (3H, s), 7.44 (2H, t, *J*=8 Hz), 7.57 (1H, t, *J*=8 Hz), and 7.89 (2H, d, *J*=8 Hz); IR ($CHCl_3$) 3315 and 1665 cm^{-1}.

2-Hydroxyimino-3-pentanone (5b): Mp 68—69 °C (lit,[19] mp 70—71 °C); ^1H NMR ($CDCl_3$) δ=1.10 (3H, t, *J*=7 Hz), 2.00 (3H, s), and 2.80 (2H, q, *J*=7 Hz); IR (KBr) 3328 and 1670 cm^{-1}.

2-Hydroxyimino-1-phenyl-1-butanone (5c):[20] Mp 116—119 °C; ^1H NMR ($CDCl_3$) δ=1.09 (3H, t, *J*=7 Hz), 2.69 (2H, q, *J*=7 Hz), 7.40 (2H, t, *J*=8 Hz), 7.53 (1H, dt, *J*=2 and 8 Hz), and 7.85 (2H, dd, *J*=2 and 8 Hz); IR ($CHCl_3$) 3316 and 1665 cm^{-1}.

3-Hydroxyimino-2-decanone (5d): Mp 52—54 °C (lit,[21] mp 51—52 °C); ^1H NMR ($CDCl_3$) δ=0.88 (3H, t, *J*=7 Hz), 1.29 (8H, m), 1.44 (2H, m), 2.38 (3H, s), and 2.55 (2H, t, *J*=7 Hz); IR ($CHCl_3$) 3298 and 1692 cm^{-1}.

3-Hydroxyimino-4-methyl-2-pentanone (5e): Mp 77—78 °C (lit,[22] 78—79 °C); ^1H NMR ($CDCl_3$) δ=1.21 (6H, d, *J*=7 Hz), 2.32 (3H, s), and 3.42 (1H, septet, *J*=7 Hz); IR ($CHCl_3$) 3294 and 1692 cm^{-1}.

2-(Hydroxyimino)propanenitrile (7a):[23] E-Form; ^1H NMR ($CDCl_3$) δ=2.20 (3H, s) and 9.53 (1H, br); IR (neat) 3308, 2234, and 1624 cm^{-1}: Z-Form; ^1H NMR ($CDCl_3$) δ=2.13 (3H, s) and 8.75 (1H, br); IR (neat) 3332, 2244, and 1624 cm^{-1}.

2-(Hydroxyimino)pentanenitrile (7b):[23] E-Form; ^1H NMR ($CDCl_3$) δ=1.01 (3H, t, *J*=7 Hz), 1.69 (2H, sextet, *J*=7 Hz), 2.51 (2H, t, *J*=7 Hz), and 9.25 (1H, br); IR (neat) 3344, 2230, and 1623 cm^{-1}: Z-Form; ^1H NMR ($CDCl_3$) δ=0.99 (3H, t, *J*=7 Hz), 1.68 (2H, sextet, *J*=7 Hz), 2.43 (2H, t, *J*=7 Hz), and 9.45 (1H, br); IR (neat) 3336, 2238, and 1625 cm^{-1}.

***N*-Methyl-2-(hydroxyimino)propionanilide (9a):** E-Form; mp 146—148 °C; ^1H NMR ($CDCl_3$) δ=1.87 (3H, s), 3.35 (3H, s), and 6.80—7.45 (5H); IR ($CHCl_3$) 3320 and 1648 cm^{-1}. Found: C, 62.75; H, 6.52; N, 14.44%. Calcd for $C_{10}H_{12}N_2O_2$: C, 62.49; H, 6.29; N, 14.57%. Z-Form; mp 115—118 °C; ^1H NMR ($CDCl_3$) δ=1.76 (3H, s), 3.35 (3H, s), 7.12 (1H, br), and 7.32 (5H, m); IR ($CHCl_3$) 3150 and 1651 cm^{-1}. Found: C, 62.62; H, 6.22; N, 14.44%. Calcd for $C_{10}H_{12}N_2O_2$: C, 62.49; H, 6.29; N, 14.57%.

***N*-Methyl-2-(hydroxyimino)butyranilide (9b):** E-Form; mp 83—84 °C; ^1H NMR ($CDCl_3$) δ=1.07 (3H, t, *J*=7 Hz), 2.38 (2H, q, *J*=7 Hz), 3.37 (3H, s), 7.20—7.50 (5H, m), and 8.70 (1H, br); IR ($CHCl_3$) 3320 and 1647 cm^{-1}. Found: C, 64.15; H, 6.76; N, 13.20%. Calcd for $C_{11}H_{14}N_2O_2$: C, 64.06; H, 6.84; N, 13.58%. Z-Form; ^1H NMR ($CDCl_3$) δ=0.93 (3H, t, *J*=7 Hz), 2.07 (2H, q, *J*=7 Hz), 3.37 (3H, s), 7.35 (5H, m), and 7.77 (1H, br); IR (neat) 3304 and 1640 cm^{-1}. Found: C, 64.45; H, 6.99; N, 13.30%. Calcd for $C_{11}H_{14}N_2O_2$: C, 64.06; H, 6.84; N, 13.58%.

Reaction of *N*-Methylacrylanilide (8a) with Triethylsilane in the Presence of Co(eobe) (Scheme 3). Triethylsilane (349 mg, 3.0 mmol) was added to a solution of *N*-methylacrylanilide (**8a**) (161 mg, 1.0 mmol) and Co(eobe) (20 mg, 0.05 mmol) in 1,2-dichloroethane (5 ml). After stirring for 48 h at room

temperature under an argon atmosphere, the solvent was removed under reduced pressure. After purification by silica gel TLC (hexane-EtOAc, 1 : 1), *N*-methylpropionanilide (**10**) and (E)-*N,N'*-dimethyl-1-butene-1,3-dicarboxanilide (**11**) were obtained in 5% and 24% yields, respectively. **10**: Mp 55—56 °C (lit,[24] mp 56 °C). ^{1}H NMR and retention time in GC analysis of this sample were identical with those of the authentic sample.

11: ^{1}H NMR ($CDCl_3$) δ=1.08 (3H, d, *J*=7 Hz), 3.10 (1H, quintet, *J*=7 Hz), 3.17 (3H, s), 3.32 (3H, s), 5.56 (1H, d, *J*=17 Hz), 6.81 (1H, dd, *J*=17 and 7 Hz), and 7.00—7.50 (10H); IR ($CHCl_3$) 1664, 1634, and 1596 cm^{-1}. Found: C, 74.93; H, 6.99; N, 8.30%. Calcd for $C_{20}H_{22}N_2O_2$: C, 74.51; H, 6.88; N, 8.69%.

References

1) For example: J. Tsuji and M. Takahashi, *J. Mol. Cat.*, **10**, 107 (1981); S.-I. Murahashi, T. Shimamura, and I. Moritani, *J. Chem. Soc., Chem. Commun.*, **1974**, 931; Y. Tanigawa, K. Nishimura, A. Kawasaki, and S.-I. Murahashi, *Tetrahedron Lett.*, **23**, 5549 (1982); S.-I. Murahashi, Y. Tanigawa, Y. Imada, and Y. Tanigawa, *ibid.*, **27**, 227 (1986); T. Okamoto, K. Kobayashi, S. Oka, and S. Tanimoto, *J. Org. Chem.*, **52**, 5089 (1987).

2) A. O. Chong, K. Oshima, and K. B. Sharpless, *J. Am. Chem. Soc.*, **99**, 3420 (1977).

3) F. Minisci, R. Galli, and G. Pollina, *Chem. Ind. (Milano)*, **47**, 736 (1965); F. Minisci, R. Galli, and M. Cecere, *ibid.*, **48**, 347 (1966); F. Minisci, *ibid.*, **49**, 705 (1967); F. Minisci, *Tetrahedron Lett.*, **5**, 546 (1964).

4) K. Kato and T. Mukaiyama, *Chem. Lett.*, **1990**, 1395.

5) R. Fischer and T. Wieland, *Chem. Ber.*, **93**, 1387 (1960); A. Dornow and D. D. Jordan, *ibid.*, **94**, 76 (1961).

6) S. M. Ali, Y. Matsuda, and S. Tanimoto, *Synthesis*, **1988**, 805.

7) K. Kato and T. Mukaiyama, *Chem. Lett.*, **1990**, 1917.

8) D. Shemin and R. M. Herbst, *J. Am. Chem. Soc.*, **60**, 1951 (1938); M. W. Tijhuis, J. D. M. Herscheid, and H. C. J. Ottenheijm, *Synthesis*, **1980**, 890.

9) W. Ziegenbein, A. Schaffler, and R. Kaufhold, *Chem. Ber.*, **88**, 1906 (1955).

10) W. H. Hartung and F. Crossley, *Org. Synth.*, Coll. Vol. II, 363 (1943).

11) M. Hayashi and T. Mukaiyama, *Chem. Lett.*, **1987**, 1283.

12) G. W. Everett and R. H. Holm, *J. Am. Chem. Soc.*, **88**, 2442 (1966).

13) K. Kato, T. Yamada, T. Takai, S. Inoki, and S. Isayama, *Bull. Chem. Soc. Jpn.*, **63**, 179 (1990).

14) Y. Nishida, K. Hayashida, N. Oishi, and S. Kida, *Inorg. Chim. Acta*, **38**, 213 (1980).

15) E. G. Jager, *Z. Chem.*, **8**, 30, 392, and 475 (1968).

16) M. Milone and F. Ferrero, *Gazz. Chim. Ital.*, **77**, 348 (1947).

17) L. A. Carpino, *J. Org. Chem.*, **29**, 2820 (1964).

18) J. G. Wood, M. R. Hone, M. E. Mattner, and C. P. Symons, *Aust. J. Sci. Res., Ser. B*, **1**, 38 (1948).

19) J. K. Rasmussen and A. Hossner, *J. Org. Chem.*, **39**, 2558 (1974).

20) R. Bartnik and B. Orlowska, *Pol. J. Chem.*, **62**, 151, 159, 427, and 433 (1988).

21) Y. N. Matyushin, V. I. Pepekin, A. D. Nikolaeva, N. M. Lyapin, L. V. Nikolaeva, A. V. Artyushin, and A. Y. Apin, *Izv. Akad. Nauk SSSR, Ser. Khim.*, **1973**, 842.

22) A. F. Ferris, *J. Org. Chem.*, **24**, 1726 (1959).

23) L. W. Kissinger and H. E. Ungnade, *J. Org. Chem.*, **25**, 1471 (1960).

24) R. E. Carter, *Acta Chem. Scand.*, **21**, 75 (1967).

Substituent Effects in the Solvolysis of *p*-(2-Substituted Cyclopropyl)-α-Methylbenzyl Chlorides[1)]

Yoshiaki KUSUYAMA,* Takako KUBO, Masami IYO, Tamami KAGOSAKU, and Kenjiro TOKAMI
Department of Chemistry, Faculty of Education, Wakayama University, Sakaedani 930, Wakayama 640
(Received March 28, 1991)

The solvolysis rates of *p*-(*cis*- or *trans*-2-substituted cyclopropyl)-α-methylbenzyl chlorides including electron-donating and electron-attracting substituents relative to a hydrogen substituent were measured in 80% aqueous acetone. The trans isomers were more reactive than the corresponding cis derivatives where cyclopropyl and phenyl groups could not get a most favorable "bisected" conformation for the cyclopropyl group to release electrons to the benzene ring. The relative rates of the trans isomers at 45 °C were best correlated by means of σ_m values with a ρ value of −3.14 and a correlation coefficient of 0.97, indicating that the cyclopropane ring was a poor transmitter of a resonance effect. The substituent effects were analyzed by means of the LSFE equation.

The C–C bonds of the cyclopropane ring have, to a greater or lesser degree, the characteristics of C–C double bonds, including more *p*-orbital character than expected for saturated C–C bonds.[2)] The cyclopropyl group can enter into conjugated systems[3,4)] and can become a strong electron donor when it is directly attached to the electron-deficient center.[5)] The superior electron-donating ability of the cyclopropyl group is evidenced quantitatively by the more negative σ^+ value (−0.41—−0.54)[6–8)] than that of isopropyl (−0.28) and other alkyl groups (−0.25 to −0.32).[9)]

In a previous paper,[6)] we reported the kinetics of the solvolysis of *p*-substituted α-methylbenzyl chlorides in 80% aqueous acetone; the *p*-cyclopropyl derivative reacted 353 times faster than the parent chloride, indicating the strong contribution of a resonance effect in the transition state. However, the relative rate of the *p*-(2,2-dichlorocyclopropyl) derivative to the unsubstituted α-methylbenzyl chloride was only 1.24. The σ^+ value for the 2,2-dichlorocyclopropyl group estimated from the solvolysis of *p*-(2,2-dichlorocyclopropyl)-α-methylbenzyl chloride and the dissociation of *p*-(2,2-dichlorocyclopropyl)phenylacetic acid in 50% ethanol by means of the LArSR equation[10)] presented by Yukawa and Tsuno, was only −0.02.[6)] Moreover, the parameter $\Delta\bar{\sigma}_R^+$ values which measure the capacities of the substituents to supply electrons by a resonance effect in the LArSR equation were −0.35 and −0.07 for the cyclopropyl and the 2,2-dichlorocyclopropyl groups, respectively. Thus, the replacement of the two hydrogens at the 2-position of cyclopropyl with two chloro substituents caused a remarkable reduction of the resonance exaltation of the cyclopropyl group. Two factors may be responsible for this reduction of the resonance effect. One is the decreasing of the polarizability of C_1–C_2 bonds due to the strongly electronegative chloro substituent. The other is the conformational change from the most favorable "bisected" conformation in order to release electrons from cyclopropyl to phenyl, due to the repulsion between the cis chlorine atom and the hydrogen atom at the ortho position of the benzene ring.[11,12)]

In order to evaluate the relative contribution of these two factors and to clarify the electronic characteristics of 2-substituted cyclopropyl groups, we have studied the solvolysis of *p*-(*cis*- and *trans*-2-substituted cyclopropyl)-α-methylbenzyl chlorides. The mechanism of this solvolysis reaction was well studied by Tsuno and co-workers.[10b)]

Results and Discussion

The solvolysis rates of *p*-(2-substituted cyclopropyl)-α-methylbenzyl chlorides in 80% aqueous acetone were determined by conductometric measurements at the initial concentrations of 10^{-5} mol dm^{-3}. The reproducibilities of the rate constants were within an accuracy of 2%. The rate constants for the bromo and the chloro

Table 1. Solvolysis Rates of *p*-(2-Substituted Cyclopropyl)-α-Methylbenzyl Chlorides in 80%(v/v) Aqueous Acetone

Substituent		$k_1\times10^5$ (s^{-1})		
		25 °C	35 °C	45 °C
H				258[a)]
F	*cis*	2.73	8.35	24.0
	trans	2.85	9.45	25.1
Cl	*cis*	0.896	2.96	8.71
	trans	1.80	5.64	16.8
Cl_2				0.905[a)]
Br	*cis*	0.89	2.80	8.75
	trans	1.73	5.30	15.8
CH_3	*cis*	12.5	36.7	105
	trans	51.5	141	387
1-CH_3		12.9	36.9	99.9
C_6H_5	*cis*	9.51	28.3	83.0
	trans	14.7	44.0	124
CH_3O	*trans*	19.7	59.9	163
$COOC_2H_5$	*cis*	0.890	2.93	9.06
	trans	1.53	4.80	14.8
[$C_6H_5CHClCH_3$]				0.729[a)], 0.726[b)]

a) Ref. 6. b) E. Berliner and N. Shieh, *J. Am. Chem. Soc.*, **79**, 3849 (1957).

derivatives thus obtained were identical to those obtained by the acid-base titration method.[6] The obtained rate constants are summarized in Table 1 together with those of the 1-methylcyclopropyl and 2,2-dichlorocyclopropyl derivatives and the parent α-methylbenzyl chloride. The relative rates of solvolysis of *p*-(2-substituted cyclopropyl)-α-methylbenzyl chloride and the activation parameters at 45 °C are listed in Table 2. The ^{1}H NMR observation revealed that the product of this solvolysis was the corresponding alcohol.

For all compounds measured, the trans isomers reacted faster than the corresponding geometrical isomers, the cis derivatives (Table 2). k_{trans}/k_{cis} values were in the range of 1.05—3.69 and increased as the van der waals radii of the substituents increased, indicating that these rate differences were caused by the repulsion between the substituent and the hydrogen atom at the ortho position in the phenyl group in the cis derivative. Our results obtained here are consistent with the solvolysis of the geometrical isomers of 2-[*p*-(2-chlorocyclopropyl)phenyl]-2-chloropropane and 2-[*p*-(2-bromocyclopropyl)phenyl]-2-chloropropane in 90% aqueous acetone reported by Kulinkovich and co-workers.[8] Thus, the cis isomers had an energetically less-favorable conformation and could not get a maximum overlap between cyclopropyl C_1–C_2 bonds and the p-orbital of the benzene ring, leading to the rate depression relative to the trans isomer. The rate deceleration effect of the 1-methyl group for the cyclopropyl group supported this explanation. The k_{trans}/k_{cis} values for a chlorine was 1.93, while k_{trans}/k_H=0.065 and k_{cis}/k_H=0.034. The rate depression by two chlorine atoms observed for the 2,2-dichlorocyclopropyl group[6] was ascribed mainly to the decreased polarizability of C_1–C_2 bonds of the cyclopropyl group, due to the electronegative behavior of the chlorine atom. These effects of the chlorine substituent obtained here were similar to those observed in the solvolysis of 2-[*p*-(2-chlorocyclopropyl)phenyl]-2-chloropropanes.[8]

It was very interesting that the methoxyl group (trans),[13] a strong electron-donating substituent by a resonance effect, retarded the reaction rate by a factor of 0.63. The phenyl group (trans) also decreased the reaction rate by a factor of 0.48. The $\log k/k_0$—$\log k/k_0$ plot of the relative rates of solvolysis between the *m*-, *p*-substituted α-methylbenzyl chlorides and the *p*-(*trans*-2-substituted cyclopropyl)-α-methylbenzyl chlorides under the same conditions showed a linear relation for the *m*-derivatives but not for the *p*-derivatives as illustrated in Fig 1. Indeed, $\log k_X/k_H$ values for *p*-(*trans*-2-substituted cyclopropyl)-α-methylbenzyl chlorides were best correlated linearly by σ_m (ρ value: −3.14, *r*:[14] 0.972) rather than σ_p and σ^+. This correlation confirmed that the cyclopropane ring was a poor transmitter of a resonance effect. There have been some experimental observations that the transmission of the conjugation through the cyclopropane ring is smaller than that through carbon-carbon double bonds.[5,15]

In a previous study, we succeeded in the estimation of the relative importance of an inductive effect and a resonance effect contributing to the dissociation of the 2-substituted 1-cyclopropanecarboxylic acids by means of Yukawa and Tsuno's treatment.[15b] A linear substituent free energy (LSFE) equation presented by Yukawa and Tsuno is considered the most useful for the estimation of the relative contribution of an inductive effect as well as a resonance effect in an extended pi-system beyond the original phenyl system.[16–18]

$$\log(k_X/k_H) = \rho_i\sigma_i + \rho_\pi^+\sigma_\pi^+$$

Here, σ_i is the inductive substituent constant and σ_π^+ is a substituent constant which measures the capability of substituents to donate electrons through electronic delo-

Table 2. The Relative Rates and the Activation Parameters of the Solvolysis of *p*-(2-Substituted Cyclopropyl)-α-Methylbenzyl Chlorides in 80%(v/v) Aqueous Acetone at 45 °C

Substituent		Relative rate	k_{trans}/k_{cis} (45 °C)	$\Delta H^{\neq}$ kcal mol^{-1}	$-\Delta S^{\neq}$ e.u.
H[a]		1		18.7	11.7
F	*cis*	0.093	1.05	19.9	10.9
	trans	0.097		19.9	12.5
Cl	*cis*	0.034	1.93	20.78	11.9
	trans	0.065		20.3	12.4
Cl_2[a]		0.0035		23.7	47.2
Br	*cis*	0.034	1.81	20.7	12.1
	trans	0.061		20.4	11.9
CH_3	*cis*	0.41	3.69	19.4	11.3
	trans	1.5		18.5	11.6
1-CH_3		0.39		18.6	13.8
C_6H_5	*cis*	0.32	1.49	19.8	10.6
	trans	0.48		19.4	10.9
CH_3O	*trans*	0.63		19.6	9.70
$COOC_2H_5$	*cis*	0.035	1.63	21.2	10.5
	trans	0.057		20.7	11.0

a) Ref. 6.

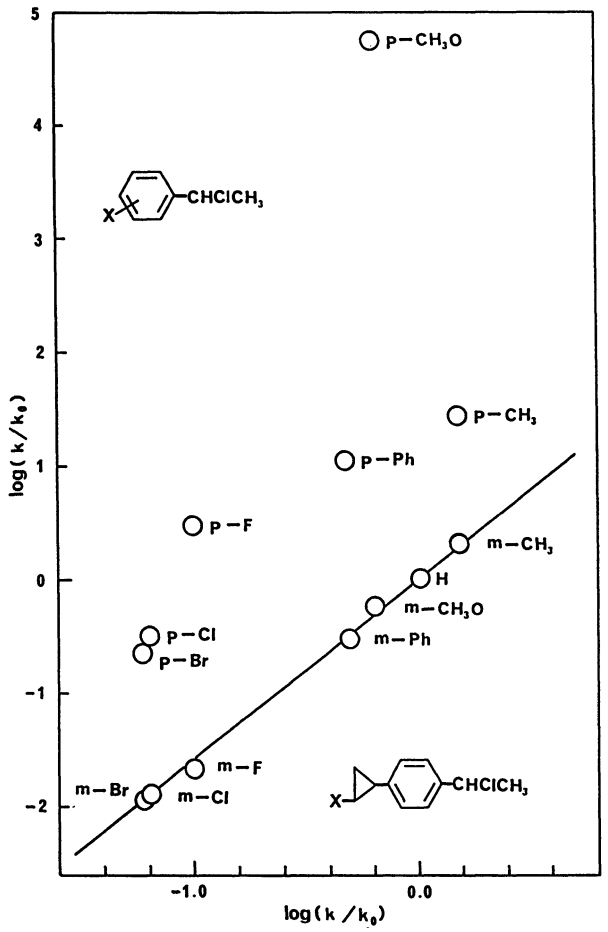

Fig. 1. Log–Log plot of relative rates of solvolysis of *m*- and *p*-substituted α-methylbenzyl chlorides against solvolysis of *p*-(*trans*-2-substituted cyclopropyl)-α-methylbenzyl chlorides in 80% aqueous acetone at 45 °C.

calization. The results of the application of the LSFE equation to the present reactivities are expressed as follows;

$$\log(k_X/k_H) = -3.52\,\sigma_i - 1.89\,\sigma_\pi^+ - 0.08 \text{ (\textit{trans}), } r = 0.996,^{14)}$$

$$\log(k_X/k_H) = -3.12\,\sigma_i - 1.30\,\sigma_\pi^+ - 0.33 \text{ (\textit{cis}), } r = 0.913.^{14)}$$

The ratios of the coefficients of σ_i and σ_π^+ (f_i and f_r, respectively) for the solvolysis of *p*-substituted α-methylbenzyl chlorides, *p*-(2-substituted cyclopropyl)-α-methylbenzyl chlorides, 1-(4′-substituted 4-biphenylyl)-ethyl chlorides,[17] and 1-(7-substituted 2-fluorenyl)ethyl chlorides[18] under the same conditions are summarized in Table 3. It appeared that the relative effectiveness of a transmitting resonance effect could be evaluated from f_r values. The intervention of the cyclopropane ring led to the deceleration of the resonance effect by a factor of 0.1. The transmitting resonance effect of the *trans*-1,2-cyclopropanediyl group was about a third that of *p*-phenylene. These results were predicted from the CNDO calculation for (2-substituted cyclopropyl) methyl cations where the LUMO of the cyclopropyl cation had small coefficients at C_2 and C_3 so the π-interaction by substituents at these positions was small.[15c] The transmitting inductive effect through the 1,2-cyclopropanediyl group was, however, larger than that through the *p*-phenylene group.

Table 3. Relative ρ_i and ρ_π^+ Values in the Solvolysis of $ArCHClCH_3$ in 80% Aqueous Acetone

Ar in $ArCHClCH_3$	Relative ρ_i (f_i)	Relative ρ_π^+ (f_r)
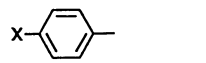 a)	2.17	2.78
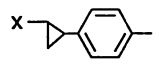 b)	1.54	0.28
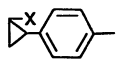 b)	1.37	0.19
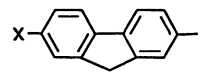 c)	1.00	1.00
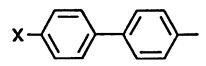 d)	0.70	0.69

a) Ref. 10b. b) Present study. c) Ref. 18. d) Ref. 17.

Experimental

All melting points were measured on a YANACO mp hot-stage melting-point apparatus and were uncorrected. The boiling points were also uncorrected. GLC analyses of liquid materials were performed on a YANACO GL80 gas chromatograph. High-performance liquid chromatography was carried out with a JASCO TRIROTOR-V by means of a Finepak SIL column with a Shodex RI SE-51 detector. Preparative-scale LC separations were carried out on a Shodex LC PR100 packed with a MERCK Lichroprep Si60 gel. A mixture of hexane and ethyl acetate was used as an eluent. The geometrical isomers were conveniently separated by this method. The mass spectra were determined at 70 eV using a JEOL D300 instrument. The IR spectra were measured using a JASCO A100 spectrometer. The NMR spectra were determined as a solution in $CDCl_3$ unless otherwise stated, with TMS as an internal standard on a JEOL EX90 spectrometer (90 MHz for ^1H and 22.4 MHz for ^{13}C) and a JEOL FX60 spectrometer (60 MHz for ^1H and 15 MHz for ^{13}C). The assignment of the structure for the geometrical isomers of substituted cyclopropanes was made from the ^{13}C NMR spectra, where the cis isomer always resonated at higher fields than did the corresponding trans isomer.[4,19]

All the *p*-(2-substituted cyclopropyl)-α-methylbenzyl chlorides were prepared from the corresponding substituted benzyl alcohols by chlorination with hydrogen chloride in dichloromethane at 3 °C. The obtained chlorides were used for the kinetic measurements without further purification after the removal of dichloromethane under reduced pressure. All the *p*-(2-substituted cyclopropyl)-α-methylbenzyl alcohols were prepared from the corresponding ketones by reduction with $NaBH_4$ in 2-propanol at room temperature or with $LiAlH_4$ in ether at 3 °C.

(2-Bromo-2-fluorocyclopropyl)benzene: Sodium *t*-butoxide (100 g) was added over 2 h to a solution of dibromofluoro-

methane (50 g, 0.26 mol) and styrene (52 g, 0.5 mol) in 150 ml of hexane cooled to 3 °C. After the addition had been completed, the mixture was stirred at room temperature for 1 h. The reaction was quenched with 500 ml of water. The reaction mixture was extracted with hexane, washed, dried ($MgSO_4$) and filtered. After the removal of hexane under reduced pressure, the remaining styrene was distilled through a Widmer column fitted with a glass spiral core and the product was distilled carefully through a short column (10 cm): yield 18.5 g (33%); bp 88 °C (7 mmHg, 1 mmHg=133.322 Pa),[20] lit,[21] 71—72 °C (5 mmHg);[20] ^{1}H NMR (CCl_4) δ=1.52—2.3 (m, 2H, CH_2), 2.35—3.1 (m, 1H, CH), and 6.9—7.4 (s, 5H).

(2-Fluorocyclopropyl)benzene: This was obtained by the reduction of (2-bromo-2-fluorocyclopropyl)benzene with $LiAlH_4$ in THF.[22] Yield 77%; bp 96—104 °C (40 mmHg).[20] Fractional distillation through a Hempel column gave a geometrical isomer of 80% purity by GC measurements. *Cis:* bp 55—58 °C (10 mmHg),[20] *trans*: bp 96—104 °C (26 mmHg).[20]

***p*-(2-Fluorocyclopropyl)acetophenone:** Iron(III) chloride (1.62 g, 0.01 mol) was added at 10 °C over 10 minutes to a mixture of (2-fluorocyclopropyl)benzene [(1.36 g, 0.01 mol), isomer ratio (4 : 1)], acetyl chloride (0.79 g, 0.01 mol), and carbon disulfide (15 ml). After the addition had been completed, the mixture was stirred at room temperature for an additional hour. The produced complex was hydrolyzed by adding diluted hydrochloric acid. The usual work-up gave *p*-(2-fluorocyclopropyl)acetophenone. Yield 0.86 g (48%). Bp 120—140 °C (6 mmHg).[20] *Cis* isomer: mp 42 °C; ^{1}H NMR δ=0.9—2.8 (m, 3H, cyclopropyl), 2.6 (s, 3H, CH_3), 4.15—4.5 and 5.15—5.60 (m, 1H, CHF), 7.38 (d, *J*=10 Hz, 2H, PhH), and 7.98 (d, *J*=10 Hz, 2H, PhH); ^{13}C NMR δ=12.53 (d, ^2J=10.28 Hz), 21.65 (d, ^2J=11 Hz), 26.54, 72.59 (d, *J*=223.1 Hz), 128.15, 128.40, 142.05, and 197.59. *Trans* isomer: Oil; ^{1}H NMR δ=0.9—2.8 (m, 3H, cyclopropyl), 2.60 (s, 3H, CH_3), 4.1—4.4 and 5.0—5.4 (m, 1H, CHF), 7.1 (d, *J*=10 Hz, 2H, PhH), and 7.9 (d, *J*=10 Hz, 2H, PhH); ^{13}C NMR δ=15.65 (d, ^2J=9.8 Hz), 22.68 (d, ^2J=11.5 Hz), 26.48 (CH_3), 75.34 (d, *J*=228.7 Hz), 126.05 (CH), 128.49 (CH), 135.21, 144.98, and 197.36.

***p*-(*cis*-2-Fluorocyclopropyl)-α-methylbenzyl Alcohol:** Bp 118 °C (3 mmHg).[20] ^{1}H NMR δ=0.8—1.3 (m, 2H, CH_2), 1.4 (d, *J*=8 Hz, 3H, CH_3), 1.6—2.3 (m, 1H, cyclopropyl), 2.43 (s, 1H, OH), 3.9—4.3 and 5.1—5.41 (m, 1H, CHF), 4.5—6.0 (q, *J*=8 Hz, 1H, CH–O), and 7.1 (s, 4H, PhH); ^{13}C NMR δ=11.62 (d, ^2J=10.3 Hz, CH_2), 21.13 (d, ^2J=11.1 Hz, CH), 24.97 (CH_3), 69.90 (CH–O), 72.34 (d, *J*=247.7 Hz, CF), 125.16 (CH), 128.45 (d, ^3J=1.3 Hz), 134.97 (d, ^3J=3.0 Hz), and 143.84.

***p*-(*trans*-2-Fluorocyclopropyl)-α-methylbenzyl Alcohol:** Mp 24 °C. ^{1}H NMR δ=0.7—1.3 (m, 2H, CH_2), 1.35 (d, *J*=8 Hz, CH_3), 1.8—2.6 (m, 1H, PhCH), 2.35 (s, 1H, OH), 3.9—4.1 and 4.9—5.2 (m, 1H, CHF), 4.7 (q, *J*=8 Hz, 1H, CH–O), 6.9 (d, *J*=7 Hz, 2H, PhH), and 7.22 (d, *J*=7 Hz, 2H, PhH); ^{13}C NMR δ=14.80 (d, ^2J=11.56 Hz, CH_2), 22.24 (d, ^2J=11.13 Hz, PhCH), 25.09 (CH), 69.84 (CH–O), 75.31 (d, *J*=226.95 Hz), 125.48 (CH), 126.21 (CH), 138.23, and 143.86.

***p*-(*cis*-2-Fluorocyclopropyl)-α-methylbenzyl Chloride:** Mp 43 °C; ^{1}H NMR δ=0.8—1.2 (m, 3H, cyclopropyl), 1.78 (d, *J*=8 Hz, 3H, CH_3), 4.0—4.4 and 5.0—5.5 (m, 1H, CHF), 5.42 (q, *J*=7 Hz, 1H, CHCl), and 7.3—8.0 (m, 4H, PhH); ^{13}C NMR δ=11.93 (d, ^2J=10.27 Hz, CH_2), 21.20 (d, ^2J=10.71 Hz, PhCH), 26.42 (CH_3), 58.60 (CHCl), 72.39 (d, *J*=222.0 Hz), 126.27 (CH), 128.65 (d, ^4J=1.29 Hz), 136.18 (d, ^3J=3.42 Hz), and 140.77. Found: C, 67.16; H, 6.09%. Calcd for $C_{11}H_{12}FCl$: C, 66.49; H, 6.09%.

***p*-(*trans*-2-Fluorocylopropyl)-α-methylbenzyl Chloride:** Mp 26 °C; ^{1}H NMR δ=0.5—1.9 (m, 2H, CH_2), 1.9 (d, *J*=7 Hz, 3H, CH_3), 2.0—2.8 (m, 1H, PhCH), 3.9—4.2 and 5.0—5.3 (m, 1H, CHF), 4.05 (q, *J*=7 Hz, 1H, CHCl), 7.0 (d, *J*=9 Hz, 2H, PhH), and 7.3 (d, *J*=9 Hz, 2H, PhH); ^{13}C NMR δ=14.88 (d, ^2J=9.85 Hz), 22.25 (d, ^2J=11.56 Hz), 26.37 (CH_3), 58.42 (CHCl), 75.15 (d, *J*=226.95 Hz), 126.38 (d, ^4J=1.0 Hz), 126.56 (CH), 139.31, and 140.79.

***p*-(*cis*-2-Chlorocyclopropyl)-α-methylbenzyl Alcohol:** This was obtained by the reduction of the corresponding acetophenone[12] with $LiAlH_4$ in ether. Bp 119 °C (2 mmHg);[20] ^{1}H NMR δ=1.0—1.7 (m, 2H, CH_2, cyclopropyl), 1.4 (d, *J*=7 Hz, 3H, CH_3), 1.8 (s, 1H, OH), 2.0—2.6 (m, 1H, CH), 3.1—3.5 (m, 1H, CH), 4.6—5.1 (q, *J*=7 Hz, CHOH), and 7.2 (s, 4H, Ph); ^{13}C NMR δ=14.24 (CH_2), 22.52, 25.00, 34.45, 70.10 (CHOH), 125.00 (CH), 129.26 (CH), 135.21, and 144.12.

***p*-(*trans*-2-Chlorocyclopropyl)-α-methylbenzyl Alcohol:** Bp 135 °C (5 mmHg);[20] mp 39 °C; ^{1}H NMR δ=1.2—1.9 (m, 2H, CH_2), 1.6 (d, *J*=7 Hz, 3H, CH_3), 2.0 (s, 1H, OH), 2.1—2.7 (m, 1H, CH), 3.1—3.5 (m, 1H, CH), 4.8—5.3 (q, *J*=7 Hz, 1H, CHOH), 7.2 (d, *J*=8 Hz, 2H, PhH), and 7.5 (d, *J*=8 Hz, 2H, PhH); ^{13}C NMR δ=18.56 (CH_2), 25.11, 26.45, 35.00, 70.01, 125.51 (CH), 126.10 (CH), 138.80, and 144.01.

***p*-(*cis*-2-Chlorocyclopropyl)-α-methylbenzyl Chloride:** Mp 43 °C; ^{1}H NMR δ=0.9—1.7 (m, 2H, CH_2), 1.93 (d, *J*=7 Hz, CH_3), 2.0—2.6 (m, 1H, CH), 3.1—3.6 (m, 1H, CH), 4.8—5.4 (q, *J*=7 Hz, 1H, CHCl), and 7.0—7.5 (m, 4H, PhH); ^{13}C NMR δ=14.43 (CH_2), 22.55, 26.40, 34.40, 58.57, 126.10 (CH), 129.38 (CH), 136.21, and 141.08; Found:C, 61.73; H, 5.22%. Calcd for $C_{11}H_{12}Cl_2$: C, 61.39, H, 5.62%.

***p*-(*trans*-2-Chlorocyclopropyl)-α-methylbenzyl Chloride:** Mp 35 °C; ^{1}H NMR δ=1.2—1.6 (m, 2H, CH_2), 1.8 (d, *J*=7 Hz, 3H, CH_3), 2.0—2.5 (m, 1H, CH), 2.9—3.3 (m, 1H, CH), 4.8—5.3 (q, *J*=7 Hz, 1H, CHCl), 7.0 (d, *J*=9 Hz, 2H, PhH), and 7.3 (d, *J*=9 Hz, 2H, PhH); ^{13}C NMR δ=18.68 (CH_2), 26.37, 35.00, 58.34, 126.16 (CH), 126.56 (CH), 139.65, and 140.93. Found: C, 62.18; H, 5.30%. Calcd for $C_{11}H_{12}Cl_2$: C, 61.39; H, 5.62%.

(2-Bromocyclopropyl)benzene: This was obtained by the treatment of (2,2-dibromocyclopropyl)benzene[23] with diethyl phosphonate in the presence of trimethylamine and water at 90 °C.[24] Bp 100—101 °C (10 mmHg).[20]

(*cis*-2-Bromocyclopropyl)benzene: ^{1}H NMR (CCl_4) δ=1.1—1.7 (m, 2H, CH_2), 1.9—2.5 (m, 1H), 3.0—3.4 (m, 1H), and 6.9—7.3 (m, 5H); ^{13}C NMR δ=14.2 (CH_2), 22.1 (PhC), 23.9 (CBr), 126.7, 127.8, 129.1, and 137.0 (ipso).

(*trans*-2-Bromocyclopropyl)benzene: ^{1}H NMR (CCl_4) δ=1.2—1.6 (m, 2H, CH_2), 2.1—2.5 (m, 1H), 2.7—3.1 (m, 1H), and 6.7—7.3 (m, 5H); ^{13}C NMR δ=18.8 (CH_2), 21.5 (CBr), 26.8 (CPh), 125.8, 126.4, 128.4, and 139.6 (ipso).

***p*-(*cis*-2-Bromocyclopropyl)acetophenone:** This was prepared by the Friedel–Crafts reaction using aluminium(III) chloride as a catalyst and carbon tetrachloride as solvent. Mp 151 °C; ^{1}H NMR δ=0.9—1.5 (m, 1H), 1.0—1.8 (m, 2H, CH_2), 2.5 (s, 3H, CH_3), 3.0—3.5 (m, 1H), 7.1—7.4 (d, 2H, *J*=7 Hz, Ph), and 7.7—8.0 (d, *J*=7 Hz, 2H, PhH); ^{13}C NMR δ=14.72 (CH_2), 22.12 (CH), 23.75 (CH), 26.51 (CH_3), 127.87 (CH), 129.18 (CH), 135.58, 142.73, and 197.42 (C=O); MS *m/z* 240, 238, 159, and 43.

***p*-(*trans*-2-Bromocyclopropyl)acetophenone:** This was prepared by the same method described above for the cis isomer. Mp 53 °C; ^{1}H NMR δ=1.2—1.7 (m, 2H, CH_2), 2.1—2.6 (m, 1H, CH), 2.45 (s, 3H, CH_3), 2.8—3.1 (m, 1H, CH), 6.8—7.1 (d,

J=8 Hz, PhH), and 7.6—7.8 (d, J=8 Hz, 2H, PhH). ^{13}C NMR δ=19.73 (CH_2), 21.52 (CH), 26.45, 26.91, 125.85, 128.52 (CH), 135.44, 145.38, and 197.11 (C=O); MS m/s 240, 238, 159, and 43.

***p*-(*cis*-2-Bromocyclopropyl)-α-methylbenzyl Alcohol:** Mp 53.5 °C; ^{1}H NMR δ=1.1—1.7 (m, 2H, CH_2), 1.4 (d, J=7 Hz, 3H, CH_3), 1.9 (s, 1H, OH), 2.0—2.5 (m, 1H, CH), 3.0—3.4 (m, 1H, CH), 4.5—4.9 (q, J=7 Hz, 1H, CH), and 6.9—7.3 (m, 4H, PhH); ^{13}C NMR δ=14.40, 21.87, 23.86, 25.00, 70.16, 125.00 (CH), 129.26 (CH), 136.33, and 144.35.

***p*-(*trans*-2-Bromocyclopropyl)-α-methylbenzyl Alcohol:** Oil; ^{1}H NMR δ=1.2—1.6 (m, 2H, CH_2), 1.38 (d, J=7 Hz, 3H, CH_3), 2.1—2.5 (m, 1H, CH), 2.6 (s, 1H, OH), 2.75—3.05 (m, 1H, CH), 4.65 (q, J=7 Hz, 1H, CH), 6.8 (d, J=12 Hz, 2H, PhH), and 7.1 (d, J=12 Hz, 2H, PhH); ^{13}C NMR δ=18.79, 21.41, 25.06 (CH_3), 26.59, 69.93 (CH), 125.79 (CH), 126.02 (CH), 138.88, and 144.12.

***p*-(*cis*-2-Bromocyclopropyl)-α-methylbenzyl Chloride:** Oil; ^{1}H NMR δ=1.1—1.8 (m, 2H, CH_2), 1.82 (d, J=7 Hz, CH_3), 2.0—2.5 (m, 1H, CH), 3.1—3.5 (m, 1H, CH), 4.8—5.3 (q, J=7 Hz, 1H, CHCl), and 7.3—7.6 (m, 4H, PhH); ^{13}C NMR δ=14.46 (CH_2), 21.75 (CH), 23.86 (CH), 26.34 (CH_3), 58.51 (CHCl), 126.02 (CH), and 129.76 (CH); MS m/z 262, 260, 225, 223, 181, and 179.

***p*-(*trans*-2-Bromocyclopropyl)-α-methylbenzyl Chloride:** Oil; ^{1}H NMR δ=1.2—1.8 (m, 2H, CH_2), 1.8 (d, J=7 Hz, 3H, CH_3), 2.0—2.6 (m, 1H, CH), 2.7—3.2 (m, 1H, CH), 4.8—5.3 (q, J=7 Hz, 1H, CHCl), 7.0 (d, J=11 Hz, 2H, PhH), and 7.3 (d, J=12 Hz, 2H, PhH); ^{13}C NMR δ=18.96 (CH_2), 21.50, 26.33 (CH_3), 26.50, 58.34 (CHCl), 126.07 (CH), 126.59 (CH), 139.86 (CH), and 141.00 (CH); MS m/z 262, 260, 259, 258, 225, 223, 181, and 179.

(*trans*-2,2-Dichloro-3-methylcyclopropyl)benzene: This was prepared by dichlorocarbene addition to *trans*-β-methylstyrene. Bp 119 °C (16 mmHg);[20] ^{1}H NMR δ=1.4 (d, J=6 Hz, 3H, CH_3), 1.8—2.1 (m, 1H), 2.4 (d, J=11 Hz, 1H), and 7.3 (s, 5H, PhH);[6,23] ^{13}C NMR δ=14.80 (CH_3), 29.76 (CH), 41.69 (PhCH), 66.59 (CCl_2), 127.39, 128.21, 128.68, and 134.91 (ipso).

(*cis*-2,2-Dichloro-3-methylcyclopropyl)benzene: This was prepared by dichlorocarbene addition to *cis*-β-methylstyrene.[22] Bp 121 °C (16 mmHg);[20] ^{1}H NMR δ=1.10 (d, J=6 Hz, 3H, CH_3), 1.8—2.3 (m, 1H), 2.8 (d, J=11 Hz, 1H), and 7.28 (s, 5H, PhH); ^{13}C NMR δ=11.90 (CH_3), 29.43, 36.06, 65.27 (CCl_2), 127.15, 128.27 (CH), 130.47 (CH), and 133.00.

(*trans*-2-Methylcyclopropyl)benzene: This was prepared by the reduction of (*trans*-2,2-dichloro-3-methylcyclopropyl)benzene with sodium and ethanol in a 47% yield, bp 80 °C (15 mmHg);[20] ^{1}H NMR δ=0.6—1.0 (m, 3H), 1.1 (d, J=8 Hz, 3H, CH_3), 1.3—1.6 (m, 1H), and 6.8—7.3 (m, 5H); ^{13}C NMR δ=17.60 (CH_2), 17.94 (CH), 19.07 (CH_3), 24.37 (PhCH), 125.04, 125.40, 128.12, and 143.90 (ipso).

(*cis*-2-Methylcyclopropyl)benzene: This was obtained by the reduction of (*cis*-2,2-dichloro-3-methylcyclopropyl)benzene using sodium and ethanol in an 8% yield. The reduction of (*cis*-2-chloro-3-methylcyclopropyl)benzene, itself prepared from $LiAlH_4$ reduction in THF from the dichloro derivative,[23] afforded a better yield (25%). Bp 75—77 °C (12 mmHg);[20] ^{13}C NMR δ=10.8 (CH_2), 12.6 (CH), 13.6 (CH_3), 21.1 (C-Ph), 125.5, 127.7 (CH), 129.2 (CH), and 139.4 (ipso).

***p*-(*cis*-2-Methylcyclopropyl)acetophenone:** Anhydrous aluminium(III) chloride (2.1 g, 15 mmol) was added at −35 °C for 1 h to a mixture of (*cis*-2-methylcyclopropyl)benzene (2.1 g, 15 mmol), acetyl chloride (1.2 g, 15 mmol) and chloroform (10 ml). After the usual work-up, *p*-(*cis*-2-methylcyclopropyl)-acetophenone (1.2 g) was obtained in a 40% yield. Bp 106—109 °C (4 mmHg);[20] ^{1}H NMR δ=0.5—1.7 (m, 3H), 0.76 (d, J=6 Hz, 3H, CH_3), 1.8—2.7 (m, 1H), 2.57 (s, 3H, CH_3), 7.25 (d, J=8 Hz, 2H, PhH), and 7.87 (d, J=8 Hz, 2H, PhH); ^{13}C NMR δ=11.56 (CH_2), 13.32 (CH), 13.67 (CH_3), 21.41 (CH), 26.48 (CH_3), 127.90 (CH), 129.04 (CH), 134.67, 145.78, and 197.59 (CO); MS m/z 174, 159, and 43.

***p*-(*trans*-2-Methylcyclopropyl)acetophenone:** This was obtained by the same method used for the *cis* isomer in a 43% yield. Bp 115 °C (6 mmHg);[20] ^{1}H NMR δ=0.75—1.85 (m, 4H), 1.35 (m, 3H, CH_3), 2.58 (s, 3H, CH_3), 7.15 (d, J=14 Hz, 2H, PhH), and 7.95 (d, J=14 Hz, 2H, PhH); ^{13}C NMR δ=18.73, 18.96, 19.25 (CH_3), 24.60 (CH), 26.37 (CH_3), 125.22 (CH), 128.35 (CH), 134.27, 150.21, and 197.26 (C=O); MS m/z 174, 159, and 43; Found: C, 81.03; H, 8.23%. Calcd for $C_{12}H_{14}O$: C, 82.72; H, 8.10%; Found: m/z 174.1043. Calcd for $C_{12}H_{14}O$: 174.1045.

***p*-(*cis*-2-Methylcyclopropyl)-α-methylbenzyl Alcohol:** Oil; ^{1}H NMR δ=0.5—1.3 (m, 3H), 1.5 (d, J=7 Hz, 3H, CH_3), 1.5—2.0 (m, 1H), 2.0 (s, 1H, OH), 4.8 (q, J=7 Hz, 1H), and 7.2 (s, 4H, PhH); ^{13}C NMR δ=10.93, 12.64, 13.58, 20.76, 24.94, 70.16, 124.85 (CH), 129.20 (CH), 138.72, and 142.87.

***p*-(*trans*-2-Methylcyclopropyl)-α-methylbenzyl Alcohol:** Oil; ^{1}H NMR δ=0.6—1.6 (m, 4H), 1.1—1.2 (m, 3H), 1.4 (d, J=7 Hz, 3H, CH_3), 2.4 (s, 1H, OH), 4.7 (q, J=7 Hz, 1H, CHOH), 6.8 (d, J=9 Hz, 2H, PhH), and 7.1 (d, J=9 Hz, 2H, PhH); ^{13}C NMR δ=17.48, 17.82, 19.02, 24.14, 25.00, 70.16, 125.28 (CH), 125.62 (CH), 142.70, and 143.27; Found: m/z 176.1198. Calcd for $C_{12}H_{16}O$: M, 176.1201.

***p*-(*cis*-2-Methylcyclopropyl)-α-methylbenzyl Chloride:** Oil; ^{1}H NMR δ=0.3—1.3 (m, 3H), 0.6—0.8 (m, 3H, CH_3), 1.4—2.1 (m, 1H), 1.8 (d, J=7 Hz, 3H, CH_3), 5.0 (q, J=7 Hz, 1H, CHCl), and 6.8—7.5 (m, 4H, PhH); ^{13}C NMR δ=11.10, 12.84, 13.61, 20.81, 26.42, 58.82, 125.93, 129.29, 139.74, and 139.88.

***p*-(*trans*-2-Methylcyclopropyl)-α-methylbenzyl Chloride:** Oil; ^{1}H NMR δ=0.6—1.6 (m, 4H), 1.2 (s, 3H, CH_3), 1.8 (d, J=7 Hz, 3H, CH_3), 5.0 (q, J=7 Hz, 1H, CHCl), 7.0 (d, J=9 Hz, 2H, PhH), and 7.3 (d, J=9 Hz, 2H, PhH); ^{13}C NMR δ=17.74 (CH_2), 18.19 (CH), 19.02 (CH_3), 24.06 (CHPh), 26.37 (CH_3), 58.77 (CHCl), 125.51 (CH), 126.30 (CH), 139.51, and 144.27; Found: m/z 194.0859. Calcd for $C_{12}H_{15}Cl$: M, 194.0862.

(1-Methylcyclopropyl)benzene: This was prepared by the reduction of (2,2-dichloro-1-methylcyclopropyl)benzene with sodium in 2-propanol.[6] Bp 84—85 °C (36 mmHg);[20] ^{1}H NMR (CCl_4) δ=0.5—0.9 (m, 4H), 1.4 (s, 3H), and 7.1 (m, 5H); ^{13}C NMR δ=15.60 19.74, 25.73, 125.38, 126.70, 128.11, and 147.02.

***p*-(1-Methylcyclopropyl)acetophenone:** This was obtained in a 60% yield by the Friedel–Crafts reaction using acetyl chloride, aluminium(III) chloride, and chloroform at 7 °C. Bp 105—112 °C (5 mmHg);[20] ^{1}H NMR (CCl_4) δ=0.7—0.9 (m, 4H, CH_2), 1.4 (s, 3H, CH_3), 7.2 (d, J=9 Hz, 2H, PhH), and 7.8 (d, J=9 Hz, 2H, PhH); ^{13}C NMR δ=16.81, 19.59, 24.85, 26.46, 126.26, 128.35, 134.44, 152.91, and 197.55.

***p*-(1-Methylcyclopropyl)-α-methylbenzyl Alcohol:** Oil; ^{1}H NMR δ=0.7—0.9 (m, 4H, CH_2), 0.8 (d, J=7 Hz, 3H, CH_3), 1.4 (t, J=3 Hz, 3H, CH_3), 3.0 (bs, 1H, OH), 4.7 (q, J=7 Hz, 1H, CHOH), and 7.2 (s, 4H, PhH); ^{13}C NMR δ=15.64 (CH_2), 19.37, 24.93, 25.65, 69.82, 125.32 (CH), 126.59 (CH), 142.99, and 146.03.

***p*-(1-Methylcyclopropyl)-α-methylbenzyl Chloride:** Oil; ^{1}H

NMR δ=0.6—0.9 (m, 4H), 1.4 (s, 3H, CH_3), 2.8 (d, *J*=8 Hz, 3H, CH_3), 5.1 (q, *J*=8 Hz, 1H, CHCl), and 7.2 (s, 4H, PhH); ^{13}C NMR δ=15.80 (CH_2), 19.42, 25.49 (CH_3), 26.37 (CH_3), 58.68 (CHCl), 126.24 (CH), 126.76 (CH), 139.74, and 147.20.

***p*-(*cis*-2-Phenylcyclopropyl)acetophenone:** This was prepared by the Friedel–Crafts reaction at −35 °C, using chloroform as a solvent. Mp 81 °C; ^{1}H NMR δ=1.1—1.8 (m, 2H, CH_2), 1.8—2.8 (m, 2H), 2.4 (s, 3H, CH_3), and 6.6—7.9 (m, 9H, PhH); ^{13}C NMR δ=11.84 (CH_2), 24.09 (CH), 25.40 (CH), 26.37 (CH_3), 125.90 (CH), 127.72 (CH), 128.47 (CH), 129.09 (CH), 134.44, 137.29, 144.69, and 197.65 (C=O); IR(neat) 1690 cm^{-1} (C=O).

***p*-(*trans*-2-Phenylcyclopropyl)acetophenone:** This was prepared by the same method for the corresponding *cis* derivative in a 36% yield. Yellow oil; ^{1}H NMR δ=1.1—1.8 (m, 2H, CH_2), 1.9—2.4 (m, 2H), 2.55 (s, 3H, CH_3), and 6.8—8.0 (m, 9H, PhH); ^{13}C NMR δ=18.85 (CH_2), 26.48 (CH_3), 28.13 (CH), 28.98 (CH), 125.56 (CH), 125.67 (CH), 125.96 (CH), 128.36 (CH), 128.52 (CH), 134.73, 141.62, 148.45, and 197.37 (C=O); ; IR (neat) 1690 cm^{-1} (C=O).

***p*-(*cis*-2-Phenylcyclopropyl)-α-methylbenzyl Alcohol:** Oil; ^{1}H NMR δ=1.2—1.7 (m, 2H, CH_2), 1.35 (d, *J*=7 Hz, 3H, CH_3), 1.80 (s, 1H, OH), 2.30—2.60 (m, 2H), 4.70 (q, *J*=7 Hz, 1H, CH), and 6.70—7.20 (m, 9H, PhH); ^{13}C NMR δ=11.47 (CH_2), 24.01 (CH), 24.39 (CH), 24.87 (CH_3), 70.06 (CH), 124.76 (CH), 125.60 (CH), 127.66 (CH), 129.00 (2CH), 137.68, 138.30, and 143.02.

***p*-(*trans*-2-Phenylcyclopropyl)-α-methylbenzyl Alcohol:** Yellow oil; ^{1}H NMR δ=1.2—1.6 (m, 2H), 1.5 (d, *J*=7 Hz, 3H, CH_3), 1.7—2.3 (m, 2H), 1.9 (s, 1H, OH), 4.8 (q, *J*=7 Hz, 1H, CH), and 6.8—7.6 (m, 9H, PhH); ^{13}C NMR δ=18.16, 25.00, 27.67, 27.96, 70.10, 125.45 (CH), 125.67 (CH), 125.79 (CH), 128.29 (CH), 141.73, 142.30, and 143.27.

***p*-(*cis*-2-Phenylcyclopropyl)-α-methylbenzyl Chloride:** Yellow oil; ^{1}H NMR δ=1.2—1.6 (m, 2H, CH_2), 1.7 (d, *J*=7 Hz, 3H, CH_3), 2.3—2.5 (m, 2H), 4.9 (q, *J*=7 Hz, 1H, CHCl), and 6.7—7.2 (m, 9H, PhH); ^{13}C NMR δ=11.73 (CH_2), 23.96 (CH), 24.55 (CH), 26.34 (CH_3), 58.66 (CHCl), 125.73 (CH), 125.85 (CH), 127.74 (CH), 129.05 (CH), 138.11, 138.80, and 140.02.

***p*-(*trans*-2-Phenylcyclopropyl)-α-methylbenzyl Chloride:** Yellow oil; ^{1}H NMR δ=1.2—1.6 (m, 2H, CH_2), 1.8 (d, *J*=8 Hz, 3H, CH_3), 1.9—2.3 (m, 2H), 4.8—5.3 (q, *J*=8 Hz, 1H), and 6.9—7.5 (m, 9H, PhH); ^{13}C NMR δ=18.22, 26.42, 27.73, 28.13, 58.60, 125.67, 125.90, 126.53, 128.35, 140.20, 142.19, and 142.70; Found: *m/z* 256.1021. Calcd for $C_{17}H_{17}Cl$: M, 256.1018.

***p*-(2-Methoxycyclopropyl)acetophenone:** Potassium (3 g, 0.75 mol) was dissolved in a mixture of methanol (25 ml) and hexane (20 ml). The upper layer of hexane was removed with a pipet. To this were added 15-crown-5 (1 ml) and (2-bromocyclopropyl)acetophenone (6.2 g, 26 mmol). The mixture was stirred and maintained at 60 °C for 1 h. After standing overnight, the reaction mixture was poured into water (300 ml) and extracted with benzene (100 ml). *p*-(2-methoxycyclopropyl)acetophenone was separated by column chromatography, using Wakogel-300 and a mixture of hexane and ethyl acetate was used as an eluent. Yield: 0.7 g, 12%. The *trans* isomer was separated by HPLC. Mp 45 °C; ^{1}H NMR δ=0.7—1.4 (m, 2H, CH_2), 1.8—2.2 (1H, CH), 2.54 (s, 3H, CH_3), 3.1—3.4 (m, 1H, C–HO), 3.38 (s, 3H, CH_3O), 6.9 (d, *J*=9 Hz, 2H, PhH), and 7.75 (d, *J*=9 Hz, 2H, PhH); ^{13}C NMR δ=16.86, 23.86, 26.37, 58.08, 63.89, 125.73 128.41, 134.84, 147.20, and 197.14.

***p*-(trans-2-Methoxycyclopropyl)-α-methylbenzyl Alcohol:** Oil; ^{1}H NMR δ=0.8—1.3 (m, 1H, CH), 0.8—1.6 (m, 2H, CH_2), 1.45 (d, *J*=7 Hz, 3H, CH_3), 1.8 (s, 1H, OH), 3.1—3.4 (m, 1H, OCH), 3.4 (s, 3H, CH_3O), 4.6—5.1 (q, *J*=7 Hz, 1H, CHOH), 7.0 (d, *J*=9 Hz, 2H, PhH), and 7.3 (d, *J*=9 Hz, 2H, PhH); ^{13}C NMR δ=15.94 (CH_2), 23.24, 25.06, 58.14, 63.77, 70.10, 125.39 (CH), 126.02 (CH), 140.47, and 143.21.

***p*-(*trans*-2-Methoxycyclopropyl)-α-methylbenzyl Chloride:** Oil; ^{1}H NMR δ=0.7—1.5 (m, 2H, CH_2), 1.6—2.3 (m, 1H, CH), 1.80 (d, *J*=7 Hz, 3H, CH_3), 3.1—3.6 (m, 1H, CH–O), 3.4 (s, 3H, CH_3), 5.0 (q, *J*=7 Hz, 1H, CHCl), 6.98 (d, *J*=9 Hz, 2H, PhH), and 7.32 (d, *J*=9 Hz, 2H, PhH); ^{13}C NMR δ=16.06 (CH_2), 23.26 (CH), 26.34 (CH_3), 58.08 (CH_3O), 58.60 (CHCl), 63.32 (CH–O), 126.02 (CH), 126.38 (CH), 140.11, and 141.39.

***p*-(*cis*-2-Ethoxycarbonylcyclopropyl)acetophenone:** This was prepared by the Friedel–Crafts reaction using ethyl *cis*-2-phenyl-1-cyclopropanecarboxylate (7 g, 37 mmol),[25] acetyl chloride (3.2 g, 41 mmol), aluminium(III) chloride (5.5 g, 41 mmol), and 1,2-dichloroethane (45 ml). The reaction was carried out at a temperature over the boiling point of 1,2-dichloroethane. Yield 0.07 g (1%). Oil; ^{1}H NMR δ=0.95 (t, *J*=7 Hz, 3H, CH_3), 1.15—2.70 (m, 4H), 2.50 (s, 3H, CH_3), 3.88 (q, *J*=7 Hz, 2H, CH_2), 7.30 (d, *J*=9 Hz, 2H, PhH), and 7.84 (d, *J*=9 Hz, 2H, PhH); ^{13}C NMR δ=11.49 (CH_2), 14.11 (CH_3), 22.19 (CH), 25.37 (CH) , 26.53 (CH_3), 60.38 (CH_2), 128.01 (CH), 129.53 (CH), 135.67, 142.39, 170.61 (C=O, ester), and 197.66 (C=O, ketone).

***p*-(*trans*-2-Ethoxycarbonylcyclopropyl)acetophenone:** This was obtained by the Friedel–Crafts reaction of ethyl *trans*-2-phenyl-1-cyclopropanecarboxylate (3.0 g, 15.8 mmol)[25] with acetyl chloride (4.9 g, 62.4 mmol) at 50 °C. Aluminium(III) chloride (3.5 g, 62 mmol) and 1,2-dichloroethane were used as a catalyst and a solvent, respectively. After the usual work-up, the obtained oil was passed through a column packed with silica gel. Oil; yield: 5 g (16%); ^{1}H NMR δ=1.28 (t, *J*=7 Hz, 3H, CH_3), 1.2—1.4 (m, 1H), 1.5—1.75 (m, 1H), 1.85—2.10 (m, 1H), 2.55 (s, 3H, CH_3), 2.45—2.7 (m, 1H), 4.20 (q, *J*=7 Hz, 2H, CH_2), 7.13 (d, *J*=9 Hz, 2H, PhH), and 7.85 (d, *J*=9 Hz, 2H, PhH); ^{13}C NMR δ=13.78, 17.03, 24.28, 25.48, 25.98, 60.38, 125.72 (CH), 128.17 (CH), 135.03, 145.50, 172.26 (COO), and 196.88 (C=O); IR 1690 cm^{-1} (C=O, ketone) and 1730 cm^{-1} (C=O, ester).

***p*-(*cis*-2-Ethoxycarbonylcyclopropyl)-α-methylbenzyl Alcohol:** This was prepared by the reduction of the corresponding ketone with $NaBH_4$ in 2-propanol. Yellow oil; ^{1}H NMR δ=0.91 (t, *J*=7 Hz, 3H, CH_3), 1.1—2.7 (m, 4H), 1.39 (d, *J*=7 Hz, 3H, CH_3), 2.31 (s, 1H, OH), 3.85 (q, *J*=7 Hz, 2H, CH_2), 4.78 (q, *J*=7 Hz, 1H), and 7.23 (s, PhH); ^{13}C NMR δ=11.23 (CH_2), 14.03 (CH_3), 21.79 (CH), 25.06 (CH_3), 25.23 (CH), 60.19 (CH_2), 70.06 (CH), 125.00 (CH), 129.40 (CH), 135.73, 144.32, and 171.03 (C=O).

***p*-(*trans*-2-Ethoxycarbonylcyclopropyl)-α-methylbenzyl Alcohol:** This was obtained by the reduction of the corresponding ketone with $NaBH_4$ in 2-propanol. Oil; ^{1}H NMR δ=1.25 (t, *J*=7 Hz, 3H, CH_3), 1.44 (d, *J*=7 Hz, 3H, CH_3), 1.2—1.7 (m, 2H, CH_2), 1.7—2.0 (m, 1H, CH), 2.30 (s, 1H, OH), 2.3—2.7 (m, 1H, CH), 4.15 (q, *J*=7 Hz, 2H, CH_2), 4.82 (q, *J*=7 Hz, 1H, CH), 7.00 (d, *J*=9 Hz, 2H, PhH), and 7.25 (d, *J*=9 Hz, 2H, PhH); ^{13}C NMR δ=14.25 (CH_3), 16.99 (CH_2), 24.15 (CH), 25.13 (CH_2), 25.90 (CH), 60.73 (CH_2), 67.00 (CH), 125.57 (CH), 126.31 (CH), 139.30, 144.23, and 173.42 (C=O); IR (neat) 3450 cm^{-1} (C=O); MS *m/z* 234 and 219.

***p*-(*cis*-2-Ethoxycarbonylcyclopropyl)-α-methylbenzyl Chlo-**

ride: Oil; ^{1}H NMR δ=0.89 (t, J=7 Hz, 3H, CH_3), 1.05—1.45 (m, 1H), 1.52—1.85 (m, 1H), 1.78 (d, J=7 Hz, 3H, CH_3), 1.88—2.23 (m, 1H), 2.32—2.70 (m, 1H), 3.84 (q, J=7 Hz, 2H, CH_2), 5.05 (q, J=7 Hz, 1H, CH), and 7.20 (s, 4H, PhH); ^{13}C NMR δ=11.24 (CH_2), 13.98 (CH_3), 21.91 (CH), 25.10 (CH), 26.39 (CH_3), 58.55 (CHCl), 60.20 (CH_2), 126.08 (CH), 129.53 (CH), 136.80, 141.13, and 170.81 (C=O).

***p*-(*trans*-2-Ethoxycarbonylcyclopropyl)-α-methylbenzyl Chloride:** Mp 39 °C; ^{1}H NMR δ=1.21 (t, J=7 Hz, 3H, CH_3), 1.02—2.0 (m, 3H), 1.78 (d, J=7 Hz, 3H, CH_3), 2.35—2.62 (m, 1H, CH), 4.13 (d, J=7 Hz, 2H, CH_2), 5.02 (q, J=7 Hz, 1H, CHCl), 7.01 (d, J=9 Hz, 2H, PhH), and 7.28 (d, J=9 Hz, 2H, PhH); ^{13}C NMR δ=14.25 (CH_3), 17.00 (CH_2), 24.22 (CH), 25.80 (CH), 26.40, 58.40 (CH), 60.70 (CH_2), 126.41 (CH), 126.65 (CH), 140.31, 141.10, and 173.14 (C=O); MS m/z 253, 255, and 218.

Kinetic Measurement. 80% aqueous acetone was prepared by mixing corresponding volumes of two components at room temperature. The solvolysis rates were followed in the usual manner according to a conductometric method. Conductivity readings were taken by using a conductivity meter (Model CM-50AT equipped with time interval unit and printer, TOA Electric Ltd.). Solvolysis was followed by taking at least 30 points at appropriate intervals for 2.5 half-lives, and an infinity reading was taken after 10 half-lives. Temperatures of the thermostat bath for the reaction rate experiments were within ±0.03 °C. The rate determination by titration was done by the same procedure as previously published.[6]

The rate constants were obtained graphically. Rate constants from repeated runs were reproducible with an accuracy of 2%.

The present work was partially supported by a Grant-in-Aid (1990) for Special Research from the Ministry of Education, Science and Culture.

References

1) Presented partly at the 8th IUPAC Conference on Physical Organic Chemistry, Tokyo (1986).

2) C. A. Coulson and W. E. Moffitt, *J. Chem. Phys.*, **15**, 151 (1947); A. D. Walsh, *Nature*, **159**, 165, 712 (1947); *Trans. Faraday Soc.*, **45**, 179 (1949); N. C. Baird and M. J. S. Dewar, *J. Am. Chem. Soc.*, **89**, 3966 (1967).

3) a) M. T. Rogers, *J. Am. Chem. Soc.*, **69**, 2544 (1947); W. W. Robertson, J. F. Music, and F. A. Matsen, *ibid.*, **72**, 5260 (1950). b) F. A. Van-Catledge, *J. Am. Chem. Soc.*, **95**, 1173 (1973); R. C. Hahn, P. H. Howard, and G. A. Lorenzo, *ibid.*, **93**, 5816 (1971); D. W. Boerth, *J. Org. Chem.*, **47**, 4085 (1982).

4) D. H. Marr and J. B. Stothers, *Can. J. Chem.*, **45**, 225 (1967); Y. Kusuyama and Y. Ikeda, *Bull. Chem. Soc. Jpn.*, **50**, 1784 (1977); Y. Kusuyama, C. D. Brenzinger, and J. D. Roberts, *Org. Magn. Reson.*, **13**, 372 (1980).

5) a) M. Charton, in "The Chemistry of Alkenes," ed by J. Zabicky, Wiley-Interscience (1970), Vol. 2, Chap. 10, and the references cited therein. b) K. B. Wiberg, B. A. Andes, and J. A. Ashe, in "Carbonium Ions," ed by G. Olah and P. V. R. Schleyer (1972), Vol. 3, Chap. 26.

6) Y. Kusuyama and Y. Ikeda, *Bull. Chem. Soc. Jpn.*, **46**, 204 (1973).

7) L. B. Jones and V. K. Jones, *Tetrahedron Lett.*, **1966**, 1493; L. B. Jones and S. S. Eng, *ibid.*, **1968**, 1431; H. C. Brown and J. D. Cleveland, *J. Org. Chem.*, **41**, 1792 (1976); P. Fischer and R. Taylor, *J. Chem. Soc., Perkin Trans. 2*, **1980**, 781; R. S. Brown and T. G. Traylor, *J. Am. Chem. Soc.*, **95**, 8025 (1973).

8) O. G. Kulinkovich, I. G. Tishchenko, I. V. Reznikov, and A. A. Pap, *Zh. Org. Khim.*, **17**, 473 (1981).

9) O. Exner, in "Advances in Linear Free Energy Relationships," ed by N. B. Chapman and J. Shorter, Plenum Press, New York and London (1972), Chap. 1.

10) a) Y. Yukawa and Y. Tsuno, *Bull. Chem. Soc. Jpn.*, **32**, 971 (1959); Y. Yukawa, Y. Tsuno, and M. Sawada, *ibid.*, **39**, 2274 (1966); Y. Yukawa and Y. Tsuno, *Nippon Kagaku Zasshi*, **86**, 873 (1965). b) Y. Tsuno, Y. Kusuyama, M. Sawada, T. Fujii, and Y. Yukawa, *Bull. Chem. Soc. Jpn.*, **48**, 3337 (1975); Y. Tsuji, M. Fujio, and Y. Tsuno, *ibid.*, **63**, 856 (1990).

11) W. F. Reynolds, R. H. Kohler, and G. K. Hamer, *Tetrahedron Lett.*, **1976**, 4671; M. E. Jason, P. R. Kurzweil, and K. E. Leonard, *J. Org. Chem.*, **51**, 2550 (1986).

12) Y. Kusuyama, T. Kagosaku, and T. Hasegawa, *Bull. Chem. Soc. Jpn.*, **63**, 2836 (1990).

13) We were not able to measure the solvolysis rate of the cis derivative. The chlorination of *p*-(*cis*-2-methoxycyclopropyl)-α-methylbenzyl alcohol by hydrogen chloride gave the corresponding chloride including 25% of impurities.

14) Correlation coefficient.

15) a) R. G. Pews and N. D. Ojha, *J. Am. Chem. Soc.*, **91**, 5769 (1969). b) Y. Kusuyama, *Bull. Chem. Soc. Jpn.*, **49**, 724 (1976); Y. Kusuyama and Y. Ikeda, *ibid.*, **50**, 1784 (1977); Y. Kusuyama, *ibid.*, **52**, 1944 (1979); Y. Kusuyama, K. Tokami, M. Mishima, and Y. Tsuno, *Org. Magn. Reson.*, **20**, 159 (1982). c) L. D. Kispert, C. Engelman, C. Dyas, and C. U. Pittman, Jr., *J. Am. Chem. Soc.*, **93**, 6948 (1971); C. F. Wilcox, L. M. Loew, and R. Hoffmann, *J. Am. Chem. Soc.*, **95**, 8192 (1973).

16) Y. Tsuno, M. Sawada, T. Fujii, and Y. Yukawa, *Bull. Chem. Soc. Jpn.*, **52**, 3033 (1979).

17) Y. Tsuno, W. Chong, Y. Tairaka, M. Sawada, and Y. Yukawa, *Bull. Chem. Soc. Jpn.*, **51**, 596 (1978).

18) Y. Tsuno, Y. Tairaka, M. Sawada, T. Fujii, and Y. Yukawa, *Bull. Chem. Soc. Jpn.*, **51**, 601 (1978).

19) O. A. Subbotin, A. S. Kozmin, Y. K. Grishin, N. M. Sergeyev, and I. G. Bolesov, *Org. Magn. Reson.*, **4**, 53 (1972).

20) 1 mmHg=133.322 Pa.

21) H. Yamanaka, R. Oshima, K. Teramura, and T. Ando, *J. Org. Chem.*, **37**, 1734 (1970).

22) Y. Kusuyama and Y. Ikeda, *Nippon Kagaku Zasshi*, **1977**, 290.

23) P. S. Skell and A. Y. Garner, *J. Am. Chem. Soc.*, **78**, 5430 (1956).

24) T. Hirao, S. Kohno, Y. Ohshiro, and T. Agawa, *Bull. Chem. Soc. Jpn.*, **56**, 1881 (1983); T. Hirao, M. Hagihara, and T. Agawa, *ibid.*, **58**, 3104 (1985); T. Hirao, T. Masunaga, Y. Ohshiro, and T. Agawa, *J. Org. Chem.*, **46**, 3746 (1981).

25) C. Kaiser, J. Weinstock, and M. P. Olmstead, *Org. Synth.*, Coll. Vol. VI, 913 (1988).

Ozone Fading of 2,2′-Dihydro Azo Copper Complex Dyes

Masaki MATSUI,* Kenjiro TSUBOTA, Katsuyoshi SHIBATA,
and Hiroshige MURAMATSU
Department of Chemistry, Faculty of Engineering, Gifu University, Yanagido 1-1, Gifu 501-11
(Received April 18, 1991)

The reactivities of dyes with ozone were in the following order, Acid Blue 74>disodium 1-(2-hydroxyphenylazo)-2-naphthol-3,6-disulfonate>Direct Yellow 12>Acid Orange 7>disodium 1-phenylazonaphthalene-3,6-disulfonate-2,2′-diolatocopper(II)>Mordant Red 3>Basic Green 4. The reaction of disodium 1-phenylazonaphthalene-3,6-disulfonate-2,2′-diolatocopper(II) with ozone was retarded by the introduction of electron-withdrawing groups and 8-sulfonato group. The potassium sulfonate dye was less reactive than the sodium one. Ozonization of 1-phenylazonaphthalene-2,2′-diolatocopper(II) gave phenol, 2-naphthol, and phthalic anhydride.

Reaction of dyes with ozone is of interest from the viewpoint of ozone fading of coloring matter and ozone treatment of dye wastewater.[1] It is important to evaluate the factors which affect the ozone fading of dyes. In our continuing series of studies on the reaction of ozone with dyes, ozone fading mechanism of several dyes have been proposed.[2–6] This report describes the reactivity and products in ozone fading of 2,2′-dihydro azo copper complex dyes.

Results and Discussion

Figure 1 shows dyes used in this study. 2-Hydroxybenzenediazonium chloride, prepared from 2-aminophenol, sodium nitrite, and hydrochloric acid, was reacted with 1- and 2-naphthol derivatives to afford metal free **1** and **2**, which were treated with copper sulfate to give **1** and **2**.

It is of interest to compare the reactivity of metal complex dyes with those of the other dyes whose ozone fading mechanisms have been reported.[2–6] In order to estimate the reactivity, the reaction in the initial stage was applied to first-order rate kinetics. For example, Fig. 2 shows the plots of logarism of A_0/A_t vs. time, where A_0 and A_t are absorbance at 0 and t sec at maximum wavelength, respectively. The plots of **1a** were linear and the rate constant (k) was calculated to be 0.0057 s^{-1}.

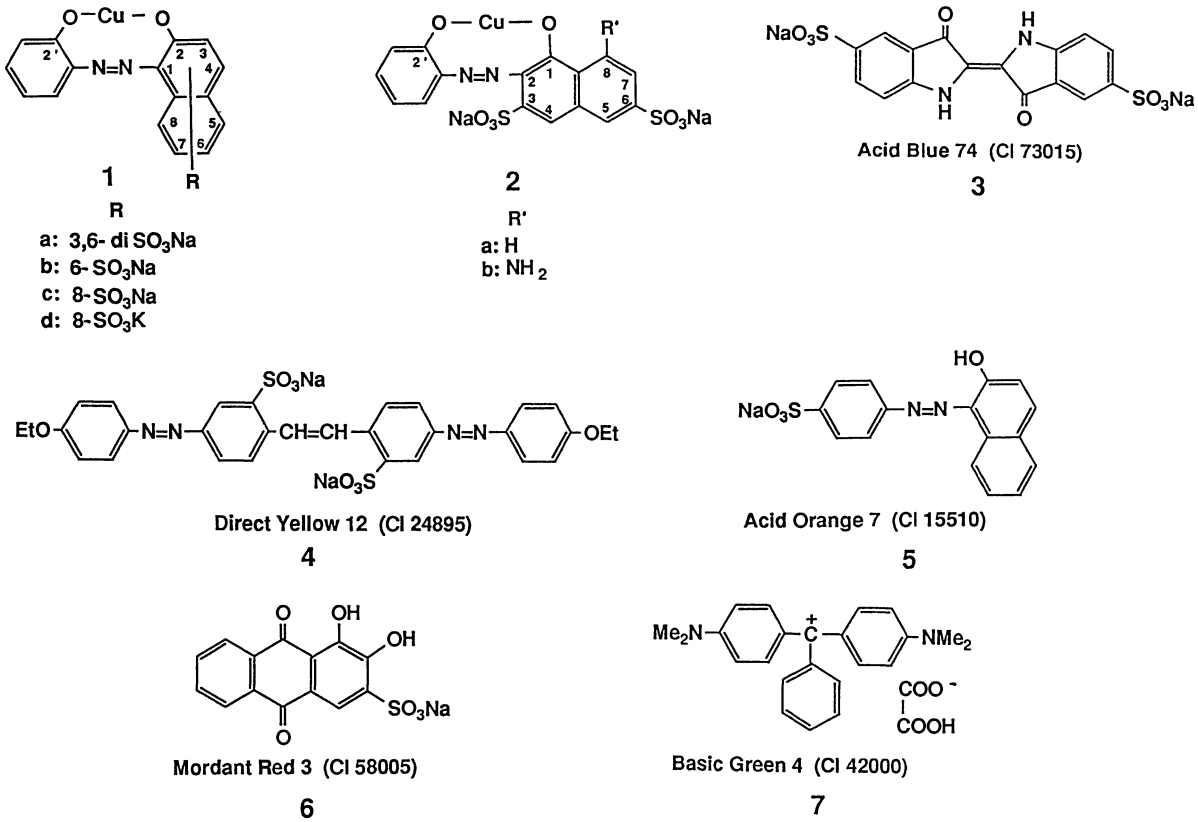

Fig. 1. Materials.

Table 1. Reactivities of Dyes with Ozone

Run	Dyes	$k\times10^3$ (s^{-1})
1	**3**	13.0±0.3
2	Metal free **1a**	12.3±0.3
3	**4**	9.6±0.0
4	**5**	6.6±0.1
5	**1a**	5.7±0.1
6	**6**	5.2±0.6
7	**7**	4.6±0.4
8	**1b**	6.8±0.1
9	**1c**	5.5±0.3
10	**1d**	4.0±0.2
11	**2a**	4.9±0.1
12	**2b**	6.0±0.1

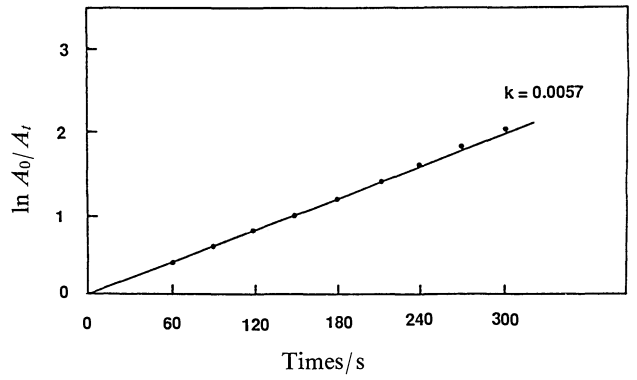

Fig. 2. Reactivity of disodium 1-phenylazonaphthalene-3,6-disulfonate-2,2′-diolatocopper(II) with ozone.

Table 1 shows the reactivities of dyes with ozone. The rate constants of dyes were in the following order, Acid Blue 74 (**3**)>metal free **1a**>Direct Yellow 12 (**4**) >Acid Orange 7 (**5**)>**1a**>Mordant Red 3 (**6**)>Basic Green 4 (**7**) (Runs 1—7). Ozone reacts easily with double bonds such as C=C and C=N. Ozonolyses of central olefinic bonds of 2-(1,3-dihydro-3-oxo-2*H*-indol-2-ylidene)-1,2-dihydro-3*H*-indol-3-one (Vat Blue 1, CI 73000) and Direct Yellow 12 (**4**) have been reported to give carbonyl compounds.[2,3] Ozone fading of 2-hydroxyazo dyes have been reported to proceed via the hydrazone isomers on the basis of substituent and solvent effects.[4] It has been reported that 1,2-dihydroxyanthraquinone (Pigment Red 83, CI 58000) was ozonized to give phthalic anhydride.[5] Although ozone attacked both the dimethylamino and olefinic moieties of aminotriphenylmethane dyes, it attacked mainly the dimethylamino moiety in the case of Basic Green 4 to give the formylmethylamino derivative.[6] Since the product is still colored, the rate constant of ozone fading is apparentely small. Aromatic azo compounds are fairly stable for ozone.[7,8] Since **1a** has bulky and electron-withdrawing copper atom in a molecule, the rate constant was smaller than the metal free **1a**.

Figure 3 shows the substituent effect on ozone fading of **1a**. The plots of logarism (k_R/k_H) vs. Hammett's σ constants, where k_R and k_H are rate constants of substituted and unsubstituted dyes respectively, were linear, whose slope (ρ) was calculated to be −0.22 (r=0.95). This result suggested that ozone attacked electrophilically the substrate and that introduction of electron-withdrawing groups into diazo component improved stability of dyes for ozone.

The reaction rates of some 2,2′-dihydro azo copper complex dyes, whose couplers consisted of 1- and 2-naphthol derivatives are summarized in Table 1. The results indicated that 1) electron-withdrawing sulfonato group (σ: 0.09 (p), 0.05 (m)) inhibited the reaction (Runs 5, 8); 2) bulky sulfonato group at the 8 position retarded the reaction (Runs 8, 9); 3) greater potassium ion (ionic radius, K=1.38 Å, Na=1.02 Å) inhibited the reaction (Runs 9, 10); and 4) electron-releasing amino group of the coupler accelerated the reaction (Runs 11, 12).

Ozonization of 1-phenylazonaphthalene-2,2′-diolatocopper(II) (**8**) gave phenol (**9**), 2-naphthol (**10**), and

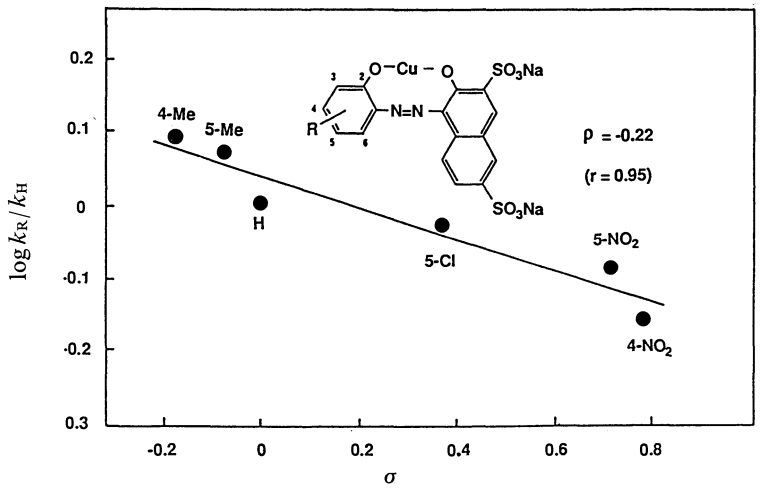

Fig. 3. Hammett's plots for the ozone fading of disodium 1-phenylazonaphthalene-3,6-disulfonate-2,2′-diolatocopper(II).

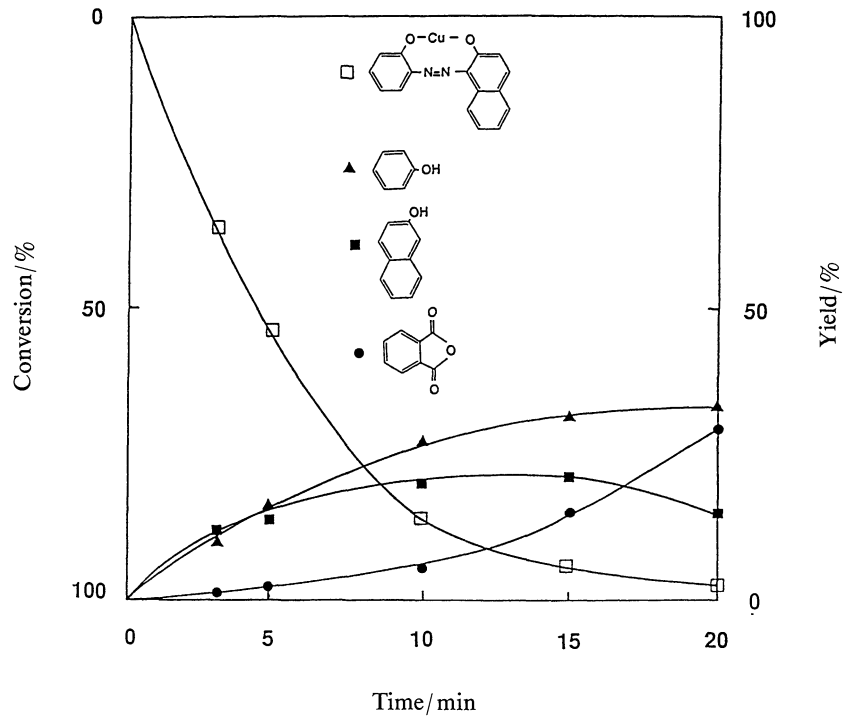

Fig. 4. Ozonization of 1-phenylazonaphthalene-2,2'-diolatocopper(II). Ozonization was carried out with an ozone–oxygen mixture (O_3: 0.068 mmol min^{-1}, O_2: 200 ml min^{-1}) on 1-phenylazonaphthalene-2,2'-diolatocopper(II) (1.6 mmol) in DMSO (2 ml) at 30 °C.

phthalic anhydride (**11**). Figure 4 shows the time-dependence of products. The ozonization of **8** gave **9** and **10**, which was further ozonized to afford **11**. Ozonization of phenol has been reported to give formic acid as a main product.[9] The reaction of 2-naphthol with ozone gave phthalic anhydride. Ozone attacked the azo linkage of **8** to give unstable azoxy intermediates which is followed by the hydrolysis of Cu–O bond to give **9** and **10**. Ozone could attack also the C=N bond of the hydrazone isomer of **8** to give the products.

Experimental

Instruments. Ozone was generated with a Nihon Ozon 0-1-2 type ozonizer. Melting points were measured with a Yanagimoto micro melting point apparatus and uncorrected. NMR, UV, and mass spectra were obtained with JEOL JUM GX 270, JASCO 410, and Shimadzu QP-1000 spectrometers, respectively. Gas chromatography was performed on a Shimadzu 4C-PF gas chromatograph.

Materials. Acid Blue 74 (**3**), Direct Yellow 12 (**4**), Acid Orange 7 (**5**), and Basic Green 4 (**7**) were purchased from Tokyo Kasei Co., Ltd. Mordant Red 3 (**6**) was obtained from Aldrich Chemical Co., Ltd. They were used without further purification.

2,2'-Dihydro azo compounds were prepared as follows; to 50% hydrochloric acid solution of 2-aminophenol (3.2 g, 29 mmol) was added 30% aqueous solution (8 ml) of sodium nitrite at 0 °C. The mixture was stirred for 1 h. To the diazotized solution was added 20% aqueous sodium hydroxide solution (35 ml) of a coupler (30 mmol). The mixture was stirred at 0 °C for 1 h. The product was obtained by salting-out techniques. Physical and spectral data of 1-(2-hydroxyphenylazo)-2-naphthol are shown below. Mp 194.0—195.0 °C (lit,[10] 193 °C); ^{1}H NMR ($CDCl_3$) δ=7.0—8.2 (m, 10H), 12.4 (s, 1H), and 14.5 (s, 1H); EIMS (70 eV) m/z (rel intensity) 264 (M^+, 100).

2,2'-Dihydro azo copper complex dyes were synthesized as follows; in the case of **1** and **2**, to an aqueous solution (150 ml) of 2,2'-dihydro azo compound (10 mmol) was added an aqueous solution of copper sulfate penta hydrate (10 mmol). The mixture was stirred at room temperature. In the case of **8**, the reaction was carried out in an acetone solution. The resulting precipitate was collected and washed with water or acetone. Found: C, 54.19; H, 3.26; N, 7.89%. Calcd for $C_{16}H_{10}N_2O_2Cu \cdot H_2O$: C, 55.89; H, 3.52; N, 8.15%.

Reactivity of Dyes with Ozone. Ozonization was carried out with an ozone–oxygen mixture (O_3: 0.068 mmol min^{-1}, O_2: 200 ml min^{-1}) on dye (0.1 mmol) in phosphate buffer solution (pH=6.8, 500 ml) at 30 °C. The rate constants were calculated on the basis of the changes of the absorbance at λ_{max} of the solution during the reaction.

Ozonization of 1-Phenylazonaphthalene-2,2'-diolatocopper-(II). Ozonization was carried out with an ozone–oxygen mixture (O_3: 0.068 mmol min^{-1}, O_2: 200 ml min^{-1}) on 1-phenylazonaphthalene-2,2'-diolatocopper(II) (1.6 mmol) in DMSO (2.0 ml) at 30 °C. After the reaction, the mixture was allowed to stand overnight. The disappearance of peroxide activity was checked by a KI test. Products were identified by GC-mass analysis and determined by gas chromatography. The conditions of gas chromatography are shown below. GLC 1: column 2% OV-1 on Gaschrom Q (60—80 mesh), 3 mm×1 m; column temperature 80—240 °C (10 °C min^{-1});

injection temperature 250 °C; detector temperature 250 °C; detection FID. GLC 2: column 2% FFAP on Gaschrom Q (80—100 mesh), 3 mm×1 m; column temperature 80—210 °C (10 °C min^{-1}); injection temperature 220 °C; detector temperature 220 °C; detection FID.

Authors would like to express their gratitude to Mr. Hiroshi Takimoto of Mitsubishi Kasei Co. for his valuable discussion.

References

1) M. Matsui, *Shikizai Kyokai Shi,* **64**, 29 (1991).
2) M. Matsui, M. Morita, K. Shibata, and Y. Takase, *Nippon Kagaku Kaishi,* **1982**, 1268.
3) M. Matsui, T. Hibino, K. Shibata, and Y. Takase, *Am. Dyest. Rep.,* **72**, 40 (1983).
4) M. Matsui, A. Konda, K. Shibata, and Y. Takase, *Bull. Chem. Soc. Jpn.,* **58**, 2829 (1985).
5) D. Grosjean, P. M. Whitmore, C. P. De Moor, and G. R. Cass, *Environ. Sci. Technol.,* **21**, 635 (1987).
6) M. Matsui, H. Nakabayashi, K. Shibata, and Y. Takase, *Bull. Chem. Soc. Jpn.,* **57**, 3312 (1984).
7) R. E. Miller, *J. Org. Chem.,* **26**, 2327 (1961).
8) M. Matsui, Y. Iwata, T. Kato, and K. Shibata, *Dyes Pig.,* **9**, 109 (1988).
9) Y. Yamamoto, E. Niki, H. Shiokawa, and Y. Kamiya, *J. Org. Chem.,* **44**, 2137 (1979).
10) S. Niementowski, *Chem. Zentralbl., Neue Folge,* **1902**, 938.

Preparation and Reactivities of (η^3-1- and 2-Trimethylsiloxyallyl)$Fe(CO)_2NO$ Complexes. Intermediates Functioning as Equivalents of β- and α-Acyl Carbocations and Acyl Carbanions

Keiji Itoh, Saburo Nakanishi,† and Yoshio Otsuji*,†
Department of Industrial Chemistry, Osaka Prefectural College of Technology, Saiwaicho, Neyagawa, Osaka 572
†Department of Applied Chemistry, College of Engineering, University of Osaka Prefecture, Mozu-Umemachi, Sakai, Osaka 591
(Received April 22, 1991)

(η^3-1- and 2-Trimethylsiloxyallyl)$Fe(CO)_2NO$ complexes were prepared by the reaction of the corresponding siloxyallylic halides with $Bu_4N[Fe(CO)_3NO]$. These complexes reacted with both of carbon nucleophiles and carbon electrophiles preferentially at the less hindered sites of the allylic ligands. In these reactions, (η^3-1-trimethylsiloxyallyl)$Fe(CO)_2NO$ complexes served as synthetically equivalent synthons for both of β-acyl carbocations and β-acyl carbanions and (η^3-2-trimethylsiloxyallyl)$Fe(CO)_2NO$ complexes as both of α-acyl carbocations and α-acyl carbanions. The stereochemical courses of the reactions are described.

π-Allyl transition metal complexes have been shown to be useful intermediates in organic synthesis.[1] In most cases, these complexes have been used as a synthetically equivalent synthon for allylic carbocations. An exceptional case is π-allyl nickel complexes. They react with carbon electrophiles such as organic halides in polar media to produce alkylated allyl compounds.[2] However, the synthetic applicability of π-allyl iron complexes has been less explored, compared with the other transition metal complexes such as π-allyl nickel and palladium complexes. Nicholas et al. have reported that cationic π-allyl iron complexes of the type, (η^3-allyl)$Fe(CO)_4BF_4$, react with carbon nucleophiles preferentially at the less hindered site of the allylic ligands to produce alkylated allyl compounds.[3] Roustan et al. have shown that allylic acetates and halides couple with carbon nucleophiles in the presence of a catalytic amount of $Na[Fe(CO)_3NO]$ also to produce alkylated allyl compounds.[4] In this catalytic reaction, the attack of nucleophiles occurs preferentially at the leaving group-bearing carbons of the allylic ligands. They proposed that this reaction proceeds via (η^3-allyl)$Fe(CO)_2NO$ complexes. Xu and Zhou have reported a similar type of coupling reactions using n-$Bu_4N[Fe(CO)_3NO]$ as catalyst, but they proposed σ-allyl iron complexes as a key intermediate in this catalytic reaction.[5] However, no systematic studies have so far been made for the reactivities of (η^3-allyl)$Fe(CO)_2NO$ complexes. Previously, we reported a convenient procedure for preparation of the tetrabutylammonium ferrate, n-$Bu_4N^+[Fe(CO)_3NO]^-$ (TBAFe), and have shown that this ferrate complex can be utilized as a useful reagent for the synthesis of a variety of (η^3-allyl)$Fe(CO)_2NO$ complexes.[6] We also found that (η^3-allyl)$Fe(CO)_2NO$ complexes derived from allylic halides react with carbon electrophiles such as allyl, acyl and alkoxycarbonyl halides to give 1,5-dienes and β,γ-unsaturated carbonyl compounds, respectively.[6] In our previous communications,[7] we showed that (η^3-1-trimethylsiloxyallyl)$Fe(CO)_2NO$ complexes react with both of carbon nucleophiles and electrophiles at the same position of the allylic ligands. Therefore, these iron complexes are envisaged to serve as a synthetically equivalent synthon for both of β-acyl carbocations and β-acyl carbanions. Since then, we have extensively investigated the chemical reactivities of iron complexes of this sort. In this paper, we report the preparation of (η^3-1- and 2-trimethylsiloxyallyl)$Fe(CO)_2NO$ complexes and their reactivity features. These complexes have a dual reactivity and react with both of carbon nucleophiles and electrophiles at the same position of the allylic ligands of the complexes, preferentially at the less hindered sites. The stereochemical courses of the reactions are also discussed.

Results and Discussion

Preparation of (η^3-Trimethylsiloxyallyl)$Fe(CO)_2NO$ Complexes. The reaction of 3-halo-2-trimethylsiloxy-1-propenes **1a**—**d** with one equiv of TBAFe in CH_2Cl_2 at room temperature gave (η^3-2-trimethylsiloxyallyl)$Fe(CO)_2NO$ complexes **2a**—**d** with evolution of one equiv of CO. The results are given in Scheme 1 and Table 1. The complexes were fairly stable to air and moisture, and they could be isolated by column chromatography on slica gel.

The structures of **2a**—**d** were established from their spectral data. The IR spectra showed characteristic absorption due to two CO ligands and one NO ligand in 1950—2050 and 1720—1730 cm^{-1} regions, respectively. The ^1H NMR spectra exhibited signals assignable to the allylic ligands. The ^1H NMR spectrum of **2c** revealed that this complex is actually a 1:1 mixture of two isomers in which the allylic ligand has a different configuration; i,e. the one isomer has the *syn*-methyl and *anti*-ethyl configuration and the other isomer has the *syn*-ethyl and *anti*-methyl configuration. The methyl proton signal of the former isomer appeared at a lower field (δ=2.07) than that of the later isomer (δ=1.51). In the case of **2d**, chlorine atom on the allylic ligand was found to be oriented to the anti-direction.

(η^3-1-Trimethylsiloxyallyl)$Fe(CO)_2NO$ complexes

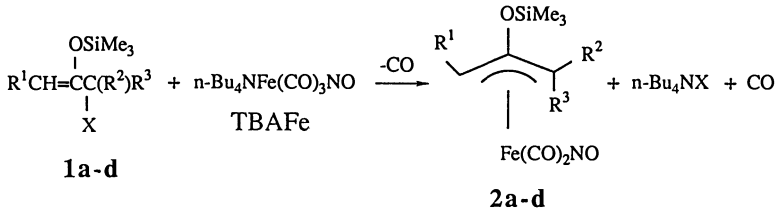

Scheme 1.

Table 1. Preparation of (η^3-2-Trimethylsiloxyallyl)Fe(CO)$_2$NO Complexes

Allylic halide	Iron complex	Isolated Yield[a)]/%
1a: R^1=R^2=R^3=H, X=Cl	**2a**	57
1b: R^1=H, R^2=R^3=Me, X=Br	**2b**	68
1c: R^1=H, R^2=Me, R^3=Et, X=Br	**2c**	72
1d: R^1=Cl, R^2=R^3=H, X=Cl	**2d**	37

a) Isolated yields based on the allylic halides used.

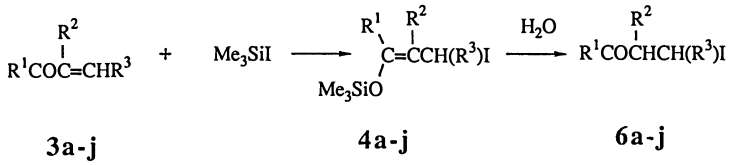

Scheme 2.

5a—**j** were synthesized by the reaction of TBAFe in CH_2Cl_2 at room temperature with one molar equiv of 3-iodo-1-trimethylsiloxy-1-propenes **4a**—**j**, which had been prepared in situ from α,β-unsaturated carbonyl compounds **3a**—**j** and Me_3SiI. Complexes **5a**—**j** were unable to isolate in pure forms because of their sensitivity to air and moisture. However, formation of the iron complexes was supported by their chemical properties and spectral data.

The reaction of **3a**—**j** with Me_3SiI in CH_2Cl_2, followed by acid hydrolysis, gave the β-iodo ketones and esters **6a**—**j**. This reaction is likely to proceed via silyl enol ethers **4a**—**j**.[8)] In separate experiments, **4a**—**j**, which were prepared from **3a**—**j** and Me_3SiI, were first treated with TBAFe, and then hydrolyzed with 4 M (1 M=1 mol dm^{-3}) HCl. This treatment gave quantitatively the starting ketones and esters **3a**—**j**. All of these results can be explained in terms of the reaction pathways shown in Scheme 2. A more direct support for the formation of **5a**—**j** was secured from the IR spectra of the reaction mixtures. The IR spectrum of the reaction mixture obtained from **3a**, Me_3SiI and TBAFe showed the characteristic bands for **5a** at 2060 and 1980 cm^{-1} due to two CO ligands, 1745 cm^{-1} due to the NO ligand, and 870 cm^{-1} due to the O–Si bond of the allylic ligand. Similar spectral data were obtained for **5b**—**j** which were prepared in a similar manner.

Reactions of (η^3-Trimethylsiloxyallyl)Fe(CO)$_2$NO Complexes. Ligand Exchange. The reactions of (η^3-trimethylsiloxyallyl)Fe(CO)$_2$NO complexes **2b** and **5b** with one equiv of allylic halides, acetates, and carbonates **7a**—**h** in CH_2Cl_2 resulted in the ligand exchange to give (η^3-allyl)Fe(CO)$_2$NO complexes **8a**—**d**. In these reactions, small amounts of ketones **9** and **3b**, which were obtained by hydrolysis of the trimethylsiloxyallylic ligands, were produced as by-products. The results are summarized in Scheme 3 and Table 2. Noteworthy is that allylic acetates and carbonates have little reactivity toward TBAFe, but they react with (η^3-trimethylsiloxyallyl)Fe(CO)$_2$NO complexes to form (η^3-allyl)-Fe(CO)$_2$NO complexes via the ligand exchange reaction. The reactivity in the ligand-exchange reaction

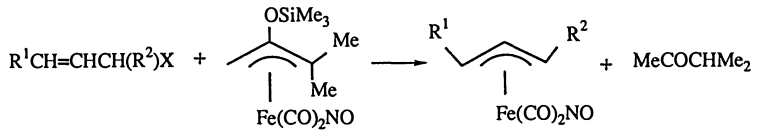

7a-h **2b** **8a-d** **9**

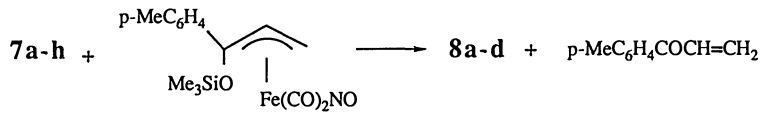

5b **3b**

Scheme 3.

Table 2. Ligand Exchange of (η^3-Trimethylsiloxyallyl)Fe(CO)$_2$NO Complexes[a)]

Allylic compound			Iron complex	Product	Yield[b)]/%
R^1	R^2	X			
7a: H	H	Br	**2b**	**8a**: R^1=R^2=H	75
7b: Ph	H	Br	**2b**	**8b**: R^1=Ph, R^2=H	68
7b: Ph	H	Br	**5b**	**8b**	73
7c: Ph	H	OAc	**5b**	**8b**	28
7d: Ph	H	OCO_2Me	**5b**	**8b**	56
7e: Me	H	Cl	**2b**	**8c**: R^1=Me, R^2=H	26
7e: Me	H	Cl	**5b**	**8c**	38
7f: Me	H	OAc	**5b**	**8c**	26
7g: $-(CH_2)_3-$		Br	**2b**	**8d**: R^1—R^2=$-(CH_2)_3-$	76
7g: $-(CH_2)_3-$		Br	**5b**	**8d**	71
7h: $-(CH_2)_3-$		OAc	**5b**	**8d**	25

a) Solvent: CH_2Cl_2, Temperature: 40 °C, Time: 5 h. b) Isolated yields based on the allylic compounds used.

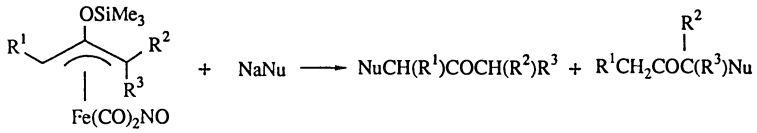

2 **10** **11**

Scheme 4.

Table 3. Reaction of the Iron Complexes **2a**—**d** with Carbon Nucleophiles

Iron complex	Nucleophile	Substituents on **10** and **11**			Yield[a)]/%	
		R^1	R^2	R^3	**10**	**11**
2a	$NaCH(CO_2Et)_2$	**a**: H	H	H	57	(**10a**=**11a**)
2a	$NaCH(COMe)CO_2Et$	**b**: H	H	H	43	(**10b**=**11b**)
2b	$NaCH(CO_2Et)_2$	**c**: H	Me	Me	46	16
2b	$NaCH(COMe)CO_2Et$	**d**: H	Me	Me	30	7
2b	$NaCH(CN)_2$	**e**: H	Me	Me	18	6
2c	$NaCH(CO_2Et)_2$	**f**: H	Me	Et	52	16
2c	$NaCH(COMe)CO_2Et$	**g**: H	Me	Et	40	9
2c	$NaCH(CN)_2$	**h**: H	Me	Et	46	4
2d	$NaCH(CO_2Et)_2$	**a**: H	H	H	53	(**10a**=**11a**)
2d	$NaCH(COMe)CO_2Et$	**b**: H	H	H	43	(**10b**=**11b**)

a) Isolated yields based on the iron complexes used.

Table 4. Reaction of the Iron Complexes **5** with Carbon Nucleophiles in THF

Iron complex	Nucleophile	Product	Yield[a]/%
5a: R=Ph	$NaCH(CO_2Et)_2$	**12a**: R=Ph, Nu=$CH(CO_2Et)_2$	95
5a:	$NaCH(COMe)CO_2Me$	**12b**: R=Ph, Nu=$CH(COMe)CO_2Me$	42
5d: R=Et	$NaCH(CO_2Et)_2$	**12c**: R=Et, Nu=$CH(CO_2Et)_2$	75
5e:[b]	$NaCH(CO_2Et)_2$	**12d**:[b]	90
5h: R=MeO	$NaCH(CO_2Et)_2$	**12e**: R=MeO, Nu=$CH(CO_2Et)_2$	95
5h:	$NaCH(COMe)CO_2Me$	**12f**: R=MeO, Nu=$CH(COMe)CO_2Me$	60
5h:	$NaCH(CN)_2$	**12g**: R=MeO, Nu=$CH(CN)_2$	92
5h:	1-morphilinocyclohexene	**12h**:[b]	89

a) Isolated yields based on the iron complexes used.

b) **5e**: 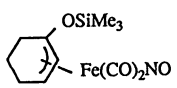 **12d**: 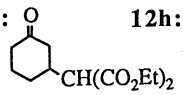 **12h**: 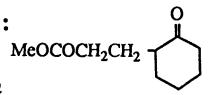

5a,d,e,h **12a-h**

Scheme 5.

implies that the stability of (η^3-allyl)$Fe(CO)_2NO$ complexes depends upon substituents on the allylic ligands and decreases in the order: alkyl, aryl>2-trimethylsiloxy>1-trimethylsiloxy.

Reactions with Carbon Nucleophiles. The iron complexes **2a**—**d** reacted with carbon nucleophiles such as $NaCH(CO_2Et)_2$, $NaCH(COMe)CO_2Et$ and $NaCH(CN)_2$ in THF at room temperature to give α-alkylated ketones **10a**—**h** along with small amounts of the regioisomers **11a**—**h** (**10a**=**11a**, **10b**=**11b**) after acid hydrolysis of the reaction mixtures. The results are shown in Scheme 4 and Table 3. In these reactions, the attack of carbon nucleophiles occurred predominantly at the less hindered sites of the allylic ligands. In the cases of **2d**, the reductive elimination of chlorine atom occurred concurrently to give the corresponding α-alkylated products. Consequently, the iron complexes **2a**—**d** can be regarded as a synthetically equivalent synthon for α-acyl carbocations.

The iron complexes **5a,d,e,h** also reacted with carbon nucleophiles in THF at room temperature to give β-alkylated ketones **12a,d,e,h** after acid hydrolysis of the reaction mixtures. The results are shown in Scheme 5 and Table 4. The regioselectivity in these reactions was extremely high, so that the nucleophiles reacted only at the less hindered sites of the allylic ligands, giving a single product in every case. Thus, the iron complexes **5a,d,e,h** can be regarded as a synthetically equivalent synthon for β-acyl carbocations.

Reactions with Carbon Electrophiles. Iron complexes **2a**—**c** reacted with 2-propynyl bromide in *N,N*-dimethylformamide (DMF) or *N*-methyl-2-pyrrolidinone (NMP) at 80 °C. In these reactions, the attack of 2-propynyl bromide occurred regioselectively also at the less hindered sites of the allylic ligands of the iron complexes. The acid hydrolysis of the reaction mixtures gave 3-butynyl ketones **13a**—**c** as sole isolable products. The results are given in Scheme 6 and Table 5.

Treatment of 3-halo-2-trimethylsiloxy-1-propenes **1a**—**c** with a half molar equiv of TBAFe in toluene at 110 °C, followed by acid hydrolysis of the reaction mixtures, gave two regioisomeric mixtures of 1,4-diketones, **14a**—**c** and **15a**—**c** (**14a**=**15a**). The results

Table 5. Reaction of the Iron Complexes **2a**—**c** with 2-Propynyl Bromide in DMF

Complex **2**	Product	Yield[a]/%
2a	**13a**	18
2b	**13b**	65
2b	**13b**	63[b]
2c	**13c**	55

a) Isolated yields based on the substrates **1** used.
b) NMP was used as solvent.

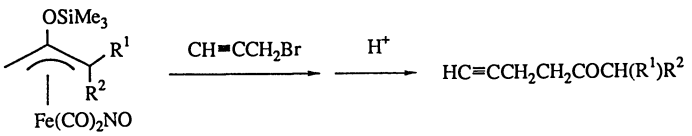

2a-c **13a-c**

Scheme 6.

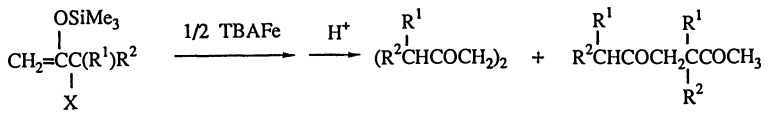

1a-c **14a-c** **15a-c**

Scheme 7.

Table 6. Formation of 1,4-Diketones

Substrate	Products: Yield[a]/%	
	14	**15**
1a	**14a**: 28	**(14a=15a)**
1b	**14b**: 69	**15b**: 22
1c	**14c**: 62	**15c**: 12

a) Isolated yields based on the substrates **1** used.

are shown in Scheme 7 and Table 6.

This reaction probably proceeds via an electrophilic attack of **1a—c** toward the intermediary produced iron complexes **2a—c**. With **1b,c**, the formation of **14b,c** predominated, indicating that a coupling at the less hindered sites of both of **1a—c** and **2a—c** is favored. Mechanistically, this reaction may involve an oxidative addition of the C–X bonds of **1a—c** on the Fe atom of the iron complexes **2a—c** as a key step. The detailed mechanistic feature of the reaction of the allylic iron complexes with allylic halides will be discussed later.

The above results strongly imply that the iron complexes **2a—c** serve as a synthetically equivalent synthon for α-acyl carbanions. Previously, Hegedus and Stiverson have demonstrated that η^3-2-methoxyallyl nickel complexes also serve as a synthetically equivalent synthon for α-acyl carbanions.[9]

The iron complexes **5a—g,i,j**, which were prepared in situ from **3a—g,i,j**, Me_3SiI and TBAFe, reacted regioselectively with 2-propynyl bromides in DMF or NMP at 80 °C to give β-propynylated ketones and esters **16a—g,i,j**, after acid hydrolysis of the reaction mixtures. The results are given in Scheme 8 and Table 7. The yields of the products were appreciably improved by pretreating **5a—g,i,j** with one equiv of triphenyl phos-

Table 7. Reaction of (η^3-1-Trimethylsiloxyallyl)Fe(CO)$_2$NO Complexes with 2-Propynyl Bromide in DMF[a]

	Complex			Additive	Product	Yield[b]/%
	R^1	R^2	R^3			
5a:	C_6H_5	H	H	None	**16a**	81
5a:				$P(OPh)_3$	**16a**	93
5b:	*p*-$CH_3C_6H_4$	H	H	None	**16b**	35
				$P(OPh)_3$	**16b**	83
				$P(OPh)_3$	**16b**	80[c]
5c:	*p*-ClC_6H_4	H	H	None	**16c**	66
				$P(OPh)_3$	**16c**	87
5d:	C_2H_5	H	H	$P(OPh)_3$	**16d**	58
5e:	$-(CH_2)_3-$	H	—[d]	$P(OPh)_3$	**16e**[e]	56
5f:	C_6H_5O	H	H	None	**16f**	12
				$P(OPh)_3$	**16f**	50
5g:	CH_3O	H	C_6H_5	None	**16g**	30
				$P(OPh)_3$	**16g**	62
5i:	C_6H_5	CH_3	H	$P(OPh)_3$	**16i**	76
5j:	C_6H_5O	CH_3	H	$P(OPh)_3$	**16j**	73

a) Reaction conditions: **5**; 2 mmol, $CH{\equiv}CCH_2Br$; 4 mmol, $P(OPh)_3$; 2 mmol, Temp; 80 °C, Time; 15 h.
b) Isolated yields based on iron complexes used.
c) NMP was used as solvent.
d) **5e**: 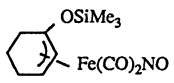
e) **16e**: 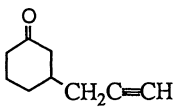

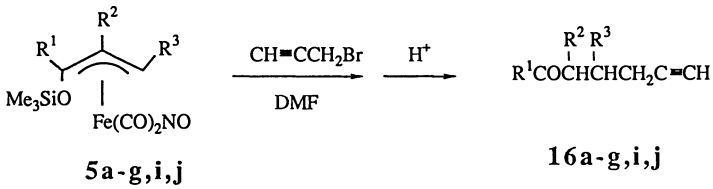

5a-g,i,j **16a-g,i,j**

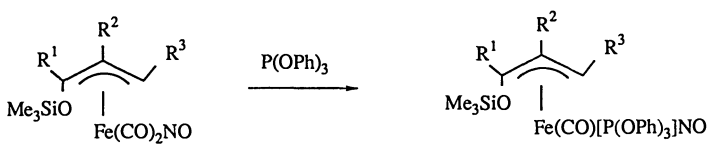

5a-g,i,j **5'a-g,i,j**

Scheme 8.

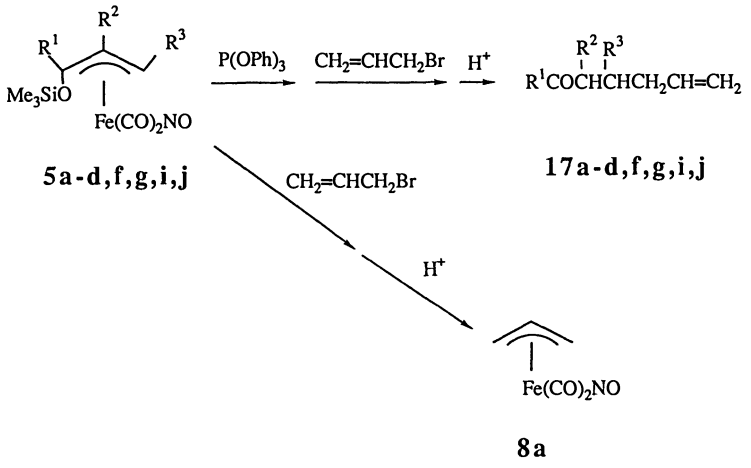

Scheme 9.

phite before adding 2-propynyl bromide to the reaction mixtures. In these cases, it is conceivable that the iron complexes **5** are first converted into the corresponding (η^3-1-trimethylsiloxyallyl)Fe(CO)[P(OPh)$_3$]NO complexes **5′**, although they were not isolated in pure forms.

Table 8. Reaction of (η^3-1-Trimethylsiloxyallyl)Fe(CO)$_2$NO Complexes with Allyl Bromide in the Presence of P(OPh)$_3$ in DMF[a)]

	Complex			Product	Yield/%
	R^1	R^2	R^3		
5a:	C_6H_5	H	H	**17a**	61
5a:		H	H	**17a**	66[b)]
5b:	*p*-$CH_3C_6H_4$	H	H	**17b**	48
5c:	*p*-ClC_6H_4	H	H	**17c**	52
5d:	C_2H_5	H	H	**17d**	25
5f:	C_6H_5O	H	H	**17f**	48
5g:	CH_3O	H	C_6H_5	**17g**	30
5i:	C_6H_5	CH_3	H	**17i**	60
5j:	C_6H_5O	CH_3	H	**17j**	42

a) Reaction conditions: **5**; 2 mmol, CH_2=$CHCH_2Br$; 4 mmol, P(OPh)$_3$; 2 mmol, Temp; 80 °C, Time; 15 h. b) NMP was used as solvent.

The iron complexes **5a—d,f,g,i,j** also reacted in DMF or NMP with allyl bromide after treating the complexes with triphenyl phosphite to give β-allylated ketones and esters **17a—d,f,g,i,j**. In the absence of triphenyl phosphite, the complexes did not react with allyl bromide at room temperature, but the ligand-exchange reaction occurred to give (η^3-allyl)Fe(CO)$_2$NO complex **8a**. The results are shown in Scheme 9 and Table 8. When the reaction was carried out at 80 °C, 1,5-hexadiene was obtained by the coupling of the allyl ligand of the complex **8a**.

All the above results strongly support the assumption that the actual reactive complexes in the reactions of the iron complexes **5** in the presence of triphenyl phosphite are **5′**, and indicate that the nucleophilic reactivity of the iron complexes **5** is increased by converting the electron-withdrawing CO ligand in the complexes to the electron-donating P(OPh)$_3$ ligand. A more detailed mechanistic feature for the reaction of the iron complexes with allylic halides was obtained from the following experiments.

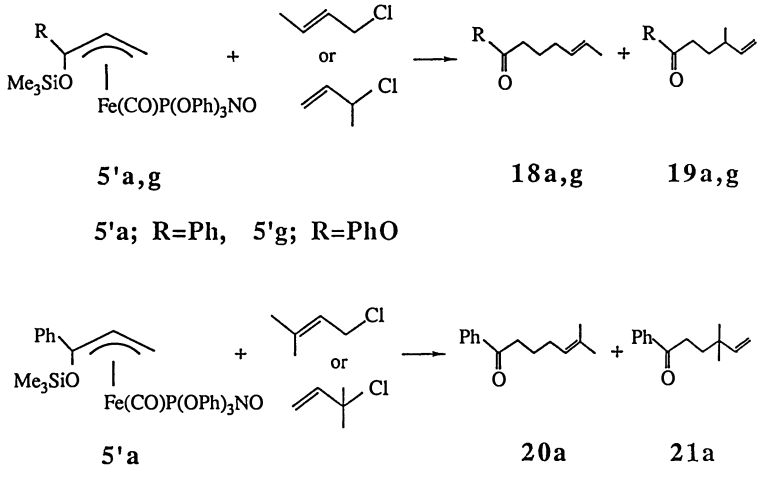

Scheme 10.

Table 9. Reaction of the Iron Complexes **5'a** and **5'g** with Allylic Chlorides in DMF

Iron complex	Allylic halide	Yield of products[a]/%	Ratio of **18**/**19** or **20**/**21**
5'a	1-Chloro-2-butene	51	38/13
5'a	3-Chloro-1-butene	48	34/14
5'g	1-Chloro-2-butene	43	32/11
5'g	3-Chloro-1-butene	50	36/14
5'a	1-Chloro-3-methyl-2-butene	58	56/ 2
5'a	3-Chloro-3-methyl-1-butene	52	50/ 2

a) Isolated yields based on the iron complexes used.

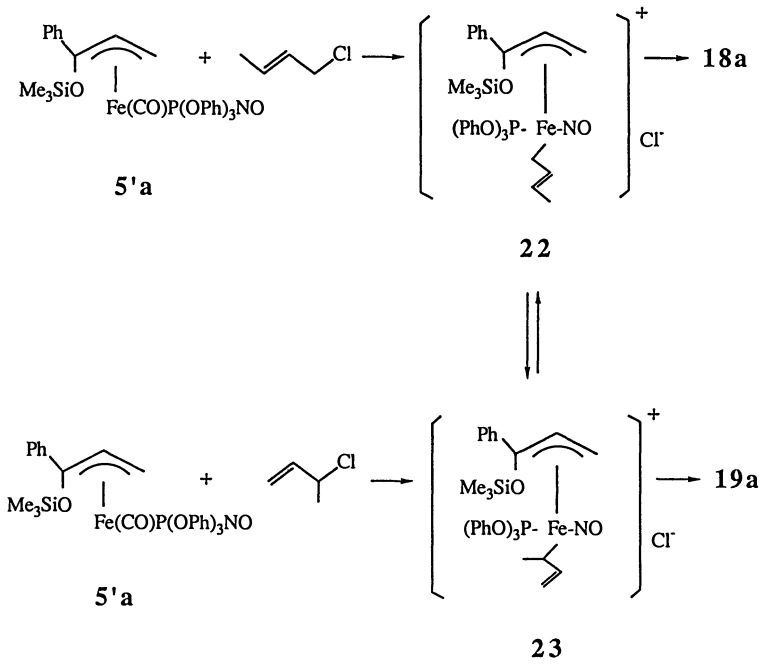

Scheme 11.

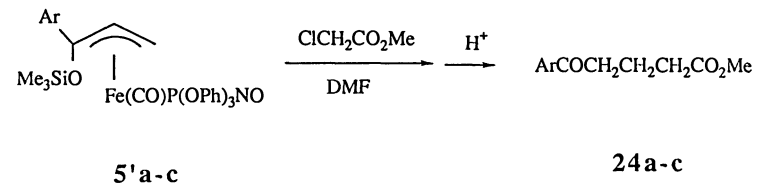

Scheme 12.

The reaction of **5'a** and **5'g** with 1-chloro-2-butene and 3-chloro-1-butene in DMF afforded a mixture of δ,ε-unsaturated ketones **18a** and **19a** and a mixture of **18g** and **19g**, respectively, essentially in the same ratio from both of the allylic halides. The reaction of **5'a** with 1-chloro-3-methyl-2-butene and 3-chloro-3-methyl-1-butene also afforded a mixture of two unsaturated ketones **20a** and **21a** almost in the same ratio. The results are given in Scheme 10 and Table 9. These results can be accounted for in terms of the reaction pathway shown in Scheme 11. The first step is the oxidative addition of allylic halides on the Fe atom of the iron complexes to form iron complexes **22** and **23** which are in equilibrium with each other. The reductive elimination of two allylic moieties gives the products.

The other example for the electrophilic addition on the iron complexes is the reaction of methyl chloroacetate with **5'a—c** in DMF. This reaction gave δ-keto esters **24a—c** in moderate yields. The results are given in Scheme 12 and Table 10.

All the above results indicate that the iron complexes **5** and **5'** serve as a synthetically equivalent synthon for β-acyl carbanions. Since β-acyl carbanions are useful intermediates in organic synthesis, several methods have already been developed for the generation of these inter-

Table 10. Reaction of (η^3-1-Trimethylsiloxyallyl)-Fe(CO)[P(OPh)$_3$]NO Complexes with Methyl Chloroacetate in DMF

Complex		Product	Yield/%
5'a:	Ar=C_6H_5	**24a**	32
5'b:	Ar=*p*-$CH_3C_6H_4$	**24b**	48
5'c:	Ar=*p*-ClC_6H_4	**24c**	28

Reaction conditions: **5'**; 2 mmol, $ClCH_2CO_2Me$; 4 mmol, Temp; 80 °C, Time 15 h.

mediates.[10–14] An approach is the desilylative ring cleavage of siloxycyclopropanes with metal salts.[12] The other approach is based on the preparation of heteroatom-substituted allylic carbanions.[13,14] By utilizing our method, carbon electrophiles can be introduced at β-position of α,β-unsaturated ketones and esters with high regioselectivity via (η^3-1-trimethylsiloxyallyl)Fe(CO)[P(OPh)$_3$]NO complexes in a one-pot manner.

Stereoselectivities. 2,6-Dibromo-4-(*t*-butyl)-1-trimethylsiloxycyclohexene (**25**) was converted to the iron complex **26** by treating with TBAFe in THF. This complex reacted smoothly with $NaCH(CO_2Me)_2$ in THF at room temperature to give exclusively *cis*-4-*t*-butyl-2-[bis(methoxycarbonyl)methyl]cyclohexanone (**27**) in a 76% yield (Scheme 13). The ^{1}H NMR spectrum of **25** showed that the hydrogen atom on C-6 was oriented to the axial direction; its proton appeared as a double doublet centered at δ=4.72 (*J*=12.01 and 5.24 Hz). The ^{1}H NMR spectrum of the final product showed that the $CH(CO_2Me)_2$ group on C-2 of **27** was oriented to the equatorial direction and the hydrogen atom on the same carbon to the axial direction; the proton signal on C-2 appeared as a triple doublet centered at δ=3.22 (*J*=13.29, 9.26, and 5.23 Hz). This result suggests that 1) the ferrate ion of TBAFe attacks the C-6 carbon of **25** via a SN_2 like process with inversion of configuration at the reaction center to form iron complex **26**, and 2) the attack of the nucleophile on the allylic ligand of **26** occurs from the opposite side of the coordinated Fe atom and causes inversion of the configuration at the reaction center. During this reaction, the reductive elimination of bromine atom occurs to produce **27**. Trost et al. have proposed a similar stereochemical course for the Pd-catalyzed reaction of *cis*-3-acetoxy-5-(methoxycarbonyl)cyclohexene with carbon nucleophiles.[2,15]

The reaction of the iron complex **26** with 2-propynyl bromide gave *trans*-4-(*t*-butyl)-2-(2-propynyl)cyclohexanone (**29**) in a 36% yield when the reaction was carried out in DMF at 75 °C after treating **26** with triphenyl phosphite (Scheme 14). The ^{1}H NMR spectrum showed that the propynyl group on C-2 of **29** was oriented to the axial direction and the hydrogen atom on the same carbon to the equatorial direction; the proton signal of the hydrogen on C-2 appeared as a qd pattern centered at δ=2.45 (*J*=7.66 and 4.42 Hz). In this reaction, **26** produced from **25** is first converted to the triphenyl phosphite complex **28**, and then react with

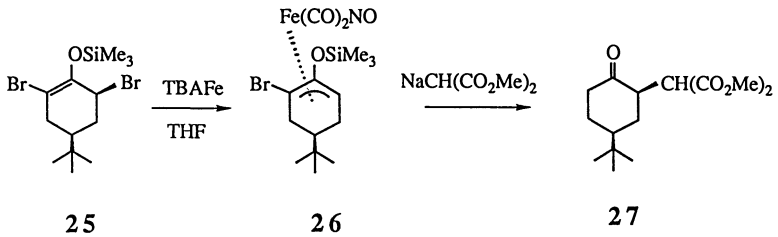

25 **26** **27**

Scheme 13.

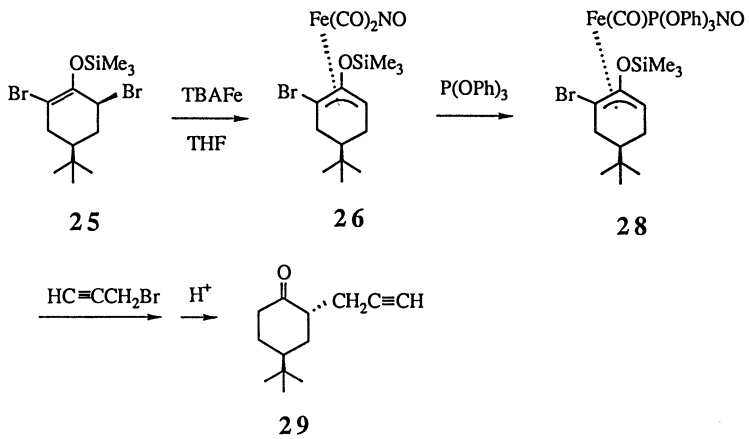

25 **26** **28**

29

Scheme 14.

2-propynyl bromide to produce **29**. The final step occurs via the oxidative addition of 2-propynyl bromide on Fe atom of **28** and subsequent reductive elimination of the organic moieties.[1] As a result, the configuration of C-2 of **25** is inverted.

Experimental

General. IR spectra were taken on a Shimadzu IR 24 spectrometer. NMR spectra were recorded with a Hitachi 24B or a JEOL FT-270 in $CDCl_3$ using tetramethylsilane as an internal standsard. Column chromatography was carried out with a Wako-gel C-200 (Wako Pure Chemical Industries). GLC analyses were performed on a Shimadzu GC 4CPF chromatograph using a column packed with SE 30 (10%) (3 mm×1 m). Elemental analyses were carried out on a Yanaco MT-3 elemental analyzer.

Materials. Tetrabutylammonium tricarbonylnitrosylferrate (TBAFe), $Bu_4N[Fe(CO)_3NO]$, was prepared by modification of the method previously reported.[6]

A solution of $Fe(CO)_5$ (60 mmol) in CH_2Cl_2 (20 cm^3) was added to a mixture of $NaNO_2$ (60 mmol) and Bu_4NBr (60 mmol) in water (20 cm^3). The resulting mixture was stirred under argon at room temperature for 2 h. The organic layer was separated, washed with water, and dried over anhydrous Na_2SO_4. Removal of the solvent under reduced pressure gave $Bu_4N[Fe(CO)_3NO]$ (TBAFe) as yellow crystals in 86% yield; mp 56—56.5 °C; IR (KBr) 1980, 1850 cm^{-1} (CO), 1630 cm^{-1} (NO). Found: C, 55.60; H, 8.96; N 6.58%. Calcd for $C_{19}H_{36}N_2O_4Fe$: C, 55.35; H, 8.80; N, 6.79%.

1-Penten-3-one, 2-cyclohexen-1-one, 3-bromo-1-phenyl-1-propene, methyl acrylate, methyl cinnamate, 1-chloro-2-butene, 3-chloro-1-butene, and 1-chloro-3-methyl-2-butene were commercial products and purified before use.

3-Chloro-2-trimethylsiloxy-1-propene (**1a**),[16] 3-bromo-3-methyl-2-trimethylsiloxy-1-butene (**1b**),[17] 3-bromo-3-methyl-2-trimethylsiloxy-1-pentene (**1c**),[17] 1,3-dichloro-2-trimethylsiloxy-1-propene (**1d**),[18] *cis*-2,6-dibromo-4-*t*-butyl-1-(trimethylsiloxy)cyclohexene (**25**),[18] and 3-chloro-3-methyl-1-butene[19] were prepared by the literature methods.

1a: Bp 61—63 °C/35 mmHg (1 mmHg=133.322 Pa); IR (neat) 2960, 2900, 1635, 1315, 1260, 1225, 1160, 1030, 915, 850 cm^{-1}; ^{1}H NMR ($CDCl_3$) δ=0.40 (9H, s), 3.92 (2H, t, J=0.9 Hz), 4.28 (1H, dt, J=2.0, 0.9 Hz), 4.50 (1H, dt J=2.0, 0.9 Hz).

1b: Bp 79 °C/22 mmHg; IR(neat) 1620, 1060, and 875 cm^{-1}; ^{1}H NMR ($CDCl_3$) δ=0.40 (9H, s), 1.95 (6H, s), 4.10 (1H, d, J=2.0 Hz), 4.60 (1H, d, J=2.0 Hz).

1c: Bp 80—82 °C/15 mmHg; IR (neat) 1620, 1060, and 875 cm^{-1}; ^{1}H NMR ($CDCl_3$) δ=0.40 (9H, s), 1.04 (3H, t J=7.0 Hz), 1.95 (3H, s), 2.17 (2H, q, J=7.0 Hz), 4.20 (1H, d, J=2.0 Hz), 4.53 (1H, d, J=2.0 Hz).

1d: Bp 55—56 °C/5 mmHg; IR (neat) 1620, 1310, 1246, 1212, 980, 841 cm^{-1}; ^{1}H NMR ($CDCl_3$) δ=0.34 (9H, s), 3.89 (2H, s), 5.70 (1H, s).

25: Bp 98—100 °C/2 mmHg; IR (neat) 1620, and 868 cm^{-1}; ^{1}H NMR ($CDCl_3$) δ=0.25 (9H, s), 0.87 (9H, s), 1.74 (1H, m), 1.92 (1H, m), 2.14 (1H, m), 2.38 (1H, dd, J=16.92, 11.28 Hz), 2.52 (1H, dd, J=16.92, 6.64 Hz), 4.61 (1H, dd, J=12.02, 5.04 Hz). ^{13}C NMR ($CDCl_3$) δ=0.98, 27.1, 34.3, 36.2, 40.8, 52.0, 108.9, 145.9. The proton signal of CHBr at C-6 appeared at δ=4.61 (dd, J=12.02, 5.04 Hz), confirming that this material has the assigned configuration.

Phenyl vinyl ketone (**3a**),[20] *p*-tolyl vinyl ketone (**3b**),[20] *p*-chlorophenyl vinyl ketone (**3c**),[20] 2-methyl-1-phenyl-2-propen-1-one (**3i**),[20] Phenyl acrylate (**3f**),[21] and phenyl methacrylate (**3j**)[21] were also prepared by the method of the literatures.

3a: IR(neat) 1670 cm^{-1}; ^{1}H NMR ($CDCl_3$) δ=5.72 (1H, dd, J=3.0, 10.3 Hz), 6.25 (1H, dd, J=3.0, 17.2 Hz), 7.06 (1H, dd, J=10.3, 17.2 Hz), 7.33 (3H, m), 7.76 (2H, m).

3b: IR (neat) 1676 cm^{-1}; ^{1}H NMR ($CDCl_3$) δ=2.31 (3H, s), 5.72 (1H, dd, J=2.7, 10.3 Hz), 6.27 (1H, dd, J=2.7, 17.1 Hz), 7.00 (1H, dd, J=10.3, 17.1 Hz), 7.08 (2H, d, J=7.9 Hz), 7.67 (2H, d, J=7.9 Hz).

3c: IR (neat) 1680 cm^{-1}; ^{1}H NMR ($CDCl_3$) δ=5.73 (1H, dd, J=2.4, 10.8 Hz), 6.23 (1H, dd, J=2.4, 17.3 Hz), 6.98 (1H, dd, J=10.8, 17.3 Hz), 7.28 (2H, d, J=8.3 Hz), 7.73 (2H, d J=8.3 Hz).

3f: IR (neat) 1726 cm^{-1}; ^{1}H NMR ($CDCl_3$) δ=5.88 (1H, m), 6.29 (2H, m), 7.02 (5H, m).

3i: IR (neat) 3030, 2940, 1646 cm^{-1}; ^{1}H NMR ($CDCl_3$) δ=2.01 (3H, s), 5.52 (1H, d, J=1.0 Hz), 5.78 (1H, d, J=1.0 Hz), 7.28 (3H, m), 7.58 (2H, m).

3j: IR (neat) 1724 cm^{-1}; ^{1}H NMR ($CDCl_3$) δ=1.95 (3H, s), 5.57 (1H, d, J=1.0 Hz), 6.10 (1H, d, J=1.0 Hz), 7.02 (5H, m).

Preparation of (η^3-Trimethylsiloxyallyl)Fe(CO)$_2$NO Complexes. General Procedure. A mixture of one of 3-halo-2-trimethylsiloxy-1-propenes (**1**) (2 mmol) and $Bu_4N[Fe(CO)_3NO]$ (TBAFe, 2 mmol) in CH_2Cl_2(5 cm^3) was stirred at room temperature for 2 h. During this period, one molar equiv of CO to TBAFe evolved. The solvent was removed under reduced pressure. Chromatography of the residue on silica gel with pentane solvent gave the corresponding (η^3-2-trimethylsiloxyallyl)Fe(CO)$_2$NO complex.

2a: IR (neat) 2020 and 1955 cm^{-1} (CO), 1720 cm^{-1} (NO), 835 cm^{-1} (OSi); ^{1}H NMR ($CDCl_3$) δ=0.18 (9H, s, $SiMe_3$), 3.47 (2H, d, J=4.0 Hz, *anti*-H), 3.90 (2H, d, J=4.0 Hz, *syn*-H). ^{13}C NMR ($CDCl_3$) δ=0.0, 51.0, 136, 218.

2b: IR (neat) 2010 and 1945 cm^{-1} (CO), 1725 cm^{-1} (NO), 845 cm^{-1} (OSi); ^{1}H NMR ($CDCl_3$) δ=0.17 (9H, s, $SiMe_3$), 1.53 (3H, s, *anti*-Me), 2.07 (3H, s, *syn*-Me), 3.51 (1H, d, J=4.2 Hz, *anti*-H), 3.98 (1H, d, J=4.2 Hz, *syn*-H). ^{13}C NMR ($CDCl_3$) δ=0.0, 24.1 (*anti*-CH_3), 28.3 (*syn*-CH_3), 46.8, 86.9, 136, 220.

2c: IR (neat) 2030 and 1950 cm^{-1} (CO), 1720 cm^{-1} (NO), 845 cm^{-1} (OSi). The ^{1}H NMR spectrum showed that this complex contains two isomers with respect to the configuration of the alkyl substituents on the allylic ligand in a 1 : 1 ratio. For the *anti*-methyl and *syn*-ethyl isomer; ^{1}H NMR ($CDCl_3$) δ=0.19 (9H, s, $SiMe_3$), 1.33 (3H, t, J=7.0 Hz, *syn*-$CH_2\underline{CH_3}$), 1.51 (3H, s, *anti*-CH_3), 2.53 (2H, q, J=7.0 Hz, *syn*-$\underline{CH_2}CH_3$), 3.47 (1H, d, J=4.2 Hz, *anti*-H), 4.00 (1H, d, J=4.2 Hz, *syn*-H). ^{13}C NMR, ($CDCl_3$) δ=0.0 ($OSi\underline{Me_3}$), 16.8 (*syn*-CH_2 $\underline{CH_3}$), 23.9 (*anti*-$\underline{CH_3}$), 33.6 (*syn*-$\underline{CH_2}CH_3$), 46.8, 87.2, 137, 219. For the *syn*-methyl and *anti*-ethyl isomer; ^{1}H NMR($CDCl_3$) δ=0.19 (9H, s, $SiMe_3$), 1.19 (3H, t, J=7.0 Hz, *anti*-$CH_2\underline{CH_3}$), 1.75 (2H, q, J=7.0 Hz, *anti*-$\underline{CH_2}CH_3$), 2.09 (3H, s, *syn*-CH_3) 3.61 (1H, d, J=4.2 Hz, *anti*-H), 4.10 (1H, d, J=4.2 Hz, *syn*-H). ^{13}C NMR($CDCl_3$) δ=0.0 ($OSi\underline{Me_3}$), 15.0 (*anti*-$CH_2\underline{CH_3}$), 28.5 (*syn*-$\underline{CH_3}$), 31.5 (*anti*-$\underline{CH_2}CH_3$), 46.8, 87.2, 137, 219.

2d: IR (neat) 2030 and 1965 cm^{-1} (CO), 1725 cm^{-1} (NO), 840 cm^{-1} (OSi); ^{1}H NMR ($CDCl_3$) δ=0.30 (9H, s, $SiMe_3$), 3.84 (1H, d, J=2.5 Hz, *anti*-H), 3.92 (1H, d, J=2.5 Hz, *syn*-H), 5.60 (1H, s, *syn*-C$\underline{H}$Cl). ^{13}C NMR ($CDCl_3$). δ=2.0, 48.5, 60.6, 128, 224.

Preparation of (η^3-1-Trimethylsiloxyallyl)Fe(CO)$_2$NO Com-

plexes. General Procedure. A mixture of one of vinyl ketones **3**, (2 mmol) with Me_3SiI (2.2 mmol) in CH_2Cl_2 (5 cm^3) was stirred at room temperature for 2 h. This reaction gave one of the corresponding 3-iodo-1-trimethylsiloxy-1-propenes (**4**). Without isolating the siloxypropenes, a solution of TBAFe (2 mmol) in CH_2Cl_2 (2.5 cm^3) was added to each of the above reaction mixtures, and the resulting mixtures were stirred under argon atmosphere at room temperature for 2 h. During this period, one equiv of CO to TBAFe evolved.

The iron complexes **5a**—**j** thus produced were unable to isolate in pure forms because of their high sensitivity to moisture and air. But, support for the formation of **5a**—**j** was furnished by IR spectra of the reaction mixtures and their chemical transformation as described in text.

Ligand Exchange of (η^3-Allyl)Fe(CO)$_2$NO Complexes. A Typical Procedure. A mixture of (η^3-2-trimethylsiloxyallyl)-Fe(CO)$_2$NO complex **2b** (2 mmol) prepared in situ and allyl bromide **7a** (2 mmol) in CH_2Cl_2 (5 cm^3) was refluxed with stirring for 2 h. After cooling, the reaction mixture was chromatographed on silica gel. Elution with hexane gave the iron complex **8a** and subsequent elution with hexane–ethyl acetate (95/5) gave 3-methyl-2-butanone (**9**).

8a: IR (neat) 2030, 1980, 1740 cm^{-1}; ^1H NMR ($CDCl_3$) δ=3.12 (2H, d, J=12.0 Hz), 3.96 (2H, d, J=6.0 Hz), 5.72 (1H, m).

8b: IR (neat) 2030, 1970, 1740 cm^{-1}; ^1H NMR ($CDCl_3$) δ=2.91 (1H, d, J=11 Hz), 3.85 (1H, d, J=6.0 Hz), 4.90 (2H, m), 7.20 (5H, m).

8c: IR (neat) 2030, 1970, 1740 cm^{-1}; ^1H NMR ($CDCl_3$) δ=1.95 (3H, d, J=5.0 Hz), 2.76 (1H, d, J=12.0 Hz), 3.68 (1H, d, J=6.0 Hz), 4.1 (2H, m).

8d: IR (neat) 2030, 1970, 1740 cm^{-1}; ^1H NMR ($CDCl_3$) δ=1.6—2.7 (m, 6H), 4.5—5.7 (m, 3H).

These spectral data of the iron complexes were essentially identical with those of the same complexes previously reported.[6]

Reaction of (η^3-Trimethylsiloxyallyl)Fe(CO)$_2$NO Complexes with Carbon Nucleophiles. General Procedure. Iron complexes **2a**—**d** (2 mmol) were prepared from 3-halo-2-trimethylsiloxy-1-propenes and TBAFe by the procedure described above. These complexes were used without isolation for the following reactions.

A mixture of an iron complex and one equiv of a carbon nucleophile in THF was stirred at room temperature for 15 h. The resulting mixture was extracted with ether. The extract was washed successively with 4 M hydrochloric acid and water, and then dried over Na_2SO_4. The solvent was removed under reduced pressure. Chromatography of the residue with hexane–ethyl acetate (9/1) gave the corresponding mixture of each one of α-alkylated ketone **10a**—**h** and **11c**—**h**.

Similarly, treatment of mixtures of (η^3-1-trimethylsiloxyallyl)Fe(CO)$_2$NO complexes **5** and carbon nucleophiles gave the corresponding β-alkylated ketones and esters **12a**—**h**.

10a: IR (neat) 1745, 1725 cm^{-1}; ^1H NMR ($CDCl_3$) δ=1.27 (6H, t, J=7.0 Hz), 2.16 (3H, s), 2.91 (2H, d, J=7.0 Hz), 3.72 (1H, t, J=7.0 Hz), 4.17 (4H, q, J=7.0 Hz). Found: C, 55.32; H, 7.46%. Anal. Calcd for $C_{10}H_{16}O_5$: C, 55.54; H, 7.46%.

10b: IR (neat) 1745, 1725 cm^{-1}; ^1H NMR ($CDCl_3$) δ=1.26 (3H, t, J=7.0 Hz), 2.10 (3H, s), 2.22 (3H, s), 2.87 (2H, d, J=7.0 Hz), 3.83 (1H, t, J=7.0 Hz), 4.09 (2H, q, J=7.0 Hz). Found: C, 57.98; H, 7.41%. Calcd for $C_9H_{14}O_4$: C, 58.05; H, 7.58%.

10c: IR (neat) 1740, 1720 cm^{-1}; ^1H NMR ($CDCl_3$) δ=1.09 (6H, d, J=7.0 Hz), 1.25 (6H, t, J=7.0 Hz), 2.62 (1H, m), 2.90 (2H, d, J=7.0 Hz), 3.71 (1H, t, J=7.0 Hz), 4.14 (4H, q, J=7.0 Hz). Found: C, 58.78; H, 7.99%. Calcd for $C_{12}H_{20}O_5$: C, 59.00; H, 8.25%.

10d: IR (neat) 1745, 1720 cm^{-1}; ^1H NMR ($CDCl_3$) δ=1.10 (6H, d, J=7.0 Hz), 1.27 (3H, t, J=7.0 Hz), 2.28 (3H, s), 2.62 (1H, m), 2.89 (2H, d, J=7.0 Hz), 3.72 (1H, t, J=7.0 Hz), 4.15 (2H, q, J=7.0 Hz). Found: C, 61.63; H, 8.22%. Calcd for $C_{11}H_{18}O_4$: C, 61.66; H,8.47%.

10e: IR (neat) 2210, 1710, 1210 cm^{-1}; ^1H NMR ($CDCl_3$) δ=1.10 (6H, d, J=7.0 Hz), 2.56 (1H, m), 2.85 (2H, d, J=7.0 Hz), 3.48 (1H, t, J=7.0 Hz). Found: C, 63.81; H, 6.72; N, 18.55%. Calcd for $C_8H_{10}N_2O$: C, 63.98; H, 6.71; N, 18.66%.

10f: IR (neat) 1745, 1715 cm^{-1}; ^1H NMR ($CDCl_3$) δ=1.02—1.34 (14H, m), 2.55 (1H, m), 2.90 (2H, d, J=7.0 Hz), 3.71 (1H, t, J=7.0 Hz), 4.10 (4H, q, J=7.0 Hz). Found: C, 60.18; H, 8.61%. Calcd for $C_{13}H_{22}O_5$ C, 60.45; H, 8.59%.

10g: IR (neat) 1745, 1720 cm^{-1}; ^1H NMR ($CDCl_3$) δ=0.90—1.40 (11H, m), 2.31 (3H, s), 2.56 (1H, m), 2.78 (2H, d, J=7.0 Hz), 3.78 (1H, t, J=7.0 Hz), 4.12 (2H, q, J=7.0 Hz). Found: C, 63.09; H, 8.68%. Calcd for $C_{12}H_{20}O_4$: C, 63.14; H, 8.83%.

10h: IR (neat) 2210, 1720 cm^{-1}; ^1H NMR ($CDCl_3$) δ=0.88—1.46 (8H, m), 2.60 (1H, m), 2.85 (2H, d, J=7.0 Hz), 3.48 (1H, t, J=7.0 Hz). Found: C, 65.77; H, 7.35; N, 16.89%. Calcd for $C_9H_{12}N_2O$: C, 65.77; H, 7.35; N, 17.06%.

11c: IR (neat) 1745, 1710 cm^{-1}; ^1H NMR ($CDCl_3$) δ=1.26 (6H, t, J=7.0 Hz), 1.30 (6H, s), 2.08(3H, s), 3.80 (1H, s), 4.06 (4H, q, J=7.0 Hz). Found: C, 58.95; H, 8.03%. Calcd for $C_{12}H_{20}O_5$: C, 59.00; H, 8.25%.

11d: IR (neat) 1745, 1720 cm^{-1}; ^1H NMR ($CDCl_3$) δ=1.21 (3H, t, J=7.0 Hz), 1.30 (6H, s), 2.06 (3H, s), 2.28 (3H, s), 3.72 (1H, s), 4.15 (2H, q, J=7.0 Hz). Found: C,61.47; H, 8.22%. Calcd for $C_{11}H_{18}O_4$ C, 61.66; H, 8.47%.

11e: IR (neat) 2210, 1710 cm^{-1}; ^1H NMR ($CDCl_3$) δ=1.21 (6H, s), 2.08 (3H, s), 3.45 (1H, s). Found: C,63.76; H, 6.68; N, 18.61%. Calcd for $C_8H_{10}N_2O$: C, 63.98, H, 6.71; N, 18.66%.

11f: IR (neat) 1745, 1710 cm^{-1}; ^1H NMR ($CDCl_3$) δ=1.02—1.33 (14H, m), 2.10 (3H, s), 3.75 (1H, s), 4.08 (4H, q, J=7.0 Hz). Found: C, 60.33; H,8.59%. Calcd for $C_{13}H_{22}O_5$: C, 60.45; H, 8.59%.

11g: IR (neat) 1745, 1720 cm^{-1}; ^1H NMR ($CDCl_3$) δ=1.02—1.34 (11H, m), 2.06 (3H, s), 2.28 (3H, s), 3.78 (1H, s), 4.18 (2H, q, J=7.0 Hz). Found: C, 63.11; H, 8.69%. Calcd for $C_{12}H_{20}O_4$: C, 63.14; H, 8.83%.

11h: IR (neat) 2210, 1720 cm^{-1}; ^1H NMR ($CDCl_3$) δ=1.02—1.34 (8H, m), 2.10 (3H, s), 3.45 (1H, s). Found: C, 65.77; H, 7.22; N, 16.89%. Calcd for $C_9H_{12}N_2O$: C, 65.83; H, 7.37; N, 17.06%.

12a: IR (neat) 1745, 1690 cm^{-1}; ^1H NMR ($CDCl_3$) δ=1.09 (6H, t, J=7.0 Hz), 2.10 (2H, q, J=7.0 Hz), 3.10 (2H, t, J=7.0 Hz), 3.30 (1H, t, J=7.0 Hz), 3.98 (4H, q, J=7.0 Hz), 7.09—7.79 (5H, m). Found: C, 65.55; H, 6.78%. Calcd for $C_{16}H_{20}O_5$: C, 65.73; H, 6.90%.

12b: IR (neat) 1745, 1728, 1682 cm^{-1}; ^1H NMR ($CDCl_3$) δ=2.04 (2H, q, J=7.0 Hz), 2.10 (3H, s), 3.13 (2H, t, J=7.0 Hz), 3.48 (1H, t, J=7.0 Hz), 3.80 (3H, s), 7.28 (3H, m), 7.70 (2H, m). Found: C, 67.81; H, 6.40%. Calcd for $C_{14}H_{16}O_4$: C, 67.72; H, 6.50%.

12c: IR (neat) 1745, 1728 cm^{-1}; ^1H NMR ($CDCl_3$) δ=1.19 (3H, t, J=7.0 Hz), 1.26 (6H, t, J=7.0 Hz), 2.12 (2H, q, J=7.0 Hz), 2.34 (2H, q, J=7.0 Hz), 2.80 (2H, t, J=7.0 Hz), 3.11 (1H,

t, J=7.0 Hz), 4.02 (4H, q, J=7.0 Hz). Found: C, 58.92; H, 8.28%. Calcd for $C_{12}H_{20}O_5$: C, 59.00; H, 8.25%.

12d: IR (neat) 1745, 1725 cm^{-1}; ^{1}H NMR ($CDCl_3$) δ=1.22 (6H, t, J=7.0 Hz), 1.50—1.98 (5H, m), 2.13—2.25 (4H, m), 3.15 (1H, d, J=7.0 Hz), 4.08 (4H, q, J=7.0 Hz). Found: C, 60.79; H, 7.71%. Calcd for $C_{13}H_{20}O_5$: C, 60.92; H, 7.87%.

12e: IR (neat) 1746 cm^{-1}; ^{1}H NMR ($CDCl_3$) δ=1.18 (6H, t, J=7.0 Hz), 2.08 (2H, q, J=7.0 Hz), 2.91 (2H, t, J=7.0 Hz), 3.34 (1H, t, J=7.0 Hz), 3.49 (3H, s), 4.02 (4H, q, J=7.0 Hz). Found: C, 53.42; H, 7.41%. Calcd for $C_{11}H_{18}O_6$: C, 53.65; H, 7.37%.

12f: IR (neat) 1745, 1718 cm^{-1}; ^{1}H NMR ($CDCl_3$) δ=1.98 (2H, q, J=7.0 Hz), 2.10 (3H, s), 3.08 (2H, t, J=7.0 Hz), 3.32 (1H, t, J=7.0 Hz), 3.49 (3H, s), 3.59 (3H, s). Found: C, 53.56; H, 6.74%. Calcd for $C_9H_{14}O_5$: C, 53.46; H, 6.98%.

12g: IR (neat) 2120, 1746 cm^{-1}; ^{1}H NMR ($CDCl_3$) δ=2.02 (2H, q, J=7.0 Hz), 2.88 (2H, t, J=7.0 Hz), 3.42 (1H, t, J=7.0 Hz), 3.49 (3H, s). Found: C, 55.02; H, 5.32; N, 18.22%. Calcd for $C_7H_8N_2O_2$: C, 55.26; H, 5.30; N, 18.41%.

12h: IR (neat) 1746, 1726 cm^{-1}; ^{1}H NMR ($CDCl_3$) δ=1.20—1.82 (8H, m), 2.10—2.46 (5H, m), 3.46 (3H, s). Found: C, 65.11; H, 8.78%. Calcd for $C_{10}H_{16}O_3$: C, 65.19; H, 8.75%.

Reaction of (η^3-2-Trimethylsiloxyallyl)Fe(CO)$_2$NO Complexes with 2-Propynyl Bromide. A Typical Procedure. A mixture of 3-chloro-2-trimethylsiloxy-1-propene (**1a**, 2 mmol) and TBAFe (2 mmol) in DMF (or NMP, 10 cm^3) was stirred at room temperature for 2 h, and 2-propynyl bromide (4 mmol) was then added. The resulting mixture was heated at 80 °C for 15 h. The mixture was hydrolyzed with 4 M hydrochloric acid and extracted with ether. The extract was washed with water, dried over Na_2SO_4, and the solvent was evaporated under reduced pressure. The residue was chromatographed on silica gel with hexane–ethyl acetate (95/5) to give α-alkynyl ketones **13a**. Similar treatments of **1b,c** gave **13b,c**.

13a: IR (neat) 3300, 2100, 1710 cm^{-1}; ^{1}H NMR ($CDCl_3$) δ=1.89 (1H, t, J=2.0 Hz), 1.98 (2H, td, J=7.0, 2.0 Hz), 2.09 (3H, s), 2.52 (2H, t, J=7.0 Hz). Found: C, 74.72; H, 8.50%. Calcd for C_6H_8O: C, 74.97; H, 8.39%.

13b: IR (neat) 3300, 2120, 1710 cm^{-1}; ^{1}H NMR ($CDCl_3$) δ=1.07 (6H, d, J=7.0 Hz), 1.88 (1H, t, J=2.0 Hz), 1.98 (2H, td, J=7.0, 2.0 Hz), 2.54 (1H, m), 2.68 (2H, t, J=7.0 Hz). Found: C, 77.28; H, 9.66%. Calcd for $C_8H_{12}O$: C, 77.38; H, 9.74%.

13c: IR (neat) 3300, 2120, 1710 cm^{-1}; ^{1}H NMR ($CDCl_3$) δ=1.02 (3H, t, J=7.0 Hz), 1.09 (3H, d, 17.0 Hz), 1.24 (2H, m), 1.89 (1H, t, J=2.0 Hz), 1.98 (2H, td, J=7.0, 2.0 Hz), 2.54 (1H, m), 2.60 (2H, t, J=7.0 Hz). Found: C,78.01; H, 10.05%. Calcd for $C_9H_{14}O$: C,78.21; H, 10.21%.

Formation of 1,4-Diketones via (η^3-1-Trimethylsiloxyallyl)-Fe(CO)$_2$NO Complexes. General Procedure. A mixture of 3-halo-2-trimethylsiloxy-1-propenes **1a—c** (4 mmol) and a half equiv of TBAFe (2 mmol) in toluene (10 cm^3) was heated at 110 °C for 15 h. The mixture was hydrolyzed with 4 M hydrochloric acid and then extracted with ether. The extract was washed with water, dried over Na_2SO_4 and the solvent was evaporated under reduced pressure. 1,4-Diketones **14a—c** and **15a—c** were isolated by chromatography of the residue on silica gel with hexane–ethyl acetate (95/5).

14a: IR (neat) 1720 cm^{-1}; ^{1}H NMR ($CDCl_3$) δ=2. 22 (6H, s), 2.71 (4H, s). Found: C, 63.21; H, 8.78%. Calcd for $C_6H_{10}O_2$: C, 63.14; H, 8.83%.

14b: IR (neat) 1720 cm^{-1}; ^{1}H NMR ($CDCl_3$) δ=1.06 (12H, d, J=7.0 Hz), 2.52 (2H, m), 2.62 (4H, s). Found: C, 70.48; H, 10.48%. Calcd for $C_{10}H_{18}O_2$: C, 70.54; H, 10.66%.

14c: IR (neat) 1720 cm^{-1}; ^{1}H NMR ($CDCl_3$) δ=0.92—1.24 (16H, m), 2.52 (2H, m), 2.62 (4H, s). Found: C, 72.63; H, 11.05%. Calcd for $C_{12}H_{22}O_2$: C, 72.68; H, 11.18%.

15b: IR (neat) 1720 cm^{-1}; ^{1}H NMR ($CDCl_3$) δ=1.06 (6H, d, J=7.0 Hz), 1.12 (6H, s), 2.08 (3H, s), 2.52 (1H, m), 2.64 (2H, s). Found: C, 70.44; H, 10.57%. Calcd for $C_{10}H_{18}O_2$: C, 70.54; H, 10.66%.

15c: IR (neat) 1720 cm^{-1}; ^{1}H NMR ($CDCl_3$) δ=0.90—1.24 (16H, m), 2.08 (3H, s), 2.52 (1H, m), 2.64 (2H, s). Found: C, 72.70; H, 11.15%. Calcd for $C_{12}H_{22}O_2$: C, 72.68, H, 11.18%.

Reaction of (η^3-1-Trimethylsiloxyally1)Fe(CO)$_2$NO Complexes with Organic Halides. General Procedure. A mixture of one of α,β-unsaturated ketones or esters (**3a—g,i,j**, 2 mmol) and Me_3SiI (2.2 mmol) in CH_2Cl_2 (10 cm^3) was stirred at room temperature for 2 h. A solution of TBAFe (2 mmol) in CH_2Cl_2 (2.5 cm^3) was added, and the resulting mixture was stirred at the same temperature for 2 h. After removal of the solvent under reduced pressure, DMF or NMP (10 cm^3) was added as a new solvent, and an organic halide (4 mmol), 2-propynyl bromide, was added to this solution. The resulting mixture was heated at 80 °C for 15 h, cooled, and extracted with ether (30 cm^3). The extract was washed successively with 4 M hydrochloric acid, aqueous $NaHSO_3$ and water, and then dried over Na_2SO_4. The solvent was removed and the residue was chromatographed on silica gel. Elution with hexane–ethyl acetate (97.5/2.5) gave the β-alkylated ketone or ester, **16a—g,i,j**.

A Typical Procedure of the Reaction in the Presence of P(OPh)$_3$. A mixture of phenyl vinyl ketone (**3a**, 2 mmol) and Me_3SiI (2.2 mmol) in CH_2Cl_2 (10 cm^3) was stirred at room temperature for 2 h. A solution of TBAFe (2 mmol) in CH_2Cl_2 (2.5 cm^3) was added, and the resulting mixture was stirred at the same temperature for 2 h. $P(OPh)_3$ (2.0 mmol) was then added, and the mixture was heated at 50 °C for 1 h. After removal of the solvent under reduced pressure, DMF (10 cm^3) was added as a new solvent, and 2-propynyl bromide (4 mmol) was added to the DMF solution. The mixture was heated at 80 °C for 15 h, cooled, and extracted with ether (30 cm^3). The extract was washed successively with 4 M hydrochloric acid, aqueous $NaHSO_3$ and water, and then dried over Na_2SO_4. The solvent was removed, and the residue was chromatographed on silica gel. Elution with hexane–ethyl acetate (97.5/2.5) gave the β-alkylated ketone **16a** in good yield. In a similar manner, **3a—g,i,j** were converted to the corresponding β-alkylated ketones and esters, **16b—g,i,j**, **17a—d,f,g,i,j**, **18a,g**, **19a,g**, **20a**, **21a**, and **24a—c** via the reactions of the iron complexes **5′** with organic halides, such as 2-propynyl bromide, allyl bromide, and methyl chloroacetate.

16a: Oil; IR (neat) 3300, 2100, 1680 cm^{-1}; ^{1}H NMR ($CDCl_3$) δ=1.84—2.00 (3H, m), 2.14—2.40 (2H, m), 3.04 (2H, t, J=6.9 Hz), 7.30—7.38 (3H, m), 7.74—7.88 (2H, m). ^{13}C NMR ($CDCl_3$) δ=17.9, 22.7, 37.0, 69.1, 83.7, 127.9, 128.0, 128.6, 136.9, 199.5. Found: C, 83.32; H, 6.99%. Calcd for $C_{12}H_{12}O$: C, 83.69; H, 7.02%.

16b: Oil; IR(neat) 3300, 2100, 1690 cm^{-1}; ^{1}H NMR ($CDCl_3$) δ=1.90 —1.99 (3H, m), 2.11—2.45 (2H, m), 2.41 (3H, s), 3.04 (2H, t, J=6.9 Hz), 7.14 (2H, d, J=8.4 Hz), 7.78 (2H, d, J=8.4 Hz). ^{13}C NMR ($CDCl_3$) δ=17.8, 21.6, 22.9, 36.9, 69.1, 83.7, 128.1, 129.3, 135.8, 202.0. Found: C, 83.61; H, 7.46%. Calcd for $C_{13}H_{14}O$: C, 83.83; H, 7.58%.

16c: Oil; IR(neat) 3300, 2100, 1690 cm^{-1}; ^{1}H NMR ($CDCl_3$) δ=1.85—1.99 (3H, m), 2.00—2.30 (2H, m), 3.04 (2H,

t, J=6.9 Hz), 7.33 (2H, d, J=8.0 Hz), 7.84 (2H, d, J=8.0 Hz). Found: C, 69.54; H, 5.31%. Calcd for $C_{12}H_{11}ClO$: C, 69.73; H, 5.37%.

16d: Oil; IR(neat) 3300, 2100, 1730 cm^{-1}; ^{1}H NMR ($CDCl_3$) δ=1.06 (3H, t, J=6.9 Hz), 1.63—1.98 (3H, m), 2.00—2.58 (6H, m). Found: C,77.18; H, 9.55%. Calcd for $C_8H_{12}O$: C, 77.38; H, 9.74%.

16e: Oil; IR (neat) 3300, 2100, 1710 cm^{-1}; ^{1}H NMR ($CDCl_3$) δ=1.66—1.80 (5H, m), 1.92—2.38 (7H, m). Found: C, 79.21; H, 8.56%. Calcd for $C_9H_{12}O$: C, 79.37; H, 8.88%.

16f: Oil; IR (neat) 3300, 2100, 1750 cm^{-1}; ^{1}H NMR ($CDCl_3$) δ=1.92—2.02 (3H, m), 2.21—2.33 (2H, m), 2.54 (2H, t, J=6.9 Hz), 7.03—7.10 (5H, m). Found: C, 76.64; H, 6.59%. Calcd for $C_{12}H_{12}O$: C, 76.57; H, 6.43%.

16g: Oil; IR (neat) 3300, 2100, 1745 cm^{-1}; ^{1}H NMR ($CDCl_3$) δ=1.93 (1H, t, J=2.4 Hz), 2.42—2.54 (2H, m), 2.60—2.78 (3H, m), 3.50 (3H, s), 7.02—7.20 (5H, m). Found: C, 76.94; H, 6.93%. Calcd for $C_{13}H_{14}O_2$: C, 77.20; H, 6.98%.

16i: Oil; IR (neat) 3300, 2100, 1680 cm^{-1}; ^{1}H NMR ($CDCl_3$) δ=1.21 (3H, d, J=6.9 Hz), 1.99 (1H, t, J=2.82 Hz), 2.11 (2H, q, J=6.9 Hz), 2.25 (2H, td, J=7.25, 2.82 Hz), 3.73 (1H, m), 7.49 (3H, m), 7.98 (2H, m). ^{13}C NMR ($CDCl_3$) δ=16.3, 17.2, 31.7, 39.1, 69.1, 76.6, 128.4, 128.7, 130.0, 136.5, 203.7. Found: C, 83.81; H, 7.51%. Calcd for $C_{13}H_{14}O$: C, 83.83; H, 7.58%.

16j: Oil; IR (neat) 3300, 2100, 1720 cm^{-1}; ^{1}H NMR ($CDCl_3$) δ=1.27 (3H, d, J=7.0 Hz), 1.98 (2H, q, J=7.0 Hz), 2.02 (1H, t, J=2.4 Hz), 2.35 (2H, td, J=7.0, 2.4 Hz), 3.03 (1H, m), 7.35 (5H, m); ^{13}C NMR ($CDCl_3$) δ=14.4, 16.8, 27.8, 36.5, 69.0, 78.3, 115.3, 121.5, 125.9, 129.4, 174.8. Found: C, 77.38; H, 6.88%. Calcd for $C_{13}H_{14}O_2$: C,77.20; H, 6.98%.

17a: Oil; IR (neat) 1680, 990, 910 cm^{-1}; ^{1}H NMR ($CDCl_3$) δ=1.85 (2H, quintet, J=7.0 Hz), 2.17 (2H, q, J=7.0 Hz), 2.98 (2H, t, J=7.0 Hz), 4.94—5.13 (2H, m), 5.69—5.88 (1H, m), 7.47—7.51 (3H, m), 7.90—8.00 (2H, m); ^{13}C NMR ($CDCl_3$) δ=23.3 (t), 33.1 (t), 37.7 (t), 115.2 (t), 128.0 (d), 128.0 (d), 128.5 (d), 132.8 (s), 136.0 (d), 200.2 (s). Found: C, 82.49; H, 7.92%. Calcd for $C_{12}H_{14}O$: C, 82.72; H, 8.10%.

17b: Oil; IR (neat) 1680, 990, 910 cm^{-1}; ^{1}H NMR ($CDCl_3$) δ=1.83 (2H, quintet, J=7.0 Hz), 2.12 (2H, br q, J=7.0 Hz), 2.40 (3H, s), 2.95 (2H, t, J=7.0 Hz), 4.92—5.06 (2H, m), 5.68—5.79 (1H, m), 7.24 (2H, d, J=8.13 Hz), 7.85 (2H, d, J=8.13 Hz); ^{13}C NMR ($CDCl_3$) δ=23.5 (q), 24.7 (t), 33.3 (t), 35.4 (t), 115.5 (t), 126.0 (d), 126.7 (d), 131.4 (s), 134.2 (d), 138.8 (s), 200.0 (s). Found: C, 82.61; H, 8.71%. Calcd for $C_{13}H_{16}O$: C, 82.93; H, 8.57%.

17c: Oil; IR (neat) 1685, 990, 910 cm^{-1}; ^{1}H NMR ($CDCl_3$) δ=1.83 (2H, quintet, J=7.2 Hz), 2.12 (2H, br q, J=7.2 Hz), 2.95 (2H, t, J=7.2 Hz), 4.93—5.12 (2H, m), 5.68 (1H, m), 7.48 (2H, d, J=8.79 Hz), 7.89 (2H, d, J=8.79 Hz); ^{13}C NMR ($CDCl_3$) δ=25.2 (t), 33.4 (t), 36.4 (t), 115.8, 127.3, 127.5, 133.6, 135.2, 139.0, 200.2. Found: C,68.97; H, 6.02%. Calcd for $C_{12}H_{13}ClO$: C, 69.06; H, 6.28%.

17d: Oil; IR (neat) 1726, 990, 910 cm^{-1}; ^{1}H NMR ($CDCl_3$) δ=1.00 (3H, t, J=7.0 Hz), 1.80 (2H, m), 2.02 (2H, q, J=7.0 Hz), 2.23 (2H, q, J=7.0 Hz), 2.30 (2H, t, J=7.0 Hz), 5.09 (2H, m), 5.70 (1H, m); ^{13}C NMR ($CDCl_3$) δ=12.4, 21.9, 31.2, 46.6, 47.1, 120.2, 129.9, 202.2. Found: C, 75.87; H, 11.21%. Calcd for $C_8H_{14}O$: C, 76.14; H, 11.18%.

17f: Oil; IR (neat) 1708, 990, 910 cm^{-1}; ^{1}H NMR ($CDCl_3$) δ=1.97 (2H, m), 2.17 (2H, q, J=7.0 Hz), 2.72 (2H, t, J=7.0 Hz), 5.04 (2H, m), 5.81 (1H, m), 7.22 (5H, m); ^{13}C NMR ($CDCl_3$) δ=17.8, 23.6, 33.0, 115.7, 121.5, 121.6, 125.7, 125.8, 150.7, 171.6. Found: C, 75.41; H, 7.02%. Calcd for $C_{12}H_{14}O$: C, 75.76; H, 7.42%.

17g: Oil; IR (neat) 1746, 990, 910 cm^{-1}; ^{1}H NMR ($CDCl_3$) δ=2.37 (2H, m), 2.89 (1H, m), 3.39 (2H, d, J=7.0 Hz), 3.81 (3H, s), 5.13 (2H, m), 5.95 (1H, m), 7.38 (5H, m); ^{13}C NMR ($CDCl_3$) δ=31.8, 48.0, 51.8, 63.5, 116.1, 127.2, 128.0, 128.8, 135.7, 140.4, 168.4. Found: C, 76.45; H, 7.81%. Calcd for $C_{13}H_{16}O_2$: C, 76.45; H 7.81%.

17i: Oil; IR (neat) 1676, 990, 910 cm^{-1}; ^{1}H NMR ($CDCl_3$) δ=1.20 (3H, d, J=7.0 Hz), 1.97 (2H, q, J=7.0 Hz), 2.09 (2H, qt, J=7.0, 1.21 Hz), 3.50 (1H, m), 4.94 (2H, m), 5.85 (1H, ddt, J=15.0, 10,2, 7.0 Hz), 7.47 (3H, m), 7.93 (2H, m); ^{13}C NMR ($CDCl_3$) δ=17.3, 31.5, 32.6, 39.8, 115.2, 128.3, 128.6, 132.8, 136.7, 138.1, 204.5. Found: C, 82.56; H, 8.57%. Calcd for $C_{13}H_{16}O$: C, 82.93; H, 8.57%.

17j: Oil; IR (neat) 1712, 990, 910 cm^{-1}; ^{1}H NMR ($CDCl_3$) δ=1.29 (3H, d, J=7.0 Hz), 1.96 (2H, q, J=7.0 Hz), 2.16 (2H, q, J=7.0 Hz), 2.71 (1H, m), 5.12 (2H, m), 5.83 (1H, m), 7.12 (5H, m); ^{13}C NMR ($CDCl_3$) δ=18.4, 32.8, 38.2, 43.5, 114.9, 121.5, 121.6, 125.7, 127.1, 129.4, 171.2. Found: C, 76.33; H, 7.78%. Calcd for $C_{13}H_{16}O_2$: C,76.43; H, 7.90%.

18a: Oil; IR (neat) 1686, 960 cm^{-1}; ^{1}H NMR ($CDCl_3$) δ=1.56 (3H, br d, J=7.0 Hz), 1.72—2.10 (4H, m), 2.81 (2H, t, J=7.0 Hz), 5.31 (2H, m), 7.30 (3H, m), 7.75 (2H, m); ^{13}C NMR ($CDCl_3$) δ=20.2, 24.8, 32.3, 37.6, 121.0, 121.6, 128.6, 132.8, 136.7, 138.4, 202.0. Found: C, 82.72; H, 8.61%. Calcd for $C_{13}H_{16}O$: C, 82.93; H, 8.57%.

19a: Oil; IR (neat) 1684, 990, 910 cm^{-1}; ^{1}H NMR ($CDCl_3$) δ=0.98 (3H, d J=7.0 Hz), 1.70—2.15 (3H, m), 2.81 (2H, t, 7.0 Hz), 4.98 (2H, m), 5.60 (1H, m), 7.30 (3H, m), 7.75 (2H, m); ^{13}C NMR ($CDCl_3$) δ=17.9, 24.7, 30.9, 33.7, 115.7, 125.6, 128.5, 129.0, 136.0, 138.4, 203.0. Found: C, 82.69; H, 8.46%. Calcd for $C_{13}H_{16}O$: C, 82.93; H, 8.57%.

18g: Oil; IR (neat) 1708, 965 cm^{-1}; ^{1}H NMR ($CDCl_3$) δ=1.68 (3H, d, J=7.0 Hz), 1.84 (2H, m), 2.12 (2H, q, J=7.0 Hz), 2.57 (2H, t J=7.0 Hz), 5.47 (2H, m), 7.36 (5H, m); ^{13}C NMR($CDCl_3$) δ=20.2, 31.4. 32.3, 37.6, 113.9, 121.6, 125.8, 129.4, 129.7, 143.3, 172.3. Found: C, 76.42; H, 7.79%. Calcd for $C_{13}H_{16}O_2$; C,76.43; H, 7.90%.

19g: Oil; IR (neat) 1708, 990, 910 cm^{-1}; ^{1}H NMR ($CDCl_3$) δ=1.10 (3H, d J=7.0 Hz), 1.73 (2H, q, J=7.0 Hz), 2.20 (1H, m), 2.55 (2H, t, J=7.0 Hz), 5.07 (2H, m), 5.69 (1H, m), 7.25 (5H, m); ^{13}C NMR ($CDCl_3$) δ=17.9, 24.7, 30.9, 33.7, 121.6, 125.2, 125.7, 126.2, 129.2, 129.4, 172.3. Found: C, 76.21; H, 7.92%. Calcd for $C_{13}H_{16}O_2$: C, 76.43; H, 7.90%.

20a: Oil; IR (neat) 1685 cm^{-1}; ^{1}H NMR ($CDCl_3$) δ=1.66 (6H, br s), 1.78—2.27 (4H, m), 2.79 (2H, t, J=7.0 Hz), 5.30 (1H, m), 7.20 (3H, m), 7.75 (2H, m); ^{13}C NMR ($CDCl_3$) δ=23.4, 26.1, 28.3, 29.8, 41.6, 119.8, 128.0, 128.3, 128.5, 128.6, 132.8, 203.7. Found: C, 83.05; H, 8.89%. Calcd for $C_{14}H_{18}O$: C, 83.12; H, 8.97%.

21a: Oil; IR (neat) 1682, 990, 910 cm^{-1}; ^{1}H NMR ($CDCl_3$) δ=1.12 (6H, s), 1.70 (2H, t, J=7.0 Hz), 2.80 (2H, t, J=7.0 Hz), 5.08 (2H, m), 5.70 (1H, dd, J=16.2, 10.6 Hz), 7.21 (3H, m), 7.75 (2H, m); ^{13}C NMR ($CDCl_3$) δ=17.6, 26.2, 33.2, 41.2, 115.4, 125.2, 128.0, 128.6, 132.8, 202.4. Found: C, 82.88; H, 8.78%. Calcd for $C_{14}H_{18}O$: C, 83.12; H, 8.97%.

24a: Oil; 1726, 1680 cm^{-1}; ^{1}H NMR ($CDCl_3$) δ=2.12 (2H, quintet, J=7.0 Hz), 2.46 (2H, t, J=7.0 Hz), 3.07 (2H, t, J=7.0 Hz), 3.70 (3H, s), 7.52 (3H, m), 7.92 (2H, m); ^{13}C NMR ($CDCl_3$) δ=23.3, 32.9, 37.0, 51.6, 127, 128, 133, 141, 174, 200. Found: C, 69.67; H, 6.74%. Calcd for $C_{12}H_{14}O_3$: C, 69.88; H, 6.84%.

24b: Oil; IR (neat) 1746, 1678 cm^{-1}; ^{1}H NMR ($CDCl_3$) δ=2.07 (2H, quintet, J=7.2 Hz), 2.41 (3H, s), 2.44 (2H, t, J=7.25 Hz), 3.03 (2H, t, J=7.25 Hz), 3.68 (3H, s), 7.27 (2H, d, J=8.02 Hz), 7.85 (2H, d, J=8.02 Hz); ^{13}C NMR ($CDCl_3$) δ=19.5, 21.6, 33.2, 37.3, 51.6, 120.1, 128.2, 129.9, 138.4, 173.8, 199.1. Found: C, 70.77; H, 7.16%. Calcd for $C_{13}H_{16}O_3$: C, 70.89; H, 7.32%.

24c: Oil; IR (neat) 1730, 1680 cm^{-1}; ^{1}H NMR ($CDCl_3$) δ=2.02 (2H, m), 2.46 (2H, t, J=7.0 Hz), 3.63 (2H, t, J=7.0 Hz), 3.70 (3H, s), 7.18 (2H, d, J=8.3 Hz); 8.02 (2H, d, J=8.3 Hz); ^{13}C NMR ($CDCl_3$) δ=22.6, 33.0, 37.8, 51.6, 129, 130, 138, 140, 172, 206. Found: C, 59.77, H, 5.42%. Calcd for $C_{12}H_{13}ClO_3$: C, 59.88; H, 5.44%.

Stereoselectivity in the Reaction of (η^3-Allyl)Fe(CO)$_2$NO Complexes with a Carbon Nucleophile. A mixture of *cis*-2,6-dibromo-4-*t*-butyl-1-(trimethylsiloxy)cyclohexene (**25**, 3 mmol) and TBAFe (4 mmol) in THF (10 cm^3) was stirred at room temperature for 3 h and then $NaCH(CO_2Me)_2$ (6 mmol) in THF (5 cm^3) was added. The resulting mixture was stirred at the same temperature for 15 h, hydrolyzed with 4 M hydrochloric acid, and extracted with ether. The extract was washed with water and dried over Na_2SO_4. After removal of the solvent under reduced pressure, the residue was chromatographed on silica gel. Elution with hexane–ethyl acetate (9/1) gave the alkylated product, **27**: Oil; IR (neat) 1746, 1724, 1280, 1060 cm^{-1}; ^{1}H NMR ($CDCl_3$) δ=0.91 (9H, s), 1.30—1.50 (2H, m), 1.65 (1H, tt, J=2 84, 12.1 Hz), 2.00—2.42 (4H, m), 3.22 (1H, ddd, J=5.24, 9.26, 13.29 Hz), 3.68 (1H, d, J=9.26 Hz), 3.74 (3H, s), 3.75 (3H, s); ^{13}C NMR ($CDCl_3$) δ=27.3, 27.6, 28.5, 32.0, 32.5, 41.1, 46.8, 49.7, 52.6, 52.7, 168.8, 168.9, 210.0. Found: C, 63.35; H, 8.33%. Calcd for $C_{15}H_{24}O_5$: C, 63.36; H, 8.50%.

A mixture of *cis*-2,6-dibromo-4-*t*-butyl-1-(trimethylsiloxy)-cyclohexene (**25**, 3 mmol) and TBAFe (4 mmol) in DMF (10 cm^3) was stirred at room temperature. To the mixture, triphenyl phosphite (3 mmol) was added and then the mixture was heated at 50 °C for 1 h. To the resulting mixture, the carbon electrophile, 2-propynyl bromide (6 mmol), was added and then the mixture was heated at 75 °C for 15 h. The mixture was hydrolyzed with 4 M hydrochloric acid, and extracted with ether. The extract was washed with 4 M NaOH aqueous solution and then water, dried over Na_2SO_4. After removal of the solvent under reduced pressure, the residue was chromatographed on silica gel. Elution with hexane–ethyl acetate (97.5/2.5) gave the alkylated product, **29**: Oil; IR (neat) 3200, 2100, 1700 cm^{-1}; ^{1}H NMR ($CDCl_3$)δ=0.94 (9H, s), 1.47 (1H, m), 1.58 (1H, m), 1.65 (1H, tt, J=12.10, 2.82 Hz) 1.97 (1H,t, J=2.82 Hz), 2.10 (1H, ddd, J=16.52, 12.10, 4.42 Hz), 2.18 (1H, ddd, J=16.52, 7.66, 2.82 Hz), 2.42 (2H, dd, J=7.66, 2.82 Hz), 2.45 (1H, qd, J=7.66, 4.42 Hz), 2.50 (1H, m), 2.65 (1H, ddd, J=16.52, 4.43, 2.42 Hz); ^{13}C NMR ($CDCl_3$) δ=18.9 (t), 27.7 (q), 28.6 (t), 32.6 (s), 34.3 (d), 41.3 (t), 46.9 (t), 48.7 (d), 69.5 (d), 82.7 (s), 211.1 (s). Found: C, 81.06; H, 10.31%. Calcd for $C_{12}H_{20}O$: C, 81.20; H, 10.48%.

Isolation of Iron Complex 26. A mixture of **25** (2 mmol) and TBAFe (2 mmol) in CH_2Cl_2 (5 cm^3) was stirred at room temperature for 3 h. The resulting mixture was chromatographed on silica gel. Complex **26** was isolated from the fraction eluted with hexane; IR (neat) 2020, 1960 cm^{-1} (CO), 1725 cm^{-1} (NO), 850 cm^{-1} (OSi); ^{1}H NMR ($CDCl_3$) δ=0.12 (9H, s), 0.92 (9H, s), 1.93 (1H, m), 2.22 (1H, m), 2.52—2.80 (3H, m), 5.30 (1H, m); ^{13}C NMR ($CDCl_3$) δ=1.8, 27.2, 31.6, 34.2, 36.2, 40.8, 47.1, 52.0, 129, 214.

This work was partially supported by a Grant-in Aid for Scientific Research No. 02640403 from the Ministry of Education, Science and Culture.

References

1) J. P. Collman, L. S. Hegedus, J. R. Norton, and R. G. Finke, "Principles and Applications of Organotransition Metal Chemistry," University Science Books, Mill Valley, California (1987).

2) B. M. Trost and T. R. Vorhoeven, "Comprehensive Organometallic Chemistry," ed by G. Wilkinson, Pergamon Press, Oxford (1982), Vol. 8, pp. 799—938.

3) G. S. Stiverman, S. Strickland, and K. M. Nicholas, *Organometllics,* **5**, 2117 (1986).

4) J. L. Roustane, J. Y. Merour, and F. Houlihan, *Tetrahedron Lett.,* **20**, 3721 (1979).

5) Y. Xu and B. Zhou, *J. Org. Chem.,* **52**, 974 (1987); B. Zhou and Y. Xu, *ibid.,* **53**, 4419 (1988).

6) T. Ueda, M. Kawakita, and Y. Otsuji, *Nippon Kagaku Kaishi,* **1985**, 271.

7) K. Itoh, S. Nakanishi, and Y. Otsuji, *Chem. Lett.,* **1987**, 2103; *ibid.,* **1988**, 473.

8) R. D. Miller and D. R. Mackean, *Tetrahedron Lett.,* **20**, 2305 (1979).

9) L. S. Hegedus and R. K. Stiverson, *J. Am. Chem. Soc.,* **96**, 3250 (1974).

10) I. Ryu and N. Sonoda, *Yuki Gosei Kagaku Kyokai Shi,* **43**, 112 (1985), and references cited therein.

11) D. Hoppe, *Angew. Chem., Int. Ed. Engl.,* **23**, 932 (1984).

12) E. Nakamura, H. Oshino, and I. Kuwajima, *J. Am. Chem. Soc.,* **108**, 3745 (1986).

13) E. Ehlinger and P. Magunus, *J. Am. Chem. Soc.,* **102**, 5004 (1980).

14) J. Fang, B. Hong, and L. Lio, *J. Org. Chem.,* **52**, 855 (1987).

15) G. Consiglio and R. M. Waymouth, *Chem. Rev.,* **89**, 257 (1989), and references cited therein.

16) A. Hosomi, A. Shirahata, Y. Araki, and H. Sakurai, *Tetrahedron Lett.,* **21**, 2325 (1980).

17) N. Shimizu, M. Tanaka, and Y. Tsuno, *J. Am. Chem. Soc.,* **104**, 1330 (1982).

18) H. Sakurai, A. Shirahata, and A. Hosomi, *Angew. Chem., Int. Ed. Engl.,* **18**, 163 (1979).

19) E. W. Collington and A. I. Meyers, *J. Org. Chem.,* **36**, 3044 (1971).

20) G. Kinast and L. F. Tietze, *Angew. Chem.,* **88**, 261 (1976); J. L. Roberts, P. S. Borromeo, and C. D. Poulter, *Tetrahedron Lett.,* **1977**, 1621.

21) M. S. Newman and L. K. Lala, *Tetrahedron Lett.,* **1967**, 3267.

Effect of Unpaired Terminal Nucleotides of Substrate RNAs on the RNA Ligation with T4 RNA Ligase

Naoki SUGIMOTO,* Akiko MATSUMURA, Keiko HASEGAWA, and Muneo SASAKI
Department of Chemistry, Faculty of Science, Konan University, Okamoto, Higashinada-ku, Kobe 658
(Received May 27, 1991)

The effect of double-helix formations and unpaired terminal nucleotides of RNA oligomer substrates on a RNA ligation with T4 RNA ligase has been investigated by using high-performance liquid chromatography (HPLC), UV absorbance, and circular dichroism (CD) measurements, and the energy calculation for the double-helix stability of RNAs. In the 1-hour reaction of single-stranded RNA acceptors, the yield of the product increased in the order of pyrimidine donors pCp>pUp and purine donors pAp>pGp. In the reaction of a double-stranded RNA acceptor, UGCGCA, the yield also increased in the same order of the donors. On the other hand, in the reaction of double-stranded RNA acceptors containing unpaired terminal nucleotides (dangling ends), pUp and pGp donors gave the largest yields of the products in the reactions of AUGCGCA and CAUGCAU acceptors, respectively. Furthermore, the yield of the product is the largest for CAUGCAU acceptor within the acceptors having A, C, G, and U dangling ends in the reaction of pGp donor. These results sugggest that the formation of the terminal base pairs of the donors and the dangling ends may affect the RNA ligation with T4 RNA ligase.

Unpaired terminal nucleotides (dangling ends) play very important roles in the structure and interaction of ribonucleic acids (RNAs). It is well-known that the dangling ends determine the stability of codon–anticodon associations[1,2] and are responsible for some codon context effects.[3] It is also known that the nucleotides determine important tertiary structures of a transfer RNA (tRNA)[4] and a catalytic core of *Tetrahymena* ribozyme.[5,6] Recently, the effect of the dangling ends on the stability of RNA duplexes has been studied energetically.[7,8] The result showed that both 3′ and 5′ terminal nucleotides stabilized the core duplexes. However, little is known about the effect of the unpaired terminal nucleotides on biochemical reactions such as ligase and nuclease reactions.

In this work, we have investigated the effect of the unpaired terminal nucleotides of substrate RNAs on the RNA ligation with T4 RNA ligase of which the overall reaction is shown in Scheme 1. The study can provide insight into the contribution of the formation of a substrate double-helix and terminal base-pair to the RNA ligation.

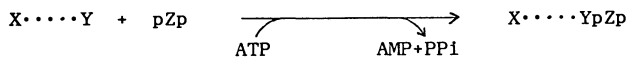

X,Y,Z : rA,rC,rG, or rU
p : phosphate

Scheme 1.

Experimental

Materials. UGCGCA, AUGC, AUGCA, AUGCG, and XAUGCAU (X=A, U, G, C) were synthesized chemically on a solid support with phosphoramidite procedures[9] and purified with high-performance liquid chromatography (HPLC) after deblocking. AUG was purchased from Sigma Chemical Co. These oligomers were further purified and desalted with a C-18 Sep-Pak cartridge. Final purity of the oligomers was checked by HPLC and was greater than at least 95%. The concentration of the oligomers was determined as described previously.[10]

Nucleotides 3′,5′-bisphosphates (pZp), albumin from bovine serum (BSA), and T4 RNA ligase were purchased from Pharmacia, Sigma Chem. Co., and BRL Inc., respectively. Adenosine 5′-triphosphate (ATP) and dithiothreitol (DTT) were products of Wako Chem. Ind.

T4 RNA Ligase Reaction. The RNA ligase reaction mixture contained 2×10^{-1} mol dm^{-3} Tris-HCl (pH 7.5), 2×10^{-2} mol dm^{-3} $MgCl_2$, 7.5×10^{-3} mol dm^{-3} ATP, 5×10^{-3} mol dm^{-3} DTT, 25×10^{-9} g dm^{-3} BSA, 1×10^{-3} mol dm^{-3} acceptor RNA oligomer, and 25 to 90 unit/ml (U/ml) of the enzyme. At the assay for the reaction, 4×10^{-3} mol dm^{-3} donor pZp was also present in the reaction mixture. After incubation for adequate times, mainly for 1 h at 37 °C, the reaction mixture was heated for 2 min at 100 °C and treated with alkaline phosphatase for 20 min at 65 °C.[11]

The analysis was performed by HPLC using a Tosoh LC System and a Cosmosil Packed Column 5C18-AR onto which aliquots from the reaction mixtures were injected. The analysis was done at a flow rate of 1 ml min^{-1} with a 50-min linear gradient from 0 to 25% methanol containing 10^{-1} mol dm^{-3} NaH_2PO_4. The peaks at 254 nm corresponding to the substrates, intermediates, and products were integrated using a Tosoh Sic Chromatocorder 12. The extent of reaction was determined by the ratio of the peak area of the product to that of the substrate. The HPLC analysis indicated no significant loss of the substrate due to contaminating nucleases.

Spectroscopy. UV absorbance spectra of the RNA oligomers were measured on a Tosoh UV 8011 spectrophotometer. Their UV melting curves (absorbance vs. temperature curves) were measured on a Hitachi U-3200 programmable spectrophotometer equipped with a Hitachi SPR-7 temperature controller. The heating rate was 0.5 or 1 °C min^{-1}. A melting temperature, T_m, at each oligomer concentration of 10^{-3} mol dm^{-3} was determined by Eq. 1:[12]

$$T_m = \Delta H^\circ / (\Delta S^\circ + R \ln(C_t)), \quad (1)$$

where ΔH° and ΔS° were the enthalpy and entropy changes for the double-helix formation of the oligomer,[7] R was the gas constant, and C_t was 10^{-3} mol dm^{-3}. Circular dichroism (CD) spectra of the oligomers were measured on a JASCO J-600 spectropolarimeter equipped with the temperature controller.

Stability Calculation of RNA Duplexes. The stability energy of the oligomer duplexes was obtained from nearest-neighbor thermodynamic parameters[7,12] as described previously.[13] For example, the entropy change ΔS° for the formation of the self-complementary UGCGCA duplex was calculated as follows:

$$\begin{aligned}\Delta S^\circ &= \Delta S^\circ(\text{initi}) + \Delta S^\circ(\text{sym}) + \Delta S^\circ(\text{UG/AC}) \\ &\quad + \Delta S^\circ(\text{GC/CG}) + \Delta S^\circ(\text{CG/GC}) \\ &\quad + \Delta S^\circ(\text{GC/CG}) + \Delta S^\circ(\text{CA/GU}) \\ &= (-10.8) + (-1.4) + (-27.8) + (-34.9) + (-19.4) \\ &\quad + (-34.9) + (-17.8) \\ &= -157.0 \text{ cal K}^{-1} \text{ mol}^{-1},\end{aligned}$$

where ΔS°(initi) was an entropy change for the initiation of making the first base pair in the region, ΔS°(sym) was the correction entropy-factor for the self-complementary sequence, and ΔS°(UG/AC), ΔS°(GC/CG), ΔS°(CG/GC), ΔS°(GC/CG), and ΔS°(CA/GU) were propagation entropy-changes for making each subsequent base pair. Similarly, the enthalpy change

$$\Delta H^\circ = -57.4 \text{ kcal mol}^{-1}.$$

Therefore, the free-energy change at 37 °C, ΔG°_{37}, which was the stability energy of the UGCGCA duplex, was obtained as follows:

$$\begin{aligned}\Delta G^\circ_{37} &= \Delta H^\circ - T\Delta S^\circ \\ &= (-57.4) - (273 + 37) \times (-157.0 \times 10^{-3}) \\ &= -8.7 \text{ kcal mol}^{-1}.\end{aligned}$$

The value of ΔG°_{37} gives the equilibrium constant, K, of the transition of the single-stranded RNA to the double-helix 1.4×10^6 mol^{-1} dm^3 at 37 °C in Eq. 2:

$$K = \exp(-\Delta G^\circ_{37}/RT) = 1.4 \times 10^6 \text{ mol}^{-1} \text{ dm}^3. \quad (2)$$

Results and Discussion

HPLC Chromatograms of Substrate and Product at Each Reaction Time. The ligations as shown in Scheme 1 were performed under the standard conditions of an 1-hour to 20-hour incubation at 37 °C with an acceptor : donor ratio of 1 : 4. Figure 1 shows the HPLC chromatograms of the ligation mixture of AAUGCAU to pUp at several reaction times. As shown in Fig. 1, only two peaks which are due to the substrate AAUGCAU and the product AAUGCAUUp can be detected after a 40-min flow, although the peaks of pUp, ATP, ADP, and AMP are observed before a 30-min flow. The yields of the product were 51, 90, and 100% at 1, 4, and 8 h, respectively.

Ligation of Single-Stranded Acceptors to Pyrimidine and Purine Donors. The yields of the products in the reaction of single-stranded RNA acceptors to pyrimidine and purine donors are listed in Table 1 with the results of Romaniuk et al.[14] The melting temperatures of AAU and AUGCA which have the possibility of the formation of the self-complementary double-helix are calculated to be less than 0 and 29 °C, respectively, suggesting these oligomers are mainly single-stranded at 37 °C. In the case of pyrimidine donors in the ligation of AUG acceptor, the yield of the product for pCp donor is larger than that for pUp donor. The same tendency for the pyrimidine donors is observed in the reaction of AAU acceptor. In the reaction of the acceptors containing a different sequence and a different strand length (Entry Nos. 5—8 in Table 1), pCp donor also gives the larger yield than pUp.

In the case of purine donors in the ligation of AUGC acceptor, pAp donor gives the larger yield than pGp. The same tendency for the donors is detected in the reaction of AAU acceptor having a different sequence and a different strand length (Nos. 11 and 12 in Table 1).

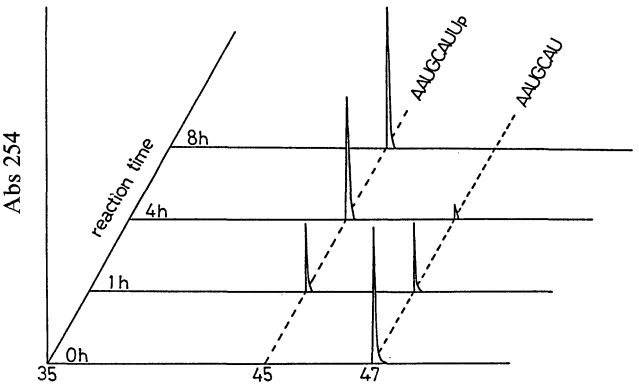

Fig. 1. HPLC chromatograms of AAUGCAU and AAUGCAUUp in the reaction mixture of the T4 RNA ligase reaction at 0, 1, 4, and 8 h.

Table 1. The Yield of the Product in the Reaction of Single-Stranded RNA Acceptors with pZp

Entry No.	Acceptor X···Y	Donor pZp	Enzyme concn U/ml	Time h	Yield %
1	AUG	C	30	1.5	31
2	AUG	U	50	2.5	12
3[a)]	AAU	C	175	1	98
4[a)]	AAU	U	175	1	75
5	AUGCA	C	30	1	55
6	AUGCA	U	30	1	18
7	AUGCG	C	50	1	62
8	AUGCG	U	50	1	3
9	AUGC	A	40	1	34
10	AUGC	G	50	1	9
11[a)]	AAU	A	175	1	63
12[a)]	AAU	G	175	1	17

a) Conditions: acceptor, 0.5 mM; donor, 1.0 mM; ATP, 3.3 mM; incubated at 37 °C in Ref. 14.

Ligation of Double-Stranded Acceptor to Pyrimidine and Purine Donors. Table 2 shows the stabilization energies at 37 °C, ΔG°_{37}, the melting temperatures, T_m, and the equilibrium constants, K, for the self-complementary double helices of UGCGCA, AUGCGCA, AUGCAU, and XAUGCAU (X=A, U, G, C). In Table 2, the calculated and observed T_m value for UGCGCA of 62.6 and 63.1 °C, respectively, suggests that the acceptor forms the self-complementary duplex at 37 °C which is the temperarure of the ligation in this work. The ΔG°_{37} value of −8.7 kcal mol^{-1} and the K value of 1.4×10^6 mol^{-1} dm^3 indicate that the oligomer exists almost as the duplex at 37 °C. In addition, the duplex of the oligomer may form an A-type double helix,[15] because, in Table 2, the T_m value calculated using A-type nearest-neighbor parameters[7,12] is consistent with the observed value. Therefore, all the results support the UGCGCA acceptor is not single-stranded but double-stranded at the reaction temperature.

The yields of the products in the reaction of double-stranded UGCGCA acceptor to pyrimidine and purine donors are listed in Table 3. In the case of pyrimidine donors, the yield of the product for pCp donor is larger than that for pUp donor. On the other hand, in the case of purine donors, pAp donor gives the larger yield than pGp. These are the same results observed in the case of the single-stranded RNA acceptor as shown in Table 1. Therefore, whether the acceptor is single-stranded or double-stranded does not affect the efficiency of the RNA ligation.

Ligation of Double-Stranded Acceptors Containing Dangling Ends to pZp Donors. In Table 2, the values of ΔG°_{37}, T_m, and K for AUGCGCA and XAUGCAU (X=A, C, G, U) show that these oligomers exist almost as the self-complementary duplexes at 37 °C as well as UGCGCA and AUGCAU. CD spectra of these oligomers support the above consideration: Figure 2 shows a typical CD spectrum of 10^{-3} mol dm^{-3} AAUGCAU in a 2×10^{-1} mol dm^{-3} Tris-HCl (pH 7.5), 2×10^{-2} mol dm^{-3} $MgCl_2$ buffer at 37 °C. The CD spectrum indicates a large positive peak at 278 nm and a small negative peak at 237 nm which are well-known to be due to a A-type RNA double helix.

In Table 2, the T_m value of AUGCGCA is 3.6 °C higher than that of UGCGCA. Also, in the case of the dangling ends on AUGCAU in the same table, the T_m values of XAUGCAU are about 4—6 °C higher than that of AUGCAU. The values of ΔG°_{37} in Table 2 show that the double helix having each dangling end is about 0.2 or 0.3 kcal mol^{-1} more stable than the core double helix of UGCGCA or AUGCAU. These results suggest the dangling nucleotide stabilizes the core double helix with its stacking interaction.[7]

In the ligation of purine donors to the AUGCGCA double-stranded acceptors having the A dangling end, the yield of the product for pAp donor is higher than that for pGp donor as shown in Entry Nos. 3 and 4 in Table 4. The result is the same in the cases of the single-stranded RNA acceptors and the double-stranded UGCGCA acceptor. In contrast, in the case of pyrimidine donors, pUp donor gives the yield of 12% higher than pCp, even under the lower enzyme unit of 25 U/ml, in Nos. 1 and 2 in Table 4, which is the opposite tendency as observed in the above cases, that is, the cases of the single-stranded and double-stranded accep-

Table 2. The Stabilization Energies, the Melting Temperatures, and the Equilibrium Constants of the Self-Complementary RNA Double Helixes

Oligomer	$-\Delta G^\circ_{37}$	T_m[a]	T_m[b]	K
	kcal mol^{-1}	°C	°C	mol^{-1} dm^3
UGCGCA	8.7	63.1	62.6	1.37×10^6
AUGCGCA	9.0		66.2	2.20×10^6
AUGCAU	5.1	42.9	40.6	4.12×10^3
AAUGCAU	5.4		46.3	6.71×10^3
CAUGCAU	5.4		45.3	6.71×10^3
GAUGCAU	5.4		46.4	6.71×10^3
UAUGCAU	5.3		44.6	5.70×10^3

a) The calculated melting temperature for the oligomer of 10^{-3} mol dm^{-3}. b) The measured melting temperature for the oligomer of 10^{-3} mol dm^{-3}.

Table 3. The Yield of the Product in the Reaction of Double-Stranded UGCGCA Acceptors with pZp

Entry No.	Acceptor X···Y	Donor pZp	Enzyme concn U/ml	Time h	Yield %
1	UGCGCA / ACGCGU	C	50	1	70
2	UGCGCA / ACGCGU	U	50	1	22
3	UGCGCA / ACGCGU	A	50	1	42
4	UGCGCA / ACGCGU	G	50	1	13

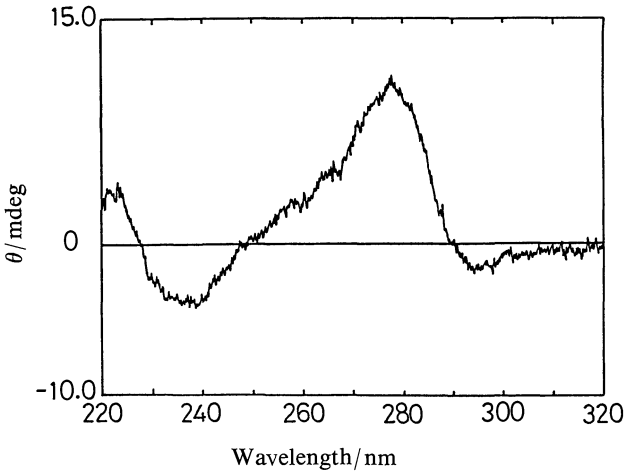

Fig. 2. CD spectrum of 10^{-3} mol dm^{-3} AAUGCAU in a buffer containing 2×10^{-2} mol dm^{-3} $MgCl_2$ and 2×10^{-1} mol dm^{-3} Tris-HCl (pH 7.5) at 37 °C.

Table 4. The Yield of the Product in the Reaction of Self-Complementary Double-Stranded AUGCGCA and CAUGCAU Acceptors Having Dangling Ends with pZp

Entry No.	Acceptor X···Y	Donor pZp	Enzyme concn U/ml	Time h	Yield %
1	AUGCGCA / ACGCGUA	C	50	1	69
2	AUGCGCA / ACGCGUA	U	25	1	81
3	AUGCGCA / ACGCGUA	A	50	1	49
4	AUGCGCA / ACGCGUA	G	90	1	17
5	CAUGCAU / UACGUAC	C	50	1	84
6	CAUGCAU / UACGUAC	U	50	1	42
7	CAUGCAU / UACGUAC	A	50	1	73
8	CAUGCAU / UACGUAC	G	50	1	100

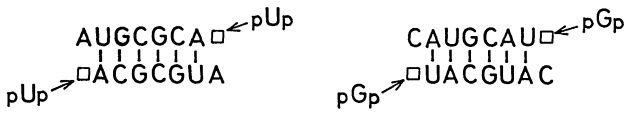

Fig. 3. The schematic illustrations of pUp and pGp donors approaching the dangling **A** and **C** nucleotide on AUGCGCA and CAUGCAU self-complementary duplexes, respectively.

tors. Even in comparison with pyrimidine donors, the pUp donor gives the highest yield of the product for 1 h. The result leads to the consideration that the pUp donors can approach most easily the dangling **A** nucleotide with a base-pair interaction[15] between the U and A nucleotides as shown in Fig. 3.

In the reaction of the double-stranded CAUGCAU acceptor having the **C** dangling end, pyrimidine donors show the same tendency observed in the single-stranded and double-stranded acceptors having no dangling end, but purine donors indicate the opposite tendency, that is, pGp gives the yield of the product 27% higher than pAp (Nos. 5—8 in Table 4). The yield of the product for pGp is the highest value for all the donors. The result supports the consideration that a base-pair interaction between the **G** and **C** nucleotides in Fig. 3 has a large effect on the ligation. Therefore, the base-pair interaction in the case of the **A** and **C** dangling ends accelerates the RNA ligation.

It follows that the base-pair formation in the reaction of the acceptors having different dangling ends to the same donor should accelerate the reaction rate more than the mismatch interactions such as GA, GU, and GG interactions.[16] In order to examine the above idea, the ligation of the pGp donor to the double stranded XAUGCAU (X=A, C, G, U) acceptors were

Table 5. The Yield of the Product in the Reaction of Double-Stranded RNA Acceptors Having Dangling Ends with pGp

Entry No.	Acceptor X···Y	Donor pZp	Enzyme concn U/ml	Time h	Yield %
1	AAUGCAU / UACGUAA	G	50	1	50
2	CAUGCAU / UACGUAC	G	50	1	100
3	GAUGCAU / UACGUAG	G	50	1	37
4	UAUGCAU / UACGUAU	G	50	1	41

studied. In Table 5, the 100% yield of the product for CAUGCAU is the largest value in comparison with the 50, 37, and 41% yield for AAUGCAU, GAUGCAU, and UAUGCAU, respectively. The result suggests the base-pair interaction between the dangling X nucleotide on the core double helix and the pZp donor, in general, accelarate the rate of the RNA ligation by its making the donor approaching easily the ligation site of the acceptor. Therefore, the study in this paper suggests that the interaction between the substrates such as the base-pair interaction between the unpaired terminal nucleotide on the double helix of the RNA acceptor and the donor as well as the interaction of the substrates with the enzyme,[17] plays a very important role in the RNA ligation with T4 RNA ligase.

The authors thank Professor D. H. Turner and Dr. S. M. Freier, University of Rochester, for their help in getting started. This work was partly supported by a Grant-in-Aid for Scientific Research on Priority Areas from the Ministry of Education, Science and Culture.

References

1) H. Grosjean, D. G. Soll, and D. M. Crothers, *J. Mol. Biol.*, **103**, 499 (1976).
2) K. Yoon, D. H. Turner, I. Tinoco, Jr., F. von der Haar, and F. Cramer, *Nucleic Acids Res.*, **3**, 2233 (1976).
3) D. Ayer and M. Yarus, *Science*, **231**, 393 (1986).
4) D. H. Turner, N. Sugimoto, and S. M. Freier, *Annu. Rev. Biophys. Biophys. Chem.*, **17**, 167 (1988).
5) A. A. Beaudry and G. F. Joyce, *Nature*, **344**, 467 (1990).
6) N. Sugimoto and M. Sasaki, *Chem. Lett.*, **1991**, 395.
7) N. Sugimoto, R. Kierzek, and D. H. Turner, *Biochemistry*, **26**, 4554 (1987).
8) N. Sugimoto, K. Hasegawa, A. Matsumura, and M. Sasaki, *Chem. Lett.*, **1991**, 1291.
9) R. Kierzek, M. H. Caruthers, C. E. Longfellow, D. Swinton, D. H. Turner, and S. M. Freier, *Biochemistry*, **25**, 7840 (1986).
10) N. Sugimoto, R. Kierzek, and D. H. Turner, *Biochemistry*, **25**, 5755 (1986).
11) B. Weiss, A. Thompson, and C. C. Richardson, *J. Biol. Chem.*, **243**, 4556 (1968).
12) S. M. Freier, R. Kierzek, J. A. Jaeger, N. Sugimoto, M.

H. Caruthers, T. Neilson, and D. H. Turner, *Proc. Natl. Acad. Sci. U.S.A.*, **83**, 9373 (1986).
13) N. Sugimoto and M. Sasaki, *Bull. Chem. Soc. Jpn.*, **62**, 3745 (1989).
14) E. Romaniuk, L. W. McLaughlin, T. Neison, and P. J. Romaniuk, *Eur. J. Biochem.*, **125**, 639 (1982).
15) W. Saenger, "Principles of Nucleic Acid Structure," Springer-Verlag, New York (1984).
16) N. Sugimoto, R. Kierzek, and D. H. Turner, *Biochemistry*, **26**, 4559 (1987).
17) D. Beckett and O. C. Uhlenbeck, "Oligonucleotide Synthesis," ed by M. J. Gait, IRL Press, Oxford (1984), Chap. 8.

Synthesis of 14,14-Difluoro-4-demethoxydaunorubicin[1)]

Fuyuhiko MATSUDA, Teruyo MATSUMOTO, Masako OHSAKI, and Shiro TERASHIMA*
Sagami Chemical Research Center, Nishi-Ohnuma, Sagamihara, Kanagawa 229
(Received May 29, 1991)

The title compound, (+)-14,14-difluoro-4-demethoxydaunorubicin hydrochloride (**9**), was prepared starting from the readily available (−)-hydroxy ester (**10**). This synthesis featured the efficient synthetic route to (−)-14,14-difluoro-4-demethoxy-7-deoxydaunomycinone (**20**) employing the Reformatsky reaction of ethyl bromodifluoroacetate with the (−)-siloxy aldehyde (**14**) and previously developed glycosylation method in which trimethylsilyl trifluoromethanesulfonate was used as an activator. In P388 *in vitro* test, **9** was found to be fifty times more active than adriamycin (**1**). Prominent antitumor activity was also observed for **9** in P388 *in vivo* test.

The anthracyclines, represented by adriamycin (**1**) and daunorubicin (**2**), are important anticancer agents exhibiting clinical effectiveness against leukemia and solid tumors.[2,3)] However, their utility for cancer chemotherapy is seriously restricted by various undesired side effects, the most notable of which is dose-related cardiotoxicity. Thus, numerous attempts have been made to prepare various structural types of congeners by chemical synthesis with an aim to overcome these disadvantages. Among synthetically elaborated analogues of **1** and **2**, unnatural 4-demethoxyadriamycin (**3**) and 4-demethoxydaunorubicin (**4**) have been reported to show better therapeutic indices than natural **1** and **2**.[2–4)]

On the other hand, a large number of the fluorinated biologically active compounds have been synthesized in the last decade to improve therapeutic property of the parent compounds or to explore novel pharmacological activity.[5)] In the field of anthracyclines, some derivatives possessing fluorinated sugar[6)] or D-ring[7)] have been synthesized. In conjunction with our program directed toward the development of novel synthetic anthracycline congeners as anticancer agents, we achieved the first synthesis of the 14-fluoroanthracyclines (**5**—**8**) which had a fluoroacetyl group as their C-9 side chain. Furthermore, these novel anthracyclines showed potent antitumor activity against P388 murine leukemia *in vitro* and *in vivo*.[8)] Thus, taking into account of these results, we are interested in evaluating the antitumor activity of 14,14-difluoro-4-demethoxydaunorubicin (**9**), the most representative member of 14,14-difluoroanthracyclines. Recently, the first synthesis of **9** has been accomplished by employing the Reformatsky reaction of ethyl bromodifluoroacetate as a key step. Moreover, **9** was found to exhibit prominent *in vitro* cytotoxicity and *in vivo* antitumor activity against P388 murine leukemia.[1)] This report deals with full details of the synthesis and antitumor activity of the novel 14,14-difluoroanthracycline (**9**).

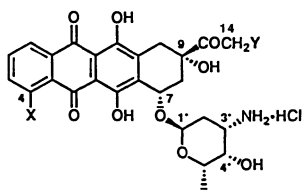

1 X=OMe, Y=OH
2 X=OMe, Y=H
3 X=H, Y=OH
4 X=Y=H

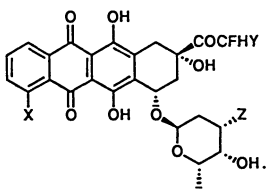

5 X=OMe, Y=H, Z=NH_2•HCl
6 X=Y=H, Z=NH_2•HCl
7 X=OMe, Y=H, Z=OH
8 X=Y=H, Z=OH
9 X=H, Y=F, Z=NH_2•HCl

Fig. 1.

Results and Discussion

Preparation of 14,14-Difluoro-4-demethoxydaunomycinone. Numerous preliminary experimentations were carried out using racemic anthracyclinone derivatives to construct a difluoroacetyl side chain at the C-9 position. At the outset of this work, introduction of fluorine atom into the C-14 position of racemic 14-fluoro-4-demethoxy-7-deoxydaunomycinone (*dl*-**15**) was examined according to the fluorination method previously explored for 7-deoxydaunomycinones.[8)] However, attempted bromination of *dl*-**15** always produced complex mixtures of reaction products. Accordingly, the Reformatsky reaction of ethyl bromodifluoroacetate[9)] was next studied, which had been frequently used to introduce a difluorinated carbon chain.[10)] Although the Reformatsky reaction with the hydroxy aldehyde (*dl*-**13**) or the acylimidazole derivative generated from the hydroxy acid (*dl*-**16**)[11)] resulted in decomposition or recovery of the starting material respectively, it was finally uncovered that the reaction with the siloxy aldehyde (*dl*-**14**) successfully produced the addition product, β-hydroxy ester (*dl*-**17**). In contrast, *dl*-**17** could not be obtained from *dl*-**14** when methyl difluoroiodoacetate[12)] was employed instead of ethyl bromodifluoroacetate probably due to instability of the zinc enolate generated *in situ*. The racemic aldehydes (*dl*-**13** and *dl*-**14**) could be prepared from the hydroxy ester (*dl*-**10**)[11)] according to the same procedures as described for optically active compounds (vide infra). On the basis of these results, an efficient synthetic method of 14,14-difluoro-4-demethoxy-7-deoxydaunomycinone (**20**) as described below was eventu-

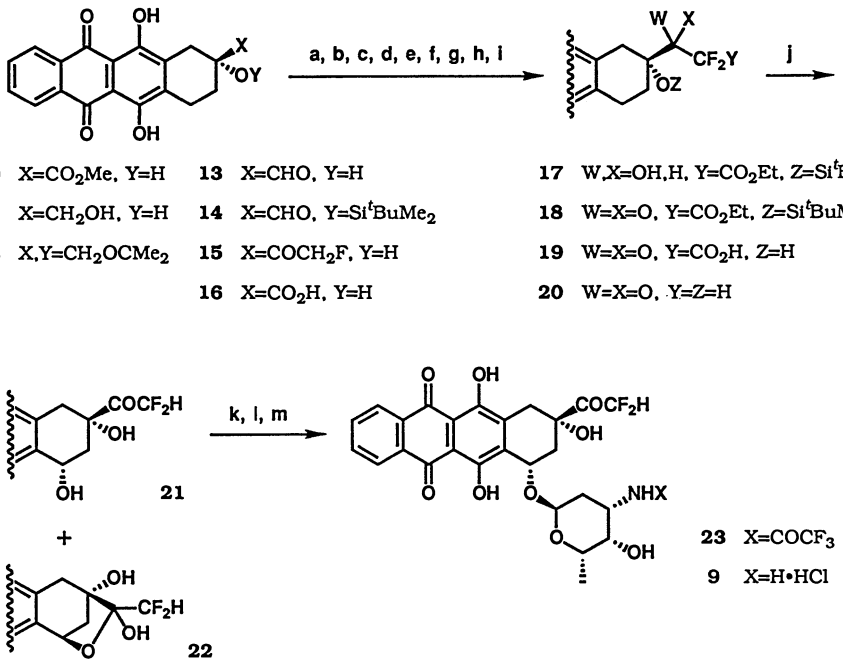

10 X=CO_2Me, Y=H
11 X=CH_2OH, Y=H
12 X,Y=CH_2OCMe_2
13 X=CHO, Y=H
14 X=CHO, Y=Si^tBuMe_2
15 X=$COCH_2F$, Y=H
16 X=CO_2H, Y=H
17 W,X=OH,H, Y=CO_2Et, Z=Si^tBuMe_2
18 W=X=O, Y=CO_2Et, Z=Si^tBuMe_2
19 W=X=O, Y=CO_2H, Z=H
20 W=X=O, Y=Z=H
21
22
23 X=$COCF_3$
9 X=H•HCl

Scheme 1. a) $NaBH_4$, $CeCl_3 \cdot 7H_2O$, $CHCl_3$–MeOH, 0 °C→rt, 3 h b) CSA, $Me_2C(OMe)_2$–acetone–THF, rt, 4 h, 78% (2 steps) c) 12 mol dm^{-3} HCl, THF, 0 °C, 4 h, 90% d) $SO_3 \cdot$Py, Et_3N, DMSO, rt, 10 min, 79% e) TBDMSOTf, 2,6-Lu, CH_2Cl_2, 0 °C→rt, 5.5 h, 86% f) $BrCF_2CO_2Et$, Zn, THF, reflux, 30 min, 42% g) Dess–Martin reagent, CH_2Cl_2, 0 °C→rt, 20 min, 45% h) 0.5 mol dm^{-3} KOH, THF–MeOH, 0 °C, 30 min, then 1 mol dm^{-3} HCl i) DMF, 60 °C, 35 min, 73% (2 steps) j) 1) Br_2, *hν*, CCl_4–$CHCl_3$–H_2O, rt, 2.5 h, 2) 2.5 mol dm^{-3} NaOH, 0 °C, 15 min, then 1 mol dm^{-3} HCl, 26% (**21**), 31% (**22**) k) L-Daunosamine derivative, TMSOTf, 4A-MS, CH_2Cl_2–Et_2O–THF, −10 °C, 5.5 h l) 0.1 mol dm^{-3} NaOH, MeOH, rt, 20 min, then 2 mol dm^{-3} AcOH, 89% (2 steps) m) 1) 0.05 mol dm^{-3} NaOH, THF, rt, 50 min, then 1 mol dm^{-3} HCl 2) 0.25 mol dm^{-3} HCl, MeOH, 40% (2 steps).

ally explored employing the Reformatsky reaction of ethyl bromodifluoroacetate with **14** as a key step.

The synthesis of optically pure **14** was carried out by utilizing the readily available optically pure (−)-hydroxy ester (**10**),[11] mp 214—215 °C, $[\alpha]_D^{20}$ −63.6° (*c* 0.110, $CHCl_3$), as the starting material. Reduction of **10** with sodium borohydride in the presence of cerium(III) chloride heptahydrate yielded the (−)-diol (**11**). The reduction product (**11**) was purified by silica-gel chromatography in a form of the corresponding (−)-acetonide (**12**), mp 220—223 °C, $[\alpha]_D^{20}$ −51.0° (*c* 0.050, $CHCl_3$), because of its sparing solubility in usual organic solvents. According to this procedure, **12** could be obtained in a higher yield (78% from **10**) than that previously reported for the reduction of **10** with lithium tri-*t*-butoxyaluminum hydride (55% from **10**).[11] Acidic hydrolysis of **12** yielded a pure sample of **11**, mp 260—263 °C, $[\alpha]_D^{20}$ −50.0° (*c* 0.060, dioxane). The (−)-siloxy aldehyde (**14**), mp 251—252 °C, $[\alpha]_D^{20}$ −76.9° (*c* 0.104, $CHCl_3$), was derived from **11** by sequential oxidation and silylation of the resulting (−)-hydroxy aldehyde (**13**), mp 248—249 °C, $[\alpha]_D^{20}$ −54.5° (*c* 0.110, dioxane).

The Reformatsky reaction of ethyl bromodifluoroacetate with **14** took place cleanly under the usual conditions,[9] giving rise to the β-hydroxy ester (**17**) as an epimeric mixture. The ratio of two epimers estimated by the ^1H NMR spectra of the mixture was 2 : 1. Without separation of the epimers, **17** was oxidized to the (−)-β-keto ester (**18**), mp 119—121 °C, $[\alpha]_D^{20}$ −91.8° (*c* 0.098, $CHCl_3$), using the Dess–Martin periodinane[13] as an oxidizing reagent. The oxidation of **17** appeared to be exceptionally difficult. Oxidants other than the Dess–Martin reagent resulted in complete recovery of **17**.[14] Sequential hydrolysis of the ethyl ester and decarboxylation of the formed β-keto acid (**19**) afforded (−)-14,14-difluoro-4-demethoxy-7-deoxydaunomycinone (**20**),[16] mp 225—228 °C, $[\alpha]_D^{20}$ −26.1° (*c* 0.153, dioxane).

Next, preparation of 14,14-difluoro-4-demethoxydaunomycinone (**21**) from **20** was examined. Since all the attempts to protect the ketonic function of **20** in a form of acetal met with failure probably due to the adjacent two fluorine atoms, direct introduction of the C_7-hydroxyl group was studied. Bromination of **20** with bromine under irradiation followed by immediate treatment of the resulting unstable C_7-bromide with aqueous alkali gave (+)-14,14-difluoro-4-demethoxydaunomycinone (**21**),[16] mp 210—213 °C, $[\alpha]_D^{20}$ +44.2° (*c*

0.113, dioxane), along with its $C_{7\beta}$-epimer in a form of the (−)-hemiacetal (**22**), mp 253—255 °C, $[\alpha]_D^{20}$ −153° (*c* 0.157 dioxane). The mixture of **21** and **22** could be separated by preparative TLC on silica gel. The stereochemistry of the C_7-position of **21** was established by the ^{1}H NMR spectrum ($CDCl_3$) which showed a W_H value of 8.0 Hz for the signal of the $C_{7\beta}$-H [δ=5.36—5.45 (m)]. On the other hand, in the ^{1}H NMR spectrum ($CDCl_3$) of **22**, a single triplet assignable to the C_{14}-methine proton appeared at δ=5.58 (J=54 Hz). Thus, it becomes apparent that **22** consists of a single hemiacetal whose stereostructure at the hemiacetal carbon could not be determined. All the attempts to epimerize **22** under acidic conditions[17] resulted in simple recovery of the starting material. Additionally, 14,14-difluoro-7-deoxydaunomycinone (**20**) could be obtained only in low yield (32%) by hydrogenolysis of **22** following the reported procedure (H_2, Pd–$BaSO_4$, MeOH, rt, 2 h).[18] These phenomena might originate from the electron-withdrawing effect accumulated by the two fluorine atoms making the hemiacetal form highly stable.

Preparation of 14,14-Difluoro-4-demethoxydaunorubicin. With **21** in hand, glycosylation was attempted using the L-daunosamine derivative according to the procedure previously reported by us.[19] Thus, **21** was allowed to react with 3-*N*-trifluoroacetyl-1,4-bis-*O*-(*p*-nitrobenzoyl)-L-daunosamine[19] in the presence of trimethylsllyl trifluoromethanesulfonate. The formed glycoside was treated with dilute alkali to effect hydrolysis of the 4′-*O*-*p*-nitrobenzoyl group, affording (+)-3′-*N*-trifluoroacetyl-14,14-difluoro-4-demethoxydaunorubicin (**23**),[16] $[\alpha]_D^{20}$ +117° (*c* 0.163, dioxane), as a sole product. The α-glycoside structure of **23** could be readily confirmed by the coupling pattern of the $C_{1'}$-H [δ=5.53 (d, J=4.2 Hz)] in the ^{1}H NMR spectrum ($CDCl_3$) of **23**. The assigned structure was further supported by comparison of the ^{1}H NMR spectrum with that of 3′-*N*-trifluoroacetyl-4-demethoxydaunorubicin.[19] Further alkaline hydrolysis of the 3′-*N*-trifluoroacetyl group followed by salt formation furnished (+)-14,14-difluoro-4-demethoxydaunorubicin hydrochloride (**9**), mp 168—171 °C, $[\alpha]_D^{20}$ +111° (*c* 0.090, MeOH). The ^{1}H NMR and ^{19}F NMR spectra (DMSO-d_6+D_2O) of **9** proved that this compound was composed of a mixture of the ketonic and the hydrate forms (3:1 by ^{1}H NMR).[16] Representative NMR spectral data are as follows; **9**: ^{1}H NMR δ=6.04 (t, J=55.8 Hz, CHF_2, hydrate), 6.85 (t, J=52.9 Hz, CHF_2, ketone); ^{19}F NMR δ=−128.0 (d, J=52.9 Hz, ketone), −131.2 (d, J=55.8 Hz, hydrate).

Antitumor Activity of 14,14-Difluoro-4-demethoxydaunorubicin. 14,14-Difluoro-4-demethoxydaunorubicin (**9**) was subjected to P388 murine leukemia *in vitro* assay along with its 3′-*N*-trifluoroacetyl derivative (**23**). While **23** showed comparable cytotoxicity (IC_{50}= 1.1×10^{-3} μg ml^{-1})[20] to that of adriamycin (**1**) (IC_{50}= 2.5×10^{-3} μg ml^{-1}), **9** was found to be at least fifty-fold more active (IC_{50}=4.6×10^{-5} μg ml^{-1}) than **1**. Since cytotoxicity of 14-fluoro-4-demethoxydaunorubicin (**6**) has already been disclosed to be compared well with that of **1**,[8] it appeared that **9** was obviously more cytotoxic than **6**. Furthermore, in P388 *in vivo* test,[21] it turned out that **9** exhibited potent inhibitory activity [T/C=161% (1.0 mg kg^{-1})].[22]

Further investigations aimed at characterizing antitumor activity of **9** are in progress and will be reported shortly.

Experimental

General. All melting points were determined with a Yamato MP-21 melting point apparatus and are uncorrected. Measurements of optical rotations were carried out by using a Horiba SEPA-200 automatic digital polarimeter. IR spectral measurements were performed with a JASCO A-202 IR spectrometer. ^{1}H NMR spectra were measured with a Hitachi R-90H spectrometer (90 MHz) and a Bruker AM-400 spectrometer (400 MHz). Measurement of ^{19}F NMR spectra were carried out with a Varian XL-100 spectrometer (94 MHz). All ^{1}H and ^{19}F-signals were expressed as ppm downfield from tetramethylsilane ($SiMe_4$) and trichlorofluoromethane ($CFCl_3$), respectively, used as an internal standard (δ-value). The following abbreviations are used: singlet (s), doublet (d), triplet (t), quartet (q), multiplet (m), broad (br). Assignments of peaks are indicated according to the numbering of IUPAC nomenclature. Mass spectra (MS) were taken with a Hitachi RMU-6MG mass spectrometer (EI-MS) and a Hitachi M-80A mass spectrometer (SI-MS). Wako Gel C-200 and Merck Silica Gel $60F_{254}$ were used for column chromatography and preparative thin-layer chromatography (TLC), respectively. All reactions were performed by using anhydrous solvents. In particular, tetrahydrofuran and ether freshly distilled from sodium benzophenone ketyl, and commercially available dichloromethane stabilized with 2-methyl-2-butene were used. The following abbreviations are used for solvents; acetic acid (AcOH), carbon tetrachloride (CCl_4), chloroform ($CHCl_3$), dichloromethane (CH_2Cl_2), *N,N*-dimethylformamide (DMF), dimethyl sulfoxide (DMSO), ethyl acetate (AcOEt), methanol (MeOH), tetrahydrofuran (THF), toluene (PhMe).

(*R*)-6,8,11-Trihydroxy-8-hydroxymethyl-7,8,9,10-tetrahydro-5,12-naphthacenedione (11). $NaBH_4$ (8.11 g, 214 mmol) was added in small portions to a stirred solution of (*R*)-6,8,11-trihydroxy-8-methoxycarbonyl-7,8,9,10-tetrahydro-5,12-naphthacenedione (**10**),[11] mp 214—215 °C, $[\alpha]_D^{20}$ −63.6° (*c* 0.110, $CHCl_3$), (7.89 g, 21.4 mmol) and $CeCl_3\cdot7H_2O$ (40.0 g, 107 mmol) in a mixture of $CHCl_3$ (400 ml) and MeOH (160 ml) cooled at 0 °C. The reaction mixture was allowed to warm up to ambient temperature and stirring was continued at the same temperature for 3 h. After further amounts of $CeCl_3\cdot7H_2O$ (40.0 g, 107 mmol) and $NaBH_4$ (8.11 g, 214 mmol) were successively added at room temperature, the reaction mixture was further stirred at the same temperature for 4 h. The mixture was poured into 1 mol dm^{-3} HCl, and extracted with a mixture of AcOEt and THF. The combined organic extracts were washed with H_2O, and dried over anhydrous $MgSO_4$. Filtration and concentration in vacuo gave crude **11**, which was dissolved in a mixture of THF (420 ml) and acetone (210 ml). After 2,2-dimethoxypropane (830 ml) and *d*-10-camphorsulfonic acid (800 mg, 3.44 mmol) were successively added to the solution at ambient temperature, the mixture was stirred at the same temperature for 4 h, poured

into saturated $NaHCO_3$, and extracted with $CHCl_3$. The organic layers were combined, washed successively with H_2O and brine, dried over anhydrous $MgSO_4$, filtered, then concentrated in vacuo. The residue was purified by column chromatography (SiO_2, PhMe–AcOEt 200:1) to give (*R*)-5′,12′-dihyroxy-2,2-dimethyl-3′,4′-dihydrospiro[1,3-dioxolane-4,2′(1′*H*)-naphthacene]-6′,11′-dione (**12**) as a red solid (6.37 g, 78%), mp 220—223 °C, $[\alpha]_D^{20}$ −51.0° (*c* 0.050, $CHCl_3$) [lit,[11] mp 222—223 °C, $[\alpha]_D^{20}$ −52.0° (*c* 0.050, $CHCl_3$)]. Spectral and chromatographic comparison showed that **12** was identical with an authentic sample.[11]

Twelve mol dm^{-3} hydrochloric acid (160 ml) was added to a suspension of **12** (6.37 g, 16.9 mmol) in THF (640 ml) at room temperature. After stirring at the same temperature for 4 h, the mixture was poured into ice-water, and extracted with a mixture of AcOEt and THF. The combined extracts were washed successively with H_2O and saturated $NaHCO_3$. dried over anhydrous $MgSO_4$, filtered, then concentrated in vacuo. Trituration of the residue with ether gave pure **11** as a dark orange solid (5.12 g, 90%), mp 260—263 °C, $[\alpha]_D^{20}$ −50.0° (*c* 0.060, dioxane) [lit,[11] mp 265—267 °C, $[\alpha]_D^{20}$ −52.0° (*c* 0.050, dioxane)]. The spectra and chromatographic behaviors of this sample were identical with those of an authentic sample.[11]

(*R*)-8-Formyl-6,8,11-trihydroxy-7,8,9,10-tetrahydro-5,12-naphthacenedione (13). A suspension of sulfur trioxide pyridine complex (467 mg, 2.93 mmol) in DMSO (1.0 ml) was added with stirring under an Ar atmosphere to a solution of **11** (49.8 mg, 0.146 mmol) and triethylamine (0.61 ml, 4.38 mmol) in DMSO (3.0 ml) at ambient temperature. After stirring at the same temperature for 10 min, the mixture was poured into 1 mol dm^{-3} HCl, and extracted with AcOEt. The combined organic layers were washed successively with H_2O and brine, and dried over anhydrous Na_2SO_4. Filtration and concentration in vacuo gave the crude product, which was purified by column chromatography (SiO_2, PhMe–AcOEt 20:1→10:1), affording pure **13** as a red powder (39.0 mg, 79%). This was recrystallized from PhMe, giving an analytical sample of **13** as red crystals, mp 248—249 °C, $[\alpha]_D^{20}$ −54.5° (*c* 0.110, dioxane). IR (KBr) 3500, 1730, 1620, 1580 cm^{-1}. ^{1}H NMR ($CDCl_3$) δ=1.80—2.00 (2H, m, C_9–H_2), 2.50 (1H, s, C_8–OH), 2.97—3.20 (4H, m, C_7–H_2, C_{10}–H_2), 7.77—7.93, 8.30—8.50 (each 2H, m, ArH×4), 9.75 (1H, s, CHO), 13.50 (2H, s, ArOH×2). EI-MS *m*/*z* 338 (M^+), 309 (M^+ −CHO), 291. Anal. Calcd for $C_{19}H_{14}O_6$: C, 67.45; H, 4.17%. Found: C, 67.18; H, 4.22%. The racemic hydroxy aldehyde (*dl*-**13**) prepared by the same procedure as described above, showed mp 251—253 °C. The ^{1}H NMR spectrum ($CDCl_3$) of *dl*-**13** was identical with that of the optically active compound.

(*R*)-8-*t*-Butyldimethylsilyloxy-8-formyl-6,11-dihydroxy-7,8,9,10-tetrahydro-5,12-naphthacenedione (14). 2,6-Lutidine (25.2 ml, 216 mmol) and *t*-butyldimethylsilyl trifluoromethanesulfonate (50.5 ml, 220 mmol) was successively added under an Ar atmosphere to a stirred suspension of **13** (3.69 g, 10.9 mmol) in CH_2Cl_2 (80 ml) at 0 °C. After stirring was continued at the same temperature for 30 min, the reaction mixture was allowed to warm up to room temperature, then stirred at the same temperature for 5 h. The mixture was poured into saturated $NaHCO_3$, and extracted with $CHCl_3$. The extracts were combined, washed successively with H_2O and brine, dried over anhydrous Na_2SO_4, filtered, then concentrated in vacuo. Recrystallization of the residue from PhMe gave pure **14** as orange crystals (4.23 g, 86%), mp 251—252 °C, $[\alpha]_D^{20}$ −76.9° (*c* 0.104, $CHCl_3$). IR (KBr) 3450, 2880, 1730, 1620, 1590 cm^{-1}. ^{1}H NMR ($CDCl_3$) δ=−0.10, 0.15 (each 3H, s, $SiMe_2$), 0.83 (9H, s, ^{t}Bu), 1.63—2.20 (2H, m, C_9–H_2), 2.83—3.20 (4H, m, C_7–H_2, C_{10}–H_2), 7.70—7.90, 8.23—8.47 (each 2H, m, ArH×4), 9.30 (1H, s, CHO), 12.95, 12.98 (each 1H, s, ArOH×2). EI-MS *m*/*z* 452 (M^+), 437 (M^+ −Me) 395 (M^+ −^{t}Bu). Anal. Calcd for $C_{25}H_{28}O_6Si$: C, 66.35; H, 6.24%. Found: 66.57; H, 6.25%. The racemic siloxy aldehyde (*dl*-**14**) prepared by the same procedure as described above, showed mp 255—257 °C. The ^{1}H NMR spectrum ($CDCl_3$) of *dl*-**14** was identical with that of the optically active compound.

(*R*)-8-*t*-Butyldimethylsilyloxy-8-(2-ethoxycarbonyl-2,2-difluoro-1-hydroxyethyl)-6,11-dihydroxy-7,8,9,10-tetrahydro-5,12-naphthacenedione (17). A mixture of Zn (1.28 g, 19.5 mmol) and ethyl bromodifluoroacetate[9] (4.22 g, 20.8 mmol) in THF (60 ml) was heated at reflux under an Ar atmosphere for 1 min. After a solution of **14** (588 mg, 1.30 mmol) in THF (60 ml) was added under reflux to the reaction mixture, stirring was continued under reflux for 30 min. After cooling, the mixture was poured into 1 mol dm^{-3} $KHSO_4$ cooled in an ice bath, and extracted with AcOEt. The combined extracts were washed with brine, and dried over anhydrous Na_2SO_4. Filtration and concentration in vacuo gave the crude product, which was chromatographed (SiO_2, PhMe–AcOEt 50:1→30:1) to give pure **17** (a 2:1 mixture of the diastereomers by ^{1}H NMR) as a red amorphous powder (313 mg, 42%). IR (KBr) 3500, 1760, 1620, 1580 cm^{-1}. ^{1}H NMR ($CDCl_3$) δ=0.00, 0.20 (each 3H, s, $SiMe_2$), 0.90, 0.92 (total 9H, each s, ^{t}Bu), 1.33 (3H, t, *J*=6.0 Hz, CH_2*Me*), 1.80—2.50 (2H, m, C_9–H_2), 2.60—3.67 (4H, m, C_7–H_2, C_{10}–H_2), 3.70—4.20 (1H, m, $C_{1'}$–H), 4.35 (2H, q, *J*=6.0 Hz, CH_2Me), 7.60—7.93, 8.20—8.40 (each 2H, m, ArH×4), 13.40, 13.46, 13.44 (total 2H, each s, ArOH×2). ^{19}F NMR ($CDCl_3$) δ=−106.4 (d, *J*=260.0 Hz), −106.7 (d, *J*=257.0 Hz), −124.3 (dd, *J*=260.0, 20.0 Hz), −125.9 (dd, *J*=257.0, 22.5 Hz). EI-MS *m*/*z* 577 (M^+ +H), 519 (M^+ −^{t}Bu).

(*R*)-8-*t*-Butyldimethylsilyloxy-8-ethoxycarbonyldifluoroacetyl-6,11-dihydroxy-7,8,9,10-tetrahydro-5,12-naphthacenedione (18). Dess–Martin reagent (428 mg, 1.01 mmol) was added under an Ar atmosphere to a stirred solution of **17** (116 mg, 0.202 mmol) in CH_2Cl_2 (20 ml) at 0 °C. The reaction mixture was allowed to warm up to room temperature, stirred at the same temperature for 20 min, poured into saturated $NaHCO_3$ containing excess $Na_2S_2O_3$, and extracted with ether. The organic layers were combined, washed successively with saturated $NaHCO_3$ and brine, dried over anhydrous Na_2SO_4, filtered, then concentrated in vacuo. The residue was purified by column chromatography (SiO_2, PhMe–AcOEt 30;1), giving pure **18** as an orange solid (52.0 mg, 45%). This was recrystallized from hexane–PhMe to afford an analytical sample of **18** as orange crystals, mp 119—121 °C, $[\alpha]_D^{20}$ −91.8° (*c* 0.098, $CHCl_3$). IR (KBr) 3450, 1790, 1740, 1620, 1600 cm^{-1}. ^{1}H NMR ($CDCl_3$) δ=0.01, 0.19 (each 3H, s, $SiMe_2$), 0.85 (9H, s, ^{t}Bu), 1.36 (3H, t, *J*=7.2 Hz, CH_2*Me*), 2.19 (1H, dt, *J*=13.2, 6.2 Hz, $C_{9\text{-ax}}$–H), 2.33 (1H, dt, *J*=13.2, 6.2 Hz, $C_{9\text{-eq}}$–H), 2.88 (1H, ddd, *J*=19.2, 7.4, 6.2 Hz, $C_{10\text{-ax}}$–H), 3.00 (1H, d, *J*=18.6 Hz, $C_{7\text{-aq}}$–H), 3.09 (1H, dt, *J*=19.2, 6.2 Hz, $C_{10\text{-eq}}$–H), 3.44 (1H, d, *J*=18.6 Hz, $C_{7\text{-eq}}$–H), 4.38 (2H, q, *J*=7.2 Hz, CH_2Me), 7.80—7.85, 8.34—8.38 (each 2H, m, ArH×4), 13.44, 13.50 (each 1H, s, ArOH×2). ^{19}F NMR ($CDCl_3$) δ=−109.1 (s). EI-MS *m*/*z* 575 (M^+ +H), 559 (M^+ −Me), 517 (M^+ −^{t}Bu). Anal. Calcd for $C_{29}H_{32}O_8F_2Si$: C, 60.61; H, 5.61%. Found: C, 60.57; H, 5.69%.

(*R*)-8-Difluoroacetyl-6,8,11-trihydroxy-7,8,9,10-tetrahydro-5,12-naphthacenedione(14,14-difluoro-4-demethoxy-7-deoxydaunomycinone) (20). A 0.53 mol dm^{-3} solution of KOH (0.74 ml, 0.392 mmol) was added to a solution of **18** (102 mg, 0.177 mmol) in a mixture of THF (5.0 ml) and MeOH (5.0 ml) cooled in an ice bath. After stirring at 0 °C for 30 min, the mixture was neutralized with 1 mol dm^{-3} HCl (pH 7), diluted with brine, and extracted with AcOEt. The combined organic layers were washed with brine, and dried over anhydrous Na_2SO_4. Filtration and concentration in vacuo gave crude (*R*)-8-carboxydifluoroacetyl-6,8,11-trihydroxy-7,8,9,10-tetrahydro-5,12-naphthacenedione (**19**), which was dissolved in DMF (10 ml). The solution was heated at 60 °C for 35 min, poured into brine, extracted with AcOEt. The combined extracts were washed with brine, dried over anhydrous Na_2SO_4, filtered, then concentrated in vacuo. The residue was purified by preparative TLC (SiO_2, PhMe–AcOEt 1 : 1) and successive azeotropic removal of H_2O using PhMe[16] to afford pure **20** as a red powder (50.5 mg, 73%). Recrystalllzation from PhMe gave an analytical sample of **20** as red crystals, mp 225—228 °C, $[\alpha]_D^{20}$ −26.1° (*c* 0.153, dioxane). IR (KBr) 3500, 1750, 1620, 1590 cm^{-1}. ^{1}H NMR ($CDCl_3$) δ=2.00—2.30 (2H, m, C_9–H_2), 2.72 (1H, s, C_8–OH), 2.57—3.55 (4H, m, C_7–H_2, C_{10}–H_2), 6.40 (1H, t, *J*=4.3 Hz, CHF_2), 7.67—8.06, 8.20—8.57 (each 2H, m, ArH×4), 13.41 (2H, s, ArOH×2). ^{19}F NMR ($CDCl_3$) δ=−127.1 (d, *J*=54.3 Hz). EI-MS *m/z* 388 (M^+), 309,291. Anal. Calcd for $C_{20}H_{14}O_6F_2$: C, 61.86; H, 3.63%. Found: C, 61.67; H, 3.54%.

(8*S*,10*S*)-8-Difluoroacetyl-6,8,10,11-tetrahydroxy-7,8,9,10-tetrahydro-5,12-naphthacenedione (14,14-Difluoro-4-demethoxydaunomycinone) (21) and (1*R*,3*S*)-13—Difluoromethyl-3,5,12,13-tetrahydroxy-1,2,3,4-tetrahydro-1,3-(epoxymethano)-6,11-naphthacenedione (22). A 0.083 mol dm^{-3} solution of Br_2 in CCl_4 (0.57 ml) was added with stirring to a mixture of **20** (30.5 mg, 0.0785 mmol) in a two-layer mixture of CCl_4 (3.1 ml), $CHCl_3$ (6.1 ml), and H_2O (4.6 ml) at ambient temperature, then the reaction mixture was stirred under irradiation with a 60 W tungsten lamp at the same temperature for 2.5 h. Further amounts of 0.083 mol dm^{-3} solution of Br_2 in CCl_4 (0.19 ml×7, total 1.90 ml, 0.158 mmol) were added after 15, 20, 25, 30, 35, 40, and 45 min. After cooling in an ice bath, 2.5 mol dm^{-3} NaOH (0.19 ml, 0.475 mmol) was added, and stirring was continued at 0 °C for 15 min. The mixture was neutralized with 1 mol dm^{-3} HCl (pH 7), and extracted with AcOEt. The combined organic layers were washed successively with H_2O and brine, dried over anhydrous Na_2SO_4, filtered, then concentrated in vacuo. The residue was separated by preparative TLC (SiO_2, $CHCl_3$–MeOH 10 : 1), affording pure **21** (containing a small amount of the hydrate form by ^{1}H NMR)[16] as a red powder (8.3 mg, 26%) and pure **22** as a red powder (9.8 mg, 31%). Recrystallizations of these from PhMe gave analytical samples of **21** and **22** as red crystals, respectively.

21: Mp 210—213 °C, $[\alpha]_D^{20}$ +44.2° (*c* 0.113, dioxane). IR (KBr) 3450, 1750, 1620, 1590 cm^{-1}. ^{1}H NMR ($CDCl_3$) δ=2.18 (1H, dd, *J*=14.8, 4.8 Hz, $C_{9\text{-aq}}$–H), 2.60 (1H, d, *J*=14.8 Hz, $C_{9\text{-eq}}$–H), 3.03 (1H, d, *J*=18.8 Hz, $C_{7\text{-ax}}$–H), 3.34 (1H, brs, C_{10}–OH), 3.40 (1H, dd, *J*=18.8, 2.3 Hz, $C_{7\text{-eq}}$–H), 4.76 (1H, s, C_8–OH), 5.36—5.45 (1H, m, C_{10}–H), 6.60 (1H, t, *J*=53.1 Hz, CHF_2), 7.79—7.94, 8.30—8.43 (each 2H, m, ArH×4), 13.27, 13.58 (each 1H, s, ArOH×2). ^{19}F NMR ($CDCl_3$) δ=−129.5, −130.0 (each dd, *J*=315.0, 53.1 Hz). EI-MS *m/z* 404 (M^+), 386, 368, 317, 307, 289. High-resolution MS, Found: *m/z* 404.0706. Calcd for $C_{20}H_{14}O_7F_2$: M, 404.0706.

22: Mp 253—255 °C, $[\alpha]_D^{20}$ −153° (*c* 0.157, dioxane). IR (KBr) 3500, 1625, 1590 cm^{-1}. ^{1}H NMR ($CDCl_3$) δ=2.04 (1H, dd, *J*=11.2, 1.8 Hz, $C_{2\text{-ax}}$–H), 2.78 (1H, ddd, *J*=11.2, 5.7, 1.8 Hz, $C_{2\text{-eq}}$–H), 3.24 (1H, d, *J*=19.5 Hz, $C_{4\text{-ax}}$–H), 3.40 (1H, d, *J*=19.5 Hz, $C_{4\text{-eq}}$–H), 5.58 (1H, t, *J*=54.5 Hz, CHF_2), 5.74 (1H, dd, *J*=5.7, 1.0 Hz, C_1–H), 7.82—7.88, 8.32—8.39 (each 2H, m, ArH×4), 13.15, 13.23 (each 1H, s, ArOH×2). ^{19}F NMR ($CDCl_3$) δ=−1287, −136.3 (each dd, *J*=347.0, 54.5 Hz). EI-MS *m/z* 404 (M^+), 368, 308, 290. High-resolution MS, Found: *m/z* 404.0703. Calcd for $C_{20}H_{14}O_7F_2$: M, 404.0706.

Preparation off 20 from 22. A mixture of **22** (9.8 mg, 0.0243 mmol) and 10% Pd–$BaSO_4$ (11.2 mg) in MeOH (2.5 ml) was stirred under a H_2 atmosphere at room temperature for 2 h. The catalyst was filtered off and washed with MeOH. The combined filtrates were concentrated in vacuo. Purification of the residue by preparative TLC (SiO_2, PhMe–AcOEt, 1 : 1) afforded pure **20** as a red powder (3.0 mg, 32%). Spectral and chromatographic comparisons revealed that this was identical with an authentic sample synthesized as described above.

(8*S*,10*S*)-10-*O*-(2,3,6-Trideoxy-3-trifluoroacetoamido-α-L-*lyxo*-hexopyranosyl)-8-difluoroscetyl-6,8,11-trihydroxy-7,8,9,10-tetrahydro-5,12-naphthacenedione (3′-*N*-Trifluoroacetyl-14,14-difluoro-4-demethoxydaunorubicin) (23). A 1.0 mol dm^{-3} solution of trimethylsilyl trifluoromethanesulfonate in CH_2Cl_2 (0.17 ml, 0.170 mmol) was added under an Ar atmosphere to a mixture of 1,4-bis-*O*-(*p*-nitrobenzoyl)-3-*N*-trifluoroacetyl-L-daunosamine[19] (46.0 mg, 0.0850 mmol) and molecular sieves 4A (257 mg) in a mixture of ether (3.7 ml) and CH_2Cl_2 (4.6 ml) at −40 °C. The mixture was stirred at 0 °C for 40 min, then cooled to −20 °C. After a solution of **21** (9.2 mg, 0.0228 mmol) in THF (4.0 ml) was added to the reaction mixture, stirring was continued at −10 °C for 5.5 h. The mixture was poured into a two-layer mixture of AcOEt and saturated $NaHCO_3$, and extracted with AcOEt. The combined extracts were washed successively with H_2O and brine, dried over Na_2SO_4, filtered, and concentrated in vacuo. The residue was dissolved in MeOH (20 ml), and 0.1 mol dm^{-3} NaOH (0.2 ml) was added to the solution cooled in an ice bath. After stirring at the same temperature for 20 min, the mixture was neutralized with 2 mol dm^{-3} AcOH, diluted with H_2O, and extracted with AcOEt. The organic layers were combined, washed successively with H_2O and brine, dried over Na_2SO_4, filtered, then concentrated in vacuo. The crude residue was purified by column chromatography (SiO_2, $CHCl_3$→$CHCl_3$–acetone 10 : 1) followed by trituration with ether and azeotropic removal of H_2O using PhMe,[16] giving pure **23** as a red amorphous powder (12.8 mg, 89%), $[\alpha]_D^{20}$ +117° (*c* 0.163, dioxane). IR (KBr) 3450, 1750, 1720, 1625, 1590 cm^{-1}. ^{1}H NMR ($CDCl_3$) δ=1.31 (3H, d, *J*=6.6 Hz, $C_{5'}$–Me), 1.86 (1H, dt, *J*=13.2, 4.2 Hz, $C_{2'\text{-ax}}$–H), 1.93—1.98 (1H, m, $C_{4'}$–OH), 2.03 (1H, dd, *J*=13.2, 5.3 Hz, $C_{2'\text{-eq}}$–H), 2.12 (1H, dd, *J*=14.7, 4.0 Hz, $C_{9\text{-ax}}$–H), 2.63 (1H, d, *J*=14.7 Hz, $C_{9\text{-eq}}$–H), 3.16 (1H, d, *J*=19.1 Hz, $C_{7\text{-ax}}$–H), 3.40 (1H, dd, *J*=19.1, 1.9 Hz, $C_{7\text{-eq}}$–H), 3.65—3.72 (1H, m, $C_{4'}$–H), 4.16—4.26 (1H, m, $C_{3'}$–H), 4.25 (1H, q, *J*=6.6 Hz, $C_{5'}$–H), 4.67 (1H, s, C_8–OH), 5.28 (1H, dd, *J*=4.0, 1.9 Hz, C_{10}–H), 5.53 (1H, d, *J*=4.2 Hz, $C_{1'}$–H), 6.60 (1H, t, *J*=54.6 Hz, CHF_2), 6.67 (1H, brd, *J*=8.5 Hz, NH), 7.80—7.90, 8.32—8.41 (each 2H, m, ArH×4), 13.32, 13.59 (each 1H, s, ArOH×2). EI-MS *m/z* 629 (M^+), 404, 386, 368, 317, 307. High-resolution MS, Found: *m/z* 629.1334. Calcd for $C_{28}H_{24}NO_{10}F_5$: M, 629.1318.

(8*S*,10*S*)-10-*O*-(3-Amino-2,3,6-trideoxy-α-L-*lyxo*-hexopyranosyl)-8-difluoracetyl-6,8,11-trihydroxy-7,8,9,10-tetrahydro-5,12-naphthacenedione Hydrochloride and (8*S*,10*S*)-10-*O*-(3-Amino-2,3,6-trideoxy-α-L-*lyxo*-hexopyranosyl)-8-(2,2-difluoro-1,1-dihydroxyethyl)-6,8,11-trihydroxy-7,8,9,10-tetrahydro-5,12-naphthacenedione Hydrochloride [14,14-Difluoro-4-demethoxydaunorubicin Hydrochloride] (9). A 0.05 mol dm^{-3} solution of NaOH (4.3 ml) was added to a solution of **23** (22.5 mg, 0.0357 mmol) in THF (0.9 ml) at ambient temperature. After stirring was continued at the same temperature for 50 min, the mixture was neutralized (pH 9) with 1 mol dm^{-3} HCl, and extracted with $CHCl_3$. The combined extracts were washed with H_2O, dried over anhydrous Na_2SO_4, filtered, and concentrated in vacuo to ca. 0.5 ml in volume. When 0.25 mol dm^{-3} HCl in MeOH (0.7 ml) and ether (ca. 20 ml) was successively added to the concentrated solution, a red powder separated. This was collected by decantation and triturated with ether. The upper ethereal layer was removed, and the precipitation was dried over KOH in vacuo, giving pure **9** (a 3 : 1 mixture of ketonic and hydrate forms by ^{1}H NMR) as a red powder (8.1 mg, 40%), mp 168—171 °C, $[\alpha]_D^{20}$ +111° (*c* 0.090, MeOH). IR (KBr) 3450, 1620, 1590 cm^{-1}. ^{1}H NMR (DMSO-d_6+D_2O) δ=1.15 (3H, d, *J*=6.6 Hz, $C_{5'}$–Me), 1.62—2.24 (3H, m, $C_{2'}$–H_2, $C_{9\text{-ax}}$–H), 2.36 (0.75H, d, *J*=14.9 Hz, $C_{9\text{-eq}}$–H, ketone), 2.43 (0.25H, d, *J*=14.9 Hz, $C_{9\text{-eq}}$–H, hydrate), 2.86 (0.25H, d, *J*=18.8 Hz, $C_{7\text{-ax}}$–H, hydrate), 3.05 (0.75H, d, *J*=18.8 Hz, $C_{7\text{-ax}}$–H, ketone), 4.11—4.23 (1H, m, $C_{5'}$–H), 4.96—5.04 (1H, m, C_{10}–H), 5.29—5.35 (1H, m, $C_{1'}$–H), 6.04 (0.25H, t, *J*=55.8 Hz, CHF_2, hydrate), 6.85 (0.75H, t, *J*=52.9 Hz, CHF_2, ketone), 7.96—8.04, 8.26—8.35 (each 2H, m, ArH×4). ^{19}F NMR (DMSO-d_6 +D_2O) δ=−128.0 (d, *J*=52.9 Hz, ketone), −131.2, (d, *J*=55.8 Hz, hydrate). SI-MS *m*/*z* 552 (M^+ +H−HCl+H_2O), 534 (M^+ +H−HCl), 495, 405, 387, 369, 308.

We are grateful to Drs. Kunikazu Sakai and Kaoru Yamada, Sagami Chemical Research Center, Drs., Shigeru Tsukagoshi, Takashi Tsuruo, and Tazuko Tashiro, Cancer Chemotherapy Center, Japanese Foundation for Cancer Research, for evaluation of *in vitro* cytotoxicity and *in vivo* antitumor activity against P388 murine leukemia. Thanks are given to Professors Takeo Taguchi and Yoshiro Kobayashi, Tokyo College of Pharmacy, for providing us with a sample of methyl difluoroiodoacetate.

References

1) Part of this work has been the subject for a preliminary communication: F. Matsuda, T. Matsumoto, M. Ohsaki, and S. Terashima, *Tetrahedron Lett.*, **30**, 4259 (1989).

2) a) F. Arcamone, *Lloydia,* **40**, 45 (1977); b) *idem.*, "Topoics in Antibiotic Chemistry," ed by P. G. Sammes, Ellis Horwood, Chichester (1978), Vol. 2, p. 99; c) *idem.*, "Anticancer Agents Based on Natural Product Models," ed by J. M. Cassady and J. D. Douros, Academic Press, New York (1980), p. 1; d) *idem.*, "Doxorubicin Anticancer Antibiotics," Academic Press, New York (1981); e) R. C. Young, R. F. Ozols, and C. E. Myers, *New Eng. J. Med.,* **305**, 139 (1981); f) R. B. Weiss, G. Sarosy, K. Clagett-Carr, M. Russo, and B. Leyland-Jones, *Can. Chem. Pharm.,* **18**, 185 (1986).

3) M. B. Naff, J. Plowman, and V. L. Narayanan, "Anthracycline Antibiotics," ed by H. S. El Khadem, Academic Press, New York (1982), p. 1.

4) a) F. Arcamone, L. Bernardi, P. Giardino, B. Patelli, A. Di Marco, A. M. Cassaza, G. Pratesi, and P. Reggiani, *Cancer Treat. Rep.,* **60**, 829 (1976); b) F. Arcamone, L. Bernardi, B. Patelli, P. Giardino, A. Di Marco, A. M. Cassaza, C. Soranzo, and G. Pratesi, *Experientia,* **34**, 1255 (1978); c) F. Ganzina, M. A. Pacciarini, and N. Di Pietro, *Invest. New. Drugs,* **4**, 85 (1986).

5) a) A. Negishi, *Fine Chemicals,* **13**, 3, (1984); b) I. Kumadaki, *Yuki Gosei Kagaku Kyokai Shi,* **42**, 786 (1984); c) *idem., Yakugaku Zasshi,* **105**, 713 (1985); d) N. Ishikawa, *Kagaku To Seibuti,* **22**, 93 (1984); e) K. Ura, *Kagaku Kogyo,* **38**, 179 (1987); f) J. T. Welch, *Tetrahedron,* **43**, 3123 (1987).

6) a) S. Castillon, A. Dessingers, R. Faghih, G. Lukacs, A. Olesker, and T.-T. Thang, *J. Org. Chem.,* **50**, 4913 (1985); b) T. Tsuchiya, Y. Takagi, K.-D. Ok, S. Umezawa, T. Takeuchi, N. Wako, and H. Umezawa, *J. Antibiot.,* **39**, 731 (1986); c) H. H. Baer and L. Siemsen, *Can. J. Chem.,* **66**, 187 (1988); d) T. Tsuchiya, Y. Takagi, S. Umezawa, K. Komuro, C. Nosaka, H. Umezawa, S. Fukatsu, and T. Yoneta, *J. Antibiot.,* **41**, 988 (1988).

7) G. W. Morrow, J. S. Swenton, J. A. Filppi, and R. L. Wolgemuth, *J. Org. Chem.,* **52**, 713 (1987).

8) a) T. Matsumoto, M. Ohsaki, F. Matsuda, and S. Terashima, *Tetrahedron Lett.,* **28**, 4419 (1987); b) T. Matsumoto, M. Ohsaki, K. Yamada, F. Matsuda, and S. Terashima, *Chem. Pharm. Bull.,* **36**, 3793 (1988).

9) E. A. Hallinan and J. Fried, *Tetrahedron Lett.,* **25**, 2301 (1984).

10) R. W. Lang and B. Schaub, *Tetrahedron Lett.,* **29**, 2943 (1988), and references cited therein.

11) M. Suzuki, T. Matsumoto, M. Ohsaki, Y. Kimura, and S. Terashima, *Chem. Pharm. Bull.,* **35**, 3658 (1987).

12) O. Kitagawa, T. Taguchi, and Y. Kobayashi, *Tetrahedron Lett.,* **29**, 1803 (1988).

13) a) R. J. Linderman and D. M. Graves, *Tetrahedron Lett.,* **28**, 4259 (1987); b) *idem., J. Org. Chem.,* **54**, 661 (1989).

14) Synthesis of 14,14,14-trifluoro-4-demethoxy-7-deoxydaunomycinone (**i**) according to the same synthetic strategy was also examined. Thus, fluoride-induced trifluoromethylation of *dl*-**13** with trifluoromethyltrimethylsilane using tetrabutylammonium fluoride as a fluoride source[15] [CF_3SiMe_3, Bu_4NF, THF, rt, then 1 mol dm^{-3} HCl, 35%] afforded 14,14,14-trifluorodaunomycinol (*dl*-**ii**) (a 1 : 1 epimeric mixture by ^{1}H NMR) as a red powder, ^{1}H NMR ($CDCl_3$) δ=1.62—2.54 (4H, m, C_8–H_2, OH×2), 2.80—3.20 (4H, m, C_7–H_2, C_{10}–H_2), 3.75—4.25 (1H, m, $CHCF_3$), 7.62—8.01, 8.12—8.50 (each 2H, m, ArH×4), 13.44, 13.47 (each 1H, s, ArOH×2). ^{19}F NMR ($CDCl_3$) δ=−72.66, −72.73 (each d, *J*=7 Hz). EI-MS *m*/*z* 408 (M^+), 388, 309. However, attempted oxidation of *dl*-**ii** with various oxidizing reagents including the Dess–Martin periodinane resulted in simple recovery of the starting material.

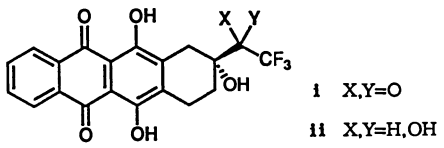

i X,Y=O

ii X,Y=H,OH

Fig. 2.

15) G. K. S. Prakash, R. Ktrishnamurti, and G. A. Olah, *J. Am. Chem. Soc.*, **111**, 393 (1989).

16) Measurements of the ^{1}H- and ^{19}F NMR spectra ($CDCl_3$) with the samples of **20**, **21**, and **23** purified by silica-gel chromatography made it clear that these compounds consisted of a mixture of the ketonic and the hydrate forms in which the former predominated (ca. 10:1). After azeotropic removal of water using toluene, signals corresponding to the hydrate form disappeared. Formation of the hydrate form may be rationalized by considering electron-withdrawing property of the two fluorine atoms. Representative NMR spectral data are as follows; **20**: ^{1}H NMR δ=6.01 (t, J=52.7 Hz, CHF_2, hydrate), 6.40 (t, J=54.3 Hz, CHF_2, ketone); ^{19}F NMR δ=127.1 (d, J=54.3 Hz, ketone). **21:** ^{1}H NMR δ=5.97 (t, J=55.2 Hz, CHF_2, hydrate), 6.60 (t, J=53.1 Hz, CHF_2, ketone); ^{19}F NMR δ=−129.5, −130.0 (each, dd, J=315.0, 53.1 Hz, ketone), −133.2 (d, J=55.2 Hz, hydrate). **23:** ^{1}H NMR δ=6.00 (t, J=55.3 Hz, CHF_2, hydrate), 6.60 (t, J=54.6 Hz, CHF_2, ketone).

17) a) H. Brockmann and J. Niemeyer, *Chem. Ber.*, **100**, 3578 (1967); b) A. S. Kende, Y.-G. Tsay, and J. E. Mills, *J. Am. Chem. Soc.*, **98**, 1967 (1976); c) T. H. Smith, A. N. Fujiwara, D. W. Henry, and W. W. Lee, *J. Am. Chem. Soc.*, **98**, 1969 (1976); d) J. S. Swenton, D. K. Anderson, D. K.Jackson, and L. Narasimhan, *J. Org. Chem.*, **46**, 4825 (1981).

18) F. Arcamone, G. Franceschi, P. Orezzi, G. Cassinelli, W. Barbieri, and R. Mondelli, *J. Am. Chem. Soc.*, **86**, 5334 (1964).

19) Y. Kimura, M. Suzuki, T. Matsumoto, R. Abe, and S. Terashima, *Bull. Chem. Soc. Jpn.*, **59**, 423 (1986).

20) Concentration ($\mu g\,ml^{-1}$) necessary to inhibit cell growth (initial cell density: 5×10^4 cells ml^{-1}) by 50% after incubation for 48 h at 37 °C.

21) Evaluated by the same method as employed at the Drug Evaluation Branch, National Cancer Institute (NCI), NIH, U.S.A. P388 murine leukemia cells (10^6) were inoculated into CDF_1 mice (6 mice/group) intraperitoneally. Drugs were administered intraperitoneally, starting 24 h after inoculation, at day 1 and 5.

22) Median survival time of test animals×100/median survival time of control animals.

Michael Addition of Acyclic Lithium 1,3-Dien-2-olates with α,β-Unsaturated Esters, Ketones, and Diesters

Shuji KANEMASA,* Masahiro KUMEGAWA,† Eiji WADA, and Masafumi NOMURA†
Institute of Advanced Material Study, Kyushu University, Kasugakoen, Kasuga 816
†Department of Molecular Science and Technology, Interdisciplinary Graduate School of Engineering Sciences, Kyushu University, Kasugakoen, Kasuga 816
(Received April 30, 1991)

The Michael addition of lithium 1,3-dien-2-olates with α,β-unsaturated carbonyl compounds is described. With α,β-unsaturated esters the reaction was reversible even at −78°C, while kinetically controlled with α,β-unsaturated ketones or alkylidenemalonates. At room temperature, the initially formed Michael adducts undergo subsequent intramolecular Michael addition to give substituted cyclohexanone derivatives in a highly stereoselective manner. Mostly *anti*-selectivity has been observed for the initial Michael addition, and the intramolecular cyclization was *cis*-selective.

1,3-Dien-1-olates, generated by the deprotonation of α,β-unsaturated carbonyl compounds, have enjoyed wide synthetic applications in alkylation,[1,2] acylation,[2c] aldol addition,[1d] Michael addition,[3,4] and other fields of organic synthesis.[5] Limited papers have been reported, however, about the reaction of 1,3-dien-2-olates; alkylation,[2,6a,b] aldol addition,[6c] and Michael addition[7] are among them. One exception is the cyclization reaction of cyclic 1,3-dien-2-olates with α,β-unsaturated esters or ketones. Since such reaction proceeds stereoselectively under mild reaction conditions to produce Diels–Alder type cyclization products, wide applications to natural product synthesis have been studied.[8]

The *endo*-selectivities observed in these six-membered ring-forming reactions[7a,8,9] were the same as those of the *endo*-selective Diels–Alder reactions of related dienes such as cyclic 2-silyloxy-1,3-dienes.[10] This is why anion-accelerated Diels–Alder reaction is taken into account as a possible mechanism for the sequential double Michael reaction.[7a,8] Although there is known an example in which the Michael reaction between cyclic 1,3-dien-2-olates and α,β-unsaturated lactones resulted in a different stereoselectivity,[7b,c] high *endo*-selectivity is usually observed in the Michael addition of cyclic 1,3-dien-2-olates.

We assumed that the high stereoselectivity observed in the cyclization reaction of cyclic 1,3-dien-2-olates could be due to the attractive secondary orbital interaction just like the *endo*-selective Diels–Alder reaction. If this is true, such interaction would be generally utilized in the stereocontrol of Michael addition employing acyclic 1,3-dien-2-olates and α,β-unsaturated carbonyl compounds. In contrast with the many reported examples of *endo*-selective Diels–Alder type cyclization of cyclic 1,3-dien-2-olates, it is very surprising that few example is known for the Michael reaction of acyclic 1,3-dien-2-olates.[11]

Results and Discussion

Preparation of Lithium 1,3-Dien-2-olates. Lithium (1*Z*,3*E*)-1,3-dien-2-olates **3a**—**e** were generated from enones **1a**—**e** via 2-silyloxy-1,3-dienes **2a**—**e** as follows: Horner–Emmons olefination of 2-oxoalkylphosphonates using lithium bromide/triethylamine in tetrahydrofuran (THF) gave (*E*)-enones **1b**—**d** as single isomers (Scheme 1, **1b**: 71%, **1c**: 91%, **1d**: 78%); other enones **1a**,**e** were commercially available. Attempted lithiation of enones **1a**,**b** with lithium diisopropylamide (LDA) at −78 °C in THF produced the formal dimer[12] of **1** along with a complex mixture of many products,[13] indicating that the indirect generation method should be applied. Accordingly, enones **1a**—**e** were first silylated with chlorotrimethylsilane and 1,8-diazabicyclo[5.4.0]-undec-7-ene (DBU)[14] to give **2a**—**e** (**2a**: 71%, **2b**: 87%, **2c**: 64%, **2d**: 92%, **2e**: 78%) after vacuum distillation, among which **2c**—**e** were obtained as single isomers. Treatment of these 2-silyloxy-1,3-dienes **2a**—**e** with butyllithium,[3a] at room temperature for 30 min in THF generated lithium 1,3-dien-2-olates **3a**—**e** in excellent yields.

To determine the structure of **2d** by comparison with its stereoisomer **2d′**, silylation of **1d** was performed according to the Danishefsky's method[15] using chrolotrimethylsilane, triethylamine, and zinc chloride in benzene to produce an 89 : 11 mixture (GLC) of **2d** and **2d′** (Scheme 2); the major isomer **2d** was assigned the *Z*,*E*-isomer on the basis of NOE spectrum in which the

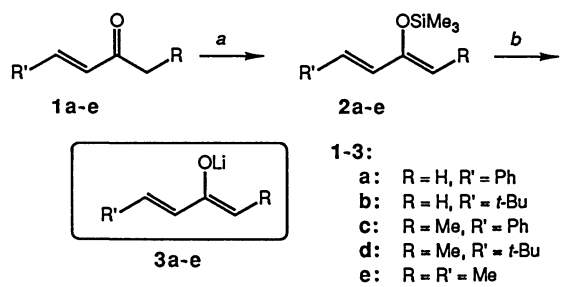

Scheme 1.

notable signal enhancement was observed between H-2 and H-4. Other 2-silyloxy-1,3-dienes **2c,e** were assigned also as the *Z,E*-structures by analogy.

Acetylation of **3d**, generated from **2d** and butyllithium by the method described above, with acetic anhydride gave acetate **4** in 85% yield as the sole *Z,E*-isomer, indicating the full retention of the *Z,E*-stereochemistry during the lithiation of **2d**. The use of THF containing hexamethylphosphoric triamide (HMPA, 10 vol%) as co-solvent in the above procedure provided essentially the equivalent result (**4**: 87%, single), confirming that the *Z*-isomer of **3d** is thermodynamically more stable.[16]

Direct lithiation of ethyl ketone **1d** with various lithium amides provided a mixture of isomeric lithium enolates, lithium *Z,E*-**3d** and *E,E*-enolate **3d'**. The *Z*/*E* ratios **3d**/**3d'** were determined after the mixtures of the lithium enolates **3d** and **3d'** were acetylated with acetic anhydride, while the yields of **4** were not always satisfactory (Scheme 3 and Table 1). The use of bulky lithium amides such as lithium hexamethyldisilylamide (LHMDS) and lithium 2,2,6,6-tetramethylpiperidide (LTMP), which are in general known to favor the formation of *E*-enolates, did not effect the selective generation of *E,E*-enolate **3d'**. The *Z,E*-isomer **3d** was still the major isomer (Table 1, Entries 6—9).[17]

Michael Reactions of Lithium 1,3-Dien-2-olates. Michael Addition to α,β-Unsaturated Esters. The reaction of lithium (2*Z*,4*E*)-6,6-dimethyl-2,4-heptadien-3-olate (**3d**) with methyl crotonate in THF was monitored on thin-layer chromatography (TLC). Within the reaction for 48 h at −78 °C, one clear new spot appeared and grew up along with the spot of **3d**, showing the occurrence of a clean reaction at a low temperature. Although this new spot was expected to correspond to the Michael adduct **6**, actually no trace of **6** was isolated after the usual hydrolytic quench of the reaction mixture. The starting enone **1d** was recovered quantitatively. Use of some other quenching agents such as saturated aqueous ammonium chloride, solid ammonium chloride, wet silica gel, methanol, *p*-toluenesulfonic acid, acetic acid, chlorotrimethylsilane, and iodomethane also resulted in the quantitative recovery of **1d**.

However, the cyclohexanone derivative **5a** was obtained in 49% yield as a single stereoisomer when the reaction temperature was raised to room temperature and continued for 26 h (Scheme 4 and Table 2, Entry 3). Assignment of the structure of **5a** will be discussed below. The stereoselective formation of **5a** seemed to

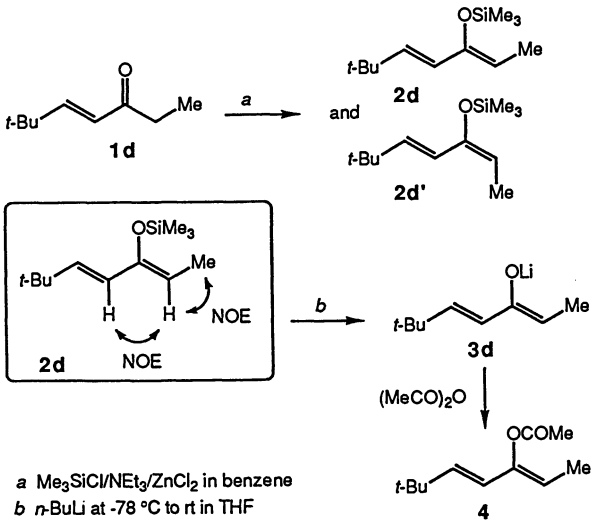

Scheme 2.

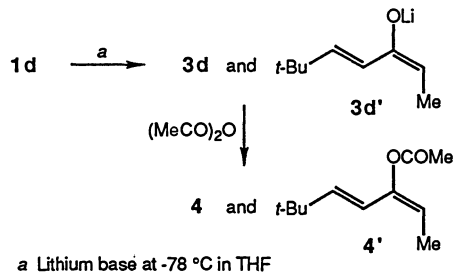

Scheme 3.

Table 1. Generation of 1,3-Dien-2-olates **3a—d**

Entry	Enone	Silyl enol ether (yield)	Lithium base	Lithium enolate	Isomer ratio (*Z*/*E*)[a]	Yield of **4**[b]
1	**1a**	**2a** (71%)	*n*-BuLi	**3a**	—	—
2	**1b**	**2b** (87%)	*n*-BuLi	**3b**	—	—
3	**1c**	**2c** (64%)	*n*-BuLi	**3c**	Single[c,d]	—
4	**1d**	**2d** (82%)	*n*-BuLi	**3d**	Single[d]	85
5	**1e**	**2e** (54%)	*n*-BuLi	**3e**	Single[c,d]	—
6	**1d**		LDA	**3d**	87:13	37
7	**1d**		LDA	**3d**	67:33[e]	51
8	**1d**		LHMDS	**3d**	88:12[e]	55
9	**1d**		LTMP	**3d**	67:33[e]	32

a) Determined by ^{1}H NMR spectrum after the *O*-acetylation with acetic anhydride. b) Isolated yield based on **2d** (Entry 4) or **1d** (Entries 6—9). c) The exclusive formation of (1*Z*,3*E*)-1,3-dien-2-olates was assumed on the basis of the observed full retention of *Z,E*-stereochemistry of the starting 2-silyloxy-1,3-diene **2d**. d) Pure (1*Z*,3*E*)-1,3-dien-2-olate. e) To the freshly prepared lithium bases in THF was added **1d** in a period of 25 min at −78 °C.

be deeply related with the appearance of a single spot on TLC during the aforementioned reaction at −78 °C. Employment of methyl (*E*)-4-bromo-2-butenoate, instead of methyl crotonate, in the reaction with **3d** at −78 °C in THF produced cyclopropane **7** as a single stereoisomer in 50% yield. It is clear that the formation of **7** took place through the intramolecular alkylation of the stereoselectively formed Michael adduct enolate **B**.

The following points are clear on the basis of these results: (1) the Michael addition of **3d** with methyl crotonate is a reversible process,[18] (2) As readily anticipated from the decreased length of conjugation, the Michael adduct enolate **A** is less stabilized than the starting enolate **3d** so that the equilibrium lies in favor for **3d**, (3) the adduct enolate **A** rapidly decomposes into each components on quenching, (4) the irreversible cyclization of the minor contributor **A** takes place around room temperature to produce the cyclized product **5a**, and (5) the reversible process and the irreversible cyclization are both stereoselective.

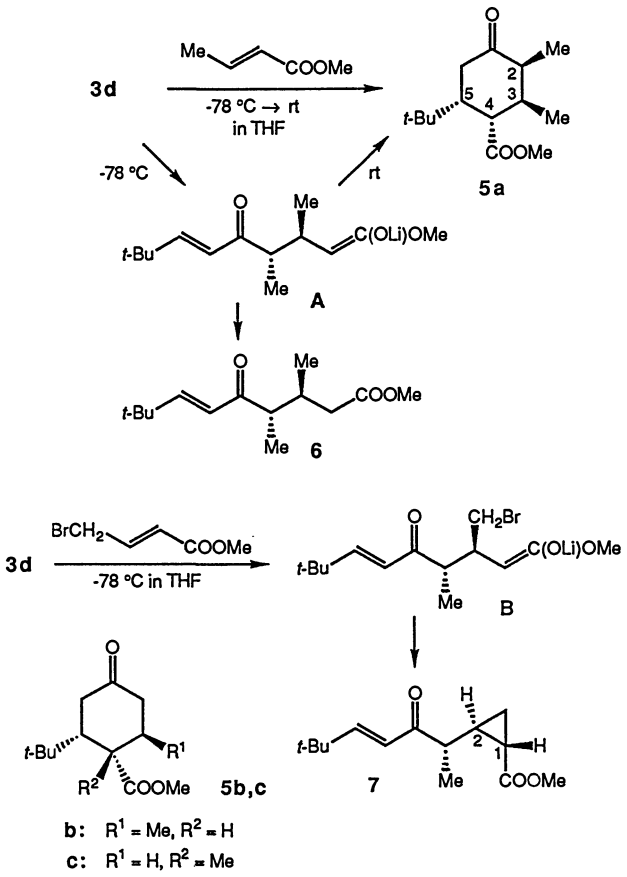

Scheme 4.

To stabilize the Michael adduct enolate **A**, the lithium enolate **3d** was first treated with zinc(II) chloride[19] at −20 to −30 °C and then allowed to react with methyl crotonate at room temperature[20] to give the Michael adduct **6** as a single diastereomer, albeit in a low yield (18%). Based on the reversible nature of the reported aldol reaction of zinc enolates with carbonyl compounds,[21] it is likely that the Michael reactions of lithium enolate **3d** and its zinc derivative are both reversible. The *anti*-configuration of **6** was tentatively assigned on the basis of the structure of **5a** which was derived from **A** presumably under thermodynamic control.

Similar reactions of lithium (1*Z*,3*E*)-5,5-dimethyl-1,3-hexadien-2-olate (**3d**) with methyl crotonate (4 h) and methacrylate (15 h) at room temperature produced cyclohexanone derivatives **5b** (87%) and **5c** (20%), respectively, both as single stereoisomers again (Scheme 4 and Table 2, Entries 1, 2).

The skeletons of **5a**—**c** correspond to the formal Diels–Alder cycloadducts of lithium 1,3-butadien-2-olates **3b,d** with methyl crotonate and methacrylate.[10] With an expectation to obtain the corresponding Diels–Alder cycloadduct, whose stereostructure may be readily assigned on the basis of the well-established stereochemical dignity of Diels–Alder reaction, enone **2d** was heated with methyl crotonate in benzene at 130 °C in a sealed tube for 6 d. However, the quantitative recovery of **2d** resulted, and the stereostructures of **5a**—**c** were assigned only on the spectroscopic basis.

The most bulky *t*-butyl substituent of **5a** must occupy the equatorial position in its stable chair conformation. That the axial H-5 showed only one big vicinal coupling with H-6$_{ax}$ (J_{5-6ax}=14.3 Hz) and the other two couplings were small (J_{5-6eq}=4.0 and J_{5-4}=3.8 Hz) indicates the 4,5-*cis* relationship. Notable NOEs were observed between H-6$_{ax}$/H-2 and H-2/H-3, showing the axial and equatorial positions of H-2 and H-3, respectively. Thus, **5a** was determined as *r*-2,*c*-3,*t*-4,*t*-5-configuration. Similar structural analysis was applied to **5b** (Scheme 4).

Table 2. Reiterative Michael Addition of Lithium 1,3-Dien-2-olates **3** with α,β-Unsaturated Esters

Entry	Enolate	α,β-Unsaturated ester	Solvent	Temp/°C[a]	Time/h[a]	Product	Yield/%[b]	Isomer ratio[c]
1	**3b**	Methyl crotonate	THF	−78→rt	2.3→1.5	**5b**	87	Single
2	**3b**	Methyl methacrylate	THF	−78→rt	2.5→22	**5c**	20	Single
3	**3d**	Methyl crotonate	THF	−78→rt	1.5→26	**5a**	49	Single
4	**3d**[d]	Methyl crotonate	THF	−78→rt	20→52	**6**	18	Single
5	**3d**	Methyl 4-bromocrotonate	THF	−78	17	**7**	50	Single

a) Each reaction time corresponds to each reaction temperature. b) Isolated yield based on **2**. c) Based on ^{1}H NMR spectrum. d) The lithium enolate **3d** was treated with zinc(II) chloride (1 equiv) at −20 to −30 °C for 20 min before methyl crotonate was added.

Structure assignment of **5c** was mainly based on the analogy of reaction mode to that of the above two cases.

As a result, the reaction of (1*Z*,3*E*)-1,3-dien-2-olate **3d** with methyl crotonate led to the stereoselective formation of *anti*-adduct enolate **A**, which was in an equilibrium with the starting components, **3d** and methyl crotonate. Stereoselectivity in the retro-Michael reaction process is not important because thermodynamically more stable *Z*-enolate **3d** and methyl crotonate are released from **A** in this retro process, and hence the retro Michael reaction process would not affect the stereoselectivity of the whole reaction. The 4,5-*cis*-selective intramolecular Michael addition pathway from the initially formed *anti*-Michael adduct enolates **A** leading to **5a—c** corresponds to that observed previously in the second cyclization step of the Michael addition of cyclic 1,3-dien-2-olates.[8] Probably the role of metal chelation is important.[9,22]

Although the *trans*-substitution of the cyclopropane ring of **7** was determined by its small vicinal coupling constant between H-1/H-2 (J_{1-2}=4.4 Hz), the configuration at the third chiral center could not be assigned only on the spectroscopic basis. Since *anti*-adduct enolate **A** was confirmed to be the intermediate involved in the reaction of **3d** with methyl crotonate, a similar *anti*-adduct enolate **B** was proposed as the intermediate involved in this reaction. Stereochemistry of **7** was tentatively assigned as shown in Scheme 4.

Michael Addition to 1-Phenyl-2-buten-1-one, (*E*)-3-Penten-2-one, or (*E*)-4-Phenyl-3-buten-2-one. To suppress the retro-Michael reaction pathway, α,β-unsaturated ketones were employed as Michael acceptors in the reactions with 1,3-dien-2-olate **3d**. Stabilization of a carbanionic center by the attaching α-acyl substituent is much higher than the stabilization by the α-ester moiety. As expected, a smooth Michael reaction took place between **3d** and 1-phenyl-2-buten-1-one (*Z*:*E*=10:90 by ^{1}H NMR) in THF; this reaction was completed in 1 h at −78 °C. An 87:13 mixture (^{1}H NMR) of Michael adducts **8** and **8′** was obtained in 73% of combined yield, after quenching with *p*-toluenesulfonic acid (Scheme 5, Table 3, Entry 1).

It was clear by the following observation that no retro-Michael reaction took place in the stage of

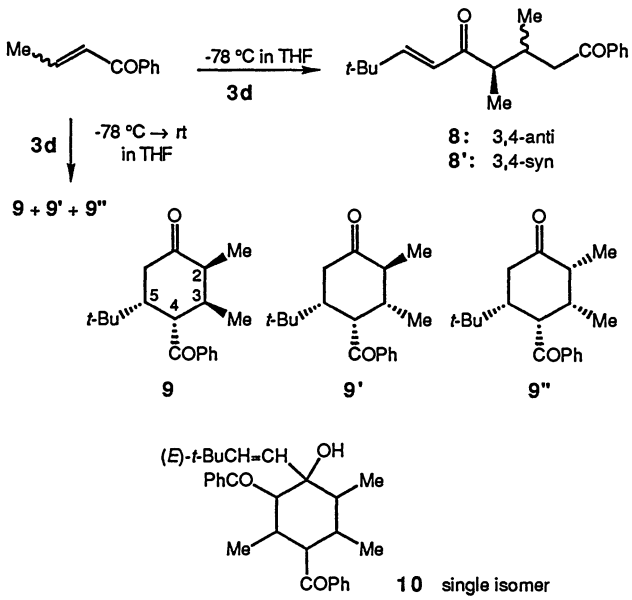

Scheme 5.

Table 3. Reaction of Enolate **3d** and/or **3d′** with 1-Phenyl-2-buten-1-one

Entry	1-Phenyl-2-buten-1-one *Z*/*E*	Dienolate[a] **3d**/**3d′**	Solvent/additive[b]	Temp °C	Time h	Product	Yield[c] %	Isomer ratio[d] *anti*/*syn*
1	10:90	**3d**	THF	−78	1	**8**+**8′**	73	87:13
2	9:91	**3d**	THF/HMPA	−78	0.5	**8**+**8′**	84	95:5
3	9:91	**3d**	THF/18-Crown-6	−78	2.5	**8**+**8′**	81	95:5
4	1:99	**3d**	THF	−78	0.5	**8**+**8′**	83	85:15
5	1:99	**3d**	THF/HMPA	−78	0.5	**8**+**8′**	87	95:5
6	99:1	**3d**	THF	−78	1	—		
7	99:1	**3d**	THF/HMPA	−78	1.5	—		
8	99:1	**3d**	THF	−78	18	**8**+**8′**	51	62:38
9	99:1	**3d**	THF/HMPA	−78	18	**8**+**8′**	50	59:41
10	1:99	**3d**+**3d′** (87:13)[e]	THF	−78	0.5	**8**+**8′**	87	78:22
11	1:99	**3d**+**3d′** (67:33)[f]	THF	−78	0.5	**8**+**8′**	72	67:33
12	1:99	**3d**+**3d′** (88:12)[g]	THF	−78	0.5	**8**+**8′**	75	89:11
13	1:99	**3d**+**3d′** (67:33)[h]	THF	−78	0.5	**8**+**8′**	57	58:42
14	1:99	**3d**+**3d′** (67:33)[e]	THF/HMPA	−78	0.5	**8**+**8′**	67	63:37
15	10:90	**3d**	THF	rt	42	**9**+**9′**+**9″**	71	62:16:22 (84:16)[i]
16	10:90	**3d**	THF/HMPA	rt	18	**9**+**9′**+**9″**	79	73:11:16 (89:11)[i]
17	99:1	**3d**	THF	rt	18	**9**+**9′**+**9″**	79	47:9:44 (91:9)[i]

a) Unless otherwise referred, enolates **3d** and **3d′** were generated from **2d** and LDA. b) HMPA (12 vol% to THF) or 18-cown-6 (1 equiv) was added as an additive. c) Isolated yield based on **2d** or **1d**. d) Determined by HPLC. e) Generated from **1d** and LDA. f) To the freshly prepared LDA in THF was added **1d** in a period of 25 min at −78 °C. g) Generated from **1d** and LHMDS. h) Generated from **1d** and LTMP. i) The calculated *anti*/*syn*-selectivity based on the ratios of **9**, **9′**, and **9″**.

Michael adduct formation at −78 °C as confirmed. Thus, when the Michael adduct enolate derived from **3d** and 1-phenyl-2-buten-1-one was treated with dimethyl ethylidenemalonate, no corresponding Michael adduct to the ethylidenemalonate acceptor was detected. The details of the reaction of **3d** with alkylidenemalonates will be described below. The Michael reaction of **3d** with 1-phenyl-2-buten-1-one (*Z*: *E*=1 : 99 to 9 : 91) in the presence of HMPA or 18-crown-6 showed satisfactorily high *anti*-selectivity (Table 3, Entries 2, 3, 5).

Next examined was the Michael reaction of (*E*)-1-phenyl-2-buten-1-one (99% pure) with the lithium 1,3-dien-2-olate with several **3d**/**3d′** ratios. As shown in Table 3 (Entries 10—13), the stereoselectivity **8**/**8′** was related with the enolate ratio **3d**/**3d′**, *anti*- **8** and *syn*-adduct **8′** being formed mainly from the *E*- and *Z*-enolate, respectively. Addition of HMPA increased the *anti*-selectivity, but only by 5% (Entry 14), making a striking contrast with the highly *anti*-selective Micahel addition of **3d** (Entries 2,5).

On the other hand, (*Z*)-1-phenyl-2-buten-1-one[23] was found to be much less reactive toward **3d**. No formation of the Michael adduct was detected on TLC after 1 h at −78 °C (Entry 6); addition of HMPA to activate the enolate **3d** was also totally ineffective (90 min at −78 °C, Entry 7). Finally, (*E*)-1-phenyl-2-buten-1-one was added to this reaction mixture and allowed to react for additional 1 h to give an 83 : 17 mixture of **8** and **8′** (65%) along with the single stereoisomer of the cyclized product **10** (28%), whose stereochemistry remained unsolved. Thus, the diastereomer ratio **8**/**8′** was independent of the *Z*/*E* ratio of the acceptor molecule, 1-phenyl-2-buten-1-one (Table 3, Entries 1—5). This is because (*E*)-1-phenyl-2-buten-1-one was the only reactive isomer. The lack of full conjugation between the carbon–carbon double bond and the carbonyl moiety may be the major reason for the decreased reactivity of (*Z*)-1-phenyl-2-buten-1-one.

When the reaction time was prolonged, (*Z*)-1-phenyl-2-buten-1-one reacted with **3d** at −78 °C to give a mixture of **8** and **8′** albeit in a poor isomer ratio (**8** : **8′**=62 : 38, Entry 8); essentially the equivalent result (**8** : **8′**=59 : 41, Entry 9) was obtained in a similar reaction in the presence of HMPA. The low *anti*-selectivity in the presence of HMPA and no dramatic change of the isomer ratio were again surprising. Although the products obtained were in cyclized forms, high stereoselectivity and satisfactory yield were observed when the same reaction was carried out at room temperature (Entry 17, 91 : 9). The poor *anti*/*syn*-selectivity observed in the reactions at −78 °C would be due to the slow Michael addition of (*Z*)-1-phenyl-2-buten-1-one. This *Z*-isomer presumably underwent partial isomerization to (*E*)-1-phenyl-2-buten-1-one in the course of Michael addition through the retro-Michael addition pathway.

At room temperature, three isomers of the cyclized products **9**, **9′**, and **9″** were obtained in the reaction of **3d** with (*Z*)-1-phenyl-2-buten-1-one (Entry 17). Since these products were assigned, mainly on the basis of NOE spectra, *r*-2,*c*-3,*t*-4,*t*-5- for **9**, *r*-2,*t*-3,*t*-4,*t*-5- for **9′**, and *r*-2,*c*-3,*c*-4,*c*-5-isomer for **9″**, the stereoselectivity of the intermolecular Michael addition was calculated to be *anti*/*syn*=91 : 9. The reactions with (*E*)-1-phenyl-2-buten-1-one at room temperature afforded the comparable results (Entries 15, 16). The equally high *anti*-selectivities observed in these reactions (Entry 17 and Entries 15, 16), regardless of the *Z*/*E* ratio of the acceptor molecules employed, would be due to the ready isomerization of (*Z*)-1-phenyl-2-buten-1-one to the (*E*)-1-phenyl-2-buten-1-one at room temperature.

Stereostructures of the cyclized products, **9** and **9′**, were determined on the basis of ^{1}H NMR spectra: Based on the small couplings for J_{5-4}(4.0 Hz) and J_{2-3}(6.2 Hz) as well as the notable NOEs between H-2/H-3, H-2/H-6$_{ax}$, and H-5/3-Me, the major stereoisomer **9** was confirmed to be the 2,3-*cis*-3,4-*trans*-4,5-*cis* structure. On the other hand, the small coupling for J_{5-4}(3.7 Hz) and big coupling for J_{2-3}(12.4 Hz) indicated the axial positions of H-2, H-3, and H-5 and the equatorial position of H-4, minor isomer **9′** being assigned the 2,3-*trans*-3,4-*cis*-4,5-*cis* structure.

The points to be noteworthy are: (1) at a low temperature (−78 °C) *anti*-**8** and *syn*-Michael adduct **8′** are mainly formed from (2*Z*,4*E*)-**3d** and (2*E*,4*E*)-1,3-dien-2-olate **3d′**, respectively, (2) the stereospecific cyclization of the resulting Michael adduct enolates leads to the cyclization products **9** and **9′** at room temperature, (3) the Michael addition at a low temperature is kinetically controlled, (4) (*Z*)-1-phenyl-2-buten-1-one is much less reactive than the (*E*)-1-phenyl-2-buten-1-one in the reaction with **3d**, (5) the presence of HMPA does not alter the transition state, (6) the fast retro process is involved in the reaction at room temperature, while this process is less important at −78 °C.

The reaction of lithium (1*Z*,3*E*)-1,3-dien-2-olate **3d** with (*E*)-3-penten-2-one at room temperature produced two cyclized products **11a** and **12** in 5 and 49% yields, respectively, while the same reaction at −78 °C resulted in the formation of complex products (Scheme 6). The structures of **11a** and **12** were determined on the basis of spectral data and also of the assumed reaction mode, and the 4,5-*cis*-configuration of **12** was confirmed by the small J_{4-5} value (3.7 Hz). The initial *anti*-Michael adduct enolate **C** went to the equilibration with the terminal enolate **D** whose irreversible aldol condensation produced **12**. Slow cyclization of enolate **C** into **11a**, even at room temperature, probably allowed the equilibration with **D**.

Similarly, reactions of **3b** and **3a** with (*E*)-3-penten-2-one and (*E*)-4-Phenyl-3-buten-2-one at room temperature gave stereoselectively cyclized products **11b** (31%) and **11c** (31%), respectively.

Michael Addition to Alkylidenemalonates. As discussed above, the reactions of lithium 1,3-dien-2-olates **3** with α,β-unsaturated esters were thermodynamically

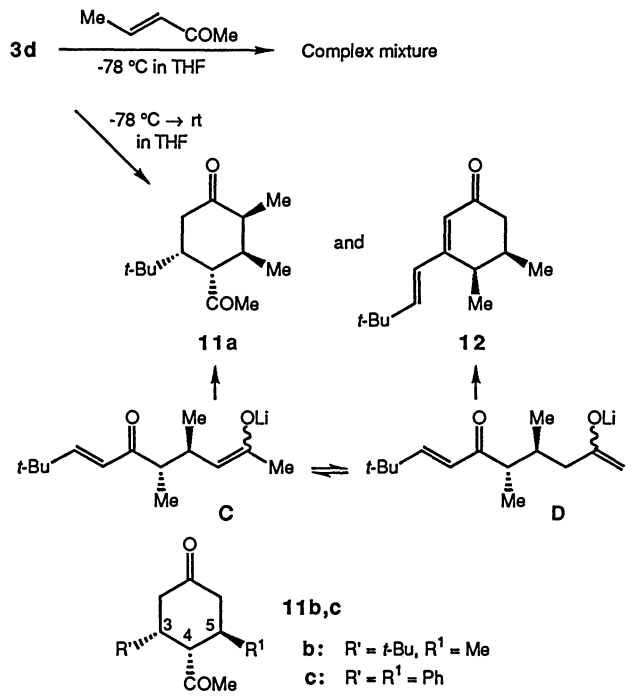

Scheme 6.

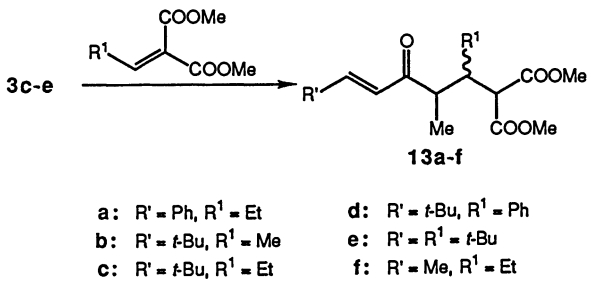

Scheme 7.

controlled even at −78 °C, no Michael adducts having been isolated on quenching. Although α,β-unsaturated ketones and **3** formed stable adducts at a low temperature (−78 °C), they underwent ready equilibration with the starting substrates at room temperature. On the other hand, alkylidenemalonates bear two electron-withdrawing ester groups at the same sp^2 carbon so that high stabilization of the adduct enolates is expected. Therefore their Michael addition should be kinetically controlled.

One of two ester moieties of alkylidenemalonates is cis to the β-substituent R^1 and the other trans, and therefore the study of Michael addition of **3** with alkylidenemalonates would provide some useful informations to solve the transition state. The question on the aforementioned rate difference of Michael additions to the *Z*- and *E*-enone acceptors, e.g. (*Z*)- and (*E*)-1-phenyl-2-buten-1-one and that on the kinetic stereoselectivity of the *Z*- and *E*-isomers of α,β-unsaturated carbonyl acceptors would be also answered.

The reactions of **3c—e** with alkylidenemalonates went to full completion within 30 min at −78 °C to give, after usual hydrolytic workup, the corresponding Michael adducts **13a—f** in excellent yields (Scheme 7 and Table 4). One exception was the reaction with dimethyl (2,2-dimethylpropylidene)malonate bearing a bulky *t*-butyl β-substituent. A higher reaction temperature and a longer reaction time were required (11 days at room temperature) and the Michael adduct **13e** was obtained only in 36% yield (Entry 9). When the β-substituent R^1 of the alkylidenemalonates was small, e.g. R^1=Me or Et, the diastereomer ratios were extremely poor (70 : 30 to 52 : 48) regardless of the nature of the terminal substituent R′ of the donor molecules **3** (Entries 1—6, 10). On the other hand, selectivities better than 90% were achieved when a bulky β-substituent R^1 such as Ph or *t*-Bu was attached at the β-position (Entries 7—9). Improvement of the stereoselectivity by adding HMPA was observed, but again only a little (Entries 2, 4, 6, 8).

It was found that the reactions with alkylidenemalonates were all kinetically controlled on the basis of the following cross reaction. Treatment of the Micahel adduct enolate between **3d** and dimethyl propylidenemalonate with dimethyl ethylidenemalonate produced no adduct to the latter acceptor.

Stereochemistry of the major isomer of **13d** was determined by its chemical conversion shown in Scheme 8

Table 4. Reaction of Enolates **3** with Dimethyl Alkylidenemalonates

Entry	Dienolate **3**	Alkylidenemalonate R^1	Solvent/additive[a]	Temp/°C	Time/h	Product	Yield/%[b]	Isomer ratio *anti*/*syn*[c]
1	**3c**	Et	THF	−78	0.5	**13a**	85	55 : 45
2	**3c**	Et	THF/HMPA	−78	0.5	**13a**	83	62 : 38
3	**3d**	Me	THF	−78	0.5	**13b**	83	52 : 48
4	**3d**	Me	THF/HMPA	−78	0.5	**13b**	87	60 : 40
5	**3d**	Et	THF	−78	0.5	**13c**	80	60 : 40
6	**3d**	Et	THF/HMPA	−78	0.5	**13c**	82	70 : 30
7	**3d**	Ph	THF	−78	0.5	**13d**	64	92 : 8
8	**3d**	Ph	THF/HMPA	−78	0.5	**13d**	89	95 : 5
9	**3d**	*t*-Bu	THF	rt	11d	**13e**	36	93 : 7
10	**3e**	Et	THF	−78	0.5	**13f**	60	64 : 36

a) HMPA (12 vol% to THF) was added as an additive. b) Isolated yield based on **2**. c) Determined by HPLC or ^{1}H NMR.

and also on the basis of spectral analysis of the derivatives. The 95:5 mixture of **13d** was purified through column chromatography to give pure sample of the major isomer of **13d**. Catalytic reduction of **13d** over palladium/carbon was followed by the carbonyl reduction with zinc borohydride in ether to give the expected lactone **15** (41%, 85:15) along with hemilactal **16** (37%, 76:24) as an overreduction product. Although these products **15** and **16** were derived from the diastereomeric alcohols produced from **14**, their different reactivity toward the zinc borohydride reduction is uncertain. It was clear that **15** consisted of two 3-epimers and **16** was a mixture of the 2- or 3-epimers, because they were converted into **17** and **18**, respectively, as single stereoisomers by the followed demethoxycarbonylation and oxidative demethoxycarbonylation. Thus, **15** and **16** were treated with aqueous sodium hydroxide in methanol at room temperature to give **17** (66%, single isomer) and **18** (94%, single isomer), respectively.

Structures of **17** and **18** were easily distinguished from each other on the basis of the observed NOE spectra (**17**: H-4/H-5, 4-Ph/5-Me, and 4-Ph/H-6; **18**: H-3_{ax}/Ph, H-3_{eq}/H-4, H-4/H-5, H-4/H-6, and H-5/H-6). Thus, the major isomer of **13d** was determined to be the *anti*-configuraion, and therefore the other major diastereoisomers **13a**—**f** obtained in the reactions of **3c**—**e** with alkylidenemalonates were assigned *anti*-stereochemistry by analogy.

Nature of Transition State. After the transition state model recently proposed by Heathcock and co-workers for the Michael addition of amide and thioamide enolates,[24] transition states **E**, **F**, **E′** and **F′** were drawn in Fig. 1. The reaction between **3d** and (*E*)-1-phenyl-2-buten-1-one was chosen as the representative example for the Michael addition of lithium 1,3-dien-2-olates to α,β-unsaturated carbonyl compounds.

From the viewpoint of stabilization of the chelating bond, the chelation between the lithium atom of **3d** and the carbonyl oxygen of the acceptor molecule should be most favorably built with the nonbonding orbital of the oxygen (models **E′** and **F′**). However, **E′** and **F′** were not the transition states actually involved in the reactions because there are serious steric repulsions between the *t*-butyl and the phenyl substituents (**F′**) or between the eclipsed three substituents (**E′**). The second favorable models were constructed with the pai orbital of the carbonyl moiety (models **E** and **F**).

The transition state **F** leading to the *syn*-adduct **8′** is nearly identical with **F′** where the only difference is the location of the lithium atom, and so **F** is also suffering from the serious steric repulsion. Without such steric repulsion between the *t*-butyl and phenyl substituents, **F** and **F′** should have been highly stabilized by chelate formation as well as the secondary orbital interaction that is often very important in the *endo*-transition state of Diels–Alder reaction. It was finally concluded that the anticipated transition state **F** or **F′** was not included in the Michael additions of lithium 1,3-dien-2-olates **3** to α,β-unsaturated carbonyl compounds. The participation of the sterically most favored transition state **E** led to the *anti*-adduct **8** as major diastereomers.

In the reaction of **3d** with alkylidenemalonates bearing a small β-substituent R^1, there are two possible

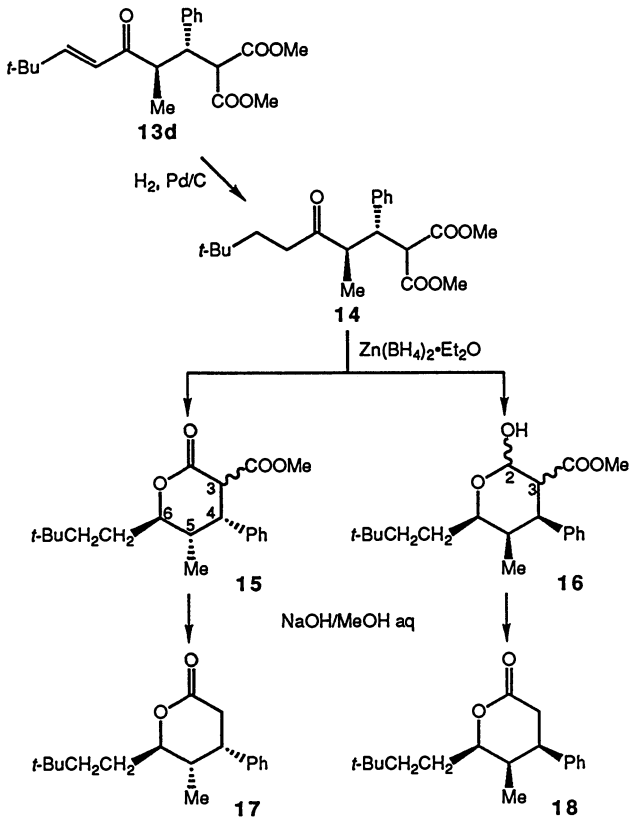

Scheme 8.

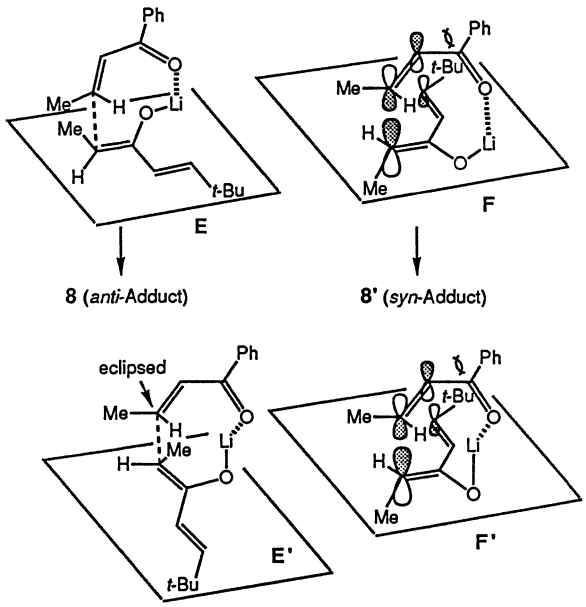

Fig. 1. Chelated treansition state for the Michael addition of lithium 1,3-dien-2-olate **3d** to (*E*)-1-phenyl-2-buten-1-one.

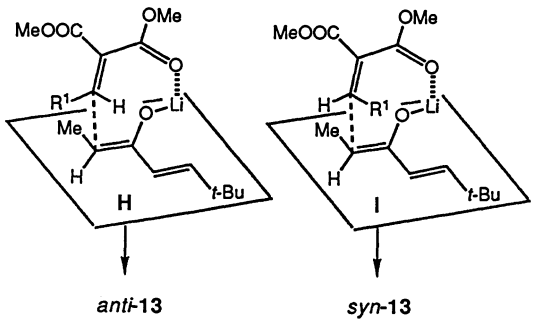

Fig. 2. Chelated transition state for the Michael addition of lithium 1,3-dien-2-olate **3d** to dimethyl alkylidenemalonates.

chelated transition states **H** and **I** with comparable stabilization energies (Fig. 2). When R^1 becomes bulky, the transition state model **I** becomes less favored sterically. Thus, it is now understood that poor stereoselectivities were observed in the reaction with the alkylidenemalonates bearing a small β-substituent R^1.

We assume that the role of chelate formation would be quite important in the Michael addition of lithium enolates to α,β-unsaturated carbonyl compounds. Little change of stereoselectivity by adding HMPA to the reaction system was observed throughout the present work. Although this seems to be inconsistent with the importance of chelation, an increased reactivity of the chelated acceptor molecule may be a key clue. The metal atom of the enolates would work as a Lewis acid catalyst to lower the LUMO (lowest unoccupied molecular orbital) level of the acceptor molecule when they come into chelation so that only the chelated acceptors are activated. The addition of a polar additive like HMPA to the reaction system does decrease the concentration of chelating molecules, but the chelating acceptors are preferentially allowed to undergo the Michael addition. There is no doubt that the reaction was chelation-controlled.

Experimental

General. Melting points were recorded on a Yanagimoto melting point apparatus and are uncorrected. IR spectra were taken with JASCO IRA-1 and A-702 spectrometers. ^{1}H and ^{13}C NMR spectra were measured with Hitachi R-40 (^{1}H NMR: 90 MHz) and JEOL GSX-270 (270 MHz for ^{1}H NMR and 67.94 MHz for ^{13}C NMR) instruments. Chemical shifts are recorded in parts per million downfield from internal tetramethylsilane. Mass spectra and high-resolution mass spectra (HRMS) were taken with a JEOL-01SG-2 spectrometer at an ionization energy of 70 eV. Elemental analyses were performed with a Hitachi 026 CHN analyzer. For preparative column chromatography, Wakogel C-200, C-300, and Merck silica gel 60 were employed. Flash chromatography was performed with an Eyera EF-10 apparatus with a 20×180 mm column packed with silica gel 60 (0.04—0.063 mm). Gas liquid chromatography (GLC) was accomplished with a Yanaco G-2800 gaschromatograph with an ionization flame detector using a 3×2000 mm glass column (SE-30) or a 0.25×50000 mm glass capillary column (Silicone GE, SE-30). Micro vacuum distillation was carried out on a Sibata GTO-250R Kugelrohr distilling apparatus.

Materials. Enones **1a** and **1e** are commercially available, and **1b**[25] and **1c,d**[26] were prepared according to the reported procedures. Zinc borohydride was prepared as follows: A solution of $ZnCl_2$ (2 g, 14.7 mmol) in dry diethyl ether (25 ml) was refluxed under nitrogen for 3 h. After cooling to room temperature, the solution was separated by decantation. This solution was added to a solution of $NaBH_4$ (1.31 g, 34.5 mmol) in ether (75 ml) and the solution was stirred under nitrogen for 18 h. The solution separated by decantation contains $Zn(BH_4)_2$ in the concentration of 0.36 M (1 M=1 mol dm^{-3}).

General Procedure for the Preparation of 2-Silyloxy-1,3-dienes 2a—e. Silylation of **1d** is described as a typical procedure. A mixture of **1d** (3.31 g, 23.6 mmol), Me_3SiCl (3.6 ml, 28.3 mmol), and DBU (4.59 ml, 30.7 mmol) in dry CH_2Cl_2 (10 ml) was refluxed for 2 h under nitrogen. After cooled to room temperature, the mixture was poured into hexane (450 ml). The colorless solid (DBU · HCl) precipitated was filtered off, the filtrate was quickly washed with ice water, and dried over magnesium sulfate. The solvent was evaporated in vacuo and the residue (5.93 g) was distilled under reduced pressure to give **2d** (4.63 g, 92%) as pale yellow liquid.

The other 2-silyloxy-1,3-dienes **2a**—**c** and **2e** were similarly prepared in the yields shown in Table 1.

(*E*)-1-Phenyl-3-(trimethylsilyloxy)-1,3-butadiene (2a): Prepared according to the reported method.[14]

(*E*)-5,5-Dimethyl-2-(trimethylsilyloxy)-1,3-hexadiene (2b): Pale yellow liquid; bp 108 °C/60 mmHg (1 mmHg=133.322 Pa) (bulb-to-bulb); IR (neat) 2950, 1600, 1460, 1310, 1260, 1030, and 900 cm^{-1}; ^{1}H NMR (C_6D_6) δ=0.19 (9H, s, $SiMe_3$), 0.99 (9H, s, *t*-Bu), 4.32, 4.35 (each 1H, each br s, H-1), 5.93 (1H, d, J_{3-4}=15.4 Hz, H-3), and 6.25 (1H, d, J_{4-3}=15.4 Hz, H-4); ^{13}C NMR (C_6D_6) δ=0.10 ($SiMe_3$), 29.59 (*t*-Bu), 32.79 (*t*-Bu), 94.55 (C-1), 123.50 (C-3), 142.30 (C-4), and 155.78 (C-2); MS *m/z* (rel intensity, %) 199 (M^++1, 10), 198 (M^+, 57), 183 (63), 155 (23), 141 (base peak), 93 (22), 75 (51), and 73 (80). HRMS Found: *m/z* 198.1440. Calcd for $C_{11}H_{22}OSi$: M, 198.1439.

(1*E*,3*Z*)-1-Phenyl-3-(trimethylsilyloxy)-1,3-pentadiene (2c): Pale yellow liquid; bp 140 °C/27 mmHg (bulb-to-bulb); IR (neat) 2950, 1620, 1400, 1370, 1320, 1240, 1190, 1020, 930, 820, 740, and 680 cm^{-1}; ^{1}H NMR (C_6D_6) δ=0.23 (9H, s, $SiMe_3$), 1.67 (3H, d, J_{5-4}=7.0 Hz, H-5), 4.89 (1H, q, J_{4-5}=7.0 Hz, H-4), 6.58 (1H, d, J_{2-1}=15.8 Hz, H-2), 6.84 (1H, d, J_{1-2}=15.8 Hz, H-1), and 7.01—7.30 (5H, m, Ph); ^{13}C NMR (C_6D_6) δ=0.73 ($SiMe_3$), 12.15 (C-5), 110.98 (C-4), 126.84, 127.12, 127.47, 127.92, 128.88, 137.65 (C-2, C-3, and Ph), and 150.45 (C-1); MS *m/z* (rel intensity, %) 233 (M^++1, 21), 232 (M^+, base peak), 231 (28), 217 (46), 203 (39), 75 (36), and 73 (68). Found: C, 72.47; H, 8.33%. Calcd for $C_{14}H_{20}OSi$: C, 72.34; H, 8.68%.

(2*Z*,4*E*)-6,6-Dimethyl-3-(trimethylsilyloxy)-2,4-heptadiene (2d): Pale yellow liquid; bp 150 °C/40 mmHg (bulb-to-bulb); IR (neat) 2950, 1620, 1450, 1330, 1240, 1200, 1030, 840, and 750 cm^{-1}; ^{1}H NMR (C_6D_6) δ=0.23 (9H, s, $SiMe_3$), 1.01 (9H, s, *t*-Bu), 1.65 (3H, d, J_{1-2}=7.0 Hz, H-1), 4.75 (1H, q, J_{2-1}=7.0 Hz, H-2), 5.89 (1H, d, J_{4-5}=15.8 Hz, H-4), and 5.98 (1H, d, J_{5-4}=15.8 Hz, H-5); NOE: H-2/H-4; ^{13}C NMR (C_6D_6) δ=0.85 ($SiMe_3$), 11.84 (C-1), 29.79 (*t*-Bu), 32.80 (*t*-Bu), 107.70 (C-2), 124.34 (C-4), 139.59 (C-5), and 150.26 (C-3); MS *m/z* (rel

intensity, %) 213 (M^++1, 20), 212 (M^+, base peak), 197 (53), 183 (39), 169 (21), 155 (51), 107 (32), 75 (34), and 73 (91). HRMS Found: m/z 212.1597. Calcd for $C_{12}H_{24}OSi$: M, 212.1595.

(2*Z*,4*E*)-3-(Trimethylsilyloxy)-2,4-hexadiene (2e); Pale yellow liquid; bp 100 °C/18 mmHg; IR (neat) 2950, 1620, 1430, 1360, 1330, 1250, 1200, 1030, 910, 830, and 740 cm^{-1}; ^1H NMR (C_6D_6) δ=0.19 (9H, s, $SiMe_3$), 1.61—1.64 (6H, m, H-1 and H-6), 4.69 (1H, q, J_{2-1}=7.0 Hz, H-2), and 5.84—5.88 (2H, m, H-4 and H-5); ^{13}C NMR (C_6D_6) δ=0.75 ($SiMe_3$), 11.76 (C-1), 17.62 (C-6), 107.14 (C-2), 123.08 (C-4), 130.81 (C-5), and 150.07 (C-3); MS m/z (rel intensity, %) 171 (M^++1, 11), 170 (M^+, 65), 155 (base peak), 141 (57), 75 (98), and 73 (93); HRMS Found: m/z 170.1132. Calcd for $C_9H_{18}OSi$: M, 170.1126.

Generation of 1,3-Dien-2-olates 3a—e and 3d′. A) From 2a—e and Butyllithium: As a typical procedure the generation of **3d** from **2d** is described: To a solution of **2d** (0.212 g, 1 mmol) in dry THF (2 ml) was added, at −78 °C under nitrogen, *n*-BuLi (1.6 M in hexane, 0.63 ml, 1 mmol). The mixture was stirred at −78 °C for 30 min and the stirring was continued for additional 30 min at room temperature to provide the THF solution of **3d**. We refer to the solution thus prepared as the standard solution of **3d**, and also the standard solutions of **3a**—**c** and **3e** were prepared by similar methods.

B) From 1d and LDA: To a solution of diisopropylamine (0.168 ml, 0.121 g, 1.2 mmol) in THF (3 ml) was added, at −78 °C under nitrogen, *n*-BuLi (1.6 M in hexane, 0.75 ml, 1.1 mmol). After stirring for 20 min, **1d** (0.14 g, 1 mmol) in THF (5 ml) was slowly added (in a period of 25 min by the aid of a Micro Feeder) and the stirring was continued at −78 °C for additional 15 min to give a solution of **3d** and **3d′** (67 : 33).

C) From 1d and LHMDS: To a solution of 1,1,1,3,3,3-hexamethyldisilazane (0.232 ml, 0.177 g, 1.1 mmol) in THF (3 ml) was added, at −78 °C under nitrogen, *n*-BuLi (0.66 ml, 1.05 mmol). After stirring for 20 min, **1d** (0.14 g, 1 mmol) in THF (5 ml) was slowly added (in a period of 25 min by the aid of a Micro Feeder) and the stirring was continued at −78 °C for additional 15 min to give a solution of **3d** and **3d′** (88 : 12).

D) From 1d and LTMP: To a solution of 2,2,6,6-tetramethylpiperidine (0.186 ml, 0.155 g, 1.1 mmol) in THF (3 ml) was added, at −78 °C under nitrogen, *n*-BuLi (0.66 ml, 1.05 mmol). After stirring for 20 min, **1d** (0.14 g, 1 mmol) in THF (5 ml) was slowly added (in a period of 25 min by the aid of a Micro Feeder) and the stirring was continued at −78 °C for additional 15 min to give a solution of **3d** and **3d′** (67 : 33).

Generation of 3d Followed by Acetylation Leading (2*Z*,4*E*)-3-Acetoxy-6,6-dimethyl-2,4-heptadiene (4). To a solution of **2d** (0.106 g, 0.5 mmol) in THF (I ml) was added, at −78 °C under nitrogen, *n*-BuLi (1.6 M in hexane, 0.32 ml, 0.5 mmol). After 30 min at −78 °C, the stirring was continued for additional 30 min at room temperature, and then cooled to −78 °C. Acetic anhydride (0.057 ml, 0.6 mmol) was added and the mixture was stirred for 40 min. The resulting mixture was poured into saturated aqueous NH_4Cl and extracted with CH_2Cl_2 (15 ml×3). The combined extracts were dried ($MgSO_4$) and evaporated in vacuo. The residue (0.091 g) was chromatographed on silica gel using hexane–EtOAc (15 : 1) to give **4** (0.077 g, 85%). Pale yellow liquid; IR (neat) 2950, 1750, 1430, 1360, 1190, 1010, 950, 900, and 770 cm^{-1}; ^1H NMR (C_6D_6) δ=0.97 (9H, s, *t*-Bu), 1.49 (3H, d, J_{1-2}=7.0 Hz, H-1), 1.80 (3H, s, OCOMe), 5.07 (1H, q, J_{2-1}=7.0 Hz, H-2), 5.79, and 5.89 (each 1H, each d, J_{4-5}=15.8 Hz, H-4 and H-5); ^{13}C NMR (C_6D_6) δ=11.40 (C-1), 19.91 (OCOMe), 29.60 (C-7), 32.86 (*t*-Bu), 114.57 (C-2), 121.13 (C-4), 139.55 (C-5), 147.53 (C-3), and 166.89 (OCOMe); MS m/z (rel intensity, %) 183 (M^++1, 4), 182 (M^+, 31), 140 (89), 125 (31), 111 (base peak), and 43 (33). HRMS Found: m/z 182.1308. Calcd for $C_{11}H_{18}O_2$: M, 182.1306.

General Procedure for the Reactions of Lithium 1,3-Dien-2-olates 3 with α,β-Unsaturated Esters Leading to 5a—c. The reaction of **3d** with methyl crotonate is described as a typical example: To the standard solution of **3d** generated from **2d** (0.425 g, 2 mmol) was added, at −78 °C under nitrogen, methyl crotonate (0.2 g, 2 mmol) in THF (1 ml). After stirring at −78 °C for 1.5 h and then at room temperature for 26 h, the mixture was poured into saturated aqueous NH_4Cl and then extracted with CH_2Cl_2 (20 ml×3). The combined extracts were dried ($MgSO_4$) and evaporated in vacuo. The residue (0.546 g) was chromatographed on silica gel with hexane–EtOAc (30 : 1, v/v) to give **5a** (0.235 g, 49%).

***c*-5-*t*-Butyl-*t*-4-(methoxycarbonyl)-*r*-2,*c*-3-dimethylcyclohexanone (5a):** Pale yellow liquid; IR (neat) 2950, 1730, 1705, 1440, 1360, 1300, 1160, and 1110 cm^{-1}; ^1H NMR ($CDCl_3$) δ=0.89 (3H, d, J_{Me-3}=7.3 Hz, 3-Me), 0.90 (9H, s, *t*-Bu), 0.96 (3H, d, J_{Me-2}=7.0 Hz, 2-Me), 1.89 (1H, ddd, J_{5-4}=3.8, J_{5-6eq}=4.0, and J_{5-6ax}=14.3 Hz, H-5), 2.26—2.39 (2H, m, H-3 and H-6_{eq}), 2.81 (1H, dd, J_{4-3}=3.3 and J_{4-5}=3.8 Hz, H-4), 2.99 (1H, dd, J_{gem}=13.2 and J_{6ax-5}=14.3 Hz, H-6_{ax}), 3.33 (1H, dq, J_{2-Me}=J_{2-3}=7.0 Hz, H-2), and 3.72 (3H, s, COOMe); ^{13}C NMR ($CDCl_3$) δ=11.63 (3-Me), 15.55 (2-Me), 27.96 (*t*-Bu), 33.00 (C-3), 39.65, 39.81 (C-5 and *t*-Bu), 43.45 (C-6), 45.76, 46.68 (C-2 and C-4), 51.56 (COOMe), 175.42 (COOMe), and 213.63 (C-1); MS m/z (rel intensity, %) 241 (M^++1, 8), 240 (M^+, 31), 184 (21), 183 (base peak), 127 (44), and 126 (15). Found: C, 69.94; H, 10.00%. Calcd for $C_{14}H_{24}O_3$: C, 69.96; H, 10.07%.

***r*-3-*t*-Butyl-*c*-4-(methoxycarbonyl)-*t*-5-methylcyclohexanone (5b):** Similar procedure using **2b** (0.397 g, 2 mmol), *n*-BuLi (2 mmol), and methyl crotonate (0.2 g, 2 mmol) under stirring at −78 °C for 2.3 h and then at room temperature for 1.5 h followed by silica-gel column chromatography with hexane–EtOAc (6 : 1, v/v) gave **5b** (0.392 g, 87%): Pale yellow liquid; IR (neat) 2950, 2900, 1700, and 1400 cm^{-1}; ^1H NMR ($CDCl_3$) δ=0.91 (9H, s, *t*-Bu), 1.06 (3H, d, J_{Me-5}=7.3 Hz, 5-Me), 1.93 (1H, dt, J_{3-2eq}=J_{3-4}=3.8 and J_{3-2ax}=13.9 Hz, H-3), 2.03 (1H, br dd, J_{6eq-5}=2.2 and J_{gem}=14.3 Hz, H-6_{eq}), 2.27 (1H, br dd, J_{2eq-3}=3.8 and J_{gem}=13.9 Hz, H-2_{eq}), 2.43 (1H, dtq, J_{5-6eq}=J_{5-4}=2.2 Hz, J_{5-6ax}=6.6, and J_{5-Me}=7.3 Hz, H-5), 2.77 (1H, br dd, J_{4-5}=2.2 and J_{4-3}=3.8 Hz, H-4), 2.93 (1H, t, J_{gem}=J_{2ax-3}=13.9 Hz, H-2_{ax}), 3.04 (1H, dd, J_{6ax-5}=6.6 and J_{gem}=14.3 Hz, H-6_{ax}), and 3.70 (3H, s, COOMe); ^{13}C NMR ($CDCl_3$) δ=20.65 (5-Me), 27.83 (*t*-Bu), 32.92 (C-5), 33.30 (C-3), 39.39 (*t*-Bu), 43.84, 44.71, 44.88 (C-2, C-4, and C-6), 51.40 (COOMe), 175.19 (COOMe), and 211.27 (C-1); MS m/z (rel intensity, %) 227 (M^++1, 8), 226 (M^+, 15), 170 (23), 169 (base peak), 127 (10), and 110 (23). HRMS Found: m/z 226. 1575. Calcd for $C_{13}H_{22}O_3$: M, 226.1568.

***r*-3-*t*-Butyl-*c*-4-(methoxycarbonyl)-*t*-4-methylcyclohexanone (5c):** Similar procedure using **2b** (0.397 g, 2 mmol), *n*-BuLi (2 mmol), and methyl methacrylate (0.2 g, 2 mmol) under stirring at −78 °C for 2.5 h and then at room temperature for 22 h followed by silica-gel column chromatography with hexane–EtOAc (7 : 1, v/v) gave **5c** (0.045 g, 20%): Pale yellow liquid; IR (neat) 2950, 1720, 1450, 1200, and 1110 cm^{-1}; ^1H NMR ($CDCl_3$) δ=0.95 (9H, s, *t*-Bu), 1.45 (3H, s, 4-Me),

1.74—1.86 (2H, m, H-3_{eq} and H-5), 2.16—2.88 (5H, m, H-2, H-6, and H-3_{ax}), and 3.72 (3H, s, COOMe); ^{13}C NMR ($CDCl_3$) δ=27.33 (4-Me), 29.62 (*t*-Bu), 35.10 (C-5), 35.85 (C-3), 36.92 (*t*-Bu), 40.72 (C-2), 44.28 (C-6), 51.62 (COOMe), 53.46 (C-4), 176.83 (COOMe), and 212.72 (C-1); MS *m/z* (rel intensity, %) 227 (M^++1, 5), 226 (M^+, 1), 171 (17), 170 (57), 169 (47), 138 (15), 111 (40), and 110 (base peak). Found: C, 69.14; H, 9.65%. Calcd for $C_{13}H_{22}O_3$: C, 68.99; H, 9.80%.

Reaction of 3d with Methyl Crotonate in the Presence of $ZnCl_2$ Leading to Methyl (3*RS*,4*RS*,6*E*)-3,4,8,8-Tetramethyl-5-oxo-6-nonenoate (6). To a solution of **2d** (0.425 g, 2 mmol) in THF (1 ml) was added, at −78 °C under nitrogen, *n*-BuLi (1.6 M in hexane, 1.25 ml, 2 mmol). After stirring at −78 °C for 20 min and at room temperature for additional 30 min, the mixture was cooled down to −20 to −30 °C and a solution of $ZnCl_2$ (0.273 g, 2 mmol) in THF (1.5 ml) was added. After 20 min, the mixture was cooled down to −78 °C and methyl crotonate (0.2 g, 2 mmol) in THF (1 ml) was added. Stirring was continued at −78 °C for 20 h and at room temperature for 52 h. The mixture was poured into saturated aqueous NH_4Cl and extracted with CH_2Cl_2 (15 ml×3). The combined extracts were dried ($MgSO_4$) and evaporated in vacuo. The residue (0.366 g) was chromatographed on silica gel using hexane–EtOAc (15 : 1) to give **6** (0.087 g, 18%): Pale yellow liquid; IR (neat) 2950, 1740, 1630, and 1460 cm^{-1}; ^{1}H NMR ($CDCl_3$) δ=0.97 (3H, d, J_{Me-3}=6.2 Hz, 3-Me), 1.07 (3H, d, J_{Me-4}=7.0 Hz, 4-Me), 1.09 (9H, s, *t*-Bu), 2.12 (1H, dd, J_{2-3}=8.8 and J_{gem}=14.7 Hz, one of H-2), 2.29—2.46 (2H, m, H-3 and the other of H-2), 2.74 (1H, quint, J_{4-3}=J_{4-Me}=7.0 Hz, H-4), 3.67 (3H, s, COOMe), 6.08 (1H, d, J_{6-7}=16.1 Hz, H-6), and 6.87 (1H, d, J_{7-6}=16.1 Hz, H-7); ^{13}C NMR ($CDCl_3$) δ=13.36 (3-Me), 18.33 (4-Me), 28.74 (*t*-Bu), 29.62 (C-3), 32.41 (C-2), 33.79 (*t*-Bu), 37.75 (C-4), 51.46 (COOMe), 124.32 (C-6), 157.42 (C-7), 173.36 (COOMe), and 203.52 (C-5); MS *m/z* (rel intensity, %) 241 (M^++1, 3), 240 (M^+, 5), 140 (17), and 111 (base peak). HRMS Found *m/z* 240.1723. Calcd for $C_{14}H_{24}O_3$: M, 240.1724.

Reaction of 3d with Methyl (*E*)-4-Bromo-2-butenoate Leading to Methyl (1*RS*,2*SR*)-2-[(1*RS*,3*E*)-1,5,5-Trimethyl-2-oxo-3-hexenyl]-1-cyclopropanecarboxylate (7). To a solution of **2d** (0.212 g, 1 mmol) in THF (1 ml) was added, at −78 °C under nitrogen, *n*-BuLi (1.6 M in hexane, 0.63 ml, 1 mmol). After 20 min at −78 °C, stirring was continued for additional 20 min at room temperature, and then cooled to −78 °C. To this mixture was added a solution of methyl (*E*)-4-bromo-2-butenoate (0.179 g, 1 mmol) in THF (1 ml). The mixture was stirred at −78 °C for 17 h, poured into saturated aqueous NH_4Cl, and then extracted with CH_2Cl_2 (15 ml×3). The combined extracts were dried over $MgSO_4$ and evaporated in vacuo. The residue (0.205 g) was chromatographed on silica gel with hexane–EtOAc (15 : 1) to give **7** (0.118 g, 50%): Pale yellow liquid; IR (neat) 2950, 1730, 1700, 1660, 1620, 1450, 1210, 1170, 990, and 920 cm^{-1}; ^{1}H NMR ($CDCl_3$) δ=0.86 (1H, ddd, J_{3-1}=4.4, J_{3-2}=6.2, and J_{gem}=8.4 Hz, one of H-3), 1.10 (9H, s, *t*-Bu), 1.13—1.28 (1H, m, the other of H-3), 1.20 (3H, d $J_{Me-1'}$=7.0 Hz, Me), 1.49 (1H, dt, J_{1-2}=J_{1-3}=4.4, and J_{1-3}=8.4 Hz, H-1), 1.60 (1H, dddd, J_{2-1}=4.4, J_{2-3}=6.2, $J_{2-1'}$=9.2, and J_{2-3}=10.6 Hz, H-2), 2.20 (1H, dq, $J_{1'-Me}$=7.0 and $J_{1'-2}$=9.2 Hz, H-1′), 3.70 (3H, s, COOMe), 6.12 (1H, d, $J_{3'-4'}$=15.8 Hz, H-3′), and 6.88 (1H, d, $J_{4'-3'}$=15.8 Hz, H-4′); ^{13}C NMR ($CDCl_3$) δ=14.85 (Me), 16.27 (C-3), 18.98 (C-2), 25.20 (C-1), 28.70 (*t*-Bu), 33.87 (*t*-Bu), 47.62 (C-1′), 51.78 (COOMe), 123.18 (C-3′), 157.89 (C-4′), 174.23 (COOMe), and 201.91 (C-2′); MS *m/z* (rel intensity, %) 239 (M^++1, 2), 238 (M^+, 12), and 111 (base peak). HRMS Found: *m/z* 238.1571. Calcd for $C_{14}H_{22}O_3$: M, 238.1568.

Reaction of 3d with 1-Phenyl-2-buten-1-one Leading to 8 and 8′. A) To the standard solution of **3d** prepared from **2d** (0.106 g, 0.5 mmol) was added under nitrogen at −78 °C a solution of 1-phenyl-2-buten-1-one (0.073 g, 0.5 mmol, *Z*: *E*=10 : 90). After stirring at −78 °C for 1 h, the mixture was poured into saturated aqueous NH_4Cl and extracted with CH_2Cl_2 (10 ml×3). The combined extracts were dried ($MgSO_4$) and evaporated in vacuo. The residue (0.16 g) was chromatographed on silica gel with hexane–EtOAc (10 : 1, v/v) to give an inseparable mixture of **8** and **8′** (0.104 g, 73%, **8** : **8′**=87 : 13 by ^{1}H NMR).

B) To a solution of **2d** (0.212 g, 1 mmol) in dry THF/HMPA (4 ml/0.5 ml) was added under nitrogen at −78 °C *n*-BuLi (1.6 M in hexane, 0.63 ml, 1 mmol). After 20 min, a solution of 1-phenyl-2-buten-1-one (0.146 g, 1 mmol, *Z*: *E*=9 : 91) was added, and the reaction was continued for 30 min. Similar workup and chromatographic purification gave **8** and **8′** (0.239 g, 84%, **8** : **8′**=95 : 5 by ^{1}H NMR).

C) To the standard solution of **3d** prepared from **2d** (0.212 g, 1 mmol) was added under nitrogen 18-Crown-6 (0.264 g, 1 mmol) in dry THF (2 ml). After 15 min, a solution of 1-phenyl-2-buten-1-one (0.146 g, 1 mmol, *Z*: *E*=9 : 91) was added, and the reaction was continued for 2.5 h. Similar workup and chromatographic purification gave **8** and **8′** (0.233 g, 81%, **8** : **8′**=95 : 5 by ^{1}H NMR).

3,4,8,8-Tetramethyl-1-phenyl-6-nonene-1,5-dione (8+8′): Isomer 8: Pale yellow liquid; IR (neat) 2950, 1660, 1610, 1450, 1360, 1260, 1200, and 980 cm^{-1}; ^{1}H NMR ($CDCl_3$) δ=1.01 (3H, d, J_{Me-3}=6.6 Hz, 3-Me), 1.07 (9H, s, *t*-Bu), 1.13 (3H, d, J_{Me-4}=7.0 Hz, 4-Me), 2.51—2.66 (1H, m, H-3), 2.71 (1H, dd, J_{2-3}=9.3 and J_{gem}=15.8 Hz, one of H-2), 2.86 (1H, dq, J_{4-3}=5.1 and J_{4-Me}=7.0 Hz, H-4), 3.08 (1H, dd, J_{2-3}=3.3 and J_{gem}=15.8 Hz, the other of H-2), 6.11 (1H, d, J_{6-7}=16.1 Hz, H-6), 6.89 (1H, d, J_{7-6}=16.1 Hz, H-7), 7.41—7.58, and 7.91—8.00 (3H and 2H, m, Ph); ^{13}C NMR ($CDCl_3$) δ=12.60 (3-Me), 18.40 (4-Me), 28.71 (*t*-Bu), 31.46 (C-3), 33.78 (*t*-Bu), 41.55 (C-4), 48.67 (C-2), 124.23 (C-6), 128.10, 128.56, 132.98, 137.14 (each Ph), 157.40 (C-7), 199.76 (C-5), and 203.69 (C-1); MS *m/z* (rel intensity, %) 287 (M^++1, 8), 286 (M^+, 36), 230 (12), 167 (40), 140 (34), 111 (base peak), and 105 (25). Found: C, 79.46; H, 9.08%. Calcd for $C_{19}H_{26}O_2$: C, 79.67; H, 9.16%.

Isomer 8′: Its formation was deduced on the basis of ^{1}H and ^{13}C NMR spectra of the crude reaction mixture because **8′** could not be separated from the mixture with **8**: Partial ^{1}H NMR ($CDCl_3$) δ=0.92 (3H, d, J_{Me-3}=6.6 Hz, 3-Me), 1.07 (3H, d, J_{Me-4}=7.0 Hz, 4-Me), 1.09 (9H, s, *t*-Bu), 6.13 (1H, d, J_{trans}=15.8 Hz, H-6), 6.94 (1H, d, J_{trans}=15.8 Hz, H-7), 7.41—7.60, and 7.92—8.00 (5H, m, Ph). Other signals are overlapping with those of **8**. Partial ^{13}C NMR ($CDCl_3$) δ=12.08 (3-Me), 16.08 (4-Me), 28.71 (C-9), 31.42 (C-3), 33.79 (C-8), 43.67 (C-4), 47.86 (C-2), 124.14 (C-6), 128.16, 128.62, 133.07, 137.06 (each Ph), 157.56 (C-7), 199.69 (C-5), and 203.90 (C-1).

Reaction of 3d with 1-Phenyl-2-buten-1-one Leading to 9+9′+9″. To the standard solution of **3d** prepared from **2d** (0.106 g, 0.5 mmol) was added, under nitrogen at −78 °C, 1-phenyl-2-buten-1-one (0.074 g, 0.5 mmol, *Z*: *E*=10 : 90 by ^{1}H NMR) in THF (1 ml). After stirring at −78 °C for 30 min and then at room temperature for 42 h, the mixture was poured into saturated NH_4Cl and extracted with CH_2Cl_2 (10 ml×3). The combined extracts were dried ($MgSO_4$) and

evaporated in vacuo. The residue (0.137 g) was chromatographed on silica gel with hexane–EtOAc (20 : 1, v/v) to give a mixture of **9**, **9′**, and **9″** (0.101 g, 71%, 62 : 16 : 22 by GLC), which were separated from each other by careful chromatographic operation.

***t*-4-Benzoyl-*t*-5-*t*-butyl-*r*-2,*c*-3-dimethylcyclohexanone (9):** Pale yellow solid; mp 65—68 °C; IR (KBr) 2900, 1660, 1200, and 970 cm^{-1}; ^1H NMR ($CDCl_3$) δ=0.87 (9H, s, *t*-Bu), 0.93 (3H, d, J_{Me-2}=6.6 Hz, 2-Me), 1.05 (3H, d, J_{Me-3}=7.3 Hz, 3-Me), 2.06 (1H, dt, $J_{5-6eq}=J_{5-4}$=4.0 and J_{5-6ax}=13.9 Hz, H-5), 2.27 (1H, ddq, J_{3-4}=1.5, J_{3-2}=6.2, and J_{3-Me}=7.3 Hz, H-3), 2.40 (1H, ddd, J_{6eq-4}=1.1, J_{6eq-5}=4.0, and J_{gem}=13.9 Hz, H-6_{eq}), 3.07 (1H, dq, J_{2-3}=6.2 and J_{2-Me}=6.6 Hz, H-2), 3.43 (1H, t, $J_{6ax-5}=J_{gem}$=13.9 Hz, H-6_{ax}), 3.86 (1H, ddd, J_{4-6eq}=1.1, J_{4-3}=1.5, and J_{4-5}=4.0 Hz, H-4), 7.48—7.65, and 7.79—8.02 (3H and 2H, m, Ph); NOE: H-2/H-3, H-2/H-6_{ax}, 2-Me/H-5, and 3-Me/H-5; ^{13}C NMR ($CDCl_3$) δ=11.68 (2-Me), 15.69 (3-Me), 28.94 (*t*-Bu), 33.36 (*t*-Bu), 39.34, 40.68 (C-3 and C-5), 42.94 (C-6), 46.72, 46.81 (C-2 and C-4), 128.12, 128.98, 133.24, 137.22 (each Ph), 203.28 (COPh), and 214.15 (C-1); MS *m/z* (rel intensity, %) 286 (M^+, 26), 230 (35), 229 (46), 174 (71), 173 (56), 111 (32), 105 (base peak), 83 (24), and 77 (34). Found: C, 79.37; H, 8.96%. Calcd for $C_{19}H_{26}O_2$: C, 79.67; H, 9.16%.

***t*-4-Benzoyl-*t*-5-*t*-butyl-*r*-2,*t*-3-dimethylcyclohexanone (9′):** Pale yellow solid; mp 108—111 °C; IR (KBr) 2900, 1650, 1440, 1200, and 970 cm^{-1}; ^1H NMR ($CDCl_3$) δ=0.82 (9H, s, *t*-Bu), 0.97 (3H, d, J_{Me-2}=7.0 Hz, 2-Me), 1.03 (3H, d, J_{Me-3}=7.0 Hz, 3-Me), 1.81—1.96 (2H, m, H-3 and H-5), 2.43 (1H, ddd, J_{6eq-4}=1.1, J_{6eq-5}=3.7, and J_{gem}=13.4 Hz, H-6_{eq}), 2.87 (1H, dq, J_{2-Me}=7.0 and J_{2-3}=12.4 Hz, H-2), 3.30 (1H, t, $J_{6ax-5}=J_{gem}$=13.4 Hz, H-6_{ax}), 4.16 (1H, br t, $J_{4-3}=J_{4-5}$=3.7 Hz, H-4), 7.48—7.64, and 8.04—8.08 (3H and 2H, m, Ph); ^{13}C NMR ($CDCl_3$) δ=11.71 (2-Me), 18.23 (3-Me), 28.51 (*t*-Bu), 33.74 (*t*-Bu), 39.55, 43.57 (C-3 and C-5), 44.66 (C-6), 45.59 (C-2), 53.35 (C-4), 128.49, 128.89, 133.20, 139.49 (each Ph), 204.53 (COPh), and 213.87 (C-1); MS *m/z* (rel intensity, %) 286 (M^+, 23), 230 (37), 229 (31), 174 (63), 173 (52), 167 (25), 140 (14), 111 (94), 105 (base peak), 83 (28), and 77 (42). HRMS Found: *m/z* 286.1932. Calcd for $C_{19}H_{26}O_2$: M, 286.1931.

***c*-4-Benzoyl-*c*-5-*t*-butyl-*r*-2,*c*-3-dimethylcyclohexanone (9″):** Pale yellow liquid; IR (neat) 3400, 2950, 1660, 1590, 1570, 1440, 1360, 1280, 1200, 1060, 990, and 690 cm^{-1}; ^1H NMR ($CDCl_3$) δ=0.86 (9H, s, *t*-Bu), 1.08 (3H, d, J_{Me-2}=6.6 Hz, 2-Me), 1.33 (3H, d, J_{Me-3}=7.0 Hz, 3-Me), 1.64 (1H, ddq, J_{3-4}=1.8, J_{3-Me}=7.0, and J_{3-2}=8.4 Hz, H-3), 2.15 (1H, dq, J_{2-Me}=6.6 and J_{2-3}=8.4 Hz, H-2), 2.26—2.88 (3H, m, H-5 and H-6), 3.68 (1H, br s, H-4), 7.45—7.60, and 7.91—7.94 (3H and 2H, m, Ph); ^{13}C NMR ($CDCl_3$) δ=13.59 (2-Me), 22.02 (3-Me), 28.45 (*t*-Bu), 33.04 (*t*-Bu), 38.21,40.24 (C-3 and C-5), 44.48, 45.34 (C-2 and C-6), 47.44 (C-4), 128.17, 128.88, 133.11, 137.50 (each Ph), 204.23 (COPh), and 212.91 (1-C); MS *m/z* (rel intensity, %) 287 (M^++1, 3), 286 (M^+, 8), 259 (28), 230 (73), 174 (base peak), 173 (31), and 105 (24). HRMS Found: *m/z* 286.1934. Calcd for $C_{19}H_{26}O_2$: M, 286.1931.

2,4-Dibenzoyl-3,5,6-trimethyl-1-[(*E*)-3,3-dimethyl-1-butenyl]cyclohexanol (10). To the standard solution of **3d** prepared from **2d** (0.182 g, 0.86 mmol) were added, under nitrogen at −78 °C, 1-phenyl-2-buten-1-one (0.125 g, 0.86 mmol, *Z* : *E*=1 : 99 by ^1H NMR) in THF (1 ml) and HMPA (0.5 ml) in THF (1 ml). After stirring at −78 °C for 1 h, the mixture was poured into saturated NH_4Cl and extracted with CH_2Cl_2 (10 ml×3). The combined extracts were dried ($MgSO_4$) and evaporated in vacuo. The residue (0.675 g) was triturated with hexane to give **10** (0.104 g, 28%). The filtrate was evaporated in vacuo and the residue was chromatographed on silica gel with hexane–EtOAc (15 : 1, v/v) to give **8** and **8′** (0.159 g, 65%, **8** : **8′**=83 : 17 by ^1H NMR). **10**: Colorless solid; mp 218—220 °C (decomp); IR (KBr) 3400, 2850, 1200, and 970 cm^{-1}; ^1H NMR ($CDCl_3$) δ=0.63 (9H, s, *t*-Bu), 0.83 (3H, d, J_{Me-3}=6.2 Hz, 3-Me), 0.92 (3H, d, J_{Me-6}=7.0 Hz, 6-Me), 0.97 (3H, d, J_{Me-5}=7.3 Hz, 5-Me), 1.90 (1H, dq, J_{6-5}=4.8 and J_{6-Me}=7.0 Hz, H-6), 2.17 (1H, ddq, J_{5-4}=4.4, J_{5-6}=4.8, and J_{5-Me}=7.3 Hz, H-5), 2.98 (1H, ddq, J_{3-Me}=6.2, J_{3-4}=11.0, and J_{3-2}=11.4 Hz, H-3), 3.53 (1H, dd, J_{4-5}=4.4 and J_{4-3}=11.0 Hz, H-4), 3.53 (1H, d, J_{2-3}=11.4 Hz, H-2), 4.01 (1H, br s, OH), 5.04, 5.48 (each 1H, each d, J_{trans}=15.8 Hz, =CH), 7.43—7.61, and 7.92—8.00 (3H and 2H, m, Ph); ^{13}C NMR ($CDCl_3$) δ=10.87, 13.42, 18.79 (3-, 5-, and 6-Me), 27.79 (C-5), 29.17 (*t*-Bu), 32.21 (*t*-Bu), 36.57 (C-6), 42.94 (C-3), 56.70,57.71 (C-2 and C-4), 75.20 (C-1), 128.06, 128.49, 128.61, 128.72, 129.95, 132.88, 133.55, 137.20, 138.79, 140.77 (=CH and Ph), 201.00, and 207.05 (2- and 4-COPh); MS *m/z* (rel intensity, %) 432 (M^+, 1), 414 (10), 294 (16), 268 (20), 267 (base peak), 266 (30), 147 (28), and 140 (50). Found: C, 80.74; H, 8.26%. Calcd for $C_{29}H_{36}O_3$: C, 80.51; H, 8.39%.

Reaction of 3d with (*E*)-3-Penten-2-one Leading ot 11a and 12. To the standard solution of **3d** prepared from **2d** (0.212 g, 1 mmol) was added under nitrogen at −78 °C (*E*)-3-penten-2-one (0.084 g, 1 mmol) in THF (1 ml). After stirred at −78 °C for 1 h and then at room temperature for 20 h, the mixture was poured into saturated NH_4Cl and extracted with CH_2Cl_2 (15 ml×3). The combined extracts were dried ($MgSO_4$) and evaporated in vacuo. The residue (0.197 g) was chromatographed on silica gel with hexane–EtOAc (15 : 1, v/v) to give **12** (0.101 g, 49%) and then **11a** (0.012 g, 5%).

***t*-4-Acetyl-*t*-5-butyl-*r*-2,*c*-3-dimethylcyclohexanone (11a):** This product could not be separated from the mixture with **12** because of the low yield. Its partial ^1H NMR spectrum was abstracted ($CDCl_3$) δ=0.91 (9H, s, *t*-Bu), 0.93 (3H, d, J_{Me-3}=7.3 Hz, 3-Me), 0.94 (3H, d, J_{Me-2}=6.2 Hz, 2-Me), 1.83 (1H, dt, $J_{5-4}=J_{5-6eq}$=3.8 and J_{5-6ax}=14.3 Hz, H-5), 2.18—2.23 (1H, m, H-3), 2.30 (1H, br dd, J_{6eq-5}=3.8 and J_{gem}=13.8 Hz, H-6_{eq}), 2.35 (3H, s, COMe), 2.95 (1H, quint, $J_{2-Me}=J_{2-3}$=6.2 Hz, H-2), 3.00 (1H, dd, J_{4-3}=1.8 and J_{4-5}=3.8 Hz, H-4), and 3.17 (1H, dd, J_{gem}=13.8 and J_{6ax-5}=14.3 Hz, H-6_{ax}).

***cis*-4,5-Dimethyl-3-[(*E*)-3,3-dimethyl-1-butenyl]-2-cyclohexen-1-one (12):** Pale yellow liquid; IR (neat): 2950, 1660, 1640, 1590, 1460, 1300, 1250, 1190, and 980 cm^{-1}; ^1H NMR ($CDCl_3$) δ=1.06 (3H, d, J_{Me-4}=7.3 Hz, 4-Me), 1.07 (3H, d, J_{Me-5}=6.2 Hz, 5-Me), 1.10 (9H, s, *t*-Bu), 2.23—2.35 (3H, m, H-5 and H-6), 2.67 (1H, dq, J_{4-5}=3.7 and J_{4-Me}=7.3 Hz, H-4), 5.83 (1H, s, H-2), 6.00, and 6.25 (each 1H, each d, J_{trans}=16.1 Hz, =CH); ^{13}C NMR ($CDCl_3$) δ=12.43 (5-Me), 18.57 (4-Me), 29.19 (*t*-Bu), 32.14 (C-6), 40.49 (C-4), 125.04 (C-1′), 125.44 (C-2), 149.15 (C-3), 164.33 (C-2′), and 200.41 (C-1); MS *m/z* (rel intensity, %) 207 (M^++1, 15), 206 (M^+, 79), 191 (base peak), 150 (24), 135 (20), 121 (55), and 107 (21). HRMS Found: *m/z* 206.1673. Calcd for $C_{14}H_{22}O$: M, 206.1670.

***c*-4-Acetyl-*r*-3-*t*-butyl-*t*-5-methylcyclohexanone (11b):** A similar procedue using the standard solution of **3b** prepared from **2b** (0.397 g, 2 mmol) and (*E*)-3-penten-2-one (0.168 g, 2 mmol) at room temperature for 4.5 h followed by chromatographic purification (silica gel, hexane–EtOAc (7 : 1, v/v)) gave **11b** (0.131 g, 31%): Pale yellow liquid; IR (neat) 2940, 1700, 1470, 1360, and 1120 cm^{-1}; ^1H NMR ($CDCl_3$) δ=0.91

(9H, s, *t*-Bu), 0.95 (3H, d, J_{Me-5}=6.2 Hz, 5-Me), 1.87 (1H, ddd, J_{3-4}=3.7, J_{3-2eq}=4.0, and J_{3-2ax}=14.3 Hz, H-3), 2.04 (1H, br d, J_{gem}=13.9 Hz, H-2_{eq}), 2.34 (3H, s, COMe), 2.24—2.41 (2H, m, H-5 and H-6_{eq}), 2.76 (1H, br dd, J_{6ax-5}=6.2 and J_{gem}=14.5 Hz, H-6_{ax}), 2.94 (1H, br s, H-4), and 3.15 (1H, dd, J_{gem}=13.9 and J_{2ax-3}=14.3 Hz, H-2_{ax}); ^{13}C NMR ($CDCl_3$) δ=20.88 (5-Me), 28.39 (COMe), 28.71 (*t*-Bu), 32.15 (C-5), 39.06 (*t*-Bu), 40.07 (C-3), 43.38, 45.99 (C-2 and C-6), 50.78 (C-4), 212.32, and 212.72 (C-1 and COMe); MS *m/z* (rel intensity, %) 211 (M^++1, 8), 210 (M^+, 24), 210 (24), 195 (21), 154 (24), 153 (base peak), 139 (14), 112 (34), and 111 (25). Found: C, 73.97; H, 10.57%. Calcd for $C_{13}H_{22}O_2$: C, 74.24; H, 10.54%.

***c*-4-Acetyl-*r*-3,*t*-5-diphenylcyclohexanone (11c):** A similar procedure using the standard solution of **3a** prepared from **2a** (0.473 g, 2 mmol) and (*E*)-4-phenyl-3-buten-2-one (0.292 g, 2 mmol) at room temperature for 1.5 h followed by chromatographic purification (silica gel, hexane–EtOAc (5:1, v/v)) gave **11c** (0.183 g, 31%): Pale yellow liquid; IR (neat) 3250, 1770, 1560, 1520, 1430, and 1240 cm^{-1}; ^{1}H NMR ($CDCl_3$) δ=1.63 (3H, s, COMe), 2.68 (1H, dd, J_{6eq-5}=5.1 and J_{gem}=15.4 Hz, H-6_{eq}), 2.73 (1H, dd, J_{2eq-3}=7.7 and J_{gem}=15.8 Hz, H-2_{eq}), 3.01 (1H, dd, J_{2ax-3}=6.2 and J_{gem}=15.8 Hz, H-2_{ax}), 3.20 (1H, dd, J_{6ax-5}=9.9 and J_{gem}=15.4 Hz, H-6_{ax}), 3.45 (1H, dd, J_{4-5}=5.5 and J_{4-3}=5.9 Hz, H-4), 3.55 (1H, ddd, J_{5-6eq}=5.1, J_{5-4}=5.5, and J_{5-6ax}=9.9 Hz, H-5), 3.62 (1H, ddd, J_{3-4}=5.9, J_{3-2ax}=6.2, and J_{3-2eq}=7.7 Hz, H-3), and 7.01—7.40 (10H, m, Ph); ^{13}C NMR ($CDCl_3$) δ=31.94 (COMe), 40.93, 41.12, 42.89, 44.22 (C-2, C-3, C-5, and C-6), 58.70 (C-4), 127.07, 127.22, 127.34, 127.66, 128.72, 128.97, 140.17, 143.09 (each Ph), 210.60, and 210.79 (C-1 and COMe); MS *m/z* (rel intensity, %) 293 (M^++1, 3), 292 (M^+, 6), 146 (85), 145 (55), 131 (base peak), 103 (84), and 86 (45). HRMS Found: *m/z* 292.1461. Calcd for $C_{20}H_{20}O_2$: M, 292.1462.

General Procedure for the Reactions of 3 with Dimethyl Alkylidenemalonates Leading to 13a—f. As a typical procedure the reaction of **3d** with dimethyl ethylidenemalonate is described: To the standard solution of **3d** prepared from **2d** (0.212 g, 1 mmol) was added under nitrogen at −78 °C dimethyl ethylidenemalonate (0.158 g, 1 mmol) in THF (0.5 ml). After stirring for 30 min at −78 °C, the mixture was poured into saturated aqueous NH_4Cl and extracted with CH_2Cl_2 (10 ml×3). The combined extracts were dried ($MgSO_4$) and evaporated in vacuo. The residue was chromatographed on silica gel with hexane–EtOAc (15:1, v/v) to give **13c** (0.25 g, 80%, *anti*/*syn*=60:40 by ^{1}H NMR). These isomers were separated and purified by careful chromatographic operation.

Dimethyl [(*E*)-1-Ethyl-2-methyl-3-oxo-5-phenyl-4-pentenylidene]malonate (13a): Two isomeric adducts were separated and purified through column chromatography on silica gel with hexane–EtOAc (15:1, v/v).

anti-**13a:** Pale yellow liquid; IR (neat) 2950, 1720, 1680, 1600, 1420, 1190, 1140, and 1020 cm^{-1}; ^{1}H NMR ($CDCl_3$) δ=0.96 (3H, t, *J*=7.3 Hz, Me of Et), 1.17 (3H, d, $J_{Me-2'}$=7.0 Hz, 2′-Me), 1.50 (2H, dq, $J_{CH2-1'}$=5.9 and *J*=7.3 Hz, CH_2 of Et), 2.66 (1H, ddt, $J_{1'-CH2}$=$J_{1'-2}$=5.9 and $J_{1'-2'}$=7.0 Hz, H-1′), 3.10 (1H, dq, $J_{2'-Me}$=$J_{2'-1'}$=7.0 Hz, H-2′), 3.62 (1H, d, $J_{2-1'}$=5.9 Hz, H-2), 3.70, 3.75 (each 3H, each s, COOMe), 6.83 (1H, d, J_{trans}=15.8 Hz, H-4′), 7.37—7.65 (5H, m, Ph), and 7.60 (1H, d, J_{trans}=15.8 Hz, H-5′); ^{13}C NMR ($CDCl_3$) δ=12.74 (Et), 13.23 (2′-Me), 23.93 (Et), 41.99 (C-1′), 46.10 (C-2′), 52.34, 52.37, 52.48 (COOMe and C-2), 125.01 (C-4′), 128.40, 128.92, 130.49, 134.55, 142.72 (Ph and C-5′), 169.31, 169.54 (each COOMe), and 202.25 (C-3′); MS *m/z* (rel intensity, %) 333 (M^++1, 2), 332 (M^+, 8), 201 (21), 200 (43), 160 (76), and 131 (base peak); Found: C, 68.83; H, 7.41%. Calcd for $C_{19}H_{24}O_5$: C, 68.64; H, 7.28%.

syn-**13a:** Pale yellow liquid; IR (neat) 2950, 1720, 1690, 1430, 1200, and 1140 cm^{-1}; ^{1}H NMR ($CDCl_3$) δ=0.84 (3H, t, *J*=7.3 Hz, Me of Et), 1.09 (3H, d, $J_{Me-2'}$=7.0 Hz, 2′-Me), 1.26—1.58 (2H, m, CH_2 of Et), 2.68—2.77 (1H, m, H-1′), 3.03 (1H, dq, $J_{2'-Me}$=4.4 and $J_{2'-1'}$=7.0 Hz, H-2′), 3.54 (1H, d, $J_{2-1'}$=8.1 Hz, H-2), 3.73, 3.78 (each 3H, each s, COOMe), 7.00 (1H, d, J_{trans}=15.8 Hz, H-4′), 7.39—7.64 (5H, m, Ph), and 7.69 (1H, d, J_{trans}=15.8 Hz, H-5′); ^{13}C NMR ($CDCl_3$) δ=10.99 (Et), 12.80 (2′-Me), 21.43 (Et), 41.01 (C-1′), 46.20 (C-2′), 52.48, 52.57 (each COOMe), 54.53 (C-2), 124.76 (C-4′), 128.48, 128.91, 130.42, 134.68, 142.86 (Ph and C-5′), 169.25, 169.41 (each COOMe), and 202.04 (C-3′); MS *m/z* (rel intensity, %) 333 (M^++1, 4), 332 (M^+, 21), 201 (21), 200 (26), 160 (84), and 131 (base peak). Found: C, 68.28; H, 7.42%. Calcd for $C_{19}H_{24}O_5$: C, 68.64; H, 7.28%.

Dimethyl [(*E*)-1,2,6,6-Tetramethyl-3-oxo-4-heptenylidene]malonate (13b): Obtained as a 52:48 inseparable mixture of *anti*-**13b** and *syn*-**13b** (by ^{1}H NMR) after column chromatography on silica gel using hexane–EtOAc (15:1, v/v). Colorless liquid; IR (neat) 2950, 1750, 1740, 1620, 1440, and 1200 cm^{-1}; ^{1}H NMR ($CDCl_3$) *anti*-isomer δ=1.01 (3H, d, $J_{Me-1'}$=7.0 Hz, 1′-Me), 1.09 (9H, s, *t*-Bu), 1.12 (3H, d, $J_{Me-2'}$=7.0 Hz, 2′-Me), 2.50—2.63 (1H, m, H-1′), 2.85—2.97 (1H, m, H-2′), 3.59 (1H, d, $J_{2-1'}$=6.2 Hz, H-2), 3.75, 3.76 (each 3H, each s, COOMe), 6.06 (1H, d, J_{trans}=15.8 Hz, H-4′), and 6.86 (1H, d, J_{trans}=15.8 Hz, H-5′); *syn*-isomer δ=0.88 (3H, d, $J_{Me-1'}$=7.0 Hz, 1′-Me), 1.00 (3H, d, $J_{Me-2'}$=7.0 Hz, 2′-Me), 1.11 (9H, s, *t*-Bu), 2.68—2.81 (1H, m, H-1′), 2.85—2.97 (1H, m, H-2′), 3.41 (1H, d, $J_{2-1'}$=8.4 Hz, H-2), 3.73, 3.74 (each 3H, each s, COOMe), 6.12 (1H, d, J_{trans}=16.1 Hz, H-4′), and 6.94 (1H, d, J_{trans}=16.1 Hz, H-5′); ^{13}C NMR ($CDCl_3$) *anti*-isomer δ=12.44 (1′-Me), 14.86 (2′-Me), 28.73 (*t*-Bu), 33.84 (*t*-Bu), 36.11 (C-1′), 46.55 (C-2′), 52.24, 52.41 (each COOMe), 53.66 (C-2), 124.60 (C-4′), 157.68 (C-5′), 169.01, 169.08 (each COOMe), and 202.69 (C-3′); *syn*-isomer δ=11.00 (1′-Me), 15.36 (2′-Me), 28.73 (*t*-Bu), 33.84 (*t*-Bu), 34.34 (C-1′), 45.59 (C-2′), 52.34, 52.50 (each COOMe), 55.20 (C-2), 123.77 (C-4′), 157.89 (C-5′), 168.92, 169.45 (each COOMe), and 203.09 (C-3′); MS *m/z* (rel intensity, %) 299 (M^++1, 2), 298 (M^+, 8), 167 (21), 140 (30), and 111 (base peak). HRMS Found: *m/z* 298.1782. Calcd for $C_{16}H_{26}O_5$: M, 298.1779.

Dimethyl [(*E*)-1-Ethyl-2,6,6-trimethyl-3-oxo-4-heptenylidene]malonate (13c): *anti*-**13c:** Colorless liquid; IR (neat) 2980, 1755, 1735, 1620, and 1460 cm^{-1}; ^{1}H NMR ($CDCl_3$) δ=0.92 (3H, t, *J*=7.3 Hz, Me of Et), 1.07 (3H, d, $J_{Me-2'}$=7.0 Hz, 2′-Me), 1.10 (9H, s, *t*-Bu), 1.38—1.58 (2H, m, CH_2 of Et), 2.53—2.62 (1H, ddt, $J_{1'-2}$=5.9 and $J_{1'-2'}$=$J_{1'-CH_2}$=7.0 Hz, H-1′), 3.01 (1H, dq, $J_{2'-1'}$=7.0 and $J_{2'-Me}$=7.0 Hz, H-2′), 3.58 (1H, d, $J_{2-1'}$=5.9 Hz, H-2), 3.70, 3.74 (each 3H, each s, COOMe), 6.08 (1H, d, J_{trans}=16.1 Hz, H-4′), and 6.86 (1H, d, J_{trans}=16.1 Hz, H-5′); ^{13}C NMR ($CDCl_3$) δ=12.74 (Et), 13.33 (2′-Me), 23.86 (Et), 28.74 (*t*-Bu), 33.79 (*t*-Bu), 41.96 (C-1′), 45.54 (C-2′), 52.25, 52.30 (each COOMe), 52.44 (C-2), 124.11 (C-4′), 157.24 (C-5′), 169.35, 169.57 (each COOMe), and 203.06 (C-3′); MS *m/z* (rel intensity, %) 313 (M^++1, 2), 312 (M^+, 4), 180 (10), 140 (base peak), and 111 (89). Found: C, 65.55; H, 9.02%. Calcd for $C_{17}H_{28}O_5$: C, 65.34; H, 9.04%.

syn-**13c:** Colorless liquid; IR (neat) 2950, 1750, 1730, 1620, 1455, and 1430 cm^{-1}; ^{1}H NMR ($CDCl_3$) δ=0.83 (3H, t, *J*=7.3 Hz, Me of Et), 1.03 (3H, d, $J_{Me-2'}$=7.0 Hz, 2′-Me), 1.11 (9H, s,

t-Bu), 1.23—1.54 (2H, m, CH_2 of Et), 2.57—2.67 (1H, m, H-1′), 2.92 (1H, dq, $J_{2'-1'}$=4.8 and $J_{2'-Me}$=7.0 Hz, H-2′), 3.49 (1H, d, $J_{2-1'}$=8.1 Hz, H-2), 3.73, 3.75 (each 3H, each s, COOMe), 6.21 (1H, d, J_{trans}=16.1 Hz, H-4′), and 6.93 (1H, d, J_{trans}=16.1 Hz, H-5′); ^{13}C NMR ($CDCl_3$) δ=11.46 (Et), 12.90 (2′-Me), 21.48 (Et), 28.74 (*t*-Bu), 33.81 (*t*-Bu), 41.08 (C-1′), 45.73 (C-2′), 52.38, 52.48 (each COOMe), 54.44 (C-2), 123.71 (C-4′), 157.52 (C-5′), 169.27, 169.35 (each COOMe), and 202.87 (C-3′); MS *m/z* (rel intensity, %) 313 (M^++1, 2), 312 (M^+, 7), 181 (12), 140 (91), and 111 (base peak). Found: C, 65.36; H, 8.87%. Calcd for $C_{17}H_{28}O_5$: C, 65.34; H, 9.04%.

Dimethyl [(*E*)-2,6,6-Trimethyl-1-phenyl-3-oxo-4-heptenylidene]malonate (13d): Only *anti*-isomer was isolated and purified by column chromatography on silica gel with hexane–EtOAc (15 : 1, v/v). Pale yellow liquid; IR (neat) 2950, 1750, 1730, 1620, 1430, and 1160 cm^{-1}; ^{1}H NMR ($CDCl_3$) δ=0.98 (9H, s, *t*-Bu), 1.14 (3H, d, $J_{Me-2'}$=7.0 Hz, 2′-Me), 3.40 (1H, dq, $J_{2'-Me}$=7.0 and $J_{2'-1'}$=7.3 Hz, H-2′), 3.46, 3.71 (each 3H, each s, COOMe), 3.75 (1H, dd, $J_{1'-2'}$=7.3 and $J_{1'-2}$=8.8 Hz, H-1′), 4.01 (1H, d, $J_{2-1'}$=8.8 Hz, H-2), 5.83 (1H, d, J_{trans}=15.8 Hz, H-4′), 6.69 (1H, d, J_{trans}=15.8 Hz, H-5′), and 7.20 (5H, s, Ph); ^{13}C NMR ($CDCl_3$) δ=15.31 (2′-Me), 28.61 (*t*-Bu), 33.69 (*t*-Bu), 47.26 (C-2′), 47.92 (C-1′), 52.28, 52.55 (each COOMe), 54.92 (C-2), 123.97 (C-4′), 127.18, 128.09, 129.15, 139.03 (each Ph), 157.19 (C-5′), 168.37, 168.86 (each COOMe), and 202.30 (C-3′); MS *m/z* (rel intensity, %) 361 (M^++1, 9), 360 (M^+, 34), 328 (11), 269 (12), 230 (10), 229 (54), 140 (16), and 111 (base peak). HRMS Found: *m/z* 360.1939. Calcd for $C_{211}H_{28}O_5$: M, 360.1935.

Dimethyl [(*E*)-1-*t*-Butyl-2,6,6-trimethyl-3-oxo-4-heptenylidene]malonate (13e): Only *anti*-isomer was isolated and purified by column chromatography on silica gel with hexane–EtOAc (15 : 1, v/v). *anti*-isomer: Pale yellow liquid; IR (neat) 2950, 1730, 1620, 1430, 1350, and 1150 cm^{-1}; ^{1}H NMR ($CDCl_3$) δ=0.88, 1.10 (each 9H, each s, *t*-Bu), 1.12 (3H, d, $J_{Me-2'}$=7.0 Hz, 2′-Me), 3.00 (1H, dd, $J_{1'-2}$=3.3 and $J_{1'-2'}$=8.8 Hz, H-1′), 3.30 (1H, dq, $J_{2'-Me}$=7.0 and $J_{2'-1'}$=8.8 Hz, H-2′), 3.74 (6H, s, 2×COOMe), 3.81 (1H, d, $J_{2-1'}$=3.3 Hz, H-2), 6.10 (1H, d, J_{trans}=16.1 Hz, H-4′), and 6.90 (1H, d, J_{trans}=16.1 Hz, H-5′); ^{13}C NMR ($CDCl_3$) δ=16.57 (2′-Me), 28.74, 29.17 (each *t*-Bu), 33.79, 35.02 (each *t*-Bu), 43.92 (C-1′), 48.49 (C-2′), 50.81 (C-2), 52.19, 52.61 (each COOMe), 123.88 (C-4′), 157.09 (C-5′), 170.17, 171.37 (each COOMe), and 203.52 (C-3′), MS *m/z* (rel intensity, %) 341 (M^++1, 2), 340 (M^+, 7), 283 (16), 242 (10), 208 (15), and 111 (base peak). Found: C, 67.22; H, 9.28%. Calcd for $C_{19}H_{32}O_5$: C, 67.01; H, 9.48%.

Dimethyl [(*E*)-1-Ethyl-2-methyl-3-oxo-4-hexenylidene]malonate (13f): Obtained as a 64 : 36 inseparable mixture of *anti*-**13f** and *syn*-**13f** (by ^{1}H NMR) after column chromatography on silica gel using hexane–EtOAc (10 : 1 to 15 : 1, v/v). Pale yellow liquid: IR (neat) 2900, 1720, 1690, 1620, 1420, 1190, and 1140 cm^{-1}; ^{1}H NMR ($CDCl_3$) *anti*-isomer δ=0.92 (3H, t, *J*=7.3 Hz, 1′-Et), 1.06 (3H, d, $J_{Me-2'}$=7.0 Hz, 2′-Me), 1.24—1.58 (2H, m, 1′-Et), 1.91 (3H, dd, $J_{6'-4'}$=1.8 and $J_{6'-5'}$=7.0 Hz, H-6′), 2.53—2.68 (1H, m, H-1′), 2.99 (1H, dq, $J_{2'-1'}$=$J_{2'-Me}$=7.0 Hz, H-2′), 3.56 (1H, d, $J_{2-1'}$=6.2 Hz, H-2), 3.69, 3.73 (each 3H, each s, COOMe), 6.21 (1H, dq, $J_{4'-6'}$=1.8 and J_{trans}=15.8 Hz, H-4′), and 6.89 (1H, dq, $J_{5'-6'}$=7.8 and J_{trans}=15.8 Hz, H-5′); *syn*-isomer δ=0.82 (3H, t, *J*=7.3 Hz, 1′-Et), 1.02 (3H, d, $J_{Me-2'}$=7.0 Hz, 2′-Me), 1.24—1.58 (2H, m, 1′-Et), 1.92 (3H, dd, $J_{6'-4'}$=1.8 and $J_{6'-5'}$=7.0 Hz, H-6′), 2.53—2.68 (1H, m, H-1′), 2.89 (1H, dq, $J_{2'-1'}$=4.4 and $J_{2'-Me}$=7.0 Hz, H-2′), 3.49 (1H, d, $J_{2-1'}$=8.1 Hz, H-2), 3.73, 3.76 (each 3H, each s, COOMe), 6.34 (1H, dq, $J_{4'-6'}$=1.8 and J_{trans}=15.8 Hz, H-4′), and 6.96 (1H, dq, $J_{5'-6'}$=7.0 and J_{trans}=15.8 Hz, H-5′); ^{13}C NMR ($CDCl_3$) *anti*-isomer δ=12.69 (Et), 12.96 (2′-Me), 18.30 (C-6′), 23.90 (Et), 41.83 (C-1′), 45.08 (C-2′), 52.31, 52.35, 52.40 (COOMe and C-2), 130.68 (C-4′), 142.73 (C-5′), 169.32, 169.56 (each COOMe), and 202.30 (C-3′); *syn*-isomer δ=11.07 (Et), 12.80 (2′-Me), 18.30 (C-6′), 21.44 (Et), 40.95 (C-1′), 45.43 (C-2′), 52.45, 52.54 (each COOMe), 54.53 (C-2), 130.25 (C-4′), 142.95 (C-5′), 169.28, 169.40 (each COOMe), and 201.97 (C-3′); MS *m/z* (rel intensity, %) 271 (M^++1, 3), 270 (M^+, 15), 139 (27), 98 (base peak), and 69 (41). HRMS Found: *m/z* 270.1467. Calcd for $C_{14}H_{22}O_5$: M, 270.1466.

Catalytic Hydrogenation Followed by $Zn(BH_4)_2$ Reduction of 13d Leading to 15 and 16. A solution of **13d** (0.67 g, 1.86 mmol) in EtOH (10 ml) in the presence of palladium/carbon (10 wt%) was stirred under hydrogen at room temperature for 12 h. The catalyst was filtered off through cerite and the filtrate was evaporated in vacuo to give **14** (0.679 g, 100%) as colorless oil [**14:** IR (neat) 2950, 1710, 1430, 1230, 1150, and 1010 cm^{-1}; ^{1}H NMR ($CDCl_3$) δ=0.74 (9H, s, *t*-Bu), 1.14 (3H, d, $J_{Me-2'}$=7.3 Hz, 2′-Me), 1.12—1.26 (2H, m, H-5′), 1.97—2.21 (2H, m, H-4′), 3.15 (1H, dq, $J_{2'-Me}$=7.3 and $J_{2'-1'}$=7.7 Hz, H-2′), 3.47, 3.71 (each 3H, each s, COOMe), 3.73 (1H, dd, $J_{1'-2'}$=7.7 and $J_{1'-2}$=9.2 Hz, H-1′), 4.03 (1H, d, $J_{2-1'}$=9.2 Hz, H-2), and 7.15—7.29 (5H, m, Ph); ^{13}C NMR ($CDCl_3$) δ=14.92 (3-Me), 29.01 (*t*-Bu), 29.63 (*t*-Bu), 36.66 (C-5′), 37.87 (C-4′), 47.79, 49.70 (C-1′ and C-2′), 52.31, 52.61 (each COOMe), 54.56 (C-2), 127.31, 128.29, 128.95, 139.16 (each Ph), 168.36, and 168.91 (each COOMe), and 213.43 (C-3′), MS *m/z* (rel intensity, %) 363 (M^++1, 24), 362 (M^+, base peak), 231 (79), 221 (59), and 113 (68). HRMS Found: *m/z* 362.2094. Calcd for $C_{21}H_{30}O_5$: M, 362.2092]. An ethereal solution of freshly prepared $Zn(BH_4)_2$ (0.36 M in diethyl ether, 8.3 ml, 3 mmol) was added to **14** (0.13 g, 0.375 mmol) in ether (1 ml) and the mixture was stirred at 0 °C for 21.5 h. The reaction was quenched with aqueous HCl (1 equiv) and extracted with CH_2Cl_2 (15 ml×2). The combined extracts were dried ($MgSO_4$) and evaporated in vacuo. The residue (0.12 g) was chromatographed on silica gel with hexane–EtOAc (10 : 1 to 4 : 1, v/v) to give **15** (0.046 g, 37%, 85 : 15 by ^{13}C NMR) and then **16** (0.046 g, 37%, 78 : 22 by ^{13}C NMR).

Methyl *c*-5-Methyl-*t*-6-(3,3-dimethylbutyl)-*r*-4-phenyl-2-oxoperhydropyran-3-carboxylate (15): Only the major isomer was isolated from the mixture. Colorless solid; mp 74—77 °C; IR (KBr) 2950, 1720, 1430, 1150, and 740 cm^{-1}; ^{1}H NMR ($CDCl_3$) δ=0.80 (3H, d, J_{Me-5}=7.3 Hz, 5-Me), 0.91 (9H, s, *t*-Bu), 1.12—1.29 (2H, m, two of H-1′ and H-2′), 1.49—1.80 (2H, m, the other of H-1′ and H-2′), 2.26 (1H, ddq, J_{5-6}=4.8, J_{5-4}=5.5, and J_{5-Me}=7.3 Hz, H-5), 3.67 (1H, dd, J_{4-5}=5.5 and J_{4-3}=7.0 Hz, H-4), 3.93 (1H, d, J_{3-4}=7.0 Hz, H-3), 4.17 (1H, dt, J_{6-5}=4.8, $J_{6-1'}$=4.8, and 7.3 Hz, H-6), and 7.12—7.38 (5H, m, Ph); ^{13}C NMR ($CDCl_3$) δ=14.34 (5-Me), 28.75 (C-2′), 29.24 (*t*-Bu), 30.06 (*t*-Bu), 34.34 (C-1′), 38.62 (C-5), 43.86 (C-4), 51.10, 52.94 (C-3 and COOMe), 84.33 (C-6), 127.53, 128.19, 128.72, 138.09 (each Ph), 167.64, and 169.21 (C-2 and COOMe); MS *m/z* (rel intensity, %) 332 (M^+, 75), 288 (50), 287 (39), 273 (base peak), 214 (35), 199 (37), 190 (25), 189 (23), 162 (23), 143 (41), 131 (63), 129 (29), 118 (53), 117 (25), 103 (24), 91 (44), 69 (29), 57 (54), and 41 (33). Found: C, 72.48; H, 8.43%. Calcd for $C_{20}H_{28}O_4$: C, 72.25; H, 8.49%.

Methyl 2-Hydroxy-*c*-5-methyl-*c*-6-(3,3-dimethylbutyl)-*r*-4-phenylperhydropyran-3-carboxylate (16): Only the major isomer was isolated from the mixture. Colorless solid; mp

132—134 °C; IR (KBr) 3300, 2850, 1680, 1420, 1250, 1060, and 1000 cm^{-1}; ^1H NMR ($CDCl_3$) δ=0.68 (3H, d, J_{Me-5}=7.0 Hz, 5-Me), 0.89 (9H, s, *t*-Bu), 1.08—1.81 (5H, m, H-1′, H-2′, and H-5), 3.05 (1H, dd, J_{3-2}=8.1 and J_{3-4}=12.5 Hz, H-3), 3.37 (1H, dd, J_{4-5}=4.0 and J_{4-3}=12.5 Hz, H-4), 3.53 (3H, s, COOMe), 3.69—3.75 (1H, m, H-6), 4.96 (1H, d, J_{2-3}=8.1 Hz, H-2), and 7.10—7.33 (5H, m, Ph); ^{13}C NMR ($CDCl_3$) δ=6.41 (5-Me), 27.63 (C-2′), 29.30 (*t*-Bu), 30.14 (C-1′), 37.02 (*t*-Bu), 39.86 (C-5), 48.34 (C-3 and C-4), 51.86 (COOMe), 80.11 (C-6), 97.79 (C-2), 126.69, 128.06, 128.29, 140.14 (each Ph), and 172.98 (COOMe); MS *m/z* (rel intensity, %) 334 (M^+, 2), 288 (29), 209 (15), 164 (16), 163 (base peak), 162 (34), and 118 (13). Found: C, 71.77; H, 8.88%. Calcd for $C_{20}H_{30}O_4$: C, 71.81; H, 9.05%.

Demethoxycarbonylation of 15 (or 16) Leading to 17 (or 18). To a solution of **15** (0.046 g, 0.138 mmol) in MeOH (1.5 ml) was added dropwise at room temperature aqueous NaOH (3%, 1 ml). This solution was stirred for 2 h, poured into aqueous HCl (1N), and extracted with dichloromethane (10 ml×3). The combined extracts were dried ($MgSO_4$) and evaporated in vacuo. The residue was chromatographed on silica gel with hexane–EtOAc (3 : 1, v/v) to give **17** (0.025 g, 66%). A similar procedure using **16** (0.046 g, 0.137 mmol) gave **18** (0.041 g, 93%).

***c*-5-Methyl-*t*-6-(3,3-dimethylbutyl)-*r*-4-phenyl-2-oxoperhydropyran (17):** Pale yellow liquid; IR (neat) 2900, 1710, 1450, 1360, 1210, 990, 750, and 690 cm^{-1}; ^1H NMR ($CDCl_3$) δ=0.82 (3H, d, J_{Me-5}=7.0 Hz, 5-Me), 0.89 (9H, s, *t*-Bu), 1.12—1.80 (4H, m, H-1′ and H-2′), 2.14 (1H, ddq, J_{5-4}=4.8, J_{5-6}=7.0, and J_{5-Me}=7.0 Hz, H-5), 2.79—2.92 (2H, m, H-3), 3.29 (1H, m, H-4), 4.07 (1H, ddd, $J_{6-1'}$=4.0, 7.8, and J_{6-5}=7.0 Hz, H-6), and 7.11—7.38 (5H, m, Ph); NOE: H-4/H-5, 4-Ph/5-Me, and 4-Ph/H-6; ^{13}C NMR ($CDCl_3$) δ=14.53 (5-Me), 28.74 (C-2′), 29.26 (*t*-Bu), 30.05 (*t*-Bu), 34.50 (C-1′) 35.61 (C-5), 38.56 (C-4), 40.53 (C-3), 83.24 (C-6), 127.15, 128.15, 128.52, 139.59 (each Ph), and 171.57 (C-2); MS *m/z* (rel intensity, %) 275 (M^++1, 7), 274 (M^+, 32), 142 (22), 131 (27), 118 (base peak), 104 (28), and 91 (22). HRMS Found: *m/z* 274.1933. Calcd for $C_{18}H_{26}O_2$: M, 274.1931

***c*-5-Methyl-*c*-6-(3,3-dimethylbutyl)-*r*-4-phenyl-2-oxoperhydropyran (18):** Pale yellow solid; mp 85—87 °C; IR (KBr) 2950, 1720, 1450, 1360, 1220, 1060, 990, and 900 cm^{-1}; ^1H NMR ($CDCl_3$) δ=0.72 (3H, d, J_{Me-5}=7.0 Hz, 5-Me), 0.91 (9H, s, *t*-Bu), 1.12—1.84 (4H, m, H-1′ and H-2′), 2.19 (1H, ddq, J_{5-4}=3.5, J_{5-Me}=7.0, and J_{5-6}=10.1 Hz, H-5), 2.79 (1H, ddd, J_{3eq-5}=0.7, J_{3eq-4}=6.6, and J_{gem}=18.3 Hz, H-3_{eq}), 2.92 (1H, dd, J_{3ax-4}=12.5, J_{gem}=18.3 Hz, H-3_{ax}), 3.41 (1H, ddd, J_{4-5}=3.5, J_{4-3eq}=6.6, and J_{4-3ax}=12.5 Hz, H-4), 4.44—4.50 (1H, m, H-6), and 7.18—7.40 (5H, m, Ph); NOE: H-3_{ax}/Ph, H-3_{eq}/H-4, H-4/H-5, H-4/H-6, and H-5/H-6; ^{13}C NMR ($CDCl_3$) δ=4.95 (5-Me), 28.06 (C-2′), 29.24 (*t*-Bu), 29.69 (*t*-Bu), 30.08 (C-1′), 35.98 (C-5), 39.48 (C-4), 41.83 (C-3), 85.50 (C-6), 127.07, 128.66, 140.30 (each Ph), and 170.98 (C-2); MS *m/z* (rel intensity, %) 275 (M^++1, 3), 274 (M^+, 15), 119 (11), 118 (base peak), and 104 (10). Found: C, 78.58; H, 9.35%. Calcd for $C_{18}H_{26}O_2$: C, 78.78; H, 9.56%.

References

1) a) J. A. Katzenellenbogen and A. L. Crumrine, *J. Am. Chem. Soc.*, **96**, 5662 (1974); b) C. N. Lam, J. M. Mellor, P. Picard, M. F. Rawlins, and J. H. A. Stibbard, *Tetrahedron Lett.*, **1978**, 4103; c) M. Ishiguro, M. Hirayama, H. Saito, A. Kajiwara, and N. Ikegawa, *Heterocycles,* **15**, 823 (1981); d) A. S. Kende and B. N. Toder, *J. Org. Chem.*, **47**, 163 (1982); e) S. G. Davies, R. J. C. Easton, A. Gonzalez, S. C. Preston, K. H. Sutton, and J. C. Walker, *Tetrahedron,* **42**, 3987 (1986); f) S. G. Davies, R. J. C. Easton, K. H. Sutton, and J. C. Walker, *J. Chem. Soc., Perkin Trans. 1,* **1987**, 489.

2) a) R. A. Lee, C. McAndrews, K. M. Patel, and W. Reusch, *Tetrahedron Lett.*, **1973**, 965; b) A. B. Smith, III and R. M. Scarborough, Jr., *ibid.*, **1978**, 4193; c) Y. Thebtaranonth and C. Yenjai, *ibid.*, **26**, 4097 (1985).

3) a) G. A. Kraus and N. Sugimoto, *Tetrahedron Lett.*, **1977**, 3929; b) R. W. Stevens and T. Mukaiyama, *Chem. Lett.*, **1985**, 855.

4) W. Oppolzer, R. Pitteloud, G. Bemardinelli, and K. Baettig, *Tetrahedron Lett.*, **24**, 4975 (1983); M. Yamaguchi, M. Hamada, S. Kawasaki, and T. Minami, *Chem. Lett.*, **1986**, 1085.

5) Y. Yamamoto, S. Hatsuya, and I. Yamada, *Tetrahedron Lett.*, **30**, 3445 (1989); Y. Yamamoto, S. Hatsuya, and J. Yamada, *J. Org. Chem.*, **55**, 3118 (1990).

6) a) M. Tanabe and D. F. Crowe, *J. Chem. Soc., Chem. Commun.*, **1973**, 564; b) C. Agami, J. Levisalles, and B. L. Cicero, *Tetrahedron,* **35**, 961 (1979); c) J. S. Panek and O. A. Bula, *Tetrahedron Lett.*, **29**, 1661 (1988).

7) a) K. B. White and W. Reusch, *Tetrahedron,* **24**, 2439 (1978); b) M. E. Krafft, R. M. Kennedy, and R. A. Holton, *Tetrahedron Lett.*, **27**, 2087 (1986); c) R. A. Holton, R. M. Kennedy, H.-B. Kim, and M. E. Krafft, *J. Am. Chem. Soc.*, **109**, 1597 (1987).

8) As recent reviews, M. Ihara and K. Fukumoto, *Yuki Gosei Kagaku Kyokaishi,* **44**, 96 (1986). See also the references cited therein.

9) R. A. Lee, *Tetruhedron Lett.*, **1973**, 3333; E. G. Gibbons, *J. Org. Chem.*, **45**, 1540 (1980); M. R. Roberts and R. H. Schlessinger, *J. Am. Chem. Soc.*, **103**, 724 (1981); E. G. Gibbons, *ibid.*, **104**, 1767 (1982).

10) T. Kametani, T. Honda, K. Fukumoto, M. Toyota, and M. Ihara, *Heterocycles,* **16**, 1673 (1981); M. E. Jung, C. A. McCombs, Y. Takeda, and Y.-G. Pan, *J. Am. Chem. Soc.*, **103**, 6677 (1981); M. Ihara, M. Toyota, K. Fukumoto, T. Kametani, and T. Honda, *J. Chem. Res., Synop.*, **1984**, 252.

11) An example of the Michael reaction of 2-silyloxy-1,3-dienes with enones is known, where the enolates of methyl ketones were only used and therefore provided no information on the stereoselectivity for the initial carbon-carbon bond formation (T. Mukaiyama, Y. Sagawa, and S. Kobayashi, *Chem. Lett.*, **1986**, 1821).

12) A. J. Bellamy, *J. Chem. Soc. B,* **1969**, 449.

13) Direct lithiation of 2-oxo-3-alkenylphosphonates with LDA or lithium bromide/amine bases resulted in the undesired polymerization of the starting enones (E. Wada, J. Funakoshi, and S. Kanemasa, unpublished results).

14) Y. Taniguchi, J. Inanaga, and M. Yamaguchi, *Bull. Chem. Soc. Jpn.*, **54**, 3229 (1981).

15) S. Danishefsky and C.-F. Yan, *J. Am. Chem. Soc.*, **101**, 7001 (1979).

16) R. E. Ireland, R. H. Muller, and A. K. Willard, *J. Am. Chem. Soc.*, **98**, 2868 (1976); Z. A. Fataftah, I. E. Kopka, and M. W. Rathke, *ibid.*, **102**, 3959 (1980).

17) D. A. Evans, "Stereoselective Alkylation Reactions of Chiral Metal Enolates," in "Asymmetric Synthesis," ed by J. D. Morrison, Academic Press, Inc., New York (1984), Vol. 3, Part B, Chap. 1, pp. 1—110.

18) P. Ballester, A. Costa, R. A. Garcia, and R. Mestres, *Tetrahedron Lett.*, **28**, 3853 (1987); E. D. Bergmann, D. Ginsburg, and R. Pappo, "The Michael Reaction," in "Organic Reactions," ed by R. Adams, New York (1959), Vol. 10, Chap. 3, pp. 179—555.

19) H.O. House, D. S. Crumrine, A. Y. Teranishi, and H. D. Olmstead, *J. Am. Chem. Soc.*, **95**, 3310 (1973).

20) Reactivity of the resulting zinc enolate was less than the corresponding lithium enolate. A somewhat higher reaction temperature was required.

21) C. H. Heathcock, C. T. Buse, W. A. Kleschick, M. C. Pirrung, J. E. Sohn, and J. Lampe, *J. Org. Chem.*, **45**, 1066 (1980).

22) M. Ihara, M. Toyota, K. Fukumoto, and T. Kametani, *Tetrahedron Lett.*, **25**, 2167 (1984).

23) (*Z*)-1-Phenyl-2-buten-1-one was synthesized by the MnO_2 oxidation of 1-phenyl-2-buten-1-ol followed by separation and purification by column chromatography.

24) D. A. Oare, M. A. Henderson, M. A. Sanner, and C. H. Heathcock, *J. Org. Chem.*, **55**, 132 (1990); D. A. Oare and C. H. Heathcock, *J. Org. Chem.*, **55**, 157 (1990).

25) R. C. Larock and J. C. Bernhardt, *J. Org. Chem.*, **43**, 710 (1978); D. B. Carr and J. Schwartz, *J. Am. Chem. Soc.*, **101**, 3521 (1979).

26) M. Takaya, P. Hong, and H. Yamazaki, *Chem. Lett.*, **1982**, 405.

Synthesis and Fluorescence Properties of Selectively Metallated Diporphyrins with Electron-Accepting Moieties

Toshi NAGATA
Department of Chemistry, Faculty of Science, Kyoto University, Kyoto 606
(Received May 29, 1991)

Synthesis of selectively metallated diporphyrins with electron-accepting moieties is described. Steady-state fluorescence spectra of these compounds showed substantial quenching of the fluorescence of the free-base porphyrin. A possible "superexchange" mechanism of long-range electron transfer is discussed.

At the initial stage of photosynthesis, an electron travels from the photoexcited (bacterio-)chlorophylls to the acceptor quinone producing a high-energy charge-separation state[1] which is utilized in the following dark processes. In the case of purple bacteria, the primary charge separation process consists of two (or three, as argued in recent reports[2]) consecutive electron transfer processes, with a bacteriopheophytin as an intermediate acceptor. The X-ray structures of bacterial photosynthetic reaction centers have been reported for several species,[3] and spatial arrangement of the chromophores is now known. However, it is still unclear what structural features are critically important for the complexes to function properly.

Many artificial chlorophyll- (or porphyrin-) quinone model compounds are being studied in order to relate

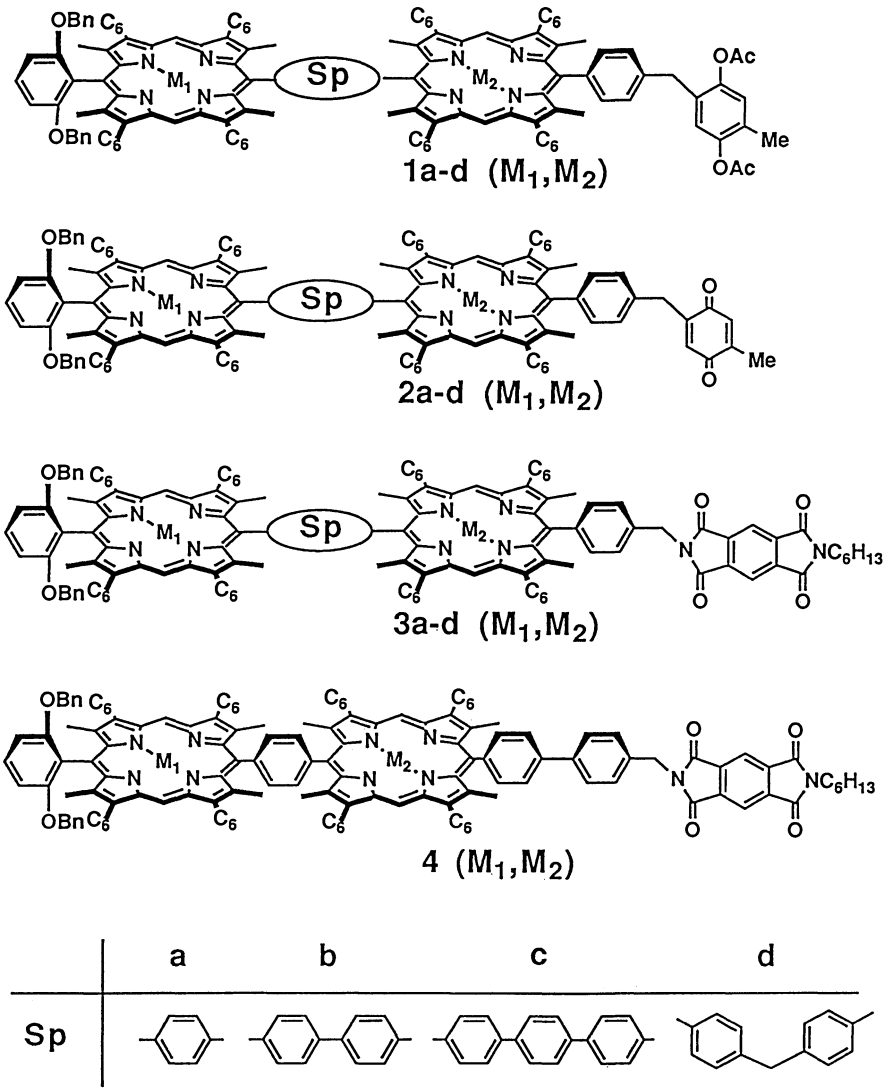

Chart 1.

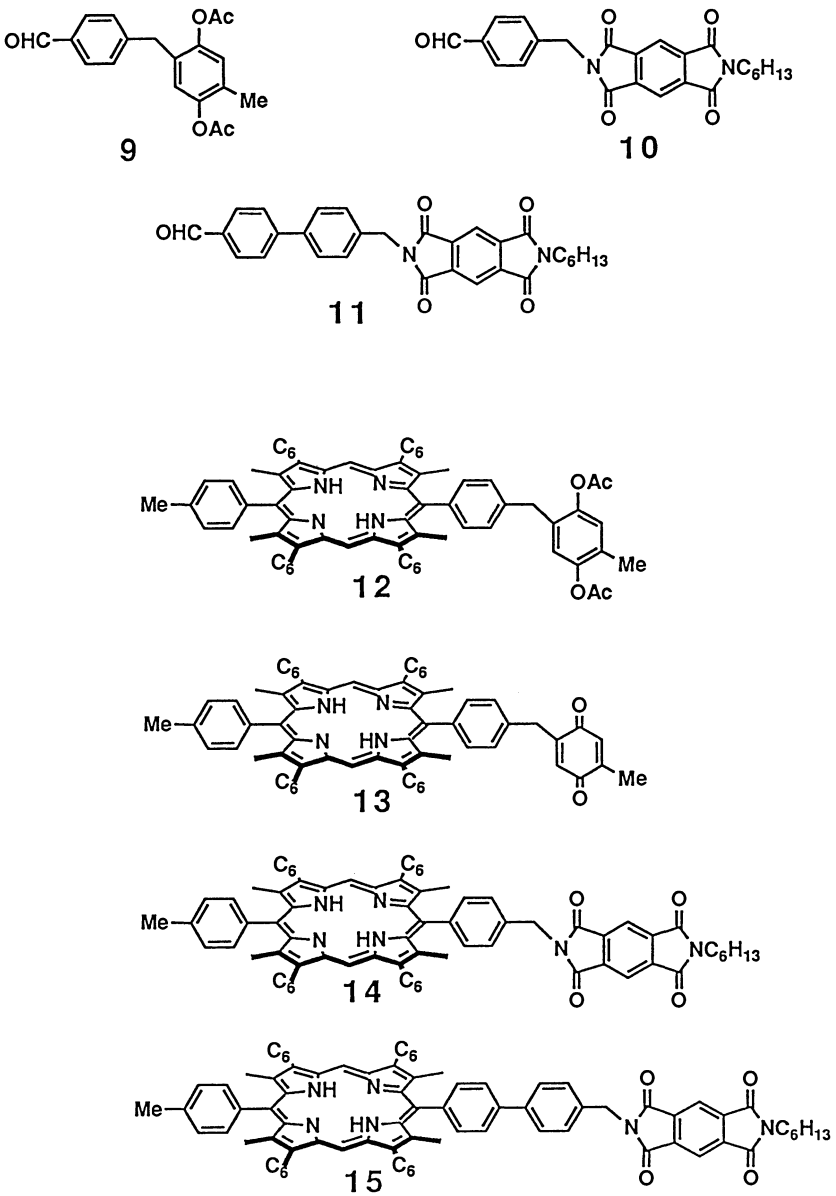

Chart 2.

the photophysical properties to the structural parameters.[4] In the course of our study on new photosynthetic model systems,[5] we designed partially metallated functionalized diporphyrins **1a**—**d** (H_2, Zn), **2a**—**d** (H_2, Zn), and **3a**—**d** (H_2, Zn) (Chart 1), as models for studying long-range electron-transfer reactions. The compounds **2a**—**d** and **3a**—**d** have the electron-accepting benzoquinone and 1,2:4,5-benzenebis (dicarboximide) (pyromellitic diimide) moieties, while the compounds **1a**—**d** are the reference compounds with the non-electron-accepting 1,4-diacetoxybenzene (hydroquinone diacetate) moiety. For each of these series, four compounds were prepared (**a**—**d**) with different types of bridging groups between the two porphyrins; 1,4-phenylene, 4,4′-biphenylylene, 4,4″-terphenylylene, and methylenebis(1,4-phenylene). The compound **4** was also prepared, in which the distance between the diimide moiety and the "distant" porphyrin (i.e. the one which is not directly bound to the diimide moiety) is the same as that in **3b** but the distances between the neighboring chromophores are different from those in **3b**. In these systems, it was expected that the photoinduced electron transfer would occur from the free-base porphyrin to the terminal acceptor, and that the intervening zinc porphyrin might play an important role during this electron transfer, as the "accessory" bacteriochlorophyll in the natural photosynthetic system might do.[6]

In this paper, the synthesis and steady-state fluorescence spectra of these compounds are reported and discussed. The keypoint in the synthetic strategy is to introduce a bulky 2,6-bis(benzyloxy)phenyl group on one end of the diporphyrin core. This group offered some regioselectivity of metal insertion which prefers the less hindered porphyrin ring. The steady-state

fluorescence spectra showed that the singlet excited state of the free-base porphyrin was quenched by the electron-accepting group. A possible "superexchange" mechanism of long-range electron transfer is also discussed.

Results and Discussion

Synthesis of Selectively Metallated Diporphyrins. The synthesis of functionalized free-base diporphyrins **1**, **2**, and **3** is shown in Scheme 1. Acid-catalyzed condensation[5e] of dipyrrolylmethane **5** with 2,6-bis(benzyloxy)-benzaldehyde and monoprotected aromatic dialdehyde **6** gave a mixture of three porphyrins. The cross-coupling product **7** was separated by column chromatography. The acetal **7** was hydrolyzed to give the corresponding aldehyde **8**, which was allowed to condense with dipyrrolylmethane **5** and functionalized aldehyde **9** (or **10**, **11**). The 1,4-diacetoxybenzene-linked diporphyrin **1** (or the diimide-linked diporphyrins **3**, **4**) was separated by column chromatography. The quinone-linked diporphyrin **2** was derived from **1**, by acidic hydrolysis of phenolic esters followed by oxidation with lead dioxide (Scheme 2). The functionalized monomeric porphyrins **12**, **14**, and **15** were synthesized by condensation of **5** with *p*-tolualdehyde and appropriate functionalized aldehyde, and separated and purified by column chromatography. The quinone-linked porphyrin **13** was derived from **12** in a similar manner as **1**.

Selectively metallated diporphyrins were synthesized by partial metallation followed by chromatographic separation. Treatment of free base of **1**, **2**, or **3** with a limited amount of zinc acetate (molar ratio $Zn(OAc)_2$/diporphyrin=0.5—1.0) in dichloromethane gave a mixture of four species, (Zn, Zn), (H_2, Zn), (Zn, H_2), and (H_2, H_2), which could be separated by flash column chromatography. The dizinc complex and the starting

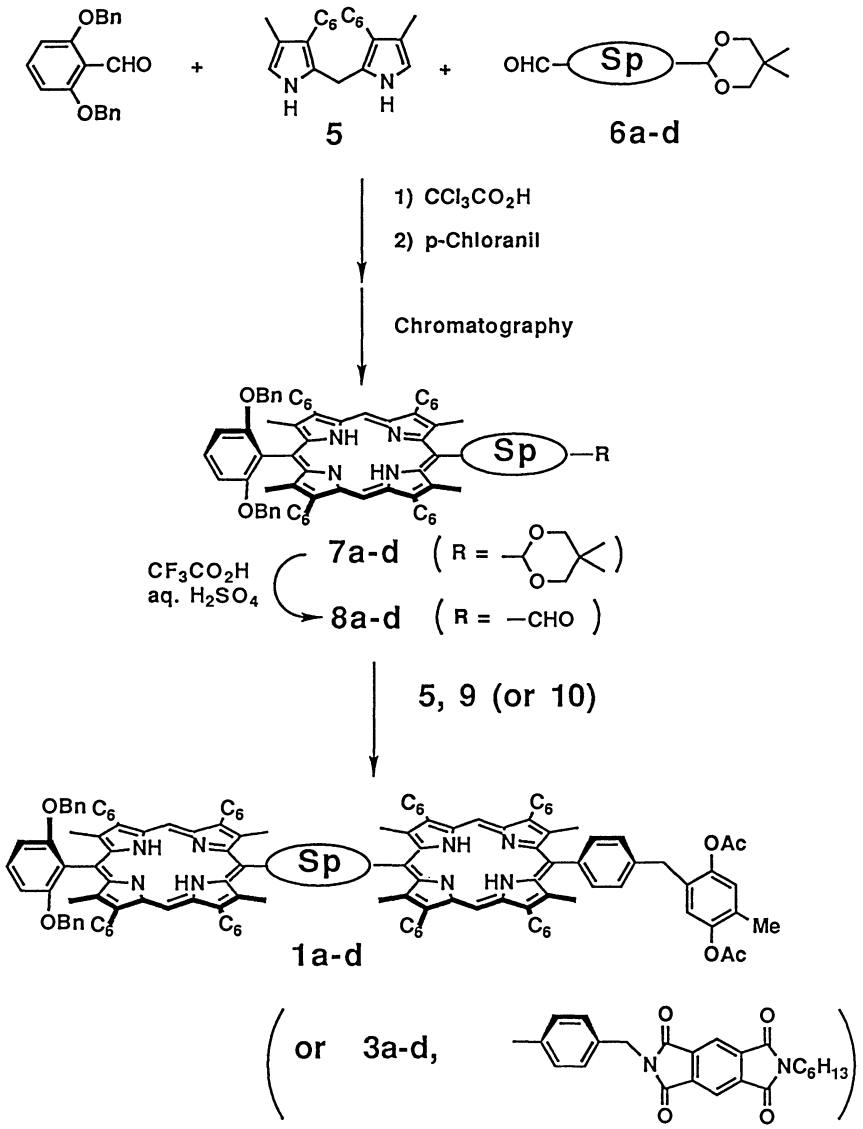

Scheme 1.

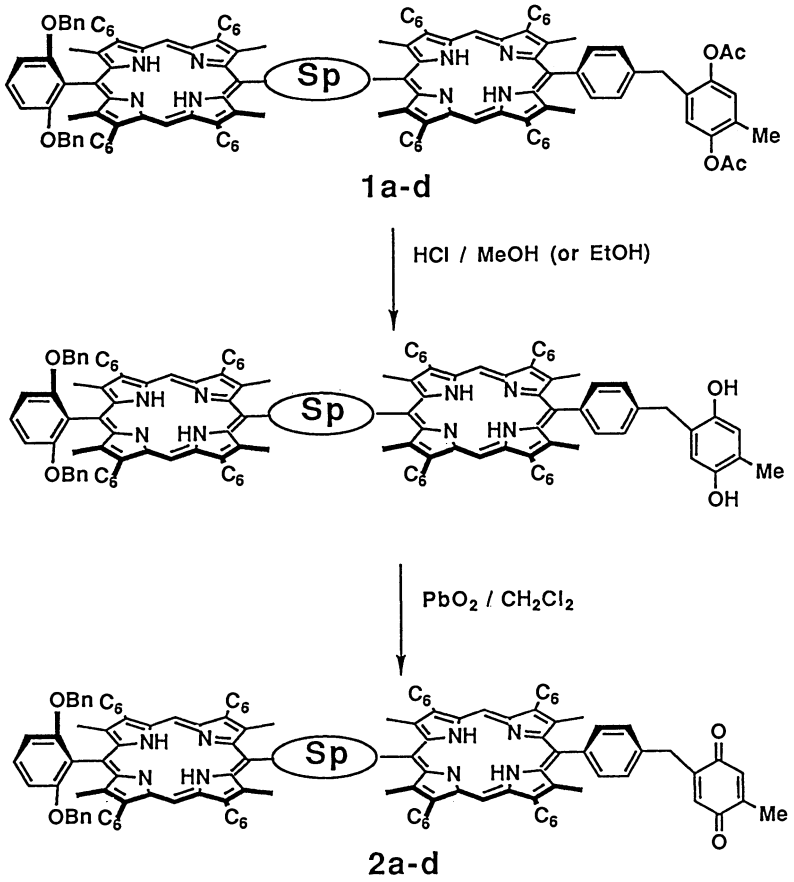

Scheme 2.

metal-free material were easily characterized using UV-visible spectroscopy. The remaining two species were characterized as monozinc complexes. Typical UV-spectra of dizinc complex, monozinc complex and metal-free diporphyrin are shown in Fig. 1. The Q-band (460 to 650 nm) absorption spectra of the free-base and dizinc diporphyrins showed the characteristic features of the monomeric free-base and zinc porphyrins, respectively (Fig. 1, A). On the other hand, the Q-band spectra of the monozinc complex was identical to the sum of those of monomeric free-base and zinc porphyrins (Fig. 1, B). The FAB (fast atom bombardment) mass spectra of these diporphyrins also showed the correct molecular weights of dizinc, monozinc, and free-base species.

Identification of the two monozinc species was a more subtle problem. In every experiment, one species (which moves slower on TLC than the other) was obtained in larger amount than the other (about 2.5 : 1). This major species was identified as the (H_2, Zn) complex based on the ^{1}H NMR spectral patterns of the porphyrin-NH protons. Figure 2 shows the high-field regions of ^{1}H NMR Spectra of metal-free **3d**, two monometallated **3d**'s (major and minor species), and monomeric porphyrins **8d** and **14**. The NH signals of **8d** appeared in lower field than those of **14**, probably due to the substituent effect of the 2,6-bis(benzyloxy)-phenyl group. The metal-free **3d** showed four signals in the NH region. The two signals in the lower field were assigned to the NH-protons of the bis(benzyloxy)-phenyl substituted ring, and the two signals in the higher field to those of the other ring. Comparison of the spectra of the two monozinc species with that of the free-base led to the conclusion that the "major" one is the (H_2, Zn) complex.

Sessler et al. reported synthesis of quinone-substituted monometallated diporphyrins.[4h] They observed complete regioselectivity in metallation of their systems, but this was not the case in the systems described here. Partial zinc insertion of **1**, **2**, and **3** always gave mixtures of all the four possible products, which were separated by column chromatography. Among the two monometallated species, one species was always obtained in higher yield, and this was identified as the (H_2, Zn) complex. Apparently, the porphyrin ring on the right side (in the drawings in Chart 1) was preferentially metallated over the ring on the left side. When the 2,6-bis(benzyloxy)phenyl group is replaced by a 2,6-dimethoxyphenyl group, the selectivity of metallation was much lower, and when the group is replaced by a hydrogen atom, essentially no selectivity was observed (data not shown). It is likely that the regioselectivity in metallation of **1**, **2**, and **3** (although not very high) is due to the bulkiness of the 2,6-bis(benzyloxy)phenyl group.

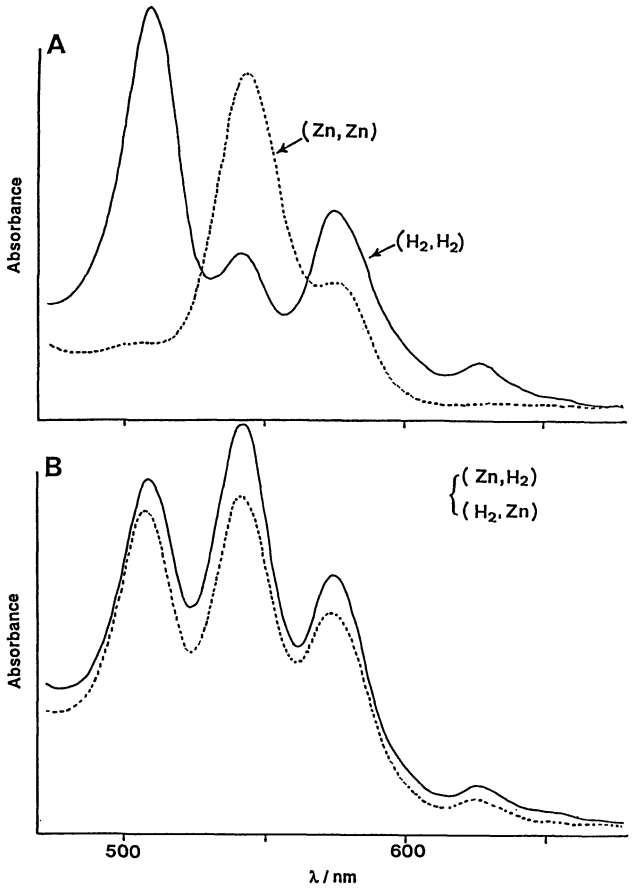

Fig. 1. Visible absorption spectra of metallated diporphyrins in THF. (A) **3d** (H_2, H_2) and **3d** (Zn, Zn). (B) Two isomeric monozinc complexes of **3d**. Solid line is the "major" complex, i.e. **3d** (H_2, Zn).

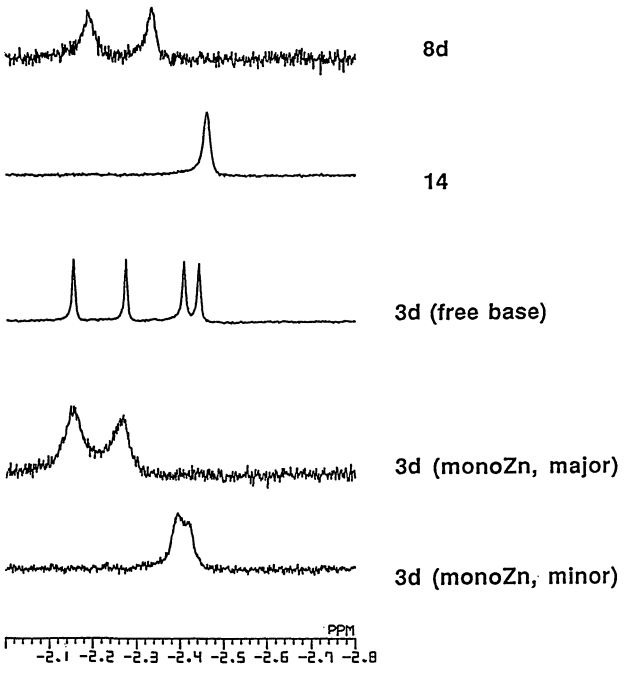

Fig. 2. ^{1}H NMR spectra of monomeric porphyrins and partially metallated diporphyrins in the high-field region.

Steady-State Fluorescence Spectra. In order to investigate the photophysical properties of monometallated diporphyrins, the fluorescence emission spectra were measured under steady-state conditions. The (H_2, Zn) compounds with attached acceptor moieties are of particular interest because of the possible long-range electron transfer from the free-base porphyrin to the acceptor.

When a THF solution of an (H_2, Zn) complex was irradiated by the 507 nm light (or 510 nm light in the case of **1a**, **2a**, and **3a**),[7] which was mainly absorbed by the free-base porphyrin moiety, characteristic emission spectrum of the free-base porphyrins was observed. Figure 3 shows the typical fluorescence spectra of the (H_2, Zn) diporphyrins with the diacetoxybenzene, quinone, and diimide moieties. The spectral shapes were essentially invariant with the various bridging groups and acceptor moieties, while the relative fluorescence intensities varied significantly. Table 1 shows the relative fluorescence intensities of these compounds (the

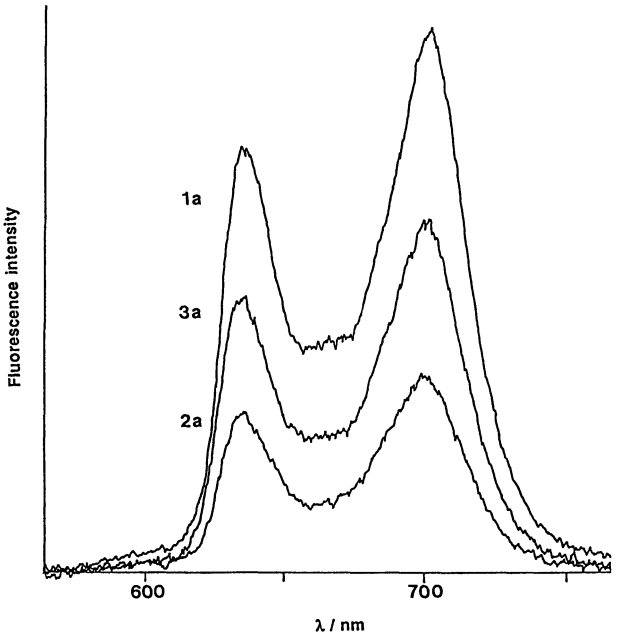

Fig. 3. Steady-state fluorescence spectra of **1a** (H_2, Zn), **2a** (H_2, Zn) and **3a** (H_2, Zn) in THF at 25 °C. Excitation at 510 nm.

Table 1. Relative Fluorescence Intensities of (H_2, Zn) Diporphyrins. Excitation at 507 nm (or 510 nm, Where Indicated). Emission at 700 nm. In THF, at 25 °C

	a	b	c	d
1	1[a)]	1	1	1
2	0.40[a)]	0.86	0.99	0.79
3	0.66[a)]	0.88	1.01	0.83
4	1.02[a)]			

a) Excitation at 510 nm.

corresponding 1,4-diacetoxybenzene-linked diporphyrins **1a**—**d** (H_2, Zn) were chosen as the references).[8] Two points should be noticed: (1) the fluorescence intensity is decreased when an acceptor moiety is present; the quinone moiety has a greater effect than the diimide moiety, and (2) the effect of the acceptor moiety is increased as the bridging group between the two porphyrin rings varies in the order 4,4″-terphenylylene< 4,4′-biphenylylene<methylenebis(1,4-phenylene)<1,4-phenylene.

It is reasonable to assume that the fluorescence of the free-base porphyrin is quenched through the electron transfer (ET) from the excited porphyrin to the acceptor quinone or diimide. A number of studies about porphyrin-quinone systems have confirmed that quinones readily accept an electron from excited molecules of porphyrins.[9] Recent transient-absorption studies have shown that quenching of porphyrin excited states by a diimide moiety also proceeds through an ET process.[10] Considering an ET quenching in the systems described here, one can explain why the quinone moiety worked as a more efficient quencher than the diimide moiety, as the ET reaction is more exothermic for the quinone than the diimide.[11] However, it is curious that the rate of "electron transfer" is unusually large for the very long donor-to-acceptor distance; k_{ET} was estimated to be 1.4×10^8 s^{-1} for **2a** (center-to-center distance 21 Å), while a rate constant less than 10^7 s^{-1} was reported for the bis(bicyclooctane) linked porphyrin-quinone system (center-to-center distance 18.8 Å).[12] It is very likely that a "superexchange" mechanism is working, in which the intervening zinc porphyrin acts as a mediator.[13]

The quenching efficiency clearly depends on the bridging group between the two porphyrins. As a general, the quenching becomes less efficient as the donor-to-acceptor distance becomes larger. However, the compound **4** offers a problem; although **4** has the same donor-to-acceptor distance as **3b**, **4** showed practically no quenching while **3b** showed quenching of 12% efficiency. The theory of superexchange can explain such a difference. It has been shown[12] that the rate of superexchange electron transfer in a D–I–A system (D, I, and A denote donor, intermediate, and acceptor) depends on the product of two transfer integrals V_{DI} and V_{IA}. In the present case, D is the free-base porphyrin, I is the zinc porphyrin, and A is the acceptor. The compound **3b** has a shorter distance between D and I and a longer distance between I and A than the compound **4**. Although there is no estimation for the values of V_{DI} and V_{IA} from the experimental data at present, the reported rates of electron transfer between two chromophores with similar geometries may be suggestive. Osuka et al. reported the rates of electron transfer in zinc–iron(III) hybrid diporphyrins;[14] 7.4×10^{10} s^{-1} for the 1,4-phenylene bridged diporphyrin and 1.6×10^{10} s^{-1} for the 4,4′-biphenylylene bridged one. The same authors also reported the rates of energy transfer in zinc–(free base) hybrid diporphyrins;[15] 6.6×10^{10} s^{-1} for the 1,4-phenylene bridged one and 7.8×10^9 s^{-1} for the 4,4′-biphenylylene bridged one. Insertion of one additional 1,4-phenylene group resulted in the decrease of the rate by a factor of 4.6 (electron transfer) or 8.5 (energy transfer). On the other hand, the fluorescence quantum yields of the two imide-linked (mono)porphyrins **14**-Zn and **15**-Zn were measured (relative values to **12**-Zn), and it was found that the fluorescence quenching in the latter was 100 times slower than in the former. These results show that, when one additional phenyl group is inserted between the two chromophores, the effect of this insertion upon the rates of electron (or energy) transfer is greater for the porphyrin–imide systems than for the porphyrin–porphyrin systems. Thus it may be possible that V_{IA} drops more severely in **4** than V_{DI} rises and hence the rate of electron transfer is smaller in **4** than in **3b**, only if it can be generally stated that the porphyrin–imide interaction is more sensitive to the distance than the porphyrin–porphyrin interaction.

Conclusion

A new series of selectively metallated diporphyrin-acceptor systems **1**, **2**, and **3** were synthesized. Introduction of a bulky substituent at one end of the diporphyrin led to preferential formation of the (H_2, Zn) isomer over the (Zn, H_2) isomer, when metallated with a limited amount of zinc acetate. Although the selectivity was not complete, the (H_2, Zn) isomers of **1**—**3** were readily purified by column chromatography, with sufficient purity for spectroscopic studies.

The (H_2, Zn) complexes of **2** and **3** showed substantial quenching of the fluorescence of the free-base porphyrin moiety. It is likely that a long-distance, superexchange electron transfer is responsible for this quenching. Synthesis and spectroscopic studies of other "partially metallated" functionalized oligoporphyrins are currently under way.

Experimental

General. For synthetic use, tetrahydrofuran (THF), dichloromethane, acetonitrile, and acetone were refluxed over and distilled from sodium benzophenone ketyl, P_2O_5, CaH_2, and $CaSO_4$, respectively. *N,N*-Dimethylformamide (DMF) was distilled under reduced pressure and stored over molecular sieves. Other solvents and reagents were reagent grade. Melting points were measured on a Yanagimoto micro melting point apparatus and are uncorrected. Preparative separations were usually performed by flash column chromatography on silica gel (Merck, Kieselgel 60H, Art. 7736).

UV-visible spectra were obtained with a Shimadzu UV-3000 spectrometer. Steady-state fluorescence spectra were taken on a Shimadzu RF-502A spectrofluorimeter. ^1H NMR spectra were recorded on a JEOL GX-400 spectrometer (operating at 400 MHz), chemical shifts being reported in the delta scale (ppm) relative to Me_4Si. Mass spectra were recorded on JEOL DX-300 and HX-110 spectrometers. For porphyrin

compounds, the positive-FAB (fast atom bombardment) ionization method was used (accelerating voltage 1.5 kV and 10 kV, Xe atom as the primary ion source). The FAB matrix was 3-nitrobenzyl alcohol/chloroform.

2,6-Bis(benzyloxy)benzaldehyde. Synthesized from 2,6-dihydroxybenzoic acid by the following sequence: (1) conversion to the methyl ester (diazomethane in THF, r.t., 98%), (2) conversion to the bis(benzyloxy) derivative by treatment with benzyl bromide (2.2 equiv) in the presence of K_2CO_3 (2.5 equiv) in acetone (reflux overnight, 71%), (3) reduction to the primary alcohol ($LiAlH_4$ in THF, r.t., 96%), and finally (4) oxidation to the aldehyde (1.2 equiv of PCC (pyridinium chlorochromate) in CH_2Cl_2, r.t., 5.5 h, 98%). Pale yellow needles, mp 76—77 °C (EtOH). ^{1}H NMR δ=10.66 (1H, s), 7.47 (4H, d, J=7.0 Hz), 7.40 (5H, m), 7.32 (2H, m), 6.63 (2H, d, J=8.5 Hz), 5.19 (4H, s). Found: H, 5.63; C, 79.16%. Calcd. for $C_{21}H_{18}O_3$: H, 5.70; C, 79.23%.

Bis(3-hexyl-4-methyl-2-pyrrolyl)methane (5). The compound **5** was synthesized from ethyl 3,5-dimethyl-4-hexyl-2-pyrrolecarboxylate[16] by the following sequence: (1) conversion to bis(5-ethoxycarbonyl-3-hexyl-4-methyl-2-pyrrolyl)-methane, via 5-acetoxymethyl derivative of the starting pyrrole,[17] (2) alkaline hydrolysis of the ester groups and decarboxylation.[18] The compound **5** was purified by passing its solution in CH_2Cl_2 through a short column of silica gel. Dark brown oil, which can be stored for about a month in the freezer. Purity was checked by ^{1}H NMR before use. ^{1}H NMR δ=7.39 (2H, br), 6.37 (2H, s), 3.81 (2H, s), 2.40 (4H, t, J=7.8 Hz), 2.04 (6H, s), 1.46 (4H, m), 1.30 (12H, m), 0.89 (6H, t, J=6.9 Hz).

4-(5,5-Dimethyl-1,3-dioxan-2-yl)benzaldehyde (6a). This aldehyde was synthesized from methyl 4-formylbenzoate by the following sequence: (1) protection of the formyl group by 2,2-dimethyl-1,3-propanediol (1.1 equiv, 0.1 equiv of *p*-toluenesulfonic acid, benzene, reflux, 2 h, 100%), (2) reduction to the primary alcohol (2 equiv of $LiAlH_4$, THF, 0 °C to r.t., 4 h, 75%), (3) oxidation to the aldehyde (1.5 equiv of PCC, 0.4 equiv of anhydrous sodium acetate, CH_2Cl_2, r.t., 3 h, 92%). Mp 60—63 °C (lit,[19] 59—62 °C).

4′-(5,5-Dimethyl-1,3-dioxan-2-yl)-[1,1′-biphenyl]-4-carbaldehyde (6b). [1,1′-Biphenyl]-4,4′-dicarbaldehyde (2.0 g, 9.5 mmol) was treated with 2,2-dimethyl-1,3-propanediol (1.0 g, 9.5 mmol) in the presence of *p*-toluenesulfonic acid (0.19 g, 1.0 mmol) in 150 ml of benzene (reflux, 2 h). The reaction mixture was cooled and shaken with saturated aqueous solution of $NaHCO_3$ (30 ml). The orange solution turned colorless and white precipitates appeared. The precipitates (bis-acetal compound) were removed by filtration and the filtrate was washed with water, dried and evaporated. The mixture was then treated with $LiAlH_4$ (360 mg, 9.5 mmol) in THF. After usual workup, the mixture was separated by column chromatography (eluted with CH_2Cl_2/Et_2O). The second fraction was collected (380 mg) and treated with PCC (388 mg, 1.8 mmol) in the presence of sodium acetate (40 mg). The monoprotected aldehyde **6b** was obtained (329 mg, 12%). ^{1}H NMR δ=10.06 (1H, s), 7.95 (2H, d, J=8.5 Hz), 7.74 (2H, d, J=8.2 Hz), 7.63 (4H, ABq), 5.46 (1H, s), 3.80 (2H, d, J=9.9 Hz), 3.68 (2H, d, J=10.7 Hz), 1.32 (3H, s), 0.82 (3H, s).

The compound **6c** and **6d** was synthesized in a similar manner as **6b**. The compound data are listed below:

6c: ^{1}H NMR δ=10.04 (1H, s), 7.94 (2H, d, J=8.6 Hz), 7.77 (2H, d, J=8.2 Hz), 7.68 (4H, s), 7.60 (4H, ABq), 5.43 (1H, s), 3.78 (2H, d, J=11.3 Hz), 3.66 (2H, d, J=10.6 Hz), 1.30 (3H, s), 0.80 (3H, s).

6d: ^{1}H NMR δ=9.96 (1H, s), 7.77 (2H, d, J=7.8 Hz), 7.45 (2H, d, J=7.8 Hz), 7.31 (2H, d, J=7.8 Hz), 7.19 (2H, d, J=8.0 Hz), 5.37 (1H, s), 4.05 (2H, s), 3.76 (2H, d, J=10.8 Hz), 3.64 (2H, d, J=11.0 Hz), 1.29 (3H, s), 0.79 (3H, s).

Methyl 4-[(2,5-Dimethoxy-4-methylphenyl)methyl]benzoate. The precursor ketone, methyl 4-(2,5-dimethoxy-4-methylbenzoyl)benzoate, was prepared from 4-methoxycarbonylbenzoyl chloride and 2,5-dimethoxytoluene ($SnCl_4$, CH_2Cl_2, reflux). A mixture of this ketone (2.04 g, 6.49 mmol), KOH (1.82 g, 32 mmol), hydrazine monohydrate (4.87 g, 97 mmol), and diethylene glycol (50 ml) was heated to 200 °C. The color of the solution changed from yellow via red-orange to colorless. After 5.5 h, the reaction mixture was poured into ice water, and acidified by hydrochloric acid. The white precipitates were collected, washed with water, dissolved again in aqueous NaOH solution, and precipitated again by adding dilute hydrochloric acid. The precipitates were filtered and washed with water, and dissolved in chloroform. The solution was dried over Na_2SO_4 and evaporated, to give 4-[(2,5-dimethoxy-4-methylphenyl)methyl]benzoic acid (1.77 g, 6.18 mmol, 95%). This was converted to the methyl ester by treatment with methyl iodide (1.6 equiv) and potassium carbonate (2.5 equiv) in acetone (reflux, overnight). The inorganic substance was removed by filtration, and acetone and excess MeI were removed by rotary evaporation. The residue was dissolved in CH_2Cl_2, washed with water, dried, and evaporated. The residual yellow oil crystallized on standing. Yield: 96%. Mp 79—80 °C (EtOH). ^{1}H NMR δ=7.92 (2H, d, J=8.2 Hz), 7.25 (2H, d, J=7.9 Hz), 6.70 (1H, s), 6.57 (1H, s), 3.98 (2H, s), 3.89 (3H, s), 3.73 (3H, s), 3.72 (3H, s). Found: H, 6.70; C, 71.79%. Calcd for $C_{18}H_{20}O_4$: H, 6.71; C, 71.98%.

4-[(2,5-Diacetoxy-4-methylphenyl)methyl]benzaldehyde (9). The methyl ester derivative (see above) was converted to the corresponding aldehyde in two steps ($LiAlH_4$ in THF, 0 °C to r.t., 6.5 h, 89%; PCC in CH_2Cl_2, r.t., 3 h, 89%). This aldehyde (1.25 g, 4.6 mmol) was dissolved in 50 ml of acetonitrile (reagent grade), and a solution of cerium(IV) ammonium nitrate (5.5 g, 10.1 mmol) in 20 ml of water was dropwise added over 30 min. After 2 h, water (50 ml) was added to the bright yellow solution, and the mixture was extracted with CH_2Cl_2. The extract was washed with water and evaporated. The residual orange oil was purified by flash column chromatography (R_f=0.5, CH_2Cl_2). This product (826 mg, 3.4 mmol) was dissolved in 15 ml of acetic anhydride, and this solution was added dropwise to a suspension of zinc dust (530 mg, 8 mmol) and anhydrous sodium acetate (290 mg) in acetic anhydride (5 ml) at 0 °C (under N_2). The mixture was stirred overnight, filtered to remove inorganic salts. The solvent was removed in vacuo, and the residual white solid was dissolved in ethyl acetate, washed with water and brine, dried, and evaporated. Yield: 1.06 g (3.2 mmol, 96%). Mp 107—108 °C (EtOH). ^{1}H NMR δ=9.97 (1H, s), 7.79 (2H, d, J=8.3 Hz), 7.31 (2H, d, J=8.3 Hz), 6.96 (1H, s), 6.80 (1H, s), 3.92 (2H, s), 2.28 (3H, s) 2.17 (3H, s), 2.15 (3H, s). Found: H, 5.48; C, 69.31%. Calcd for $C_{19}H_{18}O_5$: H, 5.56; C, 69.93%.

***N*-Hexyl-*N*′-[(4-formylphenyl)methyl]-1,2 : 4,5-benzenebis(dicarboximide) (10).** A precursor of this compound, 4-(5,5-dimethyl-1,3-dioxan-2-yl)benzylamine was synthesized in 2 steps from 4-cyanobenzaldehyde: (1) protection of the formyl group (1.1 equiv of 2,2-dimethyl-1,3-propanediol, 0.1 equiv of *p*-toluenesulfonic acid, benzene, reflux 1.5 h, 98%), (2) reduc-

tion to the primary amine ($LiAlH_4$, ether/THF, 0 °C, 5 h, 96%). This amine (6.6 g, 30 mmol) and hexylamine (9.1 g, 90 mmol) was dissolved in 150 ml of DMF, and a solution of 1,2:4,5-benzenetetracarboxylic dianhydride (13.1 g, 60 mmol) in 80 ml of DMF was added. The mixture was heated to reflux overnight and cooled. The precipitates were collected by filtration. TLC showed three products (CH_2Cl_2), and the second one was collected by column chromatography. This product (2.2 g, 4.4 mmol, 15%) was treated with acid to hydrolyze the acetal protecting group ($CHCl_3$ 50 ml, trifluoroacetic acid 20 ml, 5% aqueous H_2SO_4 15 ml, r.t., overnight). The mixture was poured into water and the organic layer was separated, washed with $NaHCO_3$ solution and water, dried and evaporated. Yield: 1.4 g (3.2 mmol, 73%). Mp>300 °C (benzene). ^1H NMR δ=9.99 (1H, s), 8.28 (2H, m), 7.86 (2H, d, J=8.3 Hz), 7.59 (2H, d, J=8.0 Hz), 4.96 (2H, s), 3.73 (2H, t, J=7.4 Hz), 1.69 (2H, m), 1.31 (6H, m), 0.87 (3H, m). Found: H, 5.05; C, 68.86; N, 6.72%. Calcd for $C_{24}H_{22}N_2O_5$: H, 5.30; C, 68.89; N, 6.69%.

4′-(5,5-Dimethyl-1,3-dioxan-2-yl)-[1,1′-biphenyl]-4-methanamine. To a solution of the monoprotected aldehyde **6b** (445 mg, 1.5 mmol) in a mixture of ethanol (50 ml) and CH_2Cl_2 (10 ml) was added a solution of hydroxylamine hydrochloride (118 mg, 1.7 mmol) and sodium carbonate (95 mg, 0.9 mmol) in 2.5 ml of water. The solution became opaque and white precipitates appeared. The mixture was stirred overnight at room temperature, then poured into 100 ml of water, extracted with CH_2Cl_2, washed with water, dried, and evaporated. The white solid was washed with hexane and dried in vacuo to give an oxime (346 mg, 1.1 mmol, 74%). This oxime (1 mmol) was treated with $LiAlH_4$ (2 mmol) in 17 ml of THF (70 °C, 6 h). After cooling, 1 ml of water and 1 ml of 10% NaOH solution was added, the solid was removed by filtration (washed by ether), and the filtrate was washed with brine, dried, and evaporated. Yield: 240 mg (0.81 mmol, 81%). ^1H NMR δ=7.58 (6H, m), 7.37 (2H, d, J=8.3 Hz), 5.44 (1H, s), 3.90 (2H, s), 3.79 (2H, d, J=11.3 Hz), 3.67 (2H, d, J=10.7 Hz), 1.31 (3H, s), 0.81 (3H, s).

***N*-Hexyl-*N*′-[[4′-formyl-[1,1′-biphenyl]-4-yl]methyl]-1,2:4,5-benzenebis(dicarboximide) (11).** This compound was synthesized from the above-described amine (0.67 mmol), hexylamine (6.0 mmol) and 1,2:4,5-benzenetetracarboxylic dianhydride (6.7 mmol) in a similar manner as **10**. Yield: 144 mg (0.29 mmol, 43%). ^1H NMR δ=10.05 (1H, s), 8.28 (2H, s), 7.93 (2H, d, J=8.2 Hz), 7.71 (2H, d, J=8.5 Hz), 7.61 (2H, d, J=8.5 Hz), 7.56 (2H, d, J=8.3 Hz), 4.95 (2H, s), 3.73 (2H, t, J=7.3 Hz), 1.69 (2H, m), 1.31 (6H, m), 0.88 (3H, m).

Synthesis of Formyl Porphyrins. 5-[2,6-Bis(benzyloxy)-phenyl]-15-(4-formylphenyl)-2,8,12,18-tetrahexyl-3,7,13,17-tetramethylporphine (8a). 2,6-Bis(benzyloxy)benzaldehyde (425 mg, 1.33 mmol), 4-(5,5-dimethyl-1,3-dioxan-2-yl)benzaldehyde **6a** (294 mg, 1.33 mmol), and bis(3-hexyl-4-methyl-2-pyrrolyl)methane **5** (913 mg, 2.67 mmol) were dissolved in 35 ml of acetonitrile. Trichloroacetic acid (131 mg, 0.80 mmol) was added, and the mixture was stirred overnight (room temperature, under nitrogen, in the dark). A solution of *p*-chloranil (1.0 g, 4.1 mmol) in a minimum amount of tetrahydrofuran was added, and the mixture was stirred for 5 h. The solvent was evaporated and the residue was taken up in chloroform, washed with saturated $NaHCO_3$ solution and water, and dried over Na_2SO_4. To this chloroform solution was added 5 ml of saturated solution of zinc acetate in methanol, and the mixture was heated to reflux for 2 h. After cooling, the reaction mixture was washed with water, dried over Na_2SO_4 and evaporated. TLC showed three products (R_f=0.8, 0.5, and 0.3, benzene) and the second was separated by column chromatography (benzene). Yield of **7a** (zinc complex): 612 mg (0.492 mmol, 37%).

The compound **7a** zinc complex (419 mg, 0.337 mmol) was dissolved in a mixture of trifluoroacetic acid (10 ml), acetic acid (20 ml) and 5% aqueous sulfuric acid (5 ml). After being heated at 100 °C for 1.5 hours, the mixture was poured into 150 ml of water and extracted with CH_2Cl_2. The organic phase was washed with saturated $NaHCO_3$ solution (effervescence!), dried over Na_2SO_4, and evaporated. The residue was triturated and washed in methanol and dried in vacuo. Yield of **8a**: 303 mg (0.277 mmol, 82%). Mp 163—167 °C. ^1H NMR δ=10.40 (1H, s, CHO), 10.22 (2H, s, meso), 3.97 (8H, m, hexyl-1), 2.57 (6H, s, Me), 2.46 (6H, s, Me), 2.19 (8H, m, hexyl-2), 1.73 (8H, m, hexyl-3), 1.46 (8H, m, hexyl-4), 1.37 (8H, m, hexyl-5), 0.90 (12H, m, hexyl-6), −2.2 (2H, br, NH); 5-Ph: 7.62 (1H, t, J=8.5 Hz), 7.00 (2H, d, J=8.8 Hz); 15-Ph: 8.28 (4H, AB quartet); benzyloxy: 6.85 (2H, t, J=7.3 Hz), 6.72 (4H, t, J=7.9 Hz), 6.58 (4H, d, J=7.3 Hz), 4.94 (4H, s).

The compounds **8b**, **8c**, and **8d** was prepared in the similar manner as **8a**. The compound data are listed below:

8b: Yield (2 steps) 24%. Mp. 195—200 °C. ^1H NMR δ=10.22 (2H, s, meso), 10.18 (1H, s, CHO), 3.99 (8H, m, hex-1), 2.57 (6H, s, Me), 2.56 (6H, s, Me), 2.20 (8H, m, hex-2), 1.74 (8H, m, hex-3), 1.48 (8H, m, hex-4), 1.35 (8H, m, hex-5), 0.90 (12H, m, hex-6), −2.3 to −2.5 (2H, br, NH); 5-Ph: 7.62 (1H, t, J=8.3 Hz), 7.01 (2H, d, J=8.8 Hz); biphenylylene: 8.20 (2H, d, J=8.3 Hz), 8.13 (4H, s), 7.61 (2H, d, J=8.3 Hz) benzyloxy: 6.85 (2H, t, J=7.8 Hz), 6.72 (4H, t, J=7.6 Hz), 6.58 (4H, d, J=7.3 Hz), 4.94 (4H, s).

8c: Yield (2 steps) 20%. Mp 181—185 °C. ^1H NMR δ=10.22 (2H, s, meso), 10.12 (1H, s, CHO), 4.00 (8H, m, hex-1), 2.58 (6H, s, Me), 2.57 (6H, s, Me), 2.21 (8H, m, hex-2), 1.74 (8H, m, hex-3), 1.48 (8H, m, hex-4), 1.38 (8H, m, hex-5), 0.90 (12H, m, hex-6), −2.15 (1H, s, NH), −2.26 (1H, s, NH); 5-Ph: 7.62 (1H, t, J=8.3 Hz), 7.01 (2H, d, J=8.3 Hz); terphenyl: 8.18 (2H, d, J=8.3 Hz), 8.10 (2H, d, J=8.3 Hz), 8.07 to 8.03 (4H, 2 doublets), 7.92 (2H, d, J=8.3 Hz), 7.90 (2H, d, J=8.3 Hz); benzyloxy: 6.85 (2H, t, J=7.3 Hz), 6.72 (4H, t, J=7.9 Hz), 6.58 (4H, d, J=7.3 Hz), 4.94 (4H, s).

8d: Yield (2 steps) 32%. Mp 52—58 °C. ^1H NMR δ=10.20 (2H, s, meso), 10.10 (1H, s, CHO), 3.98 (8H, m, hex-1), 2.57 (6H, s, Me), 2.51 (6H, s, Me), 2.19 (8H, m, hex-2), 1.74 (8H, m, hex-3), 1.46 (8H, m, hex-4), 1.36 (8H, m, hex-5), 0.90 12H, m, hex-6), −2.2 (2H, NH); 5-Ph: 7.62 (1H, t), 7.00 (2H, d, J=8.3 Hz); $PhCH_2Ph$: 8.02 (2H, d, J=7.8 Hz), 7.98 (2H, d, J=7.8 Hz), 7.62 (2H, d), 7.55 (2H, d, J=7.3 Hz), 4.44 (2H, s); benzyloxy: 6.84 (2H, t, J=7.3 Hz), 6.71 (4H, t, J=7.6 Hz), 6.57 (4H, d, J=7.8 Hz), 4.93 (4H, s).

Synthesis of Free-Base Diporphyrins. 15-[2,6-Bis(benzyloxy)phenyl]-15′-[4-[(2,5-diacetoxy-4-methylphenyl)methyl]-phenyl]-5,5′-(1,4-phenylene)bis[2,8,12,18-tetrahexyl-3,7,13,17-tetramethylporphine] (1a). The formylporphyrin **8a** (147 mg, 0.13 mmol) was dissolved in 15 ml of acetonitrile containing 57 mg (0.35 mmol) of trichloroacetic acid. The aldehyde **9** (261 mg, 0.80 mmol) in 5 ml of CH_3CN and **5** (319 mg, 0.93 mmol) in 5 ml of CH_3CN were added, and the mixture was stirred overnight (room temperature, under N_2, dark). A solution of *p*-chloranil (344 mg, 1.4 mmol) in a minimum amount of tetrahydrofuran was added, and the mixture was stirred for additional 3 h. The reaction mixture was poured into 100 ml

of water, extracted with CH_2Cl_2, washed with $NaHCO_3$ solution and dried over Na_2SO_4. This dichloromethane solution was treated with a saturated solution of zinc acetate in methanol (5 ml, 2 h reflux), washed with water, dried and evaporated. At this stage, all porphyrinic products were separated from tarry materials by column chromatography (CH_2Cl_2, R_f=0.8 to 1.0). This mixture of zinc porphyrins were dissolved in dichloromethane and shaken with two portions of 4 M (1 M=1 mol dm^{-3}) hydrochloric acid, neutralized with $NaHCO_3$ solution, dried and evaporated, to give a mixture of free-base porphyrins. The mixture was separated by column chromatography (CH_2Cl_2+Et_2O) to give two products (R_f=0.6 and 0.3, CH_2Cl_2/Et_2O (v/v)=100/5). The second fraction was the diporphyrin **1a**. Yield: 116 mg (56 mmol, 43%). Mp 134—140 °C. ^{1}H NMR δ=10.34 (2H, s, meso), 10.32 (2H, s, meso), 4.15 (8H, m, hex-1), 4.04 (8H, m, hex-1), 3.20 (12H, s, Me), 2.61 (6H, s, Me), 2.54 (6H, s, Me), 2.32 (8H, m, hex-2), 2.25 (8H, m, hex-2), 1.86 (8H, m, hex-3), 1.78 (8H, m, hex-3), 1.6—1.4 (m, hex-4 and hex-5), 1.0—0.9 (24H, m, hex-6); bridging phenylene: 8.58 (4H, s); 15-phenyl: 7.64 (1H, t, J=8.3 Hz), 7.03 (2H, d, J=8.8 Hz); benzyloxy: 6.88 (2H, t, J=7.3 Hz), 6.76 (4H, t, J=7.6 Hz), 6.62 (4H, d, J=7.3 Hz), 4.98 (4H, s); 15′-substituent: 8.02 (2H, d, J=8.3 Hz), 7.55 (2H, d, J=7.8 Hz), 7.12 (1H, s), 7.10 (1H, s), 4.24 (2H, s, benzylic), 2.44 (3H, s, acetyl), 2.43 (3H, s, acetyl), 2.27 (3H, s). MS m/z 2065 ($M+H^+$), 1032 (doubly charged ion).

The compounds **1b**, **1c**, and **1d** were prepared in the similar manner as **1a**. The compound data are listed below:

1b: Yield 69%. Mp 279—283 °C. ^{1}H NMR δ=10.29 (2H, s, meso), 10.27 (2H, s, meso), 4.0 (16H, m, hex-1), 2.75 (12H, s, Me), 2.60 (6H, s, Me), 2.53 (6H, s, Me), 2.24 (16H, m, hex-2), 1.77 (16H, m, hex-3), 1.5 (m, hex-4), 1.40 (m, hex-5), 0.93 (m, hex-6), −2.12 (1H, br, NH), −2.18 (1H, br, NH), −2.29 (1H, br, NH), −2.35 (1H, br, NH); bridging biphenylylene: 8.34 (8H, m); 15-phenyl: 7.64 (1H, t), 7.02 (2H, d, J=8.3 Hz); benzyloxy: 6.87 (2H, t, J=6.8 Hz), 6.74 (4H, t, J=7.8 Hz), 6.61 (4H, d, J=7.3 Hz), 4.96 (4H, s); 15′-substituent: 8.02 (2H, d, J=7.8 Hz), 7.54 (2H, d, J=7.8 Hz), 7.11 (1H, s), 7.09 (1H, s), 4.23 (2H, s, benzylic), 2.44 (3H, s, acetyl), 2.43 (3H, s, acetyl), 2.26 (3H, s). MS m/z 2141 ($M+H^+$).

1c: Yield 55%. Mp>300 °C. ^{1}H NMR δ=10.27 (2H, s, meso), 10.25 (2H, s, meso), 4.02 (16H, m, hex-1), 2.65 (12H, 2s, Me), 2.59 (6H, s, Me), 2.52 (6H, s, Me), 2.22 (16H, m, hex-2), 1.76 (16H, m, hex-3), 1.5 (m, hex-4), 1.39 (m, hex-5), 1.92 (m, hex-6), −2.2 (1H, br, NH), −2.3 (1H, br, NH), −2.4 (2H, br, NH); bridging terphenyl: 8.23 (12H, m); 15-phenyl: 7.63 (1H, t), 7.02 (2H, d, J=8.8 Hz); benzyloxy: 6.86 (2H, t, J=6.8 Hz), 6.73 (4H, t, J=7.6 Hz), 6.60 (4H, d, J=7.4 Hz), 4.95 (4H, s); 15′-substituent: 8.01 (2H, d, J=7.8 Hz), 7.54 (2H, d, J=7.8 Hz), 7.11 (1H, s), 7.08 (1H, s), 4.23 (2H, s, benzylic), 2.46 (3H, s, acetyl), 2.42 (3H, s, acetyl), 2.26 (3H, s, Me). MS m/z 2217 ($M+H^+$).

1d: Yield 76%. Mp 100—105 °C. ^{1}H NMR δ=10.26 (2H, s, meso), 10.24 (2H, s, meso), 4.00 (16H, m, hex-1), 2.64 (12H, s, Me), 2.59 (6H, s, Me), 2.52 (6H, s, Me), 2.20 (16H, m, hex-2), 1.75 (16H, m, hex-3), 1.49 (m, hex-4), 1.36 (16H, m, hex-5), 0.88 (m, hex-6), −2.1 to −2.4 (4H, br, NH); bridging group: 8.15 (4H, 2d), 7.85 (2H, 2d), 4.72 (2H, s); 15-phenyl: 7.63 (1H, t), 7.01 (2H, d, J=8.8 Hz); benzyloxy: 6.86 (2H, t, J=7.3 Hz), 6.73 (4H, t, J=7.8 Hz), 6.60 (4H, d, J=7.3 Hz), 4.95 (4H, s); 15′-substituent: 8.01 (2H, d, J=8.3 Hz), 7.54 (2H, d, J=8.3 Hz), 7.11 (1H, s), 7.08 (1H, s), 4.22 (2H, s, benzylic), 2.26 (3H, s, Me). MS m/z 2155 ($M+H^+$).

15-[2,6-Bis(benzyloxy)phenyl]-15′-[4-[(4-methyl-3,6-dioxo-1,4-cyclohexadienyl)methyl]phenyl]-5,5′-(1,4-phenylene)-bis-[2,8,12,18-tetrahexyl-3,7,13,17-tetramethylporphine] (2a). The diporphyrin **1a** (43 mg, 0.020 mmol) was dissolved in a mixture of 20 ml of methanol and 3 ml of concentrated hydrochloric acid. The mixture was heated under gentle reflux for 2.5 h (under N_2), poured into aqueous $NaHCO_3$ solution, extracted with CH_2Cl_2, dried and evaporated. The residue was dissolved again in CH_2Cl_2 (10 ml) and treated with 90 mg (0.38 mmol) of PbO_2 at room temperature for 2 h. The mixture was filtered through Celite to remove the inorganic material and evaporated. The crude product was purified as the dizinc complex (treatment with large excess of $Zn(OAc)_2$) by column chromatography (benzene). The free-base **2a** was recovered from the dizinc complex by treatment of the dichloromethane solution with 4 M hydrochloric acid. Yield: 30 mg (0.015 mmol, 75%). ^{1}H NMR δ=10.35 (2H, s, meso), 10.32 (2H, s, meso), 4.13 (8H, m, hex-1), 4.04 (8H, m, hex-1), 3.21 (12H, s, Me), 2.61 (6H, s, Me), 2.55 (6H, s, Me), 2.33 (8H, m, hex-2), 2.24 (8H, m, hex-2), 1.87 (8H, m, hex-3), 1.78 (8H, m, hex-3), 1.6 to 1.3 (m, hex-4 and hex-5), 0.98 to 0.90 (m, hex-6), −1.5 to −2.2 (br, NH); bridging phenylene: 8.57 (4H, s); 15-phenyl: 7.64 (1H, t), 7.03 (2H, d, J=8.3 Hz); benzyloxy: 6.88 (2H, t, J=7.8 Hz), 6.76 (4H, t, J=7.6 Hz), 6.62 (4H, d, J=7.3 Hz), 4.98 (4H, s); 15′-substituent: 8.08 (2H, d, J=7.8 Hz), 7.58 (2H, d, J=7.8 Hz), 6.79 (1H, s), 6.66 (1H, s), 4.13 (2H, s, benzylic), 2.17 (3H, s, Me). MS m/z 1981 ([M+3H]$^+$), 991 (doubly charged ion).

The compounds **2b**, **2c**, and **2d** were prepared in the similar manner as **2a**. The compound data are shown below:

2b: Yield 88%. Mp 290—295 °C. ^{1}H NMR δ=10.30 (2H, s, meso), 10.27 (2H, s, meso), 4.03 (16H, m, hex-1), 2.75 (12H, s, Me), 2.60 (6H, s, Me), 2.53 (6H, s, Me), 2.14 (16H, m, hex-2), 1.77 (16H, m, hex-3), 1.5 (m, hex-4), 1.40 (16H, m, hex-5), 0.9 (m, hex-6), −2.1 (1H, br, NH), −2.2 (1H, br, NH), −2.3 to −2.4 (2H, br, NH); bridging biphenylylene: 8.3 (8H, m); 15-phenyl: 7.64 (1H, t), 7.03 (2H, d, J=8.3 Hz) benzyloxy: 6.88 (2H, t, J=7.3 Hz), 6.75 (4H, t, J=7.8 Hz), 6.61 (4H, d, J=7.3 Hz), 7.55 (2H, d, J=7.8 Hz), 6.78 (1H, s), 6.65 (1H, s), 4.11 (2H, s, benzylic), 2.16 (3H, s, Me). MS m/z 2057 ([M+3H]$^+$), 1028 (doubly charged ion).

2c: Yield 90%. Mp 285—290 °C. ^{1}H NMR δ=10.28 (2H, s, meso), 10.25 (2H, s, meso), 4.02 (16H, m, hex-1), 2.65 (12H, s, Me), 2.59 (6H, s, Me), 2.53 (6H, s, Me), 2.23 (16H, m, hex-2), 1.77 (16H, m, hex-3), 1.51 (16H, m, hex-4), 1.38 (16H, m, hex-5), 0.93 (24H, m, hex-6), −2.1 (1H, br, NH), −2.26 (1H, br, NH), −2.35 (2H, br, NH); bridging terphenyl: 8.21 (8H, d and s), 8.15 (4H, 2 doublets); 15-phenyl: 7.63 (1H, t), 7.02 (2H, d, J=8.8 Hz); benzyloxy: 6.86 (2H, t), 2.74 (4H, t, J=7.6 Hz), 6.60 (4H, d, J=7.8 Hz), 4.96 (4H, s); 15′-substituent: 8.05 (2H, d, J=7.8 Hz), 7.55 (2H, d, J=7.8 Hz), 6.77 (1H, m, J<2 Hz), 6.64 (1H, s), 4.11 (2H, s, benzylic), 2.15 (3H, m, J<2 Hz). MS m/z 2133 ([M+3H]$^+$), 1066 (doubly charged ion).

2d: Yield 83%. Mp 143—148 °C. ^{1}H NMR δ=10.27 (2H, s, meso), 10.24 (2H, s, meso), 4.00 (16H, m, hex-1), 2.64 (12H, s, Me), 2.58 (6H, s, Me), 2.52 (6H, s, Me), 2.22 (16H, m, hex-2), 1.75 (16H, m, hex-3), 1.48 (16H, m, hex-4), 1.36 (16H, m, hex-5), 0.88 (m, hex-6), −2.15 (1H, br, NH), −2.26 (1H, m, NH), −2.35 (2H, br, NH); bridging group: 8.15 (4H, 2 doublets), 7.85 (4H, 2 doublets), 4.71 (2H, s, benzylic); 15-phenyl: 7.63 (1H, t), 7.01 (2H, d, J=8.8 Hz); benzyloxy: 6.86 (2H, t, J=7.3 Hz), 6.73 (4H, t, J=7.6 Hz), 6.59 (4H, d, J=7.3 Hz), 4.97 (4H, s); 15′-substituent: 8.06 (2H, d, J=7.8 Hz), 7.56 (2H, d,

J=8.3 Hz), 6.78 (1H, m, J<2 Hz), 6.65 (1H, m, J<2 Hz), 4.11 (2H, s, benzylic), 2.16 (3H, m, J<2 Hz, Me). MS m/z 2071 ($[M+3H]^+$).

15-[2,6-Bis(benzyloxy)phenyl]-15′-[4-(6-hexyl-1,3,5,7-tetrahydro-1,3,5,7-tetraoxobenzo[1,2-*c*:4,5-*c*′]dipyrrol-2-yl)phenyl]-5,5′-(1,4-phenylene)bis[2,8,12,18-tetrahexyl-3,7,13,17-tetramethylporphine] (3a). The formyl porphyrin **8a** (60 mg, 0.055 mmol) and the *N*-(formylphenyl)diimide **10** (161 mg, 0.385 mmol) were dissolved in a mixture of 10 ml of dry acetonitrile and 10 ml of dry benzene containing 33 mg (0.2 mmol) of trichloroacetic acid. To this solution, bis(3-hexyl-4-methyl-2-pyrrolyl)methane **5** (151 mg, 0.44 mmol) in 10 ml of acetonitrile was added, and the mixture was stirred for 5 h (dark, under N_2, room temperature). A solution of *p*-chloranil (162 mg, 0.66 mmol) in THF was added, and stirring was continued for 2 h. The solvent was removed by rotary evaporation, and the residue was taken up in dichloromethane and washed with aqueous $NaHCO_3$ solution. At this point, red precipitates appeared from the organic phase. Methanol was added to complete precipitation, and the solids were collected by filtration and washed with methanol. The red-violet solids were dissolved again in dichloromethane and treated with excess zinc acetate to give a mixture of zinc porphyrins, which was separated by column chromatography to give two products (R=0.6 and 0.4, CH_2Cl_2). The second fraction was the dizinc complex of **3a**, from which the free-base **3a** was obtained by successive treatment with 4 M hydrochloric acid and aqueous $NaHCO_3$. Yield 79 mg (0.036 mmol, 67%). ^{1}H NMR δ=10.33 (4H, s, meso), 4.17 (8H, m, hex-1), 4.03 (8H, m, hex-1), 3.21 (12H, s, Me), 2.62 (6H, s, Me), 2.46 (6H, s, Me), 2.34 (8H, m, hex-2), 2.25 (8H, m, hex-2), 1.88 (8H, m, hex-3), 1.60 (8H, m, hex-3), 1.6 to 1.3 (m, hex-4 and hex-5), 1.0 to 0.9 (m, hex-6), −1.82 (2H, br, NH), −1.91 (1H, br, NH), −2.09 (1H, br, NH); bridging phenylene: 8.59 (4H, s); 15-phenyl: 7.65 (1H, t), 7.04 (2H, d, J=8.8 Hz); benzyloxy: 6.89 (2H, t, J=7.3 Hz), 6.77 (4H, t, J=7.6 Hz), 6.64 (4H, d, J=6.8 Hz), 4.99 (4H, s); 15′-substituent: 8.2 (2H, br, imide-aromatic H), 8.08 (2H, d, J=7.8 Hz), 7.76 (2H, d, J=7.8 Hz), 5.21 (2H, s, benzylic), 3.74 (2H, t, hex-1), 1.7 (2H, m, hex-2), 1.3 (m, hex-3, 4, 5), 1.0 to 0.9 (m, hex-6). MS m/z 2157, 1078.

The compounds **3b**, **3c**, and **3d** were prepared in the similar manner as **3a**. The compound data are listed below:

3b: Yield 47%. ^{1}H NMR δ=10.28 (2H, s, meso), 10.27 (2H, s, meso), 4.1 to 4.0 (16H, m, hex-1), 2.75 (12H, s, Me), 2.60 (6H, s, Me), 2.45 (6H, s, Me), 2.3 to 2.2 (16H, m, hex-2), 1.8 to 1.7 (18H, m, hex-3 and imide-hex-2), 1.6 to 1.5 (m, hex-4), 1.5 to 1.3 (m, hex-5 and imide-hex-3, 4, and 5), 1.0 to 0.9 (m, hex-6 and imide-hex-6), −2.12 (1H, br, NH), −2.21 (1H, br, NH), −2.35 (1H, br, NH), −2 .38 (1H, br, NH); bridging biphenylylene: 8.33 (8H, m); 15-phenyl: 7.63 (1H, t), 7.03 (2H, d, J=8.8 Hz); benzyloxy: 6.88 (2H, t, J=7.8 Hz), 6.75 (4H, t, J=7.6 Hz), 6.62 (4H, d, J=7.8 Hz), 4.97 (4H, s); 15′-substituent: 8.26 (2H, br, imide-aromatic), 8.08 (2H, d, J=8.3 Hz), 7.76 (2H, d, J=7.8 Hz), 5.23 (2H, s, benzylic), 3.76 (2H, t, hex-1). MS m/z 2233, 1117.

3c: Yield 65%. Mp 116—121 °C. ^{1}H NMR δ=10.25 (4H, 2 singlets, meso), 4.0 (16H, m, hex-1), 2.66 (6H, s, Me), 2.65 (6H, s, Me), 2.60 (6H, s, Me), 2.44 (6H, s, Me), 2.23 (16H, m, hex-2), 1.77 (18H, m, hex-3 and imide-hex-2), 1.5 (m, hex-4), 1.4 (m, hex-5 and imide-hex-3,4,5), 0.9 (m, hex-6 and imide-hex-6), −2.14 (1H, s, NH), −2.26 (1H, s, NH), −2.39 (1H, s, NH), −2.42 (1H, s, NH); bridging terphenyl: 8.24 (10H, m, overlapping with imide-aromatic), 8.17 (4H, 2 doublets); 15-phenyl: 7.64 (1H, t), 7.02 (2H, d, J=8.8 Hz); benzyloxy: 6.87 (2H, t, J=7.3 Hz), 6.74 (2H, d, J=8.8 Hz), 6.87 (2H, t, J=7.3 Hz), 6.74 (t, J=7.8 Hz), 6.61 (4H, d, J=7.3 Hz), 4.96 (4H, s); 15′-substituent: 8.07 (2H, d, J=7.8 Hz), 7.75 (2H, d, J=7.8 Hz), 5.22 (2H, s, benzylic), 3.98 (2H, t, hex-1). MS m/z 2309, 1155.

3d: Yield 47%. Mp 140—145 °C. ^{1}H NMR δ=10.24 (4H, 2 singlets, meso), 4.0 (16H, m, hex-1), 2.65 (12H, s, Me), 2.59 (6H, s, Me), 2.43 (6H, s, Me), 2.2 (16H, m, hex-2), 1.8 (18H, hex-3 and imide-hex-2), 1.5 (m, hex-4), 1.3 (m, hex-5 and imide-hex-3,4,5), 0.9 (m, hex-6 and imide-hex-6), −2.16 (1H, s, NH), −2.28 (1H, s, NH), −2.41 (1H, s, NH), −2.44 (1H, s, NH); bridging group: 8.16 (6H, 2 doublets, overlapping with imide-aromatic), 7.86 (4H, 2 doublets), 4.72 (2H, s, benzylic); 15-phenyl: 7.63 (1H, t), 7.01 (2H, d, J=8.3 Hz); benzyloxy: 6.87 (2H, t, J=7.3 Hz), 6.74 (4H, t, J=7.6 Hz), 6.61 (4H, d, J=7.3 Hz), 4.96 (4H, s); 15′-substituent: 8.06 (2H, d, J=7.8 Hz), 7.74 (2H, d, J=7.8 Hz), 5.20 (2H, s, benzylic), 3.73 (2H, t, hex-1). MS m/z 2247, 1123.

15-[2,6-Bis(benzyloxy)phenyl]-15′-[4′-(6-hexyl-1,3,5,7-tetrahydro-1,3,5,7-tetraoxobenzo[1,2-*c*:4,5-*c*′-]dipyrrol-2-yl)[1,1′-biphenyl]-4-yl]-5,5′-(1,4-phenylene)bis[2,8,12,18-tetrahexyl-3,7,13,17-tetramethylporphine] (4). Synthesized from the formyl porphyrin **8a**, the aldehyde **11** and **5** in a similar manner as **3a**. Yield: 55%. Mp>300 °C, ^{1}H NMR δ= 10.35 (2H, s, meso), 10.32 (2H, s, meso), 4.16 (8H, m, hex-1), 4.04 (8H, m, hex-1), 3.18 (12H, s, Me), 2.62 (6H, s, Me), 2.54 (6H, s, Me), 2.34 (8H, m, hex-2), 2.26 (8H, m, hex-2), 1.88 (8H, m, hex-3), 1.78 (8H, m, hex-3), 1.59 (8H, m, hex-4), 1.5 to 1.3 (m, hex-4,5 and imide-hex-3,4,5), 1.0 to 0.9 (m, hex-6 and imide-hex-6), −1.78 (2H, br, NH), −1.89 (1H, br, NH), −2.03 (1H, br, NH); bridging phenylene, biphenylylene and imide-aromatic: 8.50 (4H, m), 8.18 (2H, m), 8.10 (2H, m), 7.92 (4H, m), 7.67 (2H, d); 15-phenyl: 7.65 (1H, t, J=8.6 Hz), 7.04 (2H, d, J=8.8 Hz); benzyloxy: 6.88 (2H, t, J=7.3 Hz), 6.76 (4H, t, J=7.6 Hz), 6.62 (4H, d, J=7.3 Hz), 4.98 (4H, s); imide: 5.00 (2H, s, benzylic CH_2), 3.73 (2H, t, hex-1), 1.71 (2H, m, hex-2). MS m/z 2233, 1117.

5-(4-Methylphenyl)-15-[4-[(2,5-diacetoxy-4-methylphenyl)-methyl]phenyl]-2,8,12,18-tetrahexyl-3,7,13,17-tetramethylporphine (12). Synthesized from the aldehyde **9**, *p*-tolualdehyde and **5** in a similar manner as **7a** (see the synthesis of **8a**). The zinc porphyrin was converted to the free-base **12** by treatment with 4 M hydrochloric acid. Yield: 32%. Mp 140—142 °C. ^{1}H NMR δ=10.22 (2H, s), 7.98 (2H, d, J=8.3 Hz), 7.92 (2H, d, J=7.8 Hz), 7.53 (2H, d, J=7.8 Hz), 7.52 (2H, d, J=7.8 Hz), 7.10 (1H, s), 7.07 (1H, s), 4.21 (2H, s), 3.97 (8H, t, J=7.8 Hz), 2.72 (3H, s), 2.503 (6H, s), 2.498 (6H, s), 2.42 (3H, s), 2.41 (3H, s), 2.25 (3H, s), 2.18 (8H, quint, J=7.4 Hz), 1.72 (8H, quint, J=7.5 Hz), 1.47 (8H, quint, J=7.2 Hz), 1.36 (8H, sext, J=7.3 Hz), 0.90 (12H, t, J=7.4 Hz), −2.41 (2H, s). MS m/z 1090.

The compound **14** (or **15**) was also synthesized from the aldehyde **10** (or **11**), *p*-tolualdehyde and **5** in a similar manner as **12**. The compound data are shown below:

14: Yield: 39% (solvent: CH_3CN+C_6H_6=2 : 1). Mp 120—124 °C. ^{1}H NMR δ=10.20 (2H, s), 8.31 (2H, s), 8.04 (2H, d, J=7.8 Hz), 7.92 (2H, d, J=7.8 Hz), 7.74 (2H, d, J=7.8 Hz), 7.54 (2H, d, J=7.8 Hz), 5.24 (2H, s), 3.95 (8H, m) 3.76 (2H, t, J=7.3 Hz), 2.72 (3H, s), 2.50 (6H, s), 2.41 (6H, s), 2.17 (8H, m), 1.72 (10H, m), 1.47 (8H, m), 1.35 (14H, m), 0.89 (15H, m), −2.46 (2H, s). MS m/z 1181.

15: Yield: 30% (solvent: $CH_3CN+CH_2Cl_2=4:3$). Mp 275—278 °C. ^1H NMR δ=10.22 (2H, s), 8.22 (2H, s), 8.12 (2H, d, J=7.8 Hz), 7.94 (6H, m), 7.68 (2H, d, J=8.3 Hz), 7.54 (2H, d, J=7.8 Hz), 5.01 (2H, s), 3.97 (8H, m), 3.73 (2H, t), 2.72 (3H, s), 2.52 (6H, s), 2.51 (6H, s), 2.17 (8H, m), 1.72 (10H, m), 1.53 (8H, m), 1.36 (14H, m), 0.89 (15H, m), −2.43 (2H, s). MS m/z 1257.

5-(4-Methylphenyl)-15-[4-[(3,6-dioxo-4-methyl-1,4-cyclohexadienyl)methyl]phenyl]-2,8,12,18-tetrahexyl-3,7,13,17-tetramethylporphine (13). Synthesized from the diacetoxyphenyl porphyrin **12** in a similar manner as **2a**. Yield: 91%. Mp 190—193 °C. ^1H NMR δ=10.27 (1H, s), 8.03 (2H, d, J=7.8 Hz), 7.96 (2H, d, J=7.3 Hz), 7.57 (2H, d, J=7.8 Hz), 7.50 (2H, d, J=7.8 Hz), 6.75 (1H, s), 6.59 (1H, s), 4.02 (10H, m, benzylic and hex-1), 2.76 (3H, s), 2.55 (6H, s), 2.52 (6H, s), 2.23 (8H, m), 2.15 (3H, s), 1.78 (8H, m), 1.53 (8H, m), 1.42 (m), 0.96 (12H, m), −2.35 (2H, s). MS m/z 1006 ($[M+3H]^+$).

Procedure for Selective Metallation. The free-base diporphyrin (0.015 mmol) was dissolved in 20 ml of CH_2Cl_2, and a 30 mM solution of zinc acetate in $MeOH/CH_2Cl_2$ (0.4 ml, 0.012 mmol) was added. The mixture was stirred at room temperature for 15 min, and washed with water and dilute $NaHCO_3$ solution, dried and evaporated. The residue was separated by column chromatography ($CH_2Cl_2+Et_2O$) to four fractions, and each was checked by UV-visible, MS and ^1H NMR spectra (see text). The (H_2, Zn) complex was obtained in 12—33% yield. Purity was checked by TLC and ^1H NMR spectra.

The author expresses heartful thanks to Professor Kazuhiro Maruyama and Dr. Atsuhiro Osuka of Kyoto University for their encouragement and helpful discussion. The author is also grateful to Professor Ikuo Yamashina of Kyoto Industrial University for his kind permission to use the JEOL HX-110 mass spectrometer.

References

1) "The Photosynthetic Bacterial Reaction Center, Structure and Dynamics," ed by J. Breton and A. Vermeglio, in "NATO ASI Series A (Life Science), Vol. 149," Plenum Press (1987).

2) W. Holzapfel, U. Finkele, W. Kaiser, D. Oesterhelt, H. Scheer, H. U. Stilz, and W. Zinth, *Chem. Phys. Lett.*, **160**, 1 (1989).

3) a) J. Deisenhofer, O. Epp, K. Miki, R. Huber, and H. Michel, *J. Mol. Biol.*, **180**, 385 (1984); b) C.-H. Chang, D. M. Tiede, J. Tang, J. Norris, and M. Schiffer, *FEBS Lett.*, **205**, 82 (1986).

4) a) M. R. Wasielewski, *Photochem. Photobiol.*, **48**, 923 (1988), and references therein; b) G. L. Gaines, III, M. P. O'Neil, W. A. Svec, M. P. Niemczyk, and M. R. Wasielewski, *J. Am. Chem. Soc.*, **113**, 719 (1991); c) M. R. Wasielewski, M. P. Niemczyk, D. G. Johnson, W. A. Svec, and D. W. Minsek, *Tetrahedron*, **45**, 4785 (1989); d) Y. Sakata, S. Nakashima, Y. Goto, H. Tatemitsu, S. Misumi, T. Asahi, M. Hagihara, S. Nishikawa, T. Okada, and N. Mataga, *J. Am. Chem. Soc.*, **111**, 8979 (1989); e) J. S. Lindsey, J. K. Delaney, D. C. Mauzerall, and H. Linschitz, *J. Am. Chem. Soc.*, **110**, 3610 (1988); f) D. Gust, T. A. Moore, A. L. Moore, G. Seely, P. Liddell, D. Barrett, L. O. Harding, X. C. Ma, S.-J. Lee, and F. Gao, *Tetrahedron*, **45**, 4867 (1989); g) K. Hasharoni, H. Levanon, J. Tang, H. K. Bowman, J. R. Norris, D. Gust, T. A. Moore, and A. L. Moore, *J. Am. Chem. Soc.*, **112**, 6477 (1990); h) J. L. Sessler, M. R. Johnson, S. E. Creager, J. C. Fettinger, and J. A. Ibers, *J. Am. Chem. Soc.*, **112**, 9310 (1990); i) J. L. Sessler, M. R. Johnson, and T.-Y. Lin, *Tetrahedron*, **45**, 4767 (1989); j) J. Rodriguez, C. Kirmaier, M. R. Johnson, R. A. Friesner, D. Holton, and J. L. Sessler, *J. Am. Chem. Soc.*, **113**, 1652 (1991); k) K. Maruyama and A. Osuka, *Pure Appl. Chem.*, **62**, 1511 (1990); l) A. Osuka, H. Tomita, and K. Maruyama, *Chem. Lett.*, **1988**, 1205.

5) a) A. Osuka, F. Kobayashi, T. Nagata, and K. Maruyama, *Chem. Lett.*, **1990**, 287; b) A. Osuka, K. Ida, T. Nagata, K. Maruyama, I. Yamazaki, N. Tamai, and Y. Nishimura, *Chem. Lett.*, **1989**, 2133; c) A. Osuka, T. Nagata, and K. Maruyama, *Chem. Lett.*, **1991**, 481; d) K. Maruyama, T. Nagata, N. Ono, and A. Osuka, *Bull. Chem. Soc. Jpn.*, **62**, 3167 (1989); e) T. Nagata, A. Osuka, and K. Maruyama, *J. Am. Chem. Soc.*, **112**, 3054 (1990).

6) M. Bixon, J. Jortner, M. Plato, and M. E. Michel-Beyerle, pp. 399—419 in Ref. 1.

7) In the case of the 1,4-phenylene bridged diporphyrins, the UV-visible absorption spectra were slightly (about 3 nm) red-shifted due to the exciton interaction between the two porphyrins.

8) The photophysics of the (H_2, Zn) diporphyrins are somewhat complicated because of the singlet energy transfer from the zinc porphyrin to the free-base porphyrin. When the acceptor moiety is present, the excited state of the zinc porphyrin (which is formed by absorption of the incident light; ε(free-base):ε(zinc)=6.3:1 at 507—510 nm) should be also quenched by the acceptor. Therefore, decrease of the fluorescence intensity of the free-base porphyrin can be partly attributed to the quenching of the zinc porphyrin. Analysis of the photo-steady state led to the estimation that the free-base fluorescence would be decreased through this effect by a factor of $(\varepsilon_H+k_{EN}\varepsilon_Z/(k_{EN}+k_0+k_q))/(\varepsilon_H+k_{EN}\varepsilon_Z/(k_{EN}+k_0))$, where ε_H, ε_Z are extinction coefficients of free-base and zinc porphyrins, k_{EN} is the rate of energy transfer, k_0 is the decay rate constant of the zinc porphyrin, and k_q is the rate of electron transfer from the zinc porphyrin to the acceptor. Using the values of $k_0=6.3\times10^8$ s^{-1}, $k_q=7.1\times10^{10}$ s^{-1} (for **2**), 1.3×10^{10} s^{-1} (for **3**), 8.5×10^7 s^{-1} (for **4**), and the reported values of k_{EN} (Ref. 15), the factor was estimated to be in the range of 0.89 to 1.0. The values shown in Table 1 have been compensated by these factors, thus their deviation from unity can be ascribed simply to the interaction of the free-base and the acceptor moiety.

9) See Ref. 4 and the following reviews: a) S. G. Boxer, *Biochim. Biophys. Acta*, **726**, 265 (1983); b) J. S. Connolly and J. R. Bolton, "Photoinduced Electron Transfers," ed by M. A. Fox and M. Channon, Elsevier, Amsterdam (1988), Part D, pp. 303—393.

10) a) R. J. Harrison, B. Pearce, G. S. Beddard, J. A. Cowan, and J. K. M. Sanders, *Chem. Phys.*, **116**, 429 (1987); b) A. Osuka, S. Nakajima, K. Maruyama, T. Asahi, and N. Mataga, *Chem. Lett.*, **1991**, 1003.

11) The ΔG's for electron transfer are −0.37 eV (for the quinone-linked **2a**) and −0.14 eV (for the diimide-linked **3a**).

12) B. A. Leland, A. D. Joran, P. M. Felker, J. J. Hopfield, A. H. Zewail, and P. B. Dervan, *J. Phys. Chem.*, **89**, 5571 (1985).

13) M. Plato, K. Moebius, M. E. Michel-Beyerle, M. Bixon, and J. Jortner, *J. Am. Chem. Soc.*, **110**, 7279 (1988).

The "superexchange" mechanism in electron transfer in porphyrin–quinone systems has been discussed. See Ref. 4c, 4i, and 4j.

14) A. Osuka, K. Maruyama, N. Mataga, T. Asahi, I. Yamazaki, and N. Tamai, *J. Am. Chem. Soc.*, **112**, 4958 (1990).

15) A. Osuka, K. Maruyama, I. Yamazaki, and N. Tamai, *Chem. Phys. Lett.*, **165**, 392 (1990).

16) C. K. Chang, *J. Am. Chem. Soc.*, **99**, 2819 (1977).

17) A. W. Johnson, I. T. Kay, E. Markham, R. Price, and K. B. Shaw, *J. Chem. Soc.*, **1959**, 3416.

18) P. S. Clezy and A. W. Nichol, *Aust. J. Chem.*, **11**, 1835 (1965).

19) J. S. Lindsey, I. C. Schreiman, H. C. Hsu, P. C. Kearney, and A. M. Marguerettaz, *J. Org. Chem.*, **52**, 827 (1987).

 © 1991 The Chemical Society of Japan Bull. Chem. Soc. Jpn., 64, 3017—3022 (1991)

Photochemical Hydroformylation of Olefins in the Cobalt-Phosphine Catalyst System

Sadayuki MORI,* Shunji TATSUMI, Masaki YASUDA, Kiyoshi KUDO, and Nobuyuki SUGITA
Institute for Chemical Research, Kyoto University, Gokanosho, Uji 611
(Received April 19, 1991)

Cobalt-catalyzed hydroformylation of olefins was found to proceed even at ambient temperature under UV irradiation in the presence of phosphine. Extremely high selectivity toward straight-chain aldehyde (99% in case of 1-hexene) was obtained by lowering the partial pressure of carbon monoxide at ambient temperature. A catalytic species different from the well-known species under high pressure of carbon monoxide and high temperature contributed to the highly selective formation of straight-chain aldehydes. Two photochemical processes were suggested to be involved in the photochemical hydroformylation reaction, that is, the formation of $HCo(CO)_3PBu_3$ from the cationic cobalt species, $[Co(CO)_3(PBu_3)_2]^+$, and then the formation of the coordinatively unsaturated hydride, $HCo(CO)_2PBu_3$.

Organometallic photochemistry is an area of growing interest in homogeneous transition-metal catalysis.[1] Photochemical hydroformylation of olefins was first reported by Mirbach and co-workers[2] They have examined the effects of UV irradiation on hydroformylation in some different cobalt catalyst systems. With $Co(OAc)_2$ or $Co_2(CO)_8$ as catalyst precursor in the presence of excess tributylphosphine, olefin hydroformylation proceeds photochemically under the conditions where no reaction could take place thermally (85 °C), and yields linear aldehydes in a relatively high selectivity.

$$\text{1-octene} \xrightarrow[Co(OAc)_2/PBu_3]{h\nu,\ CO/H_2,\ 85\,^\circ C} \underset{79\%}{\text{nonanal}} + \underset{9\%}{\text{2-methyloctanal}} + \underset{12\%}{\text{octane}}$$

In the absence of phosphine the thermal reaction with $Co(OAc)_2$ catalyst at 85 °C has a long induction period of 15 h, whereas the reaction under UV irradiation is initiated within 1 h. Based on the observed high pressure IR and UV absorption spectra, they have suggested the photogeneration of active catalytic species, $HCo(CO)_3PBu_3$ or $HCo(CO)_4$ in the presence or absence of phosphine, respectively.

Later, they found rhodium catalysts to be also photochemically active for the hydroformylation of olefins in the presence of norbornadiene.[3]

Recently E. M. Gordon and R. Eisenberg reported that Ru(0) complexes such as $Ru(CO)_3(PPh_3)_2$, $Ru(CO)_4PPh_3$ and $Ru_3(CO)_{12}$ are effective for the photochemical hydroformylation of ethylene and propene under mild conditions.[4]

We found the cobalt-catalyzed photochemical hydroformylation proceeds even at ambient temperature, and extremely high selectivity toward linear aldehyde is achieved at low CO partial pressure. Here we report the influence of reaction temperature and CO partial pressure on the reaction rate and selectivity toward straight-chain products, and discuss the photochemical processes and catalytic species.

Experimental

Photochemical Experiments. The photochemical reactions were performed in a 10 mL home-made UV autoclave as shown in Fig. 1. Inside of the autoclave is coated with Teflon to avoid the contact of the solution with stainless steel. If necessary, this can be used as a high-pressure UV cell for UV spectroscopy. Mixing of the liquid and gases was achieved by a magnetically driven up-and-down stirrer. The reaction solution in the autoclave was irradiated with an external high-pressure mercury lamp (500 W, Ushio USH500D) through a

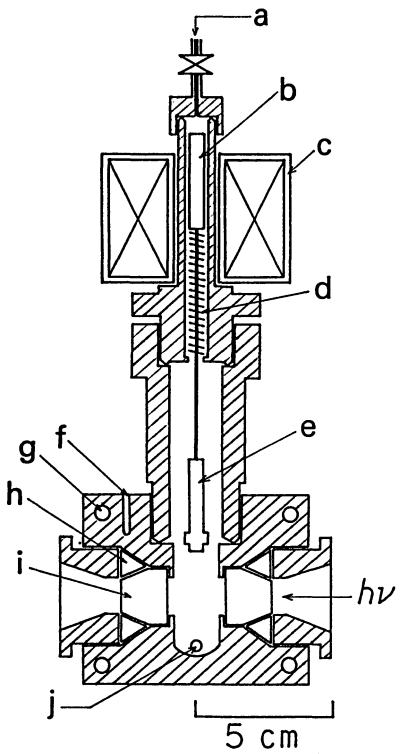

Fig. 1. High pressure UV autoclave (schematic).
a; gas inlet, b; magnet, c; solenoid, d; spring, e; up-and-down stirrer, f; thermocouple hole, g; heater or coolant, h; Teflon packing, i; quartz window, j; sample outlet.

quartz lens and a cooled water filter (2 cm thickness).

In a typical run, methanol solution (5 mL) of olefin (3.2 mol dm^{-3}), $Co(OAc)_2 \cdot 4H_2O$ (0.016 mol dm^{-3}), and PBu_3 (0.16 mol dm^{-3}) was introduced into the autoclave. The autoclave was flushed with synthesis gas (CO/H_2=1/1) three times and then pressurized to a desired pressure. The reaction mixture was stirred and then irradiated after the autoclave had been thermostated to a desired temperature. When the gas mixture of low CO content was employed, the fresh gas mixture was introduced continuously into the solution through the sample outlet portion (j in Fig. 1), and released from the gas inlet valve (a in Fig. 1) with keeping a constant pressure. The product solution was taken out through the sample outlet valve to a cooled bottle. Product analysis was performed by GLC with internal standards (Shimadzu GC-5A). A back flush system fitted with tandem column of PEG 20M and *n*-Octane/Poracil C was used for a concurrent analysis of hydrocarbons and hydroformylation products. GC-MS (NEVA TE-600) was also used to identify the products. UV absorption spectra of cobalt species such as Co^{2+}, $[Co(CO)_3(PBu_3)_2]^+$, and $Co_2(CO)_6(PBu_3)_2$ were measured by JASCO UVDEC-1 spectrometer.

Thermal Reaction with $HCo(CO)_3PBu_3$. $HCo(CO)_3PBu_3$ was prepared according to Piacenti and co-workers,[5] except for the addition of free phosphine which can avoid the concomitant formation of $HCo(CO)_4$.[6] Without isolating $HCo(CO)_3PBu_3$, a solution containing the hydride was used for the reaction, that is, $Co_2(CO)_6(PBu_3)_2$ (0.35 mmol), PBu_3 (0.35 mmol) and pentane (15 mL) were placed in a 50 mL rocking type autoclave and pressurized with 7 atm of CO and 22 atm of H_2. The autoclave was heated at 120 °C for 2 h, then cooled immediately at −70 °C. Two milliliter (16 mmol) of 1-hexene was injected into the autoclave by means of a plunger pump under −70 °C. The autoclave was rapidly heated to a desired temperature, and the reaction was started.

Materials. Commercially available $Co(OAc)_2 \cdot 4H_2O$, olefins and methanol were used without further purification. Tributylphosphine was distilled under vacuum. Hydrogen was obtained commercially. Carbon monoxide was prepared by decomposing formic acid in hot sulfuric acid. Its purity was above 98%, and impurity was mainly hydrogen. $Co_2(CO)_6(PBu_3)_2$ and $HCo(CO)_2(PBu_3)_2$ were prepared according to the procedures described in literatures.[7,8]

Results and Discussion

The results of the photochemical hydroformylation of 1-hexene with cobalt acetate and tributylphosphine in methanol are summarized in Table 1. The reaction proceeds even at ambient temperature and surprisingly the rate of hydroformylation at 30 °C is nearly the same at 80 °C and 120 °C. Heptanal via CO addition to the terminal carbon atom of 1-hexene is a principal product, and total of branched aldehydes (2-methylhexanal and 2-ethylpentanal) is about 1/10 of normal aldehyde (n/i=10, the ratio of straight-chain product to branched products is expressed by n/i hereafter). 2-Ethylpentanal is still less than 1/6 of 2-methylhexanal. The n/i ratio in isomeric aldehydes decreases slightly at 120 °C. Alcohols are minor products under these conditions, though a conventional hydroformylation with the phosphine-modified cobalt catalysts at higher temperature leads to the alcohol formation due to the highly reductive character of $HCo(CO)_3PBu_3$. Hydrogenation of olefinic substrate occurs in small extent and isomerization becomes significant only at higher temperature.

Total yield of hydroformylation products increases with the period of irradiation such as 13.6% for 18 h, 24% for 40 h, and 34% for 68 h at 30 °C, but the reaction ceases completely when the light is turned off. Thus the reaction is photocatalytic. Reactions of 1-pentene, 1-hexene, and 1-octene give almost the same results in the yield and the distribution of the corresponding

Table 1. Photochemical Hydroformylation of 1-Hexene[a]

Temp	Product yield[b]/%							
°C	*n*-Ald[c]	*i*-Ald[d]	*n*-Alc[e]	*i*-Alc[f]	Acetal[g]	Ester[h]	Hexane	2- and 3-Hexenes
30	11.9	1.12	0.17	0.03	0.01	0.35	1.3	0.1
80	13.4	1.27	0.78	0.07	0.11	0.32	1.6	2.3
120	10.3	1.30	1.83	0.13	1.79	0.15	1.5	15.1

a) Reaction conditions: $Co(OAc)_2 \cdot 4H_2O$, 0.0164 mol dm^{-3}; PBu_3, 0.163 mol dm^{-3}; 1-hexene, 3.20 mol dm^{-3}; solvent, methanol; total pressure, 80 atm (CO/H_2=1/1); reaction time, 18 h. b) Based on starting 1-hexene. c) Heptanal. d) Branched aldehyde: total of 2-methylhexanal and 2-ethylpentanal. e) 1-Heptanol. f) Branched alcohol: 2-methyl-1-hexanol. g) Heptanal dimethyl acetal. h) Methyl heptanoate.

Table 2. Photochemical Hydroformylation of Hexene Isomers[a]

Hexene	Product yield/%				
	Heptanal	2-Methylhexanal	2-Ethylpentanal	*n*-Alc[b]	*i*-Alc[b]
1-Hexene	23.6	1.96	0.31	0.39	0.08
trans-2-Hexene	18.4	2.18	0.58	0.53	0.23
trans-3-Hexene	17.4	1.86	1.41	0.61	0.31

a) Reaction conditions: Hexene, 1.60 mol dm^{-3}; temperature, 30 °C; others are the same as in Table 1. b) See footnotes in Table 1.

hydroformylation products.

In the hydroformylation of hexene isomers, the formyl group preferentially adds to the terminal carbon atom of each olefin, though the position of double bond in starting olefins affects slightly on the isomeric distribution of produced aldehydes as seen in Table 2. These results are similar to those in the conventional cobalt-catalyzed hydroformylation at higher temperature.[9] It has been assumed that fast isomerization of π-olefin complex via σ-π interconversion takes place without releasing isomerized olefins.

$$\underset{\mathrm{HCo(CO)}_m\mathrm{L}_n}{\mathrm{RCH{=}CH{-}CH_3}} \rightleftarrows \underset{\mathrm{H}\quad\mathrm{Co(CO)}_m\mathrm{L}_n}{\mathrm{RCH{-}CH{-}CH_3}} \rightleftarrows \underset{\mathrm{HCo(CO)}_m\mathrm{L}_n}{\mathrm{RCH_2{-}CH{=}CH_2}}$$

(L=phosphine)

On steric grounds, the preferable π-olefin complex is that involving the terminal olefins, thus the production of straight-chain aldehydes predominates. It is rather interesting that 2-propylhexanal was reported as the main product in the photochemical hydroformylation of 4-octene with $Co_2(CO)_8$ catalyst at 80 °C, CO/H_2=40 atm/40 atm,[10] though the thermal hydroformylation of 4-octene preferentially afforded nonanal (150 °C, CO/H_2=100 atm/100 atm).[9]

Influence of Phosphine Ligand. The influence of phosphine on the hydroformylation of 1-hexene is summarized in Table 3. At 30 °C both the presence of phosphine and UV irradiation are essential to initiate the hydroformylation reaction, and even at higher temperature (80 °C) the reaction in the presence of phosphine is still photochemical. The photochemical reaction in the absence of phosphine is faster than that in the presence of phosphine, but the n/i value is low ($n/i \approx 2$). This value is similar to that in a typical $Co_2(CO)_8$ catalyzed hydroformylation. In the absence of phosphine, aldehydes are obtained mainly as dimethyl acetals. $HCo(CO)_4$, a well-known active species in a $Co_2(CO)_8$ catalyzed hydroformylation, dissociates to H^+ and $Co(CO)_4^-$ in methanol solvent, and high acidity of the solution promotes the acetal formation. On the other hand, $HCo(CO)_3L$ (L=phosphine) in a cobalt-phosphine catalyst system is a very weak acid (K_a=1×10^{-7} for L=PBu_3[11]), thus aldehydes cannot be converted into acetals. The thermal reaction without phosphine scarcely occurs under these conditions due to a long induction period as reported previously.[2] The thermal reaction in cobalt-phosphine catalyst system at 120 °C is still very slow, whereas the photochemical reaction proceeds with a similar rate to that at 30 °C. In the absence of phosphine the reaction proceeds thermally as well as photochemically, and the n/i ratios in both thermal and photochemical reactions are low.

Table 3. Influence of Phosphine on Hydroformylation[a]

Temp	PBu_3	Product yield[b]/%	
°C	mol dm^{-3}	Photochemical	Thermal
30	0.163	13.6 (10.5)[c]	0
30	0	0	0
80	0.163	16.0 (10.6)	0
80	0	59.3[d] (2.2)	0.75[d] (2.0)
120	0.163	15.5 (8.0)	3.3 (7.8)
120	0	94.3[d] (1.8)	97.6[d] (1.8)

a) Conditions as in Table 1. b) Total yield of hydroformylated products (Aldehydes, alcohols, acetals, and ester). c) Values in parentheses indicate the n/i ratio in (aldehydes+acetals). d) Obtained mostly as dimethyl acetals.

Consequently, the characteristic of the photochemical hydroformylation is that the reaction proceeds at ambient temperature when phosphine-modified cobalt catalysts are employed.

Photochemical Process. Reductive carbonylation of $Co(ClO_4)_2\cdot6H_2O$ in the presence of phosphines affords $[Co(CO)_3L_2]^+$ (L=PBu_3) in alcoholic media under ambient conditions.[12] On the basis of UV and IR absorption spectra from the reaction of $Co(OAc)_2$ with PBu_3 under the elevated pressure of synthesis gas, Mirbach and co-workers ascertained the formation of $[Co(CO)_3(PBu_3)_2]^+$ at room temperature.[2]

$$Co^{2+} + 2PBu_3 \xrightarrow[20\,^\circ C,\ \text{in MeOH}]{H_2/CO,\ 80\ \text{atm}} [Co(CO)_3(PBu_3)_2]^+$$

As the cation $[Co(CO)_3(PBu_3)_2]^+$ has a large absorption coefficient in UV region (λ_{max}=245 nm, ε=80000), they believed that this cation is a sole photoactive species and is converted into a phosphine-coordinated hydridocarbonylcobalt under the photochemically hydroformylating conditions (Eq. 1). They assumed that the hydride initiates *thermally* the hydroformylation reaction in a similar manner proposed in a conventional hydroformylation reaction (Eqs. 2—4).

$$[Co(CO)_3(PBu_3)_2]^+ \xrightarrow[+H_2,\ -H^+,\ -PBu_3]{h\nu} HCo(CO)_3PBu_3 \quad (1)$$

$$HCo(CO)_3PBu_3 \rightleftarrows HCo(CO)_2PBu_3 + CO \quad (2)$$

$$HCo(CO)_2PBu_3 + \text{olefin} \xrightarrow{CO} RCOCo(CO)_2PBu_3 \quad (3)$$

$$RCOCo(CO)_2PBu_3 + H_2 \longrightarrow RCHO + HCo(CO)_2PBu_3 \quad (4)$$

We also observed immediate appearance of UV absorption maximum at 245 nm when a methanol solution of $Co(OAc)_2$ and PBu_3 was pressurized with 80 atm of synthesis gas. Upon irradiation to the solution the absorption at 370 nm, which can be assigned to $Co_2(CO)_6(PBu_3)_2$, appeared as a shoulder. It is probable that $HCo(CO)_3PBu_3$ was generated photochemically under the conditions employed. However, it is doubtful whether the phosphine-coordinated hydridocarbonylcobalt *thermally* initiates the hydroformylation reaction under Mirbach's conditions (85 °C) and especially under our conditions (30 °C). Because $HCo(CO)_3PBu_3$ is known to react with olefins only above 100—120 °C, in contrast to the behavior of $HCo(CO)_4$ which is active at room temperature.[5,13] Thermal reaction of $HCo(CO)_3PBu_3$ with 1-hexene was examined, and the

Table 4. Reaction of $HCo(CO)_3PBu_3$ with 1-Hexene[a]

Temp	Time	Product yield[b]/%			
°C	h	*n*-Ald[c]	*i*-Ald[c]	*n*-Alc[c]	*i*-Alc[c]
30	4	0	0	0	0
80	4	0.8	0.1	0.2	0
80	15	1.0	0.1	0.4	0
100	4	24.7	2.3	5.0	0.6
100[d]	4	2.3	0.2	0.3	0
120	4	142.7	19.8	27.3	3.3

a) Conditions and procedure: See Experimental in the text. b) Based on $Co_2(CO)_6(PBu_3)_2$. c) See footnotes in Table 1. d) Without pretreatment at 120 °C for 2 h.

results are shown in Table 4. The thermal hydroformylation of 1-hexene by $HCo(CO)_3PBu_3$ catalyst occurs only above 100 °C, and scarcely below 80 °C. No increase in the yield with prolonged reaction time (15 h) at 80 °C implies that $HCo(CO)_3PBu_3$ decomposes rather than reacts with olefin as reported earlier (Eq. 5).[5]

$$2HCo(CO)_3PBu_3 \longrightarrow Co_2(CO)_6(PBu_3)_2 + H_2 \quad (5)$$

In these experiments the formation of $HCo(CO)_3PBu_3$ is confirmed by no reaction taking place at 100 °C without the pretreatment at 120 °C for 2 h (see experimental section). Thus, absorption of light by the hydride should be required for the initiation of the reaction below 80 °C, though its steady concentration will be low.

$$HCo(CO)_3PBu_3 \xrightarrow{h\nu} HCo(CO)_2PBu_3 + CO \quad (6)$$

The photochemistry and UV spectral feature of the hydride have not been investigated. With respect to $HCo(CO)_4$, its photolysis in a matrix isolation system has been studied, in which the major process was the liberation of CO,

$$HCo(CO)_4 \xrightarrow[\text{Ar matrix}]{h\nu(254\text{ nm})} HCo(CO)_3 + CO$$

and $HCo(CO)_4$ had a absorption maximum at 227 nm with a large absorption coefficient (ε=ca. 55000).[14] A similar spectral feature may be expected for $HCo(CO)_3PBu_3$.

Consequently, two photochemical processes must be included in the photochemical hydroformylation reaction below 80 °C: First, the formation of $HCo(CO)_3PBu_3$ from the ionic species $[Co(CO)_3(PBu_3)_2]^+$ (Eq. 1), and second, the formation of the coordinatively unsaturated cobalt hydride $HCo(CO)_2PBu_3$ (Eq. 6).

Temperature Dependence. The reaction with $Co(OAc)_2/PBu_3$ catalyst affords the hydroformylation products almost in the same yield at different temperatures of 30, 80, and 120 °C as seen in Table 1. It seems to be rather unusual that the reaction rate does not change with temperature. Detailed temperature dependence on the product yield (or the reaction rate) was examined in the range of 0 °C and 140 °C, and shown in Fig. 2. The reaction proceeds slowly even at

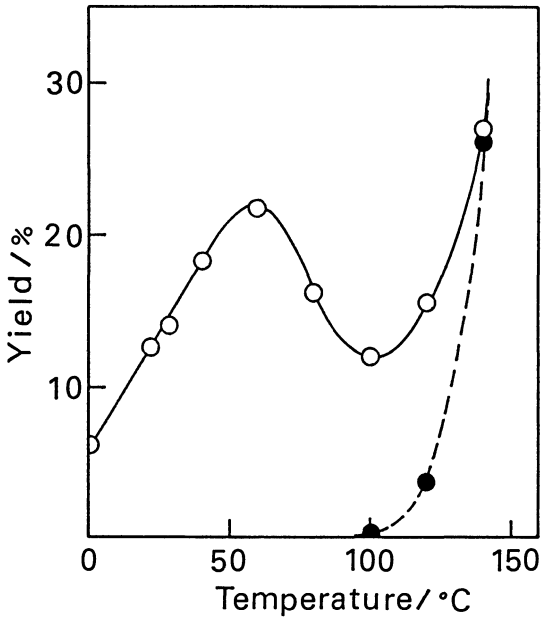

Fig. 2. Influence of reaction temperature on the hydroformylation of 1-hexene.
Reaction conditions as in Table 1, ○; photochemical, ●; thermal.

0 °C. The yield increases with temperature up to 60 °C, then decreases and again begins to increase at 100 °C. It can be seen that the yields at 30, 80, and 120 °C happened to lie on a similar value in the curve. Similar temperature dependence was found in the reactions of other substrates such as 1-pentene, 2- and 3-hexene, and 1-octene. The yield curve obtained in the thermal reaction is shown together in dotted line in Fig. 2. Thermal hydroformylation occurs above 120 °C, and at 140 °C no enhancement by irradiation is found. Thus, the reaction can be classified in two temperature regions of the photocatalytic reaction below 100 °C and the thermal reaction above 120 °C. In the photocatalytic region, the reaction is retarded above 60 °C. No detailed mechanistic consideration can be made here, but a most probable assumption is as follows: Photochemically generated $HCo(CO)_3PBu_3$ mostly decomposes to $Co_2(CO)_6(PBu_3)_2$ (Eq. 5), and regeneration of the hydride by the reverse reaction of Eq. 5 does not occur over the photocatalytic temperature range. If the photochemical generation of $HCo(CO)_3PBu_3$ has little temperature effect, then the steady concentration of the hydride will be lower at higher temperature. Although $Co_2(CO)_6(PBu_3)_2$ formed in Eq. 5 is consumed by the disproportionation in a polar solvent such as methanol,[15]

$$Co_2(CO)_6(PBu_3)_2 \xrightarrow{CO} [Co(CO)_3(PBu_3)_2]^+[Co(CO)_4]^- \quad (7)$$

small amounts of $Co_2(CO)_6(PBu_3)_2$ prevent largely the photochemical hydroformylation reaction due to its large absorption coefficient (ε=21500 at 370 nm).[16] The disappearance of the dicobalt species by disproportionation is more facile at higher temperature, then the

expected photochemical reactions become more favorable with increasing temperature.

Unsaturated hydride species $HCo(CO)_2PBu_3$, which is probably generated photochemically as described before (Eq. 6), reacts with olefins to lead to hydroformylation, or reacts with CO or phosphine to return to the saturated species.

$$HCo(CO)_2PBu_3 \xrightarrow{\text{olefin}} HCo(CO)_2(PBu_3)(\text{olefin}) \quad (8)$$

$$\xrightarrow{CO} HCo(CO)_3PBu_3 \quad (9)$$

$$\xrightarrow{PBu_3} HCo(CO)_2(PBu_3)_2 \quad (10)$$

These reactions may have different temperature dependence. Hydroformylation cycle (Eqs. 3 and 4) will have positive temperature effects, though the activation energies in each step may be low as the alkyl and acyl cobalt complexes readily react with CO and H_2, respectively, at room temperature.[5] Complex sequence of these reactions under applied conditions would result in the observed yield curve.

Thermal generation of $HCo(CO)_3PBu_3$ by the reverse reaction of Eq. 5 will become substantial above 120 °C, and thermal equilibrium (Eq. 2) has been assumed under the hydroformylating conditions. Then the irradiation becomes less effective, and at 140 °C the light has little effect on the hydroformylation reaction.

Effect of CO Partial Pressure. In conventional hydroformylation reactions, it is known that both the reaction rate and the n/i ratio in the products increase with lowering the CO partial pressure.[13,17] The former has been explained by the equilibria (Eqs. 2 and 11),

$$HCo(CO)_4 \rightleftarrows HCo(CO)_3 + CO \quad (11)$$

and the latter by the equilibrium between the phosphine substituted and unsubstituted hydride (Eq. 12), respectively.

$$HCo(CO)_3PBu_3 + CO \rightleftarrows HCo(CO)_4 + PBu_3 \quad (12)$$

In the photochemical hydroformylation of 1-hexene, similar dependence of CO partial pressure was observed as shown in Table 5. The yields of aldehydes and alcohols, and the selectivities toward normal products increased with lowering CO partial pressure. Here, following characteristic aspects are found: a) At 80 °C, the n/i ratio obtained under low CO pressure is only 1.5 times larger than that under high CO pressure. On the other hand, at 30 °C, it shows a extremely high value of 77, which corresponds to 98.7% of normal aldehyde and 1.3% of branched aldehydes. Such high selectivity has never been reported with cobalt catalysts except for the case of propene in the photochemical hydroformylation.[2] b) When high CO pressure is employed, lowering the temperature causes no increase in the n/i ratio (n/i=10 at 30 and 80 °C). c) Considerable hydrogenation of olefinic substrate is accompanied under low CO pressure, especially at 30 °C.

Thus, the high selectivity is achieved only at low pressure and low temperature. This can not be ascribed to only the above equilibrium (Eq. 12), since its equilibrium constant has been reported to have negative temperature dependence.[18] Existence of other catalytic species besides $HCo(CO)_3PBu_3$ can be expected under the conditions of low CO pressure and low temperature. Bis(phosphine) species $HCo(CO)_2(PBu_3)_2$ is most probable as the formation of about 1 : 1 mixture of $HCo(CO)_3PBu_3$ and $HCo(CO)_2(PBu_3)_2$ has been suggested in the photolysis of the cationic cobalt(I) complex $[Co(CO)_3(PBu_3)_2]^+$ under 50 atm of hydrogen.[19]

In order to ensure the contribution of $HCo(CO)_2(PBu_3)_2$ in the photochemical hydroformylation in the $Co(OAc)_2/PBu_3$ system, the hydroformylation of 1-hexene with $HCo(CO)_2(PBu_3)_2$ was carried out, and the results are summarized in Table 6. In the photochemical reaction, surprisingly high value of the n/i ratio was obtained at 30 °C and CO/H_2=1.5 atm/40 atm (n/i =215). However, when the temperature was raised to 80 °C, the n/i ratio largely decreased (n/i=25) to

Table 5. Effects of CO Partial Pressure on the Photochemical Hydroformylation of 1-Hexene[a]

P_{CO}	Temp	Product yield[b]/%						n/i[d]	n/i[e]
atm	°C	*n*-Ald[c]	*i*-Ald[c]	*n*-Alc[c]	*i*-Alc[c]	Hexane	2- and 3-Hexenes	(ald)	(alc)
1.5	30	21.6	0.28	2.02	0.05	11.7	2.8	77	41
2	30	19.2	0.37	1.46	0.05	5.9	1.4	52	30
4	30	14.3	0.52	0.67	0.04	1.9	0.3	23	15
8	30	11.1	0.76	0.26	0.03	1.5	0.3	15	9
16	30	9.5	0.75	0.16	0.03	1.3	0.2	13	7
40	30	9.3	0.95	0.11	0.01	1.1	0.1	10	8
1.5	80	12.8	0.85	5.01	0.21	5.8	12.2	15	24
2	80	14.1	0.96	3.95	0.17	4.8	8.2	15	23
4	80	14.6	1.06	2.81	0.13	3.9	7.6	14	21
8	80	13.0	1.14	1.30	0.07	2.4	4.9	11	18
16	80	10.2	0.93	0.74	0.05	2.2	3.4	11	16
40	80	10.1	1.04	0.45	0.03	1.4	2.4	10	13

a) Conditions: P_{H_2}, 40 atm; $Co(OAc)_2 \cdot 4H_2O$, 0.0170 mol dm^{-3}; PBu_3, 0.180 mol dm^{-3}; 1-hexene, 3.20 mol dm^{-3}; solvent, methanol; reaction time, 16 h. b) Based on starting 1-hexene. c) See footnotes in Table 1. d) The n/i ratio in aldehydes. e) The n/i ratio in alcohols.

Table 6. Hydroformylation of 1-Hexene with $HCo(CO)_2(PBu_3)_2$[a]

P_{CO}/P_{H_2}	Temp	Photochem	Product yield[b]/%			
atm/atm	°C	or dark	*n*-Ald[c]	*i*-Ald[c]	Alc[d]	Hexane
1.5/40	30	*hν*	30.2	0.14 (215)[e]	3.0	14.0
1.5/40	80	*hν*	17.1	0.68 (25)	1.2	5.2
1.5/40	80	Dark	0	0	0	0
40/40	30	*hν*	23.3	1.65 (14)	0.5	1.3
40/40	80	Dark	<0.1	0	0	0

a) Conditions: $HCo(CO)_2(PBu_3)_2$, 0.022 mol dm^{-3}; PBu_3, 0.21 mol dm^{-3}; 1-hexene, 0.80 mol dm^{-3}; solvent, methanol; reaction time, 6 h. b) Based on 1-hexene. c) See footnotes in Table 1. d) 1-Heptanol (2-methyl-1-hexanol was not detected). e) Values in parentheses indicate the *n*/*i* ratio in produced aldehydes.

approach to the value obtained in the $Co(OAc)_2/PBu_3$ catalyst system (*n*/*i*=15 in Table 5). Similar situation is found at high CO pressure and low temperature. Hydrogenation of olefin is remarkable only at low CO pressure and low temperature. No reaction occurs without irradiation under the conditions employed.

Predominant photochemical reaction of $HCo(CO)_2(PBu_3)_2$ is perhaps ligand dissociation, mainly of CO.

$$HCo(CO)_2(PBu_3)_2 \xrightarrow{h\nu} HCo(CO)(PBu_3)_2 + CO$$

This coordinatively unsaturated hydride will afford exclusively normal aldehyde owing to its highly steric crowding. Decrease in the *n*/*i* ratio with increasing CO pressure is due to the known equilibrium (Eq. 13).[8]

$$HCo(CO)_2(PBu_3)_2 + CO \rightleftarrows HCo(CO)_3PBu_3 + PBu_3 \quad (13)$$

Low *n*/*i* value obtained at 80 °C under much low CO pressure suggests that the above equilibrium shifts to the right-hand side at higher temperature. Lower hydrogenation activity at higher temperature also suggests the conversion of $HCo(CO)_3(PBu_3)_2$ to $HCo(CO)_3PBu_3$ under these conditions, because the hydrogenation activity of phosphine-coordinated cobalt hydrides increases with increasing the number of phosphine coordinated to the hydride.[8]

The results obtained in the reaction of $HCo(CO)_2(PBu_3)_2$ under various conditions are in accord with those in the reaction with $Co(OAc)_2/PBu_3$ catalyst. Thus, $HCo(CO)_2(PBu_3)_2$ will largely contribute to the high selectivity toward normal aldehyde as observed in the photochemical hydroformylation reaction with $Co(OAc)_2/PBu_3$ catalyst under low CO pressure and low temperature. $HCo(CO)_2(PBu_3)_2$ is known to be fairly stable up to 140 °C in various organic solvents,[8] then it can not contribute to the thermal hydroformylation reaction because higher temperature must be required to initiate the reaction and under such conditions $HCo(CO)_2(PBu_3)_2$ will be readily converted into $HCo(CO)_3PBu_3$ even under much low CO pressure. Consequently, the highly selective hydroformylation can be achieved only by the photochemical reaction which is able to proceed readily at low temperature.

References

1) E. A. Koerner von Gustorf, L. H. G. Leenders, I. Fischler, and R. N. Perutz, *Adv. Inorg. Chem. Radiochem.*, **19**, 65 (1976); G. L. Geoffroy and M. S. Wrighton, "Organometallic Photochemistry," Academic Press, New York (1979); G. W. Parshall, "Homogeneous Catalysis," John Wiley & Sons, New York (1980), p. 229; R. G. Salomon, *Tetrahedron*, **39**, 485 (1983).

2) M. J. Mirbach, M. F. Mirbach, A. Saus, N. Topalsavoglou, and T. N. Phu, *J. Am. Chem. Soc.*, **103**, 7594 (1981).

3) A. Saus, T. N. Phu, M. J. Mirbach, and M. F. Mirbach, *J. Mol. Catal.*, **18**, 117 (1983).

4) E. M. Gordon and R. Eisenberg, *J. Organomet. Chem.*, **306**, C53 (1986).

5) F. Piacenti, M. Bianchi, and E. Benedetti, *Chim. Ind. (Milan)*, **49**, 245 (1967).

6) G. F. Pregaglia, A. Andreetta, G. Gregorio, G. Montrasi, and G. F. Ferrari, *Chim. Ind. (Milan)*, **54**, 405 (1972).

7) A. R. Manning, *J. Chem. Soc. A*, **1968**, 1135.

8) G. F. Pregaglia, A. Andreetta, and G. F. Ferrari, *J. Organomet. Chem.*, **30**, 387 (1971).

9) B. Fell, W. Rupilius, and F. Asinger, *Tetahedron Lett.*, **1968**, 3261.

10) M. J. Mirbach, N. Topalsavoglou, T. N. Phu, M. F. Mirbach, and A. Saus, *Chem. Ber.*, **116**, 1422 (1983).

11) J. Falbe, "New Syntheses with Carbon Monoxide," Springer-Verlag, Berlin (1980), p. 40.

12) P. Rigo, M. Bressan, and A. Morvillo, *J. Organomet. Chem.*, **105**, 263 (1976).

13) I. Wender and P. Pino, "Organic Syntheses via Metal Carbonyls," John Wiley & Sons, New York (1977), Vol. 2, p. 105.

14) R. L. Sweany, *Inorg. Chem.*, **19**, 3512 (1980).

15) A. Andreetta, G. Montrasi, G. F. Ferrari, G. F. Pregaglia, and R. Ugo, *Nouv. J. Chim.*, **2**, 463 (1978).

16) R. W. Wegman and T. L. Brown, *Inorg. Chem.*, **22**, 183 (1983).

17) F. Piacenti, M. Bianchi, E. Benedetti, and P. Frediani, *J. Organomet. Chem.*, **23**, 257 (1970).

18) M. van Boven, N. Alemdaroglu, and J. M. L. Penninger, *J. Organomet. Chem.*, **84**, 65 (1975).

19) M. F. Mirbach, M. J. Mirbach, and R. W. Wegman, *Organometallics*, **3**, 900 (1984).

 © 1991 The Chemical Society of Japan Bull. Chem. Soc. Jpn., 64, 3023—3028 (1991)

Hydrates of Organic Compounds. XVI. Determination of the Melting Points and Hydration Numbers of the Hydrates of Tetrabutyl(or Tetraisopentyl)ammonium Alkanesulfonates

Haruo NAKAYAMA,* Masashi YAMANOBE, and Kei BABA
Division of Materials Science and Chemical Engineering, Faculty of Engineering,
Yokohama National University, Tokiwadai, Hodogaya-ku, Yokohama 240
(Received May 23, 1991)

The solid-liquid phase diagrams of binary mixtures of water with tetraisopentylammonium alkanesulfonates, $[(i\text{-}C_5H_{11})_4N][n\text{-}C_nH_{2n+1}SO_3]$ (n=1—8), bis(tetrabutylammonium) alkanedisulfonates, $[(n\text{-}C_4H_9)_4N]_2[O_3S(CH_2)_nSO_3]$ (n=2—5), and with bis(tetraisopentylammonium) alkanedisulfonates, $[(i\text{-}C_5H_{11})_4N]_2[O_3S(CH_2)_nSO_3]$ (n=2—5), were examined in order to confirm the formation of hydrates. For all of the sulfonates examined the formation of hydrates has been newly confirmed. The hydrates of the tetraisopentylammonium alkanesulfonates have hydration numbers of around 37—40 and fairly high melting points (lie between 13 and 19 °C). The typical hydrates formed by the bis(tetrabutylammonium) alkanedisulfonates have hydration numbers of around 52 and those by the bis(tetraisopentylammonium) alkanedisulfonates around 76. The former disulfonate hydrates have low melting points (between 1.0 and 10 °C). However, the latter disulfonate hydrates have fairly high melting points (between 13 and 18 °C). A salt with n=4 forms the most stable hydrate for both series of alkanedisulfonates. Judging from the hydration numbers and melting points, these hydrates seem to be clathrate-like.

It is well-known that some tetrabutylammonium and tetraisopentylammonium salts, such as $(n\text{-}C_4H_9)_4NF$ and $(i\text{-}C_5H_{11})_4NF$, can form unusual hydrates which have a large number of water molecules per one ammonium ion (hydration numbers) as well as fairly high melting points between 0 °C and room temperature.[1-3] According to a single-crystal X-ray examination by Jeffrey and co-workers[2-5] these hydrates were semi-clathrate hydrates, similar to the so-called gas hydrates:[4] The water structure is a hydrogen-bonded framework, and is essentially a regular arrangement of polyhedra, such as pentagonal dodecahedra and tetrakaidecahedra; each alkyl group of an ammonium cation is incorporated into one of the polyhedra.[2-3]

The formation of similar types of hydrates has also been known for various tetrabutylammonium (or tetraisopentylammonium) salts which have organic anions like alkanoates[5-11] and dialkanoates.[11,12] These hydrates are of special interest, since their atability and structure are affected not only by the type of tetraalkylammonium cation, but also by the hydrocarbon portion of the anion. Recently, from the fact that tetrabutylammonium alkanedioates, $[(n\text{-}C_4H_9)_4N]_2[OOC(CH_2)_n\text{-}COO]$, can form a stable clathrate-like hydrate when n=3,[12] the possibility to form a hydrate of tetrabutylammonium polyacrylate was both anticipated and verified.[13] The formation of a hydrate of such a polymeric salt has never been known before.

Another polyanion which is expected to possibly form a similar type hydrate is a polysulfonate anion, such as the poly(ethenesulfonate) anion and the poly(styrenesulfonate) anion. However, there is no basic information about the formation of hydrates of tetraalkylammonium alkanesulfonates and alkanedisulfonates, except for a series of tetrabutylammonium alkanesulfonates.[14] Thus, in this work, phase-diagrammatic studies regarding binary mixtures of water with tetraisopentylammonium alkanesulfonates, bis(tetrabutylammonium)alkanedisulfonates, or bis(tetraisopentylammonium) alkanedisulfonates were carried out in order to confirm the formation of clathrate-like hydrates and, when formed, to determine the effect of the hydrocarbon portion of the anion on the melting points and hydration numbers.

Experimental

Aqueous solutions of tetraisopentylammonium alkanesulfonates, $[(i\text{-}C_5H_{11})_4N][n\text{-}C_nH_{2n+1}SO_3]$ (n=1—6, and 8), bis(tetrabutylammonium) alkanedisulfonates, $[(n\text{-}C_4H_9)_4N]_2[O_3S(CH_2)_nSO_3]$ (n=2—5), and of bis(tetraisopentylammonium) alkanedisulfonates, $[(i\text{-}C_5H_{11})_4N]_2[O_3S(CH_2)_nSO_3]$ (n=2—5), were prepared by neutralization of either an aqueous tetrabutylammonium hydroxide solution or an aqueous tetraisopentylammonium hydroxide solution with the corresponding sulfonic acid solutions. The hydroxide solutions were obtained by treating either tetrabutylammonium iodide or tetraisopentylammonium iodide with freshly prepared silver(I) oxide in water followed by filtration of the AgI precipitate. Tetrabutylammonium iodide was prepared by precipitation from an aqueous solution of tetrabutylammonium bromide (purchased from Tokyo Kasei Kogyo Co., Ltd.) with the addition of sodium iodide, followed by washing with water and air-drying in a desiccator. The iodide was purified by repeated recrystallization from ethyl acetate. Tetraisopentylammonium iodide was synthesized and purified in the same manner as described in a previous paper.[11] All of the sulfonic acid solutions, except for CH_3SO_3H and $C_2H_5SO_3H$, were obtained by passing each sodium salt solution through a column of cation-exchange resin (Amberlite IR-120B) converted, in advance, into the acid form by about a 2 mol dm^{-3} hydrochloric acid solution. Two acids, CH_3SO_3H and $C_2H_5SO_3H$, and the sodium salts $n\text{-}C_nH_{2n+1}SO_3Na$ with n=5, 6, and 8, were purchased either from Tokyo Kasei Kogyo Co., Ltd. or Aldrich Chemical Co., Inc.. Two sodium salts, $n\text{-}C_nH_{2n+1}SO_3Na$ with n=3 and 4, were synthesized in the manner reported by Reed et al.[15] A half mole of the corre-

sponding alkyl iodide was slowly added to a hot saturated aqueous solution of one mole of sodium sulfite. The mixture was refluxed for a few days. After the water had been evaporated under reduced pressure, the reaction product was extracted with hot ethanol. The sodium salt was purified by repeated recrystallization from ethanol. Two sodium alkanedisulfonates, $NaO_3S(CH_2)_nSO_3Na$ with n=2 and 4, were purchased from Tokyo Kasei Kogyo Co., Ltd., and two other sodium salts with n=3 and 5 were synthesized using the corresponding dibromide, $Br(CH_2)_nBr$ (n=3 or 5), by a similar manner as discribed above.[16] All of the synthesized disodium salts were confirmed by their NMR and IR spectra.

The solid-liquid phase diagrams for the binary systems of water-each sulfonate mentioned above were determined in the same manner as described in previous papers.[8-11] The concentration of each mother solution was determined by measuring the amount of either tetrabutylammonium cation or tetraisopentylammonium cation by titration with a sodium tetraphenylborate solution standardized by pure $(n\text{-}C_4H_9)_4NI$ solid.

Results and Discussion

(1) The Formation of Hydrates of Tetraisopentylammonium Alkanesulfonates. The solid-liquid phase diagrams for the binary systems, water-$[(i\text{-}C_5H_{11})_4N][n\text{-}C_nH_{2n+1}SO_3]$, where n=1—3, are shown in Fig. 1. The

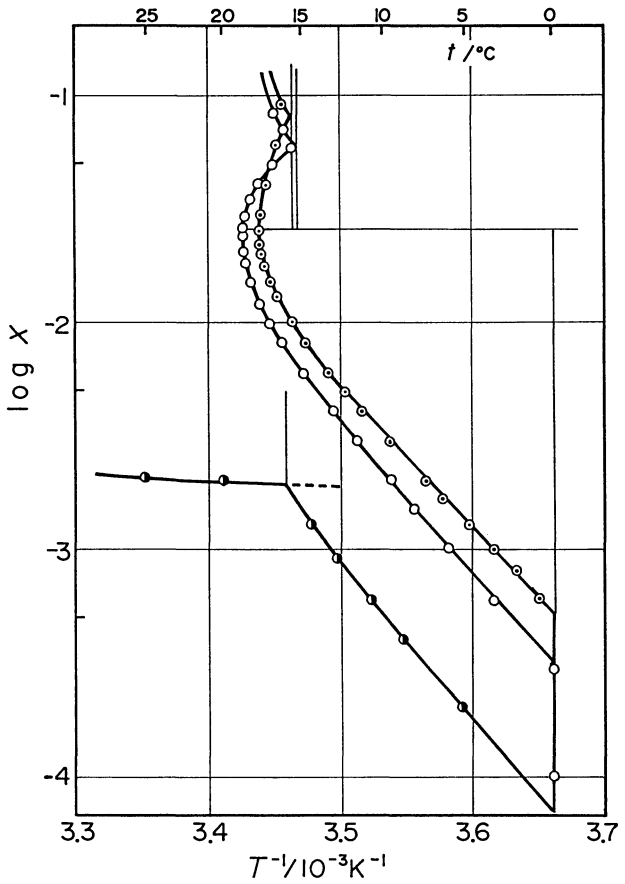

Fig. 1. Solid-liquid phase diagrams for the water-$[(i\text{-}C_5H_{11})_4N][n\text{-}C_nH_{2n+1}SO_3]$ systems. ○: n=1; ⊙: n=2; ◑: n=3.

logarithm of the concentration, expressed as the mole fraction, X, is plotted against the reciprocal of the absolute temperature. The phase diagrams of the salts with n=1 and 2 exhibit congruent melting points at concentrations near X=0.025, indicating that these two salts form a hydrate with hydration numbers around 39. These hydrates are fairly stable: The melting points are 18.7 °C (n=1) and 17.6 °C (n=2), respectively. It is interesting to note that the formation of these hydrates occurs in very dilute solutions (around $X=5\times10^{-4}$), just as found for other tetraisopentylammonium salt hydrates.[11,17]

In the n=3 system, two kinds of solid-liquid equilibrium lines intersect each other at around X=0.002 and 16.1 °C. The line at temperatures below 16.1 °C may be regarded as being an equilibrium line between a hydrate solid and an aqueous solution, just as in the case of the other two salts with n=1 and 2, since the slopes $-\partial \log X/\partial(1/T)$ are almost the same for these three systems: It has been verified that this slope is approximately proportional to the hydration numbers of the hydrate.[18] Thus, it can be concluded that the salt with n=3 forms a hydrate with hydration numbers around 39 at temperatures below 16.1 °C. Its melting point is estimated to be 22—23 °C if the hydrate were stable above 16.1 °C. The line at temperatures above 16.1 °C seems to exhibit an equilibrium between an anhydrous $[(i\text{-}C_5H_{11})_4N][n\text{-}C_3H_7SO_3]$ solid and a saturated solution. It is interesting to note that although the salt with n=3 can form a fairly stable hydrate, its anhydrous salt is more stable at temperatures above 16.1 °C.

The phase diagrams for the salts with n=4 and 5 are essentially the same as those of n=1 and 2 shown in Fig. 1, except that for the salt with n=5; in this case a region in which two liquid phases are in equilibrium appears above 20.9 °C. The critical concentration is almost the same as the congruent composition of its hydrate (X=0.025).

The phase diagrams for the salts with n=6 and 8 are shown in Fig. 2. For these two systems, the liquid-liquid equilibrium region extends towards the wide-concentration range and the low-temperature region. The solid-liquid phase diagram for the n=6 system intersects with its liquid-liquid phase diagram at X=0.067, which is greater than its congruent composition (X=0.024). However, for the n=8 system these two lines intersect at a concentration (X=0.01) before the solid-liquid line reaches its congruent composition. As a result of this, the melting point and hydration numbers for the hydrate of the n=8 salt cannot be determined exactly, though a similar hydrate to that of the n=6 salt is undoubtedly formed at concentrations below X=0.01 for the same reason as mentioned regarding the n=3 system. Its melting point is estimated to be 14—15 °C.

All of the melting points and hydration numbers, determined from each congruent melting point and congruent composition, are summarized in Table 1,

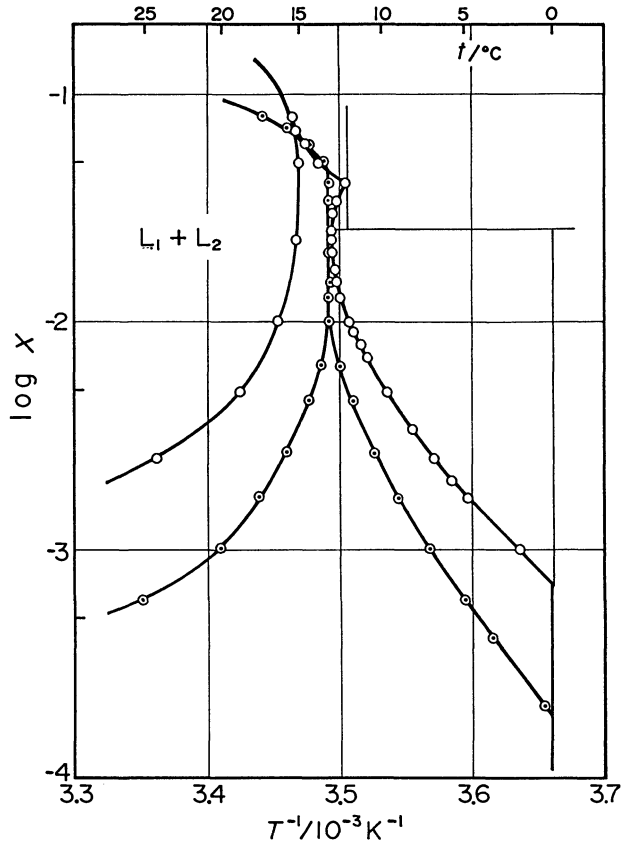

Fig. 2. Solid–liquid phase diagrams for the water–[(i-C_5H_{11})$_4$N][n-$C_nH_{2n+1}SO_3$] systems. ○: n=6; ⊙: n=8.

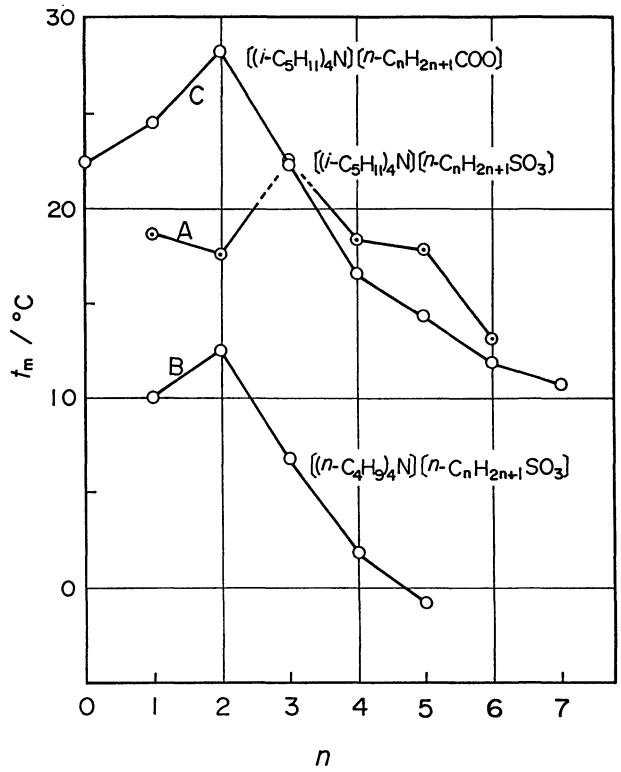

Fig. 3. Relationships between the melting points, t_m, of the hydrates of tetraisopentylammonium alkanesulfonates (A), tetrabutylammonium alkanesulfonates (B), and of tetraisopentylammonium alkanoates (C) and the number of carbon atoms, n, of either alkanesulfonate or alkanoate anion.

Table 1. Melting Points and Hydration Numbers of the Clathrate-Like Hydrates Formed by a Series of Tetraisopentylammonium Alkanesulfonates, [(i-C_5H_{11})$_4$N][n-$C_nH_{2n+1}SO_3$]

n	Melting point t_m/°C	Hydration numbers
1	18.7	39±2
2	17.6	39±2
3	(22—23)[a)]	—
4	18.3	37±2
5	17.8	40±2
6	13.1	37±2
8	(14—15)[a)]	—

a) See text.

together with estimated melting points for the hydrates of the salts with n=3 and 8. The existence of these hydrates has been newly confirmed in this study. From Table 1 it is clear that all of the hydrates have hydration numbers around 39. As mentioned above, the hydrates formed by the salts with n=3 and 8 presumably have similar hydration numbers. It is interesting to note that the same type of hydrate is formed regardless of the chain length of the alkyl group in the alkanesulfonate anion. The melting points of these hydrates are fairly high (higher than 17 °C, except for the hydrates of n=6 and 8) and the effect of the chain length of the $C_nH_{2n+1}SO_3^-$ anion on the melting points of these hydrates is not so marked. Judging from the values of the hydration numbers and the melting points, these hydrates seem to be an isostructural clathrate-like hydrate with a well-known (i-C_5H_{11})$_4$NF·39H_2O hydrate, whose structure has been examined in detail by Jeffrey and his co-worker.[3)]

In Fig.3 the relationships between the melting points (t_m) of the hydrates and the number of carbon atoms of the alkyl group in the anion (n) is shown (A), together with those of two related salts of [(n-C_4H_9)$_4$N][n-$C_nH_{2n+1}SO_3$] (B)[14)] and [(i-C_5H_{11})$_4$N][n-C_nH_{2n+1}COO] (C).[11)] A comparison of line A with line B clearly indicates that the hydrates of tetraisopentylammonium alkanesulfonates are more stable than those of tetrabutylammonium alkanesulfonates: The melting points of the former hydrates are more than 15 degrees higher than those of the latter hydrates when n is larger than 3. This fact suggests that a hydrogen-bonded framework of water molecules surrounding an (i-C_5H_{11})$_4$N$^+$ cation is fairly stable, compared with that around an (n-C_4H_9)$_4$N$^+$ cation, as has been pointed out in other studies.[11,18)] It is interesting to note that when n=1 and 2 the melting points of a series of tetraisopentylammonium alkanesulfonates (A) are 6—10 °C lower than those of a series of tetraisopentylammonium alkanoates (C). As discussed

in an earlier paper,[11] the highest melting point of the [(i-C_5H_{11})$_4$N][C_2H_5COO] hydrate is explained by the best fit of the $C_2H_5COO^-$ anion to a pentagonal dodecahedron, which exists in a gap between the arrangement of larger polyhedra filled by one of the isopentyl groups of a tetraisopentylammonium cation. For the sulfonate hydrates with n=1 and 2, however, the distortion of the hydrogen-bonded water network which incorporates sulfonate anions, like $CH_3SO_3^-$ and $C_2H_5SO_3^-$, will be greater than when incorporates such alkanoate anions as CH_3COO^- and $C_2H_5COO^-$ because of the bulkiness of the SO_3^- group, compared with the COO^- group. This leads to a lowering of the melting points of the hydrates of [(i-C_5H_{11})$_4$N][CH_3SO_3] and [(i-C_5H_{11})$_4$N]-[$C_2H_5SO_3$].

Another feature which can be seen from a comparison of lines A and C in Fig.3 is the fact that when n is larger than 3 the melting points of both series of hydrates decrease with increasing n, and the difference between them become less than 4 degrees. This behavior may be explained, at least partly, as follows: When n is larger than 3, both the $C_nH_{2n+1}SO_3^-$ anion and the $C_nH_{2n+1}COO^-$ anion can no longer be accommodated in a small cage, like a single pentagonal dodecahedron, because of their increased ionic volume. As a result, they must be accommodated in a larger polyhedron. For such a large polyhedron the distortion of the water network due to the SO_3^- group and COO^- group does not play an important role concerning the stability of the hydrates.

(2) The Formation of Hydrates of Bis(tetrabutylammonium) Alkanedisulfonates and of Bis(tetraisopentylammonium) Alkanedisulfonates. Solid-liquid phase diagrams for the binary systems, water-[(n-C_4H_9)$_4$N]$_2$-[$O_3S(CH_2)_nSO_3$], where n=2—5, are shown in Fig. 4 in the same manner as in Figs. 1 and 2. Three systems with n=2—4 exhibit congruent melting points at concentrations of around X=0.019, indicating that these three salts form a hydrate with hydration numbers of about 52. The melting points of these hydrates, however, are fairly low: they lie between 5.7 and 9.9 °C. The system with n=5 shows two congruent melting points at 1.0 and 1.4 °C at concentrations of around X=0.016 and 0.032, indicating that two kinds of hydrates with hydration numbers of around 61 and 30 are formed. The latter hydrate is also formed by a salt with n=4. In addition, in systems with n=2—4 there are incongruent melting points at concentrations of around X=0.014—0.015; the hydration numbers of the hydrates formed at concentrations below the incongruent compositions seem to be the same as that formed for the n=5 salt, around 61, because of a similarity in the slope ($\partial \log X/\partial(1/T)$) in all systems with n=2—5.

All of the melting points, hydration numbers, which are determined from each congruent composition and the congruent melting point, are summarized in Table 2. As mentioned above, three types of hydrates with hydration numbers of around 30, 52, and 61 are formed. The existence of these hydrates has been newly confirmed in this study. No information about the structure of these hydrates is present at this stage. However, hydrates with hydration numbers of about 61 seem to be isostructural with a well-known (n-C_4H_9)$_4$NF·30H_2O hydrate,[2] since the number of the water molecules per one (n-C_4H_9)$_4$N$^+$ cation is almost the same in both hydrates. Although the formation of several types of tetrabutylammonium salt hydrates which have hydration numbers less than 30 per one (n-C_4H_9)$_4$N$^+$ cation and fairly high melting points (higher than 10 °C) is known at pres-

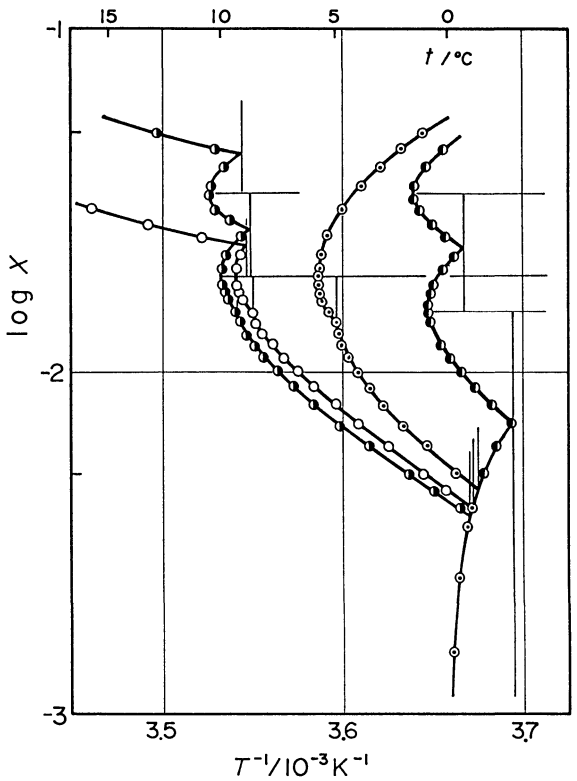

Fig. 4. Solid-liquid phase diagrams for the water-[(n-C_4H_9)$_4$N]$_2$[$O_3S(CH_2)_nSO_3$] systems. ○: n=2; ⊙: n=3; ◑: n=4; ◐: n=5.

Table 2. Melting Points and Hydration Numbers of the Clathrate-Like Hydrates Formed by a Series of Bis(tetrabutylammonium) Alkanedisulfonates, [(n-C_4H_9)$_4$N]$_2$[$O_3S(CH_2)_nSO_3$]

n	Melting point t_m/°C	Hydration numbers
2	8.7 (incong.)	—
	9.3	52±2
3	5.0 (incong.)	—
	5.7	52±3
4	9.1 (incong.)	—
	9.9	52±2
	10.4	30±2
5	1.0	61±3
	1.4	30±2

ent,[10] the correlation between these hydrates and those found in this study with hydration numbers of 30 and 52 is uncertain. Another interesting feature of Table 2 is the fact that the melting points of the hydrates of the salt with a short methylene chain of n=2 and with a somewhat long methylene chain of n=4 are higher than those of the n=3 and 5 hydrates. This may be explained by assuming that the n=2 hydrate comprises a sequence of $[(n\text{-}C_4H_9)_4N^+ \cdots {}^-O_3S(CH_2)_2SO_3^-]+[(n\text{-}C_4H_9)_4N^+]$, and that the n=4 hydrate $[(n\text{-}C_4H_9)_4N^+ \cdots {}^-O_3S(CH_2)_4SO_3^- \cdots (n\text{-}C_4H_9)_4N^+]$ in which the central ${}^-O_3S(CH_2)_4SO_3^-$ anion is surrounded by a large polyhedron made of hydrogen-bonded water networks; in the n=3 hydrate the distortion effect of the ${}^-O_3S(CH_2)_3SO_3^-$ anion on the hydrogen-bonded water network surrounding an $(n\text{-}C_4H_9)_4N^+$ cation will increase compared with that of the ${}^-O_3S(CH_2)_2SO_3^-$ anion in the n=2 hydrate; in the n=5 hydrate the distortion effect of the ${}^-O_3S(CH_2)_5SO_3^-$ anion become larger than that of the ${}^-O_3S(CH_2)_4SO_3^-$ anion in the n=4 hydrate.

The solid–liquid phase diagrams for the binary systems, water–$[(i\text{-}C_5H_{11})_4N]_2[O_3S(CH_2)_nSO_3]$, where n=2—5, are shown in Fig. 5. The phase diagram of the system with n=2 is shown by a broken line because of the similarity of data with those of the n=3 salt. It is clear from this figure that all four systems exhibit congruent melting points at around X=0.013, indicating that these four salts form a hydrate with hydration numbers around 76. Furthermore, the two systems with n=2 and 4 exhibit other congruent melting points around X=0.042—0.043, corresponding to hydrates with hydration numbers of 22—23. All of the melting points and hydration numbers determined are summarized in Table 3, together with some incongruent melting points. These hydrates were newly confirmed in this study. The hydrates with hydration numbers of around 76 seem to be isostructural with a well-known $(i\text{-}C_5H_{11})_4NF \cdot 39H_2O$ hydrate,[3] since the number of water molecules per one $(i\text{-}C_5H_{11})_4N^+$ cation is almost the same in both hydrates. The interesting features of Table 3 are summarized as follows: (1) The melting points of hydrates with hydration numbers of around 76 are 7—12 °C higher than those of the hydrates formed by a series of bis(tetrabutylammonium) alkanedisulfonates (shown in Table 2), suggesting that a hydrogen-bonded framework of water molecules around an $(i\text{-}C_5H_{11})_4N^+$ cation is more stable than that around an $(n\text{-}C_4H_9)_4N^+$ cation, as is often pointed out;[11,18] (2) The order of the melting points with respect to n is 4>2>3>5, which is the same as in the case of bis(tetrabutylammonium) alkanedisulfonate hydrates (shown in Table 2). The reason for this can be explained in the same manner as mentioned above; and (3) For the n=2 and 4 salts hydrates with hydration numbers of 22—23 are slightly stable compared with those of around 76.

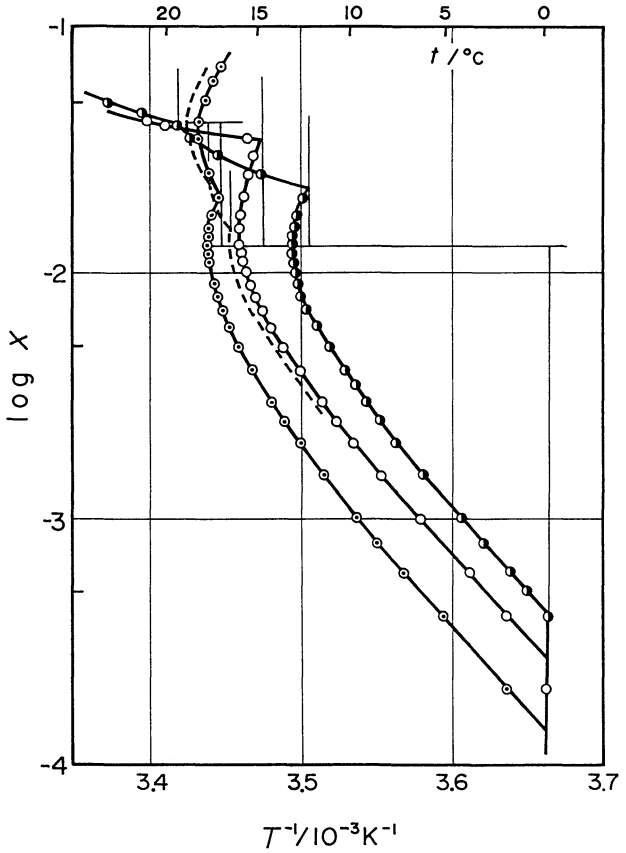

Fig. 5. Solid–liquid phase diagrams for the water–$[(i\text{-}C_5H_{11})_4N]_2[O_3S(CH_2)_nSO_3]$ systems. ○: n=3; ⊙: n=4; ◑: n=5; broken line: n=2.

Finally, in Fig. 6 the melting points of the two series of hydrates of alkanedisulfonates, $[(n\text{-}C_4H_9)_4N]_2[O_3S(CH_2)_nSO_3]$ and $[(i\text{-}C_5H_{11})_4N]_2[O_3S(CH_2)_nSO_3]$, are compared with those of the hydrates of the corresponding alkanedioates,[11] $[(n\text{-}C_4H_9)_4N]_2[OOC(CH_2)_nCOO]$ and $[(i\text{-}C_5H_{11})_4N]_2[OOC(CH_2)_nCOO]$, respectively. The dependence of the melting points on the number of n for the latter two series of hydrates has been discussed in a previous paper.[11] It is obvious from this figure that when the kind of cation is the same, either $(n\text{-}C_4H_9)_4N^+$ or $(i\text{-}C_5H_{11})_4N^+$, the melting points of the alkanedioate hydrates are fairly high compared with those of the alkanedisulfonate hydrates: The melting-

Table 3. Melting Points and Hydration Numbers of the Clathrate-Like Hydrates Formed by a Series of Bis(tetraisopentylammonium) Alkanedisulfonates, $[(i\text{-}C_5H_{11})_4N]_2[O_3S(CH_2)_nSO_3]$

n	Melting point t_m/°C	Hydration numbers
2	16.6	76±4
	17.6 (incong.)	—
	18.9	22±2
3	16.0	76±4
4	17.7	76±3
	18.2	23±2
5	13.1	76±5
	19.6 (incong.)	—

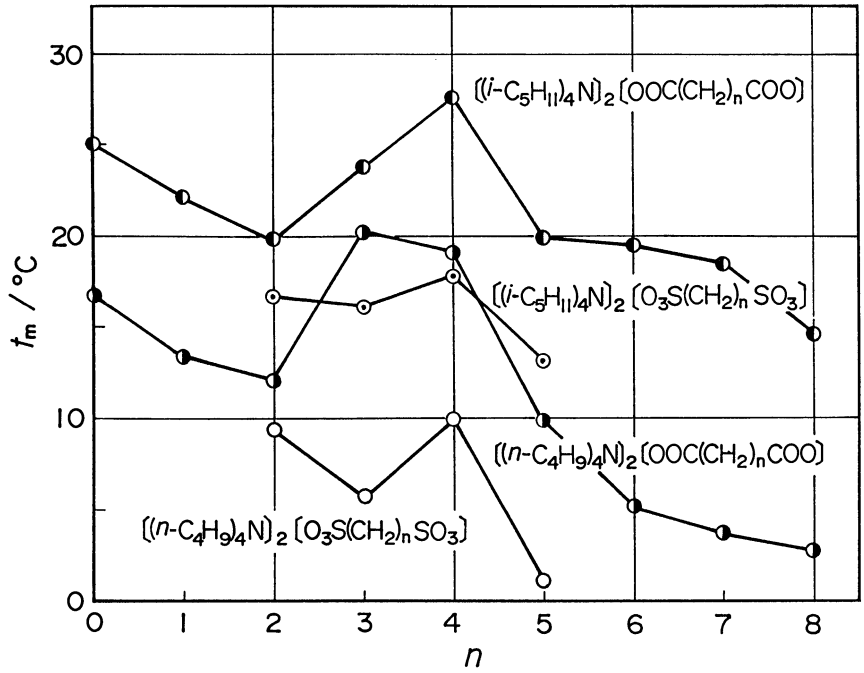

Fig. 6. Relationships between the melting points, t_m, of the hydrates of four series of salts and of the number of carbon atoms, n, of the methylene chain of the anion. ○: $[(n\text{-}C_4H_9)_4N]_2[O_3S(CH_2)_nSO_3]$; ⊙: $[(i\text{-}C_5H_{11})_4N]_2[O_3S(CH_2)_nSO_3]$; ◑: $[(n\text{-}C_4H_9)_4N]_2[OOC(CH_2)_nCOO]$; ◐: $[(i\text{-}C_5H_{11})_4N]_2[OOC(CH_2)_nCOO]$.

point differences are 9—14 °C for the tetrabutylammonium salt hydrates and 7—10 °C for the tetraisopentylammonium salt hydrates for n=3—5, although when n=2 the difference is somewhat slight (about 3 °C) for both hydrates. The high stability of the alkanedioate hydrates probably indicates that a distortion effect of the bulky alkanedisulfonate anion $[O_3S(CH_2)_nSO_3]^{2-}$ on the hydrogen-bonded water networks is larger than that of the alkanedioate anion $[OOC(CH_2)_nCOO]^{2-}$, just as discussed concerning the difference in curves A and C when n=1 and 2 in Fig. 3.

References

1) D. L. Fowler, W. V. Loebenstein, D. B. Pall, and C. A. Kraus, *J. Am. Chem. Soc.*, **62**, 1140 (1940).
2) R. K. McMullan, M. Bonamico, and G. A. Jeffrey, *J. Chem. Phys.*, **39**, 3295 (1963).
3) D. Feil and G. A. Jeffrey, *J. Chem. Phys.*, **35**, 1863 (1961).
4) W. F. Clausen, *J. Chem. Phys.*, **19**, 259, 662 (1951). L. Pauling and R. E. Marsh, *Proc. Natl. Acad. Sci. U.S.A.*, **38**, 112 (1952).
5) R. K. McMullan and G. A. Jeffrey, *J. Chem. Phys.*, **31**, 1231 (1959).
6) M. Bonamico, G. A. Jeffrey, and R. K. McMullan, *J. Chem. Phys.*, **37**, 2219 (1962).
7) Yu. A. Dyadin, L. S. Aladko, L. A. Gaponenko, and T. M. Polyanskaya, *Izv. Sib. Otd. Akad. Nauk SSSR, Ser. Khim. Nauk*, **1981** (9), 19.
8) H. Nakayama and S. Torigata, *Bull. Chem. Soc. Jpn.*, **57**, 171 (1984).
9) H. Nakayama and H. Usui, *J. Inclusion Phenom.*, **2**, 249 (1984).
10) H. Nakayama, T. Saitoh, and H. Uchida, *J. Inclusion Phenom.*, **8**, 177 (1990).
11) H. Nakayama, K. Nakamura, Y. Haga, and Y. Sugiura, *Bull. Chem. Soc. Jpn.*, **64**, 358 (1991).
12) H. Nakayama and K. Watanabe, *Bull. Chem. Soc. Jpn.*, **51**, 2518 (1978).
13) H. Nakayama, *Bull. Chem. Soc. Jpn.*, **60**, 2319 (1987).
14) H. Nakayama and H. Usui, *Bull. Chem. Soc. Jpn.*, **59**, 833 (1986).
15) R. M. Reed and H. V. Tartar, *J. Am. Chem. Soc.*, **57**, 570 (1935).
16) G. C. H. Stone, *J. Am. Chem. Soc.*, **58**, 488 (1936). S. M. McElvain, A. Jelinek, and K. Rorig, *ibid.*, **67**, 1578 (1945).
17) H. Nakayama, *Bull. Chem. Soc. Jpn.*, **54**, 3717 (1981).
18) H. Nakayama, *Bull. Chem. Soc. Jpn.*, **55**, 389 (1982).

 © 1991 The Chemical Society of Japan Bull. Chem. Soc. Jpn., 64, 3029—3034 (1991)

Coated Wire Electrodes Sensitive to Local Anesthetic Cations and Their Application to Potentiometric Determination

Hiromu SATAKE,* Takahiro MIYATA, and Shoji KANESHINA
Department of Biological Science and Technology, Faculty of Engineering,
The University of Tokushima, Minamijosanjima-cho, Tokushima 770
(Received February 6, 1991)

Coated wire electrodes sensitive to procaine(PC), tetracaine(TC), lidocaine(LC), dibucaine(DC), mepivacaine(MC), and bupivacaine(BC), based on ion-pair formation between tetraphenylborate ions and the corresponding local anesthetic cations in a plasticized poly(vinyl chloride) membrane were prepared. The electrodes showed linear responses with Nernstian slopes (55—58 mV/decade) over concentration ranges of 4×10^{-5}—10^{-2}, 4×10^{-5}—10^{-2}, 10^{-4}—10^{-2}, 4×10^{-5}—10^{-2}, 5×10^{-5}—10^{-2}, and 2×10^{-4}—10^{-2} mol dm^{-3} for PC, TC, LC, DC, MC, and BC, respectively. The change in pH did not affect the electrode performance within ranges of 3.2—7.4, 3.2—7.4, 2.1—7.7, 2.5—7.4, 3.5—7.0, and 2.4—5.6 for PC, TC, LC, DC, MC, and BC, respectively. The reproducibility, stability, response time, and selectivity were also investigated. The electrodes were applied satisfactorily to the determination of local anesthetics by potentiometry.

Many local anesthetics in clinical use are basically tertiary amine compounds, and are classified as being of the ester type [procaine (PC), tetracaine (TC), benzocaine etc.] and amide type [lidocaine (LC), dibucaine (DC), mepivacaine (MC), bupivacaine (BC) etc.]. These drugs exist in both positively charged and uncharged forms under normal in vivo conditions.[1] Both species apparently have different biological activities. The establishment of analytical methods for both species will provide useful information concerning the molecular mechanism of local anesthetic action.[2,3]

Although many methods[4-10] (including polarography, spectrophotometry, HPLC, and fluorometry) have been reported for the determination of local anesthetics, these are generally used for measuring the total concentration of local anesthetics. Potentiometry[11-17] using an ion-selective electrode has an advantage in that the electrode enables estimates of free cationic anesthetics. An ion-selective electrode comprising a poly(vinyl chloride) (PVC) membrane is the most suitable type for use as a sensor in the potentiometric determination of organic cations like local anesthetics. So far reported have been a liquid-membrane electrode[12] incorporating PC–tetraphenylborate (TPB^-) and a PVC membrane electrode with a PC–TPB ion pair[11,16] and crown ether[15] used as the sensor elements; these electrodes have complicated structures and electrodes preparation is time consuming. On the other hand, a coated wire electrode based on a PVC membrane can easily be prepared in various shapes and miniaturized. Coated wire electrodes have been used as sensors in the potentiometric titration of PC by K. Vytras et al;[13,14] other local anesthetics were not studied.

This paper discusses the preparation of PVC-membrane coated wire electrodes sensitive to PC, TC, LC, DC, MC, and BC, as well as some of the properties of the resulting electrodes. The concerned electrodes were used successfully as sensors in direct potentiometry and potentiometric titration of local anesthetics.

Experimental

Reagents. All of the reagents used in the preparation of the electrode and solution were of analytical grade. The hydrochloride salts of local anesthetics used were purchased from Sigma Chemical Co., except for lidocaine hydrochloride (Fujisawa Yakuhin Co.). The chemical structures of the local anesthetics used are shown in Fig. 1. Sodium tetraphenylborate (NaTPB) (Aldrich), dioctyl phthalate (DOP) (Tokyo Kasei), PVC (Wako) of high molecular weight, and tetrahydrofuran (THF) (Wako) were used; the THF solvent was dehydrated with molecular sieves (Wako). Ion-pairs of PC–TPB, TC–TPB, LC–TPB, DC–TPB, MC–TPB, and BC–TPB were prepared according to the same method described previously for an ion pair of tetraphenylphosphonium–tetraphenylborate,[18] and were identified by elemental analysis. Water was purified by triple distillation, once from an alkaline potassium permanganate solution.

Construction of Electrode. A coated wire electrode sensitive to local anesthetic cations was prepared by the same method described previously.[18] The copper wire (0.8 mm diameter) was coated with a PVC-membrane of ca. 0.4 mm thickness. The solution used for the PVC-membrane usually included ion pairs, DOP, PVC, and THF with various compositions. The electrode was allowed to stand for at least ten hours in contact with air; it was then conditioned by soaking in 10^{-3} mol dm^{-3} of a local anesthetic drug solution or water prior to measurements.

Potential Measurement. The electrochemical system was as follows: A local anesthetic coated wire electrode/test solution/1 mol dm^{-3} sodium nitrate agar-bridge/saturated potassium chloride/Ag–AgCl electrode.

The electromotive force (EMF) was measured at 25 °C with a multi-ion monitor (Yamashita Giken) in a constantly stirred solution. The temperature of the test solution was controlled by circulating water from a thermostatic bath (Komatu Yamato) through a double-wall beaker.

Calibration curves of the EMF vs. the logarithm of the anesthetic concentration were made as follows: The EMF values were recorded after suitable increments of standard local anesthetic solution was added to 50 cm^3 of water, so as to cover the concentration range 10^{-6}—10^{-2} mol dm^{-3}. The

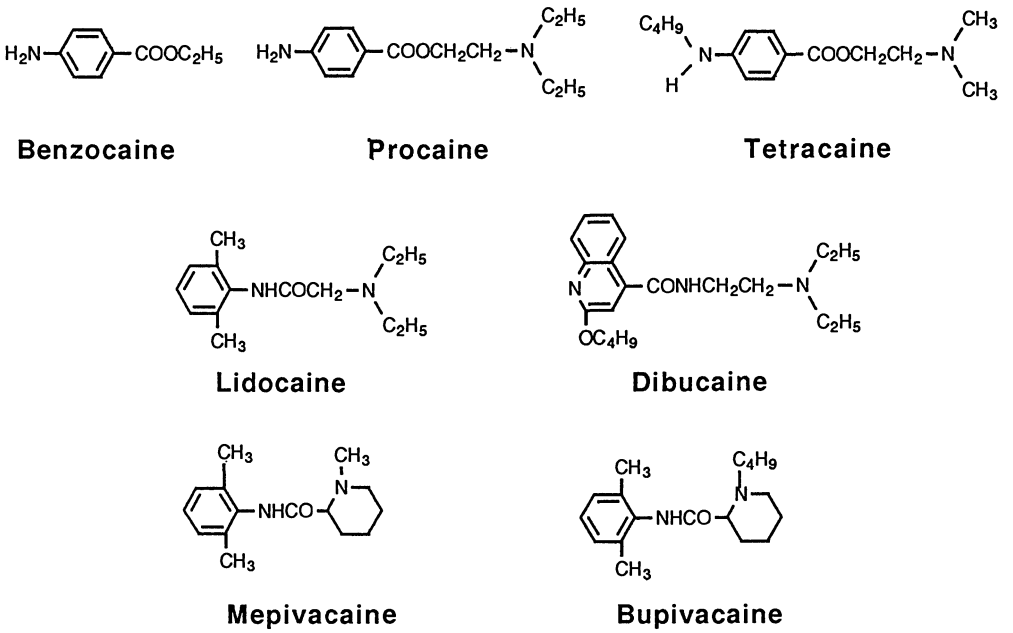

Fig. 1. Chemical structure of local anesthetics.

local anesthetic coated wire electrode and the sodium nitrate agar-bridge connected to a reference electrode was immersed in each test solution; the EMF values were recorded after each addition.

Potentiometric Titration. The anesthetic solutions for potentiometric titration were prepared in three ways. Ten cm^3 of test solution was transferred into a 100 cm^3 beaker; distilled water was added until obtaining a total volume of 50 cm^3. The resulting solution was titrated with 10^{-2} mol dm^{-3} standard NaTPB solution using the respective electrode as the sensor.

Results and Discussion

Response of the Electrode. Since the potential response of the coated wire electrode is considered to be similar to that of a liquid-membrane electrode,[19,20] the membrane potential of the electrodes depends on the ion-exchange process at the membrane/solution interface, the mobilities of anesthetic cations in the membrane, and the potentials at the membrane/electrode copper interface. Provided that both the potential at the copper/PVC membrane interface and the diffusion potential in the PVC membrane are constant, and the anesthetic cations (A^+) and TPB^- (X^-) in the membrane are in chemical equilibrium with the anesthetic-TPB ion pairs (AX) in the membrane, the membrane potential of the electrode (E_M) can be represented by

$$E_M = \text{Const} + \frac{RT}{Z_A F} \ln \frac{a_{A^+}}{\bar{C}_{A^+}}$$
$$= \text{Const} + \frac{RT}{Z_A F} \ln a_{A^+} + \frac{RT}{Z_A F} \ln K_{AX} \cdot \bar{C}_{X^-}$$
$$- \frac{RT}{Z_A F} \ln \bar{C}_{AX}, \quad (1)$$

where a_{A^+} is the activity of the anesthetic cation in the test solution, and Z_A is the charge of anesthetic cation. $\bar{C}_{A^+}$, C_{X^-} and $\bar{C}_{AX}$ represent the concentrations of the anesthetic cation, TPB^- and ion pairs in the membrane, respectively. K_{AX} is the association constant of the ion pair. F, R, and T are the Faraday constant, gas con-

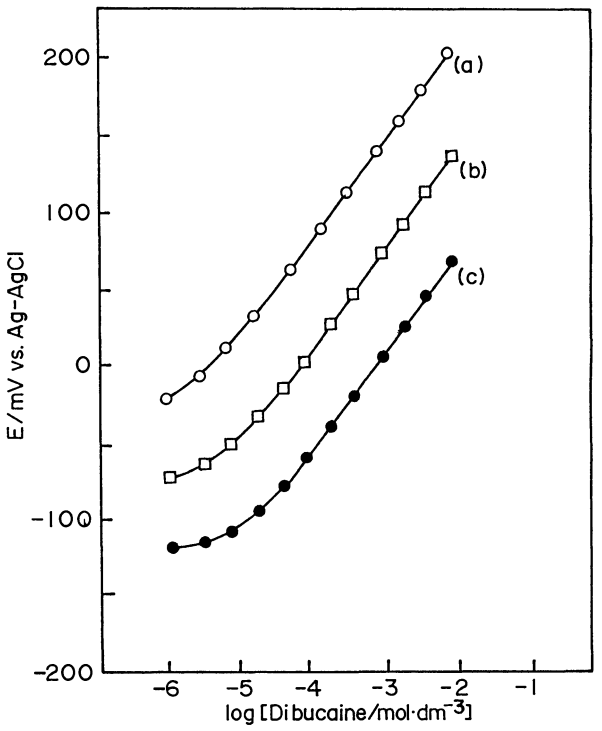

Fig. 2. Effect of the number of ion pairs in a PVC membrane on the potential of a dibucaine electrode. (a) Ion pair 1 mg+PVC 110 mg+DOP 100 mg, (b) Ion pair 5 mg+PVC 110 mg+DOP 100 mg, (c) Ion pair 50 mg+PVC 110 mg+DOP 100 mg.

stant and absolute temperature, respectively.

Equation 1 means that the higher is the concentration of the anesthetic–TPB ion pairs in PVC membrane, the lower is the membrane potential. Figure 2 shows the response curve for a dibucaine electrode containing various amounts of the dibucaine–TPB ion pairs in the PVC membrane. The potential response curve shifts to the negative side with increasing number of ion pairs in the PVC membrane, as expected from Eq. 1. Consequently, the membrane potential was defined as the activity of the anesthetic cations in solution in the case of a constant concentration of anesthetic–TPB ion pairs in the PVC membrane.

If interfering ions (B^+) exist, when the concentration of anesthetic–TPB ion pairs in the PVC membrane is kept constant, the membrane potential of the electrode is empirically given by

$$E_M = \text{Const} + \frac{RT}{Z_A F} \ln (a_{A^+} + K_{AB} \cdot a_{B^+}^{\frac{Z_A}{Z_B}}), \quad (2)$$

where K_{AB} is the selectivity coefficient of the B^+ ions for the anesthetic electrode, and a_{B^+} and Z_B are the activity and charge of a B^+ ion.

Composition of Electrode Membrane. Coated wire electrodes sensitive to local anesthetics with various membrane compositions were prepared, and the effect of the membrane composition on both the response time of the electrode and the slope of the EMF vs. concentration curve was investigated. A suitable PVC-membrane composition is shown in Table 1. The best results were obtained with an electrode membrane prepared from mixtures of local anesthetic–TPB ion pairs (5 mg), DOP (100 mg), PVC (110 mg) and 1.5 cm^3 of THF. Typical calibration curves of PC, TC, LC, DC, MC, and BC are shown in Fig. 3. The usable concentration range determined by the linear region of the calibration curves was 4×10^{-5}—10^{-2}, 4×10^{-5}—10^{-2}, 10^{-4}—10^{-2}, 4×10^{-5}—10^{-2}, 5×10^{-5}—10^{-2}, and 2×10^{-4}—10^{-2} mol dm^{-3} for PC, TC, LC, DC, MC, and BC, respectively. The response of the concerned electrodes was Nernstian (57.7, 56.6, 55.9, 58.6, 54.8, and 58.2 mV/decade for PC, TC, LC, DC, MC, and BC, respectively) and the standard relative deviation (%) of the slopes was less than 1%. The electrode can be used to determine the concentration of local anesthetic cations over a period of one month. When the contents of DOP (<50 mg) and ion-pairs (<1 mg) decreased, the electrode potential became unstable because of the high resistance of the membrane. A large excess of DOP and ion pairs in the membrane caused the surface of the copper wire to gradually become black, thus shortening the electrode lifetime and decreasing the slope of the potential curves.

Response Time and Reproducibility. The response time of the local anesthetic electrode was less than 30 seconds for a local anesthetic concentration range of 10^{-2} to 10^{-5} mol dm^{-3} and 2 min for 10^{-6} mol dm^{-3}. The reproducibility of the electrode potential was checked by either increasing or decreasing the local anesthetic concentration. The fluctuation of the electrode potentials was within a 1% standard relative deviation, with a concentration range from 10^{-4} to 10^{-2} mol dm^{-3} or from 10^{-2} to 10^{-4} mol dm^{-3}. Even after a

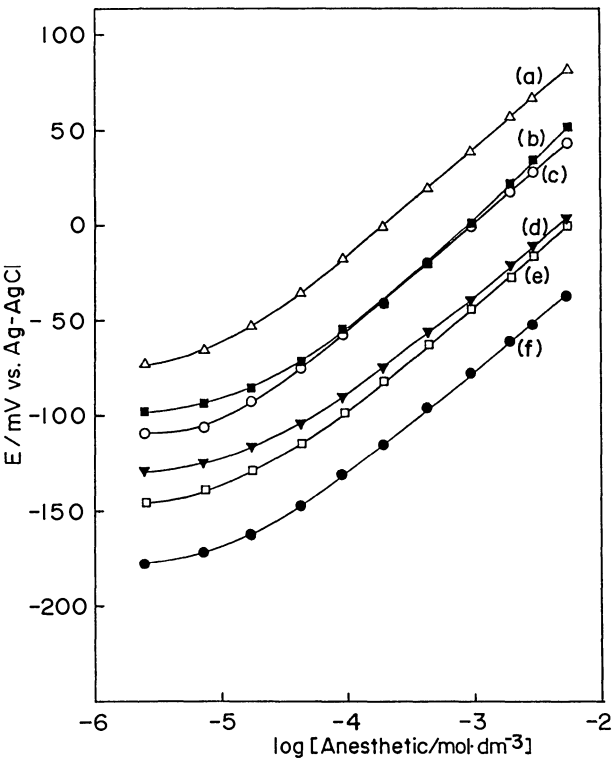

Fig. 3. Relationship between the local anesthetic concentration and the electrode potential: (a) Dibucaine; (b) Bupivacaine; (c) Tetracaine; (d) Lidocaine; (e) Mepivacaine; (f) Procaine.

Table 1. Suitable Composition of a PVC Membrane

Electrode	Ion-pair	DOP	PVC	THF	Slope	
	mg	mg	mg	ml	(mV/decade)	S.R.D (%)
Procaine	1-12 (5)	100	110	1.5	57.7	0.5
Tetracaine	1-10 (5)	100	110	1.5	56.6	0.5
Dibucaine	1-25 (5)	100	110	1.5	58.6	0.3
Lidocaine	1-25 (5)	100	110	1.5	55.9	0.9
Mepivacaine	1-10 (5)	100	110	1.5	56.8	0.6
Bupivacaine	1-25 (5)	100	110	1.5	58.2	0.5

S.R.D; Standard relative deviation. ( ): Suitable amount.

Table 2. Effect of the Ionic Strength on the Performance Characteristic of a Procaine Electrode

Ionic strength[a)]	Slope	Intercept at log[PC]=0.0	Usable log[PC] range	Correlation coefficient
0.0	56.3	76.4	−4.8—−2.2	0.9999
0.06	56.2	70.8	−4.5—−2.2	0.9998
0.107	56.3	70.5	−4.5—−2.2	0.9999
0.167	55.9	69.1	−4.2—−2.2	0.9999

a) NaCl added.

continuous measurement of the electrode potential over a period of eight hours, the change of the electrode potential was within 3 mV.

Effect of Ionic Strength. The performance characteristics of the PC electrode at various ionic strengths were examined by adding sodium chloride as the supporting electrolyte. The results are given in Table 2. The slope was almost independent of the ionic strength. The usable range of the calibration curve became slightly narrow.

Effect of pH. The effect of the pH on the electrode potential was examined for 10^{-3} mol dm^{-3} test solutions of local anesthetics, except for dibucaine (10^{-4} mol dm^{-3}). Figure 4 shows the variation in the electrode potential with changes in the pH by the addition of 10^{-1} mol dm^{-3} hydrochloric acid and/or sodium hydroxide solutions which included a corresponding local anesthetic of 10^{-3} mol dm^{-3}. The results indicate that the change in the pH did not affect the potential reading within the pH ranges 3.2—7.4, 3.2—7.4, 2.1—7.7, 2.5—7.4, 3.5—7.0, and 2.4—5.6 for PC, TC, LC, DC, MC, and BC, respectively. In acidic media of lower pH than these ranges, the electrode potential decreased as the pH value decreased. This may be attributed to a disappearance of the protonated local anesthetic, since they transformed to a diprotonated species.[11] The negative shift of the electrode potential at pH higher than about 7.5[11] may be due to a decrease in the concentration of the protonated species as a result of the precipitation of uncharged species of the local anesthetic.[11,21] In the case of the BC electrode, positive shifts of the electrode potential were observed at pH higher than 5.6. This phenomenon needs further clarification.

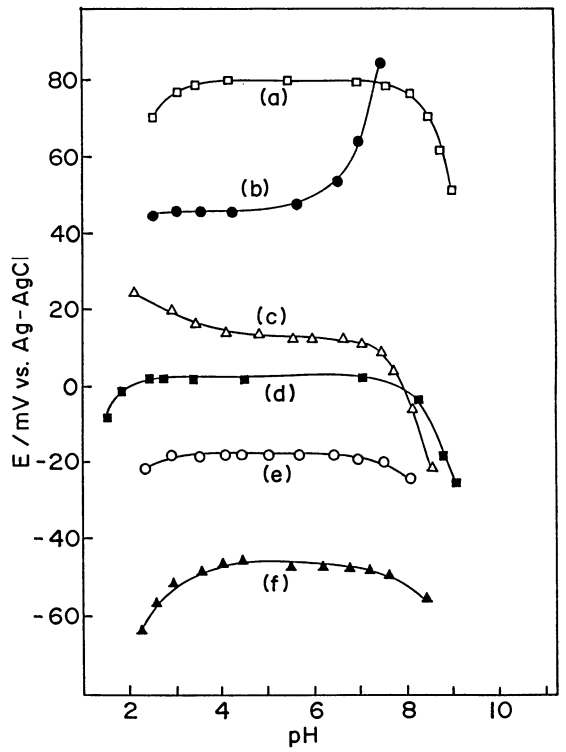

Fig. 4. Effect of pH on the response of a local-anesthetic coated wire electrode: (a) Tetracaine (9.92×10^{-4} mol dm^{-3}); (b) Bupivacaine (9.92×10^{-4} mol dm^{-3}); (c) Mepivacaine (9.92×10^{-4} mol dm^{-3}); (d) Lidocaine (9.92×10^{-4} mol dm^{-3}); (e) Dibucaine (9.98×10^{-5} mol dm^{-3}); (f) Procaine (10^{-3} mol dm^{-3}).

Selectivity of Electrodes. The selectivity of a membrane electrode based on ion-pair formation depends on the selectivity of ion-exchange at the membrane-test solution interface, the mobilities of the respective ions in the membrane, and hydrophobic interactions between the anesthetic cation and the organic membrane. The influence of some inorganic and organic cations, as well as the various substances contained in a tablet or injection solution of the local anesthetic drug, on the electrodes were investigated. The selectivity coefficients determined by a separate solution method[22,23] using 10^{-2} mol dm^{-3} of local anesthetic and interferent solution are summarized in Table 3. None of the investigated species (in Table 3) were found to interfere, as shown by the very small values of the selectivity coefficients, except for atropine, to the PC electrode. It is known that an atropine reacts with TPB^- to form an atropine-TPB ion pair.[24] The low selectivity of the PC electrode toward atropine is attributable to the partial ion-exchange of PC in a PC-TPB ion pair with atropine. The selectivity coefficients of each electrode toward other anesthetic cations was determined (summarized in Table 4). None of the electrodes were interfered with benzocaine. The DC electrode was found to have the most significant selectivity toward other local anesthetics, and the selectivity coefficients decreased in the order TC=BC>MC=LC>PC>benzocaine. The PC electrode has the lowest selectivity toward other local anesthetics. The PC electrode can therefore be used to measure the PC, TC, LC, DC, and BC concentration, as is shown in Fig. 5, even though its response is very slow. The difference in the hydrophobic property of local anesthetic molecules seems to be responsible for the difference in the electrode potential and the selectivity

Table 3. Selectivity Coefficient of Procaine, Tetracaine, Lidocaine, Dibucaine, Mepivacaine, and Bupivacaine Electrodes

Interferent	Procaine	Tetracaine	Lidocaine	Dibucaine	Mepivacaine	Bupivacaine
Sodium nitrate	−3.25	−2.98	−3.22	−2.50	−2.64	−2.76
Sodium chloride	−4.16	−4.05	−3.56	−3.62	−3.11	−3.43
Potassium nitrate	−3.21	−2.79	−2.89	−3.58	−2.39	−3.29
Disodium hydrogenphosphate	−3.36	−3.04	−4.05	−4.48	−2.93	−3.28
Calcium chloride	−4.49	−3.02	−4.40	−4.62	−3.45	−3.62
Leucine	−3.32	−2.80	−3.14	−3.91	−3.13	−2.35
Nicotinic acid	−3.34	−3.78	−2.19	−3.91	−2.39	−2.35
Atropine	−0.85	−3.20	−1.45	−3.16	−2.48	−2.98
Piperazine	−3.15	−1.91	−5.33	−4.05	−4.11	−4.95
Urea	−3.18	−3.93	−4.28	−4.26	−3.14	−2.98
Benzoic acid	−3.23	−3.41	−4.04	−4.00	−2.60	−2.83
Triethanolamine	−3.13	−3.14	−3.65	−3.80	−2.52	−2.48
Caffeine	−3.26	−3.01	−3.52	−4.10	−2.65	−2.27

Table 4. Selectivity Coefficient of Procaine, Tetracaine, Lidocaine, Dibucaine, Mepivacaine, and Bupivacaine Electrodes

Interferent	Procaine	Tetracaine	Lidocaine	Dibucaine	Mepivacaine	Bupivacaine
Benzocaine	−1.03	−2.28	−1.79	−3.40	−1.26	−1.98
Procaine	—	−1.49	−0.85	−2.59	−0.17	−1.40
Tetracaine	1.59	—	1.05	−0.92	1.10	0.01
Lidocaine	0.34	−1.05	—	−2.09	0.05	−1.28
Dibucaine	2.50	0.85	1.97	—	1.74	0.77
Mepivacaine	0.22	−1.36	0.05	−1.99	—	−1.46
Bupivacaine	1.59	−1.28	1.30	−0.78	1.50	—

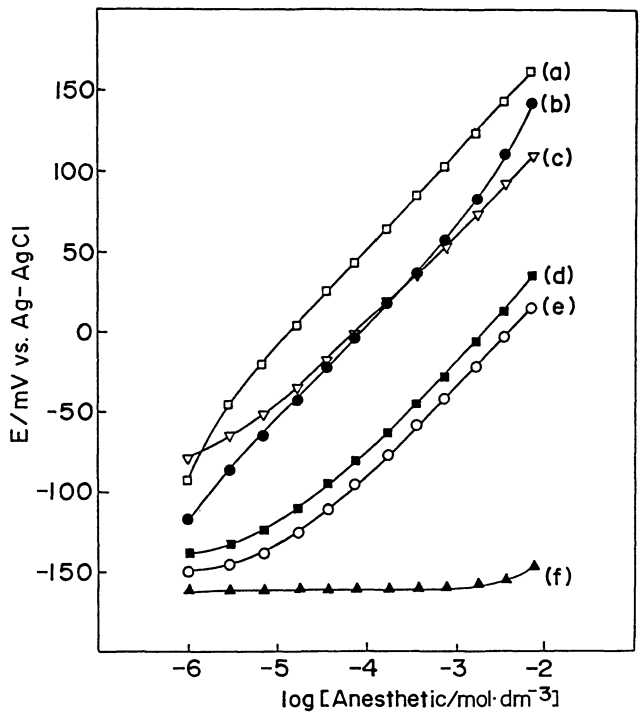

Fig. 5. Relationship between the electrode potential of a PC electrode and the local-anesthetic concentration: (a) Dibucaine; (b) Bupivacaine; (c) Tetracaine; (d) Lidocaine; (e) Procaine; (f) Benzocaine.

coefficients among the anesthetics appearing in Fig. 5 and Table 4. The distribution coefficients between 1-octanol and a buffer solution (pH 7.4), which reflect the hydrophobicity of anesthetic molecules, are known to be 1.7 for PC, 221 for TC, 43 for LC, 21 for MC, and 346 for BC.[21] The hydrophobicity of anesthetic molecules was closely related to the binding affinity of anesthetics with protein.[1] The binding affinity increased in the order PC<LC<MC<TC<BC. The larger is the distribution coefficient of the anesthetic, the higher is the electrode potential and selectivity to other anesthetics. As can be seen from Table 4, the high selectivity of the DC electrode toward other anesthetics accurately reflects differences in the distribution constant or ion-exchange ability between anesthetics. The difference in the selectivity of each electrode toward various local anesthetic can therefore be closely related to the hydrophobicity of local anesthetic molecules and the stability of anesthetic–TPB ion pair.

Analytical Application. It was proved by both potentiometric titration and direct potentiometry that PC, TC, and DC electrodes are useful sensors for the potentiometric determination of local anesthetic drugs in either pure forms or in pharmaceutical preparation. The results are shown in Tables 5 and 6. Potentiometric titration, which offers higher precision and accuracy than does a direct method, was applied to determining the purity of DC, PC, and TC reagents. PC, TC, and DC were quantitatively analyzed at a standard relative

Table 5. Potentiometric Titration of Procaine, Tetracaine, and Dibucaine

Sample	Purity (%)	S.R.D (%)
Procaine	99.18	0.2
Tetracaine	100.4	0.1
Dibucaine	98.53	0.5

a) S.R.D: Standard relative deviation; Sample: 2×10^{-3} mol dm^{-3}, 50 cm^3; Titrant: 10^{-2} mol dm^{-3} Sodium tetraphenylborate.

Table 6. Determination of Procaine in an Aqueous Injectable Solution and a Tablet

Sample	Taken (mg)	Titration[a)]		Direct method
		Found (mg)	S.R.D (%)	Found (mg)
I	100.3	100.2	0.4	104.7
II	100.5	100.5	0.4	101.9
III	100.3	100.6	0.3	101.5

I: 100 mg of procaine · HCl+6 mg of benzoic acid+5 mg of potassium disulfite+1 mg of disodium hydrogenphosphate+distilled water to 50 cm^3.
II: 100 mg of procaine · HCl+64 mg of glutamic acid+6 mg of benzoic acid+24 mg of potassium hydroxide+5 mg of potassium disulfite+0.5 mg of disodium hydrogenphosphate+distilled water to 50 cm^3.
III: 100 mg of procaine · HCl+6 mg of benzoic acid+5 mg of potassium disulfite+0.5 mg of disodium hydrogenphosphate+30 mg of vitamin B_6+200 mg of meso-inositol+distilled water to 50 cm^3.
a): Sample volume: 5 cm^3; titrant: 10^{-2} mol dm^{-3} sodium tetraphenylborate.

deviation (%) less than 0.5% by potentiometric titration using the respective electrode as the sensor, and NaTPB as a titrant (Table 5). The determination of PC in a tablet (sample I) and two aqueous injection solutions (samples II and III)[12] was carried out by potentiometric analysis. The preparation of pharmaceutical solutions and the results of analysis are shown in Table 6. It was found that PC in pharmaceutical drugs can be determined with good precision without the influence of added ingredients.

This work was supported in part by a Grant-in-Aid for General Scientific Research No. 02455015 from the Ministry of Education, Science and Culture.

References

1) B. G. Covino, *Br. J. Anaesth.*, **58**, 701 (1986).
2) F. J. Biebuyck and M. B. Dphil, *Anesthesiology,* **72**, 711 (1990).
3) J. M. Ritchie and P. Greengard, *J. Pharmacol. Exp. Ther.*, **133**, 241 (1961).
4) V. V. Ogurtsov and L. P. Yavors'ka, *Farm. Zh.*, **1986**, 62.
5) M. E. El-Kommos and K. M. Emara, *Analyst,* **112**, 1253 (1987).
6) M. A. Korany, A. M. Wahbi, M. A. Elsayed, and S. Mondour, *Anal. Lett.*, **17**, 1373 (1984).
7) H. Murakita, M. Hayashi, H. Mikami, and Y. Ishida, *Bunseki Kagaku,* **35**, 236 (1986).
8) M. L. Lyuta and A. F. Mynka, *Farm. Zh.*, **5**, 32 (1983).
9) Y. Shen, J. Fan, and M. Dong, *Yaowu. Fenxi. Zazhi.*, **8**, 91 (1988).
10) V. V. Cosofret, P. G. Zugravescu, and G. E. Baiulescu, *Talanta,* **24**, 461 (1979).
11) A. F. Shoukry, Y. M. Issa, R. El-Sheik, and M. Zareh, *Microchem. J.*, **37**, 299 (1988).
12) D. Negoiu, M. S. Ionescu, and V. V. Cosofret, *Talanta,* **28**, 377 (1981).
13) K. Vytras, M. Dajkova, and V. Mach, *Anal. Chim. Acta,* **127**, 165 (1981).
14) J. Dohnal and K. Vytras, *Farm. Obz.*, **54**, 405 (1985).
15) K. Shirahama, H. Kamaya, and I. Ueda, *Anal. Lett.*, **16**, 1485 (1983).
16) W. Liu, C. Yang, A. Li, and X. Zhou, *Yaoxue Xuebao,* **23**, 688 (1988).
17) M. S. Ionescu, S. Sitarn, G. E. Baiulescu, and V. V. Cosofret, *Rev. Chem.*, **38**, 256 (1987).
18) H. Satake, H. Hori, and S. Kaneshina, *Anal. Lett.*, **24**, 295 (1991).
19) H. James, G. Carmack, and H. Freiser, *Anal. Chem.*, **44**, 856 (1972).
20) K. Suzuki, H. Ishiwada, T. Shirai, and S. Yanagisawa, *Bunseki Kagaku,* **30**, 751 (1981).
21) G. R. Strichartz, V. Sanchez, G. R. Arthur, R. Chafetz, and D. Martin, *Anesth. Analg.*, **71**, 158 (1990).
22) K. Srinivasan and G. A. Rechnitz, *Anal. Chem.*, **41**, 1203 (1969).
23) V. V. Cosofret and R. P. Buck, *Analyst,* **109**, 1321 (1984).
24) H. Wachsmuth and E. Mertens, *J. Pharm. Belg.*, **13**, 58 (1958); *Chem. Abstr.*, **52**, 14080 (1958).

 © 1991 The Chemical Society of Japan Bull. Chem. Soc. Jpn., 64, 3035—3038 (1991)

A Further Modification of the Born Equation

Takehiro ABE
College of General Education, Tohoku University, Kawauchi, Aoba-ku, Sendai 980
(Received May 9, 1991)

By considering the distance-dependent relative permittivity of a solvent, the Born equation has been modified for a diatomic ion in which the charge is located on an atom deviating from the center of a spherical cavity. The new equation has been successfully applied to the diatomic ions of OH^-, SH^-, and CN^-.

The Born equation[1] has long been widely applied in many fields regarding the solvation free energies of ions. The Born equation is written for 1 mol of ions of point charge Ze (where Z is the formal charge and e the charge of proton) located in a spherical cavity embedded in a continuous dielectric medium of solvent as

$$\Delta G_m^\circ = \frac{e^2LZ^2}{2a} \times \left(\frac{1}{\varepsilon_r} - 1\right), \quad (1)$$

where ΔG_m° is the increase in the standard molar Gibbs function due to electrostatic interactions when one transfers the ions from a vacuum to a solution at infinite dilution of the ionic species. Here, L is the Avogadro constant, ε_r the relative permittivity of the solvent, and a the radius of the spherical cavity. In the Born model, the charge is located in the center of the spherical cavity and the local relative permittivity in the immediate neighborhood of the ion is assumed to be equal to the bulk relative permittivity (ε_r) of the solvent. The latter defect was overcome by Abe[2] by considering a distance-dependent relative permittivity of the solvent. In Abe's model, the point charge is still assumed to be located in the center of the spherical cavity, as in the case of the Born equation. This model is certainly valid for a monoatomic ion but is not valid for a polyatomic ion in which the charge located on an atom is not necessarily in the center of the cavity. In the case of a polyatomic ion, such as a diatomic ion, the point charge usually deviates from the center. Recently, Rashin and Namboodiri[3] have presented a general method for calculating the hydration enthalpy for a single charged molecule of arbitrary shape, using the Born equation and the boundary element technique. They obtained excellent results. However, applying the boundary element technique employed to obtain a numerical solution of the Poisson equation is not easy. Recently, Zhou and Stell[4] have obtained analytical equations for the pair correlation functions in the mean spherical approximation for the case of two hard-sphere ions in a model solvent of dipolar dumbbells and an expression for a single ion by letting the number density of the ionic species be infinitesimally small. The expression is similar to an empirical formula used for fitting experimental data to Eq. 1, and is currently not applicable to the present problem. In this paper, therefore, an attempt has been made to derive a simple equation that is easily applicable to a single diatomic ion in which the point charge deviates from the center of the spherical cavity, by considering the distance-dependent relative permittivity of the solvent.

Theory

As shown in Fig. 1, the point charge of Ze is located at position O in a spherical cavity (of radius a) embedded in a continuous dielectric medium of solvent whose bulk relative permittivity is ε_r. Inside the cavity, the relative permittivity is assumed to be equal to that of a vacuum. Let the origin be at position O, which deviates from the center (C) of the cavity by r_0. The z-axis is taken in the direction of line $\overline{CO}$. The distance of an arbitrary point (P) from O is denoted by r. The point at which line of $\overline{OP}$ crosses the cavity surface is denoted by Q. The angle between $\overline{OP}$ and the z-axis is denoted by θ. Then, one can write line $\overline{OQ}$ as

$$\overline{OQ} = \frac{-2r_0\cos\theta \pm \{(2r_0\cos\theta)^2 + 4(a^2 - r_0^2)\}^{1/2}}{2}, \quad (2)$$

since $a^2 = r_0^2 + \overline{OQ}^2 - 2r_0\overline{OQ}\cos(\pi - \theta)$. Here, $\overline{OQ}$ should be positive. From Eq. 2, therefore, one obtains

$$\overline{OQ} = -r_0\cos\theta + (a^2 - r_0^2\sin^2\theta)^{1/2}. \quad (3)$$

The electric field caused by Ze within the cavity is

$$E = \frac{Ze}{r^2}, \quad (4)$$

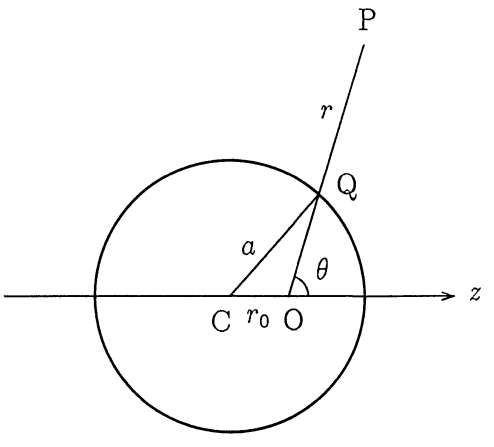

Fig. 1. Model.

while the electric field in the medium is written as

$$E_s=\frac{Ze}{\varepsilon(r)r^2}, \tag{5}$$

where $\varepsilon(r)$ is the distance-dependent relative permittivity. Here, the same formula for $\varepsilon(r)$ as was used in a previous paper[2] is adopted,

$$\varepsilon(r)=e_r\exp(-\kappa/r), \tag{6}$$

where κ is determined under the condition $\varepsilon(r)=1$ for $r=\overline{OQ}$, i.e., $1=\varepsilon_r\exp(-\kappa/\overline{OQ})$ as

$$\kappa=\overline{OQ}\ln\varepsilon_r. \tag{7}$$

When $\varepsilon(r)$ is written as $\varepsilon(r)=\varepsilon_r\exp\{-(\overline{OQ}\ln\varepsilon_r)/r\}$, the potential Φ_i (due to Ze) inside the cavity can be written simply as Ze/r, which is the same expression as in a vacuum. The potential (Φ_o) outside the cavity is $Ze/\varepsilon(r)r$. These potentials obviously satisfy the two boundary conditions of $\Phi_i=\Phi_o$ and $(\partial\Phi_i/\partial r)\cos\theta'=\varepsilon(r)(\partial\Phi_o/\partial r)\cos\theta'$ (for the normal line ($\overline{CQ}$) components, where $\theta'=\angle CQO$) for $r=\overline{OQ}$, since $\varepsilon(r)=1$ for $r=\overline{OQ}$. This simple expression for Φ_i may be due to the fact that the polarization (P) given by $P=\{\varepsilon(r)-1\}\times E_s/4\pi$ is zero for $r=\overline{OQ}$ (i.e. on the cavity surface) in this case.

By following the same procedure that Slater and Frank[5] used to calculate the total energy of an electron using a Poynting vector, the Born equation will be further modified. The infinitesimal area of the cavity surface contained in the solid angle between θ and $(\theta+d\theta)$ is given by $2\pi(a\sin\theta)(ad\theta)$. As in a previous paper,[2] therefore, one can write the solvation free energy of 1 mol of ions with the charge Ze by using a Poynting vector as follows:

$$\Delta G_m^\circ=\frac{L}{8\pi}\int_0^\pi\int_Q^\infty\{\varepsilon(r)E_s^2-E^2\}\times 2\pi(r\sin\theta)(rd\theta)dr$$
$$=\frac{L}{4}\int_0^\pi d\theta\sin\theta\int_Q^\infty\{\varepsilon(r)E_s^2-E^2\}r^2dr. \tag{8}$$

Using Eqs. 4, 5, 6, and 7, one obtains the following integral calculation:

$$\int_Q^\infty\{\varepsilon(r)E_s^2-E^2\}r^2dr=-\frac{Z^2e^2}{\varepsilon_r\kappa}\times\{1-\exp(\kappa/\overline{OQ})\}-\frac{Z^2e^2}{\overline{OQ}}$$
$$=-Z^2e^2\times\left(\frac{1-\varepsilon_r}{\varepsilon_r\ln\varepsilon_r}+1\right)\times\frac{1}{\overline{OQ}}. \tag{9}$$

Using Eqs. 3 and 9, one can rewrite Eq. 8 as follows:

$$\Delta G_m^\circ=-\frac{Z^2Le^2}{4}\times\left(\frac{1-\varepsilon_r}{\varepsilon_r\ln\varepsilon_r}+1\right)\times\int_0^\pi\frac{\sin\theta d\theta}{(a^2-r_0^2\sin^2\theta)^{1/2}-r_0\cos\theta}$$
$$=\frac{Z^2Le^2}{4a}\times\left(\frac{1}{\ln\varepsilon_r}-\frac{1}{\varepsilon_r\ln\varepsilon_r}-1\right)$$
$$\times\left\{\frac{1}{1-(r_0/a)^2}+\frac{1}{2(r_0/a)}\ln\frac{1+(r_0/a)}{1-(r_0/a)}\right\}, \tag{10}$$

where $e^2L/2=69.45$ nm kJ mol^{-1}.

Discussion

When $r_0=0$ is put into Eq. 10, one should obtain the modified equation given in a previous paper.[2] However, some modification of Eq. 10 is necessary for obtaining the ΔG_m° value for $r_0=0$, because it is impossible to put $r_0=0$ directly into Eq. 10. Expanding the terms of $1/\{1-(r_0/a)^2\}$ and $\ln\{1+(r_0/a)\}/\{1-(r_0/a)\}$ in Eq. 10 in series, one finally obtains

$$\Delta=\frac{1}{2}\times\left\{\frac{1}{1-(r_0/a)^2}+\frac{1}{2(r_0/a)}\ln\frac{1+(r_0/a)}{1-(r_0/a)}\right\}$$
$$=1+\frac{1}{2}\sum_{n=1}^{\infty}\left(1+\frac{1}{2n+1}\right)\left(\frac{r_0}{a}\right)^{2n}. \tag{11}$$

This is obviously convergent, since $a>r_0$. Thus, one can write Eq. 10 as

$$\Delta G_m^\circ=\frac{Z^2Le^2}{2a}\times\left(\frac{1}{\ln\varepsilon_r}-\frac{1}{\varepsilon_r\ln\varepsilon_r}-1\right)$$
$$\times\left\{1+\frac{1}{2}\sum_{n=1}^{\infty}\left(1+\frac{1}{2n+1}\right)\left(\frac{r_0}{a}\right)^{2n}\right\}. \tag{12}$$

When $r_0=0$, Eq. 12 is reduced to

$$\Delta G_m^\circ=\frac{Z^2Le^2}{2a}\times\left(\frac{1}{\ln\varepsilon_r}-\frac{1}{\varepsilon_r\ln\varepsilon_r}-1\right). \tag{13}$$

This is a modified equation given in a previous paper.[2] Ehrenson[6] has shown that the solvent parameter of $\{1/\ln\varepsilon_r-1/(\varepsilon_r\ln\varepsilon_r)-1\}$ in Eq 13 is the best in the inverse exponential radial dielectric function family of the modified Born equations for correcting the free energies of solvation. In a comparison of Eq. 12 with Eq. 13, Δ (Eq. 11) is a factor which indicates the degree of deviation of the position of the charge from the center of the spherical cavity for ΔG_m°.

A plot of the Δ values vs. the r_0/a values is given in Fig. 2. This figure shows that the Δ value is approximately unity over the range of r_0/a values smaller than

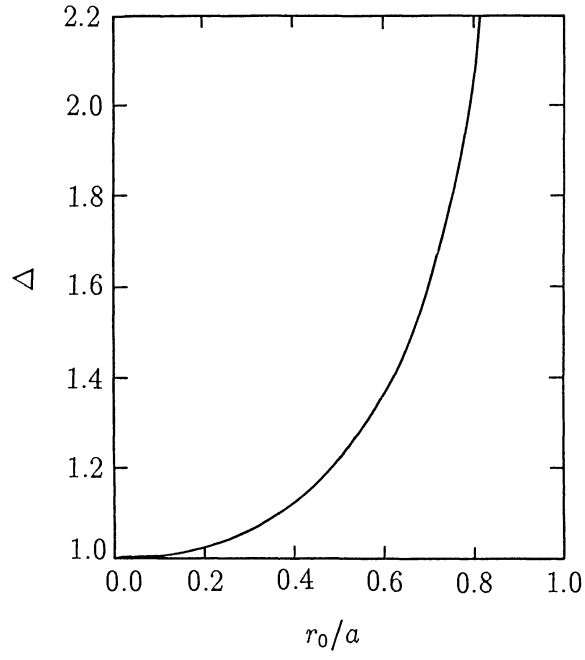

Fig. 2. Plot of Δ vs. r_0/a.

0.2. Therefore, Eq. 13 may be approximately used for an r_0/a value smaller than 0.2. However, Fig. 2 shows that the deviation of the Δ value from unity can not be ignored for r_0/a values larger than ca. 0.25. In this case, therefore, Eq. 10 should be used instead of Eq. 13.

When the constant bulk relative permittivity of ε_r is used instead of $\varepsilon(r)$, one can easily obtain the following expression for ΔG_m° in the same way as in the derivation of Eq. 10:

$$\Delta G_m^\circ = \frac{e^2LZ^2}{2a} \times \left(\frac{1}{\varepsilon_r} - 1\right) \times \Delta. \tag{14}$$

This corresponds to a modified equation of Eq. 1 for the case of a deviation of the charge from the center of the cavity by r_0. In this case, the charges are induced on the cavity surface, since $P=(\varepsilon_r-1)E_s/4\pi \neq 0$ for $r=\overline{OQ}$, where $E_s=Ze/\varepsilon_r r^2$. From the continuity of potentials at Q, the potential inside the cavity may be written as $\Phi_i=Ze/r+(1/\varepsilon_r-1)Ze/\overline{OQ}$. The second term of $(1/\varepsilon_r-1)Ze/\overline{OQ}$ (the reaction field) does not contribute to the electric field ($E=-\partial\Phi_i/\partial r=Ze/r^2$), since the term does not contain r, according to Eq. 3.

On the assumptions that only the electrostatic contribution is dominant and that a does not depend on the temperature, one can easily derive the following equations for the increase of standard molar entropy of solvation of a diatomic ion from Eqs. 1, 13, 14, and 10 according to $\Delta S_m^\circ = -(\partial \Delta G_m^\circ/\partial T)_p$ (where sufffix p denotes the constant pressure and T is the thermodynamic temperature (K)):

$$\Delta S_m^\circ = \frac{e^2LZ^2}{2a} \times \frac{1}{\varepsilon_r^2} \times \frac{d\varepsilon_r}{dT}, \tag{15}$$

$$\Delta S_m^\circ = \frac{e^2LZ^2}{2a} \times \frac{\varepsilon_r - \ln\varepsilon_r - 1}{\varepsilon_r^2(\ln\varepsilon_r)^2} \times \frac{d\varepsilon_r}{dT}, \tag{16}$$

$$\Delta S_m^\circ = \frac{e^2LZ^2}{2a} \times \frac{1}{\varepsilon_r^2} \times \frac{d\varepsilon_r}{dT} \times \Delta, \tag{17}$$

and

$$\Delta S_m^\circ = \frac{e^2LZ^2}{2a} \times \frac{\varepsilon_r - \ln\varepsilon_r - 1}{\varepsilon_r^2(\ln\varepsilon_r)^2} \times \frac{d\varepsilon_r}{dT} \times \Delta, \tag{18}$$

respectively, since the Δ factor is independent of the temperature.

Applications

The present equations have been applied to the hydration of OH^-, SH^-, and CN^-, in order to compare with the experimental ΔG_m° values (298.15 K) for the hydration of these ions reported by Marcus,[7] as shown in Table 1. In these diatomic ions the negative charges are probably located on the atoms of O, S, and N, because the electronegativities of these atoms are larger than those of the corresponding bonding atoms and the negative charge of each ion may be located at one atom according to the adjacent charge rule of Pauling.[8]

In applying Eqs. 1, 10, 13, and 14, the reported data for a (Table 1)[7] and $\varepsilon_r=78.46$ (298.15 K)[7] were used and the r_0 values were approximated by the half values of the bond lengths of these diatomic ions, based on the assumption that the center of the bond length for each diatomic ion is located at the center of the spherical cavity. The values used for the bond lengths of OH^-, SH^-, and CN^- were 0.0970, 0.1336, and 0.11718 nm,[9] respectively. The results of calculations are listed in Table 1. The table clearly shows that the values calculated by both the Born equation (Eq. 1) and its modified equation (Eq. 14) derived by considering the deviation of r_0 are in worse agreement with the experimental values than those calculated by the modified equation (Eq. 13) derived by considering only the distance-dependent relative permittivity of the solvent; it also shows that a further modified equation (Eq. 10) derived by considering both the distance-dependent relative permittivity of a solvent and the deviation of r_0 best reproduces the experimental values among the 4 equations. Thus, Eq. 10 should be used instead of Eq. 13 for an ion in which the charge is located on one atom considerably deviating from the center of the spherical cavity.

Table 1. ΔG_m° Values

Ion	a[a]/nm	ΔG_m°/kJ mol^{-1}				
		Eq. 1	Eq. 13	Eq. 14	Eq. 10	Exp.[a]
OH^-	0.140	−490	−384	−534	−418	−439
SH^-	0.195	−352	−276	−382	−300	−303
CN^-	0.191	−359	−281	−384	−301	−305

a) Ref. 7.

Table 2. ΔS_m° Values

Ion	ΔS_m°/J K^{-1} mol^{-1}				
	Eq. 15	Eq. 16	Eq. 17	Eq. 18	Exp.[a]
OH^-	−29	−111	−32	−121	−161
SH^-	−21	−80	−23	−87	−101
CN^-	−21	−82	−23	−87	−80

a) Ref. 7.

The experimental ΔS_m° values (298.15 K) for the hydration of these ions are reported also by Marcus,[7] as shown in Table 2. In applying Eqs. 15—18, the $d\varepsilon_r/dT$ value[10] of −0.3595 K^{-1} for water was used. The results calculated for ΔS_m° are shown in Table 2. The table shows that Eq. 18 best reproduces the experimental values among the 4 equations.

References

1) M. Born, *Z. phys.*, **1**, 45 (1920).
2) T. Abe, *J. Phys. Chem.*, **90**, 713 (1986).
3) A. A. Rashin and K. Namboodiri, *J. Phys. Chem.*, **91**, 6003 (1987).
4) Y. Zhou and G. Stell, *J. Chem. Phys.*, **91**, 4869 (1989).
5) a) J. C. Slater and N. H. Frank, "Introduction to Theoretical Physics," McGraw-Hill, New York (1933), Chap. 22. b) J. C. Slater and N. H. Frank, "Electromagnetism," McGraw-Hill, New York (1947), Chap. VIII.

6) S. Ehrenson, *J. Phys. Chem.*, **91**, 1868 (1987).
7) Y. Marcus, "Ion Solvation," John Wiley and Sons, Chichester (1985), pp. 47, 88, 108, 126.
8) L. Pauling, "The Nature of the Chemical Bond," 3rd ed, Cornell University Press, Ithaca (1960), Chap. 8.
9) "Kagaku Binran," 3rd ed, ed by the Chemical Society of Japan, Maruzen Publishing Co., Tokyo (1984), Kisohen, pp. II-650, 714.
10) M. H. Abraham and J. Liszi, *J. Chem. Soc., Faraday Trans. 1,* **74**, 2858 (1978).

Syntheses and Spectral Properties of New Nitrosyl-[poly(1-pyrazolyl)borato]ruthenium Complexes†

Masayoshi ONISHI
Department of Industrial Chemistry, Faculty of Engineering,
Nagasaki University, Bunkyo-machi, Nagasaki 852
(Received February 4, 1991)

Trichloro(nitrosyl)ruthenium(III) was treated with alkali-metal or thallium poly(1-pyrazolyl)borates $M(BRPz_3)$ (Pz=1-pyrazolyl) to give new nitrosyl[poly(1-pyrazolyl)borato]ruthenium(III) complexes $[RuCl_2(BRPz_3)(NO)]$ (**1**, R=Pz; **2**, R=H). A similar reaction with thallium tris(3,5-dimethyl-1-pyrazolyl)hydroborate $TlBH(3,5\text{-}Me_2Pz)_3$ (3,5-Me_2Pz=3,5-dimethyl-1-pyrazolyl) afforded the complex $[RuCl_2\{BH(3,5\text{-}Me_2Pz)_3\}(NO)]$ (**3**) as the minor product and the 3,5-dimethylpyrazole complex $[RuCl_3(NO)(3,5\text{-}Me_2PzH)_2]$ as the major one. The observation of ν(NO) bands over the range 1870 to 1900 cm^{-1} determined the NO^+ linear coordination mode in these complexes, rather than NO^- bent one. The ν(NO) values of **1**—**3** were larger than those of the corresponding known π-cyclopentadienyl analogues by ca. 90 cm^{-1}, indicating a smaller degree of π-back donation of metal–NO bonds in the former complexes. ^1H, ^{13}C, and ^{11}B NMR data of the new complexes are described. In ^1H NOE measurements of **1**, irradiation at a chemical shift of 5-H protons in the coordinated pyrazolyl groups induced a positive NOE on the 5-H proton in the uncoordinated group, and individual assignments of the pyrazolyl protons were carried out with the help of ^1H–^1H and ^{13}C–^1H COSY.

The utility of poly(1-pyrazolyl)borato ligands $BH_nPz_{(4-n)}^-$ (Pz=1-pyrazolyl),[1-3] which were first discovered by Trofimenko,[2] has been demonstrated in synthesizing a variety of transition-metal complexes. The ligands, especially in the tripodal coordination mode, have been shown to confer considerable stability on organometallic complexes and novel fluxionality in NMR spectroscopy, and have been compared to π-cyclopentadienyl ligands from the standpoint that both types of ligands are uninegative and can occupy three facial coordination sites on a metal ion. Moreover, it has been generally accepted that substituent introduction on boron and pyrazolyl carbons can significantly change the chemical reactivities, as well as other properties of their transition-metal complexes.[1-3]

In addition to the early studies concerning first-row transition-metal and molybdenum complexes, many papers have been published concerning various second- and third-row complexes in recent years,[1] regarding ruthenium, however, only a handful of poly(1-pyrazolyl)borato complexes are known,[3] in spite of the well-known potentiality of ruthenium for affording highly efficient catalytic species in a variety of homogeneous catalytic reactions. As part of our objectives in developing their catalytic reaction systems, the present author has prepared some new nitrosyl[poly(1-pyrazolyl)borato]ruthenium(III) as catalyst precursors. The dual nature of the nitrosyl ligands as NO^- and NO^+ coordination modes in transition-metal complexes is well-known, and the catalytic potential has been expected, which this duality provides.[4] For some nitrosyl complexes effective as catalysts in such reactions as olefin disproportionation and hydrogenation, their catalytic activities have been assumed to result from a facile redox process between metal and the nitrosyl ligand, which causes favorable stereochemical or structural changes about the metals.[4]

Concerning the NMR assignment of 3- and 5-H protons in the poly(1-pyrazolyl)borato ligands, there have been some arguments about uncertainty.[5] Therefore, ^1H NOE (Nuclear Overhauser Effect) measurements were carried out for the first time in order to prevent any obscurity in the assignment.

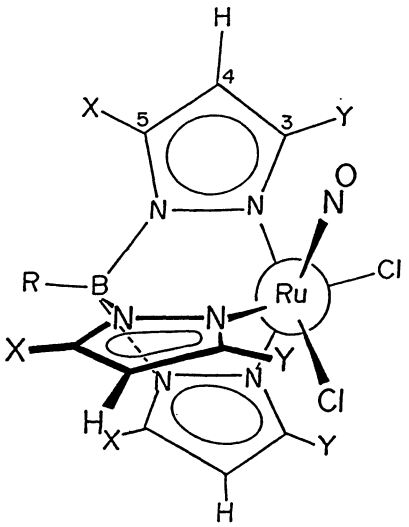

Fig. 1. New (nitrosyl) [poly(1-pyrazolyl)borato]ruthenium complexes.
1, R=1-pyrazolyl, X=Y=H; **2**, R=X=Y=H; **3**, R=H, X=Y=CH_3.

† Following the publication of "Nomenclature of Inorganic Chemistry" by IUPAC, the nitrosyl ligand is considered as being neutral in counting the formal oxidation number of ruthenium for the representation of its complexes in this paper. However, as described later, the nitrosyl ligand in the present new ruthenium(III) complexes was found to be in a NO^+ linear coordination mode, indicating an actual second-valent state of ruthenium.

Results and Discussion

Syntheses of New Ruthenium Complexes. Sodium tetrakis(1-pyrazolyl)borate $NaBPz_4$ was added to an ethanol solution of trichloro(nitrosyl)ruthenium(III). Recrystallization of the resulting precipitates from dichloromethane and benzene gave brown microcrystals of $[RuCl_2(BPz_4)(NO)]$ (**1**) in 26% yield. The microcrystals were soluble in dichloromethane, chloroform, and THF, but were sparingly soluble in benzene, diethyl ether, and ethanol.

In the case of hydrotris(1-pyrazolyl)borate anion $BHPz_3^-$, its potassium salt was treated with the trichloro(nitrosyl)ruthenium in THF to afford a mixture of some reaction products. Only brown microcrystals of $[RuCl_2(BHPz_3)(NO)]$ (**2**) were isolated after silica-gel column chromatographic separation. The yield was only 14%. The use of the thallium(I) salt of this anion increased the yield to 27%.

Thallium tris(3,5-dimethyl-1-pyrazolyl)hydroborate $TlBH(3,5\text{-}Me_2Pz)_3$ (3,5-Me_2Pz=3,5-dimethyl-1-pyrazolyl) gave the complex $[RuCl_2\{BH(3,5\text{-}Me_2Pz)_3\}(NO)]$ (**3**) as the minor product. The major one was found to be a 3,5-dimethylpyrazole complex of $[RuCl_3(NO)(3,5\text{-}Me_2PzH)_2]$ (**4**). Only the latter complex was isolated from a similar reaction of the potassium analogue. These findings indicated that bond cleavage between boron and pyrazolyl-nitrogen atoms in the tris(3,5-dimethyl-1-pyrazolyl)hydroborate anion occurred to a considerable extent in the course of the reaction with trichloro(nitrosyl)ruthenium, affording the boron-free pyrazole complex **4**. Fairly low yields of **1**—**3** were possibly due to the occurrence of the analogous cleavage of the respective poly(1-pyrazolyl)borate anions. King and Bond described similar cleavage of the poly(1-pyrazolyl)borato ligands in reactions with $[Fe(\pi\text{-}C_3H_5)I(CO)_3]$ and $[Co(\pi\text{-}C_5H_5)R_fI(CO)]$ (R_f=perfluoroalkyl).[6] From the analogous reaction of thallium tetrakis(3-*t*-butyl-1-pyrazolyl)borate, no distinguishable products were isolated.

Spectroscopic equivalence of the two 3,5-dimethylpyrazole ligands in **4** was observed in its ^1H and ^{13}C NMR spectra (vide infra, Tables 4 and 5). Figure 2 shows two probable configurations, i.e. *mer*, *trans*-configuration A and *facial*, *cis* one B. For a comparison, the complex $[RuCl_3(NO)(Pz_2CMe_2)]$ (**5**) {Pz_2CMe_2= 2,2-bis(1-pyrazolyl)propane} was prepared, where two neutral pyrazole-subunits form a *cis*-bidentate chelate to ruthenium. In contrast to **4**, this complex was insoluble in common organic solvents, and NMR observation was not possible. Although configuration determination of **4** should be deferred until X-ray analyses elucidate the molecular structure, it is tempting to suggest the *mer*, *trans*-configuration A for **4**. Among the known complexes $[RuCl_3(NO)L_2]$ (L=monodentate neutral ligands),[7] only the *mer*, *trans*-configurations of phosphine, sulfide, and selenide complexes have been determined by means of detailed spectroscopic and single crystal X-ray studies.

Spectroscopic Studies of the New Ruthenium Complexes. As summarized in Table 2, these complexes showed IR ν(NO) bands in the range 1870 to 1900 cm^{-1}. The ν(NO) bands have been reported to be in 2000—1600 and 1725—1525 cm^{-1} for the NO^+ coordination mode with linear metal–N–O bonds and the NO^- mode with bent ones, respectively.[4a,4c,8] The ν(NO) values given in Table 2 determine the NO^+ linear coordination mode in these complexes.

Similarly to the case of ν(CO) bands in metal carbon-

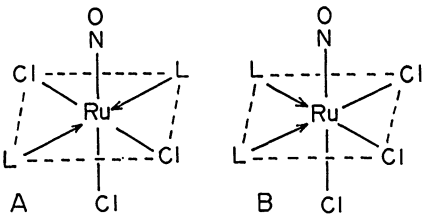

Fig. 2. Possible configurations for $[RuCl_3(NO)L_2]$ under the condition of two spectroscopically equivalent L ligands.
A, *mer, trans* configuration; B, *facial, cis* configuration.

Table 1. Syntheses of New Ruthenium Complexes

	Complex	Analysis (%)[a]			Mp[b]
		C	H	N	θ_m/°C
(**1**)	$[RuCl_2(BPz_4)(NO)]$	30.37 (29.96)	2.60 (2.51)	26.05 (26.21)	>300[c]
(**2**)	$[RuCl_2(BHPz_3)(NO)]\cdot THF$	29.54 (29.29)	3.17 (3.13)	21.74 (21.74)	168—177
(**3**)	$[RuCl_2\{BH(3,5\text{-}Me_2Pz)_3\}(NO)]\cdot 0.25C_6H_6$	38.29 (38.21)	4.44 (4.57)	18.96 (18.90)	292
(**4**)	$[RuCl_3(NO)(3,5\text{-}Me_2PzH)_2]\cdot THF$	30.42 (30.95)	4.09 (4.33)	15.02 (15.04)	258—260
(**5**)	$[RuCl_3(NO)(Pz_2CMe_2)]\cdot 0.5H_2O$	25.59 (25.58)	3.05 (3.10)	16.30 (16.57)	264

a) Calculated values in parentheses. b) Measured on plate, unless noted otherwise. With decomposition. c) In evacuated sealed capillaries.

Table 2. IR Data of New Ruthenium Complexes[a]

Complex	ν(NO)	ν(BH)	ν(NH)
1	1894		
2	1893	2522	
3	1886	2560	
4	1874		3376
5[b]	1887		

a) In cm^{-1}. Measured in CH_2Cl_2, unless noted otherwise. b) In KBr disk.

yls, the values ν(NO) have been correlated to the extent to which π-back donation from metals occurs in nitrosyl complexes.[4,8] The complexes $[Ru(\pi\text{-}C_5R_5)Cl_2(NO)]$, i.e. π-cyclopentadienyl analogues to the poly(1-pyrazolyl)boratoruthenium **1**—**3**, have been described to show ν(NO) bands at 1809 and 1790 cm^{-1} for H and CH_3 as R, respectively.[9] The ν(NO) values of the present poly(1-pyrazolyl)borato complexes are larger than those of the π-cyclopentadienyl analogues by ca. 90 cm^{-1}, indicating a smaller degree of π-back donation of metal–NO bonds in **1**—**3**. Similar phenomena were noticed in the series of (carbonyl)ruthenium(II)[3b,3c] (Table 3) and (nitrosyl)molybdenum(III)[10] complexes reported previously.

On the contrary, it has also been described that Bruce's (carbonyl)[poly(1-pyrazolyl)borato]copper(I) complexes[11] show ν(CO) bands at lower wavenumbers than those of their π-cyclopentadienyl analogues, for example, 2083 cm^{-1} for $[Cu(BHPz_3)(CO)]$ vs. 2093 cm^{-1} for $[Cu(\pi\text{-}C_5H_5)(CO)]$,[11a] and considerable stability of the Bruce's carbonyls has been recognized to result primarily from the strong σ-donor character of the poly(1-pyrazolyl)borato ligands. The copper complexes have an essentially sp^3-hybrid four-coordinate structure with a d^{10}-electron configuration, free of unoccupied d-orbitals, whereas the ruthenium complexes have an essentially d^2sp^3-hybrid six-coordinate structure with a d^6-electron configuration.

Accordingly, delocalization of the π-electron system extended to the CO or NO ligand in the ruthenium complexes was expected to occur to a more significant extent than that in the copper complexes, and the π-donor ability of the poly(1-pyrazolyl)borato ligands was revealed to be not as large as that of the π-cyclopentadienyl ligands.[12,13].

Tables 4 and 5 summarize the NMR spectral data of the new complexes observed in $CDCl_3$.[14] Complexes **2** and **3** showed ^{13}C NMR resonances of three pyrazolyl groups,[14] which are classified into two groups in a 2 : 1 ratio. The classification was readily interpretable by

Table 3. ν(CO) Described for $BRPz_3$ and π-Cyclopentadienyl Ruthenium Complexes

Complex	ν(CO) (cm^{-1})
$[Ru(azb)(BHPz_3)(CO)_2]$[a]	2048 and 1988 (Nujol)
$[Ru(\pi\text{-}C_5H_5)(azb)(CO)_2]$[a]	2033 and 1976 (C_6H_{12})
$[RuCl(BHPz_3)(CO)_2]$[b]	2071 and 2011
$[RuCl(\pi\text{-}C_5H_5)(CO)_2]$[b]	2056 and 2008

a) azb=(phenylazo)phenyl. Ref. 3b. b) Ref. 3c.

Table 5. ^1H NMR Data of New Ruthenium Complexes[a]

Complex	Class[b]	3-H	4-H	5-H	CH_3	BH or NH
1	X[c]	8.00	6.45	7.87		
	Y[c]	8.28	6.33	7.87		
	Z[d]	7.98	6.68	7.95		
2	X[e]	7.91	6.44	7.80		ca. 4.6
	Y[f]	8.16	6.28	7.59		
3	X		5.92		2.65, 2.40	ca. 4.6
	Y		5.85		2.80, 2.34	
4	X		5.97		2.60, 2.33	10.77

a) δ Values from TMS. In $CDCl_3$. NMR data of solvent molecules of solvation, incorporated on crystallization, are omitted. b) Classes of pyrazolyl groups; X, two spectroscopically equivalent coordinated pyrazolyl groups; Y, unique coordinated pyrazolyl group; Z, uncoordinated pyrazolyl group. c) $J_{3,4}$=2.2 Hz, $J_{4,5}$=2.6 Hz, $J_{3,5}$=0.7 Hz. d) $J_{3,4}$=1.5 Hz, $J_{4,5}$=2.2 Hz, $J_{3,5}$=0.7 Hz. e) $J_{3,4}$=1.8 Hz, $J_{4,5}$=2.4 Hz. f) $J_{3,4}$= $J_{4,5}$=2.4 Hz.

Table 4. ^{13}C and ^{11}B NMR Data of New Ruthenium Complexes[a]

Compd.	^{13}C NMR[b]					^{11}B NMR[d]
	Class[c]	3-C	4-C	5-C	CH_3	
1	X	144.26	108.06	137.21		−18.4
	Y	145.81	106.74	135.26[e]		
	Z	142.78	ca. 108.16	135.61[e]		
2	X	143.24	107.86	136.86		−22.3 (117Hz)
	Y	144.53	106.58	135.15		
3	X	152.32	108.84	145.46	14.46 12.51	−27.7 (105Hz)
	Y	156.13	108.99	143.79	15.86 12.51	
4	X	153.70	107.85	142.88	14.56 11.13	

a) In $CDCl_3$. b) δ Values from TMS. NMR data of solvent molecules of solvation, incorporated on crystallization, are omitted. c) Classes of pyrazolyl groups; X, two spectroscopically equivalent coordinated pyrazolyl groups; Y, unique coordinated pyrazolyl group; Z, uncoordinated pyrazolyl group. d) δ Values from $B(OMe)_3$. Coupling constants J(BH) shown in parentheses. e) Maybe interchangeable.

an end-on view (i.e. Newman projection along the B–Ru axis) of the tridentate $BHPz_3$ and $BH(3,5\text{-}Me_2Pz)_3$ ligands with local C_{3v} symmetry (Fig. 1), since the normal disposition of two chlorine atoms and the nitrosyl group with regards to the ligands would make two of the three coordinated pyrazolyl groups identical and different from the third one. The complex **1** exhibited ^{13}C NMR resonances of the uncoordinated pyra-

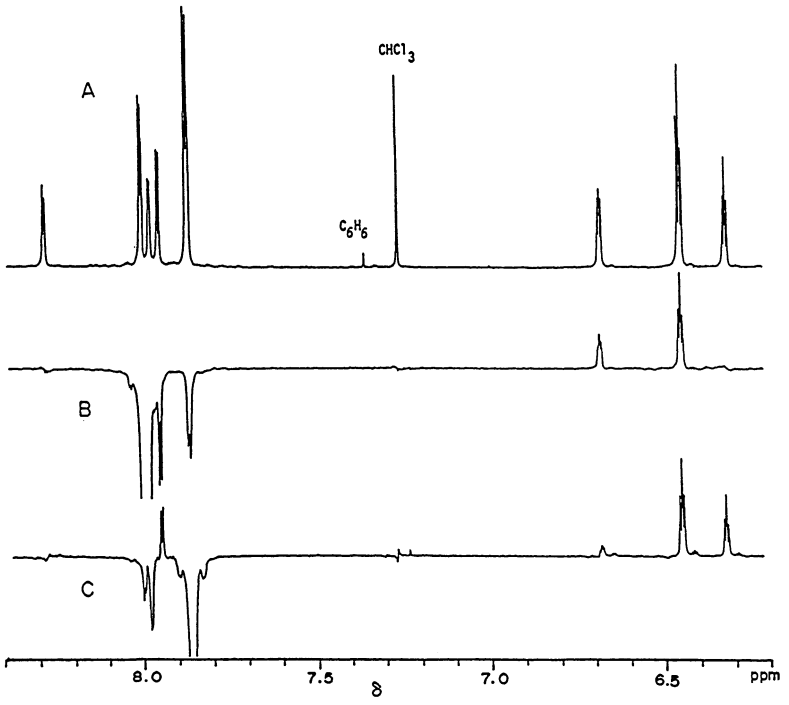

Fig. 3. ^1H NMR spectrum of the BPz_4 complex **1** and NOE observation.
A, ^1H NMR spectrum; B, NOE observation on irradiation at δ=8.00; C, NOE observation on irradiation at δ=7.87.

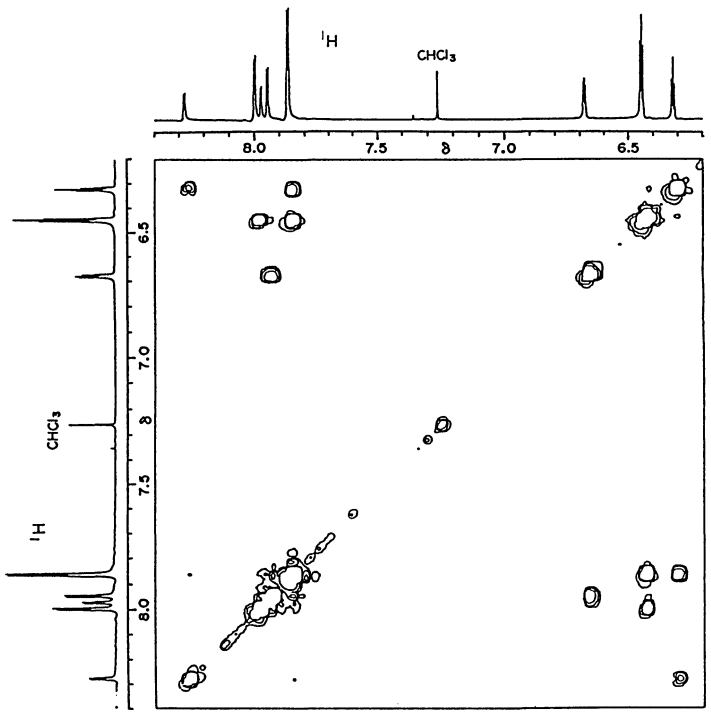

Fig. 4. The ^1H–^1H COSY spectrum of the BPz_4 complex **1**.

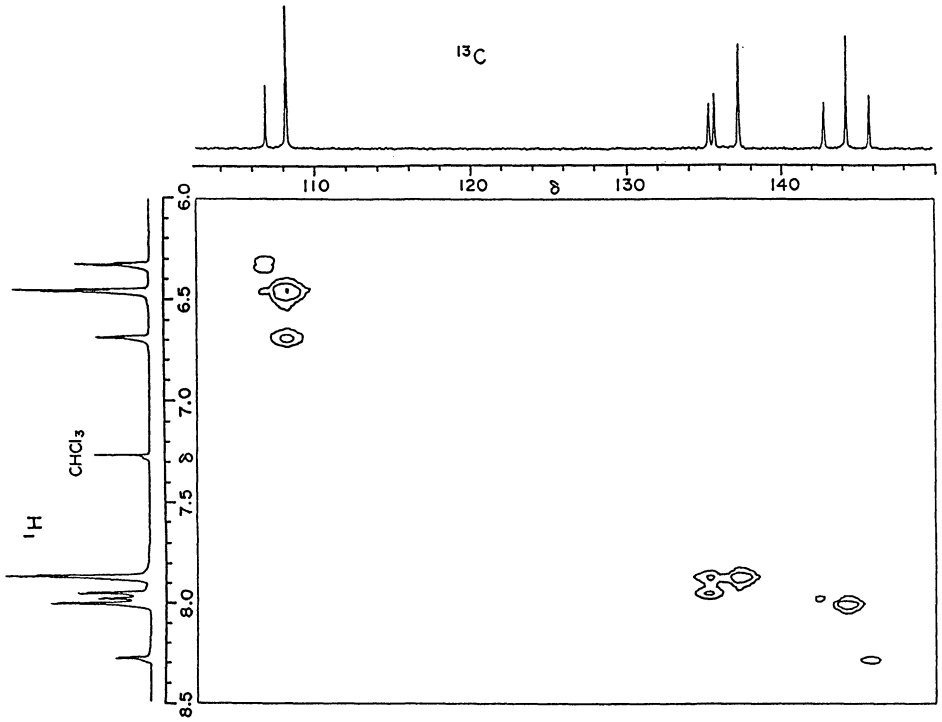

Fig. 5. The ^{13}C–^{1}H COSY spectrum of the BPz_4 complex **1**.

zolyl group, in addition to those of the three coordinated ones.

The ^{1}H NMR spectrum of the BPz_4 complex **1** is shown in Fig. 3-A. Four pyrazolyl groups were classified into three by a 2 : 1 : 1 ratio, similar to the ^{13}C NMR data, with the help of ^{1}H–^{1}H COSY (Correlation Spectroscopy) (Fig. 4) and a ^{1}H–^{1}H selective decoupling technique. Two stereochemically equivalent coordinated pyrazolyl groups (Fig. 1) gave the signal set X at δ=6.45 (2H), 7.87 (2H, overlapping), and 8.00 (2H). The remaining two unique groups were associated with a set Y of the signals at δ=6.33 (1H), 7.87 (1H, overlapping), and 8.28 (1H), and the other set Z at δ=6.68 (1H), 7.95 (1H), and 7.98 (1H).

Signals in the range δ=5.8 to 6.8 were obviously 4-H protons in the respective sets of the pyrazolyl groups. In order to prevent any obscurity in the NMR assignment of the 3- and 5-H protons, NOE measurements of **1** were carried out in this study. No similar work has so far been described concerning known poly(1-pyrazolyl)borato complexes. The NOE difference-spectra (B and C in Fig. 3) were obtained by saturating signals at δ=8.00 and 7.87, respectively. The irradiation at δ=8.00 (set X) accompanied unavoidably some simultaneous partial irradiation of the signal at δ=7.98 (set Z) owing to their close chemical shifts, and did not give any positive NOE signals except for the neighboring 4-H protons attached to the same pyrazolyl rings.[15] On the contrary, irradiation at δ=7.87 in the set(s) of X (and Y)[16] brought about a positive NOE signal at δ=7.95, belonging to the set Z. NOE value is defined as the percent variation of the intensity of a signal when another signal is saturated, and the value obtained at δ=7.95 was +5.4%. This finding clearly revealed the stereochemically close positions of the protons for the signals at δ=7.87 and 7.95. These protons were assigned to 5-H, and the set Z, which includes the signal at δ=7.95, was determined for the uncoordinated pyrazolyl group (Fig. 1).[16] The remaining set Y was attributed to the coordinated but also unique group. The signal at δ=8.00 was associated with the 3-H protons in the set X. Other NMR signals of **1** were assigned readily,[17] and the results are listed in Table 5. The ^{1}H NMR assignment was consistent with the above-described ^{13}C NMR data, as can be seen from ^{13}C–^{1}H COSY in Fig. 5. Thus, the present work demonstrated for the first time the utility of ^{1}H NOE measurements with the help of ^{1}H–^{1}H and ^{13}C–^{1}H COSY, in the assignment of 3- and 5-H protons of the poly(1-pyrazolyl)borato complexes. NMR data of **1** were helpful in analogous assignments of the other complexes, **2**—**4**.

As for the NMR fluxionality of the poly(1-pyrazolyl)borato ligands,[1c,2b,2e] the ^{1}H NMR spectra of **1** and **2** did not show any significant temperature-dependent change from −60 to 55 °C. The lack of fluxionality was in sharp contrast to the case of Trofimenko's complexes of $[Mo(\pi\text{-allyl})(BRPz_3)(CO)_2]$ with temperature-dependent trigonal-twist-rotation around the B–Mo axis.[2b,2e]

Further studies are currently in progress to apply these poly(1-pyrazolyl)boratoruthenium complexes as catalyst precursors to some homogeneous catalytic reactions, and results will be published elsewhere.

Experimental

General Procedures. Alkali-metal poly(1-pyrazolyl)-borates[2a,2c,2f] and 2,2-bis(1-pyrazolyl)propane[18] were prepared according to methods described in the literature. Trichloro-(nitrosyl)ruthenium monohydrate is commercially available or its pentahydrate was obtained by reported methods.[19] Wakogel C-200 was used for silica-gel column chromatography. Preparative operations were performed under nitrogen.

IR spectra were obtained by a JASCO A-100 spectrometer. ^1H, ^{13}C, and ^{11}B NMR spectra were recorded on a JEOL model JNM GX-400 spectrometer operating at 399.7, 100.4, and 128.2 MHz, respectively, by use of tetramethylsilane as an internal standard for the former two nuclei and trimethyl borate as an external standard for the third. The chemical shifts δ are reported in parts per million from these standards, and downfield shifts are noted as positive in all cases. Melting points were determined on a Yanagimoto MP-S3 micro-stage apparatus and are uncorrected.

Conversion of Potassium Poly(1-pyrazolyl)borates to Thallium Analogues. The conversion of the $BHPz_3$ salt has been performed using thallium formate and water as a solvent,[3b] and this procedure was also applicable to the BPz_4 salt. On the other hand, the solubility properties of the $BH(3,5\text{-}Me_2Pz)_3$ and $B(3\text{-}t\text{-}BuPz)_4$ (3-*t*-BuPz=3-*t*-butyl-1-pyrazolyl) salts are slightly different, and it thus seems to be noteworthy to describe their conversion procedures in more detail.[2c,2f]

Potassium tris(3,5-dimethyl-1-pyrazolyl)hydroborate (520 mg, 1.55 mmol), washed well with hexane to remove any free 3,5-dimethylpyrazole impurity, was dissolved in methanol and mixed with thallium formate (390 mg, 1.55 mmol) in methanol. After stirring for 2 h, the solvent was evaporated under reduced pressure, and the dichloromethane extract of the residue was washed with methanol to give white microcrystals of thallium tris(3,5-dimethyl-1-pyrazolyl)hydroborate (410 mg, 0.82 mmol) in 53% yield. Mp 273 °C (melt with sublimation).

The reaction of potassium tetrakis(3-*t*-butyl-1-pyrazolyl)-borate was performed in methanol in a manner similar to that of the $BH(3,5\text{-}Me_2Pz)_3$ salt. At the working-up stage, hexane extract was collected to afford a white powder of thallium tetrakis(3-*t*-butyl-1-pyrazolyl)borate in 56% yield. Mp 174—175 °C.

Reaction of the BPz_4 Anion with $RuCl_3(NO)$. Sodium tetrakis(1-pyrazolyl)borate (150 mg, 0.50 mmol) was added to an ethanol solution (10 ml) of trichloro(nitrosyl)ruthenium (120 mg, 0.50 mmol). After stirring overnight at room temperature, the resulting precipitates were recrystallized from dichloromethane and benzene to give brown microcrystals (63 mg, 0.13 mmol) of $[RuCl_2(BPz_4)(NO)]$ in 26% yield. For further purification, silica-gel column chromatographic separation was effective by elution with dichloromethane. The reaction of the potassium salt showed similar results.

Reaction of the $BHPz_3$ Anion with $RuCl_3(NO)$. Thallium hydrotris(1-pyrazolyl)borate (190 mg, 0.46 mmol) was mixed with trichloro(nitrosyl)ruthenium (104 mg, 0.44 mmol) in THF (20 ml). The mixture was stirred for 4 h. After removing the solvent under reduced pressure, a dichloromethane extract of the residue was chromatographed on a silica-gel column, eluting with dichloromethane to give a brown solid upon evaporation. Recrystallization from THF and diethyl ether afforded brown microcrystals (60 mg, 0.12 mmol) of $[RuCl_2(BHPz_3)(NO)]\cdot THF$ in 27% yield. A similar reaction of the potassium salt gave the same product in 14% yield.

Reaction of the $BH(3,5\text{-}Me_2Pz)_3$ Anion with $RuCl_3(NO)$. Trichloro(nitrosyl)ruthenium (130 mg, 0.55 mmol) in THF (15 ml) was treated with thallium tris(3,5-dimethyl-1-pyrazolyl)-hydroborate (280 mg, 0.56 mmol) and the mixture was stirred for 3 h at ambient temperature. Silica-gel column chromatographic separation was performed for the dichloromethane extract from the reaction mixture. A brown band upon elution with benzene and dichloromethane (1/1) gave green-tinged brown microcrystals (26 mg, 0.050 mmol) of $[RuCl_2\{BH(3,5\text{-}Me_2Pz)_3\}(NO)]\cdot 0.25C_6H_6$ in 9% yield. The dichloromethane eluate of the ensuing reddish-pink band was evaporated, and recrystallization of the residue from THF and hexane afforded reddish-brown microcrystals (39 mg, 0.078 mmol), which were characterized as $[RuCl_3(NO)(3,5\text{-}Me_2PzH)_2]\cdot THF$ (14% yield).

Reaction of 2,2-Bis(1-pyrazolyl)propane. Trichloro(nitrosyl)ruthenium (74 mg, 0.31 mmol) was allowed to react with 2,2-bis(1-pyrazolyl)propane (70 mg, 0.40 mmol) in ethanol (15 ml). The mixture was stirred overnight and the resulting precipitates were collected and washed with diethyl ether. Pale-yellow microcrystals (81 mg, 0.19 mmol) were obtained and assigned to the complex $[RuCl_3(NO)(Pz_2CMe_2)]\cdot 0.5H_2O$ (62% yield).

The present work was partially supported by the Asahi Glass Foundation. Special thanks are due to Professor Katsuma Hiraki, Mr. Yushichiro Ohama, and Mr. Kazuto Ikemoto in this Department for helpful discussions.

References

1) a) A. Shaver, "Comprehensive Coordination Chemistry," ed by G. Wilkinson, Pergamon Press, Oxford (1987), Vol. 2, Chap. 13.6, p. 245; b) *idem., J. Organomet. Chem. Libr.*, **3**, 157 (1977); c) M. Onishi, K. Hiraki, M. Shironita, Y. Yamaguchi, and S. Nakagawa, *Bull. Chem. Soc. Jpn.*, **53**, 961 (1980).

2) a) S. Trofimenko, *J. Am. Chem. Soc.*, **89**, 3170 (1967); b) *idem., ibid.*, **91**, 3183 (1969); c) *idem., ibid.*, **89**, 6288 (1967); d) *idem., Prog. Inorg. Chem.*, **34**, 115 (1986); e) P. Meakin, S. Trofimenko, and J. P. Jesson, *J. Am. Chem. Soc.*, **94**, 5677 (1972); f) S. Trofimenko, J. C. Calabrese, and J. S. Thompson, *Inorg. Chem.*, **26**, 1507 (1987).

3) a) M. O. Albers, S. Francesca, A. Crosby, D. C. Liles, D. J. Robinson, A. Shaver, and E. Singleton, *Organometallics*, **6**, 2014 (1987); b) M. I. Bruce, M. Z. Iqbal, and F. G. A. Stone, *J. Chem. Soc. A*, **1971**, 2820; c) M. I. Bruce, D. N. Sharrocks, and F. G. A. Stone, *J. Organomet. Chem.*, **31**, 269 (1971); d) D. J. O'Sullivan and F. J. Lalor, *ibid.*, **57**, C-58 (1973); e) A. M. McNair, D. C. Boyd, and K. R. Mann, *Organometallics*, **5**, 303 (1986); f) M. M. de V. Steyn, E. Singleton, S. Hietkamp, and D. C. Liles, *J. Chem. Soc., Dalton Trans.*, **1990**, 2991.

4) a) B. F. G. Johnson, B. L. Haymore, and J. R. Dilworth, "Comprehensive Coordination Chemistry," ed by G. Wilkinson, Pergamon Press, Oxford (1987), Vol. 2, Chap. 13.3, p. 99; b) G. B. Richter-Addo and P. Legzdins, *Chem. Rev.*, **88**, 991 (1988); c) M. W. Schoonover and R. Eisenberg, *J. Am. Chem. Soc.*, **99**, 8371 (1977); d) S. T. Wilson and J. A. Osborn, *ibid.*, **93**, 3068 (1971); e) L. K. Bell, J. Mason, D. M.

P. Mingos, and D. G. Tew, *Inorg. Chem.*, **22**, 3497 (1983).

5) a) W. H. McCurdy, Jr., *Inorg. Chem.*, **14**, 2292 (1975); b) C. Lopez, R. M. Claramunt, D. Sanz, C. F. Foces, F. H. Cano, R. Faure, E. Cayon, and J. Elguero, *Inorg. Chim. Acta,* **176**, 195 (1990).

6) a) R. B. King and A. Bond, *J. Am. Chem. Soc.*, **96**, 1334 (1974); b) *idem., ibid.*, **96**, 1343 (1974).

7) E. A. Seddon and K. R. Seddon, "The Chemistry of Ruthenium," Elsevier, Amsterdam (1984), Chap. 14, p. 1105.

8) a) B. L. Haymore and J. A. Ibers, *Inorg. Chem.*, **14**, 2610 (1975); b) *idem., ibid.*, **14**, 3060 (1975).

9) a) A. Efraty and G. Elbaze, *J. Organomet. Chem.*, **260**, 331 (1984); b) J. Chang, M. D. Seidler, and R. G. Bergman, *J. Am. Chem. Soc.*, **111**, 3258 (1989).

10) a) J. A. McCleverty, D. Seddon, N. A. Bailey, and N. W. J. Walker, *J. Chem. Soc., Dalton Trans.*, **1976**, 898; b) J. A. McCleverty and D. Seddon, *ibid.*, **1972**, 2526.

11) a) M. I. Bruce and A. P. P. Ostazewski, *J. Chem. Soc., Dalton Trans.*, **1973**, 2433; b) N. Kitajima, K. Fujisawa, C. Fujimoto, and Y. Moro-oka, *Chem. Lett.*, **1989**, 421.

12) R. H. Crabtree, "The Organometallic Chemistry of the Transition Metals," John Wiley & Sons, New York (1988), p. 104.

13) The complexes $[RuCl_2(BHPz_3)(NO)]$ and $[RuCl(BHPz_3)(CO)_2]$[3c] in C_6D_6 showed ^{11}B NMR resonances at $\delta=-22.6$ {J(BH)=111 Hz} and $\delta=-22.3$ {J(BH)=113 Hz}, respectively, which were a little higher fields than that of $[Cu(BHPz_3)(CO)]$[11a] at $\delta=-20.3$ {J(BH)=103 Hz]. The present author suggests some negative charge was retained on boron in **1**—**3**, at the expense of the electron delocalization to the nitrosylruthenium moiety, and was associable with the above-mentioned easy cleavage of the poly(1-pyrazolyl)borate anions in the reactions with trichloro(nitrosyl)ruthenium. Alkali-metal salts of poly(alkyl-substituted 1-pyrazolyl)borate, where alkyl substituents increase electron density on boron, were hydrolyzed gradually upon exposure to moist air with release of some alkyl-substituted pyrazoles.

14) For ruthenium and some other transition-metal complexes with tridentate poly(1-pyrazolyl)borates, ^{13}C NMR signals of 3-C were observed usually at lower fields than those of 5-C. A subsequent paper is in preparation concerning a reinvestigation of the ^1H and ^{13}C NMR assignment of known poly(1-pyrazolyl)borato complexes. A similar short description has appeared concerning alkali-metal poly(1-pyrazolyl)borates.[5b]

15) Negative NOE signals were observed for some interrelations between the 3- and 5-H protons on the same pyrazolyl rings.

16) In the case where the uncoordinated pyrazolyl group does not rotate around the axis through the 1-nitrogen atom of the group and the boron atom, two 5-H protons in the coordinated pyrazolyl groups are conceivably located at the close positions to the 5-H proton in the uncoordinated group under consideration (Fig. 1), and are thought to be responsible for the positive NOE signal of the latter proton. However, the present author presumed the other case, in which the uncoordinated pyrazolyl group rotates freely around the axis, since the ^1H NMR spectra of **1** did not show any significant temperature-dependent change from −60 to 55 °C. In this case, all three 5-H protons in the coordinated pyrazolyl groups are responsible on the average, for the positive NOE observed. Similar free rotation of the terminal uncoordinated pyrazolyl group was described for some BPz_4 complexes.[2e]

17) By considering ^{13}C–^1H COSY in Fig. 5, the present author distinguished between 3- and 5-H proton signals in the set Y.

18) S. Trofimenko, *J. Am. Chem. Soc.*, **92**, 5118 (1970).

19) J. G. Muller and K. J. Takeuchi, *Inorg. Chem.*, **29**, 2185 (1990).

Structural, Magnetic, and Spectroscopic Characterization of the Pyridine Complexes of Copper(II) Triphenylacetate: A Dimeric Copper(II) Triphenylacetate–Pyridine Complex with Distorted Trigonal Bipyramidal Geometry Around Copper[1)]

Omar W. Steward,* Michinobu Kato,*,† Shih-Chi Chang, Martin Sax,†† Chong-Hwan Chang,††
C. Frederick Jury, Yoneichiro Muto,††† Tadashi Tokii,††† Toshiaki Taura,†
James F. Pletcher,†† and Chung Soo Yoo††

Department of Chemistry and Physics, Duquesne University, Pittsburgh, Pennsylvania 15282, U.S.A.
†Department of Chemistry, Aichi Prefectural University, Mizuho-ku, Nagoya 467
††Biocrystallography Laboratory, V A Medical Center, Pittsburgh, Pennsylvania 15240 and Department of Crystallography, University of Pittsburgh, Pittsburgh, Pennsylvania 15260 U.S.A.
†††Department of Chemistry, Faculty of Science and Engineering, Saga University, Saga 840

(Received March 11, 1991)

The synthesis and characterization of three copper(II) triphenylacetate–pyridine complexes are reported along with their magnetic and spectral properties: $[Cu_2(O_2CCPh_3)_4(py)_2]\cdot C_6H_6$ (**1**), $[Cu_2(O_2CCPh_3)_4(py)_2]$ (**2**), and $Cu(O_2CCPh_3)_2\cdot 2py$ (**3**). Crystal structure analyses of **1** and **3** have revealed unusual geometries around copper: **1**, triclinic, space group $P\bar{1}$ with a=19.558(7) b=16.605(6), c=14.997(5) Å, α=114.55(2)°, β=97.11(2)°, γ=111.65(2)°, and Z=2; **3**, monoclinic, space group $P2_1/c$ with a=8.931(1), b=12.602(1), c=19.578(1) Å, β=118.17(0.4)°, and Z=2. The coordination sphere around each copper in the dimeric complex **1** is a highly distorted trigonal bipyramid with bridging triphenylacetato ligands spanning the apical and equatorial positions, resulting in a long Cu–Cu distance of 3.086(1) Å. Temperature-dependent magntic susceptibility measurements on **1** indicate that the two coppers are antiferromagnetically coupled with $-2J$=187 cm^{-1}. The structure of the monomeric complex **3** is unusual in that the out-of-plane carboxylate oxygen is twisted 12° from the normal. Two solid modifications are observed for **2**. The magnetic and spectral properties of **2a** ($-2J$=173 cm^{-1}) resemble those of **1**, and **2b** ($-2J$=321 cm^{-1}) those of copper(II) acetate monohydrate. Magneto-structural correlations are presented. The novel structural features of these complexes are suggested to arise from steric effects resulting from the spatial relationships both between and within the molecules in the crystal environment.

The structures of a large number of dimeric copper(II) complexes with the formula $[Cu_2(O_2CR)_4(L)_2]$, where R is an organic group and L is a Lewis base, have been determined.[2–6)] Almost all of these complexes have the classical copper(II) acetate monohydrate-type structure in which the ligand atoms in the coordination sphere around copper(II) are located near the corners of a square pyramid. Recently, some members of two families of these complexes have been observed to have a variation of this structure, in which the arrangement of the ligands around copper(II) can best be described as being distorted trigonal bipyramidal: complexes with bridging triphenylacetato ligands[7–10)] and complexes with bridging trichloroacetato ligands.[10–16)]

In this paper we report on the first complete structural analysis of a complex from the family containing triphenylacetato ligands, [tetrakis(μ-triphenylacetato-*O,O'*)bis(pyridine)dicopper(II)]–benzene(1/1), $[Cu_2(O_2CCPh_3)_4(py)_2]\cdot C_6H_6$ (**1**). In **1**, the coordination geometry around each of the two copper atoms is that of a highly distorted trigonal bipyramid. The factors which cause the unusual geometry around copper(II) in this binuclear complex are attributed to steric effects resulting from the spatial relationships both between and within the molecules in the crystal environment, the former being of prime importance.

Two different solid modifications of the dimeric complex, [tetrakis(μ-triphenylacetato-*O,O'*)bis(pyridine)dicopper(II)], $[Cu_2(O_2CCPh_3)_4(py)_2]$ (**2a** and **2b**), have been prepared and found to exhibit different magnetic and spectral properties. We report on the first study concerning the effect of the ligand arrangement around copper, distorted trigonal bipyramidal and square pyramidal, on the magnetic and spectral properties of these binulear conformers.

The conversion of **1** to *trans*-bis(triphenylacetato-*O,O'*)bis(pyridine)copper(II), $Cu(O_2CCPh_3)_2\cdot 2py$ (**3**), in the crystalline state is discussed. The crystal structure of the monomeric complex **3** reveals a structural modification from the reported structures for complexes of the type $Cu(O_2CR)_2\cdot 2L$, where L represents a nitrogeneous base, resulting from steric effects in which the out-of-plane carboxylate oxygen is twisted 12° from the normal. The so-called "dimer spectral band", which is observed for the complexes **1**, **2a**, and **2b**, is not observed for **3**.

Experimetal

General Procedures. All calculations for copper(II) carboxylates are based on formula weights, unless indicated otherwise. Analyses were performed by Analytische Laboratorien, Elbach, West Germany, with the exception of some copper analyses that were performed in our laboratories by atomic absorption and EDTA titration.

Materials. The starting materials (and sources) are as follows: triphenylacetic acid, benzene-d_6, ethanol-*d* (Aldrich Chemical Co.); copper(II) acetate monohydrate, pyridine (Fisher Scientific Co.).

Preparation of the Complexes. (a) $[Cu_2(O_2CCPh_3)_4(py)_2]\cdot C_6H_6$ (1) Crystals. A Büchner funnel with a fritted disk (30 mL-30 M) was placed in a beaker (100 mL). A melting-point tube open at both ends was bent and then inserted so that the air pocket which formed under the filter could be minimized. Into the beaker was added a solution of absolute ethanol–pyridine (50 : 1 v/v). $Cu(O_2CCPh_3)_2\cdot 2H_2O$ (0.3 g, 0.4 mmol), prepared by the method of Steward et al.,[17] was dissolved in hot benzene (25 mL) and poured into the Büchner funnel. The solution developed the characteristic green color of $Cu(O_2CCPh_3)_2\cdot py$ at this time. The height of the outer solution was then adjusted to ca. 1 cm above the level of the inner solution. The entire apparatus was placed in a desiccator. After four days, blue-green crystals of **1** had formed on the fritted disk in the filter. Anal. Calcd for $C_{48}H_{38}O_4CuN$: C, 76.22; H, 5.06; Cu, 8.40; N, 1.85%. Found: C, 76.15; H, 5.00; Cu, 8.45; N, 1.88%.

(b) $Cu(O_2CCPh_3)_2\cdot py$ (2a): Procedure 1. $Cu(O_2CCPh_3)_2\cdot 2H_2O$ (1.29 g, 1.91 mmol) was dissolved in benzene (150 mL). Warming on the steam bath reduces the time required for the complex to dissolve. Pyridine (0.59 g, 7.46 mmol) was added, resulting in a color change from blue to green. After filtering, the complex was precipitated by adding petroleum ether, bp 30—60 °C (700 mL). The light-green precipitate was collected in a Büchner funnel with a fritted disk (reduced-pressure filtration). The precipitate was washed with a benzene–petroleum ether mixture (1 : 9 v/v, 100 mL) and allowed to dry in air for several days, yielding 1.16 g, 1.62 mmol, (84.8% yield) of **2a**. Anal. Calcd for $C_{45}H_{35}O_4CuN$: C, 75.35; H, 4.92; Cu, 8.86; N, 1.95%. Found: C, 75.46; H, 5.00; Cu, 8.94 (EDTA titration), 8.52 (atomic absorption); N, 1.86%.[18]

Procedure 2. A mixture of $Cu(O_2CCPh_3)_2\cdot 2H_2O$ (0.67 g, 1.0 mmol) and pyridine (87 mg, 1.1 mmol) in chloroform (60 mL) was stirred on a hot plate for 0.5 h. The chloroform solution was then filtered, and the filtrate was concentrated to one-third of its volume. After standing overnight at ca. 5 °C, the concentrated solution afforded yellow-green crystals of **2a**. The crystals were washed with petroleum ether and dried in vacuo. Anal. Calcd for $C_{45}H_{35}O_4CuN$: C, 75.35; H, 4.92; Cu, 8.86; N, 1.95%. Found: C, 75.15; H, 4.65; Cu, 8.59; N, 2.12%.

(c) $Cu(O_2CCPh_3)_2\cdot py$ (2b). A mixture of $Cu(O_2CCPh_3)_2\cdot 2H_2O$ (0.67 g, 1.0 mmol) and pyridine (0.12 g, 1.5 mmol) in ethanol (50 mL) was heated with stirring on a hot plate for ca. 2 h. The resulting yellow-green precipitate was collected, washed repeatedly with ethanol and dried in vacuo. Anal. Calcd for $C_{45}H_{35}O_4CuN$: C, 75.35; H, 4.92; Cu, 8.86; N, 1.95%. Found: C, 74.62; H, 4.92; Cu, 9.11; N, 1.84%.

(d) $Cu(O_2CCPh_3)_2\cdot 2py$ (3), Crystals. Crystals of **1** were placed in a screw-capped vial containing an absolute ethanol–pyridine (50 : 1 v/v) solution. After one day, mixed crystals containing both blue-green and dark blue areas had formed. After three days, the blue-green crystals had been completely transformed into dark-blue crystals of **3**. Anal. Calcd for $C_{50}H_{40}O_4CuN_2$: C, 75.42; H, 5.06; Cu, 7.97; N, 3.51%. Found: C, 75.28; H, 4.99; Cu, 8.08; N, 3.50%.

Preparation of Triphenylacetic Acid-*d*. A small amount of triphenylacetic acid was dissolved with warming in ethanol-*d* (99.5+ atom % D). The solvent was removed by evaporation under a stream of dry nitrogen. The resulting solid was dried in a desiccator under reduced pressure.

X-Ray Procedure. (a) Collection and Reduction of the Data. The crystal of **1** selected was mounted on a glass fiber and coated with an epoxy resin. A crystal of **3** having the dimensions 0.15×0.19×0.32 mm was similarly mounted. Refined cell constants were obtained by a least-squares fit to the observed 2θ angles of 110 high-angle reflections. Data concerning the crystals are given in Table 1. The intensity data were collected using a Picker FACS-1 four-circle diffractometer to a 2θ limit of 90° for **1** and 125° for **3** using graphite-monochromated Cu $K\alpha$ radiation; a $\theta : 2\theta$ scanning technique over the range 2.5° for **1** and 2.2° for **3**; a scan rate of 1° min^{-1} was used. The background was counted for 20 s at each end of the scan range. For **1**, three standard reflections were monitored after each 100 reflections; their intensities decreased by ca. 9%. For **3**, three standard reflections were monitored after each 50 reflections; their intensities showed no fluctuations greater than ±2%. The intensities for **1** were scaled and assigned variances, $\sigma^2(I)$, according to the statistics of the scan and background counts plus the correctional term, $(0.03\ S)^2$, S being the scan count. The intensities and their variance were corrected for both Lorentz and polarization factors. For **3**, corrections were made for both absorbance and secondary extinction.[19]

Table 1. Crystallographic Data for $[Cu_2(O_2CCPh_3)_4(py)_2]\cdot C_6H_6$ (1) and $Cu(O_2CCPh_3)_2\cdot 2py$ (3)

	1	3
Formula	$C_{96}H_{76}Cu_2N_2O_8$	$C_{50}H_{40}CuN_2O_4$
Fw	1512.76	796.42
Space group	$P\bar{1}$	$P2_1/c$
a/Å	19.558(7)	8.931(1)
b/Å	16.605(6)	12.602(1)
c/Å	14.997(5)	19.578(1)
α/deg	114.55(2)	
β/deg	97.11(2)	118.17(0.4)
γ/deg	111.65(2)	
V/Å^3	3890.2	1942.5
λ/Å	1.54178	1.54178
Z	2	2
ρ_c/g cm^{-3}	1.297	1.401
μ/cm^{-1}	19.89	20.40
No. of unique data	6522	3107
No. of data with $I \geq 3\sigma(I)$	5599	2771
R	0.045	0.030
R_w	0.055	0.026

Solution and Refinement of the Structures. (a) $[Cu_2(O_2CCPh_3)_4(py)_2]\cdot C_6H_6$ (1). The triclinic unit cell was first determined from Weissenberg photographs and the $P\bar{1}$ space group was confirmed by the subsequent structure solution and refinement. The phase problem was solved by direct methods using the MULTAN program.[20] Two copper and 34 non-hydrogen atoms were located from the most probable E map. The corresponding Cu–Cu vectors were confirmed on an E^2-1 Patterson synthesis. After two difference Fourier syntheses, 102 atoms had been located. The 102 atom model, assumed to be complete, was subjected to full-matrix least-squares refinement using a program called QWKREF.[21] On the difference Fourier map, the benzene of solvation was revealed. Two more difference Fourier syntheses revealed all 71 hydrogen atoms bonded to the molecule. The hydrogen positions for the solvent ring were generated by a program called GENATM.[22] The atomic positional parameters and iso-

tropic thermal parameters for hydrogen (3.7 Å) were included in the structure factor calculations, but were not refined. Four more cycles of refinement with anisotropic thermal parameters for all of the nonhydrogen atoms converged to R=0.045. The atomic scattering factors (Cu, C,·N, and O) and the anomalous dispersion corrections (Cu and O) were taken from Ref. 23a. The scattering factors for hydrogen were taken from Stewart et al.[23b] The observed and calculated structure factors are included in the supplementary material.[24]

(b) $Cu(O_2CCPh_3)_2 \cdot 2py$ (3). The structure was solved by the multi-solution tangent-refinement method.[20] The best E map with 350 reflections (E>1.45) and 5000 phase relationships gave all of the nonhydrogen atom positions. The copper atom was located and the position confirmed by an origin removed Patterson synthesis. The positional parameters and isotropic thermal parameters of the nonhydrogen atoms were refined by several cycles of full-matrix least-squares using QWKREF program,[21] yielding R=0.115. After conversion to anisotropic thermal paramters, several further cycles reduced R to 0.069. At this point, the hydrogen atoms were located and included in the refinement. After changing the weighting scheme from counting statistics to a scheme based on an analysis of the variance,[25] the extinction correction was applied. Further refinement with the new weights converged to R=0.030. The atomic-scattering factors and anomalous-dispersion corrections employed are the same as those described in part (a). The observed and calculated structure factors are included in the supplementary material.[24]

Physical Measurements. IR spectra were recorded on a Perkin-Elmer 1430 ratio recording spectrophotometer, polystyrene standard. Reflectance spectra were obtained on a Hitachi recording spectrophotometer (323). ESR spectra were obtained from polycrystalline samples in quartz tubes, DPPH standard, as described previously,[17] except for samples of **2a**[26] and **2b**.[27]

Magnetic moments were determined in solution by the Evans method, as described previously.[17] Magnetic susceptibilities over the temperature range of 80 to 300 K were determined by the Faraday method. Corrections for the diamagnetic contributions were made using Pascal's constants.[28] The cryomagnetic data of complexes **1**, **2a**, and **2b** were fitted to the Bleaney-Bowers equation allowing for the presence of paramagnetic impurities,[29]

$$\chi_A = \frac{Ng^2\beta^2}{3kT}\left[1+\left(\frac{1}{3}\right)\exp\left(\frac{-2J}{kT}\right)\right]^{-1}(1-P)+\frac{Ng_i^2\beta^2}{4kT}P+N\alpha, \quad (1)$$

where P is the mole fraction of the noncoupled copper(II) impurity and g_i is the average g factor for the impurity. The values of g_i=2.2 and $N\alpha$=60×10^{-6} emu (1 cgs emu=4π×10^{-6} m^3) were used throughout this study. The other symbols have their usual meanings. The best-fit parameters (−2J, g, and P) were obtained by using a nonlinear least-squares program[30] on a FACOM M-200 computer at the Nagoya University Computation Center. As a convenient statistical indicator of the quality of the least-squares fit, the discrepancy index, σ_{dis}, was employed,

$$\sigma_{dis} = \left[\frac{\sum(\chi_{obsd}-\chi_{calcd})^2}{\sum\chi_{obsd}^2}\right]^{1/2}. \quad (2)$$

The Curie law was employed to correlate the cryomagnetic data for **3** assuming no monomeric impurities and $N\alpha$= 60×10^{-6} emu.

Results and Discussion

Structures. Single-crystal X-ray structures have been determined for $[Cu_2(O_2CCPh_3)_4(py)_2]\cdot C_6H_6$ (**1**), Figs. 1a and 1b, and $Cu(O_2CCPh_3)_2\cdot 2py$ (**3**), Fig. 2. The atomic positional and isotropic thermal parameters for all atoms, except hydrogen, in the complexes are

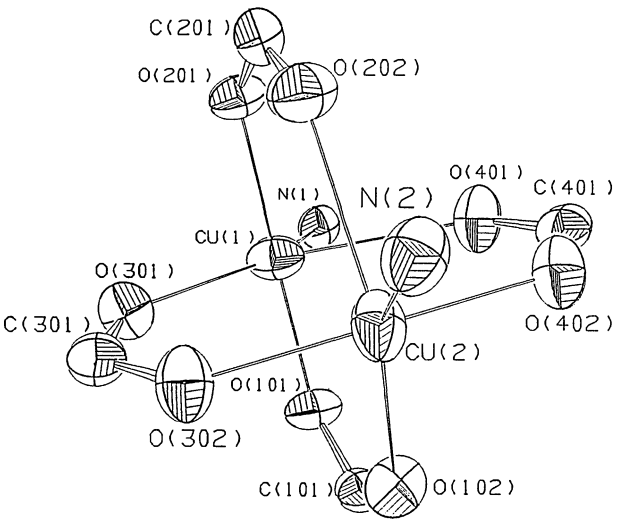

Fig. 1a. View of the cage structure of $[Cu_2(O_2CCPh_3)_4(py)_2]\cdot C_6H_6$ (**1**). N(1) and N(2) are in py(P11) and py(P21) respectively. Thermal ellipsoids are drawn to the 50% probability level.

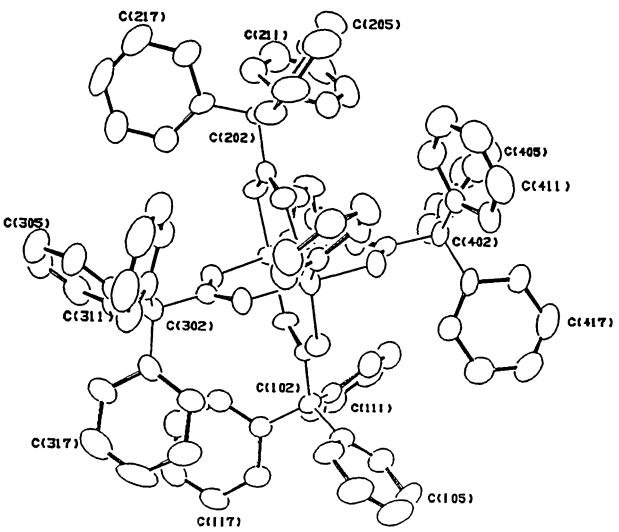

Fig. 1b. View of the structure of $[Cu_2(O_2CCPh_3)_4(py)_2]\cdot C_6H_6$ (**1**). The orientation of the cage is the same as that shown in Figure 1a. For clarity, only a few atoms in the triphenylmethyl groups have been numbered, and the hydrogen atoms and the benzene of crystallization are omitted. Thermal ellipsoids are drawn to the 50% probability level.

listed in Tables 2 and 3; listings of the positional parameters for the hydrogen atoms are included in the supplementary material (Tables 1S and 7S). Selected bond distances and bond angles are given in Tables 4 and 5; complete tables are included in the supplementary material (Tables 3S and 9S).

The structure of **1** contains two crystallographically independent copper atoms and is novel in that the five atoms in the coordination sphere around copper(II) are arranged near neither the corners of a square pyramid nor the corners of a trigonal bipyramid. Each copper atom is coplanar with two oxygen atoms and a nitrogen

Table 2. Positional Parameters ($\times 10^4$) and Equivalent Isotropic Thermal Parameters ($Å^2 \times 10$) and Their Standard Deviations for $[Cu_2(O_2CCPh_3)_4(py)_2] \cdot C_6H_6$ (**1**)

Atom	x	y	z	B_{eq}[a)]	Atom	x	y	z	B_{eq}[a)]
Cu(1)	1561(0)	9646(0)	9873(0)	30(0)	C(303)	1609(3)	8141(3)	11985(4)	27(2)
Cu(2)	3155(0)	9694(0)	9884(0)	30(0)	C(304)	1778(3)	8486(4)	13024(4)	43(3)
O(101)	1216(2)	8441(2)	8592(2)	30(1)	C(305)	1187(4)	8389(5)	13484(4)	56(3)
O(102)	2352(2)	8448(2)	8505(2)	30(1)	C(306)	428(4)	7937(4)	12879(6)	51(3)
O(201)	1941(2)	10854(2)	11162(2)	29(1)	C(307)	247(3)	7594(4)	11846(5)	44(3)
O(202)	3142(2)	11030(2)	11288(2)	34(2)	C(308)	831(3)	7684(3)	11387(4)	35(3)
O(301)	1734(2)	8940(2)	10655(2)	29(2)	C(309)	3062(3)	8727(4)	12257(3)	29(3)
O(302)	2862(2)	8915(2)	10542(2)	30(1)	C(310)	3463(3)	8226(4)	12397(4)	39(3)
O(401)	2323(2)	10572(2)	9116(2)	38(2)	C(311)	4220(4)	8793(6)	13132(5)	52(4)
O(402)	3425(2)	10449(2)	9215(2)	30(2)	C(312)	4563(3)	9812(6)	13695(4)	51(4)
N(P11)	726(2)	9918(3)	9265(3)	26(2)	C(313)	4161(3)	10303(4)	13560(4)	47(3)
N(P21)	4310(2)	10342(3)	10742(3)	25(2)	C(314)	3405(3)	9761(4)	12845(4)	36(3)
C(101)	1627(3)	8073(3)	8160(3)	26(2)	C(315)	2046(3)	7067(3)	10699(4)	31(3)
C(102)	1137(2)	7043(3)	7118(3)	27(2)	C(316)	1698(4)	6335(4)	10954(5)	59(3)
C(103)	1664(3)	6735(3)	6516(4)	31(2)	C(317)	1543(4)	5355(5)	10326(7)	77(4)
C(104)	1546(3)	6506(4)	5489(4)	42(3)	C(318)	1735(4)	5093(4)	9439(6)	72(4)
C(105)	1992(4)	6122(4)	4935(4)	57(3)	C(319)	2076(4)	5795(5)	9172(4)	58(3)
C(106)	2536(4)	5968(4)	5406(6)	59(3)	C(320)	2233(3)	6774(4)	9792(4)	42(3)
C(107)	2662(3)	6192(4)	6414(5)	52(3)	C(401)	2961(3)	10747(3)	8961(3)	29(2)
C(108)	2232(3)	6569(4)	6971(4)	41(3)	C(402)	3262(3)	11362(3)	8406(3)	29(2)
C(109)	567(3)	7203(4)	6486(3)	28(2)	C(403)	2746(3)	11836(4)	8239(4)	36(3)
C(110)	−223(3)	6548(3)	6034(4)	34(2)	C(404)	3070(3)	12819(4)	8454(4)	50(3)
C(111)	−718(3)	6731(4)	5473(4)	45(3)	C(405)	2577(5)	13181(5)	8183(5)	67(4)
C(112)	−435(4)	7553(5)	5349(4)	51(3)	C(406)	1788(5)	12580(6)	7719(5)	65(4)
C(113)	369(4)	8223(4)	5800(4)	50(3)	C(407)	1475(3)	11622(5)	7512(5)	58(4)
C(114)	849(3)	8035(4)	6356(4)	39(3)	C(408)	1939(3)	11228(4)	7745(4)	46(3)
C(115)	692(2)	6214(3)	7356(4)	27(2)	C(409)	4108(3)	12149(3)	9122(4)	32(3)
C(116)	491(3)	5227(4)	6663(4)	39(3)	C(410)	4759(3)	12129(4)	8843(4)	41(3)
C(117)	83(3)	4466(4)	6851(4)	47(3)	C(411)	5505(3)	12831(5)	9566(6)	56(4)
C(118)	−132(3)	4660(4)	7719(5)	47(3)	C(412)	5608(4)	13533(5)	10534(5)	61(3)
C(119)	53(3)	5627(5)	8411(4)	51(3)	C(413)	4967(4)	13550(5)	10818(4)	64(4)
C(120)	461(3)	6403(3)	8238(4)	41(3)	C(414)	4229(3)	12856(4)	10110(5)	51(3)
C(201)	2675(3)	11333(3)	11606(3)	28(3)	C(415)	3235(3)	10646(4)	7326(3)	28(3)
C(202)	2963(3)	12370(3)	12605(3)	27(2)	C(416)	3454(3)	11041(4)	6687(4)	45(3)
C(203)	3856(3)	13011(4)	12979(3)	30(2)	C(417)	3466(3)	10429(6)	5709(5)	57(4)
C(204)	4197(3)	14012(4)	13233(4)	41(3)	C(418)	3276(3)	9452(5)	5372(4)	47(3)
C(205)	5019(4)	14580(4)	13655(4)	49(3)	C(419)	3039(3)	9048(4)	5986(4)	43(3)
C(206)	5480(3)	14162(5)	13794(4)	52(3)	C(420)	3015(3)	9650(4)	6960(4)	34(3)
C(207)	5138(3)	13178(4)	13540(4)	47(3)	C(P11)	150(3)	9221(4)	8366(4)	39(3)
C(208)	4336(3)	12599(4)	13144(4)	41(3)	C(P12)	−382(3)	9427(4)	7929(4)	44(3)
C(209)	2526(3)	12863(3)	12284(4)	30(2)	C(P13)	−341(3)	10346(4)	8406(4)	42(3)
C(210)	2010(3)	13111(4)	12744(4)	45(3)	C(P14)	242(3)	11054(4)	9338(4)	45(3)
C(211)	1600(4)	13501(5)	12367(6)	63(4)	C(P15)	770(3)	10825(4)	9740(4)	37(3)
C(212)	1684(4)	13626(4)	11536(6)	63(4)	C(P21)	4568(3)	9957(4)	11236(4)	37(3)
C(213)	2198(4)	13366(4)	11064(4)	53(3)	C(P22)	5337(3)	10389(4)	11826(4)	44(3)
C(214)	2609(3)	12988(4)	11433(4)	39(3)	C(P23)	5867(3)	11251(4)	11911(4)	38(3)
C(215)	2769(3)	12208(4)	13501(3)	31(2)	C(P24)	5610(3)	11650(4)	11402(4)	44(3)
C(216)	3049(3)	13046(4)	14481(4)	55(3)	C(P25)	4822(3)	11190(4)	10830(4)	42(3)
C(217)	2894(4)	12958(5)	15317(4)	67(4)	C(BZ1)	4999(8)	3548(14)	7115(23)	130(9)
C(218)	2454(4)	12026(6)	15188(5)	60(4)	C(BZ2)	5105(14)	3182(10)	6199(17)	150(10)
C(219)	2172(3)	11183(4)	14225(5)	50(3)	C(BZ3)	5832(19)	3319(15)	6230(17)	150(13)
C(220)	2328(3)	11282(4)	13392(4)	34(3)	C(BZ4)	6368(9)	3788(16)	7090(26)	184(15)
C(301)	2263(3)	8718(3)	10828(3)	26(2)	C(BZ5)	6291(16)	4123(14)	8014(17)	211(13)
C(302)	2232(2)	8153(3)	11451(3)	25(2)	C(BZ6)	5561(18)	4013(12)	7955(12)	156(11)

a) B_{eq} equals one-third of the trace of the orthogonalized B_{ij} matrix.

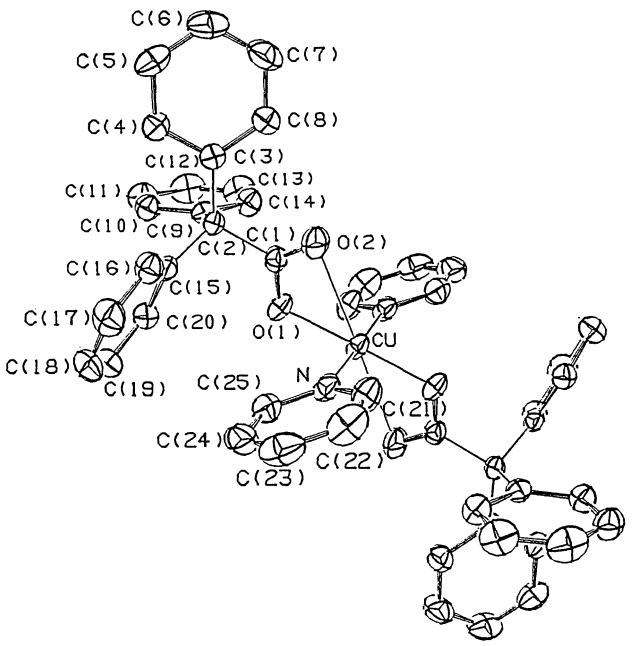

Fig. 2. View of the molecular structure of $Cu(O_2CCPh_3)_2 \cdot 2py$ (**3**). For clarity, the hydrogen atoms are omitted. Thermal ellipsoids are drawn to the 50% probability level.

Table 3. Positional Parameters ($\times 10^4$) and Equivalent Isotropic Thermal Parameters ($Å^2 \times 10$) and Their Standard Deviations for $Cu(O_2CCPh_3)_2 \cdot 2py$ (**3**)

Atom	x	y	z	B_{eq} [a]
Cu	0(0)	5000(0)	5000(0)	25(0)
O(1)	514(2)	6393(1)	5509(1)	28(0)
O(2)	−234(2)	5510(1)	6271(1)	44(1)
N	−2517(2)	5281(1)	4507(1)	29(1)
C(1)	266(2)	6319(2)	6102(1)	25(1)
C(2)	535(2)	7379(1)	6567(1)	20(1)
C(3)	527(2)	7220(2)	7348(1)	23(1)
C(4)	39(3)	8036(2)	7674(1)	29(1)
C(5)	132(3)	7930(2)	8400(1)	39(1)
C(6)	731(3)	7013(2)	8814(2)	43(1)
C(7)	1269(3)	6203(2)	8515(1)	43(1)
C(8)	1175(3)	6304(2)	7787(1)	33(1)
C(9)	2283(2)	7871(2)	6781(1)	22(1)
C(10)	2540(3)	8960(2)	6867(1)	29(1)
C(11)	4142(3)	9391(2)	7090(1)	38(1)
C(12)	5501(3)	8738(2)	7251(2)	43(1)
C(13)	5278(3)	7660(2)	7192(1)	40(1)
C(14)	3679(3)	7225(2)	6957(1)	30(1)
C(15)	−950(2)	8056(2)	5979(1)	23(1)
C(16)	−2549(3)	8010(2)	5943(1)	30(1)
C(17)	−3934(3)	8519(2)	5348(2)	42(1)
C(18)	−3762(3)	9073(2)	4788(2)	45(1)
C(19)	−2201(3)	9122(2)	4811(1)	39(1)
C(20)	−815(3)	8617(2)	5401(1)	29(1)
C(21)	−3574(3)	4479(2)	4434(1)	37(1)
C(22)	−5299(3)	4620(3)	4128(2)	47(1)
C(23)	−5982(3)	5594(3)	3874(2)	49(1)
C(24)	−4934(4)	6421(3)	3946(1)	47(1)
C(25)	−3196(3)	6242(2)	4269(1)	37(1)

a) B_{eq} equals one-third of the trace of the orthogonalized B_{ij} matrix.

atom: Cu(1), O(301), O(401), N(1) and Cu(2), O(102), O(202), N(2).[31] The O–Cu–X angles, where X is N or O, between coplanar atoms for Cu(1) and Cu(2) are 82°, 136°, 142° and 84°, 136°, 139° respectively. There are six O–Cu–X angles for each copper in the range 88—92° and one large O–Cu–O angle between 178—179°. The Cu–O bond distances for each copper vary over a considerable range, Cu(1) 1.90—2.46 Å and Cu(2) 1.88—2.35 Å.[32] The out-of-plane Cu–O bonds are very short, Cu(1) 1.90—1.91 Å and Cu(2) 1.88—1.90 Å respectively. One in-plane Cu–O bond to each copper is unusually long, 2.46 and 2.35 Å for Cu(1) and Cu(2) respectively. These Cu–O bonds are the longest that have been observed for a bridging carboxylato ligand in a dimeric copper(II) complex.[5] The Cu–N bonds are somewhat shorter than those previously observed for apical ligands in dimeric copper(II) carboxylates.

In **1**, where the ligands bonded to copper(II) do not assume a configuration which coincides with or is closely related to one of the usual five-coordinate geometries, square pyramidal or trigonal bipyramidal, one cannot readily decide by inspection whether to describe the arrangement of the ligands as distorted square pyramidal or distorted trigonal bipyramidal. Zemann[33] has described a test which allows one to make a rational choice between these two alternatives by considering the sum of the deviations of the angles between the ligands and the central metal atom in the complex from the angles in the idealized structures. Based on this test, the arrangement of the ligands in **1** is best described as distorted trigonal bipyramidal.

The cage structure of **1** is very unusual as a result of the ligand arrangement around each copper(II). The structure of the cage is depicted in Fig. 1a. The two distorted trigonal bipyramids formed by the ligands around each copper(II) are linked through the four bridging carboxylato ligands, spanning the apical and equatorial positions, to form a cage in which the dihedral angle between the equatorial planes is 88.8°. There are two adjacent short and long bridge distances in the cage: 6.48, 6.49, 6.78, and 6.86 Å. While the two short bridge distances are in the range reported for the complexes with copper(II) acetate monohydrate-type structures,[3,4] the distances of the other two bridges are the longest observed to date. The long bridge distances are primarily the result of the long Cu–O bonds, one to each copper(II). A considerable variation in the Cu–O–C angles is observed, 116—140°, with the two largest angles encompassing the long Cu–O bonds. However, there is no corresponding opening of the O–C–O angle; the mean value is 125°. As a result of the two long bridge distances, the Cu–Cu distance (3.086 Å) across the cage is much longer than that encountered in complexes where the four carboxylate bridges are of approximately the same length.[5]

The spatial relationships between the two pyridine rings which lie within the molecule, py(P11) and py(P21), and the corresponding two pyridine rings in

Table 4. Selected Bond Distances (Å) and Angles (deg) for $[Cu_2(O_2CCPh_3)_4(py)_2]\cdot C_6H_6$ (**1**)

		Distances	
Cu(1)–Cu(2)	3.086(1)	O(101)–C(101)	1.264(5)
Cu(1)–O(101)	1.907(3)	O(102)–C(101)	1.252(5)
Cu(1)–O(201)	1.905(3)	O(201)–C(201)	1.271(5)
Cu(1)–O(301)	2.049(3)	O(202)–C(201)	1.251(5)
Cu(1)–O(401)	2.458(3)	O(301)–C(301)	1.252(5)
Cu(1)–N(1)	2.053(4)	O(302)–C(301)	1.272(5)
Cu(2)–O(102)	2.065(3)	O(401)–C(401)	1.248(5)
Cu(2)–O(202)	2.349(3)	O(402)–C(401)	1.271(5)
Cu(2)–O(302)	1.903(3)	C(101)–C(102)	1.576(6)
Cu(2)–O(402)	1.883(3)	C(201)–C(202)	1.567(6)
Cu(2)–N(2)	2.062(4)	C(301)–C(302)	1.568(6)
		C(401)–C(402)	1.569(6)
		Angles	
O(101)–Cu(1)–O(201)	178.0(1)	Cu(1)–O(101)–C(101)	127.7(4)
O(101)–Cu(1)–O(301)	89.3(1)	Cu(1)–O(201)–C(201)	116.2(4)
O(101)–Cu(1)–O(401)	88.5(1)	Cu(1)–O(301)–C(301)	132.3(3)
O(101)–Cu(1)–N(1)	90.1(1)	Cu(1)–O(401)–C(401)	136.1(4)
O(201)–Cu(1)–O(301)	89.9(1)	Cu(2)–O(102)–C(101)	131.1(4)
O(201)–Cu(1)–O(401)	90.8(1)	Cu(2)–O(202)–C(201)	140.1(4)
O(201)–Cu(1)–N(1)	91.6(1)	Cu(2)–O(302)–C(301)	126.1(3)
O(301)–Cu(1)–O(401)	136.3(1)	Cu(2)–O(402)–C(401)	119.1(3)
O(301)–Cu(1)–N(1)	141.7(1)	O(101)–C(101)–O(102)	125.6(4)
O(401)–Cu(1)–N(1)	82.0(1)	O(101)–C(101)–C(102)	113.7(4)
O(102)–Cu(2)–O(202)	136.4(1)	O(102)–C(101)–C(102)	120.7(4)
O(102)–Cu(2)–O(302)	88.0(1)	O(201)–C(201)–O(202)	124.4(4)
O(102)–Cu(2)–O(402)	91.0(1)	O(201)–C(201)–C(202)	114.1(4)
O(102)–Cu(2)–N(2)	139.3(1)	O(202)–C(201)–C(202)	121.5(4)
O(202)–Cu(2)–O(302)	89.4(1)	O(301)–C(301)–O(302)	125.7(4)
O(202)–Cu(2)–O(402)	90.9(1)	O(301)–C(301)–C(302)	120.7(4)
O(202)–Cu(2)–N(2)	84.2(1)	O(302)–C(301)–C(302)	113.6(4)
O(302)–Cu(2)–O(402)	178.8(1)	O(401)–C(401)–O(402)	124.7(4)
O(302)–Cu(2)–N(2)	90.8(1)	O(401)–C(401)–C(402)	122.0(5)
O(402)–Cu(2)–N(2)	90.4(1)	O(402)–C(401)–C(402)	113.3(4)

Table 5. Selected Bond Distances (Å) and Angles (deg) for $Cu(O_2CCPh_3)_2\cdot 2py$ (**3**)

		Distances	
Cu–O(1)	1.964(1)	C(1)–C(2)	1.570(3)
Cu–O(2)	2.673(2)	C(2)–C(3)	1.545(3)
Cu–N	2.015(2)	C(2)–C(9)	1.543(3)
O(1)–C(1)	1.284(2)	C(2)–C(15)	1.540(3)
O(2)–C(1)	1.220(2)		
		Angles	
N–Cu–O(1)	91.51(6)	O(1)–C(1)–O(2)	123.2(2)
N–Cu–O(2)	80.99(6)	O(1)–C(1)–C(2)	114.7(2)
O(1)–Cu–O(2)	54.15(6)	O(2)–C(1)–C(2)	122.0(2)
Cu–O(1)–C(1)	107.2(1)		

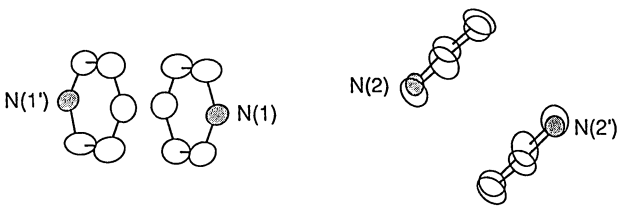

Fig. 3. View of the two intramolecular pyridine rings, py(P11) and py(P21), and the adjacent intermolecular pyridine rings, py(P11′) and py(P21′), along the *a* crystal axis of $[Cu_2(O_2CCPh_3)_4(py)_2]\cdot C_6H_6$ (**1**). N(1), (N1′), N(2), and N(2′) are in py(P11), py(P11′), py(P21), and py(P21′) respectively.

adjacent molecules, py(P11′) and py(P21′), along the *a* crystal axis, are shown in Fig. 3. The two intramolecular pyridine rings are tilted with respect to the Cu–Cu axes [Cu(2)–Cu(1)–N(1), 144.5°; Cu(1)–Cu(2)–N(2), 146.3°] toward the long Cu–O bonds, and the dihedral angles between the planes of the pyridine rings and the planes of the long bridging carboxyl groups are: py(P11)–carboxyl[O(401)C(401)O(402)], 81° and py(P21)–carboxyl[O(202)C(201)O(201)], 72°. The dihedral angle between the pyridine rings is 49.1°. The pyridine rings on adjacent molecules abut these rings resulting in parallel alignments (required by symmetry), as shown in Fig. 3. The intermolecular distances between the least-squares planes of the two intramolecular pyridine rings and the atoms of the adjacent rings are given in Table 6.

The conformations of the triphenylacetato ligands are of interest since intergroup repulsions could, in part, account for the unusual geometry around copper(II). The C–CO_2^- bond lengths (mean of 1.570 Å) are unusually long for an sp^3–sp^2 C–C bond. The triphenylmethyl groups C(101)–C(120) and C(301)–C(320) have left-

Table 6. Intermolecular Distances between the Least-Squares Planes of the Two Intramolecular Pyridine Rings, py(P11) and py(P21) and the Atoms of the Adjacent Pyridine Rings, py(P11′) and py(P21′), along the *a* Crystal Axis in $[Cu_2(O_2CCPh_3)_4(py)_2]\cdot C_6H_6$ (**1**)[a,b]

py(P11)–py(P11′)		py(P21)–py(P21′)	
Atom	Distance (Å)	Atom	Distance (Å)
N(1′)	3.418	N(2′)	3.471
C(P11′)	3.409	C(P21′)	3.471
C(P12′)	3.417	C(P22′)	3.478
C(P13′)	3.422	C(P23′)	3.476
C(P14′)	3.405	C(P24′)	3.466
C(P15′)	3.421	C(P25′)	3.483

a) The prime designates the adjacent pyridine ring. b) py(P11)–py(P21), dihedral angle, 49.1°.

handed twist propeller conformations while the twists for the groups C(201)–C(220) and C(401)–C(420) are right-handed. Jeffery et al.[34] has reported the simultaneous occurrence of two conformations in one molecule in bis(triphenylmethyl) sulfide. The angles between the phenyl rings exhibit a better threefold symmetry in the left-handed conformations than in the right-handed ones. All of the phenyl rings are coplanar with a maximum deviation of 0.142 Å. The torsion angles for defining these groups are given in Table 5S. The intramolecular distances between the ligands in **1** of < 3.7 Å are listed in Table 6S.

The benzene of crystallization is held in the crystal structure by van der Waals interactions and is lost when the crystal is allowed to stand in an open container. The ring shows considerable thermal motion.

The structure of the complex, $[Cu_2(O_2CCPh_3)_4(py)_2]$, can vary, depending on the method of preparation (see Experimental Section). The crystal structures of the two forms of $[Cu_2(O_2CCPh_3)_4(py)_2]$ (**2a**, **2b**) have not been determined; however, some conclusions concerning their molecular structures can be formulated based on their magnetic and spectral properties, vide infra. The molecular structures of **2a** and **1** must be closely related since both complexes give similar magnetic and spectral data; therefore, **2a** is assigned a distorted trigonal bipyramidal structure similar to that of **1**. The method of preparation of **2a** (Procedure 1 or 2) may result in small structural differences. The molecular structure of **2b** is more closely akin to the classical copper(II) acetate monohydrate-type structure. The magnetic and spectral data observed for **2b** are in agreement with this assignment.

The structure of $Cu(O_2CCPh_3)_2\cdot 2py$ (**3**), Fig. 2, is a variation of the *trans*-bis(acetato-*O,O′*)diamminecopper(II) type.[35] In this structure, the two triphenylacetato and two pyridine ligands are bonded to copper(II); the copper(II) lies at a center of symmetry. The coordination plane around copper(II) consists of two triphenylacetate oxygen atoms, O(1) and O′(1) and two nitrogen atoms N and N′ in a nearly square planar arrangement. The second carboxyl oxygens, O(2) and O(2′), are weakly bonded to copper(II) above and below the plane: the weak Cu–O bond distance is 2.673 Å, the O(1)–Cu–O(2) angle is 54.1°, and the N–Cu–O(2) angle is 81.0°. The dihedral angle between the coordination plane around copper(II) and the plane of the carboxyl group is 78.0°. The coordination geometry around copper(II) is best described as distorted octahedral.

In the triphenylacetato ligands, the carboxyl O(1)–C(1)–O(2) angle is 123.2°. The C–O bond lengths are significantly different: C(1)–O(1), 1.284 Å and C(1)–O(2), 1.220 Å, which suggests that the shorter C–O bond has considerably more double-bond character. The dihedral angle between the plane of the pyridine ring and carboxyl group is 80.6°. As in **1**, the $C-CO_2^-$ bond length (1.570 Å) is unusually long for an sp^3–sp^2 C–C bond. The triphenylmethyl group has a non-propeller conformation and a pseudo bisector plane passing through the atoms, C(1), C(2), C(15), and C(18).

The molecules of **3** are packed only by van der Waals forces. A stereoscopic ORTEP packing diagram is included in the supplementary material (Fig. 1S) along with the following tables: least-squared planes (Table 10S), torsion angles (Table 11S), and intramolecular nonbonded distances <3.26 Å (Table 12S).

Magnetic Susceptibility. The magnetic susceptibility data of the dimeric complexes **1**, **2a**, and **2b** were correlated using Eq. 1 (see Fig. 4). The best-fit parame-

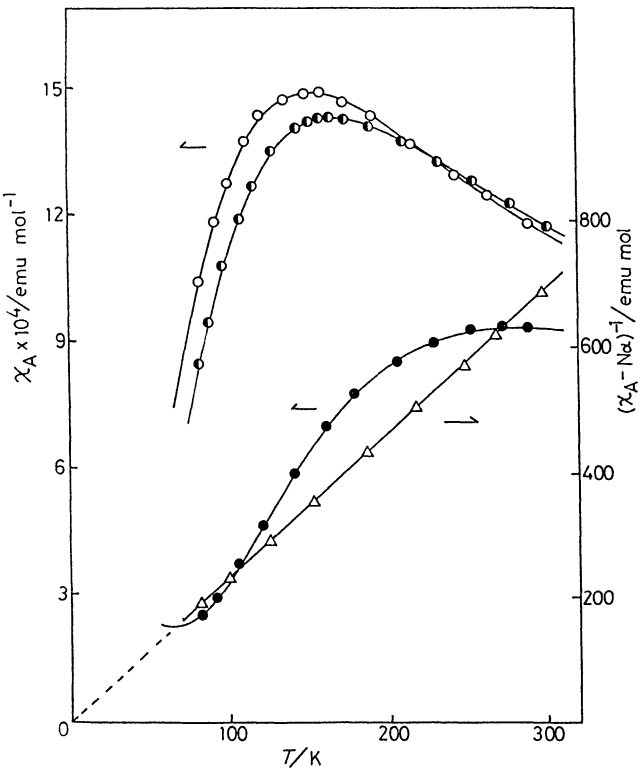

Fig. 4. Variation of the magnetic susceptibilities of the complexes with temperature: $[Cu_2(O_2CCPh_3)_4(py)_2]\cdot C_6H_6$ (**1**) (◐); $[Cu_2(O_2CCPh_3)_4(py)_2]$ (**2a**) (○), (**2b**) (●); $Cu(O_2CCPh_3)_2\cdot 2py$ (**3**) (△).

ters are given in Table 7 along with the discrepancy index (Eq. 2). The $-2J$ values of complexes **1** and **2a** are considerably smaller than the values reported for a large number of copper(II) carboxylates with a square pyramidal metal geometry, ca. 300 cm^{-1}.[5] The anomalously small $-2J$ values observed for these dimeric complexes are undoubtedly related to the novel geometry around copper, distorted trigonal bipyramidal. The small singlet-triplet separation in these complexes may be interpreted in terms of their unusual cage structure. In a bridged structure similar to that observed for **1**, in which each copper has a distorted trigonal bipyramidal metal geometry, the two ends of a Cu–O–C–O–Cu exchange pathway would connect with different metal d orbitals: one end with the $d_{x^2-y^2}$, d_{xy} orbitals having paired electrons and the other with the d_{z^2} orbital having an unpaired electron.[36]. The copper(II) carboxylates with a square pyramidal metal geometry are known to have $-2J$ values of ca. 300 cm^{-1}, as observed for copper(II) acetate monohydrate, while theoretically, those with a regular trigonal bipyramidal metal geometry should have $-2J$ values close to zero (ferromagnetic). Thus, complexes **1** and **2a**, which have intermediate $-2J$ values, are expected to have a metal geometry in between a regular square pyramidal and a regular trigonal bipyramidal arrangement. The $-2J$ value determined for **2b** is consistent with a structure for this complex, which is closely related to the classical copper(II) acetate monohydrate type.

The magnetic behavior of **3** is consistent with the monomeric structure determined in the present study (see Figs. 2 and 4, Table 7).

Electron Spin Resonance. The X-band ESR spectra of polycrystalline samples of the $Cu(O_2CCPh_3)_2 \cdot n$py complexes have been recorded. The ESR data for these complexes at ambient temperature are given in Table 8.

Table 7. Magnetic Parameters for the $Cu(O_2CCPh_3)_2 \cdot n$ py Complexes, Faraday Method

Complex	$-2J/cm^{-1}$	$\overline{g}$	$P\times10^2$	$\sigma_{dis}\times10^3$
1	187	2.20	1.04	3.17
2a[a]	173	2.14	2.56	2.00
2b	321	2.29	2.10	5.51
3	—	2.15	—	4.53

a) Prepared by Procedure 2.

Table 8. ESR Parameters for Polycrystalline $Cu(O_2CCPh_3)_2 \cdot n$ py Complexes[a]

Complex	$g_{\parallel}$	$g_{\perp}$	$\overline{g}$	D/cm^{-1}
1[b]	2.26	2.06	2.13	0.198
2a[c,d]	2.25	2.06	2.13	0.201
2b[e]	2.38	2.07	2.18	0.366
3[f]	2.28	2.06	2.14	

a) Ambient temperature. b) H_{dq}=2777 G and H_m=3150 G at 9.06 GHz. c) Prepared by Procedure 1. d) H_{dq}=2910 G at 9.34 GHz. e) H_m=3300 G at 9.46 GHz; $A_{\parallel}$=0.0070 cm^{-1}. f) $A_{\parallel}$=0.0175 cm^{-1}.

The X-band ESR spectrum of **1** is different from the spectra reported for dimeric copper(II) carboxylates in which the metal geometry is square pyramidal. The difference arises as a result of the small zero-field splitting, D, in **1** which is less than the microwave energy ($h\nu$); whereas, $D>h\nu$ for dimeric copper(II) carboxylates with approximately square pyramidal geometry. The ESR spectrum of **1** at ambient temperature (9.05 GHz) is shown in Fig. 5. The spectrum consists of two $H_{\parallel}$ lines (927, 4790 G) and two $H_{\perp}$ lines (1780, 4050 G) as well as a line resulting from a double quantum transition (2780 G) and a weak line from a monomeric impurity (3150 G). The number and positions of the lines are consistent with theoretical calculations for randomly oriented molecules in the triplet state.[37] The isotropic double quantum absorption is observed when $1/2\ h\nu<D<h\nu$.[38] The ESR spectrum of **1** at 133 K is essentially the same as at ambient temperature, except for the relative intensities of the monomer and dimer lines. Since our initial report,[8] two other copper(II) carboxylates have been observed to have similar ESR spectra.[10,13]

The small zero-field splitting parameter (D) undoubtedly is the result of the novel geometry of **1**. This parameter consists of a dipolar term (D_{dip}) which is a function of the Cu–Cu distance, and a pseudo-dipolar term (D_{ex}) which results from an exchange coupling via the orbitals of the cage.[38,39] For **1**, the smaller D parameter can be related to the geometry of the cage in which the long Cu–Cu distance and the two very long bridging distances are contributing factors.

The ESR spectrum of **2a** at ambient temperature is similar to the spectrum of **1** with nearly identical ESR parameters. The spectral similarity between **1** and **2a** suggests that removing the benzene of crystallization from **1** has little effect on the dimer structure. These

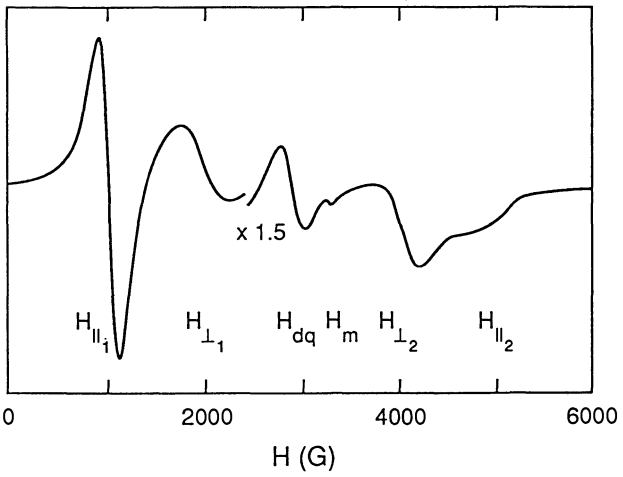

Fig. 5. The ESR spectrum (X-band, 9.05 GHz) of polycrystalline $[Cu_2(O_2CCPh_3)_4(py)_2] \cdot C_6H_6$ (**1**) at ambient temperature.

data suggest that the crystal structures of **1** and **2a** are similar, except for the benzene of crystallization.

The ESR spectrum of **2b** at 130 K shows three absorption lines which are typical of a dimeric copper(II) carboxylate when $D>h\nu$[3,4] and a line attributed to a monomer impurity. The hyperfine splitting of the low-field absorption line yields a seven-line pattern. The spectrum at ambient temperature is essentially the same, except that the hyperfine structure is not as well resolved. These data, along with the magnetic susceptibility data, suggest that the structure of **2b** is more closely aligned with the copper(II) acetate monohydrate-type structure than **1** and **2a**.

The ESR spectra of **3** at 133 K and ambient temperatures are quite typical of a monomeric copper(II) complex with a distorted octahedral geometry, showing two spectral lines resulting from the parallel and perpendicular alignments of the complex with the field;[40] the hyperfine coupling splits the low-field absorption, yielding a four-line pattern, of which only three are resolved.

Electronic Spectra. The reflectance spectra of the four copper(II) triphenylacetate-pyridine complexes are shown in Fig. 6, and the spectral data are reported in Table 9.

The most striking difference in the spectral features of the three dimeric complexes (**1**, **2a**, and **2b**) is the separation of the two peaks in the d–d band region. The peak separations in **1** and **2a**, which have a distorted trigonal bipyramidal metal geometry, are about 2000 cm^{-1}, while this separation in **2b** is 5000 cm^{-1}, a value observed for copper(II) carboxylates with the common square pyramidal geometry.[10,13] Thus, the electronic spectral data augments the proposal that complex **2b** has a structure which is closely aligned with the classical copper(II) acetate monohydrate type.

Another salient feature of the electronic spectra of the dimeric complexes **1**, **2a**, and **2b** is that the d–d band energies are about the same, **1** and **2a** having only slightly higher band energies, in spite of the structural differences. This same type of behavior has been reported for the copper(II) trichloroacetate adducts.[10–13] The d–d band energy of copper(II) complexes with trigonal bipyramidal metal geometry is reported to be lower than the band energy of the corresponding complexes with square pyramidal metal geometry.[36] The anomalously high d–d band energy observed for complexes **1** and **2a** may be ascribed to the short Cu–O bonds in the axial coordination sites which raise the energy of the d_{z^2} orbital.

The d–d band of **3**, ca. 17×10^3 cm^{-1}, occurs at higher energy than that observed for **1**, **2a**, and **2b** (ca. 13×10^3 cm^{-1}), indicating that the ligand field in complex **3** is stronger than in the latter complexes. This shift to higher energy of the d–d band of **3** undoubtedly reflects the difference in the number of coordinating atoms and the metal geometry, distorted octahedral.[41]

The so-called "dimer band" is observed as a shoulder in the near-ultraviolet region for complexes **1**, **2a**, and **2b**. This band has been reported for a large number of dimeric copper(II) carboxylates and other dimeric copper(II) systems.[42–44] The spectrum of the monomeric complex **3** does not show an absorption band in this region.

Infrared Spectra. The carbon–oxygen stretching frequencies of the copper(II) triphenylacetate–pyridine complexes are given in Table 10. The splitting of the RCO_2^- stretching frequencies, $\Delta\bar{\nu}=\bar{\nu}_{asym}-\bar{\nu}_{sym}$, is related to the symmetry of the carboxylato group: the greater the deviation from C_{2v} symmetry, the larger the $\Delta\bar{\nu}$

Table 9. Reflectance Spectral Data for the $Cu(O_2CCPh_3)_2\cdot n$ py Complexes

Complex	$\bar{\nu}_{max}\times10^{-3}/cm^{-1}$		$\Delta\bar{\nu}\times10^{-3}/cm^{-1}$
1	13.68	11.75	1.93
2a[a]	13.51	11.49	2.02
2b	13.53	8.53	5.00
3	17.48	15.38	2.10

a) Prepared by Procedure 2.

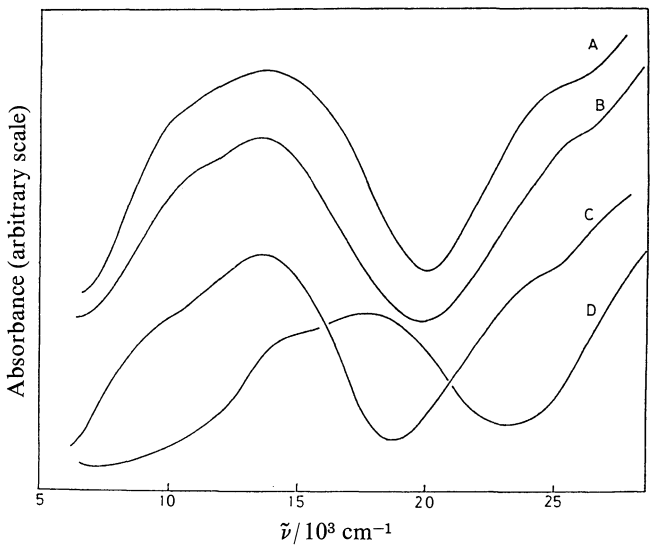

Fig. 6. Reflectance spectra of the complexes: $[Cu_2(O_2CCPh_3)_4(py)_2]\cdot C_6H_6$ (**1**) (A); $[Cu_2(O_2CCPh_3)_4(py)_2]$ (**2a**) (B); (**2b**) (C); $Cu(O_2CCPh_3)_2\cdot 2py$ (**3**) (D).

Table 10. Carbon–Oxygen Stretchig Frequecies of the Triphenylacetato Ligand for the $Cu(O_2CCPh_3)_2\cdot n$ py Complexes[a,b]

Complex	$\bar{\nu}_{asym}/cm^{-1}$	$\bar{\nu}_{sym}/cm^{-1}$	$\Delta\bar{\nu}/cm^{-1}$
1	1639	1369	270
2a[c]	1638	1367	271
2b	1627	1371	256
3	1613	1320	293

a) KBr disk. b) The following stretching frequencies were obtained for the conjugate acid form of the ligand, Ph_3CCO_2H: (C=O) 1696, (C–O) 1271; Ph_3CCO_2D: (C=O) 1692, (C–O) 1300 cm^{-1}. c) Prepared by Procedure 1.

values.[45–47] The order observed for $\Delta\bar{\nu}$ for the copper(II) triphenylacetate-pyridine complexes is **3**>**1**, **2a**>**2b**. This is the order expected from symmetry considerations for the carboxylato ligands in these complexes based on the structural, magnetic, and spectral properties given above. The C–O bond distance data (Tables 4 and 5) for complexes **1** and **3** show that there is a greater difference in the C–O bond lengths in the carboxylato ligands in **3** than in **1**. In complex **2b**, which is proposed to have a structure more closely aligned with the copper(II) acetate monohydrate type than **1**, the bridging carboxylato groups are expected to be more symmetrical than in **1**, where there is a considerable variation in the C–O bond lengths in each bridging group.

Discussion of Structures. The first reports of dimeric copper(II) carboxylates with a distorted trigonal bipyramidal geometry around copper are for $[Cu_2(O_2CCPh_3)_4(py)_2]\cdot C_6H_6$ (**1**)[7,8] and $[Cu_2(O_2CCCl_3)_4(L)_2]$, where L=tempo and proxyl.[11,12] The main structural differences between **1** and the above-mentioned trichloroacetate complexes are: in **1**, the carboxylato bridging distances are longer and the equatorial angles show larger deviations from the ideal trigonal bipyramidal geometry. Thus, in **1**, there is considerably more distortion of the geometry around copper. Recently, preliminary reports of additional dimeric complexes with distorted trigonal bipyramidal metal geometry have appeared: $[Cu_2(O_2CCPh_3)_4(\gamma\text{-picoline})_2]\cdot$2toluene,[9] $[Cu_2(O_2CCPh_3)_4(\gamma\text{-picoline})_2]\cdot$2benzene,[9] $[Cu_2(O_2CCCl_3)_4(caffeine)_2]$,[14,16] $[Cu_2(O_2CCCl_3)_4(2,5\text{-}Cl_2\text{-py})_2]\cdot$benzene,[16] $[Cu_2(O_2CCCl_3)_4(3,5\text{-}Cl_2\text{-py})_2]\cdot$toluene.[16]

The structural transformation of **1** from the usual square pyramidal arrangement of ligands around copper(II), as observed in the classical copper(II) acetate-type structure, to a distorted trigonal bipyramidal arrangement, can best be explained in terms of steric effects in the crystal environment which can arise from both inter- and intramolecular forces. The crystal-structure data for **1** suggest that crystal-packing forces play an important role in this transformation. Along the *a* crystal axis, the pyridine rings at the opposite ends of the molecule form a dihedral angle of 49.1°. The pyridine rings on adjacent molecules abut these rings resulting in a parallel alignment (cf. Fig. 3 and Table 6). The intermolecular distances between the pyridine rings and the atoms of the adjacent rings are ca. 3.41 Å for py(P11)–py(P11′) and 3.47 Å for py(P21)–py(P21′) respectively. These distances approach the value reported by Pauling[48] for the effective thickness of an aromatic ring, 3.4 Å. Cu(1) which shows the largest distortion from a square pyramidal structure, N(1)–Cu(1)–O(401), 82.0°; Cu(2)–Cu(1)–N(1), 144.50°; Cu(1)–O(401), 2.458 Å, is bonded to the py(P11) with the smallest intermolecular distance, while Cu(2) which is bonded to py(P21) shows less distortion, N(2)–Cu(2)–O(202), 84.2°; Cu(1)–Cu(2)–N(2), 146.3°; Cu(2)–O(202), 2.349 Å. These data indicate that crystal packing forces are an important factor in determining the geometry around copper(II).

The complex, $[Cu_2(O_2CCPh_3)_4(py)_2]$, exists in two crystalline modifications which exhibit different magnetic and spectral properties. Form **2a** was prepared by allowing **1** to lose the benzene of crystallization upon standing in an open container (Procedure 1) or by crystallizing the complex from a chloroform solution (Procedure 2). The magnetic and spectral properties of **2a** are nearly identical to those of **1**, suggesting that the crystal structures are similar with or without the benzene of crystallization. Form **2b** was prepared by crystallization of $[Cu_2(O_2CCPh_3)_4(py)_2]$ from an ethanol solution. The magnetic and spectral properties of **2b** are similar to those of the copper(II) carboxylates which have the classical copper(II) acetate-type structure.[5] While the crystal structure of **2b** has not been determined, the structure is certainly more closely related to complexes with a square pyramidal metal geometry than **1** and **2a**.

Further evidence which supports the above conclusion, that crystal packing forces play an important role in determining the geometry around copper(II) in **1** and **2a**, is provided by magnetic-moment data (see Table 11). Crystalline **1** and powder **2a** have the same magnetic moments at 308 K, 1.68 μ_B, both of which have similar magnetic properties that are consistent with a distorted trigonal bipyramidal structure around each copper(II) in which there is one very long Cu–O bond (2.3—2.5 Å), vide supra. The magnetic moments of these complexes in benzene solution at the same temperature are 1.56 μ_B and 1.53 μ_B, respectively. This decrease in the magnetic moments towards the value obtained for crystalline **2b** (1.51 μ_B), for which magnetic measurements are consistent with a cage structure more closely aligned with the copper(II) acetate type, suggests that on dissolution in benzene the forces which cause the molecular distortion are diminished.

The question arises as to what is structurally different

Table 11. Comparison of the Magnetic Properties of $Cu(O_2CCPh_3)_2\cdot n$ py Complexes at 308 K

Complex	$\chi_A\times10^6$ / emu mol^{-1}	μ_{eff} / μ_B	Form
1	1150[a,b]	1.68	Cryst
	1047[c]	1.56	Soln, C_6H_6
2a[d]	1150[a,b]	1.68	Powder
	1011[c]	1.53	Soln, C_6H_6
2b	930[a,b]	1.51	Cryst
3	1390[b,e]	1.85	Cryst

a) Corrected for constituent atom diamagnetism and temperature independent paramagnetism, 60×10^{-6} emu mol^{-1} of Cu(II). b) Calculated from variable temperature data, Faraday method. c) Evans method; not corrected for paramagnetic impurities. d) Prepared by Procedure 1. e) Corrected for temperature independent paramagnetism of Cu(II).

about the bridging triphenylacetato ligand which leads to the structural transformation. The triphenylacetato ligand is bulkier than other carboxylato ligands in complexes $[Cu_2(O_2CR)_4(py)_2]$ of known structure.[5] An examination of a model of **1** based on crystal-structure data, reveals that there is an area of space around each of the pyridine rings which is void of atoms. Thus, more efficient crystal packing can be obtained if the pyridine rings are angled away from the apical positions to make room for the pyridine rings on adjacent dimer units.

At the same time, the intramolecular forces between the bulky bridging triphenylacetato ligands may also have some effect on the structure. Steric repulsions between the bridging ligands could be reduced by staggering two adjacent triphenylacetato ligands with respect to the horizontal plane in D_{4h} symmetry. The out-of-plane ligands, i.e., the ligands which form the long bridges (which have right-handed conformations of the phenyl groups) show the largest deviations from threefold symmetry. These observations suggest that intramolecular steric forces could be responsible for some of the staggering of the ligands, as well as for the larger deviations from threefold symmetry. Porter et al.[12] have suggested that intramolecular steric crowding is responsible for determining the copper coordination geometry in the copper(II) trichloroacetate complexes. However, intramolecular steric crowding cannot be the major factor which controls the geometry of the dimeric copper(II) triphenylacetate–pyridine complexes, since all indications are that the structure of complex **2b** is closely akin to the classical copper(II) acetate monohydrate type.

Recently, crystal structures have been reported for the complexes, $[Cu_2(O_2CMPh_3)_4(L)_2]$ (where M=Si, L=α-picoline; M=Ge, L=quinoline), both of which have carboxylato ligands with three α-phenyl groups.[49] It is interesting to note that these complexes, while maintaining the square pyramidal metal geometry, show considerably more variation in the Cu–O bond distances than observed for complexes in which the carboxylato ligand has fewer than three α-phenyl groups. On inspection, their structures show a slight distortion of the type observed for **1**, resulting in one slightly longer Cu–O bonds to each copper in the adjacent bridging groups. One would expect less distortion by intramolecular forces in silicon and germanium complexes than in **1** as a result of the longer C–M distances in the carboxylato ligands.

The 1:2 dark blue crystalline complex, $Cu(O_2CCPh_3)_2 \cdot 2py$ (**3**), is formed from **1** by placing the blue-green crystals of **1** in an ethanol–pyridine solution and allowing the reaction to proceed for several days. The interesting aspect of this conversion is that it appears to occur in the solid phase. After one day, mixed crystals are obtained which contain both blue-green and dark-blue areas.[50] Apparently, pyridine molecules are able to diffuse into the crystal, perhaps replacing the benzene of crystallization, where the reaction occurs. Crystal-packing maps of **1** indicate that there is considerable space between molecular units. It is interesting to note that the volume of the unit cell for **3** is about one-half the volume of **1** with the *a* unit-cell distance in **3** being about one-half the *b* distance in **1**, while the other unit cell distances are comparable.

The structure of $Cu(O_2CCPh_3)_2 \cdot 2py$ (**3**) is a variation of the *trans*-bis(acetato-*O,O'*)diamminecopper(II) type.[35] Several other structures of this type, $Cu(O_2CR)_2 \cdot 2L$, where L is a nitrogeneous base, have been reported.[51–54] In comparing **3** with these structures, one observes that the Cu–O(2) distance (2.673 Å) is the shortest and the N–Cu–O(2) angle (81.0°) is the smallest so far reported. Also, the N–Cu–O(1) angle (91.5°) is greater than 90°, indicating a small deviation from a square planar arrangement of the atoms around copper in the coordination plane. In the other complexes of this type, the angles corresponding to the N–Cu–O(2) angle are close to 90° except for $Cu(O_2CCH_3)_2$-(imidazole)$_2$ (86°) where intermolecular hydrogen bonding occurs between imidazole and O(2).[12] These data indicate that in **3** the steric effects resulting from the bulky triphenylmethyl groups cause a twisting of the carboxyl groups relative to the coordination plane around copper.[55] The dihedral angle between the carboxyl ligand and the coordination plane is 78.0°.

Davey and Stephens[56] have reported the crystal structure for $Cu(O_2CCHCl_2)_2(\alpha\text{-picoline})_2$. In this complex, the *cis* conformation of the α-picoline ligands results in an asymmetric arrangement of the chelating dichloroacetato ligands. The geometry around copper(II) is distorted from a square planar arrangement, the angles formed by the out-of-plane Cu–O bonds with the plane are different, and the out-of-plane Cu–O distances vary.

In conclusion, the geometry of the coordination sphere around copper in monomeric and dimeric copper(II) carboxylates can vary considerably, depending on the size and shape of the ligands. Crystal packing forces and intramolecular repulsion forces are responsible for these structural changes. The flexibility of the coordination sphere around copper(II) has been noted.[12,36,40] Thus, one would expect to find other variations from the classical copper(II) acetate monohydrate-type and the *trans*-bis(acetato-*O,O'*)diamminecopper(II)-type structures as the spatial relationships both within and between the molecules are changed.

We greatfully acknowledge the contributions of Professor Y. Saito and Dr. S. Ohba, Keio University, for their fruitful discussions and suggestions in the preparation of this paper. We also wish to thank Professor D. W. Pratt, University of Pittsburgh, for the use of his ESR facilities, Drs. I. B. Goldberg and T. M. McKinney, Rockwell International, for running the ESR spectra of **2b**, and Professor J. W. Whittaker, Carnegie-Mellon University, for running an ESR spec-

trum of **2a**. The authors also wish to acknowledge Dr. C. E. Taylor's (formerly of our group) contribution in determining the magnetic moments by the Evans method.

References

1) Presented in part at the 23rd International Conference on Coordination Chemistry, Boulder, CO, July 29—Aug. 3 1984.

2) D. H. Hendrickson, "Magneto-Structural Correlations in Exchange Coupled Systems," ed by R. D. Willett, D. Gatteschi, and O. Kahn, D. Reidel Publishing Co., Dordrecht (1985), pp. 523—554.

3) J. Catterick and P. Thornton, *Adv. Inorg. Chem. Radiochem.*, **45**, 291 (1977).

4) R. J. Doedens, *Prog. Inorg. Chem.*, **21**, 209 (1976).

5) M. Melnik, *Coord. Chem. Rev.*, **42**, 259 (1982).

6) R. C. Mehrotra and R. Bohra, "Metal Carboxylates," Academic Press, London (1983), pp. 286—295.

7) Chang, C.-H. Ph. D. Thesis, University of Pittsburgh, Pittsburgh, PA, 1982; *Diss. Abstr. B,* **43**, 1467B, (1982).

8) O. W. Steward, M. Kato, S.-C. Chang, M. Sax, C.-H. Chang, T. Taura, C. F. Jury, Y. Muto, T. Tokii, J. F. Pletcher, and C. S. Yoo, 23rd International Conference on Coordination Chemistry, Boulder, CO, July 29—Aug. 3 1984, Abstr., p. 247.

9) M. Yamanaka, S. Ohba, Y. Saito, O. W. Steward, M. Kato, T. Tokii, Y. Muto, and I. Suzuki, 39th Symposium on Coordination Chemistry, Mito, Japan, Sept. 26—28 1989, Abstr., 1BP02.

10) M. Kato and Y. Muto, *Coord. Chem. Rev.*, **92**, 45 (1988).

11) L. C. Porter, M. H. Dickman, and R. J. Doedens, *Inorg. Chem.*, **22**, 1962 (1983).

12) L. C. Porter, M. H. Dickman, and R. J. Doedens, *Inorg. Chem.*, **25**, 678 (1986).

13) Y. Muto, M. Nakashima, T. Tokii, M. Kato, and I. Suzuki, *Bull. Chem. Soc. Jpn.*, **60**, 2849 (1987).

14) H. Uekusa, S. Ohba, Y. Saito, O. W. Steward, M. Kato, T. Tokii, and Y. Muto, 39th Symposium on Coordination Chemistry, Mito, Japan, Sept. 26—28 1989, Abstr., 1BP01.

15) H. Horie, S. Husebye, M. Kato, E. A. Meyers, Y. Muto, I. Suzuki, T. Tokii, and R. A. Zingaro, *Acta Chem. Scand. A,* **40**, 579 (1986).

16) H. Uekusa, S. Ohba, Y. Saito, T. Tokii, Y. Muto, M. Kato, S. Husebye, and O. W. Steward, 28th International Conference on Coordination Chemistry, Gera, GDR, Aug. 3—18 1990, Abstr., 6—33.

17) O. W. Steward, R. C. McAfee, S.-C. Chang, S. R. Piskor, W. J. Schreiber, C. F. Jury, C. E. Taylor, J. F. Pletcher, and C.-S. Chen, *Inorg. Chem.*, **25**, 771 (1986).

18) The benzene of crystallization is easily lost from the crystals; therefore, the analysis can vary depending on how the crystals are dried.

19) W. H. Zachariasen, *Acta Crystallogr.*, **16**, 1139 (1963).

20) P. Main, S. E. Hall, L. Lessinger, G. Germain, J. P. Declercq, and M. M. Woolfson, "MULTAM 78, A System of Computer Programs for the Automatic Solutions of Crystal Structures from X-Ray Diffraction Data," University of York, England (1987).

21) W. Furey, Jr., B. C. Wang, and M. Sax, *J. Appl. Crystallogr.*, **15**, 160 (1982).

22) R. Shiono, Tech. Rep. No. 48, Crystallography Department, University of Pittsburgh, Pittsburgh, PA.

23) a) "International Tables for X-Ray Crystallography," Kynoch Press, Birmingham (1974), Vol. III. b) R. F. Stewart, E. R. Davidson, and W. T. Simpson, *J. Chem. Phys.*, **42**, 3175 (1965).

24) Tables of observed and calculated structure factors, positional parameters for the hydrogen atoms, anisotropic thermal parameters, bond distances and angles, least-squares planes, torsion angles, nonbonding intramolecular distances for **1** and **3** along with a stereoscopic ORTEP packing diagram of **3** are deposited as Document No. 8963 at the Office of the Editor of Bull. Chem. Soc. Jpn.

25) R. A. Lalancette, M. Cefola, W. C. Hamilton, and S. J. LaPlaca, *Inorg. Chem.*, **6**, 2127 (1967).

26) Recorded on a Bruker model ER-300 ESR spectrometer.

27) Recorded on a Bruker model 220D ESR spectrometer with a 031 microprocessor field controller equipped with an Eldorado model 989 frequency counter. Temperature was controlled via a modified Varian TE "Dual" cavity equipped with a Varian Dewer insert and a model V-4540 temperature controller.

28) P. W. Selwood, "Magnetochemistry," Interscience, New York (1956), pp. 78, 91.

29) E. K. Hyde, G. Gordon, and G. F. J. Kokoszka, *Inorg. Nucl. Chem.*, **30**, 2155 (1968).

30) T. Nakagawa (University of Tokyo) and Y. Oyanagi (University of Tsukuba), SALS (model D).

31) Data for the least-squares planes are listed in Table 4S. The average estimated standard deviation of the atoms from the planes is 0.003 Å.

32) This range is much larger than is reported for complexes with the copper(II) acetate monohydrate-type structure, Ref. 5.

33) J. Zemann, *Z. Anorg. Allg. Chem.*, **324**, 241 (1963).

34) G. A. Jeffery and A. Robbins, *Acta Crystallogr., Sect. B,* **36**, 1820 (1980).

35) Yu. A. Simonov, A. V. Ablov, and T. I. Malinovski, *Kristallografiya,* **8**, 270 (1963).

36) N. Ray, L. Hulett, R. Sheahan, and B. Hathaway, *Inorg. Nucl. Chem. Lett.*, **14**, 305 (1978).

37) E. Wasserman, L. C. Snyder, and W. A. Yager, *J. Chem. Phys.*, **41**, 1763 (1964).

38) T. D. Smith and J. R. Pilbrow, *Coord. Chem. Rev.*, **13**, 173 (1974).

39) H. J. Price, J. R. Pilbrow, K. S. Murray, and T. D. Smith, *J. Chem. Soc. A,* **1970**, 968.

40) B. J. Hathaway and D. E. Billing, *Coord. Chem. Rev.*, **5**, 143 (1970).

41) A. B. P. Lever, "Inorganic Electronic Spectroscopy," 2nd ed, Elsevier, Amsterdam (1984), pp. 554—572.

42) R. W. Jotham, S. F. A. Kettle, and J. A. Marks, *J. Chem. Soc., Dalton Trans.*, **1972**, 428.

43) S. R. Desjardins, D. E. Wilcox, R. L. Musselman, and E. I. Solomon, *Inorg. Chem.*, **26**, 288 (1987).

44) P. K. Ross, M. D. Allendorf, and E. I. Solomon, *J. Am. Chem. Soc.*, **111**, 4009 (1989).

45) K. Nakamoto, "Infrared and Raman Spectra of Inorganic and Coordination Compounds," 4th ed, Interscience, New York (1986), pp. 231—233.

46) R. C. Mehrotra and R. Bohra, "Metal Carboxylates," Academic Press, London (1983), pp. 48—60.

47) S. Emori, K. Ohishi, H. Kurihara, and Y. Muto, *Bull. Chem. Soc. Jpn.*, **61**, 4439 (1988).
48) L. Pauling, "The Nature of the Chemical Bond," 3rd ed, Cornell University Press, Ithaca (1960), p. 262.
49) H. Uekusa, S. Ohba, Y. Saito, M. Kato, O. W. Steward, T. Tokii, and Y. Muto, *Acta Crystallogr., Sect. C,* **46**, 1805 (1990).
50) The first crystal on which diffraction data were collected to determine the structure of **3** turned out to be a mixed crystal.
51) G. Davey and F. S. Stephens, *J. Chem. Soc. A,* **1971**, 1917.
52) H. A. Henriksson, *Acta Crystallogr. Sect. B,* **33**, 1947 (1977).
53) N. E. Heimer and L. Y. Ahmed, *Inorg. Chem. Acta,* **64**, L65, (1982).
54) A. Busnot, F. Busont, A. Laclaire, and M. Bernard, *Z. Anorg. Allg. Chem.*, **503**, 207 (1983).
55) The intramolecular distances between the ligands in **3** of <3.8 Å are given in Table 10S.
56) G. Davey and F. S. Stephens, *J. Chem. Soc. A,* **1971**, 2578.

 © 1991 The Chemical Society of Japan Bull. Chem. Soc. Jpn., 64, 3059—3062 (1991)

Chromium(VI) Complexation with Triisooctylamine in Organic Solvents

Yaou-Huei HUANG, Chuh-Yung CHEN, and Jen-Feng KUO*
Department of Chemical Engineering, National Cheng Kung University, Tainan, Taiwan 70107, R.O.C.
(Received November 26, 1990)

Liquid–liquid extraction of chromium(VI) from chromic acid solutions with triisooctylamine (tris(6-methylheptyl)amine, abbrev. to TIOA) dissolving in various organic solutions has been studied. The reaction between chromium(VI) and TIOA in *o*-xylene has been discussed in detail. It has been found that dichromate ion and hydrogen chromate ion coexist in the system, based on the extraction data and the IR and UV-visible spectra of the TIOA-chromium salt. The chromium extraction equilibria can be expressed as:

$$\overline{\text{TIOA}} + \text{H}^+ + \text{HCrO}_4^- \rightleftarrows \overline{(\text{TIOAH})\text{HCrO}_4}$$

$$2\overline{\text{TIOA}} + 2\text{H}^+ + \text{Cr}_2\text{O}_7^{2-} \rightleftarrows \overline{(\text{TIOAH})_2\text{Cr}_2\text{O}_7}$$

The extraction constants are obtained.

It is well-known that chromate and dichromate ions can be extracted using TBP or an amine as an extractant. Many workers used tertiary amines to extract chromium(VI) from various acid solutions.[1–16] The extraction mechanism proposed by them is confusing. for example, Fedorov et al.[11] reported that trioctylamine extracts chromium(VI) as CrO_4^{2-} from H_2SO_4 solutions. Depula[12] reported that trioctylamine extracts chromium(VI) as $Cr_2O_7^{2-}$ from H_3PO_4 solutions and it probably involves $HCr_2O_7^-$ from $HClO_4$ and concentrated HNO_3 solutions in addition to $Cr_2O_7^{2-}$. Recently Takahashi et al.[16] used 3-(4-pyridyl)-1,5-dipheylpentane (a tertiary amine) to extract chromium(VI) from sulfuric acid solutions. They reported that $HCrO_4^-$ was extracted into organic phase. Henkel corporation[9] indicated that tertiary amines may extract chromium(VI) by solvating:

$$2\overline{\text{R}_3\text{N}} + 2\text{H}^+ + \text{Cr}_2\text{O}_7^{2-} \rightleftarrows \overline{(\text{R}_3\text{NH})_2\text{Cr}_2\text{O}_7},$$

or by ion exchange:

$$\overline{(\text{R}_3\text{NH})_2\text{X}} + 2\text{H}^+ + \text{Cr}_2\text{O}_7^{2-} \rightleftarrows \overline{(\text{R}_3\text{NH})_2\text{Cr}_2\text{O}_7},$$

$X=SO_4^{2-}$ or $2Cl^-$.

In order to realize the behavior of chromium(VI) extracted by amines from various acid solutions, it is necessary to extract chromium(VI) from chromic acid at first. In the study, it was decided to identify amine–chromium(VI) species and determine extraction constants for triisooctylamine–chromic acid extraction system.

Experimental

Reagents: 1.92×10^{-2} M (M=mol dm^{-3}) stock solutions (1000 ppm chromium) were prepared by dissolving 1.923 g of chromium trioxide (99.0%) in distilled deionized water and diluting to volume in a 1 dm^3 standard flask. Appropriate amouuts of TIOA (98%) were diluted with organic solvents (E.P. grade) to obtain the desired TIOA concentrations.

Procedure: Both aguecus and organic phases were vigorously mixed in a 50 cm^3 dark centrifugal tube more than six minutes at 24±1 °C. After centrifuging, the tube was settled in a water bath at 25±0.1 °C for more than three hours. The pH value of the aqueous phase was measured by a PHM 85 precision pH meter (Radiometer & Copehagen Co.). Chromium concentrations in the aqueous phase were determined using an IL-551 type atomic absorption spectrophotometeter (Instrumentation Laboratory Inc.). The concentration of chromium in the organic phase was calculated from the difference in chromium content in the aqueous phase before and after extraction multiplied by the phase A/O ratio (volume ratio of aqueous and organic phases). The free TIOA concentration was calculated by the subtraction of chromium concentration in the organic phase from initial TIOA concentration used.

Results and Discussion

Extraction Equilibrium of Chromium(VI): Figure 1 shows the log–log plots of $[\overline{\text{Cr}}]$ vs. $[\overline{\text{TIOA}}](\text{H}^+)(\text{HCrO}_4^-)$ in *o*-xylene. The initial chromium concentration is varied from 2.5×10^{-4} M to 4.0×10^{-2} M. The

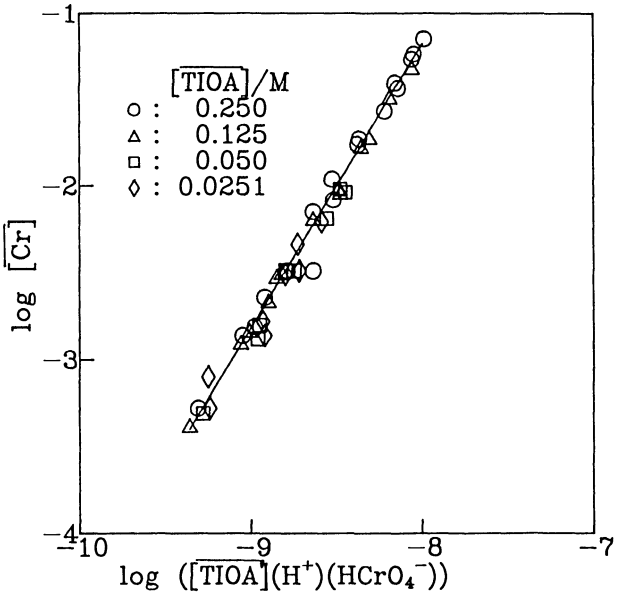

Fig. 1. Plots of $\log[\overline{\text{Cr}}]$ vs. $\log([\overline{\text{TIOA}}](\text{H}^+)(\text{HCrO}_4^-))$ for TIOA in *o*-xylene.

bar overhead in the equations denotes organic phase. It is seen from Fig. 1 that a straight line of the slope 1.6 was obtained. The result indicates that the extraction mechanism can not be described just using a single species either $HCrO_4^-$ or $Cr_2O_7^{2-}$. It is plausible that both $HCrO_4^-$ and $Cr_2O_7^{2-}$ were extracted by TIOA into the organic phase. An extraction model for the equilibria with the two components is proposed. The model involves dissociation and association of Cr(VI) species (Eqs. 1—5) in the aqueous phase, and chromium(VI) extraction equilibria (Eqs. 6 and 7) by TIOA. The values of the dissociation constants of chromic acid in Eqs. 1—5 were obtained by Neuss and Rieman,[22] Davis and Prue,[21] Takahashi et al.,[16] Hala et al.,[8] and Deptula.[2]

$$H_2Cr_2O_7 \rightleftarrows H^+ + HCr_2O_7^-, \quad (1)$$

$$K_1 = (H^+)(HCr_2O_7^-)/(H_2Cr_2O_7), \quad K_1 = 1\times10^6$$

$$HCr_2O_7^- \rightleftarrows H^+ + Cr_2O_7^{2-}, \quad (2)$$

$$K_2 = (H^+)(Cr_2O_7^{2-})/(HCr_2O_7^{2-}), \quad K_2 = 0.85$$

$$H_2CrO_4 \rightleftarrows H^+ + HCrO_4^-, \quad (3)$$

$$K_3 = (H^+)(HCrO_4^-)/(H_2CrO_4), \quad K_3 = 1.21$$

$$HCrO_4^- \rightleftarrows H^+ + CrO_4^{2-}, \quad (4)$$

$$K_4 = (H^+)(CrO_4^{2-})/(HCrO_4^-), \quad K_4 = 3.2\times10^{-7}$$

$$2HCrO_4^- \rightleftarrows Cr_2O_7^{2-} + H_2O, \quad (5)$$

$$K_5 = (Cr_2O_7^{2-})/(HCrO_4^-)^2, \quad K_5 = 98$$

$$2\overline{TIOA} + 2H^+ + Cr_2O_7^{2-} \rightleftarrows \overline{(TIOAH)_2Cr_2O_7}, \quad (6)$$

$$K_6 = [\overline{(TIOAH)_2Cr_2O_7}]/[\overline{TIOA}]^2(H^+)^2(Cr_2O_7^{2-}),$$

$$\overline{TIOA} + H^+ + HCrO_4^- \rightleftarrows \overline{(TIOAH)HCrO_4}, \quad (7)$$

$$K_7 = [\overline{(TIOAH)HCrO_4}]/[\overline{TIOA}](H^+)(HCrO_4^-).$$

The symbols [ ] and ( ) represent the molar concentration and molar activity, respectively. The activity coefficient in the organic phase is assumed to be unity for convenience. Combining the constant of Eq. 5 with that of Eq. 6 gives:

$$K_8 = [\overline{(TIOAH)_2Cr_2O_7}]/[\overline{TIOA}]^2(H^+)^2(HCrO_4^-)^2. \quad (8)$$

The total concentration of chromium in the organic phase can be expressed as:

$$[\overline{Cr}] = [\overline{(TIOAH)HCrO_4}] + 2[\overline{(TIOAH)_2Cr_2O_7}]. \quad (9)$$

Substituting Eqs. 7 and 8 into Eq. 9 and rearranging gives:

$$[\overline{Cr}]/\{[\overline{TIOA}](H^+)(HCrO_4^-)\} = K_7 + 2K_8[\overline{TIOA}](H^+)(HCrO_4^-). \quad (10)$$

Equation 10 indicates that the plot of $[\overline{Cr}]/\{[\overline{TIOA}](H^+)(HCrO_4^-)\}$ vs. $[\overline{TIOA}](H^+)(HCrO_4^-)$ will give a linear line. The slope of it is $2K_8$ and the intercept is K_7.

Figure 2 shows the plots of $[\overline{Cr}]/\{[\overline{TIOA}](H^+)(HCrO_4^-)\}$ vs. $\{[\overline{TIOA}](H^+)(HCrO_4^-)\}$. The activity coefficient of chromium in the aqueous phase was calculated by Guntelberg expression.[19] The total activity of chromium in aqueous phase ($(Cr)_{aq,total}$) is as follows:

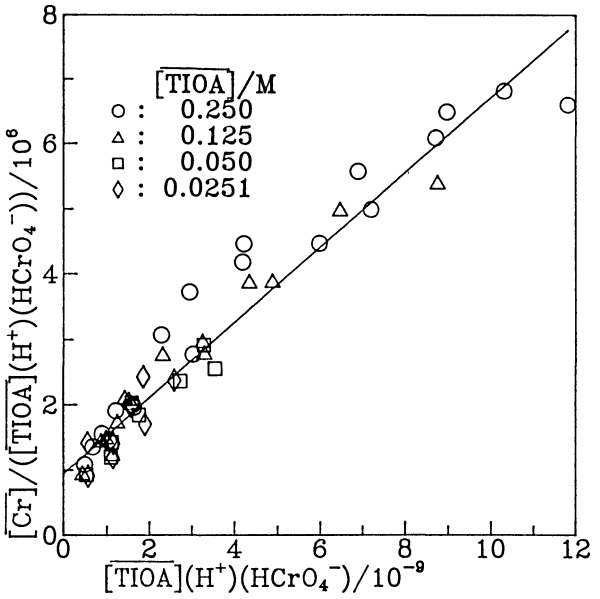

Fig. 2. Plots of $[\overline{Cr}]/([\overline{TIOA}](H^+)(HCrO_4^-))$ vs. $[\overline{TIOA}](H^+)(HCrO_4^-)$ for TIOA in *o*-xylene.

$$(Cr)_{aq,total} = 2(H_2Cr_2O_7) + 2(HCr_2O_7^-) + 2(Cr_2O_7^{2-}) + (H_2CrO_4) + (HCrO_4^-) + (CrO_4^{2-}). \quad (11)$$

Then, from Eqs. 1—5, $(Cr)_{aq,total}$ can be expressed in terms of $(HCrO_4^-)$ as well as the appropriate equilibrium constants involved.

$$\begin{aligned}(Cr)_{aq,total} &= 2\{(H^+)^2/K_1K_2 + (H^+)/K_2 + 1\}(Cr_2O_7^{2-}) \\ &\quad + \{(H^+)/K_3 + 1 + K_4/(H^+)\}(HCrO_4^-) \\ &= \{2K_5/K_1K_2\}\{(H^+)^2 + K_1(H^+) + K_1K_2\}(HCrO_4^-)^2 \\ &\quad + \{1/K_3(H^+)\}\{(H^+)^2 + K_3(H^+) + K_3K_4\}(HCrO_4^-). \quad (12)\end{aligned}$$

The activity of $HCrO_4^-$ in the aqueous phase was calculated from Eq. 12. As shown in Fig. 2, a linear line confirms the extraction model suggested. The values of $\log K_7 = 6.01$ and $\log K_8 = 14.5$ were obtained in *o*-xylene, and those in other solvents are shown in Table 1.

Table 1. Extraction Constants of Triisooctylamine-Chromium System in Various Organic Diluents

Diluent	$\log K_7$[a]	$\log K_8$[b]	ε[c]	δ[d]
Chloroform	7.73	17.1	4.90	9.3
Benzene	6.62	15.6	2.28	9.15
Toluene	6.49	14.7	2.24	8.9
o-Xylene	6.01	14.5	2.56	9.0
Carbon tetrachloride	5.62	13.7	2.21	8.6
Hexadecane	5.35	12.9	2.10	—
Hexane	4.59	12.7	1.89	7.3

a) $K_7 = [\overline{(TIOAH)HCrO_4}]/[\overline{TIOA}](H^+)(HCrO_4^-)$. b) $K_8 = [\overline{(TIOAH)_2Cr_2O_7}]/[\overline{TIOA}]^2(H^+)^2(HCrO_4^-)^2$. c) From Ref. 23. d) From Ref. 24.

Using these two equilibrium values, we can obtain the concentrations of $(TIOAH)HCrO_4$ and $(TIOAH)_2Cr_2O_7$ in the organic phase. The molar ratio of $(TIOAH)HCrO_4$ to $(TIOAH)_2Cr_2O_7$ in the organic phase can be expressed as:

$$[\overline{(TIOAH)HCrO_4}]/[\overline{(TIOAH)_2Cr_2O_7}] = K_7/\{K_8[\overline{TIOA}](H^+)(HCrO_4^-)\}, \quad (13)$$

which indicates that increasing value of $[\overline{TIOA}](H^+)(HCrO_4^-)$ will increase the molar fraction of $(TIOAH)_2Cr_2O_7$ in the organic phase.

IR and UV-visible Absorption Spectra Studies: It has been reported that the UV absorption spectra of $HCrO_4^-$ and $Cr_2O_7^{2-}$ anions show the maximum at 350 and 370 nm, respectively.[8,17] Figure 3 shows absorption spectra of TIOA-chromium salt solutions in *o*-xylene. As shown in Fig. 3, the absorption maxima of solutions 1 to 4 appear at 352.0, 353.5, 364.5, and 366.0 nm, respectively, suggesting the presence of $HCrO_4^-$ ion in solutions 1 and 2, and $Cr_2O_7^{2-}$ ion in solutions 3 and 4 as main species. Indeed, the values of $[\overline{TIOA}](H^+)(HCrO_4^-)$ in solutions 1 to 4 are estimated as $10^{-9.52}$, $10^{-9.25}$, $10^{-8.16}$ to $10^{-7.93}$, respectively, and by substituting these values into Eq. 13, we obtained the molar ratios of $(TIOAH)HCrO_4$ to $(TIOAH)_2Cr_2O_7$ to be 10.7, 5.6, 0.46, and 0.27, respectively. Consequently, the coexistence of both $HCrO_4^-$ and $Cr_2O_7^{2-}$ in the organic phase may be concluded.

The vibration spectrum of the dichromate ion had been studied. According to Stammreich et al.,[18] a weak symmetric stretching Cr–O–Cr vibration appears at 567 cm^{-1} and antisymmetric Cr–O–Cr vibrations appears at 762 cm^{-1} (strong) and 795 cm^{-1} (weak). Figure 4 shows the IR spectrum for solution 4 in Fig. 3. For comparison, the IR spectrum of pure TIOA was also shown in Fig. 4. The peaks appearing at 562, 762, and 800 cm^{-1} make sure that $(TIOAH)_2Cr_2O_7$ exits in the organic phase.

Solvent Effect: The extraction of chromium by TIOA was examined in various diluents, toluene, benzene, chloroform, carbon tetrachloride, hexane, and hexadecane. For the former four extraction systems, linear lines are obtained in the plots of $[\overline{Cr}]/$

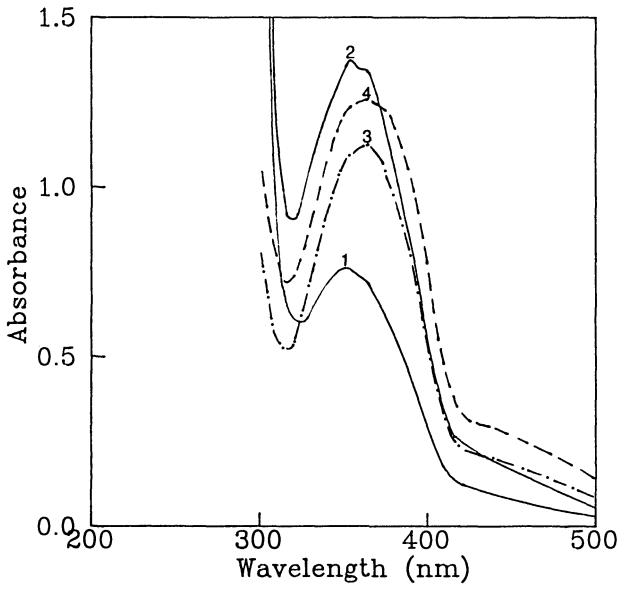

Fig. 3. UV/vis absorption spectra of Cr(VI) in the organic phase.
1 and 2: $[Cr]_i$=0.00192 M; [TIOA]=0.025 M; V_A/V_O=0.25 and 0.5 respectively.
3 and 4: $[Cr]_i$=0.0192 M; [TIOA]=0.25 M; V_A/V_O=2 and 4, respectively.

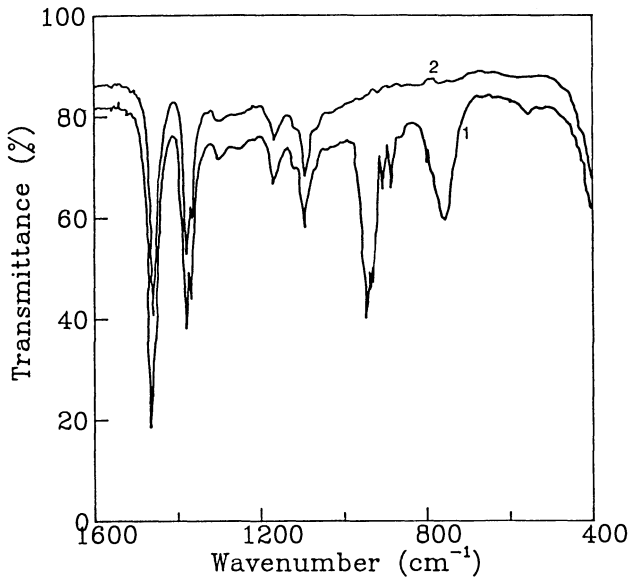

Fig. 4. IR absorption spectra of Cr(VI) in the organic phase.
Curve 1: TIOA-chromate salt. Curve 2: pure TIOA.

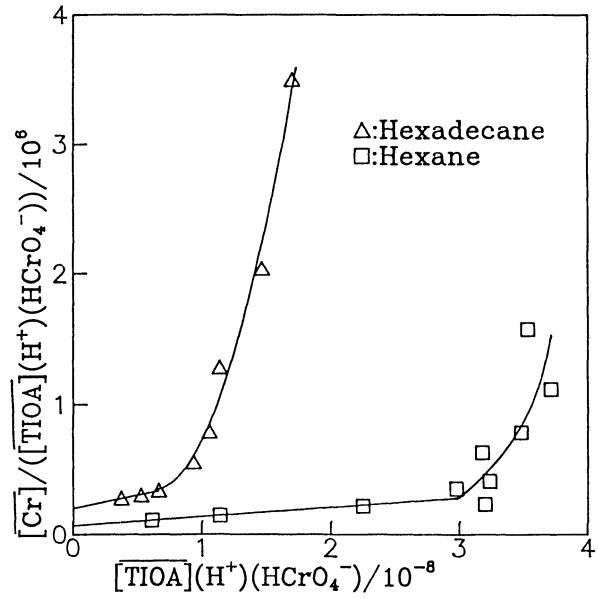

Fig. 5. Plots of $[\overline{Cr}]/([\overline{TIOA}](H^+)(HCrO_4^-))$ vs. $[\overline{TIOA}](H^+)(HCrO_4^-)$ for 0.25 M TIOA in hexane and hexadecane.

$\{[\overline{TIOA}](H^+)(HCrO_4^-)\}$ vs. $\{[\overline{TIOA}](H^+)(HCrO_4^-)\}$. However, for the latter two diluents, as shown in Fig. 5, the linear line only suits for a limited range. Beyond the linear range the slope of the lines tremendously increases. The phenomenon may be attributed to the aggregation of TIOA–chromium salt in the high chromium concentration in the organic phase. The aggregation may be caused from the low dielectric constant or low solubility parameter of hexane and hexadecane. The values of log K_7 and log K_8 for the reaction between chromium(VI) and TIOA in the diluents studied are shown in Table 1. Diamond[20] used trilaurylamine to extract HBr from aqueous phase. He found that in general, the higher the dielectric constant of the organic solvent, the better the extraction. For comparison, the dielectric constants of the solvents are also shown in Table 1. It is seen that except for the *o*-xylene system, the values of K_7 and K_8 obtained decrease with the decrease of the dielectric constant of the solvent, i.e.: chloroform>benzene>toluene>carbon tetrachloride> hexadecane>hexane. This tendency is in good agreement with that indicated by Diamond.[20] In this work, we also attempt to correlate extraction constant with the solubility parameter of solvent. As shown in the last column of Table 1, obviously a similar result as the dielectric constant was obtained.

References

1) J. P. Cuer, W. Stuckens, and N. Texier, *Proc. Int. Solvent Extr. Conf.*, **2**, 1185 (1974).
2) C. Deptula, *J. Inorg. Nucl. Chem.*, **30**, 1309 (1968).
3) E. L. Smith and J. E. Page, *J. Soc. Chem. Ind. (London)*, **67**, 48 (1948).
4) F. L. Moore, *Anal. Chem.*, **29**, 1660 (1957).
5) F. L. Moore, *Anal. Chem.*, **30**, 908 (1958).
6) W. J. Maeck et al., *Anal. Chem.*, **33**, 1775 (1961).
7) W. J. Maeck, Maxine E. Kussy, and James E. Rein, *Anal. Chem.*, **34**, 1602 (1962).
8) J. O. Hala, O. Navratil, and V. Nechuta, *J. Inorg. Nucl. Chem.*, **28**, 553 (1966).
9) Henkel Corporation (General Mills Inc.), "Chromium," Technical Bulletin S1-6 (1961).
10) I. A. Shevchuk and T. N. Simonova, *Anal. Abstr.*, **13**, 141 (1966).
11) I. A. Fedorov and Yu. F. Zhdanov, *Zh. Neorg. Khim.*, **13**, 2227 (1968).
12) C. Deptula, *Rocz. Chem.*, **41**, 3 (1967).
13) I. A. Tserkovnitskaya, G. I. Il'inskaya, and V, P. Belyaev, *Anal. Abstr.*, **20**, 1605 (1971).
14) Jiri Adam and Rudolf Pribil, *Talanta,* **18**, 91 (1971).
15) M. Verhaehe, J. Sinnesael, and A. Van Peteghem, *Bull. Soc. Chim. Belg.*, **93**, 1107 (1984).
16) K. Takahashi, K. Hirayama, and H. Hakeuchi, *Solvent Extr. Ion Exch.*, **5**, 393 (1987).
17) C. W. Davies and J. E. Prue, *Trans. Faraday Soc.*, **51**, 1045 (1955).
18) H. Stammreich, D. Bassi, O. Sala, and H. Siebert, *Spectrochim. Acta,* **13**, 192 (1958).
19) E. Z. Guntelberg, *Phys. Chem.*, **123**, 199 (1926).
20) R. M. Diamond, Solvent Extraction Chemistry, Proceedings of the International Conference on Solvent Extraction Chemistry, Goteborg, Amsterdam, North Holland 1967, Abstr., p. 349.
21) W. G. Davis and J. E. Prue, *Trans. Faraday Soc.*, **51**, 1045 (1955).
22) J. D. Neuss and W. Rieman, *J. Am. Chem. Soc.*, **56**, 2238 (1934).
23) T. Sekine and Y. Hasegawa, *Solvent Extr. Chem.*, **1977**, 48.
24) W. Smueek and S. Siekierski, *J. Inorg. Nucl. Chem.*, **24**, 1651 (1962).

 © 1991 The Chemical Society of Japan Bull. Chem. Soc. Jpn., 64, 3063—3066 (1991)

Extraction-Spectrophotometric Determination of Osmium Using 4-(2-Pyridylazo)resorcinol

Shayessteh DADFARNIA and Mojtaba SHAMSIPUR*
Department of Chemistry, Shiraz University, Shiraz, Iran
(Received January 5, 1991)

An extraction-spectrophotometric method for the determination of trace amounts of osmium(VIII) is described. Osmium is quantitatively extracted from aqueous solutions at pH 3.0—3.5 into a 10:1 chloroform–methyl isobutyl ketone mixture with tetrabutylammonium bromide, followed by spectrophotometric determination, using 4-(2-pyridylazo)resorcinol as a metallochromic indicator. The orange-red mixed complex of osmium absorbs light at λ_{max}=530 nm with a molar absorptivity of 2.5×10^4 $dm^3\,mol^{-1}\,cm^{-1}$. Beer's law is obeyed over the range 0.5—18 $\mu g\,cm^{-3}$. The method has a wide range and is sensitive and free from interferences from many anions and cations, including some platinum metals.

Because of the increasing use of osmium oxides as popular oxidizing agents in organic chemistry, and as effective catalysts for a wide variety of chemical reactions,[1–5] the separation and determination of osmium in trace levels are of special interest. Thiocyanate,[6,7] Bismuthiol II,[8] 9,10-phenanthrenequinone monoxime,[9] 1-(2-pyridylazo)-2-phenanthrol(II),[10] and 7-amino-1-hydroxynaphthalene-3,6-disulfonic acid[11] are among the spectrophotometric reagents used for the extraction and determination of osmium. However, there are some difficulties associated with the presence of interfering ions, especially platinum metals, which cannot be eliminated uisng the direct methods. On the other hand, although the catalytic methods seem to be more sensitive than extraction-spectrophotometric procedures, there is a need for rigid control of temperature, acidity, reagent, impurities, etc.[12,13]

4-(2-Pyridylazo)resorcinol (PAR) has also been used for the determination of osmium, but it suffers from the poor selectivity for osmium over the several commonly associated interfering ions.[14] In this paper we report a sensitive method for the selective extraction of Os(VIII) with tetrabutylammonium bromide (TBAB) from acidic aqueous solutions into a 10:1 chloroform–methyl isobutyl ketone mixture, which is followed by spectrophotometric determination of osmium in organic phase using PAR as a chromogenic indicator.

Experimental

Reagents. All of the chemicals used were of the highest purity available and were used without further purification.

Tetrabutylammonium bromide (TBAB, Merck) solution, 1.5% w/v. Prepared with triply distilled water.

Organic Phase. Prepared by mixing appropriate amounts of methyl isobutyl ketone (MIBK, Merck) and chloroform (Merck) to form a 1 to 10 v/v mixture.

Osmium Stock Solution. A 1 g sealed ampul of osmium tetraoxide (Fluka) dissolved in about 100 cm^3 of 0.20 M (1 M=1 $mol\,dm^{-3}$) sodium hydroxide solution and then diluted to 1 dm^3 with triply distilled water.[15] The solution was then standardized by the Klobbie's method[16] as follows: 15 cm^3 of 6 M sulfuric acid and 2 g of potassium iodide were added to 25 cm^3 of the solution and the liberated iodine was titrated against a 0.250 normal solution of sodium thiosulfate. The end-point was determined using starch paper externally as indicator. Working solutions were prepared by suitable dilution of the stock solution.

4-(2-Pyridylazo)resorcinol (PAR, Merck) solution, 0.1% w/v. Prepared with absolute methanol (Merck).

Potassium chloride (Merck) solution, 3.5 M. Prepared with triply distilled water.

Apparatus. All spectra were obtained with a Beckman DK-2A ratio recording spectrophotometer and the absorbance measurements were made with a Perkin–Elmer 35 spectrophotometer. The pH values were determined with a Corning 125 pH meter using a combined electrode.

Procedure. An aliquot of the sample solution containing 5—180 μg of Os(VIII) was placed in a 10-cm^3 flask. One cm^3 of 1.5% TBAB and 3 cm^3 of 3.5 M KCl solution were added and pH was adjusted between 3.0 and 3.5 with dilute HCl. The solution was diluted to the mark with triply distilled water. Next, the solution was transferred into a 60-cm^3 separatory funnel, 10 cm^3 of 1:10 MIBK–chloroform solvent was added and the mixture was shaken vigorously for 10 min. The phases were allowed to separate and the organic layer was collected in a 25-cm^3 flask. To ensure the complete extraction of osmium, the aqueous layer was treated with another 5-cm^3 protion of fresh organic solvent. To the combined organic extracts 1 cm^3 of 0.1% PAR solution and 3 cm^3 of methanol were added and the mixture was diluted to the mark with chloroform. For complete color development, the solution was heated in a thermostated water-bath at 50 °C for 2 h. The absorbance of the orange-red solution was measured at 530 nm against a reagent blank.

Results and Discussion

Absorption Spectra. The absorption spectra of the mixed complex of osmium with PAR and blank reagent are shown in Fig. 1. As it is seen, the orange-red complex shows a maximum at 530 nm with a molar absorptivity of 2.5×10^4 $dm^3\,mol^{-1}\,cm^{-1}$, whereas the reagent blank shows a negligible absorbance at this wavelength.

Effect of pH. The extraction of Os(VIII) with TBAB was carried out over the pH range 0.8—12.6 and the results are given in Fig. 2. It is seen that the extraction is quantitative at pH range of about 1—4, the percent of

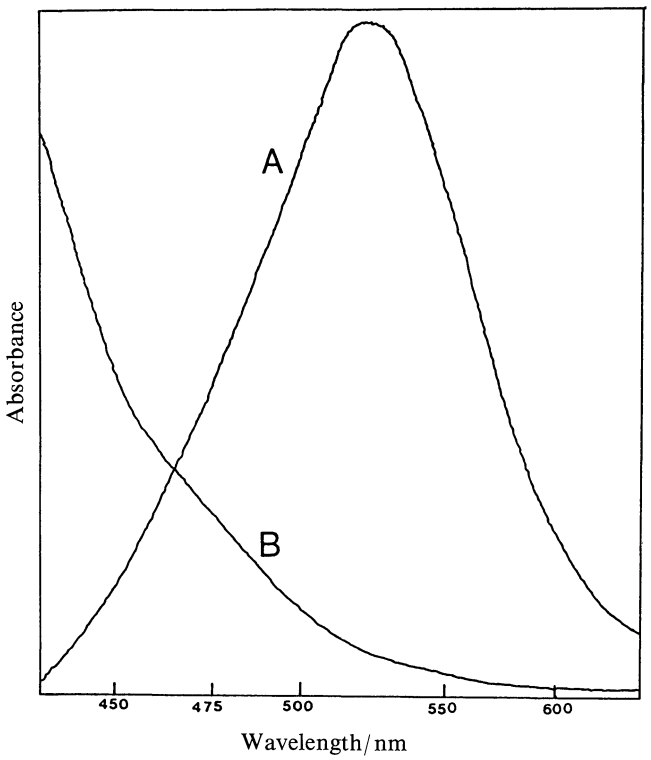

Fig. 1. Absorption spectra of the mixed complex of Os(VIII) with PAR (A) and the reagent blank (B) in organic phase.

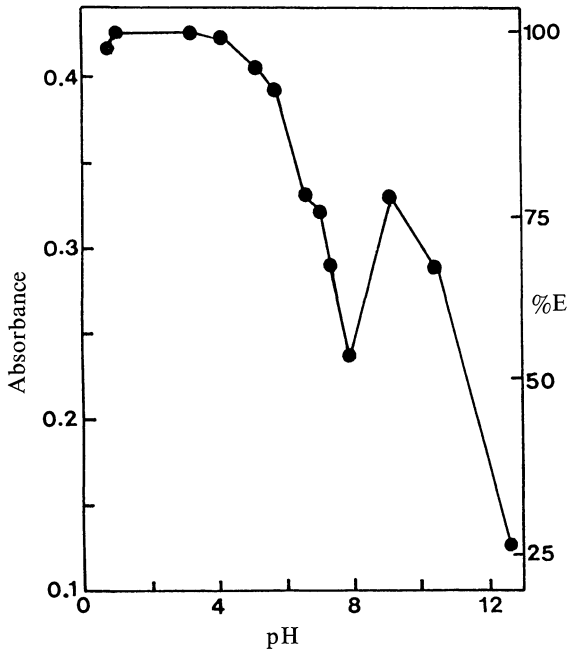

Fig. 2. Effect of pH on the extraction of Os(VIII). Conditions: Os, 10.24 μg cm^{-3}; TBAB, 3 cm^3 of 0.5% in H_2O; PAR, 1 cm^3 of 0.1% in CH_3OH; λ_{max}, 530 nm; color, orange-red.

extraction (%E) decreases drastically by an increase in pH from 4 to 12.6.

Effect of TBAB Concentration. The influence of the

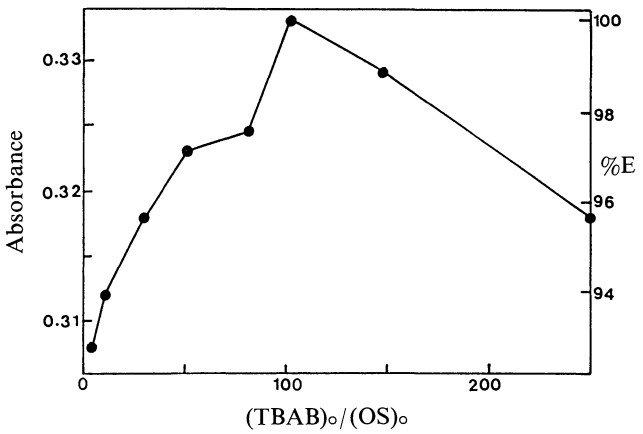

Fig. 3. Effect of TBAB concentration on the extraction of Os(VIII). Conditions: Os, 8.0 μg cm^{-3}; PAR, 1 cm^3 of 0.1% in CH_3OH; pH, 3.2; λ_{max}, 530 nm.

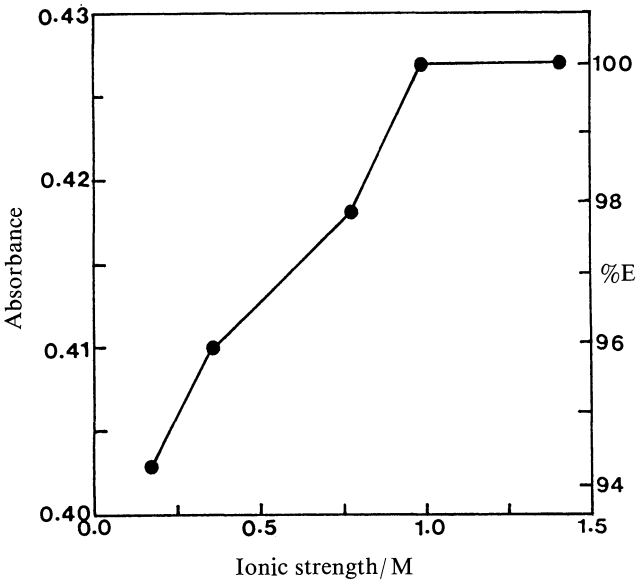

Fig. 4. Effect of ionic strength on the extraction of Os(VIII). Conditions: Os, 10.24 μg cm^{-3}, TBAB, 1 cm^3 of 0.1% in CH_3OH; pH, 3.2; λ_{max}, 530 nm.

TBAB concentration on the extraction of osmium is shown in Fig. 3. The extraction was found to be quantitative when the TBAB to osmium mole ratio is about 100. A further excess of TBAB would cause a decrease in %E, probably due to a change in the extent of ion pairing.

Effect of Ionic Strength. The ionic strength of aqueous solution was found to influence the extraction process (Fig. 4). There is an increase in %E with ionic strength of the solution, maintained by addition of KCl; quantitative extraction results at ionic strength 0.99 M. No change in %E was observed upon further addition of the KCl solution.

Effect of Organic Solvent. The extraction process was performed in a single stage at optimal condition with pure MIBK and pure chloroform. The amount of

remaining osmium in aqueous phase was checked by the reported catalytic methods.[12,13] It was found that the exctraction was more complete with MIBK, but the color intensity of the resulting complex with PAR was much higher in chloroform. However, a 1 : 10 MIBK–chloroform mixture was chosen in this study in which the effect of MIBK on the color intensity was negligible, while in a single stage process the %E was found to be >97.

Effect of Shaking Time. The extraction of osmium(VIII) under the conditions recommended in the procedure is rapid. A shaking time of 8—12 min was found sufficient for the complete extraction.

Effect of PAR Concentration. Addition of methanolic solution of PAR to the chloroform extract of osmium forms a turbid red adduct. In order to overcome the turbidity, absolute methanol was added to the solution until a 5 : 1 v/v ratio of chloroform to CH_3OH is reached and a completely clear solution was obtained. Studies with various concentration of PAR showed that 1.0 cm^3 of a 0.1% (w/v) of PAR in methanol was adequate for the complete color development (Fig. 5). A further excess of PAR increased the absorbance of reagent blank.

Effect of Temperature and Time. The influence of temperature on the color development of osmium–PAR system was studied. There is an increase in the rate of complex formation, and hence in the color development, with temperature. However, 50 °C was chosen in the procedure because of the considerable evaporation of the solvent at higher temperatures. Measurements of absorbance against time at 50 °C showed that, a duration of about 2 h is needed for complete color development. Absorbance of the resulting colored solution was found to remain unchanged for 48 h, if it was protected from the direct sunlight.

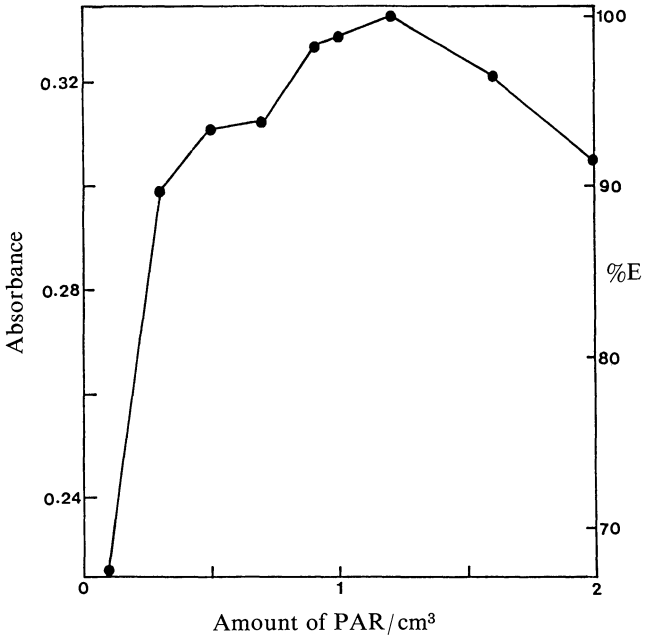

Fig. 5. Effect of PAR concentration on the absorbance of Os–PAR complex. Conditions: Os, 8.0 μg cm^{-3}; TBAB, 1 cm^3 of 1.5% in H_2O; pH, 3.2; λ_{max}, 530 nm.

Beer's Law Study. A calibration graph for osmium was obtained under the recommended conditions in procedure. Beer's law was obeyed over the concentration range 0.5—18 μg cm^{-3} of Os(VIII) and Sandell's sensitivity[17] for 0.001 absorbance was 0.0076 μg cm^{-2}. The relative error (95% confidence level) for 10.24 μg cm^{-3} of osmium was ±1.3% (12 replicates).

Stoichiometry of the Complex. The ratio of osmium to PAR in the resulting complex in organic phase was studied by continuous variations method,[18] and found to be 1 : 2.

Effect of Diverse Ions. Osmium(VIII) was extracted according to the recommended procedure in the presence of several other ions to determine the sensitivity and validity of the method. The results are shown in Table 1. An error of ±2% in the absorbance reading was considered tolerable. As it is seen, most of the common anions and cations associated with osmium did not interfere in the extraction of Os(VIII), except Ag^+, Cd^{2+}, Hg^{2+}, Zn^{2+}, and Pd^{2+}. Interferences form these cations were eliminated by either in situ masking or preseparation using appropriate methods indicated in Table 1.

Conclusion. The method described provides a reliable means of determining trace amounts of osmium. It has a wide range and is free from interferences from many anions and cations, including some platinum

Table 1. Tolerance of the Os(VIII)–TBAB–PAR System to Diverse Ions. Conditions: Os, 10.24 ppm, TBAB, 1 cm^3 of 1.5% in H_2O; PAR 1 cm^3 of 0.1% in CH_3OH; pH, 3.2; λ_{max}, 530 nm

Foreign ion	Molar ratio	Foreign ion	Molar ratio
Ag(I)	72[a,b]	W(VII)	300[a]
Al(III)	1000	Zn(II)	600[c]
Bi(III)	94[a]	Br^-	933[a]
Cd(II)	330[c]	BrO_3^-	146
Co(II)	831	CH_3COO^-	63
Cr(III)	1072	Cl^-	2097[a]
Cu(II)	614	ClO_4^-	94
Hf(III)	417[a]	CO_3^{2-}	310[a]
Hg(II)	100[d]	F^-	3913[a]
Mn(II)	39	$H_2PO_4^-$	153
Mo(VII)	465[a]	I^-	586[a]
Ni(II)	1260	IO_3^-	106[a]
Pb(II)	50[a]	NO_2^-	404
Pd(II)	17[e]	NO_3^-	150
Pt(IV)	97[a]	OCN^-	88
Rh(III)	723[a]	SCN^-	128
V(V)	40	SO_4^{2-}	775[a]

a) Above of which was not tested. b) After centrifugation and separation of the resulting precipitate with Cl^-. c) After masking with 3.0 cm^3 of 0.1 M EDTA at pH=4. d) After addition of 3.0 cm^3 of 10000 μg cm^{-3} of I^- and removal of the precipitate. e) Preliminary extraction with tetrabutylammonium iodide in a highly acidic media into chloroform, Ref. 19.

metals. The method compares favorably in sensitivity with most published methods for the determination of osmium by use of ion-association compounds, and it can certainly be classed among the most sensitive.

The support of this work by the Shiraz University Research Council is gratefully acknowledged.

References

1) P. Chaudhary, R. R. Nogoriand, R. N. Mehrotra, *Indian J. Chem., Sect. A,* **25**, 1123 (1986).
2) C. L. O'Young and J. R. Katzer, *J. Phys. Chem.,* **91**, 6013 (1987).
3) R. A. Sanches-Delgado and B. A. Oramas, *J. Mol. Catal.,* **36**, 283 (1986).
4) P. Mishra and N. C. Khandual, *Indian J. Chem., Sect. A,* **25**, 902 (1986).
5) I. Willner, R. Maidan, D. Mandler, H. Durr, G. Dorr, and K. Zengerle, *J. Am. Chem. Soc.,* **109**, 6080 (1987).
6) J. H. Wiersma and P. E. Lott, *Anal. Chem.,* **39**, 674 (1967).
7) B. K. Pal, R. P. Chowdhury, and B. K. Mitra, *Talanta,* **28**, 62 (1981).
8) A. K. Majumdar and S. K. Bhowal, *Anal. Chim. Acta,* **62**, 233 (1972).
9) A. Wasey, R. K. Bansal, and B. K. Puri, *Michrochim. Acta,* **1**, 211 (1984).
10) K. B. Pandeya, R. P. Singh, and Y. K. Bhoon, *Ann. Chim. (Rome),* **65**, 735 (1975).
11) B. U. Agarawala and A. K. Ghose, *Talanta,* **20**, 129 (1973).
12) A. A. Ensafi and A. Safavi, *Anal. Chim. Acta,* in press.
13) C. S. P. Sastry and K. V. S. S. Murly, *J. Indian Chem. Soc.,* **60**, 72 (1983).
14) M. Siroki and M. Koren, *Michrochim. Acta,* **1**, 75 (1983).
15) G. H. Ayres and W. N. Wells, *Anal. Chem.,* **32**, 317 (1950).
16) E. A. Klobbie, *Chem. Zentralbl.,* **11**, 65 (1898).
17) E. B. Sandell, "Colorimetric Determination of Trace of Metals," Interscience, New York (1956), p. 84.
18) W. Likussar and D. F. Boltz, *Anal. Chem.,* **43**, 1262 (1971).
19) S. Dadfarnia and M. Shamsipur, submitted for publication.

 © 1991 The Chemical Society of Japan Bull. Chem. Soc. Jpn., 64, 3067—3069 (1991)

Spectrophotometric Determination of Trace Amounts of Selenium Based on Catalytic Reduction of Toluidine Blue by Sulfide Ion

Hooshang PARHAM and Mojtaba SHAMSIPUR*
Department of Chemistry, Shiraz University, Shiraz, Iran
(Received January 16, 1991)

A simple, rapid, and sensitive kinetic method for the determination of trace selenium (0.03—1.5 $\mu g\,cm^{-3}$) based on its catalytic effect on the reduction reaction of toluidine blue and sodium sulfide is reported. The reaction is monitored spectrophotometrically by measuring the decreasing absorbance of toluidine blue at 605 nm by the variable time method. The detection limit is 8 $ng\,cm^{-3}$ and the relative standard deviation for 1 $\mu g\,cm^{-3}$ selenium is 1.4%. The procedure was successfully applied to the determination of selenium in real samples.

Because of the increasing industrial use of selenium,[1,2] in one hand, and its serious toxicity and cumulative effect in body,[3,4] in the other, the separation and determination of the metal ion in trace levels is of special interest. Several extraction-spectrophotometric,[5,6] and spectrophotometric catalytic[7,8] methods for the determination of selenium have been reported recently. Despite the need for rigid control of experimental parameters in the catalytic methods, they have shown very promissing features for the determination of metal ion in ultratrace levels.

In this paper we wish to report a simple, rapid, and sensitive spectrophotometric method for the determination of Se(IV) based on its catalysis of the reduction of toluidine blue by sodium sulfide in neutral solutions.

Experimental

Reagents. All chemicals were of the highest purity available and used without further purification except for vacuum drying over P_2O_5. Triply distilled deionized water was used throughout.

Selenium (IV) stock standard solution (1000 $\mu g\,cm^{-3}$) was prepared by dissolving 3.3308 g of $Na_2SeO_3 \cdot 5H_2O$ (Merck) in water and diluting to 1 dm^3 in a volumetric flask. The solution was standardized iodometrically.[9] Working solutions were prepared by appropriate dilution of the stock solution with water.

Sodium sulfide solution (1000 $\mu g\,cm^{-3}$) was prepared by dissolving 1.8750 g of $Na_2S \cdot 9H_2O$ (Hopkin and Williams) in water and diluting to 250 cm^3 in a volumetric flask. This solution was prepared daily and standardized.[9]

A 3.27×10^{-4} M (1 M=1 $mol\,dm^{-3}$) stock solution of toluidine blue (Merck) was prepared by dissolving the dyestuff in water.

Apparatus. Absorption spectra were recorded on a Beckman DK-2A ratio recording spectrophotometer and the absorbance measurements were made on a Perkin-Elmer model 35 spectrophotometer. Measurements of pH was made using a corning 125 pH-meter. A Gallen Kamp BJH-400-010D thermostirrer in which the temperature could be fixed to ±0.1 °C was used.

Procedure. The catalyzed reaction was monitored spectrophotometrically by measuring the change in absorbance at 605 nm. An appropriate amount of sample solution containing 0.30 to 1.50 $\mu g\,cm^{-3}$ of Se(IV) was transferred into a 10 cm^3 flask. Then 1 cm^3 of a 100 $\mu g\,cm^{-3}$ solution of sodium sulfide and 0.3 cm^3 of 0.01 M HCl solution (to adjust pH between 6.5—7.5) and enough water for diluting the solution to ca. 8 cm^3 were added. The solution was kept in water bath at 25 °C for 20 min. Then, 2 cm^3 of 3.27×10^{-4} M solution of toluidine blue was added when diluted to the mark and time was measured from just after the addition of toluidine blue. A portion of solution was transferred into a glass cell immediately for the absorbance measurements. The time required for the absorbance to decrease to A=0.500 was then measured.

Results and Discussion

Catalytic Reduction of Toluidine Blue by Sulfide Ion. It was found that sulfide ion at neutral pH, where it is mostly in hydrogen sulfide form HS^-, reduces toluidine blue only slowly. The half-reaction for the reduction of the dyestuff is as follows:

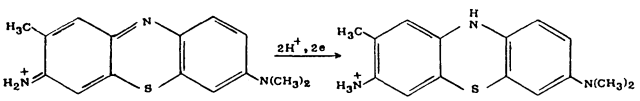

Figure 1 shows the change in the absorption spectrum of toluidine blue in the presence of sulfide ion at pH=7. However, trace amounts of Se(IV) catalyzes the reaction so that it will proceed much faster.

The catalytic effect of selenium(IV) has been explained by the formation of SeS^{2-}, after the initial reduction of Se(IV) to its elemental state.[10] This compound can then reduce the dye molecule and reform Se(IV).

Effect of Variables on the Catalyzed Reaction. The rate of the reduction reaction both in the presence and absence of Se(IV) was found to increase by increasing temperature. A temperature of 25 °C was used as the most suitable.

The rate of the catalyzed reaction was investigated over the pH range of 4—12 and the results are shown in Fig. 2. It is seen that the largest difference between the

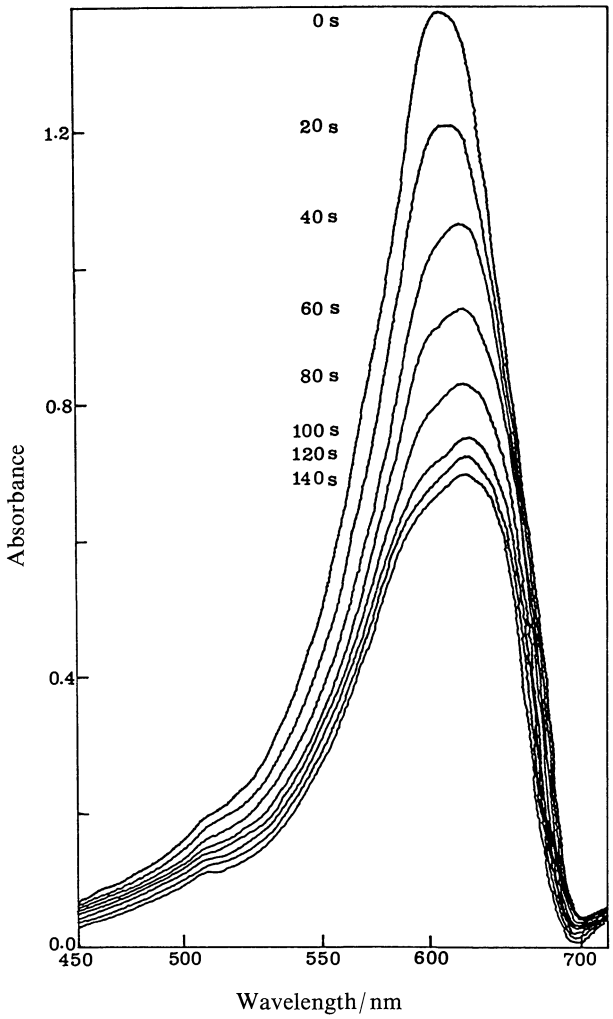

Fig. 1. Absorption spectra of 6.5×10^{-5} M toluidine blue in the presence of 3.1×10^{-4} M sodium sulfide at pH=7. Time intervals 20 s.

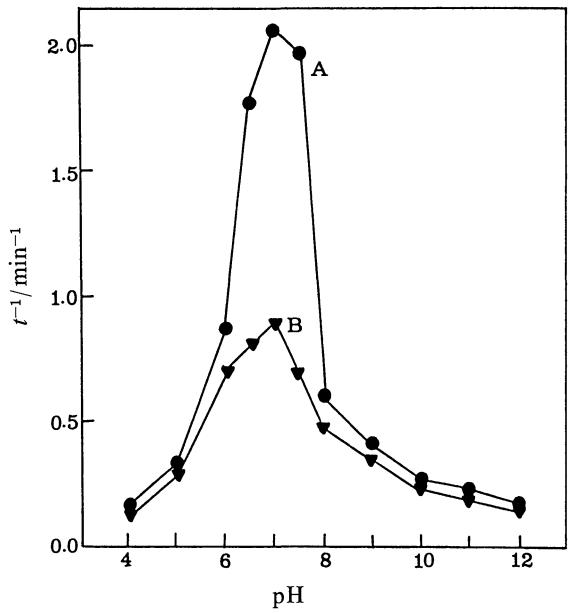

Fig. 2. Effect of pH on the reaction rate. A, sample; B, blank. Conditions: sodium sulfide, 3.13×10^{-4} M; Selenium (IV), 1 μg cm^{-3}; toluidine blue, 6.54×10^{-5} M. The letter t denotes the time required for absorbance to decrease to 0.500.

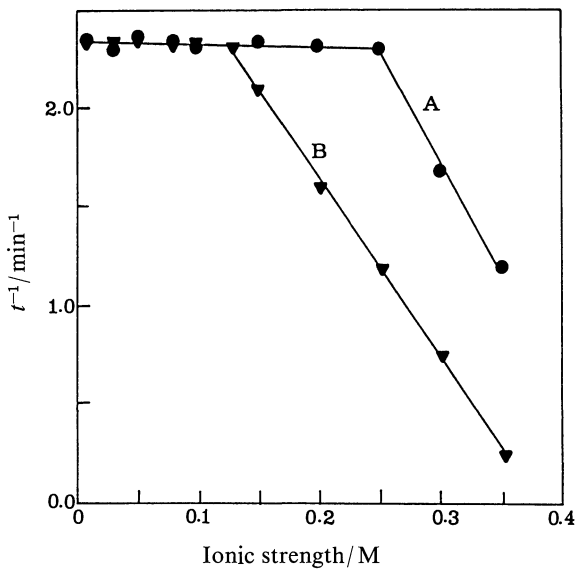

Fig. 3. Effect of ionic strength on the reaction rate. A, NaCl; B, $NaClO_4$. Conditions: Sodium sulfide, 3.13×10^{-4} M; Selenium (IV), 1 μg cm^{-3}; pH, 7; toluidine blue, 6.54×10^{-5} M.

reaction rate of the catalyzed reaction and blank occurs at pH 6.5—7.5.

Effect of ionic strength on the rate of catalyzed reaction was studied (Fig. 3). The ionic strength of solution varied from 0.01 to 0.35 M using NaCl and $NaClO_4$ solutions. As it is seen, change in the ionic strength of solution has no considerable effect on the reaction rate up to a value of about 0.15 M of $NaClO_4$ and 0.25 M NaCl. A further increase in the ionic strength would cause a drastic decrease in the reaction rate.

The influence of the concentration of sulfide ion and toluidine blue was also studied. The best results were obtained at about 3.13×10^{-4} M of sulfide ion and 6.45×10^{-5} M of the dyestuff.

Calibration. Under the optimum conditions described above, in the concentration range of 0.03—1.50 μg cm^{-3} the following regression equation is obtained:

$$1/t\ (\text{min}^{-1}) = 0.9685 + 1.2045\ \ \text{Se(IV)}$$
$$(r = 0.99968)$$

The limit of detection obtained from $Y_{DL}=Y_B+3s_B$[11] is 8 ng cm^{-3}, where Y_B is the average blank signal (0.9623 min^{-1} for ten replicate determinations) and s_B is the standard deviation of the blank signal (0.00520). The relative standard deviation of eight replicate determinations is 1.4% for a 1 μg cm^{-3} selenium(IV) solution.

Effect of Diverse Ions. In order to study the effect of various anions and cations on the determination of Se(IV), a fixed amount of selenium (1 μg cm^{-3}) was

Table 1. Tolerance Limits of Diverse Ions on the Determination of 1 μg cm^{-3} Selenium

Ion	Tolerated radio of foreign ion to Se(IV)
NO_3^-, Cl^-, Br^-, I^-, F^-, $C_2H_3O_2^-$, PO_4^{3-}, HPO_4^{2-}, SO_4^{2-}, HSO_4^-, NO_2^-, CO_3^{2-}, $S_2O_3^{2-}$, ClO_4^-, SO_3^{2-}, HSO_3^-, $S_2O_5^{2-}$, IO_3^-, EDTA	250
OCN^-, CN^-, SCN^-	20
Na(I), K(I), Li(I), Ca(II), Mg(II), Ba(II), Sr(II), Hf(IV), Zr(IV), Al(III), Ce(III), Cr(III)	500
Mo(VI), W(VI), V(V), As(V), Te(IV), Os(VIII)	250
Hg(II), Hg(I), Pb(II), Pd(II), Cu(II), Co(II), Bi(III), Mn(II), Cd(II), Zn(II), Fe(II), Ag(I)	Interfere

Table 2. Determination of Selenium in Kjeldal Tablets

Sample taken	Se/μg cm^{-3}		Recovery/%
cm^3	Contained	Found	
0.5	0.250	0.261	104.3
1.0	0.500	0.524	104.8
1.0	0.500	0.489	97.9
1.5	0.750	0.750	100.0
2.5	1.000	0.975	97.5

taken with different amounts of foreign ions and the recommended procedure was followed. A relative error of 3% was considered tolarable. The results are summarized in Table 1. As it is seen, all the anions and a large number of cations used have no considerable effect on the determination of Se(IV). However, as it is expected, the presense of cations which can form insoluble precipitates with sulfide ion would interfere the selenium determination. These cations were successfully removed from the solution by passing it from a column containing a strongly acidic cation exchanger of H^+ form (Merck, R-SO_3^- type).

It is interesting to note that, by this method Se(IV) can be determined in the presence of Se(VI), which has no catalytic effect on the reduction reaction of toluidine blue by sulfide ion. However, determination of total selenium in different samples would also be possible by the recommended procedure after the conversion of Se(VI) fo Se(IV), which can easily be done by using hydrochloric acid. It is interesting to note that, Se(VI) showed no catalytic effect on the reduction reaction of toluidine blue and sulfide ion.

Application. In order to evaluate the applicability of the method to the real samples, it was applied to the determination of selenium in Kjeldal tablets. One tablet (1.1142 g) containing 0.05 g selenium was dissolved, using a suitable procedure[12] and diluted with water to 1 dm^3 in a volumetric flask. It should be noticed that the final stage of the dissolution process involves the boiling of sample in 4 M HCl, which completely converts Se(VI) to Se(IV).[13] Then 10 cm^3 of this solution was diluted to 100 cm^3 with water and selenium content in different portions of the resulting solution was determined by the recommended procedure. The results are given in Table 2.

The support of this work by the Shiraz University Research Council is gratefully acknowledged.

References

1) J. W. Mellor, "A Comprehensive Treatise on Inorganic and Theoretical Chemistry," Longman, London (1961).
2) K. W. Bagnal, "The Chemistry of Selenium, Tellurium, and Polonium," Elsevier, Amsterdam (1966).
3) I. L. Lambert, P. Arthur, and T. E. Moor, *Anal. Chem.*, **23**, 1101 (1951).
4) E. P. Dimandis and T. P. Hadjiioannou, *Anal. Chim. Acta*, **123**, 143 (1981).
5) Y. K. Agrawal and K. H. Desai, *Anal. Lett.*, **19**, 25 (1986).
6) N. Singh and A. K. Garg, *Analyst*, **111**, 247 (1986).
7) W. C. Hawkes, *Anal. Chim. Acta*, **183**, 197 (1986).
8) A. Safavi, A. Afkhami, and A. Massoumi, *Anal. Chim. Acta*, **232**, 351 (1990).
9) A. I. Vogel, "A Text Book of Quantitative Inorganic Analysis," 3rd ed, Longman, London (1961).
10) G. A. Cutter, *Anal. Chem.*, **57**, 2951 (1985).
11) J. C. Miller and J. N. Miller, "Statistics for Analytical Chemistry," Ellis Horwood (1984).
12) F. Feigl and P. W. West, *Anal. Chem.*, **19**, 351 (1947).
13) R. A. Nadkarni and B. C. Haldar, *J. Indian Chem. Soc.*, **41**, 813 (1964).

Thermodynamic Studies of Copper(II) Sulfate in Aqueous Mannitol from Electromotive Force Measurements

Ratan L. BLOKHRA* and Anil K. SHARMA
Department of Chemistry, Himachal Pradesh University, Summer Hill, Shimla 171005, India
(Received February 18, 1991)

Electromotive force measurements of the cell Cu-Hg/$CuSO_4$(m)/Hg_2SO_4(s)/Hg have been made at 288, 298, 308, and 318 K for mannitol composition X=5, 15, and 25% (w/w) in water. The standard emf values of the cell at different temperatures and at different composition of mannitol+water mixtures have been determined by an extrapolation method. These have been utilized to evaluate the mean activity coefficient of copper(II) sulfate. The standard free energy for the cell reaction, and the primary medium effects upon $CuSO_4$ have been evaluated. The standard thermodynamic quantities for the process of transfer of $CuSO_4$ from water to the mannitol solution have been calculated from the values of the standard potential. The transfer parameters have been split into the electrostatic and chemical contributions and the results have been explained in the light of ion-solvent interactions and structural contributions to solvents.

The behavior of electrolytes in aqueous carbohydrate solutions has recently been a subject of interest.[1-6] The study of electrolytes in carbohydrate solutions is of great importance in the understanding of the physiological and biological processes associated with life. Blokhra et al.[7-9] have reported the transfer energetics of copper(II) sulfate in diethylene glycol-water, ethylene glycol-water, dioxane-water mixtures, and urea-water solutions. In continuation with the previous study, the present investigations have been carried out by using copper(II) sulfate in different mannitol+water mixtures. By setting a suitable cell, we carried out electromotive force measurements. The temperature variation of the standard potential was used to calculate different thermodynamic quantities. From these quantities and transfer energetics, we can obtain information about the thermodynamic properties of $CuSO_4$ in these solvents and about the properties and structure of the solvents. The activity coefficients of copper(II) sulfate in various mannitol+water mixtures have also been calculated.

Experimental

Mannitol and copper(II) sulfate were of analytical grade and were used without further purification. Water used was triply distilled having specific conductance of the order of 10^{-14} $m^{-1}\,\Omega^{-1}$. Solvents of various compositions were made by weight.

The emf cell used for the present study was as previously described.[7-9] Copper amalgam was prepared by electrolyzing a copper(II) perchlorate solution with a mercury pool as cathode, as described elsewhere.[10] At room temperature, a two-phase amalgam is formed between 0.0032 and 24.1% copper (w/w).[11,12] Within this range the potential will be independent of composition, and the exact composition of copper is therefore unimportant.[13] All precautions taken earlier[7] were observed in the present investigation as well.

The emf measurements were made with a digital potentiometer (Equip Tronics, Bombay) having precision of ±0.1 mV. All measurements were made in water thermostat having fluctuation of $<\pm 0.1$ °C. The cell attained equilibrium after about one hour in all the solvent mixtures. The concentrations of the solutions were occassionally checked with a conductivity bridge and no significant change was detected.

Results and Discussion

The emf (E) values of the cell are reported in Table 1.

Table 1. Electromotive Force Measurements of the Cell Used (E/V) in Various Mannitol+Water Mixtures at Different Temperatures

Concentration	T/K			
10^{-3} mol kg^{-1}	288	298	308	318
	5% mannitol			
4.00	0.4078	0.4070	0.4048	0.4038
6.00	0.4068	0.4048	0.4030	0.4018
8.00	0.4038	0.4028	0.4018	0.4010
10.00	0.4018	0.4010	0.3988	0.3978
20.00	0.3938	0.3918	0.3898	0.3878
40.00	0.3858	0.3828	0.3798	0.3768
60.00	0.3820	0.3788	0.3758	0.3718
80.00	0.3788	0.3748	0.3718	0.3688
100.00	0.3768	0.3730	0.3688	0.3658
	15% mannitol			
4.00	0.4068	0.4048	0.4020	0.3998
6.00	0.4028	0.4008	0.3988	0.3968
8.00	0.4010	0.3990	0.3968	0.3948
10.00	0.3988	0.3968	0.3948	0.3918
20.00	0.3888	0.3868	0.3848	0.3828
40.00	0.3840	0.3818	0.3788	0.3758
60.00	0.3788	0.3758	0.3728	0.3698
80.00	0.3758	0.3730	0.3698	0.3668
100.00	0.3728	0.3698	0.3668	0.3640
	25% mannitol			
4.00		0.4018	0.3990	0.3968
6.00		0.3978	0.3958	0.3938
8.00		0.3948	0.3928	0.3908
10.00		0.3920	0.3898	0.3878
20.00		0.3848	0.3818	0.3788
40.00		0.3798	0.3768	0.3748
60.00		0.3738	0.3718	0.3688
80.00		0.3698	0.3678	0.3648
100.00		0.3678	0.3648	0.3620

Assuming copper(II) sulfate to be dissociated in the solutions studied, the standard molal potentials, $E^{\ominus}_{m}$, of the cell:

$$\text{Cu–Hg/CuSO}_4\text{(m), mannitol + water mixtures/Hg}_2\text{SO}_4\text{(s)/Hg}$$

in different solutions have been estimated satisfactorily from the Hitchcock[14] type equation because concentration of solutions is <0.1 m.

$$E'_{o} = E + k\log m - k\left(\frac{AZ^{+}Z^{-}I^{1/2}}{1+Ba_{o}I^{1/2}}\right) = E^{\ominus}_{m} - kB'I, \quad (1)$$

where I is the ionic strength of the solution, m is the molal concentration of the solution, A and B are the Debye–Hückel constants, a_o is the ion-size parameter, Z^+ and Z^- are the valencies of the cation and anion, respectively, and k equals 2.3026 RT/F. B' is a constant quantity and it is a measurement of the interaction energy.[14] For each solvent at any temperature $E^{\ominus}_{m}$ was obtained by the usual extrapolation technique and the procedure is essentially the same as that used in our previous determinations.[7–9]

The dielectric constant (D_s) for the various mannitol + water mixtures were taken from the literature.[15] The densities (ρ_o) and the Debye parameters were determined experimentally[16] and from the expressions given in standard electrochemistry book.[17] The parameters A, B, and D_s are given in Table 2.

The values of activity coefficients, $\lambda_{\pm}$, can be evaluated from the relation.[18]

$$E = E^{\ominus}_{m} - k\log m\lambda_{\pm}. \quad (2)$$

From Eq. 1 it is expected that E'_o should be linear function of I when a suitable value of the ion-size parameter is chosen. The intercept of the plot at I=0 gives the value of $E^{\ominus}_{m}$. The a_o values for the various solvent mixtures at different temperatures are chosen in such a way that the deviation from linearity of the plot of E'_o against I is minimum. The following a_o values were selected for the different mannitol + water mixtures:

Mannitol (wt%)	5	15	25
a_o/Å	5.0	5.1	5.2

The values of $E^{\ominus}_{m}$ have average standard deviation of ±0.3 mV, these values at different temperatures for various mannitol + water mixtures are given in Table 3. The values of $E^{\ominus}_{m}$ could be expressed as a function of temperature in the following form:

$$E^{\ominus}_{m} = a - b(T-298.15) - c(T-298.15)^2, \quad (3)$$

where T is the temperature in K. The constants a, b, and c are given in Table 4.

The mean activity coefficient $\lambda_{\pm}$ of copper(II) sulfate

Table 2. Parameters for the Evaluation of E'_o in Mannitol + Water Mixtures at Different Temperatures

T/K	D_s	A/mol$^{-1/2}$kg$^{1/2}$	10^{-10} B/m^{-1}mol$^{-1/2}$kg$^{1/2}$
		5% mannitol	
288	81.35	0.509	0.329
298	77.83	0.517	0.330
308	74.23	0.529	0.333
318	70.80	0.540	0.335
		15% mannitol	
288	79.95	0.522	0.331
298	76.30	0.532	0.334
308	72.70	0.545	0.336
318	69.10	0.568	0.341
		25% mannitol	
298	74.77	0.549	0.336
308	71.05	0.564	0.339
318	67.55	0.580	0.343

Table 4. Values of the Constants a, b, c in Eq. 3

Mannitol/wt%	a/V	$b/10^{-4}$ V K^{-1}	$c/10^{-6}$ V K^{-2}
0	0.2659	7.25	0.00
5	0.2605	6.63	6.25
15	0.2561	6.50	6.25
25	0.2508	7.25	2.50

Table 5. Mean Molal Activity Coefficient of $CuSO_4$ in Various Mannitol + Water Mixtures at 298 K

Concentration	Mannitol (wt%)			
10^{-3} mol kg^{-1}	0	5	15	25
4.00	0.559	0.864	0.760	0.690
6.00	0.509	0.628	0.592	0.537
8.00	0.501	0.509	0.476	0.453
10.00	0.451	0.437	0.415	0.404
20.00	0.333	0.313	0.307	0.267
40.00	0.236	0.222	0.186	0.163
60.00	0.191	0.173	0.157	0.137
80.00	0.168	0.152	0.131	0.120
100.00	0.151	0.130	0.119	0.104

Table 3. Standard Molal Potentials of the Cell Used in Mannitol + Water Mixtures at Various Temperatures (The Values in Parentheses are Calculated from Constants a, b, and c of Eq. 3)

Mannitol	$E^{\ominus}_{m}$/V			
wt%	288 K	298 K	308 K	318 K
0	0.2730 (0.2732)	0.2655 (0.2660)	0.2585 (0.2587)	0.2515 (0.2514)
5	0.2655 (0.2665)	0.2615 (0.2615)	0.2540 (0.2533)	0.2470 (0.2449)
15	0.2620 (0.2620)	0.2560 (0.2560)	0.2490 (0.2490)	0.2405 (0.2419)
25	—	0.2505 (0.2505)	0.2435 (0.2434)	0.2350 (0.2358)

in different solvent was calculated with the help of Eq. 2 and these values at 298 K are listed in Table 5. An error of ±0.1 mV in emf values results in an error of ±0.002 in the value of $\lambda_{\pm}$.

The values of the activity coefficient in water (0% mannitol) are comparable with the literature values[23,24] at 298 K e.g. it is 0.153[23] and 0.150[24] for 0.1 m $CuSO_4$, 0.438[23] for 0.01 m $CuSO_4$, showing thereby that there is consistency in the measurements and the estimation of the molal activity coefficient of copper(II) sulfate. The values of the activity coefficient at a particular molality have been found to decrease with increasing mannitol content in the medium except 4.00, 6.00, and 8.00 m solutions in water. The decrease in the values may be attributed to the lowering of the dielectric constant of the medium and the abnormal lower values at lower concentration in water may be attributed to the increase in the ion-ion interactions or partial hydrolysis of the copper sulfate solution.

The standard thermodynamic function $\Delta G^{\ominus}$ for the cell reaction:

$$Hg_2SO_4(s) + Cu\text{-}Hg(s) \rightleftarrows 3\ Hg(s) + CuSO_4\ (solvated)$$

has been calculated from the temperature variation of the standard molal potential in mannitol + water solvent using

$$\Delta G^{\circ} = -nFE^{\ominus}_{m} = -2F[a - b\,(T-298.15) - c(T-298.15)^2]. \quad (4)$$

The calculated thermodynamic functions of the cell at 288—318 K in 0, 5, 15, and 25% (w/w) of mannitol + water solvents are recorded in Table 6. It is evident from Table 6 that all the thermodynamic functions are negative. The magnitude of the standard free energy changes increases with an increase in either the mannitol content in the solvent mixture or the temperature of the solvent system which may be attributed to the decrease in the dielectric constant of the medium. As the dielectric constant decreases, more work is required to keep the ions apart, and therefore, less work is produced by the electrode reaction and more positive free energy changes results. There is less spontaneity, because of decrease dissociation at lower dielectric constants.

Table 6. Standard Molal Free Energy of the Cell Reaction in Various Mannitol + Water Solvents at 288—318 K

T/K	Mannitol/wt%			
	0	5	15	25
	$-\Delta G^{\circ}$/kJ mol^{-1}±0.020			
288	52.69	51.24	50.57	—
298	51.24	50.47	49.41	48.35
308	49.89	49.02	48.06	46.99
318	48.54	47.67	46.42	45.36

The primary medium effect represents the difference in ion solvent interaction for copper(II) sulfate at the standard state in the particular solvent and in water. It is a measure of the change of Gibbs free energy which accompanies the transfer of one mole of copper(II) sulfate from the standard state in water to the standard state in respective solvent. Thus the primary medium effect measures the change in escaping tendency of copper(II) sulfate in the transfer from a standard state in one solvent to a standard state in another solvent. The primary medium effect, $\log {}^{s}_{w}\gamma^{\ominus}_{\pm}$ (mole fraction scale), of the mannitol + water solvents upon $CuSO_4$ were computed by the usual relation[19,20] at 288—318 K. The results are given in Table 7. It is seen from Table 7 that addition of mannitol changes the behavior of the medium upon the ions and the effect upon the ions is greater at higher concentrations of mannitol. Further it shows a decreasing tendency with increasing temperature. This suggests that the escaping tendency of $CuSO_4$ is greater in mannitol + water solvents than in water.

The standard thermodynamic quantities for the transfer of one mole of copper(II) sulfate from the standard state in water (w) to the standard state of respective solvents (s) were evaluated at 288—318 K with the help of usual relations.[19,20]

$$-2F[(E_m)_s - (E_m)_w] - 2\times 2.3026RT\log(M_s/M_w) = \Delta G^{\ominus}_{t} = O - PT + QT^2 \quad (5)$$

and the corresponding values for solutions of copper(II) sulfate in the various solvent media at 288—318 K are given in Table 8.

It is quite evident from Table 8 that the standard Gibbs free energy of transfer, $\Delta G^{\ominus}_{t}$, becomes more and more positive with the increase of mannitol content in the medium. The positive $\Delta G^{\ominus}_{t}$ values suggest that the elactrolyte is in higher free energy state in mannitol + water mixtures than in water so that copper(II) sulfate has more affinity for water than mannitol + water mixtures. The transfer of copper(II) sul-

Table 7. Primary Medium Effect, $\log {}^{s}_{w}\gamma^{\ominus}_{\pm}$ (Mole Fraction Scale), of Mannitol + Water Solvents upon $CuSO_4$ at 288—318 K and the Values of the Constants O, P, and Q of Eq. 5 for Evaluation of Thermodynamic Quantities for Transfer of $CuSO_4$ from Water to Mannitol + Water Media

Mannitol	$\log {}^{s}_{w}\gamma^{\ominus}_{\pm}$				$O\times10^{-3}$	$P\times10^{2}$	Q
wt%	288 K	298 K	308 K	318 K	J mol^{-1}	J K^{-1} mol^{-1}	J K^{-2} mol^{-1}
5	0.0656	0.0381	0.0368	0.0357	135.890	8.910	1.4450
15	0.0963	0.0846	0.0777	0.0872	113.441	7.366	1.2075
25	—	0.1311	0.1228	0.1308	91.738	5.905	0.9675

Table 8. Standard Thermodynamic Quantities for the Transfer of Copper(II) Sulfate from Water to Mannitol + Water Mixtures at Various Temperatures

T/K	Mannitol/wt%		
	5	15	25
	$\Delta G_t^\ominus$/kJ mol^{-1}		
288	1.15	1.46	—
298	0.71	1.17	1.68
308	0.56	1.13	1.64
318	0.70	1.32	1.79
	$\Delta H_t^\ominus$/kJ mol^{-1}		
288	18.03	13.29	—
298	9.56	6.21	5.82
308	0.81	−1.11	−0.43
318	−8.24	−8.67	−6.10
	$\Delta S_t^\ominus$/J K^{-1} mol^{-1}		
288	58.60	41.05	—
298	29.70	16.90	13.90
308	0.80	−7.25	−5.45
318	−28.10	−31.40	−24.00
	$-\Delta C_p$/J K^{-1} mol^{-1}		
288	832	696	—
298	861	720	576
308	890	744	596
318	919	768	615

fate from water to mannitol + water mixture is, therefore, not a spontaneous process with the solute in standard state in either medium. Ahluwalia and Sharma[21] suggested that the transfer of structure breaking solutes should be accompanied by a positive free energy change thereby making the transfer of there solutes from water to the mixed solvents thermodynamically unfavorable. The positive $\Delta G_t^\ominus$ values, therefore suggests that copper(II) sulfate behaves as a structure breaker in water. The positive $\Delta G_t^\ominus$ values also suggest that water is more basic than mannitol + water solvents and basicity decreases with increasing the mannitol concentration in the solvents. This view is also consistant with the fact that the escaping tendency of copper(II) sulfate is greater in mannitol + water solvent than in the pure aqueous solutions (Table 7, medium effect). The effect of temperature on $\Delta G_t^\ominus$ shows decrease in the contribution for the effects of the ions on the structure of the solvents.

The values of the transfer entropy and enthalpy reflect the complicated nature with regard to the contributions from the effects of the ions on the structure of the solvents. The values of $\Delta H_t^\ominus$ and $\Delta S_t^\ominus$ are negative at 318 K and at 15% and 25% mannitol at 308 K, while values at other temperatures and concentration are positive. The negative values suggest that the tendency of order created by copper(II) sulfate in 15% and 25% mannitol + water mixtures at 308 K and 5%, 15%, and 25% mannitol + water mixtures at 318 K is more than in pure water. However this tendency is less in 5% (w/w) mannitol + water mixture at 308 K and in all the solvents at 288 and 298 K in comparison with pure water. This shows reintroduction of some order in mannitol + water mixtures at higher temperatures. Copper(II) sulfate thus breaks more structure in water than in mannitol + water solvent at higher temperatures.

The process of transfer is associated with the transfer of charged species i.e. Cu^{2+} and SO_4^{2-} ions from water to the aqueous mannitol medium. It may, therefore, be possible to split the $\Delta G_t^\ominus$ values into two parts as suggested earlier[22] an electrostatic part, $\Delta G_{t,el}^\ominus$ corresponding to a change in dielectric constant of the medium, and a nonelectrostatic or chemical part, $\Delta G_{t,ch}^\ominus$, arising from specific chemical interactions between the ions and the solvent. Thus

$$\Delta G_t^\ominus = \Delta G_{t,el}^\ominus + \Delta G_{t,ch}^\ominus. \quad (6)$$

The electrostatic contribution $\Delta G_{t,el}^\ominus$, $\Delta H_{t,el}^\ominus$, $\Delta S_{t,el}^\ominus$, and the chemical contributions $\Delta G_{t,ch}^\ominus$, $\Delta H_{t,ch}^\ominus$, $\Delta S_{t,ch}^\ominus$ have been calculated as described earlier.[7-9] These values so calculated at 298 K are presented in Table 9. It is obvious from Table 9 that $\Delta G_{t,ch}^\ominus$ and $\Delta G_{t,el}^\ominus$ are increasingly positive in all mannitol + water mixtures. This indicates that transfer of $CuSO_4$ from water to mannitol + water mixtures is not favored as far as chemical interactions are concerned. This suggests that all mannitol + water mixtures are less basic than pure water and this enhances with increasing mannitol concentration. The electrostatic contribution of enthalpy and entropy of transfer goes on decreasing with increase in mannitol concentration. Same is the trend for chemical contribution. Taking an overall view it can be inferred that the chemical contribution or solvation predominates over electrostatic factor, resulting in an overall unfavorable effect on the transfer process from water to mannitol + water mixtures. The negative values of these parameters may be due to the introduction of order in mannitol + water mixtures.

Table 9. Electrical and the Chemical Parts of the Thermodynamic Quantities Accompanying the Transfer of Copper(II) Sulfate from Water to Mannitol + Water Mixtures at 298 K

Mannitol	$\Delta G_{t,el}^\ominus$	$\Delta G_{t,ch}^\ominus$	$\Delta H_{t,el}^\ominus$	$\Delta H_{t,ch}^\ominus$	$\Delta S_{t,el}^\ominus$	$\Delta S_{t,ch}^\ominus$
wt%	kJ mol^{-1}	kJ mol^{-1}	kJ mol^{-1}	kJ mol^{-1}	J K^{-1} mol^{-1}	J K^{-1} mol^{-1}
5	0.094	0.62	0.092	9.47	−1.75	31.45
15	0.410	0.76	−1.622	7.83	−6.82	23.72
25	0.738	0.94	−1.884	7.70	−8.80	22.70

References

1) O. D. Bonner, *J. Solution Chem.*, **11**, 315 (1982).
2) U. N. Dash, B. B. Das, U. K. Biswal, and T. Panda, *J. Electrochem. Soc. India,* **33**, 2390 (1984).
3) T. M. Herrington and C. P. Meurier, *J. Chem. Soc., Faraday Trans. 1,* **78**, 225 (1982).
4) J. G. Dawber and G. E. Hardy, *J. Chem. Soc., Faraday Trans. 1,* **80**, 2467 (1984).
5) V. Vitagliaso, G. Borriello, D. Volbe, and O. Ortona, *J. Solution Chem.,* **15**, 811 (1986).
6) J. P. Morel, C. Chermet, and N. M. Deroriers, *J. Chem. Soc., Faraday Trans. 1,* **84**, 2567 (1988).
7) R. L. Blokhra and S. Kohli, *J. Chem. Soc., Faraday Trans. 1,* **78**, 1071 (1982).
8) R. L. Blokhra, Y. P. Sehgal, and V. K. Kuthiala, *Electrochim. Acta,* **21**, 1079 (1976).
9) R. L. Blokhra, M. L. Parmar, and S. S. Thakur, *Electrochim. Acta,* **28**, 1201 (1983).
10) S. Ahrland and B. Tagerson, *Acta. Chem. Scand., Ser. A,* **31**, 615 (1977).
11) G. Tammann and J. Z. Stassfurth, *Inorg. Chem.,* **160**, 246 (1927).
12) G. Tammann and K. Z. Kollmann, *Inorg. Chem.,* **143**, 357 (1925).
13) S. Ahrland and J. Rawsthorne, *Acta Chem. Scand.,* **24**, 157 (1970).
14) D. J. G. Ives and G. J. Janz, "Reference Electrodes," Academic Press, New York (1961), p. 38.
15) G. Akerlaf, *H. Am. Chem. Soc.,* **54**, 4125 (1932).
16) R. L. Blokhra and S. K. Agarwal, *J. Chem. Thermodyn.,* **11**, 229 (1979).
17) R. A. Robinson and R. H. Stokes, "Electrolyte Solutions," Butterworths Scientific Publications, London (1955), p. 230.
18) D. A. MacInner, "The Principles of Electro-Chemistry," Dover Publications, New York (1967), p. 165.
19) M. M. Elsemongy, *Electrochim. Acta,* **23**, 957 (1978).
20) M. M. Elsemongy, A. S. Fouda, and M. F. Amira, *J. Chem. Soc., Faraday Trans. 1,* **77**, 1157 (1981).
21) T. S. Sharma and J. C. Ahluwalia, *J. Phys. Chem.,* **76**, 1366 (1972).
22) R. N. Roy, W. Wernon, and A. L. M. Bothwell, *Electrochim. Acta,* **17**, 5 (1972).
23) E. H. Getman, *J. Phys. Chem.,* **34**, 154 (1930).
24) R. A. Robinson and R. H. Stokes, "Electrolyte Solutions," Butterworths Scientific Publications, London (1955), p. 502.

 © 1991 The Chemical Society of Japan Bull. Chem. Soc. Jpn., 64, 3075—3078 (1991)

Spectrophotometric Determination of Palladium Using 2-(2-Hydroxyimino-1-oxoethyl)thiophene

Anoop Kumar CHHAKKAR and Lajpat Rai KAKKAR*
Department of Chemistry, Kurukshetra University, Kurukshetra 132119 (Haryana State), India
(Received February 28, 1991)

A highly sensitive and selective method for the determination of palladium in trace amounts is developed by complexation of Pd(II) with 2-(2-hydroxyimino-1-oxoethyl)thiophene (INAT) at pH 2.8—6.5, adjusted with diluted acetic acid. The colored species is quantitatively extracted into chloroform, whose absorbance is measured at 425 nm. The method is free from the interference of a large number of elements of great analytical importance. The usefulness of the method is further tested by analyzing different samples and the results obtained are quite satisfactory.

Though a number of methods using organic reagents[1-4] have been developed for the spectrophotometric determination of palladium, but most of them suffer from disadvantages[3,4] particularly due to the serious interferences from several elements of interest and poor sensitivities. Complexes potentially useful for the solvent extraction of palladium are those formed with 8-quinolinethiol[5,6] and thiocyanate.[7] There are also methods available where complexes are formed with hydroxyimino-substituted ketones[8-11] and some of their derivatives.[12] The efficiency of these extractions as separatory methods in the presence of other platinum and associated base metals has received relatively little attention. In many instances, the problem of coextraction has been related to the degree of interference with the colorimetric measurements. Taking into account all these factors, modern analytical techniques for the determination of trace amount of noble metals are growing in demand to the extent that one can deal effectively with a few μg of metals so as to achieve very acceptable results.

Consequently, it has been found while working that Pd(II), in microgram amounts, forms a yellow complex with 2-(2-hydroxyimino-1-oxoethyl)thiophene [(2-[α-(hydroxyimino)acetyl]thiophene, abbrev. to INAT] in diluted acid solutions (pH 2.8—6.5) which is extractable into chloroform whose absorbance is measured at 425 nm, where the absorbance of the reagent blank is minimal.

Experimental

Reagents. A stock solution of palladium containing 1 mg Pd ml^{-1} is prepared by dissolving an accurately weighed amount of $PdCl_2$ (Johnson Metthey & Co,, London) in a minimum volume of hydrochloric acid and is standardized gravimetrically.[13] Stock solutions with lower concentrations of the metal ion at the μg ml^{-1} level are prepared by suitable dilutions therefrom.

Preparation of 2-(2-Hydroxyimino-1-oxoethyl)thiophene:

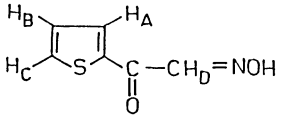

Sodium metal (1.15 g) is dissolved in 23 ml absolute ethanol and to the solution 6.7 ml of isopentyl nitrite are added slowly under cooling and stirring at the same time. This is followed by the addition of 5.4 ml of 2-acetylthiophene. The mixture is kept overnight at 0 °C. The brown sodium salt thus obtained is washed well with diethyl ether and dried in air. It is then dissolved in ice-water and neutralized with glacial acetic acid. The creamish solid is filtered, dried and crystallized from ethanol, (70% yield): Mp 115 °C; IR (Nujol) 3186 (ν_{O-H}, intramolecular hydrogen bonding), 1592 ($\nu_{C=O}$, intramolecular hydrogen bonding) cm^{-1}; ^1H NMR ($CDCl_3$) δ=7.00—7.18 (1H, m, H_B), 7.65 (1H, d, $J_{C,B}$=5.4 Hz, H_C), 7.89 (1H, s, H_D), 8.03 (1H, d, $J_{A,B}$=3.6 Hz, H_A); Found: C, 46.23; H, 3.13; N, 8.95%. Calcd for $C_6H_5NO_2S$: C, 46.45; H, 3.22; N, 9.03%. 0.1% solution of INAT in ethanol is used.

Buffer solution is prepared with sodium acetate–acetic acid (1 mol dm^{-3}).

Sample solutions are obtained by mixing the solutions of palladium(II) and other metal ions in a suitable proportion as shown in Table 2.

Pd-Charcoal Catalyst (Aldrich 20, 568-0): A weighed amount of the sample is brought into solution by heating with HCl and HNO_3 (3:1). Charcoal is filtered off from the solution and the excess of HNO_3 is decomposed completely by evaporating it to dryness. The residue is treated with water and diluted HCl and processed for the determination of palladium as described below in the procedure.

Procedure for the Determination of Palladium. To the sample solution containing 50 μg Pd(II) and/or other ions in a 100 ml separatory funnel, add 1 ml of the 0.1% INAT, 5 ml of buffer solution and the volume is made to 20 ml with distilled water (pH 4.75—4.78). The contents are gently mixed and equilibrated once with an equal volume of chloroform for one min. The two phases are allowed to separate. The organic phase is filtered through a Whatman's filter paper (No. 41) into a 25 ml volumetric flask which is then filled upto the mark with the pure chloroform. The absorbance of the yellow complex is measured at 425 nm against reagent blank on UV-visible 140-02 spectrophotometer (Shimadzu, Japan) using 1 cm cells and the amount of the metal ion is determined from the standard curve obtained by plotting different concentrations of Pd(II) and the corresponding absorbance values.

Results and Discussion

The extractability of the palladium(II)–INAT complex is affected by the kind of acid. The extractability

Table 1. Effect of Various Parameters on the Absorbance of Palladium-INAT Complex

pH[a]	2.10	2.5	2.8—6.5	7.5	8.6	9.6	10.1	10.65
Absorbance	0.595	0.605	0.63	0.605	0.595	0.58	0.56	0.52
2-(2-hydroxyimino-1-oxoethyl) thiophene[b] (ml)	0.0	0.1	0.2	0.3	0.4	0.5	0.7—5.0	
Absorbance	0.002	0.375	0.585	0.61	0.62	0.625	0.63	
Equilibration time[c] (sec)	5	10	20	30	45	60—240		
Absorbance	0.61	0.62	0.625	0.63	0.63	0.63		

a) Conditions: Pd(II)=50 μg, INAT (0.1%)=1 ml, aqueous volume=solvent volume=20 ml, solvent=chloroform, equilibration time=1 min, number of extractions=1, pH=variable. b) Conditions: pH=4.75—4.78; other conditions are the same as in (a) except variation in the INAT content. c) Conditions: INAT (0.1%)=1 ml; other conditions are the same as in (b) except the variation in equilibration time.

Table 2. Analysis of Different Samples by the Proposed Method

Sr. No.	Composition of sample: Matrix[a]	Pd(II) added	Pd(II) found
		μg	μg
1.	Pt(4), Rh(5)	45	45.0
2.	Pt(0.6), Rh(0.5), Ru(0.5), Os(0.7)	28	28.0
3.	Pt(5), Rh(4), Ru(3), Os(3)	65	65.0
4.	W(5), Mo(5), V(4)	20	20.0
5.	U(5), Ni(4), Mn(6)	40	39.5
6.	Cu(5), Co(5), Fe(4)	10	10.0
7.	Zn(4), Hg(5), Cd(6)	30	30.0
8.	Cr(4), Ce(2), Zr(2)	35	34.5
9.	Ti(4), Se(4), Be(5)	55	54.0
10.	Re(5), Ag(2)	15	15.0
11.	Ca(5), Ba(3), Sr(4)	60	61.0
12.	Bi(2), Sb(1), As(2)	17	16.0
13.	[Ag(0.053)][b]	80	80.0
14.	[Pt(0.05), Ni(0.15), V(0.025)][b]	50	50.0
15.	[Ru(0.004), Rh(0.001)][b]	100	100.0
16.	[Pt(2.85)][b]	90	90.0
17.	[Pt(0.071), Ni(0.0034)][b]	25	25.0
18.	Pd-charcoal catalyst (50 mg) Aldrich 20, 568-0	5%[c]	4.8%

a) Figure in brackets indicates the amount of the metal ion in mg. b) Sample Nos. 13, 14, 15, 16, and 17 are analogous to palladium-silver, palau, jewellery alloys, cooperite, and braggite ores, respectively. c) Reported value.

at constant acidity decreases in the following order $CH_3COOH > H_2SO_4 > HNO_3 > HClO_4 > H_3PO_4 > HCl$. Therefore, acetic acid is preferred for adjustment of pH of the solution.

The effect of various parameters namely, pH, reagent concentration and equilibration time on the absorbance of Pd(II) complex is depicted in Table 1. It is evident from the study of these variables, that for getting optimal absorbance for 50 μg Pd, pH 2.8—6.50, 0.7—5.0 ml (0.1% INAT in ethanol), 0.5—5 min shaking time are the necessary conditions to transfer quantitatively the colored species into chloroform, whose λ_{max} lies at 425 nm. The absorbance shows a downward trend if 1,2-dichloroethane, ethyl acetate, benzene, toluene, carbon tetrachloride, dichloromethane, and 1-pentanol, respectively, are used as extractant in place of chloroform.

Effect of Diverse Ion. Under the optimum conditions as given in the procedure, Os(VIII), Re(VII), Mo(VI), W(VI), Cr(III,VI), V(V), Ce(IV), Ti(IV), Se(IV), Pt(IV), Rh(III), As(III), Fe(II,III), Ni(II), Cu(II), Co(II), Mn(II), Zn(II), Cd(II), Hg(II), Be(II), Sr(II), Ba(II), Ca(II), Ag(I), each 1 mg ml^{-1}; in 20 ml aqueous volume, do not show any absorbance and hence are noninterfering.

Chloride (150), sulfate (400), nitrate (500), phosphate (100), acetate (100), citrate (150), tartrate (200), fluoride (75), oxalate (10), added initially to the aqueous phase, do not affect the absorbance of the Pd(II)-INAT complex. The figure in parentheses indicates the amount of sodium salt of the anion in milligram.

Spectral Studies and Stoichiometry of the Complex. The spectrum of the Pd(II)-INAT complex shows absorption maxima at 425 nm. Beer's law is obeyed in the range 0—4 μg Pd ml^{-1} with molar absorptivity of 3.27×10^4 $dm^3\,mol^{-1}\,cm^{-1}$ and Sandell's sensitivity is 0.003 μg Pd cm^{-2}. The ratio of metal to INAT in the extracted species is determined by Job's method of continuous variations[14] as modified by Vosburgh and Cooper[15] by taking equimolar solutions (1.8793×10^{-4} M, 1 M=1 mol dm^{-3}) of both Pd and INAT at three different wavelengths, namely, 400, 425, and 450 nm. The sharp break in the three curves obtained indicates that metal and INAT are present in the ratio of 1:2 in the complex. This is further confirmed by mole ratio method.[16]

Back Extraction. The metal ion of the Pd(II)-INAT complex in the organic phase can be easily stripped by shaking the organic phase with an equal volume of 0.5 M HCl.

Applications. The proposed method for the

Table 3. Comparison of the Proposed Method with the Existing Methods for Palladium Determination

Sr. No.	Aqueous conditions	Extractant λ_{max}	i) Beer's law range ii) Molar absorptivity iii) Sandell's sensitivity	Interfering ions	Comments	Reference
1.	10—100 μg Pd, 1 ml 2.5 M Perchloric acid, 10 ml *N,N*-dimethylformamide, 1 ml 0.1% (w/v) 3-nitroso-2,6-pyridinediol (in 9:1 water: *N,N*-dimethylformamide), heating for 20 min, in 25 ml volume	— 430 nm	i) 0.8—3.5 ppm of Pd ii) 2.6×10^4 $dm^3\ mol^{-1}\ cm^{-1}$ iii) 0.004 μg Pd cm^{-2}	Pt(IV), Ru(III) and Fe(III).	Tolerates only lower amounts of other ions of analytical interest.	17
2.	1—200 μg Pd, 2 ml 5 M acetic acid, in 10 ml volume	1% ethyl-2-(hydroxyimino)acetoacetate in $CHCl_3$ (10 ml), 400 nm	i) 0.1—20 μg Pd ml^{-1} ii) 9460 $dm^3\ mol^{-1}\ cm^{-1}$ iii) 0.011 μg Pd cm^{-2}	I^-, SCN^-, CN^-, EDTA, tartrate, citrate, oxalate, $S_2O_3^{2-}$, SO_3^{2-}, Cl^- interfere if not eliminated.	Requires different masking agents to check interference of several anions.	18
3.	Upto 50 μg Pd, 0.5 ml KI (0.1 M), 0.1 ml Hexadecyltrimethylammonium bromide (0.1 M), Pot. hydrogenphosphate–NaOH buffer (pH 6), in 10 ml volume	$CHCl_3$ (10 ml), 340 nm	i) upto 5 ppm of Pd ii) 2.038×10^4 $dm^3\ mol^{-1}\ cm^{-1}$ iii) 0.0052 μg Pd cm^{-2}	Pt(IV), Hg(II), Ag(I), SCN^-, SO_3^{2-}.	Behavior of Os(VIII), Rh(III), Ir(IV), Ru(III), not known.	19
4.	Palladium, 2-hydroxy-4-methoxy-5-chlorochalcone oxime at pH 2.5	Isobutyl alcohol, 380 nm	i) 1.4×10^{-5}—1.95×10^{-5} M (1.5—2.0 μg Pd ml^{-1}) ii) 0.73×10^4 $dm^3\ mol^{-1}\ cm^{-1}$ iii) 0.0145 μg Pd cm^{-2}	Au(III), Cr(III), Zr(IV), EDTA.	Since only C.A. is available, detailed information about the work could not be obtained.	4
5.	42 μg Pd, 3 ml of 1 M HCl, in 10 ml volume	1×10^{-3} M 2-Thiazolecarbaldehyde 2-quinolylhydrazone in C_6H_6 (10 ml), 625 nm	i) upto 4.2 μg Pd ml^{-1} ii) 1.93×10^4 $dm^3\ mol^{-1}\ cm^{-1}$ iii) 0.0055 μg Pd cm^{-2}	I^-, SCN^-, EDTA, Hg(II), Au(III), Re(VII), Ir(III), W(VI); low tolerance limits for Hg(II), Au(III), Re(VII), Ir(III), W(VI) which give yellow insoluble precipitates.	Pt(II) forms blue complex, behavior of Os(VIII), Rh(III), Ru(III) are not studied.	20
6.	50 μg Pd, 1 ml 0.1% INAT in ethanol, 5 ml buffer solution (Sodium acetate–acetic acid) pH (4.75—4.78), in 20 ml volume (PROPOSED METHOD)	$CHCl_3$ (20 ml), 425 nm	i) 0—4 μg Pd ml^{-1} ii) 3.27×10^4 $dm^3\ mol^{-1}\ cm^{-1}$ iii) 0.003 μg Pd cm^{-2}	26 Cations and 9 anions do not show any effect on the absorbance of Pd complex.	High sensitivity and selectivity, good tolerance limits, easy back extraction of the metal ion from the solvent.	(PROPOSED METHOD)

microdetermination of palladium is highly accurate and is free from the interference of a large number of elements especially the other platinum metals. The results are quite reproducible with a standard deviation of ±0.002. It compares favorably with the existing methods in terms of its sensitivity and selectivity (Table 3). Moreover, the recovery of Pd(II) from the organic solvent can be easily effected by simple back extraction. The validity of the method is further tested by analyzing satisfactorily several samples of varying complexity (Table 2).

Our sincere thanks are due to the Chairman, Department of Chemistry, Kurukshetra University, Kurukshetra for providing laboratory facilities and to UGC, New Delhi for financial support to one of us (AKC).

References

1) Y. P. Chang and N. Zhou, *Talanta,* **33**, 939 (1986).
2) G. Hernandez, R. Rodriguez, J. A. Silva, E. Chacon, and R. Mocelo, *Rev. Cubana Quim.,* **3**, 41 (1987).
3) D. Rao, K. H. Reddy, and D. V. Reddy, *Indian J. Chem., Sect. A,* **26**, 363 (1987).
4) B. K. Deshmukh and M. G. Awari, *Chem. Anal. (Warsaw),* **32**, 369 (1987).
5) J. Bankovskis and A. Ievins, *Zh. Anal. Khim.,* **13**, 507 (1958).
6) G. G. Lystsova, *Zavod. Lab.,* **28**, 543 (1962).
7) E. S. Prsheval'skii, V. I. Shlenskaya, and L. F. Maternykh, Ser. Fiz.-Mat.-i Estestven. Nauk No. 4, 71 (1954), *Chem. Abstr.,* **49**,96 (1955).
8) B. J. Desai and V. M. Shinde, *Fresenius' Z. Anal. Chem.,* **298**, 158 (1979).
9) U. B. Talwar and B. C. Haldar, *Anal. Chem.,* **38**, 1929 (1966).
10) B. J. Desai and V. M. Shinde, *Fresenius' Z. Anal. Chem.,* **295**, 412 (1979).
11) U. B. Talwar and B. C. Haldar, *Anal .Chim. Acta,* **39**, 264 (1967).
12) S. K. Majumdar, P. Chattopadhyay, and P. K. Paria, *J. Indian Chem. Soc.,* **62**, 544 (1985).
13) A. I. Vogel, "A Textbook of Quantitative Inorganic Analysis," 4th ed, Longman, London (1978), p. 474.
14) P. Job, *Ann. Chem.,* **9**, 113 (1928).
15) W. C. Vosburgh and G. R. Cooper, *J. Am. Chem. Soc.,* **63**, 437 (1941).
16) J. H. Yoe and A. L. Jones, *Ind. Eng. Chem., Anal. Ed.,* **16**, 111 (1944).
17) C. W. McDonald and J. H. Bedenbaugh, *Mikrochim. Acta,* **1970**, 474.
18) M. R. Patil and B. C. Haldar, *J. Indian Chem. Soc.,* **50**, 569 (1973).
19) T. K. Thokdar, P. K. Paria, and S. K. Majumdar, *Indian J. Chem., Sect. A,* **28**, 443 (1989).
20) T. Nakagawa, K. Doi, and M. Otomo, *Analyst,* **110**, 387 (1985).

Unusual Solvent Effect on the Cycloadditions of Aromatic Nitrile *N*-Oxide with Alkyl Substituted *p*-Benzoquinones in Ethanol-Water Systems

Yukihiko INOUE, Koji ARAKI, and Shinsaku SHIRAISHI*
Institute of Industrial Science, The University of Tokyo, Roppongi 7-22-1, Minato-ku, Tokyo 106
(Received March 18, 1991)

The second-order rate constants of 1,3-dipolar cycloaddition reactions of 2,6-dichlorobenzonitrile *N*-oxide (**1**) with 2,5-dimethyl-*p*-benzoquinone (**2a**) or 2,6-diisopropyl-*p*-benzoquinone in various solvents at 20 °C were determined by spectrophotometric method. The rate of **1** and **2a** in ethanol : water=60 : 40 solution was 5.55×10^{-2} $dm^3\,mol^{-1}\,s^{-1}$, which was fourteen folds of that in chloroform (3.9×10^{-3} $dm^3\,mol^{-1}\,s^{-1}$). This solvent effect and the low solubility of the cycloadduct in aqueous ethanol were successfully applied to the cycloadduct synthesis.

Aromatic nitrile *N*-oxides undergo 1,3-dipolar cycloaddition with alkyl di-substituted *p*-benzoquinones (**2**) at their C=C double bond to give cyclohexenedione-fused 2-isoxazoline derivatives (**3**) in good yields.[1] Some of the cycloadducts were isomerized into isoxazole derivatives by base-induced ring system transformation,[2] and subsequently by dienone–phenol rearrangement-like reaction into isoxazole-fused catechol derivatives (**4**), which exhibit barnaclecide activity.[3]

In the synthetic pathway to the potentially useful compounds, the step of the nitrile *N*-oxide cycloaddition is desirable to enhance the reaction rate and to simplify workup processes involved. In benzene solution, the reaction had to be carried out for a day to complete the reaction. The product could be obtained after chromatographic separation and subsequent recrystallization to remove unreacted quinone. The rate constants of nitrile *N*-oxide cycloaddition in various solvents were reported mostly in the early seventies.[4] In general, there is little or only a little solvent effect on the rate, and an increase of solvent polarity causes slight decrease of the rate in the cycloaddition. Chang et al. reported[5] that the rate constant of cycloaddition of 2,4,6-trimethylbenzonitrile *N*-oxide with 1,2-bis(trifluoromethyl)fumaronitrile in acetone-d_6 was fourteen times smaller than that in benzene-d_6. This is the only report of solvent effect on the cycloaddition of nitrile *N*-oxide to a C=C double bond exhibiting over ten folds difference. Recently, Breslow and Rideout reported remarkable rate acceleration for the Diels–Alder reaction in aqueous media.[6] Therefore, it is of interest to investigate the cycloaddition reactivity of nitrile *N*-oxide in aqueous solution. As far as we know, the reactions of nitrile *N*-oxides with bases or other nucleophiles in aqueous dioxane solution were the only report of the reaction of nitrile *N*-oxides in aqueous solution[7] and no report has appeared to date as to the 1,3-dipolar cycloaddition of nitrile *N*-oxides in aqueous media.

In the present research, we have examined the cycloaddition reaction of nitrile *N*-oxide with substituted *p*-benzoquinones in aqueous ethanol or other organic solvents in order to optimize the cycloaddition conditions.

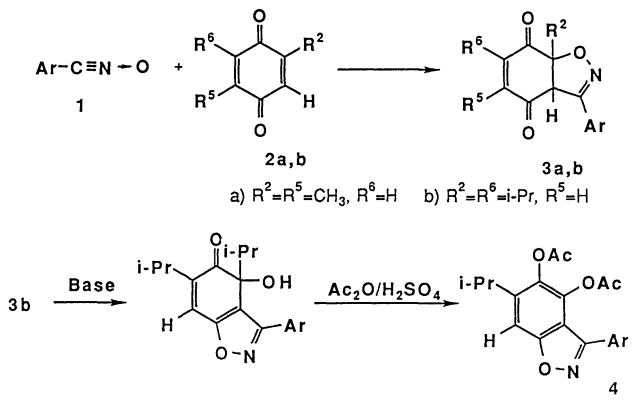

Scheme 1. Cycloaddition reaction of nitrile *N*-oxide with alkyl substituted *p*-benzoquinones (**2a**—**b**) and subsequent ring conversion reaction of the cycloadduct **3b**.

Experimental

Electronic spectra were recorded with JASCO Ubest-50 spectrometer. IR spectra of the nitrile *N*-oxide solutions were recorded with JASCO IR-700 spectrometer in KRS cell (cell length 0.1 mm). Liquid chromatography was performed with ODS column (Cica-Merck LiChrospher 100 RP-18, acetonitrile : water=70 : 30, UV 254 nm). All the reactions and measurement were carried out at 20 °C.

Reagents and Solvents. 2,6-Dichlorobenzonitrile *N*-oxide (**1**) was prepared from corresponding benzaldehyde oxime by Grundmann's method[8] and recrystallized from aqueous ethanol. All the procedures were carried out keeping temperature below 40 °C to avoid isomerization. 2,5-Dimethyl-*p*-benzoquinone (**2a**) and 2,6-diisopropyl-*p*-benzoquinone (**2b**) were synthesized from corresponding alkyl-substituted phenols by oxidation using sodium dichromate–sulfuric acid.[9] Recrystallization from hexane and vacuum distillation were used for the purification of **2a** and **2b**, respectively. Organic solvents were obtained commercially and used after distillation with desiccants. Ion-exchanged water was further purified by ultrafiltration. Composition of the water-ethanol mixture was reported in volume per cent.

The Reactions of 1 with 2a; Kinetic Study. A sample solution containing **1** and **2a** (1.00×10^{-2} mol dm^{-3} for each of the reactant) was prepared freshly, and the progress of the reaction was monitored by spectrometer at 20 °C. Amounts

of the product (**3a**) were calculated from the absorbance around 380 nm, where n–π^* absorption of **3a** was observed. The rate constants k_2 were determined according to the second-order rate equation. The same procedure was applied for determination of rate constants of **1** and **2b**.

The Reactions of 1 with 2b; Syntheses of 7-(2,6-Dichlorophenyl)-1,3-diisopropyl-8-aza-9-oxa-[4.3.0]bicyclonona-3,7-diene-2,5-dione (3b). The reactions were carried out with 1.00 mmol for each of the reactant. Stirring conditions were kept at constant throughout all experiments. The progress of the reaction was followed by HPLC analyses. In all experiments, only the formation of **3b** was observed up to 60 min. The conversions were calculated from the peak intensity of unreacted **2b**. After the reaction, precipitated **3b**, if existed, was collected by filtration, dried in vacuo, and weighed.

Results and Discussion

The Kinetic Investigation of the Cycloaddition Reaction of 1 with 2a. The reactions of **1** with **2a** were carried out in various solvents. Figure 1 represents the typical spectral change during the reaction in ethanol. In all cases, isosbestic points were observed throughout the spectral change, and the time course of the reaction followed the second-order rate equation. Therefore, contribution of side reactions such as nitrile *N*-oxide isomerization or dimerization was thought negligible under these reaction conditions. IR spectra of the product isolated from the reaction mixture was identical with that of an authentic sample of **3a**. The rate constants of these reactions were summarized in Table 1.

In the case of organic solution, the reaction was slowest in chloroform and only four folds differences were observed for the solvents examined. But in ethanol : water=60 : 40 solution, over fourteen folds of acceleration compared to that in chloroform was observed. Further increase of water content resulted in precipitation of the product (**3a**) during the reaction, and the rate constants in aqueous ethanol containing more than 60 vol% could not be determined. Logarithmic plot of the rate constants vs. solvent polarity parameters, dielectric constants (ε),[10] and E_T values,[11] are shown in Fig 2.

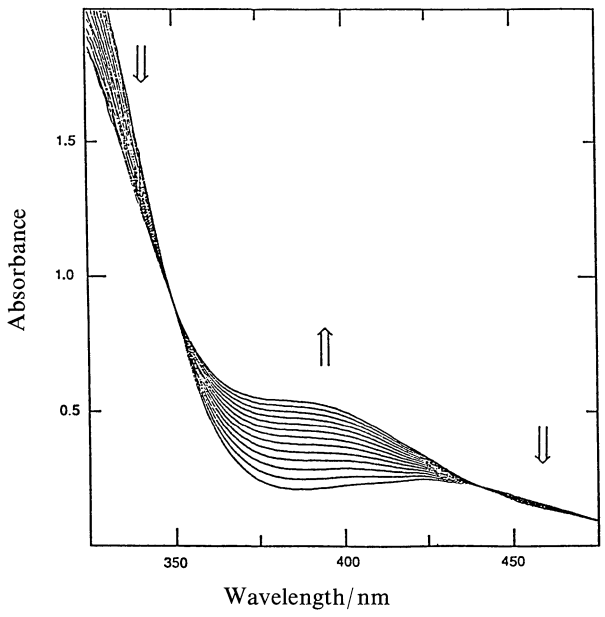

Fig. 1. Electronic spectra of **1** and **2a** in ethanol from 4 min to 64 min after the reaction was started. Substrate concentration; 1.00×10^{-2} mol dm^{-3}, Reaction temperature 20 °C.

Both curves have concave shapes, suggesting that the mode of solvent effect on the reaction is different in lower and higher region of the solvent polarity. At the lower side of the solvent polarity from cyclohexane to chloroform, the rate constants decreased as the polarity increased. In this region, rate constants exhibited normal correlation with solvent polarity.[4] But in the solvents of higher polarity, the rate constants increased as the polarity increased. Furthermore, the rate constant in ethanol : water=60 : 40 solution was fourteen times larger than that in chloroform. This solvent-induced rate acceleration is fairly large as the solvent effect on 1,3-dipolar cycloaddition reaction to C=C double bond. It is reported that the reaction of 2,4,6-trimethylbenzonitrile *N*-oxide and 1,2-bis(trifluoromethyl)fumaronitrile exhibits similar extent of solvent effect.[5] This reaction in acetone-d_6 containing water is fourteen times slower than that in benzene-d_6. In this reaction, the increase of solvent polarity caused the decrease of the rate constant. This is therefore still within the category of the normal solvent effect on 1,3-dipolar cycloaddition. However, the reaction of **1** and **2a** was accelerated in highly-polarized aqueous ethanol solvent. No other report of solvent effect exhibiting over ten folds of rate constants difference has appeared as nitrile *N*-oxide cycloaddition to C=C double or C≡C triple bond, and the results presented here are the unusual type of solvent effect on the nitrile *N*-oxide cycloaddition.

To understand this solvent effect, we tested the effect of solvation to the substrates (**1** and **2a**) and to the

Table 1. The Rate Constants of the Reactions of 2,6-Dichlorobenzonitrile *N*-Oxide (**1**) with 2,5-Dimethyl-*p*-benzoquinone (**2a**)[a] at 20 °C

Solvents	$k_2\times10^3$ [b]/dm^3 mol^{-1} s^{-1}	
Cyclohexane	17.0	(4.4)
Benzene	5.5	(1.4)
o-Xylene	8.0	(2.1)
Chloroform	3.9	(≡1)
Ethyl acetate	5.4	(1.4)
Acetonitrile	7.1	(1.8)
Dimethyl sulfoxide	14	(3.5)
N,*N*-Dimethylacetamide	11	(2.8)
Ethanol	14.6	(3.8)
Ethanol : water=80 : 20	32.8	(8.5)
Ethanol : water=60 : 40	55.5	(14.2)

a) Substrate concentrations 1.00×10^{-2} mol dm^{-3}.
b) The numbers in parentheses represents the relative rate to that in chloroform.

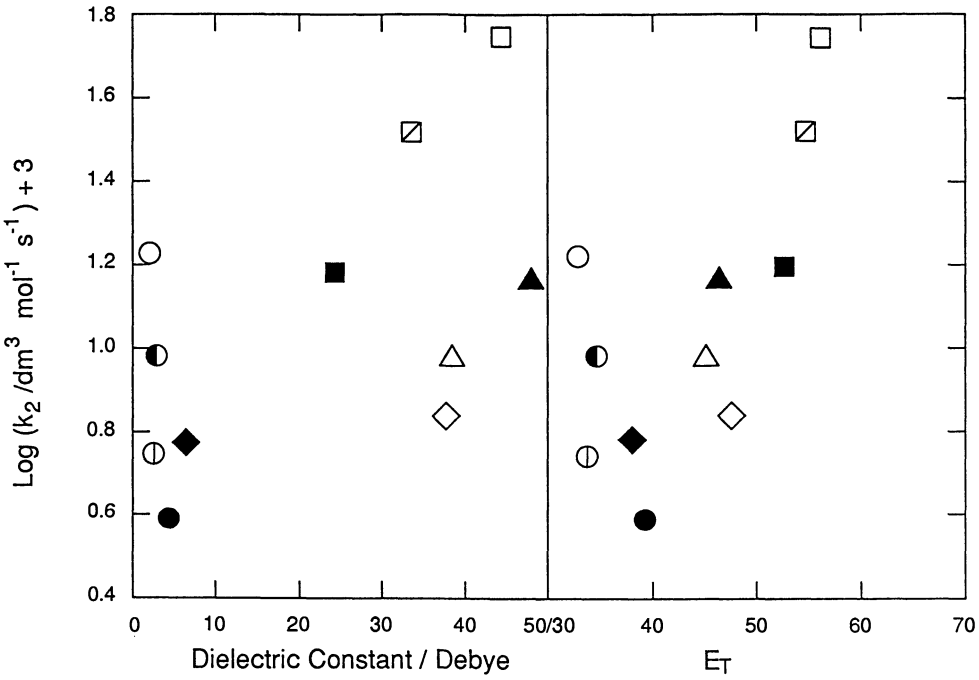

Fig. 2. The reaction of 2,6-dichlorobenzonitrile *N*-oxide (**1**) with 2,5-dimethyl-*p*-benzoquinone (**2a**); plot of log k_2 vs. dielectric constant (ε) of the solvent and solvent parameters E_T.
○; cyclohexane, ⦶; benzene, ◐; *o*-xylene, ●; chloroform, ◆; ethyl acetate, ◇; acetonitrile, △; dimethyl sulfoxide, ▲; *N,N*-dimethylacetamide, ■; ethanol, ▨; ethanol : water=80 : 20, □; ethanol : water=60 : 40.

Table 2. $\nu_{C\equiv N}$ of **1** in Solutions

Solvents	Wavenumber/cm^{-1}
Cyclohexane	2287
Benzene	2298.5
Chloroform	2306
Ethyl acetate	2301.5
Ethanol	2301
Ethanol : water=80 : 20	2303.5
Ethanol : water=60 : 40	2308.5
Solid (KBr pellet)	2306

Table 3. Absorption Maxima of **2a** in Various Solvents at 20 °C

Solvents	λ_{max}/nm (log ε)		
Cyclohexane	446(1.39)	306(2.49)	251(4.37)
Benzene	442(1.40)	a)	a)
Chloroform	432(1.45)	317(2.46)	254(4.43)
Ethyl acetate	438(1.38)	312(2.44)	a)
Ethanol	425(1.39)	313(2.44)	251(4.32)
Ethanol : water=80 : 20	425(1.45)	318(2.46)	253(4.37)
Ethanol : water=60 : 40	424(1.46)	322(2.43)	254(4.32)

a) Could not be determined due to the absorption of solvent.

product (**3a**) by spectroscopic method. Peak positions of C≡N stretching band of **1** ($\nu_{C\equiv N}$) in several solvents are summarized in Table 2, which might reflect the solvation to the nitrile *N*-oxide moiety of **1**. The $\nu_{C\equiv N}$ increase monotonously as the solvent polarity increased (except for chloroform), and the direct relationship between $\nu_{C\equiv N}$ and rate constants was not observed.

Absorption maxima of **2a** in different solvents are shown in Table 3. The band above 400 nm is assigned to be an n–π^* transition band and the stronger two bands are due to π–π^* transitions.[12] These three bands exhibited ordinary solvatochromic shifts, i.e., hypsochromic shift for n–π^* and smaller bathochromic shift for π–π^* as solvent polarity increased.

Table 4. Absorption Maxima of the n–π^* Band of **3a** in Various Solvents at 20 °C

Solvents	λ_{max}/nm (log ε)
Cyclohexane	390 (2.10)
Benzene	389 (2.11)
Chloroform	388 (2.10)
Ethyl acetate	385 (2.10)
Ethanol	384 (2.10)
Ethanol : water=80 : 20	384 (2.07)
Ethanol : water=60 : 40	383 (2.07)

The effect of solvation to the product (**3a**) was examined by electronic spectroscopy. Table 4 shows the absorption maxima of n–π^* transition of **3a**. The band exhibited hypsochromic shift monotonously and the molar extinction coefficient of the absorption slightly decreased as solvent polarity increased. These results did not reproduce the different mode of solvent effect,

and the observed rate difference could not be explained from the solvation of substrates or product. Therefore, other reasons, such as cage effect of the solvent or solvophobic effect[6] of the substrates, may play a role in this unusual solvent effect.

Synthetic Application of Unusual Solvent Effect in Aqueous Ethanol Solutions. The Reaction of 1 with 2b. In an ethanol: water=50: 50 solution, the precipitate of cycloadduct **3a** was formed soon after the solutions of **1** and **2a** were mixed, and the measurement of the time course of the reaction by electronic spectrum was unsuccessful. But this fact indicated that aqueous ethanol system offered two advantage over organic solvent systems from synthetic point of view. One is acceleration of the reaction rate and the other convenient isolation of the product. Therefore, we applied this solvent system to the cycloadduct synthesis.

For this purpose, 2,6-diisopropyl-*p*-benzoquinone (**2b**) was employed as a quinone reactant because the cycloadduct **3b** can be converted to isoxazole-fused catechol derivatives by base-catalyzed rearrangement.

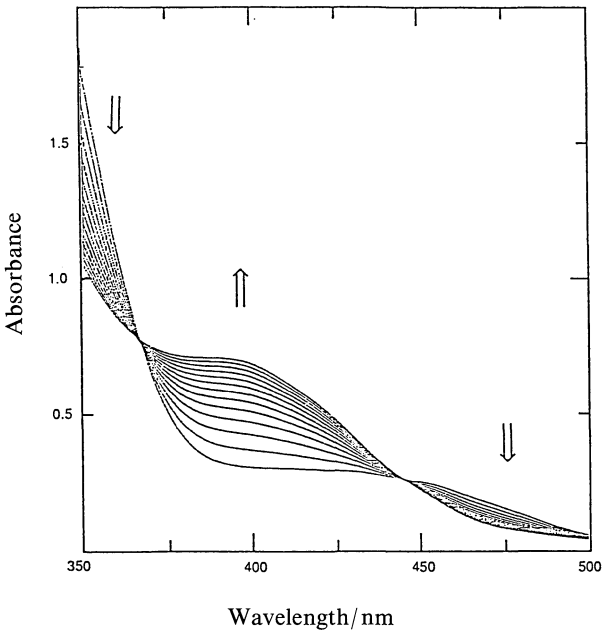

Fig. 3. Electronic spectra of **1** and **2b** in ethanol from 4 min to 64 min after the reaction was started. Substrate concentration; 1.00×10^{-2} mol dm^{-3}, Reaction temperature 20 °C.

Second order rate constants of **1** and **2b** in homogeneous media were determined by spectrophotometric method. Electronic spectra showed isosbestic points throughout the reaction, indicating the reaction proceeded without any side reactions (Fig. 3). The results are shown in Table 5. The rate constants are about twice as large as those of **1** and **2a**, and solvent effect on the rate is essentially the same as that on the reaction of **1** and **2a**. It was reported in the previous papers[13] that the reactions of **1** and **2a** or **2b** were mainly controlled by HOMO(quinone)–LUMO(nitrile *N*-oxide) interaction. Therefore, the difference between the rate constants of **1** and **2a** and those of **1** and **2b** could be ascribed to the electron donating effect of isopropyl substituents of **2b**.

In this reaction, the formation of a precipitate of **3b** was observed in ethanol: water=60: 40 system. The reaction in millimolar scale was carried out in this solvent system, and the results were shown in Table 6. Conversions determined from unreacted **2b** showed good correlation with the rate constants shown in Table 5. In the case of benzene which is frequently used as a solvent for cycloaddition of nitrile *N*-oxide, 69% of unreacted **2b** remained in the reaction mixture after 30 min. But in ethanol: water=60: 40 solvent, the reaction almost completed within 30 min and 77% of **3b** could be isolated as a precipitate by simple filtration. The filtrate was pure **3b** containing neither unreacted quinone nor nitrile *N*-oxide, and this filtrate could be used directly for the subsequent base-induced rearrangement without further purification.

In conclusion, cycloaddition reactions of nitrile *N*-oxide with quinones exhibited unusual solvent effect and were accelerated in aqueous ethanol. In this reaction, the cycloadduct could be isolated as a precipitate in pure form. Therefore the synthesis of cycloadduct was successfully optimized.

Table 5. The Rate Constants of the Reactions of 2,6-Dichlorobenzonitrile *N*-Oxide (**1**) with 2,6-Diisopropyl-*p*-benzoquinone (**2b**) at 20 °C[a]

Solvents	$k_2\times10^3$/dm^3 mol^{-1} s^{-1}
Benzene	9.8
Ethanol	29.1
Ethanol: water=80: 20	59.8

a) Substrate concentrations 1.00×10^{-2} mol dm^{-3}.

Table 6. The Reactions of 2,6-Dichlorobenzonitrile *N*-Oxide (**1**) with 2,6-Diisopropyl-*p*-benzoquinone (**2b**) at 20 °C[a]

Solvents	Conversions/%[b]		(Yield/%)
	30 min	60 min	
Benzene	31	54	(86%, 5 day[c])
Ethanol	52	63	
Ethanol: water=80: 20	64	80	
Ethanol: water=60: 40	81	87	(77% as precipitate, 1 hour)

a) Substrate concentrations 2.00×10^{-2} mol dm^{-3}. b) Calculated from unreacted **2b**. c) Ref. 1.

References

1) S. Shiraishi, B. S. Holla, and K. Imamura, *Bull. Chem. Soc. Jpn.*, **56**, 3457 (1983).

2) S. Shiraishi, B. S. Holla, and K. Imamura, 16th Congress of Heterocyclic Chemistry, Osaka, Japan, 1984, Abstr., 2B-15.

3) S. Shiraishi, Unpublished. A part of the data was presented by The Japanese–United States Congress of Pharmaceutical Sciences, Honolulu, Hawaii, 1987, Symposia Abstr., p. 130.

4) P. Caramella and P. Grünanger, in "1,3-Dipolar Cycloaddition Chemistry," ed by A. Padwa, John and Wiley Inc. (1983), Vol. 1, Chap. 3, and references sited therein.

5) Y. M. Chang, J. Sims, and K. N. Houk, *Tetrahedron Lett.*, **1975**, 4445.

6) R. Breslow and D. Rideout, *J. Am. Chem. Soc.*, **102**, 7816 (1980).

7) K. J. Dignam, A. F. Hegarty, and P. L. Quain, *J. Chem. Soc., Perkin Trans. 2*, **2**, 1457 (1977); *J. Org. Chem.*, **43**, 388 (1978).

8) C. Grundmann and J. M. Dean, *J. Org. Chem.*, **30**, 2809 (1965).

9) D. Liotta, J. Arbiser, J. W. Short, and M. Saindane, *J. Org. Chem.*, **48**, 2932 (1983).

10) G. P. Srivastava and Y. P. Varshini, *Z. Phisik. Chem.*, **213**, 304 (1960).

11) C. Reichardt and E. Harbusch-Gornert, *Liebigs Ann. Chem.*, **1983**, 721.

12) St. Berger and A. Rieker in "The Chemistry of the Quinonoid Compounds," ed by S. Patai, John Wiley & Sons Inc., New York (1974), Part 1, Chap. 4.

13) T. Hayakawa, K. Araki, and S. Shiraishi, *Bull. Chem. Soc. Jpn.*, **57**, 1643 (1984).

Absolute Stereochemistry and Novel Ring-Opening Oxidation of Methyl (*R*)-2-Hydroxysterculate

Munehiro NAKATANI and Tsunao HASE
Department of Chemistry, Faculty of Science, Kagoshima University, 1-21-35 Korimoto, Kagoshima 890
(Received March 22, 1991)

A cyclopropene-ring-containing fatty acid ester, methyl (*R*)-2-hydroxysterculate, was isolated from *Hibiscus rosa-sinensis* along with methyl sterculate and malvalate. The stereochemistry of the asymmetric carbon at C-2 was determined as *R* by applying a dibenzoate chirality method, and a mild air oxidation afforded two conjugated enone isomers accompanying a ring opening.

In continuous study on the seed germination inhibitors from *Hibiscus rosa-sinensis* (Malvaceae),[1,2] we isolated a third cyclopropene-ring-containing fatty acid ester, methyl (*R*)-2-hydroxysterculate (**1**), from the methanol extract of the root bark along with two known cyclopropenoids, methyl sterculate (**2**)[3] and malvalate (**3**).[4] Although these compounds **1**—**3** may be present as free acids or glycerides in the plant, they also showed inhibitory activites to lettuce seed germination.

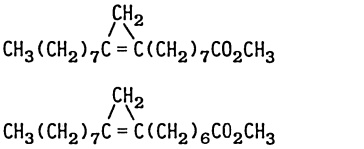

2

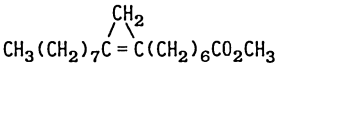

3

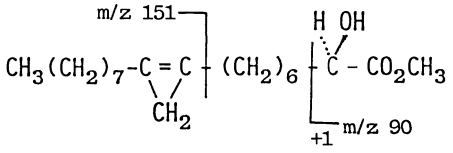

1

Compounds containing cyclopropane or cyclopropene ring in a fatty acid chain have been known to affect strongly insect metabolism.[5–9] The cyclopropenoids of sterculic acid, malvalic acid and their methyl esters (**2** and **3**), when fed to some noxious insects, sterilized their females[5,6] and reduced pupation and pupal weight of their larvae.[7,8] Therefore, 2-hydroxysterculate (**1**) is also expected to have similar activities against insects.

2-Hydroxysterculic acid was first isolated from alkaline hydrolysis products of glycerides from *Pachra* and *Bombacopsis* oil, and the stereochemistry at C-2 of the methyl ester **1** was inferred as *R* from the specific rotation ($[\alpha]_D$ −5.1°) by analogy with some α-hydroxy acid methyl esters.[10] We have now confirmed it unambiguously from the CD spectrum of a 1,2-*O*-dibenzoyl derivative **6** by applying the dibenzoate chirality method of Harada and Nakanishi.[11]

Some cyclopropenoids were known to be sensitive to air and to give polymerized mixtures.[12] A mild oxidation of **1** with air afforded a pair of conjugated enone isomers, methyl 2-hydroxy-10-methylene-9-oxooctadecanoate (**7**) and methyl 2-hydroxy-9-methylene-10-oxooctadecanoate (**8**). We also describe this novel ring opening oxidation.

Results and Discussion

Compound **1** ($C_{20}H_{36}O_3$; $[\alpha]_D$ −10°), 2.8 mg, was isolated from the root bark (1.5 kg) and identified as methyl 2-hydroxysterculate by spectrometry. It showed the presence of hydroxyl (3500 cm^{-1}) and methoxycarbonyl (1740 cm^{-1}) groups and a 1,2-disubstituted cyclopropene ring [^{1}H NMR: δ=0.77 (2H, s) and ^{13}C NMR: δ=7.4 (t), 109.2 (s), and 109.5 (s)]. The presence of the hydroxyl group on 2-position was deduced from the ^{1}H NMR and MS spectra (see Experimental). The position of the cyclopropene ring in the chain was determined by a prominent peak at *m/z* 151, corresponding to fission α to the cyclopropene ring, which was also observed (see Experimental) in the MS of methyl sterculate (**2**) and malvalate (**3**).

Stereochemistry at C-2. Several approaches to determine the configuration of chiral alcohols have been reported,[13–15] in which CD method provides better means to determine the absolute configuration of a small amount of chiral compound having suitable UV chromophores which give Cotton effects reflecting the absolute stereochemistry. We prepared a 1,2-dibenzoate **6** from **1** according to Scheme 1 and applied the dibenzoate chirality method of Harada and Nakanishi[11] for the determination of the stereochemistry of the asymmetric carbon at C-2.

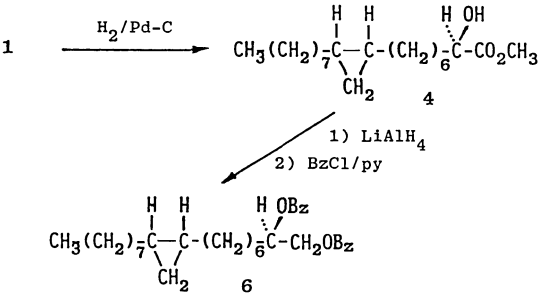

Scheme 1.

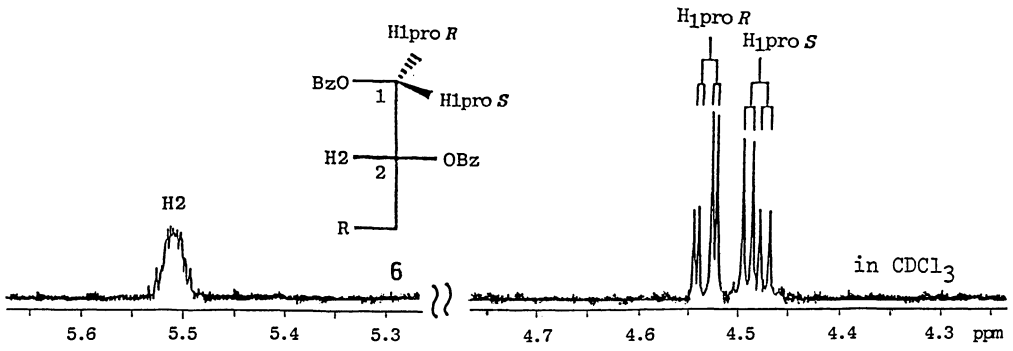

Fig. 1. The 400 MHz ^{1}H NMR spectrum of compound **6**.

The cyclopropenoid **1** was hydrogenated over palladium catalyst to give a saturated ester **4**, which should be a diastereoisomeric mixture but it showed one spot on TLC. Signals of a 1,2-disubstituted cyclopropane ring were observed at δ=−0.33 and 0.56 (1H each, $\underline{CH}_2$ / \ -CH-CH-) and 0.65 (2H, -C$\underline{H}$-C$\underline{H}$-) in the ^{1}H NMR and at δ=11.2, 16.3, and 16.3 in the ^{13}C NMR. The ester **4** was in turn reduced with lithium aluminium hydride to give a 1,2-diol **5** [^{1}H NMR: δ=3.46 and 3.65 (1H each, -CH(OH)C$\underline{H}_2$OH) and 3.72 (1H, -C$\underline{H}$(OH)-CH_2OH)]. The 1,2-dibenzoate **6** was prepared by acylation of **5** with benzoyl chloride in pyridine in the presence of a catalytic amount of 4-dimethylaminopyridine.

The ^{1}H NMR spectrum of the dibenzoate **6** showed two geminal protons due to the benzoyloxymethylene group at δ=4.48 (1H, dd, J=11.7 and 6.8 Hz) and 4.53 (1H, dd, J=11.7 and 3.4 Hz) (Fig. 1). The proton at higher field and with larger vicinal coupling constant was assigned to the H_1-pro-*S* in the case having 2*R* configuration and to the H_1-pro-*R* in 2*S*.[16] The assignment of the two prochiral protons at C_1 and an application of the Karplus type equation proposed by Haasnoot et al.[17,18] revealed that **6** existed predominantly in a *gt* conformer in the solution (see Fig. 2) and its population was 58% in $CDCl_3$ and 62% in CD_3OD (Table 1).

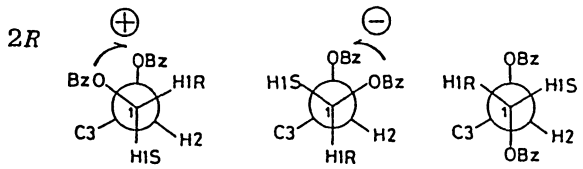

Fig. 2. Three possible conformers, *gg*, *gt*, and *tg*, in 2*R* about the C_1–C_2 bond.

The CD spectrum (Fig. 3) of **6** gave a negative exciton coupled CD having the first band at 237 nm with a negative sign and the second band at 224 nm with a positive one. The CD peaks can be attributed to the interaction between the di-*O*-benzoyl chromophores at C_1 and C_2, and the negative sign of the Cotton effect indicates that C_1–O and C_2–O bonds adopt a negative helicity, namely, *gt* conformation in 2*R* and *gg* in 2*S* (Fig. 2): there exist three kinds of staggered conformations in each case of 2*R* and 2*S*, namely, *gg*, *gt*, and *tg* about C_1–C_2 axis. In 2*R*, conformer *gt* of the C_1–C_2 bond should have a negative contribution, while conformer *gg* should have a positive contribution to the exciton coupling. On the other hand, the reverse contributions should be predictable in 2*S*. Here, the contribution of conformers *tg* with the antiperiplanar disposition of the two benzoyloxy groups will be negligible.

The results of the conformational analysis by NMR spectroscopy and the CD study revealed the absolute

Table 1. ^{1}H NMR Data of 1,2-Dibenzoate **6** (400 MHz)

Solvent	Chem. shift δ	Assign	$^1J_1$/Hz	$^1J_2$/Hz	Population (%)[a]		
					gg	*gt*	*tg*
$CDCl_3$	4.48	H_1-pro-*S*	11.7	6.8	37	58	5
	4.53	H_1-pro-*R*		3.4			
CD_3OD	4.46	H_1-pro-*S*	12.1	6.8	35	62	3
	4.62	H_1-pro-*R*		3.2			

a) Calculation from J(H_1-pro-*R*, H_2) and J(H_1-pro-*S*, H_2) values according to the following equations of Haasnoot et al. based on the Karplus equation (Refs. 17, 18).

$$2.8gg + 3.1gt + 10.7tg = J_{H_1\text{-pro-}R,\,H_2} \quad (1)$$
$$0.9gg + 10.7gt + 5.7tg = J_{H_1\text{-pro-}S,\,H_2} \quad (2)$$
$$gg + gt + tg = 1 \quad (3)$$

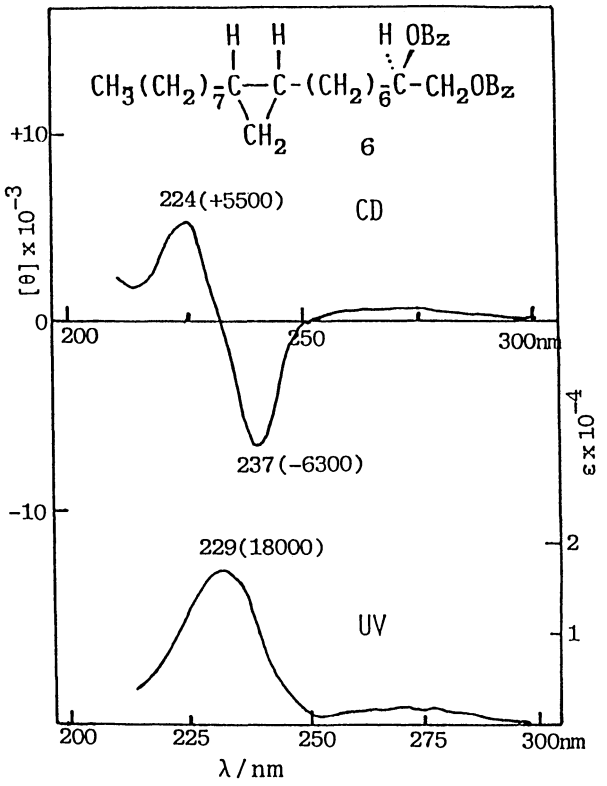

Fig. 3. CD and UV spectra of **6** in MeOH.

configuration of C-2 to be *R*.

Ring-Opening Air Oxidation. Without the bubbling air, compound **1** was slowly oxidized by air at room temperature and, after 2 weeks, completely changed to give a 1 : 1 mixture of isomers **7** and **8** (Scheme 2).

The MS spectra of **7** and **8** both indicated the same molecular formula of $C_{20}H_{36}O_4$ and their UV spectra also resembled each other to show the presence of a conjugated enone system at λ_{max} 228 nm. Signals in the ^1H and ^{13}C NMR spectra of **7** suggested the presence of a 1,1-disubstituted ethylene double bond [δ=5.70 (1H, s) and 5.97 (1H, s), and δ=124.1 and 149.2] and two carbonyl groups [δ=175.9 and 202.6] as well as a methine bearing an OH group [δ=4.21 (1H, m) and 70.4]. These data suggested that **7** had a conjugated enone system containing a side-chain methylene group instead of the cyclopropene ring in **1**. A comparison of the ^1H and ^{13}C NMR of **8** with those of **7** indicated that the two compounds had nearly identical structures and differed from one another only in the location of the enone system, and they were similar type isomers with the air-oxidation products from methyl sterculate (**2**) and malvalate (**3**) reported recently by us.[19]

Unequivocal support for their structures were obtained from their MS fragmentations. The position of the CO group in **7** has been assigned to C-9 since the significant α- and β-fission ions were obtained at m/z 167 and 182, respectively. On the other hand, **8** showed a different fragmentation to give a characteristic rearranged peak at m/z 180 and a peak at m/z 154 due to a successive loss of HC≡CH, along with a β-cleaved ion peak to the CO group at m/z 98.

These enone isomers would have been produced by a singlet oxygen attack to either of the two olefinic carbons of cyclopropene ring in **1**. Compounds **7** and **8** were also sensitive to air to give gradually a complex mixture at room temperature.

Cyclopropenoid fatty acids, sterculic acid and malvalic acid, are constituents of the seed oils of many species of the natural order Malvales and have been recognized to occur generally together, one or other being predominant according to species. The structures of these cyclopropenoid acids suggest that malvalic acid may be derived from sterculic acid by a biological α-oxidation mechanism. Evidence for this suggestion has been obtained from an incubation experiment using radioactivity labelled acetate[20] so that, if malvalic acid was derived from sterculic acid in this way, 2-hydroxysterculate (**1**) would be an intermediate to malvalate (**3**).

The occurrence of the oxidation products, **7** and **8**, in *Hibiscus* has not been observed yet, but the possibility is present at least on compound **7** because two analogs, methyl 10-methylene-9-oxooctadecanoate and 9-meth-

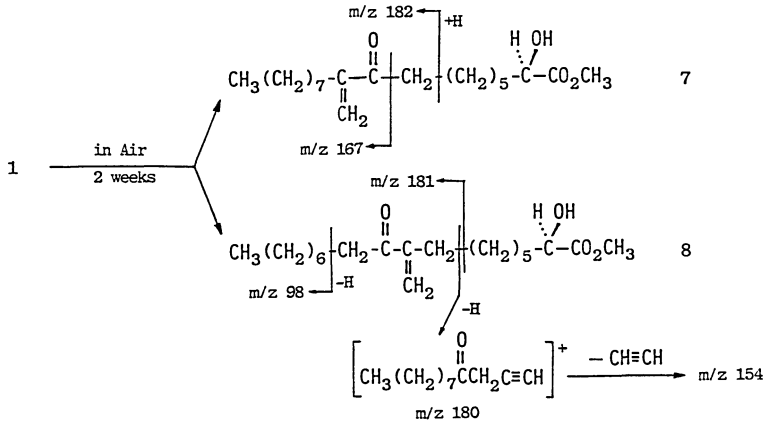

Scheme 2.

ylene-8-oxoheptadecanoate, respectively derived by air oxidation from sterculate (**2**) and malvalate (**3**), have been isolated from it.[2] The isolation study of **7** is now in progress.

Experimental

IR and UV spectra were recorded on Shimadzu IR-408 and UV-210A spectrophotometers, respectively. ^{1}H and ^{13}C NMR spectra were measured in $CDCl_3$ at 400 and 100 MHz using a JEOL FX-400 spectrometer. Mass spectra were recorded on a JEOL D-300 spectrometer. Optical rotation and circular dichroism (CD) were measured using a JASCO J-20A spectropolarimeter.

Plant Material. The root bark of *H. rosa-sinensis* was collected at Amami-Oshima (Amami Islands) in August 1988.

Isolation. The fresh root bark (1.5 kg) was extracted with MeOH. The acetone-soluble part afforded an oil containing a viscous material (Fraction A) to be separated, each of which was fractionated twice by flash chromatography on SiO_2 with CH_2Cl_2–hexane. Final purification by repeated passage through an HPLC, Waters μ-bondasphere semiprep column, using a solvent system of MeCN–H_2O gave 2.8 mg of **1** and two known cyclopropene esters **2**[3] (54.2 mg) and **3**[4] (81.6 mg). The solvent evaporation was performed at 40 °C under reduced pressure under nitrogen and the resulting products were also stored under nitrogen atmosphere.

Methyl 2-Hydroxysterculate (1). A colorless sirup; $[\alpha]_D^{24}$ −10° (*c* 0.083, $CHCl_3$); IR (liq. film) 3500, 1740, 1200 cm^{-1}; UV (MeCN) 212 nm (ε 2700); ^{1}H NMR δ=0.77 (2H, s, C$\underline{H}_2$ of cyclopropene ring), 0.88 (3H, t, *J*=6.6 Hz, 18-H), 1.25—1.37 (16H, m), 1.54 (4H, m, 7- and 12-H), 1.65 (1H, m, 3-H), 1.80 (1H, m, 3-H), 2.37 (4H, t, *J*=7.0 Hz, 8- and 11-H), 2.67 (1H, d, *J*=5.9 Hz, O$\underline{H}$, exchangeable with D_2O), 3.79 (3H, s, OC$\underline{H}_3$), 4.20 (1H, dt, *J*=4.4 and 7.0 Hz, 2-H); ^{13}C NMR δ=7.4 (C$\underline{H}_2$ of cyclopropene ring), 14.1 (C-18), 22.7 (C-17), 24.7 (C-4), 2×26.0 (C-8 and 11), 27.3 (C-7), 27.4 (C-12), 29.1, 29.3, 2×29.4, 31.9 (C-16), 34.4 (C-3), 52.5 (O$\underline{C}$H$_3$), 70.5 (C-2), 109.2 (C-9), 109.5 (C-10), 175.8 (C-1); EIMS *m/z* 324 (4, M$^+$), 265 (5), 165 (11), 151 (14), 149 (12), 109 (34), 95 (81), 90 (54), 81 (base peak), 68 (73), 67 (59), 55 (52), 42 (75). Found: *m/z* 324.2612. Calcd for $C_{20}H_{36}O_3$: M, 324.2613.

Methyl Sterculate (2). ^{13}C NMR δ=7.4, 14.1, 22.7, 25.0, 26.0, 26.1, 27.3, 27.4, 29.0, 29.1, 29.2, 29.3, 2×29.4, 31.9, 34.1, 51.5, 109.2, 109.5, 174.3; EIMS *m/z* 308 (M)$^+$, 277, 151, 109, 95, 81, 68, 55, 42.

Methyl Malvalate (3). ^{13}C NMR δ=7.4, 14.1, 22.7, 24.9, 26.0, 27.3, 27.4, 29.0, 29.1, 29.2, 29.3, 2×29.4, 31.9, 34.1, 51.4, 109.2, 109.5, 174.3; EIMS *m/z* 294 (M)$^+$, 263, 196, 151, 122, 95, 81, 68, 67, 55, 42.

Cyclopropaneoctanoic Ester 4. Cyclopropenoid **1** (1.2 mg) was hydrogenated over Pd–C in EtOH for 12 h. After removal of catalyst, the filtrate was purified by prep. TLC using ether–hexane (1:1) to give **4**. ^{1}H NMR δ=−0.33 (1H, dt, *J*=3.6 and 4.5 Hz, of cyclopropane ring), 0.56 (1H, ddd, *J*=3.6, 8.1 and 8.2 Hz, 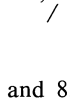 of cyclopropane ring), 0.65 (2H, m, 9- and 10-H), 0.89 (3H, t, *J*=6.7 Hz, 18-H), 1.13 (4H, m, 8- and 11-H), 1.23—1.55 (20H, m), 1.65 (1H, m), 1.79 (1H, m), 2.67 (1H, d, *J*=6.1 Hz, O$\underline{H}$), 3.79 (3H, s, OC$\underline{H}_3$, 4.20 (1H, m, 2-H); ^{13}C NMR δ=11.2 (C$\underline{H}_2$ of cyclopropane ring), 14.5 (C-18), 2×16.3 (C-9 and 10), 23.1 (C-17), 25.2 (C-4), 2×29.1, 2×29.7, 29.8, 2×30.0, 2×30.6, 32.2 (C-16), 34.9 (C-3), 53.0 (O$\underline{C}$H$_3$), 71.0 (C-2), 175.0 (C-1). Found: *m/z* 326.2815. Calcd for $C_{20}H_{38}O_3$: M, 326.2821.

8-Cyclopropyl-1,2-octanediol (5). The cyclopropane ester **4** was reduced with $LiAlH_4$ in ether to give the diol **5**. ^{1}H NMR δ=−0.32 (1H, dt, *J*=4.3 and 5.4 Hz), 0.58 (1H, dt, *J*=4.3 and 8.1 Hz), 0.66 (2H, m), 0.89 (3H, t, *J*=6.8 Hz), 1.1—1.8 (26H, m), 3.46 (1H, m, 1-H), 3.65 (1H, m, 1-H), 3.72 (1H, m, 2-H); EIMS *m/z* 298 (M)$^+$.

8-Cyclopropyl-1,2-octanediol Dibenzoate (6). A mixture of the diol **5** and 4-dimethylaminopyridine (0.3 mg) in pyridine (0.2 ml) was stirred for 0.5 h at room temperature. To the solution was added benzoyl chloride (0.2 ml), and the mixture was stirred for 12 h. TLC separation of the product using hexane–AcOEt (3:1) gave the dibenzoate **6**. ^{1}H NMR δ=−0.34 (1H, dt, *J*=4.2 and 5.5 Hz), 0.57 (1H, dt, *J*=4.1 and 8.3 Hz), 0.64 (2H, m), 0.89 (3H, t, *J*=6.7 Hz), 1.12 (4H, m), 4.48 (1H, dd, *J*=11.7 and 6.8 Hz, 1-H-pro-*S*), 4.53 (1H, dd, *J*=11.7 and 3.4 Hz, 1-H-pro-*R*), 5.51 (1H, m, 2-H), 7.34 (2H, t, *J*=8.2 Hz), 7.37 (2H, t, *J*=8.2 Hz), 7.47 (2H, dd, *J*=8.2 and 7.5 Hz), 7.93 (2H, dd, *J*=7.5 and 0.8 Hz), 7.98 (2H, dd, *J*=7.5 and 0.8 Hz); ^{1}H NMR (CD_3OD) δ=−0.35 (1H, dt, *J*=4.1 and 5.5 Hz), 0.58 (1H, ddd, *J*=4.2, 8.1, and 8.2 Hz), 0.66 (2H, m), 0.90 (3H, t, *J*=6.7 Hz), 1.15 (4H, m), 4.46 (1H, dd, *J*=12.1 and 6.8 Hz, 1-H-pro-*S*), 4.62 (1H, dd, *J*=12.1 and 3.2 Hz, 1-H-pro-*R*), 5.50 (1H, m, 2-H), 7.43 (2H, t, *J*=7.7 Hz), 7.46 (2H, t, *J*=7.7 Hz), 7.58 (1H, t, *J*=7.7 Hz), 7.60 (1H, t, *J*=7.7 Hz), 7.95 (2H, d, *J*=7.7 Hz), 8.01 (2H, d, *J*=7.7 Hz). Found: *m/z* 506.3412. Calcd for $C_{33}H_{46}O_4$: M, 506.3397.

Air Oxidation of 1. i) When air was bubbled into a CH_2Cl_2 solution of **1** (0.2 mg) for 30 min, the product was a complex mixture on HPLC. ii) Compound **1** (0.9 mg) changed to a mixture of two compounds when exposed to air at room temperature for two weeks. The products were separated by HPLC using MeCN containing 10% H_2O to give **7** (0.4 mg) and **8** (0.4 mg).

7; ^{1}H NMR δ=0.91 (3H, t, *J*=6.7 Hz, 18-H), 1.67 (1H, m, 3-H), 1.80 (1H, m, 3-H), 2.23 (2H, t, *J*=7.7 Hz, 11-H), 2.66 (2H, t, *J*=7.4 Hz, 8-H), 3.79 (3H, s, OC$\underline{H}_3$), 4.21 (1H, m, 2-H), 5.70 (1H, s,), 5.97 (1H, s,); ^{13}C NMR δ=14.1 (C-18), 22.7 (C-17), 24.6 (C-7), 28.5 (C-11), 29.0, 2×29.1, 29.3, 2×29.4, 30.9, 31.9, 34.3 (C-3), 37.8 (C-8), 52.3 (O$\underline{C}$H$_3$), 70.4 (C-2), 124.1 (=C$\underline{H}_2$), 149.2 (C-10), 175.9 (C-1), 202.6 (C-9); EIMS *m/z* 340 (5, M$^+$), 324 (6), 195 (8), 182 (36), 167 (28), 139 (7), 125 (12), 111 (47), 97 (32), 90 (2), 83 (52), 69 (75), 55 (base peak).

8; ^{1}H NMR δ=0.90 (3H, t, *J*=6.6 Hz, 18-H), 1.66 (1H, m, 3-H), 1.80 (1H, m, 3-H), 2.24 (2H, t, *J*=7.6 Hz, 8-H), 2.66 (2H, t, *J*=7.5 Hz, 11-H), 3.71 (3H, s, OC$\underline{H}_3$), 4.21 (1H, m, 2-H), 5.70 (1H, s,), 5.96 (1H, s,); ^{13}C NMR δ=14.1 (C-18), 22.7 (C-17), 24.7 (C-12), 28.4 (C-8), 2×29.1, 29.2, 29.3, 2×29.4, 30.9, 31.8, 34.1 (C-3), 37.9 (C-11), 51.6 (O$\underline{C}$H$_3$), 70.5 (C-2), 123.4 (=C$\underline{H}_2$), 149.1 (C-9), 176.6 (C-1), 202.5 (C-10); EIMS *m/z* 340 (3, M$^+$), 181 (30), 180 (33), 154 (38), 151 (44), 137 (10), 123 (30), 109 (28), 98 (26), 95 (31), 90 (3), 81 (48), 67

(59), 42 (base peak).

Seed Germination Test. Twenty seeds of lettuce (*Lactuca sativa* L.) were placed on a filter paper in a 9-cm Petri dish containing 2 ml of test solution. The dish was incubated at 23 °C in the dark room. After 3 d, the percentage germination was determined; **1**: 55% (*c* 1.5 mM), **2**: 20% (*c* 2.3 mM), and **3**: 15% (*c* 2.3 mM).

References

1) M. Nakatani, Y. Fukunaga, and T. Hase, *Phytochemistry,* **24**, 39 (1985).
2) M. Nakatani, Y. Fukunaga, and T. Hase, *Phytochemistry,* **25**, 449 (1986).
3) J. R. Nunn, *J. Chem. Soc.,* **1952**, 313.
4) J. R. Macfarlane, F. S. Shenstone, and J. R. Vickery, *Nature,* **179**, 830 (1957).
5) M. Beroza and G. C. Labreque, *J. Econ. Entomol.,* **60**, 196 (1967).
6) J. J. Lang and R. E. Treece, *J. Econ. Entomol.,* **64**, 455 (1971).
7) S. N. Thompson and J. S. Barlow, *Ann. Entomol. Soc. Am.,* **66**, 797 (1973).
8) R. G. Binder and B. G. Chan, *Entomol. Exp. Appl.,* **31**, 291 (1982).
9) M. Elliott, *Pyrethrum Post,* **2**, 18 (1951).
10) L. J. Morris and S. W. Hall, *Chem. Ind. (London),* **7**, 32 (1967).
11) N. Harada and K. Nakanishi, "Circular Dichroic Spectroscopy-Exciton Coupling in Organic Stereochemistry," University Science Books, California (1983).
12) F. L. Carter and V. L. Frampton, *Chem. Rev.,* **64**, 497 (1964).
13) A. Horeau and H. B. Kagan, *Tetrahedron,* **20**, 2431 (1964).
14) W. Schlenk, Jr., *J. Am. Oil Chem. Soc.,* **42**, 945 (1965).
15) W. Wiesler and K. Nakanishi, *J. Am. Chem. Soc.,* **111**, 3446 (1989).
16) H. Uzawa, Y. Nishida, H. Ohrui, and H. Meguro, *J. Org. Chem.,* **55**, 116 (1990).
17) C. A. G. Haasnoot, F. A. A. Lees, and C. Altona, *Tetrahedron,* **36**, 2783 (1980).
18) Y. Nishida, H. Hori, H. Ohrui, and H. Meguro, *J. Carbohydr. Chem.,* **7**, 239 (1988).
19) M. Nakatani, Y. Matsuoka, Y. Uchio, and T. Hase, *Chem. Lett.,* **1990**, 669.
20) C. Hitchcock and A. T. James, *Biochem. Biophys. Acta,* **116**, 413 (1966).

 © 1991 The Chemical Society of Japan Bull. Chem. Soc. Jpn., 64, 3089—3093 (1991)

Catalytic Oxidation of Naphthalene on Palladium in Cooperation with Copper(I)/(II) Redox Couple

Yasushi KURODA,* Atsutaka KUNAI, Michiyuki HAMADA, Tomoyuki KITANO, Sotaro ITO, and Kazuo SASAKI

Department of Applied Chemistry, Faculty of Engineering, Hiroshima University, Kagamiyama, Higashi-Hiroshima 724

(Received May 24, 1991)

Catalytic oxidation of naphthalene in moist acetic acid solutions has been studied. The catalyst used was a silica-supported palladium which works in cooperation with the Cu^{+}/Cu^{2+} redox couple. Products were 1-naphthol, 1,4-naphthoquinone and (*E*)-2-formylcinnamaldehyde with a total yield of more than 78% in which naphthoquinone shared 40%. Reaction mechanism has been discussed in comparison with that of benzene.

Among many unit processes of organic synthesis, aromatic hydroxylation reaction is one of the most difficult reactions. In recent years, we have developed a new catalytic oxidation process which works efficiently under ambient conditions and proceeds in a single batch reactor without any cumbersome treatment.[1,2] Our attention to date was, however, limited to the reaction of benzene. Since the process is expected to be applied to many aromatics other than benzene, the reaction of naphthalene has been studied tentatively. A similar study regarding the reaction of benzoic acid will appear separately.[3]

Experimental

Catalyst. For preparing catalysts, a mixture of metal salts ($CuSO_4$ and/or $PdCl_2$) and powdery silica (Merck, No. 9385, 230—400 mesh) dispersed in water was first exposed to ultrasonic wave for 90 min to homogenize the mixture. This process is necessary for achieving a high catalytic activity.[2] The mixture was then heated to dryness on a steam bath with gentle agitation. Two catalysts of different composition were prepared in this manner. They are shown as Catalyst A (1000 $CuSO_4$–50 $PdCl_2$) and B (100 $PdCl_2$), respectively, where numbers in the parentheses indicate μmol of respective metal salt per gram of silica support. In case of Catalyst B that contains no copper salt, a preliminary activation (reduction of Pd^{2+} to Pd^{0}) of the catalyst with hydrogen was done separately in benzene.

Reaction. All reactions were carried out at 25 °C under the atmospheric pressure. When catalyst A was used, the catalyst (1 g) and a mixture (20 cm^3) of benzene with a solvent given in Tables 1 and 2 were placed into an Erlenmeyer flask (100 cm^3 in volume). After replacing air in the flask with hydrogen, the flask was shaken (30 mm stroke, 140 cycle/min) or stirred magnetically for 2 h to activate the catalyst. Upon this treatment the catalyst color gets black indicating that Pd^{2+} is reduced to its metallic state. Cu^{2+} ion is also believed to be reduced to its lower valence states, at least partly. Control of the stirring rate (800 rpm) is required for attaining reproducible results. Hydrogen was then replaced by air or pure oxygen to begin the oxidation reaction.

For reactions in acetic acid, copper(II) acetate (1 mmol) and naphthalene were dissolved into the solution (25 cm^3). Reaction was performed by using Catalyst B (1 g) that contains Pd species alone and by introducing hydrogen and oxygen into the reactor flask either alternately or simultaneously.

The reaction mixture was filtered to remove the catalyst, and the solvent was removed using a rotary evaporator. Hexane was added to the residue and copper acetate was filtered off. The filtrate was concentrated, and (*E*)-2-formylcinnamaldehyde was isolated by thin-layer chromatography on silica gel: MS *m/z* 131 (M^{+} −29); ^{1}H NMR ($CDCl_3$) δ=6.67 (1H, dd, *J*=16.1, 7.8 Hz), 7.6—8.0 (4H, m), 8.58 (1H, d, *J*=16.1 Hz), 9.81 (1H, d, *J*=7.8 Hz), 10.23 (1H, s); ^{13}C NMR ($CDCl_3$) δ=128.0, 130.7, 132.3, 133.6, 133.9, 134.6, 135.4, 149.2, 192.7, 193.7.

Product Analysis. Product analysis was made by use of a high-performance liquid chromatograph equipped with a Merck Hibar column (Lichrosorb RP-18, 10×250 mm). Eluent used was a mixture of acetonitrile and a phosphate buffer solution of pH 3.5, of which the mixing ratio was varied depending on the nature of compounds to be analyzed.

Results and Discussion

1. Examination of Catalyst and Solvent. We have already demonstrated that Catalyst A shows excellent activity for producing phenol even in benzene itself.[2] We thus tried to use this catalyst for the oxidation of naphthalene. In contrast to benzene, however, naphthalene is solid at room temperature and thus needs some appropriate solvents.

We have first studied the effect of several organic solvents given in Table 1 in the reaction of benzene. The reaction was performed by using Catalyst A (1 g) in a mixture (20 cm^3) of benzene with a given solvent at several different ratio. After shaking the mixture under hydrogen for 2 h, the oxidation reaction was started and continued for 1 h by introducing air to the reactor flask. Yields of phenol are listed in Table 1. As is expected, the presence of any of the solvent hinders the oxidation of benzene appreciably. However, the hindering effect is minor in cyclohexane and this prompted us to study the oxidation of naphthalene in this solvent. Unfortunately, however, the reactivity of naphthalene in cyclohexane was unexpectedly low and produced only 0.5 μmol of 1-naphthol.

As has been reported in a previous paper,[2] the catalyst containing copper acetate was not effective when it

Table 1. Yield of Phenol (μmol) in the Oxidation of Benzene in Several Solvents

Exp.	Solvent	Volume fraction of organic solvent/%			
		80	50	20	0
1	Cyclohexane	10.5	19.3	22.0	
2	Ethyl acetate	6.9	12.5	12.2	
3	Propylene carbonate	1.1	5.1	14.7	25.9±4.3[a]
4	Acetic acid	3.2	3.8	6.8	
5	95% Acetic acid	2.4	3.6	—	

Catalyst: A (1 g), Solution volume: 20 cm^3, Gas feeding: H_2 (2 h) followed by Air (1 h).
a) Mean value of ten measurements using catalysts from five different lots. Rather a big deviation is due to the use of different lots of catalyst. Values for a given solvent were determine using a single lot of catalyst and the error was less than a few %.

Table 2. Oxidation of Benzene in Acetic Acid

Exp.	Solvent component / v/v			Product yield/μmol				Formal potential[f] (Cu^+/Cu^{2+}) /mV vs. SCE
	AN[a]	H_2O	AcOH[b]	PhOH[c]	HQ[d]	BQ[e]	Total	
1	0	0	100	4.3	0.2	1.0	5.5	—
2	0	6.5	93.5	5.7	0.4	1.2	7.3	—
3	6.5	0	93.5	4.0	4.0	3.9	11.9	625
4	6.5	6.5	87	14.8	14.0	4.8	33.6	560

Catalyst: B (1 g), Solution: Solvent (20 cm^3)+Benzene (5 cm^3)+$Cu(OAc)_2$(40 mM), Gas feeding: H_2 (15 min) followed by Air (2 h).
a) Acetonitrile, b) acetic acid, c) phenol, d) hydroquinone, e) *p*-benzoquinone. f) Formal potential was measured in a $Cu(OAc)_2$(1.3 mM) solution containing $NaClO_4$ (100 mM).

Table 3. Oxidation of Naphthalene in Acetic Acid

Exp.	Concn of naph./M	Product yield/μmol				Turnover frequency[k] /cycle h^{-1}
		1-NaphOH[h]	1,4-NaphQ[i]	Dialdehyde[j]	Total	
1[a]	0.1	2.5	5.9	2.8	11.2	0.056
2[a]	0.3	4.7	10.3	4.8	19.8	0.099
3[a]	0.5	4.8	10.4	4.7	19.9	0.100
4[b]	0.3	6.7	21.7	7.7	36.1	0.181
5[c]	0.3	21.3	50.0	18.8	90.1	0.451
6[d]	0.3	25.3	62.5	25.0	112.8	0.564
7[d,f]	0.3	25.5	72.3	22.5	120.3	0.602
8[e,g]	0.1	63.3(12.0)	209.8(39.9)	139.5(26.5)	412.6(78.4)	0.206

Catatalyst: B (1 g), Solution: $Cu(OAc)_2$ (40 mM) was dissolved in AcOH (25 cm^3) containing both AN and H_2O at 4% in volume.
a) H_2 (15 min) followed by air (2 h), b) H_2 (15 min) followed by O_2 (2 h), c) H_2 (15 min) follow by O_2 (15 min), cycle repeated 4 times, d) simultaneous (7.5 $cm^3\,min^{-1}$ for both H_2 and O_2, 2h), e) simultaneous (7.5 $cm^3\,min^{-1}$ for both H_2 and O_2, 20 h), f) CH_3COONa (50 mM) was added. g) Values in the parentheses indicate selectivity (%) based on the amount of naphthalene consumed, h) 1-naphthol, i) 1,4-naphthoquinone, j) (*E*)-2-formylcinnamaldehyde. k) Based on Pd.

was used in neat benzene. However, the catalyst became effective when a small amount of acetic acid was added to benzene. Accordingly, we next studied the reaction in acetic acid using Catalyst B that contains Pd species alone. In this case, copper(II) acetate was dissolved in the solution phase. The use of neat acetic acid resulted, however, in a poor product yield (Table 2, exp. 1). This can be attributed to the slow redox rates of the Cu(I)/Cu(II) couple in acetic acid. It is known that hydrated Cu(I) ions are oxidized readily to Cu(II) ions with dioxygen[4-7] and also that they can be stabilized with acetonitrile (AN).[4,8] We hence added both AN and water as the cosolvents. As is seen in Table 2, the presence of both the two cosolvents increased markedly the oxidation efficiency (exp. 4). Electrochemical measurements also proved that the presence of water favors the oxidation of Cu(I) to Cu(II) while AN favors the reverse reaction. The effect of water and AN is counteracting and the use of 4—7% in volume ratio for both the cosolvents seems to be optimal.

It is worth noting that under the conditions in experiment 4, nearly equal amounts of hydroquinone and phenol are produced. This is in accordance with our previous observations. In the reaction in aqueous $CuSO_4$ solutions, phenol was formed as the main product at pH 1 while hydroquinone dominated at pH 3.5.[7] Even in the reaction in neat benzene under a pressurized oxygen atmosphere, the use of the Pd–Cu composite catalyst resulted in a predominant formation of *p*-benzoquinone.[2] The present result is consistent with those and the presence of copper acetate favors the formation of hydroquinone.

2. Reaction of Naphthalene. Basic knowledges obtained for the oxidation of benzene were applied to the reaction of naphthalene by using 1 g of Catalyst B in a solution (25 cm^3) of 40 mM $Cu(OAc)_2$ (1 M=1 mol dm^{-3}) in acetic acid containing water and acetonitrile (4.0% for each). Results obtained are shown in Table 3. In experiments 1—7, the reaction was continued for 2 h. Products obtained are 1-naphthol, 1,4-naphthoquinone and (*E*)-2-formylcinnamaldehyde (which will be abbreviated as dialdehyde hereafter). A trace amount of 2-naphthol was detected among some other minor products.

The first three experiments, in which hydrogen was first supplied to the reactor for 15 min and then air followed for 2 h, indicate that the concentration of naphthalene has no remarkable effect on the yield (exps. 1—3). Replacement of air by pure oxygen results in the increase in the yield of naphthoquinone and thus total products (exp. 4).

In experiment 5, the supply of hydrogen and oxygen was alternated every 15 min and the cycle was repeated 4 times (total oxygen feeding: 1 h). The frequent alternation of gas feeding results in a marked increase of the product yield indicating that 1 h of oxidation time is unnecessarily long. The selectivity of each product remains almost unchanged. Experiment 6 was conducted under the conditions of simultaneous gas feeding i.e., both hydrogen and oxygen were supplied with an equal feed rate (7.5 $cm^3\,min^{-1}$). In comparison with the foregoing (exps. 4 and 5), the total yield increased still more by keeping the product distribution unchanged. A deliberate addition of sodium acetate increases the product yield and so that the turnover frequency (exp. 7).

In order to determine the material balance, a prolonged experiment was carried out (exp. 8), and the total selectivity with regard to the sum of the three products was found to be 78.4% and naphthoquinone shared 39.9% in it. The rest 21.4% was left undetermined. The prolonged reaction time (exp. 8) seems to increase the relative yield of dialdehyde.

Under the condition of alternate gas feeding, the product accumulation during the oxidation of naphthalene was studied. A typical example is shown in Fig. 1. It is interesting that the yield of naphthol first increases but after a short period of time it decreases gradually

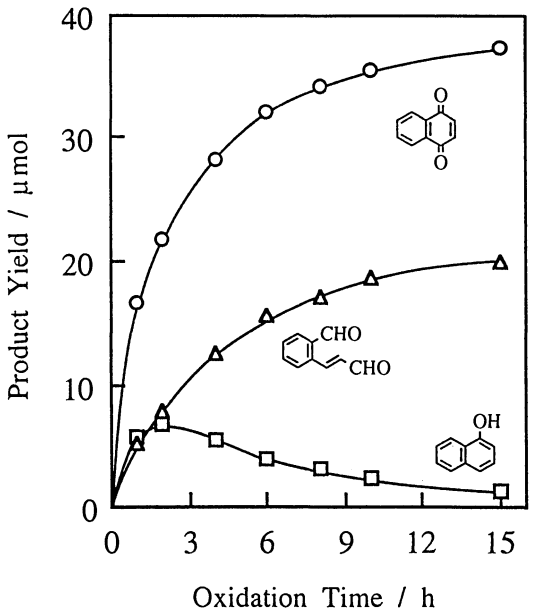

Fig. 1. Accumulation of the products during oxidation of naphthalene in acetic acid. Catalyst: B (1 g). Solution: 0.3 M Naphthalene and 40 mM $Cu(OAc)_2$ in AcOH (25 cm^3) containing both AN and H_2O at 6.5% in volume. Gas feeding: H_2 (15 min) followed by O_2.

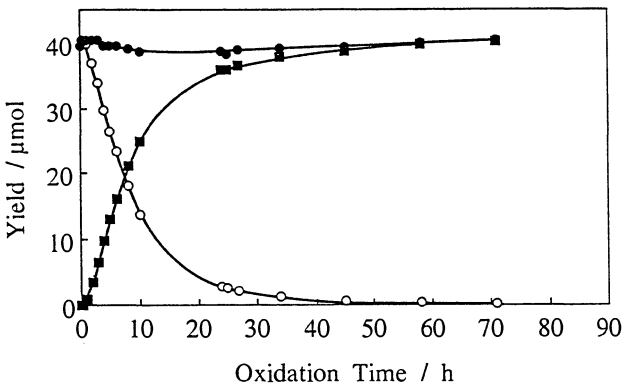

Fig. 2. Aerial oxidation of 1-naphthol to 1,4-naphthoquinone in the presence of Pd-catalyst and copper salt.
Catalyst: B (1 g). Solution: 2 mM 1-Naphthol and 10 mM $Cu(OAc)_2$ in AcOH (20 cm^3) containing both AN and H_2O at 6.5% in volume. Gas feeding: H_2 (15 min) followed by O_2.
○: 1-Naphthol, ■: 1,4-Naphthoquinone, ●: Total sum.

while other two products increases monotonously. Undoubtedly, this suggests that 1-naphthol is converted secondarily to some other product(s). In order to confirm what the final product was, the reaction of 1-naphthol was studied separately under similar reaction conditions as in Fig. 1. Further details are indicated in the caption of Fig. 2. As this figure indicates, 1-naphthol is converted quantitatively to 1,4-naphthoquinone. Fig. 3 shows results of another experiment in which Pd catalyst was not used but naphthol was

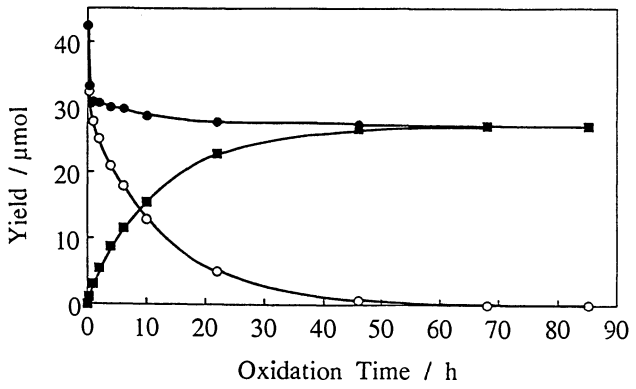

Fig. 3. Aerial oxidation of 1-naphthol in the absence of Pd-catalyst.
Solution: 2 mM 1-Naphthol and 10 mM $Cu(OAc)_2$ in AcOH (20 cm^3) containing both AN and H_2O at 6.5% in volume. The solution was kept under O_2 atmosphere with use of neither Pd-catalyst nor Cu^+ salt.
○: 1-Naphthol, ■: 1,4-Naphthoquinone, ●: Total sum.

simply dissolved in an acetic acid solution containing copper(II) acetate. In this case too, 1-naphthol was oxidized under the oxygen atmosphere to give 1,4-naphthoquinone although 35% of starting material was missed from detection by some unknown reason. In any case, it is clear that the primary product, 1-naphthol, is converted to the corresponding quinone under the conditions of the present experiments.

3. Reaction Mechanism. We have already demonstrated in the aqueous phase reactions that Cu(I) ions activate dioxygen to produce hydrogen peroxide.[5–7] Hydrogen peroxide is then reduced with Cu(I) ions to water via transient formation of hydroxyl radical. Of course, there still remain several uncertainties regarding detailed points. For instance, transient formation of a copper–oxygen complex was suggested by Zuberbuehler[9] and it might be involved in the reaction sequence. These, however, do not affect the following discussion. According to our view, the basic mechanism in the oxidation of benzene involves the formation of hydroxyl radical as the reactive species as described in our previous papers[5–7] as well as the work of several authors.[10,11] The recent publication of Okunowski[12] is in consistent with our view, particularly.

The primary intermediate is hydroxycyclohexadienyl radical, an adduct of hydroxyl radical to benzene. Under the oxygen atmosphere, the cyclohexadienyl radical readily transforms to its peroxyl radicals by adding dioxygen.[13] The peroxyl radicals are converted, depending upon the conditions of the surroundings, to either phenol or hydroquinone. We have also demonstrated that copper ions have an ability of converting efficiently a peroxyl intermediate, 4-hydroxy-2,5-cyclohexadienylperoxyl radical, to hydroquinone via, presumably, the corresponding hydroperoxyl intermediate.[5–7] These mechanisms may also be applied to the reaction of other aromatic compounds regardless of reaction media.

Generally speaking, addition of hydroxyl radical to

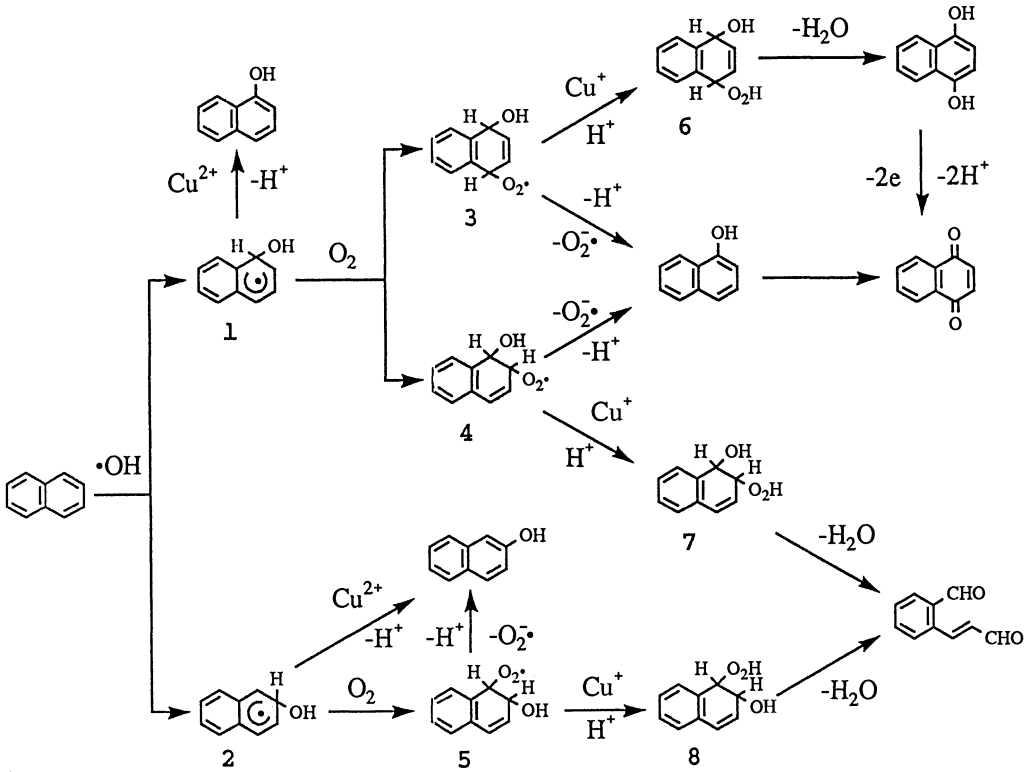

Scheme 1.

naphthalene has a possibility of occurring at either 1- or 2-position of the ring (see, Scheme 1). Considering the electrophilic nature of the reaction, however, one may conclude the preference for the 1-position, since the electron density is 0.362 at 1-position while it is 0.138 at 2-position.[14] The relative ratio of the 1- and 2-isomers will indicate the relative rate of forming 1- and 2-hydroxylated cyclohexadienyl radicals (radicals **1** and **2**, respectively), to which dioxygen adds to give peroxyl radicals (radicals **3**, **4**, and **5**). It should be noted that 1-naphthol is derived from either radical **3** or **4** by eliminating HO_2 radical (Dorfman's path[10]). Experimental results shown in Table 3 agree with this expectation and 1-naphthol is produced as the dominant product while 2-naphthol is minor. By analogy of the reaction of benzene,[5-7] direct formation of naphthols from the cyclohexadienyl radicals through the oxidative elimination of proton can be ruled out when sufficient amount of oxygen is present in the reaction medium, where radical **3** or **4** prevails.

We have shown that 1,4-naphthoquinone is certainly produced from 1-naphthol. However, this route seems to be of secondary importance in the reaction, because 1,4-naphthoquinone is produced and increases steadily from the initial stage of oxidation (see Fig. 1). The main route to lead to 1,4-naphthoquinone is believed to pass through radical **3**.

Dialdehyde may be produced through the formation of either peroxyl radical **4** or **5** derived from radical **1** or **2**, respectively. Of these, the route via radical **5** and thus hydroperoxide **8** is ruled out since radical **2** is believed to have a minor contribution. Hydroperoxide **7** derived from **4** will result in a carbon-carbon bond cleavage upon elimination of water because of the steric hindrance between hydroxyl and hydroperoxyl groups. In the oxidation of benzene, a trace amount of 2,4-hexadienedial was found in the products. In contrast, naphthalene produces dialdehyde as the second main product following to the main product, 1,4-naphthoquinone. This is due to increased stability resulted from the conjugation of an unsaturated bond in peroxyl radical **4** with a fused benzenoid system. As a result, contribution of the Dorfman's path[10] decreases and the amount of dialdehyde increases appreciably.

1,4-Naphthoquinone is formed not only by the competing reaction but also by oxidation of 1-naphthol, particularly, after the latter compound has been accumulated. As a result, the selectivity of naphthoquinone becomes more than 52% (Table 3, exp. 8). In addition, an appreciable formation of the dialdehyde from naphthalene contrasts to the negligible production of 2,4-hexadienedial from benzene. This is attributed to the difference in relative stability of oxygenated cyclohexadienyl radicals derived from benzene and naphthalene.

This work was supported financially by a Grant-in-Aid for Scientific Research on Priority Area No. 62607001 from the Ministry of Education, Science and Culture. Thanks are also due to Tokuyama Soda Co., Ltd. and Toso Co., Ltd. for their support in many respects.

References

1) A. Kunai, K. Ishihata, S. Ito, and K. Sasaki, *Chem. Lett.*, **1988**, 1967.
2) A. Kunai, T. Wani, Y. Uehara, F. Iwasaki, Y. Kuroda, S. Ito, and K. Sasaki, *Bull. Chem. Soc. Jpn.*, **62**, 2613 (1989).
3) A. Itoh, Y. Kuroda, T. Kitano, Z.-H. Guo, A. Kunai, and K. Sasaki, *J. Mol. Catal.*, (1991), in press.
4) T. Kinoshita, J. Harada, S. Ito, and K. Sasaki, *Angew. Chem., Suppl.*, **1983**, 599.
5) A. Kunai, S. Hata, S. Ito, and K. Sasaki, *J. Org. Chem.*, **51**, 3471 (1986).
6) S. Ito, T. Yamasaki, H. Okada, S. Okino, and K. Sasaki, *J. Chem. Soc., Perkin Trans. 2*, **1988**, 285.
7) S. Ito, A. Kunai, H. Okada, and K. Sasaki, *J. Org. Chem.*, **53**, 296 (1988).
8) S. Ito, H. Okada, R. Katayama, A. Kunai, and K. Sasaki, *J. Electrochem. Soc.*, **135**, 2996 (1988).
9) A. Zuberbuehler, *Helv. Chim. Acta*, **50**, 466 (1967), and related papers cited therein.
10) L. M. Dorfman, I. A. Taub, and R. E. Buhler, *J. Chem. Phys.*, **36**, 3051 (1962).
11) C. Walling and R. A. Johnson, *J. Am. Chem. Soc.*, **97**, 363 (1975).
12) J. K. Okunowski, H. E. v. Dam, and H. v. Bekkum, *Recl. Trav. Chim. Pays-Bas*, **109**, 103 (1990).
13) A. Kunai, S. Hata, S. Ito, and K. Sasaki, *J. Am. Chem. Soc.*, **108**, 6012 (1986).
14) K. Fukui, T. Yonezawa, and H. Shingu, *J. Chem. Phys.*, **20**, 722 (1952).

Anionic Surfactants with Divalent Counterions of Separate Electric Charge. III. Proton NMR Study

Yoshikiyo MOROI,* Ryohei MATUURA, and Tadashi YONEMITSU†
Department of Chemistry, Faculty of Science, Kyushu University 33, Higashi-ku, Fukuoka 812
†Department of Industrial Chemistry, Faculty of Engineering, Kyushu Sangyo University, Higashi-ku, Fukuoka 813
(Received March 22, 1991)

The proton NMR spectra of 1-tetradecanesulfonates whose cationic counterion, the 1,1′-polymethylenedipyridinium ion (with even-numbered methylene groups up to 14), is divalent with separate electric charge, were measured. From the chemical shifts the pyridine rings were found to move about in quite hydrophilic environment of micellar surface region, leading to a downfield shift of methylene groups next to head group of surfactant ion. The chemical shifts of methylene groups of micellized counterions with more than eight methylene groups are different from those of corresponding counterions in aqueous environment and are similar to those of methylene group in hydrophobic micellar interior. These results strongly support the previous conclusion that the polymethylene group with more than eight methylene groups folds and penetrates micellar interior in their micellized state.

The properties of aggregates or micelles of ionic surfactants are strongly influenced by the kind of surfactant ion and counterion. Counterions of conventional anionic surfactants so far investigated have been alkali or alkaline earth metal ions, their electrical charge being localized within a very small volume. The electrical potential of such ions seems to be energetically stabilized by coulombic interaction. This leads to smaller aqueous solubility of surfactants, resulting in higher micelle temperature range[1] or higher Krafft point.[2–4] As for organic counterions, on the other hand, the counterion binding to micelles increases with its increasing hydrophobicity and promotes a micelle formation, where the size and shape of micelles are radically affected.[5–10] Surfactants with divalent counterions whose electric charge is diffuse[11] or separate,[12,13] in particular, have physicochemical properties much different from those of conventional surfactants.

In our preceding papers on anionic surfactants with divalent counterions of separate electric charge (1,1′-polymethylenedipyridinium ion, C_nDP^{2+}), the solubility and micelle formation[14] and the micellar size and surface activity[15] have been systematically studied. The conclusion was that the polymethylene chain with eight or more methylene groups folds and penetrates the hydrophobic micellar interior. However, the questions as to how deep the penetration is and where the location of pyridinium ion is still remain unsolved. One of the promising approaches to counterion binding is to employ the NMR technique.[16–18] This technique can also indicate the solubilization site of molecules in micelle in the case where they carry the π-electrons, like the couterions of ionic surfactants used in the present study.[19–24]

This paper, then, aims to solve the above two questions using the proton NMR technique and to confirm the conclusion from the preceding works by another experimental evidence.

Experimental

Materials. Anionic surfactants with divalent cationic counterions of separate electric charge, 1,1′-polymethylenedipyridinium tetradecane-1-sulfonate were the same as those used in the previous papers,[14,15] in which the surfactants were

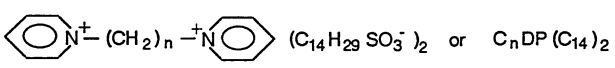

n = 2, 4, 6, 8, 10, 12, 14

named as 1,1′-(1,ω-alkanediyl)bispyridinium tetradecane-1-sulfonate or $C_nBP(C_{14})_2$. C_nDPX_2 (X=Cl, Br) were kind gifts from Prof. Kuwamura's laboratory of Gunma University and were used without further purification except those which were purified by recrystallization from acetone–ethanol mixture. Water used as a solvent is D_2O from Merck Co., Ltd.

NMR Measurement. The concentration of $C_nDP(C_{14})_2$ is 0.01 mol dm^{-3} which is about 50 times cmc for three surfactants of n=2, 4, and 6, while that of C_nDPX_2 is 0.02 mol dm^{-3}. The sample solutions were sonicated for 30 min after apparent sample dissolution. As for solutions of $C_2DP(C_{14})_2$ and $C_{14}DP(C_{14})_2$ whose Krafft points are higher than the measurement temperature the recording was made before their precipitation. The chemical shift of residual HDO signal, δ=4.5, was used as the standard of the chemical shifts, because the molar ratio of water to the divalent ion of more than 2700 is so large that the effect of the divalent ion on bulk water structure can be negligible. The NMR spectra were recorded with a JEOL GX-400 p-FT NMR spectrometer at room temperature.

Results and Discussion

The proton NMR spectra of $C_nDP(C_{14})_2$ are shown in Fig 1. The NMR spectra of C_nDPX_2 are very helpful to analysing the spectra of $C_nDP(C_{14})_2$, because C_nDP are the counterions of the latter micelles and do not form micelles by themselves at the concentration of 0.02 mol dm^{-3}: The most hydrophobic counterion $C_{14}PPCl_2$ was found to form micelles around 0.02 mol dm^{-3}.[25] In other words, their chemical shifts of every ^{1}H bound to

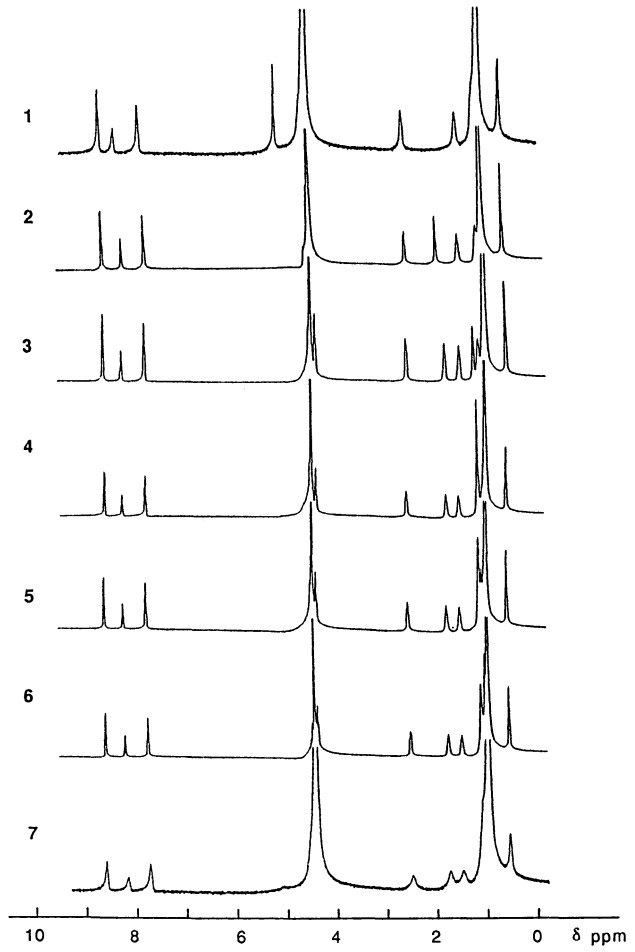

Fig. 1. ^{1}H NMR spectra of $C_nDP(C_{14})_2$: **1** n=2, **2** n=4, **3** n=6, **4** n=8, **5** n=10, **6** n=12, **7** n=14.

carbon atom are those in a very hydrophilic or an aqueous environment. The chemical shifts of C_nDPX_2 are analyzed from their intensity and position, and assigned as shown in Table 1. The chemical shifts of the ^{1}H atoms in pyridine ring are spread in the lower field as expected from the effect of π-electrons, and those of the hydrogen atoms of methylenes near the pyridine ring are found also to be influenced by the electrons as is clear from the lower chemical shifts of $=N-CH_2-$ and adjacent $-CH_2-$. The chemical shifts of ^{1}H of methylene chain in aqueous environment are 0.88—0.99 ppm.

The chemical shifts of the surfactants are also analyzed on the same ground as those of C_nDPX_2. The results are given in Table 2. More than 90% of the couterions are supposed to be bound to micelles[15] and, therefore, the spectra can be said to represent their bound state. As far as ^{1}H atoms in pyridine ring are concerned, their chemical shifts are almost the same as those of C_nDPX_2, which suggests that the cationized rings remain in an aqueous environment in micellized state. These are quite different from the chemical shifts in hydrophobic environment, for example, 8.95, 8.58, and 8.13 ppm for the α-, γ-, and β-H atoms in cyclohexane.[26] The rings connected by the longer methylene chain have been expected to be drawn toward less hydrophilic region of inner micelle, but it has turned out from the results that this is not the case. In other words, the region of micellar surface where the rings are located is very hydrophilic aqueous environment. In Fig. 2 are illustrated the difference in the chemical shifts by deducting the chemical shifts in Table 1 from those in Table 2. It is worth to mention that the down-field shift in the pyridine ring increases in the order $\alpha>\gamma>\beta$. At the same time, the enhanced down-field shift of every methylene group in polymethylene chain clearly results from concentration of pyridine rings due to micelle formation. As for PM_1, its variation is quite similar to the variation of micelle aggregation number,[15] which indicates that methylene protons of PM_1 are very sensitive to a manner of packing of surfactant ions.

The proton chemical shifts of terminal methyl and other methylenes of surfactant ion, which are referred to M_1, M_2, M_3, M_4, and M_5, change quite gradually from ca. 0.5 to 2.5 ppm. The classification of methylene groups of the alkyl chain as M_1, M_2, M_3, M_4, and M_5 is made from the chemical shifts for sodium 1-dodecanesulfonate micelles. The proton chemical shift of ca. 0.5 ppm of M_1 in inner micelle region is much smaller than the chemical shift ca. 1 ppm in aqueous environment and those of outer micellar region. The ratio of the chemical shift of M_5 to that of M_1, 5.0 is

Table 1. ^{1}H NMR Chemical Shifts of C_nDP (δ/ppm)

Compound	Pyridinium			Polymethylene			
	α	γ	β	PM_1	PM_2	PM_3	PM_4
1	8.60	8.43	7.87	5.06	—	—	—
2	8.55	8.27	7.78	4.27	1.67	—	—
3	8.55	8.25	7.77	4.27	1.68	1.05	—
4	8.56	8.25	7.77	4.30	1.68	0.99	—
5	8.53	8.25	7.77	4.33	1.69	0.98	0.93
6	8.55	8.25	7.78	4.32	1.69	0.98	0.91
7	8.55	8.25	7.75	4.30	1.68	0.98	0.88

$>N-CH_2-CH_2-(CH_2)_n-(CH_2)_m-(CH_2)_n-CH_2-CH_2-N<$
PM_1 PM_2 PM_3 PM_4 PM_3 PM_2 PM_1
n=1,2 for PM_3 m=2,4,6 for PM_4

Table 2. ^{1}H NMR Chemical Shifts of $C_nDP(C_{14})_2$ (δ/ppm)

Compound	Pyridinium			Polymethylene				M_5	M_4	M_3	M_2	M_1
	α	γ	β	PM_1	PM_2	PM_3	PM_4					
0′	—	—	—	—	—	—	—	2.66	1.57	1.13	1.07	0.67
1′	8.63	8.29	7.82	5.09	—	—	—	2.50	1.44	0.97	0.91	0.51
2′	8.63	8.23	7.78	4.54	1.87	—	—	2.47	1.43	1.03	0.90	0.50
3′	8.64	8.28	7.81	4.38	1.72	1.12	—	2.50	1.43	1.06	0.89	0.50
4′	8.65	8.26	7.82	4.38	1.69	1.08	—	2.50	1.43	0.93	0.92	0.52
5′	8.63	8.27	7.81	4.43	1.73	1.06	1.00	2.50	1.46	0.91	0.91	0.51
6′	8.65	8.26	7.82	4.43	1.74	1.04	0.96	2.38	1.49	0.91	0.91	0.51
7′	8.67	8.25	7.79	4.48	1.74	1.04	0.96	2.38	1.47	0.91	0.91	0.52

0′: CH_3-$(CH_2)_8$-CH_2-CH_2-CH_2-$SO_3^-Na^+$
M_1 M_2 M_3 M_4 M_5

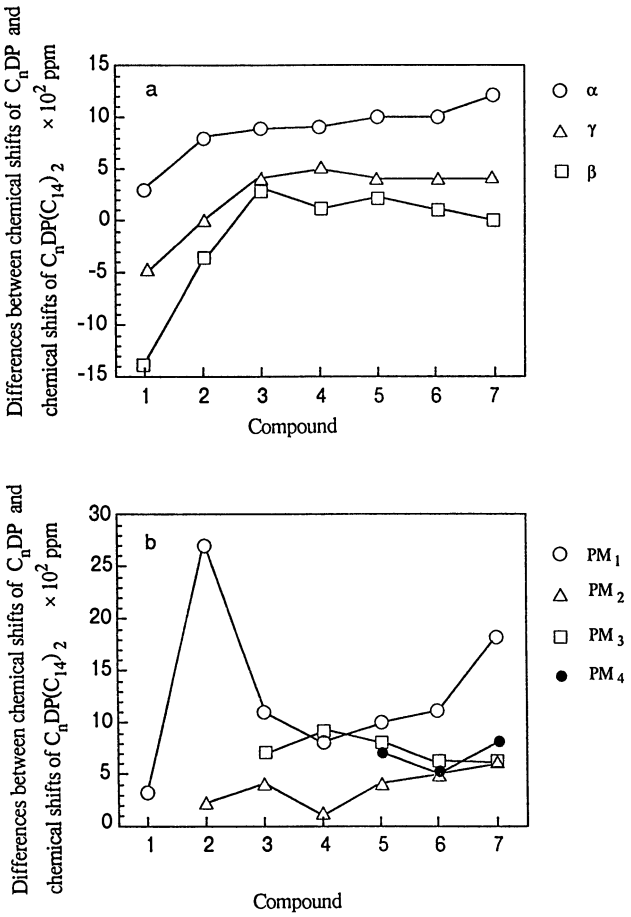

Fig. 2. The difference in the chemical shifts of counterions (a) pyridine protons, (b) polymethylene protons.

larger than that of sodium 1-dodecanesulfonate micelles, 4.0.[27] The higher ratio is due to the effect of the π-electrons of the counterions. These findings indicate the moving about of pyridine rings around the miceller surface region. The chemical shift (δ=0.96—1.08) of methylene groups (PM_3 and PM_4) of the counterions ($n \geqslant 8$) in micellized state are similar to those of methylene groups (M_2 and M_3) of surfactant ion. This suggests that PM_3 and PM_4 methylenes of counterions and M_2 and M_3 methylenes of surfactant ion are located in a similar hydrophobic environment.

The present results by ^{1}H NMR study strongly support the previous result that the polymethylene group with more than eight methylene groups folds and penetrates the hydrophobic micellar interior.

The authors are indebted to Professor Masahiko Suhara of Kanazawa University for his attention to this problem and his kind assistance in the NMR measurements.

References

1) Y. Moroi and R. Matuura, *Bull. Chem. Soc. Jpn.*, **61**, 333 (1988).
2) I. Satake, I. Iwamatsu, S. Hosokawa, and R. Matuura, *Bull. Chem. Soc. Jpn.*, **36**, 203 (1963).
3) M. Hato and K. Shinoda, *Bull. Chem. Soc. Jpn.*, **46**, 3889 (1973).
4) Y. Moroi, T. Oyama, and R. Matuura, *J. Colloid Interface Sci.*, **60**, 103 (1977).
5) P. Mukerjee, K. J. Mysels, and P. Kapauan, *J. Phys. Chem.*, **71**, 4166 (1967).
6) E. W. Anacker and A. L. Underwood, *J. Phys. Chem.*, **85**, 2463 (1981).
7) M. Almgren and S. Swarup, *J. Phys. Chem.*, **87**, 876 (1983).
8) A. L. Underwood and E. W. Anacker, *J. Colloid Interface Sci.*, **100**, 128 (1984).
9) A. L. Underwood and E. W. Anacker, *J. Phys. Chem.*, **88**, 2390 (1984).
10) M. Jansson and B. Jonsson, *J. Phys. Chem.*, **93**, 1451 (1989).
11) Y. Moroi, R. Sugii, C. Akine, and R. Matuura, *J. Colloid Interface Sci.*, **113**, 225 (1986).
12) R. Matuura, Y. Moroi, and N. Ikeda, "Surfactants in Solution," ed by K. L. Mittal and P. Bothorel, Plenum Press, New York (1986), Vol. 4, p. 289.
13) E. Lissi, E. Abuin, I. M. Cuccovia, and H. Chaimovich, *J. Colloid Interface Sci.*, **112**, 513 (1986).
14) Y. Moroi, R. Matuura, T. Kuwamura, and S. Inokuma, *J. Colloid Interface Sci.*, **113**, 225 (1986).
15) Y. Moroi, R. Matuura, M. Tanaka, Y. Murata, Y. Aikawa, E. Furutani, T. Kuwamura, H. Takahashi, and S. Inokuma, *J. Phys. Chem.*, **94**, 842 (1990).

16) H. Gustavsson and B. Lindman, *J. Am. Chem. Soc.*, **97**, 3923 (1975).
17) T. Yoshida, K. Taga, H. Okabayashi, K. Matsushita, H. Kamaya, and I. Ueda, *J. Colloid Interface Sci.*, **109**, 336 (1986).
18) M. Jansson and P. Stilbs, *J. Phys. Chem.*, **91**, 113 (1987).
19) J. H. Fendler, E. J. Fendler, G. A. Infante, P.-S. Shih, and L. K. Patterson, *J. Am. Chem. Soc.*, **97**, 89 (1975).
20) S. Miyagishi and M. Nishida, *J. Colloid Interface Sci.*, **73**, 270 (1980).
21) C. A. Bunton and C. P. Cowell, *J. Colloid Interface Sci.*, **122**, 154 (1988).
22) E. Kolehmainen, *J. Colloid Interface Sci.*, **105**, 273 (1985); **127**, 301 (1989).
23) E. Kolehmainen and R. Laatikainen, *J. Colloid Interface Sci.*, **121**, 148 (1988).
24) T. Hoshino and Y. Imamura, *Bull. Chem. Soc. Jpn.*, **63**, 502 (1990).
25) To be published in near future.
26) N. Nakagawa, "NMR Supekutoru no Kaisyaku," Kyoritsu Shuppan, Tokyo (1966), p. 91.
27) E. J. Fendler, C. L. Day, and J. H. Fendler, *J. Phys. Chem.*, **76**, 1460 (1972).

 © 1991 The Chemical Society of Japan Bull. Chem. Soc. Jpn., 64, 3098—3104 (1991) [Vol. 64, No. 10

Exothermic Reactions in C_2 Hydrocarbon Flames

Seishiro FUKUTANI,* Nílson KUNIOSHI, Keizo SAKAGUCHI, and Hiroshi JINNO†
Department of Industrial Chemistry, Faculty of Engineering, Kyoto University, Yoshida-honmachi, Sakyo-ku, Kyoto 606
†Department of Chemistry, Faculty of Science and Engineering, Sophia University, Kioicho 7-1, Chiyoda-ku, Tokyo 102
(Received June 7, 1991)

Premixed stoichiometric flames of acetylene, ethylene, and ethane with air were investigated using a chemical scheme composed of eighty-two pairs of elementary reactions to illustrate the dependence of the propagation mechanisms of C_2 hydrocarbon flames on the heat release distribution. The general role of heat release distribution through flames was depicted by means of an analytical treatment of the governing equations with the thermal properties of the gases being constant and the temperature profile given by an appropriate function of the position in the flame. It was found that the amount of heat released by chemical reactions at low-temperature regions of a flame is of fundamental importance for its propagation and that the main trigger of exothermic reactions at those zones is hydrogen atoms, which diffuses from the flame front; in the acetylene flame reactions consuming hydrogen atoms at the low-temperature region were found to yield all the heat released at that zone. Heat release distribution extended down to low-temperature regions was found to be able to lead to large burning velocities even though the amount of heat released at each position was small.

Since in the low-temperature region of a premixed flame thermal energy must increase only by the supply from the high-temperature region, the propagation mechanism of a premixed flame can be classified into two types according to the way by which the supply of energy occurs:[1] Thermal propagation and diffusion-controlled propagation. In the latter mode chemical enthalpy is carried by diffusion of active species such as hydrogen atoms and transformed to thermal energy by exothermic reactions occurring in the low-temperature region. Hydrogen–air premixed flames propagate mainly through this mode at least near stoichiometric conditions[2] and methane flames through the former mode.[3]

Acetylene, ethylene, and ethane contain two carbon atoms but different number of hydrogen atoms in their molecules. A hasty consideration may lead to the conclusion that the propagation of ethane flames is governed by the diffusion of hydrogen atoms and that of acetylene by thermal conduction. Experimental measurements of the burning velocity of those three flames,[4] however, have clarified that ethane flames possess burning velocities similar to that of methane, and acetylene flames have velocities which are less than those of hydrogen flames but considerably large among premixed flames. Those facts may warn us not to conclude rashly that the propagation mechanism of a premixed flame is simply deduced on the basis of the chemical composition of the fuel molecule.

The purposes of this paper are to elucidate the following two points by means of computer simulation using a detailed chemical reaction model: (1) What is the decisive factor to determine the propagation mechanism in the three C_2 hydrocarbon premixed flames; and (2) How heat release by chemical reactions controls the burning velocity.

Simulation Model

Some usual assumptions for models of flat flames[2] derive the following governing equations, which were used in the model in this investigation:

$$\frac{\partial \rho}{\partial t}+\frac{\partial}{\partial x}(\rho v)=0, \tag{1}$$

$$\frac{\partial}{\partial t}(c_p\rho T)+\frac{\partial}{\partial x}(c_p\rho T v)=\frac{\partial}{\partial x}\left(\lambda\frac{\partial T}{\partial x}\right)+\sum_i D_i\rho\frac{\partial h_i}{\partial x}\frac{\partial \omega_i}{\partial x}-\sum_i h_i\phi_i, \tag{2}$$

$$\frac{\partial}{\partial t}(\rho\omega_i)+\frac{\partial}{\partial x}(\rho\omega_i v)=\frac{\partial}{\partial x}\left(D_i\rho\frac{\partial \omega_i}{\partial x}\right)+\phi_i, \tag{3}$$

$$p=\rho RT\sum_i\frac{\omega_i}{m_i}, \tag{4}$$

where ρ is the density, v the flow velocity, T the temperature, p the pressure, c_p the specific heat, and λ the thermal conductivity of the gas mixture; ω_i is the mass fraction, ϕ_i the net production rate, h_i the enthalpy, m_i the molar mass and D_i the diffusion coefficient of the i-th species; and R is the gas constant.

The reaction scheme which was proposed in a previous paper[3] comprises eighty-two pairs of elementary reactions among twenty-five chemical species of C_1 and C_2 hydrocarbons and hydrogen–oxygen-containing species. The model gives valid burning velocities for methane flames with a wide range of equivalence ratio.[3]

Table 1. Stoichiometric Hydrocarbon–Air Premixed Flames

Hydrocarbons	C_2H_2	C_2H_4	C_2H_6
Burning velocity/m s^{-1}	1.56	0.76	0.49
Adiabatic flame temperature/K	2550	2380	2260
Experimental burning velocity[4]/m s^{-1}	1.56	0.78	0.48

As for the C_2 flames, however, it gives burning velocities agreed with the experimental values only for the stoichiometric and lean conditions (see Table 1); for rich conditions the calculated burning velocities are larger than the corresponding experimental velocities since the decrease in the burning velocity due to the waste of a small part of the fuel in the soot-forming process is neglected in the reaction scheme. In this work, stoichiometric flames of the C_2 hydrocarbons are, therefore, investigated by using the proposed scheme.

The boundary conditions were given as follows: at the unburned side the temperature is 298 K and the gas mixture contains only the fuel and air, and at the burned side the temperature is raised up to the adiabatic flame temperature, which is obtained by the chemical equilibrium calculation based on the total enthalpy at the unburned side, and the gas has the corresponding equilibrium composition at that temperature. A simulated flame can be kept in the steady state only when the flow velocity just agrees with the burning velocity, and this value was obtained by the trial-and-error method.

Results and Discussion

Structures of the Flames. Figure 1 shows the temperature profiles of the three C_2 hydrocarbon premixed flames. The temperature gradients increase in the order of the increasing burning velocity. In the ethane flame the temperature is elevated gradually at low temperatures just like an exponential function. In the acetylene flame, on the contrary, the temperature gradient increases steeply. The ethylene flame keeps an intermediate temperature gradient between those of the acetylene and ethane flames over the whole region.

Figure 2 shows the exothermic rates of the three flames as functions of temperature. Distinguished differences among those rates are: (1) the rate of the ethane flame is much smaller than that of the acetylene flame; (2) in the acetylene flame heat evolution starts increasing at such a low temperature as 450 K and rises with a large slope particularly at low temperatures, but in the ethane flame it increases from 700 K and keeps almost a constant gradient.

Analytical solution of the thermal energy conservation equation, Eq. 2, neglecting chemical reactions occurring at low temperatures yields the following results: if the thermal properties of the gas mixture can be treated as being constant, (1) the reaction-zone thickness of a premixed flame is inversely proportional to the burning velocity and (2) the burning velocity is proportional to the square root of the averaged reaction rate.[1] Those two predictions seem to be valid in the three C_2 flames as suggested by Figs. 1 and 2. Strictly speaking, however, the simulated burning velocity of the acetylene flame is larger than the value of the analytical prediction. The deviation comes from the indifference to the reaction-rate distribution or, correspondingly, to the exothermic rate distribution in the analytical treatment. The distribution of heat release throughout the flame, particularly at low temperatures, should be considered in order to estimate precisely the burning velocity of a premixed flame.

The inflow of chemical enthalpy into the low-temperature region of a premixed flame is substantially supported by hydrogen atoms diffused from the flame front. The second term in the right-hand side of Eq. 2

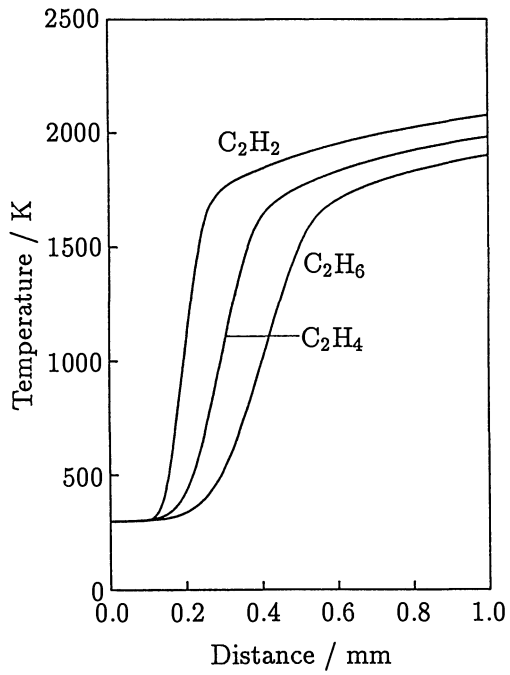

Fig. 1. Profiles of temperature in the stoichiometric C_2 hydrocarbon premixed flames.

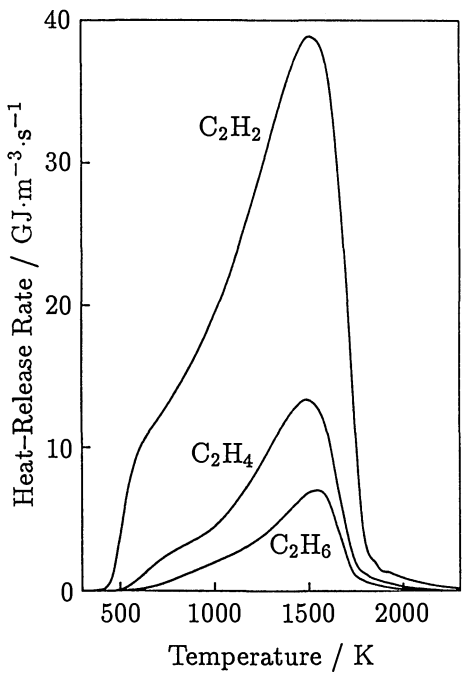

Fig. 2. Distributions of exothermic rates in the stoichiometric C_2 hydrocarbon premixed flames.

is called enthalpy transfer accompanying species diffusion. This popular designation, however, is not correct and that term does not strictly express the rate of enthalpy accumulation by species diffusion. The original enthalpy-conservation equation prescribes the conservation of total enthalpy (thermal enthalpy+chemical enthalpy):

$$\frac{\partial h}{\partial t}+\frac{\partial}{\partial x}(hv)=\frac{\partial}{\partial x}\left(\lambda\frac{\partial T}{\partial x}\right)+\sum_i\frac{\partial}{\partial x}\left(D_i\rho h_i\frac{\partial \omega_i}{\partial x}\right), \quad (5)$$

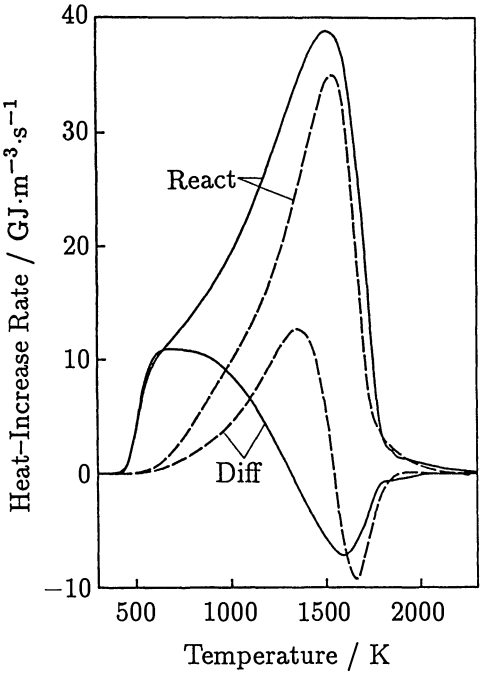

Fig. 3. Rates of the increase in enthalpy accompanying diffusion of hydrogen atoms (Diff) and those of heat release (React) in the acetylene (solid line) and ethane (dashed line) flames; the rates of the ethane flame are multiplied by a factor of 5.

where h is the total enthalpy per unit volume of the gas mixture. The second term in the right-hand side of Eq. 5 does designate the enthalpy carried by diffused species. This equation, however, does not involve explicitly an exothermic term and hence is usually transformed into the conservation equation of thermal enthalpy, Eq. 2. The so-called diffusion term appearing in Eq. 2, moreover, gives only a small contribution to the heat transfer toward low-temperature regions of premixed flames.[2,3]

Figure 3 depicts the rates of the increase in enthalpy due to diffusion of hydrogen atoms calculated according to Eq. 5 and the exothermic rates in the acetylene and ethane flames, as typical examples. In the low-temperature region of the acetylene flame the exothermic rate agrees very well with the enthalpy-increase rate due to diffused hydrogen atoms; it should be noted that the intense heat release observed between 450 K and 600 K is thoroughly ascribable to the exothermic reactions which consume all the diffused hydrogen atoms. In the ethane flame, on the other hand, diffused hydrogen atoms do not work as a direct source of the heat release but work only as a trigger for reactions occurring at low temperatures; the role as a reaction trigger is also essential because combustion reaction cannot be easily initiated in an unburned gas mixture within a short time if they are activated only by rising temperature.

The temperature-increase mode in the low-temperature region of a premixed flame, therefore, does not simply depend on the amount of hydrogen atoms contained in the fuel molecule but on the mechanisms of the reactions occurring in the high- and low-temperature regions.

Reaction Mechanisms of Production and Consumption of Hydrogen Atoms. The mechanisms of combustion reactions in the C_2 hydrocarbon flames have been discussed by many authors based on computer simulation using various reaction schemes.[5–9] Figures 4a and

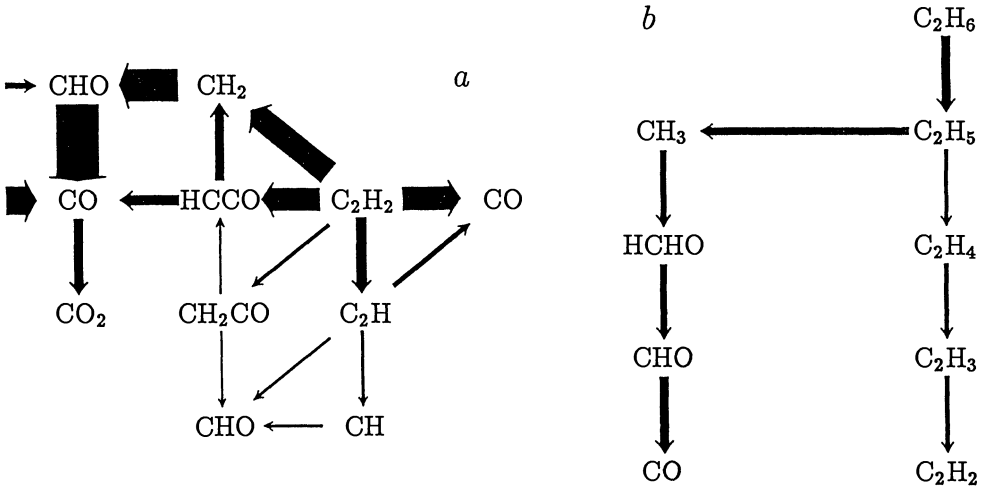

Fig. 4. Reaction pathways in the acetylene flame at 1510 K (a) and in the ethane flame at 1550 K (b). The width of the arrows is proportional to the rate of the corresponding route.

4b show the reaction pathways at the positions of the maximum exothermic rates in the acetylene and ethane flames obtained in this investigation. Carbon monoxide is slowly oxidized even at temperatures higher than 1500 K; only after conversion of all the hydrocarbons to carbon monoxide its oxidation proceeds fast.

A characteristic of the combustion reaction of the acetylene flame is that the reaction pathway from the fuel to carbon monoxide is short. Such a short span in the reaction pathway can lead to easy acceleration of the whole fuel oxidation without congestion of intermediate species. In the ethane flame, on the contrary, the main combustion route proceeds unexpectedly along the so-called C_1 route after the leap from ethyl radicals to methyl radicals through the reaction

$$C_2H_5 + H \rightarrow CH_3 + CH_3 \quad \text{(R10)}$$

at high temperatures. This is a reason why ethane flames have burning velocity similar to that of methane flames. At temperatures lower than 1200 K, however, ethyl radicals are predominantly dehydrogenated to ethylene by the reaction

$$C_2H_5 + O_2 \rightarrow C_2H_4 + HO_2. \quad \text{(R31)}$$

The ethylene flame holds the same mechanism as that of the acetylene flame since the fuel is once dehydrogenated to acetylene and reacts along the same route; the burning velocity settles down at an intermediate value between those of the acetylene and ethane flames.

In order to pursue the production and consumption of hydrogen atoms the rates of the elementary reactions in which hydrogen atoms participate are shown in Figs. 5a and 5b. Differences between the reactions of the acetylene and ethane flames are: (1) the reaction rates in the acetylene flame are much larger, as a whole, than those in the ethane flame; and (2) hydrogen atoms are consumed in a great amount in the low-temperature region of the acetylene flame.

The consumption of hydrogen atoms at low temperatures in the acetylene flame is due to the reactions

$$C_2H_2 + H + M \rightarrow C_2H_3 + M \quad \text{(R42)}$$

and

$$C_2H_3 + H \rightarrow C_2H_2 + H_2. \quad \text{(R40)}$$

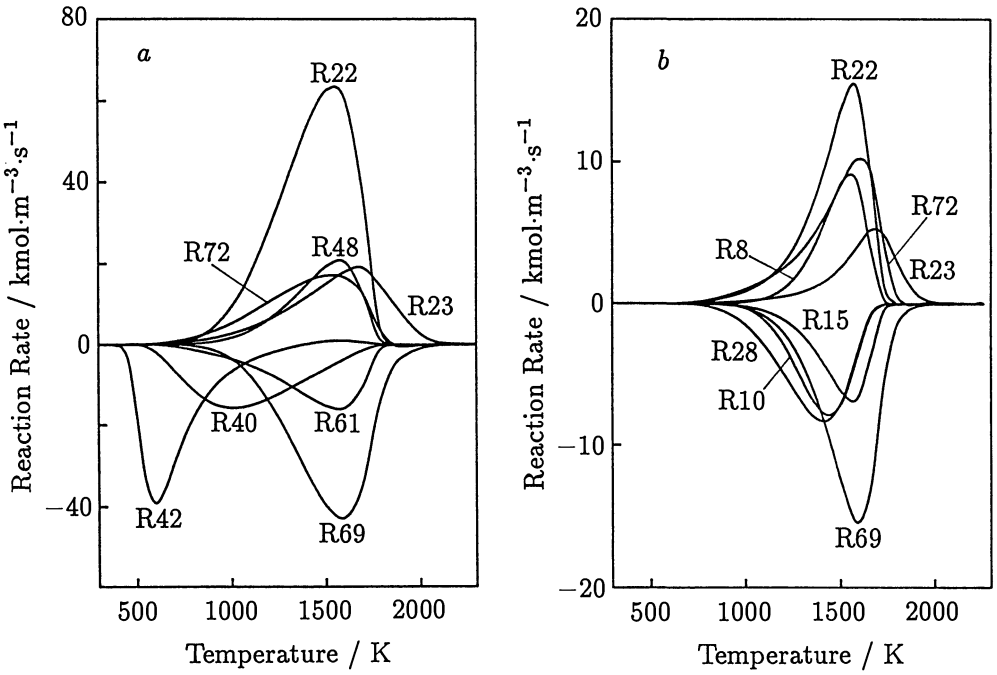

Fig. 5. Rates of the reactions in which hydrogen atoms participate in the acetylene (a) and ethane (b) flames. The negative rates express that the corresponding reactions consume hydrogen atoms.

R8: $CH_3 + O \rightarrow HCHO + H$
R10: $C_2H_5 + H \rightarrow CH_3 + CH_3$
R15: $HCHO + H \rightarrow CHO + H_2$
R22: $CHO + M \rightarrow CO + H + M$
R23: $CO + OH \rightarrow CO_2 + H$
R28: $C_2H_6 + H \rightarrow C_2H_5 + H_2$
R40: $C_2H_3 + H \rightarrow C_2H_2 + H_2$
R42: $C_2H_2 + H + M \rightarrow C_2H_3 + M$
R48: $C_2H_2 + O \rightarrow HCCO + H$
R61: $HCCO + H \rightarrow CH_2 + CO$
R69: $H + O_2 \rightarrow OH + O$
R72: $OH + H_2 \rightarrow H + H_2O$

The rate constant of reaction (R42) changes increasingly with decreasing temperature because of its negative activation energy. Hydrogen atoms diffused from the flame front, therefore, easily react with the fuel at low temperatures releasing a fairly large amount of heat, 193 kJ mol^{-1} at 500 K and 197 kJ mol^{-1} at 1000 K, for example. As temperature rises another possibility for their consumption, that is, reaction (R40) is added to the reaction mechanism. The rate constant of this reaction increases gradually with increasing temperature. This reaction also generates much heat, 249 kJ mol^{-1} at 500 K and 247 kJ mol^{-1} at 1000 K. The steep increase in exothermic rate of the acetylene flame shown in Fig. 2 is ascribed to these two reactions and the shoulder observed around 600 K comes from the intense exothermicity of reaction (R42).

The acetylene flame has thus a very effective source of heat release at low temperatures; the above described pair of reactions convert hydrogen atoms to molecular hydrogen and, at the same time, the fuel to vinyl radicals at the first stage and then the vinyl radicals back to acetylene at the second stage.

The production of hydrogen atoms is predominantly ascribable to the reaction

$$CHO + M \rightarrow CO + H + M \qquad (R22)$$

at the flame fronts of hydrocarbon flames. As described above, the reaction path from the fuel to carbon monoxide is fairly short in the acetylene flame and, therefore, hydrogen atoms are yielded in a great amount at the flame front.

Moreover, the acetylene flame has advantages for fast transport of hydrogen atoms to the low-temperature region because of the thin reaction zone shown in Fig. 1 though this condition is naturally satisfied in a flame having large burning velocity since the reaction-zone thickness is inversely proportional to burning velocity.

Consequently, when the three conditions for supply of a sufficient amount of chemical enthalpy toward the low-temperature region, that is, production of hydrogen atoms at high temperatures, their diffusion toward low-temperature region and their consumption with heat release at low temperatures, are satisfied, the amount of chemical enthalpy easily exceeds that of thermal energy carried by thermal conduction, and therefore the flame is stably maintained according to the so-called diffusion-controlled propagation mechanism.

Role of Heat Release at Low Temperatures on Flame Propagation. As pointed out in the previous subsection the effects of heat release on the burning velocity must be discussed based on the magnitude of its rate and the shape of its distribution as well. The role of the distribution of exothermic rate, particularly at low temperatures, will be investigated here.

The temperature distribution in a flame must satisfy Eq. 2. The second term in the right-hand side of that equation gives the rate of heat transfer related to species diffusion and is negligibly small as described above, and the time-dependent term in the left-hand side equals zero at steady state; therefore Eq. 2 is reduced to an ordinary differential equation

$$\frac{d}{dx}(c_p\rho Tv)=\frac{d}{dx}\left(\lambda\frac{dT}{dx}\right)-\sum_i h_i\phi_i. \qquad (6)$$

In the steady state ρv=const., and c_p and λ can be assumed to be constant in a first-order approximation, and thus Eq. 6 becomes

$$\lambda\frac{d^2T}{dx^2}-c_p\rho v\frac{dT}{dx}-\sum_i h_i\phi_i=0. \qquad (7)$$

In a low-temperature region, Eq. 7 is further simplified by neglect of the exothermic term and gives an analytical solution

$$T=\alpha\exp\left(\frac{c_p\rho v}{\lambda}x\right)+T_u, \qquad (8)$$

where T_u is the temperature of the unburned gas mixture and α is an arbitrary constant fixing the position of the flame along the x-axis. Equation 8 shows that the temperature rises exponentially in the region preceding the exothermic region in a steady premixed flame, and the temperature gradient grows as the burning velocity increases.

On the other hand the temperature of a premixed flame cannot be raised higher than its adiabatic flame temperature. The temperature, therefore, must approach asymptotically the adiabatic flame temperature and have an inflection point in its distribution. The decline of the temperature gradient toward zero should consequently be actualized by the exothermic term, that is, the last term in Eq. 7.

When exothermic reactions start at a high temperature the heat release must reduce the temperature gradient within the small temperature interval remaining before the adiabatic flame temperature; therefore chemical reactions should emit heat with a large rate. On the contrary, when they occur at low temperatures even a small rate of heat release can shift the temperature gradient toward zero. These effects of the heat release are discussed by solving Eq. 7.

Unfortunately Eq. 7 cannot be solved analytically. The subject to elucidate in this subsection is, however, how burning velocity is influenced by heat release at low temperatures. Here, in contrast with the usual method, the temperature distribution in the exothermic region is assumed, at first, as a function of position and substituted into Eq. 7, and then the exothermic term is evaluated for the given temperature distribution.

The temperature distribution is given by using a logistic function:

$$T=\frac{T_0}{1+\beta\exp(-bx)}+T_u, \qquad (9)$$

where T_0, T_u, β and b are four arbitrary constants; such a function asymptotically approaches T_u, the temperature of the unburned gases, at $x=-\infty$, $T_0+T_u\equiv T_{ad}$ at

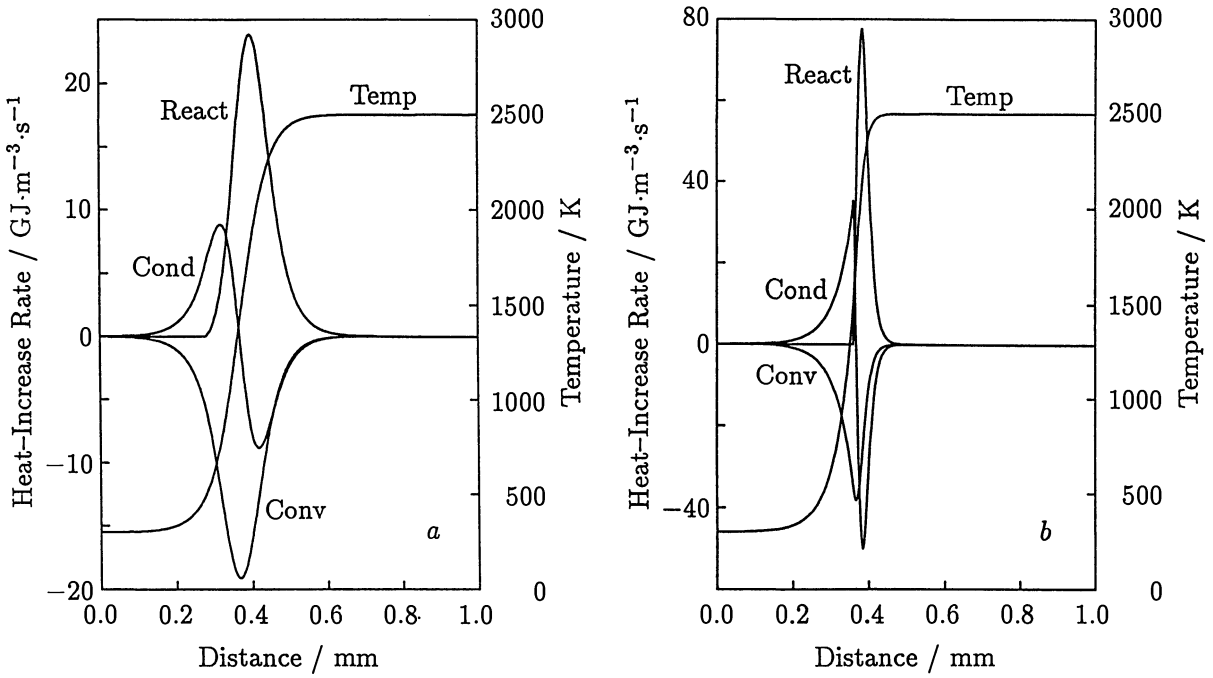

Fig. 6. Profiles of temperature (Temp) and the heat-increase rates due to convection (Conv), conduction (Cond), and the exothermic rate (React) in the flames with T_c=500 K (a) and 1500 K (b).

$x=\infty$, where T_{ad} corresponds to the adiabatic flame temperature, and has an inflection point at $x=\ln \beta/b$. The values of T determined by Eq. 9 are satisfactory for the temperature distributed in a premixed flame. The assumed logistic curve is connected with the exponential curve for the temperature distribution in the nonexothermic region, Eq. 8, in such a way that the temperature itself, and its first and second derivatives have the same values, respectively, at a certain point; the flames are distinguished by the connection temperature, which is designated as T_c. Those three conditions at the connecting point and a given T_{ad} can fix the four constants of the logistic curve.

Figures 6a and 6b show the distributions of the temperature and the heat balance in two flames with the same burning velocity, 1.0 m s^{-1}, and the same adiabatic flame temperature, 2500 K, but different connection temperatures, 500 K and 1500 K. The unburned gases of both flames have constant ρ, c_p, and λ equal to, respectively, 1.3 kg m^{-3}, 1000 J kg^{-1} K^{-1}, and 0.058 W m^{-1} K^{-1}. The two temperature distributions in the nonexothermic regions are expressed, as mentioned above, with the same exponential function of distance, but those in the exothermic regions are clearly different; the reaction zone of the flame with higher T_c is much thinner and its maximum exothermic rate is about four times as large as that of the flame with lower T_c, indicating that the flame front thickness is related to the exothermic-rate distribution.

Figure 7 depicts the exothermic-rate distributions in the various flames with a wide range of T_c. The integration of the exothermic rate of the flames in the range

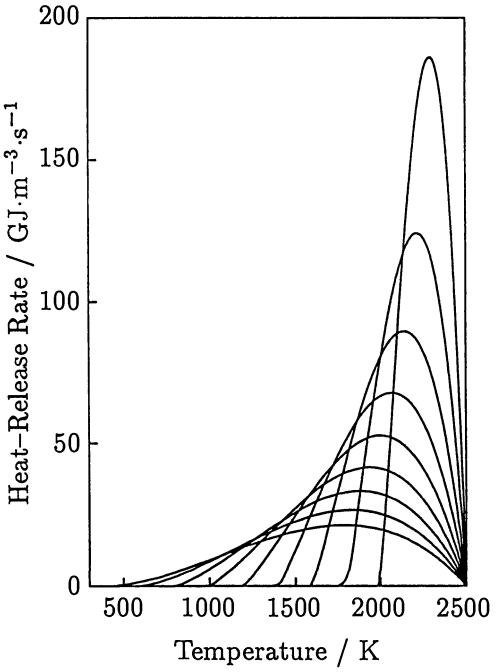

Fig. 7. Distributions of the exothermic rates of the flames having T_c ranging from 400 K to 2000 K with intervals of 200 K.

of x from $-\infty$ to $+\infty$ gives the same value since this value corresponds to the thermal energy necessary for heating the unburned gases from room temperature to the adiabatic flame temperature, 2500 K. The maximum exothermic rate of the flame with the smallest T_c, however, is about 1/9 of that of the flame with the

largest T_c; the temperature range of the exothermic region of the former flame is four times as large as that of the latter flame, and therefore the flame thickness of the former flame is larger. The result that a flame evolving heat at low temperatures can maintain stable flame propagation even if the exothermic rate is small indicates that the flame possibly possesses larger burning velocity when the exothermic rate has almost a similar magnitude.

Conclusions

Simulation of acetylene, ethylene, and ethane premixed flames was performed under the stoichiometric conditions using a detailed reaction scheme, which reproduces the combustion reactions of C_1 and C_2 hydrocarbons, and the following conclusions were obtained:

1. In the acetylene flame, enthalpy is carried into the low-temperature region as the chemical enthalpy of diffused hydrogen atoms, and converted there into thermal enthalpy by a pair of reactions which are substantially reduced to recombination of hydrogen atoms. The unburned gas is heated by those exothermic reactions. The flames where a large amount of hydrogen atoms are produced at high temperatures, diffused to the low-temperature region and consumed there with heat release can propagate according to the diffusion-controlled propagation mechanism. In the ethane flame, on the other hand, combustion reaction proceeds predominantly along the C_1 route and then this flame has the same propagation mechanism as that of a stoichiometric methane flame. In the ethylene flame the fuel is once dehydrogenated to acetylene.

2. When chemical enthalpy is carried by diffused hydrogen atoms and heat is liberated by reactions consuming them at low temperatures, the temperature distribution deviates from an exponential distribution, and the exothermic zone becomes thick. Then even small exothermic rate can maintain stably large burning velocity.

References

1) A. G. Gaydon and H. G. Wolfhard, "Flames," 4th ed, Chapman and Hall, London (1979), Chap. 5.

2) S. Fukutani, N. Kunioshi, and H. Jinno, *Bull. Chem. Soc. Jpn.*, **63**, 2191 (1990).

3) S. Fukutani, K. Sakaguchi, N. Kunioshi, and H. Jinno, *Bull. Chem. Soc. Jpn.*, **64**, 1623 (1991).

4) R. Guenther and G. Janische, *Chem. Ing. Tech.*, **43**, 975 (1971).

5) J. Warnatz, H. Bockhorn, A. Möser, and H. W. Wenz, "Nineteenth Symposium (International) on Combustion," The Combustion Institute, Pittsburgh (1982), pp. 197—209.

6) J. Warnatz, "Twentieth Symposium (International) on Combustion," The Combustion Institute, Pittsburgh (1984), pp. 845—856.

7) M. Cathonnet, F. Gaillard, J. C. Boettner, P. Cambray, D. Karmed, and J. C. Bellet, "Twentieth Symposium (International) on Combustion," The Combustion Institute, Pittsburgh (1984), pp. 819—829.

8) R. J. Hennessy, C. Robinson, and D. B. Smith, "Twenty-First Symposium (International) on Combustion," The Combustion Institute, Pittsburgh (1986), pp. 761—772.

9) C. K. Westbrook, M. M. Thornton, W. J. Pitz, and P. C. Malte, "Twenty-Second Symposium (International) on Combustion," The Combustion Institute, Pittsburgh (1988), pp. 863—871.

Cationic Self-Diffusion in Ionic Plastic Phases of Thallium Nitrite and Nitrate and in Thallium Thiocyanate

Yoshihiro FURUKAWA,* Hirokazu NAGASE, Ryuichi IKEDA,† and Daiyu NAKAMURA††
Department of Chemistry, Faculty of Science, Nagoya University, Nagoya 464-01
(Received June 11, 1991)

Cationic self-diffusion in the ionic plastic phases of $TlNO_2$ and $TlNO_3$ was investigated by measuring temperature dependences of the $^{203,205}Tl$ NMR spin-lattice relaxation time and the electrical conductivity. The NMR results showed that the Tl^+ ions in these phases undergo rapid translational diffusion with the activation energy (E_a) of 48 and 77 kJ mol^{-1} for nitrite and nitrate, respectively. The E_a values agreed well with those obtained from the electrical conductivity, indicating that the cation is the electric carrier. The diffusion constants (D) estimated from the relaxation time and conductivity data were ca. 10^{-12} m^2 s^{-1} at the respective melting point (T_m) of plastic phase. The tendency that D at T_m has the characteristic value given above is recognized for other ionic plastic phases so far reported. The Tl^+ ionic conductivity in TlSCN, which makes no plastic phase, was reported in comparison.

Plastic crystals consist of molecules whose centers of gravity form a regular crystalline lattice, whereas each molecule is in a highly movable state as in liquid. Molecular motions characteristic in the plastic crystals are the isotropic overall rotation and the translational self-diffusion which are attributable to the origin of marked plasticity observed in this phase. Systematic NMR studies on this phase of molecular crystals have revealed that the average time for the self-diffusional jump to the neighboring vacant sites observed at the melting point is independent of molecules as well as temperatures, and becomes almost the same value (ca. 10^{-7} s).[1] Similar results have been obtained in plastic phases of ionic crystals containing methylammonium cations.[2-4]

The highest-temperature solid phases of thallium nitrite and nitrate have been reported to form plastic crystals.[5-8] It has been shown from the TlNMR studies that the Tl^+ ions are diffusing in these phases.[9,10] In the present study, we intend to measure the electrical conductivity of $TlNO_2$ and $TlNO_3$ and the ^{205}Tl NMR spin-lattice relaxation time of $TlNO_3$ to get detailed information on the diffusional motions in the ionic plastic crystals.

Experimental

Commercially available $TlNO_3$ (Nacalai Tesque, GR) and $TlNO_2$ prepared by double decomposition of $Ba(NO_2)_2 \cdot H_2O$ and Tl_2SO_4 are recrystallized from aqueous solution. The ^{205}Tl spin-lattice relaxation time, T_1, was determined by the usual inversion recovery method using a homemade NMR spectrometer.[11] The electrical conductivity, σ, was measured by means of the complex impedance analysis using an Ando Denki AG-4311 LCR meter, which was interfaced to an NEC PC-9801 microcomputer by GP-IB. The impedance was determined over the frequency range between 0.1 and 100 kHz on pelletized samples with the electrodes of colloidal carbon. The sample temperatures were measured by a copper–constantan thermocouple within errors of ±1 K.

Results and Discussion

We have previously reported the temperature dependence of the spin-lattice relaxation times, T_1 and $T_{1\rho}$, in the laboratory and rotating frame, respectively, and the spin–spin relaxation time, T_2, of $^{203,205}Tl$ in $TlNO_2$.[10] These relaxation times were interpreted in terms of the reorientation of the NO_2^- ions in the low-temperature phase obtainable below the phase transitioin temperature (T_c) of 282 K and the translational self-diffusion of the Tl^+ ions in the high-temperature plastic phase above T_c. In the analysis of the relaxation times attributable to the Tl^+ ionic self-diffusion, the usual BPP-type spectral density functions were assumed.[12] A small discrepancy recognized in the motional parameters determined from T_1 and $T_{1\rho}$ analysis may be ascribed to this assumption because it has been expected that the BPP-type spectral density is a rough approximation for diffusing spins.[13]

The temperature dependence of the relaxation times in $TlNO_2$ above 263 K are represented in Fig. 1.[10] The magnetization recovery curve in the T_1 measurements of Tl nuclei usually becomes nonexponential because of the magnetic interactions between two kinds of Tl isotopes, ^{203}Tl and ^{205}Tl, which have only 1% difference in the gyromagnetic ratios.[9,10] From the observed recovery curves, we evaluated the long and short components of T_1 (T_1^l and T_1^s, respectively). The T_1^l values in the high-temperature phase of $TlNO_2$, which are known to be usually determined by lattice vibrations,[10] are ommited in Fig. 1. The T_2 increase observed on heating and the minima in both T_1^s and $T_{1\rho}$ are assignable to the translational self-diffusion of the Tl^+ ions.

The relaxation times of Tl nuclei are mainly governed by scalar (pseudo-exchange) interactions and approximated by[9,10,12]

$$(T_1^s)^{-1} = 2(\langle \delta\omega^2 \rangle_i + \langle \delta\omega^2 \rangle_j)\, j(\omega_{0i} - \omega_{0j}, \tau), \quad (1)$$

$$(T_{1\rho})_i^{-1} = \langle \delta\omega^2 \rangle_i \{ j(\omega_{1i}, \tau) + j(\omega_{0i} - \omega_{0j}, \tau) \}, \quad (2)$$

† Present address: Department of Chemistry, University of Tsukuba, Tsukuba 305.
†† Deceased on 27 February, 1991.

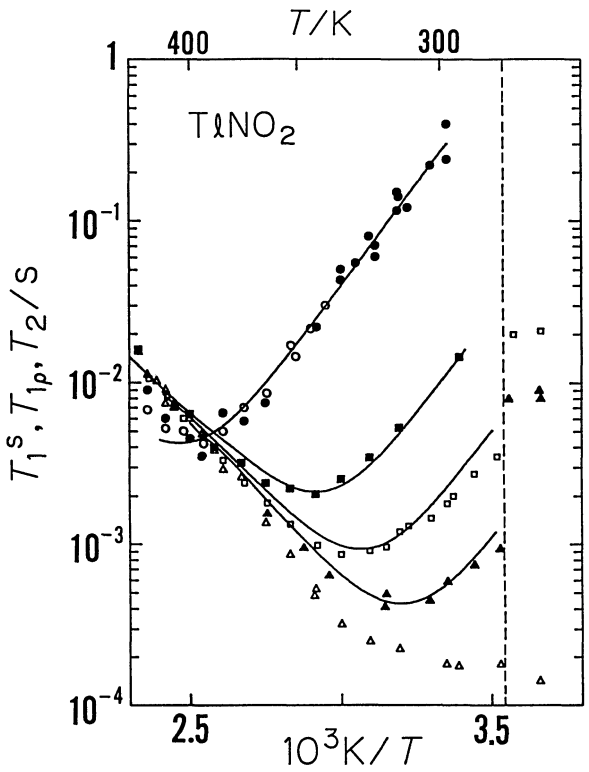

Fig. 1. Temperature dependences of T_1^s (short component), $T_{1\rho}$, and T_2 of ^{203}Tl and ^{205}Tl in $TlNO_2$ observed above 263 K.[10] T_1^s of ^{203}Tl and ^{205}Tl at 34.270 (●) and 34.613 MHz (○), respectively; ^{205}Tl $T_{1\rho}$ at ω_1=157 (■), 68 (□), and 31 krad s^{-1} (▲); ^{205}Tl T_2 (△). ^{203}Tl $T_{1\rho}$ and T_2 were omitted for simplicity. The solid lines were calculated using Eqs. 1 and 2 and the spectral density numerically given for the self-diffusion in the sc lattice.[13] The vertical broken line indicates the phase transition point.

$$(T_2)_i^{-1}=\langle\delta\omega^2\rangle_i\{j(0,\tau)+j(\omega_{0i}-\omega_{0j},\tau)\}. \quad (3)$$

Here, ω_{0i} and ω_{1i} are the Larmor frequencies of thallium-i spins (i=203 or 205) in the laboratory and rotating frame, respectively. $\langle\delta\omega^2\rangle_i$ is the NMR second moment of thallium-i spins determined by the scalar interactions with unlike thallium-j spins. Since the scalar interaction between like spins does not affect the second moment, one can obtain $0.295\langle\delta\omega^2\rangle_{203}=0.705\langle\delta\omega^2\rangle_{205}$ by referring to the natural abundances of ^{203}Tl and ^{205}Tl nuclei. This relation could be confirmed from the ratios of $T_{1\rho}$ or T_2 observed for ^{203}Tl and ^{205}Tl, indicating that the relaxations of the thallium nuclei are dominated by the scalar interactions.[10] τ is the correlation time of the Tl^+ self-diffusioin. $j(\omega,\tau)$ is the spectral density function, and under the assumption that the correlation function is exponential or of the BPP-type, it is expressed as[12]

$$j(\omega,\tau)=\tau/(1+\omega^2\tau^2). \quad (4)$$

Barton and Sholl have reported numerical results of nuclear spin relaxation times due to dipole–dipole interacions between diffusive species in fcc, bcc, and sc lattices.[13] In order to reanalyze the relaxational data given in Fig. 1, we use their numerical values of $g_{poly}(y)$, where $y=\omega\tau/2$, for the sc lattice given in Ref. 13 instead of Eq. 4 by assuming that the spectral density for the scalar interactions is the same shape as that for the dipolar ones; the fitting calculation was carried out using the T_1^s and $T_{1\rho}$ data. The determined diffusional parameters are given in Table 1. These parameters are not significantly different from those given in Ref. 10, but the present analysis can account for the temperature dependence of both T_1^s and $T_{1\rho}$ using the same parameters.

Table 1. Tl^+ Diffusional Parameters Determined from Tl NMR Relaxation Times in the Ionic Plastic Phases of $TlNO_2$ and $TlNO_3$

Compound	$C^{a)}/10^7$ s^{-2}	$\log(\tau_0/\text{s})$	E_a/kJ mol^{-1}
$TlNO_2$	6.6±0.2	−12.3±0.1	48±1
$TlNO_3$	10.2±0.5	−15.6±0.4	77±5

a) $C=(\langle\delta\omega^2\rangle_i+\langle\delta\omega^2\rangle_j)/7.5$, where the factor 7.5 was introduced by comparing the maximum values of $\omega j(\omega,\tau)$ in Eqs. 1 and 2 with that of $y\,g_{poly}(y)$ in Ref. 13.

Villa and Avogadro have studied the temperature dependences of T_1^l, $T_{1\rho}$, and T_2 of Tl nuclei in $TlNO_3$.[9] They, however, reported no T_1^s because, in most cases, it gives the same information as $T_{1\rho}$. Their derivation

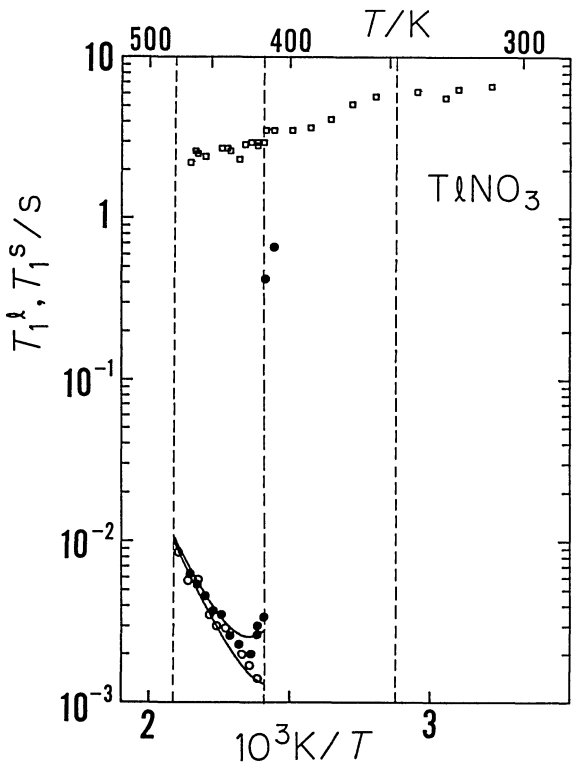

Fig. 2. Temperature dependences of ^{205}Tl T_1^l (□) and T_1^s (●) at 32 MHz, and T_1^s (○) at 16 MHz in $TlNO_3$. The solid lines for T_1^s were calculated in the same procedure as that for $TlNO_2$. Broken lines indicate the melting and two phase-transition points.

of ionic-diffusion correlation time from the $T_{1\rho}$ and T_2 is likely to be less reliable, because no $T_{1\rho}$ minimum was detected. It can be expected from their data that a T_1^s minimum in the highest-temperature phase of $TlNO_3$ will be detected, if one chooses a suitable resonance frequency. This can be derived from the fact that the NMR time scale of T_1^s $\{(\omega_{0i}-\omega_{0j})^{-1}\}$ is just between those of T_1^l (ω_0^{-1}) and $T_{1\rho}$ (ω_1^{-1}). Along this purpose, we measured the temperature dependence of T_1^s at 16 and 32 MHz. A T_1^s minimum could be observed at 32 MHz in the high-temperature plastic phase as shown in Fig. 2. The analytical procedure of the T_1^s is the same as above, and the obtained motional parameters are given in Table 1.

The diffusion constant (D_{NMR}) of the Tl^+ ions is related to the diffusion correlation times by

$$D_{NMR}=\langle l^2\rangle/6\tau, \quad (5)$$

where, $\langle l^2\rangle$ stands for the mean-square jump distance of the ions. When l is assumed to be equal to the lattice parameter of the unit cell, D_{NMR} can be derived, and the values at the melting point (T_m) of $TlNO_2$ and $TlNO_3$ are given in Table 2.

Figure 3 shows the temperature dependence of the electrical conductivity of $TlNO_2$, $TlNO_3$, and TlSCN, where the last compound forms no plastic phase.[14] The diffusion constant (D_σ) of the ions can be related to the electrical conductivity by the Nernst–Einstein equation:

$$D_\sigma=\sigma\, kT/(Ze)^2c. \quad (6)$$

Here, Ze and c are the charge and concentration of the diffusing ions, respectively. Since the Arrhenius relation is assumed for D_σ, the conductivity activation energy (E_σ) can be determined from the slope of the $\log\sigma T$ vs. $1/T$ plot.

$TlNO_2$ gave σ of 2.4×10^{-4} S m^{-1} at 296 K. With increasing temperature, the σT vs. $1/T$ plot of $TlNO_2$ increased exponentially, yielding E_σ of 46.6 kJ mol^{-1}. This is in good agreement with that determined from the relaxation measurements, indicating that the Tl^+ ions are the electric carriers in $TlNO_2$. The σ value of $TlNO_3$ shows a break in the $\log\sigma T$ vs. $1/T$ curve at both phase transition points. The decrease in σ in the intermediate-temperature phase was observed by several authors,[6,9,15] and assigned to some effect of the sample humidity.[6] The highest-temperature plastic phase has E_σ of 79 kJ mol^{-1}, which agrees with 77 kJ mol^{-1} from

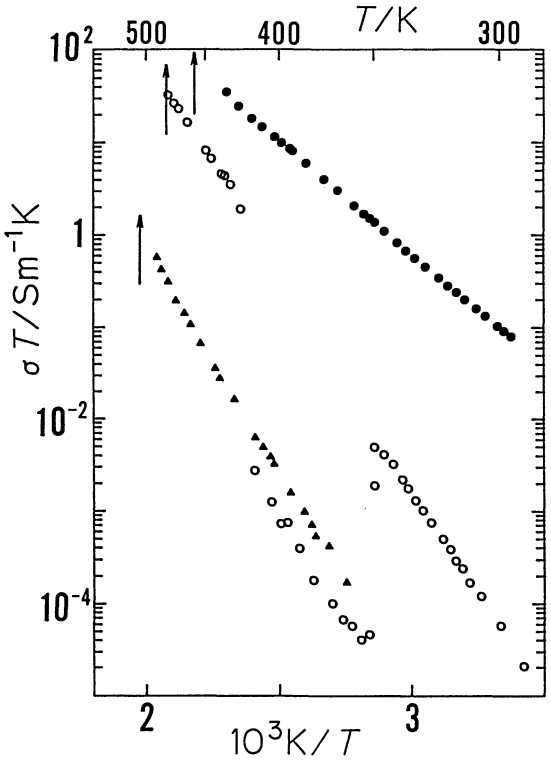

Fig. 3. Temperature dependence of the electrical conductivity (σ) in $TlNO_2$ (●), $TlNO_3$ (○), and TlSCN (▲). The $\log\sigma T$ value is plotted against $1/T$. Arrows indicate the respective melting points. The breaks in the $\log\sigma T$ vs. $1/T$ curve for $TlNO_3$ are due to the phase transitions.

Table 2. Phase Transition Temperature (T_c/K) from the Normal to Plastic Phase, Melting Point (T_m/K), Diffusion Constant ($D_m/10^{-12}$ m^{2}s^{-1}) Extrapolated to Their Melting Points of Several Ionic Plastic Crystals

Compound	$T_c(T_m)$	NMR				Conductivity		
		Nuclei	$D_{m,NMR}$	E_a	Ref[a]	$D_{m,\sigma}$	E_σ	Ref[a]
$TlNO_2$	282(459)	$^{203,205}Tl$	0.2	48	*	2.5	47	*
$TlNO_3$	417(480)	^{205}Tl	0.5	77	*	1.4	79	*
		—		77	9	—	77	9
$K[HF_2]$	470(512)	^1H,^{19}F	0.5	80	17	0.3	87	18
$[C(NH_2)_3]ClO_4$	450(525)	^1H	0.4	41	19	1.0	43	19
$[(CH_3)_4N]SCN$	455(565)[b]	^1H	1.5	110	20	2.9	100	20
$(CH_3NH_3)NO_3$	352(384)	^1H	0.4	29	2	2.5	45	2
$_{(CH3}NH_3)ClO_4$	451(528)	^1H	1.7	36	3	—	—	—
$(CH_3NH_3)I$	414(515)	^1H[c]	0.8	48	4	10	51	4
TlSCN[d]	371(507)	$^{203,205}Tl$	—	90	16	0.05	93	*

a) Asterisks represent the present work. b) Decomposition point. c) Derived from T_2 data. d) TlSCN forms no plastic phase up to T_m.

the T_1^S results. The fact that σ in TlSCN is lower than those of $TlNO_2$ and $TlNO_3$ may imply that TlSCN is not plastic. We have shown that the charge carriers in TlSCN are also the Tl^+ ions.[16] Under the assumtion that c is the total Tl^+ ion concentration, D_σ was estimated to be 2.5×10^{-12}, 1.4×10^{-12}, and 4.8×10^{-14} $m^2 s^{-1}$ at T_m of $TlNO_2$, $TlNO_3$, and TlSCN, respectively.

For many molecular plastic crystals, it has been observed that the diffusion constants at respective T_m are in the range $0.5—2.5\times10^{-13}$ $m^2 s^{-1}$ and the correlation times of the diffusion approach $10^{-7}—10^{-6}$ s.[1]

In order to see whether the diffusion constant in ionic plastic phases approaches a characteristic value at T_m, as in molecular plastic crystals, we collected experimental data on the ionic diffusions studied by electrical conductivities and NMR relaxation times. The collected data of D_{NMR} and D_σ at T_m are summarized in Table 2. Both D values of each compound are in good agreement in spite of the different methods employed to deduce them. With no exception, D_{NMR} as well as D_σ tends to converge into ca. 10^{-12} $m^2 s^{-1}$. This value is thought to be characteristic for ionic plastic phases. It is surprising that these characteristic correlation times are almost the same in both ionic and molecular plastic crystals because the weak van der Walls interaction is the main cohesive force in the molecular crystals whereas the much stronger Coulombic force is opperative in ionic crystals.

This work was partially supported by a Grant-in-Aid for Scientific Research No. 02403002 from the Ministry of Education, Science and Culture.

References

1) J. M. Chezeau and J. H. Strange, *Phys. Rep.*, **53**, 1 (1979), and the references cited therein.
2) H. Ishida, R. Ikeda, and D. Nakamura, *J. Chem. Soc., Faraday Trans. 2*, **81**, 963 (1985).
3) H. Ishida, R. Ikeda, and D. Nakamura, *Bull. Chem. Soc. Jpn.*, **60**, 467 (1987).
4) H. Ishida, R. Ikeda, and D. Nakamura, *Bull. Chem. Soc. Jpn.*, **59**, 915 (1986).
5) L. Cavalca, M. Nardelli, and I. W. Bassi, *Gazz. Chim. Ital.*, **87**, 153 (1957).
6) R. N. Brown and A. C. McLaren, *Acta Crystallogr.*, **15**, 977 (1962).
7) K. Moriya, T. Matsuo, and H. Suga, *J. Phys. Chem. Solids*, **44**, 1103 (1983).
8) K. Moriya, T. Matsuo, and H. Suga, *Thermochim. Acta*, **132**, 133 (1988).
9) M. Villa and A. Avogadro, *Phys. Status Solidi B*, **75**, 179 (1976).
10) Y. Furukawa and H. Kiriyama, *Chem. Phys. Lett.*, **93**, 617 (1982).
11) S. Gima, Y. Furukawa, R. Ikeda, and D. Nakamura, *J. Mol. Struct.*, **111**, 189 (1983).
12) A. Abragam, "The Principles of Nuclear Magnetism," Oxford University Press, London (1961).
13) W. A. Barton and C. A. Sholl, *J. Phys. C*, **9**, 4315 (1976).
14) R. Lippman and R. Rudman, *J. Chem. Phys.*, **79**, 3457 (1983).
15) J. H. Fermor and A. Kjekshus, *Acta Chem. Scand.*, **27**, 3712 (1973).
16) Y. Furukawa and D. Nakamura, *Z. Naturforsch., A*, **45**, 1211 (1990).
17) Y. Furukawa and H. Kiriyama, *Bull. Chem. Soc. Jpn.*, **51**, 3438 (1978).
18) M. L. Davis and E. F. Westrum, Jr., *J. Phys. Chem.*, **65**, 338 (1961); J. Bruinink and G. H. J. Broers, *J. Phys. Chem. Solids*, **33**, 1713 (1972).
19) S. Gima, Y. Furukawa, and D. Nakamura, *Ber. Bunsen-Ges. Phys. Chem.*, **88**, 939 (1984).
20) T. Tanabe, R. Ikeda, and D. Nakamura, *J. Chem. Soc., Faraday Trans.*, **87**, 987 (1991).

 © 1991 The Chemical Society of Japan Bull. Chem. Soc. Jpn., 64, 3109—3114 (1991)

Theoretical Study of Phenalenium Systems

Biswanath Ghosh, Debranjan Ghosh, Archana Das Gupta, and Nanda K. Das Gupta*
Department of Chemistry, Visva-Bharati University, Santiniketan, West Bengal 731235, India
(Received July 30, 1990)

Phenalenium systems have been studied using PPP method modified by Dewar et al. Ground state properties and other properties such as $\pi^* \leftarrow \pi$ spectra, ionization potential, electron affinity, half-wave reduction potential, pi-dipole moment have been predicted and correlated with experimental ones where available. Stability and resonance energy have also been discussed.

In recent years the chemistry of nonbenzenoid aromatic hydrocarbons involving the contribution of a dipolar structure in its ground state has created much interest. Azulene and its derivatives constitute the simplest case belonging to this class and they are recognized as a class of condensed and fully conjugated cyclic hydrocarbons exhibiting aromatic character with effective contribution of dipolar structures in the ground state.[1] Phenalenium systems also belong to this class having dipolar structure and they are very much interesting to synthetic organic chemists and theoretical chemists. In this paper we like to report the results of our calculations based on Pariser and Parr[2] and Pople[3] method modified by Dewar et al.[4] on the molecules (**1**—

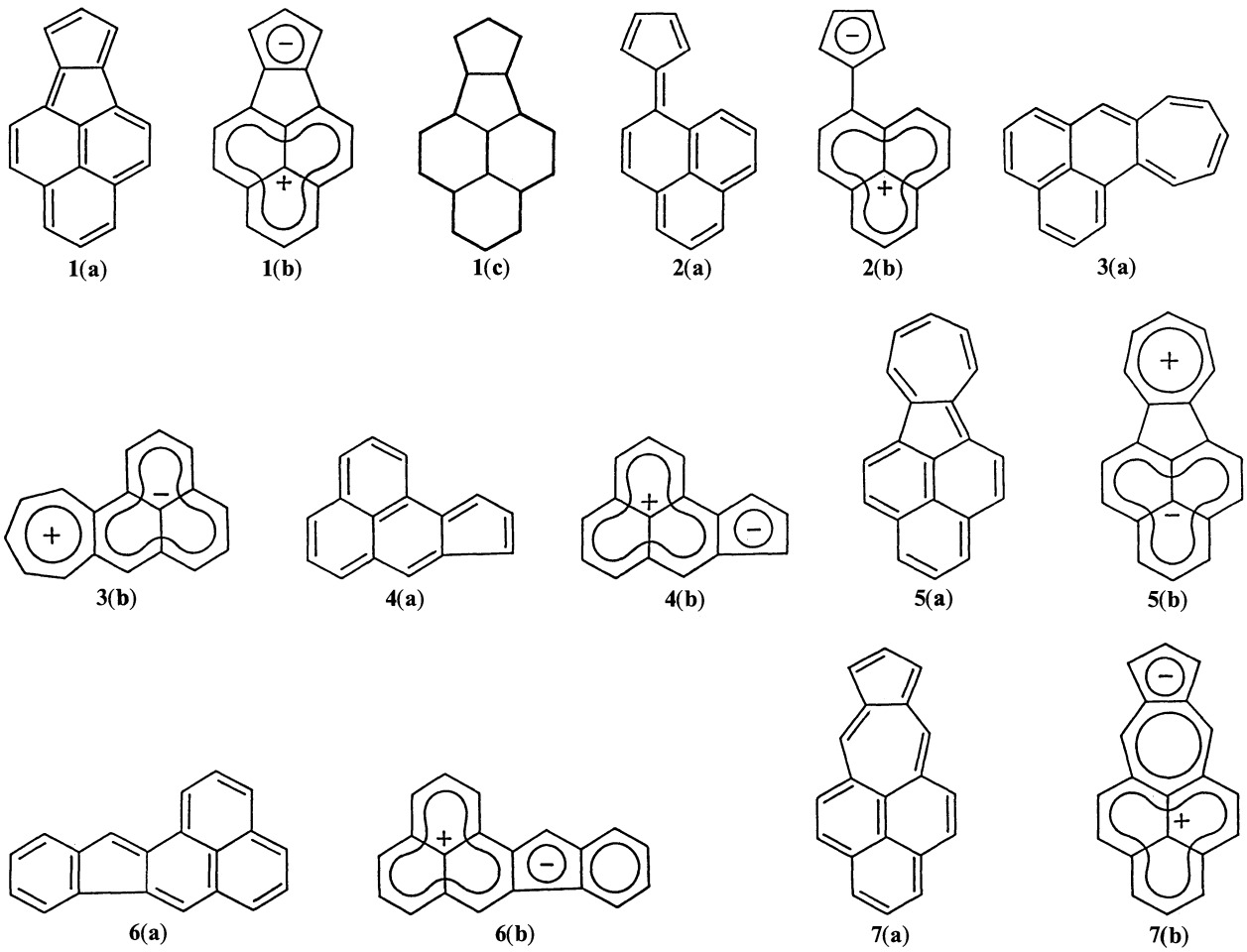

Fig. 1. Molecules studied.
Molecule **1.** a) Pentaleno[4,5,6-*cd*]phenalene, b) Dipolar form, and c) Perturbed [16]annulene.
Molecule **2.** a) Pentaphenafulvalene, b) Dipolar structure of (a).
Molecule **3.** a) Cyclohepta[*a*]phenalene, b) Dipolar structure of (a).
Molecule **4.** a) Cyclopenta[*a*]phenalene, b) Dipolar structure of (a).
Molecule **5.** a) Azuleno[1,2,3-*cd*]phenalene, b) Dipolar form of (a).
Molecule **6.** a) Indeno[2,1-*a*]phenalene, b) Dipolar structure of (a).
Molecule **7.** a) Azuleno [5,6,7-*cd*] phenalene, b) Dipolar structure of (a).

7) in Fig. 1 and predicting the ground state properties and other properties such as $\pi^* \leftarrow \pi$ spectra, ionization potential, electron affinity etc. and compare and correlate them with experimental results where available.

Although the molecule **1** has not yet been synthesized, its derivatives[5] are known. Their properties suggest that molecule **1** might be treated as a novel example of a peripheral 16π-electron model.[5b] Molecule **2**, pentaphenafulvalene is not known but its derivatives have been synthesized by Murata et al.[6] The substantial pi-electron delocalization energy (5.83 β)[7] of phenalenium cation suggests that the molecule pentaphenafulvalene (**2**) would be specially notable for its significant contribution of the resonance form (dipolar structure) and the molecule would have a high value of dipole moment. The molecules **5** and **7** are very much interesting because they contain azulene and phenalene rings and because of their unique electronic structures and their expected carcinogenic activities. The stable crystalline moss green azuleno[5,6,7-*cd*]phenalene (**7**)[8] exhibits considerable carcinogenic activity.[9] The molecule **5** has been synthesized and studied by Murata and co-workers.[10] The molecules **3** and **4** nor their derivatives are known but the molecule **6** has been synthesized and studied by Reid.[11] Some of the molecules have been theoretically studied (**1**,[11] **2**,[6] and **7**[12,13]) with different sets of parameters.

Method and Parameters

The method used here is due to Pariser and Parr[2] and Pople[3] within the zero-differential overlap approximation. The standard notations are used for the necessary parameters.[14] β_{ij} was calculated by the following four methods. SCF(a) due to the method of Lo and Whitehead.[15] SCF(b): given a value of -1.7901 eV suggested by Chung and Dewar[4a] and modified by Birss and Das Gupta.[16] In SCF(a) and (b) β_{ij} was not changed at each iteration. SCF(c): due to Dewar and Harget[4b] and SCF(d): due to Yamaguchi et al.[17] In SCF(c) and (d) β_{ij}, r_{ij}, and γ_{ij} were adjusted at each iteration according to the following relations:

In SCF(c)[4b] the relations used were

$$r_{ij}(\text{Å}) = 1.512 - 0.174\, p_{ij}, \quad (1)$$

$$\beta_{ij} = -6.927\, S_{ij}. \quad (2)$$

In SCF(d)[17] the relations used were

$$r_{ij} = 1.520 - 0.186\, p_{ij}, \quad (3)$$

$$\beta_{ij} = \beta_o \exp[a(r_o - r_{ij})], \quad (4)$$

where β_o is the resonance integral of benzene, $a = -1.7$ Å^{-1} and r_o is the bond length of benzene. The value of β_o decreased as the number of rings[18] increased.

In the SCF(a) and (b) the bond lengths were calculated using the relation of Dewar and Gleicher[19] (Eq. 5)

$$r_{ij}\,(\text{Å}) = 1.503 - 0.166\, p_{ij}, \quad (5)$$

Y_{ii} were calculated using the relation of Pariser.[20]

$$Y_{ii} = I_i - A_i. \quad (6)$$

The values of I and A have been taken from Hinze and Jaffe.[21] The values of Y_{ii} and I for carbon atom are 11.136 and 11.16 eV respectively.

For SCF(d) Y_{ij} were evaluated using the formula of Mataga and Nishimoto[22] and for other methods they were evaluated using the formula of Ohno.[23] In SCF(c) and (d) the values Y_{ij} for non bonded centers, were not varied at each iteration but kept at the values calculated from the initial geometry of the molecules which were assumed to be planar with ideal geometry and bond lengths equal to 1.40 Å.

For the prediction of spectral transitions we have used both SCF and configuration interaction (CI) methods. The final vectors, resonance integrals, and two-center two-electron repulsion integrals obtained at the end of SCF(d) procedure were transferred in the CI method. The value of β_o used in SCF(d) was -2.15 eV.[24] The configuration arising from one-electron excitation was considered. All the occupied and unoccupied orbitals were taken into consideration for the CI method.

Table 1. Correction Terms for IP and EA (in eV)

Method	Correction term for IP	Correction term for EA
SCF(a)	1.29[a]	1.49[b]
SCF(c)	1.88[c]	1.28[b]
SCF(d)	1.06[d]	1.90[d]

a) Difference between the |HOMO| and experimental value of IP of the standard molecule, chrysene (IP=8.01 eV (Ref. 28)). b) Difference between the |LUMO| and the experimental value of electron affinity of chrysene (EA=0.397 eV (Ref. 29)). c) Ref. 27. d) Ref. 30.

Table 2. IP, EA, $E_{1/2}$, and Pi-Dipole Moment of the Molecules Studied

Molecule	Method	IP/eV	EA/eV	$-E_{1/2}$/V	μ/D
1	SCF(a)	7.65	1.77		2.75
	SCF(c)	7.08	1.89	0.828	2.03
	SCF(d)	7.22	2.24		3.04
2	SCF(a)	7.60	1.74		3.84
	SCF(c)	7.30	1.44	1.194	2.14
	SCF(d)	7.49	1.74		3.63
3	SCF(a)	6.85	0.99		1.80
	SCF(c)	6.77	0.82	1.71	0.83
	SCF(d)	6.74	0.97		1.54
4	SCF(a)	7.63	1.48		2.35
	SCF(c)	7.39	1.26	1.344	1.38
	SCF(d)	7.51	1.51		2.33
5	SCF(a)	6.86	1.05		4.12
	SCF(c)	6.51	1.17	1.420	3.42
	SCF(d)	6.68	1.22		4.31
6	SCF(a)	7.45	1.39		1.53
	SCF(c)	7.21	1.20	1.393	0.93
	SCF(d)	7.33	1.40		1.49
7	SCF(a)	7.22	1.17		2.24
	SCF(c)	6.78	1.19	1.406	2.23
	SCF(d)	6.99	1.17		2.83

Results and Discussion

Molecular Properties Such as Ionization Potential, Electron Affinity, Half-Wave Reduction Potential, and π-Dipole Moment: It has been observed[26] that the values obtained from Koopmans' theorem[25] differ from the experimental values of IP and EA by 1 or 2 eV. Hence a correction term is to be added to the HOMO and LUMO so that we can obtain the correct values of IP and EA respectively. Correction terms are presented in Table 1. The half-wave reduction potential has been evaluated from the relation[27] (Eq. 7) in the context of SCF(c).

$$E_{1/2} = -0.833\, e_j - 3.46, \qquad (7)$$

where e_j is the LUMO. The values of IP, EA, and $E_{1/2}$ have been presented in Table 2. For lack of experimental values we can not compare these results with experimental ones. The values of π-dipole moment have also been included in Table 2 along with experimental values where available.

$\pi^* \leftarrow \pi$ Spectral Transitions: Theoretical spectral transitions along with oscillator strengths, f, have been presented in Table 3 which contains the experimental transitions for the molecules **1**, **2**, **5**, and **7**. Table 4 contains the theoretical transitions and f values of other molecules for which there are no experimental values. The oscillator strengths, f, were obtained from the relation.[31]

Table 3. $\pi^* \leftarrow \pi$ Spectral Transitions, ΔE (eV) and Oscillator Strength, f, of Molecules **1**, **2**, **5**, and **7**

Experimental		Sym	Theoretical								
			SCF(a)		SCF(d)		CI		Other works		
ΔE	$\log \varepsilon$[a]		ΔE	f	ΔE	f	ΔE	f	ΔE	f	ΔE
					Molecule **1**						
Ref. 5b											
2.57	3.95	A_1	2.80	1.39	2.61	1.51	2.44	0.95			
3.44	3.90	B_2	3.37	0.04	3.08	0.03	3.39	0.27			
3.88	4.04	B_2	3.96	0.57	3.78	0.16	3.75	0.01			
4.04	4.45	A_1	3.98	0.16	3.83	0.03	4.09	0.36			
4.23	4.43	A_1	4.17	0.05	4.36	0.60	4.29	0.25			
σ			0.119		0.201		0.092				
					Molecule **2**						
Ref. 6											
2.11	3.95		2.13	0.01	2.44	0.01	1.95	0.01			
3.06	3.66		2.75	1.28	2.74	1.34					
3.20	3.52		3.40	0.05			3.30	0.04			
4.06	3.80		4.06	0.44	3.90	0.37	4.19	0.12			
5.08	3.71		5.06	0.06	5.18	0.03	4.96	0.05			
σ			0.165		0.248		0.115				
					Molecule **5**						
Ref. 10											
1.63	2.52						1.51	0.02			
1.79	2.34	B_2	1.88	0.07	1.77	0.07					
2.60	4.69						2.66	0.46			
2.92	3.90	A_1	2.86	1.42	2.89	1.49					
3.53	4.85	A_1			3.64	0.86	3.63	1.83			
4.36	3.96	B_2	4.35	0.29	4.36	0.01	4.48	0.17			
4.74	4.21	B_2	4.64	0.03	4.76	0.01					
4.85	4.16						4.89	0.26			
5.08	4.12	A_1	5.17	0.07	5.14	0.05	5.17	0.01			
5.48	4.21	A_1	5.48	0.42	5.40	0.28	5.52	0.04			
σ			0.071		0.058		0.088				
					Molecule **7**[a]						
Ref. 12									Ref. 12		Ref. 13(a)
1.65	0.01	B_2	2.34	0.22	2.19	0.20	1.76	0.03	1.96	0.02	1.80
2.75	0.4	A_1	2.92	1.57	2.93	1.61	2.63	0.45	2.54	0.4	2.90
3.35	w	B_2					3.33	0.02	3.52	0.05	3.31
3.66	0.3	A_1	3.76	1.08	3.80	1.21	3.86	1.83	3.77	0.2	3.33
3.84	1.6	B_2	3.79	0.47	3.71	0.46	3.79	0.25	3.94	0.2	4.28
4.28	?	A_1	4.26	0.05	4.22	0.09	4.17	0.58	3.97	1.4	4.43
4.59	w	B_2	4.60	0.00	4.64	0.09	4.54	0.00	4.09	0.003	4.56
5.08	s	B_2	4.99	0.05	4.95	0.06	5.14	0.01	4.17	0.2	4.79
5.70	?	A_1	5.67	0.19	5.80	0.21	5.71	0.16	4.41	0.3	
σ			0.257		0.222		0.097		0.580		0.239

a) Figures in column 2 are 'f' values. 's' and 'w' stand for strong and weak.

Table 4. $\pi^* \leftarrow \pi$ Spectral Transitions, ΔE (eV) and 'f' of **3**, **4**, and **6**

SCF(a)		SCF(d)		CI	
ΔE	f	ΔE	f	ΔE	f
		Molecule **3**			
2.23	0.71	2.48	0.79	2.15	0.16
2.53	0.43	2.78	0.42	2.80	0.55
4.01	0.36	3.90	0.34	4.00	0.13
4.38	0.36	4.32	0.37	4.38	0.25
4.89	0.31	4.89	0.31	4.86	0.39
5.30	0.44	5.31	0.47	5.38	0.15
		Molecule **4**			
2.35	0.57	2.59	0.63	2.28	0.16
2.80	0.45	3.09	0.47	3.01	0.39
3.90	0.36	3.86	0.36	4.01	0.07
4.46	0.36	4.39	0.38	4.48	0.44
4.75	0.16	4.94	0.13	4.70	0.10
5.29	0.46	5.24	0.17	5.15	0.51
		Molecule **6**			
2.63	1.08	2.77	1.13	2.58	0.58
4.07	0.38	4.00	0.36	4.05	0.20
4.55	0.08	4.65	0.07	4.59	0.51
5.02	0.10	5.07	0.05	5.05	0.32
5.49	0.37	5.55	0.03	5.55	0.08

$$f = 1.085 \times 10^{-5}\, \bar{\nu}\mu^2 \qquad (8)$$

with $\bar{\nu}$ is the transition energy in cm^{-1}) and μ is the dipole length (in Å) for corresponding transition. Results of SCF(a), (d), and CI are included in the table.

From Table 3 it is clear that the correlation between the theoretical transitions and experimental ones for molecules **1** and **2** is good. However agreement between the theoretical transitions predicted by SCF(d) method is not so good. This is evident from the calculation of standard deviation, σ included in the table. For the calculation of σ, point to point correlation has been taken.

The experimental spectral transitions of molecule **5** have a large number of peak maxima many of which are not clearly resolved. Therefore the best one can do in a comparison of the theoretical and observed transitions is a general correlation over quite wide spectral regions. Table 3 displays this comparison for molecule **5**. The value of σ predicted by the SCF and CI methods suggest that the agreement between the theoretical and experimental transitions is good. Table 3 also displays the experimental transitions for molecule **7** where other theoretical works have also been included along with our work. The molecule is rich in experimental transitions and attempt has been made a point to point correlation. The values predicted by the CI method is very good compared to the values predicted by the SCF methods and other workers.[12,13a]

Stability or Aromaticity: Stability of the molecules has been studied according to the criteria of resonance energy (E_R) and resonance energy per bond (E_R/C–C) or resonance energy per π-electron (RE/PE). The values of E_R of the molecules have been calculated using the methods of Whitehead et al.,[15] Chung and Dewar,[4a] Dewar and de Llano,[32] Dewar and Harget,[4b] and Hess and Schaad.[33] The values of heat of atomization, ΔH_a and π-bond energy, resonance energy, E_R, resonance energy per carbon–carbon bond (E_R/C–C) and resonance energy per π-electron of the molecules have been presented in Table 5. Since the hydrocarbons contain benzene rings fused with five or seven membered rings, they belong to semibenzenoid systems.[34] The criteria for stability or aromaticity of this type of hydrocarbons have been discussed by Das Gupta and Das Gupta[34] and are displayed in Table 6.

The hypothetical molecule **1**, pentaleno[4,5,6-*cd*]-phenalene, can be represented by the dipolar structure. Application of Craig's rule[37] to any one of the Kekule' structure of **1** gives the result $f+g=7$ which predicts the valence-bond ground state to be nontotally symmetric and hence the molecule **1** should be pseudoaromatic. The two non-charge separated resonance forms possess a 16 π-electron moiety peripheral to the central ethylene fragment. If it is considered that the cross links are regarded to contribute only negligible perturbation the present hydrocarbon should be antiaromatic.[38] Low resonance energy and low resonance energy per carbon–carbon bond calculated by all the methods and low resonance energy per π-electron also suggest that the molecule should not be an aromatic one. Moreover, the physical properties of the derivatives of **1**, relatively high chemical shifts of the protons on the phenalene nucleus and small dipole moment [μ=2.31D (D=Debye, 1 Debye=3.3356×10^{-30} C m)][5b] of 5-ethoxy-1,3-di-*t*-butylpentaleno[1,2,3-*cd*]phenalene indicate, however, that the molecule **1** can be best represented by the perturbed [16] annulene **1(c)** rather than the dipolar form **1(b)**.

Although molecule **2** has not been synthesized, its derivatives are known. The derivative 2-ethoxy-9,10,11,12-tetrachloropentaphenafulvalene is a stable one.[6] The resonance energy, E_R/C–C and RE/PE suggest that the molecule would be a stable one in agreement with experiment. The high dipole moment of **2** (6.33 D)[6] together with the relatively low chemical shifts and the identical vicinal coupling constants[39] in its ^{1}H NMR spectrum indicates a significant participation of a dipolar resonance structure in its ground state **2(b)**.

The molecule **3** has not yet been synthesized. Its resonance energy, E_R/C–C and RE/PE which are at the lower side of the range of aromaticity and stability suggest that the molecule might not be an aromatic one.

The molecules **5** and **7** are interesting and may be considered to be composed of azulene and phenalene. Resonance energy, E_R/C–C and RE/PE suggest that they might be a stable aromatic compound. The ease of dehydrogenation during the preparation of **5** is noteworthy suggesting thermodynamic stability[10] of this compound. The diamagnetic susceptibility is 2.7.[10] The above observations furnish convincing evidence for a definite degree of aromaticity of **5**.[10]

Table 5. Heat of Atomization ΔH_a (eV), π-Bond Energy $E_{\pi b}$ (eV), Resonance Energy E_R ((eV) or in β), and Resonance Energy per Carbon–Carbon Bond E_R/C–C or Resonance Energy per π-Electron RE/PE

Molecule	Method[a)]	ΔH_a	$E_{\pi b}$	E_R	E_R/C–C or RE/PE
1	a	151.65	26.677	5.993	0.272
	b	151.85	26.253	6.035	0.279
	c	151.98	25.324	1.402	0.064
	d			0.884	0.040
	e[b)]			0.466	0.026
2	a	156.19	26.003	6.570	0.313
	b	156.36	25.590	5.534	0.264
	c	156.66	25.561	3.599	0.171
	d			0.899	0.043
	e[b)]			0.621	0.034
3	a	156.12	25.936	5.502	0.262
	b	156.30	25.522	5.466	0.260
	c	156.60	25.513	1.534	0.073
	d			0.860	0.041
	e[b)]			0.509	0.028
4	a	137.47	23.489	5.244	0.276
	b	137.63	23.118	5.237	0.276
	c	137.91	22.958	1.574	0.083
	d			0.946	0.050
	e[b)]			0.510	0.032
5	a	170.73	29.558	6.685	0.279
	b	170.94	29.086	6.793	0.284
	c	171.08	28.339	1.783	0.074
	d			1.203	0.050
	e[b)]			0.695	0.035
6	a	171.25	30.070	7.202	0.300
	b	171.45	29.601	7.208	0.300
	c	171.71	29.198	2.406	0.100
	d			1.719	0.072
	e[b)]			0.785	0.039
7	a	170.68	29.508	6.640	0.277
	b	170.89	29.040	6.647	0.277
	c	171.06	28.317	1.755	0.073
	d			1.157	0.048
	e[b)]			0.694	0.035

a) a, b, c, d, e under column method represent SCF(a), SCF(b), SCF(c), Dewar–de Llano, and Hess and Schaad methods, respectively. b) in β unit.

Table 6. Criteria of Aromaticity or Stability of Hydrocarbons

Method	Range of E_R/C–C or RE/PE for the hydrocarbons to be aromatic[35–37)]
SCF a	0.26—0.31
SCF b	0.25—0.30
SCF c	0.075—0.112
D dL[a)]	0.041—0.095
HS[b)]	0.03—0.04

a) Dewar–de Llano. b) Hess and Schaad.

Though the molecule **4** has not yet been synthesized, yet its resonance energy, E_R/C–C bond and RE/PE suggest that it might be a stable aromatic compound. It is expected that it might be synthesized in near future.

The molecule **6** has been synthesized and its chemical properties have been studied by Reid.[11)] Its high basicity, the Hammett acidity function H_o for which K' (where K' is the apparent partition coefficient) value which is unity places the molecule **6** alongside the azulenes in order of basicity.[40)] It undergoes electrophilic substitution reaction easily. The dihydroindeno-[2,1-*a*]phenalene undergoes with striking readiness to aromatization reactions.[11)] The above reactions reflect the aromatic character of molecule **6**. This is also predicted from its calculated resonance energy, E_R/C–C and RE/PE.

Conclusion

The methods SCF a, b, and c were parameterized to predict the ground state properties and stability of molecules. SCF(d) method was parameterized to predict the spectral transitions of conjugated systems. It has been observed that the methods SCF a, b, and c are also equally good, if not better than the SCF(d) method, in predicting spectral transitions as seen earlier.

Financial assistance from the Visva-Bharati University is gratefully acknowledged.

References

1) W. H. Stafford and D. H. Reid, *Chem. Ind.* (*London*), **1954**, 277.
2) R. Pariser and R. G. Parr, *J. Chem. Phys.*, **21**, 466, 767 (1953).
3) J. A. Pople, *Trans. Faraday Soc.*, **49**, 1375 (1953).
4) a) A. L. H. Chung and M. J. S. Dewar, *J. Chem. Phys.*, **42**, 756 (1965); b) M. J. S. Dewar and A. J. Harget, *Proc. R. Soc. London, Ser. A*, **315**, 443 (1970).
5) a) I. Murata, T. Nakazawa, and M. Okazaki, *Terahedron Lett.*, **1970**, 3269; b) I. Murata, M. Okazaki, and T. Nakazawa, *Angew. Chem., Int. Ed. Engl.*, **10**, 576 (1971).
6) I. Murata, T. Nakazawa, and M. Okazaki, *Tetrahedron Lett.*, **1969**, 1921.
7) M. B. Diyatkina and R. M. Shustorovitch, *Dokl. Akad. Nauk SSSR*, **117**, 1021 (1957); R. Petitt, *Chem. Ind.* (*London*), **1956**, 1306; *idem., J. Am. Chem. Soc.*, **82**, 1972 (1960); R. Zahradnik, J. Michl, and J. Koutecky, *Collect. Czech. Chem. Commun.*, **29**, 1932 (1964).
8) C. Jutz and R. Kirchlechner, *Angew. Chem., Int. Ed. Engl.*, **5**, 516 (1966); C. Jutz, R. Kirchlechner, and H. J. Seidel, *Chem. Ber.*, **102**, 2301 (1969).
9) N. P. Buu-Hoi, D. P. Hein, and C. Jutz, *Naturwissenschaften*, **54**, 470 (1967); N. P. Buu-Hoi, N. Ba Giao, and C. Jutz, *Naturwissenschaften*, **57**, 499 (1970).
10) I. Murata, K. Nakasuji, K. Yamamoto, T. Nakazawa, Y. Kayane, A. Kimura, and O. Hara, *Angew. Chem., Int. Ed. Engl.*, **14**, 170 (1975).
11) D. H. Reid, *Tetrahedron*, **3**, 339 (1958).
12) E. W. Thulstrup, J. Michl, and C. Jutz, *J. Chem. Soc., Faraday Trans. 2*, **71**, 1618 (1975).
13) a) N. K. Ray and P. T. Narashiman, *Indian J. Chem.*, **5**, 246 (1967); b) Von G. Tronger and J. Fabian, *Z. Phys. Chem., Leipzig*, **247**, 179 (1971).
14) R. G. Parr "Quantum Theory of Molecular Electronic Structure," W. A. Benjamin, New York (1963).
15) D. H. Lo and M. A. Whitehead, *Can. J. Chem.*, **46**, 2027 (1968).
16) F. W. Birss and N. K. Das Gupta, *Can. J. Chem.*, **49**, 2840 (1971).
17) H. Yamaguchi, T. Nakajima, and T. L. Kunii, *Theor. Chim. Acta*, **12**, 349 (1968).
18) K. Nishimoto and R. Fujishiro, *Bull. Chem. Soc. Jpn.*, **37**, 1660 (1964).
19) M. J. S. Dewar and G. J. Gleicher, *J. Am. Chem. Soc.*, **87**, 685, 692 (1965).
20) R. Pariser, *J. Chem. Phys.*, **21**, 568 (1953).
21) J. Hinze and H. H. Jaffe, *J. Am. Chem. Soc.*, **84**, 840 (1962).
22) M. Mataga and K. Nishimoto, *Z. Phys. Chem., Frankfurt*, **13**, 140 (1957).
23) K. Ohno, *Theor. Chim. Acta*, **2**, 219 (1964).
24) N. K. Das Gupta and F. W. Birss, *Bull. Chem. Soc. Jpn.*, **51**, 1211 (1978).
25) T. Koopmans, *Physica*, **1**, 104 (1934).
26) C. Moser, *J. Chim. Phys.*, **52**, 24 (1955).
27) F. W. Birss and N. K. Das Gupta, *Indian J. Chem., Sect. B*, **17**, 610 (1979).
28) M. E. Wacks, *J. Chem. Phys.*, **41**, 1661 (1964).
29) R. S. Becker and E. Chen, *J. Chem. Phys.*, **45**, 2403 (1966).
30) T. L. Kunii and H. Kuroda, *Theor. Chim. Acta*, **11**, 97 (1968).
31) L. Salem, "Molecular Orbital Theory of Conjugated System," W. A. Benjamin, New York (1966), p. 358.
32) I. Murata, K. Nakasuji, K. Yamamoto, T. Nakazawa, Y. Kayane, A. Kimura, and O. Hara, *Angew. Chem., Int. Ed. Engl.*, **14**, 170 (1975).
33) M. J. S. Dewar and C. de Llano, *J. Am. Chem. Soc.*, **91**, 989 (1979).
34) B. A. Hess, Jr. and L. J. Schaad, *J. Am. Chem. Soc.*, **93**, 305 (1971).
35) A. Das Gupta and N. K. Das Cupta, *Tetrahedron*, **28**, 3587 (1972); *Theor. Chim. Acta* (*Berlin*), **33**, 177 (1974).
36) A. Das Gupta, S. Chatterjee, and N. K. Das Gupta, *Bull. Chem. Soc. Jpn.*, **52**, 3070 (1979).
37) S. K. Pal, A. Das Gupta, and N. K. Das Gupta, *Bull. Chem. Soc. Jpn.*, **61**, 1749 (1988).
38) D. P. Craig, *J. Chem. Soc.*, **1951**, 3175; D. P. Craig and A. Macoll, *ibid.*, **1949**, 964.
39) M. J. S. Dewar, *J. Am. Chem. Soc.*, **74**, 3345 (1952); M. J. S. Dewar and R. Pettit, *J. Cnem. Soc.*, **1954**, 1617; D. Peters, *ibid.*, **1956**, 1023.
40) N. Jonathan, S. Gordon, and B. P. Daily, *J. Chem. Phys.*, **36**, 2443 (1962); W. B. Smith, W. H. Smith, W. H. Watson, and S. Chiranjeevi, *J. Am. Chem. Soc.*, **89**, 1438 (1967); H. Günther, *Tetrahedron Lett.*, **1967**, 2967.
41) D. H. Reid, W. H. Stafford, and J. P. Ward, *J. Chem. Soc.*, **1955**, 1193.

 © 1991 The Chemical Society of Japan Bull. Chem. Soc. Jpn., 64, 3115—3120 (1991)

Transport Studies across the Pericardial Membrane: Evaluation of Fixed Charge Density

Mohammad AHMAD,† Hasan ARIF,* Haroon Rashid KHAN, Mohammad SHOAIB, and Mohadi HASAN††
Department of Chemistry, Aligarh Muslim University, Aligarh 202002, India
†Centre of Cardiology and Cardiovascular Research, Aligarh Muslim University, Aligarh 202002, India
††Interdiscipilinary Brain Research Centre, Aligarh Mauslim University, Aligarh 202002, India
(Received September 3, 1990)

The fixed charge density, the permselectivity, and the transport number in several electrolytic solutions of varying concentration were determined across the pericardial membrane of freshly slaughtered buffalo (*Bof. Bubalis*). The irreversible thermodynamic equations originally meant for understanding the behavior of artificial membranes have been found to be equally applicable to those of the biological membranes.

The behavior of membrane systems has extensively been investigated by studying the transport properties of artificial membranes.[1-12] Some of the recent analytical and electronic techniques have added impetus to such investigations. However, in the cases of biological membranes the experimental difficulties have marred the meaningful electrophysiological studies; such as those of the membrane potential, the transport number, the permselectivity, the effective fixed charge density, the conductance, the capacitance, and the impedance.

The present study has, therefore, been undertaken with a view (i) to ascertaining as to whether or not the principle of passive transport is applicable to biological membranes, and (ii) to characterising their thermodynamic properties. Thus, the duramater, the pericardium, and the peritoneum being easily available intact biological membranes may be chosen for the purpose. Also, the transport number, the permselectivity, and the effective fixed charge density of these biological membranes are almost similar in signifying a common pattern in their behavior. In view of these facts the pericardial membrane has been taken as a test case.

Experimental

The pericardial membrane was taken out immediately after slaughtering the buffalo (*Bof. bubalis*) aged between 18—24 months, and immersed in an ice-cold Ringer solution of pH 7.4±0.2 for the preservation of the membrane tissues. The Ringer solution contained (in g dm^{-3}) NaCl: 9.00, KCl; 0.42, $CaCl_2$: 0.24, glucose: 1.00, and $NaHCO_3$: 0.15. The membrane was then washed three times with the deionized water to remove any traces of Ringer solution, prior to recording the membrane potential. The potential was developed by setting up a concentration cell of the type

S.C.E.|Solution|Membrane|Solution|S.C.E.
C_1 $C_2=10C_1$

in which S.C.E. stands for the saturated calomel electrode employed for measuring the membrane potential. The electrolytes used were the solutions of several concentrations of analytical grade (BDH, India), uni-univalent electrolytes, viz., NaCl, KCl, NH_4Cl, NaF, and KF in deionized water. The same electrolyte with different concentrations was used on both the sides of the pericardial membrane. The dilute side of the solution was taken as negative. Freshly obtained pericardial membranes were used for the potential measurements with each of these electrolytic solutions. The experiments were repeated a number of times with freshly prepared solutions of each of these electrolytes and the maximum potential values thus attained were recorded These measurements were made in a thermostated bath maintained at 25.0±0.1 °C.

Results and Discussion

The values of membrane potential ($\Delta\phi$ or E_m) measured across the pericardial membrane, separating different concentrations of 1 : 1 electrolytes are plotted as a function of $\log(C_1+C_2)/2$, with a fixed ratio of $C_2/C_1=\gamma=10$ (Fig. 1). The membrane potential after an initial increase, has been found to decrease with increase in the value of $\log(C_1+C_2)/2$. Another very important feature observed in the recording of the E_m across the pericardium, provided the concentrated side was hooked up to the positive terminal while the dilute side to that of the negative terminal. Such an observation suggests that the pericardial membrane is positively charged and is anion selective. It may also be noted, however, that for all the electrolytes below 1×10^{-3} M

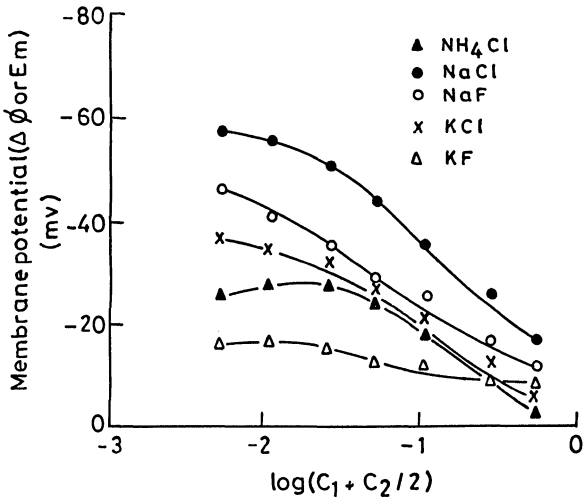

Fig. 1. Plots of observed potentials against log (C_1+C_2)/2 for various electrolytes with pericardium.

concentration (1 M=1 mol dm^{-3}) the number of ions generated matches the number of ions transferred to the other side of the membrane, thereby destroying completely the potential difference generated initially due to slight differences in the concentration of ions. Consequently, no potential differences is observed below the cited dilute concentration.

Starting with the basic flow equations Kobatake et al.[6] obtained the following relations:

$$\Delta\phi=-(RT/F)\left|\frac{1}{\beta}\ln\frac{C_2}{C_1}-\left(1+\frac{1}{\beta}-2\alpha\right)\ln\left(\frac{C_2+\alpha\beta\theta}{C_1+\alpha\beta\theta}\right)\right, \quad (1)$$

where

$$\alpha=\frac{u}{u+v} \quad (1a)$$

and

$$\beta=1+\left(\frac{KF\theta}{u}\right), \quad (1b)$$

for the membrane potential ($\Delta\phi$) which arises between two solutions of 1 : 1 electrolytes of different concentration, C_1 and C_2 ($C_1<C_2$) that are separated by a membrane.

Here, u and v are the mobilities of the positive and the negative ions, respectively, defined in terms of the mass fixed frame of reference, K is a constant, θ is the charge density, and F is the Faraday constant. These parameters are found to be independent of salt concentrations, C_1 and C_2.

For the analysis of the data, Eq. 1 can be used under two sets of conditions, namely, (a) in the dilute range, and (b) in the concentrated range; hence the two limiting forms of the above equation have been obtained as given below: (a) When concentration C_2 becomes sufficiently small, (external dilute range) Eq. 1 can be expanded[6] to given

$$\Delta\phi_r=\frac{1}{\beta}\ln\gamma-\frac{(\gamma-1)}{\alpha\beta\gamma}\left(1+\frac{1}{\beta}-2\alpha\right)\left(\frac{C_2}{\theta}\right)+0\left[\left(\frac{C_2}{\theta}\right)^2\right] \quad (2)$$

where $\Delta\phi_r$ is the absolute value of reduced potential defined by

$$\Delta\phi_r=\frac{F\Delta\phi}{-RT} \quad (3)$$

and

$$\gamma=\frac{C_2}{C_1}.$$

Equation 2, indicates that the value of β; as well as a relation between α and θ can be obtained by evaluating the intercepts and the initial slope of a plot of $\Delta\phi_r$ against C_2. Figure 2 shows a variation of reduced membrane potential, $\Delta\phi_r$ with variation in concentration in the low concentration range of the electrolyte. With an increase in concentration $\Delta\phi_r$ shows an insignificant decrease. The value may be evaluated from the slope, $1/\beta \ln\gamma$ of the above plot listed in Table 1. (b)

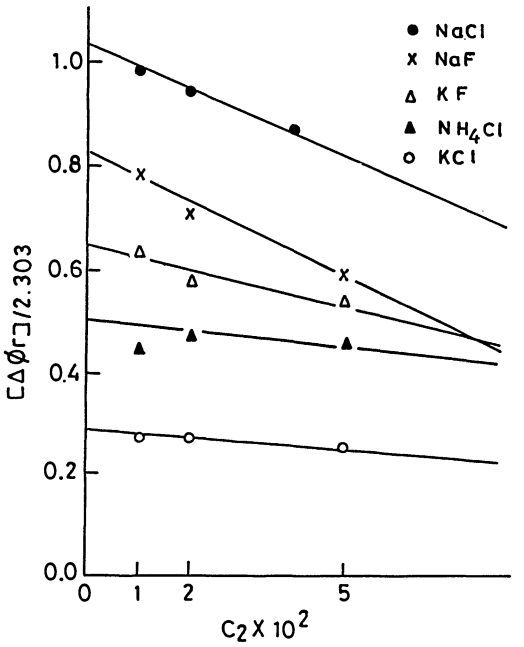

Fig. 2. Plots of $\Delta\phi_r/2.303$ versus $C_2\times10^2$ for various electrolyte with pericardium.

Table 1. Calculated Values of the Parameters α and β for Various Electrolytes at $\gamma=10$

Electrolytes	α	β
NaCl	0.56	0.97
NaF	0.55	1.22
KF	0.49	1.55
NH_4Cl	0.44	2.00
KCl	0.59	3.51

It is found experimentally that at a fixed value of γ, the inverse of an apparent transport number, t_{app}, is proportional to the inverse of concentration, C_2, in higher salt concentration range. Here, t_{app} is defined by the relation,

$$\Delta\phi_r=(1-2\,t_{app})\ln\gamma. \quad (4)$$

The values of the transport number (t_{app}), calculated from the observed membrane potentials using Eq. 4. Figure 3 shows the variation of the inverse of t_{app} of ions with that of the inverse of concentration, C_2. As the inverse of the concentration increases, the inverse of the apparent transference number also increases. This has been observed only in high concentration range. Such an observation, however, has been found to be absent in the dilute concentration range, seemingly due to an inadequate concentration for raising the required polarization.

Kobatake et al.[6] have proposed a simple method using the following approximate equation for the diffusive contribution to the emf of a cell with transport. On substituting Eq. 3 into that of Eq. 4, the following relation between $\Delta\phi$ and t_{app} is obtained:

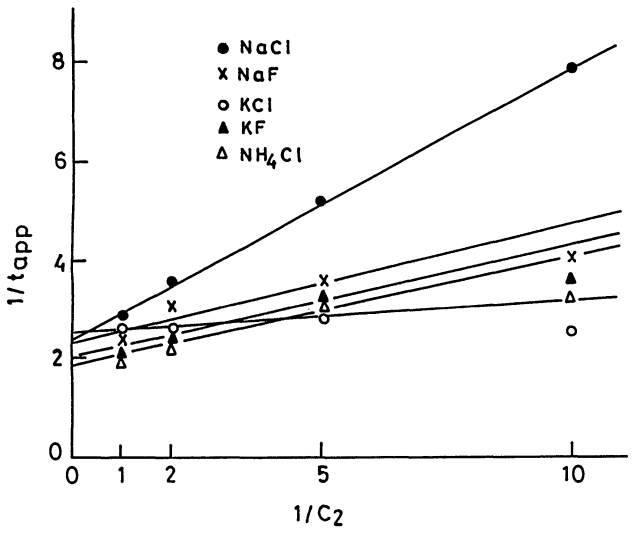

Fig. 3. Plots of $1/t_{app}$ versus $1/C_2$ for various electrolytes with pericardium.

$$\frac{F\Delta\phi}{RT}=(1-2\,t_{app})\ln\gamma, \tag{5}$$

substituting the value of $\Delta\phi$ from Eq. 1 and expanding the resultant for $1/t_{app}$, in powers of $1/C_2$, we get,

$$\frac{1}{t_{app}}=\frac{1}{1-\alpha}+\frac{(1+\beta-2\alpha\beta)(\gamma-1)\alpha}{2(1-\alpha)^2\ln\gamma}\left(\frac{\theta}{C_2}\right)+0\left[\left(\frac{\theta}{C_2}\right)^2\right]. \tag{6}$$

This indicates that the intercept for a plot of $1/t_{app}$ vs. $1/C_2$, at a fixed value of γ allows the value of α to be determined. The value of the intercept is equal to $1/(1-\alpha)$, from which α may be evaluated. Figure 3 illustrates the plots of $1/t_{app}$ vs. $1/C_2$ for various electrolytes.

For the evaluation of charge density, θ, there are two limiting cases. In the dilute range, the value of θ_d was determined by inserting the values of α and β (Table 1) in the relation between α and θ. Once α and β are known in the manner described above, the charge density θ_c (in the concentrated range), is also evaluated from the initial slope of $1/t_{app}$ against $1/C_2$ plot. The present study reveals that the charge density (θ_d) in dilute as well as in concentrated range (θ_c) agree well with each other (Table 2), thereby confirming the applicability of the Kobatake and co-worker's equation to this biological membrane.

Table 2. Charge Density (mol dm^{-3}) of Pericardial Membrane Obtained by Different Methods at γ=10

Theory	Electrolyte				
	NaCl	NaF	KCl	KF	NH_4Cl
$\theta_d\times10^2$ Kobatake's method	20.16	8.84	4.04	13.71	—
$\theta_c\times10^2$ Kobatake's method	10.7	4.93	3.94	6.58	6.71
$\theta_x\times10^2$ Kobatake's Permselectivity method, P_s vs. $\log(C_1+C_2)/2$	15.14	5.01	—	6.07	8.91
$\theta_x\times10^2$ Tasaka's method	4.11	1.29	4.76	1.64	1.90

A general method for the characterization of membranes in terms of permselectivity (P_s), which is applicable to any system, irrespective of ionic species, has been developed by Kamo et al.[9] Kobatake and Kamo[12] derived Eq. 7 for the measurement of permselectivity (P_s) for a positively charged membrane.

$$\frac{1}{(4\,\xi^2+1)^{1/2}}=P_s=\frac{[T_{app}-(1-\alpha)]}{[1-\alpha-(1-2\alpha)T_{app}]}. \tag{7}$$

It may be noted that the P_s value between zero and unity depends on the external salt concentration for the given system of membrane electrolyte pair. Now P_s can be calculated from the data of membrane potential, while the left-hand side of Eq. 7 is a function of the relative concentration $\xi=C/\phi_x$ or $(C_1+C_2)/2\phi_x$. Thus, the value of the right-hand side should be independent of the mobilities of ionic species involved. Equation 7 implies that the plot of P_s vs. $(1+4\,\xi^2)^{-1/2}$ should be a

Table 3. Calculated Values of Permselectivity (P_s), ξ, and an Arbitrary Parameter β'

Electrolytes	Concn C_2/C_1	P_s[a)]	ξ	$\beta'=n\beta$
NaCl	$1/1\times10^{-1}$	0.178	3.66	0.863
	$5\times10^{-1}/5\times10^{-2}$	0.344	1.83	0.800
	$2\times10^{-1}/2\times10^{-2}$	0.533	0.73	1.102
	$1\times10^{-1}/1\times10^{-2}$	0.689	0.36	1.784
	$5\times10^{-2}/5\times10^{-3}$	0.837	0.183	2.830
	$2\times10^{-2}/2\times10^{-3}$	0.919	0.007	8.703
	$1\times10^{-2}/1\times10^{-3}$	0.982	0.0029	10.109
NaF	$1/1\times10^{-1}$	0.09	11.00	0.778
	$5\times10^{-1}/5\times10^{-2}$	0.22	5.50	0.630
	$2\times10^{-1}/2\times10^{-2}$	0.34	2.20	0.716
	$1\times10^{-1}/1\times10^{-2}$	0.42	1.10	0.983
	$5\times10^{-2}/5\times10^{-3}$	0.53	0.55	1.601
	$2\times10^{-2}/2\times10^{-3}$	0.65	0.22	4.868
	$1\times10^{-2}/1\times10^{-3}$	0.75	0.11	12.173
KF	$1/1\times10^{-1}$	0.11	9.16	0.758
	$5\times10^{-1}/5\times10^{-2}$	0.23	4.58	0.662
	$2\times10^{-1}/2\times10^{-2}$	0.38	1.83	0.725
	$1\times10^{-1}/1\times10^{-2}$	0.46	0.91	1.033
	$5\times10^{-2}/5\times10^{-3}$	0.56	0.45	1.954
	$2\times10^{-2}/2\times10^{-3}$	0.59	0.18	8.659
	$1\times10^{-2}/1\times10^{-3}$	0.66	0.09	26.062
NH_4Cl	$1/1\times10^{-1}$	0.09	6.87	0.918
	$5\times10^{-1}/5\times10^{-2}$	0.28	3.43	0.657
	$2\times10^{-1}/2\times10^{-2}$	0.43	1.37	0.788
	$1\times10^{-1}/1\times10^{-2}$	0.51	0.68	1.286
	$5\times10^{-2}/5\times10^{-3}$	0.56	0.34	3.051
	$2\times10^{-2}/2\times10^{-3}$	0.55	0.13	18.278
	$1\times10^{-2}/1\times10^{-3}$	0.55	0.059	83.629

a) P_s values were obtained using the relation, $P_s=\frac{T_{app}-(1-\alpha)}{1-\alpha-(1-2\alpha)T_{app}}$, $\xi=\frac{c}{\phi_x}$, β' or $n\beta$ values were computed using the relation $P_s=[1/\sqrt{1+4\xi^2}]^{\beta}$.

straight line of unit slope provided the charge density is independent of salt concentration. The various values of permselectivity (Table 3) were calculated by substituting the values of α and t_{app} for pericardium. Another method of determining the charge density, based on permselectivity as developed by Kamo et al.[9] is also used here. The calculated values of P_s of pericardial membrane were plotted against log $(C_1+C_2)/2$. The curves thus obtained with various electrolytes are shown in Fig. 4. When the average concentration, $(C_1+C_2)/2$, becomes equal to the effective fixed charge density ϕ_x, the value of ξ becomes unity, i.e. $C/\phi_x=1$. Substituting this value of $\xi=1$ in $P_s=(1+4\ \xi^2)^{-1/2}$, the value of P_s becomes equal to 0.448. At this particular value (0.448), the corresponding concentration was obtained from the P_s versus log C plot. It is apparent from Fig. 4 that this value of concentration should be equal to a fixed charge density for various electrolytes. The values of charge density obtained with various electrolytes are given in Table 2. Plots of P_s vs. $(1+4\ \xi^2)^{-1/2}$ using different electrolyte is shown in Fig. 5.

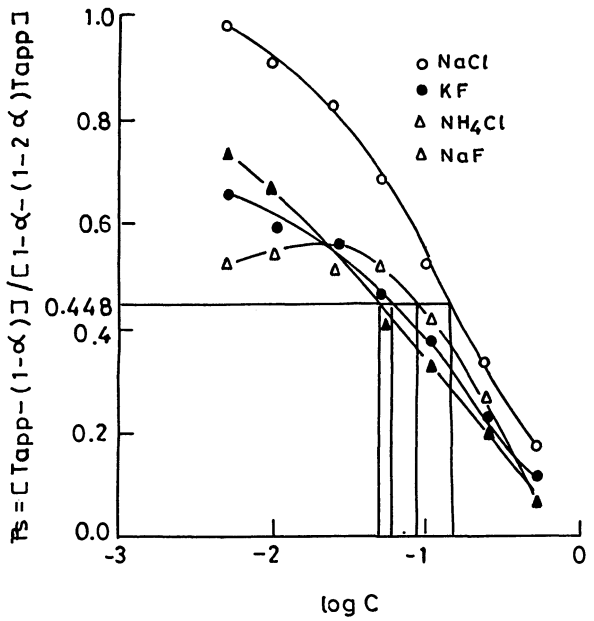

Fig. 4. Plots of P_s versus log $(C_1+C_2)/2$ for various electrolyte with pericardium.

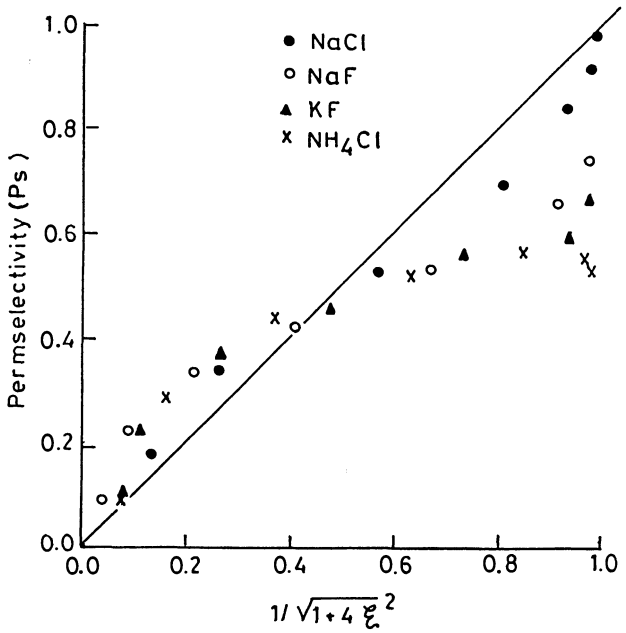

Fig. 5. Plots of P_s versus $1/\sqrt{1+4\ \xi^2}$ for various electrolytes with pericardium.

An apparent straight line of slope close to unity is the theoretical line with the assumption that the values of ϕ_x are independent of salt concentration as seemingly found for the NaCl case unlike those of the other electrolytes for which ϕ_x seems to be a function of salt concentration as apparent from the limiting values of P_s versus $(1+4\ \xi^2)^{-1/2}$ plots. An examination of Table 2 suggests that the extent to which the values of ϕ_x depend on the salt concentration is different in the cases of NaF, NaCl, KF, KCl, and NH_4Cl in which such a dependence is quite marked. Such a behavior may consequently be understood in terms of the nature as well as the concentration of the ionic species present across the pericardial membrane. Consequently, an attempt has been made to express the P_s values in terms of an arbitrary parameter, β', which turns out to be a sort of measure of the extent of deviation from linearity and is equal to $n\beta$ where n is an arbitrary parameter. This has been achieved by accounting for $(1+4\ \xi^2)^{-1/2}$ term contributing to P_s to different extent $(n\beta)$ depending upon the interaction of the solute ions with the solvent. Thus, P_s is expressed as

$$P_s=\left[\frac{1}{(1+4\ \xi^2)^{-1/2}}\right]^{\beta'}=\left[\frac{1}{(1+4\ \xi^2)^{-1/2}}\right]^{n\beta}=\frac{[T_{app}-(1-\alpha)]}{[1-\alpha-(1-2\alpha)\ T_{app}]}. \tag{8}$$

It is worthwhile to note that the proposed Eq. 8 is expected to be applicable to any type of biological membrane irrespective of the extent of deviation shown in the behavior of P_s versus $1/\sqrt{1+4\ \xi^2}$ plots. The β' values for NaCl, NaF, KF, and NH_4Cl solutions were computed (Table 3) using the rearranged form of the above equation, $\beta'=-2\log P_s/\log(1+4\ \xi^2)]$. Finally the plots of P_s against $[1/(1+4\ \xi^2)^{1/2}]^{n\beta}$ (Fig. 6) supports the above equation in which the extent of deviation has already been accounted for in terms of $n\beta$.

Tasaka et al.[13] gave two limiting forms of expressions for the membrane potential, (i) in very low concentrations, it was found that

$$\Delta\phi_r=\ln\gamma, \tag{9}$$

where $\Delta\phi_r$ is the reduced membrane potential, and (ii) at high concentration of electrolyte Eq. 10 was found to be applicable.

$$-\Delta\phi/\frac{\gamma-1}{\gamma}=\frac{RT}{F}(\phi_x/2)\frac{1}{C_1}, \tag{10}$$

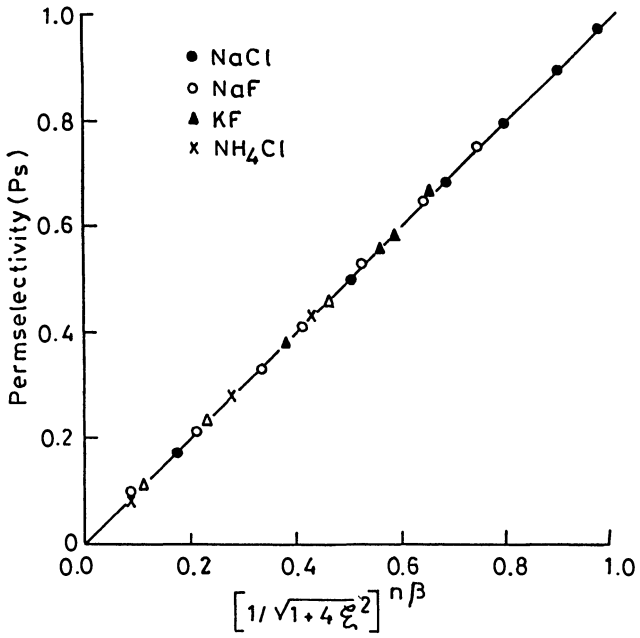

Fig. 6. Plots of P_s versus $[1/\sqrt{1+4\ \xi^2}]^{n\beta}$ for various electrolytes with pericardium.

when $\alpha=0.5$, i.e. in ordinary electrolyte solutions, Eq. 10 leads to

$$\Delta\phi_r=\frac{(2\alpha-1)}{2(1-\alpha)}\ln\gamma+\frac{(\gamma-1)\phi_x}{2(1-\alpha)\,2\gamma\,C_1}, \qquad (11)$$

In extremely high concentrations, Eq. 10 predicts a linear relationship between $\Delta\phi/[(\gamma-1)/\gamma]$ and $1/C_1$ from which the charge density (ϕ_x) can be determined. The different values of ϕ_x, derived from the initial slope of various curves of Fig. 7 are given in Table 2.

The results of these investigations show that the membrane potential can be determined with some reasonable accuracy. Also, when the pericardium separates concentrated solutions, the values of potential generated across the pericardial membrane are negative. This means that the membrane is anion selective and is positively charged. It may be noted that the anion selectivity decreases as the concentration across the membrane is increased. Again it was also observed that the apparant transport number values for the different electrolytes increases by increasing the concentration of the electrolytes across the pericardium. Furthermore, it is noted from Table 2 that the charge density values of the membrane electrolyte system are low.

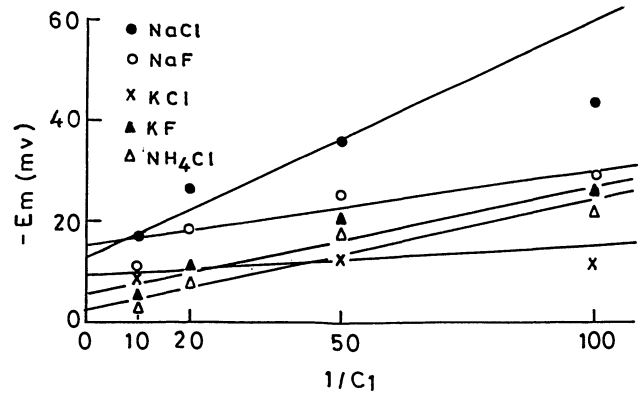

Fig. 7. Plots of E_m versus $1/C_1$ for various electrolytes with pericardium.

One would expect that the thermodynamic properties of biological membranes and those of artificial ones would be very different from each other because of the fact that the biological membranes are hitherto believed to function by active process (Ussing[14–16]), while artificial membranes are governed by the principle of passive transport. However, as stated above the present findings tend to support the contention that the laws of irreversible thermodynamics meant for passive transport are equally good for biomembranes.

The phenomenon of passive transport observed in cases of artificial membranes and that of active transport in those of biological membranes depend essentially on chemical nature of the membrane as well as on the electromotive forces developed across the cell membranes. Such a consideration has led us to examine their applicability to the biological membranes also. Consequently, it was found that the said models originally meant for explaining the behavior of artificial membranes, were equally applicable to biological membrane under investigation. As is well known, the purpose of active transport is to regulate the transfer of ions to suit the requirements of the cell. This cannot be achieved by passive transport. It seems likely that under diseased states, changes in electrolytic concentration, emotional factors etc., active transport may be inhibited and passive transport may become the dominant phenomenon. Such a situation will influence cell nutrition and its longevity because transport of essential materials and prevention of entry of toxic substances into the cell depend on the integrity of membrane function.

Thanks are due to Aligarh Muslim University, Aligarh for providing necessary facilities and to the Indian council of Medical Research, New Delhi for providing financial assistance. The cooperation and support of Professor S. A. A. Zaidi Chairman, Department of Chemistry is appreciated, We are highly indebted to Professor Nural Islam, Professor of Physical Chemistry, A.M.U. Aligarh for the help rendered in revising the manuscript.

References

1) N. Lakshminarayanaiah and F. A. Siddiqui, *Biophys. J.*, **11**, 603 (1971).

2) N. Lakshminarayanaiah and F. A. Siddiqui, *Biophys. J.*, **12**, 540 (1972).

3) S. Sheela Santhakumari and P. Radhakrishnamurty, *Bull. Electrochem.*, **1**(3), May-June, 337 (1985).

4) Y. Kobatake, *J. Phys. Chem.*, **28**, 146 (1958).
5) M. Nagasawa and Y. Kobatake, *J. Phys. Chem.*, **56**, 1017 (1952).
6) Y. Kobatake, N. Takeguchi, Y. Toyoshima, and H. Fujita, *J. Phys. Chem.*, **69**, 3981 (1965).
7) Y. Toyoshima, M. Yussa, Y. Kobatake, and H. Fujita, *Trans. Faraday Soc.*, **63**, 2803, 2814 (1967).
8) N. Kamo, Y. Toyoshima, and Y. Kobatake, *Kolloid Z. Z. Polym.*, **249**, 1061 (1971).
9) N. Kamo, Y. Toyoshima, H. Nozaki, and Y. Kobatake, *Kolloid Z. Z. Polym.*, **248**, 914 (1971).
10) N. Kamo, M. Oikawa, and Y. Kobatake, *J. Phys. Chem.*, **77**, 92 (1973); *ibid.*, **77**, 2995 (1973).
11) M. Yussa, Y. Kobatake, and H. Fujita, *J. Phys. Chem.*, **72**, 2871 (1968).
12) Y. Kobatake and N. Kamo, *Prog. Polym. Sci. Jpn.*, **5**, 257 (1972).
13) M. Tasaka, N. Aoki, Y. Konda, and M. Nagasawa, *J. Phys. Chem.*, **79**, 1307 (1975).
14) H. H. Ussing, Ion Transport Mechanism, Symp. Biol. Approaches to Cancer Chemotherapy, Louvain, June 1960.
15) H. H. Ussing, *Acta Physiol. Scand.*, **17**, 1 (1949).
16) H. H. Ussing and K. Zerhn, *Acta Physiol. Scand.*, **23**, 110 (1951).

Disproportionation of Carbon Monoxide on the Surface of Titanium and Vanadium Clusters

Arun Kumar SRIVASTAVA,* Kamla Kant TEWARI, and Isao KOJIMA†
Department of Chemistry, University of Allahabad, Allahabad, India
†Analytical Chemistry Division, National Chemical Laboratory for Industry, Tsukuba, Ibaraki 305
(Received November 26, 1990)

In the framework of CNDO (Complete Neglect of Differential Overlap method) VOIP (Valance Orbital Ionization Potential) has been evaluated using the method of Anno and Sakai and for exchange integrals Wolfsberg–Helmholtz approximation has been used. The method has been used for studying the disproportionation of carbon monoxide on titanium and vanadium clusters having two atoms respectively. A large number of theoretical models were designed, based upon various mechanistic possibilities. The bond energies between different atoms have been plotted against the distance, for the purpose of studying the formation and desorption of CO_2. The present studies suggest that the disproportionation of CO on titanium cluster may follow a dissociative path while in case of vanadium cluster this reaction may follow a disproportionation, where disproportionation involves a reaction between a 'bridge site' adsorbed CO molecule with a gas phase CO molecule.

The catalytic properties of transition metal surfaces have motivated much of the surface science research into the chemisorption of atoms and molecules.[1] The interaction of CO with metal surfaces has attracted much attention since it is considered to be a model system for understanding molecular chemisorption. The CO molecule usually bonds vertically to the surface through the carbon atom. However, there are strong-chemisorption (e.g. Nickel) and weak-chemisorption (e.g. Copper) limits, and cases of tilted and lying down molecules are also reported.[2,3] Chemisorption of carbon monoxide with Fe has been studied in detail[4–9] and anomalously low stretching mode in electron energy loss experiment has been observed.

It is thought that molecular specie is a precursor to dissociation and is important in catalytic behavior of iron.[8] Several theoretical models have been suggested to describe the chemisorption of CO.[10–14] Experimental studies based on LEED, UPS, XPS, AES, EELS,[15] and spin polarized photoemission have been reported.[16] Titanium and vanadium are known to be highly reactive transition metals relevant to problems of technological importance such as hydrogen storage[17] and also as active ingredient in some complex catalysts.[18] The adsorption of CO and subsequent build-up of carbon on the catalyst surface is of great importance since these are the key steps in methanation and Fischer–Tropsch synthesis. UPS and AES[19,20] studies have concluded that CO is dissociated on the clean titanium film at room temperature. Lee and coworkers[21] have performed molecular orbital calculation for studying molecular and dissociative chemisorption of CO on several metal surfaces.

The proceeding of a chemical reaction may be described by the splitting and formation of various bonds and therefore the changes in various bond energies may be expected to give useful information on the mechanism of the reaction. In CNDO framework the bond energy is explicitly defined and consequently the method as described here is much simpler than ab-initio method and has already been shown to be quite useful for making comparative studies.[22–24] Here we report our CNDO results on disproportionation of CO on titanium and vanadium clusters.

Method

The CNDO method is widely used and retains the main features of electron repulsion introduced by Pople, Santry, and Segal.[25] In this method the involvement of many parameters makes it less useful for the transition metal system. An effort has been made by Srivastava and Miyazaki[22,23] to reduce the number of parameters in the CNDO technique.

The local core matrix elements U_{ii} have been estimated from the atomic data using the following expression:

$$U_{ii} = -I_p(i) - (N-1)\gamma_{ss} - M\gamma_{sd}.$$

Here $I_p(i)$ is the valence state ionization potential, N denotes the total number of electrons in the valence s and p orbitals and M represents the number of electrons in d-orbital. The I_p's have been calculated by using the method of Anno and Sakai,[26] where valence orbital ionization potential (VOIP) was calculated with the help of a quadratic equation as given below:

$$\mathrm{VOIP} = A_0 + A_1 Z + A_2 Z^2,$$

where Z is the atomic number, A_0 and A_1 were evaluated with the help of the following expressions,

$$A_0 = a_0 + a_1 M + a_2 M^2,$$

$$A_1 = b_0 + b_1 M.$$

Values of a_0, a_1, a_2, b_0, and b_1 have been taken from Ref. 26. The exchange integral H_{ij} has been calculated with the help of Wolfsberg–Helmholtz approximation.[27]

$$H_{ij} = K S_{ij}(H_{ii} + H_{jj})/2.$$

The electronic configuration $3d^m4s^2$ or $3d^m4s4p$ was assumed for the ground state of titanium and vanadium atoms. Thus in the present work only $K(=1.5)$ has been used as an empirical parameter. The bond energy has been evalu-

ated from the following expression.

$$E_{AB}=\sum_{\mu}^{A}\sum_{\nu}^{B}(2P_{\mu\nu}\beta_{\mu\nu}-1/2P_{\mu\nu}{}^{2}\gamma_{AB})$$
$$+(Z_AZ_BR_{AB}{}^{-1}-P_{AA}V_{AB}-P_{BB}V_{BA}+P_{AA}P_{BB}\gamma_{AB}),$$

where all the terms have their usual meaning.

Results and Discussion

Theoretically one can predict the following mechanisms for the disproportionation of CO on the surface of titanium and vanadium.

1. Dissociative Mechanism. It claims that the dissociation of CO is first step with the formation of Ti–C and Ti–O bonds.

$$2Ti+CO\rightarrow Ti\text{-}C+Ti\text{-}O$$

followed by

$$Ti\text{-}O+CO\rightarrow CO_2$$

Similarly for vanadium formation of V–C and V–O bonds is the first step.

2. Disproportionation. It predicts reaction between the CO molecules on the surface

$$(2CO\rightarrow CO_2(g)+C_{ad}),$$

where (g) refers to a gas phase species and (ad) to an adsorbed or surface species.

Here three different possibilities have been considered for this reaction.

(i) Reaction between two adsorbed CO molecules (Model-D)

$$CO_{ad}+CO_{ad}\rightarrow CO_2(g)+C_{ad}.$$

(ii) Dissociation of CO to adsorbed C_{ad} and O_{ad} species follow by a reaction of adsorbed O_{ad} with CO either from the gas phase (Model-B) or in an adsorbed state (Model-A and Model-C)

$$CO\rightarrow C_{ad}+O_{ad},$$
$$O_{ad}+CO(g)\rightarrow CO_2(g),$$
$$O_{ad}+CO_{ad}\rightarrow CO_2(g).$$

(iii) Reaction between adsorbed CO and another CO molecule from the gas phase (Model-E)

$$CO\rightarrow CO_{ad},$$
$$CO_{ad}+CO(g)\rightarrow CO_2+C_{ad}.$$

Based upon the above three theoretically possible mechanisms different models involving Ti_2 and V_2 clusters were designed as shown in Fig. 1. For all these models the energy of interaction E_{int} of a CO molecule to the rest of cluster was calculated by using the following definition:

$$E_{int}=E_t-E_a,$$

where E_t is the total energy of the system containing all the atom as shown in each model and E_a is the total energy of the system which has one molecule of CO less than the original model.

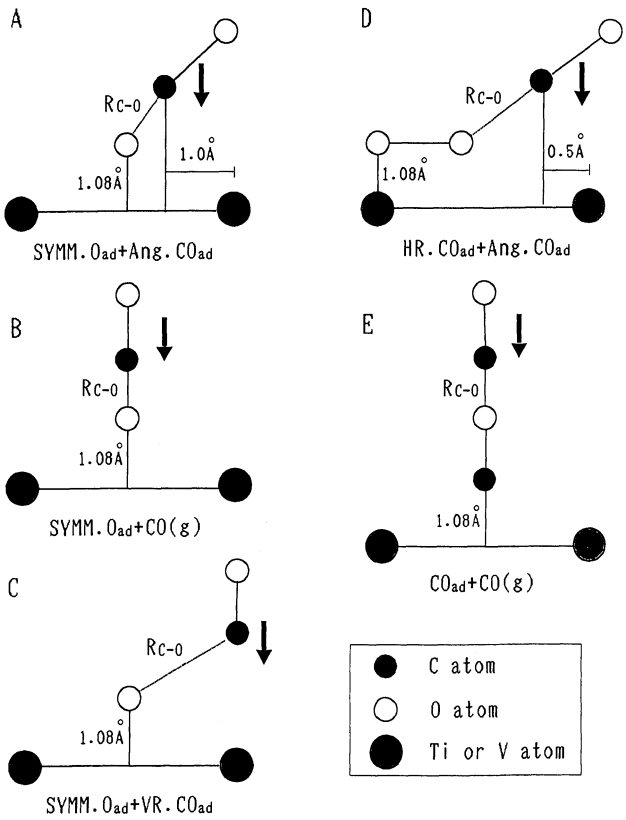

Fig. 1. Disproportionation of CO on Ti_2 or V_2 clusters.

The bond energy of CO bond (the new bond which is being formed and is essential for the formation of CO_2) i.e. E_{C-O} as well as the bond energies of the adsorbed C–O bond and Metal–O bonds were calculated. All these energies have been plotted against R_{C-O} i.e. distance between C and O atoms involved in the new bond formation. The plots of E_{int} and E_{C-O} against R_{C-O} are expected to throw light upon the formation of CO_2 and plot of $E_{metal-O}$ vs. R_{C-O} may give information regarding the desorption of the CO_2 molecules.

(a) Disproportionation of CO on Titanium Cluster (Ti_2). In Fig. 2 the energy of interaction E_{int} of carbon monoxide with rest of the cluster has been plotted against R_{C-O} and it seems that Model-C which represents a dissociative path, may be mechanistically more probable.

Figure 3 contains the plots of E_{C-O} vs. R_{C-O}. A comparative study of various curves shows that Model-C represents a pathway for the reaction which is more favorable for the formation of CO_2.

Figure 4 presents the plot of bond energy E_{Ti-O} against bond distance R_{C-O}. A close study of these curves reveals that as far as the possibility of desorption of CO_2 is concerned Model-C may be comparatively better suited.

Figure 5 presents the plot of $E_{C-O_{ad}}$ i.e. bond between O_{ad} and C against R_{C-O}.

On the basis of the qualitative studies on Ti_2 cluster, it

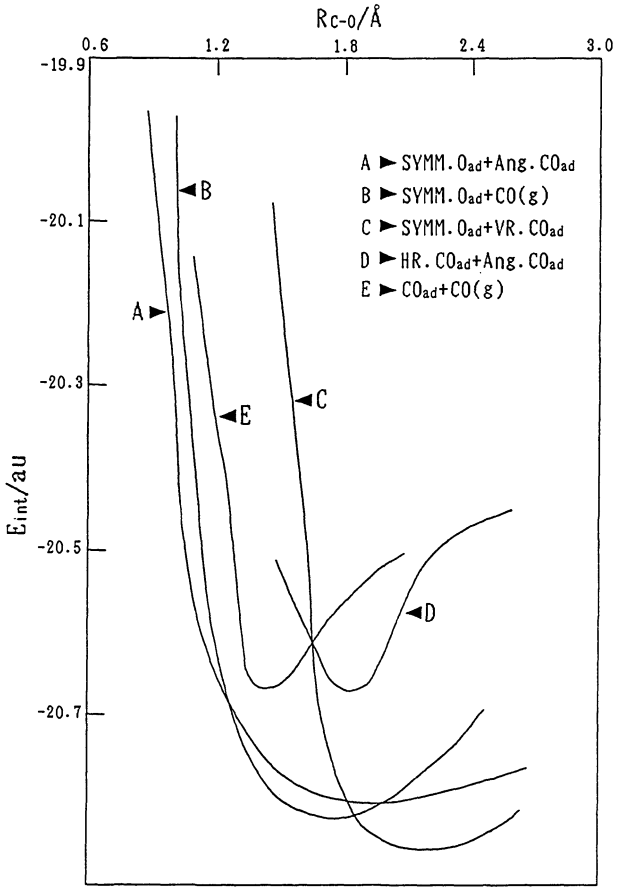

Fig. 2. Interaction energy E_{int} against R_{C-O} involving a Ti_2 cluster.

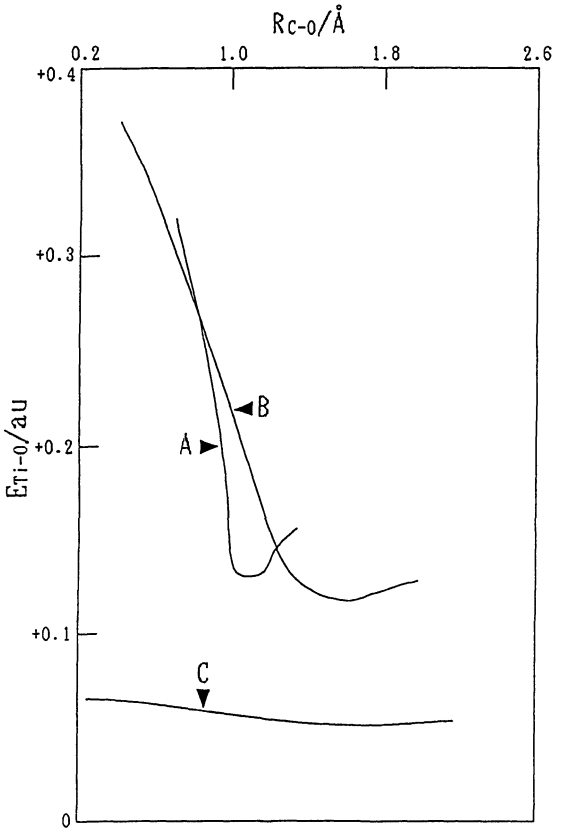

Fig. 4. Bond energy of Ti–O bond i.e. E_{Ti-O} against R_{C-O} involving a Ti_2 cluster.

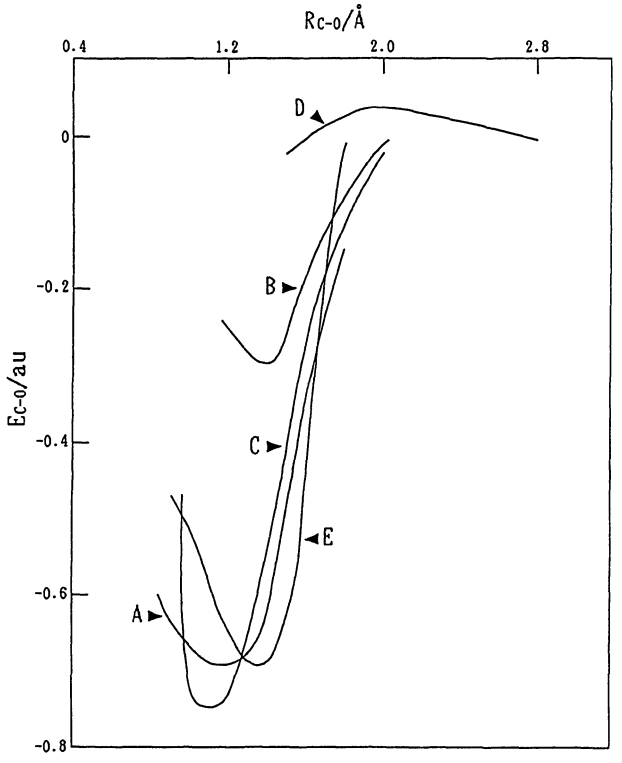

Fig. 3. Energy of C–O bond i.e. E_{C-O} against R_{C-O} involving a Ti_2 cluster.

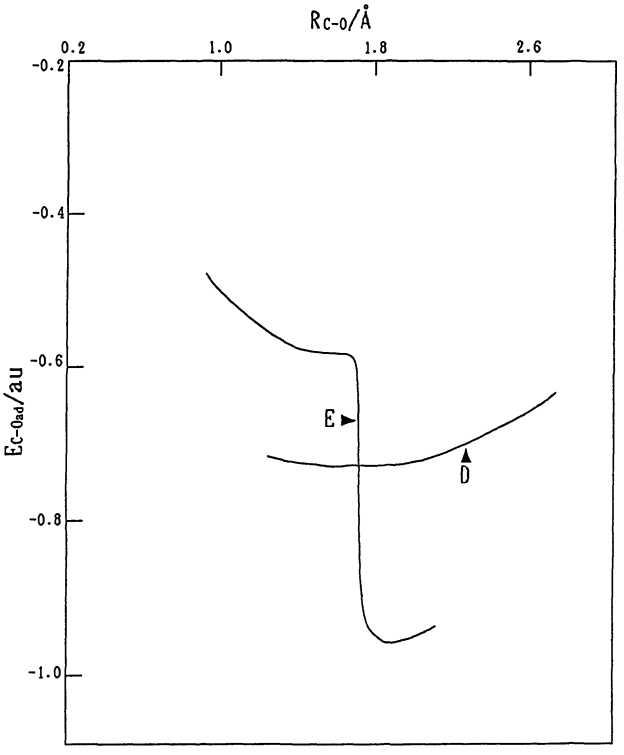

Fig. 5. Energy of $C-O_{ad}$ bond i.e. $E_{C-O_{ad}}$ against R_{C-O} involving a Ti_2 cluster.

seems that Model-C, representing the dissociative path is the only suitable path for the reaction under study. Our findings are in good agreement with the findings of Srivastava et al.[23] The dissociative mechanism for this reaction may be as given below:

$$CO \rightarrow C_{ad} + O_{ad},$$

$$O_{ad} + V : CO_{ad} \rightarrow CO_2.$$

A similar dissociative mechanism has also been proposed by Madden and Ertl,[28] on the basis of their LEED and AES studies.

(b) Disproportionation of CO on Vanadium Cluster (V_2). The energy of interaction E_{int} of carbon monoxide with rest of the cluster has been plotted against R_{C-O} in Fig. 6. From these curves it may be concluded that the Model-E represents a more suitable path for this reaction.

The plots of E_{C-O} against R_{C-O} are given in Fig. 7. A close scrutiny of these curves suggests that Model-E represents a pathway for the reaction which is more favorable for the formation of CO_2.

Plots of E_{V-O} vs. R_{C-O} are given in Fig. 8. It is interesting to note that curves A, B, and C, based upon Models-A, B, and C, respectively, show a strengthening of V–O bond, thus in case of these models there seems to be virtually no possibility of CO_2 desorption after its formation.

From Fig. 9 the weakening of C–O bond is evident in case of Model-E. So it can be concluded that the Model-E may be more favorable for the desorption of

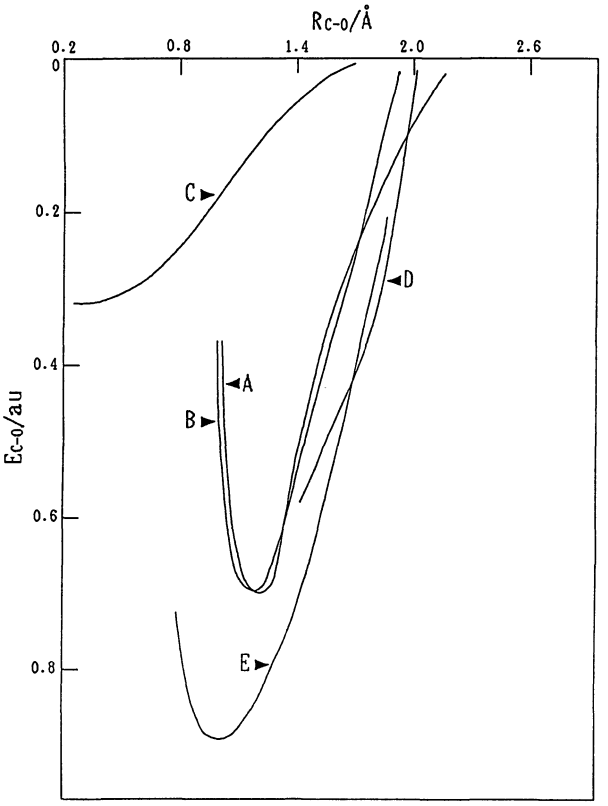

Fig. 7. Energy of C–O bond i.e. E_{C-O} against R_{C-O} involving a V_2 cluster.

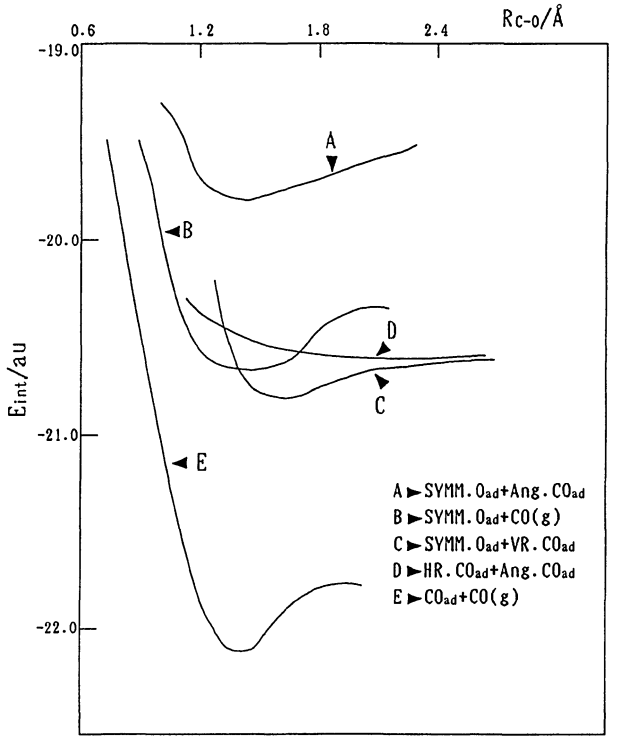

Fig. 6. Interaction energy E_{int} against R_{C-O} involving a V_2 cluster.

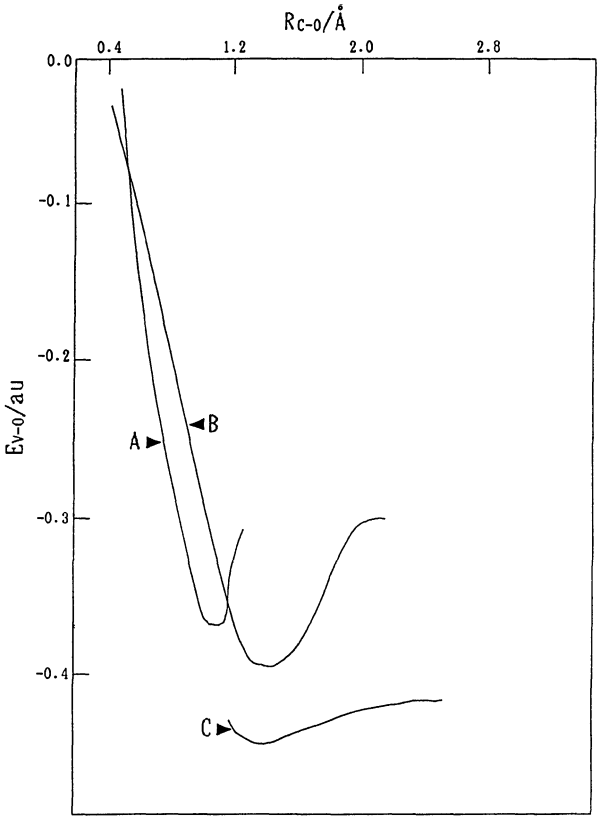

Fig. 8. Bond energy of V–O bond i.e. E_{V-O} against R_{C-O} involving a V_2 cluster.

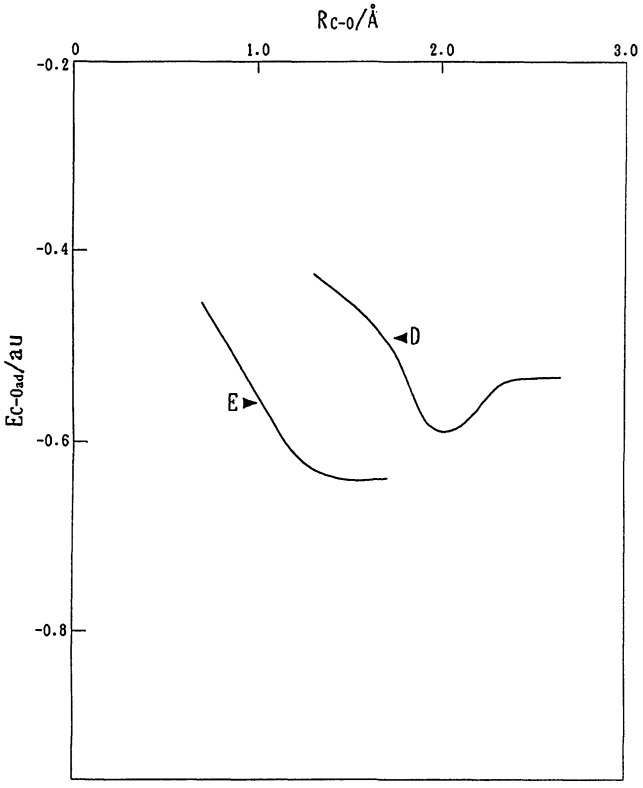

Fig. 9. Energy of C–O_{ad} bond i.e. $E_{C\text{-}O_{ad}}$ against $R_{C\text{-}O}$ involving a V_2 cluster.

CO_2.

Thus on the basis of our qualitative results, it can be suggested that Model-E offers a more suitable course for the reaction under study. The qualitative studies on V_2 cluster have shown that the following mechanism may be suggested for this reaction:

$$CO_{ad} + CO(g) \rightarrow CO_2(g) + C_{ad}.$$

A similar disproportionation mechanism has also been proposed by Keim et al.[29] on the basis of their ellipsometry and AES studies.

One of the authors (K.K.T.) is highly thankful to the CSIR, New Delhi for providing (Senior Research Fellowship) financial assistance. Thanks are also due to Computer Centre, Allahabad University for providing computer facilities in data calculation related to our present work.

References

1) D. A. King and D. P. Woodruff, "The Chemical Physics of Solid Surfaces and Heterogeneous Catalysis," Ellsevier, New York (1988), Vols. 1—4.
2) E. W. Plummer and W. Eberhardt, *Adv. Chem. Phys.*, **49**, 50 (1982).
3) H. J. Freund and M. Neumann, *Appl. Phys.*, **A47**, 3 (1988).
4) D. W. Moon, S. L. Bernasek, D. J. Dwyer, and J. L. Gland, *J. Am. Chem. Soc.*, **107**, 4363 (1985).
5) R. S. Saiki, G. S. Herman, M. Yamada, J. Osterwalder, and C. F. Fadley, *Phys. Rev. Lett.*, **63**, 283 (1989).
6) D. W. Moon, D. J. Dwyer, and S. L. Bernasek, *Surf. Sci.*, **1985**, 163.
7) F. Jona, K. O. Legg, H. D. Shih, D. W. Jepsen, and P. M. Marcus, *Phys. Rev. Lett.*, **40**, 1466 (1978).
8) D. W. Moon, S. Cameron, F. Zaera, W. Eberhardt, R. Carr, S. L. Bernasek, J. L. Gland, and D. J. Duzyer, *Surf. Sci.*, **180**, L123 (1987).
9) C. Bnndorf, B. Nieber, and B. Kruger, *Surf. Sci.*, **177**, L907 (1986).
10) G. J. Blyholder, *J. Phys. Chem.*, **68**, 2772 (1964).
11) B. Gumhalter, K. Wandelt, and Ph. Avouris, *Phys. Rev. B*, **37**, 8048 (1988).
12) E. Greuter, D. Heshelt, and E. W. Plummer, *Phys. Rev. B*, **27**, 7117 (1983).
13) C. R. Fischer, L. A. Bruke, and J. L. Whitten, *Phy. Rev. Lett.*, **45**, 344 (1982).
14) I. Kojima, A. K. Srivastava, and E. Miyazaki, *J. Chem. Phys.*, **84**, 4455 (1986).
15) J. Paul, S. D. Cameron, D. J. Dwyer, and F. M. Hoffmann, *Surf. Sci.*, **177**, 121 (1986).
16) N. B. Brookes, A. Clarkes, and P. D. Hohson, *Phys. Rev. Lett.*, **63**, 2764 (1989).
17) G. Alefeld and J. Volkl, "Hydrogen in Metals," Springer, Berlin (1978), Vols. I and II.
18) H. Morisaki, T. Watanabe, M. Iwase, and K. Yayama, *Appl. Phys. Lett.*, **29**, 338 (1976).
19) D. E. Eastman, *Solid State Commun.*, **10**, 933 (1972).
20) M. P. Hooker and J. T. Grant, *Surf. Sci.*, **62**, 21 (1977).
21) T. H. Lee and J. W. Rabalais, *Surf. Sci.*, **77**, 223 (1978).
22) A. K. Srivastava, I. Kojima, and E. Miyazaki, *Bull. Chem. Soc. Jpn.*, **59**, 3375 (1986).
23) A. K. Srivastava, E. Miyazaki, and I. Kojima, *Indian J. Chem., Sect. A*, **25**, 987 (1986).
24) A. K. Srivastava, I. Kojima, and E. Miyazaki, *Bull. Chem. Soc. Jpn.*, **62**, 3666 (1989).
25) J. A. Pople, D. P. Santry, and G. A. Segal, *J. Chem. Phys.*, **43**, 5129 (1965).
26) T. Anno and Y. Sakai, *Theor. Chim. Acta*, **18**, 208 (1970).
27) M. Wolfberg and C. Helmholtz, *J. Chem. Phys.*, **20**, 837 (1952).
28) H. H. Madden and G. Ertl, *Surf. Sci.*, **35**, 211 (1973).
29) E. G. Keim, F. Labohm, O. L. G. Gizeman, G. A. Bootsma, and J. W. Geus, *Surf. Sci.*, **112**, 52 (1981).

Raman Spectra of *N,N*-Dimethylthioacetamide Adsorbed on Silver and Copper Electrode Surfaces

Boon Hian Loo,* Yue Guey Lee, and Tamihiko Kato†
Department of Chemistry, The University of Alabama in Huntsville, Huntsville, AL 35899, USA
†Department of Applied Chemistry, Nagoya Institute of Technology, Nagoya 466
(Received January 25, 1991)

Surface-enhanced Raman (SER) spectra have been obtained from *N,N*-dimethylthioacetamide (DMTA) adsorbed on Ag and Cu electrode surfaces. Vibrational analysis of the SER spectra of DMTA is made in comparison to the bulk-phase Raman spectrum of DMTA, and the infrared data on Co, Cu, and Hg complexes of DMTA. It is concluded that the DMTA molecule is bonded through its S atom to Ag and Cu surfaces.

Previously we have studied molecular bondings of several isostructural sulfur compounds containing a thiocarbonyl C=S group, namely, thiourea (TU), thioacetamide (TA), *N,N*-dimethylthioformamide (DMTF), thiosemicarbazide (TSC), and thiocarbohydrazide (TCH) on Ag and Cu electrode surfaces.[1-5] We found that in all cases the adsorbate was bonded via its S atom to Ag and Cu surfaces. The predominantly C=S stretching bands for these molecules were shifted to lower frequencies upon adsorption on metal surfaces with amounts comparable to those observed in their organometallic complexes. We believed that there were considerable electronic interactions between the adsorbates and the substrates such that the C=S bond order was reduced, and perhaps some kind of surface complexes was formed. These surface complexes may be the surface analogs of the organometallic complexes of these molecules. In this work we extend our study to *N,N*-dimethylthioacetamide (DMTA), the second simplest tertiary thioamide. The present work is a part of our continuing effort in the understanding of molecular interactions of adsorbates with metal surfaces.[1-8]

Experimental

N,N-Dimethylthioacetamide was synthesized from *N,N*-dimethyl acetamide (Aldrich) and phosphorus pentasulfide (Aldrich), and repeatedly crystallized from hexane.[9] The experimental procedure for the in situ Raman measurements was similar to that described previously.[2,4]

Results and Discussion

Figure 1 shows the surface-enhanced Raman (SER) spectrum of DMTA adsorbed on an Ag electrode at −0.30 V vs. saturated calomel electrode (SCE), whereas Fig.2 shows the SER spectrum of DMTA adsorbed on a Cu electrode at the same potential. The SER spectra were obtained after the electrodes had undergone an oxidation-reduction cycle.

Except for some minor frequency shifts and relative band intensity differences, the general spectral features for the Ag/DMTA and Cu/DMTA systems are similar to each other. This indicates that DMTA adsorbs in a similar fashion on Ag and Cu surfaces.

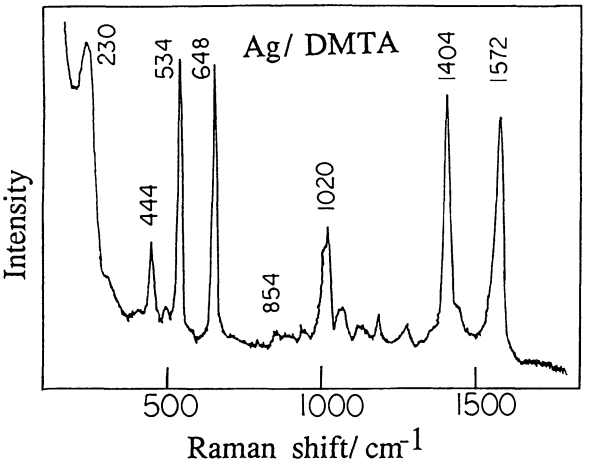

Fig. 1. Surface-enhanced Raman spectrum of DMTA adsorbed on Ag electrode at −0.3 V vs. SCE. The electrolyte was 1.4×10^{-3} M DMTA+0.1 M KCl (acidified with HCl, pH 2.5) (1 M=1 mol dm^{-3}). The electrode was anodized at 0.2 V before the spectrum was taken. The excitation wavelength was Kr^+ 647.1 nm.

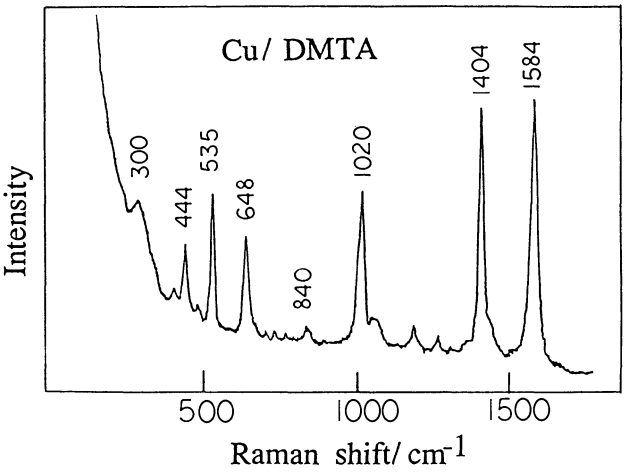

Fig. 2. Surface-enhanced Raman spectrum of DMTA adsorbed on Cu electrode at −0.3 V vs. SCE. The electrolyte was 1×10^{-4} M DMTA +0.1 M KCl (acidified with HCl, pH 2.5). The electrode was anodized at 0.1 V before the spectrum was taken. The excitation wavelength was Kr^+ 647.1 nm.

Table 1. Vibrational Frequencies (in cm^{-1}) and Potential Energy Distribution for *N,N*-Dimethylthioacetamide

Calcd	DMTA		SERS		Complexes[c]			Assignments (PED %)[d]
UBF[a]	IR[b]	Raman	Ag	Cu	CoL_2Cl_2	CuLCl	HgL_4Cl_2	
			230					ν(AgS)*
				300				ν(CuS)*
300	300 sh	302 b	—	—	290 w	306 sh	284 sh	δ(C'NC')(79)+δ(CCS)(13)
446	444 m	444 m	444	444	448 m	435 m	451 m	δ(CCS)(59)+δ(C'NC')(12)+ν(CS)(10)
495	495 m	493 m	495	495	498 m	485 w	498 w	δ(NCS)(40)+(CNC')(21)+a(C'N)(16)
—	540 vw	537 w	534	535	542 vw	540 vw	535 vw	π(C-C)(-)
661	656 s	656 vs	648	648	655 vs	635 s	640 s	ν_s(C'N)(44)+ν(CS)(25)+ν(CC)(17)
867	870 s	864 w	854	840	862 s	845 m	845 m	ν_s(C'N)(37)+ν(CS)(24)+r(C-CH_3)(15)
998	1020 vs	1014 w	1020	1020	1030 vs	1025 s	1030 vs	r(C-CH_3)(38)+r(N-CH_3)(22)+ν(CN)(11)
1004	1060 w	—	1060	1064	1060 s	1085 sh	1050 w	ν_a(C'N)(39)+r(N-CH_3)(38)
1133	1130 s	1125 w	1130	—	1130 w	1115 s	1130 s	ν_a(C'N)(26)+r(N-CH_3)(26)+ν(CC)(24)
1154	1185 s	—	1185	1185	1192 vs	1190 m	1195 m	r(N-CH_3)(36)+δ_s(N-CH_3)(14)+δ_s(N-CH_3)(12)
1279	1284 vs	1275 w	1279	1262	1285 vs	1262 vs	1270 vs	ν(CC')(28)+ν(CS)(17)+δ(NCS)(15)
1373	1370 s	—	1370	1370	1385 vs	1385 s	1370 s	δ_s(C-CH_3)(91)
1405	—	1391 w	1404	1404	—	—	—	δ_s(N-CH_3)(44)+ν(CN)(18)+δ_s(C-CH_3)(15)
1422	1430 s	1418 w	—	—	1430 s	1430 vs	1410 s	δ_s(N-CH_3)(96)
1475	1470 s	—	—	—	1465 s	1470 vs	1470 s	δ_a(N-CH_3)(80)+r(N-CH_3)(19)
1536	1540 vs	1540 b	1572	1584	1580 vs	1590 vs	1610 vs	ν(CN)(46)+δ_a(N-CH_3)(16)+r(N-CH_3)(15)

a), b), c) Ref. 10; d) Ref. 10 except *; UBF=Urey-Bradley force; L=DMTA; PED=potential energy distribution; ν=stretch; δ=deformation; r=rock; π=out-of-plane bend; s=symmetric; a=asymmetric; v=very; s=strong; m=medium; w=weak; b=broad; sh=shoulder; C's are used to denote methyl carbons next to the N atom.

The IR, Raman, and SER frequencies for DMTA, and the vibrational band assignments for DMTA and its Co, Cu, and Hg complexes are given in Table 1. The potential energy distributions (PED's) and the assignments of the bands are also given. The PED calculation was performed by Ray and Sathyanarayana using C_s point group and a Urey-Bradley force field.[10] The present assignments for the SER spectra of the DMTA adsorbed on Ag and Cu surfaces are made by comparing the SER spectra with the solid phase Raman spectrum and with the IR vibrational frequencies of its metallic complexes.[10]

Metal complexes of DMTA were not so well studied when compared to those of TU, TA, DMTF, TSC, and TCH.[11] However, useful information still can be derived from the few complexes of DMTA that had been studied. Madan and Mueller[12] reported the preparation of several Co(II) complexes of DMTA, $Co(DMTA)_2X_2$ [where X=NO_3, Cl, Br or I], and $Co(DMTA)_4$ $(ClO_4)_2$. From the electronic absorption spectra and magnetic measurements of these complexes, they concluded that the DMTA ligand was coordinated to the central Co(II) atom through the S atom. Ray and Sathyanarayana[10] studied the IR spectra of the complexes of DMTA with the chlorides of Co(II), Cu(I), and Hg(II). They found that the C-N stretching frequency occurring at 1540 cm^{-1} in DMTA was increased to 1580—1610 cm^{-1} in the complexes. Additionally, two C=S bands at 870 and 656 cm^{-1} were decreased to 862—845 and 652— 635 cm^{-1}, respectively, in metal complexes. They concluded that the bonding to the metal ions was through the S atom in these complexes. Aarts et al.[13] synthesized DMTA complexes of Au(I), Au(DMTA)X (where X=Cl, Br or I). Again, their IR results indicated that the coordination of DMTA to Au(I) was through the S atom. The ν(CN) frequency of the free molecule at 1535 cm^{-1} was shifted to higher frequencies 1557 to 1572 cm^{-1} whereas the ν(CS) frequency at 657 cm^{-1} was shifted to lower frequencies 650—648 cm^{-1}. The observed metal-sulfur stretching ν(AuS) frequency was at 300 cm^{-1}.

The experimental observations are not difficult to rationalize in view of the fact that the electronic structure of DMTA can be represented by the resonance hybrid structures **I** and **II**, with a greater contribution comes from the polar structure **II**.[14] When the bonding is through the S donor site, the ν(CS) will be shifted to a lower frequency whereas ν(CN) to a higher frequency.

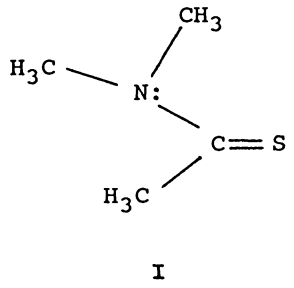

I

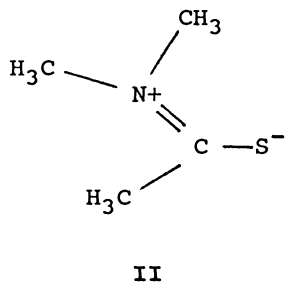

II

In the SER spectra of sulfur compounds with a thiocarbonyl group, the C-N and C=S stretching modes were most susceptible to frequency shifts upon adsorption on metal surfaces[1-5] for the same reason we have just mentioned. Thus, the C-N and C=S stretching modes will be monitored for shifts when DMTA is adsorbed on Ag and Cu electrode surfaces. In particu-

Table 2. Metal-Sulfur Vibration of Adsorbate (A) on Ag and Cu Surfaces

A	ν(AgS)/cm^{-1}	ν(CuS)/cm^{-1}
Thiourea	221	287
Thioacetamide	190	280
N,N-Dimethylthioformamide	230	288
Thiosemicarbazide	239	294
Thiocarbohydrazide	221	287
N,N-Dimethylthioacetamide	230	300

lar, the 1540 cm^{-1} Raman band with 46% PED ν(CN) is shifted to 1572 (+32) and 1584 (+44) cm^{-1}, respectively (The values in parentheses refer to the shifts from the corresponding Raman bands for DMTA). There are two bands that have a relative large contribution (about 25% PED) of the C=S stretching, one is at 656 and the other at 864 cm^{-1}. The band at 656 cm^{-1} is shifted to 648 (−8) on both Ag and Cu surfaces, whereas the 864 cm^{-1} band is shifted to 854 (−10) and 840 (−24) cm^{-1} on Ag and Cu surfaces, respectively. From this observation, we can conclude that the DMTA molecule is bonded through its S atom to the Ag and Cu electrode as was observed in previous cases.[1-5]

We assign the low-frequency vibrational modes at 230 cm^{-1} in the Ag/DMTA system and at 300 cm^{-1} in the Cu/DMTA system to the ν(AgS) and ν(CuS) modes, respectively. The intensity of these modes is increased as the applied potential becomes more cathodic, a behavior which is similar to those observed for other systems.[3,4] The frequency values of the metal to sulfur vibrations compare well with the same modes for TU, TA, DMTF, TSC, and TCH on Ag and Cu surfaces (see Table 2).

In conclusion, we have studied the adsorption of DMTA on Ag and Cu electrode surfaces. DMTA, like the other C=S compounds previously studied,[1-5] is also S-bonded to Ag and Cu surfaces.

This work was supported in part by NSF Alabama EPSCoR Grant No. RII-8610669 and International Copper Research Association Project No. 341. TK thanks the Japan Society for the Promotion of Science (JSPS) for a Visiting Fellowship (1989—90) at the University of Alabama in Huntsville under the Joint Japan-U.S. Cooperation Program in Science and Technology.

References

1) B. H. Loo, *Chem. Phys. Lett.*, **89**, 346 (1982).
2) B. H. Loo and Y. G. Lee, *Chem. Phys Lett.*, **112**, 580 (1984).
3) B. H. Loo, Y. G. Lee, and Z. Yazid, *Chem. Phys. Lett.*, **114**, 405 (1985).
4) B. H. Loo, J. Leahey, and Y. G. Lee, *Surf. Sci.*, **226**, 119 (1990).
5) B. H. Loo, J. Leahey, and Y. G. Lee, *Chem. Phys. Lett.*, **172**, 33 (1990).
6) B. H. Loo, Y. G. Lee, and Z. Yazid, *Chem. Phys. Lett.*, **115**, 134 (1985).
7) B. H. Loo, Y. G. Lee, and D. O. Frazier, *Chem. Phys. Lett.*, **119**, 312 (1985).
8) B. H. Loo, Y. G. Lee, and D. O. Frazier, *J. Phys. Chem.*, **89**, 4672 (1985).
9) A. W. Hofmann, *Ber.*, **11**, 338 (1878).
10) A. Ray and D. N. Sathyanarayana, *Bull. Chem. Soc. Jpn.*, **45**, 2712 (1972).
11) See references cited in Refs. 1—5.
12 S. K. Madan and D. Mueller, *J. Inorg. Nucl. Chem.*, **28**, 177(1966).
13) A. J. Aarts, H. O. Desseyn, and M. A. Herman, *Transition Met.Chem.*,**5**, 10 (1980).
14) H. O. Desseyn, B. J. van der Veken, and M. A. Herman, *Appl. Spectrosc.*, **32**, 101 (1978).

Adsorption-Induced Unusual Changes in the Electrical Conductivity of Some Ferrocene Derivatives

Ashis BHATTACHARJEE* and Biswanath MALLIK
Department of Spectroscopy, Indian Association for the Cultivation of Science, Jadavpur, Calcutta 700032, India
(Received January 28, 1991)

The effects of adsorption of different organic vapors on the electrical conductivity of some ferrocene derivatives have been studied using the sandwich cell technique. A conductivity peak is observed in the plot of measured current versus temperature for a sandwich cell of powdery material with some adsorbed vapors. The dependence of the intensity of the peak and the temperature at which it appears have been studied as a function of grain size of powdery materials, heating rate, amount of adsorbed vapor, and also the nature of the adsorbed vapors. At the vapor-adsorbed state these materials show very high value of activation energy and the pre exponential factor σ_o (in the usual semiconduction equation). Results indicate that the adsorption is a physical adsorption. The usual mechanisms for the adsorption-induced change in conductivity and activation energy are not suitable for explaining the observed results. Adsorption induced reversible structural phase transition seems responsible for the anomalous behavior of the adsorption-induced changes in the electrical properties of these materials. The results obtained with different ferrocene derivatives have been compared with that of ferrocene and possible reason for the adsorption induced phase transition is discussed.

Investigations on the effect of adsorption of vapors on the dark conductivity of organic as well as organometallic solid materials have been stimulated in recent years.[1–5] Adsorption or desorption of vapors changes the dark conductivity of these materials significantly. This effect of adsorption induced changes in dark conductivity can be monitored for the detection of various gases/vapors in the environment using these materials in suitable gas detectors.[1–5] The ultimate aim of such research is to find out suitable new materials that can be utilized as gas detectors for detecting specific gases, which has not yet been possible. The effect of adsorption-induced change in conductivity has shown another application also as the change in conductivity of vitamin A (alcohol and acetate) and some other linear conjugated polyenes could be involved in the primary mechanism of olfactory-transduction process.[6–7] Rosenberg et al.[6] have speculated that a week charge-transfer complex formation between vapor molecules and a semiconductor is responsible for the enhancement of conductivity and the change in activation energy in case of some polyenes. The nature of interaction between vapor or gas molecules and the solid surface is a complicated one and it is not yet clearly understood. Systematic studies are required to understand the nature of such interaction.

Recently, the studies on the effect of adsorption of vapors on ferrocene, the first synthesized organometallic compound has become a subject of great interest to us,[8] following the suggestion[9] that adsorption of minute amounts of moisture on this material may have an important role for the inconsistent results reported in the literature[10,11] regarding the pressure dependence of the electrical conductivity. In our earlier communication[8] we have discussed about the adsorption-induced unusual changes in the electrical conductivity of ferrocene. We have studied the adsorption-induced changes in the electrical conductivity of some ferrocene derivatives for eluciding the effect of substituent groups on the adsorption-induced changes. The results of this investigation are presented in this paper.

Experimental

High-purity microcrystalline ferrocenecarboxylic acid (Fc-COOH), ferrocenecarbaldehyde (Fc-CHO), acetylferrocene (Fc-$COCH_3$) in powdered form were obtained from Aldrich Chem. Co., Inc. (U.S.A.) and then were used after purification by repeated crystallization. Reagent chemicals used in this experiment were of spectrograde (E. Merck) or equivalent quality. The usual sandwich cell technique[7,12,13] with a conducting glass and a stainless steel electrode was used and the cell was placed inside a suitably designed conductivity chamber, made of brass and fashioned with teflon. The experimental arrangement for measurement of semiconduction parameters of these ferrocene derivatives with various adsorbed vapors was the same as described in earlier communications.[12,13] The finely powdered and coarsely powdered materials were used as materials of smaller grain size and larger grain size respectively. The grain size of the powdery materials taken for preparing different sample cells was kept same in each experiment. A d.c. voltage of 27 Volts was applied across the electrodes as a bias potential and a teflon spacer of 2 mil (0.005 cm) thickness was used. The conductivity chamber was first evacuated and then filled with dry nitrogen gas and its flow at a constant rate was maintained throughout the experiment. Repeated heating-cooling cycles were performed for each cell to ensure the absence of any kind of adsorbed vapors or moisture in the material before adsorption studies. For adsorption of vapors on the solid materials, dry nitrogen gas at a constant rate was bubbled through a solvent inside a bubbler kept at a fixed temperature to maintain a constant vapor pressure and then it was passed through the conductivity chamber. The cell temperature was kept at 258 K during adsorption and after obtaining saturation current the cell was further cooled down to about 250 K. Then the cell was heated with a constant heating rate of 0.01 K sec^{-1} (otherwise mentioned in the text) and the values of the dark current were noted with temperature. For current mea-

surement an electrometer (model No. EA815) of Electronic Corporation of India Ltd. was used. The temperature measurements were carried out by a Panel meter (model No. 2301) of HIL, India. It is reported that Fc-$COCH_3$ shows structural phase transition[14] near melting point. Therefore, during heat treatment the maximum temperature of the sample cell was kept much below the melting point for Fc-$COCH_3$. Similarly, in case of Fc-CHO, the maximum temperature of the cell was kept below 317K to avoid the structural phase transitions.[15]

Results and Discussion

The effect of adsorption of different vapors on the electrical conductivity (proportional to current) of the ferrocene derivatives as a function of temperature was studied. Such an effect of adsorption of toluene vapors (30 Torr vapor pressure, 1 Torr=133.322 Pa) on Fc-$COCH_3$ is illustrated in Fig. 1 [curve(1)]. At temperatures near 250 K current observed (not shown) was very low ($<10^{-14}$ A). As the temperature increases initially the current rises slowly and then rapidly; and attains a maximum value of 1.37×10^{-9} A at about 282 K. Then the current starts to decrease sharply with increasing temperature and attains a value almost equal to that of the pure sample near the room temperature. Above room temperature the current rises again with increasing temperature similar to the pure sample in nitrogen atmosphere. Thus a conductivity peak is observed at the adsorbed state by plotting the current values against temperature [curve 1, Fig. 1]. It is interesting to note that the conductivity variation [curve (2), Fig. 1; plotted in a magnified scale] in the same temperature range in pure acetylferrocene in dry nitrogen atmosphere does not show any conductivity peak and the variation is usual one as expected for a pure organic semiconductor. However, the above-mentioned conductivity peaks were also observed with different adsorbed vapors on various ferrocene derivatives.

The effect of adsorption of vapors on the dark conductivity of different ferrocene derivatives were studied under different measurement conditions such as (i) with different grain size of the powdery materials, (ii) change of heating rate, (iii) with different amounts of adsorbed vapors, and (iv) nature of adsorbed vapors. These are described below in detail.

(i) The adsorptive property of a solid surface depends on the grain boundaries of the particles constituting the surface. To investigate such a dependence in case of different polycrystalline ferrocene derivatives, qualitative experiments were performed with two different grain sizes of polycrystalline powders of these materials. The results of such a typical experiment with adsorbed ethanol vapor at 40 Torr vapor pressure on Fc-$COCH_3$ are shown in Fig. 2 for two different grain sizes. The conductivity curve corresponding to bigger grain sizes has shown a higher value of that temperature (T_{max}) at which the conductivity peak appears associated with a slightly lower value of current (I_{max}) corresponding to the conductivity peak compared to that of the smaller grain sizes. The current versus temperature curve corresponding to the former has a larger band width than that of the curve corresponding to the latter one. Dependence of I_{max} and T_{max} on the grain size was observed with other vapors and also with different ferrocene derivatives.

(ii) Similar to ferrocene (Fc-H)[8] in these derivatives also the rate of heating has an influence on the value of I_{max} as well as T_{max}. Figure 3 illustrates two conductivity curves for Fc-$COCH_3$ powders of same grain size on adsorption of ethanol vapor at 40 Torr pressure for

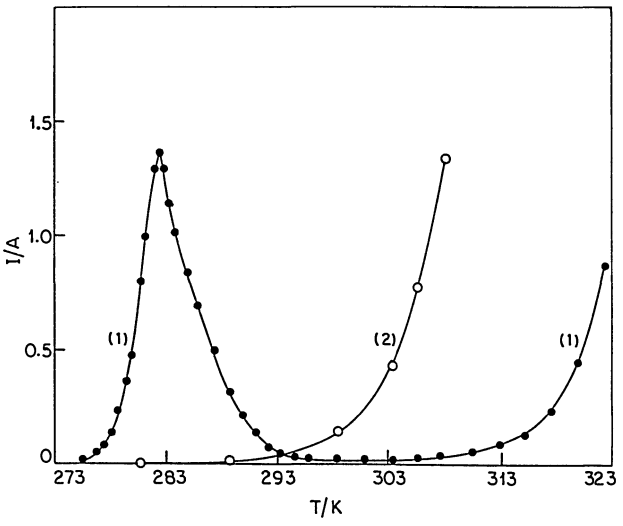

Fig. 1. Variation of dark current (conductivity) as a function of temperature in a powder cell of acetylferrocene:
1) with adsorption of toluene vapor at 30 Torr vapor pressure (left scale$\times10^{-9}$).
2) pure sample in dry nitrogen atmosphere (left scale $\times10^{-11}$).

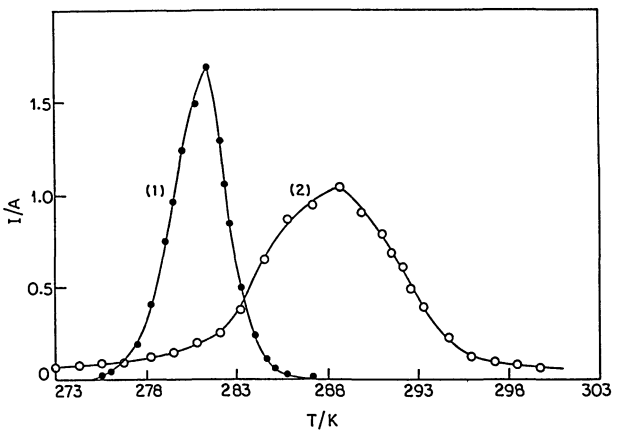

Fig. 2. Variation of dark current as a function of temperature in a powder cell of acetylferrocene with adsorbed ethanol vapor at 40 torr vapor pressure for two different grain sizes: (left scale$\times10^{-9}$)
1) smaller grain size (value of T_{max}=281.3 K),
2) bigger grain size (value of T_{max}=288.6 K).

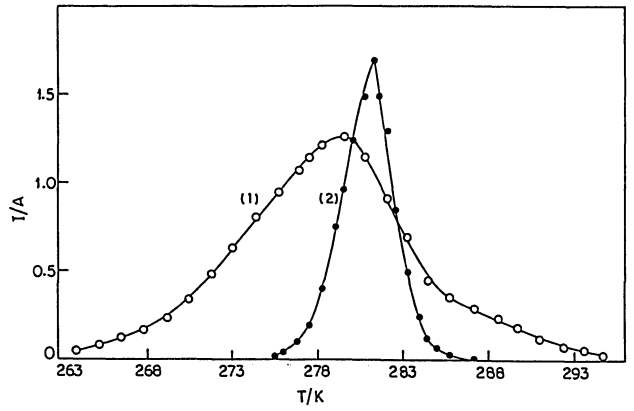

Fig. 3. Variation of dark current as a function of temperature in a powder cell of acetylferrocene with adsorbed ethanol at 40 Torr vapor pressure for two different heating rates: (left scale$\times 10^{-9}$)
1) heating rate: 0.02 K sec^{-1},
2) heating rate: 0.01 K sec^{-1}.

two different heating rates. In case of higher heating rate the conductivity peak appears at lower temperature (i.e., lower value of T_{max}) with a slightly lower value of I_{max}. But the conductivity curve in this case has a higher band width. In poly vinylalcohol, a spontaneous current emission induced by first heating run has been observed.[16] The presence of moisture in the material was thought to be the cause for such a current emission. Though the observed current versus temperature curves in case of poly vinylalcohol were very broad and different in nature from the present case, a shift of T_{max} towards lower temperature with increasing heating rate was also observed in that case as in the present experiment. The location of the conductivity peaks on the temperature scale depends on the heating rate. This is possibly due to the fact that the materials in the adsorbed state change their properties gradually over a certain temperature interval.

(iii) The dependence of I_{max} and T_{max} on the amounts of adsorbed vapors (i.e. on the vapor pressure of the adsorbed vapors) were studied for different ferrocene derivatives under study. Such a dependence is illustrated in Fig. 4 in case of Fc-$COCH_3$, where the values of dark current in a sample cell on adsorption of ethanol vapor at different vapor pressures are plotted as a function of temperature. In general it is observed that the peak value of current (I_{max}) increases with increasing vapor pressure and the temperature (T_{max}) corresponding to this peak value of current shifts a little towards the higher temperature side for larger amount of adsorbed vapors. Similar observations has been reported from the thermal desorption spectroscopic study for oxygen adsorption upon Ge surface.[17]

(iv) To study the effect of different vapors on I_{max} and T_{max} in case of a particular material experiments were performed with various vapors e.g. ethanol, methanol, 2-propanol, benzene, toluene, carbon tetrachloride etc. adsorbed at a fixed vapor pressure. (Benzene vapor solidifies at 278 K. But from the quick response of the current due to adsorption of benzene

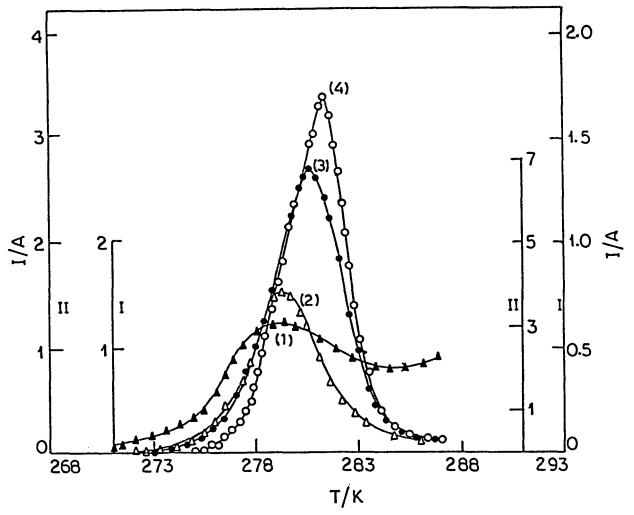

Fig. 4. Variation of dark current as a function of temperature in a powder cell of acetylferrocene with adsorption of ethanol vapor at different vapor pressures:
1) 12 Torr (left scale I$\times 10^{-12}$),
2) 22 Torr (left scale II$\times 10^{-11}$),
3) 30 Torr (right scale II$\times 10^{-11}$),
4) 40 Torr (right scale I$\times 10^{-9}$).

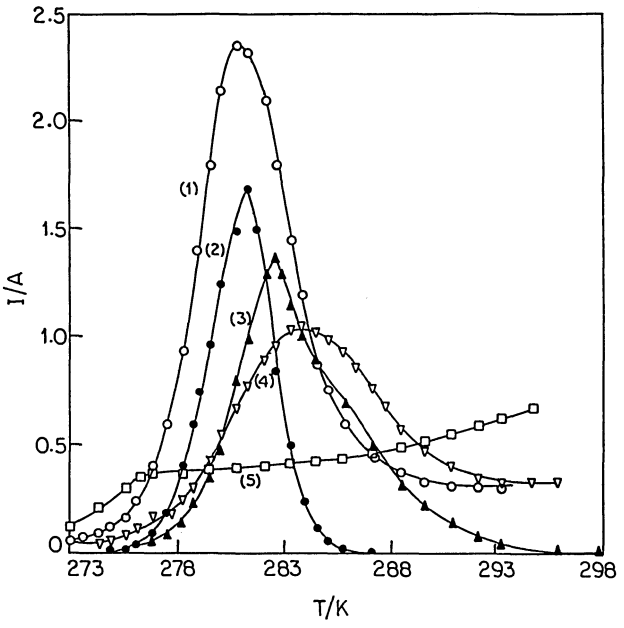

Fig. 5. Variation of dark current as a function of temperature in a powder cell of acetylferrocene with adsorption of different vapors at 40 Torr vapor pressure:
1) Benzene (left scale$\times 10^{-11}$),
2) Ethanol (left scale $\times 10^{-9}$),
3) Toluene* (left scale $\times 10^{-9}$),
4) Methanol (left scale $\times 10^{-11}$),
5) Carbon Tetrachloride (left scale$\times 10^{-12}$).
*Vapor pressure=30 Torr.

vapor upon the cell at 258 K and the similarity in the nature of the current response due to adsorption of other vapors of much lower freezing temperature it appears that the rate of adsorption is faster than the rate of freezing of benzene vapor). Results of such an experiment is shown in Fig. 5 for Fc-$COCH_3$. With the change of vapor, the change in I_{max} as well as T_{max} is evident from this figure (Fig. 5). In case of toluene vapor though the vapor pressure is less than the others, the current enhancement is comparable to (e.g. ethanol) or even higher than some other vapors (e.g. methanol, benzene). On adsorption of carbon tetrachloride vapor no sharp peak was observed. For the appearance of the conductivity peak, a particular vapor is sensitive (the sensitivity, S, may be defined as the ratio of the value of conductivity corresponding to the abovementioned peak and the value of the conductivity of the pure material without adsorption at the temperature corresponding to the peak) to different ferrocene derivatives to a different extent. This is illustrated in Fig. 6 which shows the variation of dark current with temperature for adsorption of ethanol vapor at 40 Torr vapor pressure on different materials. From this figure the effect of substituent groups on the electrical conductivity is evident. In case of Fc-H adsorbed with ethanol vapor, multiple conductivity peaks have been observed, but no such multiple peaks have been appeared in its derivatives. The effects of adsorption of various vapors on S and T_{max} in case of Fc-H and its different derivatives are summarized in Table 1 (corresponding values for Fc-H is also included for comparison). The following interesting observations may be noted from this table.

(a) For most of the adsorbed vapors the value of T_{max} as well as S in case of Fc-H is higher than the corresponding values for any derivative.

(b) In case of adsorption of different vapors in a particular compound the sequence of vapors for the enhancement of S does not correspond to the same sequence for the increase in T_{max}.

(c) For adsorption of a particular vapor in the different derivatives the increase or decrease in S is accompanied by a simultaneous increase or decrease in T_{max} (except for adsorption of benzene vapor in Fc-CHO).

(d) Either ethanol or 2-propanol shows the maximum value of S in these materials.

(e) In general, methanol shows the minimum value of S for these materials.

The experiments on adsorption of various vapors on various ferrocene derivatives under different measurement conditions indicate that the mechanism behind the appearance of the above mentioned conductivity peaks is expected to have a physical basis.

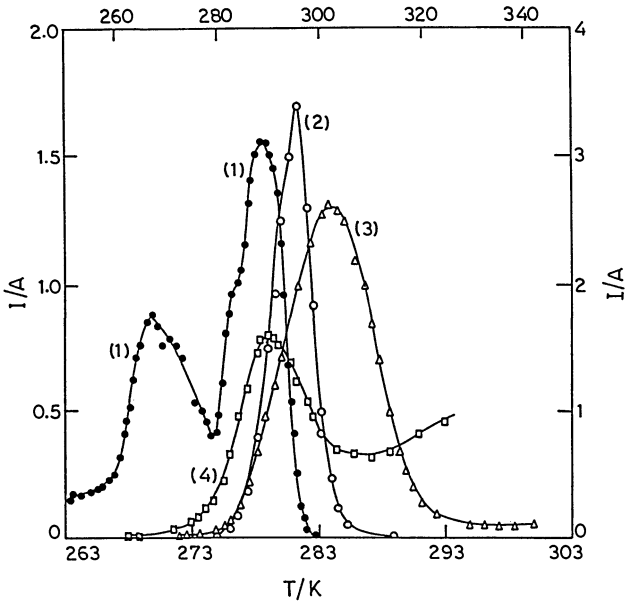

Fig. 6. Variation of dark current as a function of temperature in powder cells of different materials on adsorption of ethanol vapor at 40 Torr vapor pressure:
1) Ferrocene (right scale $\times 10^{-8}$, upper temperature scale),
2) Acetylferrocene (left scale $\times 10^{-9}$),
3) Ferrocenecarbaldehyde (right scale $\times 10^{-9}$),
4) Ferrocenecarboxylic acid (left scale $\times 10^{-11}$).

Table 1. The Values of S and T_{max}(K) for Adsorption of Different Vapors (at 40 Torr Vapor Pressure) on Ferrocene and Some of Its Derivatives at a Cell Temperature of 258 K

Vapors used	Values of ionization potential in eV [18]	Values of electron affinity in eV [19]	Values of dielectric constant at 298 K [12,20]	Different materials studied							
				Fc-H		Fc-COOH		Fc-CHO		Fc-$COCH_3$	
				S	T_{max}	S	T_{max}	S	T_{max}	S	T_{max}
Toluene[a]	8.81	0.820	2.379	4.28×10^4	298.5	5.95×10	280	2.87×10	279	3.42×10^3	282.5
Benzene	9.24	2.46	2.274	8.75×10^3	298	5.59×10^2	283	1.82×10^3	276	6.33×10	281
Ethyl acetate	10.11	—	6.02	6.25×10^2	280	1.07×10^2	279	6.15×10^2	276	—	—
Ethanol	10.5	0.594	24.0	1.5×10^5	289.5	4.76×10	279	5.65×10^3	283	4.52×10^3	281.3
2-Propanol	10.79	0.672	18.3	3.21×10^6	289	6.36×10^2	278	8.16×10^3	281	—	—
Methanol	10.85	0.377	32.63	0.045	298.5	—[b]	—	—	—	2.09×10	283.7
Carbon tetrachloride	—	1.215	2.228	3.2×10^4	295.2	1.2×10^2	280	3.25×10	279.5	1.8×10	276.3

a) Vapor pressure in this case is 30 Torr. b) A hump was observed in this case.

The electrical conductivity in organic as well as organometallic materials, charge-transfer complexes, and adsorption induced conductivity is usually expressed[7,13,21] by the Arrhenious relation

$$\sigma(T)=\sigma_0 \exp(-E/2kT), \quad (1)$$

where $\sigma(T)$ is the specific conductivity at any absolute temperature T, σ_0 is the pre exponential factor, E is the activation energy, and k is the Boltzmann constant. Experimentally E is obtained from the slope of the linear plot of $\log\sigma(T)$ or $\log I(T)$ versus $1/T$, where $I(T)$ is the current at the temperature T. As a representative curve the variation of $\log I(T)$ against reciprocal of temperature for a sample cell of Fc-$COCH_3$ with adsorbed toluene vapor is shown in Fig. 7 [curve(1)]. Usually a plot of $\log\sigma(T)$ or $\log I(T)$ versus $1/T$ gives a straight line in the low temperature region,[13,22] which shows the conduction properties of the solid material with adsorbed vapor. The slope of this line gives the activation energy of the material at the adsorbed state and the straight line at higher temperature region gives the activation energy of the pure material in vacuum or nitrogen atmosphere. Similar to the case of Fc-H,[8] in the present case also two different straight lines (AB and BC in curve 1 of Fig. 7) instead of one line have been observed at the adsorbed state and a transition from one line to another is prominent at the point B. The portion of the curve, DE represents the change in current due to desorption of vapors and the portion EF shows the conduction behavior similar to pure material in nitrogen atmosphere. The value of activation energy evaluated from the line EF is 3.7 eV which is equal to the activation energy of pure material in nitrogen atmosphere and these results show that the adsorption is a physical adsorption. The activation energy values evaluated from the portion AB and BC are 5.05 and 9.75 eV respectively. The value of σ_0 for pure Fc-$COCH_3$ is 1.76×10^{17} $\Omega^{-1}\,cm^{-1}$ and for the sample with adsorbed toluene vapor (corresponding to line BC in Fig. 7) at 30 Torr vapor pressure is about 4.48×10^{75} $\Omega^{-1}\,cm^{-1}$. Both the values of activation energy and σ_0 at the adsorbed state are anomalously high. Such an appearance of two straight lines is not a typical property for adsorption of a particular vapor only. For most of the vapors studied similar behavior was observed in each material. Figure 8 shows the appearance of such two straight lines in case of ethanol vapor adsorption on various ferrocene derivatives. The appearance of two straight lines possibly indicates that the adsorption is a two stage process.[24] Out of these two lines, the line at higher temperature (Fig. 8) gives the value of activation energy (E) which is in general much higher than the activation energy of the pure material. In Table 2 we

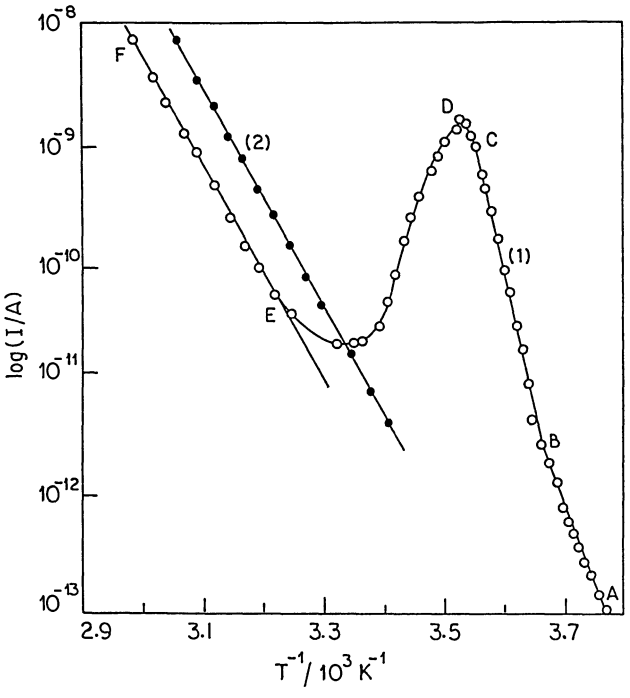

Fig. 7. Plot of logarithm of dark current vs. reciprocal of temperature for a powder cell of acetylferrocene:
1) with adsorption of toluene vapor at 30 Torr vapor pressure,
2) pure sample in dry nitrogen atmosphere.

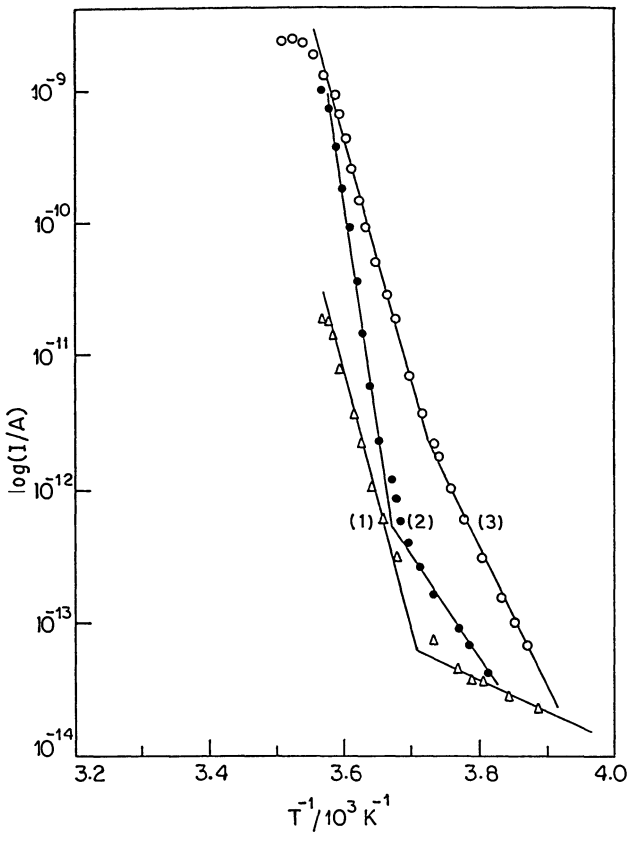

Fig. 8. Plot of logarithm of dark current vs. reciprocal of temperature at the low-temperature region for powder cell of different ferrocene derivatives with adsorption of ethanol vapor at 40 Torr vapor pressure:
1) Ferrocenecarboxylic acid,
2) Acetylferrocene,
3) Ferrocenecarbaldehyde.

Table 2. The Values of E (eV) and Corresponding σ_0 ($\Omega^{-1}\,cm^{-1}$) for Adsorption of Different Vapors (at 40 Torr Pressure) on Ferrocene and Some of Its Derivatives at a Cell Temperature of 258 K

Vapors used	Different materials studied							
	Fc-H		Fc-COOH		Fc-CHO		Fc-$COCH_3$	
	E	σ_0	E	σ_0	E	σ_0	E	σ_0
Carbon tetrachloride	10.37	9.07×10^{75}	4.33	1.99×10^{24}	3.75	5.95×10^{18}	4.3	4.34×10^{23}
Benzene	9.39	1.18×10^{68}	9.75	1.15×10^{74}	5.7	1.03×10^{39}	8.12	6.03×10^{58}
Toluene[a]	8.16	1.16×10^{58}	7.35	1.26×10^{52}	4.6	1.36×10^{27}	9.75	3.13×10^{75}
Ethyl acetate	7.5	7.87×10^{53}	7.22	1.72×10^{51}	4.75	6.11×10^{29}	—	—
2-Propanol[b]	—	—	7.3	7.09×10^{52}	5.62	3.97×10^{38}	—	—
Ethanol[b]	—	—	7.22	2.14×10^{53}	7.1	2.21×10^{51}	15.0	$>10^{99}$
Methanol	2.8	6.95×10^{18}	—	—	3.15	1.11×10^{15}	5.5	5.02×10^{44}

a) Vapor pressure is 30 Torr in this case. b) In case of ferrocene multiple peaks were observed, so these values could not be evaluated.

show the values of E evaluated from these lines along with some other parameters for adsorption of different vapors on these ferrocene derivatives. This table shows that the value of E and σ_0 are enormously high. These results are certainly unusual.

As the adsorption is a surface phenomenon the observed adsorption-induced change in the electrical conductivity of the solid materials arise mainly due to the change in surface conduction. When adsorption of vapors occurs, an exchange of charges takes place between the adsorbed molecules and the solid materials causing a change in surface electrical conductivity. It needs to be pointed out that depending on the extent of adsorption/absorption of vapors there is a possibility of formation of a solvated surface film (that may form and disappear at different temperatures) producing very high electrical conductivity. The variation of the solvated surface film with changing temperature may be related to the consequent change in conductivity. In fact, in case of the formation of solvated films, usually irreversible change is observed and it is more likely (as we have noticed also) that in a sandwich type of cell configuration due to solvation, the positive and negative electrodes will be short circuited by solvent molecules/dissolved materials. In the present experiment such a situation was carefully avoided by controlling the amount of adsorption (by adjusting the vapor pressure of the adsorbed vapor) and only the reversible adsorption-induced changes were considered. So, the appearance of the observed conductivity peak due to the formation of the solvated surface film can easily be ruled out.

The reason for the change in E in organic/organometallic semiconductors on adsorption of vapors is not yet well understood. The possible mechanism which is quite often considered is the formation of charge-transfer (CT) complexes[6,13] of adsorbed vapor molecules with the solid surface. Rosenberg et al.[23] proposed that such change in E on adsorption is associated with a change in effective dielectric constant of the material at the adsorbed state. We have checked the applicability of these theories and found that these theories are not suitable for the explanation of the change in E as well as conductivity.[8] Again the observed conductivity versus temperature curves look similar to the conventional glow curves (arise due to the thermally stimulated currents or TSC).[24] On adsorption of vapors, trapping states within the band gap of a semiconductor could be populated by charge carriers and consequently on heating TSC may appear due to detrapping of charge carriers.[25,26] But the values of trap depth calculated by the usual theory of TSC[24] are much higher than the activation energy values of the pure materials. So, the theory of TSC can not be considered as the possible mechanism behind the appearance of peak in the observed conductivity versus temperature curve under discussion.

From Eq. 1 it is clear that the increase in σ_0 is responsible for the increase in conductivity and σ_0 contains factors depending on temperature. The pre exponential factor σ_0 of the Eq. 1 can be expressed as[27]

$$\sigma_0 = qN\mu, \tag{2}$$

with

$$N = (N_A \cdot \rho \cdot Z)/M, \tag{3}$$

where q is the charge on the carrier, μ is the mobility, N_A is Avogadro's number, M is the molecular weight of the solid material, ρ is the density, and Z is the number of charge carriers available for excitation per molecule. The mobility of charge carriers for most organic and biological semiconductors usually lies[27] between 10 and 10^{-5} $cm^2\,V^{-1}\,sec^{-1}$. So a large change in σ_0 upon adsorption of vapors can not be considered due to the change in the mobility of these charge carriers in the sample in the adsorbed state. Thus the large value of σ_0 must be associated with a large density of activated charge carriers. In some organic materials an exponential temperature dependence of the charge carrier mobility has been observed.[28] The reported value of the mobility activation energy (E_μ) of a large number of organic materials lies between 0.20 and 0.77 eV.[28] Therefore, even if the exponential temperature depen-

dence of charge carrier mobility is considered, the anomalously large value of E remains unexplained.

It is known that a phase transition occurs in ferrocene under the influence of changes in external parameters like temperature[29] and pressure.[9] The ferrocene derivatives under investigation exhibit[14,15,30,31] various kinds of structural phase transitions associated with intermolecular interactions. From these observations it appears that a structural phase transition in these ferrocene derivatives due to interaction with various vapors in a suitable temperature range is not unlikely. Phase transition in the adsorption process has been reported in the literature.[32,33] It is reported[34] that as result of phase transition, the activation energy of some organic materials increases by a large amount and such phase transition is indicated by a deviation from the linearity of the $\log \sigma(T)$ or $\log I(T)$ versus $1/T$ plots. It is interesting to note that such a deviation from linearity has also been observed in the present case (Figs. 7 and 8). This adds further credence to the idea of adsorption-induced structural phase transition in these ferrocene derivatives. Such phase transitions depend on the nature of adsorbed vapors and these transitions are reversible on desorption of vapors. We have mentioned earlier that a large change in σ_0 (hence in σ) upon adsorption of vapors must be associated with a large density of activated charge carriers. The reason for such a large value of the density of activated charge carriers occuring upon a phase transition can be explained by concept of conformon,[35-37], which is considered as the activated charge carrier plus the accompanying conformational changes (here due to phase transition) carrying energy and entropy. By conformon concept Kemeny and Goklany[36] has suggested that the effective density of states for the activated charge carriers would be greatly increased due to interaction between the activated carriers and the vibrational degrees of the molecules. A change in the electronic state (as involved in transport) gives rise to an activation entropy ΔS because of a change in the vibrational frequency associated with a conformational change and this would contribute to the pre-factor σ_0. Thus, using proper thermodynamic quantities σ_0 can be written as[38]

$$\sigma_0 = A_1 \exp(\Delta S/2k) \cdot \exp(-\Delta H/2kT), \quad (4)$$

where A_1 is a constant, ΔS is known as activation entropy and ΔH is the activation enthalpy. Hence the process of current emission can be represented by the relation

$$\sigma(T) = A \exp(\Delta S/2k) \cdot \exp(-E^*/2kT), \quad (5)$$

where A is another constant and $E^* = (\Delta H + E_\mu + E)$, which accounts for the large value of activation energy in the present case.

The lattice dynamical nature of Fc-$COCH_3$, Fc-COOH, and some other ferrocene derivatives has been investigated[14,30] by some researchers in the solid state (in the tempearature range from 100 K to nearly melting point of these materials) by comparing their Mössbaur spectra with the crystal structure determined by X-ray diffraction spectroscopy. In these ferrocene derivatives the mean square amplitude of lattice vibration (thermal) of iron atoms measured from Mössbaur spectra has been observed[14,30] to be proportional to the absolute temperature nearly upto room temperature (300 K) indicating that the molecules are in harmonic lattice vibration; but a significant deviation has been found near the phase-transition temperature. From X-ray diffraction and Mössbaur spectroscopic studies Daniel et al.[31] have reported that Fc-CHO shows anomalous behavior near phase transition temperature (317 K). These results indicate a substantial modification in the lattice characteristics of the solid due to phase transition. Such phase transition has been thought[14,30,31] to be associated with a cooperative motion of different neighboring molecules. It has been suggested[14] that the orientational motion of Fc-$COCH_3$ may be hindered by interaction with neighboring molecules, for instance the steric hindrance of -$COCH_3$ groups which probably reduces the thermal motion. Two molecules of Fc-COOH have an intermolecular hydrogen bonding[30] between -COOH groups. In Fc-CHO, the -CHO side group is almost coplaner with the ring to which it is attached,[15] thus allowing conjugation of the π-electron system of the $>C=O$ bond and the aromatic cyclopentadienyl ring. As a result of different cooperative interactions, phase transition in different ferrocene derivatives (also in pure ferrocene) occurs at different temperatures. In the temperature range of present experiment the molecules of the pure ferrocene derivatives exhibit harmonic thermal vibration. But possibly due to the presence of adsorbed vapor molecules, the harmonic thermal vibration of the molecules of the ferrocene derivatives is perturbed and due to cooperative interaction such phase transition appears. As mentioned earlier, such adsorption-induced phase transition depends on the nature of the adsorbed vapor and also on the substitution group in a particular ferrocene derivative. In general methanol is less sensitive for the adsorption-induced changes. Though 2-propanol is good sensitive to most of the materials studied (Table 1), it is almost insensitive to Fc-$COCH_3$. Thus, the selectivity in the interaction of vapors with the different derivatives is evident from the observed results. In fact, the cooperative interaction which determines the phase transition is very complicated in nature[31] and it is not possible to correlate the nature of adsorption-induced phase transition with the presence of substituent group in the ferrocene derivatives at the present stage.

Thanks are due to Professor T. N. Misra of this department for his constant encouragement.

References

1) G. G. Roberts, B. Holeroft, A. Barraud, and J. Richard,

Thin Solid Films, **160**, 53 (1988).
2) A. Wilson and R. A. Collins, *Sens. Actuators,* **12**, 389 (1987).
3) H. Henrion, G. Derost, A. Ruaudel-Teixier, and A. Barraud, *Sens. Actuators,* **14**, 251 (1988).
4) P. N. Bartlett and S. K. Ling-Chung, *Sens. Actuators,* **19**, 141 (1989).
5) T. A. Jones, B. Bott, and S. C. Thorpe, *Sens. Actuators,* **17**, 467 (1989).
6) B. Rosenberg, T. N. Misra, and R. Switzer, *Nature,* **217**, 5127 (1968).
7) T. N. Misra, B. Rosenberg, and R. Switzer, *J. Chem. Phys.,* **48**, 2096 (1968).
8) B. Mallik and A. Bhattacharjee, *J. Phys. Chem. Solids,* **50**, 1113 (1989).
9) B. Karvally, B. Mallik, and G. Kemeny, *J. Mater. Sci. Lett.,* **4**, 912 (1985).
10) Y. Okamoto, J. Y. Chang, and M. A. Kantor, *J. Chem. Phys.,* **41**, 4010 (1964).
11) A. V. Maksimychev, V. A. Zhorin, A. T. Ponomerenko, and N. S. Enikolopjan, *Dokl. Acad. Nauk SSSR,* **241**, 593 (1978).
12) B. Mallik, A. Ghosh, and T. N. Misra, *Proc. Indian Acad. Sci., Sect. A, (Part 1),* **88**, 25 (1979).
13) B. Mallik, A. Ghosh, and T. N. Misra, *Bull. Chem. Soc. Jpn.,* **52**, 2091 (1979).
14) K. Sato, M. Katada, H. Sano, and M. Konno, *Bull. Chem. Soc. Jpn.,* **57**, 2361 (1984).
15) M. F. Daniel, A. J. Leadbetter, and M. A. Majid, *J. Chem. Soc., Faraday Trans. 2,* **77**, 1837 (1981).
16) A. U. Shareef, K. K. Saraf, and A. P. Srivastava, *Phys. Status Solidi A,* **77**, 381 (1983).
17) H. Froitzheim, "The Chemical Physics of Solid Surfaces and Heterogeneous Catalysis," ed by D. A. King and D. P. Woodruff, Elsevier Science Publishers, Amsterdam, Oxford, N. Y., and Tokyo (1988), Vol. 5, Chap. 5, p. 183.
18) F. Gutmann and L. E. Lyons, "Organic Semiconductors, Part A," John Wiley, New York (1967), p. 669.
19) F. Gutmann, H. Keyzer, and L. E. Lyons, "Organic Semiconductors, Part B," Robert E. Krieger Publishing Co., Malabar, Florida (1982), p. 506.
20) R. C. Weast, M. J. Astle, and W. H. Beyer, "CRC Hand Book of Chemistry and Physics," 65th ed, CRC Press, Boka Ration, Florida (1984—85), E 49.
21) H. Wotanabe, I. Motoyama, and K. Hata, *Bull. Chem. Soc. Jpn.,* **39**, 850 (1965).
22) B. Mallik, A. Ghosh, and T. N. Misra, *Phys. Status Solidi A,* **69**, 767 (1980).
23) Ref. 18, p. 497.
24) H. Mier, "Organic Semiconductor," Verlog Chemie, D-694 Weinheim (1974), p. 109.
25) A. J. G. Green, J. C. Bickerton, I. V. F. Viney, J. W. Brightwell, and B. Ray, *Solid State Commun.,* **62**, 543 (1987).
26) M. R. Grinter and C. Bowlt, *J. Phys. D, Appl. Phys.,* **9**, L61 (1976).
27) K. C. Kao and W. Hwang, "Electrical Transport in Solids," Pergamon Press, New York (1981), p. 37.
28) Ref. 19, pp. 484—492.
29) G. Calvarin, G. Clec'n, J. F. Berar, and D. Andre, *J. Phys. Chem. Solids,* **43**, 785 (1982).
30) K. Iwai, M. Katada, I. Motoyama, and H. Sano, *Bull. Chem. Soc. Jpn.,* **60**, 1961 (1987).
31) M. F. Daniel, A. J. Leadbetier, R. E. Meads, and W. G. Erker, *J. Chem. Soc., Faraday Trans. 2,* **74**, 456 (1978).
32) A. W. Adamson, "Physical Chemistry of Surfaces," John Wiley & Sons, New York, Chiechester, Brisbane, Toronto, and Singapure, p. 556.
33) L. Benedetti, M. Borsari, G. B. Gavioli, and C. Fontanesi, *J. Electroanal. Chem.,* **279**, 312 (1990).
34) Ref. 24, p. 278.
35) M. V. Volkenstein, *J. Theor. Biol.,* **34**, 193 (1972).
36) G. Kemeny and I. M. Goklany, *J. Theor. Biol.,* **40**, 107 (1973).
37) T. A. Kaplan and S. D. Mahanti, *J. Chem. Phys.,* **62**, 100 (1975).
38) D. V. Lang, "Thermally Stimulated Relaxation in Solids," ed by P. Braunlich, Springer, Berlin (1979), p. 127.

Fluorescence Quenching of Few Aromatic Amines by Chlorinated Methanes

Debabrata GOSWAMI, Ranjit S. SARPAL, and Sneh K. DOGRA*
Department of Chemistry, Indian Institute of Technology, Kanpur 208016, India
(Received February 1, 1991)

Fluorescence quenching of few aromatic amines; aniline (AB), 1-naphthylamine (1-AN), 2-naphthylamine (2-AN), 2,3-naphthalenediamine (2,3-DAN), 9-phenanthrenamine (9-AP), 1-pyrenamine (1-APy), 2-chrysenamine (2-AC), 6-chrysenamine (6-AC), and 3-fluoranthenamine (3-AF) by dichloromethane, chloroform, and carbon tetrachloride has been studied in cyclohexane and acetonitrile. The quenching rate constants (k_q) have been determined in both the solvents and these values are nearly independent of the solvent polarity. The values of k_q are nearly equal to diffusion-controlled limits (k_{diff}) for $CHCl_3$ and CCl_4 in both the solvents, whereas for CH_2Cl_2 it is three to four order of magnitude less than k_{diff}. For a given amine, k_q increases with the increase in electron affinity of the quencher, whereas for a given quencher (dichloromethane) k_q increases with the increase in singlet state energy of fluorophore. The results obtained are explained in terms of a quenching mechanism involving an intermediate donor–acceptor (DA)* complex formed between the excited aromatic amine and quencher.

In our recent study, regarding the effect of solvents on the absorption and fluorescence spectra of some aromatic amines,[1] it has been observed that the Stokes shifts [$\bar{\nu}_{abs}(max)-\bar{\nu}_{flu}(max)$], observed in the chlorinated methanes, do not follow the Lippert's equation and in some cases the fluorescence intensity was completely quenched in these solvents, especially the carbon tetrachloride. This indicates that there is some kind of specific interaction between these solvents and the aromatic amines. This kind of behavior has also been observed where the fluorescence of aromatic hydrocarbons,[2–5] ketones,[6,7] and heterocyclic[8,9] molecules has been quenched by halogenated alkanes.

In recent years, the quenching of fluorescence by these systems has been the focus of many investigations, as in the above-mentioned systems, energy transfer from aromatic hydrocarbons to halogenated alkanes are energetically not possible. In the above cases the fluorescence quenching of the fluorophores by the halogenated alkanes is observed without the appearance of any new fluorescence band. Thus in these cases, the formation of a transient excited-state complex as an intermediate in the fluorescene-quenching process is inferred on the basis of more indirect evidence. In any event, it seems clear that in those cases where the quencher possesses no low lying excited singlet state, which can be populated by dipole–dipole resonance transfer of energy from the excited fluorophore, the two molecules must approach one another at least to distances where the mutual interaction of the species is effective i.e. initial step in the fluorescence quenching process will be limited by the diffusion-limited approach of the excited fluorophore and quencher to form an encounter complex. Klein et al.[3] have postulated that halogenated alkanes form contact complexes as an intermediate which lie energetically above the S_1 state of the fluorophores and formation of this exciplex is considered as the rate-determination step in the excitation quenching process. The following equation was derived by Klein et al.[3] to express the quenching rate constant (k_q).

$$k_q \propto \exp[-(I.P.-E.A.-C-P-S_1)/k_bT], \quad (1)$$

where $I.P.$ are S_1 are the ionization potential and singlet state energy of the fluorophore, $E.A.$ is the electron affinity of the quencher, C is the coulomb energy, and P is the polarization energy of the separated charges, k_b is the Boltzman's constant.

The aim of the present study is to test the above model from two points i.e. to correlate (i) $\log k_q$ vs. ($IP-S_1$) for a single quencher and (ii) $\log k_q$ vs. $E.A.$ for a single fluorophore. For this purpose we have chosen nine aromatic amines; aniline (AB), 1-naphthylamine (1-AN), 2-naphthylamine (2-AN), 2,3-naphthalenediamine (2,3-DAN), 1-pyrenamine (1-APy), 9-phenanthrenamine (9-AP), 2-chrysenamine (2-AC), 6-chrysenamine (6-AC), and 3-fluoranthenamine (3-AF), and three different quenchers, dichloromethane, chloroform, and carbon tetrachloride.

Materials and Method

1-AN, 2-AN, 2,3-DAN, 2-AC, 6-AC, 9-AP, 3-AF, and 1-APy were procured from Aldrich Chemical Company. 1-AN, 2-AN, and 2,3-DAN were first crystallized from ethanol and were further purified by vacuum sublimation. 1-APy and 9-AP were purified by repeated crystallization from 50% ethanol (v/v) and ethanol respectively. Aniline (SD Fine Chem.) was purified by distilling under vacuum repeatedly. 2-AC, 6-AC, and 3-AF were purified by repeated crystallization from ethanol. The purity of the compounds was checked by noting the mp and comparing the spectral data with the literature data. Analytical grade cyclohexane (SD Fine Chemicals) and acetonitrile (E. Merck) were further purified according to literature procedures.[10] Spectroscopic grade dichloromethane, chloroform, and carbon tetrachloride (all BDH) were used as such. Chloranil and *p*-benzoquinone were procured from K and K Fine Chemicals. These compounds were further purified by repeated crystallization from acetone.

The absorption spectra were recorded on Shimadzu UV 190, equipped with U-135 chart recorder. Fluorescence measurements were carried out on scanning spectrofluorimeter, details are available elsewhere.[11] The concentration of the fluorophores used was of the order of 0.6—2.5×10^{-5} M (1 M=1

mol dm^{-3}), whereas those of chloroform and carbon tetrachloride varied from 0.001 to 0.7 M, except for 3-AF. Dichloromethane is a very poor quencher and thus very high concentration had to be used to get any meaningful fluorescence quenching.

Fluorescence lifetimes at 300 K were measured with the help of Applied Photophysics limited nanosecond fluorescence spectrofluorimeter (model SP-70/80) using time correlated single photon counting device. The electronic processing equipment was from Ortec. The pulse width of the flash lamp is ca. 4 ns and the convolution method was applied to determine the fluorescence lifetimes less than 10 ns.

Results and Discussion

Absorption Spectra. The absorption spectra of all the aromatic amines in cyclohexane and acetonitrile at various concentrations of chlorinated methanes do not change i.e. the band shape and full band width at half the absorbance remain same. This indicates that no complex formation between the amines and chlorinated quenchers are occuring in the ground state.

Fluorescence Spectra. The fluorescence spectra of all the aromatic amines in cyclohexane and acetonitrile at various concentration of chlorinated methanes were recorded. It has been observed that the fluorescence intensity of the fluorophore decreases with the increase of quencher concentration without the appearance of any other new fluorescence band. The fluorescence band shape and full width at half the maximum intensity did not change. Further, the fluorescence intensity as well as the absorbance of any solution containing highest concentration of quencher did not change when the spectrum was recorded after the experiment was carried out once. This indicates that no detectable photoproduct is formed under our experimental conditions. This could be due to the very small amount of quencher (less than 0.6 M) used and time used to excite the sample is also very small. Dichloromethane was the exception. In this case, the concentration of quencher used was upto 10 M. Even at such a high concentration of dichloromethane, no detectable amount of decomposition of aromatic amines is observed. Further, the Stern-Volmer plot for dichloromethane as a quencher, is linear and thus indicates that no ground state or contact complex between the fluorophore and dichloromethane is formed even at such a high concentration of the quencher.

The Stern-Volmer plot of the fluorescence quenching of 2-AN by CCl_4 is shown in Fig. 1. The plot is linear throughout the concentration of CCl_4 used.

$$\frac{I_o}{I} = 1 + K_{sv}[Q] = 1 + k_q\tau_o[Q] \quad (2)$$

where I and I_o are the fluorescence intensities of the fluorophore with and without the quencher Q, $K_{sv}=k_q\tau_o$ is the Stern-Volmer constant, k_q is the second order fluorescence quenching rate constant and τ_o is the lifetime of the fluorophore in the absence of quencher. Similar plots were observed for other fluorophores using different quenchers. The quenching rate constants k_q for the chlorinated methanes can be easily determined from K_{sv}/τ_o. The values of k_q in cyclohexane and acetonitrile as solvents are compiled in Table 1.

Different values of excitation wavelengths were used

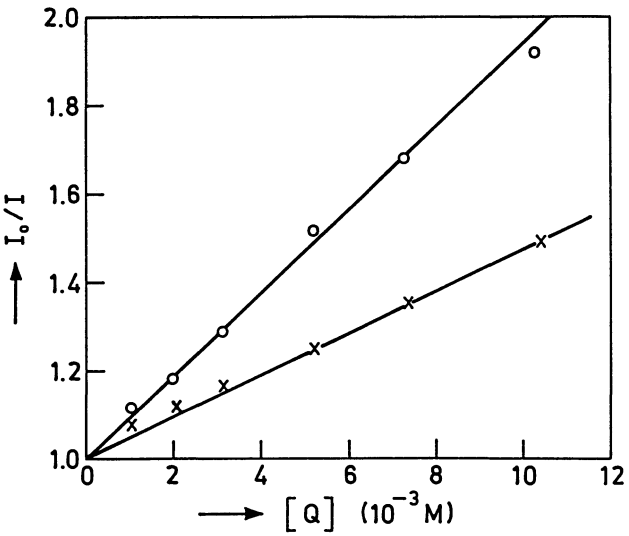

Fig. 1. Stern-Volmer plot of the fluorescence quenching of 2-AN by CCl_4 at 298K. —○—, CH_3CN; —×—, cyclohexane.

Table 1. Singlet State Energy (E_s), Lifetimes (τ_o, ns) and Quenching Rate Constants ($M^{-1}s^{-1}$) for Various Aromatic Amines in Cyclohexane and CH_3CN

S. No.	Compound	E_s	τ_o	k_q(Cyclohexane)			τ_o	k_q(CH_3CN)		
		eV	ns	CH_2Cl_2 ($\times10^6$)	$CHCl_3$ ($\times10^9$)	CCl_4 ($\times10^9$)	ns	CH_2Cl_2 ($\times10^6$)	$CHCl_3$ ($\times10^9$)	CCl_4 ($\times10^9$)
1	AB	4.1	4.3	885	13.1	15.50	5.1	212	11.83	14.20
2	1-AN	3.54	5.98	7.94	3.37	10.08	8.6	—	2.24	10.26
3	2-AN	3.72	6.2	8.82	1.89	7.59	7.3	4.52	1.12	10.11
4	2,3-DAN	3.51	6.8	2.94	2.10	11.76	4.9	2.14	4.45	10.36
5	9-AP	3.28	10.6	0.57	0.69	6.06	7.7	—	0.74	10.14
6	1-APy	3.12	5.6	0.13	0.23	10.02	4.3	3.93	0.60	10.33
7	2-AC	3.06	7.5	—	0.046	8.03	5.4	—	0.049	15.71
8	6-AC	3.06	7.5	—	0.049	6.55	6.0	—	0.0695	17.95
9	3-AF	2.80	8.1	—	0.001	0.046	8.8	—	—	0.147

for 1-AN–$CHCl_3$ system and it was found that the Stern–Volmer plot (thus K_{sv}) did not depend upon the excitation wavelength above 300 nm, (λ_{exc}=300 nm, K_{sv}=20.1 M^{-1}; λ_{exc}=325 nm, K_{sv}=19.6 M^{-1}; λ_{exc}=335 nm, K_{sv}=20.45 M^{-1}). This indicates that no distinct complex formation between $CHCl_3$ and 1-AN in the ground state is observed. Though no similar study has been carried out with other compounds, similarity of the absorption spectra of these compounds with each other does indicate that no ground-state complexes are formed in these systems also. This has also been manifested from the study of absorption characteristics as said earlier. But these results are different from those of anthracene and CCl_4,[2,3] where it has been shown that the photoproducts are formed.

A popular mechanism, generally used to explain the fluorescence quenching has the following reaction scheme:

$$A + h\nu \longrightarrow A^* \tag{2}$$

$$A^* + Q \underset{k_2}{\overset{k_1}{\rightleftarrows}} (AQ)^* \xrightarrow{k_3} A + Q \tag{3}$$

$$(AQ)^* \xrightarrow{k_f} A + h\nu_f, \qquad (AQ)^* \xrightarrow{k_I} A$$

where A, Q and $h\nu$ represent the fluorophore, quencher and the light quantum, A* and (AQ)* are the excited states of the fluorophore and of the encounter complex between A* and Q respectively, k's reaction rate constants, k_f and k_I are the rate constants for radiative and nonradiative decay processes. The apparent quenching rate constant k_q, for the collisional quenching process can be given by

$$K_q = \gamma k_1, \tag{4}$$

where γ is the efficiency of the quenching reaction, which is given by $k_3/(k_2+k_3)$ approaches unity if $k_2 \ll k_3$ (the quenching process is very fast) or it approaches k_3/k_2 when not every encounter between Q and A* results in quenching. Thus the values of $k_q=k_1$ in the former case and k_1k_3/k_2 in the latter case. As said earlier, fluorescence quenching process in the present case requires that the fluorophore and the quencher should approach each other, the maximum value of k_1 can be equal to the diffusion controlled limits. The values of k_1 thus determined, using the modified Debye equation[12] ($8RT/3000\eta$, where η is viscosity of the medium in centipoise, R is a gas constant and T the temperature in Kelvin) are found to be 9.8×10^9 $M^{-1}s^{-1}$ and 1.8×10^{10} $M^{-1}s^{-1}$ in cyclohexane and acetonitrile respectively.

The data of Table 1 clearly indicate that fluorescence quenching rate constants for all the aromatic amines by CCl_4 are nearly equal to the diffusion-controlled rate constant (k_{diff}) whereas the quenching efficiency of CH_2Cl_2 is three to four orders of magnitude less than CCl_4 and that of $CHCl_3$ is between CH_2Cl_2 and CCl_4. The quenching rate constants even in case of CH_2Cl_2 is considerably faster than can be accounted for chemical quenching (for example, the rate constant of alkyl radicals with CCl_4 does not exceed 10^4—10^5 $M^{-1}s^{-1}$, see Ref. 3). The data of Table 1 thus clearly indicate that quenching is believed to proceed via an intermediate donor-acceptor (DA)* complex formed between the excited aromatic amine and quencher and not by classical energy transfer. To test the validity of this model, Eq. 1 can be varified from two angles as mentioned below:

i) Equation 1 reduces to

$$k_q \propto \exp[-(\text{const} - E.A.)/k_bT],$$

i.e.
$$\log k_q = \text{const} + \frac{E.A.}{2.303\,k_bT}, \tag{6}$$

if the fluorophore is kept the same but quencher is varied. Figure 2 depicts the plot of $\log k_q$ vs. $E.A.$ Although the number of quenchers are only three, it is clear from Fig. 2 that plot is a curve for each amine and it levels off to a diffusion controlled rate constant. Though quantitatively we cannot get much information, qualitatively it is clear that k_q increases with increase of $E.A.$ of the quencher. Similar behavior has been observed in case of fluorescence quenching of aromatic molecules by inorganic ions.[14–17]

ii) Equation 1 reduces to Eq. 7 if we choose different fluorophores and one quencher,

$$k_q \propto \exp[-(I.P. - S_1 - \text{const})/k_bT],$$

or
$$\log k_q = \text{const} + \frac{S_1 - I.P.}{2.303\,k_bT}, \tag{7}$$

The singlet state energy of all the aromatic amines were calculated by taking the average of the long wavelength band maximum of absorption spectrum and short wavelength band maximum of fluorescence spectrum in cyclohexane. This is because in this solvent, the interactions between the solvent and the fluorophore is minimum. These values are compiled in Table 1.

The ionization potential data for all the aromatic amines are not available, except for AB, 1-AN, and 2-AN[18] (i.e. 7.7, 7.3, and 7.25 eV respectively). The experiments were carried out to calculate the ionization potentials of aromatic amines by measuring the energy of the charge-transfer band (E_{CT}) of the molecular complexes formed by these amines with different electron acceptor molecules (e.g. chloranil and benzophenone).

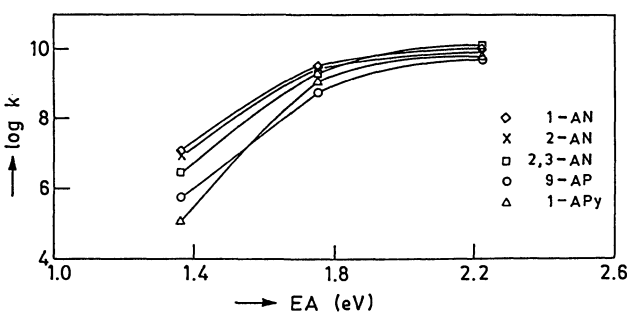

Fig. 2. Plot of $\log k_q$ vs. electron affinity of the quencher, in cyclohexane.

Unfortunately no charge-transfer bands were observed with these acceptor molecules, though simple empirical relations are available to relate the energy of the CT band and *I.P.* of donor molecule. With the limited data available, it is clear that we cannot assume that *I.P.*'s are constant for these amines. However in the absence of *I.P.* values, $\log k_q$ versus singlet state energy of the fluorophores, for CH_2Cl_2, $CHCl_3$, and CCl_4 as quenchers, in cyclohexane and acetonitrile are depicted in Fig. 3. The plots are linear for CH_2Cl_2 and $CHCl_3$ in cyclohexane and acetonitrile, with slopes 3.5 and 2.5 in the former solvent and 2.0 and 1.5 eV^{-1} in the latter solvent, whereas for CCl_4, the plots are horizontal to *x*-axis. The linear correlation suggests that *C* and *P* values are practically constant. The above results further suggest that the *I.P.* of these aromatic amines are proportional to the singlet state energy (i.e. $I.P.-S_1$), thus leading ($S_1-I.P.$) to $(1-a)\ S_1$ where '*a*' is a constant of proportionality. The above results are consistent with the fact that the values of the quenching rate constants are limited by the singlet state energy of the fluorophore so long these are less than k_{diff}. Once the value of k_q is equal to k_{diff}, k_q will be independent of either E_S or *E.A.* The values of slopes obtained in case of CH_2Cl_2 or $CHCl_3$ are much less than the theoretical value [i.e. $1/(2.303\ k_bT)=16.78\ ev^{-1}$].

Thus the above results suggest that fluorescence quenching for these aromatic amines does not occur via charge-transferred state. As said earlier quenching could proceed via an intermediate donor-acceptor (DA)* complex formed between the excited aromatic amine and quencher.

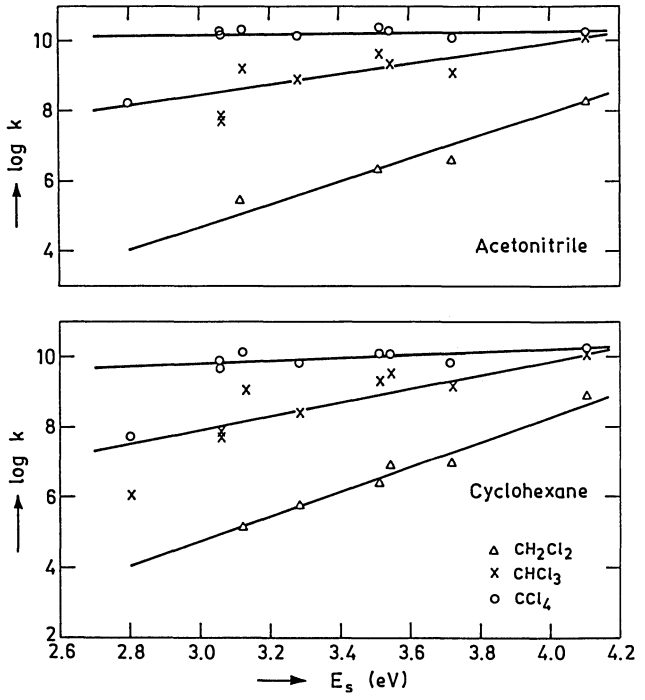

Fig. 3. Plot of log k_q vs. singlet state energy of aromatic amines. (a) Cyclohexane (b) Acetonitrile.

The value of k_q observed for 3-AF is much less than that can be predicted from the $\log k_q$ vs. S_1 plot. Our earlier results[23] have indicated that proton-induced fluorescence quenching of neutral 3-AF is much less than that generally observed in other aromatic amines,[24-28] with few exceptions.[29,30] This indicates that charge transfer character in S_1 state of 3-AF is very less and thus the transfer of charge from 3-AF to chlorinated methanes will not be efficient process.

The results of dichloromethane using as an electron acceptor have indicated that the fluorescence intensity as well as shift in fluorescence band maximum of the donor molecule is observed when the concentration of CH_2Cl_2 is more than 5 M and thus can be explained in term of a change in the rate of unimolecular photoprocesses induced by the change in solvent. At very high concentration of CH_2Cl_2 its effect as a solvent (and the decrease in k_q due to the decrease in the polarity) is more significant than the change in the quencher concentration (i.e. $k_q[Q]$ decreases with increase in [Q]). Similar dependence has also been observed in other systems.[22]

Conclusion. In conclusion, we consider that the dominant quenching pathway involves an intermediate donor-acceptor (DA)* complex formed between the excited aromatic amine and quencher molecules.

The authors are thankful to the Department of Science and Technology, New Delhi for financial support.

References

1) S. Mazumdar, R. Manoharan, and Sneh K. Dogra *J. Photochem. Photobiol. A,* **46**, 301 (1989).

2) a) C. Lewis and W. R. Ware, *Chem. Phys. Lett.*, **15**, 290 (1972). b) W. R. Ware and C. Lewis, *J. Chem. Phys.*, **57**, 3546 (1972).

3) J. Klein, V. P. Plazanet, and G. Laustriat, *J. Chim. Phys. Physiochim. Biol.*, **67**, 302 (1970).

4) D. Saperstein and E. Levine, *J. Chem. Phys.*, **62**, 3560 (1975).

5) M. V. Encinas, M. A. Rubio, and E. A. Lissi, *J. Photochem.*, **18**, 137 (1982).

6) J. O. Pavlik, P. I. Plogard, A. C. Sommsall, and J. E. Guillet, *Can. J. Chem.*, **51**, 1435 (1973).

7) R. O. Loutfy and A. C. Somersall, *Can. J. Chem.*, **54**, 760 (1976).

8) G. E. Johnson, *J. Phys. Chem.*, **84**, 2940 (1980).

9) T. Takahashi, K. Kikuchi, and H. Kokubun, *J. Photochem.*, **14**, 67 (1980).

10) J. A. Riddick and W. Bunger, "Organic Solvents," Wiley Interscience, New York (1970), pp. 632, 695, 801.

11) M. Swaminathan and S. K. Dogra, *Indian J. Chem., Sect. A,* **22**, 853 (1983).

12) J. G. Calvert and J. N. Pitts, "Photochemistry," Wiley, New York (1966), p. 627.

13) F. W. Billmeyer, "Textbook of Polymer Science," Wiley, New York (1971), pp. 293—301.

14) H. Shizuka, T. Saito, and T. Morita, *Chem. Phys. Lett.*, **56**, 519 (1976).

15) H. Shizuka, M. Nakamura, and T. Morita, *J. Phys.*

Chem., **84**, 989 (1980).
16) T. Moriya, *Bull. Chem. Soc. Jpn.*, **57**, 1723 (1984); **59**, 961 (1986).
17) K. A. Addullah and T. J. Kemp., *J. Chem. Soc., Perkin Trans. 2*, **1985**, 1279.
18) J. B. Birks, "Photophysics of Aromatic Molecules," Wiley, New York (1970), p. 408.
19) J. C. Scanio, *J. Am. Chem. Soc.*, **102**, 7747 (1980).
20) H. Leonhardt and A. Weller, *Z. Physik. Chem., N. F.*, **29**, 277 (1961); *Ber. Bunsen-Ges. Physik. Chem.*, **61**, 791 (1963).
21) T. Miwa and M. Koizumi, *Bull. Chem. Soc. Jpn.*, **38**, 529 (1965).
22) T. Miwa and M. Koizumi, *Bull. Chem. Soc. Jpn.*, **39**, 2588 (1966).
23) A. K. Mishra and S. K. Dogra, *J. Chem. Soc., Perkin Trans. 2*, **1984**, 943.
24) H. Shizuka and K. Tsutsumi, *J. Photochem.*, **9**, 304 (1978).
25) K. Tsutsumi, S. Setaguchi, and H. Shizuka, *J. Chem. Soc., Faraday Trans. 2*, **78**, 1087 (1982).
26) K. Tsutsumi and H. Shizuka, *Z. Phys. Chem.* (*Munich*), **111**, 129 (1978).
27) H. Shizuka, *Acc. Chem. Res.*, **18**, 141 (1985).
28) A. K. Mishra and S. K. Dogra, *J. Photochem.*, **23**, 163 (1983); A. K. Mishra and S. K. Dogra, *Bull. Chem. Soc. Jpn.*, **58**, 3587 (1985).
29) H. Shizuka, T. Ogiwara, and E. Kimuea, *J. Phys. Chem.*, **89**, 4302 (1985).
30) A. K. Mishra and S. K. Dogra, *Indian J. Chem., Sect. A*, **24**, 364 (1985).

 © 1991 The Chemical Society of Japan Bull. Chem. Soc. Jpn., 64, 3142—3152 (1991)

Solvatochromism and Prototropism in 2-(Aminophenyl)benzothiazoles

Joy Krishna Dey and Sneh K. Dogra*
Department of Chemistry, Indian Institute of Technology, Kanpur 208016, India
(Received February 12, 1991)

The absorption and fluorescence spectra of 2-(2-aminophenyl)-, 2-(3-aminophenyl)-, and 2-(4-aminophenyl)benzothiazoles (*o*-APBT, *m*-APBT, and *p*-APBT, respectively) have been studied in different solvents and at various acid/base concentrations. The ultraviolet and fluorescence spectra and the low pK_a value for the monocation–neutral equilibrium have indicated the presence of an intramolecular hydrogen bond (IHB) in *o*-APBT in the S_0 state. Excited state intra-molecular proton transfer (ESIPT) in *o*-APBT, gives rise to a non-fluorescent phototautomer. Large solvatochromic shifts in polar solvents have indicated the increase in the dipolemoment of *m*-APBT in S_1 state. It has been observed that in protic solvents, *m*-APBT forms a complex with solvent molecule in the S_1 state. The equilibrium constants for different prototropic equilibria of the molecules have been determined in both S_0 and S_1 states. The absorption and fluorescence spectra of the prototropic species have been explained and compared with those of 2-phenylbenzothiazole (2-PBT). The monocation (**2**) of *p*-APBT, formed by protonation at the $-NH_2$ group is found to undergo structural reorganization leading to a quinonoid structure (**2'**). The absorption and fluorescence excitation spectra (recorded at 390 nm and 460 nm fluorescence bands) indicate the simultaneous presence of species (**2**) and (**2'**), the former being more favorable in protic and the latter in nonpolar solvents. The molecular orbital calculation (PPP) has been used to calculate the absorption spectra and the charge densities at the basic centers of the neutral molecules.

The study of photophysical properties of heterocyclic organic molecules has achieved considerable importance recently because many of these molecules form an integral part of biologically important compounds and have various uses. Substituted 2-arylbenzothiazoles, although having industrial and commercial uses as fluorescence whitening agents,[1a] photoconducting materials,[1b] and as herbicides in agriculture, have not received much attention. Only 2-(2-hydroxyphenyl)-benzothiazole[2] has been studied extensively and the excited state intramolecular proton transfer (ESIPT) has been well discussed. The present study is centerd on the prototropism and solvatochromism of *o*-APBT, *m*-APBT and *p*-APBT. Since the amino group is strong electron donor in the excited state, the position of the fluorescence spectrum may exhibit a pronounced solvent dependence, but the absorption spectrum is almost insensitive to the nature of the solvent. The importance of this type of molecules (i.e. aromatic amines) in biological studies has led to intensive investigation of the origin of the polar-solvent-induced fluorescence red shift.

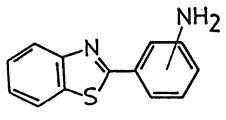

$-NH_2$ at 2'-
3'-
4'-

In our recent studies on (aminophenyl)benzimidazoles[3] and (aminophenyl)benzoxazoles,[4] it has been shown that 2-(2-aminophenyl)benzimidazole[3b] (*o*-APBI) exhibits a dual fluorescence in hydrocarbon solvents, whereas, the corresponding benzoxazole derivative[4] (*o*-APBO) gives only a single normal fluorescence band. The dual fluorescence in the former, has been attributed to a phototautomer formed by ESIPT process. The absorption spectra of the monocations of both *p*-APBI and *p*-APBO showed a large red-shifted band along with the blue-shifted band, the origin of which was unknown until the present study. The monocations of *o*-APBO, *m*-APBO, and *p*-APBO were found to undergo biprotonic phototautomerism in the S_1 state.

In order to understand these processes we have undertaken this investigation to include a detailed analysis of the electronic absorption and emission spectra of *o*-APBT, *m*-APBT, and *p*-APBT including 2-PBT and their prototropic species. In addition we have carried out molecular orbital calculation (PPP-SCF-MO-CI) to aid the interpretation of our experimental results.

Experimental

The compounds under study were synthesised by heating *o*-aminothiophenol and corresponding aminobenzoic acid in polyphosphoric acid at 200 °C and purified as described for (aminophenyl)benzoxazole.[5] The purity of the compounds was confirmed by TLC, melting point and excitation spectra recorded in methanol monitoring at different emission wavelengths. Analytical grade cyclohexane (SDS), dioxane (E. Merck), acetonitrile (E. Merck), methanol (BDH), and dichloromethane (E. Merck) were further purified as described elsewhere.[6] Analytical grade ethanediol (SDS) and glycerol (SDS) were used directly. Hexane (SRL), ethyl acetate (SDS), chloroform (SDS), and carbon tetrachloride (SDS) were all spectro grade. KOH, H_2SO_4, and ortho-H_3PO_4 used, were of analytical grade.

Aqueous pH solutions were made by mixing appropriate amounts of dilute (10^{-3} M, M=mol dm^{-3}) KOH and H_3PO_4 solutions. Solutions of pH<3 and pH>12 were made following Hammett's[7a] acidity (H_o) and Yagils[7b] basicity scales (H_-). Because of low aqueous solubility of the compounds, the solutions were prepared in methanol–water mixture containing 0.5% (v/v) methanol and the concentration of the solute was 5×10^{-6} M. Fluorescence quantum yields were calculated

for solutions having absorbance <0.1 at the excitation wavelength, and referred to the quinine sulfate in 0.05 M H_2SO_4 (ϕ_f=0.55).[7c] For fluorimetric titrations the solutions were excited at the isosbestic point.

Absorption spectra were measured in a Shimadzu UV-190U spectrophotometer equipped with a 135U chart recorder. Fluorescence spectra were recorded in a scanning spectrofluorimeter fabricated in our laboratory and the details of which are described elsewhere.[8] The pH measurements have been carried out with a Toshniwal Digital pH meter, model CL 46 fitted with a combined glass electrode (Toshniwal) operating in the range of pH 0 to 12.

Molecular orbital calculations were performed on our Institute's Dec-1090 computer. The program[9] for the calculations was obtained from QCPE, Indiana University, Blumington, USA.

Results and Discussion

1. Effect of Solvent on Absorption and Fluorescence Spectra. In Table 1, the absorption properties of the molecules in several organic solvents are indicated. Apart from the shoulder to the lower energy side of the longest wavelength band (ca. 293 nm), the absorption spectrum of *m*-APBT resembles that of 2-phenylbenzothiazole (PBT).[10] The lowest energy band of *p*-ABPT appears at a wavelength higher than that of *m*-APBT. The absorption spectrum of *o*-APBT is quite different from those of other molecules in the sense that apart from the common band (ca. 290 nm) another large red shifted band appears at 365 nm, which disappeared when the solution was made acidic (pH<3.0). These features are exactly analogous to that of *o*-APBI[3b] and *o*-APBO.[4] The second lowest energy absorption band of *o*-APBT is structured in hydrocarbon solvents and becomes broad in polar protic solvents. With the increase of solvent polarity the absorption maxima of the molecules remain almost unchanged except in *o*-APBT where the longest wavelength band shifts to the blue in protic solvents.

Fluorescence spectral data are collected in Table 2. The fluorescence spectra of *m*-APBT and *o*-APBT are broad and structureless, whereas that of *p*-APBT in hydrocarbon solvents is structured. The fluorescence spectra, unlike absorption spectra in all the cases shift to red as the solvent polarity and proton donor/acceptor capacity increased in going from cyclohexane to water. The order of emission energies, *o*-APBT<*m*-APBT<*p*-

Table 1. Absorption Band Maxima (λ_a) and Molar Extinction Coefficients ($\log\varepsilon$) of *o*-APBT, *m*-APBT, and *p*-APBT in Different Solvents and of Different Prototropic Species

Solvent	*o*-APBT		*m*-APBT		*p*-APBT		Solvent	*o*-APBT		*m*-APBT		*p*-APBT	
Species	λ_a	($\log\varepsilon$)	λ_a	($\log\varepsilon$)	λ_a	($\log\varepsilon$)	Species	λ_a	($\log\varepsilon$)	λ_a	($\log\varepsilon$)	λ_a	($\log\varepsilon$)
1	2		3		4		1	2		3		4	
Hexane	375	sh	328	sh	338	sh	1,2-Ethanediol	369		335		335	
	362	(4.12)	293		327					299			
	315	(3.68)			310								
	303	(3.89)					Glycerol	367		337		335	
	289	(4.10)								300			
	280	(4.03)					Water (pH 6.3)	351	(4.05)	325	sh	333	(4.41)
								289	(4.06)	297	(4.26)		
Cyclohexane	375	sh	328	sh	338	sh							
	363	(4.12)	294		329		Carbon tetra-	375	sh	328	sh	332	(4.49)
	315	(3.52)			310		chloride	365	(4.15)	297	(4.18)		
	304	(4.04)						300	sh				
	290	(4.12)						291	(4.16)				
	280	(4.05)						281	(4.15)				
Acetonitrile	367	(4.11)	330	sh	336	(4.54)	Dichloro-	366	(4.31)	330	sh	332	(4.56)
	315	sh	295	(4.27)			methane	300	sh	295	(4.22)		
	304	sh						291	(4.32)				
	289	(4.11)						280	sh				
	280	sh					Chloroform	366	(4.11)	329	sh	332	(4.49)
Dioxane	370	(4.16)	334	sh	337	(4.54)		300	sh	297	(4.17)		
	300	sh	296	(4.27)				291	(4.11)				
	291	(4.16)						280	sh				
	282	sh					Monocation	303[a]	(4.32)	300[b]	(4.28)	392[c]	(3.86)
Ethyl acetate	372	(4.07)	333	sh	337	(4.5)		250	—	250	—	300	(4.22)
	300	sh	295	(4.27)								251	—
	290	(4.07)											
	281	sh					Dication	310	(4.22)	320	(4.33)	320	(4.37)
							(H_0 −4.0)	252	—	256	—	257	—
Methanol	367	(4.09)	336	sh	334	(4.56)							
	315	sh	294	(4.24)									
	289	(4.14)											

a) at pH 0.5. b) at pH 2.0. c) at pH 1.5.

Table 2. Fluorescence Band Maxima, λ_f(nm) and Fluorescence Quantum Yields (ϕ_f) of *o*-APBT, *m*-APBT, and *p*-APBT in Different Solvents and of Different Prototropic Species

Solvent	*o*-APBT		*m*-APBT		*p*-APBT	
Species	λ_f	ϕ_f	λ_f	ϕ_f	λ_f	ϕ_f
Hexane	—	—	380	0.28	385(sh) 375 360(sh)	0.33
Cyclohexane	410	<0.001	380	0.29	385(sh) 375 360(sh)	0.36
Acetonitrile	435	0.074	440	0.20	400	1.0
Dioxane	425	0.07	420	0.20	395	1.0
Ethyl acetate	435	0.067	430	0.18	400	
Methanol	440	0.132	475	0.14	410	1.0
1,2-Ethanediol	443		490		415	
Glycerol	435		490		418	
Water (pH 6.2)	450	0.22	503	0.06	420	0.97
Carbon tetrachloride	420	0.001	390		385	
Dichloromethane	425	0.011	413	0.141	395	1.0
Chloroform	425	0.011	417	0.13	390	0.82
Monocation	390[a]	0.015	390[b]	0.027	443[c]	<0.001
Dication (H_o −4.0)	420		425	0.027	415	0.022

a) at pH 0.5. b) pH 2.0. c) pH 1.5.

to the resonance interaction of the lone pair of the amino nitrogen atom with the π cloud of the parent hydrocarbon. This interaction increases if an electron withdrawing group is attached at the para position. Thus the nature of electron withdrawing group at the para position decides the percentage charge transfer character in the π→π* transition as well as the value of band maximum. The large red shift observed in the longest wavelength absorption band of *p*-APBT, as compared to that in *m*-APBT, can be attributed to the presence of electron withdrawing group at the para position of aniline and thus leading to the resonance structure **II′** as shown below. This is reflected in the high absorption coefficient (ε_{max}, Table 1) of the lowest energy band, large ϕ_f value (ca. 1.0) and the structured fluorescence band in nonpolar solvents. The presence of structure **II′** can be further established from acid-base behavior of this molecule (see below).

II II′

Scheme 1.

APBT, in cyclohexane changes to the order, *m*-APBT<*o*-APBT<*p*-APBT in polar/protic solvents. The luminescence of *o*-APBT in all the solvents as well as in cyclohexane glass at 77 K exhibits a single fluorescence band at ca. 400 nm.

The fluorescence quantum yield (ϕ_f) of *p*-APBT is almost unity in all the solvents, whereas those of *o*-APBT and *m*-APBT are very rlow. *o*-APBT is weakly fluorescent (ϕ_f<0.001) in hydrocarbon solvents and the ϕ_f increases as the solvent polarity is increased. The ϕ_f value decreases for *m*-APBT with the increase of polarity.

Spectral studies of 2-arylbenzoxazoles and corresponding benzothiazoles by Passarini[10] have indicated that the aryl group acts as the main chromophore and its electronic transitions are perturbed by the benzazole moiety. Our experimental studies as well as molecular orbital (MO) calculations (CNDO/s and PPP) on 2-phenylbenzoxazole[11] have confirmed earlier results and have shown that both HOMO and LUMO are localized mostly on the phenyl ring and only partly on the oxazole ring. This means that the longest wavelength transition originates from the phenyl ring. Since benzoxazole and benzothiazole are isoelectronic, their electronic spectra are expected to be similar. Thus, the (aminophenyl)benzothiazoles can be considered as substituted anilines.

The electronic spectra of arylamines have been studied extensively[12–14] and the red shift produced in the absorption spectra of the parent hydrocarbon is due

Even though the amino group in *m*-APBT is nonconjugated with the electron withdrawing benzothiazole group, the fluorescence spectrum, in contrast to absorption spectrum, is large red shifted. This may be due to larger dipole moment of the fluorophore in the S_1 state upon excitation (section 2). The red shift observed in the fluorescence spectrum in protic polar solvents is anomalously large and could be attributed to the formation of 1 : 1 solvent–solute complex in S_1 state. This is based on the fact that (i) the Stokes shift observed in just 0.5% (v/v) methanol–cyclohexane mixture (where the properties of the solution will be close to cyclohexane) is 6210 cm^{-1} as compared to 8500 cm^{-1} in 100% methanol and (ii) full width at half maximum height of fluorescence band in cyclohexane (2959 cm^{-1}) is quite different from that in 0.5% methanol–cyclohexane solution (5640 cm^{-1}). The similar behavior has been observed in 5-aminoindazole[16a] and other aromatic amines.[16,17] This solute–solvent interaction enhances the stability of the singlet and thereby decreasing the S_1–T_1 energy gap, which in turn increases the probability of intersystem crossing.[18] This fact explains the decrease of ϕ_f value in *m*-APBT with the increase of solvent polarity in going from cyclohexane to water.

The geometry of the molecule suggests the formation of an intramolecular hydrogen bond (IHB) between the pyridinic nitrogen atom and one of the amino protons (conformer IA) in *o*-APBT. We feel that the longest wavelength band is due to the hydrogen-bonded structure IA. This is because the presence of IHB in *o*-

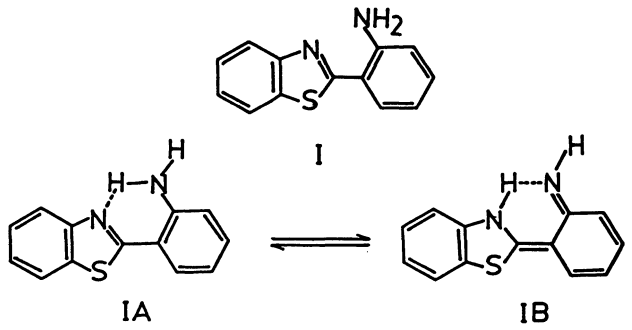

Scheme 2.

APBT will force the lone pair of the amino group to be parallel with the π-cloud and thereby increases the resonance character of this group with the benzothiazole moiety. The blue shift observed in protic solvents can be attributed to the partial breaking of the IHB as a result of competition with the intermolecular hydrogen bond formation with the solvent molecules. Similar behavior has also been observed in case of *o*-APBI[3b] and *o*-APBO[4] and can be explained on the same lines.

It is well known that the amino proton becomes strong acid and the tertiary nitrogen atom strong base in S_1 state. Along with the presence of IHB, this will facilitate the proton transfer giving rise to the phototautomer, IB. Since the rate of ESIPT is very high[2] (ca. 10^{12} s^{-1}) and the activation energy is very low (ca. 120 cm^{-1}), an emission band corresponding to the phototautomer can be expected especially in nonpolar solvents. In contrast, only a weak normal Stokes shifted broad band at 400 nm has been observed in hydrocarbon solvents, as in *o*-APBO.[4] But in case of *o*-APBI,[3b] a dual fluorescence was observed in cyclohexane. This indicates that the phototautomer IB is formed but it is nonfluorescent. It is reported[15] that the ESIPT increases the rate of internal conversion 100 times. The very low ϕ_f (<0.001) of normal Stokes shifted fluorescence band in hydrocarbon solvents proves the conversion of IA→IB. Because of the formation of a solvated complex and breaking of IHB (a prime condition for ESIPT) in polar and protic solvents, the rate of ESIPT is reduced. As a result, ϕ_f of *o*-APBT increases as the solvent polarity increases.

2. Correlation of Solvatochromic Shift with the Solvent Polarity. The variation of Stokes shift with the solvent polarity can be represented by the Lippert[19] equation

$$\bar{\nu}_{ss}=\frac{2(\mu_e-\mu_g)^2}{hca^3}f(D,n)+C, \quad (1)$$

where $\bar{\nu}_{ss}$ is the Stokes shift ($\bar{\nu}_{ss}=\bar{\nu}_a-\bar{\nu}_f$, $\bar{\nu}_a$ and $\bar{\nu}_f$ are the absorption and fluorescence maxima, respectively), μ_g and μ_e are respectively the ground and excited state dipole moments of the solute molecule, '*a*' is the "Onsager cavity radius" and $f(D,n)$ is the "Onsager polarity function" defined by the equation

$$f(D,n)=\frac{D-1}{2D+1}-\frac{n^2-1}{2n^2+1}, \quad (2)$$

where D is the static dielectric constant and n is the refractive index of the solvent; C is a constant. The other polarity parameter used is an empirical parameter $E_T(30)$; this is based on the spectral shifts of *N*-phenolbetaine,[20,21] in different solvents of varying polarity and hydrogen bonding.

In this study, the Stokes shifts of the three molecules determined in eleven solvents of varying polarity have been correlated with the $f(D,n)$[22] and $E_T(30)$[23] parameters. Table 3 gives a list of solvents, corresponding polarity parameters and the Stokes shifts. The very good linearity found in the plot of $\bar{\nu}_{ss}$ vs. $f(D,n)$, Fig. 1, in aprotic solvents (except dioxane and chloromethanes) indicates that the unspecific interactions are the key factors in shifting the fluorescence maxima to the red, for these molecules. As evident from the slopes of the plots, these interactions are large in case of *m*-APBT and may be attributed to its increase of dipole moment on excitation. Rigid molecules with limited internal degrees of freedom change the structure of the solvent cage by their dipole moment change in the excited state. This process induces a large Stokes shift in polar solvents. This is true in nonviscous solvents, where the

Table 3. Stokes Shifts of *o*-APBT, *m*-APBT, and *p*-APBT in Different Solvents and Polarity Parameters

Number	Solvent	$f(D,n)$[a]	$E_T(30)$[b]	$\bar{\nu}_{ss}/cm^{-1}$		
			kcal mol^{-1}	*o*-APBT	*m*-APBT	*p*-APBT
1	Cyclohexane	−0.001	31.07	3160	4170	3610
2	Hexane	0.002	31.0		4170	3610
3	Dioxane	0.02	36.0	3500	6130	4360
4	Ethyl acetate	0.201	38.09	3900	6690	4630
5	Acetonitrile	0.305	46.0	4260	7580	4760
6	Methanol	0.309	55.5	4520	8710	5550
7	1,2-Ethanediol	0.276	56.3	4530	9440	5850
8	Glycerol	0.264	57.0	4260	9270	5940
9	Water	0.320	63.1	6270	10770	6220
10	Dichloromethane	0.218	41.1	3800	6090	4760
11	Chloroform	0.149	39.1	3800	6410	4480

a) Values taken from Ref. 22. b) Values taken from Ref. 23.

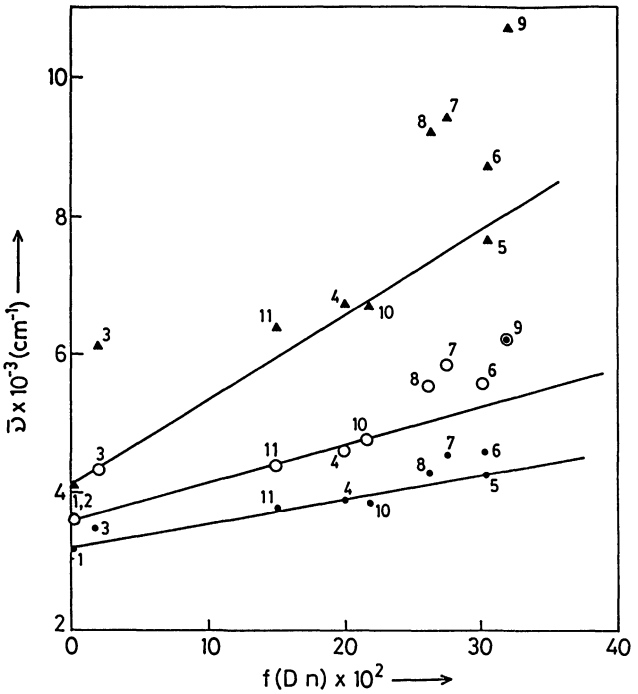

Fig. 1. Plot of $f(D,n)$ parameters revsus $\bar{\nu}_{ss}$ in different solvents: —●— *o*-APBT, —▲— *m*-APBT, and —○— *p*-APBT.

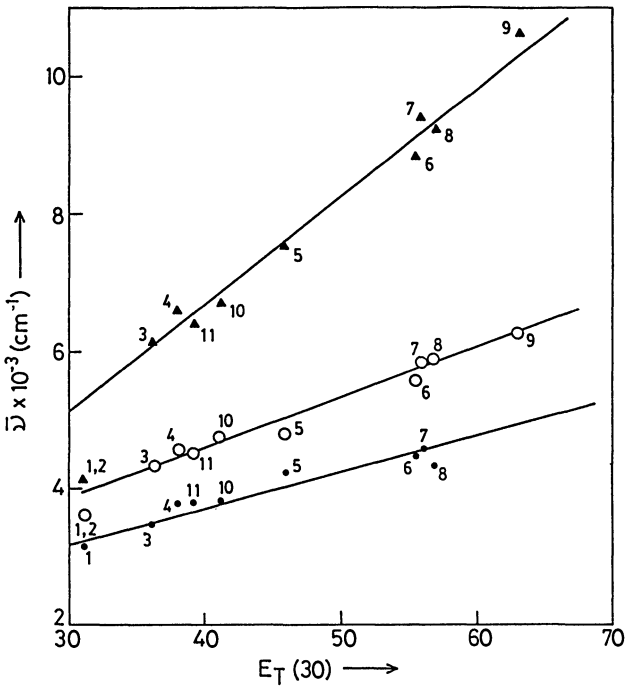

Fig. 2. Plot of $E_T(30)$ parameters versus $\bar{\nu}_{ss}$ in different solvents: —●— *o*-APBT, —▲— *m*-APBT, and —○— *p*-APBT.

rate of solvent relaxation (ca. 10^{12} s^{-1}) is faster than the fluorescence rate (10^9—10^{11} s^{-1}). But in a viscous solvent like glycerol (where the relaxation time is of the order ca. 10^{-9} s) or in a polar solvent at 77 K, the solvent relaxation can not occur during the lifetime of the excited state. The fluorescence spectrum of *m*-APBT in glycerol is broad and has the same shape as in nonviscous solvents and no blue shift is observed compared to other solvents at 300 K. This clearly indicates that the solvent relaxation is still faster than the rate of fluorescence. The anomaly in the solvatochromic shift in dioxane and protic solvents may be a result of hydrogen bond formation between the specific sites of the solute and solvent molecules giving rise to 1 : 1 complex as explained earlier.

A good correlation of Stokes shift with the $E_T(30)$ scale (Fig. 2) is indicative of the fact that the dielectric solute–solvent interactions as well as specific solute–solvent interactions, as discussed above, are responsible for the solvatochromic shifts in the molecules. The Stokes shifts observed for these molecules in chloroform and carbon tetrachloride correlate with none of the polarity scales. It is well known that chlorinated methanes quench the fluorescence of fluorophores by forming a CT in the S_1 state,[24] which may be a reason for the deviation complex of the Stokes shift from linearity of solvatochromic plots in Figs. 1 and 2.

Since the position of fluorescence maximum of *m*-APBT has shown much more solvent dependence than the other molecules, we have also investigated the fluorescence properties of this molecule in dioxane–water mixtures. The dioxane–water mixtures provide a wide range of $E_T(30)$ values and allow a convenient solvent system to probe nonspecific effects on fluorescence maximum. The solvent compositions and the corresponding $E_T(30)$ values alongwith the fluorescence maxima are listed in Table 4. A plot of $\bar{\nu}_f$ versus $E_T(30)$ values (Fig. 3) shows very good correlation. This type of effect has been reported earlier and is attributed to the increasing solvation of the solute molecules in its S_1 state by water molecules which impart an enhanced solvent structuring effect.

Table 4. Fluorescence ($\bar{\nu}_f$) Maxima of *m*-APBT in Different Dioxane–Water Mixture and Corresponding $E_T(30)$ Values

Composition number	% (v/v) Dioxane	$E_T(30)$[a] / $\times 10^3$ cm^{-1}	$\bar{\nu}_f$ / cm^{-1}
1	100	12.59	23809
2	98	14.48	22471
3	94	15.56	22222
4	92.5	15.95	21978
5	90	16.33	21505
6	80	17.14	21276
7	70	17.80	21052
8	60	18.29	20920
9	50	18.74	20618
10	40	19.44	20408
11	30	20.00	20408
12	20	20.49	20202
13	10	21.30	20000
14	0	22.00	19880

a) Values taken from Ref. 22.

3. Effect of Hydrogen Ion Concentration. The absorption and fluorescence spectra of all the molecules are studied in various acid-base concentrations in the H_0/pH/H_- range of −10.4 to 16.0 at room temperature (300 K). The spectral properties of their different prototropic species are collected in Tables 1 and 2, and the spectra are shown in Figs. 4 and 5. The behavior of these molecules in the above range of acid-base region is similar, except for *p*-APBT in the pH range of 5 to 1. This will be discussed separately.

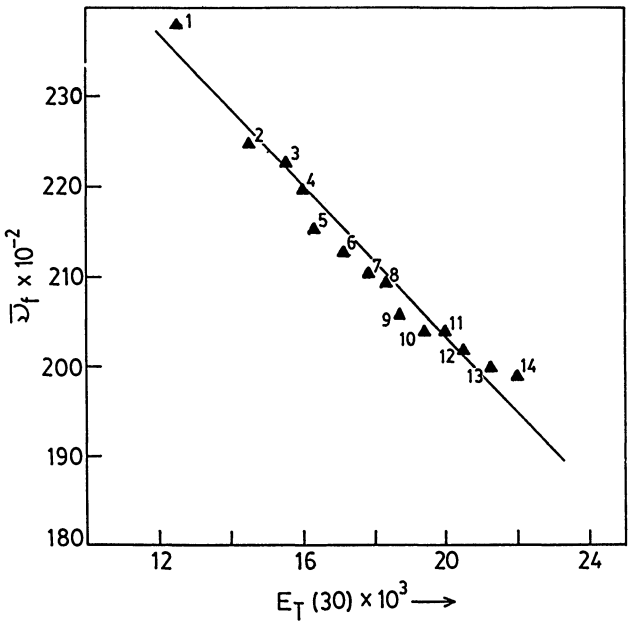

Fig. 3. Plot of $E_T(30)$ parameters versus $\bar{\nu}_f$ in dioxane-water mixtures.

The absorption spectra of *m*-APBT remains unchanged in the pH/H_- range of 5 to 16, but the fluorescence intensity decreases above pH 9. Because of insolubility, neither *o*-APBT nor *p*-APBT could not be studied in the basic media. We attribute the decrease of fluorescence intensity of *m*-APBT with increase of pH to the formation of nonfluorescent monoanion, because the anion formed by the deprotonation of amino group in general is nonfluorescent with few exceptions.[25]

All the molecules are neutral between pH 9 to 5. The blue shift in the absorption and fluorescence spectra and the resemblance of the spectra of these species with those of neutral 2-PBT at pH 4 (λ_a=299 nm, λ_f=380 nm) indicate the formation of monocation as a consequence of the protonation at the amino group. Our theoretical calculations also indicate that the charge density (Table 6) at the amino nitrogen is greater than that at the nitrogen atom of the heterocyclic ring in the S_0 and S_1

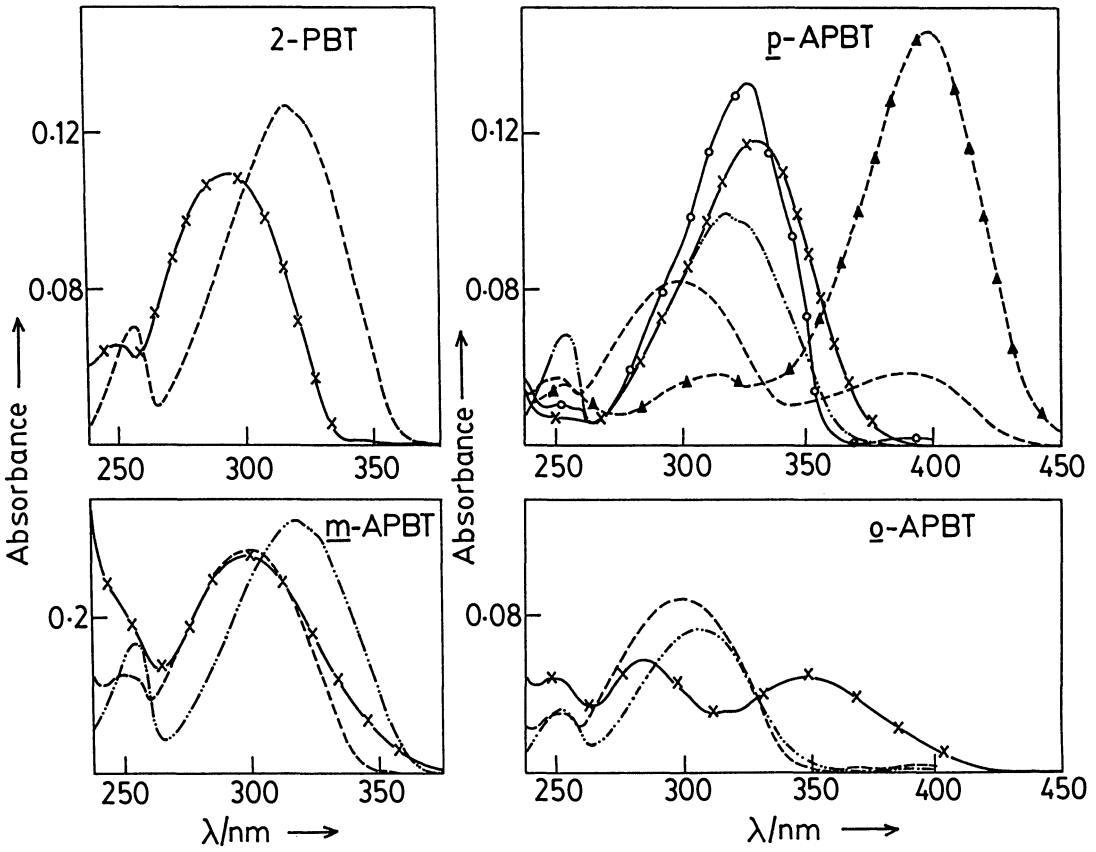

Fig. 4. Absorption spectra of the prototropic species of 2-PBT, *o*-APBT, *m*-APBT, and *p*-APBT; —×— Neutral; —— Monocation; —··— Dication; —▲— Monocation (in cyclohexane); —○— Neutral in cyclohexane.

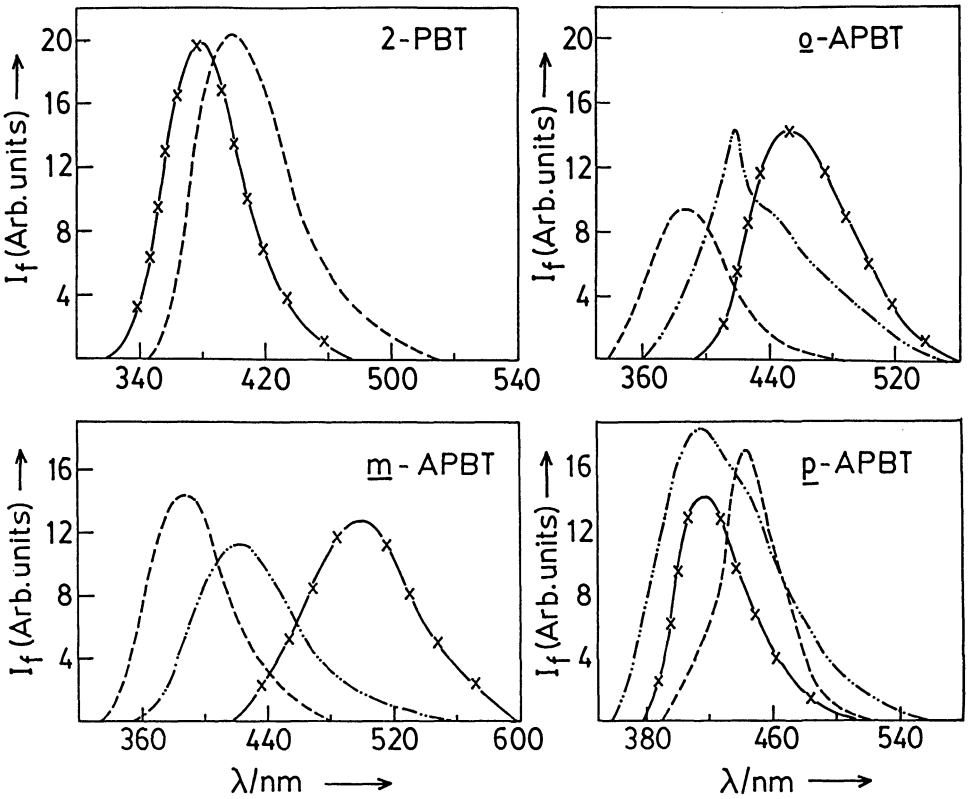

Fig. 5. Fluorescence spectra of the prototropic species of 2-PBT, *o*-APBT, *m*-APBT and *p*-APBT: —×— Neutral; —— Monocation; —··— Dication.

states. The red shift in both the absorption and fluorescence spectra of the monocation below pH 0.5 is due to the dication, formed by the protonation of the pyridinic nitrogen atom and is confirmed by their similarity with the monocation spectra of 2-PBT (λ_a=320 nm, λ_f=400 nm).

The absorption and fluorescence spectral characteristics of *p*-APBT in acidic media are interesting and quite different from those of *o*-APBT and *m*-APBT. With the increase of [H^+] (>10^{-4} M) the intensity of the 333 nm absorption band decreases and at pH 1.5, it is replaced by a large red-shifted band at 392 nm and a blue-shifted band at 300 nm. The intensity of the longest wavelength band is weak compared to the blue-shifted band in aqueous medium. The spectra exhibit two isosbestic points (300 nm and 368 nm). When the titration was carried out in cyclohexane with trifluoroacetic acid, the absorption spectrum of the species (Fig. 4) exhibits the longest wavelength band with much higher intensity compared to the blue shifted band. Further increase of acid concentration shifts the short wavelength band to red side and the lowest energy band is vanished. The absorption spectrum at H_o—4.0 resembles that of the monocation of 2-PBT.

The isosbestic points in the absorption spectra clearly indicate that only two species are involved in the equilibrium. This is also substantiated by the fact that the pK_a values calculated by measuring the intensity change at 390 and 330 nm are exactly same. The pK_a value for this equilibrium (3.0) is not very different from those of *o*-APBT (2.6) and *m*-APBT (3.4). This suggests, and also supported by the charge densities (Table 6) at the basic centers that the species at pH 1.5 is the monocation formed by protonation at the amino group. But, as can be seen from Fig. 4, the monocation spectrum does not resemble the absorption spectrum of 2-PBT. Similar behavior has also been observed in 2-, and 4-aminoquinolines,[26] 4-aminopyridine,[27] and 2-aminobenzimidazole.[28] We feel that the monocation **2** is formed by the same way as discussed in case of *o*-APBT or *m*-APBT and then undergoes a structural reorganization as shown in Scheme 3, leading to the species **2′**. In aqueous medium, the species **2** being highly solvated, this reorganization may be difficult and hence the species **2′** will have less contribution in the ground state. But in cyclohexane, the solvation is less and thus the species **2′** will be more favorable which is exhibited by the higher intensity of the longest wavelength band in

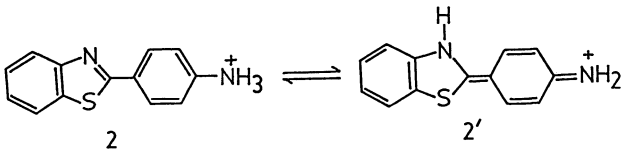

2 2′

Scheme 3.

the monocation spectrum. As the [H^+] is increased, the equilibrium is shifted towards the left and the second protonation occurs at the heterocyclic nitrogen atom giving rise to dication **3**. The resemblance between the absorption spectrum of *p*-APBT at H_o—4.0 and the absorption spectrum of the monocation of 2-PBT supports our explanation.

The fluorescence spectra, recorded for solutions in the pH range (in which the ground state equilibrium exists) by exciting at both the isosbestic points, show a gradual decrease in intensity of the 420 nm band and simultaneous appearance of 390 nm band as shoulder (only noticeable at pH 2.0) with the increase of [H^+] until pH 0.5. The band width at half maximum also increases with increase of acid concentration. When the solutions having pH<3.0 were excited at 400 nm (where the neutral molecule does not absorb) a weak fluorescence band appears at ca. 445 nm, the intensity of which increases with the decrease of pH. The fluorescence excitation spectra at pH 1.5, recorded by monitoring the fluorescence maximum at 390 and 460 nm are different from each other. The former consists of a single band matching with the monocation absorption spectrum of *o*-APBT or *m*-APBT and the latter one consists of two bands at 390 and 340 nm matching with the absorption spectrum of the monocation. The ca. 300 nm absorption band may thus be due to a mixture of species **2** and **2′**. The full width at half maximum observed for the absorption and fluorescence excitation spectra are different form each other and thus supports our conclusion. Analogous to *o*-APBT and *m*-APBT the fluorescence band at 390 nm can be assigned to the fluorescence from monocation **2** having low fluorescence quantum yield. Thus the 445 nm band may be due to the species **2′**. The increase of fluorescence intensity of the 445 nm with further increase of [H^+] can be attributed to the formation of dication **3**. This is because the fluorescence band maxima of the dications of other amines and the monocation of 2-PBT are also nearly at the same wavelength and are formed at the same acid concentration. This suggests that structural reorganization of species **2′** takes place before the dication **3** is formed and thus leading to same emission band maxima. The similar behavior has also been observed in 2-aminobenzimidazole[28] and 2- and 4-aminoquinolines.[26,27]

Table 5. Ground and Excited State pK_a Values for the Various Prototropic Reactions of *o*-APBT, *m*-APBT, *p*-APBT, and 2-PBT

Equilibrium	pK_a	pK_a^* [a]		
		Abs	Flu	Ft
o-APBT				
Dication⇄Monocation	−1.8	−0.2	2.0	
Monocation⇄Neutral	2.6	−6.9	−4.6	
Neutral⇄Monoanion	>16	—	—	
m-APBT				
Dication⇄Monocation	0.07	4.5	4.8	0.5
Monocation⇄Neutral	3.4	−3.4	−8.9	
Neutral⇄Monoanion	>16	—	—	12.4
p-APBT				
Dication⇄Monocation	0.1	—	—	
Monocation⇄Neutral	3.0	—	—	
Neutral⇄Monoanion	>16	—	—	
2-PBT				
Monocation⇄Neutral	0.7			1.0

Abs: Calculated from absorption spectra, Flu: Calculated from fluorescence spectra, Ft: Fluorimetric titration.

4. Acidity Constants. The pK_a values for different prototropic equilibria (Scheme 4) of the molecules have been determined using absorption data and are collected in Table 5. Since *p*-APBT is resonance stabilized (Scheme 1), the electron density at the amino nitrogen will be low which is reflected by the low pK_a value (3.0) for the monocation–neutral equilibrium compared to that (3.4) of *m*-APBT. The very low pK_a value for the monocation–neutral equilibrium in *o*-APBT than those of other molecules is due to the IHB formation. The pK_a value for the monocation–neutral equilibrium in 2-PBT is greater than the pK_a values for the corresponding dication–monocation equilibria of the amino derivatives. This is due to the presence of the $-\overset{+}{N}H_3$ group in their monocations, which withdraws electron density from the heterocyclic ring. Since, the $-\overset{+}{N}H_3$ group is more closer to the ⩾N atom in *o*-APBT, the decrease of electron density on ⩾N is more compared to other molecules. As a result, the pK_a for the dication-monocation equilibrium is less than that of *m*-APBT which is again lower than that of *p*-APBT.

The pK_a* values for the corresponding equilibria of the molecules including 2-PBT have also been determined by fluorimetric titrations and by Forster cycle calculations, wherever applicable. The results thus obtained are consistent with our conclusions that $-NH_2$ group becomes less basic and pyridinic nitrogen (⩾N) more basic on excitation to the S_1 state. Consequently,

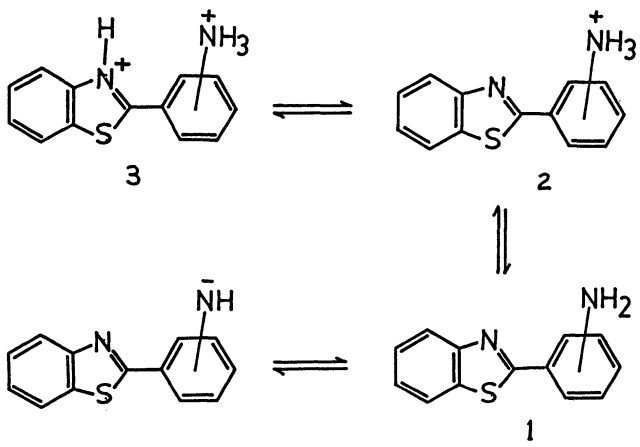

Scheme 4.

Table 6. Calculated Transition Energies (λ), Oscillator Strengths (f), Transitions Polarizations (α°) and Charge Densities at the Basic Centers of *o*-APBT, *m*-APBT, and *p*-APBT

Molecules	Transition energy(λ) (nm)	Oscillator strength (f)	Polarization (α°)[a]	π-Electron Density					
				Ground state			Excited state		
				S_1	N_3	N_{16}	S_1	N_3	N_{16}
1	2	3	4	5	6	7	8	9	10
	335	0.9286	359	1.5132	1.4332	1.9247	1.583	1.434	1.9
o-APBT(I)	303.8	0.3065	244						
	282	0.093	127						
	245.8	0.1277	98						
	346.5	0.9523	353	1.4846	1.680	1.919	1.501	1.728	1.8
o-APBT(IA)	298.0	0.189	284						
	290	0.1458	115						
	240	0.4855	312						
	327	0.9877	349	1.515	1.419	1.934	1.593	1.408	1.9
m-APBT	306	0.2855	233						
	284.9	0.1113	279						
	246	0.0682	100						
	333	1.1795	352	1.519	1.4229	1.9334	1.583	1.430	1.922
p-APBT	304	0.235	243						
	267	0.330	79						
	249	0.103	63.8						

a) α° is the angle made by the total transition moment vector with the positive direction of the long axis (directed towards the phenyl ring) of the molecule, measured anti-clockwise.

the pK_a*(1.0) is greater than pK_a(0.7) for 2-PBT. In other molecules fluorimetric titrations have resulted more or less the ground state pK_a values for the monocation–neutral equilibrium. This may be either due to the nonestablishment of the prototropic equilibrium in the S_1 state or no change occurring in pK_a value upon excitation. At present we are unable to specify which one of these mechanisms is playing the role.

The pK_a* values calculated by using the absorption band maxima and fluorescence band maxima are large and differ much from each other. This can be attributed to the difference in solvent relaxation of the conjugate acid-base pair in the S_0 and S_1 states and are consistent with the solvent relaxation data as discussed earlier. The Forster cycle method can not be used for *p*-APBT because of the failure of the assumptions made in the method.

5. Molecular Orbital Calculations. The molecular orbital calculations have been carried out for the three molecules and the hydrogen-bonded conformer of *o*-APBT by using Pariser, Parr, and Popple (PPP) method.[29–31] The parameters used for the calculations are taken from the paper by Dorr et al.[32] Other details of calculations are discussed in our earlier paper.[4]

Table 6 gives a list of values of transition energies (λ_{nm}) and the corresponding oscillator strength (f) and polarizations (α°) alongwith the π-electron densities at various basic centers. The experimental spectral data (Table 1) of *o*-APBT match more closely with those of calculated ones for its hydrogen-bonded conformation (IA). For other molecules also, the agreement between the calculated and the observed values is very good. As it is difficult to find 'f' experimentally, we are unable to compare the same with the calculated values. However, the f values for the corresponding transitions of the molecules are qualitatively consistent with the intensity ($\log\varepsilon$) of the absorption bands. As mentioned earlier, the transition moment corresponding to the longest wavelength band of the molecules is polarized towards the phenyl ring.

The data of Table 6 indicate that the π-electron density on the amino-nitrogen (N_{16}) is greater than that at the nitrogen atom (N_3) of the heterocyclic ring in both the S_0 and S_1 states. Thus, the first protonation should take place at the amino group. In the S_1 state, the electron density on N_{16} has decreased, but on N_3 it has increased, which predicts that the amino group becomes more acidic and the pyridinic nitrogen becomes more basic on excitation and are consistent with the pK_a* values of monocation–neutral and dication–monocation equilibria (Table 5). This change of charge density on the nitrogen atoms of *o*-APBT favors the formation of IHB leading to the structure IA (Scheme 2). Moreover, the calculated electron densities on the amino-nitrogen foretells that the pK_a values for monocation–neutral equilibria of the molecules will be in the order *o*-APBT (IA)<*p*-APBT<*m*-APBT and exactly the same thing can be found from Table 5.

Conclusions

The following conclusions can be made from the above study.

(i) Ultraviolet and fluorescence spectra as well as the

low pK_a value of monocation–neutral equilibrium confirm the presence of intramolecular hydrogen bonding in *o*-APBT in the S_0 and S_1 states.

(ii) Solvatochromic effects confirm that *m*-APBT is more polar in the S_1 state than *o*-APBT and *p*-APBT. Large Stokes shifts observed in protic solvents are due to the solute-solvent complex formation and the charge transfer structure of the S_1 state.

(iii) Molecular orbital calculations (PPP) as well as the pK_a values indicate that the first protonation occurs at the amino group in all the molecules. But in case of *p*-APBT, the structural reorganization of the monocation leads to the quinonoid structure. The similar study carried out in cyclohexane and trifluoroacetic acid indicates that the quinonoid form is more stable in the nonpolar solvents. The absorption, fluorescence, and excitation fluorescence spectra (recorded at 390 and 460 nm) indicate that the species **2** and **2'** are present simultaneous in both S_0 and S_1 states. The dication is formed by protonating amino as well as the tertiary nitrogen atom, having similar structure in each case.

(iv) Although the amino group becomes stronger acid and tertiary nitrogen atom more basic upon excitation, the prototropic equilibria are not established in S_1 state.

(v) Very small fluorescence quantum yield observed for normal Stokes-shifted fluorescence in nonpolar solvents indicates that the phototautomer formed in *o*-APBT is nonfluorescent. The increase of fluorescence quantum yield with hydrogen bonding solvents proves this.

The authors are thankful to the Department of Science and Technology, New Delhi for financial support to the project entitled "Proton transfer reactions in the excited states in micellar media".

References

1) a) E. Belgoderr, R. Bossio, S. Chimichi, V. Parrini, and R. Pepino, *Dyes Pigm.*, **4**, 59 (1983). b) Kalle & Co., A. G., Br. Patent 895001, April 26, 1962.

2) P. F. Barbara, L. E. Brus, and P. M. Rentzepis, *J. Am. Chem. Soc.*, **102**, 5631 (1980); D. L. Williams and A. Heller, *J. Phys. Chem.*, **74**, 4473 (1970); R. G. Brown, J. D. Hepworth, K. W. Hodgson, B. May, and M. A. West, *Chem. Ind. (London)*, **1982**, 129; R. S. Becker, C. Lenolele, and A. Zein, *J. Phys. Chem.*, **91**, 3509 (1987); R. S. Becker, C. Lenolele, and A. Zein, *J. Phys. Chem.*, **91**, 351 (1987); C. A. S. Potter and R. G. Brown, *Chem. Phys. Lett.*, **153** (1), 7 (1988) ; W. E. Brewer, M. L. Martinez, and P. T. Chou, *J. Phys. Chem.*, **94**, 1915 (1990).

3) a) P. C. Tway and L. J. Clinelove, *J. Phys. Chem.*, **86**, 5223, 5227 (1982); A. K. Mishra and S. K. Dogra, *Indian J. Phys., Sect. B*, **58**, 480 (1984); A. K. Mishra and S. K. Dogra, *Bull. Chem. Soc. Jpn.*, **58**, 3587 (1985). b) A. K. Mishra and S. K. Dogra, *J. Photochem.*, **31**, 333 (1985).

4) J. K. Dey and S. K. Dogra, *Chem. Phys.*, **143**, 97 (1990).

5) D. W. Hein, R. J. Alheim, and J. J. Leavitt, *J. Am. Chem. Soc.*, **79**, 427 (1957).

6) J. A. Riddick and W. B. Bunger, "Organic Solvents," Wiley Interscience, New York (1970), pp. 592—594, 798—805.

7) a) M. J. Jorgenson and R. D. Harter, *J. Am. Chem. Soc.*, **85**, 878 (1983). b) G. Yagil, *J. Phys. Chem.*, **71**, 1034 (1967). c) W. H. Melhuish, *J. Phys. Chem.*, **65**, 229 (1961).

8) M. Swaminathan and S. K. Dogra, *Indian J. Chem., Sect. A*, **22**, 853 (1983).

9) QCPE Program No. QCMP 007, Indiana University, Chemistry Department, U.S.A.

10) R. Passarini, *J. Chem. Soc.*, **1954**, 2256.

11) J. K. Dey and S. K. Dogra, *Indian J. Chem., Sect. A*, **29**, 1153 (1990).

12) J. N. Murrell, *Proc. Phys. Soc. London, Sect. A*, **68**, 969 (1955); H. C. Longuet-Higgins and J. N. Murrell, *Proc. Phys. Soc. London, Sect. A*, **68**, 601 (1955); M. Godfrey and J. N. Murrell, *Proc. R. Soc. London, Ser. A*, **278**, 57, 64, 71 (1964).

13) S .P. McGlynn, L. Vanquickenborne, M. Kinoshita, and D. G. Carroll, "Introduction to Applied Quantum Chemistry," ed by Holt, Rinehart, and Winston, New York, N.Y.; E. C. Lim and S. K. Chakrabarti, *J. Chem. Phys.*, **47**, 4726 (1964).

14) M. Kasha, "Light and Life," ed by W. D. McEtroy and B. Glass, John Hopkins University Press, Baltimore, Md. (1961), pp. 31—34; K. Kamura, H. Tsubomura, and S. Nagakura, *Bull. Chem. Soc. Jpn.*, **37**, 1336 (1964); K. Kamura and H. Tsubomura, *Mol. Phys.*, **11**, 349 (1966); J. C. D. Brand, D. R. Williams, and T. J. Cook, *J. Mol. Spectrosc.*, **20**, 359 (1966).

15) J. R. Merrill and R. Bennett, *J. Chem. Phys.*, **43**, 1410 (1965); J. A. Otterstedt, *J. Chem. Phys.*, **58**, 5716 (1973); H. Shizuka, K. Matsui, T. Okamura, and I. Tanaka, *J. Phys. Chem.*, **79**, 2731 (1975); W. F. Richy and R. S. Becker, *J. Phys. Chem.*, **49** (3), 2092 (1968); M. D. Cohen, G. M. J. Schmidt, and (in part) (Mrs.) S. Flavian, *J. Chem. Soc.*, **1964**, 2041; M. D. Cohen and (Mrs.) S. Flavian, *J. Chem. Soc. B*, **1967**, 317.

16) a) M. Swaminathan and S. K. Dogra, *J. Am. Chem. Soc.*, **105**, 6223 (1983). b) A. K. Mishra and S. K. Dogra, *Indian J. Chem., Sect. A*, **24**, 285 (1984). c) P. Phaniraj, A. K. Mishra, and S. K. Dogra, *Indian J. Chem., Sect. A*, **24**, 913 (1984).

17) S. G. Schulman and A. C. Capomacchia, *Anal. Chim. Acta*, **58**, 91 (1972).

18) E. C. Lim and Jack M. H. Yu, *J. Chem. Phys.*, **45**, 4712 (1966); H. Shizuka, M. Eukushima, T. Fuju, T. Kobayashi, H. Ohtani, and M. Hoshino, *Bull. Chem. Soc. Jpn.*, **58**, 2107 (1985).

19) E. Lippert, *Z. Naturforsch., A*, **10**, 541 (1955).

20) E. M. Kosower, *J. Am. Chem. Soc.*, **80**, 3253 (1958).

21) K. Dimroth, C. Reichardt, T. Siepmann, and F. Bohlmann, *Liebigs Ann. Chem.*, **661**, 1 (1983); C. Reichardt, *Angew. Chem.*, **91**, 119 (1979).

22) S. Majumdar, R. Manoharan, and S. K. Dogra, *J. Photochem. Photobiol., A: Chem.*, **46**, 301 (1989).

23) L. Coosemans, F. C. DeSchryver, and A. Van Dormael, *Chem. Phys. Lett.*, **65**, 95 (1979).

24) R. O. Loutfy and A. C. Somersall, *Can. J. Chem.*, **54**, 760 (1976); G. E. Johnson, *J. Phys. Chem.*, **84**, 2940 (1980); T. Takahashi, K. Kikuchi, and H. Kokuban, *J. Photochem.*, **14**, 67 (1980).

25) Th. Forster, *Z. Elektrochem.*, **54**, 42 (1950).

26) P. J. Kovi, A. C. Capomacchia, and S. G. Schulman,

Anal. Chem., **44**, 1611 (1972).
27) A. Albert, R. J. Goldacre, and J. Phillips, *J. Chem. Soc.*, **1948**, 2240; *J. Chem. Soc.*, **1943**, 454; *J. Chem. Soc.*, **1946**, 706; H. C. Longuet-Higgins, *J. Chem. Phys.*, **18**, 275 (1951).
28) A. K. Mishra and S. K. Dogra, *Indian J. Chem., Sect. A*, **24**, 815 (1985).
29) R. Pariser and R. G. Parr, *J. Chem. Phys.*, **21**, 466, 767 (1953).
30) J. A. Pople, *Trans. Faraday Soc.*, **49**, 1315 (1953).
31) J. Delbene and H. H. Jaffe, *J. Chem. Phys.*, **48**, 1807 (1968).
32) Von F. Dorr, G. Hohlneicher, and S. Schneider, *Ber. Bunsen-Ges. Phys. Chem.*, **70**, 803 (1966).

 © 1991 The Chemical Society of Japan Bull. Chem. Soc. Jpn., 64, 3153—3155 (1991)

Viscometry of Isothermal Urethane Polymerization

John Reji, P. Ravindran, N. R. Neelakantan, and N. Subramanian*
Department of Chemical Engineering, Indian Institute of Technology, Madras 600036, India
(Received September 20, 1990)

The viscosity values of Indian Space Research Organization's (ISRO) hydroxyl terminated polybutadiene (HTPB) at various temperatures, the isothermal viscosity changes during the curing reaction of ISRO-HTPB with dlisocyanatotoluene (TDI) with and without catalyst and with a filler, calcium carbonate have been studied. The effect of temperature on this curing reaction is determined. The viscosity-time profile has shown an anomalous behavior and an explanation is put forward on the basis of polyurethane-HTPB, TDI mixture interaction. The viscosity-time profiles are drawn using normalized coordinates, which is helpful to compare the relative viscosity build up over relative periods.

Urethane polymers have been under active development in industries since inception because of their versatile properties. Urethane elastomers and thermoplastics are two major types of raw materials which are finally fabricated into desired products. Casting is a manufacturing technique for producing the above two classes, from initial liquid reactants to final solid polymer. Before casting, the reactive components have to be precisely metered and mixed. For metering and mixing, from the standpoint of physical handling a precise konwledge of the viscosities of the individual components and also of the mixture, at various conditions of temperature, composition and reaction rate must be known. In addition, rheological considerations are necessary for the design strategies of the mixer type, mixing speed and throughout rate of the mix of the production equipment and for determining mould filling characteristics. There must be a consideration of rheology versus the reaction rate for the length limitation of the hose, which is used for transferring mixed materials from the metering cum mixing machine to the mould for casting.

The purpose of this paper is to characterize the flow behavior of an urethane reacting system involving Indian Space Research Organization's (ISRO) hydroxyl terminated polybutadiene (HTPB) under various conditions.

Experimental

Materials. Uncatalyzed, catalyzed, unfilled and filled Am+Bn liquid urethane reacting systems were used, where Am was hydroxyl terminated polybutadiene (HTPB) developed by the Indian Space Research Organization (a Patented product used for solid rocket propellant binder). Its number average molecular weight ($\bar{M}_n$) was 3000±350 and hydroxyl value was 40. "Bn" was diisocyanatotoluene (TDI) (a mixture of 80:20 2,4 and 2,6 isomers). The catalyst used was tin(II) octanoate. The filler was a fine powder of calcium carbonate with a maximum moisture content of 0.1% and specific surface area of 0.9255 $m^2 ml^{-1}$.

Procedure. HTPB and TDI were mixed according to the stoichiomerty (NCO/OH ratio) equal to one. Three tenth % of the catalyst and 10% of the filler were also added depending on the system selected (unfilled, filled, uncatalyzed and catalyzed). The reactants (also the catalyst and filler wherever necessary) were mixed well at room temperature in a beaker. One ml of the reacting sample was transferred to the plate of the Cone and Plate Brookfield digital viscometer (model DV II) provided with a constant temperature bath and recorder. For the room temperature reaction, the time required for mixing and pouring into the plate were taken into consideration, whereas for the reaction at elevated temperatures this time was neglected. The reactants were allowed to react inside the viscometer. The viscosity was recorded as a function of time at constant shear rates from the initial liquid reactants to the final nearly solid elastomer state.

All the experiments were conducted under isothermal condition using the constant temperature bath. Further because of the small sample size and the longer reaction time, non-isothermal effect due to heat of the reaction could be neglected. To check whether shear thinning was occurring, measurements were periodically made over a range of shear rates, fairly rapidly, so that any viscosity change observed would not be masked by the curing reaction.[1)]

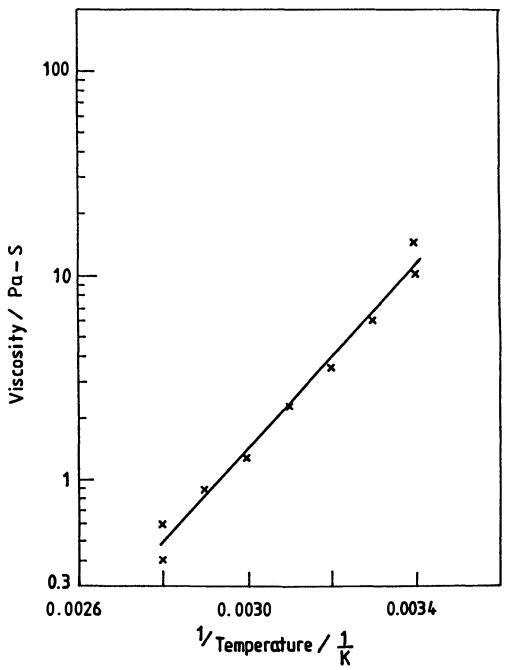

Fig. 1. Effect of temperature on viscosity for HTPB.

Results and Discussion

Figure 1 shows the effect of temperature on the viscosity of HTPB (non reacting and unfilled). The viscosity data indicate that for shear rates in the range of 1 to 40 sec^{-1}, the behavior is newtonian. The effect of temperature has been represented by Arrhenius equation, $\eta = A \exp(E/RT)$, where $A = 2.0488 \times 10^{-7}$ Pa s and $E = 43582$ J kg^{-1} mol^{-1} with η in Pa s and T in Kelvin.

Figure 2 shows the effect of temperature on the viscosity of HTPB and TDI reacting system. At higher temperatures, the initial viscosities of the reacting systems are lower, as expected. At 50 °C, the reaction effect overtakes the temperature effect on viscosity, at 70 min. At 30 and 50 °C, after a gradual increase in viscoity, at a particular time, the viscosity decreases, the decrease continues for some time and then again it increases. At lower temperatures the fall and rise are more. This is believed to be due to the solubility of the solid urethane which is already formed in the reaction medium-in the liquid polyol (HTPB)-TDI reacting system. We have separately tested the solubility of the polyurethane in the HTPB-TDI mixture and we have found that this mixture is a very good solvent for polyurethane especially for the initially formed low molecular weight type. We have separated the gel content (low molecular weight polyurethane that is formed) from sol (unreacted polyol, TDI mixture) by solvent extraction technique, using a separating funnel and benzene as a solvent (initially formed low molecular weight polyurethane is soluble in benzene also, but if we allow the reaction to advance before separation, it is possible to separate a good amount of gel from the sol). We have confirmed the mutual solubility of the gel and sol by putting these together back and seen that this sol is a very good solvent for this gel, whereas there is no dissolution when we put a finally formed polyurethane into the same sol. This shows that the dissolution of urethane in the reaction medium is dependent on its molecular weight. Then it is possible to infer that, as the reaction proceeds the dissolution occurs less readily; but because it is the relatively higher molecular weight polyurethane which dissolves, at this time, the net effect will be a decrease in the viscosity of the system; and it is possible that this effect can overtake the viscosity build up due to reaction, so that the viscosity can come down. This suggests that there may be a critical molecular weight build up above which the dissolution stops suddenly (This can be visualized more readily, if we consider the manner in which molecular weight build up takes place, in step addition polymerization, like urethane formation) and this can cause a sudden increase in viscosity. As this molecular weight build up to a critical molecular weight occurs only at the advanced stage of polymerization, and this is essentially preceded by the predominance of dissolution effect over the reaction effect, there is a fall and sudden rise of the reaction viscosity at the advanced stage of the reaction. Moreover we have seen similar observations in the isothermal viscosity changes of another ISRO-Polyol (castor oil based polyol)-TDI system also.[2] It is also further substantiated from the results of torque rheometry of urethane reacting system[3] where unreacted isocyanate acted as a plasticizer. The dissolution and reaction have two opposing effects on viscosity, the ultimate viscosity depends on which effect is dominating. At a particular point of time the former dominates over the latter, so that viscosity falls down. As time goes on, the left over HTPB-TDI mixture will react to form polyurethane and as the dissolution decreases and stops, the viscosity suddenly rises up to a large value. This is further evident from the variation of the slope after the peak. We have found that this anomalous behavior is temperature dependent. This is because the dissolution and reaction effects are temperature dependent. At higher temperatures there will be more reaction than dissolution so that the decrease in viscosity is less than that at lower temperatures. We can also

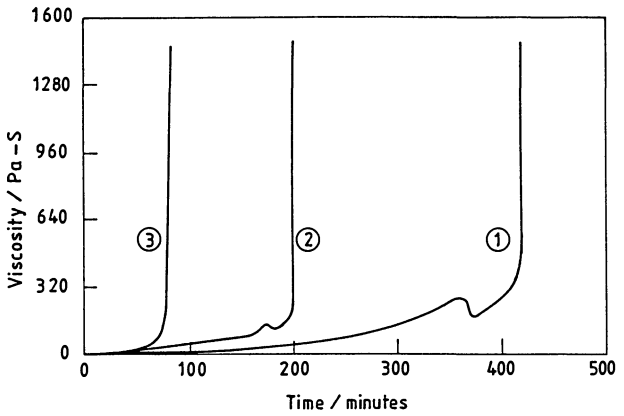

Fig. 2. Viscosity-time profiles for HTPB-TDI reactions at various temperatures; (1) 30 °C, (2) 50 °C, and (3) 70 °C.

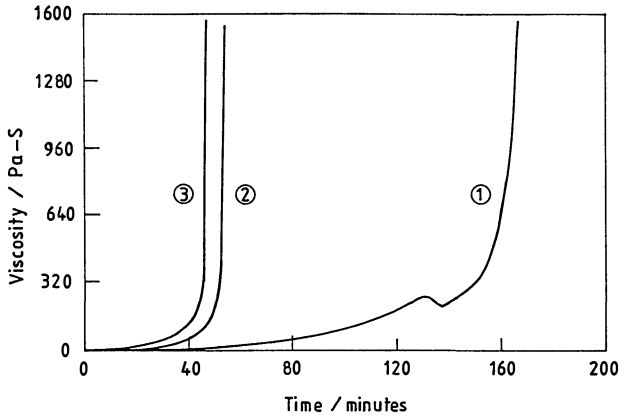

Fig. 3. Viscosity-time profiles for HTPB-TDI reactions in the presence of a catalyst, tin(II) octanoate at various temperatures; (1) 30 °C, (2) 50 °C, and (3) 70 °C.

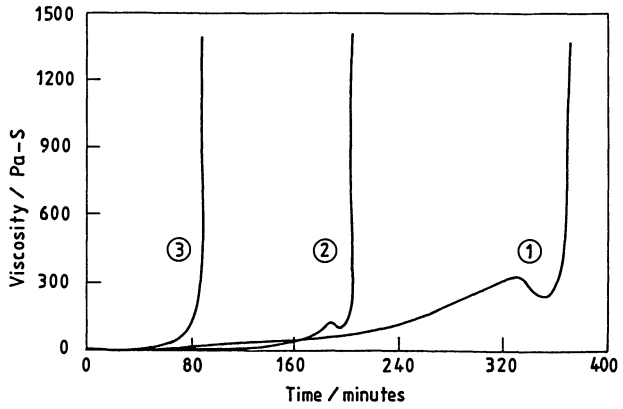

Fig. 4. Viscosity-time profiles for HTPB-TDI reactions in the presence of a catalyst, tin(II) octanoate and a filler, calcium carbonate; at (1) 30 °C, (2) 50 °C, (3) 70 °C.

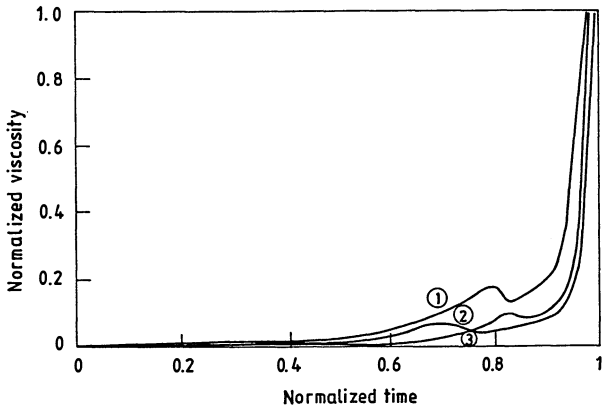

Fig. 5. Normalized viscosity-time profiles for HTPB-TDI reacting systems in the presence of catalyst, tin(II)octanoate; at (1) 30 °C, (2) 50 °C, (3) 70 °C.

obtain a viscosity-time profile where this anomalous behavior is absent, if the reaction rate is always higher than the dissolution effect. That is what happens in the reaction at 70 °C in Fig. 2 and in the reaction with catalyst at 50 °C and 70 °C in Fig. 3 and in chain extended system[4,5] at all temperatures.

Figure 4 shows that the introduction of filler increases the initial viscosity and in this case we have found that $CaCO_3$ is an inert filler, which will not interfere with the polyurethne reaction. So the introduction of a reinforcing type of filler at the reaction stage itself is helpful for better bonding of filler with the urethane matrix, which in turn will increase the mechanical properties of the final urethane polymer formed.

The viscosity data in Fig. 3 are replotted in Fig. 5 using normalized coordinates. The normalized viscosity is defined as $(\eta-\eta_o)/(\eta_{max}-\eta_o)$ where η is the viscosity at any time, t, η_o, is the viscosity at $t=t_o$ and η_{max} is the highest viscosity of this system measured using cone and plate viscometer (it is 1600 Pa s) at $t=t_{max}$, at this condition the material is nearly solid polyurethane. The normalized time is defined as $(t-t_o)/(t_{max}-t_o)$. In these normalized coordinates, the final viscosity is unity. The use of these coordinates helps to compare the relative viscosity build up over relative periods of time. The coordinates are dimensionless. The data for the HTPB-TDI catalyst tin(II) octanoate system in Fig. 5 indicate that at all temperatures the data fall almost on a single curve, till the beginning of the peak, so it is possible to draw a master curve without much deviation from the individual curves in this region and this master curve will be temperature independent.

Conclusion

The viscosity of the isothermal curing reaction of ISRO-HTPB with TDI is found to show an anomalous behavior which is not reported in literature previously. This behavior can be explained qualitatively, in terms of the opposing effects of dissolution and reaction in the system. A calcium carbonate filler does not have much effect on the curing reaction, other than its increase in initial viscosity, so fillers can be incorporated at polymerization stage itself. As the temperature increases the reaction rate can be expected to increase giving rise to an increase in the viscosity of the system; at the same time a temperature increase has a tendency to decrease the viscosity of the system; as these two effects are opposing each other, it would be interesting to follow the kinetics of the polyurethane reaction and relating the conversion to the viscosity of the system.

This work was supported by the Indian Space Research Organizaion.

References

1) R. John, N. R. Neelakantan, N. Subramanian, and S. K. Atithan, Proc. of Indian Chem. Eng. Congress, 1989, Abstr., p. 535.

2) R. John, E. T. Thachil, P. Ravindran, N. R. Neelakantan, and N. Subramanian, *Polym.-Plast. Technol. Eng.*, accepted for publication.

3) P. K. Sengupta and J. Battacharya, Proc. of International Conference on Rubber and Rubber Like Materials, RTC, IIT, Kharagpur, India, 1986.

4) R. John, N. R. Neelakantan, and N. Subramanian, *Thermochim. Acta,* accepted for publication.

5) R. John, E. T. Thachil, N. R. Neelakantan, and N. Subramanian, Proc. International Conference on Rheology and Polymer Processing, Seoul, Korea, 1990.

Interaction of Urea with *p*-Nitrophenol

Prabhat K. Das Gupta, S. P. Moulik, and A. R. Das*,†
Department of Chemistry, Jadavpur University, Calcutta 700032, India
†Polymer Science Unit, Indian Association for the Cultivation of Science, Calcutta 700032, India
(Received December 14, 1990)

Urea(U) can abstract H^+ ion from *p*-nitrophenol (PNP) forming a hydrogen bonded ion pair (proton-transfer complex $PNP^- \cdots H^+U$) of 1:1 stoichiometry with a formation constant 0.42 at 303 K. Infrared spectral measurements of the uronium phenolate and uronium nitrate have supported that the proton transferred from PNP is attached to the oxygen center of the amide. The needle shaped light yellow urea–PNP adduct is fairly stable under ordinary conditions decomposing at 398 K. The standard free energy, enthalpy, and entropy of formation determined from spectrophotometric and calorimetric methods have been found to be 3.62 kJ mol^{-1}, −13.30 kJ mol^{-1}, and −57.5 J mol^{-1} K^{-1}, respectively at 303 K.

Recent studies have indicated that urea can significantly affect the hydrogen ion activity of strong acids in aqueous medium.[1–4] It has been pointed out that the oxygen atom of the amide provides the preferential binding site for the hydrogen ion. Earlier X-ray, IR, and NMR studies have also supported that the binding of urea and strong acids occur at the oxygen rather than the nitrogen center of the amides.[5,6] However, studies on the interaction between urea and weak acids are rare and the nature of the species formed consequent to this is not specifically known. We have observed that urea can affect the dissociation of *p*-nitrophenol, PNP (pK=7.15 at 25 °C) whereas *p*-nitrosalicylic acid, PNSA (pK=10.33 at 25 °C) remains unaffected; a relatively strong base like ethylenediamine can abstract H^+ ion from PNSA yielding a hydrogen-bonded ion pair or proton transfer complex (PTC).[7,8] The formation of PTC is the result of directionally specific interaction and because of much greater charge separation its formation is favored in polar media.[9] The spectrophotometric method is incapable of differentiating between an ion pair and the PTC, therefore, the spectrum of the PTC is the same as that of the ion of the conjugate base of the weak acid.[10] We have assumed that the above arguments are valid in our acid-base system of PNP and urea. Our objective has been to study the interaction between PNP and urea using spectrophotometric, conductometric, and calorimetric methods. It will be seen that the spectral results support PTC formation rather than dissociated ionic species. The energetics of the above interaction has been presented. Besides, the urea–PNP adduct has been prepared and characterized by IR and NMR methods with reference to the nitrate adduct of the amide.

Experimental

Materials. The urea and *p*-nitrophenol used were described earlier.[3,4,8] Nitric acid used was of Anala R grade, E. Merck, Germany. Doubly distilled conductivity water of specific conductance ca. 1.5 μS cm^{-1} was used for the preparation of solution.

Methods. Spectrophotometric measurements were taken in a Carey 17D spectrophotometer in 1 cm cuvettes. Infrared spectra were taken in KBr pellets in a Perkin–Elmer Model 297 Infrared spectrophotometer. About 1.0 mg of the finely ground sample was intimately mixed with approximately 100.0 mg of dried potassium bromide powder in a mortar and pestle. The mixture was then pressed in a special die at 10000 pounds per square inch to yield a transparent disk. The disk was then held in the instrument beam for spectroscopic examination. A JEOL FT NMR FX-100 was used for NMR spectral measurements. Approximately 3.0 mg of the sample dissolved in 0.3 ml of $CDCl_3$ was used for the measurements at 100 MHz with TMS as internal standard. Conductivity measurements of aqueous PNP and PNP–urea solutions were taken with a JENWAY, U.K. conductometer in a cell of cell constant 1.02 in a thermostated bath at 303 K.

Preparation of Adducts: To prepare uronium-nitrophenolate, the amide and the PNP mixed in 1:1 mol ratio was dissolved in a small amount of water and allowed to stand in a beaker at low temperature (283 K) overnight. Fine needle shaped light yellow crystals were found to appear at the bottom. The product was carefully washed with distilled water, dried under vacuum and stored in a desiccator. The elemental analysis has shown the compound to be of 1:1 composition. The compound decomposes at 398 K.

The nitric acid adduct was prepared in the following way. In 1 mol dm^{-3} solution of urea, 1 mol dm^{-3} nitric acid solution was slowly added. Fine crystals of uronium nitrate were formed and settled at the bottom. The crystals were separated, washed with distilled water for a number of times and stored in a desiccator. Elemental analysis confirmed the adduct to be of 1:1 composition. It decomposes at 423 K (lit, value[11] 425 K).

Spectrophotometeric Measurements: Solutions of PNP and urea were prepared in a number of test tubes at constant concentration of the former (10^{-4} mol dm^{-3}) and variable concentrations of the latter from 0.05 to 6.0 mol dm^{-3}. They were placed in a constant temperature thermostated water bath at 303 K for 1 h. The spectra of the solutions were then recorded in the spectrophotometer in the wavelength range 250—450 nm at 303±0.02 K.

Conductance Measurements: The conductances of PNP at concentrations 1,2,4,6,8, and 10 mmol dm^{-3} in water as well as in 8 mol dm^{-3} aqueous urea were measured at 303 K. The conductance of the urea solution was also measured and the value subtracted from each set of the PNP–urea mixtures to compensate for the urea effect on ion transport.[1]

Calorimetric Measurements: The enthalpy of the urea–PNP interaction was determined in a Tronac 458 Isoperibol Calorimeter at 303 K. The calibration of the calorimeter was checked by measuring the heat of neutralisation of HCl with NaOH. In an actual run, urea solution was added into PNP solution keeping the final stoichiometry at least 1 : 100 and the heat liberated was determined at five urea concentrations. The heat of dilution of both the urea solution as well as the PNP solution were also determined and subtracted from the above heat of interaction to calculate the enthalpy following the procedure described elsewhere.[12,13] Since the base was directly added into the aqueous solution of PNP from a syringe in a water bath outside the Dewar flask, the heat of the interaction was calculated from the overall temperature change and the heat capacity determined after the introduction. The reported enthalpy refers to the extrapolated to zero urea concentration. The estimated standard deviation in the enthalpy value was ±0.7 kJ mol^{-1}.

Results and Discussion

The 1 : 1 stoichiometry of the reaction has been supported by the elemental analysis data of the prepared uronium *p*-nitrophenolate. The ^{1}H NMR spectrum of the PNP–urea adduct indicates the presence of the aromatic group as two double doublets centerd at δ=8.12 and 6.98 characteristic of a para substituted phenyl ring. The ^{1}H NMR spectrum of PNP and tetramethylurea[14] showed similar characteristics. In addition, the methyl proton signals appeared at δ=2.84 as a singlet. The signals were in the ratio of 1 : 3 indicating the formation of a 1 : 1 adduct. Analogically we consider that the PNP–urea adduct was also of 1 : 1 mol ratio.

The specific conductance–concentration plot in Fig. 1 suggests specific interaction between PNP and urea. Simple reduction in conductance[15] by the association of the dissociated H^+ ion as evidenced in the cases of HCl and HOAc (acetic acid) is not solely contributing to the ion transport phenomenon. A distinct departure is evidenced at higher PNP concentrations. A specific association of the migrating species PNP^- and UH^+ is anticipated which is regarded as the hydrogen-bonded ion pair.

The interaction between PNP and urea may end up into the following equilibria.

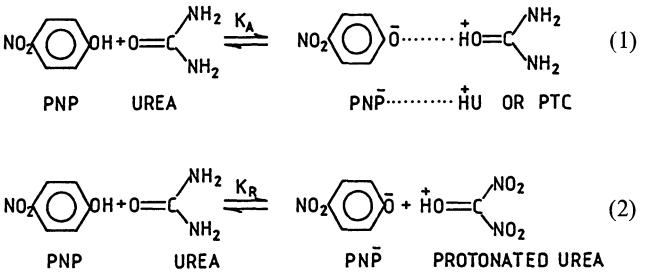

The spectra of the PNP–urea mixtures reveal decrease in the 315 nm band of the parent nondissociated PNP molecule with concomitant increase in the intensity of the 405 nm band of the phenolate anion or the PTC (Fig. 2). The reaction can thus be spectrophotometrically monitored recording the absorbance at 405 nm where PNP does absorb insignificantly. The spectra show a sharp isosbestic point at 345 nm indicating simultaneous existence of two species in equilibrium. The absorbance contributed by the self-dissociation of PNP is minor; it has been subtracted from the absorbance of all the solutions in the presence of urea to eliminate the effect. It has been established earlier[7] that both *p*-nitrosalicylate anion and the hydrogen-bonded ion pair between the said anion and protonated ethylenediamine have the same absorption maxima at 414 nm. The *p*-nitrophenolate anion (PNP^-) and the ion pair between PNP^- and the protonated urea UH^+ are considered also to absorb maximum at the same wavelength,[8] 405 nm. From fundamental considerations and following the line

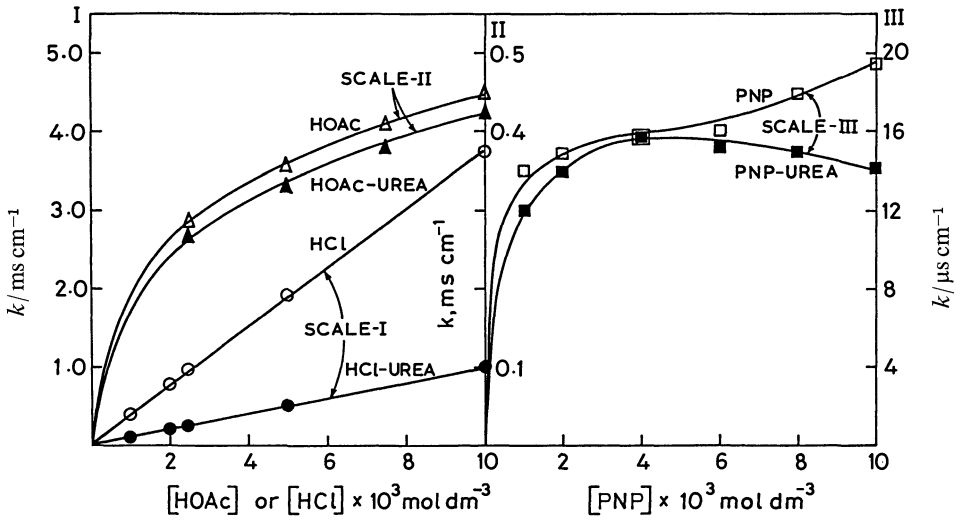

Fig. 1. Specific conductance–concentration profiles for HCl, HOAc, and PNP in aqueous and aquo-urea media at 303 K.

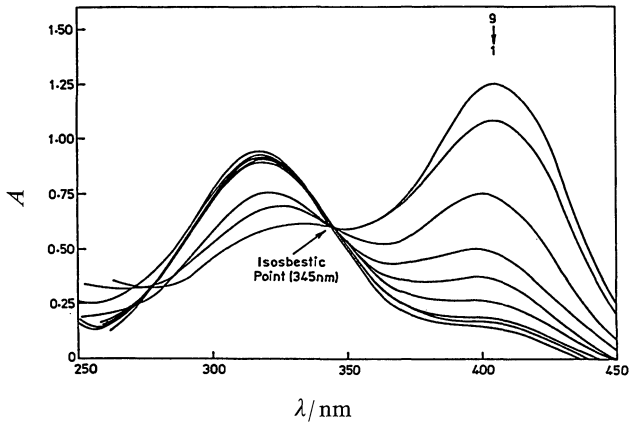

Fig. 2. Spectra of 0.1 mmol dm^{-3} PNP in aqueous urea environment at 303 K. Curves 1 to 9 are at 0, 0.05, 0.1, 0.3, 0.6, 1.0, 2.0, 4.0, and 6.0 mol dm^{-3} urea.

of arguments presented earlier,[7,8] the following Eqs. 3 and 4 can be derived for the above-mentioned Eqs. 1 and 2, respectively,

$$C_{PNP}/A = 1/\varepsilon + (1/K_A\varepsilon^2)\ 1/C_u \quad (3)$$

and

$$C_{PNP}/A = 1/\varepsilon + (1/K_R\varepsilon^2)\ A/C_u \quad (4)$$

where C_{PNP} and C_u are the stoichiometric concentrations of the *p*-nitrophenol and urea respectively, A is the absorbance of the solution at 405 nm, ε is the molar extinction coefficient of the absorbing species and K_R and K_A have significance as defined above. Since dilute solution of PNP has been used and urea is a neutral molecule, the activities of the species arising in solution are considered equal to their concentrations. The validity of Eq. 3 is examplified in Fig. 3, where a nice straight line plot is observed between C_{PNP}/A and C_u^{-1} with a correlation coefficient 0.9996 (curve 1). The ε_A and K_A derived from the slope and the intercept are $(1.78\pm0.08)\times10^4$ dm^3 mol^{-1} cm^{-1} and 0.24 ± 0.01 dm^3 mol^{-1} respectively. The value of ε of the phenolate ion[16] has been reported to be 18330 dm^3 mol^{-1} cm^{-1} at 303 K. It is seen in the figure that the results very

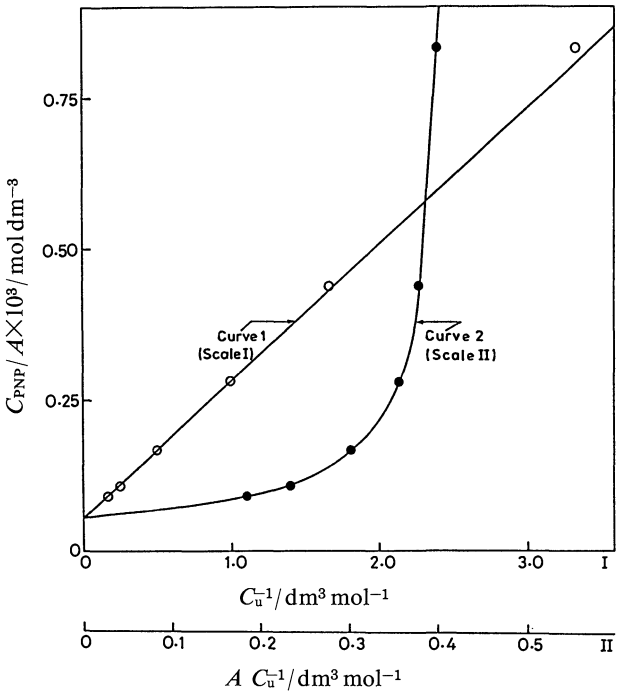

Fig. 3. C_{PNP}/A versus C_u^{-1} and C_{PNP}/A versus A/C_u plots for testing the validity of Eqs. 3 and 4 and the evaluation of the equilibrium constant, K_A and the molar extinction coefficient, ε of the complex at 303 K.

poorly fit Eq. 4. Extrapolation of the curved course (curve 2), however, yields the same intercept as produced by the curve 1, which ought to be so because the values in both the equations refer to the same species. The good correlation of the experimental results with Eq. 3 speaks in favor of the said PTC formation (Eq. 1) rather than replacement reaction (Eq. 2). From pH measurements we have reported the association constants of H^+ ion of HCl with urea to be 1.42—5.38 at 310 K in the urea concentration range of 0.5—6 mol dm^{-3}. The $PNP^- \cdots UH^+$ PTC formation constant is 0.24 dm^3 mol^{-1} at 303 K, the interaction is weaker than H^+ ion binding with the amide.

The reactant concentrations used in the experiments

Table 1. Characteristic Infrared Bands of Urea, PNP, Urea–PNP, and Uronium Nitrate

Urea ν/cm^{-1}	PNP ν/cm^{-1}	Urea–PNP[a] ν/cm^{-1}	Uronium nitrate ν/cm^{-1}	Predominant mode
3400		3400	3400	ν_{NH_2} (free)
3500		3500	3500	
	3325			ν_{OH} (H-bonded)
		1690	1700	
1685				$\nu_{C=O}$ stretch
		1650	1670	
1470		1590	1570	ν_{CN} bending
	1590	1590		$\nu_{C=C}$ (skeletal)
	1500	1500	1500	ϕ_{NO_2}
			1380	NO_3^-

a) ν_{CN} for Urea–PNP almost merges with the $\nu_{C=C}$ at 1590 cm^{-1} with a broadening effect.

were low, so the thermodynamic parameters herein reported are standard state values. The calorimetric enthalpy of the interaction (ΔH°) has been found to be -13.8 ± 0.7 kJ mol^{-1}. A value of -57 ± 3 J mol^{-1} K^{-1} has been calculated for the ΔS° from the Gibb's equation using the spectrophotometrically obtained standard free energy change ($\Delta G^\circ=3.60\pm0.01$ kJ mol^{-1}). The interaction has an overall order producing effect. The interacted species are stabilized upon complexation, the environmental solvation also adds to the ordering effect.

The characteristic IR bands of urea, PNP, urea–PNP, and uronium nitrate are given in Table 1. The amide has the following resonating structures.[17]

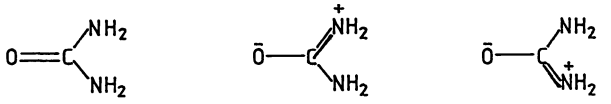

I II III

If linkage of hydrogen occurs through nitrogen then contributions of **II** and **III** will decrease and that of **I** will increase. This results in increase of the CO stretching frequency with a decrease in the CN stretching frequency. If, on the other hand, bonding occurs through oxygen then contribution of **I** decreases, the CO stretching frequency may be affected whereas that of the CN stretching should increase, the NH stretching frequency (3400—3500 cm^{-1}) should remain unaffected.

The bands of free NH_2 at 3400 and 3500 cm^{-1} in urea remain unaffected in urea–PHP and uronium nitrate, supporting noninvolvement of the linking between the nitrogen center of urea with the hydrogen of PNP and HNO_3. The stretching frequency of C=O has been little affected in the adduct whereas that of CN has been affected appreciably; in PNP adduct the shifted band of CN has overlapped with C=C skeletal response of PNP in the spectrum which is, therefore, not distinguishable. The appreciable shift in the stretching frequency of CN and nonaffected NH stretching frequency speak in favor of association of PNP and HNO_3 with the oxygen of urea. The intermolecularly bonded OH of pure PNP has shown a band at 3325 cm^{-1}, which is absent in the urea–PNP adduct indicating free OH to link with the C=O of urea. The following are the possible resonating structures of the 1 : 1 PNP adduct of urea.

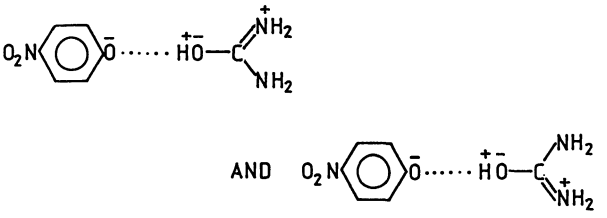

P.K.D.G. thanks U.G.C., Government of India, for awarding a Teacher Fellowship to carry out this work. We thank M. L. Das and P. K. Jana for the calorimetric and conductance measurements.

References

1) H. B. Bull, G. L. Breese, G. L. Ferguson, and C. A. Swenson, *Arch. Biochem. Biophys.*, **104**, 297 (1964).
2) O. F. Sehafer, *Chem. Ber.*, **80**, 529 (1976).
3) P. K. Das Gupta, P. K. Bhattacharyya, and S. P. Moulik, *Indian J. Chem., Sect. A*, **23**, 192 (1984).
4) P. K. Das Gupta and S. P. Moulik, *J. Phys. Chem.*, **91**, 5826 (1987).
5) C. R. Redpath and J. A. S. Smith, *Trans. Faraday Soc.*, **58**, 462 (1962).
6) I. L. Flnar, "Organic Chemistry, The Fundamental Principles," ELBS, Longman, New York (1986), Vol. 1, pp. 262—263.
7) S. P. Moulik, S. Ray, and A. R. Das, *J. Phys. Chem.*, **80**, 157 (1976).
8) S. Ray, A. R. Das, and S. P. Moulik, *Indian. J. Chem., Sect. A*, **14**, 921 (1976).
9) R. Scott, D. De Palma, and S. Vinogradov, *J. Phys. Chem.*, **72**, 3192 (1968).
10) R. Scott and S. Vinogradov, *J. Phys. Chem.*, **73**, 1890 (1969).
11) "Handbook of Chemistry and Physics," 55th ed, C.R.C. Press, Ohio (1974—1975).
12) D. H. Etough, *Anal. Chem.*, **42**, 635 (1970).
13) H. P. Hopkins, D. V. Jahagirdar, S. P. Moulik, D. H. Aue, H. M. Webb, W. R. Davidson, and M. D. Pedlev, *J. Am. Chem. Soc.*, **106**, 4341 (1984).
14) P. K. Das Gupta and S. P. Moulik, unpublished data.
15) P. K. Jana and S. P. Moulik, *Indian J. Chem., Sect. A*, **29**, 774 (1990).
16) R. A. Robinson and A. I. Biggs, *Trans. Faraday Soc.*, **51**, 901 (1955).
17) K. Nakamoto, "Infrared and Raman Spectra of Inorganic and Coordination Compounds," John Wiley & Sons, New York (1978).

The Crystal Structure of (BEDT-TTF)$_4$[Ni(CN)$_4$]

Atsushi KAWAMOTO, Masashi TANAKA,*,† and Jiro TANAKA
Department of Chemistry, Faculty of Science, Nagoya University, Chikusa, Nagoya 464-01
†Department of Chemistry, College of General Education, Nagoya University, Chikusa, Nagoya 464-01
(Received April 10, 1991)

Synopsis. The crystal of (BEDT-TTF)$_4$[Ni(CN)$_4$] (BEDT-TTF: bis(ethylenedithio)tetrathiafulvalene) belongs to the triclinic $P\bar{1}$ with the lattice constants of a=10.994(2), b=16.443(2), c=9.703(1) Å, α=97.85(1), β=115.15(1), γ=95.94(1)°. In the crystal, there exists the face to face overlap of the BEDT-TTF molecules along the [201] direction. The intermolecular interaction by the short S···S contact is also observed along the [$\bar{2}$01] direction.

Recently Saito et al. have found the superconductivity of (BEDT-TTF)$_2$[Cu(NCS)$_2$] at an ambient pressure.[1] The charge-transfer complexes between BEDT-TTF and metal complexes have many interesting properties such as the magnetic property in addition to the electrical conductivity, because such metal ion can have the incompletely occupied electron shell. From this point of view, we investigated the magnetic and electronic properties and the crystal structures of several complexes.[2-4] In the present paper, we report the crystal structure of (BEDT-TTF)$_4$[Ni(CN)$_4$].

Table 1. Positional Parameters (×10^4) and Equivalent Isotropic Thermal Parameters (Å×10^2) with e.s.d's in Parentheses

Atom	x	y	z	B_{eq}[a)]
S(1)	6982(2)	3210(1)	11779(2)	428(5)
S(2)	8571(2)	3401(1)	10025(2)	459(5)
S(3)	6248(2)	1389(1)	10876(2)	586(6)
S(4)	8086(2)	1596(1)	8720(2)	438(5)
S(5)	9547(2)	5380(1)	11662(2)	492(5)
S(6)	8027(2)	5125(1)	13483(2)	503(6)
S(7)	10730(2)	7130(1)	13153(2)	525(6)
S(8)	8964(2)	6828(1)	15350(2)	752(8)
C(9)	8067(5)	3868(3)	11372(6)	352(2)
C(10)	7076(5)	2300(3)	10692(7)	335(2)
C(11)	7781(5)	2383(3)	9871(6)	330(15)
C(12)	6651(10)	589(4)	9793(10)	879(37)
C(13)	7528(13)	707(4)	9261(15)	1629(72)
C(14)	8494(6)	4696(3)	12077(6)	367(16)
C(15)	9699(5)	6227(3)	13053(6)	358(16)
C(16)	9016(6)	6108(3)	13898(6)	417(17)
C(17)	10613(11)	7871(4)	14598(11)	1021(42)
C(18)	9622(11)	7757(4)	15057(12)	1138(47)
S(19)	2675(2)	4136(1)	2898(2)	448(5)
S(20)	4084(2)	4330(1)	954(2)	457(5)
S(21)	1677(2)	2329(1)	1741(2)	429(5)
S(22)	3359(2)	2569(1)	−596(2)	472(5)
S(23)	5052(2)	6316(1)	2528(2)	437(5)
S(24)	3673(2)	6068(1)	4483(2)	438(5)
S(25)	5891(2)	8137(1)	3626(2)	441(5)
S(26)	4317(2)	7817(1)	6048(2)	484(5)
C(27)	3675(5)	4794(3)	2377(6)	369(16)
C(28)	2594(5)	3235(3)	1664(6)	326(15)
C(29)	3234(5)	3326(3)	757(6)	352(15)
C(30)	1760(10)	1573(4)	297(10)	970(39)
C(31)	2426(15)	1673(5)	−452(15)	1712(72)
C(32)	4094(5)	5626(3)	3048(6)	356(16)
C(33)	5084(5)	7205(3)	3762(6)	344(15)
C(34)	4464(5)	7084(3)	4677(6)	344(15)
C(35)	5975(7)	8848(3)	5277(7)	534(2)
C(36)	4686(7)	8766(4)	5468(7)	517(21)
Ni(37)	10000	10000	5000	307(5)
C(38)	9613(5)	9862(3)	6665(6)	379(16)
C(39)	8128(6)	9951(3)	3776(6)	386(17)
N(40)	9358(6)	9761(4)	7665(6)	602(20)
N(41)	6978(5)	9918(3)	3054(6)	492(2)

a) $B_{eq}=\frac{8\pi^2}{3}\sum_i\sum_j U_{ij}d_i^*d_j^*\boldsymbol{a}_i\cdot\boldsymbol{a}_j$.

Experimental

Black hexagonal plate-like crystals (0.25×0.30×0.05 mm) were grown by electrochemical crystallization of BEDT-TTF in 1,1,2-trichloroethane by using K_2[Ni(CN)$_4$] as a supporting electrolyte. D_m (1.80 g dm^{-3}) was measured by flotation and D_c is 1.89 g cm^{-3} for $C_{44}H_{32}N_4S_{32}Ni$. Reflection data# were measured by Rigaku automated four-circle diffractometer AFC-5R. Crystal data: triclinic, space group $P\bar{1}$, a=10.994(2), b=16.443(2), c=9.703(1) Å, α=97.85(1), β=115.15(1), γ=95.94(1)°, and Z=1. 5473 measured reflections, $2\theta_{max}$=126°, $-13\leqslant h\leqslant 13$, $-19\leqslant k\leqslant 19$, $0\leqslant l\leqslant 11$, and R_{int}=0.03. The crystal structure was determined by the Monte-Carlo direct method with the aids of MULTAN78 program system,[5] and refined by the full matrix least squares by using 4268 non-zero unique reflections (Cu $K\alpha$, $|F_o|>3\sigma(F_o)$). Intensities were corrected for the absorption effect by the analytical method, linear absorption coefficient μ=105.45 cm^{-1} and transmission factor in the range 0.043 to 0.59. The final R value was 0.062, S=2.34, $w=1/\sigma^2(F^2)$, $(\Delta/\sigma)_{max}$=0.40 for B_{31} of C(39) atom, and $\Delta\rho_{max}$=0.7 eÅ^{-3}. The atomic parameters were given in Table 1.

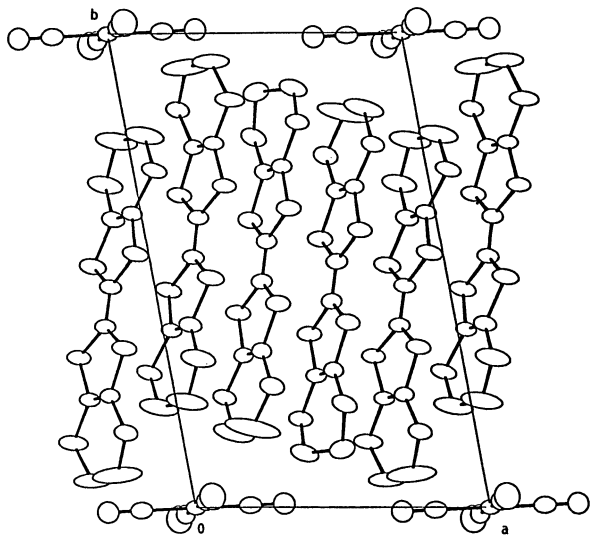

Fig. 1. Crystal structure of (BEDT-TTF)$_4$[Ni(CN)$_4$] projected on the c axis.

The complete F_o-F_c data are deposited as Document No. 8962 at the Office of the Editor of Bull. Chem. Soc. Jpn.

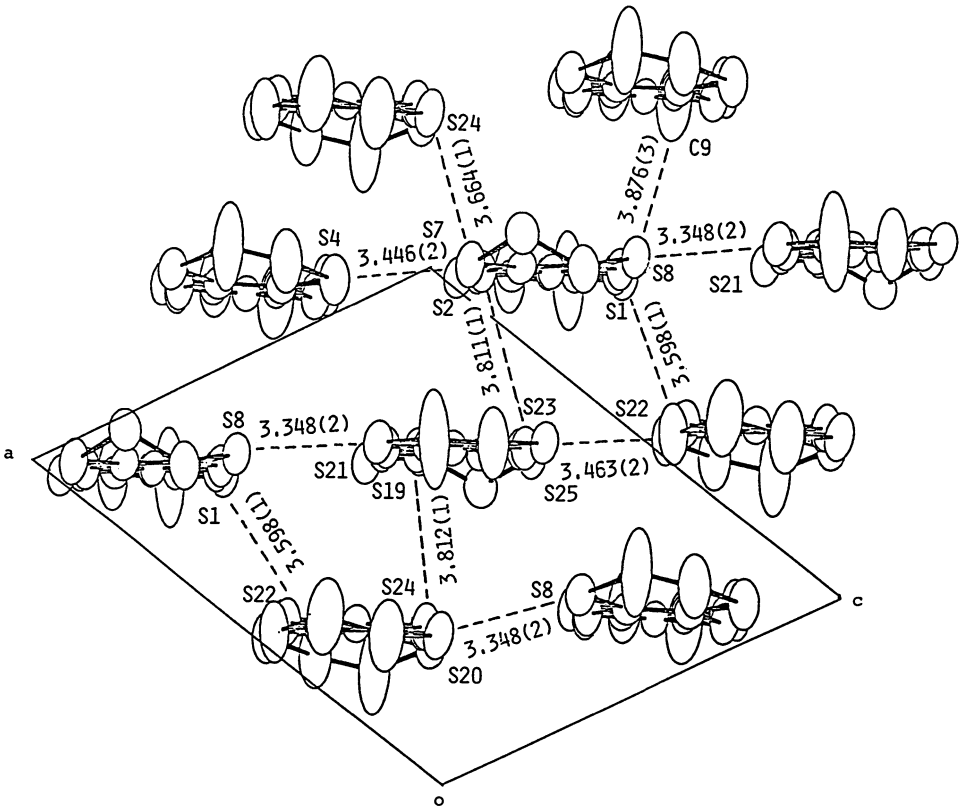

Fig. 2. Intermolecular overlaps in the BEDT-TTF sheet viewed along the molecular long axis.

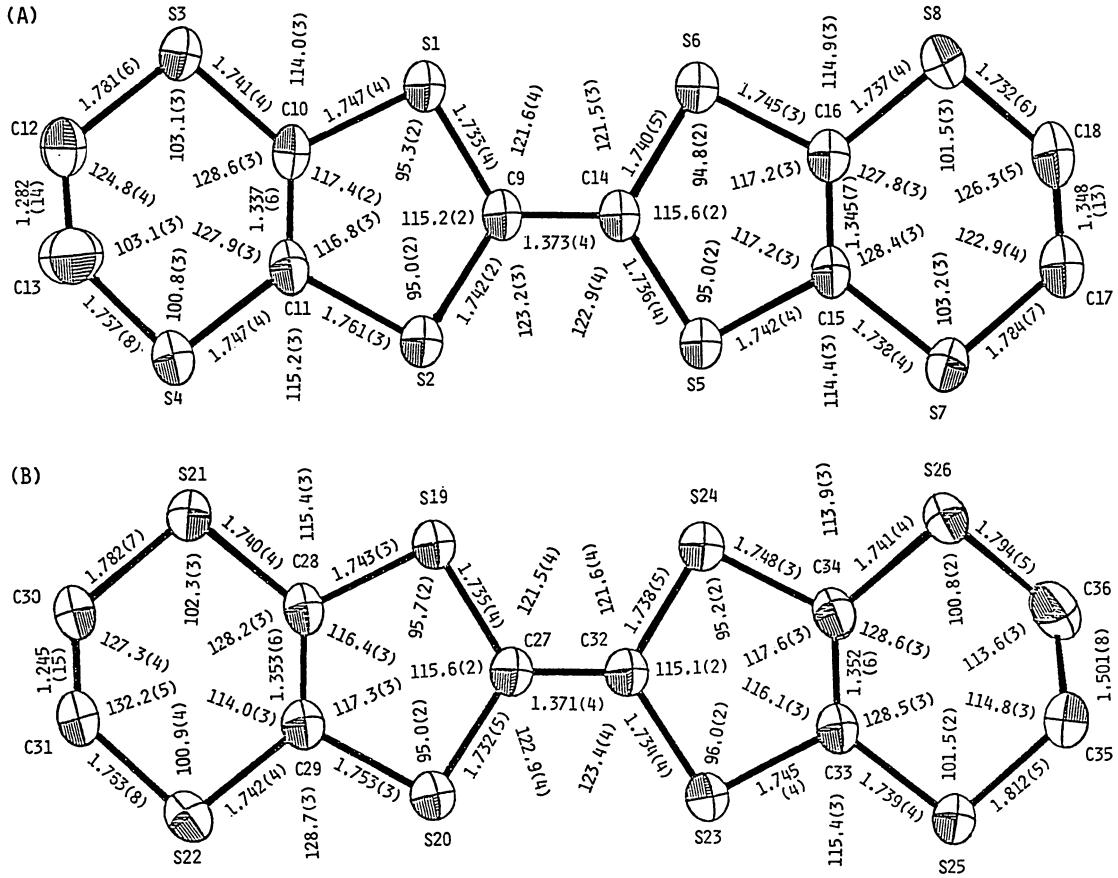

Fig. 3. Molecular dimensions for BEDT-TTF in $(BEDT\text{-}TTF)_4[Ni(CN)_4]$.

Results and Discussion

Figure 1 shows the crystal structure viewed along the *a* axis. There are two independent BEDT-TTF molecules in an asymmetric unit and the Ni atom of $[Ni(CN)_4]^{2-}$ ion is located on the inversion center. The BEDT-TTF molecules are stacked along the [201] direction. This crystal is isostructural to the crystal of $(BEDT\text{-}TTF)_4[Pt(CN)_4]$.[6] Figure 2 shows the arrangement on the (010) plane viewed nearly along the long molecular axis. The interstacking contacts are longer than the sum of the Pauling's van der Waals radii of two sulfur atoms (3.70 Å). Several S–S contacts shorter than 3.70 Å were observed along the [$\bar{2}$01] direction. The $[Ni(CN)_4]^{2-}$ anion has the square planar structure with the average Ni–C and C–N distances of 1.874(5) and 1.146(6) Å and the C–Ni–C angle of 88.3(3)°. The geometries of two crystallographycally independent BEDT-TTF molecules are shown in Fig. 3 and no significant difference could be found between them. One ethylene group of the BEDT-TTF molecule is out of the molecular plane and two carbons in the ethylene plane are located at the opposite side of the molecular plane, while another ethylene groups are in the molecular plane. In Table 2, the bond lengths of the TTF moiety in two BEDT-TTF molecules are compared with those in other BEDT-TTF salts. The average values in $(BEDT\text{-}TTF)_4[Ni(CN)_4]$ are similar to those in half-ionized BEDT-TTF and its charge can be regarded as $\rho=1/2$.

Table 2. Comparison of Averaged Bond Length (Å) of BEDT-TTF ($\rho=0$, 1/2, and 1)[7] (The bond lengths b, c, and d are averaged values)

	Molecule A	Molecule B	$\rho=0$	$\rho=1/2$	$\rho=1$
a	1.373(4)	1.371(4)	1.312(12)	1.365(4)	1.38(3)
b	1.74(1)	1.73(1)	1.757(7)	1.740(2)	1.72(1)
c	1.75(1)	1.75(1)	1.754(8)	1.750(2)	1.73(1)
d	1.34(1)	1.35(1)	1.332(7)	1.345(3)	1.37(2)

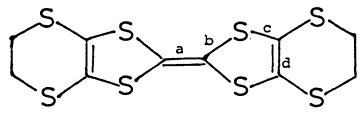

References

1) H. Urayama, H. Yamauchi, G. Saito, K. Nozawa, T. Sugano, M. Kinoshita, S. Sato, K. Oshima, A. Kawamoto, and J. Tanaka, *Chem. Lett.*, **1988**, 55.

2) A. Kawamoto, J. Tanaka, and M. Tanaka, *Acta. Crystallogr., Sect. C*, **43**, 205 (1987).

3) M. Tanaka, A. Kawamoto, J. Tanaka, M. Sano, T. Enoki, and H. Inokuchi, *Bull. Chem. Soc. Jpn.*, **60**, 2531 (1987).

4) M. Tanaka, H. Takeuchi, M. Sano, T. Enoki, K. Suzuki, and K. Imaeda, *Bull. Chem. Soc. Jpn.*, **62**, 1432 (1989).

5) P. Main, S. E. Hull, L. Lessinger, G. Germain, J.-P. Declercq, and M. M. Woolfson, MULTAN 78, A System of Computer Programs for the Automatic Solution of Crystal Structures from X-ray Diffraction Data. Univs. of York, England and Louvain, Belgium.

6) R. P. Shibaeva, R. M. Lobkovskaya, V. E. Koroykov, N. D. Kushch, E. B. Yagubskii, and M. K. Makova, *Synth. Met.*, **27**, A457 (1988).

7) H. Kobayashi, A. Kobayashi, Y. Sasaki, G. Saito, and H. Inokuchi, *Chem. Lett.*, **1984**, 183.

Effect of Proteins on the Zeta Potential of Dispersed Vesicular Globules in W/O/W Emulsions

Koichi UEDA and Sachio MATSUMOTO,*,†
Shiga Central Research Laboratories, Noevir Co., Ltd., Okada-cho, Youkaichi, Shiga 527
†Department of Agricultural Chemistry, College of Agriculture, The University of Osaka Prefecture, Sakai, Osaka 591
(Received April 30, 1991)

Synopsis. The zeta potential of dispersed vesicular globules in W/O/W emulsions was found to be reduced systematically at neutral pH by increasing the isoelectric point of proteins immobilized in the inner aqueous phase of the globules. We considered the effect of proteins on the total interactions between vesicular globules.

Dispersed globules of W/O/W emulsions can be characterized by a vesicular structure with an inner aqueous phase separated from an aqueous suspending fluid by a thin layer of the oil-phase components.[1,2] Globules of this type of emulsion also encapsulate a certain amount of water-soluble ingredients including proteins.[3–5] The authors have found that the dispersion state of the globules in W/O/W emulsions is influenced by a kind of proteins immobilized in the inner aqueous phase. Despite the fact that the globules have already been charged negatively in the aqueous phase due to differences in the affinity of the oil and the aqueous phases for ions,[6] the above finding may result from changes in the charged potential of the globules due to the surface activity of proteins, i.e. protein molecules adsorbed tightly onto the inside surface of the oil layer from the inner aqueous phase. It is the purpose of this study to obtain information concerning the correlation between the zeta potential of the vesicular globules and the isoelectric point of proteins immobilized in the globules of W/O/W emulsion systems.

Experimental

The W/O/W emulsions to be tested were divided into liquid-paraffin and olive-oil systems, respectively. The former was stabilized by Span 80 (sorbitan monooleate, produced by ICI America, Inc., U.S.A.) and Tween 80 (poly(oxyethylene) sorbitan monooleate, produced by Difico Laboratories, Inc., U.S.A.), while the latter was prepared by use of TGCR (tetraglyceryl condensed ricinolate) and DGMO (decaglyceryl monooleate). The TGCR and DGMO used were supplied by courtesy of Sakamoto Yakuhin Kogyo, Ltd., Osaka. Each system was also subdivided into four samples according to a kind of proteins immobilized in the inner aqueous phase, i.e. control (without protein), BSA (bovine serum albumin, pI: 4.4—4.9), chymotrypsin (pI: 8.1—8.6), and lysozyme (pI: 10.5—11.0) samples. The liquid paraffin and olive oil were obtained from Wako Pure Chemical Industries, Ltd., Osaka, as reagents of primary standard. BSA and chymotrypsin produced from bovine pancreas were purchased from Sigma Chemical Co., U.S.A., as a grade of biochemical reagents. Purified lysozyme from chicken egg white was provided by Wako Pure Chemical Industries, Ltd., Osaka. These materials were used without further treatment.

All of the W/O/W emulsion samples in a stable form were prepared by a combination[5] of the two separated steps of emulsification[7] and a phase-inversion technique[8,9] in order to immobilize 1 %w/w of each protein in the inner aqueous phase of the samples. According to the results of the preliminary studies, the procedure of emulsification for each sample could be summarized as follows:

(1) A range from 30 to 40 g of the oil phase containing 30 %w/w Span 80 in liquid paraffin or 30 %w/w TGCR in olive oil were placed in a vessel of a pin-mixer (described precisely in Ref. 7).

(2) An aqueous solution of 1 %w/w of each protein was then introduced successively to the oil phase in the vessel, while a stirrer unit of the pin-mixer rotated steadily at 88 rpm at room temperature so as to provide a W/O emulsion. This procedure was carried out over a range from 70 to 80 ml of the amount of the aqueous solution introduced.

(3) A definite amount of the first W/O emulsion, i.e. 90 g for the liquid-paraffin system and 54 g for another, was mixed with 45 ml of an aqueous solution of 1 %w/w Tween 80 in the liquid-paraffin system and with 36 ml of that of 1 %w/w DGMO in the olive-oil system.

(4) The mixture was finally homogenized by means of a mixer at about 5000 rpm of the armature speed for 1 min at room temperature, thus resulting a W/O/W emulsion containing one of the proteins in the inner aqueous phase of the dispersed vesicular globules. Details concerning the mixer used were also described in Ref. 7.

An optical microscopic examination indicated that almost all of the dispersed globules in freshly prepared samples have the vesicular structure with single or multiple compartments of the inner aqueous phase within a range of diameters from 2 to 30 μm.

An assembly with a rectangular cell provided by Mitamura Riken Kogyo, Ltd., Osaka, was employed for evaluating the electrophoretic mobility of the vesicular globules at neutral pH at room temperature. Each W/O/W emulsion was diluted about 100 times by the further addition of an aqueous solution of 1 mmol dm^{-3} KCl immediately before each measurement. The field strengths within a range from 3.3 to 10.0 V cm^{-1} were used to ensure that the electrophoretic mobility is independent of the actual applied voltage. A minimum of 20 readings were taken for each diluted system at any one voltage. The zeta potential (ζ) of the slipping plane of the diffused portion in the electrical double layer on the globules was calculated from the Smoluchowski equation for the electrophoresis of non-conducting spheres,[6] as follows:

$$\mu = \varepsilon_0 D\zeta / \eta, \quad (1)$$

where μ is the electrophoretic mobility, ε_0 is the permittivity of free space, and D and η are the relative permittivity and viscosity of the suspending fluid.

Results and Discussion

The values for the electrophoretic mobility and zeta potential of the vesicular globules in each sample are summarized in Table 1. The effect of proteins on the zeta potential of the globules appears in relation to the different magnitudes for the isoelectric point of the proteins immobilized in the inner aqueous phase, although the values obtained with the liquid-paraffin system are always smaller than those with the olive-oil

Table 1. Micro-Electrophoretic Data of Vesicular Globules in W/O/W Emulsions at Neutral pH at Room Temperature

Inner aqueous phase	Mobility	Zeta potential	Deviation
	$\mu m\ s^{-1}$ per $V\ cm^{-1}$	mV	mV
	Liquid paraffin system		
Without protein	−2.50	−32.1	±0.9
1% BSA	−2.14	−27.4	±0.5
1% Chymotrypsin	−1.67	−21.4	±0.4
1% Lysozyme	−1.06	−13.7	—
	Olive oil system		
Without protein	−5.56	−71.3	2.8[a)]
1% BSA	−4.30	−55.1	3.1[a)]
1% Chymotrypsin	−3.53	−45.3	2.2[a)]
1% Lysozyme	−2.27	−29.0	2.0[a)]

a) Standard deviation.

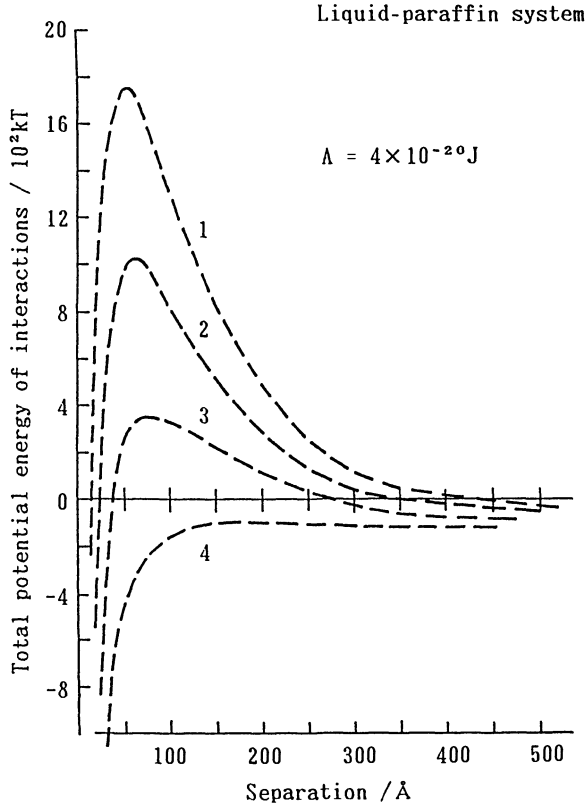

Fig. 1. Effect of proteins immobilized in the inner aqueous phase of a liquid-paraffin system on the total interactions between two vesicular globules at neutral pH at room temperature. Inner aqueous phase: Without protein (1), 1 %w/w BSA (2), 1 %w/w chymotrypsin (3), and 1 %w/w lysozyme (4).

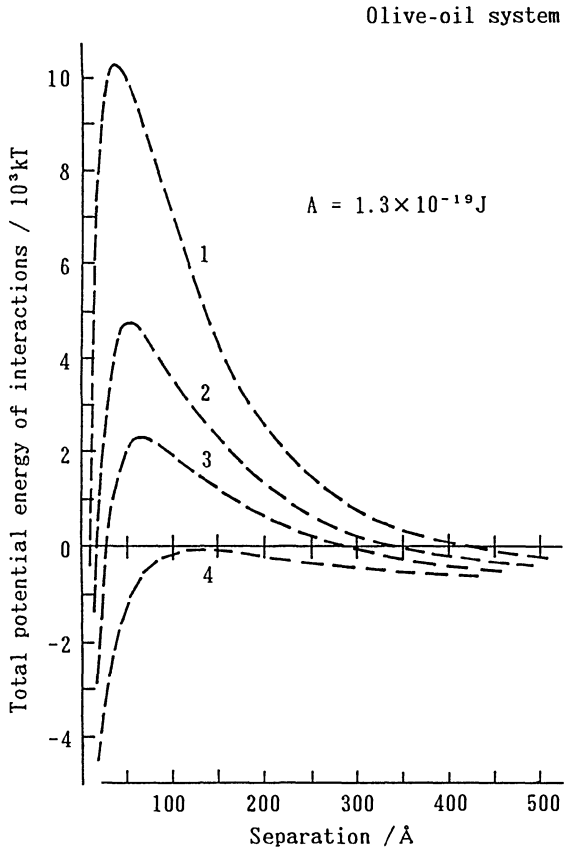

Fig. 2. Effect of proteins immobilized in the inner aqueous phase of an olive-oil system on the total interactions between two vesicular globules at neutral pH at room temperature. Inner aqueous phase: Without protein (1), 1 %w/w BSA (2), 1 %w/w chymotrypsin (3), and 1 %w/w lysozyme (4).

system. Such smaller values of the mobility and zeta potential may be brought about by the relatively longer distance to the slipping plane from the surface of the globules in the liquid-paraffin system, since the globules become to be covered by a deep hydration layer due to the existence of poly(oxyethylene) chains in the adsorbed molecules of Tween 80.[10]

Table 1, however, indicates that the zeta potential of the globules can be ranked with the magnitudes of the isoelectric point of the proteins, irrespective of the kinds of emulsifiers used, while a rapid coagulation occurs irreversively among the vesicular globules in the lysozyme samples showing the lowest zeta potential of the globules in a series of samples to be tested. The surface activity of protein molecules[11] may, more or less, result so as to form an adsorbed layer on the inside surface of the oil layer in the vesicular globules; the adsorbed protein molecules thus seem to play a role in the surface

potential of the vesicular globules according to the value of pH in the two aqueous phases. It is worth noting that the structure of the thin oil layer in a variety of W/O/W emulsions comprises the main lamellar membranes of the hydrophobic emulsifier, according to studies of the water permeation coefficient of the oil layer,[3] although the thickness of such a thin oil layer has not yet been fully investigated.

An attempt was made to estimate the total potential of interactions (V) between the two vesicular globules in each sample as a function of the separation (H) of the slipping planes in light of classical theory,[12] as follows:

$$V = 2\pi\varepsilon_0 D r\zeta^2 \ln[1+\exp(-\kappa H)] - rA/12H, \quad (2)$$

wherer r is the radius of the globules, H the separation, A the Hamaker constant, and κ the Debye-Hückel parameter given by

$$\kappa = (2ne^2z^2/\varepsilon_0 D\, kT)^{1/2}. \quad (3)$$

Here, n, e, and z are the concentration, elementary charge, and valency of counter ions, and kT is the thermal kinetic energy. The authors assumed that there is no energy barrier against the separation between the globules encapsulating lysozyme in each system because of the instability in the dispersion state, as already described. Thus, the value of the Hamaker constant could be estimated as being 4×10^{-20} J for the liquid-paraffin system and 1.3×10^{-19} J for the olive-oil system, respectively. Figures 1 and 2 compare the total potential of interactions against the separation between the two vesicular globules with each sample.

References

1) A. T. Florence and D. Whitehill, *Int. J. Pharm.*, **11**, 277 (1982).
2) S. Matsumoto, "Macro- and Microemulsions: Theory and Applications," ed by D. O. Shah, ACS Symp. Seri., ACS, Washington, DC (1985), Vol. 272, pp. 415—436.
3) S. Matsumoto, T. Inoue, M. Kohda, and K. Ikura, *J. Colloid Interface Sci.*, **77**, 555 (1980).
4) S. Magdassi and N. Garti, *J. Controlled Release*, **3**, 273 (1986).
5) S. Matsumoto and W. W. Kang, *Agric. Biol. Chem.*, **52**, 2689 (1988).
6) R. J. Hunter, "Zeta Potential in Colloid Science," Academic Press, London (1981), pp. 17—18 and pp. 59—124.
7) S. Matsumoto, Y. Kita, and D. Yonezawa, *J. Colloid Interface Sci.*, **57**, 353 (1976).
8) S. Matsumoto, *J. Colloid Interface Sci.*, **94**, 362 (1983).
9) S. Matsumoto, Y. Koh, and A. Michiura, *J. Dispersion Sci. Technol.*, **6**, 507 (1985).
10) J. Boyd, C. Parkinson, and P. Sherman, *J. Colloid Interface Sci.*, **41**, 359 (1972).
11) D. E. Graham and M. C. Phillips, "Theory and Practice of Emulsion Technology," ed by A. L. Smith, Academic Press, London (1976), pp. 75—98.
12) E. J. M. Verwey and J. Th. Overbeek, "Theory of the Stability of Lyophobic Colloid," Elsevir, Amsterdam (1948), pp. 135—185.

Correlations among One-Bond Deuterium Isotope Shifts in ^{13}C NMR and C-H Stretching Frequencies in IR for Monosubstituted Methane Derivatives

Yasuki NAKASHIMA† and Kensuke TAKAHASHI*
Department of Applied Chemistry, Nagoya Institute of Technology, Gokiso-cho, Showa-ku, Nagoya 466
†Research and Development Department, Menicon Co., Ltd., Biwajima, Nishi-ku, Nagoya 451
(Received May 29, 1991)

Synopsis. The effects of one bond deuterium isotope on ^{13}C NMR chemical shifts ($^1\Delta$) of the title compounds were found to be correlated with the corresponding C-H stretching frequencies(ν_{CH}) in IR spectroscopy, as follows: $^1\Delta$(ppb)= $-8.69\ \nu_{CH}(cm^{-1})+26500$.

The effects of the deuterium isotope on the ^{13}C NMR chemical shifts have been known for a long time. Recently, the true causes for these isotope shifts have been under intensive discussions.[1] However, for polyatomic molecules, there is no suitable model for the isotope shifts, which can be used to interpret all of the observed isotope shifts. We have systematically studied the isotope shifts on ^{13}C NMR.[2,3] As an extension of our studies, we report a correlation between $^1\Delta$ and ν_{CH}. To our knowledge, the NMR isotope shifts are related for the first time to the parameters of IR spectroscopy. Although Forsyth stated that there is no relation between $^1\Delta$ and ν_{CH} (Ref. 1b), we could find a correlation between the two parameters for a series of the title compounds.

Experimental

The isotope shifts were measured for mixtures of deuterated and undeuterated materials within an error of 3 ppb by a Varian XL-200 FT-NMR spectrometer at 50.3 MHz and about 22 °C. The IR spectra were measured for samples in the liquid phase within an error of 4 cm^{-1} using a JASCO FT/IR-8300 spectrometer. The materials were all commercially available.

Results and Discussion

The data concerning $^1\Delta$ and ν_{CH} for thirteen monosubstituted methane derivatives are given in Table 1 and are shown in Fig. 1. As can be seen in, there is a linear correlation between $^1\Delta$ and ν_{CH} with one exception. The largest deviation of CH_3NO_2 (**4**) could not yet be interpreted. The reason for this large deviation, for example, the conjugate effect or the magnetic anisotropy effect of the nitro group, can be considered.

It is well known that the C-H bond lengths can be predicted from the ν_{CH} values with high precision.[4,5] From this knowledge, $^1\Delta$ can be related to the C-H bond lengths of the observed carbons. When a C-H bond in a molecule is shorter than others, the observed ν_{CH} will be larger than that for the latter. Thus, this relation predicts that $^1\Delta$ becomes smaller for a carbon with a shorter C-H bond. This fact strongly supports an isotope shift model proposed by Jameson and Osten.[1c] This model assumes different anharmonic vibrational contributions for the C-H and C-D bonds. Although the energy surfaces for the deuterated and undeuterated materials should exactly coincide, small changes in the bond lengths and bond angles, which

Table 1. One-Bond Deuterium Isotope Shifts ($^1\Delta$) and C-H Stretching Frequencies (ν_{CH}) of Monosubstituted Methane Derivatives

No.	Substituent	$^1\Delta$[a]	Ref.	ν_{CH}[b]	Ref.
1	I	146.9	7	3029	5
2	CN	443.3	7	2979	5
3	H	579	8	2992	5
4	NO_2	684.2	7	3028	5
5	$Sn(Me)_3$	777	9	2960	5
6	SBu^n	747		2971[c,d]	
7	COMe	751[e]		2973[f]	5
8	CHO	756	10	2961	4
9	C_6H_5	825.5	11	2953	5
10	OH	849.2	7	2950[f]	5
11	CH_3	852.0	12	2950	5
12	OBu^n	903		2940[c,d]	
13	SOMe	911[e]		2955[d]	

a) $^1\Delta$ were defined as follows: $^1\Delta=\delta_{CH_3}-\delta_{CD_3}$ in ppb. Thus, high field shifts give positive $^1\Delta$. b) Measured in a gas phase (see Ref. 5) in cm^{-1}. c) Estimated values from averaged C-D stretching frequencies which are multiplied by $(13/7)^{1/2}$. See Ref. 13. d) Measured in a liquid phase in cm^{-1}. e) Measured for the d_6 compounds. Then, the contribution through three bonds was assumed to be negligible. f) Averaged for two nonequivalent C-H frequencies. See Ref. 5.

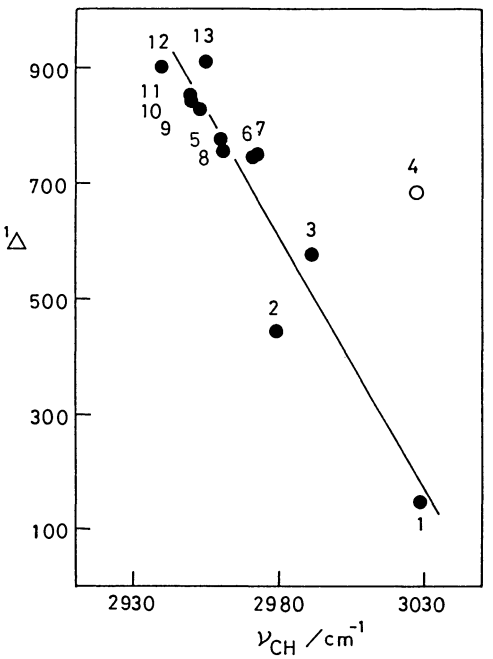

Fig. 1. Correlation of $^1\Delta$ with ν_{CH} of monosubstituted methane derivatives. With an exception of the value for CH_3NO_2, a correlated straight line is expressed as $^1\Delta$ (ppb)=26500−8.69 $\nu_{CH}(cm^{-1})$ with r=0.945 and a standard deviation of 77 ppb.

result from averaging over a vibrational motion in an anharmonic potential well, can be expected to occur.[6] This model assumes that the potential is less anharmonic for shorter, stronger bonds. With shorter bonds, the bond shortenings upon replacement of H by D are smaller, resulting in a smaller $^1\Delta$.

References

1) For recent reviews see: a) P. E. Hansen, *Ann. Rep. NMR Spectrosc.*, **15**, 105(1983); b) D. A. Forsyth, "Isotopes in Organic Chemistry," ed by Buncel and C. C. Lee, Elsevier, New York (1984), Vol. 6, Chap. 1, p.1; c) C. J. Jameson and H. J. Osten, *Ann. Rep. NMR Spectrosc.*, **17**, 1 (1985); d) S. Berger, "Isotope Effects in NMR Spectroscopy," ed by H. Günther, Springer, Berlin (1990), Vol. 22, p.1.

2) Y. Nakashima, A. Yoshino, and K. Takahashi, *Bull. Chem. Soc. Jpn.*, **62**, 1401 (1989).

3) Y. Nakashima, H. Nakane, S. Ban, and K. Takahashi, *Bull. Chem. Soc. Jpn.*, **63**, 2025 (1990).

4) H. J. Bernstein, *Spectrochim. Acta*, **18**, 161 (1962).

5) D. C. Mckean, J. L. Duncan, and L. Batt, *Spectrochim. Acta, Part A*, **29**, 1037 (1973).

6) K. L. Servis and F.-F. Shue, *J. Am. Chem. Soc.*, **102**, 7233 (1980).

7) J. R. Everett, *Org. Magn. Reson.*, **19**, 169 (1982).

8) M. Alei, Jr. and W. E. Wageman, *J. Chem. Phys.*, **68**, 783 (1978).

9) C. R. Lassigne and E. J. Wells, *J. Magn. Reson.*, **31**, 195 (1978).

10) P. E. Hansen, F. M. Nicolaisen, and K. Schaumburg, *J. Am. Chem. Soc.*, **108**, 625 (1986). The value for CD_3CHO is assumed from that for CHD_2CHO (504 ppb) which is multiplied by 3/2.

11) J. R. Wesener and H. Günther, *Tetrahedron Lett.*, **23**, 2845 (1982).

12) J. R. Wesener, D. Moskau, and H. Günther, *J. Am. Chem. Soc.*, **107**, 7307 (1985). The value for CH_2DCH_3 (284.0 ppb) is used to estimate that of CD_3CH_3 which is multiplied by 3.

13) K. Nakanishi, P. H. Solomon, and N. Furutachi, "Infrared Absorption Spectroscopy," 17th ed, Nankodo, Tokyo (1978), p.66.

New Crystalline Complexes Composed of a Fatty Acid and Nicotinamide

Shoko YOKOYAMA,* Fumio UEDA,† and Tadao FUJIE
Kyoritsu College of Pharmacy, 1-5-30, Shibakoen, Minato-ku, Tokyo 105
†Research Laboratory, Kawai Seiyaku Co., Ltd., 6-3-5, Nakano, Nakano-ku, Tokyo 164
(Received June 7, 1991)

Synopsis. New crystalline complexes composed of a fatty acid (FA) and nicotinamide (NAA) at a molar ratio of 6:5, $(FA)_6(NAA)_5$, have been isolated. The melting points of $(FA)_6(NAA)_5$ were higher than those of the corresponding equimolar complexes, $(FA)_6(NAA)_6$.

We previously reported[1] that a fatty acid (FA) forms crystalline complexes with nicotinamide (NAA), 3-pyridine carboxamide, at a molar ratio of 1:1. These FA-complexes were obtained only in 1,2-dichloroethane.[1] A fatty acid forms an association complex similar to a reversed micelle in 1,2-dichloroethane.[2] The aggregation number in the association, though not yet determined, appears to be 6.[2] Association of FA molecules in 1,2-dichloroethane may be the first step for the crystalline FA-NAA complex formation. Further, the diameter of the host cavity of $(FA)_6$ is 5.1—6.7 Å if the host structure consists of six molecules of FA.[2] This cavity size is similar to that of α or β-cyclodextrin, though cyclodextrins generally include lipophilic compounds whereas $(FA)_6$ includes water-soluble compounds.

The FA–NAA equimolar complex is suggested to be of a formula $(FA)_6(NAA)_6$, in view of the formation mechanism of FA-complexes in 1,2-dichloroethane, though the actual molecular formula of the complex has not yet been determined. The FA–NAA complex is obtained as a solid, and the complex is decomposed to FA and NAA when dissolved in solvents. The complex is partially dissociated even when it is dissolved in 1,2-dichloroethane: this is because FA forms an association complex similar to a reversed micelle in 1,2-dichloroethane and that FA is in association equilibria, monomer$\rightleftarrows$dimer$\rightleftarrows$trimer$\rightleftarrows$hexamer, in this solvent.[2] Therefore, the molecular weight of the complex cannot be determined by a general method, namely vapor pressure or freezing point depression. Though X-ray crystal structure analysis is currently envisaged, it takes a long time to attain a clear result. In the meantime, we have isolated a new crystalline complex composed of octadecanoic acid (C18) and NAA from a 1,2-dichloroethane solution.[3] The formula of the new complex was $(C18)_6(NAA)_5$, and the C18-NAA equimolar complex is transformed into $(C18)_6(NAA)_5$ at temperatures below 22 °C by releasing 16% ($\fallingdotseq$ 1/6) of NAA, when cooled in acidic aqueous medium at temperature intervals of 5 °C from 37 °C.[3] This verified that the formula of the C18-NAA equimolar complex was $(C18)_6(NAA)_6$. Hereafter we denote the FA-NAA equimolar complex as $(FA)_6(NAA)_6$.

The melting point of $(C18)_6(NAA)_5$ was higher than that of $(C18)_6(NAA)_6$.[3] In view of this, the 6:5 complexes, $(FA)_6(NAA)_5$, with various alkyl chain length were prepared, and their melting points were systematically investigated in this work. The differences in the melting point between $(FA)_6(NAA)_5$ and $(FA)_6(NAA)_6$ will be discussed.

Experimental

Materials. NAA, tetradecanoic acid (C14), pentadecanoic acid (C15), hexadecanoic acid (C16), heptadecanoic acid (C17), and octadecanoic acid (C18) were the same as those used in previous work.[1] 1,2-Dichloroethane, ethanol, and a 0.1 M KOH (M=mol dm^{-3}) ethanol solution were the same as those used previously.[1,3]

Preparation of New Complexes. FA and NAA were dissolved at a molar ratio of about 1.4:1 in warm 1,2-dichloroethane, and the solutions were left standing at 20—25, 15—20, or 5—10 °C. Crystals were then obtained by filtration and dried under reduced pressure at room temperature.

Measurement of Melting Points. Melting points were determined with an apparatus equipped with a microscope (×100).

Quantitative Analysis of FA in the Complexes. Complexes with a unique melting point were chosen for quantitative analysis. Complexes were dissolved in ethanol, and the FA contained in the solution was titrated with a 0.1 M KOH ethanol solution.[1]

Elemental Analysis. Elemental analysis of the complex for C, H, and N was carried out by the thermal conductivity method.

Results

Conditions for Preparing New Complexes. It was difficult to obtain the new crystalline complexes in pure form. Occasionally FA, NAA, or $(FA)_6(NAA)_6$ was coprecipitated by changing the experimental conditions. The preparation conditions when the new complexes were obtained pure are summarized in Table 1, though these conditions are not necessarily the most appropriate ones.

Melting Points of the New Complexes. Since the melting point of $(C18)_6(NAA)_5$ is higher than that of $(C18)_6(NAA)_6$,[3] a compound with a melting point higher than that of $(FA)_6(NAA)_6$ was regarded as a new complex. The melting points of the new complexes are summarized in Table 2.

Table 1. Conditions for $(FA)_6(NAA)_5$ Preparation

Starting material[a]		Solvent	Crystallization[b]
NAA/g	FA/g	1,2-Dichloroethane/ml	temperature/°C
1.0	C18 3.25	200	20—25
1.0	C17 3.10	180	20—25
1.0	C16 3.10	60	15—20
1.0	C15 2.80	80	5—10
1.0	C14 2.55	100	5—10

a) Molar ratios of FA to NAA are approximately 1.4:1.
b) Crystallization time is 7 h in each case.

Table 2. Melting Points of $(FA)_6(NAA)_5$

$(FA)_6(NAA)_5$	Melting point/°C
$(C18)_6(NAA)_5$	87—89
$(C17)_6(NAA)_5$	89—91
$(C16)_6(NAA)_5$	83—85
$(C15)_6(NAA)_5$	85—87
$(C14)_6(NAA)_5$	78—80

Table 3. Quantitative Analysis of FA in the New Complexes

FA	Number of determinations	FA to NAA Molar ratio[a)]
C18	6	1.20±0.00
C17	3	1.20
C16	6	1.19±0.02
C15	3	1.20
C14	6	1.19±0.01

a) Mean±SD.

Quantitative Analysis of FA in the New Complexes. The molar ratio of FA to NAA in the complex was determined by quantitative analysis of FA, and the results are shown in Table 3. As is seen, the molar ratio of FA to NAA is 1.2 : 1 for each case. This is in line with a molecular formula of $(FA)_6(NAA)_5$.

The starting mixing ratio of FA to NAA was 1.4 : 1, while the molar ratio of FA to NAA in the complex was 1.2 : 1. This is because FA exists partly as a monomer, dimer, or trimer in 1,2-dichloroethane.[2)]

Elemental Analysis of the New Complexes. The results of elemental analyses of the new complexes are given in Table 4. The experimental values are well consistent with the theoretical values based on the molecular formula $(FA)_6(NAA)_5$. This further indicates that the new complexes are of the formula $(FA)_6(NAA)_5$.

Discussion

Comparison of $(FA)_6(NAA)_5$ with $(FA)_6(NAA)_6$. The melting points of $(FA)_6(NAA)_5$, $(FA)_6(NAA)_6$, and FA are shown in Fig. 1 against the carbon number (n) of the constituent FA. The melting point of an odd-numbered FA is lower than that of an even-numbered FA with an alkyl chain longer by one carbon atom, and the relationship between the melting point of FA and n takes a zig-zag form. The melting points of $(FA)_6(NAA)_6$ are higher than those of FA, especially with odd-numbered FA, and the melting point of

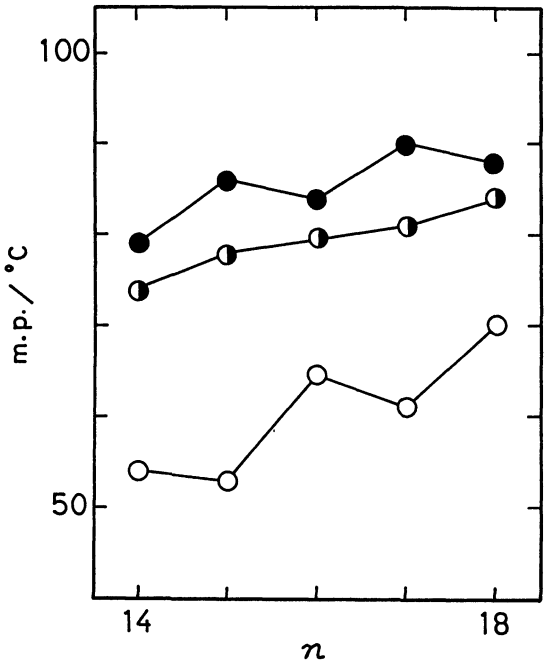

Fig. 1. Relationships between the melting point and n for $(FA)_6(NAA)_5$, $(FA)_6(NAA)_6$, and FA
●, $(FA)_6(NAA)_5$; ◑, $(FA)_6(NAA)_6$; ○, FA.

$(FA)_6(NAA)_6$ changes roughly linearly with n. The melting points of $(FA)_6(NAA)_5$ are higher than those of $(FA)_6(NAA)_6$, and the difference is larger for compounds with odd-numbered FA. The zig-zag form of the melting point curve is neatly reversed between FA and $(FA)_6(NAA)_5$: the difference in melting point between $(FA)_6(NAA)_5$ and $(FA)_6(NAA)_6$ is 4—5 °C for even-numbered FA, and 8—9 °C for odd-numbered FA. This suggests that $(FA)_6(NAA)_5$ with odd-numbered FA is more thermostable than $(FA)_6(NAA)_5$ with even-numbered FA, and is related to an observation that pure $(FA)_6(NAA)_5$ with odd-numbered FA was formed more easily than pure $(FA)_6(NAA)_5$ with even-numbered FA: namely, coprecipitation of $(FA)_6(NAA)_6$ was to a lesser extent for odd-numbered FA.

We now compare $(FA)_6(NAA)_5$ and $(FA)_6(NAA)_6$ for the preparation conditions. In preparing $(FA)_6(NAA)_5$, the mixing ratio of FA to NAA is slightly larger and the temparature for crystallization is lower. The complex formation between a FA and a water-soluble compound in 1,2-dichloroethane presumably begins with the solubilization of the water-soluble compound in the reversed micellar FA hexamer.[2)] The amount of FA hexamer

Table 4. Elemental Analysis of $(FA)_6(NAA)_5$

Formula	Analysis/% Found (Calcd)					
	C		H		N	
$(C_{18}H_{36}O_2)_6(C_6H_6N_2O)_5$	71.63	(71.52)	10.65	(10.70)	6.04	(6.05)
$(C_{17}H_{34}O_2)_6(C_6H_6N_2O)_5$	70.95	(70.99)	10.58	(10.56)	6.28	(6.27)
$(C_{16}H_{32}O_2)_6(C_6H_6N_2O)_5$	70.31	(70.41)	10.33	(10.41)	6.59	(6.52)
$(C_{15}H_{30}O_2)_6(C_6H_6N_2O)_5$	69.80	(69.79)	10.21	(10.25)	6.79	(6.78)
$(C_{14}H_{28}O_2)_6(C_6H_6N_2O)_5$	69.03	(69.12)	10.02	(10.08)	7.12	(7.07)

increases with increasing its concentration. This may have decreased the amount of NAA per FA hexamer $(FA)_6$ and have led to the formation of $(FA)_6(NAA)_5$.

The temperature also plays an important role in the crystallization of the two kinds of complexes. The temperature for crystallization may yield a difference in the tilting angle of FA molecules in the crystal structure of $(FA)_6$ which serves as a host. For example, even-numbered FA occur in three polymorphic modifications, A, B, and C.[4-6] In none of them do the chains rotate: they differ in the angle of the chains with respect to the plane of the carboxyl groups, A=chains vertical; B=chains tilted at 74°40′; C=chains tilted at 59°12′.[4] The latter two can be easily crystallized. Further, the polymorph B is obtained by slow crystallization at room temperature whereas the polymorph C is obtained by rapid crystallization at lower temperatures.[5]

The tilting angle of $(FA)_6$ in the crystal of $(FA)_6(NAA)_5$ may be different from that in $(FA)_6(NAA)_6$, similarly to the difference between the polymorphs B and C. Further, the tilting angle of $(FA)_6$ may depend on the temperature for crystallization. In view of the conditions for preparing $(FA)_6(NAA)_5$ and $(FA)_6(NAA)_6$, $(FA)_6(NAA)_5$ probably corresponds to the polymorph C of FA, while $(FA)_6(NAA)_6$ to the polymorph B. The heat of solution of the polymorph B is larger than that of the polymorph C.[5] The melting point of $(FA)_6(NAA)_5$ is higher than that of $(FA)_6(NAA)_6$, as seen in Fig. 1. These lead us to speculate that five NAA molecules are fit into the more tilted $(FA)_6$ more favorably than six NAA molecules into the less tilted $(FA)_6$, and hence $(FA)_6(NAA)_5$ is stabilized over $(FA)_6(NAA)_6$.

The reason why the thermostable $(FA)_6(NAA)_5$ was not obtained first, is related to the solubility of FA. Especially with C18, the preparing a pure complex is easier at higher temperatures, where coprecipitation of FA is well suppressed, than at lower temperatures, and the higher temperature thus favored the formation of $(FA)_6(NAA)_6$.

References

1) F. Ueda, T. Higashi, Y. Ayukawa, A. Takada, T. Fujie, A. Kaneko, and S. Yokoyama, *Bitamin,* **62**, 669 (1988).

2) S. Yokoyama and T. Fujie, *Chem. Pharm. Bull.,* **38**, 2249 (1990).

3) S. Yokoyama, F. Ueda, and T. Fujie, *Chem. Pharm. Bull.,* **39**, 1634 (1991).

4) M. Davies and B. Kybett, *Trans. Faraday Soc.,* **61**, 2646 (1965).

5) W. Beckmann, F. Rouquerol, and H. Beckmann, *Thermochim. Acta,* **66**, 295 (1983).

6) W. Beckmann, P. Boistelle, and K. Sato, *J. Chem. Eng. Data,* **29**, 111 (1984).

High-Performance Liquid Chromatographic Determination of Components in Eye Lotion Using Methoxy(3-morpholinopropyl)silanediyl Modified Silica Gel Column

Shuzo AKIYAMA,* Kenichiro NAKASHIMA, Kyoko YAMADA, and Nanako SHIRAKAWA
School of Pharmaceutical Sciences, Nagasaki University, 1-14 Bunkyo-machi, Nagasaki 852
(Received April 22, 1991)

Synopsis. A recently developed column packing material, methoxy(3-morpholinopropyl)silanediyl modified silica gel, was successfully applied to the separation and determination of components (pyridoxine, flavin adenine dinucleotide, cyanocobalamin, chlorpheniramine, naphazoline, and neostigmine) in an eye lotion, in a single analysis by a single buffer elution with UV detection.

Quite recently, we reported on the development of new column packing materials for the high-performance liquid chromatographic (HPLC) separation of water-soluble vitamins[1] as well as such substances[2] as inosinic, xanthylic, and guanylic acids related to umami. It was consequently confirmed that methoxy(3-morpholinopropyl)silanediyl modified silica gel (MPS), similar to an ion-exchange resin, is suitable for separating water-soluble compounds. On the other hand, in ophthalmologic or pharmaceutical studies, a simple and rapid determination of components in eye lotions should be useful. Although the determination of a single component, such as boric acid[3] or thimerosal,[4] in an eye lotion by HPLC is known, HPLC-analysis of multicomponents has until now been scarcely reported. In this study, we thus tried to expand on the application of MPS to the separation and determination of components in eye lotions using UV detection.

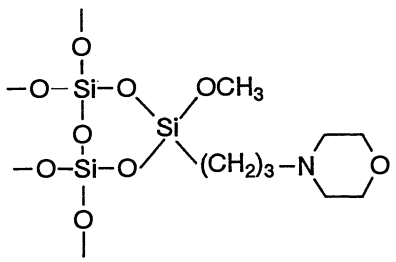

Formula.

Experimental

Material. MPS was prepared according to a previous report.[1] Pyridoxine (PY) and flavin adenine dinucleotide (FAD) were obtained from Wako Pure Chemicals Co., Ltd. Cyanocobalamin (CC), chlorpheniramine (CP) (as its maleate), naphazoline (NA), and neostigmine (NE) (as its methyl sulfate) were purchased from Sigma Chemical Co. All other reagents used were of analytical grade (Wako).

Apparatus. The chromatograph system comprised a Tosoh CCPD pump with a Rheodyne-type injector (7125) with a 100 μl loop, a Tosoh UV8011 variable-wavelength UV monitor and a Hitachi Model 561 recorder. The eluates were monitored at 270 nm.

HPLC Column and Eluent. The gel (MPS) was packed into a stainless-steel tube (150 mm×6.0 mm I.D.) using a slurry-packing technique [glycerol : methanol, 4 : 6 (v/v)] and applied to the HPLC separation at a flow rate 1.0 ml min^{-1} of 0.1 M (1 M=1 mol dm^{-3}) phosphate buffer (pH 2.3) (column temperature, 30 °C).

Preparation of a Standard Solution of the Components Contained in an Eye Lotion. Six components (PY, FAD, CC, CP, NA, and NE) in a commercially available eye lotion were separately dissolved in the eluent [0.1 M phosphate buffer (pH 2.3)]; the solutions were then arranged to 5×10^{-4} M for PY, CP, and NA, 5×10^{-5} M (CC), and 10^{-3} M (NE).

Determination. Each component was determined by the standard addition method, as follows: To a commercially available eye lotion was added a series of known concentrations of standard solution, and diluted ten times with an eluent. Aliquots (100 μl) were injected onto the HPLC.

Results and Discussion

In the separation of water-soluble components with MPS, a phosphate buffer as an eluent has been studied in detail and found to be useful.[1] We therefore used a phosphate buffer for an eluent. First of all, the effect of the eluent pH was examined in order to separate the six components (PY, FAD, CC, CP, NA, and NE). The use of a 0.1 M phosphate buffer (pH 2.3) gave a relatively good peak separation. Almost no effect was observed after the addition of sodium 1-octanesulfonate. Under the above-mentioned HPLC conditions, it was demonstrated that their water-soluble substances, including maleic acid liberated from CP maleate, can be well separated (except for CP and NA) within 15 min in a single analysis (Fig. 1). The calibra-

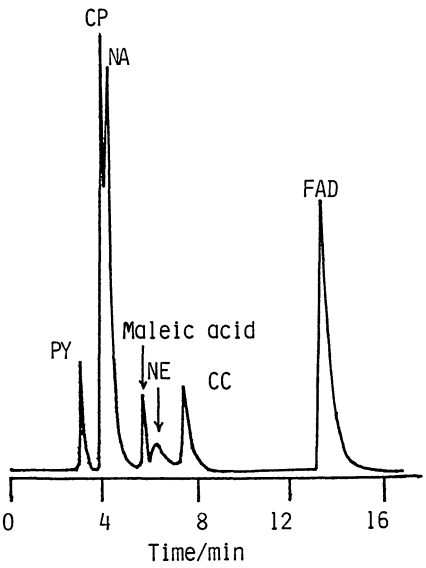

Fig. 1. Chromatogram of the components of an eye lotion.

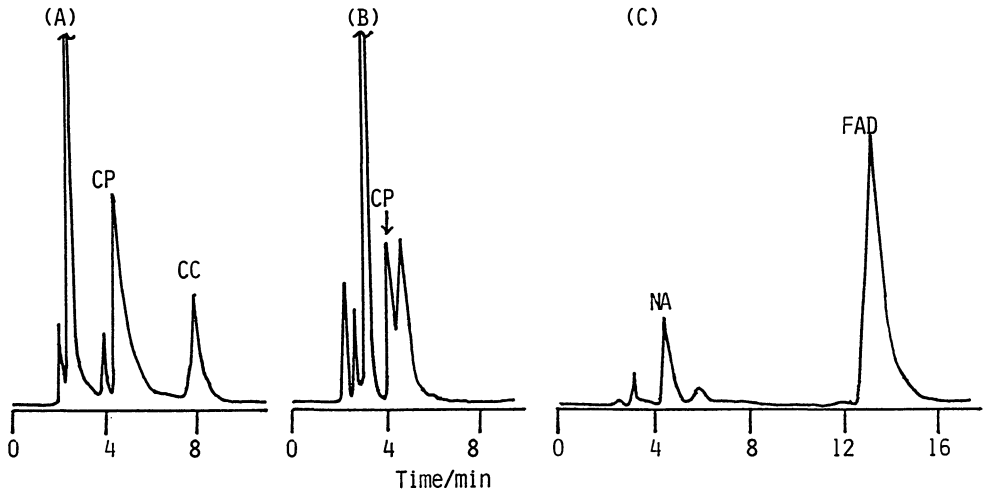

Fig. 2. Chromatograms of a commercially available eye lotion (A—C).

Table 1. Calibration Curves for the Components in Eye Lotion

Compound	Equation[a)]	r	RSD(%), n=5 (concn)
PY	Y=0.19X+0.01	0.999	3.20 (10 nmol)
FAD	Y=3.34X+0.15	0.999	1.32 (5 nmol)
CC	Y=2.24X−0.03	0.999	1.03 (1 nmol)
CP	Y=1.54X−0.08	0.999	1.28 (5 nmol)
NE	Y=0.09X−0.04	1.000	2.42 (20 nmol)
NA	Y=0.78X+0.70	0.999	1.22 (25 nmol)

a) Y=Peak height (cm), X=Concentration (nmol/injection).

Table 2. Analyses of Eye Lotion

Sample	Found (M)[a)] (w/v%)	Indicated (M) (w/v%)
Eye lotion A		
CC	7.5×10^{-5} (0.01)	7.4×10^{-5} (0.01)
CP	2.2×10^{-4} (0.01)	2.6×10^{-4} (0.01)
Eye lotion B		
CP	2.4×10^{-3} (0.09)	5.1×10^{-4} (0.02)
Eye lotion C		
FAD	5.1×10^{-4} (0.04)	4.2×10^{-4} (0.033)
NA	1.8×10^{-4} (0.004)	1.2×10^{-4} (0.003)

a) Mean of duplicate assay.

tion curves for these components obtained by using the corresponding standard solutions were linear in the nmol range of 1.75—14 (PY), 0.98—7.9 (FAD), 0.18—1.4 (CC), 0.88—7 (CP), 3.6—29 (NE), and 6.25—50 (NA). The linear regressions are shown in Table 1 with the correlation coefficients (r). As the application work, three commercially available eye lotions were assayed. Typical chromatograms are shown in Fig. 2. The peaks were confirmed by co-chromatography. Compounds CC, CP, FAD, and NA in commercially available eye lotions (A—C) were determined by the standard addition method (Table 2). Compounds PY and NE could not be determined under the experimental conditions. On the other hand, it was observed that the separation capacity of MPS gradually decreased with increasing the sample loading. This might be caused by the hydrolysis of MPS with a lower pH mobile phase. This point must be improved and is now under study.

In conclusion, MPS could be further applied to the analysis of components in commercially available eye lotions. This method might be useful for pharmaceutical studies on the stability of the components contained in eye lotions.

This work was supported in part by a Grant-in-Aid for Scientific Research No. 02453145 form the Ministry of Education, Science and Culture. We thank Daiso Co., Ltd., for providing Daiso gel and for valuable advice and discussions.

References

1) S. Akiyama, K. Nakashima, N. Shirakawa, and K. Yamada, *Bull. Chem. Soc. Jpn.*, **63**, 2809 (1990).
2) S. Akiyama, K. Nakashima, K. Yamada, N. Shirakawa, M. Sainoh, *Anal. Sci.*, **7**, 649 (1991).
3) M. Zenki, J. Ohtani, T. Ikeda, and K. Tôei, *Chem. Lett.*, **1990**, 885.
4) S. W. Lam, R. C. Meyer, and L. T. Takahashi, *J. Parenter. Sci. Technol.*, **35**, 262 (1981).

Thienylpyridines as a New Fluorescent Reagent. II.[1] Determination of Carboxylic Acid with 5-(4-Pyridyl)-2-thiophenemethanol Using HPLC

Riichiro NAKAJIMA,* Kazuhiko SHIMADA, Yasuhiro FUJII,
Akifumi YAMAMOTO, and Tadashi HARA
Department of Chemical Engineering, Faculty of Engineering, Doshisha University, Kamigyo, Kyoto 602
(Received May 9, 1991)

Synopsis. The title compound has been prepared and used as a new derivatization reagent. The reagent reacts with the carboxylic acids in chloroform in the presence of 1-isopropyl-3-(3-dimethylaminopropyl)carbodiimide to produce the corresponding fluorescent esters, which can be separated on an octadecyl-silica column. Each 5 fmol of hexadecanoic or octadecanoic acids and about 50 fmol of benzoic and *p*-anisic acids (1 μl injection) (S/N=2) were detected.

Recently, we have reported that a thienylpyridine skeleton is a new fluorophore,[2] and that 5-(4-pyridyl)-2-thiophenecarbaldehyde(**1**) is one of the useful derivatization reagents for aliphatic primary amines in HPLC.[1] The present paper deals with the preparation of a new fluorescent compound, 5-(4-pyridyl)-2-thiophenemethanol(**2**), and with its application to the determination of carboxylic acids. The detection limits of most aromatic carboxylic acids were superior to those of all known reagents,[3,4] and those of aliphatic carboxylic acids were also superior to those of known reagents, except for 3-bromomethyl-6,7-dimethoxy-1-methyl-2(1*H*)-quinoxalinone(**3**).[3] The dynamic linear range was over 4 orders of magnitude.

Experimental

Elemental analyses were performed by the Laboratory for Organic Elemental Microanalysis, Faculty of Pharmaceutical Sciences, Kyoto University. Melting points were uncorrected. The ^{1}H and ^{13}C NMR spectra were recorded on a JEOL JNM-GX400 FT spectrometer in $CDCl_3$ using TMS as the internal standard. Mass spectra were recorded on a Hitachi M-80B mass spectrometer.

Liquid chromatography experiments were conducted on a HPLC system consisting of two Tosoh CCPE pumps equipped with an MX-8010 mixer, a Rheodyne Model 7410 fixed loop injector, a Shimadzu Shim-pack CLC-ODS column (15 cm×6 mm i.d.; packed with octadecyl-silica gel), and a Shimadzu RF-535 fluorescence monitor. Chromatograms were recorded with a Shimadzu C-R3A chromatopac or with an EPSON PC-286V computer connected with the chromatopac.

Reagent. All chemicals were of reagent grade and were used as received from commercial sources, except for those noted below. Solvents were distilled and water was purified through a Milli-QII system.

Preparation of 2. Aldehyde **1**[1] (2.0 mmol) and a trace amount of Methyl Orange were dissolved in 40 ml of methanol. Sodium cyanotrihydroborate (2.6 mmol) was added, and concd hydrochloric acid–methanol (1:5) was added dropwise with stirring to maintain the red color. After 5 h, the methanol was evaporated in vacuo. The residue was taken up in 20 ml of 5% sodium hydroxide solution, and extracted with three 20-ml portions of chloroform. The combined extracts were evaporated under reduced pressure and chromatographed on silica gel (eluent, acetone:ethyl acetate=1:1), and recrystallized from chloroform to yield colorless needles **2** in a 60% yield. Mp 139.0—139.5 °C. Found: C, 62.60; H, 4.79; N 7.17%; *m/z*, 191.0404. Calcd for $C_{10}H_9NOS$: C, 62.80; H, 4.74; N, 7.32%; M, 191.0404. ^{1}H NMR (400 MHz, 40 °C) δ=2.5 (1H, br, OH), 4.86 (2H, s, CH_2), 7.01 (1H, d, *J*=3.8 Hz), 7.36 (1H, d, *J*=3.8 Hz), 7.43 (2H, dd, *J*=4.6 and 1.7 Hz, H-3 and H-5 in pyridine ring), and 8.53 (2H, dd, *J*=4.6 and 1.7 Hz, H-2 and H-6 in pyridine ring). ^{13}C NMR (100 MHz) δ=60.12 (s), 119.77 (d, 2C), 125.27 (d), 126.31 (d), 140.85 (s), 141.61 (s), 146.79 (s), and 150.25 (d, 2C). Reagent **2** was stable in the crystalline state for a year or longer in daylight at room temperature.

Derivatization Procedure. One fifth ml of chloroform containing 8.0—1.6×10^5 pmol of carboxylic acids and 0.2 ml of chloroform containing 0.8 μmol of 1-isopropyl-3-(3-dimethylaminopropyl)carbodiimide perchlorate(**4**) were added to 0.2 ml of chloroform containing 0.4 μmol of **2** and 1.6 μmol of 4-dimethylaminopyridine(**5**) in a 20-ml screw-capped reaction vial. The reaction vial was tightly closed, heated at 60 °C for 3 h, and then cooled. Each 1 μl of the solution was subjected to HPLC, and determined by monitoring the fluorescence intensities at 360 nm with excitation of 300 nm.

Results and Discussion

Preparation and Properties of 2. Reagent **2** was prepared in a 60% yield by the reduction of **1** with cyanotrihydroborate ion under the conditions described for the reduction of acetophenone;[5] its structure was proved by its ^{1}H and ^{13}C NMR spectra, MS, and elemental analysis. The alcohol **2** a stable crystalline substance, behaved as a weak base with pK_a 4.64 in 40% aqueous methanol. A nonprotonated form of **2** exhibited more excellent fluorescent properties than a protonated one. Its new carboxylic esters(**6**) also strongly fluorescenced and the pH dependence of the spectra was similar to that of 4-(2-thienyl)pyridine.[6]

Determination of Carboxylic Acids. Figure 1 shows typical chromatograms for the linear saturated fatty acid esters of **2**. The C2—C18 fatty acid esters of **2** were separated on a reversed-phase column (Shim-pack CLC-ODS) with methanol. Methanol gave a complete separation for the C12—C18 long-chain fatty acid esters, though the peaks for the esters of C2—C7 short-chain fatty acids almost overlapped those for the derivatization reagent **2** and/or an adjacent peak. When a gradient elution using 30—0%(v/v) aqueous methanol was applied, however, the esters of short-chain fatty acids were completely separated.

Three condensing reagents, i.e., **4**, dicyclohexylcarbodiimide(**7**), and diethyl phosphorocyanidate(**8**), were examined for the esterification of linear fatty acids with **2** in chloroform, since no esterification occurred in the absence of a condensing reagent; reagents **4** and **7** accelerated the esterification, but reagent **8** did not.[7] Figure 2 shows the effect of the concentration of **4** and **7** on the peak area of the esters of C2—C7 acids. The

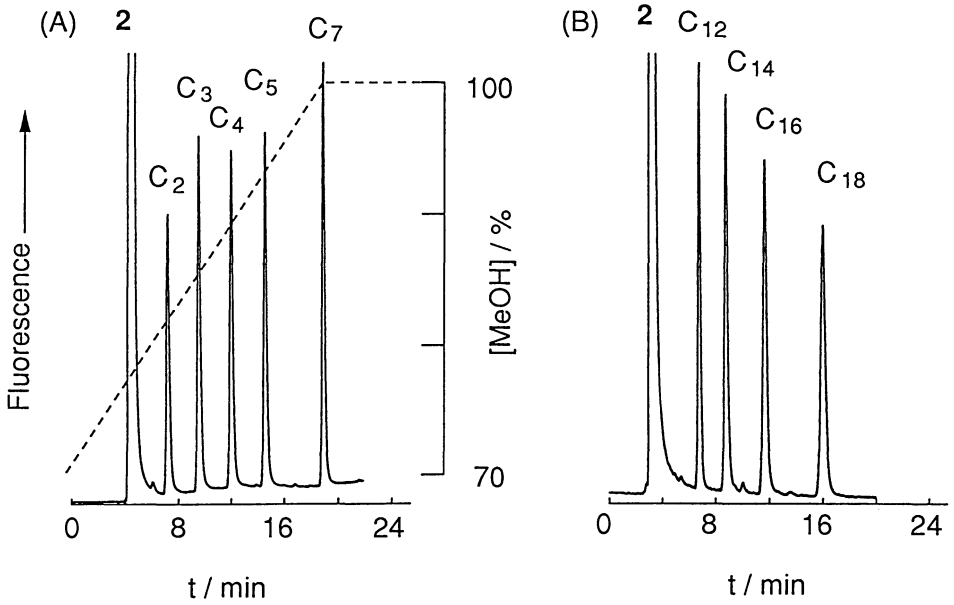

Fig. 1. Chromatograms for the esters of C2—C18 linear saturated fatty acids.
The esters are denoted by the numbers of carbon atoms of fatty acid, C*n*. Column, 150×6 mm i.d. Shim-pack CLC-ODS; eluent, (A) 30—0% (v/v) aqueous methanol and (B) methanol, 1.0 ml min^{-1}; sample size, 1 μl (70 pmol); precolumn reaction, a portion (0.2 ml) of a standard mixture of the acids (each 0.2 mmol dm^{-3}) was derivatized according to the procedure described in the experimental section.

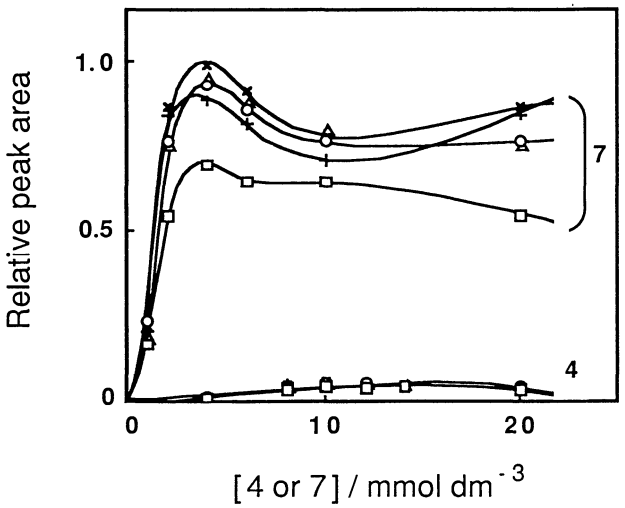

Fig. 2. Effect of the concentration of a condensing reagent, **4** or **7**, on the peak area of the esters of C2—C7 acids: (—□—) C2, (—○—) C3, (—△—) C4, (—×—) C5, and (—+—) C7 acids.
The conditions are as described in Fig. 1, except for a condensing reagent. The values of the vertical axis are represented as the ratio of the peak area of the esters to the maximum area of the C5 acid ester.

largest peaks were obtained at 4 mmol dm^{-3} of the reagent **4** solution for all the acids, where no side reaction occurred, although above this concentration other small peaks were also observed; a 4 mmol dm^{-3} **4** solution was used in subsequent work. The maximum and constant peak area were attained at temperatures higher than 60 °C and heating times longer than 3 h; heating for 3 h at 60 °C was employed in subsequent work.

Table 1. Linear Ranges and Detection Limits of Saturated Fatty Acids[a)]

Saturated fatty acid	Linear range /fmol	Detection limit (S/N=2)/fmol
Acetic acid	5.8×10^3—120×10^3	5800
Propionic acid	170—84×10^3	170
Butyric acid	420—84×10^3	420
Valeric acid	29—58×10^3	15
Heptanoic acid	27—53×10^3	13
Dodecanoic acid	110—110×10^3	110
Tetradecanoic acid	11—110×10^3	11
Hexadecanoic acid	12—120×10^3	5
Octadecanoic acid	12—120×10^3	5

a) Conditions as described in Fig. 1.

The derivatization of C18 acid with **2** went to completion under the present conditions, since both the retention time and the peak area of HPLC for a sample prepared from 2.0×10^{-5} mol dm^{-3} C18 acid solution were consistent with those of a 2.0×10^{-5}mol dm^{-3} 5-(4-pyridyl)-2-thenyl octadecanoate[6)] solution. Table 1 shows the linear ranges and detection limits (S/N=2) obtained from the calibration curves for C2—C18 acids. The linear-correlation coefficients were more than 0.9991 for all the acids within the tabulated ranges of the concentration. These limits were superior to those of the known reagents, except for **3**.[3)] The lower detection limit of C2 acid was higher than that estimated from the IFS value,[6)] because a small peak for a trace amount of the C2 acid ester and a large peak for a large excess of reagent **2** overlapped. The coefficients of

Table 2. Retention Time, Peak Area, and pK_a of Aromatic Carboxylic Acids[a)]

Aromatic carboxylic acid	Retention time/min	Relative peak area[b)]	pK_a	
o-Bromobenzoic acid	6.7	0.10	2.85[c)]	
m-Bromobenzoic acid	10.0	0.19	3.81[c)]	
p-Bromobenzoic acid	9.5	0.28	4.00[c)]	
o-Anisic acid	5.1	0.65	4.09[c)]	
m-Anisic acid	6.7	0.62	4.09[c)]	
p-Anisic acid	7.7	1.43	4.49[c)]	
Benzoic acid	6.9	1.00	4.21[c)]	5.79[d)]
p-Toluic acid	8.9	1.29		6.12[d)]

a) Conditions as stated in Fig. 1, except for the eluent (95% methanol) and concentration of the acid standard solution (each 1.5 mmol dm^{-3}). b) Expressed as a ratio of the peak area of the analyte to that of benzoic acid. c) Ref. 8. d) Ref. 9.

variation for 1.8×10^{-7} mol dm^{-3} C5 and 1.6×10^{-7} mol dm^{-3} C7 acid solutions (n=7) were 2.1 and 1.9%, respectively.

Some aromatic carboxylic acids were made to react with **2** under the derivatization conditions described above in order to produce fluorescent derivatives which could be separated by HPLC. Table 2 shows the retention time and peak area with the pK_a values of the corresponding acids. The samples prepared from 1.5 mmol dm^{-3} acid solutions were analyzed on an ODS column using 85% methanol as the moving phase. The peak area of the esters increased with increasing pK_a: the esterification of aliphatic, benzoic, and *o*-bromobenzoic acids, of which the pK_a values were 4.7—4.9, 4.21, and 2.85,[8)] occurred in 100, 20, and 3% conversions, respectively. The linear ranges for benzoic and *p*-anisic acids were 98 fmol—490 pmol and 110 fmol—550 pmol; the linear-correlation coefficients were 0.9997 and 0.9998, respectively, and the detection limits (S/N=2) were 50 and 40 fmol. The coefficients of variation for 2.5 mmol dm^{-3} benzoic and 2.8 mmol dm^{-3} *p*-anisic acid solutions (n=7) were 2.3 and 2.1%. No description has been found in the literature concerning the limits and ranges for the determination of aromatic carboxylic acids, except that by Lingeman et al.,[4)] who reported that the limit and range for benzoic acid were 100 fmol (S/N=3) and 0.1—1.0 μg (0.8—8.0 nmol), respectively. The present method was therefore superior to that reported by Lingeman et al.

We wish to express our thanks to Mr. Takashi Tamura and Mr. Kei-ichiro Ohnishi for measuring the NMR spectra and MS, respectively. The present work was partially supported by a Science and Engineering Research Grant-in-Aid from The Science and Engineering Research Institute of Doshisha University.

References

1) Part I; R. Nakajima, A. Yamamoto, and T. Hara, *Bull. Chem. Soc. Jpn.*, **63**, 1968 (1990).
2) R. Nakajima, H. Iida, and T. Hara, *Bull. Chem. Soc. Jpn.*, **63**, 636 (1990).
3) M. Yamaguchi, S. Hara, R. Matsunaga, M. Nakamura, and Y. Ohkura, *J. Chromatogr.*, **346**, 227 (1985).
4) H. Lingeman, A. Hulshoff, W. J. M. Underberg, and F. B. J. M. Offermann, *J. Chromatogr.*, **290**, 215 (1984).
5) R. F. Borch, M. D. Bernstein, and H. D. Durst, *J. Am. Chem. Soc.*, **93**, 2897 (1971).
6) R. Nakajima, K. Shimada, and T. Hara, unpublished results.
7) The esterification in the presence of **8** was carried out in *N*,*N*-dimethylformamide.
8) "Dissociation Constants of Organic Acids in Aqueous Solution," ed by G. Kortiin, W. Vogel, and K. Andrussov, Butterworths, London (1961); "Kagaku Binran Kisohen II," Rev. 2nd ed, ed by The Chemical Society of Japan, Maruzen, Tokyo (1975), pp. 994—995.
9) L. O. Sillén and A. E. Martell, "Stability Constants of Metal-Ion Complexes," Special Publication No. 17, The Chemical Society, London (1964), pp. 530, 566.

Mechanism of Reaction of *S,S*-Diphenyl-*S*-methoxythiazyne with Thiols

Toshiaki YOSHIMURA,* Eiichi TSUKURIMICHI, Yasuhisa SUGIYAMA, Hiroshi KITA, Choichiro SHIMASAKI, and Kiyoshi HASEGAWA
Department of Industrial Chemistry, Faculty of Engineering, Toyama University, Gofuku, Toyama 930
(Received March 18, 1991)

Synopsis. The reaction of *S, S*-diphenyl-*S*-methoxythiazyne with various thiols gave methyl sulfides. Kinetic investigations support a mechanism involving an initial protonation of the thiazyne nitrogen with thiol followed by a nucleophilic attack of thiolate anion on the methyl group.

Thiazynes[1] are relatively unusual compounds having an SN triple bond, and their chemistry is mostly unexplored.[2] Only a few fluoro derivatives are known.[2,3] Recently we reported the first preparation of *S,S*-diphenyl-*S*-methoxythiazyne (**1**) from the alkaline hydrolysis of *S,S*-diphenyl-N-bromosulfilimine (**2**) in methanol.[4] The structure of the compound **1** was confirmed by the fact that the compound **1** can readily react with benzenethiol to form methyl phenyl sulfide and *S,S*-diphenylsulfoximine (**3**) quantitatively. Therefore, in order to clarify the mechanism of this interesting methylation reaction, kinetic investigation was carried out.

Results and Discussion

The thiazyne **1** was prepared as a mixture with sulfoximine **3** (**1**:**3**=70:30) by the alkaline hydrolysis of *N*-bromosulfilimine **2** since the thiazyne **1** is hard to be separated.[4] The mixture was allowed to react with substituted benzenethiols, α-toluenethiol, and methyl phenyl sulfide at 30 °C in benzene. The products were analyzed by ^{1}H NMR and gas chromatography and the results are summarized in Table 1.

As shown in Table 1, both alkane- and arenethiols gave the corresponding methyl sulfides in high yields but methyl phenyl sulfide showed no reaction. Since the reaction can be readily performed under neutral conditions, this reaction is synthetically useful for methylation of SH groups as is the reaction of diazomethane. Then in order to clarify the mechanism of the reaction, kinetic investigation was carried out in benzene at 20—40 °C using substituted benzenethiols.

The reaction was followed by measuring the increasing GLPC peak of the methyl sulfide formed. The reaction was found to fit the second-order kinetic equation and the results are shown in Table 2.

A small activation energy (29 kJ mol^{-1}) and a large negative activation entropy (−184 JK^{-1} mol^{-1}) were obtained in such nonpolar solvent as benzene suggesting that the reaction involves an ion pair. Contrary to the expectation of negative trend for substituent effect for S_N2 reaction involving a nucleophilic attack of the thiol on the methyl group, a large positive ρ-value (2.63) was obtained from the Hammett plot as shown in Fig. 1.

Since methyl phenyl sulfide does not react with the thiazyne **1**, an active proton is required for this reaction.

Table 1. Reaction of *S,S*-Diphenyl-*S*-methoxythiazyne with Thiols

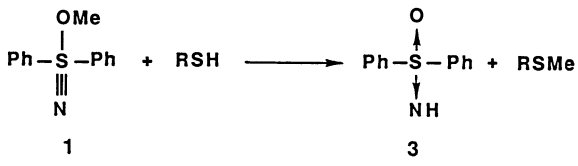

Thiol	Conditions[a]			RSMe
[RSH]	Time/h	Temp/°C	Solvent	Yield/%[b]
C_6H_5SH	10	30.0	Benzene	95
p-$CH_3C_6H_4SH$	6	30.0	Benzene	77
m-ClC_6H_4SH	7	30.0	Benzene	100
p-ClC_6H_4SH	12	30.0	Benzene	97
p-$CH_3OC_6H_4SH$	16	30.0	Benzene	83
$PhCH_2SH$	28	30.0	Benzene	52
$PhSCH_3$	3 days	50.0	Chloroform	0

a) The reactions were carried out with 2—3 equivalent amounts of thiols. b) Yields of diphenylsulfoximine are all quantitative except for the reaction with methyl phenyl sulfide.

Table 2. Kinetic Data for *S,S*-Diphenyl-*S*-methoxythiazyne with Substituted Benzenethiols

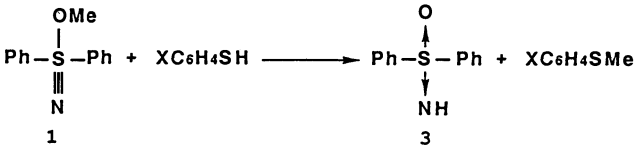

X	Temp/°C	$k\times10^2$/dm^3 mol^{-1} s^{-1}	
H	30.0	4.73±0.05	E_a=28.8±3.3 kJ mol^{-1}
H	35.0	6.30±0.16	ΔS^*=−184±8 J K^{-1} mol^{-1}
H	40.0	7.63±0.13	ρ=2.63
p-MeO	30.0	1.58±0.05	k_H/k_D=1.09
p-Me	30.0	2.67±0.06	
p-Cl	30.0	28.3 ±0.14	
m-Cl	30.0	75.2 ±0.14	
(PhSD)	30.0	4.32±0.25	

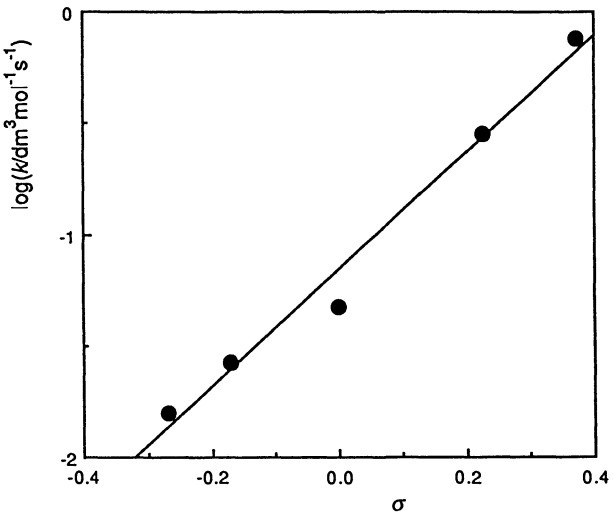

Fig. 1. The Hammett plot for the reaction of *S,S*-diphenyl-*S*-methoxythiazyne (**1**) with substituted benzenethiols.

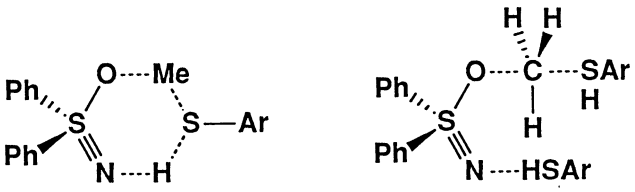

Fig. 2.

The positive ρ-value suggests that the acidity of thiol is more important than nucleophilicity. There are two possible mechanisms. One is a concerted process involving both proton transfer and nucleophilic attack of thiol sufur to the methyl group. Such a process should involve six-membered transition state or two molecules of thiol as shown in Fig. 2.

However, both mechanisms are unfavorable, because the former involves a nonlinear nucleophilic displacement on the methyl group and the latter is not consistent with present second-order kinetic results. The other one is a two-step mechanism involving an initial protonation of thiol to the nitrogen atom of the thiazyne followed by a nucleophilic attack of thiolate anion to the methyl group as shown in Scheme 1.

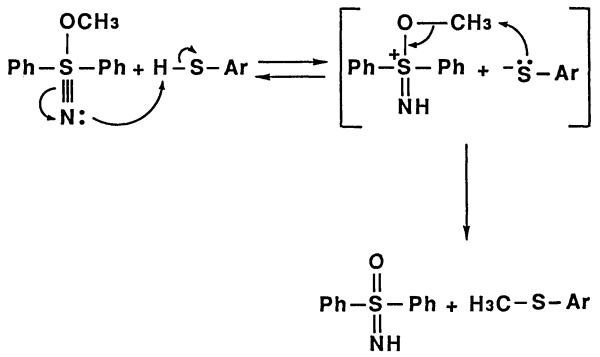

Scheme 1.

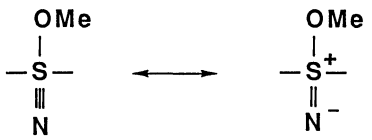

Fig. 3. Resonance structure of methoxythiazyne.

Then in order to examine a possibility of the rate-determining protonation of the nitrogen atom, isotope effect was measured using active proton-deuterated system. The rate constant of the reaction k_D using benzenethiol-*d* was found to be almost the same as k_H (k_H/k_D=1.09). Therefore the rate-determining step cannot be the first protonation step but the second nucleophilic substitution. The lack of appreciable kinetic isotope effect is also inconsistent with the concerted mechanism. The substituent effects for the acidity of benzenethiol are known to be ρ=1.81[5] in 20% EtOH, ρ=2.58[6] in 48% EtOH, and ρ=3.03[7] in 95% EtOH. Namely there is a tendency to increase the ρ-value for acidity in less polar solvent and thus the ρ-value of the predissociation in benzene can be estimated to be more than 3.0. Meanwhile, the substituent effect on benzenethiolate anion for the reaction with benzyl bromide in methanol gives relatively small ρ-values from −0.439 to −1.07 depending on the substituents on benzyl bromide.[8] Although substituent effects depend on substrates and solvents, a smaller negative ρ-value may be expected in the second step nucleophilic substitution reaction. If the substituent effect of the second step is assumed to be small, the observed positive ρ-value can be interpreted as a result of combination of a more positive ρ-value for the first equilibrium protonation step with a negative ρ-value in the second step. From the consideration of this mechanism, it is concluded that the nitrogen atom of the methoxythiazyne is basic to accept the thiol proton and to activate the carbon–oxygen bond to promote the methylation. Therefore the SN triple bond is considered to be polarized as shown in Fig. 3.

Experimental

General. IR spectra were taken on a JEOL-810 spectrometer. GLPC was performed on a Hitachi 163 using a 1-m DEGS column with N_2 gas at 50 ml min^{-1} flow rate. ^{1}H NMR spectra were obtained on a Hitachi R-24B (60MHz) in $CDCl_3$ using TMS as an internal standard.

All reagents were obtained from Wako Pure Chemical Industry Ltd., Tokyo Kasei Co., Ltd. or Aldrich Chemical Co. The reagents and solvents used were further purified by usual methods.

Preparation of *S,S*-Diphenyl-*S*-methoxythiazyne (1).[4] To a stirred solution of *N*-bromosulfilimine[9]**2** (0.4 g, 1.4 mmol) in MeOH (50 ml) was added an aqueous solution of 0.8 M-NaOH (50 ml) (1M=1 mol dm^{-3}). After the solution was warmed at 35 °C for 40 min, it was poured into a cold water, and extracted with $CHCl_3$. The combined extracts were dried over anhydrous Na_2SO_4. The residue obtained by evaporation of the solvent was found to be a mixture of *S,S*-diphenyl-*S*-methoxythiazyne (**1**) (70%) and *S,S*-diphenylsulfoximine (**3**) (30%) from the NMR spectral analysis. ^{1}H NMR and IR spectra were the same as those reported previously.[4]

Reaction of *S,S*-Diphenyl-*S*-methoxythiazyne (1) with Sub-

stituted Benzenethiols. To a solution of the thiazyne **1** in $CDCl_3$ in an NMR tube was added benzenethiol and ^1H NMR was taken immediately. The NMR spectrum showed that the methoxy signal (3.7 ppm) was already disappeared and only one methyl signal was observed at 2.35 ppm which was assigned as that of methyl phenyl sulfide. The solution was analyzed by GLPC to show retention time 52 s consistent with that of the authentic sample. (DEGS, 1 m, column temp 120 °C, injection temp 150 °C, flow rate N_2 50 ml min^{-1})

The reaction of the thiazyne **1** with substituted benzenethiols were carried out in benzene under the conditions shown in Table 1. The product sulfides were all identified by comparing their GLPC retention time with those of the authentic samples and their yields were determined by GLPC calibration curves using naphthalene or methyl phenyl sulfide as an internal standard. The solvent was removed in vacuo and residue was chromatographed on silica gel using chloroform as an eluent to give *S,S*-diphenylsulfoximine (**3**) quantitatively.

Kinetics. A benzene solution of thiazyne **1** (6.0×10^{-3} mol dm^{-3}, 10 ml) and a benzene solution of substituted benzenethiol (1.2×10^{-2} mol dm^{-3}, 10 ml) containing an internal standard (naphthalene 1.2×10^{-2} mol dm^{-3} for PhSH, *p*-$CH_3C_6H_4SH$, and *p*-$CH_3OC_6H_4SH$; methyl phenyl sulfide for *m*- and *p*-ClC_6H_4SH) were immersed in a water bath thermostated at the constant temperature (20—40 °C(±0.1 °C)). After five minutes, two solutions were mixed. At an appropriate time interval, a 0.5 ml portion of the reaction mixture was taken out, added to 1 ml of 1 M-HCl, and shaken to decompose the unreacted thiazyne **1**. The benzene solution was analyzed by GLPC (DEGS, 1 m, column temp 120 °C, injection temp 150 °C). The increasing amount of methyl-substituted phenyl sulfide was followed and the second-order rate constant was calculated by a least squares method using the equation

$$kt = 1n\,((1-fx)/(1-x))/([B]_0-[A]_0)$$

($[A]_0$ is the initial amount of thiazyne **1**, $[B]_0$ is the initial amount of substituted benzenethiol, f is the ratio $[A]_0/[B]_0$, x is the conversion of thiazyne calculated by $(a_t-a_0)/(a_\infty-a_0)$, where a_0 and a_t are the amounts of methyl phenyl sulfide at the initial time and at time t, respectively, and a_∞ is the amount at the infinite time (more than 6 h)).

Isotope Effect. The benzene solution of the thiazyne containing the sulfoximine was shaken with D_2O many times to exchange the NH group to ND and the benzene solution of benzenethiol was also treated similarly with D_2O. The H–D exchange was confirmed by ^1H NMR and IR and the kinetics was carried out similarly.

References

1) The compounds having an SN triple bond are called thiazyl compounds[2] like thiazyl trifluoride for $F_3S{\equiv}N$, but this name is not appropriate for the compounds substituted by carbon groups. Meanwhile, the name "thiazyne" is first used by Clifford et al.[3] for $Ph_2FS{\equiv}N$ as diphenylfluorothiazyne.

2) O. Glemser and R. Mews, *Angew. Chem.*, **92**, 904 (1980).

3) A. F. Clifford, J. L. Howell, and D. L. Wooton, *J. Fluorine Chem.*, **11**, 433 (1978).

4) T. Yoshimura, E. Tsukurimichi, H. Kita, H. Fujii, and C. Shimasaki, *Tetrahedron Lett.*, **30**, 6339 (1989).

5) G. Chuchani and A. Frohlich, *J. Chem. Soc.*, **1962**, 1062.

6) F. G. Bordwell and H. M. Andersen, *J. Am. Chem. Soc.*, **75**, 6019 (1953).

7) M. R. Crampton, *J. Chem. Soc. B*, **1971**, 2112.

8) R. F. Hudson and G. Klopman, *J. Chem. Soc.*, **1962**, 1062.

9) T. Yoshimura, N. Furukawa, T. Akasaka, and S. Oae, *Tetrahedron*, **33**, 1061 (1977).

Preparation of Optically Active Sulfoxides Bearing Heterocycles and Stereoselective Methylation Using Their α-Sulfinyl Carbanions

Takahiro SAGAE, Satoshi OGAWA, and Naomichi FURUKAWA*
Department of Chemistry, University of Tsukuba, Tsukuba, Ibaraki 305
(Received May 16, 1991)

Synopsis. Optically active sulfoxides bearing heterocycles i.e., (1-methyl-2-imidazolyl)methyl and 2-thienylmethyl groups were prepared and their stereoselective methylations were conducted.

Optically active sulfoxides have been widely utilized for asymmetric synthesis,[1] while only a few investigations on the preparation and utilization of optically active heteroaryl sulfoxides have been reported.[2] Recently, we reported the preparation of optically active 2-pyridylmethyl *p*-tolyl sulfoxide (**1**) and highly stereoselective methylation reaction using α-sulfinyl carbanion of **1**.[3] This carbanion also gave highly stereoselective aldol condensation products by treatment with aldehydes.[4] High stereoselectivity of the α-sulfinyl carbanion of **1** observed in the methylation below −70 °C suggests that the structure of carbanion of **1** is highly oriented by chelating Li cation by both the pyridyl nitrogen and the sulfinyl oxygen atoms.[5] This note describes the synthesis of optically active (1-methyl-2-imidazolyl)methyl and 2-thienylmethyl *p*-tolyl sulfoxides (**2** and **3** respectively) together with corresponding racemic sulfoxides and 2-furylmethyl, (1-methyl-2-benzimidazolyl)methyl, and *o*-methoxyphenylmethyl *p*-tolyl sulfoxides (**4**, **5**, and **6** respectively) and a comparison of the stereoselectivity on the methylation reaction of their α-sulfinyl carbanions with iodomethane.

Optically active sulfoxides **2** and **3** were prepared according to the Andersen's procedure[6] as shown in Scheme 1. The reaction of (1-methyl-2-imidazolyl)-

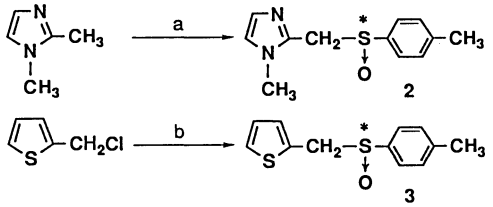

a: *n*-BuLi, THF, *l*-menthyl *p*-toluenesulfinate, b: Mg, THF, *l*-menthyl *p*-toluenesulfinate.

Scheme 1.

methyllithium and *l*-menthyl *p*-toluenesulfinate was carried out in tetrahydrofuran (THF) to give optically active sulfoxide **2** in 41% yield. However, similar treatment of 2-thienylmethyllithium with *l*-menthyl *p*-toluenesulfinate afforded not the desired sulfoxide **3** but 2-[tris(*p*-tolylsulfinyl)methyl]thiophene in quantitative yield and hence the preparation of optically active sulfoxide **3** was performed using the corresponding Grignard reagent generated from 2-(chloromethyl)thiophene. Racemic sulfoxides **2**—**6** were prepared by oxidation of corresponding sulfides with *m*-chloroperbenzoic acid (*m*CPBA) in moderate yields as shown in Scheme 2.

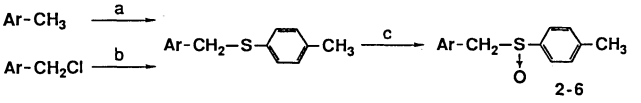

a: *n*-BuLi, THF, (*p*-Tol-S-)$_2$, b: EtOH-H_2O, *p*-Tol-SH, KOH, c: *m*CPBA, CH_2Cl_2.

Scheme 2.

In order to determine the absolute configurations of these sulfoxides **2** and **3**, their CD spectra were taken and compared with those of the sulfoxides (*R*)-(+)-[2-pyridylmethyl *p*-tolyl sulfoxide] (**1**) and (*R*)-(+)-[benzyl *p*-tolyl sulfoxide] (**7**).[7] Mislow has demonstrated that the absolute configurations of optically active compounds having similar structures can be determined by

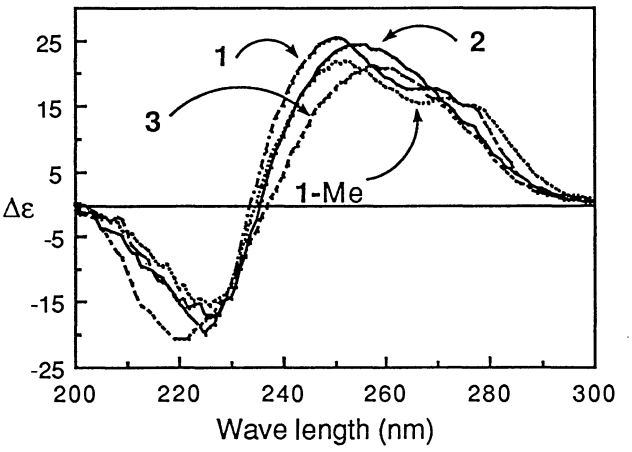

Fig. 1.

Table 1. Spectral Data of Optically Active Sulfoxides

Sulfoxide	UV		CD		
	λ_{max}(nm)	ε	λ_{ext}(nm)	Δε	$[\theta]_{max}\times10^{-4}$
1	266.0	8500	250.0	25.3	+8.4
			225.0	−20.1	−6.6
2	241.5	11500	258.0	21.1	+7.0
			220.0	−20.6	−6.8
3	254.0	8300	254.0	24.3	+8.0
			227.9	−17.4	−5.7
1-Me[a]	264.0	7800	253.0	21.8	+7.2
			223.0	−14.8	−4.9
7[b]			258.0		+7.7
			223.0		−11.7

a) (*R*,*R*)-1-(2-Pyridyl)-1-(*p*-tolylsulfinyl)ethane. b) See Ref. 7.

Table 2. Stereoselective Methylation of α-Lithio Sulfoxides Bearing Heteroaromatics with Iodomethane

Sulfoxide	Ar	Temp °C	Yield %	Diastereomeric ratio erythro : threo
2	1-Methyl-2-imidazolyl	−80	87	12.3 : 1
		−20	100	9.7 : 1
		7	100	9.5 : 1
3	2-Thienyl	−90	100	4.5 : 1
		−77	87	4.1 : 1
		−55	91	2.6 : 1
		4	97	1.4 : 1
4	2-Furyl	−90	93	5.2 : 1
		−75	73	4.3 : 1
		−55	93	2.4 : 1
		4	65	1.4 : 1
5	1-Methyl-2-benzimidazolyl	−80	24	1.3 : 1
6	*o*-Methoxyphenyl	−80	97	6.0 : 1

measurement of their CD spectra and presented the empirical rule that the sulfoxides having positive Cotton curves have *R* configuration and vice versa.[8] The CD spectra are shown in Fig. 1 and the data are summarized in Table 1. The CD spectra of **1**—**3** indicate clearly that all the sulfoxides employed in the present investigation have the same sign of Cotton curves and nearly identical magnitudes of the absorptions $[\theta]_{max}$ even by comparing their spectra with (*R*,*R*)-1-(2-pyridyl)-1-(*p*-tolylsulfinyl)ethane.[3] Therefore, the absolute configurations of sulfoxides **2** and **3** were determined to be *R*.

The methylation reaction was carried out using LDA as a base and then iodomethane in THF as shown in Scheme 3 and Table 2. In the reaction of sulfoxide **2** at −80 °C, *erythro*-1-(1-methyl-2-imidazolyl)]-1-(*p*-tolylsulfinyl)ethane was obtained more preferentially than the *threo* derivative with a ratio of 12.3 : 1. This result reveals that the reaction of the carbanion with iodomethane proceeds via a nearly identical manner with the methylation of sulfoxide **1**, namely via an initial formation of a rigid chelation complex which prevents the approach of iodomethane from its *threo* site as shown in Fig. 2. Interestingly, stereoselectivity for the methylation of the carbanion generated from **2** is rather insensitive to the reaction temperature. This result is markedly contrasted to methylations of other sulfoxides. In the case of sulfoxides **3**—**6** the ratios of isomers were found not to be as high as those obtained from **1** and **2** suggesting that their α-sulfinyl carbanions are unable to form a rigid chelation complexes. These results also support that the chelation of Li cation by the heteroatoms plays an important role in the stereoselectivity. The values of log(*erythro*/*threo*) of the methylation products shown in Table 2 were plotted against the temperatures giving straight lines and the $\Delta\Delta H^{\neq}$ and $\Delta\Delta S^{\neq}$ values were calculated by conventional Arrhenius equation; $\Delta\Delta G^{\neq}=\Delta\Delta H^{\neq}-T\Delta\Delta S^{\neq}=-RT \ln[erythro]/[threo]$. The results are summarized in Table 3.

Table 3. Activation Parameter for Methylation of Sulfoxides **2**, **3**, and **4**

Sulfoxide	$\Delta\Delta H^{\neq}$/kJ mol^{-1}	$\Delta\Delta S^{\neq}$/kJ mol^{-1} deg^{-1}
2	1.40	−13.55
3	5.48	16.93
4	6.12	19.62

The results are consistent roughly with our previous result obtained from the methylation reaction of the α-sulfinyl carbanion of **1** with iodomethane. The present results demonstrate that the carbanion generated from sulfoxide **2** is somewhat different from that of other sulfoxides bearing heterocycles. Among these heterocycles, 1-methylimidazolyl group should have highest capability for chelation with Li cation to provide a conformer which is attacked preferentially by iodomethane from the *erythro* site, thus enhancing the *erythro* stereoselectivity of its carbanion. The present investigation demonstrates the synthetic utility of the sulfoxides bearing azaheterocycles.

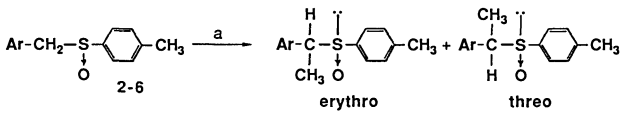

a: LDA, THF, CH_3I.

Scheme 3.

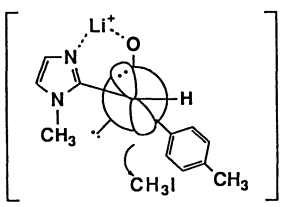

Fig. 2.

Experimental

All melting points are uncorrected. IR spectra were recorded on a JASCO A-3 spectrometer. ^{1}H NMR spectra were obtained with a Hitachi R-600 or a Bruker AM-500, or a JEOL EX-270. Preparative liquid chromatography was performed on a Japan Analytical Co., Ltd., LC-09. Elemental analyses were carried out by Chemical Analysis Center at this university. The CD spectra were measured on a JASCO J-600 spectrometer. All reagents were obtained from Wako Pure Chemical Industries Ltd., Tokyo Kasei Co., Ltd., or Aldrich Chemical Co. The solvents were purified by general methods.

Preparation of Optically Active Sulfoxides. (*R*)-(+)-[(1-Methyl-2-imidazolyl)methyl *p*-Tolyl Sulfoxide] (2). To a stirred solution of 1,2-dimethylimidazole (9.6 g, 0.1 mol) in THF (300 mL) at −78 °C was added 1.66 M *n*-BuLi (1 M=1 mol dm^{-3}) in hexane solution (65 mL, 0.11 mol). The mixture was stirred at 0 °C for 30 min and then cooled to −78 °C. The mixture was added dropwise to (*S*)-(−)-*l*-menthyl *p*-toluenesulfinate (29.5 g, 0.1 mol) in THF (300 mL) with stirring at −78 °C for 0.5 h and then −20 °C for 4 h. After hydrolysis and neutralization with aqueous ammonium chloride, the mixture was extracted with chloroform (3×500 mL). The extract was dried over anhydrous magnesium sulfate and the solvent was evaporated under reduced pressure. The residue was purified by column chromatography (silica gel; eluent, ethyl acetate–methanol=10 : 1) to give sulfoxide **2** in 41% yield. Recrystallization from benzene–hexane gave colorless crystals; mp 86—87 °C; ^{1}H NMR ($CDCl_3$) δ=7.36 (d, J=8 Hz, 2H, 2,6-ArH), 7.29 (d, J=8 Hz, 2H, 3,5-ArH), 6.99 (d, J=1 Hz, 1H, 5-ImdH), 6.82 (d, J=1 Hz, 1H, 4-ImdH), 4.26, 4.10 (ABq, J=15 Hz, 2H, CH_2), 3.45 (s, 3H, Imd-CH_3), 2.41 (s, 3H, Ar-CH_3); IR (KBr) 1050 cm^{-1} (SO); $[\alpha]_D$ +177.9° (c=0.5, acetone). Optical purity was estimated ca. 100% by ^{1}H NMR using Eu(tfc)$_3$ as a chiral shift reagent. Found: C, 61.47 H, 6.02; N, 11.92%. Calcd for $C_{12}H_{14}N_2OS$: C, 61.51; H, 6.02; N, 11.96%.

(*R*)-(+)-[2-Thienylmethyl *p*-Tolyl Sulfoxide] (3). This sulfoxide was prepared similarly as sulfoxide **2** using 2-thienylmethylmagnesium chloride. Yield 18%; mp 123—124 °C; ^{1}H NMR ($CDCl_3$) δ=7.33 (d, J=8 Hz, 2H, 2,6-ArH), 7.25 (d, J=8 Hz, 2H, 3,5-ArH), 7.23—7.22 (m, 1H, 5-ThH), 6.94—6.92 (m, 1H, 4-ThH), 6.74 (m, 1H, 3-ThH), 4.24, 4.19 (ABq, J=14 Hz, 2H, CH_2), 2.40 (s, 3H, CH_3); IR (KBr) 1040 cm^{-1} (SO); MS (m/z) 139 (M^+−97); $[\alpha]_D$ +139.7° (c=0.5, chloroform). Found: C, 60.94; H, 5.14%. Calcd for $C_{12}H_{12}OS_2$: C, 60.98; H, 5.12%.

Preparation of Racemic Sulfoxides Bearing Heterocycles. (1-Methyl-2-imidazolyl)methyl *p*-Tolyl Sulfoxide (2). Yield 52%; mp 128—130 °C; ^{1}H NMR ($CDCl_3$) δ=7.36 (d, J=8 Hz, 2H, 2,6-ArH), 7.29 (d, J=8 Hz, 2H, 3,5-ArH), 6.99 (d, J=1 Hz, 1H, 5-ImdH), 6.82 (d, J=1 Hz, 1H, 4-ImdH), 4.26, 4.10 (ABq, J=15 Hz, 2H, CH_2), 3.45 (s, 3H, Imd-CH_3), 2.41 (s, 3H, Ar-CH_3); IR (KBr) 1050 cm^{-1} (SO). Found: C, 61.44; H, 6.03; N, 11.92%. Calcd for $C_{12}H_{14}N_2OS$: C, 61.51; H, 6.02; N, 11.96%.

2-Thienylmethyl *p*-Tolyl Sulfoxide (3). Yield 93%; mp 95—96 °C; ^{1}H NMR ($CDCl_3$) δ=7.33 (d, J=8 Hz, 2H, 2,6-ArH), 7.25 (d, J=8 Hz, 2H, 3,5-ArH), 7.23—7.22 (m, 1H, 5-ThH), 6.94—6.92 (m, 1H, 3-ThH), 6.74 (m, 1H, 4-ThH), 4.24, 4.19 (ABq, J=14 Hz, 2H, CH_2), 2.40 (s, 3H, CH_3); IR (KBr) 1040 cm^{-1} (SO). Found: C, 61.02; H, 5.23%. Calcd for $C_{12}H_{12}OS_2$: C, 60.98; H, 5.12%.

2-Furylmethyl *p*-Tolyl Sulfoxide (4). Yield 74%; colorless liquid; ^{1}H NMR ($CDCl_3$) δ=7.37 (d, J=8 Hz, 2H, 2,6-ArH), 7.33 (m, 1H, 5-FurH), 7.28 (d, J=8 Hz, 2H, 3,5-ArH), 6.31 (m, 1H, 3-FurH), 6.15 (m, 1H, 4-FurH), 4.15, 4.02 (ABq, J=14 Hz, 2H, CH_2), 2.41 (s, 3H, CH_3); IR (neat) 1040 cm^{-1} (SO). Found: C, 65.30; H, 5.52%. Calcd for $C_{12}H_{12}O_2S$: C, 65.43; H, 5.49%.

(1-Methyl-2-benzimidazolyl)methyl *p*-Tolyl Sulfoxide (5). Yield 12%; mp 157—160 °C; ^{1}H NMR ($CDCl_3$) δ=7.72—7.24 (m, 8H, ArH), 4.43, 4.29 (ABq, J=15 Hz, 2H, CH_2), 3.67 (s, 3H, BzImd-CH_3), 2.40 (s, 3H, Ar-CH_3); IR (KBr) 1010 cm^{-1} (SO). Found: C, 67.75; H, 5.51; N, 9.87%. Calcd for $C_{16}H_{16}N_2OS$: C, 67.58; H, 5.67; N, 9.85%.

***o*-Methoxyphenylmethyl *p*-Tolyl Sulfoxide (6).** Yield 90%; colorless liquid; ^{1}H NMR ($CDCl_3$) δ=7.49—6.69 (m, 8H, ArH), 4.18, 4.00 (ABq, J=14 Hz, 2H, CH_2), 3.67 (s, 3H, OCH_3), 2.38 (s, 3H, Ar-CH_3); IR (neat) 1030 cm^{-1} (SO). Found : C, 68.97; H, 6.17%. Calcd for $C_{15}H_{16}O_2S$: C, 69.20; H, 6.19%.

Methylation of Lithiated Sulfoxides 2—6 with Iodomethane. Typical experimental procedure is as follows: Sulfoxide **2** (200 mg, 0.854 mmol) was dissolved into THF (10 mL) under argon atmosphere. The solution was cooled to −80 °C, and solution of LDA (0.928 mmol) in THF (2.7 mL) was added with stirring for 30 min. To this solution was added iodomethane (0.27 mL, 4.34 mmol) and the mixture was stirred for 8 h. The reaction was stopped by adding water (5 mL) and the mixture was warmed to room temperature. After hydrolysis and neutralization with aqueous ammonium chloride, the mixture was extracted with chloroform (3×30 mL) and dried over anhydrous magnesium sulfate. After removal of the solvent, the residue was purified by column chromatography (silica gel; eluent, ethyl acetate) to give 1-(1-methyl-2-imidazolyl)-1-(*p*-tolylsulfinyl)ethane in 87% yield. The products contained in 12.3 : 1 ratio of *erythro* and *threo* isomers. The *erythro* isomer was separated by preparative liquid chromatography. Mp 128—130 °C; ^{1}H NMR ($CDCl_3$) δ=7.28 (s, 4H, ArH), 7.02 (m, 1H, 5-ImdH), 6.92 (m, 1H, 4-ImdH), 4.14 (q, J=7 Hz, 1H, CH), 3.68 (s, 3H, Imd-CH_3), 2.42 (s, 3H, Ar-CH_3), 1.53 (d, J=7 Hz, 3H, CH-CH_3); IR (KBr) 1030 cm^{-1} (SO); MS (m/z) 246 (M^+). Found: C, 62.59 ; H, 6.60; N, 11.29%. Calcd for $C_{13}H_{16}N_2OS$: C, 62.87; H, 6.49; N, 11.28%. The *threo* isomer could not be isolated and was determined the structure by ^{1}H NMR chemical shifts of the mixture. Other sulfoxides were treated similarly and the ratios of isomers were determined by ^{1}H NMR spectra.

This work was supported by a Grant-in-Aid No. 02453018 from the Ministry of Education, Science and Culture.

References

1) a) M. Mikolajczyk and J. Drabowicz, "Topics in Stereochemistry," ed by N. L. Allinger and E. L. Eliel, John Wiley & Sons, New York (1982), Vol. 13, p. 333. b) G. Solladié, *Synthesis,* **1981**, 185. c) M. Cinquini, *Phosphorus Sulfur*, **24**, 39 (1985).

2) a) R. Annunziata, M. Cinquini, F. Cozzi, and A. Restelli, *J. Chem. Soc., Perkin Trans. 1,* **1985**, 2289. b) G. Demailly, C. Greck, and G. Solladié, *Tetrahedron Lett.,* **25**, 4113 (1984). c) Kai-U. Baldenius and H. B. Kagan, *Tetrahedron, Asymmetry,* **1**, 597 (1990).

3) N. Furukawa, E. Hosono, H. Fujihara, and S. Ogawa, *Bull. Chem. Soc. Jpn.,* **63**, 461 (1990).

4) N. Furukawa, T. Sagae, and S. Ogawa, *Heterorcycles,* **32**, 679 (1991).

5) a) K. Takahashi, K. Konishi, M. Takaki, and R. Asami, *J. Organomet. Chem.,* **50**, 1 (1973). b) H. Matsui, A. Yoshino, T. Yoshida, and K. Takahashi, *Bull. Chem. Soc. Jpn.,* **57**, 1052 (1984). c) R. Lett, G. Chassaing, and A. Marquet, *J. Organomet. Chem.,* **111**, C17 (1976). d) G. Chassaing and A. Marquet, *Tetrahedron,* **34**, 1399 (1978).

6) a) K. K. Andersen, *Tetrahedron Lett.,* **1962**, 93. b) K. K. Andersen, W. Gaffield, N. E. Papanikolaou, J. W. Foley, and R. I. Perkins, *J. Am. Chem. Soc.,* **86**, 5637 (1964).

7) F. D. Saeva, D. R. Rayner, and K. Mislow, *J. Am. Chem. Soc.,* **90**, 4176 (1968).

8) a) K. Mislow, A. L. Ternay, Jr., and J. T. Melillo, *J. Am. Chem. Soc.,* **85**, 2329 (1963). b) K. Mislow, M. M. Green, P. Laur, J. T. Melillo, T. Simmons, and A. L. Ternay, Jr., *J. Am. Chem. Soc.,* **87**, 1958 (1965).

Simple Preparation of (2,2′-Biphenylylene)phenylphosphine Oxide and Role of Triphenylphosphine Oxide as a Mediator for Formation of Biaryl Derivatives

Satoshi OGAWA, Yoko TAJIRI, and Naomichi FURUKAWA*
Department of Chemistry, University of Tsukuba, Tsukuba, Ibaraki 305
(Received May 16, 1991)

Synopsis. (2,2′-Biphenylylene)phenylphosphine oxide (**3**) was prepared simply by the reaction of triphenylphosphine oxide (**1**) with phenyllithium and subsequently with aqueous hydrogen peroxide in acetic acid. The oxide **3** reacted with lithium diisopropylamide (LDA) and then with several electrophiles to afford regiospecifically ortho-substituted compounds in moderate yields, which were converted to unsymmetrical 2- and 2,3′-substituted 1,1′-biaryls and triphenylphosphine oxide (**1**).

Although numerous phosphines have been utilized in modern organic synthesis, i.e., as starting materials for Wittig reagents[1] and ligands for transition metals,[2] phosphine oxides have been investigated a little and considered as undesired end products for the reactions. The P=O bond energy of triphenylphosphine oxide (**1**) is quite high (130 kcal) and is hardly reduced by simple reducing reagents.[3] This might prevent the utilization of **1** in organic synthesis. Recently, we found that triarylphosphine oxides, diaryl sulfoxides, and diaryl selenoxides underwent facile ligand exchange by the reactions with organolithium reagents.[4] On the other hand, we reported a new ortho-lithiation reaction of diaryl sulfoxides.[5] In the course of studies on the reactions of oxides derived from heteroatom (group 15 or 16 elements)-containing compounds with organolithium or Grignard reagents, we found that the ring closure reaction of triphenylphosphine oxide (**1**) on treatment with phenyllithium took place together with elimination of the oxygen atom to afford (2,2′-biphenylylene)phenylphosphine (**2**) in moderate yield. In this note, we report simple preparation of (2,2′-biphenylylene)phenylphosphine oxide (**3**) and its application for the synthesis of unsymmetrical biaryls. We also emphasize that **1** works as a mediator for the synthesis of biaryls.

When **1** was allowed to react with phenyllithium in refluxing tetrahydrofuran (THF), (2,2′-biphenylylene)-phenylphosphine (**2**) was obtained in 65% yield. Then **2** was treated with aqueous hydrogen peroxide in acetic acid to afford (2,2′-biphenylylene)phenylphosphine oxide (**3**) in 93% yield. In the reaction of **1** with phenyllithium intramolecular carbon-carbon bond formation at the ortho-positions of the two phenyl rings and reduction of phosphine oxide to phosphine took place simultaneously. Although it is hardly to argue the reaction mechanism, the following mechanism involving initial proton abstraction by phenyllithium then the incipient formation of **A** which was also suggested in the reaction of tetraphenylphosphonium salt with organolithium reagents[6] could be the probable process as shown in Scheme 1. Apparently, when one used two equivalents of phenyllithium, **2** was obtained in highest yield, namely, the reactions of **1** with one and two equivalents of phenyllithium gave **2** in 11 and 65% yields respectively. When **3** was treated with LDA and then with electrophiles at −78 °C, lithiation took place regiospecifically at the 3-position in the biphenyl ring to give monosubstituted compounds **4** in moderate yields as shown in Scheme 2 and Table 1. These 3-substituted (2,2′-biphenylylene)phenylphosphine oxides **4** reacted with phenyllithium to give the corresponding substitution products **5** in moderate yields. However, the second electrophile could not be introduced at the 2′-position in the biphenyl ring. These results seem to indicate that in the reactions of lithiated **4** with electrophiles the steric or electronic effect by the one substituent at the 3′-position prevents the approach for the second electrophile at the 2′-position. Although two substituents could not be introduced in one phenyl ring of biphenyl, **5** reacted initially with phenyllithium and subsequently with electrophiles to afford 2,3′-disubstituted 1,1′-biaryls **6** and triphenylphosphine oxide (**1**) in good yields as shown in Scheme 3 and Table 2. The recovered **1** can be used again as a starting material for

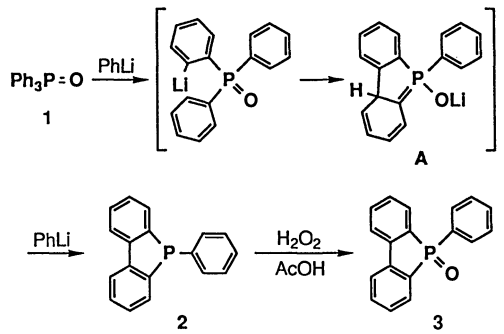

Scheme 1.

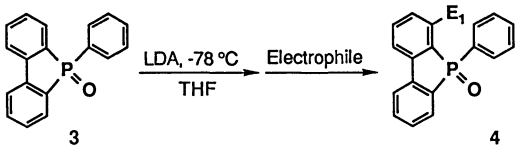

Scheme 2.

Table 1. Reactions of (2,2-Biphenylylene)phenylphosphine Oxide (**3**) with LDA and Electrophiles

LDA equiv	Electrophile	E_1	Yield/% **4**
1.0	$(CH_3)_3SiCl$	$(CH_3)_3Si$	52 (**4a**)[a]
1.0	PhCHO	PhCH(OH)	21 (**4b**)
1.0	CH_3CHO	$CH_3CH(OH)$	53 (**4c**)

a) Small amount of disubstituted product was obtained.

Table 2. Reactions of Phosphine Oxides **3** and **4a** with Phenyllithium and Electrophiles

Phosphine Oxide E_1	Yield/% **5**	Electrophile	E_2	Yield/% **6**	Yield/% **1**
H (**3**)	95 (**5a**)	—	H	69 (**6a**)	60
		$(CH_3)_3SiCl$	$(CH_3)_3Si$	46 (**6b**)	65
		PhCHO	PhCH(OH)	79 (**6c**)	62
		CH_3CHO	$CH_3CH(OH)$	55 (**6d**)	63
$(CH_3)_3Si$ (**4a**)	47 (**5b**)	—	H	99 (**6e**)	95
		$(CH_3)_3SiCl$	$(CH_3)_3Si$	16 (**6f**)	49
		CH_3CHO	$CH_3CH(OH)$	54 (**6g**)	84

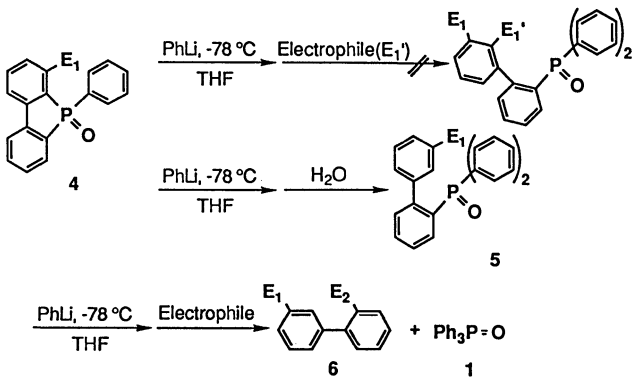

Scheme 3.

the simple reaction system to prepare unsymmetrical biaryls **6** and hence **1** plays a role of a mediator for the system. These procedures can expand the scope for the syntheses of unsymmetrical biaryls.

Experimental

All melting points are uncorrected. IR spectra were recorded on a JASCO FT/IR-5000 spectrometer. NMR spectra were obtained with a Hitachi R-600, a JEOL EX 270, or a Bruker AM-500. Mass spectra were taken with a Hitachi RMU-6MG, a Shimadzu GCMS QP-2000A, or a JEOL JMS-SX 102 mass spectrometer. Elemental analyses were carried out by Chemical Analysis Center at this University. All reagents were obtained from Wako Pure Chemical Industries, Ltd. or Aldrich Chemical Co. The reaction solvents were further purified by general methods.

Synthesis of (2,2′-Biphenylylene)phenylphophine (2). To a stirred solution of **1** (2.8 g, 10.0 mmol) in THF (80 mL) at 0 °C under N_2 atmosphere was added 1.8 M (1 M=1 mol dm^{-3}) phenyllithium (11.2 mL, 20.1 mmol). The mixture was refluxed for 12 h. After hydrolysis, the solvent was removed under reduced pressure. To the residue was added water (100 mL) and the mixture was neutralized with 1 M hydrochloric acid, extracted with dichloromethane (3×100 mL). The extract was dried with anhydrous magnesium sulfate, and the solvent was evaporated under reduced pressure. The residue was purified by column chromatography (silica gel; eluent, hexane–ethyl acetate=4:1) to give phosphine **2** in 65% yield. Recrystallization from ethyl acetate gave colorless crystals; mp 92—93 °C (lit,[7] 93—94 °C); ^{1}H NMR (500 MHz, $CDCl_3$) δ=7.18—7.25 (m, 3H, 3,4,5-PhH), 7.27—7.31 (m, 4H, 5,5′,6,6′-BiphH), 7.43 (t, J=7.8 Hz, 2H, 4,4′-BiphH), 7.66—7.71 (m, 2H, 2,6-PhH), 7.92 (d, J=7.8 Hz, 2H, 3,3′-BiphH); ^{31}P NMR (109 MHz, $CDCl_3$) δ=−11.6; MS m/z 260 (M^+).

Synthesis of (2,2′-Biphenylylene)phenylphosphine Oxide (3). To a stirred solution of **2** (260 mg, 1.0 mmol) in acetic acid (30 mL) was added 30% aqueous hydrogen peroxide (0.0168 mL, 1.47 mmol). The mixture was stirred at room temperature for 3 h, and the solvent was removed under reduced pressure. The residue was dissolved in dichloromethane (40 mL) and washed with saturated aqueous sodium hydrogencarbonate (3×30 mL) and saturated aqueous sodium chloride (2×30 mL). The organic layer was dried with anhydrous magnesium sulfate, and the solvent was evaporated under reduced pressure. The residue was recrystallized with ethyl acetate to give phosphine oxides **3** as colorless crystals in 93% yield. Mp 159—162 °C (lit,[8] 162—164.5 °C); ^{1}H NMR (500 MHz, $CDCl_3$) δ=7.37 (t, J=7.5 Hz, 2H, 4,4′-BiphH), 7.38 (t, J=7.3 Hz, 2H, 3,5-PhH), 7.48 (t, J=7.3 Hz, 1H, 4-PhH), 7.58 (t, J=7.5 Hz, 2H, 5,5′-BiphH), 7.65 (dd, J_{PCCH}=12.8, J=7.3 Hz, 2H, 2,6-PhH), 7.71 (dd, J_{PCCCH}=8.6, J=7.5 Hz, 2H, 6,6′-BiphH), 7.82 (dd, J_{PCCH}=2.9, J=7.5 Hz, 2H, 3,3′-BiphH); ^{31}P NMR (109 MHz, $CDCl_3$) δ=32.2; IR (KBr) 1195 cm^{-1} (PO); MS m/z 276 (M^+).

Reactions of (2,2′-Biphenylylene)phenylphosphine Oxide (3) with LDA and Electrophiles. To a stirred solution of **3** (276 mg, 1.0 mmol) in THF (10 mL) was added 0.17 M LDA (6.0 mL, 1.0 mmol) in THF solution under N_2 atmosphere at −78 °C for 3 h. To the mixture was added trimethylsilyl chloride (0.30 mL, 2.4 mmol) and the mixture was stirred at −78 °C for 3 h. After hydrolysis, the solvent was removed under reduced pressure. To the residue was added water (40 mL) and the mixture was neutralized with 1 M hydrochloric acid, extracted with dichloromethane (3×40 mL). The extract was dried with anhydrous magnesium sulfate, and the solvent was evaporated under reduced pressure. The residue was purified by column chromatography (silica gel; eluent, ethyl acetate) to give **4a** in 52% yield. Recrystallization from hexane–ethyl acetate gave colorless crystals; mp 189—190 °C; ^{1}H NMR (500 MHz, $CDCl_3$) δ=0.17 (s, 9H, CH_3), 7.29—7.86 (m, 12H, PhH, BiphH); ^{13}C NMR (125 MHz, $CDCl_3$) δ=0.0 (s), 120.8 (d, ^2J=9.8 Hz), 121.5 (d, ^2J=10.0 Hz), 128.6 (d, ^3J=12.3 Hz), 129.1 (d, ^3J=9.6 Hz), 129.3 (d, ^3J=10.8 Hz), 131.0 (d, ^3J=12.3 Hz), 131.4 (d, ^4J=2.6 Hz), 131.8 (d, ^4J=2.7 Hz), 132.6 (d, ^1J=106.7 Hz), 132.9 (s), 133.1 (d, ^1J=106.7 Hz), 135.8 (d, ^3J=14.0 Hz), 137.6 (d, ^1J=108.8 Hz), 140.6 (d, ^2J=21.6 Hz), 142.5 (d, ^2J=24.8 Hz), 145.7 (d, ^2J=16.3 Hz); ^{31}P NMR (109 MHz, $CDCl_3$) δ=32.9; IR (KBr) 1207 cm^{-1} (PO); MS m/z 348 (M^+). Found: C, 72.22; H, 6.06%. Calcd for $C_{21}H_{21}OPSi$: C, 72.38; H, 6.07%. Phosphine oxides **4b** and **4c** were obtained as two diastereomers by the same procedure as **4a**.

4b: One diastereomer; colorless crystals; mp 258—260 °C; ^{1}H NMR (500 MHz, $CDCl_3$) δ=6.00 (s, 1H, CH), 6.99—7.00 (m, 1H, 2′-ArH), 7.12—7.14 (m, 2H, 3′,5′-ArH), 7.19—7.22 (m, 2H, 4′,6′-ArH), 7.35—7.41 (m, 4H, 4,4′,6,6′-BiphH), 7.48 (t, J=7.4 Hz, 1H, 4-PhH), 7.59—7.65 (m, 2H, 5,5′-BiphH), 7.64 (d, J_{PCCH}=12.9 Hz, 1H, 3′-BiphH), 7.68 (t, J=7.4 Hz, 2H, 3,5-PhH), 7.79 (dd, J_{PCCH}=47.2 Hz, J=7.4 Hz, 2H, 2,6-PhH); ^{31}P NMR (109 MHz, $CDCl_3$) δ=35.8; IR (KBr) 3206 (OH), 1185 cm^{-1} (PO). Found: m/z 382.1136. Calcd for $C_{25}H_{19}O_2P$: M, 382.1123.

The other diastereomer; colorless crystals; mp 240—242.5 °C; ^{1}H NMR (500 MHz, $CDCl_3$) δ=6.05 (s, 1H, CH), 7.05—7.07 (m, 2H, 2′,6′-ArH), 7.08—7.09 (m, 1H, 4′-ArH), 7.15—7.17 (m, 2H, 3′,5′-ArH), 7.25—7.27 (m, 2H, 4,4′-BiphH), 7.34 (d, J=7.2 Hz, 2H, 6,6′-BiphH), 7.38 (t, J=7.8 Hz, 1H, 4-PhH), 7.44 (d, J=7.2 Hz, 1H, 5-BiphH), 7.46 (d, J=7.2 Hz, 1H, 5′-BiphH), 7.55 (d, J=7.8 Hz, 2H, 3,5-PhH), 7.61 (d, J_{PCCH}=15.0 Hz, 1H, 3′-BiphH), 7.79 (dd, J_{PCCH}=28.2 Hz, J=7.8 Hz, 2H, 2,6-PhH); ^{31}P NMR (109 MHz, $CDCl_3$) δ=35.7; IR (KBr) 3258 (OH), 1180 cm^{-1} (PO). Found: m/z 382.1112. Calcd for $C_{25}H_{19}O_2P$: M, 382.1123.

4c: One diastereomer; colorless crystals; mp 214—215.5 °C; ^{1}H NMR (500 MHz, $CDCl_3$) δ=1.36 (d, J=6.5 Hz, 3H, CH_3), 5.10 (q, J=6.5 Hz, 1H, CH), 7.33—7.35 (m, 2H, 4,4′-BiphH), 7.37—7.39 (m, 2H, 6,6′-BiphH), 7.46 (t, J=7.5 Hz, 1H, 4-PhH), 7.54—7.58 (m, 2H, 5,5′-BiphH), 7.62 (d, J_{PCCH}=12.4 Hz, 1H, 3′-BiphH), 7.64 (t, J=7.5 Hz, 2H, 3,5-PhH), 7.78 (dd, J_{PCCH}=33.8, J=7.5 Hz, 2H, 2,6-PhH); ^{31}P NMR (109 MHz, $CDCl_3$) δ=34.4; IR (KBr) 3292 (OH), 1193 cm^{-1} (PO). Found: m/z 320.0928. Calcd for $C_{20}H_{17}O_2P$: M, 320.0966.

The other diastereomer; colorless crystals; mp 222.5—224.5 °C; ^{1}H NMR (500 MHz, $CDCl_3$) δ=1.30 (d, J=6.2 Hz, 3H, CH_3), 5.06 (q, J=6.2 Hz, 1H, CH), 7.36—7.39 (m, 4H, 4,4′,6,6′-BiphH), 7.47 (t, J=7.8 Hz, 1H, 4-PhH), 7.55—7.58 (m, 2H, 5,5′-BiphH), 7.61 (d, J_{PCCH}=12.4 Hz, 1H, 3′-BiphH), 7.64 (t, J=7.8 Hz, 2H, 3,5-PhH), 7.78 (dd, J_{PCCH}=45.9, J=7.8 Hz, 2H, 2.6-PhH); ^{31}P NMR (109 MHz, $CDCl_3$) δ=34.9; IR (KBr) 3296 (OH), 1185 cm^{-1} (PO). Found: m/z 320.0937. Calcd for $C_{20}H_{17}O_2P$: M, 320.0966.

Reactions of (2,2′-Biphenylylene)phenylphosphine Oxide (3) and [(3-Trimethylsilyl)-2,2′-biphenylylene]phenylphosphine Oxide (4a) with Phenyllithium. In a typical run, to a stirred solution of **3** (276 mg, 1.0 mmol) in THF (15 mL) at −78 °C under N_2 atmosphere was added 1.8 M phenyllithium (0.8 mL, 1.5 mmol). The mixture was stirred at −78 °C for 30 min. After hydrolysis, the solvent was removed under reduced pressure. To the residue was added water (30 mL) and the mixture was neutralized with 1 M hydrochloric acid, extracted with dichloromethane (3×30 mL). The extract was dried with anhydrous magnesium sulfate, and the solvent was evaporated under reduced pressure. The residue was purified by column chromatography (silica gel; eluent, dichloromethane, ethyl acetate) to give **5a** in 95% yield. Recrystallization from ethyl acetate gave colorless crystals; mp 148.5—150 °C; ^{1}H NMR (500 MHz, $CDCl_3$) δ=7.01—7.58 (m, ArH); ^{13}C NMR (125 MHz, $CDCl_3$) δ=126.5 (d, ^3J=12.3 Hz), 127.1 (s), 127.2 (s), 128.0 (d, ^3J=12.0 Hz), 130.1 (s), 131.1 (d, ^4J=2.2 Hz), 131.5 (d, ^2J=9.4 Hz), 131.7 (s), 131.7 (d, ^1J=101.1 Hz), 131.9 (d, ^2J=10.1 Hz), 133.1 (d, ^1J=103.6 Hz), 134.0 (d, ^3J=12.1 Hz), 140.3 (d, ^3J=4.4 Hz), 147.7 (d, ^2J=8.9 Hz); ^{31}P NMR (109 MHz, $CDCl_3$) δ=26.3; IR (KBr) 1191 cm^{-1} (PO); MS m/z 354 (M^+). Found: C, 81.15; H, 5.40%. Calcd for $C_{24}H_{19}OP$: C, 81.34; H, 5.40%.

5b: Colorless crystals; mp 137.5—138.5 °C; ^{1}H NMR (500 MHz, $CDCl_3$) δ=0.14 (s, 9H, CH_3), 7.05—7.57 (m, 18H, ArH); ^{13}C NMR (125 MHz, $CDCl_3$) δ=−1.1 (s), 126.6 (d, ^3J=12.3 Hz), 126.7 (s), 128.0 (d, ^3J=11.7 Hz), 130.7 (s), 131.0 (d, ^4J=2.7 Hz), 131.6 (d, ^2J=9.1 Hz), 131.6 (d, ^1J=100.0 Hz), 131.7 (d, ^4J=2.3 Hz), 132.0 (d, ^2J=10.0 Hz), 132.1 (s), 133.0 (d, ^1J=104.0 Hz), 134.2 (d, ^3J=12.0 Hz), 134.7 (s), 139.1 (s), 139.7 (d, ^3J=3.8 Hz), 147.9 (d, ^2J=9.0 Hz); ^{31}P NMR (109 MHz, $CDCl_3$) δ=27.1; MS m/z 426 (M^+). Found: C, 75.97; H, 6.55%. Calcd for $C_{27}H_{27}OPSi$: C, 76.02; H, 6.38%.

Reactions of (2-Biphenylyl)diphenylphosphine Oxide (5a) and [3′-(Trimethylsilyl)-2-biphenylyl]diphenylphosphine Oxide (5b) with Phenyllithium. In a typical run, to a stirred solution of **5a** (200 mg, 0.6 mmol) in THF (10 mL) was added 1.8 M phenyllithium (1.0 mL, 1.8 mmol) in THF solution under N_2 atmosphere at −78 °C for 30 min. To the mixture was added acetaldehyde (0.05 mL, 0.9 mmol) and the mixture was stirred at −20 °C for 3 h. After hydrolysis, the solvent was removed under reduced pressure. To the residue was added water (30 mL) and the mixture was neutralized with 1 M hydrochloric acid, extracted with dichloromethane (3×30 mL). The extract was dried with anhydrous magnesium sulfate, and the solvent was evaporated under reduced pressure. The residue was purified by column chromatography (silica gel; eluent, hexane–ethyl acetate=1 : 2) to give 2-(1-hydroxyethyl)biphenyl (**6d**) and **1** in 55% and 63% yields respectively.

6d: Mp 105—107 °C (lit,[9] 111—112 °C); ^{1}H NMR ($CDCl_3$) δ=1.40 (d, J=6.6 Hz, 3H, CH_3), 4.98 (q, J=6.6 Hz, 1H, CH), 7.21—7.62 (m, 9H, ArH); IR (KBr) 3252 cm^{-1} (OH); MS m/z 198 (M^+). Found: C, 84.66; H, 7.12%. Calcd for $C_{14}H_{14}O$: C, 84.81; H, 7.12%.

6b: Colorless liquid; ^{1}H NMR ($CDCl_3$) δ=0.00 (s, 9H, CH_3), 7.15—7.70 (m, 9H, ArH); MS m/z 226 (M^+). Found: C, 79.17; H, 7.96%. Calcd for $C_{15}H_{18}Si$: C, 79.58; H, 8.01%.

6c: Mp 144—145 °C (lit,[10] 146—147 °C); ^{1}H NMR ($CDCl_3$) δ=5.93 (s, 1H, CH), 7.18—7.56 (m, 14H, ArH); IR (KBr) 3358 cm^{-1} (OH); MS m/z 260 (M^+).

6e: Colorless liquid; ^{1}H NMR ($CDCl_3$) δ=0.18 (s, 9H, CH_3), 7.30—8.90 (m, 9H, ArH); MS m/z 266 (M^+). Found: C, 79.71; H, 8.09%. Calcd for $C_{15}H_{18}Si$: C, 79.58; H, 8.01%.

6f: Colorless liquid; ^{1}H NMR ($CDCl_3$) δ=0.29 (s, 9H, CH_3), 0.35 (s, 9H, CH_3), 7.27—7.46 (m, 8H, ArH). Found: m/z 298.1539. Calcd for $C_{18}H_{26}Si_2$: M, 298.1573.

6g: Colorless liquid; ^{1}H NMR ($CDCl_3$) δ=0.28 (s, 9H, CH_3), 1.44 (d, J=6.6 Hz, 3H, CH_3), 4.44 (q, J=6.6 Hz, CH), 7.21—7.62 (m, 8H, ArH); IR (KBr): 3294 cm^{-1} (OH); MS m/z 270 (M^+). Found: C, 75.79; H, 8.38%. Calcd for $C_{17}H_{22}OSi$: C, 75.50; H, 8.20%.

This work was supported by a Grant-in-Aid No. 02453018 from the Ministry of Education, Science and Culture.

References

1) G. Wittig, *Angew. Chem.*, **68**, 505 (1956); H. J. Bestmann and R. Zimmermann, "Organic Phosphorus Compounds," ed by G. M. Kosolapoff and L. Maier, John Wiley and Sons, New York (1972), Chap. 5A.

2) G. Booth, "Organic Phosphorus Compounds," ed by G. M. Kosolapoff and L. Maier, John Wiley and Sons, New York (1972), Chap. 3A; J. G. Verkade and K. J. Coskran, Chap. 3B.

3) K. Naumann, G. Zon, and K. Mislow, *J. Am. Chem. Soc.*, **91**, 7012 (1969); L. Horner and W. D. Balzer, *Tetrahedron Lett.*, **1965**, 1157; H. Fritzsche, U. Hasserodt, and F. Korte, *Chem. Ber.*, **97**, 1988 (1964); L. Horner, H. Hoffmann, and P. Beck, *ibid.*, **91**, 1583 (1958); F. Hein, K. Issleib, and H. Rabold, *Z. Anorg. Allg. Chem.*, **287**, 208 (1956); K. Issleib and G. Grams, *ibid.*, **299**, 58 (1959).

4) N. Furukawa, "Heteroatom Chemistry," ed by E. Block, Verlag, New York (1990), p. 165; N. Furukawa, S. Ogawa, K. Matsumura, and H. Fujihara, *J. Org. Chem.*, in press.

5) S. Ogawa and N. Furukawa, *J. Org. Chem.*, in press.

6) D. Seyferth, W. B. Hughes, and J. K. Heeren, *J. Am. Chem. Soc.*, **87**, 3467 (1965).

7) G. Wittig and A. Maercker, *Chem. Ber.*, **97**, 747 (1964).

8) G. Wittig and G. Geissler, *Justus Liebigs Ann. Chem.*, **580**, 44 (1953).

9) W. F. Huber, M. Renoll, A. G. Rossow, and D. T. Mowry, *J. Am. Chem. Soc.*, **68**, 1109 (1946).

10) G. W. Gribble and R. M. Leese, *Synthesis*, **1977**, 172.

Nickel-Catalyzed Epoxidation of Olefins with NaOCl

Shigekazu YAMAZAKI* and Yasuyuki YAMAZAKI
Toyama Industrial Technology Center, 150 Futagami, Takaoka, Toyama 933
(Received May 18, 1991)

Synopsis. Nickel complexes of bidentate heterocyclic amines such as 2,2′-bipyridine and 1,10-phenanthroline have been found to be active catalysts for the epoxidation of olefins with hypochlorite as terminal oxidant. Nickel complex of 1-methylimidazole which is monodentate ligand also indicated epoxidation ability.

The development of inexpensive systems for the direct epoxidation of olefins is one of the most important theme both industrial and academic field of synthetic chemistry,[1] because epoxides are important intermediates of variety of useful products. And the design of convenient catalytic systems using simple metal complexes with inexpensive oxygen donors such as H_2O_2, *t*-BuOOH and NaOCl as terminal oxidant is current interest.[2] Epoxidation of olefins was extensively investigated in relation to the enzymatic oxygenation for the last decade with metal complex catalysts.[3] In these studies, manganese, iron, and chromium complexes of porphyrins and Schiff bases were chosen as catalysts. Recently, nickel complexes such as Ni(salen)[4] and Ni(cyclam) have been reported to act as catalysts for the epoxidation of olefins with NaOCl[5,6] and PhIO[7,8] as the terminal oxidants.[9] Here we report our results on the epoxidation of olefins catalyzed by nickel complexes of bidentate heterocyclic amine ligands such as 2,2′-bipyridine and 1,10-phenanthroline with NaOCl.

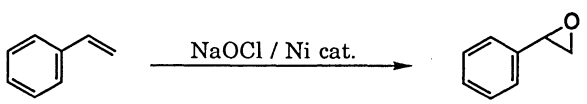

Results and Discussion

The results of the epoxidation of styrene by some nickel complexes of heterocyclic amines with NaOCl were summarized in Table 1. The epoxidation of styrene were performed typically by stirring the mixture of styrene, aqueous solution of nickel catalyst and NaOCl at room temperature. Styrene oxide was mainly obtained, and a considerable amount of benzoic acid was also produced. Among the bidentate ligands examined, 2,2′-bipyridine gave the best result on the selectivity of styrene oxide. $Ni(bpy)Cl_2$ and $Ni(bpy)_2Cl_2$ showed almost the same results (Run 3). Use of organic solvents such as CH_2Cl_2 and benzene in the epoxidation of styrene decreased the selectivity of epoxide (Run 2). Monodentate ligands such as 1-methylimidazole also indicated epoxidation ability but lowered the yield of the epoxide (Run 6).

Unlike the nickel complex catalyzed epoxidation reaction reported so far, the nickel complex described here is used as aqueous solution. Fine black precipitates which act as catalyst were appeared in a few minutes by the addition of NaOCl to the aqueous nickel complex solution. So the quaternary ammonium salts were not effective in this system as the phase-transfer catalysts.[5,6]

Table 2 showed the results of the epoxidation of styrene with various amount of $Ni(bpy)_2Cl_2$ catalyst. The best yield of styrene oxide was obtained when 2 mol% of $Ni(bpy)_2Cl_2$ was used (Run 3). The lower amount of catalyst decreased the selectivity of epoxide (Runs 4—7). On the other hand, the use of higher amount of catalyst did not increase the yield of epoxide (Runs 1, 2), and the conversion of styrene were lowered. When $Ni(bpy)_2Cl_2$ and NaOCl were mixed without styrene, NaOCl decomposed with evolution of gas. These results indicated that considerable amounts of NaOCl decomposed without the oxygen transfer to styrene, when large amount of nickel complex existed.

Epoxidations of other olefins were also investigated, and the results were summarized in Table 3. CH_2Cl_2

Table 1. Nickel Complexes-Catalyzed Epoxidation of Styrene with NaOCl[a]

Run	$Ni(L)_nCl_2$	Conv./%[b]	Yield/% Styrene oxide[b]	Yield/% Benzoic acid[c]
1	$Ni(bpy)_2Cl_2$	99	74	15
2	$Ni(bpy)_2Cl_2/CH_2Cl_2$	97	33	9
3	$Ni(bpy)Cl_2$	98	69	15
4	$Ni(dm\text{-}bpy)_2Cl_2$	99	54	30
5	$Ni(phen)_2Cl_2$	98	36	37
6	$Ni(Me\text{-}im)_4Cl_2$	85	19	27

a) 1.0 M NaOCl (12.5 mmol) was added to the mixture of styrene (5.0 mmol) and 0.050 M aq solution of catalyst (0.10 mmol), and the resulted mixture was stirred vigorously at room temperature for 5 h. b) Determined by GC. Yield based on styrene used. c) Isolated yield.

Table 2. $Ni(bpy)_2Cl_2$-Catalyzed Epoxidation of Styrene with NaOCl[a]

Run	Cat./mol%	Conv./%[b]	Turnover[c]	Yield/% Styrene oxide[b]	Yield/% Benzoic acid[d]
1	10	89	9	49(55)	24(27)
2	5	95	19	68(72)	12(12)
3	2	99	50	74	15
4	1	95	95	61(64)	19(20)
5	0.5	72	144	44(61)	13(18)
6	0.2	60	300	18(30)	11(19)
7	0.1	59	590	12(20)	23(39)

a) 0.050 M $Ni(bpy)_2Cl_2$, 2.5 equiv 1.0 M NaOCl, for 5 h, at room temperature. b) Determined by GC. The numbers in parentheses are the yield based on consumed styrene. c) Turnover=consumed styrene/nickel catalyst. d) Isolated yield.

Table 3. $Ni(bpy)_2Cl_2$-Catalyzed Epoxidation of Olefins with NaOCl[a]

Run	Olefin	NaOCl/equiv	Solvent	Time/h	Conv.[b]/%	Yield/%	
						Epoxide[b]	Benzoic acid[c]
1	Styrene	2.5	—	5	99	74	15
2	α-Methylstyrene	5	—	6	100	53	15[d]
3	*trans*-β-Methylstyrene	3.5	—	2	100	28[e]	15
4	*cis*-β-Methylstyrene	4	—	4	100	25[f]	19
5	*trans*-Stilbene	10	CH_2Cl_2	6	100	34[c,e]	21
6	*cis*-Stilbene	2.5	CH_2Cl_2	5	100	31[c,e]	19
7	Cyclohexene	6	CH_2Cl_2	3	91	10	—
8	Norbornene	5	CH_2Cl_2	3	100	14[g]	—

a) 2 mol% 0.050 M $Ni(bpy)_2Cl_2$, 1.0 M NaOCl, at room temperature. b) Determined by GC. c) Isolated yeild. d) Acetophenone 12%. e) *trans*-Epoxide. f) 8% *cis*- And 17% *trans*-epoxide. g) *exo*-Epoxide.

was used as organic solvent in the epoxidation of *trans*-stilbene and norbornene which were solid at room temperature. The epoxidation of olefins were proceeded smoothly under the same reaction conditions with styrene oxide. But the yields of the epoxides were lower than the case of styrene. In the epoxidation of α-methylstyrene, epoxide was mainly obtained in 53% yield with acetophenone and benzoic acid in 12% and 15% yields respectively. The epoxide obtained by the oxidation of *trans*-β-methylstyrene was *trans*-epoxide only. On the other hand, both *trans*- and *cis*-epoxides were obtained in the epoxidation of *cis*-β-methylstyrene in 17% and 8% yields respectively. The epoxide obtained in the epoxidation of *trans*- and *cis*-stilbene were *trans*-stilbene oxide. These results show that this epoxidation is proceeded by radical process. Contrary to the case of styrene, in the epoxidation of cyclohexene and *cis*-stilbene, use of CH_2Cl_2 as organic solvent gave better selectivities of epoxides than the reaction without organic solvent.

Conclusion

The bidentate heterocyclic amines such as 2,2′-bipyridine and 1,10-phenanthroline are good ligands for nickel-catalyzed olefin epoxidation with NaOCl. Bipyridines were more readily available than porphyrin and Schiff base ligands, so the use of catalyst having bipyridine ligand must provide synthetically useful method for the epoxidation of olefins. Since the selectivity of epoxides by the system described above were not satisfactory, we are studying to improve the selectivity of epoxides.

Experimental

cis-β-Methylstyrene was prepared by the hydrogenation of 1-phenylpropyne.[10] Epoxides other than styrene oxide, cyclohexene oxide, and α-methylstyrene oxide used as GC standards were prepared by epoxidation of the corresponding alkenes with *m*-chloroperbenzoic acid under standard conditions.[11] The other olefins, epoxides, and amine ligands were commercially available, and purified by crystallization or distillation before use. NaOCl was obtained as aqueous solution (1.9—1.5 M) and titrated before use (1 M=1 mol dm^{-3}). The NiL_nCl_2 catalysts were prepared by dissolving $NiCl_2 \cdot 6H_2O$ and *n* equivalents of the amine ligand in distilled water as 0.050 M solution. All the catalysts prepared were stand at room temperature for at least 1 day and used as aqueous solution. Analytical TLC and PTLC were performed with Merck $60F_{254}$ and $60PF_{254}$ respectively. Analyses of oxidation products were performed on a Hitachi 163 gas chromatograph attached with Shimadzu CR-5A CHROMATOPAC as integrator. ^1H NMR spectra were recorded at 60 MHz on a JEOL PMX-60Si spectrometer with tetramethylsilane as internal standard.

Styrene Oxidation. In a typical experiment, 1.0 M NaOCl (12.5 mL, 12.5 mmol) was added to the mixture of styrene (0.52 g, 5.0 mmol) and 0.050 M aqueous nickel catalyst (2.0 mL, 0.10 mmol), and the resulted mixture was stirred vigorously at room temperature. A fine black precipitate formed in a few minutes upon addition of NaOCl. After 5 h stirring, the mixture was passed through a short Celite column to remove black precipitate. The filtrate was extracted with CH_2Cl_2 (10 mL×2). The yield of styrene oxide was determined by GC analysis of the CH_2Cl_2 extract. Benzoic acid was isolated from the acidified aqueous layer by CH_2Cl_2 extraction. The oxidations of styrene in Tables 1 and 2 were performed in a same manner with appropriate amount of nickel catalyst.

Oxidations and analyses of *trans*-β-methylstyrene and *cis*-β-methylstyrene were performed in a same manner with styrene oxidation.

Oxidation of α-Methylstyrene. The oxidation was performed in a same manner with styrene oxidation under the conditions described in Table 3. The CH_2Cl_2 extract of the reaction mixture were concentrated, and then distilled by Kugelrohr under reduced pressure (80 °C, 10 mmHg, 1 mmHg=133.322 Pa). The yields of α-methylstyrene oxide and acetophenone were determined by the comparison of the ^1H NMR integration of the distillate with that of dibenzyl ether added as an internal standard. The yields of α-methylstyrene oxide and acetophenone were 53% and 12% respectively. Benzoic acid was isolated from the acidified aqueous layer by CH_2Cl_2 extraction in 15% yield.

Oxidation of *trans*-Stilbene. NaOCl (1.0 M, 20 mL, 20 mmol) was added to the mixture of *trans*-stilbene (0.36 g, 2.0 mmol) in CH_2Cl_2 (10 mL) and aqueous $Ni(bpy)_2Cl_2$ (0.050 M, 0.80 mL, 0.040 mmol). The resulted mixture was stirred vigorously at room temperature. The disappearance of *trans*-stilbene was monitored by TLC. After the complete conversion of *trans*-stilbene, the mixture was passed through a short Celite column and the filtrate was extracted twice with CH_2Cl_2. The CH_2Cl_2 extract was dried over anhydrous Na_2SO_4 and the solvent was removed out by evaporation. The residue obtained was separated on silica-gel PTLC with CH_2Cl_2 : hexane=1 : 1 as eluent. *trans*-Stilbene oxide (R_f=0.6) was obtained in 34% yield. Benzoic acid was isolated by the CH_2Cl_2 extraction of the acidified aqueous layer

in 21% yield. No *cis*-stilbene oxide was detected in the reaction mixture by TLC and ^{1}H NMR.

cis-Stilbene was oxidized and analyzed in a same manner with *trans*-isomer. Cyclohexene and norbornene were oxidized in a same manner with *trans*-stilbene under the conditions described in Table 3, and the yields of epoxides were determined by GC.

References

1) R. A. Sheldon and J. K. Kochi, "Metal-Catalyzed Oxidations of Organic Compounds," Academic Press, New York (1981).

2) R. A. Sheldon, *Bull. Soc. Chim. Belg.*, **94**, 651 (1985).

3) K. A. Jørgensen, *Chem. Rev.*, **89**, 431 (1989).

4) Abbreviations used: salen, *N,N'*-ethylenebis(salicylideneamine); cyclam, 1,4,8,11-tetraazacyclotetradecane; bpy, 2,2'-bipyridine; dm-bpy, 4,4'-dimethyl-2,2'-bipyridine; phen, 1,10-phenanthroline; Me-im, 1-methylimidazole.

5) H. Yoon and C. J. Burrows, *J. Am. Chem. Soc.*, **110**, 4087 (1988). H. Yoon, T. R. Wagler, K. J. O'Connor, and C. J. Burrows, *J. Am. Chem. Soc.*, **112**, 4568 (1990).

6) T. R. Wagler, Y. Fang, and C. J. Burrows, *Tetrahedron Lett.*, **29**, 5091 (1988). *idem.*, *J. Org. Chem.*, **54**, 1584 (1989).

7) J. F. Kinneary, J. S. Albert, and C. J. Burrows, *J. Am. Chem. Soc.*, **110**, 6124 (1988). J. F. Kinneary, T. R. Wagler, and C. J. Burrows, *Tetrahedron Lett.*, **29**, 877 (1988).

8) J. D. Koola and J. K. Kochi, *Inorg. Chem.*, **26**, 908 (1987).

9) More recently, epoxidations of olefins with O_2 catalyzed by nickel complexes of 1,3-diketones were reported; T. Mukaiyama, T. Takai, T. Yamada, and O. Rhode, *Chem. Lett.*, **1990**, 1661. T. Yamada, T. Takai, O. Rhode, and T. Mukaiyama, *ibid.*, **1991**, 1.

10) Synthesis of *cis*-β-methylstyrene, D. E. Davies, T. L. Gilchrist, and T. G. Roberts, *J. Chem. Soc., Perkin Trans. 1*, **1983**, 1275.

11) Synthesis of norbornene oxide, J. B. Lambert and L. G. Greifenstein., *J. Am. Chem. Soc.*, **96**, 5120 (1974).

Base-Induced Addition-Elimination Reactions of Electron-Deficient Vinylarenes Containing a Carbonyl or Ester Group Utilizing 4-Phenyl-3*H*-1,2,4-triazole-3,5(4*H*)-dione (PTAD)

Kazuyoshi SEGUCHI* and Satoko TANAKA
Faculty of Home Science, Mukogawa Women's University, 6-46 Ikebiraki-cho, Nishinomiya 663
(Received March 22, 1991)

Synopsis. The reaction of electron-deficient vinylarenes such as styrylketones and cinnamate with PTAD afforded double Diels-Alder products and Diels-Alder ene products; the latter underwent novel base-induced elimination of 4-phenyl-1,2,4-triazolidine-3,5-dione via a stable carbanion.

The reactions of 4-phenyl-3*H*-1,2,4-triazole-3,5(4*H*)-dione (PTAD) have been used extensively in organic syntheses, and a diversity of reactions with alkenes have been documented, such as [4+2],[1] [2+2],[2] ene,[3] and dipolar reactions.[4,5] In particular, the reactions of PTAD with electron-rich vinylarenes exemplified by styrene,[1b] vinylpyridines,[6] and benzylidenebicyclic compounds,[2,5] resulted in 1 : 2 adducts. However, no studies have described that the 3,5-dioxo-4-phenyl-1,2,4-triazolidin-1-yl group (PTAD · H) is a latent leaving group. We have found that PTAD · H served as a good leaving group in the reaction products of PTAD with styrylketones or cinnamate.

Results and Discussion

The reaction of 1-phenyl-1-penten-3-one **1a** with PTAD in dichloromethane at 25 °C afforded the double Diels-Alder product **2a** and the Diels-Alder ene product **3a** through a 1 : 1 adduct as depicted in Scheme 1 in isolated yields of 27% and 24%, respectively. Pursuit of the reaction by ^{1}H NMR spectroscopy in $CDCl_3$ at appropriate intervals failed to detect the 1 : 1 adduct because of the higher reactivity of the diene. The Diels-Alder ene product decomposed partially during purification procedures (silica-gel chromatography and recrystallization). Careful recrystallization from acetonitrile gave pure **3a** as a white powder. The spectral data and the elemental analyses supported the proposed structure. The ^{1}H NMR showed two doublet signals at δ=5.33 and 6.02 corresponding to 4-H and 5-H, respectively. The ^{13}C NMR also showed two doublet signals at δ=52.7 and 63.9. A molecular ion peak (m/z 510) was observed on the mass spectrum. When a catalytic amount of triethanolamine was added to an acetonitrile solution of **3a** at 25 °C, the solution turned yellow after a few minutes to afford yellow crystals of **4a** in 94% yield after conventional purifications. This structure was again assigned on the basis of spectral and elemental analyses. The ^{1}H NMR showed a singlet proton signal at a lower field (δ=6.21) in addition to an ethyl signal (δ=1.25 and 2.32) and a phenyl signal (δ=7.03—8.35). Compound **4a** resulted from the novel base-induced elimination of 4-phenyl-1,2,4-triazoline-3,5-dione (PTAD · H_2). This elimination reaction could be carried out in situ without isolation of **3a.**

Thus, the in situ reaction was extended to a series of electron-deficient vinylarenes such as styrylketones, cinnamate, and cinnamonitrile.[7] As shown in Table 1, similar successive addition-elimination reactions took place in all cases except for **1h** and **1j**. Concerning **1h**, unidentified products were obtained. **1j** was inert to

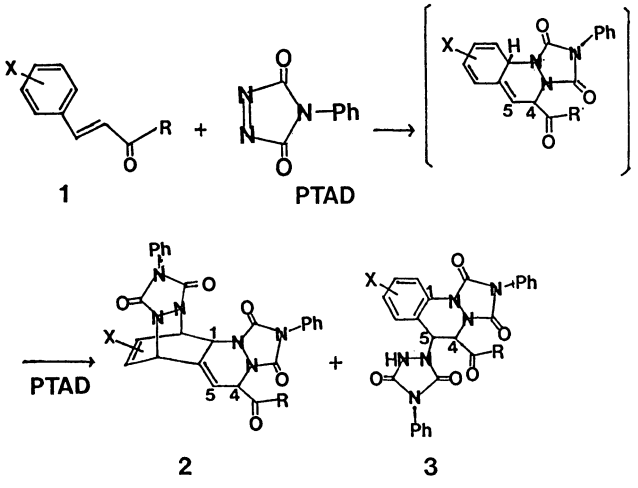

Scheme 1.

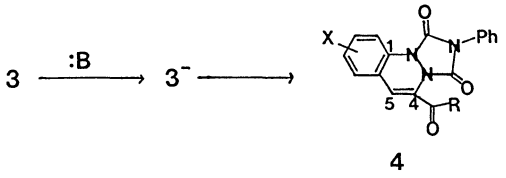

Scheme 2.

Table 1. Product Yields of **4** by Addition-Elimination Reaction in situ

	Starting compound		Yield (%) of **4**[a]
	X	R	
1a	H	Et	34 (94)
1b	H	Me	27 (90)
1c	H	Ph	16 (87)
1d	*p*-OMe	Me	52
1e	*p*-OMe	Ph	61 (92)
1f	*p*-Cl	Me	26 (70)
1g	*o*-Cl	Me	33 (68)
1h	*p*-NO_2	Me	0 (30)[b]
1i	*p*-OMe	OEt	27
1j	Cinnamonitrile		0 (78)[b]

a) Yield based on **1**. The values in parentheses show yields based on isolated crude **3**. b) The values in parentheses show recovered yields of starting materials.

PTAD possibly because of the lower electron-density of the diene.

In order to elucidate the elimination mechanism in particular, the deuterium exchange reaction of **3a** was investigated by ^{1}H NMR ($CDCl_3$) spectroscopy in the presence of deuterium oxide and a catalytic amount of sodium carbonate. Addition of sodium carbonate caused the immediate exchange at C-4 more rapidly than the formation of **4a**. Furthermore, the recovered starting material was completely deuterated at C-4. These findings suggest that the elimination reaction may proceed via a carbanion as shown in Scheme 2. Presumably, the electron-withdrawing carbonyl or ester group and amide groups each stabilize the conjugate base of **3**. In summary, the PTAD·H group is a good leaving group in the elimination reaction via a carbanion.

Experimental

Materials and Instruments. Substituted styrylketones, cinnamate, and cinnamonitrile **1a—j** were synthesized according to the reported procedures or obtained from a commercial source. PTAD was freshly prepared by Cookson's method.[8] The ^{1}H NMR and ^{13}C NMR spectra were measured in $CDCl_3$ solution using Me_4Si as an internal standard on a Hitachi R-600 or a JEOL FX-200 spectrometer. The mass spectra were recorded on a JEOL JMS DX-303 spectrometer, operating at an ionizing potential of 70 eV. The IR spectra were taken as KBr disks using a Shimadzu R-460 spectrometer. The elemental analyses were performed using a Yanagimoto Model MT-3 CHN analyzer.

Reaction of 1a with PTAD. PTAD (13.8 mmol) was added portionwise over 2 h in the dark at 25 °C to a solution of **1a** (6.59 mmol) in dichloromethane (10 ml) and the mixture was stirred overnight. The solvent was removed and the residue was flash-chromatographed on silica gel (Wakogel C-200) with dichloromethane as an eluent. **3a** from the first eluate and **2a** from the second eluate were obtained in yields of 24% and 27%, respectively.

2a; Mp 184 °C (acetone); ^{1}H NMR δ=0.99 (t, 3H), 2.52 (q, 2H), 4.10 (bs, 1H), 5.08—5.30 (m, 1H), 5.30—5.51 (m, 1H), 6.28—6.50 (m, 2H), 6.65—6.90 (m, 2H), and 7.45—7.68 (m, 10H); ^{13}C NMR δ=7.0 (q), 32.1 (t), 52.9 (d), 54.1 (d), 60.0 (d), 62.1 (d), 118.6 (d), 125.4 (d), 125.6 (d), 128.3 (d), 128.4 (d), 129.0 (d), 129.1 (d), 129.3 (d), 130.1 (s), 130.9 (s), 131.0 (d), 131.2 (d), 151.7 (s), 154.8 (s), 154.9 (s), and 200.8 (s); IR 1782, 1776, and 1709 cm^{-1}; MS *m/z* (%) 510 (6, M^+) and 333 (100, M^+—$PTADH_2$). Found: C, 63.70; H, 4.22; N, 16.44%. Calcd for $C_{27}H_{22}N_6O_5$: C, 63.50; H, 4.35; N, 16.47%.

3a; Mp 139—140 °C (acetonitrile); ^{1}H NMR δ=1.06 (t, 3H), 2.62 (q, 2H), 5.33 (d, 1H, *J*=2 Hz), 6.02 (d, 1H, *J*=2 Hz), 7.16—7.38 (m, 14H), and 8.40 (bs, 1H); ^{13}C NMR δ=7.1 (q), 32.2 (t), 52.7 (d), 63.9 (d), 114.6 (s), 116.4 (d), 124.7 (d), 125.3 (d), 126.2 (d), 128.4 (d), 128.6 (d), 129.2 (d), 129.7 (d), 130.8 (d), 131.4 (d), 133.2 (s), 146.8 (s), 151.8 (s), 153.8 (s), and 201.5 (s); IR 3160, 1764, and 1708 cm^{-1}; MS *m/z* (%) 510 (0.4, M^+) and 333 (100, M^+—$PTADH_2$). Found: C, 63.33; H, 4.27; N, 16.42%. Calcd for $C_{27}H_{22}N_6O_5$: C, 63.50; H, 4.35; N, 16.47%.

General Procedure of in situ Addition-Elimination Reaction. PTAD (13.8 mmol) was added portionwise to the stirred acetonitrile solution (10 ml) of **1** (6.59 mmol) as described above. The mixture was stirred at 25 °C overnight and then a drop of triethanolamine was added to the reaction mixture. The solution turned yellow in a few minutes. After 1 h, conventional purification procedures (concentration by a rotary evaporator, silica-gel column chromatography, and recrystallization) gave yellow crystals.

4a; Mp 202—203 °C (benzene); ^{1}H NMR δ=1.25 (t, 3H), 2.32 (q, 2H), 6.21 (s, 1H), and 7.03—8.35 (m, 9H); ^{13}C NMR δ=8.1 (q), 34.4 (t), 113.3 (d), 115.4 (d), 119.7 (s), 125.7 (d), 125.9 (d), 128.1 (d), 128.7 (d), 129.2 (d), 130.6 (s), 131.1 (d), 133.2 (s), 134.6 (s), 143.9 (s), 146.2 (s), and 194.6 (s); IR 1746 and 1638 cm^{-1}; MS *m/z*(%) 333 (100, M^+). Found: C, 68.56; H, 4.41; N, 12.56%. Calcd for $C_{19}H_{15}N_3O_3$: C, 68.44; H, 4.54; N, 12.61%.

4b; Mp 201—202 °C (benzene-hexane); ^{1}H NMR δ=2.48 (s, 3H), 6.31 (s, 1H), and 7.09—8.25 (m, 9H); ^{13}C NMR δ=28.1 (q), 114.7 (d), 115.4 (d), 119.6 (s), 125.7 (d), 125.9 (d), 128.4 (d), 128.7 (d), 129.2 (d), 130.6 (s), 131.4 (d), 133.4 (s), 134.8 (s), 144.1 (s), 146.4 (s), and 190.7 (s); IR 1746 and 1690 cm^{-1}; MS *m/z* (%) 319 (100, M^+). Found: C, 67.74; H, 3.98; N, 13.01%. Calcd for $C_{18}H_{13}N_3O_2$: C, 67.69; H, 4.11; N, 13.17%.

4c; Mp 174—175 °C (benzene-hexane); ^{1}H NMR δ=6.12 (s, 1H), and 6.99—8.38 (m, 14H); ^{13}C NMR δ=114.2 (d), 115.4 (d), 120.0 (s), 125.8 (d), 127.9 (d), 127.5 (d), 128.8 (d), 129.1 (d), 129.4 (d), 127.9 (s), 130.6 (s), 131.1 (d), 131.6 (s), 133.9 (d), 134.4 (s), 143.1 (s), 145.7 (s), and 185.5 (s); IR 1752 and 1692 cm^{-1}; MS *m/z* (%) 381 (100, M^+). Found: C, 72.52; H, 3.77; N, 10.92%. Calcd for $C_{23}H_{15}N_3O_3$: C, 72.42; H, 3.97; N, 11.06%.

4d; Mp 202—203 °C (benzene); ^{1}H NMR δ=2.48 (s, 3H), 3.85 (s, 3H), 6.44 (s, 1H), and 6.61—7.90 (m, 8H); ^{13}C NMR δ=27.7 (q), 55.7 (q), 101.5 (d), 111.7 (s), 112.1 (d), 117.0 (d), 125.1 (d), 128.8 (d), 129.3 (d), 129.9 (d), 130.7 (s), 130.8 (s), 136.6 (s), 144.0 (s), 146.8 (s), 162.5 (s), and 190.2 (s); IR 1743 and 1706 cm^{-1}; MS *m/z* (%) 349 (100, M^+). Found: C, 65.50; H, 4.24; N, 11.92%. Calcd for $C_{19}H_{15}N_3O_3$: C, 65.30; H, 4.33; N, 12.04%.

4e; Mp 209 °C (benzene-hexane); ^{1}H NMR δ=3.86 (s, 3H), 6.25 (s, 1H), and 7.33—8.10 (m, 13H); ^{13}C NMR δ=55.7 (q), 101.6 (d), 111.5 (d), 112.5 (d), 116.6 (s), 125.8 (d), 128.5 (d), 128.7 (d), 129.1 (d), 129.4 (d), 130.7 (s), 133.7 (d), 135.8 (s), 136.1 (s), 143.0 (s), 146.1 (s), 162.2 (s), and 185.3 (s); IR 1758, 1709, and 1653 cm^{-1}; MS *m/z* (%) 411 (100, M^+). Found: C, 69.81; H, 4.03; N, 10.45%. Calcd for $C_{24}H_{17}N_3O_4$: C, 70.05; H, 4.17; N, 10.22%.

4f; Mp 241—243 °C (ethanol); ^{1}H NMR δ=2.51 (s, 3H), 6.78 (s, 1H), and 7.02—7.58 (m, 8H); ^{13}C NMR δ=28.2 (q), 113.8 (d), 115.8 (d), 118.2 (s), 125.8 (d), 125.9 (d), 128.9 (d), 129.1 (d), 129.4 (d), 130.4 (s), 133.5 (s), 135.5 (s), 137.3 (s), 143.9 (s), 146.3 (s), and 190.4 (s); IR 1762, 1712, and 1682 cm^{-1}; MS *m/z* (%) 355 (39, M^++2) and 353 (100, M^+). Found: C, 61.17; H, 3.47; N, 11.67%. Calcd for $C_{18}H_{12}N_3O_3Cl$: C, 61.09; H, 3.42; N, 11.89%.

4g; Mp 216—217 °C (ethanol); ^{1}H NMR δ=2.55 (s, 3H), 6.79 (s, 1H), and 7.38—7.58 (m, 8H); ^{13}C NMR δ=28.2 (q), 110.5 (d), 113.7 (d), 118.5 (s), 125.9 (d), 126.5 (d), 128.9 (d), 129.3 (d), 130.5 (s), 131.6 (d), 133.0 (s), 134.4 (s), 143.7 (s), 146.2 (s), and 190.4 (s); IR 1757, 1717, and 1690 cm^{-1}; MS *m/z* (%) 355 (41, M^++2) and 353 (100, M^+). Found: C, 61.89; H, 3.40; N, 11.60%. Calcd for $C_{18}H_{12}N_3O_3Cl$: C, 61.09; H, 3.42; N, 11.89%.

4i; Mp 182 °C (ethanol); ^{1}H NMR δ=1.37 (t, 3H), 3.84 (s, 3H), 4.37 (q, 2H), 7.07 (s, 1H), and 7.09—7.59 (m, 8H); ^{13}C NMR δ=14.1 (q), 55.7 (q), 62.3 (t), 101.3 (d), 111.4 (d), 112.3 (d), 118.2 (d), 123.0 (s), 125.9 (d), 128.6 (d), 129.2 (d), 129.5 (d), 130.8 (s), 136.9 (s), 143.3 (s), 146.7 (s), 160.2 (s), and 162.3 (s); IR 1780, 1773, 1711, and 1707 cm^{-1}; MS *m/z* (%) 379 (100, M^+). Found: C, 63.07; H, 4.42; N, 11.05%. Calcd for $C_{20}H_{17}N_3O_5$: C, 63.30; H, 4.52; N, 11.08%.

References

1) a) M. E. Burrage, R. C. Cookson, S. S. Gupte, and I. D. R. Stevens, *J. Chem. Soc., Perkin Trans. 2*, **1975**, 1325; b) R. C. Cookson, S. S. H. Giliani, and I. D. R. Stevens, *J. Chem.*

Soc. C, **1967**, 1905.
2) W. Adam, V. Lucchini, E.-M. Peters, L. Pasquato, H. G. Schnering, K. Seguchi, H. Walter, and B. Will, *Chem. Ber.*, **122**, 133 (1989).
3) C.-C. Cheng, C. A. Seymour, M. A. Petti, and F. D. Greene, *J. Org. Chem.*, **49**, 2910 (1984).
4) W. Adam, O. De Lucchi, and K. Hill, *Chem. Ber.*, **102**, 6384 (1980).
5) W. Adam, V. Lucchini, L. Pasquato, E.-M. Peters, K. Peters, H. G. Schnering, and K. Seguchi, *Chem. Ber.*, **119**, 2932 (1986).
6) P. B. Terentev, A. N. Kost, and V. G. Kartsev, *Khim. Geterotsikl. Soedin.*, **1976**, 702; *Chem. Abstr.*, **85**, 94301 (1976).
7) The details of the cycloadditions will be published elsewhere.
8) R. C. Cookson, S. S. Gupte, I. D. R. Stevens, and C. T. Watts, *Org. Synth.*, **51**, 121 (1971).

Acceleration of the Hydrogenation of 2-Octanone with an Alkali Salt of an Organic Acid

Tsutomu OSAWA* and Tadao HARADA†
Department of Chemistry, Faculty of General Education, Tottori University, Koyamacho-minami, Tottori 680
†Department of Materials Chemistry, Faculty of Science and Technology, Ryukoku University, Seta, Otsu 520-21
(Received May 13, 1991)

Synopsis. The hydrogenation of 2-octanone over various types of nickel catalysts was found to be accelerated by the addition of small amounts of carboxylates of alkali metals such as Na, K, and Li.

It is well-documented that the tartaric acid–sodium bromide–modified nickel catalyst (TA–NaBr–MNi) gives high optical yields in the enantioface-differentiating hydrogenation of 2-alkanones,[1] as well as β-keto esters,[2] β-diketones,[3] and β-keto sulfones.[4] Optical yield over this catalyst was controlled by a number of factors. For example, we have reported that the addition of small amounts of sodium ions improved the optical yield of hydrogenation of 2-alkanones over TA–MNi in a reaction media containing both pivalic acid and tetrahydrofuran (THF),[5] whereas the addition of sodium ions resulted in no improvement of the optical yield in THF.[6]

In the course of studies on the enantioface-differentiating hydrogenation of 2-alkanones over TA–MNi, it was found that the addition of a small amount of sodium pivalate to the reaction media resulted in the acceleration of the reaction as well as an increase in the optical yield. As for the acceleration of the hydrogenation over a Raney nickel (RNi) catalyst, addition of strong bases such as sodium hydroxide or potassium hydroxide have been known to be useful.[7] However these strong bases could not be applied to sensitive

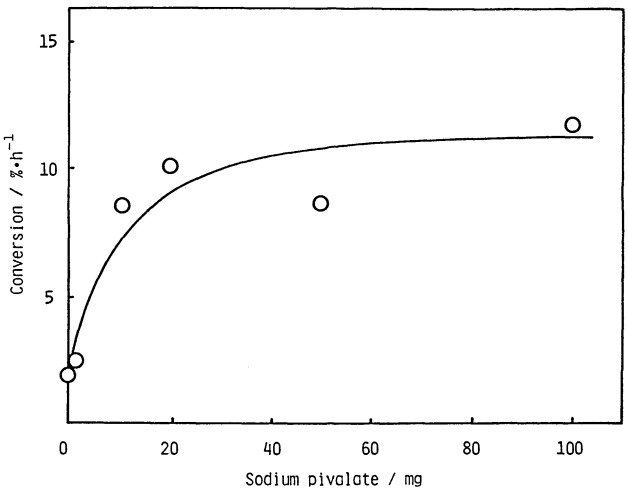

Fig. 1. Relationship between the amount of sodium pivalate in the reaction system and the rate of hydrogenation of 2-octanone.[a)]
Hydrogenation conditions: Catalyst: RNi prepared from 3.8 g of the alloy (Ni/Al=42:58) was modified with 200 ml of an aqueous solution containing TA (2 g) at 100 °C. Reaction media: a mixture of THF (20 ml) and pivalic acid (18 ml). Reaction temperature: 60 °C. Initial hydrogen pressure: 90 kg cm^{-2}.
a) The rate of the hydrogenation is represented by the conversion (%) of 2-octanone in an initial one hour.

Table 1. Effect of the Addition of an Alkali Salt on the Rate of Hydrogenation of 2-Octanone[a)]

No.	Catalyst/g	Reaction temperature/ °C	Alkali salt/mg	Hydrogenation rate[b)]
1	TA-MRNi[c)]	60	—	5
2	TA-MRNi[c)]	60	Na 2-Ethylhexanoate/20	12
3	RNi-A[d)]	60	—	11
4	RNi-A[d)]	60	Na 2-Ethylhexanoate/20	51
5	HNi/4.0[e)]	100	—	13
6	HNi/4.0[e)]	100	Na 2-Ethylhexanoate/20	31
7	Ni-FP/0.8[f)]	60	—	13
8	Ni-FP/0.8[f)]	60	Na 2-Ethylhexanoate/20	42
9	Ni-FP/0.8[f)]	60	Li 2-Ethylhexanoate/20[g)]	28
10	Ni-FP/0.8[f)]	60	K 2-Ethylhexanoate/20	30
11	Ni-FP/0.8[f)]	60	NaCl/20[h)]	17
12	MNi-FP/0.8[i)]	60	—	10

a) Hydrogenation conditions were: Substrate: 2-Octanone (10 ml), Reaction media: THF (20 ml), Initial hydrogen pressure: 90 kg cm^{-2}. b) The rate of the hydrogenation is represented by the conversion (%) of 2-octanone in an initial one hour. c) The catalyst prepared from 3.8 g of the alloy was modified with 200 ml of an aqueous solution containing TA (2 g) at 100 °C. d) The catalyst prepared from 3.8 g of the alloy was treated with 200 ml of a solution containing TA (2 g) and NaBr (12 g), at pH 3.2, 100 °C for 1h. After removal of the solution by decantation, the catalyst was treated with 1 mol dm^{-3} NaOH at 100 °C for 1 h. e) Nickel oxide was reduced at 350 °C for 1 h under a hydrogen stream. f) Nickel fine powder (mean particle size 30 nm) was reduced at 150 °C for 1 h under a hydrogen stream. g) A small amount of lithium 2-ethylhexanoate remained insoluble. h) NaCl was almost insoluble in the reaction mixture. i) Ni-FP was modified at 0 °C with 200 ml of a 0.5% aqueous solution of NaCl.

reactions such as enantioface-differentiating hydrogenation, because a small difference in reaction conditions caused great variations in the optical yield. In this paper, we shall report our findings on the effects of alkali salts on the rate of hydrogenation of 2-octanone.

Figure 1 shows the relationship between the amount of added sodium pivalate and the rate of hydrogenation of 2-octanone over the RNi catalyst modified with tartaric acid. In this experiment, the mixture of pivalic acid and THF, which was the standard reaction media for the enantioface-differentiating hydrogenation, was used as the reaction media. It was shown that the addition of the initial small amount of sodium pivalate to the reaction media resulted in a noticeable increase in the hydrogenation rate. This relationship was similar to that observed between the amount of sodium pivalate and optical yield.[8] Table 1 shows the effects of the addition of alkali ions, when THF was used as the reaction media. Hydrogenation was also accelerated by the addition of alkali ions when the reaction media did not contain pivalic acid. Among the alkali ions examined in this study, sodium ions appeared to accelerate the reaction the most. The reaction rates were enhanced approximately 5-times at maximum by the addition of sodium 2-ethylhexanoate, compared to those rates determined without sodium ions.

Potassium 2-ethylhexanoate and lithium 2-ethylhexanoate were less effective compared to sodium 2-ethylhexanoate. Lithium 2-ethylhexanoate has much less solubility in the reaction mixture than the sodium and potassium salts. When an alkali salt was almost insoluble in the reaction media (NaCl/THF), negligible acceleration effects were observed (Entry 11 in Table 1). Thus the solubility of alkali salts in the reaction mixture appeared to be one of the factors controlling the reaction rate. The cause of the difference between the reaction rate with sodium 2-ethylhexanoate and that with potassium 2-ethylhexanoate is not clear at present. The addition of sodium salts soluble in the reaction media appeared to be the most effective in promoting the reaction according to the present data.

It was found in this study that alkali carboxylates were excellent promoters for enhancing the hydrogenation of ketones over modified or unmodified Nickel catalysts. Although the mechanism of this effect is not certain, the present findings are interesting from a synthetic point of view.

Experimental

The catalysts employed in this study were prepared by the procedures reported previously.[2,8] The hydrogenation of 2-octanone was carried out in a 100-ml autoclave. The conversion (%) of 2-octanone was calculated based on the depression of hydrogen pressure and GLC analysis (5% Tween 80 on Shimalite W, 130 °C).

We thank Professor Yoshiharu Izumi of Osakagakuin University, Professor Akira Tai of Himeji Institute of Technology, and Dr. Hiroshi Ozaki of Osaka University for their many helpful discussions and suggestions in the course of this work.

References

1) T. Osawa and T. Harada, *Bull. Chem. Soc. Jpn.*, **57**, 1518 (1984).
2) T. Harada, M. Yamamoto, S. Onaka, M. Imaida, H. Ozaki, A. Tai, and Y. Izumi, *Bull. Chem. Soc. Jpn.*, **54**, 2323 (1981).
3) K. Ito, T. Harada, and A. Tai, *Bull. Chem. Soc. Jpn.*, **53**, 3367 (1980).
4) Y. Hiraki, K. Ito, T. Harada, and A. Tai, *Chem. Lett.*, **1981**, 131.
5) T. Osawa and T. Harada, *Bull. Chem. Soc. Jpn.*, **60**, 1277 (1987).
6) Unpublished results; 2-octanone (10 ml) in THF (20 ml) was hydrogenated over TA-MRNi at 60 °C. The resulting optical yields were 2% without sodium salt and 6% with sodium 2- ethylhexanoate (20 mg).
7) a) M. Dellepine and A. Horeau, *Compt. Rend.*, **201**, 1301 (1935). b)R. B. Blance and D. T. Gibson, *J. Chem. Soc.*, **1954**, 2487.
8) T. Osawa, T. Harada, and A. Tai, *J. Catal.*, **121**, 7 (1990).

A Convenient Synthesis of Monofluorobutene Derivatives

Noritada MATSUO* and Andrew S. KENDE†
Sumitomo Chemical Co., Ltd., Takarazuka Research Center, 4-2-1 Takatsukasa, Takarazuka, Hyogo 665
†Department of Chemistry, University of Rochester, Rochester, N. Y., 14627, USA
(Received May 27, 1991)

Synopsis. (*Z*)-1,4-Dibromo-1,1,2-trifluoro-2-butene (**2a**) reacts regioselectively with sodium benzenesulfinate and triethyl phosphite respectively to yield the (*Z*)-isomers of 3,4,4-trifluoro-4-bromo-2-butenyl phenyl sulfone (**3**) and diethyl (*Z*)-4-bromo-3,4,4-trifluoro-2-butenylphosphonate (**6**). These could easily be transformed to a variety of polyfunctional monofluoroalkene derivatives.

The introduction of fluorine into organic molecules often gives rise to enhancement of biological activity. There are various biologically active compounds containing a monofluoroalkene moiety,[1] in spite of the scarcity of simple, general methodology for the stereoselective synthesis of monofluoroalkene compounds.[2]

We have previously reported the versatile transformations of 1,1,2-trifluoro-1,3-butadiene (**1**) to a variety of functionalized monofluoroalkene compounds.[2]

Our continuing interest in monofluoroalkene syntheses from the diene **1** has prompted us to explore the utility of (*Z*)-1,4-dibromo-1,1,2-trifluoro-2-butene (**2a**), easily obtained by bromination of the diene **1**.[3]

In this paper we describe easier formation of C4 monofluoroalkene intermediates.

Bromination of the diene **1** in dichloromethane at −10 °C gave the mixture of (*Z*)-1,4-adduct **2a** and 1,2-adduct **2b** (**2a** : **2b**=2 : 1). The 1,2-adduct **2b** spontaneously rearranged into the (*Z*)-1,4-adduct **2a** at room temperature. The dibromide **2a** was reacted with sodium benzenesulfinate in *N,N*-dimethylformamide to give the sulfone **3** in 60% yield. The sulfone **3** underwent rapid transformation in methanolic potassium carbonate at room temperature to give in high yield the known (*Z*)-orthoester **4**, which we have previously converted[2] to monofluoro-chrysanthemic acid derivative **5**.[4]

On the other hand, the dibromide **2a** reacted with triethyl phosphite to obtain the Horner–Emmons type reagent **6**. This phosphonate was transformed to the known methyl ester **8** via the orthoester **7** by reaction with methanolic potassium carbonate at room temperature, followed by mild hydrolysis in methanol with a catalytic amount of *p*-toluenesulfonic acid.

In addition, the nitrile **9a** and various amide derivatives **9b**, **c**, **d** were easily obtained by reacting with ammonia and corresponding amines in tetrahydrofuran respectively.

The piperidide compound **9d** was transformed to the (2*Z*,4*E*)-2-fluoro analog **10b**[2] of the known insecticide piperine **10a** in high yield by reaction of the phospho-

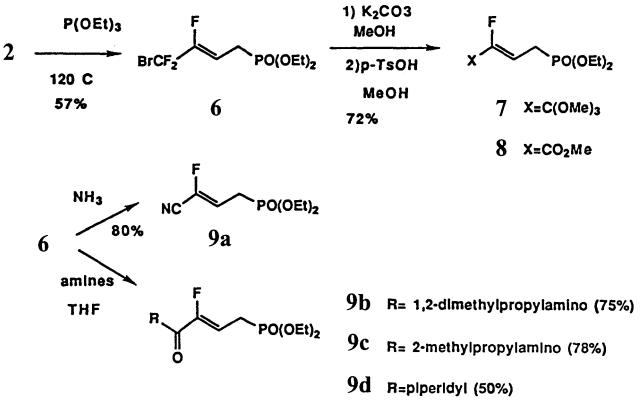

Scheme 2.

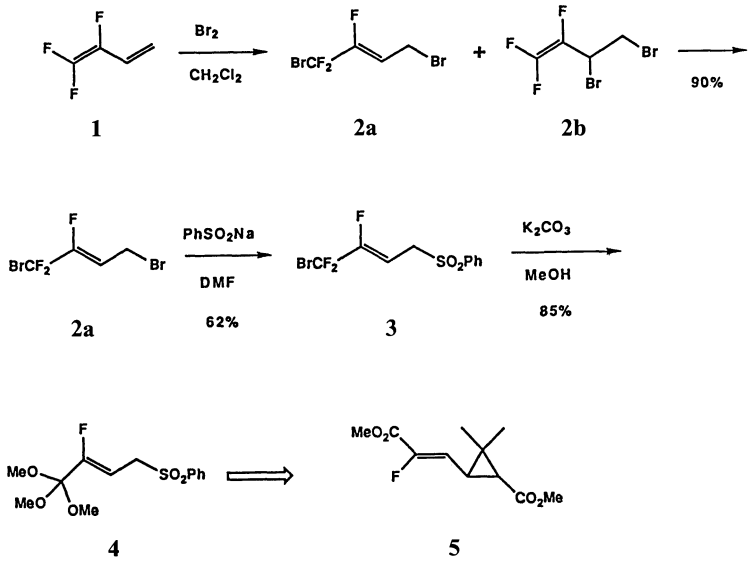

Scheme 1.

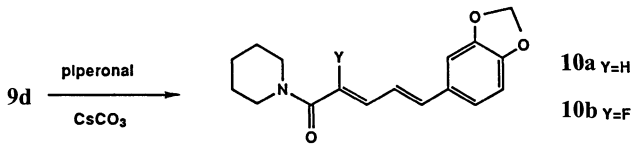

Scheme 3.

nate **9d** with piperonal in 2-propanol in the presence of cesium carbonate. Enhancement of the insecticidal activity was observed by introduction of a fluorine atom at 2 position. The details of the insecticidal activity will soon be published elsewhere.

In conclusion, by use of the 1,4-bromine adduct **2a** of 1,1,2-trifluorobutadiene **1**, important and versatile (*Z*)-monofluorobutene synthons **3** and **6** were readily obtained and these were transformed to various biologically important monofluoroalkene compounds.

Experimental

All the melting points are uncorrected. IR spectra were measured on a Hitachi Model 270-30 spectrometer. ^{1}H and ^{19}F NMR spectra were recorded on a Hitachi R-90 spectrometer in $CDCl_3$ solution, using Me_4Si as an internal standard in ^{1}H NMR and $CFCl_3$ as an external standard in ^{19}F NMR. MS spectra were recorded on a Hitachi DF/GC/MS M-80.

(*Z*)-1,4-Dibromo-1,1,2-trifluoro-2-butene (2a). To a solution of 12.9 g (119 mmol) of 1,1,2-trifluoro-1,3-butadiene in dichloromethane (150 ml) at 0 °C was slowly added 15.5 g of bromine (97 mmol). The resulting mixture was stirred for one hour at 0 °C. The mixture was poured into ice-water, and the liquid was extracted twice with dichloromethane. The organic layers were combined, washed once with brine, and then dried over anhydrous magnesium sulfate. Evaporation of solvent gave a mixture of 1,4-adduct **2a** and 1,2-adduct **2b** as a yellow oil, (**2a**:**2b**=2:1). The 1,2-adduct **2b** rearranged to the 1,4-adduct completely on standing for one day at room temperature. This was purified by distillation to give 21.9 g (84.3%) of (*Z*)-1,4-dibromo-1,1,2-trifluoro-2-butene (**2a**) as a clear oil, bp 65 °C (20 mmHg, 1 mmHg=133.322 Pa); ^{1}H NMR δ=3.96 (dq, 2H), 5.76 (dt, 1H); ^{19}F NMR δ=−57.5 (d, J=18.6), −125.4 (dt, J=28. 9, 18.6). 1,2-adduct **2b**: ^{1}H NMR δ=3.73 (m, 2H), 4.83 (dm, 1H, J=27); ^{19}F NMR δ=−98.0, −115.2, −187.5.

(*Z*)-4-Bromo-3,4,4-trifluoro-2-butenyl Phenyl Sulfone (3). To a solution of 3.1 g (11.6 mmol) of (*Z*)-1,4-dibromo-1,1,2-trifluoro-2-butene **2a** in 20 ml of *N,N*-dimethylformamide was added 2.8 g (14 mmol) of sodium benzenesulfinate. The reaction mixture was stirred for 15 h at room temperature. The contents of the flask were poured into a large excess of ice-water, and the liquid was extracted twice with ethyl acetate. The organic layers were combined, washed once with brine, and then dried over anhydrous magnesium sulfate. Evaporation of solvent gave a yellow liquid which was chromatographed on silica gel (30% ethyl acetate in hexane) to give 2.3 g (60%) of (*Z*)-4-bromo-3,4,4-trifluoro-2-butenyl phenyl sulfone as a yellow oil; ^{1}H NMR δ=3.9 (dq, 2H), 3.6 (dt, 1H), 7.4—8.0 (m, 5H); ^{19}F NMR δ=−122.39 (dt, J=18.6, 31), −57.58 (d, J=18.6).

(*Z*)-3-Fluoro-4,4,4-trimethoxy-2-butenyl Phenyl Sulfone (4). Potassium carbonate (3.8 g, 27.5 mmol) was added to a solution of 2.3 g (7 mmol) of 4-bromo-3,4,4-trifluoro-2-butenyl phenyl sulfone in 20 ml of methanol at room temperature. The resulting mixture was stirred for 12 h at room temperature. The reaction was diluted with 100 ml of diethyl ether. The contents of the flask were filtered and the white solid was washed with excess diethyl ether. The ether solution was evaporated in vacuo to give 1.8 g (85%) of the crude 3-fluoro-4,4,4-trimethoxy-2-butenyl phenyl sulfone as an oil. The physical properties were identical with those we previously reported;[2] ^{1}H NMR δ=3.1 (s, 9H), 4.0 (d, 2H, J=9), 5.5 (dt, 1H, J=9,33), 7.5—7.9 (m, 5H); ^{19}F NMR δ=−120.5 (d, J=31.1). This could be used for the next reaction without further purification.

Diethyl (*Z*)-4-Bromo-3,4,4-trifluoro-2-butenylphosphonate (6). Triethyl phosphite (6.8 g, 41.0 mmol) was added to (*Z*)-1,4-dibromo-1,1,2-trifluoro-2-butene (10.0 g, 37.3 mmol). The mixture was stirred for 10 h at 120 °C over distilling off ethyl bromide formed. The reaction mixture was distilled to obtain 6.9 g (57%) of diethyl (*Z*)-4-bromo-3,4,4-trifluoro-2-butenylphosphonate as a colorless oil; bp 96—98 °C (1 mmHg); IR (neat) 1258, 1024 cm^{-1}; ^{1}H NMR δ=2.67 (ddd, 2H), 4.1 (m, 6H), 5.57 (m, 1H); ^{19}F NMR δ=−126.97 (m), −56.44 (dd, J=20.7, 4.1); MS m/z 324 (M-1), 326 (M+1).

Diethyl (*Z*)-3-Fluoro-3-methoxycarbonyl-2-propenylphosphonate (8). Potassium carbonate (10.2 g, 73.9 mmol) was added to a solution of 6.0 g (18.5 mmol) of diethyl 4-bromo-3,4,4-trifluoro-2-butenylphosphonate in 50 ml of methanol at room temperature. The resulting mixture was stirred for 12 h at room temperature. After removal of solvent in vacuo, the residue was partitioned between 100 ml of diethyl ether and 50 ml of water. The ether layer was washed once with brine. Evaporation of the solvent gave a clear oil. Methanol (20 ml) and *p*-toluenesulfonic acid (50 mg) were added to this oil and the resulting solution was stirred for 0.5 h at room temperature. The reaction mixture was poured into water and the mixture was extracted twice with ethyl acetate. The combined organic layers were washed with brine and dried over anhydrous magnesium sulfate. Evaporation of the solvent in vacuo followed by distillation gave 3.4 g (72%) of diethyl (*Z*)-3-fluoro-3-methoxycarbonyl-2-propenylphosphonate[5] as a colorless oil; bp 125 °C (0.55 mmHg); IR (neat) 1746, 1682, 1256 cm^{-1}; ^{1}H NMR δ=1.30 (t, 6H), 2.73 (ddd, 2H), 3.8 (s, 3H), 4.1 (m, 4H), 6.13 (dq, 1H); ^{19}F NMR δ=−127.8 (dd, J=31, 12.4); MS m/z 254 (M^+).

Diethyl (*Z*)-3-Cyano-3-fluoro-2-propenylphosphonate (9a). Diethyl (*Z*)-4-bromo-3,4,4-trifluoro-2-butenylphosphonate (1.0 g, 3.1 mmol) was stirred with ammonia (15 mmol) in 10 ml of tetrahydrofuran at 0 °C for 1 h and then stirred for 12 h at room temperature. The reaction mixture was poured into ice-cooled 5% aqueous hydrochloric acid and the mixture was extracted three times with ethyl acetate after saturation of the solution with sodium chloride. The combined organic layers were washed successively with 5% sodium hydrogencarbonate solution and brine, and then dried over anhydrous magnesium sulfate. Evaporation of the solvent followed by purification with preparative TLC (hexane–ethyl acetate=1:1) gave 0.54 g (80%) of 3-cyano-3-fluoro-2-propenylphosphonate as a colorless oil: IR (neat) 2240 cm^{-1}; ^{1}H NMR δ=1.3 (t, 6H), 2.76 (ddd, 2H), 4.12 (dq, 4H), 5.81 (m, 1H); ^{19}F NMR δ=−122.34 (dd, J=12.4, 31); MS m/z 221 (M^+).

Diethyl (*Z*)-3-[(1,2-Dimethylpropyl)carbamoyl]-3-fluoro-2-propenylphosphonate (9b). 1,2-Dimethylpropylamine (0.94 g, 10.2 mmol) was added to a solution of 1.0 g (3.1 mmol) of diethyl (*Z*)-4-bromo-3,4,4-trifluoro-2-butenylphosphonate in 10 ml of tetrahydrofuran at 0 °C. The resulting mixture was stirred for 1 h at 0 °C and 12 h at room temperature. The reaction mixture was poured into ice-cooled 5% aqueous hydrochloric acid and the mixture was extracted three times with ethyl acetate after saturation of the solution with sodium chloride. The organic layers were combined, washed successively with 5% sodium hydrogencarbonate solution and brine, and then dried over anhydrous magnesium sulfate. Evaporation of the solvent followed by purification with preparative TLC (hexane–ethyl acetate=1:1) gave 0.71 g (75%) of diethyl

(*Z*)-3-[(1,2-dimethylpropyl)carbamoyl]-3-fluoro-2-propenylphosphonate as a clear oil: IR (neat) 1662 cm^{-1}; ^1H NMR δ=0.90 (d, 6H), 1.12 (d, 3H), 1.31 (t, 6H), 2.72 (ddd, 2H), 4.10 (dq, 4H), 5.7—6.4 (m, 1H); ^{19}F NMR δ=−131.08 (m, 12.4, 33); MS *m/z* 309 (M^+).

Diethyl (*Z*)-3-[(2-Methylpropyl)carbamoyl]-3-fluoro-2-propenylphosphonate (9c). (*Z*)-4-Bromo-3,4,4-trifluoro-2-butenylphosphonate (1.0 g, 3.1 mmol) was allowed to react with 2-methylpropylamine (0.74 g, 10.2 mmol) in tetrahydrofuran according to the same procedure as **9b** to give 0.71 g (78%) of (*Z*)-diethyl 3-*N*-(2-methylpropyl)carbamoyl-3-fluoro-2-propenylphosphonate: IR (neat) 1664 cm^{-1}; ^1H NMR δ=0.92 (d, 6H), 1.30 (t, 3H), 2.72 (ddd, 2H), 3.15 (t, 2H), 4.10 (dq, 4H), 5.7—6.4 (m, 1H); ^{19}F NMR δ=−131.28 (m); MS *m/z* 295 (M^+).

Diethyl (*Z*)-3-Piperidinocarbonyl-3-fluoro-2-propenylphosphonate (9d). Diethyl (*Z*)-4-Bromo-3,4,4-trifluoro-2-butenylphosphonate (1.0 g, 3.1 mmol) was allowed to react with piperidine (1.02 g, 12 mmol) in tetrahydrofuran according to the same procedure as **9b** to give 0.48 g (50%) of diethyl (*Z*)-3-piperidylcarbonyl-3-fluoro-2-propenylphosphonate: IR (neat) 1646 cm^{-1}; ^1H NMR δ=1.26 (t, 3H), 1.6 (bs, 6H), 2.68 (ddd, 2H), 3.45 (bs, 4H), 4.06 (dq, 4H), 5.2—5.9 (m, 1H); ^{19}F NMR δ=−115.3 (dd, *J*=12.4, 35.1); MS *m/z* 307 (M^+).

1-[(2*Z*,4*E*)-2-Fluoro-5-[3,4-(methylenedioxy)phenyl]-2,4-pentadienoyl]piperidine (10b). To a solution of 479 mg (1.56 mmol) of diethyl (*Z*)-3-piperidinocarbonyl-3-fluoro-2-propenylphosphonate and 257 mg (1.72 mmol) of piperonal in 5 ml of 2-propanol at 0 °C was added 1017 mg (3.02 mmol) of cesium carbonate under a nitrogen atmosphere. The reaction mixture was stirred for 3 h at 0 °C and 12 h at 20 °C. The reaction mixture was poured into ice-water and the liquid was extracted with ethyl acetate. The organic layer was washed with brine and dried over anhydrous magnesium sulfate. Evaporation of solvent gave the crude crystalline product (0.5 g). This was purified by recrystallization from hexane and ethyl acetate (3:1) to obtain 359 mg (76%) of 1-[(2*Z*,4*E*)-2-fluoro-5-[3,4-(methylenedioxy)phenyl]-2,4-pentadienoyl]-piperidine as white crystals: Mp 97.5—98.0 °C; ^1H NMR δ=1.62 (m, 6H), 3.53 (m, 4H), 5.95 (s, 2H), 6.39 (dd, 1H, *J*=10, 33), 6.62 (d, 1H, *J*=16), 6.75 (d, 1H, *J*=8), 6.84 (dd, 1H, *J*=10, 16), 6.87 (d, 1H, *J*=8), 6.98 (s, 1H); MS *m/z* 303 (M^+). Found: C, 67.22; H, 6.11; N, 4.66%. Calcd for $C_{17}H_{18}FO_3N$: C, 67.29; H, 5.99; N, 4.62%.

References

1) a) J. T. Welch, *Tetrahedron,* **43**, 3123 (1987); b) J. Mann, *Chem. Soc. Rev.*, **16**, 381 (1987).

2) N. Matsuo and A. S. Kende, *J. Org. Chem.*, **53**, 2304 (1988). Other references are cited therein.

3) D. S. Rondarev, V. P. Sass, and S. V. Sakolov, *Zh. Org. Khim.*, **11**, 937 (1975); *Chem. Abstr.*, **83**, 784685 (1975).

4) J. Tessier and J. P. Demoute, Eur. Patent Appl. EP 114012 (Roussel Uclaf); *Chem. Abstr.*, **102**, 5763k (1985).

5) A. S. Kende and N. Matsuo, Japanese Patent Kokai H2-722; U.S. Patent 4902834 (1990).

Redox Photochromism of Waterproof Viologen-Matrix Polymer System

Hiroyoshi KAMOGAWA* and Hiroshi YAMADA
Department of Applied Chemistry, Yamanashi University, Takeda 4, Kofu 400
(Received June 6, 1991)

Synopsis. A waterproof viologen-matrix polymer system exhibiting redox photochromism in thin films was devised using water-insoluble viologens embedded in *N*-vinyl-2-pyrrolidone(VP)–methyl acrylate (MA) copolymers also insoluble in water. Both the photosensitivity and the stability of the colors developed decreased with decrease in the VP-content.

In previous publications,[1–7] it has been reported that bipyridinium salts (viologens) embedded in the poly(1-vinyl-2-pyrrolidone) (PVP) matrix film reversibly develop visible intense colors with radiation of the solar level (redox photochromism).

It is required for some purposes, however, that these photochromic systems are waterproof, since both conventional viologens and PVP are water-soluble. Accordingly, waterproof thin films consisting of the viologen-matrix polymer system have been prepared and their reversible color-developing behaviors induced by near UV-irradiation of the solar level have been investigated.

Water-insoluble viologens employed in the present study were 1,1′-bis(arylmethyl)-4,4′-bipyridinium bis(tetrafluoroborate) and bis(hexafluorophosphate) (**V1**—**V4**) and *trans*-4,4′-vinylenebis[1-(*p*-methylbenzyl)pyridinium] bis(tetrafluoroborate) (**V5**) and bis(hexafluorophosphate) (**V6**).

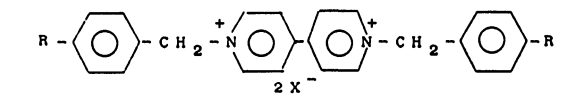

V1 – V4

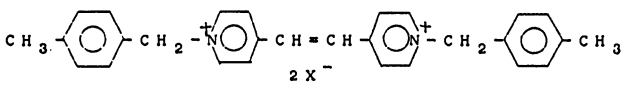

V5 – V6

	R	X
V1 :	CH_3	BF_4
V2 :	CH_3	PF_6
V3 :	Cl	BF_4
V4 :	Cl	PF_6
V5 :	–	BF_4
V6 :	–	PF_6

Viologens bearing 4,4′-bipyridinium and *trans*-4,4′-vinylenebispyridinium units were adopted as typical of exhibiting intense visible colors upon near UV irradiation.

Matrix polymers, in which the viologens were to be embedded, were copolymers of 1-vinyl-2-pyrrolidone (VP) with methyl acrylate (MA) in less than 1 : 1 molar ratios, which were insoluble in water.

Experimental

Water-Insoluble Viologens (V1—V6). 1,1′-Bis(*p*-methyl- or *p*-chlorobenzyl)-4,4′-bipyridinium dichloride or *trans*-4,4′-vinylenebis[1-(*p*-methylbenzyl)pyridinium] dichloride (11 mmol) were dissolved in water (200 ml). Aqueous HBF_4 (42 wt%; 4.8 g, 23 mmol) or aqueous HPF_6 (60 wt%; 5.6 g, 23 mmol) was then added to precipitate white to yellowish white crystalline powder (**V1**—**V6**) in more than 90% yield (mp 240, 238, 254, 249 °C for **V1**—**V4**; decomp for **V5**, **V6**). The results of IR (KBr) and elemental analyses were satisfactory.

Matrix VP-MA Copolymers. Prepared in dioxane solutions kept at 80 °C for 72 h with α,α'-azobisisobutyronitrile as initiator, in the conventional manner using glass ampules sealed under N_2. The VP-contents in copolymers were determined by elemental analyses to afford satisfactory agreements with the initial monomer ratios. Values of intrinsic viscosity $[\eta]$ in DMF at 25 °C for the 1 : 5, 1 : 7, and 1 : 10 copolymers, which were insoluble in water, were 0.22, 0.24, and 0.22 dl g^{-1}, respectively.

Films for Irradiation. Films open to air (A) and those tightly sandwiched between two glass plates (B) were prepared in the same manners as in previous studies,[6,7] except that DMF and an elevated temperature (40 °C) were employed

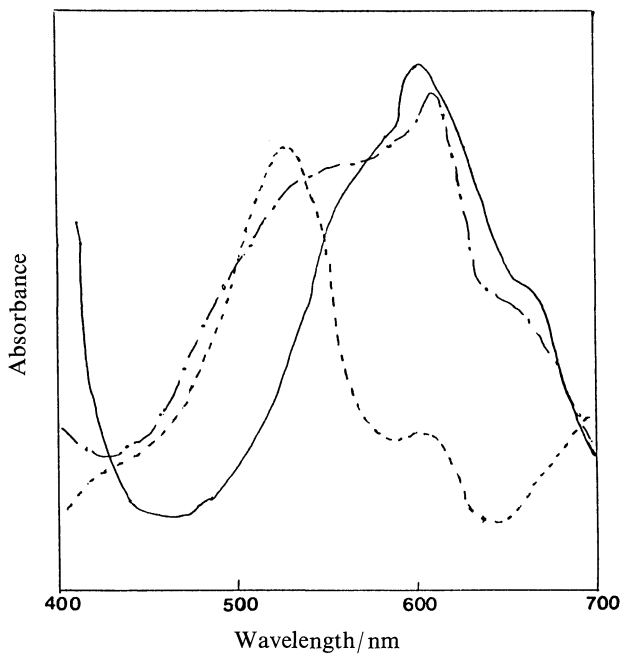

Fig. 1. Typical visible absorption spectra developed for water-insoluble viologens embedded in VP–MA copolymer matrix films with irradiation by near UV light.
—— For **V2** embedded in VP–MA (1 : 5) copolymer; ---- for **V5** in VP–MA (1 : 7) copolymer; —·— for 1, 1′-bis(*p*-methylbenzyl)-4,4′-bipyridinium dichloride in VP homopolymer. Measures of ordinates are arbitrary only to show the shapes of spectra.

instead of water as solvent and evaporation at room temperature, respectively.

Absorption Change. Radiation through a glass plate from a 75 W high pressure Hg lamp (Toshiba SHL-UV100) was applied to either films A or B placed at the distance of 5 cm from the light source, and the resulting visible absorption changes of films were determined by means of a Hitachi 200-10 recording spectrophotometer.

Results and Discussion

Viologens **V1**—**V6** were prepared by the anion exchange reaction of the respective chlorides with excess tetrafluoroboric and hexafluorophosphoric acids without any difficulty.

MA was chosen as the comonomer, since it provides not only water-proofness but also transparency and toughness to copolymer films. Films less than 0.1 mm in thickness were prepared on glass plates by evaporating DMF solutions at 40 °C. In Fig. 1 are given typical absorption spectra developed for the films upon irradiating near UV light of the solar level.

It can be recognized from Fig. 1 that the shapes and absorption maxima (λ_{max}) of the visible absorption spectra developed for the waterproof viologen–VP–MA copolymer system by near UV irradiation are almost identical with those of the radical cations produced in the water-soluble viologen–VP homopolymer one,[1–7] except that, in the latter system, absorptions attributable to associated radical cations[8] are also discernible, e.g. between ca. 500 and 600 nm for 4,4′-bipyridinium. This fact suggests that the species causing these absorption changes were also viologen radical cations generated by the photo-redox reaction, as demonstrated in previous studies.[9,10]

Equation 1 indicates this relationship in the absence

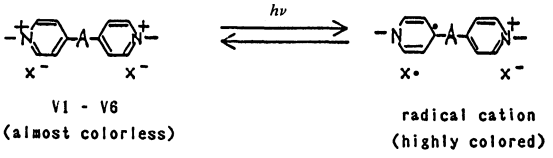

(1)

of air where A is intended to represent none and –CH=CH– for **V1**—**V4** and **V5**, **V6**, respectively.

A remarkable fact in the present case is that almost no

Table 1. Reversible Visible Absorption Change (Photochromism) for **V1**—**V4** Embedded in Matrix Polymer Film with Irradiation by UV[a]

Viologen	Matrix polymer (VP : MA) mol/mol	Film[b]	A_t[c] 3 min	A_t[c] 4 min	A_t[c] 5 min	$t_{1/2}$[d] min
V1	1 : 5	A	0.069	0.160	0.253	13
		B	0.069	0.153	0.244	27
V2	1 : 5	A	0.086	0.205	0.351	10
		B	0.087	0.194	0.351	30
V3	1 : 5	A	0.127	0.198	0.251	6
		B	0.121	0.190	0.245	60
V4	1 : 5	A	0.088	0.205	0.272	6
		B	0.113	0.206	0.275	60
V1	1 : 7	A	0.040	0.100	0.116	8
		B	0.043	0.091	0.116	30
V2	1 : 7	A	0.037	0.085	0.125	8
		B	0.037	0.099	0.127	25
V3	1 : 7	A	0.050	0.104	0.158	8
		B	0.040	0.098	0.148	70
V4	1 : 7	A	0.044	0.156	0.204	7
		B	0.049	0.160	0.206	60
V1	1 : 10	A	0.014	0.088	0.105	7
		B	0.013	0.080	0.097	10
V2	1 : 10	A	0.039	0.081	0.093	6
		B	0.040	0.086	0.102	10
V3	1 : 10	A	0.041	0.084	0.103	7
		B	0.040	0.088	0.106	40
V4	1 : 10	A	0.039	0.076	0.094	8
		B	0.044	0.083	0.103	40

a) At a distance of 5 cm from a 75 W high pressure Hg lamp, with a glass filter fitted so as to obtain the light >300 nm. b) 5% **V1**—**V4** on the basis of matrix polymer. A: Open to air; B: Tightly glass-sandwiched. c) Absorbance increase in irradiation time t. Values reduced to 0.1 mm film thickness at λ_{max} (605 nm). Absorptions were negligible for films before and long after irradiation. Irrad iation times are indicated in min. d) Half-bleaching time at 20 °C.

Table 2. Photochromism for **V5** and **V6** Embedded in Matrix Polymer Film with Irradiation by UV[a)]

Viologen	Matrix polymer (VP : MA) mol/mol	Film	A_t[b)] 15 s	A_t[b)] 30 s	$t_{1/2}$ s
V5	1 : 5	A	0.531	0.563	15
		B	0.632	0.671	20
V6	1 : 5	A	0.524	0.559	17
		B	0.789	0.801	23
V5	1 : 7	A	0.497	0.527	13
		B	0.587	0.613	16
V6	1 : 7	A	0.481	0.499	16
		B	0.630	0.660	17
V5	1 : 10	A	0.228	0.283	13
		B	0.354	0.403	16
V6	1 : 10	A	0.216	0.249	14
		B	0.370	0.428	16

a) Notations are identical with those in Table 1, unless otherwise noted. b) Values reduced to 0.1 mm thickness at λ_{max} (525 nm).

absorptions attributable to associated radical cations exist especially in the spectra for **V1**—**V4** as exemplified in Fig. 1 (——), presumably suggesting that the species are in thermodynamically less stable states when compared with those generated in VP–homopolymer (— · —). This less stable characteristic is also observed in half-bleaching time ($t_{1/2}$) in Table 1.

Thus, it is known from the values of $t_{1/2}$ that complete bleachings take place even for air-tight films (B), whereas, in the case of VP–homopolymer as matrix, the colors developed by light persist for a long term (life of months to years) under the same film-forming conditions.[7)]

The results in Tables 1 and 2 indicate that the absorbance increase (A_t) at λ_{max} in irradiation time t becomes remarkably smaller with decrease of the VP-content in the copolymers, so that the values of A_t for the 1 : 10 (VP : MA) copolymers open to air (A) amount to less than half (5 min irrad.) and approximately half (30 s irrad.) those for the 1 : 5 copolymers in the cases of **V1**—**V4** and **V5**, **V6**, respectively; $t_{1/2}$ for the tightly glass-sandwiched films (B) appear to show the same tendency.

These facts are considered to demonstrate that the principal mechanism of the photo-reaction in this case is, as shown in Eq. 1, the reductive attack of the X^- highly activated by the VP-portion of the copolymers against the photo-excited viologen dication to produce a highly colored radical cation, which is stabilized in its turn by binding to the VP-portion, by the same reason as for 1-methyl-2-pyrrolidone, a highly efficient polar aprotic solvents.[1)]

Thus, the decrease of the VP-content in polymer may lead to decreases of both reactivity of the counter anion and stability of the radical cation, thereby bringing about decreases of both A_t and $t_{1/2}$.

The photochromic behaviors investigated above were waterproof, as expected, and did not much differ among **V1**—**V4** in Table 1 and between **V5** and **V6** in Table 2 each other, with exception that **V3** and **V4** [1,1′-bis(*p*-chlorobenzyl) derivatives] provided considerably larger values of $t_{1/2}$ than **V1** and **V2** [1,1′-bis(*p*-methylbenzyl) ones] did.

Features of **V5**, **V6** in Table 2, other than providing a λ_{max} at 525 nm (red) instead of 605 nm (blue) for **V1**—**V4**,[1-7)], are high photosensitivities as well as rapid bleachings in dark. The presence of air oxygen (A) also afforded A_t always smaller than the almost absence of air (B) did.

References

1) H. Kamogawa, T. Masui, and M. Nanasawa, *Chem. Lett.*, **1980**, 1145.
2) H. Kamogawa and S. Amemiya, *Rep. Asahi Glass Found. Ind. Technol.*, **44**, 42 (1984).
3) H. Kamogawa, T. Masui, and S. Amemiya, *J. Polym. Sci., Polym. Chem. Ed.*, **22**, 383 (1984).
4) H. Kamogawa and S. Amemiya, *J. Polym. Sci., Polym. Chem. Ed.*, **23**, 2413 (1985).
5) H. Kamogawa and S. Satoh, *J. Polym. Sci., Part A; Polym. Chem.*, **26**, 653 (1988).
6) H. Kamogawa and M. Nanasawa, *Chem. Lett.*, **1988**, 373.
7) H. Kamogawa, K. Kikushima, and M. Nanasawa, *J. Polym. Sci., Part A; Polym. Chem.*, **27**, 393 (1989).
8) M. Yamana and T. Kawata, *Nippon Kagaku Kaishi*, **1977**, 941.
9) H. Kamogawa and T. Suzuki, *J. Chem. Soc., Chem. Commun.*, **1985**, 525; *Bull. Chem. Soc. Jpn.*, **60**, 794 (1987).
10) H. Kamogawa and T. Ono, *Chem. Materials*, submitted.

^1H and ^{13}C NMR Relaxation Study of Iron(III) Tetraphenylporphyrin-Imidazole Complexes

Yasuhiko YAMAMOTO,* Norishige NANAI, Riichirô CHÛJÔ, and Yoshio INOUE

Department of Biomolecular Engineering, Tokyo Institute of Technology, Meguro-ku, Tokyo 152

(Received June 10, 1991)

Synopsis. ^1H and ^{13}C nuclear relaxation of paramagnetic iron(III) tetraphenylporphyrin–imidazole complexes has been investigated in order to gain insight into the relationship between the paramagnetic relaxation rate and the electron-nucleus distance. The analysis of the nuclear spin–lattice relaxation time (T_1) in terms of the distance indicated that, for the iron porphyrin complexes used, the contribution of the electron–nucleus dipolar coupling no longer contributes significantly to the relaxation process of a proton located at more than 0.75 nm away from the iron. For the complexes studied, the electron spin–lattice relaxation time (T_{1e}) of 6.4 ps was calculated from the T_1 values measured at 26 °C.

Nuclear relaxation has been used to characterize structure and dynamics of molecules. Particularly, in the case of paramagnetic molecules, geometries of complexes in solution, determinations of coordination numbers, and calculations of correlation times have been infered from the investigation of the paramagnetic relaxation.[1–3] Nuclear spin-lattice relaxation time, T_1, in paramagnetic molecules is composed of two terms,

$$T_1^{-1} = T_{1d}^{-1} + T_{1p}^{-1}, \quad (1)$$

where T_{1d} and T_{1p} are the diamagnetic and paramagnetic spin–lattice relaxation times, respectively, and, for the nucleus in the close proximity of the unpaired electron, $T_{1d}^{-1} \ll T_{1p}^{-1}$. T_{1p} is generally expressed in terms of the dipolar and contact interactions between nucleus and unpaired electron as follows,[4–6]

$$T_{1p}^{-1} = (2/15)\gamma_I^2 g^2 \beta^2 S(S+1) r^{-6} [3\tau_c/(1+\omega_I^2\tau_c^2) + 7\tau_e/(1+\omega_S^2\tau_e^2)] + (2/3)S(S+1)(A/\hbar)^2 \tau_e/(1+\omega_S^2\tau_e^2) \quad (2)$$

and

$$\tau_c^{-1} = T_{1e}^{-1} + \tau_r^{-1} + \tau_{ex}^{-1}, \ \tau_e^{-1} = T_{1e}^{-1} + \tau_{ex}^{-1}, \quad (3)$$

where γ_I is the gyromagnetic ratio of the nucleus under consideration and T_{1e}, τ_r, and τ_{ex} are the electron spin–lattice relaxation, the molecular tumbling, and the electron exchange times, respectively. A is the hyperfine coupling constant which is related to the unpaired spin density on the resonating nucleus and the other parameters have been defined previously.[2] The Curie spin relaxation does not contribute significantly to T_{1e} for the present complex.[7–9] In large molecules with highly resolved NMR spectra, $T_{1e} \ll \tau_r$, τ_{ex}, and at high magnetic field, $\omega_I^2 T_{1e}^2 \ll 1$ and $\omega_S^2 T_{1e}^2 > 1$, the nuclear spin–lattice relaxation rate due to the electron-nucleus dipolar coupling is given as,[9,10]

$$T_1^{-1} = (2/5)\gamma_I^2 g^2 \beta^2 S(S+1) r^{-6} T_{1e} \quad (4).$$

Therefore the relaxation rate of a nucleus depends simply on the distance from the unpaired electron and γ_I.

We have measured and analyzed the T_1 values of both ^1H and ^{13}C of iron(III) tetraphenylporphyrin–imidazole complexes (structures in Fig. 1). The T_{1e} value of the complex was determined from the analysis of the observed T_1 values. The relationship between the paramagnetic relaxation rate and the electron–nucleus distance is discussed.

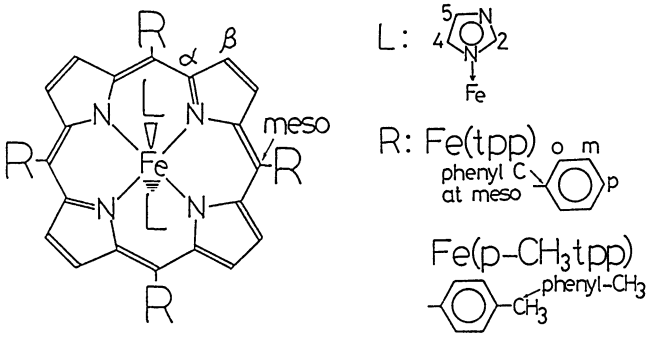

Fig. 1. Structures and numbering system of [Fe(tpp)-(Im)$_2$]Cl and [Fe(p-CH$_3$ tpp)(Im)$_2$]Cl.

Experimental

Iron(III) tetraphenylporphyrin, Fe(tpp), was purchased from Sigma Chemcal Co. and used without further purification. Iron(III) 5, 10, 15, 20-tetrakis (p-tolyl) porphyrin, Fe(p-CH$_3$ tpp), was prepared by the literature method[11] and purified using silica-gel column. Since it has been reported that the NMR spectral features of these porphyrin complexes are essentially independent of concentration (5—50 mM)[12], 10 mM iron(III) porphyrin was prepared in $CDCl_3$ with 0.2 M imidazole (Sigma) for the measurements (1M=1 mol dm^{-3}). ^1H and ^{13}C NMR spectra were recorded using a JEOL GSX-270 FT-NMR spectrometer operating at ^1H and ^{13}C frequencies of 270 and 67.8 MHz, respectively. T_1 was determined by the inversion recovery method[13] and the experimental error is <20%. Chemical shifts are given in parts per million, ppm, downfield from the signal of tetramethylsilane, with the solvent signal as internal reference.

Results and Discussion

NMR Spectra. ^{13}C NMR spectra of 10 mM iron(III) porphyrin derivatives with 0.2 M imidazole in $CDCl_3$ at 26 °C are shown in Fig. 2. The signal assignments were reported previously[12] and have been confirmed by the T_1 measurements and two-dimensional NMR spectroscopies. The resonances for free imidazole are observed at 122 and 136 ppm as indicated by asterisk in the spectra. Relatively small signal intensity for the free imidazole resonances is due to short pulsing interval used for the measurement which selectively enhances the intensity of more rapidly relaxing paramagnetic resonances. Since it has been reported that the equilibrium

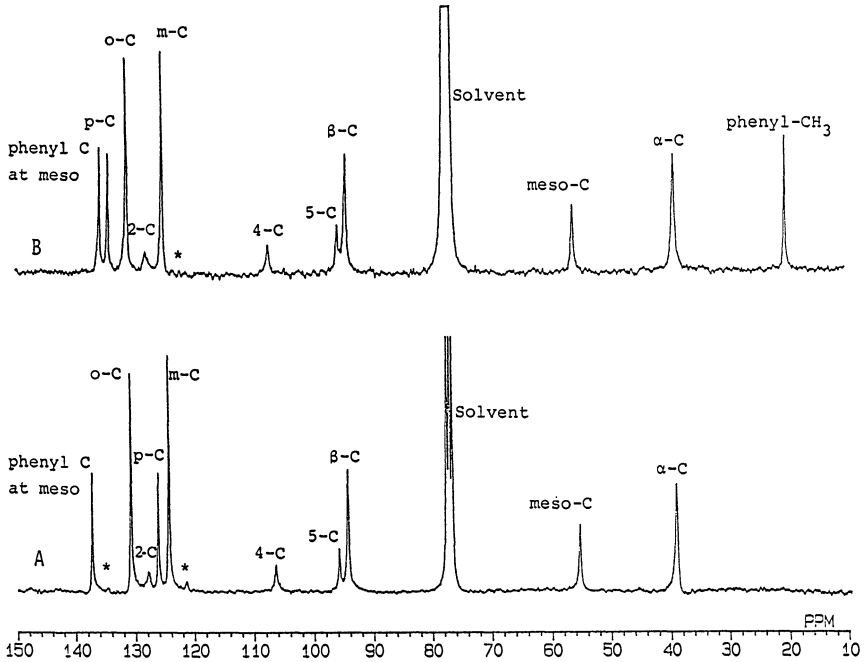

Fig. 2. 67.8 MHz ^{13}C NMR spectra of [Fe(tpp)(Im)$_2$]Cl (A) and [Fe(*p*-CH$_3$ tpp)(Im)$_2$]Cl (B) in $CDCl_3$ at 26 °C. The peak labeling corresponds to the numbering system shown in Fig. 1. The peaks indicated by * are the resonances from free imidazole.

Table 1. ^1H and ^{13}C Chemical Shifts and T_1s of [Fe(tpp)(Im)$_2$]Cl and [Fe(*p*-CH$_3$ tpp)(Im)$_2$]Cl in $CDCl_3$ at 26 °C

Resonance	[FeTPP(Im)$_2$]Cl		[FeTPP(*p*-CH$_3$)(Im)$_2$]Cl	
	δ/ppm	T_1/ms	δ/ppm	T_1/ms
^1H NMR				
β-H	−16.84	26.5	−16.72	23.2
o-H	5.17	52.1	5.10	40.5
m-H	6.28	225.2	6.03	160.3
p-H	6.22	278.6	—	—
Phenyl–CH$_3$	—	—	1.60	257.1
imidazole				
1-H	14.05	16.9	14.05	15.5
2-H	−8.45	<10	−8.35	<10
4-H	10.00	<10	10.06	<10
5-H	8.26	23.0	8.57	21.2
^{13}C NNR				
α-C	38.9	40.6	38.9	29.2
β-C	94.3	54.1	94.2	35.7
meso-C	55.2	40.7	55.9	31.7
Phenyl C at *meso*	137.3	442.5	135.6	155.7
o-C	130.7	200.8	131.0	145.3
m-C	124.3	233.6	125.0	206.2
p-C	126.1	206.6	134.2	909.1
Phenyl–CH$_3$	—	—	20.1	625.0
imidazole				
2-C	127.6	28.7	127.8	16.9
4-C	106.3	23.4	107.1	17.4
5-C	95.7	78.7	95.5	47.6

constant is of the order of 10^6 M^{-2} for imidazole binding to [Fe(tpp)]Cl in $CHCl_3$ at 25 °C,[14] the iron porphyrin should be almost completely in the bis-ligated form. In addition, the fact that both the free and bound imidazole resonances are separately observed is consistent with its slow exchange rate (ca. 10 s^{-1}).[15] ^1H NMR spectra of the complexes (not shown) were essentially identical to those reported previously.[16,17] The chemical shifts of ^1H and ^{13}C resonances are summarized in Table 1. The comparison of the shift between the two

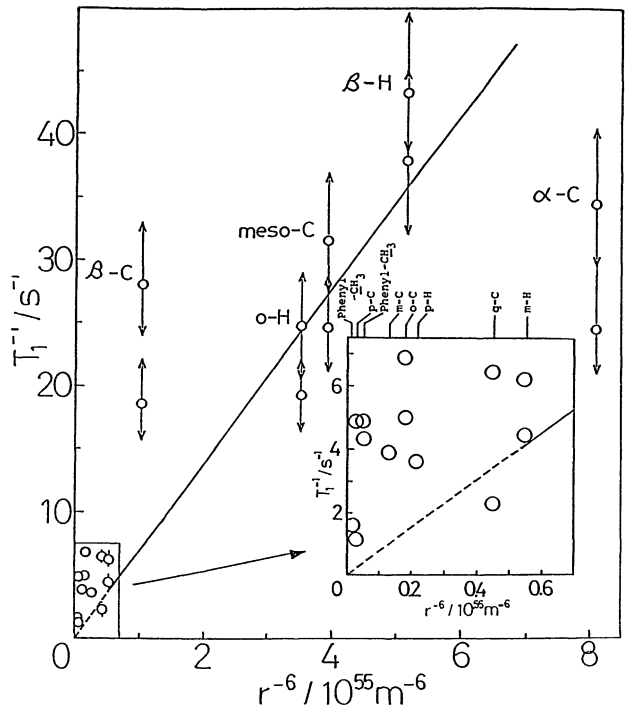

Fig. 3. The plot of T_1^{-1} against r^{-6} for ^1H of the iron porphyrin complexes studied. A straight line passing the origin was drawn with the plots for *o*- and *m*-H. For the ^{13}C data, T_1^{-1} were plotted against $r^{-6}(\gamma_C/\gamma_H)^2$. The plots near the origin was expanded in the inset.

complexes indicates that the influence of the methyl substitution on the resonance frequency is localized at the phenyl resonances.

T_1 Analysis. The observed T_1 values are included in Table 1. The T_1 values of the corresponding nuclei, except the phenyl C at *meso* and the *p*-C, between the two complexes agree within the experimental error of 20%. The difference in the T_1 value of the phenyl C at *meso* between the two complexes may be attributed to the change in the contact contribution, i.e. the second term in Eq. 2, and the presence of the unpaired spin density at this carbon has been suggested earlier.[12] The fact that the T_1 value for the *p*-C in [Fe(tpp)(Im)$_2$]Cl is considerably smaller than that in [Fe(*p*-CH_3 tpp)(Im)$_2$]Cl indicates the significance of the attached ^1H for the relaxation of this carbon. Relatively large difference in the T_1 value of the bound imidazole carbons between the two iron porphyrin complexes may be attributed to the difference in the contact contribution.

The relaxation rates of the iron porphyrin ^1H resonances are plotted against r^{-6} in Fig. 3. The plots for the ^{13}C resonances are also included in the figure in the form of T_1^{-1} vs. $r^{-6}(\gamma_C/\gamma_H)^2$, because Eq. 4 predicts that the ratio of the T_1^{-1} values for the proton and carbon located equidistantly from the metal is $(\gamma_C/\gamma_H)^2$. Since it has been already shown that the unpaired electron density on the *o*-, *m*-, and *p*-C in these complexes is negligible,[12] a straight line passing through the origin was drawn with the plots for the phenyl ^1H resonances. The T_{1e} value can then be calculated from the slope of this line using Eq, 4. The T_{1e} value of 6.4 ps was obtained and is well within the typical value for iron(III) low spin complexes (2—8 ps).[18] The interpretation of the relaxation rates for the porphyrin ring nuclei requires the knowledge about the spin density of the porphyrin skeleton. The plots in Fig. 3 do not converge to the origin as $r^{-6}\rightarrow 0$, but the relaxation rates are larger than those expected from Eq. 4 when $r^{-6}<0.5\times10^{55}m^{-6}$. These results reflect that the paramagnetic dipolar relaxation mechanism is not a predominant relaxation process for a proton located more than 0.75 nm away from the iron in the present complexes and the distance is expected to be reduced with increasing the molecular weight. It has been shown that the interpretation of the nuclear relaxation in paramagnetic hemoproteins, based on Eq. 4, tends to underestimate the iron–nucleus distance and the error becomes larger for nucleus oriented further away from the paramagnetic center.[19]

References

1) T. J. Swift,"NMR of Paramagnetic Molecules; Principles and Applications," ed by G. N. La Mar, W. D. Horrocks, Jr., and R. H. Holm, Academic Press, New York (1973), Chap. 2.
2) I. Bertini and C. Luchinat,"NMR of Paramagnetic Molecules in Biological Systems," The Benjamin/Cummings Publishing Company, Inc., (1982), Chap. 2.
3) I. Bertini, C. Luchinat, and L. Messori, *Metal Ions Biol. Syst.*, **21**, 47 (1986).
4) I. Solomon, *Phys. Rev.*, **99**, 559 (1955).
5) N. Bloembergen and L. D. Morgan, *J. Chem. Phys.*, **34**, 842 (1961).
6) N. Bloembergen, *J. Chem. Phys.*, **27**, 572 (1957).
7) M. Gueron, *J. Magn. Reson.*, **19**, 58 (1975).
8) K. Wüthrich, J. Hochmann, R. M. Keller, G. Wagner, M. Brunori, and C. Giacometti, *J. Magn. Reson.*, **19**, 111 (1975).
9) A. J. Vega and D. Fiat, *Mol. Phys.*, **31**, 347 (1976).
10) S. W. Unger, T. Jue, and G. N. La Mar, *J. Magn. Reson.*, **61**, 448 (1985).
11) R. G. Little, J. A. Anton, P. A. Loach, and J. A. Ibers, *J. Heterocyl. Chem.*, **12**, 343 (1975).
12) H. M. Goff, *J. Am. Chem. Soc.*, **103**, 3714 (1981).
13) R. L. Vold, J. S. Waugh, M. P. Klein, and D. E. Phelps, *J. Chem. Phys.*, **48**, 3831 (1968).
14) F. A. Walker, M. -W. Lo, and M. T. Ree, *J. Am. Chem. Soc.*, **98**, 5552 (1976).
15) J. D. Satterlee, G. N. La Mar, and T. J. Bold, *J. Am. Chem. Soc.*, **99**, 1088 (1977).
16) G. N. La Mar and F. A. Walker, *J. Am. Chem. Soc.*, **95**, 1782 (1973).
17) G. N. La Mar and F. A. Walker, "The Porphyrins," ed by D. Dolphin, Academic Press, New York (1979), Vol. IV, Chap. 2.
18) G. N. La Mar, "Biological Applications of Magnetic Resonance," ed. by R. G. Shulman, Academic Press, New York (1979), Chap.7.
19) Y. Yamamoto, K. Iwafune, N. Nanai, A. Ōsawa, R. Chûjô, and T. Suzuki, *Eur. J. Biochem.*, **198**, 299 (1991).

Chemical Oxidation of Tetra-*t*-butylphthalocyanine and Its Complexes with Cobalt(II), Nickel(II), Copper(II), and Zinc(II)

Ping MU, Tadahiro NAKAO, Makoto HANDA, Kuninobu KASUGA,* and Kunihisa SOGABE†
Department of Chemistry, Faculty of Science, Shimane University, Matsue 690
†Department of Chemistry, Faculty of Education, Shimane University, Matsue 690
(Received May 18, 1991)

Synopsis. While the title compounds were oxidized by $NOBF_4$, DDQ only oxidized the cobalt(II) and zinc(II) complexes in dichloromethane. To confirm their chemical oxidation, a cyclic voltammetry was measured.

It is well-known that the electrical conductivity of metallophthalocyanine complexes drastically increases in partial oxidation;[1] the single crystals grown by a slow diffusion of the complexes and oxidants or an electrochemical method exhibit a metallic conductivity, and their detailed properties have been investigated.[2,3] The conductivity also increases in partial reduction of the complexes or their analogues.[4,5] The metallophthalocyanine complexes are partially oxidized by iodine which might have difficulty oxidizing the complexes judging from their redox potentials. That is, the partial oxidation of the complexes is cooperatively promoted by a stacking effect of the oxidized complexes.

The partial oxidation of unsubstituted metallophthalocyanine complexes has been extensively investigated, but few studies have been reported on the oxidation of the complexes with peripherical substituents.[6] This paper describes the oxidation of the soluble metallophthalocyanine complexes peripherically substituted by *t*-butyl groups to investigate the effects of central metal ions and oxidants on the chemical oxidation.

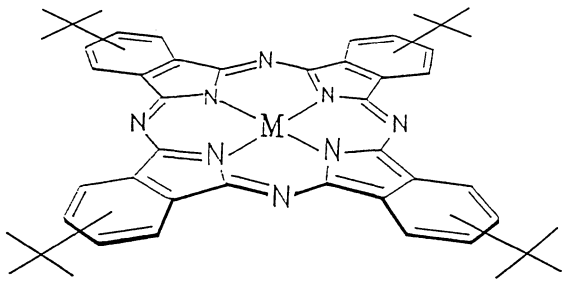

Fig. 1. Schematic representation of the $MPc(t\text{-}Bu)_4$ complex.

Experimental

Materials. Metal-free phthalocyanine and its cobalt(II), nickel(II), copper(II), and zinc(II) complexes were prepared by a method similar to that described in the literature.[6-8] 2,3-Dichloro-5,6-dicyano-*p*-benzoquinone (DDQ) was recrystallized from benzene under an argon atmosphere. Nitrosyl tetrafluoroborate ($NOBF_4$) was used without further purification.

Measurements. The electronic spectra in solution were measured on a Hitachi 200-20 spectrophotometer. The ESR spectra were measured with a JEOL-1X spectrometer. The cyclic voltammetric measurements were performed in a dichloromethane solution containing tetrabutylammonium perchlorate (0.1 mol dm^{-3}) on a Hokuto Denko HA-501 potentiostat with a Hokuto Denko HF-201 function generator. A glassy carbon disk, a platinum coil, and a saturated calomel electrode (SCE) were used as a working electrode, a counter electrode, and a reference electrode, respectively.

Results and Discussion

The metallophthalocyanine complexes are generally insoluble in common organic solvents, but the complexes which are peripherically substituted by *t*-butyl groups readily dissolve in organic solvents such as dichloromethane, chloroform, benzene, and pyridine; e.g., the solubility of $ZnPc(t\text{-}Bu)_4$ in dichloromethane is ca. 2×10^{-2} mol dm^{-3}.

Chemical Oxidation. The blue dichloromethane solution of these compounds turned reddish purple upon the addition of a strong oxidant such as $NOBF_4$. In the case of $ZnPc(t\text{-}Bu)_4$, the Q band (679 nm) extensively decreased in intensity, and new bands appeared at 528 and 721 nm. Similar spectral changes were observed in the addition of $NOBF_4$ to the dichloromethane solution of $H_2Pc(t\text{-}Bu)_4$ and its cobalt(II), nickel(II) or copper(II) complexes. It was reported that oxidation at a central metal ion slightly shifts the Q band, while ring oxidation decreases the intensity of the Q band.[9,10] The intensity of the Q bands of the compounds used in the present study decreased when the compounds were oxidized by $NOBF_4$ in dichloromethane. On the other hand, with an organic oxidant

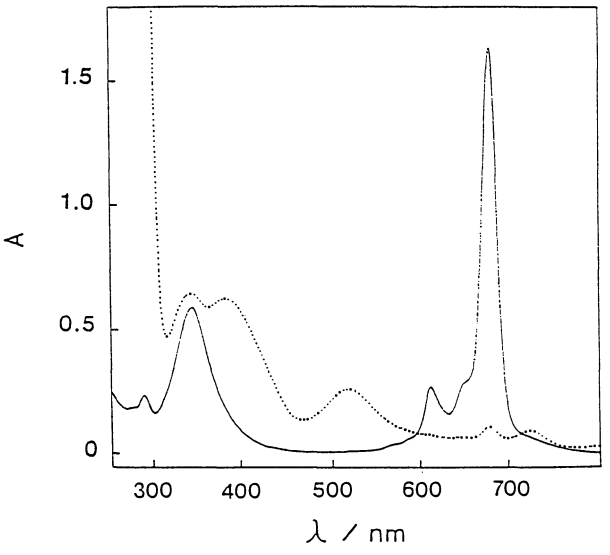

Fig. 2. Electronic spectra of $ZnPc(t\text{-}Bu)_4$ in dichloromethane: (——) [complex]=7.4×10^{-6} mol dm^{-3}; (----) [complex]=7.4×10^{-6} mol dm^{-3}, [DDQ]=1.5×10^{-5} mol dm^{-3}.

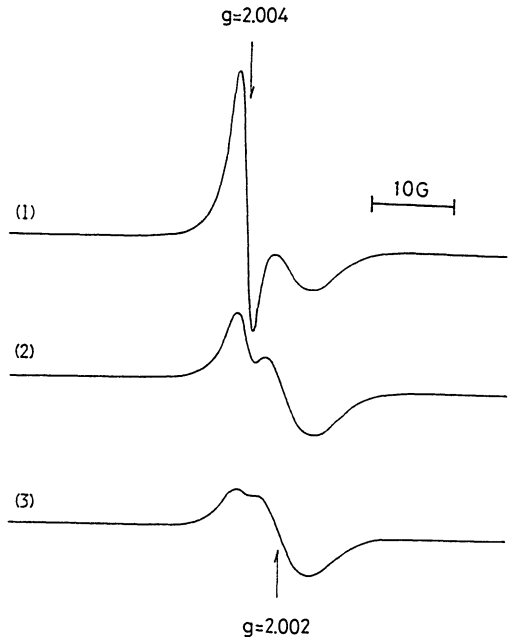

Fig. 3. ESR spectra of $ZnPc(t\text{-}Bu)_4$ oxidized by DDQ in dichloromethane at room temperature: (1) before UV irradiation; (2) irradiated for 2 min; (3) irradiated for 5 min.

such as DDQ, the blue dichloromethane solution of the cobalt(II) or zinc(II) complex turned reddish purple; e. g., the Q band (679 nm) of $ZnPc(t\text{-}Bu)_4$ decreased in intensity, and new bands appeared at 516 and 722 nm (Fig. 2). Within our knowledge, the oxidation of metallophthalocyanine with DDQ only occurs in the case of the polymer complexes of $(SnPcO)_n$ and $(AlPcF)_n$.[11,12] As soluble metallophthalocyanine complexes having simple substituents, these complexes are the first ones which could be oxidized by DDQ.

The dichloromethane solution of $ZnPc(t\text{-}Bu)_4$ oxidized by DDQ showed two ESR signals characteristic of organic radicals (Fig. 3). UV irradiation was employed to clarify the analysis of the signals. The sharp signal (g=2.004) in the lower magnetic field disappeared upon irradiation, and the g value for the signal that remained was estimated to be 2.002. On the other hand, the oxidation of the complex by $NOBF_4$ showed an ESR signal only at g=2.002. That is, the ESR signals at g=2.002 and 2.004 were assigned to those of the cationic phthalocyanine radical and the anionic DDQ radical, respectively. Furthermore, the ESR signal of the anionic DDQ radical (g=2.004) disappeared at liquid nitrogen temperature and recovered its intensity when rising to room temperature. It was reported that the anionic DDQ radicals form a dimer in the solid state, being ESR silent.[13] The concentration of the dimer in the dichloromethane solution might increase at liquid nitrogen temperature, resulting in the disappearance of the ESR signal.

Electrochemistry. The cyclic voltammograms (CV) of these compounds showed four redox couples.[14] Redox steps on the reduction side are reversible, whereas those on the oxidation side are quasi-reversible or irreversible. To confirm the behavior of the chemical oxidation, the half-wave potentials of the first step on the oxidation side are listed in Table 1. The $CoPc(t\text{-}Bu)_4$ and $ZnPc(t\text{-}Bu)_4$ complexes were easily oxidized compared with $H_2Pc(t\text{-}Bu)_4$, $NiPc(t\text{-}Bu)_4$, and $CuPc(t\text{-}Bu)_4$ in dichloromethane. By considering the potential of the first reduction step of DDQ (0.59 V vs. SCE in dichloromethane), it was obvious that only the cobalt(II) and zinc(II) complexes were oxidized by DDQ. The CV data show that the complexes are oxidized in the order of Co(II)>Ni(II) ≈Cu(II)<Zn(II). It was reported that the less the polarizing power (Ze/r) of the ion, the easier it was to oxidize the phthalocyanine ring.[15] As the ionic radii of the metal(II) ions decreased in the order of Co(II)>Ni(II)>Cu(II)<Zn(II), the order of the potentials might be explained by the polarizing power of the central ion.

Table 1. The Half-Weve Potentials of the First Oxidation Steps[a]

Compound	$E_{1/2}$[b]	$E_{1/2}$[c]
$H_2Pc(t\text{-}Bu)_4$	0.95 (irr)	0.66 (irr)
$CoPc(t\text{-}Bu)_4$	0.57 (60)	0.18 (120)
$NiPc(t\text{-}Bu)_4$	0.97 (irr)	0.89 (130)
$CuPc(t\text{-}Bu)_4$	0.82 (90)	0.81 (irr)
$ZnPc(t\text{-}Bu)_4$	0.52 (90)	0.72 (130)

a) $E_{1/2}=(E_{pa}+E_{pc})/2$ (V vs. SCE). b) In dichloromethane. c) In pyridine. Scan rate=100 mV/s^{-1}. The values in parentheses denote ΔE_p (mV). The half-wave potentials were estimated from $E_{pa}/2$ in the case of the irreversible oxidation steps.

The potential of $H_2Pc(t\text{-}Bu)_4$ in pyridine was shifted to the negative side compared with that in dichloromethane (Table 1). It was reported that the acidic protons of the phthalocyanine ring were dissociated in pyridine.[16] Then, the dissociation of the acidic protons resulted in an increase of the electron density on the phthalocyanine ring, leading to the facile oxidation of the ring. The potential of the cobalt complex was also extremely shifted to the negative side in pyridine. With the addition of $NOBF_4$ into the solution, the Q band (660 nm) of the cobalt complex shifted to 679 nm without a decrease in its intensity. That is, the central cobalt(II) ion might have been oxidized to a trivalent state.[14] The low-spin cobalt(III) ion was stabilized by the coordination of pyridine, resulting in the promotion of the oxidation of the cobalt(II) ion. Moreover, it was notable that the zinc(II) complex showed a fairly large positive shift in the potential of pyridine, but the shifts of the nickel(II) and copper(II) complexes were not so remarkable.

This work was partially supported by a Grant-in-Aid for Scientific Research No. 02453041 from the Ministry of Education, Science and Culture.

References

1) T. J. Marks, *Science*, **227**, 881 (1985), and refs. therein.
2) C. J. Schramm, R. P. Scaringe, D. R. Stojakovic, B. M. Hoffman, J. A. Ibers, and T. J. Marks, *J. Am. Chem. Soc.*, **102**, 6702 (1980).
3) K. Yakushi, H. Yamamoto, M. Yoshitake, N. Kosugi, H. Kuroda, T. Sugano, M. Kinoshita, A. Kawamoto, and J.

Tanaka, *Bull. Chem. Soc. Jpn.*, **62**, 687 (1989).
4) J. Le Moigne and R. Eren, *J. Chem. Phys.*, **83**, 6472 (1985).
5) K. Kasuga, M. Morisada, M. Handa, and K. Sogabe, *Inorg. Chim. Acta*, **174**, 161 (1990).
6) M. Hanack and R. Grosshans, *Chem. Ber.*, **122**, 1665 (1989).
7) S. Gaspard and P. Maillard, *Tetrahedron*, **43**, 1083 (1987).
8) S. A. Mikhalenko, S. V. Barkanova, O. L. Lebedev, and E. A. Luk'yanets, *J. Gen. Chem. USSR*, **41**, 2770 (1971).
9) J. F. Myeres, G. W. R. Canham, and A. B. P. Lever, *Inorg. Chem.*, **14**, 461 (1975).
10) A. E. Cahill and H. Taube, *J. Am. Chem. Soc.*, **73**, 2847 (1951).
11) J. G. Gaudiello, G. E. Kellogg, S. M. Tetrick, and T. J. Marks, *J. Am. Chem. Soc.*, **111**, 5259 (1989).
12) I. Hiromitsu, J. Takeuchi, and T. Ito, *J. Phys. Soc. Jpn.*, **59**, 2922 (1990).
13) J. S. Miller, P. J. Krusic, D. A. Dixon, W. M. Reiff, J. H. Zhang, E. C. Anderson, and A. J. Epstein, *J. Am. Chem. Soc.*, **108**, 4459 (1986).
14) Prior to the first step of the oxidation, a weak wave appeared, the details of which are unknown at the present stage.
15) A. B. P. Lever, S. Licoccia, K. Magnell, P. C. Minor, and B. S. Ramaswamy, *ACS, Symp. Ser.*, **701**, 237 (1982).
16) M. Whalley, *J. Chem. Soc.*, **1961**, 866.

Effect of Water Vapor on the Transformation of *cyclo*-Tetraphosphate

Hiroyuki NARIAI,* Itaru MOTOOKA, and Mitsutomo TSUHAKO†
Department of Chemistry, Faculty of General Education, Kobe University, Tsurukabuto, Nada-ku, Kobe 657
†Kobe Women's College of Pharmacy, Kitamachi, Motoyama, Higashinada-ku, Kobe 658
(Received May 29, 1991)

Synopsis. The effect of water vapor on the process of transformation of sodium *cyclo*-tetraphosphate $Na_4P_4O_{12}(P_{4m})$ to sodium *cyclo*-triphosphate $Na_3P_3O_9(P_{3m})$ was investigated by means of DTA-TG, X-ray diffraction analysis, isothermal heating with an electric furnace, and HPLC. The transformation of P_{4m} to P_{3m} proceeded by a radical reaction via different reaction pathways in dry and humid air.

Phosphates hydrolyze or condense on heating to form various kinds of phosphates.[1-11] These reaction processes are affected by many factors including the kind of metal, the ratio of metal to phosphorus, and the duration and rate of heating.

The water vapor pressure is also an important factor in thermal reaction of phosphates. In this study, the effect of water vapor on the thermal transformation of P_{4m} to P_{3m} was investigated.

Experimental

Chemicals. Sodium *cyclo*-tetraphosphate tetrahydrate ($P_{4m}\cdot 4H_2O$) was prepared by the method given in the literature.[1] P_{4m} was prepared by heating of its hydrate at 100 and 150 °C for 2 h and 1 h, respectively. Unless otherwise stated, guaranteed-grade reagents were used without further purification. The analytical procedures and apparatus were essentially the same as those in previous works.[12-15]

Results and Discussion

Thermal Decomposition of P_{4m} Examined by DTA-TG. Figure 1 shows the DTA-TG curves for P_{4m} at atmospheric pressure. Except for a slight decrease by dehydration of adsorbed water, there was no weight loss in the TG curve over the temperature range examined. In the DTA curve, a small exothermic peak at around 500 °C was due to the transformation of P_{4m} to P_{3m} and the endo- and exothermic peaks at about 600 °C due to decomposition of P_{3m}. The influence of water vapor was investigated under the isothermal conditions in a temperature range from 400 to 500 °C.

Isothermal Change. Figure 2 shows the X-ray diffraction patterns of the samples heated for 1 h at several temperatures and humidities. The diffraction lines of P_{4m} remained unchanged at 400 °C. At 420 °C the lines changed partially to those of P_{3m}(I) (JCPDS Card 11-0648) in dry air, while in humid air to P_{3m}(I'), which has a crystal structure different from that of P_{3m}(I).[16,17] The transformation of P_{4m} to P_{3m}(I') has not been reported. At 450 °C P_{4m} changed completely into each type of P_{3m}. Table 1 shows the changes in the amounts of phosphorus compounds in the samples heated at several temperatures. At 420 °C in a dry air atmosphere (r. h.=0%), about 56% of P_{4m} already changed to P_{3m}, while in air of 90% relative humidity at (25 °C), about 21% of P_{4m} changed to P_{3m}. Since the TG curve indicated no weight change, and since no oligophosphates were detected in the 400—500 °C region, it seems

Table 1. Changes in Phosphate Composition (Starting Material: P_{4m})

Temp	Relative humidity	P_{4m}	P_{3m}
°C	%	%	%
400	0	100.0	0
	90	100.0	0
420	0	44.3	55.7
	90	79.3	20.7
450	0	0	100.0
	90	0	100.0

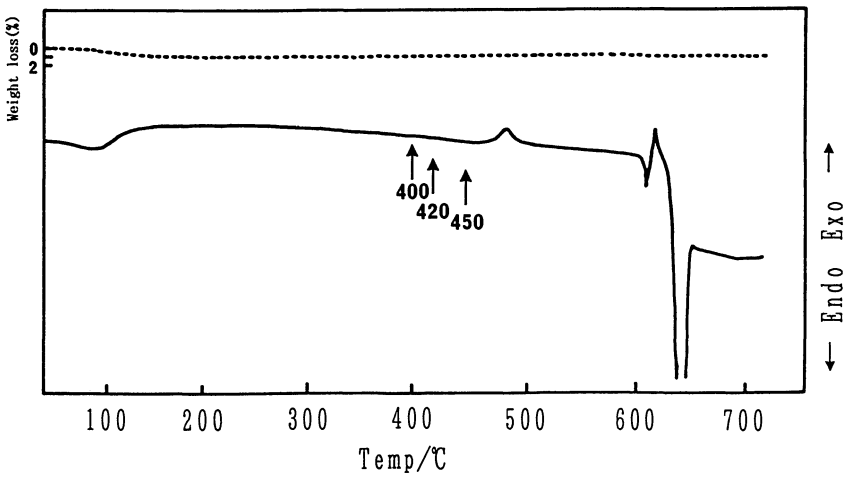

Fig. 1. DTA-TG curves for $Na_4P_4O_{12}$ anhydride. Solid line: DTA, dotted line: TG.

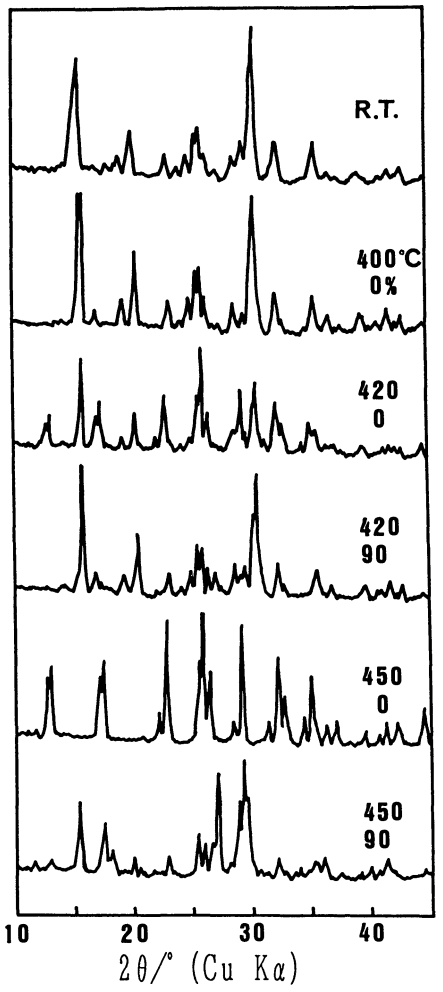

Fig. 2. X-Ray diffraction patterns of the products on heating in two different atmospheres (relative humidities of 0% and 90%). Sample: $Na_4P_4O_{12}$ anhydride. R. T., room temperature.

that the transformation of P_{4m} to P_{3m} proceeds by a radical process.[14] It is interesting to note that P_{4m} transformed to $P_{3m}(I')$ under a humid atmosphere as follows:

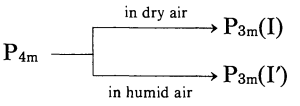

References

1) R. N. Bell, L. F. Audrieth, and O. F. Hill, *Ind. Eng. Chem.*, **44**, 568 (1952).
2) E. Thilo and I. Grunze, *Z. Anorg. Allg. Chem.*, **290**, 209 and 223 (1957).
3) E. Thilo, *Adv. Inorg. Chem. Radiochem.*, **4**, 1 (1962).
4) E. Thilo and U. Schülke, *Z. Anorg. Allg. Chem.*, **341**, 293 (1965).
5) U. Schülke, *Z. Anorg. Allg. Chem.*, **360**, 231 (1968).
6) M. Watanabe, S. Sato, and H. Saito, *Bull. Chem. Soc. Jpn.*, **48**, 896 (1975).
7) H. Worzala, *Z. Anorg. Allg. Chem.*, **445**, 27 (1978).
8) M. Watanabe, M. Matsuura, and T. Yamada, *Bull. Chem. Soc. Jpn.*, **54**, 738 (1981).
9) I. Grunze and H. Grunze, *Z. Anorg. Allg. Chem.*, **512**, 39 (1984).
10) M. Watanabe, K. Murata, and M. Maeda, *Bull. Chem. Soc. Jpn.*, **61**, 3877 (1988).
11) M. Trojan, D. Brandova, and Z. Solc, *Thermochim. Acta*, **110**, 343 (1987).
12) H. Nariai, I. Motooka, Y. Kanaji, and M. Tsuhako, *Bull. Chem. Soc. Jpn.*, **60**, 1337 (1987).
13) G. Kura, *Bull. Chem. Soc. Jpn.*, **56**, 3769 (1983).
14) H. Nariai, I. Motooka, and M. Tsuhako, *Bull. Chem. Soc. Jpn.*, **61**, 2811 (1988).
15) A. Takenaka, I. Motooka, and H. Nariai, *Bull. Chem. Soc. Jpn.*, **62**, 2819 (1989).
16) R. W. Liddell, *J. Am. Chem. Soc.*, **71**, 207 (1949).
17) J. R. Van Wazer, "Phosphorus and Its Compounds," Interscience Publishers, Inc., New York (1958), Vol. I.

Thermal Decomposition Studies on Amine Complexes of Copper(II) Nitrate in Solid State

Suresh MATHEW, C. G. R. NAIR, and K. N. NINAN*,†
Department of Chemistry, University of Kerala, Trivandrum 695034, India
†Propellant and Special Chemicals Group, Vikram Sarabhai Space Centre, Trivandrum 695022, India
(Received March 9, 1990)

Synopsis. Thermal decomposition of tetraamminecopper(II) nitrate and bis(ethylenediamine)copper(II) nitrate has been studied using TG, DTG, and DTA. The kinetic parameters for the thermal deamination of the former were evaluated. The thermal decomposition of bis(ethylenediamine)copper(II) nitrate involves the concurrent deamination and the oxidation of the liberated amine by the decomposition products of $Cu(NO_3)_2$.

Solid state thermal decomposition of different complexes and salts has been extensively studied employing both isothermal and nonisothermal methods to evaluate the kinetics of their thermal decompositions. Although transition metal amine complexes were known for a long time, investigations on their thermal decomposition behavior have been carried out only recently.[1-4] Thermal studies on the amine complexes containing nitrate anion are relatively few, because of their self oxidative decomposition.

The thermal decomposition studies on tetraamminecopper(II) nitrate and bis(ethylenediamine)copper(II) nitrate in the solid state using TG, DTA, and other accessory techniques are described in this paper. The objectives of this investigation are to explore the kinetic and thermodynamic aspects of the thermal deamination of $[Cu(NH_3)_4](NO_3)_2$ and $[Cu(en)_2](NO_3)_2$.

Experimental

Preparation of Complexes: The preparative methods of $[Cu(NH_3)_4](NO_3)_2$ and $[Cu(en)_2](NO_3)_2$ are given elsewhere.[5] Both complexes were characterized by spectral and chemical methods.

Measurements: The experimental methods and the equipments used to measure TG-DTG, DTA curves, and X-ray powder diffractograms were the same as those described in our earlier work.[3,4] The heating rates employed here are 10, 2, 0.5 °C min^{-1} and sample mass 5±0.3 mg. Area under the DTA curves was evaluated by the sigmoidal curve integration and calibrated using pure indium metal.

Mathematical Treatment of Data: Kinetic parameters were evaluated from the TG and DTA curves using four nonmechanistic methods., viz. Coats-Redfern,[6] MacCallum-Tanner,[7] Horowitz-Metzger,[8] and MKN equations.[9] The iterative determination of the order parameter 'n' is described in our earlier papers.[3,4] The entropy of activation was calculated from the equation.

$$A=[(kT_s/h)\exp(\Delta S^{\neq}/R)]$$

where k=Boltzmann constant, h=Planck's constant, and $\Delta S^{\neq}$=entropy of activation. The heat of reaction ΔH was evaluated from the DTA curve by area integration of the peak.

Results and Discussion

Thermal Decomposition of $[Cu(NH_3)_4](NO_3)_2$: The TG-DTG and DTA curves of tetraamminecopper(II) nitrate are given in Fig. 1. The TG trace revealed a clear cut decomposition state (125—225 °C) but on further heating, the complex gets exploded (ca. 257 °C) at a heating rate of 10 °C min^{-1}. This can be attributed to the presence of the reducing (NH_3) group and the oxidant nitrate group in the same compound. At a lower heating rate of 2 °C min^{-1} neat thermograms could be recorded. The phenomenological data from TG and DTA curves for each stage of decomposition are given in Table 1. From the mass loss data, the two stages of decomposition of tetraamminecopper(II) nitrate can be represented as follows:

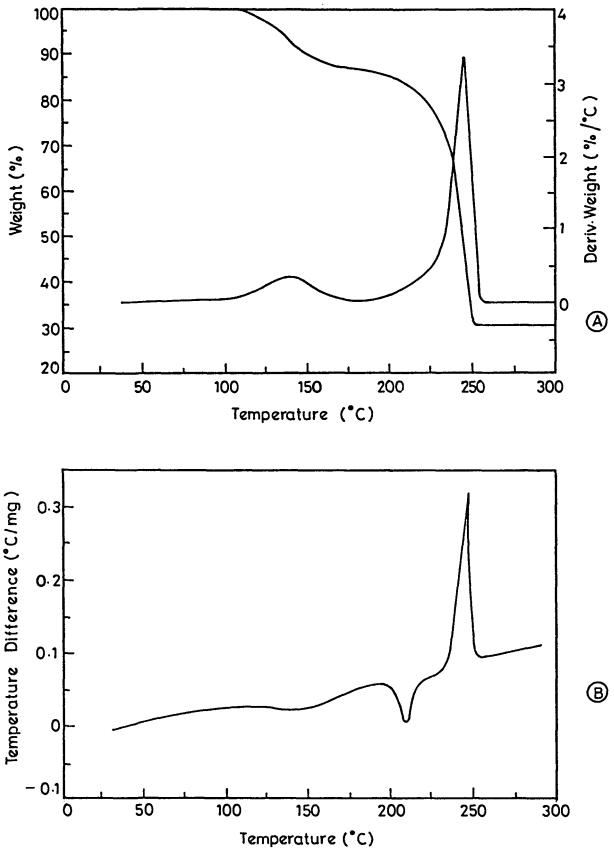

Fig. 1. A: TG and DTG curves of $[Cu(NH_3)_4](NO_3)_2$ at 2 °C min^{-1}. B: DTA curve of $[Cu(NH_3)_4](NO_3)_2$ at 2 °C min^{-1}.

$$[Cu(NH_3)_4](NO_3)_2\,(s) \longrightarrow Cu(NH_3)_2(NO_3)_2\,(s)+2NH_3\,(g)$$
$$Cu(NH_3)_2(NO_3)\,(s) \longrightarrow CuO\,(s)$$

The DTA profile of the complex shows three peaks. The first endothermic peak in the DTA curve at 146 °C is due to the first stage of deamination resulting in the formation of the diammine complex. The second

Table 1. Phenomenological Data for the Thermal Decomposition of Tetraamminecopper(II) Nitrate and Bis(ethylenediamine)copper(II) Nitrate

	Stage	$[Cu(NH_3)_4](NO_3)_2$						$[Cu(en)_2](NO_3)_2$				
		T_i	T_f	T_s	%wt loss		ΔH	T_i	T_f	T_s	%wt loss	ΔH
		°C	°C	°C	Theoretical	Observed	J gm^{-1}	°C	°C	°C	Observed	J gm^{-1}
TGA	I	90	176	140	13.31	13	—	230	252		37	—
	II	185	250	248	42.26	42	—	252	261		23	—
	III							261	272	266	3	—
	IV							276	338	296	10	—
DTA	I	98	181	146	—	—	297	230	248	245	—	−934
	II	190	218	211	—	—	180	248	258	255	—	−280
	III	227	254	249	—	—	−873	258	271	264	—	−435
	IV	—	—	—	—	—	—	271	335	293	—	−664

endothermic peak is immediately followed by a sharp exotherm, contrary to the expected enthalpy changes accompanying the decomposition of a stable complex. The exothermic peak can, however, be explained on the basis of the decomposition of $Cu(NO_3)_2$, overlapping the diammine complex. $Cu(NO_3)_2$ on decomposition gives rise to oxides of nitrogen and oxygen which in turn would oxidize the liberated ammonia. Thus the decomposition of the diammine complex initiates with a small endothermic peak (corresponding to the initial deamination), immediately followed by a sharp exotherm.

The thermal decomposition of tetraamminecopper(II) nitrate is consistent with the crystal structure of the complex.[10] The first deamination stage corresponds to the removal of two molecules of ammonia. From the single crystal study it is revealed that Cu–N bond distance for one pair is 2.03 Å and for the other pair is 2.008 Å. Hence normally the two NH_3 molecules coordinated to the copper at a distance of 2.03 Å can be expected to get liberated first. On subsequent heating, the remaining two NH_3 molecules are lost.

The intermediate diammine complex and the final residue of decomposition were identified by XRD. The final residue is found to be copper(II) oxide. The temperature values agree reasonably with the corresponding values of TG, except that the last two stages of DTA appear as a single stage in TG. However, the DTG peak temperature T_s corresponds to the T_{max} of the third stage in DTA. The ΔH for the first stage of deamination is 297 J gm^{-1} (endo), whereas for the second stage of deamination it is only 180 J gm^{-1} (Table 1). The reduction in enthalpy supports our contention that this stage corresponds only to a partial loss of ammonia. This is followed by the simultaneous loss of the rest of ammonia and the decomposition of $Cu(NO_3)_2$, leading to the exothermic oxidation of the liberated NH_3 by the decomposition products (ΔH=−873 J gm^{-1}).

Thermal Decomposition of $[Cu(en)_2](NO_3)_2$: In order to avoid the explosive decomposition due to the presence of a powerful reductant (en) and the oxidizing nitrate group the TG and DTA curves were recorded at a lower heating rate of 0.5 °C min^{-1} (Fig. 2). The decomposition temperature regime reveals that bis(ethylenediamine) complex is thermally more stable than

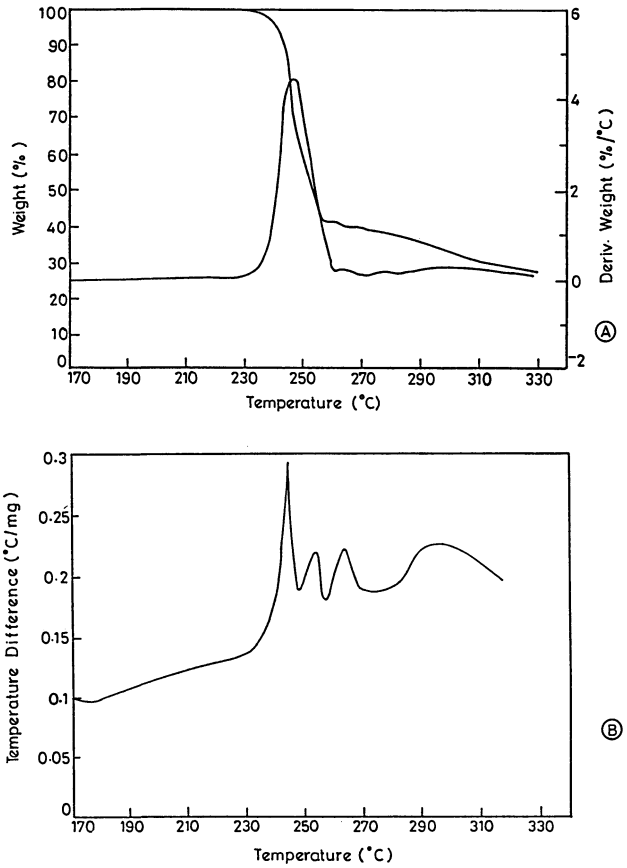

Fig. 2. A: TG and DTG curves of $[Cu(en)_2](NO_3)_2$ at 0.5 °C min^{-1}. B: DTA curve of $[Cu(en)_2](NO_3)_2$ at 0.5 °C min^{-1}.

tetraammine complex, which could be attributed to the bidentate nature of the ligand and hence a stable chelate. The weight loss corresponding to each stage of decomposition is given in Table 1. The powder diffraction pattern of the residue obtained revealed that it is pure copper(II) oxide.

The bis(ethylenediamine) complex starts decomposing at 230 °C. At this temperature, $Cu(NO_3)_2$ also starts to decompose. Due to this overlap, the whole process appears as pseudo exothermic in several steps. It is reasonable to assume that the exothermic peaks in

Table 2. Kinetic Parameters for the Deamination of $[Cu(NH_3)_4](NO_3)_2$ to $Cu(NH_3)_2(NO_3)_2$ Using Nonmechanistic Equations[a)]

		TG	DTA
n		1.56	1.56
E ($kJ\,mol^{-1}$)	CR	125.4	150.6
	MT	124.6	150.2
	HM	133.9	156.3
	MKN	125.6	150.7
A (s^{-1})	CR	2.35×10^{13}	1.26×10^{16}
	MT	1.62×10^{13}	9.65×10^{15}
	HM	2.67×10^{14}	6.09×10^{16}
	MKN	2.44×10^{13}	1.30×10^{16}
$\Delta S^{\neq}$ ($J\,K^{-1}\,mol^{-1}$)	CR	8.36	60.5
	MT	5.26	58.3
	HM	28.6	73.6
	MKN	8.67	60.8
r	CR	0.9999	0.9985
	MT	0.9999	0.9987
	HM	0.9993	0.9975
	MKN	0.9999	0.9985

a) CR: Coats-Redfern, MT: MacCallum-Tanner, HM: Horowitz-Metzger, MKN: Madhusudanan-Krishnan-Ninan.

DTA are due to the simultaneous deamination and the insitu oxidation of the liberated amine. This process takes place in four stages, and all the stages are exothermic. The first sharp exotherm corresponds probably to the loss of one en, overlapping with its partial oxidation by the decomposition products of $Cu(NO_3)_2$.

The value of ΔH computed from the area under the DTA curve along with the T_i, T_f, and T_s values for the four stages of decomposition are given in Table 1. The four exothermic peaks in DTA add upto a heat of reaction $-2313\ J\,gm^{-1}=-711\ kJ\,mol^{-1}$. The heat of combustion of ethylenediamine is $1894\ kJ\,mol^{-1}$ [11] and therefore a complete oxidation of the two moles of en would have given rise to a heat of reaction of $-3787\ kJ\,mol^{-1}$. However the minimum requirement for the complete oxidation of two ethylenediamine molecules is 16 oxygen atoms, whereas only 6 oxygen atoms are available in $Cu(NO_3)_2$. Further, some of the ethylenediamine is likely to escape oxidation in the open system. These result in only partial oxidation of the liberated ethylenediamine. This, coupled with the endothermicities of the deamination process and the decomposition of $Cu(NO_3)_2$ to CuO, leads to an overall heat of reaction much below the heat of combustion of two ethylenediamine molecules.

The kinetic parameters were evaluated for the deamination of tetraamminecopper(II) nitrate to the diammine complex. The data using the four kinetic equations from TG and DTA are tabulated in Table 2. The correlation coefficients indicate nearly perfect fits. This table shows that the order parameter for the deamination process is a fraction, as is possible.[12,13]

Table 2 shows that the kinetic parameters computed with Horowitz-Metzger equation are higher than the values from the other three equations. This is due to the inherent error involved in the approximation method employed in the derivation of the Horowitz-Metzger equation. The deamination reaction of tetraammine complex has a positive value of entropy, indicating a less ordered structure of the activated complex than the reactant and hence the reaction may be described as "faster than normal".[14] The higher values of activation energy from DTA technique may be due to the lag in the measurement of temperature as compared to mass measurement.

The authors are grateful to the authorities of Vikram Sarabhai Space Centre for providing the instrumental facilities. One of the authors (S.M) is grateful to Council of Scientific and Industrial Research, (India) for giving him a Senior Research Fellowship.

References

1) S. Kinoshita, K. Miyokawa, H. Wakita, and I. Masuda, *Bull. Chem. Soc. Jpn.*, **57**, 381 (1984).
2) N. R. Chaudhuri, M. K. Dasgupta, S. Mitra, and G. K. Patnak, *Bull. Chem. Soc. Jpn.*, **51**, 506 (1978).
3) S. Mathew, C. G. R. Nair, and K. N. Ninan, *Thermochim. Acta,* **144**, 33 (1989).
4) C. G. R. Nair, S. Mathew, and K. N. Ninan, *Thermochim. Acta,* **150**, 63 (1989).
5) I. M. Procter, B. J. Hathaway, and P. Nicholls. *J. Chem. Soc. A,* **1968**, 1678.
6) A. W. Coats and J. P. Redfern, *Nature (London)*, **201**, 68 (1964).
7) J. R. MacCallum and J. Tanner, *Eur. Polym. J.*, **6**, 1033 (1970).
8) H. H. Horowitz and G. Metzger, *Anal. Chem.*, **35**, 1464 (1963).
9) P. M. Madhusudanan, K. Krishnan, and K. N. Ninan, *Thermochim. Acta,* **97**, 189 (1986).
10) B. Morosin, *Acta Crystallogr.*, **32**, 1237 (1976).
11) C. R. C. "Hand Book of Chemistry and Physics," 68th ed, CRC Press (1988), D-276.
12) D. Blecic and Z. D. Zivkovic, *Thermochim. Acta,* **60**, 68 (1983).
13) A. C. Norris, M. I. Pope, and M. Selwood, *Thermochim. Acta,* **41**, 357 (1980).
14) J. W Moore and R. G. Pearson, "Kinetics and Mechanism," Wiley, New York (1981), p. 181.

Effect of Solvents and Acridine on Dibenzothiophene Hydrodesulfurization

Masatoshi NAGAI
Department of Chemical Engineering, Tokyo University of Agriculture and Technology, Koganei, Tokyo 184
(Received April 17, 1991)

Synopsis. A selective poisoning pattern was observed for the hydrodesulfurization of dibenzothiophene on the sulfided Mo/Al_2O_3 catalyst in the presence of acridine and the solvents xylene and tetralin, using a microreactor at 270—340 °C and 10.1 MPa total pressure.

The selective poisoning pattern is characteristic of the correlation between hydrogenation and C–S hydrogenolysis during the hydrodesulfurization (HDS) of dibenzothiophene on a sulfided Mo/Al_2O_3 catalyst.[1] When nitrogen and aromatic heterocyclic compounds were added to the feed, the compounds depressed the hydrogenation of dibenzothiophene, but not the C–S hydrogenolysis reactions during the HDS of dibenzothiophene. On the other hand, the addition of sulfur and oxygen compounds depressed the C–S hydrogenolysis of dibenzothiophene to biphenyl and of hexahydrodibenzothiophene to cyclohexylbenzene. This selective poisoning study provided a good perspective for an understanding of the nature of active sites for HDS; hydrogenation and C–S hydrogenolysis occurred on different surface sites of the sulfided molybdenum catalysts.[2]

Although the solvents are used primarily to dissolve a feed such as polynuclear aromatic sulfur compounds, there is little understanding of the effect of solvents on hydrogenation and C–S hydrogenolysis reactions during the HDS reaction. In this study, tetralin and xylene were chosen as the solvents in order to determine which type of site is inhibited by the solvent during the reaction. The present study focused on the selectivity of the sulfided Mo/Al_2O_3 catalyst for the hydrogenation and the C–S hydrogenolysis in the presence of the solvent and a poison compound, acridine, at high hydrogen pressure.

Experimental

The apparatus was a high-pressure system with an 11 mm i.d. microreactor which has been described elsewhere.[3] Hydrogen was dried by passage through a Linde 13X molecular sieve trap prior to use. Dibenzothiophene was synthesized via the same procedure as described in a previous paper.[1] Acridine and all other reagents obtained commercially were used without further purification. The 12.5% MoO_3/Al_2O_3 catalyst (0.84—1.19 mm granules) was packed in the reactor and oxidized for more than 24 h at 450 °C in air. Sulfiding was carried out with a 10% H_2S/H_2 mixture flowing at 30 L h^{-1} at atmospheric pressure and 400 °C for 3 h after reduction of the oxidized catalyst in 10 L h^{-1} hydrogen at 400 °C and 10.1 MPa pressure for 4 h. After sulfiding, the reactor was cooled to 300 °C in the H_2S/H_2 stream, and then a solution containing 5 wt% (3.53 mmol L^{-1}) of dibenzothiophene in xylene (or tetralin) was allowed to flow into the reactor. A typical reaction was carried out at 300 °C and at 28 L h^{-1} hydrogen flow and at 10.1 MPa total pressure. After the reaction had reached a steady state (in about 3 h), acridine was added to the feed at the concentration required to produce 0 to 3.1 kPa. Xylene was barely hydrogenated at 300 °C in the presence of dibenzothiophene or acridine. The liquid product samples were analyzed by FID gas chromatography.

Results and Discussion

The major products were biphenyl and cyclohexylbenzene in the dibenzothiophene HDS: the former product was formed by the direct C–S bond breakage of dibenzothiophene and the latter by the C–S hydrogenolysis of hexahydrodibenzothiophene after successive hydrogenation. The effect of acridine on dibenzothiophene HDS in xylene solvent is shown in Fig. 1. When acridine was added to the xylene solution containing dibenzothiophene, the amount of biphenyl increased in inverse proportion to the amount of cyclohexylbenzene. The addition of 0.1 wt% acridine brought about the maximum amount of 0.42 wt% biphenyl. Acridine was preferentially hydrogenated to perhydroacridine without the direct C–N hydrogenolysis of acridine on a sulfided Mo/Al_2O_3 catalyst at 300 °C, since no hydrocarbon products were observed from the acridine hydrodenitrogenation either in this reaction or in the hydrodenitrogenation of acridine alone.[4] Moreover,

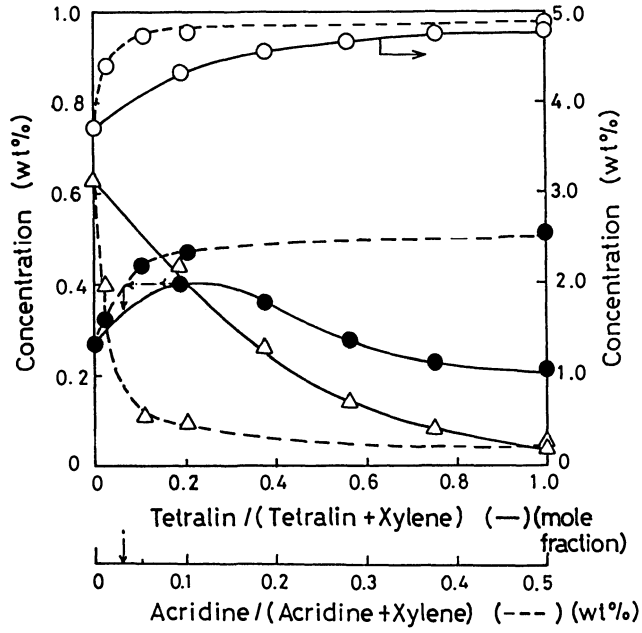

Fig. 1. Effect of xylene/(tetralin+xylene) solvent fraction (——) and of acridine (----)[1] on the major products of the HDS of dibenzothiophene at 300 °C. ○, dibenzothiophene; ●, biphenyl; △, cyclohexylbenzene.

the hydrogenation of biphenyl to cyclohexylbenzene did not occur in the presence of dibenzothiophene even on the sulfided $NiMo/Al_2O_3$ catalyst at 300 °C.[5] Therefore, the preferential hydrogenation of acridine depressed the hydrogenation of dibenzothiophene. Thus, acridine inhibited the hydrogenation sites, but not the C–S hydrogenolysis sites. The addition of acridine to the feed expelled dibenzothiophene from the hydrogenation sites. The dibenzothiophene was in turn adsorbed on the C–S hydrogenolysis sites to be desulfurized to form biphenyl. Therefore, it appeared that the decrease in cyclohexylbenzene resulted in enhanced biphenyl formation in the xylene solvent.

Changes in the ratio of xylene and tetralin in dibenzothiophene HDS are shown in Fig. 1. The amount of biphenyl was increased by increasing the tetralin-fraction and was maximized to 0.405 wt% at a 22% tetralin-fraction and was minimized to 0.2 wt% biphenyl. The amount of cyclohexylbenzene was gradually decreased to 0.035 wt% from 0.63 wt% when the tetralin-fraction was increased to 100% tetralin. The selective poisoning pattern in the presence of less than a 22% tetralin-fraction was observed for the results obtained in the presence of acridine in xylene. This suggested that less than 22% tetralin in xylene did not inhibit the C–S hydrogenolysis sites but did affect the hydrogenation sites at 300 °C. Furthermore, more than 22% tetralin inhibited both the C–S hydrogenolysis and hydrogenation sites.

The amount of a mixture of 78% xylene and 22% tetralin corresponded to the amounts of cyclohexylbenzene and biphenyl in the presence of 0.03 wt% acridine, as shown in Fig. 1. A 22% fraction of tetralin corresponded to 11.9 $mmol\,h^{-1}\,g\text{-}cat^{-1}$ of tetralin which was adsorbed on the hydrogenation sites only. The corresponding amount of acridine was 3.98×10^{-3} $mmol\,h^{-1}\,g\text{-}cat.^{-1}$. This amount was 1/3000 th the value obtained from the mixture of xylene and tetralin. These results showed that acridine was adsorbed on the hydrogenation sites 3000-fold stronger than tetralin. In a previous paper,[1] the poisoning effect of the nitrogen and aromatic compounds on the HDS of dibenzothiophene over the sulfided Mo/Al_2O_3 catalyst was studied. The strength of the adsorption constant of acridine was 67 times as great as that of phenanthrene, although tetralin was not tested in the dibenzothiophene HDS. The result suggested that tetralin was adsorbed on the hydrogenation sites 45 times less than phenanthrene.

The formation of biphenyl and cyclohexylbenzene in the HDS of dibenzothiophene in either xylene or tetralin solvent in the range of 270 to 340 °C is shown in Fig. 2. The concentrations of biphenyl and cyclohexylbenzene in the dibenzothiophene HDS in xylene solvent were 1.2 and 18 times that in tetralin at 300 °C, respectively. Tetralin inhibited both hydrogenation and C–S hydrogenolysis more than did xylene. The apparent activation energies for the formation of biphenyl were 84.9 $kJ\,mol^{-1}$ in tetralin and 76.5 $kJ\,mol^{-1}$ in xylene. The formation of cyclohexylbenzene in tetralin was much less than that in xylene. The apparent activation energies for the formation of cyclohexylbenzene were 186 in tetralin, and 157 (270—300 °C) and 58.9 (300—340 °C) $kJ\,mol^{-1}$ in xylene.[6]

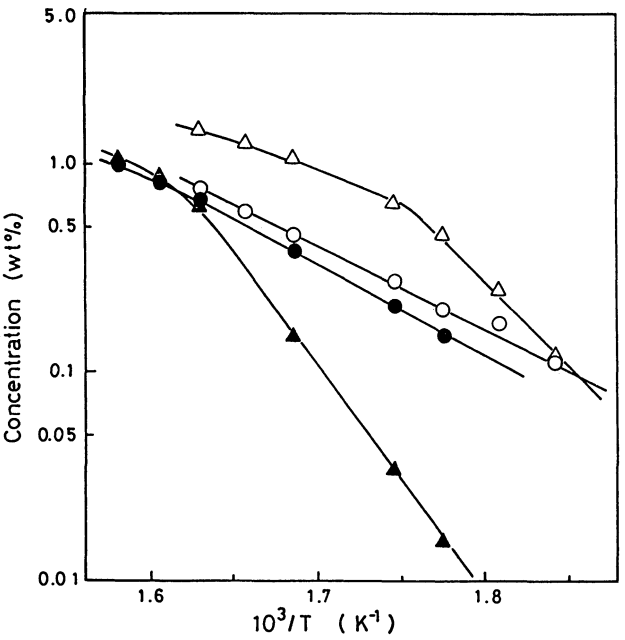

Fig. 2. Arrhenius plots of the formation of biphenyl and cyclohexylbenzene in xylene (open symbol)[6] and tetralin (closed symbol). ○●, biphenyl; △▲, cyclohexylbenzene.

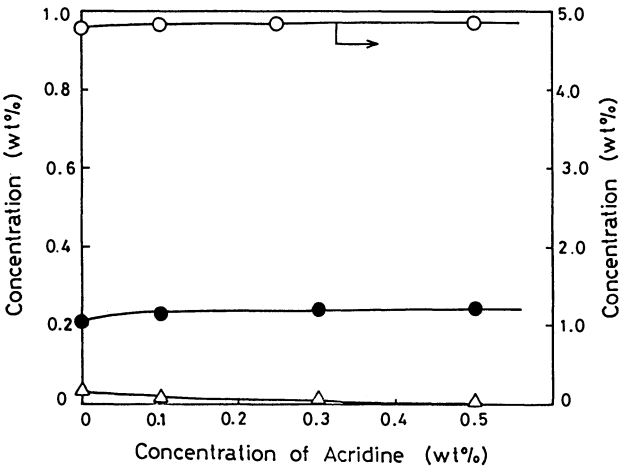

Fig. 3. Effect of acridine on the major products of the HDS of dibenzothiophene in tetralin solvent at 300 °C. The symbols are the same as those in Fig. 1.

The presence of acridine on dibenzothiophene HDS in the tetralin solvent is shown in Fig. 3. The presence of acridine lowered the amount of cyclohexylbenzene, and enhanced the amount of biphenyl, which reached constant values of 0.2% and 0.05%, respectively. The selective pattern was similar to the results of acridine addition in the xylene solvent: The presence of acridine inhibited the hydrogenation sites and resulted in increased biphenyl formation. However, more than 22% tetralin was adsorbed competitively on the active sites for the direct C–S hydrogenolysis of dibenzothiophene to biphenyl, as well as on the active sites for successive hydrogenation of dibenzothiophene. The presence of acridine slightly enhanced biphenyl formation.

In summary, the HDS of dibenzothiophene was catalyzed on two kinds of active sites on the sulfided Mo/Al_2O_3 catalyst: Site I was active for hydrogenation and was very sensitive to poisoning by nitrogen bases, while Site II was active for HDS (C–S hydrogenolysis), and was less susceptible to acridine poisoning. The presence of a small amount of tetralin hindered the hydrogenation of dibenzothiophene, but a large amount of tetralin depressed the C-S hydrogenolysis as well as the hydrogenation reaction.

Several researchers have found it necessary to postulate the existence of two kinds of catalytic sites on molybdenum sulfide catalysts. Massoth and coworkers[7–9] proposed that at least two HDS sites exist, one being poisoned and the other unaffected by pyridine. Hydrogenation was more strongly affected by pyridine than HDS. They suggested that the three reactions (HDS, hydrogenation, and cracking) appeared to take place on different sites.[7] Gates and coworkers[2,10,11] studied the HDS reaction network of dibenzothiophene and found that H_2S depressed hydrogenolysis but left hydrogenation unchanged. They also proposed that there was competitive adsorption of H_2S and the sulfur-containing reactant on one kind of catalytic site and noncompetitive adsorption of hydrogen on another kind of site. Furthermore, Shimada et al.[12] found that two-dimensional polymolybdate structures were favorable for high hydrogenation activity while electronegative molybdenum which induces Brønsted activity was required for high hydrogenolysis activity. They also reported that HDS of dibenzothiophene can be catalyzed on both kinds of active sites.

References

1) M. Nagai and T. Kabe, *J. Catal.*, **81**, 440 (1983).
2) M. Houalla, N. K. Nag, A. V. Spare, D. H. Broderick, and B. C. Gates, *AIChE J.*, **4**, 1015 (1978).
3) M. Nagai, T. Masunaga, and N. Hanaoka, *Energy Fuels*, **2**, 645 (1988).
4) M. Nagai, T. Masunaga, and N. Hanaoka *J. Catal.*, **101**, 284 (1986).
5) M. Nagai, A. Aiba, and T. Sato, *J. Catal.*, **97**, 52 (1986).
6) M. Nagai and T. Kabe, *J. Jpn. Pet. Inst.*, **23**, 82 (1980).
7) R. Ramachandran and F. E. Massoth, *Chem. Eng. Commun.*, **18**, 239 (1982).
8) J. Miciukiewicz, W. Zwierczak, and F. E. Massoth, *Bull. Soc. Chim. Belg.*, **96**, 915 (1987).
9) A. R. Saini, B. G. Johnson, and F. E. Massoth, *Appl. Catal.*, **40**, 157 (1988).
10) D. H. Broderick and B. C. Gates, *AIChE J.*, **27**, 663 (1981).
11) D. R. Kilanowski and B. C. Gates, *J. Catal.*, **62**, 70 (1980).
12) H. Shimada, T. Sato, Y. Yoshimura, J. Hiraishi, and A. Nishijina, *J. Catal.*, **110**, 275 (1988).

Addition Effect of NaF on the Deodorant Efficiency of an Iron Phthalocyanine Derivative

Koe ENMANJ,* Itsuo NISHIYAMA, Kenzo TAKAHASHI, and Muneharu SANOH
Materials and Electronic Devices Laboratory, Mitsubishi Electric Corp., Tsukaguchi-Honmachi, Amagasaki 661
(Received May 9, 1991)

Synopsis. A low temperature ESR spectrum shows that Fe(III) of an iron phthalocyanine derivative treated with NaF takes a high spin state. The deodorant efficiency of the derivative treated with NaF is three times higher than that without NaF treatment.

Hydrogen sulfide (H_2S) is one of "the eight bad smells",[1] and many reports have appeared concerning the deodorant method for it.[2] The reaction type deodorant materials containing copper(II) ion as an active substance were investigated for use in air conditioners with cleaner.[3] The lifetime of the copper(II) deodorant materials are not long enough. Biomimetic deodorant materials containing iron phthalocyanine derivatives as an enzyme-like catalyst were then studied in view of their theoretically infinite lifetimes.[4] The efficiency of these deodorant materials is not high enough for air conditioners. We improved the deodorant efficiency of a biomimetic deodorant material for H_2S by adding NaF to an iron phthalocyanine derivative. The relation between the deodorant efficiency and the high spin character of the iron phthalocyanine derivative is discussed.

Experimental

Iron(III)-4,5,4′,5′,4″,5″,4‴,5‴-octacarboxyphthalocyanine (FePc) was synthesized and purified by the method described in the literature.[5] The untreated deodorant material (UTD) was prepared by dipping 10 g of cotton in a 10 mmol dm^{-3} FePc aqueous solution followed by rinsing with 0.1 mol dm^{-3} HCl and drying at 100 °C for 1 h. The NaF-treated deodorant material (FTD) was fabricated by dipping UTD in a 1% NaF aqueous solution and drying at 100 °C for 1 h.

The deodorant efficiency, η (%) for H_2S was evaluated by the formula.[6]

$$\eta = (C_0 - C)/C_0 \times 100 \quad (1)$$

Here C_0 (170 ppb) is the H_2S concentration in the absence of the deodorant material and C the concentration passing through the deodorant material. The flow rate of air was 5 ml min^{-1}. ESR measurements were done with a JEOL JES-FX2XG spectrometer equipped with a temperature controler.

Results and Discussion

Low-temperature ESR spectra of the deodorant materials UTD and FTD are shown in Fig. 1 (a) and (b), respectively. The intensity ratio of the g=4 peak to the g=2 peak was examined. The high-spin signal at g=4 indicates that the axial symmetry of FePC is distorted.[7] Since the g value remained unchanged by addition of NaF, the symmetry arround the Fe(III) ion did not change by coordination of F^- ion to the 5th site of Fe. Because intensity ratio of the g=4 peak to g=2 peak was increased, NaF treatment may increase the ratio of the molecular number of Fe(III) in the high-spin state to that in the low-spin state. Here, g=2 peak is the overlapped signals between high spin state and low spin state.[7] The intensity ratio is 0.96 for UTD and 1.27 for FTD. The superiority of the high-spin state fraction in the FTD sample is due to the addition of F^- to the 5th coordination site of Fe(III). This phenomenon

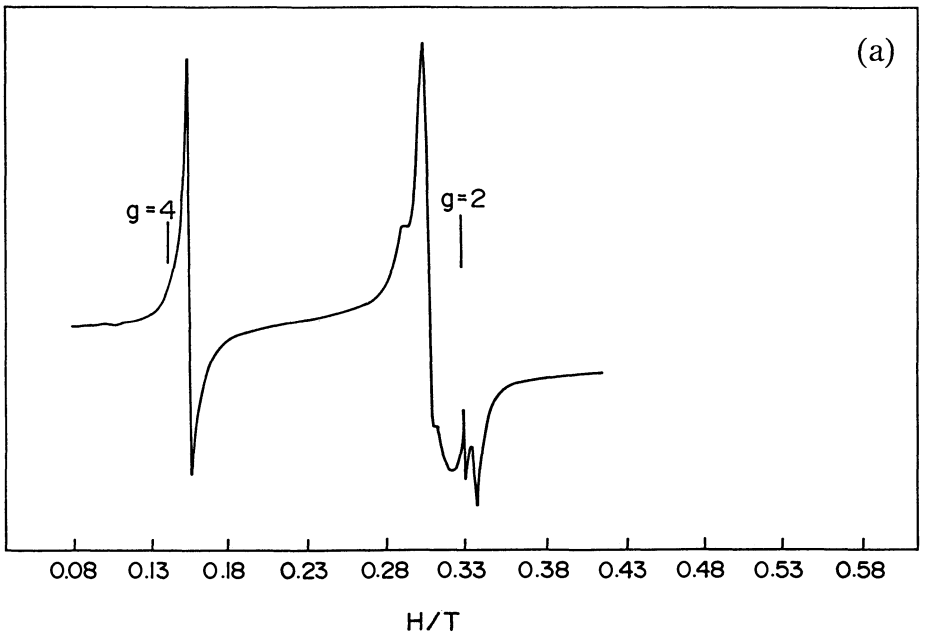

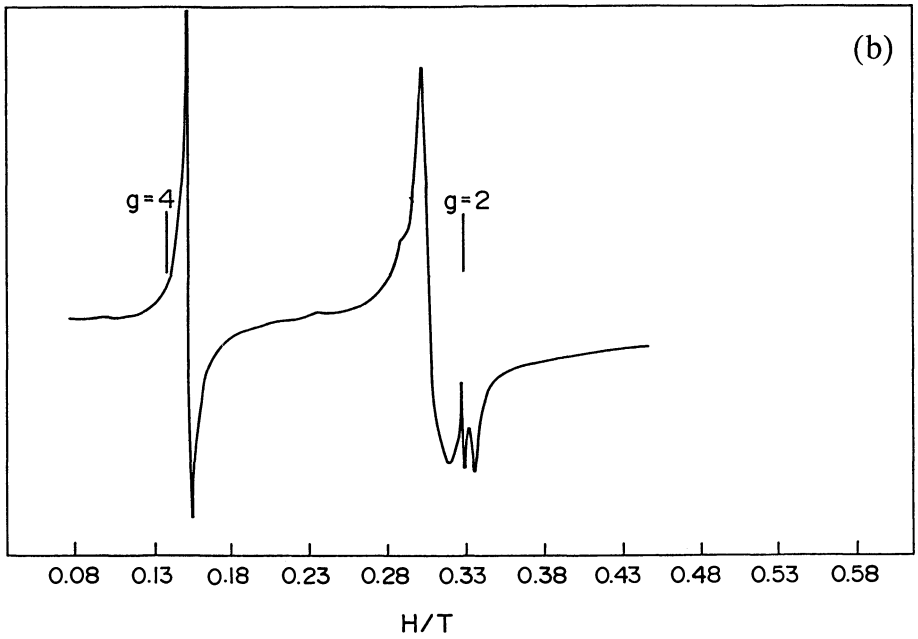

Fig. 1. (a) ESR spectrum of FePc held on cotton. (b) ESR spectrum of FePc treated with NaF and held on cotton. Temp: −143 °C, RF: 1 mW, 9.2 GHz, Field: 0.3287±0.25 T, Mod: 100 kHz, 0.63 mT, Amp: 5×10.

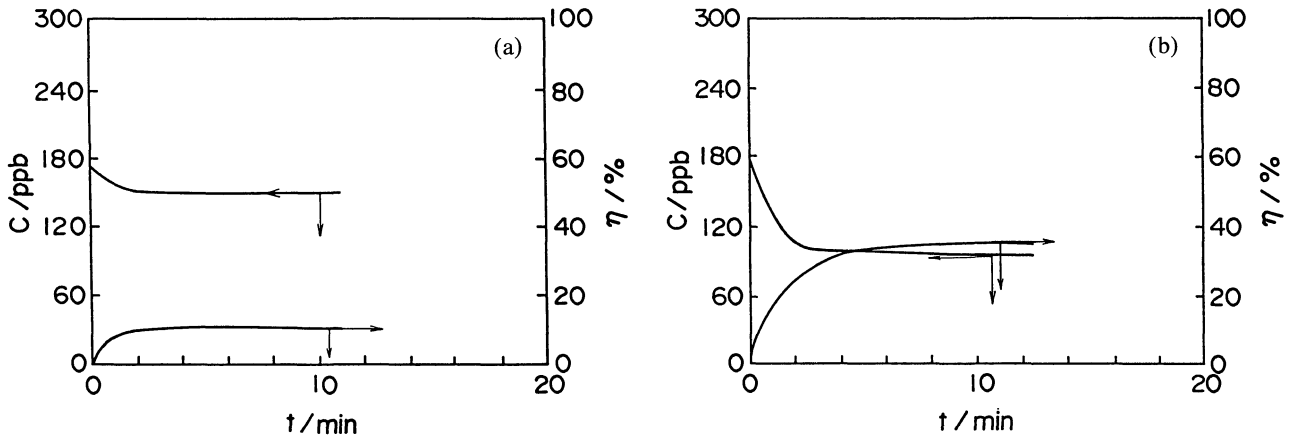

Fig. 2. (a) Time dependent deodorant efficiency of untreated deodorant material. (b) Time dependent deodorant efficiency of NaF treated deodorant material. Initial H_2S concentration, 170 ppb; Flow rate, 5 ml min^{-1}.

is related to the fact that the Bohr magnetic number of methemoglobin, whose 6th coordination site is occupied with F^-, was 5.92.[8]

The small and sharp peak at g=2.0023 originates most probable from the superoxide radical, in view of the generation of superoxide radical in the FePc systems.[4] Comparison of the peak height at g=4.0023 between UTD and FTD shows that the superoxide radical is more abundant in FTD than in UTD.

Fe(III) ion of FePc in the high-spin state has a larger reaction rate of oxidation than that in the low-spin state.[4] The results of deodorant efficiency measurements for UTD and FTD are shown in Fig. 2 (a) and (b), respectively. The efficiency of FTD was three times higher than that of UTD. This could be related to coordination of F^- to the 5th site of Fe in FePc. Details of the reaction mechanism are left for a future study.

References

1) G. Terasawa, "Development of Industrial Deodorant Materials," ed by Y. Ikari, Technology Information Association, Tokyo (1989), p. 397.
2) K. Mizushima, *Kagaku to Kogyo,* **63**, 151 (1989).
3) K. Enmanji, I. Nishiyama, and K. Takahashi, 61th Spring Meeting of the Chemical Society of Japan, Tokyo, 1991.
4) H. Shirai, "Development of Industrial Deodorant Materials," ed by Y. Ikari, Technology Information Association, Tokyo (1989), p. 227.
5) H. Shirai, H. Tsuiki, E. Masuda, T. Koyama, and K. Hanabusa, *J. Phys. Chem.,* **95**, 417 (1991).
6) *Mitsubishi Denki Giho,* **65**, 38 (1991).
7) H. Ohya and J. Yamauchi, "Eelectron Spin Resonances," Kodansha, Tokyo (1989), p. 219.
8) A. Y. Lu and M. J. Coon, *J. Biol. Chem.,* **243**, 1331 (1968).

Soccerane Derivatives of Given Symmetries

Shinsaku FUJITA
Research Laboratories, Ashigara, Fuji Photo Film Co., Ltd.,
Minami-Ashigara, Kanagawa 250-01
(Received November 26, 1990)

Symmetrical properties of soccerane and its derivatives are discussed in the light of subduction of coset representations (CRs). The 60 vertices of soccerane are equivalent and construct a single orbit governed by the CR, $\mathbf{I}_h(/\mathbf{C}_s)$. This orbit is divided into several orbits in the respective derivative, where the mode of the division is controlled by the subduction. The number of derivatives with a given formula and a given subsymmetry is calculated in terms of unit subduced cycle indices, which are derived from the subduction.

Hydrocarbons of high symmetries and related compounds have attracted continuous attention of organic chemists because of their potential properties.[1] Among them, a fully unsaturated C_{60} compound of $\mathbf{I}_h$ symmetry has once been mentioned by Osawa[2] as a theoretically interesting compound. The corresponding saturated $C_{60}H_{60}$-hydrocarbon (**1**) has been called "footballane" or "soccerane" by Castells and Serratosa.[3] They pointed out: "Since the synthesis of dodecahedrane has been recently accomplished by Paquette and his coworkers at Ohio State University, the synthesis of soccerane appears as the next goal". They later gave this complex hydrocarbon the IUPAC name,[4] i. e., hentriacontacyclo[29.29.0.$0^{2,14}$.$0^{3,29}$.$0^{4,27}$.$0^{5,13}$.$0^{6,25}$.$0^{7,12}$.-$0^{8,23}$.$0^{9,21}$.$0^{10,18}$.$0^{11,16}$.$0^{15,60}$.$0^{17,58}$.$0^{19,56}$.$0^{20,54}$.$0^{22,52}$.$0^{24,50}$.$0^{26,49}$.-$0^{28,47}$.$0^{30,45}$.$0^{32,44}$.$0^{33,59}$.$0^{34,57}$.$0^{35,43}$.$0^{36,55}$.$0^{37,42}$.$0^{38,53}$.$0^{39,51}$.$0^{40,48}$.-$0^{41,46}$]hexacontane.

Recently, a C_{60} peak has been observed in a laser vaporization of graphite by Kroto et al.,[5a] where the peak was assigned to formation of the above $\mathbf{I}_h$ molecule (a C_{60} carbon cluster).[6] This paper has stimulated a large number of theoretical studies on this carbon cluster.[7] Other compounds of $\mathbf{I}_h$ symmetry (Fig. 1) have also attracted theoretical attention of chemists.[8] A brief review has summarized predicted properties of these related compounds.[9] Geometrical properties of soccerane and other $\mathbf{I}_h$-molecules have been discussed.[10] Since soccerane has been so far detected only by physicochemical analysis, total syntheses of such high-symmetry molecules are challenging targets from the viewpoint of synthetic organic chemistry.

Since the $\mathbf{I}_h$ symmetry contains various unusual subsymmetries, derivatization of soccerane ($C_{60}H_{60}$) by substituting an appropriate set of atoms for the same number of hydrogen atoms produces molecules of the subsymmetries, which will be further targets of synthetic organic chemistry. In this connection, the number of derivatives of a given subsymmetry of this series will be of interest to organic chemists. Hosoya[10] has enumerated such soccerane derivatives by using Pólya's theorem.[11] This enumeration is, however, concerned with their molecular formulas and not with their symmetries.

We have reported a systematic enumeration of molecules in terms of unit subduced cycle indices (USCIs).[12,13] This method requires a table of marks (or the inverse) due to Burnside[14] and a table of USCIs introduced by us.[12] We have presented such tables for $\mathbf{C}_2$, $\mathbf{C}_{2v}$, $\mathbf{C}_{3v}$, $\mathbf{D}_2$, $\mathbf{D}_{2d}$, $\mathbf{D}_{2h}$, $\mathbf{D}_3$, $\mathbf{D}_{3h}$, $\mathbf{T}$, and $\mathbf{T}_d$ as well as their applications to various enumerations.[15] We have recently reported construction of such tables for the $\mathbf{I}_h$ group and applications to enumeration of dodecahedrane derivatives.[16] However, the advantage of the USCI approach for enumeration has not been fully investigated, inasmuch as the enumerations have been limited within rather simple molecules. The present paper deals with the enumeration of isomers derived from soccerane in order to exemplify the advantage and generality of the USCI approach.

1. Orbits in $\mathbf{I}_h$ Molecules. Figure 1 collects the soccerane skeleton and the related ones of $\mathbf{I}_h$ symmetry. We first examine the symmetrical properties of the skeletons. Any skeleton has several sets of equivalent positions (vertices, edges or faces). These sets are called *orbits* in accord with the terminology of permutation group. The symmetry properties of each orbit is characterized by the corresponding coset representaion (CR).[17,18] The CR is represented by the symbol $\mathbf{G}(/\mathbf{G}_i)$ that is based on a coset decomposition of $\mathbf{G}$ by $\mathbf{G}_i$, where $\mathbf{G}$ is the point group of the skeleton and $\mathbf{G}_i$ is its subgroup.

Since the $\mathbf{I}_h$ group of order 120 posesses a set of subgroups, SSG=$\{\mathbf{C}_1, \mathbf{C}_2, \mathbf{C}_s, \mathbf{C}_i, \mathbf{C}_3, \mathbf{D}_2, \mathbf{C}_{2v}, \mathbf{C}_{2h}, \mathbf{C}_5, \mathbf{D}_3,$

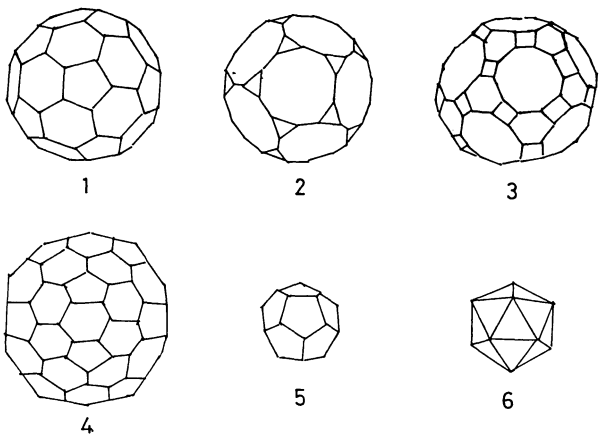

Fig. 1. Skeletons of $\mathbf{I}_h$ symmetry.

Table 1. Orbits of Several Compounds of $\mathbf{I}_h$ Symmetry

Compound	Objects	No. of objects	Coset representation	SCR notation
1	Vertices [5.6.6]	60	$\mathbf{I}_h(/\mathbf{C}_s)$	$\mathbf{I}_h[/\mathbf{C}_s([5.6.6]_{60})]$
	Edges [6:6]	60	$\mathbf{I}_h(/\mathbf{C}_s)$	
	Edges [5:6]	30	$\mathbf{I}_h(/\mathbf{C}_{2v})$	
	Hexagonal faces	20	$\mathbf{I}_h(/\mathbf{C}_{3v})$	
	Pentagonal faces	12	$\mathbf{I}_h(/\mathbf{C}_{5v})$	
2	Vertices [3.10.10]	60	$\mathbf{I}_h(/\mathbf{C}_s)$	$\mathbf{I}_h[/\mathbf{C}_s([3.10.10]_{60})]$
	Edges [3:10]	60	$\mathbf{I}_h(/\mathbf{C}_s)$	
	Edges [10:10]	30	$\mathbf{I}_h(/\mathbf{C}_{2v})$	
	Trigonal faces	20	$\mathbf{I}_h(/\mathbf{C}_{3v})$	
	Decagonal faces	12	$\mathbf{I}_h(/\mathbf{C}_{5v})$	
3	Vertices [4.6.10]	120	$\mathbf{I}_h(/\mathbf{C}_1)$	$\mathbf{I}_h[/\mathbf{C}_{3v}([4.6.10]_{120})]$
	Edges [4:6]	60	$\mathbf{I}_h(/\mathbf{C}_s)$	
	Edges [4:10]	60	$\mathbf{I}_h(/\mathbf{C}_s)$	
	Edges [10:10]	60	$\mathbf{I}_h(/\mathbf{C}_s)$	
	Tetragonal faces	30	$\mathbf{I}_h(/\mathbf{C}_{2v})$	
	Hexagonal faces	20	$\mathbf{I}_h(/\mathbf{C}_{3v})$	
	Decagonal faces	12	$\mathbf{I}_h(/\mathbf{C}_{5v})$	
4	Vertices [5.6.6]	60	$\mathbf{I}_h(/\mathbf{C}_s)$	$\mathbf{I}_h[/\mathbf{C}_s([5.6.6]_{60})$;
	Vertices [6.6.6]	20	$\mathbf{I}_h(/\mathbf{C}_{3v})$	$/\mathbf{C}_{3v}([6.6.6]_{20})]$
	Edges [6:6]	60	$\mathbf{I}_h(/\mathbf{C}_s)$	
	Edges [5:6]	60	$\mathbf{I}_h(/\mathbf{C}_s)$	
	Hexagonal faces	30	$\mathbf{I}_h(/\mathbf{C}_{2v})$	
	Pentagonal faces	12	$\mathbf{I}_h(/\mathbf{C}_{5v})$	
5	Vertices [5.5.5]	20	$\mathbf{I}_h(/\mathbf{C}_{3v})$	$\mathbf{I}_h[/\mathbf{C}_{3v}([5.5.5]_{20})]$
	Edges [5:5]	30	$\mathbf{I}_h(/\mathbf{C}_{2v})$	
	Pentagonal faces	12	$\mathbf{I}_h(/\mathbf{C}_{5v})$	
6	Vertices [3.3.3.3.3.]	12	$\mathbf{I}_h(/\mathbf{C}_{5v})$	$\mathbf{I}_h[/\mathbf{C}_{5v}([3.3.3.3.3]_{12})]$
	Edges [3:3]	30	$\mathbf{I}_h(/\mathbf{C}_{2v})$	
	Triginal faces	20	$\mathbf{I}_h(/\mathbf{C}_{3v})$	

$\mathbf{C}_{3v}$, $\mathbf{C}_{3i}$, $\mathbf{D}_{2h}$, $\mathbf{D}_5$, $\mathbf{C}_{5v}$, $\mathbf{C}_{5i}$, $\mathbf{T}$, $\mathbf{D}_{3d}$, $\mathbf{D}_{5d}$, $\mathbf{T}_h$, $\mathbf{I}$, $\mathbf{I}_h$}, the corresponding set of CRs is designated to be SCR={$\mathbf{I}_h(/\mathbf{C}_1)$, $\mathbf{I}_h(/\mathbf{C}_2)$, $\mathbf{I}_h(/\mathbf{C}_s)$, $\mathbf{I}_h(/\mathbf{C}_i)$, $\mathbf{I}_h(/\mathbf{C}_3)$, $\mathbf{I}_h(/\mathbf{D}_2)$, $\mathbf{I}_h(/\mathbf{C}_{2v})$, $\mathbf{I}_h(/\mathbf{C}_{2h})$, $\mathbf{I}_h(/\mathbf{C}_5)$, $\mathbf{I}_h(/\mathbf{D}_3)$, $\mathbf{I}_h(/\mathbf{C}_{3v})$, $\mathbf{I}_h(/\mathbf{C}_{3i})$, $\mathbf{I}_h(/\mathbf{D}_{2h})$, $\mathbf{I}_h(/\mathbf{D}_5)$, $\mathbf{I}_h(/\mathbf{C}_{5v})$, $\mathbf{I}_h(/\mathbf{C}_{5i})$, $\mathbf{I}_h(/\mathbf{T})$, $\mathbf{I}_h(/\mathbf{D}_{3d})$, $\mathbf{I}_h(/\mathbf{D}_{5d})$, $\mathbf{I}_h(/\mathbf{T}_h)$, $\mathbf{I}_h(/\mathbf{I})$, $\mathbf{I}_h(/\mathbf{I}_h)$}.

Table 1 lists orbits of each skeleton shown in Fig. 1. We have reported a method of assigning a CR to each orbit[17,18] as well as data necessary to this task.[16] For simplicity's sake, we consider the soccerane skeleton to be a truncated icosahedron, which has 60 vertices, 90 edges, and 32 faces. In order to illustrate a procedure of the assignment, we examine the 60 vertices of **1**, which are equivalent and construct a single orbit. We first count fixed points (vertices) for each subgroup during all of the operations contained in the subgroup, affording a fixed-point vector (FPV). We thus obtain an FPV= (60 0 4 0 0 0 0 0 0 0 0 0 0 0 0 0 0 0 0 0 0 0 0 0 0 0 0 0 0 0) for the vertices. This vector is multiplied by the inverse of a mark table for $\mathbf{I}_h$ group (Table 2). The resulting vector (0 0 1 0 0 0 0 0 0 0 0 0 0 0 0 0 0 0 0 0 0 0 0 0 0 0 0 0 0 0) shows the multiplicities of the subgroups listed in the SSG; in this case, there appears only one $\mathbf{I}_h(/\mathbf{C}_s)$ orbit. If the symbol $\mathbf{P}_{1(\text{vertex})}$ denotes a permutation representation concerning the 60 vertices, we have

$$\mathbf{P}_{1(\text{vertex})} = \mathbf{I}_h(/\mathbf{C}_s). \quad (1)$$

Note that the size of the orbit is equal to $|\mathbf{I}_h|/|\mathbf{C}_s|=120/2=60$. Since a 5-membered ring and two 6-membered rings meet at each vertex, we refer to this vertex as a [5.6.6] vertex. Thereby, we can obtain the SCR notation,[17] $\mathbf{I}_h[/\mathbf{C}_s([5.6.6]_{60})]$ for this skeleton, where the CR and its members are indicated.

There are two kinds of edges in **1**, which construct distinct orbits. With respect to these edges, we have an FPV=(90 2 8 0 0 0 2 0 0 0 0 0 0 0 0 0 0 0 0 0 0 0 0 0 0 0 0 0 0 0). This vector is multiplied by the inverse (Table 2), producing a row vector, (0 0 1 0 0 0 1 0 0 0 0 0 0 0 0 0 0 0 0 0 0 0 0 0 0 0 0 0 0 0). This corresponds to the following equation,

$$\mathbf{P}_{1(\text{edge})} = \mathbf{I}_h(/\mathbf{C}_s) + \mathbf{I}_h(/\mathbf{C}_{2v}), \quad (2)$$

in which the symbol $\mathbf{P}_{1(\text{edge})}$ denotes a permutation representation of the 90 edges. Note that the degree of $\mathbf{I}_h(/\mathbf{C}_s)$ is equal to $|\mathbf{I}_h|/|\mathbf{C}_s|=120/2=60$ and that of $\mathbf{I}_h(/\mathbf{C}_{2v})$ is equal to $|\mathbf{I}_h|/|\mathbf{C}_{2v}|=120/4=30$. If the symbol [6:6] denotes an edge at which two 6-membered rings fuse, Eq. 2 concludes that the sixty [6:6]edges in **1** construct an orbit that is subject to $\mathbf{I}_h(/\mathbf{C}_s)$. Similarly,

Table 2. The Inverse of the Mark Table of $\mathbf{I_h}$ Group

	Coset representation[a]																					
	$\mathbf{C_1}$	$\mathbf{C_2}$	$\mathbf{C_s}$	$\mathbf{C_i}$	$\mathbf{C_3}$	$\mathbf{D_2}$	$\mathbf{C_{2v}}$	$\mathbf{C_{2h}}$	$\mathbf{C_5}$	$\mathbf{D_3}$	$\mathbf{C_{3v}}$	$\mathbf{C_{3i}}$	$\mathbf{D_{2h}}$	$\mathbf{D_5}$	$\mathbf{C_{5v}}$	$\mathbf{C_{5i}}$	$\mathbf{T}$	$\mathbf{D_{3d}}$	$\mathbf{D_{5d}}$	$\mathbf{T_h}$	$\mathbf{I}$	$\mathbf{I_h}$	Sum[b]
$\mathbf{C_1}$	$\frac{1}{120}$	0	0	0	0	0	0	0	0	0	0	0	0	0	0	0	0	0	0	0	0	0	$\frac{1}{120}$
$\mathbf{C_2}$	$-\frac{1}{8}$	$\frac{1}{4}$	0	0	0	0	0	0	0	0	0	0	0	0	0	0	0	0	0	0	0	0	$\frac{1}{8}$
$\mathbf{C_s}$	$-\frac{1}{8}$	0	$\frac{1}{4}$	0	0	0	0	0	0	0	0	0	0	0	0	0	0	0	0	0	0	0	$\frac{1}{8}$
$\mathbf{C_i}$	$-\frac{1}{120}$	0	0	$\frac{1}{60}$	0	0	0	0	0	0	0	0	0	0	0	0	0	0	0	0	0	0	$\frac{1}{120}$
$\mathbf{C_3}$	$-\frac{1}{12}$	0	0	0	$\frac{1}{4}$	0	0	0	0	0	0	0	0	0	0	0	0	0	0	0	0	0	$\frac{1}{6}$
$\mathbf{D_2}$	$\frac{1}{12}$	$-\frac{1}{4}$	0	0	0	$\frac{1}{6}$	0	0	0	0	0	0	0	0	0	0	0	0	0	0	0	0	0
$\mathbf{C_{2v}}$	$\frac{1}{4}$	$-\frac{1}{4}$	$-\frac{1}{2}$	0	0	0	$\frac{1}{2}$	0	0	0	0	0	0	0	0	0	0	0	0	0	0	0	0
$\mathbf{C_{2h}}$	$\frac{1}{4}$	$-\frac{1}{4}$	$-\frac{1}{4}$	$-\frac{1}{4}$	0	0	0	$\frac{1}{2}$	0	0	0	0	0	0	0	0	0	0	0	0	0	0	0
$\mathbf{C_5}$	$-\frac{1}{20}$	0	0	0	0	0	0	0	$\frac{1}{4}$	0	0	0	0	0	0	0	0	0	0	0	0	0	$\frac{1}{5}$
$\mathbf{D_3}$	$\frac{1}{4}$	$-\frac{1}{2}$	0	0	$-\frac{1}{4}$	0	0	0	0	$\frac{1}{2}$	0	0	0	0	0	0	0	0	0	0	0	0	0
$\mathbf{C_{3v}}$	$\frac{1}{4}$	0	$-\frac{1}{2}$	0	$-\frac{1}{4}$	0	0	0	0	0	$\frac{1}{2}$	0	0	0	0	0	0	0	0	0	0	0	0
$\mathbf{C_{3i}}$	$\frac{1}{12}$	0	0	$-\frac{1}{6}$	$-\frac{1}{4}$	0	0	0	0	0	0	$\frac{1}{2}$	0	0	0	0	0	0	0	0	0	0	$\frac{1}{6}$
$\mathbf{D_{2h}}$	$-\frac{1}{3}$	$\frac{1}{2}$	$\frac{1}{2}$	$\frac{1}{6}$	0	$-\frac{1}{6}$	$-\frac{1}{2}$	$-\frac{1}{2}$	0	0	0	0	$\frac{1}{3}$	0	0	0	0	0	0	0	0	0	0
$\mathbf{D_5}$	$\frac{1}{4}$	$-\frac{1}{2}$	0	0	0	0	0	0	$-\frac{1}{4}$	0	0	0	0	$\frac{1}{2}$	0	0	0	0	0	0	0	0	0
$\mathbf{C_{5v}}$	$\frac{1}{4}$	0	$-\frac{1}{2}$	0	0	0	0	0	$-\frac{1}{4}$	0	0	0	0	0	$\frac{1}{2}$	0	0	0	0	0	0	0	0
$\mathbf{C_{5i}}$	$\frac{1}{20}$	0	0	$-\frac{1}{10}$	0	0	0	0	$-\frac{1}{4}$	0	0	0	0	0	0	$\frac{1}{2}$	0	0	0	0	0	0	$\frac{1}{5}$
$\mathbf{T}$	$\frac{1}{6}$	0	0	0	$-\frac{1}{2}$	$-\frac{1}{6}$	0	0	0	0	0	0	0	0	0	0	$\frac{1}{2}$	0	0	0	0	0	0
$\mathbf{D_{3d}}$	$-\frac{1}{2}$	$\frac{1}{2}$	$\frac{1}{2}$	$\frac{1}{2}$	$\frac{1}{2}$	0	0	-1	0	$-\frac{1}{2}$	$-\frac{1}{2}$	$-\frac{1}{2}$	0	0	0	0	0	1	0	0	0	0	0
$\mathbf{D_{5d}}$	$-\frac{1}{2}$	$\frac{1}{2}$	$\frac{1}{2}$	$\frac{1}{2}$	0	0	0	-1	$\frac{1}{2}$	0	0	0	0	$-\frac{1}{2}$	$-\frac{1}{2}$	$-\frac{1}{2}$	0	0	1	0	0	0	0
$\mathbf{T_h}$	$-\frac{1}{6}$	0	0	$\frac{1}{3}$	$\frac{1}{2}$	$\frac{1}{6}$	0	0	0	0	0	-1	$-\frac{1}{3}$	0	0	0	$-\frac{1}{2}$	0	0	1	0	0	0
$\mathbf{I}$	$-\frac{1}{2}$	1	0	0	$\frac{1}{2}$	0	0	0	0	$-\frac{1}{2}$	0	0	0	$-\frac{1}{2}$	0	0	$-\frac{1}{2}$	0	0	0	$\frac{1}{2}$	0	0
$\mathbf{I_h}$	$\frac{1}{2}$	-1	0	-1	$-\frac{1}{2}$	0	0	2	0	$\frac{1}{2}$	0	1	0	$\frac{1}{2}$	0	0	$\frac{1}{2}$	-1	-1	-1	$-\frac{1}{2}$	1	0

a) The symbol $\mathbf{G}_i$ is an abbreviation of $\mathbf{I_h}(/\mathbf{G}_i)$, where $\mathbf{G}_1=\mathbf{C}_1$, $\mathbf{G}_2=\mathbf{C}_2$, $\cdots$, $\mathbf{G}_s=\mathbf{I_h}$. For example, we here use $\mathbf{C}_2$ for $\mathbf{I_h}(/\mathbf{C}_2)$. b) $\mathrm{Sum}=\sum_{j=1}^{s}\bar{m}_{ji}$.

thirty [5 : 6]edges are subject to $\mathbf{I_h}(/\mathbf{C_{2v}})$.

The 32 faces of the molecule (**1**) give an FPV= (32 0 8 0 2 0 0 0 2 0 2 0 0 0 2 0 0 0 0 0 0 0). The multiplication of the FPV by the inverse (Table 2) affords a row vector (0 0 0 0 0 0 0 0 0 0 1 0 0 0 1 0 0 0 0 0 0 0), which indicates the appearence of $\mathbf{I_h}(/\mathbf{C_{3v}})$ and $\mathbf{I_h}(/\mathbf{C_{5v}})$. Hence, the 32 faces are characterized by

$$\mathbf{P}_{1(\mathrm{face})} = \mathbf{I_h}(/\mathbf{C_{3v}}) + \mathbf{I_h}(/\mathbf{C_{5v}}). \quad (3)$$

Since $|\mathbf{I_h}|/|\mathbf{C_{3v}}|=120/6=20$ and $|\mathbf{I_h}|/|\mathbf{C_{5v}}|=120/10=12$, Eq. 3 means that 20 hexagonal faces belong to an orbit governed by $\mathbf{I_h}(/\mathbf{C_{3v}})$; and that the remaining 12 pentagonal faces construct an orbit governed by $\mathbf{I_h}(/\mathbf{C_{5v}})$.

In a similar way, the orbits of the other skeletons are assigned to the respective CRs (Table 1). It should be noted that another C_{60} icosahedral skeleton (**2**) has equal numbers of vertices, edges, and faces as compared with **1** and that these are subject to the same CRs. The latter skeleton (**2**) can be differentiated from **1** by the SCR notation, $\mathbf{I_h}[/\mathbf{C_s}([3.10.10]_{60})]$.

2. Subduction of the $\mathbf{I_h}(/\mathbf{C_s})$ Orbit. The replacement of hydrogen atoms of **1** by other atoms produces a derivative of **1** that belongs to a subsymmetry of $\mathbf{I_h}$. Such a desymmetrization process is characterized in terms of subduction of the corresponding CR.[18] For manipulating the soccerane skeleton (**1**), the $\mathbf{I_h}(/\mathbf{C_s})$ CR is subduced into every subgroup. In order to illustrate such a subduction, let us examine $\mathbf{I_h}(/\mathbf{C_s})\downarrow\mathbf{C_{2v}}$, which denotes the subduction of the $\mathbf{I_h}(/\mathbf{C_s})$ representation into the $\mathbf{C_{2v}}$ group. The $\mathbf{I_h}(/\mathbf{C_s})$ row of a mark table is equal to the row vector, FPV=(60 0 4 0 0 0 0 0 0 0 0 0 0 0 0 0 0 0 0 0 0 0 0 0 0 0 0 0 0 0), the elements of which are aligned in the order of the SSG.[19] Since the SSG of the $\mathbf{C_{2v}}$ group is represented by SSG'=$\{\mathbf{C}_1, \mathbf{C}_2, \mathbf{C}_s, \mathbf{C}'_s, \mathbf{C_{2v}}\}$, we can obtain a row vector (60 0 4 4 0) by selecting from the FPV the values corresponding to the SSG'. Note that the value 4 for the $\mathbf{C}_s$ subgroup of the $\mathbf{I_h}$ is duplicated to afford the value 4 for the $\mathbf{C}'_s$ of the $\mathbf{C_{2v}}$. This vector for the $\mathbf{C_{2v}}$ group is multiplied by the inverse of a mark table for the $\mathbf{C_{2v}}$ group, i. e.,

$$(60\,0\,4\,4\,0)\begin{pmatrix} 1/4 & 0 & 0 & 0 & 0 \\ -1/4 & 1/2 & 0 & 0 & 0 \\ -1/4 & 0 & 1/2 & 0 & 0 \\ -1/4 & 0 & 0 & 1/2 & 0 \\ 1/2 & -1/2 & -1/2 & -1/2 & 1 \end{pmatrix} = (13\,0\,2\,2\,0), \quad (4)$$

Table 3. Subduction of the $\mathbf{I_h}(/\mathbf{C_s})$ Orbit

$\mathbf{G}_j$	$\mathbf{I_h}(/\mathbf{C_s}) \downarrow \mathbf{G}_j$	USCI-CF	USCI	Sum[a]
$\mathbf{C_1}$	$60\mathbf{C_1}(/\mathbf{C_1})$	b_1^{60}	s_1^{60}	1/120
$\mathbf{C_2}$	$30\mathbf{C_2}(/\mathbf{C_1})$	b_2^{30}	s_2^{30}	1/8
$\mathbf{C_s}$	$28\mathbf{C_s}(/\mathbf{C_1})+4\mathbf{C_s}(/\mathbf{C_s})$	$a_1^4c_2^{28}$	$s_1^4s_2^{28}$	1/8
$\mathbf{C_i}$	$30\mathbf{C_i}(/\mathbf{C_1})$	c_2^{30}	s_2^{30}	1/120
$\mathbf{C_3}$	$20\mathbf{C_3}(/\mathbf{C_1})$	b_3^{20}	s_3^{20}	1/6
$\mathbf{D_2}$	$15\mathbf{D_2}(/\mathbf{C_1})$	b_4^{15}	s_4^{15}	0
$\mathbf{C_{2v}}$	$13\mathbf{C_{2v}}(/\mathbf{C_1})+2\mathbf{C_{2v}}(/\mathbf{C_s})+2\mathbf{C_{2v}}(/\mathbf{C_s'})$	$a_2^4c_4^{13}$	$s_2^4s_4^{13}$	0
$\mathbf{C_{2h}}$	$14\mathbf{C_{2h}}(/\mathbf{C_1})+2\mathbf{C_{2h}}(/\mathbf{C_s})$	$a_2^2c_4^{14}$	$s_2^2s_4^{14}$	0
$\mathbf{C_5}$	$12\mathbf{C_5}(/\mathbf{C_1})$	b_5^{12}	s_5^{12}	1/5
$\mathbf{D_3}$	$10\mathbf{D_3}(/\mathbf{C_1})$	b_6^{10}	s_6^{10}	0
$\mathbf{C_{3v}}$	$8\mathbf{C_{3v}}(/\mathbf{C_1})+4\mathbf{C_{3v}}(/\mathbf{C_s})$	$a_3^4c_6^8$	$s_3^4s_6^8$	0
$\mathbf{C_{3i}}$	$10\mathbf{C_{3i}}(/\mathbf{C_1})$	c_6^{10}	s_6^{10}	1/6
$\mathbf{D_{2h}}$	$6\mathbf{D_{2h}}(/\mathbf{C_1})+\mathbf{D_{2h}}(/\mathbf{C_s})+\mathbf{D_{2h}}(/\mathbf{C_s'})+\mathbf{D_{2h}}(/\mathbf{C_s''})$	$a_4^3c_8^6$	$s_4^3s_8^6$	0
$\mathbf{D_5}$	$6\mathbf{D_5}(/\mathbf{C_1})$	b_{10}^6	s_{10}^6	0
$\mathbf{C_{5v}}$	$4\mathbf{C_{5v}}(/\mathbf{C_1})+4\mathbf{C_{5v}}(/\mathbf{C_s})$	$a_5^4c_{10}^4$	$s_5^4s_{10}^4$	0
$\mathbf{C_{5i}}$	$6\mathbf{C_{5i}}(/\mathbf{C_1})$	c_{10}^6	s_{10}^6	1/5
$\mathbf{T}$	$5\mathbf{T}(/\mathbf{C_1})$	b_{12}^5	s_{12}^5	0
$\mathbf{D_{3d}}$	$4\mathbf{D_{3d}}(/\mathbf{C_1})+2\mathbf{D_{3d}}(/\mathbf{C_s})$	$a_6^2c_{12}^4$	$s_6^2s_{12}^4$	0
$\mathbf{D_{5d}}$	$2\mathbf{D_{5d}}(/\mathbf{C_1})+2\mathbf{D_{5d}}(/\mathbf{C_s})$	$a_{10}^2c_{20}^2$	$s_{10}^2s_{20}^2$	0
$\mathbf{T_h}$	$2\mathbf{T_h}(/\mathbf{C_1})+\mathbf{T_h}(/\mathbf{C_s})$	$a_{12}c_{24}^2$	$s_{12}s_{24}^2$	0
$\mathbf{I}$	$\mathbf{I}(/\mathbf{C_1})$	b_{60}	s_{60}	0
$\mathbf{I_h}$	$\mathbf{I_h}(/\mathbf{C_s})$	a_{60}	s_{60}	0

a) The sum is obtained by summing up each row of the inverse (Table 2).

where the second 5×5 matrix is the inverse. The resulting vector indicates the multiplicity of each CR. Hence, we have

$$\mathbf{I_h}(/\mathbf{C_s})\downarrow\mathbf{C_{2v}} = 13\mathbf{C_{2v}}(/\mathbf{C_1})+2\mathbf{C_{2v}}(/\mathbf{C_s})+2\mathbf{C_{2v}}(/\mathbf{C_s'}). \quad (5)$$

Other subductions are precalculated in a similar way and collected in the second column of Table 3.

According to the subductions, we obtain unit subduced cycle indices (USCIs)[12] and USCIs with chirality fittingness (USCI-CFs).[20] In the $\mathbf{C_{2v}}$ group, we assign a variable s_4 (or c_4) to $\mathbf{C_{2v}}(/\mathbf{C_1})$, s_2 (or a_2) to $\mathbf{C_{2v}}(/\mathbf{C_s})$, and s_2 (or a_2) to $\mathbf{C_{2v}}(/\mathbf{C_s'})$, where the subscripts come from the equations, $|\mathbf{C_{2v}}|/|\mathbf{C_1}|=4$, $|\mathbf{C_{2v}}|/|\mathbf{C_s}|=2$, and $|\mathbf{C_{2v}}|/|\mathbf{C_s'}|=2$. The variable ($c_4$) is based on the chirality fittingness of the $\mathbf{C_{2v}}(/\mathbf{C_1})$ (enantiospheric);[18] the variable (a_2) stems from that of $\mathbf{C_{2v}}(/\mathbf{C_s})$ or $\mathbf{C_{2v}}(/\mathbf{C_s'})$, which is homospheric. As a result, we have a USCI ($s_2^4s_4^{13}$) and a USCI-CF ($a_2^4c_4^{13}$) in terms of Eq. 5. The other USCIs and USCI-CFs for the $\mathbf{I_h}(/\mathbf{C_s})$ CR listed in Table 3 are obtained in a similar way.

The above procedure of generating subduced representations is purely algebraic; however, the resulting coset representations of each subgroup have geometrical (or chemical) meaning. In order to convert the skeleton to a $\mathbf{C_{2v}}$-molecule, for example, we start from Eq. 5. This equation indicates that there emerge thirteen 4-membered orbits ($\mathbf{C_{2v}}(/\mathbf{C_1})$), two 2-membered orbits ($\mathbf{C_{2v}}(/\mathbf{C_s})$) and two of other 2-membered orbits ($\mathbf{C_{2v}}(/\mathbf{C_s'})$). If these orbits are occupied by different kinds of atoms, we have a $\mathbf{C_{2v}}$ molecule (**7**) with the following packing,

$$\underbrace{X_2Y_2}_{2\text{ kinds}}\quad\underbrace{Z_2W_2}_{2\text{ kinds}}\quad\underbrace{H_4\cdots B_4}_{13\text{ kinds}} \quad (6)$$

The first block of this equation corresponds to the 2-membered orbits of $\mathbf{C_{2v}}(/\mathbf{C_s})$, where ●=X and ○=Y. These vertices are fixed during a reflection concerning the mirror plane that contains ●'s and ○'s. The second block of Eq. 6 is concerned with the 2-membered orbits of $\mathbf{C_{2v}}(/\mathbf{C_s'})$, where △=Z and ▲=W. These vertices are contained in the mirror plane associated with the $\mathbf{C_s'}$ group. The third block of Eq. 6 indicates a mode of packing in the remaining 13 orbits, some of which are, for example, differentiated by distinct marks. Although there exist $\mathbf{C_{2v}}$ molecules (**8**—**10**) having the formula ($C_{60}H_{56}X_2Y_2$), their orbits are also controlled by Eq. 5. In other words, the 56 hydrogen atoms are classified into 15 equivalence classes (orbits).

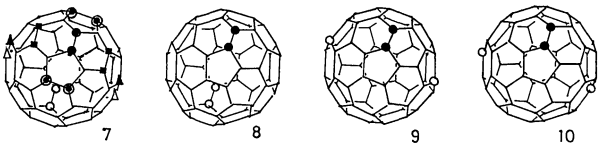

Figure 2 depicts a representative molecule for every subgroup of $\mathbf{I_h}$, where ● and ○ denote X and Y; and

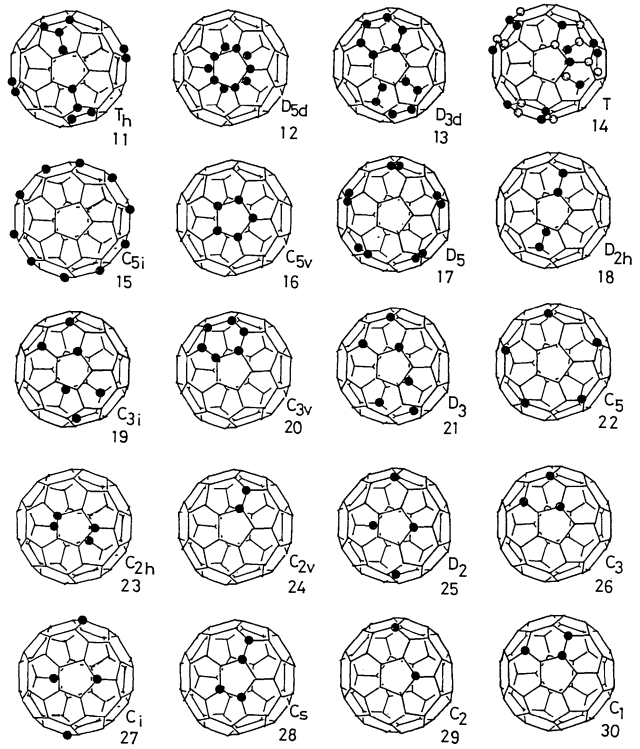

Fig. 2. Molecules derived from the soccerane skeleton (**1**).

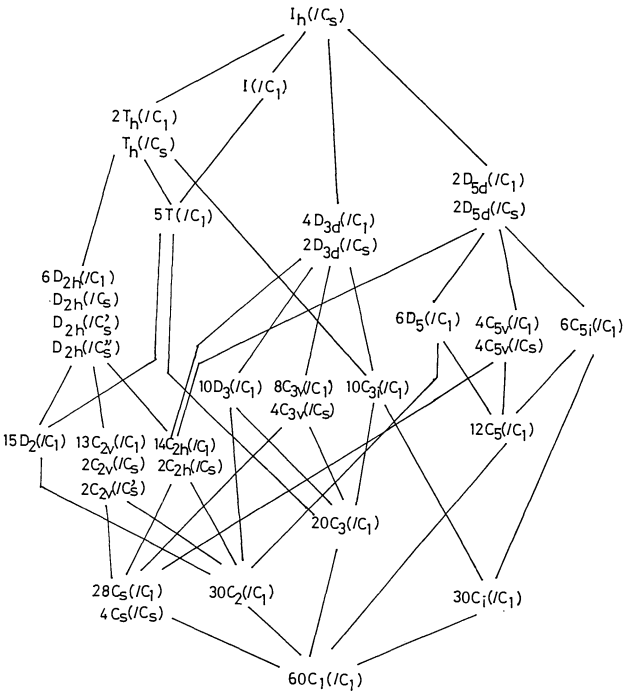

Fig. 3. Desymmetrization lattice for $\mathbf{I}_h(/\mathbf{C}_s)$.

unmarked vertices take hydrogen atoms. The orbits of each of the molecules are subject to the subduction listed in Table 1.

Since any derivation based on the soccerane skeleton (**1**) is regarded as a desymmetrization of the skeleton, the derivation can be determined systematically in terms of a desymmetrization lattice[18] for the $\mathbf{I}_h(/\mathbf{C}_s)$ (Fig. 3). This figure depicts a group-subgroup lattice for the $\mathbf{I}_h$ group which accompanies the results of subduction listed in Table 3.

The absence of a molecule of a subgroup is determined by examining its supergroups: if one of the supergroups has the same USCI as that of the subgroup at issue, the molecule does not exist. This determination can also be accomplished by using the subduction data in Fig. 3. In the present case, the CR $\mathbf{I}(/\mathbf{C}_1)$ corresponds to a 60-membered orbit, whose size is equal to that of an $\mathbf{I}_h(/\mathbf{C}_s)$ orbit. Hence, **I**-molecules are absent; all of the remaining subgroups are possible to exist for the soccerane series. This conclusion can be obtained more conveniently by comparing the corresponding USCIs; the USCI of the $\mathbf{I}(/\mathbf{C}_1)$ orbit is s_{60}, which is equl to that of the $\mathbf{I}_h(/\mathbf{C}_s)$ orbit. On the other hand, the absence of $\mathbf{C}_5$-, $\mathbf{D}_5$-, $\mathbf{C}_{5i}$-, and **I**-molecules has been reported for dodecahedrane derivatives having an $\mathbf{I}_h(/\mathbf{C}_{3v})$ orbit.[16]

3. Soccerane Derivatives with Achiral Substituents. In the preceding section, we have qualitatively examined the desymmetrizations of the soccerane skeleton (**1**) that create derivatives of various subsymmetries. The next issue is to calculate the number of such derivatives. Since the 60 vertices of saccerane (**3**) construct an orbit that is subject to $\mathbf{I}_h(/\mathbf{C}_s)$, we use the USCIs listed in Table 3 as the corresponding subduced cycle indices (SCIs).[12] We consider H and X as substituents. This corresponds to a figure inventory expressed by

$$s_d = 1 + x^d. \tag{7}$$

This was introduced into the SCIs to provide the following generating functions,

$$s_1^{60} = (1 + x)^{60} \text{ for } \mathbf{C}_1, \tag{8}$$

$$s_2^{30} = (1 + x^2)^{30} \text{ for } \mathbf{C}_2, \tag{9}$$

$$s_1^4 s_2^{28} = (1 + x)^4(1 + x^2)^{28} \text{ for } \mathbf{C}_s, \tag{10}$$

$$s_2^{30} = (1 + x^2)^{30} \text{ for } \mathbf{C}_i, \tag{11}$$

$$s_3^{20} = (1 + x^3)^{20} \text{ for } \mathbf{C}_3, \tag{12}$$

$$s_4^{15} = (1 + x^4)^{15} \text{ for } \mathbf{D}_2, \tag{13}$$

$$s_2^4 s_4^{13} = (1 + x^2)^4(1 + x^4)^{13} \text{ for } \mathbf{C}_{2v}, \tag{14}$$

$$s_2^2 s_4^{14} = (1 + x^2)^2(1 + x^4)^{14} \text{ for } \mathbf{C}_{2h}, \tag{15}$$

$$s_5^{12} = (1 + x^5)^{12} \text{ for } \mathbf{C}_5, \tag{16}$$

$$s_6^{10} = (1 + x^6)^{10} \text{ for } \mathbf{D}_3, \tag{17}$$

$$s_3^4 s_6^8 = (1 + x^3)^4(1 + x^6)^8 \text{ for } \mathbf{C}_{3v}, \tag{18}$$

$$s_6^{10} = (1 + x^6)^{10} \text{ for } \mathbf{C}_{3i}, \quad (19)$$

$$s_4^3 s_8^6 = (1 + x^4)^3(1 + x^8)^6 \text{ for } \mathbf{D}_{2h}, \quad (20)$$

$$s_{10}^6 = (1 + x^{10})^6 \text{ for } \mathbf{D}_5, \quad (21)$$

$$s_5^4 s_{10}^4 = (1 + x^5)^4(1 + x^{10})^4 \text{ for } \mathbf{C}_{5v}, \quad (22)$$

$$s_{10}^6 = (1 + x^{10})^6 \text{ for } \mathbf{C}_{5i}, \quad (23)$$

$$s_{12}^5 = (1 + x^{12})^5 \text{ for } \mathbf{T}, \quad (24)$$

$$s_6^2 s_{12}^4 = (1 + x^6)^2(1 + x^{12})^4 \text{ for } \mathbf{D}_{3d}, \quad (25)$$

$$s_{10}^2 s_{20}^2 = (1 + x^{10})^2(1 + x^{20})^2 \text{ for } \mathbf{D}_{5d}, \quad (26)$$

$$s_{12} s_{24}^2 = (1 + x^{12})(1 + x^{24})^2 \text{ for } \mathbf{T}_h, \quad (27)$$

$$s_{60} = 1 + x^{60} \text{ for } \mathbf{I}, \quad (28)$$

and

$$s_{60} = 1 + x^{60} \text{ for } \mathbf{I}_h. \quad (29)$$

After expanding these generating functions, the resulting coefficients are collected to give a matrix, each row of which consists of the coefficients of the term x^m (m=0 to 60). Since the coefficient of the term x^m is equal to that of x^{60-m}, we refer to them as being complementary. In the following discussions, therefore, we take account of the term x^m ($m \leqslant 30$) mainly. The next step is the multiplication of matrix by the inverse of the mark table.[16] For explaining this step, let us examine the term x^{12} only. The corresponding row of the matrix is equal to (1399358844975, 593775, 986895, 593775, 4845, 455, 767, 455, 0, 45, 77, 45, 19, 0, 0, 0, 5, 5, 0, 1, 0, 0). When we multiply this row vector by the inverse (Table 2), we have a row vector (11661121142, 148014, 246200, 9781, 1170, 72, 374, 213, 0, 20, 36, 19, 6, 0, 0, 0, 2, 5, 0, 1, 0, 0), which is listed in the x^{12} (or x^{48}) row of Table 4. These values are aligned in the order of the SSG of the $\mathbf{I}_h$ group. Thus, there emerge 11661121142 $\mathbf{C}_1$-, 148014 $\mathbf{C}_2$-, 246200 $\mathbf{C}_s$-, 9781 $\mathbf{C}_i$-, 1170 $\mathbf{C}_3$-, 72 $\mathbf{D}_2$-, 374 $\mathbf{C}_{2v}$-, 213 $\mathbf{C}_{2h}$-, 20 $\mathbf{D}_3$-, 36 $\mathbf{C}_{3v}$-, 19 $\mathbf{C}_{3i}$-, 6 $\mathbf{D}_{2h}$-, 2 $\mathbf{T}$-, 5 $\mathbf{D}_{3d}$-, and one $\mathbf{T}_h$-isomers, all of which have the molecular formula $C_{60}H_{48}X_{12}$. The other rows of Table 4 are calculated in a similar way. It should be emphasized that these enumerations (Table 4) produce molecules having $\mathbf{C}_5$, $\mathbf{D}_5$, and $\mathbf{C}_{5i}$ symmetries, whereas the dodecahedrane skeleton cannot produce these symmetries.[16] The absence of **I**-derivatives is verified by these enumerations.

Figure 4 depicts **T** molecules, the numbers of which are calculated to be equal to 2 for the term x^{12} and 4 for the term x^{24}. The first two molecules (**31** and **32**) correspond to x^{12}. Note that we depict an arbitrary representative selected from each pair of enantiomers. The alternate labeling in each of the four 6-membered

Table 4. The Numbers of Derivatives from **1** with H and X

Term	Numbers of derivatives in the order of SSG
1, x^{60}	0, 0, 0, 0, 0, 0, 0, 0, 0, 0, 0, 0, 0, 0, 0, 0, 0, 0, 0, 0, 0, 0, 1
x, x^{59}	0, 0, 1, 0, 0, 0, 0, 0, 0, 0, 0, 0, 0, 0, 0, 0, 0, 0, 0, 0, 0, 0, 0
x^2, x^{58}	8, 6, 6, 0, 0, 0, 2, 1, 0, 0, 0, 0, 0, 0, 0, 0, 0, 0, 0, 0, 0, 0,
x^3, x^{57}	270, 0, 27, 0, 4, 0, 0, 0, 0, 0, 2, 0, 0, 0, 0, 0, 0, 0, 0, 0, 0, 0, 0
x^4, x^{56}	3946, 98, 125, 4, 0, 2, 8, 6, 0, 0, 0, 0, 1, 0, 0, 0, 0, 0, 0, 0, 0, 0, 0
x^5, x^{55}	45310, 0, 404, 0, 0, 0, 0, 0, 2, 0, 0, 0, 0, 0, 2, 0, 0, 0, 0, 0, 0, 0, 0
x^6, x^{54}	415972, 990, 1352, 60, 40, 0, 28, 12, 0, 4, 6, 4, 0, 0, 0, 0, 0, 2, 0, 0, 0, 0
x^7, x^{53}	3216564, 0, 3654, 0, 0, 0, 0, 0, 0, 0, 0, 0, 0, 0, 0, 0, 0, 0, 0, 0, 0, 0, 0
x^8, x^{52}	21313194, 6764, 10027, 432, 0, 16, 74, 48, 0, 0, 0, 0, 3, 0, 0, 0, 0, 0, 0, 0, 0, 0
x^9, x^{51}	123180894, 0, 23733, 0, 276, 0, 0, 0, 0, 0, 18, 0, 0, 0, 0, 0, 0, 0, 0, 0, 0, 0
x^{10}, x^{50}	628236648, 35488, 55870, 2330, 0, 0, 182, 89, 12, 0, 0, 0, 0, 2, 4, 2, 0, 0, 2, 0, 0, 0
x^{11}, x^{49}	2855775000, 0, 118755, 0, 0, 0, 0, 0, 0, 0, 0, 0, 0, 0, 0, 0, 0, 0, 0, 0, 0, 0, 0
x^{12}, x^{48}	11661121142, 148014, 246200, 9781, 1170, 72, 374, 213, 0, 20, 36, 19, 6, 0, 0, 0, 2, 5, 0, 1, 0, 0
x^{13}, x^{47}	43056957720, 0, 475020, 0, 0, 0, 0, 0, 0, 0, 0, 0, 0, 0, 0, 0, 0, 0, 0, 0, 0, 0, 0
x^{14}, x^{46}	144548441676, 508404, 884780, 33748, 0, 0, 728, 364, 0, 0, 0, 0, 0, 0, 0, 0, 0, 0, 0, 0, 0, 0, 0
x^{15}, x^{45}	443283294954, 0, 1560698, 0, 3840, 0, 0, 0, 50, 0, 72, 0, 0, 0, 10, 0, 0, 0, 0, 0, 0, 0
x^{16}, x^{44}	1246734362500, 1461938, 2645692, 97213, 0, 222, 1238, 666, 0, 0, 0, 0, 11, 0, 0, 0, 0, 0, 0, 0, 0, 0
x^{17}, x^{43}	3226845176280, 0, 4292145, 0, 0, 0, 0, 0, 0, 0, 0, 0, 0, 0, 0, 0, 0, 0, 0, 0, 0, 0, 0
x^{18}, x^{42}	7708574462808, 3575230, 6682278, 237936, 9576, 0, 2002, 993, 0, 56, 112, 56, 0, 0, 0, 0, 0, 8, 0, 0, 0, 0
x^{19}, x^{41}	17040013308780, 0, 10015005, 0, 0, 0, 0, 0, 0, 0, 0, 0, 0, 0, 0, 0, 0, 0, 0, 0, 0, 0, 0
x^{20}, x^{40}	34932026335736, 7508306, 14414483, 500008, 0, 492, 2906, 1473, 110, 0, 0, 0, 17, 6, 14, 6, 0, 0, 3, 0, 0, 0
x^{21}, x^{39}	66537204356484, 0, 20029842, 0, 19296, 0, 0, 0, 0, 0, 168, 0, 0, 0, 0, 0, 0, 0, 0, 0, 0, 0
x^{22}, x^{38}	117952313908338, 13653822, 26774930, 909454, 0, 0, 4004, 2002, 0, 0, 0, 0, 0, 0, 0, 0, 0, 0, 0, 0, 0, 0
x^{23}, x^{37}	194877752875260, 0, 34597290, 0, 0, 0, 0, 0, 0, 0, 0, 0, 0, 0, 0, 0, 0, 0, 0, 0, 0, 0, 0
x^{24}, x^{36}	300436529264126, 21618198, 43090979, 1440284, 31280, 822, 5044, 2460, 0, 100, 212, 98, 21, 0, 0, 0, 4, 10, 0, 2, 0, 0
x^{25}, x^{35}	432628623838072, 0, 51895915, 0, 0, 0, 0, 0, 188, 0, 0, 0, 0, 0, 20, 0, 0, 0, 0, 0, 0, 0
x^{26}, x^{34}	582384674721528, 29935458, 60354210, 1994496, 0, 0, 6006, 3003, 0, 0, 0, 0, 0, 0, 0, 0, 0, 0, 0, 0, 0, 0
x^{27}, x^{33}	733373318255628, 0, 67863663, 0, 41864, 0, 0, 0, 0, 0, 252, 0, 0, 0, 0, 0, 0, 0, 0, 0, 0, 0
x^{28}, x^{32}	864332823097128, 36349164, 73789608, 2422115, 0, 1060, 6612, 3180, 0, 0, 0, 0, 0, 25, 0, 0, 0, 0, 0, 0, 0, 0, 0
x^{29}, x^{31}	953746586743696, 0, 77558760, 0, 0, 0, 0, 0, 0, 0, 0, 0, 0, 0, 0, 0, 0, 0, 0, 0, 0, 0, 0
x^{30}	985538119566784, 38774104, 78887120, 2583540, 45936, 0, 6864, 3416, 212, 120, 260, 120, 0, 8, 20, 8, 0, 12, 4, 0, 0, 0

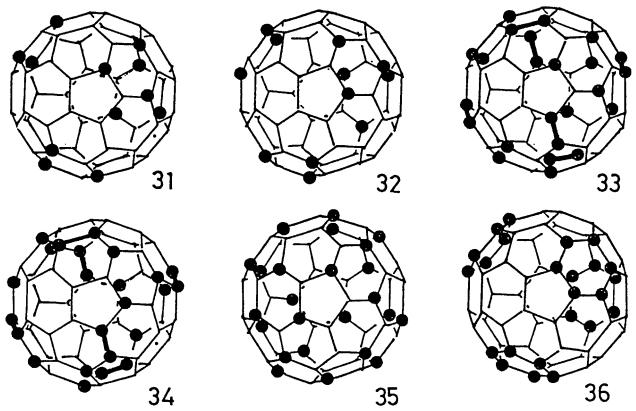

Fig. 4. **T**-Molecules derived from **1** with H and X.

rings of **31** is given just in an inverse fashion as compared with that in the counterpart of **32**. The remaining four (**33**—**36**) have the common molecular formula ($C_{60}H_{36}X_{24}$). The molecule (**33**) can be considered to come from a superposition of **11** and **31**, where heavy lines are tentatively given to show the contribution of **11**. In a similar way, the molecule (**34**) stems from a superposition of **11** and **32**. The molecule (**35**) is created by superposing **31** onto **32** so as to retain the **T**-symmetry. This superposition can be understood by focusing our attention on the eight hexagonal faces. The molecule (**36**) is generated by another mode of superposition of **31** and **32**. In accord with the qualitative discussion in the preceding section, each of these molecules has orbits that are controlled by the subduction listed in Table 3.

Molecules of $\mathbf{T}_h$ symmetry have been scarcely demonstrated by most textbooks of stereochemistry or of chemical group theory. The present enumeration provides us with suitable examples of such $\mathbf{T}_h$ molecules. Thus, there emerge three $\mathbf{T}_h$ molecules (one molecule (**11**) for x^{12} and two for x^{24}). The remaining two are depicted in Fig. 5. Comparisons of **35** (**T**) with **37** ($\mathbf{T}_h$) and with **38** ($\mathbf{T}_h$) afford their interrelation, if we pay attention to the respective eight hexagonal faces.

Figure 6 collects $\mathbf{D}_5$ molecules appearing in this enumeration. Among them, the two molecules (**17** and **39**) correspond to the term x^{10} ($C_{60}H_{50}X_{10}$) or the complementary x^{50} ($C_{60}H_{10}X_{50}$); the six isomers (**40**—**45**) are concerned with the term x^{20} ($C_{60}H_{40}X_{20}$) or the complementary x^{40} ($C_{60}H_{20}X_{40}$); and the 8 isomers (**46**—**53**) agree with the term x^{30} ($C_{60}H_{30}X_{30}$). All these molecules have a five-fold axis perpendicular to the page as well as five two-fold axes all perpendicular to the five-fold axis.

The total number of derivatives with each molecular formula is calculated in the form of a generating function.[21] Here, we give some comments to the previous results. According to Theorem 4 and Lemma 1 in our paper,[12] the number of isomers with W_θ-weight and $\mathbf{G}_i$-symmetry is represented by

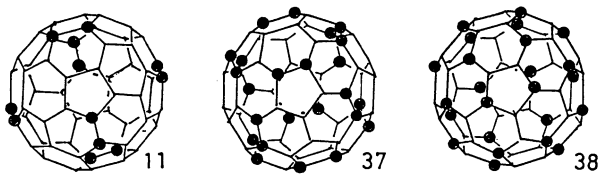

Fig. 5. $\mathbf{T}_h$-Molecules derived from **1** with H and X.

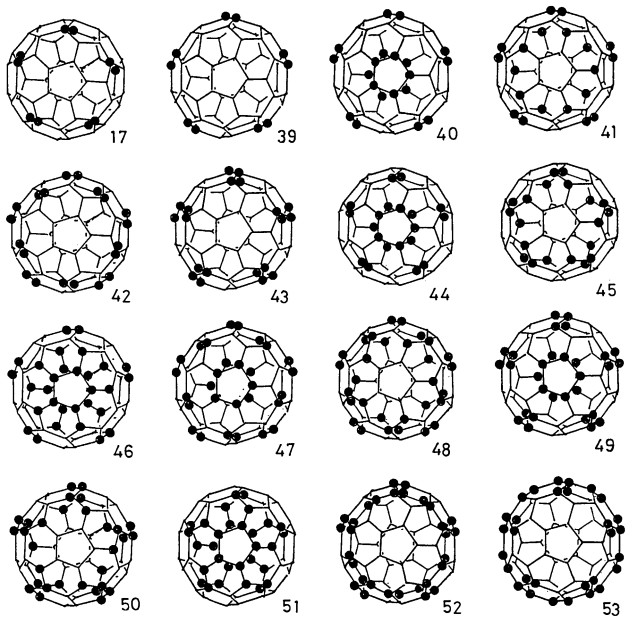

Fig. 6. $\mathbf{D}_5$-Molecules derived from **1** with H and X.

$$A_{\theta i} = \sum_{j=1}^{s} \rho_{\theta j}\overline{m}_{ji} \text{ (for } i=1,2,\cdots, s, j=1,2,\cdots,s) \tag{30}$$

where the symbol $\rho_{\theta j}$ denotes the number of fixed configurations and $\overline{m}_{ji}$ is the jith element of the inverse of the mark table for **G** group. If we tantatively fix $\mathbf{G}_i$-symmetry, then we have

$$\begin{aligned}\sum_{[\theta]} A_{\theta i}W_\theta &= \sum_{[\theta]}\sum_{j=1}^{s} \rho_{\theta j}\overline{m}_{ji}W_\theta \\ &= \sum_{j=1}^{s} \overline{m}_{ji} \sum_{[\theta]} \rho_{\theta j}W_\theta \\ &= \sum_{j=1}^{s} \overline{m}_{ji}\, ZI(\mathbf{G}_j; s_{djk}^{i\alpha}).\end{aligned} \tag{31}$$

The last equation is derived from the fact that the summation ($\sum_{[\theta]}\rho_{\theta j}W_\theta$) is a generating function of $\rho_{\theta i}$. This is in turn given by Lemma 1 of the paper[12] to be

$$\sum_{[\theta]} \rho_{\theta j}W_\theta = ZI(\mathbf{G}_j; s_{djk}^{i\alpha}), \tag{32}$$

where the right-hand side is a subduced cycle index (SCI) and $s_{djk}^{i\alpha}$ is replaced by

$$s_{djk}^{i\alpha} = \sum_{r=1}^{|X|} w_{i\alpha}(X_r)^{djk}. \tag{33}$$

We here introduce a *partial cycle index* by means of the following definition.

Definition 1. A *partial cycle index for* $\mathbf{G}_i$ *group* is defined as

$$\mathrm{PCI}(\mathbf{G}_i; s_{djk}^{i\alpha}) = \sum_{j=1}^{s} \overline{m}_{ji}\, ZI(\mathbf{G}_j; s_{djk}^{i\alpha}) (\text{for } i=1,2,\cdots, s). \tag{34}$$

When we introducte the PCI into Eq. 31, we have the following theorem.

Theorem 1. The number of isomers with W_θ-weight and $\mathbf{G}_i$-symmetry is obtained as a coefficient of the equation,

$$\sum_{[\theta]} A_{\theta i} W_\theta = \mathrm{PCI}(\mathbf{G}_j; s_{djk}^{i\alpha}) (\text{for } i=1,2,\cdots, s), \tag{35}$$

where the right-hand side a partial cycle index (PCI) and $s_{djk}^{i\alpha}$ is replaced by

$$s_{djk}^{i\alpha} = \sum_{r=1}^{|X|} w_{i\alpha}(X_r)^{djk}. \tag{36}$$

In order to count $\mathbf{C}_{2v}$-derivatives of soccerane, we have the following PCI from the data of Tables 2 and 3 by means of Eq. 34.

$$\mathrm{PCI}(\mathbf{C}_{2v}, s_d) = (1/2)s_2^4 s_4^{13} - (1/2)s_4^3 s_8^6. \tag{37}$$

In this equation, we find that the terms corresponding to the $\mathbf{C}_{2v}$- and $\mathbf{D}_{2h}$-rows are effective in the light of the $\mathbf{I}_h(/\mathbf{C}_{2v})$-column of Table 2. Introducing the figure inventory (Eq. 7) in Eq. 37, we obtain the numbers of $\mathbf{C}_{2v}$-derivatives itemized with respect to molecular formulas. They are identical to the values of the $\mathbf{C}_{2v}$ subgroup listed in Table 4. In a similar way, we can obtain a PCI and a generating function of calculating numbers of isomers for every subgroups. Since Theorem 1 is a generating-function version of Theorem 4 of the previous paper,[12] there appear no new matters beyond the previous theorem. A similar generating function has been obtained alternatively by Kerber and Thürlings,[22] though their formulation does not contain the concepts of USCIs, SCI and PCI and take no account of obligatory minimum valency.

By using the PCI, we introduce an alternative definition of a cycle index (CI):

$$\mathrm{CI} = \sum_{j=1}^{s} \mathrm{PCI}(\mathbf{G}_j; s_{djk}^{i\alpha}). \tag{38}$$

This is equivalent to our previous result,[21] i. e.,

$$\mathrm{CI} = \sum_{j=1}^{s} \left(\sum_{i=1}^{s} \overline{m}_{ji}\right) ZI(\mathbf{G}_j; s_{djk}^{i\alpha}). \tag{39}$$

The cycle index (CI) corresponding to the present case is obtained by using the data of Table 3, i. e.,

$$\begin{aligned}\mathrm{CI}(\mathbf{I}_h; s_d) = {} & (1/120)s_1^{60} + (1/8)s_2^{30} + (1/8)s_1^4 s_2^{28} + (1/120)s_2^{30} \\ & + (1/6)s_3^{20} + (1/5)s_5^{12} + (1/6)s_6^{10} + (1/5)s_{10}^6,\end{aligned} \tag{40}$$

where the coefficients of the term in the right-hand side are adopted from the rightmost column of Table 2 or 3. This derivation of the CI is based on such a theorem that is different from Pólya's one. However, these two theorems have been proven to afford the same CI in general.[21] If we introduce the figure inventory (Eq. 7) into the cycle index (Eq. 40), we have the generating function,

$$\begin{aligned}Z(x) = {} & \mathrm{CI}(\mathbf{I}_h; 1 + x^d) \\ = {} & (x^0 + x^{60}) + (x^1 + x^{59}) + 23(x^2 + x^{58}) \\ & + 303(x^3 + x^{57}) + 4190(x^4 + x^{56}) \\ & + 45718(x^5 + x^{55}) + 418470(x^6 + x^{54}) \\ & + 3220218(x^7 + x^{53}) + 21330558(x^8 + x^{52}) \\ & + 123204921(x^9 + x^{51}) + 628330629(x^{10} + x^{50}) \\ & + 2855893755(x^{11} + x^{49}) + 11661527055(x^{12} + x^{48}) \\ & + 43057432740(x^{13} + x^{47}) + 144549869700(x^{14} + x^{46}) \\ & + 443284859624(x^{15} + x^{45}) + 1246738569480(x^{16} + x^{44}) \\ & + 3226849468425(x^{17} + x^{43}) + 7708584971055(x^{18} + x^{42}) \\ & + 17040023323785(x^{19} + x^{41}) + 34932048763560(x^{20} + x^{40}) \\ & + 66537224405790(x^{21} + x^{39}) \\ & + 117952355252550(x^{22} + x^{38}) \\ & + 194877787472550(x^{23} + x^{37}) \\ & + 300436595453640(x^{24} + x^{36}) \\ & + 432628675734195(x^{25} + x^{35}) \\ & + 582384767014701(x^{26} + x^{34}) \\ & + 733373386161407(x^{27} + x^{33}) \\ & + 864332935668892(x^{28} + x^{32}) \\ & + 953746664302456(x^{29} + x^{31}) + 985538239868528x^{30}.\end{aligned} \tag{41}$$

The coefficient of each term is identical with the value that is calculated by the direct summation of the corresponding row of Table 4.

It is worthwhile mentioning the difference between Hosoya's enumeration[10] and the present one (Eq. 41). Since Hosoya has used **I** group for obtaining a CI, both enantiomers of a racemic pair are counted in as two isomers. For example, he has reported that the coefficient of the term x^2 is equal to 37, while our result (Eq. 41) contains $23x^2$. Note that our enumeration uses $\mathbf{I}_h$ group and counts each pair of enantiomers once. Since our enumeration affords such values that are itemized with respect to the terms as well as to the subsymmetries, the Hosoya's value can be calculated in terms of the data listed in Table 4. Thus, the x^2 row of Table 4 affords the expression, $8\times2+6\times2+6+2+1=37$, where the values in the left-hand side are duplicated if they are concerned with chiral subgroups. The value in the right-hand side is equal to the Hosoya's one. Compare this with $8+6+6+2+1=23$ for our result, which no such duplication is taken into account.

4. Conclusion. The 60 vertices of soccerane belong to an $\mathbf{I}_h(/\mathbf{C}_s)$ orbit. Desymmetrization of this orbit by every subgroup ($\mathbf{G}_j$) of $\mathbf{I}_h$ is characterized by the subduced representation $(\mathbf{I}_h(/\mathbf{C}_s)\downarrow\mathbf{G}_j)$. This representation is reduced to the sum of the coset representations of the $\mathbf{G}_j$ group. This subduction affords a unit subduced cycle index (USCI), which is useful for enumeration of

derivatives starting from the soccerane skeleton. The enumeration indicates the versatility of the USCI approach. Although the enumeration is restricted to the soccerane skeleton (the $\mathbf{I}_h(/\mathbf{C}_s)$ orbit), the USCI method can be applied to any other skeletons of the $\mathbf{I}_h$ symmetry (Table 1).

References

1) a) P. E. Eaton, *Tetrahedron,* **35**, 2189 (1979). b) K. Naemura, *Yuki Gosei Kagaku Kyokai Shi,* **45**, 48 (1987). c) L. A. Paquette, *Chem. Rev.,* **89**, 1051 (1989).

2) E. Osawa, *Kagaku (Kyoto),* **25**, 854 (1970).

3) J. Castells and F. Serratosa, *J. Chem. Educ.,* **60**, 941 (1983).

4) J. Castells and F. Serratosa, *J. Chem. Educ.,* **63**, 630 (1986).

5) a) H. W. Kroto, J. R. Heath, S. C. O'Brien, and R. E. Smalley, *Nature,* **318**, 162 (1985). b) Y. Liu, S. C. O'Brien, Q. L. Zhang, J. R. Heath, F. K. Tittle, R. F. Curl, H. W. Kroto, and R. E. Smalley, *Chem. Phys. Lett.,* **126**, 215 (1986). c) Q. L. Zhang, S. C. O'Brien, J. R. Heath, Y. Liu, R. F. Curl, H. W. Kroto, and R. E. Smalley, *J. Phys. Chem.,* **90**, 525 (1986).

6) We adopt the name *soccerane* for referring to this compound (or cluster) after Castells' proposal.[3] Kroto et al.[5a] have once referred to this cluster as "buckminsterfullerene"; however, Buckminster Fuller's architecture has been pointed out to be based on organized triangles, not on such a truncated icosahedron.[10]

7) a) D. J. Klein, T. G. Schmalz, G. E. Hite, and W. A. Seitz, *J. Am. Chem. Soc.,* **108**, 1301 (1986). b) Z. Slanina, J. M. Rudzinski, and E. Osawa, *Coll. Czech. Chem. Commun.,* **52**, 2831 (1987). c) R. C. Haddon, L. E. Brus, and K. Raghavachari, *Chem. Phys. Lett.,* **125**, 459 (1986). d) R. L. Disch and J. M. Schulman, *Chem. Phys. Lett.,* **125**, 465 (1986). e) P. W. Fowler, *Chem. Phys. Lett.,* **131**, 444 (1986). f) H. P. Lüthi and J. Almlöf, *Chem. Phys. Lett.,* **135**, 357 (1987). g) G. W. Hayden and E. J. Mele, *Phys. Rev. B,* **36**, 5010 (1987). h) A. J. Stone and D. J. Wales, *Chem. Phys. Lett.,* **128**, 501 (1986). i) A. D. J. Haymet, *J. Am. Chem. Soc.,* **108**, 319 (1986).

8) a) A. D. J. Haymet, *Chem. Phys. Lett.,* **122**, 421 (1985). b) P. W. Fowler and J. Woolrich, *J. Chem. Phys. Lett.,* **127**, 78 (1986). c) J. M. Schulman, R. L. Disch, M. A. Miller, and R. C. Peck, *Chem. Phys. Lett.,* **141**, 45 (1987). d) T. Shibuya and M. Yoshitani, *Chem. Phys. Lett.,* **137**, 13 (1987).

9) E. Osawa, *Kagaku (Kyoto),* **42**, 62 (1987).

10) H. Hosoya, *Gendai-Kagaku,* **201**, 38 (1987). See also O. Knop, W. W. Barker, and P. S. White, *Acta Crystallogr., Sect. A,* **31**, 461 (1975).

11) a) G. Pólya, *Acta Math.,* **68**, 145 (1937). b) G. Pólya, "Combinatorial Enumeration of Groups, Graphs, and Chemical Compounds," Springer-Verlag, New York-Berlin-Heidelberg (1987).

12) S. Fujita, *Theor. Chim. Acta,* **76**, 247 (1989).

13) For other enumeration methods, see a) J. Sheehan, *Can. J. Math.,* **20**, 1068 (1968). b) W. Hässelbarth, *Theor. Chim. Acta,* **67**, 339 (1985). c) J. Brocas, *J. Am. Chem. Soc.,* **108**, 1135 (1986). d) C. A. Mead, *J. Am. Chem. Soc.,* **109**, 2130 (1987).

14) W. Burnside, "Theory of Groups of Finite Order," 2nd ed, Cambridge Univ. Press, Cambridge (1911).

15) a) S. Fujita, *Bull. Chem. Soc. Jpn.,* **62**, 3771 (1989). b) S. Fujita, *Bull. Chem. Soc. Jpn.,* **63**, 203 (1989). c) S. Fujita, *Tetrahedron,* **46**, 365 (1989). d) S. Fujita, *Bull. Chem. Soc. Jpn.,* **63**, 1876 (1989), e) *ibid.,* **63**, 2033 (1989).

16) S. Fujita, *Bull. Chem. Soc. Jpn.,* **63**, 2759 (1990).

17) S. Fujita, *Bull. Chem. Soc. Jpn.,* **63**, 315 (1990).

18) S. Fujita, *J. Am. Chem. Soc.,* **112**, 3390 (1990).

19) A. full mark table for $\mathbf{I}_h$ group has been reported elsewhere.[16]

20) S. Fujita, *J. Math. Chem.,* **5**, 121 (1990).

21) S. Fujita, *J. Math. Chem.,* **5**, 99 (1990).

22) A. Kerber and K. -J. Thürlings, in "Lecture Notes in Mathematics," Springer, New York (1982), Vol. 969, p. 191.

Estimation of Angles between the Ground- and Excited-State Dipole Moments from Solvent Spectral Frequency Shifts

Takehiro ABE
College of General Education, Tohoku University, Kawauchi, Aoba-ku, Sendai 980
(Received April 4, 1991)

A method for estimating the angle between the ground- and excited-state dipole moments is presented on the basis of Abe's improved expressions for the solvent frequency shifts of absorption and fluorescence spectra (*Bull. Chem. Soc. Jpn.*, **54**, 327 (1981); **58**, 3415 (1985); **61**, 3797 (1988)). Applications of the method to *N,N*-dimethylaniline and aniline give angles of 39.5° and 40.0°, respectively; the excited-state dipole moments are both smaller than the corresponding ground-state dipole moments.

On the basis of theories regarding solvent effects on the frequency shifts of absorption and/or fluorescence, the dipole moments and/or polarizabilities have been estimated for the excited states of organic molecules.[1] There have, however, been a few attempts to estimate the angles between the ground- and excited-state dipole moments due to solvent spectral shifts, except for solute molecules in which both the dipole moments are obviously collinear. On the basis of the Onsager model,[15] Suppan[9,16] has presented a method used to obtain the angles between the ground- and excited-state dipole moments due to the solvent shifts of the absorption and fluorescence spectra for such organic molecules as aniline. His method requires data concerning the solvatochromic shifts in two solvents of nearly the same refractive indices. Recently, Ayachit[11] has improved Suppan's method. Upon modifying McRae's expression[17] for solvent absorption-spectral shifts, Prabhumirashi et al.[18,19] attempted to estimate the angles between the ground- and excited-state dipole moments. Later, Ayachit et al.[6] improved the method of Prabhumirashi et al. and obtained several angle values for nitroanilines.

Abe's improved expression[3,20] for the solvent absorption-spectral shift gave excited dipole moments and/or polarizabilities that were comparable to those found by electrooptical measurements.[3] Moreover, on the basis of the same treatment as in the case of the improved expression, an expression for the solvent fluorescence-spectral shift has been presented.[21] In this paper, therefore, an attempt has been made to present a method for estimating the angle between the ground- and excited-state dipole moments by combining the improved expression for the solvent absorption-spectral frequency shifts with that for the solvent fluorescence-spectral shifts.

Theory

The wave numbers of a transition from the ground state to the *i*th-excited state of a neutral solute molecule (A) in vapor and in a solvent (S) are denoted by $\sigma^{\circ}_{0i,a}$ and $\sigma_{0i,a}$ (cm^{-1}), respectively. The wave numbers of the fluorescence frequencies of the solute molecule in the vapor and in the solvent are denoted by $\sigma^{\circ}_{i0,j}$ and $\sigma_{i0,j}$ (cm^{-1}), respectively. The ground and *i*th-excited state dipole moments are denoted by $\boldsymbol{P}_{00}$ and $\boldsymbol{P}_{ii}$, respectively; α_{00} and α_{ii} are the isotropic electric polarizabilities of the ground and *i*th-excited states, respectively. The superscripts/subscripts (A and S) denote the solute and solvent molecules, respectively. Suffix f in $\alpha^{A}_{00,f}$ and $\alpha^{A}_{ii,f}$ indicates that these polarizabilities are not those which correspond ($\alpha^{A}_{00,a}$ and $\alpha^{A}_{ii,a}$ respectively) to absorption, but to fluorescence. Here, the dipole moments of the ground and *i*th-excited states concerning the fluorescence are assumed to be equal to the corresponding dipole moments regarding absorption, as has usually been assumed in all previous theories concerning fluorescence. This assumption is approximately fulfilled if the nuclear equilibrium configuration of the *i*-th excited state does not significantly differ from that of the ground state, as described in a previous paper.[21] The improved expression for $\sigma_{0i,a}$ is given by[3,20]

$$\sigma_{0i,a} = \sigma^{\circ}_{0i,a} + F \times (p^{S}_{00})^2 \times A_a + F \times \alpha^{S}_{00} \times B_a, \tag{1}$$

where

$$F = \frac{\pi}{hc}\left(\frac{4\pi L}{3}\right)^{2/3} \times \frac{(\rho^{S}/M^{S}_{r})^{2/3}}{(r_A + r_S)^4}, \tag{2}$$

$$A_a = \frac{2\{(p^{A}_{00})^2 - \boldsymbol{p}^{A}_{00}\cdot\boldsymbol{p}^{A}_{ii}\}}{3(4\pi\varepsilon_0)^2 kT} + \frac{\alpha^{A}_{00,a} - \alpha^{A}_{ii,a}}{4\pi\varepsilon_0}, \tag{3}$$

and

$$B_a = \frac{1}{4\pi\varepsilon_0} \times \{(p^{A}_{00})^2 - (p^{A}_{ii})^2 + \frac{3}{2} \times \frac{I^{S}_0 \cdot I^{A}_0}{I^{S}_0 + I^{A}_0} \times (\alpha^{A}_{00,a} - \alpha^{A}_{ii,a})\}. \tag{4}$$

Here, c is the speed of light in vacuum, h Planck's constant, L Avogadro's constant, k Boltzmann's constant, T the thermodynamic temperature, ε_0 the permittivity of a vacuum, M_r the relative molecular mass, ρ the

density, r the radius of a spherical molecule, and I_0 the ionization potential of the ground state. On the other hand, the expression for $\sigma_{i0,f}$ is given by[21]

$$\sigma_{i0,f} = \sigma^{\circ}_{i0,f} + F \times (p^{S}_{00})^2 \times A_f + F \times \alpha^{S}_{00} \times B_f, \quad (5)$$

where

$$A_f = \frac{2\{\boldsymbol{p}^{A}_{00}\cdot\boldsymbol{p}^{A}_{00} - (p^{A}_{ii})^2\}}{3(4\pi\varepsilon_0)^2 kT} + \frac{\alpha^{A}_{00,f} - \alpha^{A}_{ii,f}}{4\pi\varepsilon_0}, \quad (6)$$

and

$$B_f = \frac{1}{4\pi\varepsilon_0} \times \{(p^{A}_{00})^2 - (p^{A}_{ii})^2 + \frac{3}{2} \times \frac{I^{S}_0 \cdot I^{A}_0}{I^{S}_0 + I^{A}_0} \times (\alpha^{A}_{00,f} - \alpha^{A}_{ii,f})\}. \quad (7)$$

By combining Eq. 1 and Eq. 5, one can easily obtain the following equations:

$$\sigma_{0i,a} + \sigma_{i0,f} = a + A \times b + B \times d, \quad (8)$$

and

$$\sigma_{0i,a} - \sigma_{i0,f} = a' + C \times b' + B \times d', \quad (9)$$

where

$$A = F \times \left\{\frac{2(p^{S}_{00})^2}{3(4\pi\varepsilon_0)^2 kT} + \frac{2\alpha^{S}_{00}}{(4\pi\varepsilon_0)}\right\}, \quad (10)$$

$$B = F \times \left\{(p^{S}_{00})^2 + \frac{3\alpha^{S}_{00}}{2} \times \frac{I^{S}_0 \cdot I^{A}_0}{I^{S}_0 + I^{A}_0}\right\}, \quad (11)$$

$$C = F \times \frac{2(p^{S}_{00})^2}{3(4\pi\varepsilon_0)^2 kT}, \quad (12)$$

$$a = \sigma^{\circ}_{0i,a} + \sigma^{\circ}_{i0,f}, \quad (13)$$

$$a' = \sigma^{\circ}_{0i,a} - \sigma^{\circ}_{i0,f}, \quad (14)$$

$$b = (p^{A}_{00})^2 - (p^{A}_{ii})^2, \quad (15)$$

$$b' = (p^{A}_{00})^2 - 2(\boldsymbol{P}^{A}_{00}\cdot\boldsymbol{P}^{A}_{ii}) + (p^{A}_{ii})^2, \quad (16)$$

$$d = \frac{1}{4\pi\varepsilon_o} \times \{(\alpha^{A}_{00,a} - \alpha^{A}_{ii,a}) + (\alpha^{A}_{00,f} - \alpha^{A}_{ii,f})\}, \quad (17)$$

and

$$d' = \frac{1}{4\pi\varepsilon_o} \times \{(\alpha^{A}_{00,a} - \alpha^{A}_{ii,a}) - (\alpha^{A}_{00,f} - \alpha^{A}_{ii,f})\}, \quad (18)$$

From Eqs. 13 and 14, one obtains

$$\sigma^{\circ}_{0i,a} = \frac{1}{2} \times (a + a'), \quad (19)$$

and

$$\sigma^{\circ}_{i0,f} = \frac{1}{2} \times (a - a'). \quad (20)$$

From Eqs. 15, one obtains

$$p^{A}_{ii} = \{(p^{A}_{00})^2 - b\}^{1/2}. \quad (21)$$

When one writes $\boldsymbol{p}^{A}_{00}\cdot\boldsymbol{p}^{A}_{ii} = p^{A}_{00} p^{A}_{ii} \cos\theta$, the value of $\cos\theta$ is obtained from Eq. 16 as

$$\cos\theta = \frac{1}{2} \times \left(\frac{p^{A}_{00}}{p^{A}_{ii}} + \frac{p^{A}_{ii}}{p^{A}_{00}} - \frac{b'}{p^{A}_{00} p^{A}_{ii}}\right). \quad (22)$$

The values for F, A, B, and C can be calculated. In calculating these values, the values observed for p_{00} and I_0 in the vapor phase are used, the values for α_{00} are calculated from the sums of the bond refractions and the values for r_{AorS} may be calculated according to $r_{AorS} = (3M_r^{AorS}/4\pi L\rho^{AorS})^{1/3}$, as discussed in a previous paper.[3] Accordingly, the values for a, b, and d and those for a', b', and d' can be obtained by means of a least-squares analysis of data for the solvent absorption- and fluorescence-spectral frequency shifts, according to Eqs. 8 and 9, respectively. One can, therefore, obtain values for $\sigma^{\circ}_{0i,a}$, $\sigma^{\circ}_{i0,f}$, p^{A}_{ii}, and $\cos\theta$ according to Eqs. 19, 20, 21, and 22, respectively. Thus, one can estimate the angle of θ between the ground- and excited-state dipole moments.

Results and Discussion

The present expressions used for the solvent absorption- and fluorescence-spectral frequency shifts have been derived on the assumption that the solvent molecules form no hydrogen bonds or complexes with the solute.[20,21] In applying Eqs. 8 and 9, therefore, data for solvents which are capable of forming hydrogen bonds and complexes with solutes should be excluded. When this restriction is taken into consideration, there is no available data reported for interesting molecules, except for data regarding only *N*,*N*-dimethylaniline. The *N*,*N*-dimethylaniline molecule may be assumed not to be coplanar, since it is well-known that in the similar aniline molecule the plane containing an amino group does not lie in the plane of the benzene ring. Accordingly, the dipole moments of the ground states of *N*,*N*-dimethylaniline and aniline do not lie in the planes of the benzene rings. In view of this point *N*,*N*-dimethylaniline is appropriate for the present purpose.

Therefore, Eqs. 8 and 9 were applied to data reported by Köhler[22] regarding the solvent maximum absorption- and fluorescence-spectral shifts of *N*,*N*-dimethylaniline (22°). The data points for 8 solvents were chosen, out of his reported total of 12 solvents, by excluding protic

solvents. Unfortunately, he did not give all of the numerical values for $\sigma_{0i,a}$ except for three values for hexane, tetrahydrofuran and dioxane.. Therefore, the $\sigma_{0i,a}$ values for the 5 remaining solvents were obtained by using the Stokes shifts ($\sigma_{0i,a}-\sigma_{i0,f}$), from which values could be read off a magnified version of Fig. 1 in Ref. 22. The following values were used for *N*,*N*-dimethylaniline: r_A=0.369 nm, p_{00}^A=1.61 D (gas)[23] (1 D=3.333×10^{-30} C m), α_{00}^A=155.69×10^{-25} cm^3 (see Ref. 3) and I_0^A=7.6 eV[24] (1 eV=1.602×10^{-19} J). For convenience, the temperature was assumed to be 20 °C. Thus, the present analysis by using Eqs. 8 and 9 gives p_{ii}^A=1.02 D, θ=39.5° (cos θ=0.772), $\sigma_{0i,a}^\circ$=34100 cm^{-1} and $\sigma_{i0,f}^\circ$=31820 cm^{-1}. By applying the values of $\sigma_{0i,a}^\circ$=34100 cm^{-1} and cos θ=0.772 to Eq. 1, the same p_{ii}^A value of 1.02 D and the $\alpha_{ii,a}^A$ value of 290.6×10^{-25} cm^3 were estimated by means of Calculation 1 in Ref. 3. A similar calculation, by applying the values of p_{ii}^A=1.02 D and cos θ=0.772 to Eq. 5, gave the same $\sigma_{i0,f}^\circ$ value of 31820 cm^{-1} and $\alpha_{00,f}^A-\alpha_{ii,f}^A$=−435.4×10^{-25} cm^3 by means of a least-squares analysis. According to Eqs. 1 and 5, the values for $\sigma_{0i,a}$ and $\sigma_{i0,f}$, respectively, can be calculated by using the values so estimated for $\sigma_{0i,a}^\circ$, $\sigma_{i0,f}^\circ$, p_{ii}^A, $\alpha_{ii,a}^A$, ($\alpha_{00,f}^A-\alpha_{ii,f}^A$) and cos θ. The values ($\sigma_{0i,calcd}$) so calculated for $\sigma_{0i,a}$ and $\sigma_{i0,f}$ were compared with those ($\sigma_{0i,obsd}$) observed, as shown in Fig. 1. The correlations between the experimental and calculated frequencies are good. The estimated $\sigma_{0i,a}^\circ$ value of 34100 cm^{-1} agrees roughly with the observed value[25] of 34700 cm^{-1}. These facts may support the validity of Eqs. 8 and 9.

The p_{ii}^A value of 1.02 D, estimated in the present work, is smaller than the ground-state dipole moment of 1.61 D by 0.59 D, while the p_{ii}^A values of 3.58 D (θ=66°)[19] and 5.1 D[2] and the ($p_{ii}^A-p_{00}^A$) value of 2.0 D[22] have been estimated from solvent spectral-shift theories. Whether $p_{ii}^A>p_{00}^A$ or $p_{ii}^A<p_{00}^A$ is a serious problem for considering the electronic structure of the excited state of *N*,*N*-dimethylaniline.

In the case of a similar molecule, aniline, Lombardi[26] determined that the magnitude of the dipole moment change is $|p_{ii}^A-p_{00}^A|$=(0.85±0.15) D by a technique involving the optical Stark effect in the gas phase. As mentioned above, aniline is not appropriate for the present purpose, because the amino group of aniline is capable of forming hydrogen bonds with aprotic solvents which are high on the β scale regarding the hydrogen-bond acceptor strength.[27] For example, dioxane (β=0.37), dibutyl ether (β=0.46), diethyl ether (β=0.47), tetrahydrofuran (β=0.55) and acetonitrile (β=0.31) are involved in the solvents used by Köhler.[22] Nevertheless, an attempt has been made to apply Eqs. 8 and 9 to the 8 spectral data points[22] of Köhler for aniline in similar way in order to compare the estimated value of $|p_{ii}^A-p_{00}^A|$ with the reliable one of Lombardi. The values used for aniline are the same as those given in a previous paper:[3] r_A=0.331 nm, p_{00}^A=1.48 D(gas), α_{00}^A=117.3×10^{-25} cm^3, and I_0^A=7.68 eV. According to Eqs. 8 and 9, the results of p_{ii}^A=0.75 D, θ=40.0° (cos θ=0.766), $\sigma_{0i,a}^\circ$=34630 cm^{-1} and $\sigma_{i0,f}^\circ$=31810 cm^{-1} were estimated. By applying the values of $\sigma_{0i,a}^\circ$=34630 cm^{-1} and cos θ=0.766 to Eq. 1, the same p_{ii}^A value of 0.75 D and the $\alpha_{ii,a}^A$ value of 132.0×10^{-25} cm^3 were estimated. A similar calculation, by applying the values of p_{ii}^A=0.75 D and cos θ=0.766 to Eq. 5, gave a $\sigma_{i0,f}^\circ$ value of 34600 cm^{-1} and $\alpha_{00,f}^A-\alpha_{ii,f}^A$=−620.9×10^{-25} cm^3. The correlations between the observed and calculated values for $\sigma_{0i,a}$ and $\sigma_{i0,f}$ are shown in Fig. 2. On the whole, the correlations

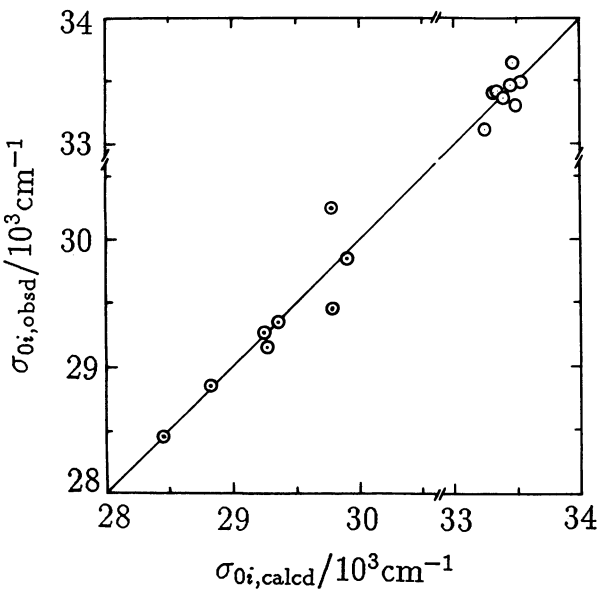

Fig. 1. Plot of the observed frequencies vs. calculated frequencies for *N*,*N*-dimethylaniline. ○, absorption frequencies; ⊙, fluorescence frequencies.

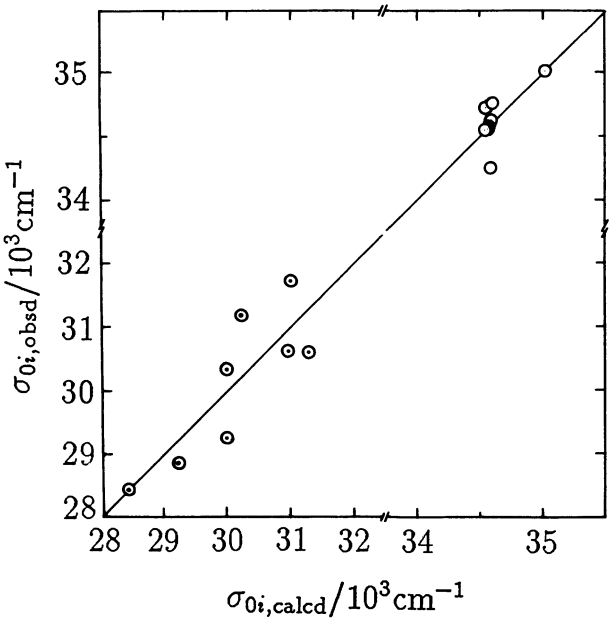

Fig. 2. Plot of the observed frequencies vs. calculated frequencies for aniline. ○, absorption frequencies; ⊙, fluorescence frequencies.

given in Fig. 2 are good, but worse than are those given in Fig. 1. The estimated $\sigma^{\circ}_{0i,a}$ value of 34630 cm^{-1} considerably deviates from the observed values of 35490[28,29] and 35500[25] cm^{-1}. Especially, the $\sigma^{\circ}_{0,f}$ value of 31810 cm^{-1}, estimated according to Eqs. 8 and 9, does not agree with that (34600 cm^{-1}) estimated from Eq. 5, although there is agreement between the corresponding values for *N*,*N*-dimethylaniline, as shown above. These worse results for aniline in comparison with the results for *N*,*N*-dimethylaniline are probably due to the use of data points for the aprotic solvents with which aniline is capable of forming hydrogen bonds. However, the p^{A}_{ii} and θ values estimated by applying Eqs. 8 and 9 for aniline may be roughly correct, since these values are close to the corresponding ones for *N*,*N*-dimethylaniline.

Here, the reliability of the θ value obtained by the present method will be investigated. Baba et al.[30] reported on the solvent effects on the absorption and fluorescence spectra of diazines, although data points for only 3 solvents could be used for the present purpose. Ony data for pyridazine are used, since the solvent spectral shifts of pyrimidine are small and pyrazine has no dipole moments in both the ground and excited states due to molecular symmetry. According to Baba et al.,[30] the cos θ value for pyridazine should be unity, since the directions of p^{A}_{00} and p^{A}_{ii} for the molecule are the same. By using r_A=0.306 nm, p^{A}_{00}=4.221 D,[24] $\alpha^{A}_{00}=91.75\times10^{-25}$ cm^3 and I^{A}_{0}=8.706 eV,[24] Eqs. 8 and 9 were applied to the data for pyridazine in 2,2,4-trimethylpentane, in diethyl ether and in acetonitrile (25 °C). The result that cos θ=1.098 was obtained. This cos θ value is approximately unity, thus leading to the suggestion that the present estimation of θ may be fairly reliable.

The p^{A}_{ii} value (0.75 D) estimated for aniline is smaller than the p^{A}_{00} value (1.48 D), as in the case of *N*,*N*-dimethylaniline. All of the p^{A}_{ii} values which have hitherto been estimated for aniline from the solvent shifts of the absorption and/or fluorescence spectra are larger than p^{A}_{00}: The p^{A}_{ii} value has been estimated by Mataga (2—2.5 D),[31] Murrell (5 D),[32] Iweibo et al. (a value nearly equal to p^{A}_{00}),[33] Suppan (5 D),[2,9,16] and Prabhumirashi et al. (2.13 and 3.30 D, θ=14°).[10,18,19] Recently, Ayachit[11] estimated the values of p^{A}_{ii}=5.3 D and θ=25° for aniline, improving on the method of Suppan.[16] In a previous paper,[3] the p^{A}_{ii} value of 2.33 D was alternatively estimated for aniline by applying Eq. 1 to only three data points for solvents. Even though only three data points are the minimum for applying the expression, it is desirable to use at least several data points. The present estimation of $p^{A}_{00}-p^{A}_{ii}$=0.75 D for aniline agrees well with the reliable value ($|p^{A}_{ii}-p^{A}_{00}|=(0.85\pm0.15)$D) of Lombardi. The discrepancy between the solvatochromic shift measurements and reliable gas phase Stark effect measurements is fundamentally due to insufficient theoretical expressions for the solvatochromic shifts, as pointed out by Lombardi.[34] As mentioned in a previous paper,[3] comparisons between the excited-state dipole moments and/or polarizabilities estimated from the solvent spectral shifts with those determined from the electrooptical measurements are necessary in order to justify the theoretical expressions used for the solvent spectral frequency shifts. Among the many theoretical expressions, those giving excited-state dipole moments and polarizability values that are comparable to those of the electrooptical measurements will survive. As described above, Abe's improved expression (Eq. 1) gave excited-state dipole moments and/or polarizabilities that were comparable to those of electrooptical measurements.[3] The present estimation that $p^{A}_{00}>p^{A}_{ii}$ for aniline can be reasonably accounted for according to MO calculations as follows: All of the MO calculations of Baba,[35] Mataga,[31] and Nagakura et al.[25,36] show a decrease in the π-electron density at the nitrogen atom in the excited state of aniline. As described in a previous paper,[3] this decrease only increases the magnitude of the excited-state dipole moment component parallel to the plane containing both the benzene ring and nitrogen atom in the same direction as that of the corresponding ground-state dipole moment component, the positive and negative terminals of which do not change sign upon excitation. Accordingly, the excited-state dipole moment component should be larger than the corresponding ground-state dipole moment component. The inclination of the calculated ground-state dipole moment (1.44 D) was obtained by Hehre et al.[37] to be 67° to the plane containing the benzene ring by means of ab initio MO theory. The corresponding inclination of p^{A}_{ii} may be smaller than that (67°) of p^{A}_{00} by 40°, since both the p^{A}_{00} and p^{A}_{ii} components parallel to the benzene ring are in the same direction. By using an inclination of 67°, the p^{A}_{00} and p^{A}_{ii} components containing the benzene ring were calculated to be 1.48 D cos 67°=0.58 D and 0.75 D cos (67°−40°)=0.67 D, respectively. These estimations satisfy the result of the above-mentioned MO calculations. Therefore, the result that the excited-state dipole moment (0.75 D) is smaller than the ground-state dipole moment (1.48 D) does not conflict with the result concerning the above-mentioned MO calculations. Accordingly, the p^{A}_{ii} value of 0.75 D estimated for aniline is reasonable.

The MO calculation of Kimura, Tsubomura, and Nagakura[25] for *N*,*N*-dimethylaniline similarly shows a decrease of the π-electron density at the nitrogen atom in the excited state of *N*,*N*-dimethylaniline. Therefore, the circumstances of *N*,*N*-dimethylaniline are the same as those of aniline. Based on the assumption of the same inclination of 67° for *N*,*N*-dimethylaniline as in the case of aniline, the p^{A}_{00} and p^{A}_{ii} components parallel to the plane containing the benzene ring were estimated as 1.61 D cos 67°=0.63 D and 1.02 D cos (67°−39.5°)=0.90 D, respectively. Also, these estimations do not conflict with the MO calculation. Thus, the present estimation of $p^{A}_{00}>p^{A}_{ii}$ for *N*,*N*-dimethylaniline may be reasonable.

As shown above, the θ values have been estimated for

N,N-dimethylaniline and aniline. Prabhumirashi et al.[19] estimated θ values of 66° and 14° for *N,N*-dimethylaniline and aniline, respectively. These θ values seem to differ too greatly. Ayachit[11] estimated a θ value of 25° for aniline. However, his estimation of p_{ii}^{A}=5.3 D is too large in comparison with the magnitude of the dipole moment change of Lombardi.[26] The present estimations using Eqs. 8 and 9 give similar θ values for similar molecules of *N,N*-dimethylaniline and aniline, as does the $|p_{ii}^{A}-p_{00}^{A}|$ value, agreeing with the reliable value of Lombardi for aniline, as described above. In conclusion, the angle between the ground- and excited-state dipole moments may be estimated by applying Eqs. 8 and 9 to data for the solvent absorption- and fluorescence-frequency shifts of a solute molecule.

References

1) For example, see the following recent papers, Refs. 2—14.

2) P. Suppan and E. Guerry-Butty, *J. Lumin.*, **33**, 335 (1985).

3) T. Abe and I. Iweibo, *Bull. Chem. Soc. Jpn.*, **58**, 3415 (1985).

4) H. Lami and N. Glasser, *J. Chem Phys.*, **84**, 597 (1986).

5) L. S. Prabhumirashi and S. S. Kunte, *Spectrochim. Acta, Part A,* **42**, 435 (1986).

6) N. H. Ayachit, D. K. Deshpande, M. A. Shashidhar, and K. S. Rao, *Spectrochim. Acta, Part A,* **42**, 585 (1986).

7) K. C. Medhi, *Spectrochim. Acta, Part A,* **42**, 1393 (1986).

8) J.-J. Aaron and M. D. Gaye, *J. Mol. Struct.*, **156**, 119 (1987).

9) D. Noukakis and P. Suppan, *Spectrochim. Acta, Part A,* **43**, 1317 (1987).

10) L. S. Prabhumirashi and S. S. Kunte, *Spectrochim. Acta, Part A,* **44**, 213 (1988); **45**, 1147 (1989).

11) N. H. Ayachit, *Chem. Phys. Lett.*, **164**, 253 (1989).

12) G. M. Anstead and J. A. Katzenellenbogen, *J. Phys. Chem.*, **92**, 6249 (1988).

13) M. Van Damme, J. Hofkens, and F. C. De Schryver, *Tetrahedron,* **45**, 4693 (1989).

14) N. Ghoneim and P. Suppan, *J. Chem. Soc., Faraday Trans.*, **86**, 2079 (1990).

15) L. Onsager, *J. Am. Chem. Soc.*, **58**, 1486 (1936).

16) P. Suppan, *Chem. Phys. Lett.*, **94**, 272 (1983).

17) E. G. McRae, *J. Phys. Chem.*, **61**, 562 (1957).

18) L. S. Prabhumirashi, *Spectrochim. Acta, Part A,* **39**, 91 (1983).

19) L. S. Parabhumirashi, D. K. N. Kutty, and A. S. Bhide, *Spectrochim. Acta, Part A,* **39**, 663 (1983).

20) T. Abe, *Bull. Chem. Soc. Jpn.*, **54**, 327 (1981).

21) T. Abe, *Bull. Chem. Soc. Jpn.*, **61**, 3797 (1988).

22) G. Köhler, *J. Photochem.*, **38**, 217 (1987).

23) L. G. Groves and S. Sugden, *J. Chem. Soc.*, **1937**, 1782.

24) "Kagaku Binran," 3rd ed, ed by The Chemical Society of Japan, Maruzen Publishing Co., Tokyo (1984), Kisohen (Fundamental Part), II, p. II-581, 721.

25) K. Kimura, H. Tsubomura, and S. Nagakura, *Bull. Chem. Soc. Jpn.*, **37**, 1336 (1964).

26) J. R. Lombardi, *J. Chem. Phys.*, **50**, 3780 (1969).

27) M. J. Kamlet, J.-L. M. Abboud, and R. W. Taft, *Prog. Phys. Org. Chem.*, **13**, 485 (1981).

28) W. W. Robertson and F. A. Matsen, *J. Am. Chem. Soc.*, **72**, 5252 (1950).

29) K. Kimura and S. Nagakura, *Mol. Phys.*, **9**, 117 (1965).

30) H. Baba, L. Goodman, and P. C. Valenti, *J. Am. Chem. Soc.*, **88**, 5410 (1966).

31) N. Mataga, *Bull. Chem. Soc. Jpn.*, **36**, 1607 (1963).

32) J. N. Murrell, *Tetrahedron,* **19**, Suppl. 2, 277 (1963).

33) I. Iweibo, R. A. Oderinde, and J. A. Faniran, *Spectrochim. Acta, Part A,* **38**, 1 (1982).

34) J. R. Lombardi, *Spectrochim. Acta, Part A,* **43**, 1323 (1987).

35) H. Baba, *Bull. Chem. Soc. Jpn.*, **34**, 76 (1961).

36) F. Hirota and S. Nagakura, *Bull. Chem. Soc. Jpn.*, **43**, 1010 (1970).

37) W. J. Hehre, L. Radom, and J. A. Pople, *J. Am. Chem. Soc.*, **94**, 1496 (1972).

Femtosecond—Picosecond Laser Photolysis Studies on Reduction Process of Excited Benzophenone with Tertiary Aromatic Amines in Acetonitrile Solution

Hiroshi MIYASAKA*, Kazuhiro MORITA, Kenji KAMADA, Toshihisa NAGATA, Manabu KIRI, and Noboru MATAGA*,†
Department of Chemistry, Faculty of Engineering Science, Osaka University, Toyonaka, Osaka 560
(Received April 30, 1991)

Photoreduction processes of benzophenone (BP)-*N*,*N*-diethylaniline (DEA) system in acetonitrile solution were studied by means of femtosecond—pecosecond laser photolysis and time resolved transient absorption spectroscopy. The reaction processes including the formation of geminate ion pairs (IP) by electron transfer (ET) between BP* and DEA at encounter followed by intra-IP proton transfer giving the ketyl radical (BPH·) were clearly observed in both triplet and singlet excited state, while the IP produced by excitation of the CT complex between BP and amine formed easily in more or less concentrated solutions did not give BPH·. In addition to the detailed investigations on the BP-DEA system, we made comparative studies on BP–tertiary aromatic amine systems including *N*,*N*-diethyl-*p*-toluidine, *N*,*N*-dimethylaniline, and *N*-methyldiphenylamine. We observed clearly the characteristic tendency that the proton transfer rate in the ^{3}IP decreased with decrease of the oxidation potential of the amine. This result was interpreted as due to the increase of the inter-ionic distance in the ^{3}IP with increase of the free energy gap for the charge separation at encounter.

Photoinduced electron transfer (ET) and related phenomena play the most fundamental and important roles in many photophysical and photochemical reactions in condensed phase.[1-4] Hydrogen abstraction of excited benzophenone (BP*) from aliphatic as well as aromatic amines in solution is one of the most important photochemical reactions related to this fundamental process and has been extensively studied for a long time.[5-19] Especially, much attention has been paid to the hydrogen abstraction of triplet benzophenone (^{3}BP*), since the rate of the intersystem crossing from the lowest excited singlet state of BP (^{1}BP*) is very large (ca. 10^{11} s^{-1}). On the basis of the experimental results that the yield of the ketyl radical in the reaction of ^{3}BP* with the amine is usually very high and that the reaction rate is rather close to that of the diffusion-controlled reaction, Cohen et al. proposed the following reaction mechanism for the hydrogen abstraction of ^{3}BP* from amines;[7]

$$^3BP^* + AH \xrightarrow[\text{Electron transfer}]{} {}^3(BP^-\cdots AH^+) \xrightarrow[\text{Proton transfer}]{} (BPH\cdot + A\cdot)$$

where $^3(BP^-\cdots AH^+)$ is the CT complex or ion pair, AH is an amine and BPH· is a ketyl radical.

For the more or less direct elucidation of the reaction mechanism, a number of investigations by using laser photolysis methods have been performed on the reduction processes of ^{3}BP*. In an early research by means of a nanosecond laser photolysis,[8,9] it was suggested that the CT or the ion pair (IP) state prior to the solvation was the species undergoing the proton transfer leading to the BPH· formation, i.e., the proton transfer in the IP state competed with the solvation leading to the ionic dissociation.

The direct measurement on the picosecond dynamics of the excited benzophenone and the amine system was reported by Peters and co-workers.[10-13] On the basis of the observed time-dependent spectral shift of the benzophenone anion radical, they concluded that the structural change of the solvent separated IP formed by the ET between ^{3}BP* and the amine to the contact IP was the key process for the proton transfer to take place. Their conclusion, however, rests upon two postulates: (1) The ET reaction proceeds exclusively between ^{3}BP* and amines (AH) even in such concentrated solutions of the amine as 1—5 M, (2) The time dependent spectral shift of the BP anion band is due to the structural change in the IP of BP^- and AH^+.

These postulates, however, do not seem valid because of the following facts. First, in addition to formation of the IP by the ET between ^{3}BP* and AH, production of the IP by the ET between ^{1}BP* and AH as well as that from the excited state of the CT complex formed between BP and AH in the ground state are inevitable in such concentrated solutions of the amine. The dynamic behaviors of IP's including their ketyl radical formation, ionic dissociation, etc. the reactivity are strongly dependent on their production pathways even if the donor-acceptor pair and the solvent are the same.[20] The different reactivity of the IP depending on the mode of its production must be taken into considerartion for the elucidation of the reaction mechanism and dynamics of the hydrogen abstraction of excited BP from AH in the concentrated solutions of amines. Second, the dynamic behaviors of these various IP's as well as the dissociated free ions produced in longer time regions (a few hundreds of picoseconds—a few nanoseconds after the excitation) in acetonitrile should be included for the interpretation of

† Dedicated to Professor K. Schaffner on the occasion of his 60th birthday.

the spectral shift, because the spectra of dissociated ions and those of IP's, especially the IP formed by CT complex excitation, are different from each other.

Along this line, we have examined the photoreduction process of excited BP by *N,N*-dimethylaniline (DMA) in acetonitrile solution by means of picosecond and femtosecond laser photolysis.[17,18] From these studies it was revealed that the IP produced by the excitation of the ground state CT complex ($^1IP_{com}$), the IP formed by CS at encounter between $^1BP^*$ and DMA ($^1IP_{enc}$), and that produced by CS at encounter between $^3BP^*$ and DMA ($^3IP_{enc}$) exhibit quite different behaviors including the rate constant of the intra-IP proton transfer (PT) and charge recombination deactivation, etc., dependent on the mode of the production. The PT rate constant of $^3IP_{enc}$ was the largest among those of the three kinds of IP's and the production yield of the ketyl radical of $^1IP_{com}$ was practically zero.

We have reported also the results of the picosecond laser photolysis studies on the reaction of the excited benzophenone with diphenylamine (DPA) in several solvents of different polarity.[16] In this case, it was demonstrated that the hydrogen abstraction and CT or IP state formation by ET reaction were competing at encounter between $^3BP^*$ and DPA both in nonpolar and polar solvent, and the CT or IP state relaxed with respect to the donor acceptor configurations and solvation did not contribute to the ketyl radical formation. Such a direct abstraction mechanism was found to be applicable also in the reaction between $^3BP^*$ and DMA in 2-propanol and in isooctane although the consecutive scheme of the ET followed by intra-IP proton transfer was confirmed for the reaction mechanism in acetonitrile.[18]

In addition, proton abstraction of the dissociated free anion of BP from the neutral amine was responsible for the BPH· formation in the photoreaction of BP–1,4-diazabicyclo[2.2.2]octane (DABCO) in acetonitrile solution,[19] where the PT process within the IP state was not observed.

Various experimental results as described above indicate that the reaction mechanism depends on the structure of the amine and the nature of the solvent. Especially, the experimental findings that the reaction mechanism depends on the solvent even if the same amine is used and that the reactivity of the IP between the same donor and acceptor in the same solvent is different depending on the mode of its production indicate that the mutual distance and orientation, including the surrounding solvents, between BP and AH at encounter are of crucial importance for the subsequent reaction processes.

In the present paper, we report the reduction process of BP* with several tertiary amines, such as *N,N*-diethylaniline (DEA), *N,N*-diethyl-*p*-toluidine (*p*-DET), and *N*-methyldiphenylamine (MDPA), in acetonitrile solution. On the basis of the experimental results obtained by picosecond and femtosecond laser photolysis as well as the previous result with DMA, we discuss the reduction process of the excited BP from the viewpoint of the structure of the transient IP which is determined by the mode of its production and by its energy level.

Experimental

A picosecond laser photolysis system with a repetitive mode-locked Nd^{3+}: YAG laser was used for transient absorption spectral measurements in the 10 ps to a few nanosecond region.[21,22] The third harmonic pulse (355 nm) with 22 ps fwhm or Raman scattering light (397 nm) obtained by focusing the 355 nm pulse into cyclohexane liquid was used for exciting the sample solutions. For the measurement of spectra in shorter time region, a femtosecond laser photolysis system was used.[4,23] In this femtosecond photolysis, second harmonics (355 nm) with 500 fs fwhm of pyridine 1 dye laser (710 nm) was used for the excitation.

Benzophenone (Wako, Special Guarantee) was purified by repeated recrystallization from ethanol and sublimation in a vacuum. *N,N*-diethylaniline (DEA) (Wako, Special Guarantee) was refluxed with acetic anhydride, washed with water, dried over potassium hydroxide, distilled under reduced pressure, and stored under vacuum. *N,N*-diethyl-*p*-toluidine (*p*-DET) (Wako, Practical Grade) was also refluxed with acetic anhydride, washed with water, dried over potassium hydroxide, and distilled under reduced pressure three times. *N*-methyldiphenylamine (MDPA) (Tokyo Kasei, Guaranteed Reagent) was distilled under reduced pressure four times. Acetonitrile (Merck Uvasol) was used without further purification for the time resolved transient absorption spectral measurements. All sample solutions were deaerated by repeated freeze-pump-thaw cycles. The BP solution and DEA were deaerated separately and DEA was added to the BP solution by distillation in a vacuum line. All measurements were performed at 22±2 °C.

The extinction coefficients used for the estimation of the reaction yields are as follows; 6500 M^{-1} cm^{-1} at ca. 525 nm for $^3BP^*$, 4600 M^{-1} cm^{-1} at 545 nm for BPH·, and 10000 M^{-1} cm^{-1} for BP^- around 700 nm. The difference of the extinction coefficient of BP^- ($\leqslant$10%) depending on the solvation and on the state such as ion pair and the dissociated free ion was taken into account in the analysis. Detailed discussion on the determination of the extinction coefficient of each species were presented in the previous paper.[16,18]

Results and Discussion

As mentioned in the introductory section and in the previous papers,[17,18] there exist at least three pathways leading to the IP formation in the photoreduction process of BP by AH:

(1) The excitation of the weak CT complex formed in the ground state, $^1IP_{com}$, (2) The ET reaction between the $^1BP^*$ and the amine, $^1IP_{enc}$, and (3) The ET reaction between $^3BP^*$ and the amine, $^3IP_{enc}$. It is of crucial importance to get precise information on the role played by each IP for the elucidation of the reaction mechanisms of the photoreduction process of BP. From such a viewpoint, we proceed to investigate those problems as

follows.

First, we examine the reaction of ^{3}BP* with DEA leading to the ketyl radical formation and make clear the role of $^3IP_{enc}$ in this reaction. Second, we demonstrate the CT complex formation between BP and DEA in the ground state and the dynamic behaviors of this complex in its excited state. Third, we show results obtained by femtosecond laser photolysis, where the ET reaction of ^{1}BP* and DEA is discussed. By summarizing these results and those obtained for the BP-DMA system,[17,18] we discuss the differences among the reactivities of ^{1}BP*, ^{3}BP*, and three kinds of IP's. Finally, we present the experimental results on the reduction process of ^{3}BP* with *p*-DET and that with MDPA. Based on the results of investigation on the ^{3}BP*-tertiary aromatic amine systems in acetonitrile solutions, we discuss the dependence of the reactivity of the $^3IP_{enc}$ on its structure which seems to be related to the energy gap for the ET reaction producing the IP.

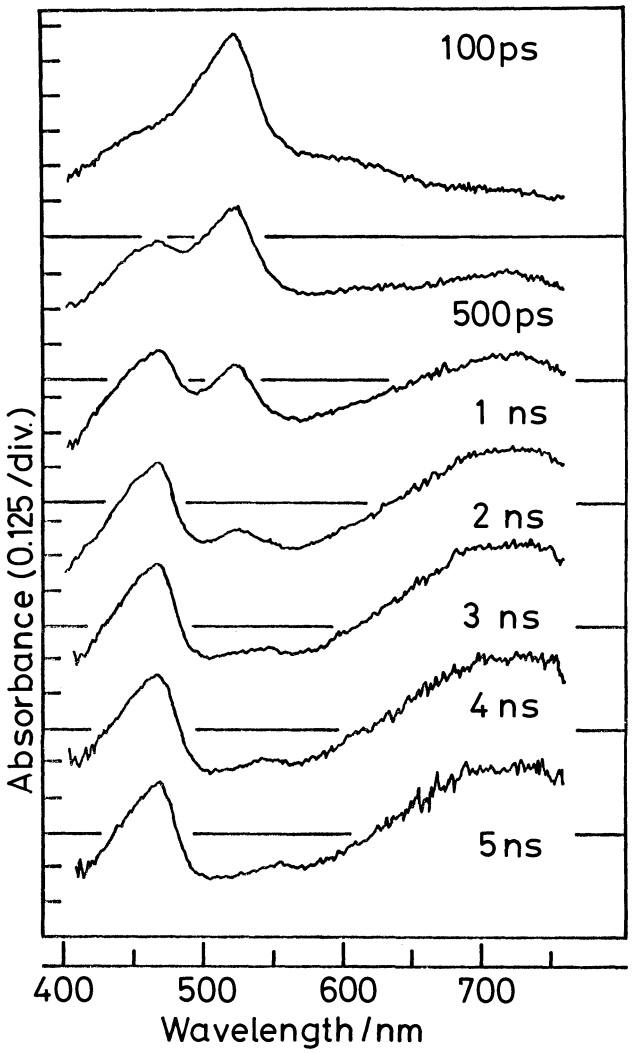

Fig. 1. Time-resolved transient absorption spectra of BP (0.01 M)–DEA (0.05 M) system in acetonitrile solution excited with a picosecond 355 nm laser pulse.

1. Reduction processes of ^{3}BP* by DEA in Acetonitrile Solution. Figure 1 shows the time resolved transient absorption spectra of BP (0.01 M)–DEA (0.05 M) (1 M=1 mol dm^{-3}) system in acetonitrile solution excited with a picosecond 355 nm laser pulse. A transient absorption spectrum with an absorption maximum at 525 nm, which is assigned to ^{3}BP*,[16-19,24,25] decreases with increase of the delay time after the excitation and new bands at 470 nm and ca. 700—720 nm appear. The new absorption band at 470 nm is assigned to DEA$^+$, and that at 700—720 nm to BP$^-$,[26] respectively. Although the absorption signal due to the BPH· radical which has an absorption maximum at 545 nm[27] is observed at longer delay times (3—5 ns) after the excitation, its yield is much smaller than those observed in cases where *N*,*N*-dimethylaniline (DMA) and diphenylamine (DPA) were used as hydrogen donors.[16,17,18] The transient absorption spectra in Fig. 1 indicate that ^{3}BP* gradually evolves with increase of the delay time into BPH· formed by the hydrogen abstraction reaction and $^3IP_{enc}$ produced through the ET reaction. No evolution of the transient absorption spectra was observed at longer delay times than 4 ns after the excitation. Taking into consideration the previous result by nanosecond laser photolysis[9] together with the present one, it may be concluded that the ionic species observed at a few nanosecond after the excitation is due to the dissociated free ions.

In order to clarify time profiles of ^{3}BP*, BPH·, and $^3IP_{enc}$, the observed absorption spectrum at each delay time was analyzed into these three species on the basis of each reference spectrum, the result of which is exhibited in Fig. 2. The ordinate represents the concentration of the individual species calculated by using each extinction coefficient given in the Experimental.

Solid lines in Fig. 2(a) represent the calculated time profiles based on the following scheme, where the BPH· and the $^3IP_{enc}$ which is dissociated into free ions at longer delay times are produced in competition with each other at the encounter of ^{3}BP* with DEA.

$$^3BP^* + DEA \longrightarrow {}^3(BP^-\cdots DEA^+)_{enc} \longrightarrow BP^-_s + DEA^+_s$$
$$\searrow\ (BPH\cdots DEA\cdot) \longrightarrow BPH\cdot + DEA\cdot$$

Scheme 1.

where DEA· indicates the neutral radical produced after the abstraction of a hydrogen atom from DEA. As is clear from Fig. 2(a), time profile of the BPH· radical and that of $^3IP_{enc}$ could not be well reproduced by Scheme 1. The deviation of the calculated time profile of the $^3IP_{enc}$ from the experimental one in such a way that the experimental result is always larger than the calculated curve in the course of the formation of the IP indicates some rapid deactivation process of the ionic species competing with the ionic dissociation. Moreover, the

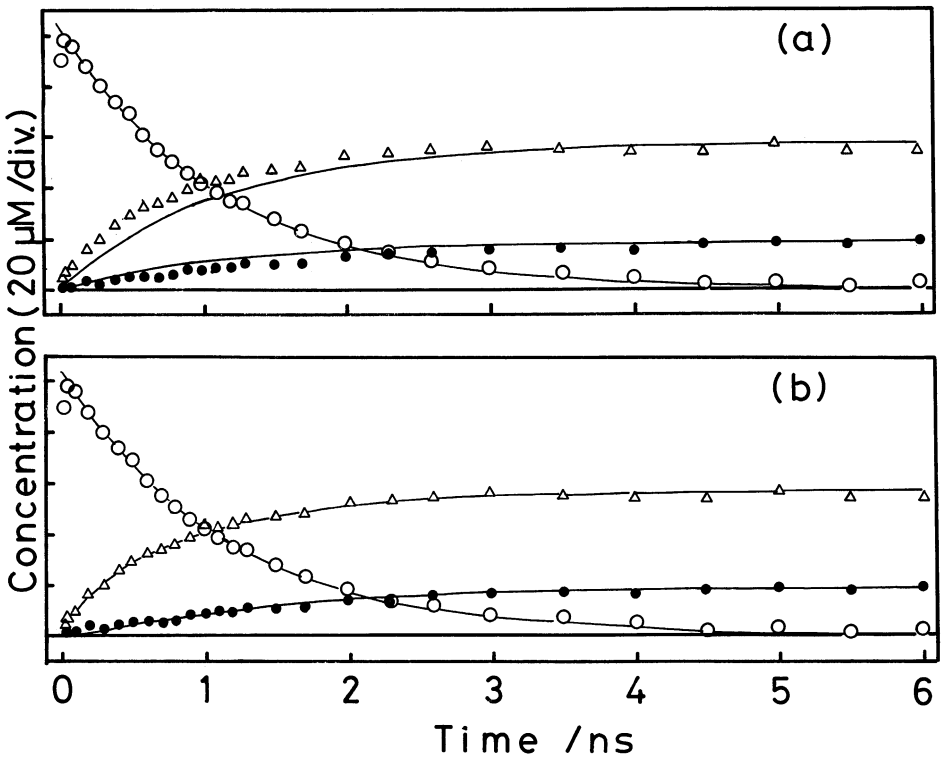

Fig. 2. Time profiles of ^{3}BP* (○), BPH· (●), and BP$^-$ and DEA$^+$ (△) of BP (0.01 M)–DEA (0.05 M) system in acetonitrile solution excited with a picosecond 355 nm laser pulse (see text). Solid lines are calculated curves based on Scheme 1(a), and on Scheme 2(b) (see text).

deviation of the time profile of the BPH· in such a way that the experimental result is always smaller than the calculated curve whose rise time is equal to the decay of ^{3}BP* indicates that the production of BPH· is not directly related to the decrease of ^{3}BP* but some intermediate species exists. Accordingly, the mechanism of Scheme 1 is not adequate for the reaction of ^{3}BP* with DEA in acetonitrile solution, although this direct abstraction mechanism competing with $^3IP_{enc}$ formation was suitable for the hydrogen abstraction process of ^{3}BP* from diphehylamine.[16]

On the other hand, the time profiles calculated on the basis of the Scheme 2 are indicated in Fig. 2(b).

$$^3BP^* + DEA \longrightarrow {}^3(BP^{-}\cdots DEA^{+})_{enc} \longrightarrow BP^-_s + DEA^+_s$$
$$\searrow\ (BPH\cdot\cdots DEA\cdot) \longrightarrow BPH\cdot + DEA\cdot$$

Scheme 2.

Scheme 2 represents the successive mechanism for the hydrogen atom transfer; the IP produced by the ET proceeds to the PT reaction competing with the ionic dissociation process. The parameters for the transient species such as the lifetime of the $^3IP_{enc}$ and reaction yields of the proton transfer and the ionic dissociation were determined respectively in such a manner that the time profiles of ^{3}BP*, BPH·, and $^3IP_{enc}$ were consistent with each other. As shown in Fig. 2(b), the time profile of each species is well reproduced by the calculated curve based on the Scheme 2. The lifetime of $^3IP_{enc}$ was 300 ps and the reaction yield of the proton transfer and that of the ionic dissociation were 0.19, and 0.55, respectively.

In order to confirm the validity of the above parameters obtained by the analysis in Fig. 2(b), we have examined several solutions containing different concentration of DEA. Fig. 3 shows time-resolved transient absorption spectra of BP(0.01 M)–DEA (0.3 M) in acetonitrile solution excited with a picosecond 355 nm laser pulse. ^{3}BP* with its absorption maximum at 525 nm decreases and those of the IP at 470 nm and 700—720 nm, and the BPH· radical at 545 nm increases with increase of the delay time after the excitation. These results are rather similar to those in Fig. 1. However, it should be noted here that the transient absorption spectrum at early stage after the excitation shows a rather large amount of the absorption signal due to IP's compared to that observed in the solution containing 0.05 M DEA. This rapid production of IP's is partly due to the formation of $^1IP_{enc}$, by the ET reaction between ^{1}BP* and DEA, and the formation of $^1IP_{com}$ by the excitation of the CT complex formed in the ground state. More details on these species will be described in the later part of the present paper.

Figure 4 shows the time profiles of three kinds of transient species, ^{3}BP*, BPH·, and IP's, of the BP (0.01 M) -DEA (0.3 M) in acetonitrile solution obtained by the same analysis as in Fig. 2. The initial yield of ^{3}BP* and the sum of yields of IP's which were produced via the excitation of the CT complex and the nonstationary quenching of ^{1}BP* by DEA was in the ratio ca. 3 : 1. In other words, almost 25% of the absorbed photon energy was used for the production of the species other than ^{3}BP*. Solid lines in Fig. 4 are calculated curves based on the consecutive reaction scheme as in Fig. 2(b) and parameters were determined in such a manner that time profiles of these three species were consistent with each other. Contributions from singlet IP's including their lifetimes and reaction yields are included in this calculation, details of which will be discussed later in the present paper.

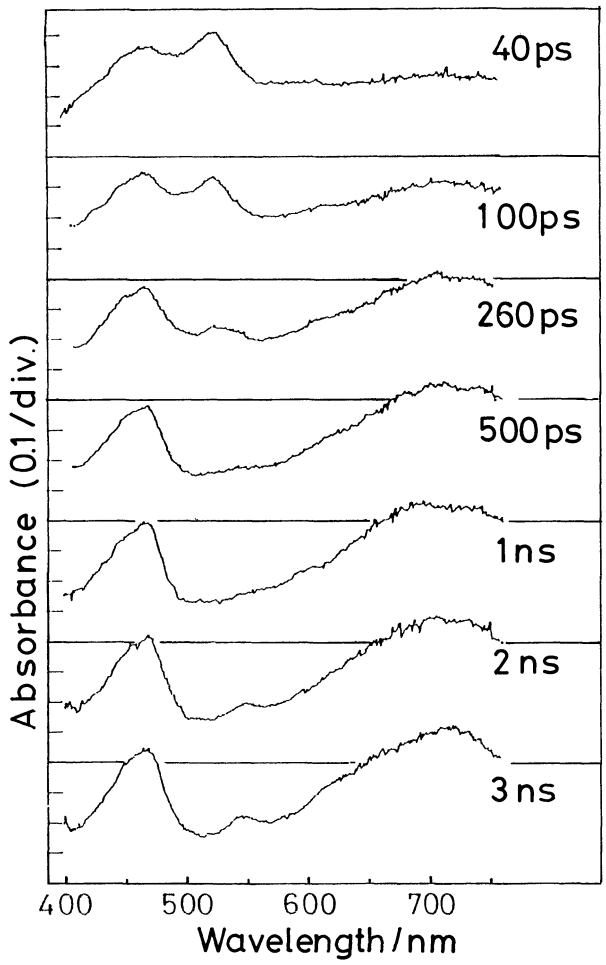

Fig. 3. Time-resolved transient absorption spectra of BP (0.01 M)-DEA (0.3 M) system in acetonitrile solution excited with a picosecond 355 nm laser pulse.

As shown in Fig. 4, experimental results are well reproduced by this calculation with following parameters; the lifetime of $^3IP_{enc}$: 290 ps, the yield of BPH·: 0.23 and that for the ionic dissociation: 0.65. The lifetime and reaction yields of $^3IP_{enc}$ agree with those obtained for the solution containing 0.05 M of DEA (Figs. 1 and 2) within the experimental error.

The consecutive reaction mechanism (Scheme 2) was found to reproduce the experimental time profiles over a wide range of DEA concentration (Table 1). Results in Table 1 clearly show that similar values were obtained for the lifetime and the reaction yields of $^3IP_{enc}$ over a wide range of the concentration of DEA by the curve-fitting procedure, indicating clearly that the reaction mechanism of the hydrogen abstraction of ^{3}BP* from DEA in acetonitrile solution can be described by Scheme 2. Moreover, the rate constant for the ionic dissociation, 2.1×10^9 s^{-1}, was similar to those obtained for a number of organic radical ion pairs produced by the electron transfer at encounter collision in acetonitrile solution at room temperature.[20,28] This result also confirms that the values of the lifetime and reaction yields of the $^3IP_{enc}$ obtained by this analysis and the extinction coefficients used here are appropriate.

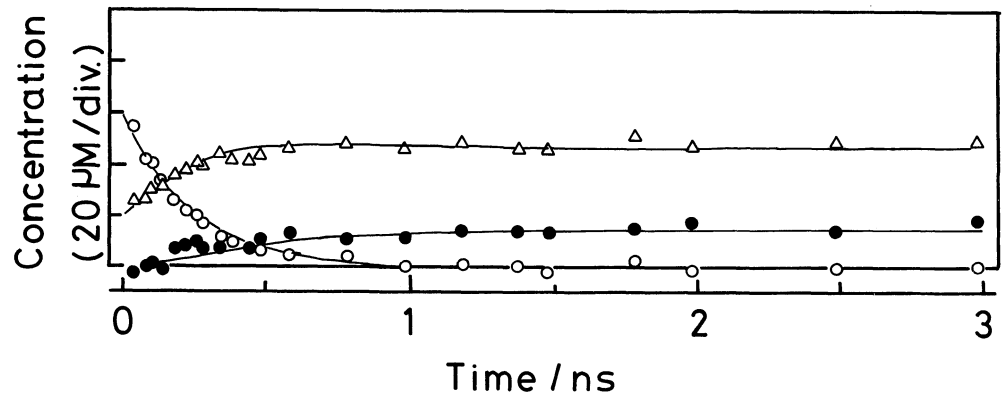

Fig. 4. Time profiles of ^{3}BP* (○), BPH· (●), and BP^- and DEA^+ (△) of BP (0.01 M)-DEA (0.3 M) system in acetonitrile solution excited with a picosecond 355 nm laser pulse (see text). Solid lines are calculated curves based on Scheme 2 (see text).

Table 1. Properties of $^3(BP^{-}\cdots DEA^{+})_{enc}$, in Acetonitrile Solutions with Various Concentrations of DEA. τ: Lifetime, ϕ_{PT} and k_{PT}: Reaction Yield and Rate Constant of the Proton Transfer, ϕ_{ID} and k_{ID}: Reaction Yield and Rate Constant for the Ionic Dissociation

[DEA]/M	τ/ps	ϕ_{PT}	ϕ_{ID}	k_{PT}/s^{-1}	k_{ID}/s^{-1}
0.05	300	0.19	0.55	6.0×10^8	1.8×10^9
0.1	280	0.19	0.62	6.8×10^8	2.2×10^9
0.3	290	0.23	0.65	7.9×10^8	2.2×10^9
0.6	290	0.21	0.60	7.2×10^8	2.1×10^9
1.0	270	0.23	0.63	8.5×10^8	2.3×10^9
Average	(286±11)	0.21±0.034	0.61±0.034	$(7.3\pm0.17)\times10^8$	$(2.1\pm0.17)\times10^9$

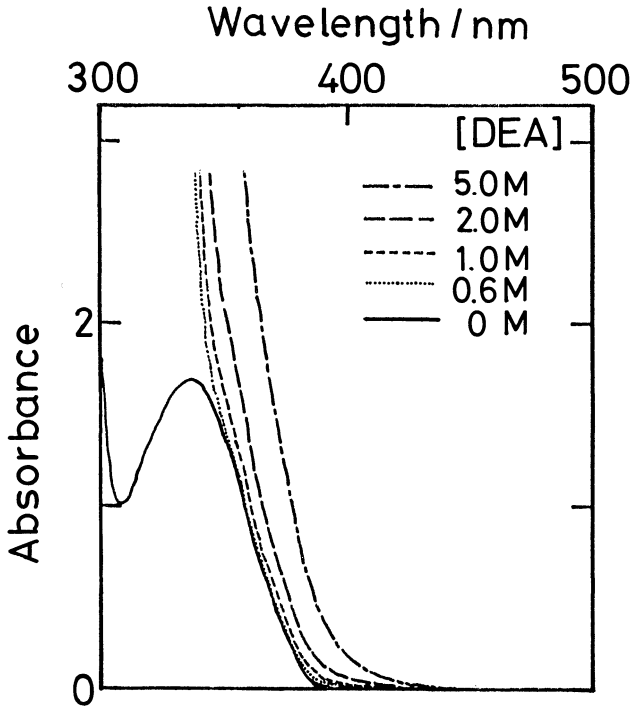

Fig. 5. Effect of DEA concentration on the ground state absorption of benzophenone in acetonitrile.

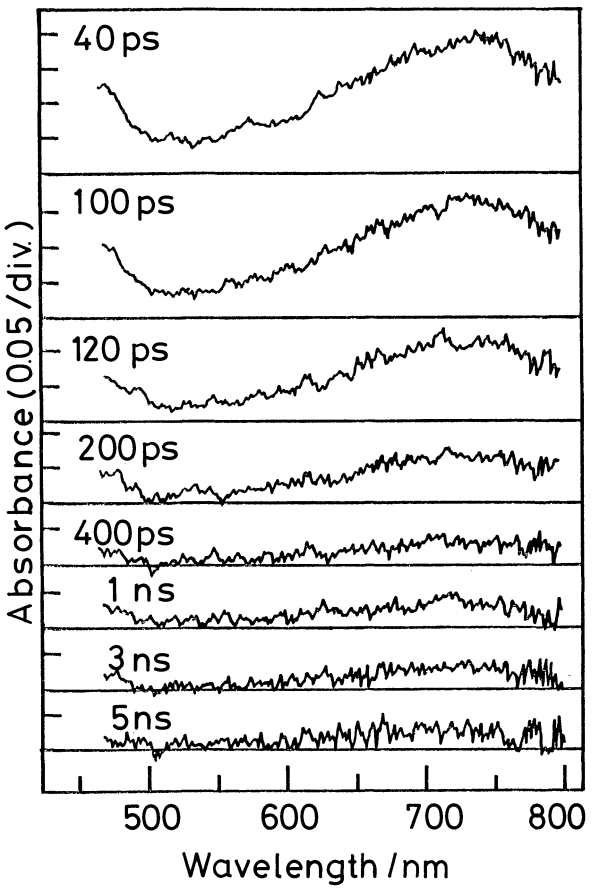

Fig. 6. Time-resolved transient absorption spectra of BP (0.5 M)–DEA (1.0 M) system in acetonitrile excited with a picosecond 397 nm laser pulse.

2. Excited State Dynamics of the Weak CT Complex between BP and DEA Formed in the Ground State in Acetonitrile Solution. In Fig. 5, we show the ground state absorption spectra of BP (0.05 M) with added DEA of various concentrations in acetonitrile solution. The increase of the absorbance in the wavelength region longer than 360 nm was observed with increase of the concentration of DEA. This change of the absorption spectrum can be attributed to the formation of weak CT complex between BP and DEA, since the selective excitation of the absorption tail leads to the immediate formation of $^1IP_{com}$ (see Fig. 6). The equilibrium constant of this complex formation, K_g, was estimated to be 0.1—0.5 by Benesi-Hildebrand plot.

Figure 6 shows transient absorption spectra of BP (0.5 M)–DEA (1.0 M) system in acetonitrile solution excited with a picosecond 397 nm laser pulse, at which wavelength the ground state complex is selectively excited as can be seen from Fig. 5. A broad absorption spectrum with an absorption maximum around 740 nm which appears immediately after the excitation can be safely assigned to BP^- in $^1IP_{com}$ on the basis of the absorption maximum and spectral shape.[18,26] The absorption in the wavelength region shorter than 500 nm, which also appears immediately after the excitation, can be ascribed to DEA^+. With increase of the delay time after the excitation, the absorption due to $^1IP_{com}$ decreases and reaches plateau value attributable to the

dissociated free ions. The decay process of the IP was approximately reproduced by the single exponential function and the time constant was obtained to be (93±5) ps. No absorption due to BPH· was detected after the decay of $^1IP_{com}$. Accordingly, it is concluded that the dominant pathway in the decay of $^1IP_{com}$ is the charge recombination (CR) process and ca. 10% of $^1IP_{com}$ dissociates into free ions.

Similar results to those of the present $^1IP_{com}$ were also observed for the excited state dynamics of the weak CT complex between BP and DMA formed in the ground state in acetonitrile solution.[17,18] Namely, short-lived transient IP state, $^1(BP^-\cdots DMA^+)_{com}$, produced by the excitation at the CT absorption band, was deactivated rapidly via the efficient CR process. The lifetime and the yield of the ionic dissociation of $^1(BP^-\cdots DMA^+)_{com}$ were (85±3) ps and <0.04, respectively. In addition, no BPH· formation was observed also in the course of the decay process of $^1(BP^-\cdots DMA^+)_{com}$. Moreover, the peak position of the absorption band due to BP^- in the IP state, $^1(BP^-\cdots DMA^+)_{com}$, was also at 740 nm, while those of $^3IP_{enc}$ and dissociated free BP^- are around 700—720 nm as shown in Fig. 1. In relation to these results, it should be noted here that the peak position of BP^- absorption changes depending on the structure of the IP and the degree of the solvation according to the previous reports.[29,30] The relation between the peak position of the BP^- absorption and the structure of IP including the surrounding solvents will be discussed in detail in the later part of the present paper.

3. Photoreduction Process of $^1BP^*$ by DEA in Acetonitrile Solution. Figure 7 shows the time resolved absorption spectra of BP (0.05 M)–DEA (0.6 M) system in acetonitrile solution excited with a femtosecond 355 nm laser pulse. The spectrum indicated by the dotted line in the first frame is due to the $S_n \leftarrow S_1$ transition of BP measured in the amine free solution.[17,18] In addition to the $S_n \leftarrow S_1$ absorption spectrum, an absorption maximum at 470 nm and broad absorption whose intensity increases toward longer wavelength region than 600 nm are observed at 1 ps after the excitation of the solution containing 0.6 M of DEA. The absorption band at 470 nm and the broad absorption in the region longer than 600 nm are assigned respectively to DEA^+ and BP^- in the IP. This rapid formation of the IP is due to the excitation at the CT band of the complex overlapping the ground state absorption band of free BP, as stated in the previous section. With increase of the delay time after the excitation, the absorption at 575 nm decreases and the absorption due to the IP gradually increases together with the increase of a new band at 525 nm due to $^3BP^*$.

The time profiles of transient absorbance at 575, 660, and 525 nm are exhibited in Fig. 8. The absorbance at 575 nm due to $^1BP^*$ arises with the time resolution of the apparatus, and shows a rapid decay with the time constant of (5.5±0.5) ps followed by a much slower decay process.

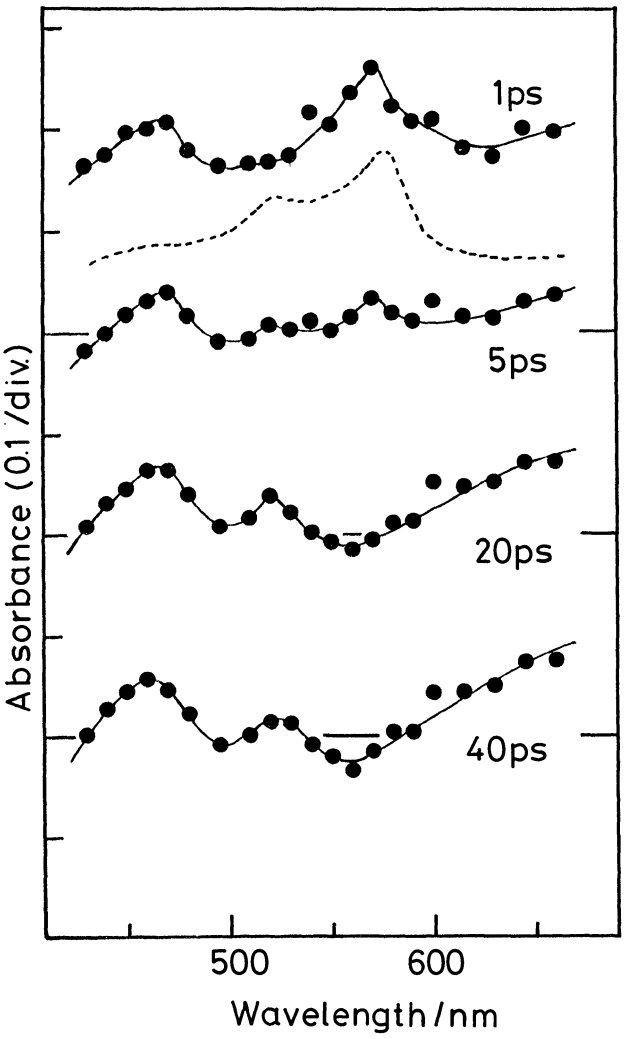

Fig. 7. Time-resolved transient absorption spectra of BP (0.05 M)–DEA (0.6 M) system in acetonitrile, measured by exciting with a 500 fs 355 nm laser pulse.

The rapid decay can be attributed to the quenching process of $^1BP^*$ by DEA on the basis of the time evolution of the spectrum in Figs. 7, 8. Since the lifetime of $^1BP^*$ in amine free solution of acetonitrile was 9.0 ps,[17,18] ca. 30—40% of $^1BP^*$ is quenched by the reaction with the neighboring DEA. On the other hand, the slower decay process with the time constant longer than a few tens of picoseconds may be attributed to the decay of $^3BP^*$ and IP's whose absorptions overlap that of $^1BP^*$ at this wavelength.

The time dependence of the absorbance monitored at 660 nm shows the rapid increase within the response of the apparatus followed by the further increase with the time constant of (5.5±0.3) ps, and then by much slower decay process. The rapid appearance of the IP immediately after the excitation is ascribed to the excitation of the CT complex formed in the ground state. On the other hand, the slower rise with the time constant of (5.5±0.3) ps is due to the IP formation via the ET

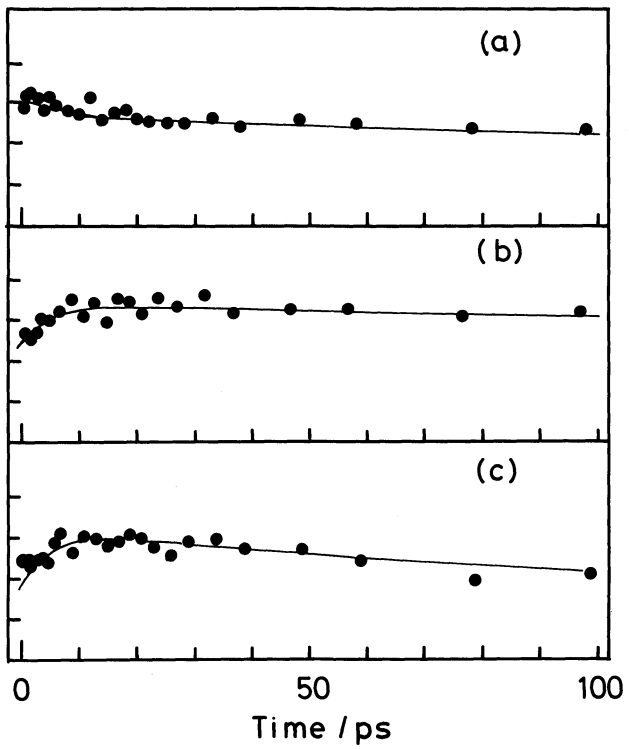

Fig. 8. Time profiles of transient absorbance of BP (0.05 M)–DEA (0.6 M) system in acetonitrile excited with a 500 fs 355 nm laser pulse and observed at 575 nm (a), 670 nm (b), and 525 nm (c).

reaction between ^{1}BP* and DEA, since the time constant of the decrease of ^{1}BP* is identical with the rise time of the IP. The quenching rate constant of ^{1}BP* by DEA, 1.6×10^{11} M^{-1} s^{-1}, is about 8—10 times as large as the diffusion controlled rate constant in acetonitrile. This rapid quenching process is probably due to the rapid reaction of ^{1}BP* with the neighboring DEA, the so-called transient effect or non-stationary quenching. Such a large reaction rate constant for the ET process between ^{1}BP* and the amine was also observed in the case of BP–DMA system.[17,18]

Time profile of the absorbance at 525 nm which is an absorption maximum of ^{3}BP* is shown in Fig. 8(c), indicating that the rapid increase of the absorbance immediately after the excitation is followed by the slower rise and much slower decay process. The rapid rise of the absorbance is ascribed to the contribution of ^{1}BP* as can be seen from Fig. 8(a). The slower increase of the absorbance is ascribed to the formation of ^{3}BP* by the intersystem crossing of ^{1}BP* on the basis of the coincidence of the time constant of the rise of ^{3}BP*, (5.4±0.5) ps, with the decay of ^{1}BP* in Fig. 8(a). Much slower decay of the absorbance may be due to the quenching of ^{3}BP* by DEA and the recombination process of IP's. The rapid quenching process of ^{1}BP* by DEA was also observed in acetonitrile solutions containing 1.0 M of DEA and that with 2.0 M of DEA. The lifetime of ^{1}BP* in the solution of [DEA]=1.0 M was 3.7 ps and that for 2.0 M DEA was 2.5 ps, respectively. With increase of [DEA], the increase of the yield of $^1IP_{enc}$ and the decrease of that of ^{3}BP* were observed.

By the analysis of the transient absorption spectrum immediately after the excitation with the femtosecond 355 nm laser pulse into two components, ^{1}BP* and $^1IP_{com}$, and by dividing each spectrum by the extinction coefficient, the fraction of $^1IP_{com}$ and that of ^{1}BP* were obtained to be 0.33 and 0.67, respectively. The fraction of $^1IP_{com}$ increases with increase of [DEA]. The fraction of $^1IP_{com}$ for 1.0 M solution of DEA and that for 2.0 M solution were 0.38 and 0.67, respectively. In addition, the contribution of the rapid quenching process of ^{1}BP* by DEA also increases with increase of [DEA] and, as a consequence, the yield of ^{3}BP* decreases. From the lifetime of ^{1}BP* and spectral evolution, we can evaluate the initial yields of $^1IP_{com}$, $^1IP_{enc}$, and ^{3}BP*, respectively. For example, only 33% of the light energy absorbed in the acetonitrile solution of BP containing 0.6 M of DEA terminated in the production of ^{3}BP*. This value decreases with increase of [DEA]; that for 1.0 M solution was 25% and that for 2.0 M solution was 10%.

From the above results and discussion, we can summarize the ET and related processes in short time regions of the excited benzophenone in the presence of DEA in acetonitrile solution as follows.

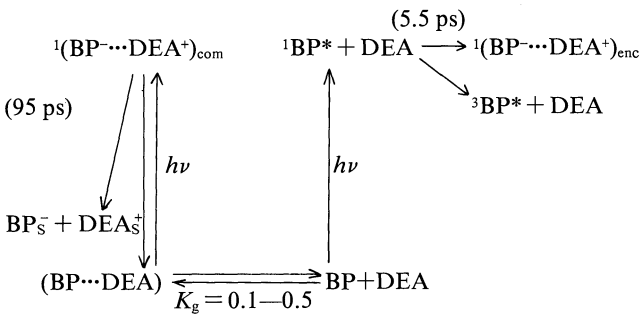

Scheme 3.

In this scheme, the $^1IP_{com}$ produced by the excitation of the CT complex formed in the ground state, is discriminated from the $^1IP_{enc}$ produced via the ET reaction between ^{1}BP* and DEA. In the case of the ET reaction in the system of BP and DMA, clear difference in the reaction processes depending on the mode of the production of IP's was observed between these two kinds of IP's.[17,18] The circumstance was similar also in the present case. The detailed discussion on this difference between two kinds of ^{1}IP's will be given in the later part of the present paper.

In order to elucidate dynamic behaviors and reaction pathways of $^1IP_{enc}$ quantitatively, transient absorption spectra of acetonitrile solutions of BP (0.01 M)–DEA (0.6 M) system in picosecond - a few nanosecond region were measured by means of the picosecond 355 nm laser pulse excitation (Fig. 9). A large amount of transient

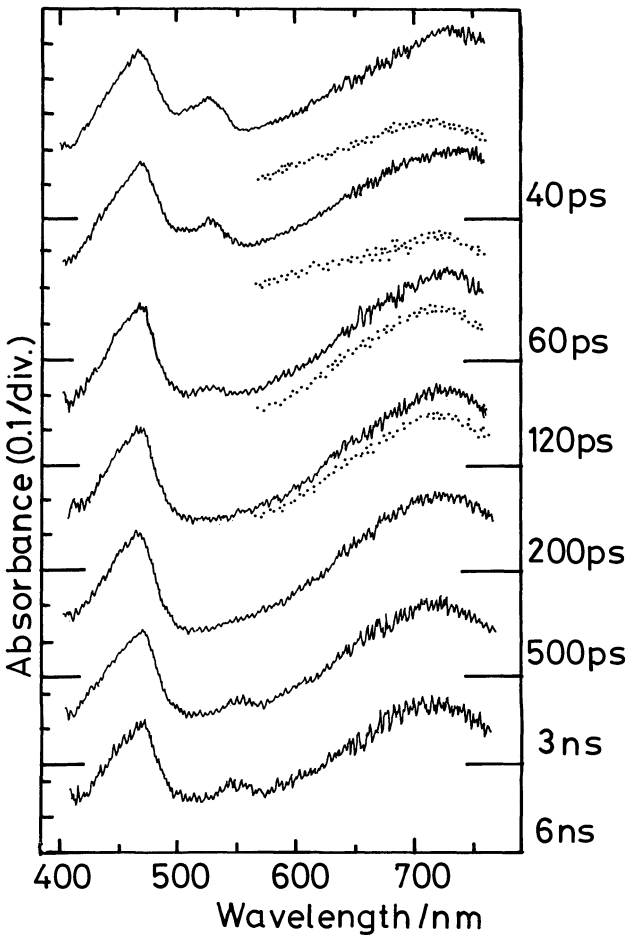

Fig. 9. Time-resolved transient absorption spectra of BP (0.01 M)–DEA (0.6 M) system in acetonitrile solution, excited with a picosecond 355 nm laser pulse. Dotted lines are the absorption spectra obtained by subtracting the contribution of the absorption bands due to $^1(BP^- \cdots DEA^+)_{com}$ from the observed spectra (see text).

absorption due to IP's which involves both $^1IP_{com}$ and $^1IP_{enc}$ was observed immediately after the excitation. In addition to the absorption bands of IP's, clear signal due to the absorption $^3BP^*$ is observed at 525 nm. The initial yield of $^3BP^*$ was 0.33 in this solution containing 0.6 M of DEA as described already in the interpretation of Figs. 7 and 8. With increase of the delay time after the excitation, the absorption of IP's also decreases and reaches a plateau value which is ascribed to the dissociated free ions. Very small absorption signal due to BPH· was observed around 550 nm at longer delay times (3—6 ns).

In Fig. 10, we show the time profiles of $^3BP^*$, BPH·, and IP's, which were obtained by the analysis of the observed spectra in Fig. 9 into these components. The initial yields of $^1IP_{com}$, $^1IP_{enc}$, and $^3BP^*$ were determined by the femtosecond laser photolysis, respectively. In addition, the reaction pathways have been elucidated and their rate constants have been determined respectively for $^3BP^*$, $^3IP_{enc}$, and $^1IP_{com}$. Hence, in principle, informations on the reactions of $^1IP_{enc}$ can be obtained by subtracting from the observed results the contributions from the reaction between $^3BP^*$ and DEA and that of $^1IP_{com}$ on the basis of their initial yields and time dependences. In the actual analysis of the time profiles of $^1IP_{enc}$, we employed the curve-fitting procedure where the lifetime and the reaction yields were varied as parameters. The solid lines in Fig. 10 were calculated curves by assuming that the lifetime, the reaction yield of the proton transfer, and the ionic dissociation yield of $^1IP_{enc}$ were 350 ps, 0.14, and 0.50, respectively. The solid curves for IP's and BPH· in Fig. 10 include the contributions from $^3IP_{enc}$ and $^1IP_{com}$. As shown in Fig. 10, the experimental results are reproduced by the calculated time dependences, and further, parameters for $^1IP_{enc}$ are almost independent of the DEA concentration as shown in Table 2. The averaged lifetime, reaction yields for the proton transfer, ionic dissociation, and charge recombination of $^1IP_{enc}$ were 343 ps, 0.15, 0.48, and 0.37, respectively.

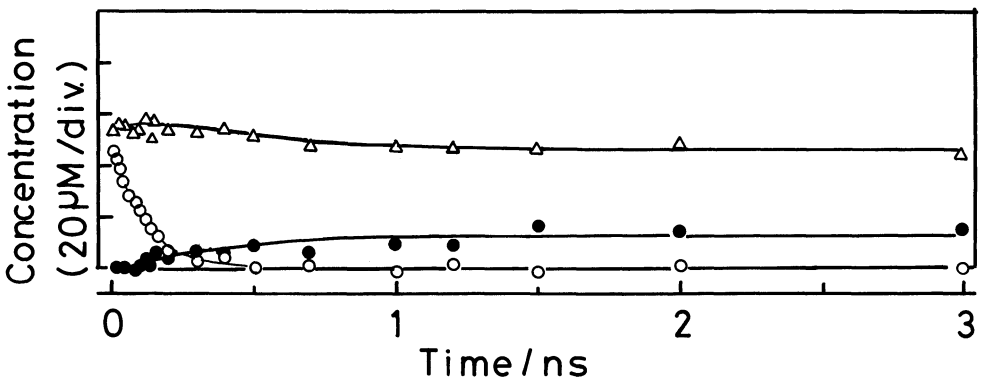

Fig. 10. Time profiles of $^3BP^*$ (○), BPH· (●), and BP^- and DEA^+ (△) of BP (0.01 M)–DEA (0.6 M) system in acetonitrile solution excited with a picosecond 355 nm laser pulse.

Table 2. Properties of the Singlet Ion Pair, $^1(BP^-\cdots DEA^+)_{enc}$, in Acetonitrile Solutions with Various Concentrations of DEA. τ: Lifetime, ϕ_{PT} and k_{PT}: Reaction Yield and Rate Constant of the Proton Transfer, ϕ_{ID} and k_{ID}: Reaction Yield and Rate Constant of the Ionic Dissociation, ϕ_{CR} and k_{CR}: Reaction Yield and Rate Constant of the Charge Recombination

[DEA]/M	τ/ps	ϕ_{PT}	ϕ_{ID}	ϕ_{CR}	k_{PT}/s^{-1}	k_{ID}/s^{-1}	k_{CR}/s^{-1}
0.3	350	0.15	0.45	0.40	4.3×10^8	1.3×10^9	1.1×10^9
0.6	350	0.14	0.50	0.36	4.0×10^8	1.4×10^9	1.0×10^9
1.0	330	0.15	0.50	0.35	4.6×10^8	1.5×10^9	1.1×10^9
Average	(343±9)	0.15±0.005	0.48±0.024	0.37±0.021	$(4.3\pm0.044)\times10^8$	$(1.4\pm0.094)\times10^9$	$(1.1\pm0.04)\times10^9$

4. Absorption Maximum of BP^- and the Structure of IP Including the Surrounding Solvents. Peters et al. reported the time-dependent blue-shift of the absorption spectrum of BP^- in the photoreduction process of excited BP with amines including DEA and they concluded that this shift was due to the structural change of the IP from the solvent-separated IP(SSIP) to the contact IP(CIP) based on the postulate that the ET reaction proceeded exclusively between $^3BP^*$ and amines.[12] As shown in Fig. 9, it was observed also in the present study that the peak position of BP^- absorption band gradually shifted from 730—740 nm to 700—710 nm region with increase of the delay time after the excitation. However, as we have pointed out in the previous sections of this paper and in the previous paper on the reduction of excited BP with DMA,[17,18] the contributions of both $^1IP_{com}$ and $^1IP_{enc}$ to the observed spectra should be taken into account for the elucidation of this spectral shift. The wavelength of the absorption peak of BP^- in $^1IP_{com}$ which decays with the time constant of (93±5) ps, was 740 nm as indicated in Fig. 6, and was different from those of $^3IP_{enc}$ and free BP^-.

In order to clarify whether the spectral shift is the intrinsic one caused by the structural change of IP or the apparent one arising from the disappearance of $^1IP_{com}$, we plotted the spectrum of BP^- obtained by subtracting the contribution of the spectrum due to $^1(BP^-\cdots DEA^+)_{com}$ overlapping those of $^1(BP^-\cdots DEA^+)_{enc}$ and $^3(BP^-\cdots DEA^+)_{enc}$ considering its fraction determined by the analysis of the time profiles of those species and its lifetime (dotted lines in Fig. 9). It is clear that the spectrum from which the contribution of $^1(BP^-\cdots DEA^+)_{com}$ was removed showed an absorption maximum around 700—720 nm although a rather broad spectrum gradually evolved into a sharper one with increase of the delay time after the excitation. From this result, we can conclude that the time dependent spectral shift was caused mainly by the disappearance of the spectrum due to $^1(BP^-\cdots DEA^+)_{com}$. This result is similar to that observed previously in the case on BP–DMA in acetonitrile solution.[17,18]

The fact that the absorption maximum of $^1IP_{com}$ is different from those of $^1IP_{enc}$, $^3IP_{enc}$, and free BP^- in both BP–DMA and BP–DEA systems may be ascribed to the difference of the structure of IP such as the mutual distance and orientation between BP^- and amine cation including the surrounding solvents. The present results clearly indicate that such assignment of the longer wavelength absorption to the SSIP and shorter one to the CIP as made by Peters et al.[12] is erroneous. Since the absorption maximum of the free BP^- was rather close to those of $^1IP_{enc}$ and $^3IP_{enc}$, ca. 700—720 nm, the structure of the solvation surrounding the BP^- in these IP_{enc}'s seems to be rather similar to those of the free BP^-. Hence, it is reasonable to assign the absorption maximum at 740 nm to the compact IP or CIP state of BP^- and amine cation and that at 700—720 nm to a more or less loose IP (LIP) or SSIP and solvated free ion state.

The above assignment is also supported by the recent investigations which demonstrate the large difference in the dynamic behaviors of IP's of various donor acceptor systems depending on the mode of their production.[2,20,28] In these studies, charge recombination (CR) rate of IP produced by the excitation of the CT complex and its dependence on the energy gap between the IP state and the ground state, $-\Delta G^\circ_{ip}$, have been examined in the case of various CT complexes covering a wide range of the energy gap by using femtosecond and picosecond laser photolysis. By these investigations, it has been revealed that the CR rate of IP produced by the CT complex excitation shows an essentially different energy gap dependence from the bell shaped one obtained in the case of IP formed by charge separation at encounter in the fluorescence quenching reaction.[2-4,20,28] Further, the CR rate of IP produced by the CT complex excitation has been confirmed, in general, to be greater than that of IP formed by charge separation at encounter for the same donor (D) and acceptor (A) pair in acetonitrile.[20] From these and related findings, it has been also suggested that the structure of IP's including the surrounding solvent is different from each other; the CIP probably with no intervening solvent molecule between A^- and D^+ would be produced in the case of the excitation of the CT complex, while LIP or SSIP with intervening solvent molecules between A^- and D^+ may be formed in the CS at encounter in the fluorescence quenching reaction. Moreover, from the results of those investigations, it has been concluded that the structures of these IP's could be maintained at least during several hundreds of picoseconds.[2-4,20,28]

Table 3. Dependence of the Reaction Rate Constants of the Ion Pairs upon the Mode of Its Production

	k_{PT}/s^{-1}	k_{ID}/s^{-1}	k_{CR}/s^{-1}
$^3(BP^-\cdots DEA^+)_{enc}$	7.3×10^8	2.1×10^9	
$^1(BP^-\cdots DEA^+)_{enc}$	4.3×10^8	1.4×10^9	1.1×10^9
$^1(BP^-\cdots DEA^+)_{com}$	$\ll10^8$	1.4×10^9	9.3×10^9
$^3(BP^-\cdots DMA^+)_{enc}$	5.4×10^9	1.4×10^9	
$^1(BP^-\cdots DMA^+)_{enc}$	6.6×10^8	9.5×10^8	5.8×10^8
$^1(BP^-\cdots DMA^+)_{com}$	$\ll10^8$	$\leqslant4\times10^8$	1.1×10^{10}

The dependence of the CR rate of IP on its mode of the production as observed in the present study on BP–DEA system as well as BP–DEA system is similar to those observed in the case of the above described various singlet IP's. In addition, we have confirmed that the relation between the CR rate and $-\Delta G^\circ_{ip}$ observed for $^1IP_{com}$ as well as $^1IP_{enc}$ in the BP–DEA and BP–DMA systems is also quantitatively in agreement with that predicted by the experimental results on various singlet IP's covering a wide range of $-\Delta G^\circ_{ip}$.[2-4,20,28] From these results regarding the $-\Delta G^\circ_{ip}$ dependence of the CR rate, the behaviors of the present $^1IP_{com}$ and $^1IP_{enc}$ are considered to be typical of the IP's produced by the excitation of the CT complex and via the ET reaction at encounter collision in the fluorescence state, respectively. By integrating the experimental results on the absorption maxima of the spectrum of BP^- in various kinds of IP's and the energy gap dependence of the CR rate of BP–DEA as well as BP–DMA IP systems, it is reasonable to assign the absorption maximum at 740 nm to the contact or compact IP state of BP^- and amine cation and that at 700—720 nm to LIP or SSIP and solvated free ion state.

5. Difference of the Reactivity between IP's Depending on the Mode of the Production. In Table 3, we list the rate constants of the proton transfer, k_{PT}, the ionic dissociation, k_{ID}, and the the charge recombination, k_{CR}, for the three kinds of IP's, $^1IP_{com}$, $^1IP_{enc}$, and $^3IP_{enc}$. In this table, the results on the IP's of BP–DMA system[17,18] are included also for the purpose of comparison. The CR rate constant of $^3IP_{enc}$ is not listed in this table, since this rate constant is very small, and hence, its quantitative determination was difficult. In both systems, clear difference of each rate constant depending on the mode of the production of the IP was observed. This result indicates that the structure of the IP is different from each other and it is approximately kept during the lifetime of the IP.

Although the rate constant of each process such as the ionic dissociation, the charge recombination, and the proton transfer is different between $(BP^-\cdots DEA^+)$ and $(BP^-\cdots DMA^+)$, the dependence of the rate constant on the mode of the production of the IP is very similar. The k_{PT}, of $^3IP_{enc}$ is the largest among these three kinds of IP's and the yield of BPH· radical of $^1IP_{com}$ was practically zero for both systems. Since the dependence of the rate constant on the production mode of the IP, $(BP^-\cdots DEA^+)$, is very similar to that of $(BP^-\cdots DMA^+)$, the interpretation in the previous paper[17,18] seems applicable also to the present result. In the following, we briefly discuss the difference of the reactivity between different IP's.

5. (a) The Difference of the Reactivity between the Singlet IP's Depending on the Mode of Their Production. In general, the geometric requirement for the proton or the hydrogen atom transfer processes seems to be more severe compared to that for the electron transfer reaction, since the conformational requirement for the latter process is dependent on the electronic molecular orbital spreading over a rather wide region, while the sites for the transfer of proton or hydrogen in the donor and the acceptor are limited within the narrow region. Hence, the difference in the structure of the IP such as the orientation and the distance seems to strongly affect the proton transfer probability.

As we have discussed in the interpretation of the spectral shift of BP^- absorption indicated in Fig. 9, $^1IP_{com}$ between BP and DEA as well as DMA may have quite different structures including the solvation from those of IP_{enc}. As a consequence of this difference in the structure, the reactivity of $^1IP_{enc}$ may be quite different from that of $^1IP_{com}$. At the present stage of the investigation, it is rather difficult to determine the precise structure of the IP composed of two molecules. However, it is strongly suggested that the initial structure of $^1IP_{com}$, especially the orientation of D^+ and A^- in the IP, is quite different from those of IP_{enc}'s. In addition, from the $-\Delta G^\circ_{ip}$ dependence of the CR rate, it is suggested that the $^1IP_{com}$ between BP and DEA or DMA has a rather rigid structure where the ions cannot reorient to take a suitable structure for the proton transfer before the recombination, while $^1IP_{enc}$ produced by the electron transfer between $^1BP^*$ and the amine at encounter has a more or less loose structure and is long-lived to form the suitable geometry for ketyl radical formation.

5. (b) The Difference of the Reactivity between $^3IP_{enc}$ and $^1IP_{enc}$. The reaction mechanism of the ketyl radical formation in the case of BP–DEA and –DMA systems in acetonitrile solutions has been confirmed to be the successive one of the IP formation followed by the proton transfer not only in the case of $^3BP^*$ but also $^1BP^*$. However, reaction rate constants in $^3IP_{enc}$ and $^1IP_{enc}$ are different from each other. The large difference of the charge recombination rate constant, k_{CR}, between two kinds of IP's can be ascribed to the difference of the spin multiplicity of the IP. On the other hand, the rate constant of the proton transfer, k_{PT}, of $^3IP_{enc}$ is larger than that of $^1IP_{enc}$, which cannot be ascribed solely to the difference of the spin multiplicity. This difference of k_{PT} between the two kinds of IP's may be related to the difference in the structure of the IP such as the mutual distance and orientations of ions in the pair including the surrounding solvents. Although it is

rather difficult at the present stage of the investigation to give any definite conclusion on the structures of these IP's, it is plausible that the IP produced by the ET reaction between ^{1}BP* and the amine has a more specific structure since the ET process is mainly due to the very rapid non-stationary reaction between the neighboring pair and, as a consequence, the shorter mutual distance and some specific orientation between the pair may be favorable for the reaction, leading to somewhat different IP structures from those produced via the stationary diffusion process. The difference in the electronic structure of ^{1}BP* from ^{3}BP* may play also some role in determining the mutual configurations favorable for ET between donor and acceptor at the encounter.

Summarizing above results and discussion on the difference of reactivity between ^{1}IP's and that between IP_{enc}'s, it may be concluded that the difference of the reactivity depending on the mode of the production of IP is related mainly to the difference of the mutual orientation of D^+ and A^- in the IP arising from the initial mutual geometry between the BP and amine undergoing the photoinduced CT or ET reaction. The relation between the distance dependence of the ET reaction and that of the intra-IP PT process and its consequence on the final hydrogen abstraction yield will be discussed in the next section.

6. The Difference of the Reactivity of Ion Pairs Depending on the Oxidation Potential of the Amine. In addition to the difference of the reactivity of the IP depending on the mode of the production, a large difference of the reactivity of $^3IP_{enc}$ was also observed between BP–DMA and BP–DEA systems. In order to clarify factors causing this difference, we have investigated photoreduction processes of BP– *N,N*-diethyl-*p*-toluidine (*p*-DET) and BP– *N*-methyldiphenylamine (MDPA) systems. We have selected these tertiary amines on the following reasons. First, the reaction mechanisms for these tertiary amines are all consecutive one of Scheme 2. Second, molecular structures of these tertiary amines are rather close to one another and have different oxidation potentials; MDPA: 0.86 V (vs. S.C.E), DMA: 0.76 V, DEA: 0.72 V, and *p*-DET: 0.69 V.[31] Although the difference of the reactivity depending on the mode of the IP production, i.e. the difference among $^3IP_{enc}$, $^1IP_{enc}$, and $^1IP_{com}$, was observed also in BP–*p*-DET and –MDPA systems[31,32] just as in BP–DEA and BP–DMA systems, we concentrate our discussion on the reduction process of ^{3}BP*.

In Fig. 11, we show transient absorption spectra of BP (0.01 M) –*p*-DET (0.05 M) system in acetonitrile solution excited with a picosecond 355 nm laser pulse. The concentration of the amine (0.05 M) was low enough to selectively observe the dynamic behaviors of ^{3}BP*. With increase of the delay time, the transient absorption spectrum due to ^{3}BP* which appeared immediately after excitaion gradually decays together with the increase of

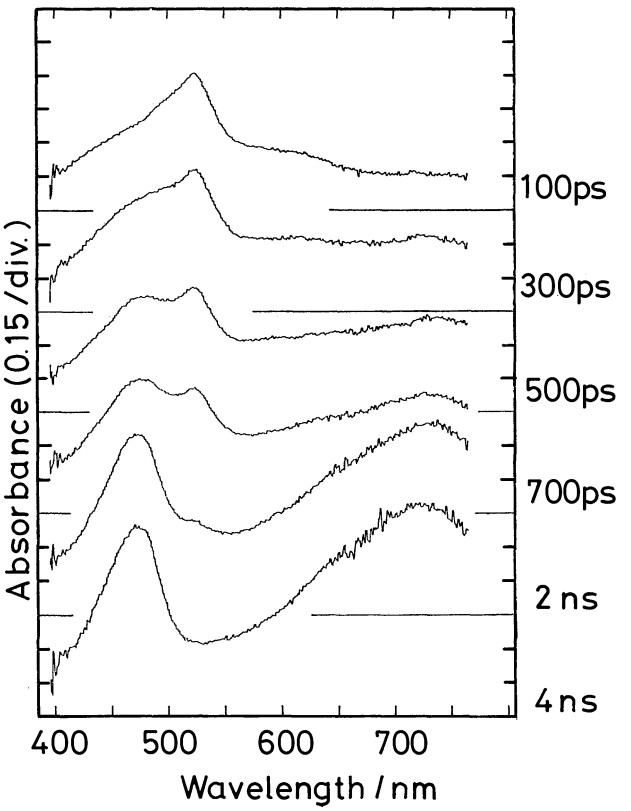

Fig. 11. Time-resolved transient absorption spectra of BP (0.01 M)–*p*-DET (0.05 M) system in acetonitrile solution, excited with a picosecond 355 nm laser pulse.

the absorbance at 700—720 nm (BP^-), and at 480 nm (*p*-DET^+). The absorbance due to BP^- and *p*-DET^+ reaches plateau value at 2—3 ns after the excitation and further evolution of the absorbance was not observed. From this result and those of the previous experiments,[9] the ionic species observed at a few ns after the excitation may be assigned to free ions. The yield of the free ions from ^{3}BP* was obtained to be 0.95±0.05 from the analysis of transient spectra in Fig. 11, where no ketyl radical formation was observed. Since neither decay process of the IP nor the formation of the ketyl radical was observed, it was not possible to determine the lifetime of $^3IP_{enc}$ by the present experiment. Hence, we estimate the lifetime and the reaction rate constants in the following manner. The rate constant for the ionic dissociation process of IP's of various donors and acceptors produced by ET at encounter in acetonitrile at room temperature (ca. 20 °C) has been determined to be $(0.5—2)\times10^9$ s^{-1}.[20,28] As listed in Table 3, k_{ID} for $^3(BP^-\cdots DEA^+)_{enc}$ and that for $^3(BP^-\cdots DMA^+)_{enc}$ were also in this range. Since the yield of the ionic dissociation of the $^3(BP^-\cdots p\text{-}DET^+)_{enc}$ was 0.95±0.05, the lifetime of the IP was estimated to be $\geqslant$500 ps assuming the similar k_{ID} value. Since the ketyl radical formation was not recognized, the rate constant for the proton transfer is estimated to be $\ll 2\times10^8$ s^{-1}. Anyhow, summarizing

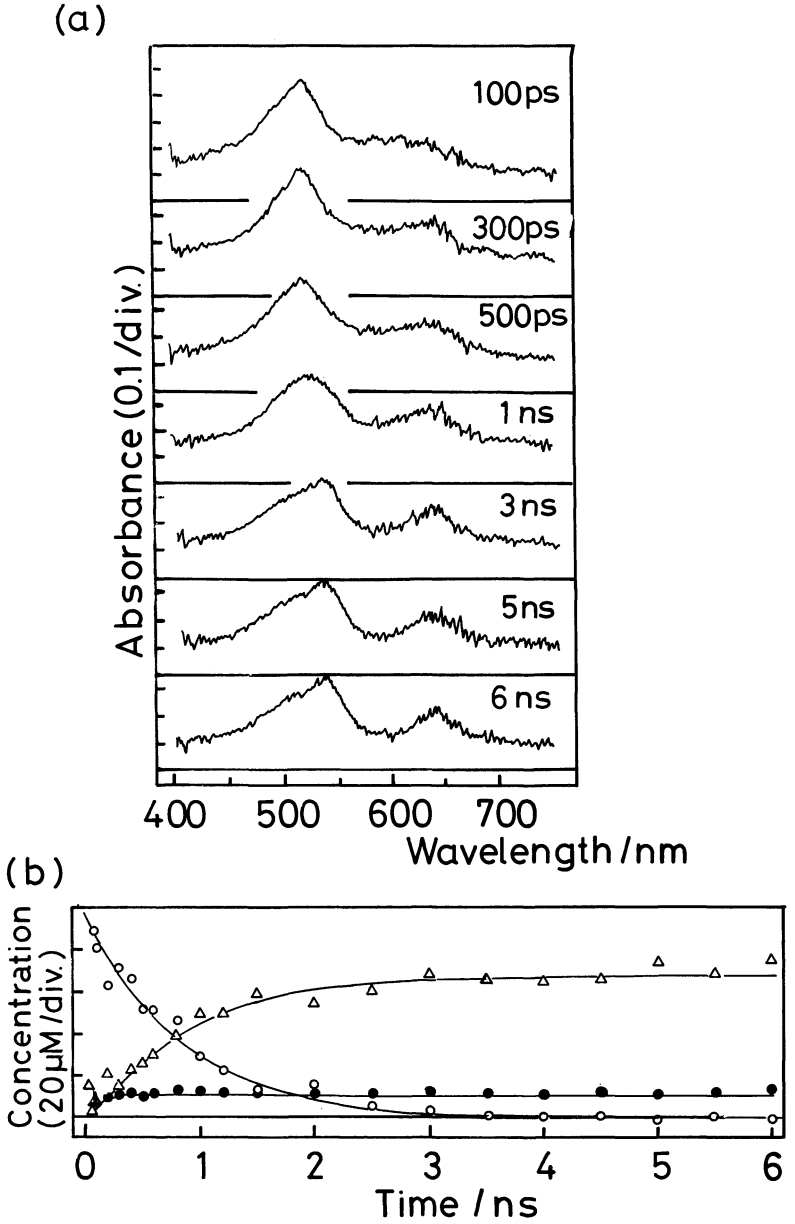

Fig. 12. a) Time-resolved transient absorption spectra of BP (0.01 M)–MDPA (0.07 M) system in acetonitrile solution, excited with a picosecond 355 nm laser pulse. b) Time profiles of ^{3}BP* (○), BPH· (△), and BP^- and $MDPA^+$ (●) of BP (0.01 M)–MDPA (0.07 M) system in acetonitrile solution excited with a picosecond 355 nm laser pulse (see text). Solid lines are calculated curves based on Scheme 2 (see text).

above results on the reduction process of ^{3}BP*-*p*-DET system, it may be concluded that the decrease of the yield of BPH· is attributable to the decrease of k_{PT}. This result indicates that, k_{PT} of $^3IP_{enc}$ between BP and the tertiary aromatic amine decreases with the decrease of the oxidation potential of the amine.

In order to confirm the effect of the oxidation potential of the amine on k_{PT} of $^3IP_{enc}$, the photoreduction process of BP–MDPA system was also investigated. Fig. 12(a) shows transient absorption spectra of BP(0.01 M)–MDPA (0.07 M) in acetonitrile excited with a picosecond 355 nm laser pulse. Although the formation of $^1IP_{com}$ and $^1IP_{enc}$ was found to increase also in this system with increase of [MDPA],[32] contributions from these IP's to the observed spectra of ionic species in Fig. 12(a) is very little. The transient absorption spectra due to ^{3}BP* observed immediately after the excitation gradually evolved in time into those of $MDPA^+$ at 645 nm, BP^- at 700—720 nm and BPH· at 545 nm. In Fig. 12(b), we exhibit the time profiles of ^{3}BP*, BPH·, and the IP.

Table 4. Dependence of the Reaction Rate Constants of the Triplet Ion Pairs upon Their Oxidation Potentials

Amine	MDPA	DMA	DEA	*p*-DET
Oxidation potential/V (vs. S.C.E.)	0.86	0.76	0.72	0.69
Lifetime of $^3IP_{enc}$/ps	90	140	290	(>500)
k_{PT}/s^{-1}	8.0×10^9	5.4×10^9	7.3×10^8	($\ll2\times10^8$)
k_{ID}/s^{-1}	1.1×10^9	1.4×10^9	2.1×10^9	(2×10^9)

Solid lines indicate the calculated curves based on the consecutive mechanisms (Scheme 2), similar to those indicated in Figs. 2 and 4. The lifetime of $^3(BP^{-}\cdots MDPA^{+})_{enc}$ was obtained to be 90 ps and the reaction yields of the proton transfer and the ionic dissociation were obtained to be 0.72 and 0.10, respectively. These values were confirmed to be almost independent of [MDPA].[32]

In Table 4, collected are the obtained values of the lifetime, k_{PT} and k_{ID} of $^3IP_{enc}$ of BP–tertiary aromatic amine systems in acetonitrile. This table shows clear dependence of each rate constant, especially k_{PT}, on the oxidation potential of the amine. This dependence of k_{PT} on the oxidation potential of the aromatic tertiary amine seems to indicate the different structure of the IP depending on the oxidation potential of the amine and seems to be closely related to the problems of the energy gap dependence of the ET reaction. Qualitatively speaking, the rate of the photoinduced ET reaction in polar solutions is regulated by:[33]
(a) Frank–Condon factor for the ET process which is related to the energy gap ($-\Delta G^\circ$) between the initial and final state of ET, (b) the reorganization energy (λ) including the intramolecular vibrational modes and the polarization of the solvent surrounding D and A, (c) the solvent dynamics, and (d) the electronic interaction responsible for ET which depends on mutual distance and orientations between D and A. When the factor (d) is not very strong and is not much different throughout a series of D, A systems, the ET rate may be determined mainly by the factor (a) and (b).

The CR decay rate constant, k_{CR}, of LIP or SSIP formed by CS at encounter in the fluorescence quenching reaction[2,3,28] as well as the phosphorescence quenching reaction[34] has been confirmed to show bell-shaped energy gap dependence. These energy gap dependences are predicted by the usual theories on the ET reaction. On the other hand, the CS rate constant, k_{CS}, at encounter in the luminescence quenching reaction rises steeply around zero energy gap and becomes diffusion-limited at favorable $-\Delta G^\circ$ regions, while no inverted effect has been experimentally confirmed yet. We have evaluated the k_{CS} values in the diffusion-limited $-\Delta G^\circ$ regions by measuring the transient effect in the fluorescence quenching reaction of a series of D, A systems in acetonitrile solutions and have demonstrated that the $-\Delta G^\circ$ dependence of k_{CS} in this top region is rather flat.[35] Such $-\Delta G^\circ$ dependence of k_{CS} in the top region can be interpreted by assuming the change of the ET distance depending on the change of $-\Delta G^\circ$ value.[35,36] That is, for larger $-\Delta G^\circ$ value, CS at a little larger distance is favorable because λ becomes larger at larger D, A distance,[36] which makes the $-\Delta G^\circ$ dependence of k_{CS} broader than that expected from the simple theoretical consideration.[37] We have made quantitative theoretical calculations on this problem, in which we have shown that the observed $-\Delta G^\circ$ dependence of k_{CS} and k_{CR} can be interpreted by assuming D, A distance distributions depending on $-\Delta G^\circ$ values in the CS reaction and also nonlinear polarization of solvent around ions.[36,38]

Along these theoretical treatments, it is expected, for the PT process following the ET reaction, that the PT rate should be drastically slowed down with the increase in the energy gap for the CS reaction in the condition where the orientation of BP^- and AH^+ and the surrounding solvation structure of IP are similar and the $-\Delta G^\circ$ value for the CS reaction is relatively large. In other words, the increase in the inter-ionic distance in the geminate IP with increase of the energy gap for the CS reaction affects the subsequent PT rate to a great extent since the rate for the PT process is much more severely dependent on the mutual distance.

The present result of the dependence of k_{PT} of $^3IP_{enc}$ on the oxidation potential of the amine is in accordance with the above considerations on the mechanism of the energy gap dependence of k_{PT}. The inter-ionic distance in those BP–amine ^3LIP will become longer to a small extent with decrease of the oxidation potential of the amine and it seems to be kept until the proton transfer taking place in competition with the ionic dissociation. The k_{PT} will decrease with decrease of the amine oxidation potential due to the increase of the proton transfer distance.

The effect of the energy gap for the CS reaction on the PT rate which is attributable to the difference in the inter-ionic distance may be expected also in the course of the $^1IP_{enc}$ formation since it is actually observed for $^3IP_{enc}$. However, because the ET between $^1BP^*$ and the amine is restricted rather severely to the pairs in the short range owing to the very short life of $^1BP^*$, such effect of the energy gap in the CS reaction will be small. Actually, k_{PT} in the $^1IP_{enc}$ does not show such energy gap dependence, but rather similar to each other for the series of $^1BP^*$–DEA, –DMA, and –MDPA systems ($k_{PT}=4.3\times10^8\ s^{-1}$, $6.6\times10^8\ s^{-1}$, and $6.0\times10^8\ s^{-1}$, respectively).

7. The Different Reaction Mechanism Depending on the Nature of the Amine. As discussed above, the mechanism of the hydrogen abstraction of ^{3}BP* from tertiary aromatic amines in acetonitrile solution is the successive reaction as given by the Scheme 2, while the hydrogen abstraction process of ^{3}BP* from primary and secondary amines such as aniline, DPA, *N*-methylaniline, and *N*-ethylaniline was the direct abstraction competing with the production of the stable IP which did not undergo the intra-IP proton transfer.[16,31] This difference of the reaction mechanism depending on the structure of the amine might be related to the existence of weak hydrogen bonding interaction between π-electrons on oxygen of the excited BP and the hydrogen directly bonded to the nitrogen of the amine. The CT interaction and this weak hydrogen bonding interaction might to closely connected with each other and facilitate the hydrogen transfer process in the encounter collision.

On the other hand, the mechanism of the hydrogen abstraction of ^{3}BP* from DMA in 2-propanol is not the successive one but can be described by the direct abstraction mechanism. The difference of the mechanism depending on the solvent may be related to the following experimental results on the singlet IP's. Concerning the structure and dynamics of the molecular complex produced by the photoinduced CT or ET reaction, it was reported that the electronic state of the typical singlet exciplex system such as pyrene–DMA was strongly dependent on the nature of the solvent such as the polarity and ability of hydrogen bonding interaction.[39,40] This dependence on the nature of the solvent was not accounted for by assuming the mere stabilization of the single electronic state by the solvation but it is necessary to take into account the change of the electronic and geometrical structures of the complex depending on the nature of the solvent.[39,40] In addition, it was revealed that, in sufficiently polar solvents, the fluorescent exciplex and nonfluorescent solvated IP's were produced competitively, depending upon the solvent polarity, from the non-relaxed CT state immediately after the electron transfer between excited singlet state of pyrene and DMA.[41] Integrating those previous results and the present ones, it is suggested that the mutual geometry such as orientation and distance including the surrounding solvent at the encounter between the reactants strongly affect the subsequent behaviors of the very short-lived transient charge transfer or the IP state.

Summarizing these various mechanisms depending on the structures of the amine, the nature of solvent, and the oxidation potential of the amine as well as the production pathways of IP, it is indicated that the transient charge transfer interaction in a short-lived intermediate formed in the excited benzophenone–amine system is of crucial importance as the factor determining the reaction mechanism.

In relation to this problem, we are now investigating the system where mutual configurations are restricted by connecting BP and amine with the methylene chain, results of which will be published in a forthcoming paper.

The present work was partially supported by a Grant-in-Aid for Specially Promoted Research No. 6265006 from the Ministry of Education, Science and Culture to N. M.

References

1) N. Mataga, *Pure Appl. Chem.*, **56**, 1255 (1984).
2) N. Mataga, *Acta Phys. Pol., A*, **71**, 767 (1987).
3) N. Mataga, "Photochemical Energy Conversion," ed by J. R. Norris and D. Meisel, Elsevier, Amsterdam (1988), p. 32.
4) N. Mataga, H. Miyasaka, T. Asahi, S. Ojima, and T. Okada, "Ultrafast Phenomena VI," Springer-Verlag, Berlin (1988), p. 511.
5) A. Beckett and G. Porter, *Trans. Faraday Soc.*, **59**, 2038 (1963).
6) G. Porter and M. R. Topp, *Proc. Roy. Soc. (London), Ser. A*, **315**, 163 (1970).
7) S. G. Cohen, A. Parola, and G. H. Rarsons, *Chem. Rev.*, **73**, 1411 (1973), and references cited therein.
8) S. Arimitsu and H. Masuhara, *Chem. Phys. Lett.*, **22**, 543 (1973).
9) S. Arimitsu, H. Masuhara, N. Mataga, and H. Tsubomura, *J. Phys. Chem.*, **79**, 1255 (1975).
10) K. S. Peters, S. C. Felich, and C. G. Shaefer, *J. Am. Chem. Soc.*, **102**, 5701 (1980).
11) C. G. Shaefer and K. S. Peters, *J. Am. Chem. Soc.*, **102**, 7567 (1980).
12) J. D. Simon and K. S. Peters, *J. Am. Chem. Soc.*, **103**, 6403 (1981).
13) L. E. Manring and K. S. Peters, *J. Am. Chem. Soc.*, **107**, 6452 (1985).
14) M. Hoshino and H. Shizuka, *J. Phys. Chem.*, **91**, 714 (1987).
15) H. Hoshino and M. Kogure, *J. Phys. Chem.*, **93**, 728 (1989).
16) H. Miyasaka and N. Mataga, *Bull. Chem. Soc. Jpn.*, **63**, 131 (1990).
17) H. Miyasaka, K. Morita, M. Kiri, and N. Mataga, "Ultrafast Phenomena VII," Springer-Verlag, Berlin (1990), p. 498.
18) H. Miyasaka, K. Morita, K. Kamada, and N. Mataga, *Bull. Chem. Soc. Jpn.*, **63**, 3385 (1990).
19) H. Miyasaka, K. Morita, K. Kamada, and N. Mataga, *Chem. Phys. Lett.*, **178**, 504 (1991).
20) a) N. Mataga, Y. Kanda, T. Asahi, H. Miyasaka, T. Okada, and T. Kakitani, *Chem. Phys.*, **127**, 239 (1988); b) T. Asahi and N. Mataga, *J. Phys. Chem.*, **93**, 6575 (1989); c) T. Asahi and N. Mataga, *ibid.*, **95**, 1956 (1991).
21) H. Masuhara, N. Ikeda, H. Miyasaka, and N. Mataga, *J. Spectros. Soc. Jpn.*, **31**, 19 (1982).
22) H. Miyasaka, H. Masuhara, and N. Mataga, *Laser Chem.*, **1**, 357 (1983).
23) H. Miyasaka, S. Ojima, and N. Mataga, *J. Phys. Chem.*, **93**, 3380 (1989).
24) E. J. Land, *Proc. Roy. Soc. (London), Ser. A*, **305**, 457 (1968).
25) R. V. Bensasson and J.-C. Gramain, *J. Chem. Soc.,*

Faraday Trans. 2, **76**, 1801 (1980).
26) T. Shida, S. Iwata, and M. Imamura, *J. Phys. Chem.,* **78**, 741 (1974).
27) H. Hiratsuka, T. Yamazaki, Y. Maekawa, T. Hidaka, and Y. Mori, *J. Phys. Chem.,* **90**, 774 (1986).
28) N. Mataga, T. Asahi, Y. Kanda, T. Okada, and T. Kakitani, *Chem. Phys.,* **127**, 249 (1988), and references there-in.
29) J. D. Simon and K. S. Peters, *J. Am. Chem. Soc.,* **105**, 4875 (1983).
30) R. K. Huddleston and J. R. Miller, *Radiat. Phys. Chem.,* **17**, 383 (1981).
31) T. Miyasaka, K. Kamada, K. Morita, M. Kiri, and N. Mataga, to be published.
32) H. Miyasaka, K. Morita, M. Kiri, T. Nagata, and N. Mataga, to be published.
33) N. Mataga, "Perspective in Photosynthesis," ed by J. Jortner and B. Pullman, Kluwer Academic, Dordrecht (1990), p. 227.
34) T. Ohno, A. Yoshimura, and N. Mataga, *Bull. Chem. Soc. Jpn.,* **94**, 4871 (1990), and references there-in.
35) S. Nishikawa, T. Asahi, T. Okada, N. Mataga, and T. Kakitani, *Chem. Phys. Lett.,* in press.
36) T. Kakitani, A. Yoshimori, and N. Mataga, "Advances in Chemistry Series," "Electron Transfer in Inorganic, Organic and Biological Systems," ed by J. R. Bolton, N. Mataga, and G. McLendon, Am. Chem. Soc. (1991), Chap. 4; *idem*, to be published.
37) R. A. Marcus, *J. Chem. Phys.,* **24**, 966 (1956); R. A. Marcus and N. Sutin, *Biochim. Biophys. Acta,* **811**, 265 (1985).
38) A. Yoshimori, T. Kakitani, Y. Enomoto, and N. Mataga, *J. Phys. Chem.,* **93**, 8316 (1989), and reference there-in.
39) N. Mataga, T. Okada, and N. Yamamoto, *Chem. Phys. Lett.,* **1**, 119 (1967).
40) N. Mataga and M. Ottolengthi, "Molecular Association Including Molecular Complexes," ed by R. Foster, Academic Press, London (1979), p. 1.
41) Y. Hirata, Y. Kanda, and N. Mataga, *J. Phys. Chem.,* **87**, 1659 (1983).

Conformational Change of Benzoquinone Crown Ether Radical Anions Induced by Complexation with Alkali Metal Cation: An ESR Study

Kiichi HASHIMOTO, Hideo TOGO, Kenji MORIHASHI, Yukihiro YOKOYAMA, and Osamu KIKUCHI*
Department of Chemistry, University of Tsukuba, Tsukuba 305
(Received June 5, 1991)

The crowned *p*-benzoquinone anion radicals, **O5**$^-$—**O8**$^-$, were generated either electrochemically or by using a reducing metal, and their ESR spectra were examined in both the absence and presence of the Na^+ or K^+ cation. The hyperfine coupling (hfc) constants of the methylene protons bonded to the quinone ring depend largely on the size of the crown ring; the orientation of the benzoquinone skeleton with respect to the crown ring was analyzed. The metal-free **O5**$^-$ has a fixed conformation in which the benzoquinone ring is nearly perpendicular to the crown ring, while **O8**$^-$ interconverts freely between two equivalent conformations. The critical case is **O6**$^-$; the line-width alternation observed in its ESR spectra was well-analyzed using the two-jump model. Temperature-dependent ESR spectra and MNDO calculations have suggested that **O6**$^-$ undergoes a restricted interconversion between two conformations in which the benzoquinone ring has an orientation similar to that of **O5**$^-$. An activation energy of 10.0 kcal mol^{-1} was determined for this motion. The ESR spectra of the ion-paired **O5**$^-$—**O8**$^-$ anion radicals have suggested that the conformational motion of the anion radicals is fixed by complexation with the Na^+ or K^+ cation. The hfc constants of the methyl protons in the benzoquinone ring increased upon complexation, indirectly confirming the interaction between the carbonyl oxygen of benzoquinone at the crown-ring side and the metal cation.

In the field of host–guest chemistry, studies of molecular switching in macrocyclic polyether systems is of great interest in relation to ion-transport phenomena in biological systems. The crown compounds including redox active functional groups, such as quinone,[1-13] nitrobenzene,[14-17] disulfide,[18] azo moieties,[19] have attracted much attention. Among them, quinone derivatives are especially interesting because they have significant properties due to the ready reversibility of the quinone–semiquinone redox system.

Our previous cyclic voltammetric study has shown that the complexation of crowned quinones, **O5**—**O8**, with alkali metal cations, Li^+, Na^+, or K^+, is enhanced by the reduction of the quinones.[6] Wolf and Cooper showed

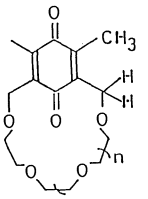

O5: $n = 1$
O6: $n = 2$
O7: $n = 3$
O8: $n = 4$

an ESR spectra which confirmed the interaction between **O6**$^-$ and the Na^+ cation.[7] Bock and Herrmann have shown that **O6**$^-$ forms a 1-to-2 complex with two alkali metal cations.[8] Delgado et al. have reported the ESR spectra of anthraquinone podands and anthraquinone crown ether anion radicals and have shown the interaction between these anion radicals and the alkali metal cation.[10-13] However, there have only been few reports[8,20] concerning the electronic structure and conformational change of the crowned anion radicals induced by interactions with alkali metal cations.

In this study, the anion radicals of **O5**—**O8**[6] were generated either electrochemically or using a reducing metal, and their ESR spectra were examined both in the absence and presence of a metal cation. From the determined hfc constants and an MNDO[21] calculation of a model anion radical, the conformational change of anion radicals induced by complexation with metal cations is discussed.

Experimental

Tetrahydrofuran (THF) was distilled from $LiAlH_4$ under an Ar atmosphere and stored over 3 Å molecular sieves. The THF was flask-to-flask distilled in a vacuum line immediately prior to use for reduction with an alkali metal. The acetonitrile (MeCN) used for electrochemical reduction was distilled from CaH_2 under an Ar atmosphere. The MeCN was stored without molecular sieves, since they contain Na^+ cations as a component. Tetrabutylammonium perchlorate (TBAP) was twice recrystallized from EtOAc and dried over vaccum pumping at room temperature for 24 h. Alkali metal perchlorate salts, $NaClO_4$ and $KClO_4$ were recrystallized from deionized water and dried over vaccum pumping at 100 °C for 24 h.

The crowned anion radicals were generated by reduction with Na or K metal in THF, and the ESR spectra of ion-paired anion radicals were recorded. The ESR spectra of "metal-free" anion radicals were obtained by the addition of a large excess amount of cryptand 221 to a sample solution prepared with Na metal. The anion radicals were also generated by electrochemical reduction in MeCN using TBAP as a supporting electrolyte. In order to obtain the ESR spectra of the ion-paired anion radicals, 1.0 or 2.0 equivalent of alkali metal perchlorate was used instead of TBAP.

The ESR spectra were recorded on an X-band JEOL JES-FE-1XG spectrometer. The temperature of the samples was controlled by means of a JEOL ES-DVT 1 variable-temperature unit. The microwave frequency was measured with an Advantest TR5212 Microwave Counter and the magnetic feld strength with an Echo Electronics EFM-2000 NMR Field Meter. Field gradients were corrected by using Fremy's salt as a reference compound.

Results

The well-resolved ESR spectra of the metal-free anion radicals and the anion radicals ion-paired with Na^+ or K^+ were obtained for **O5**—**O8**. The hfc constants were determined by simulation, and are summarized in Tables 1 and 2. In the case of the ion-paired **O5**$^-$ generated by reduction with alkali metal, the spectrum changed rapidly and the hfc constants could not be determined. The ESR spectra have the following common features: (1) each spectrum has splitting due to six methyl protons and the methylene protons attached to the quinone ring; (2) the spectra of the metal-free **O6**$^-$ and **O7**$^-$ exhibit a line-width alternation indicating restricted interconversion between conformers; and (3) the Na splitting is observed for **O5**$^-$—**O8**$^-$, while no K splitting is observed.

Reduced O5. Figure la shows the ESR spectrum of **O5**$^-$ obtained by reduction with Na metal in THF at 25 °C in the presence of cryptand 221. The ESR spectrum comprises seven main lines arising from the six equivalent methyl protons; each of these lines is further split by the methylene protons attached at the quinone ring. The hfc constants are 2.17 G (6H, 1G=10^{-4} T), 0.78 G (2H), and 0.38 G (2H). As was expected, there was no hfc by Na^+ in the presence of the cryptand, and the spectrum of the metal-free **O5**$^-$ was observed. Figure 1b shows the ESR spectra of the metal-free **O5**$^-$ observed by electrochemical reduction. The four methylene protons are equivalent in the MeCN solution. Figure 2 shows the ion-paired **O5**$^-$ observed by electrochemical reduction. The hyperfine coupling of Na was observed, while

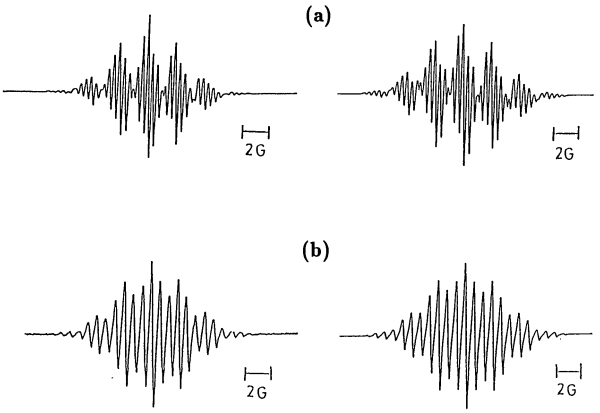

Fig. 1. ESR spectra (left) and corresponding simulated spectra (right) for reduced **O5** obtained (a) by reduction with Na metal in the presence of cryptand 221 and (b) by electrochemical reduction.

Table 1. Observed Proton Hyperfine Coupling Constants (in Gauss) upon Reduction with Alkali Metal in THF at +25°C

Ligand	M^+	$a(CH_3, 6H)$	$a(CH_2)$		a(Na)	LW[a]
O5$^-$	None[b]	2.17	0.78 (2H)	0.38 (2H)	—	0.16
O6$^-$	None[b]	2.11	0.96 (2H)	0.30 (2H)	—	0.14
	Na^+	2.75	0.72 (2H)	—	1.16	0.20
	K^+	2.61	0.72 (2H)	—	—	0.45
O7$^-$	None[b]	2.13	0.64 (4H)		—	0.30
	Na^+	2.80	0.33 (4H)		0.70	0.13
	K^+	2.65	0.36 (4H)		—	0.25
O8$^-$	None[b]	2.16	0.65 (4H)		—	0.25
	Na^+	2.79	0.40 (4H)		0.59	0.16
	K^+	2.63	0.42 (4H)		—	0.20

a) Line width (in Gauss) used for simulation. b) Measured in the presence of cryptand 221.

Table 2. Observed Proton Hyperfine Coupling Constants (in Gauss) upon Electrochemical Reduction in MeCN at +25°C

Ligand	M^+	Equiv	$a(CH_3, 6H)$	$a(CH_2)$		a(Na)	LW[a]
O5$^-$	None	—	2.02	0.65 (4H)		—	0.18
	Na^+	1.0	2.49	0.97 (2H)	—	0.97	0.23
	K^+	1.0	2.25	1.17 (2H)	—	—	0.25
O6$^-$	None	—	2.02	0.97 (2H)	0.25 (2H)	—	0.13
	Na^+	1.0	2.48	0.89 (2H)	—	1.25	0.18
	K^+	1.0	2.41	0.93 (2H)	—	—	0.31
O7$^-$	None	—	2.08	0.98 (2H)	0.26 (2H)	—	0.15
	Na^+	1.0	2.44	0.48 (4H)		0.80	0.24
	K^+	1.0	2.35	0.46 (4H)		—	0.25
O8$^-$	None	—	2.09	0.73 (4H)		—	0.25
	Na^+	2.0[b]	2.95	0.52 (4H)		—	0.20
	K^+	1.0	2.31	0.52 (4H)		—	0.28

a) Line width (in Gauss) used for simulation. b) **O8**$^-$ forms a 1-to-2 complex with Na^+ cation upon electrochemical reduction.

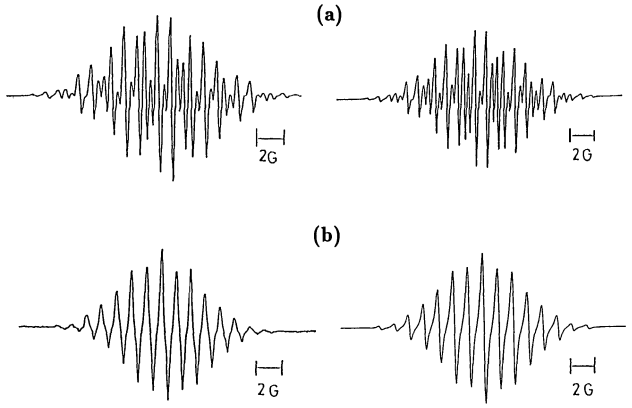

Fig. 2. ESR spectra (left) and simulated spectra (right) for reduced **O5** obtained by electrochemical reduction (a) in the presence of 1.0 equiv of Na^+ and (b) in the presence of 1.0 equiv of K^+.

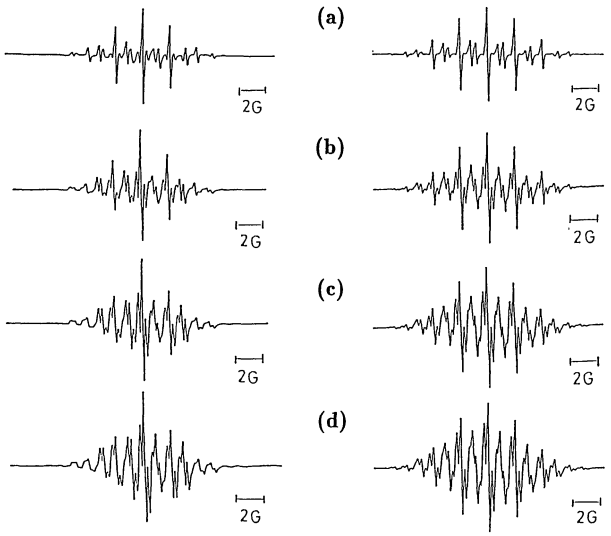

Fig. 3. Temperature-dependent ESR spectra (left) and simulated spectra (right) for metal-free $\mathbf{O6}^-$ in THF at (a) +25 °C, (b) 0 °C, (c) −20 °C, and (d) −40 °C.

that of K was not resolved.

Reduced O6. Figure 3 shows the temperature dependence of the ESR spectra of the metal-free $\mathbf{O6}^-$ obtained by reduction with Na in THF in the presence of cryptand 221. The spectra clearly exhibit an alternating line-width effect at room temperature and below, indicating a conformational interconversion of $\mathbf{O6}^-$. The temperature-dependent spectra were analyzed using a two-jump model between two conformations in which the methylene protons which bonded to the quinone ring were distinguished as being two sets of two equivalent protons. The determined hfc constants are 2.11 G (6H), 0.96 G (2H), and 0.30 G (2H). The rate constant at 25 °C was $k=2.5\times10^6$ s^{-1}. From a plot of log k against $1/T$, an activation energy of 10.0 kcal mol^{-1} was determined for the conformational interconversion.

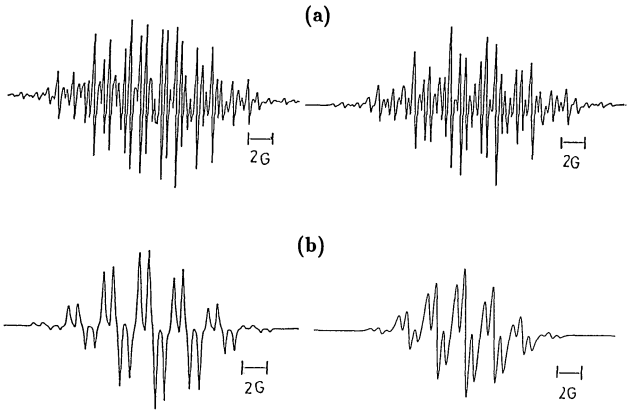

Fig. 4. ESR spectra (left) and simulated spectra (right) for reduced **O6** obtained by reduction with alkali metal (a) in the presence of Na^+ and (b) in the presence of K^+.

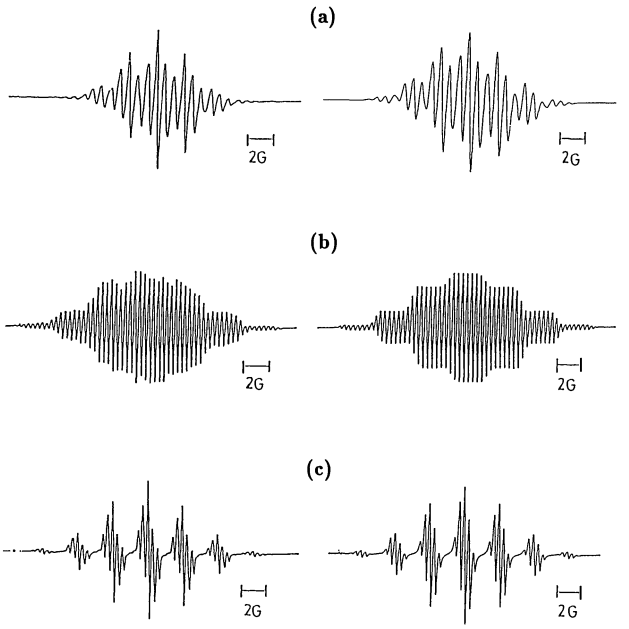

Fig. 5. ESR spectra (left) and simulated spectra (right) for reduced **O7** obtained by reduction with alkali metal (a) in the presence of Na^+ and cryptand 221, (b) in the presence of Na^+ and (c) in the presence of K^+.

Similar hfc constants were obtained for the metal-free $\mathbf{O6}^-$ generated by electrochemical reduction in MeCN.

Figure 4 shows the ESR spectra of the ion-paired $\mathbf{O6}^-$ obtained by reduction with Na or K metal; a splitting of Na was observed. No line-width alternation can be observed in the spectrum, and only one set of methylene protons (2H) has a distinct hfc constant. This characteristic of the ESR spectrum was also observed in the $\mathbf{O6}^-$–Na^+ or $\mathbf{O6}^-$–K^+ system obtained by electrochemical reduction. These results suggest that $\mathbf{O6}^-$ has a conformation in which one of the CH_2 protons lies on the quinone ring plane.

Reduced O7. Figure 5 shows the ESR spectra of $\mathbf{O7}^-$

observed by reduction with alkali metal. The metal-free **O7**$^-$ spectrum observed by reduction with Na metal has hfc constants of $a(2CH_3)$=2.13 G and $a(4H)$=0.64 G. In the metal-free **O7**$^-$ spectrum obtained by electrochemical reduction, a slight line-width alternation effect was observed; the spectrum was well reproduced by the hfc constants of $a(2CH_3)$=2.08 G, $a(2H)$=0.98 G, and $a(2H)$=0.26 G. These hfc constants of methylene protons indicate that the value of 0.64 G for 4H protons of **O7**$^-$ obtained by reduction with alkali metal is due to an average of two different sets of two protons. In the case of ion-paired **O7**$^-$, four methylene protons have the same hfc constants, irrespective of the method of radical generation.

Reduced O8. All ESR spectra of **O8**$^-$ have no line-width alternation effect, and exhibit the hfc of six equivalent methyl protons and four equivalent methylene protons. Although the hyperfine coupling of Na was observed for **O8**$^-$ ion-paired with Na^+ generated by Na metal, no Na splitting was observed when the radical anion was generated by electrochemical reduction (Fig. 6). In the latter case, 2.0 equivalents of Na^+ are present in the solution and two cations bind with **O8**$^-$; this was confirmed by a previous cyclic voltammetric study.[6]

MNDO Calculation. The orientation of the polyether groups relative to the quinone moiety plays an important role in the energy stabilization of **O5**$^-$—**O8**$^-$. Therefore, the MNDO MO calculations were carried out for the anion radical of a simple model compound, **O3**, in order to examine the conformational energy of **O5**$^-$—**O8**$^-$.

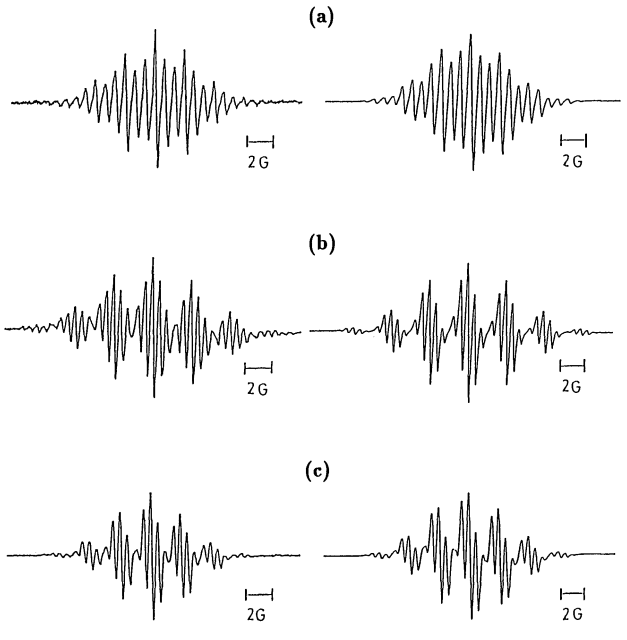

Fig. 6. ESR spectra (left) and simulated spectra (right) for reduced **O8** obtained by electrochemical reduction (a) in the absence of metal cation, (b) in the presence of 2 equivalent of Na^+ and (c) in the presence of 1 equivalent of K^+.

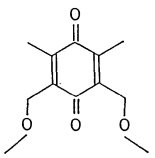

O3

The rotation angle of the CH_2OCH_3 group, ϕ, was measured from the conformation in which the C(methylene)–O(ether) bond lies on the quinone ring plane. Except for the structure of the methyl groups, which was assumed to be tetrahedral with R_{CH}=1.100 Å, all geometrical parameters were optimized under the restriction of Cs symmetry for several ϕ values. The open-shell RHF MNDO method[22] was used. The calculated energy profile is shown in Fig. 7. A similar energy profile was also obtained by a UHF MNDO calculation.

A maximum-energy structure was found at ϕ=0°, where the two C(methylene)–O(ether) bonds are in the quinone ring plane. In such a conformation, the Coulombic repulsion between the ether and carbonyl oxygen atoms becomes maximum. The increase in stabilization in going from ϕ=0° to ϕ=90° is attributed to a decrease in the Coulombic repulsion; a minimum-energy conformation was found near ϕ=90°, where the two C(methylene)–O(ether) bonds are perpendicular to the quinone ring plane. The energy difference between the maximum-energy structure (ϕ=0°) and the minimum-energy one (ϕ=90°) was calculated to be 12.0 kcal mol^{-1}.

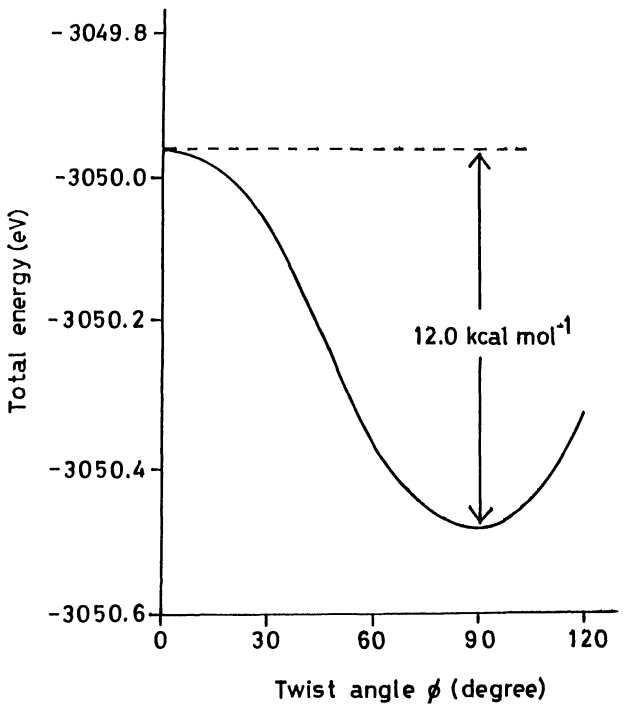

Fig. 7. Energy profile for the rotation of the CH_2OCH_3 groups of the radical anion **O3**$^-$.

Discussion

Metal-Free O6⁻. The present ESR experiment can not determine the conformation of the crown ring skeleton, since the hyperfine coupling due to the methylene protons attached at the quinone ring gives only information concerning the conformational aspects around the C(quinone)–C(methylene) bond. Since the size of the crown ring of **O6⁻** is not large enough to freely undergo a conformational interconversion, the rotation about the C(quinone)–C(methylene) bond is restricted. Because of this steric factor, the four methylene protons attached at the quinone ring are not completely equivalent over the temperature range studied, and the alternating line-width effect was observed.

In the two-jump model simulation, four methylene protons attached at the quinone ring were distinguished as being two sets of two equivalent protons: H_a=H_b and H_c=H_d (Scheme 1). We thus assumed an interconversion in which the quinone moiety turns around the C(quinone)–C(methylene) bond. The simulation along this line well reproduced the observed temperature-dependent ESR spectra of the metal-free **O6⁻** (Fig. 3), and the hfc constants listed in Tables 1 and 2 were determined.

The hfc constants of methylene protons depend on the angle, θ, between the C(methylene)–H bond and the $2p_\pi$ orbital of the quinone carbon atom. According to the McConnell–Heller equation,[23]

$$a(H_\beta) = B\cos^2\theta,$$

the orientation of the crown ring relative to the quinone moiety can be estimated. From the hfc constant of methyl protons in the duroquinone (2,3,5,6-tetramethyl-*p*-benzoquinone) anion radical, 1.9 G,[24] the empirical parameter, B, was estimated to be ca. 3.8 G for the benzoquinone radical anions. From this B value and the relative magnitude of the methylene hfc constants observed, 0.96 G and 0.30 G, the conformation of the metal-free **O6⁻** was speculated as **I**.

The MNDO calculation of the radical anion of the model compound has shown that the energy-minimum conformation exists near ϕ=90°. It may thus be said that a conformational interconversion occurs between **I** and **II**. The MNDO calculation has shown that the activation energy of this process is 12.0 kcal mol^{-1}; this value agrees well with the experimentally determined activation energy, E_A=10.0 kcal mol^{-1}.

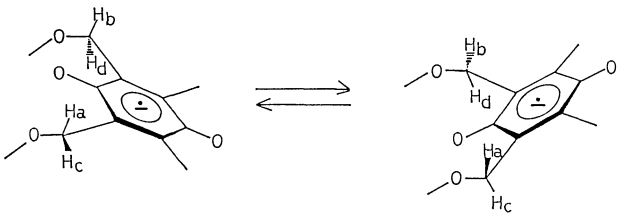

Scheme 1.

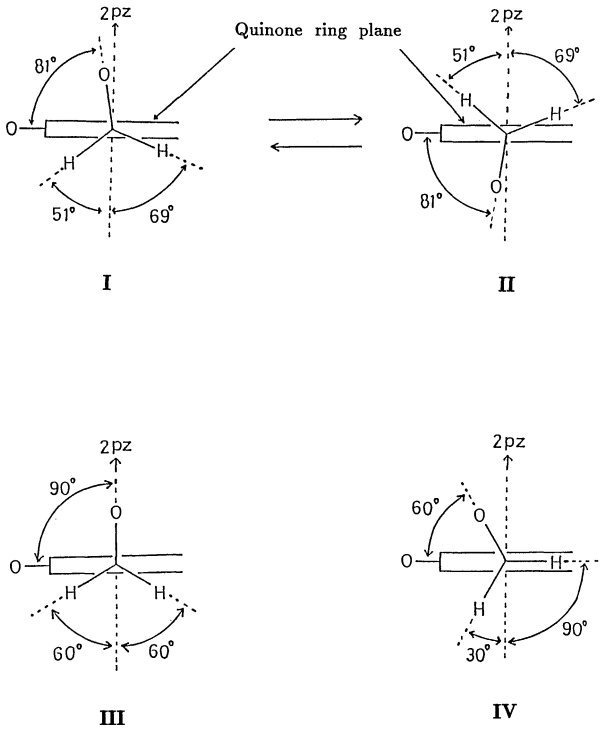

Metal-Free O5⁻. An examination of the CPK model has indicated that the size of the crown ring of the metal-free **O5⁻** is small and that the C(quinone)–C(methylene) bond is hardly allowed to rotate. No alternating line-width effect was observed in the ESR spectrum of the metal-free **O5⁻** and the hfc constants of the methylene protons in THF are similar to those of the metal-free **O6⁻**. These facts suggest that the metal-free **O5⁻** has a fixed conformation which resembles **I** or **II**.

The methylene protons of the metal-free **O5⁻** in MeCN are equivalent. Since the metal-free **O5⁻** has a fixed conformation in THF, it is reasonable to consider that the conformation of the metal-free **O5⁻** is also fixed in MeCN. In this case, the fixed conformer **III** is expected for **O5⁻**.

Metal-Free O7⁻ and O8⁻. The methylene protons of **O7⁻** and **O8⁻** are equivalent in THF. Since metal-free **O6⁻** undergoes a restricted interconversion, the metal-free **O7⁻** and **O8⁻**, which have a larger size crown ring, are expected to undergo interconversion more freely. It is thus natural to consider that the equivalency of methylene protons comes from a rapid exchange between two conformers which resemble **I** and **II**. Actually, the hfc constants of the metal-free **O7⁻** and **O8⁻** are almost the average value of two different hfc constants observed for the metal-free **O6⁻**. In the ESR spectrum of the metal-free **O7⁻** generated by an electrochemical reduction, a line-width alternation was observed; the interconversion is not rapid in this case and the rotation is slightly restricted.

Conformation of Ion-Paired Ligands. For **O5⁻** and **O6⁻** ion-paired with a Na^+ or K^+ cation, only two of four

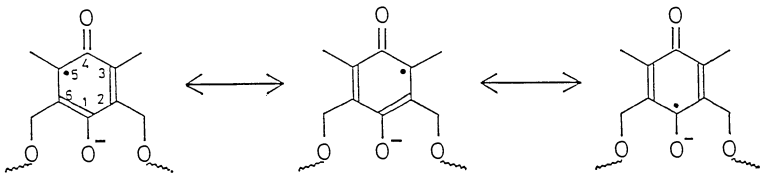

Scheme 2.

methylene protons exhibit hyperfine coupling. Thus, one of the methylene protons is expected to lie on the quinone ring plane. Therefore, conformation **IV** is suggested for the ion-paired **O5**$^-$ and **O6**$^-$.

In the case of **O7**$^-$ and **O8**$^-$ ion-paired with Na^+ or K^+, four methylene protons were equivalent. As described above, the metal-free **O7**$^-$ shows a restricted conformational interconversion in MeCN. The complexation of **O7**$^-$ with a metal cation is expected to more strongly restrict this interconversion. It is thus reasonable that the equivalency of methylene protons of **O7**$^-$ ion-paired with Na^+ comes from a fixed conformation, like **III**. From the results described above, we believe that all the ligands, **O5**$^-$—**O8**$^-$, have fixed conformations in the presence of alkali metal cations.

hfc Constants of Methyl Protons. As may be seen from Tables 1 and 2, the hfc constant of methyl protons greatly increases (20—30%) when alkali metal cations are present. This may be elucidated on the basis of an interaction between the metal cation and the quinone oxygen atom at the crown ring side. This interaction makes the resonance forms in Scheme 2 more important, and increases the spin densities of the C_1, C_3, and C_5 atoms. This is the reason why the hfc constant of the methyl protons is increased by complexaion with a cation.

It is interesting that the hfc constant of the methyl protons in **O8**$^-$ ion-paired with the Na^+ cation generated by electrochemical reduction is larger than those of other ion pairs. It has been confirmed from a cyclic voltammetric study[6] that **O8**$^-$ forms a 1-to-2 complex with the Na^+ cation. The present large hfc constant suggests that two Na^+ cations are close to the crown ring of **O8**$^-$ and interact with the oxygen atom at the crown ring side, giving a large contribution of the reasonance forms shown in Scheme 2.

Although no K splitting was observed, the hfc constants of the methyl protons increased in the presence of the K^+ cation. This fact suggests that **O5**$^-$—**O8**$^-$ interact with the K^+ cation in the same manner as with the Na^+ cation. It is thus concluded that the semiquinone oxygen atom at the crown ring side interacts with both the Na^+ and K^+ cations and that this interaction influences the spin distribution of the benzosemiquinones anion radicals.

References

1) K. Sugihara, H. Kamiya, M. Yamaguchi, T. Kaneda, and S. Misumi, *Tetrahedron Lett.*, **22**, 1619 (1981).

2) T. Kaneda, K. Sugihara, H. Kamiya, and S. Misumi, *Tetrahedron Lett.*, **22**, 4407 (1981).

3) S. Nakatsuji, Y. Ohmori, and M. Iyoda, *Bull. Chem. Soc. Jpn.*, **56**, 3185 (1983).

4) H. Bock, B. Hierholzer, F. Vögtle, and G. Hollmann, *Angew. Chem., Int. Ed. Engl.*, **23**, 57 (1984).

5) K. Maruyama, H. Shomiya, and H. Tsukube, *Tetrahedron Lett.*, **26**, 3583 (1985).

6) H. Togo, K. Hashimoto, K. Morihashi, and O. Kikuchi, *Bull. Chem. Soc. Jpn.*, **61**, 3026 (1988).

7) R. E. Wolf and S. R. Cooper, *J. Am. Chem. Soc.*, **106**, 4646 (1984).

8) H. Bock and H.-F. Herrmann, *J. Am. Chem. Soc.*, **111**, 7622 (1989).

9) L. Echegoyen, D. A. Gustowski, V. J. Gatto, and G. W. Gokel, *J. Chem. Soc., Chem. Commun.*, **1986**, 220.

10) L. Echeverria, M. Delgado, V. J. Gatto, G. W. Gokel, and L. Echegoyen, *J. Am. Chem. Soc.*, **108**, 6825 (1986).

11) D. A. Gustowski, M. Delgado, V. J. Gatto, L. Echegoyen, and G. W. Gokel, *J. Am. Chem. Soc.*, **108**, 7553 (1986).

12) D. A. Gustowski, M. Delgado, V. J. Gatto, L. Echegoyen, and G. W. Gokel, *Tetrahedron Lett.*, **27**, 3487 (1986).

13) M. Delgado, D. A. Gustowski, H. K. Yoo, V. J. Gatto, G. W. Gokel, and L. Echegoyen, *J. Am. Chem. Soc.*, **110**, 119 (1988).

14) A. Kaifer, L. Echegoyen, D. A. Gustowski, D. M. Goli, and G. W. Gokel, *J. Am. Chem. Soc.*, **105**, 7168 (1983).

15) D. A. Gustowski, L. Echegoyen, D. M. Goli, A. Kaifer, R. A. Schuitz, and G. W. Gokel, *J. Am. Chem. Soc.*, **106**, 1633 (1984).

16) C. R. Morgan, D. A. Gustowski, T. P. Cleary, L. Echegoyen, and G. W. Gokel, *J. Org. Chem.*, **49**, 5008 (1984).

17) A. Kaifer, D. A. Gustowski, L. Echegoyen, V. J. Gatto, R. A. Schultz, T. P. Cleary, C. R. Morgan, D. M. Goli, A. M. Rios, and G. W. Gokel, *J. Am. Chem. Soc.*, **107**, 1958 (1985).

18) S. Shinkai, K. Inuzuka, O. Miyazaki, and O. Manabe, *J. Am. Chem. Soc.*, **107**, 3950 (1985).

19) D. A. Gustowski, V. J. Gatto, A. Kaifer, L. Echegoyen, R. E. Godt, and G. W. Gokel, *J. Chem. Soc., Chem. Commun.*, **1984**, 923.

20) K. Tajima, M. Miyoshi, M. Furutani, Y. Fujimura, K. Mukai, and K. Ishizu, *Bull. Chem. Soc. Jpn.*, **62**, 2061 (1989).

21) M. J. S. Dewar and W. Thiel, *J. Am. Chem. Soc.*, **99**, 4899 (1977).

22) Not the approximate half-electron method but the correct open-shell RHF method for the doublet state was employed by using the MOSEMI program package written in our group.

23) C. Heller and H. M. McConnell, *J. Chem. Phys.*, **32**, 1535 (1960).

24) K. Suga, T. Takiguchi, and S. Aoyagi, *Bull. Chem. Soc. Jpn.*, **59**, 1433 (1986).

 © 1991 The Chemical Society of Japan Bull. Chem. Soc. Jpn., 64, 3251—3255 (1991)

Asymmetric Transformations of Proline and 2-Piperidinecarboxylic Acid via Formation of Salts with Optically Active Tartaric Acid

Tadashi SHIRAIWA,* Kazuyuki SHINJO, and Hidemoto KUROKAWA
Faculty of Engineering, Kansai University,
Yamate-cho, Suita, Osaka 564

(Received March 28, 1991)

The rates of racemization of optically active proline [Pro] and 2-piperidinecarboxylic acid [Pia] by using aldehydes as a catalyst tended to increase with a decrease in the acidity of the carboxylic acid used as solvent. Based on these results, the asymmetric transformations of DL-Pro and (*RS*)-Pia were carried out via formation of salts with (2*R*, 3*R*)-tartaric acid to give optically pure L-Pro in over 80% yield and (*R*)-Pia in 70% yield. The asymmetric transformation of L-Pro was more successfully achieved by using (2*S*, 3*S*)-tartaric acid to give optically pure D-Pro in 85% yield based on the starting L-Pro.

L-Proline [abbreviated as L-Pro] as an important amino acid in vivo is a cyclic amino acid with a five-membered ring and is obtained by fermentation or by isolation from protein hydrolysates. D-Pro is difficult to obtain from natural products in large quantities and has been obtained by synthetic transformations from D-glutamic acid.[1] L-Pro, therefore, is inexpensive, whereas D-Pro is significantly costly. Both D- and L-Pro are useful as chiral reagents and catalysts in asymmetric syntheses. (*S*)-2-Piperidinecarboxylic acid [(*S*)-Pia] with a six-membered ring has been synthesized from L-lysine,[2] (*R*)-Pia also from L-lysine by the Walden inversion,[3] and (*RS*)-Pia by reduction of 2-pyridinecarboxylic acid[4,5] and from *N*-benzoyl-1,2,3,6-tetrahydropyridine through cobalt-catalyzed isomerization-carboxylation.[6] (*R*)- and (*S*)-Pia, however, are extremely expensive and only (*RS*)-Pia is readily available. This paper describes easier preparations of optically active Pro and Pia.

An asymmetric transformation has a possibility of converting efficiently a racemate into a desired enantiomer and has been carried out by combination of selective crystallization of a less soluble diastereomeric salt with epimerization of the more soluble one in a solution.[7-10] Although an asymmetric transformation of *N*-butyryl-DL-proline gives L-Pro by combination of preferential crystallization with racemization,[7] such has not been reported for (*RS*)-Pia. Then the asymmetric transformation were attempted without converting Pro and Pia into their derivatives, such as *N*-acyl amino acids. Optically active amino acids are easily racemized by using aldehydes as catalyst in carboxylic acid.[11,12] In addition, optical resolutions of DL-Pro[13] and (*RS*)-Pia[14] by using (2*R*,3*R*)-tartaric acid [(*R*)-TA] as a resolving agent give the salt of L-Pro with (*R*)-TA and that of (*R*)-Pia with (*R*)-TA as a less soluble diastereomeric salt. The asymmetric transformations of DL-Pro and (*RS*)-Pia, therefore, were tried by using butanal and salicylaldehyde as the catalyst via formation of a salt with (*R*)-TA in carboxylic acids. The asymmetric transformation of L-Pro to D-Pro was also examined by using (*S*)-TA.

Experimental

Materials. DL-Pro and (*RS*)-Pia were purchased from Tokyo Kasei Kogyo Co., Ltd., L-Pro from Kokusan Chemical Works Ltd., and (*R*)- and (*S*)-TA from Wako Pure Chemicals Ind. (*R*)-Pia was obtained by asymmetric transformation.

Asymmetric Transformation. Proline: A mixture of 20.0 mmol (2.30 g) of L-Pro, 20.0 mmol (3.00 g) of (*S*)-TA, and 2.00 mmol of butanal in 30 cm^3 of butanoic acid was stirred for 1—6 h at 80 °C and subsequently for 0.5 h in an ice bath. The formed D-Pro·(*S*)-TA salt was collected by filtration, washed thoroughly with diethyl ether, and dried. After adding concentrated aqueous ammonia (0.55 cm^3 g^{-1}) to a solution of the salt in 200 cm^3 of methanol, followed by stirring the mixture for 0.5 h in an ice bath, the precipitated diammonium (2*S*, 3*S*)-tartarate was removed by filtration; the (*S*)-TA used as the resolving agent was recovered in over 90% yield as the diammonium salt; $[\alpha]_D^{20}$ −33—−32° (*c* 1.00, water): lit,[15] of diammonium (2*R*, 3*R*)-tartarate, $[\alpha]_D$ +34.0° (water). Drying of the filtrate gave D-Pro as the residue.

Similarly, the asymmetric transformation of DL-Pro was carried out by using (*R*)-TA and 0.1 mol equivalent of salicylaldehyde and butanal in butanoic acid at 90 °C. The optical purities of the obtained D-Pro·(*S*)-TA and L-Pro·(*R*)-TA salts were estimated on the basis of the specific rotations of the L-Pro·(*R*)-TA salt ($[\alpha]_D^{25}$ −24.2° (*c* 1, water)[13]) and the D-Pro·(*R*)-TA salt ($[\alpha]_D^{25}$ +44.4° (*c* 1, water))[13]) and those of D- and L-Pro from the specific rotation of L-Pro ($[\alpha]_D^{20}$ −86.2° (*c* 1.00, water)).[16]

To a solution of the D-Pro·(*S*)-TA or L-Pro·(*R*)-TA salt with over 90% optical purity in water (1 cm^3 g^{-1}) was added ethanol (20 cm^3 g^{-1}). After stirring the mixture for 1 h in an ice bath, the purified salt was collected by filtration, washed with diethyl ether, and dried. The salt was treated with concentrated aqueous ammonia similarly to the above to obtain optically pure D- and L-Pro.

(*RS*)-2-Piperidinecarboxylic Acid: A mixture of 10.0 mmol (1.29 g) of (*RS*)-Pia, 10.0 mmol (1.50 g) of (*R*)-TA, and 5.00 mmol of salicylaldehyde in 50 cm^3 of butanoic acid, pentanoic acid, or hexanoic acid was stirred for 2—10 h at 110 °C and then for 0.5 h in an ice bath. The formed (*R*)-Pia·

(*R*)-TA salt was treated with concentrated aqueous ammonia to give (*R*)-Pia.

A suspension of the (*R*)-Pia·(*R*)-TA salt with 80% optical purity in methanol (3.3 $cm^3\ g^{-1}$) was stirred for 0.5 h at 50 °C and then for 2 h at 20 °C. The purified (*R*)-Pia·(*R*)-TA salt was collected by filtration, washed with diethyl ether, and dried. Treatment of the salt with concentrated aqueous ammonia gave optically pure (*R*)-Pia; lit,[2] of (*S*)-Pia, $[\alpha]_D^{20}$ −30.6° (*c* 1, water).

Rate Constant of Racemization. After adding 4.00 mmol of butanal or salicylaldehyde to a solution of 40.0 mmol of L-Pro in 100 cm^3 of formic acid, acetic acid, propanoic acid, or butanoic acid at 80 °C, the solution was stirred at 80 °C. Two cubic centimeter portions of the solution were pipetted out at appropriate time intervals, cooled rapidly, and diluted to 10 cm^3 with acetic acid. The optical rotation at 589 nm was measured with a Union Giken PM-101 digital polarimeter equipped with a quartz cell of 5.00 cm path length. The rate constant of racemization (k_R/s^{-1}) was calculated by the least-squares method from the equation

$$\ln \alpha_0/\alpha_t = k_R\, t, \qquad (1)$$

where α_t is the optical rotation at time *t* and α_0 that extrapolated to zero time. The half-conversion period ($t_{1/2}/s$) was calculated by using the k_R value from Eq. 1.

The rate of racemization of (*R*)-Pia was measured at 110 °C for solutions of (*R*)-Pia (20.0 mmol) and butanal or salicylaldehyde (2.00 mmol) in 100 cm^3 of formic acid, acetic acid, and propanoic acid.

Results and Discussion

Racemization of L-Proline and (*R*)-2-Piperidinecarboxylic Acid. One of the major problems in an asymmetric transformation is the rate of epimerization, that is, that of racemization of an optically active substance. The rates of racemization of L-Pro and (*R*)-Pia, therefore, were measured by using butanal or salicylaldehyde in formic acid, acetic acid, propanoic acid, and butanoic acid. The rate of racemization of (*R*)-Pia in butanoic acid and those of L-Pro and (*R*)-Pia in higher carboxylic acids could not be measured because L-Pro and (*R*)-Pia did not completely dissolve in these carboxylic acids even at 110 °C. These racemizations were regarded as a first-order reaction because a linear relationship was found between $\ln \alpha_0/\alpha_t$ and time *t*. The rate constant for racemization (k_R/s^{-1}) and the half-life conversion ($t_{1/2}/s$) are summarized in Table 1.

In these racemizations, the first step is the formation of the Schiff base.[11,12] This dehydration-condensation of a cyclic amino acid with the aldehyde proceeds by protonation from the carboxylic acid used as solvent, and hence the Schiff base formed has a positive charge on the nitrogen atom.[11] The second step is proton abstraction from the α-carbon atom by the resulting carboxylate anion.[11,12]

The rate of racemization of (*R*)-Pia was extremely lower than that of L-Pro, as seen in Table 1. The four carbon and one nitrogen atoms in the five-membered ring on L-Pro lie on the approximately same plane,[17] whereas the six-membered ring on (*R*)-Pia exists in a chair form.[18] Such steric bulkiness of the ring on (*R*)-Pia may hinder the formation of the Schiff base, and hence slow down the rate of racemization compared with the pseudo-planar ring on L-Pro.

As found in racemization by using butanal, the rates of racemization of L-Pro and (*R*)-Pia were dependent on the nature of the carboxylic acid used as solvent, that is, acidity of the carboxylic acid or basicity of its carboxylate anion. The acidity constants (pK_a), estimated from the data at 0—60 °C,[19] at 80 and 110 °C tend to suggest that an order of protonation is formic acid> acetic acid>propanoic acid>butanoic acid and that of proton abstraction is butanoate anion>propanoate anion>acetate anion>formate anion. A relationship between the k_R and pK_a values is shown in Fig. 1.

The k_R value tended to increase with an increase in the pK_a value, as seen in Fig. 1. It has been reported that the rate of racemization of optically active amino acids may be most rapid in acetic acid.[11] The above result,

Table 1. Rate Constants and Half-Conversion Periods for the Racemization of L-Proline and (*R*)-2-Piperidinecarboxylic Acid

Amino acid	Aldehyde	Carboxylic acid	k_R[a] / $10^{-4}\ s^{-1}$	$t_{1/2}$[b] / 10^2 s
L-Pro[c]	Butanal	FrA[f]	0.101	686
		AcA[g]	15.3	4.53
		PrA[h]	25.6	2.71
		BuA[i]	26.2	2.65
	SA[e]	AcA[g]	3.10	22.4
(*R*)-Pia[d]	Butanal	FrA[f]	ca. 0	—
		AcA[g]	0.845	82.0
		PrA[h]	5.28	13.1
	SA[e]	AcA[g]	0.741	93.5

a) k_R: Rate constant for racemization. b) $t_{1/2}$: Half-conversion period. c) L-Proline [L-Pro] 40.0 mmol; aldehyde 4.00 mmol; carboxylic acid 100 cm^3;temperature 80 °C. d) (*R*)-2-Piperidinecarboxylic acid [(*R*)-Pia] 20.0 mmol; aldehyde 2.00 mmol; carboxylic acid 100 cm^3; temperature 110 °C. e) SA: Salicylaldehyde. f) FrA: Formic acid. g) AcA: Acetic acid. h) PrA: Propanoic acid. i) BuA: Butanoic acid.

Table 2. Asymmetric Transformation of Proline[a]

Starting proline	Aldehyde	Reaction time	Salt			Proline		
			Configuration	Yield	Optical purity	Configuration	Yield[c]	Optical purity
		h		g [%[b]]	%		%	%
DL-Pro[d]	SA[f]	1	L·(*R*)[h]	4.89 [90.9]	58.5	L	90.0	57.7
		2		5.08 [95.8]	78.7		94.4	77.4
		3		5.10 [96.2]	84.0		95.2	82.5
		4		5.07 [95.7]	88.4		94.7	87.1
		5		5.08 [95.8]	90.4		93.0	88.5
		5[g]		4.41 [83.2]	100		80.9	100
		6		5.06 [95.5]	89.2		93.2	87.9
DL-Pro[d]	Butanal	1	L·(*R*)[h]	4.98 [93.8]	73.5	L	92.1	72.0
		2		5.04 [95.0]	90.1		93.1	89.7
		3		5.03 [94.8]	90.8		94.1	91.0
		3[g]		4.49 [84.7]	100		83.3	100
L-Pro[e]	Butanal	1	D·(*S*)[i]	5.21 [98.3]	15.1	D	97.0	15.1
		2		5.15 [97.2]	82.8		96.1	84.2
		3		5.16 [97.4]	93.3		94.8	92.9
		3[g]		4.67 [88.1]	100		85.2	100
		4		5.15 [97.2]	93.3		93.2	92.5
		4[g]		4.62 [87.2]	100		84.8	100
		5		5.16 [97.4]	93.6		93.9	93.2
		6		5.18 [97.7]	94.5		95.2	93.6

a) Proline [Pro] 20.0 mmol; optically active tartaric acid [TA] 20.0 mmol; aldehyde 2.00 mmol; butanoic acid 30 cm^3. b) The yield was calculated on the basis of 20.0 mmol (5.30 g) of the salt of Pro with TA. c) The yield was calculated on the basis of 20.0 mmol (2.30 g) of Pro. d) The asymmetric transformation of DL-Pro was carried out by using (*R*)-TA as the resolving agent at 90°C. e) The asymmetric transformation of L-Pro was carried out by using (*S*)-TA as the resolving agent at 80°C. f) SA: Salicylaldehyde. g) The obtained salt was purified by recrystallization. h) L·(*R*): Salt of L-Pro with (*R*)-TA. i) D·(*S*): Salt of D-Pro with (*S*)-TA.

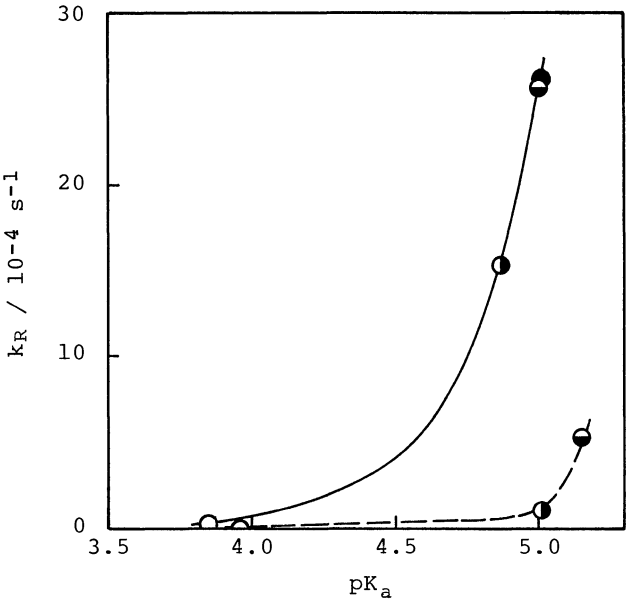

Fig. 1. Influence of the carboxylic acid used as solvent on the racemization of L-proline and (*R*)-2-piperidinecarboxylic acid.
Conditions. See footnote to Table 1. k_R: Rate constant (s^{-1}) for racemization. pK_a: The pK_a values at 80 and 110 °C were calculated by extrapolation from data at 0—60 °C; Ref. 19. —: Racemization of L-proline at 80 °C. ---: Racemization of (*R*)-2-piperidinecarboxylic acid at 110 °C. Carboxylic acid: ○ Formic acid; ◑ acetic acid; ◒ propanoic acid; ● butanoic acid.

however, suggests that the rate of racemization of optically active cyclic amino acids, such as L-Pro and (*R*)-Pia, is accelerated with a decrease in acidity of the carboxylic acid used as solvent, and hence its rate-determining step is the α-proton abstraction by the carboxylate anion.

In addition, the racemizations of L-Pro and (*R*)-Pia were more accelerated by using butanal as catalyst than salicylaldehyde.

Asymmetric Transformation of Proline. The asymmetric transformation of DL-Pro was carried out at 90 °C in butanoic acid. The result is summarized in Table 2.

When butanal was used as catalyst, the L-Pro·(*R*)-TA salt with 90% optical purity was obtained in 95% yield by allowing to react for 2 and 3 h. Although the asymmetric transformation by using salicylaldehyde required longer time than that by using butanal, as predicted from the result of racemization, those at 4—6 h gave the L-Pro·(*R*)-TA salt with 88—90% optical purity in 96% yield. These salts were purified to give optically pure L-Pro in over 80% yield based on the starting DL-Pro, as summarized in Table 2.

The asymmetric transformation of L-Pro into D-Pro was more successfully achieved by using butanal as catalyst and (*S*)-TA as the resolving agent, at 80 °C (Table 2). The D-Pro·(*S*)-TA salt with 93—95% optical purity was obtained in 97% yield by a reaction for 3—6 h. The purified salt gave optically pure D-Pro in 85% yield based on the starting L-Pro.

The rate of racemization of an optically active substance is measured under homogeneous conditions, whereas an asymmetric transformation is carried out under heterogeneous ones. Optimum conditions for the asymmetric transformation, therefore, may not always be the same as those for the racemization. However, the asymmetric transformations of DL- and L-Pro gave very good results under the conditions estimated from the result of racemization.

Asymmetric Transformation of (*RS*)-2-Piperidinecarboxylic Acid. The optical resolution of (*RS*)-Pia by using (*R*)-TA gives the (*R*)-Pia·(*R*)-TA salt as a less soluble diastereomeric salt.[14] The result of racemization of (*R*)-Pia suggests that the rate of epimerization of the Pia·(*R*)-TA salt is extremely slower than that of Pro. In addition, the result of racemization of L-Pro allows to predict that the rate of (*R*)-Pia is more rapid in butanoic acid than in acetic acid and propanoic acid. The asymmetric transformation of (*RS*)-Pia, therefore, was tried by consuming 5.00 mmol of the aldehydes per 10.0 mmol of (*RS*)-Pia in butanoic acid at 110 °C. The asymmetric transformation by using butanal, however, could not be carried out because the formed salt became a viscous mass. The asymmetric transformation of (*RS*)-Pia, therefore, was carried out by using salicylaldehyde. The result is summarized in Table 3.

The asymmetric transformation gave the (*R*)-Pia·(*R*)-TA salt with 76—80% optical purity at 3—7 h. Although the purified salt gave optically pure (*R*)-Pia in 61% yield based on the starting (*RS*)-Pia, as summarized in Table 3, the yield was not so high as expected. Such low yield seems to be due to the relatively high solubility of the salt formed in butanoic acid. The formed salt seems to be less soluble in pentanoic acid and hexanoic acid than in butanoic acid. The rates of epimerization in these carboxylic acids are estimated to be approximately equal to that in butanoic acid from the acidity constants of these carboxylic acids at 110 °C.[19,20] The asymmetric transformation was tried by a reaction for 5 h in pentanoic acid and hexanoic acid (Table 3). Comparison of the asymmetric transformations in these carboxylic acids indicated that the yield of the obtained (*R*)-Pia·(*R*)-TA salt tended to rise with an increase in the carbon number of the carboxylic acids, whereas the optical purity to fall.

One more major problem in the asymmetric transformation is the solubility of the diastereomeric salts in the solvent used. The solubility influences not only the yield of the less soluble diastereomeric salt, but its optical purity. If the solubility is too low, the asymmetric transformation in such a solvent may give the salt with low optical purity, and hence require much long time to obtain the salt with high optical purity. The asymmetric transformation in pentanoic acid, however, gave the (*R*)-

Table 3. Asymmetric Transformation of (*RS*)-2-Piperidinecarboxylic Acid[a)]

Carboxylic acid	Reaction time	(*R*)-Pia·(*R*)-TA salt		(*R*)-Pia	
		Yield	Optical purity	Yield[c)]	Optical purity
	h	g [%[b)]]	%	%	%
BuA[d)]	3	2.06 [73.8]	75.8	72.4	74.3
	4	2.06 [73.8]	77.3	72.5	76.5
	5	2.04 [73.1]	78.4	71.5	78.0
	6	2.04 [73.1]	78.1	72.1	77.9
	7	2.09 [74.9]	79.8	73.8	78.0
	7[g)]	1.76 [63.1]	100	61.4	100
PeA[e)]	2	2.41 [86.3]	41.0	84.8	39.6
	3	2.39 [85.7]	52.3	84.8	51.6
	4	2.49 [89.2]	55.5	88.0	53.2
	5	2.27 [81.4]	65.1	80.6	66.2
	6	2.24 [80.3]	73.0	79.8	73.0
	8	2.27 [81.4]	79.8	81.0	78.0
	8[g)]	1.94 [69.5]	100	68.5	100
	10	2.30 [82.4]	81.6	81.5	81.2
	10[g)]	1.99 [71.3]	100	70.2	100
HxA[f)]	5	2.31 [82.8]	52.2	81.9	51.0

a) (*RS*)-2-Piperidinecarboxylic acid [(*RS*)-Pia] 10.0 mmol; (2*R*,3*R*)-tartaric acid [(*R*)-TA] 10.0 mmol; salicylaldehyde 5.00 mmol; carboxylic acid 50 cm^3; temperature 110°C. b) The yield was calculated on the basis of 10.0 mmol (2.79 g) of the salt of (*R*)-Pia with (*R*)-TA. c) The yield was calculated on the basis of 10.0 mmol (1.29 g) of (*R*)-Pia. d) BuA: Butanoic acid. e) PeA: Pentanoic acid. f) HxA: Hexanoic acid. g) The obtained salt was purified by recrystallization.

Pia·(*R*)-TA salt with relatively high optical purity (65%) in higher yield (81%) than that (73%) in butanoic acid. The asymmetric transformation, therefore, was carried out by a reaction for 2—10 h in pentanoic acid (Table 3).

As already mentioned, the asymmetric transformation in butanoic acid gave the salt with 76—80% optical purity at 3—7 h. The yields, however, were less than 75%. The asymmetric transformations at 8 and 10 h in pentanoic acid gave the (*R*)-Pia·(*R*)-TA salt with 80% optical purity in over 80% yield. These salts recrystallized from methanol gave optically pure (*R*)-Pia in 70% yield, based on the starting (*RS*)-Pia, as summarized in Table 3.

References

1) D. Enders, H. Eichenauer, and R. Pieter, *Chem. Ber.*, **112**, 3703 (1979).
2) T. Fujii and M. Miyoshi, *Bull. Chem. Soc. Jpn.*, **48**, 1341 (1975).
3) U. Schiedt and H. G. Hoss, *Z. Physiol. Chem.*, **308**, 179 (1957).
4) P. B. Ellman, *J. Biol. Chem.*, **182**, 75 (1950).
5) A. Harris and J. R. A. Pollock, *Chem. Ind.*, **1953**, 462.
6) Y. Amino, S. Nishi, and K. Izawa, *Bull. Chem. Soc. Jpn.*, **64**, 620 (1991).
7) C. Hongo, S. Yamada, and I. Chibata, *Bull. Chem. Soc. Jpn.*, **54**, 3286 (1981).
8) C. Hongo, R. Yoshioka, M. Tohyama, S. Yamada, and I. Chibata, *Bull. Chem. Soc. Jpn.*, **56**, 3744 (1983).
9) R. Yoshioka, M. Tohyama, O. Ohtsuki, S. Yamada, and I. Chibata, *Bull. Chem. Soc. Jpn.*, **60**, 649 (1987).
10) T. Shiraiwa, K. Kataoka, S. Sakata, and H. Kurokawa, *Bull. Chem. Soc. Jpn.*, **62**, 109 (1989).
11) S. Yamada, C. Hongo, R. Yoshioka, and I. Chibata, *J. Org. Chem.*, **48**, 843 (1983).
12) R. Grigg and H. Q. N. Gunaratne, *Tetrahedron Lett.*, **24**, 4457 (1983).
13) S. Yamada, C. Hongo, and I. Chibata, *Agric. Biol. Chem.*, **41**, 2413 (1977).
14) R. J. Hemingway, *J. Pharm. Pharmacol.*, **20**, 87 (1968).
15) "Kagaku Daijiten," ed by Kagaku Daijiten Henshu Iinkai, Kyoritsu Shuppan, Tokyo (1971), Vol. 4, p. 696.
16) J. S. Davies, "Amino Acids and Peptides," Chapman and Hall, New York (1985), p. 273.
17) J. J. Verbist, M. S. Lehmann, T. F. Koetzle, and W. C. Hamilton, *Nature*, **235**, 328 (1972).
18) S. K. Bhattacharjee and K. K. Chacko, *Acta Crystallogr., Sect. B*, **35**, 396 (1979).
19) H. Ohtaki, "Youeki Kagaku," Shoukabou, Tokyo (1985), pp. 184—186.
20) R. P. Bell, "Proton in Chemistry," Cornell University Press (1959), p. 65.

Synthetic Application of Benzothiazole Ring System as an On-Off Type of Leaving Group. Synthesis of Ketones and Carboxylic Acid Derivatives from 2-(1-Substituted 1-Hydroxyalkyl)- and 2-(1-Hydroxyalkyl)benzothiazoles

Hidenori CHIKASHITA,* Masayuki ISHIHARA, Katsumi TAKIGAWA, and Kazuyoshi ITOH
Department of Applied Chemistry, Faculty of Engineering, Kansai University,
Suita,Osaka 564
(Received April 30, 1991)

A synthetic and systematic use of benzothiazole ring system as an "on-off" type of leaving group was developed for the preparation of ketones and carboxylic acid derivatives from a variety of 2-(1-substituted 1-hydroxyalkyl)- and 2-(1-hydroxyalkyl)benzothiazoles (off state) via the corresponding benzothiazolium salts (on state) obtained by the quaternization (on switch). A variety of 3-methyl-2-(1-substituted 1-hydroxyalkyl)benzothiazolium iodides (**1**) underwent a carbon–carbon bond cleavage at the 2-position to give the corresponding ketones on the simple treatment with a base under mild reaction conditions. The similar reaction of 3-methyl-2-(1-hydroxyalkyl)benzothiazolium iodides (**2**) to aldehydes proceeded less efficiently. The oxidative reaction of a variety of **2** with base and nonactivated MnO_2 in ethanol afforded the corresponding ethyl esters. This type of oxidative reaction could be also achieved in THF with different nucleophiles such as alcohol, water, thiol, and amine to give the corresponding ester, carboxylic acid, thioester, and amide, respectively.

Thiamine pyrophosphate (TPP) is a coenzyme which participates in a number of important biochemical reactions involving formation and cleavage of carbon–carbon bonds as well as oxidation reactions.[1] The catalytic unit of TPP on these reactions is the thiazolium ring. It is known that various simple thiazolium salts effect TPP type of transformations even in the absence of enzyme,[2] and up to now much interest has been focused on model reaction systems of TPP coenzyme.[3] From the standpoint of synthetic chemistry, these reactions can be regarded to offer a unique example of a heterocyclic molecule acting as an efficient leaving group because the release of the thiazolium salt unit as a thiazolium ylide by carbon–carbon bond fission is a key step and plays an essential role in the model systems. Although reaction intermediates derived from thiazolium salt catalysts have recently been of interest from a synthetic viewpoint,[4] there is little study dealing with synthetic and systematic applications of thiazole ring system by utilizing potential reactivities of the intermediate-like stable compounds themselves such as 2-(1-hydroxyalkyl)thiazolium salts. In our recent studies on benzazole field, we found several functionalities of the benzothiazole ring system available for organic synthesis and reported their applications to the novel synthetic methodologies.[5] In connection with these studies, we now investigated the preparation and reactivities of a variety of 2-(1-substituted 1-hydroxyalkyl)- and 2-(1-hydroxyalkyl)benzothiazolium salts structurally related to the intermediates on the TPP-model reactions and found that ketones and carboxylic acid derivatives were systematically obtained via these salts from the corresponding benzothiazole derivatives, revealing a novel functionality of benzothiazole ring system as an "on-off" type of leaving group. As a different type of systematic use of benzothiazole ring system in organic synthesis, we wish to report here a novel preparation method for ketones and carboxylic acid derivatives based on this concept of leaving group.

Results and Discussion

Preparation and Properties of 3-Methyl-2-(1-substituted 1-Hydroxyalkyl)- and 3-Methyl-2-(1-hydroxyalkyl)benzothiazolium Iodides (1 and 2). Benzothiazolium salts **1** and **2** were prepared as outlined in Scheme 1. The two typical procedures for large scale preparation of **1** and **2** are the following: (i) The reaction of lithiated benzothiazole (2-LiBT) with ketones and aldehydes followed by quaternization of the resulting 2-(1-substituted 1-hydroxyalkyl)- and 2-(1-hydroxyalkyl)benzothiazoles with methyl iodide in DMF; and (ii) the acylation of 2-LiBT with esters and the subsequent alkylation with organometallic reagents or hydride reduction of the resulting 2-acylbenzothiazole **3** under standard conditions, followed by the quaternization with methyl iodide in DMF. As shown in our previous paper,[5f] each step in both methods proceeds in high

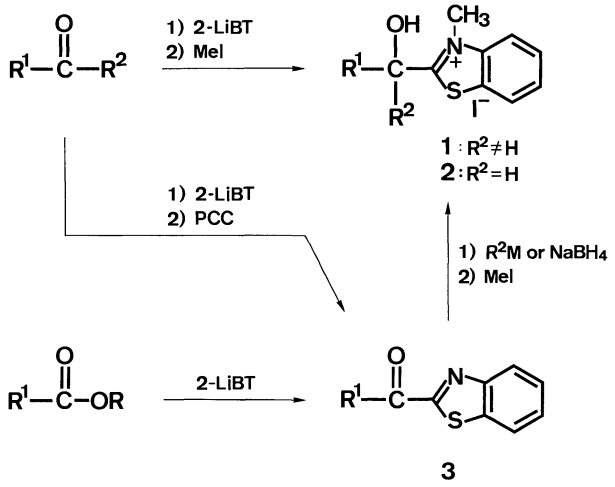

Scheme 1.

Table 1. Conversion of Benzothiazolium Salt **1a** into Acetophenone (**4a**)

Entry	Base (equiv)	Solvent	Temp/°C	Time/h	Isolated yield/%
1	K_2CO_3 (1.5)	H_2O/ethanol	Reflux	7	92
2	K_2CO_3 (1.5)	H_2O/hexane	60	2	95
3	AcONa (3.0)	H_2O/hexane	60	2	91
4	DBU (1.0)	Ethanol	r.t.	2	86
5	DBU (0.2)	Ethanol	Reflux	2	90
6	TEA (1.0)	Ethanol	r.t.	2	89
7	None	90% aq Ethanol	Reflux	72	77[a)]

a) 3-Methylbenzothiazolium iodide (**5**) was isolated in 83% yield.

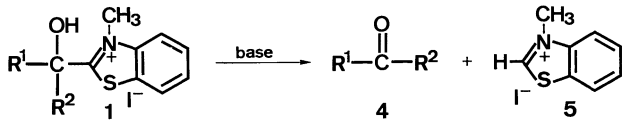

a : R^1=Ph, R^2=Me
b : R^1=Ph, R^2=Ph
c : R^1=n-C_6H_{13}, R^2=Me
d : R^1=n-Pr, R^2=Ph
e : R^1= , R^2=Me
f : R^1–R^2=$-(CH_2)_{11}-$
g : R^1–R^2=$-(CH_2)_5-$
h : R^1=PhCH=CH–, R^2=Ph

Scheme 2.

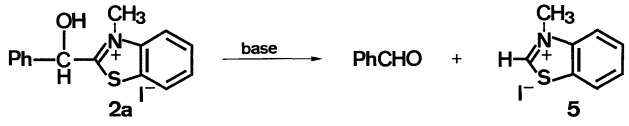

Scheme 3.

yields and benzothiazolium salts **1** and **2** are obtained in good total yields. In addition, benzothiazolium salt **1** could be easily prepared from aldehydes via 2-acylbenzothiazole **3** obtained by the reaction with 2-LiBT followed by pyridinium chlorochromate (PCC) oxidation. Benzothiazolium iodides **1** and **2** are generally obtained as very stable crystalline compounds and can be easily purified by recrystallization from methanol.

Ketone- and Aldehyde-Generating Reactions of 1 and 2. We started our studies by examining the ketone-generating reaction of the salt **1a** under a variety of reaction conditions (Scheme 2). The results are summarized in Table 1. When **1a** was homogeneously treated with 1.5 equiv of 10% aqueous K_2CO_3 in ethanol under refluxing, acetophenone (**4a**) was obtained in excellent yield after a 7-h reaction time (Entry 1). However, heterogeneous reaction by stirring the two-layer mixture consisting of **1a**, hexane, and 1.5 equiv of 10% aqueous K_2CO_3 at lower temperature was found to be more effective and ketone **4a** was obtained in nearly quantitative yield after shortened reaction time (Entry 2). In this reaction, 10% aqueous K_2CO_3 could be replaced by a weaker base such as 10% aqueous AcONa, and excellent yield of ketone **4a** was obtained under similar reaction conditions (Entry 3). On the other hand, we have found that organic bases such as 1,8-diazabicyclo[5.4.0]undec-7-ene (DBU) or triethylamine (TEA) were also effective for this type of cleavage reaction. Thus, the treatment of **1a** with 1 equiv of DBU or TEA in ethanol at room temperature afforded ketone **4a** in high yield (Entries 4,6). The use of a catalytic amount of DBU (0.2 equiv) in ethanol at refluxing temperature was also useful for producing ketone **4a** from **1a** in excellent yield (Entry 5). Furthermore, it was discovered that this acetophenone-generating reaction could proceed in the absence of bases by prolonged refluxing in 90% aqueous ethanol giving ketone **4a** in 77% yield together with 3-methylbenzothiazolium iodide (**5**) which was isolated in 83% yield (Entry 7). Although satisfactory results were obtained in all cases examined, the two-layer method using K_2CO_3 in hexane-water is the best reaction in terms of the yield of product and rapidity and cleanliness of the reaction. In fact, almost pure ketone **4a** could be obtained simply by evaporating the organic layer. In contrast to these, the cleavage of benzothiazolium salt **2a** by the methods employed for the cleavage of **1a** or by the heterogeneous reaction with aq NaOH and benzene in the presence of 6-aminohexanoic acid as a trapping agent produced benzaldehyde in generally very low yield (Scheme 3), although the homogeneous reaction in ethanol employing 10% aqueous K_2CO_3 afforded benzaldehyde in 30% isolated yield. In addition, it should be noted that the reactions employing DBU and TEA led to the formation of benzoin derived from 2 equiv of benzaldehyde. The reason for these unsuccessful results will be discussed later.

We next examined a general applicability of the ketone-generating reaction of a variety of 2-(1-substituted 1-hydroxyalkyl)benzothiazolium salts **1b**—**h** with the two-layer method using K_2CO_3 (Scheme 2). The results are summarized in Table 2. Benzothiazolium salts **1b**—**e** were all cleanly cleaved to the corresponding aliphatic and aromatic ketones **4b**—**e** and the reactions were completed within 2 h with nearly quantitative yields of the products (Entries 1—4). Cycloundecyl compound **1f** was similarly reacted to afford cycloundecanone (**4f**) in nearly quantitative yield, hence the reaction of cyclohexyl compound **1g** gave cyclohexanone (**4g**) in modest yield (Entries 5,6). On the other hand, the reaction of the benzothiazolium salt possessing a vinylic substituent, **1h**, under the present conditions did not produce the expected ketone,

Table 2. Preparation of Ketones **4** from a Variety of 2-(1-Substituted 1-Hydroxyalkyl)benzothiazolium Salts **1**[a)]

Entry	Salt **1**	Product **4**	Isolated yield/%
1	**1b**	**4b**	94
2	**1c**	**4c**	97
3	**1d**	**4d**	94
4	**1e**	**4e**	95
5	**1f**	**4f**	95
6	**1g**	**4g**	40
7	**1h**	**4h**	0

a) All reactions were carried out with the salts **1** (4 mmol) in two-layer mixture of hexane (4 ml) and 10% aqueous K_2CO_3 (8 ml) at 60 °C for 2 h under stirring.

chalcone (**4h**), at all. Thus, the present method was found to be generally applicable to the synthesis of a variety of ketones except for α,β-unsaturated ketones.

Two possible reaction mechanisms for the present cleavage reaction of **1** can be proposed as illustrated in Scheme 4. They involve deprotonation at the HO-site by the base followed by leaving the ylide **7** from the resulting zwitterion intermediate **6** (mechanism A); and hydroxylation at the benzothiazolium ring followed by leaving 2-hydroxy-3-methyl-2,3-dihydrobenzothiazole **9** from the dihydroxy intermediate **8** via 1,3-shift (mechanism B). In the chemistry of thiazolium salt catalyzed reactions, however, the mechanism involving the regeneration of a thiazolium ylide by carbon–carbon bond fission at the 2-position of the thiazolium ring in 2-(1-hydroxyalkyl)thiazolium intermediates has been accepted. In the present case, this type of mechanism is also supported by the fact that the reactions using tertiary amines in a nonaqueous system could proceed in excellent yields. Accordingly, mechanism A via active-aldehyde like intermediate **6** is most likely mechanism for the present ketone-generating reaction and well conforms to the driving force for the formation of the stable benzothiazolium ylide **7**. In addition, this type of mechanism releasing the ylide **7** has been reasonably proposed for the aldehyde formation in the reaction of **2** with organometallic reagents.[5f)] On the other hand, the reaction of **2** in the presence of a base would cause rather

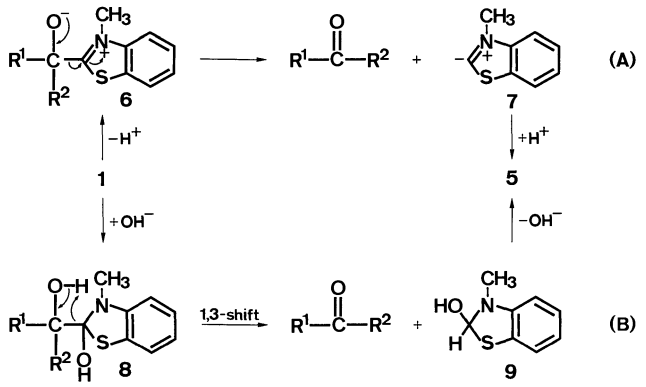

Scheme 4.

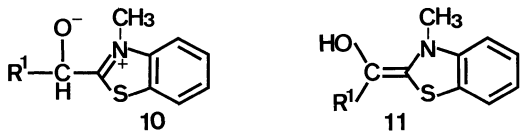

complicated equilibriums derived from the reactivity of so called "active-aldehyde" molecules **10** and **11** on the analogy of model reactions of TPP coenzyme.[2-4)] The unsuccessful results in the case of an aldehyde-generating reaction of **2** are well understood based on the formation of these complicated and indiscriminate equilibriums.

Oxidative Ester-Generating Reaction of 2. Treatment of benzothiazolium salt **2** with a base would easily produce the foregoing active-aldehyde molecules **10** and **11** which are intermediates similar to those in TPP-dependent enzymatic pathway and in its catalytic model reactions. It is well known that active-aldehyde molecules in later cases are oxidized in the presence of a variety of oxidizing agents (e.g., flavin or $K_3Fe(CN)_6$) to afford carboxylic acids, esters, or benzoin type of products depending on the reaction conditions.[3,4)] If the intermediate **10** or **11** possessing a variety of substituents can be oxidized controllably in an alcoholic solvent, this would provide a different type of useful application of benzothiazolium unit as a leaving group for the preparation of esters **12** in organic synthesis (Scheme 5). We have first examined this type of oxidative ester-generating reaction of **2a** in ethanol in the presence of a base by employing 10 equiv of nonactivated MnO_2 and $K_3Fe(CN)_6$ as convenient oxidizing agents. As shown in Table 3, all the reactions examined afforded the expected ester, ethyl benzoate (**12a**), even in the absence of a base. Among the series of reactions employing MnO_2 as an oxidizing agent (Entries 1—8), the reaction with 1 equiv of AcONa was found to give the best results affording ester **12a** in 76% isolated yield (Entry 4), while the reaction with relatively strong bases such as K_2CO_3 and Na_2CO_3 or tertiary amines such as DBU and TEA generally gave the product **12a** in modest yield. The result of the reaction in the absence of a base may indicate that compound **2a** itself can be directly oxidized under the present conditions (Entry 8). On the other hand, the reaction employing $K_3Fe(CN)_6$ in the presence of 1 equiv of AcONa proceeded less effectively

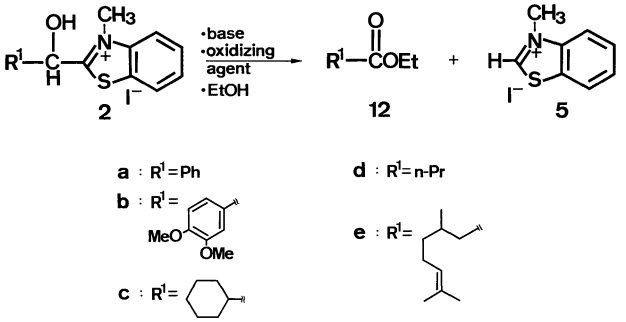

Scheme 5.

to give ester **12a** in low yield (Entries 9,10). Thus, this type of oxidative ester synthesis was then applied to several different benzothiazolium salts **2b**—**e** under the optimum conditions, with the results summarized in Table 4. Benzothiazolium salts possessing a 2-(substituted hydroxymethyl) group, **2b**,**c**,**e**, reacted well under the conditions to give the corresponding ethyl esters **12b**,**c**,**e** in good isolated yields (Entries 1,2,4), although the reaction with **2d** exceptionally showed low yield of product **12d** (Entry 3).

Table 3. Conversion of Benzothiazolium Salt **2a** into Ethyl Benzoate (**12a**)[a]

Entry	Oxidizing agent[b]	Base (equiv)	Isolated yield/%
1	MnO_2	K_2CO_3 (1.0)	49
2	MnO_2	K_2CO_3 (3.0)	53
3	MnO_2	Na_2CO_3 (1.0)	41
4	MnO_2	AcONa (1.0)	76
5	MnO_2	AcONa (3.0)	64
6	MnO_2	TEA (1.0)	45
7	MnO_2	DBU (1.0)	56
8	MnO_2	None	45
9	$K_3Fe(CN)_6$[c]	AcONa (1.0)	22
10	$K_3Fe(CN)_6$	AcONa (1.0)	28

a) All reactions were carried out in ethanol at reflux temperature for 5 h. b) Ten equiv of oxidizing agent was used unless otherwise noted. c) Two equiv of $K_3Fe(CN)_6$ was used.

Table 4. Preparation of Esters **12** from a Variety of 2-(1-Hydroxyalkyl)benzothiazolium Salts **2**[a]

Entry	Salt **2**	Product **12**	Isolated yield/%
1	**2b**	**12b**	78
2	**2c**	**12c**	52
3	**2d**	**12d**	17
4	**2e**	**12e**	70

a) All reactions were carried out with the salts **2** (2 mmol), MnO_2 (10 mmol), and AcONa (2 mmol) in ethanol (30 ml) at reflux temperature for 5 h.

Oxidative Preparation of Carboxylic Acid Derivatives from 2 in Nonnucleophilic Solvent. If it is possible that the active-aldehyde molecule **10** or **11** is also generated and oxidized efficiently in a nonnucleophilic solvent system, the reaction can be carried out in the presence of a variety of nucleophiles. To examine this possibility, we have carried out the reaction of **2** in THF in the presence of AcONa (1 equiv), MnO_2 (10 equiv), and an excess amount of alcohol at refluxing temperature. The results are summarized in Table 5. The reaction of **2a** with a large excess amount of ethanol in THF efficiently proceeded under the conditions to afford ethyl ester **12a** in good yield. Similarly, **2a**,**b**,**d**,**e** reacted with 3 equiv of 2-phenylethanol in THF to give the corresponding phenethyl esters **13a**—**d**. These results clearly show that the formation of active-aldehyde molecule **10** or **11** and its subsequent oxidation by MnO_2 followed by the reaction with an alcohol can proceed in THF as well as in ethanol solvent. We next tried the preparation of the carboxylic acid derivatives by the reaction of **2a** in the presence of several different nucleophiles as a

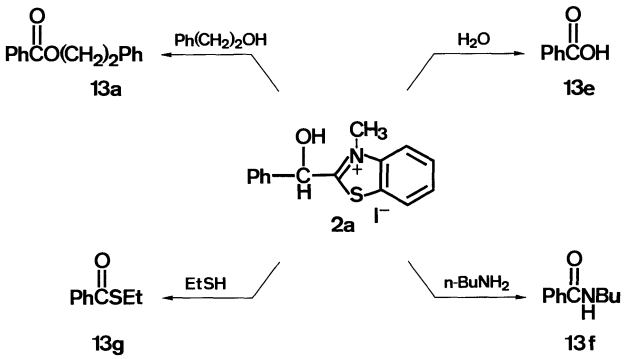

Scheme 6.

Table 5. Preparation of Esters from a Variety of 2-(1-Hydroxyalkyl)benzothiazolium Salts **2** in THF[a]

Entry	Salt **2**	Nucleophile	Product	Isolated yield/%
1	**2a**	EtOH[b]	**12a**	73
2	**2a**	$Ph(CH_2)_2OH$[c]	$PhCO_2(CH_2)_2Ph$ (**13a**)	54
3	**2b**	$Ph(CH_2)_2OH$	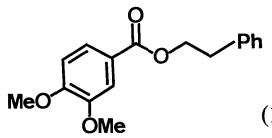 (**13b**)	35
4	**2d**	$Ph(CH_2)_2OH$	n-$C_5H_{11}CO_2(CH_2)_2Ph$ (**13c**)	21
5	**2e**	$Ph(CH_2)_2OH$	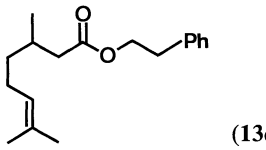 (**13d**)	52

a) All reactions were carried out with the salts **2** (2 mmol), MnO_2 (10 mmol), and AcONa (2 mmol) in THF (30 ml) at reflux temperature for 5 h. b) Large excess amount of ethanol (10 ml) was used. c) In all cases, 3 equiv of 2-phenylethanol was used.

representative example, as illustrated in Scheme 6. The reaction of **2a** in the presence of an excess amount of water at refluxing temperature gave benzoic acid (**13e**) in 76% isolated yield, while the reaction with 3 equiv of butylamine at 60 °C and the reaction with 3 equiv of ethanethiol at 38 °C also produced the corresponding amide **13f** and thioester **13g** in 42% and 57% isolated yields, respectively. However, it should be noted that the similar reaction employing a secondary amine affording a secondary amide was unsuccessful in contrast to the reaction with a primary amine.

The mechanism of the present oxidative reactions can be explained according to that proposed in a TPP-dependent enzymatic pathway and in its catalytic model reactions (Scheme 7).[3,4] However, so-called "active acyl" molecule such as **14** which is the key species to react with nucleophiles in the mechanism has not been isolated yet. We tried the direct synthesis of the active-acyl compound **15** by the *N*-methylation of 2-benzoylbenzothiazole **3a** (Scheme 8). Although the *N*-methylation of **3a** by the standard method using methyl iodide or dimethyl sulfate was very difficult due to the low nucleophilicity at the nitrogen atom, we have found that the *N*-methylation of **3a** with the powerful methylating reagent, methyl fluorosulfate, in dichloromethane at 100 °C proceeds efficiently to give the salt **15** in excellent isolated yield. The compound **15** is slightly unstable in air but can be stored in vacuo for several days. When compound **15** was treated in ethanol under refluxing, ethyl benzoate (**12a**) could be obtained in 85% isolated yield. Similarly, compound **15** reacted with an excess amount of water and butylamine in THF to give benzoic acid (**13e**) and *N*-butylbenzamide (**13f**) in 63% and 56% isolated yields, respectively. This result directly indicates that the active-acyl intermediate **14** can efficiently react with nucleophiles giving the corresponding carboxylic acid derivatives.

Summary. Synthesis of carbonyl compounds from 2-(1-substituted 1-hydroxyalkyl)- and 2-(1-hydroxyalyl)-benzothiazoles (**16** and **17**) via the corresponding benzothiazolium salts **1** and **2** developed in the present study is summarized as follows. The present study reveals that the benzothiazole ring unit can be used as an "on-off" type of leaving group in the synthesis of ketones and carboxylic acid derivatives under simple operations and mild reaction conditions. That is, benzothiazole unit (off state) was found to be able to act as a leaving group only after conversion (turning on) to benzothiazolium structure (on state) by the treatment with methylating agent (on switch). A simple advantage of this method is that the off-state compounds can be treated under a variety of severe conditions. For example, in the ketone synthesis, **16** (off state) can be regarded as a protected from for ketones because the parent ketones of **16** are regenerated via **1** (on state). In fact, benzothiazoles **16** survived the severe conditions commonly required for removal of other protecting groups.[6] This type of protection requiring an activation step for deprotection is a new method in organic synthesis and is called "locked protection" (i.e., **16** as locked form, MeI as key, **1** as delocked form, and ketones as opened form).[7] Similarly, in the ester synthesis, **17** (off state) can be considered to be a protected form for esters because the parent esters of **3** are regenerated via **2** and **14** (on states). We have already developed the synthetic application of functions of the benzothiazole ring system as a hydride- and enolates-transferring auxiliary, protecting group, and carbonyl equivalent.[5] Thus, the present chemistry of the benzothiazole ring system as an "on-off" type of leaving group should prove a useful addition of function of the system in organic synthesis.

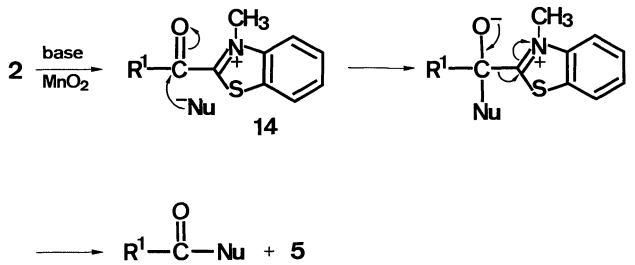

Scheme 7.

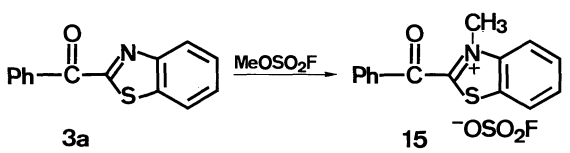

Scheme 8.

Experimental

Melting points were recorded on a Yanagimoto micro melting point apparatus and are uncorrected. ^{1}H NMR spectra were measured on a JEOL JNX PMX-60 spectrometer at 60 MHz with tetramethylsilane as an internal standard. IR spectra were recorded on a JASCO A-202 spectrophotometer. Gas chromatographic analyses were carried out on a Shimadzu Gas chromatograph GC-6AM equipped with a hydrogen flame ionization detector using glass columns (1.5 m) packed with 2% silicone OV-7 on Uniport HP (60—80 mesh). Silica gel (Wakogel C-300) was used for short-column chromatography (SCC).

Materials. 3-Methyl-2-(1-substituted 1-hydroxyalkyl)- and 3-methyl-2-(1-hydroxyalkyl)benzothiazolium iodides (**1** and **2**) and 2-benzoylbenzothiazole (**3a**) were prepared according to the previously reported methods.[5f] Methyl fluorosulfate was prepared by the literature procedure.[8] Solvents were purified according to standard procedures. The other reagents were supplied as high-grade commercial products and used without further purification.

Product Analyses. Identification of ketones and carboxylic acid derivatives obtained in the present reactions was performed by spectroscopic (^{1}H NMR and IR) and GLC methods. These spectral and GLC data were in good agreement with those of the corresponding authentic samples.

General Procedure for the Preparation of Ketone 4 from 3-Methyl-2-(1-substituted 1-Hydroxyalkyl)benzothiazolium Iodide (1). To a two-layer mixture of hexane (4 ml) and 10% aqueous K_2CO_3 (8 ml) was added the benzothiazolium salt **1** (4 mmol) and the mixture was then stirred at 60 °C for 2 h. The aqueous layer was extracted with dichloromethane and the combined organic layer and the extract was dried over $MgSO_4$. Concentration of the solution under reduced pressure afforded almost pure ketone **4**.

Reaction of Benzothiazolium Iodide 1a in Aqueous Ethanol in the Absence of Base. A solution of the benzothiazolium salt **1a** (1.59 g, 4 mmol) in 90% aqueous ethanol (20 ml) was stirred under refluxing for 3 d and then concentrated under reduced pressure. The crystalline residue was triturated with ether, filtered, and washed thoroughly with ether. Recrystallization from methanol–acetone gave pure 3-methylbenzothiazolium iodide (**5**) (0.92 g, 83%): Mp 216—217 °C (decomp) (lit,[5g] 217 °C (decomp)); ^{1}H NMR (DMSO-d_6) δ=4.38 (s, 3H, NCH_3), 7.81 (m, 2H, Arom), 8.40 (m, 2H, Arom), and 10.42 (s, 1H, CH).

The combined filtrate and washings were dried over $MgSO_4$ and concentrated under reduced pressure to give almost pure acetophenone (**4a**) as a pale yellow oil (0.37 g, 77%).

General Procedure for the Oxidative Preparation of Ethyl Ester 12 from 3-Methyl-2-(1-hydroxyalkyl)benzothiazolium Iodide (2) in Ethanol. To a solution of the benzothiazolium salt **2** (2 mmol) in dry ethanol (30 ml), MnO_2 (1.74 g, 20 mmol) and AcONa (0.16 g, 2 mmol) were added with stirring and the suspended mixture was then stirred under refluxing for 5 h. After cooling to room temperature, the insoluble materials were removed by filtration and the filtrate was concentrated under reduced pressure. The residue was diluted with hexane–dichloromethane and filtered through silica-gel pad (Wakogel C-300). Concentration of the filtrate under reduced pressure and SCC purification of the residue gave pure ester **12**.

General Procedure for the Oxidative Preparation of Carboxylic Acid Derivative 13 from 3-Methyl-2-(1-hydroxyalkyl)benzothiazolium Iodide (2) in THF. To a suspension of the benzothiazolium salt **2** (2 mmol) in dry THF (30 ml) was added MnO_2 (1.74 g, 20 mmol), AcONa (0.16 g, 2 mmol), and a nucleophile (6 mmol) and the mixture was stirred under refluxing for 5 h. After cooling to room temperature, the insoluble materials were removed by filtration and the filtrate was concentrated under reduced pressure. The residue was diluted with hexane–dichloromethane and filtered through silica-gel pad (Wakogel C-300). Concentration of the filtrate under reduced pressure and SCC purification of the residue gave pure carboxylic acid derivative **13**.

Preparation of 2-Benzoyl-3-methylbenzothiazolium Fluorosulfate (15). A solution of 2-benzoylbenzothiazole (**3a**) (1.20 g, 5 mmol) in dry dichloromethane (10 ml) was mixed with methyl fluorosulfate (1.71 g, 15 mmol) in a glass tube and the mixture was then degassed several times in vacuo. The tube was sealed in vacuo and kept at 100 °C in an oil bath for 5 h (after about 1 h, yellow needles started to separate). The yellow crystalline product was collected by suction filtration, washed thoroughly with dry dichloromethane and then dried in vacuo to give almost pure salt **15** as yellow needles (1.66 g, 94%): Mp 85—87 °C (decomp). Found: C, 50.27; H, 3.74; N, 3.76%. Calcd for $C_{15}H_{12}NO_4S_2F$: C, 50.98; H, 3.42; N, 3.96%.

The Reaction of Active-Acyl Compound 15 in Ethanol. A mixture of compound **15** (0.71 g, 2 mmol) and dry ethanol (10 ml) was refluxed with stirring for 5 h and then concentrated under reduced pressure. The residue was diluted with hexane–dichloromethane and filtered through silica-gel pad (Wakogel C-300). Concentration of the filtrate under reduced pressure and SCC purification of the residue gave pure ester **12a** in 85% yield.

The Reaction of Active-Acyl Compound 15 with Water and Buthylamine in THF. To a suspension of compound **15** (0.71 g, 2 mmol) in dry THF (30 ml) was added water (1 ml) or butylamine (0.44 g, 6 mmol) and the mixture was then stirred under refluxing for 5 h under a nitrogen atmosphere. After cooling to room temperature, the insoluble materials were removed by filtration and the filtrate was concentrated under reduced pressure. The residue was diluted with hexane–dichloromethane and filtered through silica-gel pad (Wakogel C-300). Concentration of the filtrate under reduced pressure and SCC purification of the residue gave pure carboxylic acid derivative **13e** in 63% yield or **13f** in 56% yield.

References

1) L. Stryer, "Biochemistry," 3rd ed, Freeman, New York (1988); R. Kluger, *Chem. Rev.*, **87**, 863 (1987); C. Walsh, "Enzymatic Reaction Mechanisms," Freeman, New York (1979), p. 690.

2) R. Breslow, *J. Am. Chem. Soc.*, **80**, 3719 (1958).

3) For example, see: D. Hilvert and R. Breslow, *Bioorg. Chem.*, **12**, 206 (1984); J. Castells, H. Llitjos, and M. Moreno-Manas, *Tetrahedron Lett.*, **1977**, 205; H. Inoue and K. Higashiyama, *J. Chem. Soc., Chem. Commun.*, **1980**, 549; Y. Yano, Y. Hoshino, and W. Tagaki, *Chem. Lett.*, **1980**, 749; S. Shinkai, T. Yamashita, Y. Kusano, and O. Manabe, *Tetrahedron Lett.*, **1980**, 2543; S. Shinkai, T. Yamashita, Y. Kusano, and O. Manabe, *J. Org. Chem.*, **45**, 4947 (1980); Y. Yano and Y. Tsukagoshi, *J. Chem. Res., Synop.*, **1984**, 406.

4) T. Matsumoto, H. Yamamoto, and S. Inoue, *J. Am. Chem. Soc.*, **106**, 4829 (1984); H. Inoue and S. Tamura, *J. Chem. Soc., Chem. Commun.*, **1986**, 858; F. Jordan, Z. H. Kudzin, and C. B. Rios, *J. Am. Chem. Soc.*, **109**, 4415 (1987); R. Kluger, K. Karimian, and K. Kitamura, *ibid.*, **109**, 6368 (1987); R. Breslow and E. Kool, *Tetrahedron Lett.*, **29**, 1635 (1988); H. Stetter, H. Kuhlmann, and W. Haese, *Org. Synth.*, **65**, 26 (1987); L. Jimenez and F. Diederich, *Tetrahedron Lett.*, **30**, 2759 (1989); and references cited therein.

5) a) H. Chikashita, S. Ikegami, T. Okumura, and K. Itoh, *Synthesis,* **1986**, 375; b) H. Chikashita and K. Itoh, *Bull. Chem. Soc. Jpn.*, **59**, 1747 (1986); c) H. Chikashita, H. Ide, and K. Itoh, *J. Org. Chem.*, **51**, 5400 (1986); d) H. Chikashita, M. Miyazaki, and K. Itoh, *J. Chem. Soc., Perkin Trans. 1,* **1987**, 699; e) H. Chikashita, S. Tame, and K. Itoh, *Heterocycles,* **27**, 67 (1988); f) H. Chikashita, M. Ishibaba, K. Ori, and K. Itoh, *Bull. Chem. Soc. Jpn.*, **61**, 3637 (1988); g) H. Chikashita, S. Komazawa, N. Ishimoto, K. Inoue, and K. Itoh, *ibid.*, **62**, 1215 (1989); h) H. Chikashita, N. Takegami, Y. Yanase, and K. Itoh, *ibid.*, **62**, 3389 (1989); i) H. Chikashita, S. Tame, S. Yamada, and K. Itoh, *ibid.*, **63**, 497 (1990).

6) For example, 2-(1-phenyl-1-hydroxyethyl)benzothiazole was very stable under the following conditions (recovery %=94—99): (a) 1 equiv KOH/MeOH/70 °C/7 h; (b) 20% H_2SO_4/70 °C/7 h; (c) H_2/5% Pd–C/EtOH/1 atom/r.t./18 h; (d) $NaBH_4$/EtOH/r.t./24 h; (e) CF_3COOH/r.t./24 h; (f) Al_2O_3/MeOH/reflux/10 h.

7) S. Ohta, S. Hayakawa, K. Nishimura, and M. Okamoto, *Tetrahedron Lett.*, **25**, 3251 (1984).

8) R. W. Alder, *Chem. Ind., London,* **87**, 2743 (1973).

Syntheses of Anionic Surfactants Having Two Polyfluoroalkyl Chains and Their Flocculation Ability for Dispersed Magnetite Particles in Water

Norio YOSHINO,* Noboru KOMINE, Jun-ichi SUZUKI, Yuki ARIMA, and Hidefumi HIRAI
Department of Industrial Chemistry, Faculty of Engineering, Science University of Tokyo, Kagurazaka, Shinjuku-ku, Tokyo 162
(Received July 6, 1991)

Four anionic surfactants having two polyfluoroalkyl chains in a molecule, sodium salt of bis(1*H*,1*H*,2*H*,2*H*-heptadecafluorodecyl) 2-sulfosuccinate, $CF_3(CF_2)_7(CH_2)_2OCOCH_2CH(SO_3Na)COO(CH_2)_2(CF_2)_7CF_3$, sodium salt of bis(1*H*,1*H*,9*H*-hexadecafluorononyl) 2-sulfosuccinate, $H(CF_2)_8CH_2OCOCH_2CH(SO_3Na)COOCH_2(CF_2)_8H$, sodium salt of bis(1*H*,1*H*,7*H*-dodecafluoroheptyl) 2-sulfosuccinate, $H(CF_2)_6CH_2OCOCH_2CH(SO_3Na)COOCH_2(CF_2)_6H$ and sodium salt of bis(1*H*,1*H*,5*H*-octafluoropentyl) 2-sulfosuccinate, $H(CF_2)_4CH_2OCOCH_2CH(SO_3Na)COOCH_2(CF_2)_4H$, were prepared from maleic anhydride, the corresponding alcohols having a polyfluoroalkyl chain and sodium hydrogensulfite. The flocculation and redispersion abilities of these surfactants against dispersed magnetite particles in water have been examined in comparison with other four anionic surfactants having a single polyfluoroalkyl chain in a molecule; sodium pentadecafluorooctanoate, $CF_3(CF_2)_6COONa$, sodium 9*H*-hexadecafluorononanoate, $H(CF_2)_8COONa$, sodium 7*H*-dodecafluoroheptanoate, $H(CF_2)_6COONa$, and sodium 5*H*-octafluoropentanoate, $H(CF_2)_4COONa$. These abilities were estimated by measurement of the contact angle against water using pelleted surface-modified magnetite. The abilities of the surfactants having two polyfluoroalkyl chains against flocculation-redispersion were superior to those of the surfactants having one polyfluoroalkyl chain. Especially, sodium salt of bis(1*H*,1*H*,2*H*,2*H*-heptadecafluorodecyl) 2-sulfosuccinate was the most effective surface active agent for these abilities.

It is well known that fluorocarbon polymers exhibit the properties of water and oil repellency, high lubricity, thermal and chemical stability, and so on. It is expected that new composite materials with high performance are produced by dispersing some inorganics into these fluorocarbon polymers. To disperse inorganics into organic polymers, the surface of the inorganics should be modified. Normally there are two ways, one is the use of coupling agents[1-6] and the other is the employment of surfactants such as sodium oleate.[7-11]

In this paper, the results of the syntheses and characterizations of anionic surfactants having two polyfluoroalkyl chains in a molecule and their flocculation and redispersion abilities for dispersed magnetite particles in water are reported. These abilities were compared with those of anionic surfactants having one polyfluoroalkyl chain in a molecule.

Experimental

Materials. 1*H*,1*H*,2*H*,2*H*-Heptadecafluoro-1-decanol, $CF_3(CF_2)_7(CH_2)_2OH$ (bp 88—90 °C/500 Pa), 1*H*,1*H*,9*H*-hexadecafluoro-1-nonanol, $H(CF_2)_8CH_2OH$ (bp 63 °C/53 Pa), 1*H*,1*H*,7*H*-dodecafluoro-1-heptanol, $H(CF_2)_6CH_2OH$ (bp 169—170 °C) and 1*H*,1*H*,5*H*-octafluoro-1-pentanol, $H(CF_2)_4CH_2OH$ (bp 139—140 °C), pentadecafluorooctanoic acid, $CF_3(CF_2)_6COOH$ (bp 95 °C/133 Pa), 9*H*-hexadecafluorononanoic acid, $H(CF_2)_8COOH$ (bp 92—93 °C/53 Pa), 7*H*-dodecafluoroheptanoic acid, $H(CF_2)_6COOH$ (bp 69—70 °C/120 Pa) and 5*H*-octafluoropentanoic acid, $H(CF_2)_4COOH$ (bp 40—42 °C/120 Pa) were donated from Daikin Industries, Ltd. or obtained from PCR Inc. and purified by distillation. The purity of these alcohols and carboxylic acids were checked by the use of ^1H NMR, ^{19}F NMR spectra and gas chromatography, and the impurities were not detectable. The reagent grade maleic anhydride (bp 63—65 °C/660 Pa) and solvents (toluene, 1,4-dioxane and tetrahydrofuran(THF)) were commercially obtained and purified by distillation. *p*-Toluenesulfonic acid, sodium hydrogensulfite, sodium carbonate, iron(II) chloride, and iron(III) chloride were used without further purification. Magnetite particles were made by the method of Shimoiizaka et al.[10] and the average particle size was 109 Å (by light scattering).

Measurements and Instruments. FT-IR spectra were measured in a liquid film or by a KBr method with a JEOL JIR-5300 spectrophotometer. Each spectrum was recorded at a resolution of 4 cm^{-1} with the total of 30 scans. Pulsed Fourier Transform 100-MHz ^1H NMR was run in THF-d_8, trifluoroacetic acid, or acetone-d_6 with TMS as an internal standard using a JEOL JNR-PX-100 spectrometer at room temperature. The FT mode 90-MHz ^{19}F NMR was recorded at 27 °C on a JEOL JNM-FX-90Q in THF with fluorobenzene ($\delta=-113.6$[12] from $CFCl_3$ in $CDCl_3$) as an external standard. The assignments of the ^{19}F NMR spectra were referred to in the data book.[12] Gas chromatography was performed with a Hitachi 063 (PEG-6000 supported Chromosorb A NAW 30—60 mesh 5 m packed column, TCD) or Hitachi G-3000 gas chromatograph (OV-1 25 m Fused capillary column, FID) and the intensities were measured with a Hitachi 834 chromato processor or a Hitachi D-2500 chromato integrator. The centrifuge was used with a Hitachi himac CR20B2 (10000 rpm, 10 min at 20 °C). Light scattering measurements were run with Malvern Co. 4700 Submicron Particle Analyzer (Argon Laser, 5 W, 488 nm). Ultrasonic operations were carried out using a Branson Ultrasonics Corporation Model 250 Sonifier Cell Disruptor System (200 W, 20 kHz). Potential difference was measured using Yokogawa Model PH-82 pH meter. The contact angle $\theta(°)$ was measured at 23 °C with an Elma-Kougaku Co. Gonio-type apparatus. ESCA data were taken with a Shimadzu ESCA-750.

Synthesis of Bis(polyfluoroalkyl) Maleate. Synthesis of Bis(1*H*,1*H*,2*H*,2*H*-heptadecafluorodecyl) Maleate: A mixture of 1*H*,1*H*,2*H*,2*H*-heptadecafluoro-1-decanol 30.12 g (64.9 mmol), maleic anhydride 3.03 g (30.9 mmol) and *p*-toluenesulfonic acid monohydrate 1.18 g (6.2 mmol) as a catalyst in 120 cm^3 toluene was refluxed under stirring at 110 °C for 15 h. During the reaction, the water liberated was removed azeotropically from the reaction system to shift the equilibrium of the esterification reaction. The reaction was finished when 90% or more water being formed, based on the theoretical values. After the reaction, the mixture was cooled at 70 °C and washed sufficiently with 70 °C water to remove *p*-toluenesulfonic acid and excess maleic anhydride. A white solid, bis(1*H*,1*H*,2*H*,2*H*-heptadecafluorodecyl) maleate, was obtained by fractional distillation (yield 27.1 g, 86.8%): Bp 195—197 °C/400 Pa, mp 62—63 °C; IR 3062, 2980, 2912, 1724, 1641, 1639, 1466, 1464, 1425, 1396, 1375, 1333, 1201, 1146, 1078, 1049, 1016, 1014, 972, 841, 820, 704, 658 cm^{-1}; ^{1}H NMR (in THF-d_8) δ=2.64 (CH_2CF_2, t(t)(triplet(triplet)), J=18.8 (6.7) Hz, 4H), 4.51(OCH_2, t, J=6.7 Hz, 4H), 6.40(CH, s(singlet), 2H).

Syntheses of Bis(1*H*,1*H*,9*H*-hexadecafluorononyl) Maleate, Bis(1*H*,1*H*,7*H*-dodecafluoroheptyl) Maleate, and Bis-(1*H*,1*H*,5*H*-octafluoropentyl) Maleate: The procedure and purification techniques were almost the same as those for the preparation of bis(1*H*,1*H*,2*H*,2*H*-heptadecafluorodecyl) maleate.

Bis(1*H*,1*H*,9*H*-hexadecafluorononyl) maleate was obtained by the reaction of 1*H*,1*H*,9*H*-hexadecafluoro-1-nonanol 39.3 g (90.9 mmol), maleic anhydride 4.30 g (43.9 mmol) and *p*-toluenesulfonic acid monohydrate 1.48 g (7.8 mmol) in 200 cm^3 toluene at 110 °C for 20.5 h. A colorless jelly product 15.9 g (yield 38.4%) was obtained: Bp 129—131 °C/27 Pa; IR 3097, 3076, 3022, 2981, 2960, 1747, 1655, 1454, 1412, 1350, 1288, 1201, 1144, 1088, 1039, 1038, 984, 957, 852, 816, 769, 702, 661, 636, 538 cm^{-1}; ^{1}H NMR (THF-d_8) δ=6.64 (CF_2H, t(t), J=51.0 (5.1) Hz, 2H), 4.83 (OCH_2, t, J=13.6 Hz, 4H), 6.55 (=CH, s, 2H).

Bis(1*H*,1*H*,7*H*-dodecafluoroheptyl) maleate was prepared under the following conditions: 1*H*,1*H*,7*H*-dodecafluoro-1-heptanol 37.6 g (113 mmol), maleic anhydride 5.29 g (53.9 mmol), and *p*-toluenesulfonic acid monohydrate 2.05 g (10.8 mmol) in 210 cm^3 toluene at 110 °C for 14 h. A liquid colorless product 14.8 g (yield 36.9%) was obtained: Bp 126—127 °C/13 Pa; IR 3057, 3010, 2980, 2912, 1757, 1753, 1720, 1707, 1639, 1635, 1587, 1566, 1562, 1550, 1546, 1460, 1410, 1382, 1263, 1196, 1140, 984, 949, 862, 831, 744, 715, 671 cm^{-1}; ^{1}H NMR (THF-d_8) δ=6.11 (CF_2H, t(t), J=50.8(5.0) Hz, 2H), 4.76 (OCH_2, t, J=13.6 Hz, 4H), 6.40 (=CH, s, 2H).

Bis(1*H*,1*H*,5*H*-octafluoropentyl) maleate: 1*H*,1*H*,5*H*-octafluoro-1-pentanol 37.7 g (162 mmol), maleic anhydride 7.27 g (74.1 mmol) and *p*-toluenesulfonic acid monohydrate 2.83 g (14.9 mmol) in 300 cm^3 toluene at 110 °C for 21 h. A liquid colorless product 15.4 g (yield 38.2%) was obtained: Bp 109—110 °C/40 Pa; IR 3070, 3012, 2980, 1755, 1701, 1684, 1653, 1646, 1645, 1558, 1538, 1522, 1506, 1456, 1409, 1383, 1288, 1172, 1132, 1085, 1043, 980, 904, 808, 754, 711, 605, 546, 437, 418, 415, 407, 401 cm^{-1}; ^{1}H NMR (THF-d_8) δ=6.13 (CF_2H, t(t), J=51.4 (5.4) Hz, 2H), 4.74 (OCH_2, t, J=14.0 Hz, 4H), 6.41 (=CH, s, 2H).

Synthesis of Surfactant Having Two Polyfluoroalkyl Chains. Synthesis of Sodium Salt of Bis(1*H*,1*H*,2*H*,2*H*-heptadecafluorodecyl) 2-Sulfosuccinate: Sodium salt of bis(1*H*,1*H*,2*H*,2*H*-heptadecafluorodecyl) 2-sulfosuccinate was prepared as follows. To a stirred clear solution of bis(1*H*,1*H*,2*H*,2*H*-heptadecafluorodecyl) maleate 5.00 g (5.0 mmol) in 85 cm^3 1,4-dioxane, aqueous sodium hydrogensulfite (11.9 g (7.0 mmol) of sodium hydrogensulfite in 35 cm^3 water) was added at 50 °C. The mixture was refluxed under stirring until many foams began to appear for about 10—15 h from the start of reaction. Then the reaction temperature was held at 98 °C for about 30—40 h. The white solid product precipitated was separated from the reaction mixture through a sintered glass disk, washed with 50 cm^3 hot (50 °C) 1,4-dioxane on the disk to remove the unreacted bis(1*H*,1*H*,2*H*,2*H*-heptadecafluorodecyl) maleate. The product was dispersed ultrasonically in 50 cm^3 water. This colloidal dispersion was separated by centrifugation and the upper aqueous layer was decanted off to remove the excess sodium hydrogensulfite. The purification by the water washing/centrifugation was repeated three times or more. The products free from sodium hydrogensulfite were washed with 100 cm^3 THF on a sintered glass disk to remove water. A white powder, sodium salt of bis(1*H*,1*H*,2*H*,2*H*-heptadecafluorodecyl) 2-sulfosuccinate, was obtained after vacuum drying (yield 4.74 g, 86.0%): IR 1736, 1726, 1600, 1461, 1369, 1333, 1201, 1147, 1120, 1049, 1012, 870, 836, 739, 702, 656 cm^{-1}; ^{1}H NMR (CF_3COOH) δ=2.51 (a and f, t(m(multiplet)), J=17.7 Hz, 4H), 3.36 (c, broad, 2H), 4.50 (b, d, and e, m, 5H) for $C_8F_{17}CH_2^aCH_2^bOCOCH_2^cCH^d(SO_3Na)COOCH_2^eCH_2^fC_8F_{17}$.

Syntheses of Sodium Salt of Bis(1*H*,1*H*,9*H*-hexadecafluorononyl) 2-Sulfosuccinate, Sodium Salt of Bis(1*H*,1*H*,7*H*-dodecafluoroheptyl) 2-Sulfosuccinate, and Sodium Salt of Bis-(1*H*,1*H*,5*H*-octafluoropentyl) 2-Sulfosuccinate: The synthetic method and purification techniques were almost the same as those for the preparation of sodium salt of bis-(1*H*,1*H*,2*H*,2*H*-heptadecafluorodecyl) 2-sulfosuccinate.

Sodium salt of bis(1*H*,1*H*,9*H*-hexadecafluorononyl) 2-sulfosuccinate was obtained by the reaction of bis(1*H*,1*H*,9*H*-hexadecafluorononyl) maleate 17.8 g (18.9 mmol) in 100 cm^3 1,4-dioxane with aqueous sodium hydrogensulfite (2.54 g (24.4 mmol) in 50 cm^3 water) at 98 °C for 50 h. A white powder 9.54 g (yield 48.3%) was obtained: IR 2983, 2937, 1759, 1730, 1400, 1396, 1351, 1277, 1242, 1201, 1146, 1080, 941, 874, 808, 706, 688, 654 cm^{-1}; ^{1}H NMR (CF_3COOH) δ=3.15 (c, broad, 2H), 3.8—4.9 (b, d, and e, broad, 5H), 5.50 (a and f, t(m), J=51.4 Hz, 2H) for $H^a(CF_2)_8CH_2^bOCOCH_2^cCH^d(SO_3Na)$-$COOCH_2^e(CF_2)_8H^f$.

Sodium salf of bis(1*H*,1*H*,7*H*-dodecafluoroheptyl) 2-sulfosuccinate was prepared by the reaction of bis(1*H*,1*H*,7*H*-dodecafluoroheptyl) maleate 6.63 g (8.9 mmol) in 50 cm^3 1,4-dioxane with aqueous sodium hydrogensulfite (0.93 g (8.96 mmol)/25 cm^3 water) at 98 °C for 50 h. A white powder 4.29 g (yield 56.1%) was obtained: IR 2983, 2939, 1761, 1733, 1441, 1396, 1354, 1350, 1315, 1242, 1194, 1140, 1078, 1014, 972, 928, 862, 829, 798, 739, 735, 687, 665, 655 cm^{-1}; ^{1}H NMR (CD_3COCD_3) δ=3.28 (c, d, J=6.8 Hz, 2H), 4.22 (d, t, J=6.8 Hz, 1H), 4.66 (b, t, J=14.4 Hz, 2H), 4.77 (e, t, J=14.4 Hz, 2H), 6.57 (a and f, t(t), J=51.3 (5.7) Hz, 2H) for $H^a(CF_2)_6CH_2^b$-$OCOCH_2^cCH^d(SO_3Na)COOCH_2^e(CF_2)_6H^f$.

Sodium salt of bis(1*H*,1*H*,5*H*-octafluoropentyl) 2-sulfosuccinate 5.39 g (87.9%) was synthesized as a white powder from the reaction of 1,4-dioxane solution of bis(1*H*,1*H*,5*H*-octafluoropentyl) maleate (5.15 g (9.46 mmol) in 50 cm^3 1,4-dioxane) with aqueous sodium hydrogensulfite (1.08 g

(10.4 mmol)/25 cm^3 water) at 98 °C for 50 h: IR 2985, 2939, 1763, 1741, 1483, 1441, 1433, 1405, 1354, 1315, 1263, 1240, 1165, 1132, 1049, 968, 903, 806, 758, 707, 675, 655 cm^{-1}; ^1H NMR (CD_3COCD_3) δ=3.30 (c, d, J=6.8 Hz, 2H), 4.53 (d, t, J=6.8 Hz, 1H), 4.80(b and e, t, J=14.4 Hz, 4H), 7.72(a and f, t(t), J=51.3 (5.7) Hz, 2H) for $H^a(CF_2)_4CH_2^bOCOCH_2^cCH^d(SO_3Na)COOCH_2^e(CF_2)_4H^f$.

Synthesis of Surfactant Having One Polyfluoroalkyl Chain. Syntheses of Sodium Pentadecafluorooctanoate, $C_7F_{15}COONa$, Sodium 9*H*-Hexadecafluorononanoate, $H(CF_2)_8COONa$, Sodium 7*H*-Dodecafluoroheptanoate, $H(CF_2)_6COONa$, and Sodium 5*H*-Octafluoropentanoate, $H(CF_2)_4COONa$: These surfactants were prepared from the corresponding carboxylic acids with an excess of sodium carbonate in purified THF. After the reaction at 66 °C for 10 h, the excess sodium carbonate was removed by filtration. White powdery surfactants were obtained after vaccum drying. In each case, the yield of the surfactants was higher than 95%. The purity of these surfactants was confirmed on the basis of ^1H NMR (measured in THF-d_8) and IR spectra, and the impurities were not detectable.

Sodium pentadecafluorooctanoate: IR 1695, 1425, 1365, 1325, 1234, 1205, 1147, 1105, 1020, 987, 891, 823, 777, 739, 737, 735, 671, 665, 640, 561, 530 cm^{-1}; ^1H NMR no proton.

Sodium 9*H*-hexadecafluorononanoate: IR 2933, 1697, 1659, 1425, 1342, 1288, 1196, 1151, 1083, 982, 864, 823, 771, 735, 733, 667, 650, 586, 559, 536, 507 cm^{-1}; ^1H NMR δ=6.47 (HCF_2, t(t), 50.0 (5.3) Hz), no -COOH proton.

Sodium 7*H*-dodecafluoroheptanoate: IR 2927, 2912, 2872, 1697, 1421, 1327, 1259, 1184, 1138, 1135, 1082, 945, 823, 822, 819, 769, 719, 669 cm^{-1}; ^1H NMR δ=6.22 (HCF_2, t(t), 51.0 (5.4) Hz), no -COOH proton.

Sodium 5*H*-octafluoropentanoate: IR 2919, 2862, 1696, 1428, 1403, 1303, 1240, 1172, 1126, 1082, 1050, 921, 896, 834, 819, 726, 649 cm^{-1}; ^1H NMR δ=6.58 (HCF_2, t(t), 51.7 (6.1) Hz), no -COOH proton.

Stability of Dispersed Magnetite in Water: Magnetite powder 1.00 g was put into 50 cm^3 water, and the mixture was dispersed ultrasonically for 15 min. It was confirmed that the dispersion was not sedimented and that the colloidal precipitate did not appear for 3 days or more.

Measurement of Flocculation Ability: The adsorption of the surfactants was achieved by ultrasonic irradiation (200 W, 20 kHz, 15 min) to magnetite particles (0.100 g) in 40 cm^3 aqueous solution of the surfactants at various concentrations. The ultrasonic irradiation was utilized to progress an adsorption reaction and to prevent aggregation of magnetite particles. The flocculation and redispersion abilities of the surfactants against magnetite particles were observed after leaving them standing for 24 h at room temperature.

Measurement of Contact Angles of Water on Surface-Modified Magnetite: The surface wettabilities of the modified magnetite were evaluated by the contact angle θ(°) against water on the pelleted magnetite. The pellets to measure the contact angle were prepared as follows. Pressed cellulose disks were preliminary made by pressing 40 mg cellulose powder in a die for IR pellets at 200 kg cm^{-2} for 10 min; 0.15 g of surface-modified magnetite was then placed on it. The surface-flattened pellets of magnetite were obtained by pressing again at 200 kg cm^{-2} for 15 min in the die. The contact angles were measured using 1.0×10^{-6} dm^3 of water drops. The contact angles were evaluated by extrapolating to time zero from a plot of the advancing contact angle θ(°) vs. time.[13]

Amount of Adsorbed Surfactant: The amounts of adsorbed surfactant on the surface-modified magnetite just after the beginning of flocculation and just before the beginning of redispersion were quantitated from the measurement of the potential difference of the upper clear solution, using the calibration curve obtained with an aqueous surfactant solution at various concentrations.

ESCA Measurement: The samples for ESCA measurement were obtained from the middle point of the flocculation range; the sample treated with sodium salt of bis(1*H*,1*H*,2*H*,2*H*-heptadecafluorodecyl) 2-sulfosuccinate was obtained from the ratio of [Surfactant/Magnetite]=0.07 (see Fig. 1) and another one treated with sodium pentadecafluorooctanoate was prepared from that of 0.90. These samples were washed sufficiently with water, dried in a reduced pressure and powdered with an agate mortar.

Results and Discussion

The yields of several sodium salt of bis(polyfluoroalkyl) 2-sulfosuccinate derivatives were not very high. This is probably because water-soluble surfactants, although the solubility was considerably low, had to be washed with water to remove the unreacted sodium hydrogensulfite.

The surfactants are known to change the surface properties of many substances by adsorption. We examined the surface modification ability of the surfactants having polyfluoroalkyl chain(s) by use of magnetite particles. Figure 1 shows the regions of flocculation and redispersion of magnetite particles obtained by adding the solution of the eight different surfactants at various initial concentrations. In a range of a lower surfactant concentration, the magnetite particles were flocculated with an increase in the surfactant concentration. On the contrary, the flocculated magnetite particles were dispersed again as the surfactant concentration was further increased. The region of flocculation-redispersion depended on the surfactant used. The relationship between the flocculation and the redispersion of magnetite particles is schematically illustrated in Fig. 2. The surface of magnetite particles in water is positively charged, then the surface adsorbs surfactants at a moiety of negatively charged ion ($-SO_3^-$ or $-COO^-$).[14] In a lower concentration range of surfactant, the magnetite particles adsorb the surfactants in a monolayer and the particles are surrounded by the surfactants orientating the polyfluoroalkyl chains outside. Thus, the modified magnetite particles are flocculated in water, since the surface of the modified particles have a hydrophobic property. The flocculating magnetite particles were, however, dispersed again when the surfactant concentration increased further. This means that the magnetite particles modified with a surfactant in a monolayer are surrounded by the second surfactants to make a bilayer by an interaction of polyfluoroalkyl chains, in which the second surfactants are orientated

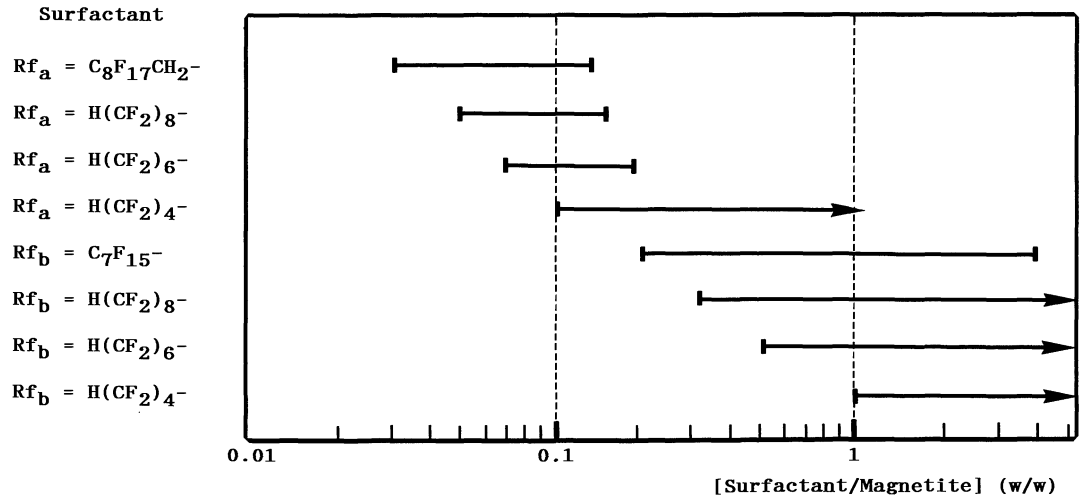

Fig. 1. Comparison of flocculation and redispersion abilities of the surfactants having polyfluoroalkyl chain(s) using magnetite particles. Rf_a and Rf_b groups are for $Rf_aCH_2OCOCH_2CH(SO_3Na)COOCH_2Rf_a$ and Rf_bCOONa, respectively.

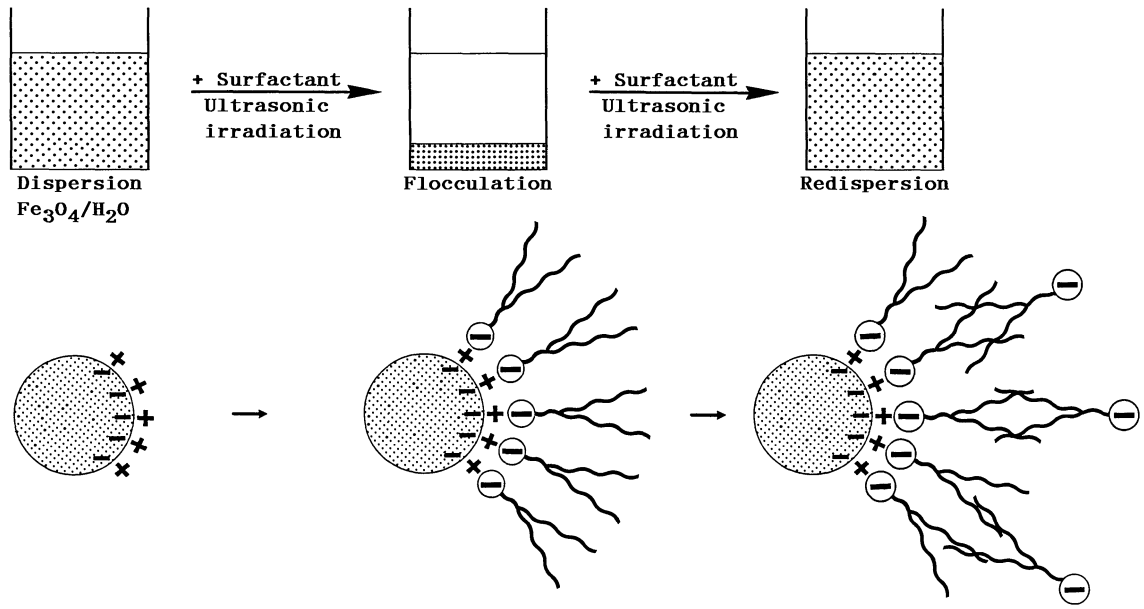

Fig. 2. Schematic illustration for flocculation and redispersion of magnetite particles.

outside at the ion moiety. From the relationship between flocculation and redispersion shown in Fig. 1, it is concluded that the ability of surfactants having two polyfluoroalkyl chains against flocculation-redispersion is superior to that of the surfactants having one polyfluoroalkyl chain. Especially, the surfactants having those two polyfluoroalkyl chains which include a trifluoromethyl group at the end of the chains were the most effective. Some of the beginning points of redispersion were incomplete to measure (drawn by the arrows in Fig. 1), because of the low solubility of these surfactants.

The results of the measurement of the contact angle against water on the modified magnetite, whose samples were obtained from the middle point in each flocculation range and pelleted, are listed in Table 1. Since the untreated magnetite pellet absorbed water drops too rapidly to determine the contact angle, the contact angle was described 0°. The values of the contact angle indicate that the surfactants having a trifluoromethyl group at the end of the chain(s) have higher hydrophobicity than the others. In the case of the surfactants having hydrogen at the end of the chain(s), the value increases with an increase in the chain length. However, these values are independent of the flocculation ability, because the amount of surfactant

Table 1. Contact Angles of Water on the Surface-Modified Magnetite Treated with the Surfactants Having Polyfluoroalkyl Chain(s)

Surfactant[a)]	Contact angle θ(°) of water
Untreated	0
$Rf_a=CF_3(CF_2)_7CH_2-$	125
$Rf_a=H(CF_2)_8-$	106
$Rf_a=H(CF_2)_6-$	80
$Rf_a=H(CF_2)_4-$	65
$Rf_b=CF_3(CF_2)_6-$	119
$Rf_b=H(CF_2)_8-$	95
$Rf_b=H(CF_2)_6-$	71
$Rf_b=H(CF_2)_4-$	64

a) $Rf_aCH_2OCOCH_2CH(SO_3Na)COOCH_2Rf_a$, Rf_bCOONa.

Table 2. Amount of Adsorbed Surfactant

Surfactant	Amount of adsorbed surfactant (mg/g magnetite)
$CF_3(CF_2)_7(CH_2)_2OCOCH_2-CH(SO_3Na)COO(CH_2)_2(CF_2)_7CF_3$	
After flocculation	29.5
Before redispersion	109
$CF_3(CF_2)_6COONa$	
After flocculation	176
Before redispersion	440

adsorbed on the magnetite surface in the middle point of the flocculation range should be different from one another.

Some of the results of the amount of adsorbed surfactant on the magnetite surface are listed in Table 2. In the case of sodium salt of bis(1*H*,1*H*,2*H*,2*H*-heptadecafluorodecyl) 2-sulfosuccinate, only 29.5 mg of surfactant were needed to flocculate 1 g of magnetite particles, and 109 mg for redispersion. On the other hand, in the case of sodium pentadecafluorooctanoate, much more surfactant was required for the flocculation (176 mg) and redispersion (440 mg). These observations also suggest that the ability of the surfactants having two polyfluoroalkyl chains for the flocculation and redispersion against the magnetite particles in water is superior to that of the surfactants having one polyfluoroalkyl chain in a molecule.

The two surface-modified magnetite samples for the ESCA measurements were obtained from the middle point of the flocculation range given in Fig. 1 ($Rf_a=C_8F_{17}CH_2-$ and $Rf_b=C_7F_{15}-$). It was found that the atomic ratio of Fe : F in the vicinity of the surface modified with sodium salt of bis(1*H*,1*H*,2*H*,2*H*-heptadecafluorodecyl) 2-sulfosuccinate was 1 : 7.53, and the ratio 1 : 4.86 was obtained from the surface treated with sodium pentadecafluorooctanoate. From these values, it was calculated that the molar ratio of Fe_3O_4: surfactant was 1 : 0.66 and 1 : 0.85, respectively. Although the initial surfactant concentration ratio (molar ratio) used to make these two samples was [sodium salt of bis(1*H*,1*H*,2*H*,2*H*-heptadecafluorodecyl) 2-sulfosuccinate] : [sodium pentadecafluorooctanoate]=1 : 33, the molar ratio obtained from these two samples was [adsorbed sodium salt of bis(1*H*,1*H*,2*H*,2*H*-heptadecafluorodecyl) 2-sulfosuccinate] : [adsorbed sodium pentadecafluorooctanoate]=0.66 : 0.85. These data also suggest that the surfactant having two polyfluoroalkyl chains has a relatively high adsorption ability; in these cases, the adsorption ability ratio is [sodium salt of bis(1*H*,1*H*,2*H*,2*H*-heptadecafluorodecyl) 2-sulfosuccinate] : [sodium pentadecafluorooctanoate]=(0.66/1) : (0.85/33)=1 : 0.04.

In conclusion, the abilities of the anionic surfactants having two polyfluoroalkyl chains for the flocculation and the redispersion against magnetite particles in water were superior to those of the surfactants having one polyfluoroalkyl chain in a molecule. Especially sodium salt of bis(1*H*,1*H*,2*H*,2*H*-heptadecafluorodecyl) 2-sulfosuccinate possessing a CF_3- group at the end of the polyfluoroalkyl chains, was the most effective surface active agent for these abilities.

The authors are grateful to Dr. Masahiko Abe of the Science University of Tokyo for the light scattering measurements. We also thank Messrs. Yukihide Shiraishi, Shin-ichi Tominaga, Tadashi Hakomori, and Munetoshi Morita for their assistance in carrying out part of the present experiments.

The present work was partially supported by a Grant-in-Aid of Scientific Research No. 62550618 from the Ministry of Education, Science and Culture, to which the authors are also grateful.

References

1) Jpn. Kokai Tokkyo Koho JP 58-172245 [83-172245].
2) E. Tsutiya and M. Takehara, *Shikizai,* **57**, 363 (1984).
3) E. Tsutiya and M. Iwatsuki, *Shikizai,* **59**, 657 (1986).
4) Jpn. Kokai Tokkyo Koho JP 59-75931 [84-75931].
5) S. J. Monte and G. Surgerman, *Rubber World,* **190(1)**, 20, 24 (1984).
6) N. Yoshino, Y. Shiraishi, and H. Hirai, *Bull. Chem. Soc. Jpn.,* **64**, 1648 (1991).
7) Jpn. Kokai Tokkyo Koho JP 58-180596 [83-180596].
8) Jpn. Kokai Tokkyo Koho JP 56-152880 [81-152880].
9) Jpn. Kokai Tokkyo Koho JP 58-89802 [83-89802].
10) Jpn. Kokai Tokkyo Koho JP 58-174495 [83-174495].
11) Jpn. Kokai Tokkyo Koho JP 52-783 [77-783].
12) K. Kushida and A. Watanabe, "Proton and Fluorine Nuclear Magnetic Resonance Spectral Data 1988 Edition," ed by Varian Instruments Ltd., Tokyo, Japan and Japan Halon Co., Ltd., Tokyo, Japan.
13) J. Kimura, T. Itoh, and M. Koishi, *Shikizai,* **50**, 431 (1977).
14) S. Kamiyama, "Jiseiryutai Nyumon," Sangyotosho, Tokyo, Japan.

Synthesis of Allyl 3-Deoxy-D-*manno*-2-octulopyranosidic Acid 4- and 5-Phosphates

Koichi FUKASE, Takashi KAMIKAWA, Yukari IWAI, Tetsuo SHIBA,†
Ernst Theodor RIETSCHEL,†† and Shoichi KUSUMOTO*
Department of Chemistry, Faculty of Science, Osaka University,
Toyonaka, Osaka 560
†† Forschungsinstitut Borstel, Parkallee 22, D-2061 Borstel, F. R. Germany
(Received June 24, 1991)

Allyl glycosides (ketosides) of pyranosidic 3-deoxy-D-*manno*-2-octulosonic acid (Kdo), phosphorylated at either positions 4 or 5 were synthesized with the aim to study the biological properties of phosphorylated Kdo. The α- and β-allyl glycosides prepared from a pyranosidic fluoride of diisopropylidene Kdo were protected at the 7- and 8-positions, and then *O*-phosphorylated at the 4- or 5-position by the phosphoramidite procedure. Separation of the positional isomers followed by deprotection afforded four compounds in pure states.

3-Deoxy-D-*manno*-2-octulosonic acid (Kdo) is a common and obligatory constituent of lipopolysaccharides (LPS) of Gram-negative bacteria.[1] It is structurally important as it forms the link between the polysaccharide region and the lipid A component of LPS.[2] Thus, Kdo is located at the reducing terminal of the polysaccharide region and α-ketosidically bound to lipid A.[3] Kdo is also of biological importance, since it modulates the endotoxic activity of lipid A[1,4] and, further, since it appears to be essential in the biosynthesis of LPS, and, thus, for the viability of Gram-negative bacteria.[5-7]

The intracatenarian Kdo-residue is, depending on the bacterial source, substituted by glycosyl or phosphoryl groups.[1,2,7] Kdo phosphate has been found in the LPS of *Bordetella pertussis*,[8] *Vibrio cholerae*,[9] *Bacteroides gingivalis*,[10] *Haemophilus influenzae*,[11] and *Vibrio parahaemolyticus*.[12] In the latter case, Kdo-4-phosphate was found to be present, whereas in the other LPS, Kdo 4-phosphate and/or Kdo 5-phosphate was identified.

As part of our synthetic work related to the elucidation of the biological significance of Kdo residues in LPS[13,14] we report here on the synthesis of α- and β-allyl glycoside (ketoside) of Kdo 4- and 5-phosphates.[15] In analogy to other Kdo derivatives these compounds are regarded as targets for serological studies aiming at the characterization of the immunoreactivity of the Kdo-containing inner core region of LPS.[16,17] The allyl groups were introduced to serve as a link for the preparation of Kdo phosphate containing antigens, i.e. the conjugation with proteins or the copolymerization with acrylamide.[17]

Results and Discussion

In the present study, the α-fluoride of diisopropylidene Kdo **4**, prepared from the Kdo ammonium salt, was employed for the formation of allyl glycosides of Kdo. The same fluoride **4** had been prepared from D-mannose in our previous work and shown to be an efficient pyranosidic glycosyl donor of Kdo.[18] In that work, it was also demonstrated that the fluoride **4** gives a mixture of α- and β-glycosides of Kdo on Lewis acid-catalyzed glycosidation when a lower alcohol is employed as the glycosyl acceptor.[18] Thus, the formation of both α- and β-allyl glycosides of Kdo could be expected in one reaction with the fluoride **4**.

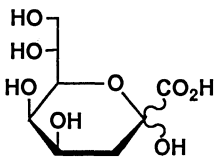

1

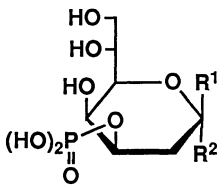

2a,b

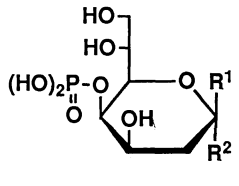

3a,b

a : $R^1 = CO_2H$, $R^2 = OCH_2\text{-}CH{=}CH_2$

b : $R^1 = OCH_2\text{-}CH{=}CH_2$, $R^2 = CO_2H$

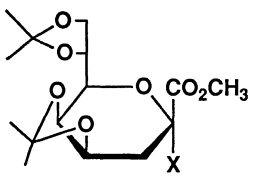

4 : X = F **5** : X = OAc

The methyl ester of Kdo, obtained from the ammonium salt, was converted to the 4,5 : 7,8-di-*O*-isopropylidene 2-acetate (**5**) of the pyranose form. Reaction of **5** with hydrogen fluoride in pyridine gave the α-fluoride (**4**) which was identical with the specimen obtained in our previous work.[18] The glycosidation

† Present address: Peptide Institute, Protein Research Foundation, 4-1-2, Ina, Minoh, Osaka 562

reaction with the fluoride using dry allyl alcohol was carried out in the presence of boron trifluoride etherate and *N*,*N*-diisopropylethylamine in dichloromethane.[19] The anomeric mixture of the allyl glycosides obtained was separated by column chromatography on silica gel to give the α-allyl glycoside **6a** (58%) and the β-anomer **6b** (24%). The former was accompanied with a small amount (2.7%) of the glycal **7** which could not be separated at this stage: the ratio of **6a** to **7** was determined spectrometrically by ^{1}H NMR.

The glycosidic configuration of these allyl glycosides was determined by examination of the differences in the chemical shift values of H_{3a} and H_{3e} in ^{1}H NMR spectra.[18,20] The large $\Delta_{3e\text{-}3a}$ value of 0.91 for **6a** assures its α-anomeric configuration, since the values are around the range of 0.6—1.19 for the various known α-anomers of 4,5 : 7,8-di-*O*-isopropylidene derivatives of Kdo. In the case of the other anomer **6b**, the corresponding $\Delta_{3e\text{-}3a}$ value was 0.24 which was close to the range of 0.26—0.28 so far observed for β-anomers.

Introduction of the phosphate moiety was first examined at the 4- or 5-position of the α-allyl glycoside. Thus, both isopropylidene groups of **6a** were once removed to give the free α-allyl glycoside methyl ester **8a**, whose 7- and 8-hydroxyl groups were again protected by selective monoisopropylidenation. When **8a** was treated with 2-methoxypropene in the presence of (+)-camphor-10-sulfonic acid (CSA) at −35 °C, TLC analysis indicated that a smooth reaction had occurred to give a monoisopropylidene derivative as the main product. This compound was assumed to be the desired 7,8-*O*-isopropylidene **9a** as judged from the result of our previous work.[14] However, the yield of purified **9a** was poor largely due to the low recovery after silica-gel column chromatography. Therefore, the crude monoisopropylidene derivative was used for the subsequent phosphorylation reaction, without any chromatographic purification.

Subsequently, the nonselective monophosphorylation of the vicinal diol function of the crude **9a** obtained above was attempted expecting that separation of the products will give both of the required 4- and 5-phosphates (**10a** and **11a**). In order to avoid the formation of a 4,5-cyclic phosphate, the phosphoramidite procedure was applied to this monophosphorylation.[21] Phosphitylation of the crude monoisopropylidene derivative **9a** with dibenzyl diisopropylphosphoramidite[22-24] and 1*H*-tetrazole at −30 °C in a mixture of dichloromethane and acetonitrile. The latter solvent was used to improve the solubility of 1*H*-tetrazole. Direct oxidation with *m*-chloroperbenzoic acid (mCPBA), without isolation of the *O*-bis(benzyloxy)phosphino derivatives, afforded a mixture of two products. Their structures were unequivocally determined as 4- and 5-phosphate of Kdo after separation by careful examination of their ^{1}H NMR spectra, where each proton signal was clearly assigned by analysis of the H–H COSY spectra. The product whose H-4 signal appeared at lower field with splitting due to the coupling with phosphorus,[25] was assigned to the 4-*O*-[bis(benzyloxy)phosphinoyl] derivative **10a**. Similarly, based on comparison of chemical shift values and H–P coupling, the other compound was the 5-*O*-[bis(benzyloxy)phosphinoyl] derivative **11a**. Both position isomers were, thus, obtained. However, their total yield was only 21% after the two-step conversion from **8a**, owing mainly to the competitive formation of the corresponding 4,5-bisphosphate and to the insufficient stability of the protecting isopropylidene group.

In order to improve the yield of the phosphorylated products, the use of a benzylidene group was next examined for the protection of the 7- and 8-hydroxyl groups. Treatment of **8a** with α,α-dimethoxytoluene and CSA at room temperature resulted in a diastereomeric mixture of the 7,8-*O*-benzylidene derivative **12a** which gave a single spot on TLC but which showed two signals (total 1H), both attributed to the benzylidene CH in its ^{1}H NMR spectrum. Reaction of this benzylidene derivative **12a** with the dibenzyl phosphoramidite and 1*H*-tetrazole was carried out as described above. The progress of the reaction was monitored by TLC and the amidite reagent was added to complete the conversion. Subsequent oxidation with mCPBA gave a mixture of products which gave two spots on silica gel TLC (R_f 0.77 and 0.54; chloroform–acetone, 9 : 1). After their separation by silica-gel column chromatography, ^{1}H NMR analysis revealed that the faster moving compound was yet a mixture composed of 5-phosphate **14a** and a diastereomer of 4-phosphate **13a**. The slower-moving compound was the other diastereomer of the 4-phosphate.

For preparative purposes, the benzylidene group of the phosphorylation product was removed with trifluoroacetic acid (TFA), prior to the separation. The debenzylidenated product was subjected to preparative HPLC on a reversed phase column to give the dibenzyl esters of 4- and 5-phosphates (**15a** and **16a**) which were identical with the products obtained by TFA treatment of the isopropylidene derivatives **10a** and **11a**, respectively. The yield was much improved by the latter route via the 7,8-*O*-benzylidene derivatives.

Cleavage of the benzyl esters of the phosphate moiety was effected quite smoothly with trimethylsilyl (TMS) bromide in dichloromethane at room temperature.[26] The hydrogenolytic removal of the benzyl group had to be avoided here because the allyl group was to be retained. The final alkaline hydrolysis of the methyl ester, and purification by HPLC on an anion-exchange resin, afforded the deprotected α-allyl glycoside 4- and 5-phosphate (**2a** and **3a**) as their ammonium salt. The purity and the structure of each product were confirmed by ^{1}H NMR and high-resolution negative FAB-mass spectra. Additional evidence excluding the possibility of mutual contamination of 4- and 5-phosphate, which may have resulted from the phosphate migration or

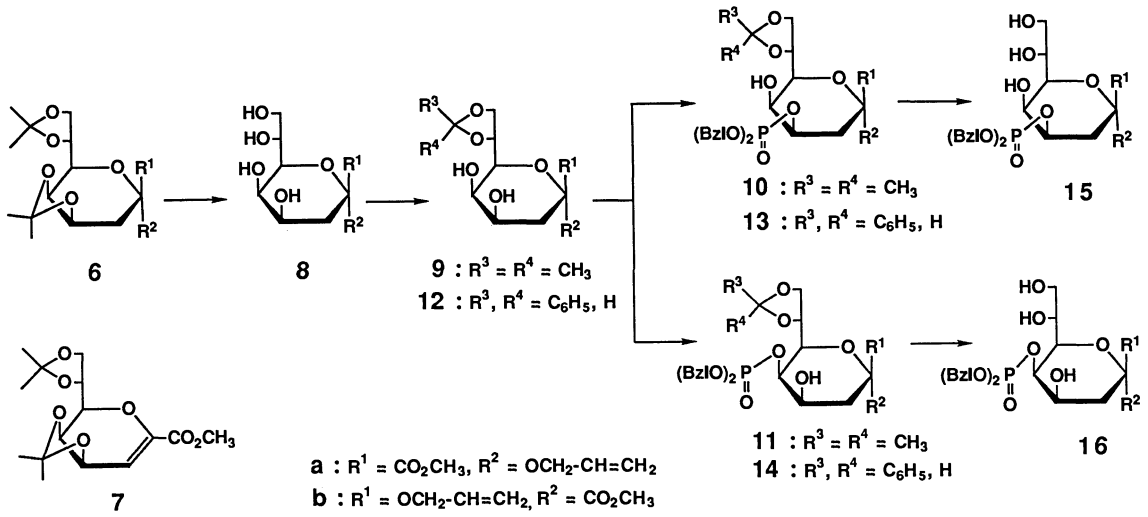

insufficient separation, was also obtained by analytical ion-pair HPLC on a reversed phase column.

The β-allyl glycoside of the Kdo methyl ester **6b** was also converted to the corresponding 4- and 5-phosphate (**2b** and **3b**) in the same way via 7,8-*O*-benzylidene derivative (**12b**).

Cleavage of the benzyl esters of the 5-phosphate **16b** proceeded satisfactorily with TMS bromide followed by sodium hydroxide to give the 5-phosphate of the β-allyl glycoside **3b**. In contrast, cleavage of the benzyl esters of the corresponding 4-phosphate **15b** with TMS bromide gave a mixture of more polar compounds, which lacked the glycosidic allyl group as judged from the positive reaction on TLC with the 2,3,5-triphenyl-2*H*-tetrazolium chloride reagent for reducing sugars.[27] In the NMR spectrum of **15b**, the signals of H-7 and H-8 appeared as rather broad peaks, most likely indicating the presence of hydrogen bonds between the bis(benzyloxy)phosphinoyl group and the two hydroxyl groups at 7- and 8-positions. Such hydrogen bonding is sterically not possible if the pyranoside ring of **15b** exists in a normal $^5C_2$ conformation, where the C7–C8 side chain and the bis(benzyloxy)phosphinoyl group are in a 1,3-diequatorial relation to each other. The ring of **15b** was therefore assumed to be distorted from the chair to $^{0,4}B$ or similar conformation, in which the benzylated phosphate moiety comes also very close to the glycosidic position. We thus anticipated that the glycosidic allyl group was cleaved by direct intramolecular attack of the acidic 4-*O*-phosphono group after the removal of the benzyl esters with TMS bromide.[28] In order to avoid such possible assistance of the free hydroxyl groups to the undesirable conformational change, the hydroxyl groups were acetylated prior to the reaction with TMS bromide. In fact, the reaction of the resultant peracetate with TMS bromide gave a single product, which, on alkaline hydrolysis, gave the desired 4-phosphate **2b** with the intact β-allyl group. The structures and the purities of both 4- and 5-phosphates of the β-allyl glycoside (**2b** and **3b**) were also confirmed in the same way as their α-anomers.

The synthetic phosphates of pyranosidic Kdo with α- and β-linked allyl groups are now being subjected to serological and other biological studies. In addition, the present work has also provided a synthetic procedure applicable to the future chemical synthesis of LPS which contains phosphorylated Kdo(s) in its inner core region.

Experimental

^{1}H NMR spectra were measured on a Varian XL-100-15 spectrometer (100 MHz) or a JEOL JNM-GSX 270, 400, or 500 spectrometer for $CDCl_3$ solutions unless otherwise noted. The chemical shifts are given in δ values either from TMS as the internal standard in $CDCl_3$ solutions or from sodium 2,2-dimethyl-2-silapentane-5-sulfonate as the external standard in D_2O solutions. High-resolution negative FAB-mass spectra were recorded on a JEOL SX-102 mass spectrometer with glycerol as the matrix, where cluster peaks of glycerol served as standards for calculation. Optical rotations were measured with a Perkin–Elmer 241 polarimeter. High-performance liquid chromatography (HPLC) was carried out with a Shimadzu LC-6A liquid chromatography apparatus with a column specified: The peaks were detected by the absorbance at 220 nm. Analytical ion-pair HPLC was carried out on a Cosmosil 5C18 column (4×250 mm) with a solvent system composed of 0.05 M (1M=1 mol dm^{-3}) *n*-Bu_4NHSO_4 and 0.05 M $(NH_4)_2SO_4$ in 3% CH_3CN at a flow rate of 1.0 ml min^{-1}. Peaks were detected at 210 nm. Kieselgel 60 (E. Merck), 0.040—0.063 mm, was used for silica-gel column chromatography at medium pressure (2—4 kg cm^{-2}). Organic solutions were dried over $MgSO_4$ and evaporated in vacuo.

Methyl 2-*O*-Acetyl-3-deoxy-4,5 : 7,8-di-*O*-isopropylidene-α-D-*manno*-2-octulosonate (5). Kdo ammonium salt (4.00 g, 15.7 mmol) was dissolved in water (15 ml) and passed through a column of Amberlite IRCG-120 (H^+ form, 40×150 mm). The column was eluted with water, and the acidic eluate was combined and lyophilized. A solution of the lyophilizate in MeOH (150 ml) was treated with an ethereal solution of CH_2N_2. The residue obtained by evaporation of the solvent was suspended in dry acetone (300 ml). After the addition of *p*-

toluenesulfonic acid monohydrate (600 mg, 3.15 mmol), the mixture was stirred at room temperature for 13 h and then neutralized by addition of Na_2CO_3 (677 mg, 6.30 mmol). The insoluble materials were filtered off, the filtrate evaporated, and the residue was dissolved in dry CH_2Cl_2 (80 ml). To the solution cooled in an ice bath were added pyridine (9.8 ml, 125 mmol), acetic anhydride (5.9 ml, 63 mmol), and 4-dimethylaminopyridine (766 mg, 6.27 mmol). The mixture was stirred at room temperature for 1 h, diluted with AcOEt (1.2 l) and worked up as usual. The crude product was subjected to column chromatography on silica gel (180 g; $CHCl_3$–acetone, 50 : 1) to give syrup; yield 4.30 g (73%). $[\alpha]_D^{18}$ +74.2° (*c* 1.12, $CHCl_3$). ^1H NMR (100 MHz) δ=4.70—3.90 (5H, m, H-4, 5, 7, 8, 8′), 3.78 (3H, s, OCH_3), 3.60 (1H, dd, *J*=8 and 2 Hz, H-6), 2.72 (1H, dd, *J*=16 and 3 Hz, H-3_{eq}), 2.10 (3H, s, $COCH_3$), 2.08 (1H, dd, *J*=16 and 3 Hz, H-3_{ax}), 1.46, 1.41. 1.39, 1.32 (each 3H, s, isopropylidene CH_3). Found: C, 54.51; H, 7.05%. Calcd for $C_{17}H_{26}O_9$: C, 54.54; H, 700%.

Methyl (3-Deoxy-4,5 : 7,8-di-*O*-isopropylidene-α-D-*manno*-2-octulopyranosyl fluorid)onate (4). To a solution of **5** (390 mg, 1.04 mmol) in pyridine (0.65 ml) cooled to −70 °C was added 70% HF–pyridine (3.0 ml) and CH_2Cl_2 (1.2 ml). The mixture was stirred at −20 °C for 10 min and at 0 °C for 10 min, and then diluted with AcOEt (70 ml). The solution was washed successively with aq solutions of 10% KF (3 times), saturated NaCl, saturated $NaHCO_3$, and NaCl and then dried. The residue obtained after evaporation of the solvent was purified by silica-gel column chromatography (10 g; $CHCl_3$–acetone, 20 : 1); yield 231 mg (66%). Mp 121—122 °C. The product was identified with the compound obtained previously.[18] $[\alpha]_D^{18}$ +11.9° (*c* 1.06, $CHCl_3$). ^1H NMR (270 MHz) δ=4.57 (1H, m, H-4), 4.43—4.35 (2H, m, H-5, 7), 4.15 (1H, dd, *J*=8.9, 5.9 Hz, H-8), 4.08 (1H, dd, *J*=8.9, 4.0 Hz, H-8′), 3.81 (3H, s, OCH_3), 3.67 (1H, ddd, *J*=8.5, 2.2, 2.2 Hz, H-6), 3.06 (1H, ddd, *J*=15.6, 3.7, $J_{3e,F}$=3.7 Hz, H-3_{eq}), 1.98 (1H, ddd, *J*=15.6, 2.8, $J_{3a,F}$=18.4 Hz, H-3_{ax}), 1.44, 1.39, 1.38, 1.33 (each 3H, s, isopropylidene CH_3). Found: C, 53.91; H, 6.96%. Calcd for $C_{15}H_{23}O_7F$: C, 53.89; H, 6.93%.

Methyl (Allyl 3-Deoxy-4,5 : 7,8-di-*O*-isopropylidene-α-D-*manno*-2-octulopyranosid)onate (6a) and Methyl (Allyl 3-Deoxy-4,5 : 7,8-di-*O*-isopropylidene-β-D-*manno*-2-octulopyranosid)onate (6b). To an ice-cooled solution of **4** (1.85 g, 5.53 mmol) in dry CH_2Cl_2 (40 ml) were successively added allyl alcohol (489 μl, 7.19 mmol), *N*,*N*-diisopropylethylamine (963 μl, 5.53 mmol) and BF_3 etherate (1.43 ml, 11.6 mmol) under N_2. The solution was stirred for 5 min at 0 °C, then cooled to −70 °C and *N*,*N*-diisopropylethylamine (1.5 ml, 8.6 mmol) was added.[29] The mixture was diluted with CH_2Cl_2 (200 ml), washed with saturated aq NaCl solution, and dried. Separation by silica-gel column chromatography (160 g; $CHCl_3$–acetone, 70 : 1) gave **6a** and **6b** as colorless syrup.

6a, yield 1.20 g (58%). This fraction was contaminated with small amount of **7** (**6a** : **7**=20 : 1 as judged from ^1H NMR data). $[\alpha]_D^{18}$ +36.5° (*c* 1.03, $CHCl_3$). ^1H NMR (500 MHz) δ=5.86 (1H, m, $-OCH_2-C\underline{H}=CH_2$), 5.26 and 5.16 (each 1H, m, $-OCH_2-CH=C\underline{H_2}$), 4.52 (1H, ddd, *J*=7.4, 4.0, 3.0 Hz, H-4), 4.39 (1H, ddd, *J*=7.9, 6.4, 4.6 Hz, H-7), 4.29 (1H, dd, *J*=7.4, 1.8 Hz, H-5), 4.16 (1H, dd, *J*=8.7, 6.4 Hz, H-8), 4.15 (1H, m, $-OC\underline{H_2}-CH=CH_2$), 3.99 (1H, dd, *J*=8.7, 4.6 Hz, H-8′), 3.82 (1H, m, $-OC\underline{H_2}-CH=CH_2$), 3.76 (3H, s, OCH_3), 3.60 (1H, dd, *J*=7.9, 1.8 Hz, H-6), 2.82 (1H, dd, *J*=15.5, 4.0 Hz, H-3_{eq}), 1.91 (1H, dd, *J*=15.5, 3.0 Hz, H-3_{ax}), 1.43, 1.41, 1.38, 1.32 (each 3H, s, isopropylidene CH_3).

6b, yield 490 mg (24%). $[\alpha]_D^{18}$ +4.0° (*c*, 1.01, $CHCl_3$). ^1H NMR (400 MHz) δ=5.89 (1H, m, $-OCH_2-C\underline{H}=CH_2$), 5.25 and 5.12 (each 1H, m, $-OCH_2-CH=C\underline{H_2}$), 4.50 (1H, ddd, *J*=7.5, 4.2, 4.2 Hz, H-4), 4.32 (1H, ddd, *J*=8.2, 6.2, 4.2 Hz, H-7), 4.29 (1H, dd, *J*=7.5, 2.0 Hz, H-5), 4.25 (1H, dd, *J*=8.7, 4.2 Hz, H-8), 4.22 (1H, m, $-OC\underline{H_2}-CH=CH_2$), 4.12 (1H, dd, *J*=8.7, 6.2 Hz, H-8′), 3.96 (1H, m, $-OC\underline{H_2}-CH=CH_2$), 3.77 (3H, s, OCH_3), 3.51 (1H, dd, *J*=8.2, 2.0 Hz, H-6), 2.29 (1H, dd, *J*=15.4, 4.2 Hz, H-3_{eq}), 2.05 (1H, dd, *J*=15.4, 4.2 Hz, H-3_{ax}), 1.50, 1.42, 1.38, 1.36 (each 3H, s, isopropylidene CH_3). Found: C, 57.94; H, 7.60%. Calcd for $C_{18}H_{28}O_8$: C, 58.05; H, 7.58%.

Methyl (Allyl 3-Deoxy-7,8-*O*-isopropylidene-α-D-*manno*-2-octulopyranosid)onate (9a). Trifluoroacetic acid (TFA) (6 ml) containing 5% of water was added to an ice-cooled solution of **6a** (680 mg, 1.83 mmol) in CH_2Cl_2 (70 ml), and the mixture stirred at the same temperature for 1 h. Evaporation under reduced pressure after addition of toluene was repeated three times followed by lyophilization from dioxane gave methyl (allyl 3-deoxy-α-D-*manno*-2-octulopyranosid)onate (**8a**) as resinous solid (yield 530 mg, 99%).

To a solution of **8a** (295 mg, 1.01 mmol) in dry acetone (40 ml) cooled to −35 °C were added 2-methoxypropene (193 μl, 2.02 mmol) and (+)-camphor-10-sulfonic acid (CSA) (23 mg, 0.10 mmol). The mixture was stirred at that temperature for 5 min, neutralized by addition of aq $NaHCO_3$ solution, and filtered. The filtrate was diluted with $CHCl_3$ (300 ml), worked up as usual, and evaporated to give colorless syrup; yield 286 mg (85%). This compound was used without purification for the subsequent reaction. ^1H NMR (270 MHz) δ=5.89 (1H, m, $-OCH_2-C\underline{H}=CH_2$), 5.28 and 5.18 (each 1H, m, $-OCH_2-CH=C\underline{H_2}$), 4.40 (1H, ddd, *J*=7.9, 6.2, 4.9 Hz, H-7), 4.17 (1H, dd, *J*=8.7, 6.2 Hz, H-8), 4.13 (1H, m, H-4), 4.10—3.80 (4H, m, H-5, 8′, and $-OC\underline{H_2}-CH=CH_2$), 3.78 (3H, s, OCH_3), 3.57 (1H, dd, *J*=7.9, 1.2 Hz, H-6), 2.19 (1H, ddd, *J*=12.9, 5.2, 0.7 Hz, H-3_{eq}), 1.91 (1H, dd, *J*=12.9, 11.4 Hz, H-3_{ax}), 1.41 and 1.37 (each 3H, s, isopropylidene CH_3).

Methyl [Allyl 4-*O*-[Bis(benzyloxy)phosphinoyl]-3-deoxy-7,8-*O*-isopropylidene-α-D-*manno*-2-octulopyranosid]onate (10a) and Methyl [Allyl 5-*O*-[Bis(benzyloxy)phosphinoyl]-3-deoxy-7,8-*O*-isopropylidene-α-D-*manno*-2-octulopyranosid]-onate (11a). A mixture of **9a** (62 mg, 0.19 mmol) and 1*H*-tetrazole (30 mg, 0.43 mmol) in dry CH_2Cl_2 (9 ml) and dry CH_3CN (0.9 ml) was cooled to −35 °C under Ar atmosphere. A solution of dibenzyl diisopropylphosphoramidite[22] (128 mg, 0.372 mmol) in dry CH_2Cl_2 (500 μl) was added to the mixture, and the whole mixture was stirred at −30 °C for 2 h. Stirring was further continued at −30 °C for 5 min after addition of a solution of mCPBA (96 mg, 0.56 mmol) in CH_2Cl_2 (2 ml). Then the mixture was diluted with CH_2Cl_2 (60 ml), washed with 10% aq $NaHSO_3$ solution, and worked up as usual. The product was subjected to separation by preparative HPLC under the following conditions and lyophilized: Cosmosil 5C18 (8×250 mm), 60—80% CH_3CN (linear gradient, 1% min^{-1}), 3 ml min^{-1}.

10a, yield 14 mg (13% from **8a**) as colorless solid. Retention time in HPLC, 9.9 min. $[\alpha]_D^{26}$ +47.1° (*c* 1.00, $CHCl_3$). ^1H NMR (270 MHz) δ=7.4—7.25 (10H, aromatic), 5.85 (1H, m, $-OCH_2-C\underline{H}=CH_2$), 5.27 (1H, m, $-OCH_2-CH=C\underline{H_2}$), 5.21—5.01 (5H, m, $-OC\underline{H_2}-CH=CH_2$, benzyl CH_2), 4.87 (1H, broad m, H-4), 4.34 (1H, ddd, *J*=8.7, 6.2, 4.5 Hz, H-7), 4.08 (1H, dd, *J*=8.7, 6.2 Hz, H-8), 3.96—3.89 (4H, m, H-5, 8′, $-OC\underline{H_2}-$

CH=CH$_2$), 3.75 (3H, s, OCH$_3$), 3.55 (1H, dd, J=8.7, 1.7, 0.5 Hz, H-6), 2.32 (1H, ddd, J=12.4, 4.2, 0.5 Hz, H-3$_{eq}$), 2.03 (1H, dd, J=12.1, 12.4 Hz, H-3$_{ax}$), 1.38 and 1.24 (each 3H, s, isopropylidene CH$_3$). Found: C, 58.05; H, 6.43%. Calcd for $C_{29}H_{37}O_{11}P\cdot 0.4H_2O$: C, 58.07; H, 6.35%.

11a, yield 10 mg (9% from **8a**) as colorless solid. Retention time in HPLC, 11.2 min. $[\alpha]_D^{26}$ +21.0° (c 1.00, CHCl$_3$). ^{1}H NMR (270 MHz) δ=7.35 (10H, aromatic), 5.87 (1H, m, -OCH$_2$-CH=CH$_2$), 5.28 and 5.18 (each, 1H, m, -OCH$_2$-CH=CH$_2$), 5.15—5.05 (4H, benzyl CH$_2$), 4.81 (1H, m, H-5), 4.27 (1H, ddd, J=8.4, 6.2, 4.4 Hz, H-7), 4.20 (1H, ddd, J=12.1, 4.9, 2.5 Hz, H-4), 4.11 (1H, dd, J=8.6, 6.2 Hz, H-8), 3.97—3.93 (3H, m, H-8′, -OCH$_2$-CH=CH$_2$), 3.77 (3H, s, OCH$_3$), 3.60 (1H, ddd, J=8.4, 3.7, 0.9 Hz, H-6), 2.24 (1H, ddd, J=13.0, 4.9, 0.7 Hz, H-3$_{eq}$), 1.87 (1H, dd, J=13.0, 12.1 Hz, H-3$_{ax}$), 1.36 and 1.23 (each 3H, s, isopropylidene CH$_3$). Found: C, 58.21; H, 6.62%. Calcd for $C_{29}H_{37}O_{11}P\cdot 0.4H_2O$: C, 58.07; H, 6.35%.

Methyl (Allyl 7,8-*O*-Benzylidene-3-deoxy-α-D-*manno*-2-octulopyranosid)onate (12a). To a solution of **8a** (50 mg, 0.17 mmol) in dry THF (1 ml) were added α,α-dimethoxytoluene (50 μl, 0.33 mmol) and CSA (5.5 mg, 24 μmol). The mixture was stirred at room temperature for 2 h and neutralized with aq NaHCO$_3$. After usual work up, the product was purified by silica-gel column chromatography (10 g; CHCl$_3$–acetone, 10 : 1) to give colorless solid; yield 37 mg (56%). $[\alpha]_D^{18}$ +58.8° (c, 1.02, CHCl$_3$). ^{1}H NMR (270 MHz) δ=7.9—7.35 (5H, aromatic), 5.93 and 5.82 (total 1H, s, benzylidene CH), 5.88 (1H, m, -OCH$_2$-CH=CH$_2$), 5.34—5.14 (2H, m, -OCH$_2$-CH=CH$_2$), 4.70—3.80 (7H, m, H-4, 5, 7, 8, 8′, -OCH$_2$-CH=CH$_2$), 3.78 (3H, s, OCH$_3$), 3.7—3.6 (1H, m, H-6), 2.30—2.15 (1H, m, H-3$_{eq}$), 1.94—1.84 (1H, m, H-3$_{ax}$). Found: C, 59.96; H, 6.27%. Calcd for $C_{19}H_{24}O_8$: 59.99; H, 6.36%.

Methyl [Allyl 4-*O*-[Bis(benzyloxy)phosphinoyl]-3-deoxy-α-D-*manno*-2-octulopyranosid]onate (15a) and Methyl [Allyl 5-*O*-[Bis(benzyloxy)phosphinoyl]-3-deoxy-α-D-*manno*-2-octulopyranosid]onate (16a). A suspension of **12a** (58 mg, 0.15 mmol) and 1*H*-tetrazole (21 mg, 0.31 mmol) in dry CH$_2$Cl$_2$ (2 ml) and dry CH$_3$CN (0.2 ml) was cooled to −35 °C under Ar atmosphere. To this cooled mixture was added a solution of dibenzyl diisopropylphosphoramidite (80 mg, 0.23 mmol) in dry CH$_2$Cl$_2$ (270 μl) with stirring. After 2 h, a solution of the amidite (40 mg, 0.12 mmol) was added and stirring was further continued for 1 h. After addition of mCPBA (61 mg, 0.35 mmol), the mixture was stirred for 5 min and then worked up as described above for the preparation of **10a** and **11a**. Column chromatography on silica gel (4 g; CHCl$_3$–acetone, 12 : 1) gave a mixture of **13a** and **14a** as solid, which was dissolved in CH$_2$Cl$_2$ (3 ml) and treated with TFA (150 μl) containing 5% of water under ice-cooling for 30 min. The mixture was worked up as described above and the products were separated by HPLC: Cosmosil 5C18 (16.7×250 mm), 40—50% CH$_3$CN (linear gradient, 1% min^{-1}), 8.0 ml min^{-1}.

15a: Resinous solid; yield 32 mg (38%). Retention time in HPLC under above conditions, 13.8 min. $[\alpha]_D^{20}$ +58.2° (c 1.00, CHCl$_3$). ^{1}H NMR (270 MHz) δ=7.35 (10H, aromatic), 5.85 (1H, m, -OCH$_2$-CH=CH$_2$), 5.25 and 5.16 (each 1H, m, -OCH$_2$-CH=CH$_2$), 5.10—4.98 (4H, benzyl CH$_2$), 4.70 (1H, broad m, H-4), 4.14 (1H, m, H-5), 4.02 (1H, m, H-7), 3.96 and 3.91 (each 1H, m, -OCH$_2$-CH=CH$_2$), 3.81 (1H, m, H-8), 3.75 (3H, s, OCH$_3$), 3.75 (1H, m, H-8′), 3.62 (1H, dd, J=7.2, 1.0 Hz, H-6), 2.25—2.05 (2H, m, H-3$_{ax\ and\ eq}$). Found: C, 55.79; H, 6.16%. Calcd for $C_{26}H_{33}O_{11}P\cdot 0.4H_2O$: C, 55.79; H, 6.09%.

16a: Resinous solid; yield 17 mg (20%). Retention time in HPLC, 15.8 min. $[\alpha]_D^{20}$ +59.6° (c 1.10, CHCl$_3$). ^{1}H NMR (400 MHz) δ=7.27 (10H, aromatic), 5.79 (1H, m, -OCH$_2$-CH=CH$_2$), 5.20 and 5.08 (each 1H, m, -OCH$_2$-CH=CH$_2$), 5.05—4.95 (4H, benzyl CH$_2$), 4.74 (1H, dd, J=2.4 Hz, $J_{H,P}$=9.4 Hz, H-5), 4.13 (1H, m, J=12.4, 4.6, 2.4, 2.4 Hz, H-4), 3.94 and 3.82 (each 1H, m, -OCH$_2$-CH=CH$_2$), 3.82—3.75 (2H, m, H-7, 8), 3.70 (3H, s, OCH$_3$), 3.67—3.62 (2H, m, H-6, 8′) 2.15 (1H, dd, J=12.4, 4.6 Hz, H-3$_{eq}$), 1.75 (1H, dd, J=12.4, 12.4 Hz, H-3$_{ax}$). Found: C, 55.99; H, 6.22%. Calcd for $C_{26}H_{33}O_{11}P\cdot 0.3H_2O$: C, 55.97; H, 6.07%.

Allyl 3-Deoxy-4-*O*-phosphono-α-D-*manno*-2-octulopyranosidonic Acid Diammonium Salt (2a). Compound **15a** (30 mg, 54 μmol) was dissolved in dry CH$_2$Cl$_2$ (2 ml) and treated with TMS bromide (43 μl, 0.33 mmol) at room temperature for 10 min. After evaporation of the mixture, the residue was lyophilized from dioxane and suspended in water (1.5 ml). The mixture was stirred with 1 M NaOH (216 μl, 216 μmol) at room temperature for 35 min and then neutralized with acetic acid, and lyophilized. The crude product was purified by HPLC: TSK-GEL DEAE-5PW (21.5×150 mm), 0.2 M ammonium formate, 7.5 ml min^{-1}. The peak with retention time of 8.4 min was collected and lyophilized to give a resinous solid; yield 19 mg (91%). Retention time in the ion-pair HPLC, 7.3 min. $[\alpha]_D^{15}$ +57.7° (c 1.00, H$_2$O). ^{1}H NMR (400 MHz, D$_2$O) δ=5.95 (1H, m, -OCH$_2$-CH=CH$_2$), 5.34 and 5.21 (each 1H, m, -OCH$_2$-CH=CH$_2$), 4.50 (1H, broad m, H-4), 4.18 (1H, broad, s, H-5), 3.97—3.90 (3H, m, H-7, 8, -OCH$_2$-CH=CH$_2$), 3.82 (1H, m, -OCH$_2$-CH=CH$_2$), 3.65—3.60 (2H, m, H-6, 8′), 2.16 (1H, dd, J=12.7, 4.4 Hz, H-3$_{eq}$), 1.92 (1H, dd, J=12.7, 12.7 Hz, H-3$_{ax}$). High resolution FAB-MS (negative). Found: m/z 357.0592. Calcd for $C_{11}H_{18}O_{11}P$: M−H, 357.0587.

Allyl 3-Deoxy-5-*O*-phosphono-α-D-*manno*-2-octulopyranosidonic Acid Diammonium Salt (3a). Compound **16a** (32 mg, 58 μmol) was treated successively with TMS bromide (48 μl, 0.35 mmol) and 1 M NaOH (174 μl, 174 μmol) as described above for **2a**. The crude product was purified by HPLC with the same column and solvent that used for **2a**: The peak with retention time of 9.6 min with a flow rate of 8.0 ml min^{-1} was collected and lyophilized to give resinous solid: Yield 18 mg (80%). Retention time in the ion-pair HPLC, 16.6 min. $[\alpha]_D^{15}$ +52.5° (c 1.00, H$_2$O). ^{1}H NMR (400 MHz, D$_2$O) δ=5.95 (1H, m, -OCH$_2$-CH=CH$_2$), 5.32 and 5.21 (each 1H, m, -OCH$_2$-CH=CH$_2$), 4.49 (1H, dd, J=2.6 Hz, $J_{H,P}$=9.2 Hz, H-5), 4.14 (1H, ddd, J=12.5, 4.8, 2.6 Hz, H-4), 3.96—3.92 (2H, m, H-7, 8), 3.90 and 3.82 (each 1H, m, -OCH$_2$-CH=CH$_2$), 3.63 (1H, dd, J=12.1, 7.1 Hz, H-8′), 3.59 (1H, d, J=8.2 Hz, H-6), 2.05 (1H, dd, J=12.5, 4.8 Hz, H-3$_{eq}$), 1.86 (1H, dd, J=12.5, 12.5 Hz, H-3$_{ax}$). High resolution FAB-MS (negative). Found: m/z 357.0552. Calcd for $C_{11}H_{18}O_{11}P$: M−H, 357.0587. Found: C, 29.31; H, 6.79; N, 6.19%. Calcd for $C_{11}H_{25}O_{11}PN_2\cdot 3H_2O$; C, 29.60; H, 7.00; N, 6.28%.

Methyl (Allyl 7,8-*O*-Benzylidene-3-deoxy-β-D-*manno*-2-octulopyranosid)onate (12b). An ice-cooled solution of **6b** (470 mg, 1.26 mmol) in CH$_2$Cl$_2$ (40 ml) was treated with 95% TFA (170 μl) and worked up as described above for the preparation of **8a** to yield **8b** (yield 366 mg, 99%) as resinous solid.

Compound **12b** was prepared from **8b** (144 mg, 0.49 mmol) with action of α,α-dimethoxytoluene (98 μl, 0.65 mmol) and CSA (8.5 mg, 37 μmol) under the same conditions described

above for **12a**. The product was purified by silica-gel column chromatography (20 g; $CHCl_3$–acetone, 10 : 1) to give colorless solid; yield 120 mg (64%). $[\alpha]_D^{20}$ +51.7° (*c* 1.00, $CHCl_3$). ^1H NMR (270 MHz) δ=7.47—7.36 (5H, aromatic), 5.90 and 5.81 (total 1H, s, benzylidene CH), 5.87 (1H, m, $-OCH_2-C\underline{H}=CH_2$), 5.25 and 5.15 (each 1H, m, $-OCH_2-CH=C\underline{H}_2$), 4.56—3.66 (10H, m, H-4, 5, 7, 8, 8′, OCH_3, $-OC\underline{H}_2-CH=CH_2$), 3.59 (1H, dd, *J*=8.5, 1.2 Hz, H-6), 2.48 (1H, m, H-3_{eq}), 1.96 (1H, m, H-3_{ax}). Found: C, 59.94; H, 6.34%. Calcd for $C_{19}H_{24}O_8$: C, 59.99; H, 6.36%.

Methyl [Allyl 4-*O*-[Bis(benzyloxy)phosphinoyl]-3-deoxy-β-D-*manno*-2-octulopyranosid]onate (15b) and Methyl [Allyl 5-*O*-[Bis(benzyloxy)phosphinoyl]-3-deoxy-β-D-*manno*-2-octulopyranosid]onate (16b). To a cooled suspension of **12b** (142 mg, 0.37 mmol) and 1*H*-tetrazole (65 mg, 0.93 mmol) in dry CH_2Cl_2 (6 ml) and dry CH_3CN (0.6 ml) were added two portions of a solution of dibenzyl diisopropylphosphoramidite (194 mg, 0.56 mmol, and 38 mg, 0.11 mmol) in dry CH_2Cl_2 under the same conditions as described for the synthesis of **15a** and **16a**. Then mCPBA (122 mg, 0.71 mmol) was added to the mixture, and the mixture worked up as described above. Column chromatography on silica gel (7 g; $CHCl_3$–acetone, 12 : 1) gave a mixture of **13b** and **14b** as syrup, which was dissolved in CH_2Cl_2 and treated with aq TFA. The products were separated by HPLC: Cosmosil 5C18 (16.7×250 mm), 55—70% CH_3CN (linear gradient, 1% min^{-1}), 8.0 ml min^{-1}.

15b: Resinous solid; yield 55 mg (27%). Retention time in HPLC under above conditions, 9.7 min. $[\alpha]_D^{18}$ +41.7° (*c* 1.06, $CHCl_3$). ^1H NMR (400 MHz) δ=7.30—7.24 (10H, aromatic), 5.75 (1H, m, $-OCH_2-C\underline{H}=CH_2$), 5.15 and 5.06 (each 1H, m, $-OCH_2-CH=C\underline{H}_2$), 5.05—4.90 (4H, benzyl CH_2), 4.21 (1H, broad m, H-4), 4.15 (1H, m, $-OC\underline{H}_2-CH=CH_2$), 4.10 (1H, broad s, H-5), 3.92 (1H, broad m, H-7), 3.88—3.78 (2H, H-8, $-OC\underline{H}_2-CH=CH_2$), 3.72 (1H, m, H-8′), 3.66 (3H, s, OCH_3), 3.31 (1H, d, *J*=8.4 Hz, H-6), 2.41 (1H, dd, *J*=12.5, 4.8 Hz, H-3_{eq}), 2.17 (1H, dd, *J*=12.5, 12.5 Hz, H-3_{ax}). Found: C, 56.11; H, 6.03%. Calcd for $C_{26}H_{33}O_{11}P$: C, 56.52; H, 6.02%.

16b: Resinous solid; yield 68 mg (33%). Retention time in HPLC, 15.8 min. $[\alpha]_D^{18}$ +40.5° (*c* 1.10, $CHCl_3$). ^1H NMR (400 MHz) δ=7.30—7.25 (10H, aromatic), 5.78 (1H, m, $-OCH_2-C\underline{H}=CH_2$), 5.18 and 5.09 (each 1H, m, $-OCH_2-CH=C\underline{H}_2$), 5.05—4.95 (4H, benzyl CH_2), 4.66 (1H, dd, *J*=2.3 Hz, J_{HP}=8.7 Hz, H-5), 4.15 and 3.85 (each 1H, m, $-OC\underline{H}_2-CH=CH_2$), 3.75—3.72 (2H, m, H-8,8′), 3.71 (3H, s, OCH_3), 3.74—3.62 (2H, m, H-4,7), 3.53 (1H, dd, *J*=9.0, 0.9 Hz, H-6), 2.43 (1H, dd, *J*=12.7, 4.7 Hz, H-3_{eq}), 1.85 (1H, dd, *J*=12.7, 12.7 Hz, H-3_{ax}). Found: C, 56.25; H, 6.20%. Calcd for $C_{26}H_{33}O_{11}P$: C, 56.52; H, 6.02%.

Allyl 3-Deoxy-5-*O*-phosphono-α-D-*manno*-2-octulopyranosidonic Acid Diammonium Salt (3b). Compound **16b** (49 mg, 89 μmol) was treated with TMS bromide (70 μl, 0.53 mmol) and 1 M NaOH, and the crude product was purified by HPLC with the same column and solvent that used for **2a**: The peak with retention time of 10.8 min at an elution rate of 8.0 ml min^{-1} was collected and lyophilized to give resinous solid; yield 25 mg (71%). Retention time in ion-pair HPLC, 13.4 min. $[\alpha]_D^5$ +26.0° (*c* 1.00, H_2O). ^1H NMR (400 MHz, D_2O) δ=5.91 (1H, m, $-OCH_2-C\underline{H}=CH_2$), 5.30 and 5.20 (each 1H, m, $-OCH_2-CH=C\underline{H}_2$), 4.41 (1H, broad d, $J_{H,P}$=8.3 Hz, H-5), 4.19 and 3.94 (each 1H, m, $-OC\underline{H}_2-CH=CH_2$), 3.92 (1H, m, H-7), 3.83—3.80 (2H, m, H-8,8′), 3.77 (1H, m, H-4), 3.75 (1H, d, *J*=9.2 Hz, H-6), 2.40 (1H, dd, *J*=12.1, 4.4 Hz, H-3_{eq}), 1.87 (1H, dd, *J*=12.4, 12.1 Hz, H-3_{ax}). High resolution FAB-MS (negative). Found: *m/z* 337.0595. Calcd for $C_{11}H_{18}O_{11}P$: M−H, 357.0587.

Allyl 3-Deoxy-4-*O*-phosphono-β-D-*manno*-2-octulopyranosidonic Acid Diammonium Salt (2b). To a solution of **15b** (45 mg, 81 mmol) in dry CH_2Cl_2 (1.0 ml) were added pyridine (51 μl, 0.65 mmol), acetic anhydride (31 μl, 0.33 mmol), and 4-dimethylaminopyridine (4.0 mg, 33 μmol). The mixture was stirred at room temperature for 1 h and worked up as usual. The acetylated product (54 mg) was dissolved in dry CH_2Cl_2 and treated with TMS bromide (42 μl, 0.32 mmol) and worked up as described above. The crude product (40 mg) was dissolved in MeOH (2 ml) without purification. To this solution was added 1 M NaOH (400 μl) under ice-cooling, and the mixture was stirred at room temperature for 1 h.

The crude product was purified by HPLC under the same conditions (elution rate, 7.0 ml min^{-1}) as described for **2a**. The peak with retention time of 7.9 min was collected and lyophilized to give a resinous solid; yield 25 mg (79%). Retention time in ion pair HPLC, 7.0 min. $[\alpha]_D^5$ +52.5° (*c* 1.00, H_2O). ^1H NMR (400 MHz, D_2O) δ=5.91 (1H, m, $-OCH_2-C\underline{H}=CH_2$), 5.30 and 5.19 (each, 1H, m, $-OCH_2-CH=C\underline{H}_2$), 4.19 (1H, m, $-OC\underline{H}_2-CH=CH_2$), 4.10 (1H, broad s, H-5), 4.06 (1H, broad m, H-4), 3.95 (1H, m, $-OC\underline{H}_2-CH-CH_2$), 3.91 (1H, ddd, *J*=8.8, 4.4, 1.7 Hz, H-7), 3.87 (1H, dd, *J*=12.1, 4.4 Hz, H-8), 3.73 (1H, dd, *J*=12.1, 1.7 Hz, H-8′), 3.63 (1H, d, *J*=8.8 Hz, H-6), 2.50 (1H, dd, *J*=12.3, 4.6 Hz, H-3_{eq}), 1.88 (1H, dd, *J*=12.3, 12.3 Hz, H-3_{ax}). High resolution FAB-MS (negative). Found: *m/z* 357.0601. Calcd for $C_{11}H_{18}O_{11}P$: M−H, 357.0587.

The authors acknowledge the partial financial support to this work by Yamada Science Foundation and Grant-in-Aid for Scientific Research on Priority Areas Nos. 01607002 and 02250107 from the Ministry of Education, Science, and Culture. Thanks are also due to Dr. B. Ekström, Astra, Sweden, for the generous gift of Kdo ammonium salt used in this work, and to Mr. H. Adachi, Osaka University, for the skillful measurement of high resolution FAB-mass spectra.

References

1) E. T. Rietschel, L. Brade, O. Holst, V. A. Kulshin, B. Lindner, A. P. Moran, U. F. Schade, U. Zähringer, and H. Brade, "Molecular Structure of Bacterial Endotoxin in Relation to Bioactivity," in "Endotoxin Research Series," ed by A. Nowotny, J. J. Spitzer, and E. J. Ziegler, Excerpta Medica, Elsevier, Amsterdam (1990), Vol. 1, pp. 15—32.

2) H. Brade, L. Brade, and E. T. Rietschel, *Zentralbl. Bakterial., Mikrobiol. Hyg., Abt. 1, Org. A,* **268**, 151 (1988).

3) U. Zähringer, B. Lindner, U. Seydel, E. T. Rietschel, H. Naoki, F. M. Unger, M. Imoto, S. Kusumoto, and T. Shiba, *Tetrahedron Lett.,* **26**, 6321 (1985).

4) J. -M. Cavaillon and N. Haeffner-Cavaillon, *Cytokine,* **2**, 313 (1990).

5) S. M. Hammond, A. Claesson, A. M. Jansson, L. -G. Larsson, B. G. Pring, C. M. Town, and B. Ekström, *Nature,* **323**, 730 (1987).

6) R. C. Goldman, W. C. Kohlbrenner, P. Lartey, and A. G. Pernet, *Nature,* **329**, 162 (1987).

7) H. Holst and H. Brade, "Chemical Structure of the Core Region of Lipopolysaccharides," in "Bacterial Endotoxic Lipopolysaccharides," ed by D. C. Morrison and J. L. Ryan, CRC Press Inc., Cleveland, Vol. 1, in press.

8) R. Chaby and L. Szabo, *Eur. J. Biochem.*, **59**, 277 (1975).

9) H. Brade, *J. Bacteriol.*, **161**, 795 (1985).

10) H. Kumada, K. Watanabe, T. Umemoto, Y. Haishima, S. Kondo, and K. Hisatsune, *FEBS Microbiol. Lett.*, **51**, 77 (1988).

11) I. M. Helander, B. Lindner, H. Brade, K. Altmann, A. A. Lindberg, E. T. Rietschel, and U. Zähringer, *Eur. J. Biochem.*, **177**, 483 (1988).

12) S. Kondo, U. Zähringer, U. Seydel, K. Hisatsune, and E. T. Rietschel, *Eur. J. Biochem.*, in press.

13) M. Imoto, N. Kusunose, S. Kusumoto, and T. Shiba, *Tetrahedron Lett.*, **29**, 2227 (1988).

14) S. Kusumoto, N. Kusunose, T. Kamikawa, and T. Shiba, *Tetrahedron Lett.*, **29**, 6325 (1988).

15) Although Kdo residues in problem are α-ketosidically linked in natural LPS, the isomeric β-allyl glycosides were also prepared in this study in order to compare the effects of the glycosidic configuration on various biological phenomena.

16) L. Brade, P. Kosma, B. J. Appelmelk, H. Paulsen, and H. Brade, *Infect. Immun.*, **55**, 362 (1987).

17) A. Rozalski, L. Brade, H. -M. Kuhn, H. Brade, P. Kosma, B. J. Appelmelk, S. Kusumoto, and H. Paulsen, *Carbohydr. Res.*, **193**, 257 (1989).

18) M. Imoto, N. Kusunose, Y. Matsuura, S. Kusumoto, and T. Shiba, *Tetrahedron Lett.*, **28**, 6277 (1987).

19) H. Kunz and W. Sager, *Helv. Chim. Acta*, **68**, 283 (1985).

20) 4,5;7,8-Di-*O*-isopropylidene derivatives of Kdo occupy the $B_{3,6}$ boat conformation, where the empirical rule described in the text is valid concerning $\Delta_{3eq\text{-}3ax}$ values (see Ref. 18). In case of Kdo derivatives which lack the 4,5-*O*-isopropylidene group and are thus expected to occupy the normal $^5C_2$ chair conformation, β-anomers have larger Δ-values than the corresponding α-anomers as described by Unger: F. M. Unger, *Adv. Carbohydr. Chem. Biochem.*, **38**, 323 (1981). This rule for chair-form Kdo applies also to the anomeric pairs of **2**, **3**, **9**, and **16**, respectively, the present assignment of the anomeric configurations being again assured. However, this rule was exceptionally not valid for one anomeric pair, i.e., **10a** and **10b** ($\Delta_{3eq\text{-}3ax}$: **10a**, 0.29; **10b**, 0.27). Presumably, this discrepancy is due to conformational change caused by the presence of the dibenzyl phosphate and the isopropylidene groups.

21) A cyclic phosphate is readily formed under base-catalyzed attack of a neighboring hydroxyl group with concomitant elimination of one of the alkoxy components of a phosphotriester; for example, see note 10) of Ref. 14.

22) Dibenzyl diisopropylphosphoramidite was prepared via (diisopropylamino)dichlorophosphine: Cf. E. Ülmann and J. Engels, *Tetrahedron Lett.*, **27**, 1023 (1986). In brief, benzyl alcohol (505 µl, 2.90 mmol) was added to a stirred solution of (diisopropylamino)dichlorophosphine (294 mg, 1.45 mmol) and *N*,*N*-diisopropylethylamine (300 µl, 2.90 mmol) in freshly distilled THF (4 ml) at 0 °C. The mixture was stirred at room temperature for 1.5 h, filtered, and the filtrate evaporated in vacuo to give a colorless syrup (499 mg), which gave one dominant spot on silica-gel TLC ($CHCl_3$–acetone 5 : 1, R_f 0.90) and very weak several other spots. The syrup was used without further purification.

23) W. Bannwarth and A. Truzeciak, *Helv. Chim. Acta*, **70**, 175 (1987).

24) K. L. Yu and B. Fraser-Reid, *Tetrahedron Lett.*, **29**, 979 (1988).

25) In the ^1H NMR spectra of many phosphorylated compounds prepared in this study, the protons on the carbon atoms bearing the phosphorylated hydroxyl groups appeared as broad signals with fine splitting but distinct $^3J_{H,P}$ values were not always obtained.

26) P. M. Chouinard and P. A. Bartlett, *J. Org. Chem.*, **51**, 75 (1986).

27) H. Metz, *Naturwissenschaften*, **48**, 567 (1961).

28) This explanation is based on the assumption that the boat-like conformation favorable for the hydrogen bonding was retained even after cleavage of the benzyl esters. However, we can not exclude the possibility that the allyl group was lost during the reaction with TMS bromide under not yet understood participation of the phosphate moiety.

29) Addition of *N*,*N*-diisopropylethylamine at higher temperature resulted in considerable cleavage of the isopropylidene groups.

Asymmetric Dipolar Cycloaddition of Nitrile Oxides to the α,β-Unsaturated Esters Bearing an Imidazolidine Chiral Controller at the β-Position

Shuji KANEMASA,* Takashi HAYASHI,† Hidetoshi YAMAMOTO,† Eiji WADA, and Tosio SAKURAI††
Institute of Advanced Material Study, Kyushu University, Kasugakoen, Kasuga 816
† Department of Molecular Science and Technology, Interdisciplinary Graduate School of Engineering Sciences, Kyushu University, Kasugakoen Kasuga 816
†† Faculty of Education, Shinshu University, Nishinagano, Nagano 380
(Received June 26, 1991)

Some α,β-unsaturated esters bearing an imidazolidine chiral controller at the β-position were employed in the asymmetric cycloaddition to nitrile oxides. Regio- and diastereoselectivities were both poor when the chiral controller was a perhydropyrrolo[1,2-*c*]imidazol-3-yl auxiliary, while the reaction of the esters bearing a C_2-symmetric imidazolidine chiral controller was exclusively regioselective or diastereoselective depending upon the nature of *N*-substituent. The transition state was briefly discussed.

Nitrile oxide is one of the 1,3-dipoles with high synthetic potential[1] because 1) their ready cycloadditions with a wide variety of dipolarophiles (electron-deficient, eletron-rich, and nonactivated types) produce 2-isoxazolines or isoxazoles bearing various functional groups, 2) these cycloadditions take place in excellent yields in a highly stereospecific and often regioselective manner, 3) the 2-isoxazolines and isoxazoles can be converted to a variety of synthetically useful functional building blocks such as β-hydroxy ketones, β-amino alcohols, α,β-unsaturated ketones, and so on.

This is why the researches directing to the development of asymmetric versions of nitrile oxide cycloaddition are now enthusiastically under way. Since there are so far few reported examples for the catalyzed nitrile oxide cycloaddition, the diastereoselective reaction by the use of chiral dipolarophiles is the only effective way to establish the asymmetric reaction. The acrylates and crotonates derived from readily available simple chiral alcohols have shown low diastereoselectivities in the cycloaddition with nitrile oxides.[2] Several recent reports presented the highly diastereoselective asymmetric cycloaddition of nitrile oxides employing the Oppolzer's sultam[3] or the chiral auxiliary derived from the Kemp's triacid.[4] However, the auxiliary-controlled asymmetric cycloaddition of nitrile oxides is still of current interest.

We have recently developed the highly diastereoselective asymmetric cycloaddition of azomethine ylide with the α,β-unsaturated esters bearing a 2-imidazolidinyl or 2-oxazolidinyl chiral controller at the β-position.[5] In the present paper, these chiral α,β-unsaturated esters were successfully applied to the asymmetric cycloaddition of nitrile oxides.

Results and Discussion

Diastereoselectivity and Regioselectivity. Reaction of benzonitrile oxide (**1**) with the α,β-unsaturated ester **3**[5a,b] bearing the (3*R*,7a*S*)-2-phenylperhydropyrrolo[1,2-*c*]imidazol-3-yl chiral controller at the β-position, in tetrahydrofuran (THF) at room temperature, produced a mixture of two regioisomeric cycloadducts **A** and **A'**, where **1** had been generated from benzohydroximoyl chloride and triethylamine (Scheme 1). The cycloadduct mixture **A** and **A'** was converted into the acetal mixture **4** and **4'** by treatment with refluxing methanol in the presence of concentrated sulfuric acid because separation of **A** and **A'** from each other or from the dimer of **1** through column chromatography was unsuccessful. The resulting acetals **4** (38%) and **4'** (14%) were separated from each other by column chromatography on silica gel (Table 1).

The relative stereochemistry and regiochemistry of **4** and **4'** were unambiguously determined by ^{1}H NMR analysis. The observed small coupling constants for J_{4-5} (4.4 Hz for both **4** and **4'**) indicated the trans relationship of H-4 and H-5. Based on the chemical shifts as well as the coupling patterns of H-4 and H-5, their regiochemistry was confirmed (the 4-ester **4**: δ=4.43

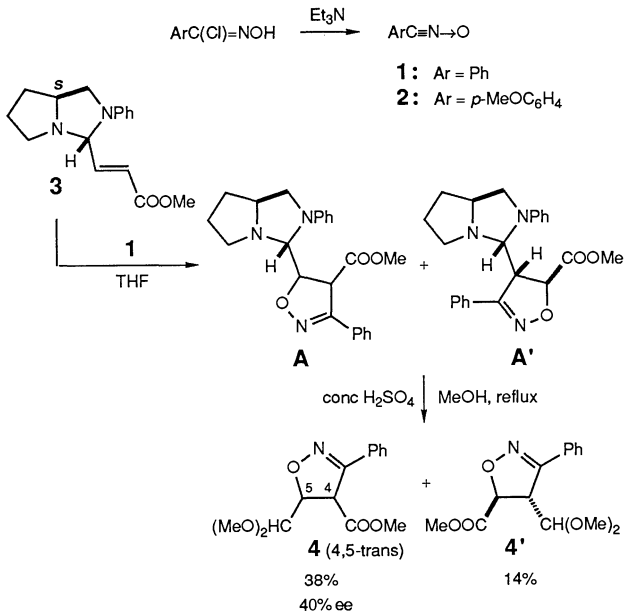

Scheme 1.

Table 1. Dipolar Cycloaddition of Benzonitrile Oxides to the α,β-Unsaturated Esters Bearing an Aminal Type Chiral Controller at the β-Position[a)]

Entry	Dipolarophile	ArCNO (equiv)	Time/h	Product (yield/%)[b)]	Selectivity (ds)[c)]
1	**3**	**1** (2)	24	**4** (38)+**4′** (14)	**4** 70:30[d)] **4′** Single
2	**5**	**1** (2)	16	**7** (52)[e)]	**7** 74:26
3	**5**	**1** (8)	57	**7** (71)	**7** 76:24
4	**5**	**2** (2)	24	**8** (64)	**8** 70:30
5	**6**	**1** (5)	23	**9** (29)+**9′** (10)	**9** Single **9′** Single
6	**6**	**1** (10)	24	**9** (34)+**9′** (16)	**9** Single **9′** Single

a) All reactions were performed in THF at room temperature. Nitrile oxides **1**, **2** were generated from the corresponding hydroximoyl chlorides and triethylamine. b) Isolated yield. c) Determined by ^{1}H NMR spectrum. d) Determined by HPLC (column: Chiral pack OD). e) Recovered **5**: 39%.

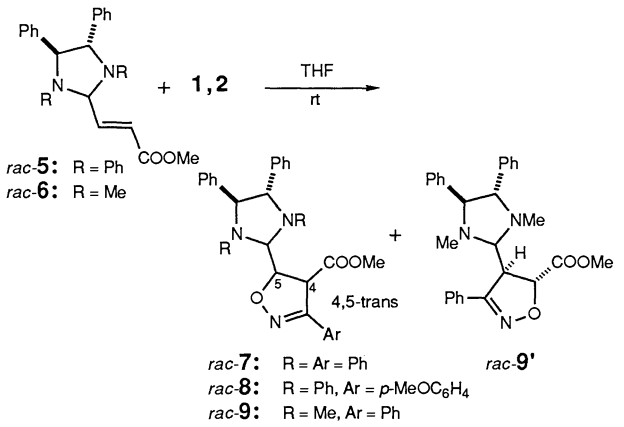

Scheme 2.

(d, H-4) and 5.01 (dd, H-5); the 5-ester **4′**: 4.29 (dd, H-4) and 5.32 (d, H-5)).

The major product **4** showed a positive optical rotation ($[\alpha]_D^{24}$=+65.9° (*c* 0.73, $CHCl_3$)) and its enantiomeric excess was determined to be 40% ee by the analysis on a high performance liquid chromatography (HPLC) using a chiral column (Daicel, Chiral pack OD). The absolute configuration of the major enantiomer of **4** was assigned to be 4*S*,5*S* by comparison of the optical rotation with that of the authentic derivative as discussed below. The minor product **4′** was found to be optically pure on the basis of the chiral HPLC analysis, whose optical rotation was recorded as $[\alpha]_D^{22}$=+133.5° (*c* 0.37, $CHCl_3$).

The α,β-unsaturated ester *rac*-**5**[5c)] bearing the 1,3,4,5-tetraphenyl-2-imidazolidinyl chiral controller at the β-position, hereafter referred to as the *N*-phenyl-substituted ester, was applied to the cycloaddition with nitrile oxide **1** at room temperature (Scheme 2). This reaction proceeded in an absolutely regioselective manner to produce a mixture of two diastereomeric 2-isoxazoline-4-carboxylates *rac*-**7** in 52% yield as the sole regioisomer (Table 1, Entry 2). This exclusively high regioselectivity was surprising because the nitrile oxide cycloaddition with α,β-unsaturated ester bearing a β-alkyl substituent is usually very poor in regioselectivity.[1a)] It is found that steric factor may be responsible for this exclusive selectivity, as mentioned later in the discussion of transition state. The diastereoselectivity of the reaction forming *rac*-**7** was only 74:26 (by ^{1}H NMR).

Since the starting α,β-unsaturated ester *rac*-**5** was partly recovered (39% yield) in the above reaction using 2-equivalents of **1**, a large excess amount of nitrile oxide **1** (8 equivalents) was used and *rac*-**7** was obtained in 71% yield (ds 76:24). A similar result was obtained in the reaction of *rac*-**5** with *p*-methoxybenzonitrile oxide **2** (Entry 4).

The reaction of **1** with the α,β-unsaturated ester *rac*-**6**[5c)] bearing the 1,3-dimethyl-4,5-diphenyl-2-imidazolidinyl chiral controller at the β-position, hereafter referred to as the *N*-methyl-substituted ester, made a striking contrast against the aforementioned reaction using the *N*-phenyl-substituted ester *rac*-**5**. Although both yield and regioselectivity were poor (the 2-isoxazoline-4-carboxylate isomer *rac*-**9**: 29%; the 2-isoxazoline-5-carboxylate one *rac*-**9′**: 10%), these regioisomers *rac*-**9** and *rac*-**9′**, separated from each other through silica-gel column chromatography, were found to be both absolutely pure diastereomers (Scheme 2 and Table 1, Entry 5).

Assignment of Absolute Configurations. The 76:24 diastereomeric mixture of **7** obtained from **1** and the optically pure (4*S*,5*S*)-(−)-**5** was treated with methanol in chloroform together with concentrated sulfuric acid to give **4** (a 75:25 mixture of enantiomers by chiral HPLC, $[\alpha]_D^{24}$=+82.8° (*c* 0.61, $CHCl_3$)) in quantitative yield (Scheme 3). The major enantiomer of so obtained 2-isoxazoline-4-carboxylate **4** was found to be identical with the major enantiomer derived from the cycloadduct **A** (Scheme 1). As a result, the same diastereotopic faces of the α,β-unsaturated ester moiety of **3** and (4*S*,5*S*)-(−)-**5** were preferred by nitrile oxide **1**.

On the other hand, the cycloadducts (+)-**9** and (+)-**9′**, obtained as the sole diastereomers from **1** and the optically pure (4*R*,5*R*)-(+)-**6**, were similarly transformed to (+)-**4** and (+)-**4′** in 73% and 96% yields, respectively.

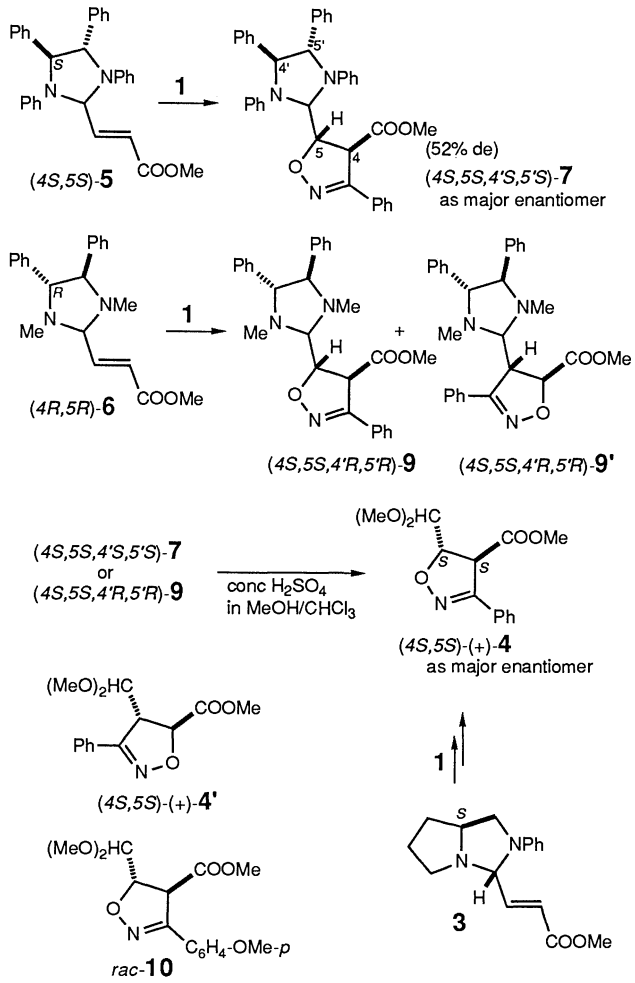

Scheme 3.

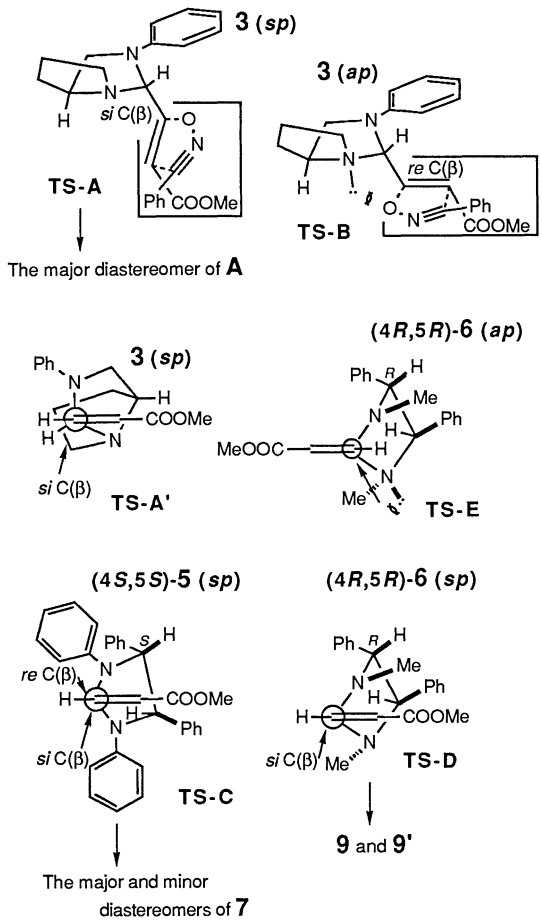

Fig. 1. Transition states for the cycloaddition of nitrile oxide **1** to **3**, **5**, or **6**.

The absolute configurations of the 2-isoxazoline-4-carboxylate skeleton of cycloadducts **A**, **7**, and **9** derived from the optically pure α,β-unsaturated esters **3**, (4*S*,5*S*)-(−)-**5**, and (4*R*,5*R*)-(+)-**6** were definitely assigned on the basis of the X-ray crystallography of *rac*-**9** and the optical rotations of 2-isoxazoline-4-carboxylates **4** derived from them. Thus, the 2-isoxazoline-4-carboxylate regioisomer *rac*-**9** derived from *rac*-**6** was assigned to be 4*RS*,5*RS*,4'*RS*,5'*SR* relative stereochemistry by X-ray crystallography. Accordingly, the 2-isoxazoline-4-carboxylate (+)-**4**, derived from *N*-methyl-substituted ester (4*R*,5*R*)-(+)-**6** via the optically pure (+)-**9**, was determined to be the 4*S*,5*S* enantiomer; the 2-isoxazoline-4-carboxylate (+)-**4**, produced as the major diastereomer from *N*-phenyl-substituted ester (4*S*,5*S*)-(−)-**5** via **7**, has the 4*S*,5*S* configuration.

Transition State. It is now clear, in the cycloaddition of nitrile oxide **1** with the α,β-unsaturated esters **5** and **6** bearing a C_2-symmetric 2-imidazolidinyl chiral controller, that the different diastereotopic faces were predominantly selected between *N*-phenyl-substituted ester **5** and *N*-methyl-substituted one **6**. The degree of diastereoselectivity also depended upon the nature of *N*-substituents of the chiral controller.

The result that the *si* C(β)-face attack of **1** to the α,β-unsaturated ester moiety of **3** was the major reaction path is explained as follows. Although the *re* C(β)-face of the thermodynamically more stable antiperiplanar conformer **3** (*ap*) is sterically open to the attack by **1**, the electrostatic repulsion working between the negative oxygen atom of **1** and the unshared electron pair at the bridgehead nitrogen of **3** would disfavor this approach (**TS-B**, Fig. 1). Accordingly, the *si* C(β)-face attack to the thermodynamically less stable synperiplanar conformer of **3** became the major approach (**TS-A**). Since the terminal oxygen atom of **1** is not so bulky, the occurrence of competitive attack of the *re* C(β)-face of **3** (*sp*) reducing the diastereoselectivity is not surprising. The partial contribution of the *re* C(β)-face attack in **TS-B** would be also a reason for the poor diastereoselectivity.

Another explanation is possible by application of the Kozikowski's "antiperiplanar effect" rule[6] or the Houk's "inside alkoxy effect" rule.[7] Three substituents are attaching to C-3 of the imidazolidine ring of **3**, a phenyl-substituted nitrogen, a bridgehead nitrogen, and a

hydrogen. The anilino type nitrogen is the bulkiest so that it occupies anti position according to the Houk's rule. The second bulky bridgehead nitrogen is inside and the smallest hydrogen is outside positions (**TS-A'**). Therefore, the nitrile oxide cycloaddition has occurred more favorably at the *si* C(β)-face.

Absolute configurations of the regioisomeric 2-isoxazoline-5-carboxylate cycloadduct **A'** and (+)-**9'** could not be assigned on the basis of spectral data and chemical conversion. In the transition state producing the cycloadduct **A'** nitrile oxide **1** has to access to the α,β-unsaturated ester moiety of **3** with the bulky phenyl substituent directing toward the bulky chiral auxiliary. As a result the only possible attack of **1** may have been at the *si* C(β)-face of **3** (*sp*) conformer, the 2-isoxazoline-5-carboxylate ring of (+)-**4'** derived from the minor regioisomers **A'** and (+)-**9'** being tentatively assigned to be 4*S*,5*S* enantiomer.

As previously reported,[5c] the perhydroimidazole ring of the *N*-phenyl-substituted ester **5** is almost flat in solution and both phenyl planes lie in the same plane as the imidazolidine ring. Since these *N*-phenyl substituents become serious steric obstacles to the approach of **1** in the transition state through which the corresponding 2-isoxazoline-5-carboxylate regioisomer is produced, the reaction of **1** with **5** produced 2-isoxazoline-4-carboxylate **7** as the exclusively regioselective cycloadduct. In **TS-C**, where two identical nitrogen substituents are located at C-2 of the imidazolidine ring of (4*S*,5*S*)-**5**, the *si* C(β)-face attack by **1** seems to be a little more favored than the *re* C(β)-face attack. The 76:24 ratio of observed diastereoselectivity is reasonable.

On the other hand, the *re* C(β)-face attack of **1** to the synperiplanar conformer of *N*-methyl-substituted ester (4*R*,5*R*)-**6** (*sp*) was totally inhibited by the top-lying *N*-methyl substituent so that the *si* C(β)-face attacks of **1** leading to (4*S*,5*S*,4'*R*,5'*R*)-**9** and (4*S*,5*S*,4'*R*,5'*R*)-**9'** became the only observed reaction (**TS-D**). Participation of the thermodynamically more stable antiperiplanar conformer **6** (*ap*) was again disfavored because of the aforementioned electrostatic repulsion (**TS-E**).

Experimental

General. Melting points were recorded on a Yanagimoto melting point apparatus and are uncorrected. IR spectra were taken with JASCO IRA-1 and A-702 spectrometers. ^{1}H and ^{13}C NMR spectra were recorded with Hitachi R-40 (^{1}H NMR: 90 MHz) and GSX-270 (270 MHz for ^{1}H NMR and 67.94 MHz for ^{13}C NMR) instruments. Chemical shifts are reported in parts per million downfield (δ) from internal tetramethylsilane. Mass spectra and high resolution mass spectra (HRMS) were recorded with a JEOL-01SG-2 spectrometer operating at an ionization energy of 70 eV. Elemental analyses were performed with a Hitachi 026 CHN analyzer. Optical rotations were recorded with a Horiba SEPA-200 polarimeter. The X-ray diffraction data were collected with graphite-monochromatized Mo $K\alpha$ radiation (λ=0.71069). Structure analyses were performed with a TEXSAN system.[8] The structure was solved by the MITHRIL[9] direct method and defined by full-matrix least squares. For preparative column chromatography, Wakogel C-200, Wako C-300, and Merck Silica gel 60 were employed. Flash chromatography was performed with an Eyera EF-10 apparatus on a 20×180 mm column packed with 0.04—0.063 mm silica gel 60.

Reaction of 1 with 3 Followed by Acetal Exchange Leading to 4 and 4'. To a solution of Et_3N (0.101 g, 1 mmol) in dry THF (4 ml) were added benzohydroximoyl chloride (0.156 g, 1 mmol) and **3** (0.136 g, 0.5 mmol) in that order. The mixture was stirred for 24 h, poured into saturated aqueous NaCl (100 ml), and extracted with Et_2O (30 ml×3). The combined extracts were dried ($MgSO_4$) and evaporated in vacuo. The residue (0.26 g) was dissolved in MeOH (10 ml) containing concentrated H_2SO_4 (1 ml). The mixture was refluxed for 24 h, neutralized with saturated aqueous $NaHCO_3$ and extracted with CH_2Cl_2 (30 ml×3). The combined extracts were dried ($MgSO_4$) and evaporated in vacuo. The residue was chromatographed (silica gel) with hexane–EtOAc (4:1 v/v) to give **4** (0.054 g, 38%) and **4'** (0.019 g, 14%). The major product **4** was found to be a 70:30 mixture of 4*S*,5*S* and 4*R*,5*R* enantiomers (HPLC, Daicel, Chiral pack OD, hexane–isopropyl alcohol (9:1 v/v) as an eluent, $[\alpha]_D^{24}$=+65.9° (*c* 0.73, $CHCl_3$)).

Methyl *trans*-5-Dimethoxymethyl-3-phenyl-2-isoxazoline-4-carboxylate (4): Colorless liquid; IR (neat) 2935, 1736, 1432, 1336, 1260, 1192, 1124, 1064, 892, and 756 cm^{-1}; ^{1}H NMR ($CDCl_3$) δ=3.47, 3.49 (each 3H, each s, 2×OMe), 3.70 (3H, s, COOMe), 4.43 (1H, d, $J_{4\text{-}5}$=4.4 Hz, H-4), 4.58 (1H, d, $J_{CH\text{-}5}$=5.5 Hz, 5-CH), 5.01 (1H, dd, $J_{5\text{-}4}$=5.5 and $J_{5\text{-}CH}$=4.4 Hz, H-5), 7.39—7.43, and 7.69—7.76 (5H, m, Ph); ^{13}C NMR ($CDCl_3$) δ=53.00 (C-4), 54.18, 55.55, 56.54 (2×OMe and COOMe), 85.38 (C-5), 103.65 (5-CH), 127.09, 128.25, 128.74, 130.33 (each Ph), 154.38 (C-3), and 169.76 (COOMe); MS *m*/*z* (rel intensity, %) 279 (M^+, 2), 76 (3), 75 (base peak). HRMS Found: *m*/*z* 279.1103. Calcd for $C_{14}H_{17}NO_5$: M, 279.1107.

Methyl *trans*-4-Dimethoxymethyl-3-phenyl-2-isoxazoline-5-carboxylate (4'): Colorless liquid; IR (neat) 3919, 1728, 1427, 1332, 1192, 1108, 1060, 880, 756, and 684 cm^{-1}; ^{1}H NMR ($CDCl_3$) δ=3.32, 3.37 (each 3H, each s, 2×OMe), 3.80 (3H, s, COOMe), 4.29 (1H, t, $J_{4\text{-}5}$=$J_{4\text{-}CH}$=4.4 Hz, H-4), 4.55 (1H, d, $J_{CH\text{-}4}$=4.4 Hz, 4-CH), 5.32 (1H, d, $J_{5\text{-}4}$=4.4 Hz, H-5), and 7.40–7.75 (5H, m, Ph); ^{13}C NMR ($CDCl_3$) δ=52.89 (C-4), 55.62, 55.75, 55.98 (2×OMe, COOMe), 79.75 (C-5), 102.95 (4-CH), 127.44, 128.36, 128.75, 130.36 (each Ph), 156.14 (C-3), and 170.87 (COOMe); MS *m*/*z* (rel intensity, %) 279 (M^+, 6), 160 (4), 76 (3), and 75 (base peak). Found: C, 60.36; H, 6.08; N, 5.11%. Calcd for $C_{14}H_{17}NO_5$: C, 60.19; H, 6.14; N, 5.02%.

Reaction of 1 with *rac*-5 Leading to *rac*-7. Triethylamine (0.14 ml, 1 mmol) was added dropwise to a solution of benzohydroximoyl chloride (0.156 g, 1 mmol) in THF (8 ml) under nitrogen at room temperature. After 5 min, the solution of *rac*-**5** (0.458 g, 1 mmol) in THF (2 ml) was added. The mixture was stirred at room temperature for 16 h, poured into saturated aqueous NH_4Cl, and then extracted with Et_2O (20 ml×3). The combined extracts were dried ($MgSO_4$) and evaporated in vacuo. The residue (0.367 g) was chromatographed (silica gel) with hexane–EtOAc (3:1 v/v) to give *rac*-**7** (0.15 g, 52%) and *rac*-**5** (0.09 g, 39%). Compound *rac*-**7** was found to be a 74:26 mixture of (4*RS*,5*RS*,4'*RS*,5'*RS*)-**7** and

(4*RS*,5*RS*,4′*SR*,5′*SR*)-**7** (by ^{1}H NMR).

From a similar reaction of **1** with optically pure (4*S*,5*S*)-**5**, a 76:24 diastereomeric mixture of (4*S*,5*S*,4′*S*,5′*S*)-**7** and (4*R*,5*R*,4′*S*,5′*S*)-**7** was obtained (by ^{1}H NMR).

Methyl *trans*-3-Phenyl-5-(*trans*-1,3,4,5-tetraphenylperhydro-2-imidazolyl)-2-isoxazoline-4-carboxylate (*rac*-**7**, a 74:26 mixture of two diastereomers): Colorless prisms (MeOH); mp 97—101 °C; IR(KBr) 3000, 1732, 1589, 1491, 1252, 984, 872, 744, and 684 cm^{-1}; ^{1}H NMR ($CDCl_3$) (4*RS*,5*RS*,4′*RS*,5′*RS*)-**7**: δ=3.63 (3H, s, COOMe), 4.67 (2H, d, J_{4-5}=$J_{4'-5'}$=8.1 Hz, H-4 and H-4′), 5.06 (1H, d, $J_{5'-4'}$=8.1 Hz, H-5′), 5.52 (1H, dd, J_{5-4}=8.1 and $J_{5-2'}$=3.3 Hz, H-5), 6.16 (1H, d, $J_{2'-5}$=3.3Hz, H-2′), 6.63—7.55 (25H, m, 5×Ph); (4*RS*,5*RS*,4′*SR*,5′*SR*)-**7**: δ=3.53 (3H, s, COOMe), 4.73 (1H, d, $J_{4'-5'}$=8.1 Hz, H-4′), 4.84 (1H, d, J_{4-5}=6.2 Hz, H-4), 5.02 (1H, d, $J_{5'-4'}$=8.1 Hz, H-5′), 5.54 (1H, dd, J_{5-4}=6.2 and $J_{5-2'}$=2.7 Hz, H-5), and 6.14 (1H, d, $J_{2'-5}$=2.7 Hz, H-2′). Other signals are overlapping with those of (4*RS*,5*RS*,4′*SR*,5′*SR*)-**7**. ^{13}C NMR ($CDCl_3$) (4*RS*,5*RS*,4′*RS*,5′*RS*)-**7**: δ=52.97 (C-4), 55.71 (COOMe), 70.58 (C-5), 75.10, 80.92 (C-4′ and C-5′), 87.47 (C-2′), 114.90, 119.41, 120.27, 120.85, 126.48, 126.68, 126.85, 127.02, 127.66, 127.75, 127.86, 128.55, 128.88, 129.25, 130.15, 138.74, 139.88, 143.13, 147.89 (each Ph), 154.53 (C-3), and 169.70 (COOMe); (4*RS*,5*RS*,4′*SR*,5′*SR*)-**7**: δ=52.83 (C-4), 69.64 (C-5), 74.44, 80.92 (C-4′ and C-5′), 88.02 (C-2′), 114.77, 119.26, 120.54, 120.74, 130.19, 138.51, 139.43, 142.59, 147.48 (each Ph), 154.28 (C-3), and 169.34 (COOMe). Other signals are overlapping with those of (4*RS*,5*RS*,4′*SR*,5′*SR*)-**7**. MS (20 eV) *m*/*z* (rel intensity, %) 548 (M^+—MeO, 0.2), 377 (4), 376 (30), 375 (base peak), 279 (2), 220 (1), 195 (1), 194 (2), 180 (4), and 103 (1). Found: C, 78.59; H, 5.86; N, 7.10%. Calcd for $C_{38}H_{33}N_3O_3$: C, 78.73; H, 5.74; N, 7.25%.

Reaction of 2 with *rac*-5 Leading to *rac*-8. Triethylamine (0.14 ml, 1 mmol) was added dropwise to a solution of *p*-methoxybenzohydroximoyl chloride (0.186 g, 1 mmol) in THF (4 ml) under nitrogen at 0 °C. After 5 min, the solution of *rac*-**5** (0.23 g, 0.5 mmol) in THF (2 ml) was added. The mixture was stirred at room temperature for 24 h, poured into saturated aqueous NH_4Cl, and then extracted with Et_2O (20 ml×3). The combined extracts were dried ($MgSO_4$) and evaporated in vacuo. The residue (0.396 g) was chromatographed (silica gel) with hexane–EtOAc (10:1 v/v) to give *rac*-**8** (0.194 g, 64%). Compound *rac*-**8** was assigned, by analogy with **7**, to be a 70:30 mixture of (4*RS*,5*RS*,4′*RS*,5′*RS*)-**8** and (4*RS*,5*RS*,4′*SR*,5′*SR*)-**8** (by ^{1}H NMR).

Methyl *trans*-3-(*p*-Methoxyphenyl)-5-(*trans*-1,3,4,5-tetraphenylperhydro-2-imidazolyl)-2-isoxazoline-4-carboxylate (*rac*-**8**, a 70:30 mixture of two diastereomers): Colorless prisms (MeOH); mp 92—94 °C; IR (KBr) 2850, 1700, 1568, 1476, 1232, 875, 820, 732, and 680 cm^{-1}, ^{1}H NMR ($CDCl_3$) major diastereomer: δ=3.61 (3H, s, COOMe), 3.76 (3H, s, OMe), 4.63 (2H, d, $J_{4'-5'}$=7.7 Hz, H-4′), 4.66 (1H, d, J_{4-5}=8.4 Hz, H-4), 5.06 (1H, d, $J_{5'-4'}$=7.7 Hz, H-5′), 5.49 (1H, dd, J_{5-4}=8.4 and $J_{5-2'}$=2.7 Hz, H-5), 6.15 (1H, d, $J_{2'-5}$=2.7 Hz, H-2′), and 6.66—7.50 (24H, m, Ar); minor diastereomer: δ=3.51 (3H, s, COOMe), 3.77 (3H, s, OMe), 4.73 (1H, d, $J_{4'-5'}$=7.7 Hz, H-4′), 4.82 (1H, d, J_{4-5}=5.9 Hz, H-4), and 5.01 (1H, d, $J_{5'-4'}$=7.7 Hz, H-5′). Other signals are overlapping with those of the major diastereomer. ^{13}C NMR ($CDCl_3$) major diastereomer: δ=52.94 (C-4), 55.26, 55.97 (OMe and COOMe), 70.54 (C-5), 75.09 and 79.93 (C-4′ and C-5′), 87.20 (C-2′), 113.99, 114.87, 120.31, 120.74, 120.85, 126.71, 127.64, 127.74, 127.89, 128.43, 128.57, 128.74, 128.87, 129.08, 129.23, 138.77, 139.92, 143.19, 147.91 (each Ar), 154.06 (C-3), 161.06 (Ar), and 169.83 (COOMe); minor diastereomer: δ=52.80 (C-4), 69.62 (C-5), 74.44 and 80.95 (C-4′ and C-5′), 87.72 (C-2′), 113.93, 114.76, 119.32, 138.54, 139.48, 142.63, and 147.54 (each Ar), 153.80 (C-3), 161.12 (Ar), and 169.47 (COOMe). Other signals are overlapping with those of the major diastereomer. MS (20 eV) *m*/*z* (rel intensity, %) 607 (M^+—2, 0.2), 376 (32), 375 (base peak), 233 (10), 196 (13), and 180 (25). Found: C, 76.69; H, 5.95; N, 6.76%. Calcd for $C_{39}H_{35}N_3O_4$: C, 76.82; H, 5.79; N, 6.89%.

Reaction of 1 with *rac*-6 Leading to *rac*-9 and *rac*-9′. Triethylamine (0.35 ml, 2.5 mmol) was added dropwise to a solution of benzohydroximoyl chloride (0.389 g, 2.5 mmol) in THF (8 ml) under nitrogen at room temperature. After 5 min, the solution of *rac*-**6** (0.168 g, 0.5 mmol) in THF (2 ml) was added. The mixture was stirred at room temperature for 23 h, poured into saturated aqueous NH_4Cl, and then extracted with Et_2O (20 ml×3). The combined extracts were dried ($MgSO_4$) and evaporated in vacuo. The residue (0.455 g) was chromatographed (silica gel) with hexane–EtOAc (20:1 v/v) to give *rac*-**9** (0.066 g, 29%) and *rac*-**9′** (0.023 g, 10%).

From a similar reaction of **1** with optically pure (4*R*,5*R*)-**6**, (4*S*,5*S*,4′*R*,5′*R*)-**9** and (4*S*,5*S*,4′*R*,5′*R*)-**9′** were obtained. Optical rotations of these (4*S*,5*S*,4′*R*,5′*R*)-**9** and (4*S*,5*S*,4′*R*,5′*R*)-**9′** were recorded as $[\alpha]_D^{22}$=+59.8 ° (*c* 2.22, $CHCl_3$) and $[\alpha]_D^{23}$=+104.9 ° (*c* 0.67, $CHCl_3$), respectively.

Methyl *trans*-5-(*trans*-1,3-Dimethyl-4,5-diphenylperhydro-2-imidazolyl)-3-phenyl-2-isoxazoline-4-carboxylate (*rac*-**9**): Colorless prisms (MeOH); mp 139—139.5 °C; IR (KBr) 2729, 1656, 1416, 1228, 1112, 952, 880, and 736 cm^{-1}; ^{1}H NMR ($CDCl_3$) δ=2.30, 2.50 (each 3H, each s, 2×NMe), 3.64 (1H, d, $J_{4'-5'}$=8.1 Hz, H-4′), 3.74 (3H, s, COOMe), 3.80 (1H, d, $J_{5'-4'}$=8.1 Hz, H-5′), 4.25 (1H, d, $J_{2'-5}$=4.4 Hz, H-2′), 4.94 (1H, d, $J_{4-5'}$=6.2 Hz, H-4), 5.35 (1H, dd, J_{5-4}=6.2 and $J_{5-2'}$=4.4 Hz, H-5), 6.95—7.31, 7.42—7.47, and 7.80—7.84 (each 10H, 3H, and 2H, m, Ph); ^{13}C NMR ($CDCl_3$) δ=33.61, 42.14 (2×NMe), 52.89 (C-4), 55.35 (COOMe), 75.25, 78.54 (C-4′ and C-5′), 84.13 (C-2′), 87.76 (C-5), 126.98, 127.30, 127.84, 128.03, 128.32, 128.45, 128.69, 128.81, 130.28, 138.38, 139.48 (each Ph), 154.55 (C-3), and 170.45 (COOMe); MS (20 eV) *m*/*z* (rel intensity, %) 424 (M^+—MeO, 0.4), 253 (2), 252 (20), 251 (base peak), 180 (2), and 103 (2). Found: C, 74.16; H, 6.44; N, 9.24%. Calcd for $C_{28}H_{29}N_3O_3$: C, 73.82; H, 6.42; N, 9.22%.

Methyl *trans*-4-(*trans*-1,3-Dimethyl-4,5-diphenylperhydro-2-imidazolyl)-3-phenyl-2-isoxazoline-5-carboxylate (*rac*-9′): Colorless liquid; IR (neat) 3700, 2800, 2340, 1720, 1445, 1200, 1020, 875, 760, and 670 cm^{-1}; ^{1}H NMR ($CDCl_3$) δ=2.18, 2.37 (each 3H, each s, 2×NMe), 3.63 (1H, d, $J_{4'-5'}$=8.1 Hz, H-4′), 3.82 (3H, s, COOMe), 3.95 (1H, d, $J_{5'-4'}$=8.1 Hz, H-5′), 4.46 (1H, d, $J_{5'-4'}$=1.5 Hz, H-2′), 4.56 (1H, dd, J_{4-5}=4.0 and $J_{4-2'}$=1.5 Hz, H-4), 5.73 (1H, d, J_{5-4}=4.0 Hz, H-5), 7.10—7.32, 7.43—7.49, and 7.77—7.82 (each, 10H, 3H, and 2H, m, Ph); ^{13}C NMR ($CDCl_3$) δ=33.55, 40.17 (2×NMe), 52.73 (C-4), 55.84 (COOMe), 75.20, 78.28 (C-4′ and C-5′), 80.67 (C-2′), 82.32 (C-5), 127.15, 127.35, 127.45, 127.84, 128.35, 128.51, 129.08, 130.42, 139.26, 139.32 (each Ph), 157.23 (C-3), and 171.57 (COOMe); Found: C, 73.98; H, 6.39; N, 9.20%. Calcd for $C_{28}H_{29}N_3O_3$: C, 73.82; H, 6.42; N, 9.22%.

X-Ray Structure Analysis of *rac*-9. A single crystal grown from MeOH had space group $P2_1/n$, a=9.13 (5), b=28.39 (1), and c=10.08 (1) Å, β=107.9 (2) °, V=2488 (1) Å^3, Z=4. The

final R factor was 0.051 for 1421 observed reflections.[10]

Removal of the Chiral Auxiliary from 7, 9, and 9′ Leading to 4 and 4′. A) **From 7:** Concentrated H_2SO_4 (0.5 ml) was added to a solution of (4*S*,5*S*,4′*S*,5′*S*)-**7** (a 76:24 diastereomeric mixture, 0.048 g, 0.083 mmol) in MeOH (3 ml) and $CHCl_3$ (2 ml). After heating under reflux for 20 h, the mixture was neutralized with saturated aqueous $NaHCO_3$, and extracted with CH_2Cl_2 (20 ml×3). The combined extracts were dried ($MgSO_4$) and evaporated in vacuo. The residue (0.041 g) was chromatographed (silica gel) with hexane–EtOAc (3:1 v/v) to give a mixture of (4*S*,5*S*)-(+)-**4** and (4*R*,5*R*)-(−)-**4** (0.023 g, 100%, a 75:25 mixture of enantiomers by HPLC using Daicel, Chiral pack OD). $[\alpha]_D^{23}=+82.8°$ (*c* 0.61, $CHCl_3$).

B) **From 9:** Concentrated H_2SO_4 (0.5 ml) was added to a solution of (4*S*,5*S*,4′*R*,5′*R*)-**9** (0.089 g, 0.195 mmol) in MeOH (5 ml) and $CHCl_3$ (3 ml). After heating under reflux for 19 h, the mixture was neutralized with saturated aqueous $NaHCO_3$ and extracted with Et_2O (40 ml×3). The combined extracts were dried ($MgSO_4$) and evaporated in vacuo. The residue (0.094 g) was chromatographed (silica gel) with hexane–EtOAc (3:1 v/v) to give (4*S*,5*S*)-(+)-**4** (0.04 g, 73%, a single enantiomer by HPLC using Daicel, Chiral pack OD, $[\alpha]_D^{22}=+166.8°$ (*c* 1.90, $CHCl_3$).

C) **From 9′**: Concentrated H_2SO_4 (0.5 ml) was added to a solution of (4*S*,5*S*,4′*R*,5′*R*)-**9′** (0.091 g, 0.2 mmol) in MeOH (5 ml) and $CHCl_3$ (3 ml). After heating under reflux for 10 h, the mixture was neutralized with saturated aqueous $NaHCO_3$ and extracted with Et_2O (30 ml×3). The combined extracts were dried ($MgSO_4$) and evaporated in vacuo. The residue (0.093 g) was chromatographed (silica gel) with hexane–EtOAc (5:1 v/v) to give (4*S*,5*S*)-(+)-**4′** (0.054 g, 96%, a single enantiomer by HPLC using Daicel, Chiral pack OD). $[\alpha]_D^{22}=+133.5°$ (*c* 0.37, $CHCl_3$).

Conversion of *rac*-8 to *rac*-10. Concentrated H_2SO_4 (0.2 ml) was added to a solution of *rac*-**8** (0.051 g, 0.084 mmol) in MeOH (3 ml) and $CHCl_3$ (2 ml). After heating under reflux for 4 h, the mixture was neutralized with saturated aqueous $NaHCO_3$, and extracted with Et_2O (40 ml×2). The combined extracts were dried ($MgSO_4$) and evaporated in vacuo. The residue (0.056 g) was chromatographed (silica gel) with hexane–EtOAc (3:1 v/v) to give *rac*-**10** (0.016 g, 64%). From the subsequent fractions *rac*-**8** (0.018 g, 35%) and *dl*-1,2-dianilino-1,2-diphenylethane (0.02 g, 65%) were obtained.

Methyl *trans*-5-Dimethoxymethyl-3-(*p*-methoxyphenyl)-2-isoxazoline-4-carboxylate (*rac*-**10**): Colorless needles (MeOH); mp 97.5—98 °C; ^{1}H NMR ($CDCl_3$) δ=3.46, 3.49 (each 3H, each s, 2×OMe), 3.71 (3H, s, COOMe), 3.83 (3H, s, *p*-OMe), 4.41 (1H, d, $J_{CH\text{-}5}$=4.8 Hz, 5-CH), 4.54 (1H, d, $J_{4\text{-}5}$= 5.1 Hz, H-4), 4.98 (1H, dd, $J_{5\text{-}4}$=5.1 and $J_{5\text{-}CH}$=4.8 Hz, H-5), 6.81, and 7.68 (each 2H, each d, Ar); ^{13}C NMR ($CDCl_3$) δ=52.99 (4-C), 54.47, 55.35, 55.53, 56.46 (2×OMe, *p*-OMe, and COOMe), 85.08 (C-5), 103.67 (5-CH), 114.16, 120.69, 128.68, 153.90 (each Ar), 161.23 (C-3), and 169.86 (COOMe); MS *m*/*z* (rel intensity, %) 309 (M^+, 8) and 75 (base peak). Found: C, 58.50; H, 6.29; N, 4.54%. Calcd for $C_{15}H_{19}NO_6$: C, 58.25; H, 6.19; N, 4.53%.

References

1) a) P. Caramella and P. Grünanger, "Nitrile Oxides and Imines," in "1,3-Dipolar Cycloaddition Chemistry," ed by A. Padwa, John Wiley & Sons, New York (1984), Vol. 1, Chap. 3, pp. 291—392; b) D. P. Curran, "Advances in Cycloaddition," ed by D. P. Curran, JAI Press, Greenwich (1988), Vol. 1, pp. 129—189; c) S. Kanemasa and O. Tsuge, *Heterocycles,* **30**, 719 (1990).

2) P. A. Wade, S. M. Singh, and M. K. Pillay, *Tetrahedron,* **40**, 601 (1984); D. P. Curran, B. H. Kim, H. P. Piyasena, R. J. Loncharich, and K. N. Houk, *J. Org. Chem.*, **52**, 2137 (1987); R. Annunziata, M. Cinquini, F. Cozzi, and L. Raimondi, *J. Chem. Soc., Chem. Commun.,* **1987**, 529; R. Annunziata, M. Cinquini, F. Cozzi, G. Dondio, and L. Raimondi, *Tetrahedron,* **43**, 2369 (1987); T. Olsson, K. Stern, and S. Sundell, *J. Org. Chem.,* **53**, 2468 (1988); R. Annunziata, M. Cinquini, F. Cozzi, and L. Raimondi, *Tetrahedron,* **44**, 4645 (1988); G. T. Le, J. P. Lellouche, L. Toupet, and J. P. Beaucourt, *Tetrahedron Lett.,* **30**, 6517 (1989); T. Gall Le, J. -P. Lellouche, L. Toupet, and J. -P. Beaucourt, *ibid.*, **30**, 6517 (1989); D. P. Curran and T. A. Heffner, *J. Org. Chem.,* **55**, 4585 (1990).

3) D. P. Curran, B. H. Kim, J. Daugherty, and T. A. Heffner, *Tetrahedron Lett.*, **29**, 3555 (1988).

4) D. P. Curran, K.-S. Jeong, T. A. Heffner, and J. Rebek, *J. Am. Chem. Soc.*, **111**, 9238 (1989).

5) a) S. Kanemasa and H. Yamamoto, *Tetrahedron Lett.*, **31**, 3633 (1990); b) S. Kanemasa, H. Yamamoto, E. Wada, T. Sakurai, and K. Urushido, *Bull. Chem. Soc. Jpn.*, **63**, 2857 (1990); c) S. Kanemasa, T. Hayashi, J. Tanaka, H. Yamamoto, and T. Sakurai, *J. Org. Chem.,* **56**, 4473 (1991); d) H. Yamamoto, S. Kanemasa, and E. Wada, *Bull. Chem. Soc. Jpn.*, **64**, 2739 (1991).

6) A. P. Kozikowski and A. K. Ghosh, *J. Am. Chem. Soc.*, **104**, 5788 (1982); A. P. Kozikowski and A. K. Ghosh, *J. Org. Chem.,* **49**, 2762 (1984).

7) K. N. Houk, S. R. Moses, Y. -D. Wu, N. G. Rondan, V. Jäger, R. Schohe, and F. R. Fronczek, *J. Am. Chem. Soc.,* **106**, 3880 (1984); K. N. Houk, H. -Y. Duh, Y. -D. Wu, and S. R. Moses, *ibid.*, **108**, 2754 (1986); D. P. Curran and S. A. Gothe, *Tetrahedron,* **44**, 3945 (1988).

8) TEXAN: TEXRAY Structure Analysis Package, Molecular Structure Corporation (1985).

9) C. J. Gilmore, *J. Appl. Crystallogr.*, **17**, 42 (1984).

10) The authors have deposited atomic coordinates for this structure with the Cambridge Crystallographic Data Centre. The coordinates can be obtained on request from The Director, Cambridge Crystallographic Data Centre, University Chemical Laboratory, Lensfield Road, Cambridge CB2 1EW, U. K.

Silicon Effects. III. Rates and Products for Solvolysis of α-(Pentamethyldisilanyl)benzyl Halides and 1,1,2,2-Tetramethyl-1,2-disilaindan-3-yl Chloride. Structure and Stability of α-(Pentamethyldisilanyl)benzyl Cation in Solution[1,2]

Nobujiro SHIMIZU,* Chieko KINOSHITA, Erika OSAJIMA, Fumie HAYAKAWA, and Yuho TSUNO
Department of Chemistry, Faculty of Science, Kyushu University, Hakozaki, Fukuoka 812
(Received July 3, 1991)

Detailed kinetic and product studies have been made on solvolysis of α-(pentamethyldisilanyl)benzyl halides (**1a-X**; X=Cl and Br) and 1,1,2,2-tetramethyl-1,2-disilaindan-3-yl chloride (**2-Cl**) in various solvents. The solvolysis of **1a-X** at 25 °C is characterized by (1) a complete 1,2-$SiMe_3$ rearrangement in the products, (2) m (sensitivity to the solvent ionizing power Y_x) values of 0.98 (X=Cl) and 0.91 (X=Br) for the solvolyses in aq acetone, (3) α-deuterium isotope effects of 1.167 and 1.163 for **1a-Cl** in 97% aq 2,2,2-trifluoroethanol (TFE) and 40% aq ethanol respectively, and (4) substituent effect expressed by a Yukawa-Tsuno LArSR equation: $\log k/k^H=-3.71$ ($\sigma^\circ+1.16\Delta\bar{\sigma}_R^+$) for the solvolysis of **1a-Cl** and the p-Me, m-Me, p-Cl, and m-Cl derivatives in 40% aq ethanol. These findings are consistent with k_c mechanism. The relative rates for **1a-Br**, α-(trimethylsilyl)benzyl bromide, and α-(*t*-butyldimethylsilyl)benzyl bromide are $1.07\times10^5:0.54:1.0$ in 97% aq TFE at 25 °C indicating solvolytic generation of α-(pentamethyldisilanyl)benzyl cation to be ca. 7 kcal mol^{-1} energetically more favorable than that of the corresponding α-(trialkylsilyl)benzyl cations. In contrast, **2-Cl** solvolyzes 0.209 times less rapidly than does 2,2-dimethyl-2-silaindan-1-yl chloride in 97% aq TFE indicating that a β-Si–Si σ bond orthogonal to the leaving group does not enhance the rate of ionization at all.

Silicon–silicon single bonds possess unusual low ionization potentials[3] and are capable of interacting with π-systems intermolecularly as well as intramolecularly.[4-6]

The Si–Si bonds are expected to interact strongly with neighboring electron-deficient centers. Eaborn and coworkers[7] have shown that p-disilanyl groups [$(Me_3Si)_nSiMe_{3-n}$] exert small and additive rate-acceleration effects in the protodestannylation of aryltrimethyltins indicative of inductive and hyperconjugative electron release from the Si–Si bonds. Kumada and coworkers[8] have reported several cationoid reactions of (halomethyl)disilanes undergoing a 1,2-silyl rearrangement from the silicon to the carbenium carbon suggestive of neighboring group participation of the Si–Si σ bond in ionization of the adjacent carbon–halogen bonds. However, neither precise mechanism for the solvolysis of the (halomethyl)disilanes nor structures of carbocations bearing α-disilanyl groups have been elucidated.

The α and β-silicon effects on stability of carbocations have received considerable mechanistic[9-11] and theoretical interests[12,13] in recent years. Previously,[1,14] we estimated the α- and β-silicon effects in the benzylic k_c solvolysis and it is of interest to compare the β-silicon effects in two benzylic cation systems, $PhHC^+$–Si–$SiMe_3$ and $PhHC^+$–C–$SiMe_3$. In order to estimate the β-silicon effect in the former system, we selected the solvolysis of α-(pentamethyldisilanyl)benzyl halides (**1a-X**; X=Br and Cl) and compared their solvolysis rates with those for structurally related α-(trialkylsilyl)benzyl halides.[14] In this paper we describe detailed kinetic and product studies on the solvolysis of **1a-X** and its cyclic analogue, 1,1,2,2-tetramethyl-1,2-disilaindan-3-yl chloride (**2-Cl**), in which the Si–Si bond is orthogonal to the leaving group, and discuss mechanistic implications on the β-silicon effects of the disilanyl groups.

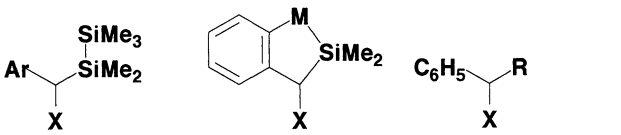

1a; Ar=C_6H_5 **2**; M=$SiMe_2$ **4**; R=Me
b; Ar=*p*-MeC_6H_4 **3**; M=CH_2 **5**; R=$SiMe_2CMe_3$
c; Ar=*m*-MeC_6H_4 **6**; R=$SiMe_3$
d; Ar=*p*-ClC_6H_4 **7**; R=CH_2SiMe_3
e; Ar=*m*-ClC_6H_4 **8**; R=CH_2CMe_3

Results

Synthesis. The bromide **1a-Br** was prepared by treatment of benzyl bromide with LDA at −78 °C in the presence of chloropentamethyldisilane.[14] The chloride **1a-Cl** and the p-Me, m-Me, p-Cl, and m-Cl derivatives (**1b-Cl-1e-Cl**) were prepared in a similar procedure. The cyclic chloride, **2-Cl**, was synthesized from *o*-bromobenzyl chloride via *o*-lithiation, a coupling reaction with 1,2-dichlorotetramethyldisilane, and ring closure of the resulting *o*-(2-chlorotetramethyldisilanyl)benzyl chloride by use of LDA, as shown in Scheme 1. 2,2-Dimethyl-2-silaindan-1-yl chloride (**3-Cl**), a reference standard for **2-Cl**, was prepared by chlorination of 2,2-dimethyl-2-silaindan with sulfuryl chloride.

Kinetic Studies. The rates of solvolysis of the halides

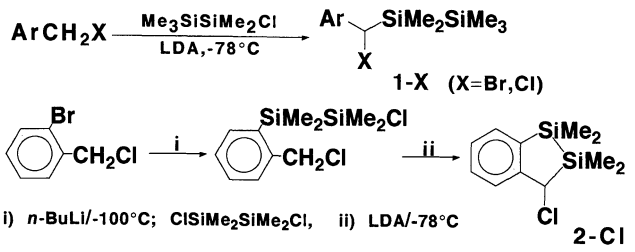

Scheme 1.

1-X, **2-Cl**, and **3-Cl** were determined UV spectrometrically in various solvents including 80/20 to 30/70 (v/v) ethanol–water (E series), 80/20 to 30/70 (v/v) acetone–water (A series), and 97/3 (w/w) to 40/60 (v/v) 2,2,2-trifluoroethanol (TFE)–water (T series) binary solvent mixtures by measuring either decrease in the reactant or increase in acid formed as its acridinium salt by using $(0.1—1.0)\times10^{-4}$ M (M= mol dm^{-3}) solutions in the presence or absence of 2—3 equiv acridine.[14] The rates were reproducible within ±3% in the both measurements and the first-order rate constants determined at 25.0±0.05 °C for **1a-Br**, **1a-Cl**, **2-Cl**, and **3-Cl** were given in Tables 1 and 2. Table 1 includes rate data for 1-phenylethyl bromide (**4-Br**) for comparison.

The solvolysis of **2-Cl** in 97% aq TFE (97T) in the presence of 2 equiv acridine also followed excellent first-order kinetics (correlation coefficient R=0.99998). Unexpectedly, however, the solvolyses in aq ethanol and aq acetone did not follow the first-order kinetics probably due to occurrence of a side reaction (vide infra) and we could not measure the rates in these solvents.

Table 3 compares the solvolysis rates of **1a-Br** in 97T and 30% aq acetone (30A) with those of its β-alkyl reference standards, α-(*t*-butyldimethylsilyl)benzyl and α-(trimethylsilyl)benzyl bromides[14] (**5-Br** and **6-Br** respectively), and the rate of solvolysis of **2-Cl** in 97T with

Table 1. Solvolysis Rates for **1a-Br**, **1a-Cl**, and **4-Br**[a]

Solvent[b]	$10^5\times k/s^{-1}$[a]		
	1a-Br	**1a-Cl**	**4a-Br**
97T	6200[c]	775 ±2.1[e]	515 ±0.12
80T	4400±26[d]	501 ±0.25	893 ±0.2
50T	5020±71[d]	500 ±4.8[d]	
30T	5590±52[d]		
30A	2060±24[d]	165 ±0.26	3100±30[d]
40A	489 ±0.3	35.5 ±0.02	876 ±0.23
50A	96.7 ±0.17	5.20 ±0.002	232 ±0.06
60A	21.8 ±0.03	0.987±0.0006	50.9 ±0.017
70A	4.30 ±0.016		12.6 ±0.001
80A	1.08 ±0.0004		
30E		437 ±0.65	
40E	668 ±1.7	59.6 ±0.51[e]	
50E	139 ±0.2	10.4 ±0.009	
60E	44.1 ±0.10	3.58 ±0.003	
70E	15.4 ±0.10		
80E	4.75 ±0.007		
90E	1.44 ±0.007		

a) At 25.0±0.05 °C. b) A: acetone–water (v/v), E: ethanol–water (v/v), and T: 2,2,2-trifluoroethanol–water (v/v) binary solvent mixtures except for 97T which is a mixture in weight percent. c) Extrapolated from other temperatures. d) Average of two runs. e) Average of three runs.

Table 2. Solvolysis Rates for **2-Cl** and **3-Cl**[a]

Solvent	$10^5\times k/s^{-1}$	
	2-Cl	**3-Cl**
97T	38.6±0.03	184±0.08
30A		189±0.11
40A		40.5±0.02
50A		6.72±0.001
40E		87.3±0.04

a) At 25±0.05 °C.

Table 3. β-Silicon Effects[a]

Substrate	β-Group	Solvent	k/s^{-1}	Relative rate
1a-Br	$SiMe_3$	97T	6.20×10^{-2}[b]	1.07×10^5
5-Br	CMe_3		5.79×10^{-7}[c,d]	1.0
6-Br	Me		3.13×10^{-7}[c]	0.54
1a-Br	$SiMe_3$	30A	2.06×10^{-2}	3.38×10^4
5-Br	CMe_3		6.10×10^{-7}[c,e]	1.0
6-Br	Me		1.02×10^{-6}[c]	1.67
2-Cl	$SiMe_2$	97T	3.86×10^{-4}	0.209
3-Cl	CH_2		1.84×10^{-3}	1.0
7-OTFA[f]	$SiMe_3$	30D[g]	4.01×10[h]	2.99×10^5
8-OTFA[f]	CMe_3	30D[g]	1.23×10^{-4}[h]	1.0
4-OTFA[f]	H	30D[g]	3.49×10^{-4}[h]	2.84

a) At 25 °C. b) Extrapolated value from other temperatures. c) Data taken from Ref. 14. d) Estimated from k(**6-Br**) and a k(**5-OTs**)/k(**6-OTs**) rate ratio of 1.85 in 97T (Ref. 14). e) Estimated from k(**6-Br**) and a k(**5-OTs**)/k(**6-OTs**) rate ratio of 0.598 in 30A (Ref. 14). f) Trifluoroacetates. g) In 30% aq dioxane. h) Data taken from Ref. 1.

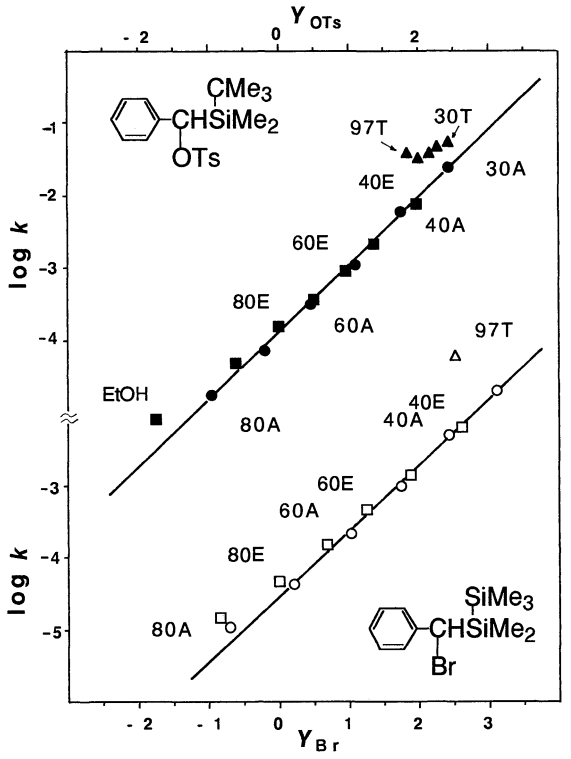

Fig. 1. Plot of log k vs. Y_{Br} for **1a-Br** (open marks) and log k vs. Y_{OTs} for **5-OTs** (closed marks) for aq acetone (circles), aq ethanol (squares), and aq TFE (triangles).

that of its standard compound **3-Cl**. Rate data[1] for 1-phenylethyl trifluoroacetate (**4-OTFA**), 1-phenyl-2-(trimethylsilyl)ethyl trifluoroacetate (**7-OTFA**), and 3,3-dimethyl-1-phenylbutyl trifluoroacetate (**8-OTFA**) were also included in Table 3 for comparison.

Figure 1 represents dependence of the solvolysis rates (log k) of **1a-Br** on solvent ionizing power Y_{Br}.[15] A separate mY plot for α-(*t*-butyldimethylsilyl)benzyl *p*-toluenesulfonate (**5-OTs**) against Y_{OTs}[16] is included for comparison. A plot of log k for **1a-Cl** vs. Y_{Cl}[15] exhibited a very similar mY plot pattern to that for **1a-Br** for the A, E, and T solvent series. Table 4 compares m values for the five different substrates, **1a-Cl**, **1a-Br**, **3-Cl**, **4-Br**, and **5-OTs**, determined from the linear correlation observed in acetone–water binary solvent mixtures.

Table 5 shows α-deuterium kinetic isotope effects (α-KIE) for the solvolysis of **1a-Cl** in 40% aq ethanol (40E) and in 97T at 25 °C.

Table 6 shows the solvolysis rates for **1a-Cl**—**1e-Cl** measured in 40E at 25 °C. The substituent effect was linearly expressed by the Yukawa-Tsuno LArSR equation (Eq. 1)[17] with an r value of 1.16 and a ρ value of −3.71 (n=5, R=0.998, SD=0.066).

$$\log k/k^{H} = \rho(\sigma^{\circ} + r\Delta\bar{\sigma}_{R}^{+}) \quad (1)$$

Table 7 shows salt effects on the solvolysis of **1a-Cl** in 40E. Neither common ion rate depression nor special salt effect was significant, indicative of unimportance of return processes. Activation parameters for the solvolyses of **1a-Br** and **1a-Cl** are given in Table 8.

Product Studies. Reductive dehalogenation of **1a-Br** and **2-Cl** with $LiAlH_4$ cleanly gave the corresponding reduction products, benzylpentamethyldisilane (**1a-H**) and 2,2-dimethyl-2-silaindan (**2-H**), suggestive of structural conservation in S_N2-type reactions. In contrast, a solvolytic reaction of **1a-Br** with ethanol in the presence or absence of a buffer base quantitatively gave a 1,2-$SiMe_3$ rearranged compound, an ethoxysilane **9a-OEt** (Scheme 2). We could not detect the formation of a structure-retained product **1a-OEt**. Similarly, buffered

Table 4. Solvent Effect

Substrate	m[a,b]
1a-Br	0.91 (n=5, R=0.996)
1a-Cl	0.98 (n=4, R=0.994)
3-Cl	0.98 (n=3, R=0.998)
5-OTs	0.94 (n=6, R=0.999)[c]
4-Br	0.87 (n=5, R=0.998)

a) Sensitivity to the solvent ionizing power; Y_{Br}, Y_{Cl} (Ref. 15), and Y_{OTs} (Ref. 16) were used for chlorides, bromides, and tosylates respectively. b) Determined from the rates in 80/20 to 30/70 (v/v) acetone/water binary mixtures. c) Data taken from Ref. 14.

Table 5. α-Deuterium Kinetic Isotope Effects[a]

Substrate	Solvent	$10^5 \times k/s^{-1}$	k_H/k_D
1a-Cl	97T	769.3 ±8.4[b]	
1a-Cl-α-d_1	97T	659.3 ±5.6[c]	1.167±0.023
1a-Cl	40E	59.61±0.50[c]	
1a-Cl-α-d_1	40E	51.27±0.50[c]	1.163±0.021

a) At 25 °C. b) Average of three runs. c) Average of two runs.

Table 6. Substituent Effect on the Solvolysis of **1-Cl**[a]

Substrate	$10^5 \times k/s^{-1}$	r[b]	ρ
1b-Cl	1100		
1c-Cl	85.2		
1a-Cl	59.6	1.16	−3.71[c]
1d-Cl	23.6		
1e-Cl	1.91		

a) In 40% aq ethanol at 25 °C. b) Resonance parameter in the Yukawa-Tsuno equation (Ref. 17). c) R=0.998; SD=0.067.

Table 7. Salt Effects on the Solvolysis of **1a-Cl**[a]

Salt	[Salt]/M	$10^5 \times k/s^{-1}$	k_{rel}
None		59.6	1.0
LiCl	0.100	62.8	1.05
LiBr	0.100	65.1	1.11
$LiClO_4$	0.040	65.6	1.11

a) In 40% aq ethanol at 25 °C.

Table 8. Activation Parameters

Substrate	Solvent	Temp °C	$10^5 \times k$ s^{-1}	$\Delta H^{\ddagger}_{298}$ kcal mol^{-1}	$\Delta S^{\ddagger}_{298}$ cal K^{-1} mol^{-1}
1a-Br	97T	25.0	6200[a]	14.5	−15.5
		20.5	4180		
		11.7	1900		
		3.7	871		
	40E	33.5	1610		
		25.0	668	17.1	−9.0
		16.0	252		
		11.7	163		
1a-Cl	40E	46.2	486		
		33.5	144		
		25.0	59.6	18.1	−12.5

a) Extrapolated value.

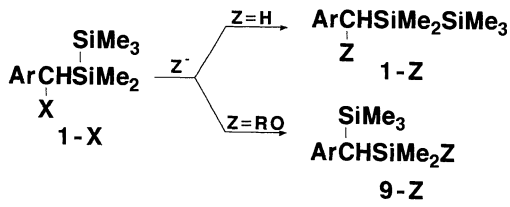

Scheme 2.

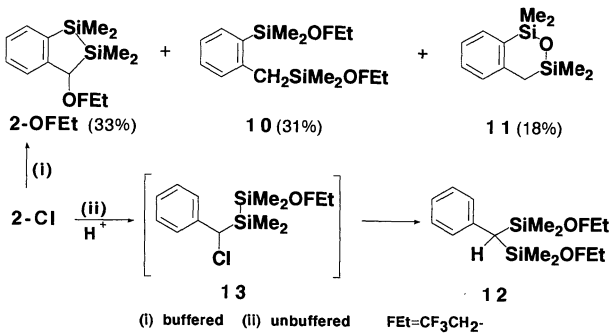

Scheme 3.

solvolyses in TFE and in 50% aq acetone respectively gave rearranged compounds, a (2,2,2-trifluoroethoxy)silane **9a-OFEt** (FEt=CH_2CF_3) and a silanol **9a-OH**, as a single product in each case. The same was true for the chlorides **1a-Cl** and **1b-Cl**. The 1,2-$SiMe_3$ migration must be directly associated with the ionization of the C–X bond of the halides **1-X**. The 1,2-silyl rearrangement has already been observed in several cationoid reactions of (halomethyl)disilanes.[8] A related 1,2-alkyl shift from the α-silicon to a carbenium carbon has also been reported by Apeloig and Stanger in the solvolysis of 2-trimethylsilyl-2-adamantyl *p*-nitrobenzoate.[18]

The solvolysis of **1b-Cl** in TFE in the presence of 1 M sodium cyanotrihydroborate gave a mixture of two rearranged products, **9b-OFEt** and a silane **9b-H**, in a ratio of 95:5, while the solvolysis in ethanol in the presence of 1 M sodium cyanotrihydroborate afforded a mixture of **9b-OEt** and a reduction product **1b-H** in the ratio 98:2. Apparently, an S_N2 reduction by the hydroborate can compete with the S_N1 solvolysis in ethanol of low ionizing power, but not in a strong ionizing solvent, TFE (Y_{OTs}=−1.75 and 1.80 for ethanol and TFE respectively). On the other hand, the hydroborate can attack a solvolysis intermediate in competition with solvent in a weakly nucleophilic solvent TFE but not in a strongly nucleophilic solvent ethanol (N_{OTs}=−3.0 and 0.0 for TFE and ethanol respectively[16]).

The halides **1-X** underwent the skeletal rearrangement thermally as well; for example, **1a-Cl** quantitatively gave a chorosilane **9a-Cl** on heating at 150 °C. We also examined a silver(I)-assisted reaction of **1a-Br**; it reacted instantaneously with silver perchlorate in THF at −78 °C and gave **9a-OEt** when ethanol was added to the mixture. Since **1a-Br** did not react with ethanol at this temperature, a precursory species must be a silyl perchlorate **9a-OClO$_3$**.

The cyclic halide **3-Cl** solvolyzed in aq acetone cleanly to give an expected alcohol **3-OH**, as does the bromide **3-Br**.[14] On the other hand, solvolytic reactions of **2-Cl** were complicated. A buffered reaction of **2-Cl** with TFE gave two solvolysis products, a structure-retained ether **2-OFEt** (33%) and an open compound **10** (31%), together with a cyclic disiloxane **11** (18%) which was presumably formed from **10** during isolation processes (Scheme 3). The result is consistent with the observed good first-order kinetics for the buffered solvolysis in 97T.

On the other hand, an unbuffered reaction with TFE led to the formation of a completely different compound, α,α-bis[dimethyl(2,2,2-trifluoroethoxy)silyl]toluene **12**. Initial protodesilylation of **2-Cl** accounts for this; as soon as hydrogen chloride is liberated on solvolysis, it must catalyze a ring opening of **2-Cl** to an α-(disilanyl)benzyl chloride **13** which would give **12** upon solvolysis (Scheme 3).

Furthermore, a buffered reaction of **2-Cl** with ethanol at 25 °C did not give solvolysis products; instead, *o*-(2-ethoxytetramethyldisilanyl)benzyl chloride **14** was ob-

tained as the major product. Although precise mechanism for the formation of **14** is not clear at present, **2-Cl** appears to undergo solvolysis only in strongly ionizing but weakly nucleophilic media like TFE; a strongly nucleophilic solvent like ethanol prefers attack on the α-silicon rather than it promotes ionization of the C–Cl bond. Oxidation of the Si–Si bond in **2-Cl** occurred predominantly at higher temperatures. For example, an attempted solvolysis in 70% aq acetone at 70 °C led to the formation of a cyclic disiloxane **15** as the major product. Compound **2-Cl** was rapidly oxidized to **15** when heated in carbon tetrachloride in the air.

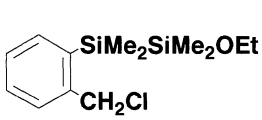

14

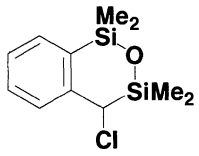

15

Discussion

Mechanism. Two observations characterizing the solvolysis of **1a-X** are a marked rate acceleration of $(0.34—1.1)\times10^5$ by the α-$SiMe_2SiMe_3$ group relative to the structurally related $SiMe_2(t\text{-Bu})$ group (Table 3) and the clean formation of the rearranged product via a 1,2-$SiMe_3$ shift. The accelerated rate coupled with the skeletal rearrangement is a general feature suggestive of neighboring group participation[19] and hence a σ-participation mechanism (k_Δ) via a bridged siliconium ion intermediate **16** is seemingly operative. However, these findings can also be accounted for by two other mechanisms. They are a concerted pathway[8] involving simultaneous solvent attack on the α-silicon, migration of an $SiMe_3$ group from the silicon to the benzylic carbon, and cleavage of the C–X bond as illustrated by the structure **17** and a simple ionization mechanism (k_c) via rate-determining formation of an open α-(pentamethyldisilanyl)benzyl cation **18** which rapidly decays to the rearranged product most likely via a silylenium ion **19** (Scheme 4).

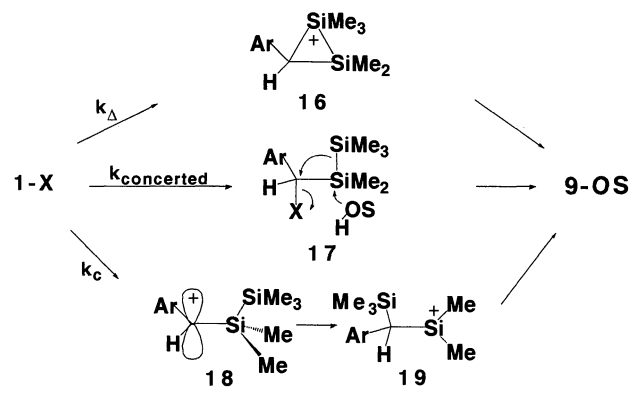

Scheme 4.

On the precise mechanism the following findings are instructive. First, the halides **1a-X** exhibit high sensitivities to the solvent ionizing power for their solvolyses in acetone–water binary solvent mixtures (Table 4), i.e., m=0.91 and 0.98 for the bromide and chloride respectively, supporting an unassisted ionization. Noteworthy is a striking resemblane in the mY plot for **1a-Br** to that for the solvolysis of the structurally related α-trialkylsilyl compound **5-OTs** (Fig. 1) indicative of a close similarity in the mechanism between the two solvolysis reactions. We have proposed the k_c mechanism for the solvolysis of **5-OTs** via a benzylic cation **20**.[14] Thus, the solvent effect is obviously more in accord with the k_c mechanism via **18** than the k_Δ and concerted mechanisms. Aq ethanol of low water content (80E and 90E) deviates upward from the aq acetone correlation line; however, this is not a result of nucleophilic solvent assistance because such interaction should lead to significant downward deviations for T solvents which are much less nucleophilic than aq acetone against the observation. The upward deviation for 97T by about one log k unit is striking but this is not associated with the 1,2-$SiMe_3$ rearrangement either because a similar large deviation of 97T is also observed for **5-OTs** which does not undergo a skeletal rearrangement. The diverging mY plot instead of a single linear correlation for A, E, and T solvent series does not mean a mechanistic shift from the k_c solvolysis but probably arises from the different responses to the ionizing power between the present benzylic derivatives and the standard adamantyl compounds.[14]

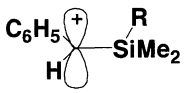

20; R=*t*-Bu

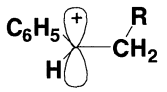

21; R=$SiMe_3$
22; R=*t*-Bu

Second, the α-KIEs (k_H/k_D) of 1.16—1.17 (Table 5) for the solvolysis of the chloride **1a-Cl** are comparable with those (1.15—1.16) for the related 1-arylethyl chlorides which undergo S_N1 solvolysis.[20] The result suggests that **1a-Cl** solvolyzes via a transition state structurally close to the cation **18**.

Thirdly, the LArSR analysis reveals that the transition state of the solvolysis of **1-Cl** requires a rather high resonance demand $r>1$ (Table 6). This is obviously incompatible with the k_Δ and concerted mechanisms and is most reasonably accommodated with the k_c mechanism. Noteworthy is a marked reduction in ρ value (−3.7) as compared to typical values around −5.5 for the S_N1 solvolysis of structurally related α-alkylbenzyl compounds.[21,22] This is undoubtedly associated with low ionization potentials of the Si–Si σ bonds.[3] The positive charge on the benzylic carbon must be significantly delocalized to the Si–Si bond mainly through hyperconjugation.[23]

Thus, the combined results lead us to conclude the k_c mechanism for the solvolysis of α-(pentamethyldisilanyl-)benzyl halides. It is worth stating that 1-phenyl-2-(trimethylsilyl)ethyl trifluoroacetate **7-OTFA** has been shown to solvolyze also by the k_c mechanism via an open benzylic cation **21**.[1] The k_c solvolysis for these benzylic systems is in agreement with recent experimental[10] and theoretical[12] results that an open bisected structure of 2-silylalkyl cations is more stable than a bridged form except for the primary cation where a bridged form is slightly more favorable than an open structure.

The absence of the common ion rate depression and special salt effect (Table 7) indicates unimportance of return processes. This is in agreement with the clean formation of the rearranged products suggestive of a rapid decay of the cation **18** to the products via a 1,2-$SiMe_3$ shift. It is of interest whether the silylenium ion **19** is really involved in the product-forming step. We have no compelling evidence for the formation of **19** but the rearrangement of **18** to **19** appears energetically favorable.[24,25]

Previously,[14] we showed the S_N1 solvolysis of 2,2-dimethyl-2-silaindan-1-yl bromide (**3-Br**). The same mechanism would probably be operative in the solvolysis of the chloride **3-Cl**. The *m* value of 0.98 (Table 4) strongly supports this. Judging from a structural similarity, we can assume the k_c solvolysis of the related chloride **2-Cl** in 97T. The formation of **2-OFEt** and **10** is compatible with intervention of 1,1,2,2-tetramethyl-1,2-disilaindan-3-yl cation **23**; the cation gives either **2-OFEt** directly or **10** after cleavage of the Si–Si bond presumably via a silene **24** or a silacyclobutene **25**.

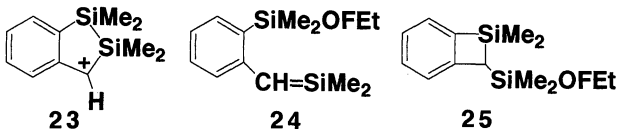

23 24 25

β-Silicon Effect. The $SiMe_2SiMe_3$ group exerts α- and β-silicon effects on the stability of the adjacent carbocations. The β-silicon effect can be estimated by comparing the rates of the α-(pentamethyldisilanyl)benzyl and the structurally related α-(trialkylsilyl)benzyl compounds. Although the rates of solvolysis of α-alkylbenzyl compounds are subjected to the steric effect of the α-alkyl group,[26] we have shown that there is little difference in the steric effect between the two α-trialkylsilyl groups, $SiMe_3$ and $SiMe_2$(*t*-Bu), in the benzylic k_c solvolysis.[14] This suggests that the steric effect of the α-$SiMe_2SiMe_3$ group is practically the same as that of $SiMe_2$(*t*-Bu) or $SiMe_3$. Thus, the k(**1a-Br**)/k(**5-Br**) rate ratios of (0.34—1.1)×10^5 (Table 3) provide a reasonable estimate for the β-silicon effect of the pentamethydisilanyl group indicating the solvolytic generation of **18** to be 6.2—6.8 kcal mol^{-1} (1 kcal= 4.18 kJ) energetically more favorable than that of **20**. A similar β-silicon effect has also been observed in the related k_c solvolysis of α-alkylbenzyl derivatives (Table 3); **7-OTFA** solvolyzes 2.99×10^5 times more rapidly than **8-OTFA** suggesting the formation of the cation **21** to be 7.5 kcal mol^{-1} more favorable than that of the corresponding β-alkyl cation **22**.[1]

It is worth stating that despite the huge β-silicon effect of the $SiMe_2SiMe_3$ group relative to $SiMe_2$(*t*-Bu), the overall effect is comparable to that of methyl (Table 1). This arises from the fact that an α-silyl group exerts a marked deactivating effect in the benzylic solvolysis. For example, **6-Br** solvolyzes (1.6—3.3)×10^4 times less rapidly than **4-Br** due to the electronic and steric effects of the trimethylsilyl group relative to methyl.[14]

Noteworthy is the fact that **2-Cl** solvolyzes slightly less rapidly than **3-Cl** (Table 3). This means that the Si–Si bond orthogonal to the leaving group does not enhance the ionization of the adjacent C–Cl bond at all. The result not only shows a striking conformational dependence of the β-silicon effect but also indicates unimportance of the inductive electron release from the β-silicon. The observed small inverse rate ratio, k(**2-Cl**)/k(**3-Cl**)=0.209, can be attributed to differences in the electronic effects and/or the steric effects between the silyl group and the alkyl group at the ortho position (*A*-value, σ_I, and σ_R° are ca. 2.5, −0.10, and 0.12 for $SiMe_3$ and 1.70, −0.01, and −0.16 for CH_3.[27,28]).

The β-silicon effect depends on the electronic demands of the carbenium carbon of the parent cation.[10,12] For example, a theoretical study indicates that the stabilization energy of a cation $R^1R^2C^+$–CH_2R^3 afforded by replacement of R^3 from hydrogen to SiH_3 increases from 15.9 kcal mol^{-1} for *t*-butyl cation (R^1=R^2=Me) to 22.1 kcal mol^{-1} for 1-methylethyl cation (R^1=Me, R^2=H) which is 18 kcal mol^{-1} less stable than *t*-butyl cation.[12] Therefore, in order to compare the β-silicon effect in the two benzylic cation systems, $PhHC^+$–$SiMe_2$–R and $PhHC^+$–CH_2–R (R=$SiMe_3$ and *t*-Bu), we must consider the stabilities of the parent cations (R=*t*-Bu) in the two systems, i.e., **20** and **22**. We can assume **22** to be 3—4 kcal mol^{-1} more stable than **20** in view of the fact that the solvolytic generation of 2,2-dimethyl-1-indanyl cation is 3—4 kcal mol^{-1} more favorable than that of 2,2-dimethyl-2-silaindan-1-yl cation.[14] Consequently, a more pronounced β-silicon effect than the observed value of 7.5 kcal mol^{-1} is expected in the $PhHC^+$–CH_2R system if **22** exhibits the same electronic demand as that of **20**; a value of more than 8.5 kcal mol^{-1} can be evaluated if we simply assume that the difference in stability between *t*-butyl cation and 1-methylethyl cation by 18 kcal mol^{-1} causes a change in the β-silicon effect by about 6 kcal mol^{-1}. Thus, it is concluded that the hyperconjugative interaction of the Si–Si bonds with the empty 2p orbital of the benzylic cation is 1—2 kcal mol^{-1} less effective than that of the corresponding C–Si bonds in agreement with the earlier suggestion that π–σ(Si–Si) conjugation is weaker than π–σ(C–Si) conjugation.[23,29]

Finally, we must point out that a direct comparison of the solvolysis rates of the two α-disilanyl compounds, **1a-Cl** and **2-Cl**, may lead to an erroneous conclusion; a k(**1a-Cl**)/k(**2-Cl**) rate ratio of 20 would suggest a very small rate enhancement by the Si–Si bond through hyperconjugation contrary to the rate enhancement of 10^5 mentioned earlier. This is obviously not justified. Since there is a marked intrinsic difference in reactivity between 1-indanyl ring system and the corresponding open benzylic system,[14,30] the k(**1a-Cl**)/k(**2-Cl**) rate ratio itself tells us nothing about the effect of the Si–Si bonds. It should be noted that a cyclic bromide **3-Br** is 7.1×10^3 times as reactive as an open compound **6-Br**.[14] If we take this rate factor as an effect of the indanyl ring system, we can estimate the rate (k_{calcd}) of solvolysis of **2-Cl** from 7.1×10^3 times k(**1a-Cl**), i.e., $k_{calcd}=56$ s^{-1} in 97T; however, **2-Cl** in fact solvolyzes with a rate constant of $k_{obsd}=3.86\times10^{-4}$ s^{-1} which is 1.5×10^5 times smaller than the expected one. The actual low reactivity of **2-Cl** undoubtedly arises from the orthogonal alignment of the Si–Si bond to the empty p-orbital of the carbenium carbon incapable of hyperconjugation. Thus, the k_{calcd}/k_{obsd} rate ratio of ca. 10^5 corresponds to a rate enhancement by the Si–Si bond mainly through hyperconjugation in the open system in good agreement with the earlier discussion.

Experimental

IR spectra were recorded on a Hitachi R-215 spectrophotometer. NMR spectra were recorded on a Hitachi R-20B spectrometer in carbon tetrachloride. Mass spectra were recorded on a Hitachi M-60 mass spectrometer. Kinetic measurements were performed with a Hitachi 220A spectrophotometer equipped with a programmed data printer. GLC analysis was performed with a Hitachi 163 gas chromatograph by using glass columns (6 mm×1.5 and 2.0 m) packed with 10% Silicone DC 550 on Chamelite CS (Column A) and 25% Apiezon grease L on Chromosorb W (Column B).

Materials. α-(Pentamethyldisilanyl)benzyl Bromide (**1a-Br**), α-(pentamethyldisilanyl)benzyl chloride (**1a-Cl**), its *p*-Me, *m*-Me, *p*-Cl, and *m*-Cl derivatives (**1b-Cl**—**1e-Cl**), and α-deuterio-α-(pentamethyldisilanyl)benzyl chloride (**1a-Cl**-d_1) were prepared by in situ coupling reaction of the corresponding benzyl halides with chloropentamethyldisilane in the presence of LDA. The following procedure for preparation of **1a-Br** is representative.

Into a stirred solution of LDA prepared from butyllithium (20 cm³, 1.7 M in hexane) and diisopropylamine (3.5 g) in THF (25 cm³) was added dropwise a solution of chloropentamethyldisilane (5.1 g) in THF (5 cm³) at −78 °C and subsequently a solution of benzyl bromide (5.2 g) in THF (5 cm³) over a period of 15 min at −78 °C. The resulting mixture was stirred overnight at that temperature. Pentane (75 cm³) was added, the mixture poured into water, and separated. Water layer was extracted with pentane (50 cm³). A combined organic layer was washed with 10% sulfuric acid, aq $NaHCO_3$, aq NaCl, and dried ($MgSO_4$). Solvent was removed on a rotary evaporator and the residual oil was distilled to give 5.32 g (58%) of **1a-Br** as a colorless oil, bp 98—99 °C (1 Torr; 1 Torr= 133.3 Pa): IR 1600, 1245, 835, 800, 695 cm^{-1}; ^{1}H NMR δ=0.0 (9H, s), 0.13 (3H, s), 0.19 (3H, s), 4.32 (1H, s), 7.20 (5H, almost s). Found: C, 48.01; H, 6.96%. Calcd for $C_{12}H_{21}BrSi_2$: C, 47.83; H, 7.02%.

1a-Cl: Bp 94—95 °C (3 Torr); IR 1595, 1245, 1065, 1025, 830, 800 cm^{-1}; UV (95% EtOH) λ_{max} (log ε) 207 (4.16), 229 (4.01); ^{1}H NMR δ=0.02 (9H, s), 0.07 (3H, s), 0.13 (3H, s), 4.38 (1H, s), 7.19 (5H, almost s). Found: C, 55.90; H, 8.17%. Calcd for $C_{12}H_{21}ClSi_2$: C, 56.10; H, 8.24%.

1a-Cl-d_1: Bp 87—88 °C (1 Torr); IR 1245, 950, 830, 795 cm^{-1}; ^{1}H NMR δ=0.02 (9H, s), 0.07 (3H, s), 0.13 (3H, s), 7.19 (5H, almost s). Found: C, 55.88; H, 8.28%. Calcd for $C_{12}H_{20}DClSi_2$: C, 55.88; H, 8.22%. ^{1}H NMR analysis indicated isotopic purity of more than 99%.

1b-Cl: Bp 106—107 °C (1 Torr); IR 1245, 1105, 830, 795 cm^{-1}; ^{1}H NMR δ=0.02 (9H, s), 0.06 (3H, s), 0.11 (3H, s), 4.33 (1H, s), 7.03 (4H, almost s). Found: C, 57.43; H, 8.42%. Calcd for $C_{13}H_{23}ClSi_2$: C, 57.63; H, 8.56%.

1c-Cl: Bp 107—108 °C (1 Torr); IR 1245, 1120, 865, 830, 800 cm^{-1}; ^{1}H NMR δ=0.02 (9H, s), 0.07 (3H, s), 0.11 (3H, s), 2.31 (3H, s), 4.33 (1H, s), 6.8—7.2 (4H, m). Found: C, 57.41; H, 8.43%. Calcd for $C_{13}H_{23}ClSi_2$: C, 57.63; H, 8.56%.

1d-Cl: Bp 92—93 °C (0.5 Torr); IR 1245, 1120, 1090, 1010, 830, 790 cm^{-1}; ^{1}H NMR δ=0.05 (12H, s), 0.11 (3H, s), 4.35 (1H, s), 7.18 (4H, A_2B_2, J=9.0 Hz). Found: C, 49.19; H, 6.86%. Calcd for $C_{12}H_{20}Cl_2Si_2$: C, 49.47; H, 6.92%.

1e-Cl: Bp 105—106 °C (1 Torr); IR 1245, 1110, 1090, 1075, 880, 830, 800 cm^{-1}; ^{1}H NMR δ=0.05 (9H, s), 0.08 (3H, s), 0.13 (3H, s), 4.34 (1H, s), 7.14 (4H, m). Found: C, 49.27; H, 6.92%. Calcd for $C_{12}H_{20}Cl_2Si_2$: C, 49.47; H, 6.92%.

1,1,2,2-Tetramethyl-1,2-disilaindan-3-yl Chloride (2-Cl): Into a solution of *o*-bromobenzyl chloride (7.65 g, 37.2 mmol) in a mixture of THF (130 cm³) and hexane (40 cm³) was added butyllithium (25 cm³, 1.6 M in hexane) at temperature around −100 °C and the mixture was stirred for 10 min at −100 °C under argon. A solution of 1,2-dichlorotetramethyldisilane (7.0 g) in THF (15 cm³) was added at such a rate as to maintain the temperature of the solution below −90 °C. The bath was removed and the mixture was allowed to warm to room temperature. Solvent was removed by distillation under reduced pressure. Dry pentane (150 cm³) was added to the residue and decanted. Pentane was removed on a rotary evaporator and the residue was distilled to give 7.02 g (68%) of *o*-(2-chlorotetramethyldisilanyl)benzyl chloride: Bp 124—125 °C (2.5 Torr); ^{1}H NMR δ=0.45 (6H, s), 0.56 (6H, s), 4.57 (2H, s), 7.18—7.56 (4H, m). Into a solution of LDA (23 mmol) in THF (20 cm³) was added a solution of this compound in THF (5 cm³) at −78 °C and the mixture was stirred for 2 h at −78 °C. Usual workup gave 2.90 g (57%) of **2-Cl** as a colorless oil: Bp 80—80.5 °C (0.5 Torr); IR 1585, 1250, 1130, 995, 860, 830, 735 m^{-1}; UV(CH_3CN) λ_{max} (log ε) 208 (4.22), 220 (shoulder, 3.92), 265 (shoulder, 2.85) 280 nm (2.55); ^{1}H NMR δ=0.20 (3H, s), 0.31 (3H, s), 0.35 (3H, s), 0.41 (3H, s), 4.46 (1H, s), 7.08—7.65 (4H, m). Found: C, 54.80; H, 7.12%. Calcd for $C_{11}H_{17}ClSi_2$: C, 54.86; H, 7.12%.

2,2-Dimethyl-2-silaindan-1-yl Chloride (3-Cl): A solution of 2,2-dimethyl-2-silaindan (3.24 g, 20 mmol),[14] sulfuryl chloride (1.35 g), and benzoyl peroxide (24 mg) in carbon tetrachloride (5 cm³) was heated under reflux for 30 min. Usual workup gave 1.2 g of **3-Cl:** Bp 86—87 °C (4 Torr); IR 1600, 1255, 1130, 1115, 850, 830, 820 cm^{-1}; UV (CH_3CN) λ_{max} (log ε) 203 (4.39), 225 (3.76), 2.77 nm (2.92); ^{1}H NMR δ=0.22

(3H, s), 0.40 (3H, s), 1.94 (1H, d, J=17.4 Hz), 2.22 (1H, d, J=17.4 Hz), 4.30 (1H, s), 6.95—7.56 (4H, m). Found: C; 60.95; H, 6.61%. Calcd for $C_{10}H_{16}ClSi$: C, 61.05; H, 6.66%.

Kinetics. Purification of solvents and kinetic procedure for rate measurements have been described elsewhere.[14] All the solvolysis reactions were followed UV spectrometrically by measuring either decrease in a reactant [243 nm for **1a-Br** and **1a-Cl** to **1e-Cl**, 245 nm for **2-Cl**, and 240 nm for **3-Cl**] or increase in a produced acid at 402.5 nm as its acridinium salt. The solvolyses followed excellent first-order kinetics over 3 to 4 half-lives (correlation coefficient R>0.9999).

Product Studies. Solvolysis of 1-X: Solvolytic reactions of **1a-Br**, **1a-Cl**, and **1b-Cl** in TFE, ethanol, and aq acetone were carried out by using 0.01—0.1 M solutions containing equimolar amounts of 2,6-dimethylpyridine at 25 °C and higher temperatures in some cases. In all cases, a single product was formed almost quantitatively and the following products were characterized.

2-Ethoxy-2,4-dimethyl-3-phenyl-2,4-disilapentane (9a-OEt): IR 1250, 1200, 1105, 1080, 1030, 940, 905, 840, 780 cm^{-1}; ^{1}H NMR δ=0.02 (12H, s), 0.06 (3H, s), 1.15 (3H, t, J=7.2 Hz), 1.52 (1H, s), 3.61 (2H, q, J=7.2 Hz), 6.6—7.3 (5H, m). Found: C, 62.80; H, 9.71%. Calcd for $C_{14}H_{26}OSi_2$: C, 63.09; H, 9.83.

2,4-Dimethyl-3-phenyl-2,4-disilapentan-2-ol (9a-OH): IR 3400, 1600, 1250, 1200, 1030, 845 cm^{-1}; ^{1}H NMR δ=0.03 (12H, s), 0.12 (3H, s), 1.35 (1H, s, disappeared on addition of D_2O), 1.51 (1H, s), 6.8—7.3 (5H, m); MS m/z 238 (M^+, 10), 223 (23), 148 (60), 147 (100), 73 (30). Found: C, 60.17; H, 9.31%. Calcd for $C_{12}H_{22}OSi_2$: C, 60.45; H, 9.30%.

2,4-Dimethyl-3-phenyl-2-(2,2,2-trifluoroethoxy)-2,4-disilapentane (9a-OFEt): IR 1600, 1300, 1285, 1255, 1160, 1030, 960, 850, 695 cm^{-1}; ^{1}H NMR δ=0.02 (9H, s), 0.09 (3H, s), 0.14 (3H, s), 1.55 (1H, s), 3.80 (2H, q, J=8.6 Hz), 6.7—7.2 (5H, m). Pure sample was obtained by GLC. Found: C, 52.80; H, 7.44%. Calcd for $C_{14}H_{23}F_3OSi_2$: C, 52.47; H, 7.23%.

2,4-Dimethyl-3-(4-methylphenyl)-2,4-disilapentan-2-ol (9b-OH): IR 3390, 1600, 1245, 1215, 1195, 1030, 850, 770 cm^{-1}; ^{1}H NMR δ=0.02 (9H, s), 0.04 (3H, s), 0.10 (3H, s), 1.47 (1H, s), 1.78 (1H, disappeared on addition of D_2O), 2.26 (3H, s), 6.88 (4H, AA′BB′, J=9.0 Hz).

2-Ethoxy-2,4-dimethyl-3-(4-methylphenyl)-2,4-disilapentane (9b-OEt): IR 1605, 1250, 1080, 1030, 945, 860, 835, 780 cm^{-1}; ^{1}H NMR δ=0.0 (12H, s), 0.03 (3H, s), 1.14 (3H, t, J=7.0 Hz), 1.44 (1H, s), 2.25 (3H, s), 3.59 (2H, q, J=7.0 Hz), 6.83 (4H, AA′BB′, J=9.0 Hz). Found: C, 71.10; H, 11.01%. Calcd for $C_{15}H_{28}OSi_2$: C, 71.37; H, 11.18%.

3-(4-Methylphenyl)-2-(2,2,2-trifluoroethoxy)-2,4,4-trimethyl-2,4-disilapentane (9b-OFEt): ^{1}H NMR δ=0.0 (9H, s), 0.07 (3H, s), 0.13 (3H, s), 1.62 (1H, s), 2.25 (3H, s), 3.81 (2H, q, J=9.0 Hz), 6.68 (4H, A_2B_2).

Solvolysis of 2-Cl: Compound **2-Cl** (399 mg) was dissolved in TFE (15 cm^3) containing acetone (1.0 cm^3) and 2,6-dimethylpyridine (182 mg) and the solution was allowed to stand for 3 d at 25 °C. A crude oil (464 mg) obtained after usual workup was shown to be a mixture of four compounds in the ratio 20:38:36:4 by GLC [Column A, 180 °C; retention time (t_R):4.0, 6.4, 13.2, and 18.4 min, respectively]. The first three components were isolated by GLC and were respectively assinged to 1,1,3,3-tetramethyl-1,3-disilaisochroman (**11**), 1,1,2,2-tetramethyl-3-(2,2,2-trifluoroethoxy)-1,2-disilaindan (**2-OFEt**), and α,o-bis[dimethyl(2,2,2-trifluoroethoxy)silyl]toluene (**10**) from the following spectral data.

2-OFEt: IR 1590, 1300, 1280, 1250, 1160, 1115, 965, 830, 670 cm^{-1}; ^{1}H NMR δ=0.04 (3H, s), 0.31 (3H, s), 0.35 (6H, s), 3.61 (2H, q, J=8.9 Hz), 4.31 (1H, s), 6.91—7.77 (4H, m). Found: C, 51.02; H, 6.30%. Calcd for $C_{13}H_{19}F_3OSi_2$: C, 51.29; H, 6.29%.

10: IR 1590, 1305, 1290, 1260, 1170, 965, 850, 840 cm^{-1}; ^{1}H NMR δ=0.14 (6H, s), 0.44 (6H, s), 2.42 (2H, s), 3.74 (2H, q, J=8.4 Hz), 3.88 (2H, q, J=8.4 Hz), 6.90—7.53 (4H, m). Found: C, 44.69; H, 5.69%. Calcd for $C_{15}H_{22}F_6O_2Si_2$: C, 44.54; H, 5.48%.

11: ^{1}H NMR δ=0.09 (6H, s), 0.31 (6H, s), 2.08 (2H, s), 6.9—7.4 (4H, m). Found: C, 59.38; H, 8.15%. Calcd for $C_{11}H_{18}OSi_2$: C, 59.41; H, 8.16%.

A solution of **2-Cl** (50 mg) in TFE (5 cm^3) was allowed to stand for 3 d at 25 °C. A crude oil (55 mg) obtained after usual workup was shown to be a mixture of 2,4-dimethyl-2,4-bis(2,2,2-trifluoroethoxy)-3-phenyl-2,4-disilapentane (**12**) and other two unidentified compounds in the GLC area ratio of 8:1:1.

12: ^{1}H NMR δ=0.13 (6H, s), 0.17 (6H, s), 1.73 (1H, s), 3.82 (4H, q, J=8.4 Hz), 6.82—7.32 (5H, m). Found: C, 45.01; H, 5.78%. Calcd for $C_{15}H_{22}F_6O_2Si_2$: C, 44.54; H, 5.48%.

The chloride **2-Cl** (420 mg) was heated in ethanol (25 cm^3) in the presence of triethylamine (185 mg) at 60 °C for 3 d. A crude oil obtained after usual workup was subjected to bulb-to-bulb distillation (130 °C, 3 Torr) to give 406 mg (81%) of 1-ethoxy-2-[o-(chloromethyl)phenyl]-1,1,2,2-tetramethyldisilane (**14**): IR 1250, 1105, 1075, 945, 830, 790, 765, 735 cm^{-1}; ^{1}H NMR δ=0.18 (6H, s), 0.44 (6H, s), 1.10 (3H, t, J=7.2 Hz), 3.54 (2H, q, J=7.2 Hz), 4.63 (1H, s), 7.04—7.56 (4H, m). Found: C, 54.72; H, 8.15%. Calcd for $C_{13}H_{23}ClOSi_2$: C, 54.42; H, 8.08%.

The chloride **2-Cl** (60 mg) was heated in 70% aq acetone (25 cm^3) at 70 °C for 4 d. A crude oil obtained after workup was subjected to chromatography over silica gel eluting with benzene to give 26 mg (40%) of 4-chloro-1,1,3,3-tetramethyl-1,3-disilaisochroman (**15**): Mp 77—78 °C; IR 1595, 1255, 1330, 1075, 990, 880, 855, 825, 790, 740 cm^{-1}; ^{1}H NMR δ=0.12 (3H, s), 0.33 (3H, s), 0.40 (3H, s), 4.18 (1H, s), 7.08—7.50 (4H, m). Found: C, 51.44; H, 6.61%. Calcd for $C_{11}H_{17}ClOSi_2$: C, 51.44; H, 6.67%.

Reactions of 1a-Br, 1b-Cl, and 2-Cl with $LiAlH_4$: A reaction of **1a-Br** (1.10 g) with $LiAlH_4$ (0.3 g) in THF (25 cm^3) (room temperature, 1 h) gave 672 mg (82%) of benzylpentamethyldisilane (**1a-H**): Bp 125—126 °C (22 Torr); IR 1600, 1250, 835, 805, 785, 695 cm^{-1}; ^{1}H NMR δ=0.0 (15H, almost s), 2.11 (2H, s), 6.75—7.30 (5H, s). Found: C, 64.77; H, 9.91%. Calcd for $C_{12}H_{22}Si_2$: C, 64.80; H, 9.97%. A reaction of **1b-Cl** with $LiAlH_4$ in THF cleanly gave **1b-H**: ^{1}H NMR δ=0.0 (15H, s), 2.06 (2H, s), 2.27 (3H, s), 6.67—7.14 (4H, m). Found: C, 65.80; H, 10.03%. Calcd for $C_{13}H_{24}Si$: C, 66.02; H, 10.23%.

A reaction of **2-Cl** (471 mg) with $LiAlH_4$ (100 mg) in THF (5 cm^3) gave 1,1,2,2-tetramethyl-1,2-disilaindan (**2-H**)[6] (353 mg, 87%).

Oxidation of 2-Cl: A solution of **2-Cl** (150 mg) in carbon tetrachloride (20 cm^3) was heated at 70 °C for 2 h, while a slow stream of oxygen being bubbled into the solution. Solvent was removed and the residue was recrystallized from pentane to give 123 mg (83%) of **15**.

Thermolysis of 1-Cl: **1a-Cl** was heated to 150 °C for 1 h in a glass ampoule. ^{1}H NMR analysis indicated clean formation of 1-chloro-2,4-dimethyl-3-phenyl-2,4-disilapentane (**9a-Cl**):

IR 1250, 1200, 1030, 840, 800, 700 cm^{-1}; ^1H NMR δ=0.07 (9H, s), 0.35 (6H, s), 1.73 (1H, s), 6.86—7.24 (5H, m). Similarly, **1e-Cl** cleanly gave **9e-Cl** on heating to 150 °C: IR 1250, 1190, 1030, 860, 830, 800, 780 cm^{-1}; ^1H NMR δ=0.06 (9H, s), 0.34 (6H, s), 1.67 (1H, s), 2.27 (3H, s), 6.72—7.05 (4H, m). Reduction of **9b-Cl** with $LiAlH_4$ in ether gave the corresponding hydrosilane **9b-H:** IR 2110, 1250, 1030, 890, 850, 830 cm^{-1}; ^1H NMR δ=0.04 (3H, s, J=3.6 Hz), 0.0 (9H, s), 0.05 (3H, d, J=3.6 Hz), 1.39 (1H, d, J=3.6 Hz), 2.23 (3H, s), 3.87—4.23 (1H, m), 6.61—7.04 (4H, m). Found: C, 65.55; H, 10.17%. Calcd for $C_{12}H_{24}Si_2$: C, 66.02; H, 10.23%.

This work was supported by a Grant-in-Aid for Scientific Research No. 01470025 from the Ministry of Education, Science and Culture.

References

1) Part II, N. Shimizu, S. Watanabe, and Y. Tsuno, *Bull. Chem. Soc. Jpn.*, **64**, 2249 (1991).

2) A part of this work has been already published: N. Shimizu, C. Kinoshita, and Y. Tsuno, *Chem. Lett.*, **1990**, 1937.

3) H. Bock and B. Solouki, "The Chemistry of Organic Silicon Compounds," ed by S. Patai and Z. Rappoport, John Wiley & Sons, New York (1989), Part I, Chap. 9, p. 555.

4) H. Sakurai, M. Kira, and T. Uchida, *J. Am. Chem. Soc.*, **95**, 6826 (1973).

5) H. Sakurai and M. Kumada, *Bull. Chem. Soc. Jpn.*, **37**, 1894 (1964); H. Gilman, W. H. Atwell, and G. L. Schwebke, *J. Organomet. Chem.*, **2**, 371 (1964); C. G. Pitt, *J. Am. Chem. Soc.*, **91**, 6613 (1969); H. Bock and H. Alt., *ibid.*, **92**, 1569 (1970); V. I. Khvostenko, B. G. Zykov, V. P. Yuriev, V. F. Mironov, G. I. Kovelzon, A. A. Panasenko, V. D. Sceludyakov, and I. A. Gailyunas, *J. Organomet. Chem.*, **218**, 155 (1981).

6) H. Sakurai, S. Tasaka, and M. Kira, *J. Am. Chem. Soc.*, **94**, 9285 (1972).

7) a) M. A. Cook, C. Eaborn, and D. R. M. Walton, *J. Organomet. Chem.*, **23**, 85 (1970); b) A. R. Bassindale, C. Eaborn, D. R. M. Walton, and D. J. Young, *ibid.*, **20**, 49 (1969).

8) a) M. Kumada, K. Tamao, M. Ishikawa, and M. Matsuno, *J. Chem. Soc., Chem. Commun.*, **1968**, 614; b) M. Kumada and M. Ishikawa., *J. Organomet. Chem.*, **1**, 411 (1964); c) M. Kumada, M. Ishikawa, and K. Tamao, *ibid.*, **5**, 226 (1966); d) K. Tamao and M. Kumada, *ibid.*, **30**, 349 (1971).

9) J. B. Lambert, G.-t, Wang, R. B. Finzel, and D. H. Teramura, *J. Am. Chem. Soc.*, **109**, 7838 (1987); J. B. Lambert and G.-t. Wang, *J. Phys, Org. Chem.*, **1**, 169 (1989); J. B. Lambert and E. C. Chelius, *J. Am. Chem. Soc.*, **112**, 8120 (1990).

10) X. Li and J. A. Stone, *J. Am. Chem. Soc.*, **111**, 5586 (1989).

11) J. Yoshida, T. Maekawa, T. Murata, S. Matsunaga, and S. Isoe, *J. Am. Chem. Soc.*, **112**, 1962 (1990).

12) S. G. Wierschke, J. Chandrasekhar, and W. L. Jorgensen, *J. Am. Chem. Soc.*, **107**, 1496 (1985); M. R. Ibrahim and W. L. Jorgensen, *ibid.*, **111**, 819 (1989).

13) Y. Apeloig, "The Chemistry of Organic Silicon Compounds," ed by S. Patai and Z. Rappoport, John Wiley & Sons, Chichester (1989), Part 1, Chap. 2.

14) N. Shimizu, E. Osajima, and Y. Tsuno, *Bull. Chem. Soc. Jpn.*, **64**, 1145 (1991).

15) T. W. Bentley and G. E. Carter, *J. Am. Chem. Soc.*, **104**, 5741 (1982).

16) F. L. Schadt, T. W. Bentley, and P. v. R. Schleyer, *J. Am. Chem. Soc.*, **98**, 7667 (1976); M. Fujio, M. Goto, K. Funatsu, Y. Tsuji, S. Ouchi, and Y. Tsuno, *Mem. Fac. Sci., Kyushu Univ., Ser. C*, **16(1)**, 85 (1987).

17) Y. Yukawa and Y. Tsuno, *Bull. Chem. Soc. Jpn.*, **32**, 971 (1959); Y. Yukawa, Y. Tsuno, and M. Sawada, *ibid.*, **39**, 5741 (1966).

18) Y. Apeloig and A. Stanger, *J. Am. Chem. Soc.*, **107**, 2806 (1985).

19) R. A. Y. Jones, "Physical and Mechanistic Organic Chemistry," Cambridge Univ. Press, Cambridge (1979).

20) V. J. Shiner, Jr., W. E. Buddenbaum, B. L. Murr, and G. Lamaty, *J. Am. Chem. Soc.*, **90**, 418 (1968).

21) Y. Tsuno, Y. Kusuyama, M. Sawada, T. Fujii, and Y. Yukawa, *Bull. Chem. Soc. Jpn.*, **48**, 3337 (1975); S. Usui, Y. Shibuya, T. Adachi, M. Fujio, and Y. Tsuno, *Mem. Fac. Sci. Kyushu Univ., Ser. C*, **14(2)**, 355 (1984).

22) M. Fujio, M. Goto, A. Murata, Y. Tsuji, M. Mishima, and Y. Tsuno, *Mem. Fac. Sci. Kyushu Univ., Ser. C*, **16(2)**, 271 (1988).

23) T. G. Traylor, W. Hanstein, H. J. Berwin, N. A. Clinton, and R. S. Brown, *J. Am. Chem. Soc.*, **93**, 5715 (1971).

24) The gas-phase data[25] suggest that trialkylsilylenium ions are as stable as 1-methyl-1-phenylethyl cation, while the solvolysis data suggest the stability of **19** to be comparable to 1-phenylethyl cation.

25) S. K. Shin and J. L. Beauchamp, *J. Am. Chem. Soc.*, **111**, 900 (1989).

26) G. Baddeley, J. Chadwick, and H. T. Taylor, *J. Chem. Soc.*, **1954**, 2405; H. Tanida and H. Matumura, *J. Am. Chem. Soc.*, **95**, 1586 (1972).

27) W. Kitching, H. A. Olszowg, G. M. Drew, and W. Adcock, *J. Org. Chem.*, **47**, 5153 (1982); E. L. Eliel, N. L. Allinger, S. J. Angyal, and G. A. Morrison, "Conformational Analysis," Interscience, New York (1965).

28) M. Charton, *Progr. Phys. Org. Chem.*, **13**, 119 (1981).

29) H. Sakurai and M. Kira, *J. Am. Chem. Soc.*, **96**, 791 (1974).

30) G. Baddeley, J. W. Rasburn, and R. Rose, *J. Chem. Soc.*, **1958**, 3168.

Preparation of New Nitrogen-Bridged Heterocycles. 27.[1] First Syntheses of 1,3-Thiazino[6,5-*b*]indolizine Derivatives

Akikazu KAKEHI,* Suketaka ITO, Tosio SAKURAI,† Kunio URUSHIDO,†
Hidetoshi ISAWA, and Manabu ENOMOTO
Department of Chemistry and Material Engineering, Faculty of Engineering,
Shinshu University, Wakasato, Nagano 380
† Department of Chemistry, Faculty of Education, Shinshu University, Nishinagano, Nagano 380
(Received April 24, 1991)

Potassium 2-indolizinethiolates, generated in situ from the treatment of dialkyl 2-[(2-ethoxycarbonylethyl)thio]indolizine-1,3-dicarboxylates with potassium *t*-butoxide in *N*,*N*-dimethylformamide, reacted smoothly with various isothiocyanates and isocyanates with the elimination of alkoxide ions to give new heterocyclic compounds, alkyl 4(3*H*)-oxo-2-thioxo- and 2,4(3*H*)-dioxo-2*H*-1,3-thiazino[6,5-*b*]indolizine-10-carboxylates, in moderate to good yields. The structures of these 1,3-thiazino[6,5-*b*]indolizine derivatives were determined mainly by elemental analyses and spectral inspections, and the structural assignment was finally confirmed by the single crystal X-ray analyses of two compounds.

Recently, we reported the simple and convenient syntheses of various indolizine derivatives possessing an active methylene group at the 2-position and electron-withdrawing groups at the 1- and 3-positions and their smooth intramolecular cyclizations to the corresponding thieno[3,2-*a*]- and thieno[2,3-*b*]indolizine derivatives in the presence of a base.[2] In particular, potassium 2-indolizinethiolate derivatives[2c] generated in situ by the treatment of the corresponding 2-[(2-ethoxycarbonylethyl)thio]- or 2-[(2-cyanoethyl)thio]indolizines with potassium *t*-butoxide were key intermediates for the syntheses of these polyfunctionalized indolizines and thiophene-fused indolizines, and their very high reactivities toward various alkylating agents were shown.[2d] The ready availability, high nucleophilicity, and wide structural versatility of these potassium 2-indolizinethiolate derivatives promped us to investigate further their reactivity toward some heterocumulenes which are well known as reactive electrophilic species.[3] In this paper, we wish to report the reactions of 2-indolizinethiolate derivatives with some isothiocyanates and isocyanates, affording new heterocycles, 2-thioxo-2*H*-1,3-thiazino[6,5-*b*]indolizin-4(3*H*)-one and 2*H*-1,3-thiazino[6,5-*b*]indolizine-2,4(3*H*)-dione derivatives.

Results and Discussion

Reactions of Potassium 2-Indolizinethiolates with Isothiocyanates and Isocyanates. The treatment of dialkyl 2-[(2-ethoxycarbonylethyl)thio]indolizine-1,3-dicarboxylates (**1a**—**e**)[2c] with potassium *t*-butoxide in *N*,*N*-dimethylformamide (DMF) at 60—70 °C, the removal of the ethyl acrylate generated, and the addition of methyl isothiocyanate (**3a**) to the resulting potassium 2-indolizinethiolate derivatives (**2a**—**e**) afforded ethyl or *t*-butyl 3-methyl-4(3*H*)-oxo-2-thioxo-2*H*-1,3-thiazino-[6,5-*b*]indolizine-10-carboxylates (**4a**—**e**) in 41—97% yields. Similar reactions of indolizine derivatives **1a**—**d** with ethyl isothiocyanate (**3b**), phenyl isothiocyanate (**3c**), and allyl isothiocyanate (**3d**) gave the corresponding 4(3*H*)-oxo-2-thioxo-2*H*-1,3-thiazino[6,5-*b*]indolizine derivatives **4f**—**q** in moderate to good yields. The reactions of **2a**—**e** with ethyl isocyanate (**3e**), and propyl isocyanate (**3f**) also provided the expected products, alkyl 3-ethyl- or 3-propyl-2,4(3*H*)-dioxo-2*H*-1,3-thiazino[6,5-*b*]indolizine-10-carboxylates **4r**—**v**, **x**—**a′**, except compound **4w**. Interestingly, no product such as 4(3*H*)-oxo-2-thioxo- or 2,4(3*H*)-dioxo-2*H*-1,3-thiazino[5,6-*a*]indolizine **5** was formed even in the reactions of heterocumulenes **3a**—**f** with dialkyl 6,8-dimethylindolizine-1,3-dicarboxylates (**1d**, **e**), in which the reactivity of the 1-alkoxycarbonyl group is fairly enhanced owing to the steric hindrance of the 8-methyl group at the peri-position (Scheme 1).[2b,d] On the other hand, the reactions of indolizines **1f**, **g** having a cyano or an acetyl group at the 1- or 3-position with reagents **3a**—**f** did not afford any products such as **7** and **8** under the reaction conditions employed here, and only the deprotected 2-indolizinethiols **6a**, **b** were obtained in 64 and 71% yields, respectively. The reactions of 2-indolizinethiols **6a**, **b**, obtained in this reaction, with **3a**—**f** were also unsuccessful. (Scheme 2)

Furthermore, any condensation products were not given in the reactions of **1a**, **b** with phenylketene and dichloroketene generated in situ by the addition of phenylacetyl chloride or dichloroacetyl chloride to the reaction mixtures.

The structural assignments for the products **4a**—**v**,**x**—**a′** were accomplised mainly by their elemental and spectral analyses and mechanistic considerations. For example, their elemental analyses coincided well with the compositions for our proposed structures and their IR spectra (see Table 5) distinctly showed the carbonyl absorption bands due to an aromatic ester and an amide group in the ranges of 1659—1721 and 1637—1664 cm^{-1}, respectively. The ^1H NMR spectra (Table 1) of **4a**—**v**, **x**—**a′** showed the presence of an alkyl, allyl, or phenyl group derived from isothiocyanates **3a**—**d** or isocyanates **3e**, **f** employed here, and the absence of an ethoxyl group of two ester alkoxyl groups which were present at the 1-

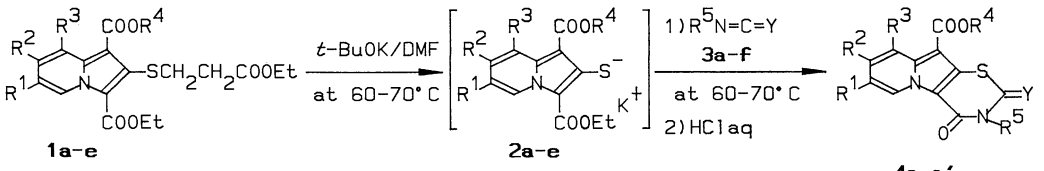

1	R^1	R^2	R^3	R^4
a	H	H	H	Et
b	H	Me	H	Et
c	H	Et	H	Et
d	Me	H	Me	Et
e	Me	H	Me	*t*-Bu

3	R^5	Y
a	Me	S
b	Et	S
c	Ph	S
d	Allyl	S
e	Et	O
f	Pr	O

4	R^1	R^2	R^3	R^4	R^5	Y
a	H	H	H	Et	Me	S
b	H	Me	H	Et	Me	S
c	H	Et	H	Et	Me	S
d	Me	H	Me	Et	Me	S
e	Me	H	Me	*t*-Bu	Me	S
f	H	H	H	Et	Et	S
g	H	Me	H	Et	Et	S
h	H	Et	H	Et	Et	S
i	Me	H	Me	Et	Et	S
j	H	H	H	Et	Ph	S
k	H	Me	H	Et	Ph	S
l	H	Et	H	Et	Ph	S
m	Me	H	Me	Et	Ph	S
n	H	H	H	Et	Allyl	S
o	H	Me	H	Et	Allyl	S
p	H	Et	H	Et	Allyl	S
q	Me	H	Me	Et	Allyl	S
r	H	H	H	Et	Et	O
s	H	Me	H	Et	Et	O
t	H	Et	H	Et	Et	O
u	Me	H	Me	Et	Et	O
v	Me	H	Me	*t*-Bu	Et	O
(w)	H	H	H	Et	Pr	O
x	H	Me	H	Et	Pr	O
y	H	Et	H	Et	Pr	O
z	Me	H	Me	Et	Pr	O
a'	Me	H	Me	*t*-Bu	Pr	O

Scheme 1.

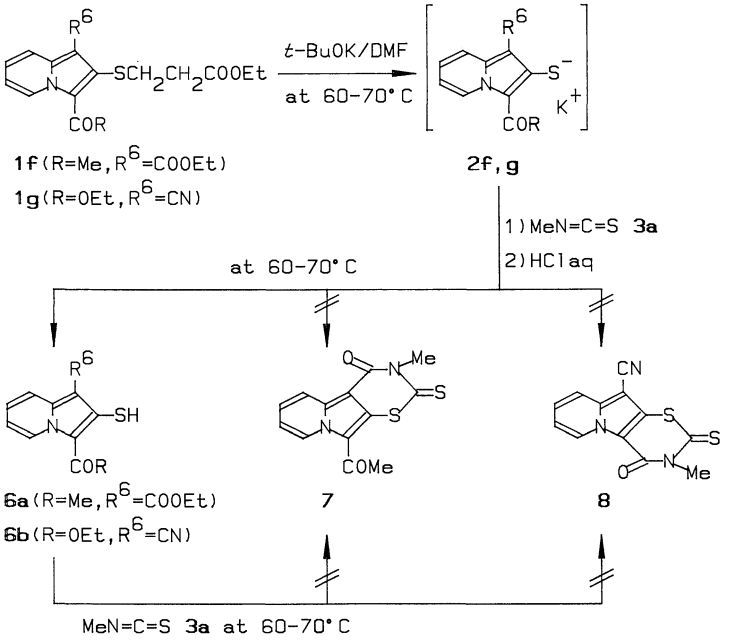

Scheme 2.

Table 1. ^{1}H NMR Spectral Data of 1,3-Thiazino[6,5-*b*]indolizines

No[a)]	C-6	C-7	C-8	C-9	R^6	R^5
4a	9.70	7.06	7.49	8.31	1.43 4.38	3.88
	br d	dt	br t	br d	t q	s
4b	9.48	6.87	2.47	8.00	1.42 4.36	3.83
	d	dd	s	br s	t q	s
4c	9.57	6.92	1.30 2.78	8.08	1.43 4.37	3.86
	d	dd	t q	br s	t q	s
4d	9.53	2.37	7.09	2.74	1.46 4.37	3.88
	br s	s	br s	s	t q	s
4e	9.59	2.38	7.11	2.74	1.66	3.91
	br s	s	br s	s	s	s
4f	9.74	7.11	7.53	8.35	1.47 4.43	1.37 4.73
	br d	dt	br t	br d	t q	t q
4g	9.52	6.92	2.49	8.08	1.43 4.38	1.33 4.72
	d	dd	s	br s	t q	t q
4h	9.56	6.94	1.31 2.80	8.08	1.43 4.36	1.31 4.68
	d	dd	t q	br s	t q	t q
4i	9.59	2.36	7.09	2.73	1.44 4.36	1.33 4.72
	br s	s	br s	s	t q	t q
4j	9.66	7.08	b)	8.40	1.48 4.45	7.1—7.7
	br d	dt		br d	t q	m
4k	9.51	6.91	2.49	8.17	1.44 4.42	7.1—7.7
	d	dd	s	br s	t q	m
4l	9.53	6.95	1.32 2.79	8.18	1.48 4.44	7.1—7.7
	d	dd	t q	br s	t q	m
4m	9.58	2.32	b)	2.80	1.47 4.42	7.0—7.7
	br s	s		s	t q	m
4n	9.66	7.05	7.48	8.27	1.43 4.38	5.0—5.5 5.6—6.4
	br d	dt	br t	br d	t q	m m
4o	9.48	6.87	2.47	8.01	1.42 4.38	5.0—5.5 5.6—6.4
	d	dd	s	br s	t q	m m
4p	9.53	6.92	1.32 2.80	8.07	1.44 4.38	5.0—5.5 5.6—6.4
	d	dd	t q	br s	t q	m m
4q	9.59	2.36	7.13	2.74	1.44 4.37	5.0—5.5 5.6—6.4
	br s	s	br s	s	t q	m m
4r	9.76	7.06	7.48	8.32	1.43 4.41	1.28 4.23
	br d	dt	br t	br d	t q	t q
4s	9.59	6.87	2.48	8.05	1.43 4.43	1.28 4.18
	d	dd	s	br s	t q	t q
4t	9.63	6.93	1.29 2.80	8.10	1.45 4.41	1.33 4.18
	d	dd	t q	br s	t q	t q
4u	9.57	2.31	7.00	2.68	1.41 4.32	1.26 4.14
	br s	s	br s	s	t q	t q
4v	9.59	2.34	7.02	2.71	1.65	1.27 4.17
	br s	s	br s	s	s	t q
4x	9.56	6.84	2.47	8.03	1.43 4.37	0.96 1.3—2.1 4.03
	d	dd	s	br s	t q	t m q
4y	9.61	6.88	1.31 2.79	8.08	1.44 4.36	0.96 1.3—2.1 4.06
	d	dd	t q	br s	t q	t m q
4z	9.59	2.34	7.06	2.72	1.44 4.37	0.97 1.3—2.1 4.06
	br s	s	br s	s	t q	t m q
4a′	9.59	2.32	7.01	2.69	1.67	0.98 1.3—2.1 4.04
	br s	s	br s	s	s	t m q

a) The coupling constants were as follows: $J_{6,7}=J_{7,8}=7.0$, $J_{8,9}=9.0$, $J_{6,8}=2.0$, and $J_{Et}=7.0$ Hz. b) Overlapped with the phenyl proton signals.

and 3-positions in starting indolizines **1a**—**e**. However, these considerations for products **4a**—**d**, **f**—**u**,**x**—**z**, except **4e**, **v**, **a′** which bear a *t*-butoxycarbonyl group, were not only true for the structures of the 1,3-thiazino[6,5-*b*]indolizines but also for an alternative structure, 1,3-thiazino[5,6-*a*]indolizine **5**. Finally, the structures of compounds **4a**—**d**, **f**—**u**, **x**—**z** were determined by analogy with the high reactivity of the 3-alkoxycarbonyl group superior to the 1-alkoxycarbonyl group[2d)] and confirmed by the X-ray analyses of compounds **4i**, **u** (see below).

Crystallography of 1,3-Thiazino[6,5-*b*]indolizines (4i,u).

Single crystals of ethyl 3-ethyl-7,9-dimethyl-4(3*H*)-

Table 2. Crystal and Structure Analysis Data of Compounds **4i**, **u**

	4i	**4u**
Formula	$C_{17}H_{18}N_2O_3S_2$	$C_{17}H_{18}N_2O_4S$
Formula weight	362.46	346.40
Crystal system	Monoclinic	Triclinic
Space group	$P2_1/a$; Z=4	$P\bar{1}$; Z=2
Lattice parameters		
a/Å	7.514 (3)	9.788 (6)
b/Å	19.469 (4)	10.571 (10)
c/Å	11.666 (4)	8.324 (10)
α/°	90	103.63 (11)
β/°	97.1 6 (3)	101.27 (8)
γ/°	90	87.74 (6)
V/Å^3	1693.4 (9)	820.9 (14)
D_{calcd}/g cm^{-3}	1.422	1.401
Crystal size/mm^3	0.12×0.08×0.80	0.10×0.10×0.60
Diffractometer	Rigaku AFC5S	Rigaku AFC5S
Radiation	Mo$K\alpha$ (λ=0.71069 Å)	Mo$K\alpha$ (λ=0.71069 Å)
Monochrometer	Graphite	Graphite
Scan type	ω–2θ	ω–2θ
2θ Max	55.0°	55.1°
Computer program	TEXSAN System[a)]	TEXSAN System[a)]
Structure solution	Direct method; SIR[b)]	Direct method; SIR[b)]
Hydrogen atom treatment	Calculated, not refined	Calculated, not refined
Refinement	Full-matrix, anisotropic	Full-matrix, anisotropic
Least-squares weight	$4F_o^2/\sigma^2$ (F_o^2)	$4F_o^2/\sigma^2$ (F_o^2)
No. of measurement ref.	Total: 4311, Unique: 4017	Total: 3981, Unique: 3750
No. of observations[c)]	1152	1932
No. of variables	217	217
Residuals R; R_w	0.062; 0.067	0.066; 0.079
Max Shift/Error	0.15	0.17
$\Delta\rho_{max}$/e$^-$ Å^{-3}	0.31	0.45

a) See Ref. 6. b) See Ref. 7. c) $I<3.00\sigma(I)$.

Table 3. Atomic Coordinates (×10^3) and Equivalent Temperature Factors for Non-Hydrogen Atoms in Compound **4i** (esd's, where given, are in parentheses)

Atom	x	y	z	B_{eq}[a)]/Å^2
S1	−66.1 (3)	190.7 (1)	−119.6 (2)	4.0 (1)
S2	−121.6 (3)	244.4 (2)	97.8 (2)	5.8 (1)
O1	−35.3 (9)	410.1 (3)	−211.4 (5)	5.4 (3)
O2	104 (1)	83.6 (4)	−428.9 (7)	8.3 (5)
O3	−38.8 (9)	85.9 (3)	−274.5 (6)	5.8 (4)
N1	31.7 (8)	305.0 (4)	−378.1 (6)	3.6 (4)
N2	−83 (1)	328.5 (4)	−77.6 (7)	4.2 (4)
C1	−87 (1)	264.1 (5)	−35.0 (7)	3.6 (4)
C2	−41 (1)	348.8 (5)	−189.7 (8)	4.0 (5)
C3	−12 (1)	294.2 (4)	−266.4 (7)	3.1 (4)
C4	54 (1)	366.3 (5)	−431.9 (9)	4.5 (5)
C5	98 (1)	367.1 (5)	−542.2 (8)	4.4 (5)
C6	116 (1)	303.8 (6)	−595.9 (7)	4.3 (5)
C7	94 (1)	242.4 (5)	−548.2 (7)	3.6 (5)
C8	53 (1)	240.5 (5)	−431.8 (8)	3.6 (4)
C9	21 (1)	190.7 (5)	−349.1 (7)	3.5 (4)
C10	−21 (1)	225.2 (4)	−250.1 (7)	3.1 (4)
C11	128 (2)	435.2 (6)	−598.8 (9)	7.1 (6)
C12	109 (1)	178.3 (5)	−615.6 (8)	5.2 (5)
C13	35 (1)	115.8 (5)	−359 (1)	5.0 (6)
C14	−28 (2)	10.9 (6)	−270 (1)	9.0 (8)
C15	−91 (2)	−13.8 (7)	−179 (1)	12 (1)
C16	−113 (1)	386.2 (5)	0.6 (8)	5.4 (5)
C17	57 (2)	414.5 (5)	59.3 (9)	6.9 (6)

a) $B_{eq}=\frac{8\pi^2}{3}\sum_{i=1}^{3}\sum_{j=1}^{3}U_{ij}a_i^*a_j^*\boldsymbol{a}_i\cdot\boldsymbol{a}_j$.

Table 4. Atomic Coordinates (×10^3) and Equivalent Temperature Factors for Non-Hydrogen Atoms in Compound **4u** (esd's, where given, are in parentheses)

Atom	x	y	z	B_{eq}[a)]/Å^2
S1	712.1 (1)	83.6 (1)	497.5 (2)	3.31 (5)
O1	909.4 (4)	−42.9 (4)	632.6 (5)	4.7 (2)
O2	625.9 (4)	−327.4 (3)	220.4 (5)	4.1 (2)
O3	552.9 (5)	289.9 (3)	439.6 (5)	5.1 (2)
O4	376.7 (4)	297.2 (3)	228.3 (5)	4.5 (2)
N1	437.8 (4)	−120.1 (4)	134.4 (5)	2.6 (1)
N2	760.4 (4)	−181.6 (4)	428.9 (5)	3.3 (2)
C1	804.7 (5)	−58.5 (5)	524.4 (7)	3.3 (2)
C2	644.2 (5)	−213.5 (5)	296.5 (6)	2.9 (2)
C3	558.3 (5)	−108.2 (4)	259.5 (6)	2.5 (2)
C4	381.5 (5)	−234.6 (5)	27.3 (6)	3.0 (2)
C5	263.7 (6)	−230.7 (5)	−87.2 (7)	3.6 (2)
C6	201.0 (5)	−111.3 (5)	−91.1 (6)	3.3 (2)
C7	252.7 (5)	4.5 (5)	15.6 (6)	2.9 (2)
C8	378.5 (5)	1.2 (4)	133.1 (6)	2.5 (2)
C9	467.3 (5)	93.0 (5)	261.4 (6)	2.7 (2)
C10	574.0 (5)	23.0 (5)	335.3 (6)	2.6 (2)
C11	201.4 (7)	−353.2 (6)	−206.9 (8)	5.1 (3)
C12	171.4 (6)	126.7 (5)	3.5 (7)	3.8 (2)
C13	469.2 (6)	235.0 (5)	317.8 (7)	3.4 (2)
C14	380.9 (7)	438.3 (6)	281 (1)	6.0 (3)
C15	260.6 (8)	488.9 (6)	184 (1)	6.6 (3)
C16	849.3 (6)	−290.2 (6)	464.9 (7)	4.1 (2)
C17	961.9 (6)	−317.9 (6)	360.8 (9)	5.7 (3)

a) $B_{eq}=\frac{8\pi^2}{3}\sum_{i=1}^{3}\sum_{j=1}^{3}U_{ij}a_i^*a_j^*\boldsymbol{a}_i\cdot\boldsymbol{a}_j$.

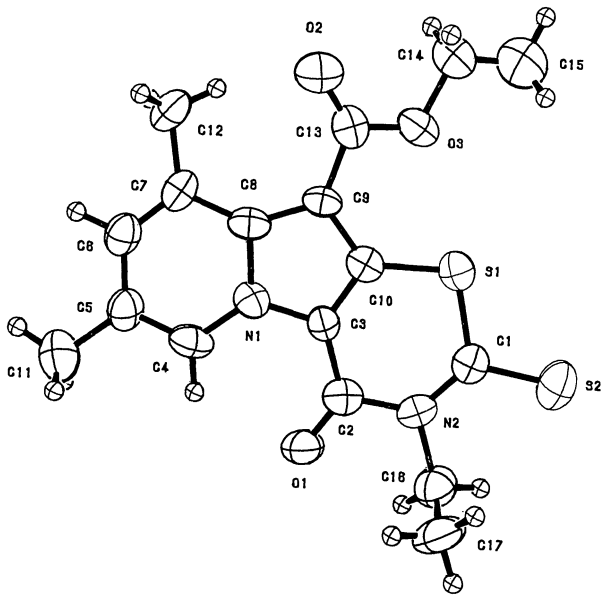

Fig. 1. ORTEP drawing of 4(3*H*)-oxo-2-thioxo-2*H*-1,3-thiazino[6,5-*b*]indolizine derivative **4i** showing the atom labeling scheme and 50% probability thermal ellipsoids.

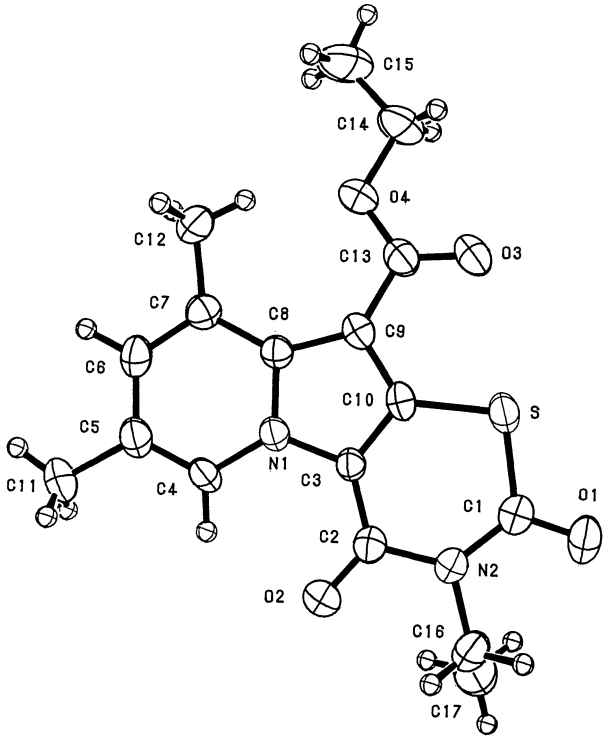

Fig. 2. ORTEP drawing of 2,4(3*H*)-dioxo-2*H*-1,3-thiazino[6,5-*b*]indolizine derivative **4u** showing the atom labeling scheme and 50% probability thermal ellipsoids.

oxo-2-thioxo- (**4i**) and ethyl 3-ethyl-7,9-dimethyl-2,4-(3*H*)-dioxo-2*H*-1,3-thiazino[6,5-*b*]indolizine-10-carboxylate (**4u**) were grown from their ethanolic solutions, respectively. A yellow monoclinic crystal for **4i** and a white triclinic crystal for **4u** were used for structure determinations. Crystal data and details of structure analyses are shown in Tables 2—4.[4] The ORTEP drawings[5] of compounds **4i**, **u** are shown in Figs. 1 and 2, respectively. Interestingly, the only difference between the structures of **4i**, **u** was observed in the conformations of their 10-ethoxycarbonyl groups, but the reason for their different packings in the crystal lattices is still unclear.

Reaction Mechanisms. These reactions were considered to proceed via the nucleophilic attack of 2-indolizinethiolate derivatives **2a**—**e** on the central carbon of heterocumulenes **3a**—**f** followed by the intramolecular nucleophilic reaction of the resulting intermediate, such as **9a**, with the elimination of an ethoxide ion. (See Scheme 3) As has been described in the transformations of 8-unsubstituted diethyl 2-(substituted methylthio)indolizine-1,3-dicarboxylates to 3-hydroxythieno[2,3-*b*]indolizines, the exclusive formation of 1,3-thiazino[6,5-*b*]indolizine derivatives **4a**—**c**, **f**—**h**, **j**—**l**,**n**—**p**, **r**—**t**, **x**, **y** from the reactions of 8-unsubstituted 2-indolizinethiolates **2a**—**c** with heterocumulenes **3a**—**f** was easily supported owing to the higher reactivity of the 3-alkoxycarbonyl group over the 1-alkoxycarbonyl group.[2b,d] However, the unavailability of 1,3-thiazino[5,6-*a*]indolizine derivatives, such as **5**, in the reactions of 6,8-dimethyl-2-indolizinethiolates **2d**, **e**, whose 1-alkoxycarbonyl group is activated by the steric hindrance of the 8-methyl group at the peri position, with **3a**—**f** was mysterious. The examination of the molecule of **5** using Dreiding models clearly showed the presence of severe repulsive interaction between the 4-oxo oxygen and the 8-methyl group. In order to avoid an unfavorable interaction like this, the exclusive intramolecular nucleophilic attack of the nitrogen anion to the carbonyl carbon of the 3-position could have occurred. On the other hand, the reason why some reactions of **2** with ketenes were unsuccessful is still unclear, but it may have been attributable in part to the bulkiness of these ketenes against the approach to the thiolate anion **2**.

In conclusion, the reactions of potassium 2-indolizinethiolate derivatives **2a**—**e** with some heterocumulenes **3a**—**f** was found to be a useful method for the preparation of new condensed indolizine derivatives.

Experimental

Melting points were measured with a Yanagimoto micromelting point apparatus and were not corrected. The microanalyses were carried out on a Perkin-Elmer 240 elemental analyzer. The ^{1}H NMR spectra were determined with a Varian EM360A spectrometer in deuteriochloroform with tetramethylsilane as an internal standard and the chemical

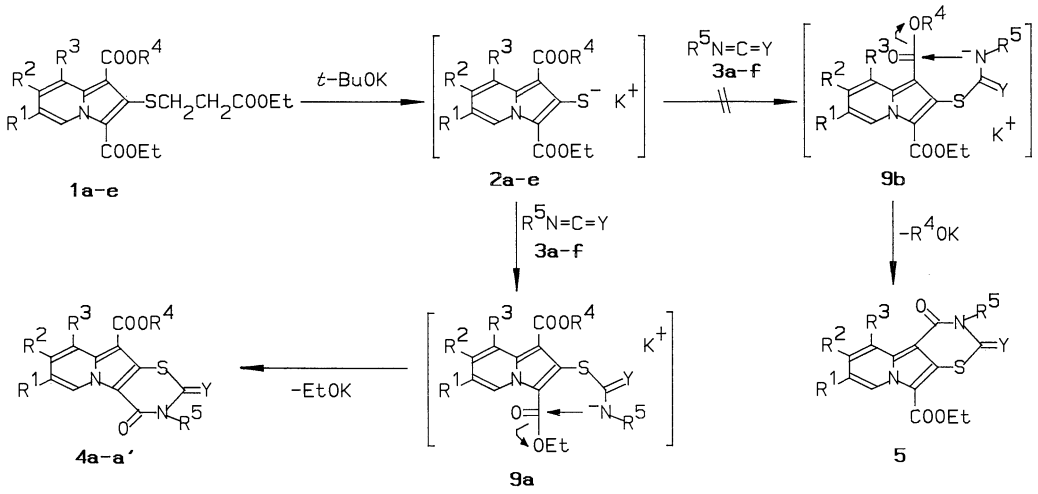

Scheme 3.

shifts are expressed in δ values. The IR spectra were taken with a Hitachi 260-10 infrared spectrophotometer.

Reaction of Indolizines with Isothiocyanates and Isocyanates in the Presence of Base. General Method. A solution of a dialkyl 2-[(2-ethoxycarbonylethyl)thio]indolizine-1,3-dicarboxylate (**1**, 1 mmol) in 2 ml of DMF was treated with potassium *t*-butoxide (0.168 g, 1.5 mmol) at 60—70 °C in a water bath for 1 h, and ethyl acrylate generated in this reaction was removed completely by a rotatory evaporator under reduced pressure. An isothiocyanate or isocyanate (**3**, 1.2 mmol) was added to the mixture and the resulting solution was allowed to react at 60—70 °C for an additional 2 h. The reaction mixture was acidified with diluted hydrochloric acid and water was then added to bring the total volume to 30 ml. The precipitates were colleted by filtration. The precipitates were then dissolved in 30 ml of chloroform and water was removed from the solution by filtration through phase-separating filter paper. The filtrate was concentrated under reduced pressure and the residue was separated by column chromatography on activated alumina using chloroform as an

Table 5. Some Data of the 1,3-Thiazino[6,5-*b*]indolizines

No[a]	React	Yield %	Mp °C	ν (KBr) cm^{-1}	Formula[b]
4a	**1a 3a**	80	234—237	1699 1657	$C_{14}H_{12}N_2O_3S_2$
4b	**1b 3a**	97	222—224	1692 1655	$C_{15}H_{14}N_2O_3S_2$
4c	**1c 3a**	41	199—201	1676 1657	$C_{16}H_{16}N_2O_3S_2$
4d	**1d 3a**	71	211—212	1718 1660	$C_{16}H_{16}N_2O_3S_2$
4e	**1e 3a**	55	232—235	1708 1661	$C_{18}H_{20}N_2O_3S_2$
4f	**1a 3b**	68	183—186	1700 1656	$C_{15}H_{14}N_2O_3S_2$
4g	**1b 3b**	82	232—235	1699 1650	$C_{16}H_{16}N_2O_3S_2$
4h	**1c 3b**	41	181—184	1694 1647	$C_{17}H_{18}N_2O_3S_2$
4i	**1d 3b**	48	210—213	1718 1659	$C_{17}H_{18}N_2O_3S_2$
4j	**1a 3c**	16	281—283	1696 1660	$C_{19}H_{14}N_2O_3S_2$
4k	**1b 3c**	19	280—283	1690 1657	$C_{20}H_{16}N_2O_3S_2$
4l	**1c 3c**	17	245—249	1693 1660	$C_{21}H_{18}N_2O_3S_2$
4m	**1d 3c**	22	283—285	1721 1661	$C_{21}H_{18}N_2O_3S_2$
4n	**1a 3d**	25	149—151	1690 1653	$C_{16}H_{14}N_2O_3S_2$
4o	**1b 3d**	61	152—155	1676 1653	$C_{17}H_{16}N_2O_3S_2$
4p	**1c 3d**	60	147—149	1691 1655	$C_{18}H_{18}N_2O_3S_2$
4q	**1d 3d**	55	172—174	1715 1663	$C_{18}H_{18}N_2O_3S_2$
4r	**1a 3e**	68	145—147	1696 1656	$C_{15}H_{14}N_2O_4S$
4s	**1b 3e**	86	188—190	1690 1661	$C_{16}H_{16}N_2O_4S$
4t	**1c 3e**	33	190—193	1691 1664	$C_{17}H_{18}N_2O_4S$
4u	**1d 3e**	42	178—181	1715 1662	$C_{17}H_{18}N_2O_4S$
4v	**1e 3e**	59	234—237	1720 1653	$C_{19}H_{22}N_2O_4S$
4x	**1b 3f**	67	159—161	1684 1660	$C_{17}H_{18}N_2O_4S$
4y	**1c 3f**	16	134—135	1698 1661	$C_{18}H_{20}N_2O_4S$
4z	**1d 3f**	34	187—188	1703 1655	$C_{18}H_{20}N_2O_4S$
4a′	**1e 3f**	34	190—191	1659 1637	$C_{20}H_{24}N_2O_4S$

a) Compounds **4a**—**q** were obtained as pale yellow needles and **4r**—**v**, **x**—**a′** as colorless needles.
b) Satisfactory analytical data (within 0.3% for C, H, and N) were obtained for all compounds.

eluent. Evaporation of the chloroform and recrystallization of the crude products from ethanol afforded the corresponding ethyl or *t*-butyl 4(3*H*)-oxo-2-thioxo- (**4a**—**q**) and 2,4(3*H*)-dioxo-2*H*-1,3-thiazino[6,5-*b*]indolizine-10-carboxylates (**4r**—**v**, **x**—**a'**). These results and some spectral data are summarized in Tables 1 and 5.

On the other hand, similar treatment of ethyl 3-acetyl-2-[(2-ethoxycarbonylethyl)thio]indolizine-1-carboxylate **1f** and ethyl 1-cyano-2-[(2-ethoxycarbonylethyl)thio]indolizine-3-carboxylate **1g** with methyl isothiocyanate **3a** gave only the corresponding 2-thiol derivatives, ethyl 3-acetyl-2-mercaptoindolizine-1-carboxylate (**6a**, mp 114—116 °C, 64% yield) and ethyl 1-cyano-2-mercaptoindolizine-3-carboxylate (**6b**, mp 130—131 °C, 71% yield), and did not afford any condensation products. Compounds **6a**, **b** were completely in accord with authentic samples in all respects.[2c] The 2-indolizinethiols **6a**, **b** did not react with reagents **3a**—**f** even under heating conditions.

The reactions of indolizines **1a**, **b** with ketene precursors such as phenylacetyl chloride and dichloroacetyl chloride under the alkaline conditions employed here were also unsuccessful.

References

1) For part 26 of this series, see A. Kakehi, S. Ito, T. Sakurai, and K. Urushido, *Chem. Pharm. Bull.*, **39**, 1949 (1991).

2) a) A. Kakehi, S. Ito, S. Matsumoto, and Y. Morimoto, *Chem. Lett.*, **1987**, 2043; b) A. Kakehi, S. Ito, T. Fujii, Y. Morimoto, S. Matsumoto, and M. Shiohara, *Bull. Chem. Soc. Jpn.*, **62**, 119 (1989); c) A. Kakehi, S. Ito, N. Yamada, and K. Yamaguchi, *Bull. Chem. Soc. Jpn.*, **63**, 829 (1990); d) *idem.*, *Chem. Pharm. Bull.*, **38**, 1527 (1990).

3) R. Richter and H. Ulrich, "The Chemistry of Functional Groups. The Chemistry of Cyanate and Their Thio Derivatives II," ed by S. Patai, John Wiley & Sons, New York (1977), Chap. 17, pp. 619—818; L. Drobnica, P. Kristian, and J. Augustin, *ibid.*, Chap. 22, pp. 1003—1221; S. Ozaki, *Chem. Rev.*, **72**, 457 (1972).

4) Bond lengths, bond and torsion angles, and F_o-F_c tables are deposited as Document No. 8965 at the Office of the Editor of Bull. Chem. Soc. Jpn.

5) C. K. Johnson, ORTEPII, Report ORNL-5138. Oak Ridge National Laboratory, Oak Ridge, Tennessee (1976).

6) TEXSAN TEXRAY, Structure Analysis Package, Molecular Structure Corporation (1985).

7) M. C. Burla, M. Camalli, G. Cascarano, C. Giacovazzo, G. Polidori, R. Spagna, and D. Viterbo, *J. Appl. Crystallogr.*, **22**, 389 (1989).

Preparation of New Nitrogen-Bridged Heterocycles. 28.[1] First Syntheses of 1,3-Oxazino[6,5-*b*]indolizine Derivatives

Akikazu KAKEHI,* Suketaka ITO, Tosio SAKURAI,† Kunio URUSHIDO,†
Susumu HATANAKA, and Kouji SUGIURA
Department of Chemistry and Material Engineering, Faculty of Engineering,
Shinshu University, Wakasato, Nagano 380
† Department of Chemistry, Faculty of Education, Shinshu University,
Nishinagano, Nagano 380
(Received May 16, 1991)

The reactions of 2-[mercapto(methylthio)methylene]-2(3*H*)-indolizinones with alkyl isothiocyanates in the presence of potassium *t*-butoxide in *N*,*N*-dimethylformamide afforded new heterocycles, 3-alkyl-2*H*-1,3-oxazino-[6,5-*b*]indolizine-2,4(3*H*)-dithione derivatives, in moderate yields. On the other hand, their reactions with phenyl isothiocyanate did not afford the corresponding 2*H*-1,3-oxazino[6,5-*b*]indolizine-2,4(3*H*)-dithiones, although the reaction of 2-[mercapto(methylthio)methylene]-1-methyl-2(3*H*)-indolizinone with phenyl isothiocyanate gave 10-methyl-3-phenyl-2-phenylimino-2,3-dihydro-4*H*-1,3-oxazino[6,5-*b*]indolizine-4-thione in a very low yield (10%). The structures of these 2*H*-1,3-oxazino[6,5-*b*]indolizine-2,4(3*H*)-dithiones and the 2-phenylimino analogue were determined by inspections of their physical and spectral data and by a single crystal X-ray analysis of one of these compounds.

In previous work, we have documented that 3-(mercaptomethylene)-2(3*H*)-indolizinones reacted with some (acyl- or cyano-substituted)methyl halides in the presence of a base to give the corresponding new heterocycles, 8,8a-dihydro[1,4]thiazino[3,4,5-*cd*]indolizin-4(1*H*)-ones, which were formed via the smooth intramolelcular Michael addition of the resulting *S*-alkylated products.[2] The high nucleophilicity of the mercapto group in these molecules[2,3] and our recent success in the preparation of 2*H*-1,3-thiazino[6,5-*b*]indolizine derivatives from potassium 2-indolizinethiolates[1] prompted us to examine the reactions between these molecules and electron-poor heterocumulenes such as isocyanate and isothiocyanate. In contrast with the smooth *S*-alkylations of 3-(mercaptomethylene)-2(3*H*)-indolizinones, their reactions with alkyl or aryl isocyanates and isothiocyanates did not proceed under ordinary reaction conditions. They reacted only with isothiocyanates under more forceful conditions in the presence of a strong base, but the products were not the initially expected 5*H*-[1,3,5]thiadiazepino[6,5,4-*cd*]indolizine derivatives. In this paper we wish to report the first synthesis of 2*H*-1,3-oxazino[6,5-*b*]indolizine derivatives by the reactions of 3-[mercapto-(methylthio)methylene]-2(3*H*)-indolizinones with some isothiocyanates in the presence of a strong base.

Results and Discussion

Reactions of 3-[Mercapto(methylthio)methylene]-2(3*H*)-indolizinones with Some Isothiocyanates. Since the high reactivity of the mercapto group of 3-(mercaptomethylene)-2(3*H*)-indolizinone derivatives toward various alkylating agents in the presence of a base was clearly shown,[2,3] their reactions with unsaturated electrophiles such as isocyanates and isothiocyanates were initially expected to form the corresponding 5*H*-[1,3,5]thiadiazepino[6,5,4-*cd*]indolizine derivatives such as **4** (see Scheme 1) via the electrophilic attack of the reagent on the sulfur atom followed by the Michael addition of the resulting aminide ion to the 5-position on the indolizine ring. Hence, the reactions of 3-[mercapto(methylthio)methylene]-2(3*H*)-indolizinones (**1a**—**e**), readily available from the alkaline treatment of 2-(substutited methyl)pyridinium bromides, carbon disulfide, and dimethyl sulfate,[3] with some isocyanates and isothiocyanates were examined carefully under various reaction conditions, and we found that, although their reactions with isocyanates did not provide any significant products, those with isothiocyanates afforded significant amounts of products when a strong base, potassium *t*-butoxide, was present. The structures of the products, however, were different from the expected ones (**4**) (See below). When a mixture of 2(3*H*)-indolizinone **1a**—**e**, methyl isothiocyanate (**2a**), and potassium *t*-butoxide was allowed to react in DMF at 70—80 °C for 20 min, the title compounds, 3-methyl-2*H*-1,3-oxazino[6,5-*b*]indolizine-2,4(3*H*)-dithiones **3a**—**e**, were obtained in 10—77% yields as orange crystals. Similar reactions of **1a**—**e** with ethyl isothiocyanate (**2b**), allyl isothiocyanate (**2c**), propyl isothiocyanate (**2d**), and butyl isothiocyanate (**2e**) in the presence of potassium *t*-butoxide gave the corresponding crystalline products **3f**—**j**, **l**—**s** except **3k**, in moderate yields. These results are shown in Scheme 1. On the other hand, the reaction of 2(3*H*)-indolizinone **1b** with phenyl isothiocyanate (**2f**) in the presence of potassium *t*-butoxide at 70—80 °C for 2 h provided an alternative product, 10-methyl-3-phenyl-2-phenylimino-2,3-dihydro-4*H*-1,3-oxazino[6,5-*b*]indolizine-4-thione **5a**, in a low yield (10%). The reactions of **1a**, **c**—**e** with the same reagent **2f** did not give any products. Furthermore, the type of product such as **5f**—**h** could not be obtained by the reactions of 2*H*-1,3-

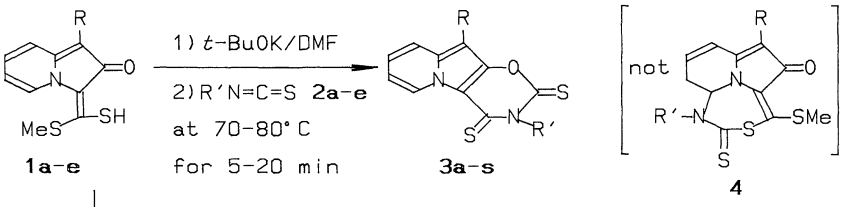

1	R
a	H
b	Me
c	Et
d	Ph
e	*p*-ClC$_6$H$_4$

2	R′
a	Me
b	Et
c	Allyl
d	Pr
e	Bu

3	R	R′
a	H	Me
b	Me	Me
c	Et	Me
d	Ph	Me
e	*p*-ClC$_6$H$_4$	Me
f	H	Et
g	Me	Et
h	Et	Et
i	Ph	Et
j	*p*-ClC$_6$H$_4$	Et

3	R	R′
(k)	H	Allyl
l	Me	Allyl
m	Et	Allyl
n	Ph	Allyl
o	*p*-ClC$_6$H$_4$	Allyl
p	Me	Pr
q	Ph	Pr
r	Me	Bu
s	Ph	Bu

Scheme 1.

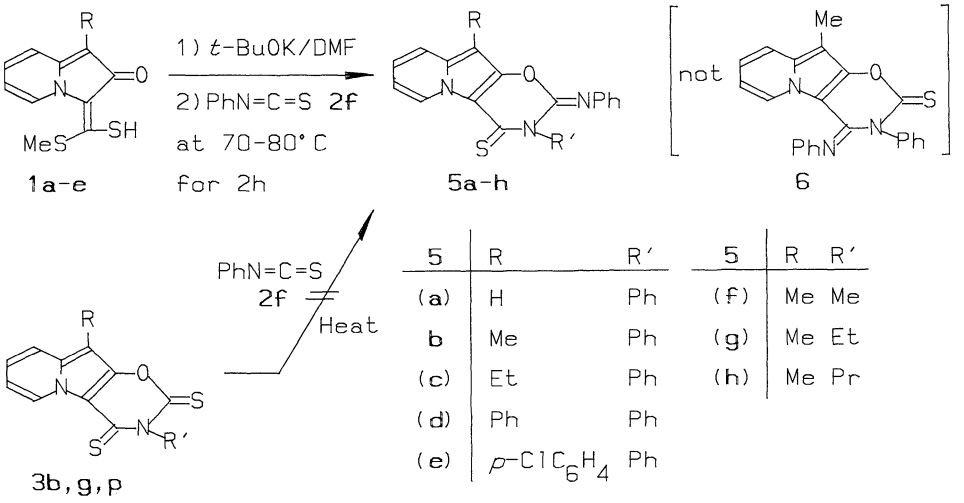

5	R	R′
(a)	H	Ph
b	Me	Ph
(c)	Et	Ph
(d)	Ph	Ph
(e)	*p*-ClC$_6$H$_4$	Ph

5	R	R′
(f)	Me	Me
(g)	Me	Et
(h)	Me	Pr

Scheme 2.

oxazino[6,5-*b*]indolizine-2,4(3*H*)-dithione (**3b**, **g**,**p**) with **2f**. (Scheme 2)

As described above, the structures of compounds **3a**—**s** were first considered to be 5*H*-[1,3,5]thiadiazepino-[6,5,4-*cd*]indolizin-5-one derivatives such as **4**, but their ^{1}H NMR (see Table 1) and mass spectra and elemental analyses clearly excluded this structure. For example, the ^{1}H NMR spectrum of compound **3a** showed only the signals due to the aromatic indolizine ring protons (δ=10.64 (1H, br d, J=7.0 Hz, 6-H), 7.2—7.7 (2H, m, 8-H and 9-H), 7.00 (1H, m, 7-H), and 6.25 (1H, s, 10-H)) and the *N*-methyl protons (δ=4.23 (3H, s)); any other signals attributable to the methylthio group were not present. The ^{1}H NMR spectra of the products **3a**—**j**, **l**—**s** were very similar to each other, and the mass spectra of **3a**,**b**,**d** and elemental analyses of **3a**—**j**, **l**—**s** were also in good accord with the proposed structures.

Furthermore, the X-ray analysis of a single crystal of 3,10-dimethyl-2*H*-1,3-oxazino[6,5-*b*]indolizine-2,4(3*H*)-dithione (**3b**) was performed and its structure was confirmed. The single crystal of this molecule **3b** was grown from an ethanolic solution. An orange monoclinic crystal for **3b** was used. Crystal data and details of the structure analysis are shown in Tables 2 and 3.[4] The ORTEP[5] drawing is shown in Fig. 1.

On the other hand, the structure of product **5b** was determined by elemental analysis and by spectral comparison with those of the 2*H*-1,3-oxazino[6,5-*b*]-

Table 1. ^{1}H NMR Spectral Data of 2*H*-1,3-Oxazino[6,5-*b*]indolizines

No[a)]	C-6	C-7	C-8	C-9	C-10	R
3a	10.64 br d	7.00 m	7.2—7.7 m		6.25 s	4.23 s
3b	10.63 br d	6.93 m	7.3—7.7 m		2.34 s	4.24 s
3c	10.52 br d	6.95 dt	7.1—7.7 m		1.26 t 2.80 q	4.18 s
3d	10.77 br d	7.05 dt	b)	7.87 br d	7.2—7.8 m	4.25 s
3e	10.72 br d	7.06 dt	b)	7.83 br d	7.2—7.8 m	4.24 s
3f	10.60 br d	7.00 m	7.2—7.7 m		6.22 s	1.44 t 5.10 q
3g	10.58 br d	7.00 dt	7.3—7.7 m		2.33 s	1.45 t 5.12 q
3h	10.58 br d	6.95 dt	7.2—7.7 m		1.29 t 2.80 q	1.40 t 5.08 q
3i	10.78 br d	7.06 dt	b)	7.88 br d	7.2—7.8 m	1.46 t 5.13 q
3j	10.50 br d	7.05 dt	b)	7.82 br d	7.2—7.8 m	1.42 t 5.14 q
3l	10.53 br d	6.95 dt	7.1—7.7 m		2.32 s	5.0—6.5 m
3m	10.62 br d	6.98 dt	7.1—7.7 m		1.26 t 2.80 q	5.0—6.5 m
3n	10.73 br d	7.03 dt	b)	7.87 br d	7.2—7.8 m	5.0—6.5 m
3o	10.72 br d	7.05 dt	b)	7.83 br d	7.2—7.8 m	5.0—6.5 m
3p	10.54 br d	6.95 dt	7.2—7.7 m		2.27 s	0.99 t 1.4—2.2 m 4.89 br t
3q	10.71 br d	7.02 dt	b)	7.84 br d	7.2—7.8 m	1.01 t 1.4—2.2 m 4.93 br t
3r	10.59 br d	6.96 dt	7.2—7.7 m		2.29 s	0.98 t 1.1—2.2 m 4.97 br t
3s	10.70 br d	7.01 dt	b)	7.83 br d	7.2—7.8 m	0.99 t 1.1—2.2 m 4.99 br t
5b	10.57 br d	b)	b)	b)	2.16 s	6.7—7.7 m

a) The coupling constants were as follows: $J_{6,7}=J_{7,8}=7.0$, $J_{8,9}=9.0$, $J_{6,8}=2.0$, and $J_{Et}=7.0$ Hz. b) Overlapped with the phenyl proton signals.

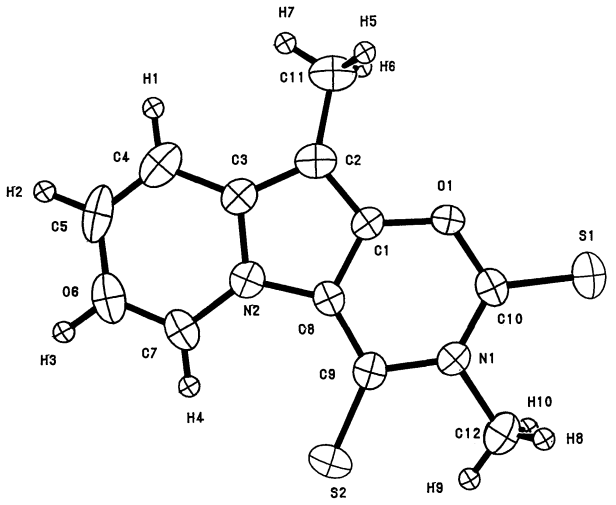

Fig. 1. ORTEP drawing of 3,10-dimethyl-2*H*-oxazino[6,5-*b*]indolizin-2,4(3*H*)-dithione (**3b**) showing the atom labeling scheme and 50% probability thermal ellipsoids.

indolizine-2,4(3*H*)-dithiones **3**. The mass spectrum (M^+ 383) and the elemental analysis of **5b** showed that the molecular formula was $C_{23}H_{17}N_3OS$ which corresponded to the subtraction of one mole of carbon disulfied from the 1:2 adduct between indolizinone **1b** and phenyl isothiocyanate (**2f**). The structural formula presumed from these findings and the mechanistic considerations was either 10-methyl-3-phenyl-2-phenylimino-2,3-dihydro-4*H*-1,3-oxazino[6,5-*b*]indolizine-4-thione **5b** or an alternative 4-phenylimino derivative **6**. The largely deshielded chemical shift (δ=10.57) attributable to the 6-H proton in **5b** was very similar to those (δ=10.53—10.78) of **3a—j**, **l—s**, indicating the similarity of the magnetic circumstances between them. Furthermore, the interpretation of the fragmentations in the mass spectra of **5b** and **3a,b,d** confirmed the structure of **5b**: The mass spectrum of **5b** exhibited *m/z* 383 (21%, M^+), 248 (13%, M^+—PhN=C=S), 189 (100%, M^+—PhN=C=NPh), 161 (3%, M^+—222), 105 (13%, M^+—278), and 78 (4%,

Table 2. Crystal and Structure Analysis Data of Compound **3b**

	3b
Formula	$C_{12}H_{10}N_2OS_2$
Formula weight	262.34
Crystal system	Monoclinic
Space group	$P2_1/m$; $Z=2$
Lattice parameters	
a/Å	9.094 (4)
b/Å	6.731 (4)
c/Å	9.859 (2)
β/°	103.47 (2)
V/Å^3	586.9 (4)
D_{calcd}/g cm^{-3}	1.484
Crystal size/mm^3	0.08×0.04×0.80
Diffractometer	Rigaku AFC5S
Radiation	Mo$K\alpha$ (λ=0.71069 Å)
Monochrometer	Graphite
Scan type	ω-2θ
2θ Max	55.0°
Computer program	TEXSAN System[a]
Structure solution	Direct method; MITHRIL[b]
Hydrogen atom treatment	Calculated, not refined
Refinement	Full-matrix, anisotropic
Least-squares weight	$4F_o^2/\sigma^2$ (F_o^2)
No. of measurement ref.	Total: 4311, Unique: 4017
No. of observations[c]	707
No. of variables	103
Residuals R; R_w	0.072; 0.107
Max Shift/Error	0.02
$\Delta\rho_{max}$/e$^-$ Å^{-3}	0.45

a) See Ref. 6. b) See Ref. 10. c) $I<3.00\sigma(I)$.

Table 3. Atomic Coordinates (×10^3) and Equivalent Temperature Factors of Compound **3b** (esd's, where given, are in parentheses)

Atom	x	y	z	B_{eq}[a]/Å^2
S1	−64.9 (4)	1/4	200.1 (4)	4.4 (2)
S2	509.1 (4)	1/4	149.5 (4)	4.3 (2)
O1	161.7 (8)	1/4	407.4 (8)	2.6 (4)
N1	228 (1)	1/4	194 (1)	2.7 (4)
N2	559 (1)	1/4	495 (1)	2.6 (4)
C1	310 (1)	1/4	473 (1)	2.5 (5)
C2	372 (1)	1/4	613 (1)	3.1 (6)
C3	529 (1)	1/4	627 (1)	2.6 (5)
C4	654 (2)	1/4	743 (2)	4.1 (7)
C5	795 (2)	1/4	725 (2)	4.3 (7)
C6	821 (1)	1/4	589 (2)	4.1 (7)
C7	706 (1)	1/4	478 (2)	3.4 (6)
C8	423 (1)	1/4	396 (1)	2.3 (5)
C9	387 (1)	1/4	250 (1)	3.1 (6)
C10	118 (1)	1/4	268 (1)	2.8 (6)
C11	292 (2)	1/4	729 (1)	4.1 (7)
C12	181 (2)	1/4	40 (2)	6(1)
H1	636.0	1/4	834.0	5.0
H2	878.2	1/4	804.4	5.2
H3	921.4	1/4	577.2	5.0
H4	723.8	1/4	386.0	4.0
H5	228.6	365.2	721.4	4.9
H6	228.6	134.8	721.4	4.9
H7	361.7	1/4	815.6	4.9
H8	117.8	364.1	9.2	7.6
H9	264.5	252.3	0.3	7.6
H10	120.7	133.6	9.0	7.6

a) $B_{eq}=\frac{8\pi^2}{3}\sum_{i=1}^{3}\sum_{j=1}^{3}U_{ij}a_i^*a_j^*\boldsymbol{a}_i\cdot\boldsymbol{a}_j$.

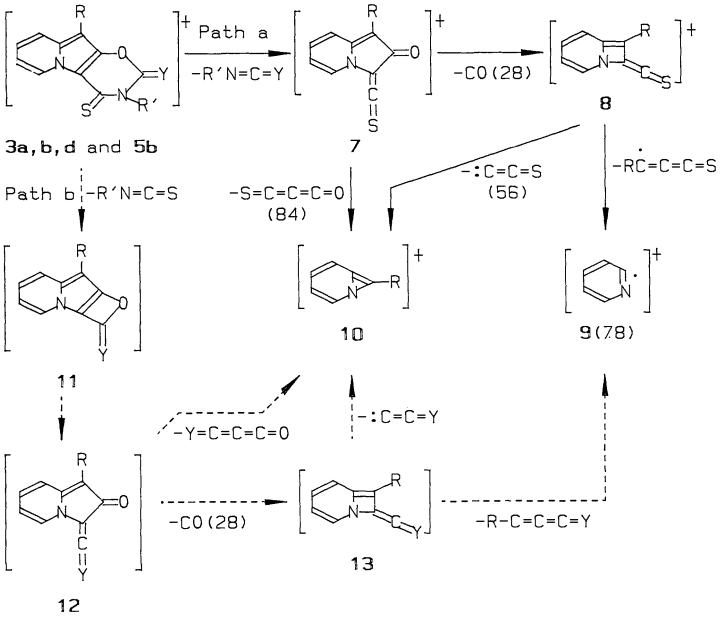

Scheme 3.

M$^+$−305), and those of **3a**,**b**,**d** showed definite peaks due to the corresponding M$^+$, (M$^+$−MeN=C=S), (M$^+$−101), (M$^+$−157), and 78 ions, respectively. The possible fragmentation patterns of the molecules **3a**,**b**,**d**, and **5b** are illustrated in Scheme 3. Although respective ions can be generally derived from both Path a (solid line) and Path b (dashed line), Path a is energetically more favorable than Path b because the fissions of any bonds

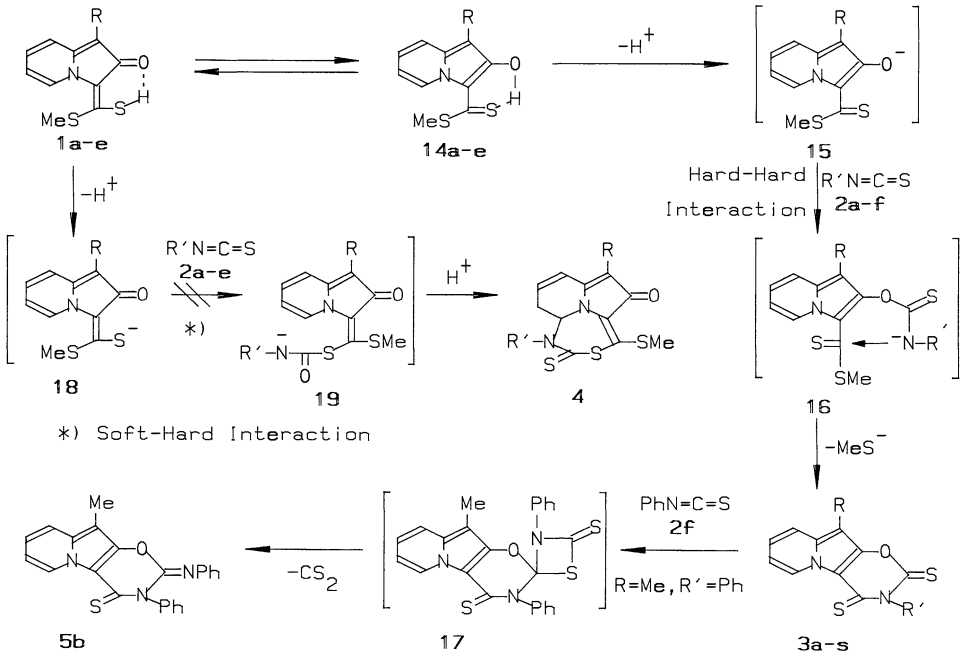

Scheme 4.

connected with the aromatic indolizine ring are not involved in this route.[6] The predominance of the *m/z* 189 ion (M^+—PhN=C=NPh) over the *m/z* 248 ion (M^+—PhN=C=S) strongly supported that this product was **5b** but not **6**.

Reaction Mechanisms. The formation of the 3-alkyl-2*H*-1,3-oxazino[6,5-*b*]indolizine-2,4(3*H*)-dithiones (**3a—j, l—s**) were explained by the initial abstraction of the active hydrogen in 3-[mercapto(methylthio)-methylene]-2(3*H*)-indolizinones **1a—e** or their 2-hydroxy tautomers **14a—e** with potassium *t*-butoxide, the electrophilic addition of isothiocyanate **2** to the resulting 2-indolizineolate ions **15**, and by the intramolecular nucleophilic attack of the aminide ion **16** to the thiocarbonyl carbon at the 3-position followed by the elimination of a methylthio anion. This mechanism is very similar to those proposed for the syntheses of 2*H*-1,3-benzoxazine-2-thiones[7] and 2*H*-1,3-thiazino[6,5-*b*]indolizin-2-thiones.[1] The reason why the initially expected product **4** could not be formed by the reaction between the alternative thiolate ion **18** and isothiocyanate **2** may be explained by considering the unfavorable interaction between this anion **18** and reagents **2** based on a HSAB principle.[8] On the other hand, 2-phenylimino derivative **5b** must be formed via the [2+2] cycloaddition of phenyl isothiocyanate (**2f**) to 10-methyl-3-phenyl-2*H*-[1,3]oxazino[6,5-*b*]indolizine-2,4(3*H*)-dithione once formed followed by the cycloreversion of the 2*H*-1,3-thiazetidine-2-thione ring in the resulting **17** with the elimination of carbon disulfide. However, the reason why other compounds **5a**, **c—h** could not be obtained by similar reactions of **1a**, **c—e** and **3b,g,p** with **2f** is still unclear. These mechanism are summarized in Scheme 4.

Experimental

Melting points were measured with a Yanagimoto micromelting point apparatus and were not corrected. The microanalyses were carried out on a Perkin-Elmer 2400 elemental analyzer. The ^{1}H NMR spectra were determined with a Varian EM360A spectrometer in deuteriochloroform with tetramethylsilane as an internal standard and the chemical shifts are expressed in δ values. The IR spectra were taken with a Hitachi 260-10 infrared spectrophotometer.

Preparations of 3-[Mercapto(methylthio)methylene]-2(3*H*)-indolizinones. The preparation of 3-[mercapto(methylthio)-methylene]-1-phenyl-2(3*H*)-indolizinone **1d**, mp 121—122 °C (Lit,[3] mp 121—122 °C), was carried out according to our previous procedure, and those of **1a—c, e** by modified procedures: **General Method.** An ethanolic solution (100 ml) of 2-methyl-, 2-ethyl-, 2-propyl-, or 2-(*p*-chlorobenzyl)pyridinium bromide (10 mmol) was treated with ethanolic sodium ethoxide at room temperature for 15—20 min. Carbon disulfide (12 mmol) and then dimethyl sulfate (11 mmol) were added to the mixture and the resulting solution was stirred for an additional 20 min. The reaction mixture was poured into 300 ml of water and was extracted with two portions of chloroform (300 ml). The chloroform layer was dried over sodium sulfate, filtered, and concentrated under reduced pressure. The residue was chromatographed on a column of alumina using chloroform as an eluent to give the crude 2(3*H*)-indolizinone, which was recrystalized from ethanol (**1a,c**) or chloroform (**1b,e**).

Some data for new compounds are as follows: **1a**, 19% yield, orange needles, mp 128—131 °C, ν (KBr) 2570 (SH) and 1570 (CO) cm^{-1}, Anal. ($C_{10}H_9NOS_2$) C,H,N.

Table 4. Some Data of the 2*H*-1,3-Oxazino[6,5-*b*]indolizines

No[a]	React	Yield %	Mp °C	ν (KBr) cm^{-1}	Formula[b]
3a	**1a 2a**	24	246—247	1560 1532	$C_{11}H_8N_2OS_2$
3b	**1b 2a**	77	283—284	1590 1533	$C_{12}H_{10}N_2OS_2$
3c	**1c 2a**	54	185—186	1580 1523	$C_{13}H_{12}N_2OS_2$
3d	**1d 2a**	40	230—232	1566 1527	$C_{17}H_{12}N_2OS_2$
3e	**1e 2a**	10	253—255	1569 1525	$C_{17}H_{11}N_2OS_2Cl$
3f	**1a 2b**	10	188—189	1560 1533	$C_{12}H_{10}N_2OS_2$
3g	**1b 2b**	23	224—225	1589 1529	$C_{13}H_{12}N_2OS_2$
3h	**1c 2b**	39	184—185	1581 1528	$C_{14}H_{14}N_2OS_2$
3i	**1d 2b**	12	189—190	1581 1531	$C_{18}H_{14}N_2OS_2$
3j	**1e 2b**	11	194—196	1570 1521	$C_{18}H_{13}N_2OS_2Cl$
3k	**1a 2c**	0			
3l	**1b 2c**	85	215—217	1587 1529	$C_{14}H_{12}N_2OS_2$
3m	**1c 2c**	41	140—142	1584 1530	$C_{15}H_{14}N_2OS_2$
3n	**1d 2c**	27	186—187	1570 1528	$C_{19}H_{14}N_2OS_2$
3o	**1e 2c**	23	209—211	1571 1527	$C_{19}H_{13}N_2OS_2Cl$
3p	**1b 2d**	17	178—180	1590 1532	$C_{14}H_{14}N_2OS_2$
3q	**1d 2d**	6	200—203	1569 1523	$C_{19}H_{16}N_2OS_2$
3r	**1b 2e**	14	167—168	1591 1537	$C_{15}H_{16}N_2OS_2$
3s	**1d 2e**	9	170—172	1568 1525	$C_{20}H_{18}N_2OS_2$

a) All compounds were obtained as orange needles. b) Satisfactory analytical data (within 0.3% for C, H, and N) were obtained for all compounds.

1b, 65% yield, orange needles, mp 134—135 °C, ν (KBr) 2580 (SH) and 1588 (CO) cm^{-1}, Anal. ($C_{11}H_{11}NOS_2$) C,H,N.

1c, 30% yield, orange needles, mp 78—80 °C, ν (KBr) 2580 (SH) and 1585 (CO) cm^{-1}, Anal. ($C_{12}H_{13}NOS_2$) C,H,N.

1e, 71% yield, orange needles, mp 153—154 °C, ν (KBr) 2520 (SH) and 1585 (CO) cm^{-1}, Anal. ($C_{16}H_{12}ClNOS_2$) C,H,N.

Reactions of 2(3*H*)-Indolizinones with Alkyl Isothiocyanates. General Method. A DMF solution (1 ml) of 3-[mercapto(methylthio)methylene]-2(3*H*)-indolizinone (**1**, 1 mmol) and isothiocyanate (**2**, 2 mmol) was treated with potassium *t*-butoxide (2 mmol) at 70—80 °C for 20 min. The reaction mixture was neutralized with diluted hydrochloric acid and then extracted with chloroform (20 ml). Water was removed from the chloroform solution by passage through phase-separating filter paper and the filtrate was concentrated under reduced pressure. The residue was separated by column chromatography on alumina using chloroform as an eluent. The chloroform solution was concentrated under reduced pressure and the recrystallization of the crude products from ethanol gave the corresponding 2*H*-1,3-oxazino[6,5-*b*]indolizine-2,4-dithione derivatives **3a**—**s** as orange needles. The results and some physical and spectral data of **3a**—**s** are listed in Tables 1 and 4.

The prolonged reactions (1—4 h) of indolizinones **1** and isothiocyanates **2** gave diminished yields of the products **3**.

Reaction of 1-Methyl-2(3*H*)-indolizinone 1b with Phenyl Isothiocyanate (2f). A DMF solution (1 ml) of **1b** (1 mmol) and **2f** (2 mmol) was heated at 70—80 °C for 2 h in the presence of potassium *t*-butoxide (2 mmol). The usual work-up of the resulting mixture gave 10-methyl-3-phenyl-2-phenylimino-2,3-dihydro-4*H*-1,3-oxazino[6,5-*b*]indolizine-4-thione (**5b**), 10% yield, orange needles, mp 266—268 °C, ν (KBr) 1675 (C=N) cm^{-1}, Anal. ($C_{23}H_{17}N_3OS$) C,H,N (See Table 1 for its ^1H NMR spectrum)

On the other hand, the reactions of indolizinones **1a**,**c**—**e** and 2*H*-1,3-oxazino[6,5-*b*]indolizine-2,4(3*H*)-dithiones **3b**,**g**,**p** with phenyl isothiocyanate (**2f**) did not afford any significant products under various reaction conditions.

References

1) For Part 27 of this series, see A. Kakehi, S. Ito, T. Sakurai, K. Urushido, H. Isawa, and M. Enomoto, *Bull. Chem. Soc. Jpn.*, **64**, 3289 (1991).

2) A. Kakehi, S. Ito, and S. Hatanaka, *Chem. Lett.*, **1989**, 2229; A. Kakehi, S. Ito, T. Fujii, T. Sakurai, K. Urushido, S. Hatanaka, T. Mabuchi, and S. Matsushita, *Bull. Chem. Soc. Jpn.*, **63**, 3571 (1990).

3) A. Kakehi, S. Ito, K. Nakanishi, K. Watanabe, and M. Kitagawa, *Bull. Chem. Soc. Jpn.*, **53**, 1115 (1980).

4) Other crystallographic data such as bond lengths, bond and torsion angles, and F_o—F_c tables are deposited as Document No. 8966 at the Office of the Editor of Bull. Chem. Soc. Jpn.

5) C. K. Johnson, ORTEP II, Report ORNL-5138, Oak Ridge National Laboratory, Oak Ridge, Tennessee (1976).

6) In the mass spectra of 2-thioxo-2,3-dihydro-4*H*-1,3-thiazino[6,5-*b*]indolizin-4-one derivatives which were recently synthesized by us (see Ref. 1), only Path a-type fragmentation was observed.

7) L. Capuano and M. Zander, *Chem. Ber.*, **99**, 3085 (1966).

8) T.-L. Ho, "Hard and Soft Acids and Bases Principle in Organic Chemistry," Academic Press (1977).

9) TEXSAN TEXRAY, Structure Analysis Package, Molecular Structures Corporation (1985).

10) C. J. Gilmore, *J. Appl. Crystallogr.*, **17**, 42 (1984).

Stereoselectivity in the Hydrogenation of 4-*t*-Butylcyclohexanone with Catalytically-Active Powder Electrodes

Yasuhisa SENDA,* Minako TATEOKA, Hiroki ITOH, and Jun-ichi ISHIYAMA†
Department of Chemistry, Faculty of Science, Yamagata University,
Koshirakawa, Yamagata 990
† Department of Engineering Science, Faculty of Engineering,
Tohoku University, Aoba, Sendai 980
(Received May 14, 1991)

The electrocatalytic hydrogenation of the title compound was examined over Raney Ni, Raney Co, Pt-carbon and Pd-carbon as hydrogen-active powder electrodes. A high conversion of ketone to alcohol was observed on the Raney catalysts when the pK_a values of the proton sources employed were around 5. The metal-on-carbon catalysts showed a relatively low conversion of ketone regardless of the proton sources. The stereochemistry of the reaction was examined.

Since Raney Ni has been known as a useful hydrogenation catalyst, its electronic properties have also allowed its use as cathodic material.[1,2] Osa et al.[3] pointed out that hydrogenation with catalytically-active powder electrodes of group VIII transition metal had several intrinsic advantage over direct, uncatalyzed electroreductions. This reaction involved the chemisorption of atomic hydrogen from the solvent on the electrodes in the first step (Fig. 1a). The potential of this step was usually much less positive than that required to reduce a functional group via an EC mechanism (Fig. 1b). Also, the electrochemical catalysis produced hydrogen in situ and avoided the need to introduce hydrogen from an external source. The reaction could be controlled by changing the electric potential and the current. In other words, the electrocatalytic hydro-

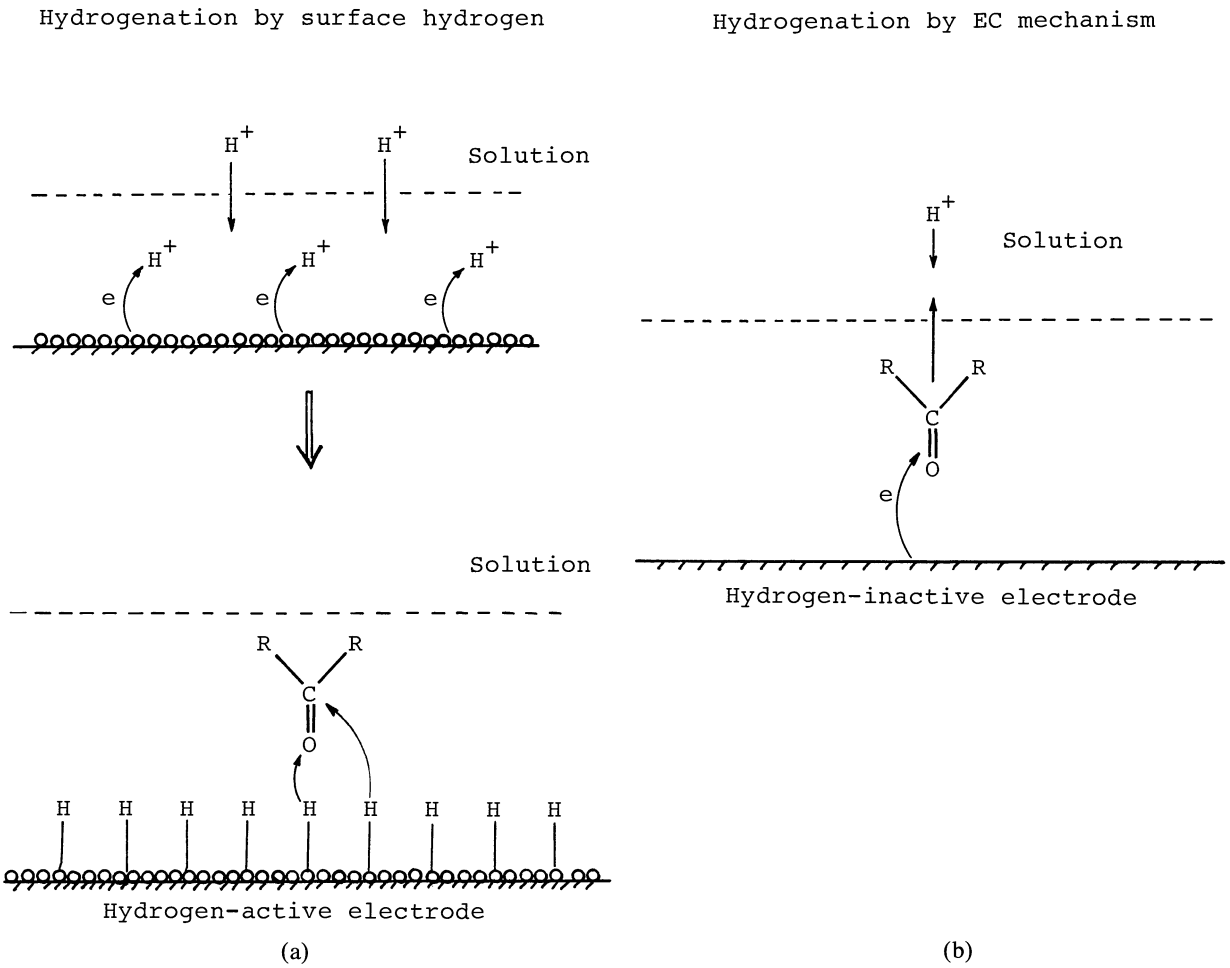

Fig. 1. Schematic representation of hydrogenation of carbonyl compounds.

Table 1. Electrocatalytic Hydrogenation of 4-*t*-Butylcyclohexanone

Catalyst proton source	pK_a	Raney Ni		Raney Co		Pt-carbon		Pd-carbon	
		Yield %	Isomer ratio (cis%)	Yield %	Isomer ratio (cis%)	Yield %	Isomer ratio (cis%)	Yield %	Isomer ratio (cis%)
CCl_3COOH	0.64	5	16	5	23	—	—	—	—
$Cl_2CHCOOH$	1.26	5	22	5	19	—	—	—	—
$ClCH_2COOH$	2.86	5	22	5	19	27	21	19	23
CH_3COOH	4.76	25	45	15	19	27	23	20	22
$(CH_3)_2CHCOOH$	4.85	68	72	78	69	25	19	18	26
CH_3CH_2COOH	4.87	42	68	66	67	23	26	21	24
$(CH_3)_3CCOOH$	5.03	59	76	59	76	—	—	—	—
C_6H_5OH	9.99	20	52	24	72	35	22	21	23
H_2O	14.0	22	35	5	35	25	22	18	23
$(CH_3)_3COH$		8	35	5	37	14	22	15	16
$(CH_3)_2CHOH$		10	40	7	33	16	22	21	22
C_2H_5OH		6	32	6	16	—	—	—	—
CH_3OH		8	30	6	18	—	—	—	—

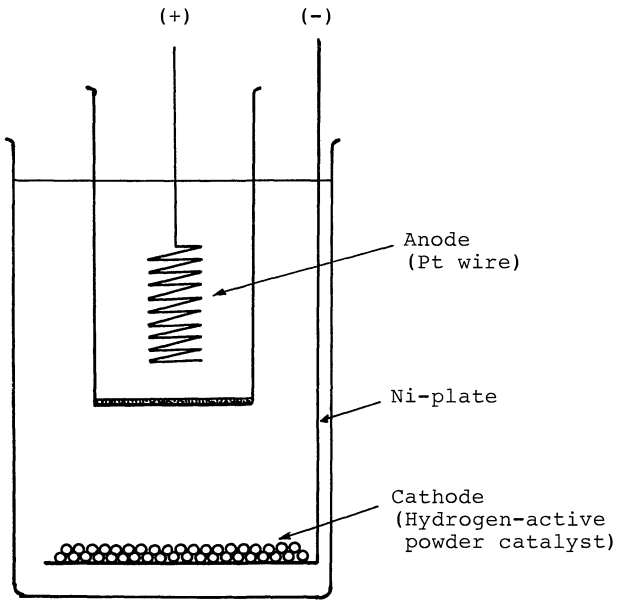

Fig. 2. Electrolysis cell.

genation on hydrogen-active powder electrodes is situated in boundaries between uncatalyzed electroreduction via an EC mechanism and ordinary catalytic hydrogenation. A number of mechanistic studies over group VIII transition metal catalysts are also found in the literature.[4)]

To the best of our knowledge, there has been no study on the stereoselective hydrogenation with active powder electrodes. 4-*t*-Butylcyclohexanone (**1**) was selected as the substrate and the stereochemistry of hydrogenation with an electrocatalytic electrode which consisted of Raney Ni, Raney Co, Pt-carbon or Pd-carbon was examined. The hydrogen adsorbed on the Raney catalyst surface was removed by treating with pentene. The electrolysis was carried out in a divided cell with the catalyst cathode and a Pt wire or graphite rod anode (Fig. 2). Table 1 tabulates the results of the electrocatalytic hydrogenation with various types of proton sources after the passage of 5×96500 C mol^{-1} of electrical charge.

Table 2. Effect of the Amount of the Catalyst on the Electrocatalytic Hydrogenation of 4-*t*-Butylcyclohexanone

Catalyst	Weight g	Yield %	Isomer ratio (cis%)
Raney Ni	1.0	68	72
	1.5	73	74
	2.0	78	70
Pt-carbon	0.02	15	19
	0.04	24	24
	0.06	23	22

The conversion of **1** to 4-*t*-butylcyclohexanol over Raney catalysts depended on the pK_a values of the proton sources. The highest conversion was 78% in a proton source with a pK_a value at around 5 under the reaction conditions employed. Decreasing or increasing the pK_a values of the proton sources reduced the conversion. The conversion was only 5% and 20%, respectively, over the Raney Ni catalyst, when chloroacetic acid and phenol were used as a proton source. When metal-on-carbon catalysts were used, the conversion of ketone to alcohol was relatively low, but no appreciable change in the conversion was observed depending on the pK_a values of the proton sources. Increasing the amount of catalyst resulted in an increase in the conversion (Table 2). In the absence of a metal catalyst, the cathodic reduction with pivalic acid as a proton source proceeded very slowly. The conversion was only 4% and the amount of *cis* alcohol was 44%.

In the ordinary catalytic hydrogenation in which sufficient hydrogen is supplied, 77 and 69% *cis* alcohol was obtained over the Raney Ni and Co catalysts, respectively, while 80% and 85% *trans* alcohol was obtained over the Pt-carbon and Pd-carbon catalysts (Table 3). In the electrocatalytic hydrogenation, the *cis*

Table 3. Comparison of the Isomeric Product Ratio between Ordinary Catalytic and Electrocatalytic Hydrogenation of 4-*t*-Butylcyclohexanone

Catalyst	Product ratio (cis%)		
	Catalytic	Electrocatalytic proton source	
		$(CH_3)_2CHCOOH$	$(CH_3)_3COH$
Raney Ni	77	72	35
Raney Co	69	69	37
Pt-carbon	20	19	22
Pd-carbon	15	26	16

alcohol was predominantly obtained at a high conversion rate over Raney catalysts (similar to ordinary catalytic hydrogenation), but the *trans* alcohol became predominant at a low conversion rate (Table 1). On the other hand, the *trans* alcohol was predominantly obtained (similar to the case of ordinary catalytic hydrogenation), and the isomeric product distribution was independent of the pK_a values of the proton sources when the carbon-supported catalysts were employed. Cathodic reduction without the electrocatalyst gave more of the *trans* alcohol than the *cis*.

The stereochemistry of the ordinary catalytic hydrogenation was interpreted in terms of the Horiuti–Polanyi mechanism which is one of the most satisfactory theories.[5] The change in the product-controlling step, depending on the catalysts, coincides with a change in the ratio of the products. The Horiuti–Polanyi formulation of the mechanism of hydrogenation of unsaturated bonds may be represented by four elementary reactions; dissociation of hydrogen, adsorption of the substrate on the catalyst, first hydrogen transfer to the adsorbed species and second hydrogen transfer to the half-hydrogenated intermediate. The proportion of the stereoisomeric products will depend upon which of the elementary reactions is a product-controlling step, because the geometry and/or composition of the several possible transition states differ from one another. When the product-controlling step is the adsorption of the substrate on the catalyst or the first hydrogen transfer from the catalyst to the adsorbed species, the stereochemistry of the reaction is controlled by the interaction between the substrate and the catalyst. On the other hand, when the product-controlling step is the second hydrogen transfer from the catalyst to the half-hydrogenated species, the stereochemistry of hydrogenation is controlled by the relative stabilities of the two epimeric half-hydrogenated species.

When the pK_a value of the proton source employed in a system was more than 5, the conversion of ketone to alcohol decreased over the Raney catalyst. Since the electron transfer to protons on the cathode is more difficult in a proton source with a higher pK_a value, an insufficient supply of active hydrogen results in a decrease in the amount of hydrogen available on the catalyst surface. This permits equilibration between the *cis* and the *trans* half-hydrogenated intermediates, thus resulting in a decrease of *cis* stereoselectivity of the reaction and the *trans* alcohol becomes predominant.

When the pK_a value of the proton source was less than 5, the conversion of ketone was also small the *trans* alcohol was preferably obtained over a Raney catalyst. The surface of the Raney catalyst is damaged in acidic conditions so that metal ions are gradually eluted from the surface and the catalyst surface poisoned by those ions. This results in a low conversion and the predominant formation of the *trans* alcohol. The optimum pK_a value of the electrocatalytic hydrogenation over a Raney catalyst is around 5. On the other hand, no poisoning under acidic conditions was observed over the metal carbon catalysts and the conversion and the isomer ratio were relatively constant under all reaction conditions employed here.

The effect of current density on the conversion of ketone to alcohol and the stereochemistry was also examined (Table 4). A change in current density had no appreciable effect on the conversion and the isomeric product distribution in the hydrogenation over Raney Ni catalyst when isobutyric acid was used as the proton source. On the other hand, the conversion was improved at a lower current density when *t*-butyl alcohol was used as the proton source. In the hydrogenation over Pt-carbon, a decrease in the current density increased the conversion of ketone to alcohol. These results indicated that a part of the produced active hydrogen by electrochemical reductrion was not used in hydrogenation but was lost as molecular hydrogen to the

Table 4. Effect of the Current Density on the Electrocatalytic Hydrogenation of 4-*t*-Butylcyclohexanone

Catalyst	Proton source	Current density	Yield	Isomer ratio
		mA cm^{-2}	%	(cis%)
Raney Ni	$(CH_3)_2CHCOOH$	26.8	62	59
		13.4	68	72
		0.67	85	60
		0.40	73	58
	$(CH_3)_3COH$	13.4	8	35
		0.67	30	31
Pt-carbon	$(CH_3)_2CHCOOH$	13.4	15	19
		0.67	33	26
		0.40	36	26

Table 5. Comparison of Pt-Wire and Graphite-Rod Anodes in the Electrocatalytic Hydrogenation of 4-*t*-Butylcyclohexanone

Anode	Pt-wire				Graphite-rod			
Catalyst	Raney Ni		Raney Co		Raney Ni		Raney Co	
Proton source	Yield %	Isomer ratio (cis%)	Yield %	Isomer ratio (cis%)	Yield %	Isomer ratio (cis%)	Yield %	Isomer ratio (cis%)
CH_3COOH	15	45	15	19	32	37	41	35
$(CH_3)_2CHCOOH$	68	72	78	69	61	60	86	60
C_6H_5OH	20	52	24	72	46	47	32	44
$(CH_3)_2CHOH$	10	40	7	33	31	36	18	22

outside of the system at a relatively high current density, while the generation of active hydrogen is moderate and is efficiently used for the hydrogenation at a low current density.

When a graphite electrode was used as the anode, no appreciable change in the results of hydrogenation was observed (Table 5).

Experimental

Electrocatalytic Hydrogenation. Metal-on-carbon catalysts were commercially available. Raney catalysts which were prepared from metal-alloy were treated with pentene to remove the hydrogen adsorbed on the catalyst surface. The electrochemical cell was a conventional divided cell with a metal catalyst cathode and a platinum coil (surface area 7.48 cm^2) or graphite rod (surface area 9.86 cm^2) anode. For making contact with the metal catalyst powder, a nickel plate electrode (surface area 12.56 cm^2) was first placed on the bottom of the flask on which a known amount of metal catalyst powder was then stacked in the presence of an electrolyte solution. The electrolyte solution consisted of 50 cm^3 of a 10% tetrahydrofuran:H_2O (9:1 volume ratio) solution containing 163 mmol of $NaClO_4$, 3.1 mmol of 4-*t*-butylcyclohexanone (**1**), and 25.0 mmol of a proton source. The electrolysis was carried out at room temperature. After the passage of 5×96500 C mol^{-1} of electrical charge, the catholyte was filtered off from the catalyst and extracted three times with ether, washed with saturated NaCl solution and analyzed by gas chromatography.

Gas Chromatographic Analysis. Analyses were performed with a Simadzu GC-8A with a glass capillary column CPB20 (0.2 mm×25 m) at 120 °C. The products were compared with the authentic sample which was prepared by the LAH reduction of **1**.

References

1) B. Sakurai and T. Arai, *Bull. Chem. Soc. Jpn.*, **35**, 93 (1962).

2) T. Chiba, M. Okamoto, H. Nagai, and Y. Tanaka, *Bull. Chem. Soc. Jpn.*, **56**, 719 (1983).

3) T. Osa, T. Matsue, A. Yokozawa, and T. Yamada, *Denki Kagaku*, **52**, 629 (1984); and the references cited therein.

4) D. Bobidn, M. Comtois, A. Martel, R. Lemieux, A. K. Cheong, G. Belot, and J. Lessard, *Can. J. Chem.*, **68**, 1218 (1990); and the references cited therein.

5) S. Siegel and B. Dmukovsky, *J. Am. Chem. Soc.*, **84**, 3132 (1962); and the references cited therin.

Neighboring Effect of a Carbonyl Group in Base-Induced Wittig-Type Rearrangements of Poly(4-nitrobenzyloxy)tropones to Bis- and Mono(α-hydroxy-4-nitrobenzyl)tropones

Bing Zhu YIN,† Akira MORI, and Hitoshi TAKESHITA*
Institute of Advanced Material Study, 86, Kyushu University,
Kasuga-koen, Kasuga, Fukuoka 816
(Received May 24, 1991)

The base-catalyzed rearrangement of bis- and tris(4-nitrobenzyloxy)tropones gave (α-hydroxy-4-nitrobenzyl)tropones through a Wittig-type mechanism. Only the 4-nitrobenzyloxy group adjacent to the carbonyl group migrated. The carbonyl group played a role in facilitating the rearrangement by chelation with the sodium on the adjacent carbanion.

To overcome severe restrictions in introducing carbon substituents into the tropone ring,[1,2] several new approaches were recently elaborated: e.g., Banwell reported efficient palladium-mediated *ipso*-substitution processes of bromotropolones with various aryl-, alkenyl-, and alkyltrimethylstannanes.[3]

Recently, we exploited a new carbon–carbon bond formation in troponoids by means of base-catalyzed rearrangements of 2-(4-cyano-, 2-nitro-, and 4-nitrobenzyloxy)tropones and 2-(2-oxo-2-phenylethoxy)tropone to 2-[α-hydroxy-(4-cyano-, 2-nitro-, and 4-nitrobenzyl)]tropones and 2-(1-hydroxy-2-oxo-2-phenylethyl)tropone, respectively, via a Wittig-type mechanism.[4] This constituted a new regio-controlled introduction of carbon substituents into a tropone ring. In this paper, we describe an extention of this base-induced rearrangement to poly(benzyloxy)tropones to prepare poly(α-hydroxy-4-nitrobenzyl)tropones, in which only the benzyloxy group adjacent to the carbonyl group rearranged.

Results and Discussion

5-Hydroxytropolone dipotassium salt (**1**) and 4-nitrobenzyl bromide (**2**) in a hexamethylphosphoric triamide (HMPA) solution gave only a single product, 2,5-bis(4-nitrobenzyloxy)tropone (**3**). However, 3-hydroxytropolone dipotassium salt (**4**) and **2** gave three products (**5**—**7**); products **5** and **6** were identified to be 2,7-bis(4-nitrobenzyloxy)- and 2,3-bis(4-nitrobenzyloxy)tropones, respectively, from the NMR spectral data and **7** was identified as monobenzylated 3-(4-nitrobenzyloxy)tropolone. Along with these, an air-oxidized by-product **8**, which was no longer a troponoid derivative, was obtained. Its ^{1}H and ^{13}C NMR spectral data indicated it was bis(4-nitrobenzyl) (*Z*,*Z*)-2,4-hexadienedioate.

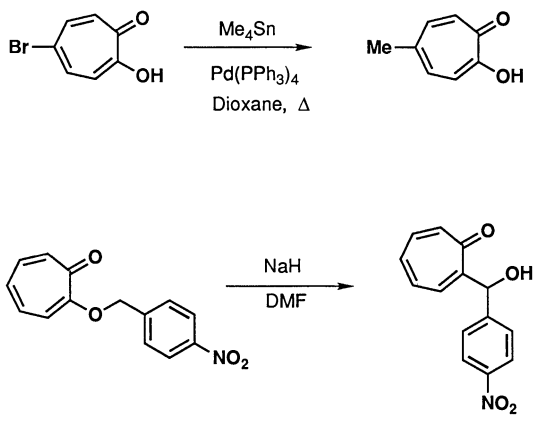

Scheme 1.

The reaction of 3,4-dihydroxytropolone tripotassium salt (**9**) with **2** gave four products (**10**—**13**): Two of them (**10** and **11**) were tris(4-nitrobenzyloxy)tropones; **10** had two singlets at a lower field (δ=5.37 and 5.40) than the other singlet at δ=5.12, whereas **11** had two singlets at a higher field (δ=5.09 and 5.16) than the other singlet at δ=5.29. Assuming that the chemical shift of benzylic methylene protons adjacent to the carbonyl group was lower, **10** was a 2,3,7-isomer, and **11** was a 2,3,4-isomer. With a similar series, chemical shifts of the methylene protons of **12** at δ=5.17 and 5.39 showed **12** to be 3,4-bis(4-nitrobenzyloxy)tropolone. The remaining isomer, **13**, was 3-hydroxy-4-(4-nitrobenzyloxy)tropolone.

When 4-isopropyltropolone potassium salt (**14**) was allowed to react with **2**, two isomeric condensates, **15** and **16**, were isolated in 66 and 34% yields, respectively. The ^{1}H NMR spectrum of **15** showed a doublet signal at δ=6.67 (*J*=9.5 Hz), which was ascribable to the proton adjacent to the benzyloxy group. The magnitude of this vicinal coupling constant indicated that the two carbons bearing these protons had a single bond character. Therefore, **15** was 6-isopropyl-2-(4-nitrobenzyloxy)tropone and **16** was a 4-isopropyl-2-(4-nitrobenzyloxy) derivative.

From 3-hydroxy-5-isopropyltropolone dipotassium salt (**17**),[5] four products (**18**—**21**) were isolated in 72, 14, 8, and 3% yields, respectively. Three of them (**18**—**20**) were isomeric bis(4-nitrobenzyloxy)tropones. The coupling constant between H-5 and H-6 (*J*=10.2 Hz) of the main product **18** showed it to be 4-isopropyl-2,7-bis(4-nitrobenzyloxy)tropone. The structures of **19** and **20**

† On leave from Yanbian University, Yanji, Jilin, People's Republic of China.

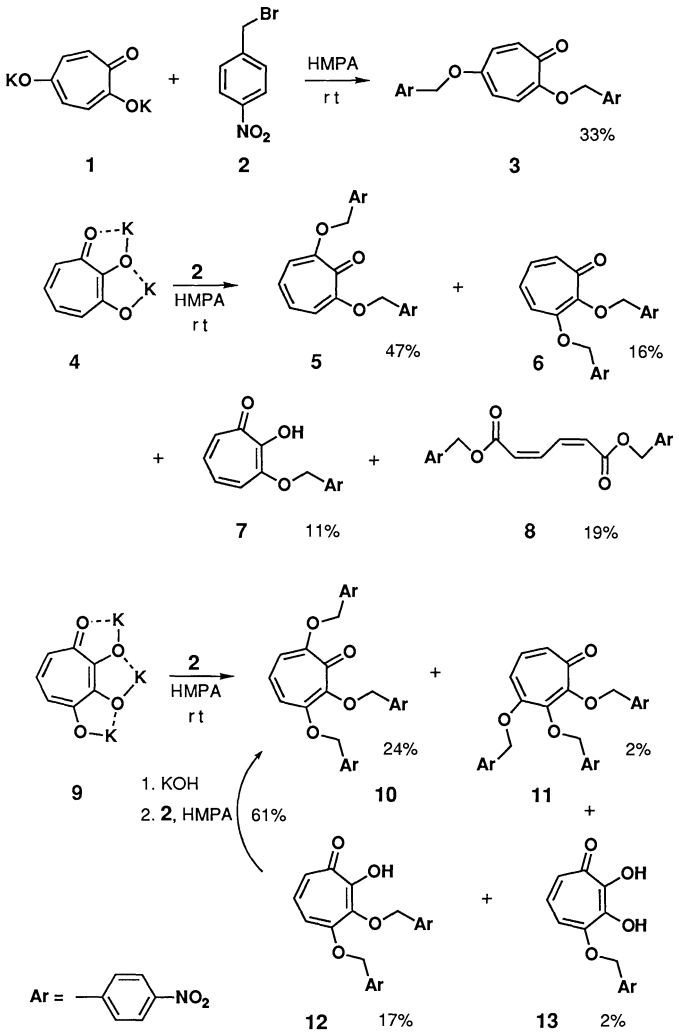

Scheme 2.

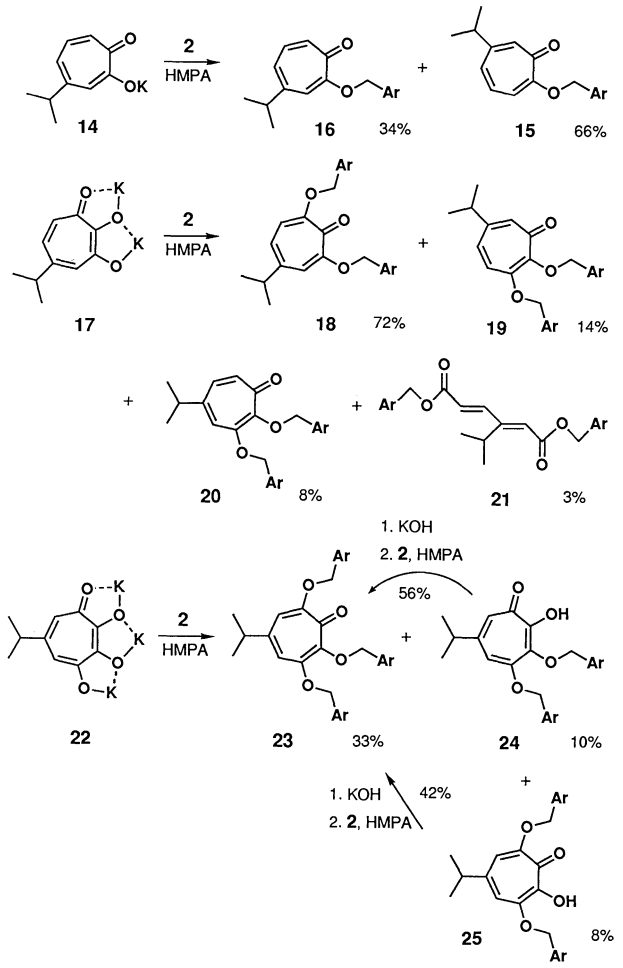

Scheme 3.

were deduced from the chemical shifts of seven-membered ring protons; **20** had a lower doublet at δ=7.21 (J=12.5 Hz) than that of **19** at δ=6.97 (J=12.0 Hz). Therefore, **19** was 6-isopropyl-2,3-bis(4-nitrobenzyloxy)-tropone and **20** was 5-isopropyl-2,3-bis(4-nitrobenzyl-oxy)tropone. The remaining **21** was an air-oxidized bis(4-nitrobenzyl) (*E*,*E*)-3-isopropyl-2,4-hexadiene-dioate.

The reaction of 3,4-dihydroxy-6-isopropyltropolone tripotassium salt (**22**) gave three products (**23**—**25**); two minor products **24** and **25** were bis(benzyloxy) derivatives and the latter was deduced to be 5-isopropyl-2,7-bis(4-nitrobenzyloxy)tropolone, whose NMR spectrum revealed an element of symmetry. Since the main product, **23**, was obtained by further reaction of **25**, it was 5-isopropyl-2,3,7-tri(4-nitrobenzyloxy)tropone. The remaining **24** is, therefore, assigned as 6-isopropyl-3,4-bis(4-nitrobenzyloxy)tropolone.

Base-Induced Rearrangements of Benzyloxytropones. When an HMPA solution of **3** was stirred in the presence of sodium hydride (NaH) at room temperature for 1 h, a single product, **26**, was obtained in 32% yield together with recovered **3** in 13% yield. The ^{1}H NMR spectrum of **26** in dimethyl-d_6 sulfoxide (DMSO-d_6) showed a singlet signal of two protons at δ=5.31 and a pair of doublet signals (J=4.4 Hz) at δ=5.92 and 6.23. One of the 4-nitrobenzyloxy groups migrated. The proton signals of the seven-membered ring of **3** appeared at δ=7.06 (d, J=11.0 Hz, H-2), which was assigned to H-2, and 6.63 (dd, J=11.0, 3.0 Hz, H-3) and those of **26** at δ=7.74 (d, J=10.3 Hz, H-2) and 6.81 (dd, J=10.3, 3.0 Hz, H-3). Therefore, **26** was 2-(α-hydroxy-4-nitrobenzyl)-5-(4-nitrobenzyloxy)tropone. Thus, the 4-nitrobenzyl group adjacent to the carbonyl group migrated exclusively.

On the other hand, a similar treatment of **5** afforded two products, **27** and **28**, in 51 and 25% yields, respectively. Pyridinium dichromate (PDC) oxidation of both **27** and **28** gave 2,7-bis(4-nitrobenzoyl)tropone (**29**). Therefore, **27** and **28** were stereoisomers. The stereochemistry of **27** and **28** was determined by liquid chromatography with a chiral stationary phase. Since the chromatogram of **27** was further separated into two peaks, **27** was a *dl*-mixture (R_f=12.2 and 16 min). On

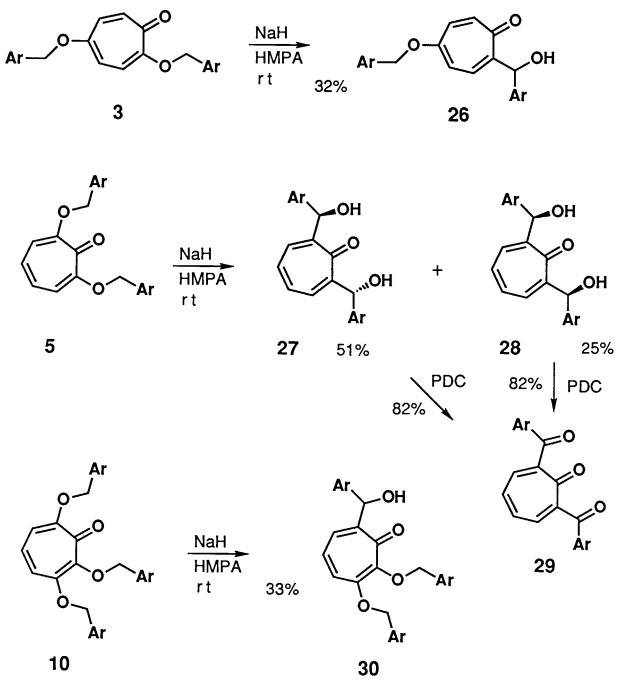

Scheme 4.

the other hand, a meso isomer, **28**, remained as a single peak (R_f=13.3 min).

The base-induced reaction of **10** gave a single product, **30**. Its ^{1}H NMR spectrum in deuteriochloroform ($CDCl_3$) revealed two singlet signals due to benzylic methylene protons at δ=5.15 and 5.25 and a singlet single at δ=6.00, a benzylic methine proton. Therefore, two benzyloxy groups were intact. The low-field-shifted H-4 (7.47 from 7.22) and H-6 (7.56 from 7.06) of **30** indicated that the benzyloxy group at C-7 migrated.

Interestingly, the ^{1}H NMR spectrum of **30** in DMSO-d_6 showed a singlet signal of benzylic methylene protons at δ=5.37 and two pairs of AB quartets at δ=5.04 and 5.13 (J=12.8 Hz) and 6.10 and 6.34 (J=4.4 Hz). In $CDCl_3$, however, it showed three singlets at δ=5.15 (2H), 5.25 (2H), and 6.00 (1H). The latter of the AB quartets in DMSO-d_6 was assigned to be a benzylic methine proton signal and a hydroxyl proton signal. The appearance of the spin-coupling in DMSO-d_6 showed the formation of an intermolecular hydrogen bond involving the hydroxyl proton. On the other hand, the former of the quartets was assigned to be benzylic methylene protons; two benzylic protons are magnetically nonequivalent. The free rotation of the benzyloxy group at C-2 was hindered by the chelation between both carbonyl and hydroxyl groups and DMSO-d_6 as shown in **A** of Fig. 1.

Similarly, base-induced reactions of **15** and **16** gave the corresponding products **31** and **32**. From **18**, a diastereoisomeric mixture of **33** and **34** was obtained in 36 and 22% yields as observed with **5**. However, their chromatographic analyses with a chiral stationary phase

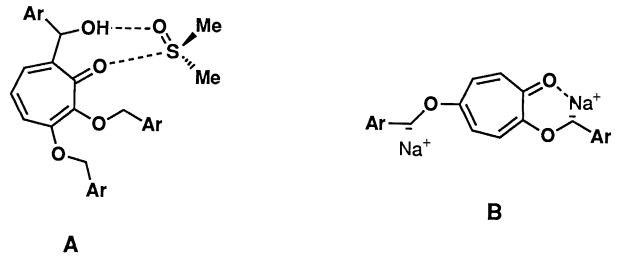

Fig. 1.

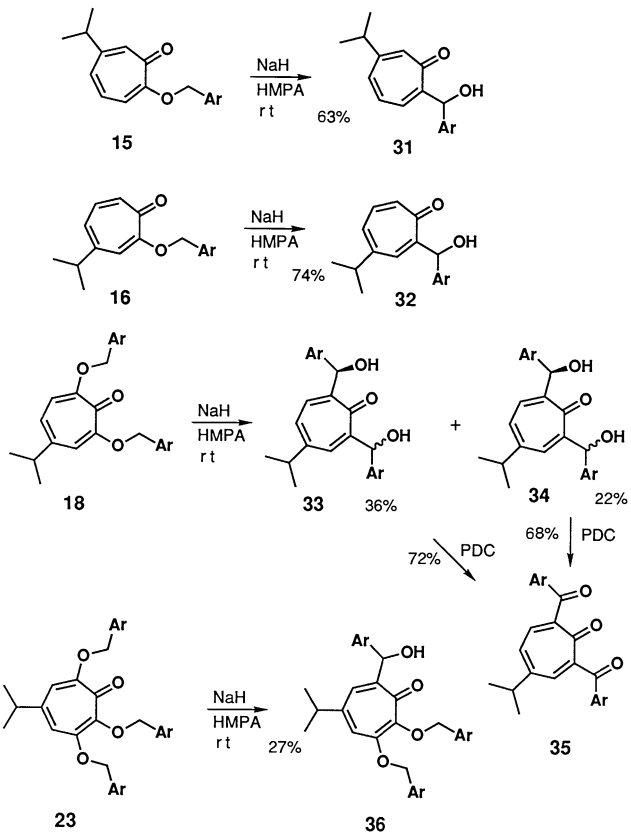

Scheme 5.

were unsuccessful. Oxidations of **33** and **34** gave the same **35**.

Finally, the reaction of **23** gave a single product, 5-isopropyl-7-(α-hydroxy-4-nitrobenzyl)-2,3-bis(4-nitrobenzyloxy)tropone (**36**).

A base-induced rearrangement of **3** gave only **26**. In 2,7-bis(4-nitrobenzyloxy)tropones, **5** and **18**, both benzyl groups migrated. Thus, the 4-nitrobenzyloxy group adjacent to the carbonyl group migrated exclusively. In tris(4-nitrobenzyloxy)tropones, **10** and **23**, only a 4-nitrobenzyloxy group at C-7 migrated. The inner benzyl group at C-2 was inactive due to the inhibition of an attack by NaH on methylene protons.

In conclusion, a Wittig-type rearrangement occurred exclusively at the benzyl group adjacent to the carbonyl

group. The carbonyl group acted as an acceptor of the sodium cation to form an active naked carbanion at the neighboring position as shown in **B** of Fig. 1. Thus, the base-catalyzed rearrangement occurred at the *ipso*-position of bis- and tris(4-nitrobenzyloxy)tropones to give (α-hydroxy-4-nitrobenzyl)tropones. This method is currently being applied to prepare a 2,7-bis(functionalized)tropone derivative, which is a versatile starting material of functioned materials such as crown ethers with a tropone skeleton.

Experimental

Elemental analyses were performed by Mrs. M. Miyazawa of this Institute, Kyushu University. Melting points were measured with a Yanagimoto micro mp apparatus and were not corrected. NMR spectra were measured by JEOL FX 100 and GSX 270H spectrometers in $CDCl_3$, unless otherwise specified, and the chemical shifts were expressed in δ units. IR spectra were taken as KBr disks for crystalline compounds or as liquid films inserted between NaCl plates for oily materials using a JASCO IR-A 102 spectrometer. UV spectra were measured by the use of Hitachi U-3200 and U-3410 spectrophotometers. Mass spectra were measured with a JEOL 01SG-2 spectrometer. The stationary phase for the column chromatography was Wakogel C-300 and the elution solvents were mixtures of hexane–ethyl acetate. HPLC was performed on a Chiralcel OJ column (Daicel Chemical Industries) by using a Waters M-45 pump and an S-301A UV detector (Soma Science) at 254 nm and by eluting with hexane–ethanol (1:2) with a flow rate of 3.5 $cm^3\ min^{-1}$.

General Procedure of Condensation Reactions of Potassium Tropolonates (1, 4, 9, 14, 17, and 22) with 2. An EtOH solution (4 cm^3) of a tropolone derivative (1 mmol) and ca. two molar equivalents of KOH was stirred at room temperature for 1 h under a nitrogen atmosphere. After removing the solvent under reduced pressure, the residue was exhaustively dried under reduced pressure to give the potassium salt. An HMPA solution (6 cm^3) of the potassium salt and **2** (577 mg) was stirred at room temperature for 2 h. The mixture was diluted with water, acidified with 5% aqueous HCl solution (pH=4), and extracted with AcOEt. The organic layer was washed with water, dried with $MgSO_4$, and removed under reduced pressure. The residue was recrystallized and/or chromatographed on a silica-gel column (AcOEt–hexane=2:1 or $CHCl_3$) to give the product.

3: Yellow needles, mp 181—183 °C (AcOEt), 33% yield. ^1H NMR (DMSO-d_6) δ=5.28 (4H, s), 6.63 (1H, dd, *J*=11.0, 3.0 Hz), 7.06 (1H, d, *J*=11.0 Hz), 7.11 (1H, d, *J*=13.2 Hz), 7.31 (1H, dd, *J*=13.2, 3.0 Hz), 7.72 (2H, d, *J*=8.8 Hz), 7.73 (2H, d, *J*=8.8 Hz), and 8.27 (4H, d, *J*=8.8 Hz); ^{13}C NMR (DMSO-d_6) δ=68.5, 68.7, 109.4, 116.7, 123.5, (2C), 123.6 (2C), 128.2 (2C), 128.3 (2C), 132.6, 137.4, 143.8, 144.3, 147.0, 147.1, 157.7, 158.2, and 178.2; IR (KBr) 3076, 1630, 1581, 1514, 1348, 1248, 1194, 1126, 1007, 846, 824, and 735 cm^{-1}; UV ($CHCl_3$) 255 (ε 24700), 267 (23200 sh), 326 (15400), and 375 nm (5700 sh); MS *m/z* (%) 408 (M^+, 8), 273 (13), 137 (100), 106 (42), 90 (50), and 78 (67).

Found: C, 61.85; H, 4.24; N, 6.86%. Calcd for $C_{21}H_{16}N_2O_7$: C, 61.76; H, 3.95; N, 6.86%.

5: Colorless powder, mp 250—251 °C ($CHCl_3$), 47% yield. ^1H NMR (TFA-*d*) δ=5.83 (4H, s), 7.83 (4H, *J*=8.4 Hz), 8.39 (4H, d, *J*=8.4 Hz), and 8.3—8.5 (4H, m); ^{13}C NMR (TFA-*d*) δ=74.6 (2C), 118.7 (2C), 126.4 (4C), 130.9 (4C), 131.9 (2C), 141.5 (2C), 142.8 (2C), 150.3 (2C), and 161.6; IR (KBr) 3075, 1628, 1599, 1555, 1513, 1348, 1250, 1222, 1153, 1103, 1081, 1017, 855, 821, and 739 cm^{-1}; UV ($CHCl_3$) 248 (ε 39400), 271 (23100 sh), 324 (12850), 351 (10700), and 363 nm (8400 sh); MS *m/z* (%) 408 (M^+, 15), 272 (100), 257 (31), and 136 (44).

Found: C, 61.98; H, 4.27; N, 7.03%. Calcd for $C_{21}H_{16}N_2O_7$: C, 61.76; H, 3.95; N, 6.86%.

6: Pale yellow powder, mp 223—225 °C ($CHCl_3$), 16% yield. ^1H NMR (TFA-*d*) δ=5.62 (2H, s), 5.74 (2H, s), 7.51 (2H, d, *J*=8.5 Hz), 7.65 (2H, d, *J*=8.5 Hz), 8.13 (2H, d, *J*=8.5 Hz), 8.23 (2H, d, *J*=8.5 Hz), 8.40 (2H, br s), and 8.48 (2H, br s); ^{13}C NMR (TFA-*d*) δ=75.4, 78.0, 125.9 (2C), 126.3 (2C), 129.6 (2C), 131.5, 132.0 (2C), 138.1, 141.8, 144.9 (2C), 145.4, 149.6, 150.5, 154.7, 170.5, and 172.3; IR (KBr) 3074, 1630, 1606, 1555, 1513, 1476, 1348, 1249, 1224, 1153, 1080, 1017, and 855 cm^{-1}; UV ($CHCl_3$) 258 (ε 34000) and 326 nm (7800); MS *m/z* (%) 408 (M^+, 7), 272 (61), 257 (18), 136 (100), 106 (38), and 78 (26).

Found: C, 61.46; H, 4.07; N, 7.04%. Calcd for $C_{21}H_{16}N_2O_7$: C, 61.76; H, 3.95; N, 6.86%.

7: Yellow prisms, mp 165—166 °C (AcOEt–hexane), 11% yield. ^1H NMR δ=5.40 (2H, s), 7.00 (1H, dd, *J*=10.3, 9.9 Hz), 7.19 (1H, t, *J*=9.9 Hz), 7.24 (1H, d, *J*=10.3 Hz), 7.43 (1H, d, *J*=9.9 Hz), 7.67 (2H, d, *J*=8.8 Hz), and 8.26 (2H, d, *J*=8.8 Hz); ^{13}C NMR δ=70.3, 118.6, 122.6, 124.0 (2C), 126.2, 127.7 (2C), 131.5, 133.0, 147.8, 158.2, 163.3, and 170.9; IR (KBr) 3438, 3116, 1608, 1558, 1510, 1424, 1343, 1261, 1092, 1090, 848, 838, 757, and 735 cm^{-1}; UV ($CHCl_3$) 248 (ε 37700), 326 (8600), 364 (7800), and 374 nm (8200); MS *m/z* (%) 273 (M^+, 70), 137 (90), 122 (100), 90 (43), and 78 (38).

Found: *m/z* 273.0637 (M^+). Calcd for $C_{14}H_{11}NO_5$: M, 273.0636.

8: Colorless needles, mp 179—179.5 °C ($CHCl_3$), 19% yield. ^1H NMR (TFA-*d*) δ=5.48 (4H, s), 6.27 (2H, dd, *J*=8.8, 1.8 Hz), 7.67 (4H, d, *J*=8.8 Hz), 7.95 (2H, dd, *J*=8.8, 1.8 Hz), and 8.36 (4H, d, *J*=8.8 Hz); ^{13}C NMR (TFA-*d*) δ=68.3 (2C), 125.5 (2C), 126.1 (4C), 130.5 (4C), 141.1 (2C), 145.2 (2C), 149.6 (2C), and 170.3 (2C); IR (KBr) 3086, 1714, 1612, 1588, 1538, 1449, 1350, 1227, 1175, 1009, 845, 830, and 733 cm^{-1}; UV ($CHCl_3$) 273 nm (ε 45300); MS *m/z* (%) 412 (M^+, 7), 232 (59), 136 (100), 106 (30), and 78 (27).

Found: C, 58.23; H, 4.03; N, 6.80%. Calcd for $C_{20}H_{16}N_2O_8$: C, 58.25; H, 3.91; N, 6.79%.

10: Pale yellow needles, mp 188—190 °C ($CHCl_3$), 24% yield. ^1H NMR (DMSO-d_6) δ=5.12 (2H, s), 5.37 (2H, s), 5.40 (2H, s), 7.06 (1H, dm, *J*=9.6 Hz), 7.15 (1H, dd, *J*=11.4, 9.6 Hz), 7.22 (1H, dm, *J*=11.4 Hz), 7.66 (2H, d, *J*=8.8 Hz), 7.72 (2H, d, *J*=8.8 Hz), 7.77 (2H, d, *J*=8.8 Hz), 8.14 (2H, d, *J*=8.8 Hz), 8.20 (2H, d, *J*=8.8 Hz), and 8.30 (2H, d, *J*=8.8 Hz); ^{13}C NMR (DMSO-d_6) δ=68.9, 70.4, 71.4, 112.5, 119.5, 123.1 (2C), 123.4 (2C), 123.6 (2C), 128.2 (2C), 128.4 (4C), 128.8, 143.8, 144.0, 145.6, 146.8, 147.0, 147.1, 151.4, 158.6, 162.9, and 172.6; IR (KBr) 3075, 1605, 1581, 1547, 1521, 1349, 1233, 1070, 842, and 737 cm^{-1}; UV ($CHCl_3$) 265 (ε 60000), 333 (10800), and 353 nm (9300 sh); MS *m/z* (%) 559 (M^+, 0.3), 424 (29), 408 (27), 289 (46), 273 (51), 153 (54), 151 (53), 137 (100), 107 (32), and 77 (12).

Found: C, 60.05; H, 4.03; N, 7.40%. Calcd for $C_{28}H_{21}N_3O_{10}$: C, 60.11; H, 3.78; N, 7.51%.

11: Pale yellow needles, mp 185—187 °C ($CHCl_3$), 2% yield. ^1H NMR (DMSO-d_6) δ=5.09 (2H, s), 5.16 (2H, s), 5.29 (2H, s), 6.64 (1H, d, *J*=9.5 Hz), 6.97 (1H, d, *J*=11.8 Hz), 7.10 (1H, dd, *J*=11.8, 9.5 Hz), 7.43 (2H, d, *J*=8.8 Hz), 7.53 (2H, d,

J=8.8 Hz), 7.61 (2H, d, J=8.8 Hz), 8.08 (2H, d, J=8.8 Hz), 8.15 (2H, d, J=8.8 Hz), and 8.22 (2H, d, J=8.8 Hz); ^{13}C NMR (DMSO-d_6) δ=70.0, 72.4, 74.2, 108.4, 123.6 (4C), 124.0 (2C), 128.0 (2C), 128.1 (2C), 128.5, 128.7 (2C), 133.1, 133.3, 141.9, 143.6, 144.1, 147.7, 148.1, 152.4, 158.5, 158.7, and 180.6; IR (KBr) 3080, 1629, 1607, 1570, 1520, 1350, 1255, 1153, 1046, 850, 738, and 709 cm^{-1}; UV ($CHCl_3$) 263 (ε 53700) and 331 nm (11700); MS m/z (%) 559 (M^+, 0.7), 424 (50), 396 (26), 288 (64), 273 (34), 153 (22), and 137 (100).

Found: C, 60.07; H, 3.97; N, 7.46%. Calcd for $C_{28}H_{21}N_3O_{10}$: C, 60.11; H, 3.78; N, 7.51%.

12: Yellow powder, mp 203—205 °C (AcOEt–hexane), 17% yield. ^{1}H NMR (DMSO-d_6) δ=5.17 (2H, s), 5.39 (2H, s), 7.08 (1H, d, J=11.4 Hz), 7.10 (1H, d, J=10.3 Hz), 7.35 (1H, dd, J=11.4, 10.3 Hz), 7.67 (2H, d, J=8.1 Hz), 7.70 (2H, d, J=8.1 Hz), 8.13 (2H, d, J=8.1 Hz), and 8.20 (2H, d, J=8.1 Hz); ^{13}C NMR (DMSO-d_6) δ=69.9, 72.0, 113.3, 117.5, 123.1 (2C), 123.4 (2C), 128.4 (2C), 128.6 (2C), 133.4, 143.6, 145.4, 146.8, 147.1 (2C), 160.6, 166.3, and 168.5; IR (KBr) 3450, 3150, 1607, 1583, 1519, 1467, 1345, 1263, 1160, 1046, 1007, and 737 cm^{-1}; UV ($CHCl_3$) 264 (ε 52000), 349 (7400), and 366 nm (6950); MS m/z (%) 424 (M^+, 8), 288 (32), 256 (6), 136 (100), 106 (31), 90 (33), and 78 (35).

Found: C, 59.29; H, 3.91; N, 6.64%. Calcd for $C_{21}H_{16}N_2O_8$: C, 59.43; H, 3.80; N, 6.60%.

13: Colorless needles, mp 178—180 °C ($CHCl_3$), 2% yield. ^{1}H NMR (DMSO-d_6) δ=5.20 (2H, s), 6.88 (1H, d, J=11.4 Hz), 6.97 (1H, d, J=9.2 Hz), 7.13 (1H, dd, J=11.4, 9.2 Hz), 7.85 (2H, d, J=8.8 Hz), and 8.25 (2H, d, J=8.8 Hz); ^{13}C NMR (DMSO-d_6) δ=70.7, 112.2, 119.7, 123.1 (2C), 128.9 (2C), 132.0, 145.3, 145.5, 146.9, 160.4, 163.5, and 169.8; IR (KBr) 3290, 3120, 1603, 1576, 1516, 1470, 1423, 1346, 1290, 1214, 1155, 1056, 1008, and 737 cm^{-1}; UV ($CHCl_3$) 259 (ε 43400), 333 (6000), and 349 nm (5500); MS m/z (%) 289 (M^+, 42), 153 (10), 137 (100), and 90 (22).

Found: m/z 289.0586 (M^+). Calcd for $C_{14}H_{11}NO_6$: M, 289.0586.

15: Colorless plates, mp 135—136 °C (AcOEt–hexane), 66% yield. ^{1}H NMR δ=1.24 (6H, d, J=7.0 Hz), 2.80 (1H, sept, J=7.0 Hz), 5.31 (2H, s), 6.67 (1H, d, J=9.5 Hz), 6.82 (1H, dd, J=11.0, 1.1 Hz), 6.93 (1H, dd, J=11.0, 9.5 Hz), 7.23 (1H, d, J=1.3 Hz), 7.64 (2H, d, J=8.8 Hz), and 8.24 (2H, d, J=8.8 Hz); ^{13}C NMR δ=23.0 (2C), 38.4, 69.4, 114.5, 124.0 (2C), 127.6 (2C), 130.6, 131.2, 135.1, 143.0, 147.7, 157.8, 163.1, and 180.2; IR (KBr) 3110, 2968, 1626, 1595, 1570, 1514, 1480, 1343, 1223, 1010, 902, 850, 787, 737, and 660 cm^{-1}; UV ($CHCl_3$) 242 (ε 30600), 270 (11900 sh), and 322 nm (9800); MS m/z (%) 299 (M^+, 61), 148 (100), 136 (15), 133 (17), 106 (20), 91 (23), and 78 (19).

Found: C, 68.51; H, 5.82; N, 4.42%. Calcd for $C_{17}H_{17}NO_4$: C, 68.21; H, 5.73; N, 4.68%.

16: Colorless needles, mp 114—115 °C (AcOEt–hexane), 34% yield. ^{1}H NMR δ=1.16 (6H, d, J=7.0 Hz), 2.77 (1H, sept, J=7.0 Hz), 5.35 (2H, s), 6.73 (1H, br s), 6.81 (1H, dm, J=10.0 Hz), 7.1—7.2 (2H, m), 7.66 (2H, d, J=8.8 Hz), and 8.26 (2H, d, J=8.8 Hz); ^{13}C NMR δ=23.2 (2C), 38.8, 69.5, 117.8, 124.0 (2C), 126.0, 127.6 (2C), 136.0, 137.0, 143.3, 147.7, 153.7, 162.9, and 180.2; IR (KBr) 3110, 2960, 1596, 1546, 1521, 1493, 1344, 1258, 1219, 1179, 1148, 998, 827, and 737 cm^{-1}; UV ($CHCl_3$) 241 (ε 30300), 269 (11700 sh), and 327 nm (10300); MS m/z (%) 299 (M^+, 36), 148 (100), 136 (15), 133 (19), 106 (18), 91 (24), 89 (13), and 78 (19).

Found: C, 68.51; H, 5.71; N, 4.57%. Calcd for $C_{17}H_{17}NO_4$: C, 68.21; H, 5.73; N, 4.68%.

18: Yellow needles, mp 154—155 °C, 72% yield. ^{1}H NMR (DMSO-d_6) δ=1.17 (6H, d, J=6.6 Hz), 2.87 (1H, sept, J=6.6 Hz), 5.32 (2H, s), 5.41 (2H, s), 6.87 (1H, dd, J=10.2, 1.1 Hz), 7.07 (1H, d, J=1.1 Hz), 7.17 (1H, d, J=10.2 Hz), 7.75 (2H, d, J=8.8 Hz), 7.79 (2H, d, J=8.8 Hz), 8.28 (2H, d, J=8.8 Hz), and 8.29 (2H, d, J=8.8 Hz); ^{13}C NMR (DMSO-d_6) δ=23.1 (2C), 37.2, 69.0, 79.1, 118.1, 118.4, 123.2, 123.5 (6C), 128.1, (4C), 144.5, 147.0, 147.3, 159.2, 160.2, and 172.3; IR (KBr) 2960, 1593, 1517, 1343, 1253, 1135, 1107, 840, and 735 cm^{-1}; UV ($CHCl_3$) 250 (ε 35300), 326 (10900), 353 (9900), and 366 nm (8000 sh); MS m/z (%) 450 (M^+, 14), 314 (59), 299 (32), 164 (12), 136 (100), 106 (31), 90 (23), and 78 (32).

Found: C, 63.80; H, 5.01; N, 6.08%. Calcd for $C_{24}H_{22}N_2O_7$: C, 63.99; H, 4.92; N, 6.22%.

19: Yellow prisms, mp 127—128 °C, 14% yield. ^{1}H NMR (DMSO-d_6) δ=1.23 (6H, d, J=7.0 Hz), 2.75 (1H, sept, J=7.0 Hz), 5.22 (2H, s), 5.26 (2H, s), 6.83 (1H, dd, J=12.0, 1.8 Hz), 6.97 (1H, d, J=12.0 Hz), 7.13 (1H, d, J=1.8 Hz), 7.52 (2H, d, J=8.8 Hz), 7.63 (2H, d, J=8.7 Hz), 8.16 (2H, d, J=8.8 Hz), and 8.21 (2H, d, J=8.7 Hz); ^{13}C NMR (DMSO-d_6) δ=22.8 (2C), 37.8, 71.9, 72.7, 123.6 (2C), 123.9 (2C), 127.8 (2C), 128.5 (2C), 129.1, 132.1, 137.2, 137.4, 143.6, 144.6, 147.6, 147.8, 155.0, 156.5, and 181.0; IR (KBr) 2965, 1604, 1512, 1348, 1240, 1175, 1105, 849, and 737 cm^{-1}; UV ($CHCl_3$) 258 (ε 30150) and 327 nm (5400 sh); MS m/z (%) 450 (M^+, 12), 314 (60), 299 (29), 164 (13), 136 (100), 106 (31), 90 (26), and 78 (34).

Found: m/z 450.1417 (M^+). Calcd for $C_{24}H_{22}N_2O_7$: M, 450.1426.

20: Pale yellow needles, mp 180—181 °C, 8% yield. ^{1}H NMR (DMSO-d_6) δ=1.21 (6H, d, J=7.0 Hz), 2.77 (1H, sept, J=7.0 Hz), 5.22 (2H, s), 5.26 (2H, s), 6.86 (1H, d, J=1.8 Hz), 7.06 (1H, dd, J=12.5, 1.8 Hz), 7.21 (1H, d, J=12.5 Hz), 7.53 (2H, d, J=8.8 Hz), 7.63 (2H, d, J=8.8 Hz); 8.16 (2H, d, J=8.8 Hz), and 8.21 (2H, d, J=8.8 Hz); ^{13}C NMR (DMSO-d_6) δ=22.9 (2C), 37.9, 72.0, 73.0, 123.6 (2C), 123.9 (2C), 126.2, 127.9 (2C), 128.6 (2C), 135.6, 140.4, 143.7, 144.6, 147.7, 147.8, 151.5, 154.4, 158.0, and 180.6; IR (KBr) 2957, 1624, 1601, 1553, 1349, 1264, 1235, 1140, 1086, 1000, 850, and 735 cm^{-1}; UV ($CHCl_3$) 257 (ε 33400) and 323 nm (10600); MS m/z (%) 450 (M^+, 9), 314 (54), 299 (17), 164 (17), 136 (100), 106 (37), 90 (34), and 78 (53).

Found: C, 63.68; H, 5.04; N, 6.01%. Calcd for $C_{24}H_{22}H_2O_7$: C, 63.99; H, 4.92; N, 6.22%.

21: Colorless needles, mp 165—166 °C, 3% yield. ^{1}H NMR δ=1.18 (6H, d, J=6.6 Hz), 2.85 (1H, sept, J=6.6 Hz), 5.28 (2H, s), 5.33 (2H, s), 6.02 (1H, s), 6.29 (1H, d, J=16.5 Hz), 7.56 (2H, d, J=8.8 Hz), 7.57 (2H, d, J=8.8 Hz), 8.23 (2H, d, J=8.8 Hz), 8.24 (2H, d, J=8.8 Hz), and 8.66 (1H, d, J=16.5 Hz); ^{13}C NMR δ=20.2 (2C), 30.8, 64.9, 65.0, 119.1, 122.3, 123.9 (5C), 128.4 (2C), 128.6 (2C), 141.2, 143.0, 143.2, 147.8, 159.2, 165.3, and 166.0; IR (KBr) 2974, 1727, 1598, 1518, 1346, 1276, 1235, 1169, 1138, 1016, 860, 833, and 735 cm^{-1}; UV ($CHCl_3$) 273 nm (ε 39100); MS m/z (%) 454 (M^+, 5), 274 (100), 136 (83), 106 (25), 90 (15), and 78 (21).

Found: C, 60.59; H, 5.15; N, 6.08%. Calcd for $C_{23}H_{22}N_2O_8$: C, 60.79; H, 4.88; N, 6.17%

23: Pale yellow crystals, mp 93—95 °C, 33% yield. ^{1}H NMR δ=1.17 (6H, d, J=6.0 Hz), 2.78 (1H, br s), 5.22 (2H, s), 5.25 (2H, s), 5.33 (2H, s), 6.70 (1H, br s), 6.78 (1H, br s), 7.54 (2H, d, J=8.8 Hz), 7.69 (4H, d, J=8.8 Hz), 8.17 (2H, d, J=8.8 Hz), 8.21 (2H, d, J=8.8 Hz), and 8.27 (2H, d, J=8.8 Hz);

^{13}C NMR δ=23.3 (2C), 31.6, 70.0, 72.4, 72.5, 115.7, 119.7, 123.5, (2C), 123.9 (3C), 124.0 (2C), 127.7 (2C), 127.9 (2C), 128.7 (2C), 143.0, 143.5, 144.8, 147.6, 147.8, 149.5, 152.2, 159.0, 162.4, and 173.8; IR (KBr) 3082, 2964, 1601, 1573, 1519, 1345, 1243, 1194, 1067, 1013, 850, and 737 cm^{-1}; UV ($CHCl_3$) 264 (ε 58100) and 334 nm (11100); MS *m/z* (%) 601 (M^+, 0.5), 466 (59), 450 (55), 330 (47), 315 (100), 303 (47), 180 (61), 167 (82), 153 (55), 151 (67), 137 (76), 107 (37), and 77 (23).

Found: C, 61.76; H, 4.65; N, 6.89%. Calcd for $C_{31}H_{27}N_3O_{10}$: C, 61.89; H, 4.52; N, 6.99%.

24: Yellow needles, mp 169—170 °C (AcOEt–hexane), 10% yield. ^{1}H NMR δ=1.20 (6H, d, *J*=7.0 Hz), 2.79 (1H, sept, *J*=7.0 Hz), 4.27 (1H, br s), 5.31 (2H, s), 5.36 (2H, s), 6.64 (1H, s), 6.93 (1H, s), 7.68 (4H, d, *J*=8.8 Hz), 8.22 (2H, d, *J*=8.8 Hz), and 8.26 (2H, d, *J*=8.8 Hz); ^{13}C NMR δ=23.1 (2C), 38.9, 69.9, 71.8, 114.7, 119.2, 123.7, 123.8 (2C), 124.0 (2C), 127.7 (2C), 129.1 (2C), 143.0, 143.9, 145.5, 147.8, 147.9, 150.7, 158.6, and 161.6; IR (KBr) 2964, 1605, 1520, 1345, 1234, 1199, 1047, 848, 822, and 738 cm^{-1}; UV ($CHCl_3$) 263 (ε 53700) and 328 nm (9800); MS *m/z* (%) 466 (M^+, 12), 422 (20), 330 (21), 303 (56), 167 (100), and 136 (22).

Found: C, 61.93; H, 4.95; N, 5.87%. Calcd for $C_{24}H_{22}N_2O_8$: C, 61.80; H, 4.75; N, 6.01%.

25: Yellow prisms, mp 180—182 °C, 8% yield. ^{1}H NMR δ=1.16 (6H, d, *J*=7.0 Hz), 2.81 (1H, sept, *J*=7.0 Hz), 5.39 (4H, s), 7.01 (2H, s), 7.68 (4H, d, *J*=8.8 Hz), and 8.26 (4H, d, *J*=8.8 Hz); ^{13}C NMR δ=23.8, 39.1, 71.0 (2C), 121.4 (2C), 123.9 (4C), 127.9 (4C), 143.6 (2C), 145.2 (2C), 147.8 (2C), 154.5 (2C), and 161.4 (2C); IR (KBr) 3100, 2966, 1604, 1542, 1518, 1469, 1402, 1344, 1226, 1094, 844, and 737 cm^{-1}; UV ($CHCl_3$) 264 (ε 51300), 330 (8400), 359 (8300), and 374 nm (8200); MS *m/z* (%) 466 (M^+, 22), 330 (34), 315 (51), 180 (26), 136 (100), 106 (41), 90 (43), and 78 (49).

Found: C, 61.76; H, 4.65; N, 5.93%. Calcd for $C_{24}H_{22}N_2O_8$: C, 61.80; H, 4.75; N, 6.01%.

Reactions of 12, 25, and 24 with 2. Under conditions similar to those described above, the reactions of **12, 25,** and **24** with **2** gave **10** (61% yield), **23** (42% yield), and **23** (56% yield), respectively.

Base-Induced Rearrangement of 4-Nitrobenzyl Ethers. A Typical Example. An HMPA solution (3.5 cm^3) of NaH (3.5 mg) and **3** (59 mg) was stirred at room temperature for 1 h. The mixture was diluted with water, acidified with 5% aqueous HCl solution (pH=3), and extracted with AcOEt. The extract was dried with $MgSO_4$ and chromatographed on a silica-gel column (AcOEt:hexane=1:1) to give 19 mg (32% yield) of **26** and 7.5 mg (13% yield) of recovered **3**.

26: Yellow powder, mp 156—158 °C. ^{1}H NMR (DMSO-d_6) δ=5.31 (2H, s), 5.92 (1H, d, *J*=4.4 Hz), 6.23 (1H, d, *J*=4.4 Hz), 6.81 (1H, dd, *J*=10.3, 3.0 Hz), 6.99 (1H, d, *J*=13.2 Hz), 7.25 (1H, dd, *J*=13.2, 3.0 Hz), 7.64 (2H, d, *J*=8.8 Hz), 7.74 (2H, d, *J*=8.8 Hz), 7.74 (1H, d, *J*=10.3 Hz), 8.15 (2H, d, *J*=8.8 Hz), and 8.28 (2H, d, *J*=8.8 Hz); ^{13}C NMR (DMSO-d_6) δ=68.6, 69.0, 110.1, 123.1 (2C), 123.6 (2C), 127.5 (2C), 128.5 (2C), 133.2, 134.0, 140.8, 143.3, 146.3, 147.2 (2C), 152.0, 161.0, and 183.2; IR (KBr) 3432, 1606, 1521, 1454, 1348, 1256, 1217, 1195, 859, and 736 cm^{-1}; UV ($CHCl_3$) 266 (ε 21500) and 326 nm (16100); MS *m/z* (%) 408 (M^+, 21), 272 (83), 244 (56), 136 (100), 106 (50), and 78 (46).

Found: C, 61.94; H, 4.16; N, 6.81%. Calcd for $C_{21}H_{16}N_2O_7$: C, 61.76; H, 3.95; N, 6.86%.

27: Yellow prisms, mp 201—203 °C (AcOEt–hexane), 51% yield. ^{1}H NMR (DMSO-d_6) δ=5.94 (2H, d, *J*=4.4 Hz), 6.24 (2H, d, *J*=4.4 Hz), 7.3—7.4 (2H, m), 7.63 (4H, d, *J*=8.8 Hz), 7.9—8.0 (2H, m), and 8.15 (4H, d, *J*=8.8 Hz); ^{13}C NMR (DMSO-d_6) δ=70.0 (2C), 123.1 (4C), 127.9 (4C), 133.7 (2C), 133.8 (2C), 146.4 (2C), 151.2 (2C), 154.2 (2C), and 182.7; IR (KBr) 3415, 1597, 1519, 1343, 1107, 1074, 1036, and 740 cm^{-1}; UV ($CHCl_3$) 272 (ε 24500) and 322 nm (12000); MS *m/z* (%) 408 (M^+, 1), 406 (7), 390 (100), 315 (9), 150 (34), and 77 (18).

Found: C, 61.81; H, 4.14; N, 6.81%. Calcd for $C_{21}H_{16}N_2O_7$: C, 61.76; H, 3.95; N, 6.86%.

28: Yellow prisms, mp 231—232 °C ($CHCl_3$), 25% yield. ^{1}H NMR (DMSO-d_6) δ=5.97 (2H, s), 6.31 (2H, br s), 7.3—7.35 (2H, m), 7.43 (4H, d, *J*=8.8 Hz), 7.85—7.9 (2H, m), and 7.97 (4H, d, *J*=8.8 Hz); ^{13}C NMR (DMSO-d_6) δ=69.8 (2C), 122.8 (4C), 127.7 (4C), 132.8 (2C), 133.5 (2C), 146.1 (2C), 151.0 (2C), 153.5 (2C), and 183.4; IR (KBr) 3280, 1599, 1564, 1515, 1345, 1109, 1059, 859, 835, and 710 cm^{-1}; UV ($CHCl_3$) 273 (ε 23800) and 322 nm (11450); MS *m/z* (%) 408 (M^+, 1), 406 (8), 390 (100), 315 (15), 165 (31), 150 (39), 104 (26), and 77 (26).

Found: C, 61.83; H, 4.07; N, 6.70%. Calcd for $C_{21}H_{16}N_2O_7$: C, 61.76; H, 3.95; N, 6.86%.

30: Yellow powder, mp 185—187 °C (AcOEt–hexane), 33% yield. ^{1}H NMR δ=5.15 (2H, s), 5.25 (2H, s), 6.00 (1H, s), 7.06 (1H, dd, *J*=12.0, 8.9 Hz), 7.16 (1H, dm, *J*=12.0 Hz), 7.47 (1H, dm, *J*=8.9 Hz), 7.51 (2H, d, *J*=8.8 Hz), 7.53 (2H, d, *J*=8.8 Hz), 7.63 (2H, d, *J*=8.8 Hz), 8.13 (2H, d, *J*=8.8 Hz), 8.18 (2H, d, *J*=8.8 Hz), and 8.20 (2H, d, *J*=8.8 Hz); ^{1}H NMR (DMSO-d_6) δ=5.04 (1H, d, *J*=12.8 Hz), 5.13 (1H, d, *J*=12.8 Hz), 5.37 (2H, s), 6.10 (1H, d, *J*=4.4 Hz), 6.34 (1H, d, *J*=4.4 Hz), 7.29 (1H, dd, *J*=11.7, 9.2 Hz), 7.47 (1H, d, *J*=11.7 Hz), 7.59 (1H, d, *J*=9.2 Hz), 7.63 (2H, d, *J*=8.8 Hz), 7.67 (2H, d, *J*=8.8 Hz), 7.84 (1H, d, *J*=8.8 Hz), 8.09 (2H, d, *J*=8.8 Hz), 8.16 (2H, d, *J*=8.8 Hz), and 8.19 (2H, d, *J*=8.8 Hz); ^{13}C NMR δ=72.2, 72.5, 75.5, 123.6 (4C), 123.7, 124.0 (3C), 127.1 (2C), 127.8 (2C), 128.4 (2C), 129.1, 129.7, 133.4, 143.0, 144.1, 147.4, 149.3, 151.4, 155.1, 158.3, and 180.1; ^{13}C NMR (DMSO-d_6) δ=69.8, 70.7, 71.2, 123.1 (4C), 123.4 (2C), 126.7, 126.9, 127.9 (2C), 128.3 (2C), 128.4 (2C), 129.8, 131.0, 144.0, 145.2, 146.7, 147.0, 151.5, 153.2, 157.6, and 177.9; IR (KBr) 3438, 1606, 1512, 1348, 1254, 1167, 853, 821, and 710 cm^{-1}; UV ($CHCl_3$) 265 (ε 48800), 329 (9800), and 357 nm (7000 sh); MS *m/z* (%) 559 (M^+, 0.5), 422 (43), 408 (24), 237 (23), 151 (100), 137 (87), 121 (26), and 107 (23)

Found: C, 60.28; H, 3.96; N, 7.62%. Calcd for $C_{28}H_{21}N_3O_{10}$: C, 60.11; H, 3.78; N, 7.51%.

31: A pale yellow oil, 63% yield. ^{1}H NMR δ=1.24 (6H, d, *J*=7.0 Hz), 2.85 (1H, sept, *J*=7.0 Hz), 3.99 (1H, br s), 5.90 (1H, s), 6.97 (1H, dd, *J*=11.7, 1.1 Hz), 6.98 (1H, dd, *J*=9.1, 1.1 Hz), 7.10 (1H, dd, *J*=11.7, 9.1 Hz), 7.47 (1H, d, *J*=1.1 Hz), 7.62 (2H, d, *J*=8.8 Hz), and 8.17 (2H, d, *J*=8.8 Hz); ^{13}C NMR δ=23.0, 23.1, 38.4, 76.0, 123.5 (2C), 127.2 (2C), 131.0, 137.6, 137.9, 139.6, 147.2, 149.6, 151.9, 155.8, and 186.6; IR (NaCl) 3367, 2977, 1628, 1598, 1520, 1346, 1108, and 860 cm^{-1}; UV (MeOH) 215 (ε 20600), 235 (20800), 277 (12200), 305 (10500), and 320 nm (9900); MS *m/z* (%) 299 (M^+, 100), 149 (93), 105 (17), 77 (23), and 43 (20).

Found: C, 68.50; H, 5.76; N, 4.74%. Calcd for $C_{17}H_{17}NO_4$: C, 68.21; H, 5.73; N, 4.68%.

32: A pale yellow oil, 74% yield. ^{1}H NMR δ=1.22 (6H, d, *J*=7.0 Hz), 2.78 (1H, sept, *J*=7.0 Hz), 3.60 (1H, br s), 5.84 (1H, s), 7.0—7.1 (3H, m), 7.37 (1H, m), 7.62 (2H, d, *J*=8.8 Hz), and 8.17 (2H, d, *J*=8.8 Hz); ^{13}C NMR δ=22.7, 22.8, 38.2, 75.2, 123.5

(2C), 127.2 (2C), 132.9, 135.4, 137.1, 138.7, 147.3, 149.4, 152.2, 158.0, and 186.9; IR (NaCl) 3375, 3027, 1628, 1606, 1552, 1526, 1348, 1090, and 842 cm^{-1}; UV (MeOH) 216 (ε 20800), 237 (20800), 276 (15700), and 316 nm (8300 sh); MS m/z (%) 299 (M^+, 100), 256 (55), 149 (23), and 77 (13).

Found: m/z 299.1157 (M^+). Calcd for $C_{17}H_{17}NO_4$: M, 299.1157.

33: Yellow crystals, mp 219—221 °C, 36% yield. ^1H NMR (DMSO-d_6) δ=1.23 (6H, d, J=7.0 Hz), 2.94 (1H, sept, J=7.0 Hz), 5.92 (1H, d, J=2.2 Hz), 5.96 (1H, d, J=2.2 Hz), 6.18 (1H, d, J=4.1 Hz), 6.28 (1H, d, J=4.1 Hz), 7.24 (1H, dd, J=9.5, 1.4 Hz), 7.63 (2H, d, J=8.8 Hz), 7.64 (2H, d, J=8.8 Hz), 7.85 (1H, d, J=9.5 Hz), 7.92 (1H, d, J=1.4 Hz), 8.14 (2H, d, J=8.8 Hz), and 8.15 (2H, d, J=8.8 Hz); ^{13}C NMR (DMSO-d_6) δ=22.8, 22.9, 37.4, 69.5, 70.2, 123.1 (4C), 127.7 (2C), 127.9 (2C), 129.5, 134.0, 134.6, 146.3, 146.4, 151.3, 151.5, 151.9, 153.4, 154.1, and 182.1; IR (KBr) 3495, 2960, 1594, 1552, 1515, 1342, 1074, 852, 831, and 703 cm^{-1}; UV ($CHCl_3$) 272 (ε 24200) and 324 nm (14000 sh); MS m/z (%) 450 (M^+, 1), 448 (9), 432 (100), 357 (11), 165 (12), 150 (35), 120 (11), 104 (26), 77 (14), and 76 (11).

Found: C, 63.91; H, 5.12; N, 6.20%. Calcd for $C_{24}H_{22}N_2O_7$: C, 63.99; H, 4.92; N, 6.22%.

34: Yellow crystals, mp 205—207 °C, 22% yield. ^1H NMR (DMSO-d_6) δ=1.22 (6H, d, J=7.0 Hz), 2.92 (1H, sept, J=7.0 Hz), 5.96 (1H, d, J=4.5 Hz), 5.98 (1H, d, J=4.5 Hz), 6.25 (1H, d, J=4.4 Hz), 6.34 (1H, d, J=4.4 Hz), 7.20 (1H, dd, J=9.5, 1.4 Hz), 7.43 (2H, d, J=8.8 Hz), 7.46 (2H, d, J=8.8 Hz), 7.78 (1H, d, J=9.5 Hz), 7.85 (1H, d, J=1.4 Hz), 7.97 (2H, d, J=8.8 Hz), and 7.98 (2H, d, J=8.8 Hz); ^{13}C NMR (DMSO-d_6) δ=22.8, 22.9, 37.3, 69.5, 70.1, 79.1, 122.8 (3C), 127.5 (2C), 127.6, 127.7 (2C), 129.2, 133.2, 133.8, 146.1 (2C), 151.1, 151.2, 151.3, 153.7, and 182.8; IR (KBr) 3485, 2965, 1598, 1519, 1344, 1080, 856, 832, and 707 cm^{-1}; UV ($CHCl_3$) 242 (ε 23200), 272 (23100), and 325 nm (12700 sh); MS m/z (%) 450 (M^+, 4), 448 (41), 432 (100), 298 (36), 150 (66), 120 (20), 104 (38), 77 (19), and 76 (19).

Found: C, 64.22; H, 5.21; N, 6.23%. Calcd for $C_{24}H_{22}N_2O_7$: C, 63.99; H, 4.92; N, 6.22%.

36: A yellow oil, 27% yield. ^1H NMR δ=1.24 (6H, d, J=6.4 Hz), 2.86 (1H, sept, J=6.4 Hz), 5.10 (2H, s), 5.24 (2H, s), 5.98 (1H, s), 7.00 (1H, br s), 7.44 (1H, br s), 7.53 (4H, d, J=8.0 Hz), 7.62 (2H, d, J=8.0 Hz), 8.11 (2H, d, J=8.0 Hz), 8.17 (2H, d, J=8.0 Hz), and 8.21 (2H, d, J=8.0 Hz); ^1H NMR (DMSO-d_6) δ=1.23 (6H, d, J=6.6 Hz), 2.98 (1H, sept, J=6.6 Hz), 5.00 (1H, d, J=11.8 Hz), 5.08 (1H, d, J=11.8 Hz), 5.39 (2H, s), 6.10 (1H, s), 6.38 (1H, br s), 7.23 (1H, s), 7.59 (2H, d, J=8.8 Hz), 7.64 (2H, d, J=8.8 Hz), 7.73 (2H, d, J=8.8 Hz), 7.81 (1H, s), 8.09 (2H, d, J=8.8 Hz), 8.16 (2H, d, J=8.8 Hz), and 8.19 (2H, d, J=8.8 Hz); ^{13}C NMR δ=23.1, 23.2, 38.6, 72.2, 72.7, 76.3, 123.6 (4C), 123.7, 123.9 (2C), 125.6, 127.0, 127.2 (2C), 127.8 (2C), 128.4 (2C), 135.3, 143.2, 144.2, 147.3, 149.5, 150.5, 151.0, 153.7, 158.7, and 179.8; ^{13}C NMR (DMSO-d_6) δ=23.1, 23.2, 38.6, 72.2, 72.7, 76.3, 123.6 (4C), 123.7, 123.9 (2C), 125.6, 127.0, 127.2 (2C), 127.8 (2C), 128.4 (2C), 135.3, 143.2, 144.2, 147.3, 149.5, 150.5, 151.0, 153.7, 158.7, and 179.8; IR (NaCl) 3380, 2962, 1605, 1522, 1348, 1260, 1167, 1110, 1013, 853, and 739 cm^{-1}; UV ($CHCl_3$) 265 (ε 39700) and 329 nm (8900); MS m/z (%) 601 (M^+, 1), 583 (2), 464 (100), 450 (93), 330 (78), 315 (45), 151 (62), and 137 (63).

Found: C, 62.12; H, 4.68; N, 7.10%. Calcd for $C_{31}H_{27}N_3O_{10}$: C, 61.89; H, 4.52; N, 6.99%.

PDC-Oxidation. A Typical Example. A CH_2Cl_2 solution (20 cm^3) of **27** (39 mg), PDC (180 mg), and celite (600 mg) was stirred at room temperature for 16 h. The mixture was chromatographed on a silica-gel column (AcOEt:hexane=1:1) to give 31.7 mg (82% yield) of **29**.

29: Pale yellow needles, mp 261—265 °C (decomp). ^1H NMR (DMSO-d_6) δ=7.55—7.6 (2H, m), 7.8—7.85 (2H, m), 8.05 (4H, d, J=9.2 Hz), and 8.29 (4H, d, J=9.2 Hz); ^{13}C NMR (DMSO-d_6) δ=123.9 (4C), 129.9 (4C), 137.2 (2C), 137.9 (2C), 140.1 (2C), 150.0 (2C), 150.7 (2C), 183.8, and 194.4 (2C); IR (KBr) 3108, 1683, 1602, 1561, 1521, 1353, 1271, 1241, 885, 850, and 749 cm^{-1}; UV ($CHCl_3$) 270 (ε 30700) 312 (11100 sh), and 343 nm (6600); MS m/z (%) 404 (M^+, 100), 376 (32), 359 (34), 329 (53), 254 (37), 226 (31), 150 (63), 104 (64), and 76 (53).

Found: C, 62.37; H, 3.11; N, 6.78%. Calcd for $C_{21}H_{12}N_2O_7$: C, 62.38; H, 2.99; N, 6.93%.

35: Pale yellow needles, mp 193—195 °C (AcOEt–hexane), 72% yield. ^1H NMR δ=1.33 (6H, d, J=7.0 Hz), 2.97 (1H, sept, J=7.0 Hz), 7.22 (1H, dd, J=9.2, 1.8 Hz), 7.46 (1H, d, J=1.8 Hz), 7.56 (1H, d, J=9.2 Hz), 7.95 (2H, d, J=8.8 Hz), 7.97 (2H, d, J=8.8 Hz), 8.26 (2H, d, J=8.8 Hz), and 8.27 (2H, d, J=8.8 Hz); ^{13}C NMR δ=22.8 (2C), 38.5, 123.9 (4C), 130.0 (2C), 130.1 (2C), 131.4, 137.9, 138.3, 140.5, 140.7, 148.7, 150.4, 150.5, 150.9, 158.7, 183.6, and 194.2 (2C); IR (KBr) 3110, 2975, 1679, 1602, 1557, 1518, 1347, 1256, and 845 cm^{-1}; UV ($CHCl_3$) 265 (ε 35800) and 316 nm (13600); MS m/z (%) 446 (M^+, 95), 418 (66), 296 (100), 150 (84), 104 (87), and 76 (53).

Found: C, 64.77; H, 4.20; N, 6.54%. Calcd for $C_{24}H_{18}N_2O_7$: C, 64.57; H, 4.06; N, 6.28%.

References

1) T. Nozoe, T. Mukai, and J. Minegishi, *Proc. Jpn. Acad.*, **27**, 419 (1951); W. von E. Doering and C. F. Haskey, *J. Am. Chem. Soc.*, **74**, 5688 (1952); T. Nozoe, T. Mukai, J. Minegishi, and T. Fujisawa, *Sci. Rep. Tohoku Univ., Ser. I*, **37**, 388 (1953); T. Mukai, *Bull. Chem. Soc. Jpn.*, **31**, 852 (1958).

2) T. Nozoe, K. Takase, and H. Matsumura, "Non-Benzenoid Aromatic Compounds, Vol. 13 of Dai Yuki Kagaku (Comprehensive Organic Chemistry), " ed by M. Kotake, Asakura Shoten, Tokyo (1960), pp. 119—133.

3) M. G. Banwell, *Aust. J. Chem.*, **44**, 1 (1991), and references cited therein.

4) H. Takeshita, A. Mori, and H. Suizu, *Bull. Chem. Soc. Jpn.*, **60**, 1429 (1987); H. Takeshita, A. Mori, and H. Suizu, *Chem. Lett.*, **1986**, 593.

 © 1991 The Chemical Society of Japan Bull. Chem. Soc. Jpn., 64, 3313—3323 (1991)

Theoretical Foundation of Prochirality. Chirogenic Sites in an Enantiospheric Orbit

Shinsaku FUJITA
Research Laboratories, Ashigara, Fuji Photo Film Co., Ltd.,
Minami-Ashigara, Kanagawa 250-01
(Received November 19, 1990)

Prochirality is one of the inherent properties of an enantiospheric orbit that is designated by a coset representation $\mathbf{G}(/\mathbf{G}_i)$. Desymmetrization of the $\mathbf{G}(/\mathbf{G}_i)$ orbit is discussed to present a new concept "**H**-chirogenic site". The chirogenic site in the $\mathbf{G}(/\mathbf{G}_i)$ orbit is capable of producing a chiral **H**-molecule under the influence of an appropriate chiral reagent. The condition for the existence of such a chirogenic site is discussed. A convenient method using a desymmetrization lattice is presented for determining chirogenic sites.

The concept of "prochirality" has been proposed by Hanson for specifying the steric course of asymmetric syntheses.[1,2] From the beginning, his definition has been polysemous; and its successor, the IUPAC rule, has afforded two distinct definitions of prochirality (rules E-4.12(a) and (b)).[3] Thus, the intrinsic meaning of the prochirality term ("pro"=before) has thus been changed to connote cases in which chiral compounds are converted into other chiral compounds (IUPAC rule E-4.12(b)). Prelog and Helmchen[4] have used the term "stereogenic" in order to get rid of confusion provided by the prochirality. Although they have carefully avoided the use of the term "prochirality", the essence of their proposal concerning prochirality is to differentiate between reflection-variant and -invariant stereogenic units. Seebach and Prelog[5] have proposed a method of specifying asymmetric syntheses. Hanson's definition and Prelog's proposal are implicity based upon permutation-group theory and play down point-group theory, though the latter is essential to discuss stereochemistry. Moreover, the prochirality has been restricted to molecular systems in which two ligands or faces are differentiated to create a chiral compound.

Mislow and Siegel[6] have discussed the prochirality concept. Their comment can be summarized as follows: Hanson's definition refers to (pro)stereogenicity rather than to prochirality. They have also proposed (pro)^p-chirality, which has been modified by Halevi.[7]

We have presented a new definition of prochirality, which is based on the concept of *chirality fittingness* derived by integrating the permutation- and point-group theories.[8] This definition affords a general approach that treats two or more ligands successfully. The renewed prochirality is one of the symmetrical properties inherent in an enantiospheric orbit. We have summarized our results in the form of a theorem.

Theorem 1.[8] *An enantiospheric orbit is capable of separating into two hemispheric orbits of the same length under a chiral environment, whether the change is reversible or irreversible.*

Then, we have defined a *prochiral* molecule as the one that has at least one enantiospheric orbit. In previous papers,[8,9] we have given a proof of this theorem in a rather intuitive fashion. We have also developed another concept *subduction of coset representations (CRs).*[10] Combining this concept with the chirality fittingness, we have clarified the prochirality to some extent. However, the previous discussion[8] are rather qualitative. In order to understand the renewed prochirality concept comprehensively, a stricter and more detailed discussion is desirable. In a continuation of the work, the present paper deals with discussions on desymmetrization of enantiospheric orbits, where more detailed results are available for formulating prochirality. In addition, the related new concept "chirogenic" is proposed.

Results

Ligands and Local Symmetry. Atoms, functional groups, and faces are three-dimensional objects to be examined in organic stereochemistry. We use the term "ligand" to comprise these objects. The chemical term "ligand" corresponds to the mathematical term "block". A set of equivalent ligands (or blocks) in a molecule is subject to a coset representation $\mathbf{G}(/\mathbf{G}_i)$, in which **G** is the global symmetry of the molecule and $\mathbf{G}_i$ denotes the local symmetry governing each ligand.[11] In this section, we briefly discuss ligands and local symmetry to obtain a minimum set of mathematical concepts.

When $\mathbf{G}_i$ is a subgroup of **G**, we have a coset decomposition,

$$\mathbf{G} = \mathbf{G}_i t_1 + \cdots + \mathbf{G}_i t_r, \tag{1}$$

where $t_1=I$. This decomposition provides a permutation representation of **G**, which is called a coset representation (CR). We use the symbol $\mathbf{G}(/\mathbf{G}_i)$ to denote the CR. The CR $\mathbf{G}(/\mathbf{G}_i)$ acts on the set of cosets represented by

$$\mathbf{G}/\mathbf{G}_i = \{\mathbf{G}_i t_1, \cdots, \mathbf{G}_i t_r\}. \tag{2}$$

Since we have

$$\mathbf{G}_i t_k (t_k^{-1} \mathbf{G}_i t_k) = \mathbf{G}_i \mathbf{G}_i t_k = \mathbf{G}_i t_k,$$

we obtain the following theorem.

Theorem 2. *The stabilizer of* $\mathbf{G}_i t_k$ *is* $t_k^{-1}\mathbf{G}_i t_k$.

If $\mathbf{G}_i$ and $t_k^{-1}\mathbf{G}_i t_k$ is conjugate within $\mathbf{G}$, then the corresponding CRs ($\mathbf{G}(/\mathbf{G}_i)$ and $\mathbf{G}(/t_k^{-1}\mathbf{G}_i t_k)$) are equivalent,i.e.,

$$\mathbf{G}(/\mathbf{G}_i) \cong \mathbf{G}(/t_k^{-1}\mathbf{G}_i t_k). \tag{3}$$

When an orbit corresponds to the CR $\mathbf{G}(/\mathbf{G}_i)$, we call the orbit a $\mathbf{G}(/\mathbf{G}_i)$ orbit. If we consider a three-dimensional object Ω_1 of $\mathbf{G}_i$ symmetry, we can provide other objects according to $t_k\Omega_1=\Omega_k$ (k=1,2,$\cdots$,r). The set of the r objects, i.e.

$$\Omega = \{\Omega_1,\Omega_2,\cdots,\Omega_r\}$$

is subject to the coset representation $\mathbf{G}(/\mathbf{G}_i)$, when Ω_k corresponds to $\mathbf{G}_i t_k$ in one-to-one fashion. We have reported the correspondence in the light of a regular body.[11] This $\mathbf{G}_i$ of $\mathbf{G}(/\mathbf{G}_i)$ is called the local symmetry that governs each member (block) of Ω.[8] Because the Ω_1 belongs to $\mathbf{G}_i$ symmetry, we have

$$g\Omega_1 = \Omega_1 \text{ (for } \forall g \in \mathbf{G}_i). \tag{4}$$

This equation affords

$$t_k g t_k^{-1}\Omega_k = t_k g t_k^{-1} t_k \Omega_1 = t_k g \Omega_1 = t_k \Omega_1 = \Omega_k \tag{5}$$

for $\forall g \in \mathbf{G}_i$ and k=1,2,$\cdots$,r. Hence, we have the following theorem.

Theorem 3. *Each* $\mathbf{G}_i$*-block* Ω_k(k=1,2,$\cdots$,r) *has stabilizer* $t_k\mathbf{G}_i t_k^{-1}$.

For emphasizing a chemical meaning, we also use the term $\mathbf{G}_i$-ligand in place of the $\mathbf{G}_i$-block. The stabilizer denotes the point group that corresponds to the local symmetry specifying the ligand.

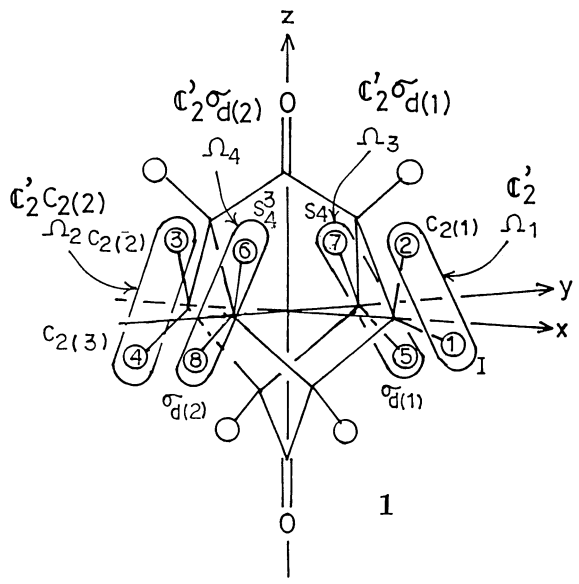

Fig. 1. $\mathbf{C}_2'$-blocks in adamantane-2,6-dione.

Eample **1**. In order to illustrate Theorem 3, let us examine $\mathbf{C}_2'$-blocks in adamantane-2,6-dione (**1**). This molecule belongs to the $\mathbf{D}_{2d}$ group, which is composed of 8 elements (symmetry operations), i.e.,

$$\mathbf{D}_{2d} = \{I,C_{2(1)},C_{2(2)},C_{2(3)},\sigma_{d(1)},S_4^3,S_4,\sigma_{d(2)}\}.$$

Consider the 8 methylene hydrogens in **1** (Fig. 1). We first assign hydrogen no. 1 to the I element. Then, hydrogen no. 2 is assigned to the $C_{2(1)}$ operation, since the action of $C_{2(1)}$ on the hydrogen no. 1 produces the hydrogen no. 2. This treatment is repeated over all of the elements of the $\mathbf{D}_{2d}$ group. As the result, we obtain the following correspondence; $1\leftrightarrow I$, $2\leftrightarrow C_{2(1)}$, $3\leftrightarrow C_{2(2)}$, $4\leftrightarrow C_{2(3)}$, $5\leftrightarrow\sigma_{d(1)}$, $6\leftrightarrow S_4^3$, $7\leftrightarrow S_4$, and $8\leftrightarrow\sigma_{d(2)}$. Let us next consider each methylene. Starting from the above results, we obtain the following correspondence;

$$\Omega_1 = \{1,2\} \leftrightarrow \mathbf{C}_2' = \{I,C_{2(1)}\}$$

$$\Omega_2 = C_{2(2)}\Omega_1 = \{3,4\} \leftrightarrow \mathbf{C}_2'C_{2(2)} = \{C_{2(2)},C_{2(3)}\}$$

$$\Omega_3 = \sigma_{d(1)}\Omega_1 = \{5,7\} \leftrightarrow \mathbf{C}_2'\sigma_{d(1)} = \{\sigma_{d(1)},S_4\}$$

$$\Omega_4 = \sigma_{d(2)}\Omega_1 = \{6,8\} \leftrightarrow \mathbf{C}_2'\sigma_{d(2)} = \{\sigma_{d(2)},S_4^3\}$$

This correspondence is associated with the coset decomposition,

$$\mathbf{D}_{2d} = \mathbf{C}_2' + \mathbf{C}_2'C_{2(2)} + \mathbf{C}_2'\sigma_{d(1)} + \mathbf{C}_2'\sigma_{d(2)}. \tag{6}$$

According to this equation, the coset representation $\mathbf{D}_{2d}(/\mathbf{C}_2')$ governs

$$\mathbf{D}_{2d}/\mathbf{C}_2' = \{\mathbf{C}_2',\mathbf{C}_2'C_{2(2)},\mathbf{C}_2'\sigma_{d(1)},\mathbf{C}_2'\sigma_{d(2)}\}.$$

as well as

$$\Omega = \{\Omega_1,\Omega_2,\Omega_3,\Omega_4\}.$$

We have four $\mathbf{C}_2'$-blocks (Ω_1 to Ω_4), the stabilizers of which are obtained by means of Theorem 3. These results are consistent with their chemical meanings.

Methylene	Stabilizer
Ω_1	$\mathbf{C}_2'=\{I,\ C_{2(1)}\}$
Ω_2	$C_{2(2)}\mathbf{C}_2'C_{2(2)}^{-1}=\mathbf{C}_2'=\{I,\ C_{2(1)}\}$
Ω_3	$\sigma_{d(1)}\mathbf{C}_2'\sigma_{d(1)}^{-1}=\mathbf{C}_2''=\{I,\ C_{2(2)}\}$
Ω_4	$\sigma_{d(2)}\mathbf{C}_2'\sigma_{d(2)}^{-1}=\mathbf{C}_2''=\{I,\ C_{2(2)}\}$

Desymmetrization of Enantiospheric Orbits. When $\mathbf{G}$ is an achiral group and $\mathbf{G}_i$ is its chiral subgroup, the $\mathbf{G}$-($/\mathbf{G}_i$) orbit is defined as an *enantiospheric* orbit.[8] The purpose of this section is to examine the desymmetrization corresponding to the subduction $\mathbf{G}(/\mathbf{G}_i)\downarrow\mathbf{G}^{\max}$, where $\mathbf{G}^{\max}$ is the subgroup that contains all of the proper

rotations of **G**. Although a general discussion on the subduction of coest representations has appeared in our previous papers,[10] the present section provides a more specified discussions concerning enantiospheric orbits.

The corresponding coset decomposition (Eq. 1) contains a transversal $\{t_1,t_2,\cdots,t_r\}$, in which $r/2$ elements are proper rotations and the remaining $r/2$ elements are improper rotations. When we designate the latter half by the symbol $u_k(k=1,2,\cdots,r/2)$, we are able to rewrite the coset decomposition as follows.

$$\mathbf{G} = (\mathbf{G}_i t_1 + \mathbf{G}_i t_2 + \cdots + \mathbf{G}_i t_k + \cdots + \mathbf{G}_i t_q) + (\mathbf{G}_i u_1 + \mathbf{G}_i u_2 + \cdots + \mathbf{G}_i u_k + \cdots + \mathbf{G}_i u_q), \quad (7)$$

where $q=r/2$ and $u_k=t_k u_1$. Note that u_1 can be an arbitrary improper rotation during the discussion in this section. The $\mathbf{G}/\mathbf{G}_i$ set is divided into two parts,

$$\mathbf{G}^+/\mathbf{G}_i = \{\mathbf{G}_i t_1, \mathbf{G}_i t_2, \cdots, \mathbf{G}_i t_q\}, \quad (8)$$

and

$$\mathbf{G}^-/\mathbf{G}_i = \{\mathbf{G}_i u_1, \mathbf{G}_i u_2, \cdots, \mathbf{G}_i u_q\}. \quad (9)$$

Obviously, each coset in $\mathbf{G}^+/\mathbf{G}_i$ contains proper rotation and $\mathbf{G}^-/\mathbf{G}_i$ is concerned with improper rotations. Because we have $\mathbf{G}_i t_k t_l \in \mathbf{G}^+/\mathbf{G}_i$, $\mathbf{G}_i t_k u_l \in \mathbf{G}^-/\mathbf{G}_i$, $\mathbf{G}_i u_k t_l \in \mathbf{G}^-/\mathbf{G}_i$ and $\mathbf{G}_i u_k u_l \in \mathbf{G}^+/\mathbf{G}_i$, the two parts, $\mathbf{G}^+/\mathbf{G}_i$ and $\mathbf{G}^-/\mathbf{G}_i$, are mirror images to each other.

Since $\mathbf{G}^{\max}$ is the subgroup that contains all of the proper rotations of **G**, we have a coset representation by using $\{t_1,t_2,\cdots,t_q\}$, i.e.,

$$\mathbf{G}^{\max} = \mathbf{G}_i t_1 + \mathbf{G}_i t_2 + \cdots + \mathbf{G}_i t_q, \quad (10)$$

because $\mathbf{G}_i$ is also a subgroup of $\mathbf{G}^{\max}$. Obviously, the subgroup $\mathbf{G}^{\max}$ is a normal subgroup of **G**, where $|\mathbf{G}^{\max}|=|\mathbf{G}|/2$.

Since any coset $(\mathbf{G}^{\max}u_k)$ contains all of the improper rotations $(k=1,2,\cdots,q)$, we can select u_1 as a representative without losing generality. Thereby, we have

$$\mathbf{G} = \mathbf{G}^{\max} + \mathbf{G}^{\max}u_1. \quad (11)$$

When Eq. 10 is introduced into Eq. 11, we have $u_k=t_k u_1(k=1,2,\cdots,q)$.

We rewrite the notation of Ω_k as follows: $\Omega_k^+=\Omega_k$ $(1\leqslant k\leqslant q)$ and $\Omega_k^-=\Omega_{q+k}$ $(1\leqslant k\leqslant q)$. Thereby, Ω is divided into two subsets,i.e.,

$$\boldsymbol{\Omega}^+ = \{\Omega_1^+,\Omega_2^+,\cdots,\Omega_q^+\}, \quad (12)$$

$$\boldsymbol{\Omega}^- = \{\Omega_1^-,\Omega_2^-,\cdots,\Omega_q^-\}, \quad (13)$$

We have the following correspondences, $\Omega_k^+ \leftrightarrow \Omega_i t_k$ and $\Omega_k^- \leftrightarrow \Omega_i u_k$, where $k=1,2,\cdots,q$. Obviously, $\boldsymbol{\Omega}^+$ and $\boldsymbol{\Omega}^-$ are mirror images to each other under the action of the **G** group. As for Example 1 (Fig. 1), we construct $\boldsymbol{\Omega}^+=\{\Omega_1,\Omega_2\}$ and $\boldsymbol{\Omega}^-=\{\Omega_3,\Omega_4\}$, which are the mirror images to each other. The two sets coincide with each other under the action of the improper rotations of $\mathbf{D}_{2d}$, but not under the action of the proper rotations of $\mathbf{D}_{2d}$.

Since Theorem 3 holds for any Ω_k^-, $u_k\mathbf{G}_i u_k^{-1}$ is the stabilzer of the Ω_k^-. Consider $u_l \in \mathbf{G}_i u_l$. Since u_l and u_k are improper rotations (i.e., $u_l,u_k\mathbf{G}^{\max}u_1$), Eq. 11 indicates that there exists a proper rotation (t_k) that satisfies $t_k=u_k u_l^{-1}\in\mathbf{G}^{\max}$. Hence, we have $u_k=t_k u_l$. It follows that

$$u_k\mathbf{G}_i u_k^{-1} = t_k u_l \mathbf{G}_i (t_k u_l)^{-1} = t_k(u_l\mathbf{G}_i u_l^{-1})t_k^{-1} \quad (14)$$

Here, we consider two cases:

Case (a) there exists an improper rotation (u_l) that satisfies $u_l\mathbf{G}_i u_l^{-1}=\mathbf{G}_i$ (i.e. $u_l\mathbf{G}_i=\mathbf{G}_i u_l$) and

Case (b) there exists no improper rotation (u_l) that satisfies $u_l\mathbf{G}_i u_l^{-1}\mathbf{G}_i$ (i.e., $u_l\mathbf{G}_i\neq\mathbf{G}_i u_l$ for $\forall u_l\in\mathbf{G}^{\max}u_1$).

In Case (a), Eq. 14 is further converted into

$$u_k\mathbf{G}_i u_k^{-1} = t_k(u_l\mathbf{G}_i u_l^{-1})t_k^{-1} = t_k\mathbf{G}_i t_k^{-1}.$$

This equation means that the stabilizer of Ω_k^- is $t_k\mathbf{G}_i t_k^{-1}$, which is identical with that of Ω_k^+. Because the stabilizer $t_k\mathbf{G}_i t_k^{-1}$ is a chiral subgroup of **G**, it is also a subgroup of $\mathbf{G}^{\max}$. Hence, all of the $t_k\mathbf{G}_i t_k^{-1}$'s are conjugate to $\mathbf{G}_i$ under the action of $\mathbf{G}^{\max}$ as well as that of **G**. Then, we have

$$\mathbf{G}^{\max}(/u_k\mathbf{G}_i u_k^{-1}) \cong \mathbf{G}^{\max}(/t_k\mathbf{G}_i t_k^{-1}) \cong \mathbf{G}^{\max}(/\mathbf{G}_i) \text{ for } \boldsymbol{\Omega}^+$$

and

$$\mathbf{G}^{\max}(/t_k\mathbf{G}_i t_k^{-1}) \cong \mathbf{G}^{\max}(/\mathbf{G}_i) \text{ for } \boldsymbol{\Omega}^-$$

for $k=1,2,\cdots,q$. It follows that the subduction $\mathbf{G}$-$(/\mathbf{G}_i)\downarrow\mathbf{G}^{\max}$ produces two $\mathbf{G}^{\max}(/\mathbf{G}_i)$ orbits (i.e. $\boldsymbol{\Omega}^+$ and $\boldsymbol{\Omega}^-$ as $\mathbf{G}^{\max}$-sets).

In case (b), $\mathbf{G}_i$ is not conjugate to any $u_l\mathbf{G}_i u_l^{-1}$ within $\mathbf{G}^{\max}$. Equation 14 indicates that $u_k\mathbf{G}_i u_k^{-1}$ $(k=1,2,\cdots,q)$ is conjugate to $u_l\mathbf{G}_i u_l^{-1}$ within $\mathbf{G}^{\max}$. Obviously, $t_k\mathbf{G}_i t_k^{-1}$ $(k=1,2,\cdots,q)$ is conjugate to $\mathbf{G}_i$ within $\mathbf{G}^{\max}$. These facts mean that $\mathbf{G}(/\mathbf{G}_i)\downarrow\mathbf{G}^{\max}$ produces two orbits according to the following equation,

$$\mathbf{G}(/\mathbf{G}_i)\downarrow\mathbf{G}^{\max} = \mathbf{G}^{\max}(/\mathbf{G}_i) + \mathbf{G}^{\max}(/\mathbf{G}_i'),$$

where $\mathbf{G}_i'=u_l\mathbf{G}_i u_l^{-1}$. As a result, $\boldsymbol{\Omega}^+$ and $\boldsymbol{\Omega}^-$ are governed by $\mathbf{G}^{\max}(/\mathbf{G}_i)$ and $\mathbf{G}^{\max}(/\mathbf{G}_i')$, respectively. The above discussions are summarized as follows.

Theorem 4. *Let* **G** *be an achiral point group. Consider an enantiospheric orbit governed by* $\mathbf{G}(/\mathbf{G}_i)$, *where* $\mathbf{G}_i$ is a chiral subgroup of **G**. *Let* $\mathbf{G}^{\max}$ *be a maximal chiral subgroup of* **G**. *Then, there are two possibilities.*

$$\text{Case (a): } \mathbf{G}(/\mathbf{G}_i)\downarrow\mathbf{G}^{\max} = 2\mathbf{G}^{\max}(/\mathbf{G}_i) \quad (15)$$

$$\text{Case (b): } \mathbf{G}(/\mathbf{G}_i)\downarrow\mathbf{G}^{\max} = \mathbf{G}^{\max}(/\mathbf{G}_i) + \mathbf{G}^{\max}(/\mathbf{G}_i'), \quad (16)$$

Table 1. Subduction of Coset Representations for $\mathbf{D}_{2d}$ Point Group

	$\downarrow\mathbf{C}_1$	$\downarrow\mathbf{C}_2$	$\downarrow\mathbf{C}_2'$	$\downarrow\mathbf{C}_s$	$\downarrow\mathbf{S}_4$	$\downarrow\mathbf{C}_{2v}$	$\downarrow\mathbf{D}_2$	$\downarrow\mathbf{D}_{2d}$
$\mathbf{D}_{2d}(/\mathbf{C}_1)$	$8\mathbf{C}_1(/\mathbf{C}_1)$	$4\mathbf{C}_2(/\mathbf{C}_1)$	$4\mathbf{C}_2'(/\mathbf{C}_1)$	$4\mathbf{C}_s(/\mathbf{C}_1)$	$2\mathbf{S}_4(/\mathbf{C}_1)$	$2\mathbf{C}_{2v}(/\mathbf{C}_1)$	$2\mathbf{D}_2(/\mathbf{C}_1)$	$\mathbf{D}_{2d}(/\mathbf{C}_1)$
$\mathbf{D}_{2d}(/\mathbf{C}_2)^{a)}$	$4\mathbf{C}_1(/\mathbf{C}_1)$	$4\mathbf{C}_2(/\mathbf{C}_2)$	$2\mathbf{C}_2'(/\mathbf{C}_1)$	$2\mathbf{C}_s(/\mathbf{C}_1)$	$2\mathbf{S}_4(/\mathbf{C}_2)$	$2\mathbf{C}_{2v}(/\mathbf{C}_2)$	$2\mathbf{D}_2(/\mathbf{C}_2)$	$\mathbf{D}_{2d}(/\mathbf{C}_2)$
$\mathbf{D}_{2d}(/\mathbf{C}_2')$	$4\mathbf{C}_1(/\mathbf{C}_1)$	$2\mathbf{C}_2(/\mathbf{C}_1)$	$\mathbf{C}_2'(/\mathbf{C}_1)+2\mathbf{C}_2'(/\mathbf{C}_2)$	$2\mathbf{C}_s(/\mathbf{C}_1)$	$\mathbf{S}_4(/\mathbf{C}_1)$	$\mathbf{C}_{2v}(/\mathbf{C}_1)$	$\mathbf{D}_2(/\mathbf{C}_2')+\mathbf{D}_2(/\mathbf{C}_2'')$	$\mathbf{D}_{2d}(/\mathbf{C}_2')$
$\mathbf{D}_{2d}(/\mathbf{C}_s)$	$4\mathbf{C}_1(/\mathbf{C}_1)$	$2\mathbf{C}_2(/\mathbf{C}_1)$	$2\mathbf{C}_2'(/\mathbf{C}_1)$	$\mathbf{C}_s(/\mathbf{C}_1)+2\mathbf{C}_s(/\mathbf{C}_s)$	$\mathbf{S}_4(/\mathbf{C}_1)$	$\mathbf{C}_{2v}(/\mathbf{C}_s)+\mathbf{C}_{2v}(/\mathbf{C}_s')$	$\mathbf{D}_2(/\mathbf{C}_1)$	$\mathbf{D}_{2d}(/\mathbf{C}_s)$
$\mathbf{D}_{2d}(/\mathbf{S}_4)^{a)}$	$2\mathbf{C}_1(/\mathbf{C}_1)$	$2\mathbf{C}_2(/\mathbf{C}_2)$	$\mathbf{C}_2'(/\mathbf{C}_1)$	$\mathbf{C}_s(/\mathbf{C}_1)$	$2\mathbf{S}_4(/\mathbf{S}_4)$	$\mathbf{C}_{2v}(/\mathbf{C}_2)$	$\mathbf{D}_2(/\mathbf{C}_2)$	$\mathbf{D}_{2d}(/\mathbf{S}_4)$
$\mathbf{D}_{2d}(/\mathbf{C}_{2v})$	$2\mathbf{C}_1(/\mathbf{C}_1)$	$2\mathbf{C}_2(/\mathbf{C}_2)$	$\mathbf{C}_2'(/\mathbf{C}_1)$	$2\mathbf{C}_s(/\mathbf{C}_s)$	$\mathbf{S}_4(/\mathbf{C}_2)$	$2\mathbf{C}_{2v}(/\mathbf{C}_{2v})$	$\mathbf{D}_2(/\mathbf{C}_2)$	$\mathbf{D}_{2d}(/\mathbf{C}_{2v})$
$\mathbf{D}_{2d}(/\mathbf{D}_2)^{a)}$	$2\mathbf{C}_1(/\mathbf{C}_1)$	$2\mathbf{C}_2(/\mathbf{C}_2)$	$2\mathbf{C}_2'(/\mathbf{C}_2)$	$\mathbf{C}_s(/\mathbf{C}_1)$	$\mathbf{S}_4(/\mathbf{C}_2)$	$\mathbf{C}_{2v}(/\mathbf{C}_2)$	$2\mathbf{D}_2(/\mathbf{D}_2)$	$\mathbf{D}_{2d}(/\mathbf{D}_2)$
$\mathbf{D}_{2d}(/\mathbf{D}_{2d})$	$\mathbf{C}_1(/\mathbf{C}_1)$	$\mathbf{C}_2(/\mathbf{C}_2)$	$\mathbf{C}_2'(/\mathbf{C}_2)$	$\mathbf{C}_s(/\mathbf{C}_s)$	$\mathbf{S}_4(/\mathbf{S}_4)$	$\mathbf{C}_{2v}(/\mathbf{C}_{2v})$	$\mathbf{D}_2(/\mathbf{D}_2)$	$\mathbf{D}_{2d}(/\mathbf{D}_{2d})$

a) Forbidden CR.

where $\mathbf{G}_i$ *and* $\mathbf{G}_i'$ *are conjugate in* $\mathbf{G}$ *but not conjugate in* $\mathbf{G}^{max}$

This thorem is the basis of Theorem 1, since it indicates that the enantiospheric $\mathbf{G}(/\mathbf{G}_i)$ orbit behaves differently under $\mathbf{G}$ and $\mathbf{G}^{max}$.

Table 1 is a subduction table for $\mathbf{D}_{2d}$ group, which lists all of the subductions concerning the $\mathbf{D}_{2d}$ group by its subgroups. From the data of this table, we select the following examples that illustrate the two possibilities described in Theorem 4.

Example **2.** Let us consider $\mathbf{D}_{2d}(/\mathbf{C}_1)\downarrow\mathbf{D}_2$. Since the $\mathbf{D}_{2d}(/\mathbf{C}_1)$ is a regular representation, each coset consists of each symmetry operation of $\mathbf{D}_{2d}$. All of the eight cosets (symmetry operations) are commutable with $\mathbf{C}_1$; hence, this case is an example of Case (a). We obtain

$$\mathbf{D}_{2d}(/\mathbf{C}_1)\downarrow\mathbf{D}_2 = 2\mathbf{D}_2(/\mathbf{C}_1). \tag{17}$$

This equation exemplifies Theorem 4.

In order to illustrate the chemical meaning of this equation, let us consider derivation of adamantane-2,6-dione (**1**). The 8 methylene hydrogen atoms (○) are taken into consideration (Fig. 2). A replacement of four hydrogen atoms (○) with other atoms (●) produces a $\mathbf{D}_2$-molecule (**2a**), in which ○'s and ●'s construct $\mathbf{D}_2(/\mathbf{C}_1)$ orbits (Fig. 2). This is an example of case (a), which is algebraically represented by Eq. 17. If ○ and ● are interchanged, the resulting molecule (**2b**) is enantiomeric to **2a**.

Example **3.** Let us examine $\mathbf{D}_{2d}(/\mathbf{C}_2')\downarrow\mathbf{D}_2$(See Example 1). We have obtained the coset decomposition represented by Eq. 6. Since we have $\mathbf{C}_2'\ \sigma_{d(1)} \neq \sigma_{d(1)}\mathbf{C}_2'$ and $\mathbf{C}_2'\ \sigma_{d(2)} \neq \sigma_{d(2)}\mathbf{C}_2'$, Theorem 4 indicates that this is an

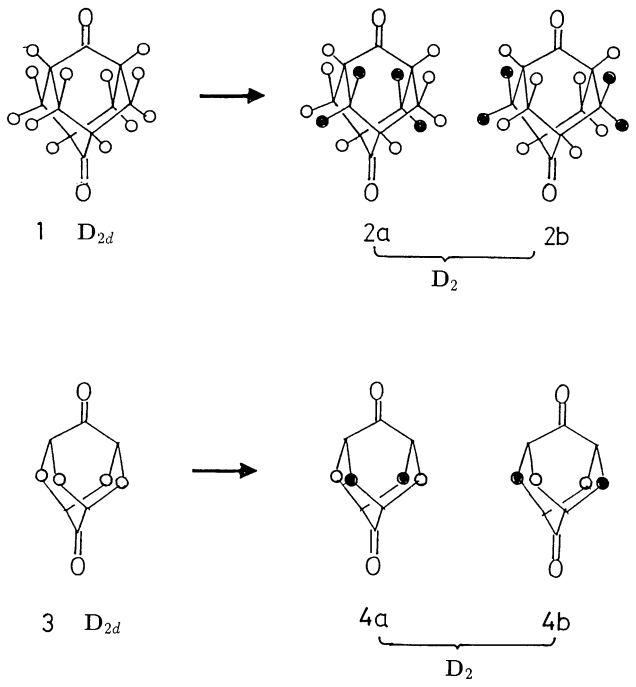

Fig. 2. $\mathbf{D}_2$ molecules derived from a $\mathbf{D}_{2d}$ molecule.

example of Case (b). In fact, we obtain

$$\mathbf{D}_{2d}(/\mathbf{C}_2')\downarrow\mathbf{D}_2 = \mathbf{D}_2(/\mathbf{C}_2') + \mathbf{D}_2(/\mathbf{C}_2''), \tag{18}$$

as shown in the intersection between the $\mathbf{D}_2(/\mathbf{C}_2')$-row and the the $\downarrow\mathbf{D}_2$-column (Table 1).

Chemically speaking, this equation corresponds to such a conversion as the desymmetrization of **3** into **4a** (or **4b**). The four methylene carbons of **3** construct an orbit governed by $\mathbf{D}_{2d}(/\mathbf{C}_2')$. This orbit is divided into a $\mathbf{D}_2(/\mathbf{C}_2')$ orbit and $\mathbf{D}_2(/\mathbf{C}_2'')$ orbit in each of the desymmetrized compounds (**4a** and **4b**).

Example **4**. Let us consider $\mathbf{S}_8(/\mathbf{C}_2)\downarrow\mathbf{C}_4$. We have the following coset decomposition,

$$\mathbf{S}_8 = \mathbf{C}_2 + \mathbf{C}_2\mathbf{C}_4 + \mathbf{C}_2S_8 + \mathbf{C}_2S_8^3. \tag{19}$$

Among the four cosets, the $\mathbf{C}_2S_8$ satisfies the relationship, $\mathbf{C}_2S_8=S_8\mathbf{C}_2$; hence, this case is an example of Case (a). We obtain

$$\mathbf{S}_8(/\mathbf{C}_2)\downarrow\mathbf{C}_4 = 2\mathbf{C}_4(/\mathbf{C}_2). \tag{20}$$

This equation exemplifies Theorem 4. Consider $\mathbf{A}=\mathbf{C}_2+\mathbf{C}_2S_8$. This set is not a group as shown later. Note that $S_8S_8\in\mathbf{C}_2C_4(S_8S_8\notin\mathbf{C}_2)$.

Further Desymmetrization of Enantiospheric Orbits. For Case (a) of Theorem 4, consider the subduced representation (SR) $\mathbf{G}^{max}(/\mathbf{G}_i)\downarrow\mathbf{G}_j$, where $\mathbf{G}_j$ is a subgroup of $\mathbf{G}^{max}$. Suppose that we obtain the following equation

$$\mathbf{G}^{max}(/\mathbf{G}_i)\downarrow\mathbf{G}_j = \sum_{k=1}^{\nu_j}\gamma_k^{(ij)}\mathbf{G}_j(/\mathbf{G}_k^{(j)}), \tag{21}$$

where the multiplicities ($\gamma_k^{(ij)}$'s) are non-negative integers.[10] Since both $\mathbf{G}_i$ and $\mathbf{G}_j$ are subgroups of $\mathbf{G}$ as well as those of $\mathbf{G}^{max}$, Eqs. 15 and 21 afford the following theorem. Note that $(\mathbf{G}(/\mathbf{G}_i)\downarrow\mathbf{G}^{max})\downarrow\mathbf{G}_j=\mathbf{G}(/\mathbf{G}_i)\downarrow\mathbf{G}_j$.

Theorem 5, *Supose that an enantiospheric orbit follows Case (a) of Theorem 4. Then, any chiral subduction,* $\mathbf{G}(/\mathbf{G}_i)\downarrow\mathbf{G}_j$, *is represented by*

$$\mathbf{G}(/\mathbf{G}_i)\downarrow\mathbf{G}_j = \sum_{k=1}^{\nu_j}(2\gamma_k^{(ij)})\mathbf{G}_j(/\mathbf{G}_k^{(j)}), \tag{22}$$

wherein $\mathbf{G}$ *contains proper and improper rotations; and its subgroups,* $\mathbf{G}_i$ *and* $\mathbf{G}_j$, *consist of proper rotations only.* As a result, any $\mathbf{G}_k^{(j)}$ is a proper rotation and any $\mathbf{G}_j(/\mathbf{G}_k^{(j)})$ represents a hemispheric orbit.

This theorem is exemplified by the following examples, which are selected from the data of Tables 1 and 2.

Example **5**. We take the equations,

$$\mathbf{D}_2(/\mathbf{C}_1)\downarrow\mathbf{C}_2 = 2\mathbf{C}_2(/\mathbf{C}_1) \text{ and}$$

$$\mathbf{D}_2(/\mathbf{C}_1)\downarrow\mathbf{C}_2' = 2\mathbf{C}_2'(/\mathbf{C}_1),$$

from Table 2. When we introduce these equations into Eq. 17, we have

$$\mathbf{D}_{2d}(/\mathbf{C}_1)\downarrow\mathbf{C}_2 = 4\mathbf{C}_2(/\mathbf{C}_1) \text{ and}$$

$$\mathbf{D}_{2d}(/\mathbf{C}_1)\downarrow\mathbf{C}_2' = 4\mathbf{C}_2'(/\mathbf{C}_1).$$

As for Case (b) of Theorem 4, consider the SR $\mathbf{G}^{max}(/\mathbf{G}_i)\downarrow\mathbf{G}_j$ where $\mathbf{G}_j$ is a subgroup of $\mathbf{G}^{max}$. Then, we obtain following equations.

$$\mathbf{G}^{max}(/\mathbf{G}_i)\downarrow\mathbf{G}_j = \sum_{k=1}^{\nu_j}\gamma_k^{(ij)}\mathbf{G}_j(/\mathbf{G}_k^{(j)}), \tag{23}$$

$$\mathbf{G}^{max}(/\mathbf{G}_i')\downarrow\mathbf{G}_j = \sum_{k=1}^{\nu_j}\delta_k^{(ij)}\mathbf{G}_j(/\mathbf{G}_k^{(j)}), \tag{24}$$

where the multiplicities ($\gamma_k^{(ij)}$'s and $\delta_k^{(ij)}$'s) are non-negative integers. Since $\mathbf{G}_i$, $\mathbf{G}_i'$ and $\mathbf{G}_j$ are subgroups of $\mathbf{G}$ and of $\mathbf{G}^{max}$, Eqs. 23 and 24 are combined with Eq. 15 to afford the following theorem.

Theorem 6. *Suppose that an enantiospheric orbit follows Case (b) of Theorem 4. Then, any chiral subduction,* $\mathbf{G}(/\mathbf{G}_i)\downarrow\mathbf{G}_j$, *is represented by*

$$\mathbf{G}^{max}(/\mathbf{G}_i)\downarrow\mathbf{G}_j = \sum_{k=1}^{\nu_j}(\gamma_k^{(ij)}+\delta_k^{(ij)})\mathbf{G}_j(/\mathbf{G}_k^{(j)}), \tag{25}$$

wherein $\mathbf{G}$ *contains proper and improper rotations; and its subgroups,* $\mathbf{G}_i$ *and* $\mathbf{G}_j$, *consist of proper rotations only.* As a result, any $\mathbf{G}_k^{(j)}$ is a proper rotation and any $\mathbf{G}_j(/\mathbf{G}_k^{(j)})$ represents a hemispheric orbit.

Theorem 6 is verified as follows.

Example **6**. When we introduce

$$\mathbf{D}_2(/\mathbf{C}_2')\downarrow\mathbf{C}_2 = \mathbf{C}_2(/\mathbf{C}_1) \text{ and}$$

$$\mathbf{D}_2(/\mathbf{C}_2'')\downarrow\mathbf{C}_2 = \mathbf{C}_2(/\mathbf{C}_1)$$

Table 2. Subduction Table of $\mathbf{D}_2$ Group

	$\downarrow\mathbf{C}_1$	$\downarrow\mathbf{C}_2$	$\downarrow\mathbf{C}_2'$	$\downarrow\mathbf{C}_2''$	$\downarrow\mathbf{D}_2$
$\mathbf{D}_2(/\mathbf{C}_1)$	$4\mathbf{C}_1(/\mathbf{C}_1)$	$2\mathbf{C}_2(/\mathbf{C}_1)$	$2\mathbf{C}_2'(/\mathbf{C}_1)$	$2\mathbf{C}_2''(/\mathbf{C}_1)$	$\mathbf{D}_2(/\mathbf{C}_1)$
$\mathbf{D}_2(/\mathbf{C}_2)$	$2\mathbf{C}_1(/\mathbf{C}_1)$	$2\mathbf{C}_2(/\mathbf{C}_2)$	$\mathbf{C}_2'(/\mathbf{C}_1)$	$\mathbf{C}_2''(/\mathbf{C}_1)$	$\mathbf{D}_2(/\mathbf{C}_2)$
$\mathbf{D}_2(/\mathbf{C}_2')$	$2\mathbf{C}_1(/\mathbf{C}_1)$	$\mathbf{C}_2(/\mathbf{C}_1)$	$2\mathbf{C}_2'(/\mathbf{C}_2)$	$\mathbf{C}_2''(/\mathbf{C}_1)$	$\mathbf{D}_2(/\mathbf{C}_2')$
$\mathbf{D}_2(/\mathbf{C}_2'')$	$2\mathbf{C}_1(/\mathbf{C}_1)$	$\mathbf{C}_2(/\mathbf{C}_1)$	$\mathbf{C}_2'(/\mathbf{C}_1)$	$2\mathbf{C}_2''(/\mathbf{C}_2)$	$\mathbf{D}_2(/\mathbf{C}_2'')$
$\mathbf{D}_2(/\mathbf{D}_2)$	$\mathbf{C}_1(/\mathbf{C}_1)$	$\mathbf{C}_2(/\mathbf{C}_2)$	$\mathbf{C}_2'(/\mathbf{C}_2)$	$\mathbf{C}_2''(/\mathbf{C}_2)$	$\mathbf{D}_2(/\mathbf{D}_2)$

into Eq. 18, we have

$$\mathbf{D}_{2d}(/\mathbf{C}_2')\downarrow\mathbf{C}_2 = 2\mathbf{C}_2(/\mathbf{C}_1).$$

This result is identical with the equation listed in the intersection between $\mathbf{D}_{2d}(/\mathbf{C}_2')$-row and $\downarrow\mathbf{D}_2$-column of Table 1. This example produces a result similar to Theorem 5, though the process is different. A more typical example is as follows. Since we have

$$\mathbf{D}_2(/\mathbf{C}_2')\downarrow\mathbf{C}_2 = 2\mathbf{C}_2'(/\mathbf{C}_2) \text{ and}$$

$$\mathbf{D}_2(/\mathbf{C}_2'')\downarrow\mathbf{C}_2 = \mathbf{C}_2''(/\mathbf{C}_1)$$

in Table 2, we introduce these equations into Eq. 18 to obtain

$$\mathbf{D}_{2d}(/\mathbf{C}_2')\downarrow\mathbf{C}_2' = 2\mathbf{C}_2'(/\mathbf{C}_2) + \mathbf{C}_2'(/\mathbf{C}_1).$$

Example 7. For illustrating Theorem 6, let us examine an enantiospheric orbit ($\mathbf{T}_h(/\mathbf{C}_3)$) appearing in the compound (**5**) of $\mathbf{T}_h$ symmetry. The subduction of this orbit into **T** is represented by

$$\mathbf{T}_h(/\mathbf{C}_3)\downarrow\mathbf{T} = 2\mathbf{T}(/\mathbf{C}_3). \tag{26}$$

This subduction is realized by compounds **6a** and **6b**, which belong to **T** symmetry (Fig. 3). These compounds are enantiomeric to each other. The occupation of the orbit is changed from $\mathbf{T}_h(/\mathbf{C}_3(A_8)]$ to $\mathbf{T}[/\mathbf{C}_3(A_4, B_4)]$.[12]

The subduction of the orbit into $\mathbf{C}_2$ is represented by

$$\mathbf{T}_h(/\mathbf{C}_3)\downarrow\mathbf{C}_2 = 4\mathbf{C}_2(/\mathbf{C}_1). \tag{27}$$

This equation is obtained according to Theorem 6 by introducting

$$\mathbf{T}(/\mathbf{C}_3)\downarrow\mathbf{C}_2 = 2\mathbf{C}_2(/\mathbf{C}_1)$$

into Eq. 26.

The chemical meaning of Eq. 27 is illustrated as follows. If we replace appropriate A_2 with B_2 according to this subduction, there appear **7a** and **7b** (Fig. 4). The resulting packing of the divided orbit is expressed by $\mathbf{C}_2[/\mathbf{C}_1(3A_2, B_2)]$.[12]

On the other hand, we introduce the equation,

$$\mathbf{T}(/\mathbf{C}_3)\downarrow\mathbf{C}_3 = \mathbf{C}_3(/\mathbf{C}_1) + \mathbf{C}_3(/\mathbf{C}_3), \tag{28}$$

into Eq. 26. Thereby, we obtain

$$\mathbf{T}_h(/\mathbf{C}_3)\downarrow\mathbf{C}_3 = 2\mathbf{C}_3(/\mathbf{C}_1) + 2\mathbf{C}_3(/\mathbf{C}_3). \tag{29}$$

Figure 5 shows examples of the subduction into $\mathbf{C}_3$. The hemispheric orbits in the products (**8a** and **8b**) are filled in a way of $\mathbf{C}_3[/\mathbf{C}_1(2A_3), /\mathbf{C}_3(A,B)]$, which is in agreement with Eq. 29.

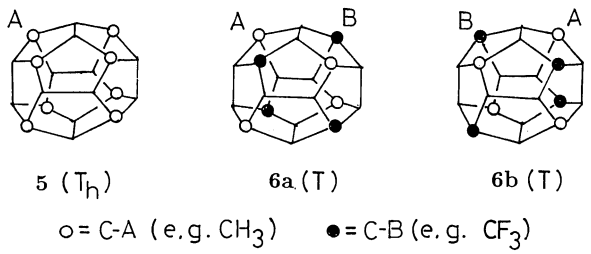

Fig. 3. **T** molecules derived from a $\mathbf{T}_h$ molecule.

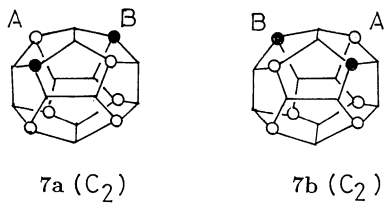

Fig. 4. $\mathbf{C}_2$ molecules derived from a $\mathbf{T}_h$ molecule.

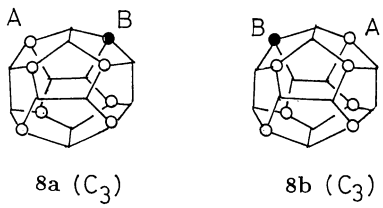

Fig. 5. $\mathbf{C}_3$ molecules derived from a $\mathbf{T}_h$ molecule.

Chirogenic Sites in Direct Chiral Synthesis. We are able to differentiate the two halves (Ω^+ and Ω^-) of an enantiospheric $\mathbf{G}(/\mathbf{G}_i)$ orbit (Ω) under chiral environment. Thereby, we obtain either one of enantiomeric $\mathbf{G}^{max}$-molecules. If we differentiate an appropriate part of the one half from the corresponding mirror image contained in the other half, we can obtain a chiral molecule. However, it is a problem to determine which subsymmetry is realized in this operation. This section deals with this problem. If the differentiation of the parts produces a chiral **H**-molecule, we call the part an **H**-*chirogenic site*. Each chirogenic site is always accompanied with the mirror image counterpart.

To begin with, we examine two extreme cases. The discussions in the preceding section afford the following theorem.

Theorem 7. *Each of the two halves of a* $\mathbf{G}(/\mathbf{G}_i)$ *orbit is a* $\mathbf{G}^{max}$*-chirogenic site.*

When $\mathbf{G}_1=\mathbf{C}_1=\{I\}$, the corresponding $\mathbf{G}(/\mathbf{G}_1)$ is a regular representation of **G**. In this case, we have a simple result as follows.

Theorem 8. *An orbit governed by the regular representation* $\mathbf{G}(/\mathbf{G}_1)$ *has a chirogenic site that corresponds every subgroup.*

Proof. When $\mathbf{G}_1=\mathbf{C}_1$, we have

$$\mathbf{G}(/\mathbf{G}_1)\downarrow\mathbf{G}_i = \frac{|\mathbf{G}|}{|\mathbf{G}_i|}\mathbf{G}_i(\mathbf{G}_1^{(i)}),$$

where $\mathbf{G}_i(/\mathbf{G}_1^{(i)})$ is the regular representation of the $\mathbf{G}_i$ group. This equation indicates that every subduction is accompanied with the division of respective orbits. Hence, the $\mathbf{G}_i(/\mathbf{G}_1^{(i)})$ part in the $\mathbf{G}(/\mathbf{G}_1)$ orbit is $\mathbf{G}_i$-chirogenic.

In order to formulate general cases other than the extreme ones, we should examine division (or conservation) of an orbit through a desymmetrization process. For this purpose, we prove the following theorem.

Theorem 9. *Let $\mathbf{G}_i$ and $\mathbf{G}_j$ be any subgroups of $\mathbf{G}$. If $\mathbf{G}(/\mathbf{G}_i)\downarrow\mathbf{G}_j$ is transitive, then we have $\mathbf{G}_i\mathbf{G}_j=\mathbf{G}$. Conversely, if we have $\mathbf{G}_i\mathbf{G}_j=\mathbf{G}$, then $\mathbf{G}(/\mathbf{G}_i)\downarrow\mathbf{G}_j$ is transitive.*

Proof. (a) Consider a coset $\mathbf{G}_it_\alpha$ appearing in the coset decomposition (Eq. 1). Then, we obtain another coset, $\mathbf{G}_it_\alpha g$, which obviously constructs a double coset, $\mathbf{G}_it_\alpha\mathbf{G}_j$, when g runs over all $g\in\mathbf{G}_j$. Obviously, the double coset corresponds to an orbit produced by the subduction, $\mathbf{G}(/\mathbf{G}_i)\downarrow\mathbf{G}_j$. If $\mathbf{G}(/\mathbf{G}_i)\downarrow\mathbf{G}_j$ is transitive, all of the double cosets should be identical, i.e. $\mathbf{G}_it_\alpha\mathbf{G}_j=\mathbf{G}_it_\beta\mathbf{G}_j$ for $\forall t_\alpha$ *and* $\forall t_\beta$. Let t_β be equal to I. Then, we have $\mathbf{G}_it_\alpha\mathbf{G}_j=\mathbf{G}_i\mathbf{G}_j$. Hence, we have

$$\bigcup_{\alpha=1}^{r}\mathbf{G}_it_\alpha\mathbf{G}_j = \bigcup_{\alpha=1}^{r}\mathbf{G}_i\mathbf{G}_j. = \mathbf{G}_i\mathbf{G}_j.$$

Since the left-hand side contains all of the elements of $\mathbf{G}$ (i.e., $\mathbf{G}=\bigcup_{\alpha=1}^{r}\mathbf{G}_it_\alpha\mathbf{G}_j$), the equation is converted into

$$\mathbf{G} = \mathbf{G}_i\mathbf{G}_j. \tag{30}$$

(b) Conversely, suppose that $\mathbf{G}_i\mathbf{G}_j=\mathbf{G}$. Then, we have $\mathbf{G}_it_1\mathbf{G}_j=\mathbf{G}$ for $t_1=I$. This equation indicates the double coset $\mathbf{G}_it_1\mathbf{G}_j$ contains all of the elements of $\mathbf{G}$. Hence, there appears one orbit during the subduction, $\mathbf{G}(/\mathbf{G}_i)\downarrow\mathbf{G}_j$; that is to say, $\mathbf{G}(/\mathbf{G}_i)\downarrow\mathbf{G}_j$ is transitive.

It should be noted that this thorem holds for any $\mathbf{G}_i$, $\mathbf{G}_j$, and $\mathbf{G}$, no matter whether they are proper or improper. The following examples clarify the scope of the theorem.

Example **8.** (a) For $\mathbf{T}_d(/\mathbf{C}_s)\downarrow\mathbf{T}$, we have $\mathbf{C}_s\mathbf{T}=\mathbf{T}_d$. Hence, Theorem 9 indicates that there emerges no division of the orbit; i.e., $\mathbf{T}_d(/\mathbf{C}_s)\downarrow\mathbf{T}=\mathbf{T}(/\mathbf{C}_1)$.

(b) For $\mathbf{T}_d(/\mathbf{C}_{3v})\downarrow\mathbf{D}_{2d}$, we have $\mathbf{C}_{3v}\mathbf{D}_{2d}=\mathbf{T}_d$. Hence, Theorem 9 indicates that there emerges no division of the orbit; i.e., $\mathbf{T}_d(/\mathbf{C}_{3v})\downarrow\mathbf{D}_{2d}=\mathbf{D}_{2d}(/\mathbf{C}_s)$.

(c) For $\mathbf{T}_d(/\mathbf{C}_{3v})\downarrow\mathbf{D}_{3v}$, we have $\mathbf{C}_{3v}\mathbf{C}_{3v}=\mathbf{C}_{3v}\neq\mathbf{T}_d$. Hence, Theorem 9 indicates that the orbit is divided during the process as follows; $\mathbf{T}_d(/\mathbf{C}_{3v})\downarrow\mathbf{C}_{3v}=\mathbf{C}_{3v}(/\mathbf{C}_s)+\mathbf{C}_{3v}(/\mathbf{C}_{3v})$.

(d) For $\mathbf{T}(/\mathbf{C}_3)\downarrow\mathbf{C}_3$, we have $\mathbf{C}_3\mathbf{C}_3=\mathbf{C}_3\neq\mathbf{T}$. Hence, Theorem 9 indicates that the orbit is divided during the process as follows; $\mathbf{T}(/\mathbf{C}_3)\downarrow\mathbf{C}_3=\mathbf{C}_3(/\mathbf{C}_1)+\mathbf{C}_3(/\mathbf{C}_3)$.

Let $\mathbf{G}(/\mathbf{G}_i)$ be enantiospheric. Then, $\mathbf{G}_i$ and $\mathbf{G}^{\max}$ are chiral subgroups; hence, $\mathbf{G}_i\mathbf{G}^{\max}=\mathbf{G}^{\max}\neq\mathbf{G}$. In this case, Theorem 9 is converted into a corollary.

Corollary 1. *An enantiospheric orbit $\mathbf{G}(/\mathbf{G}_i)$ is divided during $\mathbf{G}(/\mathbf{G}_i)\downarrow\mathbf{G}^{\max}$.*

The concrete form of the division has been given by Theorem 4.

Let $\mathbf{H}$ be a nearest subgroup of $\mathbf{G}_j$. The term "nearest" is used when there is no subgroup of $\mathbf{G}_j$ between $\mathbf{G}_j$ and $\mathbf{H}$. Thus, $\mathbf{H}$ is one of the nearest subgroups of $\mathbf{G}_j$ and $\mathbf{G}_j$ is one of the nearest supergroups of $\mathbf{H}$. Since $\mathbf{G}_j$ is chiral, $\mathbf{H}$ is also chiral. Suppose that each CR in Eq. 21 is subduced by means of

$$\mathbf{G}_j(/\mathbf{G}_k^{(j)})\downarrow\mathbf{H} = \sum_{l=1}^{\nu_l}\zeta_l^{(ij)}\mathbf{H}(/\mathbf{H}_l)$$

We have derived Eq. 21 for Case (a) and Eq. 23 for Case (b). Thereby, we derive the following equation from Eq. 21.

$$\begin{aligned}\mathbf{G}^{\max}(/\mathbf{G}_i)\downarrow\mathbf{H} &= \mathbf{G}^{\max}(/\mathbf{G}_i)\downarrow\mathbf{G}_j\downarrow\mathbf{H}\\ &= \sum_{k=1}^{\nu_j}\gamma_k^{(ij)}\mathbf{G}_j(/\mathbf{G}_k^{(j)})\downarrow\mathbf{H}\\ &= \sum_{k=1}^{\nu_j}\gamma_k^{(ij)}\sum_{l=1}^{\nu_\mathbf{H}}\zeta_l^{(ik)}\mathbf{H}(/\mathbf{H}_l)\\ &= \sum_{l=1}^{\nu_\mathbf{H}}\eta_l^{(ij)}\mathbf{H}(/\mathbf{H}_l),\end{aligned} \tag{32}$$

where

$$\eta_l^{(ij)} = \sum_{k=1}^{\nu_j}\gamma_k^{(ij)}\zeta_l^{(ik)}. \tag{33}$$

We arrive at the following theorem.

Theorem 10. *Let $\mathbf{H}$ be a nearest subgroup of $\mathbf{G}_j$. If there is an appropriate CR $(\mathbf{G}_j(/\mathbf{G}_k^{(j)}))$ that satisfies $\mathbf{G}_k^{(j)}\mathbf{H}\neq\mathbf{G}_j$, then the site governed by $\mathbf{H}(/\mathbf{H}_l)(l=1,2,\cdots,\nu_l)$ is an $\mathbf{H}$-chirogenic site during the desymmetrization process $(\mathbf{G}\rightarrow\mathbf{G}_j\rightarrow\mathbf{H})$.*

Proof. If there is an appropriate CR $(\mathbf{G}_j(/\mathbf{G}_k^{(j)}))$ that satisfies $\mathbf{G}_k^{(j)}\mathbf{H}\neq\mathbf{G}_j$, then the subduction represented by Eq. 31 produces two or more orbits (Theorem 9). This means that the site governed by $\mathbf{H}(/\mathbf{H}_l)(l=1,2,\cdots,\nu_\mathbf{H})$ is an $\mathbf{H}$-chirogenic site.

This theorem also holds for Case (b), since Eqs. 23 and 24 of Case (b) are essentially identical with Eq. 21 of Case (a). It is the next problem to determine whether the $\mathbf{H}(/\mathbf{H}_l)$ part is an $\mathbf{H}$-chirogenic site during all of the desymmetrization processes toward $\mathbf{H}$. For this purpose, we should examine all of the nearest chiral supergroups of $\mathbf{H}$. If there exists such a chiral synthesis, we call the synthesis a $\mathbf{G}(/\mathbf{G}_i)\downarrow\mathbf{H}$-ligand-differentiating reaction.

Example **9.** Let us consider $\mathbf{T}_h(/\mathbf{C}_3)\downarrow\mathbf{C}_2$. We take account of $\mathbf{D}_2$ group as a nearest chiral supergroup of $\mathbf{C}_2$.

$$\mathbf{T}_h(/\mathbf{C}_3)\downarrow\mathbf{D}_2 = 2\mathbf{D}_2(/\mathbf{C}_1) \text{ and}$$

$$\mathbf{D}_2(/\mathbf{C}_1)\downarrow\mathbf{C}_2 = 2\mathbf{C}_2(/\mathbf{C}_1)$$

We apply Theorem 10 to $\mathbf{G}_j=\mathbf{D}_2$, $\mathbf{G}_k^{(j)}=\mathbf{C}_1$ and $\mathbf{H}=\mathbf{C}_2$.

Since we have $C_1C_2=C_2\neq D_2$, there emerge two or more orbits during the conversion of D_2 into C_2. Theorem 10 indicates that the resulting $C_2(/C_1)$ parts are C_2-chirogenic. The overall process is represented by

$$T_h(/C_3)\downarrow C_2 = 4C_2(/C_1). \quad (34)$$

This conclusion is illustrated by a potential chiral synthesis (Fig. 6). Consider the attack of a chiral reagent (containing two chiral active sites) onto the molecule (**5**). One of the C_2-chirogenic sites of the T_h-$(/C_3)$ orbit is represented by the symbol (①) in **9a**, which is generated by the attack. The attack of the mirror-image part (①) creates the diastereomeric intermediate (**9b**). If **9a** is energetically preferred, the corresponding C_2-molecule is created preferably.

If all of the CRs in Eq. 21 ($G_j(/G_k^{(j)})$'s) satisfy $G_k^{(j)}H=G_j$, then each subduction represented by Eq. 31 produces one orbit (Theorem 9). This means that there appears no division of each orbit during the process of converting G_j into H_j. Thus, the site governed by G_j-$(/G_k^{(j)})$ is converted, with no division, into the one governed by $H(/H_l)$(for $\exists l$), where $|G_j|/|G_k^{(j)}|=|H|/|H_l|$. Hence, this site is not an **H**-chirogenic site but $\geqslant G_j$-chirogenic site.

The following corollary is practically important, since its chemical meaning is quite concrete.

Corollary 2. *Each G_i-ligand in a $G(/G_i)$ orbit is a G_i-chirogenic site.*

Proof. Let G_i and G_j be chiral subgroups of **G**. Suppose that G_j is an arbitrary nearest supergroup of G_i. We consider a coset representation acting on G_it_1 or $\Omega_1(t_1=I)$. The stabilizer of $G_it_1(\Omega_1)$ is G_i, under the actions of **G**, of G_j and of G_i. Hence, the orbit containing G_it_1 (or Ω_1) is subject to $|G|/|G_i|$-membered $G(/G_i)$ in the case of **G**; to $|G_j|/|G_i|$-membered $G_j(/G_i)$ in the case of G_j; and to one-membered $G_i(/G_i)$ in the case of G_i. If the second step of the desymmetrization ($G\rightarrow G_j\rightarrow G_i$ (i.e. $G_j(/G_i)\downarrow G_i$)) produces no division of the orbit, then Theorem 9 affords $G_iG_i=G_j$. It follows that $G_i=G_j$. Hence, there exists no such G_j.

This corollary indicates that we can produce a G_i molecule by differentiating one of the G_i-ligands in Ω^+ from the counterpart in Ω^+. Although there are $|G|/|G_i|$ ways for selecting such a chirogenic site, they produce homomers that are chemically identical.

It is rather tedeous task to determine chirogenic sites by means of Theorem 10. A desymmetrization lattice[8] is effective to determine such chirogenic sites of an orbits. Figure 7 depicts the desymmetrization lattice of $D_{2d}(/C_2')$. Compare $D_2(/C_2')+D_2(/D_2'')$ and $2C_2(/C_1)$. Thus, the orbits of the D_2 are not divided in the process of converting into the C_2. This fact is equivalent to the fact that Theorem 10 holds for this case. Hence, the $C_2(/C_1)$ part in the $D_{2d}(/C_2')$ orbit is not a C_2-chirogenic site. This means that there is no direct method of generating a C_2-molecule from the $D_{2d}(/C_2')$ orbit.

On the other hand, there is a direct method of generating a C_2'-molecule from the $D_{2d}(/C_2')$ orbit by the inspection of the desymmetrization lattice. This result is alternatively verified by Corollary 2.

Special Cases. In the preceding discussion, the chiral subgroup **H** ($\leqslant G_j$) is examined. The **H** part in Ω^+ can be differentiated from the mirror image in Ω^-, if Theorem 10 holds for all of the nearest supergroups G_j. It should be

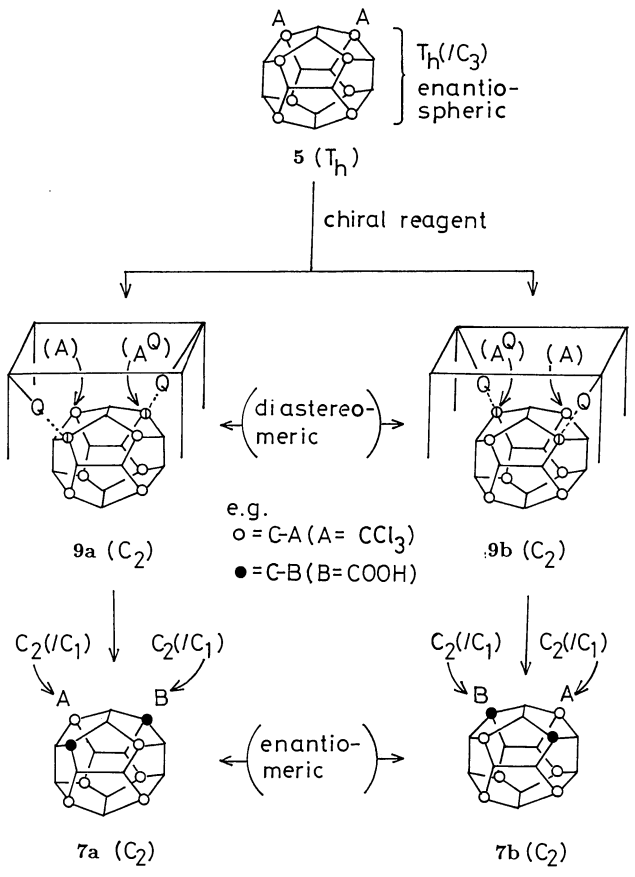

Fig. 6. A potential chiral synthesis generating C_2 molecules from a T_h molecule.

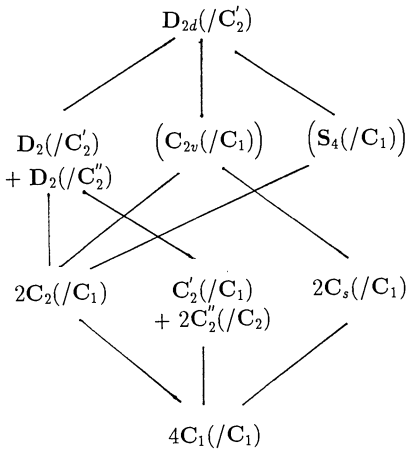

Fig. 7. Desymmetrization lattice of $D_{2d}(/C_2')$.

noted that the combination of the two parts does not always construct a group.

With respect to this point, we have the following theorem in general.

Theorem 11. *Let* $\mathbf{H}$ *be a chiral subgroup of an achiral group* $\mathbf{G}$ *and* u_1 *be an improper rotation contained in* $\mathbf{G}$. *If* $\widetilde{\mathbf{H}}=\mathbf{H}+\mathbf{H}u_1$ *is a subgroup of* $\mathbf{G}$, *then we have* $u_1\mathbf{H}=\mathbf{H}u_1$ *and* $u_1u_1\in\mathbf{H}$. *Conversely, if the relations* $u_1\mathbf{H}=\mathbf{H}u_1$ *and* $u_1u_1\in\mathbf{H}$ *hold, then* $\widetilde{\mathbf{H}}$ *is a subgroup of* $\mathbf{G}$.

Proof. (a) Suppose that $u_1\mathbf{H}=\mathbf{H}u_1$ and $u_1u_1\in\mathbf{H}$. (i) For $\forall a,b\in\mathbf{H}$, we have $ab^{-1}\in\mathbf{H}\subseteq\widetilde{\mathbf{H}}$, since $\mathbf{H}$ is a group. (ii) Consider $\forall a\in\mathbf{H}$ and $\forall b\in\mathbf{H}u_1$. There exists $b'\in\mathbf{H}$ that satisfies $b=b'u_1\in\mathbf{H}u_1$. By means of the above assumption, we have $u_1u_1=c\in\mathbf{H}$ for $\exists c\in\mathbf{H}$, $u_1c^{-1}=c'u_1$ for $\exists c'\in\mathbf{H}$, and $u_1(b')^{-1}=b''u_1$ for $\exists b''\in\mathbf{H}$. It follows that $ab^{-1}au_1^{-1}(b')^{-1}au_1c^{-1}(b')^{-1}=ac'b''u_1\in\mathbf{H}u_1\subseteq\widetilde{\mathbf{H}}$. (iii) If $a\in\mathbf{H}u_1$ and $b\in\mathbf{H}u_1$, then there exist $a',b'\in\mathbf{H}$ that satisfy $a=a'u_1\in\mathbf{H}u_1$ and $b=b'u_1\in\mathbf{H}u_1$. It follows that $ab^{-1}=a'u_1u_1^{-1}(b')^{-1}=a'(b')^{-1}\in\mathbf{H}\subseteq\widetilde{\mathbf{H}}$, On the basis of (i), (ii), and (iii), $\mathbf{H}$ is a group.

(b) Suppose that $\widetilde{\mathbf{H}}=\mathbf{H}+\mathbf{H}u_1$ is a subgroup of $\mathbf{G}$. Since $\mathbf{H}u_1$ is the set of all improper rotations in $\widetilde{\mathbf{H}}$ and $u_1\mathbf{H}$ is also the set of all improper rotations $\widetilde{\mathbf{H}}$, they must be equal. It follows that $\mathbf{H}u_1=u_1\mathbf{H}$. Since u_1 is an improper rotation, we have $u_1^{-1}\in\mathbf{H}u_1$. Since we take $u_1u_1=c$, we have $cu_1^{-1}=u_1\in\mathbf{H}u_1$. This means that $c\in\mathbf{H}$. Hence, we have $u_1u_1=c\in\mathbf{H}$.

In continuation of the preceding section, suppose that $\mathbf{H}$ is the nearest subgroup of $\mathbf{G}_j$ and $\mathbf{H}\leqslant\mathbf{G}_j\leqslant\mathbf{G}^{\max}\leqslant\mathbf{G}$. Suppose that $\mathbf{G}$ contains u_1 satisfying $u_1u_1\in\mathbf{H}$ as an improper rotation and that $\mathbf{H}u_1=u_1\mathbf{H}$. Then, Theorem 11 indicates that we are able to obtain the point group $\widetilde{\mathbf{H}}$ ($\leqslant\mathbf{G}$) that contains $\mathbf{H}$ as the maximum chiral subgroup; i.e., $\widetilde{\mathbf{H}}$ $\{h,hu_1|\forall h\in\mathbf{H}\}=\mathbf{H}+\mathbf{H}u_1$. Let us examine a subduction represented by $\mathbf{G}(/\mathbf{G}_i)\downarrow\widetilde{\mathbf{H}}$, where $\mathbf{G}(/\mathbf{G}_i)$ is enantiospheric. Since the relationship between $\widetilde{\mathbf{H}}(/\mathbf{H}_l)$ and $\mathbf{H}(/\mathbf{H}_l)$ is the same as that between $\mathbf{G}(/\mathbf{G}_i)$ and $\mathbf{G}^{\max}$-$(/\mathbf{G}_i)$, we arrive at the following theorem by means of Eq. 31.

Theorem 12. *Suppose that an enantiospheric orbit* $\mathbf{G}$-$(/\mathbf{G}_i)$ *is in accord with Case* [*a*] *of Theorem 4. If we can construct* $\widetilde{\mathbf{H}}$ *as above, the subduction* $\mathbf{G}(/\mathbf{G}_i)\downarrow\widetilde{\mathbf{H}}$ *is represented by*

$$\mathbf{G}(\mathbf{G}_i)\downarrow\widetilde{\mathbf{H}}=\sum_{l=1}^{{}^{v}\mathbf{H}}\eta_l^{(ij)}\widetilde{\mathbf{H}}(/\mathbf{H}_l), \tag{35}$$

where $\mathbf{H}_l$ *is chiral subgroups.*

The $\widetilde{\mathbf{H}}(/\mathbf{H}_l)$ orbits appearing in the right-hand side of Eq. 35 are enantiospheric. This theorem is exemplified by comparing $\mathbf{D}_{2d}(/\mathbf{C}_1)\downarrow\mathbf{C}_{2v}$ with $\mathbf{D}_{2d}(/\mathbf{C}_1)\downarrow\mathbf{C}_2$. Note that the summation in Eq. 35 is concerned with the chiral $\mathbf{H}$, not with $\widetilde{\mathbf{H}}$. In Eq. 35, $\widetilde{\mathbf{H}}(/\mathbf{H}_l)$ may be equivalent to $\widetilde{\mathbf{H}}_j$-$(/\mathbf{H}_l')$ if $\mathbf{H}_l$ is conjugate to $\mathbf{H}_l'$ as subgroups of $\widetilde{\mathbf{H}}$ and if they are not conjugate as subgroups of $\mathbf{H}$. For example, compare the subduction $\mathbf{T}_d(/\mathbf{C}_2)\downarrow\mathbf{D}_{2d}=\mathbf{D}_{2d}(/\mathbf{C}_2)+2\mathbf{D}_{2d}$-$(/\mathbf{C}_2')$ with $\mathbf{T}_d(/\mathbf{C}_2)\downarrow\mathbf{D}_2=\mathbf{D}_2(/\mathbf{C}_2)+\mathbf{D}_2(/\mathbf{C}_2')+\mathbf{D}_2(/\mathbf{C}_2'')$. It should be noted that, if there appears no division during the subduction $\mathbf{G}(/\mathbf{G}_i)\downarrow\widetilde{\mathbf{H}}$ as compared with the subduction to its supergroup(s), this process is not effective in chiral synthesis. For example, Fig. 7 contains such non-effective cases ($\mathbf{C}_{2v}$ and $\mathbf{S}_4$).

By means of Theorem 12, we have the following corollary.

Corollary 3. *a)* Let $\mathbf{G}(/\mathbf{G}_i)$ *be enantiospheric. If* $\mathbf{G}$ *contains* $\mathbf{C}_s$ *(a mirror plane) and* $\mathbf{C}_i$ *(inversion), then we have*

$$\mathbf{G}(/\mathbf{G}_i)\downarrow\mathbf{C}_s=\frac{|\mathbf{G}|}{2|\mathbf{G}_i|}\mathbf{C}_s(/\mathbf{C}_1), \tag{36}$$

$$\mathbf{G}(/\mathbf{G}_i)\downarrow\mathbf{C}_i=\frac{|\mathbf{G}|}{2|\mathbf{G}_i|}\mathbf{C}_i(/\mathbf{C}_1). \tag{37}$$

Discussion

In preceding section, we have presented the theoretical foundation of asymmetric syntheses. In the light of the resulting logical framework, we reexamine asymmetric syntheses reported so far and propose alternative possibilities of chiral syntheses. Figure 8 illustrates a potential experiment in which an enantiospheric orbit is subject to $\mathbf{C}_s(/\mathbf{C}_1)$. The starting material (**10**) of the $\mathbf{C}_s$ symmetry has two CH_2OH ligands. We regard each ligand as A in the lump. Then the two A's are subject to $\mathbf{C}_s(/\mathbf{C}_1)$, belonging to an enantiospheric orbit. In order to obtain a chiral product, we must differentiate only two ligands belonging to the orbit. Suppose that a chiral reagent (Q) attacks either of ligands. Then, such an interaction as $CH_2OH\cdots Q$ (A^Q) appears; the attack produces a chiral environment. Either one of such possible intermediates (**11a** or **11b**) is energetically predominant and yields a final product of $\mathbf{C}_1$.

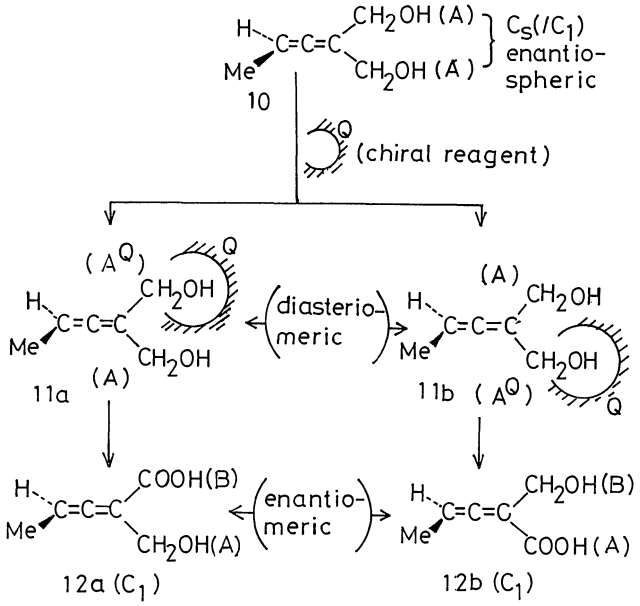

Fig. 8. A potential chiral synthesis generating $\mathbf{C}_1$ molecules from a $\mathbf{C}_s$ molecule.

All of the asymmetric syntheses reported so far[13] are classified to the above-described simple case, in which an enantiospheric orbit is governed by $C_s(/C_1)$. For an example of this type, Fuji[14] reported an asymmetric protonation of a dicarboxylate, in which two carboxylate groups belonging to an enantiospheric orbit are differentiated. These reactions have been classified into enantiotopic-group-differentiating reactions.[15] In the light of the present notation, they are characterized as $C_s(/C_1)\downarrow C_1$-ligand-differentiating reactions. An enantiospheric orbit of the faces of a carbonyl group or of the related functional group, which is subject to the $C_s(/C_1)$ representation, undergoes a chiral synthesis. For example, hydrogen transfers from chiral reducing agents to achiral substrates, asymmetric additions to alkenes, asymmetric syntheses at hetero atoms, and so forth have been reported.[13] Additional examples have been recently reviewed.[16] These reactions have been classified into enantiotopic-face-differentiating reactions.[15] They are characterized more specifically as $C_s(/C_1)\downarrow C_1$-face-differentiating reactions in terms of the present terminology.

The discussions in the previous section indicate that there can exist more general cases, in which an enantiospheric orbit is subject to a coset representation other than $C_s(/C_1)$. Figure 9 shows a potential experiment that produces a C_2 molecule (**15a** or **15b**) from an S_4 molecule (**13**). The two carbonyl groups belong to an enantiospheric orbit subject to $S_4(/C_2)$. The attack of a chiral reducing agent perturbs the carbonyls to belong to disteromeric environments (**14** and **14b**), either of which is energetically preferred. Hence, either one of an enantiomeric pair (**15a** and **15b**) is produced predominantly. This is characterized as an $S_4(/C_2)\downarrow C_2$-group-differentiating reaction. The reaction is a novel type of chiral reaction in the sense that it involves no explicit faces to be differentiated. Thus, the two carbonyl groups in **13** are associated with each other not by a mirror plane, but by S_4 operation. To the best of our knowledge, this type of reactions has never been reported. The mode of the differentiation of **13** (Fig. 9) is different from that of **10** (Fig. 8).

Example 9 (Fig. 6) illustrates a $T_h(/C_3)\downarrow C_2$-group-differentiating reaction. It is to be noted that $T_h(/C_3)\downarrow T$-group-differentiating reactions (e.g. **5**→**6a** or **6b**) and $T_h(/C_3)C_3$-group-differentiating reactions (e.g. **5**→**8a** or **8b**) are also possible. It is challenging problems to realize such novel chiral syntheses. In

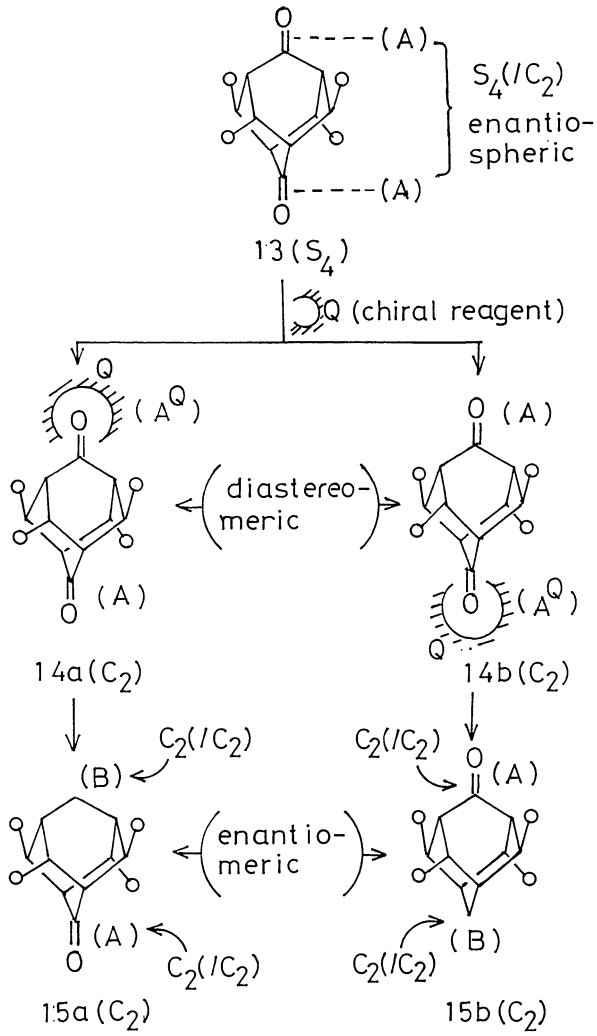

Fig. 9. A potential chiral synthesis generating C_2 molecules from a S_4 molecule.

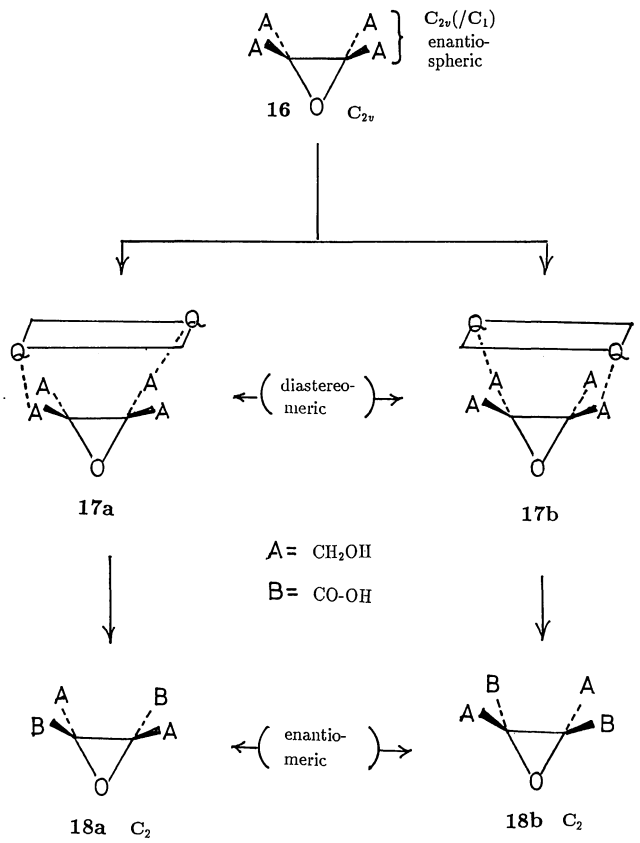

Fig. 10. A potential chiral synthesis generating C_2 molecules from a C_{2v} molecule.

particular, the $\mathbf{T}_h(/\mathbf{C}_3)\downarrow\mathbf{C}_3$-group-differentiating reaction can be accomplished if the reaction is ceased at the point that only one group of the eight functional groups (Fig. 6) has been attacked. Note that this reaction is based on Corollary 2.

Let us examine the $\mathbf{C}_{2v}$-molecule (**16**), in which four CH_2OH ligands construct an orbit subject to $\mathbf{C}_{2v}(/\mathbf{C}_1)$. This orbit is enantiospheric and active to a chiral synthesis. Figure 10 indicates a model of chiral synthesis which produces a $\mathbf{C}_2$-molecule from a $\mathbf{C}_{2v}$-molecule. This process corresponds to the subduction represented by $\mathbf{C}_{2v}(/\mathbf{C}_1)\downarrow\mathbf{C}_2=2\mathbf{C}_2(/\mathbf{C}_1)$. We can consider a potential chiral reagent that has two chiral units (Q) in diagonal positions, which are concerned with a $\mathbf{C}_2$-chirogenic site of the substrate. Since the resulting intermediates (**17a** and **17b**) are diastereomeric, the energetically predominant intermediate yields either of enantiomeric products (**18a** or **18b**). We refer to this reaction as a $\mathbf{C}_{2v}(/\mathbf{C}_1)\downarrow\mathbf{C}_2$-group-differentiating reaction.

Conclusion

Prochirality is defined logically by examining the desymmetrization of an enantiospheric orbit. A chirogenic site in the enantiospheric orbit provides a basis of operating chiral syntheses.

References

1) K. R. Hanson, *J. Am. Chem. Soc.*, **88**, 2731 (1966).
2) H. Hirschmann and K. R. Hanson, *J. Org. Chem.*, **36**, 3293 (1971).
3) IUPAC rule. Section E(1974); *Pure Appl. Chem.*, **45**, 11 (1976).
4) V. Prelog and Helmchen, *Angew. Chem., Int. Ed. Engl.*, **21**, 567 (1982).
5) D. Seebach and V. Prelog, *Angew. Chem., Int. Ed. Engl.*, **21**, 654 (1982).
6) K. Mislow and J. Siegel, *J. Am. Chem. Soc.*, **106**, 3319 (1984).
7) E. A. Halevi, *J. Chem. Res., Synop.*, **1985**, 206.
8) S. Fujita, *J. Am. Chem. Soc.*, **112**, 3390 (1990).
9) S. Fujita, *J. Math. Chem.*, **5**, 121 (1990).
10) S. Fujita, *Theor. Chim. Acta*, **76**, 247 (1989).
11) S. Fujita, *Theor. Chim. Acta*, **78**, 45 (1990).
12) S. Fujita, *Bull. Chem. Soc. Jpn.*, **63**, 315 (1990).
13) a) J. D. Morrison and H. S. Mosher, "Asymmetric Organic Reactions," Prentic-Hall, Englewood Ciffis (1971). b) K. B. Kagan and J. C. Fiaud, *Top. Stereochem.*, **10**, 175 (1978). c) R. Bentley, "Molecular Asymmetry in Biology," Academic, New York–London (1969), Vol 1; (1970), Vol. 2. d) K. Fuji, *Yuki Gosei Kagaku Kyukaishi*, **44**, 623 (1986).
14) K. Fuji, M. Node, S. Terada, M. Murata, and H. Nagasawa, *J. Am. Chem. Soc.*, **107**, 6404 (1985).
15) a) Y. Izumi, *Angew. Chem., Int. Ed. Engl.*, **10**, 871 (1971). b) Y. Izumi and A. Tai, "Stereodifferentiating Reactions. the Nature of Asymmetric Reactions," Academic, New York (1977).
16) K. Yamamoto, *Yuki Gosei Kagaku Kyokaishi*, **47**, 122 (1989).

Proton ENDOR Studies on Zinc-Doped Copper(II) Acetate Monohydrate Single Crystal

Shouich KITA,* Kengo UCHIDA, Ryo MIYAMOTO,† and Masamoto IWAIZUMI†
Department of Chemistry, Faculty of Science, Hirosaki University,
Bunkyocho 3, Hirosaki 036
† Institute for Chemical Reaction Science, Tohoku University,
Katahira 2-chome, Aobaku, Sendai 980
(Received February 27, 1991)

The proton ENDOR spectra of the zinc-doped copper(II) acetate monohydrate single crystal were measured at 20 K. Hyperfine coupling tensors have been determined for the two protons of the water molecule at the axial position of the paramagnetic copper ion and a proton of the water forming the hydrogen bond with carboxylate oxygen at the equatorial plane of the copper ion. The axial water protons have small positive isotropic hyperfine couplings owing to the pseudo-contact interaction, and the equatorial water proton has a small negative one due to the spin polarization effect of the positive spin on the acetate oxygen through the hydrogen bond. The anisotropic hyperfine tensors of the former protons are interpreted by the dipolar interaction with the unpaired spin on the copper $d_{x^2-y^2}$ orbital. The anisotropic interaction of the latter protons indicates that the spin delocalizes onto the oxygen atoms of the acetate bridges. Based on these observed hyperfine interactions, the mechanism of the spin–spin interaction in the dimer complex is discussed.

Magnetic exchange interactions in metal dimer complexes continue to be a subject of much interest among chemists.[1] Copper(II) acetate monohydrate involving an antiferromagnetic coupled dimer has been widely studied, resulting in a long controversy concerning the exchange pathway in the dimer. Figgis and Martin initially proposed that the antiferromagnetic interaction is due to the existence of a δ-bond between the copper(II) ions.[2] Forster and Ballhausen employed a molecular orbital treatment, showing the importance of the copper–copper σ-bond.[3] Later, Hansen and Ballhausen used a weakly coupled chromophore model which included no direct copper–copper interaction to explain the antiferromagnetism.[4] Goodgame et al. considered that the direct metal–metal bond is not important for the antiferromagnetism and that the spin coupling occurs by a superexchange via the carboxylate bridge.[5] Since then, the superexchange mechanism has been favored by most authors. Much current research is being directed toward the development of a more complete understanding of the exchange mechanism; various physical methods (EPR,[6a] NMR,[6b] NQR,[6c] etc.) have been employed.

Revealing the spin distribution in the dimer would be useful in clarifying the mechanism of the antiferromagnetism. Copper(II) acetate monohydrate doped with zinc(II) ions shows paramagnetism with $S=1/2$ of the Cu–Zn dimer at a temperature below 50 K, since the host Cu–Cu dimer becomes completely diamagnetic. An unpaired electron occupies one of the so-called "magnetic orbitals" which is centered on a copper atom. Kokoszka et al. investigated a zinc-doped copper acetate monohydrate single crystal by EPR.[7] They found that the unpaired electron on the copper $d_{x^2-y^2}$ orbital interacts weakly with the zinc ion. Since the superexchange interaction appears to occur through the ligand orbitals, the ligand hyperfine (hf) couplings provide useful information concerning the mechanism of the antiferromagnetic interaction. The EPR spectra show a well-resolved copper hf structure, which lacks resolution of the ligand hf splittings.

In this paper we report on the proton ENDOR of single crystal of zinc-doped copper(II) acetate monohydrate. The observed proton hf coupling tensors are compared to those of the other monomeric copper(II) complexes and the exchange interaction mechanisms are discussed.

Experimental

Single crystals of zinc-doped copper(II) acetate monohydrate were obtained in the same manner as that described in a reference.[7] Isotope-enriched ^{63}Cu acetate (99%) was used to simplify the EPR and ENDOR spectra. A copper acetate monohydrate crystal is monoclinic with a space group $C2/c$, containing four dimeric molecules in a unit cell. There are two independent intermolecular hydrogen bonds between the hydrogen atom of the water and oxygen atom of the acetate bridge, as shown in Fig. 1.[8]

The EPR spectra were recorded on a Varian E112 X-band EPR spectrometer. The magnetic fields and microwave frequencies were measured by an Echo Electronic EFM 2000 NMR field meter and a Takedariken TR 5204 frequency counter, respectively. The ENDOR spectra were recorded on an EPR spectrometer equipped with a Varian E1700 ENDOR unit and an ENI 550L RF power amplifier. These measurements were carried out at 20 K using an Oxford ESR 9 cryostat. At this temperature the host copper-copper dimers became completely diamagnetic ($S=0$) and the only copper–zinc dimers ($S=1/2$) were observed in the EPR spectra.

Results

The angular dependence of the proton ENDOR spectra observed for the magnetic field in the bc^* plane are shown in Fig. 2. A large number of proton ENDOR signals were observed, and some ENDOR signals were split into doublet lines by nuclear spin–spin couplings at

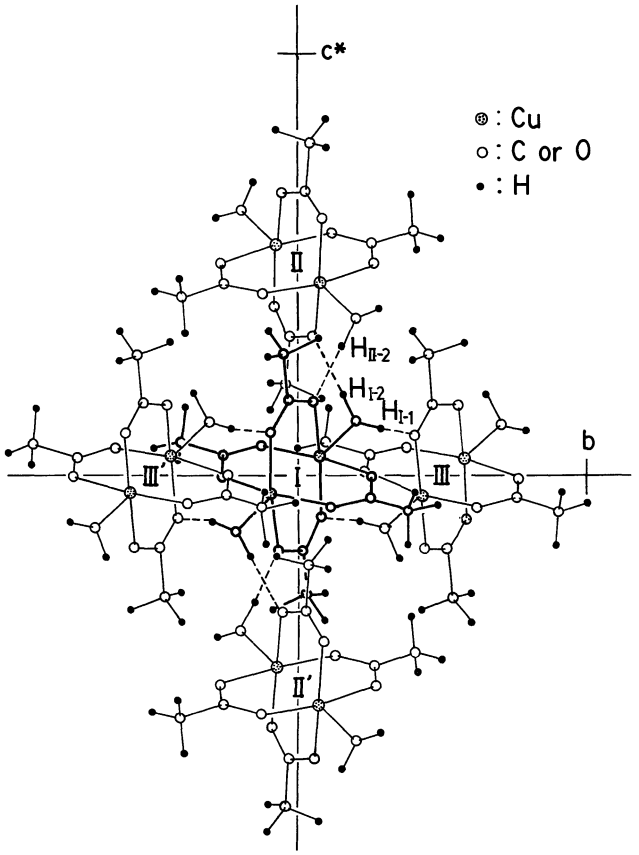

Fig. 1. Crystal structure of copper(II) acetate monohydrate projected onto the *bc** plane.

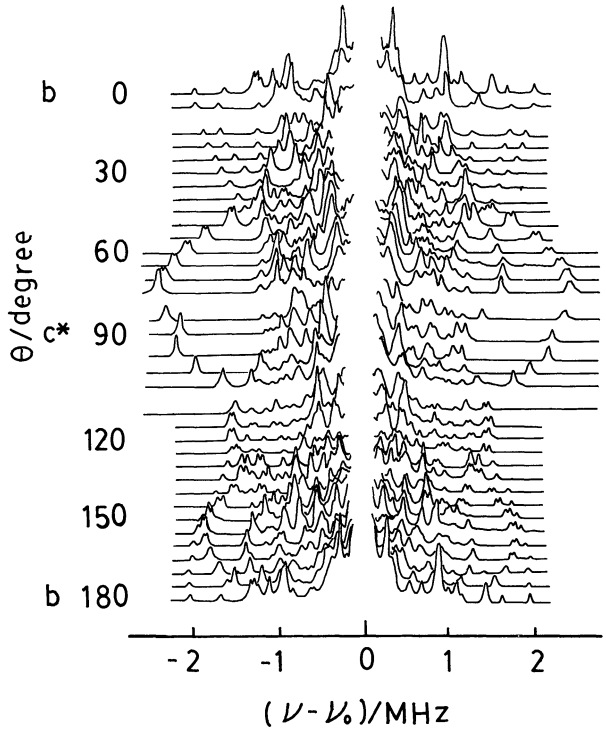

Fig. 2. Angular-dependence of ^{1}H ENDOR signals when the magnetic fields are in the *bc** plane.

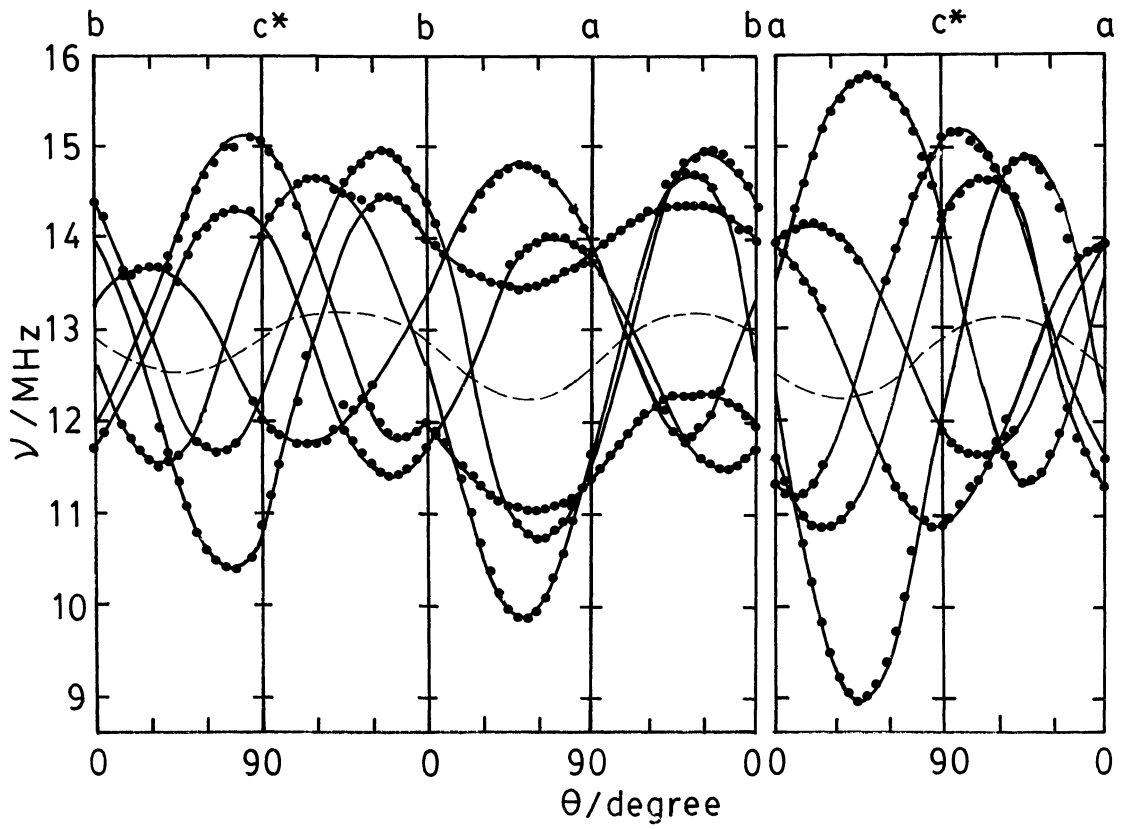

Fig. 3. Angular-dependence of ^{1}H ENDOR frequencies for rotations around the *a*-, *c**-, and *b*-axis. The broken line indicates the free proton frequency; the solid lines were calculated using the tensors of Table 1 and Eq. 1.

some crystal orientations. The ENDOR frequencies are given by

$$h\nu^{H}(M_s)=K^{H}(M_s)+h\nu(\text{2nd})+h\nu(\text{dipole}). \quad (1)$$

Although a full expression of each term was given in our previous paper,[9] it must be noted that $h\nu$(2nd) denotes a second order correction of the ENDOR frequencies due to an indirect coupling with the copper nuclei;[10] the $h\nu$(dipole) is the effect of nuclear spin–spin coupling between protons. This last term was not expressly included in the present analysis for the angular dependence of the ENDOR frequencies; however, the frequency of the center of the doublet splitting by the spin–spin coupling was used. Figure 3 shows the observed ENDOR frequencies for rotation about the *a*-, *c**-, and *b*-axis and the angular-dependent ENDOR frequencies computed by Eq. 1 and the parameters in Table 1. The signs of the hf couplings are not determinable from the conventional ENDOR technique and, hence, an assumption was made that the largest anisotropic hf principal value must be positive, since the anisotropic part of the proton hf coupling would be dominated by the dipole interaction with the spin on the metal ion. The assignment of the observed proton hf couplings to the proton positions was made by comparing their direction cosines with those of the Cu–H vectors calculated from the crystallographic data, since the principal axes of the proton hf couplings are considered to orient along the respective Cu–H directions. Three proton hf couplings could be assigned. Two of them were assigned to the protons of the water molecule coordinated to the copper ion (I-1 and I-2); the other was assigned to the proton of the water molecule which is coordinated to the neighboring complex and is involved in the hydrogen bond with the acetate oxygen (II-2). The agreement between the direction cosines of the hf coupling tensors and the crystallographic Cu–H vectors is satisfactory. The Cu–H distances calculated from the anisotropic dipolar couplings by the use of the point-dipole approximation also agree with those from the crystallographic data.

Discussion

Isotropic hf Coupling. The protons at I-1 and I-2 positions have small positive isotropic hf coupling constants, whereas the II-2 proton has a small negative one (Table 2). Similar results have been reported for $[Cu(H_2O)_6]^{2+}$ in the zinc Tutton salt by Atherton and Horsewill.[10] They found that the protons of the axial waters in $[Cu(H_2O)_6]^{2+}$ have small positive isotropic hf couplings (mean value a_{av}=0.15 MHz), and the protons of the equatorial one have negative couplings (mean value a_{av}= −0.9 MHz).

The observed hf coupling matrix ($\boldsymbol{A}$) is the sum of three contributions,

$$\boldsymbol{A}=a\boldsymbol{E}+\boldsymbol{A}^{\circ}+\boldsymbol{A}^{L}, \quad (2)$$

where the first term is the Fermi contact coupling, the second the anisotropic dipolar interaction between the electron spin and the nucleus and the third the orbital contribution to the hf couplings. Although the anisotropic spin-only coupling matrix ($\boldsymbol{A}^{\circ}$) is traceless, its orbital counterpart ($\boldsymbol{A}^{L}$) is not. The isotropic part of $\boldsymbol{A}^{L}$ is usually called the pseudo-contact interaction. Atherton and Horsewill interpreted the negative hf couplings of the equatorial protons as being the result of

Table 1. Proton Hyperfine Coupling Parameters of Zinc Doped Copper Acetate Monohydrate Single Crystal

Position[a]		Coupling constants/MHz[b]		Direction cosines			Distances/Å	
Molecule	Proton	Isotropic	Traceless	l_a	l_b	l_c*	ENDOR	X-ray
			6.15	0.727	0.591	0.350		
I	1	0.24	−2.65	−0.686	0.624	0.373	3.1	2.9
			−3.49	0.002	−0.511	0.859		
			7.61	0.677	0.296	0.674		
I	2	0.36	−3.48	0.509	0.423	−0.719	2.9	2.7
			−4.13	−0.509	0.830	0.169		
			4.81	−0.073	0.259	0.963		
II	2	−0.18	−2.36	0.998	−0.113	0.105	3.4	3.3
			−2.44	0.136	0.959	0.373		

a) Positions are indicated in Fig. 1 and the EPR active copper is the one coordinated by H_2O(I). b) Estimated error is ±0.03 MHz.

Table 2. Estimated Fermi and Pseudo-Contact Hyperfine Couplings

Proton	Experimental/MHz	Fermi/MHz	Pseudo-contact/MHz
I-1	0.24	−0.04	0.28
I-2	0.36	0.04	0.32
II-2	−0.18	−0.19	0.01

spin polarization through the OH bond by unpaired spin delocalized on the water nonbonding orbital due to an overlap with the copper unpaired spin orbital; the positive coupling of the axial protons was interpreted as arising mainly from a pseudo-contact hf interaction. In the present case the small negative spin density ($\rho_H = -0.00013$) at proton II-2 may be attributed to a spin polarization effect through the hydrogen bond due to the positive spin on the acetate oxygen, which is introduced by an overlap with the singly occupied copper 3d-orbital; this is similar to the case of protons 3 and 3′ in copper-doped zinc(II) acetate dihydrate.[11] On the other hand, the spin densities at the protons in the axial water molecule are nearly zero, indicating that neither spin delocalization nor spin polarization effects exist at the axial water molecule.

Anisotropic Coupling. The anisotropic parts of the hf tensors arise from dipolar interactions between the electron spin centered on the copper ion and the nuclear spin of the protons. However, a conventional point-dipole approximation used to evaluate the anisotropic hf tensor is not suitable for the case in which the metal-ligand distance is less than about 0.3 nm. In such a case, it is necessary to calculate the following matrix element:[12]

$$A_{\text{aniso}} = \langle \psi \mid H_{\text{dipole}} \mid \psi \rangle ; \quad (3)$$

here, H_{dipole} denotes the dipole–dipole interaction Hamiltonian and ψ is the unpaired electron orbital. Taking the $d_{x^2-y^2}$ or d_{z^2} orbital for ψ, three principal values of the tensor can be expressed in a first-order approximation as follows:

$$A_{\xi\xi} = 2PR^{-3}[1 - ((12/7)\cos^2\theta - (6/7)\sin^2\theta)R^{-2}\langle r^2\rangle_{3d}]$$

$$A_{\eta\eta} = -PR^{-3}[1 - ((12/7)\cos^2\theta - (9/7)\sin^2\theta)R^{-2}\langle r^2\rangle_{3d}] \quad (3)$$

$$A_{\zeta\zeta} = -PR^{-3}[1 - ((12/7)\cos^2\theta - (3/7)\sin^2\theta)R^{-2}\langle r^2\rangle_{3d}],$$

for $d_{x^2-y^2}$, and

$$A_{\xi\xi} = 2PR^{-3}[1 + ((6/7)\cos^2\theta - (3/7)\sin^2\theta)R^{-2}\langle r^2\rangle_{3d}]$$

$$A_{\eta\eta} = -PR^{-3}[1 + ((6/7)\cos^2\theta - (9/14)\sin^2\theta)R^{-2}\langle r^2\rangle_{3d}] \quad (4)$$

$$A_{\zeta\zeta} = -PR^{-3}[1 + ((6/7)\cos^2\theta - (3/14)\sin^2\theta)R^{-2}\langle r^2\rangle_{3d}],$$

for d_{z^2}. The principal axes ($\xi\eta\zeta$) are shown in Fig. 4, $P = g\beta_e g_n \beta_n$, R is the metal-proton distance, and θ is the angle between the z-axis and the metal-proton direction. If $R^2 \gg \langle r^2\rangle_{3d}$, the term $R^{-2}\langle r^2\rangle_{3d}$ may be ignored and Eqs. 3 and 4 are reduced to the point-dipole approximation. The anisotropic hf tensors shown in Table 3 were obtained by using $\langle r^2\rangle_{3d} = 2.88\times10^{-3}$ nm^2 for Cu^{2+} reported by Freeman et al.[13] For the protons of the I-1 and I-2 positions, the agreement between the tensors derived from the $d_{x^2-y^2}$ configuration and the experimentally determinations are satisfactory, but the

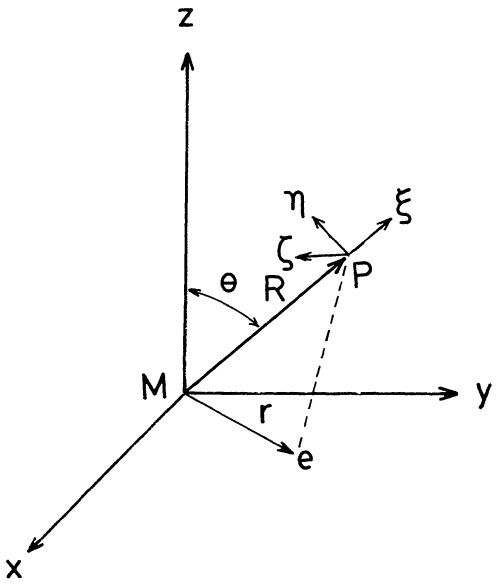

Fig. 4. Coordinate systems used for calculating the dipolar interaction between the electron spin (e) on the metal ion (M) and the nuclear spin of the proton (P). The (xyz) Cartesian coordinate system is the molecular axes of the metal complex. The (ξ, η, ζ) Cartesian coordinate system is the principal axes of the dipolar coupling tensor determined by taking the ξ-axis to be along the M–P direction and η to be in the $z\xi$ plane.

Table 3. Observed and Calculated Anisotropic hf Tensors

Position		Principal values/MHz			Direction cosines of the largest principal value					
Molecule	Proton	A_i[a]	A_i[b]	A_i[c]	l_a[a]	l_b[a]	l_c[a]	l_a[b,c]	l_b[b,c]	l_c[b,c]
		6.15	6.11	6.65	0.727	0.591	0.350	0.766	0.575	0.287
I	1	−2.65	−3.05	−3.33						
		−3.49	−3.06	−3.33						
		7.61	7.52	8.14	0.677	0.296	0.674	0.676	0.238	0.699
I	2	−3.48	−3.75	−4.06						
		−4.13	−3.77	−4.07						
		4.81	4.53	4.46	−0.073	0.259	0.963	−0.172	0.194	0.966
II	2	−2.36	−2.24	−2.22						
		−2.44	−2.29	−2.24						

a) Observed tensor. b) Calculated for the $d_{x^2-y^2}$ configuration. c) Calculated for the d_{z^2} configuration.

d_{z^2} configuration derives large hf tensors. The calculated hf tensors with both configurations for the proton II-2 are smaller than the observed hf tensor, suggesting the presence of a significant spin delocalization on the acetate oxygen.

Spin Distribution and Exchange Mechanism. In the copper(II) acetate monohydrate, two singly occupied electrons on each Cu atom interact with each other, making the triplet state energy become higher by 284 cm^{-1} than that of the singlet state.[2] In Cu–Zn dimers one unpaired electron centered on the copper atom is present. Since the unpaired electron orbital of the Cu–Zn dimer corresponds to the magnetic orbital of Cu–Cu dimer, the spin distribution of Cu–Zn dimer provides useful information concerning the magnetic orbital. The ground state configuration was initially assigned to $d_{x^2-y^2}$ by Figgis and Martin[2] and Ross;[14] they suggested that the antiferromagnetisum can be ascribed to a Cu–Cu interaction through the δ-bond; in the sustained by Forster and Ballhausen,[3] however, a Cu–Cu interaction through the σ-bond were proposed, based on the d_{z^2} ground state configuration. The isotropic proton hf couplings of the axial water molecule indicate that the spin density on the axial water molecule expected for the d_{z^2} configuration is not substantial, and that the anisotropic hf couplings of the protons are in favor of the $d_{x^2-y^2}$ ground state. Also, the isotropic and anisotropic hf coupling of the proton II-2 indicates the presence of a significant spin delocallization onto the acetate oxygen atoms from the copper $d_{x^2-y^2}$ orbital, and the spin polarization effect of the acetate ligands in the Cu–Zn dimer leads to a double-spin polarization contribution in the Cu–Cu dimer.[15] The results of the proton ENDOR study strongly support a superexchange interaction propagated by acetate bridges.

This work was partially supported by a Hirosaki University Special Research Grant.

References

1) R. D. Willett, D. Gatteschi, and O. Kahn, "Magneto-Structural Correlations in Exchange Coupled Systems," Reidel, Dordecht, The Netherlands (1985).
2) B. N. Figgis and R. L. Martin, *J. Chem. Soc.*, **1956**, 3837.
3) L. S. Forster and C. J. Ballhausen, *Acta Chem. Scand.*, **16**, 1385 (1962).
4) A. E. Hansen and C. J. Ballhausen, *Trans. Faraday Soc.*, **61**, 631 (1965).
5) D. M. L. Goodgame, N. J. Hill, D. F. Marshall, A. C. Skapski, M. L. Smart, and P. G. H. Troughton, *J. Chem. Soc., Chem. Commun.*, **1969**, 629.
6) a) A. Bencini and D. Gatteschi, "EPR of Exchange Coupled Systems," Springer-Verlag, Berlin, Heidelberg, and New York (1990), references are there in. b) M. Inoue and M. Kubo, *Inorg. Chem.*, **9**, 2310 (1970); R. A. Zelonka and M. C. Baird, *ibid.*, **11**, 134 (1972). c) A. Kawamori and G. Soda, *Mol. Phys.*, **29**, 1085 (1975); A. Kawamori, *J. Magn. Reson.*, **31**, 423 (1978).
7) G. F. Kokoszka, H. C. Allen, Jr., and G. Gordon, *J. Chem. Phys.*, **42**, 3693 (1965).
8) G. M. Brown and R. Chidambaram, *Acta Crystallogr., Sect. B*, **1973**, 2393.
9) S. Kita, M. Hashimoto, and M. Iwaizumi, *Inorg. Chem.*, **18**, 3432 (1979).
10) N. M. Atherton and A. J. Horsewill, *Mol. Phys.*, **37**, 1349 (1979).
11) N. M. Atherton and A. J. Horsewill, *Mol. Phys.*, **42**, 985 (1981).
12) B. A. Goodman and J. B. Raynor, "Advances in Inorganic Chemistry and Radiochemistry," ed by H. J. Emeleus and A. G. Sharpe, Academic Press, New York and London (1970), p. 135.
13) A. J. Freeman and R. E. Watson, "Magnetism," ed by G. T. Rado and H. Suhl, Academic Press, New York (1965), Vol. IIA, p. 167.
14) I. G. Ross, *Trans. Faraday Soc.*, **55**, 1057 (1959).
15) P. de Loth, P. Cassoux, J. P. Daudey, and J. P. Malrieu, *J. Am. Chem. Soc.*, **103**, 4007 (1981).

Equations of State for the Lennard-Jones Mixtures at High Temperatures

Shin-ichi WAKAYAMA, Mitsuo KOSHI,* and Hiroyuki MATSUI
Department of Reaction Chemistry, The University of Tokyo, 7-3-1 Hongo, Bunkyo-ku, Tokyo 113
(Received March 25, 1991)

The virial coefficients for binary mixtures at high temperatures were directly calculated up to the fifth term by use of a Monte-Carlo integration technique and the various empirical mixing rules that have been proposed for estimating mixture virial coefficients were tested. It was found that these empirical mixing rules tend to fail as the molecular size differences increased. Accurate compressibility of the Lennard-Jones binary mixtures were also calculated by adopting Metropolis Monte-Carlo simulations in order to examine validity of the fifth order virial equation of state. At high temperature (T^*=20), the compressibility factors calculated by the fifth order virial equation of state were in good agreement with the results of the simulations in the range of $V/b \geq 0.4$ ($b=2\pi\sigma^3 N_a/3$). It was also found that the van der Waals one fluid theory could provide accurate compressibility factors even for mixtures of molecules with large size differences at high temperatures.

Although detailed knowledge of the equation of state (EOS) for mixtures is required for the calculations of equilibrium properties of high density multi-component systems such as chemical equilibrium behind detonation waves, precise theoretical determination of the EOS for high density mixtures still remains very difficult. Because of this, various types of empirical or semi-empirical EOS have been widely used in many practical applications. Recent progress in Monte-Carlo and molecular dynamics simulations enables the direct calculations of properties of dense mixtures and the validity of empirical EOS has been examined against these simulation results.[1-4] However these examinations are often limited to relatively low temperature region. The accuracy of empirical EOS for dense mixtures at high temperatures still remains unclear. The primary purpose of the present study is to test the applicability of the virial EOS and the van der Waals one fluid theory to the prediction of properties of dense mixtures at high temperatures. Such examinations are especially important in exploring an adequate EOS for the calculations of detonation properties.

The virial EOS,

$$\frac{pV}{RT}=1+\frac{B(T)}{V}+\frac{C(T)}{V^2}+\frac{D(T)}{V^3}+\frac{E(T)}{V^4}+\cdots, \quad (1)$$

has several advantages for many practical applications. Its simple analytical form is well suitable to the determination of complex chemical equilibrium composition by minimizing the Gibbs free energy. In principle, the virial coefficients can be calculated theoretically on the basis of intermolecular potentials. However calculations of virial coefficients for mixtures are rather difficult; specially, exact calculation of the third and higher order virial coefficients for mixtures has not been performed. Although various empirical mixing rules for mixture virial coefficients[5-7] have been used in the past, these mixing rules have weak theoretical basis and therefore their validity has to be tested by comparing with exact mixture virial coefficients.

In the present study, the virial coefficients for binary mixtures of molecules interacting with Lennard-Jones (L-J) 12-6 potentials were calculated numerically up to fifth term. Calculations were performed with a hypothetical Lorentz-Berthelot rule for unlike L-J parameters. Although this rule is very simple, relathionship of mixing rule between the unlike L-J parameters and the virial coefficients is not straightforward. Resulting virial coefficients were compared with those derived from empirical mixing rules over wide ranges of interaction potential parameters. In addition, exact compressibility of binary L-J mixtures were directly calculated by the use of Metropolis Monte-Carlo simulation and results were compared with compressibility factors calculated by the fourth order virial EOS for the binary mixtures.

An effective one component treatment of dense mixtures is generally used in many practical EOS. Among these, the van der Waals one-fluid (vdW1) theory is the most popular and its validity at low temperatures has been investigated by comparing with the results of Monte-Carlo[8] or Molecular Dynamics[9] computer simulations. These investigations suggested that applicability of the vdW1 theory was questionable for systems that contain molecules having quite different intermolecular potential parameters. Although the vdW1 theory has been frequently applied to the calculations of detonation properties,[10] its validity has to be examined. Compressibility factors obtained from the vdW1 theory were also compared with the results of the Metropolis Monte-Carlo simulations in order to clarify the applicability of the vdw1 theory at high temperatures.

1. Virial Coefficients for Binary L-J Mixtures

1-1 Calculation of Virial Coefficients. The virial coefficients for mixtures can be written as,

$$\begin{aligned} B_m &= \sum\sum X_i X_j B_{ij}, \\ C_m &= \sum\sum\sum X_i X_j X_k C_{ijk}, \\ D_m &= \sum\sum\sum\sum X_i X_j X_k X_l D_{ijkl}, \\ E_m &= \sum\sum\sum\sum\sum X_i X_j X_k X_l X_m E_{ijklm}, \end{aligned} \tag{2}$$

here X_i is the mole fraction of component i, and B_{ij}, C_{ijk},$\cdots$ are the virial coefficients which depend on intermolecular potentials for i, j, k,$\cdots\cdots$ molecules. For example, the coefficient D_{ijkl} depends on the potential energy functions between four molecules, i, j, k, and l, and can be expressed as a sum of the cluster integral. By using notations given by Rowlinson[11] for the irreducible cluster integral, the following expression for D_{ijkl} can be derived:

$$D_{ijkl} = -(D_4 + D_5 + D_6)/8. \tag{3}$$

Here, D_4, D_5, and D_6 are the integral of the product of Mayer F-functions. For an example, a term D_4 is expressed as follows,

$$D_4 = D_{4a} + D_{4b} + D_{4c}, \tag{4}$$

$$D_{4a} = \iiint f_{01} f_{12} f_{23} f_{30}\, dR_1 dR_2 dR_3, \tag{5a}$$

$$D_{4b} = \iiint f_{01} f_{13} f_{32} f_{20}\, dR_1 dR_2 dR_3, \tag{5b}$$

$$D_{4c} = \iiint f_{02} f_{21} f_{13} f_{30}\, dR_1 dR_2 dR_3, \tag{5c}$$

$$f_{ij} = \exp\left(-\frac{U_{ij}}{kT}\right) - 1. \tag{6}$$

Here, f_{ij} is a Mayer F-function, U_{ij} is the potential between molecules i and j, and R_i ($i \neq 0$) is the position vector between molecule i and molecule 0. It is noted that the values of D_{4a}, D_{4b}, and D_{4c} are all the same for a pure fluid, but they are different each other for the multi-component system. Similar expressions for other virial coefficients can also be derived by adopting the diagrams for the irreducible cluster integral given by Rowlinson.

Calculations of virial coefficients were performed for the Lennard-Jones (L-J) binary mixtures. Although the L-J potential is known to be inaccurate as a representation of the intermolecular interaction for high energy collisions, the L-J fluid provides a convenient model for testing various mixture theories. In the present calculations, the Lorentz-Berthelot mixing rule was used for unlike intermolecular interactions; i.e., the potential energy between unlike molecules i and j is given by the equation;

$$U_{12} = 4\varepsilon_{12}((\sigma_{12}/r)^{12} - (\varepsilon_{12}/r)^6). \tag{7}$$

The L-J parameters for unlike interaction, ε_{12} and σ_{12} are calculated from the L-J parameters for a pure fluid;

$$\varepsilon_{12} = (\varepsilon_{11}\varepsilon_{22})^{1/2} = \varepsilon_{11}\alpha^{1/2}, \tag{8}$$

$$\sigma_{12} = (\sigma_{11} + \sigma_{22})/2 = \sigma_{11}(1 + \eta)/2, \tag{9}$$

here, $\alpha = \varepsilon_{22}/\varepsilon_{11}$ and $\eta = \sigma_{22}/\sigma_{11}$.

The second virial coefficient for the binary mixture, B_{12}, is directly obtained form the reduced second virial coefficient, $B^*(T^*)$, for the pure fluid;

$$B_{12}(T^*_{12}) = b_{12} B^*(T^*_{12}), \tag{10}$$

here $T^*_{12} = kT/\varepsilon_{12}$ and $b_{12} = 2\pi\sigma_{12}^3 N_a/3$ (N_a is the Avogadro number). In order to obtain higher-order virial coefficients for mixtures, various types of irreducible cluster integrals such as given in Eq. 5 have to be calculated. Although Barker et al.[12] have used the Simpson's formula to integrate these cluster integrals for a pure fluid, it is quite difficult to apply their method to a multi-component system. A numerical integration technique proposed by Conroy[13] was employed in the present calculation. Points are selected at random in space of the integration variables and the integrands are evaluated at these points. It was found that the mean value of the integrands did not converge well to the integral unless large number of points were used. However, the calculations were speeded up by employing a stratified sampling technique. For the calculation of the third virial coefficients, the intermolecular distance in the range of 0.001σ to 10σ was divided into 4 regions. These segments of intermolecular distance construct 4^2 sub-spaces of the integration variables (*strata*). Sampling points in each strata were selected by using quasi-random numbers.[13] In case of fourth and fifth virial coefficients, intermolecular distances were divided into 9 and 10 regions so that 9^3 and 10^4 strata were composed for fourth and fifth virial coefficients, respectively. It was found that total numbers of 1.6×10^6, 7.29×10^6, and 1×10^8 sampling points were required for the calculation of the third, forth, and fifth virial coefficients in order to achieve the relative accuracy within 1%.

The fifth virial coefficient for a pure fluid at $T^*=20$ were also calculated to test the integration scheme. A value of 0.0207 for the normalized fifth virial coefficient, $E_{11111}^* = E_{11111}/b_{11}^4$, is in good agreement with a value of 0.0209 calculated by Barker et al.[12] The normalized virial coefficients for unlike interactions, C^*_{ijk}, D^*_{ijkl}, and E^*_{ijklm}, were calculated at $T^*_{11}=20$ for 'σ-equal' fluid ($\eta=1$) and 'ε-equal' fluid ($\alpha=1$); results are summarized in Tables 1 and 2, respectively. Calculations of the fifth virial coefficient were only performed for parameter sets of $\alpha=1$, $\eta=2$ and $\alpha=3$, $\eta=1$, since these calculations needed very long CPU time (120 min on Cray X-MP/416).

1-2 Comparisons with Empirical Virial Coefficients for Mixtures. Although several empirical virial coefficients for unlike interactions have been proposed in

Table 1. Normalized Virial Coefficients for the ε-Equal Fluid ($\varepsilon_{11}=\varepsilon_{22}$) at $T^*_{11}=20$
(Values for a pure fluid are taken from Ref. 12.)

$\eta=\sigma_{11}/\sigma_{22}$	1	1.25	1.5	1.75	2.0
B^*_{11}	0.5254	0.5254	0.5254	0.5254	0.5254
B^*_{12}	0.5254	0.7480	1.0260	1.3650	1.7728
B^*_{22}	0.5254	1.0260	1.7732	2.8158	4.2032
C^*_{111}	0.2464	0.2464	0.2464	0.2464	0.2464
C^*_{112}	0.2464	0.3895	0.5764	0.8100	1.1008
C^*_{122}	0.2464	0.6088	1.3019	2.5133	4.4992
C^*_{222}	0.2464	0.9399	2.8067	7.0773	15.770
D^*_{1111}	0.0832	0.0832	0.0832	0.0832	0.0832
D^*_{1112}	0.0832	0.1386	0.2157	0.3186	0.4413
D^*_{1122}	0.0832	0.2295	0.5382	1.1053	2.1504
D^*_{1222}	0.0832	0.3777	1.3301	3.9000	10.086
D^*_{2222}	0.0832	0.6199	3.1985	12.808	42.598
E^*_{11111}	0.0209	0.0209	0.0209	0.0209	0.0209
E^*_{11112}	0.0209				0.1282
E^*_{11122}	0.0209				0.7578
E^*_{11222}	0.0209				4.6694
E^*_{12222}	0.0209				18.268
E^*_{22222}	0.0209				85.606

Table 2. Normalized Virial Coefficients for the σ-Equal Fluid ($\sigma_{11}=\sigma_{22}$) at $T^*_{11}=20$
(Values for a pure fluid are taken from Ref. 12.)

$\alpha=\varepsilon_{11}/\varepsilon_{22}$	1	2	3	4
B^*_{11}	0.5254	0.5254	0.5254	0.6254
B^*_{12}	0.5254	0.5058	0.4833	0.4609
B^*_{22}	0.5254	0.4609	0.3608	0.2433
C^*_{111}	0.2464	0.2464	0.2464	0.2464
C^*_{112}	0.2464	0.2601	0.2672	0.2716
C^*_{122}	0.2464	0.2734	0.2857	0.2924
C^*_{222}	0.2464	0.2861	0.3038	0.3151
D^*_{1111}	0.0832	0.0832	0.0832	0.0832
D^*_{1112}	0.0832	0.0910	0.0956	0.0989
D^*_{1122}	0.0832	0.0992	0.1087	0.1151
D^*_{1222}	0.0832	0.1075	0.1210	0.1291
D^*_{2222}	0.0832	0.1156	0.1327	0.1341
E^*_{11111}	0.0209	0.0209	0.0209	0.0209
E^*_{11112}	0.0209		0.0257	
E^*_{11122}	0.0209		0.0315	
E^*_{11222}	0.0209		0.0385	
E^*_{12222}	0.0209		0.0458	
E^*_{22222}	0.0209		0.0546	

the past, these have weak theoretical basis and the validity of empirical formulae for the fourth and fifth coefficients has never been tested against results of strict numerical calculations. Among these, following three approximations for mixture virial coefficients were tested.

(i) Based on the statistical mechanical expression of the third virial coefficient, Orentlincher et al.[5] proposed the following expression,

$$C_{ijk}=(C_{ij}C_{jk}C_{ki})^{1/2}. \tag{11}$$

The coefficient C_{ij} is defined by a similar relation to Eq. 10:

$$C_{ij}=b_{ij}^2C^*(T^*_{ij}). \tag{12}$$

Here C^* is the reduced virial coefficient for a pure fluid.

(ii) Rowlinson et al.[6] have examined several scaling approximations for mixture virial coefficients by comparing with exact values of C_{112}. They recommended to use the following expressions:

$$C_{ijk}=(b_{ij}b_{jk}b_{ki})^{2/3}C^*(kT/\varepsilon_{ijk}), \tag{13}$$

$$\varepsilon_{ijk}=(\varepsilon_{ij}\varepsilon_{jk}\varepsilon_{ki})^{1/3}. \tag{14}$$

(iii) McHenry[7] proposed an empirical formula given below:

$$C_{ijk}=b_{ijk}^2C^*(kT/\varepsilon_{ijk}), \tag{15}$$

$$b_{ijk}=2\pi[(\sigma_{ij}+\sigma_{jk}+\sigma_{ki})/3]^3N_a/3. \tag{16}$$

Extension of these mixing rules (i)—(iii) to higher order virial coefficients is straightforward. In the above equations, the reduced virial coefficients for a pure fluid, $B^*(T^*)$, $C^*(T^*)$,$\cdots$, are required to calculate mixture virial coefficients. These values were obtained by a spline interpolation of the pure-component virial coefficients given by Barker et al.[12] Resulting third and fourth virial coefficients based on the approximations (i) and (ii) are compared with the values calculated by the direct numerical integration in Fig. 1 for 'σ-equal' fluid as a function of α. It is noted that the approximations (ii) and (iii) give the same results for σ-equal fluid. As can be seen in the figure, the approximation (ii) generally gives better agreement with the results of direct numerical calculations than the approximation (i). However, errors in approximations (i) and (ii) are within 5% in the range of $\varepsilon\leqslant 4$. Figure 2 shows comparisons of mixture virial coefficients based on the approximations (ii) and (iii) with those obtained by the numerical calculations for 'ε-equal' fluid as a function of the size parameter ratio, η. In this case, the approximation (ii) is also better than (iii), but its error is more than 10% at $\eta=2$ and is rapidly increasing with increasing the difference in molecular size.

At high temperature ($T^*_{11}=20$), it can be concluded that these empirical mixing rules (i)—(iii) for binary L-J mixtures give relatively small errors ($\leqslant 5\%$) for the mixture which contains molecules of similar size even if the L-J energy parameters of these molecules are quite different. However none of these approximations can

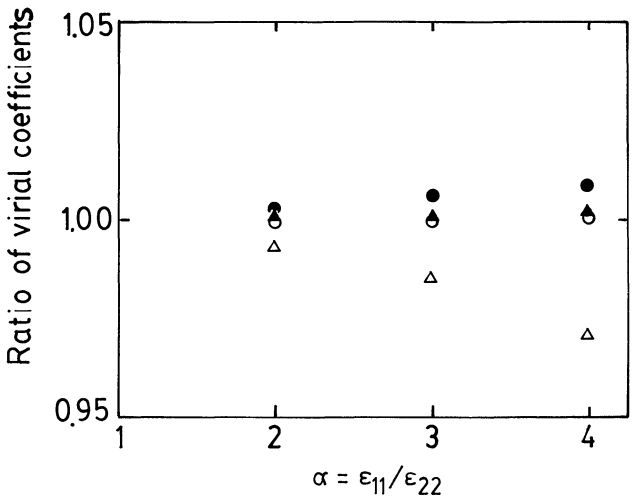

Fig. 1. Comparison of the unlike virial coefficients, C_{122}(closed points) and D_{1122}(open points), at $T^*_{11}=20$ for the σ-equal fluid calculated by the empirical mixing rules with Monte-Carlo calculations. Vertical axis is the ratio of [empirical virial coefficient]/[exact Monte-Carlo virial coefficient]. Triangles: mixing rule (i), Circles: mixing rule (ii).

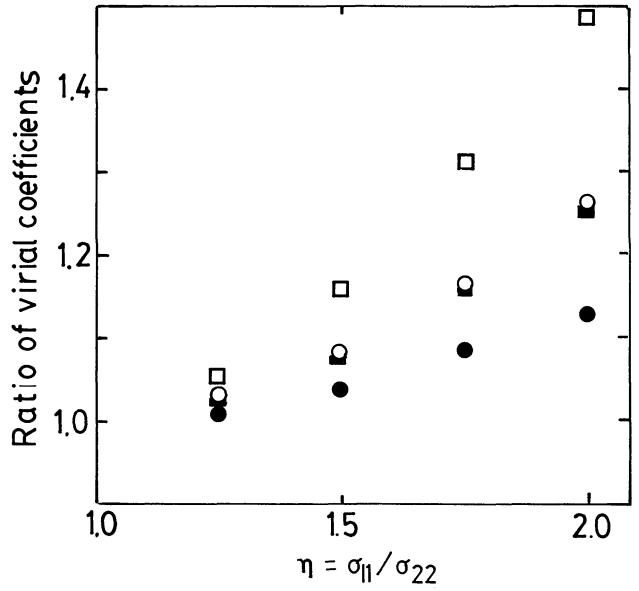

Fig. 2. Comparison of the unlike virial coefficients, C_{122}(closed points) and D_{1122}(open points), at $T^*_{11}=20$ for the ε-equal fluid calculated by the emprical mixing rules with Monte-Carlo calculations. Vertical axis is the ratio of [empirical virial coefficient]/[exact Monte Carlo virial coefficient]. Circles: mixing rule (ii), Squares: mixing rule (iii).

provide the precise third and fourth virial coefficients for mixtures containing molecules which have large difference in size.

2. Compressibility Factors at High Temperatures

2-1 Metropolis Monte-Carlo Calculation of Compressibility Factors. The compressibility factors for the L-J fluid of a single component has been widely studied by using Monte-Carlo[14-17] or molecular dynamics[18-22] simulations. Nicolas, Gubbins, Street, and Tildesley (NGST) proposed the EOS for L-J pure fluid which had 33 parameters.[14] These parameters were determined by fitting the compressibility factors to the results of their own molecular dynamics simulations together with many other results of Monte-Carlo and molecular dynamics calculations at $T^*\leqslant 6$ and $V/b\geqslant 0.4$ (V is the specific volume). Although the applicability of these simulations with limited number of molecules to much higher density range is not clear, Wood and Parker[1] showed that the Metropolis Monte-Carlo simulation[23] could be useful for the region of $V/b\geqslant 0.2$ at the temperature of $2T_c$ (T_c=the critical temperature). Since this density region is high enough for the application to many detonation problem, it might be interesting to calculate the high temperature compressibility factors by the Metropolis Monte-Carlo simulation.

In the present study, compressibility factors at high temperatures both for pure and multi-component systems were calculated by using Metropolis Monte-Carlo technique and the results were compared with the compressibility factors calculated by the virial EOS. The results presented here employed 256 particles in a cubic cell with periodic boundary conditions. A chain length of 10^5 was generated to achieve the convergence of the calculated pressures after first 6×10^4 chains were discard in order to ensure the complete relaxation of the system from the fcc initial configuration. A new configuration in the chains was constructed by moving a particle in the cell. A particle to be moved and its displacement were determined by random numbers. The rate of convergence with chain length was governed by a value of the maximum displacement of a particle to construct a new configuration in the chains. Optimum value for this maximum displacement was found to be 0.075σ.

Results of the Metropolis Monte-Carlo simulations for pure L-J fluid at $T^*=2.5$ and 20 are compared with compressibility factors calculated by the fifth order virial EOS in Fig. 3. As can be seen in the figure, the fifth order virial EOS is only valid in very low density region at $T^*=2.5$, whereas the virial series is readily converged at $T^*=20$ in the range of $V/b\leqslant 0.2$. At high temperatures, less terms seem to be needed to achieve the convergence of the virial series. In Fig. 3 compressibility factors calculated by the NGST EOS are also shown for comparison. Although the NGST EOS were derived from simulation data in the range of $0.5\leqslant T^*\leqslant 6$ and $0.4\leqslant V/b\leqslant 1.4$, results of the present Metropolis Monte-Carlo simulations are in good agreement with the NGST EOS in the range of $V/b\geqslant 0.2$ even at $T^*=20$. This indicates that the NGST EOS can be applicable at high temperatures for the calculation of detonation properties.

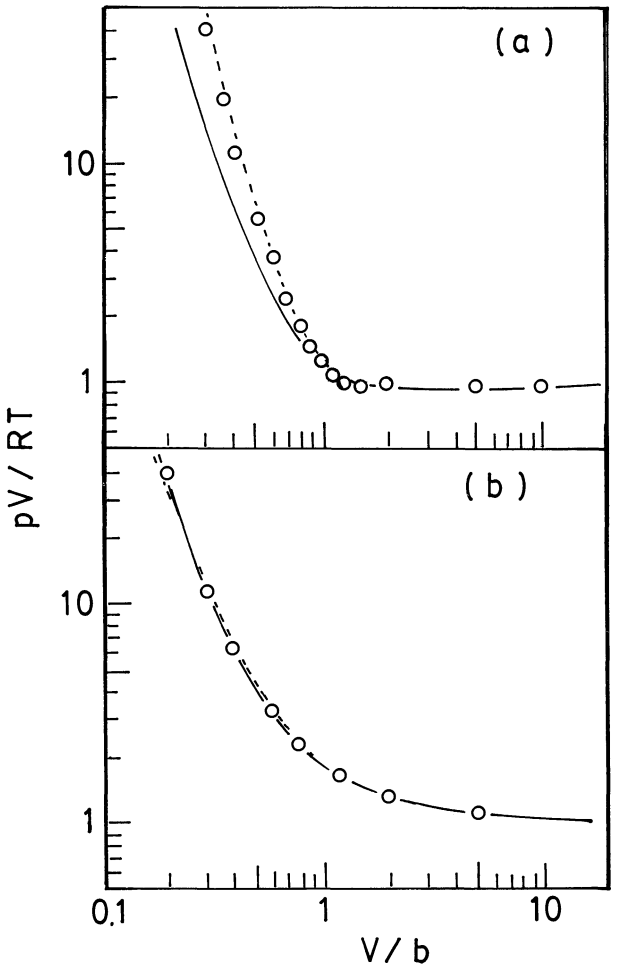

Fig. 3. Compressibility factor of the L-J pure fluid at $T^*=2.5$ (a) and $T^*=20$ (b). Circles: Metropolis Monte-Carlo simulation, solid line: the fifth order virial equation of state, broken line: the NGST equation of state (Ref. 14).

The compressibility factors for the equimolar L-J binary mixture obtained by the present Metropolis Monte-Carlo simulations at $T^*_{11}=20$ are shown in Fig. 4 for the ε-equal mixture with $\eta=2$ and in Fig. 5 for the σ-equal mixture with $\alpha=3$. In both cases the fifth order virial EOS gives excellent agreement with the present simulation results. These results suggest that the virial EOS converges much faster at high temperatures than at low temperatures in the range of $V/b \geqslant 0.2$.

2-2 Effective One Component Treatment of Dense Mixtures. The fifth order virial EOS gives accurate compressibility factors both for a single and multi-component systems at high temperatures, if the density is not too high. However, in many practical applications of the virial EOS such as calculations of chemical equilibrium in Chapman-Jouguet detonation, temperature derivatives of the virial coefficients are required. Since calculation of derivatives of virial coefficients by the Monte-Carlo or other numerical integration method is quite difficult, the analytical expression of the EOS is desirable for dense mixtures. The van der Waals one

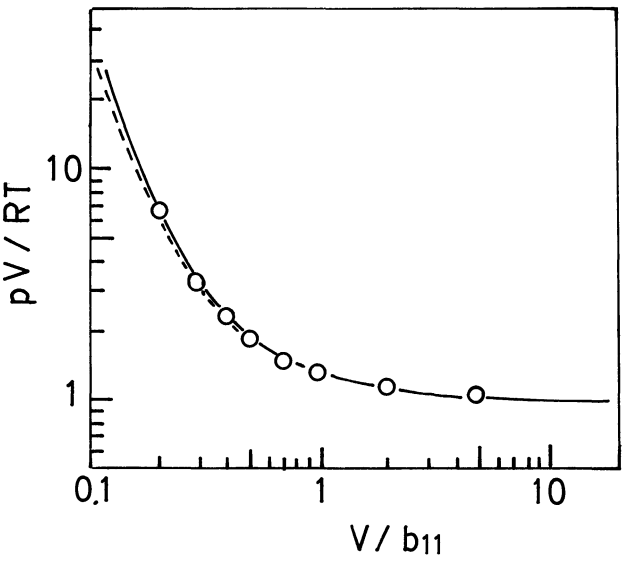

Fig. 4. Compressibility factor of the L-J binary mixture at $T^*_{11}=20$. $\alpha=\varepsilon_{11}/\varepsilon_{22}=1$ and $\eta=\sigma_{11}/\sigma_{22}=2$. Circles: Metropolis Monte-Carlo simulation, solid line: the fifth order virial equation of state, broken line: the vdW1 theory with the NGST equation of state (Ref. 14).

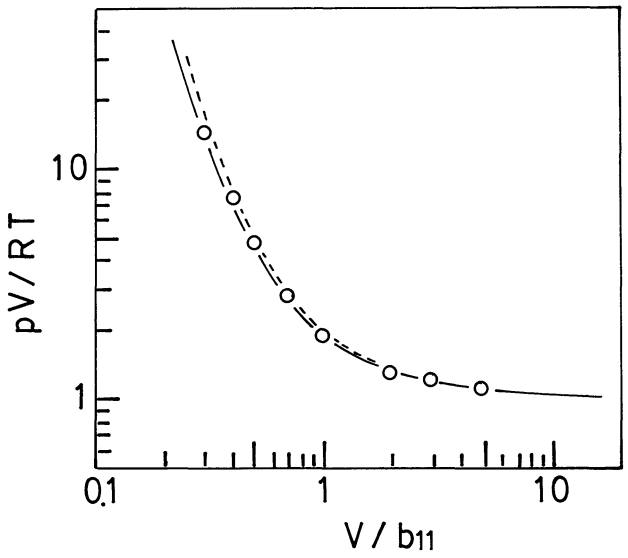

Fig. 5. Compressibility factor of the L-J binary mixture at $T^*_{11}=20$. $\alpha=\varepsilon_{11}/\varepsilon_{22}=3$ and $\eta=\sigma_{11}/\sigma_{22}=1$. Circles: Metropolis Monte-Carlo simulation, solid line: the fifth order virial equation of state, broken line: the vdW1 theory with the NGST equation of state (Ref. 14).

fluid theory is the one of the most widely used analytical expression of the equation of state in which a hypothetical effective one component potential is used for all of the intermolecular interactions. The parameters of this effective one component L-J potential, σ_m and ε_m, is given by following equations:

$$\sigma_m^3=\sum\sum X_i X_j \sigma_{ij}^3, \tag{17}$$

$$\varepsilon_m=\sum\sum X_i X_j \varepsilon_{ij} \sigma_{ij}^3 / \sigma_m^3. \tag{18}$$

By adopting the NGST EOS to define the EOS for this effective one component fluid, the compressibility factors were calculated and results are compared in Figs. 4 and 5. The van der Waals theory gives good agreement with the simulation results for ε-equal fluid and slightly higher values than the simulations for the mixtures of $\alpha=3$ and $\eta=1$. However the disagreement in this case is less than 10% in the range of $V/b \geqslant 0.4$.

It has been shown that the prediction of van der Waals mixture theory deteriorates as the molecular size difference between the species of the mixture increases at low temperatures.[2,4,24] Our results in Figs. 4 and 5 indicate that the accuracy of the van der Waals one fluid theory is considerably improved at high temperatures.

Recently Hamad and Mansoori[24] proposed a new dense fluid theory of mixtures which can be applicable for mixtures of molecules with large size and energy differences. Their theory is based on the effective one component treatment and the L-J parameters for mixtures are obtained by solving the following set of equations:

$$\frac{C^*(kT/\varepsilon_m)}{B^{*2}(kT/\varepsilon_m)} = \frac{\sum\sum\sum X_i X_j X_k C_{ijk}}{(\sum\sum X_i X_j B_{ij})^2}, \tag{19}$$

$$\sigma_m{}^3 = \frac{\sum\sum X_i X_j \sigma_{ij}{}^3 B^*(kT/\varepsilon_{ij})}{B^*(kT/\varepsilon_m)}. \tag{20}$$

The use of Eqs. 19 and 20 in calculating the mixture L-J parameters requires knowledge of the unlike interaction third virial coefficients. They used empirical mixing rules (i)—(iii) for C_{ijk} to solve Eqs. 19 and 20 and found their theory gave accurate values of Henry's constant, pressure, and internal energy of dense mixtures at low temperatures. At high temperatures, empirical mixing rules (i)—(iii) are not accurate, as shown in the previous section. We tried to solve Eqs. 19 and 20 with the exact unlike interaction third virial coefficients calculated by the Monte-Carlo integrations at $T^*{}_{11}=20$. However the attempt was failed because of the numerical instability. It is also noted that a value of σ_m in Eq. 20 is different from $\sigma_{11}=\sigma_{22}$ for the σ-equal mixtures if $\alpha \neq 1$. The applicability of Eqs. 19 and 20 at high temperatures seems to be limited unless the precise analytical expressions for C_{ijk} are available.

3. Conclusions

The virial coefficients for unlike intermolecular interactions were calculated up to the fifth order term by the direct numerical integration of cluster integral. Several empirical mixing rules for the unlike interaction virial coefficients were tested at high temperature against the results of the numerical integration. The accuracy of these approximate virial coefficients were found to be not enough for the mixtures which contained species having different molecular size.

Although the fifth order virial equation of state understimates the compressibility factors at low temperatures, it gives accurate compressibility factors of dense fluid mixtures in the range of $V/b \geqslant 0.4$ at $T^*=20$. It is also found that the van der Waals one fluid theory can provide good approximation for compressibility of mixtures regardless the difference in molecular size at high temperatures. The van der Waals one fluid theory with accurate analytical equation of state for a pure fluid such as the NGST equation of state is promising for predicting properties of high temperature dense mixtures.

The authors are grateful to Dr. T. Saito and Dr. Y. Watanabe (Cray Research Japan Ltd.) for helpful comments and discussions on our Monte-Carlo programs. A part of this work was supported by the 20th Research Grant of the Foundation for the Promotion of the Industrial Explosives Technology.

References

1) W. W. Wood and F. R. Parker, *J. Chem. Phys.*, **27**, 720 (1957).
2) D. Henderson, *Ann. Rev. Phys. Chem.*, **25**, 461 (1974).
3) K. S. Shing and K. E. Gubbins, *Mol. Phys.*, **46**, 1109 (1982).
4) K. E. Gubbins, K. S. Shing, and W. B. Streett, *J. Phys. Chem.*, **87**, 4573 (1983).
5) M. Orentlicher and J. M. Prausnitz, *Can. J. Chem.*, **45**, 373 (1967).
6) J. S. Rowlinson, F. H. Summer, and J. R. Sutton, *Trans. Faraday Soc.*, **50**, 1 (1954).
7) J. T. Henry, *Aust. J. Chem.*, **21**, 565 (1968).
8) K. S. Shing and K. E. Gubbins, *Mol. Phys.*, **49**, 1121 (1983).
9) K. C. Mo, K. E. Gubbins, G. Jacucci, and I. R. McDonald, *Mol. Phys.*, **27**, 1173 (1974).
10) F. H. Ree, *J. Chem. Phys.*, **81**, 1251 (1984).
11) J. S. Rowlinson, *Proc. R. Soc. London, Ser. A*, **279**, 147 (1964).
12) J. A. Barker, P. J. Leonard, and A. Pompe, *J. Chem. Phys.*, **44**, 4206 (1966).
13) H. Conroy, *J. Chem. Phys.*, **47**, 5307 (1967).
14) J. J. Nicolas, K. E. Gubbins, W. S. Street, and D. J. Tildesley, *Mol. Phys.*, **37**, 1429 (1979).
15) J. -P. Hansen, *Phys. Rev. A*, **2**, 221 (1970).
16) M. N. Rosenblush and A. W. Rosenblush, *J. Chem. Phys.*, **22**, 881 (1954).
17) L. R. McDonard, *Chem. Phys. Lett.*, **3**, 241 (1969).
18) J. D. Johnson, M. S. Shaw, and B. L. Holian, *J. Chem. Phys.*, **80**, 1279 (1984).
19) L. Verlet, *Phys. Rev.*, **159**, 98 (1967).
20) H. Nakanishi and K. Toukubo, *J. Chem. Phys.*, **70**, 5848 (1979).
21) H. Nakanishi, H. Narusawa, and K. Toukubo, *J. Chem. Phys.*, **72**, 3089 (1980).
22) D. L. Jolly and R. J. Bearman, *Mol. Phys.*, **41**, 137 (1980).
23) R. J. Bearman and D. L. Jolly, *Mol. Phys.*, **44**, 665 (1981).
24) E. Z. Hamad and G. A. Mansoori, *J. Chem. Phys.*, **87**, 6046 (1987).

 © 1991 The Chemical Society of Japan Bull. Chem. Soc. Jpn., 64, 3335—3339 (1991)

Cadmium (5^3P_1)-Photosensitized Luminescence of Some Aliphatic Diamines

Shunzo YAMAMOTO,* Yoshimi SUEISHI, and Norio NISHIMURA
Department of Chemistry, Faculty of Science, Okayama University, 3-1-1, Tsushima-naka, Okayama 700
(Received May 29, 1991)

The cadmium(5^3P_1)-photosensitized luminescence of some aliphatic diamines was studied by a steady-illumination method at temperatures between 230 and 330 °C. It was found that 1,2-ethylenediamine, *N*,*N*,*N*′,*N*′-tetramethyl-1,2-ethylenediamine, 1,3-propanediamine, and *N*,*N*,*N*′,*N*′-tetramethyl-1,3-propanediamine have two emission bands (wavelengths at the peaks of these bands are about 450 and 550 nm), while *N*,*N*,*N*′,*N*′-tetramethylmethanediamine, *N*,*N*′-dimethylpiperazine, and triethylenediamine have only a short-wavelength band. From the temperature and pressure dependences of the emission intensities of the two bands, it had been concluded previously that these bands could be assigned to two kinds of 1 : 1 exciplexes between an excited cadmium atom and a diamine molecule. From the temperature dependence of the equilibrium constants between the two exciplexes which had been obtained from the ratio of the emission intensities of the two bands, the enthalpy and entropy changes of the equilibrium were evaluated. The cyclic exciplexes assigned to the long-wavelength band have smaller enthalpies and entropies than do the noncyclic exciplexes assigned to the short-wavelength band.

It is well known that excited triplet cadmium[1-4] and mercury[5,6] atoms react with the some compounds which contain a nitrogen or an oxygen atom (NH_3, H_2O, aliphatic amines, alcohols, and ethers) to form exciplexes, and that these exciplexes fluoresce. Recently, we have studied the cadmium-photosensitized reactions of some aliphatic diamines.[7] Two emission bands were observed in the blue and green regions for *N*,*N*,*N*′,*N*′-tetramethyl-1,2-ethylenediamine (TMEDA) and *N*,*N*,*N*′,*N*′-tetramethyl-1,3-propanediamine (TMPDA), while only a short-wavelength band was observed for *N*,*N*′-dimethylpiperazine (DMP) and triethylenediamine (TEDA). From the temperature and pressure dependences of the emission intensities of these two bands, we have concluded that these bands can be assigned to two kinds of 1:1 exciplexes between an excited cadmium atom and a diamine molecule. The cyclic and noncyclic exciplexes which are shown in Scheme 1 were suggested for the long- and short-wavelength bands respectively. DMP and TEDA can not form cyclic exciplexes because of their rigid structures.

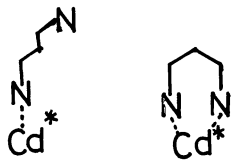

Scheme 1.

In the present study, the equilibrium constants between the two exciplexes were determined over the temperature range 230—330 °C, from which the enthalpy and entropy changes of the equilibrium can be estimated. The present paper reports on details conserning the cadmium-photosensitized luminescence of diamines and the quenching of the 326.1 nm resonance radiation by them.

Experimental

The experimental apparatus and the procedures for the measurements of resonance radiation at 326.1 nm and sensitized luminescence were similar to those used previously.[7,8] A part of the vacuum line was constructed using greaseless stopcocks in order to prevent any adhesion of sample gases to stopcock grease. A cylindrical quartz cell (17 mm in internal diameter and 20 cm in length) was kept in an electric furnace, the temperature of which was varied from 230 to 330 °C. A spiral cadmium discharge lamp made of Pyrex glass was placed in another furnace kept at 250 °C. The 228.8 nm resonance line was completely absorbed by the Pyrex glass. The visible lines from the lamp were removed with a glass band-pass filter (Toshiba, UV-D33S). The 326.1 nm resonance line was used to excite Cd($^3P_1$) atoms from cadmium vapor in the cell. The resonance radiation at 326.1 nm and the sensitized luminescence were monitored with a Hitachi spectrophotometer (Model 139). The wavelength dependence of the sensitivity of the monochromator-photomultiplier combination was determine by using standard fluorescence solutions of quinine sulfate and *N*,*N*-dimethyl-*m*-nitroaniline.[9]

N,*N*,*N*′,*N*′-Tetramethylmethanediamine (TMMDA), 1,2-ethylenediamine (EDA), TMEDA, 1,3-propanediamine (PDA), TMPDA, DMP, and TEDA were obtained from commercial sources (G. R. grade). These diamines were used after drying by potassium hydroxide and repeated trap-to-trap distillation. The cadmium metal used was of high-purity grade (99.9999%).

Results

Figure 1 shows the emission spectra obtained in the cadmium-photosensitized reaction of DMP and PDA at various temperatures between 230 and 300 °C. These spectra were corrected for the wavelength dependence of the sensitivity of the detection system. As is shown in Fig. 1, two emission bands are evident for PDA (broken lines show a separation of two bands for the spectra at 230 °C). The spectra for the PDA obtained at 230, 260, and 300 °C were adjusted to the same total intensity at two peaks. The profiles have an isosbestic point. The intensity of the short-wavelength band (band I) increases and that of the long-wavelength band (band II) decreases with increasing temperature. DMP shows one emission

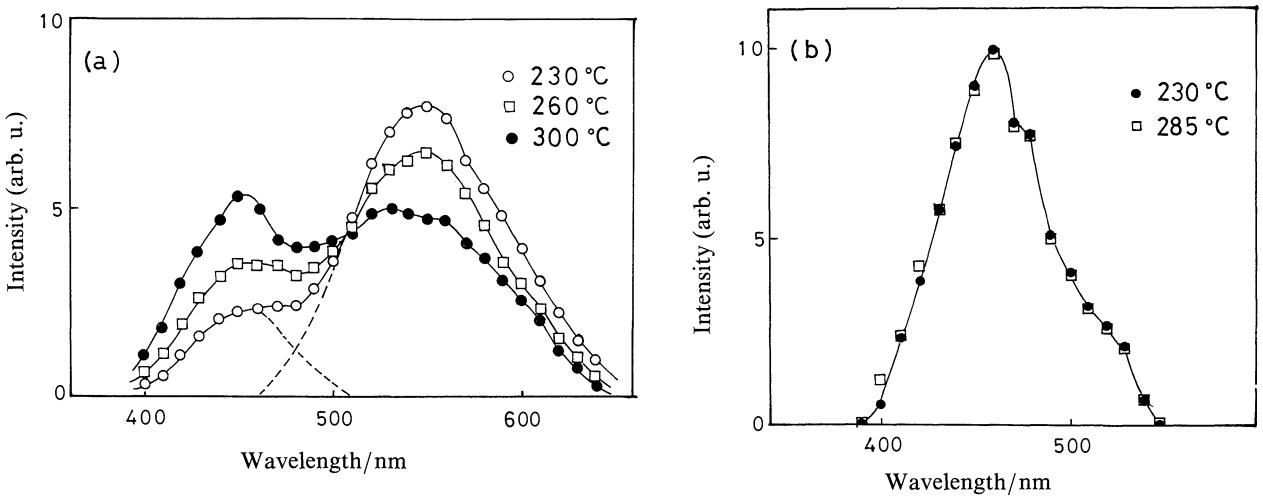

Fig. 1. Emission spectra for cadmium-photosensitized luminescence of PDA (a) and DMP (b).

Table 1. Half-Quenching Pressure for Quenching of 326.1 nm Resonance Radiation, Wavelength at Peak of Emission Bands, and Quantum Yield of Luminescence

Diamine	$P_{1/2}$	λ/nm		Quantum yield	
	Pa	Band I	Band II	Band I	Band II
TMMDA	66.0±2.6	480	—	0.24	—
EDA	8.9±0.1	460	570	0.040	0.27
TMEDA	11.1±0.2	460	550	0.020	0.16
PDA	12.7±0.2	450	550	0.044	0.17
TMPDA	15.5±0.2	452	570	0.040	0.17
DMP	12.0±0.2	460	—	0.060	—
TEDA	10.3±0.2	442	—	0.29	—

band and the spectrum is independent of temperature. EDA, TMEDA, and TMPDA have two emission bands and the temperature dependences of their emission spectra are very similar to that for PDA, while TMMDA and TEDA have only the short-wavelength band and their spectra are also independent of the temperature, like that for DMP. The position and shape of band I of EDA, TMEDA, PDA, and TMPDA are similar to those of the bands of TMMDA, DMP, and TEDA, and of the bands reported for the Cd($^3P_1$)-aliphatic amine systems. Band II has not been reported for other systems.

The quantum yields of the luminescence were determined by comparing the integrated intensity of the emission bands with that for ammonia under the same conditions. The quantum yield of the luminescence for ammonia was reported to be 0.67.[1,2] The quantum yields obtained at 230 °C are listed in Table 1.

In order to estimate the efficiencies of quenching of the 326.1 nm resonance radiation, the emission intensity at 326.1 nm was measured at various pressures of diamines. Stern-Volmer plots for some diamines are shown in Fig. 2. The half-quenching pressures obtained from the slope of the straight lines in Fig. 2 are listed in Table 1. The measurements were carried out in the absence of any

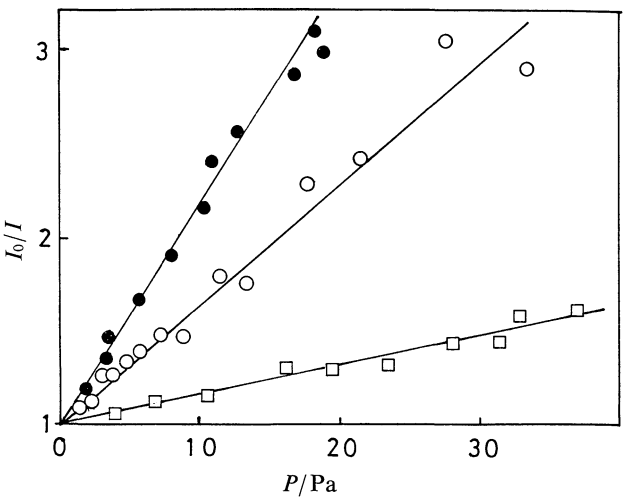

Fig. 2. Stern-Volmer plots for quenching of resonance radiation by EDA (●), TMPDA (○), and TMMDA (□) at 230 °C.

buffer gas. It is not necessary to take into account the effect of pressure broadening, since the pressures of the diamines were very low.

The pressure dependences of the relative intensities at the peaks of the emission bands for PDA are shown in Fig. 3. Slightly different pressure dependence from those presented in a previous letter[7] was obtained by using greaseless stopcocks in this study. As Fig. 3 shows, the intensities increase rapidly with increasing PDA pressure in the low-pressure region, and then leveled off to a constant value. The intensities are constant at higher pressures than 200 Pa (I_{440}/I_{550}=0.28). The pressure dependence of the relative emission intensity at 450 nm is very similar to that at 550 nm. Similar pressure dependences of the emission intensities of the two bands were obtained for EDA, TMEDA, and TMPDA.

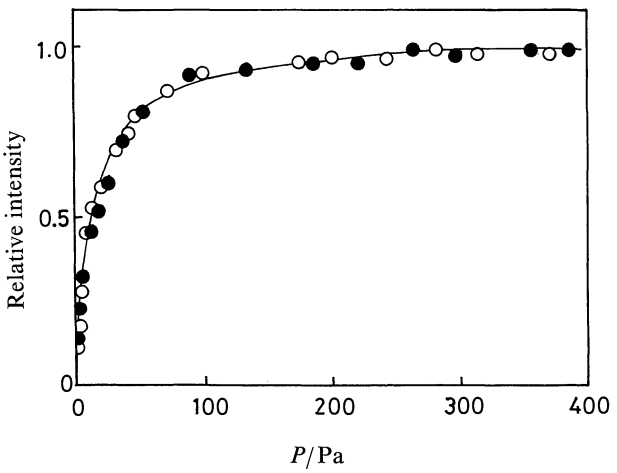

Fig. 3. Pressure dependences of emission intensities at 450 (○) and 550 nm (●) for PDA at 230°C.

Discussion

In a previous letter[7] we concluded that the two emission bands can be assigned to two kinds of 1:1 exciplexes between an excited cadmium atom and a diamine molecule from the pressure and temperature dependences of the emission intensities of the two bands as well as the dependence of the emission intensities on the intensity of the exciting light. From the temporal profiles of the intensities of the two emission bands and that of the 326.1 nm resonance radiation measured for TMPDA under pulsed excitation conditions, it has been suggested that two exciplexes are formed directly from $Cd(^3P_1)$, and that there are collision-induced mixing processes between these exciplexes.[10] The following reaction scheme has been proposed:

$$Cd(^1S_0) + h\nu(326.1\text{ nm}) \longrightarrow Cd(^3P_1) \quad (1)\ I^\circ$$

$$Cd(^3P_1) \longrightarrow Cd(^1S_0) + h\nu(326.1\text{ nm}) \quad (2)\ k_2$$

$$Cd(^3P_1) + DA \longrightarrow CdDA^* \quad (3)\ k_3$$

$$Cd(^3P_1) + DA \longrightarrow CdDA^{**} \quad (4)\ k_4$$

$$Cd(^3P_1) + DA \longrightarrow \text{other reactions} \quad (5)\ k_5$$

$$CdDA^* + DA \rightleftharpoons CdDA^{**} + DA \quad (6)(-6)\ k_6, k_{-6}$$

$$CdDA^* \longrightarrow Cd(^1S_0) + DA + h\nu(450\text{ nm}) \quad (7)\ k_7$$

$$CdDA^{**} \longrightarrow Cd(^1S_0) + DA + h\nu(550\text{ nm}). \quad (8)\ k_8$$

Here, DA represents a diamine, CdDA* stands for an exciplex which fluoresces band I, while CdDA** stands for another exciplex which fluoresces band II. As has been discussed in a previous paper,[10] it was concluded that the production of $Cd(^3P_0)$ is a minor process for the Cd/TMPDA system from the finding that the decay profile of the resonance radiation is consistent with the quenching rate constant determined from the slope of the Stern–Volmer plot. If $Cd(^3P_0)$ is produced and the equilibration between $Cd(^3P_1)$ and $Cd(^3P_0)$ is rapid, as in the Cd/ammonia system,[4] the slope of the Stern–Volmer plot should correspond to the population-weighted sum of the quenching rate constants of the $^3P_1$ and $^3P_0$ states, while the rate constant determined by the decay profiles of the resonance radiation must be equal to the weighted average; there must be a difference by a factor of more than two between the weighted sum and the weighted average at 500 K. The minor production of $Cd(^3P_0)$ in this system can be attributed to the large quenching efficiency of TMPDA. The production of $Cd(^3P_0)$ is not involved in the above-mentioned reaction mechanism, since the other diamines used also had large quenching efficiencies.

A steady-state treatment leads to the following equation:

$$\frac{I_0}{I} = 1 + \frac{k_Q}{k_2}[DA], \quad (9)$$

where I_0 and I represent the intensities of the resonance radiation (defined as k_2 $[Cd(^3P_1)]$) in the absence and presence of diamines, respectively; k_Q is the quenching rate constant: $k_Q = k_3 + k_4 + k_5$. The Stern–Volmer plots given in Fig. 3 are expressed by this equation.

In a previous paper[10] the value of $4.0\times10^5\ s^{-1}$ for k_2 (the effective radiation lifetime of $Cd(^3P_1)$ is somewhat lengthened by radiation imprisonment) was used in a simulation of temporal profile of the resonance radiation in the cadmium–TMPDA system at 230°C. From the half-quenching pressures, the values of k_Q can be estimated; they are listed in Table 1.

The following equations for the intensities of the exciplex emissions are derived by the steady-state treatment based on the assumption that fast equilibrium between two exciplexes is attained:

$$I_s = \alpha k_7[CdDA^*] = \alpha I^\circ \frac{(k_3 + k_4)[DA]}{k_2 + k_Q[DA]} \frac{k_6 k_7}{(k_6 + k_{-6})(k_7 + k_8)}, \quad (10)$$

$$I_I = \beta k_8[CdDA^{**}] = \beta I^\circ \frac{(k_3 + k_4)[DA]}{k_2 + k_Q[DA]} \frac{k_6 k_8}{(k_6 + k_{-6})(k_7 + k_8)}, \quad (11)$$

where I_s and I_I are the emission intensities at the peaks of bands I and II, I° is the intensity of the 326.1 nm resonance radiation absorbed by cadmium atoms, and α and β are proportional factors between the total emission intensities of bands I and II and the intensities at the peaks. As was mentioned above, the emission intensities at the peaks of bands I and II level off to constant values at high pressures. If I_s^∞ and I_I^∞ denote the constant intensities at high pressures, the following equation is

obtained:

$$\frac{I_s}{I_s^\infty}=\frac{I_l}{I_l^\infty}=\frac{k_Q[DA]}{k_2+k_Q[DA]}. \quad (12)$$

The solid line in Fig. 3 shows the values calculated according to Eq. 12 by using the values of k_2 and k_Q shown above. The calculated values are in good agreement with the observed ones within the limits of experimental error. Similar good agreements between the calculated and experimental values were obtained for other diamines. This demonstrates that the above reaction scheme and the assumption mentioned above are reasonable.

The equilibrium constant, K, between two exciplexes is expressed by

$$K=\frac{[CdDA^{**}]}{[CdDA^{*}]}=\frac{\alpha}{\beta}\frac{k_7}{k_8}\frac{I_l}{I_s}. \quad (13)$$

The ratios of α/β were obtained for the four diamines which show the two emission bands at some temperatures by comparing the values of I_l/I_s to the ratios of the integrated intensities of the emission bands (Table 2), and found to be independent of the temperature. Since both k_7 and k_8 are the rate constants for radiation processes, the ratio k_7/k_8 must be independent of the temperature. In a previous paper,[10] it was shown that a simulation of the temporal profiles of the two emission bands gave the results that $k_7=k_8=1.9\times10^5$ s^{-1} for TMPDA. Since we have no information concerning the values of k_7 and k_8 for other diamines, it is assumed that the values of k_7/k_8 for other diamines are also equal to unity as a first approximation. Although the k_7- and k_8-values should depend on the kind of diamine, they may be expected to vary in a somewhat similar manner to one another, since the two exciplexes for EDA, TMEDA, PDA, and TMPDA have similar structures, respectively (as will be shown later, the enthalpy changes between the two exciplexes are very similar for these diamines). The values of K can be obtained by Eq. 13 at various temperatures for EDA, TMEDA, PDA, and TMPDA. The values of ΔH° and ΔS° were obtained from the slopes and the intercepts of the straight lines between $\ln K$ and $1/T$ shown in Fig. 4 and are listed in Table 2, together with the K-values at 230 °C.

In conclusion, the exciplexes for the long-wavelength bands have a smaller enthalpy and entropy than do the exciplexes for the short-wavelength bands. This results seem to give another kind of evidence that the former are cyclic, because of the general tendency that cyclic compounds have smaller entropy than do chain compounds.[11] The energy differences between the two exciplexes obtained above are smaller than the energy differences between the wavelengths of the peaks of the two emission bands (about 48 kJ mol^{-1}). This shows that the potential energy surfaces of the ground state for

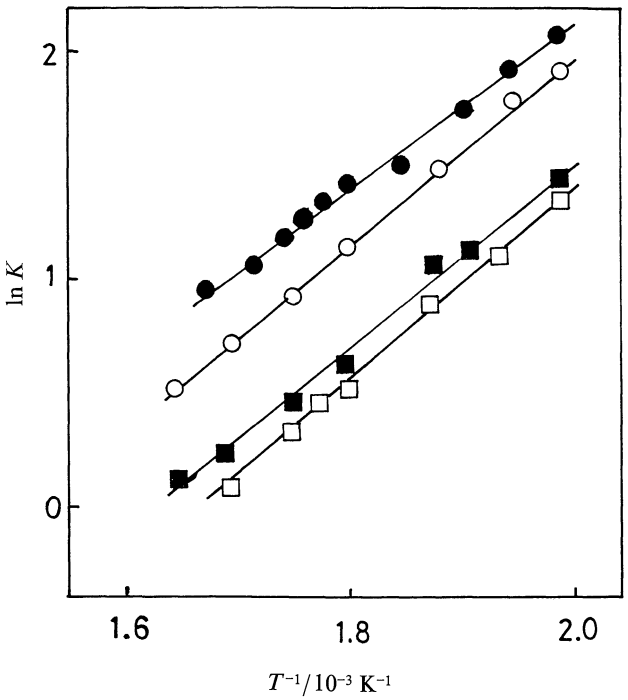

Fig. 4. Plots of $\ln K$ against $1/T$. EDA (○), TMEDA (●), PDA (□), and TMPDA (■).

Table 2. Values of k_Q, α/β, K, ΔH°, and ΔS°

Diamine	$10^{10}k_Q$ / cm^3 mol^{-1} s^{-1}	α/β	K[a]	ΔH° / kJ mol^{-1}	ΔS° / J Kmol^{-1}
TMMDA	0.51±0.02	—	—	—	—
EDA	3.8 ±0.1	0.82	6.8	−34.7±0.5	−53±1
TMEDA	3.0 ±0.1	0.84	8.0	−30.8±0.5	−44±1
PDA	2.6 ±0.1	0.87	3.9	−34.5±0.6	−57±1
TMPDA	2.2 ±0.1	0.56	4.3	−33.7±0.5	−55±1
DMP	2.8 ±0.1	—	—	—	—
TEDA	3.3 ±0.1	—	—	—	—

a) At 230 °C.

the cyclic exciplexes must be more repulsive than that for the noncyclic exciplexes; this is shown schematically in Fig. 5.

Callear et al.[12,13] observed two emission bands in mercury(6^3P_0)-*t*-butylamine and diethylamine systems. They pointed out that the short-wavelength band is due to the HgA* monomer, and that the long-wavelength band can be assigned to the HgA_2* dimer. Although they did not described the structures of the dimers, two amine molecules may attach directly to an excited mercury atom. If this is the case, the HgA_2 dimers are closely related to the cyclic exciplexes observed in the present study. Indeed, both species have a common feature of having long-wavelength bands. More experimental work is needed to clarify this point.

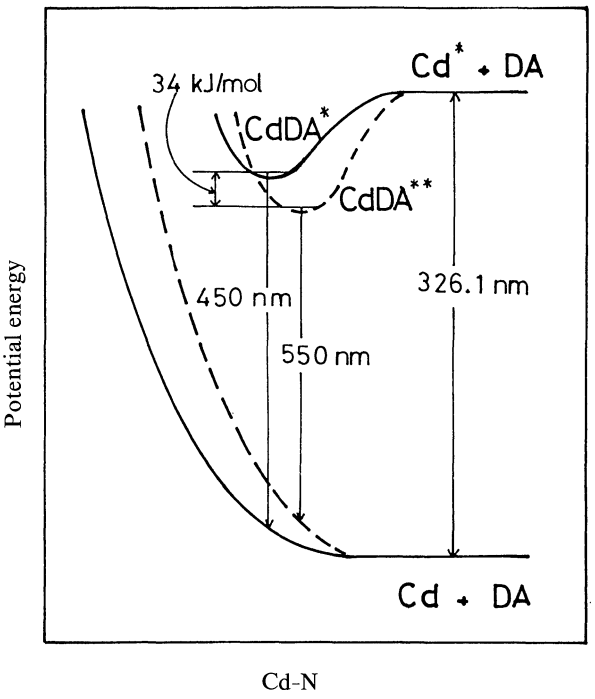

Fig. 5. Schematic potential energy diagram of diamine–Cd($^3P_1$) complexes.

References

1) S. Tsunashima and S. Sato, *Rev. Chem. Intermed.*, **2**, 201 (1979).
2) S. Yamamoto and S. Sato, *Bull. Chem. Soc. Jpn.*, **48**, 1382 (1975).
3) H. Umemoto, S. Tsunashima, and S. Sato, *Bull. Chem. Soc. Jpn.*, **51**, 1951 (1978).
4) C. J. Nokes and L. F. Phillips, *J. Chem. Soc., Faraday Trans. 2*, **78**, 2001 (1982).
5) L. F. Phillips, *Acc. Chem. Res.*, **7**, 135 (1974).
6) A. B. Callear, *Chem. Rev.*, **87**, 355 (1987).
7) S. Yamamoto, M. Itami, Y. Sueishi, and N. Nishimura, *Chem. Lett.*, **1990**, 1109.
8) S. Yamamoto, M. Yasunobu, N. Nishimura, and S. Hasegawa, *Mol. Photochem.*, **9**, 277 (1979).
9) E. Lippert, W. Nagele, I. Seibo-Blankenstein, U. Stager, and W. Voss, *Z. Anal. Chem.*, **170**, 1 (1959).
10) H. Umemoto, K. Kuwahara, T. Ohnuma, A. Masaki, and S. Yamamoto, *J. Chem. Soc., Faraday Trans.* (1991), in press.
11) S. W. Benson, "Thermochemical Kinetics," John Wiley & Sons, New York (1968), p. 51.
12) A. B. Callear, D. R. Kendall, and L. Krause, *Chem. Phys.*, **29**, 415 (1978).
13) A. B. Callear and D. P. Devonport, *J. Chem. Phys.*, **78**, 3738 (1983).

Intersystem Crossing of Radical Pair in Solvent Cage. External Heavy Atom Effect on Dual Photoreactions of Phthalazine[1)]

Hiroyasu INOUE,* Tadamitsu SAKURAI, Toshihiko HOSHI,†
Jun OKUBO,†† and Isao ONO†
Department of Applied Chemistry, Faculty of Technology, Kanagawa University,
Kanagawa-ku, Yokohama 221
† Department of Chemistry, College of Science and Engineering, Aoyama Gakuin University,
Setagaya-ku, Tokyo 157
†† Department of Natural Science for General Education, Tokyo Denki University,
Inzai-machi, Inba-gun, Chiba 270-13
(Received June 7, 1991)

The effects of the temperature, initial concentration, and chemical quenchers on dual photoreactions of phthalazine were investigated. The results give further supporting evidence for a previously proposed reaction mechanism, i.e., phthalazine in the lowest excited singlet and triplet states affords singlet and triplet radical pairs, respectively, in the initial hydrogen abstraction process from 2-propanol. The singlet radical pair gives a reduction product in a solvent cage, whereas the radicals produced in the triplet state escape from the solvent cage, causing dimerization. On the basis of the reaction mechanism of dual photoreactions, external heavy-atom effects on the radical pairs within a solvent cage have been studied. The results indicate that heavy-atom perturbations bring about an enhancement of the intersystem crossing efficiency from the triplet-state radical pair to the singlet one, including a spin inversion of the radical pair in the solvent cage, rather than $S_1 \rightarrow T_1$ intersystem crossing induced within a single molecule of phthalazine.

The spin multiplicities of a caged radical pair formed during the initial step of photochemical reactions govern the reactivities of the subsequent reactions of the radicals, affecting the product distribution. In general, singlet radical pairs undergo cage reactions efficiently, while triplet ones do so inefficiently.[2)] In the latter case, the triplet radical pairs must undergo a spin inversion to singlet radical pairs prior to cage reactions. Thus, the intersystem crossing of this type concerning radical pairs in a solvent cage competes with the escape of radicals from the cage.[3)] In this connection, the effects of an external magnetic field on caged reactions have been widely investigated.[2,4-6)] However, studies on the internal and external heavy-atom effects on the intersystem crossing process of a radical pair in a solvent cage have scarcely been reported. A 2-propanol solution of phthalazine may serve as a relevant reaction system for studying the above-mentioned effects.[7)]

In a previous paper[7)] we reported that phthalazine (P) simultaneously undergoes dual photoreactions to afford 1,2-dihydrophthalazine (**1**) and 1,1′,2,2′-tetrahydro-1,1′-biphthalazine (**2**) upon ultraviolet light irradiation in a 2-propanol solution. From the observed photochemical behavior and the phosphorescence characteristics under the influence of a quencher, sensitizer, and surfactant, the following reaction mechanism has been proposed. During the initial step of the dual photoreactions, phthalazine (P) abstracts a hydrogen atom from the 2-propanol(RH) used as a solvent to form a radical pair of the 1,2-dihydro-1-phthalazinyl radical (PH·) and the 1-hydroxy-1-methylethyl radical (R·) in a solvent cage. The resulting singlet radical pair (^{1}[PH·+R·]), derived from the lowest excited singlet state (S_1) of the substrate, participates in a subsequent hydrogen abstraction to produce **1** in a solvent cage. On the other hand, the same radical, PH·, derived from the lowest triplet state (T_1) of the substrate, escapes from the solvent cage, causing dimerization to afford product **2** (Scheme 1).

In the current work, studies of the temperature and initial concentration effects on the photochemical reactivities of phthalazine, and chemical quenching in 2-propanol, were carried out in order to obtain further supporting evidence concerning the reaction mechanism. On the basis of the reaction mechanism presented in Scheme 1, the observed external heavy-atom effects on the reactivities and phosphorescence are discussed, and an example of an intersystem crossing process that includes spin inversion from the triplet to the singlet radical pair within a solvent cage is presented.

Experimental

Materials. Phthalazine (Aldrich Chem. Co.) was purified by recrystallization from a mixture of benzene and hexane. 1,2-Dibromoethane and bromoform were purified by repeated fractional crystallizations. 2-Allylphenol and cinnamyl alcohol (Wako Pure Chemical Ind.) were used as received.

Measurements. The phosphorescence spectra were taken with a Shimadzu RF-500 spectrofluorimeter equipped with a cylindrical rotating sector at 77 K. The triplet lifetimes were determined with a previously described method in a mixture of ethanol and methanol (1:1 v/v) at 77 K.[8)]

Light Source and Irradiation. A 450 W high-pressure mercury lamp (Ushio UM-452) and a set of filters comprising a solution (1% K_2CO_3 aqueous solution containing 10^{-2} mol dm^{-3} K_2CrO_4) and a Corning glass filter (CS-7-54) were used for 313-nm light irradiation. A 70 W low-pressure mercury lamp (Ushio UL1-7SQ) and a solution filter ($NiSO_4$ 500 g dm^{-3}) were

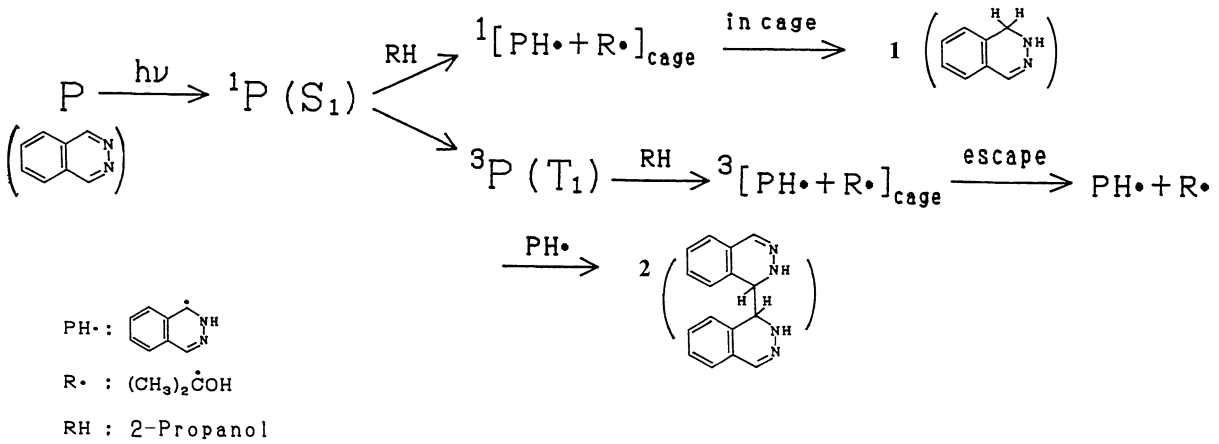

Scheme 1.

used for 254-nm light irradiation. 2-Propanol solutions of phthalazine in a 5×10^{-2} dm^3 quartz cylindrical reaction cell were flushed with nitrogen passed through a pyrogallol solution and a silica-gel column both before and during irradiation. The temperatures of the reaction system were controlled by passing temperature-controlled water into a reaction cell with a jacket.

Actinometry and Analysis of Photoproducts. Actinometry was performed by using a potassium trioxalatoferrate(III) solution.[9] The amounts of the photoproducts were spectrophotometrically determined by the same manner described previously.[7]

Results and Discussion

Temperature and Concentration Dependence of the Dual Photoreactions. In addition to the results reported earlier, the effects of the temperature and initial substrate concentrations on the formations of products **1** and **2** have been examined in order to obtain a further confirmation of the mechanism of the dual photoreactions.

In Fig. 1, the concentrations of the produced **1** and **2** are plotted against the irradiation times for reactions at various temperatures. It can be seen from this figure that product **2** is formed in higher yields at higher temperatures, while the yield of **1** is not affected by the temperature.[10] In addition, the dependence of the reactivity on the initial substrate concentrations can be seen from Table 1. The quantum yield for the formation of **1** is not altered with a change in the concentration of phthalazine, while that for **2** increases with increasing concentration.

These observed effects of the initial concentrations and temperature can be considered to give further supporting evidence for the reaction mechanism proposed earlier. That is, because the formation of **1** occurs in a solvent cage, which includes 1,2-dihydro-1-phthalazinyl radical (PH·) and alcohol radical (R·) produced in the initial hydrogen abstraction reaction, the yield of **1** may be influenced inefficiently by both the concentration and

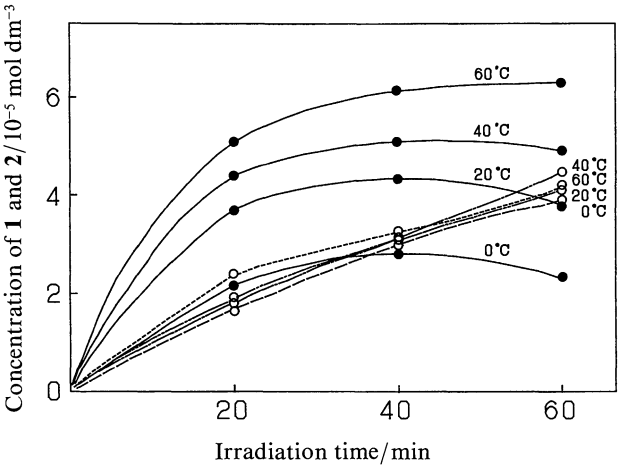

Fig. 1. Temperature dependence of the formations of **1** (○) and **2** (●). [Phthalazine]=4×10^{-4} mol dm^{-3}, Solvent: 2-Propanol, Excitation wavelength: 253.7 nm.

Table 1. Quantum Yield for the Formation of **1** (Φ_1) and **2** (Φ_2) at Room Temperature

[Phthalazine]/mol dm^{-3}	Φ_1	Φ_2	Φ_2/Φ_1
4×10^{-4}	0.010	0.041	4.1
5×10^{-3}	0.0095	0.069	7.2

temperature. Moreover, from the temperature dependence, it is demonstrated that the efficiency of the escape process of the radicals from the solvent cage of the present system is not subjected to the effect of temperature in the range 0 to 60 °C.

On the contrary, the formation of **2** is susceptible to concentration and temperature effects, since it takes place in a bulk solution through encounters of 1,2-dihydro-1-phthalazinyl radicals escaping from the solvent cage.

Quenching for the Formation of 2 by Olefins. The in-cage (S_1) and out-of-cage (T_1) reaction mechanisms for

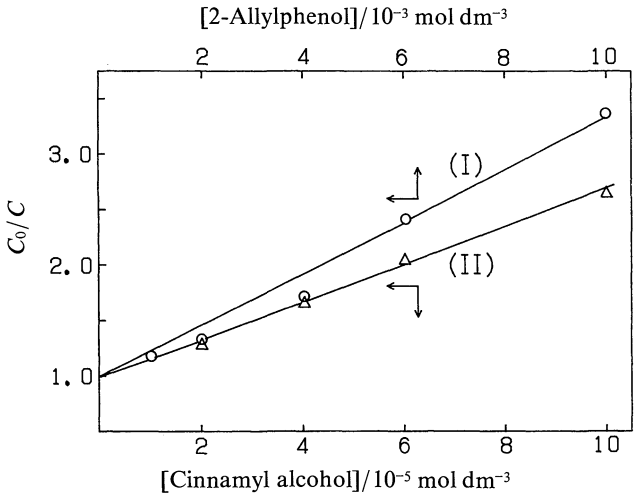

Fig. 2. Quenching for the formation of **2** by 2-allylphenol (I) and cinnamyl alcohol (II). [Phthalazine]=2×10^{-3} mol dm^{-3}, Solvent: 2-Propanol, Excitation wavelength: 313 nm. C_0 and C are the concentrations of **2** formed without and with the quenchers, respectively.

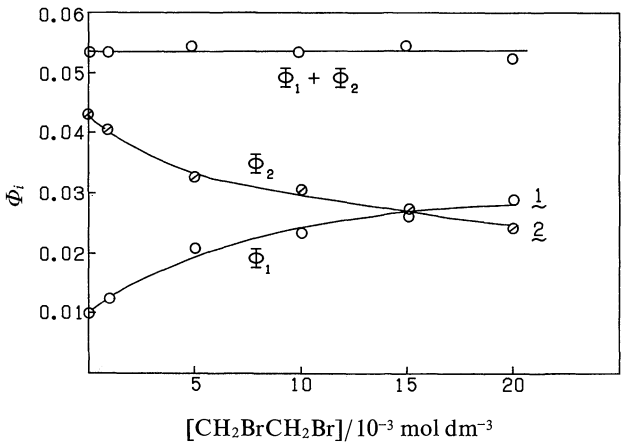

Fig. 3. External heavy-atom effect on the quantum yields by 1,2-dibromoethane. [Phthalazine]=4×10^{-4} mol dm^{-3}, Solvent: 2-Propanol, Excitation wavelength: 313 nm Φ_1: **1**, Φ_2: **2**.

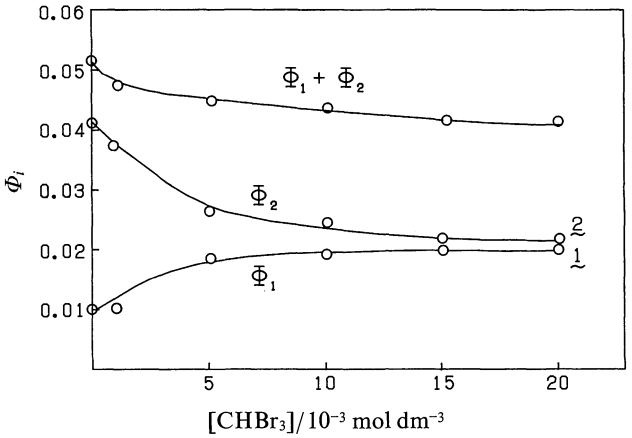

Fig. 4. External heavy-atom effect on the quantum yields by bromoform. [Phthalazine]=4×10^{-4} mol dm^{-3}, Solvent: 2-Propanol, Excitation wavelength: 313 nm Φ_1: **1**, Φ_2: **2**.

the respective **1** and **2** formations can also be demonstrated by the chemical quenching using olefinic compounds such as 2-allylphenol and cinnamyl alcohol. These compounds quench the formation of **2**, but not the formation of **1**. Stern-Volmer quenching plots are presented in Fig. 2. Since the lowest triplet energies of the above-mentioned compounds are not available, they have been estimated from their phosphorescence spectra as being 289 kJ mol^{-1} (69.2 kcal mol^{-1}) and 303 kJ mol^{-1} (72.4 kcal mol^{-1}) for 2-allylphenol and cinnamyl alcohol, respectively. These values are larger than the lowest triplet energy values of phthalazine (256 kJ mol^{-1}, 61.2 kcal mol^{-1});[11] thus, the observed quenching can not be regarded as being to a triplet–triplet energy transfer from phthalazine to the quenchers. In fact, the intensity of the phthalazine phosphorescence is not affected by these quenchers. Accordingly, the results can be explained as a sort of chemical quenching of the 1,2-dihydro-1-phthalazinyl radical by the olefinic compounds in a bulk solution. The absence of quenching for the formation of **1** is attributed to an in-cage reaction of this radical.

External Heavy Atom Effect. It has been found that the dual photoreactions of phthalazine are affected by added bromine-containing compounds, such as 1,2-dibromoethane and bromoform.[12] The quantum yields for the formations of **1** (Φ_1), **2** (Φ_2), and **1**+**2** ($\Phi_1+\Phi_2$) are plotted as a function of the concentrations of these bromo compounds in Figs. 3 and 4. The addition of bromo compounds brings about an increase in the yield of **1**, together with a decrease in the yield of **2**. This indicates that the efficiency of an intersystem crossing which is associated with the photoreactions is altered through an enhancement of the spin-orbit coupling. Moreover, it has been found that the emission intensity of phthalazine phosphorescence (with a maximum at 482 nm and a lifetime (τ=0.51 s) of the phosphorescent lowest triplet state at 77 K in a 1:1 mixture of ethanol and methanol) is not influenced by the addition of 2×10^{-2} mol dm^{-3} of the bromine compounds (1,2-dibromoethane: 0.49 s, bromoform: 0.56 s).

From the following considerations, the present observations can not be explained in terms of external heavy-atom effects on the $S_1\rightarrow T_1$ and the $T_1\rightarrow S_0$ intersystem crossing processes occurring in a single molecule of phthalazine. First, if the $S_1\rightarrow T_1$ intersystem crossing in an excited phthalazine molecule could be affected by heavy-atom perturbations, the addition of bromine compounds might lead to an increase in the yield of **2**, together with an enhancement of the phosphorescence intensity. This is clearly not the case for the present system. Second, the possible heavy-atom enhanced $T_1\rightarrow S_0$ intersystem crossing decay process of

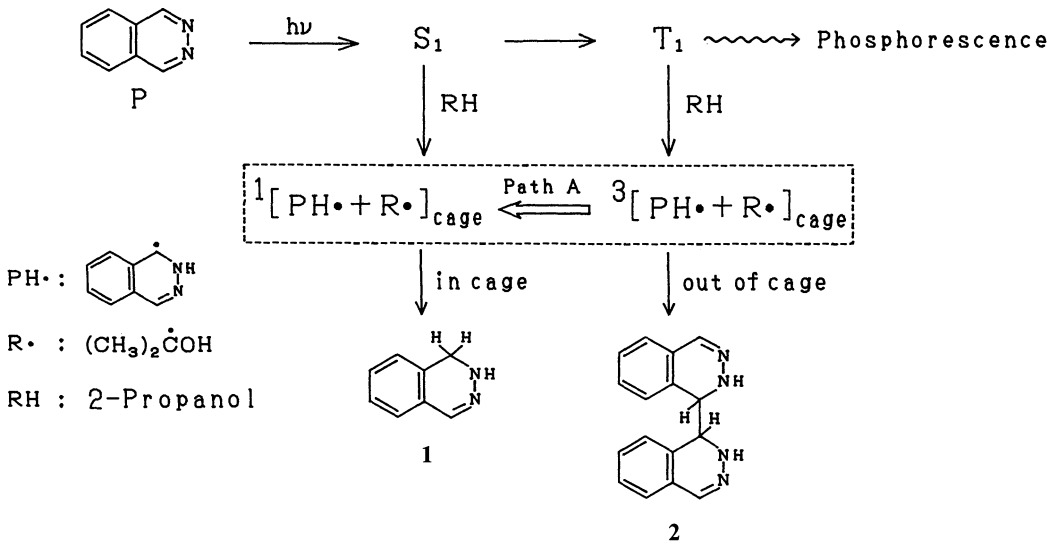

Scheme 2.

triplet phthalazine can not be responsible for the observed variation in the photoreactivity. That is, although the observed change in Φ_2 may reflect the $T_1 \rightarrow S_0$ mechanism, the observed increase in Φ_1 can not be interpreted from this mechanism, which predicts no change for a reaction occurring prior to the $T_1 \rightarrow S_0$ intersystem crossing. Third, the constancy of the phosphorescence intensity and the lifetime indicates the absence of a heavy-atom induced variation in the efficiencies of the formation and decay of the T_1 species of the phthalazine molecule.

Consequently, we have reached the following conclusion on the basis of a spin-correlated reaction mechanism in which **1** is formed from a singlet radical pair within a solvent cage as well as the findings, described above. In the present photoreaction systems including bromine compounds, the observed change in the reactivity and phosphorescence characteristics of phthalazine can be reasonably ascribed to the enhancement of an intersystem crossing process, involving a radical pair within a solvent cage formed during the initial step of the dual photoreactions; no events occurred in a single phthalazine molecule. The spin inversion from the triplet state (^{3}[PH·+R·]) of the radical pair to the singlet one (^{1}[PH·+R·]) in a solvent cage is induced under the influence of a heavy-atom spin-orbit interaction. The proposed reaction pathways are illustrated according to Scheme 2. In this scheme Path A is the proposed spin inversion (intersystem crossing) of the radical pair within the solvent cage; it competes with the escape of radicals and a back reaction to the starting materials, phthalazine (P) and 2-propanol (RH). A similar spin inversion has been revealed in several photoreactions by studies on photoreactions under an external magnetic field.[1,3-5] In this case, however, the inversion of the spin state is dominated by electron-molecular hyperfine interactions. Few descriptions are available concerning the spin inversion resulting from a spin-orbit coupling in a radical pair. Turro et al.[4] reported that the bromine-substituted dibenzyl ketone showed an internal heavy-atom effect on intersystem crossing in its radical pair. Recently, Tanimoto et al.[13] have reported that the photolysis of 2-naphthylphenyldiazomethane involves a spin inversion in a radical pair within a solvent cage under an external magnetic field. Accordingly, the results presented here are examples of photochemical reactions in which heavy-atom perturbed intersystem crossing between the singlet and triplet states of the radical pair in the solvent cage plays an important role in the product distribution and reactivity. It, therefore, seems that in some cases the selective formation of a desired product from dual photochemical reactions involving different spin-correlated radical pairs may be attained by using a heavy-atom containing compound.

References

1) A part of the results has been preliminary presented: H. Inoue, T. Sakurai, T. Hoshi, J. Okubo, and I. Ono, *Chem. Lett.*, **1990**, 1059.

2) N. J. Turro and B. Kraeutler, *Acc. Chem. Res.*, **13**, 369 (1980).

3) G. L. Closs and A. D. Trifunac, *J. Am. Chem. Soc.*, **91**, 4552 (1969).

4) N. J. Turro, C.-J. Chung, G. Jones. II, and W. G. Becker, *J. Phys. Chem.*, **86**, 3677 (1982).

5) N. J. Turro and G. C. Weed, *J. Am. Chem. Soc.*, **105**, 1861 (1983).

6) N. J. Turro, M. B. Zimmt, and I. R. Gould, *J. Phys. Chem.*, **92**, 433 (1988).

7) H. Inoue, T. Sakurai, K. Tomiyama, K. Sano, M. Oshio, T. Hoshi, and J. Okubo, *Bull. Chem. Soc. Jpn.*, **61**, 893 (1988).

8) H. Inoue, T. Sakurai, T. Hoshi, J. Okubo, and T. Kawanishi, *J. Chem. Soc., Faraday Trans. 2,* **82**, 523 (1986).
9) C. G. Hatchard and C. A. Parker, *Proc. R. Soc. London, Ser. A,* **235**, 518 (1956).
10) The product **2** is in equilibrium with phthalazine at photostationary state after an appropriate irradiation time.
11) H. Rau, *Ber. Bunsen-Ges. Phys. Chem.,* **72**, 408 (1968).
12) It was confirmed that the bromo compounds used here did not participate in the hydrogen abstraction.
13) Y. Tanimoto, C. Jinda, Y. Fujiwara, M. Itoh, K. Hirai, H. Tomioka, R. Nakagaki, and S. Nagakura, *J. Photochem. Photobiol. A,* **47**, 269 (1989).

Effect of Bromotrifluoromethane on the Ignition in Methane and Ethane-Oxygen-Argon Mixtures behind Shock Waves

Akimichi SUZUKI, Tadaaki INOMATA,* Hiroshi JINNO, and Takao MORIWAKI
Department of Chemistry, Faculty of Science and Technology,
Sophia University, Kioi-cho, 7-1, Chiyoda-ku, Tokyo 102
(Received April 2, 1991)

The ignition delay times behind shock waves in CH_4–, and C_2H_6–O_2–Ar systems containing CF_3Br were measured for a range of temperatures between 1400 and 2100 K and pressures between 1.5 and 3.5×10^5 Pa. These measurements indicated that CF_3Br promotes the ignition of CH_4 but inhibits the ignition of C_2H_6. Although the inhibition effect for C_2H_6 increases with increasing CF_3Br concentration and decreasing temperature, the promotion effect in CH_4 was independent of both the CF_3Br concentration and the temperature in this experiment. We calculated the induction times for conditions similar to the experiments using a model which included 49 elementary reactions related to CF_3Br. Calculations using this model gave induction times that were in good agreement with the experiments. The calculated values, however, depended on several effective reactions among the 49 reactions.

Ignitions of methane and ethane in shock tubes under various experimental conditions have been investigated since 1959.[1-21] It is well-known that methyl halides accelerate the ignition of CH_4 but retard the ignition of C_2H_6; these effects are due to chemical reasons.[22-23] Methyl bromide was the most effective substance as an ignition promoter for CH_4 and methyl iodide had the greatest effect as an ignition inhibitor for C_2H_6. The different effects in CH_4 and C_2H_6 ignitions have been clarified from the rates of reactions involving halogen species as well as the differences of predominant reactions in both fuels. We have already reported the effect of CH_3Br addition on the ignition of CH_4 and C_2H_6.[22-24]

In this study, in order to examine the influence of the substitution of hydrogen by fluorine, we investigated the effect of CF_3Br addition on the ignition of CH_4 or C_2H_6, compared with the effect of CH_3Br addition. Although this species has received much attention in experimental studies regarding flame inhibition,[25-29] the number of reports concerning its effects on ignition has been extremely small. We therefore provide new experimental information concerning addition effects of CF_3Br in methane- and ethane-oxygen-argon mixtures, as well as a numerical analysis of the mechanism.

Experimental

Measurements. The shock tube used in this experiment was made of 8.0 cm i.d. stainless-steel pipe. The reaction and driver sections were 450 and 80 cm in length, respectively. Thus, dwell times of about 500 microseconds behind a reflected shock wave could be obtained using helium driver gas. A poly(ethylene-terephthalate) diaphragm was ruptured by increasing the driver gas pressure up to a certain value. The reaction gases were mixtures of methane or ethane, bromotrifluoromethane, and oxygen diluted with argon (Table 1). The shock wave velocities were controled by changing the pressure ratio of helium and nitrogen gas in the driver section. The incident shock velocities were measured by PZT-type pressure transducers placed along the reaction section and a digital counter. The state of the test gas behind the shock wave was determined using ideal one-dimensional shock equations with thermodynamic properties. The onsets of ignition were detected by OH radical absorption with a photomultiplier fitted with a 306 nm interference filter on the end of reaction section. A typical oscillograph is shown in Fig. 1. The ignition delay times, defined as the time interval between the pressure rise due to the arrival of a shock wave and the rise of an optical signal by the photomultiplier, were obtained under various conditions.

Calculations: In order to discuss the effect of CF_3Br on the reaction mechanism for methane and ethane oxidations, we calculated the ignition delay times using a model. The model used for methane and ethane oxidations are described in Refs. 30—33. This mechanism consists of 35 species and 113 elementary reactions, including forward and reverse reactions.

Table 1. Test Gas Mixture Composition (%)

No.	CH_4	C_2H_6	CF_3Br	CH_3Br	O_2	Ar
1	2.0				4.0	94.0
2	2.0		0.1		4.0	93.9
3	2.0		0.2		4.0	93.8
4		1.0			3.5	95.5
5		1.0	0.1		3.5	95.4
6		1.0	0.2		3.5	95.3
7	2.0			0.1	4.0	93.9
8	2.0			0.2	4.0	93.8
9		1.0		0.1	3.5	95.4

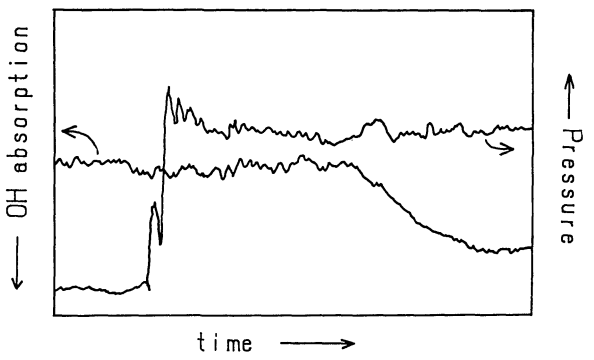

Fig. 1. Typical oscillograms of pressure and OH absorption.

Considering that the pressure is constant within the induction time (Fig. 1), a model calculation was performed that assumed a constant pressure.

We calculated the OH concentration and defined the calculated ignition delay time as being the time interval of a sudden rise in the OH concentration. This gives ignition delay times closer to the observed values.[23] Elementary reactions related to CF_3Br were obtained from the literature.[34] (Table 2)

Results and Discussion

CH_4 System. The ignition delay times of mixtures 2 and 3 including CF_3Br are slightly short compared with those of mixture 1, excluding CF_3Br over the entire temperature region, as shown in Fig. 2. The points are the observed values and the lines are the calculated values. It is obvious that CF_3Br has a promotion effect for methane ignition. The concentration dependence of

Table 2. Reaction Mechanisms and Rate Constants[a]

Reaction	Forward			Reverse		
	A	n	E	A	n	E
(A1) $CH_3Br=CH_3+Br$	1.5849E+13	0.000	71.70	2.8853E+08	0.928	2.91
(A2) $CH_3Br+H=CH_3+HBr$	1.7378E+14	0.000	6.90	1.0000E+13	0.000	5.50
(A3) $CH_3Br+Br=CH_3+Br_2$	5.0119E+13	0.000	22.90	1.0000E+13	0.000	1.00
(A4) $CH_4+Br=CH_3+HBr$	1.0000E+14	0.000	18.30	1.3183E+12	0.000	0.93
(A5) $HBr+H=H_2+Br$	7.5858E+11	0.500	1.11	3.4674E+10	1.000	16.64
(A6) $Br_2+H=Br+HBr$	6.4565E+12	0.500	1.11	6.4565E+10	1.000	42.52
(A7) $Br+Br+M=Br_2+M$	1.0000E+16	0.000	0.00	1.4454E+18	−0.500	46.05
(A8) $Br+H+M=HBr+M$	1.0000E+18	−0.710	0.00	6.4565E+21	−1.710	90.55
(A9) $C_2H_5Br+H=C_2H_5+HBr$	3.4674E+14	0.000	5.90	5.6234E+13	0.000	28.67
(A10) $C_2H_5Br+Br=C_2H_5+Br_2$	1.0000E+14	0.000	19.00	2.5119E+13	0.000	0.00
(A11) $C_2H_6+Br=C_2H_5+HBr$	7.9433E+13	0.000	13.40	1.1482E+13	0.000	3.47
(A12) $C_2H_3Br+H=C_2H_3+HBr$	3.4674E+14	0.000	7.00	1.0000E+13	0.000	25.00
(A13) $C_2H_3Br+Br=C_2H_3+Br_2$	5.0119E+13	0.000	20.00	1.0000E+13	0.000	0.00
(A14) $CF_3Br+H=CF_3+HBr$	2.1850E+14	0.000	9.46	6.9420E+12	0.000	31.32
(A15) $CF_3Br=CF_3+Br$	5.0100E+13	0.000	66.30	3.8020E+11	0.000	0.50
(A16) $CF_3Br+Br=CF_3+Br_2$	6.0256E+13	0.000	23.00	1.8620E+12	0.000	1.00
(A17) $CF_3Br+CH_3=CH_3Br+CF_3$	9.7723E+12	0.000	5.20	1.3489E+13	0.000	12.59
(A18) $CF_3+H=CF_2+HF$	3.9811E+12	0.000	0.00	5.0118E+13	0.000	110.00
(A19) $CF_3+O=CF_2+FO$	1.2882E+14	0.000	2.00	5.0118E+14	0.000	83.42
(A20) $CF_3+OH=CF_2O+HF$	3.9811E+12	0.000	0.00	4.8977E+13	0.000	115.65
(A21) $CF_3+CH_4=CF_3H+CH_3$	1.0000E+12	0.000	11.00	3.8905E+11	0.000	11.75
(A22) $CF_3+CH_3=CH_2CF_2+HF$	6.7608E+13	0.000	0.00	6.4565E+15	0.000	95.67
(A23) $CF_3+O_2=CF_2O+FO$	6.9183E+11	0.000	9.06	3.8905E+11	0.000	23.43
(A24) $CF_3H+M=CF_3+H+M$	2.8184E+15	0.000	110.30	5.0118E+13	0.000	4.00
(A25) $CF_3H=CF_2+HF$	1.2022E+12	0.000	63.00	7.4131E+05	1.000	5.87
(A26) $CF_3H+H=CF_3+H_2$	5.0118E+12	0.000	5.00	4.8978E+11	0.000	3.78
(A27) $CF_3H+O=CF_3+OH$	1.9953E+13	0.000	9.20	8.7096E+11	0.000	5.88
(A28) $CF_3H+OH=CF_3+H_2O$	3.2359E+12	0.000	3.77	1.4125E+12	0.000	17.70
(A29) $CF_3H+Br=CF_3+HBr$	1.9952E+13	0.000	23.00	6.7608E+11	0.000	4.88
(A30) $CH_2CF_2+OH=CF_2O+CH_3$	1.0000E+13	0.000	1.00	1.2882E+12	0.000	20.99
(A31) $CH_2CF_2+O=CF_2O+CH_2$	1.5136E+13	0.000	0.00	1.7378E+11	0.000	13.19
(A32) $CH_2CF_2+O=CF_2+CH_2O$	1.5135E+13	0.000	0.00	1.7378E+11	0.000	13.19
(A33) $CF_2O+H=FCO+HF$	1.2882E+11	0.000	0.00	2.3442E+09	0.000	8.50
(A34) $CF_2O+O=FCO+FO$	5.0118E+12	0.000	4.60	5.3703E+10	0.000	0.00
(A35) $CF_2O+OH=FCO+HOF$	7.5858E+11	0.000	0.00	3.4673E+10	0.000	0.00
(A36) $CF_2+CH_3=CH_2CF_2+H$	1.9953E+13	0.000	0.00	1.5849E+16	0.000	44.14
(A37) $FCO+M=F+CO+M$	1.4454E+14	0.000	30.00	1.0000E+10	1.000	0.00
(A38) $FCO+H=HF+CO$	1.9953E+14	0.000	0.00	3.6308E+14	0.000	105.00
(A39) $FCO+O=CO+FO$	1.0000E+14	0.000	0.00	1.0000E+14	0.000	19.96
(A40) $FCO+OH=CO+HOF$	1.0000E+14	0.000	0.00	4.6774E+14	0.000	19.18
(A41) $FCO+OH=CO_2+HF$	1.0000E+14	0.000	0.00	1.0000E+14	0.000	128.00
(A42) $Br+HO_2=HBr+O_2$	5.0119E+12	0.000	0.50	1.0000E+13	0.000	41.31
(A43) $HBr+OH=H_2O+Br$	1.0000E+14	0.000	0.00	1.2882E+14	0.000	31.80
(A44) $HBr+O=OH+Br$	1.0000E+14	0.000	0.00	1.2885E+13	0.000	14.90
(A45) $H_2O_2+Br=HBr+HO_2$	1.0000E+13	0.000	5.00	1.2589E+12	0.000	4.83
(A46) $CF_2+H=HF+CF$	1.0000E+13	0.000	0.00	9.1201E+11	0.000	14.89
(A47) $CF_2+O=FCO+F$	1.0000E+13	0.000	0.00	5.8884E+12	0.000	38.38
(A48) $CF_2+OH=FCO+HF$	1.0000E+13	0.000	0.00	1.8621E+13	0.000	72.62
(A49) $CF_2+OH=CF_2O+H$	1.0000E+13	0.000	0.00	1.0000E+15	0.000	64.12

a) Rate constants in the form $A=T^n\exp(-E/RT)$, in cm, mol, s, kcal, and K units.

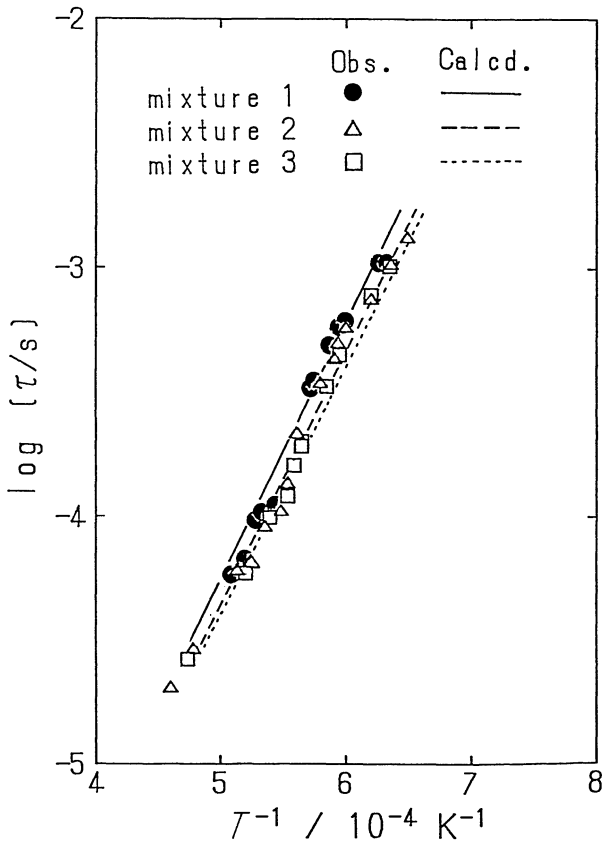

Fig. 2. Comparison of the calculated and observed ignition delay times in CH_4 systems. T is temperature behind shock wave.

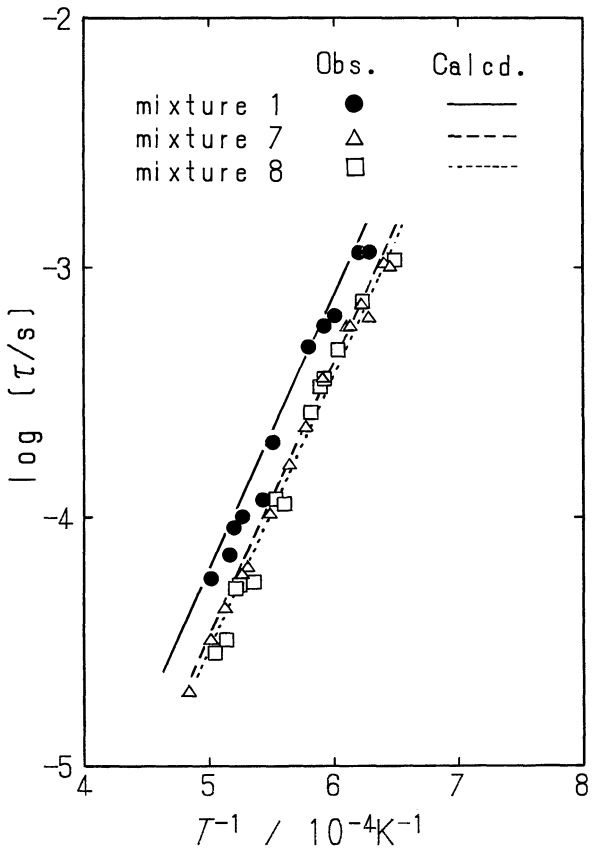

Fig. 3. Comparison of the calculated and observed ignition delay times in CH_4 systems.

CF_3Br, however, is small. These experimental data can be expressed by the least-square method as follows:

$$\log \tau = -9.85 + 1.08\ (10^4/T) \quad \text{for mixture 1,}$$

$$\log \tau = -9.48 + 1.02\ (10^4/T) \quad \text{for mixture 2,}$$

and

$$\log \tau = -9.55 + 1.03\ (10^4/T) \quad \text{for mixture 3.}$$

The slopes of mixtures 1—3 are almost the same, indicating that the promotion effect at high temperature is almost the same as that at low temperature. The ignition delay times of CH_4–O_2–Ar–CH_3Br are shown in Fig. 3 together with those of mixture 1. The tendency was the same for mixtures 7 and 8 including CH_3Br. Accordingly, we try to analyze the kinetics of methane combustion including CF_3Br in comparison with that including CH_3Br.

When comparing the results in Figs. 2 and 3 we considered that the concentration dependence of CF_3Br is smaller than that of CH_3Br.

The reaction mechanism of the CH_4–O_2–Ar system has already been studied. In order to realize a difference in the addition effects between both fuels, we express the consumption route of CH_4 according to the induction time.[35,36] An initiation reaction of this system is a thermal decomposition of fuel, as follows:

$$CH_4 = CH_3 + H. \quad \text{(R1)}$$

Though the time interval during which reaction (R1) effects the ignition delay times is short, this reaction is important, considering the fact that no ignition occurs without reaction (R1). CH_3 produced by the initiation reaction reacts with O or O_2, as follows:

$$CH_3 + O_2 = CH_3O + O \quad \text{(R2)}$$

and

$$CH_3 + O = CH_2 + OH. \quad \text{(R3)}$$

Since O atoms are scarcely produced during the early stage of the induction period, reaction (R2) is dominant. The route in flame, however, is reaction (R3), since O atoms are produced in a region of high temperature. The CH_3O produced by reaction (R2) decomposes immediately, as follows:

$$CH_3O = CH_2O + H. \quad \text{(R4)}$$

Any H atoms produced react with CH_4 and O_2:

$$CH_4 + H = CH_3 + H_2 \quad (R5)$$

and

$$H + O_2 = OH + O. \quad (R6)$$

The reaction with O_2 as a chain-branching reaction produces two radicals. Of the two radicals the O atom reacts with CH_3; on the other hand, the OH radical reacts with CH_4, as follows:

$$CH_4 + OH = CH_3 + H_2O. \quad (R7)$$

As mentioned above, CH_4 is consumed within the early stage of the induction period by a chain mechanism comprising reactions (R2), (R4), (R5) or reactions (R2), (R4), (R6), (R7).

During the ignition CF_3Br effects the chain mechanism. As shown in Figs. 2 and 3, the calculated ignition delay times agree with the observed values for all mixtures at both low and high temperatures. We therefore considered that the assumed scheme is reasonable. To make sure which reactions are effective, we performed sensitivity analysis. These were performed on 49 reactions involving F or Br-containing species by increasing both the forward and reverse rate constants, multiplying them by ten times and by deleting each reaction at 1866 and 1517 K. From this sensitivity test, the reactions which had some effects on the ignition delay times are shown in Table 3. We also performed this sensitivity test at 1517 K, as shown in Table 3. Reactions (A4) and (A15) are very sensitive in deleting, but not sensitive in increasing these rate constants. In this study we considered these reactions to be effective, owing to the high sensitivity in deleting.

Time profiles of the rates of these effective reactions involving Br-containing species at both 1517 and 1866 K

Table 3. Percentage Change of the Ignition Delay Times ($\tau_{deleted}$, $\tau_{k\times10}$) to Those (τ) Calculated by Using the Complete Mechanism in Mixture 2

Reaction	1866 K		1517 K	
	$\tau_{deleted}$[a)]	$\tau_{k\times10}$[b)]	$\tau_{deleted}$	$\tau_{k\times10}$
(A1)	+22	−19	+24	−31
(A2)	+31	−23	+67	−12
(A4)	+50	−3	+27	+1
(A5)	+1	+3	+1	+7
(A15)	+57	0	+107	−5
(A21)	+7	−11	+3	−5
(A22)	−13	+6	−11	+6
(A23)	+7	−9	+3	−4
(A31)	+5	−10	+6	−10
(A32)	0	+4	0	+4
(A34)	−2	+3	0	+4
(A44)	−1	+8	−1	+10

a) $\frac{(\tau_{deleted}-\tau)\times100}{\tau}$, b) $\frac{(\tau_{k\times10}-\tau)\times100}{\tau}$.

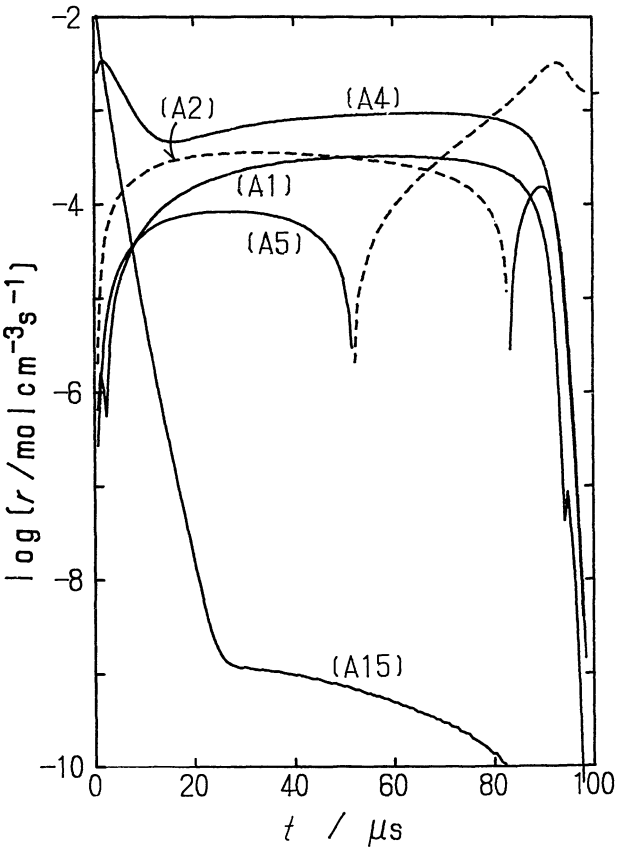

Fig. 4. Net reaction rates at 1866 K in mixture 2. t is the time after the arrival of a shock wave. The solid lines indicate that the net reaction proceeds in the forward direction; the dotted lines indicate the reverse direction.

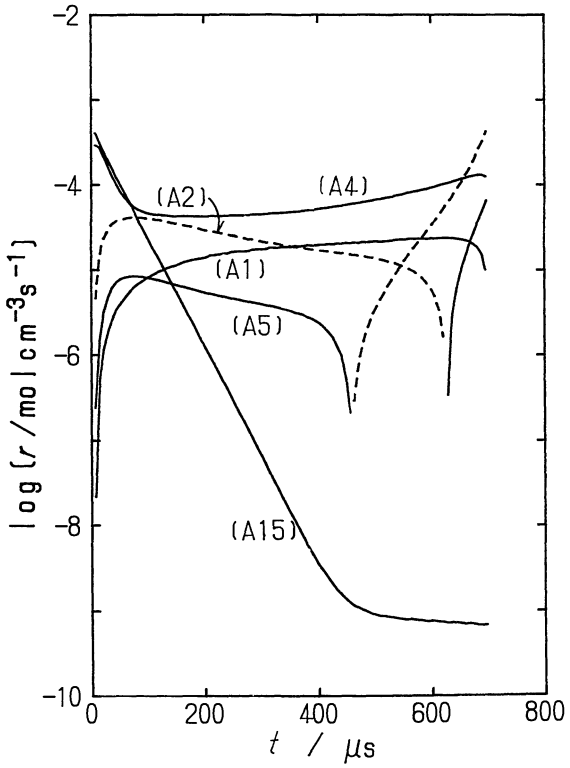

Fig. 5. Net reaction rates at 1517 K in mixture 2.

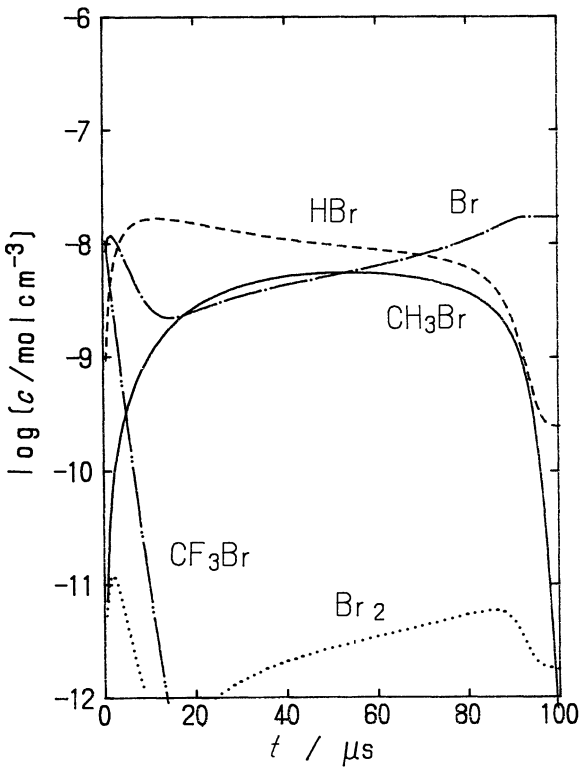

Fig. 6. Calculated concentration profiles of Br-containing species for mixture 2 at 1866 K.

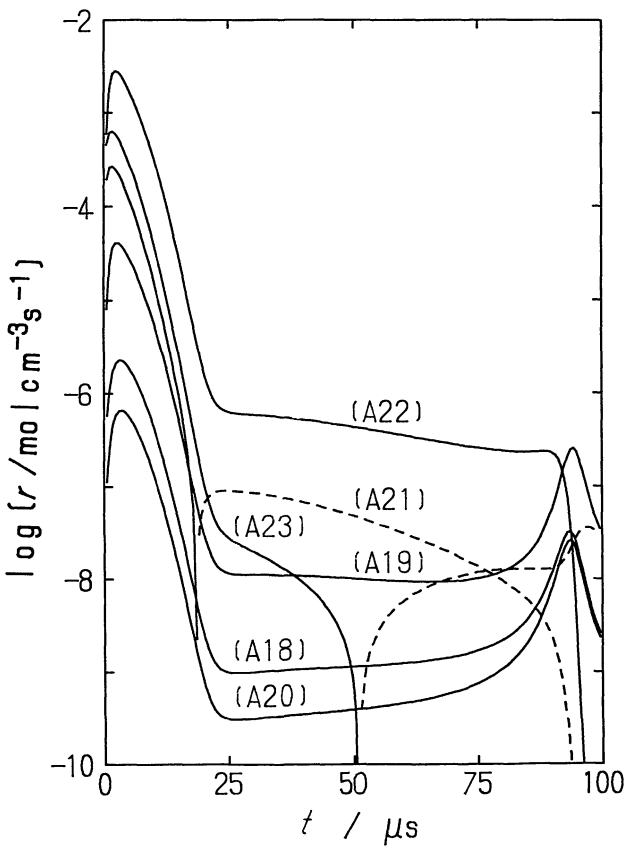

Fig. 7. Net reaction rates at 1866 K in mixture 2.

are shown in Figs. 4 and 5. Also, the time profiles of the main species including Br are shown in Fig. 6. During the early stage of the induction period reaction (A15) is the fastest of these five reactions at both 1517 and 1866 K. Further, since reaction (A15) is faster than reaction (R1), the former reaction acts as an initiation reaction. This may be reasonable, considering that the bond energy of C–Br is smaller than those of C–H and C–F.

As time passes, the rate of reaction (A15) becomes smaller. This means that CF_3Br decomposes during an earlier stage of the induction period. From Fig. 6 we realize that CF_3Br changes into CH_3Br within the ignition delay times.

Lifshitz has shown that most oxidation mechanisms for simple molecules involve closed-loop reactions that determine the behavior of the overall oxidation mechanism. In his investigation he identified the reactions that comprise this closed loop by examining the net reaction rates at half the induction time.[37] In the present study, during the induction period reactions (A1), (A2), and (A4) had high reaction rates. These reactions thus form a loop, as follows:

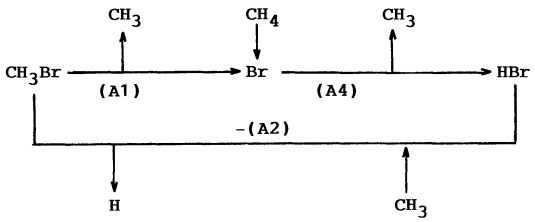

The total reaction of these reactions is

$$CH_4 = CH_3 + H,$$

which provides H atoms that are the active species during combustion. We considered that this loop has a dominant effect on methane ignition. This loop is the same as that obtained in the CH_4–O_2–CH_3Br system.

To make sure how CF_3 produced by the decomposition of CF_3Br effects the ignition delay times, we calculated the time profiles of the reaction rates which had higher values among the reactions involving the F-containing species at 1866 K (Fig. 7). It was found that reactions (A19), (A21), (A22), and (A23) have high reaction rates during the induction period. Especially, reaction (A22) has the fastest rate during the induction period, ten-times larger than other reactions. According to a sensitivity analysis, reaction (A22) has a high inhibition effect on the ignition delay times at both 1517 and 1866 K.

In this system CH_3 is produced from CH_4 by an attack of Br atoms (reaction (A4)), and CH_3 (reaction (A2)) reacts with HBr to produce H atoms, which are the active species during combustion. CH_3 thus plays an important role as a chain carrier in this system. It is further reported that reaction (A22) is also effective in flame.[34] It is therefore reasonable that reaction (A22), which consumes CH_3 as a chain carrier, has a large

inhibition effect in sensitivity analysis. By the reason that the effect suppresses any promotion effect by an attack of Br atoms, we considered that the promotion effect of CF_3Br is smaller than that of CH_3Br. From Fig. 7, the main route of CF_3Br decomposition is as follows:

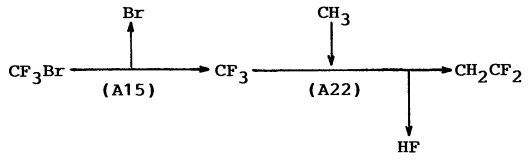

C_2H_6 System. As shown in Fig. 8, CH_3Br has an inhibition effect on ethane ignition. The lines indicate the calculated results and the points are the observed values. The observed ignition delay times of mixture 4—6 are shown, as follows, by least-squares methods:

$$\log \tau = -9.40 + 0.81\ (10^4/T) \qquad \text{for mixture 4,}$$

$$\log \tau = -9.76 + 0.91\ (10^4/T) \qquad \text{for mixture 5,}$$

and

$$\log \tau = -9.63 + 0.96\ (10^4/T) \qquad \text{for mixture 6.}$$

As the concentration of CF_3Br increases, the slopes of these lines become large. This means that this inhibition effect at high temperature is smaller than that at low temperature. The concentration dependence of CF_3Br was large in comparison with methane ignition. Since this tendency was the same for CH_3Br,[22,23] we analyzed the kinetics of the C_2H_6–O_2–CF_3Br system in comparison with the C_2H_6–O_2–CH_3Br system (already reported).

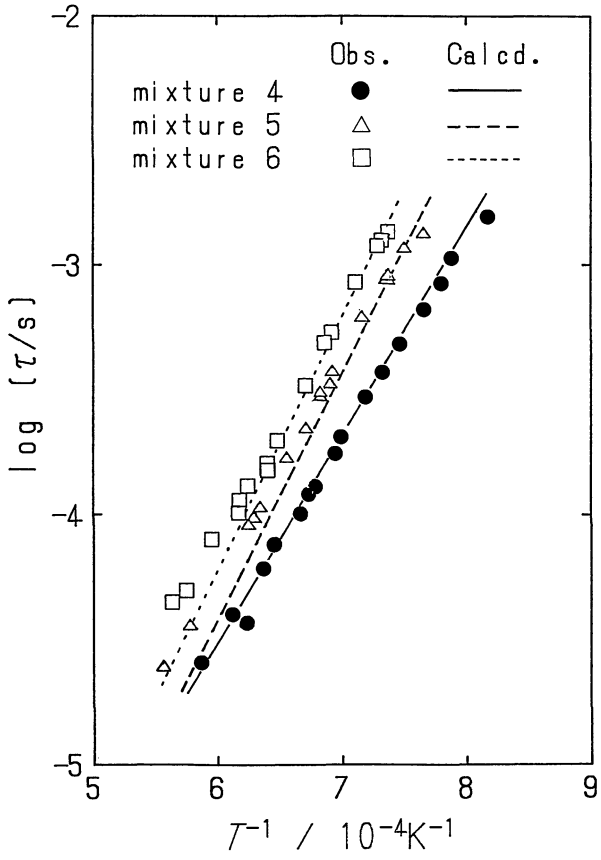

Fig. 8. Comparison of the observed and calculated ignition delay times.

In the C_2H_6–O_2–Ar system we express the consumption route of C_2H_6 during the early stage of the induction period.[35,36] In this system the initiation reaction is a thermal decomposition of C_2H_6,

$$C_2H_6 = CH_3 + CH_3. \qquad \text{(R8)}$$

The gratest part of CH_3 produced reacts with C_2H_6, as follows:

$$C_2H_6 + CH_3 = C_2H_5 + CH_4. \qquad \text{(R9)}$$

The C_2H_5 produced by reaction (R9) decompose immediately,

$$C_2H_5 = C_2H_4 + H, \qquad \text{(R10)}$$

and a part of the H atoms produced react with C_2H_6; some part of the H atoms react with O_2:

$$C_2H_6 + H = C_2H_5 + H_2 \qquad \text{(R11)}$$

and

$$H + O_2 = OH + O. \qquad \text{(R6)}$$

Reaction (R6), which is a chain-branching reaction, produces O atoms and OH radicals. OH radicals react with C_2H_6 and the O atoms react with CH_3:

$$C_2H_6 + OH = C_2H_5 + H_2O. \qquad \text{(R12)}$$

As mentioned above most of the C_2H_6 is consumed by a chain mechanism comprising reactions (R10) and (R11) or ractions (R10), (R6), and (R12).

CF_3Br effects the chain mechanism of C_2H_6 consumption. In this system we also performed a sensitivity analysis at both 1565 and 1717 K in order to realize how CF_3Br effects the mechanism. From this analysis the effective reactions are shown in Table 4. The time profiles of the reaction rates of the effective reactions which contian Br-atom are shown in Figs. 9 and 10. We also show the time profiles of the important reactions in the C_2H_6–CH_3Br system in Fig. 11 (already reported). The reactions which can be considered as an initiation type are reactions (A15) and (R8) in C_2H_6–CF_3Br, and reactions (A1) and (R8) in C_2H_6–CH_3Br. The calculated rate of reaction (R8) during the very early stage is about three times as large as that of reaction (A15) at 1500 K. The calculated rate of reaction (R8) is

Table 4. Percentage Change of the Ignition Delay Times ($\tau_{deleted}$, $\tau_{k\times10}$) to Those (τ) Calculated by Using the Complete Mechanism in Mixture 5

Reaction	1565 K		1717 K	
	$\tau_{deleted}$ [a)]	$\tau_{k\times10}$ [b)]	$\tau_{deleted}$	$\tau_{k\times10}$
(A2)	−6	+1	−6	0
(A5)	+3	−4	+1	−5
(A11)	+6	−7	+4	−9
(A14)	−13	+20	−6	+12
(A15)	+15	−13	+16	−10
(A17)	−4	+13	−4	+12
(A19)	−3	+10	0	+4
(A22)	+8	−3	+9	−2
(A30)	−4	+8	−3	+6
(A31)	+3	−11	+2	−9
(A32)	−5	+26	−4	+17
(A34)	−1	+5	0	+3
(A35)	−1	+5	−1	+2
(A36)	+7	−4	+3	−3

a) $\frac{(\tau_{deleted}-\tau)\times100}{\tau}$, b) $\frac{(\tau_{k\times10}-\tau)\times100}{\tau}$.

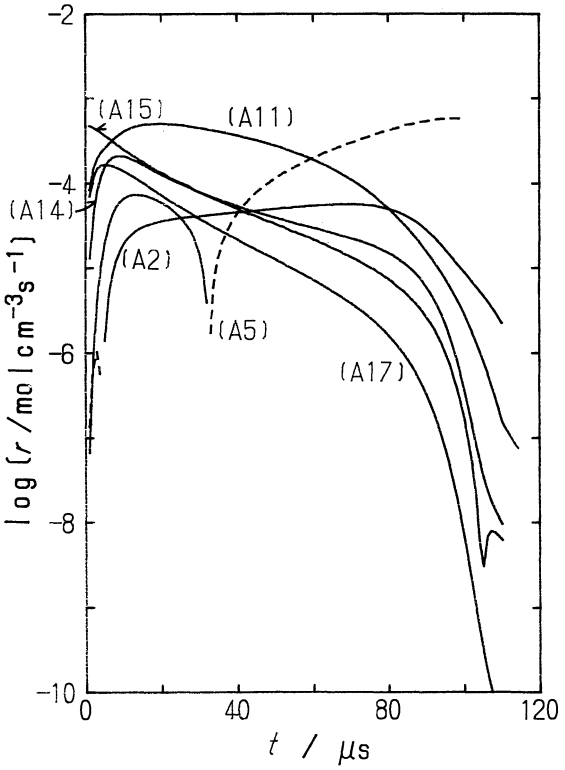

Fig. 9. Net reaction rates at 1565 K in mixture 5. The calculated reactions are those involving Br-containing species.

much faster than that of (A1). Thus, in both systems, reaction (R8) may act as the initiation reaction. However, reaction (A15), which is a thermal decomposition, also has a sufficiently large reaction rate in the C_2H_6–CF_3Br systems.

In C_2H_6–CH_3Br (already reported) CH_3Br reacts with

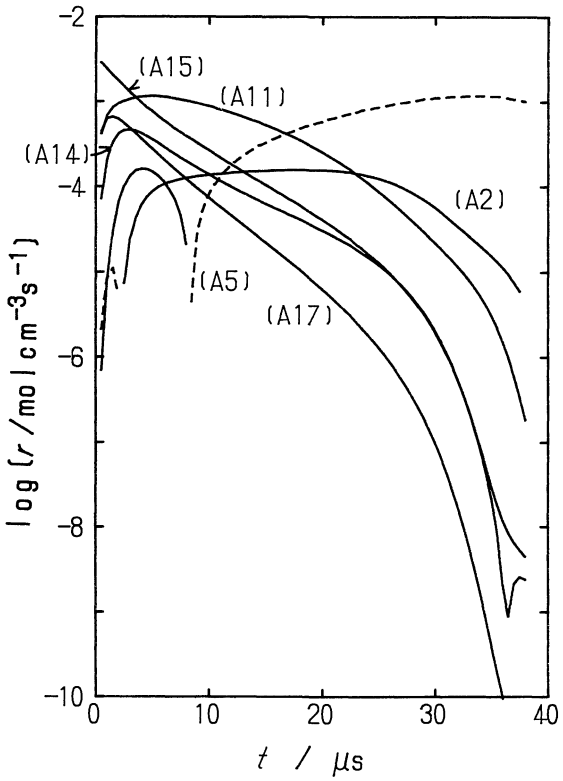

Fig. 10. Net reaction rates at 1717 K in mixture 5. The calculated reactions are those involving Br-containing species.

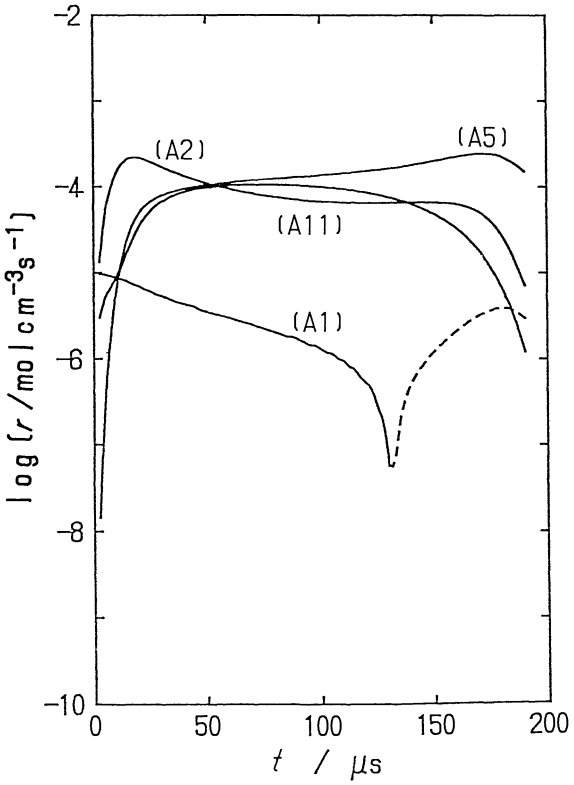

Fig. 11. Net reaction rates at 1500 K in mixture 9. The calculated reactions are those involving Br-containing species.

H produced by ethane decomposition, as follows:

$$CH_3Br + H = CH_3 + HBr, \quad (A2)$$

$$HBr + H = H_2 + Br, \quad (A5)$$

and

$$C_2H_6 + Br = C_2H_5 + HBr. \quad (A11)$$

Most of the CH_3Br is consumed by reaction (A2). This fact is reasonable considering that the ignition temperature in the C_2H_6–O_2 system is lower than that in the CH_4–O_2 system, and that the concentration of H atoms in the C_2H_6 system is larger than that in the CH_4 system. Reaction (A5), which follows reaction (A2), has a large inhibition effect, since the HBr produced by reactions (A2) and (A11) consumes H as the active species. These three reactions can be expressed by the following loop:

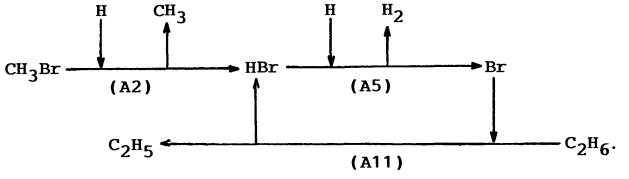

In the C_2H_6–CF_3Br system, although reaction (R8) is dominant during the early stage, the rate of reaction (A15) is sufficiently large. Further, since the H and CH_3 concentrations increase in this system, reactions (A14) and (A17) became faster, as shown in Figs. 9 and 10. It is thus considered that reactions (A14), (A15), and (A17) are competitive. Reactions (A14) and (A17) have large inhibition effects and reaction (A15) has a promotion effect according to sensitivity analysis. If CF_3Br is consumed by reaction (A14), the HBr produced by reaction (A14) may react through the same route mentioned above in the C_2H_6–CH_3Br system. However, considering that reaction (A5) has a small promotion effect, this route may not be the main one. It is interesting that reaction (A5), which has a large inhibition effect in C_2H_6–CH_3Br, has a promotion effect in C_2H_6–CF_3Br. This might be caused by a difference in the relative concentration ([HBr]/[Br]), as shown in Figs. 12 and 13. [HBr]/[Br] in a mixture including CH_3Br is much larger than that in a mixture including CF_3Br. This indicates that in a CF_3Br mixture the concentration of Br is larger than that of HBr; in this system the reverse reaction rate thus becomes larger after the middle of induction period, as shown in Figs. 9 and 10.

To summarise our interpretation of the results, we can say that the total inhibition effect in this system depends on a balance of the consumption reactions of CF_3Br (reactions (A14), (A15), and (A17)) during the early stage of the induction period. Thus, in this system the

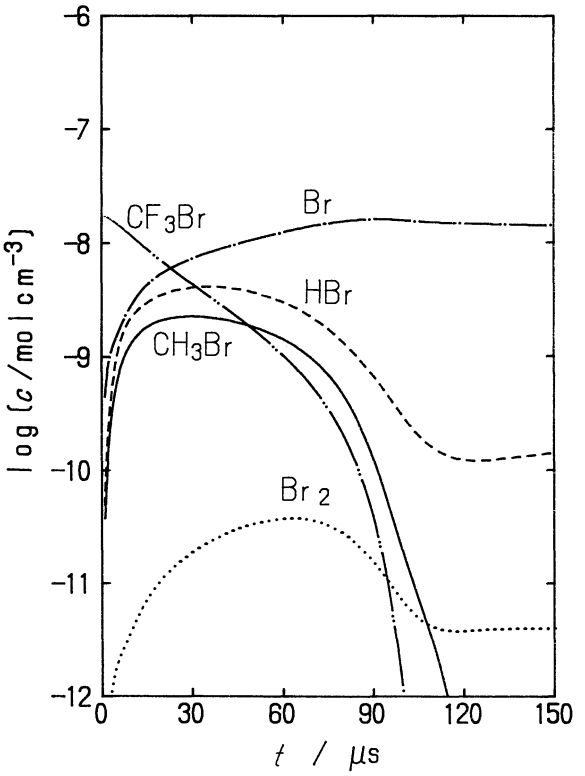

Fig. 12. Calculated concentration profiles of Br-containing species at 1565 K in mixture 5.

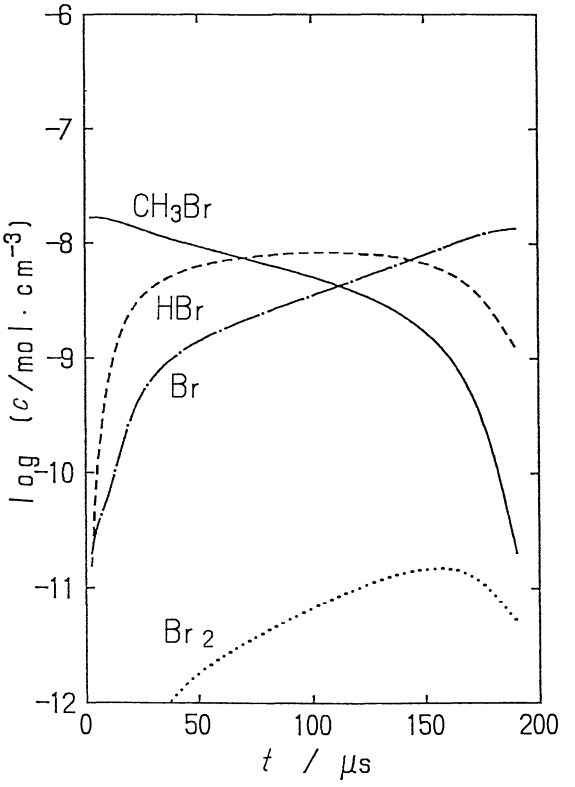

Fig. 13. Calculated concentration profiles of Br-containing species at 1500 K in mixture 9.

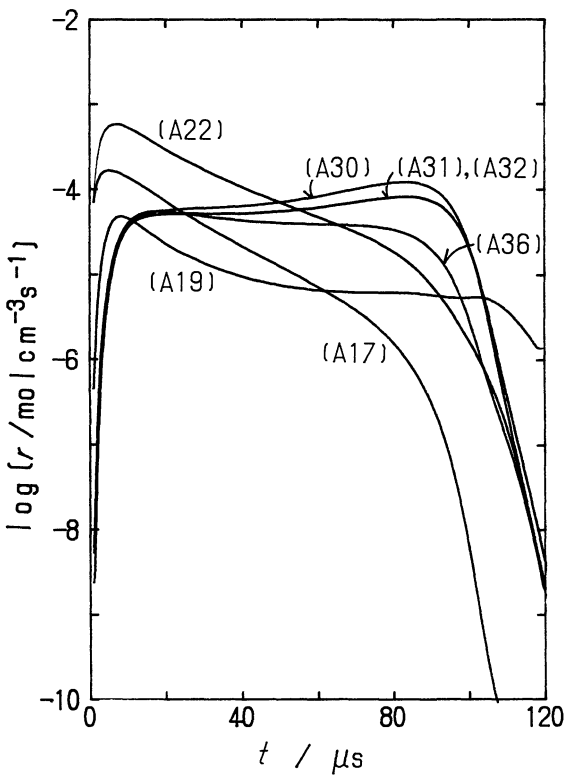

Fig. 14. Net reaction rates at 1565 K in mixture 5. The calculated reaction are the effective reactions involving F-containing species.

inhibition effects of reactions (A14) and (A17) surpass any promotion effect of reaction (A15). To make sure how CF_3 effects ethane ignition and how CF_3 is consumed, the rates of the effective reactions at 1565 K (which involve F-containing species) are shown in Fig. 14. This result indicates that reactions (A22), (A30), and (A36) have large rates during the induction period. During the earlier stage of the induction period, reaction (A22) has the fastest reaction rate.

In this system CH_3 is produced by the decomposition of C_2H_6. CH_3 is the source of active species, H. It is thus reasonable that reaction (A22), which consumes CH_3 radicals as the source of H atoms, has an inhibition effect in sensitivity analysis. This may show that the rate of reaction (A14) in this system is slower than reaction (A2) in the CH_3Br system.

CF_3 is consumed in a similar way as in the CH_4–CF_3Br system, considering that the effective reactions involving F-containing species are almost the same as in the CH_4–CF_3Br system.

Conclusion

In this study the ignition delay times were dependent on the reactions during the earlier stage. This may indicate that during the induction times the decomposition of fuel is important. Therefore, we can think that the effective reactions which formed loops didn't include O-containing reactions in the same reasons. In this study it is especially important to identify the initiation reaction. Although in the CH_4 system CF_3Br decomposition is an initiation reaction, in the C_2H_6 system C_2H_6 decomposition is an initiation reaction. This deference may cause these opposite effects.

In order to make the mechanism clearer, modifications of the used model and the concentration measurements of radicals during the induction time are essential.

References

1) A. Burcat, A. Lifshitz, and K. Scheller, *Combust. Flame,* **16**, 29 (1971).
2) D. F. Cooke and A. Williams, "Thirteenth Symp. (Int.) on Combust.," The Combustion Institute, Pittsburgh (1971), p. 757.
3) C. T. Bowman, *Combust. Sci. Technol.,* **2**, 161 (1970).
4) G. B. Skinner and R. A Ruhrwein, *J. Phys. Chem.,* **63**, 1736 (1959).
5) G. B. Kistiakowsky and L. W. Richards, *J. Chem. Phys.,* **36**, 1707 (1962).
6) T. Asaba, K. Yoneda, N. Kakihara, and T. Hikita, "Ninth Symp. (Int.) on Combust.," The Combustion Institute, Pittsburgh (1969), p. 193.
7) T. Takeyama, *J. Chem. Phys.,* **40**, 2049 (1964).
8) G. B. Kistiakowsky, J. V. Michael, and H. Niki, "Tenth Symp. (Int.) on Combust.," The Combustion Institute, Pittsburgh (1965), p. 513.
9) D. J. Seerly and C. T. Bowman, *Combust. Flame,* **14**, 37 (1970).
10) D. W. Walker, L. A. Diehl, W. A. Strauss, and R. Edse, "Rept. AFAPLTR-69-82," Air Force Aero Propulsion Lab., Air Force Systems Command, W. P. A. F. B., Ohio.
11) D. R. White, "ARL Rept. 70-0107," Wright Patterson Airforce Base, Ohio.
12) A. Lifshitz, K. Scheller, A. Burcat, and G. Skinner, *Combust. Flame,* **16**, 311 (1971).
13) D. F. Cooke and A. Williams, *Combust. Flame,* **24**, 245 (1975).
14) T. Tsuboi and H. Gg. Wargner, "Fifteenth Symp. (Int.) on Combust.," The Combustion Institute, Pittsburgh (1975), p. 883.
15) K. S. Krishnan and R. Ravikumar, *Combust. Sci. Technol.,* **24**, 245 (1975).
16) R. W. Crossely, E. Dorko, K. Scheller, and A. Burcat, *Combust. Flame,* **19**, 373 (1972).
17) E. A. Dorko, D. M. Crossely, and K. Scheller, *Combust. Flame,* **24**, 173 (1975).
18) A. Grillo and N. W. Slack, *Combust. Flame,* **27**, 107 (1976).
19) R. Ravikumar and K. A. Bhaskaran, *Combust. Flame,* **27**, 107 (1976).
20) E. K. Dobora, *Combust. Flame,* **25**, 181 (1975).
21) A. Burcat, *Combust. Flame,* **28**, 319 (1977).
22) K. Takahashi, T. Inomata, T. Moriwaki, and S. Okazaki, *Bull. Chem. Soc. Jpn.,* **62**, 2138 (1989).
23) K. Takahashi, T. Inomata, T. Moriwaki, and S. Okazaki, *Bull. Chem. Soc. Jpn.,* **61**, 3307 (1988).
24) T. Inomata, T. Moriwaki, and S. Okazaki, *Combust. Flame,* **62**, 183 (1985).

25) J. C. Biordi, C. P. Lazzara, and J. F. Rapp, *J. Phys. Chem.*, **81**, 1139 (1977).
26) J. C. Biordi, C. P. Lazzara, and J. F. Papp, *J. Phys. Chem.*, **80**, 1042 (1976).
27) J. C. Biordi, C. P. Lazzara, and J. F. Papp, *J. Phys. Chem.*, **82**, 125 (1978).
28) J. C. Biordi, C. P. Lazzara, and J. F. Papp, "Sixteen Symposium (Int.) on Combust.," The Combustion Institute, Pittsburgh (1977), p. 1097.
29) G. B. Skiner, "ACS Symposium Series, No. 16, Halogenated Fire Suppressants," ed by R. G. Gann, American Chemical Society (1975), p. 295.
30) C. K. Westbrook, *Combust. Sci. Technol.*, **20**, 5 (1979).
31) C. K. Westbrook, F. L. Dryer, and K. P. Schug, *Combust. Flame*, **52**, 299 (1983).
32) C. K. Westbrook and F. L. Dryer, *Prog. Energy Combust. Sci.*, **10**, 1 (1984).
33) C. K. Westbrook, F. L. Dryer, and K. P. Schug, "Nineteenth Symp. (Int.) on Combust.," The Combustion Institute, Pittsburgh (1982), p. 153.
34) C. K. Westbrook, "Nineteenth Symp. (Int.) on Combust.," The Combustion Institute, Pittsburgh (1982), p. 127.
35) C. K. Westbrook, *Combust. Sci. Technol.*, **23**, 191 (1980).
36) J. Warnatz, *Combust. Sci. Technol.*, **34**, 177 (1983).
37) A. Lifshitz, in "Fast Reactions in Energetic Systems," ed by C. Capellos and R. F. Walker, Reidel (Dordrecht), Dordecht (1981), p. 19.

 © 1991 The Chemical Society of Japan Bull. Chem. Soc. Jpn., 64, 3355—3362 (1991)

Triplet Intermediates in Cis-Trans Photoisomerization of 3-Chrysenylethylenes

Takashi KARATSU,*,† Tatsuro HIRESAKI, Tatsuo ARAI, Hirochika SAKURAGI, Katsumi TOKUMARU,* and Jakob WIRZ††

Department of Chemistry, The University of Tsukuba, Tsukuba, Ibaraki 305
† College of Arts and Sciences, Chiba University, Yayoi-cho, Chiba 260
†† Institut für Physikalische-Chemie der Universität Basel, Klingelbergstrasse 80, CH-4056 Basel, Switzerland

(Received June 24, 1991)

The effect of substitution of 3-chrysenyl group (Ar) on unsaturated double bonds in their triplet sensitized isomerization was investigated for Ar–CH=CH–R, R=^{t}Bu (BC) and Ph (SC) by means of stationary irradiations, laser flash photolyses, and MO calculations. Both olefins undergo mutual isomerization between their cis- and trans-isomers. However, BC has a unique triplet energy surface with two decay funnels at the planar trans (^{3}t*) and twisted (^{3}p*) conformations, which are in equilibrium with each other; ^{3}t* undergoes either unimolecular decay to the ground-state trans isomer or triplet energy transfer to the cis isomer (quantum chain process) and ^{3}p* decays to the ground state to give the cis and trans isomers. $T_n \leftarrow T_1$ absorptions observed for BC and SC are mainly attributed to ^{3}t* and ^{3}p*, respectively, on the basis of semiempirical MO calculations. The populations at ^{3}t* and ^{3}p* are estimated.

Recently, we demonstrated that the mode of photoisomerization, one-way (solely from cis to trans) or two-way (mutually between cis and trans) of aromatic olefins, Ar–CH=CH–R, in the triplet state is governed by the nature of substituents on the double bond, and proposed that the triplet energy of an aromatic group (Ar) and the conjugative property of substituent R (aryl or alkyl) play important roles in determining the mode of their isomerization by affecting the relative location of the trans and twisted triplets on their energy surface.[1-4] The lower the triplet energy of Ar, the more stabilized the trans triplet (^{3}t*) compared to the perpendicularly twisted triplet (^{3}p*) tending to result in one-way isomerization. However, a phenyl group on the β-ethylenic carbon (R=Ph) stabilizes of ^{3}p*, which favors two-way isomerization.[2-4] 2-Anthrylethylenes[5,6] and stilbenes[7,8] are extreme cases undergoing the one-way and two-way isomerizations, respectively.

Substitution of 1-pyrenyl[3] (triplet energy; E_T= 48 kcal mol^{-1}) and 8-fluoranthenyl[4] (52 kcal mol^{-1}) as Ar whose triplet energies are slightly or moderately higher than that of anthracene (42 kcal mol^{-1}) on an ethylenic carbon led to new mode of isomerization when R=Ph. These results in intermediate behavior between typical one-way and two-way isomerizations, whereas, with R=^{t}Bu, one-way isomerization takes place.[3] In the intermediate mode, the triplet states have two minima at ^{3}t* and ^{3}p* in equilibrium, and the deactivation takes place from ^{3}t* and from ^{3}p*.

These findings have led us to investigate the effect of substitution of 3-chrysenyl group on an unsaturated bond, Ar–CH=CH–R, as Ar whose triplet energy (57 kcal mol^{-1}) is slightly lower than that of naphthalene (61 kcal mol^{-1}),[9] with R=^{t}Bu, 3-(3,3-dimethyl-1-butenyl)chrysene (BC), and R=Ph, 3-styrylchrysene (SC).

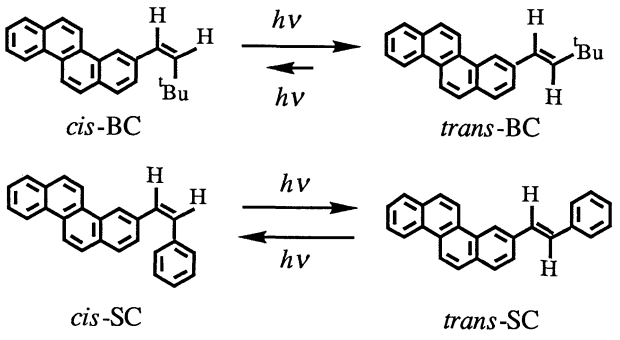

Experimental

Materials. Sensitizers (thioxanthone, benzophenone, 1- and 2-acetylnaphthalene, anthraquinone, benzil, 9-fluorenone, and biacetyl) were purified by crystallization or distillation. Solvent benzene was distilled over calcium hydride before use.

1-(Bromomethyl)naphthalene. Refluxing a mixture of 1-methylnaphthalene (25.0 g, 0.176 mol) and *N*-bromosuccinimide (30.0 g, 0.169 mol) in CCl_4 in the presence of dibenzoyl peroxide gave 1-(bromomethyl)naphthalene (37.5 g, 96%).[10] ^{1}H NMR ($CDCl_3$) δ=4.64 (s, 2H, CH_2Br), 7.2—8.2 (m, 7H, ArH).

(1-Naphthylmethyl)triphenylphosphonium Bromide. 1-(Bromomethyl)naphthalene (37.5 g, 0.17 mol) was treated with triphenylphosphine (46.0 g, 0.18 mol) in refluxing toluene to give (1-naphthylmethyl)triphenylphosphonium bromide (69.5 g, 85%).

1-(*p*-Methylstyryl)naphthalene. 1-(*p*-Methylstyryl)-naphthalene was synthesized in a similar manners with those reported for 2-styrylnaphthalene.[11] *p*-Methylbenzaldehyde (25.0 g, 0.21 mol) was allowed to react with (1-naphthylmethyl)triphenylphosphonium bromide (38 g, 0.08 mol) in the presence of sodium ethoxide (39.0 g, 0.58 mol) in absolute ethanol under dry nitrogen to give 1-(*p*-methylstyryl)naphthalene (11.9 g, 62%).

3-Methylchrysene. 3-Methylchrysene was prepared by

photochemical cyclization of 1-(*p*-methylstyryl)naphthalene. The procedures were essentially the same as those described for chrysene in the literature.[12] 1-(*p*-Methylstyryl)naphthalene (2.5 g, 0.01 mol) was irradiated by 400 W HPML (3 h) in cyclohexane (1 dm^3) in the presence of iodine (0.13 g, 0.5 mmol) under oxygen atmosphere to give 3-methylchrysene (1.97 g, 79%); mp 171—172 °C; ^1H NMR ($CDCl_3$) δ=2.68 (s, 3H, CH_3), 7.39—8.03 (m, 7H, ArH), 8.57—8.79 (m, 4H, ArH).

3-(Bromomethyl)chrysene. 3-(Bromomethyl)chrysene was prepared by bromination of 3-methylchrysene (5.8 g, 24 mmol) with *N*-bromosuccinimide (4.3 g, 24 mmol) in carbon tetrachloride in the presence of dibenzoyl peroxide. 3-(Bromomethyl)chrysene was purified by crystallization from benzene (3.4 g, 44%); mp 176—177 °C; ^1H NMR ($CDCl_3$) δ=4.81 (s, 2H, CH_2), 7.57—8.07 (m, 7H, ArH), 8.61—8.85 (m, 4H, ArH).

(3-Chrysenylmethyl)triphenylphosphonium Bromide. 3-(Bromomethyl)chrysene (3.4 g, 11 mmol) was treated with triphenylphosphine (3.2 g, 12 mmol) in refluxing toluene to give (3-chrysenylmethyl)triphenylphosphonium bromide (5.0 g, 82%).

3-(3,3-Dimethyl-1-butenyl)chrysene (BC). (3-Chrysenylmethyl)triphenylphosphonium bromide (5.0 g, 8.6 mmol) was suspended in absolute ether (200 ml) with mechanical stirring under dry nitrogen. To this solution was gradually added a solution of butyllithium in hexane (15%, 15 ml). The stirring was continued for 30 min, and then a solution of 2,2-dimethylpropanal in ether (70%, 20 ml) was added to this solution. The reaction mixture was refluxed gently for 30 min. The precipitate was filtered off and the filtrate was washed with water. After drying of extract with anhydrous sodium sulfate, evaporation of the solvent gave an isomeric mixture of 3-(3,3-dimethyl-1-butenyl)chrysene (1.4 g, 54%). The cis isomer was separated by column chromatography (SiO_2) with petroleum ether (bp<69 °C) and the trans isomer was obtained by irradiating a benzene solution of the isomeric mixture with a tungsten-halogen lamp in the presence of iodine under argon.

cis-BC: Mp 166—167 °C; ^1H NMR ($CDCl_3$) δ=1.06 (s, 9H, CMe_3), 5.82 (d, 1H, *J*=12 Hz, C=CH), 6.71 (d, 1H, *J*=12 Hz, C=CH), 7.40—8.05 (m, 7H, ArH), 8.60—8.86 (m, 4H, ArH); UV (cyclohexane) λ_{max} 228 nm (ε 20200), 264 (53100), 273 (86800), 298 (13100), 310.5 (13500), 324.5 (13200), 347 (680), 365 (530). Calcd for $C_{24}H_{22}$: C, 92.85; H, 7.14%. Found: C, 92.74; H, 7.12%.

trans-BC: Mp 158—159 °C; ^1H NMR ($CDCl_3$) δ=1.22 (s, 9H, CMe_3), 6.56 (d, 1H, *J*=16 Hz, C=CH), 6.60 (d, 1H, *J*=16 Hz, C=CH), 7.50—8.07 (m, 7H, ArH), 8.58—8.81 (m, 4H, ArH); UV (cyclohexane) λ_{max} 237 nm (ε 28900), 274 (87500), 283 (79600), 304.5 (16800), 317.5 (23100), 332 (23000), 354 (1100), 374 (730). Calcd for $C_{24}H_{22}$: C, 92.85; H, 7.14%. Found: C, 92.81; H, 7.31%.

3-Styrylchrysene (SC). Benzaldehyde (0.55 g, 5.2 mmol) was allowed to react with (3-chrysenylmethyl)triphenylphosphonium bromide (1.2 g, 2.1 mmol) in the presence of sodium ethoxide (1.4 g, 20.6 mmol) in absolute ethanol under dry nitrogen to give 3-styrylchrysene (0.66 g, 70%). The cis and trans isomers were separated by column chromatography (SiO_2) with benzene:hexane (=1:9) mixture, then purified by crystallization from benzene.

cis-SC: Mp 176—177 °C; ^1H NMR ($CDCl_3$) δ=6.80 (d, 1H, *J*=12 Hz, C=CH), 6.85 (d, 1H, *J*=12 Hz, C=CH), 7.05—8.04 (m, 7H, ArH), 8.32—8.83 (m, 4H, ArH); UV (benzene) λ_{max} 326 nm (ε 21600), 335 (21700). Calcd for $C_{26}H_{18}$: C, 94.55; H, 5.45%. Found: C, 94.83; H, 5.58%.

trans-SC: Mp 225—227.5 °C; ^1H NMR ($CDCl_3$) δ=7.30—8.08 (m, 14H, C=CH and ArH), 8.60—8.83 (m, 4H, ArH); UV (benzene) λ_{max} 294 nm (ε 47000), 306 (45000), 327 (31000), 341 (42000), 355 (35000), 380 (4500). Calcd for $C_{26}H_{18}$: C, 94.55; H, 5.45%. Found: C, 94.64; H, 5.63%.

Stationary Irradiation. Photostationary isomer ratios were measured in degassed benzene solutions (three freeze-pump-thaw cycles) in the presence of a desired concentration of a sensitizer in a 1-cm diameter quartz tube. The irradiation was performed with 366- and 405-nm light isolated through a Toshiba UV-D36B and an L-39 glass filter, respectively, from a 400-W high-pressure mercury lamp. The light intensity was determined using potassium tris(oxalato)ferrate(III) actinometry,[13] and the concentrations of olefins in the reaction mixtures were determined by GLPC or HPLC analysis.

Phosphorescence Measurement. Phosphorescence spectra were measured at 77 K in deaerated 3-methylpentane or EPA (ether:isopentane:ethanol=5:5:2) on Hitachi F-4000 or F-4010 spectrofluorimeter equipped with phosphorescence accessories.

Laser Flash Photolyses. Laser flash photolyses were performed by using an excimer laser (Lambda Physik EMG101, XeCl, 308 nm, 150±7 mJ, 10-ns fwhm) or an excimer laser-pumped dye laser (Lambda Physik FL-3002, 425 nm, 3.5±0.3 mJ, Stilbene 3) and a pulsed xenon arc (Wacom KXL-151, 150 W) as a monitoring light source.[4] Sample solutions (benzene or carbon tetrachloride) were deaerated by three freeze-pump-thaw cycles or argon purging.

Calculation. Oscillator strengths and transition energies of $T_n \leftarrow T_1$ absorptions of chrysene and 3-chrysenylethylenes and $D_n \leftarrow D_1$ absorptions of 3-chrysenylmethyl radicals were calculated by the semiempirical PPP-SCF-SCI method.[14]

Results

Isomerization Behavior on Stationary Irradiation. On triplet sensitization both BC and SC underwent two-way isomerization mutually between their cis- and trans-isomers.

However, in the isomerization of BC sensitized with anthraquinone (1×10^{-2} mol dm^{-3}) in deaerated benzene as Fig. 1 (plot a) shows, the photostationary state isomer ratios $([t]/[c])_s$ increased linearly with increasing concentration of *cis*-BC in $(2.5—10.0)\times10^{-3}$ mol dm^{-3}. As Table 1 indicates, the composition of the trans isomer at the photostationary state [(% trans)$_s$] ([BC]=1.0×10^{-3} mol dm^{-3}) was increased with lowering of the triplet energy of the sensitizers employed.

Moreover, $(\%\text{trans})_s$ decreased with increase of the concentration of the sensitizers. Thus, on 9-fluorenone sensitization, $(\%\text{trans})_s$ decreased from 8.2% at 5×10^{-3} mol dm^{-3} to negligible amounts at higher than 5×10^{-2} mol dm^{-3}, indicating that the isomerization proceeds almost one-way at 5×10^{-2} mol dm^{-3} of the sensitizer.

Addition of azulene in the range of $(3.3—13)\times10^{-4}$ mol dm^{-3} linearly increased $([t]/[c])_s$ as illustrated in Fig. 1 (plot b) on anthraquinone (1×10^{-2} mol dm^{-3}) sensitization.

Table 1. The Effect of Triplet Sensitizers on the Composition of the trans Isomer at the Photostationary State $(\%trans)_s$ of BC (1.0×10^{-3} mol dm^{-3}) in Benzene

Sensitizer	E_T/kcal mol^{-1} [a)]	Concn/mol dm^{-3}	λ_{ex}/nm [b)]	$(\%trans)_s$
Benzophenone	69	0.01	366	62
Anthraquinone	62	0.01	405	75
1-Acetylnaphthalene	56	0.07	366	74
Benzil	53	0.05	405	93
9-Fluorenone	52	0.05	405	>99

a) Ref. 15. b) Wavelengths of light used for irradiation.

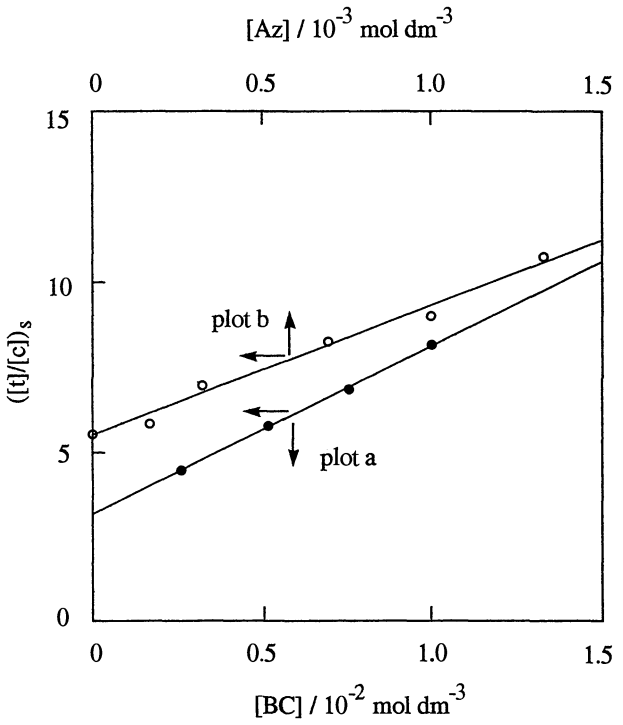

Fig. 1. Plots of the photostationary state isomer ratios against concentration of BC (plot a; closed circles) or azulene (plot b; open circles).

On the other hand, in the isomerization of SC $([t]/[c])_s$ was not changed at all with its concentration in $(0.8—3.3)\times10^{-4}$ mol dm^{-3}, however, $(\%trans)_s$ was varied among the sensitizers; 37.0 and 29.4% on sensitization with biacetyl (E_T=56.3 kcal mol^{-1},[15] 0.1 mol dm^{-3}) and benzil (0.14 mol dm^{-3}), respectively.

Phosphorescence Spectra.

cis-BC, *trans*-BC, and *trans*-SC exhibited phosphorescence in 3-methylpentane and EPA (ether:isopentane: ethanol=5:5:2) at 77 K. However, *cis*-SC did not phosphoresce at all.

As Fig. 2 illustrates, *trans*- (Fig. 2a) and *cis*-BC (Fig. 2b) exhibited different spectra. However, as depicted in Fig. 2b, the spectrum of *cis*-BC was changed very rapidly during the measurement; the weak band at 500 nm decreased and the strong bands at 515 and 560 nm increased in intensity for each scanning of the spectrum,

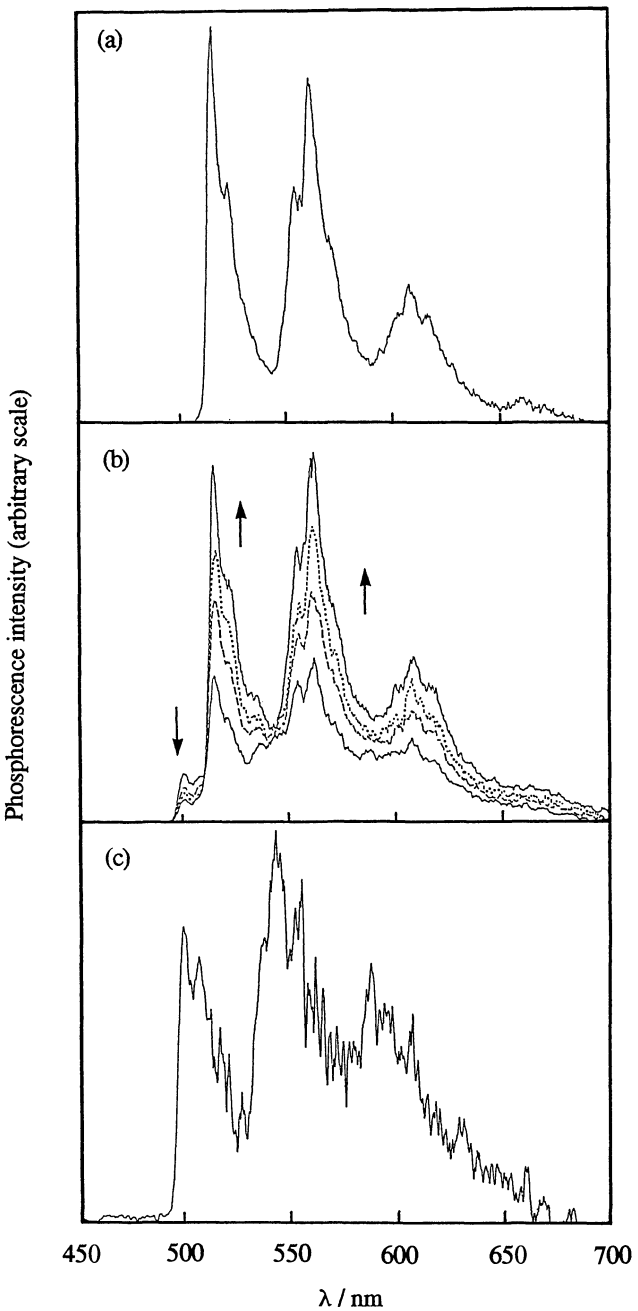

Fig. 2. Phosphorescence spectra obtained on excitation of *trans*-BC (a) and *cis*-BC (b) in 3-methylpentane at 77 K, and a difference spectra (c, subtracted a from b). Solid lines indicate the first and the 4th scans, and dashed and dotted lines indicate the second and the third scans, respectively (see text).

and finally, the spectrum became identical with that of *trans*-BC.

Therefore, the observed phosphorescence spectrum of *cis*-BC is reasonably assigned to a mixture of the cis and trans isomers. The phosphorescence spectrum due to *cis*-BC is obtained by the subtracting the spectrum of the trans isomer from that of the mixture multiplied by an adequate factor (Fig. 2-c). The lifetime measurement was unsuccesful and also it is not clear whether the emission comes from adiabatic isomerization on the triplet energy surface or re-excitation of the trans isomer after diabatic isomerization through $^3p^*$. However it should be noted that the isomerization of BC takes place even in rigid media at 77 K in spite of the presence of two relatively large substituents on both of it's ethylenic carbons. This is a property of it's T_1 potential energy surface.

The phosphorescence excitation spectrum showed the same behavior. The excitation spectrum of *trans*-BC was identical with its absorption spectrum irrespective of the monitoring wavelength either 515 or 560 nm (Fig. 3). On the other hand, the excitation spectrum of *cis*-BC was also identical, when monitored at 500 nm (Fig. 3), but not identical, when monitored at 515 nm, with its absorption spectrum, and the spectral profile was changed during

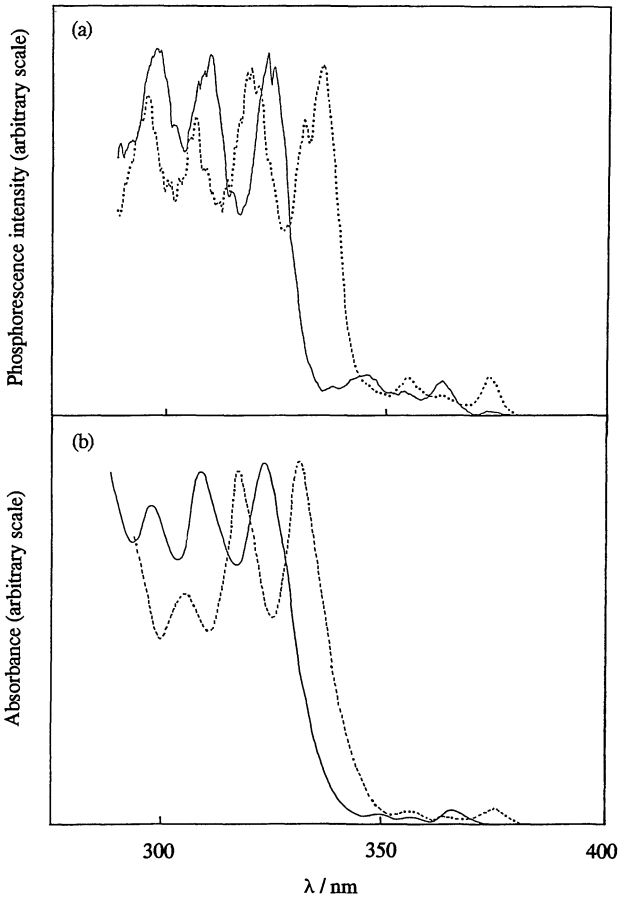

Fig. 3. Phosphorescence excitation spectra of *cis*-BC monitored at 500 nm (—) and *trans*-BC monitored at 520 nm (·····) in EPA at 77 K (a), and absorption spectra of *cis*-BC (—) and *trans*-BC (·····) in benzene at ambient temperature (b).

Table 2. Phosphorescence Spectral Data of Chrysenyl Compounds in 3-Methylpentane and EPA (indicated in parentheses) at 77 K

Compound	0,0 Band/nm	E_T/kcal mol^{-1}	Lifetime/s
Chrysene	498 (497)	57.4 (57.5)	2.6
trans-BC	516 (515)	55.4 (55.5)	1.5
cis-BC	500 (500)	57.2 (57.2)	—
trans-SC	521	54.9	2.0
cis-SC	—	—	—

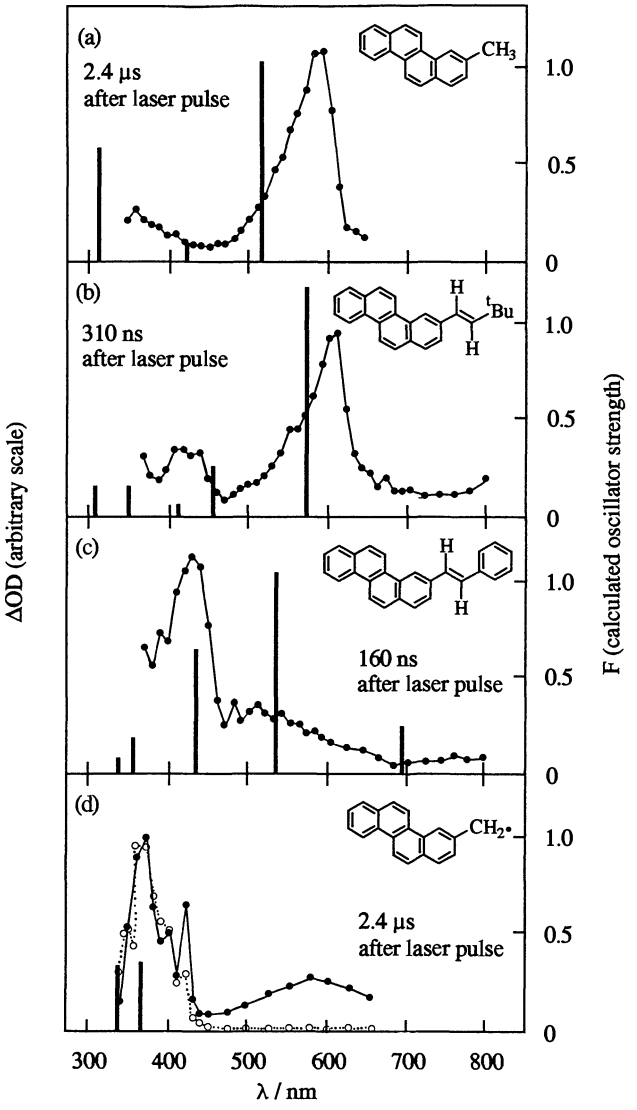

Fig. 4. $T_n \leftarrow T_1$ and $D_n \leftarrow D_1$ absorption spectra and calculated oscillator strengths (see text) of 3-methylchrysene (a), 3-(3,3-dimethyl-1-butenyl)chrysene (b), 3-styrylchrysene (c), and 3-chrysenylmethyl radical (d). Solid line was measured in deaerated benzene and dotted line was measured in deaerated CCl_4. The calculation was made for 3-vinylchrysene instead of BC.

measurement.

Table 2 summarizes the triplet energies of *trans*- and *cis*-BC, *trans*-SC along with chrysene estimated from the 0-0 band of their phosphorescence spectra.

Transient Absorption Spectra. Figure 4 depicts transient absorption spectra of the triplet state of BC, SC and related species. *trans*-BC exhibited two major $T_n \leftarrow T_1$ absorption bands around 430 and 580 nm, and *trans*-SC a strong band at 430 nm and a weak broad band around 500 nm in deaerated benzene (Fig. 4b and 4c) on sensitized excitation with biacetyl or thioxanthone (as a triplet sensitizer) with 425-nm laser pulses. The decay profiles of their absorption bands were essentially independent of wavelength and single-exponential with lifetimes of 810 ns for *trans*-BC and of 210 ns for *trans*-SC. On excitation under similar conditions *cis*-BC and *cis*-SC also exhibited almost the same absorptions with the same lifetimes as the corresponding trans isomers.

3-Methylchrysene showed almost identical $T_n \leftarrow T_1$ absorption around 580 nm with 17 μs lifetime under similar conditions (Fig. 4a) as chrysene[16] (the lifetime was determined to be 30 μs). 3-Chrysenylmethyl radical,[17] a model of the triplet olefins with a twisted conformation, generated by photolysis of 3-(bromomethyl)chrysene with 308-nm laser pulses, showed an absorption around 360 nm (Fig. 4d).

The oscillator strengths and transition energies of $T_n \leftarrow T_1$ or $D_n \leftarrow D_1$ absorptions were calculated for chrysene, 3-vinylchrysene, *trans*-SC and 3-chrysenylmethyl radicals by the semiempirical PPP-SCF-SCI method,[14] and are included in Fig. 4 as bar indications. The length of the bars indicates the relative oscillator strength.

Estimation of Extinction Coefficients of $T_n \leftarrow T_1$ Absorption for $^3t^*$ and $^3p^*$. The molar extinction coefficients (ε_T) of $T_n \leftarrow T_1$ absorption of $^3t^*$ and $^3p^*$ were determined by comparison with that of anthracene triplets (ε_T=46000 dm^3 mol^{-1} cm^{-1} at 430 nm).[18] The triplet states of the chrysenylethylenes were produced by energy transfer from thioxanthone triplets in deaerated benzene. The sensitizer was irradiated at a fixed concentration with laser pulses of a constant intensity with changing concentration of the substrates, anthracene and the chrysene derivatives to measure the optical densities (ΔOD) of their resulting triplet states. The ΔOD values increased with increasing concentration of the substrate and attained a plateau at higher concentrations. By assuming the energy transfer efficiency to be unity, ε_T value of the triplet 3-methylchrysene was determined to be 20000 dm^3 mol^{-1} cm^{-1} at 580 nm. The $T_n \leftarrow T_1$ absorption of BC exhibited ε_T=2900 and 10000 dm^3 mol^{-1} cm^{-1} at 430 and 580 nm, respectively, and that of SC showed ε_T=5900 and 1300 dm^3 mol^{-1} cm^{-1} at 430 and 580 nm, respectively.

Quenching Rate Constants of Olefin Triplets by Azulene and Oxygen. The $T_n \leftarrow T_1$ absorptions of BC and SC were efficiently quenched in benzene by azulene and oxygen without change of spectral profiles. The decay rate constant, k_d ($=1/\tau_T$) value increased linearly with increasing concentration of azulene or oxygen, and the slope gave a quenching rate constant by azulene (k_{az}^{obsd}) or oxygen (k_{ox}^{obsd}). The k_{az}^{obsd} values were obtained as 9.5×10^9, 6.8×10^9, and 3.5×10^9 mol^{-1} dm^3 s^{-1} for chrysene, BC, and SC, respectively. The k_{ox}^{obsd} values were 2.0×10^9, 3.5×10^9, and 5.6×10^9 mol^{-1} dm^3 s^{-1} for chrysene, BC, and SC, respectively.

Discussion

On anthraquinone sensitization of BC, the observed increase of the photostationary isomer ratio, $([t]/[c])_s$, linearly with BC concentration (Fig. 1) and with lowering of the triplet energies of the sensitizer employed indicates the following two things. The first, trans ($^3t^*$) and twisted triplets ($^3p^*$) are in equilibrium ($K_{tp}=k_{tp}/k_{pt}$), and the second, $^3t^*$ has a sufficient lifetime to transfer its triplet energy to the cis isomer leading to quantum chain process and $^3p^*$ decays to the ground state to give the cis and trans isomers (Scheme 1). Therefore, BC undergoes a mutual isomerization between the cis and trans isomers accompanied by quantum chain isomerization from cis to trans isomers.

In contrast to BC, the lack of concentration effects of the olefin and triplet sensitizer on $([t]/[c])_s$ for the SC isomerization indicates that SC undergoes typical two-way isomerization with a single-decay funnel at $^3p^*$.

In the transient absorption, the band around 580 nm observed for BC can be assigned to the planar trans triplet, $^3t^*$, and those around 430 nm (strong in SC and weak in BC) to $^3p^*$ by comparison with $T_n \leftarrow T_1$ absorptions of the model compounds and based on MO calculations. First, the band around 580 nm is very close in wavelength to the $T_n \leftarrow T_1$ absorptions of chrysene and 3-methylchrysene, and the other band at 430 nm to the absorption of 3-chrysenylmethyl radicals. The long tail observed for SC at longer wavelengths is likely to be due to $^3t^*$ in equilibrium with $^3p^*$. Second the observed absorption wavelengths for BC fit well with the calculated values. For SC, however, the observed spectrum around 500 nm did not fit well with the calculated result for $^3t^*$, and can be ascribed to $^3p^*$. The

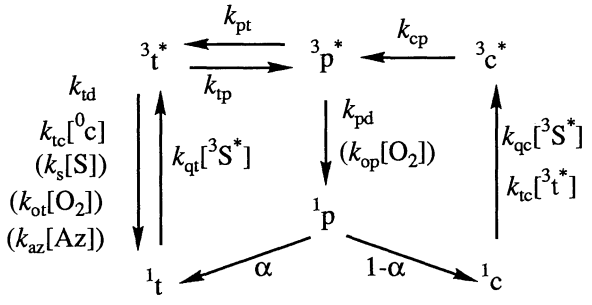

Scheme 1. Photoisomerization scheme of BC and SC.

absorption band of ^{3}p* is at longer wavelengths ($\lambda_{max}\approx$430 nm) than that of 3-chrysenylmethyl radicals ($\lambda_{max}\approx$360 nm) and this might imply some kind of interaction between the two chromophores of twisted "1,2-biradicals".

Furthermore when one assumes that the planar triplets (^{3}t*) of the olefins have the same ε_T values as the 3-methylchrysene triplets at the peak wavelength, the observed ΔOD values of these olefin triplets at 580 nm are to be obtained when ^{3}t* is populated in 50% among the triplet state of BC and in 7% for SC. Accordingly, the population of ^{3}p* is to be 50% for BC and 93% for SC in triplet state. Based on these populations, ε_T at 430 nm for ^{3}p* is estimated as 5800 and 6300 for BC and SC, respectively, and these values are in excellent agreement with each other. This is quite reasonable, because ^{3}p*'s of BC and SC may have similar twisted structures.

The observed apparent quenching rate constants of the triplet states with azulene, k_{az}^{obsd}, and by oxygen, k_{ox}^{obsd}, enable one to estimate K_{tp}. The k_{az}^{obsd} and k_{ox}^{obsd} values are related with K_{tp} as expressed by Eqs. 1 and 2,[9] where k_{ot} and k_{op} are the rate constants for quenching of ^{3}t* and ^{3}p* by oxygen, respectively.

$$k_{az}^{obsd} = \frac{k_{az}}{1 + K_{tp}}, \quad (1)$$

$$k_{ox}^{obsd} = \frac{k_{ot} + k_{op}K_{tp}}{1 + K_{tp}}. \quad (2)$$

When we assume that k_{az} for ^{3}t* of BC and SC are the same as that for chrysene, 9.5×10^9 mol^{-1} dm^3 s^{-1}, K_{tp} is estimated as 0.39 (^{3}t* 72%) for BC and 1.7 (^{3}t* 37%) for SC from Eq. 1. Likewise, reasonable assumption of $k_{ot}=2\times10^9$ as for chrysene and $k_{op}=9\times10^9$ dm^3 mol^{-1} s^{-1} as for stilbene ^{3}p*,[8] affords K_{tp} as 0.23 (^{3}t* 81%) and 0.83 (^{3}t* 55%) for BC and SC, respectively. The population of ^{3}t* is estimated here from the quenching rate constants are slightly higher than those estimated from the extinction coefficients (^{3}t* 50% for BC and 7% for SC). The difference in K_{tp} between the methods of estimation may be attributed to difficulty in assumption of the quenching rate constants, k_{az}, k_{op}, k_{ot}, and ε. However, for the convenience of the subsequent discussion, one could assume the average population of ^{3}t* as 68% and 33% for BC and SC, respectively.

Triplet energy of ^{3}t* is estimated for BC and SC from the population of ^{3}t* and ^{3}p* by using an equation $\Delta G=-RT\ln([^3p^*]/[^3t^*])$. ^{3}t* of BC is 0.5 kcal mol^{-1} lower in energy than ^{3}p* for BC ($[^3p^*]/[^3t^*]=32\%/68\%=0.47$) and ^{3}t* of SC is 0.4 kcal mol^{-1} higher in energy than ^{3}p* ($[^3p^*]/[^3t^*]=67\%/33\%=2.0$). These results together with the results of phosphorescence (Table 2) enable us to propose the potential energy surfaces along the twisting of the double bond for BC and SC as depicted in Fig. 5.

According to Scheme 1, the change of $([t]/[c])_s$ with [*cis*-BC] (plot a in Fig. 1) is expressed by Eq. 3,[2] the slope (5.3×10^2 mol^{-1} dm^3) corresponds to $k_{tc}/(1-\alpha)K_{tp}k_{pd}$ and the intercept denotes $([t]/[c])_s$ value (population of 74.8% of the trans isomer) when quantum chain process does

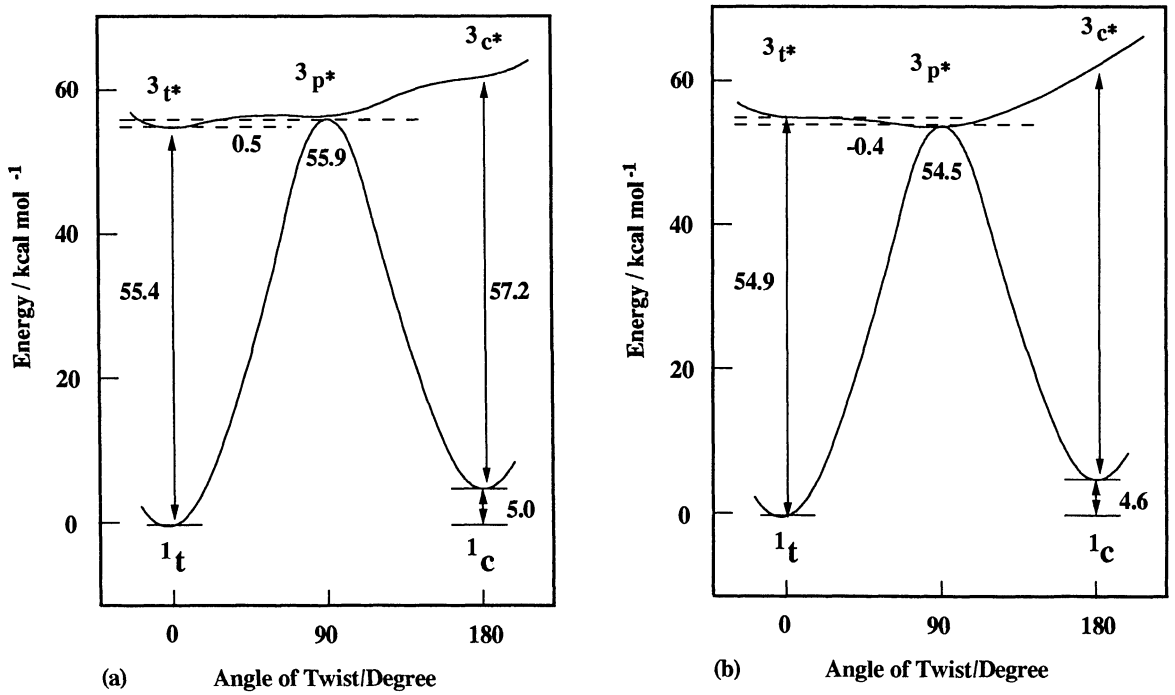

Fig. 5. Estimated potential energy surfaces for BC (a) and SC (b) plotted against rotational angle around the C–C double bond.

not participate at all.

$$([t]/[c])_s = \frac{\alpha K_{tp} k_{pd} + k_{td} + k_{tc}[cis\text{-BC}]}{(1-\alpha) K_{tp} k_{pd}}, \quad (3)$$

where we assume that the equilibrium between $^3t^*$ and $^3p^*$ is accomplished, that is $k_{tp} \gg k_{td}$, $k_{tc}[cis\text{-BC}]$ and $k_{pt} \gg k_{pd}$.

The observed triplet lifetime of BC is expressed by Eq. 4.

$$\tau_T = \frac{1 + K_{tp}}{K_{tp} k_{pd} + k_{td}}. \quad (4)$$

The rate constant for deactivation of the trans triplets, k_{td}, can be reasonably assumed to be similar to that for 3-methylchrysene (3.3×10^4 s^{-1}). Substitution of the observed values for K_{tp}(=0.67) and τ_T(=810 ns) into Eq. 4 gives k_{pd} as 3.0×10^6 s^{-1}. This is lower than the deactivation rate constant reported for stilbene (2×10^7 s^{-1}).[8]

Furthermore, Eq. 3 and Fig. 1 (plot a) give two important results. The intercept corresponds to $([t]/[c])_s = \alpha/(1-\alpha)$ when [BC]=0, since $k_{td}/(1-\alpha)K_{tp}k_{pd}$ is negligible, therefore, the observed value, [$([t]/[c])_s$=3] gives α as 0.75. The slope, $k_{tc}/(1-\alpha)K_{tp}\ k_{pd}$, ($5.3\times10^2$ mol^{-1} dm^3) combined with K_{tp} and k_{pd} gives a rate constant, k_{tc}, for the energy transfer from $^3t^*$ to cis isomer (quantum chain process) as $k_{tc}=2.7\times10^8$ mol^{-1} dm^3 s^{-1}. According to the triplet energies of *trans*- and *cis*-BC determined by their phosphorescence, 55.4 and 57.2 kcal mol^{-1}, the energy transfer from $^3t^*$ to *cis*-BC is 1.8 kcal mol^{-1} endothermic. The above value for k_{tc} is in good agreement with a value (2.5×10^8 mol^{-1} dm^3 s^{-1}) estimated for 1.8 kcal mol^{-1} endothermic energy transfer from the following well-accepted equation:[19]

$$k_{tc} = A \exp(-E_a/RT), \quad (5)$$

where, $A=5\times10^9$ mol^{-1} dm^3 s^{-1}, and $-E_a=\Delta E_T=E_T$(*trans*-BC)$-E_T$(*cis*-BC)=1.8 kcal mol^{-1} (Table 2).

In the presence of azulene, $([t]/[c])_s$ is expressed by Eq. 6,[3]

$$([t]/[c])_s = \frac{\alpha K_{tp} k_{pd} + k_{td} + k_{tc}[cis\text{-BC}] + k_{az}[Az]}{(1-\alpha) K_{tp} k_{pd}}, \quad (6)$$

where k_{az} is quenching rate constant of $^3t^*$ by azulene. The slope of plot b in Fig. 1, $k_{az}/(1-\alpha)K_{tp}k_{pd}$, 3.8×10^3 mol^{-1} dm^3, combined with α, K_{tp}, and k_{pd} values gives k_{az} as 1.9×10^9 mol^{-1} dm^3 s^{-1}. This value is quite reasonable since energy transfer from triplet state of *trans*-BC (E_T=55.4 kcal mol^{-1}, Table 2) to azulene (39.8 kcal mol^{-1})[20] is exothermic.

The $([t]/[c])_s$ values for BC depends on the triplet energy (Table 1) and concentration of the sensitizers, and the isomerization is seemingly almost one-way on sensitization with high concentration of 9-fluorenone, 0.05 mol dm^{-3}. This fact is attributed to an equilibrium between $^3t^*$ and the triplet state of the sensitizer employed (S),

$$^3S^* + {}^1t \rightleftarrows S + {}^3t^*, \quad (7)$$

because of their small difference in triplet energy. Therefore, $([t]/[c])_s$ is expressed by Eq. 8, where k_s denotes the rate constant for the energy transfer from $^3t^*$ to S, as previously reported for the isomerization of 2-(3,3-dimethyl-1-butenyl)naphthalene (BN) using sensitizers of low triplet energy.[21]

$$([t]/[c])_s = \frac{\alpha K_{tp} k_{pd} + k_{td} + k_{tc}[cis\text{-BC}] + k_s[S]}{(1-\alpha) K_{tp} k_{pd}}. \quad (8)$$

From the above arguments, triplet and ground state potential energy surfaces for BC and SC are proposed as depicted in Fig. 5.

For BC (Fig. 5-a), the triplet energies of $^3t^*$ and $^3c^*$ were estimated to be 55.4 and 57.2 kcal mol^{-1}, respectively, from their 0-0 bands of phosphorescence spectra. The triplet energy of $^3p^*$ was estimated relatively to $^3t^*$ using an equation $\Delta G=-RT\ \ln([^3p^*]/[^3t^*])$ based on the population of $^3t^*$ and $^3p^*$ ($[^3p^*]/[^3t^*]=0.47$) obtained from ε_T and quenching rate constant by azulene, thus $^3t^*$ of BC is 0.5 kcal mol^{-1} lower in energy than $^3p^*$. Ground state energy difference between cis and trans isomers due to steric hindrance is estimated as 5 kcal mol^{-1}, the same as 2-(3,3-dimethyl-1-butenyl)anthracene.[22]

For SC (Fig. 5-b), the triplet energies of $^3t^*$ (54.9 kcal mol^{-1}) and $^3p^*$ (0.4 kcal mol^{-1} lower in energy than $^3t^*$, $[^3p^*]/[^3t^*]=2.0$) are estimated similarly as for BC. However, the triplet energy of $^3c^*$ is supposed not to be lower than that for $^3t^*$, 54.9 kcal mol^{-1}, and not higher than that of chrysene, 57.4 kcal mol^{-1}, because of its lack of phosphorescence. Ground state energy difference between cis and trans isomers is estimated 4.6 kcal mol^{-1}, the same as reported to stilbene.[7]

The differences of phtochemical behavior and triplet potential energy surfaces between BC and SC may originate from the stabilization of $^3p^*$ of SC due to conjugation with diaryl substituents compared to that of BC.

Conclusion

In the triplet sensitized isomerization of 3-chrysenylethylenes, 3-styrylchrysene (SC) shows the typical two-way mode, whereas 3-(3,3-dimethyl-1-butenyl)chrysene (BC) behaves by intermediate mode with "dual decay funnel". The SC triplet decays only at the twisted geometry. On the other hand, BC triplet decays at both of the twisted and planar trans conformations leading to a quantum chain process from

the latter. Therefore in the (3,3-dimethyl-1-butenyl)-arene series, Ar–CH=CH–^{t}Bu, BC with 3-chrysenyl group (E_T of chrysene=57 kcal mol^{-1}) is located at a boundary position between typical two-way mode with Ar=2-naphthyl (E_T of naphthalene=60 kcal mol^{-1}) and cis→trans one-way mode with Ar=8-fluoranthenyl (E_T of fluoranthene=53 kcal mol^{-1}) derivative.

The present work contributes to revealing that the mode of photoisomerization of aromatic olefins, Ar–CH=CH–R, in the triplet state is controlled by the relative location of the trans and twisted triplets on the energy surface which is defined by the triplet energy of an aromatic group (Ar) and the nature of substituent R (aryl or alkyl).

The authors thank Dr. Shigero Oishi, Kitasato University, for valuable suggestions regarding the transient absorption measurements. This work was partially supported by Grant-in-Aid for Special Project Research Nos. 61123001, 62113001, and 63104001 (K.T.) and Grant-in-Aid for Scientific Research Nos. 61740242, 01740255 (T.A.), and 02453091 (K.T.) from the Ministry of Education, Science and Culture.

References

1) T. Arai, T. Karatsu, H. Misawa, Y. Kuriyama, H. Okamoto, T. Hiresaki, H. Furuuchi, H. Zeng, H. Sakuragi, and K. Tokumaru, *Pure Appl. Chem.*, **60**, 989 (1988), and references cited therein.

2) T. Arai, T. Karatsu, M. Tsuchiya, H. Sakuragi, and K. Tokumaru, *Chem. Phys. Lett.*, **149**, 161 (1988).

3) a) T. Arai, H. Okamoto, H. Sakuragi, and K. Tokumaru, *Chem. Phys. Lett.*, **157**, 46 (1989); b) H. Okamoto, T. Arai, H. Sakuragi, and K. Tokumaru, *Bull. Chem. Soc. Jpn.*, **63**, 2881 (1990); c) H. Okamoto, T. Arai, H. Sakuragi, K. Tokumaru, and Y. Kawanishi, *Bull. Chem. Soc. Jpn.*, **64**, 216 (1991).

4) a) T. Arai, Y. Kuriyama, T. Karatsu, H. Sakuragi, K. Tokumaru, and S. Oishi, *J. Photochem.*, **36**, 125 (1987); b) H. Furuuchi, T. Arai, Y. Kuriyama, H. Sakuragi, and K. Tokumaru, *Chem. Phys. Lett.*, **162**, 211 (1989).

5) T. Arai, T. Karatsu, H. Sakuragi, and K. Tokumaru, *Tetrahedron Lett.*, **24**, 2873 (1983).

6) T. Karatsu, T. Arai, H. Sakuragi, and K. Tokumaru, *Chem. Phys. Lett.*, **115**, 9 (1985).

7) J. Saltiel and J. L. Charlton, in "Rearrangement in Ground and Excited States," ed by P. de Mayo, Academic Press, New York (1980), Vol. 3, p. 25.

8) H. Görner and D. Schulte-Frohlinde, *J. Phys. Chem.*, **85**, 1835 (1981).

9) T. Arai, H. Sakuragi, K. Tokumaru, Y. Sakaguchi, J. Nakamura, and H. Hayashi, *Chem. Phys. Lett.*, **98**, 40 (1983).

10) M. Bullpitt, W. Kitching, D. Doddrell, and W. Adcock, *J. Org. Chem.*, **41**, 760 (1976).

11) G. S. Hammond, S. C. Shim, and S. P. Van, *Mol. Photochem.*, **1**, 89 (1969).

12) C. S. Wood and F. B. Mallory, *J. Org. Chem.*, **29**, 3373 (1964).

13) S. L. Murov, "Handbook of Photochemistry," Marcel Dekker, New York (1973), p. 119.

14) M. Gisin and J. Wirz, *Helv. Chim. Acta*, **66**, 1556 (1983).

15) Ref. 13, p. 3.

16) G. Porter and M. W. Windsor, *Proc. R. Soc. London, Ser. A*, **245**, 233 (1958).

17) a) D. Weir, L. J. Johnston, and J. C. Scaiano, *J. Phys. Chem.*, **92**, 1742 (1988); b) L. J. Johnston and J. C. Scaiano, *J. Am. Chem. Soc.*, **107**, 6368 (1985).

18) R. Bensasson and E. J. Land, *Trans. Faraday Soc.*, **67**, 1904 (1971).

19) W. G. Herkstroeter and G. S. Hammond, *J. Am. Chem. Soc.*, **88**, 4769 (1966).

20) A. A. Gorman, I. Hamblett, M. Irvine, P. Raby, M. C. Standen, and S. Yeates, *J. Am. Chem. Soc.*, **107**, 4404 (1985).

21) T. Arai, H. Sakuragi, and K. Tokumaru, *Chem. Lett.*, **1980**, 1335.

22) T. Karatsu, M. Tsuchiya, T. Arai, H. Sakuragi, and K. Tokumaru, *Chem. Phys. Lett.*, **169**, 36 (1990).

 © 1991 The Chemical Society of Japan Bull. Chem. Soc. Jpn., 64, 3363—3371 (1991)

Formation of Halide Complexes of Methyl- and Inorganic Germaniun(IV) in Aqueous Hydrohalogenic Acid Solutions

Yoshiki SOHRIN
Institute for Chemical Research, Kyoto University,
Uji, Kyoto 611
(Received May 31, 1991)

The reaction of methyl- and inorganic germanium(IV) hydroxides ($(CH_3)_nGe(OH)_{4-n}$; n=0, 1, 2, or 3) with halide ions (X^-=Cl^-, Br^-, or I^-) to form halide complexes ($(CH_3)_nGeX_{4-n}$) in aqueous acidic solution has been investigated by liquid–liquid extraction, solid–liquid distribution (ion exchange), and ^1H NMR spectrometry. It has been found that methylgermanium moieties are hard Lewis acids similarly to inorganic germanium(IV), because the stability constant of the halide complexes decreases in the order $Cl^->Br^->I^-$. The stability constant for an X^- ion increases as the number of methyl groups attached to the germanium atom increases. The species of inorganic-, monomethyl-, and dimethylgermanium are nonionic and have a tetrahedral structure in HX solution, and OH^- ions attached to the germanium atom are stepwise substituted by X^- ions with an increase in HX activity. Trimethylgermanium alone forms a cation, when the activity of HX is not sufficiently high. These facts suggest that the transfer of a negative charge from methyl groups to the central germanium atom lowers the stability of the bond between the germanium atom (hard acid) and an OH^- ion (hard base).

Organogermanium(IV) compounds generally have a tetrahedral configuration and are expressed as R_nGeL_{4-n} (n=1, 2, 3, or 4), where R is a σ-bonded organic ligand and L is the other ligand bonding to the germanium atom via an atom other than carbon.[1,2] The germanium–carbon (Ge–C) bond is highly inert and stable to water or air, and methylgermanium species ($n\leqslant 3$) have been found in natural waters.[3] The aqueous solution chemistry of organogermanium, however, is only slightly known.

Inorganic germanium(IV) (Ge_i) is an extremely hard and strong Lewis acid. Ge_i of low concentration is thoroughly hydrolyzed and dissolved in water as $Ge(OH)_4$, which is sometimes mentioned as GeO_2. The hydroxide complex is transformed into the halide complex (GeX_4; X=Cl, Br, or I) in hydrohalogenic acid (HX) solution, which is extracted into nonpolar organic solvents.[4,5] Although it is reported that organogermanium compounds also dissolve in water as $R_nGe(OH)_{4-n}$ and form R_nGeX_{4-n} in HX solution,[6-8] there is no quantitative knowledge of the reaction.

While studies on the structure of germanium species in aqueous solution are also rare, it appears that the tetrahedral structure is common not only for the halide complexes but also for the hydroxide complexes. Raman spectra suggested that Ge_i is present as tetrahedral $[O_2Ge(OH)_2]^{2-}$ in nearly saturated aqueous KOH,[9] and that $(CH_3)_2Ge(OH)_2$ has a tetrahedral structure in water.[8]

In order to clarify the effect of methyl groups on the Lewis acid nature of the central germanium atom, a study on halide complexing of methyl- and inorganic germanium in HX solution by liquid–liquid extraction was undertaken. In the present paper, the data of liquid–liquid extraction have been analyzed based on the information on the charge and structure of the germanium species, which is obtained from solid–liquid distribution (ion exchange) and NMR chemical shift of the methyl protons.

Experimental

Reagents. Standard solutions of monomethylgermanium (MeGe), dimethylgermanium (Me_2Ge), and trimethylgermanium (Me_3Ge) (1×10^{-2} M; 1 M=1 mol dm^{-3}) were prepared by alkaline hydrolysis of their chlorides (Alfa or Aldrich) as described previously.[10] (Caution: Although the toxicity of organogermanium compounds is thought to be low,[1] handling of these compounds should be carried out in a hood to avoid inhalation). A standard solution of 1×10^{-2} M Ge_i was prepared from germanium dioxide (Wako) according to Shimomura et al.[11] These standard solutions were stable over a year. Other chemicals were of analytical reagent grade. Distilled water was used throughout.

Resins. The resins used were a strong basic anion-exchange resin, Muromac MSA-1 (100—200 mesh, Cl^- form, Muromachikagakukogyo), a strong acidic cation-exchange resin, Muromac MSC-1 (100—200 mesh, Na^+ form, Muromachikagakukogyo), and a CHP20P resin (200—400 mesh, Mitsubishi Chemicals) that had no ion-exchange groups. These resins were macroreticular styrene–divinylbenzene copolymers. The anion-exchange resin was washed successively with distilled water, methanol, 1 M HCl, and 1 M NaOH, changed into Cl^- form by soaking the resin in ten times volume of 2 M HCl overnight, and washed with distilled water until the effluent was free from Cl^- ions. The cation-exchange resin was washed in the same way, and converted to H^+ form in 4 M HCl. The CHP20P resin was washed successively with methanol, 1 M NaOH, 1 M HCl, and methanol. These resins were dried to a constant weight in a vacuum drying oven and stored in a desiccator.

Procedure. Liquid–Liquid Extraction: An aliquot of aqueous solution containing various concentrations of HX and 5×10^{-5}—1×10^{-3} M of a germanium compound was shaken with an aliquot of CCl_4 for 30 min in a 30 ml centrifuge tube at 25±0.1 °C, using a Taitec bio-shaker BR-30L. After phase separation, the germanium concentration in both the phases was determined with a Japan Jarrel Ash ICAP-500 inductively

coupled argon plasma emission spectrometer. The precise procedure was described previously.[10]

When HI solution was used as the aqueous phase, following precautions were taken to make the solution free from I_3^-. The experiment was done under red light, and aqueous and organic solutions were deaerated with nitrogen. The I_3^- ions were removed from an HI stock solution just before its use by passing the solution through the column in which an I^- form anion-exchange resin was packed. In spite of the above precautions, it was shown by absorbance measurement at 351 nm that I_3^- ions were formed during the extraction experiment. For example, 7.0×10^{-5} M and 2.2×10^{-3} M of I_3^- were found in 0.725 M and 5.90 M HI solutions, respectively. Thus Me_3Ge alone that was extracted into the organic phase in the lowest acid concentration range was examined in the HI–CCl_4 system.

Solid-Liquid Distribution: Nine ml of aqueous solution containing various concentrations of HCl and 0.50 g of a dried ion-exchange resin were placed in a 30 ml centrifuge tube. After the addition of 1 ml of a 1×10^{-2} M germanium standard solution, the tube was shaken gently for 24 h at 25±0.1 °C with the bio-shaker. The resin was separated by filtration, and shaken with 10 ml of 1 M NaOH for 24 h to elute the germanium compound. The germanium compound concentrations in the HCl solution and the eluate were determined with the ICAP-500. From these concentrations, the distribution coefficient

$$K_d = \text{Amount of germanium in resin (mol g}^{-1})/\text{Amount of germanium in HCl solution (mol ml}^{-1}) \quad (1)$$

was calculated.

Since the CHP20P resin is hydrophobic, 0.50 g of the dried resin was first suspended in 5 ml of methanol. After the addition of 10 ml of distilled water, the resin was shaken with the methanol–water mixture for 30 min, and separated by filtration. The resin was shaken with distilled water, and finally with an HCl solution of which HCl concentration was the same as that in the distribution experiment. Then the resin was filtered and immediately used for the experiment. The subsequent procedure was similar to that for ion-exchange resins.

^{1}H NMR Spectra: ^{1}H NMR spectra were obtained in D_2O or $CDCl_3$ at 25±1 °C on a Varian VXR200 spectrometer with a Varian VXR4000 data station. Germanium compound concentrations were 10^{-1}—10^{-3} M. Chemical shifts were measured relative to the resonance of sodium 3-(trimethylsilyl)propionic-2,2,3,3-d_4 acid in D_2O and tetramethylsilane in $CDCl_3$.

Mean Activity of HX. The acid concentration in aqueous solution was measured by titration with an NaOH solution, using a Toa Electronics automatic titrator AUT-1 equipped with a glass electrode. The mean activity of HX ($a_\pm$), which was expressed on the molarity scale, was calculated from the measured concentration using a table described by Hamer and Wu[12] and the density data.[13] The initial and equilibrium concentrations of the acid agreed within 1% in solution containing more than 1 M of HX. For more dilute HX solution, however, the equilibrium concentration of the acid was lower than the initial concentration. This decrease was mainly caused by NaOH contained in the added germanium standard solution. Since the change in X^- ion concentration was negligible, the average of $a_\pm$ calculated from the initial and equilibrium concentrations of the acid was adopted as data. The error in log $a_\pm$ brought about by the above treatment is possibly a maximum of 0.2 for 10^{-3} M HX solution.

Results and Discussion

Liquid–Liquid Extraction. The results of liquid–liquid extraction are illustrated in Fig. 1. The distribution ratio of a germanium compound (D) is plotted against $a_\pm$ on log–log scale. The D is defined as

$$D = C_{Ge,o}/C_{Ge} \quad (2)$$

where $C_{Ge,o}$ and C_{Ge} mean the analytical molar

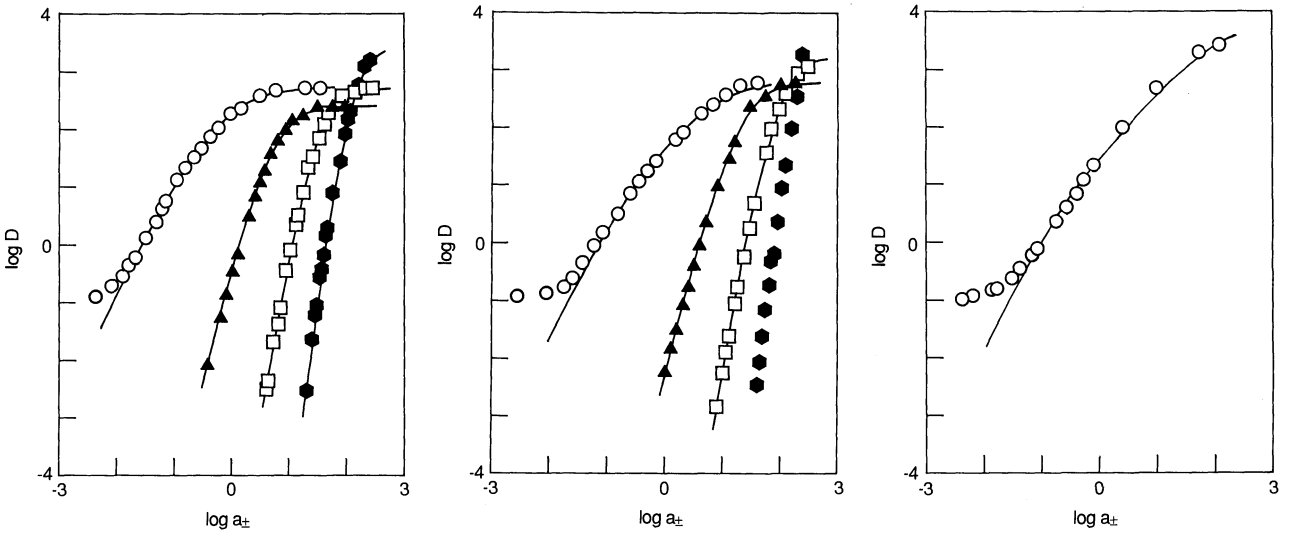

Fig. 1. Plots of log D vs. log $a_\pm$ for 5×10^{-5}—1×10^{-3} M germanium compounds. Solid curves are calculated using the partition constants (Table 1) and stepwise stability constants (Table 2). Only a portion of the experimental points are shown. (a, left) HCl–CCl_4 system; (b, center) HBr–CCl_4 system; (c, right) HI–CCl_4 system; ●, Ge_i; □, MeGe; ▲, Me_2Ge; ○, Me_3Ge.

concentration of the germanium compound in the organic phase and the aqueous phase, respectively. Cleavage of the Ge–C bonds did not occur under the experimental conditions. Distribution equilibrium was reached in a few minutes for all germanium compounds. The recovery was a minimum of 95%.

Log D did not depend on the initial concentration of germanium compounds in the aqueous phase which varied between 5×10^{-5} and 1×10^{-3} M. This fact suggests that germanium species are monomeric in both the aqueous and organic phases. While the log D vs. log $a_{\pm}$ plot of Me_3Ge is sigmoid, the plateau in the lower log $a_{\pm}$ range does not appear for the other germanium compounds. Germanium compounds should exist as nonionic hydroxides ($(CH_3)_nGe(OH)_{4-n}$; hereafter n=0, 1, 2, or 3) in water.[4,7,8] When the formation and distribution of halide complexes ($(CH_3)_nGeX_{4-n}$) are negligible in the low log $a_{\pm}$ range, D is independent of log $a_{\pm}$ and equal to the partition constant of the hydroxide:

$$P_{OH} = [(CH_3)_nGe(OH)_{4-n}]_o/[(CH_3)_nGe(OH)_{4-n}], \quad (3)$$

where brackets signify the molar concentration. Log P_{OH} of Me_3Ge is -0.95. The formation of oligomers of Me_2Ge, MeGe, and Ge_i is unlikely in the low log $a_{\pm}$ range, because log D of these compounds is much lower than the log P_{OH} of Me_3Ge.

Log D increases with the increase in log $a_{\pm}$. This is caused by the formation and distribution of the germanium halide complex. Benoit and Clerc[4] investigated the liquid–liquid extraction of Ge_i in the HCl–CCl_4 system, and found that the analytical ratio of Ge:Cl in the organic phase was 1:4. When log $a_{\pm}$ is sufficiently high, log D does not depend on log $a_{\pm}$, which implies that $(CH_3)_nGeX_{4-n}$ is the dominant species in both the aqueous and organic phases. Then, D agrees with the partition constant of the halide complex:

$$P_x = [(CH_3)_nGeX_{4-n}]_o/[(CH_3)_nGeX_{4-n}]. \quad (4)$$

It is obvious from Fig. 1 that P_x is much higher than P_{OH} for each germanium compound.

The analysis of the data is carried out on the assumption that $(CH_3)_nGeX_{4-n}$ alone is extracted into the organic phase. With regard to Me_3Ge, the D corrected by subtracting P_{OH} from the apparent D is used for the analysis. The log D vs. log $a_{\pm}$ plot is linear in the low log $a_{\pm}$ range for all systems. The slope is almost 2 for Me_3Ge, 4 for Me_2Ge, 6 for MeGe, and 8 for Ge_i (Table 1). The extraction equilibrium, overall stability constant, and extraction constant can be expressed as

$$(CH_3)_nGe(OH)_{4-n} + (4-n)H^+ + (4-n)X^- \rightleftharpoons (CH_3)_nGeX_{4-n} + (4-n)H_2O, \quad (5)$$

$$(CH_3)_nGeX_{4-n} \rightleftharpoons (CH_3)_nGeX_{4-n,o}, \quad (6)$$

$$\beta^0 = ((CH_3)_nGeX_{4-n})(H_2O)^{4-n}/((CH_3)_nGe(OH)_{4-n})(H^+)^{4-n}(X^-)^{4-n}, \quad (7)$$

$$K_{ex}{}^0 = ((CH_3)_nGeX_{4-n})_o(H_2O)^{4-n}/((CH_3)_nGe(OH)_{4-n})(H^+)^{4-n}(X^-)^{4-n} = \beta^0 P_x{}^0, \quad (8)$$

where parentheses represent the activity and superscript 0 denotes the thermodynamic constant. The following are also assumed: (i) the activity coefficients are unity for germanium species in both the aqueous and organic

Table 1. Extraction Constants, Partition Constants, and Overall Stability Constants for Halide Complexes of Methyl- and Inorganic Germanium at 25 °C

	log D vs. log $a_{\pm}$ Slope[a]	log $K_{ex}{}^0$[b]	log $P_x{}^0$	log β^0
		HCl[c]		
Ge_i	7.99±0.56[d] (5)[e]	−12.99±0.04	3.42±0.23[f]	−16.41±0.23
MeGe	5.94±0.27 (7)	−6.22±0.03	2.70±0.03 (4)	−8.92±0.04
Me_2Ge	3.77±0.01 (4)	−0.44±0.02	2.39±0.03 (5)	−2.83±0.04
Me_3Ge	1.93±0.03 (12)	3.03±0.01	2.73±0.01 (4)	0.30±0.01
		HBr		
Ge_i	7.98±0.72 (8)	−15.20±0.04	4.4[g]	−19.6
MeGe	5.42±0.17 (8)	−8.24±0.03	3.20±0.08[f]	−11.44±0.09
Me_2Ge	3.58±0.05 (9)	−2.31±0.04	2.78±0.03 (3)	−5.09±0.05
Me_3Ge	1.84±0.10 (8)	2.32±0.03	2.83±0.02 (3)	−0.51±0.04
		HI		
Me_3Ge	1.59±0.03 (6)	2.12±0.05	3.69±0.15[f]	−1.57±0.16

a) Calculated using points adopted from a linear portion in the low log $a_{\pm}$ range, where the variation in log D is about 2. b) Equation 10 was fitted to the same points which were used to calculate the slope. c) Ref. 10. d) Standard deviation. e) Number of points. f) Evaluated by the curve fitting. g) Estimated from Fig. 2.

phases; (ii) the activity of water is unity; (iii) the activities of H^+ and X^- ions are equal to $a\pm$. Then,

$$D = ((CH_3)_nGeX_{4-n})_o/((CH_3)_nGe(OH)_{4-n}), \quad (9)$$

$$\log D = 2(4-n)\log a\pm + \log K_{ex}^0. \quad (10)$$

The observed slopes can be rationalized by Eq. 10.

When $\log a\pm$ is sufficiently high,

$$\log D = \log P_x^0. \quad (11)$$

Thus, β^0 can be estimated from the extraction data. The values of $\log K_{ex}^0$, $\log P_x^0$, and $\log \beta^0$ obtained by a linear least-squares method are listed on Table 1. The plateau in the higher $\log a\pm$ range was not observed for Ge_i in the HCl and HBr systems, MeGe in the HBr system, and Me_3Ge in the HI system. $\log P_x^0$ of $GeCl_4$, CH_3GeBr_3, and $(CH_3)_3GeI$ is obtained as a parameter in the estimation of stepwise stability constants which is described later. This estimation can not be applied to $GeBr_4$, because the $\log P_x^0$ is very high. Figure 2 shows the relationship between $\log P_x^0$ and van der Waals volumes (V_w) of the germanium halide complexes that are calculated according to Bondi.[14] A fairly good correlation is observed among MeGe, Me_2Ge, and Me_3Ge, and the regression line is

$$\log P_x^0 = 0.100\ V_w - 3.18 \qquad (r = 0.890). \quad (12)$$

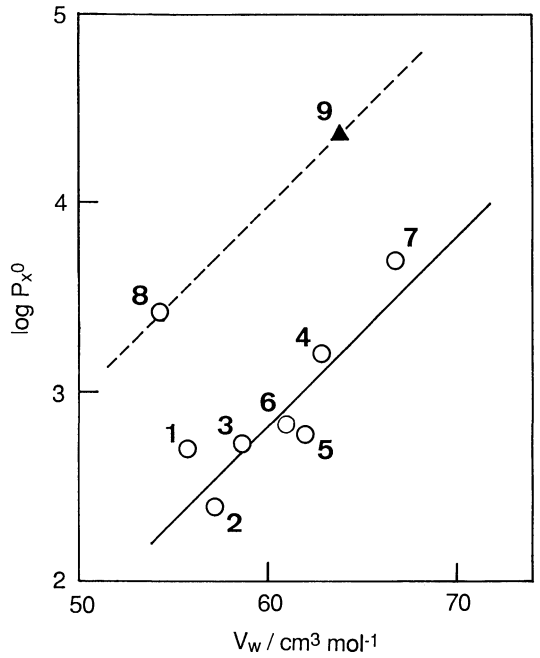

Fig. 2. Plots of $\log P_x^0$ vs. V_w for germanium halides. The solid line shows Eq. 12. ○, determined from the liquid–liquid extraction data; ▲, estimated; 1, CH_3GeCl_3; 2, $(CH_3)_2GeCl_2$; 3, $(CH_3)_3GeCl$; 4, CH_3GeBr_3; 5, $(CH_3)_2GeBr_2$; 6, $(CH_3)_3GeBr$; 7, $(CH_3)_3GeI$; 8, $GeCl_4$; 9, $GeBr_4$.

Log P_x^0 of $GeCl_4$ is higher than that expected from this correlation, which is attributable to that the molecule has no dipole moment and is highly soluble in CCl_4. Assuming that the same extent of departure from the regression line occurs for $GeBr_4$, the log P_x^0 is evaluated to be 4.4. Although application of the regular solution theory[15] was tried, no improvement over the above estimation of log P_x^0 was made because of increased number of unknown parameters.

Solid–Liquid Distribution. The dependence of $\log K_d$ on $\log a\pm$ of HCl is realized in Fig. 3. The recovery of germanium compounds was poorer (minimum 80%) and the experimental error was larger than that in the liquid–liquid extraction.

Although distribution of Ge_i, MeGe and Me_2Ge to the ion-exchange resins is negligible in the low $\log a\pm$ range, that to the CHP20P resin is significant. The value of $\log K_d$ for the CHP20P resin is enhanced in the order Ge_i<MeGe<Me_2Ge<Me_3Ge. These facts support that the germanium compounds are dissolved as the nonionic hydroxides in water. Log K_d for the CHP20P resin rises with increasing $\log a\pm$, which is ascribed to the formation and distribution of the germanium chlorides.

Log K_d of Ge_i, MeGe, and Me_2Ge for the anion- and cation-exchange resins also increases with the increase in $\log a\pm$, while the value of $\log K_d$ is lower than that for the CHP20P resin. It is probable that the distribution of these compounds is caused not by ionic interaction but by hydrophobic adsorption on the resin substrate. Hence, the dominant dissolved species of Ge_i, MeGe, and Me_2Ge are nonionic in HCl solution. The coordination number of the germanium atom in these compounds remains at four, and OH^- ions bonded to the germanium atom are stepwise substituted by Cl^- ions with increasing $\log a\pm$.

It has been supposed that Ge_i forms anionic species, such as $[Ge(OH)_xCl_{5-x}]^-$ or $[Ge(OH)_xCl_{6-x}]^{2-}$, in HCl solution (>5 M; $\log a\pm$>1.2).[4,16–18] Distribution of Ge_i to an anion-exchange resin was given as a piece of the evidence.[16] However, $\log K_d$ of Ge_i for the CHP20P resin is higher than that for the anion-exchange resin, and the distribution to the cation-exchange resin is significant above 6.5 M of HCl ($\log a\pm$>1.6), as shown in Fig. 3. Although it was stated that electrophoresis of the Ge_i anion was observed in 6 M HCl ($\log a\pm$=1.4),[17] the conclusion was based on the concentration difference of less than 5%, of which significance was doubtful from an analytical point of view. Everest and Harrison[18] claimed the presence of Ge_i anion in 6—9 M HCl solution saturated with Ge_i, because solubility of Ge_i and its adsorption on an anion-exchange resin had the maximum in this [HCl] range. They also reported that the solubility maximum did not occur in HBr solution and that no Ge_i bromo complexes were formed. In dilute Ge_i solution, however, the distribution to the anion-exchange resin shows no maximum in 6—9 M HCl (Fig. 3: 1.4—2.2 in $\log a\pm$), and the nature of log D vs.

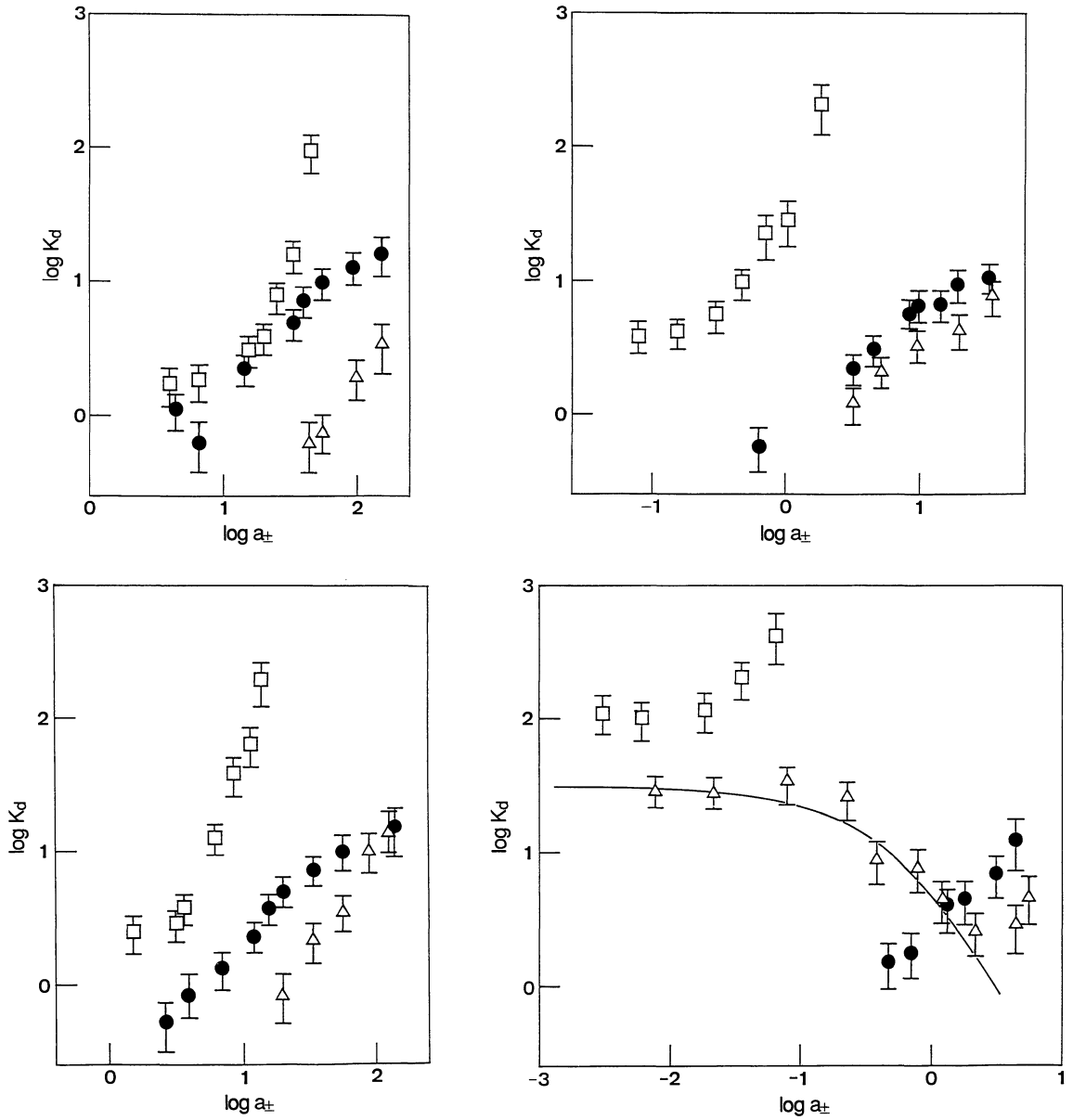

Fig. 3. Plots of log K_d vs. log $a_\pm$ for 1×10^{-3} M germanium compounds in HCl solution. Vertical bars show the 1 standard deviation. The solid curve is calculated from Eq. 20. (a, top left) Ge_i; (b, bottom left) MeGe; (c, top right) Me_2Ge; (d, bottom right) Me_3Ge; ●, anion-exchange resin; △, cation-exchange resin; □, CHP20P resin.

log $a_\pm$ plots for Ge_i in the HCl and HBr systems is identical (Fig. 1). Benoit and Clerc[4] gave the solvent extraction data in evidence of the Ge_i anion. They extracted $GeCl_4$ from aqueous phases which contained a constant total molality of HCl–$HClO_4$ or HCl–LiCl into an organic phase of CCl_4, to investigate the dependence of log D on log (Cl^-) or log (H^+). When the total molality was 12.0 mol kg^{-1} (log $a_\pm$=2.32), d log D/d log (Cl^-)=−0.2 and d log D/d log (H^+)=0.7 were found, and the Ge_i species was thought to be $[GeCl_4(OH)(H_2O)]^-$. However, the activity coefficients of Cl^- and H^+ ions are likely to vary with the change in the solute composition, when the total molality is high. Figure 1 shows that d log D/d log $a_\pm$ is 1.90 for 12.0 mol kg^{-1} HCl, which can not be explained on the presence of $[GeCl_4(OH)(H_2O)]^-$. The previously reported evidence of the Ge_i anion is controvertible as described above. Consequently, it is presumed that Ge_i does not form anionic species and retains a tetrahedral configuration in HX solution similarly to Me_2Ge and MeGe.

A remarkable difference of cation-exchange behavior for Me_3Ge from that for the other germanium compounds appears in Fig. 3. Me_3Ge is highly adsorbed by the cation-exchange resin in the low log $a_\pm$ range, whereas it is not adsorbed by the anion-exchange resin. This indicates that Me_3Ge forms a cation in HCl solution.

^{1}H NMR Spectra. Methyl protons of each germanium compound gave a singlet resonance line in D_2O

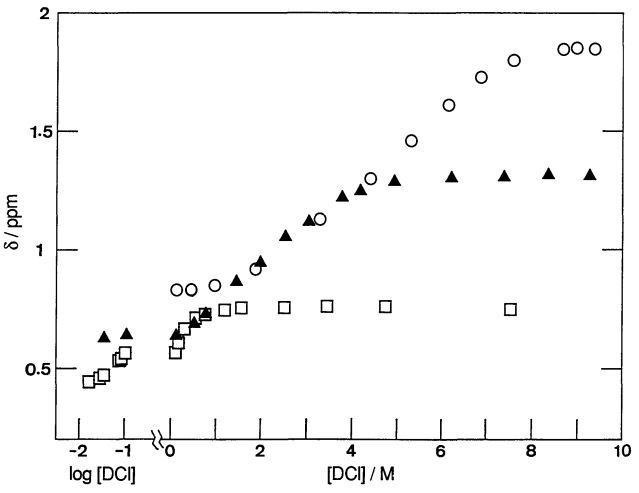

Fig. 4. Chemical shift of the methyl protons of 10^{-3}—10^{-1} M germanium compounds in D_2O as a function of [DCl]. ○, MeGe; ▲, Me_2Ge; □, Me_3Ge.

and $CDCl_3$ except one case that is mentioned later. The chemical shift of the methyl protons in D_2O is plotted against [DCl] in Fig. 4. The chemical shifts remain constant in the low [DCl] range, increase with the increase in [DCl], and reach to maximums. The maximums are the same as the chemical shifts for germanium chlorides in $CDCl_3$, which are 1.68 ppm for CH_3GeCl_3, 1.23 ppm for $(CH_3)_2GeCl_2$, and 0.72 ppm for $(CH_3)_3GeCl$. This supports that the dissolved species of methylgermanium in D_2O containing sufficiently high concentration of DCl are the chloride complexes with a tetrahedral configuration. The slight difference between the chemical shifts in D_2O and $CDCl_3$ is attributable to solvent effect.

The chemical shift of methyl protons for $(CH_3)_3GeOH$ was 0.44 ppm in D_2O and 0.42 ppm in $CDCl_3$, and that for $(CH_3)_3GeCl$ was 0.76 ppm in D_2O and 0.72 ppm in $CDCl_3$. The chemical shift was 1.22 ppm for $(CH_3)_3COH$, 1.60 ppm for $(CH_3)_3CCl$, 0.16 ppm for $(CH_3)_3SiOH$, and 0.42 ppm for $(CH_3)_3SiCl$ in $CDCl_3$. The absolute values of the chemical shift and the chemical shift changes caused by replacement of an OH^- ion bonded to the central atom by a Cl^- ion are similar among these compounds. Since the central carbon and silicon atoms in these compounds are sp^3 hybridized, it is assumed that the germanium atom of $(CH_3)_3GeOH$ and $(CH_3)_3GeCl$ is also sp^3 hybridized in both $CDCl_3$ and D_2O. With regard to the Me_3Ge cation that is suggested by the ion-exchange experiment, an sp^3d hybrid orbital is another possibility. A trimethyltin cation, $[(CH_3)_3Sn(H_2O)_2]^+$ has a bipyramidal sp^3d configuration, of which carbon atoms form a planar triangle.[19] It is difficult to presume the structure of Me_3Ge cation from the present data.

The chemical shift difference between the hydroxide and chloride complexes for Me_2Ge (0.67 ppm) and MeGe (1.02 ppm) in D_2O is twice and three times as great as that for Me_3Ge (0.32 ppm), respectively. This implies that the central germanium atoms of Me_2Ge and MeGe are also sp^3 hybridized, and that the effect of ligand exchange on the chemical shift is an additive property. Since the chemical shift increases monotonously, the formation of chloro complex anions in the intermediate [DCl] range is very unlikely.

When $(CH_3)_3GeOH$ was extracted from aqueous solution into $CDCl_3$, two singlet lines were found at 0.42 and 0.36 ppm in the organic phase. The peak area ratio was dependent on $C_{Me_3Ge,o}$, and the latter peak became large with increasing $C_{Me_3Ge,o}$. These peaks are assigned to $(CH_3)_3GeOH$ and $(CH_3)_3GeOGe(CH_3)_3$, respectively. The dimerization is written as

$$2(CH_3)_3GeOH_{,o} \rightleftharpoons (CH_3)_3GeOGe(CH_3)_{3,o} + H_2O. \quad (13)$$

Since the reaction does not proceed at an appreciable rate after separation of the aqueous and organic phases, the two lines are observed separately. The equilibrium constant for the reaction (13) is estimated at 13 from $C_{Me_3Ge,o}$ and the peak area ratio. This value indicates that the dimer comprises only 2.5% of 10^{-3} M of Me_3Ge in $CDCl_3$ which is equilibrated with water, and that the dimerization is negligible in the analysis of the liquid–liquid extraction data. When Me_2Ge and MeGe were extracted from aqueous solution into $CDCl_3$, no methyl resonance lines other than those for $(CH_3)_2GeCl_2$ and CH_3GeCl_3 were found. Although the formation of Me_2Ge oligomers in CCl_4 has been reported,[20] it is also negligible in the liquid–liquid extraction.

Stepwise Stability Constants. Based on the above discussion, the germanium species in HX solution are presumed as follows. The species of Ge_i, MeGe, and Me_2Ge have a tetrahedral structure and are nonionic. Hydroxide ions attached to the central germanium atom are stepwise substituted by X^- ions with the increase in $\log a_\pm$. Me_3Ge forms a cation when the $\log a_\pm$ is not sufficiently high. Now, stepwise stability constants for these species are estimated from the liquid–liquid extraction data.

For Ge_i, MeGe, and Me_2Ge, the stepwise reaction and stability constant are written as

$$(CH_3)_nGe(OH)_{i+1}X_{j-1} + H^+ + X^- \rightleftharpoons (CH_3)_nGe(OH)_iX_j + H_2O, \quad (14)$$

$$K_j^0 = ((CH_3)_nGe(OH)_iX_j)(H_2O)/((CH_3)_nGe(OH)_{i+1}X_{j-1})(H^+)(X^-), \quad (15)$$

where $n+i+j=4$. For Me_3Ge, the stepwise reaction and stability constant can be defined as

$$(CH_3)_3GeOH + H^+ \rightleftharpoons [(CH_3)_3Ge(H_2O)]^+ \quad (16)$$

Table 2. Stepwise Stability Constants for Methyl- and Inorganic Germanium Species in HX Solution at 25°C

	n[a]	log K_1^0	log K_2^0	log K_3^0	log K_4^0	log β^{0}[b]
			HCl			
Ge_i	21	−3.02±0.29[c]	−3.84±0.31	−4.82±0.51	−5.09±0.56	−16.77±0.87
MeGe	25	−2.31±0.10	−2.95±0.12	−3.81±0.06	—	− 9.07±0.17
Me_2Ge	17	−0.71±0.04	−2.15±0.03	—	—	− 2.86±0.05
			HBr			
MeGe	22	−2.57±0.10	−4.32±0.21	−4.67±0.23	—	−11.56±0.33
Me_2Ge	16	−1.59±0.06	−3.49±0.04	—	—	−5.08±0.07
	n	log K_{1p}^0			log K_{1x}^0	log β^0
			HCl			
Me_3Ge	27	0.55±0.04			−0.18±0.03	0.37±0.05
			HBr			
Me_3Ge	28	0.72±0.04			−1.16±0.02	−0.44±0.04
			HI			
Me_3Ge	15	0.71±0.09			−2.21±0.18	−1.50±0.20

a) Number of points. b) Calculated from the stepwise stability constants. c) Standard deviation.

$$K_{1p}^0 = ([(CH_3)_3Ge(H_2O)]^+)/((CH_3)_3GeOH)(H^+) \quad (17)$$

$$[(CH_3)_3Ge(H_2O)]^+ + X^- \rightleftharpoons (CH_3)_3GeX + H_2O \quad (18)$$

$$K_{1x}^0 = ((CH_3)_3GeX)(H_2O)/([(CH_3)_3Ge(H_2O)]^+)(X^-) \quad (19)$$

The assumptions that were made in the evaluation of K_{ex}^0 are adopted in a non-linear least-squares computation, except that the activity of water is calculated from the acid concentration and osmotic coefficient,[12] because wide ranges of [HX] are concerned in the computation. Resulting values are listed on Table 2. Log P_x^0 of $GeCl_4$, CH_3GeBr_3 and $(CH_3)_3GeI$ is also determined as a parameter by the computation (Table 1). The computation is inapplicable to Ge_i in the HBr system, because the bending on the log D vs. log $a\pm$ plot is not observed. The solid curves in Fig. 1 are calculated using the partition and stepwise stability constants.

Values of log β^0 listed on Table 2 are calculated from the stepwise stability constants, and in agreement with those on Table 1. Figure 5 shows the equilibrium composition of the germanium species in aqueous solution as a function of [HCl]. It is apparent from Figs. 4 and 5 that the [DCl] range where the variation in the chemical shift occurs is coincident with the [HCl] range where the composition of the germanium species changes. Moreover, the distribution of Me_3Ge to the cation-exchange resin is reproduced using the stepwise stability constants. When the Me_3Ge cation is the only species that is adsorbed by the cation-exchange resin,

$$K_d = 10^{-3}[[(CH_3)_3Ge(H_2O)]^+]_r/$$
$$\{[(CH_3)_3GeOH] + [[(CH_3)_3Ge(H_2O)]^+] + [(CH_3)_3GeCl]\}$$
$$= 10^{-3}K_H^{Me_3Ge}[H^+]_r/\{1/K_{1P}^0 + a\pm + K_{1X}^0(a\pm)^2/(H_2O)\}, \quad (20)$$

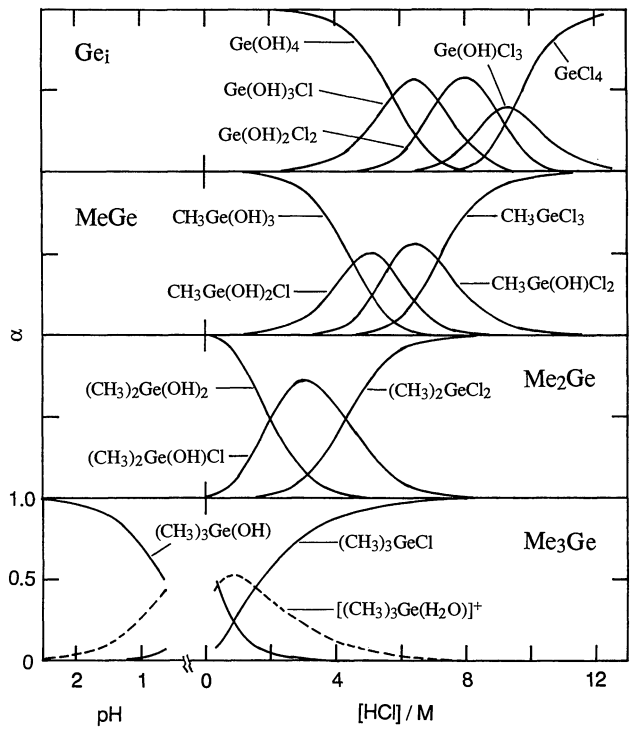

Fig. 5. Equilibrium composition of germanium species in aqueous solution as a function of [HCl].

where subscript r implies the concentration in the resin (mol g^{-1}) and

$$K_H^{Me_3Ge} = (H^+)[[(CH_3)_3Ge(H_2O)]^+]_r/[H^+]_r[[(CH_3)_3Ge(H_2O)]^+]. \quad (21)$$

Assuming that $K_H^{Me_3Ge}=1.7\times10^3$ and $[H]_r=5.0\times10^{-3}$, the solid curve in Fig. 3 is obtained. These results indicate the validity of the stepwise stability constants estimated here.

Effect of Methyl Groups on the Lewis Acid Nature of the Central Atom. Log β^0 for a methylgermanium moiety decreases in the order $Cl^->Br^->I^-$ (Tables 1 and 2). This indicates that the methylgermanium moieties are hard Lewis acids similarly to Ge_i.[8] Log β^0 for an X^- ion increases as the number of methyl groups attached to the germanium atom increases. The same tendency appears in the stepwise stability constants for an equivalent coordination site (Table 2). For chloride complexes, log $K_4^0=-5.09$ for Ge_i, log $K_3^0=-3.81$ for MeGe, log $K_2^0=-2.15$ for Me_2Ge, and log $K_{1p}^0K_{1x}^0=0.37$ for Me_3Ge. Thus an OH^- ion bound to a germanium atom is easily replaced by an X^- ion, when methyl groups are attached to the germanium atom. This feature is clearly shown in Fig. 5. The [HCl] range where the species composition changes shifts to a lower concentration range with the increase in the number of methyl groups.

Since the charge and structure of germanium compounds do not alter in the present reaction, solvent effects are not serious. The tetrahedral configuration around the central germanium atom implies that the steric strain between the ligands bonded to the germanium atom is hardly affected by the size of the ligands investigated in this paper. Consequently, the dominant factor is an inductive effect. The transfer of a negative charge from a soft base CH_3^- to the central germanium atom increases the electron density on the germanium atom, and weakens the ionic interaction between the germanium atom and a hard base, such as an OH^- ion.[21]

The inductive effect is most pronounced for Me_3Ge. The acidity of the central germanium atom of Me_3Ge is remarkably reduced by methylation. The Me_3Ge moiety can not cause hydrolysis in dilute HX solution, and forms a hydrated cation. Such a hydrated cation is not formed by Ge_i, MeGe, and Me_2Ge in HCl and HBr solutions. However, since log P_{1x}^0 of Me_3Ge decreases in the order $Cl^->Br^->I^-$, the Me_3Ge moiety is still a hard acid. Hence, the electron donation from methyl groups that reduces the bond stability between the germanium atom and a hard base does not result in stabilization of the bond between the germanium atom and a soft base, such as an I^- ion.

Cassol et al.[22] reported a similar effect by methylation on complex formation between methyltin(IV) cations, which are also hard, but are weaker Lewis acids, and F^- or Cl^- ions. According to their data, the number of methyl groups bonded to the tin atom hardly affects the tendency to bind Cl^- in equivalent coordination places: as an example, log $K_3=-0.25$ for CH_3Sn^{3+}, log $K_2=-0.23$ for $(CH_3)_2Sn^{2+}$, and log $K_1=-0.17$ for $(CH_3)_3Sn^+$. The tendency to bind F^-, however, decreases with the increase in the number of the methyl groups: log $K_3=4.12$ for CH_3Sn^{3+}, log $K_2=2.87$ for $(CH_3)_2Sn^{2+}$, and log $K_1=2.27$ for $(CH_3)_3Sn^+$. The structure of methyltin cations is different from that of methylgermanium compounds: The dimethyltin cation has an octahedral configuration containing linear C–Sn–C and the trimethyltin cation has a bipyramidal configuration.[19] Accordingly, the inductive effect of methyl groups on the tin atom is similar to that on the germanium atom despite the distinction of hybridization.

Quite a different effect has been reported on a methylmercury(II) cation, of which the central atom has a d^{10} electronic configuration similarly to germanium(IV) and tin(IV) atoms. Since the halide complex stability constant of Hg^{2+} and CH_3Hg^+ decreases in the order $I^->Br^->Cl^->F^-$,[19,23] these cations are soft acids. In this case, methylation reduces stability of the bond between the mercury atom and a soft base. For example, the stability constants of iodides are log $K_1=12.87$, log $K_2=10.95$ for Hg^{2+}, and log $K_1=8.60$ for CH_3Hg^+, whereas those of fluorides are log $K_1=1.03$ for Hg^{2+}, and log $K_1=1.50$ for CH_3Hg^+.[19,23] An explicit and extensive explanation of the effect by methylation on the Lewis acid nature of the various atoms has not been given yet.

The author wishes to thank Professor Masakazu Matsui, Dr. Sorin Kihara, and Dr. Eiichiro Nakayama for helpful discussions.

References

1) B. J. Aylett, "Organometallic Compounds," 4th ed, Chapman and Hall, London (1979), Vol. 1, Part 2, Chap. 3.
2) R. C. Poller, in "Comprehensive Organic Chemistry," ed by D. N. Jones, Pergamon Press, Oxford (1979), Vol. 3, pp. 1061—1073.
3) B. L. Lewis, M. O. Andreae, and P. N. Froelich, *Mar. Chem.*, **27**, 179 (1989).
4) R. L. Benoit and P. Clerc, *J. Phys. Chem.*, **65**, 676 (1961).
5) S. Siekierski and R. Olszer, *J. Inorg. Nucl. Chem.*, **25**, 1351 (1963).
6) C. A. Kraus and E. A. Flood, *J. Am. Chem. Soc.*, **54**, 1635 (1932).
7) E. G. Rochow and A. L. Allred, *J. Am. Chem. Soc.*, **77**, 4489 (1955).
8) R. S. Tobias and S. Hutcheson, *J. Organomet. Chem.*, **6**, 535 (1966).
9) G. E. Walrafen, *J. Chem. Phys.*, **42**, 485 (1965).
10) Y. Sohrin, *Anal. Chem.*, **63**, 811 (1991).
11) S. Shimomura, H. Sakurai, H. Morita, Y. Mino, and M. Inoue, *Anal. Chim. Acta*, **91**, 421 (1977).
12) W. J. Hamer and Y. C. Wu, *J. Phys. Chem. Ref. Data*, **1**, 1047 (1972).
13) O. Söhnel and P. Novotný, "Physical Sciences Data 22, Densities of Aqueous Solutions of Inorganic Substances," Elsevier, Amsterdam (1985).
14) A. Bondi, *J. Phys. Chem.*, **68**, 441 (1964).
15) J. H. Hildebrand and R. L. Scott, "The Solubility of Nonelectrolytes," 3rd ed, Dover Publications, New York (1964).
16) Y. Yoshino, *Bull. Chem. Soc. Jpn.*, **28**, 382 (1955).
17) A. W. Laubengayer, O. B. Billings, and A. E. Newkirk, *J. Am. Chem. Soc.*, **62**, 546 (1940).
18) D. A. Everest and J. C. Harrison, *J. Chem. Soc.*, **1957**,

1820.
19) R. S. Tobias, *Organomet. Chem. Rev.*, **1**, 93 (1966).
20) K. Moedritzer, *J. Organomet. Chem.*, **5**, 254 (1966).
21) R. G. Pearson, *J. Am. Chem. Soc.*, **85**, 3533 (1963).
22) A. Cassol, L. Magon, and R. Barbieri, *Inorg. Nucl. Chem. Lett.*, **3**, 25 (1967).
23) L. G. Sillén and A. E. Martell, "Stability Constants of Metal-Ion Complexes, Special Publication No. 17," The Chemical Society, London (1964).

Kinetic Studies of Oxygen Atom Transfer Reactions between Various *cis*-Dioxobis(dithiocarbamato)molybdenum(VI) Complexes and Triphenylphosphine

Kei UNOURA,* Yoshikiyo KATO,† Katsuaki ABE, Akio IWASE, and Hiroshi OGINO††
Department of Chemistry, Faculty of Science, Yamagata University,
Kojirakawa-machi 1-4-12, Yamagata 990
† Department of Chemistry, Faculty of General Education, Yamagata University,
Kojirakawa-machi 1-4-12, Yamagata 990
†† Department of Chemistry, Faculty of Science, Tohoku University,
Aoba-ku, Aoba, Aramaki, Sendai 980
(Received June 17, 1991)

The kinetics of the oxygen atom transfer reactions between *cis*-$[MoO_2(R_2dtc)_2]$ [R=CH_3, C_2H_5, *i*-C_3H_7, *i*-C_4H_9, $C_6H_5CH_2$ (Bz), C_6H_5 (Ph)] and PPh_3 (coupled reactions 1 and 2) have been investigated.

$$[MoO_2(R_2dtc)_2] + PPh_3 \xrightarrow{k_1} [MoO(R_2dtc)_2] + OPPh_3 \quad (1)$$

$$[MoO_2(R_2dtc)_2] + [MoO(R_2dtc)_2] \overset{K_d}{\rightleftharpoons} [Mo_2O_3(R_2dtc)_4] \quad (2)$$

The rate constants (k_1) of oxygen atom transfer reaction 1 correlate with the formal potentials of $[MoO_2(R_2dtc)_2]^{0/-1}$ except for R=Bz and Ph. The equilibrium constant values (K_d) of dimerization reaction 2 decrease with increase of the electron-donating ability of the substituents on the dithiocarbamate ligands.

Barral et al. reported that the *cis*-dioxobis(dithiocarbamato)molybdenum(VI) complexes $[MoO_2(R^1{}_2dtc)_2]$ (R^1=Et, *n*-Pr, and *i*-Bu)[1] undergo an oxygen atom transfer reaction to tertiary phosphine ($PR^2{}_3$; R^2=*n*-Bu and Ph) giving Mo(IV) complexes $[MoO(R^1{}_2dtc)_2]$ and $OPR^2{}_3$.[2] However, the reaction is complicated by the intervention of an Mo(V) dinuclear complex according to the following equations:

$$[MoO_2(R^1{}_2dtc)_2] + PR^2{}_3 \xrightarrow{k_1} [MoO(R^1{}_2dtc)_2] + OPR^2{}_3 \quad (1)$$

$$[MoO_2(R^1{}_2dtc)_2] + [MoO(R^1{}_2dtc)_2] \overset{K_d}{\rightleftharpoons} [Mo_2O_3(R^1{}_2dtc)_4] \quad (2)$$

Among these molybdenum complexes, only the Mo(V) dinuclear complexes have large extinction coefficients in the vicinity of 510 nm.[3,4] Thus, if the reaction is followed at this wavelength, biphasic kinetic behavior may be observed.

This oxygen atom transfer reaction has attracted much attention, especially as models of enzymic reactions.[5] Kinetic invesitgations have been made by several reseachers.[2,6-8] Barral et al.[2] reported kinetic studies of the $[MoO_2(n\text{-}Pr_2dtc)_2]/PPh_3$ system in *o*-dichlorobenzene at 41 °C; McDonald et al.[6] studied the kinetics of the $[MoO_2(Et_2dtc)_2]/PPh_3$ system in benzene at 24 °C, and Durant et al.[7] investigated the kinetics of $[MoO_2(Et_2dtc)_2]/PPh_3$ system in acetonitrile solution by the stopped-flow technique at temperatures between 15 and 45 °C. However, the kinetic results of these investigations were contradictory.

Holm et al.[8] extensively investigated the kinetics of reactions between $[MoO_2(Et_2dtc)_2]$ and $PPh_n(Et)_{3-n}$ (n=0—3) in 1,2-dichloroethane and developed a general treatment of the kinetics which provided a satisfactory explanation for the biphasic kinetic behavior. The rate constant k_1 was found to increase with increasing nucleophilicity of $PPh_n(Et)_{3-n}$.

Chemical properties of dithiocarbamate complexes are sensitive to the nature of the substituent on the dithiocarbamate ligand because of the existence of two resonance forms.[9]

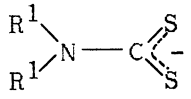
(I)

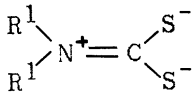
(II)

An increase of the electron-donating ability of the R^1 group favors resonance form II and hence leads to the increase of the electron density on the sulfur atoms bound to the metal atom.

Hitherto, the effect of the substituents on the dithiocarbamate ligands on the kinetics of the oxygen atom transfer reactions has not been investigated. This is the motive of this work in which the kinetics of the reactions between *cis*-$[MoO_2(R^1{}_2dtc)_2]$ (R^1=Me, Et, *i*-Pr, *i*-Bu, Bz, and Ph) and PPh_3 are dealt with. Kinetic traces were analyzed by essentially the same procedure that developed by Holm et al.[8]

Experimental

Materials. 1,2-Dichloroethane ($1,2\text{-}C_2H_4Cl_2$), obtained from Wako Pure Chemicals Industries, was purified by fractional distillation over P_2O_5. Triphenylphosphine (Nacalai Tesque Inc.) was purified twice by recrystallization from ethanol–water. Sodium salts of dithiocarbamates $R^1{}_2dtc^-$

(R^1=*i*-Pr, *i*-Bu, Bz, Ph) were prepared by literature methods.[10,11] Sodium salts of dimethyldithiocarbamate and diethyldithiocarbamate were purchased from Nacalai Tesque Inc. The complexes $[MoO_2(R^1{}_2dtc)_2]$ were prepared according to literature methods.[12,13]

Apparatus and Procedures. Procedures for kinetic measurements were almost identical with those reported previously.[8] The change of absorbance vs. time was measured with a UV-160 spectrophotometer (Shimadzu Co.).

Calculations in the kinetic analysis were performed by an ACOS 630/10 computer. For the nonlinear least-squares fitting between experimental data and theoretical values, the SALS (Statistical Analysis with Least Squares fitting) program developed by Nakagawa and Oyanagi[14] was used.

Results and Discussion

Biphasic kinetic behavior was observed for all $[MoO_2(R^1{}_2dtc)_2]/PPh_3$ systems, and is due to the formation and decay of $[Mo_2O_3(R^1{}_2dtc)_4]$ (Fig. 1). The kinetic traces are also found to be sensitive to the nature of substituents on the dithiocarbamate ligands.

The kinetic analysis of coupled reactions 1 and 2 was developed by Holm et al.[8] The absorbance of the reaction solution is expressed by equation 3 ($L=R^1{}_2dtc_2^-$).

$$A = l\left(\varepsilon_4 \frac{(C-[MoO_2L_2])}{1+2K_d[MoO_2L_2]} + \varepsilon_5 \frac{K_d[MoO_2L_2]\,(C-[MoO_2L_2])}{1+2K_d[MoO_2L_2]} + \varepsilon_6[MoO_2L_2]\right) \quad (3)$$

where l and C denote the optical path length and the initial concentration of $[MoO_2L_2]$, respectively. Symbols ε_4, ε_5, and ε_6 are the molar extinction coefficients of $[MoOL_2]$, $[Mo_2O_3L_4]$, and $[MoO_2L_2]$, respectively, the lattermost of which can be determined independently by spectroscopic measurement of $[MoO_2L_2]$. The time dependence of $[MoO_2L_2]$ is given by

$$-k_1t = \frac{1+K_dC}{P-C}\ln\left(\frac{[MoO_2L_2]}{C}\right) + 2K_d\ln\left(\frac{2K_d[MoO_2L_2]+1}{2K_dC+1}\right) - \frac{1+K_d(2P-C+Q^{1/2})}{2(P-C)}\times \ln\left(\frac{1+K_d(2[MoO_2L_2]+2P-C-Q^{1/2})}{1+K_d(2P+C-Q^{1/2})}\right) - \frac{1+K_d(2P-C-Q^{1/2})}{2(P-C)}\times \ln\left(\frac{1+K_d(2[MoO_2L_2]+2P-C+Q^{1/2})}{1+K_d(2P+C+Q^{1/2})}\right), \quad (4)$$

where $P \neq C$ and $Q=K_d^{-2}+4P^2+C^2+2K_d^{-1}C-4PC$. Here, k_1 is the rate constant for the forward reaction of reaction 1 and P is the initial concentration of PPh_3. The time dependence of $[MoO_2L_2]$ was numerically obtained from equation 4 by the Newton–Raphson method, and the absorbance vs. time curve was calculated from equation 3. The kinetic parameters are obtained by the nonlinear least-sqaures fitting between the observed data and the values calculated from equation 3. The fitting parameters are k_1, K_d, ε_4, and ε_5 in this study.

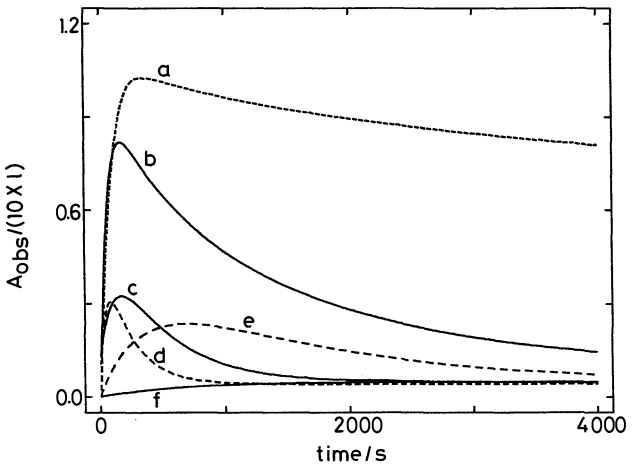

Fig. 1. Change of absorbance as a function of time for the reaction between 1.0 mM $[MoO_2(R^1{}_2dtc)_2]$ and 50.0 mM PPh_3 in 1,2-dichloroethane at 25°C. (a) R^1=Ph, (b) R^1=Bz, (c) R^1=Et, (d) R^1=Me, (e) R^1=*i*-Bu, (f) R^1=*i*-Pr. Absorbance (A_{obs}) was measured in a quartz cell with optical path length (l)=0.1 cm for (a)—(e) and 1 cm for (f).

The results of kinetic analysis are summarized in Table 1. Most of the kinetic runs were obtained under the conditions $[MoO_2(R^1{}_2dtc)_2]_0$=1.0 mM and $[PPh_3]_0$=50.0 mM (1 M=1 mol dm^{-3}). However, in the $[MoO_2(Bz_2dtc)_2]/PPh_3$ system, the initial concentrations of $[MoO_2(Bz_2dtc)_2]$ and PPh_3 were varied to confirm the validity of the kinetic analysis. The agreements among the parameters obtained are satisfactory. Furthermore, the parameters k_1, K_d, ε_4, and ε_5 determined for the system $[MoO_2(Et_2dtc)_2]/PPh_3$ in this study are in fair agreement with the values reported by Holm et al.[8]

The rate constant for oxygen atom transfer reaction 1 is influenced by the nature of the substituents on the dithiocarbamate ligands. As shown in Fig. 2, the log k_1 values correlate linearly with the formal potentials for the one-electron reduction of $[MoO_2(R^1{}_2dtc)_2]$,[15] except for R^1=Bz and Ph. This suggests that one-electron transfer from PPh_3 to $[MoO_2(R^1{}_2dtc)_2]$ plays an important role in the rate determining step of the oxygen atom transfer reactions. The values of log k_1 for the systems $[MoO_2(Bz_2dtc)_2]/PPh_3$ and $[MoO_2(Ph_2dtc)_2]/PPh_3$ deviate from the correlation line between log k_1 and the formal potentials. This may be due to the electron-withdrawing effect of the benzyl and phenyl groups; in these cases, the contribution of resonance form I becomes more important than that of form II.

Table 1. Kinetic Data for the Oxygen Atom Transfer Reaction between $[MoO_2(R^1{}_2dtc)_2]$ and PPh_3 in 1,2-$C_2H_4Cl_2$ at 25 °C[a)]

R^1	$k_1/M^{-1}\,s^{-1}$	K_d/M^{-1}	$\varepsilon_4/M^{-1}\,cm^{-1}$	$\varepsilon_5/M^{-1}\,cm^{-1}$	$\varepsilon_6/M^{-1}\,cm^{-1}$[b)]
i-Pr[c)]	0.0120(1)	$5(3)\times10^1$	$4.60(2)\times10^2$	$1.7(8)\times10^4$	30
i-Bu	0.0241(5)	$5.0(8)\times10^2$	$5.2(5)\times10^2$	$2.4(3)\times10^4$	17
Et	0.085(3)	$7.9(4)\times10^2$	$4.8(2)\times10^2$	$2.44(6)\times10^4$	17
Et[d)]	0.071(3)	$5.9(10)\times10^2$	4.3×10^2[b)]	$2.80(25)\times10^4$	18
Me	0.203(7)	$1.18(6)\times10^3$	$4.7(2)\times10^2$	$2.12(9)\times10^4$	12
Bz	0.15(1)	$1.47(6)\times10^4$	$7.1(3)\times10^2$	$2.5(2)\times10^4$	13
Bz[e)]	0.155(9)	$1.27(3)\times10^4$	$7.7(5)\times10^2$	$2.43(7)\times10^4$	13
Bz[f)]	0.138(1)	$1.43(4)\times10^4$	$6.9(3)\times10^2$	$2.39(2)\times10^4$	13
Ph	0.113(9)	$4(2)\times10^5$	$4.7(2)\times10^2$	$2.2(2)\times10^4$	57

a) Each value is the average of four determinations, unless otherwise stated. Standard deviations are given in parentheses. Initial concentrations of $[MoO_2(R^1{}_2dtc)_2]$ and PPh_3 are 1.0 and 50.0 mM, respectively, unless otherwise stated. The symbols ε_4, ε_5, and ε_6 denote molar extinction coefficients at 512 nm of $[MoO(R^1{}_2dtc)_2]$, $[Mo_2O_3(R^1{}_2dtc)_4]$, and $[MoO_2(R^1{}_2dtc)_2]$, respectively. b) The extinction coefficient values were determined by independent spectroscopic measurements. c) Average of two determinations. d) From Ref. 8. e) $[MoO_2(Bz_2dtc)_2]$= 0.5 mM; $[PPh_3]$=50 mM. f) $[MoO_2(Bz_2dtc)_2]$=1.0 mM; $[PPh_3]$=100 mM.

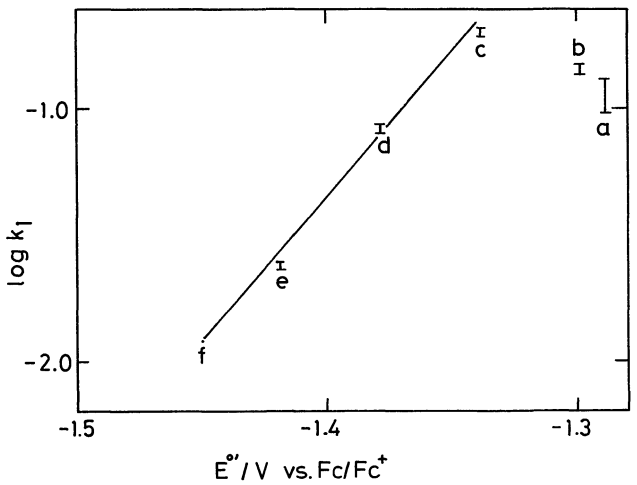

Fig. 2. Correlation between $\log k_1$ and the formal potentials for the one-electron reduction of $[MoO_2(R^1{}_2dtc)_2]$.[15] (a) R^1=Ph, (b) R^1=Bz, (c) R^1=Me, (d) R^1=Et, (e) R^1=*i*-Bu, (f) R^1=*i*-Pr.

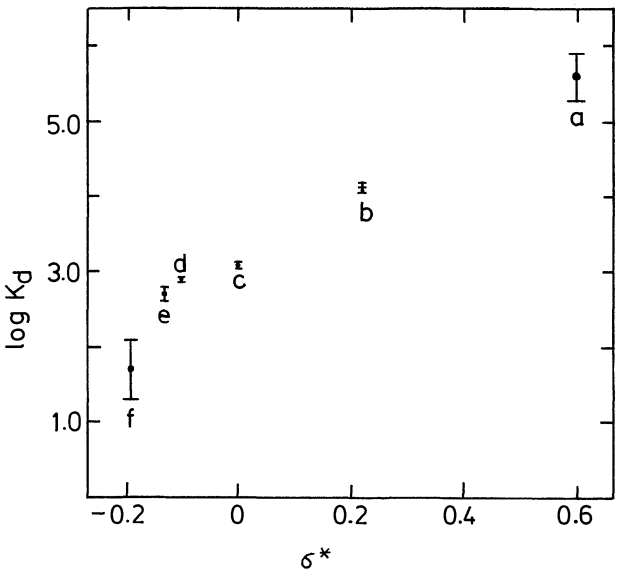

Fig. 3. Plots of $\log K_d$ vs. Taft's polar substituent constant of the substituents on dithiocarbamate ligands. (a) R^1=Ph, (b) R^1=Bz, (c) R^1=Me, (d) R^1=Et, (e) R^1=*i*-Bu, (f) R^1=*i*-Pr.

The equilibrium constant of reaction 2, K_d, also varies with the nature of the substituents on the dithiocarbamate ligands. The $\log K_d$ value correlates well with Taft's polar substituent constant (σ^*)[16] as shown in Fig. 3: The $\log K_d$ value decreases with increase of the electron-donating ability of substituents.

The $[Mo_2O_3]^{4+}$ moiety in $[Mo_2O_3(n\text{-}Pr_2dtc)_4]$ has a nearly linear Mo–O–Mo linkage and the two terminal-oxygen atoms are in the cis-positions.[17] The electronic structure of the $[Mo_2O_3]^{4+}$ moiety was described by Cotton et at.[18] Two electrons from oxygen and one electron from each molybdenum atom fill bonding and nonbonding orbitals derived by the interaction between the d_{xz} orbitals of each Mo atom and the p_x orbital of bridging oxygen to form a three-center π-bond over the Mo–O–Mo linkage. The energy level of the bonding orbital of the three-center π-bond rises with the increase of electron-donating ability of the substituents on the dithiocarbamate ligands. Censequently, $[Mo_2O_3(R^1{}_2dtc)_4]$ becomes less stable with increasing electron-donating ability of the substituents.

References

1) Abbreviations, R_2dtc^-=dithiocarbamate, Et=C_2H_5, Me=CH_3, Bz=$C_6H_5CH_2$, Ph=C_6H_5, *i*-Bu=*i*-C_4H_9, *n*-Bu=*n*-C_4H_9, *i*-Pr=*i*-C_3H_7, *n*-Pr=*n*-C_3H_7.

2) R. Barral and C. Bocard, *Tetrahedron Lett.*, **17**, 1693 (1972).

3) R. Colton and G. R. Scollary, *Aust. J. Chem.*, **21**, 1427 (1968).

4) R. N. Jowitt and P. C. H. Mitchell, *J. Chem. Soc. A,* **1970**, 1702.
5) R. H. Holm, *Coord. Chem. Rev.,* **100**, 183 (1990).
6) D. B. McDonald and J. I. Schulman, *Anal. Chem.,* **47**, 2023 (1975).
7) R. Durant, C. D. Garner, M. R. Hyde, and F. E. Mabbs, *J. Chem. Soc., Dalton Trans.,* **1977**, 955.
8) M. S. Reynolds, J. M. Berg, and R. H. Holm, *Inorg. Chem.,* **23**, 3057 (1984).
9) D. Coucouvanis, "Progress in Inorganic Chemistry," ed by S. J. Lippard, Wiley-Interscience, New York (1979), Vol. 26, p. 301.
10) H. L. Klopping and G. L. M. Van Der Kerk, *Recl. Trav. Chim. Pays-Bas,* **70**, 917 (1951).
11) E. J. Kupchik and P. J. Calabretta, *Inorg. Chem.,* **4**, 973 (1965).
12) F. W. Moore and M. L. Larson, *Inorg. Chem.,* **6**, 998 (1967).
13) K. G. Moloy, *Inorg. Chem.,* **27**, 677 (1988).
14) T. Nakagawa and Y. Oyanagi, "Recent Developments in Statistical Inference and Data Analysis," ed by K. Matsushita, North-Holland Publishing Co., Amsterdam (1980), p. 221.
15) K. Unoura, A. Iwase, and H. Ogino, *J. Electroanal. Chem.,* **295**, 385 (1990).
16) R. W. Taft, Jr., *J. Am. Chem. Soc.,* **75**, 4231 (1953).
17) L. Ricard, J. Estienne, P. Karagiannidis, P. Toledano, J. Fischer, A. Mitschler, and R. Weiss, *J. Coord. Chem.,* **3**, 277 (1974).
18) A. B. Blake, F. A. Cotton, and J. S. Wood, *J. Am. Chem. Soc.,* **86**, 3024 (1964).

Four- and Five-Coordinated Nickel(II) Isocyanide Complexes and Donor-Acceptor Complexes Containing Nickel and Mercury††

Yasuhiro YAMAMOTO,* Kazuko EHARA, Katsuo TAKAHASHI,† and Hiroshi YAMAZAKI†
Toho University, Faculty of Science, Miyama, Funabashi-shi, Chiba 274
†RIKEN, The Institute of Physical and Chemical Research, Wako-shi, Sitama 351-01
(Received June 18, 1991)

Reaction of $NiI_2(RNC)_2$ (**1**) (**a**: R=2,6-$Me_2C_6H_3$; **b**; 4-Br-2,6-$Me_2C_6H_2$; c: 2,4-*t*-Bu_2-6-MeC_6H_2: d: 2,4,6-*t*-$Bu_3C_6H_2$ with RNC or PPh_3 gave $NiI_2(RNC)_3$ (2) or $NiI_2(PPh_3)(RNC)_2$ (**3**) (a: R=2,6-$Me_2C_6H_3$; b: 2,6-Me_2-4-BrC_6H_2). An X-ray analysis of (**3a**) showed that the complex has a trigonal bipyramidal structure; crystal data: Space group $Pna2_1$; a=21.577(2), b=9.440(1), c=17.075(1) Å, $\alpha=\beta=\gamma=90.0°$, V=3477.7(6) Å^3, R=0.0444. The bromide and chloride complexes, $NiX_2(2,6\text{-}Me_2C_6H_3NC)_2$ (**1e**: X=Cl; **1f**: X=Br) did not produce five-coordinated species. When complexes (**1a**, **1b**, **1e**, or **1f**) were treated with Hg in the presence of isocyanide, the donor-acceptor complexes $[Ni(RNC)_4HgX_2]_2$ (X=I, Br, or Cl) (**4**) were formed. An X-ray analysis of (**4b**) (R=4-Br-2,6-$Me_2C_6H_2$) was undertaken; crystal data: Space group: $P\bar{1}$ (triclinic); a=12.709(3), b=16.145(3), c=12.614(3) Å, α=96.11(2), β=107.67(2), γ=73.11(2)°, V=2359.5(10) Å^3, R=0.0686. The complex is a donor-acceptor complex containing the Ni–Hg bond and has a dimeric structure bridged by two I atoms. The configuration around Ni is the trigonal bipyramid and around Hg, distorted tetrahedron.

The low-valent metal complexes often show an instability that is related to the electron-releasing capability of ligands. This instability can be improved by the release of the excess electron density from the metal center. One possibe way to reduce the electron density on the metal atom without changing its oxidation state is formation of a donor–acceptor complex. A general preparation of donor–acceptor complexes is arising from interaction of zerovalent complexes with Group 2 metal dihalides.[1] Dixneuf et al have reported that carbene–iron derivatives which were easily oxidized were stabilized by formation of carbene–Fe(O) Hg(II) donor–acceptor complexes on treatment with HgX_2.[2]

When $NiX_2(RNC)_2$ were treated with mercury metal in the presence of isocyanide, an initial electron transfer from Hg^0 to Ni^{2+} occurred, and finally the Ni–Hg donor–acceptor complex was formed. Here we reported preparation and characterization of donor–acceptor complexes and related ones.

Experimental

Isocyanides[3] and $NiI_2(RNC)_2$[4] were prepared by literature methods, some with modification. Electronic and infrared spectra were recorded on Hitachi 330 and JASCO 442 spectrometers, respectively. ^{1}H NMR spectra were recorded on a JEOL FX100 instrument. Electric conductivities were measured by the Ando Electronic Co. LCR-10 impedance bridge.

Preparation of *trans*-NiI_2(2,4,6-*t*-$Bu_3C_6H_2NC)_2$ (1d). A mixture of NiI_2 (0.57 g, 1 mmol) and 2,4,6-*t*-$Bu_3C_6H_2NC$ (0.12 g, 0.44 mmol) in CH_2Cl_2 (5 ml) was stirred at room temperature. After 1 h, the mixture was filtered and the solvent was removed in vacuo. The residue was crystallized from CH_2Cl_2–hexane to give the title complex (0.16 g, 86%). Found: C, 53.45; H, 6.82; N, 3.25%. Calcd for $C_{38}H_{58}N_2I_2Ni$: C, 53.36; H, 6.83; N, 3.27%. IR (KBr): 2174 cm^{-1}. ^{1}H NMR ($CDCl_3$) δ=1.31 (s, *p*-*t*-Bu), 1.58 (s, *o*-*t*-Bu), and 7.33 (s, aromatic protons).

Other nickel(II) complexes were prepared by a similar procedure mentioned above.

trans-$NiI_2(2,6\text{-}Me_2C_6H_3NC)_2$ (**1a**) (88%): Found: C, 37.59; H, 3.25; N, 4.89%. Calcd for $C_{18}H_{18}N_2I_2Ni$: C, 37.61; H, 3.16; N, 4.87%. IR (KBr) 2163 cm^{-1}. ^{1}H NMR ($CDCl_3$) δ=2.52 (s, Me), and ca. 7.2 (m, aromatic protons). ^{1}H NMR (a mixture of **1a** and RNC)($CDCl_3$) δ=2.45 (s, *o*-Me), and ca. 7.2 (aromatic protons). Electronic spectrum (CH_2Cl_2) λ_{max} 387 (5500 dm^3 mol^{-1} cm^{-1}), 342 (3700), 296 (36700), and 237 (23500) nm.

trans-NiI_2(2,4-*t*-Bu_2-6-$MeC_6H_2NC)_2$ (**1c**) (73%): Found: C, 49.84; H, 6.01; N, 3.63%. Calcd for $C_{32}H_{46}N_2I_2Ni$: C, 50.07; H, 6.12; N, 3.67%. IR (nujol) 2168 cm^{-1}. ^{1}H NMR ($CDCl_3$) δ=1.30 (s, *p*-*t*-Bu), 1.50 (s, *m*-*t*-Bu); 2.49 (s, *m*-Me), and ca. 7.2 (aromatic protons). ^{1}H NMR ($CDCl_3$) (a mixture of **1c** and RNC) δ=1.30 (s, *p*-*t*-Bu), 1.50 (s, *m*-*t*-Bu), 2.45 (s, *m*-Me), and ca. 7 (aromatic protons). Electronic spectrum (CH_2Cl_2) λ_{max} 453 (1700), 388 (10900), 340 sh (8000), 290 (65700), 262 (40000), and 247.5 (49200) nm.

trans-NiI_2(4-Br-2,6-$Me_2C_6H_2NC)_2$ (**1b**) (90%): Found: C, 29.66; H, 2.17; N, 3.73%. Calcd for $C_{18}H_{16}N_2Br_2I_2Ni$: C, 29.51; H, 2.20; N. 3.82%. IR (nujol) 2171 cm^{-1}. Electronic spectrum (CH_2Cl_2) λ_{max} 450 (900), 389 (5900), 346 (4700), 304 (43700), 296 (42800), and 248 (24400) nm.

Preparation of *cis*-$NiCl_2(2,6\text{-}Me_2C_6H_3NC)_2$ (1e). To a solution of $NiCl_2(PPh_3)_2$ (0.16 g, 0.25 mmol) in CH_2Cl_2 (10 ml) was added 2,6-xylyl isocyanide (0.075 g, 0.57 mmol) at room temperature. After 1 h, the solution was filtered and the solvent was removed in vacuo. Crystallization of the residue from CH_2Cl_2 and hexane gave orange yellow crystals (0.064 g, 65%). Found: C, 55.05; H, 4.59; N, 7.11%. Calcd for $C_{18}H_{18}N_2Cl_2Ni$: C, 55.16; H, 4.63; N, 7.15%. IR (nujol) 2208, and 2195 cm^{-1}. ^{1}H NMR ($CDCl_3$) δ=2.42 (s, *o*-Me), and ca. 7.0 (aromatic protons). ^{1}H NMR ($CDCl_3$) (a mixture of **3a** and RNC) δ=2.41 (s, *o*-Me), and ca. 7 (aromatic protons).

trans-$NiBr_2$ (2,6-$Me_2C_6H_3NC)_2$ (**1f**), was prepared from a metathesis of (**1e**) with KBr. Found: C, 44.88; H, 3.89; N, 5.77%. Calcd for $C_{18}H_{18}N_2Br_2Ni$: C, 44.96; H, 3.77; N, 5.83%.

†† Studies on the Interaction of Transition-Metal Complexes 34. For Part 33, see Y. Yamamoto and H. Yamazaki, *J. Chem. Soc., Dalton Trans.*, **1989**, 2161.

^{1}H NMR ($CDCl_3$) δ=2.45 (s, *o*-Me), ca. 7 (aromatic protons). ^{1}H NMR ($CDCl_3$) (**2a** and RNC) δ=2.40 (s, *o*-Me), ca. 7 (aromatic protons). IR (nujol) 2194 cm^{-1}.

Preparation of $NiI_2(2,6\text{-}Me_2C_6H_3NC)_3$ (2a). 2,6-Xylyl isocyanide (0.07 g, 0.53 mmol) was added to a brown solution of *trans*-$NiI_2(2,6\text{-}Me_2C_6H_3NC)_2$ (0.20 g, 0.35 mmol) in CH_2Cl_2 (5 ml) at room temperature. The solution color turned blue. Addition of hexane to the solution gave blue crystals (0.21 g, 85.0%) of the title complex. Found: C, 45.63; H, 3.76; N, 5.94%. Calcd for $C_{27}H_{27}N_3I_2Ni$: C, 45.93; H, 3.85; N, 5.95%. IR (nujol) 2162 cm^{-1}. ^{1}H NMR ($CDCl_3$) δ=2.50 (s, Me), and ca. 7.13 (c, aromatic protons). Electronic spectrum (CH_2Cl_2) λ_{max} 450 sh (680), 386 (5900), 343 (4200), and 295 (37700) nm.

$NiI_2(4\text{-Br-}2,6\text{-}Me_2C_6H_2NC)_3$ (**2b**) (75%). Found: C, 34.77; H, 2.43; N, 4.61%. Calcd for $C_{27}H_{24}N_3Br_3I_2Ni$: C, 34.40; H, 2.57; N, 4.46%. IR (nujol) 2160 cm^{-1}.

Preparation of $NiI_2(PPh_3)(2,6\text{-}Me_2C_6H_3NC)_2\cdot 1/3CH_2Cl_2$ (3a). To an orange solution of *cis*-$NiCl_2(PPh_3)_2$ (0.3 g, 0.46 mmol) and 2,6-xylyl isocyanide (0.13 g, 1.0 mmol) in CH_2Cl_2 (10 ml) was added an excess of KI in H_2O (5 ml) at room temperature and the mixture was stirred for 1 h. Organic layer was dried over Na_2SO_4. Removal of the solvent and crystallization of the residue from CH_2Cl_2 and hexane gave blue crystals (0.26 g, 67.5%). Found: C, 50.25; H, 3.95; N, 3.21%. Calcd for $C_{36+(1/3)}H_{33+(2/3)}N_2PCl_{(2/3)}I_2Ni$: C, 50.42; H, 3.92; N, 3.24%. IR (nujol) 2160 and 2187 cm^{-1}. ^{1}H NMR ($CDCl_3$) δ=2.20 (s, Me), 5.29 (s, CH_2), and ca. 7.6 (c, aromatic protons). Electronic spectrum (CH_2Cl_2) λ_{max} 570 (1700), 384 (5100), ca. 340 (7500), and 291 (38000) nm.

4-Bromo-2,6-dimethylphenyl isocyanide complex was also prepared by a similar procedure.

$NiI_2(PPh_3)$ (4-Br-2,6-$Me_2C_6H_2NC)_2$ (**3b**) (75%): Found: C, 43.44; H, 3.31; N, 2.84%. Calcd for $C_{36}H_{31}N_2Br_2I_2PNi$: C, 43.46; H, 3.14; N, 2.82%. IR (nujol) 2160 cm^{-1}.

Preparation of $[Ni(2,6\text{-}Me_2C_6H_3NC)_4][PF_6]\cdot CH_2Cl_2$. When $[NH_4][PF_6]$ was added to a brown solution of $NiBr_2$ (0.32 g, 1.47 mmol) and 2,6-xylyl isocyanide (0.393 g, 3.0 mmol) in THF (15 ml), the solution turned wine red. After the mixture was heated at 60 °C for 2 h, the solvent was removed in vacuo and the residue was extracted with CH_2Cl_2. The solvent was removed to ca. 5 ml and hexane was added, giving brown crystals (0.38 g, 53%) containing one molecule of CH_2Cl_2 as a solvated molecule. Found: C, 46.87; H, 4.02; N, 5.93%. Calcd for $C_{37}H_{38}N_4P_2F_{12}Cl_2Ni$: C, 46.38; H, 4.00; N, 5.85%. IR (nujol) 2176 and 2192 cm^{-1}. ^{1}H NMR ($CDCl_3$) δ=2.53 (s, Me), 5.30 (s, CH_2), and ca. 7.1 (aromatic protons).

Preparation of $[Ni(2,6\text{-}Me_2C_6H_3NC)_4HgI_2]_2$ (4a). (a) Reaction of *trans*-$NiI_2(2,6\text{-}Me_2C_6H_3NC)_2$ with mercury in the presence of 2,6-xylyl isocyanide. A mixture of *trans*-$NiI_2(2,6\text{-}Me_2C_6H_3NC)_2$ (0.11 g, 0.19 mmol), 2,6-xylyl isocyanide (0.03 g, 0.23 mmol) and Hg (ca. 2 ml) in CH_3CN (10 ml) was stirred for 2.5 h at room temperature, forming the dark yellow precipitate. The organic layer was dried and the residue was extracted with benzene. The solvent was dried to ca. 3 ml and hexane was added, giving brown crystals (0.14 g, 71%) of the title complex. Found: C, 41.58; H, 3.44; N, 5.27%. Calcd for $C_{72}H_{72}N_8I_4Hg_2Ni_2$: C, 41.66; H, 3.50; N, 5.40%. IR (nujol) 2139 and 2081 cm^{-1}. ^{1}H NMR ($CDCl_3$) δ=2.50 (s, Me), ca. 7 (aromatic protons). Electronic spectrum (CH_2Cl_2) λ_{max} ca. 360 sh (10400), 305 (20700), 237 sh (27700), and 231 (29400) nm.

(b) Reaction of $Ni(2,6\text{-}Me_2C_6H_3NC)_4$ with HgI_2. 2,6-Xylyl isocyanide. To a suspension of $Ni(2,6\text{-}Me_2C_6H_3NC)_4$ (0.26 g, 0.45 mmol) in CH_3CN (15 ml) was added HgI_2 (0.2 g, 0.44 mmol). After stirring for 5 h at room temperature, the mixture was filtered and the solvent was removed in vacuo. Recrystallization of the residue from CH_2Cl_2–hexane gave brown crystals.

The following complexes were prepared by the procedure (a).

4-Bromo-2,6-dimethyl isocyanide complex, $[Ni(4\text{-Br-}2,6\text{-}Me_2C_6H_3NC)_4HgI_2]_2$ $(C_6H_6)_2$ (**4b**) (87%), was also prepared from the reaction of *trans*-$NiI_2(4\text{-Br-}2,6\text{-}Me_2C_6H_3NC)_2$ with mercury in the presence of 4-bromo-2,6-dimethylphenyl isocyanide. Found: C, 35.15; H, 2.69; N, 3.91%. Calcd for $C_{84}H_{76}N_8Br_8I_4Hg_2Ni_2$: C, 35.24; H, 2.68; N, 3.91% . IR (nujol) 2141 and 2082 cm^{-1}. ^{1}H NMR ($CDCl_3$) δ=1.55 (s, 6H, Me), 2.44 (s, 18H, Me), and 7.37 (benzene and aromatic protons). Electronic spectrum (CH_2Cl_2) λ_{max} ca. 360 sh (11300) and 313 (20300) nm.

$[Ni(2,6\text{-}Me_2C_6H_3NC)_4HgCl_2]_2$ (**4e**) (65%). Found: C, 50.05; H, 4.21; N, 6.47%. Calcd for $C_{36}H_{36}N_4Cl_2HgNi$: C, 50.58; H, 4.24; N, 6.55%. IR (nujol) 2165 and 2104 cm^{-1}. ^{1}H NMR ($CDCl_3$) δ=2.49 (s, Me), and ca. 7.0 (aromatic protons). Electronic spectrum (CH_2Cl_2): λ_{max} 330 sh (9500) and 280 (15000) nm.

$[Ni(2,6\text{-}Me_2C_6H_3NC)_4HgBr_2]_2$ (**4f**) (68%). Found: C, 45.83; H, 3.85; N, 5.76%. Calcd for $C_{36}H_{36}N_4Br_2HgNi$: C, 45.80; H, 3.84; N, 5.94%. IR (nujol) 2165 and 2101 cm^{-1}. ^{1}H NMR ($CDCl_3$) δ=2.58 (s, Me), ca. 7.0 (aromatic protons). Electronic spectrum (CH_2Cl_2) λ_{max} 312 sh (19000).

Preparation of $[Ni(PPh_3)(4\text{-Br-}2,6\text{-}Me_2C_6H_2NC)_3HgI_2]_2$ (5b). Mercury was added to a blue solution of $NiI_2(PPh_3)$ (4-Br-2,6-$Me_2C_6H_3NC)_2$ (0.14 g, 0.14 mmol) and 4-bromo-2,6-dimethylphenyl isocyanide (0.03 g, 0.14 mmol) in benzene (10 ml) and the mixture was stirred for 0.5 h at room temperature, changing an orange solution. The mixture was filtered and the solvent was removed to ca. 3 ml. Hexane was added, giving orange crystals (0.134 g, 68%) of the title complex. Found: C, 38.51; H, 2.77; N, 3.01%. Calcd for $C_{90}H_{78}N_6Br_6I_4P_2Hg_2Ni_2$: C, 38.45; H, 2.80; N, 2.99%. IR (nujol) 2075 and 2085 cm^{-1}. ^{1}H NMR ($CDCl_3$) δ=2.14 (s, Me), and ca. 7.3 (aromatic protons). Electronic spectrum (CH_2Cl_2) λ_{max} 396 (15500), 323 (27400), and 260 sh (37800) nm.

$[Ni(PPh_3)(2,6\text{-}Me_2C_6H_3NC)_3HgI_2]_2(CH_2Cl_2)_3$ (**5a**) was recrystallized from CH_2Cl_2 and hexane. Found: C, 43.33; H, 3.44; N, 3.14%. Calcd for $C_{93}H_{90}N_6Cl_6P_2I_4Hg_2Ni_2$: C, 43.08; H, 3.50; N, 3.24%. IR (nujol) 2082 cm^{-1}. ^{1}H NMR ($CDCl_3$) δ=2.23 (s, Me), 5.29 (s, CH_2), and ca. 7.3 (aromatic protons). Electronic spectrum (CH_2Cl_2) λ_{max} 394 (10000), 314 (18600), and 260 (46800) nm.

Data Collection and Solution of the Structure. Complex (**3a**) was recrystallized from CH_2Cl_2–benzene, and **4b**, from benzene–hexane, respectively. Weissenberg photographs indicated that the crystals of **3a** were orthorhombic with space group $Pna2_1$ and those of **4b**, triclinic with the space group $P\bar{1}$. Cell constatns of **3a** were determined from 18 reflections ($11°<2\theta<22°$), and those of **4b** from 20 reflections ($12°<2\theta<25°$) on a Rigaku automated diffractometer. Details of the crystal parameters along with data collection are summarized in Table 1. Intensities were corrected for Lorentz and polarization effects. No absorption corrections were made; the absorption coefficient of **4b** is large, but the crystal used for data collection was not well-shaped one to make correction. The positions of the heacy atoms were determined by a Patterson map using the UNICS III program system.[5]

The remaining atoms were located in succeeding different Fourier syntheses. The positions of all atoms for **3a**, and of Hg, Ni, and Br atoms for **4b** were refined anisotropically by using block-diagonal least-squares methods. Final difference Fourier maps of **3a** and **4b** showed smaller residual peaks than 0.6 e A^{-3}. No attempts were made to locate the hydrogen atoms. The positional parameters are given in Tables 2 and 3. Anomalous dispersion effects and atomic scattering factors

Table 1. Crystal Data and Experimental Details

Compd	**3a**	**4b**[a]
Formula	$C_{36}H_{33}N_2PI_2Ni$	$C_{84}H_{76}N_8Br_8I_4Hg_2Ni_2$
F. W.	837.2	2363.1
Crystal system	Orthorhombic	Triclinic
Space group	$Pna2_1$	$P\bar{1}$
a/Å	21.577(2)	12.709(3)
b/Å	9.440(1)	16.145(3)
c/Å	17.075(1)	12.614(3)
α/deg	90.0	96.11(2)
β/deg	90.0	107.67(2)
γ/deg	90.0	73.11(2)
V/Å^3	3477.7(6)	2359.5(10)
Z	4	2
Crystal size/mm	0.2×0.17×0.30	—[b]
D_x/g cm^{-1}	1.60	2.01
μ (Mo $K\alpha$)/cm^{-1}	23.9	83.3
Radiatn	Mo$K\alpha$ (λ=0.71073 Å from graphite monochromator)	
Scan speed/deg	4 in 2θ min^{-1}	4 in 2θ min^{-1}
2θ limits/deg	3.0—45.0	3.0—50.0
Scan mode	ω scan for $2\theta \leqq 30$	ω–2θ scan for $2\theta > 30$
Unique data measd	2739	4789
Unique data used ($F_o > 3\sigma(F_o)$)	2639	4555
No. of variables	380	258
F(000)	1648	1344
R[c]	0.0444	0.0686
R_w[d]	0.0457	0.0728

a) Measurement was carried out in a capilary. Benzene is contained as a solvated molecule. b) The well-shaped crystal to measure the crystal size was not obtained. c) $R=\Sigma\|\|F_o|-|F_c\|/\Sigma|F_o|$. d) $R_w=[\Sigma w(|F_o|-|F_c|)^2/\Sigma wF_o^2]^{1/2}$.

Table 2. Atomic Parameters of $[NiI_2(PPh_3)(2,6\text{-}Me_2C_6H_3NC)_2]$ (**3a**)[a]

Atom	x	y	z	B_{eq}	Atom	x	y	z	B_{eq}
Ni	3474(1)	302(2)	627(1)	3.1(0.0)	C(26)	344(1)	−328(2)	−166(1)	5.0(0.4)
I(1)	2783(0)	2321(1)	0(0)	4.6(0.0)	C(27)	339(1)	66(2)	−223(1)	5.6(0.5)
I(2)	2773(0)	−1735(1)	1213(1)	4.9(0.0)	C(28)	351(1)	−412(2)	−92(1)	7.2(0.7)
P	4507(1)	404(4)	807(2)	3.1(0.1)	C(31)	489(1)	150(1)	8(1)	3.4(0.3)
N(10)	330(1)	170(1)	218(1)	4.0(0.3)	C(32)	556(1)	178(2)	13(1)	5.4(0.5)
C(10)	335(1)	117(1)	159(1)	3.2(0.3)	C(33)	582(1)	266(2)	−43(1)	5.7(0.5)
C(11)	325(1)	243(2)	290(1)	3.9(0.4)	C(34)	547(1)	322(2)	−106(1)	6.1(0.5)
C(12)	318(1)	159(2)	355(1)	4.7(0.4)	C(35)	485(1)	294(2)	−111(1)	5.2(0.5)
C(13)	312(1)	229(2)	427(1)	5.9(0.5)	C(36)	456(1)	209(2)	−54(1)	4.1(0.4)
C(14)	310(1)	380(2)	429(1)	6.0(0.5)	C(41)	474(1)	114(2)	174(1)	3.7(0.4)
C(15)	317(1)	462(2)	361(1)	5.1(0.5)	C(42)	484(1)	261(2)	183(1)	4.6(0.4)
C(16)	324(1)	394(2)	288(1)	3.5(0.3)	C(43)	495(1)	319(2)	258(1)	6.0(0.5)
C(17)	315(1)	−0.5(0.2)	352(1)	6.0(0.5)	C(44)	494(1)	230(2)	323(1)	6.1(0.6)
C(18)	333(1)	472(2)	213(1)	5.7(0.5)	C(45)	486(1)	88(2)	314(1)	6.2(0.6)
N(20)	350(0)	−112(1)	−91(1)	3.4(0.3)	C(46)	474(1)	25(2)	241(1)	5.0(0.4)
C(20)	351(1)	−58(2)	−31(1)	3.5(0.3)	C(51)	489(1)	−132(1)	78(1)	4.1(0.4)
C(21)	344(1)	−180(2)	−166(1)	4.7(0.4)	C(52)	552(1)	−147(2)	97(1)	5.9(0.5)
C(22)	338(1)	−86(2)	−231(1)	4.8(0.4)	C(53)	580(1)	−278(2)	95(1)	7.2(0.6)
C(23)	328(1)	−160(2)	−305(1)	6.9(0.6)	C(54)	548(1)	−396(2)	80(1)	7.0(0.6)
C(24)	329(1)	−310(2)	−305(1)	6.6(0.6)	C(55)	486(1)	−391(2)	62(1)	6.8(0.6)
C(25)	335(1)	−397(2)	−241(1)	6.2(0.6)	C(56)	455(1)	−254(2)	64(1)	5.7(0.5)

a) Positional parameters are multiplied by 10^3 except atoms from Ni to P. The equivalent temperature factors, $B_{eq}=(4/3)\Sigma\Sigma\beta_{ij}(a_ia_j)$ are multiplied by 10^2.

Table 3. Atomic Parameters of $[Ni(4\text{-}Br\text{-}2,6\text{-}Me_2C_6H_2NC)_4HgI]_2$ (**4b**)[a]

Atom	x	y	z	B_{eq}	Atom	x	y	z	B_{eq}
Hg	−427(1)	1175(1)	4306(1)	4.9(0.0)	C28	405(2)	122(2)	566(2)	7.2(0.6)
Ni	53(2)	2492(1)	5565(2)	3.8(0.1)	C30	52(2)	171(1)	674(2)	4.8(0.4)
I1	−1306(1)	1449(1)	2069(1)	5.7(0.1)	N30	88(1)	138(1)	758(1)	5.1(0.4)
I2	1642(1)	−314(1)	4758(1)	5.1(0.0)	C31	139(2)	101(1)	864(2)	5.2(0.4)
Br10	−7578(2)	4599(2)	4152(4)	13.2(0.2)	C32	65(2)	98(1)	928(2)	4.6(0.4)
Br20	5845(3)	1651(2)	2526(3)	9.5(0.1)	C33	113(2)	64(1)	1033(2)	5.4(0.5)
Br30	3000(3)	−99(2)	12160(2)	9.3(0.1)	C34	232(2)	35(1)	1033(2)	5.4(0.5)
Br40	2184(8)	6163(3)	11011(5)	28.5(0.5)	C35	305(2)	37(1)	1008(2)	6.0(0.5)
C10	−151(2)	286(1)	501(2)	5.0(0.4)	C36	256(2)	70(1)	902(2)	5.3(0.5)
N10	−253(1)	315(1)	478(1)	5.4(0.4)	C37	−65(2)	131(2)	879(2)	7.1(0.6)
C11	−374(2)	350(1)	462(2)	5.4(0.5)	C38	328(3)	72(2)	824(3)	9.1(0.8)
C12	−434(2)	395(2)	369(2)	6.4(0.5)	C40	35(2)	345(1)	642(2)	4.3(0.4)
C13	−558(2)	431(2)	353(2)	7.1(0.6)	N40	59(1)	400(1)	703(1)	5.0(0.3)
C14	−590(2)	412(2)	439(2)	7.9(0.7)	C41	93(2)	453(1)	792(2)	5.5(0.5)
C15	−536(2)	364(2)	531(2)	8.2(0.7)	C42	104(2)	535(1)	776(2)	5.4(0.5)
C16	−410(2)	330(2)	546(2)	6.9(0.6)	C43	144(2)	585(2)	866(2)	8.3(0.7)
C17	−385(3)	415(2)	285(3)	9.5(0.8)	C44	164(3)	557(2)	965(3)	11.5(1.0)
C18	−341(2)	274(2)	643(2)	8.5(0.7)	C45	148(4)	477(3)	994(4)	14.8(1.3)
C20	110(2)	227(1)	477(2)	4.1(0.4)	C46	123(3)	421(2)	898(3)	11.2(1.0)
N20	183(1)	213(1)	433(1)	4.8(0.3)	C47	77(2)	563(1)	661(2)	6.1(0.5)
C21	278(2)	199(1)	385(2)	4.3(0.4)	C48	102(4)	329(3)	914(4)	15.7(1.5)
C22	253(2)	228(1)	283(2)	4.7(0.4)	C1	−597(4)	309(3)	−197(4)	14.7(1.3)
C23	348(2)	216(2)	239(2)	6.6(0.5)	C2	−503(4)	234(3)	−149(4)	14.3(1.3)
C24	456(2)	175(1)	310(2)	6.0(0.5)	C3	−429(4)	230(3)	−50(4)	15.6(1.5)
C25	478(2)	147(1)	409(2)	6.1(0.5)	C4	−432(7)	295(5)	5(7)	28.2(3.1)
C26	387(2)	154(1)	454(2)	5.5(0.5)	C5	−513(6)	382(5)	−36(6)	27.5(3.0)
C27	131(2)	270(2)	210(2)	7.3(0.6)	C6	−592(4)	381(3)	134(4)	14.5(1.3)

a) Positional parameters are multiplied by 10^4 (from Hg to Br40) and by 10^3 (from C10 to C6). The atoms from Hg to Br40 were anisotropically defined and other atoms were isotropically defined. The equivalent temperature factors, $B_{eq}=(4/3)\Sigma\Sigma\beta_{ij}(a_ia_j)$ are multiplied by 10^2.

were taken from the usual tabulation.[6]

Results and Discussion

Preparation of *trans*- and *cis*-$NiX_2(RNC)_2$ and Related Complexes. Organge or brown complexes, $NiI_2(RNC)_2$ (**1a**: R=2,6-$Me_2C_6H_3$; **1b**: R=4-Br-2,6-$Me_2C_6H_2$; **1c**: R=2,4-*t*-Bu_2-6-MeC_6H_2; **1d**: 2,4,6-*t*-$Bu_3C_6H_2$) were prepared from reactions of NiI_2 with isocyanides, according to literature methods.[4] The chloride complex, $NiCl_2(RNC)_2$ (R=2,6-$Me_2C_6H_3$) (**1e**) was preparated by a substitution reaction of dichlorobis(triphenylphosphine)nickel(II) with isocyanide. The bromide, $NiBr_2(RNC)_2$ (R=2,6-$Me_2C_6H_3$) (**1f**) was obtained by a metathesis of the chloride complex with KBr. The infrared spectra showed only one sharp band at ca. 2100 cm^{-1} (ν(N≡C)) for iodide and bromide complexes, and two peaks for the chloride one. The iodide and bromide complexes have a trans-configuration and the latter, a cis-one.

The reaction of **1a** or **1b** with an appropriate isocyanide or PPh_3 gave blue complexes formulated as $NiI_2(RNC)_3$ (**2a**: R=2,6-$Me_2C_6H_3$; **2b**; R=4-Br-2,6-$Me_2C_6H_2$) and $NiI_2(PPh_3)(RNC)_2$ (**3a**: R=2,6-$Me_2C_6H_3$, **3b**: R=4-Br-2,6-$Me_2C_6H_2$), respectivley. It was supported by an X-ray analysis of **3a** that complexes **2** and **3** have the trigonal bipyramidal structure (Fig. 1).

The basal plane has been occupied by two I's and a phosphine, and two isocyanide ligands have been in the apical positions. The ^1H NMR spectrum of **2a** showed only one singlet at δ=2.50 for *o*-methyl protons, suggesting an intramolecular exchange between apical and basal isocyanide ligands. In the ^1H NMR spectrum of a mixture of **2a** and 2,6-xylyl isocyanide only one singlet due to *o*-methyl groups appeared at δ=2.45, and the electric conductivity of the mixture showed to be a nonelectrolyte. This behavior is due to an inter- and intramolecular ligand exchange.

Brown solution of **1f** changed blue reminiscent of a five-coordinated species, when 2,6-xylyl isocyanide was added to **1f** in CH_2Cl_2. Some attempts to isolate a blue species were unsuccessful with recovery of **1f**. A similar reaction was carried out for the chloride complex **1e**. Color change has not been observed and the electronic spectrum of the mixture is similar to that of **1e**, showing that a five-coordinate species does not exist. Five-coordinated species with I are more stable than those with Br and Cl, probably due to higher coordination ability than the other halogens.

In the reaction of **1c** or **1d** containing bulky isocyanide, no assignment responsible for the formation of five-coordinated species was observed, and the starting complex was recovered, due to steric bulkiness.

Donor–Acceptor Complexes. When mercury was added to a solution of **1b** in CH_3CN, brown crystals

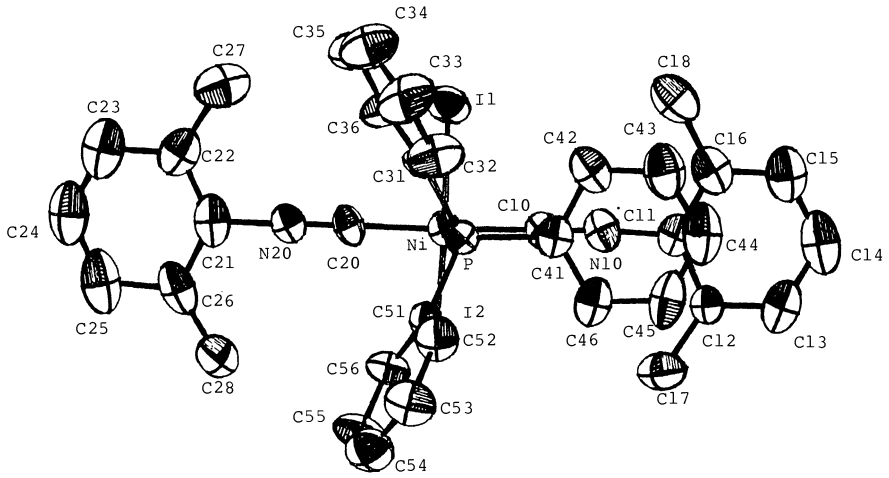

Fig. 1. Molecular structure of $[NiI_2(PPh_3)(2,6\text{-}Me_2c_6H_3NC)_2]$ (**3a**).

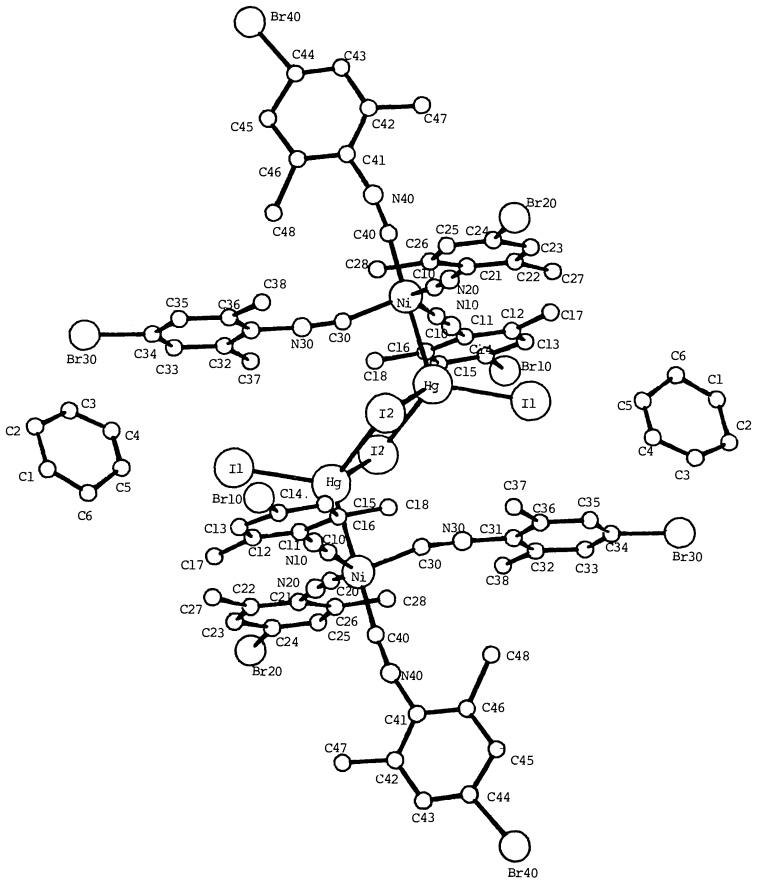

Fig. 2. Molecular structure of $[Ni(4\text{-Br-}2,6\text{-}Me_2C_6H_2NC)_4HgI_2]_2$ (**4b**).

formulated as $[Ni(4\text{-Br-}2,6\text{-}Me_2C_6H_2NC)_4HgI_2]_2$ (**4b**) were obtained. A similar reaction

$$2NiX_2(RNC)_2 + 4RNC + 2Hg \longrightarrow [Ni(RNC)_4HgX_2]_2 \quad (1)$$

occurred in the presence of 4-bromo-2,6-dimethylphenyl isocyanide to give **4b** quantitatively. The structure was determined by an X-ray analysis (Fig. 2).

The spectroscopic studies of **4b** were in good agreement with the crystal structure. The infrared sepctrum showed two ν (N≡C) peaks at 2050—2150 cm^{-1}, being in higher energy region than those of the parent zerovalent complexes and in lower energy than those of divalent complexes, suggesting partical charge transfer from nickel to mercury. Similar infrared behaviors have been noted in the molybdenum–mercury bonded

complexes.[7]

The ^{1}H NMR spectrum showed two characteristic peaks at δ=1.55 and 2.44 consisting of a 1:3 intensity ratio, assigned to the apical and basal isocyanide ligands, respectively. The ^{1}H NMR spectrum of a mixture of **4b** and 4-bromo-2,6-dimethylphenyl isocyanide showed two singlets at δ=1.56 and 2.44 for *o*-methyl protons. The former intensity increased with added isocyanide, showing that ligand exchange between the apical and free isocyanide ligands has occurred. The ligand in a trans-position to a Ni–Hg bond is more labile than the basal ones. It has been known that isocyanide ligands in a trans position to M–M bond were preferentially replaced by PPh_3 in the reactions of $[L_3M-ML_3]^{2+}$ (M=Pd, Pt; L=RNC) with triphenylphosphine.[8] Similar donor–acceptor complexes $[Ni(2,6\text{-}Me_2C_6H_3NC)_4HgX_2]_2$ (**4a**: X=I; **4e**: X=Cl; **4f**: X=Br) were prepared from **1a**, **1e**, or **1f** with mercury in the presence of 2,6-xylyl isocyanide. The ^{1}H NMR spectra of these complexes showed only one singlet at ca. δ=2.50 for *o*-methyl protons, suggesting an intermolecular ligand exchange. 2,6-Xylyl isocyanide ligand is more labile than 4-bromo-2,6-dimethylphenyl isocyanide, related with an electron-acceptor ability. These donor–acceptor complexes were also obtianed by the usual treatment of $Ni(RNC)_4$ with HgI_2.

$$2\,Ni(RNC)_4 + 2\,HgI_2 \longrightarrow [Ni(RNC)_4HgI_2]_2. \quad (2)$$

The phosphine complexes, $[Ni(PPh_3)(RNC)_3HgI_2]_2$ (**5a**: R=2.6-$Me_2C_6H_3$; **5b** R=4-Br-2,6-$Me_2C_6H_2$) were prepared by the reaction of $NiI_2(PPh_3)(RNC)_2$ with mercury in the presence of isocyanide. The infrared spectrum showed two N≡C stretching frequencies at 2070 and 2090 cm^{-1}, in lower energy region than those of the parent complex, due to greater σ-donor ability of triphenylphosphine than isocyanide. The ^{1}H NMR spectrum showed a singlet at δ=ca. 2.17 for *o*-methyl protons. We tentatively assumed that the apical isocyanide was replaced by triphenylphosphine, because of labile property of the apical ligand as shown in the ^{1}H NMR spectrum of **4b**.

Rossi and Hoffmann have concluded from a molecular orbital treatment of five-coordinated d^8 complexes that good σ-donor ligands will prefer axial site, while good π-acceptor will prefer the equatorial sites.[9] The configuration of these complexes is in agreement with the proposal.

Electronic Spectra. The electronic spectrum of a 1.25×10^{-4} M (M=mol dm^{-3}) solution of **3a** in CH_2Cl_2 showed two peaks at 569 and 367 nm, and two shoulder peaks at ca. 455 and 340 nm. With decrease of the solution concentration (2.51×10^{-5} M), the peak at 569 nm disappeared and the shoulder at ca. 340 nm decreased. Finally the spectrum consisted with that of **1a**, suggesting that triphenylphosphine in the basal plane is more labile than isocyanide ligands in the apical plane. Similar spectroscopic changes have been observed in **2a**. When RNC or PPh_3 (ca. 20 times per the complex) was added to a ca. 10^{-5} M solution of $NiI_2(RNC)_2$ or $NiI_2(RNC)_3$ in CH_2Cl_2, a new peak appeared at ca. 570 nm. The similar behavior was observed in a mixture of **1f** and 2,6-xylyl isocyanide (1: ca. 100 ratio), but the complex (**1e**) did not showed formation of a five-coordinated species even in the presence of a large excess of 2,6-xylyl isocyanide. These results showed the presence of the following equilibrium (trigonal bipyramidal⇌square planar), where L is RNC or PPh_3.

$$NiI_2(RNC)_2(L) \rightleftharpoons NiI_2(RNC)_2 + L. \quad (3)$$

The equilibrium of **2** or **3** lies far to the left in a high concentration or in the presence of an appropriate ligand. The electronic spectrum of **4** showed two peaks at ca. 250 and 310 nm, shifted to shorter wavelength than that of the parent zerovalent complex, probably accompanied with Ni→π*(CNR). The λ_{max} values of **4** red-shifted with Cl, Br, and I. Bathochromic shift was observed in the triphenylphosphine derivative **5**. These are related with the electron acceptor ability.

Structures of $NiI_2(PPh_3)(2,6\text{-}Me_2C_6H_3NC)_2$ (3a) and $[Ni(4\text{-}Br\text{-}2,6\text{-}Me_2C_6H_2NC)_4HgI_2]_2$ (4b). Sructure of 3a. The blue complex (**3a**) has a distorted trigonal bipyramidal structure, in which two isocyanide ligands occupied apical positions, and two I atoms and a phosphine, a basal plane. This structure is in disagreement with Rossi and Hoffmann's result.[9] The average bond angle of I–Ni–P is 124°, wider than a theoretical angle and the I–Ni–I angle is 110°, narrower than an ideal angle. The bond angle of C(10)–Ni–C(20) is 174°, bent away from triphenylphosphine. These are responsible for steric influence of bulky phosphine. The average Ni–I bond is 2.645 Å, comparable with usual Ni–I bond distance. The Ni–C(10) bond length of 1.85(1) Å is longer than 1.81(1) Å of the Ni–C(20) bond. Phenyl rings of apical isocyanide ligands are almost parallel to one phenyl ring of triphenylphosphine (C41–C46) [172.4(6) and 164.1(6)°]. These likely minimized steric interaction between aromatic rings of isocyanide and triphenylphosphine. Diherdal angles between the NiI_2P plane and phenyl rings of apical ligands (C11–C16 and C21–C26) are 92.1(4) and 78.4(5)°, respectively, again due to releasing of steric interaction.

Structure of 4b. The geometry around nickel atom is a distorted trigonal bipyramid. The Hg–Ni–C(40) bond is linear. The nickel atom is occupied upward by 0.33 Å from the triangular C(10)C(20)C(30) plane (a mean angle of C(40)–Ni–C: 100.0°), and the average C–Ni–C angle associated with the triangle C(10)C(20)C(30) are ca. 117°. The plane [C(10)C(20)C(30)] is almost parallel to phenyl rings of isocyanide ligands in the apical sites, minimizing repulsive interaction with axial ligands. The geometry around mercury atom was essentially tetrahedral with the main distortion. The Ni–Hg–I and

I–Hg–I bond angles except the I(2)–Hg–I(2′) bond angle of 92.1(5)° containing a bridged ligands, is in the range 108.8—116.6°. The bond length of Hg–Ni is 2.619 (3) Å, being comparable with the sum (2.59 Å) of the covalent radii. The Hg–I (bridged) distances (2.954(1) and 2.900(2) Å) are longer than that of Hg–I (terminal) bond (2.734(2) Å). They were shorter than the terminal and bridged Hg–I distances (2.681(1) (terminal) and 2.982(1) and 2.937(1) (bridged) in $[(Ph_3PC_5H_4)Hg(\mu\text{-}I)I]_2$.[10] The C–N triple bond length are usual. The Ni–C–N and C–N–C bond angles are similar to those found in usual isocyanide complexes. The Hg–I(2)–Hg bond angle is 87.9°, comparable with that in $[(Ph_3PC_5H_4)Hg(\mu\text{-}I)I]_2$.[10]

Supplemental Materials.

Thermal parameters (Tables 1 and 3), bond distances and angles (Tables 2 and 4), and Tables of F_o-F_c are available. The tables of thermal parameters, all the bond distances and angles, and observed and calculated structural factors are deposited as Document No. 8969 at the Office of the Editor of Bull. Chem. Soc. Jpn.

Table 4. Selected Bond Distances and Angles of **3a**

	Bond distance (Å)		
Ni–I(1)	2.646(2)	Ni–I(2)	2.644(2)
Ni–P	2.252(3)	Ni–C(10)	1.849(13)
Ni–C(20)	1.806(13)	C(10)–C(20)	1.135(17)
C(20)–N(20)	1.142(16)	N(10)–C(11)	1.414(19)
N(20)–C(21)	1.440(18)		
	Bond angle (deg)		
I(1)–Ni–I(2)	110.71(6)	I(1)–Ni–C(10)	87.57(39)
I(1)–Ni–C(20)	90.01(43)	I(1)–Ni–P	125.63(12)
I(2)–Ni–C(10)	84.49(39)	I(2)–Ni–C(20)	91.53(43)
I(2)–Ni–P	123.11(12)	C(10)–Ni–C(20)	174.29(53)
C(10)–Ni–P	90.21(37)	C(20)–Ni–P	95.40(40)
Ni–C(10)–N(10)	177.0(11)	C(10)–N(10)–C(21)	177.3(14)
Ni–C(20)–N(20)	176.2(11)	C(20)–N(20)–C(21)	175.4(12)

This work was partially supported by a Grant-in Aid for Scientific Research No. 0260484 from the Ministry of Education, Science and Culture.

References

1) J. M. Burlitch, "Comprehensive Organometallic Chemistry," ed by G. Wilkinson, F. G. A. Stone, and E. W. Abel, Pergamon Press, New York (1982), Vol. 6, Chap. 42, p. 983.

2) D. V. Khasnis, H. L. Bozec, and P. H. Dixneuf, *Organometallics,* **5**, 1772 (1986).

3) a) H. M. Walborsky and G. E. Niznik, *J. Org. Chem.,* **37**, 187 (1972). b) Y. Yamamoto, K. Aoki, and H. Yamazaki, *Inorg. Chem.,* **18**, 1681 (1979).

4) S. Otsuka, A. Nakamura, and Y. Tatsuno, *J. Am. Chem. Soc.,* **91**, 6994 (1969).

5) T. Sakurai and K. Kobayashi, UNICSIII System (I), 1978.

6) "Intenational Tables for X-Ray Crystallography," Kynoch Press, Birmingham (1962), Vol. 3.

7) a) M. Panizo and M. Cano, *J. Organomet. Chem.,* **266**, 247 (1984). b) M. P. Pardo and M. Cano, *J. Organomet. Chem.,* **247**, 293 (1983). c) D. J. Cook, J. L. Daws, and R. D. W. Kemmitt, *J. Chem. Soc. A,* **1967**, 1547. d) I. N. Nowell and D. R. Russell, *J. Chem. Soc., Chem. Commun.,* **1967**, 817. e) P. D. Brotherton, J. M. Epstein, A. H. White, and S. B. Wild, *Aust. J. Chem.,* **27**, 2667 (1974). f) P. N. Brier, A. A. Chalmers, J. Lewis, and S. B. Wild, *J. Chem. Soc. A,* **1967**, 1889.

Table 5. Selected Bond Distances and Angles of **4b**

	Bond distance (Å)		
Hg–Ni	2.619(3)	Hg–I(1)	2.734(2)
Hg–I(2)	2.954(1)	Hg–I(2′)	2.900(2)
Ni–C(10)	1.836(19)	Ni–C(20)	1.837(22)
Ni–C(30)	1.884(21)	Ni–C(40)	1.853(19)
C(10)–N(10)	1.195(26)	N(10)–C(11)	1.428(28)
C(20)–N(20)	1.174(29)	N(20)–C(21)	1.460(30)
C(30)–N(30)	1.145(26)	N(30)–C(31)	1.409(26)
C(40)–N(40)	1.164(25)	N(40)–C(41)	1.364(26)
	Bond angle (deg)		
Ni–Hg–I(1)	116.62(7)	Ni–Hg–I(2)	108.84(6)
Ni–Hg–I(2′)	111.1(6)	I(1)–Hg–I(2)	110.24(5)
I(1)–Hg–I(2′)	115.1(3)	I(2)–Hg–I(2′)	92.1(5)
Hg–Ni–C(10)	77.5(6)	Hg–Ni–C(20)	78.5(6)
Hg–Ni–C(30)	84.3(6)	Hg–Ni–C(40)	178.0(5)
C(10)–Ni–C(20)	126.7(9)	C(10)–Hg–C(30)	84.3(6)
Hg–Ni–C(40)	178.0(5)	C(10)–Ni–C(20)	126.7(9)
C(10)–Ni–C(30)	112.3(10)	C(10)–Ni–C(40)	100.8(8)
C(20)–Ni–C(30)	111.7(8)	C(20)–Ni–C(40)	101.9(10)
C(30)–Ni–C(40)	97.4(9)	Ni–C(10)–N(10)	171.0(18)
Ni–C(20)–N(20)	175.3(15)	Ni–C(30)–N(30)	166.1(19)
Ni–C(40)–N(40)	173.9(16)	C(10)–N(10)–C(11)	175.0(22)
C(20)–N(20)–C(21)	175.8(18)	C(30)–N(30)–C(31)	175.2(23)
C(40)–N(40)–C(41)	168.3(22)		

8) Y. Yamamoto, K. Takahashi, and H. Yamazaki, *J. Am. Chem. Soc.*, **108**, 2458 (1986). b) Y. Yamamoto, K. Takahashi, K. Matsuda, and H. Yamazaki, *J. Chem. Soc., Dalton Trans.*, **1987**, 1833.

9) A. R. Rossi and R. Hoffman, *Inorg. Chem.*, **14**, 365 (1975).

10) a) N. L. Holy, N. C. Baenziger, R. M. Flynn, and D. C. Swenson, *J. Am. Chem. Soc.*, **98**, 7823 (1976). b) N. C. Baenziger, R. M. Flynn, D. C. Swenson, and N. L. Holy, *Acta Crystallogr., Sect. B*, **34**, 2300 (1978).

The Reaction of 2-Substituted Cycloalkanones with Aldehydes under Acidic Conditions

Tadashi SATO* and Kengo HAYASE
Department of Applied Chemistry, Waseda University, Ookubo 3, Shinjuku-ku, Tokyo 169
(Received May 27, 1991)

The title reaction proceeded with either ring enlargement or bicyclic compound formation, as well as the aldol reaction, depending upon the types of the reactants and reaction conditions.

The aldol reaction between ketones and aldehydes generally affords a mixture of many products, due to the involvement of self-condensation, reverse reaction, dehydration followed by Michael addition, among others. Therefore, the cross aldol reaction is usually carried out using some derivatives equivalent to the substrates, such as enol ethers for ketones, and acetals for aldehydes.[1)]

During our studies on the chemistry of β-stannyl ketones with Lewis acids, we noticed that 2-methylcyclopentanone reacted with benzaldehyde cleanly to undergo a ring enlargement under a Lewis acid treatment. Inspired by the results, we investigated the reactions of 2-substituted cycloalkanones with aldehydes under various conditions without any prior derivatization. It was found that the reaction proceeded fairly cleanly, affording several types of products depending upon the kinds of Lewis acids and aldehydes.

Results

When 2-methylcyclopentanone (**1**) was reacted with benzaldehyde **2a** or unsaturated aldehydes **2b**—**2e** under Lewis acid treatment, cyclohexenones **4a**—**4e** were obtained as major products (Eq. 1). The ring enlargement was also effected from **5** by the reaction with **2a** and **2b** (Eq. 2). The results are summarized in Table 1 (Runs a—j).

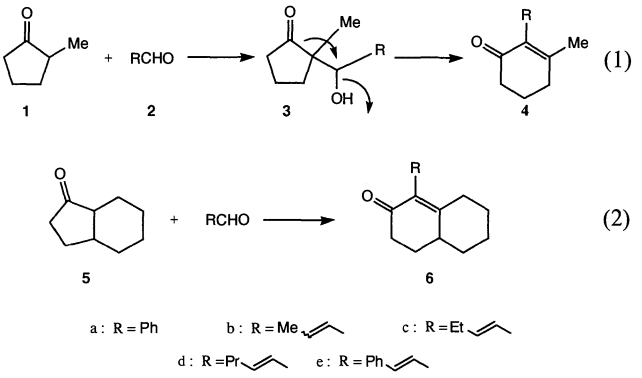

The reaction could be schemed as initiated by the aldol reaction producing **3**, followed by the elimination of the hydroxyl group and acyl migration. Expectedly the aldol **3a**, prepared according to the reported method,[2)] gave **4a** when treated with trimethylsilyl trifluoromethanesulfonate (TMSOTf) treatment (Run k).

Although the acyl migration was exclusive in Runs a, f,

Table 1. Lewis Acid-Induced Reaction of Cycloalkanones or Aldols with Aldehydes

Run	Starting material	Aldehyde	Lewis acid	Product (yield %)[a)]				
a	**1**	**2a**	$AlCl_3$	**4a**	(62)			
b	**1**	**2a**	TMSOTf	**4a**	(67)	**7**	(ca. 15)	
c	**1**	**2a**	*n*-Bu_2BOTf	**4a**	(48)	**7**	(10)	**16f** (8)
d	**1**	**2a**	$BF_3{\cdot}OEt_2$	**4a**	(29)	**16f**	(ca. 20)	
e	**1**	**2b**	TMSOTf	**4b**-*trans*	(79)	**4b**-*cis*	(9)	
f	**1**	**2c**	TMSOTf	**4c**	(62)			
g	**1**	**2d**	TMSOTf	**4d**	(70)			
h	**1**	**2e**	TMSOTf	**4e**	(51)	**8**	(10)	
i	**5**	**2a**	TMSOTf	**6a**	(50)			
j	**5**	**2b**	TMSOTf	**6b**	(70)			
k	**3a**	—	TMSOTf	**4a**	(26)	**7**	(tr)	
l	**1**	**2a**	$TiCl_4$	**3a**	(12)			
m	**12f**	**13**	TMSOTf	**15f**	(26, 40[b)])			
n	**12f**	**13**	$AlCl_3$	**14f**	(75)			
o	**12g**	**2a**	TMSOTf	**16g**	(65)			
p	**12g**	**13**	TMSOTf	**15g**	(41, 52[b)])			
q	**12g**	**13**	$AlCl_3$	**14g**	(74)			
r	**14f**	—	TMSOTf	**15f**	(16)			
s	**14f**	**13**	TMSOTf	**15f**	(30)			
t	**14g**	—	TMSOTf	**15g**	(49)			

a) Yields are on the cycloalkanone basis. b) Using two equivalents of **13**.

g, i, and j, the methyl migration also occurred in Runs b and c, producing **7** as a minor product. An aldol condensation at the 5-position was also observed as a side reaction in Runs c and d, producing **16f** (Eq. 4). A small amount of by-product was isolated in Run h, to which the structure **8** was assigned in view of the spectroscopic data.[3] Presumably **8** was formed through an intramolecular S_N2' type reaction on the side chain of **3e** with C5 of the cyclopentanone ring. No products involving methyl migration, nor methylene migration were identified in the reactions with the unsaturated aldehydes. The minor product in Run e was assigned as a cis isomer, since it showed exactly the same mass spectrum as that of the major product, while it lacked the IR peak for the trans double bond at 969 cm^{-1} found in the major product.

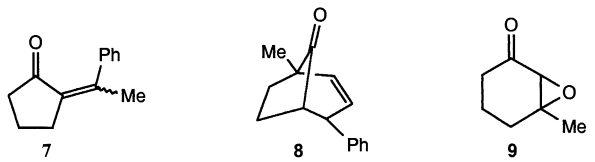

7 **8** **9**

10 **11**

The structure of **4a** was confirmed by comparing with the authentic sample, prepared from **9** according to the reported method.[4] The structure of **7** (*trans–cis* mixture) was confirmed by the catalytic hydrogenation to afford **10** (diastereomer mixture), which indicated the IR absorption at 1736 cm^{-1}, suggesting the presence of five-membered ketone system. The attempted dehydration of **11**, obtained in small amount from the corresponding silyl enol ether and acetophenone,[5] resulted only in retro-aldol reaction to give acetophenone, without affording any amount of **7**.

The reaction terminated at the stage of aldol formation **3a**, when a mixture of **1** and **2a** was treated with $TiCl_4$ (Run l). However, no reaction proceeded with AgOTf, Et_3B, $SnCl_4$, or $FeCl_3 \cdot 6H_2O$. Characteristically $AlCl_3$ and BF_3–etherate did not induce the reaction of the unsaturated aldehydes **2b** and **2d** with **1**, contrary to the cases of benzaldehyde (Runs a and d).

In contrast to the ring enlargement with the aromatic or unsaturated aldehydes described above, the reaction type changed entirely when acetaldehyde **13** was used. The TMSOTf-induced reaction of **12f** (=**1**) with **13** afforded a bicyclic compound **15f** (Eq. 3), even with the use of only one equivalent of the aldehyde. The involvement of two molecules of the aldehyde was evident in view of the mass spectroscopic data. Presumably the reaction proceeded through a double aldol reaction at 2 and 5-positions of **12f**, followed by

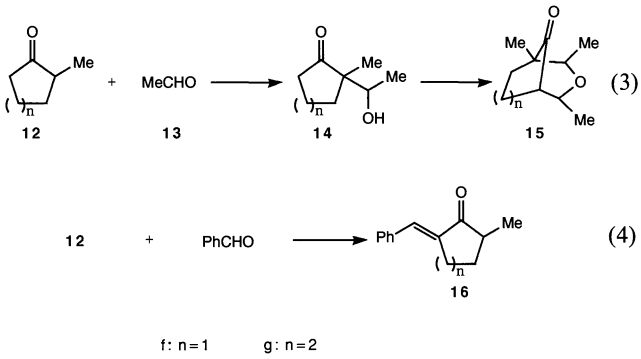

(3)

(4)

f: n=1 g: n=2

cyclization. Expectedly, the yield was improved by using two equivalents of **13** (Run m). The same type of the reaction occurred with **12g** upon treatment with TMSOTf, affording **15g** (Run p). Notably, **15f** was a single diastereomer as revealed from ^1H NMR (400 MHz) and ^{13}C NMR spectra, while **15g** was evidently a mixture of diastereomers in view of ^1H NMR analysis. Presumably, the whole reaction is controlled thermodynamically to afford the products as the most stable form. The bicyclic compounds **15f** and **15g** were also obtained from the respective mono-aldols **14f** and **14g** upon treatment with TMSOTf, irrespective of whether acetaldehyde was added or not (Runs r—t). Apparently the reactions in Runs r and t involved the retro-aldol reaction. The aldols **14f** and **14g** (diastereomer mixture) were prepared from the corresponding silyl enol ethers with **13** under the $TiCl_4$ treatment.[2]

Unlike the cases of the five-membered ketone described above, no ring enlargement was observed in case of the six-membered ring system even with benzaldehyde. When **12g** was treated with **2a** in the presence of TMSOTf, the product was an α,β-enone **16g**, identical with the authenic sample prepared by the reported method.[7] (Eq. 4, Run o).

The reaction terminated at the stage of mono-aldols **14f** and **14g**, when the reactions of **12f** and **12g**, respectively, were induced with $AlCl_3$ (Runs n and q). The diastereoselectivity in these cases was a little higher than that obtained in the $TiCl_4$-induced aldol reaction of the corresponding silyl enol ethers.[2]

Discussion

It appears that all the reactions described in the present paper proceed through the initial aldol reaction at the more substituted α-position (2-position) of the cycloalkanones. It has been known that the reactions of 2-methylcyclohexanone and 2-methylcyclopentanone with some aldehydes in protic solvents proceed at the unsubstituted position (5- or 6-position) of the cycloalkanones followed by dehydration under both acidic and basic conditions.[6,7] Generally the benzylidene derivatives (*exo*-enones) are obtained under basic conditions, while benzyl derivatives (*endo*-enones)

are obtained under acidic conditions.[8] It has been well documented that the aldol reaction is reversible and accompanied by a facile dehydration in protic solvents. Thus the thermodynamically most stable compounds might be the product under these conditions. On the other hand, the kinetic aldols can be isolated without being dehydrated, by starting from the corresponding derivatives of the substrates in aprotic solvents under mild conditions. Under these conditions, the reaction site is controlled by the regiochemistry of the enolates. The regioselective aldol reaction at the substituted position of the 2-substituted cycloalkanones has been elaborated by starting from the more substituted silyl enol ethers.[1] The silyl enol ethers or other metal enolates derived therefrom react with aldehydes to produce regiospecific aldols. The aldol reaction of the persubstituted enolates prepared in this way has been extensively studied, particularly from view point of the stereochemistry.[9] The formation of the persubstituted enolates has also been achieved from 2-bromo-2-methylcyclohexanone by treating with Zn-Et_2AlCl.[10]

The regiochemistry of the aldol reaction of the unsymmetrical cycloalkanones in aprotic solvents has received less attention. It is known that the aldol reaction of 2-methylcycloalkanones with benzaldehyde proceeds at the less hindered site, when promoted by tetraalkoxysilane/fluoride anion in dimethylformamide or without solvent.[11] The diethylaluminum tetramethylpiperidide-induced aldol reaction of 2-methylcyclohexanone in tetrahydrofuran is also known to react at the 6-position,[12] indicating that the enolization proceeds to afford the less substituted enolate. Therefore it is remarkable that the present reaction proceeded at the more hindered position. Although the aldols **3** and **14** were actually isolated in Runs 1, n, and q, the aldols underwent further reaction to result in either ring enlargement or retro-aldol reaction in other cases. Conceivably the ring enlargement reaction proceeded through (1) elimination of the hydroxyl group from the aldol, (2) concomitant 1,2-acyl migration, and (3) deprotonation, as shown in Eq. 1. Probably the series of the steps proceed only when elimination of the hydroxyl group (step 1) is facilitated through the cation-stabilizing effect by phenyl or alkenyl group, and the ring enlargement (step 2) does not give rise to the unfavorable strain, as would possibly be encountered in the *trans*-formation from six- to seven-membered ring system. Unless these requirements are fulfilled, the retro-aldol reaction proceeds to produce either **15** or **16**, depending upon whether the aldehyde is acetaldehyde or benzaldehyde, respectively. The γ-pyrone formation from 2,6-dialkylcyclohexanones under acidic conditions has been reported.[13]

The 1,2-acyl migration will be discussed next. A reaction scheme involving cyclopropoxyl radical or anion, resulted from the intramolecular addition of alkyl radical or anion to the carbonyl group is a well-

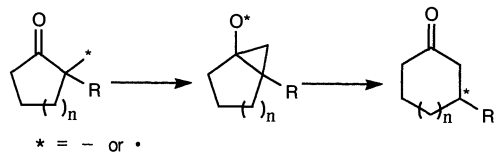

(5)

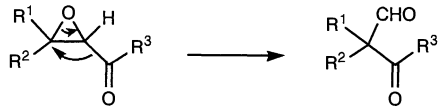

(6)

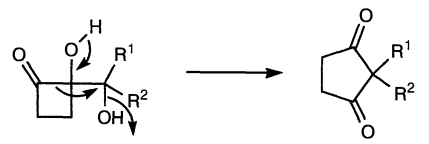

(7)

documented process of 1,2-acyl migration (Eq. 5).[14] It seems likely, however, that the present ring enlargement involves a direct 1,2-acyl migration to the electron deficient carbon terminus rather than through the cyclopropoxy intermediates. This type of the acyl migration was first studied by House in the Lewis acid-induced reactions of α,β-epoxy ketones, and has been a target of many researchers (Eq. 6).[15] The unusually high migratory aptitude of the acyl group, as compared with that of methylene or hydride, has been established.[16] The 1,2-acyl migration proceeds concertedly with inversion of configuration at the migration terminus. Another instance of the Lewis acid-induced 1,2-acyl migration has been observed with pinacol–aldol system (Eq. 7).[17] Since the epoxy ketone could be looked as an equivalent to the aldol in a sense that the β-position of the carbonyl group has an oxygen leaving group, these examples could be assigned as precedence for the 1,2-acyl migration in the aldol system. However, it is highly likely that the acyl migration in these systems is effectively drived by the opening of oxirane or cyclobutanone ring, and also by the presence of a carbocation-stabilizing oxygen substituent at the migration origin carbon. Thus the present reaction is notable in that the 1,2-acyl migration is induced only with the participation of the alkenyl and aryl groups in stabilizing the cationic intermediates.

The base-induced reaction of the tosylate of **14g** has been reported to afford a mixture of cyclobutanone derivatives as well as a ring-opened product. However, neither acyl migration nor retro-aldol reaction has been observed.[18]

Remarkably the products from the unsaturated aldehydes have a unique system of 2-acyl-1,3-diene unit. To our best knowledge, only two cases have been reported for the preparation of this cross-conjugated electron-deficient diene system: the vinylation at α-position of α,β-epoxy ketones,[4] and the Robinson annulation of cycloalkanones with divinyl ketone.[19]

The phenylation at the α-position of α,β-epoxy ketones affording **6a** has been demonstrated as an example of α-alkylation and α-arylation of α,β-enones.[20,21]

Experimental

General Procedure and Instrumentation. GLC experiments were carried out on a 2.5 m×3 mm stainless steel column packed with Silicone SE 30 or Carbowax 20 M on silanized Chromosorb W. Column chromatography was carried out on Kieselgel 60, Art. 7734 (70—230 mesh ASTM). All the spectroscopic data were determined on a pure sample obtained by column chromatography. ^{1}H NMR spectra (60 MHz) were recorded on a Hitachi R-24 or JEOL PMX60 SI spectrometer. ^{1}H NMR (90 MHz) and ^{13}C NMR (22.5 MHz) spectra were measured on a Hitachi JNM-PMX 60 S R-90 H spectrometer, and 400 MHz ^{1}H NMR spectra on a JEOL GSX-400 spectrometer. GC-MS spectra were taken on a Shimadzu QP-1000 mass spectrometer, and high-resolution mass spectra on a JEOL DX-300 mass spectrometer. IR spectra were recorded on a Shimadzu IR-400 spectrometer. Unless otherwise stated, CH_2Cl_2 was used as a solvent for the column chromatography, CCl_4 solutions for ^{1}H NMR (60 MHz), $CDCl_3$ solutions for ^{1}H NMR (400 MHz) and ^{13}C NMR, and liquid film for IR measurement.

Reaction of 1 with 2a in the Presence of $AlCl_3$ (Run a). To a suspension of $AlCl_3$ (0.333 g, 2.5 mmol) in CH_2Cl_2 (10 ml) was added dropwise a CH_2Cl_2 solution (20 ml) of **1** (0.245 g, 2.5 mmol) and **2a** (0.265 g, 2.5 mmol) at room temperature during a period of 20 min. After stirred for additional 3 h at this temperature, aqueous $NaHCO_3$ was added and the products were extracted with CH_2Cl_2. The extract was dried over Na_2SO_4, and the solvent was removed in vacuo. The product was purified on a column chromatography to afford **4a** (0.287 g, 62%). IR 1665 and 1622 cm^{-1}. ^{1}H NMR δ=1.7—2.65 (m, 6H), 1.87 (s, 3H), and 6.8—7.45 (m, 5H). The compound **4a** was identical with the authentic sample prepared according to the reported method.[4]

Reaction of 1 with 2a in the Presence of TMSOTf (Run b). To a solution of **1** (0.245 g, 2.5 mmol) and **2a** (0.265 g, 2.5 mmol) in CH_2Cl_2 (20 ml) was added dropwise a CH_2Cl_2 solution (10 ml) of TMSOTf (0.555 g, 2.5 mmol) at room temperature during a period of 20 min. After stirred for additional 3 h, the reaction mixture was worked-up in the same way as described above. The column chromatography afforded **4a** (0.311 g, 67%) and **7** (0.102 g, 9%). In view of the ^{13}C NMR spectrum, **7** was a *trans-cis* mixture. For **7**, MS *m/z* 186 (M$^+$, base), 171, 153, 143, 128, 115, 91, 77, and 65. IR 1698, 1636, and 701 cm^{-1}. ^{1}H NMR δ=1.5—3.5 (m, 6H), 1.67 (d, *J*=2 Hz, 3H), and 7.11 (s, 5H). ^{13}C NMR[22] δ=[9.97*, 16.02], [31.17, 32.36*], [35.23, 36.77*], [39.68, 46.07*], 125.80, 127.93, 128.38, 139.09, 140.56, 156.56, and [210.24,* 210.74], (1:4). Found: *m/z* 186.1015. Calcd for $C_{13}H_{14}O$: M, 186.1044.

Upon catalytic hydrogenation (5% Pd-C/1 atm H_2/AcOEt, 35 h), **7** gave **10** in almost pure state as a diastereomer mixture (77% yield), as evident from ^{13}C NMR analysis. For **10**, MS *m/z* 188 (M$^+$), 173, 145, 117, 110, 97, 91 (base), and 65. IR 1736, 1453, and 699 cm^{-1}. ^{1}H NMR δ=0.96 and 1.20 (two doublets, *J*=8 Hz, 3H), 1.3—3.3 (m, 8H), and 7.10 (s, 5H). ^{13}C NMR[22] δ=[14.45*, 14.91], [25.67, 27.15*], [28.75, 29.74*], 36.01, [42.84, 44.35*], [49.62. 50.60], 125.94, 128.16, 128.75, and 139.68, (1:2). Found: *m/z* 188.1171. Calcd for $C_{13}H_{16}O$: M, 188.1201.

Reaction of 1 with 2a in the Presence of (*n*-Bu)$_2$BOTf, BF_3·OEt_2 (Runs c, d). The reactions were carried out in the same way as described for the TMSOTf-induced reaction (Run b). The respective produts and yields are shown in the Table 1. For **16f**,[11] ^{1}H NMR δ=1.13 (d, *J*=6 Hz, 3H), 1.3—3.5 (m, 6H), and 6.8—7.7 (m, 6H).

Reaction of 3a in the Presence of TMSOTf (Run k). The aldol **3a** was prepared according to the reported method.[2] ^{1}H NMR (diastereomer mixture) δ=0.67 (s, 1/4H), 0.98 (s, 3/4H), 1.15—2.20 (m 6H), 4.10 (br. s, 1H), 4.62 (s, 1H) 7.16 (s, 5H).

To a CH_2Cl_2 solution (45 ml) of **3a** (1.169 g, 5.73 mmol) was added dropwise a CH_2Cl_2 solution (23 ml) of TMSOTf (1.273 g, 5.73 mmol) in the ssme way as described for Run b. The products were **4a** (0.278 g, 26%) and **7** (trace).

Reaction of 1 with 2a in the Presence of $TiCl_4$ (Run 1). The reaction was carried out in the same way as in Run b, from **1** (0.245 g, 2.5 mmol) and **2a** (0.265 g, 2.5 mmol) with $TiCl_4$ (0.480 g, 2.5 mmol). The product was indentical with the authentic **3a** prepared above, with the diastereomer showing at δ=0.67 as the major product.

Reaction of 1 with 2b, 2c, 2d, or 2e in the Presence of TMSOTf (Runs e, f, g, h). To a solution of **1** (0.245 g, 2.5 mmol) in CH_2Cl_2 (5 ml) was added dropwise a CH_2Cl_2 solution (5 ml) of TMSOTf (0.555 g, 2.5 mmol) at room temperature during a period of 15 min. After 15 min, a solution of **2b** (*trans*+*cis*), **2c** (*trans*), **2d** (*trans*), or **2e** (*trans*) (3 mmol) in CH_2Cl_2 (30 ml) was added during a period of 3.5 h. After stirred for additional 45 min at this temperature, the reaction mixture was worked-up in the same way as in Run a. While the products **4c**, **4d**, and **4e** were obtained as single isomers, **4b** was a mixture of *trans* and *cis* isomers, which were separated into each fraction on the column chromatography in yields as specified in the Table 1.

For *trans*-**4b**, MS *m/z* 150 (M$^+$), 135, 117, 107, 91, 79 (base), and 77. IR 1666, 1613, 1375, and 969 cm^{-1}. ^{1}H NMR δ=1.76 (d, *J*=6 Hz, 3H), 1.97 (s, 3H), 2.15—2.55 (m, 6H), and 5.9—6.1 (m, 2H). Found: *m/z* 150.1059. Calcd for $C_{10}H_{14}O$: M, 150.1045.

For *cis*-**4b**, MS same as that for the trans isomer. IR 1666, 1616, 1375, and 787 cm^{-1}. ^{1}H NMR δ=1.45 (d, *J*=6 Hz, 3H), 1.80 (s, 3H), 1.95—2.5 (m, 4H), and 5.4—6.0 (m, 2H). Found: *m/z* 150.1073. Calcd for $C_{10}H_{14}O$: M, 150.1045.

For **4c**, MS *m/z* 164 (M$^+$), 149, 135 (base), 131, 121, 107, 93, 91, 79, and 77. IR 1670, 1375, and 970 cm^{-1}. ^{1}H NMR δ=1.03 (t, *J*=6 Hz, 3H), 1.7—2.6 (m, 6H), 1.97 (s, 3H), and 5.8—6.1 (m, 2H). Found: *m/z* 164.1182. Calcd for $C_{11}H_{16}O$: M, 164.1201.

For **4d**, MS *m/z* 178 (M$^+$), 163, 149, 135 (base), 121, 107, 91, and 80. IR 1670, 1611, and 970 cm^{-1}. ^{1}H NMR δ=0.92 (dist. t, *J*=6 Hz, 3H), 1.1—2.7 (m, 10H), 1.97 (s, 3H), and 5.7—6.1 (m, 2H). Found: *m/z* 178.1361. Calcd for $C_{12}H_{18}O$: M, 178.1357.

For **4e**, MS *m/z* 212 (M$^+$), 197 (base), 179, 169, 155, 141, 115, 91, 77, and 65. IR 1668, 1626, 1375, and 970 cm^{-1}. ^{1}H NMR δ=1.97 (s, 3H), 1.5—2.5 (m, 6H), 6.77 and 6.93 (ABq, *J*=17 Hz, 2H), and 7.0—7.5 (m, 5H). Found: *m/z* 212.1175. Calcd for $C_{15}H_{16}O$: M, 212.1201.

For **8**,[3] MS *m/z* 212 (M$^+$, base), 197, 183, 155, 141, 128, 115, 91, and 77. IR 1732, 1236, and 1053 cm^{-1}. ^{1}H NMR δ=1.33 (s, 3H), 1.4—2.5 (m, 5H), 2.48 (d, *J*=6 Hz, 1H), 6.11 and 6.33

(ABq, J=15 Hz, 2H; upper halves further split to doublets with J=6 Hz), and 6.9—7.6 (m, 5H). ^{13}C NMR δ=16.54, 26.40, 29.22, 31.61, 45.28, 83.68, 123.58, 125.97, 127.24, 128.31, 134.06, 136.78, and 170.63. Found: m/z 1212.1216. Calcd for $C_{15}H_{16}O$: M, 212.1201.

Reaction of 5 with 2a in the Presence of TMSOTf (Run i). To a solution of **5**[23] (0.298 g, 2.16 mmol) and **2a** (0.229 g, 2.16 mmol) in CH_2Cl_2 (20 ml) was added dropwise a CH_2Cl_2 solution (10 ml) of TMSOTf (0.480 g, 2.16 mmol) at room temperature during a period of 20 min. After stirred for additional 3 h, the reaction mixture was worked-up and purified as in Run a, to afford **6a**[20] (0.243 g, 50%). MS m/z 226 (M^+, base), 198, 169, 153, 141, 129, 104, 91, and 77. IR 1671 cm^{-1}. ^{1}H NMR δ=0.60—2.83 (m, 13H) and 6.63—7.53 (m, 5H). ^{13}C NMR[24] δ=24.99†, 26.78†, 28.01†, 32.11†, 34.59†, 36.06†, 38.18, 126.10, 127.07, 129.28, 134.88†, 135.45†, 160.73†, and 196.72†. Found: m/z 226.1366. Calcd for $C_{16}H_{18}O$: M, 226.1358.

Reaction of 5 with 2b in the Presence of TMSOTf (Run j). To a solution of **5** (0.204 g, 1.48 mmol) in CH_2Cl_2 (5 ml) was added dropwise a CH_2Cl_2 solution (5 ml) of TMSOTf (0.329 g, 1.48 mmol) at room temperature during a period of 15 min. After 15 min, a solution of **2b** (0.124 g, 1.78 mmol) in CH_2Cl_2 (30 ml) was added during a period of 3.5 h. After stirred for additional 45 min at this temperature, the reaction mixture was worked-up and purified as above, to afford **6b** (0.197 g, 70%). MS m/z 190 (M^+, base), 175, 161, 147, 119, 105, 91, and 79. IR 1670, 1612, 1488, and 967 cm^{-1}. ^{1}H NMR δ=1.20—2.50 (m, 13H), 1.78 (d, J=5.2 Hz, 3H), and 5.40—6.17 (m, 2H). ^{13}C NMR[24] δ=18.09, 24.95†, 26.67†, 27.64†, 31.19†, 34.50†, 35.99†, 38.49, 123.27, 129.94, 130.53†, 159.16†, and 197.48†. Found: m/z 190.1352. Calcd for $C_{13}H_{18}O$: M, 190.1358.

Reaction of 12f with 13 in the Presence of TMSOTf (Run m). To a solution of **12f** (0.245 g, 2.5 mmol) in CH_2Cl_2 (10 ml) was added dropwise a CH_2Cl_2 solution (10 ml) of TMSOTf (0.278 g, 1.25 mmol) at room temperature during a period of 10 min. After 15 min, a solution of **13** (0.110 g, 2.5 mmol) in CH_2Cl_2 (10 ml) was added during a period of 30 min, and stirred for additional 1.2 h at this temperature. The same work-up as above afforded **15f** (0.109 g, 26%). MS m/z 168 (M^+), 124, 96, 71, 69 (base), and 55. IR 1745, 1379, and 1082 cm^{-1}. ^{1}H NMR (400 MHz, $CDCl_3$) δ=0.93 (s, 3H), 1.20 (d, J=6.2 Hz, 3H), 1.26 (d, J=6.2 Hz, 3H), 1.39—1.48 (m, 1H), 1.69—1.79 (m, 1H), 1.95—2.40 (m, 1H), 2.15—2.24 (m, 2H), 3.55 (q, J=6.2 Hz, 1H), and 3.93 (q, J=6.2 Hz, 1H). ^{13}C NMR δ=13.87, 15.27, 16.55, 18.66, 24.60, 51.00, 52.39, 78.88, 82.93, and 218.49. Found: m/z 168.1158. Calcd for $C_{10}H_{16}O_2$: M, 168.1150.

The yield was improved to 40%, when 5.0 mmol (2 equiv) of **13** was used.

In the same way, **12g** afforded **15g**, in yields shown in the Table 1 (Run p). MS m/z 182 (M^+), 138, 123, 110, 95, 82 (base), 81, 69, 68, and 67. IR 1718, 1380, and 1124 cm^{-1}. ^{1}H NMR δ=0.83 (s, 3H), 1.21 (d, J=6 Hz, 3H), 1.23 (d, J=6 Hz, 3H), 1.4—2.9 (m, 7H), 3.44 (q, J=6 Hz, 1H), and 3.82 (q, J=6 Hz, 1H). Found: m/z 182.1321. Calcd for $C_{11}H_{18}O_2$: M, 182.1307.

Reaction of 12f with 13 in the Presence of $AlCl_3$ (Run n). To a suspension of $AlCl_3$ (0.333 g, 2.5 mmol) in CH_2Cl_2 (10 ml) was added dropwise a CH_2Cl_2 solution (10 ml) of **12f** (0.246 g, 2.5 mmol) at room temperature during a period of 10 min. After 15 min, a CH_2Cl_2 solution (10 ml) of **13** (0.110 g, 2.5 mmol) was added during a period of 20 min. After stirred for additional 3.5 h at this temperature, the reaction mixture was worked-up in the same way as above to afford **14f** (0.298 g, 75%). The product was identical with that prepared according to the reported method,[2] which was separated into two diastereomers on a column chromatography (silica gel, hexane–ether=3/1). For diastereomer-I, IR 3446, 1731, and 1059 cm^{-1}. ^{1}H NMR δ=1.00 (s, 3H), 1.06 (d, J=6 Hz, 3H), 1.2—2.5 (m, 6H), 3.68 (q, J=6 Hz, 1H), and 3.67 (s, 1H). For diastereomer-II, ^{1}H NMR δ=0.83 (s, 3H), 1.09 (d, J=6 Hz, 3H), 1.2—2.5 (m, 6H), 3.55 (br. s, 1H), and 3.82 (q, J=6 Hz, 1H).

In the same way, **12g** (0.140 g, 1.25 mmol) gave **14g** (0.746 g, 74%)[18] as a diastereomer mixture (Run q), which was identical with that prepared according to the reported method.[2] ^{1}H NMR δ=0.9—1.15 (a couple of singlets and doublets, 6H), 1.5—2.7 (m, 8H), 3.47 (bs. s, 1H), and 3.9—4.3 (m, 1H).

Reaction of 12g with 2a in the Presence of TMSOTf (Run o). Using **12g** (0.280 g, 2.5 mmol), the reaction was carried out in the same way as in Run b, to afford **16g** (0.324 g, 65%). The product was identical with that prepared by the reported method.[7] ^{1}H NMR, δ=1.12 (d, J=7 Hz, 3H), 1.3—3.2 (m, 7H), 7.25 (s, 6H).

Reaction of 14f in the Presence of TMSOTf (Run r). To a CH_2Cl_2 solution (20 ml) of **14f** (0.336 g, 2.36 mmol) was added dropwise a CH_2Cl_2 solution (10 ml) of TMSOTf (0.524 g, 2.36 mmol) at room temperature during a period of 30 min. The mixture was worked-up in the same way as above to give **15f** (0.061 g, 16%). The yield was improved when the reaction was carried out in the otherwise same way with **13** added (Run s).

In the same way, **14g** (0.390 g, 2.5 mmol) gave **15g** (0.224 g, 49%) (Run t).

Financial support from The Asahi Glass Foundation is greatly acknowledged. We also would like to thank Shin-Etsu Chemical Co., Ltd. and Toray Silicone Co., Ltd. for generous gift of silyl reagents.

References

1) T. Mukaiyama, "Organic Reactions," John Wiley & Sons, Inc., New York (1982), Vol. 28, p. 203.

2) T. Mukaiyama, K. Banno, and K. Narasaka, *J. Am. Chem. Soc.*, **96**, 7503 (1974); E. Negishi and S. Chatterjee, *Tetrahedron Lett.*, **24**, 1341 (1983).

3) We could not rule out the structure of possible isomer, 5-methyl-4-phenyl[3.2.1]oct-2-en-8-one, in view of these data alone.

4) P. A. Wender, J. M. Erhardt, and L. J. Letendre, *J. Am. Chem. Soc.*, **103**, 2114 (1981).

5) Cf. E. Ghera and S. Shoua, *J. Org. Chem.*, **37**, 1292 (1972).

6) A. T. Nielsen, "Organic Reactions," John Wiley & Sons, Inc., New York (1968), Vol. 16, p. 247—248.

7) A. T. Rowland, M. W. Brechbiel, and A. Sykes-Gerelus, *J. Chem. Educ.*, **62**, 908 (1985).

8) A. Hassner and T. C. Mead, *Tetrahedron*, **20**, 2201 (1964).

9) S. Yamago, D. Machii, and E. Nakamura, *J. Org. Chem.*, **56**, 2098 (1991).

10) K. Maruoka, S. Hashimoto, Y. Kitagawa, H. Yamamoto, and H. Nozaki, *J. Am. Chem. Soc.*, **99**, 7705 (1977).

11) C. Chuit, R. J. P. Corriu, and C. Reye, *Synthesis*, **1983**, 294.

12) H. Nozaki, K. Oshima, K. Takai, and S. Ozawa, *Chem. Lett.*, **1979**, 379.
13) A. Haller and R. Cornubert, *Bull. Soc. Chim. Fr.*, **39**, 1621 (1926).
14) For recent references: D. L. Boger and R. J. Mathvink, *J. Org. Chem.*, **55**, 5442 (1990); T. Shono, N. Kise, N. Uematsu, S. Morimoto, and E. Okazaki, *J. Org. Chem.*, **55**, 5037 (1990); T. Sato, T. Watanabe, T. Hayata, and T. Tsukui, *Tetrahedron*, **45**, 6401 (1989).
15) R. D. Bach and J. M. Domagala, *J. Org. Chem.*, **43**, 4181 (1984), and references cited therein.
16) H. O. House and D. J. Reif, *J. Am. Chem. Soc.*, **79**, 6491 (1957).
17) J. Shimada, K. Hashimoto, B. H. Kim, E. Nakamura, and I. Kuwajima, *J. Am. Chem. Soc.*, **106**, 1759 (1984).
18) F. Nerdel, D. Frank, and H. Marschall, *Chem. Ber.*, **100**, 720 (1967).
19) I. G. Tischenko and V. V. Berezovskii, *Vestn. Akad. Navuk BSSR, Ser. Khim. Navuk*, **1979**, 98; *Chem. Abstr.*, **91**, 192883 (1979).
20) P. L. Fuchs, *J. Org. Chem.*, **41**, 2935 (1976).
21) G. Stork and A. A. Ponaras, *J. Org. Chem.*, **41**, 2937 (1976).
22) Signals shown in the brackets appear as a pair, with asterisk on the stronger peaks. The averaged ratio of each pair is shown in parenthesis.
23) H. O. House and G. H. Rasmusson, *J. Org. Chem.*, **28**, 31 (1963).
24) Signals with dagger (†) appeared as inverted signals in J-modulated spectrum.

Determination of the Absolute Configuration and Enantiomeric Purity of Allylic and Acetylenic Alcohols

Fujiko YASUHARA,*†† Shozo YAMAGUCHI,††† Masayuki TAKEDA,†

Department of Chemistry, College of General Education, Tohoku University, Kawauchi, Aoba-ku, Sendai 980

† Department of Biochemistry and Engineering, Faculty of Engineering, Tohoku University, Aramaki-Aoba, Aoba-ku, Sendai 980

(Received June 10, 1991)

The relative magnitude of steric bulk of saturated vs. unsaturated substituents in the title compounds has been estimated by a lanthanoid induced shift (LIS) study of these (*R*)-(+)-α-methoxy-α-(trifluoromethyl)phenylacetate esters [(*R*)-(+)-MTPA esters] by ^{1}H NMR spectroscopy:

CH_2=C(Me)–>Pentyl>*n*-Pr>Et≃CH_2=CH–>Me>CH≡C–; Ph>Cyclohexyl

These results allow the assignment of the absolute configurations of both cyclic and acyclic unsaturated alcohols. Furthermore, the relative intensity of well-separated OMe signals for those diastereomeric MTPA esters can be used for the determination of the %ee of the original alcohols.

The phenomenon of the chemical shift nonequivalence of diastereomeric esters and amides has been widely used for determinations of the absolute configuration and enantiomeric purity of alcohols and amines. The method using α-methoxy-α-(trifluoromethyl)phenylacetic acid (MTPA; Mosher acid) is especially useful and has been most widely employed for this purpose.[1a] This procedure, however, is not applicable when the ^{1}H NMR signals of the respective diastereomers are not sufficiently separated, or when the crucial signals overlap with other resonances. In such cases, the use of a lanthanoid shift reagent, such as Eu(fod)$_3$ (fod=6,6,7,7,8,8,8-heptafluoro-2,2-dimethyl-3,5-octanedione), with MTPA derivatives (MTPA/LSR method[1b]) often enhances the substancial separation of signals from the OMe and phenyl groups in the MTPA moiety and the methine proton in the alcohol moiety so that useful analyses can be performed.

In the course of continuing LIS studies,[2] we have become interested in extending the MTPA/LSR method to the title compounds, since these chiral unsaturated alcohols (**1** and **2**) and their related compounds are widely distributed in natural products as well as key intermediates for the synthesis of various biological active substances. In order to obtain an NMR configurational correlation scheme (Fig. 2) for predicting the absolute configuration of these alcohols by the MTPA/LSR method, it is essential to clarify the effective steric bulk of saturated vs. unsaturated substituents (R_1 vs. R_2) of the alcohol moiety in the MTPA esters for the coordinating Eu(fod)$_3$.

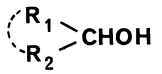

R_1: Alkyl, R_2: –CH=CHR (1)

R_1: Alkyl, R_2: –C≡CR (2)

Results and Discussion

The partially active alcohols employed in this study were prepared by an asymmetric reduction of the corresponding ketones with the Darvon/$LiAlH_4$ complex[3] in good enantioselectivity (e.g., 68% ee for 3-butyn-2-ol). The alcohols, thus obtained, were purified by preparative GLC, if necessary. It is worthwhile noting that the Darvon/LAH complex reduction of α,β-unsaturated carbonyl compound affords an excellent regioselectivity, giving a 1,2-addition product similar to that with $NaBH_4$/$CeCl_3$.[4] Some of them were obtained by the hydride reduction of the corresponding homochiral ketones with $NaBH_4$/$CeCl_3$ or by the optical resolution of racemic alcohols via (*S*)-1-phenylethylamine salts of phthalic acid half esters. *cis*- and *trans*-4-*p*-Menthen-3-ols (Entries 20 and 21) were separated by preparative GLC from a mixture (*cis*/*trans*=88/12) obtained by an LAH reduction of (−)-4-*p*-menthen-3-one ($[\alpha]_D^{20}$ −62.5°, neat).

Shift studies were carried out on diastereomeric mixture of the MTPA esters, as previously reported.[5] Generally, the signal due to the OMe group in the diastereomeric MTPA esters appears as a single peak, thus giving no stereochemical information about the chiral center in question. The signal, however, gave a sufficient separation by the progressive addition of Eu(fod)$_3$. Figure 1 shows a typical example of an LIS study of the (*R*)-MTPA ester of (+)-2-cyclohexen-1-ol. The results are summarised in Table 1.

It is well-known that the order of the steric requirement of the alkyl, alkenyl and alkynyl groups varies appreciably with the reaction mode; for instance, the magnitude of the conformational free energy of the substituent on the cyclohexane ring is of the order of

†† Present adress: Sendai National College of Technology, Kami-ayashi, Aoba-ku, Sendai 989-31.

††† Present adress: Tohoku Gakuin University, Ichinasaka, Izumi-ku, Sendai 981-31.

Et>Me>CH_2=CH–>CH≡C–; *t*-Bu>Ph.[6]

On the other hand, a partly reversed order,

Ph>*t*-Bu; CH≡C–>CH_2=CH–>Et>Me,[7]

has been observed for the chiral hydride reduction of carbonyl compounds by modified $LiAlH_4$ complexes, probably because of an electronic effect which plays a more important role than does the van der Waals repulsion. However, it has been reported that the relative magnitude of the steric requirement of several substituents in the MTPA/LSR study is of the order of

Ph>*t*-Bu>*i*-Pr>Et>Me;[5] COOMe>Ph>Alkyl;[8]

Table 1. Lanthanoid Induced Shift of Methoxyl Group in the Acid Moiety for Diastereomeric (*R*)-MTPA Esters of Allylic and Acetylenic Alcohols

Entry	(*R*)-MTPA-O-CH(L)(M) L	M	LIS_{OMe} LIS^A	LIS^B	ΔLIS_{OMe} LIS^A-LIS^B	Config. with Larger LIS_{OMe}	Remarks
1	Me	CH≡C–	7.8		0	—	
			(0.16)[a]	(−0.22)[a]	(0.38)[a]	(*S*)[a]	
2	Et	CH≡C–	4.8	3.8	1.0	(*S*)	
			(0.07)[a]	(−0.19)[a]	(0.26)[a]	(*S*)[a]	
3	CH_2=CH–	Me	6.8	5.8	1.0	(*R*)	
4	Et ≃	CH_2=CH–	14.8		0	—	
5	*n*-Pr	CH_2=CH–	9.7	9.5	0.2	(*S*)	
6	*i*-Pr	CH_2=CH–	6.8	5.8	1.0	(*S*)	
7	Pentyl	CH_2=CH–	7.1	6.4	0.7	(*S*)	
8	Hexyl	CH_2=CH–	10.5	9.6	1.0	(*S*)	
9	CH_2=CHCH_2–	Me	8.2	6.8	1.4	(*R*)	
10	CH_2=C(Me)–	Et	8.8	6.9	1.9	(*R*)	
11	Ph	Cyclohexyl	8.8	7.7	1.1	(*R*)	
12	···CH_2–CH_2–	···CH=CH–	8.7	7.4	1.3	(*S*)	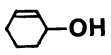
13	···CH(Me)–CH_2–	···CH=CH–	9.3	8.6	0.7	(*S*) (*cis*)	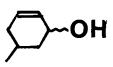
14	···CH(Me)–CH_2–	···CH=CH–	10.1	7.8	2.3	(*S*) (*trans*)	
15	···CH_2–CH_2–	···CH=CH–	8.0	7.5	0.5	(*S*)[b] (*cis*)	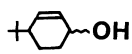
16	···CH_2–CH_2–	···CH=CH–	7.4	6.9	0.5	(*S*)[b] (*trans*)	
17	···CH=C(Me)–	···CH_2–CH_2–	10.1	9.2	0.9	(*R*)[c]	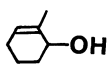
18	···CH=C(Me)–	···(*i*-Pr*)CH–CH_2–	11.4	7.9	3.5	(*R*) (*cis*)	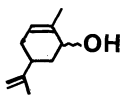
19	···CH=C(Me)–	···(*i*-Pr*)CH–CH_2–	14.1	18.3	−4.2	(*S*) (*trans*)[d]	
	(*i*-Pr*: *i*-Propenyl)						
20	···CH=C(*i*-Pr)–	···CH(Me)–CH_2–	13.9	6.8	7.1	(*R*) (*cis*)	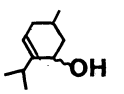
21	···CH=C(*i*-Pr)–	···CH(Me)–CH_2–	11.5	10.5	1.0	(*R*) (*trans*)	
22	···C(···C=C(Me)–)(···CH_2–CH_2–)		[6.3] [4.9] (Racemate)		|1.4|		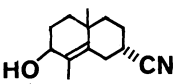
23	···CH_2–CH_2–	···CH=CH–	8.3	8.9	−0.6	(*R*)	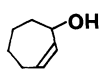
24	···CH_2–CH_2–	···CH=CH–	8.4	8.5	−0.1	(*R*)	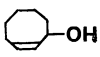

a) Determined by LIS value of the ethynyl proton. b) Configurations not previously reported. These configurations agrees with those predicted from the sense of asymmetric induction by Darvon/LAH complex.[3] c) The assignment is consistent with that presumed from the steric course of asymmetric reduction via hydrosilylation (T. Kogure and I. Ojima, *J. Organomet. Chem.*, **234**, 249 (1982)). d) The result was obtained by repeated run (Ref. 5).

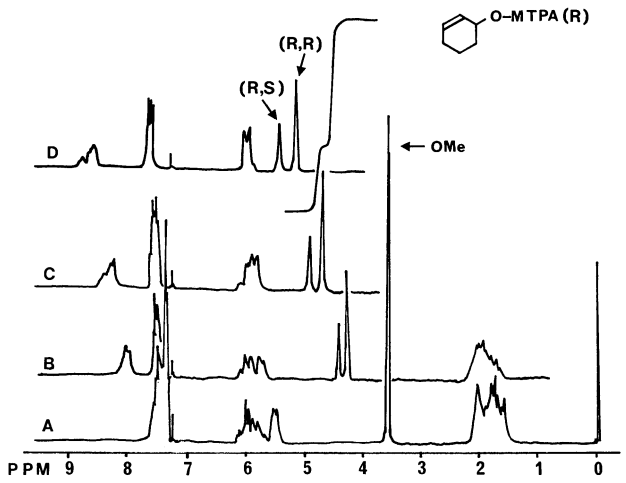

Fig. 1. ^{1}H NMR spectra of the (*R*)-(+)-MTPA ester of 2-cyclohexen-1-ol [(*R*)-(+), 27% ee] in the presence of a specified molar ratio of Eu(fod)$_3$ to the MTPA ester in $CDCl_3$. A, 0; B, 0.1; C, 0.16; D, 0.22.

no systematic investigation has been carried out for those of unsaturated substituents.

The results given in Table 1 clearly indicate that, in contrast to the above two cases,[6,7] the order of effective steric bulk of the substituents in coordination with Eu(fod)$_3$ is as follows:

(a) acyclic alcohols

CH_2=C(Me)->Pentyl>*n*-Pr>Et≃CH_2=CH->Me>CH≡C-; CH_2=$CHCH_2$->Et, Me; Ph>Cyclohexyl

(b) cyclic alcohols

···CH=C(*i*-Pr)->···CH=C(Me)->···CH(Me)-CH_2-, CH_2-CH_2-; ···CH_2-CH(Me)->···CH_2-CH_2->···CH=CH-

These observations strongly suggest that the electronic interaction between the unsaturated substituent and the three heptafluoropropyl groups in Eu(fod)$_3$ is not a dominant factor, but that an extension effect[9] of the substituents is effective (e.g the ethynyl and vinyl groups vs. the methyl group; Entries 1 and 3).

As reported previously,[5] since Eu(fod)$_3$ approaches to the *si*-face side of the ester carbonyl group, the LIS_{OMe} due to compounds (**A**) is consistently larger than that of the compounds (**B**). This correlation scheme enables the determination of the absolute configuration of original alcohols by considering the relative magnitude of the substituents.

Furthermore, the relative intensity of well-separated OMe signals for the diastereomeric MTPA esters can be used to determine the diastereomeric ratio of MTPA esters and, hence, the enantiomeric purity of the original alcohols. The experimental deviations from those obtained by measurements of specific rotation were within ±2%.

Previously,[5] we have observed that substrates with a quasi-axial hydroxyl group, such as *trans*-carveol (Entry 19), do not follow the correlation scheme and that the steric bulk of the substituent on the carbinyl carbon atom of the original alcohol is of the order of

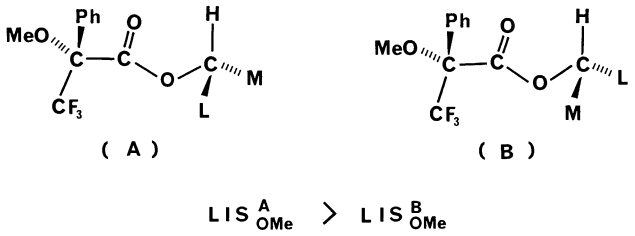

Fig. 2. NMR configurational correlation scheme.

···(*i*-Pr*)CH-CH_2->···CH=C(Me)-,

contrary to the usual order. As can be seen in the case of *trans*-4-*p*-menthen-3-ol (Entry 21), however, this irregularity disappeared when the methyl group was substituted by a more bulky isopropyl group.

In cases where only one enantiomer of the concerned alcohol is available (as is often the case with natural products) two diastereomeric MTPA esters can be generated from the same alcohol using both (*R*)-(+)- and (*S*)-(−)-MTPA. Since the NMR spectra of (*R*,*S*) and (*S*,*R*) or (*R*,*R*) and (*S*,*S*) enantiomers are indistinguishable, an application of symmetry principles should provide the necessary information.

Entries 23 and 24 are clear exceptions to this correlation scheme. Although the preferred conformation of these substrates seems to be responsible for this irregularity,[10] a further detailed study would be necessary for an elucidation of this problem.

An MTPA ester of 3,5,5-trimethyl-2-cyclohexen-1-ol (**3**) decomposed immediately upon the addition of a catalytic amount of Eu(fod)$_3$ to a $CDCl_3$ solution, giving three elimination products [one of which was separated (GLC), and identified as 2,6,6-trimethyl-1,3-cyclohexadiene (**4**)[11]] under ordinary NMR measurement conditions ($CDCl_3$, at ambient temperature).

A similar phenomenon was also observed for the MTPA esters of 3-methyl-2-cyclohexen-1-ol, *cis*- and *trans*-piperitols, β-ionol, 2,3,4,4a,5,6,7,8-octahydro-4a-

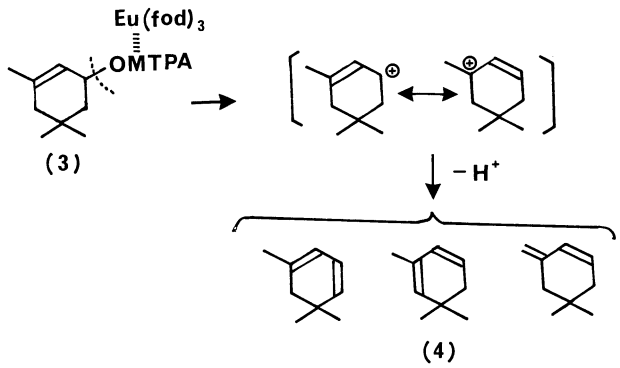

methyl-2-naphthol, and 4-methyl-3-penten-2-ol. Although this mild elimination reaction caused by the Lewis acid character of $Eu(fod)_3$ is strictly a characteristic of the compounds which afford a tertiary carbocation intermediate, the reaction seems to be inhibited by the adjacent alkyl group on the sp^2 carbon atom (Entry 22), which prevents access[12] of $Eu(fod)_3$. A further investigation of this unique elimination reaction is in progress.

Experimental

Instruments. NMR spectra were taken on a Hitachi R-90H FT spectrometer in $CDCl_3$ with TMS as an internal standard. Optical rotations were determined on Perkin-Elmer 241 electronic polarimeter using 1-dm and 0.1-dm thermostated microcells. GLC analyses were made on Shimadzu GC-7A using PEG 20M column (3 mm×2.0 m). Preparative GLC was carried out on a Varian Aerograph (model 700) using the same stationary phase (column: 4 mm×2.0 m).

Solvents and Reagents. Ether was distilled over $LiAlH_4$. Pyridine was dried over BaO and distilled. All of the solvents were stored over a Linde molecular sieve 4A. A stock $LiAlH_4$ solution in ether was passed through a glass filter under nitrogen and stored in a flask closed with a rubber septum. It was analyzed by iodometry immediately prior to use.[13] Aliquots were removed by a syringe, as needed.

Synthesis of Substrate (Representative Example). Optically active (+)-(1*R*,4*S*)- and (+)-(1*R*,4*R*)-4-*t*-butyl-2-cyclohexen-1-ols (a) 2-Bromo-4-*t*-butylcyclohexanones (**5**). To a stirred solution of 15.4 g of 4-*t*-butylcyclohexanone in 50 ml of CCl_4 was added dropwise 15.1 g of bromine in 15 ml CCl_4. The reaction flask was cooled to 15—30 °C and the rate of addition was adjusted so as to maintain a faint coloration of bromine at all times (ca. 2 h). The reaction product was washed with water, sodium carbonate solution, and saturated brine, successively, and dried over magnesium sulfate. The solvent was evaporated to give 20.5 g of crude (**5**) as a yellow oil.

(b) dl-4-*t*-Butyl-2-cyclohexen-1-one (**6**). The dehydrobromination was carried out as described by Miyano.[14] Under a nitrogen atmosphere, to a hot stirred suspension (140 °C) of 1.6 g of magnesium oxide in 45 ml *N*,*N*-dimethylformamide was added 7.0 g of (**5**) in 5 ml of *N*,*N*-dimethylformamide; the reaction mixture was stirred for 1 h. After it was cooled with an ice-bath, the magnesium oxide was dissolved by adding 100 ml of dil. hydrochloric acid and extracted several times with ether. The combined ether extract was washed with brine, sodium carbonate, and saturated brine, successively, and the solution was dried over magnesium sulfate. After the solvent was evaporated, the residue was distilled under reduced pressure to give 3.7 g of crude product as a colorless oil (bp 80—83 °C/8 Torr, 1 Torr=133.322 Pa). GLC analysis showed that the product contains 11% of 4-*t*-butylcyclohexanone and 89% of (**6**); it was purified by liquid chromatography (silica gel; hexane–ethyl acetate=10/2) to give (**6**). Compound (**6**): Colorless oil, ^1H NMR ($CDCl_3$) δ=0.98 (s, 9H), 6.02 (d of d, J=10 and 2 Hz, 1H), 7.00 (d of t, J=10 and 2 Hz, 1H). These spectra data were consistent with the literature.[15]

(c) (+)-(1*R*,4*S*)-(**7**) and (+)-(1*R*,4*R*)-4-*t*-Butyl-2-cyclohexen-1-ol(**8**). These alcohols were obtained by an asymmetric reduction of (**6**) with a Darvon/LAH complex according to the procedure reported previously.[3] GLC analysis indicated that the product contains sole 1,2-addition products [**7**: 15%, **8**: 85%]; and no other isomer was detected. The separation of *cis* and *trans* mixture was performed by preparative GLC.{(**7**): $[\alpha]_D^{25}$ +31.7° (*c* 0.68 methanol), mp 54.5 °C. Found: C, 77.36: H, 11.85%. Calcd for $C_{10}H_{18}O$: C, 77.86; H, 11.76%. ^1H NMR ($CDCl_3$) δ=0.91 (s, 9H), 4.02—4.19 (m, 1H), 5.91 (s, 2H); (**8**): $[\alpha]_D^{25}$ +5.14° (*c* 1.07 methanol) mp 38 °C. Found: C, 77.57; H, 11.91%. Calcd for $C_{10}H_{18}O$: C, 77.86; H, 11.76%. ^1H NMR ($CDCl_3$) δ=0.87 (s, 9H), 4.02—4.31 (m, 1H), 5.74 (s, 2H)].

MTPA Esters. 0.1 mmol of partially active unsaturated alcohols were converted to a diastereomeric mixture of (*R*)-(+)-MTPA esters with excess MTPA chloride made from (*R*)-(+)-MTPA according to the usual method.[1]

NMR Shift Studies (Representative Example). NMR spectra of the (*R*)-(+)-MTPA ester of partially active 2-cyclohexen-1-ol ($[\alpha]_D^{25}$ +40.3° (*c* 1.11, $CHCl_3$) 27% ee) were taken with a molar ratio of $Eu(fod)_3$ to the MTPA ester ranging over 0.1—0.3 in $CDCl_3$ (Fig. 1); the magnitudes of the induced chemical shift of the OMe signals were plotted vs. the molar ratio [$Eu(fod)_3$/MTPA ester]. In this range the induced shifts were essentially linear with respect to the molar ratio of the reagent. The ratio of the peak areas of well-separated OMe signals with larger and smaller LIS values was (36/64). From the results of Table 1, (-CH=CH-<-CH_2-CH_2-), (+)-2-cyclohexen-1-ol has the *R*-configuration.[16]

The authors express their sincere thanks to Dr. Masayoshi Ando for his generous gift of valuable samples (Entry 22 and 2,3,4,4a,5,6,7,8-octahydro-4a-methyl-2-naphthol).

References

1) a) J. A. Dale and H. S. Mosher, *J. Am. Chem. Soc.*, **95**, 512 (1973). b) S. Yamaguchi, "Asymmetric Analysis," ed by J. D. Morrison, Academic Press, New York (1983). Vol. 1, p. 125.

2) Previous Communication: *Tetrahedron Lett.*, **25**, 5801 (1984).

3) S. Yamaguchi and H. S. Mosher, *J. Org. Chem.*, **38**, 1870 (1973).

4) J. L. Luche, *J. Am. Chem. Soc.*, **100**, 2226 (1987).

5) S. Yamaguchi, F. Yasuhara, and K. Kabuto, *Tetrahedron*, **32**, 1363 (1976).

6) J. A. Hirsh, *Top. Stereochem.*, **1**, 199 (1967).

7) H. Haubenstock, *Top. Stereochem.*, **14**, 231 (1983).

8) F. Yasuhara and S. Yamaguchi, *Tetrahedron Lett.*, **21**, 2827 (1980).

9) S. Yamaguchi, J. A. Dale, and H. S. Mosher, *J. Org. Chem.*, **37**, 3174 (1972); S. Yamaguchi and K. Kabuto, *Bull. Chem. Soc. Jpn.*, **50**, 3033 (1977).

10) A similar anomalous stereochemical observation has been reported in the Simmons-Smith reaction in which the sense of asymmetric induction was reversed for 2-cycloocten-1-ol and 2-cyclohepten-1-ol: C. D. Polter, E. C. Friedrich, and S. Winstein, *J. Am. Chem. Soc.*, **91**, 6982 (1969).

11) C. Arnaud and J. Huet, *Bull. Soc. Chim. Fr.*, **18**, 4170 (1972).

12) Since 2'-methoxy-1,1-binaphthyl-2'-carboxylic acid has a considerable large steric effect, the esters of these alcohols are

not subject to elimination reaction and can substitute for Mosher Reagent. [S. Miyano, S. Okada, H. Hotta, M. Takeda, T. Suzuki, C. Kabuto, and F. Yasuhara, *Bull. Chem. Soc. Jpn.*, **62**, 3886 (1989).]

13) H. Felkin, *Bull. Soc. Chim. Fr.*, **18**, 347 (1951).

14) M. Miyano and L. R. Dorn, *J. Org. Chem.*, **37**, 268 (1972).

15) J. P. Konopelski, P. Sudararaman, G. Barth, and C. Djerassi, *J. Am. Chem. Soc.*, **102**, 2737 (1980).

16) R. K. Hill and J. W. Morgan, *J. Org. Chem.*, **33**, 927 (1968).

 © 1991 The Chemical Society of Japan Bull. Chem. Soc. Jpn., 64, 3395—3401 (1991)

Effect of Alkylammonium Ions on the Photochemical Behaviors of γ-Stilbazolium Aggregates in Clay Interlayers

Hisanao USAMI, Katsuhiko TAKAGI, and Yasuhiko SAWAKI*
Department of Applied Chemistry, Faculty of Engineering, Nagoya University,
Chikusa-ku, Nagoya 464-01
(Received June 10, 1991)

Effect of alkylammonium ions (C_n^+) has been studied on the clusterization and photochemical behaviors of γ-stilbazolium (4-(2-phenylvinyl)pyridinium) ion (**1**) adsorbed on clay interlayers. The aggregates of **1** were shown to be dissociated by the coadsorption of C_n^+ with molecular length longer than that of **1**. The major photoreaction was changed from cyclodimerization to *E–Z* isomerization on coadsorbing C_n^+'s longer than **1**. The efficient excimer emission from intercalated **1** was dramatically reduced by coadsorbing alkylammonium ions. The resulting concentration dependence of excimer emission intensity is nicely simulated by a Monte Carlo method for two-dimensional lattice site models.

A marked interest has been focused on the photochemistry and photophysics of molecules in heterogeneous systems including micelles, vesicles, and so on.[1,2] On the other hand, only a little has been studied for photochemistry in heterogeneous systems such as silica gel,[3] zeolites,[4] and layered clay minerals.

Smecite clays consist of planar polyanionic sheets and exchangeable sodium ions, providing a stable electrostatic field. An interesting point to be noted is such that the restricted space, i.e., clearance space, in clay layers is variable depending on the size of organic cations to be intercalated.[5] In clay systems, a unique absorption behavior has been reported where different guest molecules are adsorbed separately from each other.[6] It is also reported that the coadsorption of alkylammonium ions induces a significant conformational change of adsorbents.[7]

However, little is known about a possibility, scope, and limitation of photoreaction in clay interlayers. We have been interested in applying the interlayer space of clay as a unique reaction field for spatially controlled photoreactions. We have recently reported that a clay-intercalated stilbazolium ion (**1**) undergoes a selective photodimerization to give *syn* head-to-tail type cyclodimer.[8] It has been also shown that the intercalation is quite efficient and the molecules are relatively immobile.[9] The present paper discloses an interesting effect of alkylammonium ions (C_n^+) on the photochemical behaviors of intercalated aggregates, which are adequately simulated by a Monte Carlo method for a two-dimensional lattice model.

Results and Discussion

In the previous report,[8] the intercalation of γ-stilbazolium (4-(2-phenylvinyl)pyridinium) ion (**1**) on clay interlayers was shown to result in a quite efficient photochemical dimerization affording *syn* head-to-tail (Eq. 1). The selective cyclodimerization was discussed on the basis of antiparallel packing of intercalated molecules.

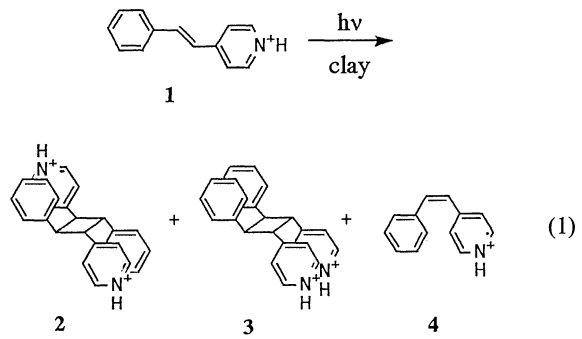

(1)

Effect of Alkylammonium Ions (C_n^+) on the Photoreaction of Intercalated 1. The effect of alkylammonium ions (C_n^+) on the photochemical behaviors of intercalated **1** was determined in order to examine the formation and dissociation of molecular aggregates in clay interlayers. Irradiations of **1** intercalated on Saponite clay were carried out in the presence of various amounts of C_n^+. The photochemical reaction of **1** was found to be remarkably affected by certain kinds of C_n^+. As shown in Fig. 1, octylammonium ion (C_8^+) heavily retarded the dimerization, while butyl homolog (C_4^+) was practically of no effect. For the case of C_8^+, the *E–Z* isomerization became the predominant photoreaction.

Two possibilities are conceivable as an origin for the inefficient cyclodimerization in the presence of longer chain ammonium ions. One is such that stibazolium ions in the clay layers are substituted by ammonium ions and extracted into the bulk solution, resulting in the efficient *E–Z* photoisomerization. The other one is that coadsorbed C_n^+ ions may cause a significant change in the packing mode of **1** favorable for the isomerization. In order to differentiate the two possibilities, the effect of chain length of ammonium ions on the adsorption of **1** was examined as described in the followings.

Substitution of Intercalated 1 with C_n^+. Adsorption equilibrium and its constant, K_{ad}, for the adsorption of C_n^+ on clay interlayers are expressed as Eqs. 2 and 3, respectively. The K_{ad} values have been shown to increase

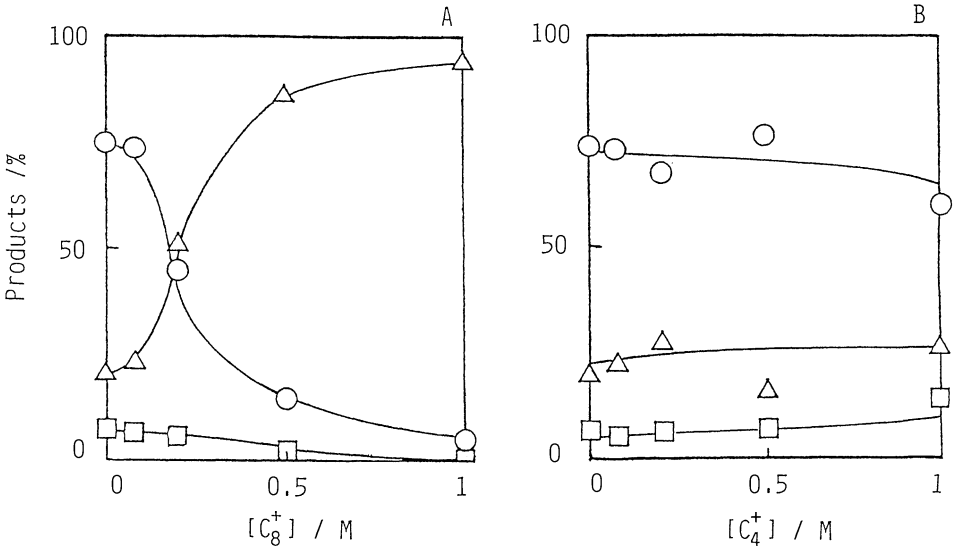

Fig. 1. Effect of alkyl ammonium ions on photoreactivity of pre-intercalated **1** on clay; —○—, *syn* head-to-tail dimer (**2**); —□—, *syn* head-to-head dimer (**3**); —△—, *Z*-**1** (**4**). Intercalated **1**-clay complex (40 mg or 6.8 mM based on CEC; i.e., 100% adsorption) was suspended in 5 ml of aqueous solution of alkylammonium ions; A, octylammonium (C_8^+); B, butylammonium (C_4^+). After stirring overnight, irradiation was carried out for 30 min with a 300 WHg lamp through a Pyrex filter.

Table 1. Substitution of Stilbazolium Ions (**1**) by Alkylammonium Ions (C_n^+) in Clay Interlayer[a]

Alkylammonium ions		K_{ad}[c]	Substituted stilbazolium ions[d]/%
Alkyl group	Molecular length[b]/Å		
—[e]	—	—	1
Butyl (C_4^+)	6.7	0.72	1
Pentyl (C_5^+)	7.9	0.96	2
Hexyl (C_6^+)	9.2	1.99	4
Heptyl (C_7^+)	10.4	3.92	87
Octyl (C_8^+)	11.7	9.2	86
Decyl (C_{10}^+)	14.2	35.7	—

a) In aqueous solution of C_n^+ (0.5 M and 0.6 M HCl, 5 ml) 40 mg of **1**-clay complex was dispersed and stirred overnight. The ratio of $[C_n^+]/[\mathbf{1}]$ was 74. b) Calculated for the all staggered conformers using the following bond lengths: 1.54 Å (C–C), 1.47 Å (C–N), 1.09 Å (C–H), 1.01 Å (N–H). All of the bond angles were assumed to be 109.5°. The molecular length of **1** is 10.4 Å. c) Equilibrium constants of adsorption of C_n^+ on clay.[10] d) Estimated from uv absorption of filtrate through a membrane filter. See experimental section for details. e) No additives.

with increasing chain lengths of C_n^+;[10] e.g., K_{ad}=0.7 for C_4^+ and 9.2 for C_8^+ as listed in Table 1.

$$C_n^+ + Na^+\text{-clay}^- \overset{K_{ad}}{\rightleftharpoons} C_n^+\text{-clay}^- + Na^+ \quad (2)$$

$$K_{ad} = [C_n^+\text{-clay}^-][Na^+]/[C_n^+][Na^+\text{-clay}^-] \quad (3)$$

Stilbazolium ion (**1**) was shown to be effectively intercalated with K_{ad}=ca. 490.[9] Attempted substitution of intercalated **1** by excess amount of C_n^+ added was carried out. As shown in the last column of Table 1, the substitution with C_n^+ where $n \leqslant 6$ was practically negligible, but that with C_7^+ or C_8^+ was quite effective. The expelling effect of C_7^+ and C_8^+ is not explicable in terms of the K_{ad} value of C_n^+ itself, since the increase of one methylene in C_n^+ results in an increase of K_{ad} values only by a factor of two, despite of discontinuous increase of substitution efficiencies at n=6 and 7 (see the third column in Table 1). It is interesting to note that the substitution is most effective when the molecular length of C_n^+ ions is close to that of **1** (i.e., 10.4 Å). The origin of the dramatic effect is unclear at present and remains to be explored. However, the apparent retardation of photodimerization by adding octylammonium ion, as shown in Fig. 1, is mainly due to the effective substitution of **1** by C_8^+.

Effect of C_n^+ on Aggregation Mode of 1. Effect of alkylammonium ions on the photoreaction of intercalated **1** was studied and the results are summarized in Table 2. Hereafter, the amounts of C_n^+ ions were adjusted not to exceed the clay CEC in order to assure the coadsorption of **1** and C_n^+ on clay interlayers. The cyclodimer formation was decreased and the *E*–Z isomerization became predominant by increasing chain length in C_n^+. These features are more apparent in Fig. 2, which demonstrates an alteration of photoproduct distributions by changing the chain lengths. Notable here is that the critical length of C_n^+ is again comparable

Table 2. Effect of Coadsorbed Alkylammonium Ions on the Photoreaction of **1**

$C_n^{+a)}$	Conversion/%	Products/%		
		2	**3**	**4**
—	47	60	14	26
C_4^+	50	58	4	38
C_6^+	56	58	4	38
C_8^+	50	45	4	51
C_{10}^+	61	36	3	61
C_{12}^+	63	44	3	53
C_{14}^+	65	45	4	51

a) Mixed solutions of **1** (0.16 mM, 4% adsorption), C_n^+ (3.2 mM, 80% adsorption), and Saponite clay (4 mM, vs. CEC) were stirred for two hours and irradiated.

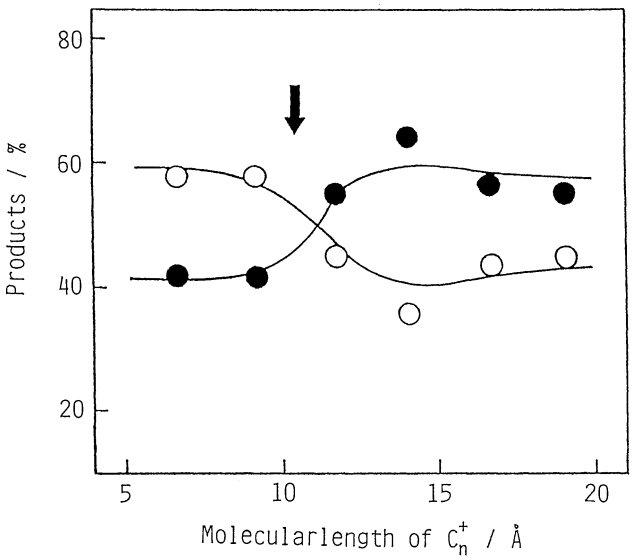

Fig. 2. Effect of molecular lengths of C_n^+ on the photoreaction of intercalated **1**; —○—, cyclodimer (**2**+**3**); —●—, *Z*-**1** (**4**). Suspended solution of **1** (0.16 mM; 4% adsorption) and C_n^+ (3.2 mM; 80% adsorption) intercalated on clay (4 mM) were irradiated by a 300 WHg lamp through a Pyrex filter. The bold arrow represents the molecular length of **1**.

to that of **1** (10.4 Å) as shown by an arrow in Fig. 2.

It is known that the anionic sites of Saponite clay interlayers are scattered on every five angstroms as an average distance.[8,12] The stereochemistry of cyclodimers and emissions from **1** suggested the intercalation of **1** in an alternative antiparallel fashion.[8] The present effect of alkylammonium ions suggests that clusters of **1** are homogenized by the C_n^+ ions of molecular length similar to that of **1** to yield isolated stilbazolium ions responsible for *E*–*Z* isomerization. This fact could be interpreted by a phase separation affected by molecular size, shape and the polar functional groups as known in the case of micelles, microemulsions[11] and clay interlayers.[6] It is tentatively proposed that the present photodimerization is significantly affected by the degree of homogenization of **1** and C_n^+. The addition of

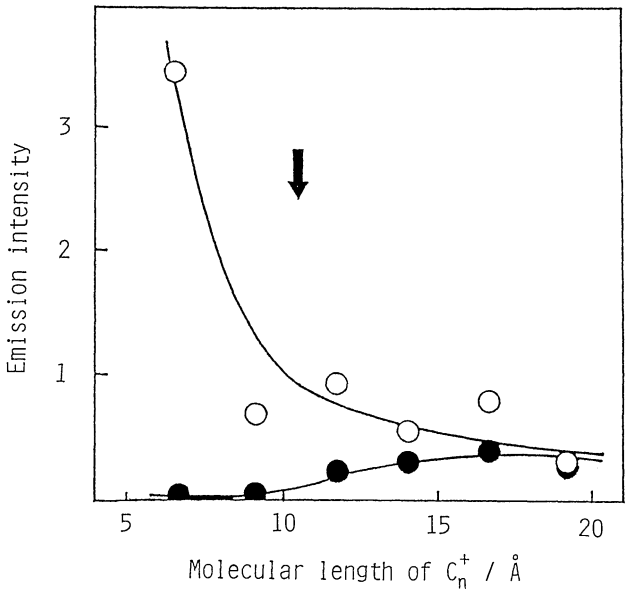

Fig. 3. Effect of molecular lengths of C_n^+ on the emission of **1** intercalated on clay; (a) —○—, excimer fluorescence monitored at 495 nm; (b) —●—, monomer fluorescence monitored at 423 nm. Colloidal suspensions of **1** (5 μM; 5% adsorption) and C_n^+ (95 μM, 95% adsorption) intercalated on clay (100 μM) were excited at 330 nm under Ar. The bold arrow represents the molecular length of **1**.

octylammonium ion would decompose a cluster of **1** by homogenized coadsorption.

Effect of C_n^+ on Monomer and Excimer Fluorescence of 1. In order to get a further insight in the molecular aggregates of **1**, the effect of alkylammonium ions was examined from the monomer and excimer fluorescence of intercalated **1**. Fig. 3 shows the effect of chain lengths of C_n^+ on the fluorescences from **1** in clay layers. The excimer fluorescence was efficiently inhibited by C_n^+'s with longer chain length, and the monomer fluorescence increased with the increasing length. These facts indicate that C_n^+ ions higher than octylammonium ion effectively dissociate the molecular aggregates of **1**. The resulting relative intensity of monomer and excimer fluorescence may be a probe for the aggregation and dissociation of adsorbents.

As shown in Fig. 4, the excimer fluorescence from intercalated **1** is nearly constant in a wide range of 0.1 to 20% adsorption, which indicates an efficient cluster formation or a heterogeneous adsorption of stilbazolium ions.[8] Then, it is interesting to examine the effect of alkylammonium ions on the concentration dependence of fluorescences from **1**. The results with C_8^+ are quite interesting as shown in Fig. 4B. That is, the excimer fluorescence was effectively reduced by coadsorption of C_8^+ and was practically negligible in case of the adsorption of **1** below 5%. This fact suggests that the molecular cluster of **1** was dissociated by C_8^+ and that the two adsorbents of **1** and C_8^+ were homogeneously

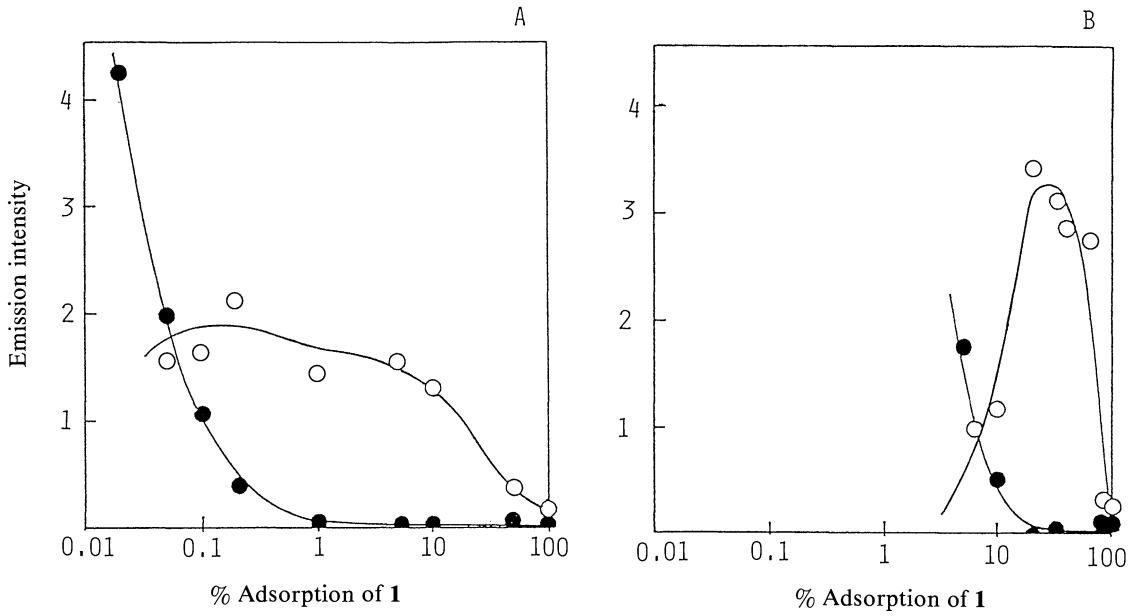

Fig. 4. Effect of C_8^+ on the fraction dependence of fluorescence intensity from **1**; (a) —○—, excimer fluorescence monitored at 495 nm; (b) —●—, monomer fluorescence monitored at 423 nm on the excitation at 330 nm. A: Colloidal suspension of **1** (5 μM and 6 μM of aqueous HCl) intercalated on clay.[8] B: Colloidal suspension of **1** (5 μM and 6 μM aqueous HCl) intercalated on clay, where the remaining sodium ions were completely exchanged by C_8^+.

adsorbed on the clay interlayer.

Simulation of Intercalation on Two-Dimensional Lattice. The effective cluster formation even with 0.1% adsorption of **1** and its dissociation by coadsorbed C_8^+ may be understood more quantitatively by the following simulation behavior for intercalation. It is established that cationic species are adsorbed electrostatically on anionic sites of clay interlayers. The adsorbed species may scramble among any available sites on clay layers. Thus, the adsorbed species aggregate with guest molecules to form clusters depending on their strength of interaction.

A Monte Carlo simulation can treat a mutual interaction of adsorbent on homogeneously dispersed sites. Put n particles of adsorbent (S_1) on a flat surface with a two-dimensional lattice, assuming that the S_1 particles are free to change their adsorbing sites but confined within the lattice. In this model, S_1 can associate with S_n to form an aggregate S_{n+1} with an equilibrium constant K_n, as expressed in case of micelles, in Eqs. 4—6.[2] Here, S_2, S_3, and S_n denote dimer, trimer, and n-mer of S_1, respectively.

$$S_1 + S_1 \overset{K_1}{\rightleftharpoons} S_2 \tag{4}$$

$$S_1 + S_2 \overset{K_2}{\rightleftharpoons} S_3 \tag{5}$$

$$S_1 + S_n \overset{K_n}{\rightleftharpoons} S_{n+1} \tag{6}$$

For the simplicity, K_1, K_2, and K_n could be assumed to be equal to K as the case of the association of surfactant molecules, where the total concentration of S_1 is put

$$[S_1] + 2[S_2] + 3[S_3] + \cdots + n[S_n] + \cdots = 1 \tag{7}$$

unity as Eq. 7. Here, $[S_1]$, $[S_2]$, ···, and $[S_n]$ indicate the fractions of S_1, S_2, ···, and S_n, respectively.

When the two-dimensional lattice possesses a large number of sites, the fractions of n-mers with $n \geqslant 4$ are negligibly small, and Eq. 7 is reduced to Eq. 8.

$$[S_1] + 2[S_2] + 3[S_3] = 1 \tag{8}$$

The fractions of $[S_1]$, $[S_2]$, and $[S_3]$ are calculated as a function of K on the basis of Eqs. 4—6, according to Eq. 9 (See experimental section for details). For example, $[S_1]:[S_2]:[S_3]=1.0:0:0$, $0.56:0.16:0.04$, and $0.42:0.18:0.07$ when $K=0$, 0.5, and 1.0, respectively.

When the number of lattice sites is not of large excess, a more complicated treatment is needed. Suppose that n particles of S_1 are scattered over the two-dimensional lattice. The extent of attractive interaction between the particles could be estimated by means of a probability for an added S_1 particle to be settled on a site without neighboring S_1 particles; the details are described in Experimental section.

In case of 10% intercalation, typical distribution patterns are shown with $K=0$, 0.5, 2, and 20 in Figs. 5A—D. As apparent from these Figures, adsorbent clusters appear and grow with increasing K values. Fig. 6 shows simulation curves for a relationship between %-adsorp-

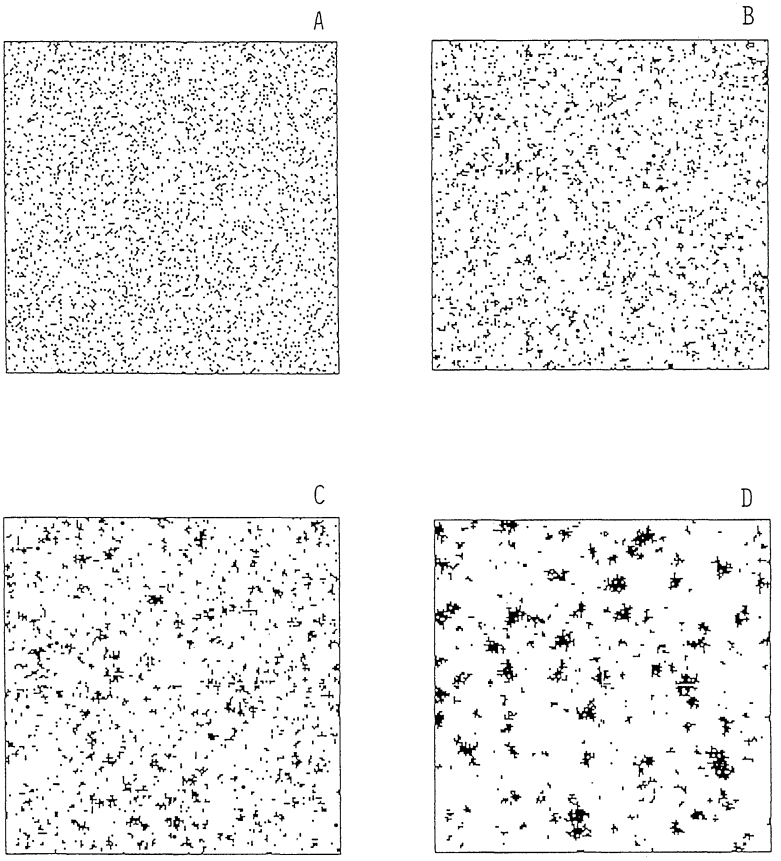

Fig. 5. Adsorption model of S_n on two-dimensional lattice as simulated by a Monte Carlo method; (A) K=0; (B) K=0.5; (C) K=2; (D) K=20. See text for details.

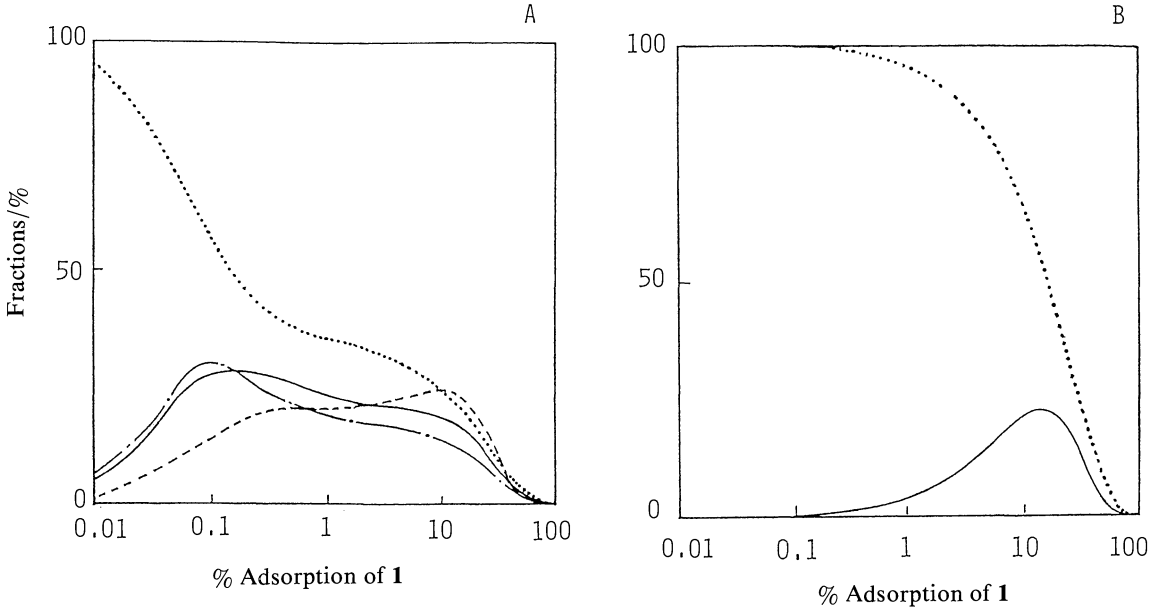

Fig. 6. Computer simulation of fractions of monomer and dimeric aggregates depending on the %-adsorption. A: [S_2] with K=0.1 (----), K=0.5 (—), and K=1.0 (—·—). [S_1] with K=0.5 (·····). B: [S_2] (—) and [S_1] (·····) with K=0.

tion and fractions of S_1 and S_2 in case of K=0 and 0.5. The resulting profiles of S_1 and S_2 fractions in Fig. 6A are quite comparable with the observed monomer and excimer fluorescence intensities in Fig. 4A. The adequate simulation with K=0.5 was confirmed by comparing with the S_2 fraction curves in case of K=0.1 and 1 in Fig. 6A. The coincidence between the two Figures implies a moderate interaction between stilbazolium ions, i.e., K=0.5.

As shown in Fig. 6B, profiles of $[S_1]$ and $[S_2]$ against %-adsorption with K=0 are very close to the features of Fig. 4B for the relative intensities of the monomer and excimer emissions of **1**, where C_8^+ is coadsorbed with **1**. This definitely suggests that specific interaction between the stilbazolium ions is canceled by the coadsorption of C_8^+.

Conclusion. The efficient formation of clusters of stilbazolium ions in clay interlayer is retarded or inhibited by adding alkylammonium ions, C_n^+, with comparable chain length. This is evidenced by an effect of C_n^+ upon the photochemical cyclodimerization and fluorescence intensities. The formation of dimer or cluster of adsorbent is adequately simulated by a Monte Carlo method for a two-dimensional lattice site model.

Experimental

Emission spectra were measured using a Hitachi 650-10S spectrophotometer. Product analyses were carried out with a JASCO UVIDEC-100-III HPLC instrument. Fractions were monitored at 250 nm using a Sil-NH_2 column (30 cm) and the mixed solvent of hexane, ethanol, and 25% aqueous ammonium hydroxide (450 : 50 : 1, v/v) as an eluent flowed at 1 cm^3 min^{-1}.

Materials. A synthetic Saponite clay, Sumecton SA (>110 mesh), was kindly gifted by Kunimine Ind. Co.; the cation-exchange capacity (CEC) is 99.68 mequiv/100 g. Synthesis of stilbazolium (**1**) and the identification of products, *syn* head-to-tail (**2**) and head-to-head (**3**) dimers, and *Z*-stilbazolium ion (**4**), were carried out as reported previously.[8,13] Alkylamines of extra pure grade were used as received from Tokyo Kasei Co.

Irradiations. The irradiation of **1** intercalated on clay layers in the presence of akylammonium ion (C_n^+) was carried out according to following two procedures.

I) Suspended System: The **1**-adsorbed sample were prepared by stirring for 2 h the mixed solutions of **1** (5 mM and 6 mM HCl aq, 100 ml) (1 M=1 mol dm^{-3}) and Saponite clay (10 mM aq, 50 ml). The resulting pale yellow precipitates were filtered out using a membrane filter (Advantech, pore size: 0.45 μm), dried overnight in vacuo, and were ground up with a mortar. From the absorbance of the filtrate, the %-adsorption of **1** on the clay was easily determined. Forty milligrams of the powdered clay-intercalated **1** were dispersed in 5 ml of alkylamine solution (0—1 M and 1.2 equivalents of HCl aq) and were stirred overnight. The irradiation was carried out with a 300 W high-pressure mercury lamp through a Pyrex filter for 30 minutes under Ar. The resulting reaction mixtures were added to concd HCl (10 ml), kept overnight, neutralized with NaOH aq, extracted by CH_2Cl_2, and analyzer by HPLC.

II) Colloidal System: The aqueous solution of **1** (2 mM and 2.4 mM HCl aq, 2 ml) was added to the mixture of aqueous clay (10 mM, 10 ml) and an alkylamine (40 mM and 48 mM HCl aq, 2 ml); the mixed solution was made 25 ml by volume by adding water. After the similar irradiation for 30 min, the products were analyzed as described above.

Emission Spectra. Aqueous solutions of **1** (50 μM and 60 μM HCl aq, 1 ml) and the clay (1000 μM, 1 ml) and/or alkylamines (950 μM, 1 ml) were mixed, made 10 ml by adding water, and stirred overnight. The mixed solution was taken in 1 cm cell, purged with Ar for five minutes. The emission spectra of intercalated **1** were measured by exciting at 330 nm and monitoring at 423 and 495 nm for the monomer and excimer emissions, respectively.

Simulation of Adsorption Modes on Clay Layers. The aggregation modes of **1** on clay layers were simulated on the basis of algorithm noted in the text using a Monte Carlo method. The random numbers for the method were generated using the subroutine of BASIC language program for a NEC PC-9801 microcomputer.

In order to estimate an extent of the attractive interaction between the particles, the Monte Carlo simulation was carried out under the following restrictions. A probability for an added S_1 particle to be settled on a site without neighboring S_1 particles is adjusted so as to be coincident with the fraction, $[S_1]$, obtained from Eq. 9 derived from Eq. 8, when K is fixed on 0 to 20. If not, the S_1 particle is again

$$[S_1] + 2K[S_1]^2 + 3K[S_1]^3 = 1 \quad (9)$$

resettled, until it is adsorbed as an isolated one, with maximum limit of 20 times retrials. This treatment means that the $[S_1]$ is equal to that in the presence of large number of sites.

This work was partly supported by a Grant-in-Aid for Scientific Research from the Ministry of Education, Science and Culture.

Reference

1) J. K. Thomas, "The Chemistry of Excitation at Interfaces," ACS Monograph 181, The American Chemical Society, Washington, DC (1984).

2) K. Kalyanasundaram, "Photochemistry in Microheterogeneous Systems," Academic Press, New York (1987).

3) For an example; D. Oelkrug, S. Reich, F. Wilkinson, and P. A. Leicester, *J. Phys. Chem.*, **95**, 269 (1991).

4) V. Ramamurthy, D. R. Corbin, C. V. Kumar, and N. J. Turro, *Tetrahedron Lett.*, **31**, 47 (1990).

5) S. L. Swartzen-Allen and E. Matijević, *Chem. Rev.*, **74**, 385 (1974), and the references therein; G. Lagaly, *Angew. Chem., Int. Ed. Engl.*, **15**, 575 (1976).

6) P. K. Ghosh and A. J. Bard, *J. Phys. Chem.*, **88**, 5519 (1984).

7) R. A. Della Guardia and J. K. Thomas, *J. Phys. Chem.*, **87**, 3550 (1983); T. Nakamura and J. K. Thomas, *J. Phys. Chem.*, **90**, 641 (1986); J. Wheeler and J. K. Thomas, *Langmuir*, **4**, 543 (1988); K. Viaene, R. A. Shoonheydt, M. Crutzen, B. Kunyima, and F. C. DeSchryver, *Langmuir*, **4**, 749 (1988).

8) H. Usami, K. Takagi, and Y. Sawaki, *J. Chem. Soc., Perkin Trans. 2*, **1990**, 1723.

9) H. Usami, K. Takagi, and Y. Sawaki, *J. Chem. Soc.,*

Faraday Trans., in press.

10) C. T. Cowan and D. White, *Trans. Faraday Soc.*, **54**, 691 (1958).

11) As a review; P. H. Elworthy, A. T. Florence, and C. B. Macfarlane, "Solubilization by Surface-Active Agents," Chapman and Hall, London (1968), Chap.2, pp. 61—116.

12) C. P. Herrero, J. Sanz, and J. M. Serratosa, *J. Phys. Chem.*, **93**, 4311 (1989).

13) F. H. Quina and D. G. Whitten, *J. Am. Chem. Soc.*, **99**, 877 (1977); K. Takagi, B. R. Suddaby, S. L. Vadas, C. A. Backer, and D. G. Whitten, *J. Am. Chem. Soc.*, **108**, 7865 (1986).

 © 1991 The Chemical Society of Japan Bull. Chem. Soc. Jpn., 64, 3402—3410 (1991) [Vol. 64, No. 11

Laser Photolysis Studies on [2+2]-Photocycloreversion and Photoisomerization Reactions of *trans*- and *cis*-1,2-Di(1-pyrenyl)cyclobutane Dimers through Radical Ion Intermediates

Akira TSUCHIDA, Masahide YAMAMOTO,* and Yasunori NISHIJIMA
Department of Polymer Chemistry, Faculty of Engineering, Kyoto University,
Yoshida, Sakyo-ku, Kyoto 606
(Received June 10, 1991)

Transient radical ion intermediates of [2+2]-photocycloreversion and photoisomerization reactions of the 1-vinylpyrene (**1**) cyclobutane dimers, *trans*- and *cis*-1,2-di(1-pyrenyl)cyclobutanes (**2t** and **2c**, respectively), were studied by nanosecond laser photolysis measurements; the reaction quantum yields were determined by photoproduct analysis. The excited singlet state of dimers **2t** and **2c** was quenched by an electron acceptor, 1,4-dicyanobenzene, with a diffusion-controlled rate in a polar acetonitrile solvent. The transient absorption spectra of the dimers in the system showed the formation of a dimer radical cation of pyrene chromophores, whose positive charge was delocalized in the two pyrene rings. The dimers were cleaved to form **1** through the dimer radical cation. By contrast, the formation of a dimer radical anion could not be observed in quenching by an electron donor, *N*,*N*-dimethyl-*p*-toluidine. The cleavage yield of the dimers from the anionic species was low. The decrease in the electron density in the cyclobutane bond in the cationic state promotes the cycloreversion reaction of dimers. In the absence of an electron donor or acceptor in the nonpolar benzene solvent, the direct photocleavage of **2t** and **2c** to **1** through the singlet excited state occurred efficiently, whereas in polar acetonitrile the cleavage was reduced to half by solvation of the excited states. A photocleavage of dimers also occurred in their triplet states.

The fragmentation reactions of cyclobutane compounds into two olefins, and of oxetane into a carbonyl group and an olefin, have been considered to be good prototypes of [2+2]-cycloreversion reactions.[1-17] If two bonds of the cyclobutane ring are broken simultaneously according to the Woodward–Hoffmann rule, the cleavage reaction proceeds in one step without any transient intermediate.[2] In this case, the stereoselective cycloreversion of cyclobutanes, similar to the case of cycloaddition of olefins, is allowed in their photoexcited states. A photoinduced [2+2]-cycloreversion reaction of cyclobutanes has occasionally been used as the simplest case for theoretical studies of the principle of orbital symmetry conservation.[3,4]

Recently, many reports concerning photocycloreversion reaction have been devoted to two fields. The photocleavage of pyrimidine dimers of DNA is of biological interest.[1,14] UV-Irradiation of DNA produces pyrimidine dimers; this damaged DNA is photoreactivated by the cycloreversion of the dimers caused by a photoreactivating enzyme. Secondly, chemically stored energy in the strained molecules is important from the standpoint of solar-energy storage.[10-13] For this purpose, the valence isomerizations of norbornadiene to quadricyclene and cage compounds have been extensively studied in this field.

As for the recent mechanistic studies concerning the photocycloreversion of the cyclobutane ring, many transient intermediates have been reported to exist.[1,7-17] 1,4-Diradical intermediates are occasionally found in the pyrolysis or photocleavage via the excited triplet state of cyclobutanes.[7-9,11,15,18] Photochemically produced excited complexes, such as excimers and exciplexes, are also reported to initiate cleavage.[11-17] The cycloreversions via the radical cation or anions are mainly studied by using gamma-ray irradiation and pulse radiolysis.[15] The behavior of the cyclobutane radical cations in the cycloreversion reaction has also been studied by theoretical calculations as well as by chemically induced magnetic polarization (CIDNP) experiments.[19,20]

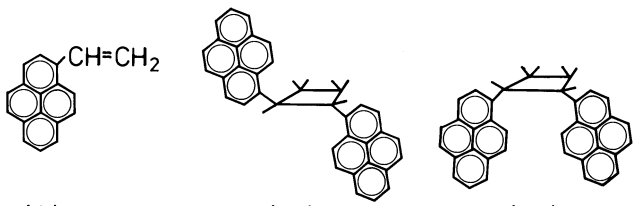

(1) (2t) (2c)

In the present work, we studied the radical cation and anion formation of cyclobutane compounds by nanosecond laser photolysis, and tried to understand the transient intermediates which participate in the cleavage and isomerization reactions via the ionic states. The two isomers of the 1-vinylpyrene (**1**) dimers, *trans*- and *cis*-1,2-di(1-pyrenyl)cyclobutanes (**2t** and **2c**, respectively), have two pyrenyl (Py) groups in the vicinal position of a cyclobutane ring. The chromophore Py is well-known for excimer and dimer radical cation formations:[21-23] In this report, the term "dimer radical ion" is used for the dimeric radical ion whose positive or negative charge delocalizes between two chromophores, whereas the term "radical ion of dimer" is used for the radical ion of one chromophore in cyclobutanes.[23-29] By the measurement of laser photolysis, the "dimer radical ions" and "radical ion of dimers" of **2t** and **2c** were well distinguishable with the transient absorption spectra. Besides the laser photolysis measurements, the reaction quantum yields of photoinduced cycloreversion and isomerization were determined by product analysis,

and are discussed with regard to the transient intermediates observed in the transient absorption spectra.

Experimental

Chemicals. 1-Vinylpyrene **1** was synthesized from 1-pyrenecarbaldehyde by a Wittig reaction. Purification was made by recrystallization and silica-gel column chromatography with hexane–dichloromethane (5:1, v/v) as the eluent. Care was taken to eliminate pyrene, which was an impurity in 1-pyrenecarbaldehyde. Pyrene (Py, Tokyo Kasei Kogyo Co.) was purified twice by recrystallization and once by column chromatography. 1,4-Dicyanobenzene (DCNB, Wako Pure Chem. Ind.) and benzophenone (BP, Wako) were purified three times by recrystallization. *N*,*N*-Dimethyl-*p*-toluidine (DMT, Wako) was purified by distillation under reduced pressure prior to use.

Benzene (Wako) and 2-chlorobutane (Tokyo Kasei) were dried over $CaCl_2$ and purified by distillation. Acetonitrile (MeCN, Wako) was dried by refluxing over P_2O_5 several times and was fractionally distilled. 2-Methyltetrahydrofuran (MTHF, Tokyo Kasei) was filtered using an Al_2O_3 column and then dried. Purification was achieved by distillation under N_2 and subsequent vacuum distillation.

1-Vinylpyrene **1** cyclobutane dimers, **2t** and **2c**, were photochemically produced: The photodimerization of **1** in a MeCN solution produces *trans*- and *cis*-cyclobutane dimers.[30] Photoirradiation of a degassed MeCN solution of **1** (0.027 mol dm^{-3}) in a Pyrex tube by a 300-W high-pressure mercury lamp (Toshiba) for 3 h at room temperature gave both dimers. The products were fractionated by liquid chromatography (Waters, 3000 type) on a silica-gel column (Micro PORASIL) by eluting with CH_2Cl_2–hexane (4:100, v/v). The cis dimer has a larger retention time than the trans dimer. The conformation of **2t** and **2c** was determined by NMR chemical shifts.[31,32]

***trans*-1,2-Di(1-pyrenyl)cyclobutane 2t:** Mp 162—164 °C; ^{1}H NMR (90 MHz; C_6D_6; Me_4Si) δ=2.00—2.49 (4H, m, CH_2), 4.68—5.03 (2H, m, CH), and 7.58—8.37 (18H, m, aromatic); MS *m*/*z* 456 (10 %, M^+), 428 (2, $M^+-C_2H_4$), and 228 [100, **1**$^+$].

***cis*-1,2-Di(1-pyrenyl)cyclobutane 2c:** Mp 81—83 °C; IR (KBr) 3050 m, 2930 m, 2850 w, 1600 m, 1580 w, 1490 w, 1430 w, 1410 w, 1180 s, 840 vs, 750 s, 710 s, 695 s, 675 m, and 495 m cm^{-1}; ^{1}H NMR (90 MHz; C_6D_6; Me_4Si) δ=2.48—2.90 (4H, m, CH_2), 4.98—5.24 (2H, m, CH), and 7.38—8.22 (18H, m, aromatic); MS *m*/*z* 456 (0.5%, M^+), 428 (0.1, $M^+-C_2H_4$), and 228 [100, **1**$^+$].

Cyclobutane dimers were purified by liquid chromatography prior to use; the purity of both dimer was found to be more than 99%. Care was taken to prevent the dimers from thermal or photochemical decomposition.

Quantum Yield Measurements of Photoreactions. The quantum yields of the cycloreversion and isomerization of dimers were determined by photoirradiation under the monochromatic light of a spectrofluorophotometer. A 5-cm^3 sample solution of the dimers (5.0×10^{-5} mol dm^{-3}) in a 1-cm quartz cell was freed from oxygen by N_2 bubbling for 15 min. The samples were photoexcited in a temperature-controlled (297 K) sample chamber of an RF-501 spectrofluorophotometer (Shimadzu). The number of photons of the monochromatic Xe lamp measured by potassium ferrioxalate actinometry[33,34] was 2.0×10^{-9} E s^{-1} at 330 nm (slit width: 19 nm). The Py chromophore was selectively photoexcited at 330 nm, and the system with a DMT additive was photoexcited at 350 nm, since DMT has an absorption tail at 330 nm. For a system of triplet photosensitization, BP was selectively excited at 375 nm. After photoirradiation, the samples were analyzed immediately by liquid chromatography. In all measurements, the photoreaction yield was limited to less than 30% and the absorption of the exciting light by the products was corrected. For all systems, the contribution of thermal reactions, which was practically negligible, was corrected for by a blank experiment. The values of the determined reaction quantum yield were reproducible within ±5%.

Optical Measurements. All sample for the absorption and emission measurements were degassed ($<10^{-5}$ mmHg, 1 mmHg=133.322 Pa) by repeated freeze-pump-thaw cycles in a Pyrex ampoule fitted with a 1-cm quartz cell. The absorption spectra were measured by a UV-200S spectrophotometer (Shimadzu) at a 2-nm slit width. The emission spectra were obtained with an RF-501 spectrofluorophotometer (Shimadzu), whose spectral response was calibrated using a standard tungsten lamp. The quantum yield of emission was determined relative to that of quinine sulfate in sulfuric acid.[35]

The transient absorption was obtained by a nanosecond ruby laser photolysis apparatus, as described elsewhere.[36] The measurements were made at 297 K. The exciting laser light pulse at 347.1 nm has a 10-mJ pulse energy and a 14-ns pulse duration. Samples for the laser photolysis were freed from oxygen by N_2 bubbling for 15 min. The optical density of all samples at 347.1 nm was adjusted to be nearly the same (ca. 1.0) in order to attain homogeneous excitation.

The reference absorption spectra of the radical ions were measured by gamma-ray irradiation from a ^{60}Co source (2×10^6 rad h^{-1}) using a degassed 1-mm quartz cell in glass matrices at 77 K. Radical cations and radical anions were produced in glass matrices of 2-chlorobutane and MTHF, respectively.[37]

Results

Absorption and Emission of Dimers. The absorption-band shape of the chromophore Py is sensitive to the environmental conditions.[38] The cyclobutane dimers, **2t** and **2c**, have the Py groups in the vicinal position of the cyclobutane ring. The absorption spectra thus reflect the degree of the ground-state interaction between two neighboring Py chromophores.

Figure 1 shows the absorption spectra of dimers obtained in the MeCN solvent at 297 K and normalized at 290 nm. The absorption bands at around 290—360 nm are ascribed to the S_2—S_0 transition of the Py chromophore.[22] In Fig. 1, *trans*-dimer **2t** shows practically the same band shape as does that of reference 1-ethylpyrene (EPy); that is, two neighboring Py chromophores at the trans position of cyclobutane ring show no evidence of interaction in the shape of the absorption bands. However, the spectrum of *cis*-dimer **2c** is different from that of **2t**, indicating the existence of an interaction between two Py groups. In the spectrum of **2c**, the vibrational structure becomes less clear: The ratios of the absorption peak to valley for **2c** were smaller than those of **2t**. The molar extinction coefficient of **2t** at the 348.0 nm peak was ca. 8×10^4, whereas that of **2c**

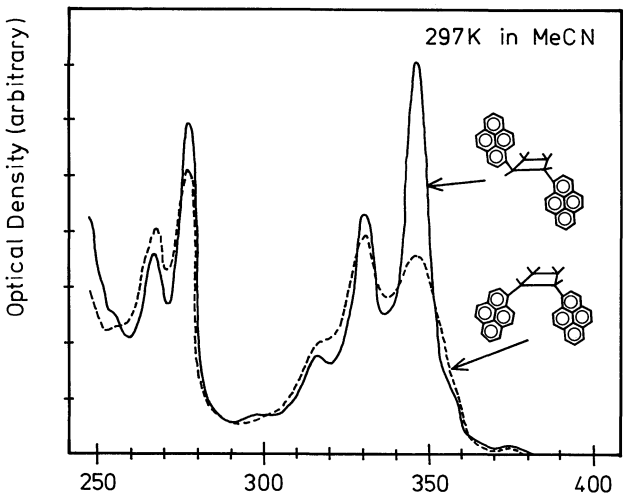

Fig. 1. Absorption spectra of 1-vinylpyrene **1** cyclobutane dimers (**2t**: solid line, and **2c**: broken line) measured in MeCN solvent at 297 K. The spectra were normalized at 290 nm.

was decreased to ca. 3×10^4. This shows that the distance of two Py chromophores of **2t** is too far to interact in the ground state, while for **2c** two Py groups take a sandwich-like conformation and interact with each other. This interaction of chromophores induced broadening of the absorption band with no peak shift, but with a slight hypochromicity.

As for the emission of the dimers, it was very weak due to intramolecular quenching in solution: The emission quantum yield of the intramolecular excimer of **2c** was less than 0.002 at 297 K in benzene solvent; the clear excimer emission of **2t** could not be observed, as has been reported for the emission of tetraphenylcyclobutanes.[11] The pure emission spectra of dimers in solution were difficult to measure due to the contamination of **1**, which shows strong fluorescence and was easily produced by photocleavage, even under the weak exciting light of a spectrofluorophotometer.[16,30] The excited state of the dimers is deactivated by the cleavage reaction and the emission is considerably quenched.

Photoreaction Quantum Yield of Dimers. Table 1 shows the absolute reaction quantum yields of the photoinduced cycloreversion and isomerization of dimers **2t** and **2c**, in several conditions. The O_2-freed sample solutions in the temperature-controlled sample chamber of a spectrofluorophotometer at 297 K were photoirradiated by monochromatic Xe light for a few minutes; the products were then analyzed immediately by liquid chromatography. The Py chromophore was selectively excited by 330 nm light and 1-vinylpyrene **1** was exclusively produced by the [2+2]-cycloreversion of the dimers. Together with the photocleavage reaction, the photoisomerization reaction from *cis*- to *trans*- and *trans* to *cis*-cyclobutane also occurred. Table 1 shows the values of the quantum yields of the cycloreversion and isomerization in nonpolar benzene and polar MeCN solvents. An electron donor, *N*,*N*-dimethyl-*p*-toluidine (DMT), as an additive produces radical anions of **2t** and **2c**, whereas the additive electron acceptor, 1,4-dicyanobenzene (DCNB), produces radical cations of the dimers.[39,40] The concentrations of DMT (1.0×10^{-2} mol dm^{-3}) and DCNB (1.0×10^{-2} mol dm^{-3}) were enough to quench the excited state of Py within 10 ns. An additive, benzophenone (BP, 2.5×10^{-2} mol dm^{-3}), was used as a triplet sensitizer; in this case, BP was selectively photoexcited at 375 nm. The triplet energies of Py and BP are 201 kJ mol^{-1},[33] and 290 kJ mol^{-1},[33] respectively. In this energy relationship, the triplet energy transfer from ^{3}BP* to Py is expected to be diffusion-controlled. In this sensitized system, the reaction quantum yields include both the intersystem crossing efficiency of ^{1}BP* to ^{3}BP* and the triplet energy transfer quantum efficiency from ^{3}BP* to Py. However, both efficiencies are expected to be quantitative at this concentration of Py and, therefore, the values in Table 1 are equivalent to the reaction quantum yields of ^{3}**2t*** and ^{3}**2c***.

Reference Absorption Spectra. For an interpretation of the transient spectra in laser photolysis, reference absorption spectra were obtained by gamma-ray ionization[37] at 77 K in rigid matrices (2-chlorobutane and MTHF) and by laser photolysis at 297 K in solution.

Figure 2 shows two T–T ([I] and [II]) and six radical ion ([III]—[VIII]) absorption spectra with their peak wavelengths. The three spectra obtained at 297 K ([I]—[III]) were measured by the laser photolysis in liquid solvents, whereas five radical ion spectra obtained at

Table 1. Photocycloreversion and Photoisomerization Quantum Yields of Cyclobutane Dimers

Solvent/Additive	Photocycloreversion		Photoisomerization	
	2t	**2c**	**2t**	**2c**
MeCN/DMT[a]	0.033	0.046	0.005	0.033
MeCN/DCNB[b]	0.073	0.061	<0.001	0.071
Benzene	0.15	0.17	0.025	0.080
MeCN	0.093	0.077	0.007	0.033
MeCN/BP[c]	0.060	0.12	0.007	0.099

a) *N*,*N*-Dimethyl-*p*-toluidine (DMT, 1.0×10^{-2} mol dm^{-3}) was added as an electron donor. b) 1,4-Dicyanobenzene (DCNB, 1.0×10^{-2} mol dm^{-3}) was added as an electron acceptor. c) Benzophenone (BP, 2.5×10^{-2} mol dm^{-3}) was added as a triplet sensitizer, and was selectively photoexcited.

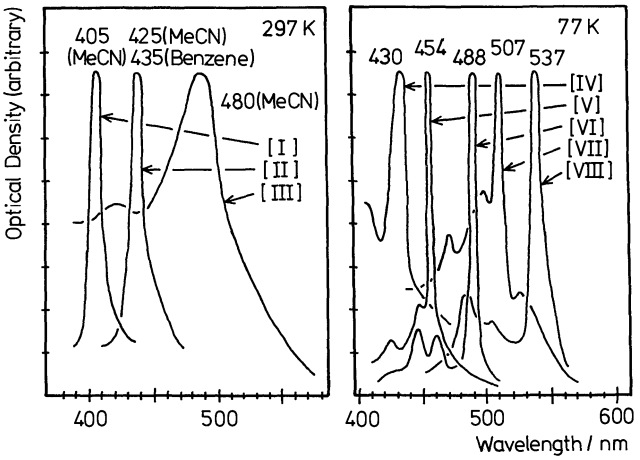

Fig. 2. Absorption spectra of triplet states and radical ions with the peak wavelengths. Spectra [I]—[III] were measured by the laser photolysis at 297 K. Spectra [IV]—[VIII] were obtained by the gamma-ray irradiation in rigid matrices at 77 K. [I]: ^{3}Py*, [II]: ^{3}**1***, [III]: DMT‡, [IV]: DCNB$^{\cdot-}$, [V]: Py‡, [VI]: Py$^{\cdot-}$, [VII]: **1**‡, and [VIII]: **1**$^{\cdot-}$.

77 K ([IV]—[VIII]) were measured by gamma-ray irradiation in rigid matrices. The radical ions and triplet states of the Py chromophore had sharp absorption bands at both temperatures, and the substitution by a vinyl group appreciably induced the red-shift of the peaks. For example, ^{3}Py* has an absorption peak at 405 nm, whereas ^{3}**1*** has a peak at 425 nm in the MeCN solvent. Hence, we can distinguish the Py triplet state (405 nm) formed in the cyclobutanes from the triplet state of **1** (425 nm) which is the product of photocleavage.

Figure 3 shows the absorption spectra of the radical ions of **2t** and **2c** produced by gamma-ray irradiation in rigid matrices at 77 K. The irradiation in the 2-chlorobutane matrix produces the radical cation of the solute, whereas in the MTHF matrix the radical anion is formed. Figures 3 [A] and [C] show the absorption spectra of **2t**‡ and **2c**‡, respectively. They show almost the same characteristics: Both have a broad peak at around 480 nm, which is quite different from that of Py‡ (454 nm). The absorption band shown in spectra [A] and [C] resembles that of intramolecular Py$_2^{\ddagger}$ in shape as well as in position. Such an absorption band

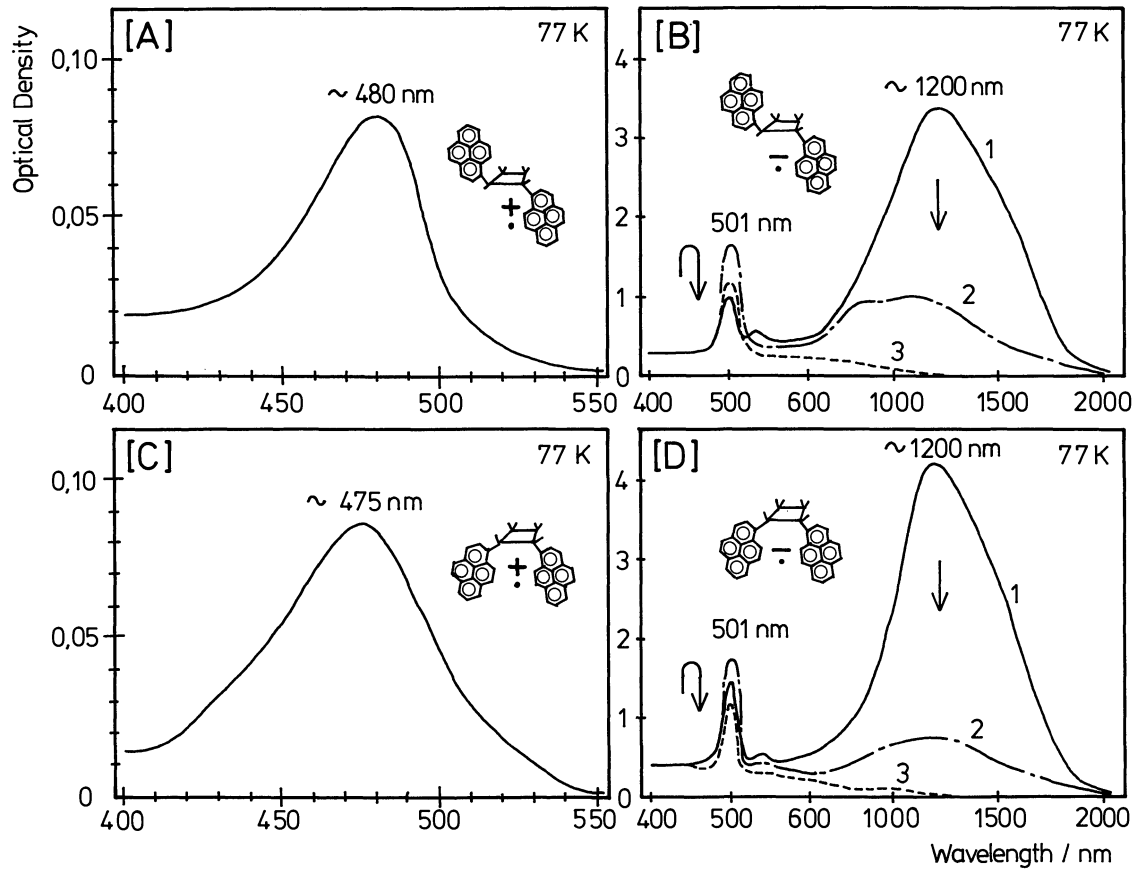

Fig. 3. Absorption spectra of radical ions of 1-vinylpyrene **1** cyclobutane dimers (**2t**: [A] and [B], and **2c**: [C] and [D]) with the peak wavelengths. Spectra were obtained by the gamma-ray irradiation in rigid matrices at 77 K. Immediately after irradiation (spectra No. 1), after warming (spectra No. 2), and after further warming (spectra No. 3). [A]: **2t**‡, [C]: **2c**‡, [B]: **2t**$^{\cdot-}$, and [D]: **2c**$^{\cdot-}$.

was observed for poly(1-vinylpyrene) or for the dimer models.[41] Therefore, these spectra are ascribed to the dimer radical cation of the intramolecular Py ($Py_2^{+\cdot}$) whose positive charge is delocalized between two py rings. The absorption spectrum of intramolecular $Py_2^{+\cdot}$ is less clear in vibrational structure compared to that of the dimer radical cation formed intermolecularly from pyrene.[23]

Radical anions of **2t** and **2c** were produced in MTHF at 77 K and the absorption spectra are shown in Fig. 3 [B] and [D], respectively. Both spectra are almost identical and the curves numbered 1 were taken immediately after gamma-ray irradiation. Two absorption bands are recognized in the spectra: The band at 501 nm is ascribed to the radical anion of Py ($Py^{-\cdot}$) formed in the dimers, and the band at around 1200 nm is assigned to the absorption of trapped electrons.[42] A slight warming of the MTHF matrix increased the band intensity at 501 nm, as shown in spectra No. 2; further warming decreased the absorption (spectra No. 3). The initial increase of this band is explained by a recapturing of trapped electrons to Py chromophores. This absorption band at 501 nm is very sharp compared with that of broad $Py_2^{+\cdot}$, and is similar to $Py^{-\cdot}$ (488 nm) in Fig. 2. The small spectral shift and the sharp band shape show the weaker interaction of Py chromophores in the anionic states of **2t** and **2c** than do those in the cationic states.[28,29]

Laser Photolysis Measurements. Nanosecond ruby-laser photolysis was carried out in order to study the transient intermediates of photocleavage reactions. Figure 4 shows the transient absorption spectra of dimers in benzene and MeCN solutions at 297 K. As shown in spectra [A] and [B], only ^{3}**1*** can be recognized by the photolysis of dimers in the benzene solvent. The transient absorption immediately after laser excitation (<50 ns) was hardly measured due to the overlap of the emission and the absorption of Py excimer could not be observed.[43] In the polar solvent MeCN, the spectra were the same as those in benzene, except for the shift of the absosrption maximum of ^{3}**1*** from 435 nm to 425 nm, which is due to the solvent effect as shown in the reference absorption spectra of Fig. 2. As shown in Fig. 4 [C] and [D], the addition of DMT as an electron donor to the dimers in MeCN solvent produced several transient species, which are ascribed to ^{3}**1*** (425 nm), $DMT^{+\cdot}$ (470 nm), $\mathbf{1}^{-\cdot}$ (500 nm), and $Py^{-\cdot}$ (530 nm). Since DMT has an absorption tail at 347.1 nm, the concentration of DMT in these systems was lowered to 1.0×10^{-3} mol dm^{-3}, which was a tenth of the concentration for the steady-state measurements of Table 1. Next, the effect of an electron acceptor DCNB was examined; the results are shown in spectra [E] and [F], where a strong absorption band of $Py_2^{+\cdot}$ was found at around 480 nm. The concentration of DCNB in these systems was the same as that for the steady-state experiment of Table 1, and the absorption of $DCNB^{-\cdot}$ appeared at 430 nm, overlapping with that of ^{3}**1***. In the figures, the dimer radical cations of **2t** and **2c** gave almost the same spectra.

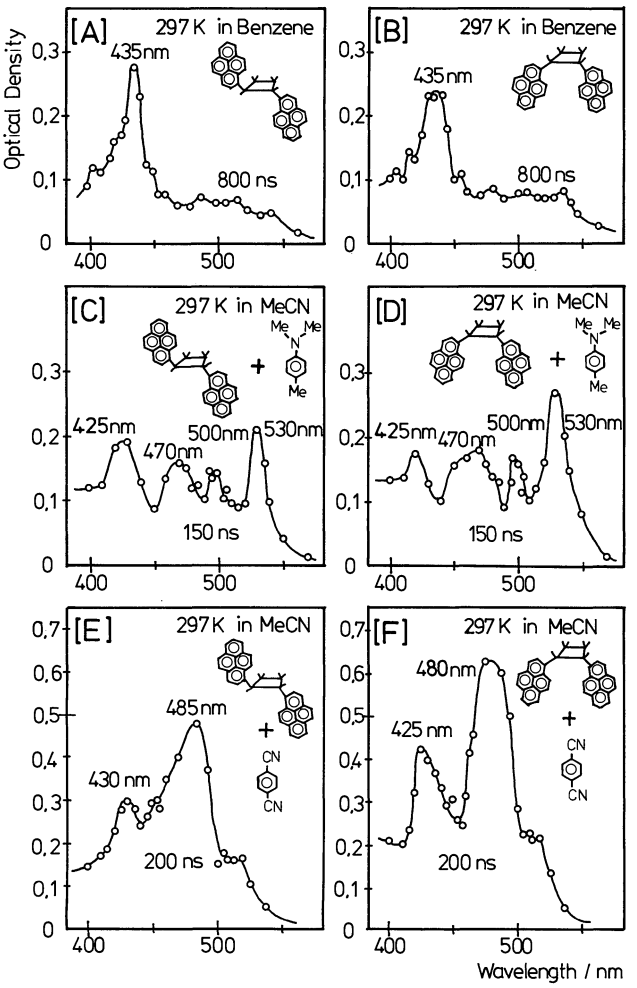

Fig. 4. Transient absorption spectra of 1-vinylpyrene **1** cyclobutane dimers **2t** ([A], [C], and [E]) and **2c** ([B], [D], and [F]) measured by the laser photolysis in benzene ([A] and [B]) or MeCN ([C], [D], [E], and [F]) solvent at 297 K. [A]: **2t** obtained at 800 ns after excitation, [C]: **2t** with DMT at 150 ns, [E]: **2t** with DCNB at 200 ns, [B]: **2c** at 800 ns, [D]: **2c** with DMT at 150 ns, and [F]: **2c** with DCNB at 200 ns. [DMT]= 1.0×10^{-3} mol dm^{-3}, and [DCNB]=1.0×10^{-2} mol dm^{-3}.

Table 2. Observed Transient Intermediates by Laser Photolysis Measurements

Solvent/Additive	2t	2c
MeCN/DMT[a]	^{3}**1***, $Py^{-\cdot}$, $\mathbf{1}^{-\cdot}$, $DMT^{+\cdot}$	^{3}**1***, $Py^{-\cdot}$, $\mathbf{1}^{-\cdot}$, $DMT^{+\cdot}$
MeCN/DCNB[b]	(^{3}**1***)[c], $Py_2^{+\cdot}$, $DCNB^{-\cdot}$	(^{3}**1***)[c], $Py^{+\cdot}$, $DCNB^{-\cdot}$
Benzene	^{3}**1***	^{3}**1***

a) *N*,*N*-Dimethyl-*p*-toluidine (DMT, 1.0×10^{-3} mol dm^{-3}) was added. b) 1,4-Dicyanobenzene (DCNB, 1.0×10^{-2} mol dm^{-3}) was added. c) Absorption band of ^{3}**1*** overlapps with that of $DCNB^{-\cdot}$.

Table 2 summarizes the transient species observed in Fig. 4. In every system, the formation of ^{3}**1*** was

recognized but ^{3}Py* could not be found in the time range of our measurements. In a system with an additive, DCNB, the absorption of the dimer radical cation ($Py_2^{+\cdot}$) was observed, whereas in the system with DMT, there was no noticeable evidence of dimer radical anion ($Py_2^{-\cdot}$) formation.

Discussion

Figure 1 shows a broader absorption band shape of **2c** than that of **2t**, indicating that two neighboring Py chromophores interact in the cis position of the cyclobutane ring. This interaction in the ground state was not found for the cyclobutanes having naphthyl groups. The absorption spectra of *trans*- and *cis*-1,2-di(2-naphthyl)cyclobutanes resemble those of 2-ethylnaphthalene.[44] The Py ring seems to be large enough to interact in the cis position of cyclobutane. The trans dimer **2t** showed almost the same absorption spectrum as that of EPy; that is, the Py chromophores in the trans position of cyclobutane are too far to interact. By contrast, as for the cyclobutane which has an electron donor and an acceptor in the trans position, a chromophore interaction was found in the absorption spectrum; the absorption bands of the Py chromophore for the *trans*-cycloadduct of *trans*-1-(4-dimethylaminophenyl)-2-(1-pyrenyl)cyclobutane were slightly different from that of EPy.[16] The interaction distance of the electron donor–acceptor pair seems to be long enough to reach in the trans position of the cyclobutane ring in the ground state.

Photocycloreversion of Dimers via Ionic Intermediates. The cycloreversion and isomerization of dimers, **2t** and **2c**, via the ionic intermediates were examined by the addition of an electron donor DMT or an electron acceptor DCNB to the solution. The chromophore pairs of DMT–Py and of Py–DCNB are known to form exciplexes in nonpolar solvents; their photophysical characteristics have been extensively studied.[39,40] In such polar solvents as MeCN, an electron transfer from a donor to an acceptor is followed by photodissociation into solvated free radical ions; in this case, electron transfer from DMT to Py produces $DMT^{+\cdot}$ and $Py^{-\cdot}$ and that from Py to DCNB produce $Py^{+\cdot}$ and $DCNB^{-\cdot}$.

Spectra [C] and [D] of Fig. 4 show the transient absorption obtained 150 ns after excitation in an MeCN solvent at 297 K. Photoexcited **2t** and **2c** were quenched by DMT to give the four transient absorption bands. As shown in the figures, the two dimers show similar spectra. In these systems, the concentration of DMT was lowered to one tenth of that in the quantum yield measurements, as mentioned before. By dilution, the electron-transfer quenching of dimers by DMT becomes slightly insufficient. The formations of ^{3}**1*** (425 nm) and $\mathbf{1}^{-\cdot}$ (500 nm), as shown in the spectra, are considered to be caused by this low DMT concentration. The quenching by DMT cannot effectively compete with the direct photocleavage which produces **1**. Then, successive photoabsorption of the same exciting laser pulse tail by product **1** forms ^{1}**1***, which is converted to ^{3}**1*** by intersystem crossing; and $\mathbf{1}^{-\cdot}$ was produced by an electron transfer from DMT to ^{1}**1***. The fact that the lifetime of ^{3}**1*** did not change with the concentration of DMT indicates that the quenching of ^{3}**1*** by DMT is negligible.

The $Py^{-\cdot}$ can be recognized at 530 nm in transient spectra [C] and [D]. The absorption band shape and the peak wavelength of the $Py^{-\cdot}$ are in accord with those obtained by gamma-ray irradiation, as shown in Figs. 3 [B] and [D]. This $Py^{-\cdot}$, whose charge is localized to one Py ring, is produced by electron transfer quenching of ^{1}**2t*** and ^{1}**2c*** with DMT. In the present study, no absorption band which can be ascribed to $Py_2^{-\cdot}$ could be found. As for the formation of the aromatic dimer radical anion, there has been no report,[25] except for a special case.[26] The charge resonance energy in the dimer radical anion seems to be weaker than that of the dimer radical cation. The results that the lifetime of the $Py^{-\cdot}$ is in the microsecond order and that it decays mostly by the recombination with $DMT^{+\cdot}$ (470 nm) indicate that the fraction of the cleavage of dimers through the $Py^{-\cdot}$ is not so large.

Table 1 shows that the quantum yields of photocleavage of dimers through the quenching by DMT are low (0.033 for **2t** and 0.046 for **2c**). This is because $\mathbf{2t}^{-\cdot}$ and $\mathbf{2c}^{-\cdot}$ are deactivated by the recombination with $DMT^{+\cdot}$ and their cleavage is not a major process. On the other hand, the cleavage quantum yields of dimers quenched by DCNB are higher (0.073 for **2t** and 0.061 for **2c**) than the systems of the DMT additive. In the transient absorption spectra as shown in Figs. 4 [E] and [F], the strong absorption of $Py_2^{+\cdot}$ (ca. 480 nm), which was identified by the reference spectra of Figs. 3 [A] and [C], was found as a main band, and this $Py_2^{+\cdot}$ seems to be cleaved. In Figs. 4 [E] and [F], the small absorption band of ^{3}**1*** can also be recognized through it overlaps with that of $DCNB^{-\cdot}$ (430 nm), but it is not a major product.

It is interesting that the photocleavage via $\mathbf{2t}^{+\cdot}$ and $\mathbf{2c}^{+\cdot}$, whose positive charge is delocalized to $Py_2^{+\cdot}$, is more efficient than that via $\mathbf{2t}^{-\cdot}$ and $\mathbf{2c}^{-\cdot}$, whose negative charge is localized to $Py^{-\cdot}$. Ledwith et al. proposed that an open-chain type radical cation of *trans*-1,2-di(9-carbazolyl)cyclobutane (DCzB) participates in the cycloaddition reaction.[45] The laser photolysis experiments of the DCzB showed that the two carbazole (Cz) chromophores in the trans position of the cyclobutane ring give the absorption of the dimer radical cation ($Cz_2^{+\cdot}$).[27] In our system of $\mathbf{2t}^{+\cdot}$, the formation of the dimer radical cation has been confirmed, as mentioned above. Recently, a theoretical calculation and experiments concerning CIDNP have suggested the existence of a "long-bonded cyclobutane" structure:[19,20] The one bond of a radical cation cyclobutane ring becomes long by the deficiency of the electron density.

The finding that the cleavage quantum yields of $\mathbf{2t}^{\pm\cdot}$ and $\mathbf{2c}^{\pm\cdot}$ are larger than those of $\mathbf{2t}^{-\cdot}$ and $\mathbf{2c}^{-\cdot}$ is in agreement with the reactivity tendency of the "long-bonded cyclobutane" structure. The decrease in the electron density in the cyclobutane bond is considered to promote the cleavage reaction.

As for the isomerization reactions of dimers via ionic intermediates, the isomerization from **2c** to **2t** was found to be favorable. This is considered to be caused by the steric factor of the cyclobutane ring.

Photocycloreversion of Dimers from Singlet and Triplet Excited States. As shown in Table 1, the reaction quantum yields of cycloreversion and isomerization of **2t** and **2c** without an additive in the nonpolar benzene solvent are larger than those in the polar MeCN solvent. The polar excited singlet state of cyclobutanes seems to be stabilized in a polar MeCN solvent by solvation, and deactivation processes become dominant. Similar solvent effects could also be seen in our previous study.[16] As for the effects of different configurations of **2t** and **2c**, the quantum yields of cycloreversion of both dimers were nearly the same, whereas those of isomerization were larger for **2c** than for **2t**. The latter seems to be due to the "cis effect" of the Py chromophores.[1,8] The "cis effect" occurs due to a strain of the cyclobutane ring when the cyclobutane ring is substituted by large chromophores, or when the cyclobutane ring is a part of a bi- or polycycle. The photocleavage reaction in the latter case has often been reported to proceed by a chain mechanism.[13,14] In the present system, however, the effect is not so large. Furthermore, the quantum yields of cycloreversion for **2t** and **2c** are nearly the same. It seems that a cycloreversion in the excited state is effective for the large Py chromophore in the trans position of cyclobutane, as well as in the cis position.

The cycloreversion and isomerization from the excited triplet state of dimers, **2t** and **2c**, were observed by the use of triplet sensitizer of benzophenone (BP) as shown in Table 1. As mentioned before, these quantum yields in Table 1 are regarded as being the quantum yield of cleavage or isomerization of the dimers from their triplet state. They show that the dimer **2c** has a higher reactivity of cycloreversion and isomerization compared with that for **2t**. In triplet sensitized photocycloreversion, a diradical intermediate is most popular.[9,15] Probably, this is also ascribed to the cis effect.

In laser photolysis measurements, the transient absorption spectra of [A] and [B] in Fig. 4 gave only the band of $^3\mathbf{1}^*$. This formation of $^3\mathbf{1}^*$ was recognized in all transient spectra as shown in Table 2, and further the system which gave a large cleavage quantum yield showed stronger absorption of $^3\mathbf{1}^*$. These facts suggest that $^3\mathbf{1}^*$ is formed through a two step photo-excitation process.[16] The exciting laser light of our laser photolysis has a pulse duration of 14 ns. If the rate of cycloreversion is fast enough, the photoproduct **1** can be excited again by the same exciting light pulse tail, and then the produced $^1\mathbf{1}^*$ converts to $^3\mathbf{1}^*$. Overlapping of the fluorescence in the short time region (<50 ns) after the excitation hindered the observation of short-lived transient species, such as an excimer or zwitterion in the systems of Figs. 4 [A] and [B]. As for the anthracene dimer, the excimer was proposed as the transient intermediate of the cycloreversion.[11] Similarly, the excimer intermediate may participate in the cycloreversion of **2t** and **2c** in consideration of the fact that the chromophore Py easily forms the excimer.[21,22] As for the cyclobutane compounds, the most stable conformation of a cis cyclobutane ring is considered to be in a puckered form. The planar form, where two aromatic rings take the nearest conformation, has a slightly higher energy state, ca. 6.3 kJ mol^{-1} than the puckered form.[46] Furthermore, two aromatic rings cannot take a parallel-sandwich arrangement, even in the planar form of cyclobutane by the framework of cyclobutane ring.[44] Therefore, the excimer formed in cyclobutane compounds is unstable, and this is probably one of the reasons for the weak excimer emission and short lifetime.

Conclusion

The transient states of photocycloreversion and isomerization reactions of 1-vinylpyrene **1** cyclobutane

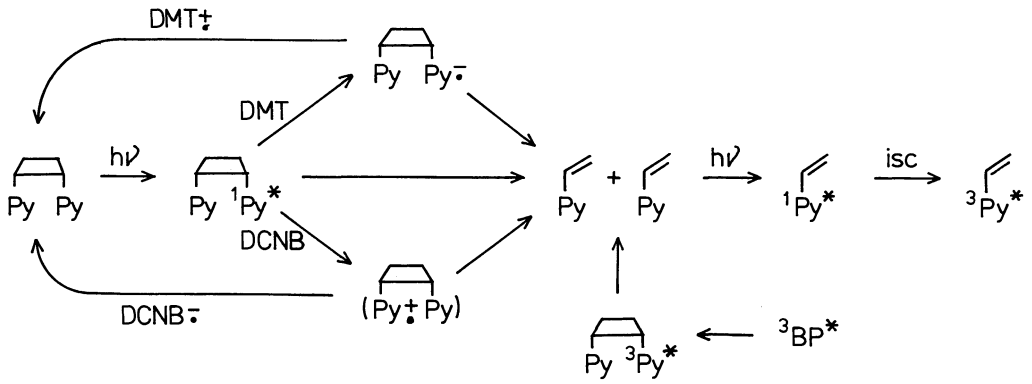

Scheme 1.

dimers, **2t** and **2c**, were discussed from the absorption spectra of laser photolysis and by the reaction quantum yields under the steady-state photoirradiation. The results are summarized in the Scheme. An efficient cycloreversion of dimers was found from their singlet and triplet states, though the solvation of the excited state by a polar solvent decreased the cycloreversion yields. The intramolecular dimer radical cation formation was observed for the dimers and the $\mathbf{2t}^{\cdot+}$ and $\mathbf{2c}^{\cdot+}$ were found to cleave in a yield comparable to that of direct photocleavage. An electron deficiency in the dimers is considered to be responsible for the cleavage. No formation of the dimer radical anion was observed. The cleavage of $\mathbf{2t}^{\cdot-}$ and $\mathbf{2c}^{\cdot-}$ to **1** was inefficient.

We thank Professor Hitoshi Yamaoka of the Research Reactor Institute, Kyoto University, for his help in determining the reference absorption spectra of the ion radicals.

References

1) Reviews: a) E. Schaumann and R. Ketcham, *Angew. Chem., Int. Ed. Engl.,* **21**, 225 (1982). b) A. A. Lamola, *Mol. Photochem.,* **4**, 107 (1972). c) J. J. McCullough, *Chem. Rev.,* **87**, 811 (1987). d) M. C. Lasne and J. L. Ripoll, *Synthesis,* **1985**, 121. e) K. C. Bishop, III, *Chem. Rev.,* **76**, 461 (1976). f) C. Pac, *Pure Appl. Chem.,* **58**, 1249 (1986).

2) R. B. Woodward and R. Hoffmann, "The Conservation of Orbital Symmetry," Academic Press, New York (1970).

3) K. N. Houk, *Pure Appl. Chem.,* **54**, 1633 (1982).

4) a) T. Bally, E. Haselbach, Z. Lanyiova, and P. Baertschi, *Helv. Chim. Acta,* **61**, 2488 (1978). b) E. Haselbach, T. Bally, and Z. Lanyiova, *Helv. Chim. Acta,* **62**, 577 (1979). c) E. Haselbach, T. Bally, Z. Lanyiova, and P. Baertschi, *Helv. Chim. Acta,* **62**, 583 (1979).

5) N. Yonezawa, T. Yoshida, and M. Hasegawa, *J. Chem. Soc., Perkin Trans. 1,* **1983**, 1083, and other references are sited therein.

6) C. Kaneko, N. Katagiri, K. Uchiyama, and T. Yamada, *Chem. Pharm. Bull.,* **33**, 4160 (1985).

7) a) L. M. Stephenson and J. I. Brauman, *J. Am. Chem. Soc.,* **93**, 1988 (1971). b) L. M. Stephenson and T. A. Gibson, *J. Am. Chem. Soc.,* **96**, 5624 (1974).

8) a) G. Kaupp and M. Stark, *Chem. Ber.,* **110**, 3084 (1977). b) G. Kaupp, M. Stark, and H. Fritz, *Chem. Ber.,* **111**, 3624 (1978).

9) a) H. Shizuka, I. Seki, T. Morita, and T. Iizuka, *Bull. Chem. Soc. Jpn.,* **52**, 2074 (1979). b) H. Kobashi, H. Ikawa, R. Kondo, and T. Morita, *Bull. Chem. Soc. Jpn.,* **55**, 3013 (1982).

10) S. Murov and G. G. Hammond, *J. Phys. Chem.,* **72**, 3797 (1968).

11) a) G. Jones, II and V. L. Chow, *J. Org. Chem.,* **39**, 1447 (1974). b) G. Jones, II and S. -H. Chiang, *Tetrahedron,* **37**, 3397 (1981). c) G. Jones, II, W. Schwarz, and V. Malba, *J. Phys. Chem.,* **86**, 2286 (1982). d) G. Jones, II, S. -H. Chiang, W. G. Becker, and J. A. Welch, *J. Phys. Chem.,* **86**, 2805 (1982). e) L. E. Manring, K. S. Peters, G. Jones, II, and W. R. Bergmark, *J. Am. Chem. Soc.,* **107**, 1485 (1985).

12) G. N. Taylor, *Z. Phys. Chem. (Wiesbaden),* **101**, 237 (1976).

13) a) T. Mukai and Y. Yamashita, *Tetrahedron Lett.,* **19**, 357 (1978). b) K. Okada, K. Hisamitsu, and T. Mukai, *Tetahedron Lett.,* **22**, 1251 (1981). c) T. Miyashi, K. Wakamatsu, T. Akiya, K. Kikuchi, and T. Mukai, *J. Am. Chem. Soc.,* **109**, 5270 (1987). d) Y. Yamashita, H. Ikeda, and T. Mukai, *J. Am. Chem. Soc.,* **109**, 6682 (1987), and other references are sited therein.

14) a) T. Majima, C. Pac, J. Kubo, and H. Sakurai, *Tetrahedron Lett.,* **21**, 377 (1980). b) T. Majima, C. Pac, and H. Sakurai, *J. Am. Chem. Soc.,* **102**, 5265 (1980). c) C. Pac, J. Kubo, T. Majima, and H. Sakurai, *Photochem. Photobiol.,* **36**, 273 (1982). d) C. Pac, T. Ohtsuki, Y. Shiota, S. Yanagida, and H. Sakurai, *Bull. Chem. Soc. Jpn.,* **59**, 1133 (1986), and other references are sited therein.

15) a) S. Takamuku, B. Dinh-Ngoc, and W. Schnabel, *Z. Naturforsh., Teil A,* **33**, 1281 (1978). b) S. Takamuku and W. Schnabel, *Chem. Phys. Lett.,* **69**, 399 (1980). c) S. Takamuku, H. Kigawa, H. Suematsu, S. Toki, K. Tsunori, and H. Sakurai, *J. Phys. Chem.,* **86**, 1861 (1982). d) H. Nishino, S. Toki, and S. Takamuku, *J. Am. Chem. Soc.,* **108**, 5030 (1986), and other references are sited therein.

16) A. Tsuchida, M. Yamamoto, and Y. Nishijima, *J. Chem. Soc., Perkin Trans. 2,* **1987**, 507.

17) a) J. M. Masnovi and J. K. Kochi, *J. Am. Chem. Soc.,* **107**, 6781 (1985). b) J. M. Masnovi and J. K. Kochi, *J. Phys. Chem.,* **91**, 1878 (1987).

18) a) R. D. Small, Jr. and J. C. Scaiano, *Chem. Phys. Lett.,* **50**, 431 (1977). b) R. D. Small, Jr. and J. C. Scaiano, *Chem. Phys. Lett.,* **59**, 246 (1978). c) D. H. R. Barton, B. Charpiot, K. U. Ingold, L. J. Johnston, W. B. Motherwell, J. C. Scaiano, and S. Stanforth, *J. Am. Chem. Soc.,* **107**, 3607 (1985).

19) a) D. J. Bellville, D. D. Wirth, and N. L. Bauld, *J. Am. Chem. Soc.,* **103**, 718 (1981). b) R. A. Pabon, D. J. Bellville, and N. L. Bauld, *J. Am. Chem. Soc.,* **106**, 2730 (1984). c) D. J. Bellville, R. A. Pabon, and N. L. Bauld, *J. Am. Chem. Soc.,* **107**, 4978 (1985), and other references are sited therein.

20) a) H. D. Roth, in "Chemically Induced Magnetic Polarization," ed by L. T. Muus, P. W. Atkins, K. A. McLauchlan, and J. B. Pedersen, Reidel, Dordrecht (1977). b) H. D. Roth and M. L. M. Schilling, *J. Am. Chem. Soc.,* **103**, 1246 (1981). c) H. D. Roth and M. L. M. Schilling, *J. Am. Chem. Soc.,* **103**, 7210 (1981).

21) T. Förster and K. Kasper, *Z. Phys. Chem. (Munich),* **1**, 275 (1954).

22) J. B. Birks, "Photophysics of Aromatic Molecules," Wiley, New York (1970).

23) a) A. Kira, S. Arai, and M. Imamura, *J. Chem. Phys.,* **54**, 4890 (1971). b) S. Arai, A. Kira, and M. Imamura, *J. Chem. Phys.,* **56**, 1777 (1972). c) A. Kira, S. Arai, and M. Imamura, *J. Phys. Chem.,* **76**, 1119 (1972). d) A. Kira, M. Imamura, and T. Shida, *J. Phys. Chem.,* **80**, 1445 (1976).

24) a) I. C. Lewis and L. S. Singer, *J. Chem. Phys.,* **43**, 2712 (1965). b) M. A. J. Rogers, *Chem. Phys. Lett.,* **9**, 107 (1971). c) R. E. Bühler and W. Funk, *J. Phys. Chem.,* **79**, 2098 (1975). d) A. K. Chandra, K. Bhanuprakash, V. C. Jyoti Bhasu, and D. Srikanthan, *Mol. Phys.,* **52**, 733 (1984).

25) a) B. Badger and B. Brocklehurst, *Trans. Faraday Soc.,* **65**, 2588 (1969). b) B. Badger and B. Brocklehurst, *Trans. Faraday Soc.,* **65**, 2939 (1969). c) B. Badger, B. Brocklehurst, and R. D. Russell, *Chem. Phys. Lett.,* **1**, 122 (1967).

26) a) T. Shida and S. Iwata, *J. Am. Chem. Soc.,* **95**, 3473 (1973). b) T. Shida, *J. Phys. Chem.,* **82**, 991 (1978).

27) a) H. Masuhara, J. Vandendriessche, K. Demeyer, N. Boens, and F. C. De Schryver, *Macromolecules,* **15**, 1471 (1982). b) H. Masuhara, N. Tamai, N. Mataga, F. C. De Schryver, and J. Vandendriessche, *J. Am. Chem. Soc.,* **105**, 7256 (1983). c) H. Masuhara, J. A. Tanaka, N. Mataga, F. C. De Schryver, and P. Collart, *Polym. J.,* **15**, 915 (1983). d) H. Masuhara, K. Yamamoto, N. Tamai, K. Inoue, and N. Mataga, *J. Phys. Chem.,* **88**, 3971 (1984).

28) a) S. Arai, A. Kira, and M. Imamura, *J. Phys. Chem.,* **81**, 110 (1977). b) T. Shida and S. Iwata, *J. Chem. Phys.,* **56**, 2858 (1972).

29) A. Tsuchida, N. Masuda, M. Yamamoto, and Y. Nishijima, *Macromolecules,* **19**, 1299 (1986).

30) I. Tsushi, Y. Shirota, and H. Mikawa, *Polym. Prepr. Jpn.,* **23**, 109 (1974).

31) a) M. Yamamoto, T. Asanuma, and Y. Nishijima, *J. Chem. Soc., Chem. Commun.,* **1975**, 53. b) T. Asanuma, M. Yamamoto, and Y. Nishijima, *J. Chem. Soc., Chem. Commun.,* **1975**, 56. c) T. Asanuma, M. Yamamoto, and Y. Nishijima, *J. Chem. Soc., Chem. Commun.,* **1975**, 608.

32) a) A. Tsuchida, M. Yamamoto, and Y. Nishijima, *J. Chem. Soc., Perkin Trans. 2,* **1986**, 239. b) A. Tsuchida, M. Yamamoto, and Y. Nishijima, *Bull. Chem. Soc. Jpn.,* **60**, 2899 (1987).

33) S. L. Murov, "Handbook of Photochemistry," Marcel Dekker, New York (1973).

34) C. G. Hatchard and C. A. Parker, *Proc. R. Soc. London, Ser. A,* **235**, 518 (1956).

35) J. N. Demas and G. A. Crosby, *J. Phys. Chem.,* **75**, 991 (1971).

36) A. Tsuchida, M. Yamamoto, and Y. Nishijima, *J. Phys. Chem.,* **88**, 5062 (1984).

37) W. H. Hamill, in "Radical Ions," ed by E. T. Kaiser and L. Kevan, Interscience, New York (1968), Chap. 9.

38) a) K. Kalyanasundaram and J. K. Thomas, *J. Am. Chem. Soc.,* **99**, 2039 (1977). b) A. Nakajima, *Bull. Chem. Soc. Jpn.,* **50**, 2473 (1977).

39) a) N. Mataga, T. Okada, and N. Yamamoto, *Chem. Phys. Lett.,* **1**, 119 (1967). b) N. Mataga and T. Kubota, "Molecular Interactions and Electronic Spectra," Dekker, New York (1970). c) H. Masuhara and N. Mataga, *Acc. Chem. Res.,* **14**, 312 (1981).

40) a) K. G. Grellmann, A. R. Watkins, and A. Weller, *J. Phys. Chem.,* **76**, 469 (1972). b) H. Schomburg, H. Staerk, and A. Weller, *Chem. Phys. Lett.,* **21**, 433 (1973). c) H. Schomburg, H. Staerk, and A. Weller, *Chem. Phys. Lett.,* **22**, 1 (1973). d) H. Schomburg, H. Staerk, A. Weller, and H. J. Werner, *Chem. Phys. Lett.,* **56**, 399 (1978).

41) a) J. A. Tanaka, H. Masuhara, and N. Mataga, *Polym. J.,* **18**, 181 (1986). b) J. A. Tanaka, H. Masuhara, N. Mataga, R. Goedeweeck, and F. C. De Schryver, *Polym. J.,* **18**, 331 (1986).

42) L. F. Dorfman and F. Y. Jou, in "Electrons in Fluids," ed by J. Jortner and N. R. Kestner, Springer-Verlag, Berlin (1973).

43) M. F. M. Post, J. Langelaar, and J. D. W. Voorst, *Chem. Phys. Lett.,* **10**, 468 (1971).

44) S. Ito, M. Yamamoto, and Y. Nishijima, *Bull. Chem. Soc. Jpn.,* **57**, 3295 (1984).

45) a) P. Beresford, M. C. Lambert, and A. Ledwith, *J. Chem. Soc., Chem. Commun.,* **1970**, 2508. b) A. Ledwith, *Acc. Chem. Res.,* **5**, 133 (1972).

46) R. M. Moriarty, in "Topics in Stereochemistry," ed by E. L. Eliel and N. L. Allinger, Interscience, New York (1974), Vol. 8, p. 271.

 © 1991 The Chemical Society of Japan Bull. Chem. Soc. Jpn., 64, 3411—3416 (1991)

Acid-Promoted Oxidations of an NAD(P)H Model with Hydrogen Peroxide and Molecular Oxygen

Seizo TAMAGAKI, Takashi MIMURA, and Waichiro TAGAKI*
Department of Bioapplied Chemistry, Faculty of Engineering, Osaka City University, Sugimoto 3-3-138, Sumiyoshi-ku, Osaka 558
(Received June 24, 1991)

The $HClO_4$-catalyzed H_2O_2- and O_2-oxidations of a dihyropyridine in acetonitrile were mechanistically investigated; the H_2O_2-oxidation under nitrogen followed a heterolytic course to yield the corresponding pyridinium salt along with a monooxygenated product, while the O_2-oxidation produced the pyridinium salt and H_2O_2 via a radical-chain pathway in which H_2O_2 is not only merely the product but also an initiator.

NAD(P)H pyridine coenzyme is used as a versatile reductant in a living cell,[1] and numerous examples exist of reductions of many organic functional groups such as C=O, C=C, and N=O bonds with NAD(P)H and its model compounds.[2] Meanwhile, peroxides occur in a living body in connection with production or removal of peroxidic compounds and activation of oxygen.[3] Although the oxidations of NAD(P)H by peroxides are potentially important in biology, model studies on the oxidation of NAD(P)H with peroxidic compounds have been only a few. For examle, 1-methyl-1,4-dihydro-3,5-bis(ethoxycarbonyl)-2,6-lutidine was oxidized at high temperatures with diacyl peroxides by a free-radical chain mechanism to the corresponding pyridinium cation.[4] Thus, noncatalytic reactions are generally very slow despite the inherent reducing ability of an NAD(P)H ring itself. Recently, we have reported on the rate-enhancing effect of some bivalent metals in the O_2- and H_2O_2-oxidations of an NAD(P)H model (1-benzyl-3,5-bis(1-pyrrolidinylcarbonyl)-1,4-dihydropyridine (BPDH)); these reactions were found to proceed via a radical chain mechanism.[5]

In continuing our study of oxidations of a dihydropyridine ring, acid-catalyzed oxidation of BPDH with H_2O_2 under N_2 or O_2 has been thoroughly investigated in this work and we have found that, unlike bivalent metal-facilitated oxidations, the acid-catalyzed H_2O_2-oxidation proceeds via different courses depending on the reaction atmosphere. The acid-catalyzed oxidations of a closely-related NADH model with oxygen were previously studied under special conditions,[6] and by using an acid-stable NADH model (BPDH), where H_2O_2 is a final product.[7]

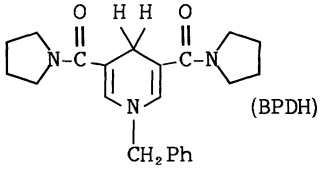

(BPDH)

Experimental

Materials. BPDH was prepared by reducing 1-benzyl-3,5-bis(1-pyrrolidinylcarbonyl)pyridinium chloride with $Na_2S_2O_4$ in a two-phase aqueous Na_2CO_3–CH_2Cl_2 system in a blanket of nitrogen as described in the preceding paper.[8] Acetonitrile was distilled from P_2O_{10}. H_2O_2 (30%) and $HClO_4$ (70%) were obtained from Wako Pure Chemical Industry and used as received.

Kinetics. The acid-catalyzed oxidations have been studied at 25 °C in CH_3CN in the presence of $HClO_4$ as the catalyst by monitoring the variation of the absorbance at 355 nm due to BPDH with time. Unless otherwise stated, the concentrations of BPDH, $HClO_4$, and H_2O_2 were 0.1 mM, 0.1—20 mM, and 0.5—15 mM, respectively. (mM=10^{-3} M, 1M=1 mol dm^{-3}). An $HClO_4$- and an H_2O_2-stock solution were prepared by diluting commercially available 70 and 30% aqueous solutions, respectively, with MeCN.

H_2O_2-Oxidation of BPDH. Product Analysis. BPDH (0.55 g, 1.5 mmol) was dissolved in 20 ml of CH_3CN. To this solution 2.0 mmol of H_2O_2 (30%) and 2.0 mmol of $HClO_4$ (70%) were added under nitrogen. After stirring for 24 h at room temperature, hydrochloric acid (1 equiv, 20 ml) was added. The acetonitrile was evaporated under reduced pressure, the resulting mixture was extracted with $CHCl_3$, and then the solvent was evaporated. The residue was subjected to preparative TLC on a silica plate eluting with 10:1 $CHCl_3$–MeOH to give the oxidized form of BPDH (BPD^+Cl^-) (50%) and 1-Benzyl-3,5-bis(1-pyrrolidinylcarbonyl)-3,4-dihydro-2(1*H*)-pyridinone (47%): Mp 188—192 °C; UV (MeCN) 274 (ε 8800); ^1H NMR ($CDCl_3$) δ=1.85 (8H, m, $N(CH_2)_2(C\underline{H}_2)_2$), 2.87 (2H, m(ABX), 4-$C\underline{H}_2$), 3.47 (8H, m, $N(C\underline{H}_2)_2(CH_2)_2$), 3.77 (1H, q(ABX), 3-H), 4.68 (2H, dd, Ph-$C\underline{H}_2$), 6.52 (1H, s, 6-H), and 7.18 (5H, s, Ph); MS (70 eV) *m/z* (rel intensity) 381 (M^+; 0.7), 311 (1.1), 283 (73), and 91 (100). Elemental Anal: Found: C, 69.11; H, 7.10; N, 10.72 %. Calcd for $C_{22}H_{27}N_3O_3$: C, 69.27; H, 7.13; N, 11.02 %.

O_2-Oxidation of BPDH. Product Analysis. The reaction with O_2 was performed with 0.50 mmol BPDH and 0.5—50 mmol $HClO_4$ in pure oxygen-saturated MeCN (50 ml) for 24 h. To evaluate the yield of the H_2O_2 produced, excess PPh_3 and AcOH was added and the reaction mixture was kept standing at room temperature for another 24 h. An excess of hydrochloric acid was added, the solvent was evaporated, and the residue was subjected to preparative TLC eluting with 5:1 $CHCl_3$–MeOH, giving $Ph_3P=O$ and the corresponding pyridinium chloride (BPD^+Cl^-, I). The results are collected in Table 1.

BPDH–$HClO_4$ 1:1 Adduct. Addition of an approximate excess of aqueous 70 % $HClO_4$ to a solution of BPDH (0.5 mmol) in 25 mL of CH_3CN gave immediate precipitation of a yellow solid; decompn. 153—155 °C; its ^1H NMR spectrum

Table 1. O_2-Oxidation of BPDH in the Presence of Perchloric Acid

Catalyst	M	Isolated yield/%	
		H_2O_2[a)]	BPD^+Cl^-
$HClO_4$	0.01	70.8	95.0
$HClO_4$	0.20	67.7	96.0
$HClO_4$	1.00	50.5	86.9
$Ca(ClO_4)_2$[5)]	0.05	89.4	94.9

Conditions: [BPDH]=1.0×10^{-2} M; in O_2-saturated MeCN (50 mL) at 25°C. a) The amount of produced H_2O_2 was determined as $Ph_3P=O$.

in DMSO-d_6 indicated that the adduct dissociated into the original components, $HClO_4$ and BPDH, in a molar ratio of 1:1. The resonance due to the liberated $HClO_4$ appeared at δ=10.0.

Results and Discussion

The oxidation of BPDH by H_2O_2 under nitrogen in $HClO_4$-containing acetonitrile afforded the monooxygenated (II) as well as dehydrogenated (I) products being isolated in a 1:1 ratio. In order to disclose the reaction mechanism, the reaction was kinetically examined in

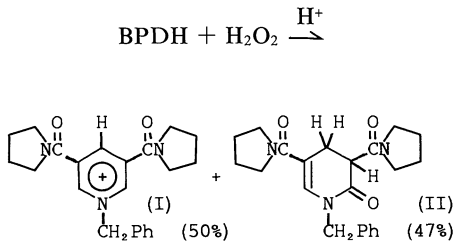

detail. The progress of reaction was followed spectroscopically by monitoring the disappearance of BPDH. The BPDH oxidation of an equiv of H_2O_2 under nitrogen was so much slow that a 100-fold excess of H_2O_2 was employed to retain the practical reaction rate. The reaction followed the first-order kinetics in each [BPDH] and [H_2O_2] (Fig. 1). The rate variation with changing [$HClO_4$] (<10 mM) was complicated but interesting; the rate was linear with regard to [$HClO_4$] in the region of less than 1.5 mM and, after passing through the maximum, the rate seems to approach slowly zero (Fig. 2); such a characteristic feature of acid-dependency of the rate can not be accounted for in terms of a decreasing activity of $HClO_4$ with its increasing concentrations because dissociation of $HClO_4$ to H^+ and ClO_4^- in acetonitrile is almost complete in such a low [$HClO_4$] region (pK_a<2 in MeCN).[9)] Another explanation might be possible by considering participation of water inevitably involved in 70% $HClO_4$, but it also seems unlikely, because no substantial influence was observed by addition of up to a 100-fold excess of water over $HClO_4$. Similarly, the abnormal rate-[$HClO_4$] profile can not be interpreted, of course, by a mechanism, involving a protonation

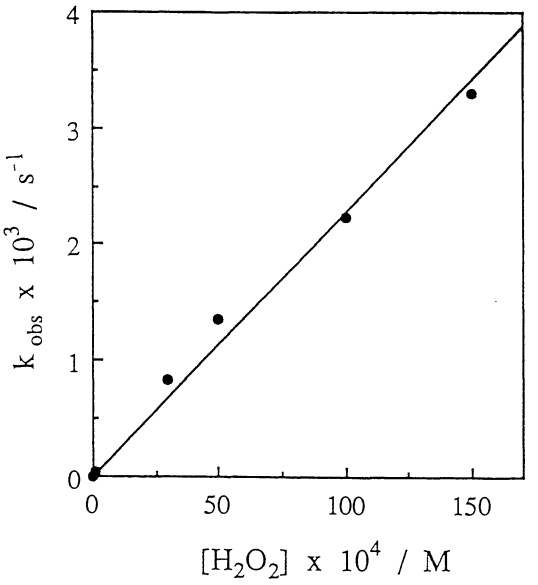

Fig. 1. Dependence of k_{obs} upon H_2O_2 concentration for H_2O_2-oxidation of BPDH under nitrogen in MeCN at 25°C; $[BPDH]_0$=0.1 mM; [$HClO_4$]=2.0 mM.

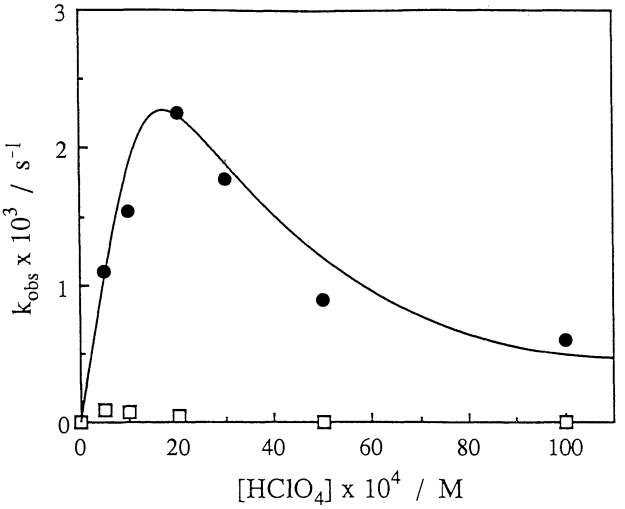

Fig. 2. H_2O_2-oxidation of BPDH in the presence of changing $HClO_4$ concentrations under nitrogen; $[BPDH]_0$=0.1 mM; ●: $[H_2O_2]_0$=10 mM, □: $[H_2O_2]_0$=0.1 mM.

equilibrium between free BPDH and monoprotonated BPDH, where H^+ activates H_2O_2 and only the free BPDH is active for oxidation. Such a mechanism leads to yielding merely a saturation curve.

Meanwhile, the UV-absorption maximum for BPDH (355 nm) shifted stepwise to higher wavelengths when [$HClO_4$] was increased (Figs. 3a and 3b); the first shift to 390 nm occurring around [$HClO_4$]=1 mM is attributed to the formation of the BPDH-$HClO_4$ 1:1 adduct and the second shift to 410 nm around [$HClO_4$]=3.5 mM is attributed to that of the 1:2 adduct. The former adduct

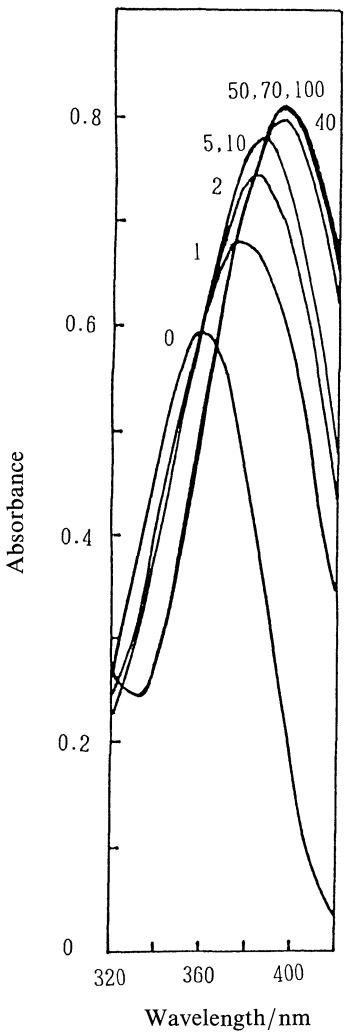

Fig. 3a. UV spectra of BPDH in the presence of $HClO_4$; the numbers indicate the concentrations of $HClO_4$ in 10^{-4} M.

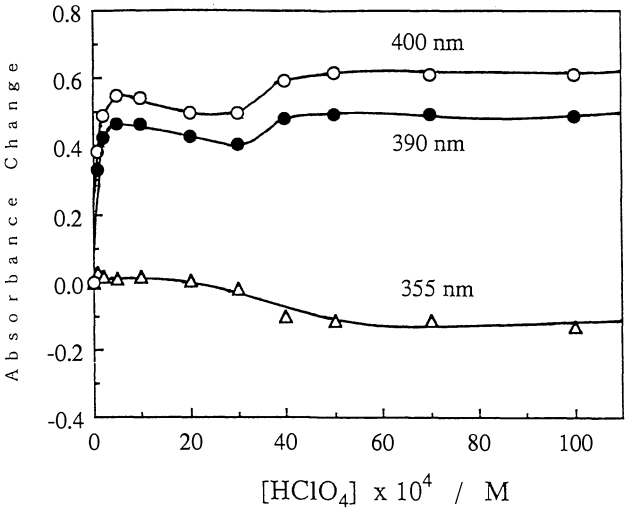

Fig. 3b. Change of absorbance due to BPDH with increasing $HClO_4$ concentrations at various wavelengths under nitrogen.

itself could be isolated quantitatively as a yellow precipitate from the acetonitrile solution of a mixture of BPDH and $HClO_4$. The complex exhibits two carbonyl stretching vibration frequencies with almost equal intensities at 1660 and 1690 cm^{-1} which are due to the protonated and the not protonated carbonyl groups in a BPDH molecule, respectively. The absorption due to BPDH itself appears at 1670 cm^{-1}. Thus, the overall protonation events may be expressed as equation 1.

$$\text{BPDH} \underset{\text{HClO}_4}{\overset{K_{a1}}{\rightleftharpoons}} \text{BPDH}\cdot\text{H}^+\text{ClO}_4^- \underset{\text{HClO}_4}{\overset{K_{a2}}{\rightleftharpoons}} \text{(III)} \quad (1)$$

The site of the second protonation is not yet defined. However, we tentatively propose the structure III which bears a proton on each carbonyl oxygen in solution. We can safely say, therefore, that the singly and doubly protonated BPDHs have to coexist, both being virtually inactive toward this oxidation. Furthermore, no influence was observed by a 100-fold addition of a well-known radical chain inhibitor, 2,6-di-*t*-butyl-4-methylphenol (BHT). All these findings allow us to conclude that the oxidation proceeds through an ionic pathway (Scheme 1); namely, the reaction is initiated by rate-determining electrophilic attack of a protonated H_2O_2 at the 3-position of the BPDH ring with the highest

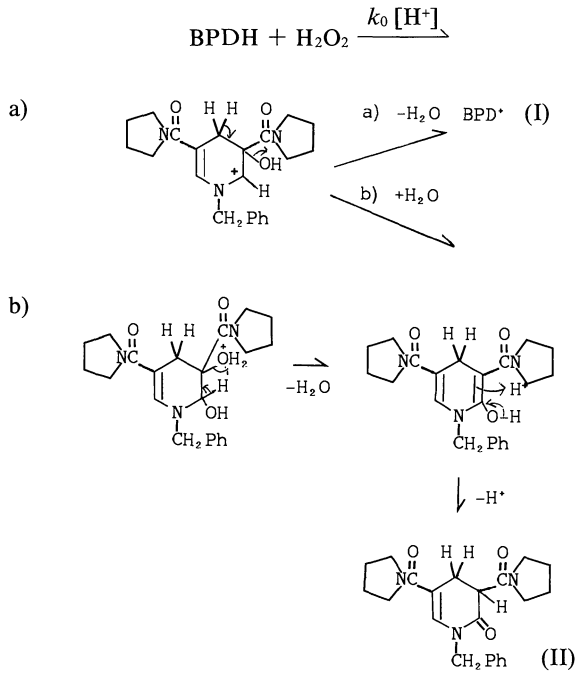

Scheme 1.

HOMO coefficient, followed by partition either to the pyridinium cation (I) via dehydration (path a) or to the monooxygenated compound (II) via hydration followed by dehydration (Path b).

Upon taking the acid-equilibria (1) into consideration explicitly, we obtain the rate equation (2) as a function of [$HClO_4$] well-accounting for the experimental data. From a set of data given in Fig. 2, K_{a1}, K_{a2}, and k' values were estimated by a nonlinear curve-fitting program to be 800 M^{-1}, 300 M^{-1}, and 4 $M^{-1}\,s^{-1}$, respectively. The rate constant k' means $k_0[H_2O_2]$, and is treated as a valuable independent of [H^+].

$$V = -\,d[BPDH]/dt = k_o[H_2O_2][BPDH]_T[H^+]/(1 + K_{a1}[H^+] + K_{a1}K_{a2}[H^+]^2) = k_{obs}[BPDH]_T \quad (2)$$

$$k_{obs} = k'[H^+]/(1 + K_{a1}[H^+] + K_{a1}K_{a2}[H^+]^2)$$

In contrast to the slow oxidation between BPDH and an equiv of H_2O_2 under nitrogen, the same quantity of H_2O_2 under oxygen was found to remarkably enhance the BPDH oxidation. In order to disclose the reaction mechanism, the progress of the O_2-oxidation was followed spectroscopically by monitoring the disappearance of BPDH and the effect of H_2O_2 on rate was examined at first; the results thus obtained are given in Fig. 4, which shows that the rate increased with increasing added H_2O_2 but the addition of H_2O_2 was not necessarily required for the smooth oxidation to occur. Table 1 reveals also that the oxidation of BPDH under an oxygen atmosphere in $HClO_4$-containing acetonitrile afforded BPD^+ (I) and H_2O_2 in quantitative and good yields, respectively. Thus, from now on, we will discuss on the results of the reactions performed under oxygen with no H_2O_2 added. In Fig. 5 is shown a typical ln (A–A_∞) vs. time plot, where a short lag period appeared, indicative of occurrence of a radical chain reaction; in fact, addition of a radical scavenger BHT strongly retarded the overall rate (Fig. 6). A following rapid BPDH consumption was first-order in BPDH; the linearity of the rate vs. $[BPDH]_0$ plot also confirmed this conclusion (data not shown). For simplifying rate evaluation, the rate constant (k_{obs}) for the BPDH-consuming phase was calculated by assuming pseudo-first-order kinetics with respect to BPDH throughout this work. As addition of a trace of H_2O_2 eliminated the lag period, one of the tasks of the H_2O_2 appears to be in enhancing the rate of the initiation step through its homolytic O–O cleavage at the start of the reaction.

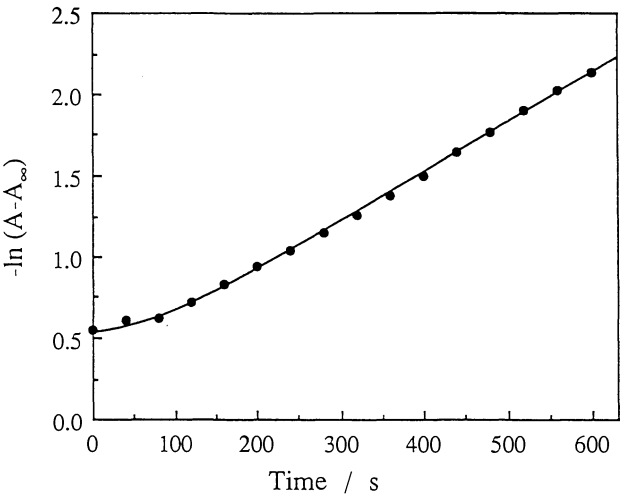

Fig. 5. ln ($A-A_\infty$) vs. time plot for pure O_2-oxidation of BPDH in the presence of $HClO_4$ in MeCN at 25 °C; [$HClO_4$]=5.0 mM; $[BPDH]_0$=0.1 mM.

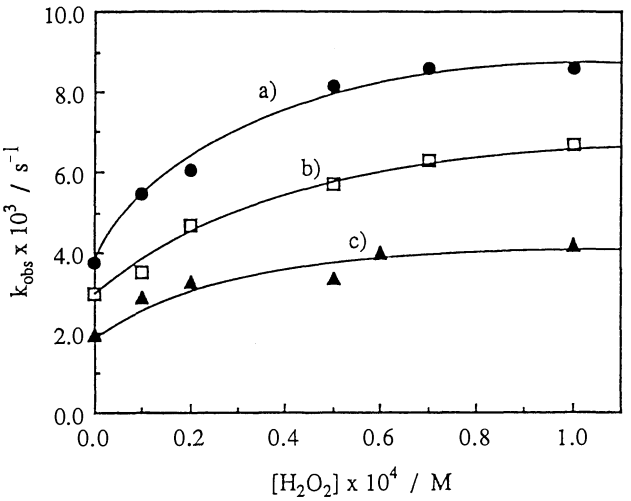

Fig. 4. Effect of H_2O_2 concentrations on the BPDH oxidation in oxygen-saturated MeCN at 25 °C; [$HClO_4$]=2.0 mM (a), 1.0 mM (b), 10 mM (c); $[BPDH]_0$=0.1 mM.

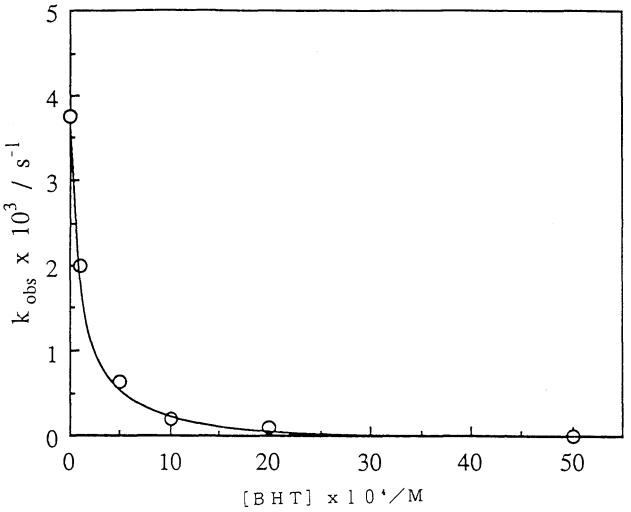

Fig. 6. Effect of altering concentrations of BHT on the rate of pure O_2-oxidation of BPDH; [$HClO_4$]= 2.0 mM; the other conditions were the same as those of Fig. 1.

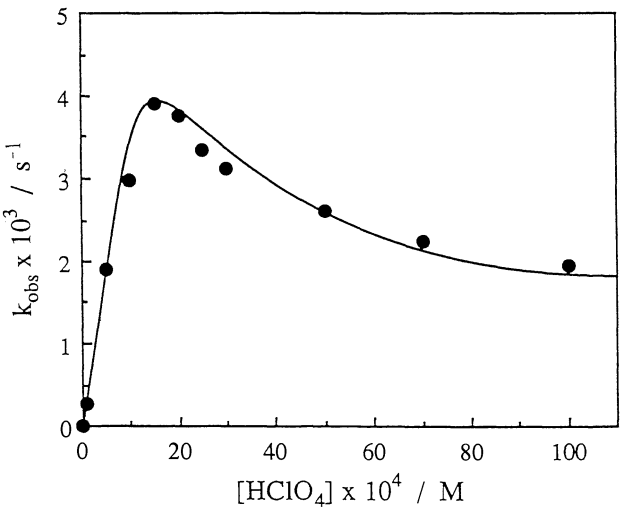

Fig. 7. Pure O_2-Oxidation of BPDH in the presence of various concentrations of $HClO_4$.

The effect of changing amounts of $HClO_4$ on rate exhibited the same characteristic feature as in the H_2O_2-oxidation under N_2 (Fig. 7), indicating that the virtually inactive singly- and doubly-protonated BPDHs are involved here also. When the rate constants were plotted as a function of the percent oxygen content ($\eta = P_{O_2}/(P_{O_2}+P_{N_2})$) of the O_2–N_2 mixture used to saturate the solution, a downward curvature was obtained; the rate was essentially independent of the concentration of the dissolved oxygen in solution at $\eta > 0.2$. Recently, Fukuzumi et al have kinetically studied closely related O_2-oxidation for an acid-stable NADH model, 10-methyl-9,10-dihydroacridine, in the presence of concentrated $HClO_4$; the reaction was first-order in each [$AcrH_2$] and [O_2]. They proposed a mechanism involving the rate-determining acid-catalyzed electron-transfer from $AcrH_2$ to O_2 followed by direct hydrogen transfer from $AcrH_2^{\cdot+}$ to $HO_2\cdot$ in the solvent cage to yield $AcrH^+$ and H_2O_2.[7] In contrast with $AcrH_2$, BPDH undergoes an autoxidation. In order to explain the observed effects of concentrations of BPDH and O_2 on the rate, therefore, we will propose the following Scheme 2 consisting of a set of reactions (3),(4),(5),(6),(7),(8), and (9); H_2O_2-producing reaction (3) is taken into consideration to explain the appearence of the induction period in the absence of added H_2O_2. As for the initiation in the radical chain sequence, we are forced to assume a set of reactions (4), (5), and (6) being the only reactions of importance to be compatible with the experimental data. Solvents and reagents have been reported to be inevitably contaminated with adventitiuos metal ions,[10] therefore, a reactive radical species capable of triggering the chain reaction might be produced according to the Fenton-like reaction. "M" here is used to denote an adventituous metal ion, maybe Fe^{2+}, which undergoes the Fenton reaction to give an $HO\cdot$ radical. This inference would be supported by the fact that addition of an 0.1 equiv of $Fe(ClO_4)_2$ to an O_2-saturated MeCN solution of BPDH removed the induction phase and accerelated the reaction by 1.5-fold.

At high O_2 concentrations ($\eta > 0.2$) the most important termination process must be the disproportionation of $HOO\cdot$ to H_2O_2 and O_2 since reaction (7) would become faster than reaction (8) under such conditions.

During the induction period:

$$\mathrm{BPDH} + O_2 \xrightarrow[\text{slow}]{H^+} \mathrm{BPD^+} + H_2O_2 \qquad (3)$$

Chain-initiating reaction:

$$H_2O_2 + \mathrm{M} \xrightarrow{k_1[H^+]\ (\sim 10^2)} \mathrm{HO\cdot} + \mathrm{M^+} \qquad (4)^{11}$$

$$2\mathrm{M^+} + \mathrm{BPDH} \xrightarrow{(>10^5)} 2\mathrm{M} + \mathrm{BPD^+} + H^+ \qquad (5)^{12}$$

$$\mathrm{HO\cdot} + \mathrm{BPDH} \xrightarrow{k_2\ (\sim 10^{10})} \mathrm{BPD\cdot} + H_2O \qquad (6)^{13}$$

Chain-propagating reaction:

$$\mathrm{BPD\cdot} + O_2 + H^+ \xrightarrow{k_3\ (\sim 10^9)} \mathrm{BPD^+} + \mathrm{HO_2\cdot} \qquad (7)^{14}$$

$$\mathrm{HO_2\cdot} + \mathrm{BPDH} \xrightarrow{k_4\ (\sim 10^9)} H_2O_2\cdot + \mathrm{BPD\cdot} \qquad (8)^{15}$$

Chain-terminating reaction:

$$2\,\mathrm{HO_2\cdot} \xrightarrow{k_5\ (8\times 10^5)} H_2O_2\cdot + O_2 \qquad (9)^{16}$$

Scheme 2. The figures in parentheses are presumed second-order-rate constants ($M^{-1}\,s^{-1}$) in water.

The combination of the individual steps, with assuming a long chain length for the major propagation process, affords the net reaction (Eq. 10):

$$\mathrm{BPDH} + O_2 \xrightarrow{H^+} \mathrm{BPD^+} + H_2O_2 \qquad (10)$$

According to the steady state treatment for intermediates $HO\cdot$, $BPD\cdot$, and $HO_2\cdot$, we arrive at the following equation (11) for the overall rate at given time t (the protonation equilibria (Eq. 1) are not taken into account):

$$V = k_{obs}[\mathrm{BPDH}]$$

$$k_{obs} = k_4\{(k_1/k_5)[H_2O_2][Fe^{2+}][H^+]\}^{1/2} \qquad (11)$$

The proposed mechanism satisfactorily explains the

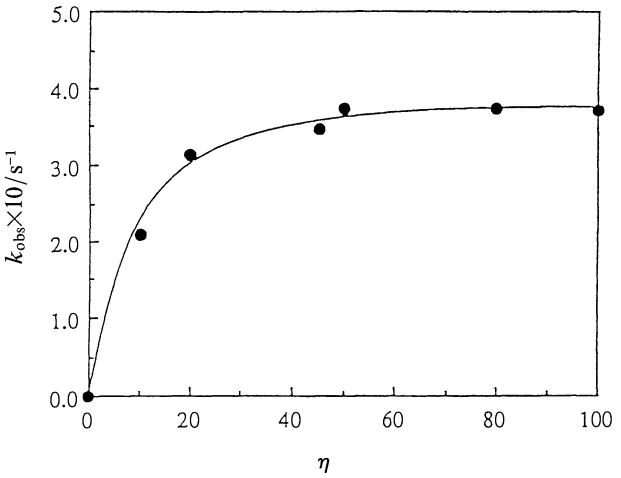

Fig. 8. Effect of partial pressures of oxygen (η) on k_{obs} for oxidation of BPDH; [$HClO_4$]=2.0 mM.

influence of changing O_2-concentrations; namely, the rate is independent of the percent O_2 content when the concentration of dissolved O_2 in solution is significantly high as compared with that of BPDH (Fig. 8). Furthermore, the equation (11) shows that the rate should increase with the square root of H_2O_2 concentrations. Actually, as Fig. 4 reveals, the plot of the observed rate constant (k_{obs}) vs. H_2O_2 concentrations affords a downward curvature.

Meanwhile, H_2O_2 not only caused the induction time to decrease but also H_2O_2 would be employed to initiate another series of chain reactions involving HO· radical as a chain-carrying species, which resulted in depression of the H_2O_2 yield (equations (12) and (13)).

$$BPD\cdot + H_2O_2 \xrightarrow{H^+} BPD^+ + HO\cdot \quad (12)$$

$$HO\cdot + BPDH \longrightarrow H_2O + BPD\cdot \quad (13)$$

The real overall mechanism might become so complicated accordingly that no quantitative evaluation of the rate constant for each step was not attempted.

In conclusion, 1-benzyl-3,5-bis(1-pyrrolydinylcarbonyl)-1,4-dihydropyridine (BPDH) underwent H_2O_2-oxidation in the presence of $HClO_4$ to give BPD^+ and the monooxygenated product in a 1 : 1 ratio through an ionic process, while the O_2-oxidation of the same substrate afforded the BPD^+ and H_2O_2 through a radical-chain pathway including HOO· and BPD· radicals as the chain carriers.

References

1) C. -I. Brändén, H. JÖrnvall, H. E. Eklund, and B. Furugren, "Alchol Dehydroganases," in "The Enzymes," ed by P. D. Boyer, Academic Press, New York (1975), Vol. 2; C. Williams, Jr., "The Redox Chemistry of 1,4-Dihydronicotinic Acid Derivatives," in "The Enzymes," ed by P. D. Boyer, Academic Press, New York (1976), Vol. 13.

2) D. M. Stout and A. I. Mayers, *Chem. Rev.*, **82**, 223 (1982).

3) H. Okamoto, M. Nozaki, and O. Hayaishi, *Biochem. Biophys. Res. Commun.*, **32**, 30 (1968); R. H. White-Stevens and H. Kamin, *ibid.*, **38**, 882 (1970); J. F. G. Vliegenthart and G. A. Veldink, "Lipoxygenases," in "Free Radicals in Biology," ed by W. A. Pryor, Academic Press, New York (1982), Vol. V.

4) E. S. Huyser, J. A. K. Harmony, and F. L. McMillian, *J. Am. Chem. Soc.*, **94**, 3176 (1972).

5) S. Tamagaki, T. Mimura, and W. Tagaki, *J. Chem. Soc., Perkin Trans. 2*, **1990**, 1645.

6) J.H. Bechara and G. Cilento, *Biochemistry*, **10**, 1831 (1971).

7) S. Fukuzumi, M. Chiba, M. Ishikawa, K. Ishikawa, and T. Tanaka, *J. Chem. Soc., Perkin Trans. 2*, **1989**, 1417.

8) H. Awano, K. Takemoto, H. Ohya, M. Tomio, S. Tamagaki, and W. Tagaki, *Bull. Chem. Soc. Jpn.*, **60**, 1887 (1986).

9) J. F. Coetzee and G. R. Padmanabhan, *J. Phys. Chem.*, **69**, 3193 (1965); J. F. Coetzee, *Prog. Phys. Org. Chem.*, **4**, 45 (1967).

10) H. W. Richter and W. H. Waddell, *J. Am. Chem. Soc.*, **104**, 4630 (1982); H. W. Richter, M. A. Fetrow, R. E. Lewis, and W. H. Waddell, *ibid.*, **104**, 1666 (1982).

11) k=76 M^{-1} s^{-1} for the reaction $H_2O_2+Fe^{2+}\rightarrow HO\cdot+Fe^{3+}+HO^-$.

12) k for the reaction between BPDH and $Fe(ClO_4)_3$ in MeCN was 10^5 M^{-1} s^{-1}.

13) Anbar and Neta, *Int. J. Appl. Radiat. Isot.*, **18**, 493 (1967).

14) 1.9×10^9 M^{-1} s^{-1} for the reaction $NAD\cdot+O_2\rightarrow NAD^++O_2^-$.

15) A. Nadezhdin and H. B. Dunford, *J. Phys. Chem.*, **83**, 1957 (1979).

16) D. T. Sawyer and J. S. Valentine, *Acc. Chem. Res.*, **14**, 393 (1981).

Synthesis of Naphth[1,2,3-*cd*]indol-6(2*H*)-one Derivatives and Their Fluorescence Properties

Sadao ARAI,* Shigeaki YAMAUCHI, Yuriko MORIYA, Tei-ichi TANAKA, Yoko YAMAZAKI, Haruo INOUE, Takamichi YAMAGISHI, and Mitsuhiko HIDA*
Department of Industrial Chemistry, Faculty of Technology, Tokyo Metropolitan University, 1-1 Minami-osawa, Hachioji, Tokyo 192-03
(Received June 29, 1991)

Highly fluorescent 1-phenylnaphth[1,2,3-*cd*]indol-6(2*H*)-one (**3b**) and its 7-chloro and 7-amino derivatives were synthesized by reaction of 1-aminoanthraquinones with benzyl chloride in KOH–DMSO system, followed by treatment with aluminium chloride. The compound **3b** was easily *N*-alkylated with various alkyl halides in KOH–DMSO system. The fluorescence quantum yields (Q_f) of naphth[1,2,3-*cd*]indol-6(2*H*)-one derivatives **3** were high (0.5—0.7), except for 7-amino derivatives which did not fluoresce. The Q_f of 7-chloro derivative (**3d**) was strongly dependent on solvent: 0.37 in ethanol; 0.02 in acetonitrile; 0 in benzene. The compounds **3** were demonstrated to be efficient laser dyes for 500—550 nm region.

Fluorescent dyes attract continuous attention because of their application in various field.[1] Especially dye laser applications are growing. In our previous paper we reported a new synthetic method of highly fluorescent naphthindolone derivatives.[2] Thus the reaction of 1-aminoanthraquinone (**1a**) with benzyl chloride in the presence of powdered potassium hydroxide (KOH) in dimethyl sulfoxide (DMSO) afforded 3,11b-dibenzyl-2-phenyl-3,11b-dihydroanthra[1,9-*de*]-1,3-oxazin-7(2*H*)-one (**2a**). Then, the compound **2a** was treated with concd hydrochloric acid in ethanol or aluminium chloride in benzene to give 2-benzyl-1-phenylnaphth[1,2,3-*cd*]indol-6(2*H*)-one (**3a**) or 1-phenylnaphth[1,2,3-*cd*]indol-6(2*H*)-one(**3b**), respectively. Although naphth[1,2,3-*cd*]indol-6(2*H*)-one derivatives have been known to be good fluorophores,[3] little has been reported concerning their properties so far. We report herein the synthesis of new naphth[1,2,3-*cd*]indol-6(2*H*)-one derivatives and their fluorescence properties and lasing behavior.

Results and Discussion

Synthesis of Naphth[1,2,3-*cd*]indol-6(2*H*)-one Derivatives. In order to synthesize new substituted 1-

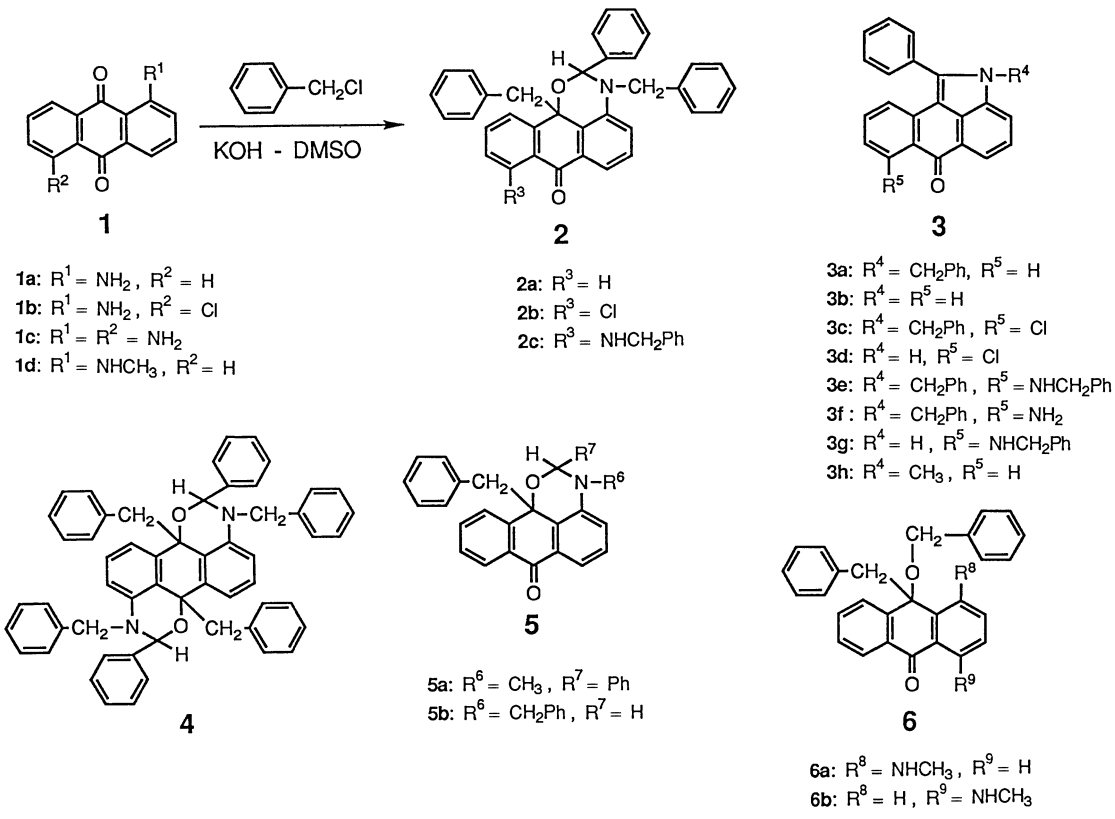

Scheme 1.

phenylnaphth[1,2,3-*cd*]indol-6(2*H*)-one derivatives, 1-amino-5-chloroanthraquinone (**1b**), 1,5-diaminoanthraquinone (**1c**), and 1-methylaminoanthraquinone (**1d**) were used as starting compounds. The aminoanthraquinone was first treated with powdered KOH in DMSO to yield green solution of the corresponding amide ion. Then excess benzyl chloride was added to the amide ion solution. In the reaction of **1b**, 3,6-dihydro-2*H*-1,3-oxazine compound (**2b**) was obtained in 53% yield. The reaction of **1c** also gave 3,6-dihydro-2*H*-1,3-oxazine compound (**2c**) in 16% yield, and compound **4**, which would be derived from **2c** by the further reaction, was not observed. In the case of the reaction of **1d**, mass spectrum of the isolated product does not show the signals of expected 3,6-dihydro-2*H*-1,3-oxazine compound (**5a** or **5b**: M 417) but does *m*/*z* 419. Its IR spectrum shows the presence of N–H group at 3400 cm^{-1}. ^1H NMR also suggests the presence of N–H group at around 6.3 ppm: By the addition of CD_3OD, the peak of *N*-methyl group (doublet at 2.90 ppm) was changed to singlet and the peaks at around 6.3 ppm was disappeared. ^1H NMR also shows two sets of benzylic protons, which had different chemical shifts with doublet at 4.10 ppm and AB quartet at 3.57 ppm. These results and analytical data suggest that the product is not the expected 3,6-dihydro-2*H*-1,3-oxazine compound (**5a** or **5b**) but benzyl ether-type compound: 10-benzyl-10-benzyloxy-4-methylamino-9(10*H*)-anthracenone (**6a**). Treatment of compound **6a** with concd hydrochloric acid gave compound **3h** (*vide infra*). This fact excludes the possibility of the isomeric structure, 10-benzyl-10-benzyloxy-1-methylamino-9(10*H*)-anthracenone (**6b**).

The 3,6-dihydro-2*H*-1,3-oxazine compound (**2b**) was treated with concd HCl in ethanol to afford 2-benzyl-7-chloro-1-phenylnaphth[1,2,3-*cd*]indol-6(2*H*)-one (**3c**) in 36% yield. In the reaction of **2b** with aluminium chloride in refluxing benzene the debenzylated product (**3d**) was obtained in 53% yield together with **3c** (12% yield). The reaction of **2c** with $AlCl_3$ in refluxing benzene gave the 7-amino derivatives **3e**, **3f**, and **3g** in 41, 18, and 22% yields, respectively. Treatment of **2c** with $AlCl_3$ or $FeCl_3$ at room temperature afforded only **3e** in 24 and 39% yields, respectively. The 7-benzylamino derivative **3g** was also obtained by the nucleophilic reaction of **3d** with benzylamine in 8% yield. It is noteworthy that reaction of benzyl ether-type compound **6a** with concd HCl in ethanol afforded 1-phenyl-2-methylnaphth[1,2,3-*cd*]indol-6(2*H*)-one (**3h**) in 66% yield, which was identical with *N*-methylation product of **3b** in KOH–DMSO system (see Table 1).

The *N*-alkylation in KOH–DMSO system[4] was applied to **3b** using various alkyl halides in order to examine the properties of the *N*-alkylated compounds as fluorophore, and the alkyl substituent affected largely the lasing behavior (vide infra). After the compound **3b** was deprotonated by KOH in DMSO, alkyl halide was added. Table 1 shows that the *N*-alkylation of **3b** in KOH–DMSO system afforded the corresponding *N*-alkyl derivatives in good yields. The reaction of **3b** with 2-bromoethanol, protected with tetrahydropyranyl group, afforded the corresponding *N*-alkyl derivative (**3l**), which was easily converted to the alcohol (**3m**) by the treatment with *p*-toluenesulfonic acid.

Table 1. *N*-Alkylation of **3b** in KOH–DMSO System

RX	Time/h	Product	Yield/%
$PhCH_2Cl$	5	**3a**	89
CH_3Br	2.5	**3h**	13
n-C_4H_9I	1	**3i**	92
$Br(CH_2)_8Br$	1	**3j**	79
$C_{16}H_{33}Br$	11	**3k**	90
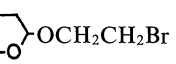	18	**3l**	47

Table 2. Absorption and Fluorescence Properties of 1-Phenylnaphth[1,2,3-*cd*]indol-6(2*H*)-ones **3** in Ethanol

	R^4	R^5	λ_a/nm[a]	λ_f/nm[b]	Q_f[c]
3a	CH_2Ph	H	426	498	0.65±0.05
3b	H	H	430	496	0.51
3c	CH_2Ph	Cl	430	498	0.30
3d	H	Cl	433	500	0.37
3e	CH_2Ph	$NHCH_2Ph$	491	—	0
3f	CH_2Ph	NH_2	477	—	0
3g	H	$NHCH_2Ph$	493	—	0
3h	CH_3	H	431	505	0.59
3i	$(CH_2)_3CH_3$	H	430	501	0.64
3j	$(CH_2)_8Br$	H	431	501	0.61
3k	$(CH_2)_{15}CH_3$	H	431	501	0.65
3l	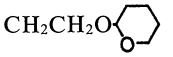	H	425	499	0.70
3m	CH_2CH_2OH	H	428	504	0.56

a) Absorption maximum. b) Fluorescence maximum. c) Fluorescence quantum yield.

Fluorescence Properties. Table 2 shows the wavelength of absorption and fluorescence maxima of the compounds **3** in ethanol. Varying the substituent in the 2-position does not result in large shifts in both absorption and fluorescence: The compounds **3** have their absorption maxima (λ_a) at around 430 nm and fluorescence maxima (λ_f) at around 500 nm. In the cases of 7-amino derivatives (**3e**, **3f**, and **3g**) the absorption maxima appeared at the longer wavelength region of 477—493 nm which could be assigned as an intramolecular charge-transfer band between the amino group in the 7-position and the carbonyl group. The fluorescence quantum yield (Q_f) of **3a** was found to be 0.65±0.05, 0.68±0.02, and 0.62 by using three different fluorescence standard of quinine sulfate, fluorescein, and 9,10-diphenylanthracene, respectively. Hence, in Table 2 the Q_f of compounds **3** in ethanol was compared using quinine sulfate as a standard. The Q_f are generally high (0.51—0.70). The substitution of chlorine for H at 7-position resulted in a decrease in Q_f, suggesting

Table 3. Solvent Effect on Absorption and Fluorescence Maxima and Fluorescence Quantum Yields

R^4	R^5	Solvent	λ_a/nm	λ_f/nm	Q_f
3a CH_2Ph	H	C_2H_5OH	426	498	0.65±0.05
		CH_3CN	429	479	0.65
		C_6H_6	428	461	0.24
3b H	H	C_2H_5OH	430	496	0.51
		CH_3CN	420	479	0.49
		C_6H_6	407	456	0.11
3d H	Cl	C_2H_5OH	433	500	0.37
		CH_3CN	429	479	0.02
		C_6H_6	410	—	0
3e CH_2Ph	$NHCH_2Ph$	C_2H_5OH	491	—	0
		CH_3CN	485	—	0
		C_6H_6	485	—	0
3h CH_3	H	C_2H_5OH	431	505	0.59
		CH_3CN	433	487	0.59
		C_6H_6	433	467	0.41
3i *n*-C_4H_9	H	C_2H_5OH	430	501	0.64
		CH_3CN	433	486	0.59
		C_6H_6	432	463	0.34

appreciable deactivation from lowest excited singlet (S_1) state due to internal heavy atom effect. The 7-amino derivatives (**3e—g**) were almost nonfluorescent. This result could be ascribable to the intramolecular CT nature of the S_1 state.[5] As shown in Table 3, the absorption spectra of 2-alkyl derivatives (**3a**, **3h**, and **3i**) showed no significant solvent dependence, while in the cases of the derivatives (**3b**, **3d**, and **3e**) bathochromic shift was observed with increasing solvent polarity. Fluorescence emissions also underwent bathochromic shifts with increasing solvent polarity. Larger Stokes shifts were observed in polar solvents than in nonpolar solvents. These results indicate the excited states of compounds **3** are more stabilized by polar solvents. Fluorescence quantum yield of the 7-chloro derivative (**3d**) was largely dependent on solvent polarity: It has a diminished Q_f in acetonitrile and was almost non-fluorescent in benzene. Hence **3d** would be a useful probe for examining the polarity of the environment around the fluorescent species.

Lasing Behavior. Highly fluorescent compounds **3** were examined for application to laser dyes. The excimer laser operating on XeCl at 308 nm was used as an excitation source. By using this pump laser radiation with 13 ns pulse width, the lasing pulse of **3b** at 506 nm with 7.8 ns was observed, indicating a pulse compressing effect by lasing phenomena. The methanol solution of **3l** and **3m** also exhibited intense laser radiation by XeCl pumping. The tuning curves for **3b**, **3l**, and **3m** in methanol are shown in Fig. 1. The lasing maxima of compound **3b**, **3l**, and **3m** were 506, 508, and 512 nm, respectively. The compound **3m** exhibits a lasing action over a wide range of a 50 nm (500—550 nm). The compound **3l**, which shows a similar tunability to **3b**, has relatively good efficiency of energy conversion from the pump source.

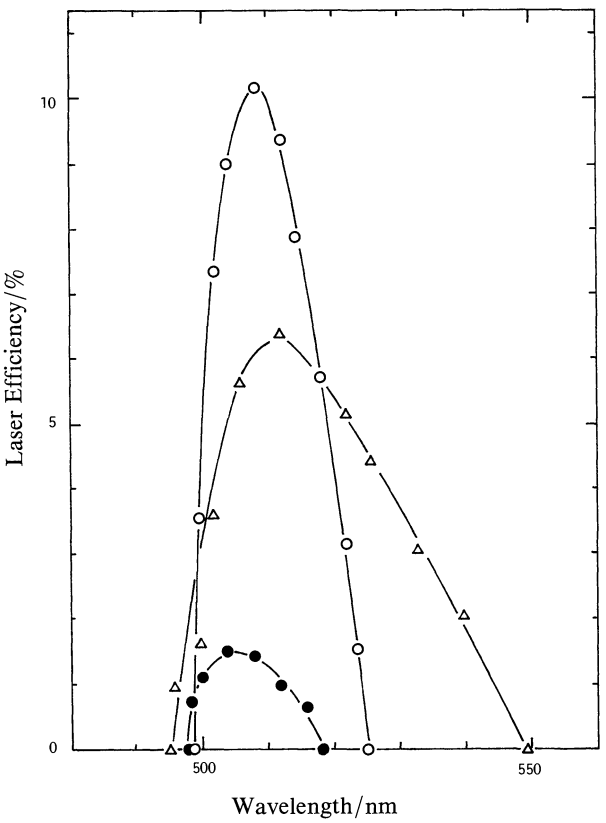

Fig. 1. Tuning curves for naphth[1,2,3-*cd*]indol-6(2*H*)-one derivatives (**3b**, **3l**, and **3m**) in Methanol. ●: **3b**, ○: **3l**, △: **3m**.

Experimental

Materials. 1-Amino-5-chloroanthraquinone was prepared as follows: The mixture of sodium anthraquinone-1-sulfonate (4.68 g, 15.4 mmol), 95% H_2SO_4 (16 cm^3), and nitric acid (Sp. Gr. about 1.38; 2 cm^3) was heated at 95 °C for 5 h to afford 5-

nitroanthraquinone-1-sulfonic acid, which was treated with sodium chlorate (0.28 g) in hydrochloric acid to give 1-chloro-5-nitroanthraquinone. The reduction of the crude 1-chloro-5-nitroanthraquinone was carried out with sodium sulfide (11 g) in aqueous NaOH solution at 80 °C for 10 h. The product was purified by silica-gel column chromatography with benzene as eluent, followed by recrystallization from benzene to afford 1-amino-5-chloroanthraquinone as red crystals (1.428 g, 36% from sodium anthraquinone-1-sulfonate): Mp 217—219 °C (lit,[6] 219 °C); Found: C, 65.22; H, 2.97; N, 4.94%. 1,5-Diaminoanthraquinone and 1-methylaminoanthraquinone (Sumitomo Chemical Co.) were purified by recrystallization from toluene. Dimethyl sulfoxide was distilled twice under reduced pressure and stored under a nitrogen atmosphere. Benzyl chloride was distilled under a nitrogen atmosphere.

The solvents used in all spectroscopic and lasing measurements were spectrograde or purified according to the literature procedure.[7]

Instruments. Melting points obtained on a Mitamura melting point apparatus are uncorrected. UV and visible spectra were recorded with a Hitachi 220A spectrometer. ^{1}H NMR data were recorded on a Hitachi R-24 (60 MHz) and JEOL FX90Q (90 MHz) spectrometers with Me_4Si as an internal standard. IR spectra were measured on a JASCO IRA-1 spectrometer. Mass spectra were recorded with a JEOL JMS-DX 300 spectrometer by the electron impact (EI) ionizing technique at 70 eV and by the fast-atom bombardment (FAB) with *m*-nitrobenzyl alcohol as a matrix. Elemental analyses were performed on a Yanaco MT2 CHN corder. Fluorescence spectra were measured on a Hitachi MPF-4 spectrofluorometer. Quinine sulfate (Q_f=0.55 in 0.5 mol dm^{-3} sulfuric acid aqueous solution),[8] fluorescein (Q_f=0.79 in 0.1 M NaOH aqueous solution),[9] or 9,10-diphenylanthracene (Q_f=1.0 in cyclohexane)[10] was used as a standard for the determination of fluorescence quantum yields.

Lasing experiments were performed using excimer laser (Lumonics Hyper EX-400) operating on XeCl at 308 nm as excitation source. The dye laser (Lumonics HyperDye-300) output was measured using a joule meter (Scientech model 38-0101).

The compounds **2** and **3** were obtained by the two-step method described previously.[2]

8-Chloro-3,11b-dibenzyl-2-phenyl-3,11b-dihydroanthra[1,9-*de*]-1,3-oxazin-7(2*H*)-one (2b). 1-Amino-5-chloroanthraquinone (**1b**: 513 mg, 1.99 mmol) was reacted with benzyl chloride (2.69 g, 21.2 mmol) in the presence of powdered KOH (1.03g, 18.4 mmol) in DMSO (60 cm^3) at 30 °C for 1 h. The reaction mixture was poured into water (1000 cm^3) and extracted with benzene. After the benzene extract was concentrated, the residue was purified by silica-gel column chromatography with benzene as eluent, followed by recrystallization from ethanol to afford **2b** (316 mg, 53%) as yellow crystals: Mp 194—195 °C; IR (KBr) 1670, 1595, 1580, 1480, 1447, 1295, and 700 cm^{-1}; ^{1}H NMR ($CDCl_3$) δ=3.1—4.8 (4H, m, CH_2) and 6.1—7.9 (22H, m, ArH); MS *m*/*z* 527 and 529 (M^+); Found: C, 79.48; H, 4.71; N, 2.53%. Calcd for $C_{35}H_{26}NO_2Cl$: C, 79.61; H, 4.96; N, 2.65%.

8-Benzylamino-3,11b-dibenzyl-2-phenyl-3,11b-dihydroanthra[1,9-*de*]-1,3-oxazin-7(2*H*)-one (2c). After the mixture of 1,5-diaminoanthraquinone (477 mg, 2 mmol) and KOH (1.12 g, 20 mmol) in DMSO (60 cm^3) was stirred for 30 min, benzyl chloride (5.06 g, 40 mmol) was added to the mixture. The solution was stirred overnight at RT. The reaction mixture was poured into water (1000 cm^3) and the organic materials were extracted with benzene. The benzene extract was evaporated. The residue showed 5 spots on TLC (SiO_2, benzene). The largest spot (R_f=0.70) was separated by column chromatography (SiO_2, benzene), followed by recrystallization from ethanol to afford **2c** (192 mg, 16%) as orange crystals: Mp 174.4 °C; UV (C_2H_5OH) 417 (log ε 3.96) and 244 nm (4.41); IR (KBr) 1630, 1590, 1520, 1493, 1282, 792, and 698 cm^{-1}; ^{1}H NMR ($CDCl_3$) δ=3.47 (2H, ABq, *J*=12 Hz, CH_2), 4.39 (2H, ABq, *J*=16 Hz, NCH_2), 4.46 (2H, d, *J*=6 Hz, $NHC\underline{H}_2$), 6.2—7.2 (27H, m, ArH), and 9.63 (1H, t, *J*=6 Hz, NH); MS *m*/*z* 598 (M^+); Found: C, 84.06; H, 5.62; N, 4.31%. Calcd for $C_{42}H_{34}N_2O_2$; C, 84.25; H, 5.73; N, 4.68%.

2-Benzyl-7-chloro-1-phenylnaphth[1,2,3-*cd*]indol-6(2*H*)-one (3c). A mixture of **2b** (211 mg, 0.4 mmol) and concd HCl (5 cm^3) in ethanol (35 cm^3) was refluxed for 3 h. The mixture was concentrated and the residue was purified by column chromatography (SiO_2, benzene), followed by recrystallization from ethanol to afford **3c** (47 mg, 36%) as pale orange crystals: Mp 245—246 °C; UV (C_2H_5OH) 430 (log ε 4.13), 352 (3.61), 310 (sh), and 279 nm (4.24); IR (KBr) 1640, 1606, 1588, 1330, 1192, and 708 cm^{-1}; ^{1}H NMR ($CDCl_3$) δ=5.2 (2H, s, CH_2) and 6.5—8.2 (16H, m, ArH); MS *m*/*z* 419 and 421 (M^+); Found: C, 80.22; H, 4.51; N, 3.46%. Calcd for $C_{28}H_{18}NOCl$: C, 80.09; H, 4.32; N, 3.34%.

7-Chloro-1-phenylnaphth[1,2,3-*cd*]indol-6(2*H*)-one (3d). A mixture of **2b** (517 mg, 0.98 mmol) and $AlCl_3$ (932 mg, 7 mmol) in benzene (180 cm^3) was refluxed for 1 h. The mixture was poured into ice-water. The benzene extract was evaporated and the residue was purified by column chromatography (SiO_2, benzene), followed by recrystallization from ethanol to afford **3d** (171 mg, 53%) as yellow crystals: Mp 330.5—331.5 °C; UV (C_2H_5OH) 433 (log ε 4.13), 357 (sh), 313 (3.88), 280 (4.15), and 248 nm (4.45); IR (KBr) 3200, 1640, 1610, 1590, 1382, 1293, 1042, and 793 cm^{-1}; ^{1}H NMR ($CDCl_3$) δ=7.3—8.0 (11H, m, ArH) and 12.3 (1H, br s, NH); MS *m*/*z* 329 and 331 (M^+); Found: C, 76.23; H, 3.51; N, 4.40%. Calcd for $C_{21}H_{12}NOCl$: C, 76.48; H, 3.67; N, 4.25%.

2-Benzyl-7-benzylamino-1-phenylnaphth[1,2,3-*cd*]indol-6(2*H*)-one (3e). A mixture of **2c** (261 mg, 0.44 mmol) and $AlCl_3$ (382 mg, 2.9 mmol) in benzene (75 cm^3) was refluxed for 35 min. The mixture was poured into ice-water. The benzene extract was evaporated. The residue showed 3 spots (R_f=0.20, 0.10, and 0.05) on TLC (SiO_2, benzene). These products were separated by column chromatography (SiO_2, benzene), followed by recrystallization from ethanol to afford compounds **3e** (87 mg, 41%), **3f** (31 mg, 18%), and **3g** (39 mg, 22%). **3e** (R_f=0.20) as orange crystals: Mp 230.0—230.5 °C (decomp); UV (C_2H_5OH) 491 (log ε 4.13), 383 (sh), 350 (3.87), and 317 nm (3.70); IR (KBr) 3200, 1637, 1575, 1375, 1244, 790, and 700 cm^{-1}; ^{1}H NMR ($CDCl_3$) δ=4.51 (2H, d, *J*=6 Hz, NCH_2), 5.17 (2H, s, CH_2), 6.3—8.2 (21H, m, ArH), and 11.96 (1H, t, *J*=6 Hz, NH); MS *m*/*z* 490 (M^+); Found: C, 85.41; H, 5.20; N, 5.66%. Calcd for $C_{35}H_{26}N_2O$: C, 85.68; H, 5.34; N, 5.71%.

7-Amino-2-benzyl-1-phenylnaphth[1,2,3-*cd*]indol-6(2*H*)-one (3f). (R_f=0.05) as orange crystals: UV (C_2H_5OH) 477 (log ε 3.99), 347 (3.83), and 289 nm (4.04); IR (KBr) 3440, 3030, 1630, 1592, 1268, and 710 cm^{-1}; ^{1}H NMR ($CDCl_3$) δ=5.22 (2H, s, CH_2) and 6.1—8.2 (18H, m, ArH and NH_2); MS *m*/*z* 400 (M^+); Found: C, 83.69; H, 4.80; N, 7.15%. Calcd for $C_{28}H_{20}N_2O$: C, 83.97; H, 5.03; N, 7.00%.

7-Benzylamino-1-phenylnaphth[1,2,3-*cd*]indol-6(2*H*)-one

(3g). A mixture of **3d** (345 mg, 1.05 mmol) and benzylamine (10 cm^3) was heated at 100 °C for 130 h. The mixture was evaporated and the residue was purified by column chromatography (SiO_2, benzene), followed by recrystallization from ethanol to afford **3g** as red crystals (34 mg, 8%): Mp 244.0—245.0 °C; UV (C_2H_5OH) 493 (log ε 3.66), 367 (3.52), 288 (4.16), and 264 nm (4.21); IR (KBr) 3200, 2930, 2850, 1600, 1570, 1388, 1200, and 700 cm^{-1}; ^1H NMR (60 MHz, $CDCl_3$) δ=4.55 (2H, d, *J*=4.8 Hz, CH_2), 6.2—8.8 (17H, m, ArH and NH), and 10.8 (1H, t, *J*=4.8 Hz, $NHCH_2$); MS *m/z* 400 (M^+); Found: C, 83.71; H, 5.22; N, 6.91%. Calcd for $C_{28}H_{20}N_2O$: C, 83.97; H, 5.03; N, 7.00%.

10-Benzyl-10-benzyloxy-4-methylamino-9(10*H*)-anthracenone (6a). 1-Methylaminoanthraquinone (**1d**: 475 mg, 2 mmol) was reacted with benzyl chloride (3.2 g, 25 mmol) in the presence of powdered KOH (1.1 g, 20 mmol) in DMSO (60 cm^3) at 30 °C for 1 h. The reaction mixture was poured into water (1000 cm^3) and extracted with benzene. After the benzene extract was concentrated, the residue was purified by silica-gel column chromatography with benzene as eluent, followed by recrystallization from ethanol to afford **6a** (344 mg, 41%) as pale orange crystals: Mp 162.1—163.2 °C (decomp); UV (C_2H_5OH) 397 nm (log ε 3.32); IR (KBr) 3390 (NH) and 1660 (C=O) cm^{-1}; ^1H NMR ($CDCl_3$) δ=2.90 (3H, d, *J*=5 Hz, CH_2), 3.57 (2H, ABq, *J*=13 Hz, CH_2), 4.10 (2H, d, *J*=2 Hz, CH_2), and 5.9—8.1 (18H, m, ArH and NH); MS *m/z* 419 (M^+); Found: C, 83.16; H, 5.90; N, 3.47%. Calcd for $C_{29}H_{25}NO_2$: C, 83.03; H, 6.01; N, 3.34%.

2-Methyl-1-phenylnaphth[1,2,3-*cd*]indol-6(2*H*)-one (3h). A mixture of **6a** (195 mg, 0.46 mmol) and concd HCl (10 cm^3) in ethanol (50 cm^3) was refluxed for 3 h. The mixture was concentrated and the residue was purified by column chromatography (SiO_2, benzene), followed by recrystallization from ethanol to afford **3h** (94 mg, 66%): UV (C_2H_5OH) 431 nm (log ε 4.10); IR (KBr) 3060, 1628, 1590, 1480, 1292, 992, 762, and 700 cm^{-1}; ^1H NMR (DMSO-d_6) δ=3.58 (3H, s, CH_3) and 6.8—8.5 (12H, m, ArH); MS *m/z* 309 (M^+); Found: C, 85.29; H, 4.78; N, 4.49%. Calcd for $C_{22}H_{15}NO$, C, 85.41; H, 4.89; N, 4.53%.

***N*-Alkylation of 3b.** A typical procedure is described for the reaction of **3b** with butyl iodide. The compound **3b** (295 mg, 1 mmol) was stirred with powdered KOH (561 mg, 10 mmol) in DMSO (30 cm^3) for 30 min at 30 °C. Then butyl iodide (1.84 g, 10 mmol) was added to the mixture and the solution was stirred for 1 h at 30 °C. The reaction was quenched with water (700 cm^3). The mixture was extracted with benzene, washed with water, and evaporated. The residue was submitted to column chromatography on silica gel using benzene as eluent. The yellow fractions (R_f=0.08) were concentrated and recrystallized from ethanol to afford **2-butyl-1-phenylnaphth[1,2,3-*cd*]indol-6(2*H*)-one (3i)** (323 mg, 92%) as yellow needles; mp 179.5—180.0 °C; UV (C_2H_5OH) 242 (log ε 4.42), 275 (4.24), 304 (4.07), 355 (3.61), and 430 nm (4.09); IR (KBr) 3070, 2980, 2950, 2880, 1635, 1595, 1290, 772, and 707 cm^{-1}; ^1H NMR ($CDCl_3$) δ=0.5—1.9 [m, 7H, $-(CH_2)_2CH_3$], 3.97 (t, 2H, N-CH_2), and 7.0—8.6 (m, 12H, ArH); MS *m/z* 351 (M^+); Found: C, 85.68; H, 6.00; N, 3.89%. Calcd for $C_{25}H_{21}NO_2$: C, 85.44; H, 6.02; N, 3.99%.

2-(8-Bromooctyl)-1-phenylnaphth[1,2,3-*cd*]indol-6(2*H*)-one (3j): Yellow needles from ethanol; mp 88.0—88.5 °C; UV (C_2H_5OH) 242 (sh, log ε 4.47), 275 (4.27), 303 (4.10), 354 (3.65), and 431nm (4.10); IR (KBr) 3060, 2940, 2860, 1630, 1595, 1335, 1278, 770, and 702 cm^{-1}; ^1H NMR ($CDCl_3$) δ=0.8—2.0 [m, 12H, $-(CH_2)_6$], 3.38 (t, 2H, Br-CH_2), 4.18 (t, 2H, N-CH_2), and 7.0—8.7 (m, 12H, ArH); MS *m/z* 485 and 487 (M^+); Found: C, 72.16; H, 5.90; N, 2.86%; Calcd for $C_{29}H_{28}NO_2Br$: C, 71.90; H, 5.80; N, 2.88%.

2-Hexadecyl-1-phenylnaphth[1,2,3-*cd*]indol-6(2*H*)-one (3k): Yellow crystals from ethanol; mp 82.5—83.0 °C; UV (C_2H_5OH) 243 (log ε 4.45), 275 (4.26), 304 (4.09), 354 (3.64), and 431 nm (4.10); IR (KBr) 3070, 2930, 2860, 1630, 1598, 1480, 1290, and 708 cm^{-1}; ^1H NMR ($CDCl_3$) δ=0.4—1.9 [m, 31H, $-(CH_2)_{14}CH_3$], 4.05 (t, 2H, N-CH_2), and 7.2—8.7 (m, 12H, ArH); MS *m/z* 519 (M^+); Found: C, 85.84; H, 8.67; N, 2.71%. Calcd for $C_{37}H_{45}NO_2$: C, 85.50; H, 8.73; N, 2.69%.

1-Phenyl-2-[2-(tetrahydropyranyloxy)ethyl]naphth[1,2,3-*cd*]indol-6(2*H*)-one (3l): The reaction of **3b** with 1-bromo-2-tetrahydropyranyloxyethane, which was obtained by the reaction of 2-bromoethanol with dihydropyrane in the presence of *p*-toluenesulfonic acid, afforded **3l** as pale brown oil (47%): UV (C_2H_5OH) 425 nm (log ε 4.05); IR (KBr) 2940, 1635, 1288, 1122, 1033, and 700 cm^{-1}; ^1H NMR ($CDCl_3$) δ=1.1—1.6 (6H, m), 3.1—4.5 (m, 7H), and 7.1—8.4 (H, m, ArH); FABMS *m/z* 424 $(M+1)^+$; Found: C, 79.26; H, 5.79; N, 3.19%. Calcd for $C_{28}H_{25}NO_3$: C, 79.41; H, 5.95; N, 3.31%.

2-(2-Hydroxyethyl)-1-phenylnaphth[1,2,3-*cd*]indol-6(2*H*)-one (3m). A methanol (10 cm^3) solution of **3l** (111 mg, 0.26 mmol) and *p*-toluenesulfonic acid (53.2 mg, 0.27 mmol) was stirred for 16 h at RT. After the mixture was dried, the residue was recrystallized from methanol to afford **3m** as yellow needles (61.8 mg, 69%); mp 216—217 °C; UV (C_2H_5OH) 428 nm (log ε 3.97); IR (KBr) 3400, 1610, 1580, 1474, 1275, 1080, and 702 cm^{-1}; ^1H NMR ($CDCl_3$+CD_3OD) δ=3.84 (2H, t, *J*=5.6 Hz, NCH_2), 4.21 (2H, t, *J*=5.6 Hz, CH_2O), and 7.1—8.5 (12H, m, ArH); FAB-MS *m/z* 340 $(M+1)^+$; Found: C, 81.20; H, 5.11; N, 4.17%. Calcd for $C_{23}H_{19}NO_2$: C, 81.39; H, 5.05; N, 4.13 %.

We wish to express our thanks to Messrs. Masao Usui and Tsutomu Shinoda of Tokyo Metropolitan Industrial Technology Center for mass spectral measurements (EI).

References

1) H. Zollinger, "Color Chemistry," VCH publishers, New York (1987).

2) S. Arai, T. Yamagishi, and M. Hida, *Chem. Lett.*, **1981**, 1789, and *Bull. Chem. Soc. Jpn.*, **64**, 324 (1991).

3) J. Houben, "Das Anthracen und Die Anthrachinone," Georg Thieme, Verlag (1929), pp. 615—617.

4) S. Arai, S. Kato, and M. Hida, *Bull. Chem. Soc. Jpn.*, **58**, 1458 (1985).

5) H. Inoue, M. Hida, N. Nakashima, and K. Yoshihara, *J. Phys. Chem.*, **86**, 3184 (1982).

6) T. Maki and H. Seki, *Bull. Chem. Soc. Jpn.*, **27**, 613 (1954).

7) D. D. Perrin and W. L. F. Armarego, "Purification of Laboratory Chemicals," Pergammon, Oxford (1988).

8) W. H. Melhuish, *J. Phys. Chem.*, **64**, 762 (1960).

9) L. S. Forster and R. Livingston, *J. Chem. Phys.*, **20**, 1315 (1952).

10) R. F. Chen, *J. Res. Natl. Bur. Stand., Sect. A*, **76**, 593 (1972).

Structures of Diterpenoid Tropolones, Salviolone and Miltipolone, from the Root of *Salvia miltiorrhiza* Bunge

Ginda HARO, Masahito MORI, Midori O. ISHITSUKA, Takenori KUSUMI, Yoshinobu INOUYE, and Hiroshi KAKISAWA*
Department of Chemistry, University of Tsukuba, Tsukuba, Ibaraki 305
(Received July 8, 1991)

New types of a bisnorditerpenoid and a norditerpenoid possessing a benzotropolonoid and a tropolonoid moieties, salviolone (**8**) and miltipolone (**15**), respectively, have been isolated and their structures were determined by spectroscopic methods. The structure of salviolone was confirmed by a total synthesis. These compounds exhibit cytotoxic activities against cultured cells.

The dried roots of *Salvia miltiorrhiza* Bunge (Labiatae), known as "Tanjin" in Japanese or "Danshen" in Chinese, have been used in these countries as a folk medicine to treat a wide variety of diseases.[1] Chemical constituents of this root were extensively investigated since 1934,[2] and surveys of minor metabolites were further continued in order to identify more potently active constituents, for the activity of the crude extract often exceeds that of the identified constituents. This Chinese drug is colored reddish-orange and many coloring constituents, mainly quinones[3] with abietane skeleton, as represented by transhione-I (**1**)[4] and isocryptotanshinone (**2**),[5] have been identified. Some of these compounds seemed to be the artifacts produced during drug preparation. We studied on pharmaceutically active compounds in the fresh roots of *S. miltiorrhiza* and found colorless new compounds, designated salviolone (**8**)[6] and miltipolone **15**)[9] besides norsalvioxide (**3**),[6] secodialdehyde (**4**),[7] abietatriene (**5**),[7] cryptoacetalide (**6**),[8] and isomanool (**7**).[7] The new compounds, salviolone and miltipolone, were found to possess unique diterpenoid benzotropolone and tropolone chromophores, respectively. Although many tropolonoid terpenes possessing mono- and sesquiterpenoid skeletons have been known, to the best our knowledge, these are the first diterpenoid tropolones found from the nature. Present report deals with structure elucidation of these compounds.[9]

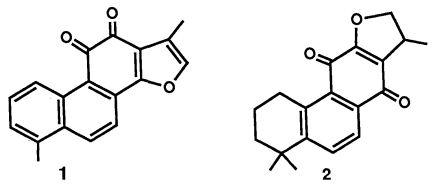

Chart 1.

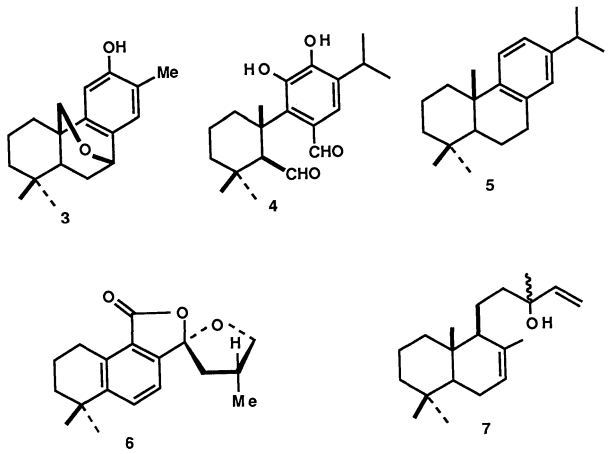

Chart 2.

The fresh roots were soaked in methanol just after the collection and the methanol extract was repeatedly separated by chromatographies to afford new compounds, salviolone (**8**) and miltipolone (**15**), as pale yellow and colorless crystals, respectively.

The molecular composition of salviolone (**8**) was determined to be $C_{18}H_{20}O_2$ from the high resolution mass spectrum. The ^1H NMR spectrum showed a rather downfield aliphatic triplet at δ=3.10 (2H, t, J=7 Hz), which was assignable to a benzylic methylene group and was found to couple with a perturbed quintet at δ=1.95 (2H). This quintet is further coupled with a deformed triplet at δ=1.72 (2H). A singlet at δ=1.36 (6H), possibly due to a *gem*-dimethyl group, exhibits an NOE cross peak in the NOESY spectrum to the methylene signal at δ=1.72, implicating the presence of Ar-CH_2-CH_2-CH_2-CMe_2-group. The IR spectrum shows the bands ascribable to a phenolic OH at 3270 and 1240 cm^{-1}. An intense absorption at 1630 cm^{-1} and an upfield carbonyl signal (δ=179.9) in the ^{13}C NMR spectrum indicated the presence of a carbonyl group involved in a highly conjugated system. Appearance of eleven downfield signals at δ=127.1—179.9 in the ^{13}C NMR spectrum and four downfield proton signals at δ=7.53 (1H, d, J=8.5 Hz), 7.58 (1H, d, J=8.5 Hz), 7.95 (1H, s), and 8.05 (1H, s) as well as the downfield methyl singlet at δ=2.49, and deep blue coloration by iron(III) chloride suggested the existence of some particular phenolic moiety such as an acetylnaphthol or a methylbenzotropolonoid structure. The benzotropolonoid structure seemed to be more probable because of the presence of the cross peak (long-range coupling) between the methyl protons at δ=2.49 and an aromatic proton δ=7.95 in the COSY

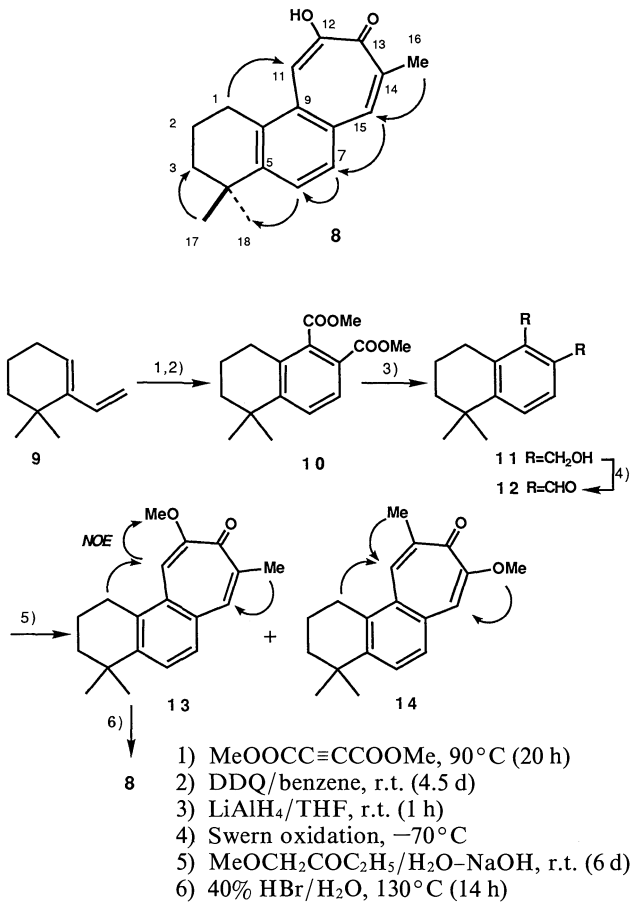

Chart 3.

spectrum. This was further supported by the UV spectrum; the absorption maxima of salviolone [λ_{max} 388 (log ε 3.23), 368 (3.28), 312 (3.60), 285 (4.42), 249 (4.20), 242 nm (4.18)] were quite similar to those of 2-methyl-4,5-benzotropolone.[10] Structure **8** was deduced from these properties and biogenetic considerations. This structure was supported by finding the NOE's in the NOE difference and NOESY spectra (indicated on the structure by arrows). Finally this structure was unequivocally confirmed by a total synthesis.

The Diels–Alder reaction between 3,3-dimethyl-2-vinylcyclohexene (**9**)[11] and methyl acetylenedicarboxylate proceeded smoothly by heating the mixture to give an adduct, which without isolation was treated with DDQ to afford a phthalic ester **10**. The ester **10** was reduced to a diol **11**, which was then subjected to the Swern oxidation at −70 °C to give a dialdehyde **12**. As the dialdehyde was unstable, the crude **12** was immediately used in the following step. The suspension of the dialdehyde **12** and 1-methoxy-2-butanone[12] in an aqueous sodium hydroxide solution[13] was stirred for six days to afford a mixture of salviolone methyl ether **13** and its regioisomer **14** (**13**:**14**=2:1) in 28% yield from the diol **11**. Both products were separated, and characterized by the ^{1}H NMR spectra and NOE experiments (indicated by arrows on the structures). The reactions of the dialdehyde and methoxybutanone did not proceed at all in aqueous alcoholic media.[13,14] The major isomer **13** was heated in aqueous hydrobromic acid to give salviolone (**8**). The spectroscopic properties (^{1}H and ^{13}C NMR, IR, and UV spectra) of synthetic and natural salviolone were identical in all respects.[9]

Miltipolone (**15**) was found to have the molecular formula $C_{19}H_{24}O_3$ from the high resolution FAB mass peak (MH^+). Spectral properties of this compound were partially very close to those of norsalvioxide (**3**)[6] and salviolone (**8**).[6] The IR spectrum showed the band ascribable to a hydrogen bonded OH group at 3000—3300 cm^{-1}. An intense absorption at 1620 cm^{-1} and a rather upfield signal at δ=171.97 in the ^{13}C NMR spectrum indicated the presence of a carbonyl group involved in a conjugated system similar to that of salviolone (**8**). Appearance of six olefinic carbon signals at δ=120.0—166.37 in the ^{13}C NMR spectrum and two downfield proton signals at δ=7.28 and 7.40 as well as very downfield methyl signal at δ=2.42 in the ^{1}H NMR spectrum and deep violet coloration by ferric chloride suggested the existence of some particular phenolic moiety such as an *o*-hydroxyacetophenone or a tropolonoid group. The tropolonoid chromophore was reinforced by the presence of the cross peak between the methyl protons at δ=2.42 and an aromatic proton at δ=7.28 in the COSY spectrum as well as the UV absorption maxima characteristic for the tropolone.[15] The presence of the methyltropolone moiety was confirmed by determining the connectivity of six aromatic carbon atoms and one upfield carbonyl carbon by the COLOC spectrum (Table 1); for example the proton at δ=7.28 on C-15 (δ=136.37) was correlated with C-7 (δ=74.38), C-9 (δ=155.99), C-13 (δ=166.37), and C-19 (δ=21.3), and the proton at δ=7.40 on C-11 (δ=120.02) to C-8 (δ=138.67), C-12 (δ=171.97) and C-13 (δ=166.37).

Two of three oxygen atoms in miltipolone are involved in the tropolonoid moiety and the remaining one oxygen atom was supposed to be included in an ether linkage from the ^{13}C NMR signal at δ=74.38 (d, C-7) and 67.35 (t, 16-C), and the ^{1}H NMR signals on the oxymethylene

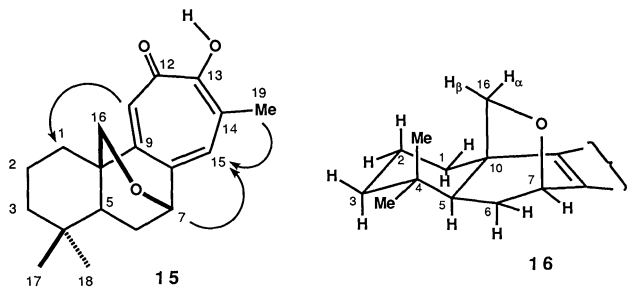

Chart 4.

Table 1. The ^1H and ^{13}C NMR Data (δ; $CDCl_3$) for **15**

No. of carbon	^{13}C NMR (125 MHz)	^1H NMR (500 MHz, J in Hz)	δ ^1H coupling with J^3 (COLOC)
1	29.92 (t)	α-H 1.95 (dt, 4.5, 13.4)	1.60
		β-H 1.72 (dtd, 13.4, 3.1, 1.9)	
2	18.98 (t)	1.62 (m), 1.70 (m)	
3	40.99 (t)	α-H 1.20 (dt, 4, 13)	0.86, 1.23, 1.72
		β-H 1.60 (dtd, 1.9, 3.6, 13)	
4	34.39 (s)		1.62, 1.66, 2.11
5	41.47 (d)	1.23 (ddd, 2.0, .2, 12.0)	0.86, 1.16, 1.60, 1.72, 4.68
6	29.24 (t)	α-H 1.66 (ddd, 2.0, 12.0, 13.9)	
		β-H 2.11 (ddd, 3.8, 6.2, 13.9)	
7	74.38 (d)	4.68 (dd, 2.0, 3.8)	7.28
8	138.67 (s)		2.11, 7.40
9	155.99 (s)		4.36, 4.68, 7.28
10	40.62 (s)		1.72, 7.40
11	120.02 (d)	7.40 (s)	
12	171.97 (s)		7.40
13	166.37 (s)	9.6 (OH, br)	2.42, 7.28, 7.40
14	131.31		2.42
15	136.37 (d)	7.28 (s)	2.42, 4.68
16	67.35 (t)	α-H 2.99 (dd 2.0, 9.1)	
		β-H 4.36 (d 9.1)	
17	21.3 (q)	3H 1.16 (s)	0.86, 1.23
18	32.7 (q)	3H 0.86 (s)	1.16
19	21.3 (q)	3H 2.42 (s)	7.28

protons (16-CH_2) appearing at δ=2.99 and 4.36 as well as the oxymethine proton at δ=4.68 (7-H). Except for the two aromatic proton chemical shifts, the ^1H NMR patterns of miltipolone were almost superimposable to those of norsalvioxide **3**. This similarity inferred the presence of the partial structure **16** in miltipolone, and the structure was firmly established by the extensive analyses of two dimensional and double resonance NMR spectra. The existence of *geminal* dimethyl group was confirmed by the detections of a *J*-cross peak in the COSY and an NOE cross peak in the NOESY spectra between the two aliphatic methyl signals at δ=0.86 and 1.16. The COLOC spectrum showed the ^3J cross peaks between 5-C (δ=41.47) and 1-H (δ=1.72), 3-H (δ=1.60), 7-H (δ=4.68), 17-H_3 (δ=1.16), and 18-H_3 (δ=0.86). A W-type coupling between 16-H_α and 5-H indicated their anticoplanar orientation. Noteworthy is the fact that the chemical shifts of methylene protons (δ=2.99 and 4.36) at 16-C are considerably different each other due to an anisotropic effect of the tropolonoid group. The presence of *J*-coupling of the proton at δ=4.68 (7-H) to the aromatic proton signal at δ=7.28 (15-H) suggested the connectivity of the partial structure **16** to the tropolonoid moiety. This was further confirmed by observing the NOE's in the NOESY spectrum as indicated in the structure.

Biogenetically,[16] miltipolone (**15**) seems to be a precursor of norsalvioxide (**3**) and salviolone (**8**); oxidative decarbonylation would give the phenolic norsalvioxide (**3**) as in the case that the mild oxidation of a tropolonoid alkaloid, colchicein, produces a corresponding phenolic compound, colchinol:[17] Oxidative deoxymethylenation from miltipolone (**15**) would afford salviolone (**8**).

Salviolone exhibited a cytotoxic activity (TD_{50}) against Vero cells at 3.3 μg ml^{-1}, while miltipolone was active against murine melanoma cell (B16F10) and human colon carcinoma (HCT-116) with TD_{50} 0.16 and 0.003 μg ml^{-1}, respectively.

Experimental

Infrared spectra were recorded on a Hitachi 360 spectrophotometer and ultraviolet spectra were recorded on a Hitachi 340 spectrophotometer. Optical rotation was recorded on a JASCO DIP-181 polarimeter using a 10 cm microcell. ^1H and ^{13}C NMR spectra were taken on JEOL JNM-FX-90Q or Bruker AM-500 spectrometers. Proton chemical shifts are reported in ppm relative to internal TMS and carbon shifts relative to the center peak of $CDCl_3$ (δ=77.1).

Extraction and Isolation. The roots of *Salvia miltiorrhiza* Bunge were collected in June 1984 at Dalian, China. The roots were soaked in MeOH immediately after collection and allowed to stand for 2 weeks. The MeOH extract was concentrated and the residue washed with CH_2Cl_2. The CH_2Cl_2 solution was dried over Na_2SO_4 and concentrated to give a dark brown residue and this material was repeatedly separated by column chromatography on silica gel (Merck, Kieselgel 60 and Wako, Wakogel C-300). Further separations by preparative TLC (Merck GF 254, 0.5 mm) afforded norsalvioxide (**3**), salviolone (**8**), miltipolone (**15**), cryptoacetalide (**6**), and secodialdehyde (**4**).

Salviolone (8): Pale yellow solid, high resolution MS, Found: m/z 268.1490. Calcd for $C_{18}H_{20}O_2$: M, 268.1464. IR (KBr) ν_{max} 3270, 1630, 1566, 1240 cm^{-1}. UV λ_{max} (hexane) 388

(log ε 3.23), 368 (3.28), 312 (3.60), 285 (4.42), 249 (4.20), 242 nm (4.18). ^{1}H NMR δ=1.36 (6H, s, 17,18-Me$_2$), 1.72 (2H, m, 3-H$_2$), 1.95 (2H, quint, J=7 Hz, 2-H$_2$), 2.49 (3H, bs, 16-Me), 3.10 (2H, t, J=7 Hz, 1-H$_2$), 7.53 (1H, d, J=8.5 Hz, 6-H), 7.58 (1H, d, J=8.5 Hz, 7-H), 7.95 (1H, brs, 15-H), 8.05 (1H, s, 11-H), 8.45 (1H, brs, OH); ^{13}C NMR δ=19.7, 22.3, 28.9, 31.7 (×2), 35.0, 38.1, 113.2, 127.1, 131.3, 132.4, 134.0, 134.1, 136.0, 144.1, 148.8, 153.9, 179.9.

Miltipolone (15): Colorless crystals, mp 132 °C, high resolution MS, Found: m/z 301.1837. Calcd or $C_{19}H_{25}O_3$, MH$^+$: m/z 301.1803, $[\alpha]_D^{25}$ −77.8° (c 0.20, $CHCl_3$). UV λ_{max} (EtOH) 244 (log ε 4.52), 324 (3.89), 350 (3.89), 368 nm (3.80).

Methyl 5,5-Dimethyl-5,6,7,8-tetrahydro-1,2-naphthalenedicarboxylate (10). A mixture of 341 mg (2.50 mmol) of 6,6-dimethyl-1-vinylcyclohexene (**9**)[11] and 382 mg (2.69 mmol) of methyl acetylenedicarboxylate was heated at 90 °C for 20 h under an argon atmosphere. The crude product, ^{1}H NMR ($CDCl_3$) δ=5.38 (t, 1H), 3.79 (s, 3H), 3.74 (s, 3H), 3.1—2.9 (m, 2H), 1.7—1.2 (m, 4H), 1.09 (s, 3H), and 1.03 (s, 3H), was dissolved in 20 ml of benzene and 571 mg (2.52 mmol) of DDQ was added and the whole was stirred at room temperature for 4.5 d. The mixture was filtered through an alumina column eluted by benzene and pure **10** was obtained by Kugelrohr distillation (bath temp: 180—190 °C/0.3 mmHg, 1 mmHg=133.322 Pa) in 37% yield. **10**: ^{1}H NMR ($CDCl_3$) δ=1.32 (s, 6H), 2.6—2.8 (m, 2H), 3.81 (s, 6H), 7.34 (d, 1H, J=8.6 Hz), and 7.71 (d, 1H, J=8.6 Hz). Found: C, 69.24; H, 7.38%. Calcd for $C_{16}H_{20}O_4$: C, 69.55; H, 7.30%.

5,5-Dimethyl-5,6,7,8-tetrahydro-1,2-naphthalenebis(methanol) (11). To an ice-cooled solution of 205 mg (0.74 mmol) of the diester **10** in 12 ml of dry THF was added 840 mg of lithium aluminium hydride and the mixture was stirred at room temperature for 1 h. A usual work-up gave crude products, which were purified by flash chromatography with dichloromethane–methanol (24 : 1) to give 139 mg (85%) of **11**; mp 83.5—85.0 °C (from benzene); ^{1}H NMR ($CDCl_3$) δ=1.28 (s, 6H), 1.5—2.0 (m, 4H), 2.8—3.0 (m, 2H), 4.78 (s, 2H), 4.82 (s, 2H), 7.10 (d, 1H, J=8 Hz), and 7.30 (d, 1H, J=8 Hz). Found: C, 76.27; H, 9.14%. Calcd for $C_{14}H_{20}O_2$: C, 76.33; H, 9.15%.

Salviolone Methyl Ether (13) and Its Isomeric Methyl Ether (14). To a 112 μg (1.27 mmol) of oxalyl dichloride in 1.86 ml of dichloromethane was added a solution of 185 μl (2.60 mmol) of DMSO in 0.56 ml of dichloromethane at −78 °C drop by drop. After 5 min, 100 mg (0.45 mmol) of the diol **11** in 0.82 ml of dichloromethane was added and the mixture was stirred at that temperature for 45 min. After triethylamine (700 μg, 5.02 mmol) had been added, the whole was stirred for 10 min and then warmed to room temperature. After 1 h, ethyl ether was added to the solution and the whole was filtered through a magnesium sulfate-layer and the filtrate was evaporated to give a crude dialdehyde **12**; ^{1}H NMR ($CDCl_3$) δ=1.1 (s, 6H), 1.2—1.7 (m, 4H), 2.4—2.7 (m, 2H), 7.2 (d, 1H, J=10 Hz), 7.4 (d, 1H, J=10 Hz), 10.0 (s, 1H), and 10.4 (s, 1H). As the aldehyde **12** was unstable, the crude one was used immediately in a subsequent step without further purification. A mixture of the crude dialdehyde **12** and 71 mg (0.70 mmol) of 1-methoxy-2-butanone[12] in 0.3 ml of 2 M NaOH (1 M=1 mol dm^{-3}) and 11.7 ml of distilled water was stirred at room temperature for 6 d;[13] the flask was occasionally ultrasonicated to disperse the syrup produced. The products were taken in diethyl ether and then dichloromethane, and the extracts were washed with saline and dried over anhyd Na_2SO_4. The crude materials were purified by flash chromatography with hexane–ethyl acetate (7 : 3) followed by a preparative TLC (hexane : AcOEt=8 : 2, 14 times development) to afford 28.5 mg of **13** and 18.7 mg of **14**. Total yield from the diol **11** was 28%. **13**; mp 177—178 °C (from benzene); ^{1}H NMR (500 MHz, $CDCl_3$) δ=1.34 (s, 6H), 1.71 (m, 2H), 1.94 (m, 2H), 2.37 (s, 3H), 3.04 (t, 2H, J=6.4 Hz), 3.93 (s, 3H), 7.34 (s, 1H), 7.47 (d, 1H, J=8.5 Hz), 7.50 (d, 1H, J=8.5 Hz), and 7.71 (s, 1H); NOE 2.37 vs. 7.71, 3.93 vs. 7.34, and 3.04 vs. 7.34; ^{13}C NMR (125 MHz, $CDCl_3$) δ=19.8, 22.9, 29.0, 31.8, 34.9, 38.2, 56.0, 111.2, 127.0, 131.1, 131.5, 134.1, 138.9, 140.8, 148.2, 156.3, and 181.6. Found: C, 80.61; H, 7.83%. Calcd for $C_{19}H_{22}O_2$: C, 80.93; H, 7.85%. **14**: Oil; ^{1}H NMR ($CDCl_3$) δ=1.33 (s, 6H), 1.69 (m, 2H), 1.92 (m, 2H), 2.43 (s, 3H), 3.07 (t, 2H, J=6.4 Hz), 3.93 (s, 3H), 7.01 (s, 1H), 7.48 (d, 1H, J=8.5 Hz), 7.54 (d, 1H, J=8.5 Hz), and 8.14 (s, 1H); NOE: δ=8.14 vs. 3.07, δ=2.43 vs. 8.14, and δ=3.93 vs. 7.01.

Synthesis of Salviolone (15). A mixture of 5.9 mg of **13** and 0.75 ml of 40% aqueous HBr was heated at 130 °C for 14 h. The products were taken in chloroform and purified by preparative TLC (dichloromethane : hexane=4 : 1, 3 times development) to give 2.4 mg of **15** in 43% yield.

The authors are grateful to Dr. Guo Yong Tian, Dalian Institute of Medical and Pharmaceutical Science, Dalian, China, for the collection of fresh roots of the plant used in this study. We also thank Bristol-Myers Squibb Research Institute for bioassay.

References

1) H. M. Chang, "Pharmacology and Application of Chinese Materia Medica," ed by P. But, Vol. 1, p. 255 (1986).
2) M. Nakao and T. Fukushima, *J. Pharm. Soc. Jpn.*, **5**, 154 (1934).
3) R. H. Thomson, "Naturally Occurring Quinones, Vol. I", Academic Press, New York (1971), pp. 640—648, and Vol. III, Chapmann and Hall, New York (1987), p. 609.
4) F. von Wessely and A. Bauer, *Ber.*, **75**, 958 (1942); K. Takiura, *J. Pharm. Soc. Jpn.*, **61**, 482 (1941).
5) H. Kakisawa, T. Hayashi, and T. Yamazaki, *Tetrahedron Lett.*, **1969**, 301.
6) H. Ginda, T. Kusumi, M. O. Ishitsuka, and H. Kakisawa, *ibid.*, **29**, 4603 (1988).
7) Unpublished result.
8) F. Asari, T. Kusumi, G. -S. Zheng, Y. -Z Cen, and H. Kakisawa, *Chem. Lett.*, **1990**, 1885.
9) Some parts of these studies were reported as preliminarily communications; Ref. 6: G. Haro and H. Kakisawa, *Chem. Lett.*, **1990**, 1599; and M. Mori, Y. Inouye, and H. Kakisawa, *Chem. Lett.*, **1989**, 1021.
10) H. Christol, M. Y. Delhoste, and M. Mousseron, *Bull. Soc. Chim. Fr.*, **1959**, 1238.
11) H. Kakisawa and I. Ikeda, *J. Chem. Soc. Jpn.*, **88**, 4761 (1967).
12) P. D. Bartlett and S. D. Ross, *J. Am. Chem. Soc.*, **70**, 926 (1948).
13) H. Fernholz, E. Hartwig, and J. C. Salfeld, *Justus Liebig Ann. Chem.*, **576**, 131 (1952); D. S. Tarbell and J. C. Bill, *J. Am. Chem. Soc.*, **74**, 1234 (1952).
14) D. S. Tarbell, G. F. Scott, and A. D. Kemp, *J. Am. Chem. Soc.*, **72**, 379 (1950).

15) A. I. Scott, "Interpretation of the Ultraviolet Spectra of Natural Products," Pergamon Press, Oxford (1964), p. 309.

16) The absolute configuration of miltipolone (**15**) has not been determined experimentally, but it has been tentatively assigned as seen in structure **15** by consideration of the cooccurrence of secodialdehyde (**4**), abietatriene (**5**), and isomanool (**7**), the absolute configurations of which have been already established.

17) J. Cech and F. Santary, *Collect. Crech. Chem. Commun.*, **14**, 532 (1949).

High Thermodynamic Diastereoselection in the Equilibration of Acyclic γ-Alkoxy α-Amino Nitriles

Takashi INABA,† Makoto FUJITA, and Katsuyuki OGURA*
Department of Applied Chemistry, Faculty of Engineering, Chiba University,
1-33 Yayoicho, Chiba 260
† Graduate School of Science and Technology, Chiba University,
1-33 Yayoicho, Chiba 260
(Received July 24, 1991)

An equilibrium between two diastereomers of an acyclic γ-alkoxy α-amino nitrile was attained in chloroform, and the major component is always its (*R**, *S**)-isomer with high diastereoselectivity.

In acyclic systems, there have been many reports on kinetically controlled 1,3-asymmetric induction, where high stereoselectivity can be realized with aid of metal chelation.[1] On the contrary, high stereoselectivity is unlikely under thermodynamic conditions. Recently we reported a highly selective thermodynamic 1,3-stereocontrol in α-amino nitriles (**1**) derived from α-alkylbenzylamines and aldehydes.[2] In this system, the chiral center of the parent α-alkylbenzylamines controls the stereochemical structure of the α-amino nitrile.

Here we wish to report the second example of high 1,3-asymmetric induction in an acyclic system, i.e., the equilibration between two diastereomeric isomers of an acyclic γ-alkoxy α-amino nitrile (**3**) which, on treatment with an acid, produces a synthetic precursor of the corresponding γ-hydroxy α-amino acid, i.e. α-methyl α-amino γ-lactone (**4**).

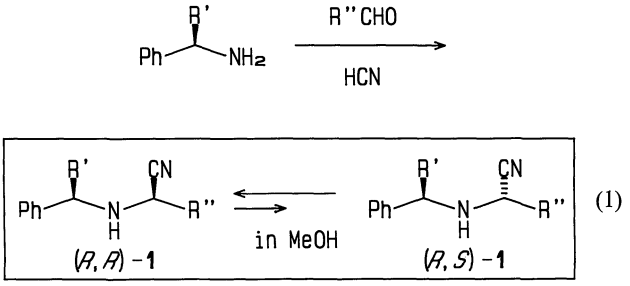

(1)

Results and Discussion

The α-amino nitriles **3a** and **3c** were prepared by the Strecker-type reaction of the corresponding **2** with benzylamine (10 mol equiv), KCN (10 equiv), $NaHSO_3$ (15 equiv) in water or methanol–water (1:3) at room temperature for ca. 20 h. By the reaction of **2b** with benzylamine hydrochloride (1.0 mol equiv) and KCN (1.1 mol equiv) in water, **3b** was obtained. Under these conditions, insoluble **3** separated out as an oil. Yields of **3a**, **3b**, and **3c** were 64%, 63%, and 76%, respectively. The compound (**3d**) which has two methyl groups at its β-position was synthesized in 55% yield by silylcyanation of the Schiff base derived from **2d** and benzylamine and subsequent hydrolytic desilylation. The product (**3**), which consists of two diastereomers, is so labile that we cannot isolate it in pure form except for a major isomer of **3a**. In chromatographic separation on silica gel or Florisil, **3** decomposed. Recycling high-performance gel permeation chromatography made it possible to isolate **3** in a nearly pure form. Recrystallization of **3a** from hexane afforded (*R**, *S**)-**3a** as colorless crystals.

Equilibration between (*R**,*S**)-**3** and (*R**,*R**)-**3**

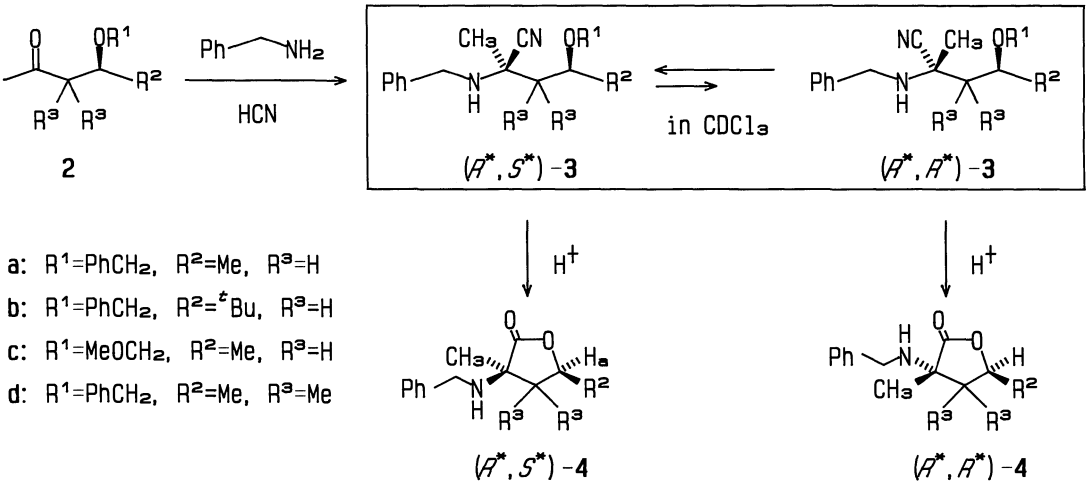

Scheme 1.

occurred in chloroform, probably via the corresponding Schiff base (**5**) or its protonated form. In methanol, **3** decomposed slowly because **5** reacts with methanol.

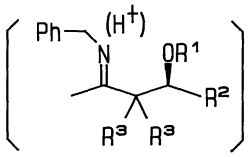

5

This behavior is in contrast with that of **1**, which does not undergo epimerization in chloroform, but in methanol. When the $CDCl_3$ solution of pure (*R**,*S**)-**3a** was allowed to stand at room temperature, epimerization took place. After about 1 d, the ratio of (*R**,*S**)-**3a** and (*R**, *R**)-**3a** was 84:16 (^{1}H NMR). Since this value remained unchanged by elongation of the reaction time, the value of 84:16 was concluded to be the equilibrium ratio of **3a**. The equilibrium ratios of **3b**—**d** were determined after the freshly prepared diastereomeric mixtures were allowed to stand in $CDCl_3$ for 1 d.[3] As summarized in Scheme 2, (*R**, *S**)-**3** is a major component in all cases. Considering that the present 1,3-asymmetric induction is thermodynamically controlled in an acyclic system, the observed concentrations of (*R**, *S**)-**3** are high.

In the IR spectrum of (*R**,*S**)-**3a**, intramolecular hydrogen bonding was observed between the amino hydrogen and the ethereal oxygen. Thus, a dilute $CHCl_3$ solution (0.013 M, 1 M=1 mol dm^{-3}) of (*R**,*S**)-**3a** exhibited an IR absorption at 3340 cm^{-1}. Further the lone pair of the amino nitrogen of an α-amino nitrile is widely recognized to be placed antiperiplanar to its cyano group (stereoelectronic effect).[2,4,5] Therefore the favorable conformers of (*R**,*S**)-**3** and (*R**,*R**)-**3** are assumed to be **[A]** and **[B]**, respectively. Since R^2 group is located at equatorial position in **[A]** and **[B]** has an axial R^2 group, (*R**, *S**)-**3** is more stable than the corresponding (*R**, *R**)-**3**. The important role of the intramolecular hydrogen bonding in high diastereoselection of **3** is supported by a low equilibrium ratio of (*R**, *S**)-**3a** and (*R**, *R**)-**3a** (66:34) in DMSO. The lower

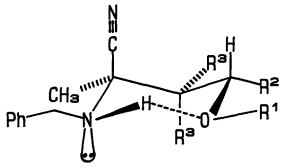

[A] ≡ (*R**, *S**)-**3**

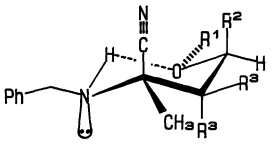

[B] ≡ (*R**, *R**)-**3**

stereoselectivity (69:31) in the equilibration of **3c** is consistent with the decreased electron density of the OR^1 group (R^1=CH_2OCH_3) to make the hydrogen bonding weak.

Finally we describe an acid-catalyzed conversion of **3** into the coresponding α-methyl-α-benzylamino-γ-butyrolactone (**4**) which is brought about by the protonation of the cyano group, the attack of the resulting cation ($-\overset{+}{C}$=NH) on the ethereal oxygen, and the subsequent cleavage of the R^1–O bond. The mechanistic consideration indicates that this reaction is stereospecific. Indeed, (*R**,*S**)-**4a** was given as a single isomer in 65% yield when pure (*R**,*S**)-**3a** was treated with 95% sulfuric acid at room temperature for 15 h. On similar treatment of a diastereomeric mixture of **3a** (84:16), the diastereomeric ratio of **4a** was almost unchanged (82:18). Analogously, **3b** (its diastereomeric ratio=84:16) and **3c** (69:31) also afforded **4b** (75:25) and **4a** (67:33), respectively. In the case of **3d** (79:21), an initial product was 4,5-dihydro-2(3*H*)-furanimine (**6**) (68% yield; 74:26) which was transformed into a 74:26 mixture (96% yield) of (*R**,*S**)-**4d** and (*R**,*R**)-**4d** with *p*-toluenesulfonic acid (PTS) in wet THF. In ^{1}H NMR spectrum of

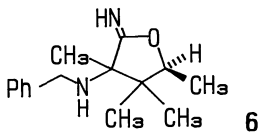

6

(*R**,*S**)-**4**, strong NOE was observed between methine proton (H_a) and α-methyl protons (**4a** ca. 4%; **4b** 4.8%; **4d** 3.6%), whereas no NOE was detected in those of (*R**,*R**)-

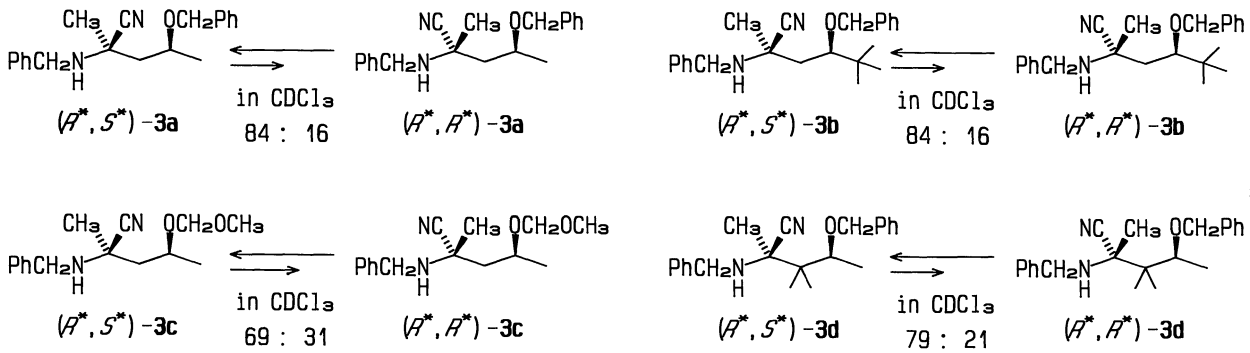

Scheme 2.

4. These facts did not determine only the configurations of **4**, but also those of **3**.

In conclusion, thermodynamically controlled acyclic 1,3-asymmetric induction with high efficiency was realized in the equilibration between two diastereomers of **3**. The conversion of **3** to **4** shows that the present asymmetric induction provides a tool for preparing optically active α-amino acids bearing γ-hydroxy and α-methyl groups from easily available optically active 4-alkoxy-2-alkanones.[6,7]

Experimental

General Procedures. Melting points were determined on a hot-stage microscope apparatus (Yanagimoto) and are uncorrected. ^{1}H NMR spectra were obtained on Hitachi R-600 (60 MHz), JEOL JNM-FX 270 (270 MHz) and JEOL JNM-GSX 500 (500 MHz) spectrometers. Chemical shifts are reported in ppm down field from TMS as the internal standard (δ scale). Infrared spectra were determined with a JASCO A-200 spectrometer and data are presented in cm^{-1} for important diagnostic absorptions. Mass spectra (MS) were determined on a Hitachi RMU-7M spectrometer at 70 eV. Microanalytical data were provided by the Analysis Center of Chiba University.

Preparation of β-Alkoxy Ketones (2). 4-Benzyloxy-2-pentanone (**2a**) and 4-benzyloxy-5,5-dimethyl-2-hexanone (**2b**) were prepared by the "Moffatt–Pfitzner" oxidation[8] of the corresponding alcohols with pyridine, trifluoroacetic acid, and dicyclohexylcarbodiimide in dimethyl sulfoxide.

2a: A colorless oil; bp 103—105°C/133 Pa; ^{1}H NMR ($CDCl_3$; 60 MHz) δ=7.31 (s, 5H), 4.60 (d, 1H, *J*=12 Hz), 4.45 (d, 1H, *J*=12 Hz), 4.06 (m, 1H), 2.72 (dd, 1H, *J*=16, 7 Hz), 2.47 (dd, 1H, *J*=16, 6 Hz), 2.12 (s, 3H), and 1.25 (d, 3H, *J*=6 Hz); IR (neat) 1715 cm^{-1}. Found: *m/z* 192.1160. Calcd for $C_{12}H_{16}O_2$: M, 192.1150.

2b: A colorless oil; bp 117°C/200 Pa; ^{1}H NMR ($CDCl_3$, 270 MHz) δ=7.35—7.21 (m, 5H), 4.58 (d, 1H, *J*=11.2 Hz), 4.52 (d, 1H, *J*=11.2 Hz), 3.71 (dd, 1H, *J*=3.3, 7.9 Hz), 2.69 (dd, 1H, *J*=7.9, 16.5 Hz), 2.57 (dd, 1H, *J*=3.3, 16.5 Hz), 2.17 (s, 3H), and 0.94 (s, 9H); IR (neat) 1720 cm^{-1}. Found: C, 77.05; H, 9.47%. Calcd for $C_{15}H_{22}O_2$: C, 76.88; H, 9.46%. Found: *m/z* 234.1623. Calcd for $C_{15}H_{22}O_2$: M, 234.1618.

4-Methyoxymethyl-2-pentanone (**2c**) was prepared by methoxymethylation of 4-hydroxy-2-pentanone with chloromethyl methyl ether and *i*-Pr_2NEt.[9]

Hydrolysis of 2-(1,1-dimethyl-2-benzyloxypropyl)-2-methyl-1,3-dioxolane, which was prepared by addition of methyllithium to 2-(1-formyl-1-methylethyl)-2-methyl-1,3-dioxolane[10] and subsequent benzylation with benzyl bromide and NaH, gave 4-benzyloxy-3,3-dimethyl-2-pentanone (**2d**): A colorless liquid; ^{1}H NMR ($CDCl_3$, 270 MHz) δ=7.36—7.23 (m, 5H), 4.61 (d, 1H, *J*=11.5 Hz), 4.36 (d, 1H, *J*=11.5 Hz), 3.76 (q, 1H, *J*=6.3 Hz), 2.12 (s, 3H), 1.16 (s, 3H), 1.13 (d, 3H, *J*=6.3 Hz), and 1.07 (s, 3H); IR (neat) 1700 cm^{-1}. Found: C, 76.50; H, 9.19%. Anal. Calcd for $C_{14}H_{20}O_2$: C, 76.33; H, 9.15%.

Preparation of 2-Benzylamino-4-benzyloxy-2-methylpentanenitrile (3a) and Its Lactonization. A Typical Procedure: To a suspension of **2a** (384 mg, 2.00 mmol) in water (30 ml) were added $NaHSO_3$ (3.12 g, 30.0 mmol), KCN (1.30 g, 20.0 mmol) and a solution of benzylamine (2.12 g, 20.0 mmol) in MeOH (10 ml) under cooling with ice. After the reaction mixture was stirred at room temperature for 20 h, a deposited oil was extracted with CH_2Cl_2 (30 ml×1, 10 ml×2). The combined organic layers were dried ($MgSO_4$) and evaporated in vacuo. After quick chromatography (within 10 min) on silica gel [hexane–ethyl acetate (5:1)], HPLC separation[11] afforded a colorless oil (393 mg, 64%) which was shown by ^{1}H NMR to consist of (*R**,*S**)-**3a** (84%), (*R**,*R**)-**3a** (16%), and **2a** (trace). The major diastereomer was isolated in a pure form by recrystallization from hexane.

(*R**,*S**)-**3a**: Colorless crystals; mp 35.5°C (hexane); ^{1}H NMR ($CDCl_3$, 270 MHz) δ=7.36—7.07 (m, 10H), 4.61 (d, 1H, *J*=10.6 Hz), 4.40 (d, 1H, *J*=10.9 Hz), 4.18 (m, 1H). 3.80 (d, 1H, *J*=12.0 Hz), 3.73 (d, 1H, *J*=12.0 Hz), 3.11 (br s, 1H, NH), 2.03 (dd, 1H, *J*=14.5, 10.6 Hz), 1.81 (dd, 1H, *J*=14.5, 2.6 Hz), 1.48 (s, 3H), and 1.27 (d, 3H, *J*=5.9 Hz); IR (KBr) 3350 and 2220 cm^{-1}. Found: C, 77.85; H, 7.98; N, 9.10%. Calcd for $C_{20}H_{24}N_2O$: C, 77.98; H, 7.84; N, 9.08%.

^{1}H NMR of (*R**,*R**)-**3a** ($CDCl_3$–D_2O, 270 MHz), which was assigned from spectra of the diastereomeric mixture: δ=7.36—7.07 (m, 5H), 4.61 (d, 1H, *J*=11.2 Hz), 4.43 (d, 1H, *J*=11.2 Hz), 3.88 (m, 1H), 3.86 (s, 2H), 2.08 (dd, 1H, *J*=9.2, 14.5 Hz), 1.85 (dd, 1H, *J*=3.3, 14.5 Hz), 1.55 (s, 3H), and 1.30 (d, 3H, *J*=6.3 Hz).

A diastereomeric mixture (84:16) of **3a** (376 mg, 1.22 mmol) was added to concd sulfuric acid (95%, 5.0 ml) under cooling with ice. After being stirred for 15 h at room temperature, the resulting mixture was poured onto ice containing aqueous NH_3 (28% concn; 15 ml). After extraction with CH_2Cl_2 (30 ml×1, 10 ml×2), the combined organic layers were dried ($MgSO_4$), evaporated in vacuo, and subjected to flash chromatography on silica gel [hexane–ethyl acetate (7:2—2:1)] to give (*R**,*S**)-**4a** (101 mg, 38%) and (*R**,*R**)-**4a** (22.0 mg, 8.2%).

(*R**,*S**)-**4a**: A colorless oil; ^{1}H NMR (500 MHz, $CDCl_3$) δ=7.37—7.24 (m, 5H), 4.53 (qt, 1H, *J*=5.9, 10.1 Hz), 3.80 (d, 1H, *J*=12.1 Hz), 3.68 (d, 1H, *J*=12.1 Hz), 2.19 (dd, 1H, *J*=5.9, 13.0 Hz), 2.06 (dd, 1H, *J*=10.1, 13.0 Hz), 1.72 (br s, 1H, NH), 1.45 (d, 3H, *J*=6.0 Hz), and 1.43 (s, 3H); IR (neat) 3340 and 1770 cm^{-1}. Found: C, 71.16; H, 7.84; N, 6.39%. Calcd for $C_{13}H_{17}NO_2$: C, 71.21; H, 7.81; N, 6.39%.

(*R**,*R**)-**4a:** Colorless crystals; mp 39—40°C (hexane–Et_2O); ^{1}H NMR ($CDCl_3$, 500 MHz) δ=7.33—7.24 (m, 5H), 4.70 (qt, 1H, *J*=6.3, 8.5 Hz). 3.89 (d, 1H, *J*=12.1 Hz), 3.74 (d, 1H, *J*=12.1 Hz), 2.47 (dd, 1H, *J*=6.6, 13.5 Hz), 1.80 (dd, 1H, *J*=8.5, 13.5 Hz), 1.49 (br s, 1H, NH), 1.47 (s, 3H), and 1.42 (d, 3H, *J*=6.3 Hz); IR (KBr) 3290 and 1750 cm^{-1}. Found: C, 71.26; H, 7.85; N, 6.36%. Calcd for $C_{13}H_{17}NO_2$: C, 71.21; H, 7.81; N, 6.39%.

Similarly, treatment of pure (*R**,*S**)-**3a** (110 mg, 0.357 mmol) with sulfuric acid gave (*R**,*S**)-**4a** (51.1 mg, 65%). In this reaction mixture, we could not detect (*R**,*S**)-**4a**.

2-Benzylamino-4-methoxymethoxy-2-methylbutanenitrile (3c) and Its Lactonization: In a similar manner, **3c** (418 mg, 76%) was obtaind from **2c** (292 mg, 2.00 mmol) as a colorless oil, which was shown by ^{1}H NMR to consist of (*R**,*S**)-**3c** (66%), (*R**,*R**)-**3c** (30%), and **2c** (4%): ^{1}H NMR ($CDCl_3$, 270 MHz) δ=7.41—7.23 (m, 5H), 4.71 (d, 0.30×1H, *J*=7.3 Hz), 4.70 (d, 0.66×1H, *J*=6.9 Hz), 4.65 (d, 0.30×1H, *J*=7.3 Hz), 4.63 (d, 0.66×1H, *J*=6.9 Hz), 4.20 (m, 0.66×1H), 4.01 (m, 0.30×1H), 3.88 (br m, 0.96×2H), 3.352 (s, 0.30×3H), 3.345 (s, 0.04×3H), 3.32 (s, 0.66×3H), 2.83 (br s, 0.96×1H, NH), 2.18 (s, 0.04×3H), 2.06 (dd, 0.30×1H, *J*=5.3, 14.8 Hz), 2.00 (dd, 0.66×1H, *J*=7.9,

14.5 Hz), 1.82 (dd, 0.30×1H, J=3.6, 14.5 Hz), 1.78 (dd, 0.66×1H, J=2.7, 14.5 Hz), 1.57 (s, 0.30×3H), 1.50 (s, 0.66×3H), 1.26 (d, 0.30×3H, J=6.3 Hz), 1.24 (d, 0.66×3H, J=5.9 Hz), and 1.22 (d, 0.04×3H, J=6.3 Hz); IR (neat) 3350 and 2220 cm^{-1}.

When a 69:31 mixture of (*R**,*S**)- and (*R**,*R**)-**3c** was treated with sulfuric acid, a 67:33 mixture of (*R**,*S**)- and (*R**,*R**)-**4a** was given in 37% yield.

2-Benzylamino-4-benzyloxy-2,5,5-trimethylhexanenitrile (3b) and 2-Benzylamino-4-(*t*-butyl)-2-methyl-γ-butyrolactone (4b): To a stirring suspension of **2b** (234 mg, 1.00 mmol) in water (0.50 ml) were added benzylamine hydrochloride (145 mg, 1.01 mmol) and KCN (72.0 mg, 1.11 mmol) at room temperature. After the reaction mixture was stirred at the same temperature for 20 h, CH_2Cl_2 (20 ml) and anhydrous $MgSO_4$ to remove the water were added, and the solvent was evaporated in vacuo. A short-column chromatography on silica gel (eluent: ethyl acetate) followed by HPLC separation[11] afforded a colorless oil (229 mg, 63%) which was shown by ^1H NMR to consist of (*R**,*S**)-**3b** (84%) and (*R**,*R**)-**3b** (16%); ^1H NMR ($CDCl_3$, 270 MHz) δ=7.37—7.03 (m, 10H, ArH), 4.82 (d, 0.84×1H, J=11.2 Hz, $OC\underline{H}_2Ph$), 4.78 (d, 0.84×1H, J=11.5 Hz, $OC\underline{H}_2Ph$), 3.91 (d, 0.16×1H, J=9.6 Hz, $NC\underline{H}_2Ph$), 3.90 (d, 0.16×1H, J=9.6 Hz, $NC\underline{H}_2Ph$), 3.74 (br s, 0.84×2H, $NC\underline{H}_2Ph$), 3.68 (dd, 0.84×1H, J=3.3, 10.2 Hz, $OC\underline{H}CH_2$), 3.37 (dd, 0.16×1H, J=3.6, 6.9 Hz, $OC\underline{H}CH_2$), 1.98 (dd, 0.84×1H, J=10.2, 14.5 Hz, $OCHC\underline{H}_2$), 1.88 (dd, 0.84×1H, J=3.3, 14.5 Hz), 1.57 (s, 0.16×3H, $C\underline{H}_3CCN$), 1.50 (s, 0.84×3H, $C\underline{H}_3CCN$), 0.99 (s, 0.84×9H, $C(C\underline{H}_3)_3$), and 0.98 (s, 0.84×9H, $C(C\underline{H}_3)_3$); IR (neat) 3340 cm^{-1}.

Treatment of thus obtained **3b** with sulfuric acid resulted in formation of **4b** with a diastereomeric ratio of 75:25 in 51% yield.

(*R**,*S**)-**4b:** Colorless crystals; mp 74°C (hexane); ^1H NMR ($CDCl_3$, 500 MHz) δ=7.38—7.24 (m, 5H), 4.10 (dd, 1H, J=6.1, 11.0 Hz), 3.78 (d, 1H, J=12.1 Hz), 3.68 (d, 1H, J=12.1 Hz), 2.24 (dd, 1H, J=11.0, 12.9 Hz), 1.92 (dd, 1H, J=6.1 Hz, 12.9 Hz), 1.76 (br s, 1H, $N\underline{H}$), 1.44 (s, 3H), 0.97 (s, 9H); IR (KBr) 3340, 1760 cm^{-1}. Found: C, 73.75; H, 8.94; N, 5.23%. Calcd for $C_{16}H_{23}NO_2$: C, 73.53; H, 8.87; N, 5.36%. Found: m/z 217.1837. Calcd for $C_{15}H_{23}N$: M−CO_2, 217.1829.

(*R**,*R**)-**4b:** Colorless crystals; mp 78°C (hexane); ^1H NMR ($CDCl_3$, 500 MHz) δ=7.35—7.24 (m, 5H), 4.28 (dd, 1H, J=6.6, 9.9 Hz), 3.80 (d, 1H, J=12.1 Hz), 3.76 (d, 1H, J=12.1 Hz), 2.18 (dd, H, J=6.6, 13.8 Hz), 1.95 (dd, 1H, J=9.9, 13.8 Hz), 1.55 (br s, 1H, $N\underline{H}$), 1.45 (s, 3H) and 0.94 (s, 9H); IR (KBr) 3340 and 1740 cm^{-1}. Found: C, 73.46; H, 8.93; N, 5.17%. Calcd for $C_{16}H_{23}NO_2$: C, 73.53; H, 8.87; N, 5.36%. Found: m/z 217.1837. Calcd for $C_{15}H_{23}N$: M−CO_2, 217.1829.

2-Benzylamino-4-benzyloxy-2,3,3-trimethylpentanenitrile (3d): The mixture of **2d** (440 mg, 2.00 mmol), benzylamine (856 mg, 8.00 mmol), and $BF_3{\cdot}OEt_2$ (20 mg) was stirred at 80°C for 16 h under an atmosphere of nitrogen. After removal of the unreacted benzylamine under reduced pressure (100°C/67 Pa), the residue was dissolved in CH_2Cl_2 (6.0 ml) and then trimethylsilyl cyanide (0.40 ml, 3.0 mmol) and $ZnCl_2$ (20 mg) were added at room temperature. After being stirred at the same temperature for 4 h, the reaction mixture was passed through a short column on silica gel (5 g) using Et_2O as an eluent. Purification by recycling HPLC[11] gave a colorless oil (504 mg) which was shown by ^1H NMR to comprise (*R**,*S**)-**3d** (63%), (*R**,*R**)-**3d** (17%), and the Schiff base (**5**; R^1=$PhCH_2$, R^2=R^3=Me) (20%) which might be produced from **3d** by elimination of a HCN moiety during workup. The yield of **3d** was calculated to be 55%. ^1H NMR of **3d** ($CDCl_3$, 270 MHz): δ=7.36—7.03 (m, 10H), 4.623 (d, 0.20×1H, J=11.9 Hz), 4.617 (d, 0.17×1H, J=11.5 Hz), 4.60 (d, 0.63×1H, J=10.6 Hz), 4.51 (br s, 0.20×2H, $NC\underline{H}_2Ph$), 4.42 (d, 0.63×1H, J=10.5 Hz, $OC\underline{H}_2Ph$), 4.37 (d, 0.20×1H, J=11.9 Hz, $OC\underline{H}_2Ph$), 4.29 (d, 0.17×1H, J=11.5 Hz, $OC\underline{H}_2Ph$), 3.98 (q, 0.63×1H, J=6.3 Hz, $OC\underline{H}CH_3$), 3.82 (br s, 0.17×2H, $NC\underline{H}_2Ph$), 3.74 (d, 0.63×2H, J=6.3 Hz, $NC\underline{H}_2Ph$), 3.74 (q, 0.20×1H, J=6.3 Hz, $OC\underline{H}CH_3$), 3.57 (q, 0.17×1H, J=6.3 Hz, $OC\underline{H}CH_3$), 3.32 (br t, 0.80×1H, J=6.6 Hz, $N\underline{H}$), 1.84 (s, 0.20×3H), 1.46 (s, 0.17×3H), 1.39 (s, 0.63×3H), 1.30 (d, 0.17×3H, J=6.3 Hz), 1.25 (d, 0.63×3H, J=6.3 Hz), 1.21 (s, 0.17×3H), 1.19 (s, 0.17×3H), 1.13 (s, 0.20×6H), 1.12 (d, 0.20×3H, J=6.3 Hz), 1.03 (s, 0.63×3H), and 1.00 (s, 0.63×3H); IR (neat) 3350 and 2220 cm^{-1}.

3-Benzylamino-3,4,4,5-tetramethyl-4,5-dihydro-2(3*H*)-furanimine (6): The similar procedure gave 3-benzylamino-3,4,4,5-tetramethyl-4,5-dihydro-2(3*H*)-furanimine (**6**) as a diastereomeric mixture (200 mg, 68%; (*R**,*S**):(*R**,*R**)=79:21) from the equilibrium mixture of (*R**,*S**)-**3d** and (*R**,*R**)-**3d** (504 mg, 80% purity, 1.20 mmol). **6** was colorless crystals; mp 67—71°C; ^1H NMR ($CDCl_3$, 270 MHz) δ=7.41—7.21 (m, 5H, ArH), 4.63 (q, 0.26×1H, J=6.6 Hz, $OC\underline{H}CH_3$), 4.14 (q, 0.74×1H, J=6.3 Hz, $OC\underline{H}CH_3$), 4.04 (d, 0.74×1H, J=12.5 Hz, $NC\underline{H}_2Ph$), 3.85 (d, 0.74×1H, J=12.2 Hz, $NC\underline{H}_2Ph$), 3.83 (s, 0.26×2H, $NC\underline{H}_2Ph$), 1.40 (s, 0.74×3H, $NCC\underline{H}_3$), 1.27 (s, 0.26×3H, $NCC\underline{H}_3$), 1.24 (d, 0.74×3H, J=6.6 Hz, $OCHC\underline{H}_3$), 1.20 (d, 0.26×3H, J=6.6 Hz, $OCHC\underline{H}_3$), 1.10 (s, 0.74×3H, $C(C\underline{H}_3)_2$), 0.95 (s, 0.74×3H, $C(C\underline{H}_3)_2$), 0.94 (s, 0.26×3H, $C(C\underline{H}_3)_2$), and 0.85 (s, 0.26×3H, $C(C\underline{H}_3)_2$); IR (KBr) 3340, 3290, and 1675 cm^{-1}. Found: C, 73.26; H, 9.02; N, 11.36%. Calcd for $C_{15}H_{22}N_2O$: C, 73.13; H, 9.00; N, 11.37%.

2-Benzylamino-2,3,3,4-tetramethyl-γ-butyrolactone (4d): To the solution of **6** (269 mg, 1.09 mmol) in THF (8 ml) were added *p*-toluenesulfonic acid monohydrate (560 mg, 2.95 mmol) and H_2O (0.8 ml). After reflux for 16 h, the reaction mixture was neutralized with saturated aqueous $NaHCO_3$ and extracted with Et_2O (40 ml). The organic layer was washed with brine, dried ($MgSO_4$), and evaporated in vacuo. Flash chromatography on silica gel [hexane–ethyl acetate (5:1)] afforded a 74:26 mixture (*R**,*S**)-**4d** and (*R**,*R**)-**4d** (258 mg, 96% yield), which was separated by recycling HPLC[12] [eluent: hexane–ethyl acetate (2:1)].

(*R**,*S**)-**4d:** Colorless crystals; mp 60—61°C; ^1H NMR ($CDCl_3$, 500 MHz) δ=7.40—7.23 (m, 5H), 4.25 (q, 1H, J=6.4 Hz), 4.13 (d, 1H, J=12.3 Hz), 3.82 (br d, 1H, J=11.5 Hz), 1.40 (s, 3H), 1.29 (d, 3H, J=6.6 Hz), 1.05 (s, 3H), and 0.99 (s, 3H); IR (KBr) 3320 and 1760 cm^{-1}. Found: C, 72.96; H, 8.62; N, 5.58%. Calcd for $C_{15}H_{21}N_2O_2$: C, 72.84; H, 8.56; N, 5.66%.

(*R**,*R**)-**4d:** Colorless crystals; mp 49—50°C; ^1H NMR ($CDCl_3$, 500 MHz) δ=7.33—7.22 (m, 5H), 4.71 (q, 1H, J=6.4 Hz), 3.87 (d, 1H, J=12.6 Hz), 3.71 (d, 1H, J=12.6 Hz), 1.26 (d, J=6.4 Hz, 3H), 1.25 (s, 3H), 0.97 (s, 3H), and 0.89 (s, 3H); IR (KBr) 3330 and 1760 cm^{-1}. Found: C, 72.83; H, 8.64; N, 5.54%. Calcd for $C_{15}H_{21}N_2O_2$: C, 72.84; H, 8.56; N, 5.66%.

References

1) Reviews: a) M. T. Reetz, "Organotitanium Reagents in Organic Synthesis," Springer-Verlag, Berlin (1986), pp. 140—144. b) D. Schinzer, "Selectivities in Lewis Acid Promoted Reactions," Kluwer Academic Publishers, Dordrecht (1989),

pp. 73—105.

2) T. Inaba, M. Fujita, and K. Ogura, *J. Org. Chem.*, **56**, 1274 (1991).

3) These ratios were nearly equal to those of the crude products.

4) A review: P. Deslongchamps, "Stereoelectronic Effects in Organic Chemistry," Pergamon, Oxford (1983), pp. 215—216.

5) a) M. Petrzilka, D. Felix, and A. Eschenmoser, *Helv. Chim. Acta,* **56**, 2950 (1973). b) M. Riediker and W. Graf, *Helv. Chim. Acta,* **62**, 2053 (1979). c) R. H. Mueller and R. M. Dipardo, *J. Chem. Soc., Chem. Commun.*, **1975**, 565.

6) Reviews: a) C. H. Heathcock, "The Aldol Addition Reaction," in "Asymmetric Synthesis. Vol. 3," ed by J. D. Morrison, Academic Press, Inc., New York (1984), pp. 111—212. b) M. Braun, *Angew. Chem., Int. Ed. Engl.*, **26**, 24 (1987).

7) a) H. Eichenauer, E. Friedrich, W. Lutz, and D. Enders, *Angew. Chem., Int. Ed. Engl.*, **17**, 206 (1978). b) K. Narasaka, T. Miwa, H. Hayashi, and M. Ohta, *Chem. Lett.*, **1984**, 1399. c) M. T. Reetz, F. Kunisch, and P. Heitmann, *Tetrahedron Lett,* **27**, 4721 (1986). d) I. Paterson and J. M. Goodman, *Tetrahedron Lett.*, **30**, 997 (1989).

8) K. E. Pfitzner and J. G. Moffatt, *J. Am. Chem. Soc.*, **85**, 3027 (1963); *ibid.*, **87**, 5670 (1965).

9) T. Sato, H. Matsuoka, T. Igarashi, M. Minomura, and E. Murayama, *J. Org. Chem.*, **53**, 1207 (1988).

10) O. P. Vig, G. Singh, O. P. Chugh, and K. L. Matta, *J. Indian Chem. Soc.*, **46**, 363 (1969).

11) With LC-908 (Japan Analytical Industry, Co., Ltd.) equipped with JAIGEL-1H (i.d. 20×600 mm) and JAIGEL-2H (i.d. 20×600 mm); eluent, 0.5% NEt_3 containing $CHCl_3$.

12) With LC-908 (Japan Analytical Industry, Co., Ltd.) equipped with D-SIL-5-06-B (S-5 60A SIL) (i.d. 30×250 mm) (YMC Co., Ltd.).

 © 1991 The Chemical Society of Japan Bull. Chem. Soc. Jpn., 64, 3432—3437 (1991) [Vol. 64, No. 11

Mechanistic Study of the Hydrogenation of Carbon Dioxide to Methanol over Supported Rhenium and Copper-Zinc Catalysts

Zheng Xu,† Zaihu Qian,† and Hideshi Hattori*
Department of Chemistry, Faculty of Science, Hokkaido University, Sapporo 060
† Department of Chemistry, Jilin University, Changchun, China
(Received March 1, 1991)

The reaction of a mixture containing ^{13}CO, CO_2, and H_2 was carried out in order to elucidate the reaction mechanisms of carbon dioxide hydrogenation to methanol over supported Re catalysts as well as Cu–Zn oxide catalysts. The reactions of formic acid and formaldehyde with hydrogen were also examined. From the incorporation of ^{13}C in the product methanol, it could be distinguised whether the carbon dioxide hydrogenation to methanol proceeds through formation and successive hydrogenation of CO or by direct hydrogenation of CO_2. Methanol is formed almost exclusively by direct hydrogenation of CO_2 over CuO–ZnO based catalysts. However, the two reaction routes operate over Re/ZrO_2 and Re/CeO_2, the contribution of route via CO being higher over Re/ZrO_2 than over Re/CeO_2. The reactions of formic acid and formaldehyde with hydrogen suggest that the surface formate and the adsorbed formaldehyde are involved in the methanol formation, and that the conversion of the formate to the adsorbed formaldehyde is a key step.

In sharp contrast to the extensive studies involving hydrogenation of CO to methanol, hydrogenation of CO_2 to methanol has left some uncertainties regarding the mechanisms. One of the discussion points concerning the mechanism of methanol synthesis is the reaction intermediates. The other point to be discussed is the source of carbon for the product methanol. One candidate is CO_2 and the other is CO resulting from a reverse water–gas shift reaction of CO_2 and H_2.

Two kinds of catalysts used for the methanol synthesis from CO_2 and H_2 are supported transition metals and CuO–ZnO based catalysts. The mechanisms of methanol synthesis seem to be dependent upon the type of catalyst.

As the intermediate of methanol synthesis, surface formate species has been proposed for both supported transition metal catalysts and Cu–Zn oxide catalysts. Ramaroson et al. studied the mechanisms of the formation of C_1 products from CO_2 and H_2 over Pd/SiO_2 and Pd/Al_2O_3 by a chemical trapping method.[1] They proposed that the first step involves the formation of formate by CO_2 insertion into a hydroxide site. Solymosi et al. confirmed by IR spectroscopy the formation of formate in the hydrogenation of CO_2 over supported Rh catalysts.[2] They proposed that hydrogen activated on the Rh migrates onto the support and reacts with hydrocarbonate to yield the formate ion.

Over CuO–ZnO based catalysts, Kieffer et al.[3] and Ramaroson et al.[4] have reported that the formation of formate as an intermediate for the methanol synthesis from CO_2 and H_2 was observed by a chemical trapping method. Amenomiya et al. observed the formation of formate during CO_2 hydrogenation.[5] They proposed that the formate is formed by the insertion of CO_2 into a hydroxide site, and that the formate species is a common intermediate to methanol synthesis as well as to CO formation by a reverse water–gas shift.

To clarify whether methanol is formed directly from CO_2 or through the formation of CO followed by hydrogenation, isotope-labeling studies were performed. Chinchen et al. used $^{14}CO_2$ or ^{14}CO in a mixture of $CO_2/CO/H_2$, and found that CO_2 is the major reactant for methanol synthesis over $CuO–ZnO–Al_2O_3$ under industrial conditions.[6] Liu et al. used ^{18}O-labeled CO_2 for methanol synthesis over a Cu–Zn oxide catalyst.[7] Their results have indicated that there are at least four parallel reactions: $CO–CO_2$ exchange, CO hydrogenation, CO_2 hydrogenation, and a water–gas shift.

Erdoeheloyi et al. studied the hydrogenation of CO_2 over supported Pd.[8] The results failed to suppoort the idea that methanol is produced in a direct reaction of CO_2 and not through the formation of CO and its consecutive hydrogenation.

It seems that over CuO–ZnO based catalysts, methanol is formed directly from CO_2. However, it is not certain whether the same conclusion can be made regarding methanol synthesis over supported transition metal catalysts.

In our previous papers, methanol syntheses from CO_2 and H_2 were carried out over supported Re catalysts and Cu–Zn oxide supported on various metal oxides in order to examine the support effects.[9,10] The activity and selectivity depend on the type of support for both the Re and Cu–Zn oxide catalysts. It is also suggested that different mechanisms are operating in methanol formation over Re/ZrO_2 and Re/CeO_2. In the present study, the mechanisms of hydrogenation of CO_2 were studied regarding both supported Re and Cu–Zn oxide catalysts by the use of ^{13}C-labeled CO in order to clarify the origin of carbon in the products. The reaction of formic acid or formaldehyde with hydrogen was carried out in order to examine the intermediates for methanol.

Experimental

Preparation of Catalysts. Supported Re catalysts were prepared by impregnating CeO_2 and ZrO_2 (20—40 mesh) with an NH_4ReO_4 solution (1 M, 1 M=1 mol dm^{-3}), followed by drying in a vacuum and successively reducing with hydrogen first at 200°C for 2 h, then 400°C for 4 h, and finally at a reaction temperature of 200°C for 2 h before use. The content of Re was adjusted to be 1.5 wt% for both catalysts.

The Cu–Zn oxide catalyst was prepared by the hydrolysis of a mixed solution containing 1 M $Cu(NO_3)_2$ and 1 M $Zn(NO_3)_2$ with 1 M aqueous solution, followed by washing and drying. The dried catalyst was calcined in air at 350°C for 3 h and then at 500°C for 1 h. The mole percents of CuO was adjusted to be 50%.

The Cu–Zn oxide catalysts supported on ZrO_2, MgO, Al_2O_3, and Cr_2O_3 were prepared by the direct addition of $Zr(OH)_4$, $Mg(OH)_2$, $Al(OH)_3$, and $Cr(OH)_3$, respectively, to the $Cu(OH)_2$–$Zn(OH)_2$ coprecipitates obtained as above; this was followed by drying and calcining also in a manner similar to the above. The mole percents of CuO, ZnO, and support metal oxides were adjusted to be 42, 47, and 11% for CuO–ZnO–ZrO_2, 47, 47, and 6% for CuO–ZnO–MgO and CuO–ZnO–Al_2O_3, 34.5, 34.5, and 11% for CuO–ZnO–Cr_2O_3.

Isotope Labeling Reaction. A mixture containing CO_2 (140 Torr, 1 Torr=133.322 Pa), H_2 (420 Torr) and ^{13}CO (10 Torr) was used as a reactant. The ^{13}CO was purchased from Cambridge Isotope Laboratories; its isotopic purity was 99%. Hydrogen was purified by passage through 13X molecular sieves. The CO_2 was purified by freeze-thaw cycles. A recirculation reactor having a volume of 267 cm^3 was employed. A catalyst sample (0.30 g) was placed in the reactor and reduced with hydrogen flow at 300°C for 6 h. After evacuating the hydrogen for 30 min, the reactant was introduced into the reaction system. All reactions were carried out at 200°C. During the reaction, a trap placed in the loop of the recirculation reactor was kept at −78.5°C, so that the formed methanol could be trapped so as to keep the vapor pressure of methanol negligibly low in order to avoid a reverse reaction. For product analysis, the catalyst bed was closed from the recirculation loop and the trap was heated to room temperature. The reaction mixture was then withdrawn. A part of the withdrawn reaction mixture was analyzed by gas chromatography. The other part was subjected to mass spectrometric analysis.

Reaction of Formic Acid or Formaldehyde with Hydrogen. For the reaction of formic acid or formaldehyde with hydrogen, the same recirculation reactor was employed. After pretreatment, the catalyst was exposed to 12 Torr formic acid or formaldehyde at room temperature for 30 min. Then, 420 Torr hydrogen was introduced, and the catalyst was heated to a reaction temperature of 200°C. The products were analyzed by a gas chromatograph using Porapak-Q column.

XPS Measurements. XPS were measured by using an Escalab MK II spectrometer equipped with an in situ reaction cell inside the pretreatment chamber. Mg $K\alpha$ was used as a radiation source. A plate sample was evacuated at room temperature in the pretreatment chamber, then transferred to a small reactor where the reduction with hydrogen stream was carried out at 300°C for 2 h. After the prereduced sample was transferred to the pretreatment chamber, evacuated, and transferred to the analyzing chamber, the Cu2p spectra were measured.

Results and Discussion

Regarding the reaction of the mixture containing CO_2, ^{13}CO and H_2, the experimental results are shown in Table 1. Over Re catalysts, methane was produced as well as methanol. In particular, the formation of methane exceeded to a considerable extent over Re/ZrO_2. In contrast to the case of the Re catalysts, methane was not formed over Cu–Zn oxide catalysts. Practically no reaction was appreciable over CuO–ZnO–Cr_2O_3.

The percentages of the ^{13}C content in each product are plotted against the reaction time in Figs. 1 and 2 for Re/ZrO_2 and Re/CeO_2, respectively. If the product is formed directly from CO_2, the ^{13}C content in the product will be 0% at a conversion of 0%. On the contrary, the

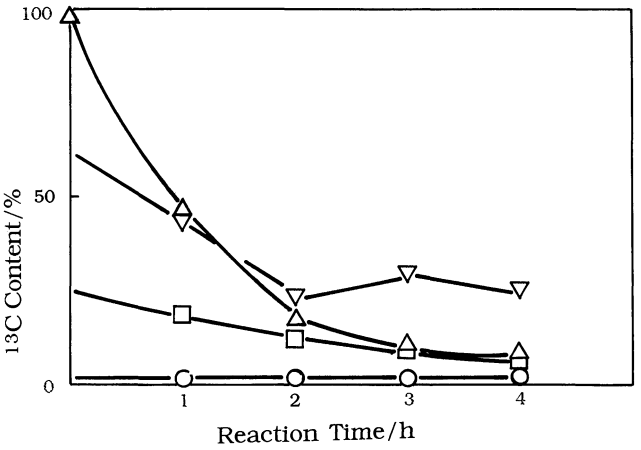

Fig. 1. Variations in the ^{13}C contents of each product in the reaction of $H_2+CO_2+^{13}CO$ over Re/ZrO_2 as a function of the reaction time. △: CO, ○: CO_2, □: CH_3OH, ▽: CH_4.

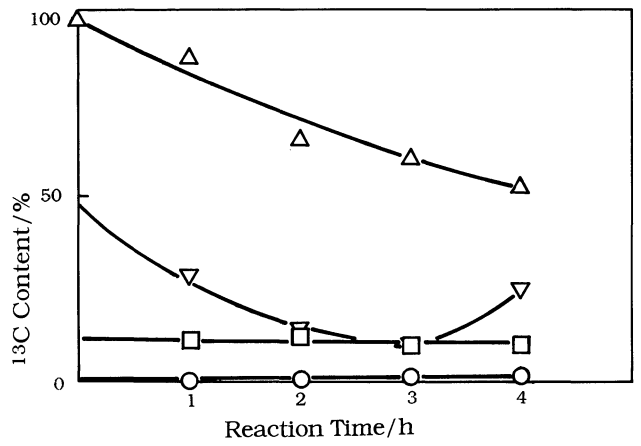

Fig. 2. Variations in the ^{13}C contents of each product in the reaction of $H_2+CO_2+^{13}CO$ over Re/CeO_2 as a function of the reaction time. △: CO, ○: CO_2, □: CH_3OH, ▽: CH_4.

Table 1. Product Distribution and ^{13}C Isotopic Distribution in the Reaction of H_2, CO_2, and ^{13}CO[a)]

Catalyst	Reac. time	Product composition/%					^{13}C Content in each product/%			
	h	CO	CH_4	CH_3OH	CO_2	C_2	CO	CH_4	CH_3OH	CO_2
Re/CeO_2	1	7.7	0.2	0.1	92.0	0.1	80.7	28.5	11.0	0.5
	2	8.0	0.6	0.3	91.0	0.1	65.3	13.4	11.9	0.9
	3	8.6	0.8	0.5	90.1	0.1	60.2	9.4	9.6	1.3
	4	9.2	1.0	0.6	89.1	0.2	52.6	24.5	9.6	1.7
Re/ZrO_2	1	4.4	3.0	0.2	92.1	0.3	46.5	42.2	18.5	1.2
	2	4.2	6.1	0.3	88.8	0.6	17.6	23.4	11.5	1.4
	3	4.5	8.6	0.4	85.7	0.9	10.7	29.0	9.7	1.7
	4	9.5	10.6	0.4	78.5	1.1	8.2	25.1	7.1	2.0
CuO–ZnO	1	11.8	0	0.2	86.2	0	37.7	—	2.8	0
	2	13.0	0	0.6	84.2	0	37.4	—	2.1	0.4
	3	14.5	0	0.8	81.4	0	34.0	—	2.3	0.8
	4	16.0	0	1.0	79.3	0	31.4	—	2.0	0.8
CuO–ZnO–MgO	0.5	7.7	0	0.6	89.4	0	61.1	—	0.9	0.1
	1.0	10.4	0	0.9	85.4	0	43.5	—	1.8	0.4
	1.5	13.3	0	1.2	80.6	0	37.6	—	2.0	0.5
	2.0	16.0	0	1.0	76.3	0	26.5	—	1.9	0.7
CuO–ZnO–Al_2O_3	0.5	7.4	0	0.4	91.3	0	80.3	—		0
	1.0	8.8	0	1.2	88.1	0	66.6	—	1.3	0
	1.5	10.5	0	2.0	84.2	0	58.5	—	0.8	0.1
	2.0	12.3	0	2.7	80.3	0	46.6	—	0.5	0.2
CuO–ZnO–ZrO_2	0.5	9.6	0	0.2	88.9	0	81.9	—	1.0	0.2
	1.0	11.2	0	1.7	84.9	0	69.4	—	1.1	0.3
	1.5	12.9	0	2.0	80.8	0	59.9	—	1.8	0.3
	2.0	14.5	0	2.7	77.6	0	52.6	—	1.8	0.4
CuO–ZnO–Cr_2O_3	1	8.6	0	0	91.3	0	91.7	—	—	0.2
	2	8.4	0	0	91.5	0	90.3	—	—	0.2
	3	8.5	0	0	91.5	0	88.1	—	—	0.2
	4	8.9	0	0	91.0	0	81.4	—	—	0

a) Reaction conditions: Reactant: H_2 (420 Torr)+CO_2 (140 Torr)+^{13}CO (10 Torr), Catalyst: 300 mg, Reaction temperature: 200°C.

^{13}C content will be 100% if the product is formed from CO. Although the values obtained by extrapolation to 0 conversion have some uncertainties, these are useful for determining the reaction route. Over a Re/ZrO_2 catalyst, the ^{13}C content in CH_4 was about 60—70% at a conversion of 0%, while that of CH_3OH was in the range of more than 25%. It is thus suggested that CH_4 is formed predominantly via CO, while CH_3OH is formed predominantly by a direct reaction of CO_2.

Over a Re/CeO_2 catalyst, the ^{13}C contents in both CH_4 and CH_3OH were low, compared to those produced over Re/ZrO_2. The percentages of the ^{13}C contents in CH_4 and CH_3OH at a conversion of 0% were about 50% and 10%, respectively. It is, therefore, suggested that the contributions of the routes via CO and via CO_2 are almost equivalent for CH_4 formation, and that CH_3OH is predominantly formed from CO_2. This indicates that the catalytic behavior is different over Re/ZrO_2 and Re/CeO_2 in CO_2 hydrogenation.

One more difference between Re/ZrO_2 and Re/CeO_2 was observed regarding the rate of a CO–CO_2 carbon exchange. Over both catalysts, the rate of incorporation of ^{12}C into CO was fast compared to the formation rates of CH_4 and CH_3OH. The rate of CO–CO_2 carbon exchange was much faster for Re/ZrO_2 than for Re/CeO_2.

The distribution of ^{13}C in the products produced over Cu–Zn oxide catalysts were quite different from those observed over the supported Re catalysts, such as CuO–ZnO–ZrO_2, as shown in Fig. 3. The ^{13}C contents in CH_3OH produced over Cu–Zn oxide catalysts were close to 0%. This demonstrates that product methanol is directly formed from CO_2. The contribution from the route via CO is negligible. This coincides with the conclusion reported by Chinchen et al. for Cu–Zn/Al_2O_3 catalyst.[6)]

Although the incorporation of ^{13}C into methanol was negligible, a CO–CO_2 carbon exchange occurred to a considerable extent. Two possibilities which account for the fast CO–CO_2 exchange against a negligible incorporation of ^{13}C into methanol are as follows. One possibility is that the intermediates for the formation of

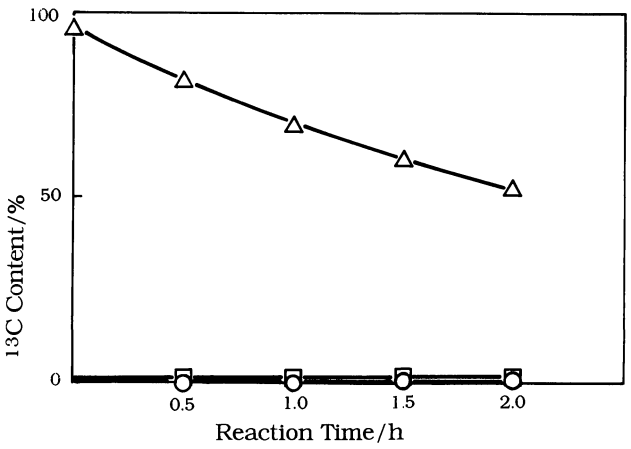

Fig. 3. Variations in the ^{13}C contents of each product in the reaction of $H_2+CO_2+^{13}CO$ over CuO–ZnO–ZrO_2 as a function of the reaction time. △: CO, ○: CO_2, □: CH_3OH.

methanol from CO_2 are not common to those for a CO–CO_2 carbon exchange. The other possibility is that the intermediates are common, but that the slow step in the formation of methanol is a conversion of the intermediates, leading to methanol.

Reactions of Formic Acid and Formaldehyde with Hydrogen. Formic acid is supposed to be adsorbed on the surface in the form of formate. The purpose of the reactions was to determine how the formate and the adsorbed formaldehyde are involved in the hydrogenation of carbon dioxide by a comparison of the product distribution with those obtained in the hydrogenation of carbon dioxide. In the reactions of formic acid and formaldehyde with hydrogen, all of the formic acid and formaldehyde were completely consumed within 1 h; the conversions were 100%. The product distributions in the reactions of formic acid and formaldehyde with hydrogen are given in Tables 2 and 3, respectively.

Over the Re/CeO_2 catalyst, the products in the reaction of adsorbed formic acid with H_2 comprised of CO_2, CH_4, and CO. No methanol formation was observed. Over the Re/ZrO_2 catalyst, however, the products comprised of CH_4 and CO, neither CO_2 nor methanol was observed. It should be noted that CO_2 was not formed over Re/ZrO_2 at all, though CO_2 was the main product over Re/CeO_2.

Over Cu–Zn oxide catalysts, CO, CO_2, and methanol were produced; no methanol was formed over CuO–ZnO–Cr_2O_3. The production of methanol was the highest for CuO–ZnO–ZrO_2.

For all of the catalysts examined, the product distributions in the reaction of formic acid with hydrogen and in the hydrogenation of CO_2 show common features regarding the following three points: (1) The amount of methane greatly exceeded that of methanol over Re catalysts. (2) Over Cu–Zn oxide catalysts, methanol was formed; no methane was formed. (3) Over CuO–ZnO–Cr_2O_3, neither methanol nor methane were formed.

The reaction of formaldehyde with hydrogen gave product distribution quite different from that of formic acid with hydrogen. Over Re/ZrO_2 and Re/CeO_2 catalyst, methanol was formed considerably. In addition, the formation of CO_2, which was the main product in the reaction of formic acid with hydrogen on Re/CeO_2, was not observed.

Over Cu–Zn oxide catalysts, the products comprised mostly of methanol. Only small amounts of CO_2 and CO were formed in the reaction of formaldehyde with hydrogen. It is to be noted that with Cu–Zn oxide

Table 2. Product Distribution of the Reaction of Formic Acid with Hydrogen

Catalyst	Reaction time/h	Yield/%				
		CO	CH_4	CO_2	C_2	CH_3OH
Re/CeO_2	1	8.6	3.8	87.6	0	0
	2	12.9	12.5	74.1	0.5	0
Re/ZrO_2	1	4.3	94.8	0	0.9	0
	2	6.5	93.1	0	0.5	0
CuO–ZnO	1	32.6	0	62.7	0	4.7
	3	28.8	0	60.2	0	11.0
CuO–ZnO–Al_2O_3	1	19.6	0	70.2	0	10.2
	2	34.7	0	40.0	0	25.3
CuO–ZnO–ZrO_2	1	15.7	0	44.9	0	39.4
	2	20.3	0	34.1	0	45.6
CuO–ZnO–Cr_2O_3	1	56.4	0	43.6	0	0
	2	56.7	0	42.3	0	0

a) Reaction conditions: Reactant: HCOOH (12 Torr)+H_2 (420 Torr), Catalyst: 300 mg, Reaction temperature: 200°C.

Table 3. Product Distribution of the Reaction of Formaldehyde with Hydrogen[a)]

Catalyst	Reaction time/h	Yield/%				
		CO	CH_4	CO_2	C_2	CH_3OH
Re/CeO_2	1	7.2	59.7	0	0.8	32.1
	2	10.3	77.9	0	0.9	11.0
Re/ZrO_2	1	7.3	85.2	0	0	7.5
	2	0	95.4	0	0	0
CuO–ZnO	1	6.2	0	11.9	0	81.9
	2	5.3	0	5.9	0	88.7
$CuO–ZnO–Al_2O_3$	1	2.0	0	0	0	98.0
	2	3.2	0	0.8	0	96.0
$CuO–ZnO–ZrO_2$	1	2.1	0	1.0	0	96.9
	2	6.5	0	1.6	0	91.8
$CuO–ZnO–Cr_2O_3$	1	3.4	0	1.9	0	94.6
	2	6.1	0	3.0	0	90.9

a) Reaction conditions: HCHO (12 Torr)+H_2 (420 Torr), Catalyst: 300 mg, Reaction temperature: 200°C.

catalysts methanol was formed, even over CuO–ZnO–Cr_2O_3, over which no methanol was formed from formic acid. This indicates that the conversion of adsorbed formic acid to adsorbed formaldehyde is very slow over CuO–ZnO–Cr_2O_3 catalysts.

Some common features between CO_2 hydrogenation and the reaction of formic acid with hydrogen and the predominant formation of methanol in the reaction of formaldehyde suggest the following reaction route. At first, formate is formed from CO_2 and hydrogen; the formate converts into the adsorbed formaldehyde. The adsorbed formaldehyde is hydrogenated to yield methanol. The formation of formate may proceed by the insertion of CO_2 into the hydroxide site, as suggested by Amenomiya et al.[5)] A scheme for methanol formation may be as shown below:

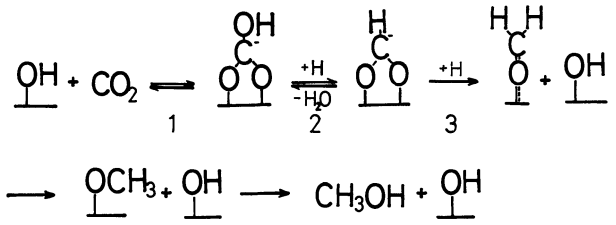

Scheme 1.

Since CO–CO_2 carbon exchange is fast, and essentially no incorporation of ^{13}C into methanol was observed in the reaction of ^{13}CO, CO_2, and H_2, a CO–CO_2 carbon exchange proceeds by intermediates which are different from the formate shown above.

The conversion of the formate into the adsorbed formaldehyde (step 3) is the key step in methanol synthesis. Once the adsorbed formaldehyde is formed, methanol is easily yielded, as is evidenced by the selective formation of methanol in the reaction of formaldehyde with hydrogen.

Over a CuO–ZnO–Cr_2O_3 catalyst, methanol was not formed, neither in CO_2 hydrogenation nor in the reaction of formic acid with hydrogen; methanol, however, was selectively formed in the reaction of formaldehyde with

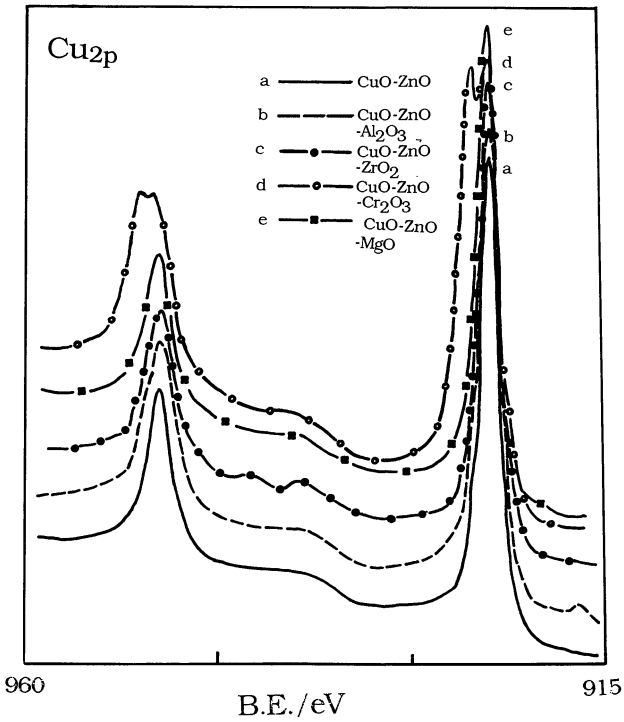

Fig. 4. XPS spectra of various Cu–Zn oxide catalysts after reduction with H_2 at 300°C.

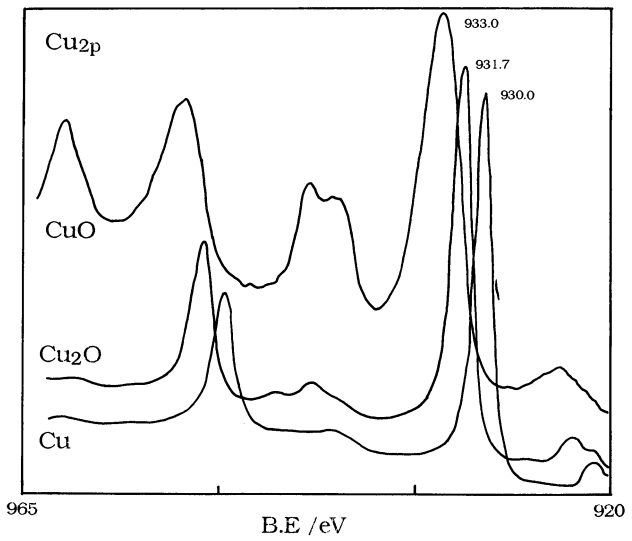

Fig. 5. XPS spectra of standard oxides of Cu.

hydrogen. The conversion of formate into the adsorbed formaldehyde is very slow over $CuO–ZnO–Cr_2O_3$. The state of Cu on $CuO–ZnO–Cr_2O_3$ should be different from those on the other supported CuO–ZnO catalysts. To examine the states of Cu, XPS was measured with $CuO–ZnO–Cr_2O_3$ together with the other Cu–Zn oxide catalysts. As shown in Fig. 4, $CuO–ZnO–Cr_2O_3$ showed two peaks in the Cu_{2p} region, while the other Cu–Zn oxide catalysts showed a single peak. The peaks are assigned to Cu^+, compared with the peaks for CuO, Cu_2O, and Cu^0, as shown in Fig. 5. The peak at 932.7 eV is positioned between those for Cu^{2+} and Cu^+. It is not certain why $CuO–ZnO–Cr_2O_3$ showed two peaks, but it can be said that Cu in the $CuO–ZnO–Cr_2O_3$ tends to stay at a higher oxidation state, compared with the other Cu–Zn oxide catalysts.

In our previous paper,[10] we proposed that Cu^+ in a Cu–Zn oxide solid solution is an active site for methanol formation from CO_2 and H_2.[10] The state of Cu in $CuO–ZnO–Cr_2O_3$ may be either partly oxidized Cu^+ or partly reduced Cu^{2+}. This causes the conversion of the formate to the adsorbed formaldehyde difficult.

With the Re/ZrO_2 catalyst, most of the methanol is formed through the reaction of CO with H_2, though the selectivity to methanol is very low under the reaction condition of subatomospheric pressure. With the Re/CeO_2 catalyst, one of the routes to methanol is considered to proceed by a direct hydrogenation of CO_2 in a similar manner to that shown in Scheme 1.

References

1) E. Ramaroson, R. Kieffer, and A. Kiennemann, *J. Chem. Soc., Chem. Commun.*, **1982**, 645.
2) F. Solymosi, A. Erdohelyi, and T. Bansagi, *J. Chem. Soc., Faraday Trans. 1*, **77**, 2645 (1981).
3) R. Kiffer, E. Ramaroson, A. Deluarche, and Y. Trambouze, *React. Kinet. Catal. Lett.*, **16**, No. 2—3, 207 (1981).
4) E. Ramaroson, R. Kiffer, and A. Kiennemann, *Appl. Catal.*, **4**, 211 (1982).
5) Y. Amenomiya and T. Tagawa, *Proc. Int. Congr. Catal., 8th, Berlin*, **1982**, Vol. 2, p. 577.
6) G. C. Chinchen, P. J. Denny, D. G. Parker, M. S. Spencer, and D. A. Whan, *Appl. Catal.*, **30**, 333 (1987).
7) G. Liu, D. Willcox, M. Garland, and H. H. Kung, *J. Catal.*, **96**, 251 (1985).
8) A. Erdoheloyi, M. Pasztor, and F. Solymosi, *J. Catal.*, **98**, 166 (1986).
9) Z. Xu, Z. H. Qian, H. Hattori, and K. Tanabe, *Bull. Chem. Soc. Jpn.*, **64**, 1664 (1991).
10) Z. Xu, Z. H. Qian, L. Q. Mao, K. Tanabe, and H. Hattori, *Bull. Chem. Soc. Jpn.*, **64**, 1658 (1991).

Reaction of Cyanoguanidine with Formaldehyde. V. Properties of Cyanoguanidine-Formaldehyde Resin as a Coagulating Agent of Anionic Colloidal Particles

Ryuichi SHIBA,* Miyuki TAKAHASHI, Toichi EBISUNO,†
Yoichi SHINDOU,† and Michiaki TAKIMOTO†
Department of Applied Science, Faculty of Technology, Tokyo Denki University,
Kanda, Chiyoda-ku, Tokyo 101
† Department of Chemistry, Faculty of Science, Toho University,
Miyama 2-2-1, Funabashi, Chiba 274
(Received March 7, 1991)

The coagulation of anionic colloidal particles by the cyanoguanidine (CG)–formaldehyde resin has been reported to be caused by an electrostatic interaction of the (diaminomethylene)urea (DU) cation with an anionic surface charge of particles. Our results show that neither DU·HCl nor di-hydrochlorides of *N*,*N*'-methylenebis [*N*'-(diaminomethylene)urea] (Bis-DU·2HCl), itself, nor the resinous products of DU·HCl or Bis-DU·2HCl with formaldehyde, are such effective coagulating agents as the CG–formaldehyde resin and are not explicable only in terms of the electrostatic interaction. Gel-permeation chromatograms of the resins have revealed that the coagulation efficiency increased in proportion to the increase of the fraction of components having higher molecular weight, suggesting that components having higher molecular weight play an important role in coagulation due to the CG–formaldehyde resin.

The resinous products of cyanoguanidine (CG) with formaldehyde under acidic conditions are useful as commercial coagulating agents.[1] The reaction of CG with formaldehyde under acidic conditions is complicated, since the transform of CG into (diaminomethylene)urea (DU) is simultaneously accompanied by the hydroxymethylation and codensation of CG with formaldehyde, as well as the hydroxymethylation and condensation of DU with formaldehyde.[2-6] The coagulation of anionic colloidal particles by CG–formaldehyde resin (CG-resin) has since been explained to be due caused by neutralization of surface charge with cationic DU.[7] However, the detailed mechanism of coagulation has not yet been solved.

In order to elucidate the coagulation mechanism, the composition of the CG-resin was analyzed by gel-permeation chromatography under various conditions, together with those resinous products of DU·HCl and di-hydrochlorides of *N*,*N*'-methylenebis [*N*'-(diaminomethylene)urea] (Bis-DU·2HCl) with formaldehyde, which are hereafter referred to as the DU·HCl-resin and Bis-DU·2HCl-resin. The amounts of formaldehyde bound to DUs or released from the CG-resin by acid-hydrolysis were quantitatively measured, as well as the viscosity change, in order to confirm the reactions. The relationship between the distribution of the molecular weight of these resins and the coagulation efficiency was analyzed.

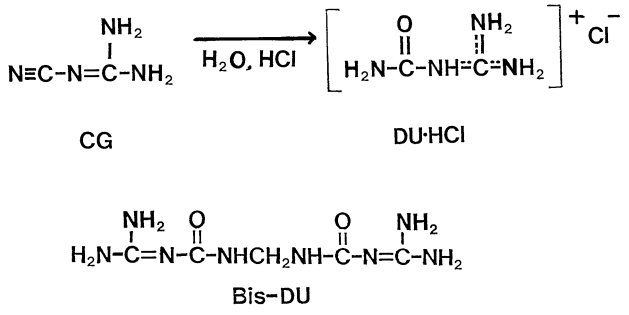

Scheme 1.

Results and Discussion

Since CG was easily converted into DU·HCl by reacting it with equimolar H_2O and HCl, the CG-resin was considerd to have an analogous structure to that of the DU·HCl-resin. However, the reaction patterns of CG+HCl and DU·HCl with formaldehyde were different from each other. Figure 1 shows the time courses of the reaction of formaldehyde with CG- and DU·HCl-resins, respectively. A linkage of $-CH_2-O-CH_2-$ was scarcely formed in both resins. The amont of formaldehyde reacted tended to be underestimated when determined through iodometry, due to the formation of an insoluble product. More formaldehyde reacted with CG than with DU·HCl, and was incorporated to the methylene moiety of resious products. The amounts of the bound formaldehyde in the CG-resin increased for 2—3 h and were nearly saturated at 3 h. Gel-permeation chromatograms of CG- and DU·HCl-resins, as shown in Fig. 2, revealed that the CG-resin was enriched with components having higher molecular weight, compared with that of other resins. This was supported by the fact that the solution of the CG-resin is more viscous than that of the DU·HCl-resin. The distribution of molecular weight ranges from 200 to 1200 for the CG-resin which is wider than 150—400 for the DU·HCl resin. A similar result was also obtained when a Shodex Q801 column was used instead of TSK gel columns.

The results concerning the coagulation measurement

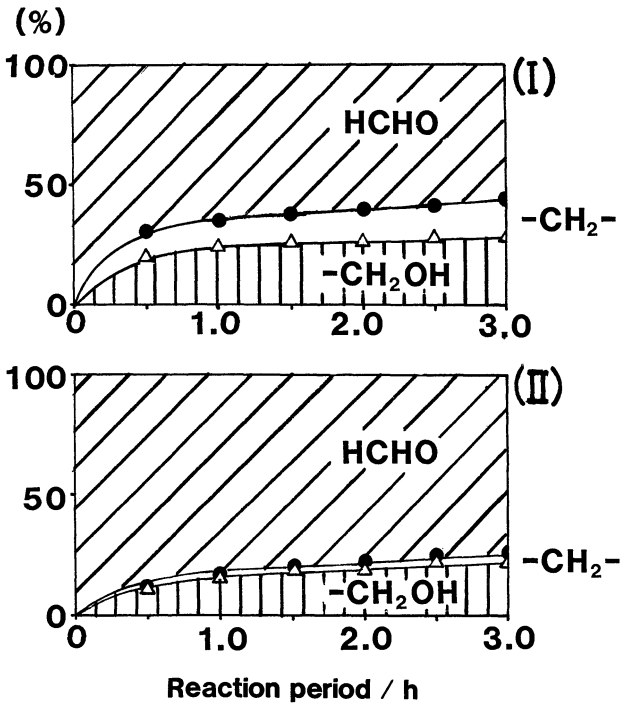

Fig. 1. Time courses of the reactions of cyanoguanidine (CG) and hydrochloride of (diaminomethylene)-urea (DU·HCl) with formaldehyde at 70°C. (I) CG+Formaldehyde+HCl=(1/2/1), (II) DU·HCl+Formaldehyde=(1/2). At 30-min intervals, aliquots of the reaction solutions were withdrawn, and the amounts of several types of formaldehyde were analysed by the Na_2SO_3 method (A) and the iodometry (B). ▨: HCHO=(A), ▥: $-CH_2OH$=(B)−(A), □: $-CH_2-$= (initial amount of formaldehyde)-(B).

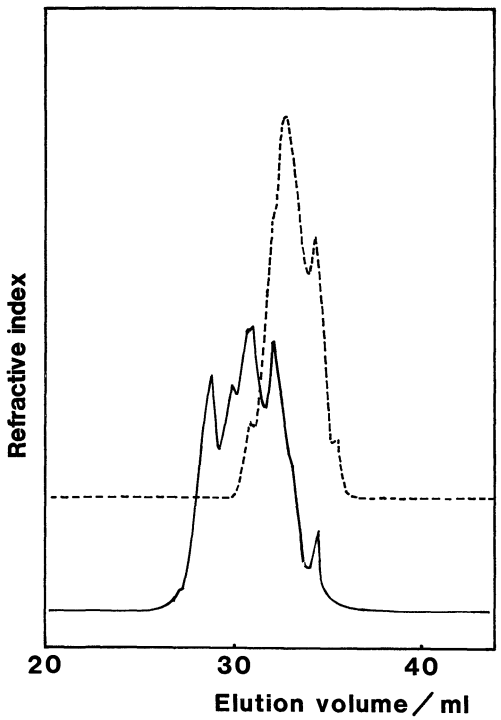

Fig. 2. Gel-permeation chromatograms of the CG- and DU·HCl-resins on combination columns comprising TSK gel $G2500PW_{XL}$ and $G3000PW_{XL}$. The resinous products of CG+Formaldehyde+HCl=(1/2/1)(—) and DU·HCl+Formaldehyde=(1/2)(----), were eluted by a mixed solution of 0.5 mol dm^{-3} acetic acid and 0.5 mol dm^{-3} sodium acetate (1:1) at 40°C.

are summarized in Fig. 3. Neither DU·HCl nor Bis-DU·2HCl, itself, nor the DU·HCl- or Bis-DU·2HCl-resin was such an effective coagulating agent as the CG-resin. Particles of Kaolin having anionic charges were also coagulated by these resins, which were virtually idnetical to polystyrene latex. These results were not explicable in terms of only the mechanisms hitherto presented, that the DU and/or Bis-DU cations should play decisive roles in the coagulation process of latex particles by the CG-resin. This suggests that the components having higher molecular weight in the CG-resin play an important role in the coagulation (flocculation) of latex particles. This was supported by the fact that the flocculation efficiency is improved with an increase of the fraction of components having higher molecular weight, that is, the flocculation efficiency of the CG-2.0F-HCl resin is superior to that of the CG-1.0F-HCl or CG-0.5F-HCl resin.

In order to obtain a clue for elucidating the structure of the CG-resin, its absorption spectrum in the UV region and ^{13}C NMR spectrum were measured. The CG-resin was acid-hydrolyzed under the same conditions as described in the experimental section. While the spectrum of the solution of CG was not affected by the pH, that of DU·HCl was different between acidic and alkaline pH. The spectrum of a solution of the CG-resin resembled that of DU (Fig. 4), suggesting that CG might be transformed into DU during the early stage of resinification. The ^{13}C NMR spectrum of the CG-resin also elucidated an early transformation of CG into DU, since the signal of δ=115.9 (-CN) disappeared and a new signal of δ=150.9 ($-CO-NH_2$) appeared during the early stage of resinification.

As shown in Fig. 5, the released formaldehyde molecules were classified into three categories, as described in the experimental section. The CG-resin has three types of methylene moieties, such as =C(NHR)-NH-CH_2-NH-C(NHR)=, -CO-NH-CH_2-NH-CO-, and =C(NHR)-NH-CH_2-NH-CO-.

These results suggested that the CG-resin has the structure of DU as the mother structure, and comprises a mixture of various condensates having three types of the methylene moieties. Our results suggest that the coagulation of anionic colloidal particles by the CG-formaldehyde resin is not explicable only in terms of its cationic charge, and that the components of the CG-formaldehyde resin having higher molecular weight are considered to play an important role in coagulation (fluocculation).

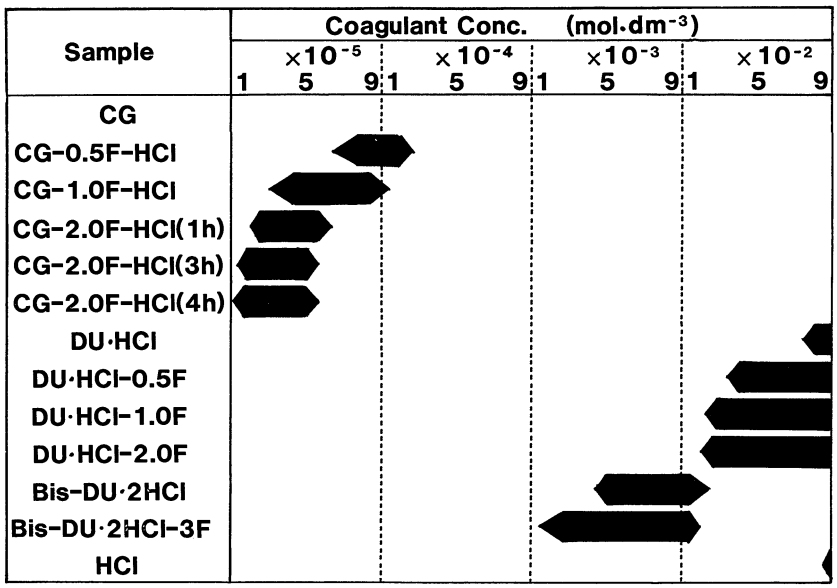

Fig. 3. Coagulation of polystyrene latex by CG, DU·HCl, Bis-DU·2HCl, and their resinous products with formaldehyde. Polystyrene latex: radius, 0.8—1.0 μm; final concentration 0.1%. The length and width of the band simultaneously represent the range of the concentration and the strength of the coagulating activity. CG-0.5F-HCl, CG-1.0F-HCl and CG-2.0F-HCl represent the resinous products of CG with formaldehyde (F) under acidic conditions (the feed mole ratios: CG/F/HCl=1/0.5/1, 1/1/1 and 1/2/1, respectively). DU·HCl-0.5F, DU·HCl-1.0F, DU·HCl-2.0F, and Bis-DU·2HCl-3.0F are the resinous products of DU·HCl/F=0.5, 1/1, and 1/2 and Bis-DU·2HCl/F=1/3, respectively. These products were obtained from the reactions for 4 h, unless otherwise noted.

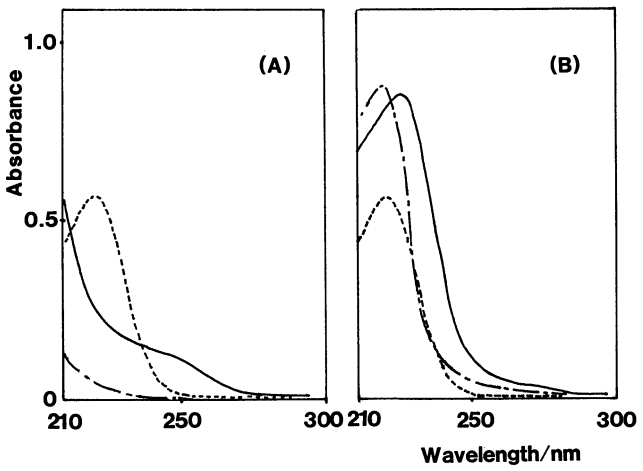

Fig. 4. UV spectra of CG, DU·HCl and the CG-resin under acidic and alkaline conditions. (A) Acidic: in 0.1 mol dm^{-3} HCl soln. (B) Alkaline: in 0.1 mol dm^{-3} aq NaOH soln. CG, ----: DU·HCl, —·—·: the CG-resin, ——. The CG-resin was prepared from CG and formaldehyde (CG/F/HCl=1/2/1) at 70°C for 4 h.

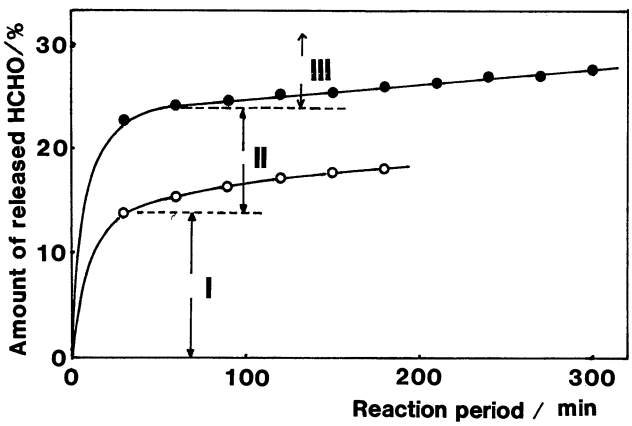

Fig. 5. Acid-hydrolysis of the CG-resin. The CG-resin used was the same as described in Fig. 4. The amounts of the released formaldehyde molecules were determined colorimetrically by the use of acetylacetone. The aq 1% solution of the CG-resin was hydrolyzed in 1.0 mol dm^{-3} HCl at 50°C (—○—) and in 1.0 mol dm^{-3} H_2SO_4 at 90°C (—●—). The numerals, I, II, and III each represents the type of released formaldehyde. I, the hydroxymethyl group: II, the methylene moiety in =C(NHR)-NH-CH_2-NH-C(NHR)= and/or in =C(NHR)-NH-CH_2-NH-CO-: III, the methylene moiety in -CO-NH-CH_2-NH-CO-.

Experimental

Preparation of Bis-CG, Bis-DU, and Resins. Bis(*N'*-cyanoguanidino)methane (Bis-CG) and Bis-DU were prepared by the same procedures already described.[8-10] Various CG-, DU·HCl-, Bis-DU·2HCl-resins were prepared by varying the reaction conditions, such as the feed mole ratios of CG, DU·HCl, Bis-DU·2HCl/formaldehyde, reaction temperature, and reaction periods. The typical preparations for CG- and DU·HCl-resins were as follows.

CG-resin: Forty two grams (0.5 mol) of CG were added to a mixture of 75 ml of 37% formalin (neuralized) (1.0 mol formaldehyde) and 66.3 ml of distilled water. After CG was thoroughly dissolved, 85.2 ml of 6 mol dm^{-3} HCl were added dropwise to the solution, the temperature of which was kept at 70 °C for 4—6 h.

DU·HCl-resin: The preparation procedure for DU·HCl-resin was virtually identical with that for CG-resin except for 69.4 g of DU·HCl and 75.7 ml of distilled water were used instead of 42 g of CG and 66.3 ml of distilled water.

Determination of Amounts of Formaldehyde. (I) Formaldehyde in the Reaction Solution. At 30 min intervals, aliquots of the solution were withdrawn, and the amounts of formaldehyde were determined by the Na_2SO_3 method (A) and iodometry (B). Residual amounts of formaldehyde (HCHO in Fig. 1)=(A); the amounts of formaldehyde in hydroxymethyl groups (-CH_2OH in Fig. 1)=(B)−(A); the amounts of formaldehyde incorporated into the form of methylene moiety (-CH_2- in Fig. 1)=(the initial amount of formaldehyde)−(B) were calculated.

(II) Formaldehyde in the Acid Hydrolysates. In order to obtain a clue to the structure of resins, a few standard samples (Bis-CG, Bis-DU and their hydroxymethyl derivatives) and resins were acid-hydrolyzed with 1.0 mol dm^{-3} HCl at 50 °C or 1.0 mol dm^{-3} H_2SO_4 at 90 °C and the amounts of formaldehyde were determined colorimetrically by the use of acetylacetone.[11] Further details were the same as described in our previous paper.[8] From the results on the standard samples the released formaldehyde molecules were classified into three categories, as follows: The most easily released formaldehyde (type I), from the hydroxymethyl groups; the moderately released ones (type II), from the methylene moiety in =C(NHR)-NH-CH_2-NH-C(NHR)=; and the ones hard to release (type III), from the methylene moiety in -CO-NH-CH_2-NH-CO-.

The Measurement of the Coagulation Efficiency. To carry out the coagulation measurement, 10 ml of a colloidal solution of 0.1% of polystyrene latex of 0.8—1.0 μm radius (or 25 ml of 600 mg dm^{-3} of Kaolin having anionic charges) and the resinous products solution containing 10^{-6}—10^{-2} mol dm^{-3} (the final concentration) were introduced to a stoppered test tube; the total volume was then adjusted to 20 ml (or 50 ml). The depth of the supernatant over the suspended layer was measured at 10-min intervals for 2 h. The coagulation efficiency of the resinous products was evaluated in terms of their minimum concentration in which the most rapid coagulation occurred.

Gel-Permeation Chromatography. A chromatographic separation of an aliquot of the resinous products was carried out on a combination columns comprising TSK gel G2500PW_{XL} and G3000PW_{XL}, eluting by the mixed solution of 0.5 mol dm^{-3} acetic acid and 0.5 mol dm^{-3} sodium acetate (1 : 1) at 40 °C. The molecular weight of the components of the resins were estimated by calibration curves with polyethylene glycol.

^{13}C NMR Spectrometry. The NMR spectra of the products were measured in a D_2O solution with dioxane as the internal standard at 90 MHz on a JOEL FX 90Q instrument.

The authors wish to thank Dr. Takaaki Arai of Nihon University for generous gift of polystyrene latex.

References

1) S. Sakai, *Kobunshi,* **8**, 612 (1959).
2) M. Hamada, *Rep. Lab. Toho Reiyon,* **1**, 28 (1954).
3) U. Miyaoka and T. Matsui, *Rep. Fac. Tech. Fukui Univ.,* **2**, 85 (1955).
4) E. Yamada, *Kogyo Kagaku Zasshi,* **62**, 1161 (1959).
5) M. Hamada, *Rep. Lab. Toho Reiyon,* **2**, 85 (1955).
6) M. Takimoto, T. Ebisuno, and R. Shiba, *Bull. Chem. Soc. Jpn.,* **56**, 3319 (1983).
7) M. Nakajima and K. Kuwahara, *Kogyoyosui,* **1975**, 54.
8) R. Shiba, M. Takahashi, T. Ebisuno, and M. Takimoto, *J. Thermosetting Plast., Jpn.,* **10**, 141 (1989).
9) W. -D. Spiethoff, *Chem. Ber.,* **100**, 4050 (1967).
10) R. Shiba, M. Takahashi, T. Ebisuno, and M. Takimoto, *Bull. Chem. Soc. Jpn.,* **61**, 2197 (1989).
11) B. J. Comption and W. C. Purdy, *Anal. Chim. Acta,* **119**, 349 (1980).

Effect of Anions on the Epoxidation of Styrenes with H_2O_2 in the Presence of Ammonium Heptamolybdate(VI)-Dioctyltin Oxide Catalysts

Masami INOUE,* Eiichi NAKAYAMA, Yuuko NAKAMURA, Seichi RENGAKUJI, and Keiichi NISHIBE
Faculty of Engineering, University of Toyama, Gofuku, Toyama 930
(Received May 18, 1991)

The epoxidation of styrene, α-methylstyrene, β-methylstyrene, *p*-chlorostyrene, and *m*-divinylbenzene with H_2O_2 in the presence of ammonium heptamolybdate(VI)–dioctyltin oxide catalysts in $CHCl_3$–H_2O was studied. The addition of neutral salts, such as $NaNO_3$ or Na_2SO_4, to the catalyst system prevented the successive hydration of styrene oxide once formed. The presence of KCl or NaCl almost suppressed the oxidation, while no substantial effect was observed in $NaClO_4$. The various effects of these anions were related to the results concerning the coordination of anions to Mo(VI)-ions.

The epoxidation catalysts and agents for alkenes provided various kinds of epoxides.[1] Among those, styrene oxide and its derivatives are useful materials for polymer chemistry and organic synthesis. The use of aqueous H_2O_2 as an oxidation agent is easy to handle and clean since H_2O_2 is reduced to give water. In our present reaction conditions, the hydration of styrene oxide to 1-phenyl-1,2-ethanediol was a chief side reaction.

Previously, we proposed ammonium heptamolybdate-(VI)–dioctyltin oxide catalysts for the selective epoxidation of styrene as well as aliphatic alkenes with H_2O_2 in $CHCl_3$–H_2O.[2] In this two-layer solvent system, a longer reaction time (24 h) decreased the yield of styrene oxide after reaching a maximal yield. During the investigation of the effect of anions on the catalytic activity, we found that the addition of a small amount of neutral salts, such as $NaNO_3$ or Na_2SO_4, prevented the hydration of styrene oxide. On the other hand, in the case of KCl and NaCl, the rate of oxidation was decreased remarkably.

In this report, the epoxidation of styrene, α-methylstyrene, β-methylstyrene, *p*-chlorostyrene, and *m*-divinylbenzene was carried out and the effect of anions was studied from the standpoint of the activity of catalysts and the selectivity in epoxide formation.

Experimental

Materials. Styrene (Wako Pure Chemicals Co.), α-methylstyrene, β-methylstyrene, *p*-chlorostyrene, *m*-divinylbenzene (Tokyo Kasei Co.), and dioctyltin oxide (Kyodo Yakuhin Co., Tokyo) were used as received. Aqueous 60% H_2O_2 was kindly supplied from Tokai Denka Kogyo Co., Tokyo. KCl was used after twice recrystallizations. Neutral salts and other materials of GR grade were used for this experiment.

General Procedures. In a 300 ml round-bottom flask equipped with a condenser, the catalyst was prepared in situ by mixing ammonium heptamolybdate(VI) (0.57 mmol), neutral salts (4.8 mmol in H_2O 8.0 ml), and dioctyltin oxide (8.0 mmol). The reaction was carried out by the addition of $CHCl_3$ (8 ml), styrenes (350 mmol), and H_2O_2 (318 mmol) under stirring with TEFLON (poly(tetrafluoroethylene))-covered magnetic stirring bar at 30 °C in a thermostatted water bath. Dioctyltin oxide, dispersed in $CHCl_3$, gradually dissolved and the reaction was started. At intervals, a small portion (0.5 ml) was pipetted out of the $CHCl_3$-layer and diluted with $CHCl_3$ (5 ml). To the solution was added *m*-xylene in acetonitrile solution (0.5 ml) as an internal standard.

Gas-liquid chromatography (GLC) was carried out on a Shimadzu GC-8A instrument using a glass column (2 m) packed with a 2%-Silicone OV-17 (2 m) under programmed oven temperature from 50 to 150 °C (3 °C min^{-1}). In the case of divinylbenzene, the temperature range from 50 to 230 °C (4 °C min^{-1}) was used. In the preparation of authentic epoxides, styrene, α-methylstyrene, β-methystyrene, *p*-chlorostyrene, and *m*-divinylbenzene were oxidized with *m*-chloroperbenzoic acid (mcpba) according to a method described in the literature,[3] and the corresponding epoxides were obtained by column chromatography (Kieselgel 60, Merck Co.) with pentane followed by pentane–diethyl ether (2:1) as eluents. The purities of these epoxides were 85 to 95% according to GLC analysis. The *m*-divinylbenzene monoepoxide separated from the solution was unstable and polymerized upon standing at room temperature for a few days.

Results and Discussion

Effect of Salts in the Epoxidation of Styrene. The oxidation of styrene with H_2O_2 was carried out in a two-phase solvent of $CHCl_3$–H_2O in the presence of ammonium heptamolybdate(VI)–dioctyltin oxide and an equivalent amount of such neutral salts as $NaNO_3$, Na_2SO_4, $NaClO_4$, KCl, or NaCl to Mo(VI) ions. In the absence of salts, the yield of styrene oxide reached a maximum of 60% after 8 h; further reaction (24 h) gradually decreased the yield to as low as a 34%.

Figure 1 shows the time course of the epoxidation of styrene with H_2O_2 in the presence of various salts. The addition of these salts changed the color of the aqueous layer from yellow to orange. When such salts as Na_2SO_4 or $NaNO_3$ were added, the hydration of styrene oxide, once formed, was delayed.

Unexpectedly, although the addition of NaCl and KCl

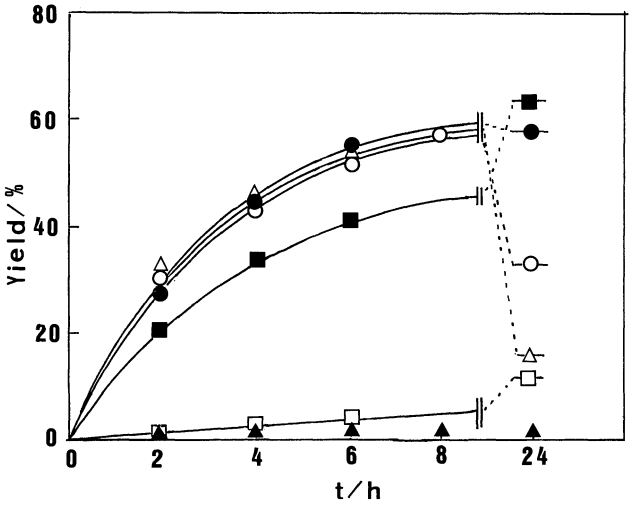

Fig. 1. Effect of salts in the epoxidation of styrene (**1**) at 30°C. ○; none ●; Na_2SO_4, ■; $NaNO_3$, △; $NaClO_4$, □; KCl, ▲; NaCl. **1** (43.7 mmol), 60% H_2O_2 (39.7 mmol), $(NH_4)_6Mo_7O_{24}\cdot 4H_2O$ (0.07 mmol), dioctyltin oxide (1.0 mmol), salts (0.6 mmol in H_2O 1 ml), and $CHCl_3$ (5 ml) were used. Yield were based on H_2O_2.

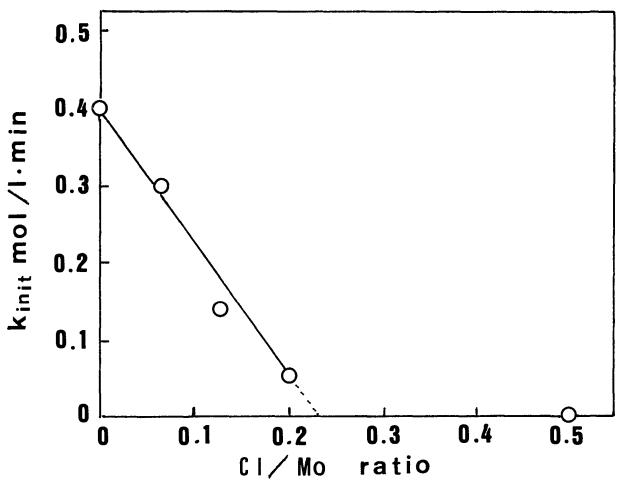

Fig. 2. Relation between the initial rate of the epoxidation of styrene (**1**) and the ratio of Cl^- to Mo(VI) ion.[a]
a) **1** (350 mmol), 60% H_2O_2 (318 mmol), $(NH_4)_6Mo_7O_{24}\cdot 4H_2O$ (0.57 mmol), dioctyltin oxide (8 mmol), KCl (8 mmol in H_2O 8 ml), and $CHCl_3$ (40 ml) were used. Reactions were carried out at 30°C.

Table 1. Initial Rate of the Epoxidation of Styrene (**1**) in the Presence of Various Salts[a] at 30°C

Salts	Initial rate / mol l^{-1} s^{-1}
None	2.9×10^{-2}
ClO_4^-	2.8×10^{-2}
SO_4^{2-}	1.6×10^{-2}
NO_3^-	1.3×10^{-2}
Cl^-	ca. 0

a) **1** (350 mmol), 60% H_2O_2 (318 mmol), $(NH_4)_6Mo_7O_{24}\cdot 4H_2O$ (0.57 mmol), dioctyltin oxide (8 mmol), salts (4.8 mmol in H_2O 8 ml), and $CHCl_3$ (40 ml) were used.

strongly suppressed the oxidation, the presence of NaBr and NaI decomposed H_2O_2 vigorously. In the case of $NaClO_4$, no substantial effect upon the yield of epoxide was observed.

Phenylacetaldehyde as a by-product was not found in our reaction products when GLC was carried out on a glass column packed with PEG (2m) with the programmed oven temperature from 50 to 150°C (3°C min^{-1}).

The effect of salts was confirmed quantitatively by taking the initial rates for the oxidation to styrene oxide (Table 1). In all experiments, the selectivities to styrene oxide were >90%, except during the initial stage of a reaction lower than 10% conversion. The rates of epoxidation considerably differed depending on the kinds of anions, as shown by the following order:

$$H_2O,\ ClO_4^- > SO_4^{2-} > NO_3^- > Cl^-.$$

This tendency, except for ClO_4^-, was in accord with that of well-known spectrochemical series observed in the spectral shifts of metal complexes in the presence of various anions.[4] Although the precise structure of Mo(VI) complexes in solution is still unknown, it was supposed that anions such as SO_4^{2-}, NO_3^-, or Cl^- are tightly coordinated on Mo(VI) ions and affected both the oxidation of styrene and the hydration of styrene oxide by decreasing the Lewis acidity of the catalyst. From a practical standpoint, the addition of Na_2SO_4 or $NaNO_3$ is usable as a kind of stabilizer of styrene oxide.

It was interesting that the addition of KCl to Mo(VI) ions in a 1:1 ratio almost suppressed the oxidation. The oxidation rate was decreased in proportion to the amount of KCl to Mo(VI) ions. Figure 2 shows a linear relationship between the initial rate of the oxidation and the amount of KCl to Mo(VI) ions. The extrapolation of the rate of oxidation to zero velocity gave the ratio of KCl:Mo(VI) ion =1:4.

Therefore, from the obtained results, two possible cases were considered. In the first, the amount of active species was only 1/4 of ammonium heptamolybdate(VI) used. The other case was that one active complex molecule was formed from four Mo(VI) ions. In any case, tightly coordinated Cl^- on Mo(VI) ions decreased the activity for the oxidation of styrene. From the obtained results, we supposed that these anions, except ClO_4^-, are also coordinated on Mo(VI) ions as a ligand.

Effect of Salts in the Epoxidation of Styrene Derivatives. The effect of salts on the stabilization of epoxide was also examined for several styrene derivatives. As shown in Table 2, the addition of $NaNO_3$ also stabilized β-methylstyrene oxide and *m*-divinylbenzene monoepoxide. On the other hand, under our reaction conditions,

Table 2. Effect of $NaNO_3$ on the Epoxidation of Styrene Derivatives with H_2O_2[a)]

Styrenes	Temp. °C	Salts	Time h	Yield %	Time h	Yield %
Styrene	30	$NaNO_3$	12	60.4	24	52.0
		None		61.7		25.8
p-Chlorostyrene	30	$NaNO_3$	10	42.5	24	57.1
		None		58.1		71.4
α-Methylstyrene	35	$NaNO_3$	10	46.3	24	54.3
		None		52.1		58.6
β-Methylstyrene	30	$NaNO_3$	10	52.8	24	76.5
		None		67.1		47.9
m-Divinylbenzene	40	$NaNO_3$	6	57.5[b,c)]	8	56.2[b,e)]
		None		40.3[b,d)]		10.5[b,f)]

a) Styrenes (4.3 mol l^{-1} $CHCl_3$), styrenes : 60% H_2O_2 : $(NH_4)_6Mo_7O_{24}\cdot 4H_2O$: Oct_2SnO : $NaNO_3$=100 : 100 : 1 : 2 : 1. b) Yield of monoepoxide. c) Diepoxide 9.9%. d) Diepoxide 1.8%. e) Diepoxide 5.4%. f)No diepoxide was detected.

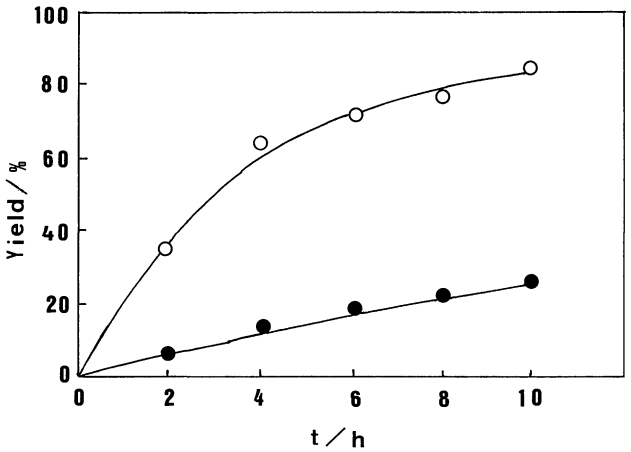

Fig. 3. Effect of stirring on the epoxidation of styrene (**1**) at 30°C,[a)] ○; under stirring, ●; without stirring, a) **1** (394 mmol), 60% H_2O_2 (187 mmol), $(NH_4)_6Mo_7O_{24}\cdot 4H_2O$ (0.57 mmol), dioctyltin oxide (8 mmol), $NaNO_3$ (4.8 mmol in H_2O 5 ml), and $CHCl_3$ (45 ml) were used. Yields were based on H_2O_2.

α-methylstyrene oxide and *p*-chlorostyrene oxide, once formed, were sufficiently stable, even under a lack of such salts as $NaNO_3$ or Na_2SO_4. In the case of *m*-divinylbenzene, the oxidation was almost stopped when one of two vinyl groups was oxidized.

The effect of the concentration of styrene or H_2O_2 upon the epoxidation rate also gave information concerning the Mo(VI) complexes under oxidation: The rates were approximately first-order with respect to both the styrene and H_2O_2 concentrations. Therefore, the coordination of these substrates to Mo(VI) ions might be very weak. The stirring procedure (150 rpm) increased the oxidation rate by as large as 6 times (Fig. 3). The evaporation of water from the aqueous layer of the reaction solution gave ammonium heptamolybdate(VI) as yellow crystals, while a pale-yellow syrup of organotin compounds was obtained from the $CHCl_3$ layer. However, both of the separated compounds were inactive for epoxidation.

In our catalyst system, the instability of styrene oxide and the denaturalization of Mo(VI) complexes were serious drawbacks. The former could be improved with a slight sacrifice of the catalyst activity by the addition of salts, such as $NaNO_3$ or Na_2SO_4.

The present work was supported in part by The Tamura Foundation for Encouragement of Science and Technology.

References

1) K. A. Joergensen, *Chem. Rev.*, **89**, 431 (1991).
2) T. Kamiyama, M. Inoue, H. Kashiwagi, and S. Enomoto, *Bull. Chem. Soc. Jpn.*, **63**, 1559 (1990).
3) M. Imuta and H. Ziffer, *J. Org. Chem.*, **44**, 1351 (1979).
4) R. Tsuchida, M. Kobayashi, and S. Yamada, *Bull. Chem. Soc. Jpn.*, **13**, 388 (1938).

Direct Synthesis of Trimethoxysilane from Methanol and Hydrogen-Treated Silicon Using Copper(II) Chloride as a Catalyst

Eiichi SUZUKI, Takatsugu KAMATA, and Yoshio ONO*
Department of Chemical Engineering, Tokyo Institute of Technology,
2-12-1 Ookayama, Meguro-ku, Tokyo 152
(Received April 9, 1991)

Synopsis. When silicon, on which copper(II) chloride was supported, was pretreated under a hydrogen stream at 533 K and brought in contact with methanol at 533 K, trimethoxysilane was formed with an 89% selectivity and a complete silicon conversion in 5.5 h. Pits were formed on the silicon surface, and grew with increasing silicon conversion.

Trimethoxysilane is an important chemical, since various organosilicon compounds can be derived by the reactions of trimethoxysilane and organic compounds. By using a copper compound as a catalyst, trimethoxysilane has been obtained selectively from silicon and methanol. A selectivity of 80—90% for trimethoxysilane has been attained by adding methanol dropwise into a suspension of silicon and copper(I) chloride[1] or copper(II) hydroxide[2] in e.g. dodecylbenzene. By passing methanol vapor through a mixture of silicon–copper(I) chloride–zinc[3] or that of silicon–copper(I) chloride,[4] which was pretreated at 623 K, trimethoxysilane with a selectivity of 84—98% was also yielded.

It is presumed that the reduction of copper(I) chloride powder by silicon (Eq. 1) at the pretreatment stage is involved in the formation of active sites in a silicon–methanol reaction,[3,4] just as in the direct synthesis of methylchlorosilanes from methyl chloride and silicon–copper(I) chloride mixture:[5-8]

$$4\,CuCl + Si \longrightarrow 4\,Cu + SiCl_4. \quad (1)$$

The copper thus formed in the atomic form must be very reactive towards silicon to form the alloy on the silicon surface. Copper compounds other than copper(I) chloride can therefore be used as a catalyst if they can be reduced to the active form.

This work concerns a direct synthesis of trimethoxysilane from silicon and methanol in which a copper-based catalyst is supported on silicon. Copper(II) chloride is chosen as the catalyst since it dissolves in methanol. We wish to report here that if the silicon–copper(II) chloride is pretreated under a hydrogen stream, a complete reaction of silicon with methanol to yield trimethoxysilane with high selectivity can be attained.

Experimental

Silicon (Soekawa Chemical Co., Ltd., 99.5% in purity) was used without any cleaning. The silicon was sieved into grains of 45-63 μm, washed with water, and immersed in a methanol solution of copper(II) chloride (Kanto Chemical Co., Inc., guaranteed reagent grade). Evaporation of methanol at room temperature gave a "silicon–copper(II) chloride contact mass", a 0.5 g portion of which was loaded in a fixed-bed flow reactor. After the pretreatment at 533—723 K for 1 h under a helium or hydrogen stream, methanol was fed at 533—553 K by a motor-driven syringe at a rate of 87 mmol h^{-1}. The effluent gas was analyzed automatically every 2.5 min with a gas chromatograph (2 m-long SE-30 column).

Scanning electron micrographs (SEM) were taken using a Hitachi S-510 instrument with an acceleration voltage of 25 kV.

Results and Discussion

Silicon grains both before and after copper(II) chloride (Cu=2.5 wt.%) was supported were examined by a scanning electron microscopy. The silicon grains exhibited a rather smooth surface (Fig. 1a), while each grain of the contact mass had deposits of copper(II) chloride, as exemplified in Fig. 1b.

The formation of copper from the silicon–copper(II) chloride contact mass may be facilitated by hydrogen during the pretreatment stage, since hydrogen may reduce copper(II) chloride directly to copper or copper(I) chloride, which then undergoes reduction to copper, according to Eq. 1. Such an efficient conversion of copper(II) chloride to copper would lead to an enhanced

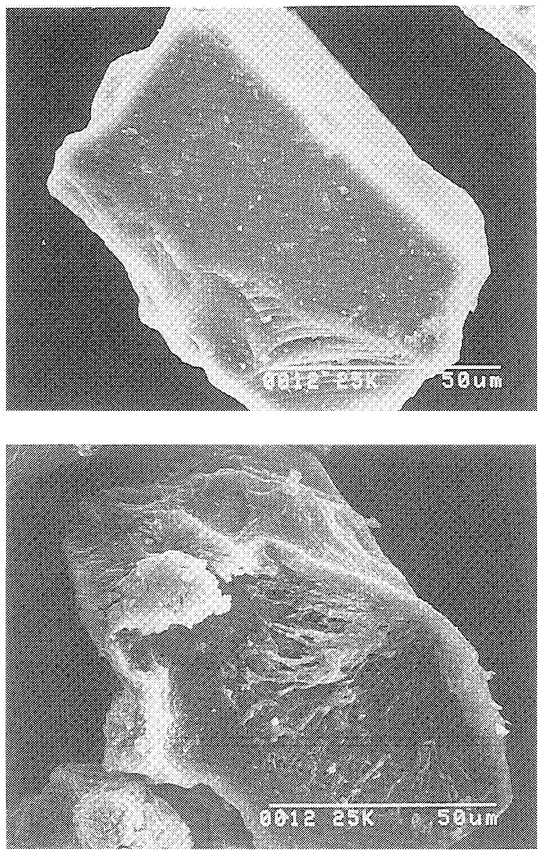

Fig. 1. Scanning electron micrographs of silicon and the silicon–$CuCl_2$ contact mass. Silicon (a), silicon–$CuCl_2$ contact mass (Cu=2.5 wt.%) (b). At 1000 magnifications.

reactivity of silicon. Then, the silicon–copper(II) chloride contact mass (Cu=2.5 wt%) was pretreated under a hydrogen stream at several temperatures (533—723 K) and tested for a reaction with methanol at 533 K. The enhancing effect of the hydrogen-pretretreatment on the reactivity of silicon is striking when the pretreatment is carried out at 533 K. Thus, with the hydrogen-pretreatment, a complete silicon conversion was attained in a reaction time of 5.5 h (Fig. 2a); with the helium-pretreatment, however, only 56% silicon conversion was obtained.

In Fig. 3, the rates of formation of methoxysilanes ($(CH_3O)_3SiH$+$(CH_3O)_4Si$) are plotted against the reaction time. For a pretreatment at 533 K, after an induction period the rate increased and attained a maximum beyond which it decreased, the silicon conversion attaining 100% in 5.5 h. With increasing temperature of the hydrogen-pretreatment, the induction period became shortened and eventually disappeared, and the conversions of silicon to methoxysilanes decreased. The silicon conversion at 5 h was 72, 35, and 4% at 573, 623, and 723 K of the pretreatment temperature, respectively.

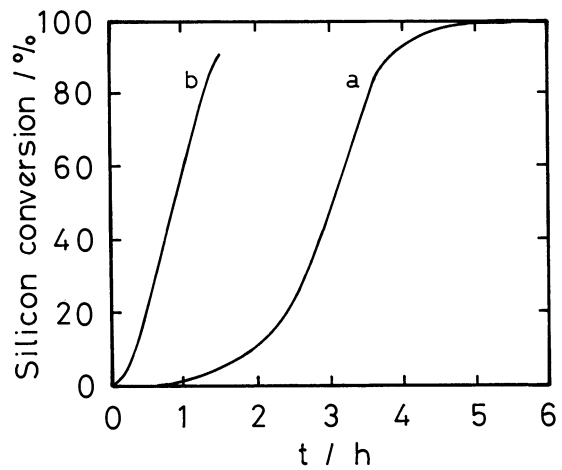

Fig. 2. Change in the cumulative silicon conversion with the reaction time. Pretreatment conditions: Silicon–$CuCl_2$ contact mass (Cu=2.5 wt.%) was pretreated under a hydrogen stream at 533 K (a) and 553 K (b) for 1 h. Reaction conditions: Reaction temperature=533 K (a) and 553 K (b), and CH_3OH= 99 kPa.

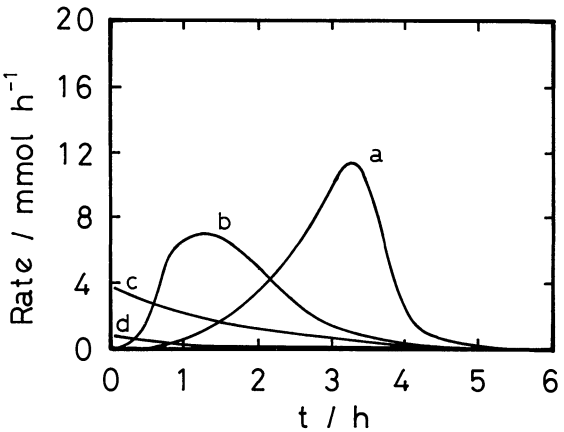

Fig. 3. Effect of hydrogen-pretreatment temperature on the change in the rate of formation of methoxysilanes ($(CH_3O)_3SiH$+$(CH_3O)_4Si$) with reaction time. Pretreatment conditions: Silicon–$CuCl_2$ contact mass (Cu=2.5 wt%) was pretreated under a hydrogen stream at 533 K (a), 573 (b), 623 K (c), and 723 K (d) for 1 h. Reaction conditions: Reaction temperature=533 K and CH_3OH=99 kPa.

We suppose that hydrogen facilitates the formation of copper on the silicon surface and that such a lower pretreatment temperature as 533 K is favorable for avoiding the agglomeration of the atomic copper and thus for the efficient reaction of the copper with silicon to form active sites for silicon–methanol reaction. A change in the morphology of the contact mass by the hydrogen-pretreatment at 533 K, however, was not detected by a SEM examination.

The selectivity for trimethoxysilane averaged over 5 h was 89, 93, 96, and 94% for pretreatments at 533, 573, 623, and 723 K, respectively.

A very efficient conversion of silicon was achieved at a higher reaction temperature of 553 K. Here, the contact mass (Cu=2.5 wt.%) was pretreated under a hydrogen stream at 553 K. Thus, as shown in Fig. 2b, in only a reaction time of 1.5 h, the silicon conversion attained 91%, the selectivity for trimethoxysilane averaged over the reaction time being 90%.

The change in the morphology of the reacting silicon grains with various levels of silicon conversion was examined. The silicon–copper(II) chloride contact mass (Cu=2.5 wt.%) was pretreated under a hydrogen stream at 533 K for 1 h and brought into contact with methanol vapor at 533 K for 0.6, 1, 3, and 4 h, the silicon conversion being 0.1, 1, 48, and 95%, respectively. The SEM images of the samples are shown in Fig. 4. A striking change in the morphology of silicon grains upon exposure to methanol was observed. Thus, the sample with a 0.1% of silicon conversion contained silicon grains with a pit, as exemplified in Fig. 4a.

With an increase in the silicon conversion, the number of silicon grains having detectable pits increased; silicon grains with irregular outlines accounted for the majority part of silicon grains, as shown Figs. 4b—d. The size of the pits develops with increasing silicon conversion. The silicon–methanol reaction does not occur uniformly on the silicon surface, but starts at areas scattered on the surface. The observation of pits on the silicon surface has a similarity to that in a silicon–methanol[9] or –methyl chloride[7,8] reaction using powdered copper(I) chloride as a catalyst, where active-site formation at the defects or pinholes of SiO_2 overlayer is postulated.

References

1) Japan Kokai Tokkyo Koho 55-28928 (1980); 55-76891 (1980); 57-108094 (1982); 62-96433 (1987).
2) United States Patent 4727173 (1988).
3) United States Patent 3072700 (1963); Deutsche Patent 1127338 (1960).
4) E. Suzuki and Y. Ono, *Chem. Lett.*, **1990**, 47.
5) R. J. H. Voorhoeve and J. C. Vlugter, *J. Catal.*, **4**, 123 (1965).
6) R. J. H. Voorhoeve, "Organohalosilanes: Precursors to

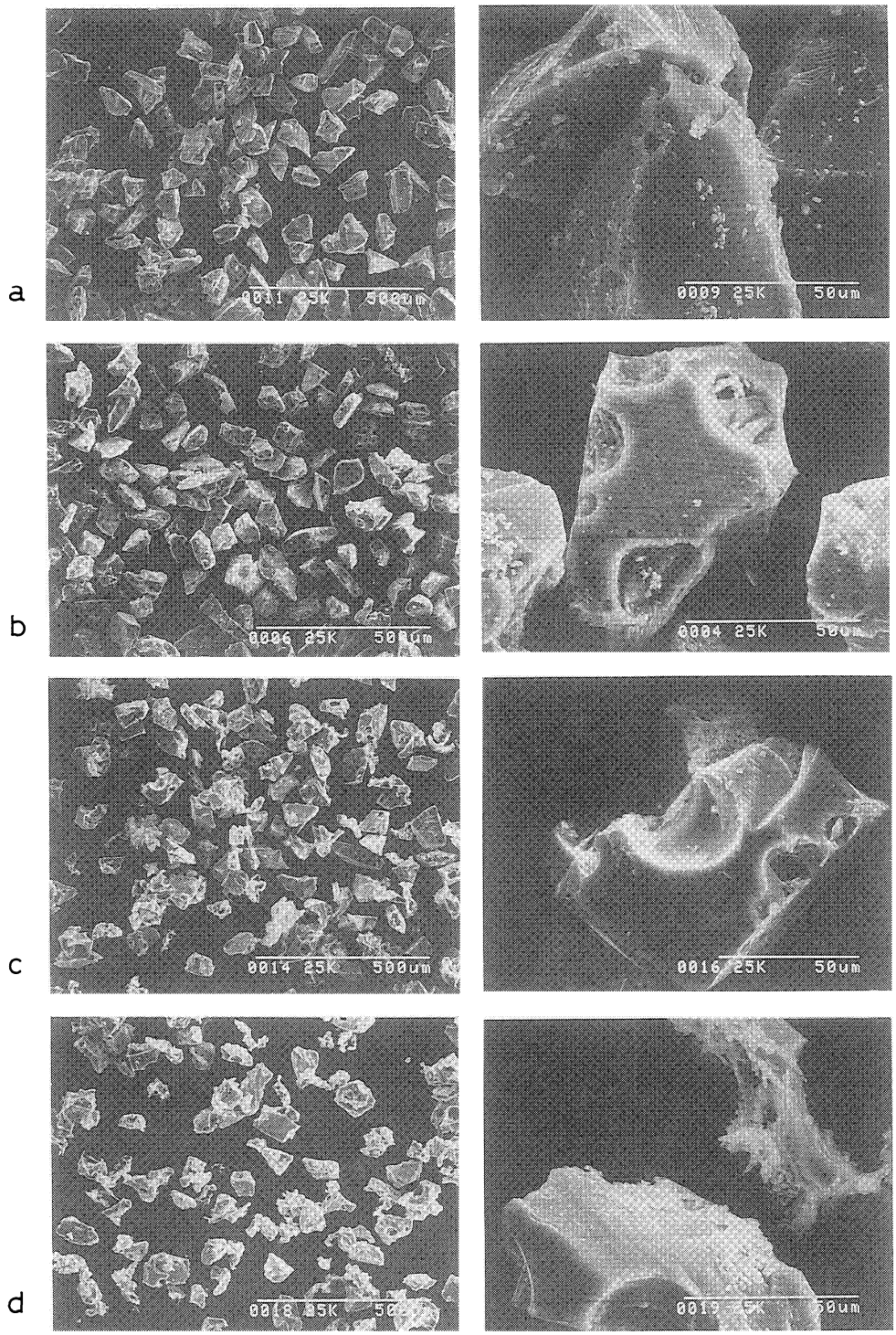

Fig. 4. Scanning electron micrographs of reacting silicon grains with various levels of silicon conversion. Pretreatment conditions: Silicon-$CuCl_2$ contact mass (Cu=2.5 wt%) was pretreated under a hydrogen stream at 533 K for 1 h. Reaction conditions: CH_3OH=99 kPa, reaction temperature=533 K, and reaction time=0.6 h (a), 1 h (b), 3 h (c), and 4 h (d). The left and right plates were obtained at 40 and 1000 magnifications, respectively.

Silicone," Elsevier, Amsterdam (1967).
7) W. F. Banholzer, N. Lewis, and W. Ward, *J. Catal.*, **101**, 405 (1986).
8) W. F. Banholzer and M. C. Burrell, *J. Catal.*, **114**, 259 (1988).
9) E. Suzuki and Y. Ono, *J. Catal.*, **125**, 390 (1990).

Ab Initio Study of Pyridyl Cations, Anions, and Radicals

Osamu KIKUCHI,* Yuji HONDO, Yukihiro YOKOYAMA, Kenji MORIHASHI, and Mitsunobu NAKAYAMA
Department of Chemistry, University of Tsukuba, Tsukuba 305
(Received April 26, 1991)

Synopsis. Ab initio calculations were carried out for the 2-, 3-, and 4-pyridyl cations, anions, and radicals in order to examine their molecular structures and relative energies among three isomers. The 4-31G//3-21G calculations have predicted that 2-pyridyl cation, 4-pyridyl anion, and 2-pyridyl radical are most stable among the isomers.

Pyridyl is derived formally from pyridine by the CH bond cleavage, and three types of species, cations, anions, and radicals, exist depending on the number of electrons involved in the carbon centered orbital. For the radical, 2-, 3-, and 4-pyridyl radicals have been detected by ESR,[1,2] and the reactivity of 2-pyridyl has been discussed.[3] The pyridyl anions and cations have been considered as the intermediates in chemical reactions.[4-7] Only a few theoretical works have been reported on these species.[8,9] In this note, we report the molecular and electronic structures of pyridyl cations, anions, and radicals determined by ab initio calculations and compare the relative stability among the 2-, 3-, and 4-isomers.

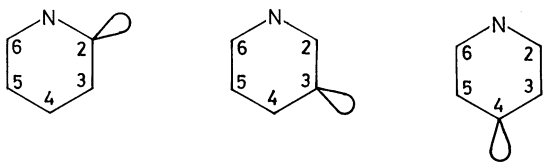

2 3 4

The closed-shell SCF method was used for the cations and anions, while the open-shell RHF method was used for the radicals. The molecular structures were optimized with the 3-21G basis set[10] under the restriction of the planarity for all species. All calculations were carried out using ABINIT program written in our group. The optimized molecular structures are shown in Figs. 1—3 and the relative energies among the isomers are listed in Table 1.

Pyridyl Cations. The calculated bond angles at the cationic carbon center of pyridyl cations are almost constant, 140°—142°, in three isomers. These bond angles are close to that calculated for the phenyl cation by Bernardi et al.[11] as is shown in Fig. 4-b. Since 2-pyridyl cation is isoelectronic with *o*-benzyne, it is interesting to compare the structures between them. Fig. 4-c is the structure of *o*-benzyne reported by Scheiner et al.[12] As may be seen from Fig. 4-c, the distortion of the carbon skeleton from hexagon is not large in *o*-benzyne, while a significant distortion is observed in the 2-pyridyl cation. This is due to the large bond angle at the carbon center in 2-pyridyl cation which is adjacent to the nitrogen atom and has the strong cationic character.

The 2-pyridyl cation is calculated to be more stable than the other isomers. This may simply be understood by the interaction between the cationic center and the nitrogen lone-pair electrons in 2-pyridyl. In spite of this large interaction, the large positive charge remains at the cationic carbon atom in 2-pyridyl; the value of +0.704

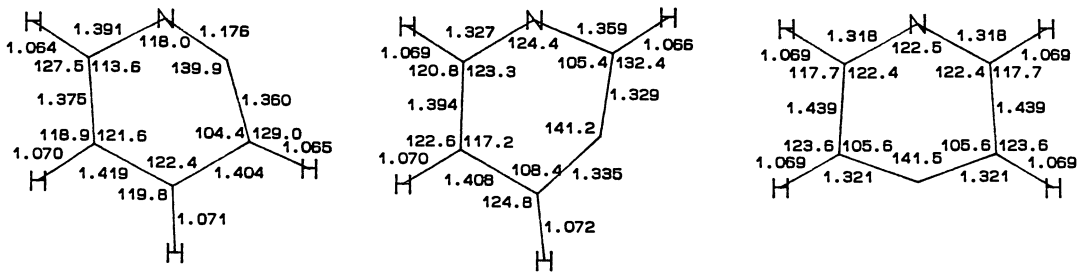

2 3 4

Fig. 1. Molecular structures of pyridyl cations optimized with the 3-21G basis set. Bond lengths are shown in Å and bond angles are in degrees.

Table 1. 4-31G//3-21G Energies (au) of Three Isomers of Pyridyl Cations, Anions, and Radicals[a]

	Pyridyl cations	Pyridyl anions	Pyridyl radicals
2	−245.398005 (0.0)	−245.643669 (10.0)	−245.682080 (0.0)
3	−245.353832 (27.7)	−245.654192 (3.4)	−245.675981 (3.8)
4	−245.357490 (25.4)	−245.659626 (0.0)	−245.678910 (2.0)

a) Values in parentheses are relative energies among three isomers in kcal mol^{-1}.

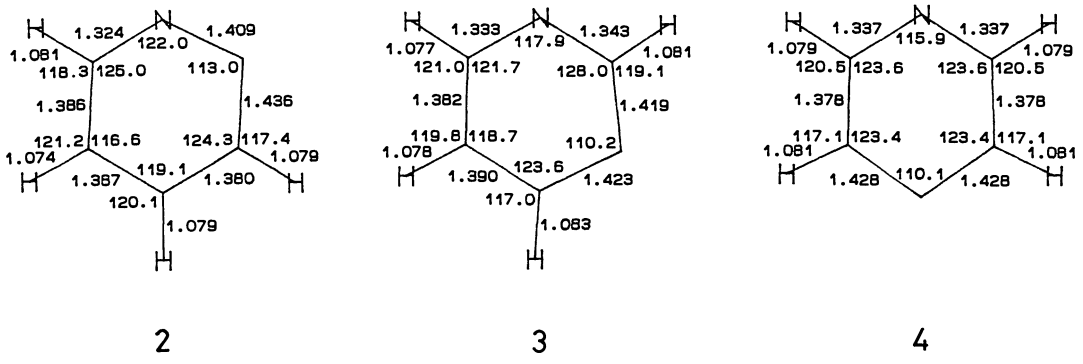

Fig. 2. Molecular structures of pyridyl anions optimized with the 3-21G basis set. Bond lengths are shown in Å and bond angles are in degrees.

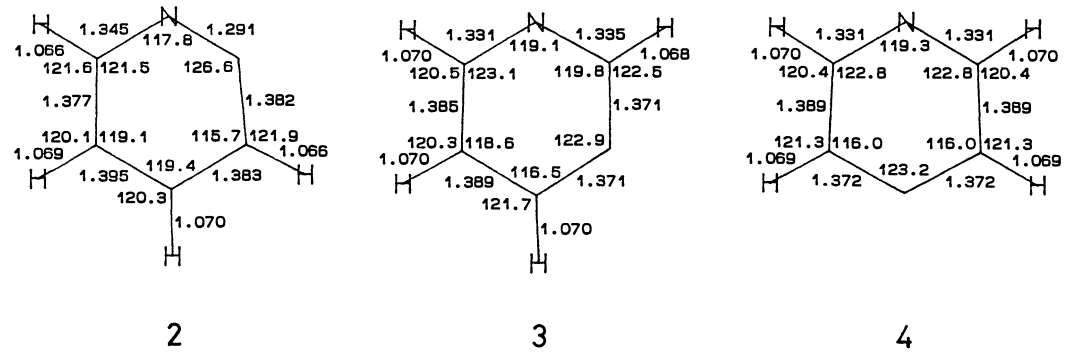

Fig. 3. Molecular structures of pyridyl radicals optimized with the 3-21G basis set. Bond lengths are shown in Å and bond angles are in degrees.

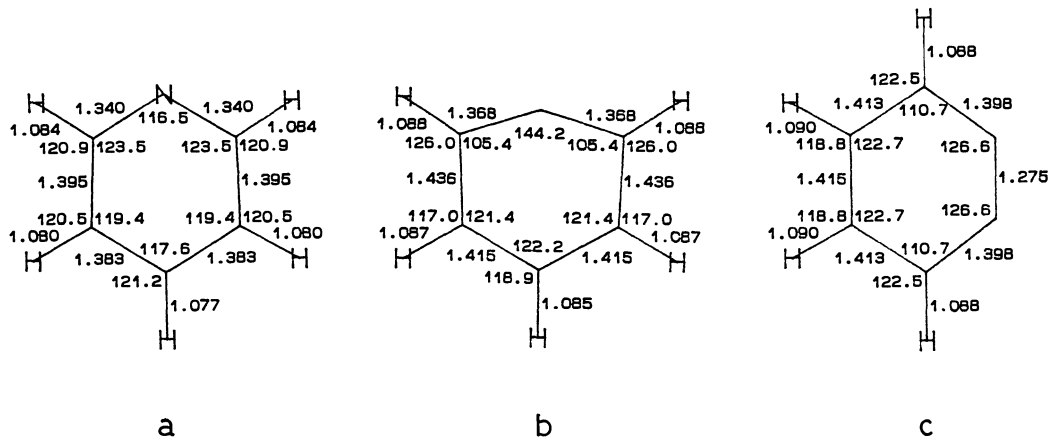

Fig. 4. Molecular structures of a) pyridine from experiment,[13] b) phenyl cation optimized with MCSCF/STO-3G,[11] and c) *o*-benzyne optimized with MP2/DZ+P.[12]

may be compared with those of the cationic centers in other isomers, +0.189 (3-pyridyl) and +0.410(4-pyridyl). This indicates that the stabilization expected in 2-pyridyl is due to the electrostatic interaction.

Pyridyl Anions. The angle at the anionic carbon atom is 110°—113° for three isomers. As may be understood from Fig. 2 and Fig. 4-a, the local structure around the nitrogen atom in 3- and 4-isomers is not largely disturbed by deprotonation of pyridine. In the case of 2-pyridyl anion, a remarkable distortion is observed at the anionic center. This is due to the repulsive interaction between two lone-pair electorns at the adjacent nitrogen and carbon atoms. This interaction makes the 2-pyridyl anion unstable. The 4-pyridyl

anion is calculated to be most stable, although the energy differences among three isomers are not large.

The 6-31G*//AM1 calculations gave the same trend in the relative stabilities among three anions, although AM1 calculations gave incorrect results for the relative energies of these anions.[9]

Pyridyl Radicals. Although the 4-31G//STO-3G calculations of pyridyl radicals have been reported earlier,[8] it may be worth to show the structures and energies obtained by the same level of calculations as for the cations and anions. The molecular structures (Fig. 3) and the relative stabilities of three isomers (Table 1) are parellel to the 4-31G//STO-3G results.

References

1) H. J. Bower, J. A. McRae, and M. C. R. Symons, *Chem. Commun.*, **1967**, 542; *J. Chem. Soc. A*, **1968**, 2696.

2) P. H. Kasai and D. McLeod, Jr., *J. Am. Chem. Soc.*, **92**, 6085 (1970); **94**, 720 (1972).

3) J. A. Zoltewicz and G. A. Locko, *J. Org. Chem.*, **48**, 4214 (1983).

4) T. Kauffmann and R. Wirthwein, *Angew. Chem., Int. Ed. Engl.*, **10**, 20 (1971).

5) J. A. Zoltewicz and C. L. Smith, *J. Am. Chem. Soc.*, **89**, 3358 (1967).

6) J. F. Bennett and P. Singh, *J. Org. Chem.*, **46**, 4567 (1981).

7) K. Ohkura, K. Seki, M. Terashima, and Y. Kanaoka, *Tetrahedron Lett.*, **30**, 3433 (1989).

8) O. Kikuchi, Y. Hondo, K. Morihashi, and M. Nakayama, *Bull. Chem. Soc. Jpn.*, **61**, 291 (1988).

9) M. Meot-Ner and S. A. Kafafi, *J. Am. Chem. Soc.*, **110**, 6297 (1988).

10) J. S. Binkley, J. A. Pople, and W. J. Hehre, *J. Am. Chem. Soc.*, **102**, 939 (1980).

11) F. Bernardi, F. Grandinetti, A. Guarino, and M. A. Robb, *Chem. Phys. Lett.*, **153**, 309 (1988).

12) A. C. Scheiner, H. F. Schaefer, III, and B. Liu, *J. Am. Chem. Soc.*, **111**, 3118 (1989).

13) L. E. Sutton, "Tables of Interatomic Distances and Configuration in Molecules and Ions," The Chemical Society, London (1965).

Spin-Lattice Relaxation Time Measurements of Ions and Water Molecules Containing Spin 1 Nuclei in Lyotropic Liquid Crystalline Systems

Masayasu IIDA*,† and Alan S. TRACEY
Department of Chemistry, Simon Fraser University,
Burnaby, B. C. V5A 1S6, Canada
(Received May 31, 1991)

Synopsis. The Jeener-Broekaert pulse sequence was applied to the ^{14}N and ^{2}H NMR measurement for studying the dynamic behavior of ions (ammonium and nitrate ions) and water molecules, respectively in lyotropic nematic liquid crystal solutions. The results showed that, in all cases except for the ammonium ion in alkaline solutions, the water molecules and the ions measured gave NMR spectra with properties characteristic of extreme narrowing conditions.

The behavior of ions and water molecules in amphiphilic solutions have been of interest for many years. Nuclear magnetic resonance spectroscopy has provided a powerful tool for the study of specific interactions occuring at the water-amphiphile interface of isotropic micellar and liquid crystalline detergent systems. Relaxation time measurements have been utilized for most investigations on the study of interactions in micellar solutions while the direct observation of quadrupole spittings have been useful in liquid crystalline solutions.[1] When water molecules or ions strongly interact with amphiphiles, two kinds of relaxation times are observed, indicating that a fast anisotropic motion is superposed on a more extensive slow motion.[2] In relaxation studies on liquid crystal systems an application of a phase-shifted, double-quantum pulse sequence on the basis of the Jeener-Broekaert excitation has been known to be useful to determine simultaneously the spectral densities $J_1(\omega_0)$ and $J_2(2\omega_0)$,[3,4] where ω_0 is the nuclear precession frequency. This pulse sequence is applicable to $I=1$ spin systems and most of the studies hitherto performed have been concentrated on deuterium relaxation of water or of amphiphiles.[5-7] In the present work, the Jeener-Broekaert pulse sequence measurements of the ^{2}H relaxation times of water molecules and of the ^{14}N ones of the NH_4^+ and NO_3^- ions have been carried out to reveal their dynamic behavior at water-amphiphile interfaces in aligned lyotropic liquid crystal systems. The present study is the first example of applying the Jeener-Broekaert pulse sequence to the ions containing ^{14}N nucleus to study their interactions with amphiphiles. The extent of the interactions of the water molecules or the ions with the amphiphiles can be seen through the quadrupole splittings and the activation energies of their rotational motions.

Experimental

Materials. The potassium dodecanoate was prepared from the dodecanoic acid by neutralization with aqueous KOH solution followed by a recrystallization several times from 95% ethanol. Sodium and ammonium decyl sulfates and decylammonium chloride were prepared by the standard methods.[8,9] 1-Decanol was obtained commercially and distilled before use. Ammonium nitrate and $^{2}H_2O$ (99.8% ^{2}H) were also obtained commercially and used directly. The solvent used for the $^{2}H_2O$ dynamic study was 5% $^{2}H_2O$ which was prepared by mixing the above $^{2}H_2O$ with a twice distilled H_2O. For the NO_3^- and NH_4^+ dynamic studies, a twice distilled water was used as a solvent.

NMR Measuements. NMR spectra were obtained on a Bruker WM-400 NMR spectrometer using a multinuclear probe operating at 61.48 MHz for deuterium and at 28.94 MHz for ^{14}N. The spin-lattice relaxation times, T_{1Z} (associated with the return of the Zeeman energy to its equilibrium value) and T_{1Q} (the decay of the quadrupolar energy) were measured using the $(\pi/2)_y$-τ-$(\pi/4)_x$-t_1-$(\alpha)_x$ pulse sequence. This is commonly called the Jeener-Broekaert sequence and has been applied according to the method performed by Vold et al.,[3] where $\tau=1/(2\Delta\nu_Q)$ and $\Delta\nu_Q$ is quadrupolar coupling constant. T_{1Z} and T_{1Q} can be determined from the sum and difference of the line intensities measured as a function of evolution time t_1 where α is fixed as 0.31π. In addition to this, the T_1 (I. R.) value for each sample solution was also determined by the conventional inversion-recovery method. The temperature was maintained with an accuracy of ±0.5 °C by a nitrogen gas flow.

Components of Liquid Crystals. The lyotropic mesophases used in this study had the general components of detergents, stock solutions containing salts in H_2O (or 5% $^{2}H_2O$) and 1-decanol (except for the decylammonium chloride system). The liquid crystal systems consisted of: 1) Ammonium decyl sulfate/Sodium decyl sulfate/DeOH/H_2O=362 mg/368 mg/81 mg/1008 mg. 2): Decylammonium chloride/ammonium nitrate/acidic (0.04 mol dm^{-3} pyridine-0.06 mol dm^{-3} HCl) H_2O=600 mg/80 mg/1010 mg. 3) Potassium dodecanoate/ammonium nitrate/DeOH/basic (0.08 mol dm^{-3} ethylenediamine-0.03 mol dm^{-3} HBr) H_2O=298 mg/50 mg/50 mg/1010 mg. The pH values of the 1) solution were 5.3 and 10.3 which are controlled by pyridine-HBr in the acidic region or by ethylenediamine-HBr in the alkaline region, respectively. The pH values were 2.5 for the 2) solution and 10.0 for the 3) solution.

Results and Discussion

The quadrupole splittings, $\Delta\nu_Q$, for the $^{14}NH_4^+$, $^{14}NO_3^-$, and $^{2}H_2O$ were measured in the range where a single phase of the nematic lyotropic liquid crystal is present and were used to decide the τ values as stated above. The $\Delta\nu_Q$, values linearly decreased with increasing temperatures. For each system we calculated $\Delta\nu_Q(0)$ ($\Delta\nu_Q$ extrapolated to $t=0$ °C) and the results are listed in Table 1. For the $^{2}H_2O$ molecule and the counterion in a liquid crystal system, it is generally considered that the magnitude of the $\Delta\nu_Q(0)$ is proportional to the extent of the hydration or the ion-binding if we compare between similar component systems.[1]

† Present address: Department of Chemistry, Nara Women's University, Nara 630

Table 1. Quadrupole Splittings Being extrapolated to t=0 °C for ^{14}N of NH_4^+, NO_3^-, and ^2H_2O in Some Liquid Crystalline Systems

a) Potassium dodecanoate system (pH 10.0)			
	i) $^{14}NH_4^+$	ii) $^{14}NO_3^-$	iii) ^2H_2O
$\Delta\nu_Q(0)$/kHz=	4.2±0.3[a]	0.31±0.01	0.15±0.01
b) Decylammonium chloride system (pH 2.5)			
	i) $^{14}NH_4^+$	ii) $^{14}NO_3^-$	iii) ^2H_2O
$\Delta\nu_Q(0)$/kHz=	1.2±0.1	46±2	0.24±0.02
c) Sodium/ammonium decyl sulfate system			
i) $^{14}NH_4^+$	(pH 5.3)	(pH 10.3)	
$\Delta\nu_Q(0)$/kHz=	1.3±0.1	2.2±0.1[a]	
ii) ^2H_2O (pH 5.3)			
$\Delta\nu_Q(0)$/kHz=0.43±0.02 kHz			

a) These values include the values for the ammonia molecule.

For a single I=1 nucleus, application of the Jeener–Broekaert pulse sequence provides two kinds of the spin-lattice relaxation times associated with the return of the Zeeman energy to its equilibrium value T_{1Z} and the decay of the quadrupolar energy T_{1Q}. These two relaxation times can be expressed by the spectral densities ($J_1(\omega_r)$ and $J_2(\omega_r)$) as follows.[3,4]

$$R_{1Z} = 1/T_{1Z} = (e^2qQ/h)^2 3/80(J_1(\omega_r) + 4J_2(2\omega_r)), \quad (1)$$

$$R_{1Q} = 1/T_{1Q} = (e^2qQ/h)^2 3/80(3 \cdot J_1(\omega_r)) \quad (2)$$

where (e^2qQ/h) is the quadrupolar coupling constant.

The usefulness of the application of this method is the ability to simultaneously determine the individual spectral densities of motion, $J_1(\omega_0)$ and $J_2(2\omega_0)$. If water molecules or ions form ion-pairs with amphiphiles so that their motion is restricted, their relaxation times should be frequency dependent and the two spectral densities will have different values. If the interactions do not strongly restrict the motional properties, the relaxation times should be independent of the nuclear precession frequency (extreme narrowing condition), so that J_1 equals J_2. In this case the T_{1Q}/T_{1Z} ratio should be 1.67.

According to the method proposed by Vold and Vold,[3,4] we obtained values of T_{1Q} and T_{1Z} for ^2H_2O and $^{14}NH_4^+$ in various systems with varying temperatures. The results are listed in Tables 2—5 together with T_1 values obtained by the inversion-recovery method. A correspondence between the T_{1Z} and the T_1 (I.R.) value in all cases are satisfactory. We can thus use two kinds of the spin-lattice relaxation times to calculate the T_{1Q}/T_{1Z} ratios and to check whether the extreme narrowing condition is fulfilled or not. The values obtained (listed in the bottom rows of Tables 2—5) show that the ratios coincide with 1.67 within the experimental error in all the cases. It has also been shown for some micellar solutions[10] and for an aqueous sodium dibutyl phosphate lamellar mesophase[11] that the extreme narrowing condition is fulfilled for counterions or water molecules. To compare the extent of the ion binding or the hydration, we calculated activation energies for effective correlation times, τ_{eff}, related with the relaxation rates, R_1. The temperature dependency of R_1 will correspond to that of τ_{eff},[12] which may show an Arrhenius behavior. We obtained the activation energy for τ_{eff} from the Arrhenius plot of $1/T_1$, where we used T_1 values obtained through inversion-recovery method because these values

Table 2. Temperature Dependences of ^{14}N Relaxation Times of NH_4^+ and NO_3^- in the Potassium Dodecanoate Liquid Crystals

i) $^{14}NH_4^+$ (pH 10.0)[a]		ii) $^{14}NO_3^-$ (pH 10.0)[b]		
T/K	T_1(I.R.)/ms	T_1(I.R.)/ms	T_{1Q}/ms	T_{1Z}/ms
288	11	68	125	71
290	11	75	130	72
293	13	—	—	—
295	13	88	135	91
300	14	96	148	100
302	14	—	—	—
305	15	112	189	110

a) ΔE_a/kJ mol^{-1}=13±2. b) ΔE_a/kJ mol^{-1}=20±2; T_{1Q}/T_{1Z}=1.7±0.1.

Table 3. Temperature Dependences of ^{14}N Relaxation Times of NH_4^+ in the Decylammonium Chloride Liquid Crystals (pH 2.5)

T/K	T_1(I.R.)/s	T_{1Q}/s	T_{1Z}/s
285	0.84	1.43	0.85
288	0.88	1.51	0.90
290	0.93	1.55	0.94
293	0.99	1.57	1.00
296	1.03	1.65	1.00
298	1.05	1.68	1.03

ΔE_a/kJ mol^{-1}=13±2; T_{1Q}/T_{1Z}=1.6±0.1.

Table 4. Temperature Dependences of the Relaxation Times of $^{14}NH_4^+$in Sodium/Ammonium Decyl Sulfate Liquid Crystal

T/K	i) pH=5.3[a] T_1(I.R.)/s	T_{1Q}/s	T_{1Z}/s	ii) pH=10.3[b] T_1(I.R.)/ms
281	0.18	0.30	0.17	3.3
285	0.23	0.42	0.25	3.6
289	0.29	0.45	0.27	4.0
293	0.31	0.53	0.33	4.4
297	0.40	0.61	0.36	4.8
300	0.45	0.73	0.41	5.1

a) ΔE_a/kJ mol^{-1}=33±2; T_{1Q}/T_{1Z}=1.7±0.1. b) ΔE_a/kJ mol^{-1}=16±3.

Table 5. Temperature Dependences of the Relaxation Times of ^2H_2O in the Decylammonium Chloride Liquid Crystal (pH 2.5)

T/K	T_1(I.R.)/s	T_{1Q}/s	T_{1Z}/s
285	0.24	0.40	0.25
288	0.28	0.49	0.29
293	0.33	0.51	0.32
296	0.36	0.58	0.34
299	0.43	0.71	0.42

ΔE_a/kJ mol^{-1}=28±4; T_{1Q}/T_{1Z}=1.65±0.05.

Table 6. Temperature Dependences of the Relaxation Times of ^2H_2O in the Sodium Decyl Sulfate Liquid Crystal (pH 5.3)

T/K	T_1(I.R.)/s
285	0.22
289	0.25
293	0.28
297	0.31
300	0.35

ΔE_a/kJ mol^{-1}=22±1.

will be of higher accuracy than the corresponding T_{1Z} values. The Arrhenius plots for all the systems were approximately linear in the temperature range utilized here and the activation energies were obtained as listed in the bottom rows of Tables 2—6. We can generally say, when comparing similar component systems, that larger activation energies are required for the reorientation of the ions or molecules if they interact with the amphiphiles as for instance, NH_4^+/decylammonium mesophase (pH 2.5), E_a=13±2 kJ mol^{-1} vs. NH_4^+/decyl sulfate mesophase (pH 5.3), E_a=33±2 kJ mol^{-1}. Clearly the activation energies increase if the ions or molecules interact more strongly and also the $\Delta\nu_Q$ values of the nuclei of interest also increase with increasing interactions with the amphiphiles.

Only in the case of the ammonium ion in alkaline solutions where formation of the ammonia is appreciable,[13] the ratios obtained were significantly smaller than 1.67 and were around 1.3—1.4. Since the ammonia molecules can be considered to be also under extreme narrowing condition, the T_{1Q}/T_{1Z} ratio for the ammonium ion in alkaline solution is also expected to be close to 1.67. The significantly smaller values of the ratio obtained here may, therefore, arise from the effect of the rapid exchange between the ammonium ion and the ammonia molecule, whose ^{14}N nuclear quadrupolar coupling constants are quite different.[14] Since the coincidence of the T_{1Z} values with the corresponding T_1 (I.R.) values was better than that of the T_{1Q}/T_{1Z} values with 1.67 in these cases, the difference in the latter values can be attributed to a larger effect of the exchange on the T_{1Q} values than the T_{1Z} values. The T_{1Q} value obtained for the ammonium ion in the alkaline solution thus may be different from that defined in Eq. 2. Although the analysis of the result for this system in detail seems to be complicated, the activation energy for the ^{14}N relaxation rate obtained by the inversion-recovery method can be a measure for the extent of the interaction of the ammonium ions with the amphiphiles: As shown in Table 4, the activation energy in the acidic solution is appreciably larger than that in the alkaline solution and this result is consistent with the fact that the interaction of the ammonia molecules with the anionic amphiphiles is slight due to an absence of the electrostatic interactions.

In conclusion, this application of the Jeener-Broekaert pulse sequence to study the dynamic behavior of the nitrate and ammonium ions and the water molecules showed that these systems in most cases undergo the extreme narrowing of their NMR signals. It was not possible to ascertain if they undergo slow motions within the water-amphiphile interface. The activation energies for their reorientational motions, however, described the extent of the binding of the ions and water molecules to the amphiphiles.

The authors are grateful to Professor Hideo Yamatera (Daido Institute of Technology) for helpful discussion. Thanks are gratefully extended to NSERC Canada for its financial support of this work.

References

1) B. Lindman, "NMR of Newly Accessible Nuclei," Vol. 1, (1983).
2) T. C. Farrar and E. D. Becker, "Pulse and Fourier Transform NMR," Academic Press, New York (1971), Chap. 4.
3) R. R. Vold, "NMR of Liquid Crystals," ed by J. W. Emsley, D. Reidel, Dondrecht (1985), pp. 260—275.
4) R. R. Vold and R. L. Vold, "Liquid Crystals and Ordered Fluids,," ed by A. C. Griffin and J. F. Johnson, Plenum, New York (1984), Vol. 4, pp. 561—578.
5) J. P. Jacobson and K. Schaumburg, *J. Magn. Reson.*, **24**, 173 (1976).
6) T. C. Wong and K. R. Jeffrey, *Mol. Phys.*, **46**, 1 (1982).
7) K. R. Jeffrey, T. C. Wong, and A. P. Tulloch, *Mol. Phys.*, **52**, 307 (1984).
8) L. W. Reeves and A. S. Tracey, *J. Am. Chem. Soc.*, **97**, 5729 (1975).
9) K. Radley and A. S. Tracey, *Mol. Cryst. Liq. Cryst. Lett.*, **1**, 95 (1985).
10) E. Sjöblom and U. Henriksson, *J. Phys. Chem.*, **86**, 4451 (1982).
11) C. Chachaty and J. P. Quaegebeur, *Mol. Phys.*, **52**, 1081 (1984).
12) A. M. de P. Nicholas and R. E. Wasylishen, *J. Phys. Chem.*, **89**, 5446 (1985); A. M. de P. Nicholas and R. E. Wasylishen, *Can. J. Chem.*, **65**, 951 (1987).
13) "Stability Constants of Metal-Ion Complexes," ed by Silllén; The Chemical Society; Burlington House, London (1964), p. 150.
14) "Multinuclear NMR," ed by J. Mason, Plenum, New York (1987), p. 346.

Graph-Theoretical Analysis of the Cyclic Bicalicene Conjugated Systems

Jun-ichi AIHARA
Department of Chemistry, Faculty of Science, Shizuoka University,
Oya, Shizuoka 422
(Received June 5, 1991)

Synopsis. The so-called cyclic bicalicene is aromatic although it can be regarded as a perturbed [16]annulene. Graph-theoretical analysis shows that the aromaticity of this molecule arises primarily from three- and five-membered circuits and their combinations. The peripheral sixteen-membered circuit presumably destabilizes the conjugated system to a very slight extent.

In 1981 Yoshida and co-workers synthesized a novel pentacyclic conjugated hydrocarbon **1a**, and chose the appropriate name cyclic bicalicene for it.[1-5] It is stable in air at room temperature for several weeks. Its structural isomer in the form of **2a** has not been prepared yet. Since these two cyclic bicalicenes can be viewed as perturbed [16]annulenes, they are expected to be antiaromatic in nature. However, at least **1a** is aromatic in its chemical behavior.[2-5] Further, it exhibits neither strong first- nor second-order double-bond fixation.[6]

In general, aromaticity is associated straightforwardly with cyclic conjugation of π-electrons. All possible cyclic paths in a mono- or polycyclic conjugated system are responsible for aromaticity.[7-10] Such cyclic paths have been termed ring components or circuits in chemical graph theory.[7-10] Then, what kind of circuits contribute much to the aromaticity of **1a** and **2a**? In this paper, we make a graph-theoretical analysis of total π-electron energy for these cyclic bicalicenes, aiming at clarifying the role of peripheral conjugation. Hückel molecular orbital (HMO) theory is employed.

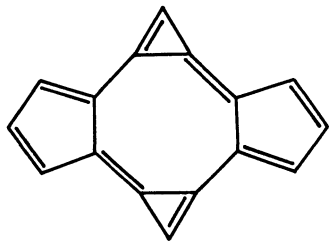

1a

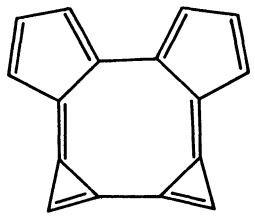

2a

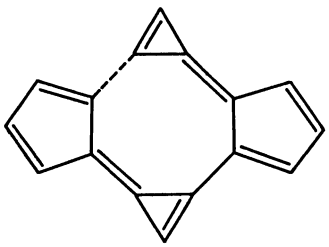

1b

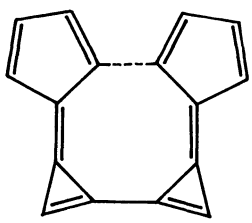

2b

Results and Discussion

Not only the Dewar resonance energy (DRE) but also the topological resonance energy (TRE) has been used as a good index for determining the degree of aromaticity for cyclic conjugated systems.[7-12] The TREs defined by the simple Hückel model and the ω-technique (ω=1.4) will be denoted by TRE(ω=0) and TRE(ω=1.4), respectively. For alternant hydrocarbons the TRE(ω=0) is equal to the TRE(ω=1.4), whereas for non-alternant hydrocarbons the TRE(ω=1.4) is more or less smaller than the TRE(ω=0). The TRE(ω=1.4) proved more realistic as an aromaticity index for non-alternant hydrocarbons such as cyclic bicalicenes **1a** and **2a**.[10]

The TREs of **1a**, **2a**, and related structures are listed in Table 1. There is no doubt about regarding **1a** as an aromatic species since both the TRE(ω=0) and the TRE(ω=1.4) are large and positive in sign. In contrast, **2a** has a smaller positive TRE(ω=0) and a negative TRE(ω=1.4), which suggest that this molecule is nonaromatic or antiaromatic in its chemical behavior. The DREs of **1a** and **2a** were calculated to be 15.75 and 6.71 kcal mol^{-1}, respectively. Here, the conjugated system of **1a** was assumed to be of D_{2h} symmetry. These DREs are fairly consistent with the corresponding TREs. For comparison, the TRE and the DRE for benzene are $0.273|\beta|$[7,8] and 20.0 kcal mol^{-1},[12] respectively.

If Kekulé structures can be written for a subsystem of any cycle conjugated system, obtained by deleting a given circuit from the system, this very circuit is called a conjugated circuit. In 1976 Randić pointed out that the conjugated circuits are the main source of aromaticity in polycyclic aromatic molecules.[13,14] He successfully estimated the DREs of many polycyclic systems simply by enumerating every type of conjugated circuits.[13,14]

Table 1. Stabilization Energies (SEs) due to Type-II Circuits

Species	Total π-electron energy/β	SE/$\lvert\beta\rvert$	TRE/$\lvert\beta\rvert$
	A. Simple Hückel model (ω=0)		
1a	22.783	−0.020	0.657
1b	22.824	0.020	0.697
2a	22.599	−0.030	0.471
2b	22.659	0.030	0.531
	B. ω-Technique (ω=1.4)		
1a	22.319	−0.017	0.192
1b	22.352	0.017	0.226
2a	21.940	−0.030	−0.188
2b	22.000	0.030	−0.128

The peripheral sixteen-membered circuit is only one conjugated circuit in cyclic bicalicenes **1a** and **2a**. Accordingly, these molecules might be thought to be as antiaromatic as a sixteen-membered conjugated circuit. The DRE value estimated on this basis is −0.06 eV, which is obviously inconsistent with the positive DRE or TREs of **1a**.

Such an inconsistency can be settled by graph-theoretically analyzing the total π-electron energies of each cyclic bicalicene and its Möbius isomer. Here, a Möbius isomer is a hypothetical molecule, obtained by changing the sign of the resonance integral for one of the C–C bonds connecting the three- and five-membered rings in **1a**. A C–C bond with a resonance integral of $-\beta$ is identical with a twisted C–C bond because $-\beta$ usually represents a C–C bond twisted by 180°.[15] Möbius isomers thus defined for **1a** and **2a** are given in **1b** and **2b**, respectively, in which dashed lines indicate twisted C–C bonds. Each has a Möbius-type peripheral conjugated subsystem.

Twenty circuits can be chosen from each cyclic bicalicene conjugated system. Eleven non-identical circuits in **1a** are presented in Fig. 1. Three- and five-membered circuits in **1a** and **2a** will be referred to as type-I circuits with all other ones referred to as type-II circuits. In Fig. 1, A and B are type-I circuits, while all others, including the peripheral conjugated circuit K, are type-II circuits. Type-I circuits in **1a** and **2a** are identical with those in **1b** and **2b**, respectively, whereas type-II circuits in each cyclic bicalicene become singly twisted in the Möbius isomer.

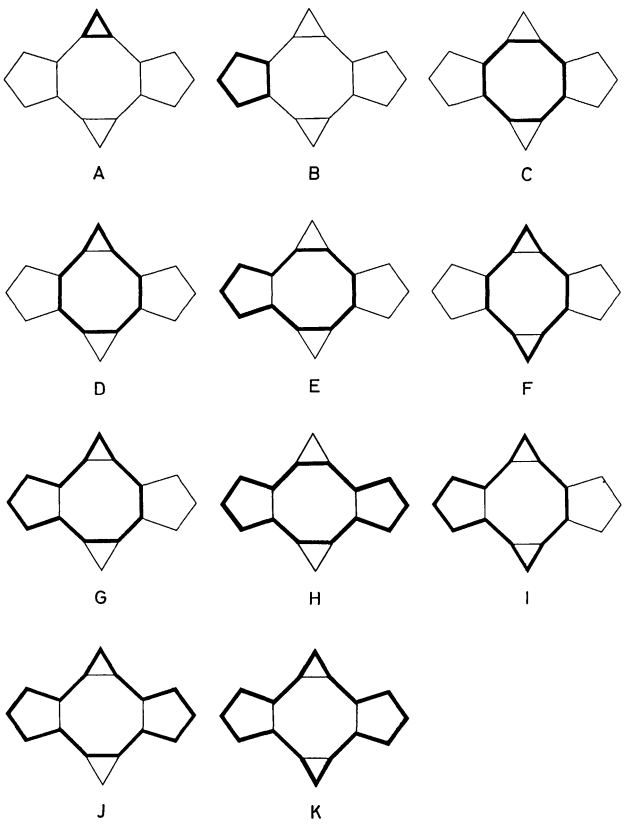

Fig. 1. Non-identical circuits in **1a**.

The total π-electron energy of a molecule can be expressed formally as a function of all circuits.[7–10,16] Some circuits lower the energy of the molecule, while others raise it. The former circuits are classified as aromatic circuits, and the latter ones as antiaromatic circuits. Every type-I circuit in **1a** and **2a** retains essentially the same aromatic character in **1b** and **2b**, respectively. However, aromatic and antiaromatic type-II circuits become antiaromatic and aromatic, respectively, on going from each cyclic bicalicene to its Möbius isomer.[17,18] Therefore, it follows that the energy difference between each cyclic bicalicene and the Möbius isomer represents the change in aromaticity of all type-II circuits.

HMO calculations revealed that each cyclic bicalicene and its Möbius isomer have similar total π-electron energies. For example, **1a** is less stable than **1b** only by $0.041|\beta|$. This fact indicates that type-II circuits, as a whole, destabilize **1a** to a very slight extent, and stabilize **1b** to a similar extent. Therefore, the stabilization energy (SE) of each cyclic bicalicene due to type-II circuits must be about half the energy difference between it and the Möbius isomer. The SE is about $-0.020|\beta|$ for **1a**, the negative sign of which indicates the predominant contribution of antiaromatic $4n$-membered type-II circuits. However, its absolute value is less than 10 percent of the TRE(ω=1.4). The same is essentially true of **2a**. In view of the very small SEs, it seems unlikely that peripheral conjugated subsystems in **1a** and **2a** have large annulenoid character.

It is worthy of note that **1a** has a large positive DRE and TRE although it does not have aromatic $(4n+2)$-membered conjugated circuits. It is type-I circuits such as three- and five-membered ones and their combinations that are important for characterizing electronic properties of **1a** and **2a**. These odd-membered circuits are never conjugated ones in Randić's sense.[13,14] His concept of conjugated circuits must somehow be modified in order to explain aromatic properties of cyclic bicalicenes.

Concluding Remarks

The Hückel $4n+2$ rule was originally proposed for monocyclic conjugated systems.[19] The idea that cyclic bicalicenes (**1a** and **2a**) may be regarded as perturbed [16]annulenes has been based on the unjustified assumption that this rule is applicable to polycyclic conjugated systems. We previously proved that the Hückel $4n+2$ rule in principle holds for monocyclic conjugated systems.[20] However, there is no reason to believe that annulenoid conjugation is important in such polycyclic conjugated systems as **1a** and **2a**. The peripheral conjugated subsystems in these species are so heavily perturbed that it is difficult to treat them naively as perturbed [16]annulenes. The present results are fully consistent with previous graph-theoretical considerations on **1a**.[2–5]

References

1) Systematic name: pentacyclo[11.3.0.$0^{2,4}$.$0^{5,9}$.$0^{10,12}$]-hexadeca-1,3,5,7,9,11,13,15-octaene

2) Z. Yoshida, *Pure Appl. Chem.*, **54**, 1059 (1982).

3) S. Yoneda, M. Shibata, S. Kida, Z. Yoshida, Y. Kai, K. Miki, and N. Kasai, *Angew. Chem., Int. Ed. Engl.,* **23**, 63 (1984).
4) T. Sugimoto, M. Shibata, S. Yoneda, Z. Yoshida, Y. Kai, K. Miki, N. Kasai, and T. Kobayashi, *J. Am. Chem. Soc.,* **108**, 7032 (1986).
5) T. Sugimoto and Z. Yoshida, *Pure Appl. Chem.,* **62**, 551 (1990).
6) A. Toyota and T. Nakajima, *Chem. Lett.,* **1982**, 1049.
7) J. Aihara, *J. Am. Chem. Soc.,* **98**, 2750 (1976).
8) M. Milun, I. Gutman, and N. Trinajstić, *J. Am. Chem. Soc.,* **99**, 1692 (1977).
9) A. Graovac, I. Gutman, and N. Trinajstić, "Topological Approach to the Chemistry of Conjugated Molecules," Springer, Heidelberg (1977).
10) J. Aihara, *Bull. Chem. Soc. Jpn.,* **53**, 2689 (1980).
11) M. J. S. Dewar and G. J. Gleicher, *J. Am. Chem. Soc.,* **87**, 685, 692 (1965).
12) M. J. S. Dewar and C. de Llano, *J. Am. Chem. Soc.,* **91**, 789 (1969).
13) M. Randić, *Chem. Phys. Lett.,* **38**, 68 (1976).
14) M. Randić, *J. Am. Chem. Soc.,* **99**, 444 (1977).
15) E. Heilbronner, *Tetrahedron Lett.,* **1964**, 1923.
16) H. Hosoya, K. Hosoi, and I. Gutman, *Theor. Chim. Acta,* **38**, 37 (1975).
17) N. Mizoguchi, *J. Phys. Chem.,* **92**, 2754 (1988).
18) N. Mizoguchi, *Chem. Phys. Lett.,* **158**, 383 (1989).
19) E. Hückel, *Z. Phys.,* **70**, 204 (1931).
20) J. Aihara and H. Ichikawa, *Bull. Chem. Soc. Jpn.,* **61**, 223 (1988).

Determination of Methane Concentration in Air Extracted from Antarctic Ice Core Samples

Yasunori TOHJIMA,*,† Takeshi TOMINAGA, Yoshihiro MAKIDE,†† and Yoshiyuki FUJII†††
Department of Chemistry, Faculty of Science, The University of Tokyo,
Hongo, Bunkyo-ku, Tokyo 113
†† Radioisotope Center, The University of Tokyo,
Yayoi, Bunkyo-ku, Tokyo 113
††† National Institute of Polar Research, Kaga, Itabashi-ku, Tokyo 173
(Received April 12, 1991)

Synopsis. A convenient method was developed for detrmination of methane concentration in old air trapped in Antarctic ice core samples. The air was extracted with a stainless steel bellows pump after quick refreezing of melted ice samples and the methane was measured with a gas chromatograph with an FID. The averaged methane concentration in the Mizuho ice core at a depth of 330 m (ca. 3600 BP, 11 samples) was 750±20 ppbv.

Great concern has been expressed about the increasing concentrations of trace gases in the atmosphere and their effects on the global environment. The atmospheric concentrations in ancient times give us information on their natural background concentrations and the contribution of human activities.

In polar regions, snow is consolidated to firn, which contains permeable pore space for the air. When the firn turns into ice through densification and recrystallization over the course of 100 to 3000 years, the air in the ice pores becomes isolated from the atmosphere and enclosed in the ice as bubbles. A typical ice sample contains about 100 ml air (STP) per kg ice. Analyses of the air trapped in ice bubbles have revealed the historical changes of carbon dioxide[1-4] and methane concentrations.[5-10]

For extraction of the air in ice core samples, the ice block placed in a flask must be either crushed in a vacuum at temperatures below 0 °C (dry extraction method) or thawed (melt extraction method). The melt extraction method has advantages over the dry extraction method because the air in the sample is recovered quantitatively with a very simple apparatus. The dry extraction method requires a sophisticated apparatus with an inevitably large dead volume to extract only the air in bubbles. Moreover, the extracted air was reported to become contaminated by methane when ice was ground by a milling cutter.[7,8]

We, therefore, developed a new melt extraction method in which an ice sample was thawed and quickly refrozen. To transfer the extracted air we used an all-stainless-steel bellows pump instead of a mercury Toepler pump or liquid helium condensation, which may cause contamination and is expensive.

Experimental

Analytical Procedure for Ice Samples. The setup for the extraction and analysis of air is shown in Fig. 1. An ice core sample was cut into several pieces and weighed after removal of the surface layer (1 cm) at −20 °C in the cold room of the National Institute of Polar Research (NIPR). Ice blocks (about 100 g) were placed in a thick-walled, cylindrical glass flask (230 ml) sealed with a Viton O-ring and equipped with a glass-Teflon valve at the top. The flask was first evacuated for one hour at Dry Ice temperature; then the valve was closed and the ice was thawed in a water bath at 80 °C. When about 80% of the ice was thawed, the water bath was removed and the melt water was stirred with a magnetic spinner placed inside to bring the air in gas phase into equilibrium with that in liquid phase. Then it was quickly frozen at liquid nitrogen temperature so as to trap the dissolved gases. It took about 45 min to refreeze 100 g of melt water. The air in the gas phase was extracted, dried by being passed through a cold trap at −100 °C, and transferred into a preevacuated stainless steel sample loop (20 ml) or a small flask by an all-stainless steel bellows pump (specially made by GL Science, Co., using the excellent stainless-steel bellows material AM350) with no polymer parts inside. The gas was eventually analyzed with a gas chromatograph (Shimadzu GC-8A) equipped with a Polapak Q column (3 mm i.d., 4 ml length) and a flame ionization detector (FID).

The methane peak area in the chromatogram was compared with that of the clean air sample in a stainless steel flask calibrated in our laboratory.

Selection of Extraction Conditions. Each component of

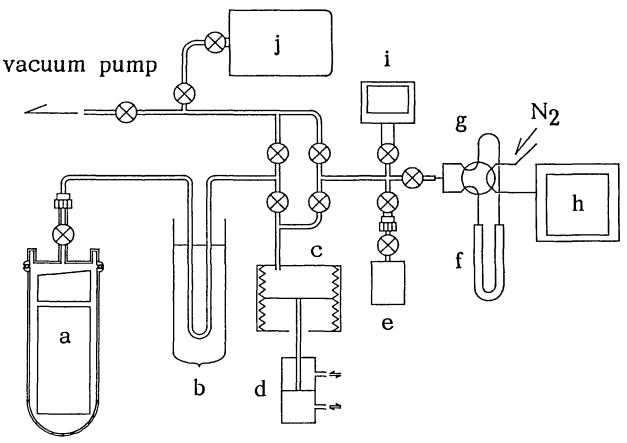

Fig. 1. Schematic diagram of air extraction from ice core sample and methane measurement system. a: sample flask; b: water vapor trap (−100 °C); c: all-stainless-steel bellows pump; d: actuator for pump; e: small flask; f: sampling loop (20 ml); g: 6-way valve; h: gas chromatograph (Shimadzu GC8A): i: pressure gauge (Datametrics Barocel Pressure Sensor); j: secondary standard.

† Present address: Laboratory for Earthquake Chemistry, Faculty of Science, The University of Tokyo, Bunkyo-ku, Tokyo 113.

the air released from the melted sample is distributed differently between liquid and gas phases depending on its particular solubility in water. Since the water solubility of methane is greater than that of nitrogen or oxygen, the methane mixing ratio is depleted in the gas phase. If we could refreeze the melt water again extremely slowly from the bottom of the flask, most air dissolved in the water might be purged due to its negligible solubility in ice crystals, and the original air composition might be closely reproduced in the head space. However, it would take many hours to free the ice completely of air, or it is almost impossible to do so.

In quick freezing, the air purged from the growing ice crystals condenses at the ice-water interface. When the air at the interface cannot be dissolved in the water, nucleation of air bubbles occurs, and the air bubbles are trapped in the growing ice. Hence, if the growth of ice is faster than the air diffusion in the water, the ice incorporates the initially dissolved air almost completely. In this work, the ice grew at the rate of about 3×10^{-3} cm s^{-1}, which was much larger than the rate of diffusion of air in water (the diffusion coefficient: about 10^{-5} cm^2 s^{-1}), and in practice the ice contained many bubbles. Accordingly, we assume that the dissolved air can be preserved in the quickly refrozen ice and that the air in the gas phase has the same composition with that in equilibrium with the melted water.

It was reported that the air in the bubbles of Camp Century ice from Greenland had almost the same composition as to nitrogen, oxygen and argon as that in the present air.[11] Assuming that the main components are of the same composition as that in the present air and follow Henry's law, we can calculate the methane concentration in the head space air. The methane concentration (C) in the head space of the sample flask is given by

$$C=\frac{(V_a/V_w+\alpha_{air}T/T_0)}{(V_a/V_w+\alpha_{CH_4}T/T_0)}\times C_0$$

where C_0 is the initial methane concentration in ice bubbles; α_{air} and α_{CH_4} are Bunsen solubility coefficients of air and methane, respectively; T is the temperature at which the thawed water was equilibrated; T_0 is 273 K; V_a is the volume of head space of sample flask; and V_w is water volume. Figure 2 shows the ratio of C to C_0 calculated at several equilibrium temperatures as a function of the volume ratio of V_a to V_w. If the volume ratio is <1, methane concentration decreases sharply with the decrease in the volume ratio. If the volume ratio is >1, methane concentration approaches the original concentration in ice bubbles (C_0). In this work, we kept the volume of the sample vessel constant so that V_a/V_w remained at about 1, or the methane concentration was depleted by about 2%.

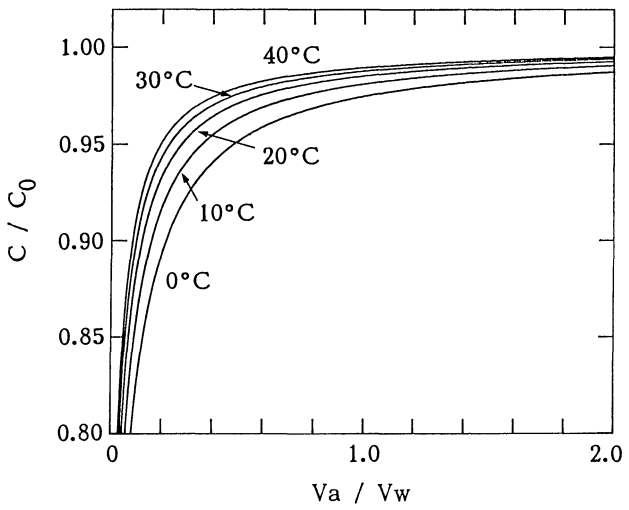

Fig. 2. Relation between the ratio of methane concentration in the air equilibrated with sample water (C) to that in ice bubbles (C_0) and the ratio of volume of headspace (V_a) to that of the water (V_w). The curves correspond to samples equilibrated at indicated temperatures.

Results and Discussion

Contamination and Correction of Methane Concentration. When the air was transferred with a bellows pump, the methane concentration was found to increase with a pumpling motion. In order to estimate the amount of methane emitted from the bellows pump, methane-free nitrogen was introduced into the pump and analyzed after some pumping motions. The amount of methane released from the stainless steel bellows increased linearly with the pumping time. Since this pump had been carefully baked and evacuated before its use, the methane released could not be explained by the desorption of the adsorbed methane from the metal surface. Since the frictional contact between metals is known to produce trace amounts of methane,[7,8] deformation of even the most excellent metal bellows (AM 350) may have produced the methane.

However, in practice, sufficient air can be obtained by one or two strokes of pumping motion to measure methane concentration, and contamination can be kept below 20 ppbv. For correction of the methane contamination during the analysis of ice samples, blank tests were carried out as follows:

(1) Ice prepared under air-free conditions was placed in the sample flask and evacuated. Methane-free nitrogen was then introduced into the sample flask at the same pressure as that for the air released from ice core samples. Following the same thaw-and-freeze procedure, methane concentration was determined.

(2) The same procedure as described above in (1) was used, but in the absence of ice. Blank values obtained were 40±20 ppbv and 20±5 ppbv, respectively. The former was slightly larger than the contamination arising from the bellows pump: even if the ice contained no air bubbles visually, a small amount of methane may have been included in the ice lattice. The latter value was consistent with the contamination from the bellows pump. As has been reported by Rasmussen and Khalil on snow samples from Mt. Hood,[12] we can assume that no methane is contained in falling snow in the Antarctica. Thus it is likely that almost all the contamination was caused by the bellows metal; correction was made for such unavoidable and reproducible contamination. In addition, methane concentration was corrected for change in concentration due to the gas–liquid distribution.

Application to Antarctic Core Samples. Methane concentration in the ice core drilled at Mizuho Station in 1984 was determined by the melt extraction method. The core sample for analysis (30 cm in length) was obtained at 330 m depth and was estimated to be about 3600 years old;[13] a 30 cm span at the depth of 330 m

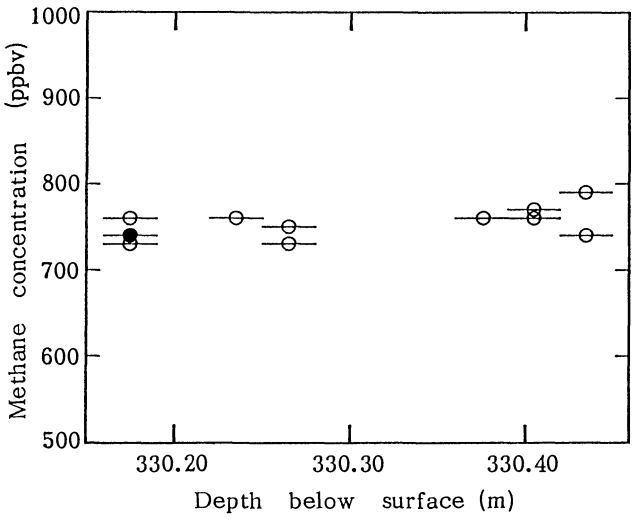

Fig. 3. Observed methane concentrations in the Mizuho core sample drilled in 1984 at 330-m depth below the surface. The solid circle shows the sample from the surface of the core.

corresponds to about 4 years. The core sample (13 cm in diameter) was first sliced horizontally into 3 cm thick disks, which were then divided into two halves after their rims, about 1 cm below the surface, had been removed. We took eleven sections of ice blocks from the core sample; one of them was the surface ice of the sample. The result of the analysis is shown in Fig. 3; the solid circle shows the concentration in the surface ice. The methane concentrations were observed to be uniform over the period studied, and the concentration at the surface was not necessarily higher than the others. The averaged methane concentration of the eleven samples was found to be 750±20 ppbv, a slightly higher value than those previously reported for similar ages.[5,6,10] After the presentation of our results,[14] Nakazawa et al. reported that the methane concentrations of several Mizuho core samples near the depth of 330 m were 690 to 750 ppbv.[15] Since the preesent core sample had many horizontal cracks probably produced during thermal core boring, we cannot exclude the possibility that the air in the ice core sample was contaminated by modern air.

We have developed a technique for extrication of air in polar ice. The precision of the methane analysis with 100 g core samples was about 20 ppbv. Although the bellows pump released negligible amounts of methane during operation, the current analytical system and procedures are simple and convenient; with improvements in the pump, or for analysis of te other components, this method will be quite useful.

References

1) R. J. Delmas, J. M. Ascencio, and M. Legrand, *Nature,* **284**, 155 (1980).
2) A. Neftel, H. Oeschger, J. Schwander, B. Stauffer, and R. Zumbrunn, *Nature,* **295**, 220 (1980).
3) A. Neftel, E. Moor, H. Oeschger, and B. Stauffer, *Nature,* **315**, 45 (1985).
4) J. M. Barnola, D. Raynaud, Y. S. Korotkevich, and C. Lorius, *Nature,* **329**, 408 (1987).
5) H. Craig and C. C. Chou, *Geophys. Res. Lett.,* **9**, 1221 (1982).
6) R. A. Rasmussen and M. A. K. Khalil, *J. Geophys. Res.,* **89**, 11599 (1984).
7) B. Stauffer, G. Fischer, A. Neftel, and H. Oeschger, *Science,* **229**, 1368 (1985).
8) G. I. Pearman, D. Etheridge, F. de Silva, and P. J. Fraser, *Nature,* **320**, 248 (1986).
9) D. Raynaud, J. Chappellaz, J. M. Barnola, Y. S. Korotkevich, and C. Lorius, *Nature,* **333**, 655 (1988).
10) B. Stauffer, E. Lochbronner, H. Oeschger, and J. Schwander, *Nature,* **332**, 812 (1988).
11) W. Berner, B. Stauffer, and H. Oeschger, *Nature,* **276**, 53 (1978).
12) R. A. Rasmussen and M. A. K. Khalil, *J. Air Pollut. Control. Assoc.,* **32**, 176 (1982).
13) M. Nakawo, H. Ohmae, F. Nishio, and T. Kameda, *Proc. NIPR Symp. Polar Meteorol. Glaciol.,* **2**, 105 (1989).
14) Y. Tohjima, T. Tominaga, Y. Makide, and Y. Fujii, 12th Symposium on Polar Meteorology and Glaciology, Tokyo, July 1989, Abstr., No.9.
15) T. Nakazawa, et al., 13th Symposium on Polar Meteorology and Glaciology, Tokyo, July 1990, Abstr., No. 55.

The Magnetic Properties of the 2-Pyridone Adducts of Copper(II) Benzoates and Related Copper(II) Compounds

Shuji EMORI,* Hiroyuki SUENAGA, and Naomi GOTO
Department of Chemistry, Faculty of Science and Engineering,
Saga University, Honjo-machi, Saga 840
(Received June 19, 1991)

Synopsis. The 2-pyridone adducts of copper(II) benzoate, copper(II) 2-pyridinolate, and bis(adenine)copper(II) sulfate were prepared, and then characterized by means of magnetic susceptibility and IR spectroscopy. Their magnetic properties were correlated with the basicities and coordinate-bond lengths of the bridging ligands.

Like copper(II) alkanoates, most copper(II) benzoate,[1] copper(II) 2-pyridinolate,[2,3] copper(II) pyrrolo[2,3-*b*]pyridinate,[4] and bis(adenine)copper(II) compounds[5,6] may have dinuclear structures similar to that of copper(II) acetate monohydrate.[7,8] Through the bridging ligands between the copper(II) ions, superexchange couplings operate, and the room-temperature magnetic moments vary with the strength of the spin-exchange couplings (the Bleaney–Bowers equation).[1-6] Naturally, the magnetic moments or the strength of the spin-exchange couplings for these dinuclear compounds have been discussed with reference to the basicity of the bridging ligands (pK_{a1} or pK_{a2}).[9,10] On the other hand, for series of transition metal oxides and fluorides, a correlation between the strength of the spin-exchange couplings and the coordinate-bond lengths has been proposed,[11,12] and rationalized with an exchange perturbation treatment of cation–anion–cation in a three-center, four-electron model.[13] Also, in copper(II) acetate-type dinuclear compounds, the coordinate-bond length must play a role in determining the strength of the superexchange couplings. In order to investigate concurrently the basicity and bond length dependence, we prepared some 2-pyridone adducts of copper(II) benzoates, copper(II) 2-pyridinolates, and bis(adenine)-copper(II) sulfate, and measured their magnetic susceptibilities at room temperature.

The adducts were prepared by heating the hydrates of copper(II) acetate, copper(II) 3- and 5-substituted benzoates, and bis(adenine)copper(II) sulfate with excesses of molten 2-pyridones for 30 min (mp 107, 165, and 185°C for 2-pyridone and 5-chloro- and 5-nitro-2-pyridones, respectively). The excess 2-pyridones were removed by sublimation.[3] The effective magnetic moments were evaluated from the magnetic susceptibilities, which were corrected for the diamagnetic contribution using the Pascal constants[14] and for temperature-independent paramagnetism using the value 60×10^{-6} emu mol^{-1} (1 emu$=4\pi\times10^{-6}$ m^3). The IR spectra of the solid compounds were recorded using nujol mulls in the 4000—600 cm^{-1} range.

The obtained compounds show magnetic moments of 1.25—1.45 BM, similar to those of well-characterized dinuclear copper(II) compounds.[8-10,15] All of the benzoates show COO stretching bands of ca. 1675—1615 and 1435—1405 cm^{-1}, characteristic of bridging carboxylate anions.[16] The magnetic and IR spectral data indicate that the present compounds have copper(II) acetate-type dinuclear structures with 2-pyridones occupying the axial positions (Fig. 1). Although the 2/3 adducts have structures with a partial lack of axial ligands, their magnetic moments are assumed to be practically the same as those of the monoadducts.

For several series of dinuclear copper(II) compounds,[9,10] it has been reported that the room-temperature magnetic moments decrease linearly with the basicities of the bridging ligands. In order to demonstrate the linear correlation for the present compounds, their magnetic moments (in BM), together with literature data regarding related copper(II) com-

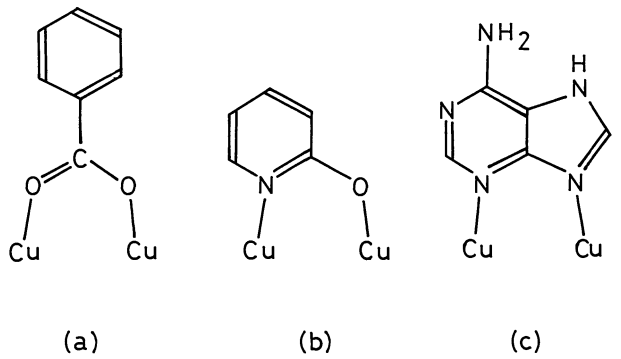

Fig. 1. Bonding arrangements in dinuclear copper(II) benzoate (a), copper(II) 2-pyridinolate (b), and bis(adenine)copper(II) (c) compounds.

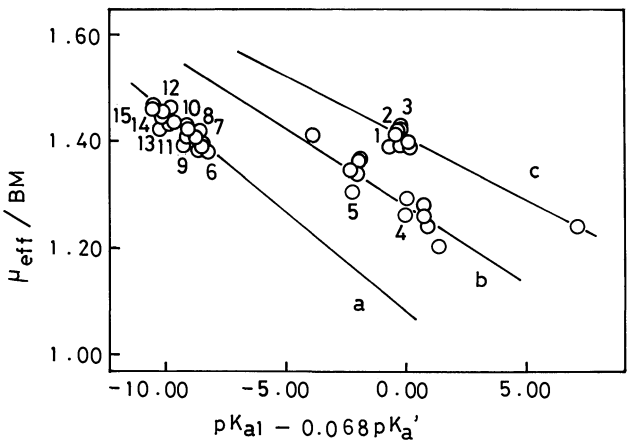

Fig. 2. Magnetic moments at 20°C for copper(II) benzoate (a), copper(II) 2-pyridinolate (b), and bis(adenine)copper(II) (c) compounds plotted against the acidities of the ligands.

Table 1. Analytical Data and Effective Magnetic Moments at 20°C

Compound		Found (Calcd)/%				μ_{eff}/BM
		Cu	C	H	N	
$CuSO_4(Haden)_2 \cdot PyOH \cdot H_2O$	(1)	11.86 (11.70)	32.70 (33.18)	3.05 (3.16)	28.10 (28.38)	1.41
$CuSO_4(Haden)_2(5\text{-}ClPyOH)_{2/3}$	(2)	12.26 (12.31)	30.98 (31.02)	2.50 (2.47)	28.88 (28.94)	1.42
$CuSO_4(Haden)_2 \cdot 5\text{-}NO_2PyOH$	(3)	11.16 (11.15)	31.44 (31.61)	2.50 (2.48)	29.36 (29.49)	1.43
$Cu(5\text{-}ClpyO)_2 \cdot 5\text{-}ClPyOH$	(4)	14.31 (14.12)	39.98 (40.02)	2.23 (2.24)	9.31 (9.33)	1.26
$Cu(5\text{-}NO_2pyO)_2 \cdot 5\text{-}NO_2PyOH$	(5)	12.93 (13.19)	37.29 (37.39)	2.03 (2.09)	17.43 (17.44)	1.31
$Cu(C_6H_5COO)_2 \cdot PyOH$	(6)	15.77 (15.85)	56.95 (56.93)	3.78 (3.77)	3.51 (3.49)	1.38
$Cu(3\text{-}ClC_6H_4COO)_2 \cdot PyOH$	(7)	13.65 (13.53)	48.59 (48.58)	2.80 (2.79)	2.99 (2.98)	1.41
$Cu(3\text{-}ClC_6H_4COO)_2(5\text{-}ClPyOH)_{2/3}$	(8)	13.71 (13.78)	45.18 (45.16)	2.35 (2.33)	2.01 (2.03)	1.40
$Cu(3\text{-}NO_2C_6H_4COO)_2 \cdot 5\text{-}ClPyOH$	(9)	12.19 (12.10)	43.45 (43.44)	2.31 (2.30)	8.02 (8.00)	1.39
$Cu(3\text{-}NO_2C_6H_4COO)_2(5\text{-}NO_2PyOH)_{2/3}$	(10)	13.08 (12.99)	42.58 (42.56)	2.22 (2.20)	9.52 (9.54)	1.43
$Cu(3,5\text{-}Cl_2C_6H_3COO)_2(PyOH)_{2/3}$	(11)	12.68 (12.53)	41.13 (41.07)	1.89 (1.86)	1.83 (1.84)	1.43
$Cu(3,5\text{-}Cl_2C_6H_3COO)_2(5\text{-}ClPyOH)_{2/3}$	(12)	11.98 (11.99)	39.31 (39.29)	1.66 (1.65)	1.74 (1.76)	1.46
$Cu[3,5\text{-}(NO_2)_2C_6H_3COO]_2(PyOH)_{4/3}$	(13)	10.30 (10.37)	40.55 (40.52)	2.09 (2.08)	12.23 (12.20)	1.42
$Cu[3,5\text{-}(NO_2)_2C_6H_3COO]_2 \cdot 5\text{-}ClPyOH$	(14)	10.53 (10.33)	37.13 (37.09)	1.65 (1.64)	11.40 (11.38)	1.44
$Cu[3,5\text{-}(NO_2)_2C_6H_3COO]_2(5\text{-}NO_2PyOH)_{4/3}$	(15)	9.51 (9.45)	36.91 (36.91)	1.73 (1.70)	13.96 (13.88)	1.44

pounds,[4,8-10,15] are plotted in Fig. 2 against the basicities of the bridging ligands ($pK_{a1}-0.068\,pK_a'$), where $-0.068\,pK_a'$ is the correction term for the axial ligation. K_{a1} and K_a' are the acid constants of the conjugate cation acids of the bridging and axial ligands, respectively.[17,18] The points for each series of the copper(II) benzoate, copper(II) 2-pyridinolate, and bis(adenine)copper(II) compounds give a straight line with slopes of $K=-0.037$, -0.029, or -0.023, respectively. The slope obtained for the benzoates is in fair agreement with that ($K=-0.052$) for plots of the magnetic moments of dinuclear copper(II) carboxylates[9] against $pK_{a2}-0.068\,pK_a'$, when the linear relationship for carboxylic acids, $pK_{a1}=1.40\,pK_{a2}-13.8$, is taken into account.[19] Three lines intersect at a point, enabling us to summarize them as

$$\mu_{eff} = 1.94[1 + K(pK_{a1} - 0.068pK_a' + 23.0)]. \quad (1)$$

The reasonably good correlation for each series confirms that the strength of spin-exchange couplings is undoutedly affected by the basicity of the bridging ligands; the different slopes for the three series indicate that it is also affected by factors other than basicity.

Although the variation in the slopes seems to be attributable to bondings between pairs of copper(II) ions, this is not consistent concerning the trend in copper(II)-copper(II) separations.[1-6] The coordinate-bond lengths of the present bridging ligands are typically Cu-O(1), 1.967(6)—1.981(6) Å and Cu-O(2), 1.950(10)—1.965(6) Å in dinuclear copper(II) benzoates,[1] Cu-N, 2.000(6)—2.015(10) Å and Cu-O, 1.950(10)—1.959(6) Å in dinuclear copper(II) 2-pyridinolates,[2,3] and Cu-N(1), 2.038(6)—2.043(11) Å and Cu-N(2), 2.008(11)—2.012(6) Å in dinuclear bis(adenine)copper(II) compounds,[5,6] respectively. The longer coordinate bond of each bridging ligand is selected for a comparison, because the strength of the superexchange coupling is determined by the weakest bond in the coupling pathway.[10] Apparently, the above-obtained slopes become steeper as the coordinate-bond lengths decrease; the variation in the K's is in good quantitative agreement with the theoretical prediction regarding the distance dependence of the strength of the spin-exchange coupling.[11] The basicity and bond length dependence was collaborated and evaluated separately. These relations suggest that the spin-exchange couplings in the present compounds operate through the sp^2-orbitals more strongly than through the p_π-orbitals of the bridging ligands.

References

1) M. Melnik, M. Dunaj-Jurco, and M. Handlovic, *Inorg. Chim. Acta,* **86**, 185 (1984); and references therein.

2) Y. Nishida and S. Kida, *Bull. Chem. Soc. Jpn.,* **58**, 383 (1985).

3) S. Yeh, D. Liaw, and S. Peng, *Bull. Inst. Chem., Acad. Sin.,* **34**, 49 (1987).

4) S. Peng and Y. Lin, *Acta Crystallogr., Sect. C,* **42**, 1725 (1986).
5) A. Terzis, A. L. Beauchamp, and R. Rivest, *Inorg. Chem.,* **12**, 1166 (1973).
6) P. de Meester and A. C. Skapski, *J. Chem. Soc. A,* **1971**, 2167.
7) J. N. von Niekerk and F. R. L. Schoening, *Acta Crystallogr.,* **6**, 227 (1953).
8) G. M. Brown and R. Chidambaram, *Acta Crystallogr., Sect. B,* **29**, 2393 (1973).
9) S. Emori, S. Matsunaga, and M. Goto, *Bull. Chem. Soc. Jpn.,* **62**, 4047 (1989).
10) S. Emori, R. Furukawa, and S. Nakashima, *Bull. Chem. Soc. Jpn.,* **63**, 2426 (1990).
11) D. Broch, *J. Phys. Chem. Solids,* **27**, 881 (1966).
12) K. C. Johnson and A. J. Slevers, *Phys. Rev. B,* **10**, 1027 (1974).
13) L. J. DeJongh and R. Block, *Physica* (*B*+*C*), **79**, 568 (1975).
14) G. Foex, "Constants Sélectionées, Diamagnétisms et Paramagnetisme," Masson, Paris (1957).
15) T. Asakawa, M. Inoue, K. Hara, and M. Kubo, *Bull. Chem. Soc. Jpn.,* **45**, 1054 (1972).
16) L. J. Bellamy, "The Infrared Spectra of Complex Molecules," 3rd ed, Chapman and Hall, London (1975).
17) R. Stewart and K. Yates, *J. Am. Chem. Soc.,* **82**, 4059 (1960).
18) E. Spinner and J. C. B. White, *J. Chem. Soc. B,* **1966**, 991.
19) M. Liler, *J. Chem. Soc.,* **1965**, 4300.

Preparation and Properties of Oxo-Centered Trinuclear Chromium(III) Complexes with Bridging Optically Active Amino Acids, $[Cr_3(\mu_3\text{-}O)(\mu\text{-}O,O'\text{-amino-acid})_6(H_2O)_3]^{7+}$ [1)]

Hisashi KATO, Kou NAKATA, Akira NAGASAWA,† Tadashi YAMAGUCHI, Yoichi SASAKI,*,†† and Tasuku ITO*
Department of Chemistry, Faculty of Science, Tohoku University, Aoba, Aramaki, Aoba-ku, Sendai 980
(Received July 10, 1991)

Synopsis. Trinuclear chromium(III) complexes with optically active amino acids as bridging groups, $[Cr_3(\mu_3\text{-}O)(\mu\text{-}RCH(NH_3)COO)_6(H_2O)_3]X_7$ (R=CH_3, $(CH_3)_2CH$, $(CH_3)_2CHCH_2$, $C_6H_5CH_2$; X=Cl^-, NO_3^-), were prepared, and the X-ray structure of the L-valine complex was determined. Their electronic spectra and magnetic moments are similar to those of analogous carboxylate-bridged trichromium(III) complexes.

Oxo-centered triangular trinuclear metal complexes with bridging carboxylates ($RCOO^-$) between each pair of metal ions are known for various tervalent metal ions such as V, Cr, Mn, Fe, Co, Ru, Rh, and Ir.[2)] They have a general formula, $[M_3(O)(RCOO)_6L_3]^+$ (hereafter abbreviated as M_3, and L stands for a monodentate ligand such as H_2O, pyridine, and so on). Amino acids are also known as bridging ligands (μ-O,O'-$RCH(NH_3)COO$) for the Fe_3 complexes[3-7)] and some mixed Fe_nCr_{3-n} analogs.[8-10)] Complexes with bridging amino acids are important to extend the chemistry of trinuclear complexes. The Fe_3 amino acid complexes are not stable in aqueous solution,[11)] and not suitable for extending their chemistry further particularly in solution. We thought it important to prepare amino acid bridged derivatives of the trinuclear metal complexes with substitution inert metal ions such as Cr(III), Ru(III), and Rh(III). Amino acid complex for these metal ions reported before we started the present study was only $[Cr_3(\mu_3\text{-}O)(\mu\text{-}O,O'\text{-glyH})_6(H_2O)_3]^{7+}$ (Hgly=glycine).[9)] The present paper describes the preparation and some properties of new trinuclear chromium(III) complexes with optically active amino acid bridges. Very recently, alanine and α-aminobutane chromium(III) complexes were reported by Fisher et al.[12,13)]

Experimental

Preparation of the Complexes. L-Alanine Complex, $[Cr_3(\mu_3\text{-}O)(\mu\text{-}O,O'\text{-}CH_3CH(NH_3)COO)_6(H_2O)_3]Cl_7\cdot 5H_2O$ (1). $Cr(NO_3)_3\cdot 9H_2O$ (4.00 g, 0.01 mol) dissolved in absolute ethanol (20 cm^3) was added to the suspension of L-alanine (1.78 g, 0.02 mol) in water (20 cm^3). After pH was adjusted to 2 with diluted nitric acid, the mixture was kept at 70—80 °C for 10 h, during which time L-alanine was dissolved completely. Volume of the solution was then reduced to ca. 20 cm^3 on a rotatory evaporator. The solution was then treated with Sephadex G-10 column chromatography (35 mmϕ×400 mm). The green eluate of 0.1 M HCl (1 M=1 mol dm^{-3}) was concentrated to dryness. The green residue was dissolved in a small amount of ethanol. Green powder was obtained on addition of diethylether, and was collected by filtration and dried under vacuum. Yield, 1.02 g (26%). Anal. Found: C, 19.87; H, 4.68; N, 7.37%. Calcd for $C_{18}H_{58}N_6O_{21}Cl_7Cr_3$: C, 19.67; H, 4.59; N, 7.65%. IR (cm^{-1}): $COO(\nu_a)$, 1655; $COO(\nu_s)$, 1436.

L-Valine Complex, $[Cr_3(\mu_3\text{-}O)(\mu\text{-}O,O'\text{-}(CH_3)_2CHCH(NH_3)COO)_6(H_2O)_3](NO_3)_7\cdot 5H_2O$ (2). This was prepared similarly as **1** by using L-valine (2.38 g, 0.02 mol) in place of L-alanine. After reducing the volume to ca. 20 cm^3, the solution was set aside for a few days at room temperature instead of treating with the column. Large green crystals were collected by filtration and dried under vacuum. Yield, 1.78 g (36%). Anal. Found: C, 24.53; H, 5.26; N, 13.16%. Calcd for $C_{30}H_{82}N_{13}O_{42}Cr_3$: C, 24.80; H, 5.69; N, 12.53%. IR (cm^{-1}): $COO(\nu_a)$, 1658; $COO(\nu_s)$, 1452.

L-Leusine Complex, $[Cr_3(\mu_3\text{-}O)(\mu\text{-}O,O'\text{-}(CH_3)_2CHCH_2CH(NH_3)COO)_6(H_2O)_3]Cl_7\cdot H_2O$ (3), and L-Phenylalanine Complex, $[Cr_3(\mu_3\text{-}O)(\mu\text{-}O,O'\text{-}C_6H_5CH_2CH(NH_3)COO)_6(H_2O)_3]Cl_7\cdot 6H_2O$ (4). These compounds were synthesized in a similar way to the preparation for **1**. Yield of green powder, 1.08 g (26%) for **3** and 0.33 g (7%) for **4**. Anal. Found for **3**: C, 32.42; H, 7.02; N, 6.53%. Calcd for $C_{36}H_{92}N_6O_{20}Cl_7Cr_3$: C, 32.43; H, 6.95; N, 6.30%. Found for **4**: C, 41.21; H, 5.37; N, 5.32%. Calcd for $C_{54}H_{84}N_6O_{22}Cl_7Cr_3$: C, 41.21; H, 5.34; N, 5.34%. IR (cm^{-1}): $COO(\nu_a)$ 1655, $COO(\nu_s)$ 1445 for **3**; $COO(\nu_a)$ 1660, $COO(\nu_s)$ 1450 for **4**.

Measurements. Electronic and CD spectra were measured with a Hitachi 340 spectrophotometer and a JASCO J-40A spectropolarimeter, respectively. Infrared absorption spectra were recorded on a JASCO IR-810 spectrophotometer by KBr method. Magnetic susceptibilities at room temperature were measured in methanol-d_4 by the Evans method.[14)]

X-Ray Structure Determination for 2. A green crystal of the L-valine complex (**2**) with dimensions 0.3×0.3×0.4 mm was used for the X-ray work. X-Ray data were collected on a Rigaku AFC-5R four circle diffractometer equipped with a rotating Mo anode (40 kV, 200 mA, λ=0.71069 Å). Intensity data were corrected for Lorentz and polarization factors. No absorption correction was applied. Crystallographic data are: monoclinic, $P2_1$, a=13.104(5), b=21.460(7), c=12.218(4) Å, β=110.99(3)°, V=3207(2) Å^3, Z=2, ρ_{obsd}=1.47, ρ_{calcd}=1.50 g cm^{-3}.

The structure was solved by the direct method and refined by use of the block-diagonal least-squares method. All the non-hydrogen atoms were refined anisotropically. Hydrogen atoms were not included in the calculation. Final R value was 0.099 for 6394 independent reflections ($F_o \geqslant 3\sigma(F_o)$) and 794 parameters.[15)] All the calculations were performed with the Universal Crystallographic Computer Program System UNICS III[16)] on an ACOS-1000 computer at the Computer Center of Tohoku University.

Results and Discussion

Preparation and Stability of the New Complexes. Desired complexes with neutral amino acid (zwitter ion

† Present address: Department of Chemistry, Faculty of Science, Saitama University, Shimo-okubo, Urawa 338.

†† Present address: Department of Chemistry, Faculty of Science, Hokkaido University, Kita-ku, Sapporo 060.

form) bridges have high electric charge of 7+. In spite of this, preparation and isolation of the complexes were straightforward. Chromium(III) ions and amino acids appear to undergo self-assembly to give desired trinuclear complexes in acidic aqueous ethanol solution. Similar trinuclear complexes would be easily prepared with other amino acids than those used in this study. The complexes are stable in acidic solution. However they decompose slowly in neutral solution and immediately in alkaline solution as evidenced by electronic spectral change. They are soluble in certain organic solvents such as methanol and ethanol. Attempts to prepare complexes with pyridine ligands at the terminal positions were unsuccessful. It is probabbly because the compounds are unstable in basic media.

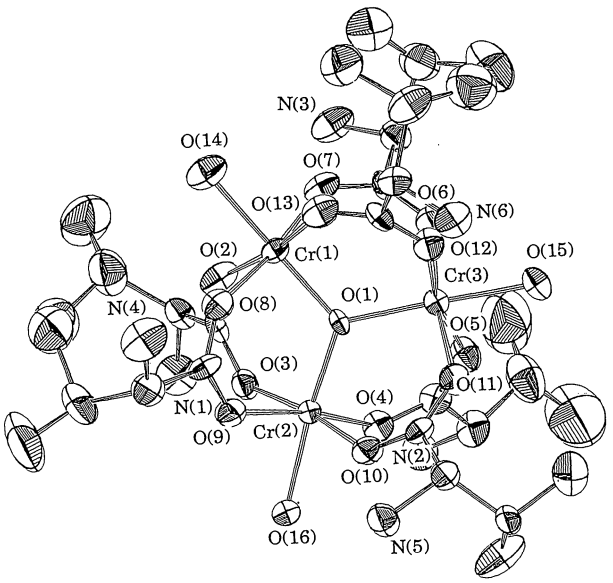

Fig. 1. Structure of $[Cr_3(\mu_3\text{-}O)(\mu\text{-}O,O'\text{-}(CH_3)_2CHCH(NH_3)COO)_6(H_2O)_3]^{7+}$ (**2**) and atomic labelling scheme.

The Structure of the L-Valine Complex. Figure 1 shows the structure of the complex cation. Selected bond distances and angles are summarized in Table 1.[15] The complex contains a triangular Cr_3 unit with an oxide ion in the center of the triangle. Each pair of Cr atoms are doubly bridged by carboxylate groups of two L-valine ligands. Overall skeletal structure is very similar to those of other trinuclear chromium carboxylates.[17-19] Each chromium ion takes slightly distrorted octahedral geometry, shifting towards the central oxide ion from the plane defined by four carboxylate oxygens (0.13—0.20 Å). This is also seen in other trichromium complexes. The Cr···Cr distance is 3.30(2) Å and the Cr–(μ_3-O) distance is 1.90(1) Å. The core structure is similar to amino-acid-bridged trinuclear iron(III) complexes.[20] No regularity is found in the orientation of $(CH_3)_2CHCH$ residue of the bridged L-valine.

Electronic and Circular Dichroism Spectra. Table 2 summarizes electronic absorption and circular dichroism spectral data of the new complexes in aqueous solutions. Spectra of the L-valine and L-phenylalanine complex are shown in Fig. 2. Two absorption peaks in visible region are seen as other trichromium complexes,[21] and are assigned from longer wavelengths to $^4A_{1g}\rightarrow{}^4T_{2g}$ and $^4A_{1g}\rightarrow{}^4T_{1g}$ transitions of octahedral chromium(III) center. Circular dichroism peaks are weak as expected from the fact that the asymmetric centers are apart from the chromophoric center. It is noted that the main CD peaks corresponding to the $^4A_{1g}\rightarrow{}^4T_{2g}$ transition is negative for the L-valine and L-leusine complexes, whereas positive for other two complexes. The reason

Table 1. Selected Bond Distances (Å) and Angles (°) for $[Cr_3(\mu_3\text{-}O)(\mu\text{-}O,O'\text{-}(CH_3)_2CHCH(NH_3)COO)_6(H_2O)_3](NO_3)_7\cdot 5H_2O$ (**2**)

Distances/Å				Angles/°			
Cr(1)-O(1)	1.880(9)	Cr(1)-O(8)	1.979(10)	O(1)-Cr(1)-O(14)	177.38(46)	O(1)-Cr(2)-O(10)	91.27(38)
Cr(2)-O(1)	1.961(12)	Cr(1)-O(13)	1.976(12)	O(1)-Cr(1)-O(2)	92.92(45)	O(1)-Cr(3)-O(15)	178.54(41)
Cr(3)-O(1)	1.942(9)	Cr(2)-O(3)	1.996(10)	O(1)-Cr(1)-O(7)	93.04(43)	O(1)-Cr(3)-O(5)	96.52(39)
Cr(1)-Cr(2)	3.273(3)	Cr(2)-O(4)	1.951(10)	O(1)-Cr(1)-O(8)	94.66(39)	O(1)-Cr(3)-O(6)	94.46(41)
Cr(2)-Cr(3)	3.317(3)	Cr(2)-O(9)	1.993(10)	O(1)-Cr(1)-O(13)	96.61(43)	O(1)-Cr(3)-O(11)	93.86(40)
Cr(1)-Cr(3)	3.298(3)	Cr(2)-O(10)	1.948(10)	O(1)-Cr(2)-O(16)	175.00(39)	O(1)-Cr(3)-O(12)	96.02(40)
Cr(1)-O(14)	2.038(13)	Cr(3)-O(5)	1.955(10)	O(1)-Cr(2)-O(3)	96.49(38)	Cr(1)-O(1)-Cr(2)	120.68(45)
Cr(2)-O(16)	2.048(10)	Cr(3)-O(6)	1.952(11)	O(1)-Cr(2)-O(4)	94.89(39)	Cr(1)-O(1)-Cr(3)	119.26(44)
Cr(3)-O(15)	2.005(11)	Cr(3)-O(11)	1.968(10)	O(1)-Cr(2)-O(9)	96.06(40)	Cr(2)-O(1)-Cr(3)	120.06(44)
Cr(1)-O(2)	1.961(12)	Cr(3)-O(12)	1.955(10)				
Cr(1)-O(7)	1.963(11)						

Table 2. Electronic Absorption (A) and Circular Dichroism (B) Spectral Data of the New Complexes in Aqueous Solution

Complex	(A) λ/nm (ε/M^{-1} cm^{-1})	(B) λ/nm ($\Delta\varepsilon$/M^{-1} cm^{-1})
$[Cr_3O(L\text{-ala})_6(H_2O)_3]Cl_7\cdot 5H_2O$[a]	712(14)[s] 664(46)[s] 588(90) 438(113)	658(+0.15) 602(+0.36) 486(−0.14) 426(+0.11) 350(+0.07)
$[Cr_3O(L\text{-val})_6(H_2O)_3]Cl_7\cdot 5H_2O$[b]	714(10)[s] 665(37)[s] 589(89) 440(104)	600(−0.50) 540(+0.11) 482(−0.03) 428(+0.10) 355(−0.05)
$[Cr_3O(L\text{-leu})_6(H_2O)_3]Cl_7\cdot 5H_2O$[c]	714(9)[s] 664(40)[s] 588(86) 440(106)	606(−0.24) 550(+0.14) 488(−0.12) 430(+0.13)
$[Cr_3O(L\text{-phe})_6(H_2O)_3]Cl_7\cdot 6H_2O$[d]	714(13)[s] 666(47)[s] 589(104) 442(136)	660(+0.23) 592(+0.41) 488(−0.24) 426(+0.17) 362(+0.05)

s=shoulder. a) L-ala=*O,O'*-$CH_3CH(NH_3)COO$. b) L-val=*O,O'*-$(CH_3)_2CHCH(NH_3)COO$. c) L-leu=*O,O'*-$(CH_3)_2CHCH_2CH(NH_3)COO$. d) L-phe=*O,O'*-$C_6H_5CH_2CH(NH_3)COO$.

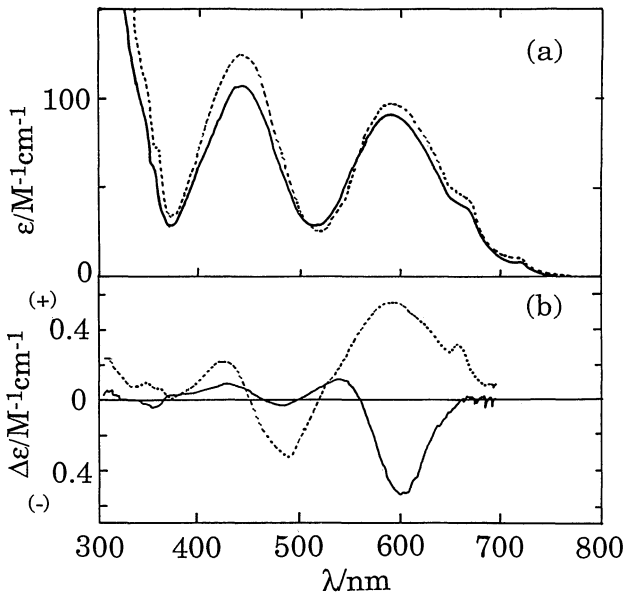

Fig. 2. Electronic absorption (a) and circular dichroism (b) spectra of (**2**) (—) and (**4**) (-----) in aqueous solution.

for this phenomena is not clear. CD spectra in other region are similar for all the four complexes.

Magnetic Properties. The μ_{eff} values obtained by the Evans method at room temperature were 3.39, 3.31, 3.37, and 3.38 (BM per Cr) for the L-alanine, L-valine, L-leusine, and L-phenylalanine complexes, respectively. These values are close to those reported for the carboxylate-bridged trichromium complexes (3.13–3.48 BM)[22] and glycine complex (3.34 BM).[10] These values are somewhat smaller than the spin-only value (3.87 BM), and may suggest weak antiferromagnetic interactions among the three chromium ions.[22]

Redox Properties. Cyclic voltammograms in methanol of the new complexes were measured in the range from −3.0 to +1.0 V vs. Ag/Ag^+ (0.1 M $AgClO_4$). No redox wave was observed in the range studied.

This work was supported by a Grant-in-Aid for Scientific Research No. 02245106 on Priority Area of "Molecular Approaches to Non-equilibrium Processes in Solutions" and a Grant-in-Aid for Scientific Research No.01430009 from the Ministry of Education, Science and Culture. The authors are indebted to Dr. C. Kabuto of this Department for the X-ray intensity data collection.

References

1) H. Kato, K. Nakata, A. Nagasawa, Y. Sasaki, and T. Ito, 59th National Meeting of the Chemical Society of Japan, Yokohama, April 1990, Abstr., No. 1P13.
2) R. D. Cannon and R. P. White, *Progr. Inorg. Chem.*, **36**, 195 (1988).
3) E. M. Holt, S. L. Holt, W. F. Tucker, R. O. Asplund, and K. J. Watson, *J. Am. Chem. Soc.*, **96**, 2621 (1974).
4) W. F. Tucker, R. O. Asplund, and S. L. Holt, *Arch. Biochem. Biophys.*, **166**, 433 (1975).
5) R. Thundathil and S. L. Holt, *Inorg. Chem.*, **15**, 745 (1976).
6) R. N. Puri, R. O. Asplund, and S. L. Holt, *J. Coord. Chem.*, **11**, 125 (1981).
7) R. N. Puri and R. O. Asplund, *J. Coord. Chem.*, **11**, 73, (1981); *Inorg. Chim. Acta*, **54**, L187 (1981); **66**, 7, 49 (1982).
8) W. Clegg, O. M. Lam, and B. P. Straughan, *Angew. Chem., Int. Ed. Engl.*, **23**, 434 (1984); *Inorg. Chim. Acta*, **90**, L75 (1984).
9) B. P. Straughan and O. M. Lam, *Inorg. Chim. Acta*, **98**, 7 (1985).
10) B. P. Straughan, O. M. Lam, and A. Earnshaw, *J. Chem. Soc., Dalton Trans.*, **1987**, 97.
11) K. Nakata, A. Nagasawa, Y. Sasaki, and T. Ito, *Chem. Lett.*, **1989**, 753.
12) V. R. Fisher, T. A. Nasonova, Kh. M. Yakubov, V. R. Voronkova, L. V. Mosina, and Yu. V. Yablokov, *Russ. J. Inorg. Chem.*, **35**, 1298 (1990).
13) In the paper by Fisher et al.,[12] synthetic procedures for L-alanine complex have been described. However, they are different from our method described in this paper.
14) D. F. Evans, *J. Chem. Soc.*, **1959**, 2003.
15) Tables of positional and anisotropic thermal parameters, calculated and observed structure factors, and complete bond lengths and angles are deposited as Document No. 8968 at the Office of the Editor of Bull. Chem. Soc. Jpn.
16) T. Sakurai and K. Kobayashi, *Rikagaku Kenkyusho Hokoku*, **55**, 69 (1979).
17) S. C. Chang and G. A. Jeffrey, *Acta Crystallogr., Sect. B*, **26**, 673 (1970).
18) J. E. Bradshow, D. A. Grossie, D. F. Mullica, and D. E. Pennington, *Inorg. Chim. Acta*, **141**, 41 (1989).
19) E. Gonzalez-Vergara, J. Hegenauer, and P. Saltman, *Inorg. Chim. Acta*, **66**, 115 (1982).
20) R. V. Thundathil, E. M. Holt, S. L. Holt, and K. J. Watson, *J. Am. Chem. Soc.*, **99**, 1818 (1977).
21) L. Dubicki and P. Day, *Inorg. Chem.*, **11**, 1868 (1972).
22) A. Earnshaw, B. N. Figgis, and J. Lewis, *J. Chem. Soc. A*, **1966**, 1656.

A Facile Reduction of Certain Schiff Bases with Di- and Trichlorosilanes

Hidenori OKAMOTO* and Shozo KATO
Tsukuba Research Lab., Tokuyama Soda Co., Ltd., 40 Wadai, Tsukuba, Ibaraki 300-42
(Received March 29, 1991)

Synopsis. The reduction of *N*-[(3-methoxy-2-thienyl)methylene]-2,6-dimethylaniline (**2**) by use of trichlorosilane proceeded smoothly in the presence of a catalytic amount of BF_3·Et_2O. The trichlorosilane/BF_3·Et_2O combination was applicable to the reduction of various Schiff bases. In the case of dichlorosilane, the reduction of **2** proceeded with a 90% yield without any catalysts.

Recently we have found a highly active chloroacetamide herbicide (**1**) for paddy field rice.[1] Compound **1** has been synthesized in two steps from *N*-[3-methoxy-2-thienyl)methylene]-2,6-dimethylaniline (**2**) which involved a reducing step and a chloroacetylating step as shown in the following scheme.

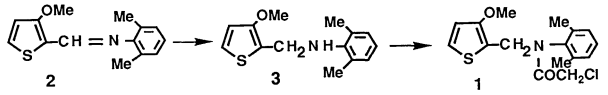

On a laboratory scale, the above reduction proceeded easily by the use of $LiAlH_4$. However, $LiAlH_4$ is not suitable for industrial use because of the relatively high cost and the difficulty in handing. Common reducing agents such as hydrogen with a catalyst, sodium in methanol, and formic acid, did not afford the amine **3** in satisfactory yield probably due to the steric hindrance around the carbon–nitrogen double bond. In some cases, desulfurization in the thiophene ring was observed.

In this paper, we wish to report an excellent and economical reduction of the Schiff base **2** to the amine **3** by use of di- and trichlorosilanes.

Results and Discussion

According to the literature, reduction of Schiff bases to the corresponding amines has been accomplished by various di- and tri-substituted silanes such as Et_3SiH/CF_3COOH,[2] Et_2SiH_2/Rh,[3] and $HSiCl_3$.[4] At first, we tried to reduce the Schiff base **2** using trichlorosilane in acetonitrile without any catalyst according to Benkeser's method.[4] However, the reaction mixture turned black and the desired amine **3** was not obtained at all after hydrolysis. This result indicated that Benkeser's method could not be applied to certain Schiff bases.

During the course of our investigation, we have found that the reduction of **2** with trichlorosilane proceeds to some extent with the use of benzene as a solvent and more smoothly on the addition of a Lewis acid (e.g. BF_3·Et_2O) as a catalyst. Thus, **2** was reduced with trichlorosilane in the presence of BF_3·Et_2O to afford **3** in a 61% yield.

$$\mathbf{2} \xrightarrow[C_6H_6]{HSiCl_3/BF_3\cdot Et_2O} \xrightarrow{KOH/aq\ EtOH} \mathbf{3}$$

We have extended this reduction with trichlorosilane to other Schiff bases. The results are shown in Table 1. As can be seen in the Table, the reduction of Schiff bases with trichlorosilane was proved to proceed satisfactorily

Table 1. Reduction of Schiff Bases to Amines with Trichlorosilane[a]

Entry	Schiff base	Catalyst	Amine	Yield/%[b]
1	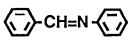	None	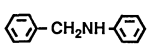	17
2	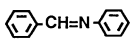	BF_3·Et_2O	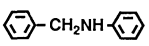	40
3	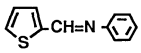	BF_3·Et_2O	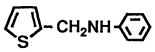	37
4	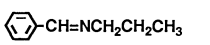	BF_3·Et_2O	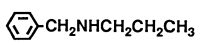	89
5	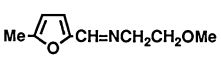	BF_3·Et_2O	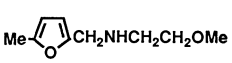	82
6	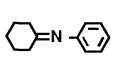	BF_3·Et_2O	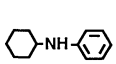	81
7	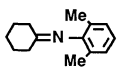	BF_3·Et_2O	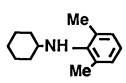	61

a) The reactions were carried out in benzene for 4 h, followed by hydrolysis using KOH in aqueous EtOH.
b) Yield was determined by GC and ^1H NMR.

in benzene in the presence of $BF_3 \cdot Et_2O$. The Schiff bases derived from alkylamines were converted into the corresponding amines in a better yield than those derived from arylamines (Entries 2, 3, 4, and 5). The reduction of the Schiff base prepared from cyclohexanone proceeded easily, in contrast to the Schiff base prepared from benzaldehyde (Entries 2 and 6). These results might be explained by considering that the lone pair of electrons on the nitrogen atom of the Schiff bases should play a role in complexing with trichlorosilane. A steric effect was noted in the comparison of Entry 6 and 7. The combination of trichlorosilane/$BF_3 \cdot Et_2O$ in benzene was found to be applicable to various Schiff bases.

When the Schiff base **2** was treated with dichlorosilane instead of trichlorosilane, the desired amine **3** was obtained in a 90% yield without a catalyst as described below.

$$2 \xrightarrow[C_6H_6]{H_2SiCl_2} \xrightarrow{KOH/aq\ EtOH} 3$$

The proposed mechanism of the addition of trichlorosilane to a Schiff base in acetonitrile was that the lone pair of electrons of the Schiff base nitrogen reacted with trichlorosilane to form a complex, followed by an intramolecular hydride transfer to give a *N*-trichlorosilyl compound.[4] To clarify this reduction mechanism, we have measured the ^1H NMR spectrum in C_6D_6. When $BF_3 \cdot Et_2O$ was mixed with trichlorosilane, the spectrum was a mere combination of each signal ascribed to both compounds. However, when $BF_3 \cdot Et_2O$ was mixed with **2**, the signal at 8.48 ppm (CH=N) disappeared and a signal appeared at 9.32 ppm. A small amount of solid, which was regarded as a Schiff base-BF_3 complex, was obtained. On the basis of these facts, a rational mechanism can be proposed in the following Scheme.

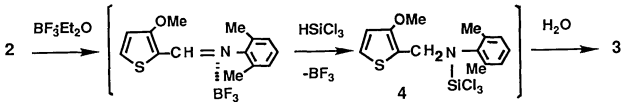

At first, $BF_3 \cdot Et_2O$ would locate close to the Schiff base to form a certain complex which then reacts with trichlorosilane to form the *N*-silyl compound **4** which affords the amine by hydrolysis. On the other hand, dichlorosilane can form **4** smoothly without a catalyst probably due to the steric factor.

The method described in this report might be useful for the synthesis of a secondary amine from a Schiff base.

Experimental

The ^1H NMR spectra were measured with a Hitachi R1500 spectrometer using tetramethylsilane as an internal standard. The GC Mass spectra were obtained on a Hitachi M80 spectrometer.

Reduction of 2 to 3 with Trichlorosilane. A one-hundred milliliter flask containing **2** (2.48 g, 10 mmol) in benzene (15 ml) was cooled in an ice bath. After trichlorosilane (3.98 g, 29 mmol) and $BF_3 \cdot Et_2O$ (0.1 ml) were added slowly, the resulting mixture was heated to reflux temperature for 7 h. After being cooled to room temperature, the mixture was treated with KOH (3.3 g) in 80% aqueous EtOH (45 ml) in an ice bath and stirred at room temperature for 12 h. The organic layer was extracted with ether and dried over anhydrous sodium sulfate. The solvent was then distilled out and the resulting pale yellow liquid (1.50 g, 61% yield) was composed of **3** which boiled at 122 °C/0.15 mmHg (1 mmHg=133.322 Pa). ^1H NMR ($CDCl_3$) δ=2.25 (6H, s, CH_3), 3.30 (1H, brs, NH), 3.71 (3H, s, OCH_3), 4.14 (2H, s, CH_2), and 6.68—7.03 (5H, aromatic H); IR (KBr) 3380 cm^{-1} (NH); MS *m/z* 247 (M^+). Found: C, 68.08; H, 6.78; N, 5.58%. Calcd for $C_{14}H_{17}NOS$: C, 68.01; H, 6.88; N, 5.67%.

Reduction of Various Schiff Bases with Trichlorosilane. A typical procedure is as follows. A flask containing *N*-benzylidenepropylamine (1.47 g, 10 mmol) in benzene (8 ml) was cooled in an ice bath. After trichlorosilane (1.60 g, 12 mmol) in benzene (2 ml) and $BF_3 \cdot Et_2O$ (0.1 ml) were added slowly, the resulting mixture was heated to reflux temperature for 4 h. After being cooled to room temperature, the mixture was treated with KOH (4.0 g) in 80% aqueous EtOH (35 ml) in an ice bath and stirred at room temperature for 12 h. The organic layer was extracted with ether and dried over anhydrous sodium sulfate. Removal of the solvent in vacuo gave *N*-benzylpropylamine as a pale yellow liquid (1.33 g). The yield was 89% (Table 1, Entry 4).

Other reductions were carried out in a manner similar to that described above and the products were comfirmed by GC, GCMS, and ^1H NMR. In the cases of the reactions resulting in good yields (Entries 4, 5, and 6), the obtained amine was obtained in pure form without any purification. In each case of the reaction resulting in a low yield (Entries 1, 2, 3, and 7), unreacted Schiff base was recovered along with the expected amine.

Reduction of 2 to 3 with Dichlorosilane. A one-hundred milliliter glass autoclave was charged with **2** (2.48 g, 10 mmol) in benzene (15 ml) and cooled in a dry ice–methanol bath. Dichlorosilane (2.81 g, 28 mmol) was introduced and the resulting solution was warmed to room temperature. The reaction mixture was stirred for 8 h in an oil bath (50 °C), treated with KOH (4.0 g) in 80% aqueous MeOH (35 ml) in an ice bath and stirred at room temperature for 12 h. The organic layer was extracted with ether and dried over anhydrous sodium sulfate. The solvent was removed in vacuo and the residue was distilled to give **3** as a pale yellow liquid (2.22 g, 90% yield).

References

1) M. Ogasawara, M. Konnai, T. Takematsu, S. Kato, and M. Ishizaki, *Weed Res., (Tokyo),* **32**, 131 (1989).
2) D. N. Kursanov, Z. N. Parnes, and N. M. Loin, *Synthesis,* **1974**, 633.
3) I. Ojima and T. Kogure, *Tetrahedron Lett.,* **1973**, 2475.
4) R. A. Benkeser and D. C. Snyder, *J. Organomet. Chem.,* **225**, 107 (1982).

Photochemical Lumiketone-Type Rearrangement of 3-Methoxyphenol Promoted by $AlBr_3$

Kiyomi KAKIUCHI,* Masaki UE, Bunji YAMAGUCHI, Atsushi NISHIMOTO, and Yoshito TOBE*
Department of Applied Fine Chemistry, Faculty of Engineering,
Osaka University, Suita, Osaka 565
(Received April 15, 1991)

Synopsis. Irradiation of 3-methoxyphenol in the presence of 2 equiv of $AlBr_3$ in CH_2Cl_2 gave 4-methoxybicyclo[3.1.0]hex-3-en-2-one in a 38% yield. 3-Methoxy-2-methylphenol also yielded the lumiketone rearrangement product. On the other hand, 3-methoxy-4-methyl-, 3-methoxy-5-methyl-, and 5-methoxy-2-methylphenol underwent transposition of the methyl group to give equilibrium mixtures of the three methoxycresols.

Protonated alkyl-substituted phenols have been shown to undergo lumiketone-type photorearrangement which was effected by a Brønsted acid (FSO_3H, CF_3SO_3H) or a Lewis acid ($AlBr_3$, aluminosilicates) giving bicyclo[3.1.0]hex-3-en-2-ones.[1] This rearrangement is analogous to the well-known isomerizations of 2,5-cyclohexadienones[2] and provides a useful method for the preparation of bicyclo[3.1.0]hex-3-en-2-ones. Although a variety of methyl-substituted phenols undergo this transformation successfully, there seems to be no reports on those with functional groups other than alkyl moieties on the phenol ring. In the present paper, we describe the isomerization of 3-methoxyphenols **1a** and **1b** to the corresponding 4-methoxybicyclo[3.1.0]hex-3-en-2-ones **2a** and **2b**.[3] Since the products **2a** and **2b** possess a β-methoxy-α,β-enone functionality, they could serve as versatile synthetic intermediates for further manipulation.

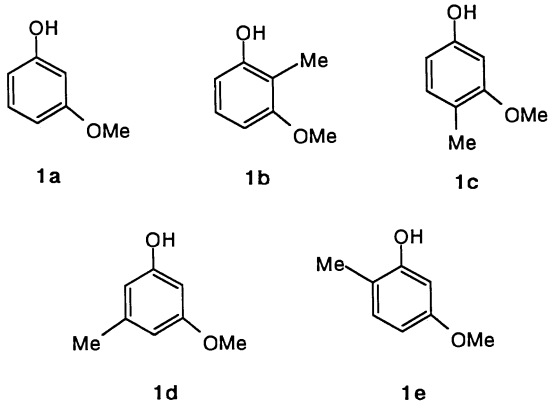

When a solution of **1a** and 2 equiv of $AlBr_3$ in CH_2Cl_2 was irradiated through a Pyrex filter, 4-methoxybicyclo[3.1.0]hex-3-en-2-one (**2a**) was obtained in a 38% isolated yield (74% yield based on **1a** consumed) along with unreacted **1a** (43% conversion).[4] The conversion of **1a** to **2a** reached maximum after about 4.5 h irradiation and by prolonged irradiation the relative ratio of **2a** decreased gradually due to photochemcal cycloreversion to **1a**. Similar cycloreversion of bicyclo[3.1.0]hex-3-en-2-ones has been reported.[5] Indeed, independent irradiation of **2a** showed that **2a** isomerized to **1a** efficiently irrespective of the presence of $AlBr_3$. While irradiation of **2a** in the presence of $AlBr_3$ (2 equiv) gave an equilibrium mixture of **2a** and **1a**, the cycloreversion of **2a** was irreversible in the absence of $AlBr_3$ to afford **1a** in a 83% yield.

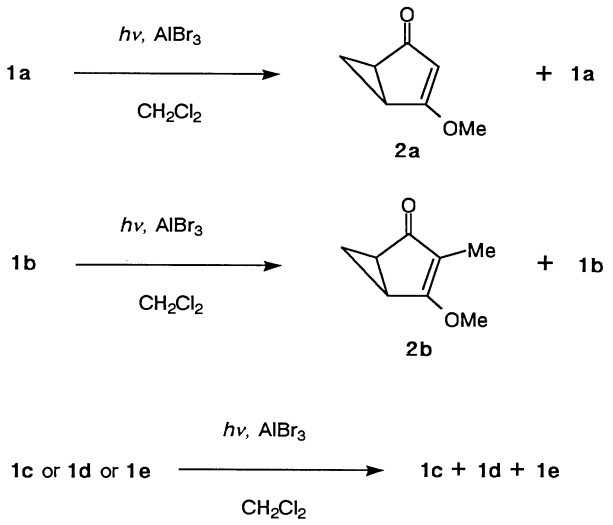

On the other hand, irradiation of the 4-methyl derivative **1c** with $AlBr_3$ (2 equiv) gave an equilibrium mixture composed of **1c**, 3-methoxy-5-methylphenol (**1d**), and 5-methoxy-2-methylphenol (**1e**)(**1c**:**1d**:**1e**= 24:36:39). Similarly, irradiation of **1d** and **1e** with $AlBr_3$ gave mixtures of **1c**, **1d**, and **1e** (7:34:59 from **1d**, 3:26:70 from **1e**). No bicyclohexenones were detected in these cases. It became apparent that the mode of isomerization, i.e., lumiketone-type rearrangement or methyl transposition, of the methyl derivatives **1b**—**1e** is critically dependent on the position of the methyl group.

The above reactivity difference is explained in terms of the reaction pathways shown in Scheme 1 and 2. In view of the previous work done by Childs,[1] it is reasonable to assume that the lumiketone-type rearrangement of **1a** and **1b** proceeds through the para protonated complexes **3a** and **3b**, respectively (Scheme 1). On the other hand, the methyl transposition of **1c**—**1e** is explained by positing the respective complexes **3c**—**3e** which are protonated on the methyl-bearing carbons of the phenol ring. These are interconverted by 1,2-migration of the methyl group, which is located adjacent to the carbocation centers (Scheme 2).

Although the lumiketone-type transformation was successful only for **1a** and **1b**, it should be pointed out

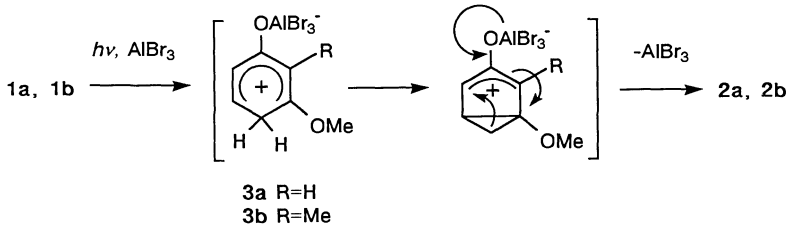

Scheme 1.

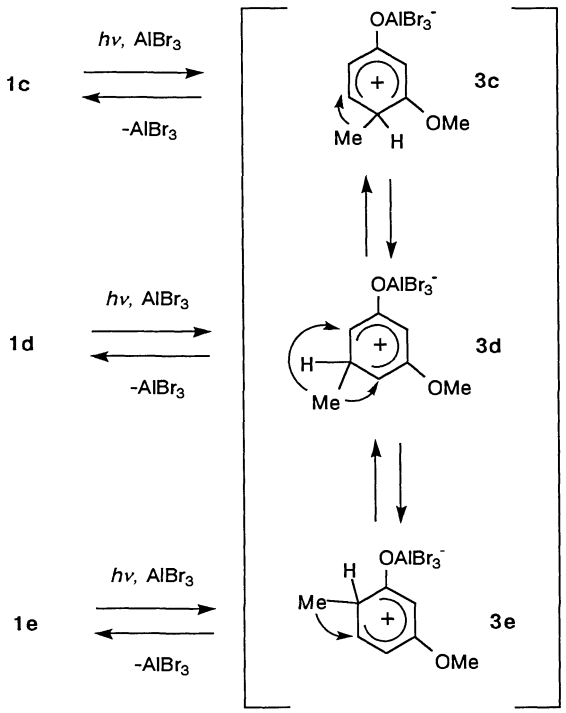

Scheme 2.

that products **2a** and **2b** possess a β-methoxy-α,β-enone functionality which is a versatile synthon for further functional group transformation. Moreover, although isolated yields of **2a** and **2b** were only moderate, the products were isolated in an almost pure state by simple extraction and the starting material can be recovered from the alkaline extract. Therefore, despite its limitations, the present transformation provides a useful way to prepare bicyclo[3.1.0]hex-3-en-2-one derivatives from readily available 3-methoxyphenols.

Experimental

IR spectra were recorded on a Hitachi 260-10 spectrometer. ^{1}H NMR (400 MHz) and ^{13}C NMR (100 MHz) spectra were measured with a JEOL JNM-GSX-400 spectrometer. Mass spectra were obtained with a JEOL JMS-DX303 spectrometer. GLC was undertaken with Hitachi G-3000 chromatograph with a capillary column of FFAP (6 m).

3-Methoxyphenol (**1a**) was commercially available and was distilled before use. 3-Methoxy-2-methylphenol (**1b**),[6] 3-methoxy-4-methylphenol (**1c**),[7] 3-methoxy-5-methylphenol (**1d**),[8] and 5-methoxy-2-methylphenol (**1e**)[9] were prepared according to the reported procedures.

Photoisomerization of 3-Methoxyphenol (1a) to 2a. A solution of 500 mg (4.03 mmol) of **1a** and 2.15 g (8.06 mmol) of $AlBr_3$ in 25 ml of CH_2Cl_2 was irradiated with a 500 W high pressure mercury lamp through a Pyrex filter at room temperature. The progress of the reaction was monitored by GLC. After 4.5 h, the mixture was carefully added to ice water and extracted three times with ether. The ether extract was washed with 10% NaOH solution, brine, and dried with $MgSO_4$. Evaporation of the solvent followed by chromatography on silica gel (elution with ether) gave 159 mg (38% yield; 74% based on consumed **1a**) of **2a**. The alkaline washing was acidified with HCl and extracted with ether. The extract was washed with brine, dried, and evaporated. Chromatography on silica gel (elution with 20% ether in petroleum ether) afforded 286 mg (57% recovery) of unreacted **1a**.

2a: IR (neat) 1680, 1580, 1240, and 960 cm^{-1}; ^{1}H NMR ($CDCl_3$) δ=4.65 (s, 1H), 3.80 (s, 3H), 2.29 (m, 1H), 2.17 (m, 1H), and 1.4—1.5 (m, 2H); ^{13}C NMR ($CDCl_3$) δ=203.3 (s), 191.2 (s), 95.7 (d), 58.8 (q), 31.4 (t), 24.2 (d), and 20.5 (d); MS *m/z* (rel intensity) 124 (M^+, 100), 96 (45), 81 (36), and 53 (57). Found: C, 67.62; H, 6.44%. Calcd for $C_7H_8O_2$: 67.73; H, 6.50%.

Photoisomerization of 3-Methoxy-2-methylphenol (1b) to 2b. A solution of 100 mg (0.724 mmol) of **1b** and 386 mg (1.45 mmol) of $AlBr_3$ in 5 ml of CH_2Cl_2 was irradiated as above for 30 min. The reaction was worked up as above to give 19 mg (19% yield; 33% based on **1b** consumed) of **2b** and 42 mg (58% conversion) of unreacted **1b**.

2b: IR (neat) 1680, 1620, 1280, 1240, 1000, and 930 cm^{-1}; ^{1}H NMR ($CDCl_3$) δ=3.98 (s, 3H), 2.28 (m, 1H), 2.12 (ddd, *J*=3.9, 6.8, and 8.3 Hz, 1H), 1.47 (ddd, *J*=3.9, 4.9, and 7.8 Hz, 1H), 1.44 (s, 3H), and 1.31 (dd, *J*=3.9 and 7.3 Hz, 1H); ^{13}C NMR ($CDCl_3$) δ=203.4 (s), 185.1 (s), 108.2 (s), 57.0 (q), 33.1 (t), 23.1 (d), 16.1 (d), and 5.6 (q); MS *m/z* (rel intensity) 138 (M^+, 100), 107 (30), 95 (23), 79 (26), and 67 (35). HR MS Found: *m/z* 138.0678. Calcd for $C_8H_{10}O_2$: M, 138.0681.

Photoisomerization of 3-Methoxy-4-methylphenol (1c), 3-Methoxy-5-methylphenol (1d), and 5-Methoxy-2-methylphenol (1e). Irradiation of 100 mg (0.75 mmol) of **1c** or **1d** or **1e** and 398 mg (1.5 mmol) of $AlBr_3$ in 5 ml of CH_2Cl_2 was undertaken as above for 10 h. The mixture was worked up as above and the subsequent flash chromatography on silica gel (ether–hexane=10 : 90 eluent) gave a mixture of **1c**, **1d**, and **1e**. Yields and the ratio of the products (GLC) are as follows: From **1c**: 71 mg (71% yield), **1c** : **1d** : **1e**=24 : 36 : 39. From **1d**: 71 mg (71% yield), **1c** : **1d** : **1e**=7 : 34 : 59. From **1e**: 61 mg (61% yield), **1c** : **1d** : **1e**=3 : 26 : 70. The products were identified by GLC and ^{1}H NMR spectra.

1c: ^{1}H NMR ($CDCl_3$) δ=6.94 (d, *J*=8.3 Hz, 1H), 6.37 (s, 1H), 6.31 (d, *J*=8.3 Hz, 1H), 5.01 (s, 1H), 3.77 (s, 3H), and 2.12 (s, 3H).

1d: ^{1}H NMR ($CDCl_3$) δ=6.31 (br s, 1H), 6.26 (br s, 1H), 6.23 (t, *J*=2.5 Hz, 1H), 5.59 (br s, 1H), 3.74 (s, 3H), and 2.25 (s, 3H).

1e: ^{1}H NMR ($CDCl_3$) δ=6.99 (d, J=8.3 Hz, 1H), 6.41 (dd, J=2.5 and 8.3 Hz, 1H), 6.38 (d, J=2.5 Hz, 1H), 5.28 (br s, 1H), 3.74 (s, 3H), and 2.16 (s, 3H).

Photocycloreversion of 4-Methoxybicyclo[3.1.0]hex-3-en-2-one (2a). A solution of 80 mg (0.65 mmol) of **2a** in 4 ml of CH_2Cl_2 was irradiated for 1 h until the starting material was consumed completely. The solvent was evaporated and the subsequent flash chromatography gave 66 mg (83% yield) of **1a**.

A solution of 80 mg (0.65 mmol) of **2a** and 344 mg (1.3 mmol) of $AlBr_3$ in 4 ml of CH_2Cl_2 was irradiated for 1 h. The mixture was worked up as described for the isomerization of **1a** to **2a**. After chromatography, 40 mg (50% yield) of **1a** and 19 mg (24% yield) of unreacted **2a** were obtained. By prolonged irradiation, while the ratio of **1a** and **2a** did not change appreciably, their yields decreased due to the formation of a small amount of unidentified side products.

We are grateful to the Ministry of Education, Science and Culture for the support of the NMR and Mass Spectral facilities used in this work at the Instrumental Analysis Center of the Faculty of Engineering, Osaka University and for partial support of this work through a Grant-in-Aid.

References

1) a) R. F. Childs, B. D. Parrington, and M. Zeya, *J. Org. Chem.*, **44**, 4912 (1979). b) P. Baeckstrom, U. Jacobsson, B. Koutek, and T. Norin, *ibid.*, **50**, 3728 (1985). c) S. K. Chadda and R. F. Childs, *Can. J. Chem.*, **63**, 3449 (1985). d) R. F. Childs and B. E. George, *ibid.*, **66**, 1343 (1988).

2) For reviews: P. J. Kropp, "Organic Photochemistry," ed by O. L. Chapman, Marcel Dekker, New York (1967), Vol. 1, p. 1; K. Schaffner and M. Demuth, "Rearrangements in Ground and Excited States," ed by P. de Mayo, Academic Press, New York (1980), Vol. 3, p. 281.

3) For a Lewis acid-mediated photoreaction of 2-naphthols: M. Ue, M. Kinugawa, K. Kakiuchi, Y. Tobe, and Y. Odaira, *Tetrahedron Lett.*, **30**, 6193 (1989).

4) Although it has been reported that similar photoisomerization of methyl-substituted phenols is dependent on the irradiation wavelength,[1a] irradiation of **1a** through a solution filter of 1,4-diphenylbutadiene in tetrahydrofuran (0.15 mol dm^{-3}; λ>350 nm) resulted in essentially the same results as that from irradiation through a Pyrex filter. Moreover, CF_3SO_3H[1b,c] was found to be uneffective for this transformation.

5) J. W. Wheeler and R. H. Eastman, *J. Am. Chem. Soc.*, **81**, 2361 (1959); H. E. Zimmerman, R. Keese, J. Nasielski, and J. S. Swenton, *ibid.*, **88**, 4895 (1966); L. Barber, O. L. Chapman, and J. D. Lassila, *ibid.*, **90**, 5933 (1968).

6) A. Rashid and G. Read, *J. Chem. Soc. C*, **1967**, 1323.

7) R. N. Mirrington and G. I. Feutrill, *Org. Synth.*, **53**, 90 (1973).

8) M. Tomita and S. Ueda, *Yakugaku Zasshi*, **80**, 353 (1960).

9) J. Wu, J. L. Beal, and R. W. Doskotch, *J. Org. Chem.*, **45**, 208 (1980).

Preparation of Stable 5,15-Dihydroporphyrin

Noboru ONO,* Hiroshi KAZIRO,† and Kazuhiro MARUYAMA†
Department of Chemistry, Faculty of Science, Ehime University, Matsuyama 790
† Department of Chemistry, Faculty of Science, Kyoto University, Kyoto 606
(Received May 13, 1991)

Synopsis. Very stable 5,15-dihydroporphyrin was perpared by the acid catalyzed reaction of dipyrromethane with two benzaldehyde molecules which were linked by an appropriate linkage.

Porphyrin macrocycles constitute an important class of compounds of particular interest owing to their role in biological systems.[1] Recent work has been devoted to the design of new porphyrin ligands with specific properties, or new structural analogues of porphyrins.[2] Dihydroporphyrins, which have two additional hydrogen atoms on the porphyrin nucleus, have also been the subjects of intense study.[3] 5,15-Dihydroporphyrins are intermediates in the formation of porphyrins, but they have not been isolated in the preparation of porphyrins, for they are readily oxidized to porphyrins. The most general synthetic procedure for stable 5,15-dihydroporphyrins is the reductive alkylation of metalloporphyrins. Various 5,15-dihydroporphyrins have been prepared by this method, and they have been used as effective ligands for various metals.[4] In this paper we wish to report a novel method for the preparation of a very stable strapped 5,15-dihydroporphyrin which was not oxidized to the corresponding porphyrins by strong oxidizing agents such as *p*-chloranil. Such strapped 5,15-dihydroporphyrins can not be prepared by the alkylation of an anion of metalloporphyrin with a dihalide.[4]

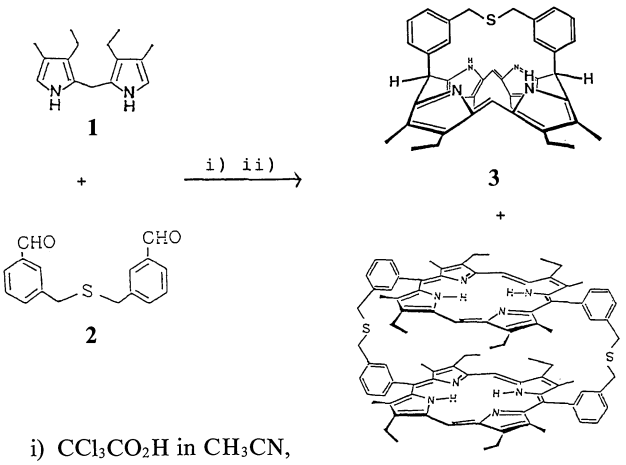

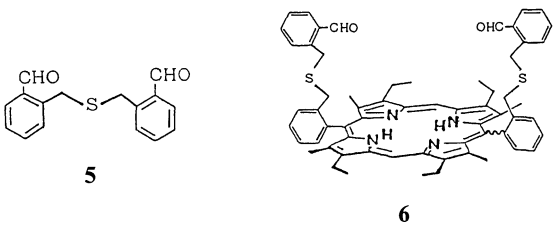

The acid-catalyzed reaction of dipyrromethane (**1**) with a dialdehyde linked by a thioether group was carried out in order to generate thioether strapped porphyrins or face-to-face dimeric porphyrins bridged by a thioether linkage. The thioether linkage is important, because the sulfur atom may be removed by the procedure established in cyclophane chemistry.[5] Thioether strapped porphyrin can also be regarded as a model of the active electron transporting site of cytochrome c.[6] The two benzaldehyde molecules are linked by CH_2SCH_2 at the *o*- or *m*-position. Such aldehydes were prepared by the reaction of the corresponding bromethylbenzaldehydes with sodium sulfide. The reaction of **1** with dialdehyde (**2**) linked at the *m*-position gave strapped 5,15-dihydroporphyrin (**3**) and face-to-face dimeric porphyrin (**4**) in 65% and 3% yields, respectively. The high yield of **3** was remarkable. On the other hand, the reaction of **1** with dialdehyde (**5**), in which two aldehyde moieties were linked at the *o*-position, gave a complex set of products. It was impossible to isolate any pure products. The mass spectra of the products suggested the formation of porphyrin **6**, but further characterization was very difficult due to the instability and complexity of the products. However, the mass spectra of the corresponding 5,15-dihydroporphyrin and porphirin dimers were not detected. Compound **3** was extremely stable to oxidizing agents, and it was not oxidized to the corresponding porphyrins by chloranil or oxygen. Thus, the formation of stable 5,15-dihydroporphyrins depended on the linkage which connected the two aldehyde moieties. When a longer linkage was used, the strapped porphyrin and face-to-face porphyrin dimers were formed by the similar reaction.[7] The CPK model of **3** showed that the bond angles around the 5 and 15 positions of the tetrapyrrole macrocycle were ideal for the formation of stable 5,15-dihydroporphyrins. The bond angles of the tetrapyrrole which may be obtained from 5 were unfavorable for the formation of 5,15-dihydroporphyrin. 5,15-Dihydroporphyrins were not isolated from the reaction of dialdehydes linked by longer linkages, for they were readily oxidized to the corresponding porphyrins. When the thioether linkage of **3** was cleaved, tetrapyrrole should have been readily oxidized to porphyrins. In fact, treatment of **3** with Raney Ni gave porphyrin **7** in a good yield, which may provide a useful method for the stereoselective synthesis of 5,15-diarylporphyrins.

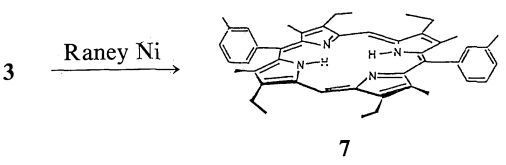

Compound **3** was an orange solid (λ_{max} 427.5 nm) and has a strong affinity to various metals like porphyrins. Preliminary experiments using an ion selective electrode showed a strong affinity to Ni or Cu. The use of **3** as a ligand is now being studied.

Experimental

Mass spectra were recorded on a JEOL DX-300 spectrometer using the FAB method; the FAB matrix was $CHCl_3$+trifluoroacetic acid/*m*-nitrobenzyl alcohol/glycerol.

Bis(3-formylbenzyl) Sulfide (2). A mixture of *m*-bromomethylbenzadehyde[8] (1.25 g, 6.3 mmol) and $Na_2S \cdot 9H_2O$ (0.87 g, 7.5 mmol) in *N*,*N*-dimethylformamide (80 ml) was stirred for 30 h under Ar at room temperature. The reaction mixture was then poured into water and extracted with CH_2Cl_2. The organic layer was washed with water and dried over anhydrous magnesium sulfate. Evaporation of the solvent gave crude **2**, which was purified by column chromatography (silica gel/hexane–ethyl acetate 3:1) to give pure **2** as a white solid, mp 74—76 °C, 0.64 g (75% yield). ^{1}H NMR (400 MHz, $CDCl_3$) δ=3.68 (s, 4H). 7.48 (t, J=4 Hz, 2H), 7.54 (d, J=4 Hz, 2H), 7.75 (s, 2H), 7.76 (d, J=4 Hz, 2H), and 10.0 (s, 2H). Found: C, 71.05; H, 5.90%. Calcd for $C_{16}H_{14}O_2S$: C, 71.08; H, 5.96%.

Bis(2-formylbenzyl) Sulfide (5). This compound was prepared from *o*-bromomethylbenzaldehyde by the same procedure as the preparation of **2**, mp 60—62 °C, ^{1}H NMR (400 MHz, $CDCl_3$) δ=4.15 (s, 4H), 7.36 (d, J=4 Hz, 2H), 7.45 (t, J=4 Hz, 2H), 7.52 (t, J=4 Hz, 2H), 7.83 (d, J=4 Hz, 2H), and 10.2 (s, 2H). Found: C, 71.12; H, 5.88%. Calcd for $C_{16}H_{14}O_2S$: C, 71.08; H, 5.96%.

Preparation of 5,15-Dihydroporphyrin (3) and Porphyrin (4). A solution of trichloroacetic acid (10 mg) in dry acetonitrile (30 ml) was added to a stirred solution of bis(3-ethyl-4-methyl-2-pyrrolyl)methane[9] (**1**, 0.65 mmol) and dialdehyde (**2**, 0.32 mmol) in dry acetonitrile (30 ml) under N_2 in the dark. After stirring the solution at room temperature for 12 h, *p*-chloranil (0.45 g) in dry tetrahydrofuran (10 ml) was added and the resulting mixture was stirred for 12 h at room temperature. After removing the solvent, the residue was subjected to column chromatography (alumina Woelm N-I/CH_2Cl_2) to give **3** and **4**, respectively. Recrystallization from CH_2Cl_2–CH_3OH gave pure **3** as an orange solid in a 65% yield. Mp 250 °C (decomp), UV-vis (CH_2Cl_2) 427.5 nm. ^{1}H NMR (400 MHz, $CDCl_3$) δ=1.11 (t, J=7 Hz, 12H), 2.11 (s, 12H), 2.53 (q, J=7 Hz, 8H), 3.35 (s, 4H), 5.46 (s, 2H), 6.99 (s, 2H), 7.26—7.36 (m, 8H), and 9.20 (br, 2H, NH). MS (FAB) m/z 691 ($M+H^+$). Found: C, 79.84; H, 7.36; N, 8.02%. Calcd for $C_{46}H_{50}N_4S$: C, 79.96; H, 7.29; N, 8.11%. Porphyrin **4**: 3% yield as a purple solid, UV-vis (CH_2Cl_2) 395, 507, 540, 578, and 627 nm. MS (FAB) m/z 1377 ($M+H^+$). NMR spectra were too complicated to be characterized. The absorption spectra indicated interaction between two chromopheres; the soret band is blue-shifted and the Q bands are red-shifted compared to the monomeric 5,15-diarylporphyrin.

The reaction of **5** with **1** was carried out in the same way as described above. Several unstable products were detected by TLC. All attempts to isolate pure compounds by column chromatography or recrystallization were unsuccessful. MS (FAB) m/z 959, which suggested that porphyrin **6** may have been involved in a complex set of products. However, further charaterization of the products was impossible due to instability of the products.

Preparation of 5,15-Di-*m*-tolyl-2,8,12,18-tetraethyl-3,7-13,17-tetramethylporphyrin (7). A mixture of **3** (30 mg) and Raney Ni W-7 (500 mg) in ethanol (1 ml) and CH_2Cl_2 (15 ml) was heated at reflux temperature for 24 h. The reaction mixture was poured into water and extracted with CH_2Cl_2. The extract was washed with water and dried with anhydrous magnesium sulfate. After the removal of the solvent, the residue was subjected to column chromatography (silica gel/CH_2Cl_2) to give **7** (20 mg, 80% yield). Uv-vis (CH_2Cl_2) λ_{max} 408, 506, 538, 571, and 625 nm. ^{1}H NMR (400 MHz, $CDCl_3$) δ=2.24 (br, 2H, NH), 1.76 (t, J=7 Hz, 12H), 2.20 (s, 6H), 2.43 (s, 12H), 4.00 (m, 8H), 7.8—8.2 (m, 8H), and 10.18 (s, 2H). MS (FAB) m/z 657 ($M+H^+$).

This work was partially supported by Grants-in-Aid for Scientific Research No. 02353022 from the Ministry of Education, Science and Culture and the Nippon Shouken Foundation.

References

1) "The Porphyrins," ed by D. Dolphin, Academic Press, New York (1978—1979), Vols. 1—7.

2) Heteroporphyrins: M. J. Broadhurst, R. Crigg, and A. W. Johnson, *J. Chem. Soc. C*, **1971**, 3681; A. Ulman and J. Manasen, *J Am. Chem. Soc.*, **97**, 6540 (1975).
Homoporphyrins: H. J. Callot, T. Tschamber, and E. Schaeffer, *J. Am. Chem. Soc.*, **97**, 6138 (1975).
Pentapyrrolic macrocycles: V. J. Bauer, D. L. J. Clive, D. Dolphin, J. B. Paine, F. L. Harris, M. M. King, J. Loder, S. W. Chien Wang, and R. B. Woodward, *J. Am. Chem. Soc.*, **105**, 6429 (1983); J. L. Sessler, M. J. Cyr, V. Lynch, and J. A. Ibers, *J. Am. Chem. Soc.*, **112**, 2810 (1990).
Hexaphyrin: A. Gossauer, *Chimia*, **37**, 341 (1983).
Porphycene: E. Vogel, M. Kocher, A. Schmickler, and J. Lex, *Angew. Chem., Int. Ed. Engl.*, **25**, 257 (1986).

3) J. W. Buchler, C. Dreher, K. L. Lay, Y. J. A. Lee, and W. R. Scheidt, *Inorg. Chem.*, **22**, 888 (1983), and references therein.

4) A. Botulinski, J. W. Buchler, K. L. Lay, and H. Stoppa, *Leibigs Ann. Chem.*, **1984**, 1259; J. W. Buchler and L. Puppe, *ibid.*, **740**, 142 (1970).

5) V. Boekelheide and R. A. Hollins, *J. Am. Chem. Soc.*, **92**, 3512 (1970); F. Vogtle and L. Rossa, *Angew. Chem., Int. Ed. Engl.*, **18**, 515 (1972).

6) B. Morgan, D. Dolphin, R. H. Jones, and F. W. B. Einstein, *J. Org. Chem.*, **52**, 4628 (1987), and references therein.

7) A. Osuka, F. Kobayashi, and K. Maruyama, *Bull. Chem. Soc. Jpn.*, **64**, 1213 (1991).

8) B. S. Bookser and T. C. Bruice, *J. Am. Chem. Soc.*, **113**, 4208 (1991).

9) P. S. Clezy and A. W. Nicol, *Aust. J. Chem.*, **11**, 1835 (1965).

Asymmetric Reduction of Carbon-Carbon Double Bonds of Conjugated Enones with Fermenting Bakers' Yeast

Takashi SAKAI,* Syuji MATSUMOTO, Syukou HIDAKA, Norihisa IMAJO, Sadao TSUBOI, and Masanori UTAKA*
Department of Applied Chemistry, Faculty of Engineering, Okayama University, Tsushima, Okayama 700
(Received May 23, 1991)

Synopsis. Bakers' yeast reduction of α-substituted or β,β-disubstituted α,β-unsaturated ketones gave saturated chiral ketones with excellent optical purity, while the β,β-disubstituted derivative remained intact.

A number of bakers' yeast reductions of carbon–carbon double bonds, which are functionalized with hydroxymethyl,[1a] formyl,[1b] or nitro group,[1c] have been reported.[1d] However, less attention has been paid on the conjugated enones. For example, the carbonyl group of 4-phenyl-3-buten-2-one is reduced predominantly to give the corresponding (*S*)-allyl alcohol.[2] In contrast, we previously reported the bakers' yeast reduction of the carbon-carbon double bond of functionalized enones such as 3-chloro-3-alken-2-ones[3a] and 3-(1-hydroxyalkyl)-3-buten-2-ones,[3b] both of which afforded the corresponding saturated ketones with high optical purity. The effects of the chloro or the hydroxyl group on the reaction were obscure. We report here the reduction of simple enones such as 3-alkyl-3-buten-2-ones and 3- or 4-phenyl-3-buten-2-one. The α-substituted enones are reduced to the saturated ketones with excellent optical purity. The results are discussed as compared with those of 3-(1-hydroxyalkyl)-3-buten-2-ones.[3b]

Table 1 shows the reduction of 3-alkyl-3-buten-2-ones (**1a—e**) by use of pressed bakers' yeast (PBY). Enones **1b—d** having an alkyl chain of C_6 to C_{11} gave saturated ketones **2b—d** with high enantiomeric excess (ee) (Scheme 1). (2*S**,3*R**)-3-Methyl-2-alkanols **3b**[4] (1% yield) and **3c**[4] (6% yield) were also isolated as a minor component.[5] The absolute configuration for **2b-d** was assigned to be (*R*) by comparison of the rotation with that for authentic (*R*)-**2b**.[6] Interestingly, the enone **1c** was reduced in 30% yield with a rather shorter reaction time (11 h), while the yield could not be increased further even by extension of the time to 22 h. The shorter-chain homolog **1b** and the longer-chain one **1d** required much prolonged reaction times, 64 h and 90 h respectively, to give **2b** and **2d** in rather lowered yields. The shortest homolog **1a** (R=C_5H_{11}) gave neither reduction product nor substrate recovered. The longest one **1e** (R=$C_{12}H_{25}$) remained intact. Thus the yeast reduction of the enones having α-alkyl group **1** was found to be highly dependent on the length of the α-alkyl chain.

The results mentioned above are in contrast to those for the 3-(1-hydroxyalkyl)-3-buten-2-ones:[3b] 1) 3-Pentyl-3-buten-2-one (**1a**) was not reduced nor recovered at all after 87 h incubation, but the 3-(1-hydroxypentyl)-3-buten-2-one was reduced in 56% yield after 69 h. 2) 3-Hexyl-3-buten-2-one (**1b**) was reduced in 24% yield by 64 h incubation without recovery of the starting enone, but 3-(1-hydroxypentyl)-3-buten-2-one was reduced in 72% yield for 114 h. Thus the 1-hydroxy group in the alkyl substituent seems to enhance the yield and prevent the loss of substrate during the incubation.

The substrate was then replaced to the aromatic

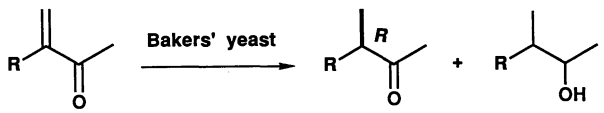

1 **2** (2S*,3R*)-**3**

a: R = C_5H_{11}, **b**: R = C_6H_{13}, **c**: R = C_8H_{17}, **d**: R = $C_{11}H_{23}$, **e**: R = $C_{12}H_{25}$

Scheme 1.

Table 1. Bakers' Yeast Reduction of 3-Alkyl-3-buten-2-ones (**1a—e**)

	1	Time	**1**	(*R*)-**2**		
	R	h	Recovery/%	Yield/%	$[\alpha]_D$ (*c*, $CHCl_3$)	ee[a]/%
a	C_5H_{11}	87	0	0	—	—
b	C_6H_{13}	16	26	15	—	—
b	C_6H_{13}	25	18	16	—	—
b	C_6H_{13}	64	0	24[b]	−15.7° (1.4)[c]	>99
c	C_8H_{17}	11	5	30	—	—
c	C_8H_{17}	22	0	29[d]	−16.4° (2.8)	>98
d	$C_{11}H_{23}$	20	30	13	—	—
d	$C_{11}H_{23}$	50	34	21	—	—
d	$C_{11}H_{23}$	90	20	22	−12.7° (1.3)	>98
e	$C_{12}H_{25}$	74	78	0	—	—

a) Determined by 200 MHz (for **2b**) or 100 MHz (for **2c** and **2d**) ^1H NMR spectra in the presence of (+)-Eu $(hfc)_3$. b) Alcohol **3b** was obtained in 1% yield. c) Reported rotation: $[\alpha]_D$ −12.03°. (neat) for the (*R*) enantiomer (99% ee) (Ref. 6b). d) Alcohol **3c** was produced in 6% yield.

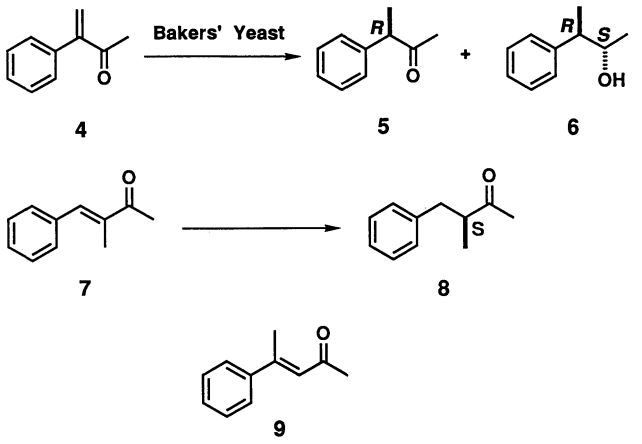

Scheme 2.

analogues. The reduction of 3-phenyl-3-buten-2-one (**4**) was carried out by use of immobilized bakers' yeast (IMBY) to afford (*R*)-(−)-3-phenyl-2-butanone (**5**)[7] (24% yield, 95% ee) and (2*S*,3*R*)-(+)-3-phenyl-2-butanol (**6**)[8] (6% yield) (Scheme 2). The IMBY method required 30 times as much bakers' yeast as the substrate by weight, showing a sharp contrast to the free bakers' yeast method which needed 110 times yeast to give **5** in only 4% yield with 56% ee. The substrate **4** showed a remarkable inhibitory feature to the fermentation.

The reduction of 3-methyl-4-phenyl-3-buten-2-one (**7**) with IMBY gave (*S*)-(+)-3-methyl-4-phenyl-2-butanone (**8**) in 52% yield. However, the optical purity was lowered to 72% ee. The β,β-disubstituted enone such as 4-phenyl-3-penten-2-one (**9**) was recovered unchanged. Thus, the bakers' yeast reduction is found to suffer with the β-substituent(s) of the α,β-unsaturated ketones.

Experimental

Ir spectra were recorded with a Jasco A-102 spectrometer. ^{1}H NMR spectra at 60 and 100 MHz were obtained on JEOL PMX-60SI and JEOL FX-100 spectrometers, respectively, and those at 200 and 500 MHz as well as ^{13}C NMR spectra (50 MHz) were measured on Varian VXR spectrometers. Preparative column chromatography was carried out by using silica gel (Merck Silica Gel 60). Purification by HPLC was performed by use of Hitachi 655 apparatus with Unisil Q column (10.7 mm i.d.×250 mm l). Compounds **7**[9] and **9**[10] were prepared by the reported methods. Elemental analyses were carried out by Eiichiro Amano of this laboratory.

3-Alkyl-3-buten-2-ones (1a—e). These compounds were prepared by the palladium-catalyzed decarboxylation-deacetoxylation of allyl α-acetoxymethyl β-keto carboxylates which were derived from allyl acetoacetate via three steps[11] (method A). Enone **1b** was also synthesized by the formaldehyde-K_2CO_3 promoted deacetylation-methylenation[12] of 3-hexyl-2,4-pentanedione (95% yield), which was prepared by Bu_4NHSO_4 catalyzed alkylation[13] of acetylacetone with 1-iodohexane (70% yield) (method B). The overall yields of **1a—e** (method A) after purification by column chromatography and their spectral and physical data are shown below.

3-Pentyl-3-buten-2-one (1a):[11] 24.9% yield; IR (neat) 1680, 1630 cm^{-1}; ^{1}H NMR (CCl_4) δ=0.75—1.10 (m, 3H), 1.10—2.24 (m, 8H), 2.24 (s, 3H), 5.61 (s, 1H), 5.85 (s, 1H).

3-Hexyl-3-buten-2-one (1b):[14a] 5.6% yield; IR (neat) 1680, 1630 cm^{-1}; ^{1}H NMR (CCl_4) δ=0.65—1.05 (m, 3H), 1.09—1.90 (m, 14H), 2.23 (s, 3H), 5.60 (s, 1H), 5.83 (s, 1H).

3-Octyl-3-buten-2-one (1c):[14b] 22% yield; IR (neat) 1680, 1630 cm^{-1}; ^{1}H NMR (CCl_4) δ=0.70—1.15 (m, 3H), 1.10—1.80 (m, 14H), 2.22 (s, 3H), 5.57 (s, 1H), 5.81 (s, 1H).

3-Undecyl-3-buten-2-one (1d):[14c] 9.7% yield; IR (neat) 1680, 1630 cm^{-1}; ^{1}H NMR (CCl_4) δ=0.70—1.07 (m, 3H), 1.07—1.90 (m, 14H), 2.24 (s, 3H), 5.61 (s, 1H), 5.84 (s, 1H).

3-Dodecyl-3-buten-2-one (1e): 10.5% yield; bp 160 °C (7.5 mmHg, 1 mmHg=133.322 Pa); IR (neat) 1680, 1620 cm^{-1}; ^{1}H NMR (CCl_4) δ=0.70—1.07 (m, 3H), 1.07—1.90 (m, 14H), 2.24 (s, 3H), 5.61 (s, 1H), 5.84 (s, 1H). Found: C, 80.32; H, 12.45%. Calcd for $C_{15}H_{28}O$: C, 80.29; H, 12.58%.

Typical Reduction of 1a—e with Pressed Bakers' Yeast. (*R*)-(−)-3-Methyl-2-undecanone (2c) and (2*S,3*R**)-3-Methyl-2-undecanol (3c):**[4] To a 500 ml round bottomed flask were added boiled water (110 ml), pressed bakers' yeast (7.0 g), and glucose (10.0 g). The suspension was stirred for 20 min at 30 °C and then enone **1c** (275 mg, 1.51 mmol) was added. After stirring for additional 7 h at 30 °C, glucose (10 g) was added and the stirring was continued for 22 h in total. Celite (12 g) was added and the mixture was stirred further for 6 h. After filtration under suction, the filtrate was extracted with ethyl acetate and the residue was washed with ethyl acetate. The combined organic layer was dried over $MgSO_4$ and concentrated under reduced pressure. Fractionation of the crude products with column chromatography on silica gel (30 g, hexane:ethyl acetate=30:1) followed by purification by HPLC (hexane:ethyl acetate 30:1, 1.7 ml min^{-1}) gave ketone **2c** (3.5 min, 80 mg, 29% yield) and alcohol **3c** (7.0 min, 16 mg, 6% yield).

2c: IR (neat) 1720 cm^{-1}; ^{1}H NMR ($CDCl_3$) δ=0.70—2.02 (m, 17H), 1.07 (d, 3H, *J*=7 Hz), 2.09 (s, 3H), 2.01—2.60 (m, 1H); ^{13}C NMR ($CDCl_3$) δ=14.1 (q), 16.2 (q), 22.7 (t), 27.3 (t), 28.0 (q), 29.3 (t), 29.5 (t), 29.7 (t), 31.9 (t), 47.3 (d), 212.9 (s). Found: C, 78.44; H, 13.34%. Calcd for $C_{12}H_{24}O$: C, 78.20; H, 13.12%.

3c:[4] IR (neat) 2800—3000 cm^{-1}; ^{1}H NMR ($CDCl_3$) δ= 0.84 (d, 3H, *J*=6.0 Hz), 0.85 (t, 3H, *J*=7.0 Hz), 1.10—1.60 (m, 15H), 1.10 (d, 3H, *J*=6.5 Hz); 3.63 (dq, 1H, *J*=6.0 and 6.0 Hz); ^{13}C NMR ($CDCl_3$) δ=14.1 (q), 14.5 (q), 19.3 (q), 22.7 (t), 27.3 (t), 29.4 (t), 29.7 (t), 30.0 (t), 31.9 (t), 32.6 (t), 40.1 (d), 71.8 (d). Found: C, 77.42; H, 14.01%. Calcd for C: 77.35; H, 14.06%.

(*R*)-(−)-3-Methyl-2-nonanone (2b)[6] **and (2*S**,3*R**)-3-Methyl-2-nonanol (3b).**[15] **2b:** IR (neat) 1715 cm^{-1}; ^{1}H NMR ($CDCl_3$) δ=0.86 (t, 3H, *J*=6.8 Hz), 1.06 (d, 3H, *J*=6.8 Hz), 1.25 (m, 10H), 2.11 (s, 3H); 2.48 (dq, 1H, *J*=6.8 Hz and 6.8 Hz).

3b: 1% yield; ^{1}H NMR ($CDCl_3$) δ=0.87 (d, 3H, *J*=6.6 Hz), 0.89 (bt, 3H), 1.13 (d, 3H, *J*=6.3 Hz), 1.05—1.70 (m, 11H), 3.67 (dq, 1H *J*=6.0 and 6.0 Hz).

(*R*)-(−)-3-Methyl-2-tetradecanone (2d): IR (neat) 1715 cm^{-1}; ^{1}H NMR ($CDCl_4$) δ=0.70—1.90 (m, 23H), 1.03 (d, 3H, *J*=7 Hz), 2.01 (s, 3H), 2.01—2.65 (m, 1H). Found: C, 79.41; H, 13.33%. Calcd for $C_{15}H_3O$: C, 79.58; H, 13.35%.

Determination of ee for (*R*)-2b—d. The ee of **2b** was determined by use of the ^{1}H NMR (200 MHz, $CDCl_3$) spectrum recorded in the presence of 30 mol% of (+)-Eu(hfc)$_3$ at 30 °C. Under the conditions, the singlet due to the terminal methyl group of (±)-**2b**, prepared as described below, resolved to a pair of singlets at δ=3.130 (for *S*) and δ=3.111 (for *R*). Similar ^{1}H NMR (100 MHz) experiments were carried out for **2c** and **2d** by using 50 mol% of (+)-Eu(hfc)$_3$.

Preparation of (±)-2b—d. These compounds were prepared for the references in the ^{1}H NMR shift reagent experiments. A mixture of 3-hexyl-3-buten-2-one (212 mg, 1.37 mmol) and 5% Pd-C (110 mg) was stirred at room temperature under hydrogen atmosphere overnight. Filtra-

tion of the mixture followed by concentration gave a crude product, which was purified by column chromatography (hexane:ethyl acetate=30:1) to give (±)-**2b** in 74% yield. Compounds (±)-**2c** (52% yield) and (±)-**2d** (40% yield) were obtained in a similar way.

3-Phenyl-3-buten-2-one (4).[16] The following method is newly developed here. 1-Phenylvinylmagnesium bromide was prepared by the reaction of α-bromostyrene (2.75 g, 15 mmol) and magnesium turnings (413 mg, 0.017 g-atom) in 10 ml of THF.[17] The dark brown suspension of the Grignard reagent was introduced dropwise to a solution of acetic anhydride (1.53 g, 5 mmol) in 5 ml of THF at −78 °C. After being stirred for 1 h at the temperature, the cooling bath was removed and the mixture was stirred further for 2.5 h. Water was added and the solvent was removed under reduced pressure. The organic layer was extracted with ethyl acetate and washed with aqueous $NaHCO_3$ and brine, dried over $MgSO_4$, concentrated under reduced pressure. The crude product was distilled under vacuum to give 1.40 g (64% yield) of enone **4**: Bp 100—105 °C (5 mmHg); IR (neat) 3070, 1680 cm^{-1}; ^1H NMR ($CDCl_3$) δ=2.45 (s, 3H), 5.98 (s, 1H), 6.19 (s, 1H), 7.25—7.45 (5H, m); ^{13}C NMR ($CDCl_3$) δ=27.4 (q), 125.7 (t), 128.1 (d), 128.4 (d), 137.0 (s), 149.5 (s), 199.4 (s).

Bakers' Yeast Reduction of Enone (4). (*R*)-(−)-3-Phenyl-2-butanone (5)[7] **and (2*S*,3*R*)-(+)-3-Phenyl-2-butanol (6).**[8] Immobilized bakers' yeast (dry bakers' yeast: sodium alginate= 4:1 in w/w) was prepared by the procedure described previously.[18] To a mixture of the immobilized bakers' yeast (78 ml including 6 g of bakers' yeast), glucose (20 g), and boiled water (150 ml) was stirred at 35 °C for 30 min. Enone **4** (963 mg, 6.59 mmol) was added and the mixture was stirred for 48 h. In the course of the reaction, 110 g of glucose was consumed. The combined ethyl acetate extracts both from the aqueous layer and from the gels were treated in a usual manner[18] and the crude product was purified by column chromatography (hexane:ethyl acetate, 20—10:1) to give ketone **5** (236 mg, 24% yield) and (2*S*,3*R*)-alcohol **6** (55 mg, 6% yield).

5: ($[\alpha]_D$−333° (*c* 0.75, benzene), lit[7] $[\alpha]_D$+368° (benzene) for 3*S*); IR (neat) 3050, 1720, 1500 cm^{-1}, ^1H NMR ($CDCl_3$) δ=1.38 (d, 3H, *J*=7.0 Hz), 2.04 (s, 3H), 3.74 (q, 1H, *J*=7.0 Hz), 7.18—7.36 (m, 5H).

6: ($[\alpha]_D$+17.7° (*c* 3.53, EtOH), [lit,[8] $[\alpha]_D$+16.2 (*c* 3.6, EtOH, 81% ee)]; ^1H NMR ($CDCl_3$) δ=1.23 (d, 3H, *J*=6.2 Hz), 1.26 (d, 3H, *J*=7.2 Hz), 1.58 (s, 1H, OH), 2.67 (dq 1H, *J*=7.2 Hz, 7.2 Hz), 3.85 (dq, 1H, *J*=7.2 Hz, 6.2 Hz), 7.2—7.4 (m, 5H).

Optical purity of **5** was determined as 95% ee in a similar manner to that dscribed for aliphatic ketone **2b-d**.

(±)-3-Phenyl-2-butanone (±)-(5). A mixture of enone **4** (200 mg, 1.37 mmol), palladium chloride (23 mg, 0.13 mmol), silica gel (100 mg) in ethanol (3 ml) was stirred under hydrogen at room temperature for 2 d. A usual workup followed by distillation [bp 100—105 °C (5 mmHg)] gave ketone (±)-**5** (152 mg, 75% yield).

(*S*)-(+)-4-Phenyl-3-methyl-2-butanone (8).[19] Incubation was carried out at 35 °C for 82 h by use of enone **7** (160 mg, 1.88 mmol), glucose (90 g in all), water (400 ml), and the immobilized yeast (150 ml, including 18 g of bakers' yeast). Workup in a usual way followed by purification with preparative TLC (20 cm×20 cm, silica-gel plate with 2 mm thickness, hexane:ether 5:1) gave ketone **8** (110 mg, 37% yield): $[\alpha]_D$+33.6° (*c* 2.74, EtOH) (lit, $[\alpha]_D$+45.5° (EtOH) for **8**); IR (neat) 1710 and 1600 cm^{-1}; ^1H NMR (CCl_4) δ=1.02 (d, 3H, *J*=6 Hz), 1.95 (s, 3H), 2.28—3.10 (m, 3H), 7.05 (s, 5H). Optical purity was determined to be 72% ee by a similar ^1H NMR (200MHz) method to that described above.

The authors are grateful to the SC-NMR Laboratory of Okayama University for obtaining ^1H (200 and 500 MHz) and ^{13}C (50 MHz) NMR spectra.

References

1) a) P. Gramatica, P. Manitto, D. Monti, and G. Speranza, *Tetrahedron,* **43**, 4481 (1987). b) C. Fuganti, P. Grasselli, S. Servi, and H. E. Högberg, *J. Chem. Soc., Perkin Trans.,* **7**, 3061 (1988). c) H. Ohta, N. Kobayashi, and K. Ozaki, *J. Org. Chem.,* **54**, 1802 (1989). d) Current review: S. Servi, *Synthesis,* **1990**, 1.

2) C. Fuganti, P. Grasselli, S. Servi, F. Spreafico, C. Zirotti, and P. Casati, *J. Chem. Res., Synop.,* **1984**, 112.

3) a) M. Utaka, S. Konishi, and A. Takeda, *Tetrahedron Lett.,* **27**, 4737 (1986). b)M. Utaka, S. Onoue, and A. Takeda, *Chem. Lett.,* **1987**, 971.

4) The assignment was ascertained by the preparation of (±)-syn- and (±)-anti-**3b** independently: Treatment of (±)-**2b** with an equimolar amount of $LiAlH_4$ in THF at room temperature gave a 42 (syn: $J_{2,3}$=4.3 Hz): 58 (anti: $J_{2,3}$=6.0 Hz) mixture of (±)-**3b** (92% yield), which were separated by the HPLC (hexane : ethyl acetate=5 : 1). ^1H NMR for (±)-syn-**3b** ($CDCl_3$) δ=0.883 (t, 3H, *J*=7.0 Hz, C_3-Me), 0.886 (d, 3H, *J*=7.0 Hz), 1.146 (d, 3H, *J*=6.5 Hz, C_1), 1.20—1.47 (m, 11H), 3.700 (dq, 1H, *J*=6.5, 4.3 Hz).

5) We examined that the enone **2b** was not reduced to **3b** by further treatment with RBY, being recovered intact.

6) a) D. Seebach, D. Steinmüller, and F. Demuth, *Angew. Chem., Int. Ed. Engl.,* **7**, 620 (1968). b) J. P. Collman, S. R. Winter, and D. R. Clark, *J. Am. Chem. Soc.,* **94**, 1788 (1972).

7) C. Fuganti, P. Grasseli, F. Sprefico, and C. Zirotti, *J. Org. Chem.,* **49**, 534 (1984).

8) H. C. Brown, P. K. Jadhav, and A. K. Mandal, *J. Org. Chem.,* **47**, 5074 (1982).

9) H. Muller, *Ber.,* **35**, 970 (1902).

10) S. N. Hückein and L. Weiler, *Can. J. Chem.,* **52**, 2157 (1974).

11) J. Tsuji, M. Nisar, and I. Minami, *Tetrahedron Lett.,* **27**, 2483 (1986).

12) S. Tsuboi, T. Uno, and A. Takeda, *Chem. Lett.,* **1978**, 1325.

13) A. Brändström and U. Junggeren, *Tetrahedron Lett.,* **1972**, 473.

14) a) D. F. Taber and B. P. Gunn, *J. Org. Chem.,* **44**, 450 (1979). b) J.-L. Gras, *Tetrahedron Lett.,* **1978**, 2955. c) T. Mandai, M. Takeshita, M. Kawada, and J. Otera, *Chem. Lett.,* **1984**, 1259.

15) Racemic compound: M. Baratchart, R. Lalande, and B. Millard, and J. Moulines, *Bull. Soc. Chim. Fr.,* **1976**, 953.

16) D. L. Boger and M. D. Mullican, *J. Org. Chem.,* **45**, 5002 (1980).

17) W. D. Lubell and H. Rapoport, *J. Am. Chem. Soc.,* **110**, 7447 (1988).

18) T. Sakai, T.Nakamura, K. Fukuda, E. Amano, and A. Takeda, *Bull. Chem. Soc. Jpn.,* **59**, 3185 (1986).

19) a) T. Kashiwagi, K. Fujimori, S. Kozuka, and S. Oae, *Tetrahedron,* **26**, 3647 (1970). b) W. Smadja, S. Czernecki, G. Ville, and C. Georgoulis, *Organometallics,* **6**, 166 (1987).

Preparation of 3,3-Bis(phosphoryl)cyclopropenes

Hiroshi YOSHIDA,* Masanori AOYAMA, Fumitaka UTSUMI,
Tsuyoshi OGATA, and Kiyoshi MATSUMOTO†
Department of Applied Chemistry, Faculty of Engineering, Shizuoka University, Hamamatsu 432
† Graduate School of Human and Environmental Studies, Kyoto University, Sakyo-ku, Kyoto 606
(Received May 24, 1991)

Synopsis. The reaction of 1,2-diphenyl- and 1-methyl-2-phenyl-3,3-dichloro- or dibromocyclopropenes with trialkyl phosphites, dialkyl phenylphosphonites, and alkyl diphenylphosphinites afforded cyclopropenes with 3,3-diorganophosphorous substituents in moderate yields via double Arbuzov type reactions.

In a continuation of our studies on the chemistry of cyclopropenium salts and cyclopropenes possessing heteroatom substituents[1] we have tried to prepare cyclopropenium salts with organophosphorus substituents. The reaction of 1-ethoxy-2,3-diphenylcyclopropenium tetrafluoroborate with diethyl phospite or triethylphosphite provided no good results, yielding the original diphenylcyclopropenone. The reaction with dihalocyclopropene, however, proved to be a new easy route to cyclopropenes substituted with 3,3-diorganophspophorous substituents. The dialkoxyphosphinyl derivatives of the general structure, P–CH_2–P or P–CHR–P, have attracted considerable attention because of their biological activities,[2] chelation to metals,[3] and roles as synthetic tools.[4]

The reactions of cyclopropenones (**1**) with thionyl halides afford 3,3-dihalocyclopropenes (**2**) in good yield.[5] Since **2** are unstable to moisture they were used without isolation.

A mixture of 3,3-dichloro-1,2-diphenylcyclopropene (**2aa**) and trimethyl phosphite (**3a**, mole ratio 1 : 1.1) in dichloromethane at 40 °C for 1 d gave 3,3-bis(dimethoxyphosphinyl)-1,2-diphenylcyclopropene (**4aa**) in 37% yield. The use of a mole ratio of 1 : 2.2 afforded **4aa** in 68% yield. The structure of **4aa** was assigned from IR, ^1H, ^{13}C, ^{31}P NMR, and mass spectroscopic studies and chemical transformation. The cyclopropene **4aa** was stable under acidic conditions in a stirring mixture of $HClO_4$–CH_2Cl_2 at room temperature for 2 h. In contrast, upon heating at 50 °C with sodium hydroxide in methanol for 4 h **4aa** provided **5** in 88% yield, indicating the presence of a cyclopropene ring (Scheme 1). A similar treatment of **2** at 40 °C with 2.2 times excess moles of **3** yielded cyclopropenes with 3,3-diorganophosphorous substituents **4** in moderate yields, as listed in Table 1. No 1 : 1 addition product could be isolated. The yields of **4** decreased in the order OMe>OEt>OPr^{-i} with the substituent of phosphorous esters.

It has been shown that the reaction of 1,1-dibromocyclopropanes with trialkyl phosphite at 90 °C in the

Table 1. Reaction of **2** with **3** at 40 °C in CH_2Cl_2

Reaction		Time/h	Product (Yield/%)
2aa	**3a**	24	**4aa** (68)
	3b		**4ab** (48)
	3c		**4ac** (19)
	3d		**4ad** (46)
	3e		**4ae** (35)
	3f	48	**4af** (48)
	3g		**4af** (34)
2ab	**3a**	24	**4aa** (17)
	3b		**4ab** (15)
2ba	**3a**		**4ba** (31)

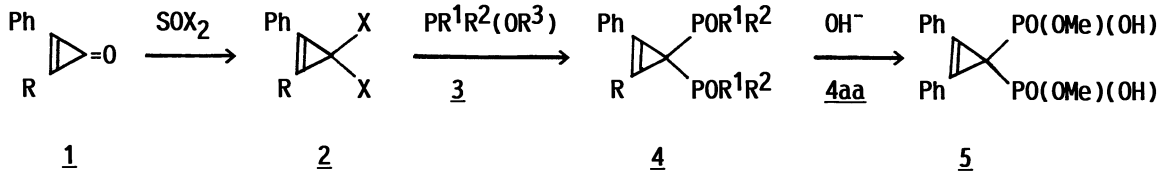

1 2 4 5

1	R
a	Ph
b	Me

2	R	X
aa	Ph	Cl
ab	Ph	Br
ba	Me	Cl

3	R^1	R^2	R^3
a	OMe	OMe	Me
b	OEt	OEt	Et
c	OPr^{-i}	OPr^{-i}	Pr^{-i}
d	Ph	OMe	Me
e	Ph	OEt	Et
f	Ph	Ph	Me
g	Ph	Ph	Et

4	R	R^1	R^2
aa	Ph	OMe	OMe
ab	Ph	OEt	OEt
ac	Ph	OPr^{-i}	OPr^{-i}
ad	Ph	Ph	OMe
ae	Ph	Ph	OEt
af	Ph	Ph	Ph
ba	Me	OMe	OMe

Scheme 1.

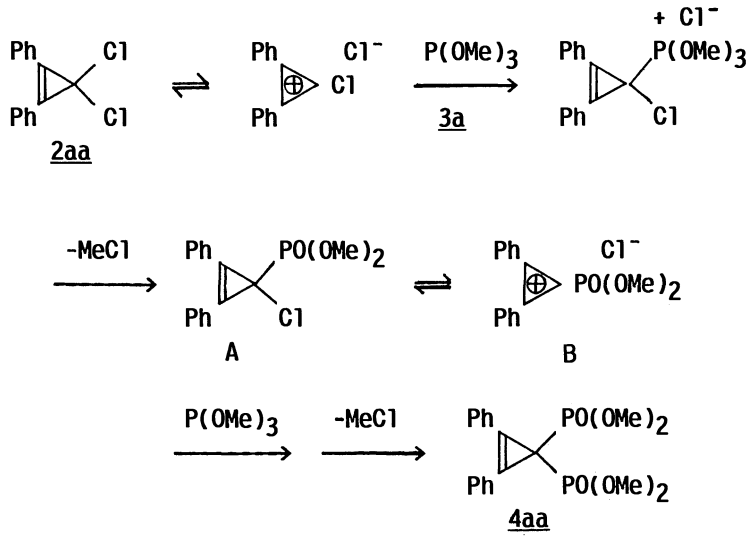

Scheme 2.

presence of triethylamine and water provides cyclopropylphosphonates via reductive phosphonation with dialkyl phosphonates.[6]

Considering the results, we obtained a plausible mechanism for the generation of a representative compound **4aa**, as shown in Scheme 2. Although the isolation of 3-chloro-3-dimethoxylphosphinyl-1,2-diphenylcyclopropene **A**, a mono-Arbuzov reaction product,[7] failed, the intermediacy of mono-adduct **A** was clear from the final product **4**. The reaction of the possible intermediate cyclopropenium salt **B** with **3a** would yield two types of substitution products. One isomer **4** was obtained as stable crystals (Table 1). The formation of another isomer might be prevented by the bulky phenyl group inhibiting substitution onto C-2 with **3** or the subsequent Arbuzov reaction to collapse to the starting reagents. The high activity of the halocyclopropenes was attributed to their aromatic nature.

Experimental

General. The melting points were uncorrected. The ^{1}H NMR spectra were recorded on a Hitachi R-24B (60 MHz) and ^{13}C and ^{31}P NMR spectra on a JEOL JNM FX-90Q (22.40 MHz). NMR spectra were recorded in $CDCl_3$, unless otherwise stated, using TMS (^{1}H and ^{13}C) as an inner or H_3PO_4 (^{31}P) as an external standard. The IR spectra were obtained on a JEOL JIR 100.

The Reaction of 3,3-Dichloro-1,2-diphenylcyclopropene (2aa) with Trimethyl Phosphite (3a). A mixture of 1,2-diphenylcyclopropenone (**1a**) (0.50 g 2.4 mmol) and thionyl chloride (40 mmol) was heated at 40 °C for 2 h; excess of thionyl chloride was removed in vacuo to afford orange crystals of **2aa**. A solution of **2aa** and **3a** (5.3 mmol) in dichloromethane (10 ml) was heated at 40 °C for 24 h. The reaction mixture was condensed in vacuo to dryness, and the obtained crystals washed with petroleum ether; recrystallization from benzene–petroleum ether afforded **4aa** in 68% yield.

4aa: Mp 127—129 °C; IR (KBr) 1860, 1240, and 1030 cm^{-1}; ^{1}H NMR δ=3.72 (dd, J_{POCH}=5.4 and 5.4 Hz, 12H, $4CH_3$) and 7.2—8.1 (m, 10H, 2Ph); ^{13}C NMR δ=23.3 (C-3), 53.0 (CH_3), 104.9, 125.6, 128.8(d), 129.8(d), and 130.1(d); ^{31}P NMR δ=25.26; MS (*m*/*z*) 408 (M^+). Found: C, 55.85; H, 5.36%. Calcd for $C_{19}H_{22}O_6P_2$: C, 55.88; H, 5.43%.

2ab was prepared from **1a** (2.4 mmol) and thionyl bromide (2.9 mmol) in dichloromethane (5 ml) at room temperature for 10 min. Chlorination of **1b** (2.4 mmol) with thionyl chloride (2.4 mmol) was performed at 0 °C for 5 min in dichloromethane (5 ml) to yield **2ba**.

A similar treatment of **2** with **3** yielded **4** in moderate yields, as summarized in Table 1. The physical properties of the products are as follows:

4ab: Mp 99—102 °C; IR (KBr) 1860, 1240, and 1020 cm^{-1}; ^{1}H NMR δ=1.20 (t, *J*=7.2 Hz, 12H, $4CH_3$), 3.8—4.4 (m, 8H, $4CH_2$), and 7.2—8.1 (m, 10H, 2Ph); ^{13}C NMR δ=16.3 (CH_3), 24.3 (C-3), 62.2 (CH_2), 105.4, 126.0, 128.7(d), 129.6(d), and 130.2(d); ^{31}P NMR δ=22.93; MS (*m*/*z*) 464 (M^+). Found: C, 59.43; 6.54%. Calcd for $C_{23}H_{30}O_6P_2$: C, 59.48; H, 6.51%.

4ac: Mp 80—81 °C; IR (KBr) 1840, 1220, and 980 cm^{-1}; ^{1}H NMR δ=1.20 (dd, *J*=6.0 and 6.0 Hz, 24H, $8CH_3$), 4.3—5.0 (m, 4H, 4CH), and 7.2—8.1 (m, 10H, 2Ph); ^{13}C NMR δ=25.9 (CH_3), 26.3 (CH_3), 27.6 (C-3), 72.8(CH), 107.9, 128.4, 130.6(d), 131.4(d), and 132.3(d); ^{31}P NMR δ=21.47; MS (*m*/*z*) 520 (M^+). Found: C, 62.18; H, 7.43%. Calcd for $C_{27}H_{38}O_6P_2$: C, 62.29; H, 7.35%.

4ad: Mp 154—157 °C; IR (KBr) 1820, 1220, and 1020 cm^{-1}; ^{1}H NMR δ=3.5—3.9 (m, 6H, $2CH_3$) and 6.9—7.9 (m, 20H, 4Ph); ^{13}C NMR δ=30.7 (C-3), 51.7 (CH_3), 105.6(d), 125.9(s), 127.6(d), 127.9(d), 128.4(d), 129.5(d), 129.9(d), 131.7(s), and 132.2(d); ^{31}P NMR δ=42.10; MS (*m*/*z*) 500 (M^+). Found: C, 69.65; H, 4.98%. Calcd for $C_{29}H_{26}O_4P_2$: C, 69.59; H, 5.23%.

4ae: Mp 95—97 °C; IR (KBr) 1830, 1230, and 1030 cm^{-1}; ^{1}H NMR δ=1.0—1.5 (m, 6H, $2CH_3$), 3.7—4.5 (m, 4H, $2CH_2$), and 6.9—8.9 (m, 20H. 4Ph); ^{13}C NMR δ=16.4 (CH_3), 18.3 (C-3), 61.2 (CH_2), 106.1 (s), 125.9(d), 127.6(d), 128.3(d), 129.4(d), 130.0(d), 130.2(d), 131.7(s), and 132.5(d); ^{31}P NMR δ=9.88; MS (*m*/*z*) 528 (M^+). Found: C, 70.21; H, 5.82%. Calcd for $C_{31}H_{30}O_4P_2$: C, 70.44; H, 5.72%.

4af: Mp 184—185 °C; IR (KBr) 1190 cm^{-1}; ^{1}H NMR δ=6.8—8.1 (m); ^{13}C NMR δ=36.6(C-3). 108.3(s), 126.5, 127.2, 127.5, 127.8, 128.3, 129.5, 129.8, 131.0, 131.7, 131.9. 132.1, and 133.8; ^{31}P NMR δ=33.68; MS (*m*/*z*) 592 (M^+). Found: C, 79.13; H, 5.01%. Calcd for $C_{39}H_{30}O_2P_2$: C, 79.04; H, 5.10%.

4ba: Mp 83—85 °C; IR (KBr) 1885, 1240, and 1020 cm^{-1}; ^{1}H NMR δ=2.45 (s, 3H, CH_3), 3.6—4.0 (m, 12H, $4CH_3$), and 7.2—7.8 (m, 5H, Ph); ^{13}C NMR δ=11.8 (CH_3), 23.7 (C-3), 54.0 (OCH_3), 103.8(s), 105.1, 126.5, 130.0(d), 130.6(d), and 131.0(d);

MS (m/z) 348 (M^+). Found: C, 48.41; H, 6.13%. Calcd for $C_{14}H_{22}O_6P_2$: C, 48.28; H, 6.36%.

Hydrolysis of 4aa. A solution of **4aa** (0.5 mmol) in ethanol (15 ml) containing 2.5 mmols of sodium hydroxide was heated at 50 °C for 5 h. The reaction mixture was quenched to ice water and acidified with hydrochloric acid. Precipitated crystals were collected and recrystallized from ethanol to yied **5** in 88% yield.

5: Mp 239—242 °C; IR (KBr) 2650, 1210, and 1040 cm^{-1}; ^1H NMR ($CDCl_3$+CF_3CO_2H, 10:1) δ=3.79 (dd, J=5.4 Hz, $2CH_3$) and 7.2—8.0 (m, 10H, 2Ph); ^{13}C NMR ($CDCl_3$+CF_3CO_2H, 10:1) δ=23.2 (C-3), 53.6 (CH_3), 94.1, 124.1(s), 129.2(d), 130.1(d), and 130.9(d); ^{31}P NMR ($CDCl_3$+CF_3CO_2H, 10:1) δ=26.86; MS (m/z) 380 (M^+). Found: C, 53.31; H, 4.51%. Calcd for $C_{17}H_{18}O_6P_2$: C, 53.69; H, 4.77%.

References

1) H. Yoshida, K. Yoshida, Y. Totani, T. Ogata, and K. Matsumoto, *Bull. Chem. Soc. Jpn.*, **63**, 3579 (1990), and references cited therein.

2) R. Engel, *Chem. Rev.*, **77**, 349 (1977); D. W. Hutchinson and D. M. Thornton, *Synthesis*, **1990**, 135, and references cited therin.

3) N. A. Bondarenko, M. V. Rudomino, and E. N. Tsvetkov, *Synthesis*, **1991**, 125, and references cited therin.

4) R. C. Gatrone, *J. Org. Chem.*, **54**, 4272 (1989).

5) S. W. Tobey and R. West, *J. Am. Chem. Soc.*, **86**, 4215 (1964); R. West, D. C. Zecher, and S. W. Tobey, *J. Am. Chem. Soc.*, **92**, 168 (1970).

6) T. Hirao and T. Ohshiro, *J. Synth. Org. Chem. Jpn.*, **45**, 784 (1987); T. Hirao, M. Hagikara, Y. Ohshiro, and T. Agawa, *Synthesis*, **1984**, 60.

7) A. K. Bhattacharya and G. Thyagarajan, *Chem. Rev.*, **81**, 415 (1981).

S_H2' Type Reactions of Arenesulfonyl Chlorides with Allylic Compounds Catalyzed by a Ruthenium(II) Complex

Nobumasa KAMIGATA,* Kimiko ISHII, Takeshi OHTSUKA, and Haruo MATSUYAMA
Department of Chemistry, Faculty of Science, Tokyo Metropolitan University,
Minami-Ohsawa, Hachioji, Tokyo 192-03
(Received June 6, 1991)

Synopsis. In the presence of a catalytic amount of dichlorotris(triphenylphosphine)ruthenium(II), the reactions of arenesulfonyl chlorides with allyl phenyl sulfide and allyl phenyl selenide proceeded smoothly to give allyl phenyl sulfone in high yield as well as the corresponding diphenyl disulfide or diphenyl diselenide. An S_H2'-type mechanism involving the arenesulfonyl radical is proposed.

We previously reported that the reactions of alkane- and arenesulfonyl chlorides with olefins in the presence of a catalytic amount of ruthenium(II) phosphine complex gave the corresponding 1:1 adducts in high yields. A radical mechanism in the coordination sphere of the metal complex is proposed since the reactions were suppressed by the addition of radical inhibitors, such as galvinoxyl, *p*-benzoquinone or DPPH.[1] However, there was no further experimental evidence for the radical process; i.e. we failed to detect the radical intermediates by ESR and CIDNP methods. By the way, Kosugi and Migita first reported the S_H2'-type reactions of the allyl sulfides and halides as being characteristic free radical reactions.[2] We have thus studied the ruthenium(II)-catalyzed reactions of arenesulfonyl chlorides with allyl sulfide and selenide, expecting to obtain the S_H2'-type reaction products; the results should provide good evidence to support the radical mechanism previously proposed by us.

When a solution of tosyl chloride (**1**) (2.0 mmol), allyl phenyl sulfide (**2a**) (4.0 mmol), and a catalytic amount of dichlorotris(triphenylphosphine)ruthenium(II) in benzene was degassed and heated at 140 °C for 24 h, the reaction proceeded smoothly, yielding allyl *p*-tolyl sulfone (**3a**) (89%), diphenyl disulfide (**4a**) (5%), 2-chloro-1,3-bis(phenylthio)propane (**5a**) (51%), and 1-chloro-2,3-bis(phenylthio)propane (**5b**) (17%). No such 1:1 adduct as 2-chloro-3-phenylthio-1-tosylpropane was detected in the reaction products. Similarly, the reactions of benzene-, *p*-chlorobenzene-, and methanesulfonyl chlorides with **2a** in the presence of ruthenium(II) catalyst were also carried out. The results are summarized in Table 1.

Table 1. Reaction of Arene- and Methanesulfonyl Chlorides with Allyl Aryl Sulfide

R in RSO_2Cl	Products, yields[a]/%			
	3	**4a**	**5a**	**5b**
1a *p*-$CH_3C_6H_4$	**3a** 89	5	51	17
1b Ph	**3b** 71	2	54	18
1c *p*-ClC_6H_4	**3c** 71	3	55	18
1d CH_3	**3d** 68	2	48	16

a) Yields were determined by GC based on **1** used.

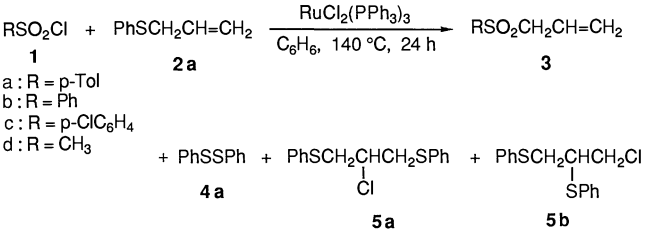

The formation of these reaction products can be accounted for by the radical mechanism shown in Scheme 1. The S_H2' reaction of the arenesulfonyl radical, formed by the interaction of arenesulfonyl chloride with the ruthenium(II) catalyst, with allyl phenyl sulfide gives allyl aryl sulfone (**3**) and phenylthiyl radical (**6**). Although the dimerization of radical **6** affords diphenyl disulfide (**4a**), this represents a minor reaction course. Alternatively, phenylthiyl radical (**6**) adds to excess allyl phenyl sulfide (**2a**), coexisting in the reaction media, to give carbon radical (**7a**) which is considered to lie in equilibrium with radical (**7b**).[3] The transformation of the chlorine atom from the ruthenium(III)–Cl species to radical intermediate **7** gives products **5a** and **5b**.

The reaction of tosyl chloride (**1a**) with allyl phenyl selenide (**2b**) in the presence of the ruthenium(II) catalyst was also studied under similar conditions. In this case, allyl *p*-tolyl sulfone (**3a**), diphenyl diselenide (**4b**), and allyl chloride (**8**) were obtained in high yields. Similarly, the reactions of benzene- and *p*-chlorobenzenesulfonyl chloride (**1b** and **1c**) with **2b** under the ruthenium(II) catalyst were also studied. The results are summarized in Table 2.

The formation of product **3** is accounted for by a S_H2' reaction of the arenesulfonyl radical with allyl phenyl selenide (**2b**). The dimerization of the phenylseleno

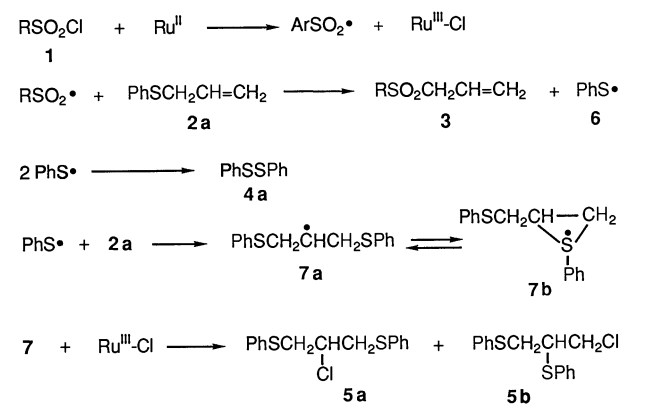

Scheme 1.

Table 2. Reaction of Arenesulfonyl Chlorides with Allyl Aryl Selenide

R in RSO_2Cl	Products, yields[a]/%		
	3	**4b**	**8**
1a *p*-$CH_3C_6H_4$	**3a** 78	98	67
1b Ph	**3b** 75	73	60
1c *p*-ClC_6H_4	**3c** 72	83	62

a) Yields were determined by GC based on **1** used.

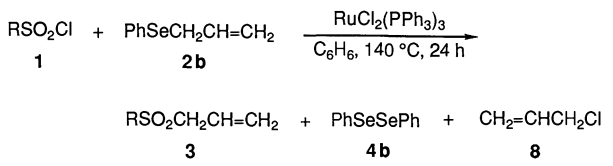

radical to afford diphenyl diselenide (**4b**) is a minor course. In this case, the phenylseleno radical attacks on the selenium atom of excess allyl phenyl selenide coexisting in the reaction media gives diphenyl diselenide (**4b**) and allyl radical (**9**). The allyl radical abstracts the chlorine atom from the Ru(III)–Cl to afford allyl chloride and regenerate Ru(II) (Sheme 2).

The reason why the phenylseleno radical attacks the selenium atom of allyl selenide (**2b**), whereas the phenylthiyl radical reacts with the carbon–carbon double bond of allyl phenyl sufide (**2a**), is accounted for as follows. Although a soft phenylseleno radical reacts selectively with the soft atom (selenium atom) of **2b**, a hard phenylthiyl radical attacks the hard atom (carbon atom) of **2a**.

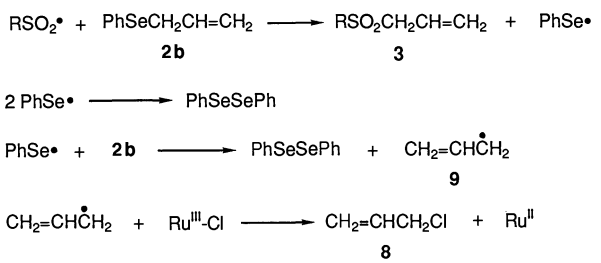

Scheme 2.

In order to obtain further evidence for the S_H2' reaction, the reactions of arenesulfonyl chlorides with (*E*)-2-butenyl phenyl sulfide (**10a**) or (*E*)-2-butenyl phenyl selenide (**10b**) catalyzed by the ruthenium(II) complex were studied. As shown in Table 3, aryl 1-methyl-2-propenyl sulfones (**11**) were formed together with aryl (*E*)-2-butenyl sulfones (**12**). The formation of **11** can be accounted for by the S_H2' reaction. Product **12** is considered to be formed by a secondary reaction of the arenesulfonyl radical with aryl 1-methyl-2-propenyl sulfone (**11**), once formed.

In any case, the fact that the S_H2' reaction products were obtained in high yields strongly supports the radical mechanism in the ruthenium(II)-catalyzed reaction of sulfonyl chloride with olefins, as we proposed previously.

Table 3. Reaction of Arenesulfonyl Chlorides with Aryl (*E*)-2-Butenyl Sulfide and Selenide

R in RSO_2Cl	Z in **10**	Products, yields[a]/%		
1a *p*-$CH_3C_6H_4$	**10a** S	**11a** 22	**12a** 7	**4a** 14
1b *p*-ClH_6H_4	**10a** S	**11b** 34	**12b** 13	**4a** 22
1a *p*-$CH_3C_6H_4$	**10b** Se	**11a** 29	**12a** 28	**4b** 77
1b *p*-ClC_6H_4	**10b** Se	**11b** 41	**12b** 28	**4b** 84

a) Yields were determined by GC based on **1** used.

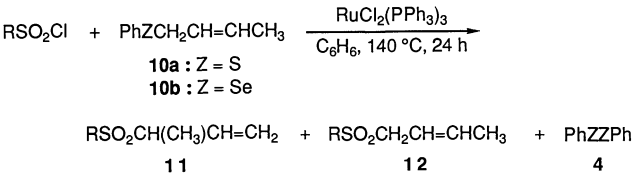

Experimental

Measurement. The melting points were determined on a Yamato MP-21 apparatus and are uncorrected. The infrared absorption spectra were determined on a Hitachi Model 260-10 spectrophotometer with samples as either neat liquids or KBr disks. The proton magnetic resonance spectra were taken with JEOL-PMX 60SI (60 MHz) and Varian XL-200 (200 MHz) spectrometers. The mass spectra were determined with a JEOL JMS-DX 300 mass spectrometer with a JEOL JMA 5000 Mass Data System at an ionizing voltage of 20—70 eV. Gas chromatography was performed using a Hitachi 263-30 gas chromatograph with a SE-30 (10%) 1 m stainless-steel column. Gel-permeation chromatography was performed using a JAI LC-08 liquid chromatograph with two JAIGEL-1H columns (20 mm×600 mm) with chloroform as the eluent.

Materials. Allyl phenyl sulfide (**2a**) (bp 73 °C/4 mmHg, 1 mmHg=133.322 Pa) and allyl phenyl selenide (**2b**) (bp 71 °C/3 mmHg) were prepared by the reaction of allyl bromide with sodium benzenethiolate and sodium benzeneselenolate, respectively. (*E*)-2-Butenyl phenyl sulfide (**10a**) (bp 88 °C/4 mmHg) and (*E*)-2-butenyl phenyl selenide (**10b**) (bp 88 °C/3 mmHg) were prepared by the treatment of (*E*)-2-butenyl bromide with sodium benzenethiolate and sodium benzeneselenolate, respectively. Distillation was performed using a precission-distillation apparatus (Kyowa VI-DL Concentric-Tube Fractionator); the regioisomers formed as the by-products, 1-methyl-2-propenyl phenyl sulfide and 1-methyl-2-propenyl phenyl selenide, were completely removed, respectively. Methanesulfonyl chloride and benzenesulfonyl chloride of Tokyo Kasei Chemicals were purified by distillation under nitrogen prior to use. *p*-Toluenesulfonyl chloride (Tokyo Kasei Chemicals) and *p*-chlorobenzenesulfonyl chloride (Wako Chemicals) were recrystallized prior to use. Dichlorotris(triphenylphosphine)ruthenium(II) was prepared by the method described in the literature.[4]

General Procedure for the Reaction of Sulfonyl Chlorides with Allyl Sulfide or Selenide. A solution containing arenesulfonyl chloride (2.0 mmol), allyl phenyl sulfide (4.0 mmol) or allyl phenyl selenide (6.0 mmol), and dichlorotris-(triphenylphosphine)ruthenium(II) (0.1 mmol) in 4.0 cm^3 of benzene was degassed by a freeze-pump-thaw cycle, sealed in an ampoule, and heated at 140 °C for 24 h. The reaction mixture was subjected to short-column chromatography on Florisil with ethyl acetate to remove the metal complex. The products were isolated from the reaction mixture by the use of gel-

permeation chromatography and/or column chromatography over silica gel (Wakogel C-60), and were identified by IR, NMR, and MS. The yields of the products were determined by GC with eicosane as an internal standard. The physical and spectral data of allyl aryl sulfones (**3a**—**3c**) and allyl methyl sulfone (**3d**) were identical to authentic samples. 2-Chloro-1,3-bis(phenylthio)propane (**5a**) IR (neat) 3050, 1480, 1275, 918, and 740 cm^{-1}; ^1H NMR ($CDCl_3$; 200 MHz) δ=3.32 (2H, dd, J=3.75 and 1.92 Hz), 3.47 (2H, dd, J=3.75 and 1.98 Hz), 4.05 (1H, quint, J=1.92 Hz), and 7.13—7.56 (10H, m); MS m/z 294 (M^+), 185, 149, 109, and 77.

1-Chloro-2,3-bis(phenylthio)propane (5b): IR (neat) 3050, 1480, 1275, 920, and 720 cm^{-1}; ^1H NMR ($CDCl_3$; 200 MHz) δ=3.14—3.58 (3H, m), 3.86 (1H, dd, J=3.03 and 1.80 Hz), 4.02 (1H, dd, J=3.03 and 1.17 Hz), and 7.13—7.56 (10H, m); MS m/z 294 (M^+), 185, 149, 135, 123, 116, 109, and 77.

3-Methyl-3-tosylpropene (11a): Mp 63 °C, IR (KBr) 2980, 2260, 1640, 1598, 1315, 1145, and 1085 cm^{-1}; ^1H NMR ($CDCl_3$) δ=1.41 (3H, d, J=6.6 Hz), 2.41 (3H, s), 3.42—3.90 (1H, m), 4.84—6.11 (3H, m), and 7.26 and 7.63 (4H, ABq, J=8.4 Hz), MS m/z 210 (M^+), 156, 140, and 91.

3-(*p*-Chlorophenylsulfonyl)-1-butene (11b): IR (neat) 3100, 2090, 1645, 1585, 1315, 1145, and 1090 cm^{-1}; ^1H NMR ($CDCl_3$) δ=1.42 (3H, d, J=7.2 Hz), 3.45—3.94 (1H, m), 4.85—6.12 (3H, m), and 7.46 and 7.72 (4H, ABq, J=9.0 Hz); MS m/z 230 (M^+), 175, 160, 144, and 112.

1-Tosyl-2-butene (12a): IR (neat) 2920, 1735, 1665, 1585, 1320, 1130, and 1085 cm^{-1}; ^1H NMR ($CDCl_3$) δ=1.69 (3H, d, J=4.2 Hz), 2.43 (3H, s), 3.71 (2H, d, J=5.4 Hz), 5.35—5.60 (2H, m) and 7.32 and 7.70 (4H, ABq, J=8.4 Hz); MS m/z 210 (M^+), 156, 135, and 92.

1-(*p*-Chlorophenylsulfonyl)-2-butene (12b): IR (neat) 3080, 2910, 1690, 1665, 1585, 1320, 1145, and 1090 cm^{-1}; ^1H NMR ($CDCl_3$) δ=1.68 (3H, d, J=4.2 Hz), 3.70 (2H, d, J=6.0 Hz), 5.25—5.63 (2H, m), and 7.47 and 7.73 (4H, ABq, J=8.4 Hz); MS m/z 230 (M^+), 197, 175, and 112.

References

1) N. Kamigata, H. Sawada, N. Suzuki, and M. Kobayashi, *Phosphorus Sulfur,* **19**, 199 (1984); N. Kamigata, H. Sawada, J. Ozaki, and M. Kobayashi, *Sulfur Lett.,* **1**, 131 (1983); N. Kamigata, N. Suzuki, and M. Kobayashi, *Phosphorus Sulfur,* **20**, 139 (1984); N. Kamigata, H. Sawada, and M. Kobayashi, *J. Org. Chem.,* **48**, 3793 (1983); N. Kamigata, J. Ozaki, and M. Kobayashi, *J. Org. Chem.,* **50**, 5045 (1985); M. Kameyama, N. Kamigata, and M. Kobayashi, *Chem. Lett.,* **1986**, 527; M. Kameyama, N. Kamigata, and M. Kobayashi, *J. Org. Chem.,* **52**, 3312 (1987); M. Kameyama and N. Kamigata, *Bull. Chem. Soc. Jpn.,* **60**, 3687 (1987).

2) M. Kosugi, K. Kurino, K. Takayama, and T. Migita, *J. Organomet. Chem.,* **56**, C11 (1973); T. Migita, M. Kosugi, K. Takayama, and Y. Nakagawa, *Tetrahedron,* **29**, 51 (1973); M. Kosugi, Y. Shimizu, and T. Migita, *J. Organomet. Chem.,* **129**, C36 (1977).

3) P. D. Readio and P. S. Skell, *J. Org. Chem.,* **31**, 759 (1966).

4) T. A. Stephenson and G. Wilkinson, *J. Inorg. Nucl. Chem.,* **28**, 945 (1966); P. S. Hallam, T. A. Stephenson, and G. Wilkinson, *J. Chem. Soc. A,* **1970**, 2497.

Reactivity of Alkaneselenenyl Bromide: Conversion of Alcohols into the Corresponding Alkyl Bromides with Dialkylselenium Dibromide

Sadatoshi AKABORI* and Yoshinori TAKANOHASHI
Department of Chemistry, Faculty of Science, Toho University, Funabashi-shi, Chiba 274
(Received June 7, 1991)

Synopsis. The reaction of alcohols with dialkylselenium dibromide gave the corresponding bromides in moderate to high yields. Alkaneselenyl bromide, produced by the thermal decomposition from dialkylselenium dibromide, acts as a brominating agent. The reaction of alcohols with dialkylselenium dichloride also afforded the corresponding chlorides, although the yields were relatively low compared with those of the bromide.

Although organoselenium compounds have been known for a long time, some compounds being described at the end of the last century, the use of selenium reagents or intermediates has only been recent.[1] Although the structures of the organoselenium functions are similar to those of organic sulfur compounds, the use of selenium reagents often facilitates the reaction to proceed under simpler and milder conditions. It is also well known that alkyl halides can be obtained by the reaction of alcohols with many kinds of halogenating agents.[2] For example, hydrogen halide, phosporous halide, thionyl halide, etc. have been used as halogenating agents. Recently, Furukawa et al.[3] also reported the conversion of alcohols to alkyl bromides using the bromine adduct of dimethyl sulfide (Me_2SBr_2). In a previous paper, we reported a new procedure for the highly selective reduction of tertiary amides to the corresponding amines with $NaBH_4$–diethylselenium dibromide **2a** as the reducing agent in tetrahydrofuran.[4] We also reported a convenient one-pot procedure for the synthesis of symmetric tricalcogena[3]metallocenophanes using **2a** as the selenium insertion reagent.[5] In connection with these results we report here a new procedure for the convenient conversion of alcohols to alkyl halides using dialkylselenium dihalide **2** as the halogenating agent.

Results and Discussion

The reaction was carried out as follows. The reaction of **2a** with a large excess of 1-octanol at 80 °C for 7 h afforded 1-bromooctane in 98% yield together with 1,2-dibromoethane (75%). Similar reactions were carried

$$\underset{\mathbf{1}}{ROH} \xrightarrow{2} \underset{\mathbf{3}}{RX}$$

out using **2b**, **2c**, and **2d** as brominating agents. These results are summarized in Table 1. At room temperature this reaction did not proceed, and the starting materials were recovered quantitatively. Furthermore, among the examined dialkylselenium dibromides used as brominating agents **2a**, **2b**, **2c**, and **2d**, **2a** usually gave the best results; the yields of 1-bromooctane using **2b**, **2c**, and **2d** had nearly similar values. These results suggest that the bromine atom in **2a** may act as an electron-attracting group, and the cleavage of the Se–C bond in **2a** occurred more easily compared with those in **2b**, **2c**, and **2d**. The following bromination of several kinds of alcohols was therefore carried out using **2a** as the bromination reagent. These results are summarized in Table 2. Primary alcohols could be converted to the corresponding bromides in much higher yields compared with those of secondary alcohols. The yields of primary bromides **3a**—**c** were also much higher than that obtained by the methods already reported.[2] In contrast with the above bromination reaction, the reaction of the alcohols with bis(2-chloroethyl)selenium dichloride **4** gave the corresponding alkyl chlorides **5a**—**d**, although the yields were relatively low compared with those for bromination (Table 2). This result may be attributed to the strong Se–Cl bond compared to the Se–Br bond.[6] Furthermore, a similar reaction of alcohols was carried out using diethylselenium diiodide **6** as the iodinating reagent. However, the corresponding alkyl iodides could not be obtained in any cases. The differences in the halogenating abilities between the bromine or

Table 1. Bromination of 1-Octanol **1a** with Dialkylselenium Dibromides **2**

Brominating agent R_2SeBr_2	Yield (%) of 1-bromooctane **3a**
2a: R=$BrCH_2CH_2$–	98
2b: R=CH_3CH_2–	35
2c: R=$(CH_3)_2CH$–	45
2d: R=C_6H_{13}–	40

a) Determined by GLC based on **2**.

Table 2. Halogenation of Alcohols with Bis(2-haloethyl)selenium Dihalides **2a** and **4**

Alcohol R=	Reagent	Product X=	Yield/%
1a: C_8H_{17}–	**2a**	**3a** (X=Br)	98
1a: C_8H_{17}–	**4**	**5a** (X=Cl)	39
1b: C_5H_{11}–	**2a**	**3b** (X=Br)	78
1b: C_5H_{11}–	**4**	**5b** (X=Cl)	35
1c: C_4H_9–	**2a**	**3c** (X=Br)	96
1c: C_4H_9–	**4**	**5c** (X=Cl)	34
1d: $C_3H_7CHCH_3$	**2a**	**3d** (X=Br)	52
1d: $C_3H_7CHCH_3$	**4**	**5d** (X=Cl)	8
1e: $C_2H_5CHCH_3$	**2a**	**3e** (X=Br)	50
1f: $C_2H_5C(CH_3)_2$	**2a**	**3f** (X=Br)	52
1g: $(CH_3)_3C$–	**2a**	**3g** (X=Br)	41

a) The yields were determined by GLC.

chlorine adducts and the iodine adduct are attributable to these structures. Indeed, it was reported that the chlorine and bromine adducts of dialkyl selenide are trigonal bipyramidal structures, while the iodine adduct is a molecular complex.[7,8] The iodine adduct could therefore not react with alcohol, while the reaction of the bromine and chlorine adducts with alcohol gave alkaneselenyl halides and an alkyl halide. In fact, Behagel et al.[9] and Edwards et al.[10] reported that the thermal decomposition of dialkylselenium dibromide easily gave alkaneselenenyl bromide and alkyl bromide. This finding was also confirmed by the following experiments. After a solution of diethylselenium diiodide **6** in methanol-d_4 was refluxed for 7 h, the ^{1}H NMR spectrum of the solution was measured. However, no spectral changes were observed.

In order to investigate the chemical species in this reaction, the change conversion of 1-octanol **1a** versus the reaction time in the reaction with **2b** and with ethaneselenenyl bromide **7** (which was obtained by the reaction of diethyl diselenide with bromine in quantitative yield) was measured. Very similar results were obtained (yields ca. 30%) in both reactions. Similar results were also obtained in a comparison of the reactions of 1-butanol with **2b** and **7**. The yields of the alkyl bromide using ethaneselenenyl bromide **7** are comparable with those using **2a**, although the reason cannot be detailed at present. However, these finding suggests that bromination occurred as follows: i) after thermal decomposition of **2b** in alcohol gives **7**, the negatively charged bromine atom of **7** attacks the carbon atom attached to the hydroxyl group; ii) perhaps the initial reaction is the formation of alkaneselnenyl bromide and the resulting alkaneselenenyl bromide rapidly reacts with nucleophile to form HBr and RSeOR′. The next step is a nucleophilic replacement of the hydroxyl group of alcohol by the bromine anion. Support for the reaction mechanism (ii) is, however, based on the following. It is well known that the reaction of alkaneselenenyl bromide with methanol gave HBr and a stable selenium compound.[11,12] Furthermore, the reaction of 1-octanol **1a** with bis(2-bromoethyl)selenium dibromide **2a** in the presence of hydrogen chloride gave 1-chlorooctane **5a** together with 1-bromooctane **3a** in 77% yield. Also, as previously described, the relatively higher reactivity of **2a** in comparison with **2b**—**d** has been ascribed to a facile generation of the corresponding alkaneselenenyl bromide from **2a**. This means that the rate-determining step is the generation of the alkaneselenenyl bromide, rather than the brominating step.

This reaction mechanism is completely different from that of the bromination methanism of alcohol using Me_2SBr_2, in which dimethylbromosulphonium bromide plays an important role as the brominating agent.[3]

Experimental

Gas chromatography was performed on a Shimadzu G. C-8APF gas chromatography with a PEG20M (2.0%) 2m glass column.

Materials. Diethylselenium dibromide **2b**,[13] diethylselenium diiodide **6**,[14] bis(2-bromoethyl)selenium dibromide **2a**,[15] bis(2-chloroethyl)selenium dichloride **4**,[16] dihexylselenium dibromide **2d**,[17] diisopropylselenium dibromide **2c**,[17] diethyl diselenide and ethaneselenenyl bromide **7**[18] were prepared according to methods described in the literature. All of the alcohols and alkyl halides purchased from commercial sources were used without further purification; all solvents were purified by distillation in the usual manner.

General Procedure for the Halogenation of Alcohols with Dialkylselenium Dihalide. The following procedure used for the preparation of the alkyl halides is representative. A mixture of bis(2-bromoethyl)selenium dibromide **2a** (2.25 g, 5 mmol) and alcohol **1a** (10 ml) was stirred for 7 h at 80 °C. The reaction mixture was cooled to room temperature and then the supernatant solution was analyzed by GLC. The yield of 1-bromooctane **3a** was 98%.

All products, thus obtained, were known compounds, and were identified by the bp's as well as by comparisons of the NMR and IR spectra and/or the GLC retention times with those of authentic samples prepared independently.

A similar reaction was also carried out at room temperature. However, the brominating products could not be obtained and the starting materials were recovered in quantitative yields.

Preparation of Ethaneselenenyl bromide 7 in 1-Octanol or Tetrachloromethane. Bromine (0.40 g, 2.5 mmol) was rapidly added to a solution of diethyl diselenide (0.78 g, 2.5 mmol) in 1-octanol **1a** (10 ml). After the solution was stirred for 30 min at 0 °C, ethaneselenenyl bromide **7** was obtained in quantitative yield according to a method described in the literature.[18]

The resulting ethaneselenenyl bromide **7** was used without isolation in the following reaction with alcohols, as described below.

General Procedure for the Bromination of Alcohols with Ethaneselenenyl Bromide 7 in Tetrachloromethane. To a tetrachloromethane solution (10 ml) containing diethyl diselenide (1.56 g, 5 mmol) bromine (0.8 g, 5 mmol) was quickly added at 0 °C. After stirring 30 min at 0 °C, 1-octanol **1a** (1.30 g, 10 mmol) was rapidly added to the resulting tetrachloromethane solution of ethaneselenenyl bromide **7**. The reaction mixture was stirred for a further 7 h at 80 °C. After the reaction mixture was cooled to room temperature, the supernatant solution was analyzed by GLC. The yield of 1-bromooctane **3a** was 35%.

General Procedure for the Bromination of Alcohols with Ethaneselenenyl Bromide 7 in Alcohol. A mixture of diethyl diselenide (0.78 g, 2.5 mmol) and bromine (0.40 g, 2.5 mmol) in 1-octanol **1** (10 ml) was stirred for 30 min at 0 °C and then refluxed for a further 7 h at 80 °C. After the reaction mixture was cooled to room temperature, the supernatant solution was analyzed by GLC. The yield of 1-bromooctane **3a** was 35%.

Reaction of 1-Octanol 1a with 2a in the Presence of HCl. A solution of **2a** (2.25 g, 5 mmol) in 10 ml of 1-octanol **1a** containing dry HCl was stirred at 80 °C for 7 h. The reaction mixture was then analyzed. The GLC analyses revealed the presence of **3a** (3.9 mmol, 77%) and 1-chlorooctane **5a** (1.1 mmol).

The authors wish to express their thanks to Professor Naoki Inamoto of the Juntendo University for useful discussion.

References

1) C. Paulmier, "Selenium Reagents and Intermediates in Organic Syntheses," ed by J. E. Baldwin, Pergamon Press, New York (1986).

2) C. A. Buehler and D. E. Pearson, "Survey of Organic Syntheses," Wiley-Interscience, New York (1970).

3) N. Furukawa, T. Inoue, T. Aida, and S. Oae, *J. Chem.*

Soc., Chem. Commun., **1973**, 212.
4) S. Akabori and Y. Takanohashi, *Chem. Lett.,* **1990**, 251, *J. Chem. Soc., Perkin Trans. 1,* **1991**, 479.
5) S. Akabori, Y. Takanohashi, and S. Takagi, *Synth. Commun.,* **20**, 3187 (1990).
6) K. A. Jensen and A. Kajaer, "The Chemistry of Organic Selenium and Tellurium Compounds," ed by S. Patai and Z. Rappoport, John Wiley and Sons, New York (1986), Vol. 1, p. 15.
7) W. Nakanishi, Y. Yamamoto, Y. Kusuyama, Y. Ikeda, and H. Iwamura, *Chem. Lett.,* **1983**, 675.
8) a) S. Akabori, Y. Takanohashi, S. Aoki, and S. Sato, the 61th Annual Meeting of Chemical Society of Japan, Yokohama, 1991, Abstr. II, p. 1623. b) *idem., J. Chem. Soc., Perkin Trans. 1,* in press.
9) O. Behagel and K. Hoffman, *Ber.,* **72B**, 582 (1939).
10) O. K, Edward, W. R. Gaythwaite, J. Kenyon, and H. Phillips, *J. Chem. Soc.,* **1928**, 2293.
11) W. Jenny, *Hev. Chim. Acta,* **35**, 1591 (1952).
12) W. S. Cook and R. A. Donia, *J. Am. Chem. Soc.,* **73**, 2275 (1951).
13) L. B. Marjorie and C. Frederick, *J. Chem. Soc.,* **1942**, 570.
14) D. K. Safin and G. A. Chmutova, *Zh. Obshch. Khim.,* **55**, 2564 (1985).
15) H. C. Bell and C. S. Gibson, *J. Chem. Soc.,* **1925**, 1877.
16) G. Bell, *J. Chem. Soc.,* **1927**, 1882.
17) M. Schmidt and H. D. Block, *Chem. Ber.,* **103**, 3705 (1979).
18) D. N. Brattesami and C. H. Heathcock, *Tetrahedron Lett.,* **26**, 2279 (1974).

Alumina-Catalyzed Addition of Thiols to Methyl Propiolate

Mitsuo KODOMARI,* Goroh SAITOH, and Suehiko YOSHITOMI
Department of Industrial Chemistry, Faculty of Engineering, Shibaura Institute of Technology, Shibaura, Minato-ku, Tokyo 108
(Received June 10, 1991)

Synopsis. The addition of thiols to methyl propiolate was remarkably accelerated in the presence of alumina to give the *Z*-isomer of the 1:1 adducts stereoselectively, in which alumina acts as a bifunctional catalyst of acid and base.

Recently, a significant improvement of the reagent activity or selectivity has been achieved for a variety of organic reactions by the use of reagents supported on an inorganic solid or by the adsorption of substrates onto the surface of an inorganic solid.[1] The application of an inorganic solid (e.g., silica gel,[2] alumina,[3], zeolite[4]) as a solid base and an acid catalyst for organic reactions in the liquid phase has also attracted the attention of organic chemists. We previously reported that addition of phenols to dimethyl acetylenedicarboxylate adsorbed on alumina in the absence of a base gives *cis*-addition products selectively.[5] Although the addition of phenol to methyl propiolate under similar conditions did not occur, thiols reacted with methyl propiolate in the presence of alumina to give the *Z*-isomer of the 1:1 adducts in high yield. Herein, we report on these results.

Results and Discussion

The reaction of thiols, especially aliphatic thiols, with esters of propiolic acid is very slow in the absence of catalysts, but is remarkably accelerated by a base, giving 1:1 adducts which are a mixture of both the *E*- and *Z*-isomer. The ratio of the *E*- and *Z*-isomer is dependent on the nature of the solvents. The reaction in a protic polar solvent gives predominantly the *Z*-isomer and in an aprotic solvent mainly the *E*-isomer.[6]

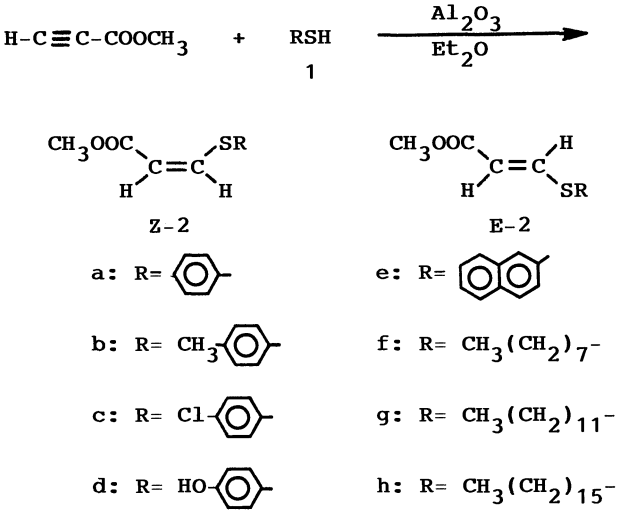

Scheme 1.

A reaction of 2-naphthalenethiol (**1e**) with methyl propiolate was carried out in diethyl ether in the absence of a base at 10 °C for 1 h to give a 19% yield of methyl 3-(2-naphthylthio)acrylate (**2e**), which was a mixture of the iosmers (*Z*/*E* 50/50). By adding triethylamine as a catalyst the reaction was accelerated to give a 85% yield of **2e**. The *Z*/*E* ratio of the product isomers, however, was about the same as in the absence of a catalyst. In contrast, the reaction in the presence of neutral alumina under similar conditions gave a 96% yield of **2e**; the *Z*/*E* ratio of the product isomers was 90/10. Neutral alumina was most effective in promoting the reaction. Silica gel and a molecular sieve (5A) were entirely ineffective. The yield of **2e** and the ratio of the product isomers obtained in a variety of solvents are about the same as in diethyl ether (see Table 1). These results suggest that the reaction occurs on the sulface of alumina rather than in the solution. Substituted aromatic thiols also reacted with methyl propiolate in the presence of alumina under similar conditions to give the corresponding *Z*-isomer of **2** in high yields. The reaction with aliphatic thiols, which are less reactive than aromatic thiols, required a long reaction time; the stereoselectivity is slightly lower than in a reaction with aromatic thiols. Neutral alumina showed a higher catalytic activity than that of basic alumina; acidic alumina was ineffective (see Table 2). Although thiol is readily oxidized to disulfide in the presence of alumina under mild conditions,[7] disulfides were not detected under these reaction conditions. It is well-known that *cis*-(2-substituted vinyl) sulfides are isomerized by thiyl radical to an equilibrium mixture consisting mainly of the *E*-isomer.[8] A mixture of *Z*-**2b** and catalytic amounts of *p*-toluenethiol in diethyl ether was stirred at 10 °C for 10 h. However, no isomerization of the *Z*-

Table 1. Addition of 2-Naphthalenethiol (**1e**) to Methyl Propiolate[a]

Catalyst	Solvent	Yield of **2e**/%[b]	Ratio of *Z*-**2e**/*E*-**2e**[c]
None	Et_2O	19	50/50
Al_2O_3[d]	Et_2O	96	90/10
	$CHCl_3$	97	90/10
	CH_3CN	99	94/6
	EtOH	98	91/9
SiO_2[e]	Et_2O	20	55/45
MS-5A[f]	Et_2O	20	58/42
NEt_3[g]	Et_2O	85	42/58

a) A mixture of **1e** (1 mmol), methyl propiolate (1 mmol) and a catalyst (0.5 g) in diethyl ether was stirred at 10 °C for 1 h. b) By GLC. c) Determined by ^1H NMR. d) Neutral alumina for column chromatography. e) For column chromatography. f) Powder. g) 0.1 mmol.

Table 2. Alumina-Catalyzed Addition of Thiols to Methyl Propiolate[a)]

Thiol/**1**	Time/h	Yield of **2**/%[b)]	Ratio of *Z*-**2**/*E*-**2**[c)]
1a	1	97 (7)	87/13 (63/37)
1b	1	97 (20)	88/12 (59/41)
1c	1	98 (21)	91/ 9 (59/41)
1d	1	90 (9)	84/16 (57/43)
1e	1	96 (19)	90/10 (50/50)
1f	48	86 (2)	83/17 (43/57)
1g	48	89 (3)	78/22 (39/61)
1g[d)]	48	65	80/20
1g[e)]	48	13	68/32
1h	48	81 (3)	70/30 (5/95)

a) All reactions were carried out at 10 °C in diethyl ether under nitrogen. b) By GLC. c) By ^{1}H NMR. b, c) Figures in parentheses show the yield and the *Z*/*E* ratio obtained in the reaction without alumina. d) Basic alumina. e) Acidic alumina.

isomer to the *E*-isomer occurred. *Z*-**2b** was isomerized to the *E*-isomer upon heating in the presence of *p*-toluenethiol at 80 °C in benzene. These results show that the *E*-isomer of the product isomers does not arise from the *Z*-isomer by post-isomerization under these reaction conditions. It has been reported that the nucleophilic ring opening of epoxides is catalyzed by zeolite, in which the cooperative function of both the acid and base sites on its surface is thougt to be essential for effective catalysis.[4)] The effective catalysis of neutral alumina in the addition of thiols to methyl propiolate is also likely to be due to the cooperative function of acid and base sites on the alumina surface. Thus, the nucleophilicity of thiol is enhanced by a base site, and methyl propiolate can be activated by an acid site. The interaction between a acid site and a carbonyl group of methyl propiolate facilitates the formation of an enol during an attack by the nucleophile (RS^-) at the triple bond. The stereoselectivity in the reaction with aromatic thiols was higher than that in a reaction with aliphatic thiols, and the *Z*/*E* ratio of the product isomers in the reaction with aliphatic thiols decreased with incresing length of the alkyl group. These observations indicate that the *Z*-isomer is formed preferentially when the thiol molecule is strongly adsorbed on the surface of alumina. The resonance-stabilized anion intermediate, which is formed by the coordination of the thiolate ion at the β-carbon of methyl propiolate, is adsorbed on its surface. The intermediate therefore accepts a proton from thiol on its least hindered side to give the *Z*-isomer (see scheme 2).

Experimental

Methyl (*Z*)-3-(2-Naphthylthio)acrylate (*Z*-2e). General Procedure. Neutral alumina (ICN Biomedicals, N-Super 1, 2.5 g) was added to a solution of methyl propiolate (5 mmol, 0.42 g) in diethyl ether (40 ml), and stirred at 10 °C for 20 min. To the mixture was added a solution of 2-naphthalenethiol (5 mmol, 0.80 g) in diethyl ether (20 ml); stirring continued at 10 °C for 1 h under nitrogen. The product mixture was filtered, and the solid was washed with diethyl ether. The combined filtrate was washed with 5% aqueous sodium hydroxide and water, and dried. Evaporation of the solvent under reduced pressure yielded 1.21 g of **2e** as a white solid. The *Z*/*E* ratio of the product isomers was determined by ^{1}H NMR. The *Z*/*E* ratio was 90/10. Pure *Z*-isomers of **2b**, **2c**, **2d**, **2e**, **2g**, and **2h** were readily obtained by recrystallization of the crude products from appropriate solvents. The melting point and spectrum data for these *Z*-isomers are shown below.

Methyl (*Z*)-3-(*p*-Tolylthio)acrylate (2b). Mp 53—54 °C (lit,[9)] 54—55 °C) (from hexane); ^{1}H NMR ($CDCl_3$) δ=2.31 (3H, s, CH_3), 3.73 (3H, s, OCH_3), 5.86 (1H, d, *J*=9.9 Hz, =CHO–), 7.12 (2H, d, *J*=10 Hz, PhH), 7.34 (1H, d, *J*=9.9 Hz, =CHS–), 7.35 (2H, d, *J*=10 Hz, PhH).

Methyl (*Z*)-3-(*p*-Chlorophenylthio)acrylate (2c). Mp 99—100 °C (from hexane); IR (KBr) 1696, 1222, 1170, 1094, 817 cm^{-1}; ^{1}H NMR ($CDCl_3$) δ=3.76 (3H, s, OCH_3), 5.93 (1H, d, *J*=9.9 Hz, =CHCO–), 7.19 (1H, d, *J*=9.9 Hz, =CHS–), 6.98—7.65 (4H, m, PhH); MS *m*/*z* (%) 228 (M^+; 100), 197 (75), 169 (58), 143 (44), 134 (43), 125 (9), 117 (24), 108 (45). HRMS. Found: *m*/*z* 228.0006. Calcd for $C_{10}H_9O_2SCl$: M, 228.0012.

Methyl (*Z*)-3-(*p*-Hydroxyphenylthio)acrylate (2d). Mp 114—115 °C (from benzene–hexane); IR (KBr) 3287, 1671, 1228, 1168, 802 cm^{-1}; ^{1}H NMR ($CDCl_3$) δ=3.71 (3H, s, OCH_3), 5.87 (1H, d, *J*=10.8 Hz, =CHCO–), 6.91 (2H, d, *J*=9.5 Hz, PhH), 7.29 (1H, d, *J*=10.8 Hz, =CHS–), 7.37 (2H, d, *J*=9.5 Hz, PhH), 8.73 (1H, s, –OH); MS *m*/*z* (%) 210 (M^+, 100), 179 (52),

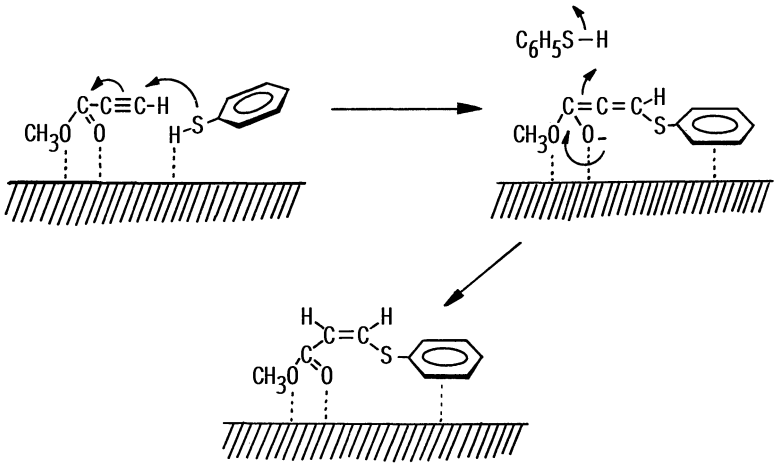

Scheme 2.

151 (46), 133 (10), 125 (42), 107 (12), 97 (14), 81 (15). HRMS. Found: m/z 210.0326. Calcd for $C_{10}H_{10}O_3S$: M, 210.0351.

Methyl (*Z*)-3-(2-Naphthylthio)acrylate (2e). Mp 73—74 °C (from hexane); IR (KBr) 1697, 1564, 1080, 865, 740 cm^{-1}; ^1H NMR ($CDCl_3$) δ=3.74 (3H, s, OCH_3), 5.91 (1H, d, J=10.8 Hz, =CHCO–), 7.28 (1H, d, 10.8 Hz, =CHS–), 7.31—7.90 (7H, m, arom.); MS m/z (%) 244 (M^+; 57), 213 (15), 185 (100), 159 (8), 152 (10), 141 (8), 127 (12), 115 (53). HRMS. Found: m/z 244.0558. Calcd for $C_{14}H_{12}O_2S$: M, 244.0558.

Methyl (*Z*)-3-(Dodecylthio)acrylate (2g). Mp 47—48 °C (from methanol); IR (KBr) 2920, 2850, 1698, 1470, 804 cm^{-1}; ^1H NMR ($CDCl_3$) δ=0.89 (3H, t, $-CH_3$), 1.10—1.78 (20H, m, $-(CH_2)_{10}-$), 2.76 (2H, t, $-SCH_2-$), 3.72 (3H, s, $-OCH_3$), 5.84 (1H, d, J=10.8 Hz, =CHCO–), 7.11 (1H, d, J=10.8 Hz, =CHS–). MS m/z(%) 286 (M^+; 22), 225 (15), 213 (20), 199 (20), 117 (40), 100 (21), 87 (46), 69 (26), 55 (71), 43 (100). HRMS. Found: m/z 286.1996. Calcd for $C_{16}H_{30}O_2S$: M, 286.1967.

Methyl (*Z*)-3-(Hexadecylthio)acrylate (2h). Mp 63—64 °C (from methanol); IR (KBr) 2921, 2850, 1697, 1471, 804 cm^{-1}; ^1H NMR ($CDCl_3$) δ=0.88 (3H, t, $-CH_3$), 1.14—1.78 (28H, m, $-(CH_2)_{14}-$), 2.75 (2H, t, $-SCH_2-$), 3.72 (3H, s, $-OCH_3$), 5.84 (1H, d, J=9.9 Hz, =CHCO–), 7.10 (1H, d, J=9.9 Hz, =CHS–); MS m/z (%) 342 (M^+; 11), 311 (10), 269 (14), 255 (26), 117 (26), 87 (36), 69 (19), 55 (67), 43 (100). HRMS. Found: m/z 342.2589. Calcd for $C_{20}H_{38}O_2S$: M, 342.2593.

References

1) For reviews, see a) A. Mckillop and D. W. Young, *Synthesis,* **1979**, 401; b) G. H. Posner, *Angew. Chem., Int. Ed. Engl.,* **17**, 487 (1978); c) A. Cornelis and P. Laszlo, *Synthesis,* **1985**, 909.

2) Y. Kamitori, M. Hojo, R. Masuda, T. Izumi, and S. Tsukamoto, *J. Org. Chem.,* **49**, 4161 (1984).

3) S. W. Pelletier, A. P. Venkov, J. F. Moore, and N. V. Mody, *Tetrahedron Lett.,* **21**, 809 (1980).

4) M. Onaka, M. Kawai, and Y. Izumi, *Chem. Lett.,* **1985**, 779.

5) M. Kodomari, T. Sakamoto, and S. Yoshitomi, *J. Chem. Soc., Chem. Commun.,* **1990**, 701.

6) P. D. Halphen and T. C. Owen, *J. Org. Chem.,* **38**, 3507 (1973).

7) K. T. Liu and Y. C. Tong, *Synthesis,* **1978**, 669.

8) A. A. Oswald, K. Griesbaum, B. E. Hudson, Jr., and J. M. Bergman, *J. Am. Chem. Soc.,* **86**, 2877 (1964).

9) W. E. Truce and G. J. W. Tichenor, *J. Org. Chem.,* **37**, 2391 (1972).

Photochemistry of Substituted 2-Benzoylcyclohexanones

Tadashi HASEGAWA,* Yiming YANG, and Michikazu YOSHIOKA†
Department of Chemistry, Tokyo Gakugei University,
Nukuikitamachi, Koganei, Tokyo 184
† Department of Chemistry, Saitama University,
Shimo-okubo, Urawa, Saitama 338
(Received June 28, 1991)

Synopsis. The photoreactivities of substituted 2-benzoylcyclohexanones were distinguished as three different types; 1) the exclusive Norrish Type II cleavage when there were no alkyl groups on the 2- nor on the ortho-position, 2) the benzoyl group shift from the 2- to the 4-position when an alkyl group was present on the 2- and not on the ortho-position, and 3) 1,2,3,4,4a,9a-hexahydro-9(10*H*)-anthracenone derivative formation when an ortho-methyl group was present.

The Norrish Type II photoreactions of alkyl phenyl ketones have been investigated extensively.[1] In the Type II reaction, the cleavage generally competes with the cyclization. We have reported that 2-benzoylcyclohexanone (**1a**) underwent an exclusive Type II cleavage reaction to give **2a** and that the enol from of **2a** acted as an effective internal filter.[2] A 1-phenyl-1,3-alkanedione has been utilized to prevent the coloration of polymers, and ability and efficiency as a preventer are known to be affected by the alkyl chain length of the diketone and alkyl substituents on the chain.[3] Compound **2a** may be utilized as a good preventer with a C=C double bond at the end of the alkyl chain. The Type II cleavage reaction of substituted 2-benzoylcyclohexanones **1** is expected to be a useful method for the preparation of substituted 1-phenyl-6-heptene-1,3-diones **2**. The ratio of the cleavage to the cyclization in the Type II reaction was reported to be affected by α- and β-substituents.[4] We recently found that the introduction of a methyl group to the 2-position of **1a** resulted in a remarkable changeover in the reaction course.[5] We report here a substituent effect on the product distribution in the Type II reaction of substituted 2-benzoylcyclohexanones.

The substituted 2-benzoylcyclohexanones **1c**, **d**, **f**, and **g** have no 2- nor ortho-alkyl substituents. Irradiation of these compounds in benzene under nitrogen with a 450 W high-pressure mercury lamp through a Pyrex filter gave the corresponding Type II cleavage products in high yields as in the case of **1a**.[2] The photoreactions are applicable to the synthesis of **2** because of high product yields.

On the other hand, irradiation of **1i** and **1j**, both of which have 2-methyl groups, gave a pair of isomers of the 1,4-aroyl shift products **3i** and **3j**, respectively. Irradiation of **1k**, which has a 4-methyl group in addition to the 2-methyl group, gave an intractable mixture. Formation of **3** can be explained in terms of the Type II cyclization followed by the cyclobutanol ring opening as reported in the case of **1b**.[5] The enhanced cyclization caused by the 2-methyl group can be explained in terms of the presence of an unfavourable nonbonding interaction in the transition state during the elimination.[6] The 4-methyl group may prevent the recombination of the radical centers in the 1,4-biradical intermediate **5k** because of steric repulsion so as to reduce the yield of the Type II product **3k**. Two isomers of **3**, cis and trans isomers with respect to the C4-aroyl and C2-methyl groups, might be produced in the process of the cyclobutanol ring opening.[5] The major isomer seems to be the more stable trans isomer.

Compound **11** has two γ-hydrogens, one on the ethyl group and one on the cyclohexanone ring. However, only the γ-hydrogen on the ring was abstracted by the excited benzoyl oxygen. Irradiation of **11** gave **31** in a

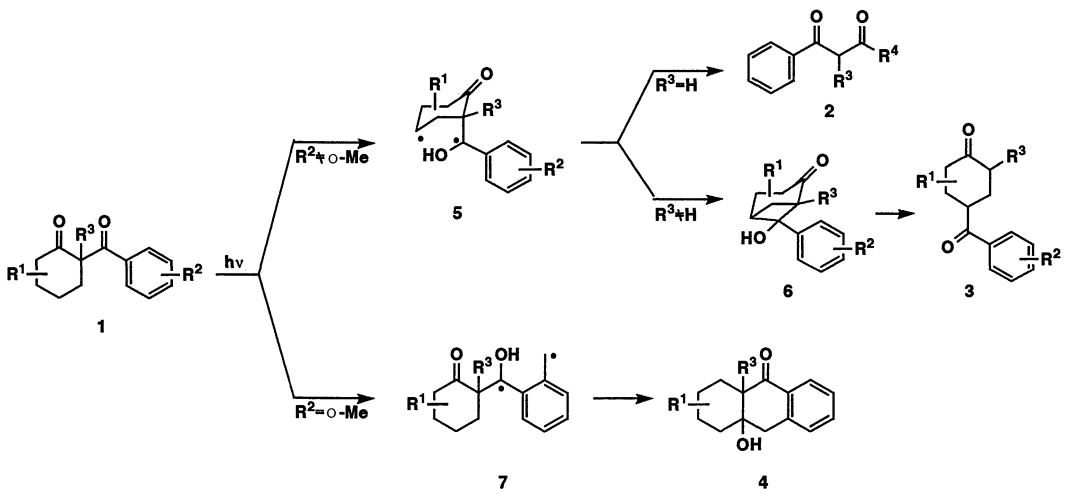

Scheme 1.

Table 1. Product Yields in the Type II Reaction of **1**

Ketone	R^1	R^2	R^3	R^4	Yield/%			Ref.
					2	**3**[a)]	**4**	
a	H	H	H	$CH_2CH_2CH=CH_2$	82	0	—	2)
b	H	H	Me		0	79/11	—	5)
c	4-Me	H	H	$CH_2CH_2CMe=CH$	68	0	—	
d	6-Me	H	H	$CHMeCH_2CH=CH_2$	72	0	—	
e	H	*o*-Me	H		0	0	57	7)
f	H	*m*-Me	H	$CH_2CH_2CH=CH_2$	97	0	—	
g	H	*p*-Me	H	$CH_2CH_2CH=CH_2$	99	0	—	
h	H	*o*-Me	Me		0	0	93	
i	H	*m*-Me	Me		0	78/20	—	
j	H	*p*-Me	Me		0	70/17	—	
k	4-Me	H	Me	$CH_2CH_2CMe=CH_2$	x	x	x[b)]	
l	H	H	Et		0	75/16	—	

a) Two isomers with respect to C4-aroyl and C2-alkyl groups were isolated. b) An intractable mixture was formed.

91% yield. No products derived from ethyl hydrogen abstraction were detected. The axial hydrogen at the 4-position seemed to be more favored for abstraction by the benzoyl carbonyl group than γ-hydrogen on the ethyl group because of geometical preference.

The excited aroyl oxygen in **1** could abstract a γ-hydrogen on the ortho-methyl group when the group was present.[7,8)] Hornback *et al.* reported that photolysis of **1e** gave **4e** in a 57% yield via intramolecular hydrogen abstraction from the ortho-methyl group.[7)] Compound **1h** had a methyl group on C2 as well as the ortho-position. The presence of the 2-methyl group was expected to affect the direction of hydrogen abstraction. However, irradiation of **1h** gave only the product via the ortho-methyl hydrogen abstraction in a 93% yield. No products arising from abstraction of the C4-hydrogen could be detected. Formation of **4** may be explained in terms of trapping of the benzyl radical center by the cyclohexanone carbonyl.[7)] The 2-methyl group seemed to promote the trapping process.

Experimental

The IR spectra were recorded with a JASCO A-3 spectrometer, ^1H and ^{13}C NMR spectra were measured with a JEOL FX90Q spectrometer using tetramethylsilane as an internal standard. An Ushio 450 W high-pressure mercury lamp was used as an irradiation source. The substituted 2-benzoylcyclohexanones without a 2-methyl group were prepared from the corresponding morpholinocyclohexanone and aroyl chloride[9)] and 2-methylation was performed using a phase-transfer catalyst.[5)]

General Procedure for Irradiation of 1. A solution of the substituted 2-benzoylcyclohexanone **1** (ca. 2 mmol) in 50 cm^3 of benzene was irradiated under nitrogen with a 450 W high-pressure mercury lamp through a Pyrex filter. After removing the solvent the residue was chromatographed on a silica-gel column. Elution with a mixture of benzene and ethyl acetate gave **2**, **3**, or **4**.

4-Benzoyl-2-methylcyclohexanone (3b): Major isomer: 79%[5)] yield. Minor isomer: 11% yield; bp 120—121 °C/3 mmHg (1 mmHg=133.322 Pa); IR (neat) 1680 and 1710 cm^{-1}; ^1H NMR ($CDCl_3$) δ= 1.09 (3H, d, J=6.7 Hz, CH_3), 1.7—2.9 (7H, m, CH and CH_2), 3.81 (1H, quint, J=5.1 Hz, CHCOPh), 7.4—7.7 (3H, m, aromatic), and 7.9—8.1 (2H, m, aromatic); ^{13}C NMR ($CDCl_3$) δ=15.2 (q), 28.4 (t), 36.2 (t), 38.0 (t), 39.7 (d), 41.6 (d), 128.4 (d, 2C), 128.8 (d, 2C), 132.8 (d), 135.9 (s), 202.5 (s), and 212.9 (s). Found: C, 77.65; H, 7.61%. Calcd for $C_{14}H_{16}O_2$: C, 77.75; H, 7.46%.

6-Methyl-1-phenyl-6-heptene-1,3-dione (2c): 68% yield; bp 112—115 °C/2 mmHg; IR (neat) 1600 cm^{-1}; ^1H NMR ($CDCl_3$) δ=1.79 (3H, s, CH_3), 2.3—2.8 (4H, m, CH_2), 4.11 (0.14H, s, CH_2), 4.78 (2H, s, olefinic), 6.22 (0.93H, s, olefinic), 7.3—7.6 (3H, m, aromatic), 7.8—8.0 (2H, m, aromatic), and 16.23 (0.93H, bs, OH). Found: C, 77.69; H, 7.39%. Calcd for $C_{14}H_{16}O_2$: C, 77.75; H, 7.46%.

4-Methyl-1-phenyl-6-heptene-1,3-dione (2d): 72% yield; bp 110—113 °C/2 mmHg; IR (neat) 1600 cm^{-1}; ^1H NMR ($CDCl_3$) δ=1.21 (3H, d, J=6.6 Hz, CH_3), 2.1—2.7 (3H, m, CH and CH_2), 4.11 (0.14H, s, CH_2), 5.01 (1H, d, J=1.3 Hz, olefinic), 5.12 (1H, d, J=5.3 Hz, olefinic), 5.6—6.0 (1H, m, olefinic), 6.16 (0.93H, s, olefinic), 7.4—7.6 (3H, m, aromatic), 7.8—8.0 (2H, m, aromatic), and 16.31 (0.93H, bs, OH). Found: C, 77.49; H, 7.69%. Calcd for $C_{14}H_{16}O_2$: C, 77.75; H, 7.46%.

1-(3-Methylphenyl)-6-heptene-1,3-dione (2f): 97% yield; bp 115—120 °C/2 mmHg; IR (neat) 1600 cm^{-1}; ^1H NMR ($CDCl_3$) δ=2.3—2.8 (4H, m, CH_2), 2.36 (3H, s, CH_3), 4.02 (0.18H, s, CH_2), 4.94 (1H, d, J=1.4 Hz, olefinic), 5.10 (1H, d, J=7.5 Hz, olefinic), 5.7—6.1 (1H, m, olefinic), 6.13 (0.91H, s, olefinic), 7.3—7.5 (2H, m, aromatic), 7.6—7.8 (2H, m, aromatic), and 16.33 (0.91, s, OH). Found: C, 77.73; H, 7.59%. Calcd for $C_{14}H_{16}O_2$: C, 77.75; H, 7.46%.

1-(4-Methylphenyl)-6-heptene-1,3-dione (2g): 99% yield; bp 115—120 °C/2 mmHg; IR (neat) 1580 cm^{-1}; ^1H NMR ($CDCl_3$) δ=2.3—2.6 (4H, m, CH_2), 2.34 (3H, s, CH_3), 3.99 (0.2H, s, CH_2), 4.93 (1H, bs, olefinic), 5.08 (1H, d, J=8.5 Hz, olefinic), 5.7—6.1 (1H, m, olefinic), 6.10 (0.9H, s, olefinic), 7.17 (2H, d, J=8.4 Hz, aromatic), 7.73 (2H, d, J=8.4 Hz, aromatic), and 16.29 (0.9H, bs, OH). Found: C, 77.76; H, 7.30%. Calcd for $C_{14}H_{16}O_2$: C, 77.75; H, 7.46%.

4a-Hydroxy-9a-methyl-1,2,3,4,4a,9a-hexahydro-9(10*H*)-anthracenone (4h): 93% yield; mp 127.5—135 °C; IR (KBr) 1670, 1685, 3480, and 3520 cm^{-1}; ^1H NMR ($CDCl_3$) δ=1.13 (3H, s, CH_3), 1.3—2.1 (8H, m, CH_2), 1.19 (1H, s, OH), 2.93 (2H, ABq, J=17.6 Hz, CH_2), 7.0—7.6 (3H, m, aromatic), and 7.95 (1H, d, J=5.8 Hz, aromatic); ^{13}C NMR ($CDCl_3$) δ=19.8 (t), 20.7 (t), 20.8 (q), 27.6 (t), 34.3 (t), 40.5 (t), 49.3 (s), 75.0 (s), 126.6 (d), 127.5 (d), 129.2 (d), 131.7 (s), 133.0 (d), 138.6 (s), and 202.1 (s). Found: C, 78.32; H, 7.74 %. Calcd for $C_{15}H_{18}O_2$: C, 78.23; H, 7.88%.

4-(3-Methylbenzoyl)-2-methylcyclohexanone (3i): Major isomer: 78% yield; bp 130—135 °C/2 mmHg; IR (neat) 1680 and 1710 cm^{-1}; ^1H NMR ($CDCl_3$) δ=1.07 (3H, d, J=6.2 Hz, CH_3), 1.4—2.8 (7H,m, CH and CH_2), 2.43 (3H, s, CH_3), 3.82 (1H, tt,

J=3.9 and 11.5 Hz, CHCOPh), 7.3—7.5 (2H, m, aromatic), and 7.7—7.9 (2H, m, aromatic); ^{13}C NMR ($CDCl_3$) δ=14.4 (q), 21.3 (q), 30.0 (t), 38.1 (t), 40.3 (t), 43.9 (d), 44.5 (d), 125.3 (d), 128.7 (d), 128.8 (d), 133.9 (d), 136.0 (s), 138.5 (s), 201.3 (s), and 210.6 (s). Found: C, 78.16; H, 7.88%. Calcd for $C_{15}H_{18}O_2$: C, 78.23; H, 7.88%.

Minor isomer: 20% yield; bp 120—125°C/2 mmHg; IR (neat) 1680 and 1710 cm^{-1}; ^{1}H NMR ($CDCl_3$) δ=1.08 (3H, d, J=6.7 Hz, CH_3), 1.6—2.9 (7H, m, CH and CH_2), 2.43 (3H, s, CH_3), 3.77 (1H, quint, J=4.8 Hz, CHCOPh, 7.4—7.5 (2H, m, aromatic), and 7.7—7.9 (2H, m, aromatic); ^{13}C NMR ($CDCl_3$) δ=15.3 (q), 21.3 (q), 28.3 (t), 36.1 (t), 37.9 (t), 40.0 (d), 41.6 (d), 125.5 (d), 128.7 (d), 128.9 (d), 133.7 (d), 136.5 (s), 138.6 (s), 202.4 (s), and 211.8 (s). Found; C, 78.24; H, 7.81%. Calcd for $C_{15}H_{18}O_2$: C, 78.23; H, 7.88%.

4-(4-Methylbenzoyl)-2-methylcyclohexanone (3j): Major isomer: 70% yield; mp 74—74.5°C; IR (KBr) 1675 and 1710 cm^{-1}; ^{1}H NMR ($CDCl_3$) δ=1.08 (3H, d, J=5.9 Hz, CH_3), 1.4—2.7 (7H, m, CH and CH_2), 2.45 (3H, s, CH_3), 3.83 (1H, tt, J=7.2 and 11.7 Hz, CHCOPh), 7.37 (2H, d, J=8.7 Hz, aromatic), and 7.94 (2H, d, J=8.7 Hz, aromatic); ^{13}C NMR ($CDCl_3$) δ=13.9 (q), 21.0 (q), 29.6 (t), 37.8 (t), 39.8 (t), 43.4 (d), 43.8 (d), 127.9 (d, 2C), 129.0 (d, 2C), 133.4 (s), 143.4 (s), 200.2 (s), and 209.7 (s). Found: C, 78.21; H, 7.81%. Calcd for $C_{15}H_{18}O_2$: C, 78.23; H, 7.88%.

Monor isomer: 17% yield; bp 120—123°C/2 mmHg; IR (neat) 1670 and 1710 cm^{-1}; ^{1}H NMR ($CDCl_3$) δ=1.08 (3H, d, J=6.7 Hz, CH_3), 1.6—3.0 (7H, m, CH and CH_2), 2.45 (3H, s, CH_3), 4.93 (1H, quint, J=5.1 Hz, CHCOPh), 7.29 (2H, d, J=8.7 Hz, aromatic), and 7.90 (2H, d, J=8.7 Hz, aromatic); ^{13}C NMR ($CDCl_3$) δ=15.1 (q), 21.4 (q), 28.3 (t), 36.2 (t), 37.9 (t), 39.7 (d), 41.6 (d), 128.4 (d, 2C), 129.4 (d, 2C), 133.9 (s), 143.7 (s), 201.8 (s), and 211.9 (s). Found: C, 78.25; H, 7.80%. Calcd for $C_{15}H_{18}O_2$: C, 78.23; H, 7.88%.

4-Benzoyl-2-ethylcyclohexanone (31): Major isomer: 75% yield; bp 125—128°C/2 mmHg; IR (neat) 1680 and 1710 cm^{-1}; ^{1}H NMR ($CDCl_3$) δ=0.91 (3H, t, J=7.2 Hz, CH_3), 1.1—2.6 (9H, m, CH and CH_2), 3.83 (1H, tt, J=7.2 and 11.6 Hz, CHCOPh), 7.4—7.7 (3H, m, aromatic), and 8.0—8.2 (2H, m, aromatic); ^{13}C NMR ($CDCl_3$) δ=11.5 (q), 22.2 (t), 30.0 (t), 35.5 (t), 40.6 (t), 44.5 (d), 50.7 (d), 128.2 (d, 2C), 128.8 (d, 2C), 133.0 (d), 136.5 (s), 201.3 (s), and 210.6 (s). Found: C, 77.97; H, 7.83 %. Calcd for $C_{15}H_{18}O_2$: C, 78.23; H, 7.88%.

Minor isomer could not be separated completely from the major isomer. 16% yield (based on the ^{1}H NMR analysis); ^{1}H NMR ($CDCl_3$) δ=0.91 (3H, t, J=7.2 Hz, CH_3), 1.2—2.6 (9H, m, CH and CH_2), 3.83 (1H, quint, J=5.8 Hz, CHCOPh), 7.4—7.7 (3H, m, aromatic), and 7.9—8.1 (2H, m, aromatic); ^{13}C NMR ($CDCl_3$) δ=11.5 (q), 23.4 (t), 28.4 (t), 33.7 (t), 38.1 (t), 39.8 (d), 49.1 (d), 128.2 (d, 2C), 128.8 (d, 2C), 133.0 (d), 136.5 (s), 202.5 (s), and 212.8 (s).

References

1) P. J. Wagner, *Acc. Chem. Res.*, **4**, 168 (1971); "Rearrangements in Ground and Excited States," ed by P. de Mayo, Academic Press, New York (1980), Vol. 3, p. 381.

2) T. Hasegawa, M. Nishimura, and M. Yoshioka, *J. Phys. Org. Chem.*, **3**, 230 (1990).

3) N. Kamiya, *Enkabiniru to Porima*, **25**, 7 (1985).

4) For instance, F. D. Lewis, and T. A. Hillard, *J. Am. Chem. Soc.*, **92**, 6672 (1970); *ibid.*, **94**, 3852 (1972).

5) T. Hasegawa, M. Nishimura, Y. Kodama, and M. Yoshioka, *Bull. Chem. Soc. Jpn.*, **63**, 935 (1990); we have not been able to assign the structure of the minor isomer of **3b**.

6) F. D. Lewis, R. W. Johnson, and R. A. Ruden, *J. Am. Chem. Soc.*, **94**, 4292 (1972).

7) J. M. Hornback, M. L. Poundstone, B. Vadlamani, S. M. Graham, J. Gabay, and S. T. Patton, *J. Org. Chem.*, **53**, 5597 (1988).

8) M. Yoshioka, K. Nishizawa, M. Arai, and T. Hasegawa, *J. Chem. Soc., Perkin Trans. 1*, **1991**, 541.

9) R. S. Monson, "Advanced Orbanic Synthesis," Academic Press, New York (1971), p. 81.

Synthesis of Antiprismatic [5.5]Ferrocenophane ([5](1,1′)[5](3,4′)Ferrocenophane)

Masao HISATOME,* Shuichi YOSHIDA, and Koji YAMAKAWA
Faculty of Pharmaceutical Sciences, Science University of Tokyo, 12 Ichigaya-Funagawara, Shinjuku-ku, Tokyo 162
(Received July 8, 1991)

Synopsis. The title compound **2**, which is the first example of a C_2 symmetric dibridged ferrocenophane, has been synthesized via a base-catalyzed condensation of 3,4′-diacyl-[5]ferrocenophane. The spectroscopic properties of **2** are briefly discussed by comparing them with the corresponding prismatic [5,5]ferrocenophane having C_{2v} symmetry.

In intramolecularly 1,3-dibridged ferrocenes with two polymethylene chains, there are, in principle, two geometric isomers bridged at the 1,1′- and 3,3′-positions and at the 1,1′- and 3,4′-positions of the cyclopentadienyl (Cp) rings, which are called "prismatic" and "antiprismatic" ferrocenophanes,[1] respectively. Although a number of 1,3-dibridged ferrocenophanes have been prepared thus far,[1-7] all of them are bridged in a prismatic form. There has been only one report on the preparation of [5](1,1′)[5](3,4′)ferrocenophane derivative (**3**) by Nesmeyanov,[8] though its configuration has not be determined. The reason that no example exists of a structurally confirmed antiprismatic ferrocenophane may arise from the following problems: (i) Bridging of [*n*](1,1′)ferrocenophane-3-propanoic acids ($n>2$) by a heteroannularly cyclization reaction, which is usually employed for the preparation of dibridged ferrocenophanes, selectively gives 3′-bridged compounds, but no 4′-bridged compound. (ii) A spectroscopic distinction between prismatic and antiprismatic structures is not easy. This article describes the preparation of [5](1,1′)[5](3,4′)ferrocenophane (**2**) via a linking between the substituents of the two Cp rings, a determination of its antiprismatic configuration and a spectroscopic characterization of **2**, compared with the corresponding prismatic compound **1**.

An acylation of 3-acetyl[5]ferrocenophane (**4**)[4] with 3-chloropropanoyl chloride and $AlCl_3$ gave three isomeric diacylferrocenophanes, **5a**—**5c**, which were easily convertible to enone **6a**—**6c** by elimination. The α′-substituted structures of **5a** and **5c** were ascertained by means of their ^{1}H NMR spectra, in which the 3′- and 4′-proton signals, respectively, appeared as triplets with ortho coupling constants (J=2.6 and 2.7 Hz). The desired β′-substituted compound **5b** was so unstable in solvents that it could not be characterized by ^{1}H NMR spectrometry. Compound **5b** was readily converted to stable enone **6b**, even by a treatment with neutral alumina in benzene. The ^{1}H NMR spectrum of **6b** showed a triplet signal with a meta coupling constant (J=1.4 Hz); its β′-substituted form was confirmed. At this stage it could not be determined whether **5b** and **6b** were 3,3′- or 3,4′-acylated phanes, although 3,4′-substituted structures were predictable due to a substitution disadvantage just below the position of the acyl group in ferrocenophanes.[9] No other possible β′-acylated compound was isolated in the present reaction.

A second bridge formation was carried out according to a modified procedure in the preparation of [5](1,1′)ferrocenophane-1,5-dione reported by Barr and Watts.[10] A crude mixture, obtained by acylation of **4**, without separating into each component, was treated by aq NaOH; dibridged diketone **7** was isolated (16% from **4**) from the many products by chromatography. An intramolecular Michael condensation of enone **6b** was also attempted, but the yield of **7** could not be improved (9%). The desired antiprismatically bridged structure of **7** was determined by ^{1}H NMR spectrometry in the

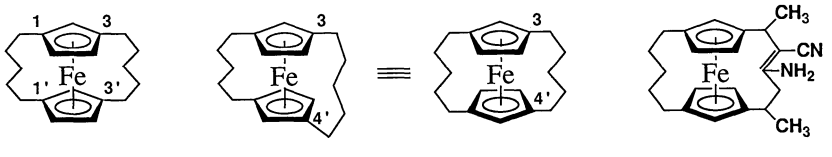

1 2 3

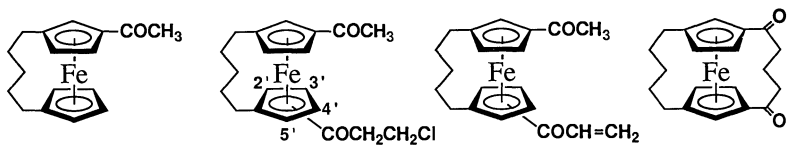

4 5 6 7

a: 2′-substituted
b: 4′-substituted
c: 5′-substituted

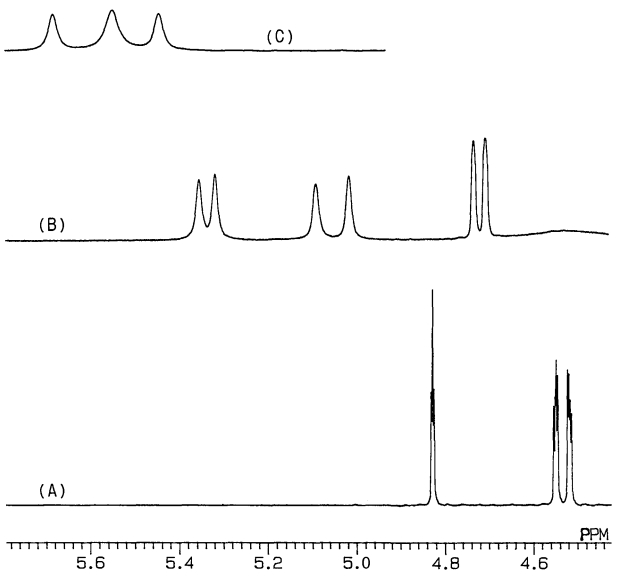

Fig. 1. Cp ring proton region in the ^{1}H NMR spectra of **7** in $CDCl_3$ without any additive (A), with tris[3-(trifluoromethylhydroxymethylene)-*d*-camphorato]-europium(III) [Eu(tfmc)] (B), and with tris[(heptafluorobutanoyl)pivaloylmethanato]europium(III) [Eu(fod)] (C).

presence of a chiral shift reagent. [5](1,1′)[5](3,4′)Ferrocenophane-1,5-dione (**7**) is a racemic mixture of two chiral molecules, while the corresponding isomeric [5](1,1′)[5](3,3′)ferrocenophane-1,5-dione is a *meso* compound possessing two symmetric planes through the central iron atom. Accordingly, each proton signal of the former in the ^{1}H NMR spectrum should split into two signals due to diastereomeric interactions between a pair of enantiomers and a chiral shift reagent, but that of the latter prismatic diketone does not under the same conditions. The spectra of **7** in $CDCl_3$ without any additive, with chiral a shift reagent, [Eu(tfmc)], and with an achiral shift reagent, [Eu(fod)], are shown in Fig. 1. The desired bridging feature of **7** was proven in terms of the spectral behavior.

The reduction of the two carbonyl groups of **7** gave the antiprismatic [5.5]ferrocenophane **2**. The ^{1}H and ^{13}C NMR spectra of **2** are obviously distinguished from those of ferrocenophane **1**, of which the pprismatic structure was already confirmed.[7] It is interesting that the d–d* band of **2** in the electronic absorption spectrum in tetrahydrofuran (THF) shifted to a longer wavelength (456 nm) than that of **1** (444 nm; ferrocene, 440 nm in THF). The shift value of **2** resembles that of tetra-bridged [5$_4$](1,2,3,4)-ferrocenophane (460 nm).[11] A linear relationship between the hypsochromic shift of the d–d* band and a compression of the Cp–Fe–Cp distance has been found in multibridged ferrocenophanes.[12] An elongation of the Cp–Fe–Cp distance in [5$_4$]ferrocenophane (3.336 Å;[11] ferrocene, 3.32 Å[13]) was observed in an X-ray crystal analysis. It would therefore be suggested that the distance of the two Cp rings of **2** is a little longer than that of **1**, and that the two pentamethylene bridges in antiprismatic manner elongate the distance. A consideration using a Dreiding molecular model supports this assumption, that is, the molecule of **2** is somewhat strained by avoiding steric hindrance among the hydrogens of the polymethylene chains in a zigzag conformation, while that of **1** is in a relaxed conformation.

Experimental

Melting points were uncorrected. IR, mass and electronic spectra were obtained on the same instruments as those used in a previous report,[11] except for NMR spectra, which were measured on a JEOL JNM GSX500 spectrometer relative to tetramethylsilane as an internal standard.

Acylation of 3-Acetyl[5]ferrocenophane (4) with 3-Chloropropanoyl Chloride. A mixture of 3-chloropropanoyl chloride (2.52 g, 20.6 mmol) and $AlCl_3$ (3.10 g, 23.3 mmol) in dichloromethane (50 ml) was prepared under an Ar atmosphere and stirred at room temperature for 2 h. To the resulting suspension was added dropwise 3-acetyl[5]ferrocenophane (**4**)[4] (3.00 g, 10.1 mmol) in dichloromethane (30 ml). The reaction mixture was stirred at room temperature for 22 h, and then quenched with water. The hydrolysate was extracted with dichloromethane; and the extracts were washed with water, dried over $CaCl_2$, and evaporated. The crude was column-chromatographed over silica gel with benzene–ethyl acetate (10:1). The starting material **4** was recovered from first band. The second band yielded 3-acetyl-2′-(3-chloropropanoyl)[5](1,1′)ferrocenophane (**5a**) (0.11 g, 2.8%) as a red solid. IR (KBr) 1650 and 1670 (C=O) cm^{-1}; ^{1}H NMR ($CDCl_3$) δ=1.64, 1.86, 2.24, 2.33, 2.53, and 3.05 (2H, 4H, 1H, 1H, 1H, and 1H, each m, $-CH_2-$ of bridge), 2.42 (3H, s, $-COCH_3$), 2.94 and 3.23 (each 2H, dt, J=6.2, 18.0 Hz, $-COCH_2-$), 3.90 (2H, t, J=6.2 Hz, $-CH_2Cl$), 4.28, 4.30, 4.57 and 4.67 (1H, 2H, 1H, and 1H, each m, Cp-H), 4.64 (1H, t, J=2.6 Hz, 4′-H of Cp); MS m/z (rel intensity) 386 (25, M$^+$), 350 (100, [M−Cl]$^+$).

The third band yielded 3-acetyl-5′-(3-chloropropanoyl)[5](1,1′)ferrocenophane (**5c**) (0.31 g, 7.9%) as a red solid. IR (KBr) 1640 (C=O) cm^{-1}; ^{1}H NMR ($CDCl_3$) δ=1.67, 1.82, 1.90, 2.30, 2.45, and 2.99 (1H, 1H, 3H, 2H, 2H, and 1H, each m, $-CH_2-$ of bridge), 2.38 (3H, s, $-COCH_3$), 3.04 and 3.28 (each 1H, m, $-COCH_2-$), 3.80 and 4.00 (each 1H, m, $-CH_2Cl$), 4.20 (1H, t, J=2.7 Hz, 3′-H of Cp), 4.27, 4.59, 4.75 and 4.88 (each 1H, dd, J=1.3, 2.7 Hz, 4-, 5-, 2′-, and 4′-H of Cp), 4.54 (1H, t, J=1.3 Hz, 2-H of Cp).

These two compounds, **5a** and **5c**, could not be sufficiently purified due to the easy occurrence of elimination in solvents.

The fourth band yielded 3-acetyl-4′-(3-chloropropanoyl-[5](1,1′)ferrocenophane (**5b**) (1.16 g, 30%) as a red solid. The ^{1}H NMR spectrum of **5b** was contaminated with the many signals of enone **6b** generated by a rapid elimination in $CDCl_3$, and could not be sufficiently analyzed. The structure of **5b** was inferred from a structural determination of **6b** derived by the elimination of **5b**, as mentioned below.

3-Acetyl-4′-propenoyl[5](1,1′)ferrocenophane (6b). A crude mixture obtained by the acylation of **4** (1.00 g, 3.38 mmol) with 3-chloropropanoyl chloride (0.88 g, 7.21 mmol) and $AlCl_3$ (1.03 g, 7.77 mmol) according to the procedure described above was treated with alumina in benzene–ethyl acetate. The mixture was eluted and evaporated. The residue was column-chromatographed over alumina with benzene–ethyl acetate (10:1) to be separated into five bands. The third and fourth bands yielded 2′- and 5′-propenoyl-[5](1,1′)ferrocenophanes (**6a**, 0.06 g, 5% from **4**; **6c**, 0.14 g, 12%), respectively, as red oils.

The fifth band yielded 3-acetyl-4′-propenoyl[5](1,1′)ferrocenophane (**6b**) (0.63 g, 53%), which was recrystallized from hexane–ethyl acetate to give red prisms; mp 113—113.5°C. IR (KBr) 1640 and 1660 cm^{-1}; ^{1}H NMR ($CDCl_3$) δ=1.84, 1.99

and 2.38 (4H, 2H and 4H, each m, $-CH_2-$ of bridge), 2.35 (3H, s, $-COCH_3$), 4.38, 4.70, 4.53 and 4.55 (each 1H, dd, J=1.4, 2.6 Hz, 4-, 5-, 2'-, and 3'-H of Cp), 4.59 and 4.61 (each 1H, t, J=1.4 Hz, 2- and 5'-H of Cp), 5.78 (1H, dd, J=1.8, 10.4 Hz, $=CH_2$ of propenoyl), 6.48 (1H, dd, J=1.8, 16.9 Hz, $=CH_2$ of propenoyl), 6.76 (1H, dd, J=10.4, 16.9 Hz, vinyl-H of propenoyl).

Found: C, 68.28; H, 6.27%. Calcd for $C_{20}H_{22}O_2Fe$: C, 68.59; H, 6.33%.

[5](1,1')[5](3,4')Ferrocenophane-1,5-dione (7). (1) The crude mixture obtained by acylation of **4** (3.00 g, 10.1 mmol) with 3-chloropropanoyl chloride (2.52 g, 20.6 mmol) and $AlCl_3$ (3.10 g, 23.3 mmol) was dissolved to ethanol (400 ml), and 10% aq NaOH (400 ml) was added. After the solution was stirred at room temperature for 12 h, a large excess of water was added. The mixture was extracted with dichloromethane, and the extracts was washed with saturated aq NaCl, dried over $CaCl_2$ and evaporated. The residue was column-chromatographed over silica gel to be separated into many bands. The seventh band eluted with benzene–ethyl acetate (20:1) yielded [5.5]ferrocenophane-1,5-dione (**7**) (0.43 g, 16% from **4**), which was recrystallized from hexane–ethyl acetate to give red needles; mp 246—246.5°C. IR (KBr) 1670 (C=O) cm^{-1}; ^1H NMR ($CDCl_3$) δ=1.66, 1.74, 1.94, 2.53 and 2.86 (each 2H, m, $-CH_2-$ of aliphatic bridge), 2.08, 2.11, 2.24, 2.28, 2.35 and 2.38 (each 1H, m, $-CH_2-$ of dioxo-bridge), 4.52 and 4.55 (each 2H, dd, J=1.5, 2.7 Hz, 4-, 5-, 2'-, and 3'-H of Cp), 4.83 (2H, t, J=1.5 Hz, 2- and 5'-H of Cp); ^{13}C NMR ($CDCl_3$) δ=23.83, 25.82, 26.00, 27.17, and 34.41 ($-CH_2-$), 68.67, 73.45 and 95.56 (Cp–C), 205.70 (C=O); MS m/z (rel intensity) 350 (100, M^+).

Found: C, 68.16; H, 6.25%. Calcd for $C_{20}H_{22}O_2Fe$: C, 68.59; H, 6.33%.

(2) To a solution of enone **6b** (80 mg, 0.23 mmol) in ether (5.0 ml) was added dropwise a solution of KOH (0.17 g) in ethanol (1.5 ml) at 0°C. The mixture was stirred for 2 h, and then extracted with dichloromethane. The extracts were washed with saturated aq NaCl, dried over $CaCl_2$ and evaporated. Column chromatography on silica gel with benzene/ethyl acetate afforded two bands. The first band yielded diketone **7** (7 mg, 9%). The second band (24 mg) was an unknown red oil.

Both reactions of **6b** with aq KOH in ethanol (without ether) and with EtONa in ethanol gave no bridged diketone **7**.

[5](1,1')[5](3,4')Ferrocenophane (2). Diketone **7** (200 mg, 0.57 mmol) in ether (50 ml) was added dropwise to a suspension of $LiAlH_4$ (60 mg, 1.6 mmol) and $AlCl_3$ (230 mg, 1.7 mmol) in ether (20 ml) at 20°C. The mixture was decomposed with wet ether, and the hydrolysate was extracted with ether. The extracts were washed with saturated aq NaCl, dried over Na_2SO_4 and evaporated. Column chromatography on silica gel with benzene provided [5](1,1')[5](3,4')ferrocenophane (**2**) (0.171 mg, 93%) as the main band. An analytical sample was obtained by recrystallization from hexane–ethyl acetate as yellow needles; mp 122—123°C. ^1H NMR ($CDCl_3$) δ=1.72, 1.99, 2.23, 2.34 and 2.37 (8H, 4H, 4H, 2H, and 2H, $-CH_2-$ of bridge), 3.75 (2H, t, J=1.5 Hz, 2- and 5'-H of Cp), 3.98 (4H, d, J=1.5 Hz, 4-, 5-, 2'-, and 3'-H of Cp); ^{13}C NMR ($CDCl_3$) δ=23.56, 26.25, and 26.53 ($-CH_2-$), 68.04, 68.71 and 87.92 (Cp–C); MS (m/z rel intensity) 322 (100, M^+); λ_{max} (THF) 456 nm (ε=119).

Found: C, 75.15; H, 8.16%; M^+, 322.1389. Calcd for $C_{20}H_{26}Fe$: C, 74.54, H, 8.13%; M, 322.1383. Calcd for $C_{20}H_{26}Fe \cdot 1/6\ (C_6H_{14})$: C, 74.89; H, 8.49%. (Hexane, C_6H_{14}, may originate in the solvent used in recrystallization.)

[5](1,1')[5](3,3')Ferrocenophane (1). The spectra of **1** previously reported (mp 86—87°C[7]) were also measured on the same instruments in order to compare them with those of **2**. ^1H NMR ($CDCl_3$) δ=1.82, 2.00, 2.13, and 2.36 (8H, 2H, 2H and 8H, each m, $-CH_2-$ of bridge), 3.78 and 3.88 (2H and 4H, t and d, Cp-H); ^{13}C NMR ($CDCl_3$) δ=23.69, 24.60 and 25.94 ($-CH_2-$), 66.87, 68.74 and 87.01 (Cp–C); λ_{max} (THF) 444 nm (ε=124).

References

1) W. E. Watts, *Organomet. Chem. Rev.*, **2**, 231 (1967).
2) K. Schlögl and M. Peterlik, *Monatsh. Chem.*, **93**, 1328 (1962).
3) K. L. Rinehart, Jr., D. E. Bublitz, and D. H. Gustafson, *J. Am. Chem. Soc.*, **85**, 970 (1963).
4) A. D. Brown, Jr. and J. K. Winstead, *J. Org. Chem.*, **36**, 2832 (1971).
5) M. Hisatome, T. Sakamoto, and K. Yamakawa, *J. Organomet. Chem.*, **107**, 87 (1976); M. Hisatome, N. Watanabe, T. Sakamoto, and K. Yamakawa, *ibid.*, **125**, 79 (1977).
6) D. Astruc, R. Dabard, M. Martin, P. Batail, and D. Grandjean, *Tetrahedron Lett.*, **1976**, 829.
7) M. Hisatome and M. Hillman, *J. Organomet. Chem.*, **212**, 217 (1981).
8) A. N. Nesmeyanov, M. I. Rybinskaya, G. B. Schul'pin, and M. V. Tolstaya, *Dokl. Akad. Nauk SSSR*, **229**, 1124 (1976).
9) M. Hisatome, J. Watanabe, and K. Yamakawa, *J. Organomet. Chem.*, **266**, 159 (1984).
10) T. H. Barr and W. E. Watts, *Tetahedron Lett.*, **24**, 3219 (1968).
11) M. Hisatome, R. Yamashita, J. Watanabe, K. Yamakawa, and Y. Iitake, *Bull. Chem. Soc. Jpn.*, **61**, 1687 (1988).
12) M. Hisatome, J. Watanabe, K. Yamakawa, K. Kozawa, and T. Uchida, *Nippon Kagaku Kaishi*, **1985**, 572.
13) F. Takusagawa and T. F. Koetzle, *Acta Crystallogr., Sect. B*, **35**, 867 (1979).

Synthesis of (*E*)- and (*Z*)-2,3-Bis(trifluoromethyl)allyl Alcohols by γ-Ray Irradiation of Hexafluoro-2-butyne with Alcohols and Some Reactions

Masakazu NISHIDA, Yoshio HAYAKAWA, Masaki MATSUI,†
Katsuyoshi SHIBATA,† and Hiroshige MURAMATSU*,†
Government Industrial Research Institute, Nagoya, Hirate-cho, Kita-ku, Nagoya 462
† Department of Chemistry, Faculty of Engineering, Gifu University, Yanagido, Gifu 501-11
(Received July 9, 1991)

Synopsis. Radiation-induced addition reaction of alcohols to hexafluoro-2-butyne provided (*E*)- and (*Z*)-2,3-bis(trifluoromethyl)allyl alcohols, which were dehydrated to afford 1,2-bis(trifluoromethyl)-1,3-butadienes. Thermal cyclization of 3-methyl-1,2-bis(trifluoromethyl)-1,3-butadiene afforded 1-methyl-2,3-bis(trifluoromethyl)cyclobutene.

Although radical addition is one of the most useful reactions to synthesize organic compounds,[1] little is known on the reaction of polyfluoroalkynes. In our continuing series of studies on the radical addition reaction of polyfluoro compounds,[2-8] the reaction of hexafluorobutyne with alcohols to give 1:1 adducts, 2,3-bis(trifluoromethyl)allyl alcohols, and a few reactions of the adducts have been examined in this investigation.

Irradiation of hexafluoro-2-butyne (**1**) with alcohols (**2**) in Freon 113 afforded (*E*)- and (*Z*)-2,3-bis(trifluoromethyl)allyl alcohols **3** (Table 1). The stereoisomers were identified based on the ^{19}F NMR spectroscopy (*E*: J_{CF_3,CF_3}=1 Hz, *Z*: J_{CF_3,CF_3}=12 Hz).[9]

A reasonable reaction path for the formation of **3** is shown in Eqs. 1—3.

$$RR'CHOH\ (\mathbf{2}) \xrightarrow{\gamma\text{-ray}} RR'\dot{C}OH\ (\mathbf{4}) \quad (1)$$

$$RR'\dot{C}OH\ (\mathbf{4}) + CF_3C{\equiv}CCF_3\ (\mathbf{1}) \longrightarrow CF_3\dot{C}{=}C(CF_3)CRR'OH\ (\mathbf{5}) \quad (2)$$

$$CF_3\dot{C}{=}C(CF_3)CRR'OH\ (\mathbf{5}) + RR'CHOH\ (\mathbf{2}) \longrightarrow CF_3CH{=}C(CF_3)CRR'OH\ (\mathbf{3}) + RR'\dot{C}OH\ (\mathbf{4}) \quad (3)$$

More stable 1-hydroxyalkyl radical **4** can give the products **3** in good yields (stability, primary<secondary <tertiary). Radical intermediate **5** is in equilibrium between *E*-**5** and *Z*-**5** (Scheme 1). Steric hindrance between the CF_3 group at the 3-position and an alkyl group at the 2-position can control the product distribution, i.e., the bulky alkyl group at the 2-position may shift the equilibrium to *Z*-**5** to increase the yield of *Z*-**3**.

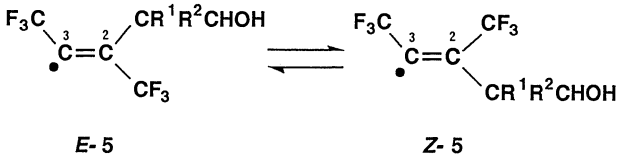

E-**5** *Z*-**5**

Scheme 1.

Dehydration of a mixture of *E*- and *Z*-**3** gave a mixture of *E*- and *Z*-**6** in 60—95 % yields (Table 2). In the case of **3b** and **3d**, the *E*/*Z* ratio of the products **6** concerning with the double bond with two CF_3 groups was the same as that of starting materials, suggesting that *E*- and *Z*-**3** afforded the corresponding *E*- and *Z*-**6**, respectively. In the case of **3c**, the formation of four isomers was confirmed by gas chromatography.

Thermal cyclization of **6d** gave 1-methyl-2,3-bis(trifluoromethyl)cyclobutene (**7d**) in 25% yield (Scheme 2).

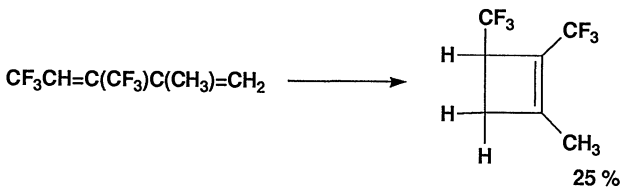

6d **7d**

Scheme 2.

Table 1. Synthesis of 2,3-Bis(trifluoromethyl)allyl Alcohols

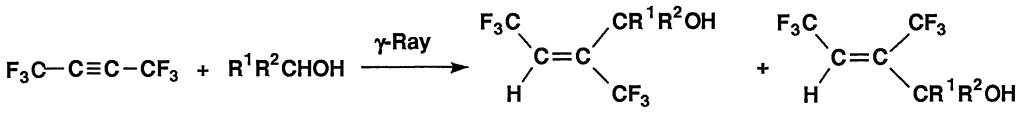

1 **2** *E*-**3** *Z*-**3**

Compd	R^1	R^2	Total irradiation / Mrad	Yield of **3** / %	*E*/*Z* Ratio
a	H	H	197	29	100/0
b	H	CH_3	98	67	55/45
c	H	C_2H_5	98	26	47/53
d	CH_3	CH_3	98	88	9/91

Table 2. Dehydration of 2,3-Bis(trifluoromethyl)allyl Alcohols

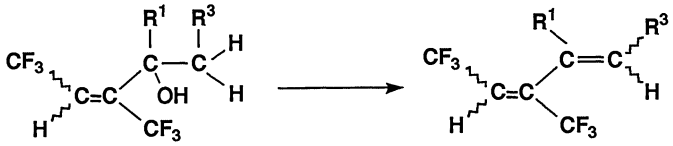

3 6

Compd	R^1	R^3	Reaction time	Yield of **6**
			min	%
b	H	H	90	79
c	H	CH_3	50	60
d	CH_3	H	90	95

The structure of **7d** was confirmed by its ^{1}H NMR spectrum, i.e., δ values of methylene (5.01—5.23 ppm) and methine (5.95—6.14 ppm) protons of **6d** shifted to 2.57 and 3.90 ppm in **7d**, respectively. The same reaction of **6b** gave an amorphous polymer.

Experimental

Instruments. ^{1}H NMR spectra were measured with a Hitachi R-22 instrument (90 MHz) in carbon tetrachloride and chemical shifts were given as δ ppm relative to tetramethylsilane (TMS) as an internal standard. ^{19}F NMR spectra were obtained with a Hitachi R-20B (56.45 MHz) in carbon tetrachloride and chemical shifts were given as δ ppm relative to trifluoroacetic acid as an external standard. The IR spectra were recorded on a Hitachi EPI-2 grating spectrometer.

General procedure for γ-Ray Irradiation of Hexafluoro-2-butyne with Alcohols. Hexafluoro-2-butyne (**1**, 16.28 g, 0.10 mol), ethanol (**2b**, 5.57 g, 0.12 mol), and Freon 113 (20.15 g, 0.11 mol) were placed in a glass ampoule (100 ml). The ampoule was degassed by a freeze-thaw cycle and was sealed under reduced pressure. The γ-ray irradiation was carried out at 6.2×10^4R h^{-1} by ^{60}Co for 158 h at ambient temperature (total irradiation, 98.2 Mrad). After the reaction, were evaporated the starting material, ethanol, and Freon 113. The residual liquid was distilled to give a mixture (14 g) of (*E*)- and (*Z*)-3,4-bis(trifluoromethyl)-3-buten-2-ol (*E*-**3b** and *Z*-**3b**), which were separated using a preparative gas chromatograph. The physical and spectral data are shown below.

(*E*)-2,3-Bis(trifluoromethyl)-2-propen-1-ol (*E*-3a): Bp 110°C; d_4^{20} 1.501; n_D^{20} 1.3368; IR (neat) 1690 (C=C) cm^{-1}; ^{1}H NMR δ=3.58 (br s, 1H, OH), 4.42 (br s, 2H, CH_2), and 6.35 (qq, *J*=7.8 and 1.8 Hz, 1H, C=CH); ^{19}F NMR δ=11.1 (dq, *J*=2 and 1 Hz, 2-CF_3) and 20.8 (dq, *J*=8 and 1 Hz, 3-CF_3); Found: C, 31.06; H, 2.06 %. Calcd for $C_5H_4F_6O$: C, 30.95; H, 2.08 %.

(*E*)-3,4-Bis(trifluoromethyl)-3-buten-2-ol (*E*-3b): Bp 115°C; d_4^{20} 1.408; n_D^{20} 1.3484; IR (neat) 1682 (C=C) cm^{-1}; ^{1}H NMR δ=1.49 (d, *J*=6.0 Hz, 3H, CH_3), 3.79 (br s, 1H, OH), 5.02 (q, *J*=6.0 Hz, 1H, 1-CH), and 6.22 (qq, *J*=8.4 and 1.2 Hz, 1H, 3-CH); ^{19}F NMR δ=15.6 (dq, *J*=1 and 1 Hz, 2-CF_3) and 21.6 (dq, *J*=8 and 1 Hz, 3-CF_3); Found: C, 34.57; H, 3.04 %. Calcd for $C_6H_6F_6O$: C, 34.63; H, 2.91%.

(*Z*)-3,4-Bis(trifluoromethyl)-3-buten-2-ol (*Z*-3b): Bp 128°C; d_4^{20} 1.427; n_D^{20} 1.3500; IR (neat) 1691 (C=C) cm^{-1}; ^{1}H NMR δ=1.45 (d, *J*=6.0 Hz, 3H, CH_3), 3.23 (br s, 1H, OH), 4.58 (q, *J*=6.0 Hz, 1H, 1-CH), and 6.37 (q, *J*=8.4 Hz, 1H, 3-CH); ^{19}F NMR δ=18.0 (q, *J*=12 Hz, 2-CF_3) and 21.6 (dq, *J*=8 and 12 Hz, 3-CF_3); Found: C, 34.63; H, 2.66%. Calcd for $C_6H_6F_6O$: C, 34.63; H, 2.91%.

(*E*)-1,2-Bis(trifluoromethyl)-1-penten-3-ol (*E*-3c): Bp 126°C; d_4^{20} 1.343; n_D^{20} 1.3579; IR (neat) 1678 (C=C) cm^{-1}; ^{1}H NMR δ=1.02 (t, *J*=6.6 Hz, 3H, CH_3), 1.67 (dq, *J*=6.6 and 6.0 Hz, 2H, CH_2), 3.63 (br s, 1H, OH), 4.74 (d, *J*=6.0 Hz, 1H, 1-CH), and 6.37 (q, *J*=7.8 Hz, 1H, 3-CH); ^{19}F NMR δ=16.8 (q, *J*=1 Hz, 2-CF_3) and 22.8 (dq, *J*=8 and 1 Hz, 3-CF_3); Found: C, 37.56; H, 3.80%. Calcd for $C_7H_8F_6O$: C, 37.70; H, 3.62%.

(*Z*)-1,2-Bis(trifluoromethyl)-1-penten-3-ol (*Z*-3c): Bp 139°C; d_4^{20} 1.360; n_D^{20} 1.3589; IR (neat) 1687 (C=C) cm^{-1}; ^{1}H NMR δ=1.00 (t, *J*=6.6 Hz, 3H, CH_3), 1.62 (br, 2H, CH_2), 2.83 (br s, 1H, OH), 4.37 (br, 1H, 1-CH), and 6.34 (q, *J*=9.0 Hz, 1H, 3-CH); ^{19}F NMR δ=17.6 (q, *J*=12 Hz. 2-CF_3) and 20.4 (dq, *J*=9 and 12 Hz, 3-CF_3); Found: C, 37.85; H, 3.67%. Calcd for $C_7H_8F_6O$: C, 37.70; H, 3.62%.

(*E*)-3,4-Bis(trifluoromethyl)-2-methyl-3-buten-2-ol (*E*-3d): Bp 119°C; d_4^{20} 1.360; n_D^{20} 1.3604; IR (neat) 1673 (C=C) cm^{-1}; ^{1}H NMR δ=1.58 (br s, 6H, CH_3), 2.86 (br s, 1H, OH), and 6.27 (qq, *J*=9.6 and 1.8 Hz, 1H, CH); ^{19}F NMR δ=14.8 (dq, *J*=2 and 2 Hz, 2-CF_3) and 24.8 (dq, *J*=10 and 2 Hz, 3-CF_3); Found: C, 37.73; H, 3.58%. Calcd for $C_7H_8F_6O$: C, 37.70; H, 3.62%.

(*Z*)-3,4-Bis(trifluoromethyl)-2-methyl-3-buten-2-ol (*Z*-3d): Bp 134°C; d_4^{20} 1.356; n_D^{20} 1.3596; IR (neat) 1679 (C=C) cm^{-1}; ^{1}H NMR δ=1.52 (br s, 6H, CH_3), 2.61 (br s, 1H, OH), and 6.56 (q, *J*=8.4 Hz, 1H, CH); Found: C, 37.63; H, 3.62%. Calcd for $C_7H_8F_6O$: C, 37.70; H, 3.62%.

Dehydration of 2,3-Bis(trifluoromethyl)allyl Alcohols (3). In a flask (100 ml) equipped with a distillation apparatus, were placed a mixture of (*E*)- and (*Z*)-3,4-bis(trifluoromethyl)-3-buten-2-ol (**3b**, 12.3 g, 0.06 mol) and phosphorus pentaoxide (24 g, 0.17 mol). The mixture was heated at 100°C. As the reaction proceeded, was distilled out a mixture of (*E*)- and (*Z*)-1,2-bis(trifluoromethyl)-1,3-butadiene (**6b**, 8.9 g), which were separated using a preparative gas chromatograph. The physical and spectral data are shown below.

(*E*)-1,2-Bis(trifluoromethyl)-1,3-butadiene (*E*-6b): Bp 53°C; d_4^{20} 1.302; n_D^{20} 1.3321; IR (neat) 1613 and 1668 (C=C) cm^{-1}; ^{1}H NMR δ=5.4—6.7 (m, 3H, CH=CH_2) and 6.15 (q, *J*=9.0 Hz, 1H, CF_3CH); ^{19}F NMR δ=12.6 (d, *J*=1 Hz, 2-CF_3) and 19.4 (dq, *J*=9 and 1 Hz, 1-CF_3); Found: C, 37.86; H, 2.07%. Calcd for $C_6H_4F_6$: C, 37.91; H, 2.12%.

(*Z*)-Bis(trifluoromethyl)-1,3-butadiene (*Z*-6b): d_4^{20}1.350; n_D^{20} 1.3410; IR (neat) 1691 (C=C) cm^{-1}; ^{1}H NMR δ=5.3—6.7 (m, 3H, CH=CH_2) and 6.00 (q, *J*=7.8 Hz, 1H, CF_3CH); ^{19}F NMR δ=15.2 (q, *J*=11 Hz, 2-CF_3) and 19.7 (dq, *J*=8 and 11 Hz, 1-CF_3); Found: C, 37.49; H, 2.16%. Calcd for $C_6H_4F_6$: C, 37.91; H, 2.12%.

(*E*)-1,2-Bis(trifluoromethyl)-3-methyl-1,3-butadiene (*E*-6d): Bp 67.0°C; d_4^{20} 1.221; n_D^{20} 1.3277; IR (neat) 1641 and 1681 (C=C) cm^{-1}; ^{1}H NMR δ=1.94 (br s, 3H, CH_3), 5.01 (br s, 1H, CH_2), 5.23 (q, *J*=1.2 Hz, 1H, CH_2), and 6.14 (qq, *J*=7.2 and 1.8 Hz, 1H, CH); ^{19}F NMR δ=9.7 (br s, 2-CF_3) and 18.3 (br d, 1-CF_3); Found: C, 40.67; H, 2.87%. Calcd for $C_7H_6F_6$: C, 41.19; H, 2.96%.

(*Z*)-1,2-Bis(trifluoromethyl)-3-methyl-1,3-butadiene (*Z*-6d): Bp 89°C; d_4^{20}1.280; n_D^{20} 1.3441; IR (neat) 1648 and 1669 (C=C) cm^{-1}; ^{1}H NMR δ=1.96 (q, *J*=8.2 Hz, 3H, CH_3), 5.21 (br s, 2H, CH_2), and 5.95 (q, *J*=8.4 Hz, 1H, CH); ^{19}F NMR δ=17.0 (q, *J*=13 Hz, 2-CF_3) and 19.8 (dq, *J*=8 and 13 Hz, 1-CF_3); Found: C, 40.90; H, 2.92%, Calcd for $C_7H_6F_6$: C, 41.19; H, 2.96%.

Cyclization of 1,2-Bis(trifluoromethyl)-1,3-butadiene (6d). In a stainless steel autoclave (100 ml) was placed a mixture of (*E*)- and (*Z*)-1,2-bis(trifluoromethyl)-3-methyl-1,3-butadiene (**6d**, 5.9 g, 28.9 mmol) and *dl*-limonene (1.0 g, a polymerization inhibitor). After heating the reaction mixture at 200°C for 24 h, the product was distilled and purified using a preparative gas chromatograph to afford 1-methyl-2,3-bis(trifluoromethyl)cyclobutene (**7d**, 1.5 g) in 25% yield.

1-Methyl-2,3-bis(trifluoromethyl)cyclobutene (7d): Mp 107°C; d_4^{20} 1.305; n_D^{20} 1.3362; IR (neat) 1694 (C=C) cm^{-1}; ^1H NMR δ=1.90 (br s, 3H, CH_3), 2.57 (br s, 2H, CH_2), and 3.90 (br s, 1H, CH); ^{19}F NMR δ=5.7 (dq, J=8 and 2 Hz, CCF_3) and 13.8 (br, $CHCF_3$); Found: C, 40.90; H, 2.88%, Calcd for $C_7H_6F_6$: C, 41.19; H, 2.96%.

References

1) C. Walling and E.S. Huyser, "Free Radical Addition to Olefins to Form Carbon–Carbon Bonds," in "Organic Reaction," ed by C. Cope, John Wiley & Sons, Inc., New York (1963), Vol. 13, pp. 91—376.
2) K. Inukai, T. Ueda, and H. Muramatsu, *J. Org. Chem.*, **29**, 2224 (1964).
3) H. Muramatu and K. Inukai, *J. Org. Chem.*, **30**, 544 (1965).
4) H. Muramatsu, K. Inukai, and T. Ueda, *J. Org. Chem.*, **30**, 2546, (1965).
5) H. Muramatsu, S. Moriuchi, and K. Inukai, *J. Org. Chem.*, **31**, 1306 (1966).
6) H. Muramatsu, K. Inukai, and T. Ueda, *Bull. Chem. Soc. Jpn.*, **40**, 903 (1967).
7) H. Muramatsu, H. Kimoto, and K. Inukai, *Bull. Chem. Soc. Jpn.*, **42**, 1155 (1969).
8) T. Ueda, K. Inukai, and H. Muramatsu, *Bull. Chem. Soc. Jpn.*, **42**, 1684 (1969).
9) G. V. D. Tiers, *J. Phys. Chem.*, **66**, 1192 (1962).

Oxidation of 4,6,8-Trimethylazulene and Guaiazulene with Hydrogen Peroxide in Pyridine[1)]

Yoshiharu MATSUBARA, Masanori MORITA,† Shin-ichi TAKEKUMA,* Tomohiro NAKANO, Hiroshi YAMAMOTO,*,†† and Tetsuo NOZOE†††

Department of Applied Chemistry, Faculty of Science and Engineering, Kinki University, Kowakae, Higashi-Osaka 577

† Kinki University Cooperative Laboratories Center, Kowakae , Higashi-Osaka 577

†† Department of Chemistry, Okayama University, Okayama 700

††† Tokyo Research Laboratories, Takasago Corporation, Kamata, Ohta-ku, Tokyo 144

(Received July 12, 1991)

Synopsis. Oxidation of 4,6,8-trimethylazulene (**1**) with hydrogen peroxide in pyridine at 25°C for 18 h gave 4,6,8-trimethyl-1,5- and -1,7-azulenequinones, their 2-(4,6,8-trimethyl-1-azulenyl) derivatives, and 2,3-dihydro-4,6- and -4,7-dimethyl-2-(4,6,8-trimethyl-1-azulenyl)-1*H*-inden-1-ones in much higher yields than those by autoxidation of **1** in DMF at 120°C. The same oxidation of guaiazulene afforded sixteen separable products, among which there were three new dimeric condensates.

We have undertaken a systematic investigation on autoxidation of various azulenes for the past several years and isolated a wide variety of interesting products.[2)] Oxidation of guaiazulene (**2**) with peracetic acid was also conducted recently, and three dimeric compounds **3**, **4**, and **5** were isolated in good yields.[3-5)] These compounds were proved to be important intermediates for the autoxidation products of **2**. We now wish to report on oxidation of two representative trialkyl azulene derivatives, 4,6,8-trimethylazulene (**1**) and guaiazulene (**2**), with hydrogen peroxide in pyridine, which has resulted in isolation of several 1,5- and 1,7-azulenequinone derivatives in much higher yields than those by autoxidation, as well as disclosing several new types of reaction pathways in the oxidation of azulenic hydrocarbons.

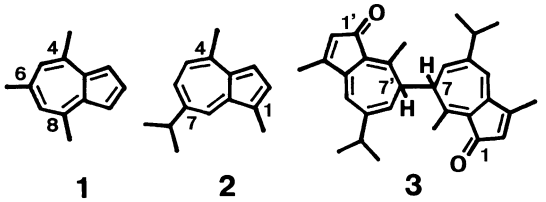

1 **2** **3**

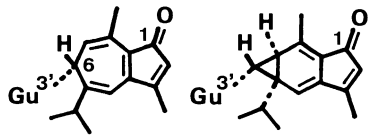

4 **5**

Gu3'= 3-guaiazulenyl

Oxidation of 4,6,8-Trimethylazulene (1). Oxidation of **1** with hydrogen peroxide in pyridine was carried out at 25°C for 18 h, during which the reaction was monitored by the use of the reversed-phase high-pressure liquid chromatography (HPLC) and silica-gel TLC. As in the case of our previous studies no oxidation of azulenes, the reaction products were carefully separated into each component by using chromatography, when about 33% of the starting material **1** was consumed. Thus, we obtained seven products (**6**—**12**); the sequence of the compound numbers corresponds to the decreasing R_f values on silica-gel TLC (15:85 AcOEt–hexane). In Chart 1 are summarized these products, whose structures were established by UV-visible, IR ^{1}H NMR, and EI MS spectroscopy as will be explained below. Yields of the isolated products, which are based on the consumed starting material **1**, totaled to 36%. Besides these, there still remained 63% (w/w) yield of unidentified polar resinous products.

Compound **6** (5% yield) (M^+: m/z 328 by EI MS) contained a carbonyl group (1695 cm^{-1}) and a 4,6,8-trimethyl-1-azulenyl moiety (^{1}H NMR). A careful analysis of the ^{1}H NMR spectra with the aid of decoupling techniques and by comparison of the parameters (δ and J values) with those of related compounds[2)] established the structure of 2,3-dihydro-4,7-dimethyl-2-(4,6,8-trimethyl-1-azulenyl)-1*H*-inden-1-one for **6**. The assignments of the ^{1}H NMR signals are recorded in the Experimental section. Compound **7** (5% yield) turned out to be the 4,6-dimethyl isomer of **6** by the similar analysis of the IR, ^{1}H NMR, and EI MS spectral data.

Compound **8** (1% yield) possesed a dimeric composition ($C_{26}H_{24}O_3$ by HR MS) and contained three carbonyl groups (1705, 1675, and 1570 cm^{-1}). The ^{1}H NMR data indicated the presence of a 2-substituted 4,6,8-trimethyl-1,5-azulenequinone[2b)] moiety and a certain nucleus ($C_{13}H_{13}O$) that exhibited three methyl groups (at δ=2.18, 2.86, and 3.18, all singlet), an olefinic proton (at δ=6.53, singlet), and three aromatic protons [at δ=6.93(2H) and 6.96, both singlet]. However, structure of **8**[6)] is not yet determined.

Compounds **9** and **10** (9% yield), a inseparable mixture, were found to be a mixture of 2-(4,6,8-trimethyl-1-azulenyl)-4,6,8-trimethyl-1,7- and -1,5-azulenequinones in a ratio of ca. 1:1, respectively. The assignment of the coupling positions (C_2–$C_{1'}$) of the two moieties in these compounds were based on an NOE

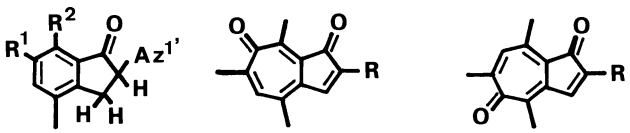

6: R^1 = H, R^2 = Me **9**: R = $Az^{1'}$ **10**: R = $Az^{1'}$

7: R^1 = Me, R^2 = H **11**: R = H* **12**: R = H*

Chart 1. Oxidation products from **1** with hydrogen peroxide in pyridine at 25°C for 18 h: $Az^{1'}$=4,6,8-trimethyl-1-azulenyl; *previously known compounds.

experiment on the Me-4 and H-3 signals of the 4,6,8-trimethyl-1,7- and -1,5-azulenequinone moieties. Compounds **11** and **12** (8% yield each) were identified by UV, IR, ^{1}H NMR, and EI MS spectroscopy as 4,6,8-trimethyl-1,7- and -1,5-azulenequinones,[2b] respectively. It is noteworthy that azulenequinones (**11** and **12** as well as **9** and **10**) were produced in significantly higher yields under the present conditions than the previous autoxidation of **1** in DMF at 120°C (1% yield each for **11** and **12**).[2b]

No oxidation was found to take place, when **1** was treated with pyridine 1-oxide[7-8] in pyridine at 25°C for 18 h. Therefore, the above results are most likely due to the lower reaction temperature and the neutral conditions that would prevent those products decomposition during the oxidation.

Oxidation of Guaiazulene (2). Compound **2** was treated with hydrogen peroxide in pyridine at 25°C for 8 h in a manner similar to that described for **1**. After separation, sixteen products (**13**—**28**) were obtained as pure compounds besides the recovered starting material **2** (60%). Structures of these products are shown in Chart 2, among which thirteen compounds (**13**, **15**, **17**, and **19**—**28**) were spectroscopically identical with those obtained previously by autoxidation of **2**.[2]

Compound **14** was found to be the 3,5′-isomer by spectroscopy. Compound **16** (M^+: m/z 394 by EI MS) contained a 3-guaiazulenyl moiety attached to a methyl group of the 7-isopropyl substituent of **2** (UV and ^{1}H NMR). Compound **18** (M^+: m/z 354 by EI MS) possessed a 3-guaiazulenyl moiety attached to C-2 of 3,7-dimethyl-1*H*-inden-1-one (UV and ^{1}H NMR).

The total yields of the isolated products from **2** were 72%, but there still remained a 20% (w/w) yield of unidentified polar resinous products. 5-Isopropyl-3,8-dimethyl-1,7-azulenequinone (**28**) was obtained in the highest yield (10%) among the isolated products. The newly isolated compounds **14** and **16** are apparently formed by two new types of bimolecular coupling reactions: Namely, coupling of the most reactive site (C-3) of guaiazulene with a seemingly far less reactive site of the seven-membered nucleus C-7 (to give **14**) and of a side-chain isopropyl group of **2** (to give **16**).

Although the exact reaction mechanism has still remained to be clarified, the present work is believed to provide notable information on potential synthetic application to the preparation of some azulenequinones.

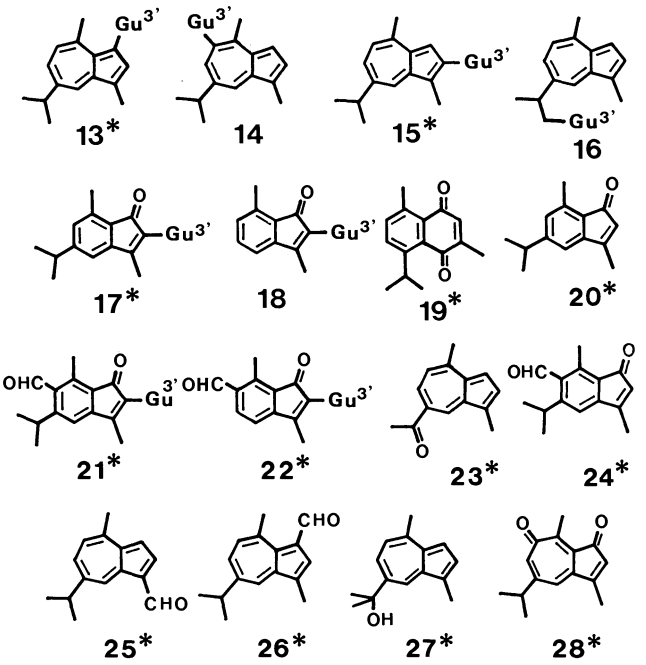

Chart 2. Oxidation products from **2** with hydrogen peroxide in pyridine at 25°C for 8 h: Gu$^{3'}$=3-guaiazulenyl; *previously known compounds.

Experimental

Melting points were determined with a Yanagimoto MP-S3 instrument and are uncorrected. Chromatographic saparation and the spectral measurement were carried out according to the procedures described before,[2a] except that ^{1}H NMR spectra were recorded with a JEOL GSX-270 (270 MHz for ^{1}H).

Oxidation of 4,6,8-Trimethylazulene (1). Compound **1**[9] (0.33 g) was added to a stirred solution of hydrogen peroxide (30% aq, 10 ml) in pyridine (20 ml). The mixture was stirred at 25°C for 18 h. The reactant was treated with cold 10% aq HCl (500 ml), carefully neutralized with aq Na_2CO_3, and extracted with hexane (3×100 ml). The extract was washed with water, dried (Na_2SO_4), and evaporated in vacuo. The residue (0.34 g) was purified by silica-gel column chromatography first with hexane (to recover the unreacted **1**), then with hexane-ethyl acetate (to separate several products), and finally with methanol (to eluate the polar substance) as the eluants. Then, each fraction of the products was further purified by preparative HPLC; when necessary, this chromatographic procedure was repeated. Thus, the following seven products were obtained as pure substances (**6**—**12**), besides the recovered starting material **1** [0.22 g (conversion: 33%); R_f=0.94] and polar resinous substances [76 mg, 63% (w/w); R_f=0.0]. The yield of each product is based on the consumed starting material (0.11 g).

2,3-Dihydro-4,7-dimethyl-2-(4,6,8-trimethyl-1-azulenyl)-1*H*-inden-1-one (6): Violet needles; 6 mg (5%); mp 154°C; R_f=0.56; IR ($CHCl_3$) 1695 cm^{-1} (C=O); ^{1}H NMR δ=2.32 (3H, brs, Me-4), 2.59 (3H, s, Me-6′), 2.64 (3H, brs, Me-7), 2.82 (3H, s, Me-4′), 3.14 (3H, brs, Me-8′), 3.17 (1H, dd, J=17.5, 4.0 Hz, H-3), 3.63 (1H, dd, J=17.5, 8.5 Hz, H-3), 4.92 (1H, brdd, J=8.5, 4.0 Hz, H-2), 6.97 (1H, s, H-5′), 6.99 (1H, s, H-7′), 7.08 (1H, brd, J=7.5 Hz, H-6), 7.26 (1H, brd, J=4.0 Hz, H-3′), 7.28 (1H, d, J=4.0 Hz, H-2′), and 7.30 (1H, brd, J=7.5 Hz, H-5); EI MS m/z 328 (M^+; 100%), 313 (39), 285 (50), 270 (54), 253 (24), 239 (20), 170 (62), 152 (15), 128 (13), 115 (21), 91 (9), 77 (4), 65 (4), and 51 (3).

2,3-Dihydro-4,6-dimethyl-2-(4,6,8-trimethyl-1-azulenyl)-1*H*-inden-1-one (7): Violet needles; 6 mg (5%); mp 182°C; R_f=0.49; IR ($CHCl_3$) 1695 cm^{-1} (C=O); ^{1}H NMR δ=2.33 (3H, brs, Me-4), 2.41 (3H, brs, Me-6), 2.59 (3H, s, Me-6′), 2.82 (3H, s, Me-4′), 3.13 (3H, brs, Me-8′), 3.14 (1H, dd, J=17.0, 4.0 Hz, H-3), 3.65 (1H. dd. J=17.0, 8.0 Hz, H-3), 4.94 (1H, brdd, J=8.0, 4.0 Hz, H-2), 6.98 (1H, s, H-5′), 6.99 (1H, s, H-7′), 7.26 (1H, brd, J=4.0 Hz, H-3′), 7.28 (1H, d, J=4.0 Hz, H-2′), 7.30 (1H, s, H-5), and 7.51 (1H, s, H-7); EI MS m/z 328 (M^+; 100%), 313 (60), 285 (38), 270 (56), 253 (26), 239 (21), 170 (45), 152 (17), 128 (14), 115 (20), 91 (11), 77 (9), 65 (4), 51 (4), and 41 (5).

4,6,8-Trimethyl-2-(4,6,8-trimethyl-1-azulenyl)-1,7- and -1,5-azulenequinone (9 and 10): (As a ca. 1:1 mixture, respectively); dark reddish violet needles; 11 mg (9%); mp 185—192°C; R_f=0.38; IR ($CHCl_3$) 1735, 1690, and 1575 cm^{-1} (C=O); ^{1}H NMR for **9** δ=2.27 (3H, brd, $J\approx$1 Hz, Me-6), 2.36 (3H, s, Me-4), 2.615 (3H, s, Me-8), 2.69 (3H, s, Me-6′), 2.72 (3H, s, Me-4′), 2.883 (3H, s, Me-8′), 7.06 (1H, s, H-5′), 7.10 (1H, s, H-7′), 7.11 (1H, brq, $J\approx$1 Hz, H-5), 7.34 (1H, d, J=4.0 Hz, H-3′), 7.62 (1H, d, J=4.0 Hz, H-2′), and 7.69 (1H, s, H-3) and

for **10** δ=2.30 (3H, brd, $J\approx1$ Hz, Me-6), 2.37 (3H, s, Me-4), 2.62 (3H, s, Me-8), 2.70 (3H, s, Me-6′), 2.73 (3H, s, Me-4′), 2.877 (3H, s, Me-8′), 7.085 (1H, s, H-5′), 7.09 (1H, brq, $J\approx1$ Hz, H-7), 7.12 (1H, s, H-7′), 7.40 (1H, d, J=4.0 Hz, H-3′), 7.66 (1H, d, J=4.0 Hz, H-2′), and 7.77 (1H, s, H-3); NOE experiment [obsd NOEs(%) by irradiation of Me-4 for **9**] H-3=29, (for **10**) H-3=38; EI MS m/z 368 (M^+; 74%), 340 (100), 325 (35), 310 (22), 297 (28), 281 (26), 267 (37), 252 (15), 239 (17), 170 (11), 152 (20), 128 (17), 115 (24), 91 (11), 77 (13), and 41 (15).

4,6,8-Trimethyl-1,7-azulenequinone[2b] **(11):** Yellow needles; 10 mg (8%); mp 118°C decomp (lit,[2b] mp 118°C decomp); R_f=0.25; UV, IR, ^{1}H NMR, and EI MS, identical with the spectra of the authentic sample.

4,6,8-Trimethyl-1,5-azulenequinone[2b] **(12):** Yellow needles; 10 mg (8%); mp 120°C decomp (lit.[2b] mp 120°C decomp); R_f=0.23; UV, IR, ^{1}H NMR, and EI MS, identical with the spectra of the authentic sample.

Oxidation of Guaiazulene (2). Oxidation of **2**[9] (0.10 g) with hydrogen peroxide (30% aq, 3 ml) in pyridine (5 ml) was carried out at 25°C for 8 h in a manner similar to that described for **1**, thus affording, after the careful chromatographic separation, sixteen products (**13**—**28**), besides the recovered starting material **2** (60 mg, 40% conversion, R_f=0.95) and polar resinous substances [8 mg, 20% (w/w); R_f=0.0]. The yield of each product is based on the consumed starting material (40 mg).

Previously Known Compounds: Comounds **13** (4 mg, 10%), **15** (3 mg, 8%), **17** (1 mg, 3%), **19** (1 mg, 3%), **20** (2 mg, 5%), **21** (1 mg, 3%), **22** (1 mg, 3%), **23** (1 mg, 3%), **24** (2 mg, 5%), **25** (1 mg, 3%), **26** (1 mg, 3%), **27** (2 mg, 5%), and **28** (4 mg, 10%) were obtained, which had also been produced by autoxidation of **2**.[2]

3,5′-Biguaiazulene (14): (As a ca. 37:63 mixture of **14** and **13**, respectively); dark greenish blue paste; R_f=0.71; ^{1}H NMR δ=1.31, 1.32 (3H each, d, J=7.0 Hz, *i*-Pr-7′), 1.40 (6H, d, J=7.0 Hz, *i*-Pr-7), 2.26 (3H, s, Me-4′), 2.50 (3H, s, Me-4), 2.70 (3H, s, Me-1), 2.71 (3H, s, Me-1′), 3.02 (1H, sept, J=7.0 Hz, Me_2CH-7′), 3.08 (1H, sept, J=7.0 Hz, Me_2CH-7), 6.82 (1H, d, J=10.0 Hz, H-5), 7.29 (1H, d, J=3.5 Hz, H-3′), 7.33 (1H, dd, J=10.0, 2.0 Hz, H-6), 7.46 (1H, s, H-2), 7.62 (1H, d, J=2.0 Hz, H-6′), 7.65 (1H, d, J=3.5 Hz, H-2′), 8.22 (1H, d, J=2.0 Hz, H-8), and 8.23 (1H, d, J=2.0 Hz, H-8′).

7-[2-(3-Guaiazulenyl)-1-methylethyl]-1,4-dimethylazulene (16): Blue prisms; 1 mg (3%); mp 117°C; R_f=0.71; UV λ_{max} (MeOH) 246, 285, 307,[sh] 352, 369, and 613 nm (log ε 4.60, 4.65, 4.52, 3.76, 3.74, and 3.03); ^{1}H NMR δ=1.35 (6H, d, J=7.0 Hz, *i*-Pr-7′), 1.37 (3H, d, J=7.0 Hz, CH_3CH-7), 2.55 (3H, s, Me-1), 2.61 (3H, s, Me-1′), 2.84 (3H, s, Me-4), 2.99 (3H, s, Me-4′), 3.01 (1H, sept, J=7.0 Hz, Me_2CH-7′), 3.24 (1H, dqd, J=8.5, 7.0, 6.0 Hz, CH-7), 3.46 (1H, dd, J=14.5, 8.5 Hz, CH–C-7), 3.66 (1H, dd, J=14.5, 6.0 Hz, CH–C-7), 6.82 (1H, d, J=10.5 Hz, H-5′), 6.99 (1H, d, J=10.5 Hz, H-5), 7.23 (1H, d, J=4.0 Hz, H-3), 7.25 (1H, dd, J=10.5, 2.0 Hz, H-6), 7.36 (1H, s, H-2′), 7.40 (1H, dd, J=10.5, 2.0 Hz, H-6′), 7.62 (1H, d, J=4.0 Hz, H-2), 8.03 (1H, d, J=2.0 Hz, H-8), and 8.16 (1H, d, J=2.0 Hz, H-8′); EI MS m/z 394 (M^+; 6%), 211 (100), 195 (4), 183 (9), 165 (4), 153 (4), and 44 (4).

2-(3-Guaiazulenyl)-3,7-dimethyl-1*H*-inden-1-one (18): Dark red paste; 2 mg (5%); R_f=0.64; UV λ_{max} (MeOH) 248, 283, 307,[sh] 352, 368,[sh] 458, and 490 nm (log ε 4.53, 4.50, 4.45, 3.65, 3.66, 3.39, and 3.38); IR ($CHCl_3$) 1695 cm^{-1} (C=O); ^{1}H NMR δ=1.33 (6H, d, J=7.0 Hz, *i*-Pr-7′), 2.08 (3H, s, Me-3), 2.56 (3H, s, Me-7), 2.64 (3H, s, Me-4′), 2.66 (3H, s, Me-1′), 3.06 (1H, sept, J=7.0 Hz, Me_2CH-7′), 6.93 (1H, d, J=11.0 Hz, H-5′), 6.98 (1H, brd, J=7.5 Hz, H-6), 7.01 (1H, brd, J=7.5 Hz, H-4), 7.27 (1H, t, J=7.5 Hz, H-5), 7.35 (1H, dd, J=11.0, 2.0 Hz, H-6′), 7.40 (1H, s, H-2′), and 8.14 (1H, d, J=2.0 Hz, H-8′); EI MS m/z 354 (M^+; 100%), 339 (19), 321 (4), 309 (6), 296 (5), 279 (5), 265 (5), 253 (6), 239 (4), 177 (3), and 165 (4).

References

1) A part of the results were presented at the 59th Meeting of the Chemical Society of Japan, Yokohama, April 1990, Abstr., No. 2 D7 30.

2) a) S. Takekuma, Y. Matsubara, H. Yamamoto, and T. Nozoe, *Bull. Chem. Soc. Jpn.*, **61**, 475 (1988). b) Y. Matsubara, S. Takekuma, K. Yokoi, H. Yamamoto, and T. Nozoe, *ibid.*, **60**, 1415 (1987), and references cited therein.

3) Y. Matsubara, S. Matsui, S. Takekuma, H. Yamamoto, and T. Nozoe, *Nippon Kagaku Kaishi*, **1988**, 1704.

4) Y. Matsubara, S. Matsui, S. Takekuma, Y. P. Quo, H. Yamamoto, and T. Nozoe, *Bull. Chem. Soc. Jpn.*, **62**, 2040 (1989).

5) Y. Matsubara, M. Morita, S. Matsui, S. Takekuma, H. Yamamoto, S. Ito, N. Morita, T. Asao, and T. Nozoe, *Bull. Chem. Soc. Jpn.*, **63**, 1841 (1990).

6) Compound **8**: Dark green prisms; 1 mg (1%); mp 205°C; R_f=0.43; IR ($CHCl_3$) 1705, 1675, and 1570 cm^{-1} (C=O); ^{1}H NMR δ=2.18 (6H, s), 2.35 (3H, s), 2.61 (3H, s), 2.86 (3H, s), 3.18 (3H, s), 6.53 (1H, s), 6.93 (2H, s), 6.96 (1H, brs), 6.99 (1H, brs), and 7.78 (1H, s); EI MS m/z 384 (M^+; 85%), 356 (3), 341 (4), 313 (6), 209 (7), 185 (6), 165 (13), 147 (100), 119 (23), and 91 (4). Found: m/z 384.1704. Calcd for $C_{26}H_{24}O_3$: M, 384.1725.

7) H. S. Mosher, L. Turner, and A. Carlsmith, *Org. Synth.*, Coll. Vol. IV, 828 (1963).

8) Hydrogen peroxide alone does not normally react with nitrogen-containg heteroaromatic compounds such as pyridine: see e.g., A. R. Katritzky and J. M. Lagowski, "Chemistry of the Heterocyclic N-Oxides," Academic Press, New York (1971), p. 56.

9) We are grateful to Konan Kako Co. (Osaka) for a generous gift of 4,6,8-trimethylazulene and guaiazulene.

Mass Transfer and Product-Selectivity in Electroreduction of *p*-Methylbenzaldehyde

Po-Chung CHENG and Tsutomu NONAKA*
Department of Electronic Chemistry, Graduate School at Nagatsuta, Tokyo Institute of Technology, 4259 Nagatsuta, Midori-ku, Yokohama 277
(Received July 4, 1991)

Synopsis. Mass transfer coefficients estimated from the formation ratio of the hydrodimeric to hydromonomeric products in electroreduction of *p*-methylbenzaldehyde in parallel plate electrode–flow cell and rotating cylinder electrode–beaker cell systems were shown in good agreement (less than 8% difference) with those obtained by ordinary current–potential and concentration–time methods.

Electroreduction of carbonyl compounds yields the corresponding hydrodimers and hydromonomers. In 1960's, Udupa and co-workers[1] found that the formation ratio of the hydrodimers to hydromonomers at a rotating electrode was larger than that at a stationary electrode. This means that mass transfer plays an important role in controlling product-selectivity in electroorganic synthesis, and it is interesting to describe such behavior by a mathematical model. In previous work,[2] we developed a mathematical reaction model for the electroreductionof *p*-methylbenzaldehyde to the hydrodimer [1,2-bis(*p*-methylphenyl)-1,2-ethanediol] and the hydromonomer (*p*-methylbenzyl alcohol) at a rotating cylinder cathode in an acidic solution, and showed that the product-selectivity (formation ratio of the former to the latter product) is predictable if substrate concentration, current density and mass-transfer coefficient are known. Using the mass transfer coefficients obtained from polarization curves, the values of product-selectivity were estimated and found to be in good agreement with the experimental ones.

Inversely, it is also expected that mass transfer coefficient can be obtained from product-selectivity as described below.

Although a rotating electrode system is conveniently used for a small scale operation and one can control precisely mass transfer to and from electrode surface in this system, a flow cell system is much more practical in view of industrization.[1] In this work, a modification of the above mathematical method devloped for a rotating electrode–beaker cell system was made to be applied to a parallel plate electrode-flow cell one.

Experimental

A parallel plate flow cell (Micro Flow cell, ElectroCell AB, Sweden) was equipped with a Pb plate cathode (3.2×3.2 cm) and a so-called USA anode with a similar dimension. The catholyte of 0.25 mol dm^{-3} H_2SO_4/50% v/v ethanol containing *p*-methylbenzaldehyde (0.08 mol dm^{-3}) was separated from the anolyte by a cationic membrane (Ionac MC-3470, Sybron Chemicals Inc., USA). The electrolytes were circulated with tubing pumps (Masterflex RA-71, Cole-Pamer, USA). Pre-electrolysis without *p*-methylbenzaldehyde was carried out for ca. 15 min before the preparative electrolysis. All the electrolyses were operated at 25±2°C.

An electrolytic cell equipped with a rotating cylinder Pb cathode is described in the previous paper.[2] The products were routinely analyzed with HPLC.

Results and Discussion

A Rotating Cylinder Electrode–Beaker Cell System. The reaction mechanism for electroreduction of *p*-methylbenzaldehyde in an acidic solution is proposed as follows:[2]

$$\mathrm{ArCHO} \underset{}{\overset{\mathrm{H^+}}{\rightleftharpoons}} \mathrm{Ar\overset{+}{C}H(OH)} \qquad \text{(I)}$$

$$\mathrm{Ar\overset{+}{C}H(OH)} \xrightarrow{\mathrm{e}} \mathrm{Ar\dot{C}H(OH)} \qquad \text{(II)}$$

$$\mathrm{Ar\dot{C}H(OH)} \longrightarrow \frac{1}{2}\ \mathrm{Ar\underset{OH}{\underset{|}{C}}H-\underset{OH}{\underset{|}{C}}HAr} \qquad \text{(III)}$$

$$\mathrm{Ar\dot{C}H(OH)} \xrightarrow{\mathrm{e}+\mathrm{H^+}} \mathrm{ArCH_2OH} \qquad \text{(IV)}$$

(Ar = CH_3–C$_6$H$_4$–)

The limiting current density (i_L) for the primary electron-transfer reaction (Eq. II), which yields the radical intermediate, is defined by

$$i_L = k_m FC, \qquad (1)$$

where k_m and C are mass transfer coefficient and bulk concentration of substrate, respectively, and F is the Faraday constant.

Under galvanostatic operation, the product-selectivity for a batch electrolysis at a rotating cylinder electrode is written according to whether current density (i) at the beginning of electrolysis is larger than i_L or not.[2]

$i_L \geqslant i$ at $t=0$: Let t_0 be the time required to decrease i_L to i, then one has

$$C_0 = i/k_m F, \qquad (2)$$

$$t_0 = VF(C_i - C_0)/iA, \qquad (3)$$

where C_i and C_0 are the concentrations of substrate at $t=0$ and $t=t_0$, respectively, A is electrode area, and V is the volume of electrolyte.

The product-selectivity (ζ), defined as the formation ratio of hydrodimer (HD) to hydromonomer (HM), is then written as

$$\zeta = \frac{[\mathrm{HD}]}{[\mathrm{HM}]} = \frac{iA(2t_0-t)/2VF+\{1-\exp[-k_m A(t-t_0)/V]\}C_0}{iA(t-t_0)/VF-\{1-\exp[-k_m A(t-t_0)/V]\}C_0} \qquad (4)$$

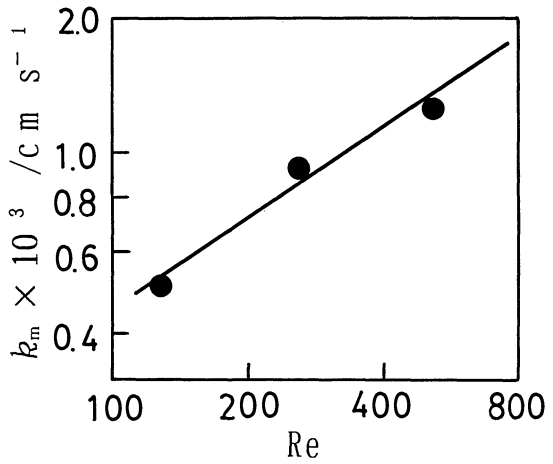

Fig. 1. Mass-Transfer coefficients (k_m) obtained by mathematical analysis of product-selectivity in a rotating cylinder electrode-beaker cell system. $Re=du_r/v$. Straight line: calculated from polarization curves. Plot: Experimentally obtained.

where [HD] and [HM] are the concentrations of HD and HM, respectively.[2]

$i_L < i$ at $t=0$: Substituting t_0 and C_0 with 0 and C_i, respectively, ζ can be calculated by Eq. 4.

If C_i, i and ζ are known, we can obtain k_m from Eq. 4 by Newton's method. Figure 1 shows the k_m values calculated at a rotating cylinder electrode using the data in the previous paper.[2] The sraight line in Fig. 1 is derived from polarization curves (Eq. 1), and it is noticeable that the k_m's obtained by both methods agree with each other. The relationship between k_m and Reynolds number (Re) can be expressed by Eq. 5.

$$k_m = 2.2 \times 10^{-5}\, Re^{0.66}\ (\mathrm{cm\ s^{-1}}), \tag{5}$$

where $Re=du_r/v$, u_r is the peripheral velocity, $v=0.0253$ cm^2 s^{-1} is the kinematic viscosity,[4] and $d=0.50$ cm is the cylinder diameter. The slope in Fig. 1 is 0.66, and the characteristic value for a rotating cylinder electrode is between 0.61 and 0.70 for $100<Re<160000$.[5-7] It must be emphasized here that the mathematical analysis of mass transfer in a rotating cylinder electrode system has not been reported for electroorganic reaction so far as we know.

A Parallel Plate Electrode-Flow Cell System. $i_L \geqq i$ at $t=0$: The concentration in the catholyte reservoir (C, i.e. the concentration at the entrance of the cell) decreases with t in the following way:

$$C = C_i - iAt/VF \qquad \text{when } t \leqslant t_0, \tag{6}$$

$$C = C_0 \exp[-p(t-t_0)] \qquad \text{when } t > t_0, \tag{7}$$

where

$$p = [1-\exp(-k_mA/Q)]Q/V,$$

and Q is the volumetric flow rate. Then Eq. 8 is derived by mathematical analysis similar to that in a rotating electrode system.

$$\zeta = \frac{iA(2t_0-t)/2VF + k_mAC_0\{1-\exp[-p(t-t_0)]\}/pV}{iA(t-t_0)/VF - k_mAC_0\{1-\exp[-p(t-t_0)]\}/pV}. \tag{8}$$

$i_L < i$ at $t=0$: Substituting t_0 and C_0 with 0 and C_i, respectively, ζ is given by Eq. 8.

Table 1 shows the experimental values of product-selectivity (ζ) obtained in the galvanostatic electrolysis of p-methylbenzaldehyde using the flow cell. Here a dimensionless parameter (q) is used instead of t. $q=1$ means that the charge passed for 1 mol of substrate is 96485 coulombs. The relation between q and t is given by

$$t = qVFC_i/iA. \tag{9}$$

As expected from Eq. 8, ζ decreases with an increase in t (i.e.q). On the other hand, ζ increases with an increase in k_m and the effect of Q is attributed to this. However, the correlation between k_m and Q (or Re) for the flow cell used is unknown, hence a numerical method similar to that in a rotating electrode system was used to calculate k_m's and their calculated values were also shown in Table 1. Then the following correlation is established:

Table 1. Product-Selectivity ζ (Hydrodimer/Hydromonomer) for the Reaction of p-Methylbenzaldehyde (Initial Concentration: 0.08 mol dm^{-3}) in a Parallel Plate Electrode-Flow Cell System and k_m Calculated by Newton's Method. $q=iAt/VFC_i$

Q/cm^3 min^{-1}	i/mA cm^{-2}	q	Exptl ζ	Calcd k_m/cm s^{-1}
150	8.0	0.2	1.06	0.000851
150	8.0	0.3	0.885	0.000860
150	8.0	0.4	0.739	0.000869
200	10.0	0.4	0.660	0.00106
250	12.0	0.2	1.05	0.00128
250	12.0	0.3	0.904	0.00130
250	12.0	0.4	0.774	0.00132
300	8.0	0.4	13.30	0.00138
300	10.0	0.4	3.40	0.00144
400	12.0	0.2	6.10	0.00160
400	12.0	0.3	4.33	0.00165
400	12.0	0.4	3.14	0.00170

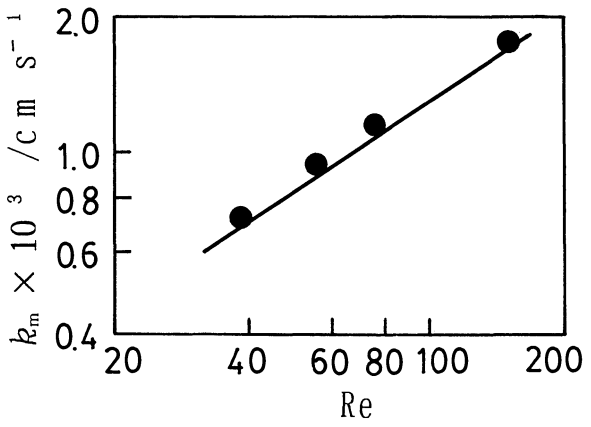

Fig. 2. Mass-Transfer coefficients (k_m) in a parallel plate electrode–flow cell system. $Re=d_e u/v$. Straight line: Eq. 10. Plot: Obtained from Eq. 7.

$$k_m = 5.84 \times 10^{-5}\ Re^{0.67}\ (\mathrm{cm\ s^{-1}}), \qquad (10)$$

where $Re=d_e u/v$, u is the linear velocity, and d_e=0.58 cm is the equivalent diameter of the flow cell.

The validity of Eq. 10 must be examined by comparing with other methods based on different principles. In stead of the information of mass transport from polarization curves (Eq. 1), Eq. 7 was used for this purpose.[8] From the relation of C and t, k_m was derived. The straight line in Fig. 2 comes from Eq. 10. Although k_m's calculated from Eq. 7 are somewhat larger than those of Eq. 10, the difference (4—8%) between them is rather small. Accordingly, the application of this mathematical reaction model to the electroreduction of *p*-methylbenzaldehyde is proven reasonable in the flow cell system.

However, flow in a range of $Re<1000$ is expected to be laminar. The experimental k_m's are larger than those of a correlation for laminar flow,[9] and the power in Eq. 10 indicates that the flow under our operating conditions is in a transition state from laminar flow to turbulent flow. It must be considered that the entrance effect introduces a measure of uncertainty into the prediction of mass-transfer rates in this type of electrolysis system.[10]

From the above discussion we conclude that the product-selectivity is itself an index of mass transport in some electrolytic systems, and mass-transfer coefficients can be estimated theoretically and experimentally in pratical parallel plate flow cell systems as well as in rotating electrode systems used for laboratory study. Furthermore, it is suggested that theoretical prediction of product-selectivity is possible by means of appropriate cell design.

References

1) H. V. K. Udupa, G. S. Subramanian, K. S. Udupa, and K. Katarajan, *Electrochim. Acta,* **9**, 313 (1964).
2) P.-C. Cheng, T. Nonaka, and T.-C. Chou, *Bull. Chem. Soc. Jpn.,* **64**, 1911 (1991).
3) For example: D. E. Danly, *Chem. Ind. (London)*, **1979**, 439.
4) A. E. Dustan and F. B. Thole, *J. Chem. Soc.,* **95**, 1556 (1909).
5) M. Eisenberg, C. W. Tobias, and C. R. Wilke, *J. Electrochem. Soc.,* **101**, 306 (1954).
6) N. R. K. Vilambi and D.-T. Chin, *J. Electrochem. Soc.,* **134**, 2501 (1987).
7) M. K. Kishinevskii and T. S. Kornienko, *Soviet Electrochem.,* **25**, 737 (1989).
8) R. M. Spotnitz, R. F. Kreh, J. T. Lundquist, and P. T. Press, *J. Appl. Electrochem.,* **20**, 209 (1990).
9) D. J. Pickett and B. R. Stanmore, *J. Appl. Electrochem.,* **2**, 151 (1972).
10) J. M. T. Clark, F. Goodridge, and R. E. Plimley, *J. Appl. Electrochem.,* **18**, 899 (1988).

Comparison of the Temperature and Location Dependence of ^1H and ^{13}C NMR Shifts between Saturated 1,3- and 1,2-Diamines Coordinated to Low-Spin Tetracyanoferrate(III)

Yoshitaka KURODA,* Masafumi GOTO,*,† and Tomoya SAKAI
Faculty of Pharmaceutical Sciences, Nagoya City University, Mizuho-ku, Nagoya 467
†Faculty of Pharmaceutical Sciences, Kumamoto University, Kumamoto 862
(Received November 26, 1990)

The temperature dependence of the ^1H NMR for low-spin iron(III) complexes, $[Fe^{III}(CN)_4(1,3\text{-diamine})]^-$, with 1,3-propanediamine, (2*R*,4*S*)-2,4-pentanediamine, and (2*R*,4*R*)-2,4-pentanediamine were measured at 323—183 K. The coordinated amine segment, $Fe\text{-}N(H_N)_2\text{-}C(H_\alpha)_2\text{-}C(H_\beta)_2$, resonated in the following magnetic field regions at 323—183 K: H_α^{ax}, 7.2—20.5; H_β^{ax}, 10.8—35.0; H_β^{eq}, 23.9—65.7; H_β^{methyl}, 1.8—9.9 ppm. All of the ^1H signals moved in the downfield direction with a decrease in the temperature, and exhibited a non-Curie behavior. The H_N shifts at 300 K were 110—279 ppm. The temperature and location dependence of the isotropic shift (δ^{iso}) for the ^1H and ^{13}C nuclei were accounted for by the combination of Fermi contact and dipolar contributions. The Fermi constants and spin populations were estimated for the ^1H and ^{13}C nuclei. Not only the spin polarization mechanism, but also a direct mechanism, were suggested for spin propagation from the Fe^{III} to the respective atoms.

Paramagnetic metal ions affect the NMR shifts of the compounds coordinated to them.[1] Such effects of metal ions have heen extensively investigated for unsaturated compounds.[2,3] On the other hand, studies of saturated compounds have almost been limited to Ni^{II} amine complexes.[4–7] Transition metal ions, such as the low-spin Fe^{III} ion, are expected to have different magnetic effects from those of Ni^{II}, according to their electronic configurations.

The ^1H and ^{13}C NMR spectra of saturated 1,2-diamines coordinated to a low-spin Fe^{III} ion, $[Fe^{III}(CN)_4(1,2\text{-diamine})]^-$, have been studied by using 1,2-ethanediamine (en), (*R*)-1,2-propanediamine (*R*-pn), (1*R*,2*R*)-1,2-cyclohexanediamine (*R*-chxn), *N*,*N*′-dimethyl-1,2-ethanediamine (s-Me$_2$en), etc.[8–10]

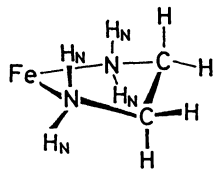

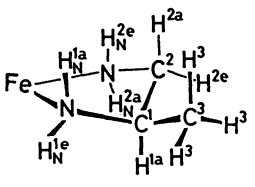

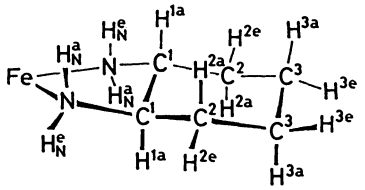

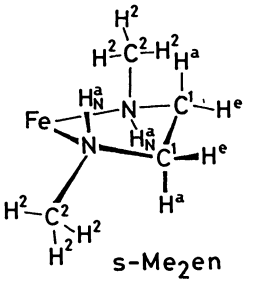

These Fe^{III} complexes do not obey the Curie law and show characteristic isotropic shifts (δ^{iso}) which are strongly dependent on the nuclear locations relative to the paramagnetic center, the Fe^{III} ion: downfield and upfield shifts were observed for the axial and equatorial protons bonded to the same carbon atom on the chelate ring, respectively. To clarify these features, δ^{iso} was separated into the Fermi contact shift (δ^{con}) and the dipolar shift (δ^{dip}), based on the electronic states obtained from a *g*-value analysis of the Fe^{III} en complex;[9] these shifts have been related to the nuclear positions.[9,10] This investigation has revealed that (1) nuclei nearer to the average plane of the chelate ring have larger δ^{con} values, and (2) that the non-Curie behavior of δ^{iso} can be accounted for by the temperature dependence of δ^{dip}.

The 1,3-diamine chelates, $[Fe^{III,II}(CN)_4(1,3\text{-diamine})]^{-,2-}$, such as (2*R*,4*S*)-2,4-pentanediamine (*meso*-ptn), 1,3-propanediamine (tn), (2*R*,4*R*)-2,4-pentanediamine (*R*-ptn), and 1,3-butanediamine (1,3-bn) assume a chair or skew-boat conformation, as shown in Fig. 1.[11] These 1,3-diamine chelates have a central methylene part which is absent in the 1,2-diamine chelates, and the nuclei of the former are further apart from the coordination plane than those of the latter with *gauche* conformations.[12–15] These structural differences are expected to make the δ^{dip} and δ^{con} values for the 1,3-diamine chelates different from those for the 1,2-diamine chelates.

The variations of the ^1H NMR shifts of the 1,3-diamine chelates with temperature were previously utilized for estimating the chair⇆chair interconversion rate,[16] though the temperature dependence was treated empirically. We now report on the C^{1}H and N^{1}H shifts of the *meso*-ptn, tn, *R*-ptn, and 1,3-bn chelates measured at 323—183 and 300 K, respectively. The δ^{iso} values for the CH and NH shifts, as well as the previously reported ^{13}C shifts,[11] are separated into δ^{dip} and δ^{con}. The δ^{con} values, thus obtained, are compared with those for the Fe^{III} 1,2-diamine chelates.[9,10]

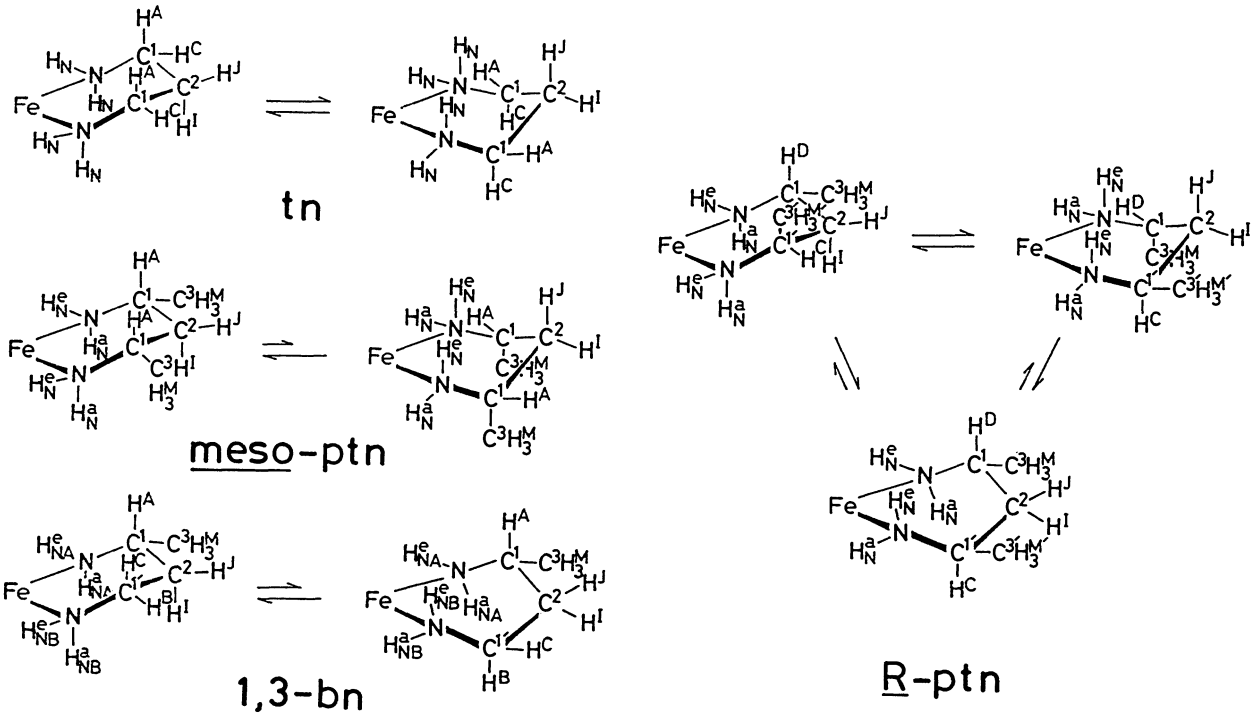

Fig. 1. Schematic structures of the chelates and the numbering of protons and carbons. Fe=Fe(CN)$_4$.

Experimental

Materials. Sodium tetracyano(1,3-diamine)ferrate(III) and ferrate(II) complexes containing 1,3-propanediamine (tn), (2*R*,4*S*)-2,4-pentanediamine (*meso*-ptn), (2*R*,4*R*)-2,4-pentanediamine (*R*-ptn), and 1,3-butanediamine (1,3-bn) as 1,3-diamines were prepared as previously reported.[11]

Measurement. The variable-temperature ^{1}H NMR spectra of the Fe^{III} 1,3-diamine complexes were recorded on a JEOL FX-100 spectrometer with ca. 0.05 M (1 M=1 mol dm^{-3}) solutions in CD_3OD containing 0.25% DCl at 323—183 K. Acidic solutions were necessary to protect the coordinated diamines against dehydrogenation.[17,18] Dilute solutions were required in order to avoid the deposition of complexes below 273 K. FID signals (pulse width: 7 μs; observation time 10 s) were collected 40 times for each sample at each temperature to obtain spectra with S/N ratios over 20/1. The probe temperature was controlled with a JNM-VT-3C temperature-control apparatus, and determined from the chemical shift difference between the methyl and hydroxyl protons of methanol.[19] The N^{1}H shifts of the Fe^{III} 1,3-diamine complexes were recorded on a JEOL FX-100 spectrometer at 300 K using 40—50 mg of the complexes dissolved in pD 2.0 DCl-D_2O (0.3 cm^3). Sodium 3-trimethylsilylpropionate-2,2,3,3-d_4 (TSP; 0.00 ppm) was used as an internal reference. The positive chemical shifts indicate downfield shifts from the standard.

Results and Discussion

Temperature Dependence of ^{1}H NMR Spectra of $[Fe^{III}(CN)_4(1,3\text{-diamine})]^-$. ^{1}H NMR spectra of $[Fe^{III}(CN)_4(tn)]^-$, $[Fe^{III}(CN)_4(meso\text{-ptn})]^-$, and $[Fe^{III}(CN)_4(R\text{-ptn})]^-$ (tn=1,3-propanediamine, *meso*-ptn=(2*R*,4*S*)-2,4-pentanediamine, *R*-ptn=(2*R*,4*R*)-2,4-pentanediamine) were measured in CD_3OD containing 0.25% DCl. The temperature range was limited to 323—183 K by the boiling and freezing points of the solvent.[16,20] Acidification of the solvent with DCl is necessary to protect the coordinated diamine molecule against dehydrogenation, which yields the corresponding Fe^{II} diimine complex under neutral or basic conditions.[17,18] The observed chemical shifts ($\delta_{Fe^{III}}$) are listed in the fifth column of Table 1.

(a) *meso*-ptn. $[Fe^{III}(CN)_4(meso\text{-ptn})]^-$ showed four CH peaks of H^J, H^I, H^A, and H^M downfield, with an area ratio of 1:1:2:6.[11] These peaks moved in the downfield direction and dispersed with a decrease in temperature. Their line-widths at half-height were broadened from 29, 47, 63, and 17 Hz at 323 K to 210, 350, 530, and 105 Hz at 183 K, respectively.

The large difference in the $\delta_{Fe^{III}}$ values of H^I and H^J, i.e. ca. 13—31 ppm at 323—183 K, indicates that the *meso*-ptn chelate is fixed in a chair conformation with two equatorial methyl groups (See Fig. 1). The H^A shift is less than the H^I and H^J shifts, whereas the corresponding axial protons of the 1,2-diamine chelates show the largest downfield shift among the CH's.[9,10,16,20] The H^A and H^M shifts are less than half the corresponding shifts for the 1,2-diamine chelates. The line-width at half-height is of the order of $H^A > H^I > H^J > H^M$, the reversed order of their distance from the Fe^{III} ion.

(b) tn. $[Fe^{III}(CN)_4(tn)]^-$ exhibited two peaks, one downfield and the other upfield, with an area ratio of 1:2. The former was assigned to H^I and H^J, and the latter to H^A and H^C. The $H^{I,J}$ shift is almost the same as the mean of the H^I and H^J shifts for the *meso*-ptn

Table 1. ^1H and ^{13}C NMR Shifts[a] and Calculated Isotropic, Dipolar, and Fermi Contact Shifts[a] for $[Fe^{III}(CN)_4(1,3\text{-diamine})]^-$

Diamine	Nucleus	Temp	$\delta_{Fe^{II}}$[b]	$\delta_{Fe^{III}}$	δ^{iso}[c]	δ^{dip}[d]	δ^{con}[e]
		K	ppm	ppm	ppm	ppm	ppm
tn	$H^{A,C}$	323	—	−6.00	−8.80	7.17	−15.97
		313	—	−6.06	−8.86	7.65	−16.51
		303	2.80	−6.15	−8.95	8.17	−17.12
		293	—	−6.19	−8.99	8.75	−17.74
		283	—	−6.27	−9.07	9.38	−18.45
		273	—	−6.34	−9.14	10.08	−19.22
		263	—	−6.44	−9.24	10.85	−20.10
		253	—	−6.53	−9.33	11.71	−21.04
		243	—	−6.65	−9.45	12.66	−22.11
		233	—	−6.80	−9.60	13.72	−23.32
		223	—	−6.97	−9.77	14.91	−24.68
		213	—	−7.09	−9.89	16.24	−26.13
		203	—	−7.21	−10.01	17.74	−27.75
		193	—	−7.36	−10.16	19.43	−29.59
		183	—	−7.62	−10.42	21.35	−31.77
	$H^{I,J}$	323	—	18.17	16.74	12.14	4.60
		313	—	19.05	17.62	12.95	4.67
		303	1.43	20.08	18.65	13.84	4.81
		293	—	21.33	19.90	14.81	5.09
		283	—	22.59	21.16	15.88	5.28
		273	—	24.08	22.65	17.07	5.58
		263	—	25.55	24.12	18.37	5.75
		253	—	27.65	26.22	19.82	6.40
		243	—	29.57	28.14	21.44	6.70
		233	—	32.24	30.81	23.23	7.58
		223	—	34.80	33.37	25.24	8.13
		213	—	37.72	36.29	27.50	8.79
		203	—	41.37	39.94	30.04	9.90
		193	—	45.49	44.06	32.90	11.16
		183	—	50.93	49.50	36.15	13.35
	H_N	300	f)	193.0	193.0	7.9	185.1
	C^1	300	42.3[g]	222.4[g]	180.1	23.0	157.1
	C^2	300	28.6[g]	29.4[g]	0.8	22.9	−22.1
meso-ptn	H^A	323	—	7.23	4.43	2.63	1.80
		313	—	7.55	4.75	2.81	1.94
		303	2.80	7.89	5.09	3.00	2.09
		293	—	8.31	5.51	3.21	2.30
		283	—	8.80	6.00	3.45	2.55
		273	—	9.24	6.44	3.70	2.74
		263	—	9.83	7.03	3.99	3.04
		253	—	10.52	7.72	4.30	3.42
		243	—	11.20	8.40	4.65	3.75
		233	—	12.11	9.31	5.04	4.27
		223	—	13.21	10.41	5.47	4.94
		213	—	14.51	11.71	5.96	5.75
		203	—	15.81	13.01	6.51	6.50
		193	—	17.77	14.97	7.14	7.83
		183	—	20.49	17.69	7.84	9.85
	H^I	323	—	10.83	9.95	7.92	2.03
		313	—	11.52	10.64	8.45	2.19
		303	0.88	12.20	11.32	9.03	2.29
		293	—	13.04	12.16	9.67	2.49
		283	—	13.92	13.04	10.37	2.67
		273	—	14.98	14.10	11.14	2.96
		263	—	16.10	15.22	11.99	3.23
		253	—	17.45	16.57	12.94	3.63
		243	—	18.80	17.92	13.99	3.93
		233	—	20.54	19.66	15.17	4.49
		223	—	22.75	21.87	16.48	5.39
		213	—	25.12	24.24	17.95	6.29
		203	—	27.77	26.89	19.60	7.29
		193	—	30.71	29.83	21.48	8.35
		183	—	34.95	34.07	23.60	10.47
	H^J	323	—	23.85	22.23	16.85	5.38
		313	—	25.07	23.45	17.97	5.48
		303	1.62	26.30	24.68	19.20	5.48
		293	—	27.82	26.20	20.56	5.64
		283	—	29.41	27.79	22.04	5.75
		273	—	31.28	29.66	23.69	5.97
		263	—	33.31	31.69	25.50	6.19
		253	—	35.71	34.09	27.51	6.58
		243	—	38.07	36.45	29.75	6.70
		233	—	41.15	39.53	32.24	7.29
		223	—	44.95	43.33	35.03	8.30
		213	—	49.07	47.45	38.16	9.29
		203	—	53.34	51.72	41.69	10.03
		193	—	58.60	56.98	45.66	11.32
		183	—	65.66	64.04	50.17	13.87
	H^M	323	—	2.52	1.31	3.64	−2.33
		313	—	2.72	1.51	3.89	−2.38
		303	1.21	2.94	1.73	4.16	−2.43
		293	—	3.21	2.00	4.45	−2.45
		283	—	3.48	2.27	4.77	−2.50
		273	—	3.79	2.58	5.13	−2.55
		263	—	4.14	2.93	5.52	−2.59
		253	—	4.56	3.35	5.96	−2.61
		243	—	4.96	3.75	6.44	−2.69
		233	—	5.56	4.35	6.98	−2.63
		223	—	6.15	4.94	7.58	−2.64
		213	—	6.86	5.65	8.26	−2.61
		203	—	7.62	6.41	9.02	−2.61
		193	—	8.60	7.39	9.89	−2.50
		183	—	9.93	8.72	10.86	−2.14
	H_N^a	300	f)	110.2	110.2	21.8	88.4
	H_N^c	300	f)	278.8	278.8	0.7	278.1
	C^1	300	49.8[g]	214.9[g]	165.1	20.9	144.2
	C^2	300	43.2[g]	50.8[g]	7.6	23.0	−15.4
	C^3	300	26.7[g]	−35.9[g]	−62.6	6.3	−68.9
R-ptn	$H^{C,D}$	323	—	−0.29	−3.29	10.29	−13.58
		313	—	−0.15	−3.15	10.97	−14.12
		303	3.00	−0.12	−3.12	11.72	−14.84
		293	—	0.32	−2.68	12.55	−15.23
		283	—	0.53	−2.47	13.46	−15.93
		273	—	0.88	−2.12	14.46	−16.58
		263	—	1.12	−1.88	15.57	−17.45
		253	—	1.44	−1.56	16.80	−18.36
	$H^{I,J}$	323	—	14.18	12.74	10.13	2.61
		313	—	14.83	13.39	10.81	2.58
		303	1.44	15.42	13.98	11.55	2.43
		293	—	16.57	15.13	12.36	2.77
		283	—	17.53	16.09	13.25	2.84
		273	—	18.63	17.19	14.24	2.95
		263	—	19.92	18.48	15.33	3.15
		253	—	21.27	19.83	16.54	3.29
		243	—	22.89	21.45	17.89	3.56
		233	—	24.92	23.48	19.38	4.10
		223	—	26.92	25.48	21.06	4.42
		213	—	29.48	28.04	22.94	5.10
		203	—	32.37	30.93	25.06	5.87

Table 1. (Continued)

Diamine	Nucleus	Temp	$\delta_{Fe^{II}}$ [b]	$\delta_{Fe^{III}}$	δ^{iso} [c]	δ^{dip} [d]	δ^{con} [e]	Diamine	Nucleus	Temp	$\delta_{Fe^{II}}$ [b]	$\delta_{Fe^{III}}$	δ^{iso} [c]	δ^{dip} [d]	δ^{con} [e]
		K	ppm	ppm	ppm	ppm	ppm			K	ppm	ppm	ppm	ppm	ppm
		193	—	35.57	34.13	27.45	6.68		H_N^c	300	f)	231.1	231.1	0.1	231.0
		183	—	40.19	38.75	30.16	5.59		C^1	300	44.9[g]	216.3[g]	171.4	26.3	145.1
	H^M	323	—	1.77	0.62	3.79	−3.17		C^2	300	40.3[g]	46.9[g]	6.6	22.4	−15.8
		313	—	1.88	0.73	4.04	−3.31		C^3	300	25.5[g]	−21.0[g]	−46.5	7.1	−53.6
		303	1.15	1.97	0.82	4.32	−3.50	1,3-bn	H_{NA}^a	300	f)	106.9	106.9	21.8	85.1
		293	—	2.12	0.97	4.62	−3.65		H_{NB}^a	300	f)	118.8	118.8	21.8	97.0
		283	—	2.27	1.12	4.95	−3.83		H_{NA}^c	300	f)	274.9	274.9	0.7	274.2
		273	—	2.38	1.23	5.32	−4.09		H_{NB}^c	300	f)	268.8	268.8	0.7	268.1
		263	—	2.54	1.39	5.73	−4.34		H^A	300	2.92[g]	6.30[g]	3.38	3.07	0.31
		253	—	2.68	1.53	6.18	−4.65		H^B	300	2.91[g]	−11.35[g]	−14.26	7.10	−21.36
		243	—	2.82	1.67	6.68	−5.01		H^C	300	2.65[g]	5.73[g]	3.08	3.07	0.01
		233	—	3.03	1.88	7.25	−5.37		H^I	300	1.03[g]	14.64[g]	13.61	9.23	4.38
		223	—	3.44	2.29	7.87	−5.58		H^J	300	1.62[g]	32.70[g]	31.08	19.62	11.46
		213	—	3.55	2.40	8.58	−6.18		H^M	300	1.24[g]	3.97[g]	2.73	4.25	−1.52
		203	—	3.68	2.53	9.37	−6.84		C^1	300	42.4[g]	202.9[g]	160.5	20.9	139.6
		193	—	3.79	2.64	10.26	−7.62		$C^{1'}$	300	49.4[g]	239.8[g]	190.4	20.9	169.5
		183	—	3.96	2.81	11.28	−8.47		C^2	300	35.7[g]	39.5[g]	3.8	23.0	−19.2
	H_N^a	300	f)	134.0	134.0	14.6	119.4		C^3	300	26.7[g]	−39.4[g]	−66.1	6.3	−72.4

a) Positive values indicate downfield shifts. b) Chemical shifts for $[Fe^{II}(CN)_4(\text{diamine})]^{2-}$ were measured in D_2O at 300 K.[11] c) Isotropic shifts calculated from Eqs. 1—3. d) Dipolar shifts calculated from Eq. 2. e) Fermi contact shifts calculated from Eq. 3. f) The NH signal for $[Fe^{II}(CN)_4(meso\text{-ptn})]^{2-}$ was observed at 2.16 ppm in pD 2.0 DCl-D_2O solution. Since this shift is small enough compared with $\delta_{Fe^{III}}$, we assumed that δ^{con} is equal to $\delta_{Fe^{III}}$. g) From Ref. 11.

chelate in the 323—183 K temperature range.[11] This signal-averaging indicates a rapid interconversion of the tn chelate between the two chair forms (See Fig. 1), the rate constant of which has been already estimated to be 6×10^8 s^{-1} at 298 K.[16]

The magnitude of the $H^{I,J}$ shifts is larger than that of the $H^{A,C}$ shifts, despite the longer distances between the former nuclei and the Fe^{III} ion. This order of $\delta_{Fe^{III}}$ is different from that for the 1,2-diamine chelates, where the nuclei nearer the Fe^{III} ion have shown larger $\delta_{Fe^{III}}$ values.[8-10]

As the temperature decreased, the magnitude of the $H^{A,C}$ and $H^{I,J}$ shifts increased. The $H^{A,C}$ peak was wider than the $H^{I,J}$ peak: The line-widths at half-height were 36 and 27 Hz at 323 K, and 590 and 470 Hz at 183 K, respectively. This broadening with a decrease in the temperature is due to a rapid exchange of the resonance sites, in addition to a reduction of the relaxation time. The expected four peaks corresponding to H^A, H^C, H^I, and H^J, however, could not be observed, even at 183 K.

(c) *R*-ptn. $[Fe^{III}(CN)_4(R\text{-ptn})]^-$ showed three signals of $H^{I,J}$, H^M, and $H^{C,D}$ downfield with an area ratio of 1:3:1. This signal-averaging is attributable to an alteration of the *R*-ptn chelate between the chair and λ-skew-boat forms shown in Fig. 1.[11] The population of the two forms has been estimated to be ca. 50:50, based on the $H^{C,D}$ shift at 300 K.[11]

All of the signals moved in the downfield direction as the temperature decreased. The overlap with the solvent signals prevented any observation of the $H^{C,D}$ signal below 243 K. The widths of the $H^{I,J}$, H^M, and $H^{C,D}$ peaks were 21, 18, and 62 Hz at 323 K, respectively. The decrease in the temperature to 183 K broadened these peaks, but was not sufficient to separate them into the peaks corresponding to the individual protons. The *R*-ptn chelate is, thus, expected to alter between the chair and λ-skew-boat forms as fast as the tn chelate, i.e. $>10^8$ s^{-1} at 298 K.[16]

The ^1H shifts of these Fe^{III} 1,3-diamine complexes are plotted against T^{-1} in Fig. 2. The nonlinearity indi-

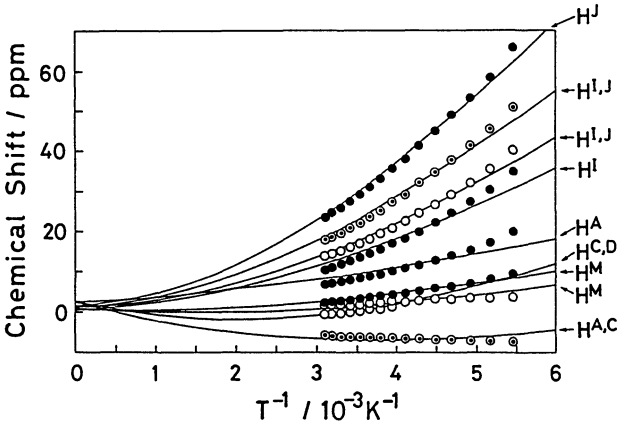

Fig. 2. Temperature dependence of ^1H NMR shifts of $[Fe^{III}(CN)_4(1,3\text{-diamine})]^-$ in CD_3OD containing 0.25% DCl. The circles indicate the observed values: *meso*-ptn (●), tn (⊙), and *R*-ptn (○). The solid curves indicate the estimated values. The chemical shifts at $T^{-1}=0$ are the shifts of the corresponding Fe^{II} complexes.

cates that the 1,3-diamine chelates, as well as the 1,2-diamine chelates,[9,10,20] do not obey the Curie law.

Amino Protons. The ^1H NMR spectra of the amino protons (NH) of $[Fe^{III}(CN)_4(1,3\text{-bn})]^-$ (1,3-bn=1,3-butanediamine), besides the Fe^{III} 1,3-diamine complexes described above, were measured in p*D* 2.0 DCl–D_2O at 300 K. The following chemical shifts and line-widths at half-height were obtained: *meso*-ptn, 110.2 (390) and 278.8 (840); tn, 193.0 (510); *R*-ptn, 134.0 (160) and 231.1 (320); 1,3-bn, 106.9 (580), 118.8 (580), 268.8 (820), and 274.9 ppm (950 Hz). The higher field peaks were assigned to the axial amino protons and the lower field peaks to the equatorial protons, as those for the 1,2-diamine complexes.[10]

The two NH peaks observed for the *meso*-ptn chelate correspond to H_N^a and H_N^e (See Fig. 1). The $\delta_{Fe^{III}}$ difference of the NH peaks amounts to 168.6 ppm, which is ca. 5 times as large as 34 ppm for the *R*-chxn chelate.[10] This large difference indicates that the *meso*-ptn chelate assumes a chair form.

The single NH peak for the tn chelate has almost the same values of chemical shift and line-width as the mean values, 194.5 ppm and 560 Hz, for the H_N^a and H_N^e peaks of the *meso*-ptn chelate. The rapid interconversion of the tn chelate between the two chair forms is, thus, demonstrated by the NH as well as CH line shapes.

The difference between the two NH shifts of the *R*-ptn chleate, 97.1 ppm, is 58% of that for the *meso*-ptn chelate, and the average NH shift of the former differs by ca. 10 ppm from those for the *meso*-ptn and tn chelates. These features are ascribed to a rapid chair⇆ λ-skew-boat alteration of the *R*-ptn chelate.[11] If the λ-skew-boat form is assumed to have the same NH shift difference, 34 ppm, as the 1,2-diamine chelates, the estimated ratio of the chair : λ-skew-boat is ca. 53 : 47. This ratio is almost the same as that reported for $[Ni(H_2O)_4(rac\text{-ptn})]^{2+}$, 54 : 46.[4]

The 1,3-bn chelate exists as an equilibrium mixture of a chair and a skew-boat form with an equatorial methyl group.[11] The population of the chair form has been estimated to be 76—96% from the H^B and H^C shifts,[11] whereas 98% is obtained from the H^A shift (see Table 1). This difference indicates that the conformation at the methyl group-side resembles that of the *meso*-ptn chelate, while the unsubstituted methylene has a different conformation from that of the latter. The four NH peaks were assigned, from downfield to upfield, to H_{NA}^a, H_{NB}^a, H_{NB}^e, and H_{NA}^e, by comparing the NH shifts of the 1,3-bn and *meso*-ptn chelates.

The typical values of $\delta_{Fe^{III}}$ and the line-width for H_N^a

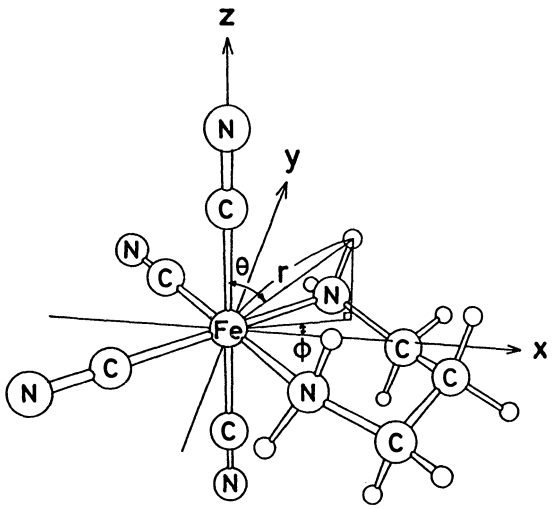

Fig. 3. Coordinate system for the analysis of isotropic NMR shift.

Table 2. Geometric Factors

Diamine	Nucleus	G_A / 10^{28} m^{-3}	G_B / 10^{28} m^{-3}	Diamine	Nucleus	G_A / 10^{28} m^{-3}	G_B / 10^{28} m^{-3}
tn	H_N	−4.898	−2.011	*meso*-ptn	H_N^a	−3.733	1.284
	$H^{A,C}$	−0.842	0.908		H_N^e	−6.391	−4.611
	$H^{I,J}$	−1.421	1.540		H^A	0.485	0.890
	C^1	−2.864	2.117		H^I	−0.821	1.080
	C^2	−2.374	2.446		H^J	−2.054	2.080
					H^M	−0.812	0.193
1,3-bn	H_{NA}^a	−3.733	1.284		C^1	−2.560	1.950
	H_{NB}^a	−3.733	1.284		C^2	−2.267	2.532
	H_{NA}^e	−6.391	−4.611		C^3	−1.088	0.370
	H_{NB}^e	−6.391	−4.611				
	H^A	0.485	0.890	*R*-ptn	H_N^a	−3.513	0.148
	H^B	−0.172	1.153		H_N^e	−5.917	−4.130
	H^C	0.485	0.890		$H^{C,D}$	−0.301	1.939
	H^I	−0.821	1.080		$H^{I,J}$	−1.214	1.265
	H^J	−2.054	2.080		H^M	−0.808	0.225
	H^M	−0.812	0.193		C^1	−3.133	2.530
	C^1	−2.560	1.950		C^2	−2.367	2.367
	$C^{1'}$	−2.560	1.950		C^3	−1.117	0.456
	C^2	−2.267	2.532				
	C^3	−1.088	0.370				

and H_N^e of the 1,2-diamine chelates are 127 (300) and 164 ppm (310 Hz) at 300 K.[10] Almost the same values were observed for H_N^a's of the 1,3-diamine chelates, but H_N^e of the *meso*-ptn chelate exhibited a wide line-width of 840 Hz and resonated at a lower magnetic field by ca. 100 ppm than H_N^e's of the 1,2-diamine chelates.

Geometric Factor. The coordinate system for the analysis of nuclear magnetic resonance is illustrated in Fig. 3, where the z-axis goes through the bonds NC–Fe–CN, and the x-axis bisects the angle N–Fe–N of the six-membered chelate ring. The location of a nucleus relative to the Fe^{III} ion can be represented by the geometric factors (G_A and G_B) defined by the equations $G_A=(3\cos^2\theta-1)/r^3$ and $G_B=\sin\theta\cos 2\phi/r^3$, where the distance r and angles θ and ϕ are defined as shown in Fig. 3.

The geometric factors for the Fe^{III} tn, *meso*-ptn, and *R*-ptn chelates were calculated by assuming that (1) these chelates have the chair, chair, and λ-skew-boat conformations shown in Fig. 1, respectively, and (2) that these conformers have the same geometries as do the complexes, $(-)_{589}$-$[Co(tn)_3Cl_3\cdot H_2O$,[12] $(+)_{510}$-$[Co(meso$-ptn$)_2(ox)]ClO_4\cdot H_2O$,[13] $(-)_{546}$-$[Co(R$-ptn$)_3]Cl_3\cdot 2H_2O$.[14]

The geometric factors for the 1,3-bn chelate were assumed to be equal to those for the *meso*-ptn chelate. The coordinates of the hydrogen atoms were calculated by assuming that these nuclei locate at the vertices of tetrahedrons with bond lengths of C–H=1.09 and N–H =1.02 Å. These bond lengths were obtained from the neutron diffraction of *trans*-$[CoCl_2(en)_2]Cl\cdot(H_5O_2)^+Cl^-$.[15]

The calculated values of G_A and G_B are listed in Table 2. The values for $H^{A,C}$ and $H^{I,J}$ of the tn chelate were taken to be equal to the mean values for the axial and equatorial protons because the alteration of the tn chelate between two chair conformations rapidly exchanges magnetic atmospheres of these protons. The values for the methyl protons of the *meso*- and *R*-ptn chelates were estimated by assuming a free rotation of the methyl groups.

Analysis of Chemical Shift. The effects of an unpaired electron on the ^1H and ^{13}C NMR shifts can be represented by an isotropic shift (δ^{iso}) defined by the difference in chemical shift between the paramagnetic Fe^{III} complex ($\delta_{Fe^{III}}$) and the diamagnetic Fe^{II} complex ($\delta_{Fe^{II}}$) with the same ligands as the Fe^{III} complex:[8–10]

$$\delta^{iso}=\delta_{Fe^{III}}-\delta_{Fe^{II}} \quad (1)$$

The δ^{iso} values for the *meso*-ptn, tn, *R*-ptn, and 1,3-bn complexes, listed in the sixth column of Table 1, were calculated by assuming that the $\delta_{Fe^{II}}$ values[11] are independent of the temperature.

The N$\underline{H}$ peak of $[Fe^{II}(CN)_4$ (*meso*-ptn$)]^{2-}$ appeared at 2.16 ppm in pD 2.0 DCl–D_2O.[11] This $\delta_{Fe^{II}}$ value is, however, negligibly small compared to the corresponding $\delta_{Fe^{III}}$ values, and the $\delta_{Fe^{III}}$ values were regarded as the δ^{iso} values for the N$\underline{H}$'s.

The δ^{iso} values can be separated into a dipolar shift (δ^{dip}) and a Fermi contact shift (δ^{con}) by using Eqs. 2 and 3:[9,20]

$$\delta^{dip}=(10^6/24\pi)[(2\chi_{zz}-\chi_{yy}-\chi_{xx})\cdot G_A+3(\chi_{xx}-\chi_{yy})\cdot G_B], \quad (2)$$

$$\delta^{con}=10^6 a_N\beta[6k_BT\gamma\hbar\sum_{i=1}^{3}\exp(-E_i/k_BT)]^{-1}\cdot\sum_{q=x,y,z}[\sum_{i=1}^{3}\exp(-E_i/k_BT)\cdot\langle\mu_q\rangle_{ii}-2k_BT\sum_{i=1}^{2}\sum_{j=i+1}^{3}Q_{ij}\ \langle\mu_q\rangle_{ij}\langle s_q\rangle_{ij}]. \quad (3)$$

Here, δ^{dip} and δ^{con} are in units of ppm, and their positive values indicate downfield shifts. The other symbols are defined as reported in a previous paper.[9]

The δ^{dip} values in the seventh column of Table 1 were estimated from Eq. 2. Here, we used the eigenvalues and eigenfunctions of the Kramers doublets obtained for $[Fe^{III}(CN)_4(en)]^-$ because the electronic and CD spectra of the 1,3-diamine complexes resemble those of the 1,2-diamine complex.[11] The δ^{con} values in Table 1 were

Table 3. Fermi Contact Coupling Constants a_N and Spin Population

Diamine	Nucleus	a_N[a] / MHz	$10^4\times$Spin population
tn	H_N	+6.20	+44
	$H^{A,C}$	−0.60±0.03	−4.2±0.2
	$H^{I,J}$	+0.19±0.03	+1.3±0.2
	C^1	+1.32	+4.3
	C^2	−0.19	−0.6
meso-ptn	H_N^a	+2.96	+21
	H_N^e	+9.36	+66
	H^A	+0.11±0.04	+0.8±0.3
	H^I	+0.12±0.04	+0.8±0.3
	H^J	+0.20±0.03	+1.4±0.2
	H^M	−0.07±0.01	−0.5±0.1
	C^1	+1.22	+3.9
	C^2	−0.13	−0.4
	C^3	−0.58	−1.9
1,3-bn	H_{NA}^a	+2.85	+22
	H_{NB}^a	+3.25	+23
	H_{NA}^e	+9.23	+65
	H_{NB}^e	+9.03	+64
	H^A	+0.01	+0.1
	H^B	−0.72	−5.0
	H^C	+0.00	+0.0
	H^I	+0.15	+1.0
	H^J	+0.38	+2.7
	H^M	−0.05	−0.4
	C^1	+1.18	+3.8
	$C^{1'}$	+1.43	+4.6
	C^2	−0.16	−0.5
	C^3	−0.61	−2.0
R-ptn	H_N^a	+4.00	+28
	H_N^e	+7.74	+54
	$H^{C,D}$	−0.50±0.01	−3.5±0.1
	$H^{I,J}$	+0.11±0.03	+0.8±0.2
	H^M	−0.14±0.02	−1.0±0.1
	C^1	+1.22	+3.9
	C^2	−0.13	−0.4
	C^3	−0.45	−1.4

a) Positive a_N indicates that δ^{con} is downfield shift. The a_N values were obtained for CD_3OD solutions containing 0.25% DCl.

obtained by substracting each δ^{dip} value from the corresponding experimental value of δ^{iso}. The Fermi constants in MHz (a_N) calculated from the δ^{con} values by Eq. 3 are summarized in Table 3.

The $\delta_{Fe^{III}}$ values were also estimated from Eqs. 1—3 by employing a_N as a variable so as to obtain the best agreement with the ^1H shifts observed at 323—183 K, and are indicated by the solid lines in Fig. 2. The insufficient agreement for H^A and H^I of the *meso*-ptn chelate is attributable to the use of a single a_N for each nucleus in order to simplify the calculation, although the a_N values vary with the individual terms in Eq. 3.[1,21]

Fermi Contact Shift and Dipolar Shift. The symbols C_α and C_β are used, for convenience, to refer to the carbon atoms in the sequence Fe–N–C_α–C_β. The axial and equatorial protons bonded to the nitrogen and carbon atoms are designated by the symbols H^a_N, H^e_N, H^a_α, H^e_β etc.

(a) Carbon Atoms. The C_α δ^{iso} values for the 1,3-diamine chelates are in the range 165—180 ppm. These δ^{iso}'s are all positive and are ca. 90% of those for the 1,2-diamine chelates.[8–10] Since the δ^{dip} values for C_α are 21—26 ppm, the δ^{iso} values mostly consist of δ^{con}. The estimated δ^{con} values are in the range 144—157 ppm, which have the same sign and are ca. 5% less than those for the 1,2-diamine chelates.[8–10]

The δ^{iso},δ^{dip}, and δ^{con} values for the methyl carbons ($C_{\beta M}$) are in the ranges −40—−63, 6—7, and −53—−69 ppm, respectively, and are ca. 90% of those for the 1,2-diamine chelates with the same sign.[8–10] The central methylene carbons ($C_{\beta C}$) of the 1,3-diamine chelates have δ^{iso} values of 0.8—8 ppm, which differ in both sign and magnitude from those for $C_{\beta M}$ as well as from those for C_β atoms of the 1,2-diamine chelates. This difference is attributed to the small $C_{\beta C}$ δ^{con} values of −15—−22 ppm, which are ca. one fourth of the δ^{con} values for $C_{\beta M}$ and C_β.

(b) C<u>H</u>. The δ^{iso} value for H^A of the *meso*-ptn chelate is about half those for H^a_α of the 1,2-diamine chelates.[8–10] This decrease in δ^{iso} is due to the small δ^{dip} and δ^{con} values for the former.

The δ^{iso} values for H_β, such as H^I and H^J of the *meso*- and *R*-ptn chelates, are ca. 1—3 times as large as those for H_β of the 1,2-diamine chelates. The δ^{con} values for the former comprise 70—80% of the δ^{iso} values, and are 2—3 times as large as the δ^{con} values for the latter. The equatorial H^J has larger δ^{con} values than does the axial H^I. The H^M protons of the *meso*- and *R*-ptn chelates show δ^{iso} values less than half those for the methyl protons of the 1,2-diamine chelates. This is because the former chelates have more negative δ^{con} values than the latter, whereas both chelates have almost the same δ^{dip} values. The δ^{con} values for H^M are opposite in sign to those for H^I and H^J, although these protons belong to the H_β group. Opposite signs of δ^{con} for H^M and $H^{I,J}$ have been reported for paramagnetic Ni^{II} complexes, $[Ni^{II}(H_2O)_4(1,3\text{-diamine})]^{2+}$, with *meso*-ptn, *rac*-ptn, and 1,3-bn.[4]

The negative δ^{iso} value for $H^{A,C}$ of the tn chelate is less than half those for the en chelate with the same sign. This reduction of δ^{iso} is attributed to the small δ^{dip} values for $H^{A,C}$. The δ^{con} value estimated for H^e_α of the 1,3-bn chelate is −21.36 ppm at 300 K, which is similar to the value, −30.2 ppm, estimated from the δ^{con} values for $H^{A,C}$ of the tn chelate and H^A of the *meso*-ptn chelate. These δ^{con} values are 80—90% of those for H^e_α of the 1,2-diamine chelates.[8–10]

(c) N<u>H</u>. The δ^{iso} for amino protons mostly consist of δ^{con} with large negative values. The differences in δ^{iso} between the 1,3- and 1,2-diamine chelates amount to more than 100 ppm for the lower field H^e_N peaks and ca. 20 ppm for the higher field H^a_N peaks.[10] The replacement of the 1,2-diamine chelates by the 1,3-diamine chelates only slightly affects the distances from H^a_N to the *xy* plane (See Fig. 3), such as 0.89—0.95 Å in the former chelates and 0.94—0.97 Å in the latter, whereas the distances with respect to H^e_N are reduced from 0.62—0.76 Å to 0.19—0.34 Å.[12–15,22,23] This correlation between the δ^{iso} values and distances supports the assignment of the amino protons described above.

Spin Population. The nuclei nearer to the *xy* plane showed larger δ^{con} values, as described above. This tendency is ascribed to the unpaired electron predominantly occupying the $3d_{x^2-y^2}$ orbital of the Fe^{III} ion, as has been reported previously for the 1,2-diamine chelates.[9] Since the 1,3-diamine chelates assume chair and/or skew-boat forms, their C_α and $C_{\beta M}$ nuclei are at a distance 0.5—0.6 Å further apart from the *xy* plane than those for the 1,2-diamine chelates with *gauche* forms. The 1,3-diamine chelates thus have smaller δ^{con} values and, accordingly, smaller spin populations than the latter.

The δ^{con} values for C_α and C_β of the 1,3-diamine chelates are opposite in sign, although these values were estimated by neglecting the contribution of ligand-centered dipolar shift (δ_L^{dip}). This suggests that the unpaired spin propagates through σ bonds by a spin-polarization mechanism,[24–26] just as the 1,2-diamine chelates,[8–10] and that the contribution of δ_L^{dip} is small.

The a_N values are related to the spin population in a 1s orbital of hydrogen (Q_{1s}) and that in a 2s orbital of carbon (Q_{2s}) by the relations $Q_{1s}=a_N/1420$ and $Q_{2s}=a_N/3110$, where 1420 and 3110 MHz are Fermi constants calculated for $^1H\cdot$ and $^{13}C\cdot$ radicals, respectively.[27] The estimated values of Q_{1s} and Q_{2s} are listed in Table 3.

The propagation of the positive spin on the Fe^{III} ion by spin-polarization mechanism is expected to give comparable negative spin-populations to both $C_{\beta C}$ and $C_{\beta M}$. However, the δ^{con} value for the former carbon is ca. one third of that for the latter. Since the $C_{\beta C}$ nucleus locates near the *xy* plane and in the direction of the lobe of the $d_{x^2-y^2}$ orbital,[12–14] $C_{\beta C}$ can directly interact with the positive spin in the d orbital (direct mechanism). This interaction yields a positive spin on $C_{\beta C}$, which compensates the negative spin propagated by spin-polarization mechanism, resulting in a decrease in the

negative spin population on $C_{\beta C}$.

The reversal of the sign of δ^{con} between the carbon atoms and protons at the α and β positions indicates that the spin-polarization mechanism is predominant not only in the C–C bonds but also in the C–H bonds. At both the α and β positions, H^e has larger δ^{con} values than H^a. The spin propagation is, thus, anisotropic and occurs more easily in the equatorial direction. This feature is the same as that observed in the 1,2-diamine chelates.[8–10]

Since H^I and H^J of the 1,3-diamine chelates locate in the direction of the lobe of the Fe $d_{x^2-y^2}$ orbital, a direct mechanism is possible for these protons, in addition to the spin-polarization mechanism. Both mechanisms produce a positive spin on these protons, resulting in an increase in their spin populations. The larger δ^{con} values for the H^I and H^J nuclei relative to the values for H_β of the 1,2-diamine chelates are thus attributable to the direct mechanism. The large δ^{con} values for H_N can also be accounted for by the contribution of the direct mechanism.

References

1) J. P. Jesson, "NMR of Paramagnetic Molecules," ed by G. N. La Mar, W. D. Horrocks, Jr., and R. H. Holm, Academic Press, New York (1973), Chap. 1.

2) D. R. Eaton, "NMR of Paramagnetic Molecules," ed by G. N. La Mar, W. D. Horrocks, Jr., and R. H. Holm, Academic Press, New York (1973), Chap. 5.

3) W. D. Horrocks, Jr.,"NMR of Paramagnetic Molecules," ed by G. N. La Mar, W. D. Horrocks, Jr., and R. H. Holm, Academic Press, New York (1973), Chap. 4.

4) J. E. Sarneski and C. N. Reilley, *Inorg. Chem.*, **13**, 977 (1974).

5) C. J. Hawkins and R. M. Peachey, *Acta Chem. Scand., Ser. A*, **32**, 815 (1978).

6) C. E. Strouse and N. A. Matwiyoff, *J. Chem. Soc., Chem. Commun.*, **1970**, 439.

7) I. Morishima, K. Yoshikawa, and K. Okada, *J. Am. Chem. Soc.*, **98**, 3787 (1976).

8) Y. Kuroda, M. Goto, and T. Sakai, *Bull. Chem. Soc. Jpn.*, **60**, 3917 (1987).

9) Y. Kuroda, M. Goto, and T. Sakai, *Bull. Chem. Soc. Jpn.*, **62**, 3614 (1989).

10) Y. Kuroda, M. Goto, and T. Sakai, to be published.

11) M. Goto, H. Nakayabu, H. Ito, H. Tsubamoto, K. Nakabayashi, Y. Kuroda, and T. Sakai, *Inorg. Chem.*, **25**, 1684 (1986).

12) R. Nagao, F. Marumo, and Y. Saito, *Acta Crystallogr., Sect. B*, **29**, 2438 (1973).

13) I. Oonishi, S. Sato, and Y. Saito, *Acta Crystallogr., Sect. B*, **30**, 2256 (1974).

14) A. Kobayashi, F. Marumo, and Y. Saito, *Acta Crystallogr., Sect. B*, **29**, 2443 (1973).

15) J. Rozire and J. M. Williams, *Inorg. Chem.*, **15**, 1174 (1976).

16) Y. Kuroda, M. Goto, and T. Sakai, *Bull. Chem. Soc. Jpn.*, **62**, 3437 (1989).

17) M. Goto, M. Takeshita, N. Kanda, T. Sakai, and V. L. Goedken, *Inorg. Chem.*, **24**, 582 (1985).

18) Y. Kuroda, N. Tanaka, M. Goto, and T. Sakai, *Inorg. Chem.*, **28**, 2163 (1989).

19) The probe temperature was calibrated by the use of the calibration chart supplied by JEOL.

20) Y. Kuroda, N. Tanaka, M. Goto, and T. Sakai, *Inorg. Chem.*, **28**, 997 (1989).

21) R. J. Kurland and B. R. McGarvey, *J. Magn. Reson.*, **2**, 286 (1970).

22) R. Kuroda and Y. Saito, *Acta Crystallogr., Sect. B*, **30**, 2126 (1974).

23) A. Kobayashi, F. Marumo, and Y. Saito, *Acta Crystallogr., Sect. C*, **39**, 807 (1983).

24) Z. Luz, *J. Chem. Phys.*, **48**, 4186 (1968).

25) W. D. Horrocks, Jr. and D. L. Johnston, *Inorg. Chem.*, **10**, 1835 (1971).

26) M. J. Scarlett, A. T. Casey, and R. A. Craig, *Aust. J. Chem.*, **23**, 1333 (1970); **24**, 31 (1971).

27) J. R. Morton, J. R. Rowlands, and D. H. Whiffen, *Natl. Phys. Lab. (U. K.), Rep. BPR*, **1962**, 13.

Solvent Effect on the ESR Parameters of Di-*t*-butyl Nitroxide and Galvinoxyl. Theoretical Application of the MNDO Effective Charge Model

Hideto TAKASE, Kenji MORIHASHI, and Osamu KIKUCHI*
Department of Chemistry, University of Tsukuba, Tsukuba 305
(Received May 30, 1991)

An effective charge model of the solvent effect was incorporated with the RHF-MNDO-CI method for free radicals, allowing the solvent effect on the hyperfine coupling constants (hfcc) and *g*-values of the di-*t*-butyl nitroxide (DTBN) and galvionxyl radicals to be examined. The calculated solvent dependences of the spin distribution and the n→π* excitation energy of DTBN have well elucidated the observed solvent effect on the hfcc and *g*-value of DTBN. The observed trend for the proton hfcc of galvinoxyl has been correctly reproduced by the present theoretical model.

The hyperfine coupling constants (hfcc) and *g*-value derived from the ESR spectra of a free radical vary with the solvent polarity; the solvent dependences of these ESR parameters have been considered theoretically.[1-4] Among the various theoretical models concerning the solvent effect, the effective charge model is one of the continuum models based on Born's solvation energy.[5] This model was first suggested by Klopman,[6] and a correct description has been given by Tapia[7] as well as by Constanciel and Contreras.[8] In our previous papers, the MNDOS method, in which the effective charge model is incorporated with the MNDO[9] method, was proposed and applied to a conformational analysis of both amine[10] and amino acids in solution,[11] as well as the solvent effect on the potential energy surface of typical S_N2 reactions.[12] In this paper we extend the MNDOS method to an open-shell RHF method for free radicals. The solvent effect was also introduced to the configulation interaction (CI) calculation, and the RHF-MNDOS-CI method was applied in order to examine the solvent effect on the hfcc and *g*-value of typical neutral free radicals, di-*t*-butyl nitroxide (DTBN) and galvinoxyl radicals.

Experimental

DTBN and galvinoxyl were purchased commercially and were used as received. The spectrograde solvents were dried on 3 or 4 Å molecular sieves which were activated before use. The dried solvents were transferred into the sample tube in the vacuum line. Fremy salt was used as the standard sample; the nitrogen hfcc and *g*-value are 13.00 G (1 G=10^{-4} T) and 2.00550, respectively.

Method of Calculation

In a previous paper[13] we reported that the RHF-MNDO-CI method gives better agreement with experiments than does the UHF-MNDO method in calculations concerning hfcc of π-radicals. In this paper the effective charge model is incorpolated with the RHF-MNDO-CI method in order to evaluate the solvent effect on the ESR parameters of π-radicals.

In the effective charge model, the solvation energy is given by a generalized Born formula, which was derived by Hoijtink et al.[14] as well as Chalvet and Jano:[15]

$$E^{\mathrm{solv}}=-\frac{1}{2}(1-\varepsilon^{-1})\sum_{\mathrm{A}}Q_{\mathrm{A}}^2/r_{\mathrm{A}}-\frac{1}{2}(1-\varepsilon^{-1})\sum_{\mathrm{A}}\sum_{\mathrm{B}}Q_{\mathrm{A}}Q_{\mathrm{B}}/R_{\mathrm{AB}}. \quad (1)$$

Here, A and B are atoms in the molecule, Q_{A} and r_{A} are the charge and the radius of the A atom, respectively, and R_{AB} is the distance between A and B. The energy of a free radical in solution (E^{S}) is the sum of the energy in its isolated state (E^0) and the solvation energy (E^{solv}):

$$E^{\mathrm{S}}=E^0+E^{\mathrm{solv}}. \quad (2)$$

E^0 is calculated using the restricted wavefunction for the doublet state:

$$\Psi_g=|\phi_1\bar{\phi}_1\cdots\phi_{m-1}\bar{\phi}_{m-1}\phi_m>. \quad (3)$$

Since the atomic population is derived under the ZDO approximation using semiempirical MO methods, the variational procedure for the solvation energy term (Eq. 1) was carried out under the ZDO approximation. The variational method gives two Fock operators (F^{c} and F^{o}) for a doubly-occupied MO and a singly-occupied MO, respectively:

$$F^{\mathrm{c}}=H_{\mathrm{core}}+\sum_l(2J_l-K_l)+\frac{1}{2}(2J_m-K_m)+G$$

and

$$F^{\mathrm{o}}=\frac{1}{2}[H_{\mathrm{core}}+\sum_k(2J_k-K_k)+G]. \quad (4)$$

The *G* term is an additional operator which reflects the solvent effect:

$$G=-(1-\varepsilon^{-1})(2\sum_l J_l+J_m-L)$$

and

$$L=\left[\sum_{\mathrm{B}}Z_{\mathrm{B}}\int d\tau_2\chi_{\mathrm{B}}^*(2)\frac{1}{r_{12}}\chi_{\mathrm{B}}(2)\right], \quad (5)$$

where Z_{B} is the core charge and χ are the atomic orbitals. The matrix elements of *G* with respect to atomic orbitals are

$$G_{rr}=<\chi_r|G|\chi_r>=(1-\varepsilon^{-1})\sum_{\mathrm{B}}Q_{\mathrm{B}}\Gamma_{\mathrm{AB}}$$

and

$$G_{rs}=\langle\chi_r|G|\chi_s\rangle=0, \tag{6}$$

where Γ_{AB} are the electron repulsion integral and are evaluated by an empirical formula.[12] The off-diagonal elements for G are zero, due to the ZDO approximation. Two Fock operators (F^c and F^o) were unified and solved according to the general SCF procedure by Hirao and Nakatsuji.[16]

In the CI calculation, only one type of singly-excited configulation function ($\Psi_{i\to k}$(II)) which mixes directly with Ψ_g, was included,[13]

$$\Psi_{i\to k}(\mathrm{II})=\frac{1}{\sqrt{6}}\{|\cdots\phi_i\bar{\phi}_k\cdots\phi_{m-1}\bar{\phi}_{m-1}\phi_m\rangle - |\cdots\phi_k\bar{\phi}_i\cdots\phi_{m-1}\bar{\phi}_{m-1}\phi_m\rangle - 2|\cdots\phi_i\phi_k\cdots\phi_{m-1}\bar{\phi}_{m-1}\bar{\phi}_m\rangle\}. \tag{7}$$

The CI matrix elements were calculated for the following operator:

$$H^S=H+\sum_i G(i), \tag{8}$$

where H is the Hamiltonian for an isolated molecule and $G(i)$ is an one-electron operator for the solvent effect. The matrix elements for $G(i)$ with respect to the MO's are related to G_{rr} in Eq. 6 by

$$\langle\phi_i|G|\phi_j\rangle=\sum_r C_{ri}C_{rj}G_{rr}, \tag{9}$$

where C_{ri} and C_{rj} are the LCAO coefficients.

The hfcc were calculated using the following equation:[17]

$$a_A=(8\pi/3)g_e\beta_e\hbar\gamma_A|\chi_S^{(A)}(0)|^2\rho_S^{(A)}, \tag{10}$$

where $\rho_S^{(A)}$ is the spin density of the s-type valence atomic orbital on atom A calculated using the CI wavefunction; the others are constants for the electron and the atom.

The g-value was obtained as an average of three principle values of a g-tensor, which were calculated using Stone's equation:[18]

$$g_{\mu\nu}=g_e\delta_{\mu\nu}+\Delta g_{\mu\nu}, \text{ where}$$

$$\Delta g_{\mu\nu}=\sum_{i=1}^{m-1}2\langle\phi_i|\sum_A L_\mu^{(A)}|\phi_m\rangle\langle\phi_m|\sum_A\xi^{(A)}L_\nu^{(A)}|\phi_i\rangle/\Delta E_{i\to m} - \sum_{k=m+1}^{n}2\langle\phi_m|\sum_A L_\mu^{(A)}|\phi_k\rangle\langle\phi_k|\sum_A\xi^{(A)}L_\nu^{(A)}|\phi_m\rangle/\Delta E_{m\to k}. \tag{11}$$

Here, ϕ_i and ϕ_k are the doubly-occupied and vacant MO obtained by the RHF-MNDOS method, respectively. In this equation, the one-electron excitation energy should be evaluated for a Hamiltonian which includes the solvent effect:

$$\Delta E_{i\to m}=\langle\Psi_{i\to m}|H^S|\Psi_{i\to m}\rangle-\langle\Psi_g|H^S|\Psi_g\rangle$$

and

$$\Delta E_{m\to k}=\langle\Psi_{m\to k}|H^S|\Psi_{m\to k}\rangle-\langle\Psi_g|H^S|\Psi_g\rangle. \tag{12}$$

In this way, an effective charge model has been introduced into both the open-shell RHF-MNDO method and the CI calculation, allowing the solvent effect on the ESR parameters to be evaluated.

Results and Discussion

DTBN. The solvent dependence of the hfcc and g-value of DTBN are listed in Table 1. Since the electronic structure of a free radical is affected by the various properties of the solvent, it may be difficult to rationalize the observed solvent dependence of the ESR parameters by any single property of the solvent. However, Table 1 shows clear trends between the ESR parameters of DTBN as well as the dielectric constant of the solvent; the hfcc of the nitrogen atom increases with an increase in the dielectric constant of the solvent (ε), while the g-value decreases with an increase in ε. These trends are characteristic of nitric oxide radicals.[4]

In the MO calculation, the t-butyl groups in DTBN were replaced by methyl groups and assumed to have C_{2v} symmetry (Fig. 1). The geometry was optimized by the RHF-MNDOS method for several ε values.

The computational results are shown in Table 2. The nitrogen hfcc (a_N) increases with an increase in ε, while the g-value decreases with an increse in ε. These trends were observed in experiments (Table 1). An analysis of the electronic structure of DTBN reveals the essential feature of the solvent dependence of the hfcc and g-value. The calculated net charges of the nitrogen and oxygen (Q_N and Q_O) are shown in Table 2. As can be seen from Table 2, Q_O becomes more negative and Q_N

Table 1. Experimental hfcc and g-Values of DTBN in Various Solvents

Solvent	ε	a_N[a)]	g-Value
Cyclohexane	2.02	15.10	2.00610
CCl_4	2.23	15.27	2.00607
Benzene	2.27	15.35	2.00603
Toluene	2.38	15.26	2.00603
THF	7.39	15.29	2.00604
Acetone	20.5	15.38	2.00599
DMF	36.7	15.57	2.00599
CH_3CN	37.5	15.51	2.00595

a) hfcc of nitrogen in gauss.

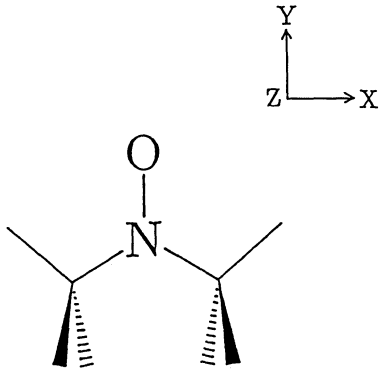

Fig. 1. DTBN model with C_{2v} planar symmetry.

slightly less negative when ε increases. Thus, DTBN is expected to be polarized in a polar solvent. The π spin density on the nitrogen atom increases with an increase in ε (Table 2). This elucidates well the observed solvent dependence of a_N, since it is propotional to the spin density of the 2s-atomic orbital of the nitrogen atom, which is generated by the spin-polarization mechanism.

Little attention has been paid to the solvent dependence of the g-value of a free radical. The present theoretical results reproduce well the solvent effect on the g-value of DTBN. In Table 3, three g-shifts are shown for ε=1 and for ε=40. From this table it is found that the Δg_{yy} is dominant and that $\delta g_{yy}(12,13)$ makes the largest contribution to Δg_{yy}. The 13th MO is the singly-occupied MO (SOMO); the 12th MO corresponds the oxygen lone-pair orbital. Hence, Δg_{yy} can be approximated by

$$\Delta g_{yy} \simeq \rho_\pi^{(O)} / \Delta E_{n\to\pi^*}. \quad (13)$$

When ε increases, $\rho_\pi^{(O)}$ decreases (Table 2), while $\Delta E_{n\to\pi^*}$ increases (Table 3). The tendency calculated for $\Delta E_{n\to\pi^*}$ has been observed in the visible spectra of DTBN in solution by Kawamura et al.[4] in which the $n\to\pi^*$ excitation energy increases with an increase in the solvent polarity. As a result, the observed solvent dependence of the g-value of DTBN is well elucidated by the present calculations.

Galvinoxyl. The solvent dependence of the g-value of galvinoxyl was found to be very small; MNDOS-CI calculations have shown that the g-value of galvinoxyl is almost constant. On the other hand, the hfcc of the methine proton and the ring protons of galvinoxyl decrease as ε increases. Thus, the solvent dependence of hfcc of galvinoxyl was examined in some detail.

In the MO calculations, the t-butyl groups in galvinoxyl were replaced by hydrogen atoms. Four representative structures of galvinoxyl are shown in Fig. 2. The X-ray analysis has shown that the galvinoxyl has a C_2 twisted structure.[19] The UHF-MNDO calculation also supported the C_2 twisted structure as the lowest-energy structure (Table 5). Thus, the C_2 twisted structure was optimized by the RHF-MNDOS method for several ε values, and the hfcc were obtained by RHF-MNDOS-CI calculations. The computational results are shown in Table 6. The hfcc of the methine proton

Table 2. Solvent Dependence of hfcc, g-Value, Atomic Charges, and π-Spin Densities for DTBN Model Calculated by RHF-MNDOS-CI Method

ε	a_N[a]	g-value	Q_N	Q_O	$\rho_\pi^{(N)}$	$\rho_\pi^{(O)}$
1.0	11.28	2.00628	−0.1633	−0.2586	0.3658	0.6059
2.0	12.58	2.00609	−0.1826	−0.3502	0.4169	0.5529
5.0	13.91	2.00582	−0.1872	−0.4472	0.4737	0.4924
10.0	14.50	2.00567	−0.1846	−0.4932	0.5009	0.4629
20.0	14.83	2.00559	−0.1816	−0.5198	0.5165	0.4458
40.0	15.01	2.00554	−0.1802	−0.5343	0.5250	0.4365

a) hfcc of nitrogen in gauss.

Table 3. Calculated g-Shifts of the DTBN Model

ε	Δg_{xx}	Δg_{yy}	Δg_{zz}	$\delta g_{yy}(12,13)$	$\Delta E_{n\to\pi^*}$
1.0	0.00126	0.01063	0.0	0.01156	1.986
40.0	0.00203	0.00763	0.0	0.00835	2.426

Table 4. Experimental hfcc and g-Value of Galvinoxyl in Various Solvents

Solvent	ε	$a_H(m)$[a]	$a_H(r)$[b]	g-Value
Cyclohexane	2.02	6.02	1.40	2.00449
CCl_4	2.23	5.96	1.40	2.00448
Benzene	2.27	5.99	1.38	2.00447
Toluene	2.38	5.83	1.36	2.00447
Et_2O	4.22	5.85	1.41	2.00448
THF	7.39	5.99	1.35	2.00445
Acetone	20.5	5.85	1.35	2.00445
DMF	36.7	5.69	1.34	2.00445
CH_3CN	37.5	5.76	1.35	2.00443

a) hfcc of methine proton in gauss. b) hfcc of ring proton in gauss.

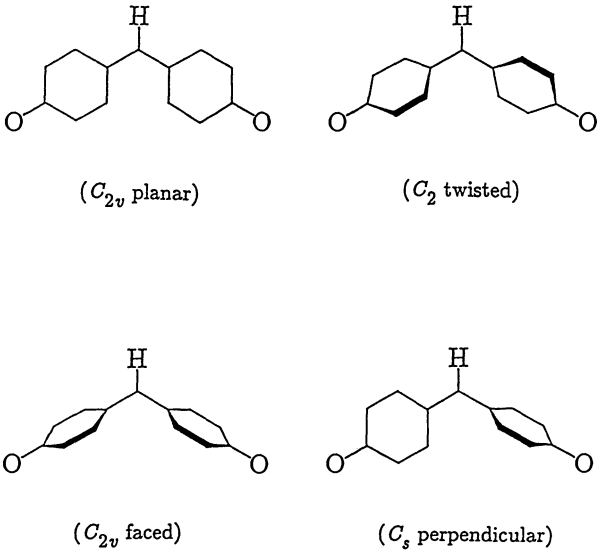

Fig. 2. Four representative structures of the galvinoxyl model.

Table 5. Calculated Total Energies (eV) and Relative Energies (kcal mol^{-1}) of Galvinoxyl[a]

Symmetry	State	RHF		UHF	
		Total	Rel	Total	Rel
C_{2v} planar	$^2A_2$	−2430.046	6.7	−2431.112	2.5
C_2 twisted	^2A	−2430.096	5.5	−2431.221	0.0
C_{2v} faced	$^2B_1$	−2428.036	53.1	···	
C_s perpendicular	$^2A'$	−2430.336	0.0[b]	−2430.982	5.5

a) The molecular structure was optimized under each symmetric restriction. b) The lowest state was predicted by RHF calculation to be the A′ state. This may be due to the doublet instability.[20]

Table 6. The Proton hfcc and π-Spin Densities of the Galvinoxyl Model Calculated by RHF-MNDOS-CI Method

ε	$a_H(m)$[a]	$a_H(i)$[b]	$a_H(e)$[c]	$\rho_\pi^{(C)}$	$\rho_\pi^{(O)}$
1.0	6.05	0.94	0.89	−0.1446	0.0487
2.0	5.98	0.93	0.87	−0.1439	0.0473
5.0	5.87	0.89	0.82	−0.1420	0.0464
10.0	5.81	0.83	0.75	−0.1399	0.0460
20.0	5.76	0.76	0.67	−0.1380	0.0453
40.0	5.70	0.69	0.60	−0.1364	0.0453

a) hfcc of methine proton in gauss. b) hfcc of interior ring proton in gauss. c) hfcc of exterior ring proton in gauss.

and two ring protons decrease with an increase in ε. These are the trends observed in experiment. The π spin density of the methine carbon atom decreases with an increase in ε. This is the reason why the hfcc of the methine proton decreases when ε increases.

In this paper, the effective charge model of the solvent effect was introduced into the open-shell RHF formalism and the CI calculations. The RHF-MNDOS-CI method, thus obtained, was used to evaluate the solvent effect on the ESR parameters of DTBN and galvinoxyl. The computational results well elucidated the observed solvent dependences of the hfcc and g-value of these radicals.

References

1) A. H. Reddoch and S. Konishi, *J. Chem. Phys.*, **70**, 2121 (1979).
2) S. Kubota and Y. Ikegami, *J. Phys. Chem.*, **82**, 2739 (1978).
3) P. Ludwig, T. Layloff, and R. N. Adams, *J. Am. Chem. Soc.*, **86**, 2568 (1964).
4) T. Kawamura, S. Matsunami, and T. Yonezawa, *Bull. Chem. Soc. Jpn.*, **40**, 1111 (1967).
5) M. Born, *Z. Phys.*, **1**, 45 (1920).
6) G. Klopman, *Chem. Phys. Lett.*, **1**, 200 (1967).
7) O. Tapia, "Quantum Theory of Chemical Reactions," ed by R. Daudel, A. Pullman, L. Salem, and A. Veillard, Reidel, Dordrecht (1981), Vol. 2, p. 25.
8) R. Constanciel and R. Contreras, *Theor. Chim. Acta*, **65**, 1 (1984).
9) M. J. S. Dewar and W. Thiel, *J. Am. Chem. Soc.*, **99**, 4899, 4907 (1977).
10) T. Kozaki, K. Morihashi, and O. Kikuchi, *J. Mol. Struct. (Theochem.)*, **168**, 265 (1988).
11) O. Kikuchi, T. Natui, and T. Kozaki, *J. Mol. Struct. (Theochem.)*, **207**, 103 (1990).
12) T. Kozaki, K. Morihashi, and O. Kikuchi, *J. Am. Chem. Soc.*, **111**, 1547 (1989).
13) K. Morihashi, H. Takase, and O. Kikuchi, *Bull. Chem. Soc. Jpn.*, **63**, 2113 (1990).
14) G. J. Hoijtink, E. de Boer, P. H. van der Meij, and W. P. Weijland, *Recl. Trav. Chim. Pays-Bas*, **75**, 487 (1956).
15) O. Chalvet and I. Jano, *C. R. Acad. Sci. Paris*, **256**, 1867 (1964); I. Jano, *C. R. Acad. Soc. Paris*, **261**, 103 (1965).
16) K. Hirao and H. Nakatsuji, *J. Chem. Phys.*, **59**, 1457 (1973).
17) A. Carrington and A. D. McLachlan, "Introduction to Magnetic Resonance," Harper and Row, New York (1967).
18) A. J. Stone, *Proc. Roy. Soc. A*, **271**, 424 (1963).
19) D. E. Williams, *Mol. Phys.*, **16**, 145 (1969).
20) O. Kikuchi, *Chem. Phys. Lett.*, **72**, 487 (1980), and references cited therein.

Kinetic Study of Casein Micelle Formation Observed by a Stopped-Flow Apparatus

Sadakatsu NISHIKAWA,* Misa TATSUSUE, Tadaomi INOUE,† and Tatsuya YASUNAGA†
Department of Chemistry, Faculty of Science and Engineering, Saga University, Saga 840
†Faculty of Engineering, Kinki University, Hiroshingai 5, Kure, Hiroshima 737-01
(Received June 10, 1991)

The time dependent optical density changes were observed when aqueous solutions (Tris buffer) of sodium casein from milk were mixed with those of calcium chloride by a newly constructed stopped-flow apparatus which was controlled by an 8-bit microcomputer. Two approaches for single exponential decay curve analysis were used, i.e. the Guggenheim analysis and an analysis according to a linear relation between the time and the logarithm of the corresponding absorbance change, at a concentration range between 0.02—0.05 wt% of the casein and in that between 10—30 mmol dm^{-3} of calcium chloride at 25 °C. The same time constants and reaction amplitudes were obtained from both analyses of the decay curves. The obtained rate parameters were found to be concentration dependent. The result was interpreted by a stepwise reaction mechanism for the formation of a casein aggregate. The rate-determining step was speculated to be the first step of the larger molecular aggregate of the casein according to the concentration dependence of the apparent rate constant and the reaction amplitude. The rate constant for the casein micellization could be approximately estimated as being of the order of 10^4 mol^{-1} dm^3 s^{-1} at 25 °C. The effects of NaCl, $MgCl_2$, and $CaBr_2$ on casein micelle formation were also examined; it was kinetically confirmed that only calcium cations played an important role in the formation of the casein micelle.

Caseins are proteins comprising several polypeptides; the characteristic properties in aqueous media have been widely studied by various methods.[1-5] It is well known that the casein molecules form the micelle, the aggregation number of which is quite large when it is compared with those of surfactants in aqueous media. The micelle formation mechanism in aqueous solutions of surfactants seems to have been established kinetically by various chemical relaxation methods.[6-8] However, few investigations concerning the dynamic characters for the casein micelles have not been carried out,[9-14] although they are very important regarding the mechanism of protein conformational change. Most of the kinetic studies have been limited to those in the time range of more than few tens of seconds, their time courses seeming to be very complex. One of the attractive procedures used to analyze the aggregation reaction of casein involves an enzymatic model using a von Smoluchowski-type reaction.[12,14,15] However, the reaction mechanisms are still unconfirmed. We have speculated that the primary step in the formation of the casein micelles exists in a shorter time range, and might be observed in dilute solutions. For observing such process, a stopped-flow method involving the observation of the optical density change might be powerful owing to a large change in the optical density which is expected when casein micelles are formed. When stopped-flow equipment is used to follow reaction the process, it is necessary that the observed time courses (the time dependence of the optical density change) are precisely analyzed in order to clarify the reaction mechanism.[16]

Under these circumstances, the present study was undertaken in the hope that an elucidation of a simple time dependence for micelle formation could provide a fundamental understanding of any structural changes in the protein. This information is also important in relation to the dynamic stabilities and solution properties of various proteins, since the protein aggregation is well known to play an important role in both denaturation and renaturation.[17]

Experimental

Apparatus: We used a newly constructed stopped-flow equipment comprising a DC lamp (100 W), a mixer, a monochrometer (Shimadzu monochrometer Grating 1200), a photomultiplier, an offset electronic circuit, an operational DC amplifier, a wave memory (NF MODEL WM-841), a digital voltmeter (Advantest TR6845) and an 8-bit microcomputer (NEC 8800). The mixer was driven by pistons with compressed air; the dead time for the mixing was about 5 ms. The temperature of the mixer and the solution reservoirs was controlled by circulating the water maintained at a constant temperature. For each run, 0.252 cm^3 solutions were mixed; after more than five run drives the data were accumulated and averaged. The absorption spectra were recorded from 370 to 600 nm by Hitachi 323 Recording Spectrophotometer and JEOL Ubest-30 spectrometer.

Chemicals: Highly purified sodium casein was supplied from Technical Research Institute, Snow Brand Milk Products, Co., Ltd. and was used without further purification. The metal contents in the sodium casein samples were analyzed and found to be Na=1200 mg/100 g, Ca=4.3 mg/100 g, P =700 mg/100 g; all other metals were less than 1 mg/100 g. The purest grade calcium chloride, magnesium chloride, calcium bromide and tris(hydroxymethyl)aminomethane [Tris] were purchased from Wako Pure Chemicals. They were used without further purification. The solutions were prepared using a Tris–HCl buffer solvent from doubly distilled water which was degassed by ultrasound under reduced pressure. The desired pH values for the solutions were obtained by changing the ratio of the Tris and HCl concentrations. Most of the experiments were carried out at pH 7.20, unless stated otherwise.

All of the experiments were carried out at least within one day after preparing the casein solutions at 25 °C.

Results

The visible absorption spectra were recorded over the concentration range 0.01 to 0.05 wt% casein. A slight absorbance was observed in solutions of casein. This might mean that the solute molecules do not dissolve in their monomer forms in an aqueous media. When calcium chloride was added, the absorbance was found to increase remarkably at all wavelengths measured. The absorbance decreased monotonously with an increase of the wavelength. No characteristic absorption peak was observed over the range of the measured wavelength. Such a broad change of the absorbance may be due to solution turbidity caused by casein aggregates. Figure 1 shows the concentration dependence of the absorbance at 440 nm. The absorbance increased linearly with concentration, and it increased more steeply when $CaCl_2$ was added. It is important that the absorbance in solutions with $CaCl_2$ is much larger than those without $CaCl_2$.

Most of the stopped-flow experiments were carried out at 440 nm, since the sensitivity of our apparatus was relatively high at this wavelength. When casein solutions were mixed with a solvent buffer, or with the similar solution of casein, no optical density change was observed over a time range of more than 20.48 ms in full scale in the wave memory. Upon mixing with $CaCl_2$ solution, clear changes were observed over the appropriate time range for the apparatus.

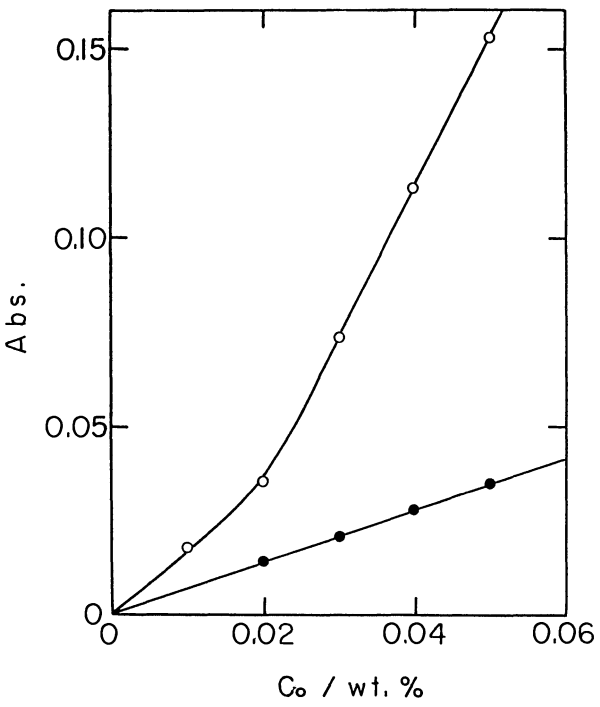

Fig. 1. Concentration dependence of absorbance for aqueous solutions of casein at 25 °C. ○: with 15 mmol dm^{-3} $CaCl_2$, ●: without $CaCl_2$.

The relation between the voltage of the signals from the photomultiplier and the product concentration, [P], is given by $\log\{(V_{100}-V_0)/(V_t-V_0)\}=\varepsilon l\,[P]$, where V_{100} is the signal voltage at the open current, V_0 that at the dark current, V_t the voltage at time t, l the effective observation cell length and ε a constant. We define $\varepsilon l\,[P_\infty]$ as the reaction amplitude where $[P_\infty]$ is the product concentration at infinite time of the reaction. The time dependence of the product is given as follows if it satisfies the first-order rate equation:

$$[P]=[P_\infty]\{1-\exp(-k_{app}t)\}, \quad (1)$$

where k_{app} is the apparent first-order rate constant. Using the relations between the observing voltage change in the signals and the concentration of the product at time t, Eq. 1 is expressed as

$$\log\{(V_t-V_0)/(V_\infty-V_0)\} = \log\{(V_{100}-V_0)/(V_\infty-V_0)\}\exp(-k_{app}t). \quad (2)$$

The voltage at infinite time, V_∞, is determined from the 2% increased values by averaging the last 10 digital signals in the wave memory and digital voltmeter. Plots of the logarithm of the left-hand side of Eq. 2 vs. time, (t), provide an apparent rate constant from the slope and the reaction amplitude from the intercept using a linear least mean-square method. The Guggenheim method can also be used to analyze the time dependence of the output signals, from which the apparent rate constant and reaction amplitude can also be obtained.[18] The appropriateness for these treatments was confirmed by numerical simulations for model calculations. The observed signals were analyzed by the two above-mentioned analytical procedures for the casein solutions in the concentration range from 0.02 to 0.05 wt% with various concentrations of $CaCl_2$. It was found that the time dependence of the optical density change is well fitted to Eq. 2. Figure 2 is one of the traces of the reactions when the casein solutions are mixed with that of $CaCl_2$. The rate constant and the reaction amplitude calculated from the above two procedures were the same. Also, the same apparent first-order rate constant, k_{app}, and the same reaction amplitude were obtained in an appropriate concentration range, even if a different sampling time in the wave memory was used. At concentrations less than 0.02 wt%, the optical density change was too small. On the other hand, upon increasing the casein concentration more than by 0.05 wt%, the reaction traces were not fitted to Eq. 2. This might indicate that more complex reactions proceeded at high concentration.

Figure 3 shows the casein concentration dependence of the apparent first-order rate constant at 10, 15, and 30 mmol dm^{-3} of $CaCl_2$. It can be seen that k_{app} at 10 and 15 mmol dm^{-3} $CaCl_2$ is apparently proportional to the casein concentration. However, at 30 mmol dm^{-3} it seems to be curved, and the rate constants obtained by the two procedures become different at high concentra-

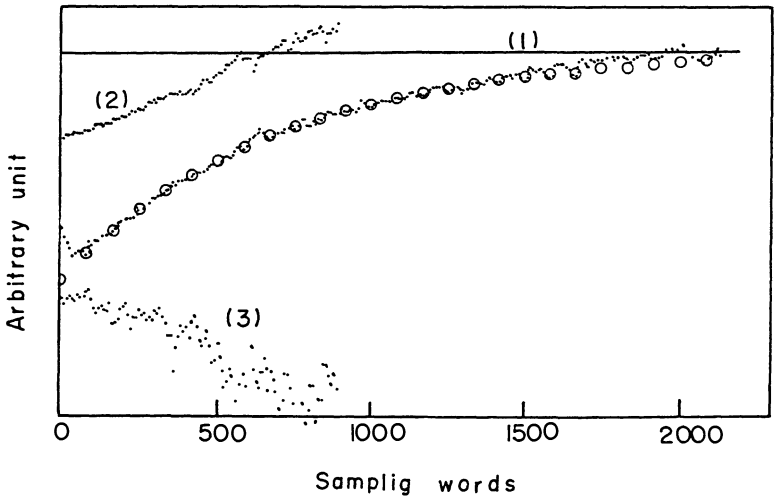

Fig. 2. Representative stopped-flow trace for an aqueous solution of casein with $CaCl_2$ (small dotted lines).
(1): Estimated infinite line.
(2): Plots of ln [log $\{(V_t-V_0)/(V_{100}-V_0)\}$] vs. time (**UA**),
(3): Guggenheim plots (**GA**).
The circles indicate the calculated values using the obtained rate parameters. In the following figure, we represent the results by the Guggenheim analytical procedure as **GA** and those by the plots of ln [log $\{(V_t-V_0)/(V_{100}-V_0)\}$] vs. t as **UA**.

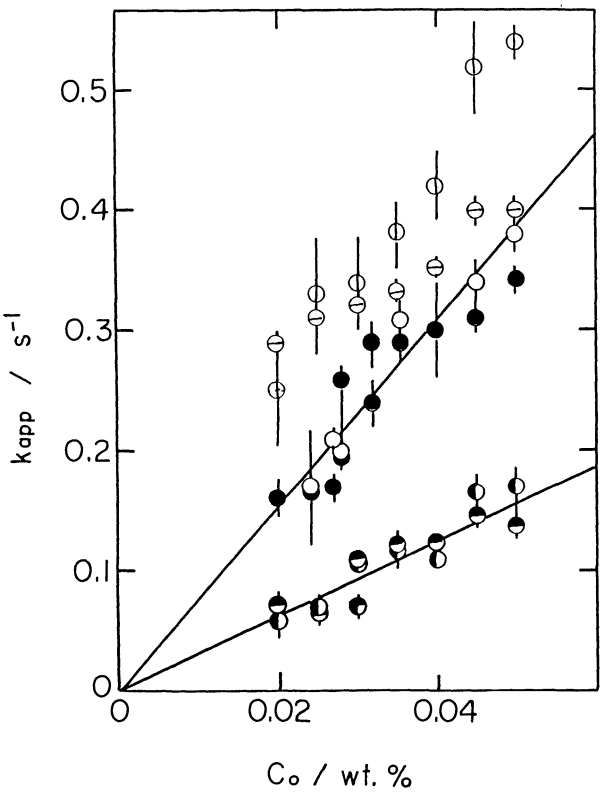

Fig. 3. Casein concentration dependence of the apparent first-order rate constant at 25 °C. ⦶: with 30 mmol dm^{-3} $CaCl_2$ by **GA**, ⊖: with 30 mmol dm^{-3} $CaCl_2$ by **UA**, ○: with 15 mmol dm^{-3} $CaCl_2$ by **GA**, ●: with 15 mmol dm^{-3} $CaCl_2$ by **UA**, ◐: with 10 mmol dm^{-3} $CaCl_2$ by **GA** and ◓: 10 mmol dm^{-3} $CaCl_2$ by **UA**.

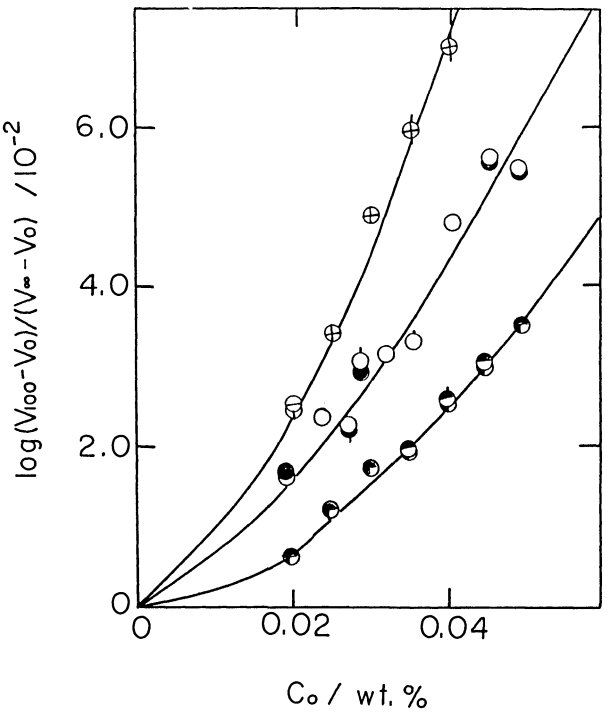

Fig. 4. Casein concentration dependence of the reaction amplitude at 25 °C. ⦶: with 30 mmol dm^{-3} $CaCl_2$ by **GA**, ⊖: with 30 mmol dm^{-3} $CaCl_2$ by **UA**, ○: with 15 mmol dm^{-3} $CaCl_2$ by **GA**, ●: with 15 mmol dm^{-3} $CaCl_2$ by **UA**, ◐: with 10 mmol dm^{-3} $CaCl_2$ by **GA** and ◓: with 10 mmol dm^{-3} $CaCl_2$ by **UA**.

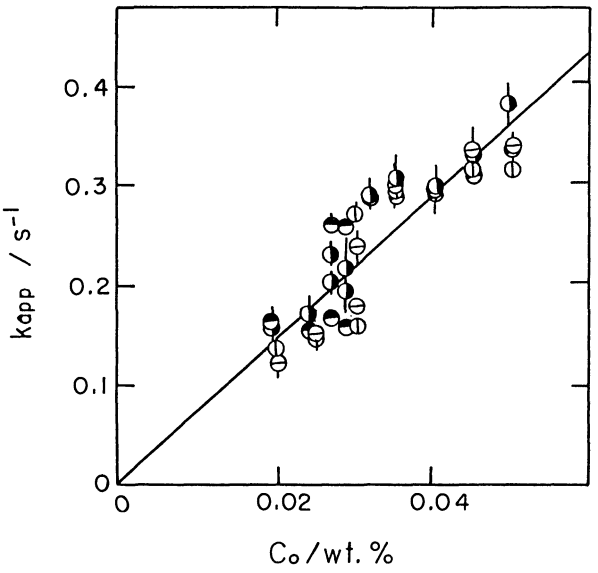

Fig. 5. Comparison of the effects of $CaCl_2$ and $CaBr_2$ on the first-order rate constant as a function of the casein concentration at 25 °C. The salt concentration was fixed at 15 mmol dm^{-3}. ◑: $CaCl_2$ solution by **GA**, ◓: $CaCl_2$ solution by **UA**, ⊖: $CaBr_2$ solution by **GA** and ⊕: $CaBr_2$ solution by **UA**.

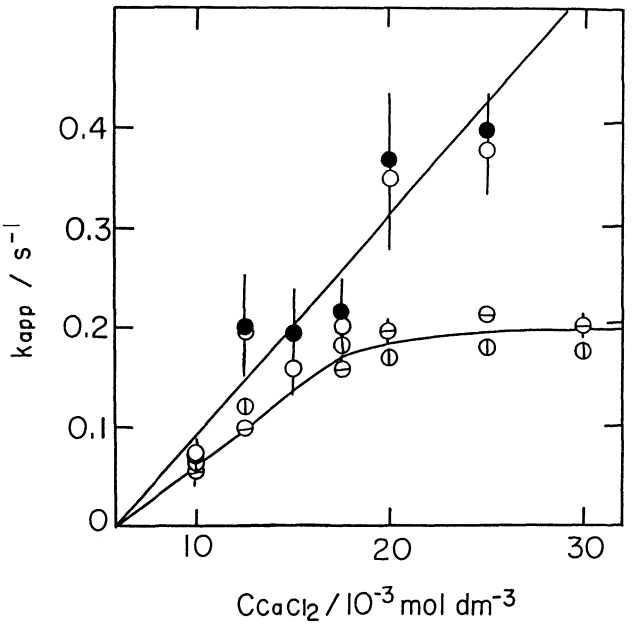

Fig. 7. Concentration dependence of $CaCl_2$ on the apparent first-order rate constant at 25 °C. ⊖: with 0.02 wt% casein by **GA**, ⊕: with 0.02 wt% casein by **UA**, ●: with 0.03 wt% casein by **GA** and ○: with 0.03 wt% casein by **UA**.

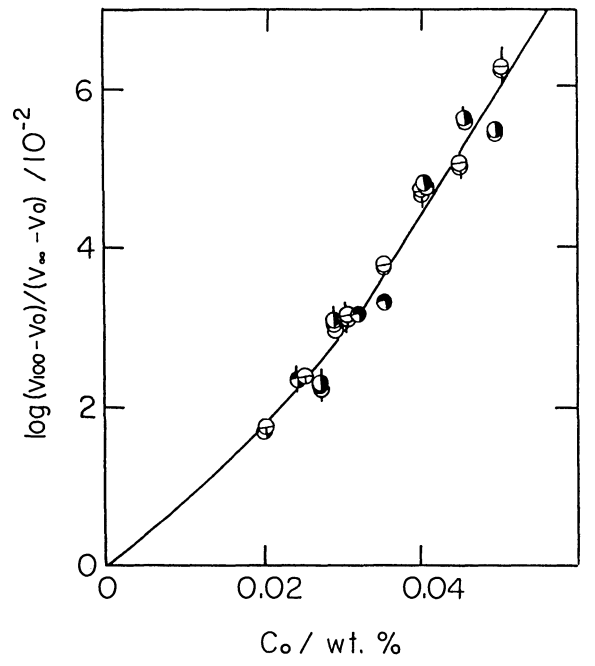

Fig. 6. Comparison of the effect of $CaCl_2$ and $CaBr_2$ on the reaction amplitude for casein solutions at 25 °C. ◑: $CaCl_2$ solution by **GA**, ◓: $CaCl_2$ solution by **UA**, ⊖: $CaBr_2$ solution by **GA** and ⊕: $CaBr_2$ solution by **UA**.

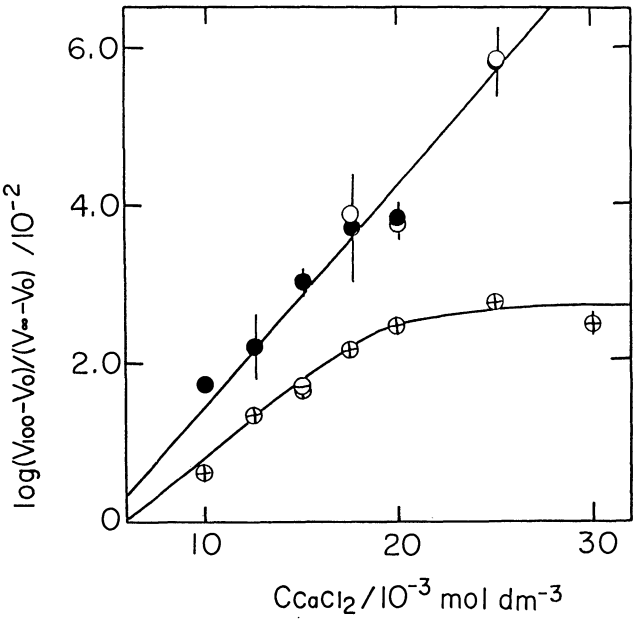

Fig. 8. Concentration dependence of $CaCl_2$ on the reaction amplitude at 25 °C. ⊖: with 0.02 wt% casein by **GA**, ⊕: with 0.02 wt% casein by **UA**, ●: with 0.03 wt% casein by **GA** and ○: with 0.03 wt% casein by **UA**.

tions of casein. Figure 4 represents the concentration dependence of the reaction amplitude. In order to observe the effect of an anion on the reaction, aqueous solutions of calcium bromide were mixed with casein solution. The results are shown in Figs. 5 and 6 together with those for solutions with $CaCl_2$. As can be seen in these figures, the dependences of the apparent first-order rate constant and the reaction amplitude on the casein concentration are very similar to those of $CaCl_2$. This means that only calcium cations play an

important role in changing the optical density.

The $CaCl_2$ concentration dependences of the apparent rate parameters are illustrated in Figs. 7 and 8. It can be seen that the apparent rate constant is also dependent on the $CaCl_2$ concentration and that the profiles depend considerably upon the casein concentration. In order to see the effects of other salts on this phenomenon, 50 mmol dm^{-3} sodium chloride and 30 mmol dm^{-3} magnesium chloride solutions were also mixed with the casein solutions. However, no optical density changes were observed. These results also indicate that the calcium cations bind specifically to the casein molecules and some conformational or structural changes of casein cause the optical density change for the casein solutions. The apparent rate constant and the reaction amplitude obtained at pH 7.2, 8.2, and 9.1 were almost independent of the solution pH.

Discussion

In kinetic experiments carried out using a stopped-flow apparatus, the method of distinguishing whether the reaction is first order or other is very important in order to consider precisely the reaction mechanisms in solutions. Only one analytical procedure of the reaction trace as a function of time might provide equivocal information. As shown above, in the present study the fact that the two analytical procedures of the time traces give the same rate constant and the same reaction amplitude shows that the observed time-dependent optical density change is due to a first-order rate process in the casein solutions, although the concentration range was restricted.

The effects of the calcium cation on the casein solution have been widely studied by various methods. It is said that the addition of the calcium ions to a casein solution promotes the formation of the casein micelle.[14,19] Not many kinetic studies, on the other hand, have been carried out regarding casein micelle formation. This may be because many complex reactions proceed quite rapidly in the concentrated solutions, even if the experiment is performed in solution with only a single polypeptide. Therefore, the time course of the reaction seems to be very complex.[9-12] It should be noteworthy that a single exponential decay phenomenon was observed in the low concentrations presently studied. It is certain that this phenomenon is associated with the casein aggregates, since the solution turbidity increases upon the addition of calcium cations. It is desired to clarify why such a simple time course is observed as in Fig. 2, and why the apparent rate constant and the reaction amplitude increase with the casein concentration, as can be seen in Figs. 3 and 4.

It has been considered that small aggregates or subunits comprising mainly α_s-, β- and κ-casein held together by hydrophobic interaction, exist in dilute solutions of casein.[4,12] Also, a sufficiently high local protein concentration is also speculated when aggregates of protein are formed.[17] As can be seen in Fig. 1, a small absorbance is observed in the solution of casein without adding $CaCl_2$. This result implies the existence of small aggregates. The absorbance increases dramatically when calcium cations are added. On the basis of the present dynamic and static experimental situations and the previous examinations conducted so far, the aggregation reaction of casein may generally proceed in stepwise processes as follows:

$$A_s + A \overset{k_1}{\rightarrow} A_{s+1} \overset{k_2}{\underset{A}{\rightarrow}} A_{s+2} \overset{k_3}{\underset{A}{\rightarrow}} \cdots\cdots \overset{k_n}{\underset{A}{\rightarrow}} A_n. \quad (3)$$

Here k_i is the rate constant for each process and A_s indicates the small aggregate which might act as a nucleus for larger aggregate formation. When the calcium cations bind specifically to free casein or small aggregate, the repulsive forces between them may be weakened, and then larger aggregates may be formed. The reaction associated with ion binding is so fast that it is far beyond the time stale of the stopped-flow method,[20] since the ion binding sites are expected to be either phosphate or carboxylic groups.[21,22] Also, it may be natural to consider that the aggregates actually consist of various molecules with different aggregation numbers, that is, they exist under a proper distribution.[4] However, we simply analyze the observed phenomenon by a conventional reaction kinetics, which may give us a legible feature of the reaction. It is very hard to decide definitely the rate determining step for such an aggregation reaction. We assume here that the rates of steps beyond the the second are so rapid that the stationary states are established. This assumption is widely used to interpret the aggregation process for relatively small molecules,[23] and may also be reasonably accepted, since such an aggregation process proceeds cooperatively once the reaction starts. Then, the reaction could be simplified as follows:

$$A_s + A \overset{k_f}{\underset{nA}{\rightarrow}} A_{s+1} \rightarrow A_{s+n+1}, \quad (4)$$

where s is the mean aggregation number for small aggregate which may grow to larger aggregate, A_{s+n+1}. For the second step in Eq. 4, we define the equilibrium constant, K, as $K=[A_{s+n+1}]/[A_{s+1}][A]^n$, which arises from the stationary state assumption. The rate equation for formation of A_{s+1} is expressed by

$$d[A_{s+1}]/dt = k_f (A_{s0} - [A_{s+1}])(A_0 - [A_{s+1}]), \quad (5)$$

where A_{s0} and A_0 bare the initial concentrations of the reactants, A_s and A, respectively. The solution of the above equation gives the time course of the reactants as

$$[A] = A_0(A_0 - A_{s0})/\{A_0 - A_{s0}\exp -(A_0 - A_{s0})k_f t\}$$

and

$$[A_{s+1}] = [A_0 A_{s0}\{\exp(A_0 - A_{s0})k_f t - 1\}]/ [A_0 \exp(A_0 - A_{s0})k_f t - A_{s0}]. \quad (6)$$

It is expected that the concentration of small aggregate, A_{s0}, is smaller than that of a free or monomer casein, A_0,

because the analytical concentration is not so high. Therfore, the condition $(A_0/A_{s0})\exp(A_0-A_{s0})k_f t \gg 1$ may be well satisfied. Using the stationary state assumption for the second step in Eq. 4, we obtain the time dependence of larger aggregate, as follows:

$$[A_{s+n+1}] = K(A_0-A_{s0})^n A_{s0}\{1-\exp -(A_0-A_{s0})k_f t\} = [\overline{A_{s+n+1}}]\{1-\exp -(A_0-A_{s0})k_f t\}, \quad (7)$$

where $[\overline{A_{s+n+1}}]$ is the concentration of the larger aggregate at an infinite time of the reaction. This equation indicates that the appearance of larger aggregates may be approximated by a single exponential factor and that the rate of the appearance of larger aggregates depends on the initial concentrations of the monomer and small aggregate casein molecules. It might be possible that the aggregate formation reaction by self-association of the small aggregates, such as $nA_s \rightarrow (A_s)_n$, causes the observed optical density change. However, the concentration dependences of the apparent first-order reaction and the reaction amplitude could not be well explained by such a reaction mechanism. The aggregation reaction associated with only free or monomer casein molecules was also considered to be the cause of the phenomenon, though the observed phenomena was not well interpreted.

The solution turbidity, τ, is related to the molecular weight of the aggregate, M_w, and the concentration, as[14]

$$\tau = QM_w[A_{s+n+1}], \quad (8)$$

where Q is a constant. Using Eqs.7 and 8, and comparing Eq. 2, the apparent rate constant, k_{app} observed by the stopped-flow method is found to be $(A_0-A_{s0})k_f$ and the reachtion amplitude, $\log\{(V_{100}-V_0)/(V_\infty-V_0)\}$, corresponds to $QM_w[A_{s+n+1}]$.

First, following the above relations, we consider the concentration dependence of the apparent rate constant, k_{app}. As can be seen in Fig. 3, plots of k_{app} vs. C_0 seems to indicate a linear increase with almost a zero intercept at 10 and 15 mmol dm^{-3} $CaCl_2$. These may mean that the concentration of small aggregates is much smaller than that of free casein molecules in a relatively dilute solution because $C_0=[A_0]+s[A_{s0}]$. From the slopes of these plots, we obtained rate constants of k_f=2.8 (wt% $s)^{-1}$ for a solution with 10 mmol dm^{-3} and k_f=7.6 (wt% $s)^{-1}$ for that with 15 mmol dm^{-3}. With increasing $CaCl_2$ concentration, the plots gave a slightly curved line and a positive intercept. Therefore, we reluctantly show the experimental results at 30 mmol dm^{-3} $CaCl_2$ without having determined the rate constant. Such an unexpected dependence might mean that an approximated analytical equation (Eq. 7) is not satisfied at higher concentrations of $CaCl_2$. Also, according to previous studies,[11,14] it is said that a von Smolucowski-type reaction proceeds for the formation of larger micelles; this process can be expressed as

$$[M_w] = [M_w(0)](1+k'C_0 t), \quad (9)$$

where $[M_w(0)]$ is the molecular weight at t=0, and k' the rate constant for the coagulation process. Then, the observed time dependence of the optical density change may deviate from single exponential decay at a relatively high concentration of $CaCl_2$. Actually, at concentrations of more than 0.05 wt% casein, the time courses of the stopped-flow could not also be fitted to the single exponential decay function. These results may indicate that more complex reactions start at around these conditions.

Small aggregates or submicelles are expected to be spongy protein particles with molecular weight, 250000.[12] It is said that they consist of 10 or 12 casein molecules. These estimations are quite reasonable if we take into account the constituting molecular structures of casein, namely α-, β- and κ-casein. The mean free casein concentration is roughly estimated from the analytical concentration. If we take the mean molecular weight of monomer casein to be 25000, the obtained rate constants, k_f, are converted to be 7×10^4 mol^{-1} dm^3 s^{-1} at 10 mmol dm^{-3} $CaCl_2$ and 1.9×10^5 mol^{-1} dm^3 s^{-1} at 15 mmol dm^{-3} $CaCl_2$. These rate constants are those for the first step for the aggregation in Eq. 3. The fact that the larger rate constant is obtained at higher concentrations of $CaCl_2$ may be considered as follows. The greater binding of Ca^{2+} ions to the casein molecule makes the repulsive interaction between the proteins decrease, thus facilitating the aggregation. This speculation is also supported by the $CaCl_2$ dependence of the rate parameters, which is considered later. The processes after the second one are considered to be very rapid since the stationary state approximation is well satisfied.

Next, the concentration dependence of the reaction amplitude is considered. As can be seen in Fig. 4, it increases monotonously with the concentration; such a dependence reflects an increase of the larger micelle concentration, $[A_{s+n+1}]$. Unfortunately, however, the quantitative analytical correlation between the absorbance measured by the static method (Fig. 1) and the amplitude of the reaction (Fig. 4) is not given at this stage because the observation cell of the stopped-flow apparatus consists of cylindrical quartz with a 2 mm diameter light pass length. The monotonous increase of the reaction amplitude is easily speculated from Eqs. 7 and 8. Qualitatively, both of the dependences observed by the static and dynamic methods are very similar eah other. This confirms that the observed time dependent phenomenon is associated with the formation of larger casein mielles induced by binding of the calcium cations.

The $CaCl_2$ concentration dependences on the apparent rate constant and the reaction amplitude seem to reflect the specificity of calcium ion binding to the casein. As can be seen in Figs. 7 and 8, they increase for lower concentrations of $CaCl_2$, but tend to reach their plateaus when the casein concentration is low. Such profiles of the rate parameters may indicate that the number of the binding sites in the casein molecule is

limited. With increasing the calcium concentration, the rate increases, which is seen in solutions with 0.03 wt% casein and in the dilute solution of $CaCl_2$ with 0.02 wt% casein. When most of the binding sites are occupied by calcium ions, the aggregation process may tend to reach a constant value.

In conclusion, it was found in the present study that there is a very rapid and simple process regarding the casein micelle formation in aqueous media during the early stage of the reaction process. The time dependence is described by a single exponential time constant, and can be well interpreted in terms of the aggregation reaction mechanism. In a concentrated solution of casein, further, more complex reactions are speculated to take place.

Further dynamical studies concerning the solutions of individual proteins in casein are desired for elucidating more details concerning molecular aggregation mechanism.

The authors gratefully acknowledge Technical Research Institute, Snow Brand Milk Products, Co., Ltd. for supplying the samples of purified sodium casein used in this work.

References

1) D. S. Horne and T. G. Parker, *J. Dairy Res.*, **50**, 425 (1983).
2) M. C. A. Griffin, *J. Colloid Interface Sci.*, **115**, 499 (1987).
3) T. Ono, T. Furuyama, and S. Odagiri, *Agric. Biol. Chem.*, **47**, 221 (1983).
4) S. C. H. Lin, R. K. Dewan, V. A. Bloomfield, and C. V. Morre, *Biochemistry*, **10**, 4788 (1971).
5) N. Mattarella and T. Richardson, *J. Dairy Sci.*, **65**, 2253 (1982).
6) E. A. G. Anianson and S. N. Wall, *J. Phys. Chem.*, **78**, 1024 (1982).
7) M. Teubner, *J. Phys. Chem.*, **83**, 2917 (1979).
8) S. Kato, H. Nomura, R. Zielinski, and S. Ikeda, *Bull. Chem. Soc. Jpn.*, **59**, 707 (1986).
9) T. Sanner and G. Kovacc-Proszt, *Biochim. Biophys. Acta*, **303**, 68 (1973).
10) D. J. McMkhon, R. J. Brown and C. A. Ernstro, *J. Dairy Sci.*, **67**, 745 (1984).
11) T. A. J. Payens, A. K. Wiersma, and J. Brinkhuis, *Biophys. Chem.*, **6**, 253 (1977).
12) T. A. J. Payens, *Biophys. Chem.*, **6**, 263 (1977).
13) D. G. Dalgleish, *Biophys. Chem.*, **11**, 147 (1980).
14) D. G. Dalgleish, *J. Dairy Res.*, **50**, 331 (1983).
15) J. Bentz and S. Nir, *J. Chem. Soc., Faraday Trans. 1*, **77**, 1249 (1981).
16) D. K. Strickland, L. Larsson, D. E. Nevenschwander, and I. Bjork, *Biochemistry*, **30**, 2797 (1991).
17) M. E. Goldberg, R. Rudolph, and R. Jaencke, *Biochemistry*, **30**, 2790 (1991).
18) The computer program is written in BASIC except that for transferring the signals from the wave memory to the computer. It is available to one of the authors on request. It may be also applicable to the analyses of the single exponential decay curves observed by the transient relaxation methods with small modifications.
19) T. Ono, M. Yahagi, and S. Odagiri, *Agric. Biol. Chem.*, **44**, 1499 (1980).
20) P. Hemmes, L. Oppenheimer, K. M. Sheer, D. Saar, F. Jordan, and S. Nishikawa, *J. Phys. Chem.*, **86**, 1434 (1982).
21) H. G. Ter-Host, *Neth. Milk Dairy J.*, **17**, 185 (1963).
22) G. T. Pyne and T. C. A. McGann, *J. Dairy Rev.*, **27**, 9 (1960).
23) F. Garland and J. Rassing, *J. Phys. Chem.*, **75**, 3182 (1971).

Extended X-Ray Absorption Fine Structure Studies on Local Structure in Amorphous $LaNi_{5.0}$ Films

Tomoyoshi SUENOBU, Hiroki SAKAGUCHI, Takaharu TSUJI, Hiroyoshi KANAI,† Satohiro YOSHIDA,†† and Gin-ya ADACHI*

Department of Applied Chemistry, Faculty of Engineering, Osaka University, Yamadaoka, Suita, Osaka 565
†Faculty of Living Science, Kyoto Prefectural University, Shimogamo, Sakyoku, Kyoto 606
††Department of Hydrocarbon Chemistry and Division of Molecular Engineering, Kyoto University, Kyoto 606

(Received July 15, 1991)

Analyses of the local structure around La and Ni atoms in amorphous $LaNi_{5.0}$ films have been performed using the extended X-ray absorption fine structure (EXAFS), and the effect of the structure on the difference of hydrogen absorption characteristics between the amorphous and crystalline $LaNi_{5.0}$ has been elucidated. The lengthening of interatomic distances for the Ni–Ni and La–Ni pairs, respectively, was observed for the amorphous samples in comparison with the crystalline ones. A part of the hydrogen sites existed in the crystalline $LaNi_5$ was distorted in the amorphous one. Since the hydrogen atoms appear to be difficult to enter these sites distorted, the hydrogen content in the amorphous $LaNi_5$ is smaller than that in the crystalline one.

Amorphous $LaNi_5$ films have attracted considerable technological and scientific interest, such as hydrogen purification, catalysis, and batteries[1–3] Their physical and chemical properties have been found to be much different from those of the crystalline sample.[4–7] The amorphous $LaNi_5$ film has been known not to pulverize after repeated hydrogenation–dehydrogenation cycling, and absorbs hydrogen less than a half of the amount taken up by the crystalline bulk.[5,7] These differences of properties appear to be closely related to the structure of the films, so that it is necessary to obtain the detailed structural information at an atomic level.

In the present study, the local structure around La and Ni atoms in the amorphous $LaNi_{5.0}$ films is clarified by means of EXAFS, and the results are compared with those in the crystalline sample. The relationship between the structure and the hydrogen absorption characteristics is discussed.

Experimental

The $LaNi_{5.0}$ amorphous films (ca. 1 μm thick which was determined by direct observation of the cross section of the sample using a scanning electron microscope.) were deposited on a polyimide membrane (Kapton, 40 μm thick, Toray-du Pont Co., Ltd.) at room temperature by using sputtering method.[4,6,7] For the sputtering, parameters of 0.395-Pa Argon pressure (99.999%) and a radio-frequency generating power of 400 W were employed for all sputtered samples. The sputtering target consisted of a disk in which 98% of the surface area is $LaNi_{4.8}$ (33.0 wt% La, 66.8 wt% Ni) and 2% is $LaNi_{3.0}$. The La–Ni alloys were supplied by Santoku Metal Industry, Kobe, Japan. X-Ray diffraction measurements were made to verify the amorphous state. Their homogeneity and stoichiometry were checked by means of X-ray fluorescent spectroscopy and X-ray photoelectron spectroscopy. The films precisely having a composition of $LaNi_{5.0}$ were used for the EXAFS measurements. The $LaNi_{5.0}$ crystalline powder and commercially available Ni foil (5 μm thick, 99.98% pure, The Japan Lamp Industries) were used as reference materials. The crystalline $LaNi_{5.0}$ alloy film with a crystallinity of 80% was prepared on a stainless-steel substrate at 530 K by sputtering. The film was peeled from the substrate with an adhesive tape, and the resulting film was applied to the EXAFS measurements. The crystallinity of the film was determined from the heat of crystallization which was estimated by the differential scanning calorimetry (DSC).[7]

The measurement of X-ray absorption spectra (XAS) were performed by means of synchrotron radiation employing the EXAFS facilities of BL-7C of the Photon Factory in the National Laboratory for High-Energy Physics, Tsukuba, Japan. An Si(111) double crystal monochromator was used to monochromatize the X-rays from a 2.5-GeV positron storage ring. The ring current was between 350.5 and 246.9 mA. EXAFS spectra were collected at the Ni K- and La L_{III}-edges. The focusing mirror was used to reduce higher harmonics at the La edge. Energy resolution of 1.4 eV can be achieved at the Ni K-edge (8331.7 eV) when a source-size is not considered. The total thickness of the $LaNi_{5.0}$ films used for the X-ray absorption measurements were about 35 and 20 μm for the La and Ni edges respectively. All the XAS data were obtained at 220 K. Analyses of the EXAFS data were performed with a "KABO" program in the FACOM M382 computer system at the Data Processing Center, Kyoto University, Japan.

The photon energy was calibrated by the characteristic inflection point at the edge of the absorption spectrum of the standard Ni foil (5 μm thick, 8331.7 eV). The EXAFS oscillatory part $\chi(E)$ above the absorption edge was extracted from the XAS data using a simple equation of $A/E^{2.75}$ instead of Victoreen formula and normalized as described elsewhere.[8–10] The photoelectron wave vector k is related to the photon energy E expressed by $k=2\pi[2m(E-E_0)]^{1/2}/h$, where m is mass of an electron, h, Planck's constant, E_0, the threshold energy of the absorption edge. E_0 was determined as $E_{inf}+\Delta E$, where E_{inf} was the inflection point where the differential coefficient of the spectrum near the absorption edge is maximum and ΔE was allowed to be various fixed values. Reconstruction of the crystalline $LaNi_{5.0}$ spectra can only be achieved using +4.5 eV as ΔE at Ni K-edge and +4.0 eV at La L-edge. Subsequently, $E_0(=E_{inf}+\Delta E)$ was determined with these ΔE values for the amorphous and 80% crystallinity films. Fourier transforms are taken over the range of 3.3—14.0 $Å^{-1}$ and 4.0—9.2 $Å^{-1}$ for the Ni and La edges respectively to obtain the

radial structure function (RSF). In order to obtain the bond distance and the coordination number, the main peaks (Ni; 1.6—2.7 Å, La; 2.4—3.4 Å) were Fourier filtered into the k space, where the inverse Fourier transform was analyzed by the single scattering formula of Stern et al.[11—13] The resulting filtered EXAFS was fitted to the formula of Stern et al., with three variables, namely, B ($=N\times S$; N, true coordination number, S, damping factor which was evaluated from the coordination number of the Ni foil.[14]), apparent coordination number, L, interatomic distance, and σ^2, Debye-Waller factor by means of the nonlinear least square curve-fitting method.[15] Theoretical phase shifts and backscattering amplitudes of Teo and Lee are used in the curve fitting analyses.[16,17] As obtained in general EXAFS measurement,[19,20] the errors in the parameters of B and L were determined as the ranges within which the R value changes by a factor of 2 from the minimum value, with the other parameters held fixed, where R is a reliability factor.

Results and Discussion

Figure 1 illustrates XANES spectra on the Ni K-edge

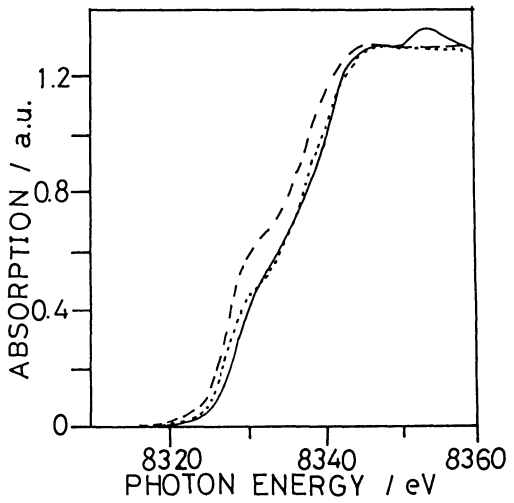

Fig. 1. Ni K-edge XANES spectra for $LaNi_{5.0}$.
——: Ni foil,
– – –: $LaNi_{5.0}$ crystalline bulk,
.....: $LaNi_{5.0}$ amorphous sputtered film.

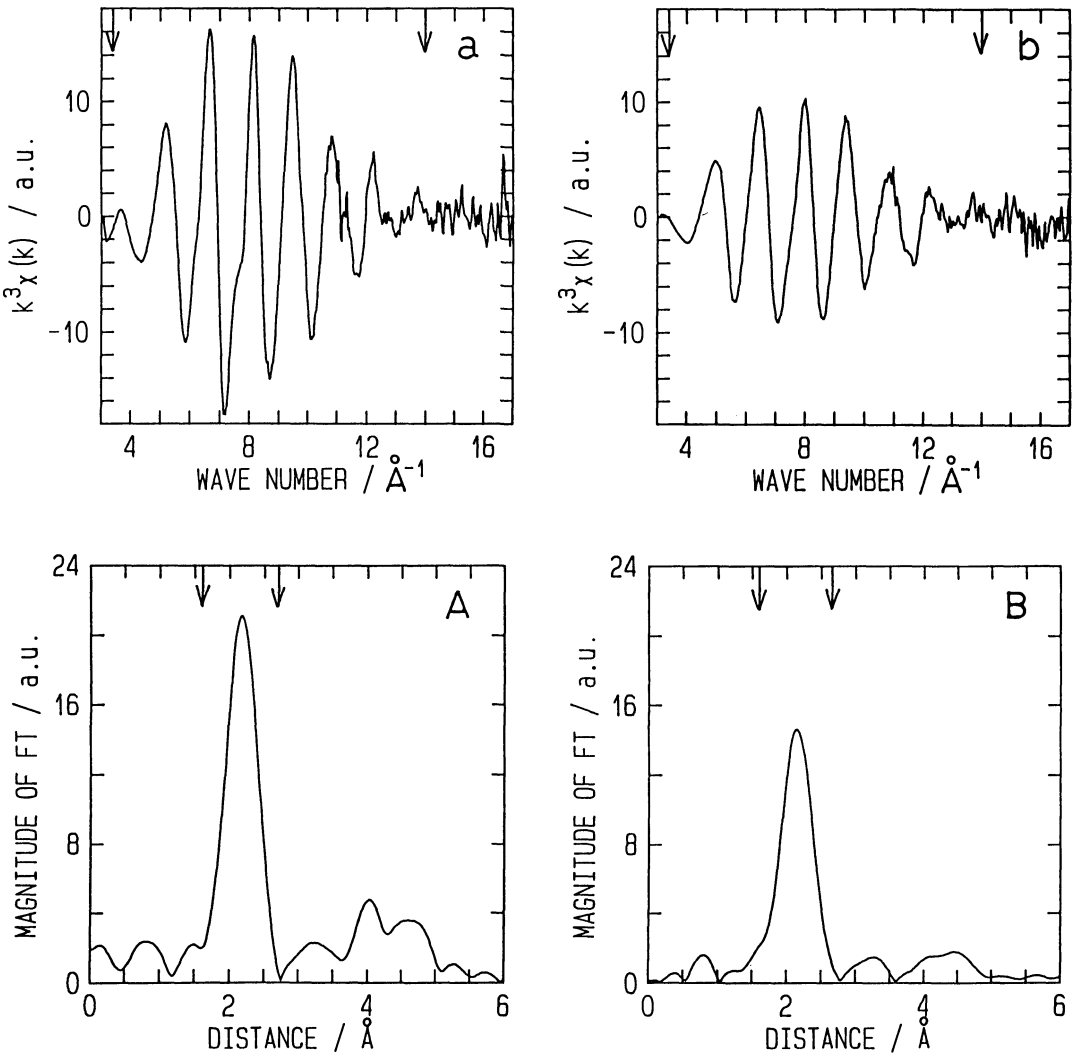

Fig. 2. Ni K-edge k^3-weighted EXAFS spectra (a—b) and magnitudes of their Fourier transforms (A—B), in the 80% crystallinity(a,A) and the amorphous sputtered(b,B) $LaNi_{5.0}$ films. (Arrows (↓) illustrated in the figures indicate the range for Fourier transforms or back Fourier transforms.)

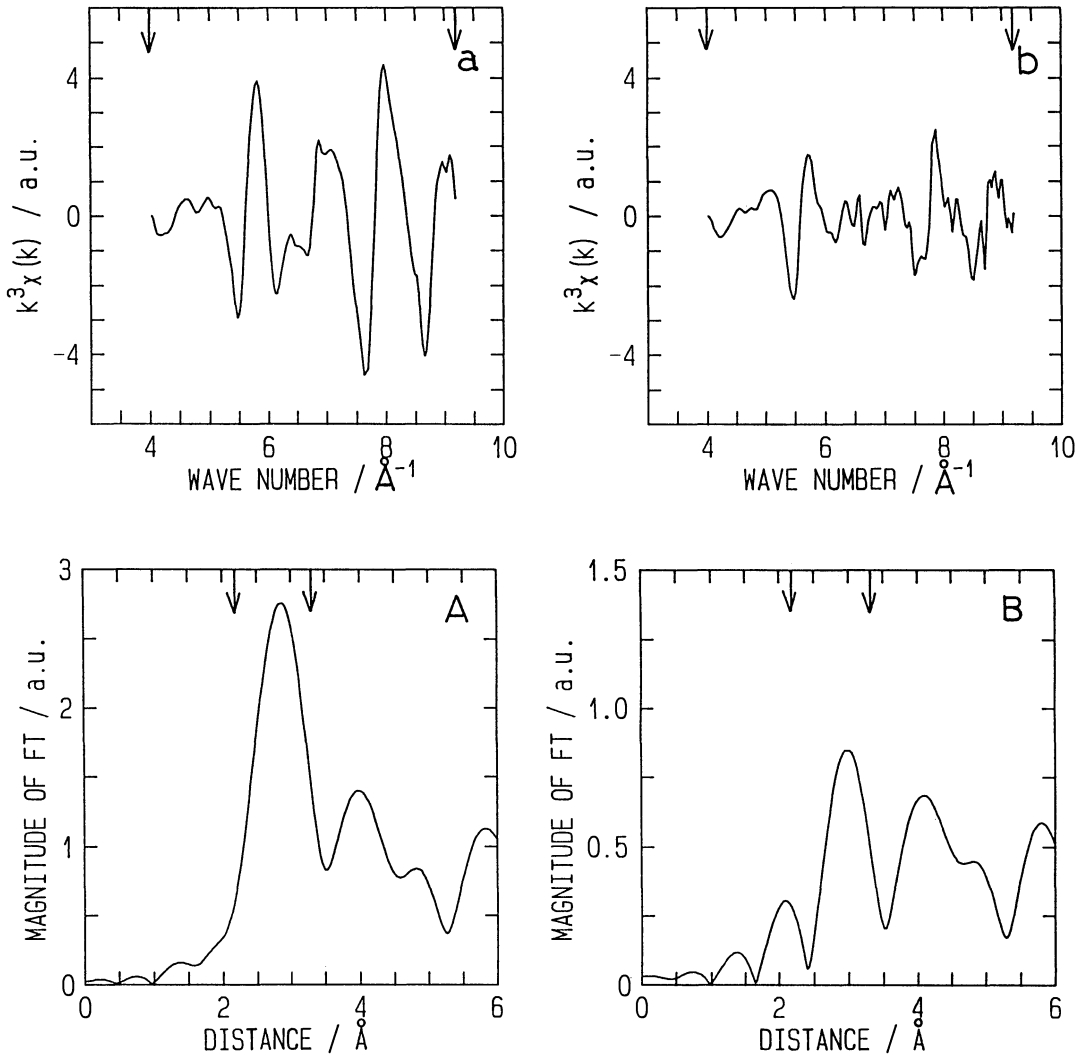

Fig. 3. La L_{III}-edge k^3-weighted EXAFS spectra (a—b) and magnitudes of their Fourier transforms (A—B), in the 80% crystallinity(a,A) and the amorphous sputtered(b,B) $LaNi_{5.0}$ films.

for the Ni foil, the $LaNi_{5.0}$ crystalline bulk and the $LaNi_{5.0}$ amorphous sputtered film. The absorption edge for the $LaNi_5$ crystalline bulk shifted about 1.5 eV to the lower energy side compared with that for the Ni foil due to the narrowing of the Ni 3d-band caused by the charge transfer from the 5d-band of La, which has smaller electronegativity than Ni, to the Ni 3d-band. As for the $LaNi_{5.0}$ amorphous film, the energy position of absorption edge was higher than that for the crystalline bulk. However, no difference of the energy position of absorption edge was observed between the amorphous $LaNi_{5.0}$ film and the Ni foil. This is because the degree of energy transfer from La to Ni for the amorphous film is lower than that for the crystalline bulk.

Figures 2 and 3 show the k^3-weighted EXAFS spectra at the Ni K- and La L_{III}-edges in the sputtered amorphous $LaNi_{5.0}$ films and the 80% crystallinity film. The amplitude of the EXAFS oscillations for the amorphous film was smaller than that for the crystalline film with a crystallinity of 80%. The damping of EXAFS oscillation for the amorphous film seems not to be caused by the decrease in the coordination number, but by the larger static disorder which increases the Debye-Waller factor.

The magnitudes of the Fourier transforms obtained by a Fourier analysis of the EXAFS data in these films are also shown in Figs. 2 and 3. A large peak appeared in these samples on the Ni edge at about 2 Å corresponding to mainly the Ni–Ni and partially Ni–La distance, while on the La edge at about 3 Å corresponding to the La–Ni distance. The profiles of transforms in the sputtered amorphous films show resemblance to that in the 80% crystallinity film, so that it was suggested that the local structures around central Ni and La atoms for the amorphous $LaNi_5$ were similar to those for the crystalline one. The weak intensity of the main peak for the amorphous films was observed on both two edges due to the larger static disorder.

The results of the curve fitting analysis on the Ni edge are presented in Table 1. As for the shortest Ni–

Table 1. Structural Parameters at the Ni K-Edge for $LaNi_{5.0}$[a]

Central atom	Crystalline bulk					80% crystallinity sputtered film				Amorphous sputtered film			
	XRD[b]		EXAFS										
	N	L(Å)	L(Å)	σ^2(Å$^2\times10^{-3}$)	R	N	L(Å)	σ^2(Å$^2\times10^{-3}$)	R	N	L(Å)	σ^2	R
Ni	4.8Ni	2.461	2.45±0.01	5.2		5.0Ni±0.6	2.46±0.01	5.2		4.6Ni±0.5	2.46±0.01	6.8	
	4 Ni	2.507	2.51±0.01	6.0	3.1×10^{-3}	4.5Ni±1.1	2.56±0.01	8.7	6.2×10^{-3}	3.5Ni±0.9	2.57±0.02	13.2	4.8×10^{-3}
	3 La	2.894	2.89±0.06	8.5		1.4La±1.2	2.90±0.06	8.8		1.7La±1.4	2.92±0.08	14.6	

a) L; interatomic distance, N; real coordination number, σ; Debye–Waller factor, $R=(\{\sum_k[\chi_{obs}(k)-\chi_{calc}(k)]^2\}/[\sum_k\chi_{obs}(k)]^2)^{1/2}$. b) Data from Ref. 18.

Table 2. Structural Parameters at the La L_{III}-Edge for $LaNi_{5.0}$[a]

Central atom	Crystalline bulk					80% crystallinity sputtered film				Amorphous sputtered film			
	XRD[b]		EXAFS										
	N	L(Å)	L(Å)	σ^2(Å$^2\times10^{-2}$)	R	B	L(Å)	σ^2(Å$^2\times10^{-2}$)	R	B	L(Å)	σ^2	R
La	6 Ni	2.894	2.91±0.03	2.1		1.7±0.1Ni	2.96±0.02	2.0		1.3±0.1Ni	3.01±0.01	2.1	
	12Ni	3.202	3.28±0.01	1.1	1.1×10^{-3}	3.8±0.1Ni	3.28±0.01	1.4	9.8×10^{-4}	2.8±0.2Ni	3.27±0.01	2.1	6.6×10^{-3}

a) L; interatomic distance, B; apparent coordination number, $B=S\times N$, S; damping factor, N; real coordination number, σ; Debye–Waller factor, $R=(\{\sum_k[\chi_{obs}(k)-\chi_{calc}(k)]^2\}/[\sum_k\chi_{obs}(k)]^2)^{1/2}$. b) Data from Ref. 18.

Ni(Ni_I–Ni_{II}) pairs with an interatomic distance of 2.461 Å, the coordination number around Ni_I atoms (CN: 6) is different from that around Ni_{II} atoms (CN: 4), since there are two kinds of Ni atoms (Ni_I and Ni_{II}) having the different symmetry in $LaNi_5$. Therefore, the coordination number for the pairs was estimated with considering the proportion of the number of each Ni atoms in a unit cell. The calculation was performed with the following equation, $(6\times2+4\times3)/5=4.8$.

A fit of the oscillations above the Ni edge was attempted for the crystalline $LaNi_5$ bulk with one shell of Ni atoms. The resulting interatomic distance of the Ni–Ni pair, 2.475 Å, was intermediate between the shortest distance, 2.461 Å, and the second shortest distance, 2.507 Å, which are obtained from XRD analyses,[18] so that it was suggested that the large peak appeared at about 2 Å in the RSF consisted of more than two subshells. When the curve fitting was performed with two subshells of Ni atoms at two different distances from the central atom, the distances of the two Ni–Ni pairs were 2.461 and 2.501 Å respectively. Although these distances were fairly fitted with those estimated from the XRD analyses, the reliability (R) and Debye–Waller (σ^2) factors were still large. Therefore, the interatomic distances were determined by adding one subshell of La atoms at a larger distance (2.89 Å) to the two subshells of Ni atoms. The combination of these three subshells could simulate the spectrum, since both R and σ^2 factors were smaller than the result obtained from the curve fitting with two Ni subshells. For the crystalline bulk, the coordination number obtained with EXAFS is not listed in the table because the XAS was not satisfactory.

The structural parameters of the amorphous film were similar to those of the crystalline bulk though there is the slight difference in the interatomic distance. This indicates that the sites accommodated with hydrogen atoms in the amorphous film were analogous to those in the crystalline bulk. The distances of second Ni–Ni pairs were found to increase about 0.06 Å for the amorphous films in comparison with those for the crystalline bulk. The parameters of interatomic distances for the amorphous sputtered film were slightly different from those for the crystalline film which has a crystallinity of 80%.

The structural parameters for the La edge are summarized in Table 2. The coordination number listed in the table is a tentative value because no adequate result for the $LaNi_{5.0}$ powder as a reference material was obtained from the EXAFS analysis due to inhomogeneities of the particle size in the sample layer.

Lanthanum atoms in the crystalline bulk are known to be coordinated by two kinds of nickel atoms (La–Ni_I; ca. 2.9 Å, La–Ni_{II}; ca. 3.2 Å). For the curve fitting analyses on La L_{III}-edges, the inverse Fourier transform of calculated EXAFS with these two subshells of La–Ni pairs fairly agree with that of experimental EXAFS. The ca. 0.1 Å lengthening of La–Ni_I pairs were found for

the amorphous films in comparison with those for the crystalline bulk. On the Ni K-edge, however, it was not possible to evaluate the differences of Ni_I–La distances between the amorphous film and the crystalline bulk because of large uncertainties in these parameters due to small contribution of the Ni_I–La third subshell to the first nearest neighbor shell consisted of Ni_I–Ni_{II}, Ni_{II}–Ni_{II}, and Ni_I–La subshells.

$LaNi_5$ crystallizes with a hexagonal $CaCu_5$-type structure ($P6/mmm$ space group). The structure consists of two alternating types of plane, the basal plane being consisted of lanthanum and nickel atoms (Ni_I), while the $z=1/2$ plane being consisted of only nickel atoms (Ni_{II}). There are at least three models used to describe the structure of $LaNi_5$ hydride.[21–23] We employed to the model reported by Lartigue et al.,[21], because the refinement of neutron powder diffraction data for their analyses gave better reliability factors. According to the model ($P6_3mc$ space group), as shown in Fig. 4, there are three types of sites (D1, D3, and D5 sites) occupied with hydrogen or deuterium atoms for the crystalline bulk. On the D1 site (2b), hydrogen atoms are found nearly at the center of the Ni_4 tetrahedra ($3Ni_I+1Ni_{II}$). On 6c sites, D3 and D5 atoms are displaced by about 0.4 Å from the center of both the tetrahedra[two lanthanum and two nickel atoms (Ni_{II})], and octahedra[two lanthanum and four nickel atoms ($2Ni_I+2Ni_{II}$)]. On the local structures obtained from the EXAFS analyses, the La and Ni environments do not vary much from the crystalline bulk to the amorphous film, as was suggested by the fact that the Fourier transforms do not change much on the La and Ni edges. Moreover, the Ni–Ni and La–Ni distributions in the amorphous film still have some resemblance to the crystalline bulk, so that the three types of hydrogen sites (D1, D3, and D5) appear to exist in the amorphous film as well as the crystalline bulk. As mentioned above, however, the Ni_{II}–Ni_{II} and La–Ni_I distances were lengthened compared with those for the crystalline bulk, consequently, a part of these three hydrogen sites existed in the crystalline bulk become somewhat distorted. Since the hydrogen atoms appears to be difficult to be stably located in the sites distorted, the amount of hydrogen taken up by the amorphous $LaNi_{5.0}$ is smaller than that by the crystalline one.

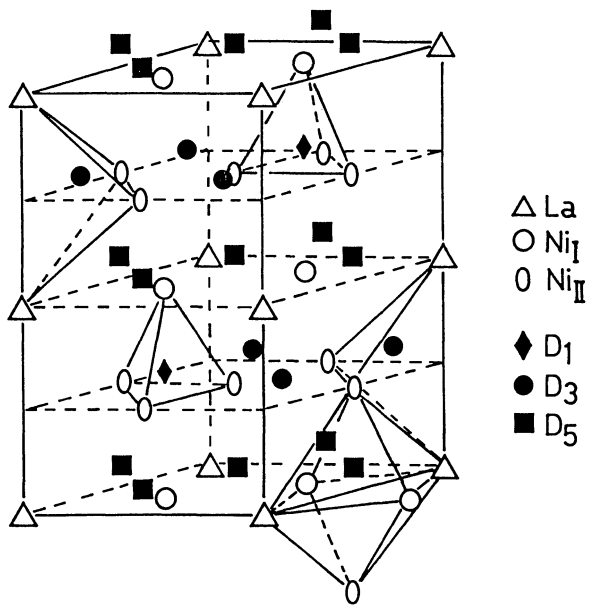

Fig. 4. Structure of the hypothetical fully ordered $LaNi_5D_7$ phase involving three types of sites occupied with hydrogen.

Conclusion

The local structures around La and Ni atoms in amorphous $LaNi_5$ films have been clarified with EXAFS. The distortion of three kinds of sites in which hydrogen atoms are considered to occupy was observed in the amorphous films due to the lengthening of interatomic distances in the Ni–Ni and La–Ni pairs. If the hydrogen atoms become difficult to be stably located in the sites, the hydrogen content in the amorphous $LaNi_{5.0}$ would be smaller than that in the crystalline one.

We thank Dr. M. Nomura and the staff of the Photon Factory at KEK for their helpful advice and technical assistance in the EXAFS measurement. This work was partially supported by a Grant in Aid for Developmental Scientific Research Nos. 63850167 and 01470074 for G. Adachi, and No. 63790311 for H. Sakaguchi, from the Ministry of Education, Science and Culture.

References

1) G. Adachi, H. Nagai, and J. Shiokawa, *J. Less-Common Met.*, **97**, L9 (1984).
2) H. Sakaguchi, G. Adachi, and J. Shiokawa, *Bull. Chem. Soc. Jpn.*, **61**, 521 (1988).
3) H. Sakaguchi, Y. Yagi, J. Shiokawa, and G. Adachi, *J. Less-Common Met.*, **149**, 185 (1989).
4) G. Adachi, H. Sakaguchi, K. Niki, H. Nagai, and J. Shiokawa, *Bull. Chem. Soc. Jpn.*, **58**, 885 (1985).
5) H. Sakaguchi, N. Taniguchi, H. Nagai, K. Niki, G. Adachi, and J. Shiokawa, *J. Phys. Chem.*, **89**, 5550 (1985).
6) H. Sakaguchi, N. Taniguchi, H. Seri, J. Shiokawa, and G. Adachi, *J. Appl. Phys.*, **64**, 888 (1988).
7) H. Sakaguchi, H. Seri, and G. Adachi, *J. Phys. Chem.*, **94**, 5313 (1990).
8) B. J. Jan, H. J. Klabunde, T. Tanaka, H. Kanai, and S. Yoshida, *J. Am. Chem. Soc.*, **110**, 5951 (1988).
9) H. Yamashita, H. Mizutani, T. Tanaka, T. Funabiki, and S. Yoshida, *J. Non-Cryst. Solids*, **95 & 96**, 419 (1987).
10) T. Tanaka, H. Yamashita, R. Tsuchitani, T. Funabiki, and S. Yoshida, *J. Chem. Soc.*, **84**, 2987 (1988).
11) E. A. Stern, *Phys. Rev. B*, **10**, 3027 (1974).
12) C. A. Ashley and S. Doniach, *Phys. Rev. B*, **11**, 1279 (1975).
13) P. A. Lee and J. B. Pendry, *Phys. Rev. B*, **11**, 2795 (1975).
14) A. Taylor, *J. Inst. Met.*, **77**, 585 (1950).
15) K. Levenberg, *Q. Appl. Math.*, **2**, 164 (1944).

16) B. K. Teo, P. A. Lee, A. L. Simons, P. Eisenberger, and B. M. Kincaid, *J. Am. Chem. Soc.,* **99**, 3854 (1977).
17) P. A. Lee, B. K. Teo, and A. L. Simons, *J. Am. Chem. Soc.,* **99**, 3856 (1977).
18) M. Gupta, *J. Less-Common Met.,* **130**, 219 (1987).
19) T. Claeson, J. B. Boyce, P. W. Lowe, and T. H. Gaballe, *Phys. Rev. B,* **29**, 4969 (1984).
20) B. Lengeler and P. Eisenberger, *Phys. Rev. B,* **21**, 4507 (1980).
21) C. Lartigue, A. Le Bail, and A. Percheron-Guegan, *J. Less-Common Met.,* **129**, 65 (1987).
22) H. Hayakawa, K. Nomura, Y. Ishido, Y. Akiba, and S. Shin, *J. Less-Common Met.,* **143**, 315 (1988).
23) P. Thompson, J. J. Reilly, L. M. Hastings, and R. Hempelmann, *J. Phys. F,* **16**, 675 (1986).

 © 1991 The Chemical Society of Japan Bull. Chem. Soc. Jpn., 64, 3528—3537 (1991)

Conformational Stability of V-Amyloses and Their Hydration-Induced Conversion to B-Type Form as Studied by High-Resolution Solid-State ^{13}C NMR Spectroscopy

Hazime SAITÔ,* Junko YAMADA,† Tohru YUKUMOTO,††
Hirofumi YAJIMA,†† and Ryuichi ENDO††
Department of Life Science, Himeji Institute of Technology,
Harima Science Garden City, Kamigori-cho, Hyogo 678-12
†Biophysics Division, National Cancer Center Research Institute,
Tsukiji 5-chome, Chuo-ku, Tokyo 104
††Department of Applied Chemistry, Science University of Tokyo,
Kagurazaka, Shinjuku-ku, Tokyo 162
(Received July 19, 1991)

We have recorded ^{13}C NMR spectra of several preparations of amorphous samples, V-amyloses and their hydrates to gain insight into their relative stability and subsequent hydration-induced conformational change. It was found that the ^{13}C NMR line width of the iodine complex prepared as a precipitate in aqueous solution was the narrowest among these preparations, including the iodine complex formed from cast film. It is noteworthy that these V-amyloses are not always stable when they are equilibrated in an atmosphere of 96% R. H. in a desiccator and converted to B-type form, consistent with previous observation by Senti and Witnauer (*J. Am. Chem. Soc.*, **70**, 1438 (1948)). ^{2}H NMR line shape and spin-lattice relaxation times were measured for partially deuterated V and B-type amylose samples containing DMSO-d_6 and deuterium oxide, respectively, to explore the dynamics of the DMSO and water molecules bound to the polymer chains. It is unlikely that any drastic conformational change such as unfolding followed by refolding and plausible change of handedness is caused by such mild physical treatment as humidification. Therefore, it appears that the resulting B-type form should be ascribed to a left-handed single helix as a consequence of a slight modification of V-amylose, in contrast to the previous interpretation based on the data of X-ray diffraction and NMR studies. Gelation mechanism of amylose gel based on this view is also discussed.

It has been shown that amyloses (I) and starches ((1→4)-α-D-glucan) exhibit the following polymorphs, as analyzed mainly by X-ray diffraction study:[1,2] V-, A-, B-, and C- forms. The V-form exists as complexes with small organic molecules, water or iodine, and have in common a left-handed, single six-residue helix.[1,3–6] The A- and B-forms are found for cereal and tuber starches, respectively.[1,2] The detailed structure of the B-form is still the subject of current debate. The B-form was initially considered as a single helical conformation,[7] since the conversion of V- to B-amylose takes place on humidification.[8] Later, the structure was refined as a right-handed double helix packed in an antiparallel fashion,[9,10] following the suggestion by Kainuma and French,[11] although two sixfold helical models were proposed from the data for similar unit cell dimension.[12] The double helical model was later questioned upon taking into account the biosynthesis mechanism[13] and optical rotation.[14] The handedness of the double helix, however, was recently revised as a left-handed one on the basis of refined X-ray diffraction and optical rotation.[15–17] In addition, it was shown that a left-handed, single-stranded helix is formed by crystalline complex between maltoheptaose and glycogen phosphorylase a.[18] An antiparallel, left-handed double-helix[19] was found in the crystal structure of the polyiodide complex, a dimer of *p*-nitrophenyl-α-maltohexaose.

In addition, a number of complementary studies on the conformations of amylose and starch have been performed by ^{13}C NMR method,[17,20–30] since X-ray fiber diffraction study provides only relatively limited information. In general, consistent results between X-ray and NMR studies have been obtained for a number of samples having V-,[20,21,24,26–28] A-, and B-forms,[17,22,23,25–27] although the NMR approach is further able to afford conformational data for less crystalline sample or gels. It seems, however, essential to analyze the process of mutual conversion among the V-, A-, and B-forms to obtain additional information on this subject. In this connection, a comparative study is indispensable to reach any definite conclusion.

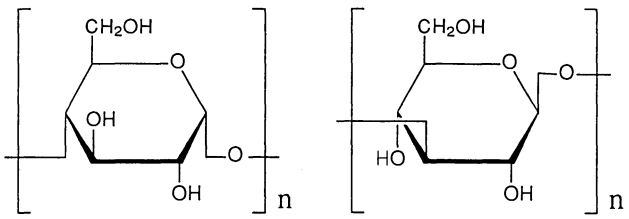

I II

(1→3)-β-D-Glucan (II) of high molecular weight is considered to be a pertinent reference compound for the present purpose, because it adopts a single helix similar to that of (1→4)-α-D-glucan[31–33] and because it posseses the ability to form multiple-stranded helices,[34,35] in relation to gel formation. We have previously demonstrated that (1→3)-β-D-glucan as well as (1→3)-β-D-

xylan can assume the three kinds of different conformations: single chain, single helix, and triple helix, depending upon sources and sample history.[36–42] We found that these forms can be mutually converted in a controlled manner by various types of physical treatments such as hydration, dehydration, annealing, etc. The resultant conformational changes are readily monitored by a characteristic displacement of conformation-dependent ^{13}C chemical shifts[43,44] as recorded by high-resolution solid-state ^{13}C NMR spectroscopy.

This sort of ^{13}C NMR study on polysaccharides with systematically manipulated conformations provides a simple and reliable means to distinguish a single chain/helix form from multiple-stranded chains. Such a distinction, however, is not always feasible by X-ray diffraction alone because distinguishing between multi-stranded coaxial helices and nested single helices is often one of the most difficult problems in interpreting fiber-diffraction data.[45,46] Instead, it is emphasized that the present ^{13}C NMR approach, utilizing physically converted samples in a controlled manner, is an excellent means for this purpose, as manifested from our studies on (1→3)-β-D-glucans,[36–41] (1→3)-β-D-xylan,[42] and agarose.[47]

We report here ^{13}C NMR studies on various preparations of V-amyloses and their hydration-induced conversion from V- to B-type forms to gain further insight into the relative stability of these preparations when being exposed to high humidity, handedness of the single or double helical B-type amylose, and distinction between the single- and double-stranded helices for the B-amylose and its consequence to a gelation mechanism of amylose gel.

Experimental

We used several types of amylose samples with different degree of polymerization from different commercial sources: DP 17 (EX-I, Seikagaku Kogyo, Tokyo), DP 100 (EX-III, Seikagaku Kogyo, Tokyo), DP 1000 (Aldrich Chemicals, USA). These samples were used without further purification. As starting materials for conversion study, we prepared either cast film (AF) or lyophilized samples by evaporating solvent from a DMSO solution. For the latter, an amylose film was prepared by casting a DMSO solution (dissolved in DMSO at 40 °C) on $(CH_3)_3SiCl_2$-coated flat dishes, followed by evaporation of DMSO at 50 °C. The preparation of the 1-butanol complex has been previously described.[20] The iodine complex from cast film (AFI) was prepared by placing AF for 3 days in a desiccator (96% R.H.) exposed to iodine vapor. The crystalline iodine complex was isolated as precipitate by addition of excess amount of iodine solution to amylose aqueous solution (ca. 1 g dm^{-3}), and dried over silica gel. The amount of iodine in the complexes was determined by a flask-combustion method. All of the hydrated samples were prepared by placing the samples in an atmosphere of 96% R.H. for 12 h. An annealed amylose sample was prepared by heating an aqueous suspension of V-amylose lyophilized from DMSO solution (DP 1000, Aldrich) at 155 °C in an autoclave for 15 min followed by slow cooling, in a similar manner to that of annealed curdlan.[37] As reference samples of the A- and B- forms, we used corn and potato starches commercially available (Nacalai Chemicals, Kyoto). Partialy deuterated V- or B-amylose samples containing DMSO-d_6 or deuterium oxide, respectively, were prepared by analogous manner, described above.

^{13}C NMR spectra of solid materials were recorded on a Bruker CXP-300 spectrometer (75.46 MHz) utilizing cross polarization-magic angle spinning (CP-MAS). All of samples were contained in a ceramic rotor with a double air bearing and spun as fast as 3 kHz. Pulse width, contact time and repetition time were 3.5 μs, 1 ms, and 4 s, respectively. Spectra were usually accumulated ca. 1000 times. ^{13}C chemical shifts were referred to TMS through ^{13}C chemical shift of carboxyl peak of glycine (176.03 ppm). High power ^2H NMR spectra were recorded on the same spectrometer at 46.08 MHz with a pulse sequence of quadrupole echo.[48]

X-Ray powder diffraction was measured on a Rigaku Denki RINT-1400 utilizing Cu $K\alpha$, 40 kV 200 mA. Samples were placed in a sealed capillary to preserve the relative humidity.

Results

In Fig. 1, we show ^{13}C NMR spectra of two typical examples of V-amyloses, iodine (A) and 1-butanol complexes (B). Five peaks are well resolved and assigned on the basis of previous work.[20] Exactly the same charac-

Table 1. ^{13}C Chemical Shifts of (1→4)-α-D-Glucans (ppm from TMS)

	DP 17 (EX-I)		DP 100 (EX-III)		DP 1000 (Aldrich)		
	Lyophilized from DMSO solution	Hydrate[a]	Lyophilized from DMSO solution	Hydrate[b]	Lyophilized from DMSO solution	Hydrate[b]	Iodine complex
C-1	101.5		102.2	101.8	102.1		101.0
		99.2	99.2	100.0		99.3	
		98.3		98.5		98.0	
(C-4)	81.2	—	81.4	80.3	82.3	—	79.6
C-2,3,4,5	71.4	73.7	74.1	74.0	71.3	72.6	73.7
		70.6	71.5	70.9	71.6	70.5	71.0
		69.2					
C-6	60.1	60.2	61.2	60.6	60.7	60.6	60.3

a) Hydrate sample of anhydrous powder. b) Hydrate samples which are lyophilized from DMSO solution.

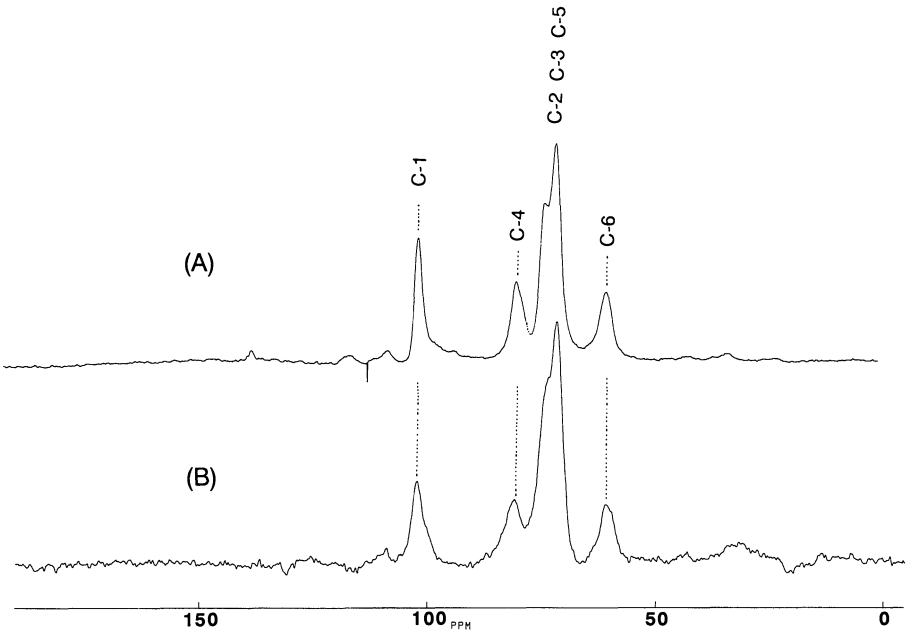

Fig. 1. ^{13}C NMR spectra of crystalline complexes of amyloses (Aldrich, DP 1000) with iodine (A) and (EX-III, DP 100) with 1-butanol (B).

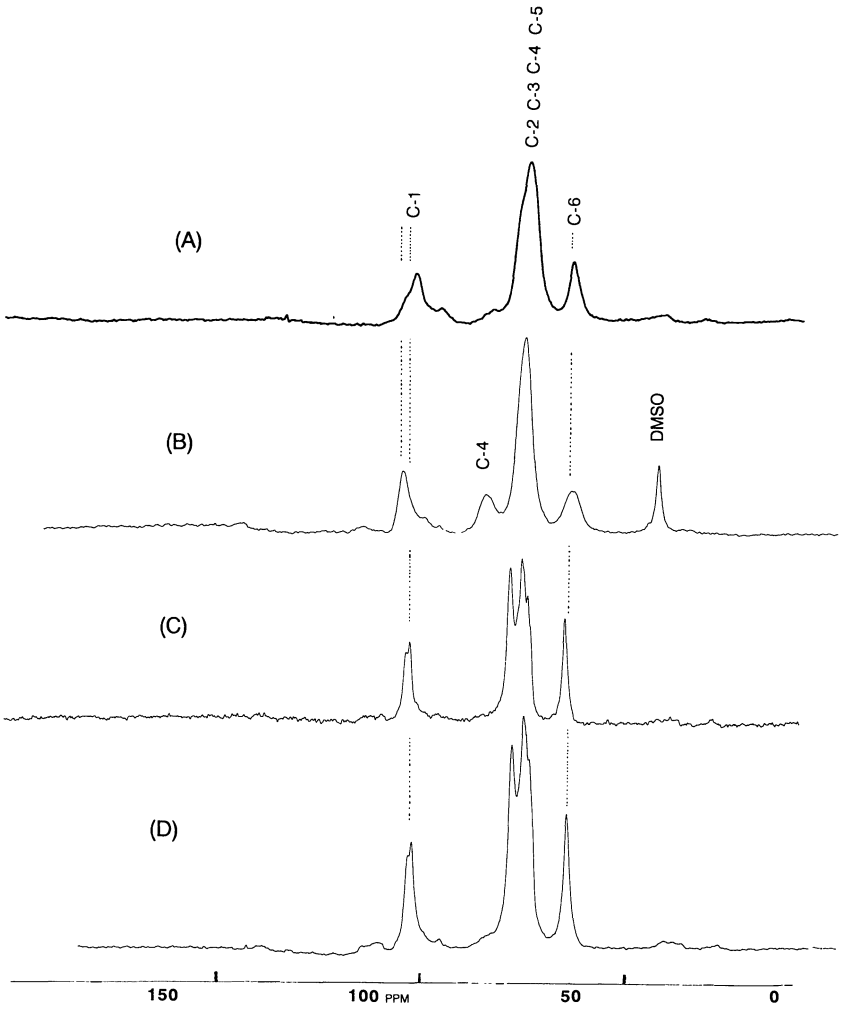

Fig. 2. ^{13}C NMR spectra of low molecular weight amylose (EX-I, DP 17) (A) anhydrous amylose powder, (B) anhydrous lyophilized powder, (C) hydrated amylose powder, and (D) hydrated iodine complex.

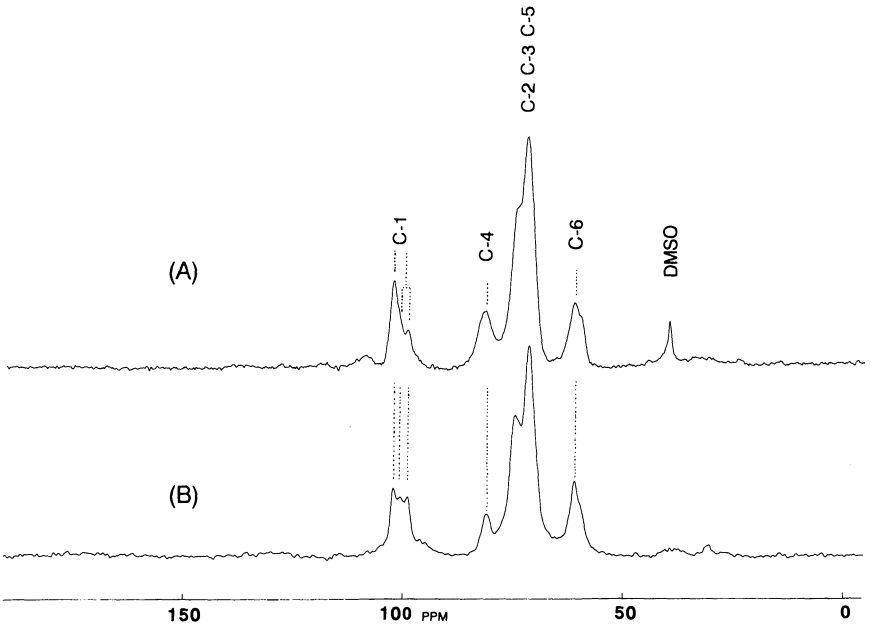

Fig. 3. ^{13}C NMR spectra of amylose with intermediate molecular weight (EX-III, DP 100) lyophilized from DMSO solution. (A) anhydrous, (B) hydrated.

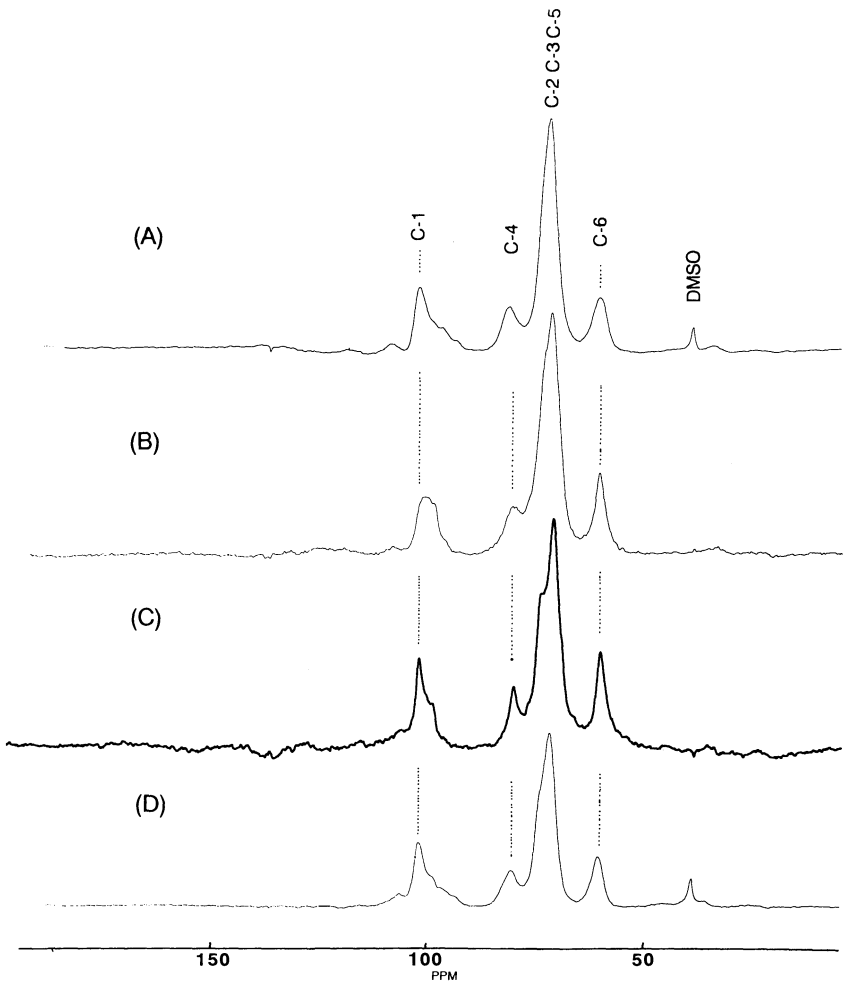

Fig. 4. ^{13}C NMR spectra of amylose with high molecular weight (Aldrich, DP 1000) lyophilized from DMSO. (A) anhydrous, (B) hydrate, (C) hydrated iodine complex and (D) anhydrous iodine complex.

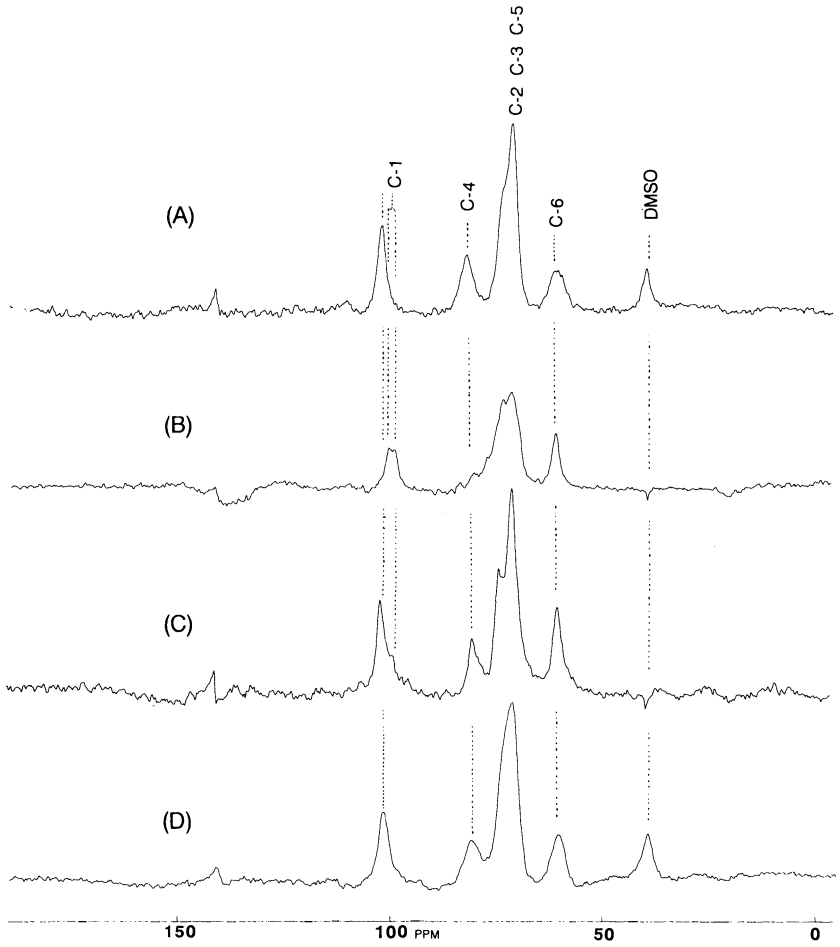

Fig. 5. ^{13}C NMR spectra of amylose film from high molecular weight sample (Aldrich, DP 1000).
(A) anhydrous, (B) hydrated, (C) hydrated iodine complex, and (D) anhydrous iodine complex.

teristic pattern was seen for both type of V-amyloses, in spite of a difference in guest molecules and molecular weight in host molecules (Aldrich, DP 1000 and EX-III, DP 100 for the former and the latter, respectively).

Figure 2 shows ^{13}C NMR spectra of amylose powder of low molecular weight (EX-I, DP 17) under various conditions. The ^{13}C chemical shifts thus obtained were summarized in Table 1. Clearly, anhydrous powder lyophilized from a DMSO solution (Fig. 2(B)) gave rise to the spectral pattern of V-form, as compared with that of the iodine complex (Fig. 1(A)), although this form might be distorted to some extent compared to that of the crystalline complex. The uppermost signal at 39 ppm is assigned to the methyl signal of DMSO molecules bound to the amylose chain. The anhydrous powder, however, has an amorphous structure distorted from the B-form, as judged from the broad envelope of the ^{13}C NMR signal in the C-1 region and the absence of the C-4 peak at 81 ppm (Fig. 2(A)). It is noteworthy that hydration of the anhydrous powder induced distinct spectral change (Fig. 2(C)). Obviously, the spectral pattern of the resulting hydrate powder (C and D) arises from that of B-amylose (doublet pattern in the C-1 region,[20-24] spectrum not shown). The spectral pattern of Fig. 2(D) is of the B-form despite being the iodine complex. The iodine content for this sample turned out to be less than 0.5%, indicating that the amount of the iodine complex (V-form) is negligible and the rest is the major B-form.

Figure 3 shows the ^{13}C NMR spectra of an amylose of an intermediate degree of polymerization (EX-III, DP 100). The C-1 peak of the lyophilized sample from DMSO solution arises from two components: the downfield singlet signal (the lowermost peak) ascribable to V-form (70%) and the upfield doublet shoulder (the middle and uppermost peak) ascribable to B-form (30%) (Fig. 3A), as estimated from comparison of the respective peak intensities. Again, the peak at 39 ppm is assigned to the methyl signal of DMSO bound to the polymer. Hydration of this sample resulted in partial conformational change from the V- to B-form, as manifested from the buildup of the upfield doublet pattern (up to 50%) in the C-1 with expense of the C-4 intensity (V-amylose) (Fig. 3B).

Table 2. Summary of Conformation Characterized by ^{13}C NMR and X-Ray Diffraction

	Anhydrous (lyophilized from DMSO solution)		Hydrate[a)]	
	NMR	X-Ray	NMR	X-Ray
DP 17 (EX-I)	V	V	B	Amorphous B[b)]
DP 100 (EX-III)	V(70%)+B(30%)	Amorphous	V(50%)+B(50%)	Amorphous
DP 1000 (Aldrich)	V	V	B	Amorphous
Iodine complex	V	V	V	V

a) Anhydrous lyophilized sample from DMSO solution was hydrated under the condition of 96% R.H. for over 12 h. b) Anhydrous powder sample was hydrated.

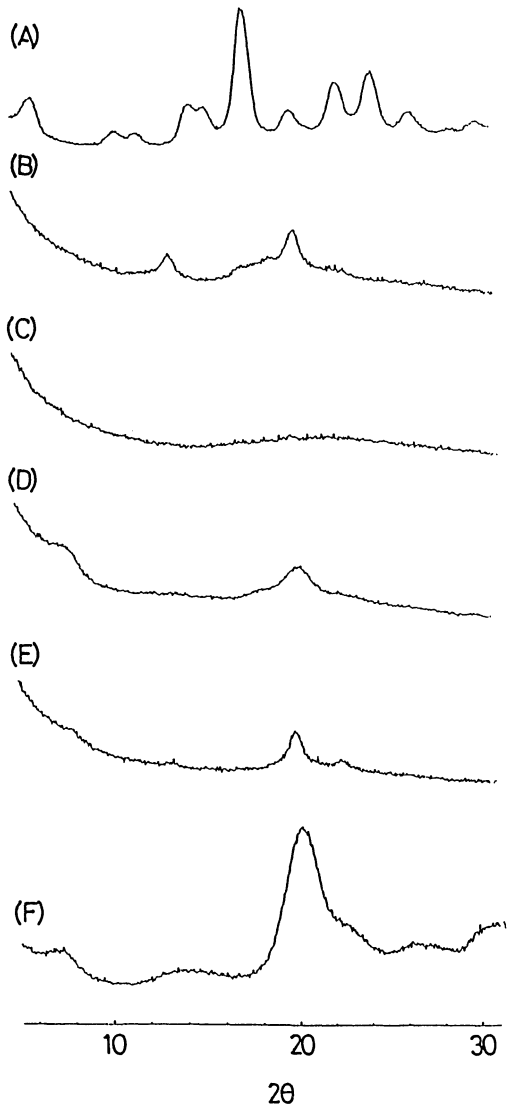

Fig. 6. Comparison of X-ray powder diffraction patterns of various types of amyloses (samples (B)—(E) correspond with the respective samples (A)—(D) of Fig. 4).
(A) hydrated amylose (DP 17) from anhydrous powder, (B) anhydrous amylose (DP 1000) lyophilized from DMSO, (C) hydrated amylose (DP 1000) lyophilized from DMSO, (D) hydrated iodine-complex (DP 1000), (E) anhydrous iodine complex (DP 1000), (F) amylose iodine complex as precipitate (DP 1000).

Similar experiments were repeated for amylose with high degree of polymerization (Aldrich, DP 1000). In contrast to the case of intermediate degree of polymerization, hydration of V-form amylose resulted in complete conversion to B-form (Figs. 4(A) and (B)). Annealing of this sample yielded a very narrow B-type spectrum comparable to that of Figure 2D, although the X-ray diffraction pattern was still a halo (spectra not shown). The iodine content in this complex is ca. 10%, as determined by the change of weight before and after the complexation. It is interesting to note that the iodine complex (Fig. 4(D)) was stable after exposure to an atmosphere of 96% R.H. (Fig. 4(C)). These experiments were also performed for samples prepared from cast film. Interestingly, the hydration-induced conformational change is incomplete but still observable as seen from the increase of the upper field doublet of the C-1 region and the decrease of the peak intensity at the C-4 for the cast film (Figs. 5(A) and (B)), in contrast to the observation for lyophilized powder (Figs. 4(A) and (B)). Again, it is found that the iodine complex prepared from a cast film is stable for the exposure to high humidity.

Typical X-ray powder diffraction patterns of the above-mentioned samples (see Fig. 4) were illustrated in Fig. 6. The resulting conformational features obtained from the X-ray and NMR studies are summarized in Table 2. The conformation revealed by X-ray diffraction is consistent with that obtained by NMR as far as V-amylose is concerned. On the other hand, the hydration-induced B-form converted from V-amylose (as judged from NMR data) turned out to be amor-

Table 3. ^{2}H Spin-Lattice Relaxation Times of DMSO-d_6 and Deuterium Oxide Bound to Amylose and Curdlan (ms)

	Temp/K	DMSO-d_6	D_2O
Amylose, V form	295	42.9	
	303	52.6	
B form	295		14.3
Curdlan, Anhydrous	295	44.2	
	303	44.8	
	314	48.5	
	323	68.3	
Hydrate	295		10.1

phous as shown by X-ray diffraction study (Table 2). The 46.08 MHz ^{2}H NMR signals of DMSO-d_6 (V-amylose) and ^2H_2O (B-amylose) were observed as single peaks with line widths of 1.9 and 2.4 kHz at ambient temperature, respectively (spectra not shown). Almost the same result was obtained for curdlan, a (1→3)-β-D-glucan as a reference compound for amylose. The ^{2}H spin-lattice relaxation times of DMSO-d_6 and D_2O are 44 and 10 ms at 22 °C, respectively, as summarized in Table 3.

Discussion

Relative Stability of V-Amyloses and Molecular Motions of Guest Molecules. The present observations clearly demonstrate that three types of amylose preparations, complexes with 1-butanol, DMSO, and iodine, exhibit similar V-type forms, consistent with the X-ray data (Fig. 6 and Table 2). In fact, previous X-ray diffraction studies showed that all V-amylose structures are almost the same with h (rise per residue) in a very narrow range from 1.32 to 1.36 Å.[1] Complexing agents such as water, small organic molecules, or iodine are found inside the helix channel on the basis of the X-ray diffraction studies.[1] Nevertheless, the relative stability of these complexes varies with the type of complexing agent: Water molecules are readily removed by lyophilization, as in the case of the amorphous form (Fig. 2(A)), and DMSO and 1-butanol (spectra not shown) molecules are readily replaced by water molecules upon exposure to high humidity as a result of a conformational change from the V- to the B-form.

For this reason, it is expected that these complexing agents are not necessarily strongly bound to the amylose chain and can undergo rapid motion in the cavity if the sizes of these molecules are smaller than that of the cavity. Such motion, if any, could be easily detected by examining how ^{2}H quadrupole splittings are averaged out by plausible molecular motions and by the extent of the ^{2}H spin-lattice relaxation times of the deuterated guest molecules.[49,50] It is expected that ^{2}H NMR signals of ^2H_2O or DMSO-d_6 complexed to amylose by forming B- or V-form are split into a doublet pattern whose separation of peaks being about 100—200 and 40 kHz (with C_3 rotation of methyl group), respectively, if they are tightly bound (static). This expectation is based on the fact that the quadrupole coupling constants, e^2qQ/h, of the former and the latter are of the order of 140—300 and 170 kHz, respectively.[49] It turned out that only a singlet signal was visible as a result of rapid isotropic averaging of the quadrupole interaction in the solid state with correlation times of the order of 10^{-6} s.[49] Also, Table 3 shows that the ^{2}H T_1 values of bound ^2H_2O and DMSO-d_6 molecules are 10 and 44 ms, respectively, at ambient temperature and are increased to 68 ms for the latter (in the case of DMSO bound to curdlan). These results indicate that the correlation times of the isotropic tumbling motions of the former and latter are in the vicinity of the T_1 minimum (10 ms),[50] namely about 10^{-8} s, and on the high temperature side of the T_1 minimum.[51]

The existence of such loosely bound guest molecules undergoing rapid isotropic motions is consistent with a view that DMSO molecules inside the cavity are readily replaced by water molecules when these samples were hydrated. Humidification of these samples results in hydration-induced conformational change. Replaced water molecules, however, are not always tightly bound to amylose chains and undergo rapid reorientation motion (correlation time being in the order of 10^{-8} s) as revealed by the present ^{2}H NMR observation, in contrast to the view from X-ray diffraction study.[16]

It is interesting to note that, in contrast, the iodine complex is stable under high humidity. This stability is indicated by the fact that these complexes are formed in the presence of water molecules. The amounts of water bound to the iodine complexes, however, are less than 50% of that of the uncomplexd amyloses.[52] The adsorbed water molecules are consumed in converting the molecular iodine in the cavity to I_3^- or I_5^- ions, which are indispensable for stabilization of the iodine complexes.[53] Consequently, approximately three iodines occupy the helix channel within one fiber repeat, but the iodines form an almost linear polyiodide chain of undetermined length.[1] This is the reason why the iodine complexes are highly stable in the presence of high humidity.

Hydration-Induced Conformational Change. It is now clear that hydration induces a conformational change of amyloses of various molecular weights from either amorphous or V- to B-type forms (Figs. 2—5), although the extent is different between powder and cast film. Here, we use the term "B-type" form instead of B-form when its X-ray diffraction pattern is a halo (Fig. 6) even if its NMR pattern exhibits the spectral feature of B-form. Nevertheless, it is emphasized that the conformation of the "B-type" form is very close to that of the B-form as far as short-range order is concerned, as will be discussed later. This observation is consistent with the previous work of Blackwell et al.[7] who previously described this hydration-induced form as B-form.

It is interesting that conversion is incomplete for amylose preparation of intermediate degree of polymerization (DP 100), as compared with that of high degree (DP 1000) or low degree of polymerization (DP 17). The conformation of amylose of intermediate molecular weight (DP 100) lyophilized from DMSO solution turned out to be a mixture of V- and B-forms. The proportion of the B-type form is increased by humidification but it is not completely converted to pure B-type form. This trend is consistent with the previous study on the effect of chain length on phase behavior and aggregation kinetics utilizing monodisperse amyloses:[54] Amyloses having chain lengths of <110 residues are found to precipitate from aqueous solution, and gela-

tion is found to predominate over precipitation for longer chains (>1100). It is probable that aggregated amylose is rather hydrophobic and can be resistant to conformational change due to hydration. Here, the following two points are noteworthy as to the conformational behavior of amylose in cast film. First, the ^{13}C NMR spectra of cast film (Fig. 5A) are generally broadened compared to those of the lyophilized powder from DMSO solution (Fig. 4A). This is readily explained on the basis that the conformation in cast film can be distorted to some extent when the liquid film was heated up to 50 °C to evaporate the DMSO. This sort of conformational distortion is accelerated when DMSO molecules inside the cavity are also removed, as manifested by the considerably reduced peak intensity of DMSO methyl signal (Fig. 5B). Second, there remains a considerable proportion of unconverted V-form (Fig. 5B) after humidification in spite of the high molecular weight sample used (DP 1000) (see also Fig. 4B). Such a distortion is not necessarily taken into account for the lyophilized sample, because DMSO molecules are removed at frozen state. It is probable that the formation of the aggregated amylose as in the case of intermediate molecular weight sample might prevent complete conformational change due to humidification.

In addition to the present observations from V- to B-change, hydration-induced conversion between amorphous and B-form has been also previously demonstrated.[17,23–27] The "amorphous" structure defined by X-ray diffraction does not necessarily indicate the presence of a completely disordered structure because there are a number of cases where secondary structure is amorphous as viewed from X-ray diffraction but is still quite ordered as viewed from the ^{13}C NMR study.[44] This situation is readily understood in that X-ray diffraction is sensitive to long range order, while NMR is sensitive to short range order. Hence, there appear several types of amorphous structures which are close to either B- or V-forms, or a mixture of both (see Table 3). For instance, the ^{13}C NMR spectrum of an anhydrous powder with a low degree of polymerization (DP 17) (Fig. 2(A)) may be ascribed to a distorted B-form. On the other hand, a number of examples have been presented for dried potato starch[23–27] whose ^{13}C NMR patterns are rather close to those of V-amylose, although dispersion of chemical shifts, especially at the C-1 region, is enormous. Accordingly, the "amorphous"→B-type or B-type→ "amorphous" conversion for samples with intermediate or high degree of polymerization can be considered as a modified V→B-type or B-type→V conversion.

The reverse B→V conversion, however, has not been realized by X-ray diffraction study. This may be one of the reasons why the single helical model of B-amylose by Blackwell et al.[7] has long been neglected. Nevertheless, it is now clear that such reverse conversion can be readily identified by solid-state NMR.[17,23–27] In addition, the B-form amyloses are completely converted to V-form by dissolving those in DMSO solution, followed by lyophilization (spectra not shown). This sort of V→B or B→V conversion is parallel with the conversion between anhydrous and hydrate state as observed for (1→3)-β-D-glucans previously reported, as summarized in Table 4.[37–41] It is emphasized that complete dissolution in aqueous solution is an essential requirement for the conversion of (1→3)-β- D-glucan from the singe helix to the triple helix.[37,39,40] This means that unfolding of the polymer chains followed by refolding in aqueous media is a necessary condition for such conversion. In this connection, it is hardly likely that simple humidification of amylose in a desiccator causes such an unfolding/refolding process leading from the single-stranded helilx (V-form) to double-stranded helix (B-form). It is therefore natural to conclude that the left-hand chirality is preserved upon humidification. The above-mentioned hydration-induced conversion is related to a change among a variety of left-handed single-stranded helices as observed for amylose, its derivative and its oligomers.[19] It is also shown that the helical parameters of an antiparallel double helix of maltohexaose are comparable to those obtained for the left-handed amylose single helix of maltoheptaose complexed with phosphorylase a.[18,19] As mentioned above, annealing of amylose at 155 °C did not induce a spectral change from the B-type form. This means that multiple-stranded helices may not be formed even after annealing followed by slow cooling. It is concluded that the B-type form thus obtained takes a left-handed single helix form, rather than the previously proposed double helix conformation, although the helical parameters should be different from those of the V-form.[18,19] Thus, it is needless to claim that the ^{13}C chemical shifts of the B-type form differ from those of V-form.

Significance of Single Helix and Gelation Mechanism. It is well recognized that biopolymer gels are usually formed by the physical association of parts of the polymer chains at regions of local order or "junction zones" to produce a continuous, three dimensional poly-

Table 4. Summary of Conformational Conversion Achieved for (1→4)-α-D- and (1→3)-β-D-Glucans

Treatment	(1→4)-α-D-Glucans	(1→3)-β-D-Glucans
Lyophilization from DMSO soln	V	Single chain
Hydration (humidification)	B	Single helix
Annealing/slow cooling	B	Triple helix

mer network.[55] So far, two different views have been presented for the gelation mechanism of amylose: Miles et al.[56] have suggested that gels are formed upon cooling molecularly entangled solutions as a result of phase separation of the polymer-rich phase, whereas Wu and Sarko[9] proposed that gelation occurs through cross-linking by double helical junction zones. As an alternative model of the former type of gelation, the presence of short segments of antiparallel double helices between single helical chains also would result in three dimensional network.[19] In principle, it is possible to distinguish which mechanism is more likely for the network structure of the amylose gel on the basis of conformational elucidation of dynamically heterogeneous network by means of variety of ^{13}C NMR technique.[24,40]

In fact, Gidley[24] showed that amylose gel contains two kinds of ^{13}C resonances: The B-type signals from motionally restricted regions as recorded by the CP-MAS technique and the signals identical to those found in aqueous solution. Obviously, the latter signals can be ascribed to the presence of mobile region in the network whose conformation is a random coil.[20] The former peaks, on the other hand, are thus ascribed to aggregated regions of the single helical chains based on our present observation, although they were ascribed to double-helical junction zone by Gidley.[17] At this point, it is worthwhile to point out that only a small amount of cross-linking agent, say 0.1—5%, is sufficient to form elastic gels, as shown by studies of chemically cross-linked gels of synthetic polymers.[57,58] To support this view, we showed that the triple-helical region as cross-links is ca. 10% at most in an elastic curdlan gel.[37,40,57] This means that the amylose gel does not necessarily consist entirely of molecular chains arising from the double-helical structure. Instead, it appears that the "solid-like" region of the amylose gel[17] might be ascribed to the presence of phase-separated aggregates of the B- type single-helical chains as cross-links. This view seems to be in favor of the gelation mechanism of Miles,[56] although alternative cross-links by the antiparallel short segments of the double-helices[19] could also exist. The latter could not be easily distinguished from the aggregated single helices, because the resulting helical parameters are comparable to those of the single-stranded helices.[19]

References

1) A. Sarko and P. Zugenmaier, *ACS Symp. Ser.*, **141**, 459 (1980).

2) D. French, "Starch: Chemistry and Technology," 2nd ed, ed by R. L. Whistler, J. N. BeMiller, and E. D. Paschall, Academic Press, New York (1984), p. 183.

3) R. E. Rundle, *J. Am. Chem. Soc.*, **69**, 1769 (1947).

4) A. D. French and H. F. Zobel, *Biopolymers*, **5**, 457 (1987).

5) W. Winter and A. Sarko, *Biopolymers*, **11**, 849 (1972).

6) B. Zaslow, V. G. Murphy, and A. D. French, *Biopolymers*, **13**, 779 (1974).

7) J. Blackwell, A. Sarko, and R. H. Marchessault, *J. Mol. Biol.*, **42**, 379 (1969).

8) F. R. Senti and L. P. Witnauer, *J. Am. Chem. Soc.*, **70**, 1438 (1948).

9) H. C. H. Wu and A. Sarko, *Carbohydr. Res.*, **61**, 7 (1978).

10) H. C. H. Wu and A. Sarko, *Carbohydr. Res.*, **61**, 27 (1978).

11) K. Kainuma and D. French, *Biopolymers*, **11**, 2241 (1972).

12) R. Cleven, C. van der Berg, and L. van der Plas, *Starch/Stärke*, **30**, 223 (1978).

13) D. A. Rees, *Pure Appl. Chem.*, **53**, 1 (1981).

14) D. L. Wild and J. M. V. Blanshard, *Carbohydr. Polym.*, **6**, 121 (1986).

15) A. Imberty, H. Chanzy, S. Perez, and A. Buleon, *J. Mol. Biol.*, **201**, 365 (1988).

16) A. Imberty and S. Perez, *Biopolymers*, **27**, 1205 (1988).

17) M. J. Gidley, *Macromolecules*, **22**, 351 (1989).

18) E. Goldsmith, S. Sprang, and R. Fletterrick, *J. Mol. Biol.*, **156**, 411 (1982).

19) W. Hinrichs, G. Buttner, M. Steifa, Ch. Betzel, V. Zabel, B. Pfannemuller, and W. Saenger, *Science*, **238**, 205 (1987).

20) H. Saitô and R. Tabeta, *Chem. Lett.*, **1981**, 713.

21) H. Saitô, G. Izumi, T. Mamizuka, S. Suzuki, and R. Tabeta, *J. Chem. Soc., Chem. Commun.*, **1982**, 1386.

22) R. H. Marchessault, M. G. Taylor, C. A. Fyfe, and R. P. Veregin, *Carbohydr. Res.*, **144**, C1 (1985).

23) R. P. Veregin, C. A. Fyfe, R. H. Marchessault, and M. G. Taylor, *Macromolecules*, **19**, 1030 (1986).

24) R. P. Veregin, C. A. Fyfe, and R. H. Marchessault, *Macromolecules*, **20**, 3007 (1987).

25) F. Horii, A. Hirai, and R. Kitamaru, *Macromolecules*, **19**, 930 (1986).

26) F. Horii, H. Yamamoto, A. Hirai, and R. Kitamaru, *Carbohydr. Res.*, **160**, 29 (1987).

27) M. J. Gidley and S. M. Bociek *J. Am. Chem. Soc.*, **107**, 7040 (1985).

28) M. J. Gidley and S. M. Bociek, *Carbohydr. Res.*, **183**, 126 (1988).

29) S. F. Tanner, S. G. Ring, M. A. Whittam, and P. S. Belton, *Int. J. Biol. Macromol.*, **19**, 219 (1987).

30) J. M. Hewitt, M. Linder, S. Perez, and A. Buleon, *Carbohydr. Res.*, **154**, 1 (1986).

31) R. H. Marchessault and Y. Deslandes, *ACS Symp. Ser.*, **126**, 221 (1980).

32) H. Takeda, N. Yasuoka, N. Kasai, and T. Harada, *Polym. J. (Tokyo)*, **10**, 355 (1978).

33) K. Okuyama, M. Otsubo, Y. Fukuzawa, M. Ozawa, T. Harada, and N. Kasai, *Carbohydr. Res.*, in press.

34) T. L. Bluhm and A. Sarko, *Can. J. Chem.*, **55**, 293 (1977).

35) T. L. Bluhm and A. Sarko, *Carbohydr. Res.*, **54**, 125 (1977).

36) H. Saitô, R. Tabeta, T. Sasaki, and Y. Yoshioka, *Bull. Chem. Soc. Jpn.*, **59**, 1957 (1986).

37) H. Saitô, R. Tabeta, M. Yokoi, and T. Erata, *Bull. Chem. Soc. Jpn.*, **60**, 4259 (1987).

38) H. Saitô and M. Yokoi, *Bull. Chem. Soc. Jpn.*, **62**, 1957 (1989).

39) H. Saitô, M. Yokoi, and Y. Yoshioka, *Macromolecules*, **22**, 3892 (1989).

40) H. Saitô, Y. Yoshioka, M. Yokoi, and J. Yamada, *Biopolymers,* **19**, 1689 (1990).
41) H. Saitô, Y. Yoshioka, N. Uehara, J. Aketagawa, S. Tanaka, and Y. Shibata, *Carbohydr. Res.,* **217**, 181 (1991).
42) H. Saitô, J. Yamada, Y. Yoshioka, Y. Shibata, and T. Erata, *Biopolymers,* **31**, 933 (1991).
43) H. Saitô, *Magn. Reson. Chem.,* **24**, 835 (1986).
44) H. Saitô and I. Ando, *Annu. Rep. NMR Spectrosc.,* **21**, 209 (1989).
45) S. Arnott and A. K. Mitra, "Molecular Biophysics of the Extracelluar Matrix," ed by S. Arnott, D. A. Rees, and E. R. Morris, Humane Press, New York(1981), Chap. 3.
46) S. A. Foord and E. D. T. Atkins, *Biopolymers,* **28**, 1345 (1989).
47) H. Saitô, M. Yokoi, and J. Yamada, *Carbohydr. Res.,* **199**, 1 (1990).
48) J. H. Davis, K. R. Jeffrey, M. Bloom, M. I. Valic, and T. P. Higgs, *Chem. Phys. Lett.,* **42**, 390 (1976).
49) H. H. Mantsch, H. Saitô, and I. C. P. Smith, *Prog. Nucl. Magn. Reson. Spectrosc.,* **11**, 211 (1978).
50) J. H. Davis, *Biochim. Biophys. Acta,* **737**, 117 (1983).
51) It is unlikely that conformational change of host molecules occurs within the temperature range studied (295—323 K), because backbone of polysaccharides is generally rigid as judged from the data of ^{13}C spin-lattice relaxation times of the laboratory frame for (1→3)-β-D-glucans and β-xylan (Refs. 38, 39, and 42).
52) H. Yajima, T. Otsuka, and R. Endo, *Rep. Prog. Polym. Phys. Jpn.,* **31**, 679 (1988).
53) R. C. Teitelbaum, S. L. Ruby, and T. J. Marks, *J. Am. Chem. Soc.,* **102**, 3322 (1980); H. Yajima, T. Nishimura, T. Ishii, and T. Handa, *Carbohydr. Res.,* **163**, 155 (1987).
54) M. J. Gidley and P. V. Bulpin, *Macromolecules,* **22**, 341 (1989).
55) P. J. Flory, *Faraday Discuss. Chem. Soc.,* **57**, 7 (1974).
56) M. J. Miles, V. J. Morris, and S. G. Ring, *Carbohydr. Res.,* **135**, 257 (1985).
57) H. Saitô, *ACS Symp. Ser.,* **150**, 125 (1981).
58) K. Yokota, A. Abe, S. Hosaka, I. Sakai, and H. Saitô, *Macromolecules,* **11**, 95 (1978).

Synthesis and Properties of Peroxy Esters Having a Benzophenone Chromophore

Hiromi KUMURA, Tomoyuki NAKAMURA, Yoshiki HIGUCHI, and Shuji SUYAMA*
Chemicals & Explosives Research Laboratory, Nippon Oil & Fats Co., Ltd.,
Taketoyo-cho, Chita-gun, Aichi 470-23
(Received March 5, 1991)

Diperoxy esters having a benzophenone chromophore have been successfully synthesized from the reaction of 3-chloro-3-phenylphthalide (**1**) with 2,5-dihydroperoxy-2,5-dimethyl-3-hexyne (**4a**) or 2,5-dihydroperoxy-2,5-dimethylhexane (**4b**). The corresponding diperoxy esters had a UV absorption above 300 nm. The free radicals produced during the photolysis of these compounds initiated the radical polymerization of methyl methacrylate at room temperature under UV light.

The isomerism of the various derivatives of 3-chloro-3-phenylphthalide (**1**), the pseudo-chloride of *o*-benzoylbenzoic acid, has been reported. Neckers[1] obtained a mixture of the pseudo-type peroxy ester (**2**) and the normal type peroxy ester (**3**) from the reaction of **1** with *t*-butyl hydroperoxide, and isolated **2** and **3** by means of column chromatography.

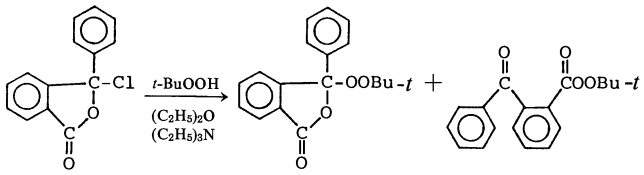

1 **2** **3** (1)

Rüchardt[2,3] and Chang[4] reported the synthesis of the pseudo-type diperoxy esters from the reaction of **1** with dihydroperoxides in the presence of amines in organic solvent. They obtained a viscous liquid as the reaction mixture of **1** with **4a** or **4b** and isolated the corresponding pseudo-type peroxy esters, 2,5-bis[(1-phenyl-3-oxo-1,3-dihydro-1-isobenzofuranyl)dioxy]-2,5-dimethyl-3-hexyne (**5a**) or 2,5-bis[(1-phenyl-3-oxo-1,3-dihydro-1-isobenzofuranyl)dioxy]-2,5-dimethylhexane (**5b**) by chromatography in poor yields.

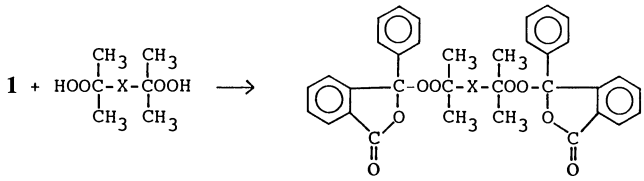

4a (X=–C≡C–)
4b (X=–CH_2CH_2–)

5a (X=–C≡C–)
5b (X=–CH_2CH_2–) (2)

However, no reports concerning the synthesis of the normal type diperoxy esters have been published. If the normal type peroxy esters can be obtained, they will be useful as photoinitiators because they have a UV absorption above 300 nm.[1,5] In the present paper, we report the successful synthesis and the properties of diperoxy esters having a benzophenone chromophore from the reaction of **1** with dihydroperoxides in 40% NaOH aqueous solution.

Results and Discussion

Synthesis in Aq NaOH Solution. When a benzene–dioxane solution of **1** and **4a** was treated with aq 40% NaOH solution at 0—5 °C for 4 h, a white slurry was formed. This was filtrated and washed with water and diethyl ether. After evaporation of the solvent under vacuum, a white powder was obtained. Its structure was ascertained by means of ^{1}H NMR, ^{13}C NMR and other spectral measurements. The ^{1}H NMR spectrum showed this product had twelve methyl and eighteen phenyl protons. The ^{13}C NMR spectrum showed a characteristic absorption at 163.6 (C=O of peroxy ester)[6] and 196.0 (C=O of benzophenone)[7] and the IR spectrum showed absorptions at 1760 (C=O of peroxy ester) and 1680 cm^{-1} (C=O of benzophenone). These data showed that this product was the normal type peroxy ester, 2,5-bis(*o*-benzoylbenzoyldioxy)-2,5-dimethyl-3-hexyne (**6a**) (Eq.3). Compound **6a** contained 5.24% active oxygen measured by iodometric titration and it was shown to be 96.7% pure. The yield of **6a** based on **1** was 62%.

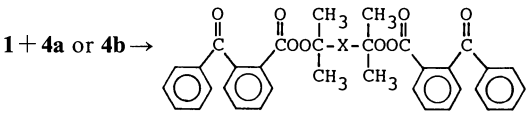

6a (X=–C≡C–)
6b (X=–CH_2CH_2–) (3)

The similar treatment of **1** with **4b** gave a white powder of 2,5-bis(*o*-benzoylbenzoyldioxy)-2,5-dimethylhexane (**6b**) in a 68.4% yield (Eq.3). The structure was also ascertained by means of spectroscopic measurements. The ^{1}H NMR spectrum indicated this prod-

uct had twelve methyl, four methylene and eighteen phenyl protons. The IR and ^{13}C NMR spectra showed the presence of a benzoyl group and a peroxy ester carbonyl group. This product contained 4.34% active oxygen and it was shown to be 80.7% pure. This was the first example of the synthesis of peroxy esters having a benzophenone chromophore in good yields.

Synthesis in Pyridine/Dioxane. In order to confirm the difference between the work of Rüchardt[2,3] and Chang[4] and the present study, we reinvestigated the reaction of **1** with **4a** under the same conditions used by Chang.[4] Thus, **1** was allowed to react with a solution of **4a** and pyridine in dioxane. The reaction mixture was diluted with water and then extracted with diethyl ether. The ether solution was treated as described in the experimental section and white crystals were obtained. The structure of this product was ascertained by means of IR, NMR, and other spectral measurements. The IR spectrum of this compound indicated absorptions at 1780 (C=O of phthalide) and 1100 cm^{-1} (cyclic C–O–C) and the ^{13}C NMR spectrum indicated characteristic absorption at 168.2 (C=O of phthalide). The mass spectrum of this compound showed the molecular weight to be 590. The lack of the absorption of a benzoyl group in the IR and ^{13}C NMR spectra apparently showed that this compound differed from the diperoxy ester **6a**. These data indicated that this compound was the pseudo-type peroxy ester **5a**. It contained 5.30% active oxygen determined by iodometric titration and it was shown to be 97.8% pure. The yield of **5a** was only 3%.

It was found that the peroxy ester **6a** was also formed under these reaction conditions. This was confirmed by HPLC analysis with an authentic sample of **6a**. However, the isolation of **6a** from this reaction mixture was unsuccessful, because only a trace amount of **6a** was formed.

Reaction Mechanism. It is known that **1** is susceptible to attack by nucleophiles at two centers. Displacement at the tetrahedral center leads to the pseudo-type derivatives, whereas an addition-elimination sequence at the phthalide carbonyl group results in opening of the phthalide ring.[8] The formation mechanism of the normal type peroxy ester in aq NaOH solution may be explained as follows. In nucleophilic displacement of esters, it has been shown that the addition-elimination reaction involves a tetrahedral intermediate.[9] The feasibility of the forward reaction depends on whether

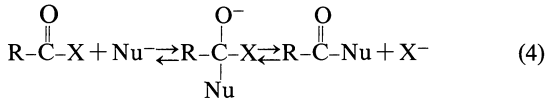

(4)

Nu^- is a stronger nucleophile than X^-. A similar situation may exist in the case of the pseudo acid chloride derivatives. Nucleophiles stronger than the PhC(O$^-$)Cl group in **7** may be able to bring about displacement at the phthalide carbonyl group (Eq. 5).

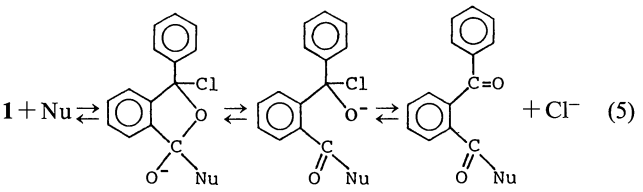

(5)

7

In aq NaOH solution, a certain amount of alkyl hydroperoxide dissociates into alkylperoxide anion (ROO^-). This ROO^- is known to be a very strong nucleophile because of its α-effect[10] and seems to be a stronger one than the PhC(O$^-$)Cl group. On the other hand, the above-mentioned reaction will not occur in pyridine-dioxane solution because of the low concentration of ROO^-. It has been reported[9] that the weaker nucleophiles like organic amines bring about displacement at the tetrahedral center to form the pseudo-type derivatives. Then, in pyridine–dioxane solution, it is expected that the reaction shown in the following scheme would occur by an S_N1 mechanism.

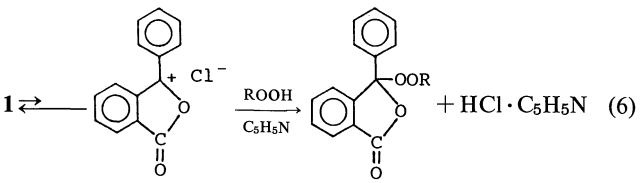

(6)

UV Absorption Spectra. The UV absorption spectra of **5a**, **6a** and benzophenone are shown in Fig. 1. Compound **6a** behaved like benzophenone with respect to the absorption, that is, a maxima in the range 300—380 nm and a typical n–π^* extinction coefficient of 2.29×10^2 $dm^3\,mol^{-1}\,cm^{-1}$. On the other hand, **5a** showed a dif-

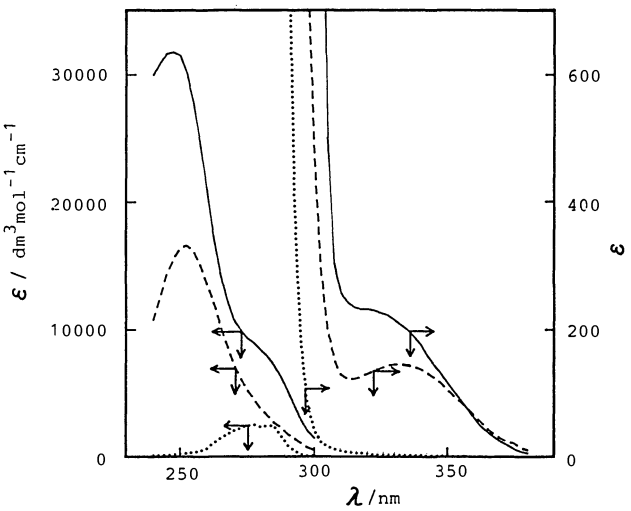

Fig. 1. UV absorption spectra of the peroxy esters and benzophenone in CH_3OH. ·····; **5a**, ——; **6a**, – – –; benzophenone.

Table 1. Photodecomposition Products of **6a**[a)]

Products	Yield[b)]/%
10	100
o-Benzoylbenzoic acid	61
Benzophenone	20
1,2-Diphenylethane	18

a) Photodecomposition was carried out in toluene at 25 °C. Initial concentration of **6a**: 0.026 mol dm^{-3}. b) Yields of products: [(moles of products)/(moles of **6a** consumed)]×100. The conversion of **6a** was 21.5%.

ferently shaped spectra than that of **6a**. Compound **5a** had a less intense absorption in the range 300—380 nm, which reflected the substituent in the phthalide.

Photodecomposition. Photodecomposition studies of **6a** were carried out in aromatic solvents at 25 °C by irradiating with 366 nm light. The decomposition products in toluene, analyzed by HPLC, were 2-(*o*-benzoylbenzoyldioxy)-5-hydroxy-2,5-dimethyl-3-hexyne (**10**), *o*-benzoylbenzoic acid and benzophenone (Table 1). The total recovery of the benzophenone moiety was 90%. The quantitative formation of **10** indicated that the photolysis of **6a** proceeded stepwise. A likely scheme leading to the products is shown by the following equations.

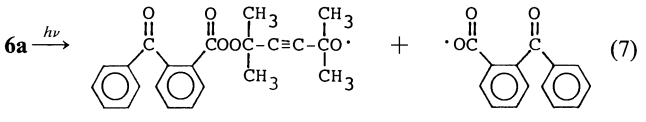

8 **9** (7)

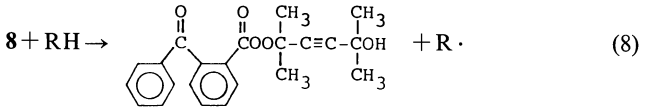

10 (8)

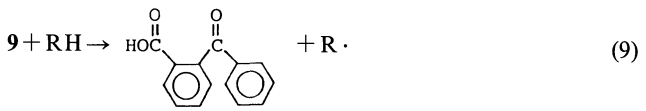

(9)

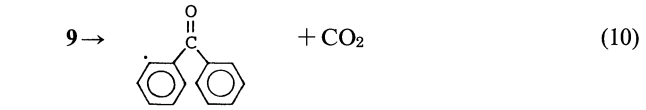

(10)

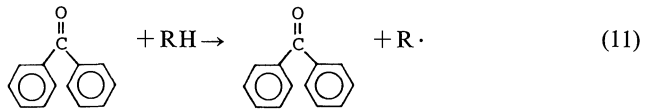

(11)

$$2\,R\cdot \rightarrow R\text{-}R \qquad (12)$$

The quantum yield of photolysis of **6a** in benzene was observed to be 0.97. Values of Φ for other peroxides in benzene have been reported by Neckers and Leffler and are 0.94 and 0.97 for *t*-butyl peroxy *p*-benzoylbenzoate (**11**)[1)] and *p*-benzoylbenzoyl peroxide (**12**),[5)] respectively. The value for **6a** was comparable to these data and it was significantly higher than that of the benzophenone-sensitized decomposition of benzoyl peroxide (Φ=0.25 in benzene).[11)] This result clearly indicated the efficacy of the intramolecular energy transfer in **6a** in contrast to the bimolecular process.

Compound **6a** gave linear Stern-Volmer plots when naphthalene was used as a triplet quencher (Fig. 2), which meant the photodecomposition of **6a** proceeded via the excited triplet state.

The resulting value of $k_q\tau$ for **6a** was 4.7 dm^3 mol^{-1}. If the rate constant k_q was assumed to be equal to the diffusion-controlled rate constant (k_q=9×10^9 dm^3 mol^{-1} s^{-1}), the lifetime of the excited triplet, τ, of **6a** was estimated to be 0.5×10^{-9} s. The present τ value for **6a**

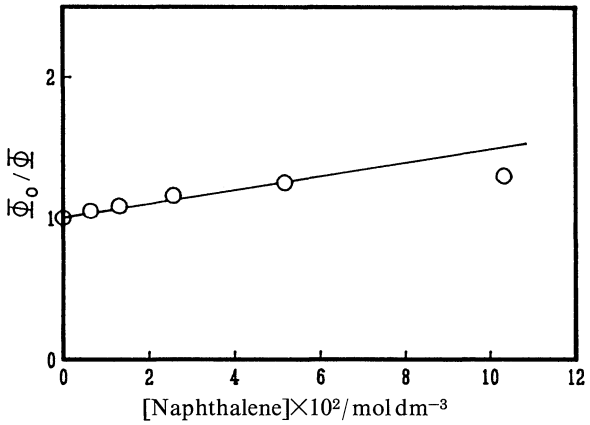

Fig. 2. Stern-Volmer plots for quenching of **6a** by naphthalene in benzene.

Table 2. Rate Constants and Activation Parameters for Thermal Decomposition of Various Peroxy Esters[a)]

Peroxy ester	Temp	Rate const.	Activation parameters	
	°C	$10^5\,k_d$/s^{-1}	$\Delta H^{\ddagger}$/kJ mol^{-1}	$\Delta S^{\ddagger}$/J K^{-1} mol^{-1}
2	110	0.83±0.03	164.1±4.6	84.1±11.7
	120	3.15±0.14		
	130	11.24±0.82		
5a	120	1.09±0.18	173.0±1.4	98.0±3.4
	130	4.26±0.16		
	140	14.9 ±1.1		
6a	110	1.49±0.11	149.4±0.1	51.0±0.14
	120	5.06±0.27		
	130	16.13±0.21		
6b	120	19.6 ±0.72		
13a	110	1.69±0.14	167.0±3.2	97.8±8.2
	120	6.90±0.35		
	130	24.8 ±1.0		
13b	120	24.15±0.30		

a) Initial concentration of peroxy esters was 0.05 mol dm^{-3}.

Table 3. Photopolymerization of MMA (at 25 °C 30 min)[a)]

Peroxy ester	Concn	Conv.	Molecular weight		M_w/M_n
	mol dm^{-3}	%	$M_n/10^4$	$M_w/10^4$	
Blank	—	0.05	194	358	1.84
2	0.010	3.9	9.35	20.1	2.15
5a	0.005	4.8	8.96	16.5	1.84
6a	0.010	14.4	1.99	5.94	2.98
	0.005	10.7	2.61	7.00	2.68
	0.0025	9.1	3.20	8.10	2.53
13a+Benzophenone	0.005	1.4	19.9	51.1	2.56

a) Light intensity $I_0=7.61\times10^{-4}$ Einstein min^{-1}.

was very close to those for **11** and **12**, that is, τ values of 4×10^{-9} s[1)] and 0.87×10^{-9} s,[12)] respectively. The lifetime of the benzophenone triplet in benzene has been reported to be 8.4×10^{-6} s,[13)] and τ of **6a** was 2×10^4 times shorter than that of benzophenone. Thus, the rates of energy transfer from the excited triplet state of benzophenone having a peroxide group to the O–O bond were about the same in these three peroxides and it was shown that the energy transfer rate was almost independent of the structure of the peroxides.

Thermal Decompositon. The thermal decomposition of the peroxy esters was also investigated to test the effect of the structure of the peroxy esters in the ground state. The thermolysis was carried out in cumene under nitrogen. The rates for the thermolysis were measured by iodometric titration and good first-order plots were obtained in all cases. The results are given in Table 2 together with the calculated activation parameters. The activation parameters for these peroxides indicate a nonconcerted homolytic cleavage of one peroxy bond.

The decomposition of the normal type peroxy ester **6a** occured 4—5 times faster than that of the pseudo-type peroxy ester **5a**. The rate constants and activation parameters of **6a** were comparable to those of *t*-butyl peroxybenzoate (i.e. $\Delta H^{\neq}=156.8$ kJ mol^{-1} and $\Delta S^{\neq}=66.0$ J K^{-1} mol^{-1}).[14)] The activation parameters of **5a** were similar to those of **2**.

In order to clarify the effect of a benzoyl group on the thermal decomposition rate of **6a** and **6b**, the thermolysis of 2,5-bis(benzoyldioxy)-2,5-dimethyl-3-hexyne (**13a**) and 2,5-bis(benzoyldioxy)-2,5-dimethylhexane (**13b**) were carried out. The rate constants of the thermal decomposition of **6a** and **6b** having an *o*-benzoyl group were a little smaller than those of the corresponding **13a** and **13b**, respectively. This could be predicted from the electron-attractive effect of the *o*-carbonyl group.[15)]

Photopolymerization. Some polymerization studies were carried out using the newly developed peroxy ester and methyl methacrylate (MMA) as a monomer. The results are given in Table 3.

Table 3 shows that MMA did not polymerize photochemically in the absence of any initiator under these conditions. Normal type peroxy ester **6a** initiated the photopolymerization of MMA effectively and the pseudo-type peroxy esters **2** and **5a** also initiated it. The rate of photopolymerization with **6a** was two times higher than **5a**. The photopolymerization with equimolar amounts of **13a** and benzophenone was also carried out and the result showed the polymerization rate with the benzophenone-sensitized **13a** was lower than that of **6a**.

In conclusion, the initiation of photopolymerization with **6a** occurred via the intramolecular energy-transfer mechanism from the n–π^* excited state of a benzoyl group to an O–O bond.

These results showed that the peroxy esters having a benzophenone functionality provided an efficient photochemical source of free radicals.

Experimental

^{1}H and ^{13}C NMR spectra were recorded on a JEOL GSX 270 FT-NMR spectrometer using $CDCl_3$ as a solvent and TMS as an internal standard. HPLC analyses were performed with a Shimadzu LC-5A liquid chromatograph by using a 6.0 mm×15 cm Shimpack CLC-ODS column. GPC analyses were performed with a Shimadzu LC-6A liquid chromatograph with a Shimadzu RID-6A refractive index detector, by using two 30 cm Shodex KF-80M columns, a 30 cm Shimadzu HSG-10S, and a 30 cm Shimadzu HSG-15SH column. Infrared spectra were obtained on a JASCO A-3 infrared spectrophotometer; peaks were reported in units of cm^{-1}. UV spectra were measured on a Shimadzu UV-2200 UV-vis spectrophotometer. Melting points were measured with a Yanaco micro melting point apparatus. Mass spectra were obtained on a JEOL JMS-D300 mass spectrometer at 200 eV under chemical ionization conditions and on a JEOL JMS-DX300 mass spectrometer at 70 eV under electron impact conditions.

Materials. Cumene was purified by distillation after washing with concentrated sulfuric acid. Methyl methacrylate was purified by distillation after washing with 5% NaOH aqueous solution. 3-(*t*-Butyldioxy)-3-phenylphthalide (**2**), 2,5-bis(benzoyldioxy)-2,5-dimethyl-3-hexyne (**13a**), and 2,5-bis(benzoyldioxy)-2,5-dimethylhexane (**13b**) were the products of Nippon Oil & Fats Co., Ltd. 3-Chloro-3-phenylphthalide (**1**) was prepared by the reaction of *o*-benzoylbenzoic acid (22.6 g, 1.0 mol) with thionyl chloride (18 g, 1.5 mol in benzene (50 ml)) for 24 h under reflux. After evaporation of the thionyl chloride, the remaining oil proved to be almost pure 3-chloro-3-phenylphthalide (Cl 14.4%, purity 99.4%, no C=O absorption around 1650 cm^{-1}, strong C=O absorption at 1790 cm^{-1}).

Preparation of 2,5-Bis[(1-phenyl-3-oxo-1,3-dihydro-1-isobenzofuranyl)dioxy]-2,5-dimethyl-3-hexyne (5a). Compound **1** (12.2 g, 0.05 mol) was added with stirring to a solution of **4a** (4.4 g, 0.025 mol) and pyridine (4.2 g, 0.052 mol) in 13 ml of dioxane at 20—25 °C. The reaction mixture was stirred at 25—35 °C for 4 h and then allowed to stand at room temperature for about 12 h. It was diluted with 25 ml of water and then extracted five times with 25 ml of diethyl ether. The ether solution was washed five times with 10 ml portions of 5% $NaHCO_3$ aqueous solution and five times with 10 ml portions of water, and dried over anhydrous $MgSO_4$. After filtration, the diethyl ether solution was allowed to stand at −23 °C overnight. A white crystalline substance was separated. Filtration and removal of solvent in a vacuum gave a white powder. Active oxygen 5.30% (calculated 5.42%); Mp 160 °C; IR($CHCl_3$) 2975, 1780, 1610, 1475, 1460, 1290, 1160, 1100, 1060, 1000, 940, 890, and 830 cm^{-1}; ^1H NMR ($CDCl_3$) δ=1.37—1.52 (CH_3, 12H, q) and 7.32—7.80 (aromatic, 18H, m); ^{13}C NMR ($CDCl_3$) δ=26.9, 27.2 (each CH_3), 77.9 (acetylenic C), 85.1 (tert C), 110.1 (tert C), 123.9, 125.1, 126.2, 126.5, 126.9, 128.7, 129.8, 130.1 , 130.4, 134.2, 135.3, 146.7 (each Ph) and 168.2 (carbonyl C of phthalide); UV(MeOH) λ_{max} nm (ε) 277(2490) and 284 (2410); MS(CI), Found : m/z 608; Calcd for $C_{36}H_{34}O_8N$:($M+NH_4$), 608.

Preparation of 2,5-Bis(*o*-benzoylbenzoyldioxy)-2,5-dimethyl-3-hexyne (6a). Finely divided **1** (31 g, 0.127 mol) was added with stirring to a mixture of **4a** (10. 3 g, 0.058 mol) and 40% NaOH aqueous solution (12.3 g, 0.124 mol) in benzene-dioxane (20 ml, 40 ml) at 5—10 °C. The reaction mixture was stirred at 0—5 °C for 4 h. A white slurry was obtained and it was filtered and then washed three times with 60 ml of water and twice with 20 ml of diethyl ether. Vacuum drying of the solvent gave a white powder (23 g) in a 62% yield, based on the amount of **1** used; it contained 5.24% active oxygen as determined by iodometric titration. This compound gave one peak on HPLC analysis. Mp 129—130 °C; IR ($CHCl_3$) 2950, 1760, 1680, 1600, 1460, 1320, 1280, 1160, 1120, 1040, 940, 880, and 820 cm^{-1}; ^1H NMR ($CDCl_3$) δ=1.42 (CH_3, 12H, s) and 7.38—7.93 (aromatic, 18H, m); ^{13}C NMR ($CDCl_3$) δ=26.4 (CH_3), 78.9 (acetylenic C), 84.7 (tert C), 126.7, 128.3, 128.5, 129.7, 129.8, 129.9, 132.7, 133.3, 136.7, 141 .6 (each Ph C), 163.6 (carbonyl C of peroxy ester), and 196.0 (carbonyl C of benzophenone); UV(MeOH) λ_{max} nm (ε) 203 (60800), 247 (31800), 280 (8400), and 320 (sh 230).

Preparation of 2,5-Bis(*o*-benzoylbenzoyldioxy)-2,5-dimethylhexane (6b). Compound **1** (12.2 g, 0.05 mol) was added with stirring to a mixture of **4b** (5.8 g, 0.025 mol) and 40% NaOH aqueous solution (5.0 g, 0.05 mol) in benzene-dioxane (5 ml, 18 ml) at 5—10 °C. The reaction mixture was stirred at 0—5 °C for 4 h and worked up as for **1a**. A white powder (15.8 g) was obtained (yield 68.4%). Active oxygen 4.34% (calculated 5.38%); Mp 154—157 °C; IR ($CHCl_3$) 2950, 1760, 1680, 1600, 1460, 1320, 1280, 1130, 1110, 940, and 880 cm^{-1} ^1H NMR ($CDCl_3$) δ=1.13 (CH_3, 12H, s), 1.57 (CH_2, 4H, s), and 7.36—7.92 (aromatic, 18H, m); ^{13}C NMR ($CDCl_3$) δ=24.2 (CH_3), 32.6 (CH_2), 85.8 (tert C), 127.1, 128.2, 128.6, 129.8, 129.9, 130.0, 132.4, 133.4, 136.6, 141.3 (each Ph C), 164.3 (carbonyl C of peroxy ester), and 196.0 (carbonyl C of benzophenone).

Photodecomposition Products. A 10 ml toluene solution of 0.026 mol dm^{-3} of **6a** was placed in Pyrex tubes (15 mm diameter), degassed by three cycles of freeze-thawing, and sealed under vacuum. The tubes were placed in a merry-go-round around a filtered UV source of 366 nm and the temperature of the tubes was controlled at 25 °C by a water-cooled bath. The light source was a TAIKA 400 W high-pressure mercury lamp combined with a Toshiba UV-D36A filter. The tubes were taken out at different predetermined intervals, and kept frozen in a freezer in the dark until analyses were done. The photolyzed solutions were analyzed by HPLC and compared with the authentic samples. The identification of 2-(*o*-benzoylbenzoyldioxy)-5-hydroxy-2,5-dimethyl-3-hexyne (**10**) was carried out by isolation from the mixture of decomposion products by means of HPLC. The fraction was collected and the removal of solvent in vacuum gave a viscous liquid. The structure was ascertained by means of IR, ^1H NMR and ^{13}C NMR spectroscopy. IR ($CHCl_3$) 2950, 1760, 1670, 1600, 1455, 1320, 1280, 1150, 1130, 1040, 940, 900, and 840 cm^{-1}; ^1H NMR ($CDCl_3$) δ=1.46 (CH_3, 12H, s) and 7.45—7.98 (aromatic, 9H, m); ^{13}C NMR ($CDCl_3$) δ=26.4, 31.0 (CH_3), 79.2, 81.7 (acetylenic C), 64.6, 89.7 (tert C) , 126.9, 128.1 , 128.3, 128.6, 129.9, 130.1, 132.5, 133.7, 136.5, 141.4 (each Ph C), 163.8 (carbonyl C of peroxy ester), and 196.6 (carbonyl C of benzophenone); MS(EI) m/z 366(M^+).

Quantum Yield. A 10 ml benzene solution of **6a** was irradiated at 25 °C. The irradiation conditions were the same as those in the decomposition products study. After irradiation, the remaining amount of peroxide was determined by iodometric titration. A tube containing an actinometric solution (benzophenone (0.1 mol dm^{-3}) and benzhydrol (0.1 mol dm^{-3}) in benzene) was irradiated in parallel with every run and light intensity was determined actinometrically.

Thermal Decomposition. A 10 ml cumene solution of 0. 05 mol dm^{-3} peroxide was placed in a glass ampule. The ampule was purged with nitrogen, sealed, and immersed in a constant-temperature bath regulated ±0.1 °C. At successive time intervals, tubes were removed from the bath and immersed in a Dry Ice–acetone bath. The concentration of peroxide in the solution was then measured by iodometric titration. The reaction was followed up to 75—80% decomposition and exhibited first order kinetics.

Iodometric Titration. 10 ml of a 0.2 mol dm^{-3} KOH–methanol solution was added to the solution of peroxide, then the mixture stood for 5 min in the dark, followed by iodometric titration. The titration procedure involved the use of a mixture (20 : 4 ml) of isopropyl alcohol and acetic acid as the solvent, and saturated potassium iodide aqueous solution as the source of iodine. After boiling for 3 min to liberate the iodide, the iodine was titrated to the end point with 0.01 mol dm^{-3} sodium thiosulfate solution. The values for the observed first-order rate constants and their standard deviations were calculated from the first-order rate equation using the least-squares method. The values for the activation parameters and their standard deviation were calculated from the absolute rate equation of Eying using the least-squares method.

Polymerization Studies. The irradiation of monomer solutions was carried out in degassed sealed Pyrex tubes of 15 mm diameter that were placed in a merry-go-round with a filtered UV source of 366 nm at the center. The light source was the same as that used in the photodecomposition studies. The temperature of the tubes was maintained at 25 °C by a water-cooled bath. The yield of the polymer was measured (below 20% conversion) gravimetrically. The average molecular weight of the purified polymers was determined by GPC.

References

1) L. Thijs, S. N. Gupta, and D. C. Neckers, *J. Org. Chem.*, **44**, 4123 (1979). D. C. Neckers, U. S. Patent 4416826 (1983).
2) G. Hamprecht and C. Rüchardt, *Tetrahedron Lett.*, **1968**, 3195.
3) C. Rüchardt and G. Hamprecht, Deut. Patent 1518128 (1965).
4) Y. G. Chang and P. S. Bailey, U. S. Patent 3654315 (1972). Y. G. Chang, U. S. Patent 3755369 (1973).
5) J. E. Leffler and J. W. Miley, *J. Am. Chem. Soc.*, **93**, 7005 (1971).
6) G. Gornar, R. Radeglia, E. Scharn, and M. Schulz, *J. Prakt. Chem.*, **325**, 333 (1983).
7) S. Tanaka, S. Toda, I. Nagoya, C. Nagata, K. Kaohta, S. Hashimoto, K. Musha, and K. Yamaguchi, *Bunseki Kagaku*, **24**, 553 (1975).
8) M. S. Newman and C. Courduvelis, *J. Am. Chem. Soc.*, **88**, 781 (1966).
9) M. V. Bhatt, K. M. Kamath, and M. Ravindranathan, *J. Chem. Soc. C*, **1971**, 1772.
10) J. O. Edwards and R. G. Pearson, *J. Am. Chem. Soc.*, **84**, 16 (1962).
11) C. Walling and M. J. Gibian, *J. Am. Chem. Soc.*, **87**, 3413 (1965).
12) E. A. Morlino, M. D. Bohorquez, D. C. Neckers, and M. A. J. Rodgers, *J. Am. Chem. Soc.*, **113**, 3599 (1991).
13) J. Saltiel, H. C. Curtis, L. Metts, J. W. Miley, J. Winterle, and M. Wrighton, *J. Am. Chem. Soc.*, **92**, 410 (1970).
14) A. T. Blomquist and I. A. Berstein, *J. Am. Chem. Soc.*, **73**, 5546 (1951).
15) D. A. Cable, J. A. Ernst, and T. T. Tidwell, *J. Org. Chem.*, **37**, 3420 (1972).

Ring Transformation of 1-Substituted 3,5-Dinitro-4-pyridones to 4-Nitro-5(2*H*)-isoxazolone by Hydroxylamine[1)]

Masahiro ARIGA,* Yasuo TOHDA, Hiroko NAKASHIMA, Keita TANI, Yutaka MORI,† and Eizo MATSUMURA
Department of Chemistry, Osaka Kyoiku University, Minamikawabori-cho, Tennoji-ku, Osaka 543
(Received May 27, 1991)

New ring transformations of 3,5-dinitro-1-(4-nitrophenyl)-4-pyridone and its homologues with hydroxylamine were found to give 4-nitro-5(2*H*)-isoxazolone. These results were rationalized by double ring transformations in sequence. The fact that the 4-position of the 4-pyridone behaved as an electrophlic site was the first example in this series of ring transfomations, and was caused by the alpha-effect of the reagent. Some reactions of the isoxazolone were carried out.

In this series of nucleophilic reactions of elctron-deficient pyridones, we have reported ring transformations of 1-substituted 3,5-dinitro-4-pyridones with either enolate anions or primary amines. Several types of ring transformations were observed depending on the combination of the enolate anion and the 1-substituent of the pyridone used.[2)] Reaction with a primary amine resulted in the exchange of the ring nitrogen moiety of the pyridone with that of the primary amine.[3)] This reaction developed the utility of the 4-pyridone as a protecting group for primary amines. Thus, a variety of amino acids were protected and deprotected by 3,5-dinitro-1-(4-nitrophenyl)-4-pyridone (**1a**) without racemization throughout the sequence.[4)] This replacement of the ring nitrogen moiety was caused by a small difference in the basicity between the primary amine used for the reagent and the liberated one.

These results prompted us to investigate the behavior of hetero bidentate nucleophilic reagents such as hydroxylamine or hydrazine toward the pyridone. The carbonyl carbon of the pyridone did not act as an electrophilic center in our previous studies of this series, but such ambident reagents were anticipated to attack the carbonyl carbon of the pyridone, because of their strong nucleophilicity caused by the alpha-effect.

In this paper we wish to report a new type of ring transformation of 1-substituted 3,5-dinitro-4-pyridones with hydroxylamine.

Results and Discussion

Reaction of 3,5-dinitro-1-(4-nitrophenyl)-4-pyridone (**1a**) with a twofold excess of hydroxylamine hydrochloride in pyridine occurred smoothly at room temperature. The dark red color of the reaction mixture faded to yellow within an hour, and product (**2**) was obtained as colorless needles together with 4-nitroaniline. Treatment of **2** with concd hydrochloric acid gave a free acid, 4-aci-nitro-5(4*H*)-isoxazolone (**3**), liberating a pyridine molecule. The pyridinium salt of **3** was identical to **2** as confirmed by mixing **3** with pyridine to give **2** quantitatively. The ^{1}H NMR spectrum of **3** showed two singlets at 8.40 and 11.0 ppm; the latter disappeared on addition of D_2O. The broad absorption with its center at about 2300 cm^{-1} (hydrogen bonded O–H) and the strong absorption at 1770 cm^{-1} (C=O) in the IR spectrum

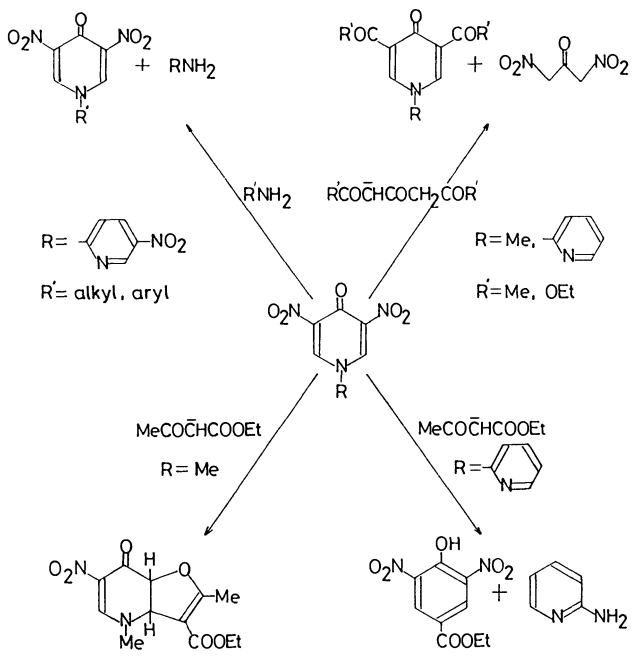

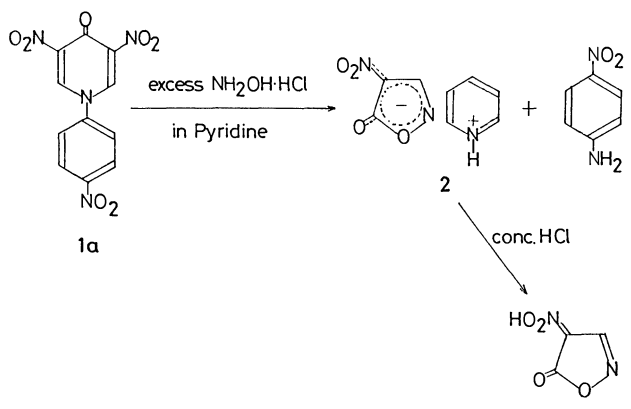

† Present address: Mukogawa Women's University, Ikebiraki-cho, Nishinomiya 663.

suggested that **3** was the aci-nitro form. These spectral characteristics of **3** were very similar to those of 3-methyl-4-aci-nitro-5(4*H*)-isoxazolone as reported by R. Nesi et al.[5]

The structure of **3** was also confirmed by independent synthesis of **3** from the reaction of methyl 2-nitro-3-ethoxypropenoate and hydroxylamine hydrochloride in the presence of pyridine.

The results apparently showed that the N and O atoms of hydroxylamine attacked at the 2- and 4-positions of the 4-pyridone ring, respectively. Concurrent formation of 4-nitroaniline, however, showed that cleavage of the N(1)–C(2) bond and the N(1)–C(6) bond of the pyridone had occurred. That is, double ring transformations in sequence were suggested to occur, and 2-nitroacetaldehyde oxime must have been produced in addition to **2** and 4-nitroaniline.

The following two reactions were examined from the above viewpoint.

The reaction of **1a** with 1.1 equimolar amounts of the reagent in pyridine yielded the complex of 1-hydroxy-3,5-dinitro-4-pyridone and pyridine in a molar ratio of 2:1 (**4**) as red columns in addition to 4-nitroaniline (Table 1, Entry 2). Product **4** easily gave 1-hydroxy-3,5-dinitro-4-pyridone (**5**) by treating with dil hydrochloric acid, and was regenerated reversibly by treating **5** with pyridine. This fact showed that hydroxylamine acted as a primary amine, and attacked at the 2- and 6-positions of the 4-pyridone to result in exchange of the *N*-substituent moiety of the 4-pyridone as reported in the previous paper.[3]

Treatment of **4** with a slight excess of hydroxylamine hydrochloride in pyridine at room temperature gave **2** in a good yield (Table 1, Entry 3). 2-Nitroacetaldehyde oxime which should supposedly have been derived from the rest of **4** in the ring transformation was not isolated directly under these conditions, but its formation was evidently confirmed by the fact that 2-nitro-2-(phenylhydrazono)acetaldehyde oxime (**6**) was isolated when the filtrate from which **2** had been filtered off was treated with aqueous benzenediazonium chloride. The oxime **6** was independently obtained from authentic 2-nitroacetaldehyde oxime[6] with benzenediazonium chloride.

A provable reaction course matching the above observations may be proposed as follows. Formation of the σ-addut was followed by ring opening to give an intermediate **7**, and the cyclization of **7** with elimination of 4-nitroaniline gave **5**. Pyridone **5** was then easily subject to attack by excess hydroxylamine to give ring-opened intermediate **8**. In the symmetrical intermediate **8**, an intramolecular attack of either oxygen atom of the two hydroxylamino functions at the carbonyl carbon atom lead to 4-aci-nitro-5(4*H*)isoxazolone **3** with liberation of 2-nitroacetaldehyde oxime. Even though either of the more nucleophilic nitrogen atoms of these hydroxylamino groups attacked at the β-position of the nitroolefin part of **8**, the intramolecular reaction resulted in

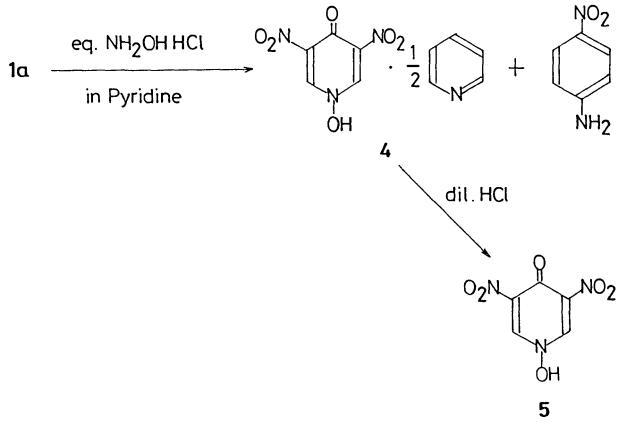

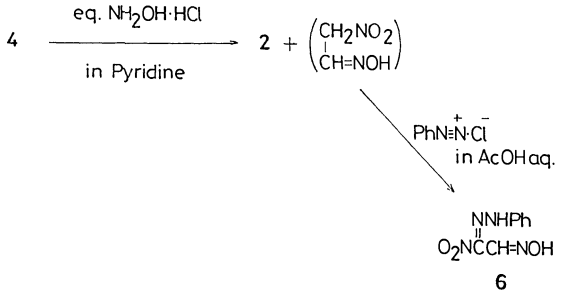

Table 1. Ring Transformations of 1-Substituted 3,5-Dinitro-4-pyridones with Hydroxylamine

Entry	4-Pyridone 1-Substituent	Reaction conditions			Products (Yield/%)		
		$NH_2OH \cdot HCl$ mol ratio	Temp °C	Time h	**2**	**4**	**1**(recovery)
1	**1a** $-C_6H_4-NO_2-4$	3.0	20	2	88	—	—
2	**1a** $-C_6H_4-NO_2-4$	1.1	20	2	—	83	—
3	**4** –OH	1.1	20	2	80	—	—
4	**1b** –2-Pyridyl	3.0	20	2	83	—	—
5	**1c** $-C_6H_5$	3.0	20	2	21	—	78
6	**1c** $-C_6H_5$	3.0	50	2	71	—	16
7	**1c** $-C_6H_5$	3.0	20	5	62	—	27
8	**1d** $-CH_3$	3.0	20	5	Trace	—	93
9	**1d** $-CH_3$	3.0	50	5	26	—	65
10	**1d** $-CH_3$	1.1	50	5	16	—	73

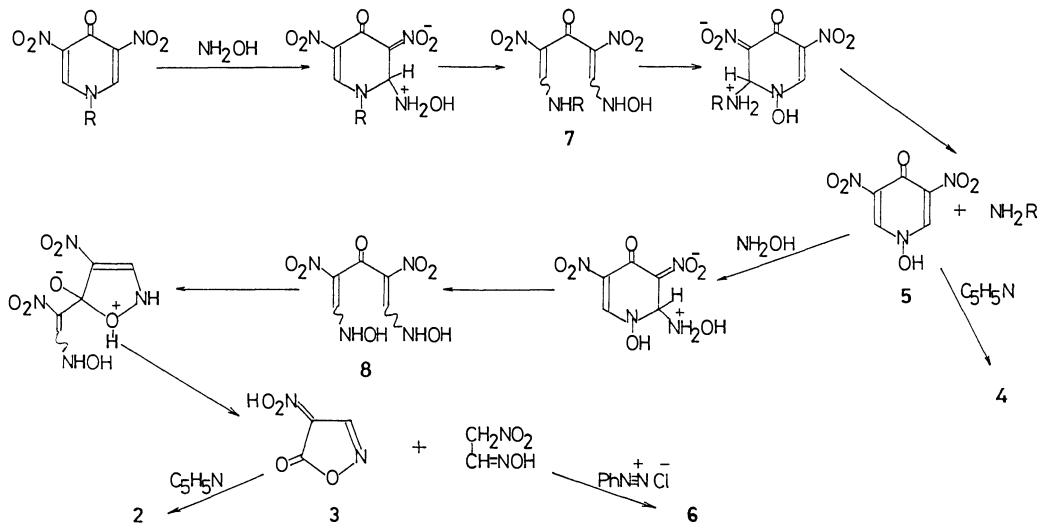

regeneration of **5**.

In order to prove the generality and limitation of the reaction, some 1-substituted 3,5-dinitro-4-pyridones (**1b**, **1c**, and **1d**) were investigated.

The order of reactivity of these pyridones in the ring transformation appeares to be **1a**≈**1b**>**1c**>**1d** from the results of the reactions shown in Table 1. The 1-methyl homologue **1d**, which was the least reactive among the four, however, gave a satisfactory result under modified reaction conditions. These results are reasonably acceptable upon reflection of the electronic effects of the 1-substituent. The electron-releasing effect of the methyl group might have suppressed the reactivity of the pyridone ring. In the case of the reactions of **1a** and **1b**, the color of the reaction mixture turned immediately to dark red when the reactants were mixed, then faded away within an hour. On the other hand, **1c**, and **1d** showed moderate or no evident change in color of the reaction mixture during the reactions. These facts show that the more basic the liberated amine moiety is the smaller the rate of the formation of **5** is. The fact that **2** rather than **4** is obtained as a product with recovery of substrate from the reaction of **1d** with equimolar hydroxylamine (Table 1, Entry 10) contrasts to the result of the reaction of **1a** (Entry 2). The reaction rate of the first step ring transformation of **1a** and **1b** appears to be larger than that of the second step ring transformation, but the rate of **1d** appears to be just the opposite.

Although, 3-methyl[5] and 3-phenyl[7] analogs of **3** have been reported, to our knowledge 3-unsubstituted 4-nitro-5(2*H*)-isoxazolones, **3** and **2**, are unknown compounds. Some reactions of the isoxazolones were carried out to examine their particular chemical properties.

The *N*-methylation of **3** was accomplished by direct treatment of **2** with dimethyl sulfate to give 2-methl-4-nitro-5(2*H*)-isoxazolone (**9**) in a good yield. Acetylation could be performed by heating **2** in excess acetyl chloride at 50 °C to give 2-acetyl-4-nitro-5(2*H*)-isoxazolone (**10**). Reaction of **9** with hydroxylamine hydrochloride in pyridine reproduced **2** quantitatively.

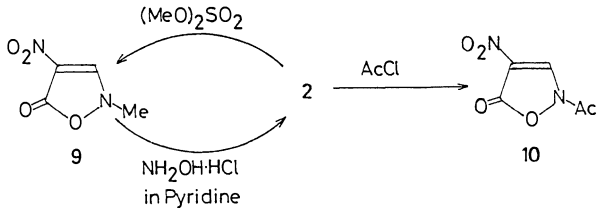

We were able to draw out a new reactivity of the 4-pyridone by the ring transformation with hydroxylamine giving 4-nitro-5(2*H*)-isoxazolone with elimination of the 2-nitroacetaldehyde derivative. The product and its derivatives, especially the *N*-methyl derivative **9**, have a variety of functionalities, such as *β*-nitro enamine, heterodiene and *α*-nitro lactone, in its ring, and are anticipated to demonstrate various types of reactivity including ring transformation. New ring transformations of **9** on the basis of this idea are currently under study.

Experimental

All melting points were measured on a Yanako melting point apparatus and were uncorrected. IR spectra were obtained on a Hitachi 260-10 spectrometer as Nujol mull, and ^{1}H NMR spectra were recorded on a Hitachi R-20B spectrometer with TMS as an internal standard.

Reaction of 3,5-Dinitro-1-(4-nitrophenyl)-4-pyridone (1a) with Excess Hydroxylamine Hydrochloride. Hydroxylamine hydrochloride (0.690 g, 10.0 mmol) was added with stirring by a magnetic stirrer to a solution of **1a** (1.00 g, 3.27 mmol) in pyridine (50 ml). The reaction mixture was allowed to stand at room temperature for 2 h. The pyridine was evaporated under reduced pressure at 35—40 °C, water (50 ml) was added to the residual solid, and the yellow precipitates were collected on a filter to give 4-nitroaniline (0.420 g, 3.04 mmol, 93% yield). The filtrate was concentrated to dryness under reduced pressure. The residual mass was dissolved in ethanol

(20 ml), and the resulting solution was cooled in an ice bath. The crystalline precipitates were collected by filtration to give **2** (0.602 g, 2.88 mmol, 88% yield) as colorless needles (recrystallized from ethanol), mp 136.0—137.0 °C (decomp). IR 2500—1950 (broad) (N–H), 1680 (C=O), 1520, and 1325 cm^{-1} (NO_2). ^1H NMR (DMSO-d_6) δ=8.2 (m, 2H), 8.41 (s, 1H), 9.0 (m, 2H), and 10.4 (broad s, 1H). Found: C, 45.93; H, 3.39; N, 20.20%. Calcd for $C_8H_7N_3O_4$: C, 45.94; H, 3.37; N, 20.09%.

Reaction of 1a with 1.1 Equimolar Amounts of Hydroxylamine Hydrochloride. One gram (3.27 mmol) of **1a** was treated with hydroxylamine hydrochloride (0.250 g, 3.60 mmol) as described above, in this case, the dark red color of the reaction mixture remained during the reaction time. After the solvent was evaporated off, the residual solid was extracted with chloroform. From the extraction, 4-nitroaniline (0.425 g, 3.08 mmol, 94% yield) was obtained. The residual solid was rinsed with a small amount of ethanol to give **4** (0.650 g, 2.70 mmol, 83% yield) as red columns (recrystallized from water), mp 202.0—203.0 °C (decomp). ^1H NMR (DMSO-d_6) δ=7.5 (m, 1H), 7.9 (m, 0.5H), 8.6 (m, 1H), 9.16 (s, 2H), and 9.5 (broad s, 1H). Found: C, 37.16; H, 2.30; N, 20.37%. Calcd for $C_{15}H_{11}N_7O_{12}$: C, 37.43; H, 2.30; N, 20.37%.

Reaction of 4 with Hydroxylamine Hydrochloride. A mixture of **4** (0.500 g, 2.08 mmol) and hydroxylamine hydrochloride (0.175 g, 2.88 mmol) in pyridine (50 ml) was allowed to stand at room temperature for 2 h. The pyridine was evaporated to dryness, ethanol (10 ml) was added to the residue, and the crystalline precipitates were collected on a filter to give **2** (0.350 g, 1.67 mmol, 80% yield). The filtrate was concentrated and the residue was dissolved in water (10 ml), then the resulting aqueous solution was cooled in an ice bath. To the solution was added an aqueous solution of benzenediazonium chloride prepared from aniline (0.250 g, 2.69 mmol) and sodium nitrite (0.220 g, 3.19 mmol) in 1 M (1 M=1 mol dm^{-3}) hydrochloric acid (10 ml) at 0 °C. The precipitates were recrystallized from water to give **5** (0.210 g, 1.01 mmol, 49% yield) as orange needles, mp 186.0—187.0 °C (decomp). ^1H NMR (DMSO-d_6) δ=7.4 (m, 5H), 8.56 (s, 1H), 12.3 (broad s, 1H), and 12.53 (s, 1H). Found: C, 46.72; H, 4.03; N, 27.04%. Calcd for $C_8H_8N_4O_3$: C, 46.15; H, 3.87; N, 25.97%.

Alternate Synthesis of 2. A mixture of methyl 3-ethoxy-2-nitropropenoate[8] (3.50 g, 20.0 mmol), hydroxylamine hydrochloride (1.81 g, 26.0 mmol), and pyridine (5.40 g, 50.6 mmol) in ethanol (75 ml) was heated at 50—60 °C for 2 h. The reaction mixture was cooled in an ice bath, and the crystalline precipitates were collected by filtration giving **2** (3.60 g, 17.2 mmol, 86% yield).

Preparation of 6 from Authentic 2-Nitroacetaldehyde Oxime. A solution of benzenediazonium chloride prepared just as described above was added to a solution of 2-nitroacetaldehyde oxime (0.200 g, 1.92 mmol) in 1 M hydrochloric acid (10 ml) at 0 °C. Yellow precipitates were recrystallized from water to give **6** (0.220 g, 1.06 mmol, 55% yield).

4-Aci-nitro-5(4*H*)-isoxazolone (3). A mixture of **2** (1.00 g, 4.78 mmol) in concd hydrochloric acid (10 ml) was heated at 50—60 °C until **2** dissolved, and then cooled in an ice bath. The precipitates were collected by filtration, rinsed with a small amount of cold water and then with diethyl ether, and were dried in a desiccator over sodium hydroxide to give **3** (0.510 g, 3.92 mmol, 82% yield) as colorless needles, mp 145.0—146.0 °C. IR 2600 (broad) (O–H) and 1700 cm^{-1} (C=O). ^1H NMR (DMSO-d_6) δ=8.40 (s, 1H) and 11.0 (s, 1H). Found: C, 27.86; H, 1.65; N, 21.33%. Calcd for $C_3H_2N_2O_4$: C, 27.70; H, 1.55; N, 21.54%.

Reaction of 1b, 1c, and 1d with Hydroxylamine Hydrochloride. One gram of 4-pyridone was treated with 3 equimolar amounts of hydroxylamine hydrochloride under the conditions shown in Table 1 according to the reaction of **1a**. The solvent was evaporated off, and the residual solid was treated with a small amount of benzene. After removal of the benzene by decantation, the residual mass was extracted with hot chloroform (30 ml×3). The combined extractions were evaporated and the residual solid was rinsed with a small portion of ethanol to give **3**.

2-Methyl-4-nitro-5(2*H*)-isoxazolone (9). A mixture of **2** (1.00 g, 4.78 mmol) and dimethyl sulfate (0.900, 7.14 mmol) was gently heated at 50—60 °C for 100 m. Water (10 ml) was added to the cold reaction mixture, and the precipitates were collected by filtration then rinsed with a small amount of cold ethanol to give **6** (0.585 g, 4.06 mmol, 85% yield) as colorless needles (recrystallized from etrhanol), mp 136.0—137.0 °C (decomp). IR 1775 (C=O), 1615 (C=N), 1510, and 1375 cm^{-1} (NO_2). ^1H NMR (DMSO-d_6) δ=3.79 (s, 3H), and 9.63 (s, 1H). Found: C, 33.44; H, 2.87; N, 19.45%. Calcd for $C_4H_4N_2O_4$: C, 33.44; H, 2.80; N, 19.44%.

2-Acetyl-4-nitro-5(2*H*)-isoxazolone (10). A mixture of **2** (0.500 g, 2.39 mmol) and acetyl chloride (3.0 g, 38.2 mmol) was heated at 50 °C for 30 min. After the acetyl chloride was evaporated, crushed ice (2 9) was added to the residue, and the crystalline precipitates were collected on filter and rinsed with a small amount of cold water to give **10**, (0.281 g, 1.50 mmol, 63% yield), mp 132.0—134.0 °C (decomp). IR 1810 (C=O), 1760 (C=O), 1570, and 1350 cm^{-1} (NO_2). ^1H NMR (DMSO-d_6) δ=1.91 (s, 3H) and 8.43 (s, 1H). Found: C, 35.09; H, 2.41; N, 16.50%. Calcd for $C_5H_4N_2O_5$: C, 34.89; H, 2.34; N, 16.28%.

Reaction of 9 with Hydroxylamine Hydrochloride. A mixture of **9** (0.500 g, 3.47 mmol) and hydroxylamine hydrochloride (0.290 g, 4.17 mmol) in pyridine (20 ml) was heated at 50 °C for 1 h. After the solvent was evaporated in vacuo, ethanol (10 ml) was added to the residue, and the crystalline precipitates were collected by filtration to give **3** (0.690 g, 3.30 mmol, 95% yield).

References

1) The Nucleophilic Reaction upon Electron-Deficient Pyridone Derivatives. XI. for the preceding paper, see Y. Tohda, M. Eiraku, T. Nakagawa, Y. Usami, M. Ariga, T. Kawashima, K. Tani, H. Watanabe, and Y. Mori, *Bull. Chem. Soc. Jpn.*, **63**, 2820 (1990).

2) E. Matsumura, M. Ariga, and Y. Tohda, *Bull. Chem. Soc. Jpn.*, **53**, 2891 (1980).

3) E. Matsumura, M. Ariga, Y. Tohda, and T. Kawashima, *Tetrahedron Lett.*, **22**, 757 (1981).

4) E. Matsumura, H. Kobayashi, T. Nishikawa, M. Ariga, Y. Tohda, and T. Kawashima, *Bull. Chem. Soc. Jpn.*, **57**, 1961 (1984).

5) R. Nesi, S. Chimichi, F. De Sio, R. Pepino, and P. Tedeschi, *Tetrahedron Lett.*, **23**, 4397 (1982).

6) W. Steinkopf, *J. Prakt. Chem.*, **81**, 224 (1910).

7) R. Nesi, S. Chimichi, D. Giomi, P. S. Fantoni, and P. Tedeschi, *J. Chem. Soc., Perkin Trans. 1*, **1987**, 1005.

8) M. J. Kamlet, *J. Org. Chem.*, **24**, 714 (1959).

 © 1991 The Chemical Society of Japan Bull. Chem. Soc. Jpn., 64, 3548—3556 (1991)

Studies on Synthetic Ionophores. IX.[1] X-Ray Crystal Structure Analysis of Potassium, Rubidium, and Cesium Salts of a Synthetic Carboxylic Ionophore

Noriko KASUGA, Seiichi NAKAHAMA, Kazuo YAMAGUCHI,*,†
Yuji OHASHI,†† and Kayako HORI†††
Department of Polymer Chemistry, Faculty of Engineering, Tokyo Institute of Technology, 2-12-1, Ohokayama, Meguro-ku, Tokyo 152
†Department of Materials Science, Faculty of Science, Kanagawa University, Tsuchiya, Hiratsuka, Kanagawa 259-12
††Department of Chemistry, Faculty of Science, Tokyo Institute of Technology, 2-12-1, Ohokayama, Meguro-ku, Tokyo 152
†††Department of Chemistry, Faculty of Science, Ochanomizu University, Otsuka, Bunkyo-ku, Tokyo 112
(Received May 30, 1991)

X-Ray crystal structure data are presented for potassium, rubidium, and cesium salts (**2**, **3**, and **4**) of 2-[[2-[2-[2-[2-[2-[2-[2-(2-hydroxyethoxy)phenoxy]ethoxy]phenoxy]ethoxy]phenoxy]ethoxy]phenoxy]methyl]benzoic acid (**1**). The crystals of the potassium salt (**2**) monohydrate dichloroform solvate ($2 \cdot H_2O \cdot 2CHCl_3$) are triclinic, space group $P\bar{1}$ with two molecules in the unit cell dimensions a=14.517(1), b=16.380(1), c=13.315(1) Å, α=72.313(8)°, β=117.313(8)°, γ=120.853(5)°. R=0.102 for 6351 observed reflections. The crystals of $3 \cdot H_2O \cdot CHCl_3$ are monoclinic, space group $P2_1/a$ with four molecules in the unit cell dimensions a=24.085(6), b=13.068(2), c=13.983(4) Å, β=105.402(32)°. R=0.068 for 5112 observed reflections. The crystals of $4 \cdot H_2O \cdot CHCl_3$ are monoclinic, space group $P2_1/n$ with four molecules in the unit cell dimensions a=24.412(7), b=13.075(2), c=14.077(4) Å, β=106.743(31)°. R=0.071 for 6153 observed reflections. The backbones of **2**, **3**, and **4** form pseudocycles by head-to-tail hydrogen bonding between the terminal carboxylato and hydroxyl groups (O···O distance, 2.672, 2.699, and 2.706 Å, respectively). The conformations about C–C and C–O bonds are gauche and trans respectively, except for two of the C–O bonds which are gauche to make the pseudocyclic backbone bend like the seam of a tennis ball resulting in the formation of cavities fitted for the size of each cation.

Naturally occurring carboxylic ionophores such as monensin and nigericin, which contain a terminal carboxyl group, one or two hydroxyl groups at the other end, and several ether oxygens provided by tetrahydrofuran and tetrahydropyran rings, mediate transport of ions across biological and artificial membranes.[2] They have been studied as antibiotics[3] and have provided an experimental tool for investigating the roles of transmembrane gradients of ions in regulating biological phenomena.[4] Complexation of an ionized ionophore with cations is capable of transporting the cations across membranes and each of the ionophores has a different specificity for various cations.

To understand the complexation properties of the ion carrier, single crystal X-ray structures of various complexes have been analyzed.[5] The conformation of silver salt of monensin in crystal form was first reported in which the monensin anion is held by the head-to-tail hydrogen bondings between the carboxylato group and the two hydroxyl functions of the terminal tetrahydropyran ring to wrap the cation in the cavity.[6] The sodium salts in anhydrous and hydrate crystal forms are nearly identical with one another, and with that of the silver salt complex. However, the structures of the complexes are somewhat different from that of the free acid in terms of the carboxylic acid conformation, the head-to-tail hydrogen bonding, and the conformation of one of the tetrahydrofuran rings.[7,8] Analogous conformations are also found in carboxylic ionophores with the backbones of 21—24 atoms and their complexes.[5,9] The pseudocyclic framework of the ionophores through head-to-tail hydrogen bonding may be called a 'ring' conformation.

However, in the molecular structures of X206 with 28-atoms backbone and its complexes as well as the methyl-substituted analogue (alborixin), the backbone is similar to that of the seam of a tennis ball rather than a ring conformation.[10] Since the backbone of X206 is much longer and more flexible by lack of sterically rigid spiro ring than those of short-chain carboxylic ionophores such as monensin, the pseudocyclic molecule with head-to-tail hydrogen bonding adopts such a 'seam' conformation to form a hydrophobic surface. A ring conformation of monensin and its complexes by head-to-tail hydrogen bonding is rather flat, but enough to form the lipophilic surface of the ionophore molecules. It appears that lipophilicity of the exterior of the complexes with a 'ring or seam' conformation enables these ionophores to transport ions through hydrophobic membranes.

A similar conformation was observed in K^+ complex of a crown ether, dibenzo-30-crown-10.[11] Typical crown ethers with smaller ring sizes have a cavity fitted for coordinated cations in a 'ring' conformation. In this case, however, the cavity size of a 'ring' conformation is too large to be wrapped round potassium ion, but a 'seam' conformation by hinge of the crown ether backbone at two sites form a cavity adjusted for size of

potassium cation resulting in a spherically lipophilic surface of the potassium complex.

We have synthesized a series of linear polyether compounds containing a carboxyl and a hydroxyl groups at one and the other ends as analogues to naturally occurring carboxylic ionophores. Transport of alkali and alkaline earth metal ions mediated by these synthetic ionophores through organic liquid membranes were investigated in terms of effect of the ionophore structures on the ion transport ability and selectivity.[1,12] It was found that the presence of the hydroxyl group, the relative position of the carboxyl group, the number of the ether oxygens, and the hydrophobicity influenced the ion transport ability and selectivity. Among the synthetic carboxylic ionophores, 2-[[2-[2-[2-[2-[2-[2-[2-(2-hydroxyethoxy)phenoxy]ethoxy]phenoxy]ethoxy]-phenoxy]ethoxy]phenoxy]methyl]benzoic acid (**1**) exhibited the highest selectivity for K^+ over Na^+.[13] The backbone of **1** consists of 30 atoms and the length is similar to that of a flexible ionophore (X206) rather than a rigid ionophore (monensin). However, no tetrahydrofuran or tetrahydropyran ring contains in the synthetic ionophore, and instead the molecule is composed of repeating units derived from catechol and ethylene glycol, which largely differs from those of natural ionophores. Therefore, conformations about C–C and C–O bonds are freely rotated except for O–C–C–O of catechol ring. Furthermore, since **1** has neither methyl substituent for aromatic or aliphatic carbon nor hydroxyl group in the backbone, the flexibility is probably higher than that of X206. In fact, the ^{1}H NMR spectra of **1** and the sodium salt show that chemically equivalent protons have the identical chemical shifts one another because of a rapid interconversion between many conformers on the NMR time scale.[13] In contrast, the separation of the chemically equivalent proton resonances was observed in the ^{1}H NMR spectra of the potassium salt (**2**),[13] and the assignments of the signals by two-dimensional NMR methods and the analysis of the proton–proton vicinal coupling constants enabled us to estimate the existing conformations in solution with the highly lipophilic exterior of **2** among many accessible conformations.[14]

Our preliminary X-ray analysis of the potassium salt of **1**, **2**, reveals that the backbone has a conformation similar to those of X206 and the salts, and K^+-alborixin.[15] In this paper we describe the structures of the potassium, rubidium, cesium salts (**2**, **3**, **4**) of the

Table 1. Crystal Data, Experimental Conditions, and Refinement Details of **2**, **3**, and **4**

	2	**3**	**4**
Lattice	Triclinic	Monoclinic	Monoclinic
Formula	$C_{40}H_{39}O_{11}K \cdot H_2O \cdot 2CHCl_3$	$C_{40}H_{39}O_{11}Rb \cdot H_2O \cdot CHCl_3$	$C_{40}H_{39}O_{11}Cs \cdot H_2O \cdot CHCl_3$
Mr	991.61	918.54	966.04
Space group	$P\bar{1}$	$P2_1/a$	$P2_1/n$
a/Å	14.517(1)	24.085(6)	24.412(7)
b/Å	16.380(1)	13.068(2)	13.075(2)
c/Å	13.315(1)	13.983(4)	14.077(4)
α/°	72.313(8)	90.0	90.0
β/°	117.313(8)	105.402(32)	106.743(31)
γ/°	120.853(5)	90.0	90.0
V/Å^3	2406.3(4)	4242.9(18)	4302.7(20)
λ/Å	1.54184	0.71073	0.71073
μ/cm^{-1}	28.53(Cu $K\alpha$)	14.94(Mo $K\alpha$)	10.18(Mo $K\alpha$)
Z	2	4	4
F(000)	938	1884.0	1956.01
D_x/g cm^{-3}	1.374	1.437	1.492
Crystal size/mm	0.8×0.3×0.25	0.3×0.3×0.3	0.3×0.3×0.3
2θ range (°) and	42—60	19—29	19—29
reflections for cell parameter	18	20	16
2θ range/°	3—125	6—50	3—50
Index ranges			
h	−20 to 20	−30 to 30	−24 to 24
k	−23 to 23	0 to 16	0 to 15
l	0 to 18	0 to 17	0 to 16
Scan rate/° min^{-1}	4	8	8
Scan width ω/°	1.0+0.15tan θ	1.0+0.35tan θ	1.0+0.35tan θ
Independent reflections	7693	6273	7864
Observed reflections with $\lvert F_o\rvert > 3\sigma(\lvert F_o\rvert)$	6351	5112	6153
Maximum Δ/σ	0.40	0.06	0.01
Maximum $\Delta\rho$/eA^{-3}	0.44	0.53	0.68
R	0.102	0.068	0.071
R_w	0.126	0.077	0.082

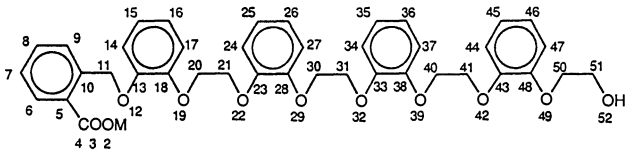

1; M=H
2; M=K
3; M=Rb
4; M=Cs

synthetic carboxylic ionophore (**1**) determined by X-ray crystallography. This study will give us very important information on how a host molecule utilizes local conformational changes to rearrange coordination sites for optimum complexation with a guest cation.

Experimental

Synthesis of carboxylic ionophore (**1**) and the potassium salt (**2**) has been previously described.[13,15] The corresponding rubidium and cesium salts (**3** and **4**) were prepared in a similar manner to that for **2**. Colorless parallelepiped crystals of $2 \cdot H_2O \cdot 2CHCl_3$, $3 \cdot H_2O \cdot CHCl_3$, and $4 \cdot H_2O \cdot CHCl_3$ were obtained from chloroform solutions and sealed in a glass capillary with a drop of chloroform. Crystal data, experimental conditions, refinement details of $2 \cdot H_2O \cdot 2CHCl_3$, $3 \cdot H_2O \cdot CHCl_3$, and $4 \cdot H_2O \cdot CHCl_3$ are shown in Table 1. Intensities of $2 \cdot H_2O \cdot 2CHCl_3$ and $4 \cdot H_2O \cdot CHCl_3$ were collected on a Rigaku AFC-4 four-circle diffractometer; graphite monochromater, Cu $K\alpha$ radiation (45 kV, 25 mA, λ=1.54184 Å) and Mo $K\alpha$ radiation (40 kV, 20 mA, λ=0.71073 Å), respectively. Intensities of $3 \cdot H_2O \cdot CHCl_3$ were collected on a Rigaku off centered four-circle diffractometer; graphite monochorometer, Mo $K\alpha$ radiation (50 kV, 150 mA, λ=0.71073 Å). Cell parameters were obtained by least-squares method. Intensities were measured by using 2θ–ω scan technique. Stationary background counts were accumulated for 5 s before and after each scan. Three standard reflections were monitored every 50 reflections. The intensities of $2 \cdot H_2O \cdot 2CHCl_3$ were not changed significantly, but those of $3 \cdot H_2O \cdot 2CHCl_3$ and $4 \cdot H_2O \cdot CHCl_3$ gradually decreased to 90% compared with their initial values. Corrections were made for Lorentz and polarization, while absorption and extinction were ignored.

The structures were solved by the direct method using the program (MULTAN 78)[16] and subsequent difference Fourier calculation. Refinements were performed by block-matrix least-squares with the program SHELX 76[17] (and block-diagonal least-squares with the program HBLS[18] for $2 \cdot H_2O \cdot 2CHCl_3$). One of the two independent chloroform molecules in $2 \cdot H_2O \cdot 2CHCl_3$ revealed highly disordered structure. Several peaks on the difference map were assigned to the Cl atoms with appropriate occupancy factors. The difference maps of $3 \cdot H_2O \cdot CHCl_3$ and $4 \cdot H_2O \cdot CHCl_3$ showed that the Cl atoms of the chloroform molecule were highly dis-

Table 2. Final Atomic Coordinates of $2 \cdot H_2O \cdot 2CHCl_3$ with Their Estimated Standard Deviations for Non-Hydrogen Atoms ($\times 10^4$) and Equivalent Isotropic Thermal Parameters

Atom		x	y	z	B_{eq}[a]	Atom		x	y	z	B_{eq}[a]
K		7316(1)	8612(1)	1574(1)	4.6	C	30	7665(5)	6989(4)	4380(5)	6.8
O	2	6107(3)	9365(2)	−496(3)	5.7	C	31	8109(5)	7893(5)	4882(4)	6.9
O	3	6819(3)	9180(2)	−1535(3)	5.9	O	32	7660(3)	8496(3)	4020(3)	5.9
C	4	6671(4)	9683(3)	−1132(4)	4.7	C	33	8003(4)	9388(4)	4278(4)	5.6
C	5	7211(4)	10744(3)	−1444(4)	4.9	C	34	8799(5)	9733(5)	5331(5)	7.3
C	6	7256(4)	11062(4)	−2530(4)	5.7	C	35	9082(6)	10636(6)	5487(7)	9.7
C	7	7699(5)	12013(4)	−2878(5)	6.8	C	36	8595(7)	11185(5)	4676(7)	9.4
C	8	8152(5)	12675(4)	−2143(6)	7.6	C	37	7788(5)	10836(4)	3593(6)	7.5
C	9	8139(5)	12387(4)	−1051(5)	6.6	C	38	7514(4)	9937(3)	3434(4)	5.2
C	10	7669(4)	11420(3)	−696(4)	5.2	O	39	6759(3)	9598(2)	2373(3)	5.1
C	11	7704(4)	11129(3)	508(4)	4.9	C	40	5558(4)	9299(4)	2110(5)	5.6
O	12	8442(2)	10664(2)	1145(3)	5.0	C	41	5007(4)	8300(4)	2602(5)	5.4
C	13	9618(4)	11232(3)	1425(4)	4.9	C	42	5018(3)	7696(2)	2038(3)	5.5
C	14	10144(5)	12179(4)	1614(5)	6.7	C	43	4680(4)	6751(3)	2442(4)	5.1
C	15	11355(5)	12716(4)	1896(6)	7.3	C	44	4275(5)	6334(4)	3322(5)	6.4
C	16	11981(4)	12278(4)	2010(5)	6.6	C	45	3971(6)	5370(4)	3684(6)	8.0
C	17	11463(4)	11324(4)	1843(5)	5.8	C	46	4070(5)	4822(4)	3169(6)	7.6
C	18	10265(4)	10798(3)	1551(4)	4.4	C	47	4474(4)	5233(3)	2259(5)	6.2
O	19	9670(2)	9850(2)	1355(3)	4.8	C	48	4770(4)	6205(3)	1914(4)	5.3
C	20	10337(4)	9408(3)	1453(4)	5.0	O	49	5182(3)	6689(2)	1050(3)	6.0
C	21	9560(4)	8384(4)	1226(4)	5.3	C	50	5218(5)	6149(3)	412(4)	5.7
O	22	9068(3)	7949(2)	2077(3)	5.2	C	51	5505(5)	6810(4)	−571(5)	6.2
C	23	8485(4)	6973(3)	2186(4)	5.4	O	52	6643(3)	7568(2)	−175(3)	5.8
C	24	8358(5)	6367(4)	1546(5)	6.7	O	101	3883(4)	8047(4)	9292(5)	9.8
C	25	7747(6)	5380(4)	1755(6)	8.3	C	102	4857(6)	1736(5)	3743(5)	7.5
C	26	7281(6)	5023(4)	2564(7)	8.9	Cl	103	5268(3)	2884(2)	3995(2)	12.0
C	27	7377(5)	5621(4)	3185(6)	7.9	Cl	104	4182(3)	911(2)	4664(2)	12.6
C	28	7983(4)	6606(3)	2972(4)	5.5	Cl	105	5986(3)	1566(3)	3905(3)	15.6
O	29	8139(3)	7294(3)	3525(3)	6.3						

a) $B_{eq}=\frac{8}{3}\pi^2\sum_i\sum_j U_{ij}a_i^*a_j^*\boldsymbol{a}_i\cdot\boldsymbol{a}_j$.

ordered All the non-hydrogen atoms except those of the disordered chloroform molecule were refined with anisotropic thermal parameter. Some hydrogen atoms found on difference Fourier maps and the others derived geometrically (C–H 1.08 Å) were refined isotropically. The quantity minimized was $\sum w(|F_o|-|F_c|)^2$ with $w=(\sigma(|F_o|)^2+0.004|F_o|)^{-1}$. Atomic scattering factors were taken from International Tables for X-ray Crystallography.[19] Calculations were carried out on HITAC M-680 computer at the Computer Center of the University of Tokyo.

Table 3. Final Atomic Coordinates of $3 \cdot H_2O \cdot CHCl_3$ with Their Estimated Standard Deviations for Rb ($\times 10^5$) and Non-Hydrogen Atoms ($\times 10^4$) and Equivalent Isotropic Thermal Parameters

Atom		x	y	z	B_{eq}[a]
Rb	1	37291(3)	6733(5)	67686(5)	4.5
O	2	2896(2)	747(3)	4762(4)	6.0
O	3	3339(2)	−463(3)	4113(4)	5.7
C	4	3166(3)	432(5)	4166(5)	4.6
C	5	3285(2)	1183(5)	3426(5)	4.3
C	6	3234(3)	846(6)	2467(5)	5.3
C	7	3310(3)	1496(7)	1733(5)	6.3
C	8	3454(3)	2512(7)	1968(6)	6.5
C	9	3522(3)	2855(6)	2926(6)	5.7
C	10	3434(2)	2209(5)	3662(5)	4.5
C	11	3524(3)	2618(5)	4701(5)	4.9
O	12	4031(2)	2152(3)	5361(3)	4.6
C	13	4566(3)	2454(5)	5277(4)	4.2
C	14	4669(3)	3381(5)	4869(5)	5.3
C	15	5235(3)	3623(5)	4845(6)	6.0
C	16	5677(3)	2969(6)	5224(6)	5.7
C	17	5572(3)	2029(5)	5636(5)	4.8
C	18	5019(3)	1774(4)	5655(4)	4.0
O	19	4874(2)	880(3)	6038(3)	4.4
C	20	5337(3)	178(5)	6429(5)	4.8
C	21	5095(3)	−779(4)	6743(5)	4.5
O	22	4869(2)	−505(3)	7564(3)	4.3
C	23	4721(2)	−1285(4)	8105(4)	3.9
C	24	4805(3)	−2316(5)	7943(5)	4.7
C	25	4657(3)	−3035(5)	8586(6)	5.6
C	26	4429(3)	−2732(5)	9334(5)	5.1
C	27	4333(3)	−1685(5)	9471(5)	4.5
C	28	4473(2)	−974(4)	8861(4)	3.8
O	29	4388(2)	58(3)	8925(3)	4.1
C	30	4138(2)	399(4)	9673(4)	3.9
C	31	4121(3)	1556(4)	9631(5)	4.3
O	32	3716(2)	1861(3)	8728(3)	4.6
C	33	3629(3)	2901(4)	8593(5)	4.4
C	34	3873(3)	3640(5)	9304(5)	5.2
C	35	3756(3)	4647(5)	9083(7)	6.3
C	36	3400(4)	4947(6)	8175(8)	7.3
C	37	3151(3)	4218(5)	7480(7)	6.3
C	38	3262(3)	3200(5)	7683(5)	4.4
O	39	3042(2)	2464(3)	6969(3)	5.1
C	40	2437(3)	2280(5)	6798(6)	6.3
C	41	2315(3)	1657(6)	7613(6)	6.2
O	42	2538(2)	649(3)	7551(4)	5.7
C	43	2584(3)	−17(6)	8321(5)	5.0
C	44	2428(3)	175(7)	9209(6)	6.5
C	45	2513(4)	−571(8)	9923(6)	7.1
C	46	2757(3)	−1475(7)	9803(6)	6.9
C	47	2898(3)	−1698(6)	8930(6)	5.7
C	48	2812(3)	−965(5)	8190(5)	4.9
O	49	2941(2)	−1088(3)	7303(3)	5.1
C	50	3104(3)	−2077(5)	7063(5)	4.8
C	51	3133(3)	−2042(5)	6001(6)	5.4
O	52	3580(2)	−1379(3)	5906(3)	5.4

a) $B_{eq}=\frac{8}{3}\pi^2\sum_i\sum_j U_{ij}a_i^*a_j^*\boldsymbol{a}_i\cdot\boldsymbol{a}_j$.

Table 4. Final Atomic Coordinates of $4 \cdot H_2O \cdot CHCl_3$ with Their Estimated Standard Deviations for Cs ($\times 10^5$) and Non-Hydrogen Atoms ($\times 10^4$) and Equivalent Isotropic Thermal Parameters

Atom		x	y	z	B_{eq}[a]
Cs	1	62964(2)	7416(4)	29961(3)	4.3
O	2	6652(2)	−417(4)	661(4)	5.3
O	3	7133(2)	819(4)	1666(4)	5.1
C	4	6836(3)	486(5)	854(5)	3.8
C	5	6695(3)	1216(5)	−33(5)	4.1
C	6	6746(3)	856(6)	−925(5)	5.2
C	7	6664(4)	1486(7)	−1759(6)	6.4
C	8	6502(4)	2498(6)	−1686(6)	6.1
C	9	6436(3)	2869(6)	−799(6)	5.4
C	10	6537(3)	2234(5)	37(5)	4.0
C	11	6441(3)	2681(6)	977(5)	4.7
O	12	5954(2)	2196(3)	1176(3)	4.1
C	13	5415(2)	2493(4)	603(5)	3.9
C	14	5301(3)	3414(5)	94(6)	4.9
C	15	4736(3)	3645(6)	−446(6)	5.5
C	16	4296(3)	2971(5)	−458(6)	5.0
C	17	4409(3)	2058(5)	58(5)	4.3
C	18	4968(2)	1813(4)	583(4)	3.5
O	19	5122(2)	908(3)	1122(3)	3.9
C	20	4660(3)	208(5)	1086(5)	4.1
C	21	4916(3)	−739(5)	1662(5)	4.7
O	22	5127(2)	−464(3)	2680(3)	3.9
C	23	5287(3)	−1269(4)	3348(4)	3.7
C	24	5215(3)	−2295(4)	3106(6)	4.8
C	25	5365(4)	−3029(6)	3857(6)	5.7
C	26	5587(3)	−2753(5)	4828(6)	5.6
C	27	5671(3)	−1713(5)	5066(5)	4.3
C	28	5522(3)	−985(4)	4324(4)	3.4
O	29	5590(2)	66(3)	4498(3)	3.6
C	30	5843(3)	386(4)	5499(4)	3.6
C	31	5857(3)	1551(5)	5504(5)	3.7
O	32	6295(2)	1857(3)	5074(4)	4.0
C	33	6386(3)	2908(4)	5050(5)	3.7
C	34	6111(3)	3619(5)	5484(6)	5.2
C	35	6234(4)	4648(5)	5404(7)	6.2
C	36	6639(4)	4953(6)	4943(8)	6.9
C	37	6912(4)	4232(5)	4522(7)	5.7
C	38	6784(3)	3219(4)	4576(5)	4.5
O	39	7038(2)	2493(4)	4112(4)	5.3
C	40	7633(3)	2290(6)	4581(7)	6.3
C	41	7688(3)	1600(5)	5477(7)	6.3
O	42	7492(3)	620(3)	5070(4)	5.1
C	43	7422(3)	−118(5)	5741(5)	4.7
C	44	7552(4)	9(7)	6766(5)	6.4
C	45	7443(5)	−793(8)	7341(7)	7.6
C	46	7202(4)	−1702(8)	6931(6)	6.6
C	47	7093(3)	−1839(6)	5912(5)	5.4
C	48	7203(3)	−1046(5)	5333(4)	4.4
O	49	7105(2)	−1118(4)	4301(3)	4.6
C	50	6920(3)	−2102(5)	3854(5)	4.9
C	51	6924(3)	−2020(6)	2774(5)	5.1
O	52	6477(2)	−1355(4)	2263(4)	5.4

a) $B_{eq}=\frac{8}{3}\pi^2\sum_i\sum_j U_{ij}a_i^*a_j^*\boldsymbol{a}_i\cdot\boldsymbol{a}_j$.

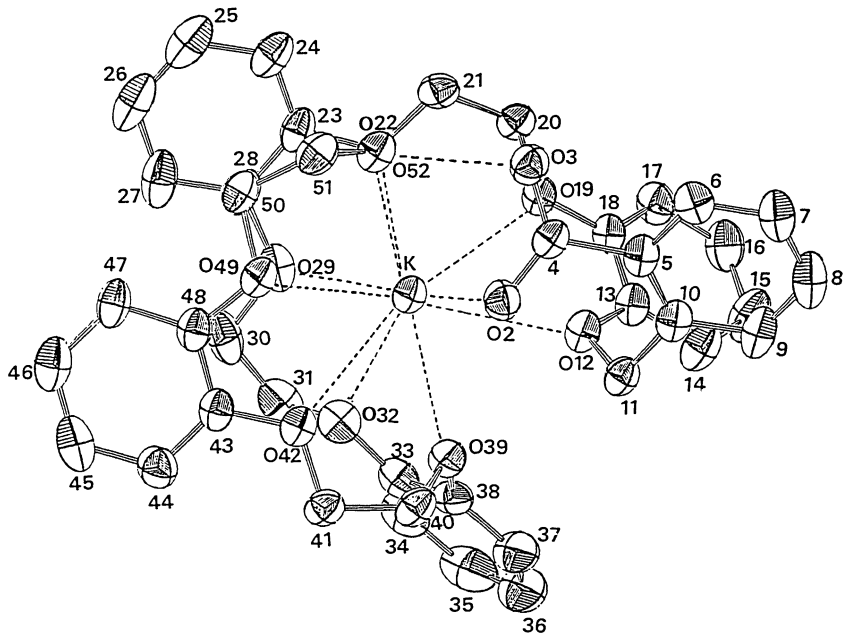

Fig. 1. Molecular structure of **2**. The thermal ellipsoid is 50% probability level. The solid and broken lines indicate coordination and hydrogen bonds, respectively.

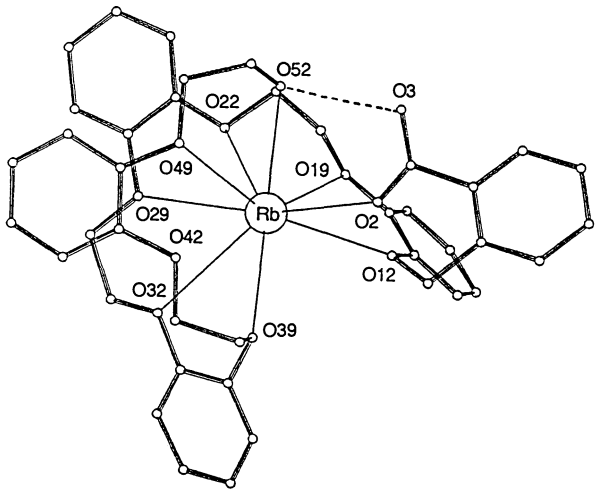

Fig. 2. Molecular structure of **3**. There is no bond between O(42) and Rb.

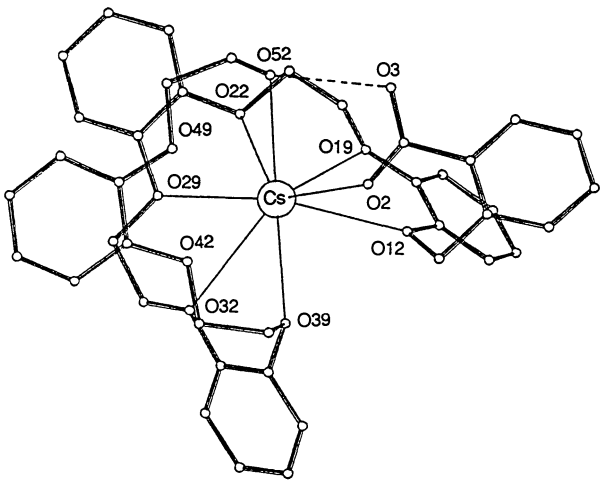

Fig. 3. Molecular structure of **4**. The O(42) has any bond with the Cs ion.

Results and Discussion

Tables 2—4 list the final atomic coordinates and equivalent isotopic thermal parameters of **2**, **3**, and **4**.[20] Molecular structures of **2**, **3**, and **4** are shown in Figs. 1, 2, and 3, respectively. Bond lengths, bond angles, and torsional angles are given in Tables 5, 6, and 7, respectively. They agree well with the usually observed corresponding parameters. In each complex, the intramolecular hydrogen bonding between the carboxylato group and the hydroxyl group at the other end of the molecule produces a pseudocyclic conformation as observed in naturally occurring carboxylic ionophores. The O···O distances are 2.672, 2.699, and 2.706 Å, respectively. As shown in Table 7, the conformations about the aliphatic C–C bonds are gauche with alternate signs through the backbone. Most of the torsion angles about the C–O bonds are close to 180°, whereas both the C(11)–O(12) and O(12)–C(13) bonds and the C(38)–O(39) and O(39)–C(40) bonds have gauche conformations, which play a role of hinges in turning the backbone abruptly. The head-to-tail hydrogen bonding and the torsional angles resulted in the molecular conformation with a thirty-one-membered pseudocycle like the seam of a tennis ball and the ligand wrapped round the potassium ion.

Table 5. Bond Length (Å) in **2**, **3**, and **4**

	2	**3**	**4**
O(2)–C(4)	1.261(7)	1.257(9)	1.243(8)
O(3)–C(4)	1.253(7)	1.250(9)	1.264(9)
C(4)–C(5)	1.506(8)	1.508(9)	1.531(9)
C(5)–C(6)	1.401(8)	1.385(10)	1.379(11)
C(5)–C(10)	1.402(8)	1.405(9)	1.397(9)
C(6)–C(7)	1.365(10)	1.380(12)	1.401(12)
C(7)–C(8)	1.375(11)	1.390(13)	1.393(13)
C(8)–C(9)	1.391(10)	1.379(12)	1.392(12)
C(9)–C(10)	1.390(9)	1.389(10)	1.402(10)
C(10)–C(11)	1.512(8)	1.509(10)	1.526(10)
C(11)–O(12)	1.435(7)	1.455(8)	1.445(9)
O(12)–C(13)	1.385(7)	1.383(8)	1.386(8)
C(13)–C(14)	1.378(9)	1.388(10)	1.387(10)
C(13)–C(18)	1.372(7)	1.397(9)	1.400(9)
C(14)–C(15)	1.420(10)	1.408(11)	1.404(12)
C(15)–C(16)	1.355(10)	1.359(11)	1.385(11)
C(16)–C(17)	1.382(9)	1.408(10)	1.383(11)
C(17)–C(18)	1.401(8)	1.381(9)	1.389(9)
C(18)–O(19)	1.376(6)	1.369(7)	1.398(8)
O(19)–C(20)	1.423(7)	1.435(8)	1.442(9)
C(20)–C(21)	1.494(8)	1.494(10)	1.514(11)
C(21)–O(22)	1.425(7)	1.441(8)	1.423(10)
O(22)–C(23)	1.369(7)	1.371(7)	1.391(8)
C(23)–C(24)	1.390(9)	1.389(9)	1.383(10)
C(23)–C(28)	1.362(9)	1.405(8)	1.378(9)
C(24)–C(25)	1.399(11)	1.412(10)	1.397(12)
C(25)–C(26)	1.356(13)	1.362(11)	1.365(12)
C(26)–C(27)	1.381(12)	1.409(10)	1.401(11)
C(27)–C(28)	1.397(10)	1.364(9)	1.383(10)
C(28)–O(29)	1.397(8)	1.370(7)	1.397(8)
O(29)–C(30)	1.428(9)	1.410(7)	1.428(8)
C(30)–C(31)	1.509(11)	1.512(9)	1.523(10)
C(31)–O(32)	1.416(9)	1.431(8)	1.428(8)
O(32)–C(33)	1.379(8)	1.381(8)	1.395(8)
C(33)–C(34)	1.395(10)	1.399(10)	1.388(11)
C(33)–C(38)	1.373(9)	1.398(10)	1.388(10)
C(34)–C(35)	1.373(13)	1.363(12)	1.391(13)
C(35)–C(36)	1.356(14)	1.387(15)	1.388(15)
C(36)–C(37)	1.430(13)	1.379(14)	1.383(15)
C(37)–C(38)	1.373(10)	1.373(11)	1.368(13)
C(38)–O(39)	1.393(7)	1.386(8)	1.395(10)
O(39)–C(40)	1.439(7)	1.433(9)	1.437(11)
C(40)–C(41)	1.494(9)	1.490(12)	1.525(13)
C(41)–O(42)	1.422(7)	1.434(10)	1.429(11)
O(42)–C(43)	1.371(7)	1.366(9)	1.394(10)
C(43)–C(44)	1.386(9)	1.413(12)	1.396(12)
C(43)–C(48)	1.377(8)	1.387(10)	1.382(10)
C(44)–C(45)	1.393(11)	1.371(14)	1.397(14)
C(45)–C(46)	1.375(11)	1.349(14)	1.376(15)
C(46)–C(47)	1.419(10)	1.382(12)	1.393(13)
C(47)–C(48)	1.402(9)	1.385(10)	1.392(11)
C(48)–O(49)	1.378(7)	1.366(8)	1.407(9)
O(49)–C(50)	1.434(8)	1.417(9)	1.446(10)
C(50)–C(51)	1.495(10)	1.506(11)	1.527(11)
C(51)–O(52)	1.430(8)	1.416(9)	1.419(9)

Similar structures with a 29-membered ring through a head-to-tail hydrogen bond are observed in X206, the Na^+ and Ag^+ complexes, and K^+ complex of alborixin.[10] The O···O distances of the hydrogen bonds are 2.91, 2.86, 2.74, and 2.66 Å, respectively. In addition, two other intramolecular hydrogen bonds exist in X206 and the derivatives. These three intramolecular bonds must play a role in the stabilization of the observed structures for the free acid as well as the complexes. In contrast, our synthetic ionophore has a single intramolecular hydrogen bonding. Since a single crystal of **1** has not been obtained so far, the conformation of **1** in the crystal is not known. The free acid may adopt a stable conformation largely different from that of the K^+ complex. X-Ray structure analysis of a crown ether with a thirty-membered ring (dibenzo-30-crown-10) and the complex with KI was reported.[11] Four of the C–C–O–C angles change trans in the free molecule to gauche in the complex. The gauche conformation provides the complex with a structure like the seam of a tennis ball, whereas the free molecule has a rather flat conformation. It appears that the flat conformation of the crown ether is more stable than the 'tennis ball' structure, and coordination of the ether oxygens to the potassium ion in the complex contributes the stabilization of the complex structure.

The overall conformation of **2**, **3**, and **4** is similar to each other as described above, but the cavity size changes by altering the backbone conformation to accommodate the cations with different diameters. Although the difference in bond lengths and angles of **2**, **3**, and **4** is not much as shown in Tables 5 and 6, the torsional angles of the ionophore backbones are significantly different among the three. Compared with the torsional angles about the aliphatic C–C bonds with gauche conformations, the absolute values of **2** are smaller than those of **3** and **4**, except for the case of O(29)–C(30)–C(31)–O(32). Most of dihedral angles about aromatic carbon and oxygen bonds are −6°—+8° except for C(11)–O(12)–C(13)–C(14) and C(37)–C(38)–O(39)–C(40). In the case of C(11)–O(12)–C(13)–C(14), the angle of **2** is larger than those of **3** and **4**. Among aliphatic carbon and oxygen bonds, C(10)–O(11)–C(12)–C(13) and C(38)–C(39)–O(40)–C(41) are gauche. The torsional angle about C(38)–C(39)–O(40)–C(41) of **2** (−98°) is larger than those of **3** and **4**. There is less difference between torsional angles of **3** and **4**. The sum of these conformational changes leads to the different distances between O(12) and O(39), 3.040 Å for **2**, 3.708 Å for **3**, and 4.235 Å for **4**, and to the variety of cavity sizes.

Distances between the ionophore oxygens and the cations are shown in Table 8. With the size of the cations ($K^+ < Rb^+ < Cs^+$), the distance becomes large. The oxygen of terminal hydroxyl group and one of the oxygens of carboxyl group at the other end are close to the cations, but another carboxyl oxygen which has the head-to-tail hydrogen bonding to the terminal hydroxyl group is too distant from the cation to coordinate with them. In addition, two ether oxygens at the hinges have short distances to the cation. Among the two terminal and two internal oxygens of the potassium salt, **2**, the closest oxygen to the potassium is O(39) at the hinge, and then the terminal two oxygens are close and O(12) at the other hinge is furthest. In the case of **3**, the

Table 6. Bond Angles (°) in **2**, **3**, and **4**

	2	**3**	**4**		**2**	**3**	**4**
O(2)-C(4)-O(3)	124.9(5)	125.9(6)	127.0(6)	C(26)-C(27)-C(28)	118.3(7)	120.0(6)	119.9(7)
O(2)-C(4)-C(5)	118.4(5)	117.9(6)	117.8(6)	C(23)-C(28)-C(27)	121.2(6)	119.9(6)	120.7(6)
O(3)-C(4)-C(5)	116.7(5)	116.2(6)	115.1(6)	C(23)-C(28)-O(29)	114.2(5)	115.8(5)	115.7(6)
C(4)-C(5)-C(6)	118.0(5)	118.2(6)	118.1(6)	C(27)-C(28)-O(29)	124.6(6)	124.3(5)	123.5(6)
C(4)-C(5)-C(10)	123.0(6)	123.0(6)	122.6(6)	C(28)-O(29)-C(30)	119.1(5)	117.4(5)	117.2(5)
C(6)-C(5)-C(10)	119.1(5)	118.8(6)	119.3(6)	O(29)-C(30)-C(31)	104.8(6)	107.4(5)	107.5(5)
C(5)-C(6)-C(7)	120.9(6)	121.9(7)	122.2(8)	C(30)-C(31)-O(32)	108.1(6)	108.6(5)	107.3(5)
C(6)-C(7)-C(8)	120.0(7)	119.1(8)	118.2(8)	C(31)-O(32)-C(33)	118.1(5)	116.0(5)	115.6(5)
C(7)-C(8)-C(9)	120.7(7)	119.8(8)	120.4(8)	O(32)-C(33)-C(34)	123.2(6)	124.2(6)	123.2(6)
C(8)-C(9)-C(10)	119.8(6)	121.3(7)	120.5(7)	O(32)-C(33)-C(38)	116.4(6)	115.8(6)	116.1(6)
C(5)-C(10)-C(9)	120.0(6)	119.0(6)	119.4(6)	C(34)-C(33)-C(38)	120.5(6)	119.9(6)	120.7(7)
C(5)-C(10)-C(11)	121.9(5)	121.7(6)	122.7(6)	C(33)-C(34)-C(35)	118.0(8)	118.9(7)	118.0(8)
C(9)-C(10)-C(11)	118.5(5)	119.2(6)	117.8(6)	C(34)-C(35)-C(36)	122.6(9)	121.4(9)	120.9(9)
C(10)-C(11)-O(12)	110.4(5)	110.1(5)	109.9(6)	C(35)-C(36)-C(37)	119.4(9)	119.8(10)	120.1(10)
C(11)-O(12)-C(13)	116.9(4)	118.1(5)	117.4(5)	C(36)-C(37)-C(38)	117.9(7)	120.0(9)	119.3(9)
O(12)-C(13)-C(14)	123.0(5)	123.8(6)	124.0(6)	C(33)-C(38)-C(37)	121.6(6)	120.0(7)	120.8(7)
O(12)-C(13)-C(18)	116.7(5)	115.9(5)	115.9(5)	C(33)-C(38)-O(39)	119.8(5)	119.3(6)	119.6(6)
C(14)-C(13)-C(18)	120.3(5)	120.3(6)	120.2(6)	C(37)-C(38)-O(39)	118.6(6)	120.5(7)	119.6(7)
C(13)-C(14)-C(15)	119.7(6)	119.1(7)	119.0(7)	C(38)-O(39)-C(40)	115.8(4)	114.5(5)	115.9(6)
C(14)-C(15)-C(16)	119.3(7)	120.8(7)	120.5(7)	O(39)-C(40)-C(41)	111.1(5)	111.2(7)	109.0(7)
C(15)-C(16)-C(17)	121.4(7)	120.1(7)	120.4(7)	C(40)-C(41)-O(42)	106.9(5)	107.6(7)	105.0(7)
C(16)-C(17)-C(18)	119.3(6)	119.8(6)	119.7(7)	C(41)-O(42)-C(43)	117.6(5)	119.4(6)	116.2(6)
C(13)-C(18)-C(17)	120.1(5)	119.9(6)	120.2(6)	O(42)-C(43)-C(44)	124.7(5)	126.5(7)	125.6(7)
C(13)-C(18)-O(19)	116.4(5)	115.9(5)	116.1(5)	O(42)-C(43)-C(48)	115.6(5)	114.7(6)	115.8(6)
C(17)-C(18)-O(19)	123.6(5)	124.2(6)	123.6(6)	C(44)-C(43)-C(48)	119.7(6)	118.8(7)	118.6(7)
C(18)-O(19)-C(20)	116.3(4)	116.2(5)	115.6(5)	C(43)-C(44)-C(45)	120.3(7)	119.4(8)	119.1(8)
O(19)-C(20)-C(21)	109.1(5)	108.8(5)	107.6(6)	C(44)-C(45)-C(46)	120.3(7)	121.2(10)	122.3(10)
C(20)-C(21)-O(22)	106.6(5)	106.6(5)	107.8(6)	C(45)-C(46)-C(47)	120.3(7)	120.8(9)	118.4(9)
C(21)-O(22)-C(23)	118.1(5)	117.6(5)	116.1(5)	C(46)-C(47)-C(48)	118.0(6)	119.4(7)	119.6(8)
O(22)-C(23)-C(24)	124.9(6)	124.1(5)	125.2(6)	C(43)-C(48)-C(47)	121.3(6)	120.3(7)	121.9(7)
O(22)-C(23)-C(28)	115.1(5)	115.1(5)	115.2(6)	C(43)-C(48)-O(49)	115.0(5)	114.7(6)	114.7(6)
C(24)-C(23)-C(28)	119.9(6)	120.8(6)	119.6(6)	C(47)-C(48)-O(49)	123.7(5)	125.0(6)	123.4(7)
C(23)-C(24)-C(25)	118.9(7)	118.0(6)	119.5(7)	C(48)-O(49)-C(50)	117.8(5)	117.8(5)	116.6(6)
C(24)-C(25)-C(26)	120.5(8)	121.2(7)	121.2(8)	O(49)-C(50)-C(51)	106.3(5)	107.1(6)	106.2(6)
C(25)-C(26)-C(27)	121.1(9)	120.0(7)	119.0(8)	C(50)-C(51)-O(52)	110.0(6)	110.3(6)	108.9(6)

Table 7. Torsion Angles (°) in **2**, **3**, and **4** Crystals

	2	**3**	**4**
C(10)-C(11)-O(12)-C(13)	+76	+73	+76
C(18)-O(19)-C(20)-C(21)	+179	−176	−177
C(20)-C(21)-O(22)-C(23)	−171	−168	−169
C(28)-O(29)-C(30)-C(31)	+175	+177	+179
C(30)-C(31)-O(32)-C(33)	−177	+177	−178
C(38)-O(39)-C(40)-C(41)	−98	−76	−78
C(40)-C(41)-O(42)-C(43)	+173	+167	+171
C(48)-O(49)-C(50)-C(51)	+171	+172	+172
C(11)-O(12)-C(13)-C(14)	+31	+23	+21
C(17)-C(18)-O(19)-C(20)	−1	−1	−1
C(21)-O(22)-C(23)-C(24)	+2	+4	+5
C(27)-C(28)-O(29)-C(30)	+1	+0	−2
C(31)-O(32)-C(33)-C(34)	+2	−5	−5
C(37)-C(38)-O(39)-C(40)	−76	−74	−73
C(41)-O(42)-C(43)-C(44)	+3	+0	+3
C(47)-C(48)-O(49)-C(50)	+5	+9	+5
O(19)-C(20)-C(21)-O(22)	−48	−66	−68
O(29)-C(30)-C(31)-O(32)	+70	+68	+73
O(39)-C(40)-C(41)-O(42)	−59	−69	−72
O(49)-C(50)-C(51)-O(52)	+57	+65	+70

Table 8. Distance (Å) between Alkali Metal Ion and Oxygen

	2	**3**	**4**
M-O(2)	2.814(4)	2.986(5)	3.144(6)
M-O(3)	3.760(5)	3.876(5)	3.937(6)
M-O(12)	2.890(4)	2.983(4)	3.106(5)
M-O(19)	3.053(4)	3.196(4)	3.296(5)
M-O(22)	2.987(4)	3.085(4)	3.178(5)
M-O(29)	3.038(4)	3.117(4)	3.213(5)
M-O(32)	3.020(4)	3.157(4)	3.270(5)
M-O(39)	2.751(4)	2.923(5)	3.058(6)
M-O(42)	3.156(4)	3.330(5)	3.486(6)
M-O(49)	3.058(5)	3.196(4)	3.330(6)
M-O(52)	2.814(4)	2.923(5)	3.006(6)

ether and terminal hydroxyl oxygens of O(39) and O(52) are closer to the rubidium than O(2) and O(12). The distance from the oxygens to the cesium of **4** increases in the order of O(52)<O(39)<O(12)<O(2). Most of the other oxygens far from the cation are also thought to coordinate with the cations.

The crystal radii (CR) which were calculated and tabulated by Shannon based on the many results of X-ray crystal structure analysis, increase with increasing

coordination number.[21] Values of CR plus van der Waals radius of oxygen (1.4 Å) could be considered as a criterion of the largest coordination distance of oxygen to cation (CD). The CD values of potassium, rubidium, and cesium ions for respective coordination number are illustrated in Table 9. M–O distances of the ionophore complexes in Table 8 are compared with the CD values. The compound, **2**, appears to have ten oxygen donor atoms for the potassium, although the distance between O(42) and K (3.156 Å) is slightly larger than the CD (3.13 Å). Only O(3) (K–O distance 3.760 Å) has no interaction with the potassium as described above. In contrast, the coordination number of **3** is nine: The ninth O(49) is nearly on the coordination sphere of Rb^+, but the distance of 3.330 Å between O(42) and rubidium is larger than the CD of 3.20 Å for ten coordination numbers. Nine oxygen atoms of **4** are also donors for the cesium ion in which the distances between the oxygens and cesium are in the range 3.006 to 3.330 Å. Rubidium and cesium cations of **3** and **4** are nonacoordinated to the oxygens except for O(42) and O(3). These results indicate that the potassium ion of **2** is more stabilized than the rubidium and cesium ions of **3** and **4**, which is consistent with the selectivity of ion transport by **1** as described above.

Compared with a centrosymmetric complex of dibenzo-30-crown-10 with KI that has a 'seam' conformation with ten K–O distances in the range 2.850(6)—2.931(6) Å,[11] the complex structure of **2** as well as **3** and **4** may be a relatively loose arrangement. However, the complex structure of **2** seems to be as stable as that of alborixin-K^+ with another 'seam' conformation in which the eight oxygens from one carboxyl and four hydroxyl groups, and three ether linkages coordinate with the potassium with the distances of 2.70—3.06 Å, while there is no interaction of the other six oxygens with the cation.[10c,d]

The crystal packing of the complex, **2**, is shown in Fig. 4. The molecules of **2** are stacked on (010) plane to generate a layer structure. Two chloroform molecules and one water per one of **2** occupy the interlayer space. One of the two nonequivalent chloroform molecules is highly disordered in a column along the *c*-axis. Crystal structures of **3** and **4** are shown in Figs. 5 and 6. Different from **2**, both of **3** and **4** contain one water and one chloroform molecules which are present between

Table 9. Estimated Largest Coordination Distances (CD) between Oxygen and Cations for Each Coordinaton Number (*n*)

n	CD/Å		
	K^+	Rb^+	Cs^+
8	3.05	3.15	3.28
9	3.09	3.17	3.32
10	3.13	3.20	3.35
11	—	3.23	3.39
12	3.18	3.26	3.42

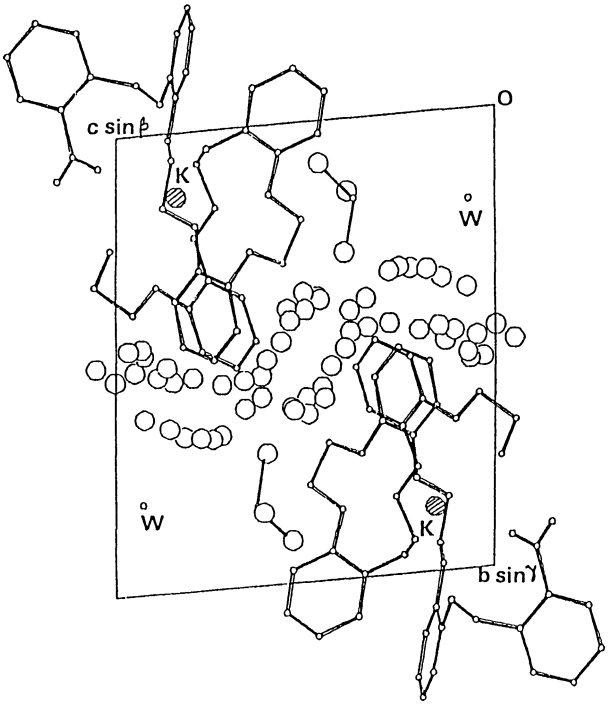

Fig. 4. Crystal structure of $2 \cdot H_2O \cdot 2CHCl_3$ viewed down the *a* axis. The large circles indicate Cl atom of the disordered $CHCl_3$ molecule.

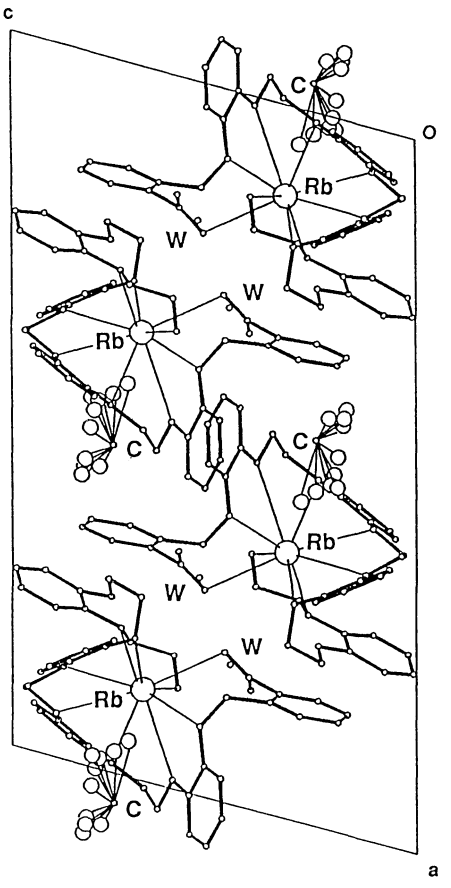

Fig. 5. Crystal structure of $3 \cdot H_2O \cdot CHCl_3$ viewed along the *b* axis.

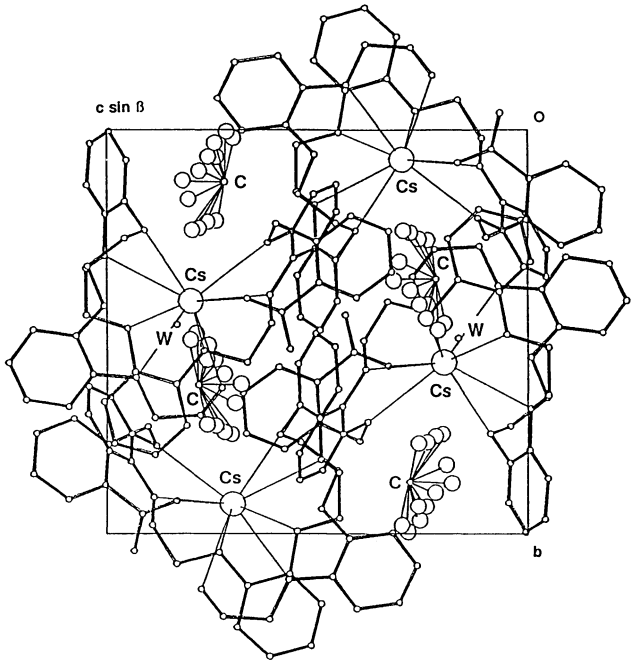

Fig. 6. Crystal structure of $4 \cdot H_2O \cdot CHCl_3$ viewed along the *a* axis. The $CHCl_3$ molecule is highly disordered.

the layer structure formed by the salts. The chloroform molecules are disordered in the interlayer as observed in **2**. These crystal structures with weak interaction between the ionophore molecules of **2**, **3**, and **4** suggest that the alkali metal salts of **1** have stable conformations in chloroform solution similar to those in the crystal.

On the basis of the conformation in the crystal, solution conformations of **2**—**4** by means of NMR spectroscopy are investigated and will be reported in near future.

References

1) Part VIII. K. Yamaguchi, H. Kuboniwa, N. Murakami, A. Hirao, S. Nakahama, and N. Yamazaki, *Bull. Chem. Soc. Jpn.*, **62**, 1097 (1988).

2) G. R. Painter and B. C. Pressman, "Topics in Current Chemistry 101. Host Guest Complex Chemistry II," ed by F. Vogtle, Springer Verlag, Berlin (1982); pp. 83—110, and references cited therein.

3) a) J. W. Westley, *Annu. Rep. Med. Chem.*, **10**, 246 (1975); b) J. W. Westley, *Adv. Appl. Microbiol.*, **22**, 177 (1977).

4) B. C. Pressman, *Annu. Rev. Biochem.*, **45**, 501 (1976).

5) R. Hilgenfelt and W. Saenger, "Topics in Current Chemistry 101. Host Guest Complex Chemistry II," ed by F. Vögtle, Springer Verlag, Berlin (1982); pp. 1—82, and references cited therein.

6) a) A. Agatrap, J. W. Chamberlin, M. Pinkerton, and L. K. Steinrauf, *J. Am. Chem. Soc.*, **89**, 5737 (1967); b) M. Pinkerton and L. K. Steinrauf, *J. Mol. Biol.*, **49**, 533 (1970).

7) W. K. Lutz, F. K. Winkler, and J. D. Dunitz, *Helv. Chim. Acta*, **54**, 1103 (1971).

8) W. L. Duax, G. D. Smith, and P. D. Strong, *J. Am. Chem. Soc.*, **102**, 6725 (1980).

9) a) L. K. Steinrauf, M. Pinkerton, and J. W. Chamberlin, *Biochem. Biophys. Res. Commun.*, **33**, 29 (1968); b) T. Kubota, S. Matsunami, M. Shiro, and H. Koyama, *J. Chem. Soc., Chem. Commun.*, **1968**, 1541; c) M. Shiro and H. Koyama, *J. Chem. Soc. B*, **1970**, 243; d) L. K. Steinrauf, E. W. Czerwinski, and M. Pinkerton, *Biochem. Biophys. Res. Commun.*, **45**, 1279 (1971); e) A. J. Geddes, B. Sheldrick, and W. T. J. Stevenson, *Biochem. Biophys. Res. Commun.*, **60**, 1245 (1974); f) P. Y. Barrans and M. Alleaume, *Acta Crystallogr., Sect. B*, **36**, 936 (1980).

10) a) J. F. Blount and J. W. Westley, *J. Chem. Soc., Chem. Commun.*, **1971**, 927; b) J. F. Blount and J. W. Westley, *ibid.*, **1975**, 533; c) M. Alleaume, B. Busetta, C. Farges, P. Gachon, A. Kergomard, and T. Staron, *ibid.*, **1975**, 411; d) P. V. Roey, W. L. Duax, P. D. Strong, and G. D. Smith, *Isr. J. Chem.*, **24**, 2183 (1984).

11) M. A. Bush and M. R. Truter, *J. Chem. Soc., Perkin Trans. 2*, **1972**, 345.

12) a) H. Kuboniwa, K. Yamaguchi, A. Hirao, S. Nakahama, and N. Yamazaki, *Chem. Lett.*, **1982**, 1937; b) K. Yamaguchi, S. Negi, S. Kozakai, R. Nagano, H. Kuboniwa, A. Hirao, S. Nakahama, and N. Yamazaki, *Bull. Chem. Soc. Jpn.*, **61**, 2047 (1988).

13) H. Kuboniwa, S. Nagami, K. Yamaguchi, A. Hirao, S. Nakahama, and N. Yamazaki, *J. Chem. Soc., Chem. Commun.*, **1985**, 1469.

14) H. Kuboniwa, K. Yamaguchi, A. Hirao, and S. Nakahama, *Magn. Reson. Chem.*, **24**, 961 (1986).

15) H. Kuboniwa, K. Yamaguchi, S. Nakahama, K. Hori, and Y. Ohashi, *Chem. Lett.*, **1988**, 923.

16) P. Main, S. E. Hull, L. Lessinger, G. Germain, J.-P. Declerq, and M. M. Woolfson, MULTAN 78. A System of Computer Programs for the Automatic Solution of Crystal Structures from X-Ray Diffraction Data. Univs. of York, England and Loivain, Belgium (1978).

17) G. M. Sheldrick, SHELX 76. A Program for Crystal Structure Determination. Univ. of Cambridge (1976).

18) T. Ashida, HBLS V, The Universal Crystallographic Computing System-Osaka, The Computation Center, Osaka University (1973), p. 53.

19) "Intrernational Tables for X-Ray Crystallography, Kynoch Press, Birmingham, England (1974), Vol. IV, p. 71.

20) The positional and thermal parameters of the solvents and hydrogen atoms, the final anisotropic thermal parameters, and F_o-F_c tables are deposited as Document No. 8971 at the Office of the Editor of Bull. Chem. Soc. Jpn.

21) R. D. Shannon, *Acta Crystallogr., Sect. A*, **32**, 751 (1976).

Reactions of 1,1-Disubstituted Alkenes with Acetoacetamides and Molecular Oxygen in the Presence of Manganese(III) Acetate

Chang-Yi QIAN, Hiroshi NISHINO, and Kazu KUROSAWA*
Department of Chemistry, Faculty of Science, Kumamoto University, Kurokami 2-39-1, Kumamoto 860
(Received June 7, 1991)

The reactions of 1,1-disubstituted ethenes with acetoacetamide or *N*-substituted acetoacetamides, and molecular oxygen in the presence of manganese(III) acetate gave a mixture of *c*-4- and *t*-4-carbamoyl-3-methyl-1,2-dioxan-*r*-3-ols in good yields. Effects of substituents in the alkenes as well as in the carbamoyl group in the acetoacetamides were observed. Stereochemistry and the reactivity of the 4-carbamoyl-3-methyl-1,2-dioxan-3-ols are discussed.

A number of cyclic peroxides having a 1,2-dioxane ring system have been isolated from natural sources and have some biological activities.[1] We recently reported that the manganese(III)-based oxidative free-radical cyclization of alkenes with 1,3-dicarbonyl compounds and molecular oxygen produced 4-acyl-1,2-dioxan-3-ols in moderate to good yields.[2] Since the reaction is extremely facile for the synthesis of 1,2-dioxan-3-ols and the products may have some biological activities, we have investigated the reaction of alkenes with acetoacetamides in the presence of manganese(III) acetate (abbreviated [$Mn(OAc)_3$]) and molecular oxygen (O_2).

Results and Discussion

The reactions were carried out at various molar ratios of alkene : acetoacetamide : [$Mn(OAc)_3$]. When a mixture of 1,1-diphenylethene (**1a**), *N*-(4-methylphenyl)-acetoacetamide (**2a**), and [$Mn(OAc)_3$] was stirred in acetic acid under a current of dried air at 23 °C, the product was found to be 4-(4-methylphenylcarbamoyl)-3-methyl-6,6-diphenyl-1,2-dioxan-3-ol (**3aa**). The structure of **3aa** was elucidated by ^1H and ^{13}C NMR, IR spectra, and elemental analysis (Fig. 1). The maximum yield for **3aa** was attained from the reaction with a molar ratio of 1 : 3 : 1 (Table 1, Entry 3). The yield of **3aa** decreased when the reaction was carried out using a small volume of acetic acid (Entry 5). The reaction under an atmosphere of O_2 gave a slightly decreased yield (Entry 6). The reaction under an atmosphere of argon gave 3-(4-methylphenylcarbamoyl)-2-methyl-5,5-diphenyl-4,5-dihydrofuran (**4aa**) along with a large amount of unchanged alkene (Entry 7). The reactions at a slightly higher or lower temperature resulted in decreased yields of **3aa** (Entries 8, 9). Benzophenone was formed in the reaction at a higher temperature. Addition of water and the use of propanoic acid as a solvent also lowered the yield (Entries 10, 12), but the reactions in the presence of acetic anhydride and potassium acetate gave **3aa** in good yields (Entries 13, 14). Other metal acetates, such as Co(II), Co(III), Mn(II), Cu(II), Ni(II), Tl(III), Pb(IV), and $FeCl_3$ were used and it was found that similar reactions at 23 °C for 12—14 h in the presence of Co(II), Co(III), or Mn(II) did yield 4-

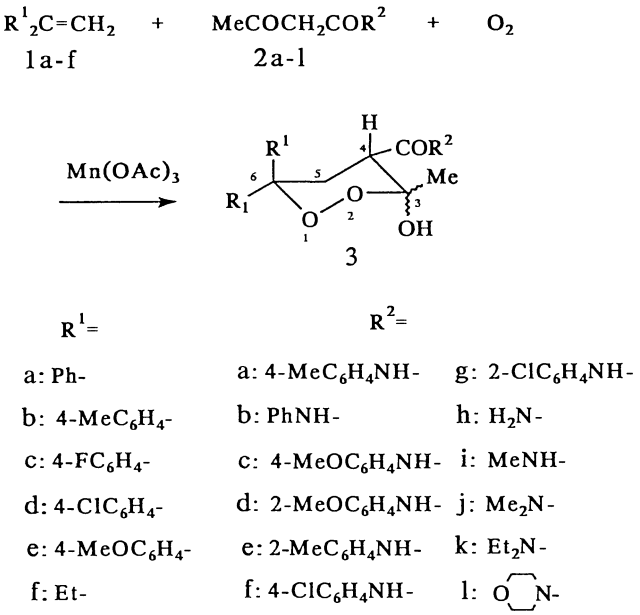

Fig. 1.

Table 1. Reactions of 1,1-Diphenylethene (**1a**) with *N*-(4-Methylphenyl)acetoacetamide (**2a**) and $[Mn(OAc)_3]$–O_2

Entry	Molar ratio[a]	Solvent[b]	Temp °C	Time h	Product composition (yield/%)[c] **1a**	**3aa**	**4aa**
1	1:1:1	AcOH	23	14		61	
2	1:2:1	AcOH	23	14		81	
3	1:3:1	AcOH	23	13		92	
4	1:3:1	AcOH[d]	23	13		89	
5	1:3:1	AcOH[e]	23	14		58	
6	1:3:1	AcOH[f]	23	14		78	
7	1:3:1	AcOH[g]	23	14	62		29
8	1:3:1	AcOH	36—42	6		34	18[h]
9	1:3:1	AcOH	15—18	15		55	
10	1:3:1	AcOH–H_2O[i]	23	14		58	
11	1:3:1	HCOOH	23	16	100		
12	1:3:1	$C_2H_5CO_2H$	23	14		51	33
13	1:3:1	AcOH–Ac_2O[j]	23	13		80	
14	1:3:1	AcOH–AcOK[k]	23	13		93	

a) **1a**:**2a**:$[Mn(OAc)_3]$. b) 25 cm^3 of solvent was used unless otherwise stated. c) Isolated yields (calculated on the basis of the alkene added). d) Acetic acid (60 cm^3) was used. e) Acetic acid (10 cm^3) was used. f) The reaction was carried out under an oxygen atmosphere. g) The reaction was carried out under an argon atmosphere and **2a** was recovered (59% yield). h) Benzophenone was obtained (5% yield). i) Water (7.5 cm^3) was added. j) Acetic anhydride (500 mg) was added. k) Potassium acetate (100 mg) was added.

Table 2. Reactions of 1,1-Disubstituted Ethenes (**1a—f**) with Acetoacetamides (**2a—l**) and $[Mn(OAc)_3]$–O_2[a]

Entry	Alkene	Acetoacetamide	Time h	Product (Yield/%)[b]	Isomer ratio
15	**1a**	**2a**	13	**3aa** (92)	59:41
16	**1a**	**2b**	12	**3ab** (96)	62:38
17	**1a**	**2c**	14	**3ac** (82)	63:36
18	**1a**	**2d**	14	**3ad** (84)	73:27
19	**1a**	**2e**	12	**3ae** (94)	83:17
20	**1a**	**2f**	12	**3af** (94)	57:43
21	**1a**	**2g**	12	**3ag** (93)	74:26
22	**1a**	**2h**	12	**3ah** (88)	56:44
23	**1a**	**2i**	13	**3ai** (85)	58:42
24	**1a**	**2j**	12	**3aj** (87)	95: 5
25	**1a**	**2k**	12	**3ak** (89)	96: 4
26	**1a**	**2l**	11	**3al** (88)	100: 0
27	**1b**	**2a**	13	**3ba** (99)	54:46
28	**1b**	**2b**	12	**3bb** (98)	56:44
29	**1b**	**2e**	12	**3be** (100)	77:23
30	**1b**	**2f**	14	**3bf** (99)	67:33
31	**1b**	**2g**	12	**3bg** (100)	94: 6
32	**1b**	**2h**	13	**3bh** (96)	59:41
33	**1c**	**2b**	12	**3cb** (94)	53:47
34	**1c**	**2j**	13	**3cj** (59)	94: 6
35	**1d**	**2g**	14	**3dg** (87)	91: 9
36	**1d**	**2j**	12	**3dj** (89)	94: 6
37	**1e**	**2g**	13	**3eg** (83)	91: 9
38	**1e**	**2j**	12	**3ej** (78)	96: 4
39	**1f**	**2b**	12	**3fb** (68)	56:44
40	**1f**	**2f**	12	**3ff** (62)	54:46

a) The reactions were carried out in acetic acid at a 1:3:1 molar ratio for alkene: acetoacetamide: $[Mn(OAc)_3]$ at 23 °C under a current of air. b) Isolated yield (calculated on the basis of alkene used).

(4-methylphenylcarbamoyl)-3-methyl-6,6-diphenyl-1,2-dioxan-3-ol (**3aa**) (Co(II), 60% yield; Co(III), 66% yield; Mn(II), 92% yield). It was thus shown that Mn(II) was as effective as Mn(III).

The reactions of 1,1-bis(4-methylphenyl)ethene (**1b**), 1,1-bis(4-fluorophenyl)ethene (**1c**), 1,1-bis(4-chloro-

phenyl)ethene (**1d**), 1,1-(4-methoxyphenyl)ethene (**1e**), and 2-ethyl-1-butene (**1f**) using acetoacetamide (**2h**) and various *N*-substituted acetoacetamides: *N*-phenyl- (**2b**), *N*-(4-methoxyphenyl)- (**2c**), *N*-(2-methoxyphenyl)- (**2d**), *N*-(2-methylphenyl)- (**2e**), *N*-(4-chlorophenyl)- (**2f**), *N*-(2-chlorophenyl)- (**2g**), *N*-methyl-(**2i**), *N,N*-dimethyl- (**2j**) and *N,N*-diethylacetoacetamide (**2k**), and *N*-(1,3-dioxobutyl)morpholine (**2l**) were then examined. The reactions were carried out in acetic acid with [$Mn(OAc)_3$] at a molar ratio of 1 : 3 : 1 at 23 °C under an air stream. The results are listed in Table 2. 1,1-Diphenylethenes (**1a**—**e**) always gave 4-carbamoyl-3-methyl-1,2-dioxan-3-ols in excellent yields, whereas 2-ethyl-1-butene (**1f**) yielded the corresponding 4-carbamoyl-3-methyl-1,2-dioxan-3-ols in a slightly lower yield (Entries 39, 40). (*E*)-1,2-Diphenylethene and triphenylethene were not reactive.

Structural Assignments. Contrary to the reactions of the 1,3-diketones which gave a single stereoisomer,[2] the reaction of acetoacetamides yielded a mixture of two stereoisomers. When recrystallized **3ab** was dissolved in DMSO-d_6 for measurement of the ^{1}H NMR spectra, two methyl proton signals appeared at δ=1.27 and 1.53. The intensity of the methyl signal at the lower field gradually increased, while that of the methyl signal at the higher field decreased. The change in the intensities was followed at intervals and it was found that the mixture reached equilibrium after 12 h at room temperature. Thus, each isomer ratio (shown in Table 2) was determined from the intensities of the two methyl signals in the ^{1}H NMR spectrum at 12 h after preparing the solution. The ^{13}C NMR spectrum in DMSO-d_6 exhibited a pair of carbon signals: carbonyl carbons at δ=168.879 and 168.640, carbons attached to two oxygens at δ=101.885 and 98.185, carbons attached to one oxygen at δ=84.894 and 84.416, methine carbons at δ=48.212 and 47.391, methylene carbons at δ=34.234 and 30.624, and methyl carbons at δ=24.239 and 20.063. The assignments were based on their DEPT-135 and -90 spectra. The methyl ^{1}H signals at δ=1.27 and 1.53 were correlated to the methyl carbon signals at δ=24.239 and 20.063, respectively, by measuring a H,C COSY spectrum. The difference of the chemical shifts for the methyl signals in the ^{13}C NMR spectrum would indicate the different conformations of these methyl groups at the C-3 position in a 1,2-dioxane ring, that is, axial and equatorial methyl groups. In order to clarify the matter, methyl and acetyl derivatives of **3ab** were prepared and their ^{13}C NMR spectra were analyzed (Table 3). Treatment of **3ab** with dimethyl sulfate and potassium carbonate in refluxing acetone yielded two isomeric methyl derivatives, **5ab** (49%) and **5ab′** (35%) which were separated on a silica-gel column. It was the methyl carbon at the C-3 position that showed a larger chemical-shift difference than others in the ^{13}C NMR spectrum, and it appeared at δ=18.918 for **5ab** and δ=14.545 for **5ab′** (Table 3). It has been assigned that the methyl carbon with the higher field shift had an axial conformation, and the one with the lower field shift had an equatorial conformation.[3] A $-CH_2-CH<$ unit in **5ab** and **5ab′** was shown as an ABX and an AB_2 spin system, respectively, in the 400 MHz ^{1}H NMR spectra. Since both spin systems had large J values: J_{AB}=13.20, J_{AX}=14.83, J_{BX}=4.57 Hz for **5ab** and J_{AB}=13.9 Hz for **5ab′**, H-4 shoud have had a large J value as an axial hydrogen. It followed that both carbamoyl groups at C-4 in **5ab** and **5ab′** could be assigned as equatorial. Thus, the structures of **5ab** and **5ab′** were shown to be *c*-4-(phenylcarbamoyl)-*r*-3-methoxy-3-methyl-6,6-diphenyl-1,2-dioxane and *t*-4-(phenylcarbamoyl)-*r*-3-methoxy-3-methyl-6,6-diphenyl-1,2-dioxane, respectively (Fig. 1).

A similar situation existed for the acetates of **3ab**, which again consisted of two isomers, **6ab**, (54%) and **6ab′** (21%). The methyl carbon at C-3 appeared at δ=21.332 for **6ab** and δ=17.424 for **6ab′** (Table 3). Therefore, the structures of *c*-4-(phenylcarbamoyl)-3-methyl-6,6-diphenyl-1,2-dioxan-*r*-3-ol acetate and *t*-4-(phenylcarbamoyl)-3-methyl-6,6-diphenyl-1,2-dioxan-*r*-3-ol acetate could be assigned to **6ab** and **6ab′**, respectively.

It was thus shown that 4-(phenylcarbamoyl)-3-methyl-6,6-diphenyl-1,2-dioxan-3-ols (**3ab**) exist as an equilibrium mixture of two epimers at the C-3 position. This made quite a contrast with the 4-acetyl-3-methyl-1,2-dioxan-3-ols which were shown to exist as a single stereoisomer having an axial hydroxyl group.[2] It seems possible that hydrogen bonds can be formed

Table 3. Spectral Data for 4-(Phenylcarbamoyl)-3-methyl-6,6-diphenyl-1,2-dioxan-3-ol (**3ab**) and Its Derivatives

Compound	^{13}C NMR (δ)								^{1}H NMR (δ)	IR(ν)	
	>C=O	C-3	C-4	C-5	C-6	Me	OMe	OAc	Me	>C=O, –OAc	
3ab	168.640	98.185	47.391	30.624	84.416	20.063 (a)[a]			1.53 (a)	1657	
	168.879	101.885	48.212	34.234	84.896	24.239 (e)[b]			1.27 (e)		
5ab	169.316	100.860	50.439	33.806	85.704	18.918 (e)	49.350		1.30 (e)	1664	
5ab′	168.463	106.556	48.243	32.863	87.208	14.545 (a)	50.018		1.34 (a)	1692	
6ab	167.538	103.259	50.555	32.833	85.790	21.332 (e)		22.212	1.70 (e)	1665	1731
	167.448										
6ab′	168.386	109.047	48.362	32.953	86.939	17.424 (a)		22.257	1.73 (a)	1690	1732
	167.657										

a) a: axial. b) e: equatorial.

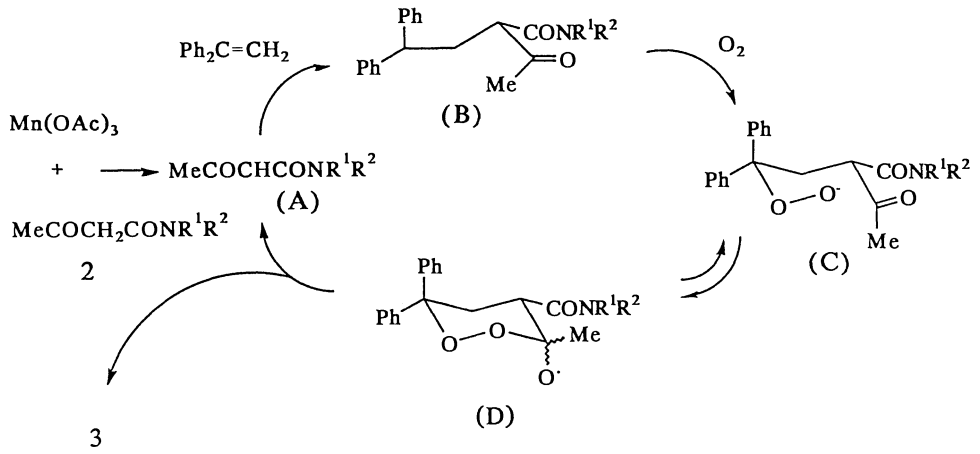

Scheme 1. The reaction mechanisms.

between the hydroxyl and carbamoyl groups in **3ab** irrespective of the conformation of the hydroxyl group, either axial or equatorial, and this could make the stability of the epimers comparable. **3ab** exhibited carbonyl absorption at ν 1657 which was compared with **5ab** (ν 1664), **5ab'** (ν 1692), **6ab** (ν 1665), and **6ab'** (ν 1690) (Table 3). This indicated the presence of hydrogen bonding between the hydroxyl and carbamoyl groups in **3ab**. On the other hand, the hydrogen bonding between the hydroxyl group and the carbonyl function in 4-acetyl-3-methyl-1,2-dioxan-3-ols may be weak, since the carbonyl absorption of this compound appeared at ν 1696 while that of the acetate appeared at ν 1701.[2] Therefore, the conformation of the hydroxyl group in 4-acetyl-3-methyl-1,2-dioxan-3-ol would be controlled mainly by an anomeric effect.[4]

Reactions of 3aa. Compound **3aa** was hydrogenated in the presence of palladium on charcoal as catalyst in ethanol to give 3-(4-methylphenylcarbamoyl)-2-methyl-5,5-diphenyl-tetrahydro-2-furanol (**7aa**), while hydrogenation in acetic acid yielded **4aa**, which was identical with that obtained in the manganese(III) acetate oxidation under an atmosphere of argon. On heating in acetic acid, **7aa** gave **4aa**. Treatment of **3aa** with aqueous potassium hydroxide solution yielded benzophenone in a moderate yield.

Reaction Mechanisms for the Formation of Compounds 3. The reaction could be accounted for in terms of a radical reaction initiated by the acetylcarbamoylmethyl radical (**A**), $\cdot CH(COCH_3)CONR^1R^2$, that was formed either by the interaction of $[Mn(OAc)_3]$ with acetoacetamide (**2**) or by the reaction of **2** with a carboxymethyl radical, $\cdot CH_2CO_2H$, which could be produced by the thermal decomposition[5] of $[Mn(OAc)_3]$. However, it seemed unlikely that the carboxymethyl radical would be formed at room temperature. Although we have not succeeded in obtaining a stable Mn(III)–acetoacetamide complex, the radical **A** could be produced by the interaction of **2** with $[Mn(OAc)_3]$. In fact, the radical **A** was trapped with xanthene to give *N*-phenyl-2-(9-xanthenyl)acetoacetamide (**8**) as in the reaction of malonamide.[6] The radical **A** attacked an alkene forming a stable tertiary carbon radical (**B**) which reacted with molecular oxygen to form a peroxyl radical (**C**), and then the alkoxyl radical (**D**), and finally gave **3** (Scheme 1). The reaction of **B** under an atmosphere of argon or reaction at an elevated temperature yielded the dihydrofuran (**4ab**).

Benzophenone was obtained in a reaction at a slightly higher temperature. The reaction of **1a** with $[Mn(OAc)_3]$ in the absence of acetoacetamide yielded 2,2-diphenyl-2-hydroxyethyl acetate (**9**) (4% yield) and benzophenone (7% yield). Thus, the formation of benzophenone could be envisaged as follows:

$$Ph_2C{=}CH_2 \xrightarrow[AcOH]{Mn(III)} Ph_2C(OH)CH_2OAc \xrightarrow{Mn(III)} Ph_2C{=}O$$
9

Alkaline degradation of **3aa** yielded benzophenone and a polymeric product which exhibited a broad multiplet at δ=3.7 together with other signals at δ=7.3 and 2.2. This could be explained as follows: a hydroxide ion attacked the proton on the $C_{(3)}$–OH to give an alkoxide anion (**E**), in which the 1,2-dioxane ring was

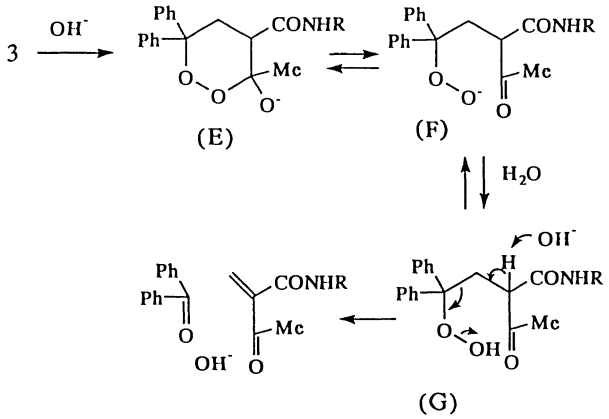

Scheme 2. R=4-methylphenyl.

opened to yield a peroxide anion (**F**). Abstraction of a proton from a solvent molecule and further decomposition of **G** yielded benzophenone and an acrylamide. The latter could not be isolated probably because of polymerization (Scheme 2).

It could thus be concluded that the facile radical reaction of an acetylcarbamoylmethyl radical with an alkene and molecular oxygen yielded a mixture of *c*-4- and *t*-4-carbamoyl-3-methyl-1,2-dioxan-*r*-3-ols (**3**) in excellent yields, although the electro-initiated formation of cyclic peroxide was reported.[7] The latter reaction seemed to be limited to the 1,3-dicarbonyl compounds which could produce only tertiary carbon radicals. Our reaction, on the other hand, has been successful with active methylenes as well as active methine compounds having an acyl and a carbamoyl group. This can be utilized in organic syntheses.

Experimental

Measurements. All the ^1H and ^{13}C NMR spectra were taken either with JNM PMX-60SI (60 MHz), JNM EX-90 FT NMR (90 MHz for ^1H, 22.4 MHz for ^{13}C) or JNM GX-400 FT NMR (400 MHz) spectrometers with tetramethylsilane used as the internal standard. Chemical shifts are shown in δ values (ppm). The IR spectra were measured on a JASCO A-102 IR spectrometer. The IR data are expressed in cm^{-1}. All melting moints were determined with a Yanaco MP-J3 micromelting point apparatus.

Materials. Manganese(III) acetate[8] was prepared according to the method in the literature. 1,1-Diphenylethenes (**1a—e**) were prepared by dehydration of the corresponding alcohols which were synthesized from substituted acetophenones and arylmagnesium bromides.[9] 2-Ethyl-1-butene (**1f**) and the acetoacetamides (**2a—2l**) were purchased from Tokyo-Kasei Co., Ltd. and used as received.

Reaction of Alkenes with Acetoacetamide in the Presence of Maganese(III) Acetate–O_2. The general procedure for the reaction of alkenes with acetoacetamide in the presence of $[Mn(OAc)_3]$–O_2 was as follows. $[Mn(OAc)_3]$ (1 mmol) was added to a stirred solution of an alkene (**1**, 1 mmol) and an acetoacetamide (**2**, 1—3 mmol) in acetic acid (25 cm^3) in a three-necked flask equipped with a dry air inlet tube. The mixture was stirred at 23 °C under an air stream for the period of time shown in Tables 1 and 2. The solvent was removed in vacuo and the residue was triturated with water, followed by extraction with benzene. The products were separated either on TLC (Wakogel B10) while eluting with chloroform, or on a silica-gel column eluting with benzene. The products were further purified by recrystallization from appropriate solvents. The yields are listed in Tables 1 and 2.

Products. 4-(4-Methylphenylcarbamoyl)-3-methyl-6,6-diphenyl-1,2-dioxan-3-ol (3aa): Mp 197—199 °C (from benzene–hexane); IR (KBr) ν 3500—3100 and 1648; ^1H NMR (60 MHz, DMSO-d_6) δ=1.23 and 1.47 (s, s, 3H), 2.22 (s, 3H), 2.71—3.02 (m, 3H), 6.83 and 7.01 (s, s, 1H), 7.05—7.81 (m, 14H), and 9.71 (br. s, 1H). Found: C, 74.38; H, 6.21; N, 3.51%. Calcd for $C_{25}H_{25}NO_4$: C, 74.42; N, 6.25; N, 3.47%.

4-(Phenylcarbamoyl)-3-methyl-6,6-diphenyl-1,2-dioxan-3-ol (3ab): Mp 168—170 °C (from benzene–hexane); IR (KBr) ν 3500—3100 and 1657; ^1H NMR (60 MHz, DMSO-d_6) δ=1.27 and 1.53 (s, s, 3H), 2.70—3.01 (m, 3H), 6.72 and 7.03 (s, s, 1H), 7.06—7.77 (m, 15H), and 9.73 (br. s, 1H). Found: C, 74.04; H, 5.85; N, 3.57%. Calcd for $C_{24}H_{23}O_4N$: C, 74.02; H, 5.95; N, 3.60%.

4-(4-Methoxyphenylcarbamoyl)-3-methyl-6,6-diphenyl-1,2-dioxan-3-ol (3ac): Mp 180—182 °C (from benzene–hexane); IR (KBr) ν 3500—3100 and 1641; ^1H NMR (60 MHz, DMSO-d_6) δ=1.23 and 1.50 (s, s, 3H), 2.60—3.01 (m, 3H), 3.69 (s, 3H), 6.75 and 6.93 (s, s, 1H), 7.15—7.71 (m, 14H), and 9.62 (br. s, 1H). Found: C, 71.98; H, 6.33; N, 3.13%. Calcd for $C_{25}H_{25}NO_5$: C, 71.58; H, 6,01; N, 3.34%.

4-(2-Methoxyphenylcarbamoyl)-3-methyl-6,6-diphenyl-1,2-dioxan-3-ol (3ad): Mp 188—190 °C (from benzene–hexane); IR (KBr) ν 3500—3100 and 1640; ^1H NMR (60 MHz, DMSO-d_6) δ=1.28 and 1.53 (s, s, 3H), 2.60—3.01 (m, 3H), 3.85 (s, 3H), 6.93 and 7.05 (s, s, 1H), 7.13—8.33 (m, 14H), and 9.67 (br. s, 1H). Found: C, 71.48; H, 6.27; N, 3.04%. Calcd for $C_{25}H_{25}NO_5$: C, 71.58; H, 6.01; N, 3.34%.

4-(2-Methylphenylcarbamoyl)-3-methyl-6,6-diphenyl-1,2-dioxan-3-ol (3ae): Mp 197—199 °C (from benzene–hexane); IR (KBr) ν 3500—3100 and 1644; ^1H NMR (60 MHz, DMSO-d_6) δ=1.34 and 1.57 (s, s, 3H), 2.23 (s, 3H), 2.70—3.01 (m, 3H), 7.01 and 7.32 (s, s, 1H), 7.68—7.90 (m, 14H), and 9.41 (br. s, 1H). Found: C, 74.62; H, 6.29; N, 3.43%. Calcd for $C_{25}H_{25}NO_4$: C, 74.42; H, 6.25; N, 3.47%.

4-(4-Chlorophenylcarbamoyl)-3-methyl-6,6-diphenyl-1,2-dioxan-3-ol (3af): Mp 192—194 °C (from benzene–hexane); IR (KBr) ν 3500—3100 and 1662; ^{1}NMR (60 MHz, DMSO-d_6) δ=1.29 and 1.51 (s, s, 3H), 2.70—3.01 (m, 3H), 6.86 and 7.18 (s, s, 1H), 7.30—7.74 (m, 14H), and 9.72 (br. s, 1H). Found: C, 68.07; H, 5.20; N, 3.34%. Calcd for $C_{24}H_{22}ClNO_4$: C, 68.00; H, 5.23; N, 3.30%.

4-(2-Chlorophenylcarbamoyl)-3-methyl-6,6-diphenyl-1,2-dioxan-3-ol (3ag): Mp 191—193 °C (from benzene–hexane); IR (KBr) ν 3500—3100 and 1656; ^1H NMR (60 MHz, DMSO-d_6) δ=1.36 and 1.52 (s, s, 3H), 2.80—3.13 (m, 3H), 7.03 and 7.16 (s, s, 1H), 7.31—7.76 (m, 14H), and 9.88 (br. s, 1H). Found: C, 67.78; H, 5.17; N, 3.30%. Calcd for $C_{24}H_{22}ClNO_4$: C, 68.00; H, 5.23; N, 3.30%.

4-Carbamoyl-3-methyl-6,6-diphenyl-1,2-dioxan-3-ol (3ah): Mp 179—181 °C (from benzene–hexane); IR (KBr) ν 3500—3100 and 1659; ^1H NMR (60 MHz, DMSO-d_6) δ=1.10 and 1.38 (s, s, 3H), 2.32—3.02 (m, 3H), 6.64 and 6.88 (s, s, 1H), 7.15 (br. s, 2H), and 7.17—7.73 (m, 10H). Found: C, 69.19; H, 6.09; N, 4.45%. Calcd for $C_{18}H_{19}NO_4$: C, 68.99; H, 6.11; N, 4.47%.

4-(Methylcarbamoyl)-3-methyl-6,6-diphenyl-1,2-dioxan-3-ol (3ai): Mp 193—195 °C (from benzene–hexane); IR (KBr) ν 3500—3100 and 1645; ^1H NMR (60 MHz, DMSO-d_6) δ=1.17 and 1.45 (s, s, 3H), 2.62 and 2.68 (s, s, 3H), 2.27—3.05 (m, 3H), 6.67 and 6.85 (s, s, 1H), 6.95—7.67 (m, 10H), and 7.82 (br. s, 1H). Found: C, 69.67; H, 6.40; N, 4.33%. Calcd for $C_{19}H_{21}NO_4$: C, 69.70; H, 6.47; N, 4.28%.

***c*-4-(Dimethylcarbamoyl)-3-methyl-6,6-diphenyl-1,2-dioxan-*r*-3-ol (3aj):** Mp 193—194 °C (from benzene–hexane); IR (KBr) ν 3260 and 1611; ^1H NMR (60 MHz, DMSO-d_6) δ=1.07 (s, 3H), 2.88 (s, 3H), 2.97 (s, 3H), 2.63—3.13 (m, 3H), 6.78 (s, 1H), and 7.16—7.78 (m, 10H); ^{13}C NMR (DMSO-d_6) δ=172.086, 143.653, 141.714, 128.288, 128.154, 127.587, 127.080, 126.304, 125.350, 98.140, 84.103, 42.304, 39.787, 37.068, 31.370, and 24.970. Found: C, 70.41; H, 6.71; N, 4.16%. Calcd for $C_{20}H_{23}NO_4$: C, 70.36; H, 6.79; N,

4.10%.

***t*-4-(Dimethylcarbamoyl)-3-methyl-6,6-diphenyl-1,2-dioxan-*r*-3-ol (3aj'):** Mp 190—191 °C (from benzene-hexane); IR (KBr) ν 3236 and 1614; ^{1}H NMR (60 MHz, DMSO-d_6) δ=1.38 (s, 3H), 2.91 (s, 3H), 3.01 (s, 3H), 2.65—3.15 (m, 3H), 6.87 (s, 1H), and 7.18—7.81 (m, 10H); ^{13}C NMR (DMSO-d_6) δ=170.202, 145.041, 142.132, 128.286, 128.169, 127.796, 127.080, 126.290, 125.171, 102.705, 84.924, 42.767, 37.334, 35.442, 35.442, and 20.286. Found: C, 70.38; H, 6.78; N, 4.11%. Calcd for $C_{20}H_{23}NO_4$: C, 70.36; H, 6.79; N, 4.10%.

4-(Diethylcarbamoyl)-3-methyl-6,6-diphenyl-1,2-dioxan-3-ol (3ak): Mp 190—191 °C (from benzene-hexane); IR (KBr) ν 3276 and 1613; ^{1}H NMR (60 MHz, DMSO-d_6) δ=0.81—1.23 (m, 6H), 1.06 and 1.23 (s, s, 3H), 2.63—2.96 (m, 3H), 3.05—3.53 (m, 4H), 6.78 and 6.97 (s, s, 1H), and 7.06—7.83 (m, 10H); ^{13}C NMR (DMSO-d_6) δ=171.445, 143.430, 141.610, 128.259, 128.140, 127.617, 127.065, 126.260, 125.410, 97.947, 84.163, 42.767, 41.917, 40.425, 32.026, 24.866, 14.439, and 12.738. Found: C, 71.59; H, 7.36; N, 3.86%. Calcd for $C_{22}H_{27}NO_4$: C, 71.52; H, 7.37; N, 3.79%.

4-(Morpholinocarbamoyl)-3-methyl-6,6-diphenyl-1,2-dioxan-3-ol (3al): Mp 196—197 °C (from benzene-hexane); IR (KBr) ν 3276 and 1612; ^{1}H NMR (60 MHz, DMSO-d_6) δ=1.33 (s, 3H), 2.61—3.11 (m, 3H), 3.12—4.01 (m, 8H), 7.03 (s, 1H), and 7.21—7.61 (m, 10H); ^{13}C NMR (DMSO-d_6) δ=168.714, 143.762, 141.982, 128.318, 128.184, 127.140, 127.095, 126.215, 125.171, 102.451, 85.043, 66.142, 46.138, 42.498, 42.051, 35.234, and 20.107. Found: C, 68.63; H, 6.58; N, 3.61%. Calcd for $C_{22}H_{25}NO_5$: C, 68.91; H, 6.57; N, 3.65%.

6,6-Bis(4-methylphenyl)-4-(4-methylphenylcarbamoyl)-3-methyl-1,2-dioxan-3-ol (3ba): Mp 165—168 °C (from benzene-hexane); IR (KBr) ν 3500—3100 and 1650; ^{1}H NMR (60 MHz, DMSO-d_6) δ=1.22 and 1.48 (s, s, 3H), 2.20 (s, 3H), 2.25 (s, 3H), 2.27 (s, 3H) , 2.57—2.98 (m, 3H) , 6.77 and 6.90 (s, s, 1H), 6.78—7.60 (m, 12H), and 9.62 (br. s, 1H). Found: C, 75.17; H, 6.77; N, 3.24%. Calcd for $C_{27}H_{29}NO_4$: C, 75.15; H, 6.77; N, 3.25%.

6,6-Bis(4-methylphenyl)-4-(phenylcarbamoyl)-3-methyl-1,2-dioxan-3-ol (3bb): Mp 193—195 °C (from benzene-hexane); IR (KBr) ν 3500—3100 and 1659; ^{1}H NMR (60 MHz, DMSO-d_6) δ=1.23 and 1.48 (s, s, 3H), 2.05 (s, 3H), 2.12 (s, 3H), 2.61—3.01 (m, 3H), 6.71 and 6.75 (s, s, 1H), 6.93—7.73 (m, 13H), and 9.83 (br. s, 1H). Found: C, 74.85; H, 6.51; N, 3.37%. Calcd for $C_{26}H_{27}NO_4$: C, 74.80; H, 6.52; N, 3.36%.

6,6-Bis(4-methylphenyl)-4-(2-methylphenylcarbamoyl)-3-methyl-1,2-dioxan-3-ol (3be): Mp 164—167 °C (from benzene-hexane); IR (KBr) ν 3500—3100 and 1624; ^{1}H NMR (60 MHz, DMSO-d_6) δ=1.27 and 1.44 (s, s, 3H), 2.17 (s, 3H), 2.21 (s, 3H), 2.29 (s, 3H), 2.61—3.01 (m, 3H) 6.98 and 7.32 (s, 1H), 7.02—7.69 (m, 12H), and 9.28 (br. s, 1H). Found: C, 75.09; H, 6.78; N, 3.24%. Calcd for $C_{27}H_{29}NO_4$: C, 75.15; H, 6.77; N, 3.25%.

4-(4-Chlorophenylcarbamoyl)-6,6-bis(4-methylphenyl)-3-methyl-1,2-dioxan-3-ol (3bf): Mp 120—123 °C (from benzene-hexane); IR (KBr) ν 3500—3100 and 1658; ^{1}H NMR (60 MHz, DMSO-d_6) δ=1.25 and 1.52 (s, s, 3H), 2.18 (s, 3H), 2.29 (s, 3H), 2.63—3.01 (m, 3H), 6.72 and 7.00 (s, s, 1H), 7.03—7.92 (m, 12H), and 9.28 (br. s, 1H). Found: C, 68.83; H, 5.80; N, 3.17%. Calcd for $C_{26}H_{26}ClNO_4$: C, 69.10; H, 5.80; N, 3.10%.

4-(2-Chlorophenylcarbamoyl)-6,6-bis(4-methylphenyl)-3-methyl-1,2-dioxan-3-ol (3bg): Mp 169—171 °C (from benzene-hexane); IR (KBr) ν 3500—3100 and 1658; ^{1}H NMR (60 MHz, DMSO-d_6) δ=1.32 and 1.51 (s, s, 3H), 2.21 (s, 3H), 2.30 (s, 3H), 2.57—3.02 (m, 3H), 7.01—8.20 (m, 13H), and 9.81 (br. s, 1H). Found: C, 68.72; H, 5.80; N, 3.18%. Calcd for $C_{26}N_{26}ClNO_4$: C, 69.10; H, 5.80; N, 3.10%.

6,6-Bis(4-methylphenyl)-4-carbamoyl-3-methyl-1,2-dioxan-3-ol (3bh): Mp 194—197 °C (from benzene-hexane); IR (KBr) ν 3500—3100 and 1641; ^{1}H NMR (60 MHz, DMSO-d_6) δ=1.18 and 1.42 (s, s, 3H), 2.22 (s, 3H), 2.27 (s, 3H), 2.78—3.02 (m, 3H), 6.67 and 6.83 (s, s, 1H), 6.92 (br. s, 2H), and 6.93—7.59 (m, 8H). Found: C, 70.38; H, 6.77; N, 4.11%. Calcd for $C_{20}H_{23}NO_4$: C, 70.38; H, 6.79; N, 4.10%.

6,6-Bis(4-fluorophenyl)-4-(phenylcarbamoyl)-3-methyl-1,2-dioxan-3-ol (3cb): Mp 185—188 °C (from benzene-hexane); IR (KBr) ν 3500—3100 and 1646; ^{1}H NMR (60 MHz, DMSO-d_6) δ=1.23 and 1.52 (s, s, 3H), 2.61—3.11 (m, 3H), 6.85 and 7.03 (s, s, 1H), 7.04—7.92 (m, 13H), and 9.81 (br. s, 1H). Found: C, 67.80; H, 4.95; N, 3.31%. Calcd for $C_{24}H_{21}F_2NO_4$: C, 67.75; H, 4.98; N, 3.30%.

6,6-Bis(4-fluorophenyl)-4-(dimethylcarbamoyl)-3-methyl-1,2-dioxan-3-ol (3cj): Mp 162—164 °C (from benzene-hexane); IR (KBr) ν 3380 and 1627; ^{1}H NMR (60 MHz, DMSO-d_6) δ=1.08 and 1.38 (s, s, 3H), 2.89 (s, 3H), 2.97 (s, 3H), 2.68—3.11 (m, 3H), 6.80 and 6.98 (s, s, 1H), and 6.92—7.86 (m, 8H); Found: C, 63.84; H, 5.65; N, 3.66%. Calcd for $C_{20}H_{21}F_2NO_4$: C, 63.65; H, 5.61; N, 3.71%.

6,6-Bis(4-chlorophenyl)-4-(2-chlorophenylcarbamoyl)-1,2-dioxan-3-ol (3dg): Mp 154—156 °C (from benzene-hexane); IR (KBr) ν 3500—3100 and 1658; ^{1}H NMR (60 MHz, DMSO-d_6) δ=1.35 and 1.51 (s, s, 3H), 2.62—3.01 (m, 3H), 7.13 and 7.25 (s, s, 1H), 7.15—8.12 (m, 12H), and 9.81 (br. s, 1H). Found: C, 57.97; H, 4.17; N, 2.91%. Calcd for $C_{24}H_{20}Cl_3NO_4$: C, 58.49; H, 4.10; N, 2.84%.

6,6-Bis(4-chlorophenyl)-4-(dimethylcarbamoyl)-3-methyl-1,2-dioxan-3-ol (3dj): Mp 191—192 °C (from benzene-hexane); IR (KBr) ν 3292 and 1617; ^{1}H NMR (60 MHz, DMSO-d_6) δ=1.18 and 1.42 (s, s, 3H), 2.58 (s, 3H), 2.65 (s, 3H), 2.66—3.13 (m, 3H), 6.75 and 6.98 (s, s, 1H), and 7.32—7.61 (m, 8H). Found: C, 58.57; H, 5.20; N, 3.37%. Calcd for $C_{20}H_{21}Cl_2NO_4$: C, 58.54; H, 5.16; N, 3.31%.

4-(2-Chlorophenylcarbamoyl)-6,6-bis(4-methoxyphenyl)-3-methyl-1,2-dioxan-3-ol (3eg): Mp 124—126 °C (from benzene-hexane); IR (KBr) ν 3500—3100 and 1655; ^{1}H NMR (60 MHz, DMSO-d_6) δ=1.30 and 1.52 (s, s, 3H), 2.66—3.04 (m, 3H), 3.71 (s, 3H), 3.77 (s, 3H) , 6.83—8.33 (m, 13H), and 9.81 (br. s, 1H). Found: C, 64.48; N, 5.47; N, 3.08%. Calcd for $C_{26}H_{26}ClNO_6$: C, 64.53; H, 5.42; N, 2.91%.

6,6-Bis(4-methoxyphenyl)-4-(dimethylcarbamoyl)-3-methyl-1,2-dioxan-3-ol (3ej): Mp 200—201 °C (from benzene-hexane); IR (KBr) ν 3192 and 1608; ^{1}H NMR (60 MHz, DMSO-d_6) δ=1.08 and 1.34 (s, s, 3H), 2.88 (s, 3H), 2.96 (s, 3H), 2.64—3.13 (m, 3H), 3.71 (s, 3H), 3.77 (s, 3H), 6.73 and 7.01 (s, s, 1H), and 6.83—7.63 (m, 8H). Found: C, 65.67; H, 6.78; N, 3.48%. Calcd for $C_{22}H_{27}NO_6$: C, 65.82; H, 6.78; N, 3.79%.

4-(Phenylcarbamoyl)-6,6-diethyl-3-methyl-1,2-dioxan-3-ol (3fb): Mp 149—152 °C (from benzene-hexane); IR (KBr) ν 3500—3100 and 1642; ^{1}H NMR (60 MHz, DMSO-d_6) δ=0.72—1.13 (m, 6H), 1.28—2.31 (m, 7H), 2.72—3.08 (m, 3H), 6.50 and 6.83 (s, s, 1H), 7.01—8.02 (m, 5H), and 9.77 (br. s, 1H); ^{13}C NMR (DMSO-d_6) δ=169.789, 169.595, 138.999, 138.701, 128.632, 128.587, 123.411, 123.142, 119.443, 119.147,

101.706, 97.499, 81.970, 80.672, 47.526, 46.064, 32.130, 29.609, 27.953, 27.867, 24.015, 22.777, 24.478, 19.868, 7.502, 7.397, 7.342, and 6.965. Found: C, 65.63; H, 7.62; N, 5.01%. Calcd for $C_{16}H_{23}NO_4$: C, 65.51; H, 7.90; N, 4.78%.

4-(4-Chlorophenylcarbamoyl)-6,6-diethyl-3-methyl-1,2-dioxan-3-ol (3ff): Mp 157—159 °C (from benzene–hexane); IR (KBr) ν 3500—3100 and 1658; ^{1}H NMR (60 MHz, DMSO-d_6) δ=0.63—1.08 (m, 6H), 1.28—2.31 (m, 7H), 2.66—3.12 (m, 3H), 6.50 and 6.83 (s, s, 1H), 7.22—7.78 (m, 4H), and 9.93 (br. s, 1H); ^{13}C NMR (DMSO-d_6) δ=169.799, 169.596, 137.927, 137.673, 128.484, 128.371, 126.962, 126.724, 120.981, 101.618, 97.456, 81.961, 80.659, 47.526, 46.214, 32.037, 29.417, 27.825, 27.821, 24.017, 22.764, 24.465, 19.885, 7.489, 7.384, 7.381, and 6.966. Found: C, 58.49; H, 6.62; N, 4.35%. Calcd for $C_{16}H_{22}ClNO_4$: C, 58.62; H, 6.73; N, 4.27%.

3-(4-Methylphenylcarbamoyl)-2-methyl-5,5-diphenyl-4,5-dihydrofuran (4aa): Mp 251—252 °C (from ethanol); IR (KBr) ν 3264 and 1657; ^{1}H NMR (60 MHz, DMSO-d_6) δ=2.23 (s, 3H), 2.30 (t, J=1.2 Hz, 3H), 3.73 (q, J=1.2 Hz, 2H), 6.98—7.68 (m, 14H), and 9.81 (br. s, 1H). Found: C, 81.34; H, 6.33; N, 3.72%. Calcd for $C_{25}H_{23}NO_2$: C, 81.26; H, 6.28; N, 3.79%.

Methylation of 4-(Phenylcarbamoyl)-3-methyl-6,6-diphenyl-1,2-dioxan-3-ol (3ab). Anhydrous potassium carbonate (180 mg) and dimethyl sulfate (170 mg) were added to compound **3ab** (389 mg) in anhydrous acetone (5 cm^3). The mixture was heated under reflux for 10 h. Water (5 cm^3) was added to the mixture after cooling and the acetone was removed. The residue was extracted with chloroform (total 60 cm^3) and the extract was dried over anhydrous magnesium sulfate. After the removal of the chloroform, the crude product was chromatographed on a silica-gel column while eluting with benzene to give *c*-4-(phenylcarbamoyl)-*r*-3-methoxy-3-methyl-6,6-diphenyl-1,2-dioxane (**5ab**) (197 mg, 49% yield), and *t*-4-(phenylcarbamoyl)-*r*-3-methoxyl-6,6-diphenyl-1,2-dioxane (**5ab′**) (141 mg, 35% yield).

***c*-4-(Phenylcarbamoyl)-*r*-3-methoxy-3-methyl-6,6-diphenyl-1,2-dioxane (5ab):** Mp 186—187 °C (from benzene–hexane); IR (KBr) ν 3308 and 1664; ^{1}H NMR (400 MHz, $CDCl_3$) δ=1.299 (s, 3H), 2.826—2.856 (m, J=13.20, 14.83, and 4.57 Hz, 2H), 2.970 (dd, J=14.83 and 4.57 Hz, 1H),3.449 (s, 3H), 7.110—7.605 (m, 15H), and 8.807 (s, 1H); ^{13}C NMR ($CDCl_3$) δ=169.316, 143.405, 140.481, 137.840, 128.979, 128.592, 128.323, 127.786, 127.592, 126.995, 125.921, 124.266, 119.820, 100.860, 85.704, 50.439, 49.350, 33.806, and 18.918. Found: C, 74.39; H, 6.33; N, 3.45%. Calcd for $C_{25}H_{25}NO_4$: C, 74.42; H, 6.25; N, 3.47%.

***t*-4-(Phenylcarbamoyl)-*r*-3-methoxy-3-methyl-6,6-diphenyl-1,2-dioxane (5ab′):** Mp 176—177 °C (from benzene–hexane); IR (KBr) ν 3340 and 1692; ^{1}H NMR (400 MHz, $CDCl_3$) δ=1.336 (s, 3H), 2.531 (t, J=13.92 Hz, 1H), 3.032—3.076 (d, J=13.92 Hz, 2H), 3.489 (s, 3H), 7.11—7.49 (m, 15H), and 7.78 (s, 1H); ^{13}C NMR ($CDCl_3$) δ=168.463, 145.684, 141.507, 137.703, 129.066, 128.514, 128.320, 127.738, 126.187, 125.799, 124.292, 119.593, 106.556, 87.208, 50.018, 48.243, 32.863, and 14.545. Found: C, 74.39; H, 6.31; N, 3.49%. Calcd for $C_{25}H_{25}NO_4$: C, 74.42; H, 6.25; N, 3.47%.

Acetylation of 4-(Phenylcarbamoyl)-3-methyl-6,6-diphenyl-1,2-dioxan-3-ol (3ab). Compound **3ab** (389 mg) was treated with a mixture of acetic anhydride (102 mg), pyridine (14 mg), and triethylamine (121 mg) at room temperature overnight. The reaction mixture was concentrated to dryness in vacuo and the residue was dissolved in benzene (30 cm^3). The benzene solution was washed with 2 M (1 M=1 mol dm^{-3}) hydrochloric acid (30 cm^3), and with a saturated aqueous sodium hydrogencarbonate solution, then dried over anhydrous magnesium sulfate. After the removal of the benzene, the residue was chromatographed on a silica-gel column while eluting with benzene, giving *c*-4-(phenylcarbamoyl)-3-methyl-6,6-diphenyl-1,2-dioxan-*r*-3-ol acetate (**6ab**) (232 mg, 54% yield), and *t*-4-(phenylcarbamoyl)-3-methyl-6,6-diphenyl-1,2-dioxan-*r*-3-ol acetate (**6ab′**) (91 mg, 21% yield).

***c*-4-(Phenylcarbamoyl)-3-methyl-6,6-diphenyl-1,2-dioxan-*r*-3-ol Acetate (6ab):** Mp 186—187 °C (from benzene–hexane); IR (KBr) ν 3320, 1731, and 1665; ^{1}H NMR (60 MHz, $CDCl_3$) δ=1.70 (s, 3H), 2.15 (s, 3H), 2.76—3.36 (m, 3H), 7.06—7.68 (m, 15H), and 7.83 (s, 1H); ^{13}C NMR ($CDCl_3$) δ=167.538, 167.448, 142.760, 140.299, 137.360, 129.170, 128.708, 128.484, 128.230, 127.664, 126.768, 125.724, 124.859, 119.966, 103.259, 85.790, 50.555, 32.833, 22.212, and 21.332. Found: C, 72.50; H, 5.85; N, 3.28%. Calcd for $C_{26}H_{25}NO_5$: C, 72.37; H, 5.84; N, 3.25%.

***t*-4-(Phenylcarbamoyl)-3-methyl-6,6-diphenyl-1,2-dioxan-*r*-3-ol Acetate (6ab′):** Mp 153—154 °C (from benzene–hexane); IR (KBr) ν 3382, 1732, and 1690; ^{1}H NMR (60 MHz, $CDCl_3$), δ=1.73 (s, 3H), 2.21 (s, 3H), 2.78—3.23 (m, 3H), 7.13—7.66 (m, 15H), and 7.83 (s, 1H); ^{13}C NMR ($CDCl_3$) δ=168.836, 167.657, 145.341, 141.051, 137.434, 129.111, 128.588, 128.365, 127.977, 127.335, 126.052, 125.575, 124.680, 119.802, 109.047, 86.939, 48.362, 32.953, 22.257, and 17.424. Found: C, 72.45; H, 5.84; N, 3.24%; Calcd for $C_{26}H_{25}NO_5$: C, 72.37; H, 5.84; N, 3.25%.

Catalytic Hydrogenation of 4-(4-Methylphenylcarbamoyl)-3-methyl-6,6-diphenyl-1,2-dioxan-3-ol (3aa). (a) In acetic acid. A mixture of **3aa** (403 mg) and 5% palladium on charcoal (20 mg) in ethyl acetate (5 cm^3) was stirred under an atmosphere of hydrogen at room temperature for 3 h. The reaction mixture was filtered and the filtrate was concentrated to dryness. The solidified residue was recrystallized from benzene, giving 3-(4-methylphenylcarbamoyl)-2-methyl-5,5-diphenyl-4,5-dihydrofuran (**4aa**) (86% yield): Mp 251—252 °C; (b) In ethanol. Hydrogenation of **3aa** similar to (a) but in ethanol yielded 3-(4-methylphenylcarbamoyl)-2-methyl-5,5-diphenyltetrahydro-2-furanol (**7aa**) (80% yield): Mp 225—227 °C (from ethanol); IR (KBr) ν 3600—3100, and 1642; ^{1}H NMR (60 MHz, DMSO-d_6), δ=1.57 (s, 3H), 2.22 (s, 3H), 2.81—3.12 (m, 3H), 6.11 (s, 1H), 7.03—7.67 (m, 14H), and 9.66 (br. s, 1H). Found: C, 77.51; H, 6.50; N, 3.60%. Calcd for $C_{25}H_{25}NO_3$: C, 77.49; H, 6.50; N, 3.61%.

Dehydration of 7aa. Compound **7aa** (194 mg) was dissolved in acetic acid (0.5 cm^3) and the solution was heated under reflux for 1 h. After the removal of the acetic acid, the residue was recrystallized from benzene, giving **4aa** (87% yield): Mp 251—252 °C, identical with that obtained from the preceding experiment (a).

Decomposition of 3aa with Methanolic Potassium Hydroxide. A mixture of **3aa** (202 mg) and 5% KOH–MeOH (10 cm^3) was heated under reflux for 2 h. After the removal of the methanol, Water (20 cm^3) was added, and the mixture was extracted with benzene (total 60 cm^3). The benzene solution was washed with dilute hydrochloric acid (30 cm^3), a saturated aqueous sodium hydrogencarbonate solution (20 cm^3), and water (20 cm^3), and then dried over anhydrous magnesium sulfate. After the removal of the benzene, the resulting mixture was chromatographed on a silica-gel plate while eluting with benzene, yielding benzophenone (66 mg, 72% yield).

Reaction of Xanthene with *N*-Phenylacetoacetamide (2b) in the Presence of Manganese(III) Acetate. [$Mn(OAc)_3$] (536 mg) was added to a solution of xanthene (180 mg) and **2b** (707 mg) in acetic acid (30 cm^3) at 100 °C. The reaction mixture was heated at the same temperature until the dark-brown color of the solution turned opaque white (approximately 3 min). After the removal of the solvent under reduced pressure, the residue was treated with 2 M hydrochloric acid (30 cm^3) and extracted with chloroform (25 $cm^3 \times 3$). The products were separated on a silica-gel column, while eluting with chloroform, and recrystallized.

***N*-Phenyl-2-(9-xanthenyl)acetoacetamide (8).** (182.1 mg, 51% yield): Mp 203—204 °C (from ethanol); IR (KBr) ν 3328, 1719, and 1659; ^1H NMR (60 MHz, DMSO-d_6) δ=1.99 (s, 3H), 3.90 (d, J=10.0 Hz, 1H), 3.87 (d, J=10.0 Hz, 1H), 6.8—7.6 (m, 13H), and 9.91 (br. s, 1H). Found: C, 77.09; H, 5.31; N, 4.09%. Calcd for $C_{23}H_{19}O_3N$: C, 77.29; H, 5.36; N, 3.92%. Xanthene (34.5 mg, 19% yield) and *N*-phenylacetoacetamide (**2a**, 69.2 mg, 10% yield) were recovered.

Reaction of 1,1-Diphenylethene (1a) with Manganese(III) Acetate. A mixture of **1a** (180 mg) and [$Mn(OAc)_3$] (268 mg) in acetic acid (30 cm^3) was stirred at 23 °C under an air stream for 12 h. The reaction mixture was worked-up in a manner similar to that described above, giving 2,2-diphenyl-2-hydroxyethyl acetate (**9**) (10.2 mg, 4% yield, mp 87—88 °C (lit,[10] mp 91 °C)), benzophenone (12.7 mg, 7% yield), and unreacted **1a** (147.6 mg, 82% yield).

References

1) I. Saito and S. S. Nittala, "Endoperoxides," in "The Chemistry of Peroxides," ed by S. Patai, John Wiley, New York (1983), pp. 311—374. L. Zhang, W.-S. Zhou, and X.-X. Ku, *J. Chem. Soc., Chem. Commun.*, **1988**, 523.

2) a) S. Tategami, T. Yamada, H. Nishino, J. D. Korp, and K. Kurosawa, *Tetrahedron Lett.*, **31**, 6371 (1990). b) H. Nishino, S. Tategami, T. Yamada, J. D. Korp, and K. Kurosawa, *Bull. Chem. Soc. Jpn.*, **64**, 1800 (1991).

3) D. K. Dalling and D. M. Grant, *J. Am. Chem. Soc.*, **89**, 6612 (1967).

4) J. T. Edward, *Chem. Ind.*, **1955**, 1102.

5) E. I. Heiba, R. M. Dessau, and P. G. Rodewald, *J. Am. Chem. Soc.*, **96**, 7977 (1974).

6) K. Tsunoda, M. Yamane, H. Nishino, and K. Kurosawa, *Bull. Chem. Soc. Jpn.*, **64**, 851 (1991).

7) J. Yoshida, K. Sakaguchi, and S. Isoe, *Tetrahedron Lett.*, **28**, 667 (1987). J. Yoshida, S. Nakatani, K. Sakaguchi, and S. Isoe, *J. Org. Chem.*, **54**, 3383 (1989). J. Yoshida, S. Nakatani, and S. Isoe, *Tetrahedron Lett.*, **31**, 2425 (1990).

8) P. Andrulis, Jr., M. J. S. Dewar, R. Dietz, and R. Hunt, *J. Am. Chem. Soc.*, **88**, 5473 (1966).

9) H. Nishino, *Bull. Chem. Soc. Jpn.*, **58**, 1922 (1985).

10) E. P. Kohler and E. M. Hygaard, *J. Am. Chem. Soc.*, **55**, 310 (1933).

Preparation of Some Polyfunctional Indenes and Indanones: The Reaction of Mercapto-Substituted Cyclopropenium Salts with Alcohols and Thiols

Hiroshi YOSHIDA,* Youko TAKAHASHI, Hiroaki KINOSHITA, Sadao UKISHIMA, Tsuyoshi OGATA, and Kiyoshi MATSUMOTO†

Department of Applied Chemistry, Faculty of Engineering, Shizuoka University, Hamamatsu 432
†Graduate School of Human and Environmental Studies, Kyoto University, Sakyo-ku, Kyoto 606

(Received June 26, 1991)

The reaction of 1-methylthio-, 1-(4-methylphenylthio)-, or 1-*t*-butylthio-2,3-diphenylcyclopropenium salts with alcohols, phenols, and thiols in the presence of triethylamine at around 80 °C gave 1*H*-indene-1-thiol derivatives in fair to moderate yields. In contrast, the same reactions at room temperature afforded 1-alkylthio- or arylthio-1-cyclopropene derivatives together with a small amount of the 3-isomer. Some 1-isomers were separated as pure crystals and produced the corresponding indenes in quantitative yields when heated. Kinetic studies of the ring-opening of cyclopropenes suggested a vinylcarbene intermediate based on the small effects of solvent polarities and phenoxyl substituents on the reaction rates. The reaction of diphenylcyclopropenone with thiol in the presence of trifluoroacetic acid yielded 1*H*-indene-1,3-dithiol detivatives via a 1,3-bis(alkylthio)-or (arylthio)-1-cyclopropene intermediate. On acidic hydrolysis of 3-alkoxyindenes and on heating of 3-allyloxy- and 3-(2-propynyloxy)indenes, polyfunctionally-substituted indanones were obtained in good yields.

In recent years, investigations of three membered carbocycles such as cyclopropane, cyclopropene, cyclopropenone, and cyclopropenium ion have been undertaken not only to satisfy physical interests but also to develop a versatile tool for organic syntheses.[1] In the series of our studies of the cyclopropenium salts bearing heteroatom substituents,[2] we have previously reported that the reaction of a mercapto-substituted cyclopropenium salt **1**, e.g. 1-methylthio-2,3-diphenylcyclopropenium bromide (**1a**) with acyclic[3] and cyclic 1,3-diketones[4] afforded pentadienols and 2*H*-pyranes, respectively. Furthermore, the reaction of **1a** with some Grignard reagents yielded a mixture of 1-methylthio- and 3-methylthiocyclopropenes, of which the former isomer lead to the ring opening products, indenes, via vinylcarbene intermediates (Scheme 1).[5]

Encouraged by these results, we undertook further studies of the reaction of **1** with other nucleophiles. We report here the reaction of **1** with alcohols, phenols, and thiols to produce polyfunctional indenes. Current interests in polysubstituted indenes have been focused on synthesis,[6] oxidation with ozone,[7] electrochemical reduction,[8] and application to medical chemistry.[9]

The salt **1a** has been prepared from methylation of diphenylcyclopropenethione,[3] whereas 1-(4-methylphenylthio)- and 1-*t*-butylthio-2,3-diphenylcyclopropenium tetrafluoroborates (**1b**, **c**) were obtained from the reaction of ethoxycyclopropenium tetrafluoroborate with thiols in good yields.

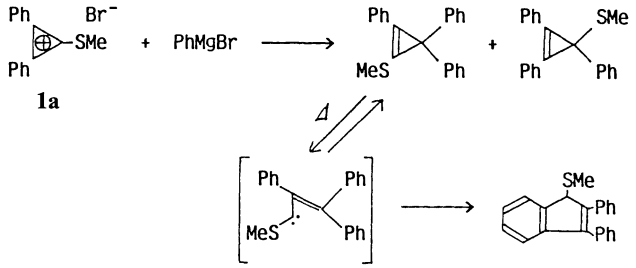

Scheme 1.

Treatment of a mixture of **1a**, methanol, and triethylamine (mole ratio, 1 : 1.1 : 3) in benzene at 80 °C afforded, after column chromatography over silica gel, 3-methoxy-1-methylthio-2-phenyl-1*H*-indene **3aa** in a 68% yield. The structure of the product was unequivocally established by ^{1}H and ^{13}C NMR and mass spectroscopic studies as well as by conversion to indanone **6a** upon standing in a hydrochloric acid–ethanol solution

Table 1. The Reaction of **1** with **2** in Benzene

1	2	Reaction conditions		Product (yield/%)
		Temp/°C	Time/h	
1a	**2a**	80	1	**3aa** (68)
	2c	80	1	**3ac** (74)
	2d	80	1	**3ad** (49)
	2e	80	1	**3ae** (52)
	2h	80	0.5	**3ah** (71)
	2i	80	0.5	**3ai** (76)
	2j	80	0.5	**3aj** (63)
	2k	80	0.5	**3ak** (61)
	2l	80	0.5	**3al** (32)
1b	**2a**	25	1.5	**3ba** (75)
	2b	80	1	**3bb** (52)
	2c	80	1	**3bc** (82)
	2d	80	1	**3bd** (69)
	2e	80	1	**3be** (91)
	2f	80	1	**3bf** (19)
	2g	80	1	**3bg** (37)
1c	**2a**	25	2	**3ca** (65)
	2b	80	1	**3cb** (59)
	2c	80	1	**3cc** (84)
	2d	80	1	**3cd** (94)

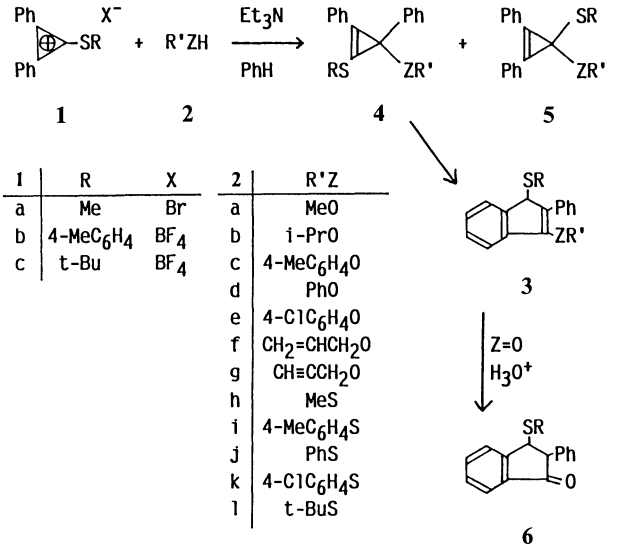

1	R	X
a	Me	Br
b	4-MeC$_6$H$_4$	BF_4
c	t-Bu	BF_4

2	R'Z
a	MeO
b	i-PrO
c	4-MeC$_6$H$_4$O
d	PhO
e	4-ClC$_6$H$_4$O
f	CH_2=$CHCH_2$O
g	CH≡CCH_2O
h	MeS
i	4-MeC$_6$H$_4$S
j	PhS
k	4-ClC$_6$H$_4$S
l	t-BuS

Scheme 2.

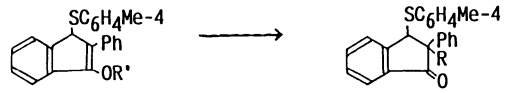

3bf: R'=–CH_2CH=CH_2 **7a**: R=–CH_2CH=CH_2
3bg: R'=–CH_2C≡CH **7b**: R=–CH=C=CH_2

Scheme 3.

at room temperature for 2 d. Similar treatment of the salts **1a**—**c** with alcohols, phenols, or thiols (**2a**—**g**) afforded indenes **3** in fair to moderate yields (Table 1).

The conversion of indenes with 3-allyloxy- and 3-(2-propynyloxy)-substituents (**3bf** and **3bg**) to indanones **7a** and **7b** was accomplished by means of heating at benzene reflux temperature via a Claisen rearrangement (Scheme 3).

In order to detect the intermediate cyclopropenes, some controlled experiments were performed. Thus, the salt **1a** was treated with methanethiol **2h** in the presence of triethylamine at room temperature for 10 min. The crude product absorbed at around 1780 cm^{-1} in the IR spectrum indicating the presence of cyclopropenes. The ^{1}H NMR spectrum showed a mixture of the cyclopropenes **4ah** and **5ah** together with a small amount of the indene **3ah** (Table 2). The ratio was determined by the integration of methylthio groups of **3ah**, **4ah**, and **5ah**, whose signals appeared at δ=1.20 and 2.12, 1.85 and 2.47, and 2.03 respectively. Attempted isolation of pure **4ah** and **5ah** by cc or tlc was unsuccessful, since **4ah** was thermally unstable and produced the corresponding indene **3ah**, while **5ah** was converted to the cyclopropenone. On cooling to −20 °C, petroleum ether was added to the crude reaction mixture and some cyclopropenes **4** were recovered as crystals (Table 2). The structure of **4** was unambiguously determined from its ^{1}H and ^{13}C NMR, and mass spectra, and transformations to the corresponding indenes **3**. As summarized in Table 2, the crude reaction mixture also contained 3-mercaptocyclopropene **5**. Only **5ak** was isolated as an oil by a short column separation. Although attempts to isolate the other **5**'s failed, ^{1}H NMR and IR spectra as well as isolation of cyclopropenone from the cc elution indicated the presence of **5**.

Cyclopropenes prepared from the reactions of the salts **1b** and **1c** with alcohols were too unstable to isolate in a pure form even by separation on short cc or at lower temperatures.

The distribution of the products **4** and **5** suggested that the employed nucleophiles preferentially attacked the carbon atom unsubstituted by sulfur. This regioselectivity was attributed to the strong electron releasing properties of alkyl- or arylthio groups and steric repulsion between the phenyl substituent of **1** and the entering nucleophiles as have been observed for the reaction between **1** and Grignard reagents.[5]

Keeping a solution of **4** at around 20 to 80 °C resulted in the formation of the corresponding indene **3** in quantitative yields. Kinetic studies were performed in order to clarify the mechanism of the ring opening of **4** (Table 3). The rate was followed at suitable time intervals by analyzing the ^{1}H NMR spectra of the methylthio groups

Table 2. The Reaction of **1a** with **2** under Controlled Conditions

2	Mole ratio **1a**:**2**:amine	Time/min	Temp/°C	Products **4**:**5**[a]	(Isolation/%)[b]
2c	1:1:3 (Et_3N)	15	25	10:1	(**4ac**, 46)
2d	1:1:3 (Et_3N)	15	25	6:1	
	1:1:3 (Et_3N)	10	10	6:1	(**4ad**, 52)
	1:1:5 (Et_3N)	10	10	6:1	
	1:1:3 (Et_2NPr-*i*)	15	10	6:1	
2e	1:1:3 (Et_3N)	15	25	6:1	(**4ae**, 57)
2h		15	25	9:1	
2i		15	25	6:1	
2j		15	25	6:1	
2k		15	25	6:1	(**4ak**, 52; **5ak**, 2)
2l		15	25	7:2	

a) The ratio was determined by ^{1}H NMR spectroscopy using SMe signals. b) Isolation by low-temperature crystallization.

Table 3. Kinetic Studies of the Themal Ring-Opening of **4**

Reactant	Solvent (ε)	Temp/°C	$10^4\ k_1/s^{-1}$	
4ac	CCl_4 (2.2)	55.5	2.24±0.20	
4ad	CCl_4 (2.2)	55.5	1.81±0.11	
4ae	CCl_4 (2.2)	45.0	0.48±0.05	a)
		50.4	0.72±0.03	
		55.5	1.42±0.07	
		60.0	2.03±0.13	
	C_6D_6 (2.3)	50.4	0.52±0.05	
	1,2-$C_6H_4Cl_2$ (9.9)	50.4	1.02±0.09	
	PhCN (25.2)	45.0	0.84±0.04	b)
		50.4	1.51±0.11	
		55.5	2.14±0.14	
		60.0	4.81±0.17	
	$PhNO_2$ (34.6)	50.4	1.01±0.07	
4ak	CCl_4 (2.2)	45.4	0.64±0.05	c)
		50.4	0.99±0.09	
		55.5	1.98±0.18	
		60.0	2.68±0.19	

a) E_a=90.1±2.0 kJ mol^{-1}, $\Delta S^{\ddagger}$=−10.1±1.3 eu.
b) E_a=89.1±5.9 kJ mol^{-1}, $\Delta S^{\ddagger}$=−10.1±4.6 eu.
c) E_a=90.1±0.3 kJ mol^{-1}, $\Delta S^{\ddagger}$=−10.1±0.1 eu.

of **4** by using methyl phenyl sulfide or dimethyl sulfone as an internal standard. The disappearance of **4** showed good first-order rate constants (k_1). Small effects of phenoxy substituents (ρ=−0.51) and solvents polarities on the rate indicated the small ionization of the intermediates of ring opening.

Tetraphenylcyclopropene has been reported to rearrange to indene with an activation energy of 167 kJ mol^{-1} (on heating at 240 °C),[10] while the activation energies of the rearrangement to **3** were only about 100 kJ mol^{-1}.

These results show that the ring opening of **4** proceeded via a vinylcarbene, stabilized by the adjacent mercapto group as shown in Scheme 1, followed by intramolecular hydrogen abstraction to produce indene **3**.

The following two reactions (Schemes 4 and 5) also provide support for the vinyl carbene intermediate for the ring opening of cyclopropenes. Treatment of **1** in methanol with triethylamine provided the methyl acetals **8a**, **b**, and **c** in 82, 86, and 85% yields respectively. Hydrolysis of **8** under acidic conditions afforded the vinyl ketones **9** in quantitative yields. Photoisomerization of **9c** in benzene yielded a 1 : 1 mixture of **9c** and **10**. The stereochemistry of **10** was assigned to *Z* on the basis of the ^{1}H NMR spectrum of the *t*-butylthio group at δ=1.39, because that of **9c** appeared at 1.33 (Scheme 4).

The cyclopropene **4ah** also reacted with refluxing methanol to give an unstable mixture of *E*- and *Z*-isomers of 3-methoxy-3-methylthio-1-propene **11** (Scheme 5). The structure was evident from the spectroscopic studies and conversion to the propenals **12** (Scheme 5). Although the two isomers could not be readily separated, high field ^{1}H NMR indicated that the *E*-isomer was the major product (10 : 3).

In our previous paper, we showed the reaction of cyclopropenone with thiol in the presence of potassium hydroxide in ethanol to yield thiolacrylates[11] (Scheme 6). Cyclopropenone is known to form a "salt"[12] with a Brönsted acid, and the salt is considered to be a hydroxy-substituted cyclopropenium.[11] It is reasonable to consider that the mercapto-substituted cyclopropenium ion would be generated in an acidic solution of cyclopropenone and thiol. This consideration was suggested by the following experiments. When a mixture of diphenylcyclopropenone **13**, methanethiol **2h**, and trifluoroacetic acid (mole ratio, 1 : 1 : 1) in benzene was heated at 60 °C, the indene **3ah** was obtained in a 15% yield along with **13** (70% recovery). The use of a mole rario of 1 : 3 : 3 resulted in better yields of **3** (Table 4). The ^{1}H NMR spectroscopic studies indicated that

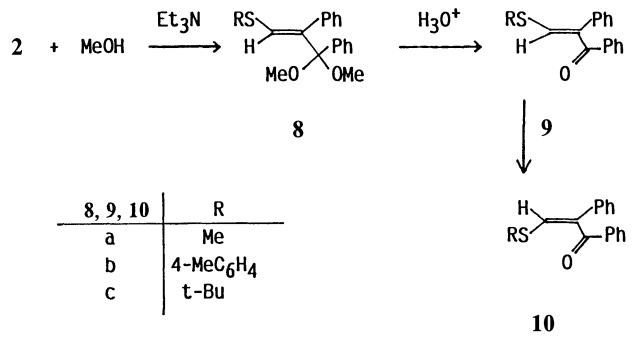

Scheme 4.

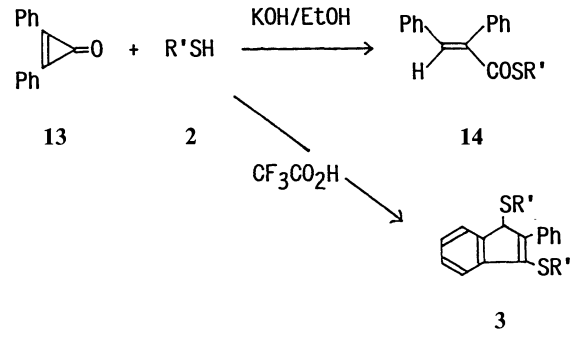

Scheme 6.

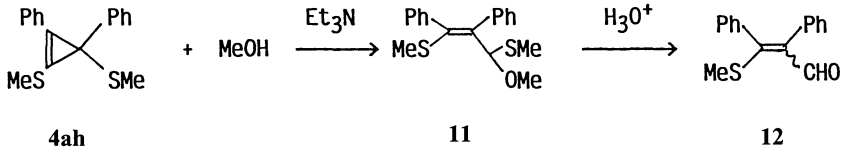

Scheme 5.

Table 4. The Reaction of Cyclopropenone **13** with Thiol **2** in the Presence of Trifluoroacetic Acid

Thiol	Solvent	Temp/°C	Time/d	Product (Yield/%)
2h	PhH	60	5	**3ah** (57)
2i	PhH	80	1	**3bi** (72)
	EtOH	80	1	(61)
2j	PhH	80	1	**3jj** (72)
2k	PhH	80	1	**3kk** (86)
	EtOH	80	1	(55)
2l	PhH	80	3	None
	EtOH	80	3	**14** (52)

the reaction mixture with a ratio 1 : 3 : 3 in benzene after 1 h at room temperature contained a mixture of **3ah**, **4ah**, and **5ah** in a mole ratio of 1 : 4 : 1.4. Whereas the bulky thiol **2l** did not yield indene **3**, but the thioacrylate **14** (R′=*t*-Bu), similar treatment of thiols **2i—k** with **13** produced indenes **3** in moderate yields (Table 4). Thus, the indenes **3** were formed from 1,3-bis(alkylthio)- or 1,3-bis(arylthio)-1-cyclopropenes **4** even under acidic conditions.

Experimental

1) General. Melting points were uncorrected. The ^{1}H NMR spectra were recorded on a Hitachi R-24B (60 MHz) and the ^{13}C NMR spectra on a JEOL JNM FX-90Q (22.49 MHz) or EX-90 (22.50 MHz) spectrometer. The IR spectra were obtained on a JEOL JIR 100 spectrometer.

2) Preparation of 1-Mercapto-2,3-diphenylcyclopropenium Salts (1). 1-Methylthio-2,3-diphenylcyclopropenium bromide (**1a**) was prepared as previously described.[3] 1-(4-Methylphenylthio)-2,3-diphenylcyclopropenium tetrafluoroborate (**1b**) was prepared as follows. A solution of triethyloxonium tetrafluoroborate (1.9 g, 10 mmol) and diphenylcyclopropenone (2.06 g, 10 mmol) in dichloromethane (10 cm^3) was stirred at room temperature for 2 h. To the mixture was added 4-thiocresol (1.24 g, 10 mmol) in one portion. 1 h later the precipitates were collected, washed with dry benzene, and dried in vacuo. **1b:** 2.8 g (85%); mp, 204—206 °C; IR (KBr) 1820 cm^{-1}; ^{1}H NMR ($CDCl_3$+CF_3CO_2H, 5 : 1) δ=2.52 (s, 3H, Me) and 7.3—8.2 (m, 14H, arom). The salt **1c** was prepared similarly. The only different point was that benzene was added to the reaction mixture to precipitate the salt. **1c:** 3.12 g (80%); mp 130—133 °C; IR (KBr) 1820 cm^{-1}; ($CDCl_3$+CF_3CO_2H, 5 : 1) δ=1.82 (s, 9H, *t*-Bu) and 7.6—8.4 (m, 10H, 2Ph).

3) The Reaction of 1 with Alcohols, Phenols, and Thiols (2). A mixture of **1** (2.0 mmol), **2** (2.2 mmol), and triethylamine (6.0 mmol) in dry benzene (15 cm^3) was stirred well at an appropriate temperature. The reactions with thiols were carried out in sealed tubes. The resulting solution was washed with aqueous sodium hydroxide (0.5% solution), dried over anhydrous sodium carbonate, and condensed in vacuo. The reactions at 80 °C yielded pure **3** on recrystallization from methanol unless otherwise stated (Table 1). The controlled reactions for shorter times at lower temperatures afforded a mixture of cyclopropenes (**4** and **5**). To the crude product was added petroleum ether and the mixture was cooled to −20 °C to afford crystalline **4**. In only one case was **5ak** provided after a short cc over silica gel (Table 2). The physical properties of **3**, **4**, and **5** were as follows.

3aa: Mp 82—84 °C; IR (KBr) 1600 cm^{-1}; ^{1}H NMR ($CDCl_3$) δ=1.25 (s, 3H, MeS), 3.74 (s, 3H, MeO), 4.58 (s, 1H, CH), and 6.8—8.0 (m, 9H, arom); MS (*m/z*), 268 (M$^+$). Found: C, 75.87; H, 5.99%. Calcd for $C_{17}H_{16}OS$: C, 76.08; H, 5.96%.

3ac: Mp 97—100 °C; IR (KBr) 1600 cm^{-1}; ^{1}H NMR ($CDCl_3$) δ=1.48 (s, 3H, MeS), 2.28 (s, 3H, Me), 4.86 (s, 1H, CH), and 6.6—8.0 (m, 13H, arom); ^{13}C NMR ($CDCl_3$) δ=9.2 (q, MeS), 20.6 (q, Me), 47.8 (d, CH), 116.1 (d), 119.6 (d), 124.2 (d), 126.4 (d), 127.2 (d), 127.6 (d), 128.1 (d), 128.2 (d), 130.1 (d), 132.1 (s), 132.2 (s), 138.7 (s), 143.1 (s), and 149.3 (s); MS (*m/z*), 344 (M$^+$). Found C, 80.25; H, 5.78%. Calcd for $C_{23}H_{20}OS$: C, 80.19; H, 5.85%.

3ad: Mp 79—80 °C IR (KBr) 1600 cm^{-1}; ^{1}H NMR ($CDCl_3$) δ=1.51 (s, 3H, MeS), 4.87 (s, 1H, CH), and 6.5—7.9 (m, 14H, arom); ^{13}C NMR ($CDCl_3$) δ=9.3 (q, MeS), 47.8 (d, CH), 116.7 (d), 119.6 (d), 122.7 (d), 124.3 (d), 126.5 (d), 127.3 (d), 127.4 (d), 128.0 (d), 128.2 (d), 128.3 (d), 130.0 (s), 132.2 (s), 138.6 (s), 143.1 (s), 149.0 (s), and 156.1 (s); MS (*m/z*), 330 (M$^+$). Found C, 79.90; H, 5.62%. Calcd for $C_{22}H_{18}OS$: C, 79.96; H, 5.49%.

3ae: Mp 142—145 °C; IR (KBr) 1600 cm^{-1}; ^{1}H NMR ($CDCl_3$) δ=1.40 (s, 3H, MeS), 4.87 (s, 1H, CH), and 6.7—7.9 (m, 13H, arom); MS (*m/z*), 364 (M$^+$). Found C, 72.54; H, 4.57%. Calcd for $C_{22}H_{17}ClOS$: C, 72.41; H, 4.69%.

3ah: Mp 94—96 °C; ^{1}H NMR ($CDCl_3$) δ=1.22 (s, 3H, Me), 2.12 (s, 3H, Me), 4.71 (s, 1H, CH), and 6.8—7.9 (m, 9H, arom); ^{13}C NMR ($CDCl_3$) δ=9.0 (q, Me), 17.1 (q, Me), 52.4 (d, CH), 120.2 (d), 123.9 (d), 126.2 (d), 127.6 (d), 127.7 (d), 127.9 (d), 129.3 (d), 133.7 (s), 134.4 (s), 142.9 (s), 144.0 (s), and 147.0 (s); MS (*m/z*), 284 (M$^+$). Found C, 71.68; H, 5.73%. Calcd for $C_{17}H_{16}S_2$: C, 71.78; H, 5.66%.

3ai: Mp 124—126 °C (hexane); ^{1}H NMR ($CDCl_3$) δ=1.38 (s, 3H, MeS), 2.20 (s, 3H, Me), 4.88 (s, 1H, CH), and 6.8—7.9 (m, 13H, arom); MS (*m/z*), 360 (M$^+$). Found C, 76.73; H, 5.52%. Calcd for $C_{23}H_{20}S_2$: C, 76.62; H, 5.59%.

3aj: Mp 128—129 °C; ^{1}H NMR ($CDCl_3$) δ=1.35 (s, 3H, MeS), 4.90 (s, 1H, CH), and 6.8—7.9 (m, 14H, arom); MS (*m/z*), 346 (M$^+$). Found C, 76.36; H, 5.29%. Calcd for $C_{22}H_{18}S_2$: C, 76.26; H, 5.24%.

3ak: Mp 119—121 °C; ^{1}H NMR ($CDCl_3$) δ=1.41 (s, 3H, MeS), 4.95 (s, 1H, CH), and 7.1—7.7 (m, 13H, arom); MS (*m/z*), 380 (M$^+$). Found C, 69.43; H, 4.54%. Calcd for $C_{22}H_{17}ClS_2$: C, 69.36; H, 4.49%.

3al: Mp 87—90 °C; ^{1}H NMR ($CDCl_3$) δ=1.08 (s, 9H, Bu-*t*), 1.23 (s, 3H, MeS), 4.76 (s, 1H, CH), and 7.0—7.6 (m, 9H, arom); MS (*m/z*), 326 (M$^+$). Found C, 73.68; H, 6.68%. Calcd for $C_{20}H_{22}S_2$: C, 73.57; H, 6.79%.

3ba: Mp 79—81 °C; IR (KBr) 1605 cm^{-1}; ^{1}H NMR ($CDCl_3$) δ=2.08 (s, 3H, Me), 3.58 (s, 3H, MeO), 4.87 (s, 1H, CH), and 6.6—7.9 (m, 13H, arom); MS (*m/z*), 344 (M$^+$). Found C, 80.04; H, 5.93%. Calcd for $C_{23}H_{20}OS$: C, 80.19; H, 5.85%.

3bb: Mp 76 °C; IR (KBr) 1605 cm^{-1}; ^{1}H NMR ($CDCl_3$) δ=1.14 (d, *J*=7 Hz, 6H, 2Me), 2.15 (s, 3H, Me), 4.35 (sept, 1H, CH), 4.96 (s, 1H, CH), and 6.5—8.1 (m, 13H, arom); MS (*m/z*), 372 (M$^+$). Found C, 80.74; H, 6.43%. Calcd for $C_{25}H_{24}OS$: C, 80.60; H, 6.49%.

3bc: Mp 198—199 °C; IR (KBr) 1605 cm^{-1}; ^{1}H NMR ($CDCl_3$) δ=2.30 (S, 6H, 2Me), 4.99 (s, 1H, CH), and 6.2—7.8 (m, 17H, arom); ^{13}C NMR ($CDCl_3$) δ=20.6 (q, Me), 21.2 (q, Me), 51.5 (d, CH), 116.1 (d), 119.7 (d), 124.6 (d), 126.1 (d),

126.3 (d), 127.1 (d), 128.0 (d), 128.3 (d), 128.4 (d), 129.0 (d), 129.9 (d), 131.8 (s), 132.6 (s), 136.0 (s), 138.5 (d), 138.7 (s), 143.8 (s), 149.5 (s), and 154.1 (s); MS (*m/z*), 420 (M^+). Found C, 82.90; H, 5.68%. Calcd for $C_{29}H_{24}OS$: C, 82.82; H, 5.75%.

3bd: Mp 131—134 °C; IR (KBr) 1600 cm^{-1}; ^1H NMR ($CDCl_3$) δ=2.26 (s, 3H, Me), 5.04 (s, 1H, CH), and 6.3—7.9 (m, 18H, arom); ^{13}C NMR ($CDCl_3$) δ=21.2 (q, Me), 51.4 (d, CH), 116.3 (d), 119.6 (d), 122.4 (d), 124.7 (d), 126.1 (d), 127.2 (d), 128.1 (d), 128.3 (s), 128.4 (d), 129.0 (d), 130.2 (s), 130.9 (s), 132.5 (d), 136.0 (d), 138.4 (s), 138.8 (s), 143.7 (s), 149.2 (s), and 156.2 (s); MS (*m/z*), 406 (M^+). Found C, 82.59; H, 5.52%. Calcd for $C_{28}H_{22}OS$: C, 82.72; H, 5.45%.

3be: Mp 192—194 °C; IR (KBr) 1595 cm^{-1}; ^1H NMR ($CDCl_3$) δ=2.25 (s, 3H, Me), 5.00 (s, 1H, CH), and 6.3—7.9 (m, 17H, arom); MS (*m/z*), 440 (M^+). Found C, 76.21; H, 4.75%. Calcd for $C_{28}H_{21}ClOS$: C, 76.26; H, 4.79%.

3bf: Mp 55—56 °C (petroleum ether); IR (KBr) 1600 cm^{-1}; ^1H NMR ($CDCl_3$) δ=2.18 (s, 3H, Me), 4.15—4.40 (m, 2H, CH_2), 4.88 (s, 1H, CH), 5.50 (m, 2H, CH_2O), and 6.4—7.8 (m, 13H, arom); MS (*m/z*), 370 (M^+). Found: C, 81.22; H, 5.91%. Calcd for $C_{25}H_{22}OS$: C, 81.04; H, 5.98%.

3bg: Mp 55—56 °C (petroleum ether); IR (KBr) 2140 and 1600 cm^{-1}; ^1H NMR ($CDCl_3$) δ=2.15 (s, 3H, Me), 2.40 (t, *J*=3 Hz, 1H, CH), 4.39 (d, *J*=3 Hz, 2H, CH_2), 4.89 (s, 1H, CH), and 6.9—7.8 (m, 13H, arom); ^{13}C NMR ($CDCl_3$) δ=21.2 (q, Me), 51.9 (d), 59.0 (t), 78.8 (s, $\underline{C}CH$), 118.8 (d), 124.1 (s), 124.4 (d), 126.3 (d), 127.1 (d), 127.4 (d), 128.2 (d), 128.7 (d), 128.9 (d), 129.8 (s), 132.2 (s), 134.9 (d), 138.3 (s), 139.3 (s), 143.6 (s), and 153.8 (s); MS (*m/z*), 368 (M^+). Found C, 81.42; H, 5.54%. Calcd for $C_{25}H_{19}OS$: C, 81.48; H, 5.47%.

3ca: Mp 116 °C; IR (KBr) 1600 cm^{-1}; ^1H NMR ($CDCl_3$) δ=1.01 (s, 9H, Bu-*t*), 3.72 (s, 3H, MeO), 4.64 (s, 1H, CH), and 7.0—8.1 (m, 9H, arom); MS (*m/z*), 310 (M^+). Found C, 77.43; H, 7.03%. Calcd for $C_{20}H_{22}OS$: C, 77.37; H, 7.14%.

3cb: Mp 76 °C; IR (KBr) 1605 cm^{-1}; ^1H NMR ($CDCl_3$) δ=1.14 (d, *J*=7 Hz, 2Me), 2.15 (s, 3H, Me), 4.35 (sept, 1H, CH), 4.96 (s, 1H, CH), and 6.5—8.1 (m, 13H, arom); MS (*m/z*), 338 (M^+). Found C, 78.14; H, 7.79%. Calcd for $C_{22}H_{26}OS$: C, 78.06; H, 7.74%.

3cc: Mp 129—130 °C IR (KBr) 1600 cm^{-1}; ^1H NMR ($CDCl_3$) δ=1.10 (s, 9H, Bu-*t*), 4.89 (s, 1H, CH), and 6.2—7.8 (m, 17H, arom); ^{13}C NMR ($CDCl_3$) δ=20.6 (q, Me), 32.3 (q, 3Me), 45.7 (s, $\underline{C}Me_3$), 48.8 (d, CH), 116.2 (d), 119.9 (d), 124.8 (d), 126.1 (d), 127.0 (d), 128.0 (d), 128.7 (d), 129.9 (s), 130.0 (d), 131.9 (s), 133.0 (s), 137.8 (s), 145.5 (s), 148.5 (s), and 154.3 (s); MS (*m/z*), 386 (M^+). Found C, 80.67; H, 6.79%. Calcd for $C_{26}H_{26}OS$: C, 80.78; H, 6.77%.

3cd: Oil; IR (KBr) 1600 cm^{-1}; ^1H NMR ($CDCl_3$) δ=1.12 (s, 9H, Bu-*t*), 4.93 (s, 1H, CH), and 6.7—7.8 (m, 13H, arom); MS (*m/z*), 372 (M^+). Found C, 80.69; H, 6.53%. Calcd for $C_{25}H_{24}OS$: C, 80.60;, H, 6.49%.

4ac: Mp 99—100 °C; IR (KBr) 1780 cm^{-1}; ^1H NMR ($CDCl_3$) δ=2.19 (s, 3H, Me), 2.56 (s, 3H, MeS), and 6.6—7.9 (m, 14H, arom); ^{13}C NMR (C_6D_6) δ=16.7 (q, MeS), 20.5 (q, Me), 69.5 (s, C_3), 118.3 (d), 118.7 (s), 119.3 (s), 126.9 (d), 128.5 (d), 128.7 (d), 128.9 (d), 130.0 (d), 130.5 (s), 142.3 (s), and 155.7 (s); MS (*m/z*), 343 (M^+−1). Found C, 80.09; H, 5.77%. Calcd for $C_{23}H_{20}OS$: C, 80.19; H, 5.85%.

4ad: Mp 107—108 °C; IR (KBr) 1790 cm^{-1}; ^1H NMR ($CDCl_3$) δ=2.59 (s, 3H, Me) and 6.5—7.9 (m, 15H, arom); ^{13}C NMR (C_6D_6) δ=16.7 (q, MeS), 69.2 (s, C_3), 118.0 (d), 118.4 (s), 119.3 (s), 121.4 (d), 126.6 (d), 126.9 (d), 128.4 (d), 128.7 (d), 128.9 (d), 129.5 (d), 129.9 (s), 142.0 (s), and 158.0 (s); MS (*m/z*), 330 (M^+). Found C, 80.06; H, 5.47%. Calcd for $C_{22}H_{18}OS$: C, 79.96; H, 5.49%.

4ae: Mp 122—124 °C; IR (KBr) 1785 cm^{-1}; ^1H NMR ($CDCl_3$) δ=2.65 (s, 3H, Me) and 6.7—7.8 (m, 14H, arom); ^{13}C NMR (C_6D_6) δ=16.8 (sm Me), 69.7 (s, C_3), 118.2 (s), 119.4 (d), 121.7 (s), 126.4 (d), 126.5 (d), 127.2 (d), 128.2 (d), 128.8 (d), 129.0 (d), 129.5 (d), 129.9 (s), 141.5 (s), and 156.6 (s); MS (*m/z*), 364 (M^+). Found C, 72.24; H, 4.55%. Calcd for $C_{22}H_{17}ClOS$: C, 72.41; H, 4.69%.

4ak: Mp 100—102 °C; IR (KBr) 1780 cm^{-1}; ^1H NMR ($CDCl_3$) δ=2.18 (s, 3H, Me) and 6.8—7.8 (m, 14H, arom); ^{13}C NMR (C_6D_6) δ=15.6 (q, Me), 30.1 (s, C_3), 122.3 (d), 127.4 (s), 127.6 (d), 128.3 (d), 128.7 (d), 129.8 (d), 130.0 (d), 132.9 (s), 134.8 (d), 135.5 (s), and 137.8 (s); MS (*m/z*), 380 (M^+). Found C, 69.31; H, 4.29%. Calcd for $C_{22}H_{17}ClS_2$: C, 69.36; H, 4.49%.

5ak: Oil; IR (KBr) 1820 cm^{-1}; ^1H NMR ($CDCl_3$) δ=2.25 (s, 3H, Me) and 6.3—8.0 (m, 14H, arom); ^{13}C NMR (C_6D_6) δ=1.3 (q, Me), 17.2 (s, C_3), 127.4 (s), 128.3 (d), 128.5 (d), 128.7 (d), 129.8 (d), 131.4 (s), 136.9 (s), 139.3 (s), and 147.3 (d); MS (*m/z*), 333 (M^+−1).

Hydrolysis of **3aa** or **3ba** (0.5 mmol) in a mixture of ethanol (10 cm^3) and 3 mol dm^{-3} aqueous HCl (15 cm^3) for 2 d at room temperature yielded 3-methylthio- or 3-(4-methylphenylthio)-2-phenyl-1-indanone [**6a**(R=Me) or **6b**(R=4-MeC_6H_4)] in 92 or 94% yields.

6a: Mp 76—77 °C (MeOH); IR (KBr) 1690 cm^{-1}; ^1H NMR ($CDCl_3$) δ=1.93 (s, 3H, Me), 3.79 (d, *J*=4 Hz, 1H, C_2H), 4.35 (d, *J*=4 Hz, 1H, and C_3H), and 6.9—7.9 (m, 9H, arom); MS (*m/z*), 254 (M^+). Found C, 75.49; H, 5.43%. Calcd for $C_{16}H_{14}OS$: C, 75.55; H, 5.54%.

6b: Mp 102—104 °C (MeOH); IR (KBr) 1710 cm^{-1}; ^1H NMR ($CDCl_3$) δ=2.19 (s, 3H, Me), 3.70 (d, *J*=4 Hz, C_2H), 4.60 (d, *J*=4 Hz, C_1H), and 6.5—7.9 (m, 13H, arom); MS (*m/z*), 330 (M^+). Found C, 79.91; H, 5.58%. Calcd for $C_{22}H_{18}OS$: C, 79.96; H, 5.49%.

Heating **3bf** and **3bg** in refluxing benzene for 2 d provided **7a** and **7b** in 95 and 92% yields, respectively, on crystallization from petroleum ether.

7a: Mp 119—122 °C; IR (KBr) 1720 cm^{-1}; ^1H NMR ($CDCl_3$) δ=2.20 (s, 3H, Me), 2.48—3.45 (m, 2H, CH_2), 4.7—5.2 (m, 2H, CH_2), 4.94 (s, 1H, C_1H), 5.2—6.1 (m, 1H, CH), and 6.4—7.8 (m, 13H, arom); MS (*m/z*), 370 (M^+). Found C, 80.89; H, 5.91%. Calcd for $C_{25}H_{22}OS$: C, 81.04; H, 5.98%.

7b: Mp 119—121 °C; IR (KBr) 1950 cm^{-1}; ^1H NMR ($CDCl_3$) δ=2.32 (s, 3H, Me), 4.81 (d, *J*=6 Hz, 2H, CH_2), 5.21 (s, 1H, C_1H), 5.70 (t, *J*=6 Hz, CH), and 6.5—8.0 (m, 13H, arom); ^{13}C NMR ($CDCl_3$) δ=21.0 (q, Me), 56.8 (d, C_3), 62.5 (s, C_2) 79.6 (t), 94.1 (d), 124.3 (s), 126.6 (s), 127.6 (d), 127.8 (d), 128.8 (d), 129.0 (d), 129.5 (d), 131.9 (d), 132.2 (d), 134.7 (s), 135.4 (d), 137.3 (s), 139.7 (s), 154.2 (s), 202.7 (s, CO), and 207.0 (s, =C=); MS (*m/z*), 368(M^+). Found C, 81.43; H, 5.55%. Calcd for $C_{25}H_{20}OS$: C, 81.48; H, 5.47%.

4) Kinetic Investigation of the Thermolysis of 4. A solution of **4** and methyl phenyl sulfide (or dimethyl sulfone) in an appropriate solvent was sealed in an NMR tube and was kept standing in a thermostated bath (±0.1 °C); the rate was followed at suitable time intervals by analyzing the ^1H NMR spectra of the methylthio groups of **3**, **4**, and the internal standard. The results are collected in Table 3.

5) Methanolysis of 1. A solution of **1** (2 mmol) and triethylamine (6 mmol) in methanol (15 cm^3) was refluxed for

1 h. The solution was quenched with aqueous NaOH (0.1%) and the organic product was extracted with benzene. The usual workup, followed by recrystallization from chloroform–petroleum ether, yielded the 2-propenalacetals **8**.

8a: 82%; mp 103—105 °C; IR (KBr) 1615 cm^{-1}; ^1H NMR ($CDCl_3$) δ=2.29 (s, 3H, MeS), 3.14 (s, 6H, 2MeO), and 6.7—7.8 (m, 11H, arom and =CH); ^{13}C NMR ($CDCl_3$) δ=17.4 (q, MeS), 49.1 (s, MeO), 103.0 (s), 126.9 (d), 127.5 (d), 129.3 (d), 131.0 (d), 136.5 (s), 137.5 (s), and 140.2 (s); MS (*m/z*), 300 (M^+). Found C, 71.83; H, 6.71%. Calcd for $C_{18}H_{20}O_2S$: C, 71.96; H, 6.71%.

8b: 86%; mp 90—93 °C: IR (KBr) 1600 cm^{-1}; ^1H NMR ($CDCl_3$) δ=2.32 (s, 3H, Me), 3.20 (s, 6H, 2MeO), and 6.7—7.5 (m, 14H, arom and =CH); ^{13}C NMR ($CDCl_3$) δ=21.0 (q, Me), 49.2 (q, MeO), 102.9 (s), 127.3 (d), 127.4 (d), 127.6 (d), 128.1 (d), 128.9 (d), 129.3 (d), 129.5 (d), 129.8 (d), 130.1 (d), 132.6 (s), 137.1 (s), 138.0 (s), and 139.9 (s); MS (*m/z*), 376 (M^+). Found C, 76.59; H, 6.24%. Calcd for $C_{24}H_{24}O_2S$: C, 76.56; H, 6.42%.

8c: 85%; mp 74—77 °C IR (KBr) 1600 cm^{-1}; ^1H NMR ($CDCl_3$) δ=1.40 (s, 9H, Bu-*t*), 3.19 (s, 6H, 2MeO), and 7.0—7.6 (m, 11H, arom and =CH); ^{13}C NMR ($CDCl_3$) δ=31.1 (q, 3Me), 43.6 (s, $\underline{C}Me_3$), 49.2 (s, MeO), 103.0 (s), 125.5 (d), 126.9 (d), 127.4 (d), 128.2 (d), 129.3 (d), 131.4 (d), 136.7 (s), 137.7 (s), and 140.3 (s); MS (*m/z*), 342 (M^+). Found C, 73.75; H, 7.87%. Calcd for $C_{21}H_{26}O_2S$: C, 73.64; H, 7.65%.

Hydrolysis of **8** (2 mmol) in a mixture of methanol (15 cm^3) and aqueous HCl (3 mol dm^{-3}, 10 cm^3) at room temperature for 1 d afforded phenyl vinyl ketones **9** in a quantitative yield from chloroform–petroleum ether.

9a: Mp 59—61 °C; IR (KBr) 1625 cm^{-1}; ^1H NMR ($CDCl_3$) δ=2.29 (s, 3H, Me) and 6.8—7.9 (m, 11H, arom and =CH); ^{13}C NMR ($CDCl_3$) δ=18.0 (q, Me), 127.7 (d), 128.0 (d), 128.2 (d), 129.2 (d), 131.4 (d), 135.9 (s), 136.4 (s), 138.6 (s), 148.9 (d), and 193.2 (s, C=O); MS (*m/z*), 254 (M^+). Found C, 75.71; H, 5.42%. Calcd for $C_{16}H_{14}OS$: C, 75.55; H, 5.54%.

9b: Mp 59—60 °C; IR (KBr) 1645 cm^{-1}; ^1H NMR ($CDCl_3$) δ=2.25 (s, 3H, Me) and 6.5—7.9 (m, 15H, arom and =CH); ^{13}C NMR ($CDCl_3$) δ=21.0 (q, Me), 128.0 (d), 128.1 (d), 128.3 (d), 129.3 (d), 129.5 (d), 130.1 (d), 130.6 (d), 130.8 (d), 131.6 (d), 135.8 (d), 136.8 (s), 138.3 (s), 138.4 (s), 146.5 (d), and 193.4 (s, C=O); MS (*m/z*), 330 (M^+). Found C, 79.88; H, 5.44%. Calcd for $C_{22}H_{18}OS$: C, 79.96; H, 5.49%.

9c: Mp 83—86 °C; IR (KBr) 1640 cm^{-1}; ^1H NMR ($CDCl_3$) δ=1.33 (s, 9H, 3Me) and 7.2—7.8 (m, 11H, arom and =CH); ^{13}C NMR ($CDCl_3$) δ=30.9 (q, 3Me), 45.4 (s, $\underline{C}Me_3$), 127.7 (d), 128.0 (d), 128.2 (d), 129.3 (d), 129.4 (d), 131.4 (d), 136.0 (s), 138.9 (s), 144.4 (d), and 193.6 (s, C=O); MS (*m/z*), 296 (M^+). Found C, 77.18; H, 6.64%. Calcd for $C_{19}H_{20}OS$: C, 76.98; H, 6.80%.

The stereochemistry of **9c** was studied under irradiation by a high pressure mercury lamp. The initial signal at δ=3.19 decreased and a new signal at δ=3.44 appeared in equal strength.

6) Methanolysis of 4ah. A crude product mixture of **4ah** and **5ah** (9 : 1, 2 mmol) (obtained from the predescribed workup) was heated at reflux temperature in methanol (10 cm^3) containing 0.5% NaOH for 1 d. The usual workup gave an acid-sensitive oil, whose ^1H NMR spectrum showed major peaks at δ=1.60, 1.79, 1.90, 2.12, 2.18 (MeS's), 3.16, 3.20, and 3.47 (MeO's). An acid hydrolysis with a solution of aqueous HCl (3 mol dm^{-3}, 5 cm^3) in ethanol (5 cm^3) at room temperature for 1 d yielded a mixture of aldehyde **12** in a 53% yield after a short column chromatography over silica gel. The separation of *E*- and *Z*- isomers was unsuccessful.

12: Oil, 1740 cm^{-1}; ^1H NMR ($CDCl_3$) δ=1.74 and 1.92 (s, 1 : 0.3, 3H, MeS), 6.8—7.7 (m, 10H, 2Ph), 9.19 and 10.35 (s, 1 : 0.3, 1H, CHO); MS (*m/z*), 254 (M^+). Found C, 75.47; H, 5.61%. Calcd for $C_{16}H_{14}OS$: C, 75.55; H, 5.54%.

7) The Reaction of Diphenylcyclopropenone 13 with Thiol 2 in the Presence of Trifluoroacetic Acid. General Procedure. A mixture of **2**, **13**, and trifluoroacetic acid (3, 1, and 3 mmol, respectively) in benzene or ethanol (5 cm^3) was heated in a sealed tube for an appropriate time. The usual workup in the manner described above yielded indene **3** or thiolacrylate **14** (R′=Bu-*t*) by recrystallization from methanol. The results are collected in Table 4.

3bi: Mp 177—178 °C; ^1H NMR δ=2.22 (s, 3H Me), 2.25 (s, 3H, Me), 5.07 (s, 1H, CH), and 6.5—7.8 (m, 17H, Ar); MS (*m/z*), 436 (M^+). Found: C, 79.62; H, 5.65%. Calcd for $C_{29}H_{24}S_2$: C, 79.76; H, 5.55%.

3jj: Mp 127—128 °C; IR (KBr) 1600 cm^{-1}; ^1H NMR ($CDCl_3$) δ=5.13 (s, 1H, CH) and 6.5—7.8 (m, 19H, arom); MS (*m/z*), 408 (M^+). Found C, 79.57; H, 4.84%. Calcd for $C_{27}H_{20}S_2$: C, 79.37; H, 4.93%.

3kk: Mp 186—187 °C; IR (KBr) 1600 cm^{-1}; ^1H NMR ($CDCl_3$) δ=5.12 (s, 1H, CH) and 6.5—7.9 (m, 17H, arom); MS (*m/z*), 476 (M^+). Found C, 67.79; H, 3.58%. Calcd for $C_{27}H_{18}Cl_2S_2$: C, 67.92; H, 3.79%.

14 (R′=Bu-*t*): Mp 109—111 °C (lit,[11] 109—111 °C).

References

1) For reviews: T. Eicher and J. L. Weber, *Fortschr. Chem. Forsch.*, **57**, 1 (1975); B. M. Trost, *Top. Curr. Chem.*, **133**, 3 (1986); P. Binger and H. M. Buch, *ibid.*, **135**, 77 (1987); M. S. Baird, *ibid.*, **144**, 137 (1988); J. Tanko and T. Hudlicky, *Chem. Rev.*, **89**, 165 (1989).

2) H. Yoshida, K. Yoshida, H. Totani, T. Ogata, and K. Matsumoto, *Bull. Chem. Soc. Jpn.*, **63**, 3579 (1990).

3) H. Yoshida, M. Nakajima, T. Ogata, and K. Matsumoto, *Bull. Chem. Soc. Jpn.*, **56**, 3015 (1983).

4) H. Yoshida, M. Nakajima, T. Ogata, and K. Matsumoto, *Bull. Chem. Soc. Jpn.*, **57**, 734 (1984).

5) H. Yoshida, H. Sano, M. Kato, T. Ogata, and K. Matsumoto, *Bull. Chem. Soc. Jpn.*, **59**, 2833 (1986).

6) P. Nicolet, J.-Y. Sanchez, A. Benaboura, and M. J. M. Abadie, *Synthesis*, **1987**, 202; A. Padwa, D. M. Cordova, and M. J. Pulwerl, *J. Org. Chem.*, **56**, 4747 (1991).

7) K. J. McCullough, N. Nakamura, T. Fujisaka, M. Nojima, and S. Kusubayashi, *J. Am. Chem. Soc.*, **113**, 1786 (1991).

8) G. Farnia, F. Marcuzzi, G. Melloni, G. Sandona, and M. V. Zucca, *J. Am. Chem. Soc.*, **111**, 981 (1989).

9) G. M. Ansteas, C. S. Peterson, K. G. Pinney, S. R. Wilson, and J. A. Katzenellenbogen, *J. Med. Chem.*, **33**, 2726 (1990).

10) M. A. Battiste, B. Halton, and R. H. Grubbs, *J. Chem. Soc., Chem. Commun.*, **1967**, 907.

11) H. Yoshida and T. Ogata, *Nippon Kagaku Kaishi*, **1982**, 534.

12) R. Breslow, T. Eicher, A. Krebs, R. A. Peterson, and J. Posner, *J. Am. Chem. Soc.*, **87**, 1320 (1965).

Studies on the Secondary Structure of Bradykinin in Aqueous Solution. Syntheses, Circular Dichroism Spectra, and Biological Activities of Bradykinin Amide and [D-Ala^4]-Bradykinin[1)]

Chikao HASHIMOTO,*,† Sukekatsu NOZAKI,†† and Ichiro MURAMATSU
Department of Chemistry, College of Science, Rikkyo University, Toshima-ku, Nishi-Ikebukuro, Tokyo 171
††Faculty of Pharmaceutical Sciences, Josai University, Sakado, Saitama 350-02
(Received July 9, 1991)

Bradykinin amide and [D-Ala^4]-bradykinin were synthesized by the 'hold-in-solution' method. The circular dichroism spectra of both peptides were measured and compared with that of bradykinin. These analogs exhibited weak activity (0.01% of bradykinin) in the increment of blood flow in a femoral artery of dog.

The secondary structure of bradykinin (BK), H–Arg–Pro–Pro–Gly–Phe–Ser–Pro–Phe–Arg–OH, has been investigated by several research groups.[2–7)] It is known that the circular dichroism (CD) spectrum of BK shows troughs at about 200 and at 234 nm, and a peak at 221 nm. In our previous papers,[8,9)] on the basis of comparison of the CD spectra of several BK analogs containing a 5-aminovaleric acid residue, the presence of an intramolecular 3→1 hydrogen bond between the carbonyl oxygen of Ser^6 and the amide proton of Phe^8, an intramolecular 4→1 hydrogen bond between the carbonyl oxygen of Pro^2 and the amide proton of Phe^5, and a salt bridge between the guanidino group of Arg^1 and the carboxyl group of Arg^9 was emphasized for the secondary structure of BK in aqueous solution. Further, it was deduced that the intramolecular 3→1 hydrogen bond contributes to the trough at 234 nm and the intramolecular 4→1 hydrogen bond and the salt bridge contribute to the peak at 221 nm. Also, it was suggested that the trough at about 200 nm arises mainly from the sequences Arg^1–Pro^2–Pro^3–Gly^4 and Phe^5–Ser^6–Pro^7. The present study was carried out to investigate further the presence of the salt bridge and the intramolecular 4→1 hydrogen bond in the secondary structure of BK in aqueous solution. The syntheses, the CD spectra, and the biological activities of BK-amide and [D-Ala^4]-BK are described.

Results and Discussion

Synthesis. The side chains of Arg and Ser were protected by Mbs[10)] and Bzl, respectively. Protected BK and [D-Ala^4]-BK were synthesized by a stepwise elongation using H–Arg(Mbs)–ONBzl as a starting material, and Boc-amino acid derivatives as acylating reagents (Z derivative for the final acylation) by the 'hold-in-solution' method.[11–13)] The protected BK and [D-Ala^4]-BK were purified by gel chromatography on a Sephadex LH-20 column and a Sephadex LH-60 column, respectively. The protected BK was converted to the corresponding BK-amide by treatment with NH_3/MeOH. The protected BK-amide and [D-Ala^4]-BK were hydrogenolyzed and then treated with methanesulfonic acid.[14)] Both of the free peptides were converted to the acetate form by a Dowex 1×2 column, and further purified by ion-exchange chromatography on a carboxymethylcellulose column, gel chromatography on a Sephadex G-10 column, and finally, partition chromatography on a Sephadex G-25 column.[15)]

Circular Dichroism Spectra. The CD spectra were measured in the region of 190—270 nm. Free BK-amide and [D-Ala^4]-BK were dissolved in water. The CD data are reported as molar ellipticity, $[\theta]$, which is expressed in degrees square centimeters per decimole.

BK-amide can not form the salt bridge proposed by Ivanov et al.[5)] because of the lack of the C-terminal carboxyl group. Our previous study suggested that the salt bridge brings about the stabilization of the intramolecular 4→1 hydrogen bond and the increment of ellipticity at 221 nm.[8,9)] Therefore, the conversion of the C-terminal carboxyl group into an amide should have resulted in a change for this peak. The CD spectrum of BK-amide in Fig. 1 indicates a trough at 232 nm, a peak at 223 nm, and a deep trough at 202 nm. The peak at 223 nm was considerably lower compared with that of BK. This change can be postulated to be a result of a decrease in the stability of the intramolecular 4→1 hydrogen bond. In regard to the peak at 223 nm, the ellipticity of BK-amide was very similar to that of [5-Ava$^{1-2}$]-BK. [5-Ava$^{1-2}$]-BK also can not form the salt bridge because of the lack of the guanidino group of Arg^1. In spite of the modification of each site remote from others in the primary structure, the similarity of the ellipticities of both the peptides in this region strongly implies the presence of a salt bridge in the BK molecule.

Venkatachalam[16)] indicated that a type-II β-turn is stabilized by the introduction of a D-amino acid residue into the third position (i+2) of the turn. Therefore, the β-turn in the N-terminal part of BK generated by the 4→1 hydrogen bond should be stabilized by replacing the Gly^4 residue with a D-Ala residue. The CD spectrum of [D-Ala^4]-BK in Fig. 2 shows a trough at 202 nm,

† Present address: Department of Chemistry, The Jikei University School of Medicine, 8-3-1, Kokuryo-cho, Chofu-shi, Tokyo 182.

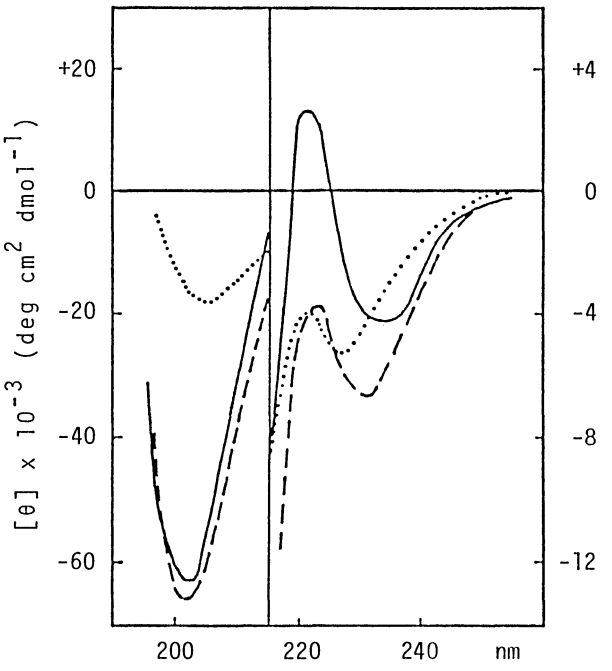

Fig. 1. CD spectra of BK-amide (----), [5-Ava$^{1-2}$]-BK (·····),[8,9] and BK (——) in water.

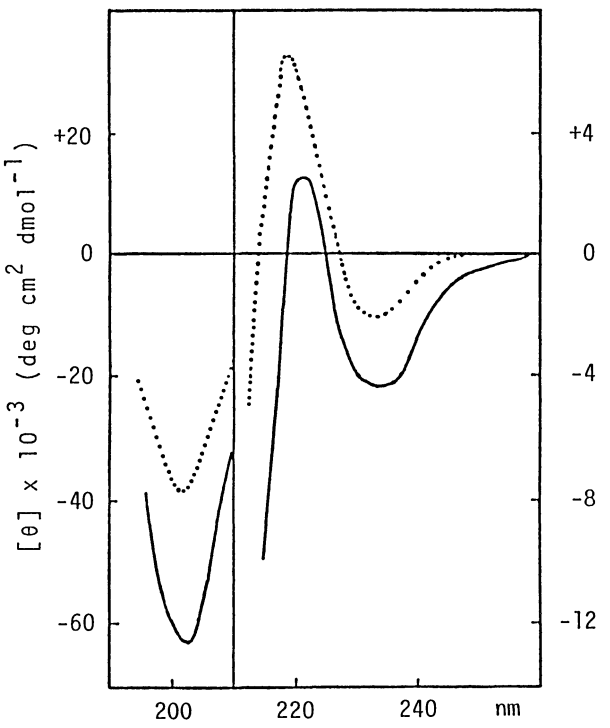

Fig. 2. CD spectra of [D-Ala^4]-BK (·····) and BK (——) in water.

a high peak at 219 nm, and a trough at 234 nm. The increment of the ellipticity at 219 nm compared with BK seems to be based on stabilization of the intramolecular 4→1 hydrogen bond between the carbonyl oxygen of Pro^2 and the amide proton of Phe^5; i.e., the β-turn. This hydrogen bond in BK has Pro and Gly residues at positions (i+1) and (i+2), respectively. It has been reported that the β-turn structure often involves Pro and Gly residues as preferable amino acids at positions (i+1) and (i+2) in the corner of the turn.[16,17] This indication does not conflict with our present conclusion.

As for the CD band near 234 nm, the troughs of BK-amide and [D-Ala^4]-BK imply the presence of the intramolecular 3→1 hydrogen bond proposed by Cann et al.[4,6] in these peptides.

Regarding the trough near 200 nm, the spectrum of BK-amide was similar to that of BK. This result suggested that the C-terminal amide group does not contribute to the trough at about 200 nm. The trough of [D-Ala^4]-BK was shallower than that of BK, that is, it may have been due to a conformational change of the amide bond of Pro^3-Gly^4 caused by replacing the Gly^4 residue with a D-Ala residue. The present results are not in conflict with the previous conclusions that both of the sequences Arg^1-Pro^2-Pro^3-Gly^4 and Phe^5-Ser^6-Pro^7 contribute to this band.[8,9]

Biological Activity. The biological activity of BK-amide and [D-Ala^4]-BK was found to be 0.01% of that of BK in the increment of blood flow in a femoral artery of dog. The low activity of BK-amide was consistent with the fact that the addition of an amino acid residue to the carboxyl terminal of BK generally results in a lowering of biological activity. It showed that the carboxyl group of Arg^9 is important for biological activity.

The analogs of luteinizing hormone-releasing hormone,[18,19] enkephaline,[20] and motiline,[21] containing a D-Ala residue instead of the Gly residue in a sequence -Tyr-Gly- corresponding to positions (i+1) and (i+2) of the β-turn, showed very large activities compared with the corresponding native peptides. However, in the case of [D-Ala^4]-BK, such a structure-activity correlation was not found.

Experimental

Melting points were measured by a capillary method and are given as uncorrected values. Optical rotations were determined with a Shimadzu polarimeter III or a DIP-370 digital polarimeter (JASCO). Amino acid analyses were performed on a JLC-6AS automatic analyzer (JEOL) or an L-8500 amino acid analyzer (Hitachi) after acid hydrolysis with 6 M (1 M=1 mol dm^{-3}) HCl in a sealed tube at 110 °C for 24 h. The theoretical values of amino acid ratios are shown in parentheses after each result.

Thin-layer chromatography was performed on TLC plates of silica gel 60 F_{254} (Merck and Co.) or cellulose (Avicel), using the following solvent systems (volume ratios): R_f^1, chloroform-methanol (95:5); R_f^2, chloroform-methanol (9:1); R_f^3, 1-butanol-acetic acid-water (4:1:1); R_f^4, 1-butanol-acetic acid-water (4:1:2); R_f^5, 1-butanol-pyridine-acetic acid-water (4:1:1:2); R_f^6, 1-butanol-pyridine-acetic acid-water (16:10:3:12); R_f^7, 1-butanol-pyridine-acetic acid-water (15:10:3:12).

The CD spectra were measured on a JASCO J-20 CD, ORD spectropolarimeter using a quartz cell with a path length of 0.50 mm. The measurements were carried out at room

temperature (24 °C) and at concentrations of 3.2×10^{-4} M and 1.5×10^{-3} M.

Biological activity was tested regarding the increment of blood flow in the femoral artery of dog according to a method similar to that in the previous paper.[9] The administration range of the analogs was $1\times(10^{-9}$—$10^{-4})$ g. The threshold dose of BK was 1×10^{-9} g, and its value was estimated as 100%. The activities of the analogs were expressed as relative activity compared with that of BK.

Z-Arg(Mbs)-Pro-Pro-Gly-Phe-Ser(Bzl)-Pro-Phe-Arg(Mbs)-ONBzl. The protected BK was synthesized from H-Arg(Mbs)-ONBzl by the 'hold-in-solution' method, that is, by successive coupling with Boc-Phe-OH, Boc-Pro-OH, Boc-Ser(Bzl)-OH, Boc-Phe-OH, Boc-Gly-OH, Boc-Pro-OH, Boc-Pro-OH, and Z-Arg(Mbs)-OH. Each amino acid residue was introduced by repeating the following five steps. (1) Acylation of the amino component (1.0 mmol) in 1,2-dichloroethane (ca. 10 ml) at room temperature for several hours with a Boc-amino acid (Z-derivative for the final acylation) (2.0 mmol), EDC·HCl[22] (2.0 mmol), and HOBt[23] (2.0 mmol). (2) Washing with 0.1 M HCl, water, 5% Na_2CO_3, and water (removed by pipetting). (3) Cleavage of the Boc group by HCl/dioxane at room temperature for ca. 30 min. (4) Addition of a slight excess of 2 M Na_2CO_3 and removal of the aqueous phase. (5) Washing with water. The crude protected BK was purified by a Sephadex LH-20 column (1.6×116.5 cm) using DMF as eluent. Fractions 19—26 (4.0 g each) were combined and concentrated. The residue was triturated with diethyl ether; overall yield 1.047 g (59%). For analysis, a part of the product was further purified by a silica-gel column and recrystallization from chloroform–diethyl ether; mp 129—132 °C, $[\alpha]_D^{27.5}$ −35.6° (*c* 1.0, $CHCl_3$); R_f^1 0.22, R_f^2 0.54 (silica gel). Amino acid ratios in acid hydrolyzate: Ser 1.00 (1), Pro 3.13 (3), Gly 1.01 (1), Phe 1.92 (2), Arg 1.95 (2). Found: C, 56.99; H, 5.72; N, 12.78%. Calcd for $C_{86}H_{102}O_{21}N_{16}S_2\cdot2.5H_2O$: C, 57.23; H, 5.97; N, 12.42%. FAB mass: *m/z* 1759 (MH^+, $C_{86}H_{103}O_{21}N_{16}S_2$).

H-Arg-Pro-Pro-Gly-Phe-Ser-Pro-Phe-Arg-NH₂. The protected BK (300 mg) was dissolved in a mixture of MeOH (3.0 ml) and DMF (2.0 ml). The solution was saturated with NH_3 gas and then stirred at room temperature overnight. After removal of the solvent, the residue was solidified by the addition of diethyl ether. The product was dissolved in a mixture of DMF (8.0 ml), water (5.0 ml), and acetic acid (1.0 ml), and then hydrogenated over palladium black in a H_2 atmosphere for ca. 3 d. Water was added in several portions during the hydrogenation. After removal of the catalyst, the solvent was evaporated. The residue was treated with methanesulfonic acid (5.5 ml) containing anisole (0.20 ml) for 50 min at room temperature. Diethyl ether was added to this mixture. The solid was dissolved in water (2.5 ml) and the solution was passed through a Dowex 1×2 column (1.28×8.0 cm) (acetate form) with water as eluent. The eluate was concentrated and the residue was dissolved in ammonium acetate buffer (0.04 M, pH 6.0) (2.5 ml). The solution was applied to a carboxymethylcellulose column (1.7×22.5 cm: Whatman CM-52), and then eluted with ammonium acetate buffers (0.04—0.40 M, pH 6.0) by a linear gradient method. Fractions 68—82 (3.0 g each) were combined and concentrated. The residue was dissolved in 4% acetic acid (2.0 ml) and the solution was subjected to a Sephadex G-10 column (1.7×38.0 cm). Fractions 11—15 (2.5 g each) were combined and concentrated to give a first crop. Fractions 16—23 were also combined and concentrated. The residue was rechromatographed on a Sephadex G-10 column (1.7×38.5 cm) to obtain an additional crop. The combined crops were dissolved in 1-butanol–pyridine–acetic acid–water (16 : 10 : 3 : 12) (1.25 ml) and applied to a Sephadex G-25 column (1.7×23.9 cm). After elution by the same solvent, fractions 9—11 (3.0 g each) were collected and concentrated. The residue was lyophilized from water; yield 82.3 mg (36%); $[\alpha]_D^{24}$ −94.7° (*c* 0.10, H_2O); R_f^4 0.53, R_f^6 0.64, R_f^7 0.54 (cellulose). Amino acid ratios in acid hydrolyzate: Ser 1.18 (1), Pro 2.95 (3), Gly 1.01 (1), Phe 1.92 (2), Arg 1.94 (2), NH_3 1.07 (1). Found: C, 49.94; H, 6.57; N, 16.52%. Calcd for $C_{50}H_{74}O_{10}N_{16}\cdot3CH_3COOH\cdot6H_2O$: C, 49.92; H, 7.33; N, 16.63%.

Z-Arg(Mbs)-Pro-Pro-D-Ala-Phe-Ser(Bzl)-Pro-Phe-Arg(Mbs)-ONBzl. The protected [D-Ala⁴]-BK was synthesized from H-Arg(Mbs)-ONBzl (1.5 mmol) by successive coupling with Boc-Phe-OH, Boc-Pro-OH, Boc-Ser(Bzl)-OH, Boc-Phe-OH, Boc-D-Ala-OH, Boc-Pro-OH, Boc-Pro-OH, and Z-Arg(Mbs)-OH (3.0 mmol each) by the same method as described above. The residue was reprecipitated from methanol–diethyl ether (2.565 g). The crude protected [D-Ala⁴]-BK was purified by a Sephadex LH-60 column (1.7×135 cm) with DMF as eluent; overall yield 1.314 g (47%). For analysis, a part of the product was purified by a silica-gel column and recrystallization from methanol–ethyl acetate–diethyl ether; mp 121–123 °C; $[\alpha]_D^{27.5}$ −35.2° (*c* 1.0, $CHCl_3$); R_f^1 0.29, R_f^2 0.63 (silica gel). Amino acid ratios in acid hydrolyzate: Ser 0.98 (1), Pro 3.14 (3), Ala 1.01 (1), Phe 1.91 (2), Arg 1.97 (2). Found: C, 57.45; H, 6.11; N, 12.66%. Calcd for $C_{87}H_{104}O_{21}N_{16}S_2\cdot2.5H_2O$: C, 57.45; H, 6.04; N, 12.32%. FAB mass: *m/z* 1773 (MH^+, $C_{87}H_{105}O_{21}N_{16}S_2$).

H-Arg-Pro-Pro-D-Ala-Phe-Ser-Pro-Phe-Arg-OH. The protected [D-Ala⁴]-BK (350 mg) was dissolved in DMF–water–acetic acid (10, 5, and 1 ml) and then hydrogenated over palladium black for 4 d. After removal of the catalyst, the solvent was evaporated. The residue was treated with methanesulfonic acid (7.0 ml) containing anisole (0.5 ml) for 50 min at room temperature. The precipitates were obtained by the addition of diethyl ether. The solid was dissolved in water (3.0 ml) and the solution was passed through a Dowex 1×2 column (1.28×7.5 cm) (acetate form) with water as eluent. The eluate was combined and concentrated. The residue was dissolved in ammonium acetate buffer (0.04 M, pH 6.0) (3.0 ml) and the solution was chromatographed on a carboxymethylcellulose column (1.7×24.0 cm: Whatman CM-52) using ammonium acetate buffers (0.04—0.40 M, pH 6.0) by a linear gradient method. Fractions 68—76 (3.0 g each) were combined and concentrated. The residue was dissolved in 4% acetic acid (2.0 ml) and the solution was applied to a Sephadex G-10 column (1.7×39.8 cm) with the same solvent as eluent. Fractions of 2.5 g each were collected. Fractions 15—21 were combined and the solvent was removed. The residue was dissolved in 1-butanol–pyridine–acetic acid–water (4 : 1 : 1 : 2) (2.3 ml) and the solution was subjected to a Sephadex G-25 column (1.7×24.5 cm) with the same solvent as eluent. Fractions 28—34 (3.0 g each) were combined and the solvent was evaporated. The residue was further purified by the same chromatographic methods. The product was lyophilized from water; yield 53.24 mg (22%); $[\alpha]_D^{24}$ −63.7° (*c* 0.10, H_2O); R_f^3 0.59, R_f^5 0.65 (cellulose). Amino acid ratios in acid hydrolyzate: Ser 0.94 (1), Pro 2.92 (3), Ala 0.98 (1), Phe 2.03 (2), Arg 2.07 (2). Found: C, 52.23; H, 6.99; N, 15.82%. Calcd for $C_{51}H_{75}O_{11}N_{15}\cdot3CH_3COOH\cdot3H_2O$: C, 52.32; H, 7.16; N,

16.06%.

We are grateful to the Research Laboratory of Toyo Jozo Co., Ltd. for the elemental, amino acid, and FAB mass analyses, and to the Research Laboratory of Nihon Kayaku Co., Ltd. for the measurement of biological activity.

References

1) The amino acids used with the exception of glycine and D-alanine were in the L-configuration. The abbreviations used are those recommended by the IUPAC-IUB Joint Commission on Biochemical Nomenclature (JCBN): *Eur. J. Biochem.*, **138**, 9 (1984). The following additional abbreviations are used: Mbs, *p*-methoxybenzenesulfonyl; Bzl, benzyl; ONBzl, *p*-nitrobenzyl ester; Boc, *t*-butoxycarbonyl; Z, benzyloxycarbonyl; EDC·HCl, 1-ethyl-3-(3-dimethylaminopropyl)carbodiimide hydrochloride; HOBt, 1-hydroxybenzotriazole; DMF, *N,N*-dimethylformamide; FAB, Fast Atom Bombardment; 5-Ava, 5-aminovaleric acid.

2) A. Bodanszky, M. Bodanszky, E. J. Jorpes, V. Mutt, and M. A. Ondetti, *Experientia,* **26**, 948 (1970).

3) A. H. Brady, J. W. Ryan, and J. M. Stewart, *Biochem. J.,* **121**, 179 (1971).

4) J. R. Cann, J. M. Stewart, and G. R. Matsueda, *Biochemistry,* **12**, 3780 (1973).

5) V. T. Ivanov, M. P. Filatova, Z. Reissman, T. O. Reutova, E. S. Efremov, V. S. Pashkov, S. G. Galaktionov, G. L. Grigoryan, and Yu. A. Ovchinnikov, "Peptides," ed by R. Walter and J. Meienhofer, Ann Arbor Publishers, Michigan (1975), p. 151.

6) R. E. London, J. M. Stewart, J. R. Cann, and N. A. Matwiyoff, *Biochemistry,* **17**, 2270 (1978).

7) G. I. Chipens, F. K. Mutulis, N. V. Myshlyakova, I. P. Misina, R. O. Vitolina, V. J. Klusha, and B. S. Katayev, *Int. J. Pept. Protein Res.,* **26**, 460 (1985).

8) C. Hashimoto, M. Tamaki, H. Uchida, S. Nozaki, S. Sofuku, and I. Muramatsu, "Peptide Chemistry 1978," ed by N. Izumiya, Protein Research Foundation, Osaka (1979), p. 115.

9) C. Hashimoto, M. Tamaki, S. Sofuku, and I. Muramatsu, *Bull. Chem. Soc. Jpn.,* **64**, 1533 (1991).

10) O. Nishimura and M. Fujino, *Chem. Pharm. Bull.,* **24**, 1568 (1976).

11) I. Muramatsu, C. Hashimoto, A. Kimura, Y. Saika, and S. Nozaki, "Peptide Chemistry 1977," ed by T. Shiba, Protein Research Foundation, Osaka (1978), p. 61.

12) S. Nozaki, A. Kimura, and I. Muramatsu, *Chem. Lett.,* **1977**, 1057.

13) S. Nozaki and I. Muramatsu, *Bull. Chem. Soc. Jpn.,* **55**, 2165 (1982).

14) H. Yajima, Y. Kiso, H. Ogawa, N. Fujii, and H. Irie, *Chem. Pharm. Bull.,* **23**, 1164 (1975).

15) D. Yamashiro, *Nature,* **201**, 76 (1964).

16) C. M. Venkatachalam, *Biopolymers,* **6**, 1425 (1968).

17) P. N. Lewis, F. A. Momany, and H. A. Scheraga, *Proc. Natl. Acad. Sci. U.S.A.,* **68**, 2293 (1971).

18) M. W. Monahan, M. S. Amoss, H. A. Anderson, and W. Vale, *Biochemistry,* **12**, 4616 (1973).

19) M. Fujino, I. Yamazaki, S. Kobayashi, T. Fukuda, S. Shinagawa, R. Nakayama, W. F. White, and R. H. Rippel, *Biochem. Biophys. Res. Commun.,* **57**, 1248 (1974).

20) D. H. Coy, A. J. Kastin, A. V. Schally, O. Morin, N. G. Caron, F. Labrie, J. M. Walker, R. Fertel, G. G. Berntson, and C. A. Sandman, *Biochem. Biophys. Res. Commun.,* **73**, 632 (1976).

21) S. Shinagawa, M. Fujino, H. Yajima, T. Segawa, and Y. Okuma, *Chem. Pharm. Bull.,* **26**, 880 (1978).

22) J. C. Sheehan, J. Preston, and P. A. Cruickshank, *J. Am. Chem. Soc.,* **87**, 2492 (1965).

23) W. König and R. Geiger, *Chem. Ber.,* **103**, 788 (1970).

Dehydrooligopeptides. XIII. Selective Enzymatic Hydrolysis of *N*-Protected α-Dehydroglutamic Acid Diesters and Their Analogs Using Papain as Catalyst[1)]

Chung-gi SHIN,* Nobuyuki TAKAHASHI, and Masashi SEKI
Laboratory of Organic Chemistry, Faculty of Technology, Kanagawa University, Rokkakubashi, Kanagawa-ku, Yokohama 221
(Received May 2, 1991)

Since the α-ester of α,γ-dimethyl *N*-benzyloxycarbonyl-α-dehydroglutamate (ΔGlu) was found to be hydrolyzed using papain, a variety of *N*-protected α-dehydroglutamates and their analogs, both esters of which were the same or different from each other, were newly synthesized and subjected to a similar hydrolysis. Although the substrates, with bulkier ester group at the γ- as well as α-positions, were found to become difficult to hydrolyze, the kind and size of the *N*-protecting group did not effect the hydrolysis. Moreover, it was found that the length of side chain of the substrate greatly influenced hydrolysis. The present study suggests that papain may become a useful tool for the hydrolysis and coupling of ΔGlu with α-amino acid or peptide.

During about the past two decades, the many successes regarding the synthesis of a number of peptides by utilizing proteolytic enzymes, such as papain and α-chymotrypsin A etc., have contributed great epochal effects to the field of organic synthetic chemistry.[2-5)] Even the complex macromolecules of useful peptide hormones could be synthesized under considerably mild conditions by the widely developed enzymatic synthetic method.[6-8)]

On the contrary, it was hardly believed up to now that the unusual α-amino acid, α-dehydroamino acid (DHA) ester, could be similarly hydrolyzed or coupled with L-α-amino acid (AA) enzymatically. Recently, however, a very selective hydrolysis of the α-ester moiety of α,γ-dimethyl *N*-benzyloxycarbonyl-α-dehydroglutamate [Cbz-ΔGlu(OMe)-OMe; **1b**] and novel peptide formation with L-Leu-NHPh by using papain (EC 3.4.22.2) have for the first time been successful and reported briefly.[9,10)] Since it was thought to be necessary to reexamine and widely develop a similar hydrolysis, we undertook a further detailed study. That is, many kinds of α-dehydroglutamates and their analogs, in which two carboxyl groups and an amino group are protected with various *C*- and *N*-protecting groups, were newly synthesized and the effects of the three protecting groups and the influence of the length of the side chain to enzymatic hydrolysis were thoroughly studied. Regarding the results, the substrate specificity of papain was broadened considerably.

Experimental

General. The melting points were determined with a Yamato Mp-21 micro-melting-point apparatus, and were uncorrected. The IR spectra were recorded with a Hitachi EPI-G2 spectrometer. The ^{1}H NMR spectra were measured with a JEOL LMN-PS-100 spectrometer in a $CDCl_3$ or DMSO-d_6 solution with tetramethylsilane used as the internal standard.

Enzyme. Papain (2.8 units mg^{-1}), purchased from Sigma Chemical Co., U. S. A., was used without further purification.

***N*-Protected α-Dehydroglutamates (1) and Their Analogs.** Cbz-ΔGlu(OMe)-OMe (**1b**), Cbz-ΔGlu(OEt)-OMe (**1c**), and Cbz-ΔGlu(OBzl)-OMe (**1e**) (Bzl=benzyl) were prepared by the γ-esterification of Cbz-ΔGlu-OMe (**1a**)[1)] with an appropriate alcohol, according to a reported method.[1)] Cbz-ΔGlu(OEt)-OEt (**1f**) and Cbz-ΔGlu(OBzl)-OBzl (**1g**) were also obtained similarly by the α,γ-diesterification of Cbz-ΔGlu-OH (**2a**)[11)] with EtOH or BzlOH. Cbz-ΔGlu(OBu^t)-OMe (**1d**) (Bu^t= *t*-butyl) was derived by the treatment of **1a** with isobutene in a sealed tubes.[12)] Similarly, Cbz-ΔGlu(OBu^t)-OBu^t(**1h**) was also obtained from **2a** and isobutene. In addition, *N*-methoxycarbonyl (Moc)-ΔGlu(OMe)-OMe (**1i**), *N*-ethoxycarbonyl (Eoc)-ΔGlu(OMe)-OMe (**1j**), *N*-isopropoxycarbonyl (Ipo)-ΔGlu(OMe)-OMe (**1k**), and *N*-*n*-butoxycarbonyl (Nbc)-ΔGlu(OMe)-OMe (**1l**) were prepared by the condensation of α,γ-dimethyl α-oxoglutarate with an appropriate alkyl carbamate.[1)] As an analog of the ΔGlu derivative, Cbz-ΔAsp(OMe)-OMe (**1m**) was obtained by the elimination of Cbz-β-(hydroxy)aspartic acid dimethyl ester.[13)] Furthermore, 2-(*N*-Cbz-amino)-2-hexenedioic acid dimethyl ester [Cbz-ΔAhx(OMe)-OMe; **1n**] and 2-(*N*-Cbz-amino)-2-heptenedioic acid dimethyl ester [Cbz-ΔAhp(OMe)-OMe; **1o**] were also derived by the condensation of 2-oxohexanedioic acid dimethyl ester and 2-oxoheptanedioic acid dimethyl ester with benzyl carbamate, respectively, by the usual method.[1)] The identification data of **1**, thus obtained, are presented in Tables 1 and 2.

Methyl 2-(*N*-Cbz-Amino)-5-hydroxy-2-pentenoate (1p). To a suspension of Cbz-ΔGlu(OMe)-OH (**2b**) (3 g, 10 mmol) and $NaBH_4$ (2.32 g, 61 mmol) in Bu^{t}OH (15 ml) was added MeOH, with stirring, at 60 °C until it became a transparent solution. After stirring for 3 h, the resulting solution was neutralized with 1 M-HCl (1 M=1 mol dm^{-3}) and concentrated under reduced pressure to give a crude residue, which was dissolved in ethyl acetate (30 ml). The resultant solution was washed with brine and dried over anhydrous Na_2SO_4. Concentration in vacuo gave crystals, which were recrystallized from $CHCl_3$ to give 2-(*N*-Cbz-amino)-5-hydroxy-2-pentenoic acid (**2p**) as colorless needles. Yield 80%, mp 114—115 °C. IR (KBr) 3250 (NH), 1655 (C=C) cm^{-1}. ^{1}H NMR (DMSO-d_6) δ=8.57 (bs, 1H, NH), 6.48 (t, 1H, *J*=7.0 Hz, -CH=). Found: C, 60.34; H, 6.04; N, 5.11%. Calcd for $C_{14}H_{17}NO_5$ C, 60.20; H, 6.14; N, 5.02%. Subsequently, the obtained **2p** (2.1 g, 7.9 mmol) was treated with MeOH (20 ml)

Table 1. The Yields and Melting Points of ROOC-$(CH_2)_n$CH=C$\langle^{COOR'}_{NHCOOX}$ (1)

Compound No.	n	X	R	R'	Yield %	Mp θ_m/°C	Formula	Found (Calcd)/% C	H	N
1b	1	Bzl	Me	Me	70	82—83[a]	$C_{15}H_{17}NO_6$	58.74 (58.63	5.50 5.78	4.53 4.56)
1c	1	Bzl	Et	Me	95	62—63[b]	$C_{16}H_{19}NO_6$	60.03 (59.80	5.78 5.96	4.37 4.36)
1d	1	Bzl	Bu^t	Me	81	Syrup	$C_{18}H_{23}NO_6$			4.20 (4.01)
1e	1	Bzl	Bzl	Me	69	Syrup	$C_{21}H_{21}NO_6$	66.00 (65.78	5.24 5.52	3.42 3.65)
1f	1	Bzl	Et	Et	87	55—56[b]	$C_{17}H_{21}NO_6$	60.69 (60.88	6.26 6.31	4.18 4.18)
1g	1	Bzl	Bu^t	Bu^t	66	62—63[c]	$C_{27}H_{25}NO_6$	70.33 (70.57	5.40 5.48	3.21 3.05)
1h	1	Bzl	Bzl	Bzl	60	71—72[c]	$C_{21}H_{29}NO_6$	64.40 (64.43	7.40 7.47	3.29 3.68)
1i	1	Me	Me	Me	52	82—83[d]	$C_9H_{13}NO_6$	46.61 (46.75	5.61 5.67	6.04 6.06)
1j	1	Et	Me	Me	80	42—43[b]	$C_{10}H_{15}NO_6$	48.86 (48.97	6.03 6.17	5.70 5.71)
1k	1	Pr^i	Me	Me	80	90—91[c]	$C_{11}H_{17}NO_6$	50.92 (50.96	6.51 6.61	5.56 5.40)
1l	1	Bu^n	Me	Me	86	Syrup	$C_{12}H_{19}NO_6$	52.88 (52.74	7.00 7.01	5.21 5.13)
1m[e]	0	Bzl	Me	Me	72	Syrup				
1n	2	Bzl	Me	Me	80	Syrup	$C_{16}H_{19}NO_6$	60.62 (60.88	6.19 6.31	4.03 4.18)
1o	3	Bzl	Me	Me	70	52—53[c]	$C_{17}H_{21}NO_6$	60.07 (59.80	6.09 5.96	4.58 4.36)

a) Colorless needles from $CHCl_3$. b) Colorless needles from hexane–ethyl acetate. c) Colorless prisms from hexane–ethyl acetate. d) Colorless needles from diisopropyl ether. e) Lit, 13.

Table 2. The IR and ^{1}H NMR Spectral Data of **1**

Compound No.	IR, ν/cm^{-1} in KBr		^{1}H NMR, δ in $CDCl_3$	
	-NH-	-C=C-	-CH= (J/Hz)	-NH-
1b	3250	1665	6.76t (7.0)	6.60bs
1c	3275	1655	6.71t (7.0)	6.63bs
1d	3340	1670	6.78t (7.0)	6.69bs
1e	3370	1665	6.76t (7.0)	6.60bs
1f	3280	1665	6.78t (7.0)	6.77bs
1g	3290	1655	6.64t (7.0)	6.54bs
1h	3345	1645	6.87t (7.0)	6.64bs
1i	3340	1670	6.68t (7.0)	6.80bs
1j	3340	1655	6.64t (7.0)	6.98bs
1k	3270	1670	6.76t (7.5)	6.38bs
1l	3330	1670	6.60t (7.0)	6.90bs
1m	3305	1640	5.44s	9.63s
1n	3330	1660	6.51t (7.0)	6.70bs
1o	3335	1660	6.46t (7.0)	7.02bs

in the presence of $SOCl_2$ (0.64 ml), with stirring, at −10 °C for 30 min. The reaction solution was further stirred at room temperature overnight and concentrated in vacuo. The obtained residue was dissolved in ethyl acetate (30 ml) and the resulting solution was washed with successively saturated $NaHCO_3$ aqueous solution and brine and then dried over anhydrous Na_2SO_4. Concentration in vacuo gave a yellow syrup, which was purified on a silica-gel column using a mixture of $CHCl_3$ and acetone (10 : 1 v/v) as the eluent. The eluate was concentrated in vacuo to give **1p** as a yellow syrup. Yield 82%. IR 3330 (NH), 1660 (C=C) cm^{-1}. ^{1}H NMR ($CDCl_3$) δ=7.00 (bs, 1H, NH), 6.59 (t, 1H, J=7.0 Hz, -CH=). Found: C, 59.03; H, 5.65; N, 5.33%. Calcd for $C_{13}N_{15}NO_5$: C, 58.86; H, 5.70; N, 5.28%.

General Enzymatic Hydrolysis of 1. A suspension (5 ml) of an appropriate **1** [100 mM and papain (30 g dm^{-3}) in the presence of 2-mercaptoethanol (0.1 ml) in McIlvaine buffer was incubated, with shaking, at pH 8.0 and at 35 °C for 24 h. The structures and yields of the hydrolyzates were identified and determined by HPLC on a Hitachi 630-50 model (column 4ϕ×250 mm). The eluent (MeOH : H_2O=60 : 40 v/v) was run with a flow rate of 1 ml min^{-1}. The peaks were determined at 230 nm by comparing the retention times with those of authentic compounds prepared chemically.[1,11] The peak intensities were used to calculate the relative concentrations. Furthermore, to isolate pure **2**, the reaction solution was treated with a saturated $NaHCO_3$ aqueous solution (50 ml) and washed twice with ethyl acetate (60 ml). The aqueous layer was acidified to pH 2.0 with 6 M-HCl and extracted three times with ethyl acetate (100 ml). The combined extracts were washed twice with brine (60 ml) and dried over anhydrous Na_2SO_4. Concentration in vacuo gave crystals or syrup, which were recrystallized from an appropriate organic solvent or purified on a silica-gel column using a mixture of $CHCl_3$ and acetone (10 : 1 v/v) as the eluent to give γ-alkyl esters of *N*-protected α-dehydroglutamic acids (**2a**—**2d** and **2i**—**l**) and their analogs (**2n** and **2o**). The identification data of **2** are summarized in Tables 3 and 4.

Table 3. The Yields and Melting Points of ROOC-$(CH_2)_n$CH=C$\langle^{COOH}_{NHCOOX}$ (2)

Compound				Yield	Mp	Formula	Found (Calcd)/%		
No.	*n*	R	X	%	θ_m/°C		C	H	N
2a	1	H	Bzl	38	146—147[c]	$C_{13}H_{13}NO_6$	56.19	4.97	4.92
							(55.91	4.70	5.02)
2b	1	Me	Bzl	94	129—130[d]	$C_{14}H_{15}NO_6$	57.58	5.12	4.80
							(57.33	5.16	4.78)
2c	1	Et	Bzl	86[a] 51[b]	132—133[d]	$C_{15}H_{17}NO_6$	58.43	5.45	4.49
							(58.63	5.58	4.56)
2d	1	Bu^t	Bzl	23	Syrup	$C_{17}H_{21}NO_6$	60.78	6.05	4.12
							(60.88	6.31	4.18)
2i	1	Me	Me	Quant	127—128[e]	$C_8H_{11}NO_6$	43.91	5.03	6.35
							(44.24	5.11	6.45)
2j	1	Me	Et	Quant	130—131[d]	$C_9H_{13}NO_6$	46.77	5.58	5.86
							(46.75	5.67	6.06)
2k	1	Me	Pr^i	Quant	154—155[d]	$C_{10}H_{15}NO_6$	48.67	5.93	5.41
							(48.97	6.17	5.71)
2l	1	Me	Bu^n	Quant	119—120[d]	$C_{11}H_{17}NO_6$	51.05	6.63	5.33
							(50.96	6.61	5.40)
2n	2	Me	Bzl	47	116—117[f]	$C_{14}H_{15}NO_6$	57.48	5.31	4.57
							(57.33	5.16	4.78)
2o	3	Me	Bzl	11	78—79[f]	$C_{15}H_{17}NO_6$	58.78	5.69	4.31
							(58.63	5.58	4.56)

a) From **1c**. b) From **1f**. c) Colorless needles from $CHCl_3$–ethyl acetate. d) Colorless needles from ethyl acetate. e) Colorless needles from hexane–ethyl acetate. f) Colorless prisms from hexane–ethyl acetate.

Table 4. The IR and ^{1}H NMR Spectral Data of **2**

Compound No.	IR, ν/cm^{-1} in KBr		^{1}H NMR, δ in DMSO-d_6		
	-NH-	-C=C-	-COOH	-CH= (J/Hz)	-CH$_2$CH=
2a	3250	1655	8.56bs	6.50t (7.0)	3.19d
2b	3285	1660	8.41bs[a]	6.88t (7.0)	3.29d
2c	3290	1665	9.21bs[a]	6.86t (7.0)	3.26d
2d	3305	1655	7.58bs	6.76t (7.0)	3.22d
2i	3300	1660	8.59bs	6.44t (7.0)	3.28d
2j	3305	1660	8.54bs	6.42t (7.0)	3.28d
2k	3300	1660	8.41bs	6.38t (7.0)	3.24d
2l	3280	1665	8.46bs	6.39t (7.0)	3.24d
2n	3285	1660	8.65bs	6.37t (7.0)	2.58—2.20m
2o	3290	1650	8.59bs	6.37t (7.0)	1.70—1.48m

a) Measured in $CDCl_3$.

Enzymatic Hydrolysis of 1p. Quite similarly, the hydrolysis of **1p** with papain was worked up to give **2p**, which was completely in accord with the compound derived by the reduction of **2b** with $NaBH_4$. Yield 80%.

Results and Discussion

In order to examine and to further develop the new catalytic action of cheaper and readily accessible papain, various DHA esters (**1**) as the substrate were submitted to the enzymatic reaction.

First of all, in particular, to obtain optimal conditions the hydrolysis of **1b** was thoroughly reexamined, since a preliminary run using papain had already been achieved to give **2b**[9] almost quantitatively. In addition to a detailed examination of the effect of the pH,[9] the effects of the reaction time and concentration of both the enzyme and substrate were studied, as shown in Figs. 1—4.

The pH of the reaction solution was changed from 3 to 9, although the optimal pH value of esterase action of papain in a McIlvaine buffer is well-known to be around 7. As a result, the yield of **2b** increased abruptly over the pH range from 6 to 8, and reached more than 90% at pH 8. Consequently, the α-ester hydrolysis of **1b** was found to be extremely dependent upon the pH. That is, Fig. 1 indicates that a rather alkaline pH may be preferred for the such hydrolysis of **1**. Subsequently, the time course of a similar hydrolysis of **1b** at 8.0 was also examined. As Fig. 2 shows, the hydrolysis is comparatively slow and the yield of the hydrolyzate reached ultimately more than 90% over 24 h.

Concerning the amount of papain, the enzyme con-

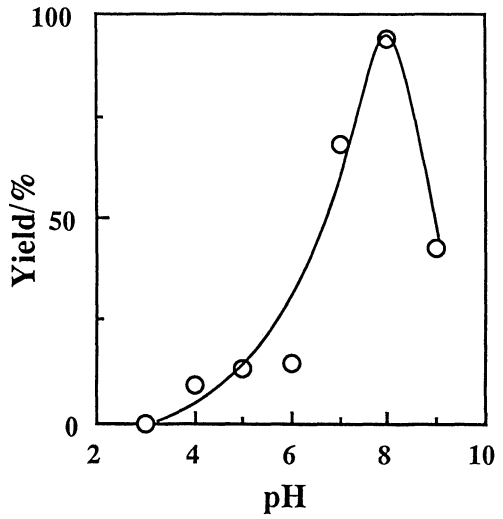

Fig. 1. Effect of pH. The reaction mixture (5 ml), containing 200 mM **1b** and 30 g dm^{-3} papain (2.8 units mg^{-1}) in McIlvaine buffer, was shaken at various pH's at 35 °C for 24 h.

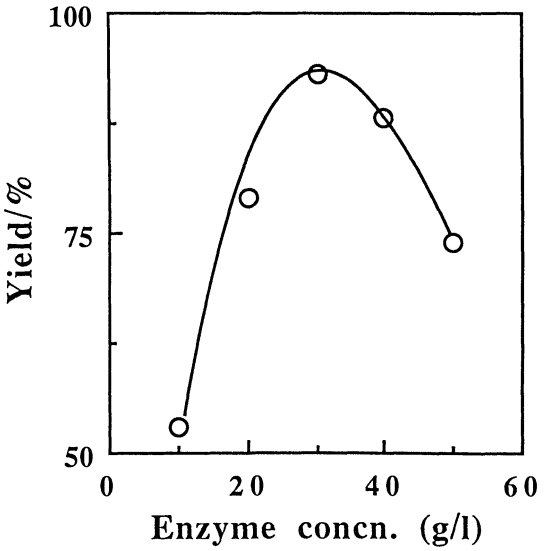

Fig. 3. Effect of enzyme concentration. The reaction mixture (5 ml), containing 200 mM **1b** and various concentrations of papain in McIlvaine buffer, was shaken at pH 8 at 35 °C for 24 h.

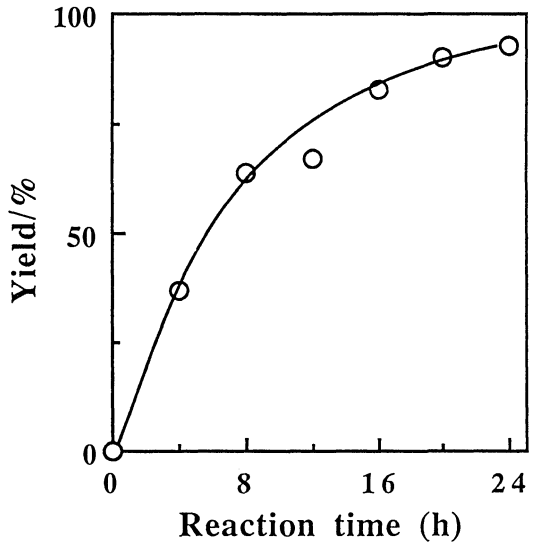

Fig. 2. Effect of reaction time. The reaction mixture (5 ml), containing 200 mM **1b** and 30 g dm^{-3} papain (2.8 units mg^{-1}) in McIlvaine buffer, was shaken at pH 8 at 35 °C for various hours.

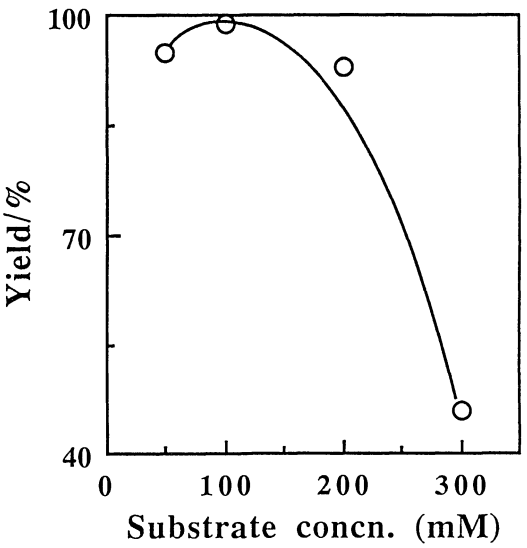

Fig. 4. Effect of substrate concentration. The reaction mixture (5 ml), containing various concentrations of **1b** and 30 g dm^{-3} papain (2.8 units mg^{-1}) in McIlvaine buffer, was shaken at pH 8 at 35 °C for 24 h.

centration at around 30 g dm^{-3} provided the highest yield. Fig. 3 indicates that a considerably large amount of enzyme is required for the hydrolysis. In addition, Fig. 4 indicates that a substrate concentration ranging from 50 to 150 mM affords a very high yield of more than 95%. Consequently, the substrate concentration of 100 mM was found to be the most effective.

As can be seen from Figs. 1—4, the results show that the enzymatic hydrolysis of **1b** requires a considerably prolonged reaction time and higher concentration of enzyme, but closely depends upon a comparatively lower substrate concentration under a slightly alkaline pH.

The optimal conditions of the hydrolysis of **1b** [papain (30 g dm^{-3}), substrate (100 mM) in McIlvaine buffer at pH 8.0 and at 35 °C for 24 h], was applied to a similar hydrolysis of all the substrates (**1**), according to Scheme 1.

From the results and the fact that other DHA esters have also been hydrolyzed,[14] our present study indicates that papain is a potent catalyst for the hydrolysis of various DHA esters. The structural characteristics of

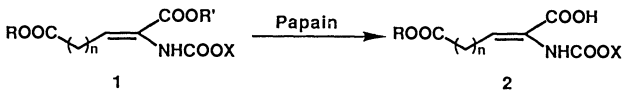

1 2

No.	n	X	R	R'
1a	1	Bzl	H	Me
1b	1	Bzl	Me	Me
1c	1	Bzl	Et	Me
1d	1	Bzl	Bu^t	Me
1e	1	Bzl	Bzl	Me
1f	1	Bzl	Et	Et
1g	1	Bzl	Bu^t	Bu^t
1h	1	Bzl	Bzl	Bzl
1i	1	Me	Me	Me
1j	1	Et	Me	Me
1k	1	Pr^i	Me	Me
1l	1	Bu^n	Me	Me
1m	0	Bzl	Me	Me
1n	2	Bzl	Me	Me
1o	3	Bzl	Me	Me

Scheme 1.

the substrates (**1**) to the substrate specificity of papain is discussed below. Particularly, as can be seen from Table 3, in the cases of **1b**, **1c**, and **1f**, when the α,γ-diester groups were comparatively small in size, the α-ester alone was readily hydrolyzed to give the corresponding γ-methyl ester (**2b**) in 94% yield and γ-ethyl ester [Cbz-⊿Glu(OEt)-OH; (**2c**)] in 85% from **1c** and 51% from **1f** yields, respectively. However, a similar hydrolysis of the γ-free ⊿Glu-OMe (**1a**) could not easily give **2a**[1] in only 38% yield.

On the other hand, since the sizes of the γ-ester (**1d** and **1e**) and α,γ-diesters (**1g** and **1h**) gradually become bulky, hydrolysis was found to become more difficult. In the case of **1d**, the hydrolysis proceeded ultimately to give Cbz-⊿Glu(OBu^t)-OH (**2d**) in 23% yield, while in the case of a bulkier γ-benzyl ester (**1e**) hydrolysis didn't take place. Accordingly, as is naturally expected, the bulky α,γ-di-*t*-butyl (**1g**) and α,γ-dibenzyl esters (**1h**) were by no means hydrolyzed. As a result, it can be seen the size and bulkiness of the γ-ester (X), as well as those of the α-ester (Y), are very important factors for the hydrolysis of such substrates [Cbz-⊿Glu(OX)-OY] with papain, except for **1a**.

In addition, besides the above-two *C*-protecting groups, the *N*-protecting groups of **1** are also thought to be another important factor. It is necessary to investigate whether or not the *N*-protecting group influences this type of hydrolysis. Being kept the both sides as methyl esters, the substrates (**1**) protected with five kinds of *N*-protecting groups [that is, from the smallest Moc (**1i**), Eoc (**1j**), Ipc (**1k**), Nbc (**1l**) to the largest Cbz group (**1b**)] were synthesized, and then applied to a similar hydrolysis. As a result, all of the esterase actions took place beautifully to give the corresponding *N*-protected ⊿Glu(OMe)-OH (**2i**—**l**) in ca 91% yields. These results clearly indicate that such enzymatic hydrolysis is not affected by the size of the *N*-protecting groups.

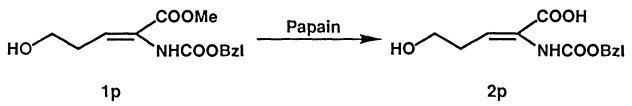

1p 2p

Scheme 2.

However, interestingly, it was found that the length of the side chain of **1** was greatly related to the hydrolysis, as shown in Table 3. Namely, dehydroaspartate (**1m**) was by no means hydrolyzed, whereas dehydroglutamate (**1b**) was hydrolyzed almost quantitatively; then, the longer the side chain from **1b** to **1o** via **1n** became, the yield decreased abruptly.

Furthermore, since a similar hydrolysis of **1b** having a hydroxyl group at the terminus of the side chain was also achieved to give 2-(*N*-Cbz-amino)-5-hydroxy-2-pentenoic acid (**2p**) in 80% yield (Scheme 2), it seems that the existence of the γ-ester group in ⊿Glu derivatives is not necessarily essential; that of the electronegative group near the γ-position, however, may be rather important. On the other hand, it is of particular interest that the results of the hydrolysis are not affected by the kinds and sizes of the *N*-protecting groups at all, but by the length of the side chain.

On the contrary, however, in the case of the treatment of **1b** with α-chymotrypsin A, interestingly, it has been already revealed that the γ-methyl ester is selectively hydrolyzed.[15]

In conclusion, besides being surprised that the enzymatic hydrolysis of the DHA ester occurred, it is very available synthetically that only the α-ester of **1** could be enzymatically hydrolyzed, whereas the selective hydrolysis of **1** was extremely difficult by the chemical method.[9] Furthermore, the results indicate that the reverse reaction, i.e., peptide-bond formation, can also be catalyzed with papain. In fact, the enzymatic synthesis of various dehydroglutamyldipeptides were successful. After all, the present study suggested that papain has become a sufficiently useful tool for organic synthesis.

References

1) C. Shin, N. Takahashi, and Y. Yonezawa, *Chem. Pharm. Bull.*, **38**, 2020 (1990).

2) Y. Isowa, M. Ohmori, M. Sato, and K. Mori, *Bull. Chem. Soc. Jpn.*, **50**, 2766 (1977).

3) K. Morihara and T. Oka, *Biochem. J.*, **163**, 531 (1977).

4) Y. Isowa, M. Ohmori, T. Ichikawa, and K. Mori, *Tetrahedron Lett.*, **1979**, 2611.

5) K. Morihara and T. Oka, *J. Biochem.*, **89**, 385 (1981).

6) For examples, W. Kullmann, *J. Biol. Chem.*, **255**, 8234 (1980); W. Kullmann, *J. Org. Chem.*, **47**, 5300 (1982).

7) For examples, K. Morihara, "Peptide Bond Synthesis Catalyzed by Various Proteases," *Protein, Nucleic Acid, Enzyme*, **26**, 1979 (1981); K. Morihara, "Enzymatic Synthesis of Peptides," *ibid.*, **29**, 49 (1984).

8) K. Morihara, "Biotechnology Series," Kodansha Co.,

Ltd., Tokyo (1987), Chap. 2, p. 75.
9) C. Shin, N. Takahashi, and Y. Yonezawa, *Chem. Lett.*, **1988**, 2001.
10) C. Shin and N. Takahashi, *Chem. Lett.*, **1989**, 747.
11) C. Shin, Y. Yonezawa, and E. Watanabe, *Tetrahedron Lett.*, **26**, 85 (1985).
12) Y. Yonezawa, T. Obara, and C. Shin, *Nippon Kagaku Kaishi*, **1987**, 838.
13) C. Shin, T. Obara, S. Morita, and Y. Yonezawa, *Bull. Chem. Soc. Jpn.*, **61**, 3265 (1988).
14) C. Shin, M. Seki, and H. Tano, The National Meeting of the Chemical Society of Japan, Yokohama, April 1991, Abstr., No. 3D104.
15) C. Shin, M. Seki, and N. Takahashi, *Chem. Lett.*, **1990**, 2089.

 © 1991 The Chemical Society of Japan Bull. Chem. Soc. Jpn., 64, 3581—3584 (1991)

The Properties of the Multistage Bioreactor Constructed by the LB Technique

Michihiro OHNISHI,* Coe ISHIMOTO, and Jun'etsu SETO
SONY Corporation Research Center, 174, Fujitsuka-cho, Hodogaya-ku, Yokohama 240
(Received June 24, 1991)

A multistage bioreactor consisting of organic ultrathin layers was successfully realized by immobilizing glucose oxidase and glucoamylase by the Langmuir–Blodgett technique (LB technique). Starch as the substrate was quickly converted into gluconic acid and hydrogen peroxide as the products in this bioreactor via the intermediate, glucose. The rate of the sequential reactions was electrochemically measured. This rate increased proportionally with increasing the concentration of starch, and also increased with increasing the amount of glucose oxidase in the LB film. This bioreactor, however, decayed soon. The reason of this decay was considered to be the structural conversion of the LB layers with glucoamylase. The multistage bioreactor constructed by the LB technique will be used not only as a super small-sized, rapid bioreactor or biosensor but also as an investigating means of the reconstitution of membrane enzyme and biomembrane.

The biomembrane is commonly a complex of lipid and protein constituting sequential enzymatic reaction systems. The same reactions may be realized in an artificially reconstructed system. A system using the microcapsule technique[1] as previously been demonstrated. Glucoamylase was adsorbed to the outside of a microcapsule within which glucose oxidase was contained. The construct functioned as an extremely small-sized bioreactor which converted starch into gluconic acid via glucose. Glucose as the intermediate, however, moved slowly into the inside of the microcapsule, and the rate of the overall reaction was not rapid.

If the enzymes are immobilized in ultrathin films the intermediates of sequential reactions will be able to move rapidly from one enzyme to the next. It is easy to immobilize protein in an organic ultrathin film if the Langmuir–Blodgett technique (LB technique) is used.[2]

The LB technique provides the following advantages: i) It is expected that the denaturation of enzymes is minimized as the technique is a wet process at normal temperature and pressure. ii) The devices constructed by this technique are so small and their that rapid diffusion of the substrate molecules of the enzymatic reactions are allowed. iii) The construction of multilayer structures is easy since the LB film is made by consecutively depositing monolayers. Onoue and Moriizumi constructed a glucose sensor by immobilizing glucose oxidase by the LB technique.[3,4] i) and ii) have already been demonstrated by these previous workers. We realized a two-step sequential reaction by constructing an LB film incorporating different enzymes in successive layers, by the introduction of the viewpoint of iii). This multistage bioreactor is a composite system combining the reaction of glucoamylase which hydrolyzes starch to glucose, and that of glucose oxidase which oxidizes glucose to gluconic acid and hydrogen peroxide.

Experimental

Materials. Enzymes: Glucose oxidase (EC 1. 1. 3. 4) from *Aspergillus niger* (Sigma Chemical) and glucoamylase (EC 3. 2. 1. 3) from *Aspergillus oryzae* (Sigma Chemical) were used. Each enzyme was dissolved in ultra pure water at a concentration of 500 mg dm^{-3}. The electric conductivity of ultra pure water produced by using Milli Q Organex-Q type (Millipore) was more than 17.5 MΩ cm.

Amphiphilic Materials: As a result of considering the surface charges of the enzymes, icosanoic acid (Applied Science) was used to adsorb glucose oxidase and a mixture of trimethyloctadecylammonium chloride (Tokyo Kasei Kogyo) and methyl icosanoate (Applied Science), weight ratio 1:4, was used to adsorb glucoamylase.[4,5] The trimethyloctadecylammonium chloride was recrystallized from hot ethanol–ether. The spreading solvents of the amphiphilic materials were prepared in chloroform (Spectrosol series of Dojindo Laboratories), at a concentration of 1 mg cm^{-3}.

Substrates: Glass substrates with two gold-evaporated electrodes were used. The area of each electrode was 10 mm^2. The surface of the substrate was treated with trichlorooctadecylsilane (Shin-etsu Chemical) and made hydrophobic.[6]

Preparations. Fromherz Method:[2] A Fromherz-type trough (Mayer–Feintechnik) was used. The trough has eight trough compartments, and two barriers can move from one trough compartment to another ad libitum. This Fromherz method was used to carry out the following process. The subphase solution is placed in several trough compartments. Then, a monolayer of amphiphilic molecules is organized on the surface of the subphase. Next, a protein solution is placed in the adjoining trough compartments. The monolayer is then moved over onto the surface of the protein solution to allow the protein to adsorb to the monolayer. This composite monolayer with adsorbed protein is returned onto the pure subphase. The composite monolayer is then deposited onto a glass substrate by the LB technique, and in this way the LB film incorporating protein can be constructed.

Conditions for Constructing the Enzyme LB Film: The Fromherz method was carried out. Ultra pure water was used as the subphase (pH approximately 6, 20 °C). The surface pressure of the monolayer of icosanoic acid was 30 dyne cm^{-1} (1 dyne=10^{-5} N) through the adsorption step, and that of the mixed monolayer described above was 20 dyne cm^{-1}. The time allowed for adsorption was 1 h. The surface pressure of the composite monolayer on the subphase was increased to 35 dyne cm^{-1} for deposition. The dipping speed

was 5 mm min^{-1}. A Y-type deposition was obtained for each composite monolayer. The transfer ratio was between 0.9 and 1.0.

The Measurement of the Enzymatic Reaction. Hydrogen peroxide generated by the enzymatic reaction was measured electrochemically.[3] The substrate was placed in a 1 cm×1 cm cell for spectroscopy containing 1 ml of 0.05 M (1 M=1 mol dm^{-3}) acetate buffer (pH 5, 20 °C).[7] The electrodes on the substrate were connected to a potentiostat with the applied potential set at 0.8 volt. The electrode current was recorded by an X-T recorder connected to the potentiostat. Glucose or soluble starch of reagent grade was used as the substrate of the enzymatic reactions. The substrate solution was prepared in acetate buffer, and 200 μl of a concentrated solution was injected into the buffer in the cell to produce the necessary concentrations.

Results and Discussion

The enzymatic reactions is following:

Glucoamylase

$$\text{starch} + (n-1)\cdot H_2O \longrightarrow n\cdot \text{D-glucose}$$

Glucose oxidase

$$\text{D-glucose} + O_2 \longrightarrow \text{D-gluconic acid} + H_2O_2$$

First, the properties of a bioreactor constructed by the deposition of an LB film incorporating glucose oxidase was studied. The response current at 1 min after injecting glucose, two LB layers incorporating glucose oxidase was directly proportional to the concentration of glucose in the range less than 3 g dm^{-3} (Fig. 1). When this bioreactor was kept at 5 °C for several months, the response current changed very little, indicating high stability. These results agreed with the results by Onoue and Moriizumi.[3]

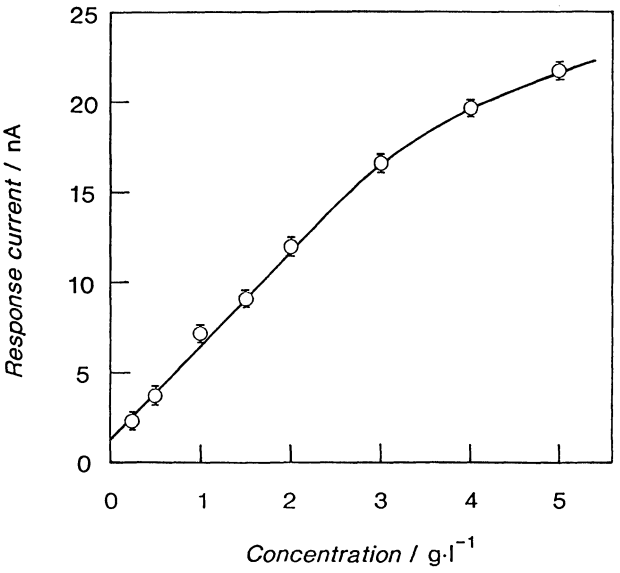

Fig. 1. Response current vs. concentration of glucose. Two LB layers incorporating glucose oxidase was measured. The value (average ±standard error) was observed at 1 min after the addition of glucose solution.

Next, the properties of a multistage bioreactor constructed by depositing two LB layers incorporating glucoamylase onto eight LB layers incorporating glucose oxidase was studied. The time-dependences of the response currents for a series of concentrations of starch are shown in Fig. 2. Rapid response was observed at each concentration of starch solution. These response currents attained steady states in a few seconds. The microcapsule-type bioreactor showed a lag time of sev-

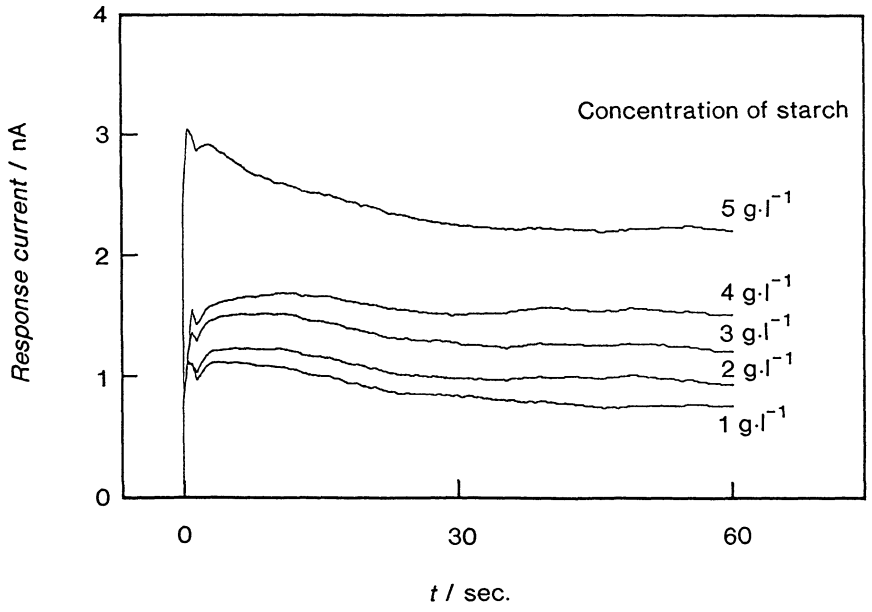

Fig. 2. Response current vs. time after addition of starch solution (t). Two LB layers incorporating glucoamylase on eight LB layers incorporating glucose oxidase were measured.

eral minutes in the reactions.[1] The very short lag time indicates that the diffusion of the intermediate species, glucose, was very rapid in the ultrathin LB film.

Greater concentrations of starch increased the response current. Figure 3 shows the dependence of the response current of the bioreactor, at 1 min after injection, on the concentration of starch. The response current was linearly related to the concentration of starch from 2 to 5 g dm^{-3}, suggesting the possibility of its use as a starch sensor. The reason the fitted line does not go through the origin is probably due to the fact that the solution is not stirred, resulting in some nonuniformity of concentration.

Figure 4 shows the response currents at 1 min after the injection of starch solution plotted against the number of the LB layers incorporating glucose oxidase. In each sample, two LB layers incorporating glucoamylase were deposited on to the LB layers incorporating glucose oxidase. The concentration of starch was 5 g dm^{-3}. The response current was proportional to the number of the glucose oxidase LB layers. As the amount of adsorbed glucose oxidase per one LB layer is constant, this indicated that the activity of the reaction was proportional to the total amount of enzyme incorporated.

The storage stability of the bioreactor constructed was investigated. The bioreactor constructed with two LB layers of glucoamylase deposited on eight LB layers of glucose oxidase was kept at 5 °C. The response current at 1 min after injection of a 5 g dm^{-3} starch solution is plotted in Fig. 5. The response current decreased significantly in five days after construction. The decrease in response current for a bioreactor incorporating only glucose oxidase was found to be very small. Thus, it is suspected that the decay was caused

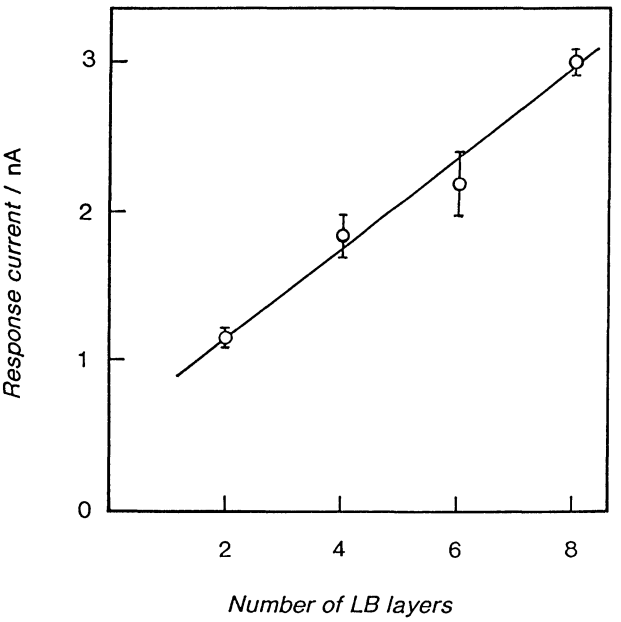

Fig. 4. Response current vs. number of LB layers incorporated with glucose oxidase.
Two LB layers incorporated with glucoamylase on LB layers incorporated with glucose oxidase were measured. The value (average ±standard error) was observed at 1 min after the addition of starch solution. The concentration of starch was 5 g dm^{-3}.

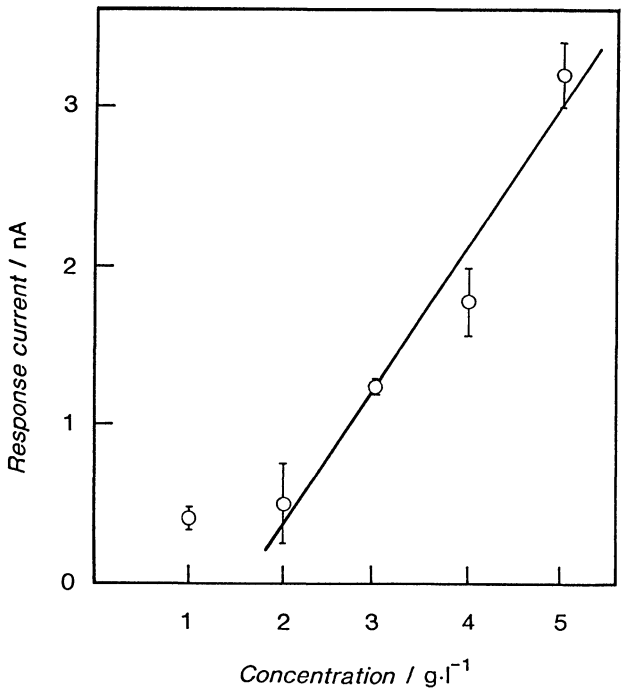

Fig. 3. Response current vs. concentration of starch.
The value (average ±standard error) was observed at 1 min after the addition of starch solution.

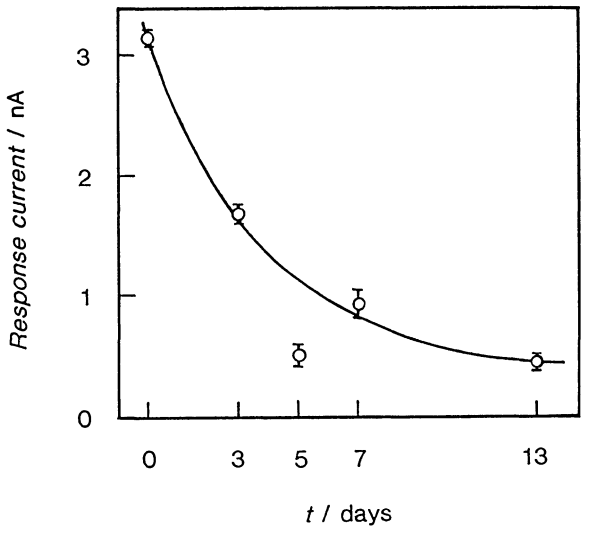

Fig. 5. Storage stability of the bioreactor. Days after preparation (t) vs. response current.
Storage temperature was 5 °C. The bioreactor was constructed with two LB layers incorporated with glucoamylase on eight LB layers incorporated with glucose oxidase. The value (average ±standard error) was observed at 1 min after the addition of starch solution. The concentration of starch was 5 g dm^{-3}.

by the LB layers incorporated with glucoamylase.

The structure of the multistage bioreactor constructed by the LB technique is similar to a biomembrane. Therefore, it will be possible to apply this approach to the study of the property of reconstructed membrane enzyme systems as well as to the construction of ultramicro or ultrarapid bioreactors or biosensors.[8,9] This approach would allow the control of the adsorbed site and the amount of enzyme.[4,10,11]

We thank Dr. Akio Yasuda for his advice about the electrochemical measurement.

References

1) T. Komori, N. Muramatsu, and T. Kondo, *Appl. Biochem. Biotechnol.*, **14**, 29 (1987).
2) P. Fromherz, *FEBS Lett.*, **11**, 205 (1970).
3) Y. Onoue and T. Moriizumi, *Trans. IEE Jpn.*, **107-A**, 97 (1987).
4) M. Sriyudthak, H. Yamagishi, and T. Moriizumi, *Thin Solid Films*, **160**, 463 (1988).
5) "Biochemicals Organic Compounds for Research and Diagnostic Regents 1990," Sigma Chemical's Catalog, p. 1544.
6) J. Sagiv, *J. Am. Chem. Soc.*, **102**, 92 (1980).
7) M. Ohnishi, G. Okada, H. Taniguchi, and Y. Sakano, *Tanpakushitu Kakusan Koso*, **30**, 489 (1985).
8) D. W. Tank, C. Miller, and W. W. Webb, *Proc. Natl. Acad. Sci. U. S. A.*, **79**, 7749 (1982).
9) T. Hamamoto, E. Muneyuki, and H. Hirata, *Saibou Kougaku*, **7**, 69 (1988).
10) T. Suzawa, "Koubunshi-Hyoumen No Kiso To Ouyou (Jyou)," ed by Y. Ikada, Kagaku-Doujin, Kyoto (1986), Chap. 11, pp. 249—259.
11) M. Ohnishi, C. Ishimoto, and J. Seto, 54th Spring Meeting of the Chemical Society of Japan, 1987, Abstr., No. 2 VIAl 6.

Back Biting Reactions during the Catalytic Decomposition of Polyethylene

Yumiko ISHIHARA,*,† Hidesaburo NANBU,†† Katsuhiko SAIDO,†††
Tadashi IKEMURA, and Tomoyuki TAKESUE
Department of Industrial Chemistry, College of Science and Technology,
Nihon University, 1-8, Kanda-Surugadai, Chiyoda-ku, Tokyo 101
†††College of Pharmacy, Nihon University, 7-7-1, Narashinodai, Funabashi-shi, Chiba 274
(Received July 15, 1991)

Isobutane and isopentane were selectively obtained by polyethylene catalytic decomposition using the NaY-type zeolite catalyst. Back biting reactions are thus essential to gas formation during the catalytic decomposition of polyethylene. Chain-end secondary carbonium ions cause back biting reactions involving intramolecular rearrnagement to form the C_9 fraction. Isobutane and isopentane are then produced by decomposition of the gasification precursor C_9 fraction.

Polymer degradation has mainly been studied for the purposes of attaining greater heat and weather stabilization.[1-4] Many reports describe the mechanisms for this based on radical reactions. However, very little study has been directed to the catalytic degradation of polymers.[5-9] As shown in previous reports,[10,11] unique reactions occur in the catalytic degradation of polyethylene and polystyrene.

For instance, branched ethylene oligomers are produced in the catalytic degradation of polyethylene in the presence of the silica-alumina catalyst.[10] Indan oligomers are produced in the catalytic degradation of polystyrene in the presence of the aluminum chloride catalyst.[11] Gasification was found to occur with the gasification precursor in polyethylene catalytic decomposition. By the zeolite catalyst, the composition of gas resulting from polyethylene catalytic decomposition is unique and differs from that by the silica-alumina catalyst. The gas is composed of isobutane (C_4) and isopentane (C_5), in equimolar amounts at low temperature. The formation mechanisms of these fractions are of interest for the practical utilization of waste polyethylene.

Back biting reactions in gas formation were noted to occur exclusively as elementary reactions. The mechanisms for these reactions are discussed in detail in the following.

Experimental

Sample and Catalyst. The sample was polyethylene (hereafter referred to as PE, $\bar{M}_n$=3.98×10⁴, manufacted by Mitsui Petrochemical Industries Co., Ltd., powder with a mesh of >80).

A NaY-type zeolite catalyst (Na-atoms replacement: Toyo CCI Co., Ltd.) with 24—26 wt% alumina content was used after being heated for 5 h in dry air at 450 °C. It was made into powders of >100 mesh. The physicochemical properties of catalyst are showen in Table 1.

Table 1. Physicochemical Properties of the Catalysts

Catalyst		Zeolite
Al_2O_3	(%)	24—26
SiO_2	(%)	74—76
Na_2O_3	(%)	<0.1
Fe_2O_3	(mmol g^{-1})	0.82
Specific surface area	(m^2 g^{-1})	510—580
Average pore size	(Å)	15—20

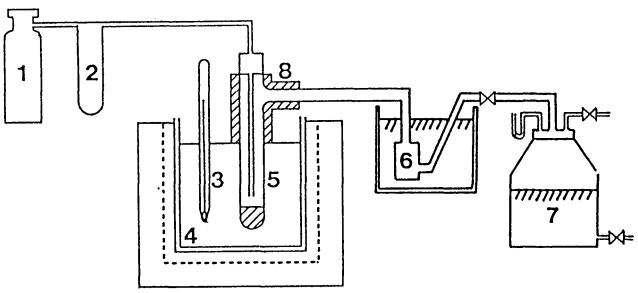

Fig. 1. Batch system reactor for catalytic decomposition. 1) N_2 cylinder, 2) Manometer, 3) Thermometer, 4) Metal bath, 5) Reactor, 6) Trap for liquid, 7) Trap for gaseous products, 8) Asbestos.

Experimental Operation and Procedure. A pyrex glass tube reactor (outer diameter: 25 mm and length: 240 mm) connected to a trap was used to recover gaseous and liquid products as shown in Fig. 1.

The experimental procedure was as follows: 2 g of the sample and 0.06 to 2 g of the catalyst were mixed by stirring. The mixture was placed on the bottom of the reactor and the reaction was conducted from 180 to 300 °C; nitrogen gas was passed through the reactor at a flow rate of 120 ml min^{-1} for 60 min and the ratio of catalyst to sample (C/S) was varied from 0.03 to 1.00.

Analysis Method. To analyze the reaction products recovered, the limiting viscosity method ($[\eta]=5.10\times10^{-4}[\bar{M}_n]^{0.725}$)[12] was used to determine the molecular weight of the degraded polymer. The molecular weight distributions of the oligomer and liquid were determined by field desorption infrared (FD-), field ionization-mass spectrometers (FI-MS)

† Present address: Inoue Biodetrioration Laboratory, 2-26-10, Sekimachi-Minami, Nerima-ku, Tokyo 177.
†† Present address: Shinnitetu Chemical Co., Ltd., 4-10-3, Nakai, Kokurakita-ku, Kitakyushu-shi, Fukuoka 803.

respectively.[13] The gaseous and liquid products were quantitatively analyzed by a gas–liquid chromatograph (GC-8A of Shimadzu).[14] Chemical structure was determined ^1H and ^{13}C NMR (JEOL, Ltd., JNM-FX100).[10]

Results and Discussion

Material Balance and Gas Yields by the Zeolite Catalyst. The relationship between reaction temperature and the reaction products of PE decomposition was investigated using the zeolite catalyst. The results are shown in Table 2. The reaction products consisted of 4 fractions, degraded polymer ($\bar{M}_n$=1000<), oligomer ($\bar{M}_w$=300—800), liquid ($\bar{M}_w$=100—250) and gas. The yield of degraded polymer decreased at higher temperature, while that of the liquid fraction containing small amounts of olefins increased rapidly. These results show close agreement with those for PE catalytic decomposition in the presence of the silica–alumina catalyst.[13] As described previously, the gas fraction is produced during liquid fraction (gasification precursor) decomposition and does not derive from chain-end carbonium ions of the oligomer and polymer fractions.[14] If the gas fraction is produced from chain-ends of molecules of the oligomer and polymer fractions, it should be obtainable in a large isobutene yield by isomerization of chain-end carbonium ions without decrease in molecular weight, as shown in Scheme 1.

The formation of 4 fractions indicates that a decrease in molecular weight occurred. From Table 2, the liquid fraction is produced by further decomposition of oligomer and polymer fractions. Gas formation takes place at the chain-ends of the liquid fraction produced by oligomer decomposition, as when using the silica–alumina catalyst.[14]

Table 3 shows the gas composition at each reaction temperature. At a low reaction temperature of 180 °C, the yields of isobutane and isopentane were about 46.5 and 46.9 mol%, respectively.

Gas composition by the silica–alumina catalyst with lower acidity was found to consist of isobutane 54.9 mol%, isopentane 5.9 mol% at 280 °C[13] and thus may possibly depend mainly on the acidity of the catalyst. Isobutane yield was much more than those of the other gaseous products. The formation mechanism of isobutane is possibly direct β-scission of chain-end tertiary carbonium ions produced by redecomposition of the liquid fraction as shown in Scheme 1:

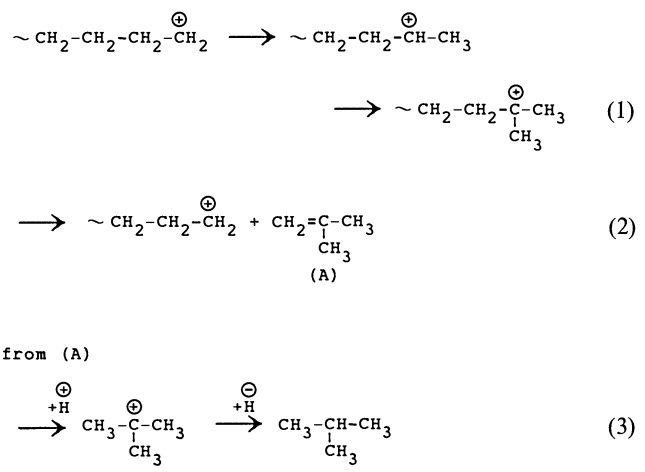

Scheme 1.

In the case of the zeolite catalyst, isopentane yield (36 mol%) was much higher that by the silica–alumina catalyst (6 mol%) at the same temperature 280 °C and isobutane and isopentane would not likely have been formed simultaneously from chain-end primary and secondary carbonium ions. Isopentane was not produced by β-scission from chain-end carbonium ions (primary, secondary and tertiary) in the presence of the zeolite catalyst.

Changes in C_4 and C_5 Fraction Yields as Function of Reaction Conditions. Effects of Reaction Temperature: Figure 2 shows the yields of C_4 and C_5 fractions.

Table 3. Components of Gaseous Products from Catalytic Degradation of PE

Temp/°C	180	200	220	240	260	280	300
Yield/mol%							
Methane	0.0	0.0	0.0	0.0	0.0	0.0	0.3
Ethane[a]	0.0	0.0	0.0	0.1	0.9	0.6	0.9
Propane	2.9	5.1	4.9	4.8	7.4	6.4	6.3
Propylene	0.0	0.5	0.9	4.6	7.4	6.4	6.3
Isobutane	46.5	47.3	41.2	39.9	34.9	44.0	40.7
Butane	3.7	4.6	5.4	4.6	4.8	4.8	4.7
Isobutene	0.0	0.0	0.0	3.3	0.5	2.7	3.8
trans-2-Butene	0.0	0.0	0.3	0.7	0.4	1.3	2.2
Isopentane	46.9	41.2	44.9	42.9	35.9	35.6	34.5
Pentane	0.0	1.3	2.4	2.1	2.0	0.9	1.4

Reaction conditions: zeolite catalyst, time=1 h, C/S =0.25.
a) Ethane, ethylene mixtures.

Table 2. Material Balance of Catalytic Degradation Products from PE

Temp/°C	180	200	220	240	260	280	300
Fraction yield/wt%							
Gas	0.2	1.2	1.7	2.7	3.2	3.1	5.6
Liquid	3.0	7.1	10.3	13.1	16.6	24.5	27.7
Oligomer	25.1	30.0	28.0	27.8	24.8	22.9	24.0
Degraded polymer	71.8	61.8	60.0	56.4	46.0	49.5	42.7
Cake	Trace	Trace	Trace	Trace	Trace	Trace	Trace

Reaction conditions: zeolite catalyst, time=1 h, C/S=0.25.

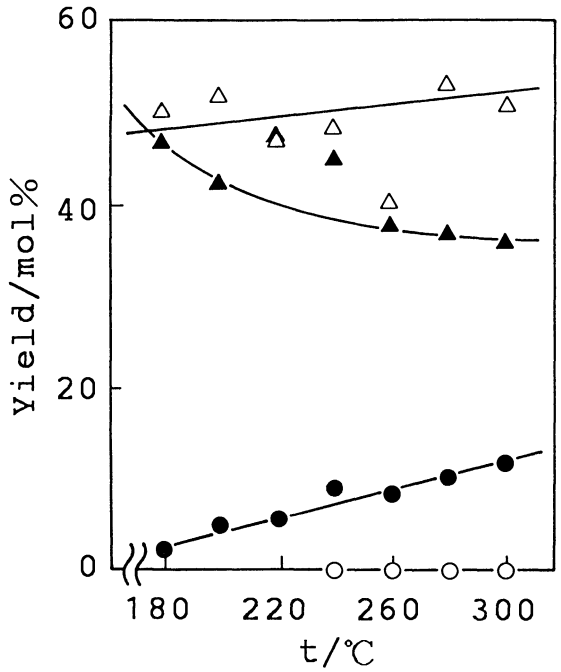

Fig. 2. Composition of gaseous products by polyethylene.
○; C_2, ●: C_3, △: C_4, ▲: C_5.
Reaction conditions; zeolite catalyst, time=1 h, C/S=0.25.

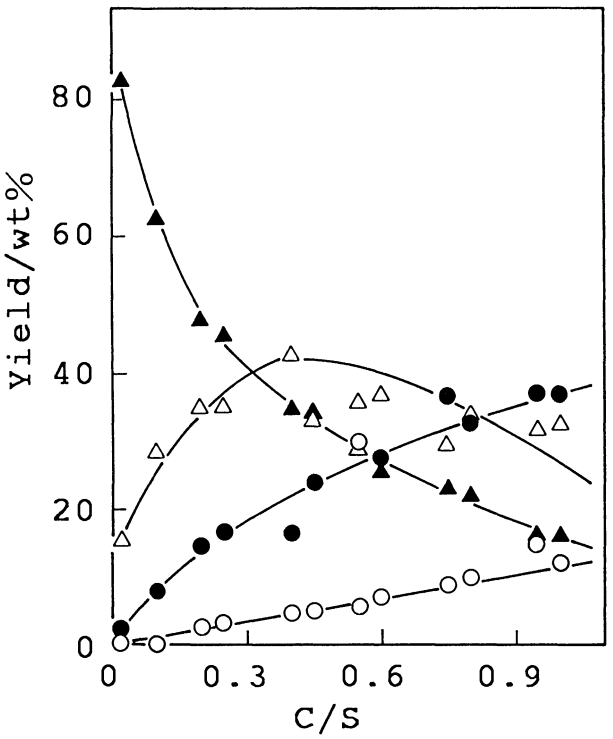

Fig. 3. Material balance of catalytic decomposition products of polyethylene.
○; gas, ●: liquid, △: oligomer, ▲: degraded polymer.
Reaction conditions; zeolite catalyst, temp=260 °C, time=1 h.

C_4 increased slightly with rise in temperature and was about 50.2 mol% at 180 °C and 51.4 mol% at 300 °C. The C_5 fraction decreased while the C_3 fraction increased at high temperature. The compositions of these fractions were independent of reaction temperature.

Table 3 shows the gas fractions to be produced mainly from the liquid fraction. The decrease in C_5 yield corresponds to the increase in C_3 and C_2 yields at high temperature. The C_5 fraction may possibly decompose into C_3 and C_2 fractions at high temperature.

On using the zeolite catalyst, isobutane and isopentane were produced preferentially. Thus, direct β-scission from chain-end carbonium ions is not important.

The stabilization of chain-end carbonium ions has generally been shown to result from rearrangement of ions (15 kcal mol^{-1}) and direct β-scission (45 kcal mol^{-1}).[15] The intramolecular rearrangement of chain-end carbonium ions thus occurs before direct β-scission. Isobutane and isopentane may possibly be formed from the gasification precursor (liquid fraction) produced by decomposition for the stabilization of internal rearranged ions.

Effects of Contact Time: Figure 3 shows the yield of each fraction at various catalyst concentrations at the same reaction temperature. Decomposition was accelerated of high catalyst concentration even though the temperature was the same. The rapid increase in oligomer yield corresponded to the decrease in degraded polymer yield and the liquid fraction also increased with decrease in oligomer yield. Figure 4 shows the yields of the C_4, C_5 and C_3 fractions at various catalyst concentrations. The composition of gas showed virtually no change with catalyst concentration and yield in each case increased with the catalyst/sample (C/S) ratio. The formation of C_4 and C_5 fractions in equimolar amounts was confirmed. Direct β-scission of secondary or primary chain-end carbonium ions with the formation of C_4 and C_5 was not important and thus, intramolecular rearrangement reactions should be required. In Fig. 4, the rates of C_4 and C_5 formation are nearly equal and these fractions may possibly derive from the same reaction intermediate. If isobutane and isopentane are produced from different reaction intermediates, their yields should also differ.

Gas and liquid yields increased with catalyst concentration at the same temperature (Fig. 3), though gas composition showed no change (Fig. 4). Only reaction temperature affected gas yield (Fig. 2). From Fig. 3, the rapid decrease in oligomer yield can be seen to correspond to increase in liquid yield. The liquid fraction (gasification precursor) is thus shown to be produced by decomposition of oligomers. Thus, changes in the molecular weight of oligomer and liquid fractions were carefully examined.

Molecular Weight and Distribution of the Oligomer Fraction. Figure 5 shows the molecular weight distri-

bution of the oligomer fraction: $\bar{M}_w$=200—1000 (top peak $\bar{M}_w$=350, 180 °C (A)),$\bar{M}_w$=200—700 (top peak $\bar{M}_w$=300, 240 °C (B)), and $\bar{M}_w$=200—500 (top peak $\bar{M}_w$=300, 280 °C (C)) were obtained by FD-MS, respectively. The molecular weight and its distribution shifted to the lower molecular weight side with rise in temperature. Figure 6 shows FI-MS spectrum of the liquid fraction recovered at 280 °C. The molecular weight distribution of M_w=100—250 (top peak M_w=130) was measured for the liquid fraction. That is, the liquid fraction for gas formation are formed during decomposition of the oligomer fraction.

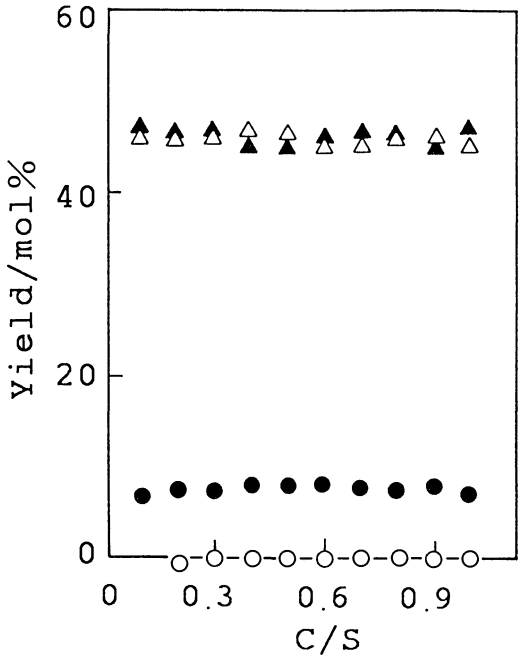

Fig. 4. Composition of gaseous products by polyethylene.
○; C_2, ●: C_3, △: C_4, ▲: C_5.
Reaction conditions; zeolite catalyst, temp=260 °C, time=1 h.

Chemical structure of the Oligomer Fraction. The oligomer structure should thus be carefully analyzed to clarify the mechanism for liquid formation. Figure 7 shows the chemical structure of the oligomer fraction by ^{1}H NMR spectrum (280 °C). The liquid fraction structure was essentially the same as that of the oligomer

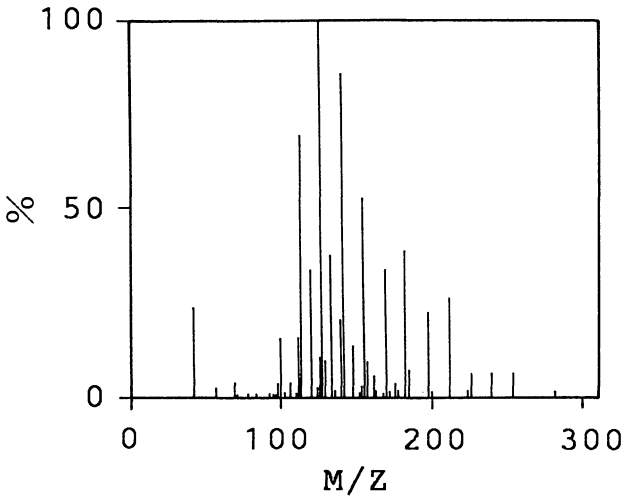

Fig. 6. FI-MS spectrum of the liquid fraction.
Reaction conditions; zeolite catalyst, temp=280 °C, time=1 h, C/S=0.25.

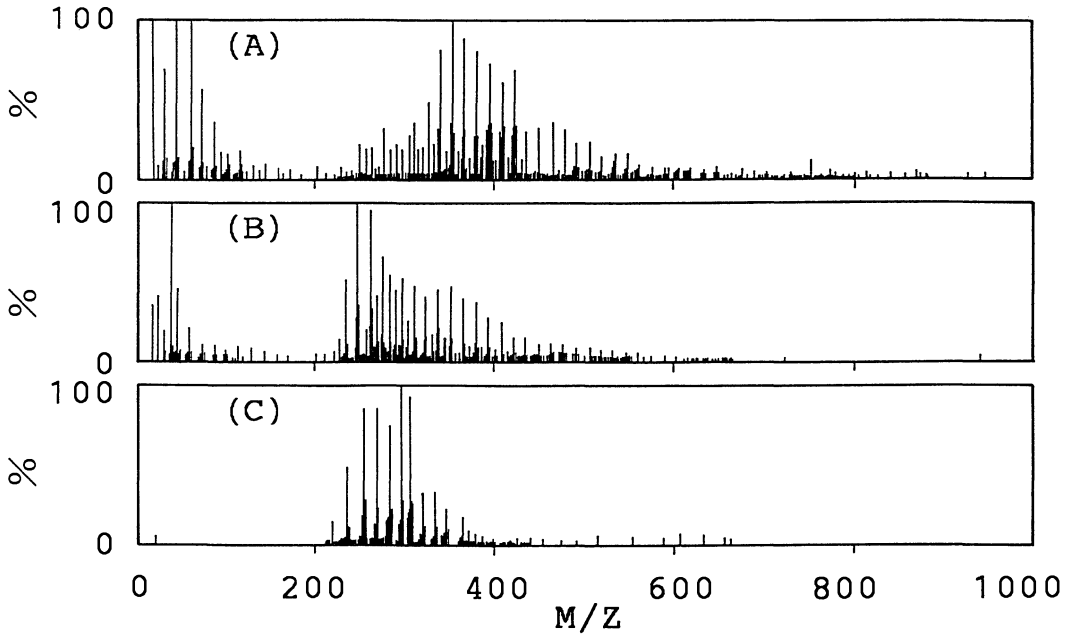

Fig. 5. FD-MS spectra of the oligomer fraction.
Reaction conditions; zeolite catalyst, temp=180 °C (A), 240 °C (B), 280 °C (C), time=1 h, C/S=0.25.

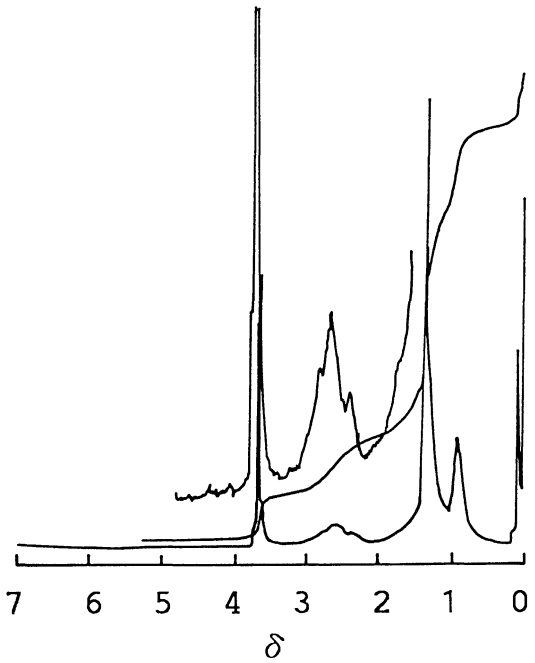

Fig. 7. ^{1}H NMR spectrum of the oligomer fraction. Reaction conditions; zeolite catalyst, temp=280 °C, time=1 h, C/S=0.25.

Table 4. Chemical Shifts of Oligomer and Degraded Polymer Mixture Observed by ^{13}C NMR and Calculated

Branched species	Carbon No.	Calcd[a)] (ppm)	Obsd (ppm)
~C-C-C-C-C	1	13.86	14.19
5 4 3 2 1	2	22.65	22.91
	3	32.40	32.27
	4	29.71	29.68
	5	29.96	30.09
4 3 2 1			
~C-C-C-C	1	22.13	22.91
C	2	27.99	27.48
1	3	39.35	39.10
	4	27.20	27.15
1 2 3 2 1			
~C-C-C-C-C~	1	27.27	27.15
C	2	36.91	36.16
4	3	32.52	32.72
	4	20.07	20.31

a) Chemical shifts calculated by Lindeman-Adams method. (L. P. Lindeman and J. Q. Adams, *Anal. Chem.*, **43**, 1245 (1971)).

fraction, though the weakest olefinic signals could be detected. The chemical structure of oligomer and degraded polymer mixture are shown in Table 4. The results of analysis of chain-end structures indicated direct β-scission of on-chain tertiary carbonium ions of oligomers. The liquid fraction also possesses these chain-ends. The β-scission is shown in following Scheme 2.

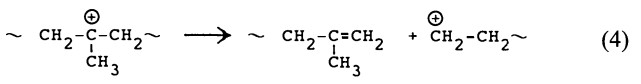

Scheme 2.

The olefinic liquid fraction flowed into the trap without hydrogenation during a short residence time with high vapor pressure, thus showing it not to possess hydrogenated components.

As shown in Table 5, the oligomer was found to have branched components each possessing short chains of C_1—C_6 6.1 per 20 carbon and $\bar{M}_w$=300 (short chain consist mainly of methyl groups). The extent of branching was essentially the same and showed the back bones of the oligomer structures to be similar to that of copolymer of propylene and 1-butene. The extent of branching has been shown to increase with molecular weight decrease.[13)] The extent of branching of further decomposed liquid from oligomers may possible be the same as that of polypropylene back bones (8 per 20 carbon).

It thus follows that secondary carbonium ions are mainly produced at chain-ends of the liquid fraction produced by β-scission of on-chain carbonium ions of the oligomer. The equimoler formation of C_4 and C_5 by direct β-scission of chain-end secondary carbonium ions from the liquid fraction is difficult and thus internal on-chain carbonium ions should be produced through intramolecular rearrangement of chain-end ions by way of least activation energy which ought to be tertiary carbonium ions. The gasification precursor for the C_4 and C_5 fraction formation may possibly be produced by β-scission of on-chain carbonium ions of the liquid fraction.

Mechanism for the Formation of Isobutane and Isopentane. The β-scission for the catalytic decomposition of the oligomer chains possessing short side chains is shown in Scheme 3.

As shown in Tables 2, 4, and 5, yields of the liquid fraction, chain-end structure of oligomer and the extent of branchings indicate that the oligomer fraction undergo random scission to produce the liquid fraction which has chain-end olefin (B) and chain-end secondary carbonium ions (C). The reactions for this are as follows:

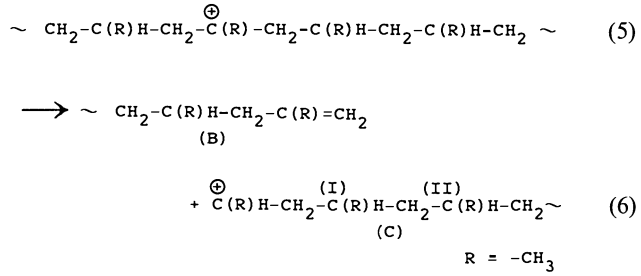

Scheme 3.

Table 5. The Branching Concentration in the Oligomer Fraction

Temp/°C	260	280	300
$CH_3/20CH_2$	2.2	4.3	6.1

Reaction conditions: zeolite catalyst, time=1 h, C/S =0.25.

Affinity of chain-end olefins for protons released from the catalyst is remarkably high. Consequently, as shown in reaction step (7), olefin (B) immediately undergoes proton addition to form tertiary carbonium ions. These ions are stabilized primarily by β-scission. Hydride ion addition (8) occurs to give the saturated liquid fraction. The reactions for this are as follows:

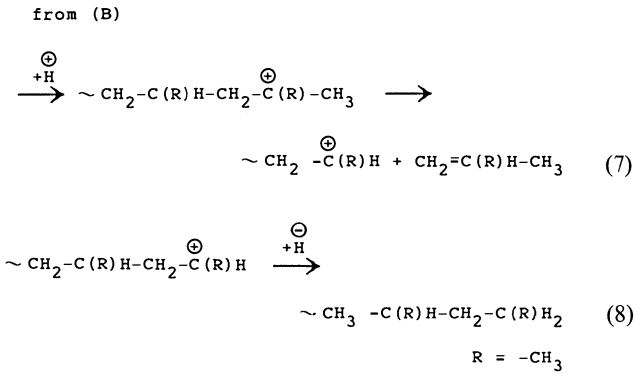

Only chain-end secondary carbonium ions are produced in the liquid fraction by decomposition of oligomers and are stabilized by an intramolecular rearrangement having the least activation energy. (10—15 kcal mol^{-1}).[15] This occurs most easily through intramolecular rearrangement (15 kcal mol^{-1})[15] rather than by β-scission (45 kcal mol^{-1}).[15] That is, secondary carbonium ions are likely converted preferentially to tertiary carbonium ions.

For example, the intramolecular rearrngement of chain-end ions (C) occurs easily on neighboring tertiary carbons by either (I) or (II) (step 6). The formation of ions (I) proceeds via a four membered transition state, while that of ions (II) by a six membered ring. The intramolecular rearrngement of ions (II) occurs exclusively by way of a more stable transition state in step (9).

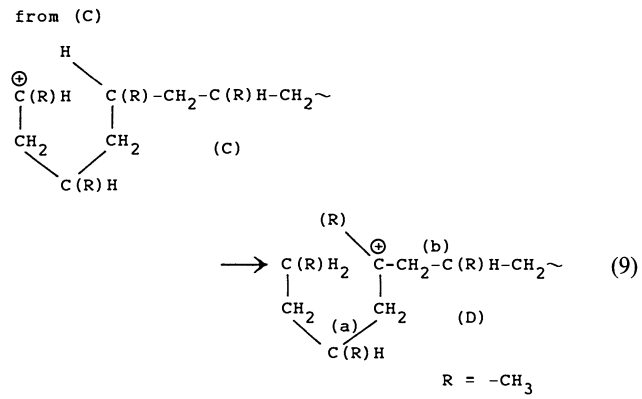

Chain-end secondary carbonium ions (C) produce internal on-chain tertiary carbonium ions (D) by back biting reactions in step (9). Stabilization of ions (D) occurs by direct β-scission, through either (a) or (b). In the case of the (a) position, 1-methylbutylium ions (E) and chain-end olefins (B) are produced, respectively (step 10). Isopentane is produced by way of hydrogenation and isomerization of (E) ions. The main product produced must thus be only isopentane and the liquid fraction in step (10).

Of course, on the case of this, equimolar yields of C_4 and C_5 could not be recorded. Virtually no gas formation from chain-end olefins occurs continuously. β-scission occurs very little or not at all at the (a) position. Elementary reactions generally lead to the formation of more stable products. The reaction of step (10) is not important.

The stabilization of on-chain carbonium ions (D) occurs through step (11). The C_9 component (F) (branched nonene) is produced by β-scission of (D) ions. From the olefinic branched C_9 fraction (F), reaction intermediate (G) is produced immediately by proton addition in step (12).

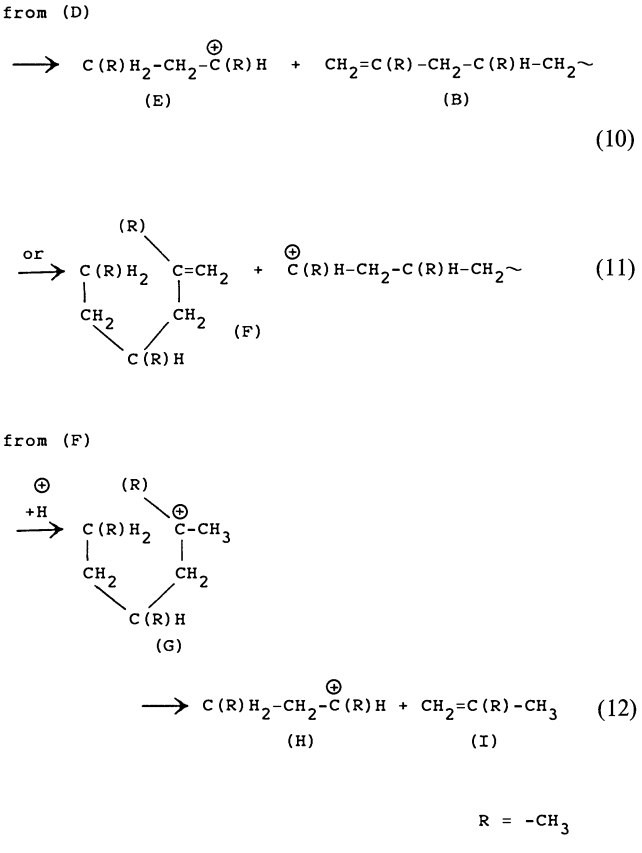

The C_4 and C_5 fractions are produced by the redecomposition of intermediate (G). Isobutene is immediately hydrogenated to give isobutane. The 1-methylbutylium ions (H) produced are stabilized by hydride ion addition following isomerization. Isopentane is produced by the hydrogenation of (H) ions.

Table 6. Quantitative Determination of Carbon Number Distribution from the GLC Analysis (Liquid Fraction)

Carbon number	Yield/%
5	0.8
6	2.9
7	6.1
8	7.4
9	17.9
10	17.5
11	20.4
12	11.7
13	13.3

Reaction conditions: zeolite catalyst, temp=260 °C, time=1 h, C/S=O.25.

These steps can be demonstrated by the results of selective formation with equimolar yields of C_4 and C_5 fractions. The continual formation of C_9 is possible only through the reaction intermediate (C) ions in step (9) and not by chain-end olefins (B) in step (10). That is, β-scisssion of (D) ions takes place mainly at the (b) position.

The C_9 fraction (gasification precursor) must first be detected as evidence that these steps actually occur. Table 6 shows the carbon number distribution of the liquid fraction determined by GLC analysis. The liquid fraction consisted of C_9—C_{13} fractions with the C_9 fraction (M_w=128) as the main product. Beltrame, et. al. found the C_9 fraction (saturated and unsaturated isomers) to be the main component in the catalytic decomposition products of PE in the presence of the silica-alumina catalyst.[16]

The C_9 fraction thus corresponds to the reaction intermediate as a gasification precursor. Chain-end secondary carbonium ions of the liquid fraction are formed during the decomposition of the oligomer fraction. These ions are mainly stabilized by back biting involving intramolecular rearrangement. Rearraged on-chain tertiary carbonium ions are also stabilized by β-scission, and consequently, the C_9 fraction is produced. The C_9 fraction cannot be produced by direct β-scission of (a) position, chain-end carbonium ions of the liquid and oligomer fractions but from internal on-chain carbonium ions produced by intramolecular rearrangement via the lowest activation energy than that by β-scission.

The manner in which isobutane and isopentane are formed is shown in Scheme 3. Back biting reactions (step (9)) are quite important to this formation. Isobutane is produced by the hydrogenation of butenes, but no pentenes could be detected in the formation of isopentane and pentane. Pentanes are not produced by hydrogenation of C_5 olefins. That no isopentene could be detected is clear indication of C_9 fraction redecomposition. In this process, only 1-methylbutylium ions are formed. Unstable C_5 ions may possibly be decomposed into the C_3 and C_2 fractions at high temperature. Reaction steps (9) and (11) are repeated. Continuative gasification takes place at step (12) by way of steps (9) and (11).

The oligomer fraction was found to have essentially the same degree of branching as the polypropylene back bone structure. Therefore, the product distribution of polypropylene catalytic decomposition was analyzed. Gas produced by polypropylene decomposition using the silica-alumina catalyst consisted of isobutane 40.4 mol% and isopentane 30.9 mol% at 280 °C.[13] As shown in Table 3, the yield of C_4 and C_5 fractions were 44 and 36 mol% at the same temperature, respectively. The present results confirm the occurrence of these steps PE catalytic decomposition by the NaY-type zeolite catalyst should certainly give rise to isobutane and isopentane as the main products. Back biting reactions are thus shown essential to the formation of the gasification precursor (C_9 fraction) in the catalytic decomposition of PE.

Conclusions

An attempt was made to determine the mechanism for the formation of gas having a peculiar composition in PE decomposition in the presence of the zeolite catalyst. Based on the results obtained, the following conclusions are drawn.

1) The production of isobutane and isopentane in nearly equimolar yields was found at low temperature.

2) The C_9 fraction of the gasification precursor is thus obtained by β-scission of rearrenged on-chain tertiary carbonium ions produced by back biting reactions of chain-end secondary carbonium ions of liquid fraction.

3) Isobutane and isopentane are also produced by redecomposition of the C_9 fraction.

References

1) S. L. Madorsky, "Thermal Degradation of Organic Polymers," Interscience Publishers, New York (1964).

2) H. H. G. Jellinek, "Aspects of Degradation and Stabilization of Polymers," Elsevier (1978).

3) K. Tibor, "Polymer Degradation," Van Nostrand Reinhold Company Inc., New York (l983).

4) N. Grassie and G. Scot, "Polymer Degradation and Stabilization," Cambridge University Press, Cambrige (1985).

5) T. Yoshida, A. Ayame, and H. Kanoh, *Bull. Jpn. Pet. Inst.*, **17**, 218 (1975).

6) Y. Uemichi, A. Ayame, T. Yoshida, and H. Kanoh, *Bull. Jpn. Pet. Inst.*, **23**, 35 (1980).

7) B. Pukanszky, J. P. Kennedy, T. Helen, and F. Tudos, *Polym. Bull.*, **5**,469 (1981).

8) G. Audiso, *J. Anal. Appl. Pyrolysis*, **8**, 87 (1985).

9) M. Langhamer and I. Luederwold, *Makromol. Chem.*, **187**, 829 (1986).

10) H. Nanbu, Y. Ishihara, H. Honma, T. Takesue, and T. Ikemura, *Nippon Kagaku Kaishi*, **1987**, 765.

11) H. Nanbu, Y. Sakuma, Y. Ishihara, T. Takesue, and T. Ikemura, *Polym. Degrad. Stab.*, **19**, 61 (1987).

12) R. Chiang, *J. Phys. Chem.*, **69**, 1645 (1965).

13) Y. Ishihara, H. Nanbu, T. Ikemura, and T. Takesue, *J. Appl. Polym. Sci.*, **38**, 1491 (1989).
14) Y. Ishihara, H. Nanbu, T. Ikemura, and T. Takesue, *Fuel*, **69**, 978 (1990).
15) "Bunkai. Sanka," ed by Japan Petroleum Institute, Asakura Shoten, Tokyo (1962), p. 23.
16) P. L. Beltrame, P. Carniti, G. Audisio, and F. Bertoni, *Polym. Degrad. Stab.*, **26**, 209 (1989).

Synthesis, Chemical Properties, and Structure of a Sterically Hindered Ketone, 2,2,5,5-Tetramethyl-4,4-diphenyl-3-thiolanone

Juzo NAKAYAMA,* Atsushi HIRASHIMA, and Yoshinobu YOKOMORI†
Department of Chemistry, Faculty of Science, Saitama University, Urawa, Saitama 338
†Department of Chemistry, The National Defense Academy, Hashirimizu, Yokosuka, Kanagawa 239
(Received July 29, 1991)

A sterically hindered ketone, 2,2,5,5-tetramethyl-4,4-diphenyl-3-thiolanone (**1**), was synthesized in two steps starting from 2,2,4,4-tetramethyl-1,5-diphenyl-3-thiapentane-1,5-dione. The carbonyl group of **1** is unreactive toward a series of nucleophiles which are bulkier than hydride or its equivalents. The observed unreactivity is ascribed to the steric hindrance enhanced by the two methyl groups on C-5 ("buttressing" effect). The result of an X-ray single crystal structure analysis of **1** is also described.

We have been investigating the synthesis using 3-thiapentane-1,5-diones and related compounds as starting materials.[1] In this connection we have synthesized a sterically hindered ketone, 2,2,5,5-tetramethyl-4,4-diphenyl-3-thiolanone (**1**), in two steps starting from 2,2,4,4-tetramethyl-1,5-diphenyl-3-thiapentane-1,5-dione (**2**). We report here the synthesis, chemical properties, and X-ray single crystal structure analysis of **1**.

Results and Discussion

Preparation of 1 and Related Compounds. Isobutyrophenone was brominated by molecular bromine in ether and the resulting crude bromide **4** was allowed to react with sodium sulfide in two ways. A two-phase mixture of sodium sulfide and **4** in water–hexane was stirred in the presence of methyltrioctylammonium chloride (a phase transfer catalyst) at room temperature. Usual work-up of the mixture afforded the expected sulfide **2** in 60% yield (based on isobutyrophenone). When an aqueous solution of sodium sulfide was added to a stirred and ice-cooled solution of **4** in acetone or ethanol, however, the disulfide **3** was obtained unexpectedly in 45% yield along with isobutyrophenone. The initial process of this reaction also must involve a nucleophilic substitution leading to **5**. In this case, however, **5** preferentially reacts with sodium sulfide, but not with **4**, to give the enolate of isobutryophenone and sodium disulfide. The reaction of sodium disulfide with **4** should give rise to the final product **3**. Supporting evidence for this mechanism comes from the finding that treatment of α-chlorodeoxybenzoin with one equiv of sodium methanethiolate at 0 °C in ethanol affords α-methylthiodeoxybenzoin, which in turn gives deoxybenzoin and dimethyl disulfide by further treatment with sodium methanethiolate.[2] We have also experienced that α-halodeoxybenzoins and related compounds are reduced to the corresponding dehalogenated products by sodium sulfide even when the reaction was carried out under phase transfer conditions in the presene of methyltrioctylammonium chloride.[1]

We have previously shown that intramolecular reductive coupling of a series of 3-thiapentane-1,5-diones with a low valent titanium reagent, prepared from titanium(IV) chloride and zinc in tetrahydrofuran (THF),[4] around 0 °C affords 3,4-thiolanediols in good yields,[1c,e–g,k] while the reduction in refluxing THF gives 2,5-dihydrothiophenes.[1b,d,f] Thus, treatment of **2** with

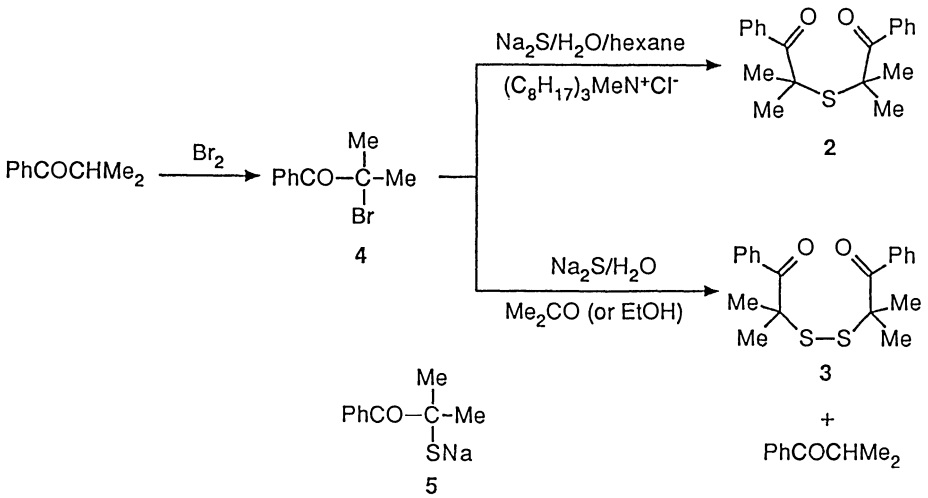

Scheme 1.

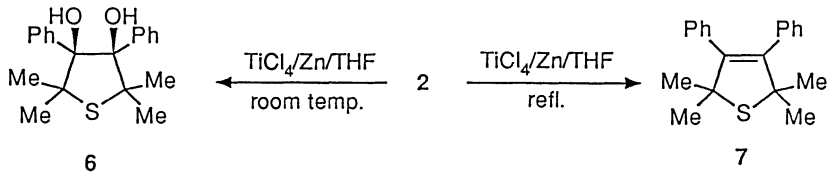

Scheme 2.

the low valent titanium reagent at room temperature affords the diol **6** in 45% yield, while the reduction in refluxing THF gives the dihydrothiophene **7** in 43% yield. Two hydroxyl groups of a number of thiolanediols prepared by the present method have a *cis*-configuration without any exception,[1e,g] and hence two hydroxyl groups of **6** must have a *cis*-configuration.

It is well documented that cyclic *cis*-1,2-diols undergo pinacol rearrangement more smoothly than the corresponding *trans*-1,2-diols do.[5] Thus, heating the diol **6** with a catalytic amount of *p*-toluenesulfonic acid (TsOH) in refluxing benzene for 2 h brings about a smooth pinacol rearrangement to give the expected ketone **1** (84%) in addition to the epoxide **8** (15%). Prolonged heating does not change the ratio of **1** to **8**, revealing that no rearrangement of **8** to **1** occurs under the applied conditions. Oxidation of **6** with 2.3 equiv of *m*-chloroperbenzoic acid (MCPBA) in dichloromethane at room temperature gives the sulfone **9** nearly quantitatively. The pinacol rearrangement of **9** is sluggish; heating **9** with TsOH in refluxing benzene for 5 h affords the ketone **10** only in 3% yield with 50% recovery of **9**, the main product being the epoxide **11** (38%). Oxidation of the ketone **1** with 2.2 equiv of MCPBA at room temperature gives the corresponding sulfoxide (24%) and the sulfone **10** (68%). No clear explanation for the difference of the ratio of ketones to epoxides produced from **6** and **9** is available. More smooth pinacol rearrangement of **6** may be ascribed to the difference of the conformation between **6** and **9** or the stabilization of the carbonium ion intermediate by the neighboring group participation of sulfur such as **12**.

Chemical Properties of 1. Reactivities toward nitrogen nucleophiles were first examined. Many sterically hindered ketones react with hydrazine in refluxing diethylene glycol to give the corresponding hydrazones in good yields.[6] However, **1** does not react with excess hydrazine under the above conditions (refl., 97 h), **1** being recovered nearly quantitatively. Heating **1** with *p*-toluenesulfonohydrazide in the presence of a catalytic amount of hydrochloric acid in refluxing ethanol for 54 h also did not bring about hydrazone formation, but unexpectedly afforded di-*p*-tolyl disulfide (4%) and *S*-*p*-tolyl *p*-toluenethiosulfonate (80%) with quantitative recovery of **1**. A separate experiment showed that heating the hydrazide alone under the above conditions gives the disulfide (32%) and thiosulfonate (48%). Although the mechanism of the reaction is not clear, this type of reaction seems unprecedented.

The ketone **1** is also inert to sulfur nucleophiles.

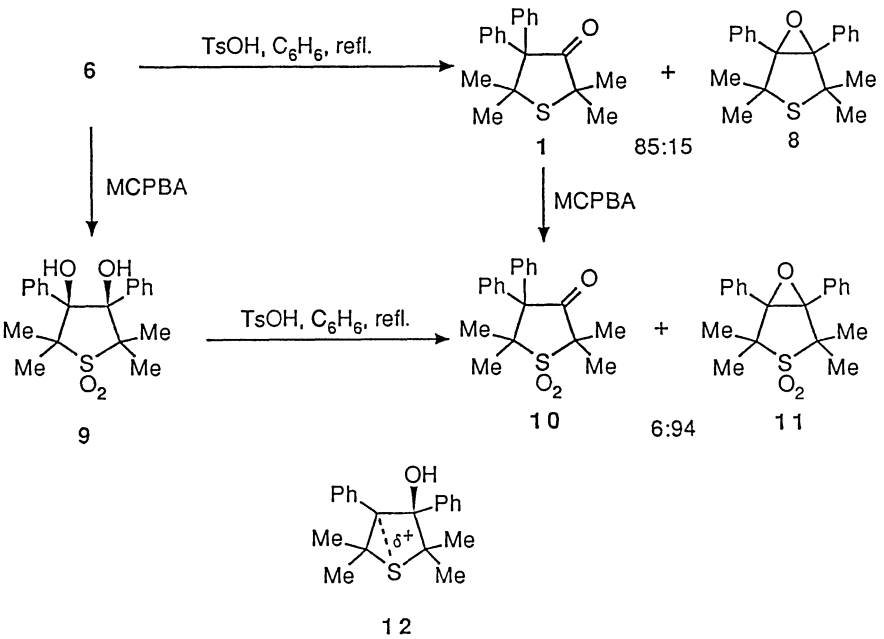

Scheme 3.

Heating **1** with excess Lawesson's reagent [2,4-bis(4-methoxyphenyl)1,3-dithia-2,4-diphosphetane-2,4-disulfide] in refluxing toluene for 12 h resulted in the quantitative revovery of **1** without formation of the corresponding thioketone. Treatment of **1** with 1,2-ethanedithiol in the presence of $BF_3 \cdot Et_2O$ in refluxing dichloromethane does not bring about dithioacetal formation.

Attempted reduction of **1** with sodium borohydride in refluxing THF resulted in the quantitative recovery of **1**. Lithium aluminum hydride reduced **1** to the corresponding alcohol **13** in 87% yield in THF at room temperature. This is the only example that a soomth reaction occurred at the carbonyl moiety.

Reaction of **1** with excess butyllithium in THF at room temperature for 24 h affords the alcohol **13** in 28% yield with 52% recovery of **1**. The formation of **13** may best be explained by assuming a cyclic transition state mechanism **14**. Such mechanim is often encountered in reactions of sterically hindered nonenolizable ketones with Grignard reagents or organolithium reagents.[7] Thus, methylmagnesium bromide which does not carry a β hydrogen and hence cannot react with **1** by the above mechanism is inactive toward **1** in refluxing THF. The reaction of **1** with excess butylmagnesium bromide in refluxing THF for 27 h affords the dihydrothiophene **7** in 54% yield with 43% recovery of **1**. The most straightforward explanation for the above result involves the initial formation of **13**; dehydration of **13** accompanied by migration of phenyl should lead to **7**. However, neither action of butylmagnesium bromide on **13** nor heating **19** with TsOH in refluxing THF affords **7**. An alternative mechanism producing **7** may, therefore, be operative.

Metallation of α-alkyl substituent of nonenolizable ketones with lithium 2,2,6,6-tetramethylpiperidide (LTMP) was recently reported.[8] Treatment of **1** with excess LTMP afforded a complex mixture containing unreacted **1** (65%), no evidence for metallation of the methyl or phenyl being obtained.

Oxidation of **1** with excess MCPBA at room temperature affords a mixture of the corresponding sulfoxide and sulfone **10** as already described. Oxidation of **1** with a large excess of MCPBA catalyzed by TsOH in refluxing dichloromethane afforded **10** quantitatively; no product due to the Baeyer–Villiger oxidation was formed.

We therefore conclude that the carbonyl of **1** is inactive toward nucleophiles which are bulkier than hydride or its equivalent (butyllithium and probably butylmagnesium bromide). The observed inactivity must be ascribed to steric hindrance. Thus, two methyls on C-2 and two phenyls on C-4 interfere the approach of nucleophiles to the carbonyl carbon. At least, in the present system, phenyl behaves as a bulkier substituent than methyl because the ketone **15** and related ones are able to react with hydrazine,[6b–d] whereas **1** is not.[9] The steric hindrance must be further enhanced by the presence of two methyls on C-5; interaction between two phenyls and these two methyls makes the former substituents conformationally more rigid and inelastic ("buttressing" effect).[10] Incidentally the spacial interaction between carbonyl carbon and sulfur such as **16** is not appreciable and thus is not the cause of the inactivity. In ^{13}C NMR the carbonyl carbon of **1** occurs at δ=215 and that of **10** at δ=205. The observed difference is not the one expected from the presence of spacial interaction. In the IR spectrum the carbonyl stretchin of **1** appears at 1728 cm^{-1}, the normal position as a five-membered ketone.[11]

X-Ray Single Crystal Structure Analysis of 1. Figure 1 shows an ORTEP drawing of the compounds **1**. The

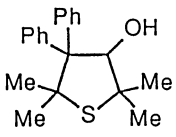

13

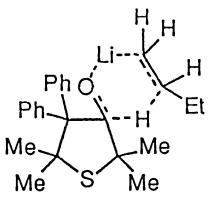

14

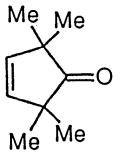

15

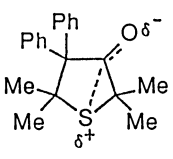

16

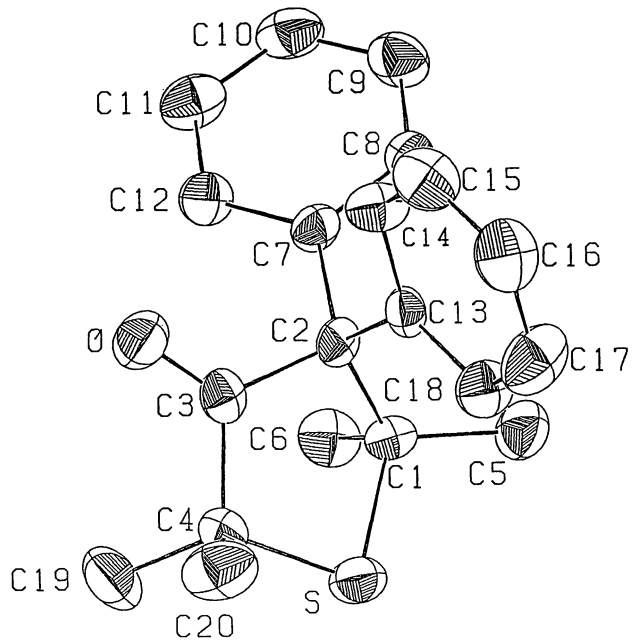

Fig. 1. An ORTEP drawing (Johnson) of compound **1**, showing the numbering scheme of the atoms (50% probability thermal ellipsoids).

Table 1. Final Atomic Coordinates ($\times 10^4$) and Equivalent Isotropic Thermal Parameters ($Å^2 \times 10^2$) with Estimated Standard Deviations in Parentheses

Atom	x	y	z	B_{eq} [a)]
S	3202(1)	314(1)	8376(1)	319(6)
O	2813(5)	−712(3)	5127(4)	401(23)
C1	2556(6)	−751(3)	8433(5)	257(25)
C2	3049(5)	−1202(3)	7305(5)	227(23)
C3	2949(6)	−554(3)	6232(6)	254(26)
C4	3128(6)	348(3)	6692(6)	277(25)
C5	3073(8)	−1113(4)	9741(6)	385(33)
C6	961(7)	−717(4)	8266(7)	345(30)
C7	2113(6)	−1964(3)	6933(5)	259(26)
C8	2336(7)	−2673(4)	7657(6)	295(28)
C9	1446(8)	−3343(4)	7469(7)	369(33)
C10	309(8)	−3315(4)	6511(7)	387(34)
C11	84(7)	−2629(4)	5741(7)	366(33)
C12	978(6)	−1958(4)	5961(6)	303(28)
C13	4600(6)	−1456(3)	7450(5)	238(24)
C14	4971(7)	−2036(4)	6602(7)	344(31)
C15	6344(8)	−2243(4)	6599(7)	411(36)
C16	7378(7)	−1874(5)	7456(8)	456(40)
C17	7036(8)	−1294(5)	8288(8)	476(40)
C18	5667(7)	−1078(4)	8281(6)	349(31)
C19	1857(9)	848(4)	6023(7)	482(39)
C20	4449(9)	717(5)	6352(7)	473(39)

a) $B_{eq}=1/3\sum_i\sum_j B_{ij}\boldsymbol{a}_i^*\boldsymbol{a}_j^*\boldsymbol{a}_i\cdot\boldsymbol{a}_j$.

Table 2. Bond Lengths and Angles with Estimated Standard Deviations in Parentheses

(a) Bond lengths (l/Å)			
S–C1	1.840(6)	C5–C1–C6	106.7(5)
S–C4	1.801(6)	C1–C2–C3	105.9(4)
O–C3	1.201(7)	C1–C2–C7	109.0(4)
C1–C2	1.562(8)	C1–C2–C13	118.2(4)
C1–C5	1.527(10)	C3–C2–C7	112.9(4)
C1–C6	1.538(9)	C3–C2–C13	100.8(4)
C2–C3	1.549(8)	C7–C2–C13	109.8(4)
C2–C7	1.545(8)	O–C3–C2	125.1(5)
C2–C13	1.550(8)	O–C3–C4	120.4(5)
C3–C4	1.543(8)	C2–C3–C4	114.4(4)
C4–C19	1.549(10)	S–C4–C3	106.0(4)
C4–C20	1.523(10)	S–C4–C19	111.8(4)
C7–C8	1.382(9)	S–C4–C20	111.5(4)
C7–C12	1.384(9)	C3–C4–C19	108.0(5)
C8–C9	1.382(10)	C3–C4–C20	110.4(5)
C9–C10	1.377(11)	C19–C4–C20	109.1(6)
C10–C11	1.380(10)	C2–C7–C8	119.2(5)
C11–C12	1.387(9)	C2–C7–C12	123.4(5)
C13–C14	1.401(9)	C8–C7–C12	117.3(5)
C13–C18	1.391(9)	C7–C8–C9	122.3(6)
C14–C15	1.382(10)	C8–C9–C10	119.3(7)
C15–C16	1.379(11)	C9–C10–C11	119.9(7)
C16–C17	1.377(12)	C10–C11–C12	119.8(6)
C17–C18	1.381(11)	C7–C12–C11	121.4(6)
		C2–C13–C14	118.1(5)
(b) Bond angles (ϕ/°)		C2–C13–C18	124.0(5)
C1–S–C4	96.2(2)	C14–C13–C18	117.6(5)
S–C1–C2	105.0(4)	C13–C14–C15	121.7(6)
S–C1–C5	109.2(4)	C14–C15–C16	119.4(7)
S–C1–C6	108.0(4)	C15–C16–C17	119.8(7)
C2–C1–C5	116.1(5)	C16–C17–C18	120.9(7)
C2–C1–C6	111.7(5)	C13–C18–C17	120.6(6)

numbering given in Fig. 1 is arbitrary and is not consistent with that of the IUPAC nomenclature. Final atomic coordinates and equivalent thermal parameters are summarized in Table 1. Bond lengths and bond angles are listed in Table 2. These results show that the five-membered ring of **1** is in a half-chair conformation. The longer bond length (1.562 Å) of the C1–C2 bond compared to usual sp^3–sp^3 carbon bonds reveals the presence of large nonbonded repulsion between two methyls on C1 and two phenyls on C2; length of the corresponding bond of the parent thiolane is 1.536 Å.[12] The bond angle C2–C3–O is as large as 125.1°, while the bond angle C4–C3–O is reduced to 120.4°. This indicates that the nonbonded repulsion mentioned above thrusts the phenyls to the carbonyl side, which in turn results in the repulsion between the phenyls and the carbonyl oxygen and thus expands the bond angle C2–C3–O. The repulsion between the carbonyl oxygen and the two methyls on C4 is avoidable by placing these groups in a noneclipsed conformation. This may agree with the fact that the C3–C4 bond (1.543 Å) is slightly shorter than the C2–C3 bond (1.549 Å). Also interesting is the fact that the S–C1 bond (1.840 Å) is longer than the S–C4 bond (1.801 Å). This probably means that the nonbonded repulsion between the phenyls on C2 and methyls on C1 thrusts the latters to the sulfur side, thus in turn making the nonbonded repulsion between the methyls and lone pair electrons on the sulfur large enough to lengthen the S–C1 bond. The C=O bond length (1.201 Å) seems to correspond to those of usual carbonyl compounds.[13] The C1–S–C4 bond angle (96.2°) is larger than the corresponding bond angle (93.4°) of the parent thiolane.[12] The distances between S and C3 and between S and O are 2.675(6) and 3.828(6) Å, respectively. The former value shows that the spacial interaction beween the sulfur and C3 is weak, if present.

Experimental

General. Melting points were measured on a MEL-TEMP capillary tube melting point apparatus and are uncorrected. IR spectra were taken on a Hitachi 270-50 spectrometer. ^{1}H NMR spectra were recorded on a JEOL PMX-60 or a JEOL FX-90Q spectrometer. ^{13}C NMR spectra were determined on a JEOL FX-90Q spectrometer. Chemical shifts are reported as δ values in parts per million relative to tetramethylsilane. Mass spectra (MS) were determined on a Shimadzu QP 1000 spectrometer. Column chromatography was conducted using E. Merck silica gel 60 (70—230 mesh). Tetrahydrofuran (THF) containing no stabilizer from a freshly opened bottle was dried over molecular sieves under nitrogen. Other materials were used as purchased unless otherwise noted. Elemetnal analyses of all new compounds were performed by the chemical analysis center of Saitama University and are consistent with the calculated values within ±0.30%.

2,2,4,4-Tetramethyl-1,5-diphenyl-3-thiapentane-1,5-dione (2). To a stirred and ice-cooled mixture of 25.1 g (0.17 mol)

of isobutyrophenone and a catalytic amount of aluminum chloride (ca. 0.3 g) in 170 ml of ether was added 27.1 g (0.17 mol) of bromine over a period of 1.5 h. After stirring for 0.5 h at room temperature the reaction was quenched by adding 300 ml of ice-water. The organic layer was separated, washed with water, dried over anhydrous magnesium sulfate, and evaporated to give 38.0 g of the crude bromide **4**.

The bromide thus obtained was dissolved in 170 ml of hexane and then mixed with a solution of 93.0 g (0.38 mmol) of sodium sulfide nonahydrate in 170 ml of water. The addition of 2 ml of methyltrioctylammonium chloride under stirring to the above two-phase mixture brought about a mildly exothermic reaction. After stirring for 6 h at room temperature the white crystals deposited were collected by filtration, washed with 20 ml of hexane and then with 20 ml of water, and dried to give 14.6 g of **2**, mp 98.5—99 °C. The filtrate and washings were combined and then the organic layer was separated, washed with water, dried, and evaporated. The residue was recrystallized from methanol to give 2.1 g of **2**, mp 99 °C (combined yield 60%, based on isobutyrophenone). **2**: ^{1}H NMR ($CDDCl_3$) δ=1.55 (12H, s, Me), 7.1—7.7 (6H, m, phenyl), 7.9—8.4 (4H, m, phenyl); MS m/z 326 (M^+). Anal. ($C_{20}H_{22}O_2S$) C, H.

2,2,5,5-Tetramethyl-1,6-diphenyl-3,4-dithiahexane-1,6-dione (3). The crude bromide **4** (22.7g, 0.1 mmol) obtained as above was dissolved in 130 ml of ethanol. To this ice-cooled and stirred solution was added a solution of 12.3 g (51 mmol) of sodium sulfide nonahydrate in 25 ml of water over a period of 0.5 h. The mixture was warmed to room temperature and stirred for 3 h. The resulting crystalline precipitate was collected by filtration, washed with water and then with 10 ml of methanol, and dried to give 7.4 g (41%) of **3**. Analyses of the filtrate by TLC and ^{1}H NMR revealed the formation of isobutyrophenone in a considerable amount. Analytically pure **3** was obtained by recrystallization from methanol: mp 59.5—60 °C; ^{1}H NMR ($CDCl_3$) δ=1.50 (12H, s, Me), 7.1—7.5 (6H, m, phenyl), 7.8—8.1 (4H, m, phenyl); MS m/z 358 (M^+), 179 (base peak). Anal. ($C_{20}H_{22}O_2S_2$)C,H.

2,2,5,5-Tetramethyl-3,4-diphenylthiolanethiolane-3,4-diol (6). To a stirred and ice-cooled suspension of 6.0 g (92 mmol) of zinc powder in 100 ml of THF was added 5 ml (46 mmol) of titanium(IV) chloride during 0.5 h. Alter stirring for 0.5 h at that temperature, a solution of 3.27 g (10 mmol) of the sulfide **2** in 70 ml of THF was added over a period of 0.5 h. The mixture was slowly warmed to room temperature and stirred for 12 h. The reaction was quenched by adding a sufficient amount of ice and a 10% aqueous sodium carbonate solution (100 ml). Dichloromethane (200 ml) was added and the mixture was stirred for 15 min and filtered through a pad of celite. The organic layer was separated, washed with water repeatedly, dried over anhydrous magnesium sulfate, and evaporated. The residue was recrystallized from hexane to afford 0.76 g of **6**, mp 128—129 °C. Purification of the mother liquor of recrystallization by silica-gel column chromatography gave a further amount (0.74 g) of **6**. Total yield, 45% (1.50 g). **6**: IR (KBr) 3556, 3512 cm^{-1} (OH); ^{1}H NMR ($CDCl_3$) δ=1.27 (6H, s, Me), 1.73 (6H, s, Me), 3.41 (2H, s, OH), 6.9—7.6 (10H, m, phenyl). Anal. ($C_{20}H_{24}O_2S$) C, H.

2,2,5,5-Tetramethyl-3,4-dipheyl-2,5-dihydrothiophene (7). A low valent titanium reagent was prepared from 10 ml (92 mmol) of titanium(IV) chloride and 12 g (184 mmol) of zinc powder in 150 ml of THF. A solution of 6.53 g (20 mmol) of **2** in 60 ml of THF was added dropwise to the above reagent which was stirred and cooled by an ice-salt bath. The mixture was slowly warmed to room temperature and then refluxed for 2 h. Treatment of the mixture in a manner silmilar to that described above gave 2.52 g (40%) of **7**: Mp 163—164 °C (from methanol); ^{1}H NMR ($CDCl_3$) δ=1.56 (12H, s, Me), 7.03 (10H, broad s, phenyl). Anal. ($C_{20}H_{22}S$) C, H.

Pinacol Rearrangment of 6. A mixture of 328 mg (1 mmol) of **6** and 30 mg of *p*-toluenesulfonic acid monohydrate in 30 ml of benzene was refluxed for 2 h. The mixture was evaporated and the residue was chromatographed on a column of silica gel. Elution with carbon tetrachloride gave 261 mg (84%) of 2,2,5,5-tetramethyl-4,4-diphenyl-3-thiolanone (**1**), 47 mg (15%) of 3,4-epoxy-2,2,5,5-tetramethyl-3,4-diphenylthiolane (**8**), and a trace amount of **6** in this order. Prolonged heating (reflux for 6.5 h) also afforded **1** and **8** in 85 and 14.5% yields, respectively, indicating that no rearrangement of **8** to **1** occurs under the applied conditions.

1: Mp 154 °C (from methanol); IR (KBr) 1728 cm^{-1} (C=O); ^{1}H NMR ($CDCl_3$) δ=1.36 (12H, s, Me), 7.13—7.34 (6H, m, phenyl), 7.39—7.59 (4H, m, phenyl); ^{13}C NMR ($CDCl_3$) δ= 29.5, 31.6, 49.5, 54.6, 71.6, 126.8, 127.4, 131.6, 140.9, 214.5 (C=O). Anal. ($C_{20}H_{22}OS$) C, H.

8: Mp 178—179 °C (from ethanol); ^{1}H NMR ($CDCl_3$) δ=1.37 (6H, s, Me), 1.64 (6H, s, Me), 6.96—7.47 (10H, m, phenyl). Anal. ($C_{20}H_{22}OS$)C, H.

Preparation of 9 and Its Acid-Catalyzed Rearrangement. A mixture of 658 mg (2 mmol) of the diol **6** and 781 mg (4.5 mmol) of MCPBA (Tokyo Kasei) in 20 ml of dichloromethane was stirred at room temperature for 4 h. The mixture was diluted with 50 ml of dichloromethane, washed with a 10% aqueous solution of sodium hydrogensulfite, a 10% aqueous solution of sodium carbonate, and water, dried over magnesium sulfate, and evaporated. Purification of the resulting crystalline residue with a short column of silica gel using dichloromethane as the eluent gave 703 mg (98%) of 3,4-dihydroxy-2,2,5,5-tetramethyl-3,4-diphenylthiolane 1,1-dioxide (**9**): Mp 169—171 °C (from cyclohexane); IR (KBr) 3404 (OH), 1268, 1102 cm^{-1} (SO_2); ^{1}H NMR ($CDCl_3$) δ=1.42 (6H, s, Me), 1.64 (6H, s, Me), 3.98 (2H, s, OH), 6.95—7.35 (10H, m, phenyl). Anal. ($C_{20}H_{24}O_4S$) C, H.

A mixture of 360 mg (1 mmol) of **9** and 30 mg of *p*-toluenesulfonic acid monohydrate in 30 ml of benzene was heated under reflux for 5 h. The mixture was evaporated and the residue was chromatographed on a column of silica gel. Elution with dichloromethane gave 8.6 mg (2.5%) of 2,2,5,5-tetramethyl-4,4-diphenyl-3-thiolanone 1,1-dioxide (**10**), 131 mg (38%) of 3,4-epoxy-2,2,5,5-tetramethyl-4,4-diphenylthiolane 1,1-dioxide (**11**), and 182 mg (50%) of **9** in this order.

10: Mp 191—192 °C (from cyclohexane); IR (KBr) 1738 (C=O), 1296, 1108 cm^{-1} (SO_2); ^{1}H NMR ($CDCl_3$) δ=1.41 (6H, s, Me), 1.48 (6H, s, Me), 7.1—7.7 (10H, m, phenyl); ^{13}C NMR ($CDCl_3$) δ=22.6, 22.9, 23.9, 24.3, 62.0, 66.7, 71.6, 126.1, 129.2, 132.3, 139.4, 207.5 (C=O). Anal. ($C_{20}H_{22}O_3S$) C, H.

11: Mp 259—260 °C (from EtOH); IR (KBr) 1298, 1108 cm^{-1} (SO_2); ^{1}H NMR ($CDCl_3$) δ=1.42 (6H, s, Me), 1.61 (6H, s, Me), 7.0—7.4 (10H, m, phenyl); ^{13}C NMR ($CDCl_3$) δ=18.0, 23.3, 62.9, 74.9, 127.6, 128.4, 128.6, 131.1. Anal. ($C_{20}H_{22}O_3S$) C, H.

Oxiation of 1 with MCPBA. To a stirred solution of 162 mg (0.52 mmol) of **1** in 10 ml of dichloromethene was added 197 mg (1.15 mmol) of MCPBA in small portions. After stirring at room temperature for 21 h, the mixture was washed

with a 10% aqueous sodium hydrogensulfite solution, a 10% aqueous sodium carbonate solution, and water, dried over magnesium sulfate, and evaporated. The residue was chromatographed on a column of silica gel. Elution with dichloromethane gave 122 mg (68%) of the sulfone **10**, which is identical with that obtained by the acid-catalyzed rearrangement of **9** in every respect. Further elution with the same solvent gave 41 mg (24%) of 2,2,5,5-tetramethyl-4,4-diphenyl-3-thiolanone 1-oxide: Mp 167 °C (from hexane); ^{1}H NMR ($CDCl_3$) δ=1.06 (3H, s, Me), 1.10 (3H, s, Me), 1.40 (3H, s, Me), 1.62 (3H, s, Me), 7.05—7.62 (10H, m, phenyl). Anal. ($C_{20}H_{22}O_2S$) C, H.

A mixture of 156 mg (0.5 mmol) of **1**, 363 mg (2 mmol) of MCPBA, and 10 mg of *p*-toluenesulfonic acid monohydrate in 20 ml of dichloromethane was stirred for several hours at room temperature and then refluxed for 32 h. Workup of the mixture gave the sulfone **10** quantitatively; no product arising from Baeyer–Villiger oxidation was detected.

Attempted Reactions of 1 with Nitrogen Nucleophiles. a) With Hydrazine. A mixture of 621 mg (2 mmol) of **1** and 1.25 ml (25.7 mmol) of hydrazine monohydrate in 10 ml of diethylene glycol was heated under reflux for 97 h. Usual workup of the resulting dark brown mixture afforded **1** in 97% yield.

b) *p*-Toluenesulfonohydrazide. A mixture of 546 mg (1.76 mmol) of **1**, 376 mg (2 mmol) of *p*-toluenesulfonohydrazide, and three drops of concentrated hydrochloric acid in 15 ml of 95% ethanol was refluxed for 54 h. The mixture was cooled and the resulting crystalline precipitate was collected by filtration to give 76% recovery of **1**. The filtrate was evaporated under reduced pressure and the residue was chromatographed on a column of silica gel. Elution with carbon tetrachloride gave 9 mg (3.7%) of di-*p*-tolyl disulfide, mp 44—45 °C, 101 mg (18.5%) of **1**, and 224 mg (80%) of *S*-*p*-tolyl *p*-toluenethiosulfonate, mp 74 °C (lit,[14] mp 76 °C), in this order.

In a separate experiment a mixture of 374 mg (2 mmol) of *p*-toluenesulfonohydrazide and three drops of concentrated hydrochloric acid in 15 ml of 95% ethanol was refluxed for 54 h. Chromatographic workup of the mixture gave the disulfide and thiosulfonate in 32 and 48% yields, respectively.

Attempted Reactions of 1 with Sulfur Nucleophiles. a) With Lawesson's Reagent. A mixture of 155 mg (0.5 mmol) of **1** and 1.03 g (2.5 mmol) of freshly prepared Lawesson's reagent in 10 ml of anhydrous toluene was refluxed for 12 h under nitrogen. Workup of the mixture gave **1** quantitatively.

b) With 1,2-Ethanedithiol. A mixture of 155 mg (0.5 mmol) of **1**, 377 mg (4 mmol) of 1,2-ethanedithiol, and 0.2 ml of boron trifluoride etherate in 5 ml of dichloromethane was refluxed for 12 h. Chromatographic workup of the mixture gave **1** quantitatively.

Hydride Reduction of 1. a) With Sodium Borohydride. To a stirred and ice-cooled solution of 226 mg (0.73 mmol) of **1** in 5 ml of THF was added 100 mg (2.7 mmol) of sodium borohydride. The mixture was warmed to room temperature and then refluxed for 8 h. Usual workup of the mixture gave **1** quantitatively.

b) With Lithium Aluminum Hydride. To a stirred and ice-cooled solution of 155 mg (0.5 mmol) of **1** in 5 ml of anhydrous THF was added 100 mg (2.6 mmol) of lithium aluminum hydride. The mixture was stirred for 0.5 h at that temperature, warmed to room temperature, and stirred for 3.5 h. The reaction was quenched by addition of wet THF and then water. The mixture was extracted with ether. The extract was washed with water, dried over anhydrous magnesium sulfate, and evaporated. The residue was chromatographed on a column of silica gel. Elution with benzene gave 5.4 mg of an unidentified product and then 135 mg (87%) of 2,2,5,5-tetramethyl-4,4-diphenyl-3-thiolanol (**13**):Mp 124 °C (from hexane); IR (KBr) 3560 cm^{-1} (OH); ^{1}H NMR ($CDCl_3$) δ=0.83 (3H, s, Me), 1.09 (3H, s, Me), 1.61 (3H, s, Me), 1.67 (3H, s, Me), 1.45 (1H, d, J=13Hz, OH), 5.14 (1H, d, J=13Hz, methine), 7.06—7.54 (8H, m, phenyl), 7.54—8.01 (2H, m, pheyl); ^{13}C NMR ($CDCl_3$) δ=23.6, 24.1, 35.8, 36.1, 49.6, 51.9, 66.4, 81.9, 126.6, 127.1, 127.8, 128.8, 133.8, 134.0, 139.8, 145.0. Anal. ($C_{20}H_{24}OS$) C, H.

Reactions of 1 with Organometallic Reagents. a) With Butyllithium. To a stirred and ice-cooled solution of 311 mg (1 mmol) of **1** in 5 ml of anhydrous THF was added 1.26 ml (2 mmol) of 1.59 M (1M=1 mol dm^{-3}) solution of butyllithium in hexane under nitrogen. The mixture was slowly warmed to room temperature and stirred for 24 h. The reaction was quenched by addition of wet THF and then water. The mixture was extracted with water, dried over anhydrous magnesium sulfate, and evaporated. Silica-gel column chromatography of the residue with carbon tetrachloride as the eluent gave **1** (52%), 88 mg (28%) of **13**, and three unidentified compounds in small amounts.

b) With Methylmagnesium Bromide. To a solution of 311 mg (1 mmol) of **1** in 5 ml of anhydrous THF was added 0.67 ml (2 mmol) of 3 M solution of methylmagnesium bromide in ether under nitrogen. The mixture was stirred for 2 h at room temperature and then refluxed for 15 h. Usual workup of the mixture gave **1** in 99% yield.

c) With Butylmagnesium Bromide. To a stirred and ice-cooled butylmagnesium bromide solution, prepared from 766 mg (5.6 mmol) of butyl bromide and 122 mg (5 mmol) of magnesium in 3 ml of THF, was added a solution of 303 mg (0.98 mmol) of **1** in 2 ml of THF under nitrogen. The mixture was slowly warmed to room temperature and then refluxed for 27 h. The reaction was quenched by addition of wet THF and then water. The mixture was extracted with ether. The extract was washed with water, dried over anhydrous magnesium sulfate, and evaporated. The residue was chromatographed on a column of silica gel. Elution with carbon tetrachloride afforded 126 mg (44%) of **7**, 109 mg of a mixture of **7** and **1** in the ratio 1 : 2.6, and 50 mg of **1**. The compound **7** obtained above is identical with that prepared by reductive coupling of **2** in every respect.

Neither action of excess butymagnesium bromide on **13** in refluxing THF for 27 h nor heating **13** with *p*-toluenesulfonic aicd monohydrate in refluxing THF for 11 h gave any **7**, **13** being recovered quantitatively.

d) With Lithium 2,2,6,6-Tetramethylpiperidide. The reagent was prepared by addition of 1.6 ml (2.54 mmol) of 1.59 M solution of butyllithium in hexane to a stirred and ice-cooled solution of 2.5 mmol of 2,2,6,6-tetramethylpiperidine in 12 ml of hexane under nitrogen.[15] To this reagent was added 155 mg (0.5 mmol) of **1** all at once. The mixture was slowly warmed to room temperature and heated under reflux for 24 h. Column chromatographic workup of the mixture allowed the isolation of several unidetified products in minute amounts and **1** in 65% yield.

X-Ray Crystal Structure Analysis of 1. A colorless crystal of **1** with dimensions of ca. 0.2×0.2×0.1 mm^3 was mounted on a Rigaku AFC-6 automated diffractometer. Systematic

absences were consistent with the space group $P\,2_1/c$. The intensity data were measured by means of ω-2θ of 60° by using graphite-monochromated Mo $K\alpha$ radiation (λ=0.7107 Å). Usual corrections were made for Lorentz and polarization effects, but no absorption correction was applied. Independent reflections with $|F_o|>4\sigma(F_o)$, 1901 reflections, were used for the structural determination.

Crystal Data: $C_{20}H_{22}OS$, F.W.=310.5, monoclinic, $P2_1/c$, a=9.764(3), b=16.174(9), c=10.755(6) Å, β=100.04(3)°, V=1672 Å^3, Z=4, D_x=1.233 g cm^{-3}, μ(Mo $K\alpha$)=1.84 cm^{-1}. The structure was solved by the direct method (MULTAN 78).[16] Positions of H atoms were fixed at calculated positions (with C–H=1.08 Å) with fixed isotropic temperature factors (B=5.0. Å^2). The structure was refined anisotropically for non-H atoms and isotropically for H atoms by full-matrix least squares method. The final discrepancy factors were R=0.090 and R_w=0.052 [w=$(\sigma^2(F_o)+0.14722|F_o|-0.0015|F_o|^2)^{-1}$], and $(\Delta/\sigma)_{max}$ in the final refinement cycle was 0.01. The scattering factors were taken from Ref 17. The calculations were carried out on a HITAC M-680H computer at the computer room of The National Defense Academy, using UNICS-Nagoya.[18,19]

References

1) For example, see a) J. Nakayama, H. Motoyama, H. Machida, M. Shimomura, and M. Hoshino, *Heterocycles,* **22**, 1527 (1984). b) J. Nakayama, H. Machida, and M. Hoshino, *Tetrahedron Lett.,* **26**, 1981 (1985). c) J. Nakayama, H. Machida, R. Saito, and M. Hoshino, *ibid.,* **26**, 1983 (1985). d) J. Nakayama, H. Machida, R. Saito, K. Akimoto, and M. Hoshino, *Chem. Lett.,* **1985**, 1173. e) J. Nakayama, S. Yamaoka, and M. Hoshino, *Tetrahedron Lett.,* **28**, 1799 (1987). f) J. Nakayama, S. Murabayashi, and M. Hoshino, *Heterocycles,* **26**, 2599 (1987). g) J. Nakayama, S. Yamaoka, and M. Hoshino, *Tetrahedron Lett.,* **29**, 1161 (1988). h) J. Nakayama, S. Yamaoka, T. Nakanishi, and M. Hoshino, *J. Am. Chem. Soc.,* **110**, 6598 (1988). i) J. Nakayama, T. Konishi, A. Ishii, and M. Hoshino, *Bull. Chem. Soc. Jpn.,* **62**, 2608 (1990). k) J. Nakayama and R. Hasemi, *J. Am. Chem. Soc.,* **112**, 5654 (1990).

2) M. Oki, W. Funakoshi, and A. Nakamura, *Bull. Chem. Soc. Jpn.,* **44**, 828 (1971).

3) J. Nakayama, H. Machida, H. Motoyama, I. Ishii, and M. Hoshino, The 12th Symposium on Organic Sulfur and Phosphorus Chemistry, Osaka, 1984, Abstr., No. 18.

4) T. Mukaiyama, T. Sato, and J. Hanna, *Chem. Lett.,* **1973**, 1041.

5) P. D. Bartlett and I. Pöckel, *J. Am. Chem. Soc.,* **59**, 820 (1937); P. D. Bartlett and A. Bavley, *ibid.,* **60**, 2426 (1938); P. D. Bartlett and R. F. Brown, *ibid.,* **62**, 2927 (1940).

6) a) D. H. R. Barton, F. S. Guziec, Jr., and I. Shahak, *J. Chem. Soc., Perkin Trans. 1,* **1974**, 1794. b) F. S. Guziec, Jr. and C. J. Murphy, *J. Org. Chem.,* **47**, 3573 (1982). c) E. R. Cullen, F. S. Guziec, Jr., and C. J. Murphy, *J. Org. Chem.,* **47**, 3563 (1982). d) F. S. Guziec, L. J. SanFilippo, C. J. Murphy, C. A. Moustakis, and E. R. Cullen, *Tetrahedron,* **41**, 4843 (1985).

7) M. T. Reetz and C. Weis, *Synthesis,* **1977**, 135; J. D. Buhler, *J. Org. Chem.,* **38**, 904 (1973); G. B. Bennett, W. J. Houlihan, and R. B. Mason, *J. Organomet. Chem.,* **99**, 185 (1975).

8) C. S. Shiner, A. H. Berks, and A. M. Fisher, *J. Am. Chem. Soc.,* **110**, 957 (1988).

9) We cannot exclude the possibility that the inertness of the compound may in part come from electrostatic repulsion between phenyls and a nucleophile.

10) F. H. Westheimer, "Steric Effects in Organic Chemistry," ed by M. S. Newman, Maruzen, Tokyo (1956), p. 523.

11) L. J. Bellamy, "The Infrared Spectra of Complex Molecules," 3rd ed, Chapman and Hall, London(1975), p. 168.

12) Z. Nahlovska, B. Nahlovska, and H. M. Seip, *Acta Chem. Scand.,* **23**, 3534 (1969).

13) G. Berthier and J. Serre, "The Chemistry of the Carbonyl Group," ed by S. Patai, Interscience, London (1966), p. 3.

14) J. L. Kice and K. W. Bowers, *J. Am. Chem. Soc.,* **84**, 605 (1962).

15) D. A. Olofson and C. M. Dougherty, *J. Am. Chem. Soc.,* **95**, 581 (1973).

16) P. Main, S. E. Hull, L. Lessinger, G. Germain, J. P. Declercq, and M. M. Woolfson (1978), MULTAN78, A System of Computer Programs for the Automatic Solution of Crystal Structure from X-Ray Diffraction Data, University of York, England and Louvain, Belgium.

17) "International Tables for X-Ray Crystallography," Kynoch Press, Birmingham (1964), Vol. IV.

18) T. Ashida, "The Universal Computing System-Nagoya," 1981.

19) The coordinates of H atoms, the anisotropic thermal parameters of non-H atoms, and F_o-F_c tables have been deposited as Document No. 8472 at the Office of Bull. Chem. Soc. Jpn.

Selective Mono- and Bis(alkoxycarbonylation)s of Olefins Catalyzed by Palladium in the Presence of Cu(I) or Cu(II) Chloride under Remarkably Mild Conditions. Application to the Synthesis of γ-Butyrolactone Derivatives

Shiho Toda, Masanori Miyamoto, Hideki Kinoshita, and Katsuhiko Inomata*
Department of Chemistry, Faculty of Science, Kanazawa University, Marunouchi 1-1, Kanazawa, Ishikawa 920
(Received August 5, 1991)

Palladium-catalyzed mono- and bis(alkoxycarbonylation)s of olefins were controlled by the use of copper(II) and copper(I) chloride, respectively, in alcohol under normal pressure of carbon monoxide and oxygen at room temperature without any other additives. 3-Buten-1-ols gave the corresponding γ-butyrolactones and 2-oxotetrahydrofuran-3-acetic acid esters, respectively, in high yields.

It is well-known that palladium chloride can catalyze the hydroesterification[1] and hydrocarboxylation[2] of olefins in acidic alcohols under mild conditions. In the course of our attempts to improve such hydroesterification reaction using various kinds of palladium catalysts in the absence of hydrochloric acid under mild conditions, we realized that palladium(0) black precipitates prior to the beginning or the completion of the reaction whenever the expected monoesters could be obtained in good yields from terminal olefins. On the basis of this observation, we eventually found that Pd–C is a favorable catalyst for the alkoxycarbonylation of olefins, and have briefly reported in the previous paper[3] that mono- and bis(alkoxycarbonylation)s of olefins can be controlled by the use of copper(II) and copper(I) chloride, respectively, together with the Pd–C catalyst in alcohol under normal pressure of carbon monoxide. However, acceleration of the reaction, which required around 8 d for completion, remained as a problem to be solved for wide synthetic applications.

We wish to report here the remarkably improved method which uses palladium(II) and copper(II) or copper(I) chloride under normal pressure of carbon monoxide and oxygen at room temperature comparing with the previous method[3] (Method A in Tables 1 and 2). The present reaction was applied to the synthesis of γ-butyrolactone derivatives.

The monocarbonylation of 1-undecene (**1b**) using various kinds of palladium catalysts (0.02 equiv) and copper(II) chloride (1.5 equiv) was first investigated under CO and O_2 (ca. 1/1, v/v, 1 atm) atmosphere in methanol at 25 °C without addition of an acid. It was found that (1) $PdCl_2$ and $[PdCl_2(CH_3CN)_2]$ are catalysts of choice, (2) the latter is better in view of selectivity of **2b**/**3b** [form of Pd catalyst, reaction time, total yields of **2b** and **3b**, and ratio of **2b**/**3b** were as follows: $PdCl_2$, 23 h, quant., 49/51; $[PdCl_2(CH_3CN)_2]$, 40 h, 90%, 86/14; $[PdCl_2(PhCN)_2]$ 42 h, 74%, 86/14; $[PdCl_2(PPh_3)_2]$,

Table 1. Mono(alkoxycarbonylation) of Terminal Olefins with $CuCl_2$

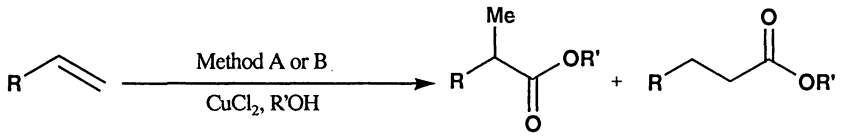

1 2 3

1	R	Method A[a] Solv.	Yield of 2+3/%	Ratio of 2/3[c]	1	Method B[b] Time/h	Yield of 2+3/%	Ratio of 2/3[c]
a,	$CH_3(CH_2)_7$	—	—	—	**a**,	24	92	85/15
b,	$CH_3(CH_2)_8$	MeOH	Quant.	81/19	**b**,	24	Quant.	80/20
c,	$CH_3(CH_2)_9$	MeOH	Quant.	78/22	**c**,	96	96	87/13
d,	$CH_3(CH_2)_{11}$	EtOH	Quant.	72/28	**d**,	74	99	85/15
e,	$CH_3(CH_2)_{15}$	EtOH	82	77/23	**e**,	73	94	83/17
f,	$Ph(CH_2)_2$	MeOH	Quant.	96/4	**f**,	43	90	90/10
g,	$PhOCH_2$	—	—	—	**g**,	96	68	85/15
h,	$TsCH_2$	—	—	—	**h**,	120	Quant.	81/19
i,	$Ts(CH_2)_2$	—	—	—	**i**,	41	91	67/33

a) Pd–C (0.11 equiv), $CuCl_2$ (3 equiv), CO (1 atm), for 8 d at 25 °C. b) $[PdCl_2(CH_3CN)_2]$ (0.02 equiv), $CuCl_2$ (1.5 equiv), CO/O_2 (ca. 1/1, v/v, 1 atm), in MeOH/THF (1/1) at 25 °C. c) Determined by 400 MHz ^1H NMR spectra.

43 h, 14%, 44/56; [$PdCl_2$(dppe)] (dppe=1,2-bis (diphenylphosphino)ethane), 42 h, no reaction; [$PdCl_2$(dppp)] (dppp=1,3-bis(diphenylphosphino)propane), 38 h, no reaction; [$Pd(PPh_3)_4$], 48 h, 37%, 25/75], and (3) phosphine ligands retarded the reaction and gave the linear esters in preference. Regarding solvent systems, it was found that the use of THF, CH_2Cl_2, ether, or benzene as co-solvent with methanol is effective probably because of high solubility of olefin in them, but polar solvents retard the reaction [solvent, reaction time, total yields of **2b** and **3b**, and ratio of **2b**/**3b** were as follows, when [$PdCl_2(CH_3CN)_2$] (0.02 equiv) and $CuCl_2$ (1.5 equiv) were used under similar conditions: MeOH, 40 h, 90%, 86/14; MeOH/THF (1/1, v/v), 24 h, quant., 79/21; MeOH/CH_2Cl_2(1/1, v/v), 30 h, 91%, 82/18; MeOH/Et_2O (1/1, v/v), 75 h, 94%, 85/15; MeOH/benzene (1/1, v/v), 29 h, 95%, 76/24; MeOH/CH_3CN (1/1, v/v), 42 h, 50%, 85/15; MeOH/DMF (1/1, v/v), 51 h, 17%, 87/13; MeOH/DMSO (1/1, v/v), 72 h, trace]. Consequently, various kinds of monoesters (**2a—i** and **3a—i**) were prepared in excellent yields from the corresponding terminal olefins including the functionalized ones (**1g—i**) with [$PdCl_2(CH_3CN)_2$] (0.02 equiv) and $CuCl_2$ (1.5 equiv) in MeOH/THF (1/1, v/v) under CO/O_2 (ca. 1/1, v/v, 1 atm)at 25 °C as summarized in Table 1 (Method B).

The predominant formation of branched monoesters (**2**) by formal Markovnikov addition of methoxycarbonyl group to olefins can be rationalized on the basis of the formation of carbonium ion intermediate,[4] or acidic decomposition of the intermediate (**4**) formed in preference to the regioisomer (**5**) by HCl evolved in the reaction. The reaction mixture using $CuCl_2$ was actually strongly acidic.

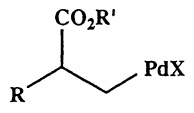

4

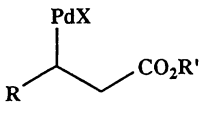

5

The treatment of 3-buten-1-ols (**6a,b**) in THF in a similar manner afforded the corresponding γ-butyrolactones (**7a,b**) in good yields as shown in the following Eqs. 1 and 2.[5]

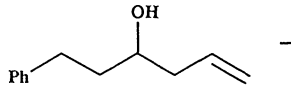

6a

in THF
70 h

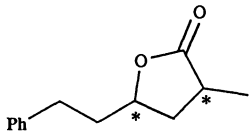

(Eq. 1)

7a, 67%
Ratio of diastereoisomers
63:37

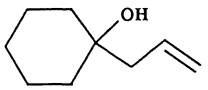

6b

in THF
70 h

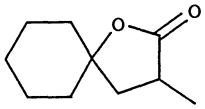

7b, 76%
Mp 67—68 °C

(Eq. 2)

Table 2. Bis(alkoxycarbonylation) of Terminal Olefins with CuCl

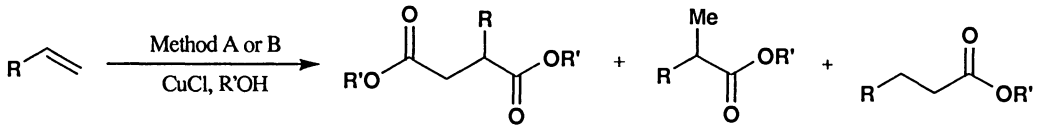

1 8 2 3

1	R	Method A[a] Solv.	Time/d	Yield of 8/%	1	Method B[b] Solv.	Time/d	Yield of 8/%	Yield of 2+3/%	Ratio of 2/3[c]
a,	$CH_3(CH_2)_7$	—	—	—	**a**,	MeOH	1	70	21	43/57
b,	$CH_3(CH_2)_8$	MeOH	9	Quant.	**b**,	MeOH	1	96	Trace	—
c,	$CH_3(CH_2)_9$	MeOH	8	89	**c**,	MeOH	3	89	11	45/55
d,	$CH_3(CH_2)_{11}$	EtOH	8.5	56	**d**,	MeOH/THF(1/1)	7	90	10	30/70
d,	$CH_3(CH_2)_{11}$	MeOH/THF(1/1)	8	84	**e**,	MeOH/THF(1/1)	7	87	12	10/90
e,	$CH_3(CH_2)_{15}$	EtOH	9	67	**f**,	MeOH	2.5	98	Trace	—
e,	$CH_3(CH_2)_{15}$	MeOH/THF(1/1)	9	92	**g**,	MeOH/THF(1/1)	6	71[d]	—	—
f,	$Ph(CH_2)_2$	MeOH	8	97	**g**,	MeOH	21 h[e]	88	—	—
g,	$PhOCH_2$	—	—	—	**h**,	MeOH/THF(1/1)	6	50[f]	—	—
h,	$TsCH_2$	—	—	—	**h**,	MeOH	18 h[g]	71	—	—
i,	$Ts(CH_2)_2$	—	—	—	**i**,	MeOH	2.5	94	—	—
					i,	MeOH	11 h[g]	87	—	—

a) Pd–C (0.11 equiv), CuCl (3 equiv), CO (1 atm), at 25 °C in the dark. b) $PdCl_2$ (0.02 equiv), CuCl (1.5 equiv), CO/O_2 (ca. 1/1, v/v, 1 atm), at 25 °C. c) Determined by 400 MHz ^{1}H NMR spectra. d) 24% of **1g** was recovered. e) Carried out at 70 °C. f) 50% of **1h** was recovered. g) Carried out at 70 °C with 3.0 equiv of CuCl.

Table 3. Preparation of γ-Butyrolactone 2-Acetic Acid Esters from 3-Butenols[a)]

Entry	3-Butenols	Time	Products	Yield/%
1	**6a**, 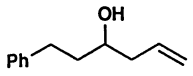	23 h	**9a**, 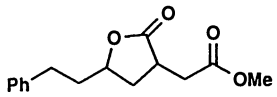	90[b)]
2	**6b**, 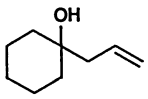	20 h	**9b**, 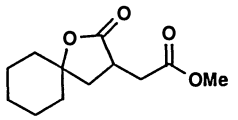	80
3	**6c**, 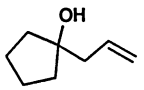	18 h	**9c**, 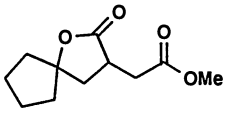	86
4	**6d**,	16 h	**9d**, 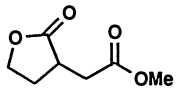	76[c)]
5	**6e**, 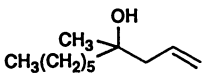	7 d	**9e**, 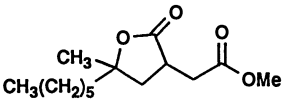	94[b)]
6	**6f**, 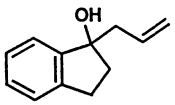	2 d	**9f**, 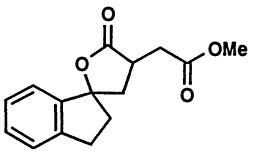	80[b)]

a) $PdCl_2$ (0.1 equiv), CuCl (1.5 equiv), CO/O_2 (ca. 1/1, v/v, 1 atm), in MeOH at 25 °C. b) Ratios of diastereoisomers were determined by 400 MHz ^1H NMR spectra as follows: **9a** (68/32), **9e** (58/42), **9f** (54/46). c) Determined by GC [OV-17, 2 m×3 mm, N_2, 20 ml min^{-1}, 100—170 °C (20 °C min^{-1})] with internal standard, 1,2,3,4-tetrahydronaphthalene.

On the other hand, when copper(I) chloride was used in place of copper(II) chloride in the above reaction, diesters (succinates, **8a**—**i**) were selectively formed in high yields as well as the case of Pd–C catalyst (Method A) as shown in Table 2 (Method B). The reaction mixture was faintly acidic in contrast to the case of copper(II) chloride. Although the active species formed from copper(I) chloride in the present reaction is not yet clear, the pale green coloration suggests the formation of copper(II) species, at least in part, by oxidation with molecular oxygen. It is likely that the copper(II) species reacts further with carbon monoxide to afford (alkoxycarbonyl)chlorocopper [Cu(Cl)COOR] which is probably involved in the carbonylation of olefins under neutral conditions as described in the literature.[6)] It is noteworthy that the carbonylation reaction was remarkably retarded by the addition of equimolar amount of LiCl, NaCl, or KCl under similar conditions.

Recently Tamaru and his co-workers reported the interesting inter- and intramolecular bis(alkoxycarbonylation) of 3-buten-1-ols catalyzed by palladium(II).[7)] It prompted us to apply the present bis(alkoxycarbonylation) system to 3-buten-1-ols (**6a**—**f**). The results are summarized in Table 3. The reaction proceeded selectively to give the corresponding 2-oxotetrahydrofuran-3-acetic acid esters (**9a**—**f**) in high yields by the use of 0.1 equiv of $PdCl_2$ and 1.5 equiv of CuCl in spite of the absence of additives such as propylene oxide, triethyl orthoacetate, or *N*,*N*,*N*′,*N*′-tetramethylurea employed in the reported procedure.[7)]

Now it has become possible to control the mono- and bis(alkoxycarbonylation)s of olefins catalyzed by palladium(0) or palladium(II) simply employing copper(II) or copper(I) chloride under remarkably mild conditions.

Mechanistic studies and applications of the present carbonylation reactions are now in progress.

Experimental

All the melting points were determined with a micro melting apparatus (Yanagimoto-Seisakusho) and were uncorrected. The ^1H NMR, IR, and MS spectra were recorded on JEOL JNM-GX 400(400 MHz) FT-NMR spectrometer, JASCO IRA-1 diffraction grating infrared spectrometer, and Hitachi M-80 mass spectrometer, respectively. The chemical shifts of NMR are reported in the δ-scale relative to TMS as an internal standard.

Materials. All the solvents were distilled and stored over a drying agent. Thin-layer chromatography (TLC) was performed on Merck's silica gel 60 PF_{254} (Art. 7749). Terminal olefins (**1a**—**e**) were purified by distillation over active

carbon before use. CuCl was freshly prepared from copper sulfate.[8]

Mono(alkoxycarbonylation) of 1b with $CuCl_2$ (Method A). In a flask equipped with a balloon containing carbon monoxide (1 atm), 1-undecene (**1b**, 39 mg, 0.25 mmol) was added to a mixed dispersion of 5% Pd-C (58 mg, 0.11 equiv of Pd) and anhydrous $CuCl_2$ (from Wako Pure Chemical Industries, Ltd., 95% purity, 106 mg, 3.0 equiv) in absolute methanol (4 ml) at 25 °C. After stirring for 8 d at 25 °C, the reaction mixture was added dropwise to aqueous 10% $NaHCO_3$ solution. The filtrate through Celite was diluted by ethyl acetate. The organic layer was separated and successively washed with water and brine, and dried over sodium sulfate. The residue obtained by evaporation of the solvent was subjected to preparative TLC (SiO_2, hexane/ethyl acetate=10/1, v/v) to afford 54 mg of a mixture of regioisomeric monoesters (**2b**/**3b**=81/19, quantitative yield) as a colorless oil. MS *m/z* 214 (M^+, 2.02%), 101 (29.47), 88(100.00), 87 (11.00), 74 (11.53), 57 (10.00), 43 (10.46); IR (neat) 2920, 2850, 1730, 1460, 1425, 1365, 1250, 1185, 1155, 725 cm^{-1};^1H NMR of **2b** (R′=Me) ($CDCl_3$) δ=0.88 (t, *J*=6.87 Hz, 3H), 1.14 (d, *J*=7.02 Hz, 3H), 1.26 (s, 14H), 1.40 (m, 1H), 1.65 (m, 1H), 2.43 (sextuplet, *J*=7.02 Hz, 1H), 3.66 (s, 3H);^1H NMR of **3b** (R′=Me) ($CDCl_3$) δ=0.88 (t, *J*=6.87 Hz, 3H), 1.26 (s, 16H), 1.65 (m, 2H), 2.31 (t, *J*=7.48 Hz, 2H), 3.66 (s, 3H).

In a similar manner, other monoesters (**2c—f**/**3c—f**) were prepared from the corresponding terminal olefins (**1c—f**).

Methyl 2-Methyldodecanoate (2c, R′=Me) and Methyl Tridecanoate (3c, R′=Me): An oil (a mixture of regioisomers); MS *m/z* 229 (M^++1, 0.89%), 228 (M^+, 3.79), 143 (7.44), 115 (5.59), 101 (33.75), 88 (100.00), 87 (15.29), 74 (6.27); IR (neat) 2920, 2840, 1730, 1455, 1420, 1370, 1185, 1150, 710 cm^{-1}; ^1H NMR of **2c** ($CDCl_3$) δ=0.88 (t, *J*=7.02 Hz, 3H), 1.14 (d, *J*=7.02, 3H), 1.26 (s, 16H), 1.40 (m, 1H), 1.65 (m, 1H), 2.43 (sextuplet, *J*=7.02 Hz, 1H), 3.67 (s, 3H); ^1H NMR of **3c** ($CDCl_3$) δ=0.88 (t, *J*=7.02 Hz, 3H), 1.26 (s, 18H), 1.65 (m, 2H), 2.31 (t, *J*=7.02 Hz, 2H), 3.67 (s, 3H); **2c**/**3c**=78/22.

Ethyl 2-Methyltetradecanoate (2d, R′=Et) and Ethyl Pentadecanoate (3d, R′=Et): An oil (a mixture of regioisomers); MS *m/z* 271 (M^++1, 18.60%), 270 (M^+, 31.28), 227 (11.02), 225 (11.97), 213 (12.90), 157 (14.59), 116 (11.24), 115 (32.30), 102 (100.00), 101 (15.93), 88 (12.68), 74 (11.18), 43 (10.07); IR (neat) 2935, 2860, 1740, 1465, 1380, 1180, 1160 cm^{-1}; ^1H NMR of **2d** ($CDCl_3$) δ=0.92 (t, *J*=7.02 Hz, 3H), 1.17 (d, *J*=7.02 Hz, 3H), 1.29 (m, 23H), 1.43 (m, 1H), 1.65 (m, 1H), 2.44 (sextuplet, *J*=7.02 Hz, 1H), 4.16 (q, *J*=7.02 Hz, 2H); ^1H NMR of **3d** ($CDCl_3$) δ=0.92 (t, *J*=7.02 Hz, 3H), 1.29 (m, 25H), 1.65 (m, 2H), 2.32 (t, *J*=7.32 Hz, 2H), 4.16 (q, *J*=7.02 Hz, 2H); **2d**/**3d**=72/28.

Methyl 2-Methyltetradecanoate (2d, R′=Me) and Methyl Pentadecanoate (3d, R′=Me): An oil (a mixture of regioisomers); MS *m/z* 257 (M^++1, 1.31%), 256 (M^+, 5.60), 101 (16.82), 88 (100.00); IR (neat) 2930, 2860, 1740, 1455, 1370, 1190, 1160 cm^{-1}; ^1H NMR of **2d** ($CDCl_3$) δ=0.88 (t, *J*=7.02 Hz, 3H), 1.14 (d, *J*=7.02 Hz, 3H), 1.26 (s, 20H), 1.40 (m, 1H), 1.65 (m, 1H), 2.43 (sextuplet, *J*=7.02 Hz, 1H), 3.66 (s, 3H); ^1H NMR of **3d** ($CDCl_3$) δ=0.88 (t, *J*=7.02 Hz, 3H), 1.26 (s, 22H), 1.65 (m, 2H), 2.30 (t, *J*=7.32 Hz, 2H), 3.67 (s, 3H); **2d**/**3d**=85/15 (by Method B).

Ethyl 2-Methyloctadecanoate (2e, R′=Et) and Ethyl Nonadecanoate (3e, R′=Et): An oil (a mixture of regioisomers); MS *m/z* 327 (M^++1, 14.03%), 326 (M^+, 31.35), 269 (12.02), 185 (13.25), 157 (22.19), 129 (19.18), 115 (45.77), 102 (100.00), 101 (22.53), 83 (14.64), 74 (17.62), 57 (21.55); IR (neat) 2920, 2850, 1725, 1460, 1370, 1175 cm^{-1}; ^1H NMR of **2e** ($CDCl_3$) δ=0.88 (t, *J*=6.72 Hz, 3H), 1.13 (d, *J*=7.02 Hz, 3H), 1.25 (m, 31H), 1.40 (m, 1H), 1.64 (m, 1H), 2.40 (sextuplet, *J*=7.02 Hz, 1H), 4.10 (q, *J*=7.02 Hz, 2H); ^1H NMR of **3e** ($CDCl_3$) δ=0.88 (t, *J*=6.72 Hz, 3H), 1.25 (m, 33H), 1.64 (m, 2H), 2.28 (t, *J*=7.32 Hz, 2H), 4.10 (q, *J*=7.02 Hz, 2H); **2e**/**3e**=77/23.

Methyl 2-Methyloctadecanoate (2e, R′=Me) and Methyl Nonadecanoate (3e, R′=Me): An oil (a mixture of regioisomers); MS *m/z* 313 (M^++1, 5.49%), 312 (M^+, 21.71), 101 (36.66), 88 (100.00); IR (neat) 2930, 2860, 1735, 1455, 1190, 1160 cm^{-1}; ^1H NMR of **2e** ($CDCl_3$) δ=0.88 (t, *J*=7.02 Hz, 3H), 1.13 (d, *J*=7.02 Hz, 3H), 1.26 (s, 28H), 1.40 (m, 1H), 1.65 (m, 1H), 2.42 (sextuplet, *J*=7.02 Hz, 1H), 3.66 (s, 3H); ^1H NMR of **3e** ($CDCl_3$) δ=0.88 (t, *J*=7.02 Hz, 3H), 1.26 (s, 30H), 1.65 (m, 2H), 2.30 (t, *J*=7.63 Hz, 2H), 3.66 (s, 3H); **2e**/**3e**=83/17 (by Method B).

Methyl 2-Methyl-4-phenylbutanoate (2f, R′=Me) and Methyl 5-Phenylpentanoate (3f, R′=Me): An oil (a mixture of regioisomers); MS *m/z* 192 (M^+, 5.96%), 105 (8.13), 104 (9.52), 91 (33.28), 88 (100.00), 57 (15.07); IR (neat) 3000, 2900, 1720, 1590, 1480, 1440, 1420, 1365, 1230, 1190, 1150, 1040, 735, 690 cm^{-1}; ^1H NMR of **2f** ($CDCl_3$) δ=1.18 (d, *J*=7.02 Hz, 3H), 1.71 (m, 1H), 2.04 (m, 1H), 2.47 (sextuplet, *J*=7.02 Hz, 1H), 2.60 (t, *J*=7.93 Hz, 2H), 3.67 (s, 3H), 7.17 (m, 3H), 7.27 (m, 2H); ^1H NMR of **3f** ($CDCl_3$) δ=1.66 (m, 4H), 2.32 (t,*J*=7.02 Hz, 2H), 2.75 (m, 1H), 2.95 (m, 1H), 2.60 (t, *J*=7.93 Hz, 2H), 3.67 (s, 3H), 7.17 (m, 3H), 7.27 (m, 2H); **2f**/**3f**=96/4.

Mono(alkoxycarbonylation) of 1a with $CuCl_2$ (Method B). In a flask equipped with balloons containing carbon monoxide (1 atm) and oxygen (1 atm), 1-decene (**1a**, 35 mg, 0.25 mmol) was added dropwise to a mixture of $[PdCl_2(CH_3CN)_2]$ (6 mg, 0.02 equiv) and anhydrous $CuCl_2$ (95% purity, 53 mg, 1.5 equiv) in absolute methanol (2 ml) and THF (2 ml) at 25 °C. After stirring for 24 h at 25 °C, the reaction mixture was added dropwise to aqueous 10% $NaHCO_3$ solution. The filtrate through Celite was treated with a small amount of aqueous KCN solution to deactivate palladium catalyst and diluted by ethyl acetate. The organic layer was separated and successively washed with water and brine, and dried over sodium sulfate. The residue obtained by evaporation of the solvent was subjected to preparative TLC (SiO_2, hexane/ethyl acetate=10/1, v/v) to afford 46 mg of a mixture of regioisomeric monoesters (**2a**/**3a**=85/15, 92% yield) as a colorless oil. MS *m/z* 200 (M^+, 5.28%), 101 (29.12), 88 (100.00), 87 (56.67), 74 (79.26); IR (neat) 2940, 2860, 1735, 1455, 1430, 1375, 1190, 1160 cm^{-1}; ^1H NMR of **2a** (R′=Me) ($CDCl_3$) δ=0.88 (t, *J*=7.02 Hz, 3H), 1.13 (d, *J*=7.02 Hz, 3H), 1.26 (s, 12H), 1.40 (m, 1H), 1.64 (m, 1H), 2.43 (sextuplet, *J*=7.02 Hz, 1H), 3.67 (s, 3H) ; ^1H NMR of **3a** (R′=Me) ($CDCl_3$) δ=0.88 (t, *J*=7.02 Hz, 3H), 1.26 (s, 14H), 1.64 (m, 2H), 2.30 (t, *J*=7.62 Hz, 2H), 3.67 (s, 3H).

In a similar manner, other monoesters (**2b—i**/**3b—i**) and lactones (**7a,b**) were prepared from the corresponding terminal olefins (**1b—i**) and 3-buten-1-ols (**6a,b**), respectively. Regioisomers, **2g—i** and **3g—i**, could be separated each other by preparative TLC. Their spectral data except **2b—f**/**3b—f**, those of which have been shown above, are given in the following.

Methyl 2-Methyl-3-phenoxypropanoate (2g, R′=Me): An oil; MS *m/z* 194 (M^+, 40.60%), 149 (99.24), 137 (46.36), 101 (29.07), 94 (30.32), 71 (44.86), 69 (100.00), 59 (40.10); IR (neat) 3030, 2980, 2950, 2880, 1730, 1595, 1580, 1490, 1460, 1430,

1240, 1195, 1165, 1030, 745, 680 cm^{-1}; ^{1}H NMR ($CDCl_3$) δ=1.30 (d, J=7.02 Hz, 3H), 2.95 (m, 1H), 3.72 (s, 3H), 3.99 (dd, J=9.16, 6.71 Hz, 1H), 4.19 (dd, J=9.16, 6.14 Hz, 1H), 6.90 (m, 2H), 6.95 (m, 1H), 7.27 (m, 2H).

Methy 2-Methyl-3-phenoxybutanoate (3g, R′=Me): An oil; MS m/z 194 (M^+, 12.63%), 163 (15.04), 101 (100.00), 94 (35.12), 59 (42.09), 28 (33.68); IR (neat) 3020, 2920, 1730, 1590, 1580, 1480, 1460, 1430, 1230, 1160, 1070, 1030, 740, 680 cm^{-1}; ^{1}H NMR ($CDCl_3$) δ=2.11 (m, 2H), 2.53 (t, J=7.32 Hz, 1H), 3.69 (s, 3H), 4.01 (t, J=6.11 Hz, 2H), 6.88 (m, 2H), 6.94 (m, 1H), 7.26 (m, 2H).

Methyl 2-Methyl-3-(*p*-tolylsulfonyl)propanoate (2h, R′=Me): Mp 86—87 °C (recrystallized from hexane/ethyl acetate); MS m/z 257 (M^++1, 1.98%), 256 (M^+, 12.28), 155 (28.25), 139 (53.38), 132 (13.80), 101 (100.00), 92 (49.40), 91 (78.49), 73 (22.33), 69 (35.37), 59 (70.00); IR (KBr) 2995, 2970, 1735, 1590, 1450, 1430, 1380, 1300, 1140, 880, 830, 810, 760, 680 cm^{-1}; ^{1}H NMR ($CDCl_3$) δ=1.31 (d, J=7.02 Hz, 3H), 2.45 (s, 3H), 3.01 (m, 1H), 3.07 (dd, J=14.04, 5.19 Hz, 1H), 3.62 (s, 3H), 3.67 (dd, J=14.04, 7.33 Hz, 1H), 7.36 (d, J=8.24 Hz, 2H), 7.78 (d, J=8.24 Hz, 2H). Found: C, 56.18; H, 6.17%. Calcd for $C_{12}H_{16}O_4S$: C, 56.23; H, 6.29%.

Methyl 4-(*p*-Tolylsulfonyl)butanoate (3h, R′=Me): An oil; MS m/z 257 (M^++1, 0.39%), 256 (M^+, 2.22), 225 (14.38), 183 (6.63), 155 (6.30), 139 (9.18), 101 (100.00), 91 (20.55), 59 (39.90); IR (neat) 2965, 2940, 1735, 1590, 1435, 1310, 1300, 1280, 1140, 1080, 810, 720 cm^{-1}; ^{1}H NMR ($CDCl_3$) δ=2.02 (m, 2H), 2.45 (s, 3H), 2.46 (t, J=7.17 Hz, 2H), 3.15 (m, 2H), 3.65 (s, 3H), 7.37 (d, J=8.24 Hz, 2H), 7.79 (d, J=8.24 Hz, 2H).

Methyl 2-Methyl-4-(*p*-tolylsulfonyl)butanoate (2i, R′=Me): An oil; MS m/z 271 (M^++1, 0.35%), 270 (M^+, 0.91), 239 (6.92), 183 (6.33), 157 (6.51), 140 (6.10), 139 (6.53), 115 (100.00), 91 (14.13), 59 (39.85); IR (neat) 3040, 2960, 1730, 1595, 1450, 1380, 1300, 1200, 1140, 1085, 1050, 810, 730 cm^{-1}; ^{1}H NMR ($CDCl_3$) δ=1.16 (d, J=7.01 Hz, 3H), 1.87 (m, 1H), 2.00 (m, 1H), 2.46 (s, 3H), 2.56 (m, 1H), 3.11 (m, 2H), 3.65 (s, 3H), 7.36 (d, J=8.09 Hz, 2H), 7.77 (d, J=8.09 Hz, 2H).

Methyl 5-(*p*-Tolylsulfonyl)pentanoate (3i, R′=Me): An oil; MS m/z 271 (M^++1, 0.28%), 270 (M^+, 1.04), 239 (8.59), 155 (5.98), 115 (100.00), 92 (12.89), 91 (17.87), 83 (26.01), 73 (40.50), 59 (13.91), 55 (41.67); IR (neat) 3040, 2960, 1735, 1600, 1440, 1300, 1285, 1145, 1095, 910, 810, 730 cm^{-1}; ^{1}H NMR ($CDCl_3$) δ=1.72 (m, 4H), 2.30 (t, J=7.02 Hz, 2H), 2.46 (s, 3H), 3.07 (t, J=7.33 Hz, 2H), 3.65 (s, 3H), 7.36 (d, J=8.24 Hz, 2H), 7.78 (d, J=8.24 Hz, 2H).

2-Methyl-6-phenyl-4-hexanolide (7a): An oil (a mixture of diastereoisomers); MS m/z 204 (M^+, 43.07%), 131 (42.27), 130 (100.00), 117 (50.72), 92 (75.94), 91 (88.26); IR (neat) 3040, 2940, 1770, 1600, 1490, 1450, 1375, 1355, 1180, 1160, 1020, 925, 745, 695 cm^{-1}; ^{1}H NMR of a major diastereoisomer (**M**) ($CDCl_3$, by COSY) δ=1.27 (d, J=7.02 Hz, 3H), 1.53 (m, 1H), 1.81—2.07 (m, 2H), 2.46 (m, 1H), 2.60—2.78 (m, 3H), 4.31 (m, 1H), 7.20 (m, 3H), 7.28 (m, 2H); ^{1}H NMR of a minor diastereoisomer (**m**) ($CDCl_3$, by COSY) δ=1.28 (d, J=7.33 Hz, 3H), 1.90—2.15 (m, 4H), 2.70—2.87 (m, 3H), 4.49 (m, 1H), 7.20 (m, 3H), 7.28 (m, 2H); **M**/**m**=63/37.

3-Methyl-1-oxaspiro[4.5]decan-2-one (7b): Mp 67—68 °C (recrystallized from hexane, lit, 68—70 °C,[9a] 70.5—71 °C[9b,c]); MS m/z 169 (M^++1, 1.47%), 168 (M^+, 10.80), 125 (100), 124 (31.11), 112 (20.87), 82 (39.66), 81 (28.22), 55 (43.90); IR (KBr) 2940, 2860, 1765, 1440, 1210, 1130, 960, 950, 920 cm^{-1}; ^{1}H NMR ($CDCl_3$) δ=1.27 (d, J=7.33 Hz, 3H), 1.39 (m, 1H), 1.45—1.65 (m, 5H), 1.58 (dd, J=12.81, 11.29 Hz, 1H), 1.65—1.82 (m, 4H), 2.34 (dd, J=12.81, 9.16 Hz, 1H), 2.78 (m, 1H).

Bis(alkoxycarbonylation) of 1b with CuCl (Method A). In a flask equipped with a balloon containing carbon monoxide (1 atm), 1-undecene (**1b**, 39 mg, 0.25 mmol) was added to a mixed dispersion of 5% Pd–C (58 mg, 0.11 equiv of Pd) and CuCl (74 mg, 3.0 equiv) in absolute methanol (4 ml) at 25 °C. After stirring for 9 d at 25 °C, the reaction mixture was added dropwise to aqueous 10% $NaHCO_3$ solution. The filtrate through Celite was diluted by ethyl acetate. The organic layer was successively washed with water and brine, and dried over sodium sulfate. The residue obtained by evaporation of the solvent was subjected to preparative TLC (SiO_2, hexane/ethyl acetate=15/1, v/v) to afford 68 mg of diesters [**8b** (R′=Me), quantitative yield] as a colorless oil. MS m/z 273 (M^++1, 3.75%), 241 (39.63), 199 (43.25), 170 (30.32), 146 (96.68), 138 (23.91), 114 (100.00), 97 (16.45), 87 (20.92), 83 (15.93), 55 (17.30); IR (neat) 2910, 2840, 1730, 1430, 1350, 1250, 1185, 1150, 995, 905, 725 cm^{-1}; ^{1}H NMR ($CDCl_3$) δ=0.88 (t, J=6.71 Hz, 3H), 1.26 (m, 14H), 1.51 (m, 1H), 1.63 (m, 1H), 2.43 (dd, J=16.48, 5.19 Hz, 1H), 2.71 (dd, J=16.48 Hz, 9.15 Hz, 1H), 2.83 (m, 1H), 3.67 (s, 3H), 3.70 (s, 3H).

In a similar manner, other diesters (**8c—f**) were prepared from the corresponding terminal olefins (**1c—f**).

Dimethyl 2-Decylsuccinate (8c, R′=Me): An oil ; MS m/z 287 (M^++1, 2.25%), 286 (M^+, 0.19), 255 (20.54), 213 (31.77), 170 (24.45), 146 (100.00), 138 (16.41), 114 (76.57), 97 (11.86), 87 (12.88), 55 (14.93); IR (neat) 2930, 2860, 1740, 1460, 1435, 1370, 1240, 1200, 1180 cm^{-1}; ^{1}H NMR ($CDCl_3$) δ=0.88 (t, J=6.72 Hz, 3H), 1.25 (s, 16H), 1.50 (m, 1H), 1.62 (m, 1H), 2.43 (dd, J=16.48, 5.19 Hz, 1H), 2.71 (dd, J=16.48, 9.16 Hz, 1H), 2.82 (m, 1H), 3.67 (s, 3H), 3.69 (s, 3H).

Diethyl 2-Dodecylsuccinate (8d, R′=Et): An oil; MS m/z 343 (M^++1, 28.34%), 297 (67.42), 255 (39.36), 184 (37.43), 174 (100.00), 138 (23.41), 128 (84.72), 101 (16.54), 97 (16.71), 55 (17.69), 43 (19.84); IR (neat) 2935, 2860, 1745, 1735, 1465, 1375, 1260, 1175, 1160, 1030 cm^{-1}; ^{1}H NMR ($CDCl_3$) δ=0.83 (t, J=6.72 Hz, 3H), 1.20 (m, 26H), 1.45 (m, 1H), 1.57 (m, 1H), 2.36 (dd, J=16.18, 5.19 Hz, 1H), 2.64 (dd, J=16.18, 9.46 Hz, 1H), 2.76 (m, 1H), 4.09 (m, 4H).

Dimethyl 2-Dodecylsuccinate (8d, R′=Me): Mp 34—35 °C (not recrystallized); MS m/z 315 (M^++1, 0.30%), 283 (10.70), 241 (21.90), 170 (26.96), 156 (10.45), 146 (100.00), 138 (17.03), 114 (60.74), 97 (10.78), 87 (9.44), 83 (9.60), 55 (8.84); IR (neat, melted) 2900, 2830, 1720, 1440, 1420, 1145 cm^{-1}; ^{1}H NMR ($CDCl_3$) δ=0.88 (t, J=6.87 Hz, 3H), 1.25 (s, 20H), 1.50 (m, 1H), 1.63 (m, 1H), 2.43 (dd, J=16.48, 4.89 Hz, 1H), 2.71 (dd, J=16.48, 9.46 Hz, 1H), 2.84 (m, 1H), 3.67 (s, 3H), 3.70 (s, 3H).

Diethyl 2-Hexadecylsuccinate (8e, R′=Et): An oil; MS m/z 399 (M^++1, 0.93%), 398 (M^+, 0.91), 353 (17.41), 311 (16.46), 184 (26.20), 174 (100.00), 138 (15.59), 128 (48.71), 101 (10.99), 97 (12.02), 83 (10.93), 57 (11.50); IR (neat) 2930, 2860, 1735, 1460, 1370, 1250, 1170, 1160, 1025 cm^{-1}; ^{1}H NMR ($CDCl_3$) δ=0.91 (t, J=6.72 Hz, 3H), 1.29 (m, 34H), 1.53 (m, 1H), 1.67 (m, 1H), 2.44 (dd, J=16.33, 5.04 Hz, 1H), 2.72 (dd, J=16.33, 9.32 Hz, 1H), 2.84 (m, 1H), 4.18 (m, 4H).

Dimethyl 2-Hexadecylsuccinate (8e, R′=Me): Mp 35 °C (not recrystallized); MS m/z 371 (M^++1, 1.03%), 370 (M^+, 1.09), 339 (15.56), 297 (23.54), 170 (34.56), 156 (12.37), 146 (100.00), 138 (14.95), 114 (37.74), 97 (10.75); IR (KBr) 2920, 2840, 1730, 1720, 1460, 1430, 1370, 1355, 1205, 1160 cm^{-1}; ^{1}H NMR ($CDCl_3$) δ=0.88 (t, J=6.87 Hz, 3H), 1.26 (s, 28H), 1.51 (m, 1H), 1.63 (m, 1H), 2.43 (dd, J=16.33, 4.88 Hz, 1H), 2.71 (dd, J=16.33, 9.46 Hz, 1H), 2.83 (m, 1H), 3.67 (s, 3H),

3.70 (s, 3H).

Dimethyl 2-(2-Phenylethyl)succinate (8f, R′=Me): An oil MS *m/z* 251 (M^++1, 5.36%), 250 (M^+, 8.96), 187 (57.43), 146 (100.00), 144 (11.01), 117 (11.51), 114 (77.49), 104 (31.50), 91 (24.76); IR (neat) 3020, 2950, 2850, 1735, 1600, 1495, 1435, 1365, 1260, 1200, 1160, 730, 700 cm^{-1}; ^1H NMR ($CDCl_3$) δ=1.83 (m, 1H), 1.98 (m, 1H), 2.48 (dd, *J*=16.48, 5.19 Hz, 1H), 2.62 (m, 2H), 2.76 (dd, *J*=16.48, 9.16 Hz, 1H), 2.88 (m, 1H), 3.66 (s, 3H), 3.70 (s, 3H), 7.17 (m, 3H), 7.27 (m, 2H).

Bis(alkoxycarbonylation) of 1a with CuCl (Method B). In a flask equipped with balloons containing carbon monoxide (1 atm) and oxygen (1 atm), 1-decene (**1a**, 35 mg, 0.25 mmol) was added to a mixed dispersion of $PdCl_2$ (1 mg, 0.02 equiv) and anhydrous CuCl (37 mg, 1.5 equiv) in absolute methanol (4 ml) at 25 °C. After stirring for 1 d at 25 °C, the reaction mixture was added dropwise to aqueous 10% $NaHCO_3$ solution. The filtrate through Celite was treated with a small amount of aqueous KCN solution to deactivate palladium catalyst and diluted by ethyl acetate. The organic layer was successively washed with water and brine, and dried over sodium sulfate. The residue obtained by evaporation of the solvent was subjected to preparative TLC (SiO_2, hexane/ethyl acetate=10/1, v/v) to afford 45 mg of diester [**8a**(R′=Me), 70%] as a colorless oil accompanied by 10 mg of monoesters (**2a**/**3a**=43/57, 21% yield). **8a**:[10] MS *m/z* 259 (M^++1, 0.59%), 227 (22.03), 185 (44.04), 170 (21.70), 146(100.00), 114 (97.01); IR (neat) 2930, 2860, 1735, 1430, 1160, 1000 cm^{-1}; ^1H NMR ($CDCl_3$) δ=0.88 (t, *J*=6.87 Hz, 3H), 1.26 (m, 12H), 1.51 (m, 1H), 1.62 (m, 1H), 2.43 (dd, *J*=16.48, 5.04 Hz, 1H), 2.71 (dd, *J*=16.48, 9.46 Hz, 1H), 2.84 (m, 1H), 3.67 (s, 3H), 3.70 (s, 3H).

In a similar manner, other diesters (**8b**—**i**) and 2-oxotetrahydrofuran-3-acetic acid esters (**9a**—**f**) were prepared from the corresponding terminal olefins (**1b**—**i**) and 3-buten-1-ols (**6a**—**f**), respectively. Their spectral data except **8b**—**f**, those of which have been shown above, are given in the following.

Dimethyl 2-(Phenoxymethyl)succinate (8g, R′=Me): An oil; MS *m/z* 253 (M^++1, 2.86%), 252 (M^+, 18.75), 189 (67.53), 160 (18.92), 159 (100.00), 127 (71.35), 99(29.69), 94 (21.59); IR (neat) 3005, 2960, 1730, 1590, 1580, 1490, 1460, 1435, 1230, 1160, 1070, 1030, 995, 900, 745, 720, 680 cm^{-1}; ^1H NMR ($CDCl_3$) δ=2.74 (dd, *J*=17.09, 5.80 Hz, 1H), 2.95 (dd, *J*=17.09, 7.93 Hz, 1H), 3.33 (m, 1H), 3.70 (s, 3H), 3.74 (s, 3H), 4.21 (d, *J*=5.81 Hz, 2H), 6.88 (d, *J*=7.63 Hz, 2H), 6.96 (t, *J*=7.33 Hz, 1H), 7.27 (m, 2H).

Dimethyl 2-(*p*-Tolylsulfonylmethyl)succinate (8h, R′=Me): An oil ; MS *m/z* 315 (M^++1, 0.51%), 314 (M^+, 1.62), 159 (100.00), 139 (25.31), 127 (65.85), 99 (20.52), 91 (26.04); IR (neat) 3020, 2960, 2840, 1730, 1660, 1585, 1430, 1400, 1360, 1310, 1290, 1280, 1200, 1140, 1080, 1030, 820, 800, 720 cm^{-1}; ^1H NMR ($CDCl_3$) δ=2.46 (s, 3H), 2.91 (d, *J*=6.10 Hz, 2H), 3.29 (m, 1H), 3.38 (dd, *J*=14.35, 7.63 Hz, 1H), 3.67 (dd, *J*=14.35, 5.19 Hz, 1H), 3.67 (s, 3H), 3.68 (s, 3H), 7.37 (d, *J*=8.09 Hz, 2H), 7.79 (d, *J*=8.09 Hz, 2H).

Dimthyl 2-[2-(*p*-Tolylsulfonyl)ethyl]succinate (8i, R′=Me): An oil; MS *m/z* 329 (M^++1, 0.09%), 328 (M^+, 0.16), 297 (13.25), 173 (100.00), 141 (26.60), 139 (13.24), 113 (28.99), 91 (9.46), 71 (18.36); IR (neat) 3000, 2960, 1730, 1590, 1430, 1400, 1310, 1295, 1280, 1200, 1160, 1140, 1080, 1010, 910, 805, 720 cm^{-1}; ^1H NMR ($CDCl_3$) δ=2.00 (m, 2H), 2.44 (dd, *J*=16.78, 5.80 Hz, 1H), 2.45 (s, 3H), 2.70 (dd, *J*=16.78, 8.24 Hz, 1H), 2.93 (m, 1H), 3.14 (m, 2H), 3.65 (s, 3H), 3.67 (s, 3H), 7.36 (d, *J*=8.09 Hz, 2H). 7.76 (d, *J*=8.09 Hz, 2H).

2-(Methoxycarbonymethyl)-6-phenyl-4-hexanolide (9a):[7b] An oil (a mixture of diastereoisomers); MS *m/z* 263 (M^++1, 5.73%), 262 (M^+, 29.12), 230 (15.66), 170 (18.43), 132 (27.07), 131 (21.43), 130 (100.00), 92 (44.47), 91 (53.42), 59 (6.81); IR (neat) 3000, 2920, 1760, 1725, 1590, 1480, 1425, 1360, 1250, 1150, 1020, 980, 900, 720, 690 cm^{-1}; ^1H NMR of a major diastereoisomer (**M**) ($CDCl_3$) δ=1.82—2.25 (m, 4H), 2.50—2.93 (m, 4H), 2.93—3.10 (m, 1H), 3.70 (s, 3H), 4.54 (m, 1H), 7.20 (m, 3H), 7.29 (m, 2H); ^1H NMR of a minor diastereoisomer (**m**) ($CDCl_3$) δ=1.82—2.25 (m, 4H), 2.50—2.93 (m, 4H), 2.93—3.10 (m, 1H), 3.70 (s, 3H), 4.38 (m, 1H), 7.20 (m, 3H), 7.29 (m, 2H); **M**/**m**=68/32.

3-(Methoxycarbonylmethyl)-1-oxaspiro[4.5]decan-2-one (9b):[7b] An oil; MS *m/z* 227 (M^++1, 13.04%), 226 (M^+, 79.63), 195 (48.56), 183 (86.10), 166 (100.00), 155 (66.80), 153 (58.32), 151 (35.84), 150 (82.71), 132 (27.67), 123 (22.69), 108 (25.87), 100 (27.57), 67 (25.13); IR (neat) 2960, 2880, 1770, 1740, 1205 cm^{-1}; ^1H NMR ($CDCl_3$) δ=1.39—1.84 (m, 10H), 1.69 (t, *J*=12.11 Hz, 1H), 2.44 (dd, *J*=12.11, 9.31 Hz, 1H), 2.53 (dd, *J*=10.04, 9.15 Hz, 1H), 2.90 (dd, *J*=17.04, 4.27 Hz, 1H), 3.13 (m, 1H).

3-(Methoxycarbonylmethyl)-1-oxaspiro[4.4]nonan-2-one (9c): An oil; MS *m/z* 212 (M^+, 1.89%), 183 (41.69), 181 (39.00), 155 (37.14), 152 (100.00), 136 (74.62), 110 (37.98), 94 (56.60), 55 (29.20); IR (neat) 2900, 2840, 1760, 1720, 1420, 1320, 1360, 1260, 1140 cm^{-1}; ^1H NMR ($CDCl_3$) δ=1.70—2.09 (m, 9H), 2.45 (dd, *J*=12.51, 8.55 Hz, 1H), 2.50 (dd, *J*=17.09, 9.16 Hz, 1H), 2.92 (dd, *J*=17.09, 3.97 Hz, 1H), 3.13 (m, 1H), 3.71 (s, 3H).

2-(Methoxycarbonylmethyl)-4-butanolide (9d):[7b] An oil; MS *m/z* 159 (M^++1, 1.97%), 127 (37.80), 114 (16.88), 82 (16.91), 72 (22.41), 59 (57.33), 55 (100.00); IR (neat) 2945, 2910, 1760, 1725, 1430, 1360, 1260, 1200, 1145, 1015 cm^{-1}; ^1H NMR ($CDCl_3$) δ=2.05 (m, 1H), 2.51—2.59 (m, 2H), 2.89—3.01 (m, 2H), 3.72 (s, 3H), 4.24 (m, 1H), 4.41 (dt, *J*=8.85, 1.83 Hz, 1H).

4-Methy1-2-(methoxycarbonylmethyl)-4-decanolide (9e): An oil (a mixture of diastereoisomers); MS *m/z* 257 (M^++1, 0.38%), 171 (100.00), 143 (25.36), 139 (13.64), 111 (10.33); IR (neat) 2950, 2880, 1770, 1745, 1460, 1440, 1385, 1290, 1240, 1190, 1175, 1140 cm^{-1}; ^1H NMR of a major diastereoisomer (**M**) ($CDCl_3$) δ=0.89 (t, *J*=7.02 Hz, 3H), 1.22—1.40 (m, 8H), 1.44 (s, 3H), 1.55—1.90 (m, 3H), 2.45 (dd, *J*=11.81, 8.85 Hz, 1H), 2.55 (dd, *J*=11.59, 8.85 Hz, 1H), 2.89 (dd, *J*=7.63, 3.96 Hz, 1H), 3.14 (m, 1H), 3.70 (s, 3H); ^1H NMR of a minor diastereoisomer (**m**) ($CDCl_3$) δ=0.89 (t, *J*=7.02 Hz, 3H), 1.22—1.40 (m, 8H), 1.37 (s, 3H), 1.55—1.90 (m, 3H), 2.30 (dd, *J*=12.52, 8.85 Hz, 1H), 2.51 (dd, *J*=11.59, 8.85 Hz, 1H), 2.93 (dd, *J*=7.63, 3.96 Hz, 1H), 3.14 (m, 1H), 3.70 (s, 3H); **M**/**m**=58/42.

4-(Methoxycarbonylmethyl)spiro[furan-2(3*H*),1′-indan]-5(4*H*)-one (9f): An oil (a mixture of diastereoisomers); MS *m/z* 261 (M^++1, 5.08%), 260 (M^+, 27.41), 229 (36.52), 216 (46.17), 184 (67.52), 143 (100.00), 133 (53.64), 128 (80.13), 100 (94.33); IR (neat) 3030, 2960, 1760, 1730, 1600, 1450, 1430, 1360, 1320, 1250, 1210, 1190, 1165, 1140, 980, 900, 750, 720 cm^{-1}; ^1H NMR of a major diastereoisomer (**M**) ($CDCl_3$) δ=2.22—2.43 (m, 2H), 2.56—2.71 (m, 2H), 2.85—3.02 (m, 3H), 3.06—3.15 (m, 1H), 3.48 (m, 1H), 3.73 (s, 3H), 7.24—7.39 (m, 4H); ^1H NMR of a minor diastereoisomer (**m**) ($CDCl_3$) δ=2.22—2.43 (m, 3H), 2.56—2.71 (m, 2H), 2.85—3.02 (m, 2H), 3.06—3.16 (m, 1H), 3.27 (m, 1H), 3.73 (s, 3H), 7.24—7.39

(m, 4H); **M**/**m**=54/46.

This work is partly supported by the Research Grant-in-Aid from The Ministry of Education, Science and Culture.

References

1) B. Despeyroux and H. Alper, *Ann. N. Y. Acad. Sci.*, **415**, 148 (1983); S. B. Fergusson and H. Alper, *J. Chem. Soc., Chem. Commun.*, **1984**, 1349.

2) H. Alper, J. B. Woell, B. Despeyroux, and D. J. H. Smith, *J. Chem. Soc., Chem. Commun.*, **1983**, 1270.

3) K. Inomata, S. Toda, and H. Kinoshita, *Chem. Lett.*, **1990**, 1567.

4) D. M. Fenton, *J. Org. Chem.*, **38**, 3192 (1973). Another mechanism involving $HPdL_nCl$ was proposed by Tsuji: J. Tsuji, *Acc. Chem. Res.*, **2**, 144 (1962).

5) H. Alper and D. Leonard, *J. Chem. Soc., Chem. Commun.*, **1985**, 511.

6) P. Bréchot, Y. Chauvin, D. Commereuc, and L. Saussine, *Organometallics*, **9**, 26 (1990), and references cited therein.

7) a) Y. Tamaru, M. Hojo, and Z. Yoshida, *Tetrahedron Lett.*, **28**, 325 (1987); b) Y. Tamura, M. Hojo, and Z. Yoshida, *J. Org. Chem.*, **56**, 1099 (1991).

8) C. S. Marvel and S. M. McElvan, *Org. Synth.*, Coll. Vol. I, 170 (1956).

9) a) A. M. El-Abbady and H. A. A. Regaila, *J. Chem., U.A.R.*, **9**, 301 (1966); *Chem. Abstr.*, **67**, 116730a (1967). b) T. H. Black and W. J. DuBay, III, *Tetrahedron Lett.*, **28**, 4787 (1987). c) T. H. Black, W. J. DuBay, III, and P. S. Tully, *J. Org. Chem.*, **53**, 5922 (1988).

10) D. E. James and J. K. Stille, *J. Am. Chem. Soc.*, **98**, 1810 (1976).

Laser-Induced Organic Transformation. Direct and Selective Synthesis of Diols from Methanol, Ethanol, and Their Mixture in the Presence of Hydrogen Peroxide

Yuichi SHIMIZU,* Shun'ichi SUGIMOTO, Shunichi KAWANISHI, and Nobutake SUZUKI
Osaka Laboratory for Radiation Chemistry, Japan Atomic Energy Research Institute, 25-1 Mii-minami, Neyagawa, Osaka 572
(Received August 12, 1991)

The laser-induced transformation of methanol (MeOH), ethanol (EtOH), and MeOH–EtOH mixture have been investigated in the presence of H_2O_2. Ethylene glycol (EG) was highly selectively produced in high quantum yield (ϕ=0.94) by KrF-laser irradiation of the N_2-saturated MeOH and the selectivity was 94% at 3.2 ml h^{-1} of H_2O_2 feeding rate (f). Butanediol (BD) and acetaldehyde (AA) were directly and selectively produced by KrF-laser irradiation of the N_2-saturated EtOH. The quantum yields of BD and AA were 0.42 and 0.29, respectively, and the combined selectivity was 97% at f=3.4 ml h^{-1}. Also, propanediols (PD) were directly produced by KrF-laser irradiation of the N_2-saturated MeOH–EtOH mixture. The quantity of 1,2-PD reached the maximum at about 64 mol% of MeOH content. EG is produced through the dimerization of hydroxymethyl radicals formed by the abstraction of a hydrogen atom from MeOH by hydroxyl radical formed in high density by the laser-photolysis of H_2O_2. Similarly, 2,3-BD is produced by the dimerization of 1-hydroxyethyl radicals formed by the abstraction of α-hydrogen atom from EtOH by hydroxyl radical and 1,2-PD is produced by the recombination between hydroxymethyl radical and 1-hydroxyethyl radical.

The direct transformation of alcohols, which are not petrochemicals, into more valuable compounds is very important from a viewpoint of effective utilization of organic resources. Ethylene glycol (EG), butanediols (BD), and propanediols (PD), present-day manufactured by a multistep process using ethylene, butene, acetaldehyde, and propylene etc. obtained in petrochemical industry,[1] are very important as raw materials for the industrial production of polyester synthetic fiber and polyester resin, and also as antifreezing agent and so on.

In the previous paper,[2,3] we reported that EG was directly and selectively synthesized by steady state UV (low-pressure mercury lamp) irradiation of the N_2-saturated MeOH containing H_2O_2. For the purpose of highly selective synthesis of EG, we have attempted to proceed more efficiently the reaction of MeOH with H_2O_2 using a KrF laser with high intensity. We found that EG was highly selectively synthesized by KrF-laser irradiation of the N_2-saturated MeOH containing H_2O_2.[4] Also, we found that BD and acetaldehyde (AA) were directly and selectively synthesized by KrF-laser irradiation of N_2-saturated EtOH containing H_2O_2.[5]

In this paper, we report in further detail with regard to the laser-induced direct synthesis of EG and BD from MeOH and EtOH, respectively, and discuss the reaction mechanism. Furthermore, we report the laser-induced direct synthesis of PD from MeOH–EtOH mixture containing H_2O_2.

Experimental

Materials. All chemicals were of reagent grade. MeOH and EtOH were purchased from Tokyo Kasei Kogyo Co., Ltd. and were used without further purification. The aqueous 30% hydrogen peroxide was purchased from Santoku Chemical Industries Co., Ltd. N_2 used was of high purity grade of above 99.9%.

Apparatus and Procedures. The laser-induced reactions were carried out in a Pyrex glass cylindrical reaction vessel (volume: 91.5 ml, diameter: 35.5 mm, length: 70 mm) with a Suprasil window for the incidence of laser beam. MeOH, EtOH, and MeOH–EtOH mixture (56—64 ml) were placed in the reaction vessel, respectively, and well-bubbled with nitrogen in order to remove oxygen. The N_2-saturated MeOH, EtOH, and MeOH–EtOH mixture were stirred magnetically (500 rpm), and irradiated with the KrF laser (Lumonics Hyper EX-460, wavelength: 248 nm, pulse energy: 350 mJ per pulse, frequency: 16 Hz, pulse duration: 12—15 ns, beam shape: 9×34 mm) at room temperature. At the same time with irradiation, the aqueous 30% H_2O_2 was added to MeOH, EtOH, and MeOH–EtOH mixture with the feeding rate (f) from 3.2 to 16.0 ml h^{-1} by using a microfeeder (Atto Corp., AC-2120). For the purpose of comparison, some experiments were carried out using a steady state UV (low-pressure mercury lamp, wavelength: mainly 253.7 nm, quantity of light: 3.38×10^{18} photons s^{-1}).

Actinometry. The quantity of light from the laser was determined by using a calorimeter (Scientech 38-4UV5). The calorimeter was also placed behind the reaction vessel to determine precisely the quantity of light absorbed by alcohol–H_2O_2 mixture during the laser irradiation. The quantity of light was 4.38×10^{17} photons per pulse.

Analysis. Products were analyzed by gas chromatography (Shimadzu GC-7A: Porapak Q column, GC-4C: Porapak N or Chromosorb 101 column, and GC-3BT: Molecular sieve 5A column) and ion chromatography (Yokogawa IC-100: SAX 1 column).

Results and Discussion

N_2-Saturated Methanol. When the N_2-saturated

MeOH containing H_2O_2 was irradiated with the KrF laser, EG was produced as a major product together with formic acid (FA), methyl formate (MF), formaldehyde, hydrogen, carbon dioxide, carbon monoxide, and methane as minor products. Figure 1 shows the quantities of EG, FA, and MF as a function of number of photon at f=3.2 ml h^{-1}. The quantity of EG increased linearly with number of photon up to about 4.1×10^{20} photons ml^{-1}. The quantities of EG, FA, and MF were 43.3, 0.4, and 0.4×10^{-2} mmol ml^{-1}, respectively, and the sum of the quantities of other products was less than 0.1×10^{-2} mmol ml^{-1} at irradiation of 4.0×10^{20} photons ml^{-1}. The quantum yield of EG formed and the selectivity were 0.94 and 94%, respectively, at irradiation of 4.7×10^{19} photons ml^{-1}. Such high quantum yield and selectivity indicate that the formation of EG proceeds efficiently in this system. Also, when the N_2-saturated MeOH alone was irradiated in the absence of H_2O_2, organic products were hardly produced even after irradiation of about 4.1×10^{20} photons ml^{-1}.

On the other hand, in the case of steady state UV irradiation, the quantum yield of EG formed was 0.73 and the selectivity was 85% at irradiation of 3.7×10^{20} photons ml^{-1}.[3] It was found from these results that the quantum yield of EG formed and the selectivity were much larger in KrF-laser irradiation than in steady state UV one. This indicates that the KrF-laser irradiation is favorable for the effective formation of EG.

Figure 2 shows the effects of H_2O_2 feeding rate on the quantities of EG, FA, and MF. The quantity of EG decreased with increasing H_2O_2 feeding rate in the range of f=3.2—14.4 ml h^{-1}. This indicates that the H_2O_2 feeding rate is an important factor for the efficient formation of EG, and that the efficient formation of EG is favorable in lower H_2O_2 feeding rate. The sum of the quantities of FA and MF was less than 1×10^{-2} mmol ml^{-1} at f=14.4 ml h^{-1}. Table 1 shows the effects of H_2O_2 feeding rate on the quantum yield of EG formed and the selectivity. The quantum yield of EG formed decreased with increasing H_2O_2 feeding rate, that is, from 0.94 at f=3.2 ml h^{-1} to 0.56 at f=14.4 ml h^{-1}. The selectivity of EG formation was 94—97% in the wide range of f=3.2—14.4 ml h^{-1}. It was found from these results that EG was highly selectively synthesized in high quantum yield by KrF-laser irradiation of the N_2-saturated MeOH in lower H_2O_2 feeding rate ranges.

N_2-Saturated Ethanol. When the N_2-saturated EtOH containing H_2O_2 was irradiated with the KrF laser, 2,3-, 1,3-BD, and AA were produced as major products together with 1,4-BD, hydrogen, carbon dioxide, carbon monoxide, and methane as minor products. Figure 3 shows the quantities of 2,3-, 1,3-, 1,4-BD, and AA as a function of number of photon at f=3.4 ml h^{-1}. The

Table 1. Effects of H_2O_2 Feeding Rate on the Quantum Yield of Ethylene Glycol Formed and the Selectivity in the Case of KrF-Laser Irradiation of N_2-Saturated Methanol

H_2O_2 feeding rate	Number of photon	Ethylene glycol	
ml h^{-1}	10^{20} photons ml^{-1}	ϕ	Selectivity/%
3.2	0.5	0.94	94
5.3	2.5	0.68	97
8.9	1.6	0.62	97
14.4	1.6	0.56	96

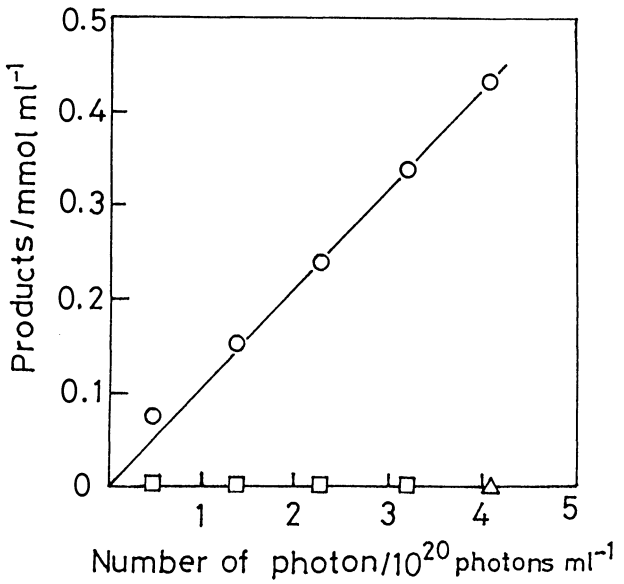

Fig. 1. Plots of the quantities of main products as a function of number of photon in the case of KrF-laser irradiation of N_2-saturated methanol.
○: Ethylene glycol, □: Methyl formate, △: Formic acid. Aqueous 30% H_2O_2 feeding rate: 3.2 ml h^{-1}.

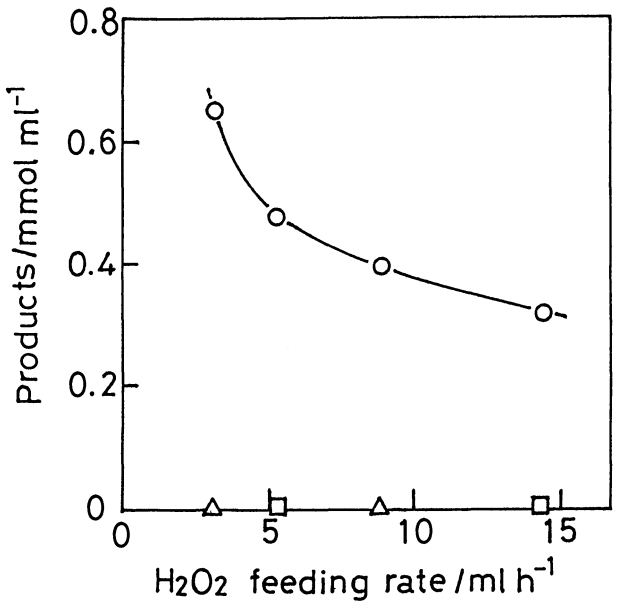

Fig. 2. Effects of H_2O_2 feeding rate on the quantities of main products in the case of KrF-laser irradiation of N_2-saturated methanol.
Symbols are the same as in Fig. 1. Number of photon: 2.8×10^{20} photons ml^{-1}.

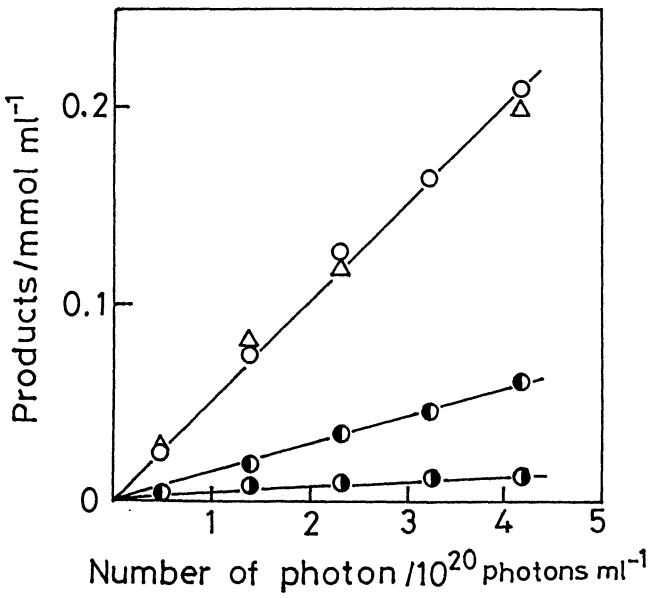

Fig. 3. Plots of the quantities of main products as a function of number of photon in the case of KrF-laser irradiation of N_2-saturated ethanol.
○: 2,3-Butanediol, ◐: 1,3-Butanediol, ◑: 1,4-Butanediol, △: Acetaldehyde. Aqueous 30% H_2O_2 feeding rate: 3.4 ml h^{-1}.

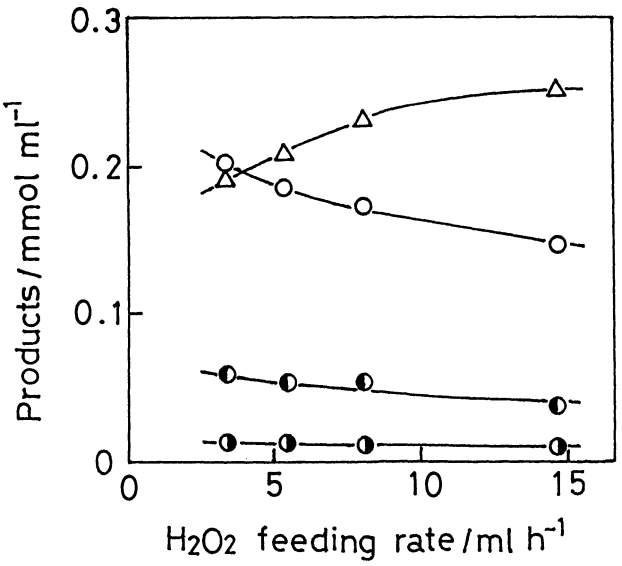

Fig. 4. Effects of H_2O_2 feeding rate on the quantities of main products in the case of KrF-laser irradiation of N_2-saturated ethanol.
Symbols are the same as in Fig. 3. Number of photon: 4.0×10^{20} photons ml^{-1}.

quantities of 2,3-, 1,3-, 1,4-BD, and AA increased linearly with number of photon up to about 4.2×10^{20} photons ml^{-1}. The quantities of 2,3-, 1,3-, 1,4-BD, and AA were 20.2, 5.8, 1.2, and 19.2×10^{-2} mmol ml^{-1}, respectively, and the sum of the quantities of other products was less than 1.6×10^{-2} mmol ml^{-1} at irradiation of 4.0×10^{20} photons ml^{-1}. The quantum yields of 2,3-, 1,3-, 1,4-BD, and AA formed were 0.31, 0.09, 0.02, and 0.29, respectively, and the selectivities were 42, 12, 3, and 40%. Also, when the N_2-saturated EtOH alone was irradiated in the absence of H_2O_2, organic products were hardly produced even after irradiation of about 4.2×10^{20} photons ml^{-1}.

On the other hand, in the case of steady state UV irradiation, the quantities of 2,3-, 1,3-, 1,4-BD, and AA were 11.6, 0.3, 0.7, and 24.7×10^{-2} mmol ml^{-1}, and the selectivities were 29, 1, 2, and 62%, respectively, at irradiation of 4.0×10^{20} photons ml^{-1}. It was found from these results that the quantity and the selectivity of BD were much larger in KrF-laser irradiation than in steady state UV one. This indicates that the KrF-laser irradiation is favorable for the effective formation of BD.

Figure 4 shows the effects of H_2O_2 feeding rate on the quantities of 2,3-, 1,3-, 1,4-BD, and AA. The quantities of BD decreased with increasing H_2O_2 feeding rate, while that of AA increased. The sum of the quantities of 2,3-BD and AA was almost constant (40×10^{-2} mmol ml^{-1}) in the wide ranges of f=3.4—14.7 ml h^{-1}. The quantity of BD was much larger than that of AA in lower f ranges, on the contrary, in higher f ranges the former was smaller than the latter. The quantum yields of BD and AA formed were 0.42 and 0.29, respectively, at f=3.4 ml h^{-1}. The combined quantum yield of BD and AA formed and the combined selectiv-

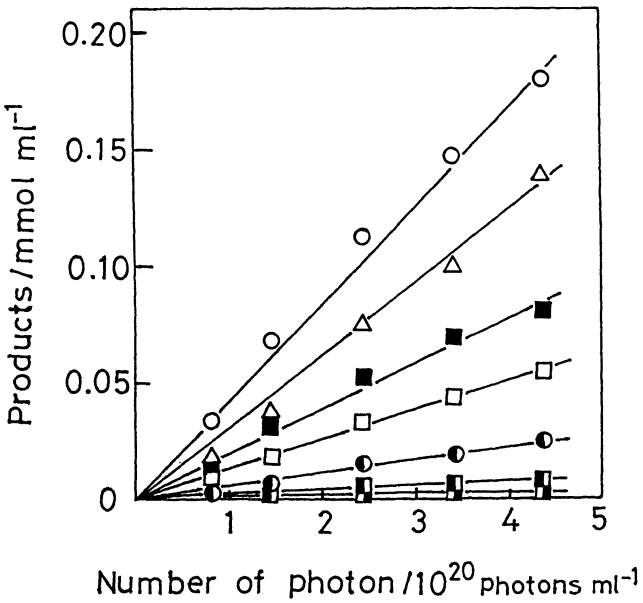

Fig. 5. Plots of the quantities of main products as a function of number of photon in the case of KrF-laser irradiation of N_2-saturated methanol-ethanol mixture.
○: 1,2-Propanediol, ◐: 1,3-Propanediol, □: 2,3-Butanediol, ◧: 1,3-Butanediol, ◨: 1,4-Butanediol, △: Ethylene glycol, ■: Acetaldehyde. Aqueous 30% H_2O_2 feeding rate: 3.6 ml h^{-1}. Methanol content: 66.7 mol%.

ity were 0.70—0.71 and 92—97%, respectively, in the wide f ranges. It was found from these results that BD and AA were directly and selectively synthesized by KrF-laser irradiation of the N_2-saturated EtOH containing H_2O_2. Such high combined quantum yield and selectivity indicate that the formations of BD and AA proceed efficiently in this system.

N_2-Saturated Methanol-Ethanol Mixture. When the N_2-saturated MeOH-EtOH mixture containing H_2O_2 was irradiated with the KrF laser, 1,2-PD, EG, 2,3-BD, and AA were produced as major products together with 1,3-PD, 1,3-BD, 1,4-BD, hydrogen, carbon dioxide, carbon monoxide, and methane as minor products. Figure 5 shows the quantities of main products as a function of number of photon at f=3.6 ml h^{-1}. The quantities of 1,2-PD, EG, 2,3-BD, 1,3-PD, 1,3-BD, 1,4-BD, and AA increased linearly with number of photon up to about 4.4×10^{20} photons ml^{-1}. The quantities of 1,2-PD, EG, 2,3-BD, 1,3-PD, 1,3-BD, 1,4-BD, and AA were 16.8, 12.8, 5.2, 2.2, 0.8, 0.3, and 7.8×10^{-2} mmol ml^{-1}, respectively, and the sum of the quantities of other products was less than 0.3×10^{-2} mmol ml^{-1} at irradiation of 4.0×10^{20} photons ml^{-1}.

On the other hand, in the case of steady state UV irradiation, the quantities of 1,2-PD, EG, 2,3-BD, and AA were 10.2, 9.4, 2.6, and 12.7×10^{-2} mmol ml^{-1}, respectively, at irradiation of 4.0×10^{20} photons ml^{-1}. It was found from these results that the quantities of PD, EG, and BD were much larger in KrF-laser irradiation than in steady state UV one. This indicates that the KrF-laser irradiation is favorable for the effective formation of PD, EG, and BD.

Figure 6 shows the effects of H_2O_2 feeding rate on the quantities of 1,2-PD, EG, 2,3-BD, and AA. The quantities of 1,2-PD, EG, and 2,3-BD decreased linearly with increasing H_2O_2 feeding rate, while that of AA increased. The quantities of 1,2-PD and EG were much larger than that of AA in lower f ranges, on the contrary, in higher f ranges the formers were smaller than the latter. This result indicates that the efficient formation of diols is favorable in lower f ranges.

Figure 7 shows the effects of MeOH content on the quantities of 1,2-PD, EG, 2,3-BD, and AA at f=3.6 ml h^{-1}. The quantity of 1,2-PD increased with MeOH content and reached the maximum at about 64 mol% of MeOH content. The quantity of EG increased linearly with MeOH content, while those of 2,3-BD and AA decreased. In the case of 64 mol% of MeOH content, the quantum yields of PD, EG, BD, and AA were 0.30, 0.17, 0.11, and 0.14, respectively, and the combined quantum yield was 0.72. The selectivities of 1,2-PD, EG, 2,3-BD, and AA were 36, 24, 13, and 19%, respectively, and the combined selectivity of diols and AA formation is 99%. It was found from these results that PD was directly synthesized by KrF-laser irradiation of the N_2-saturated MeOH-EtOH mixture containing H_2O_2. Such high combined quantum yield and selectivity indicate that the formation of diols such as PD, EG, and BD and AA proceeds efficiently in this system.

Reaction Mechanism. As described in the previous paper,[3] in the case of steady state UV irradiation of N_2-saturated MeOH containing H_2O_2, EG was produced

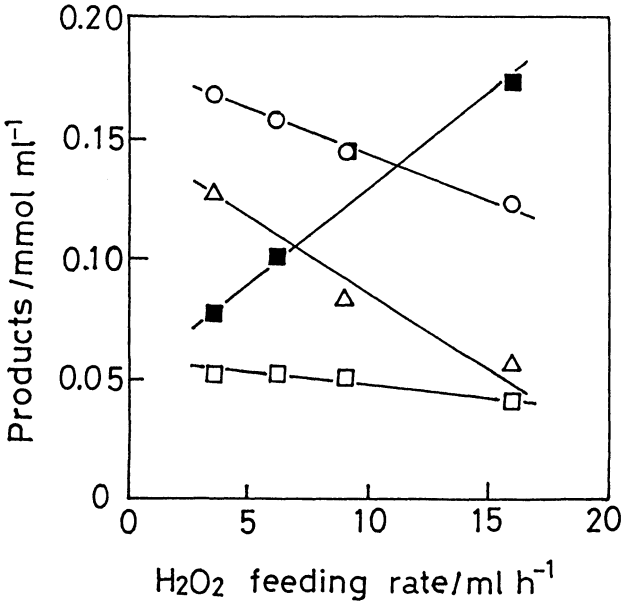

Fig. 6. Effects of H_2O_2 feeding rate on the quantities of main products in the case of KrF-laser irradiation of N_2-saturated methanol-ethanol mixture.
Symbols are the same as in Fig. 5. Number of photon: 4.0×10^{20} photons ml^{-1}. Methanol content: 66.7 mol%.

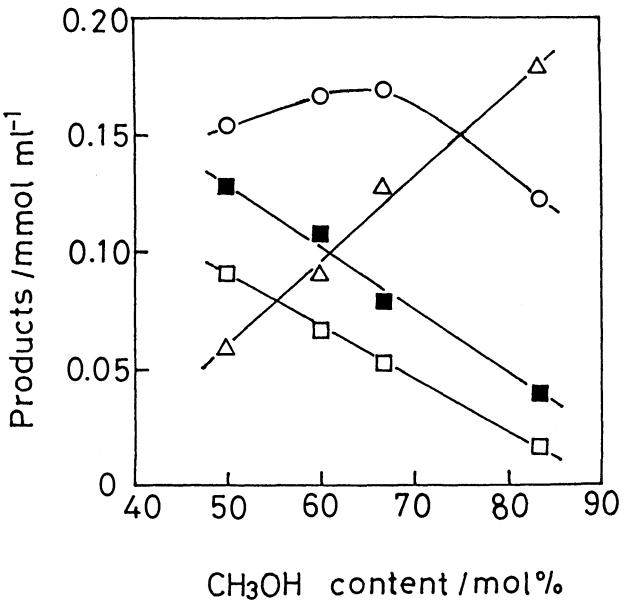

Fig. 7. Effects of methanol content on the quantities of main products in the case of KrF-laser irradiation of N_2-saturated methanol-ethanol mixture.
Symbols are the same as in Fig. 5. Aqueous 30% H_2O_2 feeding rate: 3.6 ml h^{-1}. Number of photon: 4.0×10^{20} photons ml^{-1}.

through the dimerization of hydroxymethyl radicals which were formed by the abstraction of a hydrogen atom from MeOH by hydroxyl radical formed by the photolysis of H_2O_2 as the reactions (1)—(3).

$$H_2O_2 \xrightarrow{h\nu} 2\cdot OH \quad (1)$$

$$CH_3OH + \cdot OH \longrightarrow \cdot CH_2OH + H_2O \quad (2)$$

$$2\cdot CH_2OH \longrightarrow (CH_2OH)_2 \quad (3)$$

The UV absorption spectrum of H_2O_2 gives a strong and very broad absorption band in the wavelength range of UV and vacuum UV regions below 300 nm. The absorbance of H_2O_2 at the wavelength of KrF laser (248 nm) is about 1.3 times that at the wavelength of steady state UV (253.7 nm). In analogy with the case of steady state UV irradiation,[6] H_2O_2 is very efficiently decomposed to form hydroxyl radicals by the laser irradiation. It can therefore be considered that in the case of KrF-laser irradiation of the N_2-saturated MeOH, EG would be produced through the reactions (1)—(3). As described already, quantum yield of EG formed was much larger in the KrF-laser irradiation than in steady state UV irradiation. The light intensity is about 10^7 times larger with the KrF laser than with the low-pressure mercury lamp. It is therefore considered that in KrF-laser irradiation, hydroxyl radical would be formed in high density (Eq. 1), and the abstraction of a hydrogen atom from MeOH occurs more efficiently (Eq. 2), followed by the effective dimerization of hydroxymethyl radicals (Eq. 3).

As shown in Table 1, the high quantum yield of EG formed was obtained in lower f ranges. In the case of f=3.2 ml h^{-1}, assuming the quantum yield of hydroxyl radical formed by the reaction (1) is 2.0,[6] 94% of hydroxyl radical formed is consumed to form EG. This indicates that most of hydroxyl radicals formed are very efficiently consumed by the reaction (2). It is therefore considered that such high quantum yield of EG formed in lower f ranges by KrF-laser irradiation is attributed to the effective dimerization of hydroxymethyl radical formed in high density. Also, in higher f ranges, the quantum yield of EG formed decreased. Since EG hardly has the absorption band at 248 nm, it is considered that the decrease of EG formation in higher f ranges is mainly attributed to the scavenging of hydroxyl radical by H_2O_2 to form hydroperoxyl radical (Eq. 4).[7]

$$H_2O_2 + \cdot OH \longrightarrow \cdot O_2H + H_2O \quad (4)$$

The hydroperoxyl radical formed by the reaction (4) reacts mainly with hydroxyl radical to form H_2O and O_2.[8]

In the case of KrF-laser irradiation of the N_2-saturated EtOH, the hydroxyl radical abstracts competitively α- or β-hydrogen atom from EtOH to form 1- or 2-hydroxyethyl radical (Eqs. 5 and 6).[9] It is therefore considered that 2,3- and 1,4-BD are produced by the dimerization of 1- and 2-hydroxyethyl radicals (Eqs. 7 and 8), respectively, and that 1,3-BD is produced by the recombination between 1- and 2-hydroxyethyl radicals (Eq. 9).

$$CH_3CH_2OH + \cdot OH \longrightarrow CH_3\dot{C}HOH + H_2O \quad (5)$$

$$CH_3CH_2OH + \cdot OH \longrightarrow \cdot CH_2CH_2OH + H_2O \quad (6)$$

$$2CH_3\dot{C}HOH \longrightarrow (CH_3CHOH)_2 \quad (7)$$

$$2\cdot CH_2CH_2OH \longrightarrow (CH_2CH_2OH)_2 \quad (8)$$

$$CH_3\dot{C}HOH + \cdot CH_2CH_2OH \longrightarrow CH_3CHOHCH_2CH_2OH \quad (9)$$

It is also considered that AA is mainly produced by the disproportionation of 1-hydroxyethyl radicals in competition with the dimerization (Eq. 10).[9,10]

$$2CH_3\dot{C}HOH \longrightarrow CH_3CHO + CH_3CH_2OH \quad (10)$$

The quantities of 2,3-, 1,3-BD, and AA formed via 1-hydroxyethyl radical were much larger than that of 1,4-BD formed via 2-hydroxyethyl radical. In the case of irradiation of 4.0×10^{20} photons ml^{-1}, the percentage of the quantity of products formed via 1-hydroxyethyl radical to that formed via 1- and 2-hydroxyethyl radicals was 91% at f=3.4 ml h^{-1}. This value is in excellent agreement with that (90%) obtained by the radiation-induced oxidation of aqueous EtOH solutions.[9] This supports the reaction mechanism for the formations of BD and AA in lower f ranges proposed above.

On the other hand, as shown in Fig. 4, the quantity of AA increased in higher f ranges. Assuming AA is produced by the reaction (10), the percentage of the quantity of products formed via 1-hydroxyethyl radical to that formed via 1- and 2-hydroxyethyl radicals was 94% at f=14.7 ml h^{-1} in the case of irradiation of 4.0×10^{20} photons ml^{-1}. This value is larger than that (91%) at f=3.4 ml h^{-1} described above. It is known that 1-hydroxyethyl radical reacts with H_2O_2 to form AA (Eq. 11).[9]

$$CH_3\dot{C}HOH + H_2O_2 \longrightarrow CH_3CHO + H_2O + \cdot OH \quad (11)$$

Assuming AA is produced by the reaction (11), the percentage of the quantity of products formed via 1-hydroxyethyl radical to that formed via 1- and 2-hydroxyethyl radicals was 91% at f=14.7 ml h^{-1} in the case of irradiation of 4.0×10^{20} photons ml^{-1}, and was in good agreement with the value (90%)[9] in reference. It is therefore considered from these results that AA is preferentially produced by the reaction (11) in higher f ranges.

In the case of KrF-laser irradiation of the N_2-saturated MeOH–EtOH mixture, the hydroxyl radical reacts with MeOH and EtOH to form hydroxymethyl, 1-, and 2-hydroxyethyl radicals. It is therefore considered that 1,2- and 1,3-PD are produced by the recombination between hydroxymethyl radical and 1-and 2-hydroxyethyl radicals (Eqs. 12 and 13), respectively.

$$\cdot CH_2OH + CH_3\dot{C}HOH \longrightarrow CH_3CHOHCH_2OH \quad (12)$$

$$\cdot CH_2OH + \cdot CH_2CH_2OH \longrightarrow HOCH_2CH_2CH_2OH \quad (13)$$

As shown in Fig. 7, the quantity of 1,2-PD reached a maximum at about 64 mol% of MeOH content. The ratio (1.7) of MeOH to EtOH at the maximum of 1,2-PD is in good agreement with the ratio ($k_{EtOH}/k_{MeOH}=1.5$)[11] of the rate constant of the abstraction of hydrogen atoms from MeOH and EtOH by hydroxyl radical. Also, the percentage of the quantity of 1,2-PD to that of total PD was 86% at irradiation of 4.0×10^{20} photons ml^{-1}. This value is close to the relative probability (90%)[9] of the abstraction of a hydrogen atom from α-position to that from β-position of EtOH by hydroxyl radical. These results support the reaction mechanism of the PD formation proposed above. Also, EG and 2,3-BD are produced by the dimerization of hydroxymethyl and 1-hydroxyethyl radicals, respectively, (Eqs. 3 and 7). AA is mainly produced by the disproportionation of 1-hydroxyethyl radicals in lower f ranges (Eq. 10) and the reaction of 1-hydroxyethyl radical with H_2O_2 in higher f ranges (Eq. 11).

References

1) "10889 No Kagaku Shohin," ed by the Kagaku Kogyo Nippo Sha, Tokyo (1989), p. 339, 416, 421; "Kagaku Binran, Oyo Kagaku," ed by the Chemical Society of Japan, Maruzen, Tokyo (1986), Part 1, p. 514.

2) Y. Shimizu, S. Sugimoto, and N. Suzuki, *Chem. Lett.*, **1989**, 333.

3) Y. Shimizu, S. Sugimoto, S. Kawanishi, and N. Suzuki, *Bull. Chem. Soc. Jpn.*, **63**, 97 (1990).

4) Y. Shimizu, S. Sugimoto, S. Kawanishi, and N. Suzuki, *Chem. Lett.*, **1989**, 2153.

5) Y. Shimizu, S. Sugimoto, S. Kawanishi, and N. Suzuki, *Chem. Lett.*, **1991**, 35.

6) F. S. Dainton and J. Rowbottom, *Trans. Faraday Soc.*, **49**, 1160 (1953).

7) L. F. Keyser, *J. Phys. Chem.*, **92**, 1193 (1988).

8) J. K. Thomas, *J. Phys. Chem.*, **67**, 2593 (1963).

9) C. E. Burchill and I. S. Ginns, *Can. J. Chem.*, **48**, 2628 (1970).

10) C. Anastasi, V. Simpson, J. Munk, and P. Pagsberg, *J. Phys. Chem.*, **94**, 6327 (1990).

11) "Kagaku Binran, Kiso" ed by the Chemical Society of Japan, Maruzen, Tokyo (1984), Part II, p. 423.

Molecular Motions of *t*-Butylammonium Ions and Structural Phase Transitions in Solid *t*-Butylammonium Perchlorate Studied by ^{1}H NMR and Thermal Measurements

Hiroyuki ISHIDA,* Tadashi IWACHIDO, Naomi HAYAMA,
Daiyu NAKAMURA,† and Ryuichi IKEDA††
Department of Chemistry, College of General Education, Okayama University, Okayama 700
†Department of Chemistry, Faculty of Science, Nagoya University, Nagoya 464-01
††Department of Chemistry, University of Tsukuba, Tsukuba 305
(Received June 25, 1991)

Differential thermal analysis (DTA), differential scanning calorimetry (DSC), and the temperature dependences of the ^{1}H spin-lattice relaxation time (T_1) and the second moment (M_2) of ^{1}H NMR absorptions were studied in $(CH_3)_3CNH_3ClO_4$ and its partially deuterated analogs, $(CH_3)_3CND_3ClO_4$ and $(CD_3)_3CNH_3ClO_4$. DTA and DSC studied revealed four solid phases, including a metastable phase, in the temperature range between 80 K and the melting point (414 K). The stable phases (named as I, II, and III) were obtained above 394 K, between 394 and 327 K, and below 327 K, respectively. The metastable phase II′, prepared by rapid cooling the phase II to ca. 100 K, exists below ca. 245 K. The cationic motions in each solid phase were studied by T_1 and M_2 experiments. Three kinds of motions (reorientations of the CH_3 groups about their C–C bond axes, the NH_3^+ group about its C–N bond axis, and the *t*-butyl group about the C–N bond axis) were observed in these phases and their motional parameters were determined

The solid methyl-substituted ammonium perchlorates, $(CH_3)_nNH_{4-n}ClO_4$ (n=1—4), are known to undergo polymorphic phase transitions which are interrelated with changes in the motional states of the cations and anions in crystals.[1-8] In the highest-temperature solid phases of these salts, both ions are in a highly disordered state, obtaining the greatest part of their motional freedom. Especially, in the phases of mono-, di-, and trimethylammonium perchlorates the cations were shown to perform rapid translational self-diffusion as well as isotropic rotation as a whole by NMR techniques.[2-4,6,7]

Since a *t*-butylammonium ion is expected to be easily movable in crystals because of its higher symmetry and more spherical shape than mono- and trimethylammonium ions, *t*-butylammonium perchlorate seems to be an interesting candidate for studying the relation between ionic motions and the polymorphic phase transitions expected to occur. The motions of *t*-butylammonium ions in a solid have been investigated by ^{1}H NMR techniques for *t*-butylamine tropolone adduct,[9] *t*-butylammonium halides,[10-12] and nitrate;[13] in these salts the cations have been found to be tightly fixed in the crystal lattice and to form fairly strong N–H···X type hydrogen bonds between the cation and the anion. Since a perchlorate ion is expected to form a hydrogen bond with a counter cation much weaker than halide ions, it is interesting to elucidate the molecular motions of the *t*-butylammonium ion expected to be more loosely bound in a crystal.

In the present study measurements of the temperature dependences of the ^{1}H spin-lattice relaxation time (T_1) and the second moment (M_2) of the ^{1}H NMR absorptions, differential thermal analysis (DTA), and differential scanning calorimetry (DSC) have been carried out for *t*-butylammonium perchlorate and its partially deuterated analogs to reveal the phase transitions, possible cationic motions, and their time scales in respective solid phases.

† Deceased on 27 February, 1991.

Experimental

^{1}H T_1 was determined at 32 and 8.5 MHz by means of a pulsed NMR spectrometer described elsewhere.[14] A 180°—τ—90° pulse sequence was employed. Continuous-wave ^{1}H NMR spectra were recorded at 40 MHz by using a JEOL JNM-MW-40S spectrometer. A home-made apparatus similar to that reported previously[15] was employed for DTA experiments. Differential scanning calorimetry (DSC) was carried out by use of a Perkin-Elmer 7 Series Thermal Analysis System.

$(CH_3)_3CNH_3ClO_4$ (abbreviated to (*t*-BA)ClO_4) was prepared by neutralizing *t*-butylamine with perchloric acid and recrystallized twice from isopropyl alcohol. $(CH_3)_3CND_3ClO_4$ ((*t*-BAd_3)ClO_4) was prepared from purified (*t*-BA)ClO_4 by repeated crystallization three times from heavy water and was finally purified by recrystallization from CH_3OD. $(CD_3)_3CNH_3ClO_4$ ((*t*-Bd_9A)ClO_4) was obtained from perchloric acid and $(CD_3)_3CNH_2$ purchased from MSD Isotopes and recrystallized from isopropyl alcohol. The obtained crystals were dried under high vacuum at room temperature for 24 h and then at ca. 50 °C for 24 h before elemental analysis and the measurements of NMR, DTA, and DSC. Calcd for $(CH_3)_3CNH_3ClO_4$: C, 27.67; H, 6.91; N, 8.07%. Found: C, 27.64; H, 6.82; N, 8.13%.

Results

DTA curves recorded for (*t*-BA)ClO_4 over the temperature range of 80—420 K are shown in Fig. 1. When the sample was heated from room temperature, three endothermic anomalies appeared at 327, 394, and

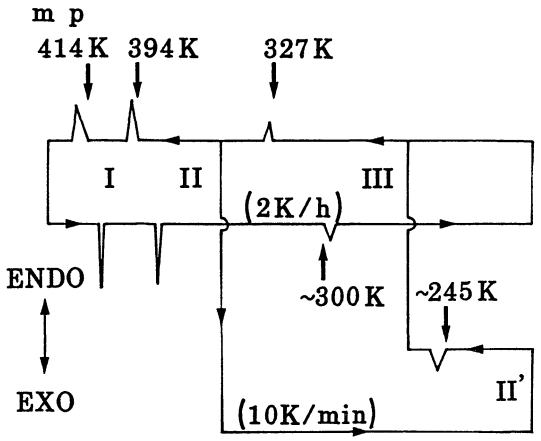

Fig. 1. DTA curves of $(CH_3)_3CNH_3ClO_4$. The cooling and heating rate is ca. 1 K min^{-1} unless otherwise noted. I, II, III, and II′ are the names of obtained solid phases.

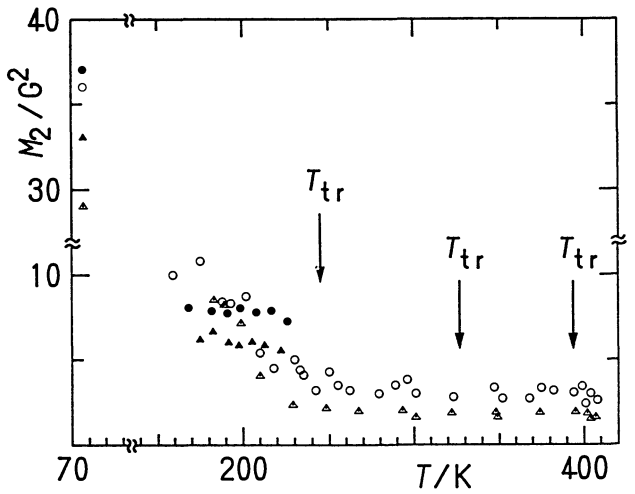

Fig. 2. Temperature dependence of the ^{1}H NMR second moment (M_2) observed for $(CH_3)_3CNH_3ClO_4$ (○ for phases I, II, and III; ● for phase II′) and $(CH_3)_3CND_3ClO_4$ (△ for I, II, and III; ▲ for II′). T_{tr}'s are transition temperatures determined for $(CH_3)_3CNH_3ClO_4$ by DTA.

414±1 K. The first two anomalies were attributed to solid-solid phase transitions and the last one to melting. The corresponding entropy changes determined by DSC were 6.9, 12, and 17 J K^{-1} mol^{-1}, respectively.

The phase obtained between 327 and 394 K could easily be supercooled down to ca. 100 K by cooling at a rate faster than 10 K min^{-1}. With increasing temperature of a rapidly cooled sample, an unusual exothermic anomaly appeared at ca. 245 K. The solid phases revealed by DTA are designated in the order of decreasing temperature as phases I, II, III, and II′, as shown in Fig. 1. The partially deuterated analogs, (*t*-BAd_3)ClO_4 and (*t*-Bd_9A)ClO_4, showed approximately the same DTA curves as in Fig. 1 and their transition temperatures are given in Figs. 4 and 5, respectively.

The temperature variation of M_2 observed for (*t*-BA)ClO_4 and (*t*-BAd_3)ClO_4 between 77 and 408 K is shown in Fig. 2. The M_2 values at 77 K determined for (*t*-BA)ClO_4 in phases III and II′ were 36 and 37±2 G^2 (1 G=1×10^{-4} T), respectively, while for (*t*-BAd_3)ClO_4, 33 and 29±2 G^2, they were of the same order. Between 170 and 220 K in phase II′, almost constant values of 7.8 and 5.9±0.3 G^2 were obtained for (*t*-BA)ClO_4 and (*t*-BAd_3)ClO_4, respectively. Above 240 K, the M_2 values for both salts were almost constant and no remarkable change was observed at the transition points, T_{tr}(III→II) and T_{tr}(II→I).

The temperature dependences of ^{1}H NMR T_1 determined at 32 and 8.5 MHz are shown in Figs. 3, 4, and 5 for (*t*-BA)ClO_4, (*t*-BAd_3)ClO_4, and (*t*-Bd_9A)ClO_4, respectively. When measured at 32 MHz, (*t*-BA)ClO_4 in phase III yielded three T_1 minima of 25, 42, and 51 ms located at 172, 235, and 323 K, respectively, while (*t*-BAd_3)ClO_4 exhibited two minima of 21 and 59 ms at 169 and 317 K, respectively. Regarding (*t*-Bd_9A)ClO_4, a T_1 minimum of 13 ms was observed at 244 K.

(*t*-BA)ClO_4 and (*t*-BAd_3)ClO_4 in phase II′ gave a broad and asymmetric T_1 minimum, considered to have resulted from superimposed two or more minima. From the T_1 data observed for (*t*-Bd_9A)ClO_4 at 8.5

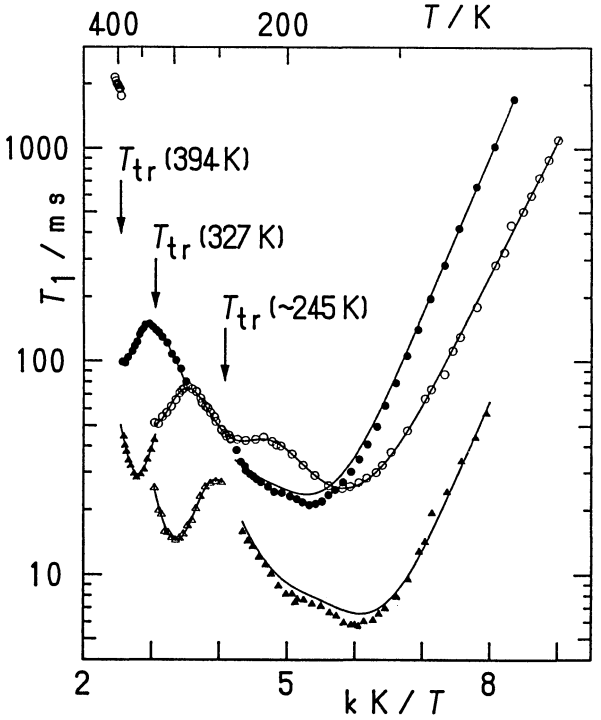

Fig. 3. Temperature dependence of the spin-lattice relaxation time (T_1) observed at 8.5 MHz (△ for phase III; ▲ for phases II and II′) and 32 MHz (○ for I and III; ● for II and II′) in $(CH_3)_3CNH_3ClO_4$. The solid lines in phases II and III indicate the best-fit theoretical values, whereas the lines in phase II′ are the calculated T_1 curves using the motional parameters determined for $(CH_3)_3CND_3ClO_4$ and $(CD_3)_3CNH_3ClO_4$.

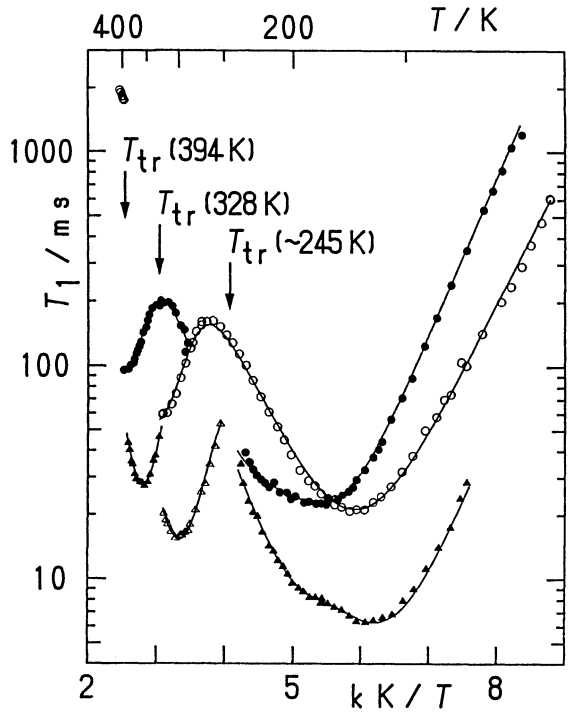

Fig. 4. Temperature dependence of the spin-lattice relaxation time (T_1) observed at 8.5 MHz (△ for phase III; ▲ for phases II and II') and 32 MHz (○ for I and III; ● for II and II') in $(CH_3)_3CND_3ClO_4$. T_{tr}'s are transition temperatures determined for $(CH_3)_3CND_3ClO_4$ by DTA. The solid lines indicate the best-fit theoretical values.

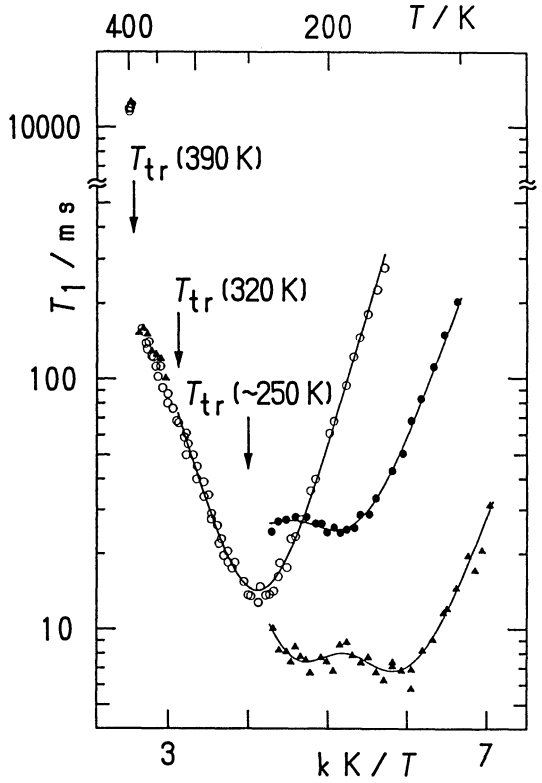

Fig. 5. Temperature dependence of the spin-lattice relaxation time (T_1) observed at 8.5 (▲) and 32 MHz (○ for phases I, II, and III; ● for phase II') in $(CD_3)_3CNH_3ClO_4$. T_{tr}'s are transition temperatures determined for $(CD_3)_3CNH_3ClO_4$ by DTA. Solid lines indicate the best-fit theoretical values.

MHz, two minima could be distinguished at 170 and 210 K.

A sudden increase of T_1 was observed for (*t*-BA)ClO_4 and (*t*-BAd_3)ClO_4 at T_{tr}(III→II), above which temperature each salt measured at 8.5 MHz showed a minimum at almost the same temperature (360 K) in phase II. T_1 of (*t*-Bd_9A)ClO_4 showed no remarkable discontinuity at the transition and increased with temperature in phase II; the gradient of T_1 vs. T^{-1} plots in this phase is slightly gentler than in phase III. At T_{tr}(II→I), of all salts increased discontinuously. In phase I, T_1 of (*t*-BA)ClO_4 and (*t*-BAd_3)ClO_4 increased with temperature, whereas a decrease of T_1 was observed for (*t*-Bd_9A)ClO_4. T_1 of each salt measured at 32 and 8.5 MHz gave the same values within the experimental error.

Discussion

Second Moments of ^{1}H NMR Absorptions. To interpret the M_2 values obtained for (*t*-BA)ClO_4 and (*t*-BAd_3)ClO_4, we calculated the M_2 values for the following motional states of the cation: 1) the rigid lattice, 2) the C_3 reorientations of the three CH_3 groups about the respective C–C bond axes, 3) the C_3 reorientation of the NH_3^+ group about the C–N bond axis in addition to the CH_3 reorientations, and 4) the C_3' reorientation of the *t*-butyl group about the C–N bond axis together with the NH_3^+ and CH_3 reorientations. Since no crystal data are available for this salt, we calculated the M_2 values arising from only intra-cationic magnetic dipole-dipole interactions. In the calculation, the bond distances of C–C, C–N, C–H, and N–H were taken to be 1.54, 1.47, 1.10, and 1.04 Å, respectively;[16,17] all bond angles were assumed to be tetrahedral. The calculated values for the above-mentioned motional modes are given in Table 1 for both *t*-BA^+ and *t*-BAd_3^+ cations.

By comparing the observed M_2 values with the calculated ones, the cations are expected to be rigid at 77 K in phases III and II'. The differences between the

Table 1. Second Moments (M_2/G^2) of ^{1}H NMR Absorptions Calculated for $(CH_3)_3CNH_3^+$ and $(CH_3)_3CND_3^+$ Cations

	$(CH_3)_3CNH_3^+$	$(CH_3)_3CND_3^+$
Rigid	25.7	22.7
CH_3 Reorientation	12.7	6.0
CH_3 and NH_3^+ Reorientation	7.0	6.0
CH_3, NH_3^+, and *t*-Butyl Reorientation	3.8	2.3

observed and calculated values seem to be attributable to intermolecular contributions. The almost constant values of M_2 observed between 170 and 220 K in phase II′ can be explained by a model of the C_3 reorientations of the CH_3 and NH_3^+ groups. Above ca. 240 K, the cations are considered to undergo the C_3 reorientations of the CH_3 and NH_3^+ groups as well as the C_3' reorientation of the *t*-butyl group. The M_2 values of 3.3±0.3 and 2.0±0.2 G^2 obtalned for (*t*-BA)ClO_4 and (*t*-BAd_3)ClO_4, respectively, above 240 K are, however, somewhat smaller than the calculated values for this motional model. This implies the existence of additional cationic motions which are activated even below 240 K. The large-amplitude librations of the cation about the C–C and C–N axes can be thought of as one such motional mode. In fact, a large-amplitude torsional motion of the cation about the C–N axis has been reported from an X-ray diffraction study of $(CH_3)_3CNH_3Cl$.[18] Since a ClO_4^- ion forms the hydrogen bond with a cation weaker than a Cl^- ion, it is expected that the cation in perchlorate librates more freely with a much larger amplitude.

The observed entropy changes (ΔS_{tr}) at T_{tr}(III→II) and T_{tr}(II→I) were considerably large, and the sum of the two ΔS_{tr} (ca. 19 $J K^{-1} mol^{-1}$) was comparable with each ΔS_{tr} value at the two transitions reported for $CH_3NH_3ClO_4$.[3] This salt undergoes two solid–solid phase transitions at 321 K (ΔS_{tr}=20.9 $J K^{-1} mol^{-1}$) and 451 K (ΔS_{tr}=16.9 $J K^{-1} mol^{-1}$) and then transforms into a plastic phase in which both cations and anions are freely movable, like in liquid phase. It has been revealed that, at both low- and high-temperature transitions, the anions and the cations, respectively, acquire the greatest part of their motional freedom.[1–5,19] One might expect, accordingly, that the cations and/or the anions in (*t*-BA)ClO_4 also obtain motional freedom to a similar extent through these two transitions. Since the motional state of the *t*-BA^+ cations is thought to be little affected at both transitions, where no marked decrease in M_2 was observed, the increase in motional freedom probably occurs only in the anions and, hence, the isotropic rotation of the anions is expected in phase I.

Room-Temperature Phase (III). Referring to the above discussion on M_2, we can assign the T_1 minimum at 240 K observed for (*t*-Bd_9A)ClO_4 to the C_3 reorientation of the NH_3^+ group. For this motion, ^1H T_1 can be expressed as[20]

$$T_1^{-1} = Cf(\tau), \tag{1}$$

$$C = (9/20)\gamma^4\hbar^2 r^{-6} \tag{2}$$

and

$$f(\tau) = \tau/(1+\omega^2\tau^2) + 4\tau/(1+4\omega^2\tau^2). \tag{3}$$

Here, γ, r, τ, and ω denote the gyromagnetic ratio of a proton, the inter-proton distance in the NH_3^+ group, the correlation time of the motion, and the angular resonance frequency, respectively. Assuming an Arrhenius-type relationship between τ and the activation energy (E_a) for the reorientation process, one obtains

$$\tau = \tau_0 \exp(E_a/RT), \tag{4}$$

where τ_0 is the correlation time at infinite temperature. Eqs. 1—4 were fitted to the T_1 data obtained for (*t*-Bd_9A)ClO_4 using a least-squares method. The optimum values of E_a, τ_0, and C obtained are listed in Table 2.

Table 2. Motional Parameters of *t*-Butylammonium Ions in $(CH_3)_3CNH_3ClO_4$, $(CH_3)_3CND_3ClO_4$, and $(CD_3)_3CNH_3ClO_4$

Compound	E_a/kJ mol^{-1}	τ_0/10^{-13} s	C/10^9 s^{-2}	Reorienting group
$(CH_3)_3CNH_3ClO_4$				
Phase I	17.3±0.5	—	—	*t*-Butyl
Phase II	41.1±0.5	0.12±0.03	1.1±0.1	*t*-Butyl(1)
	14.9±0.2	—	—	*t*-Butyl(2) and NH_3^+
Phase III	12.1±0.1	6.2 ±0.2	5.5±0.1	CH_3
	21.8±0.4	0.53±0.10	2.1±0.1	NH_3^+
	32.3±0.4	0.26±0.04	2.4±0.2	*t*-Butyl
Phase II′	14.6±0.5	—	—	CH_3 and NH_3^+
$(CH_3)_3CND_3ClO_4$				
Phase I	17.3±0.5	—	—	*t*-Butyl
Phase II	44.1±0.7	0.05±0.01	1.3±0.1	*t*-Butyl(1)
	15.3±0.5	—	—	*t*-Butyl(2)
Phase III	12.0±0.1	6.0 ±0.3	6.6±0.1	CH_3
	32.4±0.4	0.26±0.05	2.4±0.3	*t*-Butyl
Phase II′	14.1±0.1	2.6 ±0.3	5.4±0.1	CH_3(1)
	17.3±0.5	2.7 ±0.7	2.7±0.1	CH_3(2)
$(CD_3)_3CNH_3ClO_4$				
Phase II	14.8±0.8	—	—	NH_3^+
Phase III	20.1±0.2	1.5 ±0.2	9.9±0.2	NH_3^+
Phase II′	16.1±0.3	1.3 ±0.3	5.0±0.2	NH_3^+(1)
	19.6±1.0	2.2 ±0.2	4.1±0.2	NH_3^+(2)

The T_1 minimum at 172 K observed for $(t\text{-BA}d_3)ClO_4$ is attributable to the C_3 reorientation of all CH_3 groups in the cation, and the T_1 minima around 310 K observed at 8.5 and 32 MHz to the C_3' reorientation of the *t*-butyl group from the above discussion on M_2. Since the T_1 minima arising from the reorientations of the CH_3 and *t*-butyl groups are well separated, the correlation time (τ_1) for the CH_3 group motion is considered to be much shorter than that (τ_2) for the *t*-butyl group, i.e., $\tau_1 \ll \tau_2$. Thus, assuming that all CH_3 groups in this phase are crystallographically equivalent, we can express ^1H T_1 for these two motions by the sum of the two BBP equations associated with the CH_3 and the *t*-butyl group motions:[10,21,22]

$$T_1^{-1} = C(\text{Me})f(\tau_1) + C(\text{Bu})f(\tau_2), \quad (5)$$

$$C(\text{Me}) = (9/80)\gamma^4\hbar^2 r^{-6}\{(3/2)\sin^4\delta + (1/2)(8-3\sin^4\delta)\}, \quad (6a)$$

and

$$C(\text{Bu}) = \gamma^4\hbar^2\{(9/80)\, r^{-6}(\sin^2 2\delta + \sin^4\delta) + (27/20)R^{-6}\}. \quad (6b)$$

Here, C(Me) and C(Bu), r, R, and δ are the motional constants, the interproton distance in a CH_3 group, the distance between the centers of three protons in each CH_3 group, and the angle between C–C and C–N bonds, respectively. Employing an Arrhenius-type relationship as given by Eq. 4 for these two motions, the activation energies, the correlation times at infinite temperature, and the motional constants could be obtained for $(t\text{-BA}d_3)ClO_4$ by a fitting calculation of Eqs. 5 and 6 to the observed T_1 data. The best-fit motional parameters are listed in Table 2. Good agreement between the observed and calculated T_1 was obtained, as shown in Fig. 4.

From the above discussion on the two deuterated analogs, three well separated T_1 minima of $(t\text{-BA})ClO_4$ located at 172, 235, and 323 K can be assigned to the reorientations of the CH_3, NH_3^+, and *t*-butyl groups, respectively. T_1 for $(t\text{-BA})ClO_4$ can be expressed as

$$T_1^{-1} = (3/4)\{T_1(t\text{-BA}d_3)\}^{-1} + (1/4)\{T_1(t\text{-B}d_9\text{A})\}^{-1}, \quad (7)$$

where $T_1(t\text{-BA}d_3)$ and $T_1(t\text{-B}d_9\text{A})$ are given by Eqs. 5 and 1, respectively. A fitting calculation to the T_1 data of $(t\text{-BA})ClO_4$ was carried out using Eqs. 4 and 7. The results are given in Table 2.

The large activation energy (32.3 kJ mol^{-1}) obtained for the *t*-butyl reorientation implies that the cations were tightly packed in the crystal. Comparable activation energies of 26.9—32.6 kJ mol^{-1} were reported for *t*-BA bromide and iodide.[10,11] This result is reasonable in view of these three kinds of anions with about the same size and shape. E_a=12.1 kJ mol^{-1} for the CH_3 reorientation is also comparable with 9.8—11.7 kJ mol^{-1} for the less hindered CH_3 groups in the *t*-BA cation in halides.[10,11] E_a=21.8 kJ mol^{-1} for the NH_3^+ group, on the other hand, is considerably smaller than 27.3[23]—44.2 kJ mol^{-1} for the same motion in halides.[10,12] This is explainable in terms of a weak hydrogen bond of the N–H···O type formed in perchlorate; E_a in the present perchlorate, however, is much larger than 2—5 and 2—3 kJ mol^{-1} for the NH_3^+ reorientation in $CH_3NH_3ClO_4$[2-4] and for the NH_4^+ reorientation in NH_4ClO_4,[24-26] respectively, the values of which are regarded as being typical examples for perchlorates containing very weak hydrogen bonds. Accordingly, we suppose in the present salt, besides the hydrogen bonding, interionic steric interactions due to tightly packed cations and anions also give a considerable contribution to the barrier for NH_3^+ rotation.

Metastable Phase (II'). The T_1 minima observed for $(t\text{-B}d_9\text{A})ClO_4$ can be attributed to the C_3 reorientation of the NH_3^+ group. Since the two T_1 minima having almost the same values were obtained at 8.5 MHz, it is expected that there exist two crystallographically nonequivalent cations in this phase with an abundance ratio of 1 : 1. ^1H T_1 for the present motion can be expressed by superimposed two BPP equations, as

$$T_1^{-1} = C_1 f(\tau_1) + C_2 f(\tau_2). \quad (8)$$

A fitting calculation was made by use of Eqs. 8 and 4, and the results are shown in Table 2.

The broad and asymmetric T_1 minimum of $(t\text{-BA}d_3)ClO_4$ can be explained in terms of the C_3 reorientation of the nonequivalent CH_3 groups by referring to the M_2 results. When we assume two kinds of CH_3 groups in this phase, an equation similar to Eq. 8 can be used to analyze the T_1 data. A fitting calculation using this equation was successful as is shown in Fig. 4; its results are listed in Table 2. We obtained $C_1 = 5.4\times10^9$ and $C_2 = 2.7\times10^9$ s^{-2} as the optimum values for the motional constants; this implies that the nonequivalent CH_3 groups can be classified into two groups with an abundance ratio of 2 : 1. Since two kinds of cations have been revealed to exist in phase II' from the results of $(t\text{-B}d_9\text{A})ClO_4$, the above results can be interpreted in terms of one of the following two models: 1) each cation includes two kinds of nonequivalent CH_3 groups, and 2) one cation contains three equivalent CH_3 groups, while the other has nonequivalent CH_3 groups (2 : 1), one of which is embedded in almost the same circumstance as the former three CH_3 groups.

From the results of the partially deuterated analogs, the broad T_1 minimum in $(t\text{-BA})ClO_4$ is considered as resulting from at least four T_1 successively overlapped minima, two of which are attributed to CH_3 motions and the other two to NH_3^+ motions. Thus, T_1 of $(t\text{-BA})ClO_4$ can be written using a formula similar to Eq. 7, where both $T_1(t\text{-BA}d_3)$ and $T_1(t\text{-B}d_9\text{A})$ consist of two BBP equations as given by Eq. 8. Since it is difficult to fit this equation to the present data owing to too many adjustable parameters, we only evaluated the activation energy for the CH_3 and NH_3^+ reorientations from the slope of ln T_1 vs. T^{-1} plots below 150 K. In Fig. 3, the calculated T_1 curves using Eq. 7 by substituting

the parameters obtained for (*t*-BAd_3)ClO_4 and (*t*-Bd_9A)ClO_4 are shown. The agreement between the experimental and calculated T_1 is satisfactory.

It is interesting to compare the activation energies for the CH_3 and NH_3^+ groups in phase II′ with those in phase III. Table 2 shows that the activation energies of the CH_3 groups in the metastable phase (phase II′) are higher than that in the stable phase (phase III), whereas those of NH_3^+ are lower in phase II′ than in phase III. The same relation of the activation energies between metastable and stable phases is found in *t*-BA nitrate, where three solid phases (one stable and two metastable) exist below 254 K, between 95 and 350 K, and below 235 K, respectively.[13]

Intermediate Phase(II). The T_1 increase of (*t*-Bd_9A)-ClO_4 with temperature in phase II is attributed to the NH_3^+ reorientation, the activation energy of which evaluated from the slope of T_1 curve is smaller than that in phase III. Since no discontinuous change in T_1 of (*t*-Bd_9A)ClO_4 was observed at T_{tr}(III→II) determined by DTA, the reorientation of the NH_3^+ group is little affected at this transition.

On the other hand, (*t*-BAd_3)ClO_4 showed a sudden increase of T_1 at T_{tr}(III→II), above which temperature this salt yielded a T_1 maximum and a minimum at 32 MHz; measurements at 8.5 MHz gave only a minimum in phase II. From these results, we can expect the presence of the following two kinds of cationic motions which contribute to in T_1 in this phase of (*t*-BAd_3)ClO_4: 1) the motion assignable to the T_1 minima observed at 32 and 8.5 MHz, and 2) the other contributing to T_1 at 32 MHz, mainly in the low-temperature range of the T_1 maximum. Referring to the M_2 results, both of these motions can be regarded as the *t*-butyl reorientation, since the CH_3 group motion is considered to be too frequent to affect T_1 in this phase as predicted from the T_1 results in phase III. This means that there exist two kinds of *t*-butyl groups, or two kinds of cations; the T_1 minimum can be attributed to one of the two kinds of *t*-butyl groups and the T_1 decrease observed in the high-temperature side of the maximum to the motion of the other. This interpretation is supported by the fact that the minimum value of 28 ms observed at 8.5 MHz in this phase is almost twice as large as that of 15 ms in phase III; this minimum was assigned to the motions of all *t*-butyl groups in the crystal.

When the motion of one of the *t*-butyl groups contributing to T_1 at the high temperature range in phase II is sufficiently fast to allow the narrowing limit $\omega\tau_f \ll 1$, where τ_f is the correlation time for this motion, T_1 can be expressed by modifying the Eq. 8 as

$$T_1^{-1} = C_s f(\tau_s) + 5C_f\tau_f. \quad (9)$$

Here, τ_s, C_s, and C_f are the correlation time for the motion yielding the T_1 minimum, the motional constant for this motion, and that for the fast motion, respectively. Assuming an Arrhenius relationship, like that given by Eq. 4, for the two motions, we calculated the motional parameters for (*t*-BAd_3)ClO_4 listed in Table 2 by fitting Eqs. 4 and 9 to the observed T_1 data. It is interesting to note that at T_{tr}(III→II) the cations considered to be equivalent in phase III become nonequivalent and that the C_3' reorientation of half the *t*-butyl groups is slowed down while the other half is accelerated. Further, the cations in phase II seem to be disordered statically rather than dynamically. Even if the cations are dynamically disordered, the jumping rate between the disordered sites of the cations is much slower than the ^1H NMR frequency.

The T_1 minimum of (*t*-BA)ClO_4 can be assigned to the reorientation of one of the two kinds of *t*-butyl groups in accordance with the results regarding its partially deuterated analogs. T_1 in the high-temperature side of the T_1 maximum observed at 32 MHz is attributable to the reorientations of the other *t*-butyl group and the NH_3^+ group. Parameters for these motions were obtained by a fitting calculation using an equation such as that given by Eq. 9.

High-Temperature Phase (I). At T_{tr}(II→I), T_1 of all salts increased discontinuously. Since no marked change in M_2 was observed around this temperature, the discontinuous increase of T_1 is ascribable to sudden decreases in the correlation times of the NH_3^+ and *t*-butyl groups. In phase I of (*t*-BA)ClO_4 and (*t*-BAd_3)ClO_4, the *t*-butyl motion is considered to be a dominant relaxation process. The activation energies for this motion in both salts were estimated as 17.3 kJ mol^{-1} from the slope of the $\ln T_1$ *vs.* T^{-1} curves. This value is quite small as compared with that in *t*-BA halides, indicating that the cation is loosely packed in this phase.

T_1 of (*t*-Bd_9A)ClO_4 in phase I is very long and decreases with increasing temperature. This implies that the motion of the NH_3^+ group is too fast to have any discernible influence on T_1, and that another relaxation process is dominant in this region. Since no marked frequency dependence of T_1 was observed, one of the possible processes is a spin-rotation interaction[24,27-29] due to rapid rotation of the NH_3^+ group.

It is somewhat surprising that the onset of the isotropic rotation of the cation is hindered even in the highest-temperature phase, although the *t*-BA^+ cations packed with globular ClO_4^- anions are expected to be easily rotatable due to their sphere-like shape. In the highest-temperature phase of (*t*-BA)NO_3 crystals involving non-spherical anions, on the contrary, the cations are revealed to perform isotropic rotation and translational self-diffusion.[13]

References

1) M. Stammler, R. Bruenner, W. Schmidt, and D. Orcutt, *Adv. X-Ray Anal.*, **9**, 170 (1966).

2) H. Ishida, R. Ikeda, and D. Nakamura, *Chem. Lett.*, **1982**, 1943.

3) S. Jurga and H. W. Spiess, *Z. Naturforsch., Teil A*, **40**, 602 (1985).

4) H. Ishida, R. Ikeda, and D. Nakamura, *Bull. Chem. Soc. Jpn.*, **60**, 467 (1987).
5) S. Jurga, J. Seliger, R. Blinc, and H. W. Spiess, *Phys. Lett. A*, **116**, 295 (1986).
6) S. Jurga and H. W. Spiess, *Ber. Bunsen-Ges. Phys. Chem.*, **89**, 763 (1985).
7) S. Jurga, *Phys. Status Solidi A*, **81**, 77 (1984).
8) S. Jurga, G. S. Harbison, B. Blümich, H. W. Spiess, F. Fujara, and A. Olinger, *Ber. Bunsen-Ges. Phys. Chem.*, **90**, 1153 (1986).
9) C. A. McDowell, P. Raghunathan, and D. S. Williams, *J. Magn. Reson.*, **24**, 113 (1976).
10) C. I. Ratcliffe and B. A. Dunell, *J. Chem. Soc., Faraday Trans. 2*, **73**, 493 (1977).
11) R. Konieczka and Z. Pajak, *J. Chem. Soc., Faraday Trans. 2*, **77**, 2041 (1981).
12) H. Ishida, S. Inada, N. Hayama, D. Nakamura, and R. Ikeda, *Z. Naturforsch., Teil A*, **46**, 265 (1991).
13) H. Ishida, T. Iwachido, N. Hayama, R. Ikeda, M. Hashimoto, and D. Nakamura, *Z. Naturforsch., Teil A*, **44**, 71 (1989).
14) H. Ishida, T. Iwachido, N. Hayama, R. Ikeda, M. Terashima, and D. Nakamura, *Z. Naturforsch., Teil A*, **44**, 741 (1989).
15) Y. Kume, R. Ikeda, and D. Nakamura, *J. Magn. Reson.*, **33**, 331 (1979).
16) E. R. Andrew and P. C. Canepa, *J. Magn. Reson.*, **7**, 429 (1972).
17) J. Tsau and D. F. R. Gilson, *Can. J. Chem.*, **51**, 1990 (1973).
18) K. N. Trueblood, *Acta Crystallogr., Sect. C*, **43**, 711 (1987).
19) N. G. Parsonage and L. A. K. Staveley, "Disorder in Crystals," Clarendon Press, Oxford (1978), Chap. 7.
20) A. Abragam, "The Principles of Nuclear Magnetism," Oxford University Press, London (1961), Chap. VIII.
21) M. B. Dunn and C. A. McDowell, *Mol. Phys.*, **24**, 969 (1972).
22) S. Albert, H. S. Gutowsky, and J. A. Ripmeester, *J. Chem. Phys.*, **56**, 3672 (1972).
23) This activation energy for the NH_3^+ reorientation evaluated from the T_1 data of (*t*-BA)I and (*t*-BAd_3)I by Ratcliffe and Dunell[10] is considered to be underestimated because it is difficult to evaluate accurately the activation energy from overlapped T_1 minima due to the *t*-butyl and NH_3^+ reorientations as tried by these authors. A discussion about this was made in our previous paper[12] where the E_a values for the NH_3^+ group in *t*-butylammonium chloride and bromide were determined directly from the T_1 data of (*t*-Bd_9A)Cl and (*t*-Bd_9A)Br.
24) R. Ikeda and C. A. McDowell, *Chem. Phys. Lett.*, **14**, 389 (1972).
25) J. W. Riehl, R. Wang, and H. W. Bernard, *J. Chem. Phys.*, **58**, 508 (1973).
26) W. Güttler and J. U. Von Schütz, *Chem. Phys. Lett.*, **20**, 133 (1973), and references therein.
27) R. J. C. Brown, H. S. Gutowsky, and K. Shimomura, *J. Chem. Phys.*, **38**, 76 (1963).
28) P. S. Hubbard, *Phys. Rev.*, **131**, 1155 (1963).
29) J. H. Rugheimer and P. S. Hubbard, *J. Chem. Phys.*, **39**, 552 (1963).

 © 1991 The Chemical Society of Japan Bull. Chem. Soc. Jpn., 64, 3620—3626 (1991) [Vol. 64, No. 12

ENDOR and TRIPLE Studies of Diphenyl Nitroxide (DPNO)

Jun YAMAUCHI,* Hideo FUJITA, and Yasuo DEGUCHI
College of Liberal Arts and Sciences, Kyoto University, Kyoto 606
(Received July 8, 1991)

ENDOR and triple resonance (GTR) of diphenyl nitroxide (DPNO) were observed in solution; it was demonstrated that DPNO is an interesting model radical forming a three-spin system (electron and ^{1}H- and ^{14}N-nuclear spins). The detected ^{14}N-ENDOR belongs to one of the smallest hyperfine cases (A_N=0.9653 mT). Its optimum temperature was 210 K, higher than that of the ^{1}H, which is due to the large anisotropic hyperfine interaction of ^{14}N. In the ^{1}H-ENDOR spectra the effect of cross relaxation was observed, as in the case of the ^{14}N-ENDOR lines; their temperature variations of intensity showed two maximum regions, one due to the optimum energy relaxation in the ^{14}N-spin system and the other due to the energy relaxation inherent in the ^{1}H-spin system. In the triple studies new phenomena were pointed out: An enhancement saturation effect due to the large hyperfine interaction and an intensified enhancement or de-enhancement effect due to the cross relaxation.

In investigations of electron spin resonance (ESR) spectroscopy and its applications to chemistry, diphenyl nitroxide (DPNO) has been used as a model radical for a few decades. The reason may be that DPNO is not only facile in handling, but also it can afford an interesting spin system consisting of an electron spin and two nuclear spins, ^{1}H and ^{14}N. ESR experiments of DPNO were first performed using single crystals, and some variations of exchange narrowed lines were measured by changing the magnitude of magnetic dilution in crystals.[1] Then, well-resolved ^{1}H-hyperfine spectra were observed in order to calculate the linewidth of each hyperfine line.[2] It was also reported that dissolved oxygen in solvents plays a remarkable negative role in diminishing the ^{1}H-hyperfine lines.[3] Some of the present authors et al. have investigated the repulsion scheme between the two ortho-protons of DPNO and the effect of methyl substitution on the ortho-positions of DPNO.[4]

In an electron-nuclear double-resonance (ENDOR) study, on the other hand, DPNO and its methyl derivatives have been investigated in detail from the point of view of steric hindrance.[5] An extension of ENDOR to a general triple resonance (GTR) for DPNO has been attempted in order to assure a negative spin density on the carbon atoms at the meta-positions of DPNO, demonstrating the typical GTR behavior in the spectral intensity change.[6] In these double- and triple-resonance investigations, no ^{14}N signals or a responce have been observed, in spite of the largest hyperfine coupling constant (A_N=0.965 mT) in this system.

Some nitroxide radicals have been investigated extensively with regard to ^{14}N-ENDOR detections.[7] The first observation was accomplished by Leniart et al. for some alicyclic nitroxide radicals.[8] We recently reported on ^{1}H- and ^{14}N-ENDOR studies of *t*-butylphenyl nitroxide (BPNO).[9] In these investigations, the characteristic features in ^{14}N-ENDOR were pointed out, such as cross relaxations in the ^{14}N-ENDOR and the influence of the ^{14}N-spin quantum number on the ^{1}H-ENDOR patterns. In this report we focus attention on ^{14}N-ENDOR observations of DPNO, the temperature dependences of the ^{14}N- and ^{1}H-ENDOR lines, and the ^{1}H-GTR characteristics of the radio-frequency power variations; we discuss especially how the ^{1}H-ENDOR and GTR are influenced by the ^{14}N-spin system. Success involving the ^{14}N-ENDOR detection would again shed light on DPNO as an interesting model sample in both double- and triple-resonance spectroscopies, in which three interacting spins (the electron spin and ^{1}H- and ^{14}N-nuclear spins) play an important role in the energy relaxations.

Experimental

Samples were synthesized as described in a previous paper.[4] For the ENDOR measurements, freshly prepared DPNO gave satisfactory results. Therefore, we used the following procedure. The synthesized DPNO was diluted magnetically in a diamagnetic matrix of benzophenone; this solid solution was kept in a refrigerator. Just before sampling for the measurements, pure DPNO was separated by chromatography.

A broad-band ENDOR spectrometer equipped with a TM_{110} mode cavity was used as described previously.[5] Two signal generators, i.e. HP8601A (Hewlett-Packard) and VP-8179B10 (National), were used for scanning the radio-frequency with FM modulation (6.5 kHz) and pumping the radio-frequency without FM modulation, respectively.[6] The experimental conditions of the multiple resonances are as follows: for the ^{14}N-ENDOR observed at 220 K, a microwave power of 20 mW and a radio-frequency power of 100 W were used; for the ^{1}H-GTR measured at 180 K, a microwave power of 20 mW and a scanning radio-frequency power of 80 W were used. The pumping radio-frequency power was changed between 0—100 W. Ethylbenzene or toluene was used as a solvent and the temperature was controlled by a JEOL ES-DVT2 between 160—230 K.

Results

In the ENDOR measurements, although two pairs of ^{1}H signals centered at the free-proton frequency (14.196 MHz) were usually detected within the observed temperature region, the optimum temperature was found to be

180 K (see Fig. 2 in the literature[6]).

The inner pair at 13.044 and 15.348 MHz was assigned to the meta-protons with a hyperfine coupling constant, A_{Hm}=0.082 mT. The outer one at 11.512 and 16.881 MHz is attributable to the ortho- and para-protons of A_{Ho}=A_{Hp}=0.191 mT. Hereafter, the ENDOR absorption lines are designated as **a'**, **b'**, **b**, and **a** from the low-frequency side, respectively. The temperature dependence of the signal intensities of each line between 170—230 K is plotted in Fig. 1.

For the ^{14}N-ENDOR observation the experimental conditions were carefully chosen with regard to both the microwave and radio-frequency powers, temperature, and sample concentration. The solvents were not varied except for toluene and ethylbenzene. The temperature was found to be optimum at about 210 K, rather higher than in the detection of ^{1}H-ENDOR. The lower sample concentration seemed to be better for accomplishing easy saturation and low-noise detection of the 80 Hz ESR. Figure 2 shows the ^{1}H- and ^{14}N-ENDOR spectra observed at 220 K in a toluene solution. The newly appearing one pair of signals between the ^{1}H-ENDOR lines (**a'**, **b'**, and **b'**, **b**) was assigned to the ^{14}N-ENDOR lines. Spectra (a), (b), and (c) in Fig. 2 indicate ENDOR pattern variations due to the nitrogen nuclear quantum

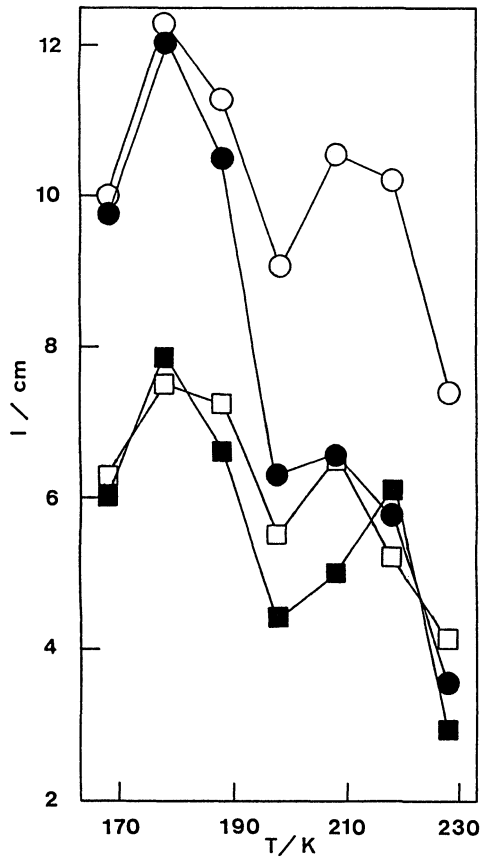

Fig. 1. Intensity variations of the ^{1}H-ENDOR lines taken as a peak-to-peak height. ○ and ● indicate the outer paired lines (**a** and **a'**), and □ and ■ the inner ones (**b** and **b'**).

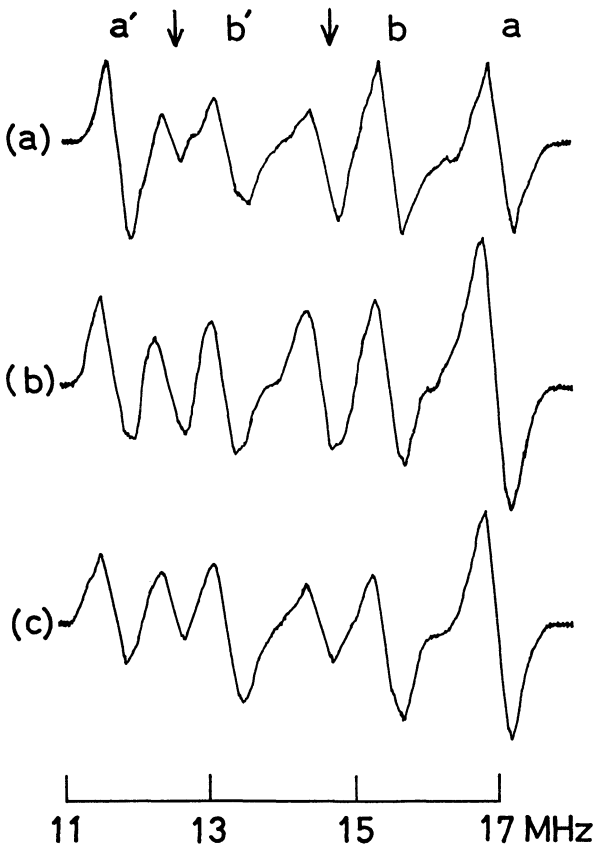

Fig. 2 ^{14}N- and ^{1}H-ENDOR spectra of DPNO observed in toluene at 220 K. The arrows indicate the ^{14}N-ENDOR lines. In these ENDOR observations ESR was monitored at the low-field ESR m_I=1 (**a**), the central ESR m_I=0 (**b**), and the high-field ESR m_I=−1 (**c**).

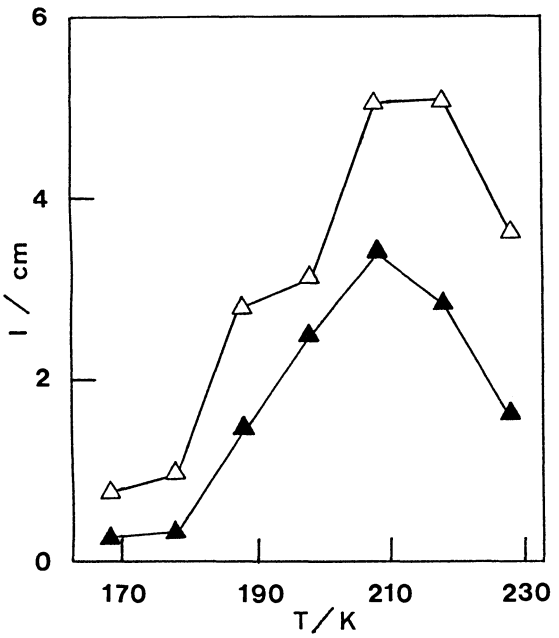

Fig. 3. Intensity variations of the ^{14}N-ENDOR lines taken as a peak-to-peak height. △ and ▲ indicate the high- and low-frequency lines, respectively.

numbers (m_I=1, 0, and −1) where the ESR was monitored.[10] The spectral intensity change of Fig. 2-(b) vs. temperature was shown in Fig. 3.

In the GTR measurements each of the ^{1}H-ENDOR lines was pumped using the second radio-frequency power; then, the other ^{1}H-ENDOR lines were influenced regarding their absorption intensity (see Fig. 2 in the literature[6]). The intensity variations measured at 180 K are plotted against the pumping radio-frequency power in Figs. 4 and 5. The GTR behaviors were the most

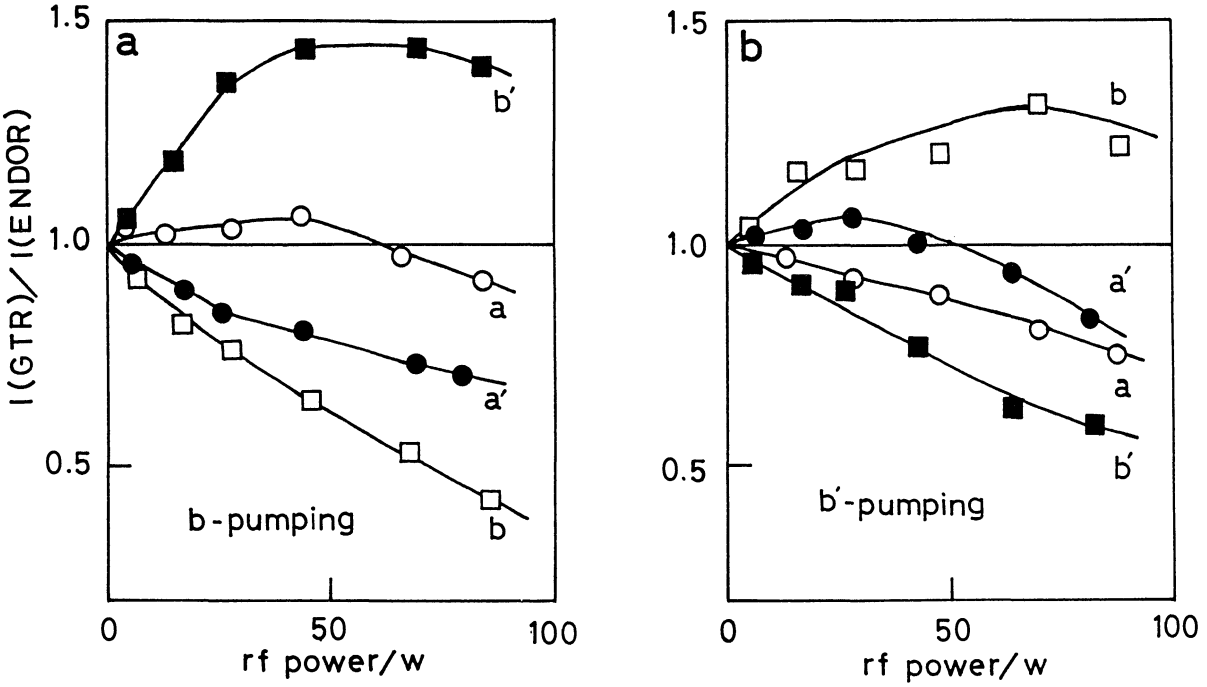

Fig. 4. Enhancement and de-enhancement of the GTR spectra with the inner paired ^{1}H-ENDOR lines (**b** and **b'**) pumped by the radio-frequency powers in the abscissa scale. ESR monitoring was set on the m_I=0 component. (See text concerning the ordinate scale.)

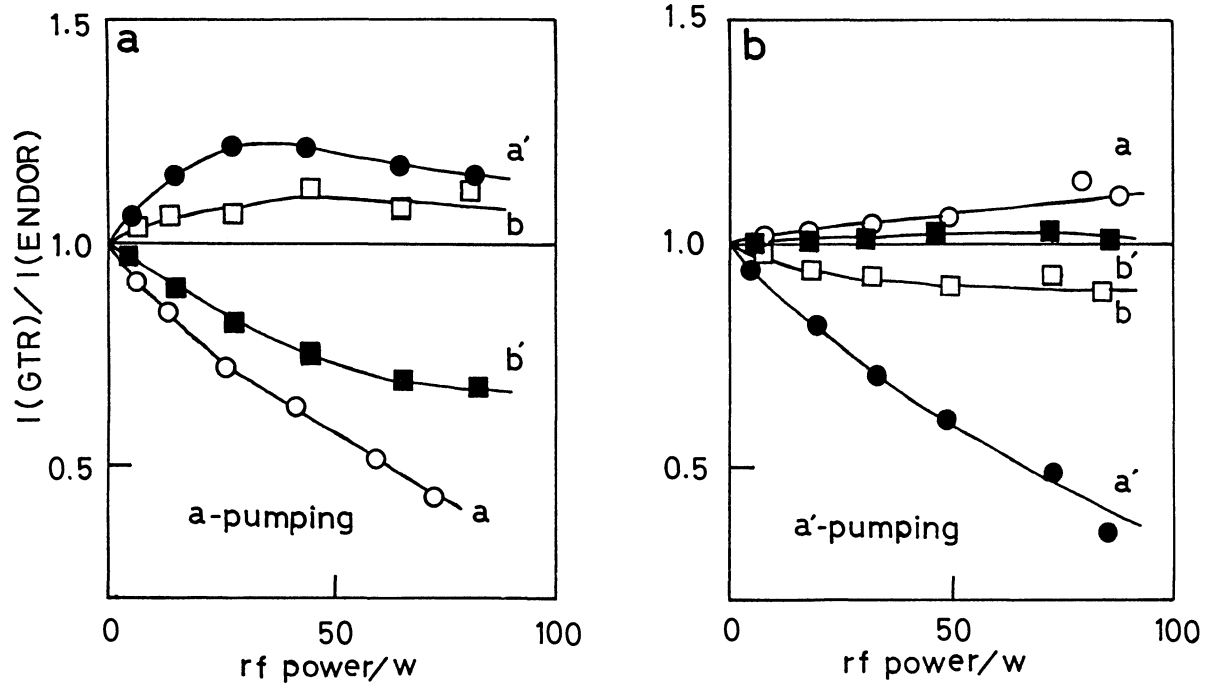

Fig. 5. Enhancement and de-enhancement of the GTR spectra with the outer paired ^{1}H-ENDOR lines (**a** and **a'**) pumped by the radio-frequency powers in the abscissa scale. ESR monitoring was set on the m_I=0 component. (See text concerning the ordinate scale.)

remarkable at the optimum temperature of the ^{1}H-ENDOR (180 K). The spectral enhancement or de-enhancement of the GTR spectra was not emphasized at the optimum temperature of the ^{14}N-ENDOR (210 K), probably due to complicated energy relaxations in the ^{14}N- and ^{1}H-nuclear spin systems, as discussed later. The data in Figs. 4 and 5 were obtained by monitoring the ESR of the m_I=0 component. If we changed the ESR observation to those of m_I=1 or −1, the intensity variations were slightly influenced, as is also discussed later.

Discussion

^{14}N-ENDOR Spectra. The newly appearing lines among the ^{1}H-ENDOR lines can be assigned to the ^{14}N-ENDOR absorptions, because of a separation of the two lines corresponding to $2\nu_N$, where ν_N is the nitrogen nuclear-magnetic-resonance frequency. Therefore, the average frequency of the paired lines is equal to the ^{14}N hyperfine coupling constant, A_N=0.9653 mT, which is in good agreement with the value A_N=0.965 mT determined from the ESR at 188 K in toluene.

The ^{14}N hyperfine coupling constant, A_N=0.9653 mT, is among the smaller values found in ENDOR observations of nitroxide radicals. It is usually true that the lower is the hyperfine coupling constant, the more difficult it is to be detected. Our observation is presently a lower-limit case of the nitroxide radicals. There have been several ^{14}N-ENDOR observations reported for other types of radicals with a smaller ^{14}N hyperfine interaction.[11,12] The difference may be associated with energy relaxation due to an anisotropic hyperfine interaction Tr $\{A'^2\}$, which is described below.

The higher optimum temperature of the ^{14}N-ENDOR (Fig. 3) is attributable to the different anisotropic hyperfine interactions of the ^{14}N and ^{1}H nuclei. In general, the calculated ENDOR signal can be expressed by τ_R and Tr$\{A'^2\}$, based on certain assumptions, where τ_R is the rotational correlation time of the molecule and Tr$\{A'^2\}$ is the trace of the squared anisotropic part of the electron-nuclear dipolar interaction.[11] The anisotropic ^{14}N hyperfine interaction, Tr$\{A'^2\}$, for nitroxide radicals, such as DPNO, is Tr$\{A'^2\}$=2200 MHz^2; whereas that of the ^{1}H, which is attached to the benzene ring, is about 30 MHz^2.[1,13] This difference explains the higher optimum temperature of the ^{14}N-ENDOR.

The ^{14}N-ENDOR lines indicated by the arrows in Fig. 2 show the spectral intensity change depending on ESR monitoring. This phenomenon was first pointed out by Leniart et al.,[8] and could be explained in terms of cross relaxation W_{X1} and W_{X2} depicted in Fig. 6. For instance, when one is sitting on the higher or lower field component of the ESR (m_I=−1 or +1) in the ENDOR observations, the energy relaxation is governed by the W_{X1}, W_{X2}, ω_{n1}, and ω_{n2} transitions associated with the central components of the energy levels. Accordingly, the high- and low-frequency ENDOR absorptions

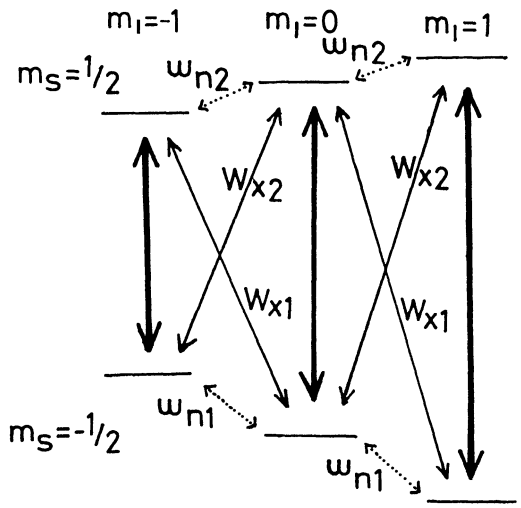

Fig. 6. Energy diagram of the unpaired electron (m_S=1/2, −1/2) and the ^{14}N nucleus (m_I=1, 0, −1). The cross relaxations W_{X1} and W_{X2} relate the transitions $\Delta(m_S+m_I)=0$ and $\Delta(m_S+m_I)=\pm2$, respectively. The high- and low-frequency ENDOR absorptions correspond to ω_{n1} and ω_{n2}, respectively. This diagram is depicted for the case of a positive hyperfine interaction $A_N>0$.

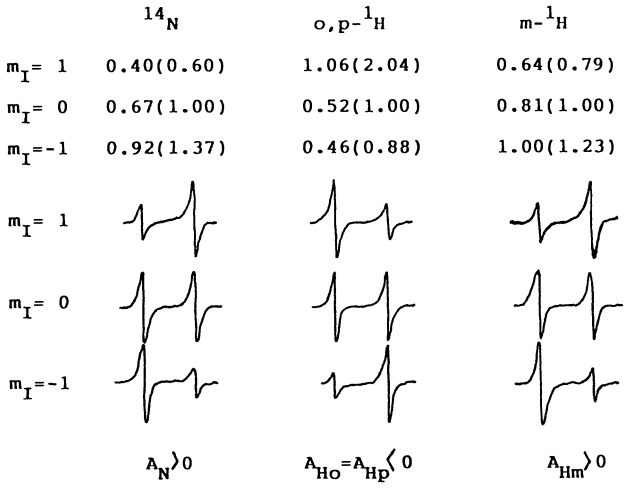

Fig. 7. Intensity ratio and its variations of each paired line for the ESR monitoring on m_I=1, 0, and −1. The schematic paired lines are depicted on the basis of the normalized intensity ratios (values in the parentheses). The meta-protons behave like the ^{14}N, whereas the ortho- and para-protons behave in an opposite way, leading to $A_{Hm}>0$ and $A_{Ho}=A_{Hp}<0$.

(ω_{n1} and ω_{n2}, respectively) show different spectral intensities due to the different W_{X1} and W_{X2} values. On the other hand, the central energy levels, which belong to m_I=0 component, can dissipate their energy to both sides. As a result, the high- and low-frequency ENDOR lines are averaged in intensity. The ^{14}N-ENDOR intensity changes with the m_I values are tabulated in Fig. 7. The values indicate the intensity ratio between the low- and high-frequency components; those

in the parentheses were normalized ones by the intensity ratio of $m_I=0$. The intensity patterns shown schematically in Fig. 7 indicate a positive hyperfine coupling constant of the ^{14}N nucleus, as is supposed in Fig. 6. Interestingly, these ^{14}N-cross relaxations also influence the ^1H-energy relaxation, as is summarized in Fig. 7. This is discussed next.

^1H-ENDOR Spectra. The ^1H-ENDOR lines are rather broad at 220 K, but the intensity changes with the m_I values are clear (Fig. 7). This effect was first pointed out by Janzen et al.[14] and independently by us,[15] and is referred to CRISP (cross relaxation intensity sequence pattern). The spectral intensity changes are opposite for the ortho- or para-protons and the meta-protons. This means the opposite signs of the hyperfine coupling constants (that is, $A_{Ho}=A_{Hp}<0$ and $A_{Hm}>0$) because the energy levels in Fig. 6 are reversed, depending on the signs of the hyperfine coupling constants. We can therefore conclude a negative spin density at the meta-positions of the phenyl rings, which agrees with the conclusion derived from the GTR results. The strong and weak intensity sequence patterns become important regarding the GTR behaviors on the spectral enhancement or de-enhancement.

The influence of the ^{14}N-energy relaxation on the ^1H-nuclear system was also ascertained by the temperature dependences of the ^1H-ENDOR lines. Figure 1 shows the intensities of the ^1H lines of the ENDOR spectra ($m_I=0$) at various temperatures. There are two characteristic features. One is the fact that there are two maximum regions; the other is the good coincidence of the intensity of each paired line at the lowest temperature region. Comparing these results with those of the ^{14}N-ENDOR lines (Fig. 3), one can easily conclude that the first maximum region around 210 K is somewhat related to the optimum temperature of the ^{14}N-ENDOR lines. This means that the effective energy relaxation in the ^{14}N-spin system at this temperature might cause a sufficient energy relaxation in the ^1H-spin system. As a matter of fact, the optimum conditions inherent in the ^1H-spin system are fulfilled at the lower temperatures, exhibiting a second maximum at 180 K. This finding implies the existence of a coupling between the ^{14}N and ^1H nuclei through the electron spin or through a direct interaction.[16] The meaningful effect of the nuclear–nuclear coupling was first pointed out concerning this ENDOR intensity. In addition to the CRISP effect, this is another interesting point regarding a three-spin system comprising one electron and two nuclear spins (^1H and ^{14}N). In the case of a three-spin system with similar nuclei (for instance, two non-equivalent protons), the energy relaxations becomes optimum at almost the same temperature regions, resulting in one maximum. The essential point in our spin system is two different nuclei (^{14}N and ^1H) which have optimum energy relaxation at different temperatures.

The second feature of Fig. 1 can also be explained by the above-mentioned interaction. At lower temperatures the ^{14}N–energy relaxation becomes ineffective and the original characteristics of the pure ^1H-spin system appear. Therefore, approaching the ^1H-optimum temperature region, the intensity of each paired line becomes the same as that shown in Fig. 1. As for this new finding, one comment is noteworthy concerning the previous experiment of BPNO.[9] The temperature dependence of the ENDOR intensities of the ^1H and ^{14}N absorptions were not analyzed in this way. The correct interpretation should be as follows. The first optimum region of the ^1H lines appeared at $-60\,^\circ C$, roughly corresponding to the maximum of the ^{14}N intensity. In BPNO, however, no second maximum, which is originally characteristic of the ^1H nuclei, was found over the observed temperature range (above $-90\,^\circ C$).

Triple Resonance Spectra. Figures 4 and 5 show the intensity variations of the GTR spectra by the pumping radio-frequency power. The spectral enhancement was defined by $I(\mathrm{GTR})/I(\mathrm{ENDOR})$, where $I(\mathrm{GTR})$ and $I(\mathrm{ENDOR})$ are the spectral intensity taken as absorption height with and without the pumping radio-frequency power, respectively. According to the results given in Figs. 4 and 5, one can conclude the opposite signs for the hyperfine coupling constants of the meta- and the ortho- or para-protons, since the inner paired lines (**b′** and **b**) as well as the outer ones (**a′** and **a**) change oppositely in intensity.[17] For instance, in Fig. 4, upon pumping one of the inner pair (**b′**), an enhancement took place on the high-frequency partner (**b**); on the outer paired lines, however, the high-frequency line **a** decreased and the low-frequency one **a′** was enhanced, though its enhancement was quite small. This situation is fully inversed to the case of pumping one of the inner lines, **b**. These observations are also the same for the cases of **a** and **a′** pumping (Fig. 5).

We next consider the enhancement or de-enhancement values. The radio-frequency pumping effect is always clear for the de-enhancement case, whereas the behavior in the enhancement situation is sometimes smeared out and the intensity enhancement is cancelled in the high radio-frequency power region, which may be referred to as enhancement "saturation". Since this tendency seems to be remarkable concerning the outer pair, one of the reasons for this enhancement saturation may be the large hyperfine coupling constant of the ortho- or para-protons, as compared with that of the meta-protons. This effect can be called a radio-frequency enhancement effect at the nucleus through a hyperfine interaction. An intensity enhancement saturation is therefore likely to occur at a relatively small radio-frequency power for nuclei with large hyperfine coupling constants.

How the GTR behavior depends on the ^{14}N-quantum number (m_I) is discussed next. The ENDOR spectral changes by the ^{14}N-quantum number is described above. The spectra were influenced like the patterns summarized in Fig. 7, that is, the intensity height of each line is either increased or decreased, depending on the ^{14}N-

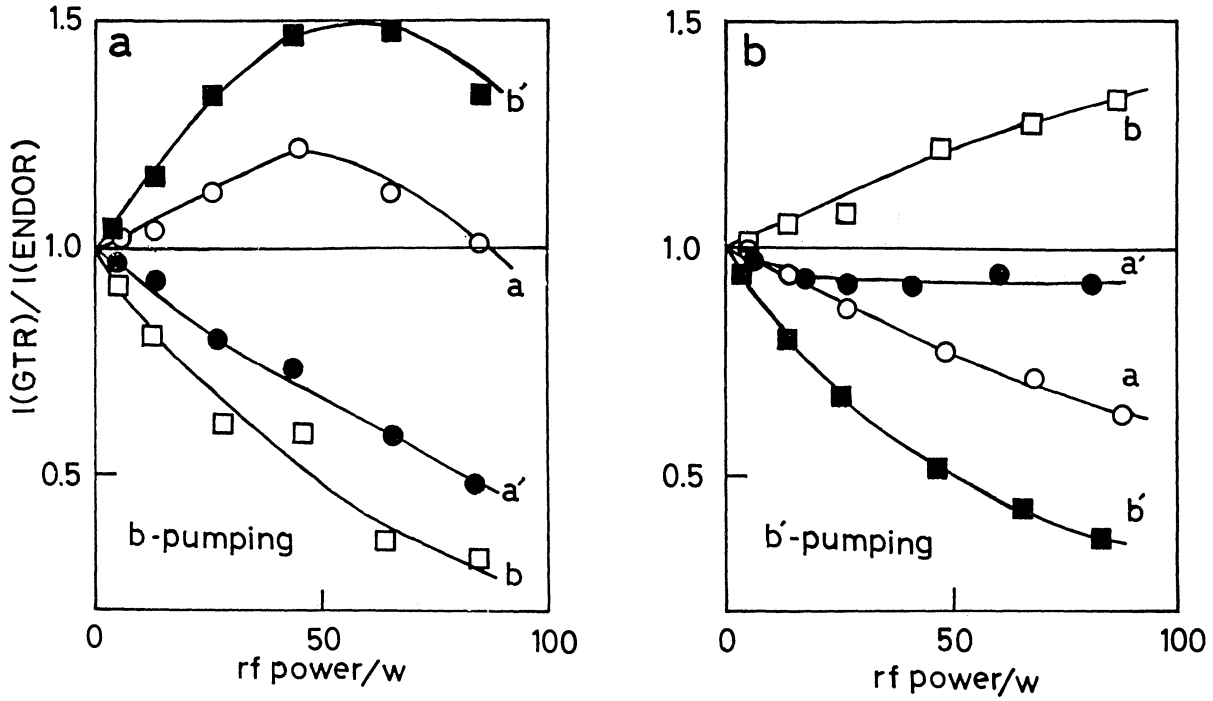

Fig. 8. Enhancement and de-enhancement of the GTR spectra with the inner paired ^{1}H-ENDOR lines (**b** and **b'**) pumped by the radio-frequency powers in the abscissa scale. ESR monitoring was set on the m_I=1 component. Compare with Fig. 4.

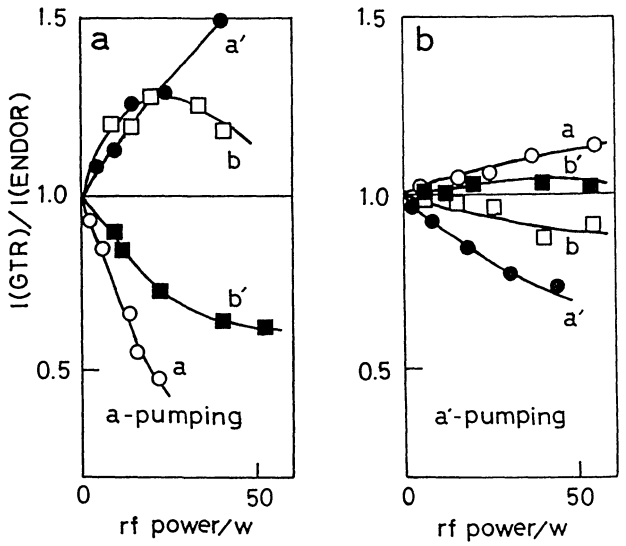

Fig. 9. Enhancement and de-enhancement of the GTR spectra with the outer paired ^{1}H-ENDOR lines (**a** and **a'**) pumped by the radio-frequency powers in the abscissa scale. ESR monitoring was set on the m_I=−1 component. Compare with Fig. 5.

quantum number (m_I) of the monitoring ESR and on the signs of the ^{1}H-hyperfine coupling constant (A_H). Regarding the GTR behavior, these cross relaxation effects should be combined, causing either more-enhanced or less-enhanced variations. This evidence is shown in Figs. 8 and 9. The experimental conditions for Fig. 8 were the same as those for Fig. 4, except for monitoring ESR. In the case of Fig. 8 the low-field ESR component (m_I=1) was monitored; line **b'** thus decreased, and line **b** increased due to the cross-relaxation effect (Fig. 7). Thus, the enhancement of the **b'** line or the de-enhancement of the b line is intensified by **b** pumping. This is the case of Fig. 8-a, which should be compared with Fig. 4-a. On the other hand, the opposite triple pumping (**b'** pumping) may give a dull behavior, like that shown in Fig. 8-b (compare with Fig. 4-b). Completely the same behaviors were also observed for high-field ESR monitoring (m_I=−1). As is hown in Fig. 9-a, enhancement of the **a'** line and the de-enhancement of the **a** line are intensified in the case of the **a** line pumping, because the line **a'** is already decreased and the line **a** increased by the cross relaxation (compare with Fig. 5-a). Fig 9-b should also be compared with Fig. 5-b. These findings belong to another type of three-spin effect in triple resonance spectroscopy.

In conclusion, by observing the ^{14}N- and ^{1}H-ENDOR spectra of DPNO, several interesting types of behavior were disclosed in ENDOR and GTR spectroscopies. The ^{14}N-hyperfine coupling constant detected by this ENDOR experiment is one of the smallest limits for the nitroxide radicals. The paired ^{14}N-ENDOR lines are distorted in intensity by cross relaxation in the ^{14}N nucleus and the unpaired electron. This effect is also present regarding the ^{1}H-ENDOR intensities. The double optimum temperatures for the ^{1}H-ENDOR lines were demonstrated, the higher one being due to the optimum energy relaxation of the ^{14}N nuclei and the

lower one due to that of the ^{1}H-spin system. These phenomena interelating two nuclei are interesting subjects concerning three-spin systems. In GTR experiments the intensity changes due to the radio-frequency-pumping power were analyzed in terms of the opposite signs of the hyperfine coupling constants, the enhancement saturation effect, and the effect of the cross relaxation. The latter two observations are pointed out here as a new interesting point concerning a three-spin system.

References

1) Y. Deguchi, *Bull. Chem. Soc. Jpn.*, **34**, 910 (1961).
2) Y. Deguchi, *Bull. Chem. Soc. Jpn.*, **35**, 260 (1962).
3) Y. Deguchi, *Bull. Chem. Soc. Jpn.*, **35**, 598 (1962).
4) J. Yamauchi, H. Nishiguchi, K. Mukai, Y. Deguchi, and H. Takaki, *Bull. Chem. Soc. Jpn.*, **40**, 2512 (1967).
5) J. Yamauchi, K. Okada, and Y. Deguchi, *Bull. Chem. Soc. Jpn.*, **60**, 483 (1987).
6) Y. Deguchi, K. Okada, J. Yamauchi, and K. Fujii, *Chem. Lett.*, **1983**, 1611.
7) H. Kurreck, B. Kirste, and W. Lubitz, "Electron Nuclear Double Resonance Spectroscopy of Radicals in Solutions," VCH Publisher, Inc., Weinheim (1988).
8) D. S. Leniart, J. C. Vedrine, and J. S. Hyde, *Chem. Phys. Lett.*, **6**, 637 (1970).
9) J. Yamauchi and Y. Deguchi, *Can. J. Chem.*, **66**, 1862 (1988).
10) The nitrogen hyperfine coupling constant is far larger than the proton ones. The ESR spectra, therefore, split into three groups which belong to m_I=1, 0, and −1 components.
11) F. Lendzian, M. Plato, and K. Mobius, *J. Magn. Reson.*, **44**, 20 (1981).
12) R. Biehl, K. Mobius, S. E. O'Connor, R. I. Walter, and H. Zimmermann, *J. Phys. Chem.*, **83**, 3449 (1979).
13) T. S. Lin, *J. Chem. Phys.*, **57**, 910 (1972).
14) E. G. Janzen and U. M. Oehler, *Chem. Lett.*, **1984**, 1233.
15) J. Yamauchi and Y. Deguchi, *Chem. Lett.*, **1985**, 111.
16) The former is the indirect ^{14}N and ^{1}H interaction through the hyperfine interactions ($A_N I_N S + A_H I_H S$) and the latter the direct ^{14}N and ^{1}H interaction of $J I_N I_H$ type.
17) K. Mobius and R. Biehl, "Multiple Electron Resonance Spectroscopy," ed by M. M. Dorio and J. H. Freed, Plenum Press, New York (1979), Chap. 14.

 © 1991 The Chemical Society of Japan Bull. Chem. Soc. Jpn., 64, 3627—3633 (1991)

Cobalt(III) Complexes with $[N_{6-n}X_n]$-Type Ligands. VII.[1] Preparation and Properties of Isomers of the (Salicylamidato)cobalt(III) Complexes with Tris(2-aminoethyl)amine, Triethylenetetramine, and Ethylenediamine Ligands

Eiko TOYOTA and Yoshihisa YAMAMOTO*
Faculty of Pharmaceutical Sciences, Higashi Nippon Gakuen University,
Ishikari-Tobetsu, Hokkaido 061-02
(Received March 7, 1991)

Title complexes of *t*- and *p*-[Co(**A**)(tren)]$Cl_2 \cdot H_2O$, *t*- and *p*-[Co(**C**)(tren)]$Cl \cdot H_2O$, *cis*-β_1 and β_2-[Co(**A**)(trien)]-$Cl_2 \cdot 2H_2O$, *cis*-β_1-[Co(**C**)(trien)]$Cl \cdot H_2O$, *cis*-β_1-[Co(**D**)(trien)]$Cl \cdot H_2O$, [Co(**A**)$(en)_2$]$Cl_2 \cdot H_2O$, [Co(**C**)$(en)_2$]$Cl \cdot H_2O$, and [Co(**D**)$(en)_2$]$Cl \cdot H_2O$ have been obtained from a reaction mixture of [$CoCl_2$L]$Cl \cdot H_2O$ [L: tren, trien, or $(en)_2$], Ag_2O, and salicylamide.

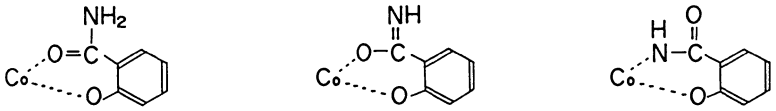

(A) (C) (D)

Separations of the **A**-, **C**-, and **D**-type complexes, and of the geometrical isomers of *t*- and *p*- or *cis*-β_1 and β_2 were attempted by using Dowex 50W-X2 column chromatography. Distinction of the **A**-, **C**-, and **D**-type complexes is described in the IR, ^1H, ^{13}C NMR, and absorption spectra; the solubility in DMSO; and the electric conductivities in aqueous solutions. The formation ratio of the **A**-, **C**-, and **D**-type complexes has been dependent upon the pH of the reaction mixture. The chemical shifts (δ=113—115) of the C-1 carbon signals for the **A**-type complexes are at a higher field than those (δ=117—122) of the **C**- and **D**-type complexes. The ε values (3400—3700) of the charge transfer band at ca. 340 nm in the absorption spectra for the **A**-type complexes are greater than those (2500—3000) of the **C**- and **D**-type complexes. The **C**-type and **D**-type complexes are a linkage isomer. A characteristic property of the linkage isomer has been observed in the absorption and ^{13}C NMR spectra as well as the solubility in DMSO.

We previously described the preparation, properties, and geometrical isomers of mixed-ligand (8-quinolinolato)-,[2-4] (salicylato)-,[5-7] (thiosalicylato)-,[8] or (salicylaldehydato)cobalt(III)[9,10] complexes with ethylenediamine (en), tris(2-aminoethyl)amine (tren), triethylenetetramine (trien), 3,7-diazanonane-1,9-diamine (2,3,2-tet), 4,7-diazadecane-1,10-diamine (3,2,3-tet), and 4,8-diazaundecane-1,11-diamine (3,3,3-tet) ligands. However, the preparation and properties of the mixed-ligand amine(salicylamidato)cobalt(III) complexes have not been of concern.

Salicylamide (*o*-hydroxybenzamide) is a very useful ligand in the field of coordination chemistry, since the $-CONH_2$ group of salicylamide can coordinate to a metal atom through the carbonyl oxygen (**A**-type) or the amide nitrogen (**B**-type), as is shown in Fig. 1. So far, bis- and tris(salicylamidato)metal complexes[11-13] of the **A**-type, $[M(A)_m]^{n+}$ [M: Fe(III), Co(II), Ni(II), Cu(II), Zn(II), Cd(II), or Hg(II); *m*: 2 or 3], have been reported concerning preparation, magnetic moments, IR spectra, and X-ray diffraction. However, the corresponding **B**-type complexes could not be prepared.

We recently succeeded in preparing the tetraamine(salicylamidato)cobalt(III) complex,[1] [Co(**D**)-$(NH_3)_4$]$Cl \cdot H_2O$, of the **D**-type, which is a bond between a cobalt atom and an imide nitrogen from a reaction mixture of $CoCl_2 \cdot 6H_2O$, aqueous ammonia, H_2O_2, and salicylamide. However, the **A**-, **B**-, and **C**-type complexes could not be obtained. Now, however, complexes of the **A**-, **C**-, and **D**-types have been prepared in this study. Thus, the present paper deals with the preparation and properties of the mixed-ligand amine-(salicylamidato)cobalt(III) complexes of [Co(**A**)L]$Cl_2 \cdot$

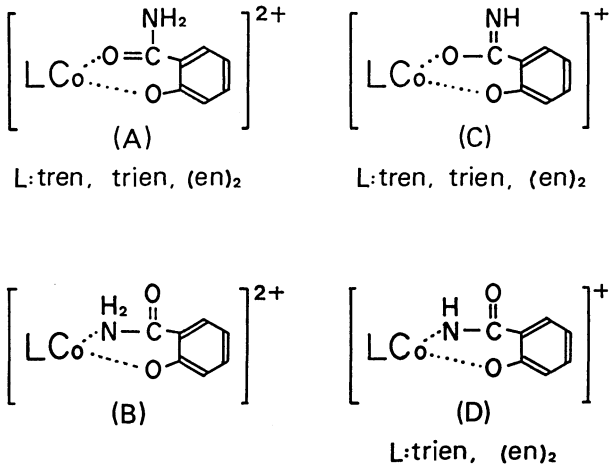

Fig. 1. Configurations of the **A**—**D**-type complexes of amine(salicylamidato)cobalt(III) complexes.

nH$_2$O [L: tren, trien, or (en)$_2$], [Co(**C**)L]Cl·H$_2$O [L: tren, trien, or (en)$_2$], and [Co(**D**)L]Cl·H$_2$O [L: trien or (en)$_2$].

Experimental

Measurements. The electric conductivities were determined by the use of a CM-40S conductivity meter (TOA) in aqueous solutions at room temperature. The IR spectra were recorded in KBr disks with a 270-30 spectrophotometer (Hitachi). The visible absorption spectra were recorded in water with a Shimadzu UV-210 recording spectrophotometer. The ^{1}H and ^{13}C NMR spectra were recorded with a JNM-FX90Q FT NMR spectrometer (JEOL). The melting points were measured on an MP-500D apparatus (Yanako).

Preparation of Complexes. *t*-(Salicylamidato-*O,O*)[tris(2-aminoethyl)amine]cobalt(III) Dichloride Hydrate (1), *p*-(Salicylamidato-*O,O*)[tris(2-aminoethyl)amine]cobalt(III) Dichloride Hydrate (2), *t*-(Salicylamidato-*O,O*)[tris(2-aminoethyl)amine]cobalt(III) Chloride Hydrate (3), and *p*-(Salicylamidato-*O,O*)[tris(2-aminoethyl)amine]cobalt(III) Chloride Hydrate (4): [CoCl$_2$tren]Cl·H$_2$O (10.0 g, 30.3 mmol) was added to moistend fresh Ag$_2$O, which was made from silver nitrate (10.3 g, 60.6 mmol) and potassium hydroxide (3.4 g, 60.6 mmol). The mixture was stirred for several minutes at room temperature; then, 10 cm^3 of water was added to the mixture. The mixture was stirred for about 30 min at 60 °C, and the precipitated silver chloride was filtered off and washed with a small amount of water. A methanol solution (60 cm^3) of salicylamide (4.15 g, 30.3 mmol) was added, drop by drop, to the reddish-violet filtrate (pH 8.6). The solution was stirred for 12 h at 58 °C and was then concentrated on a rotary evaporator, and salicylamide (ca. 0.6 g) precipitated was filtered. The separation of complexes **1**—**4** was achieved by using a column (ϕ 2.5 cm×40 cm) of ion-exchange resin (Dowex 50W-X2, 100—200 mesh). Upon elution with 0.3 mol dm^{-3} NaCl, the effluents of the first reddish-brown band (complex **3**) and second red band (complex **4**) were collected and concentrated, respectively. Then, the third red band (complex **1**) and fourth red band (complex **2**) were eluted with 0.8 mol dm^{-3} NaCl and concentrated, respectively. Complexes **1**—**4** were recrystallized from water–ethanol–ether. Yields: 2.6 g (19.9%) for **1**, 3.8 g (29.2%) for **2**, 0.53 g (4.4%) for **3**, 0.38 g (3.2%) for **4**. Found **1**: C, 36.35; H, 6.11; N, 16.44; Cl, 16.59%. **2**: C, 36.55; H, 6.27; N, 16.31; Cl, 16.70%. Calcd for $CoC_{13}H_{26}N_5O_3Cl_2$ (MW 430.22): C, 36.29; H, 6.09; N, 16.28; Cl, 16.48%. Found **3**: C, 39.59; H, 6.55; N, 17.51; Cl, 9.23%. **4**: C, 39.74; H, 6.58; N, 17.56; Cl, 9.29%. Calcd for $CoC_{13}H_{25}N_5O_3Cl$ (MW 393.76): C, 39.65; H, 6.40; N, 17.79; Cl, 9.00%. ^{1}H NMR **1**: δ=2.60—3.07 (4H, NH$_2$- side CH$_2$), 3.07—3.90 (8H, NH$_2$- and N- side CH$_2$); 4.75 (6H, NH$_2$); 6.7—7.8 (4H, salicylamidato) in 1.8 mol dm^{-3} D$_2$SO$_4$. δ=2.5—3.5 (12H, CH$_2$); 5.12 (2H), 5.85 (4H), each NH$_2$; 6.3—7.9 (4H, salicylamidato); 8.85, 8.92 (each 1H, -CONH$_2$) in DMSO-d_6. **2**: δ=2.50—2.80 (2H, NH$_2$- side CH$_2$), 2.80—3.45 (6H, NH$_2$- and N- side CH$_2$), 3.45—3.90 (4H, N- side CH$_2$); 4.69 (4H), 5.04 (2H), each NH$_2$; 6.7—7.7 (4H, salicylamidato) in 1.8 mol dm^{-3} D$_2$SO$_4$. δ=2.5—3.5 (12H, CH$_2$); 4.85 (2H), 6.14 (4H), each NH$_2$; 6.4—7.9 (4H, salicylamidato); 8.70, 8.84 (each 1H, -CONH$_2$) in DMSO-d_6. **3**: δ=2.70—3.05 (4H, NH$_2$- side CH$_2$), 3.05—3.85 (8H, NH$_2$- and N- side CH$_2$); 5.00 (6H, NH$_2$); 6.6—7.9 (4H, salicylamidato) in 1.8 mol dm^{-3} D$_2$SO$_4$. δ=2.4—3.5 (12H, CH$_2$); 4.61 (2H), 5.25 (4H), each NH$_2$; 6.2—7.9 (4H, salicylamidato) in DMSO-d_6. **4**: δ=2.44—2.77 (2H, NH$_2$- side CH$_2$), 2.77—3.39 (6H, NH$_2$- and N- side CH$_2$), 3.39—4.00 (4H, N- side CH$_2$); 4.85 (4H), 5.10 (2H), each NH$_2$; 6.5—7.9 (4H, salicylamidato) in 1.8 mol dm^{-3} D$_2$SO$_4$. δ=2.4—3.6 (12H, CH$_2$); 4.50 (2H), 5.51 (4H), each NH$_2$; 6.3—7.9 (4H, salicylamidato) in DMSO-d_6. ^{13}C NMR (D$_2$O) **1**: δ=44.3, 45.4, 45.4 (each NH$_2$- side CH$_2$), 60.8, 61.8, 61.8 (each N- side CH$_2$); δ=114.3 (C-1), 167.2 (C-2), 118.1 (C-3), 136.4 (C-4), 124.8 (C-5), 130.0 (C-6), 173.1 (C-7). **2**: δ=43.6, 45.2, 45.2 (each NH$_2$- side CH$_2$), 61.7, 62.0, 62.0 (each N- side CH$_2$); δ=113.1 (C-1), 166.7 (C-2), 117.6 (C-3), 136.1 (C-4), 125.7 (C-5), 129.6 (C-6), 173.4 (C-7). **3**: δ=44.0, 45.4, 45.4 (each NH$_2$- side CH$_2$), 60.7, 61.4, 61.4 (each N- side CH$_2$); δ=118.7 (C-1), 167.9 (C-2), 117.3 (C-3), 134.6 (C-4), 123.6 (C-5), 132.6 (C-6), 174.0 (C-7). **4**: δ=43.5, 45.3, 45.3 (each NH$_2$- side CH$_2$), 61.3, 61.6, 61.6 (each N- side CH$_2$), δ=117.4 (C-1), 167.7 (C-2), 117.0 (C-3), 134.6 (C-4), 124.8 (C-5), 132.4 (C-6), 174.6 (C-7). Mp: 242 for **1**, 207 for **2**, 238 for **3**, 250 °C for **4**.

***cis*-β_1-(Salicylamidato-*O,O*)(triethylenetetramine)cobalt(III) Dichloride Dihydrate (5), *cis*-β_2-(Salicylamidato-*O,O*)-(triethylenetetramine)cobalt(III) Dichloride Dihydrate (6), *cis*-β_1-(Salicylamidato-*O,O*)(triethylenetetramine)cobalt(III) Chloride Hydrate (7), *cis*-β_2-(Salicylamidato-*O,O*)(triethylenetetramine)cobalt(III) Chloride Hydrate (8), and *cis*-β_1-(Salicylamidato-*N,O*)(triethylenetetramine)cobalt(III) Chloride Hydrate (9):** A mixture of complexes **5**—**9** was prepared from a reaction mixture (pH 8.6) of [CoCl$_2$(trien)]Cl (10.0 g, 32.1 mmol), fresh Ag$_2$O (7.44 g, 32.1 mmol), and salicylamide (4.4 g, 32.1 mmol) according to the procedure for complexes **1**—**4**. The separation of complexes **5**—**9** was achieved by a column (ϕ 2.5 cm×30 cm) of ion-exchange resin (Dowex 50W-X2, 100-200 mesh). Upon elution with 0.2 mol dm^{-3} NaCl, the effluents of the first reddish-violet band (mixture of complexes **7** and **8**) and second red band (complex **9**) were collected and concentrated, respectively. Then, upon elution with 0.6 mol dm^{-3} NaCl, the effluents of the third red band (complex **5**) and fourth red band (complex **6**) were collected and concentrated, respectively. The separation of complexes **7** and **8** from the first reddish-violet band was achieved by a column (ϕ 2.5 cm×40 cm) of ion-exchange resin (Dowex 50W-X2, 200—400 mesh). Upon elution with 0.1 mol dm^{-3} NaCl, the effluents of the lower (**7**) and upper (**8**) layers of the reddish-violet band were collected and concentrated, respectively. Complex **7** was isolated; pure complex **8** was not obtained, however, because of isomerization to **7**. Complexes **5**—**7** and **9** were recrystallized from water–ethanol–ether or water–ethanol–acetone. Yields: 2.1 g (14.6%) for **5**, 2.3 g (16.0%) for **6**, 1.1 g (8.7%) for **7**, 0.35 g (2.8%) for **9**, recovered salicylamide: 0.85 g. Found **5**: C, 34.60; H, 6.52; N, 15.80; Cl, 15.80%. **6**: C, 34.57; H, 6.55; N, 15.66; Cl, 16.06%. Calcd for $CoC_{13}H_{28}N_5O_4Cl_2$ (MW 448.23): C, 34.83; H, 6.30; N, 15.63; Cl, 15.82%. Found **7**: C, 39.92; H, 6.57; N, 17.56; Cl, 9.14%. Calcd for $CoC_{13}H_{25}N_5O_3Cl$ (MW 393.76): C, 39.65; H, 6.40; N, 17.79; Cl, 9.00%. Found **9**: C, 39.84; H, 6.42; N, 17.88; Cl, 9.30%. Calcd for $CoC_{13}H_{25}N_5O_3Cl$ (MW 393.76): C, 39.65; H, 6.40; N, 17.79; Cl, 9.00%. IR **5**: 3108, 3130, 3184, 3200 cm^{-1} (NH stretch.); 1000, 1030, 1056, 1080 cm^{-1} (NH$_2$ twist.). **6**: 3100, 3200, 3248, 3288 cm^{-1} (NH stretch.); 1002, 1036, 1052, 1078 cm^{-1} (NH$_2$ twist.). **7**: 3090, 3150, 3200, 3240 cm^{-1} (NH stretch.); 1002, 1043, 1052, 1074 cm^{-1} (NH$_2$ twist.). **9**: 3040, 3130, 3180, 3226 cm^{-1} (NH stretch.); 999, 1038, 1077, 1100 cm^{-1} (NH$_2$ twist.). ^{1}H NMR **5**: δ=2.35—3.60 (12H, NH$_2$- and NH- side CH$_2$); 4.24 (2H,

N(1)H_2), 4.5—5.2 (2H, N(4)H_2); 6.22 (2H, N(2)H and N(3)H); 6.7—7.8 (4H, salicylamidato) in 1.8 mol dm^{-3} D_2SO_4. δ=2.15—3.28 (12H, CH_2); 3.84 (1H), 5.11 (2H), 5.51 (1H), each NH_2; 6.95, 8.20 (each 1H, NH); 6.4—7.9 (4H, salicylamidato); 8.89, 8.96 (each 1H, -$CONH_2$) in DMSO-d_6. **6**: δ=2.38—2.78 (3H, NH_2- side CH_2), 2.78—3.65 (9H, NH_2- and NH- side CH_2); 4.30 (3H, N(1)H_2 and N(4)H_2), 5.01 (1H, N(4)H_2), 5.95 (N(2)H), 6.30 (N(3)H); 6.6—7.7 (4H, salicylamidato) in 1.8 mol dm^{-3} D_2SO_4. δ=2.10—2.60 (3H), 2.60—3.27 (9H), each CH_2; 3.95, 4.69, 5.37, 5.85 (each 1H, NH_2), 7.00, 8.23 (each 1H, NH); 6.4—7.9 (4H, salicylamidato); 8.68, 8.95 (each 1H, -$CONH_2$) in DMSO-d_6. **7**: δ=2.30—3.60 (12H, NH_2- and NH- side CH_2); 4.70 (4H, N(1)H_2 and N(4)H_2), 5.90 (2H, N(2)H and N(3)H); 6.6—7.9 (4H, salicylamidato) in 1.8 mol dm^{-3} D_2SO_4. δ=2.10—3.25 (12H, CH_2); 3.7—4.3 (2H), 4.5—5.2 (2H), each NH_2; 5.52, 6.10 (each 1H, NH); 6.2—7.9 (4H, salicylamidato) in DMSO-d_6. **9**: δ=2.32—3.64 (12H, NH_2- and NH- side CH_2); 3.64—4.49 (4H, N(1)H_2, N(4)H_2, and -CONH), 4.65 (1H, N(4)H_2), 5.76 (N(2)H), 6.18 (N(3)H); 6.6—7.9 (4H, salicylamidato) in 1.8 mol dm^{-3} D_2SO_4. δ= 1.90—3.25 (13H, CH_2 and NH_2), 4.22 (1H), 4.53 (2H), each NH_2; 4.89 (1H, -CONH); 5.43, 7.61 (each 1H, NH); 6.2—7.9 (4H, salicylamidato) in DMSO-d_6. ^{13}C NMR (D_2O) **5**: δ= 42.7, 47.8 (each NH_2- side CH_2), 48.4, 49.9, 51.9, 53.0 (each NH- side CH_2); δ=115.0 (C-1), 167.3 (C-2), 117.9 (C-3), 136.3 (C-4), 125.0 (C-5), 129.8 (C-6), 173.3 (C-7). **6**: δ=42.3, 47.5 (each NH_2- side CH_2); δ=48.6, 50.0, 52.3, 52.7 (each NH- side CH_2); δ=114.2 (C-1), 167.4 (C-2), 117.6 (C-3), 136.1 (C-4), 125.4 (C-5), 129.6 (C-6), 173.0 (C-7). **7**: δ=41.4, 47.0 (each NH_2- side CH_2), 48.9, 50.0, 52.4, 53.0 (each NH- side CH_2); δ=117.3 (C-1), 165.9 (C-2), 117.6 (C-3), 133.5 (C-4), 123.6 (C-5), 130.7 (C-6), 172.9 (C-7). **9**: δ=41.4, 48.0 (each NH_2- side CH_2), 48.3, 49.3, 52.8, 53.6 (each NH- side CH_2); δ=121.5 (C-1), 166.7 (C-2), 117.0 (C-3), 133.3 (C-4), 123.7 (C-5), 130.5 (C-6), 172.5 (C-7). Mp: 217 for **5**, 225 for **6**, 230 for **7**, 244 °C for **9**.

Bis(ethylenediamine)(salicylamidato-*O,O*)cobalt(III) Dichloride Hydrate (10), Bis(ethylenediamine)(salicylamidato-*O,O*)cobalt(III) Chloride Hydrate (11), and Bis(ethylenediamine)(salicylamidato-*N,O*)cobalt(III) Chloride Hydrate (12): A mixture of complexes **10**—**12** was prepared from the reaction mixture (pH 8.6) of $[CoCl_2(en)_2]Cl$ (10.0 g, 35.0 mmol), fresh Ag_2O (8.11 g, 35.0 mmol), and salicylamide (4.8 g, 35.0 mmol) according to the procedure for complexes **1**—**4**. The separation of complexes **10**—**12** was achieved by a column (φ 2.5 cm×20 cm) of ion-exchange resin (Dowex 50W-X2, 100—200 mesh). Upon elution with 0.2 mol dm^{-3} NaCl, the effluent of the first red band (mixture of **11** and **12**) was collected and concentrated. Then, the second red band (**10**) was eluted with 0.8 mol dm^{-3} NaCl. The effluent of **10** was collected and concentrated. The separation of **11** and **12** was achieved by a column (φ 2.5 cm×40 cm) of ion-exchange resin (Dowex 50W-X2, 200—400 mesh). Upon elution with 0.1 mol dm^{-3} NaCl, the effluents of the lower (**11**) and upper (**12**) layers of the red band were collected and concentrated, respectively. Complexes **10**—**12** were recrystallized from water-ethanol-ether. Yields: 5.31 g (37.5%) for **10**, 0.6 g (4.7%) for **11**, 0.3 g (2.3%) for **12**. Found **10**: C, 32.72; H, 5.88; N, 17.19; Cl, 17.78%. Calcd for $CoC_{11}H_{24}N_5O_3Cl_2$ (MW 404.18): C, 32.69; H, 5.99; N, 17.33; Cl, 17.54%. Found **11**: C, 36.19; H, 6.52; N, 19.18; Cl, 9.78%. **12**: C, 36.04; H, 6.22; N, 18.98; Cl, 9.87%. Calcd for $CoC_{11}H_{23}N_5O_3Cl$ (MW 367.72): C, 35.93; N, 6.30; N, 19.05; Cl, 9.64%. ^{1}H NMR **10**: δ=2.76, 2.84 (each 4H, CH_2); 4.17 (2H), 4.30—4.75 (3H), 4.95 (1H), 5.16 (2H), each NH_2; 6.7—7.7 (4H, salicylamidato) in 1.8 mol dm^{-3} D_2SO_4. δ=2.3—2.8 (8H, CH_2); 4.21 (1H), 4.42 (1H), 5.00 (1H), 5.25 (1H), 5.45—6.20 (4H), each NH_2; 6.4—7.9 (4H, salicylamidato); 8.58, 8.80 (each 1H, -$CONH_2$) in DMSO-d_6. **11**: δ=2.85 (8H, CH_2); 4.26 (2H), 4.50 (2H), 4.96 (1H), 5.27 (3H), each NH_2; 6.4—7.9 (4H, salicylamidato) in 1.8 mol dm^{-3} D_2SO_4. δ=2.3—2.8 (8H, CH_2); 4.06 (2H), 4.63 (2H), 5.44 (4H), each NH_2; 6.2—7.9 (4H, salicylamidato) in DMSO-d_6. **12**: δ=2.75 (8H, CH_2); 3.93 (1H, -CONH); 4.28 (3H), 4.64 (5H), each NH_2; 6.6—7.9 (4H, salicylamidato) in 1.8 mol dm^{-3} D_2SO_4. δ=2.3—2.8 (8H, CH_2); 3.5—5.0 (7H, NH_2 and -CONH), 5.30 (2H, NH_2); 6.2—7.9 (4H, salicylamidato) in DMSO-d_6. ^{13}C NMR (D_2O) **10**: δ=43.7, 44.1, 45.6, 45.9 (each CH_2); δ=113.9 (C-1), 167.0 (C-2), 117.7 (C-3), 136.1 (C-4), 125.1 (C-5), 129.8 (C-6), 173.1 (C-7). **11**: δ=43.9, 43.9, 45.6, 45.7 (each CH_2); δ=118.1 (C-1), 167.7 (C-2), 117.2 (C-3), 134.5 (C-4), 124.0 (C-5), 132.6 (C-6), 174.2 (C-7). **12**: δ=44.8, 45.1 , 45.2, 45.4 (each CH_2); δ=120.7 (C-1), 166.4 (C-2), 117.0 (C-3), 133.2 (C-4), 123.6 (C-5), 130.6 (C-6), 172.5 (C-7). Mp: 218 for **10**, 245 for **11**, 256 °C for **12**.

Preparation of Complex 3 from 1 and of 4 from 2: Complex **1** (0.3 g, 6.97 mmol) was added to ammonia solution (6 cm^3, pH 10), and the mixture was stirred for 13 h at 62 °C. The solution was concentrated on a rotary evaporator. The purification of **3** was achieved by column chromatography on alumina. Complex **4** was also obtained from the mixture of **2** and ammonia solution. Yields: 0.22 g (80.1%) for **3**, 0.20 g (72.8%) for **4**.

Preparation of Complex 7 from 5 or 6: Complex **5** (1.0 g, 2.23 mmol) was added to an ammonia solution (15 cm^3, pH 10); the mixture was then stirred for 3 h at 62 °C, and concentrated on a rotary evaporator. The precipitated complex **7** was filtered. Yield: 0.64 g (72.9%).

Complex **6** (1.0 g, 2.23 mmol) was added to an ammonia solution (15 cm^3, pH 10); the mixture was then stirred for 12 h at 62 °C, concentrated, and the precipitated complex filtered. This complex was a mixture of complexes **7** and **8**. Complex **8** in the mixture became **7** after 5 h at 62 °C in solution, since **8** isomerizes to **7**. Yield: 0.56 g (63.7%).

Preparation of Complex 11 from 10: Complex **10** (1.0 g, 2.47 mmol) was added to an ammonia solution (15 cm^3, pH 10); the mixture was stirred for 13 h at 62 °C, and then concentrated on a rotary evaporator. The purification of **11** was achieved by column chromatography on alumina. Yield: 0.56 g (61.6%).

Solubility. All complexes were very soluble in water and soluble in methanol. For dimethyl sulfoxide (DMSO), complexes **1**, **2**, **5**, **6**, **9**, **10**, and **12** were soluble, but complexes **3**, **4**, **7**, and **11** were very slightly soluble. All of the complexes were not soluble in common organic solvents, such as acetone and ether.

Results and Discussion

The abbreviations of the octahedral amine(salicylamidato)cobalt(III) complexes in this research are listed in Table 1.

Complexes. Complexes **1**—**12** have been obtained from a reaction mixture of $[CoCl_2(L)]Cl \cdot nH_2O$ (L: tren, trien, $(en)_2$), Ag_2O, and salicylamide. Complexes **1**—**12** were separated by Dowex 50W-X2 column chromatography. The formation ratios of **1**, **2**, **3**, and **4** are ca.

Table 1. Abbreviations and Some Physical Properties of Complexes **1**—**7**, **9**—**12**, and **17**

No.	Complex	Electric conductivity of aqueous solution	IR (C=O)	^{13}C NMR[a] C-1	Absorption bands in water		
					λ/nm (ε/cm^{-1} mol^{-1} dm^3)		
		S cm^2 mol^{-1}	cm^{-1}	δ			
1	*t*-[Co(**A**)tren]Cl$_2$·H$_2$O	240	1644	114.3	340 (3720)	530 (275)	
2	*p*-[Co(**A**)tren]Cl$_2$·H$_2$O	250	1640	113.1	343 (3450)	510 (220)	
3	*t*-[Co(**C**)tren]Cl·H$_2$O	108	—	118.7	330 (2820)	535 (215)	
4	*p*-[Co(**C**)tren]Cl·H$_2$O	110	—	117.4	332 (3000)	515 (220)	
5	*cis*-β_1-[Co(**A**)trien]Cl$_2$·2H$_2$O	250	1644	115.0	340 (3410)	520 (315)	
6	*cis*-β_2-[Co(**A**)trien]Cl$_2$·2H$_2$O	245	1630	114.2	345 (3580)	512 (285)	
7	*cis*-β_1-[Co(**C**)trien]Cl·H$_2$O	115	—	117.3	320 (2500)	535 (260)	
9	*cis*-β_1-[Co(**D**)trien]Cl·H$_2$O	145	—	121.5	326 (2560)	510 (255)	535 (245)
10	[Co(**A**)(en)$_2$]Cl$_2$·H$_2$O	240	1644	113.9	342 (3600)	512 (235)	
11	[Co(**C**)(en)$_2$]Cl·H$_2$O	135	—	118.1	328 (2830)	517 (210)	
12	[Co(**D**)(en)$_2$]Cl·H$_2$O	140	—	120.7	326 (2790)	513 (210)	535 (200)
17[b]	[Co(**D**)(NH$_3$)$_4$]Cl·H$_2$O	113	—	120.0	323 (2790)	512 (185)	545 (180)

a) Solvent D$_2$O, standard dioxane (δ=67.4). b) Ref. 1.

6 : 9 : 1 : 1, respectively. The formation ratios of **5**, **6**, **7**, and **9** are ca. 5 : 6 : 3 : 1, respectively, and those of **10**, **11**, and **12** are ca. 16 : 2 : 1, respectively. The colors of **1** and **5** are russet. The colors of **2**, **4**, **7**, **10**, and **11** are red, and those of **3**, **6**, **9**, and **12** are brownish-violet, reddish-pink, reddish-violet, and reddish-brown, respectively.

The absorption spectra of all complexes were measured in water (Table 1). The absorption bands at ca. 340 nm of the complexes were assigned to the charge transfer band, while the bands at ca. 520 nm were assigned to the first absorption band[1] (Table 1). The ^{1}H NMR spectra of all complexes were measured in 1.8 mol dm^{-3} D$_2$SO$_4$ and in DMSO-d_6. The signals at δ=6.2—7.9 of the complexes were assigned to the ring protons of the coordinated salicylamidato ligand. The signals at δ=2.4—4.0 and 4.3—5.5 for **1**—**4** in 1.8 mol dm^{-3} D$_2$SO$_4$ were assigned to the methylene and amine protons of the coordinated tren ligand, respectively, by the comparisons with those of *t*- and *p*-salicylaldehydato(tren)cobalt(III) dichloride hydrate,[10] *t*-, *p*-[Co(salad)tren]Cl$_2$·H$_2$O (*t*: **13**, *p*: **14**). The methylene and amine protons of the coordinated trien ligand for **5**—**7** and **9** were assigned on the basis of those of *cis*-β_1 and β_2-salicylaldehydato(trien)cobalt(III) dichloride dihydrate,[9,10] *cis*-β_1, β_2-[Co(salad)trien]Cl$_2$·2H$_2$O (β_1: **15**, β_2: **16**). The signals at δ=2.7—2.9 and 4.1—5.3 for **10**—**12** have been assigned to methylene and amine protons of the coordinated ethylenediamine ligand, respectively. The ^{13}C NMR spectra of all complexes were measured in D$_2$O. Seven signals at δ=113—175 of the complexes were assigned to the carbons of the coordinated salicylamidato ligand by comparisons with those of tetraammine(salicylamidato)cobalt(III) chloride hydrate,[1] [Co(**D**)(NH$_3$)$_4$]Cl·H$_2$O (**17**). The signals at δ=43—45 and 60—62 for **1**—**4** were assigned to the NH$_2$- and N- side methylene carbons[7,10] of the coordinated tren ligand, respectively. The signals at δ=41—48 and 48—54 of **5**—**7** and **9** were assigned to the NH$_2$- and NH- side methylene carbons[6,10] of the coordinated trien ligand, respectively. The signals at δ=43—46 of **10**—**12** were assigned to the methylene carbons of the coordinated ethylenediamine ligand. The data are collected in the Experimental section.

The electric conductivities of **1** and **2** are ca. 240 S cm^2 mol^{-1} in aqueous solutions. The IR spectra of **1** and **2** show the C=O stretching vibration at 1640 cm^{-1}, which is lower than that (1680 cm^{-1}) of free salicylamide[13] in the solid state. This suggests that the carbonyl oxygen of the coordinated salicylamidato ligand of **1** and **2** is bonded to a cobalt atom.[11,13] The ^{1}H NMR spectra in DMSO-d_6 of **1** and **2** showed two singlet signals at δ=8.85 (1H) and 8.92 (1H) for **1** and δ=8.70 (1H) and 8.84 (1H) for **2**. Both signals were assigned to -CONH$_2$ protons of the coordinated salicylamidato ligand by the comparison with those (δ=7.5—8.7) of

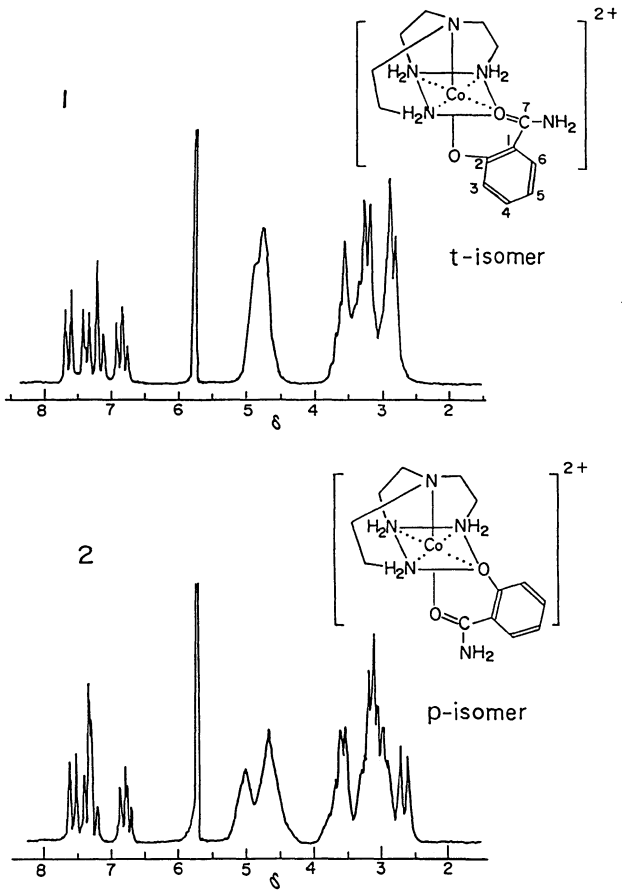

Fig. 2. ^{1}H NMR spectra of complexes **1** and **2** in 1.8 mol dm^{-3} D_2SO_4.
1: *t*-[Co(**A**)tren]$Cl_2 \cdot H_2O$. **2**: *p*-[Co(**A**)tren]$Cl_2 \cdot H_2O$.

free salicylamide.[14] Thus, complexes **1** and **2** have been assigned to **A**-type complexes, $[Co(A)tren]^{2+}$. On the other hand, the electric conductivities of **3** and **4** are ca. 110 S cm^2 mol^{-1}. The IR spectra of **3** and **4** do not show a band due to the C=O stretching vibration. Complexes **3** and **4** have been obtained from a reaction mixture (pH 10) of **1** and **2** with an ammonia solution, respectively (cf. Experimental section). Thus, complexes **3** and **4** have been assigned to **C**-type complexes, $[Co(C)tren]^+$. Complexes **3** and **4** are very slightly soluble in DMSO, though **1** and **2** are soluble. The chemical shifts of the C-1 carbon (position: cf. Fig. 2) signal for **3** and **4** are at a lower field than those of **1** and **2** (Table 1). The ε values of the charge-transfer band at ca. 340 nm in the absorption spectra for **3** and **4** are smaller than those of **1** and **2** (Table 1).

The electric conductivities of **5** and **6** are ca. 250 S cm^2 mol^{-1}. The IR spectra of **5** and **6** showed a band due to C=O stretching vibration at 1630—1644 cm^{-1}. The $-CONH_2$ proton signals of the coordinated salicylamidato ligand of **5** and **6** are observed in the region δ=8.6—9.0 in DMSO-d_6 (Fig. 3). Thus, complexes **5** and **6** are assigned to the **A**-type. The electric conductivity of **7** is 115 S cm^2 mol^{-1}. The IR spectrum of **7** does not show a band due to the C=O stretching vibration. Complex **7** is very slightly soluble in DMSO. Complex **7** was obtained from a reaction mixture (pH 10) of **5** and an ammonia solution. Thus, complex **7** is assigned to the **C**-type. Next, the electric conductivity of **9** is 145 S cm^2 mol^{-1}. The absorption spectrum of **9** shows split first bands at 510 and 535 nm. The

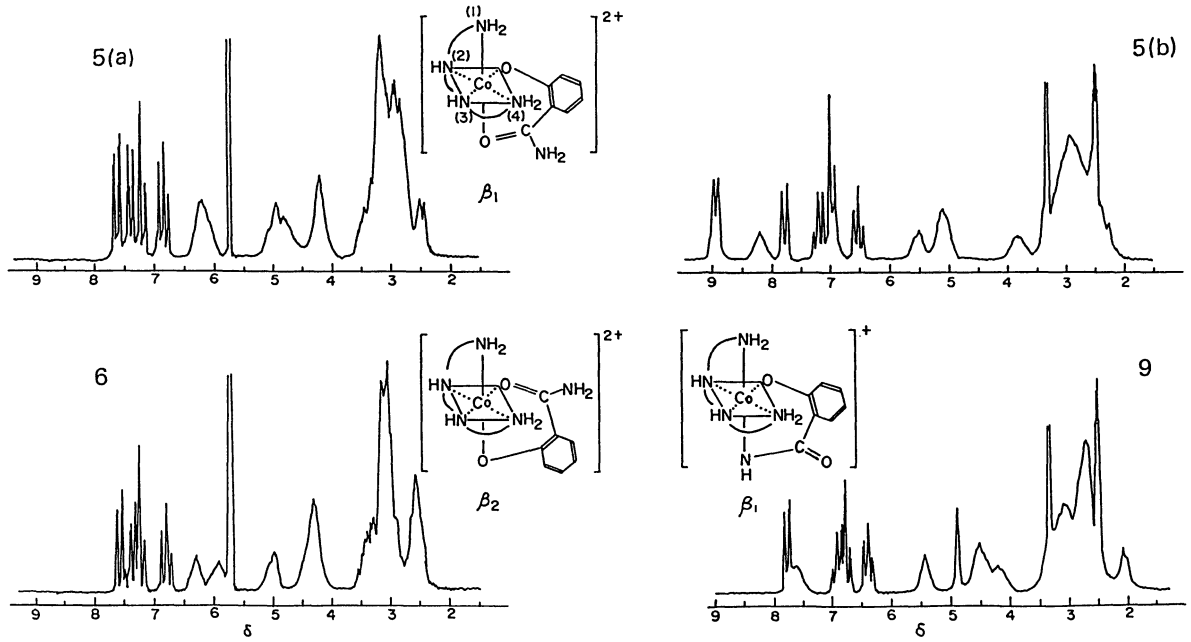

Fig. 3. ^{1}H NMR spectra of complexes **5**, **6**, and **9**.
5(a): *cis*-β_1-[Co(**A**)trien]$Cl_2 \cdot 2H_2O$ in 1.8 mol dm^{-3} D_2SO_4.
5(b): *cis*-β_1-[Co(**A**)trien]$Cl_2 \cdot 2H_2O$ in DMSO-d_6.
6: *cis*-β_2-[Co(**A**)trien]$Cl_2 \cdot 2H_2O$ in 1.8 mol dm^{-3} D_2SO_4.
9: *cis*-β_1-[Co(**D**)trien]$Cl \cdot H_2O$ in DMSO-d_6.

$-CONH^-$ proton signal of the coordinated salicylamidato ligand of **9** is observed at δ=4.89 in DMSO-d_6 (Fig. 3). The C-1 carbon signal of **9** is observed at δ=121.5. These properties of **9** are in agreement with those of **17**, which were reported previously (Table 1). Thus, complex **9** is assigned to the **D**-type, $[Co(\mathbf{D})(trien)]^+$.

The results of the electric conductivities, IR, ^1H, ^{13}C, and absorption spectra of **10**, **11**, and **12** are similar to those of (**1**, **2**, **5**, **6**), (**3**, **4**, **7**), and **9**, respectively, as shown in Table 1 and the Experimental section. Thus, **10**, **11**, and **12** are assigned to the **A**-, **C**-, and **D**-type complexes, respectively.

Isomers of the Complexes. Octahedral salicylamidato(tren)cobalt(III) complexes exist in the *t*- and *p*-isomeric forms[10,15] (Fig. 2). A distinction between **1** and **2** was found in the ^1H NMR spectra in 1.8 mol dm^{-3} D_2SO_4 (Fig. 2). The chemical shift (δ=4.69) of the proton signal of the NH_2 groups of the coordinated tren ligand of **2** is at a higher field than that (δ=4.75) of **1**, i.e., the NH_2 group of **2** is considered to be at a position trans to the phenoxyl oxygen of the coordinated salicylamidato ligand, which is more electronegative than the carbonyl oxygen.[10] Also, the signals of the methylene protons for **2** show two very sharp peaks[10] in the region δ=2.5—2.8; those for **1**, however, do not show the corresponding peaks (Fig. 2). These properties of **1** and **2** are similar to those of the corresponding complexes, **13** and **14**, respectively. Thus, **1** and **2** are assigned to the *t*- and *p*-isomers, respectively, as shown in Fig. 2. Next, the chemical shift (δ=4.85) of the proton signal of the NH_2 groups of the coordinated tren ligand of **4** in the ^1H NMR spectra in 1.8 mol dm^{-3} D_2SO_4 is at a higher field than that (δ=5.00) of **3**. The signals of the methylene protons of **4** show two very sharp peaks in the region δ=2.5—2.8, but those for **2** do not show the corresponding peaks (cf. Experimental section). In addition, complexes **3** and **4** were obtained from a reaction mixture (pH 10) of **1** and **2** with an ammonia solution, respectively. Thus, complexes **3** and **4** are assigned to the *t*- and *p*-isomers, respectively. No isomerization between *t*-isomer (**1**, **3**) and *p*-isomer (**2**, **4**) was observed in water and methanol at room temperature.

Octahedral salicylamidato(trien)cobalt(III) complexes exist in three geometrical isomers of *cis*-α, *cis*-β_1, and *cis*-β_2.[8,10] The IR spectra of **5**—**7** and **9** show four absorption bands in the NH_2 twisting region (990—1100 cm^{-1}) and four absorption bands in the NH stretching region (3000—3300 cm^{-1}) (cf. Experimental section). The ^{13}C NMR spectra of **5**—**7** and **9** show six carbon signals for the coordinated trien ligand. Thus, complexes **5**—**7** and **9** are assigned to the *cis*-β-form.[5,8] A distinction between **5** and **6** was observed in the ^1H NMR spectra in 1.8 mol dm^{-3} D_2SO_4 and the absorption spectra: the methylene proton signals of **6** were divided into two groups at δ=2.3—2.8 (3H) and 2.8—3.7 (9H) (Fig. 3); those of **5** could not be divided. The ε value of the first absorption band of **5** is greater than that of **6**. These properties for **5** and **6** are similar to those of **15** and **16**, respectively. Thus, complexes **5** and **6** were assigned to the *cis*-β_1 and β_2-isomers, respectively, as shown in Fig. 3. No isomerization between **5** and **6** was observed in water at room temperature. The methylene proton signals of **7** in 1.8 mol dm^{-3} D_2SO_4 are very close to those of **5**. Complex **7** was obtained directly from a reaction mixture (pH 10) of **5** and an ammonia solution. Thus, complex **7** was assigned to the *cis*-β_1-isomer. On the other hand, complex **7** and another complex **8** were obtained from a reaction mixture (pH 10) of **6** and an ammonia solution. Complex **8** could be assigned to the *cis*-β_2-isomer, but could not be isolated from the reaction mixture by the chromatographic method, because **8** isomerized to **7**. The methylene proton signals of **9** in 1.8 mol dm^{-3} D_2SO_4 are very close to those of **5** and **7**. Thus, complex **9** can be assigned to the *cis*-β_1-isomer.

In this study, **A**-, **C**-, and **D**-type complexes have been prepared. The formation of the **A**-type complexes is due to the bond between a cobalt atom and carbonyl oxygen of salicylamide ligand. The **C**-type complexes have been formed by the deprotonation of $-CONH_2$ of the coordinated salicylamidato ligand of the **A**-type complexes, since the **C**-type complexes have been obtained from a reaction mixture (pH 10) of the **A**-type complexes and an ammonia solution. The formation of the **D**-type complexes is due to the bond between a cobalt atom and the deprotonated imide nitrogen ($-CONH^-$) from $-CONH_2$ of the salicylamide ligand in an alkaline solution.

The different properties between the **A**-type complexes and the **C**- and **D**-type complexes are as follows: i) Yield (30—50%) of the **A**-type complexes was larger than those (4—9% for **C** and 2—3% for **D**) of the **C**- and **D**-type complexes at pH 8.6, but that (20%) of the **A**-type complexes decreases at pH 10 and those (15% for **C** and 3—5% for **D**) of the **C**- and **D**-type complexes increase. Thus, the preparation of the mixed-ligand cobalt(III) complexes with the salicylamidato ligand has been dependent upon the pH of the reaction mixture. ii) The chemical shifts (δ=113—115) of the C-1 carbon signals for the **A**-type complexes are at a higher field than those (δ=117—122) of the **C**- and **D**-type complexes. iii) The ε values (3400—3700) of the charge-transfer band at ca. 340 nm in the absorption spectra for the **A**-type complexes are greater than those (2500—3000) of the **C**- and **D**-type complexes.

The **C**-type and **D**-type complexes are a linkage isomer. A characteristic property of this linkage isomer has been observed in the absorption and ^{13}C NMR spectra as well as solubility in DMSO: i.e., the first absorption band for the **D**-type complexes shows split first bands at ca. 510 and 535 nm; that for the **C**-type complexes, however, does not show a split first band. The C-1 carbon signals of the **D**-type complexes are observed in the region δ=120—122, but those of the **C**-type complexes are observed at δ=117—118. The **D**-

type complexes are soluble in DMSO, but the **C**-type complexes are very slightly soluble.

References

1) Part VI: Y. Yamamoto and N. Shinya, *Bull. Chem. Soc. Jpn.*, **60**, 1186 (1987).
2) Y. Yamamoto, R. Kataoka, S. Imahara, and T. Amano, *Bull. Chem. Soc. Jpn.*, **54**, 2972 (1981).
3) Y. Yamamoto, E. Toyota, and Y. Yamamoto, *Bull. Chem. Soc. Jpn.*, **56**, 2721 (1983).
4) Y. Yamamoto and E. Toyota, *Bull. Chem. Soc. Jpn.*, **57**, 47 (1984).
5) Y. Yamamoto and E. Toyota, *Bull. Chem. Soc. Jpn.*, **52**, 2540 (1979).
6) Y. Yamamoto, H. Kudo, and E. Toyota, *Bull. Chem. Soc. Jpn.*, **56**, 1051 (1983).
7) E. Toyota, Y. Yamamoto, and Y. Yamamoto, *Bull. Chem. Soc. Jpn.*, **61**, 3175 (1988).
8) Y. Yamamoto, K. Yoshii, E. Toyota, and K. Konno, *Bull. Chem. Soc. Jpn.*, **62**, 724 (1989).
9) Y. Yamamoto, E. Toyota, and S. Tsukuda, *Bull. Chem. Soc. Jpn.*, **58**, 1595 (1985).
10) E. Toyota and Y. Yamamoto, *Bull. Chem. Soc. Jpn.*, **62**, 3817 (1989).
11) B. S. Pannu, S. L. Chopra, and S. S. Parmar, *Indian. J. Chem.*, **9**, 1396 (1971).
12) B. S. Pannu and S. L. Chopra, *J. Indian. Chem. Soc.*, **51**, 387 (1974).
13) B. S. Pannu and S. L. Chopra, *Z. Anorg. Allg. Chem.*, **398**, 83 (1973).
14) "Handbook of Proton-NMR Spectra and Data," ed by Asahi Research Center Co., Ltd., Academic Press, Tokyo (1985), Vol. 2, p. 292.
15) The designations *t* and *p* refer to the position of the phenoxyl oxygen trans to a tertiary (*t*) or a primary (*p*) amine nitrogen of tren, respectively.

Fluorometric Determination of Amino Acids and Proteins Utilizing a Copper(II) Catalyzed Reaction

Hisakazu MORI,* Kazue SAKAI, Kyoko YAMASHINA, Sayuri HIRATA, and Kumiko HORIE
Kyoritsu College of Pharmacy, Shibakoen, Minato-ku, Tokyo 105
(Received May 18, 1991)

Amino acids accelerated the copper(II)-catalyzed oxidation of di-2-pyridyl ketone hydrazone (DPKH) to form a fluorescent compound. With the use of this enhancement effect of catalysis, various amino acids (L-histidine, L-cysteine, L-glutamic acid, glycine, DL-serine, and L-arginine) could be determined by flow injection analysis. The detection limit of L-histidine was less than 2 pmol. On the contrary, proteins decreased the catalysis. Proteins were also determined through the utilization of this effect. In this determination, the addition of citric acid was found to be very effective. The detection limit of bovine serum albumin was less than 20 ng. The effect of protein upon the catalysis of copper(II) was considered to be ascribable to an inhibition of the coordination of DPKH to copper(II).

In trace analyses of amino acids they are usually transformed to derivatives which can be detected colorimetrically or fluorometrically at low level. One mole of the derivative corresponds to one mole of an amino acid in such reactions. Amino acids can also be determined by other methods than those with derivatisation. In these methods, two types of reactions seem to be utilized. One type is such a chemiluminescence reaction as that between luminol and hydrogen peroxide catalyzed by cobalt(II)[1] or copper(II).[2] The addition of an amino acid to this reaction system, forming a complex with a metal ion, reduces the chemiluminescence. Thus, amino acids are determined quantitatively. The other type is a fluorogenic oxidation reaction catalyzed by copper(II) in which amino acids accelerate the reaction rate. With the use of this enhancement effect of catalysis, amino acids were determined[3] by flow injection analysis (FIA). In this catalytic reaction, one mole of an amino acid may correspond to more than one mole of the fluorescent compound. Thus, a more sensitive detection would be achieved by optimizing the reaction conditions. This would also be done by the use of a reaction substrate which is oxidized to a compound having intense fluorescence.

In the present study regarding the determination of amino acids, di-2-pyridyl ketone hydrazone (DPKH) was adopted as a reaction substrate instead of phenyl 2-pyridyl ketone hydrazone (PPKH), which was used in the previous study.[3] It is known[4] that the oxidation product of DPKH shows an intense fluorescence in the acidic media. Thus, the FIA system was applied with a flow line of hydrochloric acid in order to detect the oxidation product in an acidic media. The effects of proteins on the copper(II)-catalyzed oxidation were also investigated, compared with those of amino acids. The necessary conditions for the sensitive detection of proteins were pursued.

Experimental

Chemicals. DPKH was synthesized by the reaction of di-2-pyridyl ketone with hydrazine monohydrate according to a method described in the literature.[4] Amino acids and copper(II) salts were of analytical reagent grade. Bovine serum albumin (BSA) was purchased from Sigma Chemical Co. and human serum albumin (HSA), from Wako Pure Chemical Industries, LTD.

Apparatus and Procedures. Figure 1 shows a schematic diagram of the FIA system used in the present study. It contains four flow lines (Teflon, 0.5 mm i.d.). C_1 is a 5×10^{-5} M(1 M $\equiv$1 mol dm^{-3}) aqueous solution of DPKH. C_2 is 0.1 M NaOH. C_3 is water and C_4 is 0.4 M HCl. An alkaline solution of DPKH could not be used instead of the flow lines, C_1 and C_2, because of the gradual change of the base line on the recorder. All solutions were pumped by two double-plunger-type pumps (Nihonseimitsu NP-D-322U) at a flow rate of 1.2 cm^3 min^{-1}. Samples were injected to the flow system by an injector (Nihonseimitsu NVI-3002) with a 50 mm^3 sample loop. The aerial oxidation of DPKH, catalyzed by the amino acid–copper(II) complex, was carried out in a reaction coil (150 cm) immersed in a water bath thermostated at 25 °C. The fluorescence[4] (λ_{ex} 349 nm, λ_{em} 435 nm) of the reaction

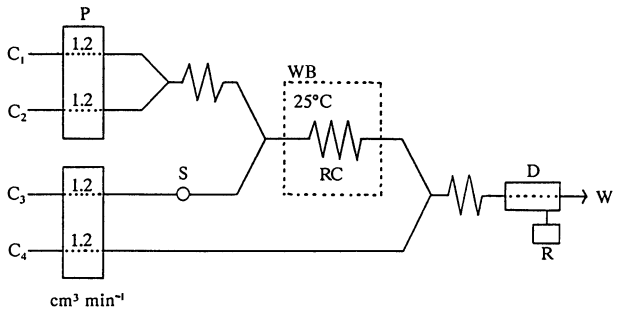

Fig. 1. Schematic diagram of the FIA system.
S: sample injector, C_1: 5×10^{-5} M aqueous solution of DPKH, C_2: 0.1 M NaOH, C_3: water, C_4: 0.4 M HCl, P: pump, RC: reaction coil, WB: water bath, D: detector, R: recorder, W: waste.

product acidified by 0.4 M HCl was monitored by a spectrofluorometer (Hitachi F-1000) with a 12 mm^3 flow cell, and recorded on a recorder (data processor, Shimadzu C-R1A). The peak height of the signal was calculated using this recorder.

The samples of amino acids were prepared in a buffer solution as mixtures of 4×10^{-7} M copper(II) and various amounts of each amino acid. After stirring for 10 min it was subjected to analysis. The samples of proteins were usually prepared in a similar manner as described above. Those in the Atkins–Pantin buffer (boric acid–potassium chloride–sodium carbonate) containing citrate were prepared as follows. A copper(II) solution in a citric acid–disodium hydrogenphosphate buffer (pH 3.0) was diluted with the Atkins–Pantin buffer. This solution was mixed with a Atkins–Pantin buffer solution of protein.

Absorption Spectra Measurements. The absorption spectra of the mixtures of copper(II), L-histidine (or BSA), and DPKH were measured at room temperature as follows. A mixture in a quartz cell of 0.5 cm^3 of 2×10^{-3} M aqueous copper(II) solution, 1 cm^3 of aqueous L-histidine (or BSA) solution, and 0.5 cm^3 of 0.05 M Clark–Lubs buffer (boric acid–potassium chloride–sodium hydroxide, pH 9.0) was bubbled with N_2 gas for 5 min. Then, into this mixture was added 1 cm^3 of a 1×10^{-3} M aqueous solution of DPKH through which N_2 gas had been previously passed. About 5 s after mixing, a measurement of the absorption spectrum was started with a spectrophotometer (Hitachi U-3210).

Results and Discussion

Determination of Amino Acids. As reported in a previous paper,[3] the amino acid–copper(II) complex in the alkaline buffer solution had shown an enhanced catalytic activity in the aerial oxidation of PPKH. In the present work using DPKH, the catalytic activities of the amino acid–copper(II) (1 : 1) complex (4×10^{-7} M) in the buffer solutions of various pH values were compared with those of copper(II). The amino acid used was L-histidine, which had given the maximum activity in a previous study.[3] Phosphate buffer (0.005 M) was employed in the pH range of 5.0 to 7.0, and Clark–Lubs buffer (0.005 M) in the pH range of 8.0 to 10.0. As shown in Fig. 2, copper(II) and the L-histidine–copper(II) complex indicated comparable catalytic activities in weakly acidic media. In more basic media, the catalytic activities of both decreased, though that of the L-histidine–copper(II) complex became superior to that of copper(II), showing that the addition of L-histidine to copper(II) in a basic media enhances the catalytic activity of copper(II), as in the case of the aerial oxidation of PPKH.[3] It was suggested that the determination of this amino acid could be made most sensitively with the use of a buffer of pH 9.0 among those of various pH values. The decrease in the catalytic activity in more basic media would be due to the formation of phosphate(s) or hydroxide(s) of copper(II); this decrease could be partly prevented by the formation of an active L-histidine–copper(II) complex.

Other reaction conditions were examined in order to detect lower amounts of L-histidine. Favorable peaks were obtained at a DPKH concentration of 5×10^{-5} M in the series of 5×10^{-4}, 5×10^{-5} and 5×10^{-6} M. Among three concentrations (0.05, 0.005, and 0.0005 M) of the Clark–Lubs buffer (pH 9.0), that of 0.005 M gave the greatest difference between the signal due to aerial oxidation with and without L-histidine. Several copper(II) salts, i.e., nitrate, chloride, perchlorate, and sulfate were examined, and the use of copper(II) nitrate gave the maximum signal. The temperature of the water bath where the reaction coil was immersed was varied (15, 25, 35, and 45 °C). Since the signal did not increase very

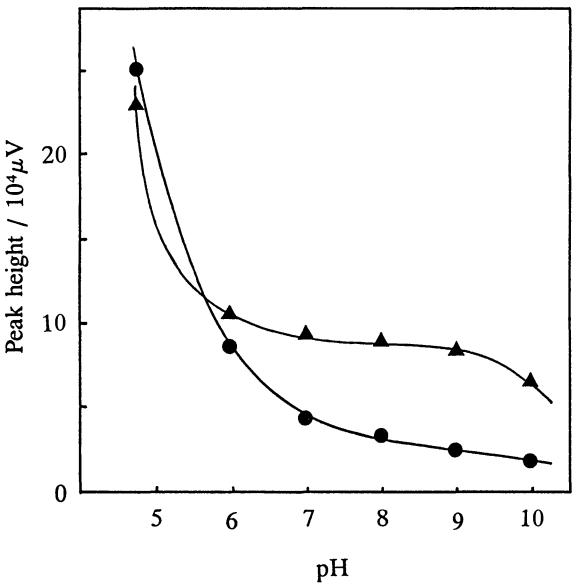

Fig. 2. Variation of the peak heights of signals with a change of the pH values of sample solutions.
●: copper(II), ▲: copper(II) + L-histidine(1 : 1).

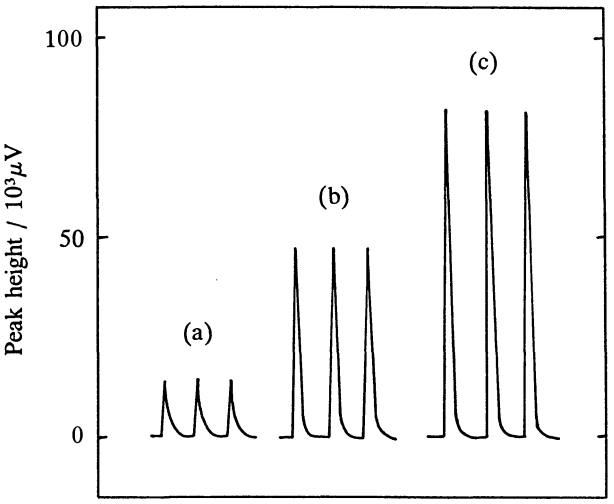

Fig. 3. Peaks with increased height by the addition of L-histidine.
(a): 0, (b): 0.4, (c): 0.8.
The amount of added L-histidine is represented by the molar ratio to copper(II).

much at temperatures greater than 25 °C, a temperature of 25 °C was adopted for the reaction. The variation of the concentration of hydrochloric acid did not change the peak height, provided that the concentration of hydrochloric acid is higher than that of the sodium hydroxide solution. Thus, concentrations of 0.4 and 0.1 M were respectively employed as those of the hydrochloric acid and sodium hydroxide solutions.

Figure 3 shows the peaks obtained when the samples containing various amounts of L-histidine were subjected to analysis. As the molar ratio of L-histidine to copper(II) was increased, the fluorescence intensity increased linearly in the molar ratio range from 0 to 1. The correlation coefficient (r) was 0.996 (n=7) and the relative standard deviation at a molar ratio of 0.4 was 2.3% (n=5). All of the amino acids investigated increased the catalysis of copper(II). In the cases of L-histidine and L-cysteine, the peak height of the signal increased linearly over a molar ratio range of about 1, but deviated from a linear relationship at a molar ratio greater than 1. The maximum molar ratio below which a linear relationship was observed was 3 for L-glutamic acid, 4 for glycine and DL-serine, and 5 for L-arginine. The calibration curves for all amino acids included the point of molar ratio 0 in the linear range. Table 1 gives the upper limits of the linear range for each amino acid. In Table 1 are also shown the slopes of the calibration curves which were defined as the difference between the peak height at a molar ratio of 1 and that at a molar ratio of 0. The slopes for L-histidine and L-cysteine are larger than those for other amino acids. A similar tendency had been observed in a determination using PPKH,[3] though this tendency was more marked in the present study.

In the determination of L-histidine, the content of this amino acid was 2 pmol in a sample with a molar ratio of 0.1. This value was less than one third of that in the case of PPKH. This difference would come from the character of the oxidation product of DPKH, which shows intense fluorescence in an acidic media.

Table 2 shows the effects of foreign metal ions in the determination of L-histidine. The relative peak height of the signal in the case of the mixture to that in the case of copper(II) was used as an indication of the effect of a foreign metal ion. Zinc(II), manganese(II), silver(I), mercury(II), and cobalt(II) increased the peak height in this order. On the other hand, nickel(II) and iron(III) decreased the peak height. EDTA at the same level as copper(II) interfered with the determination. This would be ascribed to the formation of a copper(II)–EDTA complex with a large formation constant, to which DPKH cannot coordinate.

Determination of Proteins. We further applied this method to the determination of protein which is practically important in biological studies. Preliminary

Table 1. Upper Limits of the Linear Ranges and Slopes of Calibration Curves for Various Amino Acids

Amino acid	Upper limit/10^{-7} M	Slope/10^3 μV
L-Histidine	4	69.0
L-Cysteine	3.2	73.7
L-Glutamic acid	12	15.4
Glycine	16	11.6
DL-Serine	16	6.3
L-Arginine	20	2.1

Table 2. Relative Peak Heights in the Presence of Foreign Metal Ions

Metal ion	Added Amount/[Metal ion][Cu(II)]$^{-1}$				
	0.5	1	10	100	500
None		1			
Co(II)		1.7	4.3		
Hg(II)		1.3	2.8		
Ag(I)		1.1	1.8		
Mn(II)		1.1	1.4		
Zn(II)		1.0	1.1	1.4	1.7
Al(III)		1.0	1.0	1.0	1.0
Ni(II)		0.9	0.2		
Fe(III)		0.9	0.7		
EDTA	0.5	0.1	≈0		

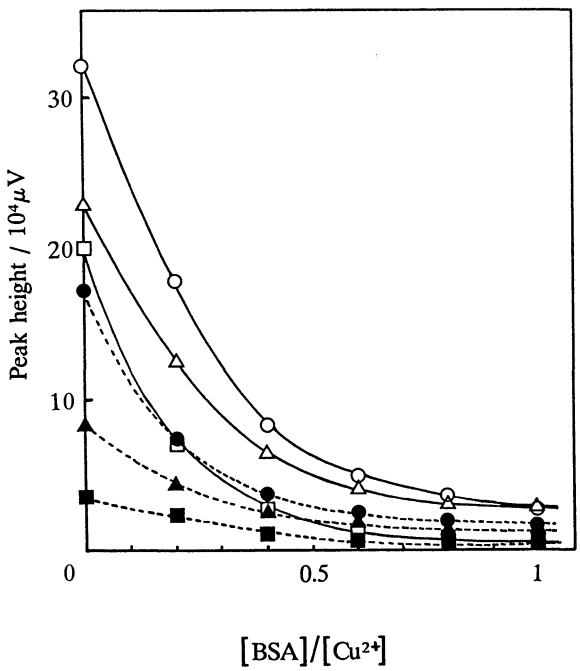

Fig. 4. Calibration curves for BSA samples in phosphate buffers (0.005 M) and citric acid–disodium hydrogenphosphate buffers of various pH values.
phosphate buffer, ●: pH 5.0, ▲: pH 6.0, ■: pH 8.0.
citric acid–disodium hydrogenphosphate buffer, ○: pH 5.0, △: pH 6.0, □: pH 8.0.
BSA samples were prepared on the assumption that the molecular weight of BSA was 69000. Thus, in the case that the molar ratio of BSA to copper(II) is unity, this sample contains 1380 ng of BSA. The samples in a citric acid–disodium hydrogenphosphate buffer contain 0.005 M citric acid.

experiments concerning BSA showed that this protein decreased the catalysis of copper(II), in contrast with amino acids. Figure 4 indicates the effects of the kinds of buffers and their pH values of BSA samples. With respect to the samples in a phosphate buffer, the catalysis of free copper(II) (that is, when no protein was added) was markedly lowered in the alkaline pH region. On the other hand, the samples in citric acid–disodium hydrogenphosphate buffer showed higher catalytic activities than those in phosphate buffer and the catalysis was not so much decreased, even in the alkaline pH region. This effect would be due to the formation of a soluble citric acid–copper(II) complex toward which DPKH can coordinate to be oxidated. Another oxyacid, tartaric acid, also showed a similar effect in the alkaline pH region, which was fairly smaller than that due to citric acid.

By experiments involving spectrum measurements (see below), it was previously confirmed that BSA reacts with greater amounts of copper(II) in more basic solutions. Thus, in order to detect lower amounts of protein, we exclusively examined samples in strongly alkaline buffers containing citrate. The Clark–Lubs buffer (pH 8.0—10.0) and the Atkins–Pantin buffer (pH 9.0—11.0) were employed for sample preparation. In the case of the Clark–Lubs buffer, that of pH 10.0 afforded the most acute decrease in signal over the range of small amounts of added protein. However, plotting of data over this range gave a calibration curve with comparatively large scattering. When the Atkins–Pantin buffer was applied, a more basic buffer reduced more extensively the signal due to free copper(II). Thus, a buffer of pH 9.0 afforded the best calibration curve, containing a linear line (r=−0.997) over the range of less than 200 ng of added protein (Fig. 5). The relative standard deviation upon the addition of 80 ng of BSA was 1.50% (n=5). Figure 5 also shows the calibration curve for HSA; it contains a linear line(r=−1.000) over the range of less than 200 ng. The relative standard deviation upon the addition of 80 ng of HSA was 1.69%, (n=5). The detection limits were less than 20 ng in the respective calibration curves. At present, the sensitivity using the present method for protein determination does not attain to that in the method using the copper(II) catalyzed chemiluminescence reaction between 1,10-phenanthroline and hydrogen peroxide.[5]

We presently have interest in the different effects of proteins from amino acids on the catalysis of copper(II). In order to elucidate this difference, the effect of L-histidine or BSA on the coordination of DPKH to copper(II) was investigated. As the absorption spectrum (a) in Fig. 6 shows, the mixing of a solution of DPKH with a solution of copper(II) in alkaline buffer (Clark–Lubs, pH 9.0) afforded a new absorption maximum at 426 nm, indicating the coordination of DPKH to copper(II). When the solution of DPKH was mixed with a copper(II) solution containing L-histidine, the spectrum was little changed in the region of a molar ratio of L-histidine to copper(II) less than 1. On the contrary, when the DPKH solution was mixed with a copper(II) solution containing BSA, the absorbance was remarkably reduced at a molar ratio less than 1 (spectrum (b)—(e) in Fig. 6). In a more basic buffer, this tendency was much more marked. These facts would

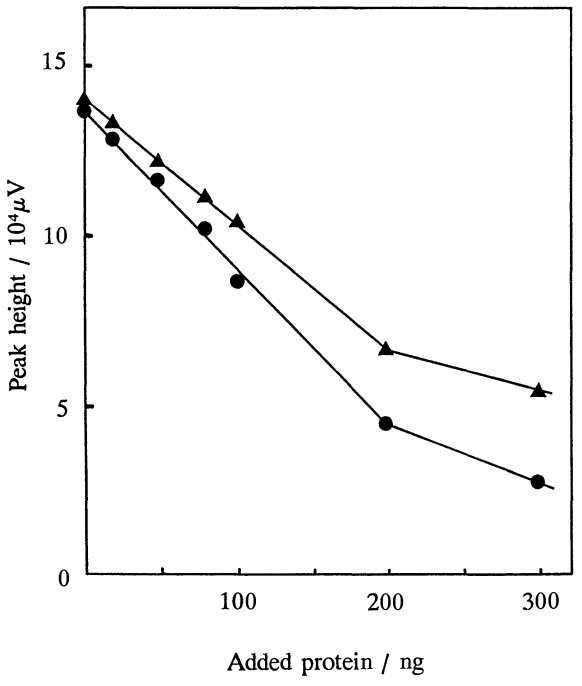

Fig. 5. Calibration curves for BSA and HSA samples in an Atkins–Pantin buffer containing citrate (pH 9.0).
●: BSA, ▲: HSA.
The sample solutions prepared contain 2×10^{-5} M citric acid, 0.05 M boric acid, 0.05 M potassium chloride, and 0.029 M sodium carbonate.

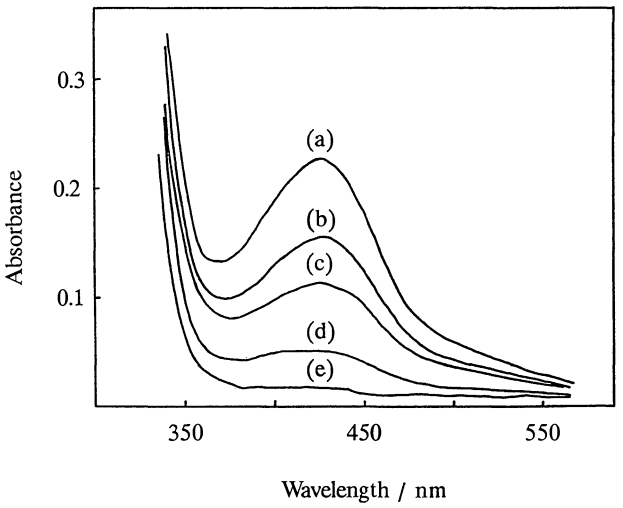

Fig. 6. Absorption spectra of the mixtures of copper(II), BSA, and DPKH with various molar ratios of BSA to copper(II).
(a): 0, (b): 0.047, (c): 0.094, (d): 0.19, (e): 0.47.

indicate that BSA firmly coordinated to copper(II) and inhibited the coordination of DPKH to copper(II), while L-histidine scarcely did so.

The determination of amino acids or proteins by the present method can be performed in 1 min. The sensitive detection of amino acids was achieved by the utilization of DPKH, owing to the intense fluorescence of the reaction product in an acidic media. The use of the compounds whose oxidation product have more intense fluorescence and/or which are oxidized with high velocity would increase the sensitivity in the detection of amino acids or proteins. The study in this direction is in progress.

References

1) A. MacDonald and T. A. Nieman, *Anal. Chem.*, **57**, 936 (1985).
2) T. Hara, M. Toriyama, T. Ebuchi, and M. Imaki, *Chem. Lett.*, **1985**, 341.
3) H. Mori and K. Natsume, *Anal. Sci.*, **3**, 581 (1987).
4) F. Grases, F. Garcia-Sanchez, and M. Valcarcel, *Anal. Chim. Acta*, **119**, 359 (1980).
5) T. Hara, T. Ebuchi, A. Arai, and M. Imaki, *Bull. Chem. Soc. Jpn.*, **59**, 1833 (1986).

Ferromagnetic Spin-Coupling between Gadolinium(III) and Copper(II) Ions in Discrete Binuclear Gd(III)-Cu(II) Complexes

Masatomi SAKAMOTO,* Masayuki HASHIMURA, Kimihiro MATSUKI, Naohide MATSUMOTO,*,† Keiji INOUE,† and Hisashi ŌKAWA†

Department of Applied Chemistry, Faculty of Engineering, Ehime University, Matsuyama 790
†Department of Chemistry, Faculty of Science, Kyushu University, Fukuoka 812

(Received May 30, 1991)

Three discrete binuclear gadolinium(III)–copper(II) complexes ($CuGd(fsadien)NO_3 \cdot 5H_2O$ (**1**), $CuGd(hsapn)NO_3 \cdot 3H_2O$ (**2**), and $[Gd(pvm)_3Cu(A)]$ (**3**)) have been synthesized; we use the notation H_4fsadien=*N,N'*-bis(3-carboxysalicylidene)diethylenetriamine, H_4hsapn=*N,N'*-bis(3-hydroxysalicylidene)-1,2-propanediamine, Hpvm= dipivaloylmethane (2,2,6,6-tetramethyl-3,5-heptanedione), and H_2A=4-(6-methyl-8-oxo-2,5-diazanona-1,5,7-trienyl)imidazole. Magnetic susceptibility measurements (4.2—300 K) have revealed that the spin coupling between the Gd(III) and Cu(II) ions is ferromagnetic with coupling constants J=+2.3 cm^{-1} for (**1**), +5.7 cm^{-1} for (**2**), and +0.5 cm^{-1} for (**3**), on the basis of the spin-Hamiltonian $H=-2JS_{Gd} \cdot S_{Cu}$.

Magnetic studies on the d-transition metal polynuclear complexes have shown tremendous progress during the latest decade regarding experimental and theoretical fields.[1,2] Procedures have become fairly well established for predicting the magnetic properties of polynuclear d-transition metal complexes.[1,2] On the other hand, magnetic investigations concerning mixed-metal complexes comprising d- and f-transition metal ions have been overlooked until recently due to the very weak interaction and the large anisotropic effect of lanthanoid ions. Characterization of the magnetic interaction between d- and f-transition metal ions is our next target for elucidation. In particular, the synthesis of ferromagnetic complexes is among the stimulating subjects. Recently, Gatteschi and his co-workers reported on the ferromagnetic interaction operating between Gd(III) and Cu(II) ions in a trinuclear $GdCu_2$ system $\{Cu(saltn)\}_2Gd(H_2O)(NO_3)_3 \cdot 2C_2H_5NO_2$ (H_2saltn=*N,N'*-di(salicylidene)-1,3-propanediamine)[3] and its related complexes[4] as well as a tetranuclear Gd_2Cu_2 system $[Gd(hfac)_3Cu(satn)(OH)]_2$ (hfac= hexafluoroacetylacetonate, Hsatn=*N*-(3-aminopropyl)-salicylideneamine).[5] However, in these complexes the antiferromagnetic interaction operating between the terminal copper ions makes it difficult to evaluate the magnetic interaction between the Cu(II) and Gd(III) ions. In order to establish the magnetic interaction between Cu(II) and Gd(III) ions, it is desirable to synthesize discrete binuclear Gd(III)–Cu(II) complexes and to investigate their magnetic properties. Recently, in a communication, we reported on the synthesis and ferromagnetic property of a discrete Gd(III)–Cu(II) complex, $CuGd(fsaen)NO_3 \cdot 4H_2O$($H_4$fsaen=*N,N'*-bis(3-carboxysalicylidene)ethylenediamine).[6] In order to provide more examples of discrete binuclear Gd(III)–Cu(II) complexes and to investigate the structural variation effects (bridging mode and coordination geometry) upon spin-coupling, we prepared in the present study complexes (**1**), (**2**), and (**3**) and investigated their magnetic properties.

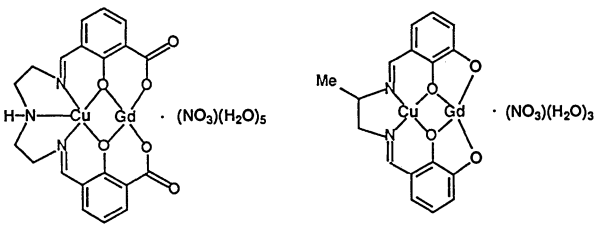

1 **2**

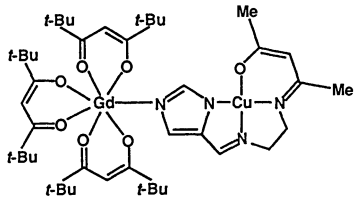

3

Experimental

Physical Measurements. Elemental analyses for C, H, and N were carried out at the Service Center of Elemental Analysis, Kyushu University. Copper and Gadolinium were determined by titration against EDTA, where NH_4F and thiourea were used as masking reagents for Gd and Cu, respectively. The magnetic susceptibilities were measured with a HOXAN HSM-D SQUID magnetometer over the temperature range 4.2—300 K under the applied magnetic field 500 G. The magnetic susceptibilities were calibrated by the use of $(NH_4)_2Mn(SO_4)_2 \cdot 6H_2O$. Data were corrected for magnetization of the sample holder and for diamagnetism contributions with Pascal's constants. The effective magnetic moments were calculated by the equation $\mu_{eff}=2.828(\chi_M T)^{1/2}$, where χ_M is the magnetic susceptibility per CuGd.

Synthesis. Starting complexes $Cu(H_2fsadien)$,[7] $[Gd(pvm)_3]$,[8] and $[Cu(A)] \cdot 0.5\ CHCl_3$[9] were prepared according to methods described in the literature; where H_4fsadien=*N,N'*-bis(3-carboxysalicylidene)diethylenetriamine, Hpvm=dipivaloylmethane (2,2,6,6-tetramethyl-3,5-heptanedione), and H_2A= 4-(6-methyl-8-oxo-2,5-diazanona-1,5,7-trienyl)imidazole.

$CuGd(fsadien)NO_3 \cdot 5H_2O$ (1). To a suspension of

Cu(H_2fsadien) (1 mmol) in 50 cm^3 of methanol was added a methanol solution (10 cm^3) of $LiOH \cdot H_2O$ (2 mmol) followed by 240 cm^3 of methanol. The mixture was then heated until it became clear. To this solution was added a methanol solution (5 cm^3) of $Gd(NO_3)_3 \cdot 6H_2O$ (1 mmol). After refluxing for 2 h, the solution volume was reduced to 50 cm^3 by a rotary evaporator. Green microcrystals precipitated were collected by suction filtration, washed with methanol and diethyl ether, and dried in air. Yield 60 %. Anal. Calcd for $C_{20}H_{27}N_4O_{14}CuGd$: C, 31.27; H,3.54; N, 7.29; Cu, 8.27; Gd, 21.32%. Found: C, 31.29; H, 3.22; N, 7.38; Cu, 8.28, Gd, 21.30%.

Bis(2-formyl-6-hydroxyphenoxy)copper(II) Monohydrate (2a). To a methanol solution (60 cm^3) of 2,3-dihydroxybenzaldehyde (20 mmol) was added an aqueous solution (50 cm^3) of copper(II) acetate monohydrate (10 mmol) in order to immediately precipitate a yellow-brown powder. After stirring for 1 h at room temperature, the precipitate was collected by suction filtration, washed with water, methanol, and diethyl ether, and dried in air. The yield was 90 %. Anal. Calcd for $C_{14}H_{10}O_6Cu \cdot H_2O$: C, 47.26; H, 3.40%. Found: C, 47.57; H, 3.5%.

[*N,N'*-Bis(3-hydroxysalicylidene)-1,2-propanediaminato-copper(II) Monohydrate Cu(H_2sapn)$\cdot H_2O$ (2b). To a suspension of **2a** (40 mmol) in ethanol (150 cm^3) was added 1,2-propanediamine (20 mmol). The mixture was first warmed on a hot plate for 2 h under stirring, and then cooled to room temperature, resulting in a brown precipitate which was collected by suction filtration, washed with water, ethanol, and diethyl ether, and finally dried in air. Yield 85—90%. Anal. Calcd for $C_{17}H_{16}N_2O_4Cu \cdot H_2O$: C, 51.84; H, 4.61; N, 7.11; Cu, 16.13%. Found: C, 52.33; H, 4.56; N, 7.08; Cu, 15.97%.

CuGd(hsapn)$NO_3 \cdot 3H_2O$ (2). To a suspension of **2b** (2.5 mmol) in 20 cm^3 of methanol was added a methanol solution (25 cm^3) of $LiOH \cdot H_2O$ (5 mmol). To the resulting clear solution was added a methanol solution (10 cm^3) of $Gd(NO_3)_2 \cdot 6H_2O$; the mixture was subsequently refluxed for 2 h. After cooling to room temperature, a brown precipitate was collected by suction filtration, washed with methanol and diethyl ether, and dried in air. Yield 95%. Anal. Calcd for $C_{17}H_{14}N_3O_7CuGd \cdot 3H_2O$:C, 31.55; H, 3.11; N, 6.49; Cu, 9.82; Gd, 24.30%. Found: C, 31.69; H, 3.05; N, 6.86; Cu, 9.48; Gd, 24.10%.

[Gd(pvm)$_3$Cu(A)] (3). To a chloroform solution (20 cm^3) of [Gd(pvm)$_3$] (0.5 mmol) was added a chloroform solution (30 cm^3) of [Cu(A)]$\cdot$0.5$CHCl_3$ (0.5 mmol). The mixture was warmed on a hot plate for 10 min and filtered. To the filtrate was added diethyl ether dropwise until the solution became cloudy. After standing overnight, silky red crystals were collected by suction filtration, washed with ether, and dried in air. Recrystallization was carried out from the mixed solution of chloroform–diethyl ether. The yield was 10 %. Anal. Calcd for $C_{44}H_{71}N_4O_7CuGd$: C, 53.44; H, 7.24; N, 5.67; Cu, 6.43; Gd, 15.89%. Found: C, 53.50; H, 7.23; N, 5.69; Cu, 6.30; Gd, 15.75%.

Results and Discussion

The temperature dependence of the magnetic susceptibility per CuGd unit (χ_M), the reciprocal magnetic susceptibility ($1/\chi_M$), and the effective magnetic moment (μ_{eff}) of CuGd(fsadien)$NO_3 \cdot 5H_2O$ (**1**) are shown in Fig. 1. The numerical magnetic data of (**1**)—(**3**)

CuGd(fsadien)$NO_3 \cdot 5H_2O$ (1).

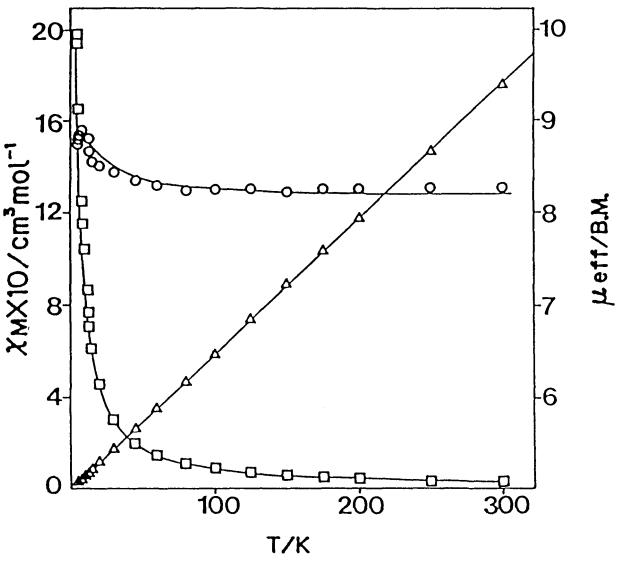

Fig. 1. Plots of χ_M vs. T(△), $1/\chi_M$ vs. T(△), and μ_{eff} vs. T(○) for (**1**), where χ_M is the magnetic susceptibility per GdCu unit, μ_{eff} the effective magnetic moment. The theoretical curve is drawn with the fitting parameters g=2.01, J=+2.3 cm^{-1}, θ=−0.12 K as solid lines.

and the plots of χ_M vs. T, $1/\chi_M$ vs. T, and μ_{eff} vs. T for (**2**) and (**3**) are reported as supplementary materials (Tables SI—SIII, Figs. S1 and S2) as Document No. 8970 at the office of the Editor of Bull. Chem. Soc. Jpn. The $1/\chi_M$ vs. T plot of (**1**) follows the Curie-Weiss law ($\chi_M = C/(T-\theta)$) with a Weiss constant θ=1.1 K, suggesting a weak ferromagnetic interaction. The effective magnetic moment at room temperature is 8.27 μ_B, which is slightly larger than the spin-only value (8.12 μ_B) in the absence of the magnetic interaction of this spin-system (S_{Cu}=1/2, S_{Gd}=7/2). It should be noted here that the ground state of Gd(III) is $^8S_{7/2}$ and that the next excited state is well separated in energy, so that its μ_{eff} value can be approximated by the spin-only equation, $\mu_{eff}=[4s(s+1)]^{1/2}$. As the temperature is lowered, the magnetic moment increasing gradually from 8.27 μ_B at 300 K, reaches a maximum value of 9.10 μ_B at 10.0 K, and then decreases to 8.73 μ_B at 4.8 K. The maximum value (9.10 μ_B) is comparable to the spin-only value (8.94 μ_B) for the spin-state S=4, which should arise from a ferromagnetic spin-coupling of the spin-system Gd(III)–Cu(II) (S_{Gd}=7/2, S_{Cu}=1/2). Thus, the observed magnetic behavior clearly demonstrates the operation of an intramolecular ferromagnetic spin-coupling between Gd(III) and Cu(II) ions. A decrease in the magnetic moment below 10 K may be attributed to an intermolecular antiferromagnetic interaction. The magnetic behaviors of (**2**) and (**3**) are essentially similar to that of (**1**). The magnetic data could be reproduced on the basis of a spin-only expression including a correction

Table 1. Coupling Constants in Gd(III)–Cu(II) Complexes

Compound	System	J_{GdCu}	θ	J_{CuCu}	Ref.
$CuGd(fsaen)NO_3 \cdot 3H_2O$	GdCu	+2.1	—	—	6
$CuGd(fsadien)NO_3 \cdot 5H_2O$ (**1**)	GdCu	+2.3[a]	−0.12	—	This work
$CuGd(hsapn)NO_3 \cdot 3H_2O$ (**2**)	GdCu	+5.7[b]	−1.5	—	This work
$Gd(pvm)_3Cu(A)$ (**3**)	GdCu	+0.5[c]	—	—	This work
$[Cu(hapen)_2Gd(H_2O)_3](ClO_4)_3$	$GdCu_2$	+2.7	—	−2.1	4
$[Cu(salen)_2Gd(H_2O)_3](ClO_4)_3$	$GdCu_2$	+3.7	—	−6.1	4
$[Cu(saltn)_2Gd(H_2O)(NO_3)_2]$	$GdCu_2$	+0.61	—	−1.8	3
$[Gd(hfac)_3Cu(satn)OH]_2$	Gd_2Cu_2	+1.42	—	−1.73	5

The spin-Hamiltonian is taken as the form $H=-2JS_{Gd} \cdot S_{Cu}$ for all the complexes. Cu(hapen) = *N,N'*-ethylenebis[1-(*o*-hydroxyphenyl)ethaniminato]copper(II). Cu(salen)=[*N,N'*-di(salicylidene)ethylenediaminato]copper(II). Cu(saltn)=[*N,N'*-di(salicylidene)-1,3-propanediaminato]-copper(II). H_4fsaen=*N,N'*-bis(3-carboxysalicylidene)ethylenediamine. a), b), c). The agreement factors $R=[\sum(\mu_{obsd}-\mu_{cald})^2/\sum\mu_{obsd}^2]^{1/2}$; a), 0.014; b), 0.015; c), 0.0068.

term of intermolecular interaction (1), where a spin-Hamiltonian is defined as $H=-2JS_{Cu} \cdot S_{Gd}$.

$$\chi_M=\frac{4Ng^2\beta^2}{kT(T-\theta)}\frac{15+7\exp(4J/kT)}{9+7\exp(4J/kT)}, \quad (1)$$

Theoretical curves using the best-fit parameters are represented as solid lines in Fig. 1. The best-fit parameters of (**1**)—(**3**) and the agreement factors $R=[\sum(\mu_{obsd}-\mu_{cald})^2/\sum\mu_{obsd}^2]^{1/2}$, along with the parameters of Gd(III)–Cu(II) oligomers reported so far are given in Table 1. The coupling between Gd(III) and Cu(II) ions are all ferromagnetic, in spite of the differences among the complexes in coordination numbers, coordination geometries, and bridging ligands (phenoxo, hydroxo, imidazolato). The coupling constants (J_{GdCu}) are small and similar to each other. The magnetic behaviors of the present discrete binuclear complexes (**1**)—(**3**) have demonstrated undoubtedly a ferromagnetic spin-coupling between the Gd(III) and Cu(II) ions.

In a superexchange mechanism which is successfully applicable to d-transition metal polynuclear complexes, a weak antiferromagnetic interaction would be expected, since the magnetic orbital of Cu(II) can overlap at least one of the seven f orbitals of Gd(III) ion and the antiferomagnetic contribution is dominat. Accidental orthogonality is also not probable due to the fact that ferromagnetic coupling is always observed in complexes with different coordination numbers, geometries, and bridging groups. One plausible mechanism that can cause a ferromagnetic coupling between Gd(III) and Cu(II) proposed by Benelli et al.[5] is the spin-polarization that occurs when the magnetic orbital of Cu(II) overlaps the empty 6s orbital of Gd(III) through a filled bridging orbital. The fraction of unpaired electron thus polarized from Cu to Gd is parallel to the f electrons due to Hund's rule, affording ferromagnetic coupling between Cu(II) and Gd(III). The fact that the 4 f orbital is shielded by the outer filled 5s and 5p orbitals, and lanthanoid ions generally form complexes using 6s, 6p, and/or 5d orbitals supports the spin-polarization mechanism.

Supplementary Material Available: Tables SI, SII, and SIII (temperatures, magnetic susceptibilities per CuGd unit, and effective magnetic moments per CuGd unit for (**1**), (**2**) and (**3**)), and Figures S1 and S2 (temperature dependence of the magnetic susceptibilities, reciprocal magnetic susceptibilities, and effective magnetic moments for (**2**) and (**3**)).

This work was partly supported by a Grant-in-Aid for Scientific Research No. 01540515 from the Ministry of Education, Science and Culture.

References

1) O. Kahn, *Struct. Bonding (Berlin)*, **68**, 89 (1986).
2) C. J. Cairns and D. H. Busch, *Coord. Chem. Rev.*, **69**, 1 (1986).
3) A. Benelli, A. Caneschi, A. Dei, and D. Gatteschi, *Inorg. Chem.*, **25**, 572 (1986).
4) A. Bencini, C. Benelli, A. Caneschi, R. L. Carlin, A. Dei, and D. Gatteschi, *J. Am. Chem. Soc.*, **107**, 8128 (1985).
5) C. Benelli, A. Caneschi, D. Gatteschi, O. Guillou, and L. Pardi, *Inorg. Chem.*, **29**, 1750 (1990).
6) N. Matsumoto, M. Sakamoto, H. Tamaki, H. Ōkawa, and S. Kida, *Chem. Lett.*, **1990**, 853.
7) U. Casellato, D. Fregona, S. Sitran, S. Tamburini, P. A. Vigato, and P. Zanello, *Inorg. Chim. Acta*, **95**, 309 (1984).
8) M. F. Richardson, D. F. Wagner, and D. E. Sands, *J. Inorg. Nucl. Chem.*, **30**, 1275 (1968).
9) N. Matsumoto, T. Akui, H. Murakami, J. Kanesaka, A. Ohyoshi, and H. Ōkawa, *J. Chem. Soc., Dalton Trans.*, **1988**, 1021.

 © 1991 The Chemical Society of Japan Bull. Chem. Soc. Jpn., 64, 3642—3646 (1991) [Vol. 64, No. 12

Studies of the Hydrous Zirconium(IV) Oxide Ion Exchanger. II. The Rate of Isotopic Exchange of Sodium Ions between the Exchanger in the Na^+ Form and Aqueous Solutions

Yasushi INOUE,* Hiromichi YAMAZAKI, and Tomonori NARITA
Department of Nuclear Engineering, Faculty of Engineering, Tohoku University, Aramaki, Aoba-ku, Sendai 980
(Received July 10, 1991)

The rate of the isotopic exchange of Na^+ between hydrous Zr^{IV} oxide in the Na^+ form and aqueous solutions of sodium salts was determined radiochemically. The rate is controlled by particle diffusion, film diffusion, or both, according to the conditions. The exchange rate is controlled by particle diffusion, when the exchanger particles are large (radius, 171 μm), the solutions are more concentrated than 0.1 mol dm^{-3} Na^+ and the flow rate through the exchanger particles is high, whereas under the opposite conditions film diffusion is the rate-controlling step. The activation energies of Na^+ diffusion are 30±3 and 18.9±0.5 kJ mol^{-1} for particle and film diffusion, respectively.

An investigation of ion-exchange kinetics is very important for understanding the ion-exchange mechanism of hydrous metal oxides. A measurement of the isotopic exchange rate of cations between ion exchangers and solutions provides fundamental data which are useful for elucidating ion-exchange kinetics. The authors undertook radiochemical experiments to measure the Na^+ isotopic exchange rates for hydrous Nb^V and Sn^{IV} oxides. The rate controlling step of the reaction was different between two oxides; for the hydrous Nb^V oxide the exchange rate was controlled by the diffusion of Na^+ in the exchanger particles,[1] while for the hydrous Sn^{IV} oxide it was controlled by the diffusion of Na^+ in the primary particles, which were formed during the initial stage of precipitation and aggregated to form an oxide gel.[2] Further investigations, therefore, should be carried out for a variety of other hydrous metal oxides in order to understand the ion-exchange kinetics of these kinds of materials.

This paper deals with the results of radiochemical experiments undertaken to measure the isotopic exchange rate of Na^+ between hydrous Zr^{IV} oxide in the Na^+ form and aqueous solutions of sodium salts.

Experimental

Preparation of the Exchanger in the Na^+ Form Spiked with ^{22}Na. The hydrous Zr^{IV} oxide prepared by a previously recommended method[3] was classified into four particle sizes by using Japan Industrial Standard sieves; it was then converted to the H^+ form by treating it with a 0.05 mol dm^{-3} HCl solution. After being washed with water, the exchanger was air-dried and stored in a desiccator containing a saturated NH_4Cl solution (relative humidity, 79% at 25 °C). Table 1 shows the particle size and some properties of each sample. These properties were determined by the methods described in a preceding paper.[1] The exchanger in the H^+ form was then converted to the Na^+ form by treating it with solutions having the same chemical composition as those used for the rate measurement. The exchanger was then labeled with ^{22}Na by equilibrating it with a ^{22}Na solution having the same chemical composition as the above mentioned solution for longer than 2 d at room temperature. After being separated from the solution by filtration under suction, the exchanger was used for a rate measurement. The Na^+ solutions used for these procedures were prepared by desired combinations of NaCl and NaOH solutions, except for the experiments carried out in 0.01 mol dm^{-3} Na^+ solutions, where 3-(cyclohexylamino)-1-propane sulfonic acid was added as a buffer reagent. The presence of the buffer reagent was confirmed by a preliminary experiment to affect neither the Na^+ exchange capacity nor the rate of the reaction.

Measurement of the Isotopic Exchange Rate. All of the rate measurements were performed in a nitrogen atmosphere by using the same apparatus as described earlier.[4] The rate was measured in a solution with the same composition as that used for converting the exchanger to the Na^+ form; otherwise, the ion-exchange reaction would occur between H^+ and Na^+ ions, since the ion-exchange capacity for Na^+ strongly depends on the pH and on the concentration of the solution. A 0.1 gram portion of the sample was placed in a cage and immersed in 200 cm^3 of a solution of the desired composition while the cage was being rotated. By rotating the cage we can contact the exchanger particles with a rapid stream of the solution

Table 1. Particle Size and Some Properties of the Samples

Average radius	Density	Composition	Specific surface area	Specific pore volume
μm	g cm^{-3}	mol H_2O(mol ZrO_2)$^{-1}$	m^2 g^{-1}	cm^3 g^{-1}
171±5	2.51±0.03	—	—	0.12±0.01
125±4	—	3.66±0.04	288±2	—
88±1	—	—	—	—
56±3	2.48±0.04	—	—	0.10±0.01

with a flow rate determined by the revolution rate, and mix the solution to keep it homogeneous. The frequency of revolution was measured with a Yokogawa, Model 2607, phototachometer. The solution had been adjusted in advance to a constant temperature within ±0.1 °C. Aliquots of the solution (0.2 cm^3) were taken out at appropriate time intervals in order to measure the radioactivity with a well-type NaI(Tl)-scintillation counter (Aroka Model ARC-361). The time of the contact of the exchanger with the solution was taken as the elapsed time between immersing the cage and withdrawing an aliquot of the solution. The fractional attainment of equilibrium $F=Q_t/Q_\infty$, was calculated from these results; here, Q_t is the total radioactivity of the solution at time t and Q_∞ at $t=\infty$. Q_∞ was calculated using $Q_\infty=Q_iM/(M+m)$, where Q_i is the initial total radioactivity of the exchanger, and m and M the total amounts of Na^+ in the exchanger and in the solution, respectively. Although the rate was measured by a batch method, the infinite solution-volume approximation was closely obeyed under the present experimental conditions; the ratio of the total amount of Na^+ in the exchanger to that in solution was less than 0.02, unless as otherwise noted.

Results and Discussion

The fractional pore volume of the hydrous Zr^{IV} oxide was found to be 0.28±0.02 on the basis of the density and the pore volume of the material (Table 1). Figure 1 shows the pore-size distribution; no significant difference was observed between samples with different particle radii. As the diameters of a large majority of the pores are around twice as large as those of hydrated Na^+ ions (reported to be 1.2 to 1.4 nm[5]), the ions (unhydrated or hydrated) can move fast along the pores in the hydrous Zr^{IV} oxide. Since the pores, functioning as the main paths of the ions, occupy a large fraction of the total volume, the particles of hydrous Zr^{IV} oxide can be regarded as being homogeneous from the standpoint of kinetics.

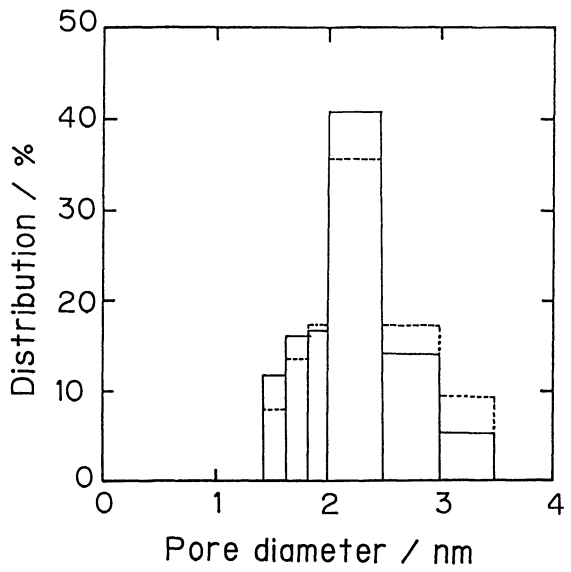

Fig. 1. Pore size distribution.
Particle radius, ----: 171 μm, ——: 125 μm.

When the isotopic exchange rate is controlled by the diffusion of ions in homogeneous spherical exchangers immersed in a well-stirred solution of approximately infinite volume (particle diffusion), the fractional attainment of equilibrium (F) can be obtained by solving the equation,[6]

$$F=1-\frac{6}{\pi^2}\sum_{n=1}^{\infty}\frac{1}{n^2}\exp(-Bn^2t), \tag{1}$$

where

$$B=\pi^2\,\bar{D}/r^2, \tag{2}$$

$\bar{D}$ is the diffusion coefficient of the ions in the exchanger, and r the radius of the particles. When F is less than about 0.3, Eq. 1 can be approximated by a simpler form,[7]

$$F=\frac{6}{r}\left(\frac{\bar{D}t}{\pi}\right)^{1/2}, \tag{3}$$

which holds to a fairly good approximation. A plot of F against the square root of the contact time, therefore, must give a straight line passing through the point of origin in the region of F less than 0.3.

When F is smaller than 0.85, the Bt values can be calculated to a fairly good approximation from the measured values of F by using an equation derived by Reichenberg,[8]

$$Bt=2-\frac{\pi^2}{3}F-2\pi\left(1-\frac{\pi}{3}F\right)^{1/2}, \tag{4}$$

In this case, a plot of Bt against t gives a straight line passing through the point of origin.

When the rate is controlled by the diffusion of the ions in the liquid film on the surface of the particles (film diffusion), F is given by

$$F=1-\exp\left(-\frac{3DCt}{r\delta\bar{C}}\right) \tag{5}$$

under infinite solution-volume conditions. D is the Na^+ diffusion coefficient in the solution, C and $\bar{C}$ the concentration of Na^+ in the solution and that in the exchanger, respectively, and δ the film thickness.[6]

Span et al. and Tsai analyzed the ion-exchange rates in the case where the diffusion of ions was about equally fast in the exchanger particles and in the film.[9,10] They suggested that any decrease in the product of $(\bar{C}/C)\times(\bar{D}/D)\times(\delta/r)$ favored particle diffusion over film diffusion control; the contribution of these processes to the overall rate can be judged according to the manner of deviation from linearity between F and $\sqrt{t}$ or between $-\log(1-F)$ and t.

Figure 2 shows the effect of the frequency of revolution of the cage on the rate of the isotopic exchange between the samples with an average radius 171 μm and 0.1 mol dm^{-3} Na^+ solutions at pH 12. The rate increased with the revolution frequency up to 1310 min^{-1}, wherefrom the linearity between F and $\sqrt{t}$ held during the initial stage of the reaction. This fact indi-

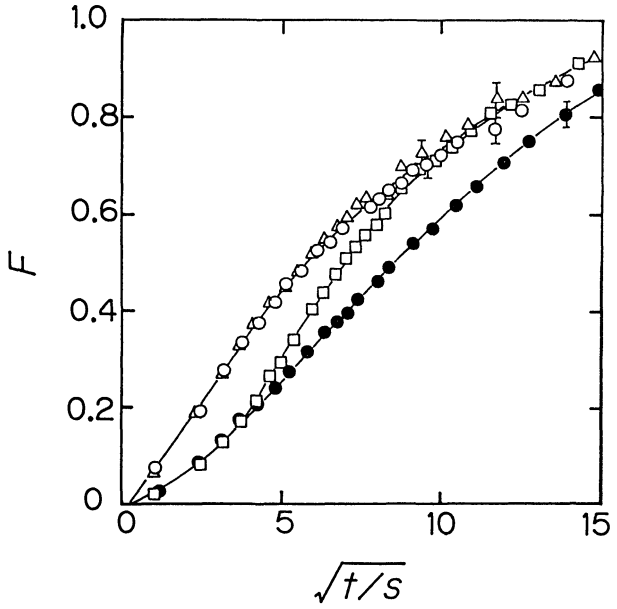

Fig. 2. Effect of agitation on the isotopic exchange rates (F vs. $\sqrt{t}$ plots).
Particle radius, 171 μm; Temperature, 1.0 °C; 0.1 mol dm^{-3} Na^+ solution; pH, 12.0.
Revolution frequency of the cage/min^{-1}, ○: 1430; △: 1310; □: 1160; ●: 860.

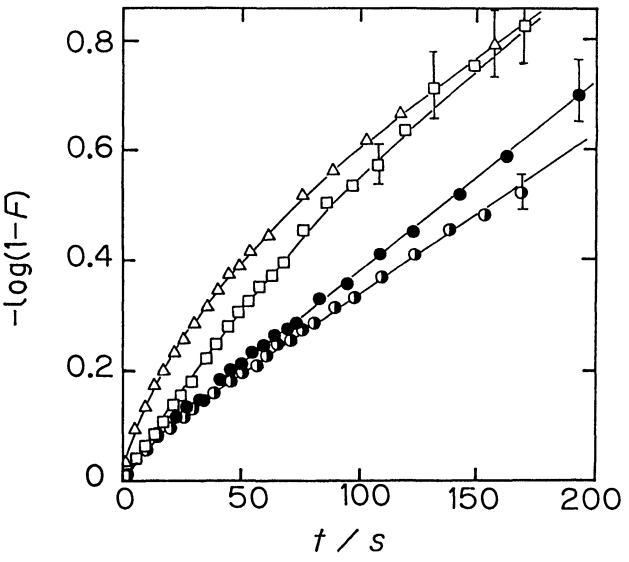

Fig. 3. Effect of agitation on the isotopic exchange rates (−log (1−F) vs. t plots).
Particle radius, 171 μm; Temperature, 1.0 °C; 0.1 mol dm^{-3} Na^+ solution; pH, 12.0.
Revolution frequency of the cage/min^{-1} △: 1310; □: 1160, ●: 860; ◑: 660.

cates that the exchange rate is controlled by Na^+ diffusion in the exchanger particles (Eq. 3). When the revolution rate was slower than 1160 min^{-1}, the plot of F against $\sqrt{t}$ became sigmoid. Hence, the rate cannot be controlled solely by particle diffusion. When the same data were plotted with t as the abscissa against

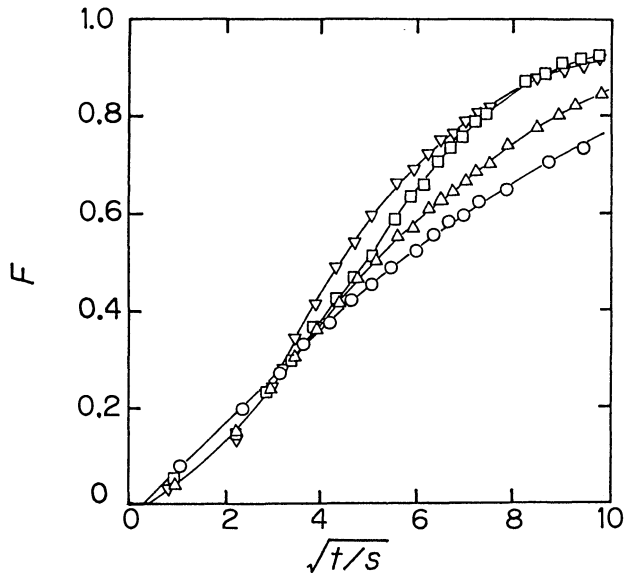

Fig. 4. Effect of particle size on the isotopic exchange rates.
Temperature, 1.0 °C; 0.1 mol dm^{-3} Na^+ solution; pH, 12.0; Revolution frequency of the cage, 1310 min^{-1}.
Particle raduis/μm, ○: 171; △: 125; □: 88; ▽: 56.

−log (1−F) as the ordinate (Fig. 3), a linear relation was obtained in the region of larger F at a revolution rate slower than 1160 min^{-1}. The linear part broadened, and its slope decreased with decreasing revolution rate of the cage. This observation suggests that an increased contribution of film diffusion to the overall exchange rate is due to an increase in δ. The rate of Na^+ diffusion in the film, however, does not entirely control the exchange rate, even at such a slow revolution rate as 660 min^{-1}, since the shoulder is observed during the early stage of the exchange reaction.

Figure 4 shows the effect of particle size on the rate in a 0.1 mol dm^{-3} Na^+ solution at a revolution frequency of 1310 min^{-1}. The overall rate increased with decreasing particle size. The relation between F and $\sqrt{t}$, initially linear at 171 μm, deviated from linearity and became sigmoid when smaller particles were used. This shows the increasing contribution of film diffusion to the overall rate with decreasing particle size, since higher δ/r favors film diffusion control. In order to realize pure particle diffusion control, particles as large as those with a radius of 171 μm should be used, even when the revolution rate of the cage is very high.

Figure 5 shows the influence of the Na^+ concentration on the exchange rate at a high revolution frequency of 1310 min^{-1}. The rate was independent of the concentration of the solutions. This fact also suggests particle diffusion control, since Eq. 1 does not involve term C.

The effect of temperature on the isotopic exchange rate was then studied under the conditions which were required to realize pure particle diffusion control. The results are shown in Fig. 6, which indicate that the rate increases with temperature. The $\bar{D}$ values were then

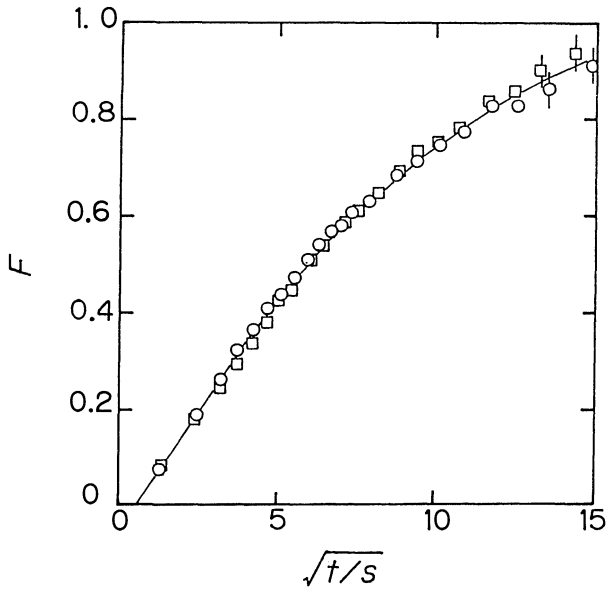

Fig. 5. Effect of Na^+ concentration on the isotopic exchange rates-1.
Temperature, 1.0 °C; pH, 12.0; Revolution frequency of the cage, 1310 min^{-1}; Particle radius, 171 μm.
Na^+ concentration in solutions/mol dm^{-3}, ○: 0.10; □: 1.0.

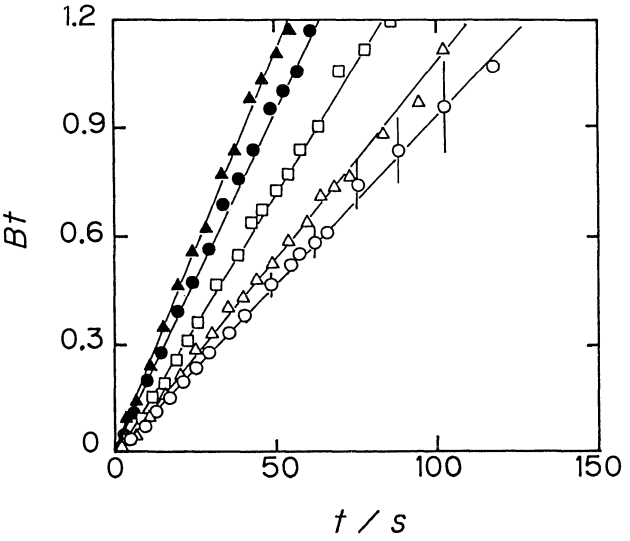

Fig. 6. Effect of temperature on the isotopic exchange rate (Particle diffusion).
0.1 mol dm^{-3} Na^+ solution; pH, 12.0; Revolution frequency of the cage, 1310 min^{-1}; Particle radius, 171 μm.
Temperature/ °C, ○: 1.0; △: 5.0; □: 10.5; ●: 15.1; ▲: 20.1.

evaluated by means of Eq. 2 from the slopes of these lines and the average radius of the particles (Table 2). When $\ln \overline{D}$ was plotted against $1/T$, good linearity was obtained. From the Arrhenius equation, $\overline{D}=\overline{D}_o \exp(-E_a/RT)$, the activation energy, E_a, and the constant, $\overline{D}_o$, were determined. The activation energy (30±3 kJ mol^{-1}) is similar to that reported for Na^+ diffusion in other hydrous metal oxides (35±2 and 27±4 kJ mol^{-1}, respectively, in the hydrous Sn^{IV} oxide and in the hydrous Nb^V oxide) and in a sulfonated polystyrene type resin (35 kJ mol^{-1}).[1,2,11] The larger $\overline{D}$ in hydrous Zr^{IV} oxide, as compared with that in other kinds of exchangers, therefore, is due to a larger $\overline{D}_o$. According to Eyring, this means either a large distance between the equilibrium positions in the process of diffusion or activation accompanied by an increase in entropy, or both.[12]

Table 2. Effect of Temperature on the Na^+ Particle Diffusion Coefficients

Temperature	$\overline{D}$	E_a	$\overline{D}_o$
°C	$cm^2 s^{-1}$	kJ mol^{-1}	$cm^2 s^{-1}$
1.0±0.1	(2.74±0.15)×10^{-7}		
5.0	(3.24±0.08)×10^{-7}		
10.5	(4.36±0.12)×10^{-7}	30±3	0.178
15.1	(5.40±0.10)×10^{-7}		
20.1	(6.35±0.12)×10^{-7}		

Particle radius, 171±4 μm. Revolution frequency of the cage, 1310 min^{-1}. 0.1 mol dm^{-3} Na(Cl, OH), pH 12.0±0.1.

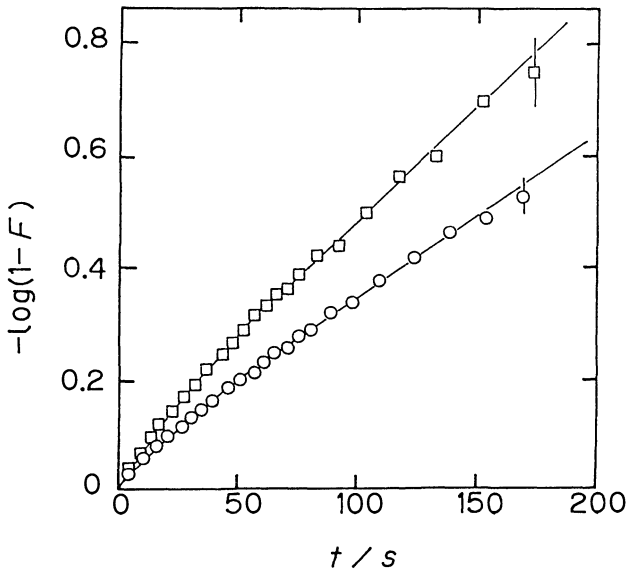

Fig. 7. Effect of Na^+ concentration on the isotopic exchange rates-2.
Temperature, 1.0 °C; pH, 12.0; Revolution frequency of the cage, 660 min^{-1}; Particle radius, 171 μm.
Na^+ concentration in solutions/mol dm^{-3}, ○: 0.10; □: 1.0.

Figure 7 shows the influence of the Na^+ concentration on the exchange rate at a slow revolution rate of the cage (660 min^{-1}). Dissimilarly to the case of a higher revolution rate, the exchange rate increased with Na^+ concentration in solution. In the region where $-\log(1-F)$ is linear with t and the film diffusion controls the rate, the rate increases with the ratio $C/\overline{C}$, as can be

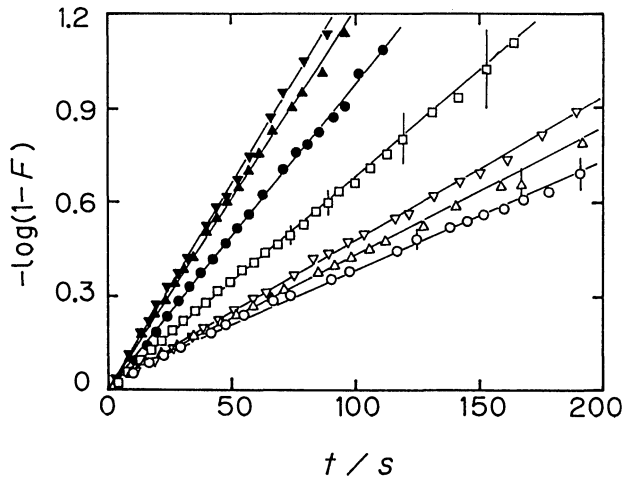

Fig. 8. Effect of temperature on the isotopic exchange rates (film diffusion).
0.01 mol dm^{-3} Na^+ solution; pH, 11.0; Revolution frequency of the cage, 104±4 min^{-1}.
Particle radius, 171 μm; Temperature/ °C, ○: 3.1; △: 5.2; ▽: 11.1; □26.3.
Particle radius, 125 μm; Temperature/ °C, ●: 15.2; ▲: 22.9, ▼: 24.6.

expected from Eq. 5. The Na^+ exchange capacity of hydrous Zr^{IV} oxide at pH 12 increased from 0.67 mmol g^{-1} in a 0.1 mol dm^{-3} Na^+ solution to 0.99 mmol g^{-1} in a 1 mol dm^{-3} Na^+ solution. The concentration dependence of the exchange rate suggests that film diffusion mainly controls the rate at a low flow rate of the solution through the exchanger particles.

In order to realize pure film-diffusion control, the experimental conditions should be such as those to minimize the value of $C/\overline{C}$ and the flow rate of the solution through the exchanger particles. The $C/\overline{C}$ ratio determined experimentally at pH 10 to 12 decreased with decreasing Na^+ concentration, reaching a minimum at 2×10^{-3} mol dm^{-3}, wherefrom it increased due to an abrupt decrease in $\overline{C}$. At this concentration, however, the infinite solution volume approximation is not obeyed in the present experimental conditions. The authors, therefore, adopted a 0.01 mol dm^{-3} Na^+ solution with pH 11.0 as a concentration to obtain a $C/\overline{C}$ as small as possible under the infinite solution volume condition. The revolution rate of the cage was set to 104±4 min^{-1}, and supplementary agitation was made by using a magnetic stirrer to keep the surrounding solution homogeneous.

The isotopic exchange rate at varying temperatures was measured as is shown in Fig. 8. The plots of $-\log(1-F)$ vs. t, except for smaller particles at 9.9 °C, were straight lines passing through the point of origin, indicating pure film diffusion control. Furthermore, the exchange rate increased with temperature and with decreasing particle size. The activation energy of Na^+ diffusion in the film (E_a') can be determined from the Arrhenius plot, since all parameters, except D, in the exponential term in Eq. 5 can be assumed to be constant over the limited temperature range studied; E_a'=18.9±0.6 and 18.8±0.5 kJ mol^{-1}, respectively, for the exchangers with r=171 and 125 μm. They agreed well with the activation energy reported for the Na^+ diffusion coefficient in a NaCl solution (18.4 kJ mol^{-1}).[13] These results indicate that the rate of Na^+ diffusion in the film governs the rate of Na^+ isotopic exchange between hydrous Zr^{IV} oxide and 0.01 mol dm^{-3} Na^+ solutions. The film thickness (δ) was estimated from the slopes of the lines in Fig. 8 by using D values which were calculated from Robinson's data.[13] In this evaluation, the exchange capacity expressed volumetrically (mmol Na^+ cm^{-3}) was used. The film thickness was 2.3×10^{-3} cm at r=171 μm and 1.6×10^{-3} cm at r=125 μm, which were compatible with the values estimated from a hydrodynamic measurement (10^{-3} to 10^{-2} cm).[6] The increase in δ with particle radius is consistent with both the theoretical and empirical relations between the film thickness and the dimensionless hydrodynamic numbers.[6]

References

1) Y. Inoue, H. Yamazaki, and M. Ikeda, *Bull. Chem. Soc. Jpn.*, **61**, 1147 (1988); **62**, 262 (1989).
2) Y. Inoue, H. Yamazaki, and A. Osawa, *Bull. Chem. Soc. Jpn.*, **59**, 169 (1986).
3) Y. Inoue and H. Yamazaki, *Bull. Chem. Soc. Jpn.*, **60**, 891 (1987).
4) Y. Inoue and Y. Yamada, *Bull. Chem. Soc. Jpn.*, **56**, 705 (1983).
5) R. Kunin, "Ion Exchange Resins," John Wiley & Sons, New York (1958), p. 27.
6) F. Helfferich, "Ion Exchange," McGraw-Hill, New York (1963), Chap. 6.
7) G. E. Boyd, A. W. Adomson, and L. S. Myers, *J. Am. Chem. Soc.*, **69**, 2863 (1947).
8) D. Reichenberg, *J. Am. Chem. Soc.*, **75**, 589 (1953).
9) J. Span and M. Ribaric, *J. Chem. Phys.*, **41** (8), 2347 (1964).
10) Fuan-Nan Tsai, *J. Phys. Chem.*, **86**, 2339 (1982).
11) G. E. Boyd and B. A. Soldano, *J. Am. Chem. Soc.*, **75**, 6091 (1953).
12) S. Glasstone, K. J. Laidler, and H. Eyring, "The Theory of Rate Processes," McGraw-Hill, New York (1941), Chap. 9.
13) R. A. Robinson and R. H. Stokes, "Electrolyte Solution," Butterworths & Co., London (1959), p. 513.

Cis-Trans Isomerism among the Octahedral Diaquabis(*N,N*- or *N,N'*-dialkylethylenediamine)nickel(II) Complexes and Their Thermal Reaction Products

Yoshinori IHARA,† Yasuhiro SATAKE, Masatatsu SUZUKI, and Akira UEHARA*
Department of Chemistry, Faculty of Science, Kanazawa University, Marunouchi 1-1, Kanazawa 920
†Laboratory of Chemistry, Faculty of Education, Kanazawa University, Marunouchi 1-1, Kanazawa 920
(Received August 7, 1991)

The thermochemical changes in coordination structure of diaquabis(*N,N*- or *N,N'*-dialkylethylenediamine)nickel(II) complexes ($[Ni(H_2O)_2(diamine)_2]X_2 \cdot nH_2O$) were reinvestigated by means of TG-DTA and electronic spectroscopy at room and elevated temperatures, where diamine is *N,N*- (or *N,N'*)-dimethylethylenediamine (*NN*- or *NN'*-dmen) or *N,N*-(or *N,N'*)-diethylethylenediamine (*NN*- or *NN'*-deen); X is Cl^-, Br^-, I^-, or NO_3^-; *n* is 0, 1, 2, or 3. The diaqua complexes prepared were all trans except for *cis*-$[Ni(H_2O)_2(NN\text{-dmen})_2]I_2$. The trans complexes with the symmetric (*N,N'*-dialkylsubstituted) diamines brought about a deaquation-anation upon heating, retaining the original trans configuration, while those with the asymmetric (*N,N*-dialkylsubstituted) diamines transformed into the cis complexes. In the case of the *NN*-dmen complexes, *cis*-halogenoaqua species were isolated as a stable intermediate during the thermal reactions. The complex nitrates changed to *trans*-dinitrato or *cis*-mononitrato species depending upon the diamines. The effects of the *N*-substituents in the diamines and of the anions on the patterns of thermal reactions were also discussed.

Nickel(II) complexes provide various informative examples of thermochromism in solid phase, which are mainly associated with a change in coordination geometry.[1] However, systematic knowledge is still lacking for the factors which govern the preference of particular coordination geometries at different temperatures.

We have studied the coordination structures of many bis(*N*- or *C*-substituted ethylenediamine)nickel(II) complexes and the products of their solid-phase thermal reactions, and the effects of *N*- or *C*-substituent group(s) upon their structural changes during the thermal treatment.[2–6] Our previous reports[2,3] clarified that the thermal reactions of the complexes containing *N,N*- or *N,N'*-dimethylethylenediamine (*NN*- or *NN'*-dmen) and *N,N*- or *N,N'*-diethylethylenediamine (*NN*- or *NN'*-deen) can be classified into either deaquation-anation(1) or deaquation(2) as shown below:

$$[Ni(H_2O)_2(diamine)_2]X_2\ (Oh) \xrightarrow{-2H_2O} [NiX_2(diamine)_2]\ (Oh') \quad (1)$$

$$[Ni(H_2O)_2(diamine)_2]X_2\ (Oh) \xrightarrow{-2H_2O} [Ni(diamine)_2]X_2\ (Sp) \quad (2)$$

where Oh (or Oh') and Sp represent octahedral and square planar species, respectively. Unfortunately, we were not able to decide whether the Oh and Oh' complexes are cis or trans in spite that the decision is fundamental for understanding the details of their thermal reactions.

The present study was therefore undertaken to reinvestigate the thermal reactions of the nickel(II) complexes containing the above four diamines especially for clarifying the details of cis-trans isomerism and the effects of *N*-substituents on the structural changes during the thermal reactions.

Experimental

Materials. Four diamines (*NN*-dmen, *NN'*-dmen, *NN*-deen, and *NN'*-deen) of commercial reagent grade were used without further purification. The complexes, $[Ni(H_2O)_2(diamine)_2]X_2 \cdot nH_2O$ (X=Cl^-, Br^-, I^-, or NO_3^-; *n*=0, 1, 2, or 3), were prepared by the known methods.[7,8] The *NN*-deen complexes, $[Ni(NN\text{-deen})_2]X_2$ (X=I^- and NO_3^-), were exclusively isolated as anhydrous square planar complexes.

Measurements. Electronic spectra in solid phase were measured by the diffuse reflectance method with a Hitachi U-3400 spectrophotometer. The spectra at elevated temperatures were monitored by use of a hand-made heating cell, which was set up on the apparatus and was controlled by a REX-C72 temperature controller equipped with a copper–constantan thermocouple. IR spectra were recorded on a JASCO A-3 spectrophotometer in Nujol mulls. The standardized cell for the apparatus was used for the IR spectral measurements at elevated temperatures. The measurements of TG-DTA and DSC were carried out with a Seiko TA station SSC 5000 apparatus under a constant flow of nitrogen (0.2 $dm^3\ min^{-1}$ for TG-DTA; 0.03 $dm^3\ min^{-1}$ for DSC). Samples (10—20 mg) were triturated into fine powders beforehand, and were heated at the rate of 2.0 °C min^{-1}.

Results

Structures of $[Ni(H_2O)_2(diamine)_2]X_2 \cdot nH_2O$. Diagnosis of cis and trans isomers of the bis(diamine)nickel(II) complexes has already been established by means of electronic spectroscopy.[9–11] The energy levels derived from F and P terms of a d^8 system (Ni^{2+}) in ligand fields of different symmetries (Oh, D_{4h}, and C_{2v}) are shown in Fig. 1, along with the rough sketches of the typical electronic spectra of *trans*- and *cis*-$[NiX_2(diamine)_2]$. In a D_{4h} system, three or sometimes four bands are practically observed in visible-near IR region. The band due to $^3B_{1g} \rightarrow {}^3E_g$ (from $^3T_{1g}(F)$) transition is

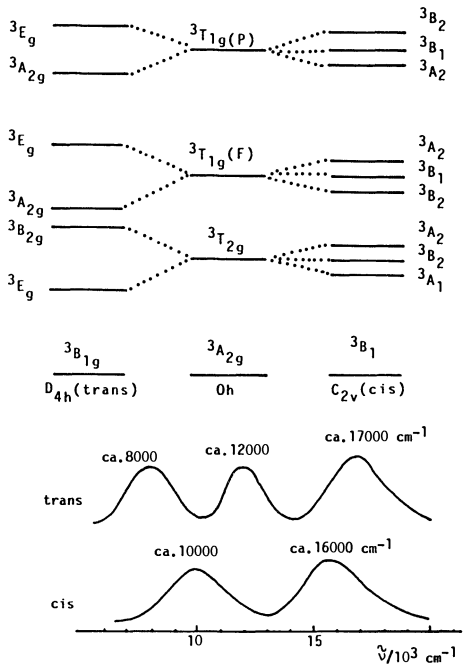

Fig. 1. Top: Energy level diagrams of a d^8 system in ligand fields of different symmetries. Bottom: Rough skeches of the electronic spectra of *trans*- and *cis*- [NiX_2(diamine)$_2$].

normally observed at ca. 17000 cm^{-1}. The band of $^3B_{1g}\rightarrow{}^3A_{2g}$ (from $^3T_{1g}$(F)) transition seems to lie very close to that of $^3B_{1g}\rightarrow{}^3B_{2g}$ transition, giving one or two peaks around ca. 12000 cm^{-1}. The band at ca. 8000 cm^{-1} is assigned to $^3B_{1g}\rightarrow{}^3E_g$ transition. On the other hand, in a C_{2v} system, the splittings of the respective terms are close so that two rather broad bands are observed at ca. 16000 cm^{-1} and ca. 10000 cm^{-1}.

Table 1 summarizes the spectral data of the diaqua complexes and the configurational assignments along with those of their thermal reaction products. At room temperature, only [$Ni(H_2O)_2$(*NN*-dmen)$_2$]I_2 gives apparently a single band in near IR region, indicating that the complex belongs to cis configuration. All the other complexes show spectral patterns characteristic of trans geometry which gives three or four bands due to d–d transitions.

Chaudhuri et al. have pointed out[12] that the complex chloride and bromide with *NN*-dmen prepared by the same methods as ours are not the diaqua species, but *trans*-halogenoaqua ones, *trans*-[$NiX(H_2O)$(*NN*-dmen)$_2$]$X\cdot nH_2O$ (X=Cl or Br), because the complexes behave as an 1 : 1 electrolyte in methanol (Λ_m=70 and 80 Ω^{-1} cm^2 dm^{-3} for the chloride and bromide, respec-

Table 1. Electronic Spectral Data and Configurational Assignments

Complex	Temp/°C	Band maxima, $\tilde{\nu}/10^3$ cm^{-1}					Configuration
trans-[$Ni(H_2O)_2$(*NN'*-dmen)$_2$]$Cl_2\cdot 3H_2O$	RT	7.8	12.0 (sh)	12.9	17.1		*trans*-Diaqua
	110	8.0	12.9		16.9		*trans*-Dichloro
trans-[$Ni(H_2O)_2$(*NN'*-dmen)$_2$]$Br_2\cdot H_2O$	RT	8.4	12.3	13.2 (sh)	17.4		*trans*-Diaqua
	80	7.4	12.8		16.9		*trans*-Dibromo
trans-[$Ni(H_2O)_2$(*NN'*-dmen)$_2$]$I_2\cdot 2H_2O$	RT	8.9	12.4	13.3	17.7		*trans*-Diaqua
	60	6.9	11.1 (sh)	12.6	16.5		*trans*-Diiodo
trans-[$Ni(H_2O)_2$(*NN'*-dmen)$_2$]$(NO_3)_2\cdot 2H_2O$	RT	9.3	12.0	13.1 (sh)	17.4		*trans*-Diaqua
	60	10.5		17.0			*cis*-Mononitrato
	130	8.5	12.3	13.3	17.8		*trans*-Dinitrato
trans-[$Ni(H_2O)_2$(*NN'*-deen)$_2$]$Cl_2\cdot H_2O$	RT	9.1	12.1	13.1	17.6		*trans*-Diaqua
	60	8.3	11.6	12.6	16.8		*trans*-Dichloro
trans-[$Ni(H_2O)_2$(*NN'*-deen)$_2$]Br_2	RT	8.9	12.1	13.2	17.4		*trans*-Diaqua
	100	7.5	13.3		16.2		*trans*-Dibromo
trans-[$Ni(H_2O)_2$(*NN'*-deen)$_2$]I_2	RT	8.9	12.5	14.9 (sh)	17.5		*trans*-Diaqua
	100	7.0	11.8		16.1		*trans*-Diiodo
trans-[$Ni(H_2O)_2$(*NN'*-deen)$_2$]$(NO_3)_2$	RT	9.2	12.1	13.4	17.5		*trans*-Diaqua
	90	10.1		17.0			*cis*-Mononitrato
trans-[$Ni(H_2O)_2$(*NN*-dmen)$_2$]$Cl_2\cdot 2H_2O$	RT	8.1	11.2	13.2	17.0		*trans*-Diaqua
	60	9.5		16.0			*cis*-Chloroaqua
	95	9.4		15.9			*cis*-Dichloro
trans-[$Ni(H_2O)_2$(*NN*-dmen)$_2$]$Br_2\cdot 2H_2O$	RT	8.3	11.2	13.2	16.8		*trans*-Diaqua
	80	9.5		16.0			*cis*-Bromoaqua
	95	9.3		15.7			*cis*-Dibromo
cis-[$Ni(H_2O)_2$(*NN*-dmen)$_2$]I_2	RT	9.9		16.4			*cis*-Diaqua
	90				20.0		Square planar
trans-[$Ni(H_2O)_2$(*NN*-dmen)$_2$]$(NO_3)_2\cdot H_2O$	RT	8.6	11.8	13.4 (sh)	17.3		*trans*-Diaqua
	70	8.5	11.5	13.2 (sh)	17.1		*trans*-Mononitrato
trans-[$Ni(H_2O)_2$(*NN*-deen)$_2$]Cl_2	RT	7.4	10.2		16.4		*trans*-Diaqua
	100	8.5		14.9			*cis*-Dichloro
trans-[$Ni(H_2O)_2$(*NN*-deen)$_2$]Br_2	RT	7.5	10.3		16.4		*trans*-Diaqua
	75				21.4		Square planar
trans-[$Ni(H_2O)_2$(en)$_2$]$(NO_3)_2$	RT	9.0	12.7	13.6	18.3		*trans*-Diaqua
	70	8.8	12.8	13.6	18.3		*trans*-Dinitrato
	170	10.5		17.5			*cis*-Mononitrato

Table 2. Results of Thermal Analyses

Complex	Dehydration		Color	
	Temp/°C	Mass loss /% (calcd)	Room temp	After dehydration
trans-$[Ni(H_2O)_2(NN'\text{-dmen})_2]Cl_2 \cdot 3H_2O$	25—75	22.79 (22.70)	Violet	Blue
trans-$[Ni(H_2O)_2(NN'\text{-dmen})_2]Br_2 \cdot H_2O$	20—50	11.53 (12.00)	Violet	Blue
trans-$[Ni(H_2O)_2(NN'\text{-dmen})_2]I_2 \cdot 2H_2O$	25—45	12.72 (12.85)	Violet	Blue
trans-$[Ni(H_2O)_2(NN'\text{-dmen})_2](NO_3)_2 \cdot 2H_2O$	30—58	16.58 (16.72)	Violet	Blue-violet
trans-$[Ni(H_2O)_2(NN'\text{-deen})_2]Cl_2 \cdot H_2O$	20—58	12.73 (12.99)	Violet	Blue
trans-$[Ni(H_2O)_2(NN'\text{-deen})_2]Br_2$	50—88	7.19 (7.40)	Violet	Blue
trans-$[Ni(H_2O)_2(NN'\text{-deen})_2]I_2$	40—96	6.23 (6.20)	Violet	Green
trans-$[Ni(H_2O)_2(NN'\text{-deen})_2](NO_3)_2$	35—90	7.77 (7.99)	Violet	Blue
trans-$[Ni(H_2O)_2(NN\text{-dmen})_2]Cl_2 \cdot 2H_2O$	25—100	19.02 (19.06)	Violet	Blue-green
trans-$[Ni(H_2O)_2(NN\text{-dmen})_2]Br_2 \cdot 2H_2O$	20—100	15.24 (15.43)	Blue-violet	Blue-green
cis-$[Ni(H_2O)_2(NN\text{-dmen})_2]I_2$	20—83	7.12 (6.86)	Blue	Orange
trans-$[Ni(H_2O)_2(NN\text{-dmen})_2](NO_3)_2 \cdot H_2O$	25—53	12.96 (13.08)	Violet	Blue
trans-$[Ni(H_2O)_2(NN\text{-deen})_2]Cl_2$	55—100	8.97 (9.05)	Blue	Yellow-green
trans-$[Ni(H_2O)_2(NN\text{-deen})_2]Br_2$	30—84	7.34 (7.40)	Blue	Orange
trans-$[Ni(H_2O)_2(en)_2](NO_3)_2$	25—50	10.08 (10.63)	Violet	Violet

tively). Indeed, our complex chloride with the same composition gave nearly the same molar conductivity (92 $\Omega^{-1}\,cm^2\,dm^{-3}$). However, the X-ray single-crystal analyses for the complex chloride[13] have revealed that the two water molecules undoubtedly occupy trans position in the octahedral environment. The low value in molar conductivity may be due to the contribution of chloroaqua species which are formed by deaquation-anation in methanol, because the violet powder slightly changed towards blue on dissolution, giving the spectrum whose peak maxima shift towards the red compared with that of the diaqua complex in solid state.

Thermal Reactions of Complex Halides Containing Symmetric Diamines. Table 2 summarizes the results of TG-DTA and the color changes upon dehydration of all the complexes. The TG-DTA curve of *trans*-$[Ni(H_2O)_2(NN'\text{-dmen})_2]Cl_2 \cdot 3H_2O$ is shown in Fig. 2. The complex loses the five moles of waters (three lattice waters plus two coordinated waters) in one step at 25—75 °C, changing to the anhydrous complex. As shown in Fig. 3, the spectral pattern of the anhydrous product remains nearly unchanged in comparison with that of the original complex except that the red shifts of the

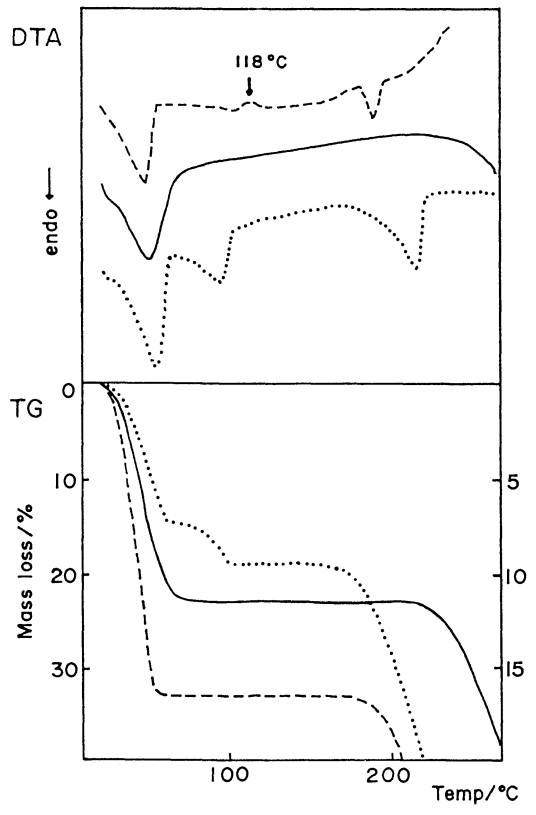

Fig. 2. TG-DTA curves for *trans*-$[Ni(H_2O)_2(NN'\text{-dmen})_2]Cl_2 \cdot 3H_2O$ (——), *trans*-$[Ni(H_2O)_2(NN\text{-dmen})_2]Cl_2 \cdot 2H_2O$ (·····), and *trans*-$[Ni(H_2O)_2(NN'\text{-dmen})_2](NO_3)_2 \cdot 2H_2O$ (----). The TG data of the last complex is illustrated against the right-hand axis.

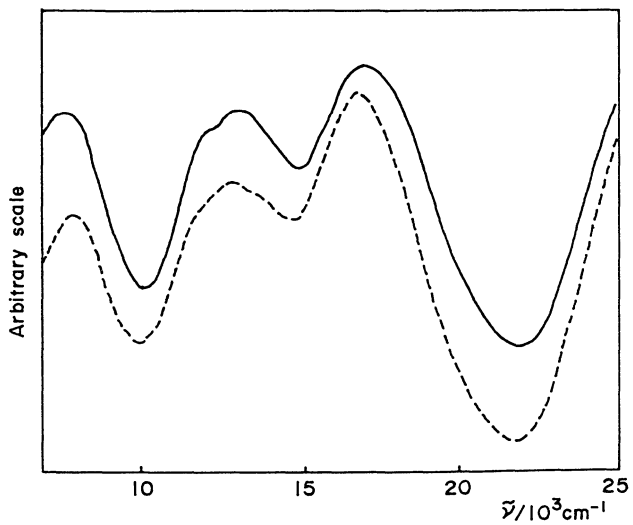

Fig. 3. Electronic spectra of *trans*-$[Ni(H_2O)_2(NN'\text{-dmen})_2]Cl_2 \cdot 3H_2O$ (——) and the product obtained by heating the *trans*-complex at 110 °C (----).

peak maxima take place because of the replacement of axial ligands ($H_2O \rightarrow Cl$). The remaining five complex halides with *NN'*-dmen and *NN'*-deen also liberate their waters below 100 °C, giving the stable anhydrous products with color changes, as summarized in Table 2. These products show three or four bands in their electronic spectra, indicating that the *trans*-octahedral configurations are still retained upon dehydration. It can thus be concluded that a simple deaquation-anation (*trans*-diaqua→*trans*-dianiono) occurs in all the complex halides with the symmetric diamines, retaining the original geometries.

Thermal Reactions of Complex Halides Containing Asymmetric Diamines. The *NN*-dmen or *NN*-deen complexes showed various patterns of thermal reactions depending on the anions. The TG-DTA curve of *trans*-$[Ni(H_2O)_2(NN\text{-dmen})_2]Cl_2 \cdot 2H_2O$ (Fig. 2) indicates that the complex dehydrates in two-steps. The violet diaqua complex loses three moles of water (two lattice waters plus one coordinated water) to become blue at 25—60 °C and then blue-green at 60—100 °C with evolution of the remaining one mole of coordinated water.

Figure 4 shows the electronic spectra of *trans*-$[Ni(H_2O)_2(NN\text{-dmen})_2]Cl_2 \cdot 2H_2O$, and the products obtained by heating the trans complex at 60 °C and 95 °C. As seen from the figure, both products display a spectral pattern characteristic of cis configuration. The corresponding bromide gives almost the same results in TG-DTA and spectral changes (Table 1). Accordingly, thermal reactions of the two complexes may proceed as follows: *trans*-diaqua→*cis*-halogenoaqua→*cis*-dihalogeno species.[14]

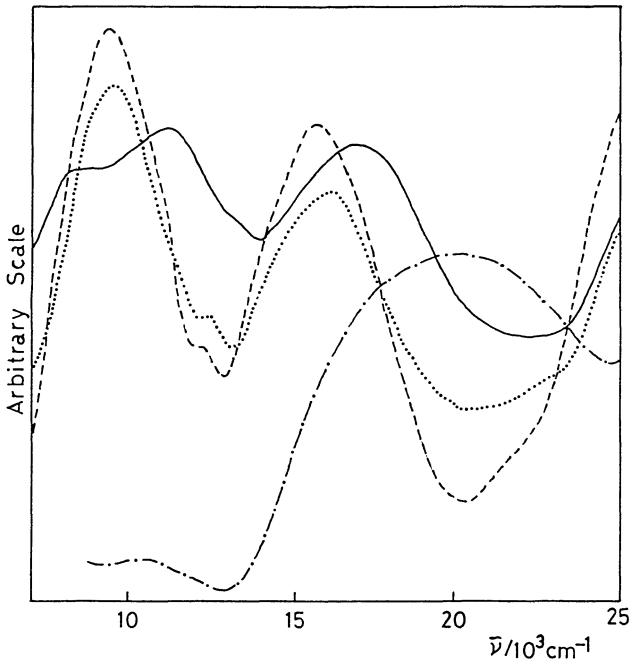

Fig. 4. Electronic spectra of *trans*-$[Ni(H_2O)_2(NN\text{-dmen})_2]Cl_2 \cdot 2H_2O$ (——), the products obtained by heating the *trans*-complex at 60 °C (·····) and 95 °C (----), and the anhydrous product obtained by heating *cis*-$[Ni(H_2O)_2(NN\text{-dmen})_2]I_2$ at 90 °C (— - —).

The blue iodide isolated as a *cis*-diaqua complex changes to orange species after thermal deaquation. The orange product obtained at 90 °C is diamagnetic and gives a broad band at ca. 20000 cm^{-1} in its spectrum (Fig. 4) assignable to $^1A_{1g} \rightarrow {}^1A_{2g}$ transition of a square planar structure.[15]

In the *NN*-deen complexes, the chloride changed to *cis*-dichloro complex at 100 °C (Table 1) with no formation of chloroaqua species. The bromide became diamagnetic square planar upon dehydration, and the iodide was anhydrous square planar even at room temperature.

Thermal Reactions of Complex Nitrates. The complex nitrate with *NN'*-deen undergoes dehydration in one-step. As seen from Table 1, the anhydrous product exhibits two bands at 10100 cm^{-1} and 17000 cm^{-1}, indicating that trans-to-cis configurational change takes place simultaneously with deaquation-anation. The coordination mode of nitrate ion was also determined IR spectrophotometrically. It is well-known that, in general, a NO_3^- ion in a metal complex gives rise to a weak combination band in the range of 1700—1800 cm^{-1}.[10,15]. In the present case, the diaqua complex shows a single peak at 1748 cm^{-1} assignable to the free NO_3^- ions. This peak splits into three peaks at 1718, 1750, and 1767 cm^{-1} in the spectrum at 100 °C. The peak at 1750 cm^{-1} indicates that a part of the NO_3^- ions remains uncoordinated, while the large separation (49 cm^{-1}) between the other two peaks indicates that the coordinated NO_3^- ion functions as a bidentate ligand. This reaction can thus be understood as shown below:

$$trans\text{-}[Ni(H_2O)_2(NN\text{-deen})_2](NO_3)_2 \longrightarrow cis\text{-}[Ni(NO_3)(NN\text{-deen})_2](NO_3)$$

The TG-DTA curve for *trans*-$[Ni(H_2O)_2(NN\text{-dmen})_2](NO_3)_2 \cdot 2H_2O$ (Fig. 2) shows that the complex gives a small but clear exothermic peak at 118 °C with no mass loss after dehydration. The complex changed in color from blue-violet to violet before and after the peak. The enthalpy change of the reaction was estimated to be −6.4 kJ mol^{-1} by means of DSC measurement.[17] The spectral differences between the blue-violet and violet products (Table 1) indicate that this exothermic peak is associated with the cis-to-trans isomerization. The IR band at 1757 cm^{-1} assignable to the free NO_3^- ions of the diaqua complex splits into three peaks at 1718, 1747, and 1767 cm^{-1} in the spectrum at 60 °C (just after dehydration): the peak at 1747 cm^{-1} is due to the free NO_3^- ions, while the other two peaks with a separation of 49 cm^{-1} show the presence of bidentate NO_3^- ions. On the other hand, the spectrum at 130 °C (after the exothermic DTA peak) is split into two peaks with a small separation (16 cm^{-1}), showing that the two NO_3^- ions are coordinated as monodentate ligands. These results are consistent with the configu-

rational assignments from the electronic spectra. This reaction can thus be described as follows: *trans*-$[Ni(H_2O)_2(NN'\text{-dmen})_2](NO_3)_2 \cdot 2H_2O$ first undergoes dehydration-anation accompanied by a trans-to-cis configurational change, yielding *cis*-$[Ni(NO_3)(NN'\text{-dmen})_2](NO_3)$, which then isomerizes to *trans*-$[Ni(NO_3)_2(NN'\text{-dmen})_2]$ at 118 °C. On the other hand, the *NN*-dmen complex shows a simple deaquation-anation, retaining the original trans configuration (Table 1).[12]

The corresponding ethylenediamine (en) complex, *trans*-$[Ni(H_2O)_2(en)_2](NO_3)_2$, was also studied, the results of which are contained in Tables 1 and 2. This complex first transformed into the violet *trans*-dinitrato complex upon deaquation-anation. Then the *trans*-dinitrato complex isomerized to blue-violet *cis*-mononitrato species at 170 °C, which is in contrast to the above case of the *NN'*-dmen complex. This isomerization was endothermic and reversible.

Discussion

Scheme 1 summarizes the thermal reaction pathways of the complex chlorides, bromides, and nitrates clarified in this work. The thermal behaviors of the complex nitrates are quite different from those of the halides, and the reactions of the complexes with the symmetric diamines are different from those of the asymmetric ones. It is thus clear that the preferred geometry of a complex depends on the combination of diamine and anion, and either trans or cis configuration is strongly stabilized for a particular combination of ligands.[18]

In the case of halides, the *NN'*-dmen and *NN'*-deen complexes undergo dehydration-anation, during which their trans configurations are retained; the anation takes place at the axial positions which are occupied by the water molecules before heating. On the other hand, the stable halogenoaqua species can be isolated for the complex halides of *NN*-dmen, since two moles of coordinated waters are liberated one by one in two separate steps. Another significant feature of the complexes with asymmetric diamines is that cis configuration is favored in both halogenoaqua and dihalogeno complexes.

Such peculiar reactions of the asymmetric diamine complexes must be associated with the structures of starting diaqua complexes. According to the X-ray structural study[13] on *trans*-$[Ni(H_2O)_2(NN\text{-dmen})_2]Cl_2 \cdot 2H_2O$ and *trans*-$[Ni(H_2O)_2(NN\text{-deen})_2]Cl_2$, both complexes take tetragonally distorted octahedrons with four in-plane neighbors ($N(H_2)N(H_2)OO$) and two remote axial ones ($N(R_2)N(R_2)$):[19] i.e., the two alkylated nitrogen atoms occupy axial sites apart from each other to minimize their mutual steric hindrance and the distances of $Ni\text{–}N(R)_2$ bonds are remarkably longer than the other. These structural results are obviously different from those of the symmetric diamine complexes with the stronger Ni–NH(R) bonds.[20,21] Thus, it appears reasonable to assume that, in the case of the complexes with asymmetric diamines, a process of the $Ni\text{–}NR_2$ bond rupture is involved in the mechanism of thermal deaquation-anation.

In the case of the nitrates, interesting thermal

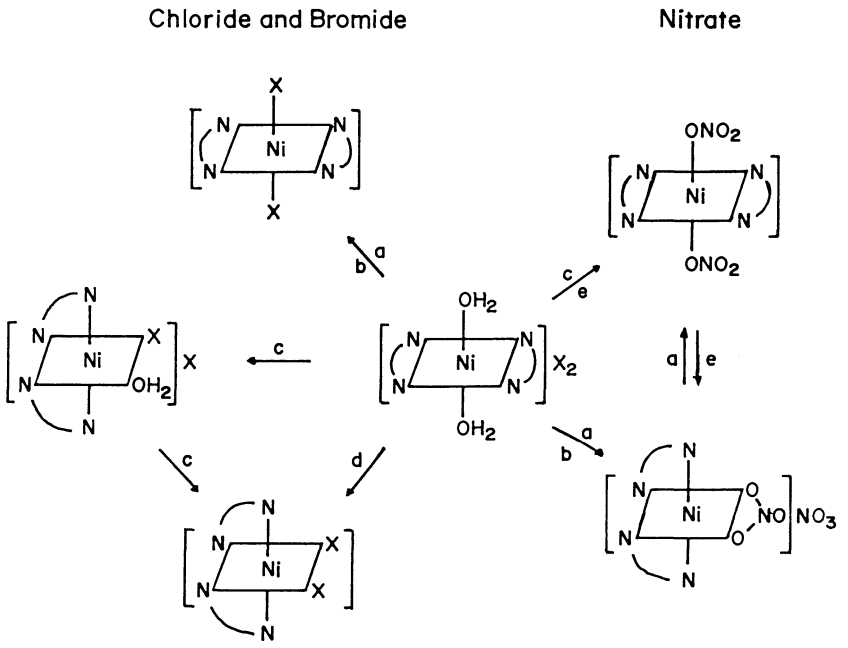

Scheme 1.

cis→trans and trans→cis isomerization were observed in the anhydrous complexes with *NN'*-dmen and en, respectively. On the other hand, only the *NN*-dmen complex kept the original geometry upon dehydration and showed no isomerization after dehydration.

References

1) D. R. Bloomquist and R. D. Willett, *Coord. Chem. Rev.*, **47**, 125 (1982).

2) R. Tsuchiya, S. Joba, A. Uehara, and E. Kyuno, *Bull. Chem. Soc. Jpn.*, **46**, 1454 (1973).

3) Y. Ihara, E. Izumi, A. Uehara, R. Tsuchiya, S. Nakagawa, and E. Kyuno, *Bull. Chem. Soc. Jpn.*, **55**, 1028 (1982).

4) Y. Ihara, T. Kamishima, and R. Tsuchiya, *Thermochim. Acta*, **67**, 23 (1983).

5) Y. Ihara, A. Wada, Y. Fukuda, and K. Sone, *Bull. Chem. Soc. Jpn.*, **59**, 2309 (1986).

6) Y. Ihara, Y. Fukuda, and K. Sone, *Inorg. Chem.*, **26**, 3745 (1987).

7) D. M. L. Goodgame and L. M. Venanzi, *J. Chem. Soc.*, **1963**, 616.

8) D. M. L. Goodgame and L. M. Venanzi, *J. Chem. Soc.*, **1963**, 5909.

9) A. B. P. Lever, "Inorganic Electronic Spectroscopy," 2nd ed, Elsevier, Amsterdam (1985).

10) Y. Ihara, Y. Fukuda, and K. Sone, *Bull. Chem. Soc. Jpn.*, **59**, 1825 (1986).

11) A. B. P. Lever, I. M. Walker, and P. J. McCarthy, *Can. J. Chem.*, **60**, 495 (1982).

12) S. Koner, A. Ghosh, and N. R. Chaudhuri, *Bull. Chem. Soc. Jpn.*, **63**, 2387 (1990).

13) Y. Ihara, Y. Satake, Y. Fujimoto, H. Senda, M. Suzuki, and A. Uehara, *Bull. Chem. Soc. Jpn.*, **64**, 2349 (1991).

14) Chaudhuri et al.[12] have also studied the thermal reactions of these complexes in solid state and identified only the final products in the two-step thermochemical changes as *cis*-$[NiX_2(NN\text{-dmen})_2]$.

15) G. Maki, *J. Chem. Phys.*, **28**, 651 (1958).

16) A. B. P. Lever, E. Mantovani, and B. S. Ramaswamy, *Can. J. Chem.*, **49**, 1957 (1971).

17) In the course of preparing this article, the thermal reaction of the complex nitrate with *NN'*-dmen has just recently been reported by Chaudhuri et al.. They estimated the enthalpy change of -7.1 kJ mol^{-1} for the thermal cis-to-trans isomerization of the *NN'*-dmen complex. S. Koner, A. Ghosh, and N. R. Chaudhuri, *J. Chem. Soc., Dalton Trans.*, **1990**, 1563.

18) Lever et al. studied the corresponding nitro complexes, in which the nitrite (NO_2^-) ions behave like the NO_3^- ions in our complexes, forming *trans*-$[Ni(NO_2)_2(NN\text{-dmen})_2]$ and *cis*-$[Ni(NO_2)(NN'\text{-deen})_2](NO_2)$. I. M. Walker, A. B. P. Lever, and P. J. McCarthy, *Can. J. Chem.*, **58**, 823 (1980).

19) The Ni–NR_2 distances (2.183 Å for the *NN*-dmen and 2.273 Å for the *NN*-deen complexes) are much longer than those of the Ni–NH_2 bonds (2.078 Å for the former and 2.061 Å for the latter) and of the Ni–OH_2 bonds (2.108 and 2.093 Å).

20) A. J. Finney, M. A. Hitchman, C. L. Raston, G. L. Rowbottom, and A. H. White, *Aust. J. Chem.*, **34**, 2047 (1981).

21) R. Birdy, D. M. L. Goodgame, J. C. McConway, and D. Rogers, *J. Chem. Soc., Dalton Trans.*, **1977**, 1730.

 © 1991 The Chemical Society of Japan Bull. Chem. Soc. Jpn., 64, 3653—3658 (1991)

Ligand-Mediated Pseudohypersensitivity of Some 4f–4f Transitions in Neodymium(III) Interaction with Fluorinated Nucleic Acid Components

Sudhindra N. Misra* and Surendra B. Mehta
Chemistry Department, Bhavnagar University, Bhavnagar 364002, India
(Received November 19, 1990)

Absorption difference and comparative absorption spectrophotometry of the systems containing Nd(III) and fluorinated nucleic bases (fluoroadenine, fluorocytosine, fluorothymine, and fluorouracil) and fluorinated nucleosides (fluoroadenosine, fluorocytidine, fluorothymidine, and fluorouridine) in ethyl acetate–water (90 : 10), have shown that certain 4f–4f transitions ($^4I_{9/2}\rightarrow{}^4G_{7/2}$, $^4F_{7/2}$, $^4F_{5/2}$, and $^4F_{3/2}$), which are generally considered to be insensitive, have been found to exhibit substantial sensitivity towards even minor changes in the coordination environment around neodymium(III). The observation has been referred to as "Ligand-Mediated Pseudohypersensitivity." The magnitude of various spectral parameters (energy interaction, Slater–Condon interelectronic repulsion F_k, spin–orbit interaction ξ_{4f}, nephelauxetic $\bar{\beta}$, b, δ, and Judd–Ofelt T_λ intensity and oscillator strength (P)), computed using regression analysis, has been used in exploring the degree of inner and outer sphere coordination, incidence of covalency and extent of involvement of metal 4f orbitals in bonding. The isolation of solid complexes and their characterization by elemental analysis, infrared spectral, and Karl Fischer titration suggested octa and nona coordinated environment around neodymium and some probable structures for these complexes have been proposed.

Complexation of lanthanoids brings about drastic changes in the intensity of certain transitions[1] which are characterized by the large values of $U^{(2)}$ matrix element and exhibit substantial increase and variation of Judd[2]–Ofelt[3] T_2 parameter while the intensities of other 4f–4f transitions are almost unaffected.[4–7] Such transitions called hypersensitive transitions and the shape, energy, and oscillator strength of these transitions have successfully been used to extract information about the degree of outer and inner sphere coordination and extent of involvement of metal 4f orbital,[9] in identifying binding sites of the biomolecules and in following the biochemical reactions involving calcium.[10,11]

During the course of our work on neodymium(III) with β-diketones, diols, and 1,10-phenanthroline, we have found unusual sensitivity of some nonhypersensitive transitions like $^4I_{9/2}\rightarrow{}^4G_{7/2}$, $^4F_{7/2}$, $^4F_{5/2}$, and $^4F_{3/2}$. These transitions were earlier considered to be almost insensitive[1–9] towards coordination changes but in this present investigation these transitions have been found to show substantial sensitivity towards even minor changes in the immediate coordination environment around neodymium(III). The name "Ligand-Mediated Pseudohypersensitivity" has been given for this observation because the coordinating ability, denticity, normalized bite, size of chelate ring of the different ligands affect the sensitivity of these nonhypersensitive transitions to different extent.[12]

The present communication describes the absorption difference, comparative absorption spectrophotometry along with the variation of various spectral parameters in exhibition of Ligand-Mediated Pseudohypersensitivity of $^4I_{9/2}\rightarrow{}^4G_{7/2}$, $^4F_{7/2}$, $^4F_{5/2}$, and $^4F_{3/2}$ using the interaction of Nd(III) with fluorinated nucleic bases like fluoroadenine, fluorocytosine, fluorouracil, and fluorothymine and fluorinated nucleosides, fluoroadenosine, fluorocytidine, fluorouridine, and fluorothymidine.

To support the absorption spectral studies, the neodymium(III) complexes with these fluorinated biomolecules have been isolated and characterized by analysis and IR. Peliminary ultrasonic studies have shown the ligating behavior of these biomolecules in aqueous as well as semi-nonaqueous (50 : 50 DMF–water) media. Probable structures have been proposed on the findings of the present study.

Experimental

Neodymium(III) oxide of 99.99% purity from Indian Rare Earths Ltd., India, was converted into nitrate and then was used for synthesis and spectral studies. Fluorocytosine, fluorouridine, and fluorocytidine were prepared by the methods described.[13] Fluoroadenosine and fluorothymidine were prepared by selective fluorination of adenosine and thymidine by xenon difluoride in genetron.

Absorption spectra in the visible region was recorded on Shimadzu FS 260 and Beckman DU-7 spectrophotometer. The hypersensitive $^4I_{9/2}\rightarrow{}^4G_{5/2}$ and pseudohypersensitive $^4I_{9/2}\rightarrow{}^4G_{7/2}$, $^4F_{7/2}$, $^4F_{5/2}$, $^4F_{3/2}$ were resolved and recorded on expanded scale and were used as Marker bands.

Preparation Complexes of Fluorouracil Fluorocytosine, and Fluorothymine with Neodymium(III). The reactions of neodymium(III) nitrate (0.001 M, 1M=1 mol dm^{-3}) and fluorinated nucleic base (0.005 M) in ethyl acetate and acetone (50 : 50) mixture with constant stirring in inert atmosphere for several hours, resulted in the separation of pinkish microcrystalline solids corresponding to the formula; $[Nd(base)_4\cdot(H_2O)_4]^{3+}$ established after elemental analysis, and analysis of water by Karl Fischer titration.

Preparation of Complexes of Fluorouridine, Fluorocytidine, Fluorothymidine, and Fluoroadenosine. The solution of neodymium(III) nitrate (0.002 M) was added to the ethyl acetate–acetone mixture containing 0.005 M nucleoside and was stirred for 6 h at 20 °C. The reaction mixture was then

placed in a vacuum desiccator and after four days, the crystalline complex slowly separated out from the liquor. These crystals were washed with ethyl acetate and dried in desiccator. The analysis of the product suggested the stoichiometry: $[Nd(nucleoside)_2 \cdot (H_2O)_3]^{3+}$. The amount of coordinated water was estimated in the complex by Karl Fischer titration. The reaction involving fluoroadenosine yielded a mixture of 1:2 and 1:3 products. These could not be separated effectively in pure state. The analytical data showed that observed and calculated percentage of Nd, C, N, H_2O of the neodymium(III) complexes with the fluorinated nucleic bases and fluorinated nucleosides tally within ±2%. The analytical data can be provided by the author on request.

Results and Discussion

The $^4I_{9/2} \rightarrow {}^4G_{5/2}$ transition of Nd(III) is universally accepted as hypersensitive transition as it obeys selection rules for quadrupole transitions and undergoes very high intensification on complexation.[1,8,9,12,14,15] Small changes in the immediate coordination environment around Nd(III) bring about wide variation of oscillator strength. Contrary to this the intensities of nonhypersensitive transitions are reported either vary slightly or not changed at all or sometimes decrease.[4-6] Iftikar[15] has reported a marginal increase (ca. 15%) in the oscillator strength of the nonhypersensitive transition, contrary to the several fold increase shown by hypersensitive $^4I_{9/2} \rightarrow {}^4G_{5/2}$ transition.

Table 2 clearly shows that the percentage variation of the oscillator strength of $^4I_{9/2} \rightarrow {}^4G_{7/2}, {}^4F_{7/2}, {}^4F_{5/2}, {}^4F_{3/2}$ which does not obey selection rule, yet these show significant sensitivity evidenced by large percentage variation of oscillator strength which is almost same as shown by the hypersensitive $^4I_{9/2} \rightarrow {}^4G_{5/2}$ transition. We are reporting the high sensitivity of these nonhypersensitive transitions for the first time. The name "Ligand-Mediated Pseudohypersensitivity" has been suggested for such observation. It appears that the nature of the ligand (denticity, number and coordinating power of ligating sites, degree of chelation, normalized bite of the ligand) and the nature, lability, and geometry of complex species, induce the unusual sensitivity to these nonhypersensitive transitions, Other factors may also be attributed to the enhancement and sensitivity of these transitions.

i) The second-order interactions which are two order magnitude less than the Coulombic interaction (generally ignored) may become prominent by the ligating characteristics of the coordinating molecule. This may lower the excited state of these pseudohypersensitive transitions and in consequence their transition possibility enhances.

ii) The nephelauxetic effect may induce some broadening of the bands and hence may contribute to the intensification of the bands.

iii) These transitions may be borrowing intensities from the neighboring transitions.

Really we are not in a position to give some concrete explanation for this unusual sensitivity of these nonhypersensitive f–f transitions.

Judd[2]–Ofelt[3] theory predicts that the intensity of 4f–4f transition arises principally from forced electric dipole mechanism. Thus the electric dipole oscillator strength (P) is expressed as the product of T_λ parameters and appropriate transition matrix element $U^{(\lambda)}$ at frequency of transition ν, of the transition J→J′

$$P_{e.d} = \sum_{\lambda=2,4,6} T_\lambda \nu (f^n \psi_J \| U^{(\lambda)} \| f^n \psi'_{J'})^2$$

The Judd–Ofelt intensity parameters are empirical, yet these show high sensitivity towards even minor changes in the coordination environment (T_2) and symmetry of the molecule (T_4, T_6).[16] These parameters have been widely used in the structure elucidation of lanthanoid coordination compounds both in the solid as well as in solution. The T_λ and P have also been computed by regression analysis and are summarized in Table 2.

The energy of a 4f–4f transition comprises of two major components: the Coulombic (represented by inter-electronic repulsion F_k Slater Condon parameter) and spin orbit (Lande-ξ_{4f}) components (Table 1). The complexation of lanthanoids brings about lowering of these components resulting in the phenomenon of nephelauxetic effect represented by nephelauxetic ratio ($\bar{\beta}$):

$$\beta_1 = \frac{F_k{}^c}{F_k{}^f};\ \beta_2 = \frac{\xi_{4f}{}^c}{\xi_{4f}{}^f};\ \bar{\beta} = \frac{\beta_1 + \beta_2}{2}$$

$$b^{1/2} = \left[\frac{1-\bar{\beta}}{2}\right]^{1/2};\ \delta = \left[\frac{1-\bar{\beta}}{\bar{\beta}}\right] \times 100$$

Bonding (b) and percentage covalency parameter (δ) which are related to nephelauxtic ratio ($\bar{\beta}$) are also used to describe the structural features of a lanthanoid complex. The significance and evaluation of these (F_k, $\bar{\beta}$, δ, ξ_{4f}, and b) parameters have been discussed in earlier publications.[12,14]

Peacock[4] has shown that the inclusion of covalency can affect the angular part of the 4f wave function and thus can affect preferentially T_2 parameter. Writing ligand wave function, as the sum of the renormalized radial wave function, multiplied with spherical harmonics with the origin at central metal ion,

$$\Phi_{Ligand} = \sum_k \bar{\alpha}_{km} \sum_m Y_{km} \text{ with } k, \text{ odd},$$

while metal wave function can be written as the sum of the original 4f wave function and ligand wave function weighted by mixing coefficient (b) also known as bonding parameter and related to nephelauxetic effect.

$$\Phi_{Metal} = (1-b)^{1/2} |4f\rangle - b^{1/2} |\Phi_{Ligand}\rangle$$

Hence the relevant term which can affect T_λ parameter is b. Generally covalency increase is accompanied by increase in T_λ parameter. Nephelauxetic effect which is caused by the lowering of the excited state, of the metal ion by surrounding ligand field, is influenced by the asymmetric part of the crystal field. The significant

Table 1. Computed Energy Interaction (F_K/cm^{-1}), Spin Orbit Interaction (ξ_{4f}), Nephelauxatic ($\overline{\beta}$), Bonding (b), and Covalency (δ) Parameters Derived from Energy Level Data of Nd(III) Complexes with Metabolites

Complex	F_2	F_4	F_6	ξ_{4f}	$\overline{\beta}_e$	$(1-\overline{\beta}_e)$	$b_e^{1/2}$	δ
(1)	(2)	(3)	(4)	(5)	(6)	(7)	(8)	
Nd-fluoroadenine								
1:1	332.94	47.957	4.960	884.00	0.958	0.042	0.107	3.143
1:2	332.94	47.957	4.960	884.00	0.958	0.042	0.107	3.242
1:3	329.167	48.132	5.630	889.00	0.988	0.012	0.107	1.052
Nd-fluorouracil								
1:1	330.867	47.957	4.96	884.0	0.958	0.042	0.107	3.280
1:2	330.942	47.957	4.96	884.0	0.958	0.042	0.108	3.258
1:3	330.942	47.957	4.96	884.0	0.958	0.042	0.107	3.242
Nd-fluorocytosine								
1:1	330.867	47.957	4.96	884.4	0.958	0.042	0.108	3.242
1:2	330.867	47.957	4.96	884.0	0.958	0.042	0.108	3.249
1:3	330.667	47.957	4.97	884.00	0.956	0.044	0.112	3.428
Nd-fluorothymine								
1:1	330.87	47.96	4.96	884.00	0.958	0.042	0.108	3.242
1:2	330.95	47.96	4.96	884.00	0.958	0.042	0.108	3.242
1:3	328.56	46.35	5.07	866.0	0.990	0.010	0.070	1.052
Nd-fluoroadenosine								
1:1	330.94	47.95	4.96	884.00	0.970	0.030	0.110	2.857
1:2	329.91	48.50	5.04	887.00	0.958	0.042	0.112	3.012
1:3	329.56	48.06	5.02	897.00	0.970	0.030	0.112	2.894
Nd-fluorouridine								
1:1	330.94	47.96	4.96	884.00	0.958	0.442	0.108	3.249
1:2	330.31	47.15	5.02	884.00	0.957	0.043	0.112	3.489
1:3	329.117	48.05	5.02	895.0	0.962	0.038	0.111	2.965
Nd-fluorocytidine								
1:1	330.91	47.55	4.97	884.0	0.963	0.037	0.109	3.472
1:2	330.94	47.95	4.96	884.00	0.964	0.036	0.107	3.242
1:3	329.56	48.05	5.02	890.0	0.968	0.032	0.108	2.894
Nd-fluorothymidine								
1:1	328.56	48.06	5.02	896.0	0.970	0.030	0.110	2.857
1:2	328.86	48.00	5.01	897.00	0.958	0.042	0.112	3.012
1:3	328.91	47.98	5.02	896.50	0.978	0.030	0.112	2.894

changes in the T_λ parameters in absence of significant nephelauxetic effect (as observed in our system) show that the unsymmetrical part of the field has major influence on these (T_λ) parameters. The chromophore present in these complexes is identical, while changes are due to the attachment of functional groups which are not directly involved in the metal ligand bonding. These appear to be most probably responsible for the distortion of the oxygen around neodymium lowering the site symmetry and thus increasing the probability of 4f–4f transition. Using Judd–Ofelt theory, above assumption can be explained where the expression for T_λ parameters is

$$T_\lambda = \chi\left[\frac{8\pi^2 m}{3h}\right](2\lambda+1)\sum_{t,p}A_{t,p}|^2\xi^2(t,\lambda)>$$

In the above equation $A_{t,p}$ (t, odd) are odd parity term in crystal field expansion depending upon the site symmetry of the complex. The quantity $\xi^2(t, \lambda)$ contains integral involving radial part of the wave function and excited parity electronic wave function measuring the symmetric part of the ligand field (amount of covalency) and does not vary appreciably in Nd(III) complexes with these fluorinated biomolecules. However, T_λ prameters vary substantially with the change and stoichiometry of the ligands. Hence the quantity $\xi^2(t, \lambda)$ which is not dependent on the nature and stoichiometry of the ligand is not the factor causing change in T_λ. Thus the remaining part of the equation ($A_{t,p}$) the asymmetric part of the ligand field expansion appears to be responsible for the variation of T_λ parameter. These remaining quantities arise therefore from the distortion of the geometry around neodymium.

Binding of Fluorinated Nucleic Bases with Neodymium(III). These fluorinated nucleic bases possess both nitrogen and oxygen as potential donor sites except fluoroadenine, which has only nitrogen as coordinating sites. The complexes isolated with fluorocytosine, fluorouracil, and fluorothymine corresponded to the composition $[Nd(Base)_4\cdot(H_2O)_4]^{3+}$. The pure compound with fluoroadenine could not be isolated, however, some ill defined complexes appear to be formed with fluoroadenine. A look at the Table 2 shows that the oscillator strength (P) of neodymium(III) fluoroadenine system was almost similar to that neodymium(III) fluorouracil system suggesting that fluoroadenine inter-

Table 2. Computed and Observed Oscillator Strengths (P) of Important 4f—4f Transition and T_λ Parameters of Nd(III) Complexes with Fluorinated Metabolites

Complex	$^4I_{9/2}\rightarrow{}^4G_{7/2}$		$^4I_{9/2}\rightarrow{}^4G_{5/2}$		$^4I_{9/2}\rightarrow{}^4F_{7/2}$		$^4I_{9/2}\rightarrow{}^4F_{5/2}$		$^4I_{9/2}\rightarrow{}^4F_{3/2}$		T_2	T_4	T_6
	Obsd	Calcd	Obsd	Calcd	Obsd	Calcd	Obsd	Calcd	Obsd	Calcd			
Nd-fluoroadenine													
1:1	1.942	1.292	4.798	4.798	5.013	5.319	5.376	5.466	0.964	0.874	179.27	251.78	327.1
1:2	1.352	1.620	6.053	6.005	5.002	5.015	4.965	5.314	0.831	1.096	224.77	315.70	410.1
1:3	1.550	1.988	7.923	7.638	3.201	3.090	4.018	3.668	0.874	1.447	300.25	418.00	543.0
Nd-fluorouracil													
1:1	1.362	1.258	4.668	4.668	4.545	3.806	3.348	4.040	0.791	0.882	175.61	245.81	319.22
1:2	2.616	1.554	5.758	5.758	4.994	4.896	5.087	5.170	0.869	1.052	215.50	302.3	393.16
1:3	2.437	1.644	7.170	7.170	5.216	4.898	5.032	5.327	1.331	1.310	268.42	377.0	489.63
Nd-fluorocytosine													
1:1	2.477	1.344	4.983	4.985	5.72	5.565	5.57	5.715	1.198	0.909	186.55	262.10	340.29
1:2	2.649	1.668	6.179	6.173	5.419	5.722	6.271	5.985	1.064	1.126	231.07	324.55	421.52
1:3	2.210	2.216	8.210	8.208	6.000	5.254	5.074	5.768	0.894	1.498	307.96	431.81	560.79
Nd-fluorothymine													
1:1	2.940	1.842	4.080	4.080	3.652	4.060	4.35	4.218	0.804	0.749	152.72	214.52	279.57
1:2	2.788	1.688	6.187	6.187	5.084	5.373	5.563	5.563	0.948	1.130	231.61	325.27	422.46
1:3	2.067	1.930	7.160	7.160	7.160	6.665	6.062	6.224	0.850	1.305	268.70	376.68	489.28
Nd-fluorodenosine													
1:1	3.348	2.378	5.110	5.110	5.484	5.620	5.603	5.780	0.990	0.932	191.28	268.70	348.93
1:2	2.456	2.221	8.221	8.221	5.442	4.970	4.970	5.518	0.658	1.532	310.78	433.48	562.98
1:3	2.081	2.994	11.124	11.124	4.968	5.111	5.384	5.938	0.686	1.031	420.6	586.00	761.76
Nd-fluorouridine													
1:1	2.248	1.426	5.294	5.292	5.389	5.598	5.78	5.776	0.911	0.966	198.11	278.26	361.37
1:2	2.265	2.523	9.379	9.377	6.368	6.124	6.124	6.514	0.804	1.718	356.21	495.16	643.05
1:3	2.758	3.010	11.274	11.274	6.342	5.343	5.343	6.588	0.962	2.053	427.20	594.82	772.50
Nd-fluorocytidine													
1:1	1.610	1.908	7.088	7.084	7.350	6.692	5.939	6.986	1.107	1.294	285.81	372.71	484.04
1:2	3.627	2.698	10.013	10.013	7.021	5.994	5.090	6.646	1.456	1.827	374.78	526.40	683.64
1:3	2.952	3.409	13.586	13.584	6.478	5.214	5.596	6.312	1.195	2.307	478.65	666.49	865.56
Nd-fluorothymidine													
1:1	1.550	2.329	8.868	8.886	5.425	5.38	5.376	5.960	0.870	1.616	336.86	468.20	607.99
1:2	1.842	3.130	11.629	11.622	6.018	5.669	5.478	6.526	0.928	2.126	440.40	613.20	796.40
1:3	2.628	3.763	14.995	13.943	6.420	5.525	4.926	6.750	2.065	2.160	528.40	735.72	955.54

acts in some way with neodymium(III), most probably involving pyrimidine or imidazole nitrogen in semi-nonaqueous 80:20 DMF:water.

The infrared spectra of the ligands in the carbonyl region show considerable changes on complexation. For fluorouracil and fluorocytosine complexes, the carbonyl absorption in the infrared region appears as a broad band, with its center of gravity shifted to lower energy as compared to corresponding ligand. Susi and Ard[17] considered the band in the 1540—1800 cm^{-1} region to $\nu(^2C{=}O)$ in phase $\nu(^4C{=}O)+\nu(C{=}O)$ and out phase $\nu(C{=}O)+\nu(C{=}O)$. In case of fluorothymine complex the bands at 1735 cm^{-1} (m), 1677 cm^{-1} (s) of fluorothymine shifted to the lower energy side indicating the participation of carbonyl oxygen in complexation with neodymium(III). Susi and Ard[17] suggested, that highest band in the region 1540—1800 cm^{-1} can be ascribed to $\nu(^2C{=}O)$, on the basis of the bond length reported for thymine hydrate by Gerdil.[18] Though the complexation can also be expected through ($^4C{=}O$), the donor capability of ($^2C{=}O$) will be more than that of ($^4C{=}O$). In fluorothymine the presence of electron-releasing CH_3 group on the fifth carbon atom will make ($^4C{=}O$) a less attractive donor. This points out clearly that the pyrimidinone oxygen atom can effectively act as donor. The weakness of the field is in accordance with the high π-electron density calculated for both oxygen in fluorouracil and fluorothymine. These atoms would be expected to act as moderate donor with ligand field at this low end of the oxygen donor range. The metal-ligand bond may well be fairly strong with very low crystal field stabilization energy. This situation in neodymium(III) complexes will make them very labile. The lability of neodymium(III) complexes with fluorinated nucleic bases will impart only weak intensities to the intra 4f-4f bands as is observed in the present study.

Preliminary ultrasonic studies of fluorouracil, fluorocytosine, fluorothymine in aqueous medium in presence of neodymium(III), have clearly shown that these fluorinated nucleic bases weaken water structures, while the same metabolite strengthen water structure in presence of aprotic solvent.[19]

(i) In water, fluorouracil, fluorocytosine, fluoroadenine, and fluorothymine gave positive values for partial metal compressibility (Φ_k°). This appears to be due to the displacement of net water molecules into the interstices, with the result these fluorinated bases in aqueous medium become highly hydrated and hence are not

readily available for coordination with neodymium.

(ii) The high dielectric constant of water induces significant ionization of metal-ligand bond hence the energies of various 4f–4f transition vary very little while the shape of the intra 4f–4f bands, specially $^4I_{9/2} \rightarrow {}^4G_{5/2}$ and $^4I_{9/2} \rightarrow {}^4F_{5/2}$ hypersensitive and pseudohypersensitive bands respectively change significantly.

(iii) The addition of aprotic solvent (DMF/DMSO) lowers the dielectric constant of the solvent mixture and decreasing the ionization of metal ligand bond. Secondly in the DMSO–water mixture these nucleic bases strengthen water structure (shown by negative values of partial molal compressibility Φ_k°),[19] hence these metabolites behave as better ligands. Thirdly the addition of DMSO also removes partly the water molecules from the coordination shell around Nd(III) and hence create different immediate coordination environment around neodymium(III).

(iv) Preliminary stability constant measurements of neodymium(III) fluorinated base systems have indicated significant stacking,[19] which also contributes towards weak intensities of intra 4f–4f bands.

Thus one can infer from infrared, absorption spectral and solution studies that these fluorinated nucleic bases act as better ligands in DMSO–water than in H_2O and their binding to neodymium is through carbonyl oxygen preferably through $\nu(^2C{=}O)$ carbonyl oxygen as unidentate manner as the bands due ν(N–H) do not appear to show any appreciable change. The presence of four water molecules of coordination and four base molecule coordinated in neutral unidentate manner through carbonyl oxygen and thus providing an octacoordinated environment around Nd(III) in these complexes.

Binding of Fluorocytidine, Fluorothymidine, Fluorouridine, and Fluoroadenosine with Neodymium(III). Significant shifts have been observed in ν(C=O) vibration which occurs around 1660—1680 cm^{-1} in fluorocytidine, fluorouridine, and fluorothymidine shifts to ca. 1700 cm^{-1} as asymmetric shaped broad band, whose center of gravity is around ca. 1700 cm^{-1} probably indicative of the participation of oxygen of the carbonyl group in bonding to neodymium(III). The presence of three water molecules have been indicated by Karl Fischer titration. The ν(OH) bands of the ligand change into broad band, suggesting the participation of ribose hydroxyl group in complexation to neodymium. These informations suggest the probable structure for $[Nd(nucleoside)_2(H_2O)_3]^{3+}$ complexes, involving nona coordinated Nd(III). Similar structure has been proposed by Brittain[20] and Richardson[21] earlier for $[Nd(uridine)_2(H_2O)_2]$ complexes. The terdentate attachment of the nucleoside to metal involves two cis hydroxyl oxygen of ribose and participation of carbonyl oxygen.

The proposed structures for Nd–adenosine complexes are given on our observations in Nd–fluorouridine/fluorothymidine/fluorocytidine systems. Since the pure 1 : 2 and 1 : 3 complexes could not be separated and hence the structure proposed are only on analytical data (C, H, N, H_2O, and Nd) and the conclusion derived from other Nd(nucleoside) complexes.

Absorption spectra of the solution containing neodymium(III) and fluoroadenosine, fluorouridine, fluorocytidine, fluorothymidine, and fluoroadenine, fluorouracil, fluorocytosine, and fluorothymine in 1 : 1, 1 : 2, and 1 : 3 stoichiometry have shown that the intensities increase with the ligand stoichiometry. However, the spectra recorded in 1 : 4 stoichiometry did not show change from that observed in 1 : 3 stoichiometry hence the data has not been included. There has been significant variation in intensity parameters while the variation in the energy interaction parameters has been insignificant. No doubt the energy interaction parameters are quite different from that of neodymium(III) aquo and more so from neodymium(III) free ion. Comparing the magnitude of spectral parameters like P and T_λ for fluorinated nucleic bases and their nucleosides, the parameters have higher values for fluorinated nucleosides as compared to these observed for corresponding to non-fluorinated nucleic base which is understandable in view of the better complexing power shown by the former biomolecule.

Conclusion

The interaction of fluorouracil, fluorocytosine, and 1fluorothymine and their nucleosides with neodymium involves participation of oxygen donor sites of the ligand. The attachment of the ligand is as neutral species. The presence of water molecules complete the nona- or octa-coordination around neodymium in presence of fluoronucleosides and fluoronucleic bases respectively. The magnitude and variation of spectral parameter shows significant changes in the intensities and intensity parameters but less prominent changes in the coulombic and spin orbit interaction parameters. These point to the fact that the changes in the symmetry of the complex play dominant role. The unusual intensification and wide variation of oscillator strength of some nonhypersensitive 4f–4f transitions was observed which was given the name 'LIGAND-MEDIATED PSEUDOHYPERSENSITIVITY'.

References

1) D. M. Gruen, C. W. Dekock, and R. L. McBeth, *Adv. Chem. Ser.*, **71**, 102 (1967); D. M. Gruen and C. W. Dekock, *J. Chem. Phys.*, **45**, 455 (1966).

2) B. R. Judd, *Phys. Rev.*, **127**, 750 (1962).

3) G. S. Ofelt, *J. Chem. Phys.*, **37**, 511 (1962).

4) a) R. D. Peacock, *Mol. Phys.*, **25**, 817 (1973); b) *Struct. Bonding (Berlin)*, **22**, 83 (1975).

5) W. F. Krupke, *Phys. Rev. A*, **145**, 325 (1966).

6) J. L. Ryan and C. K. Jorgensen, *J. Phys. Chem.*, **70**, 2845 (1966).

7) C. K. Jorgensen and B. R. Judd, *Mol. Phys.*, **8**, 281 (1964).

8) G. R. Choppin, D. E. Henrie, and K. Buijs, *Inorg.*

Chem., **5**, 1743 (1966); G. R. Choppin, D. E. Henrie, and R. L. Fellows, *Coord. Chem. Rev.*, **18**, 199 (1976).
9) K. B. Yatsimirskii and N. K. Davidenko, *Coord. Chem. Rev.*, **27**, 223 (1979).
10) E. R. Birnbaum, J. E. Gomez, and D. W. Darnall, *J. Am. Chem. Soc.*, **92**, 5287 (1970).
11) E. R. Birnbaum, C. Yoshida, J. E. Gomez, and D. W. Darnall, *Bioinorg. Chem.*, **3**, 15 (1973).
12) S. N. Misra, K. J. Shah, G. Joseph, K. Anjaiah, and Venkatasubramanian, *Indian J. Chem., Sect. A*, **29**, 266 (1990); S. N. Misra and Shaun O. Sommerer, *Can. J. Chem.*, Jan. issue of 1992.
13) R. S. Tipson and L. B. Townsend, "Nucleic Acid Chemistry," John Wiley & Sons, N. Y. (1978), Vols. I and II.
14) S. N. Misra and A. Kothari, *Can. J. Chem.*, **61**, 1775 (1983); S. N. Misra and W. N. Cabalfin, *Chem. Scr.*, **29**, 75 (1989).
15) K. Iftikar, *Inorg. Chim. Acta.*, **129**, 261 (1987).
16) W. T. Carnall, P. R. Fields, and K. Rajnak, *J. Chem. Phys.*, **49**, 4412, 4424, 4443, 4447, 4450 (1968).
17) H. Susi and J. S. Ard, *Spectrochim. Acta, Part A*, **27**, 1549 (1971); **30**, 1843 (1974).
18) R. Gerdil, *Acta Compt.*, **14**, 333 (1961).
19) J. D. Pande and K. Misra, private commun.
20) H. G. Brittain, *Coord. Chem. Rev.*, **48**, 243 (1983).
24) F. S. Richardson, *Chem. Rev.*, **82**, 541 (1982).

 © 1991 The Chemical Society of Japan Bull. Chem. Soc. Jpn., 64, 3659—3661 (1991)

Study of Various Factors Affecting the Stability of Ternary Cu(II) and Ni(II) Complexes

Mohammd Rafiqe ULLAH and Pabithrak K. BHATTACHARYA*
Department of Chemistry, Faculty of Science, M. S. University of Baroda, Baroda 390002, India
(Received September 10, 1990)

The stability constants of the ternary M(II) complexes [MAL], where M(II) refers to Cu(II) and Ni(II), A refers to 2,6-pyridinedicarboxylic acid (dpa) and iminodiacetic acid (imda) and L refers to glycine, α-alanine, phenylalanine, tyrosine, tryptophan, ethylenediamine, 1,3-propanediamine, oxalic acid, catechol, catechuic acid, tiron, pyrogallol, *o*-aminophenol, and *o*-phenylenediamine, have been determined potentiometrically by using SCOGS computer programme. Probable reasons for less negative $\Delta\log K$ values of the ternary complexes have been discussed.

The nature of the two ligands involved in the formation of the ternary complex greatly affects its stability constant.[1,2]

These effects vary with the nature of the metal ion involved. The interesting comparisons have been made of Cu(II) and Ni(II) ternary complexes.[3,4] Five main nonstatistical factors have been observed to be of significance in determining the stability of a ternary complex.

i) The charges on the two ligands leading to electrostatic repulsion.[5,6]

ii) π Acid character of one of the ligands.[7,8]

iii) Tridentate character of one of the ligands.[9,10]

iv) Large groups in the vicinity of the coordinating atoms leading to steric hindrance between the ligands.[11,12]

v) Intramolecular interligand interactions.[13,14]

It was thought of interest to study the ternary complexes involving 2,6-pyridinedicarboxylic acid (dpa=AH_2), as one of the ligands, which is subject to the effect of four of the above factors. Complexes of the type MAL have been studied where, M=Cu(II) and Ni(II) and L=glycine, α-alanine, phenylalanine, tyrosine, tryptophan, ethylenediamine, 1,3-propanediamine, oxalic acid, catechol, catechuic acid, tiron, pyrogallol, *o*-aminophenol, *o*-phenylenediamine and AH_2=dpa or iminodiacetic acid (imda). Formation constants of some of the M-imda complexes have been reported eariler,[15] but they have been redetermined to get the values under similar experimental conditions.

Experimental

All the reagents used were of A.R. grade and the titrations were carried out in aqueous medium using a G.P. Electronics pH meter (No. 8021, accuracy±0.01 pH unit). The proton-ligand formation constant of the ligands and the formation constants of the binary complexes CuL, CuL_2, NiL, NiL_2, and NiL_3 were determined in aqueous medium at 25 °C and I=0.2 M ($NaClO_4$) (1 M=1 mol dm^{-3}) using the SCOGS[16] computer programme (charges on the species have been omitted for simplicity). In the case of proton-ligand formation constants L, LH, and LH_2 and for formation constants of the binary complexes L, LH, LH_2, M, ML, ML_2 species were considered. ML_3 species was also considered in case of Ni(II) complexes. These refined values are in close agreement with the values reported earlier in literature.[17–19] These values were used as fixed parameters for the refinement of the formation constants of the ternary complexes [MAL]. For the determination of the formation constant of the ternary complexes MAL, the following sets of solutions (50 cm^3) having M : A : L in the ratio 1 : 1 : 1 and 1 : 2 : 2 were prepared and titrated against standard alkali:

i) 0.02 M $HClO_4$, 0.002 M metal perchlorate, 0.002 M ligand (A), 0.002 M ligand (L) and 0.174 M $NaClO_4$.

ii) 0.02 M $HClO_4$, 0.002 M metal perchlorate, 0.004 M ligand (A), 0.004 M ligand (L) and 0.170 M $NaClO_4$.

Titrations of each set were carried out twice to check the reproducibility of the data. In case of catechol and its derivatives titrations were carried out under nitrogen atmosphere. The pH range selected for the computer programme was 3—7 for [CuAL] and 5—9 for [NiAL] complexes. The experimental values of pH and volume of alkali used in this range were fed to the computer. Calculations were carried out using the computer programme SCOGS. The species considered for the calculation of formation constants of the ternary complexes were A, AH, AH_2, L, LH, LH_2, M, MA, MA_2, ML, ML_2, and MAL. ML_3 species were also considered in case of Ni(II) complexes. The formation constants $\log K^{M}_{MAL}$, $\Delta\log K$ and $\Delta(\Delta\log K)$ have been presented in Tables 1 and 2. The deviations in the $\log K^{M}_{MAL}$ values have been shown in brackets. These indicate random errors in the titration, dependent on the precision of the instruments.

Discussion

The stability of the ternary complexes can be quantitatively evaluated in terms of $\Delta\log K$.

$$\Delta\log K = \log K^{MA}_{MAL} - \log K^{M}_{ML}$$
$$= \log K^{ML}_{MAL} - \log K^{M}_{MA}.$$

Alternatively it can be shown as

$$\Delta\log K = \log \beta^{M}_{MAL} - (\log K^{M}_{MA} + \log K^{M}_{ML}).$$

It is observed, that in general, $\Delta\log K$ for the MAL complexes studied is negative, as expected from the statistical considerations. $\Delta\log K$ becomes more negative with increasing charge on the ligand L, e.g. oxalate$\gtrsim$glycinate~ethylenediamine. This is because imda and dpa have two negative charges. The second negatively charged ligand faces electrostatic repulsion in

Table 1. Stability Constants of Ligand Complexes in Aqueous Medium and I=0.2 M ($NaClO_4$) at 25±1 °C with Standard Deviation in Parentheses

Ligand (L)	2,6-Pyridinedicarboxylic acid–Ni–L		2,6-Pyridine carboxylic acid–Cu–L		($\Delta\log K_{Ni}-\Delta\log K_{Cu}$)
	$\log K^{Ni}_{NiAL}$	$\Delta\log K$	$\log K^{Cu}_{CuAL}$	$\Delta\log K$	$\Delta(\Delta\log K)$
Glycine	12.20 (0.04)	−0.59	15.84 (0.03)	−0.98	+0.39
α-Alanine	11.90 (0.04)	−0.56	16.00 (0.05)	−0.83	+0.27
Phenylalanine	11.78 (0.07)	+0.01	16.10 (0.06)	−0.29	+0.30
Tyrosine	11.90 (0.01)	+0.19	15.92 (0.02)	−0.28	+0.47
Tryptophan	12.39 (0.01)	+0.14	16.69 (0.02)	−0.19	+0.33
Ethylenediamine	14.36 (0.05)	−0.58	18.02 (0.04)	−0.91	+0.33
1,3-Propanediamine	13.42 (0.04)	−0.97	17.60 (0.05)	−1.01	+0.04
Oxalic acid	10.35 (0.07)	−0.69	11.69 (0.06)	−2.05	+1.36
Catechol	14.82 (0.01)	−0.51	20.90 (0.03)	−1.66	+1.15
Catechuic Acid	14.32 (0.01)	−0.71	19.98 (0.03)	−1.71	+1.00
Tiron	15.05 (0.07)	−1.50	20.89 (0.05)	−1.83	+0.33
Pyrogallol	13.40 (0.06)	−0.97	20.66 (0.07)	−1.04	+0.07
o-Aminophenol	10.50 (0.07)	−0.84	16.46 (0.07)	−0.93	+0.09
o-Phenylenediamine	—	—	12.62 (0.06)	−0.72	—

Table 2. Stability Constants of Mixed Ligand Complexes in Aqueous Medium and I=0.2 M ($NaClO_4$) at 25±1 °C with Standard Deviation in Parentheses

Ligand (L)	Iminodiacetic acid–Ni–L		Iminodiacetic acid–Cu–L		($\Delta\log K_{Ni}-\Delta\log K_{Cu}$)
	$\log K^{Ni}_{NiAL}$	$\Delta\log K$	$\log K^{Cu}_{CuAL}$	$\Delta\log K$	$\Delta(\Delta\log K)$
Glycine	13.55 (0.04)	−0.79	15.71 (0.06)	−1.73	0.94
α-Alanine	13.31 (0.04)	−0.70	15.76 (0.06)	−1.69	0.99
Phenylalanine	12.80 (0.01)	−0.52	15.73 (0.05)	−1.28	0.76
Tyrosine	12.86 (0.01)	−0.40	15.52 (0.02)	−1.30	0.90
Tryptophan	13.37	−0.43	16.14	−1.36	0.93
Ethylenediamine	15.77 (0.02)	−0.72	18.31 (0.04)	−1.24	0.52
1,3-Propanediamine	14.78 (0.01)	−1.14	16.97 (0.07)	−2.26	1.12
Oxalic acid	—	—	—	—	—
Catechol	15.42 (0.02)	−1.46	—	—	—
Tiron	15.78 (0.02)	−2.32	—	—	—
Pyrogallol	14.39 (0.04)	−1.53	—	—	—
o-Aminophenol	11.15 (0.05)	−1.74	—	—	—
o-Phenylenediamine	—	—	—	—	—

forming the ternary complex. Hence, the tendency of L^{n-} to get bound to neutral MA will be less than to get bound with charged M^{2+} ion in the formation of binary complex ML, leading to negative $\Delta\log K$ value. The electrostatic replusion is more with increasing charge on L^{n-}, resulting in more negative $\Delta\log K$ values.

However, it is observed that $\Delta\log K$ in [M–dpa–L] complexes is less negative than [M–imda–L]. This is attributable to the fact that dpa coordinates from two carboxylates and one tertiary amine nitrogen. There is π acidic character in the ligand, due to the possibility of $M\rightarrow N\pi$ bond formation. On the other hand imda coordinates from two carboxylates and one σ bonding secondary amine nitrogen. Due to the π acidic character of dpa $\Delta\log K$ is less negative as observed in [M–dipyridyl–L] complexes.[7,8]

It is interesting to observe that $\Delta\log K$ is more negative in case of Cu(II) complexes compared to Ni(II) complexes. This is due to the tridentate character of dpa and imda.

In the binary complex the tridentate ligand dpa or imda occupy the three equatorial positions around the metal ion. Hence in the formation of the termary complex, the bidentate ligand(L) has to occupy one equatorial and one axial position,[20] or the tridentate ligand has to change to two equatorial and one axial position, and there may be equilibrium between the two forms. Due to Jahn Teller effect, in case of CuAL complexes either ligand is strained in occupying the axial position and hence its tendency to coordinate with the MA is much less than in the binary complex, hence $\log K^{MA}_{MAL}$ is much less than $\log K^{M}_{ML}$ and $\Delta\log K$ is more negative. In the absence of Jahn Teller distortion in Ni(II) complexes, the bidentate or the tridentate ligand does not feel any strain in occupying one equatorial and one axial position, and hence $\Delta\log K$ is less negative.

It is interesting to observe that $\Delta(\Delta\log K)(=\Delta\log K_{NiAL}-\Delta\log K_{CuAL})$ is less in MdpaL complexes than MimdaL complexes. This can be explained by considering the fact that the stabilizing effect of π acidic character of ligand (A) is more pronounced in CuAL complexes than in NiAL complexes. Hence the destabilization of the Cu–dpa–L complexes due to J. T. effect, is compensated by the increase in stability due to greater π acidic character of dpa. Hence $\Delta(\Delta\log K)$ $(=\Delta\log K_{NiAL}-\Delta\log K_{CuAL})$ is less in case of MdpaL complexes, compared to M–imda–L complexes.

It is observed that for the complexes Cu–dpa–L and Ni–dpa–L, where L=phenylalanine, tyrosine and tryptophan, $\Delta\log K$ value is less negative than the complexes where L=glycine or α-alanine. This is because of intramolecular interligand interaction as observed by Sigel[21] in complexes of the type $M(phen)(pheCA)^{+}$ where $M=Cu^{2+}$, Zn^{2+}, phen=1,10-phenanthroline and pheCA =phenylalkane carboxylates as also by Yamauchi[22] in complexes of the type Cu(DA)(AA), where AA=amino acids with side chains and DA= diamines. In the present complexes, the amino acids are bidentate, hence occupy one equatorial and one axial position or both equatorial positions as in case of glycinate and α-alaninate. Model building shows that in case where the amino acid occupied both equatorial positions, the non-coordinated side group, phenyl, hydroxyphenyl, and indole ring of phenylalanine, tyrosine, and tryptophan respectively, come over the pyridyl ring of dpa and hence non-covalent hydrophobic interaction stabilizes the ternary complex, leading to less negative $\Delta\log K$ values. Thus in cases of M–dpa–L complexes, the bidentate amino acid L should prefer two equatorial positions.

We are thankful to the referee for helpful suggestions.

References

1) H. Sigel, "Metal Ions in Biological Systems," Marcel Dekker, New York (1973), Vol. 2; (1981), Vol. 13.
2) P. Griesser and H. Sigel, *Inorg. Chem.*, **9**, 1237 (1970).
3) B. E. Fisher and H. Sigel, *Inorg. Chem.*, **18**, 425 (1979).
4) F. A. Walker, H. Sigel, and D. B. McCormik, *Inorg. Chem.*, **11**, 1756 (1972).
5) J. I. Watters and P. Dewitt, *J. Am. Chem. Soc.*, **82**, 1333 (1960).
6) O. Yamauchi and A. Odani, *J. Am. Chem.. Soc.*, **103**, 391 (1981).
7) M. V. Chidambaram and P. K. Bhattacharya, *J. Inorg. Nucl. Chem.*, **32**, 3271 (1970).
8) P. J. Patel, V. K. Patel, and P. K. Bhattacharya, *Indian J. Chem., Sect. A*, **21**, 590 (1982).
9) H. Gampp, H. Sigel, and A. D. Zuberbuhler, *Inorg. Chem.*, **21**, 1190 (1982).
10) W. E. Hatfield and T. S. Piper, *Inorg. Chem.*, **3**, 841 (1964).
11) P. C. Parikh and P. K. Bhattacharya, *Bull. Acad. Pol. Sci.*, **23** (**4**), 289 (1975).
12) W. E. Bennett, *J. Am. Chem. Soc.*, **79**, 1290 (1957).
13) N. Emanuel and P. K. Bhattacharya, *Indian J. Chem., Sect. A*, **24**, 498 (1985).
14) Phalguni Chaudhuri and H. Sigel, *J. Am. Chem. Soc.*, **99**, 3142 (1977).
15) G. Sharma and J. P. Tandon, *Talanta*, **18**, 1163 (1971).
16) I. G. Sayce, *Talanta*, **15**, 1397 (1966). I. G. Sayce, *Talanta*, **18**, 653 (1971). I. G. Sayce and V. S. Sharma, *Talanta*, **19**, 831 (1972).
17) A. E. Martell and P. M. Smith, "Critical Stability Constants," Plenum Press, New York (1977), Vol. 3.
18) H. Sigel, P. P. Huber, and R. F. Pasternack, *Inorg. Chem.*, **10**, 222 (1971).
19) A. Odani and O. Yamauchi, *Inorg. Chem. Acta*, **93**, 13 (1984).
20) Jan G. H. du Preez and Bernardus J. A. M. Van Brecht, *J. Chem. Soc., Dalton Trans.*, **1989**, 253.
21) R. M. Balakrishnan, K. H. Scheller, U. K. Haring, R. Tribolet, and H. Sigel, *Inorg. Chem.* **24**, 2067 (1985).
22) O. Yamauchi and A. Odani, *J. Am. Chem. Soc.*, **107**, 5938 (1985).

Preliminary Polarographic Studies of Sulfur and Selenium Solutions in Hydrazine Hydrate

S. K. Srivastava, K. S. Chandra Babu, O. N. Srivastava,† and Dharam Singh*
Analytical Division, Department of Chemistry, Banaras Hindu University, Varanasi 221005, India
†Department of Physics, Banaras Hindu University, Varanasi 221005, India
(Received September 20, 1990)

The dropping mercury electrode polarographic behavior of sulfur and selenium solutions in hydrazine hydrate has been studied in highly alkaline aqueous solution containing supporting electrolyte of 0.1 M ammonium tartrate (1 M=1 mol dm^{-3}). Both the sulfur and selenium revealed a composite anodic-cathodic waves. The values of $E_{1/2}$ for sulfur and selenium solutions, taken from the cathodic wave of the polarograms corresponded to $E_{1/2}$=−0.78 and −1.03 V vs. SCE respectively. The effect of mercury pressure and concentration of depolarizer on the relative magnitude of the wave heights has also been studied on the basis of typical reactions involved at DME in this solvent medium. No maxima supressor was used in the present study for both cases.

Polarographic study of sulfur solution in pyridine and ethanol, using sodium acetate–acetic acid buffer, exhibits elemental behavior[1–4] while in strongly alkaline medium, sulfur dissolves as sulfide and polysulfide ions.[5–7] Elemental sulfur and selenium dissolve in alkaline solution of sulfides of alkali metals with the formation of selenosulfide (Se_2S^-),[11] and in concentrated alkaline solutions to give polysulfides and polyselenides.[12] This transformation of elemental sulfur and selenium into selenosulfide is a convenient method for determining these elements. Konapik and Werner[7–9] carried out the polarographic studies of polysulfide ions in 2 M (M=mol dm^{-3}) NaOH and suggested the following reaction mechanism. They proposed that the anodic wave of the polarogram is due to the oxidation of mercury by sulfide ions, and the reduction of polysulfide and elemental sulfur is responsible for the cathodic wave as:

$$Hg + S^{2-} \longrightarrow HgS + 2e$$
$$S_2^- + 2e \longrightarrow 2S^{2-}$$
$$S + 2e \longrightarrow S^{2-}$$

Lingane and Niedrach[10] reported the polarography of selenide ions in different media with pH ranging from 1 to 14. Toropova et al.[11,12] have shown that selenium dissolves in highly alkaline media, as polyselenide ions. They proposed similar reaction mechanism at DME as suggested by Konapik and Werner.[7–9] In highly alkaline solutions like hydrazine hydrate the elemental selenium and sulfur are transformed to selenosulfide and polysulfide for determination. In the case of hydrazine hydrate, it is reported that sulfur and selenium in any oxidation state is readily reduced to elemental sulfur/selenium and dissolved in hydrazine forming solvation complex. The polarographic behavior of sulfur and selenium in hydrazine hydrate solutions at DME is less studied. In the present study, hydrazine hydrate in 50–50% mole ratio with water was employed as solvent for the polarographic determination of S and Se in elemental form and in various oxidation states. In our preliminary studies it was observed that 50% hydrazine hydrate+50% water was the suitable solvent composition for analysis. The effect of mercury pressure and depolarizers on wave heights of the polarograms have also been studied and results have been discussed.

Experimental

The commercially available (BDH) analytical grade hydrazine hydrate ($N_2H_4 \cdot H_2O$) was further purified by standard distillation procedure before use. Various volume ratios of distilled hydrazine hydrate was mixed with deionized water. Since, 50 volume % $N_2H_4 \cdot H_2O$+50% H_2O was found to have high solubility for sulfur and selenium, the same ratio of the solvent was used as the solvent in the present investigation. The standard solutions of AR-grade sulfur and selenium were prepared by dissolving accurately weighed quantity of the elements in 25 ml of the solvent. Ammonium tartarate (0.1 M) was used as the supporting electrolyte. The total volume of the supporting electrolyte and the analyte was made upto 25 ml and transferred to the polarographic cell. The flow rate 'm' and time 't' of the dropping mercury electrode (DME) assembly at a mercury height of 35 cm were 1.5 mg s^{-1} and 5.0 s, respectively. All the currents and potentials reported in this work were corrected for the residual current as well as the IR drop involved. The solutions were deaerated by bubbling nitrogen and the polarograms were recorded with the Leeds and Northup Electrochemograph type E at 25±1 °C.

Results and Discussion

As evident from Figs. 1 and 2, both the sulfur and selenium solutions in hydrazine hydrate, produce a composite anodic-cathodic waves.

Hydrazine hydrate dissociates according to the equilibrium in aqueous solution.

$$N_2H_4 \cdot H_2O \rightleftarrows N_2H_5^+ + OH^-$$

Hydrazinium ions reduce sulfur to sulfide (S^{2-}) and polysulfide (S_n^{2-}) ions with the evolution of nitrogen according to the following reactions.

$$4N_2H_5^+ + S_8 + 20OH^- \longrightarrow 4N_2 + 8S^{2-} + 20H_2O$$
$$S^{2-} + nS \rightleftarrows S_n^{2-}$$

Similarly, elemental selenium produces selenide (Se^{2-})

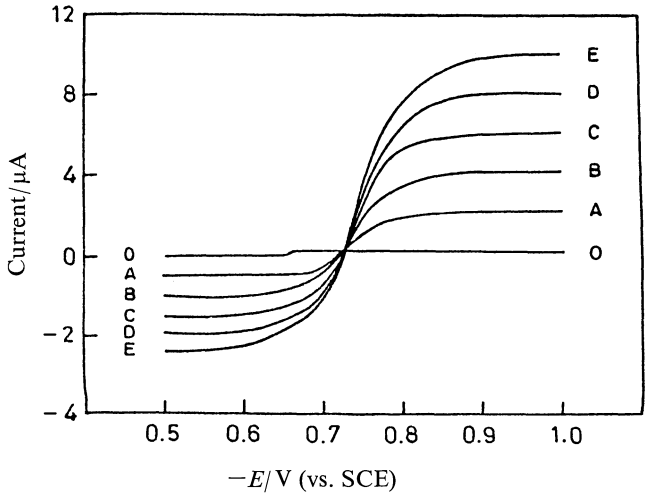

Fig. 1. Polarographic curves of sulfur solutions in hydrazine hydrate at various concentrations: A, 0.5079 mM; B, 1.0080 mM; C, 1.5000 mM; D, 1.9850 mM; E, 2.4610 mM (Line '0' is residual current, H_{Hg}=35 cm, pH=ca. 12).

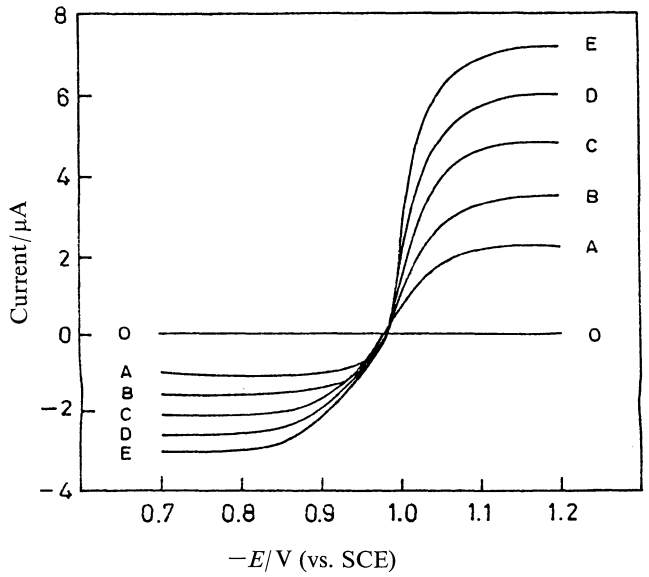

Fig. 2. Polarographic curves of selenium solutions in hydrazine hydrate at various concentrations: A, 0.6640 mM; B, 0.9911 mM; C, 1.3151 mM; D, 1.6358 mM; E, 1.9535 mM (Line '0' is residual current, H_{Hg}=35 cm, pH=ca. 12).

and polyselenide (Se_n^{2-}) ions, when dissolved in hydrazine hydrate.

The typical reaction mechanism proposed by Konopik and Werner,[7-9] and Totopova et al.[11,12] can be utilized in explaining the existence of composite anodic-cathodic waves in both cases. The sulfide (S^{2-}) and polysulphide (S_n^{2-}) ions produced in the solution react with mercury drop according to the following reactions.

$$S^{2-} + Hg \longrightarrow HgS + 2e \quad (1)$$

$$S_2^{2-} + Hg \longrightarrow HgS + S^{2-}$$
$$HgS + 2e \longrightarrow Hg + S^{2-}$$
$$S_2^{2-} + 2e \longrightarrow 2S^{2-} \quad (2)$$

and

$$Hg + S \longrightarrow HgS$$
$$HgS + 2e \longrightarrow Hg + S^{2-}$$
$$S + 2e \longrightarrow S^{2-} \quad (3)$$

The anodic wave can be attributed to the oxidation of mercury by sulfide (S^{2-}) ions, whereas the reduction of polysulfide (S_n^{2-}) ions and elemental sulfur is responsible for the cathodic step. Selenium also revealed a composite anodic-cathodic wave based on the similar mode of reaction mechanism. The values of $E_{1/2}$ for sulfur and selenium solutions taken from the cathodic wave of the polarogram correspond to $E_{1/2}$=−0.78 and −1.03 V vs. SCE, respectively. Similarly, the values reported in Tables 1 and 2 corresponded to the cathodic wave of the respective polarograms. Although there is no other direct evidence to prove this assumption, there appears to have no other options. One of the important advantages of this procedure is that the sulfur and selenium in any oxidation state can be reduced to elemental state and slowly dissolved in the hydrazine hydrate+water solvent. Therefore, this may be utilized as a new and convenient method for the determination of sulfur and selenium present in various analytes.

A plot of concentration vs. diffusion current gave a straight line, and the values calculated for diffusion current constant (I) were fairly constant (Tables 1 and 2) indicating the utility of the data for analytical purposes.

Table 1. Relationship of Diffusion Current with Sulfur Concentration and Values of Diffusion Current Constant

Curve	Sulfur concentration C/mM	Diffusion current i_d/μA	Diffusion current constant, I	Half wave potential $E_{1/2}$/V (vs. SCE)
A	0.5079	1.95	2.2	
B	1.0080	3.90	2.2	
C	1.5000	5.85	2.2	
D	1.9850	7.80	2.3	
E	2.4610	9.75	2.3	−0.78

Table 2. Relationship of Diffusion Current with Selenium Concentration and Values of Diffusion Current Constant

Curve	Selenium concentration C/mM	Diffusion current i_d/μA	Diffusion current constant, I	Half wave potential $E_{1/2}$/V (vs. SCE)
A	0.0640	2.25	2.0	
B	0.9911	3.45	2.0	
C	1.3151	4.80	2.1	
D	1.6358	6.00	2.1	
E	1.9535	7.20	2.1	−1.03

Table 3. Relationship of Diffusion Current with Mercury Height for Sulfur Solution

Mercury height H_{Hg}/cm	Diffusion current i_d/μA	$i_d/\mu A/\sqrt{H_{Hg}}$/cm
30	4.05	0.73
40	4.50	0.71
50	5.10	0.72
60	5.40	0.69

Table 4. Relationship of Diffusion Current with Mercury Height for Selenium Solution

Mercury height H_{Hg}/cm	Diffusion current i_d/μA	$i_d/\mu A/\sqrt{H_{Hg}}$/cm
35	6.00	1.01
45	6.75	1.00
55	7.50	1.01
65	8.25	1.02

The plot of $\log i_d$ vs. $\log H_{Hg}$ was a straight line with the slope closer to 0.5 and the values calculated for $i_d/\sqrt{H_{Hg}}$ at different heights of mercury column were fairly constant (Tables 3 and 4) showing that the waves were diffusion controlled in both systems.

Sincere thanks of the authors are due to Head of the Chemistry Department, Banaras Hindu University for providing necessary facilities. One of the authors (KSCB) acknowledges CSIR, Government of India for awarding Senior Research Fellowship.

References

1) G. Proske, *Naturwissenschaften,* **33**, 220 (1946).
2) M. I. Gerber and A. D. Shusherina, *Zh. Anal. Khim.,* **5**, 262 (1950).
3) G. Proske, *Anal. Chem.,* **24**, 1834 (1952).
4) M. von Stackelberg, W. Hans, and G. Hauck, *Ber. Bunsen-Ges. Phys. Chem.,* **61**, 473 (1957).
5) G. Duyckaerts, *Bull. Soc. R. Sci. Liege,* **17**, 313 (1948).
6) G. Delaure, *Chim. Anal. (Paris),* **44**, 91 (1962).
7) N. Konopik and E. Werner, *Monatsh. Chem.,* **83**, 1187 (1952).
8) E. Werner and N. Konopik, *Monatsh. Chem.,* **83**, 599 (1952).
9) E. Werner, *Monatsh. Chem.,* **83**, 1369 (1952).
10) J. J. Lingane and L. H. Niedrach, *J. Am. Chem. Soc.,* **70**, 4115 (1948).
11) V. F. Toropova, L. N., Medvedeva, and Yu. N. Polyakov, "Issledovaniya po Elektrokhimi, Magnetokhimii i Elektrokhimicheskim Metodam Analiza," Kazanskii Universitet, (1970), Vol. 3, p. 12.
12) V. F. Toropova, *Zh. Anal. Khim.,* **11**, 599 (1956).

Reaction of Tetraiodomercurate Anion with HSO_3Cl: Synthesis of and Physico-Chemical Studies on $M_2[Hg(SO_3Cl)_4]$ (M=Cu(I), K), $(Et_4N)_2[Hg(SO_3Cl)_2I_2]$, and $K_2[Hg(SO_3Cl)_nI_{4-n}]$ (n=1, 2, and 3)

Mohammad YAMIN SIDDIQI,* Zafar Ahmad SIDDIQI, and Mohammad SHAKIR
Inorganic Chemistry Division, Department of Chemistry, Aligarh Muslim University, Aligarh 202002, India
(Received February 25, 1991)

Reactions of $[M_2HgI_4]$ with excess of HSO_3Cl afford $M_2[Hg(SO_3Cl)_4]$ (M=Cu(I), K). However, the reactions of K_2HgI_4 with stoichiometric amounts of HSO_3Cl, i.e., in 1 : 3, 1 : 2, and 1 : 1 molar ratios, yield $K_2[Hg(SO_3Cl)_nI_{4-n}]$ (n=3,2,1). In these reactions HSO_3Cl acts as both chlorosulfating agent as well as medium of the reaction. Et_4NI reacts with $Cu^I_2[Hg(SO_3Cl)_4]$ suspended in CH_2Cl_2 affording $(Et_4N)_2[Hg(SO_3Cl)_2I_2]$ and $[CuSO_3Cl]_x$. All these compounds have been characterized by elemental analysis, electrical conductivity measurements, IR and electronic spectral studies.

Tetrahalometallate complex anions of the type $[MX_4]^{-2}$ ($M=Mn^{II}$, Fe^{II}, Ni^{II}, Cu^{II}, Zn^{II}, Hg^{II}; $X=Cl^-$, Br^-, and I^-) and also of $[FeX_4]^-$ are quite well known.[1-7] The halogen complex anions of Mn^{II}, Fe^{II}, Fe^{III}, and Hg^{II} have been thoroughly investigated using IR,[8,9] electronic,[10] Raman,[11] Chlorine nuclear quadrupole resonances[8] and Mössbauer spectroscopic studies for analysing molecular structure and mode of bonding in these complex anions. Tetrakis (chlorosulfato)metallate anions, $[M(SO_3Cl)_4]^-$, [$M=B^{III}$, Al^{III}, and Ga^{III} are obtained,[14-18] by utilizing either the addition reactions of sulfuric acid anhydrides or the solvolytic reactions of chlorosulfuric acid with corresponding tetrachlorometallates. The preparation and characterization of complex (chlorosulfato) metallates of heavier transition metals, i.e., $Na_2[Pd(SO_3Cl)_4]$ and $Na_2[Ir(SO_3Cl)_6]$, have been reported[19] from this laboratory. Here we are communicatingg for the first time the synthesis and characterization of $M_2[Hg(SO_3Cl)_4]$, [M=K and Cu(I)], $(Et_4N)_2[Hg(SO_3Cl)_2I_2]$ and $K_2[Hg(SO_3Cl)_nI_{4-n}]$ (n=1, 2, and 3).

Experimental

Materials. Pure chlorosulfuric acid (Riedel) was used as such; HgI_2, Et_4NI, $CuSO_4 \cdot 5H_2O$, and KI all were commercially pure samples which were used after recrystallization. However, Cu_2HgI_4 and K_2HgI_4 were synthesized according to the reported methods.[20] The solvents diethyl ether, DMSO, CH_2Cl_2, hexane, and acetonitrile were used after drying.[21]

Preparation of $Cu_2[Hg(SO_3Cl)_4]$ (1). Solid [Cu_2HgI_4] (0.9340 g or 1.11 mmol) was placed in a reaction flask and chlorosulfuric acid was added in excess (ca. 15 ml) at room temperature with magnetic stirring. A vigorous exothermic reaction took place with evolution of violet fumes. The reaction mixture was stirred for about three hours. The light brown colored solid material was filtered off through a sintered glass frit under N_2, washed with HSO_3Cl, and finally with thionyl chloride and then dried in vacuo at 60 °C to a constant weight (mp 300 °C, yield 0.75 g (ca. 80%) based on Cu_2HgI_4).

Preparation of $(Et_4N)_2[Hg(SO_3Cl)_2I_2]$ (2). Tetraethylammonium iodide (1.285 g or 5.42 mmol) was reacted with 1.9688 g (2.4 mmol) of **1** suspended in 25 ml dichloromethane and stirred for about 4 h. The wine red colored solution was filtered off leaving behind some colorless residue. The solution was then mixed with hexane and kept at ca. 10 °C for a week. Dark brown, hexagonal crystals appeared along with some dirty white powdery mass which settled at the bottom. The crystals were collected and again recrystallized in the same manner. The recrystallized material melts at 135 °C (Yield 1.38 g (ca. 70%) based on **1**). The white amorphous solid was washed several times with CH_2Cl_2 and vacuum dried. The result of the elemental analysis proved it $[CuSO_3Cl]_x$. Found: Cu, 35.12; S, 17.8; Cl, 19.90%. Calcd for $[CuSO_3Cl]_x$: Cu, 35.48; S, 18.87; Cl 19.82%, respectively.

Preparation of $K_2[Hg(SO_3Cl)_nI_{4-n}]$ [n=1, 2, 3, and 4; (6, 5, 4 and 3)]. For $K_2[Hg(SO_3Cl)_4]$ (3) solid K_2HgI_4 (0.7860 g or 0.001 mol) was mixed with excess of frozen HSO_3Cl. The temperature of the reaction mixture was slowly brought to room temperature with continuous magnetic stirring. The resulting dark red solution was poured dropwise in chilled dry diethyl ether in a closed vessel which resulted in the separation of colorless solid material. The solution was decanted off and the solid was repeatedly washed with ether till the washing did not show any color. The solid was vacuum dried, mp 197 °C, yield 0.55 g (ca. 70%) based on K_2HgI_4.

Compounds **4**, **5**, and **6** were prepared by mixing K_2HgI_4 with frozen HSO_3Cl in 1 : 3, 1 : 2, and 1 : 1 molar ratios, respectively, and the reaction mixture was allowed to warm up to room temperature with continuous stirring giving brownish-yellow colored solutions. These solutions separately resulted in the solid material when poured dropwise to chilled diethyl ether and the solid compounds were isolated in the manner as described above for **3**, melting points: **4** decomp 298—300 °C; **5** decomp 253—255 °C, **6** decomp 232—235 °C; yields: 2.7 g, 0.55 g, 3.79 g (70%, 70%, 80%, respectively based on K_2HgI_4).

Analysis. The results of C, H, N analyses were obtained from the microanalytical laboratory of I.I.T. Kanpur, whereas Cu, Hg, S, Cl, and I were determined by established methods.[22,23] The IR spectra (4000—250 cm^{-1}) were recorded as Nujol mulls using a Perkin Elmer Model 621 Spectrophotometer. Electrical conductivity was measured in 10^{-3} mol dm^{-3} solutions in DMSO or CH_3CN using a sys-

* Present address: Department of Medical Elementology/ Toxicology, Faculty of Science, Hamdard University, New Delhi 110062, India.

tronic bridge model 302 thermostated at 25±0.1 °C. The electronic spectra were recorded in DMSO or CH_3CN using a PYE Unicam 8800 spectrophotometer.

Results and Discussion

For the synthesis of **1** and **3** the solvolytic reaction of $[M_2HgI_4]$ with HSO_3Cl has been utilized where HSO_3Cl also serves as the reaction medium and the formation may be typified by the following reactions.

$$M_2HgI_4 + 4HSO_3Cl \rightarrow M_2[Hg(SO_3Cl)_4] + 4HI \quad (1)$$

$$2HI + 2HSO_3Cl \rightarrow H_2SO_4 + 2HCl + I_2 + SO_2 \quad (2)$$

(M=K, Cu(I)).

Reaction of **1** with Et_4NI in CH_2Cl_2, where both the reactants are separately insoluble, seems to be an interesting one. It was anticipated to get the replacement of copper(I) ion by the bulky cation, Et_4N^+ together with the release of Cu(I)iodide. It is noteworthy that in this reaction the final products obtained (Experimental Section) have been characterized as **2** and $[CuSO_3Cl]_x$, but only **2** is soluble in CH_2Cl_2 giving a dark brown solution. This implies that during the course of the reaction, in addition to the exchange of the cation, an anion replacement also takes place which may reasonably be due to the soft nature of iodide ion.[24-26] The reaction may be represented by the following equation.

$$Cu_2[Hg(SO_3Cl)_4] + 2Et_4NI \rightarrow (Et_4N)_2[Hg(SO_3Cl)_2I_2] + 2CuSO_3Cl \quad (3)$$

Stoichiometric amounts of $[K_2HgI_4]$ and HSO_3Cl, i.e., 1 : 1, 1 : 2, and 1 : 3 molar ratios, have been used for the preparation of **6**, **5**, and **4** where chlorosulfuric acid is an efficient chlorosulfating agent[27] effectively displacing an iodine atom as shown below.

$$K_2HgI_4 + nHSO_3Cl \rightarrow K_2[Hg(SO_3Cl)_nI_{4-n}] + nHI \quad (4)$$

(n=1, 2, and 3).

The magnitudes of the molar conductivity measured in DMSO for **3**, **4**, **5**, **6** and in CH_3CN for **1** and **2** (Table 1) suggest these to be strong electrolytes.[28]

Table 1. Elemental Analysis and Molar Conductance of the Compounds[a]

Copounds		Melting points	Found (Calcd)/%					μM^{b}	Yield
		°C	S	Cl	I	Hg	Cu	$cm^2\ S^{-1}\ mol^{-1}$	%
$Cu_2[Hg(SO_3Cl)_4]$	**1**	d.300	16.8 (17.4)	17.0 (17.2)	—	24.7 (25.4)	15.8 (16.26)	181	80
$(Et_4N)_2[Hg(SO_3Cl)_2I_2]$	**2**	130	8.1 (8.3)	8.5 (9.09)	31.6 (32.0)	25.1 (25.9)	—	140	70
$K_2[Hg(SO_3Cl)_4]$	**3**	197	18.4 (18.28)	19.1 (20.28)	—	29.3 (28.37)	—	250	70
$K_2[Hg(SO_3Cl)_3I]$	**4**	d.298—300d	12.01 (12.8)	13.77 (14.2)	18.02 (16.9)	25.4 (26.6)	—	200	70
$K_2[Hg(SO_3Cl)_2I_2]$	**5**	d.253—255d	7.99 (8.39)	8.98 (9.18)	32.80 (33.33)	25.7 (26.77)		145	70
$K_2[Hg(SO_3Cl)I_3]$	**6**	d.232—235d	4.17 (4.13)	4.39 (4.58)	49.75 (49.22)	24.1 (25.83)	—	161	80

a) Calculated values in parenthesis, d decomposition. b) for **1** and **2** in CH_3CN and for **3**, **4**, **5**, and **6** in DMSO.

Table 2. Infrared Frequencies (cm^{-1}) and Electronic Spectral Bands (nm) of Compounds[a]

Compounds		ν_6(E)	ν_2(A)	ν_3(A)	ν_5(E)	ν_1(A)	ν_4(E)	$\nu_{(Et_4N)}$	Electronic spectra		
$Cu_2[Hg(SO_3Cl)_4]$	**1**	310 w 330 w	460 m	540 s	590 s 610 s	1075 s	1280 s 1300 s		230 m, 470 mb.	260 m,	280 s,
$(Et_4N)_2[Hg(SO_3Cl)_2I_2]$	**2**	310 w 320 w	420 m	545 m	590 s 610 s	1030 s	1170 s 1225 s	2980 m 2940 m 1450 b 1365 m 1005 s	230 w, 360 mb.	260 s,	280 sh,
$K_2[Hg(SO_3Cl)_4]$	**3**	310 w 330 w	460 m	520 s	570 s 590 s	1050 s	1170 m 1250 s 1290 s		230 m, 350 s,	260 m, 470 mb	280 sh,
$K_2[Hg(SO_3Cl)_3I]$	**4**	310 w 330 w	450 m	510 s	580 s 600 s	1070 s	1230 s 1290 s		230 m, 360 sh.	260 m,	280 sh,
$K_2[Hg(SO_3Cl)_2I_2]$	**5**	320 w 340 w	450 m	530 s	600 s 610 s	1060 s	1270 s 1300 s		230 m,	290 s,	360 m
$K_2[Hg(SO_3Cl)I_3]$	**6**	310 w 330 w	460 m	520 s	590 s 610 s	1056 s	1200 s 1230 s		270 s,	300 m,	370 sh

a) w=weak, m=medium, s=strong, b=broad, sh=shoulder, ν_1(A) sym·SO_3 stretch, ν_4(E) asym·SO_3 stretch, ν_5(E) asym·SO_3 def., ν_3(A) sym·SO_3 def., ν_2(A) S–Cl stretch, ν_6(E) S–Cl wag.

The IR spectra of the compounds (Table 2) show bands which may reasonably be assigned to the characteristic SO_3Cl^- group vibrations. The chlorosulfate group is known[19,30] to coordinate to a metal ion in a uni- or bidentate manner exhibiting considerable cation–anion interaction. The free SO_3Cl^- ion has C_{3v} symmetry[27] which would comprise of six IR active fundamentals, namely ν_1(A), ν_2(A), ν_3(A), ν_3(E), ν_5(E), and ν_6(E) with three of these being degenerate. It has been observed[29–31] that ν_1(A) frequency in transition metal and rare earth metal chlorosulfates lies to a higher energy by about 35 cm^{-1} from that indicated[27] in ionic $CsSO_3Cl$, owing to an increased cation–anion interaction leading to a reduced C_s symmety. The lowering of the symmetry from C_{3v} to C_s causes the splitting of the degenerate modes exhibiting in all nine IR active fundamentals.[27] The present IR data are consistent with a covalent bonding of the SO_3Cl^- group to the Hg^{2+} ion. The nature and the positions of the bands in the IR spectra of all these compounds are identical, suggesting the formation of similar species with most likely tetrahedral geometry.

Goodgame et al.[32,33] have reported that in $K_3[Hg(NO_2)_4](NO_3)$ and $K_2[Hg(NO_2)_4]$ there are four chelating NO_2 groups surrounding the Hg^{2+} ion in an approximately tetrahedral array. The characteristic stretching frequency for (Hg–I) bond expected[34] at ca. 120 cm^{-1} could not be recorded as it occurs beyond the range of our instrument. The probable tetrahedral geometry of the anion $[Hg(SO_3Cl)_2I_{4-n}]^{2-}$ (n=1, 2, 3, and 4) may reasonably be represented as shown below, where X is I or SO_3Cl.

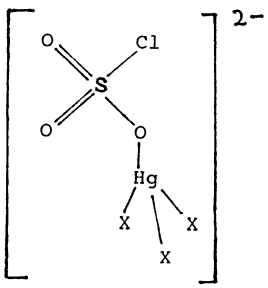

It has been reported that the two bands observed in the UV-region (250—300 nm) for transition metal chlorosulfate,[35] are due to charge transfer as well as the $n \rightarrow \sigma^*$ transition of the SO_3Cl^- group, irrespective of the IR geometry. Wolfsberg and Helmholtz[36] have proposed the LCAO-MO scheme to account the electronic spectra of the molecules like MnO_4^-, CrO_4^{2-}, $CoCl_4^{2-}$, and ClO_4^- etc. (Td symmetry). The observed lowest energy band of the $[Hg(SO_3Cl)_4]^{2-}$ anion (Table 2) in qualitative terms reasonably corresponds to the transition, HOMO [filled nonbonding π-orbital]→LUMO [unfilled antibonding π*-orbital]. The possibility of a Jahn–Teller distortion[37] in the molecule could not be ruled out as the spectrum contains closely spaced bands in the UV-region. The electronic spectra[38] of $[HgI_4]^{2-}$ and of $[HgI_3]^-$ anion[26,34] are similar showing maxima at 270 and 320 nm, characteristic of a tetrahedral geometry of the complex anion.[39] Although the exact nature of the transitions responsible for these bands has not authoritatively pronounced, they were considered to be due to promotion of a nonbonding electron to the available two unfilled orbitals. It has been indicated[40] that the substitution of halogen for oxygen atoms in CrO_4^{2-} (CrO_3F^-, CrO_3Cl^-, CrO_2Cl_2) shifts the absorption band to longer wavelengths suggesting that the $[Hg(SO_3Cl)_4]^{2-}$ anion also would exhibit a similar red-shift on substituting iodine atoms in place of a SO_3Cl^- group. However, no such information is revealed in the electronic spectra of **2**, **4**, and **5** rather the band occurring in the visible region of **1** and **3** does not appear in the former cases.

Support from CSIR, New Delhi, India (Grant No. 9/86/(138)/87-EMR-I) to MY is gratefully acknowledged.

References

1) N. S. Gill, *J. Chem. Soc.*, **1961**, 3512.
2) A. P. Grinsberg and M. B. Robin, *Inorg. Chem.*, **2**, 817 (1963).
3) D. F. C. Morris, E. L. Short, and D. N. Waters, *J. Inorg. Nucl. Chem.*, **25**, 975 (1963).
4) B. J. Hathaway and D. G. Holah, *J. Chem. Soc.*, **1964**, 2408.
5) A. Sabatini and L. Sacconi, *J. Am. Chem. Soc.*, **86**, 17 (1964).
6) J. Hiroshi and T. Shimanouch, *Spectrochim. Acta*, **22**, 1483 (1966).
7) H. Poulet and J. P. Mathiew, *J. Chim. Phys.*, **60**, 442 (1663).
8) D. E. Scaife, *Aust. J. Chem.*, **24**, 1753 (1971).
9) J. T. R. Dunsmuir and A. P. Lane, *J. Inorg. Nucl. Chem.*, **33**, 4361 (1971).
10) F. A. Cotton, M. L. Goodgame, and M. Goodgame, *J. Am. Chem. Soc.*, **84**, 167 (1962).
11) G. J. Janz and D. W. James, *J. Chem. Phys.*, **38**, 905 (1963).
12) P. R. Edwards and C. E. Johnson, *J. Chem. Phys.*, **49**, 211 (1968).
13) N. N. Greenwood and T. C. Gihb, "Mössbauer Spectroscopy," Chapman Hall, London (1971).
14) B. Vandrope and M. Drache, *Bull. Soc. Chim. Fr.*, **1971**, 2878.
15) B. Vandrope, M. Drache, and B. Dubois, *C. R. Acad. Sci. Russ., Ser. C*, **73**, 276 (1973).
16) B. Vandrope, M. Drache, and J. Neubel, *Bull. Soc. Chim. Fr.*, **1976**, 1949.
17) G. Mairesse and M. Drache, *Acta Crystallogr., Sect. B*, **34**, 1771 (1978).
18) M. C. D. Deneufeglise, M. Drache, and B. Vandrope, *J. Chim. Phys.*, **76**, 919 (1979).
19) S. A. A. Zaidi, S. R. A. Zaidi, T. A. Khan, Z. A. Siddiqi, and M. Shakir, *Synth. React. Inorg. Met-Org. Chem.*, **16**, 491 (1986).
20) G. Brauer, "Hand Book of Preparative Inorganic

Chemistry," Academic Press, New York (1965), Vol. 2, p. 1110.
21) I. Vogel, "A Text Book of Practical Organic Chemistry Including Qualitative Organic Analysis," 4th ed, Longman Group Limited, Edinburgh (1978), pp. 207—272.
22) I. Vogel, "A Text Book of Quantiative Inorganic Analysis," Longmans Green and Co., London (1954), pp. 399 and 401.
23) C. N. Reilly, R. W. Schmid, and F. A. Sadak, *J. Chem. Educ.*, **36**, 555 (1959).
24) R. G. Pearson, *J. Am. Chem. Soc.*, **85**, 3533 (1963); *Science,* **151**, 172 (1966).
25) J. G. Edwards, *J. Am. Chem. Soc.*, **76**, 1540 (1954).
26) S. Ahrland, J. Chattnand, and N. R. Dacied, *Q. Rev., Chem. Soc.*, **12**, 265 (1958).
27) E. A. Robinson and J. A. Ciruna, *Can. J. Chem.*, **46**, 1715 (1968).
28) W. G. Gearay, *Coord. Chem. Rev.*, **7**, 81, (1971).
29) Z. A. Siddiqi, Luthfullah, N. A. Ansari, and S. A. A. Zaidi, *J. Inorg. Nucl. Chem.*, **43**, 397 (1981).
30) Z. A. Siddiqi, M. Aslam, N. A. Ansari, M. Shakir, and S. A. A. Zaidi, *Synth. React. Inorg. Met-Org. Chem.*, **11**, 475 (1981).
31) S. A. A. Zaidi, S. R. A. Zaidi, M. Shakir, M. Aslam, and Z. A. Siddiqi, *Polyhedron,* **4**, 365 (1985).
32) D. M. L. Goodgame and M. A. Hitchman, *J. Chem. Soc. A,* **1967**, 612.
33) D. M. L. Goodgame and M. A. Hitchman, *Inorg. Chem.*, **4**, 731 (1965).
34) M. A. Hooper and D. W. James, *Aust. J. Chem.*, **24**, 1331 (1971).
35) Z. A. Siddiqi, M. Shakir, M. Aslam, T. A. Khan, and S. A. A. Zaidi, *Synth. React. Inorg. Met-Org. Chem.*, **13**, 397 (1983).
36) M. Wolfsberg and L. Helmholtz, *J. Chem. Phys.*, **20**, 837 (1952).
37) A. D. Liehr, *J. Chem. Educ.*, **39**, 135 (1962).
38) T. R. Griffiths, *Anal. Chem.*, **35**, 1077 (1963).
39) M. Delwaulla, *Bull. Soc. Chim. Fr.*, **1955**, 1294.
40) L. Helmholtz, H. Brennan, and M. Wolfsberg, *J. Chem. Phys.*, **23**, 853 (1955).

 © 1991 The Chemical Society of Japan Bull. Chem. Soc. Jpn., 64, 3669—3672 (1991)

Electrochemical Reactions at Sacrificial Electrodes. VII. Synthesis of Some Unique Mercury(II) Alkoxides and Glycolates and Their Coordination Compounds

Jagtar Singh BANAIT,* Rani DEVI, and Baljit SINGH
Department of Chemistry, Punjabi University, Patiala 147002, India
(Received March 22, 1991)

The electrochemical oxidation of malononitrile, diethyl malonate, ethyl cyanoacetate, cyanoacetamide, ethyl acetoacetate, and acetylacetone has been carried out in acetonitrile at sacrificial mercury anode using tetrabutylammonium chloride as supporting electrolyte. The products of these reactions have been identified by elemental analysis and IR spectral studies and are found to be mercury(II) alkoxides/glycolates. Electrochemical oxidation of these compounds in the presence of ligands like 1,10-phenanthroline and 2,2′-bipyridyl yields coordination compounds of these alkoxides/glycolates. All these reactions have been found to proceed with a very high current efficiency.

Recently in our laboratories, eleotrochemical reactions of carboxylic acids, polyhedric alcohols, and monohydric alcohols have been conducted at sacrificial copper,[1-3] mercury,[4] and cadmium[5] anodes. It has been observed that the acidic proton in these compounds has been replaced by the anode metal through these electrochemical reactions. The present paper reports the electrochemical reactions of malononitrile, diethyl malonate, ethyl cyanoacetate, cyanoacetamide, ethyl acetoacetate, and acetylacetone (H_2R) at sacrificial mercury anode. These compounds have no acidic proton but can loose protons to yield carbanions under suitable experimental conditions. Adducts of these products of the above reactions with ligands such as 1,10-phenanthroline and 2,2′-bipyridyl have also been prepared by the electrochemical technique.

Experimental

Material and Equipment. Acetonitrile was dried over phosphorus pentaoxide and distilled. Freshly distilled acetonitrile was used as solvent in all these electrochemical reactions.

Tetrabutylammonium chloride was crystallized from conductivity water and dried under reduced pressure at 100 °C and used as supporting electrolyte.

Mercury was distilled in before use. Other organic compounds (Reidel Pure) were used as supplied.

Electrolysis was carried out in an H-type cell[1-3] made of Pyrex glass. The cathode and anode compartments were separated from each other by a sintered disc of G-3 porosity. Volume of the anode compartment (ca. 200 cm^3) was almost three times as large as that of cathode compartment (ca. 65 cm^3).

Platinum foil (1×1 cm^2) was used as a cathode and mercury pool (surface area 25 cm^2) as anode.

Direct current was obtained with the help of a Toshniwal electrophoresis power supply.

Procedure. A solution of tetrabutylammonium chloride (0.5×10^{-2} mol dm^{-3}) in acetonitrile (250 cm^3) was taken in the electrolysis cell. Two grams of the organic compound (H_2R) was also added to this solution. Necessary connections were then made with the power supply and potential accross the electrodes was adjusted so that a current of about 20 mA passed through the cell. The other experimental details were essentially the same as reported earlier.[1] White/grey colored solids separated in the anode compartment after a prolonged electrolysis of about ten hours. The products were collected by filtration, washed several times with dry acetonitrile in an all glass filtration unit and dried in vacuum.

Coordination compounds of the products of the above electrolytic processes were prepared through the electrolysis of the solution of tetrabutylammonium chloride (0.5×10^{-2} mol dm^{-3}) in acetonitrile containing 2.0 g of the organic compound (H_2R) and 1.0 g of the ligand at the sacrificial mercury anode. The details of the experimental procedure are the same as above.

Current efficiencies were determined from the ratio of actual and theoretical amounts of mercury dissolved when a current of 20.0 mA was passed for 2 h through the cell in the given system.

Infrared spectra of the products in Nujol were recorded with Beckman IR-20 spectrophotometer using sodium chloride plates in the region of 4000 to 600 cm^{-1} and polyethylene plates in the region of 600 to 200 cm^{-1}.

Mercury contents in the electrochemical products were estimated potentiometrically.[6]

Results and Discussion

Products of the electrochemical reactions of malononitrile, diethyl malonate, ethyl cyanoacetate, cyanoacetamide, ethyl acetoacetate, and acetylacetone are not affected much by moisture and air and are quite stable. All these compounds are insoluble in the common organic solvents. The product of acetylacetone, however, is soluble in most of the polar solvents.

The products of these electrochemical reactions do not melt upto a temperature of 250 °C. However, in some of the cases there has been a color change of the product in the temperature range of 230 to 250 °C.

Elemental analysis (Hg, C, H, and N) of these compounds have been carried out and the data are listed in Table 1 alongwith the electrolysis characteristics. Perusal of Table 1 reveals that the elemental analysis of the products corresponds to a general formula of $Hg(HR)_2$

Table 1. Electrolysis Characteristics, Analytical and Other Relevant Data of the Electrolysis Processes of H_2R at Mercury Anode

H_2R	Potential applied	Electricity passed	Product	Color	Elemental analysis[a]/%				Current efficiencies
	V	Coulombs			Mercury	Carbon	Hydrogen	Nitrogen	%
Malononitrile	30	650	$C_6H_2N_4Hg$	White	59.6 (60.7)	23.9 (21.8)	0.5 (0.6)	15.8 (16.9)	88
Diethyl malonate	20	710	$C_{14}H_{22}O_8Hg$	Grey	35.0 (38.7)	33.0 (32.4)	3.3 (4.2)	—	78
Ethyl cyanoacetate	30	680	$C_{10}H_{12}O_4N_2Hg$	Grey	47.1 (47.2)	31.1 (28.3)	2.5 (2.8)	6.9 (6.6)	72
Cyanoacetamide	20	720	$C_6H_6O_2N_4Hg$	Grey	51.8 (53.7)	18.3 (19.6)	0.9 (1.1)	14.2 (15.3)	78
Ethyl acetoacetate	30	640	$C_{12}H_{18}O_6Hg$	White	42.9 (43.7)	30.4 (31.4)	2.9 (3.9)	—	71
Acetylacetone	30	680	$C_{10}H_{14}O_4Hg$	Grey	51.3 (50.3)	30.0 (30.1)	3.2 (3.5)	—	75

a) Results in parenthesis are the theoretical values.

which shows that a proton from the organic molecules (H_2R) has been replaced by the mercury anode.

Infrared spectral data of the electrochemical products recorded in the region of 4000 to 200 cm^{-1} reveal that the characteristic bands of all the products except that of malononitrile appear in the regions of 1020 to 1060 and 450 to 460 cm^{-1}. Survey of literature[7,8] reveals that the ν(C–Hg) stretching band appears in the region of 515 to 554 cm^{-1} and no such band has been observed in the infrared spectra of the present products.

The carbanions formed by the abstraction of proton from the present organic molecules have been reported to exist in different resonance forms:

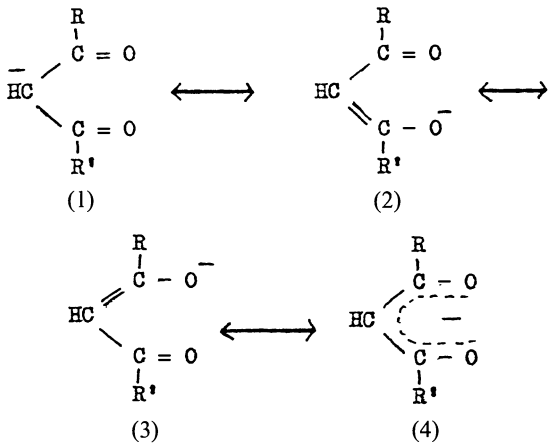

(1) (2) (3) (4)

Absence of ν(C–Hg) absorption band in the infrared spectra of the electrochemical products indicate that these products may have formed through the resonance form (4). Survey of literature[9,14] reveals that the ν(C–O)M and ν(M–O) absorption bands in various metal alkoxides appear in the regions of 1000 to 1150 cm^{-1} and 400 to 500 cm^{-1} respectively. Infrared spectra of some mercury(II) alkoxides have been reported recently from our laboratories.[4] The absorption bands in the regions 1000 to 1060 cm^{-1} and 450 to 460 cm^{-1} have been assigned to ν(C–O)Hg and ν(Hg–O) respectively. Thus the infrared studies support the formation of these products through the resonance form (4).

In case of malonitrile, a strong absorption band appears at 2180 cm^{-1}. Generally, ν(C≡N) bands appear in the region of 2240 to 2260 cm^{-1} in alkanenitriles.[15] Appearance of ν(C≡N) stretching modes in the lower region also supports the formation of the product of the electrochemical reaction of malononitrile through the resonance form (5):

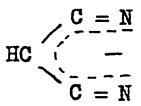

(5)

Absorption bands at 2200 and 2150 cm^{-1} have also been observed in the product of ethyl cyanoacetate and cyanoacetamide respectively in addition to the absorption bands in the regions 1010 to 1020 and 450 to 460 cm^{-1}. This also supports the formation of these products through the resonance forms of the type (4) and (5). Thus all these organic compounds except malononitrile yield mercury(II) alkoxides/glycolates through the present electrochemical reactions.

Survey of literature[9–11,16–18] reveals that the metal alkoxides, generally exist as polymers by forming bridged structure through alkoxide groups. Appearance of ν(C–O)Hg absorption bands in the lower region and comparatively broad peaks indicate the polymer structure of these compounds through alkoxyl groups. Insoluble behavior of these compounds in almost all organic solvents also supports this fact. Molecular weight of these compounds, however, could not be determined because of their insolubility in various solvents having convenient melting point.

Current efficiencies of all these reactions have been

determined and are listed in Table 1. Reactions of alcohols at sacrificial anodes[2-4] reveal that the metal alkoxide is the only product containing metal atom. The present electrochemical reactions are similar to those of alcohols as in both the cases a proton from the organic molecule is replaced by the sacrificial metal anode. Current efficiencies have, therefore, been evaluated on the basis of equivalents of metal dissolved per Faraday of electricity passed. Perusal of Table 1 reveals that crrrent efficiencies of all these reactions are quite close to 100% showing thereby that the reactions leading to the formation of mercury(II) alkoxides/glycolates are the predominant reactions of these systems. The reaction scheme may be written as:

At the cathode:

$$2\,H_2R + 2e^- \longrightarrow 2\,HR^- + H_2$$

At the anode:

$$2\,HR^- + Hg_{(+)} \longrightarrow (HR)_2Hg + 2\,e^-$$

Coordination Compounds. The electrochemical products of ethyl cyanoacetate and diethyl malonate have been refluxed with 1,10-phenanthroline and 2,2′-bipyridyl in solvents like methanol, ethanol, acetonitrile, and benzene for more than 48 h. However, the elemental analysis showed that the donor molecules could not rupture the alkoxide bridges to form their coordination compounds. It is, therefore, considered worthwhile to add the ligand molecules to these compounds before these are polymerized. Electrolysis of the organic compounds has therefore, been carried out in the presence of sufficient amount of 1,10-phenanthroline or 2,2′-bipyridyl.

The products of these electrochemical reactions are also insoluble in the common organic solvents. This indicates that these may also be polymer in nature like the parent alkoxides/glycolates. Melting points of these products are above 250 °C. Some of these compounds, however, show slight color change in the temperature range of 200 to 250 °C. These compounds are not affected by moisture or air and are quite stable.

Elemental analysis (Hg, C, H, and N) has been carried out and the data are recorded in Table 2. The analytical data of these compounds agree with the molecular formula, $Hg(HR)_2 \cdot L$.

Infrared spectral data of these compounds show the characteristic ν(C–O)Hg stretching vibrations[9-14] between 1030 and 1120 cm^{-1}. The absorption bands are slightly broad, appear in a slightly higher region as compared to the parent mercury(II) alkoxides/glycolates and distinct two or three absorption bands are observed in this region. Increase in the number of bands in this region indicates the presence of both the terminal and bridged alkoxide groups in these compounds. The presence of terminal alkoxyl groups may be attributed to the coordination of the ligand molecules and the presence of bridged alkoxyl groups shows that the present coordination compounds of mercury(II) alkoxides/glycolates have still polymeric structure. Insoluble behavior of these compounds also supports the polymeric structure of these compounds. Many such metal alkoxides in which in addition to the ligand

Table 2. Electrolysis Characteristics, Elemental Analysis and Other Related Data of the Electrolysis of H_2R+Ligand Systems at Mercury Anode

System	Potential applied	Electricity passed	Product	Color	Elemental analysis[a]/%				Current efficiencies
	V	Coulombs			Hg	C	H	N	%
Malononitrile+2,2′-Bipy.	30	640	$C_6H_2N_4Hg \cdot C_{10}H_8N_2$	Grey	40.7 (41.3)	37.9 (39.4)	2.0 (2.1)	16.9 (17.3)	80
Diethyl malonate+2,2′-Bipy.	40	510	$C_{14}H_{22}O_8Hg \cdot C_{10}H_8N_2$	Grey	29.1 (29.7)	40.9 (42.7)	4.8 (4.5)	4.9 (4.2)	62
Ethyl cyanoacetate+2,2′-Bipy.	20	720	$C_{10}H_{12}O_4N_2Hg \cdot C_{10}H_8N_2$	Grey	33.6 (34.6)	40.8 (42.1)	3.0 (3.5)	9.2 (9.8)	84
Cyanoacetamide+2,2′-Bipy.	20	700	$C_6H_6O_2N_4Hg \cdot C_{10}H_8N_2$	Light Brown	40.1 (38.4)	35.9 (36.7)	1.9 (2.6)	15.1 (16.1)	76
Ethyl acetoacetate+2,2′-Bipy.	20	720	$C_{12}H_{18}O_6Hg \cdot C_{10}H_8N_2$	Grey	31.9 (32.7)	43.2 (43.0)	3.8 (4.2)	4.5 (4.6)	67
Acetylacetone+2,2′-Bipy.	30	650	$C_{10}H_{14}O_4Hg \cdot C_{10}H_8N_2$	Grey	37.2 (36.2)	41.2 (43.3)	3.7 (4.0)	4.9 (5.1)	82
Diethyl malonate+1,10-Phen.	30	650	$C_{14}H_{22}O_8Hg \cdot C_{12}H_8N_2$	Light Green	28.4 (28.8)	43.6 (44.7)	3.6 (4.3)	3.9 (4.0)	79
Ethyl cyanoacetate+1,10-Phen.	40	500	$C_{10}H_{12}O_4N_2Hg \cdot C_{12}H_8N_2$	White	33.5 (33.2)	42.2 (43.7)	3.3 (3.3)	9.0 (9.3)	83
Cyanoacetamide+1,10-Phen.	20	680	$C_6H_6O_2N_4Hg \cdot C_{12}H_8N_2$	Grey	37.4 (36.9)	38.9 (39.5)	2.0 (2.7)	14.2 (15.3)	60
Ethyl acetoacetate+1,10-Phen.	20	650	$C_{12}H_{18}O_6Hg \cdot C_{12}H_8N_2$	White	30.9 (31.4)	43.7 (45.1)	3.9 (4.1)	4.3 (4.4)	64
Acetylacetone+1,10-Phen.	30	650	$C_{10}H_{14}O_4Hg \cdot C_{12}H_8N_2$	Grey	34.5 (34.7)	43.8 (45.6)	3.2 (3.8)	3.9 (4.8)	82

a) Results in parenthesis are the theoretical values.

molecules, alkoxyl bridging are also present have been reported in literature.[19–21]

Current efficiencies of all these systems are recorded in Table 2. It has been observed that the current efficiencies of most of the systems are quite close to 100% showing thereby that the reactions leading to the formation of coordination compounds of mercury(II) alkoxides/glycolates are the predominant reactions of these systems.

The present methods for the synthesis of mercury(II) alkoxides/glycolates and their coordination compounds are quite simple as compared to the usual multistep methods[10] for the synthesis of such compounds. These methods are associated with quite high values of current efficiencies also. Thus the electrochemical technique presents a new route for the synthesis of metal alkoxides/glycolates and their coordination compounds.

References

1) J. S. Banait, G. Singh, and P. K. Pahil, *J. Electrochem. Soc. (India)*, **33**, 173 (1984).
2) J. S. Banait, and P. K. Pahil, *Polyhedron,* **5**, 1865 (1986).
3) J. S. Banait and P. K. Pahil, *Synth. React. Inorg. Met. -Org. Chem.,* **16**, 1217 (1986).
4) J. S. Banait, S. K. Deol, and Baljit Singh, *Synth. React. Inorg. Met.-Org. Chem.,* **20**, 1331 (1990).
5) J. S. Banait and Baljit Singh, *Indian J. Chem.,* in press.
6) A. I. Vogel, "A Text Book of Quantitative Inorganic Analysis," Longman, Green and Co., Ltd., London (1961).
7) I. S. Butler and M. L. Newbury, *Spectrochim. Acta, Sect. A,* **33**, 669 (1977).
8) P. L. Goggin, G. Kerneny, and J. Mink, *J. Chem. Soc., Faraday Trans. 2,* **72**, 1025 (1972).
9) C. H. Brubaker, Jr. and M. Nicholas, *J. Inorg. Nucl. Chem.,* **27**, 59 (1965).
10) D. C. Bradley, R. C. Mehrotra, and D. P. Gaur, "Metal Alkoxides," Academic Press, New York (1978).
11) R. W. Adams, C. G. Barraclough, R. L. Martin, and G. Winter, *Aust. J. Chem.,* **20**, 2351 (1967).
12) C. E. Coates, J. A. Heslop, and D. Ridley, *J, Chem. Soc. A,* **1968**, 1118.
13) C. G. Barraclough, D. C. Bradley, J. Lewis, and I. M. Thomas, *J. Chem. Soc.,* **1961**, 2601.
14) D. C. Bradley and A. H. Westlake, Proc. Symp. Coord. Chem., Tihang, Hungary, Hungarian Acad. Sci., Budapest (1965).
15) J. R. Dyer, "Applications of Absorption Spectroscopy of Organic Compounds," Prentice-Hall of India Pvt. Ltd., New Delhi (1969).
16) G. A. Kakos and G. Winter, *Aust. J. Chem.,* **20**, 2343 (1967).
17) A. G. Krunger and G. Winter, *Aust. J. Chem.,* **23**, 1 (1970).
18) G. A. Kakos and G. Winter, *Aust. J. Chem.,* **22**, 97 (1969).
19) C. E. Coates and A. H. Fishwick, *J. Chem. Soc. A,* **1968**, 477.
20) S. Mathur, R. Ouaki, V. K. Mathur, R. C. Mehrotra, and J. C. Maire, *Indian J. Chem.,* **7**, 284 (1969).
21) R. C. Paul and H. S. Makhni, *Indian J. Chem.,* **9**, 247 (1971).

Acid-Base and Complex-Formation Properties of *N*-Hydroxy-3-pyridinecarboxamide and *N*,2-Dihydroxybenzamide in Aqueous Solution

Enrico Leporati
Istituto di Chimica Generale ed Inorganica dell'Università degli Studi di Parma, Viale delle Scienze 78, 43100-Parma, Italy
(Received April 22, 1991)

The protonation and complexation equilibria of the iron(III) and copper(II) complexes of *N*-hydroxy-3-pyridinecarboxamide (hpca) and *N*,2-dihydroxybenzamide (dhbc) have been investigated by potentiometric and spectrophotometric techniques in 0.5 mol dm^{-3} (KCl) at 25±0.1 °C. It was shown that the properties of iron(III) and copper(II) chelates under study are similar to those of corresponding chelates of simple aromatic hydroxamic acids (without any additional donor groupings in the molecule). The hydroxamate and carbonyl oxygens may also take part in coordination in the copper(II) and iron(III) systems.

Because of their pronounced chelating properties the organic derivatives of hydroxylamine are used in analytical chemistry for a long time. Beside of oximes and *N*-alkyl or *N*-aryl derivatives of hydroxylamine there are hydroxamic acids that are known to be useful in analytical praxis.[1] The occurrence of hydroxamic acid derivatives in living organisms (where they play an important role in biochemical processes as the iron binders and transfers, growth regulators, pigments and precursors of other compounds)[2,3] and especially the discovery of antibiotic properties of aspergillic acid have initiated extensive investigation of hydroxamic acids as potential antimicrobial substances. New hydroxy- and amino-substituted benzohydroxamic acids[4] were prepared and tested along with other previously reported benzohydroxamic acids (see Table 2 of Ref. 4) for enzyme inhibition and antitumor activity. Among numerous hydroxamic acids synthesized and studied up to now, the group of hydroxamic acids derived from pyridine occupies an important place. It has been shown that various ring-substituted 4-pyridinecarbohydroxamic acids exhibit an antiviral effect.[5] Derivatives of 3-pyridinecarbohydroxamic acid (acting as the inhibitor of urease) was even patented as the domestic animal and poultry feed additive which should improve the nitrogen uptake during the meat production.[6] As a loose continuation of our previous work dealing with the properties of amino-substituted aliphatic hydroxamic acids[7—10] (which are related to 3-pyridinecarbohydroxamic acid with respect to the presence of the nitrogen atom in the vicinity of the *N*-hydroxycarbamoyl group) we decided to fill the gap in the knowledge of fundamental physicochemical properties of hpca and their iron(III) chelates by the paper presented. Moreover, we extended the study to analogous aromatic hydroxamic acid (dhbc) that has not yet been described in the literature.

Experimental

Potentiometric Measurements. Potentiometric titrations were carried out using a Metrohm E 636 Titroprocessor and a combined electrode 8102SC Ross (ORION Research). The range of concentration of ligand in the potentiometric titrations was 0.0107—0.0141 mol dm^{-3} for hpca-H$^+$ (pH range 2.55—11.91; number of titrations 4); 0.00673—0.01009 mol dm^{-3} for dhbc-H$^+$ (pH range 2.51—11.50; number of titrations 6); 0.0142—0.0283 mol dm^{-3} for hpca-Fe^{3+} (pH range 1.86—6.09; number of titrations 5); 0.0105—0.0283 mol dm^{-3} for dhbc-Cu^{2+} (pH range 2.37—6.09; number of titrations 4). The metal concentration varied between 0.002124—0.007258 mol dm^{-3} for hpca-Fe^{3+} and 0.003413—0.005784 mol dm^{-3} for dhbc-Cu^{2+} systems, and potassium chloride (I=0.5 mol dm^{-3}) was used as supporting electrolyte.

Spectrophotometric Measurements. Absorption spectra in the ranges 300—700±0.3 nm for Fe^{3+}-hpca were measured with a KONTRON UVIKON 860 spectrophotometer to the fourth decimal place with a stepping of 2 nm. Solutions containing the ligand and the iron prepared and maintained under purified nitrogen at the ionic strength 0.5 mol dm^{-3} (KCl), were measured at pH from 1.83 to 8.01 at 25.0±0.1 °C using 10 mm cells.

Results and Discussion

Protonation Equilibria. Starting from several sets of potentiometric data, at first the macroscopic protonation constants of the ligands (hpca and dhbc) and the initial amounts of reagents (T_L, T_H/mmol) were refined at the same time by using the SUPERQUAD[11] computer program without introducing the liquid-junction potentials (A_j and B_j) into the calculations, as shown in previous publications.[7—10] After the refinement procedure, the variances (σ^2) as regards the initial amounts of the reagents (T_L, T_H) were 4.061×10^{-7} and 5.919×10^{-7} mmol^2 for hpca and 2.753×10^{-8} and 1.074×10^{-7} mmol^2 for dhbc, respectively. The calculated cumulative and stepwise protonation and complex-formation constants (β_{pqr}) of hpca and dhbc are reported in Table 1. The potentiometric titration curves of the protonated ligand (hpca), H_2L^+ (Scheme 1), show two distinct deprotonation centers: the pyridine nitrogen (>NH$^+$) [pH 2.5—4.5; (H^2, Scheme 1), log K_2=3.189(5)], and the hydroxyl group of the -NHOH moiety [pH 7.0—9.0; (H^1, Scheme 1), log K_1=7.986(3)]; while the dhbc ligand (dhbc=H_2L,

Table 1. Cumulative and Stepwise Protonation Complex Formation Constants of *N*-Hydroxy-3-pyridinecarboxamide (hpca) and *N*,2-Dihydroxybenzamide (dhbc) at 25 °C and I=0.5 mol dm^{-3} (KCl)

	SUPERQUAD			
	hpca		dhbc	
	H^+	Fe^{3+}	H^+	Cu^{2+}
$\log \beta_{011}$	7.986 (3)		9.722 (3)	
$\log \beta_{021}$	11.175 (6)		17.091 (5)	
$\log K_2^{H}$ a)	3.189 (5)[b]		7.369 (4)	
$\log \beta_{101}$				13.31 (3)
$\log \beta_{122}$		22.51 (10)		
$\log \beta_{112}$		20.03 (6)		
$\log \beta_{102}$		17.20 (9)		25.78 (9)
$\log \beta_{103}$		23.47 (8)		
Z[c]	185	267	317	245
χ^2[d]	43.02	17.85	6.66	21.18
U	4.85×10^1	1.94×10^3	7.91×10^1	5.17×10^2
σ[e]	0.53	2.72	0.51	3.07

a) $\log K_n=\log \beta_{0\ n\ 1}-\log \beta_{0\ n-1\ 1}$. b) $\sigma(\log K_n)=[(\sigma^2(\log \beta_{0\ n\ 1})+\sigma^2(\log \beta_{0\ n-1\ 1}))/2]^{1/2}$. c) Total number of experimental data points used in the refinement. d) Observed χ^2; calculated value (6, 0.95) should be 12.6, where 6 is the number of degrees of freedom and 0.95 is the confidence coefficient in the χ^2 distribution. e) $\sigma=\sum_{i=1}^{Z} w_i(E_i^{obsd}-E_i^{calcd})^2/(Z-m)$, where m is the number of parameters to be refined.

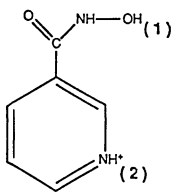

Scheme 1. (H_2L^+)=Hhpca

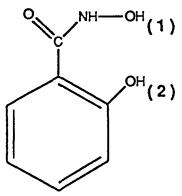

Scheme 2. (H_2L)=dhbc

Scheme 2) can only liberate two protons, one from the -OH group of the hydroxamic moiety [pH 6.1—8.2; (H^1, Scheme 2), $\log K_2$=7.369(4)] and one from the phenolic hydroxyl group [pH 8.4—10.6; (H^2, Scheme 2), $\log K_1$=9.722(3)]. The introduction of the CONHOH group into the pyridine ring (Scheme 1) resulted in a significant decrease of the basicity of the pyridine nitrogen from pK_a=5.3[12] to $\log K_2$=3.189(5) for hpca. This fact can be explained by a negative induction effect of the -CONHOH group on the nitrogen heteroatom. On the other hand, the substitution of an -NHOH group for the carboxyl OH^- group in the hydroxybenzohydroxamic acid examined (dhbc, Scheme 2) significantly lowers the protonation constant of the -OH group [$\log K_1$=9.722(3)] as compared to the analogous protonation constant of the corresponding -OH group in salicylic acid [$\log K_1$=13.4[13]] according to the electron-withdrawing character of the -NHOH moiety. The value for the protonation equilibrium of the hydroxamate moiety (-NHO^-) for the hpca is the same as obtained previously by conventional spectrophotometric method.[14] Rowland et al.[14] reported value of $\log \beta_{011}$=8.09 at I=0.1 mol dm^{-3} ($NaClO_4$) at 25 °C.

Metal-Complex Equilibria. Initial estimates of formation constants and the stoichiometries of possible complexes were obtained, in the case of the binary systems, from the features of formation curves. Following our usual approach, SUPERQUAD was employed to refine the formation constants and, on the basis of the usual numerical criteria, to select the initial sets of complexes. The final choices from the equilibrium models attempted are demonstrated by the excellent matching of the experimental and calculated potentiometric data and are reported in Table 1. The refinement included fixed contributions from the known metal hydrolysis constants of the species $[Fe(OH)]^{2+}$, $[Fe(OH)_2]^+$, $[Fe_2(OH)_2]^{4+}$, and $[Fe_3(OH)_4]^{5+}$. The relative importance of the various species in each pH range is shown by the typical distribution diagram, reported in Fig. 1. The species distribution curves show that complexation begins at low pH values: ca. 1.5 for $[FeH_2L_2]^{3+}$ (13.6%). The titration curves obtained on varying the iron and ligand concentrations were also processed by the FICS method (subprogram of STBLTY[15]) to give $(\partial C_H/\partial C_M)_{CL,pH}$ or $(\partial C_H/\partial C_L)_{CM,pH}$

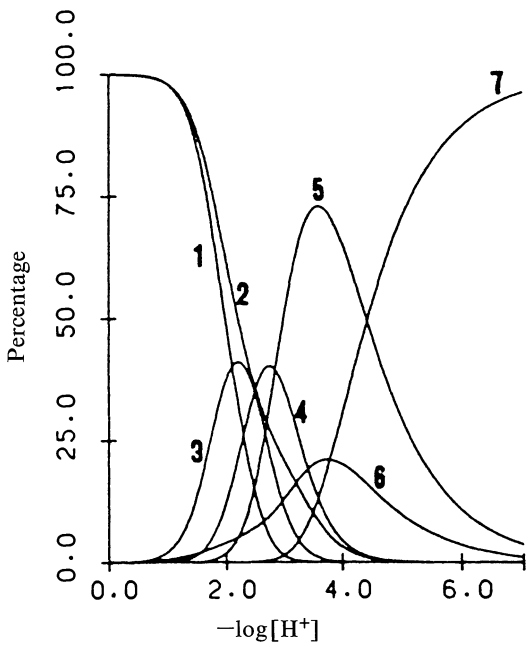

Distribution diagram for system

Fig. 1. Typical distribution diagram for Fe^{3+}-hpca system. The percentage of each species has been calculated from the data of a hypothetical solution of iron ions (0.004 mol dm^{-3}) and hpca (0.012 mol dm^{-3}) by the Haltafall program (N. Ingri, W. Kakalowicz, L. G. Sillén, and B. Warnqvist, **14**, 1261 (1967)), and using a PLOTTER Calcomp 936. The percentages of the species not containing iron were calculated as percentages of the total ligand, those containing iron as percentages of the total metal. (1) Fe^{3+}, (2) H_2L^+, (3) $FeH_2L_2^{3+}$, (4) $FeHL_2^{2+}$, (5) FeL_2^+, (6) HL, (7) FeL_3.

respectively, as a function of pH. The displacement of two protons at pH 2.2 presumably gives an $[FeH_2L_2]^{3+}$ (41.0%) species and at pH 2.7 the predominant species is $[FeHL_2]^{2+}$ (40.1%) corresponding to the displacement of two protons with neutralization of one proton residing on the pyridinic nitrogen. At pH 3.6, the proton displacement value corresponding to the iron coordination rises to about 2.0 and can be attributed to the formation of the $[FeL_2]^{+}$ (72.8%) species when the hydroxamate moiety is about 79.1% ionized. On raising the pH further, $[FeL_3]$ (max. 96.35 at pH 7.0) species is formed. At pH=7.0, approximately three protons per mol of Fe^{3+} are liberated and the hydroxamic acid group is about completely ionized.

The spectrophotometric study was carried out on solutions containing hpca and iron ion, with concentrations and pH values selected from those employed in the potentiometric titrations. Some typical absorption spectra obtained for Fe^{III}–hpca system at different pH values are reported in Fig. 2. When the pH is increased from 1.830 to 5.346 (Fig. 2), small hypsochromic and high hyperchromic shifts (from 478 to 436 nm) are observed (intense reddish brown) [maximum, 0.683 A at 478 nm(1); 0.722 A at 476 nm(2); 0.803 A at 472 nm(3); 0.884 A at 464 nm(4); 0.963 A at 454 nm(5); 1.069 A at 442 nm(6); 1.141 A at 436 nm(7); Fig. 2], revealing changes previously described qualitatively by Neilands.[16] A maximum at 436 nm (curve 7, Fig. 2) is reached at pH 5.3, which corresponds to the maximum in the concentration (75.4%) of the species, $[FeL_3]$ (Fig. 1, curve 7). As the pH is raised from 1.83 to 8.01 the λ_{max} is observed to shift from 478 to 422 nm (Fig. 2). This charge-transfer band is typical of iron(III) hydroxamates but the pH dependence of the λ_{max} is not like that of the other naturally occurring siderophores as ferrichromes and ferrioxamines. A sharp color change is observed from red-brown to orange at about pH 5.5. No further changes are seen until approximately pH 8.0 when the color lightens to yellow-orange. Above pH 10.5 the iron is observed to precipitate as the hydroxide. Elaboration of the visible spectral data (300—700 nm) by a refinement procedure with the SQUAD[17] program indicates that at least four colored species are present between pH 1.83—8.01 ($[FeH_2L_2]^{3+}$, $[FeHL_2]^{2+}$, $[FeL_2]^{+}$, and $[FeL_3]$). Our best model is in partial agreement only with those given by El-Ezaby and Hassan,[18] Brown et al.,[19] and E. Farkas et al.,[20] for the iron(III)–aha (aha=2-amino-*N*-hydroxyacetamide) and iron(III)–ahpr (ahpr=2-amino-*N*-hydroxypropanamide) systems, respectively. Since iron(III) is a typical hard ion, we assume coordination through the *O,O* atoms of the hydroxamate moiety of hpca. Accordingly, the protonated $[FeH_2L_2]^{3+}$ (Scheme 3), and $[FeHL_2]^{2+}$ (Scheme 4) complexes contain the pyridinic nitrogen in its protonated form. This assumption is supported by the spectrophotometric results, and those recorded for iron(III) hydroxamate systems.[8,21–23] The pH dependence of iron(III)–hpca system differs from that of the iron(III) trihydroxamate siderophores, which have a broad visible maximum from 420 to 440 nm and do not

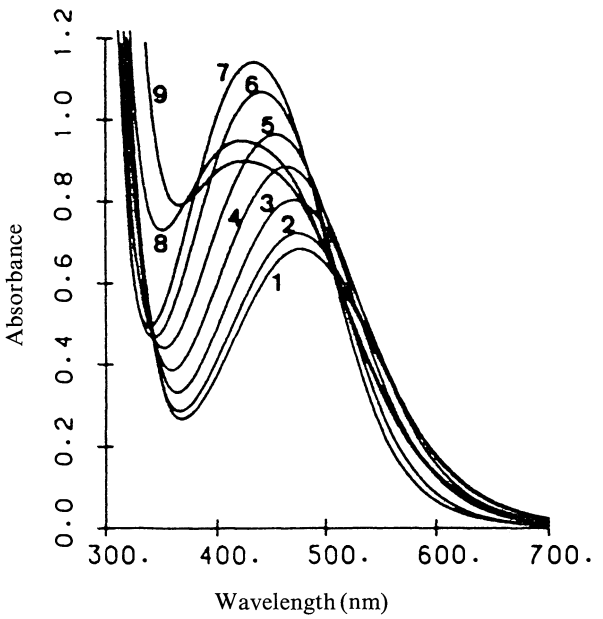

Fig. 2. Plots of experimental absorbance data versus wavelength for solutions [C_L range 2.536×10^{-2}—2.830×10^{-2} mol dm^{-3}, C_M range 3.058×10^{-3}—3.413×10^{-3} mol dm^{-3}; (1) pH=1.830, (2) pH=1.970, (3) pH=2.279, (4) pH=2.734, (5) pH=3.234, (6) pH=3.841, (7) pH=5.346, (8) pH=7.038, (9) pH=8.013] of Fe^{3+}–hpca system at 25 °C using the program VISION with the plotter Calcomp 936.

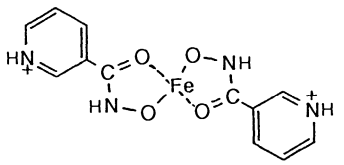

Scheme 3. $[FeH_2L_2]^{3+}$

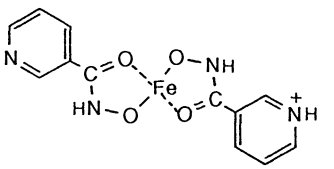

Scheme 4. $[FeHL_2]^{2+}$

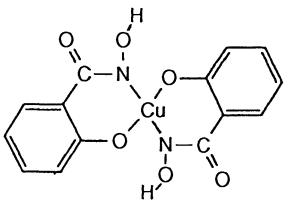

Scheme 5. $[CuL_2]^{2-}$

exhibits the marked pH-dependent spectral shifts seen for example with aerobactin.[24] Only one absorption band was observed in the pH range 1.83 to 5.35 with λ_{max} changing from 478 (pH=1.83) to 436 (pH=5.35) nm. The increase in absorption and shift to smaller wavelengths with increase in pH indicates greater complexation, and, above pH 7.3, both λ_{max} and ε_{max} remain constant, consistent with formation of the [FeL_3] species which predominates in this range. Our results concerning the main species in neutral solution of Fe^{3+}–hpca system are in good agreement with those reported earlier for iron(III) hydroxamate systems (Table 1). Nevertheless the large difference in log β_{pqr} over 5—6 log units reflects a very instable ligand structure of *N*-hydroxy-3-pyridinecarboxamide (hpca) probably due to the large variation in basicity of the only *N*-hydroxyamide grouping involved in coordination as simple aromatic hydroxamic acids. The Fe^{3+}–hpca system therefore probably satisfies different criteria for biological activities and analytical roles, strongly indicating Fe^{3+}–hpca complexes as suitable sources of iron as trace element essential in animal nutrition. However our results show clearly that, at least at physiological pH, the assumption of an uncoordinated α-amino group (heteroatom), which may be particularly active because of a possible surface-active role, is incorrect since the major species in this pH range is FeL_3.

In Cu^{II} complexes with dhbc it is certain that the copper hit on the ligand takes place following the *N,O* coordination (six membered chelate rings, Scheme 5). In comparison with the amino hydroxamic acids till now investigated, where the coordination to copper ion was *N,N* type, here the mononuclear complexes are much more stable (log K_1 and log K_2 much greater), perhaps it is due both to the kinds of atoms (*N,O* rather than *N,N*, Scheme 5) and to greater basicity of the groups involved in the coordination. The trend of potentiometric titration curves for Cu^{2+}–dhbc system has only a buffer zone (spectrophotometric titrations reveal only a intense green color), while in the systems studied till now and involving Cu^{2+} and amino hydroxamic acids were perfectly visible two buffer zones shared by inflection point, where you could observe the formation of polynuclear hydrolized species, that does not present in the Cu^{2+}–dhbc system because probably of the high stability of simple complexes.

Grateful acknowledgement is made to the Ministero dell'Università e della Ricerca Scientifica e Tecnologica (M.U.R.S.T.) and National Research Council of Italy (C.N.R.) for generous grants. I am greatly indebted to Professors P. Gans, A. Vacca, and A. Sabatini for their generous support of the program SUPERQUAD.

References

1) A. K. Majumdar, "*N*-Benzoylphenylhydroxylamine and Its Analogues," Pergamon Press, Oxford (1972).
2) J. B. Neilands, *Science,* **156**, 1443 (1967).
3) H. Maehr, *Pure Appl. Chem.,* **28**, 603 (1971).
4) B. van't Riet, G. L. Wampler, and H. L. Elford, *J. Med. Chem.,* **22(5)**, 589 (1979).
5) B. Rada, T. Hanusovskà, K. Palàt, M. Celadnìk, and L. Novàcek, *Acta Virol.,* **15**, 326 (1971).
6) Eisai Co., Ltd., Fr. Patent 2134967; *Chem. Abstr.,* **78**, 146518g (1978).
7) E. Leporati, *J. Chem. Soc., Dalton Trans.,* **1989**, 1299.
8) E. Leporati and G. Nardi, *Bull. Chem. Soc. Jpn.,* (1991), in the press.
9) E. Leporati, *Inorg. Chem.,* **28**, 3752 (1989).
10) E. Leporati and G. Nardi, *Gazz. Chim. Ital.,* **121**, 147 (1991).
11) P. Gans, A. Sabatini, and A. Vacca, *J. Chem. Soc., Dalton Trans.,* **1985**, 1195.
12) L. G. Sillèn and A. E. Martell, "Stability Constants of Metal-Ion Complexes," The Chem. Society, London (1964).
13) M. Cefola, A. S. Tompa, A. V. Celiano, and P. S. Gentile, *Inorg. Chem.,* **1**, 290 (1962).
14) R. Rowland and C. E. Meloan, *Anal. Chem.,* **36**, 1997 (1964).
15) B. Sarkar and T. P. A. Kruck, *Can. J. Chem.,* **51**, 3541 (1973).
16) C. L. Atkin and J. B. Neilands, *Biochemistry,* **7**, 3734 (1968).
17) D. J. Leggett and W. A. E. McBryde, *Anal. Chem.* **47**, 1065 (1975).
18) M. S. El-Ezaby and M. M. Hassan, *Polyhedron,* **4**, 429 (1985).
19) D. A. Brown, M. V. Chidambaram, and J. D. Glennon, *Inorg. Chem.,* **19**, 3260 (1980).
20) E. Farkas, J. Szoke, T. Kiss, H. Kozlowski, and W. Bal, *J. Chem. Soc., Dalton Trans.,* **1989**, 2247.
21) C. J. Carrano, S. R. Cooper, and K. N. Raymond, *J. Am. Chem. Soc.,***101**, 599 (1979).
22) E. Farkas and P. Buglyo, *J. Chem. Soc., Dalton Trans.,* **1990**, 1549.
23) D. A. Brown and R. Mageswaran, *Inorg. Chim. Acta,* **161**, 267 (1989).
24) W. R. Harris, C. J. Carrano, and K. N. Raymond, *J. Am. Chem. Soc.,* **101**, 2722 (1979).

Correlation between Physicochemical Characteristics of Synthetic Cationic Amphiphiles and Their DNA Transfection Ability

Tetsuyuki AKAO,* Tetsurou OSAKI, Jun-ya MITOMA,† Akio ITO,† and Toyoki KUNITAKE††
Fukuoka Industrial Technology Center, Chemical and Textile Industry Research Institute, Chikushino, Fukuoka 818
†Department of Chemistry, Faculty of Science, Kyushu University, Hakozaki, Fukuoka 812
††Department of Organic Synthesis, Faculty of Engineering, Kyushu University, Hakozaki, Fukuoka 812
(Received May 16, 1991)

Liposomes formed with synthetic double-chain ammonium amphiphiles were used for DNA transfection into eukaryotic cells. We studied the correlation between the efficiency of various cationic amphiphiles in DNA transfection and their physicochemical properties. The efficiency of amphiphiles in the transfection was examined by the transient expression of β-galactosidase from its cDNA in COS cells. Amphiphiles with a phase-transition temperature (T_c) lower than 37 °C, as measured by differential scanning calorimetry, could introduce DNA into the cells. Electron microscopic observation indicated that amphiphiles possessing DNA transfection ability form vesicular structures in aqueous solution. Thus, fluid and vesicular bilayer structures were much higher than rigid and helical bilayer structures regarding the effectiveness of amphiphiles in DNA transfection. The efficiency of didodecyl *N*-[*p*-(2-trimethylammonioethoxy)benzoyl]-L-glutamate bromide was the highest of all the synthetic amphiphiles examined.

In 1977 it was found that stable bilayer membranes were formed from dialkyldimethylammonium bromides[1] and a large number of cationic amphiphiles with long dialkyl chains were shown to form bilayer membranes.[2] As these synthetic bilayer membranes have physicochemical characteristics, such as an aggregate morphology,[3] phase transition,[4] fusio,[5] and phase separation,[5] similar to those of the biolipid bilayer membranes, possibly they can be used for various biological systems, without harmful effects. Use of synthetic amphiphiles in biological systems has the advantage in that the physicochemical characteristics of amphiphiles can be controlled by designing specific molecular structures.

Cationic liposome-mediated transfection is one of effective methods of introducing DNA into eukaryotic cells. The liposomes spontaneously interact with DNA, fuse with cultured cells and facilitate the delivery of functional DNA into the cells. A cationic liposome formed from [2,3-bis(oleoyloxy)propyl]-trimethylammonium chloride (DOTMA) was first reported to be effective in DNA transformation.[6,7] In the foregoing paper we showed that one of dialkyl ammonium amphiphiles, didodecyl *N*-[*p*-(2-trimethylammonioethoxy)-benzoyl]-L-glutamate bromide, which can form a stable bilayer membrane, had a higher DNA transfection potential than did DOTMA.[8,9]

We have examined the correlation between the efficiency of synthetic amphiphiles in DNA transfection and their physicochemical characteristics, such as membrane fluidity and aggregate morphologies. We show that amphiphiles forming fluid and vesicular bilayer are highly effective in DNA transfection.

Results and Discussion

Two series of chiral dialkylammonium amphiphiles, **1** and **2** (Fig. 1), were synthesized and the correlation between physicochemical properties and DNA transfection ability was examined. A first series of amphiphiles, **1**(*m,n*), consists of two tails (length of "tail", *m*), trifunctional glutamate and phenylene groups as a connector, methylene spacer (the length of "spacer", *n*) and ammonio group as a cationic head. A second series of amphiphiles, **2**(*m,n*), has the same basic structure as **1**, but there is no phenylene group in the connector.

Transfection Efficiency of Amphiphiles. To examine the relative efficiency of amphiphiles in the delivery of DNA into cells, we used the transient expression of plasmid pCH110 with a β-galactosidase gene in COS cells. The extent of the expression was determined

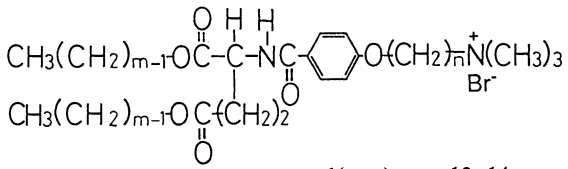

1(*m,n*) $m=12, 14$ $n=2, 4, 6, 8$

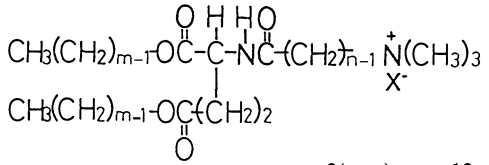

2(*m,n*) $m=12, 14$ $n=2, 4, 6$

X=Cl (n=2, 4)
=Br (n=6)

Fig. 1. Structures of the synthetic cationic amphiphiles examined.

by measuring the percentage of cells expressing β-galactosidase and by assaying enzyme activity in the cell extracts. Figure 2 shows the efficiency of various amphiphiles in the expression of β-galactosidase. COS cells were transformed with 1 to μg of pCH110 DNA using 10 μg (13 nmol) of liposomes prepared from the amphiphiles, as described under Experimental. Since less than 5% of the total cells were detached from the dish during the culture periods, in all the experiments, the amphiphiles were not cytotoxic, under the condition used. As can be seen in the figure, two measurements of the expression of β-galactosidase, the number of cells expressing the enzyme and the total enzyme activity in the cell extract, correlated fairly well, hence all the cells incorporating plasmid DNA seem to express the gene and produce the enzyme protein, to almost the same extent. In a series of **1**, the transfection efficiency varied greatly according to differences in lengths of a tail and spacer of the amphiphiles. An increase in spacer length of a series of **1**(12,*n*) caused a remarkable decrease in the transfection efficiency. A more dramatic difference was observed between series of **1**(12,*n*) and **1**(14,*n*). Change of dialkyl chains from dodecyl to tetradecyl groups resulted in an almost complete loss of transfection ability. In the second series, **2**(12,*n*) and **2**(14,*n*), all compounds listed in Fig. 1 had the ability to transfer a gene, though their efficiencies were less than a half of **1**(12,2). There seems to be no correlation between the efficiency of the amphiphiles of series **2** in gene transfection and their structural characteristics, lengths of a tail and spacer (Fig. 2). In the series of **1**(12,*n*) and **2**(12,*n*), 1-2 μg of DNA was optimum for the transfection, and 5 μg of DNA led to a marked decrease in the efficiency. Since a preliminary experiment showed that about 2 μg of DNA could bind to 10 μg of the amphiphiles, free DNA might interfere with the liposome-mediated transfection of DNA into the cells when 5 μg of DNA was used. Among the amphiphiles examined, **1**(12,2) showed the highest efficiency in DNA transfection.

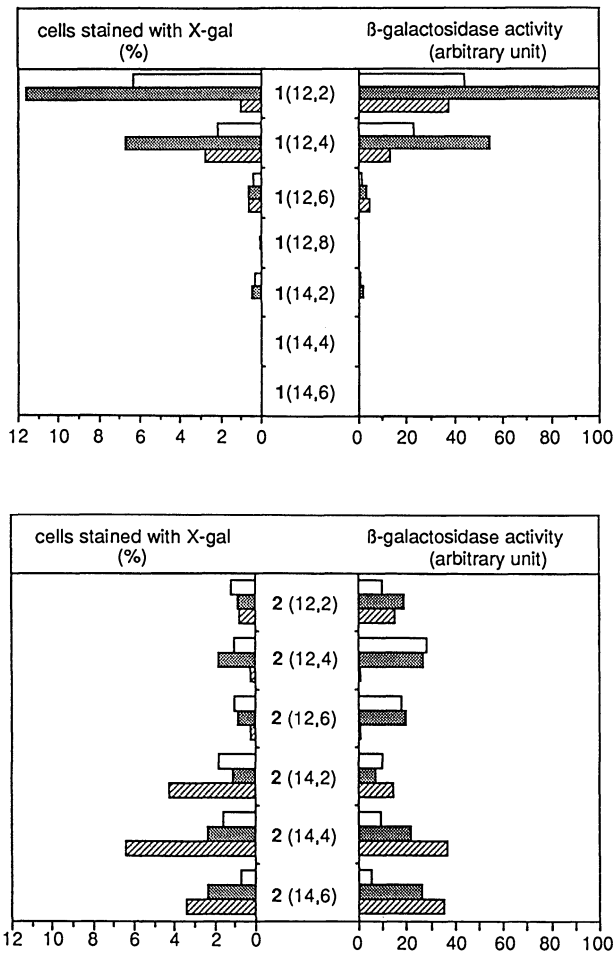

Fig. 2. Transfection efficiency of various amphiphiles. Cells were transfected with amphiphiles/DNA complexes containing 13 nmol of amphiphiles and μg (open bar), 2 μg (dotted bar), 5 μg (oblique line bar) of plasmid DNA, pCH110, per 22 mm dish. After incubation of the cells for 48 h, the cells were harvested and subjected to assay of transfection, as described under Experimental. The relative activity of β-galactosidase was expressed by setting the enzyme activity in the extract of the cell transformed with **1**(12,2) at 100.

Table 1. Phase Transition Temperature T_c and Aggregation Morphology of Amphiphiles **1** and **2**

Amphiphile (*m*, *n*)	T_c[a] (DSC peak)/°C	Aggregate morphology[b]
1 (12, 2)	24.8	Vesicle
1 (12, 4)	29.4	Vesicle
1 (12, 6)	39.4	Lamella
1 (12, 8)	39.9	Filament
1 (14, 2)	41.1	Vesicle
1 (14, 4)	45.0	Vesicle & lamella
1 (14, 6)	51.2	Filament
2 (12, 2)	N. D.[c]	Vesicle & lamella
2 (12, 4)	N. D.	Vesicle & lamella
2 (12, 6)	9.0	Vesicle & lamella
2 (14, 2)	22.0	Vesicle
2 (14, 4)	21.8	Vesicle
2 (14, 6)	25.4	Vesicle

a) Sample, 20 mM in water. Temperature was elevated from 5 °C at a rate of 1 °C min^{-1}.
b) Sample, 10 mM in water. c) N. D.: not detected.

Physicochemical Characteristics of Amphiphiles. To determine which physicochemical properties of amphiphiles are responsible for transfection efficiency, we measured thermal and morphological behavior, of amphiphiles in aqueous solution and searched for a possible correlation between transfection efficiencies and physicochemical characteristics.

Phase Transition. The transition between the crystal and liquid-crystal phases is one of the most fundamental characteristics of a bilayer membrane. The phase transition can be detected directly by differential scanning calorimetry (DSC).[4] The phase-transition temperature T_c (peak top temperature in the DSC scan) is summarized in Table 1. As pointed out d by Kunitake and Ando,[4] T_c increased with an increase in tail and spacer lengths of the amphiphiles. A series of **2** without a phenylene unit in the connector region had much lower T_c values than did a series of **1**. In a series of **1**, enhanced aromatic stacking may suppress molecular disordering in the liquid crystalline state. T_c values of **2**(12,2) and **2**(12,4) were too low to be determined by DSC measurements. These results indicate that all the amphiphiles possessing measurable DNA transfection ability, **1**(12,2), **1**(12,4), and a series of **2**, had T_c values lower than 37 °C. Since the transfection experiment was carried out at 37 °C, these amphiphiles were in the fluid liquid crystalline state in the culture medium. Thus, the primary requirement for the transfection of DNA appears to be fluidity of the liposomes.

Aggregate Morphology. Electron microscopy is a useful tool for the direct observation of bilayer formation and aggregate morphology of the amphiphiles. Some representative electron micrographs are shown in Fig. 3. All the amphiphiles had bilayer structures. However, the aggregate morphology varies with the molecular structure of the component amphiphile. Amphiphile **1**(12,2) formed well-developed vesicles with a diameter of 300—600 Å, as shown in Fig. 3a. Similar morphologies were observed for **1**(12,4), **1**(14,2), **1**(14,4), **2**(14,2), **2**(14,4), and **2**(14,6), but with different diameters of 500—3000, 400—1000, 300—600, 800—1500, 1000—2500 and 500—3000 Å, respectively. Figure 3b shows multiwalled vesicles and/or lamellae aggregates formed from **2**(12,2), with a diameter of 400—2000 Å. Amphiphiles **2**(12,4) and **2**(12,6) had similar morphologies. Amphiphile **1**(12,6) gave fragmentary lamellae (Fig. 3c), and **1**(12,8) and **1**(14,6) gave helical filaments with a length of 1—3 μm (Fig. 3d). Aggregate morphology of amphiphiles **1** and **2** are summarized in Table 1. These morphological observations indicate that amphiphiles forming vesicular structure had DNA transfection ability and that the smaller vesicles appeared to be more

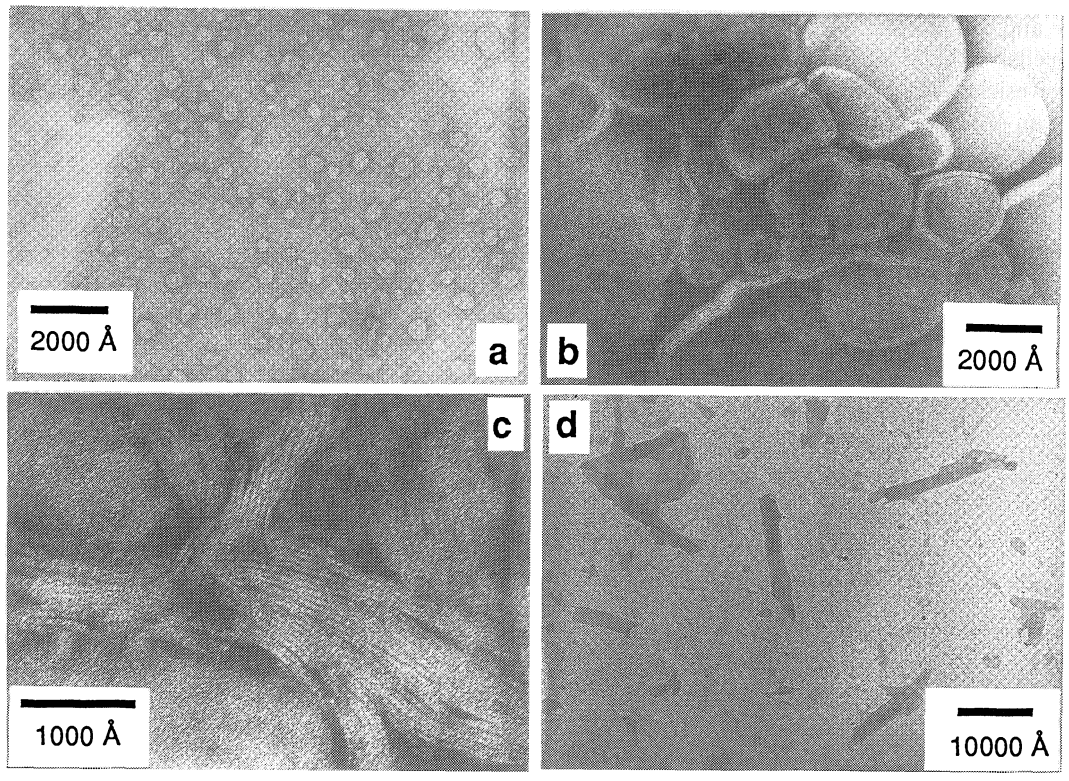

Fig. 3. Electron micrographs of aggregates formed from **1** and **2**. Amphiphiles **1** and **2** were suspended in water (10 mM), sonicated, and stained with uranyl acetate.
a. **1**(12,2), original magnification×50000
b. **2**(12,2), original magnification×50000
c. **1**(12,6), original magnification×150000
d. **1**(14,6), original magnification×10000

effective than larger ones.

Aggregate Size. Stability of the aggregates was studied by measuring change in size while standing. Aqueous dispersions of the amphiphiles were kept at room temperature (about 25 °C) for 0.5 and 24 h and size of the aggregates was measured using a dynamic light scattering apparatus (Table 2). Average size of the aggregates of the amphiphiles **1** and **2** was much the same as those determined by electron microscopy. After leaving for 24 h at room temperature, aggregate sizes of **1**(12,2), **1**(12,4), **1**(14,2), and **1**(14,4) increased by less than 20% of the original size, hence that the vesicular structures formed by these amphiphiles were stable and little fusion occurred between the vesicles. On the other hand, aggregates of **1**(12,6), **1**(12,8), and of a series of **2** increased in size by 4—20 times. In these aggregates, fusion and/or morphological change from vesicular structure to lamella, tubular, or filamentous structure, of the bilayer membranes seemed to readily occur. These results suggest that amphiphiles forming stable aggregates had a higher DNA-transfection ability.

In conclusion, we found a good correlation between the efficiency of the synthetic amphiphiles in gene transfection and their physicochemical characteristics, such as membrane fluidity and aggregate morphologies. The primary requirement of an amphiphile for DNA transfection is that the T_c value be lower than 37 °C so that it is in the fluid liquid crystalline state at the culture temperature and can interact with plasma membranes of the culture cells. The second requirement is to form a small stable vesicle. The vesicular structure might be required for an effective interaction between aggregates and DNA and/or the cells. Thus, amphiphiles that form small stable vesicles in the fluid state are suitable for DNA-transfection, and **1**(12,2) is highest in efficiency of all the amphiphiles we tested.

Table 2. Aggregate Size of Amphiphiles **1** and **2**

Amphiphile (m, n)	Aggregate size[a]/10^3 Å	
	0.5 h	24 h
1 (12, 2)	1.2	1.5
1 (12, 4)	1.6	1.9
1 (12, 6)	1.6	6.9
1 (12, 8)	4.7	25.9
1 (14, 2)	1.2	1.3
1 (14, 4)	1.3	1.4
1 (14, 6)	1.5	—[b]
2 (12, 2)	0.8	16.3
2 (12, 4)	1.3	18.7
2 (12, 6)	1.1	4.0
2 (14, 2)	0.7	11.0
2 (14, 4)	0.9	8.8
2 (14, 6)	0.8	9.4

a) Aqueous dispersion of amphiphiles (0.043 mM) were left at room temperature (about 25 °C) for 0.5 and 24 h. The measurements were carried out using dynamic light scattering spectrophotometer at 25 °C. b) Not determined.

Experimental

Chemicals. Double-chain amphiphiles **1** and **2**, listed in Fig. 1, were synthesized according to the method of Kunitake et al.[10]

Cells and Plasmids. Cos-1, a simian kidney cell line transformed with simian virus 40 (SV40), was maintained in a Dulbecco's modified Eagle Medium (DMEM) supplemented with 10% inactivated fetal calf serum in an atmosphere of 10% CO_2 at 37 °C. Plasmid DNA (pCH110) has a β-galactosidase gene (lac Z) and SV40 early promoter.

Amphiphiles-Mediated Transfection. Transfection experiments were carried out as described by Felgner et al.[6,7] with some modifications.[8,9] COS-1 cells were grown to just before confluency in 22 mm dishes and washed twice with 1 ml of Hepes-buffered saline (HBS; 20 mM Hepes-KOH buffer containing 150 mM NaCl (1 M=1 mol dm^{-3}), pH 7.4). Plasmid DNA (in 10 mM Tris-HCl, 1 mM EDTA, pH 8.0) and amphiphiles suspension (13 nmol, prepared by sonication) were diluted separately with 0.15 ml of HBS. Both solutions were combined and 0.4 ml of amphiphiles–DNA mixture was poured gently onto the cells. After incubation for 3—5 h at 37 °C, 2 ml of DMEM supplemented with 10% fetal calf serum was added and the detached cells became suspended. The medium was replaced with 2 ml of a fresh medium after 12—20 h, and the cells were incubated for 48 h from the first addition of DMEM.

Transfection Efficiency. Monolayer cells were harvested after a 48 h culture. The efficiency of amphiphiles in the expression of β-galactosidase was measured by counting the number of the cells visualized by histochemical staining of the enzyme activity and by assaying of the total enzyme activity in the extract of the cultured cells using 5-bromo-4-chloro-3-indolyl β-D-galactopyranoside (X-gal)[11] and *o*-nitrophenyl β-D-galactopyranoside[12] as the substrate, respectively.

Phase-Transition Temperature. An aqueous solution of amphiphile (20 mM) was sealed in a silver sample pan. Measurements were carried out using a Seikosha differential scanning calorimeter Model DSC-210 heating rate, 1 °C min^{-1}.[4]

Electron Microscopy. Amphiphiles suspended in distilled water (10 mM) were sonicated using a Tomy Sonifier for several minutes to give a clear solution and this solution was applied to carbon-coated grids and dried in vacuo. The sample was stained with a 2% aqueous uranyl acetate solution and subjected to electron microscopic examination[13] using a Hitachi electron microscope, Model H-7000.

Dynamic Light Scattering. Amphiphiles suspended in water (0.043 mM) were sonicated for several minutes to give a clear solution. After standing at room temperature (about 25 °C) for 0.5 and 24 h, the suspension was subjected to dynamic light scattering experiment[13] using an Otsuka Electronics Co., Model DLS-700 with a laser light source.

References

1) T. Kunitake and Y. Okahata, *J. Am. Chem. Soc.*, **99**, 3860 (1977).

2) Y. Okahata, R. Ando, and T. Kunitake, *Ber. Bunsen-Ges. Phys. Chem.*, **85**, 789 (1981).

3) T. Kunitake, Y. Okahata, and S. Tawaki, *J. Collid Interface Sci.*, **103**, 190 (1985).

4) T. Kunitake and R. Ando, *Mem. Fac. Eng., Kyushu Univ.*, **46**, 221 (1986).

5) M. Shimomura and T. Kunitake, *Chem. Lett.*, **1981**, 1001.
6) P. L. Felgner, T. R. Gadek, M. Holm, R. Roman, H. W. Chan, M. Wenz, J. P. Northrop, G. M. Ringold, and M. Danielsen, *Proc. Natl. Acad. Sci. U.S.A.*, **84**, 7413 (1987).
7) P. L. Felgner and G. M. Ringold, *Nature*, **337**, 384 (1989).
8) A. Ito, R. Miyazoe, I. Mitoma, T. Akao, T. Osaki, and T. Kunitake, *Biochem. Int.*, **22**, 235 (1990).
9) T. Akao, T. Osaki, J. Mitoma, A. Ito, and T. Kunitake, *Chem. Lett.*, **1991**, 311.
10) T. Kunitake, N. Nakashima, M. Shimomura, Y. Okahata, K. Kano, and T. Ogawa, *J Am. Chem. Soc.*, **102**, 6642 (1980).
11) J. R. Sanes, J. L. R. Rubenstein, and J. F. Nicolas, *EMBO J.*, **5**, 3133 (1986).
12) T. Edlund, M. D. Walker, P. J. Barr, and W. J. Rutter, *Science*, **230**, 912 (1985).
13) T. Kunitake and Y. Okahata, *J. Am. Chem. Soc.*, **102**, 549 (1980).

The Claisen Rearrangement of 2-Phenylsulfinyl-2-propenyl Phenyl Ethers —A New Route to Functionalized Phenols and 2-Methylbenzofurans

Muhammad Akram KHAN†
Department of Chemistry, University of Kuwait, P.O. Box 5969, Safat 13060, Kuwait
(Received December 1, 1990)

The hitherto unknown Claisen rearrangement of 2-phenylsulfinyl-2-propenyl phenyl ethers to the corresponding 2-(2-phenylsulfinyl-2-propenyl)phenols is reported. The latter compounds underwent Michael reactions with a variety of nucleophiles to provide functionalized phenolic adducts. *O*-Alkylation of the initial rearrangement products with 3-bromo-2-phenylsulfinyl-1-propene and 2,3-dibromo-1-propene followed by [3,3] sigmatropic rearrangement provided a promising route to 7-substituted 2-methylbenzofurans.

Although the [3,3] sigmatropic rearrangement of enol or phenol ethers to the corresponding *C*-alkylated products also known as the Claisen rearrangement[1] has enjoyed widespread application in organic synthesis for over seven decades, it continues to be a rewarding reaction for the construction of carbon–carbon bonds. We report here in this context a hitherto unknown Claisen rearrangement of (phenoxy-substituted alkenyl) phenyl sulfoxides (**2a—d**). Alkenyl sulfoxides are versatile molecules in organic synthesis. They act as dienophiles, Michael acceptors, and as precursors to alkenyl sulfides, chloroalkyl sulfides, ketones, allenes, enamines, and enamides.[2] The alkenyl sulfoxides (**2a—g**) were prepared efficiently by the regiospecific addition of benzenesulfenic acid to the terminal alkynes (**1a—g**). The benzenesulfenic acid was generated in situ by the thermolysis of 1-cyano-2-(phenylsulfinyl) ethane.[3]

The sulfoxides (**2a—d**) as solutions in mesitylene were very cleanly transformed upon reflux into the corresponding phenols (**3a—d**) (yields ca. 50%). The reaction progress was monitored by TLC which showed the phenolic products (**3a—d**) to have relatively lower R_f values compared with the starting ethers (**2a—d**). Using 1,2-dichlorobenzene (DCB) as the reaction solvent the yields of the products (**3a—d**) were significantly improved (80%). ^{1}H NMR and IR spectroscopies tentatively established the product structures. The appearance of OH absorptions (ca. 3200 cm^{-1}) in the IR spectra of products (**3a—d**) and the change in the chemical shift of the diastereotopic allylic methylene protons from low field (δ=4.1—4.5 in starting materials **2a—d**) to high field (δ=3.1—3.5 in products **3a—d**) were the most noticeable spectroscopic features that witnessed the rearrangement process.

Under similar reaction conditions to above the thioether (**2e**) rearranged to yield 2-methylbenzothiophen (**4**) along with *O*-phenyl and *S*-phenyl benzenethiosulfinates (PhSSOPh), a product known to arise from the intermolecular condensation of benzenesulfenic acid. 2-Methylbenzo[*b*]thiophens and 2-methylbenzofurans have previously been obtained from the Claisen rearrangement of 2-chloro-2-propenyl

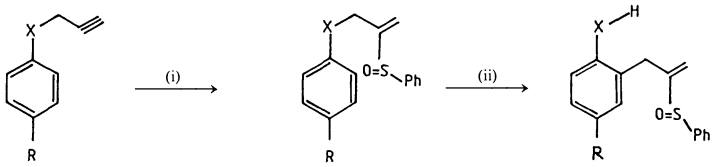

1 (**a**) R=H, X=O
(**b**) R=Cl, X=O
(**c**) R=CH_3, X=O
(**d**) R=OCH_3, X=O
(**e**) R=H, X=S
(**f**) R=H, X=NEt
(**g**) R=CH_3, X=NH

2 (**a**) R=H, X=O
(**b**) R=Cl, X=O
(**c**) R=CH_3, X=O
(**d**) R=OCH_3, X=O
(**e**) R=H, X=S
(**f**) R=H, X=NEt
(**g**) R=CH_3, X=NH

3 (**a**) R=H, X=O
(**b**) R=CH_3, X=O
(**c**) R=OCH_3, X=O
(**d**) R=Cl, X=O

Scheme 1. Reagents: (i) $PhS\overset{O}{\overset{\|}{C}}H_2CH_2CN$, 110 °C, under N_2. (ii) As solutions in mesitylene or 1,2-dichlorobenzene, 180 °C (oil bath), 18—24 h, under N_2.

† Present address: Division of Chemistry, Sheffield City Polytechnic, Pond Street, Sheffield, S1 1WB, UK.

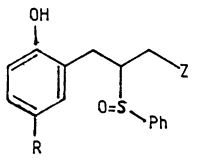

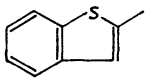

4

5 (**a**) R=H, Z=$CH(CO_2Et)_2$
(**b**) R=H, Z=$NH(CH_2)_2CO_2Et$
(**c**) R=H, Z=$-SCH_2CO_2Et$
(**d**) R=OCH_3, Z=OEt

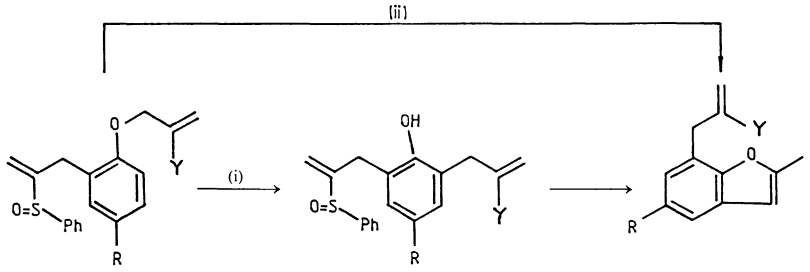

6 (**a**) R=OCH_3, Y=Br
(**b**) R=OCH_3, Y=SOPh

7 (**a**) R=H, Y=Br
(**b**) R=OCH_3, Y=SOPh

8 (**a**) R=H, Y=Br
(**b**) R=OCH_3, Y=SOPh

Scheme 2. Reagents: (i) Solution in mesitylene, 180 °C (oil bath), under N_2, 22 h. (ii) SiO_2 added to solution in mesitylene, 180 °C (oil bath), 22 h.

phenyl ethers and thioethers.[4]

The corresponding amino-substituted sulfoxides (**2f**, **2g**) resisted rearrangement under similar reactions. Although it is known that the amino Claisen rearrangement is greatly accelerated by acids and Lewis acid catalysis,[5] the use of these reagents in our case was negated by the fact that sulfoxides are decomposed by such reagents.

The (phenoxy-substituted alkenyl) sulfoxides (**3a**—**d**) underwent Michael reactions in alcoholic solutions with diethyl sodiomalonate, thiolate anions, β-alanine ethyl ester and sodium ethoxide to furnish the adducts (**5a**—**d**) in good yields. Since suitably substituted phenolic compounds are pharmacologically rewarding compounds,[6] the Michael reactions of the phenols (**3a**—**d**) provides a method for synthesizing a great variety of new hetero derivatives such as (**5a**—**d**) that otherwise are difficult to produce.

O-Alkylation of **3** with synthons 2,3-dibromo-1-propene and 2-bromo-2-phenylsulfinyl-1-propene[2] gave the ethers (**6a**) and (**6b**) respectively which underwent [3,3] sigmatropic rearrangement upon reflux in mesitylene to afford the acyclic adducts (**7a**) and (**7b**) as the only reaction products. However, rearrangement of the ethers (**6a**) and (**6b**) under catalysis by SiO_2 (Fluka 60H) resulted in the formation of 2-methylbenzofurans (**8a**) and (**8b**) respectively. Repeating the SiO_2-catalyzed reactions in DCB as the solvent resulted in decomposition and polymerization. Dark oily compounds in the case of **7b** were obtained that crystallized upon the addition of diethyl ether. Although soluble in chloroform the identification of the solid proved difficult, however. Benzofurans are biologically important molecules.[7] The Michael reactions of the 7-(phenylsulfinyl-substituted alkenyl) benzofuran (**8b**) with various nucleophiles should provide a route to a wide variety of hetero derivatives that might have interesting physiological properties.

Experimental

NMR spectra were recorded on either JEOL EX90 FT or Perkin-Elmer R34 (220 MHz) NMR spectrometers for solutions in $CDCl_3$ with $SiMe_4$ as an internal standard. IR spectra were recorded on a Perkin-Elmer 520B spectrophotometer. Mass spectra were obtained on either Finnigan MAT 311A or Nermag R10-10 connected to a Varian Vista 6000 GC. Analytical TLC was performed on Eastman Kodak Silica Chromatogram sheets using diethyl ether (ether) as the eluent. Column chromatography was performed on Fluka SiO_2 60H under pressure using the short path technique.

Preparation of Acetylenic Precursors (1a—g). The preparations of compounds **1a**,[8] **1e**,[8] **1f**,[8] and **1g**,[2] are described elsewhere.

3-(4-Chlorophenoxy)-1-propyne (1b). This was prepared (11.7 g, 70%) from NaOEt (0.1 mol) in dry EtOH (45 ml), 4-chlorophenol (12.86 g, 0.1 mol) and 3-bromo-1-propyne (12.9 g, 0.108 mol); bp 60 °C/0.2 mm Hg (1 mmHg=133.322 Pa); IR (neat) 3295 (HC≡C–), 2115 (–C≡C–) cm^{-1}; ^1H NMR δ=2.50

(1H, t, J=2 Hz acetylenic proton), 4.60 (2H, d, J=2 Hz, $-OCH_2-$), 6.80 (2H, d, J=9 Hz, ArH *ortho* to oxygen), 7.22 (2H, d, J=9 Hz, ArH *ortho* to Cl). Found: C, 64.7; H, 4.1%. Calcd. for C_9H_7OCl: C, 64.86; H, 4.20%.

3-(*p*-Tolyloxy)-1-propyne (1c). It was prepared in a similar way to above from *p*-cresol (10.8 g, 0.1 mol), 3-bromo-1-propyne (12.9 g, 0.108 M) (1 M=1 mol dm^{-3}) and NaOEt (0.1 mol); bp 50 °C/0.2 mm Hg; IR (neat) 3290 (HC≡C–), 2110 (–C≡C–) cm^{-1}; ^{1}H NMR δ=2.23 (3H, s, $-CH_3$), (1H, t, J=2 Hz, acetylenic proton), 4.57 (2H, d, J=2 Hz, $-OCH_2-$), 6.76 (2H, d, J=9 Hz, ArH *ortho* to oxygen), 7.03 (2H, d, J=9 Hz, ArH *ortho* to CH_3). Found: C, 82.0; H, 6.7%. Calcd for $C_{10}H_{10}O$: C, 82.19; H, 6.85%.

3-(4-Methoxyphenoxy)-1-propyne (1d). This was prepared (65 g, 86%) from *p*-anisole (58 g, 0.47 mol), 3-bromo-1-propyne (57 g, 0.48 mol), and NaOEt (0.47 M); bp 112—114 °C/7 mmHg; IR (neat) 3295 (HC≡C–), 2125 (–C≡C–) cm^{-1}; ^{1}H NMR δ=2.45 (1H, t, J=2 Hz, acetylenic proton), 3.63 (3H, s, $-OCH_3$), 4.50 (2H, d, J=2 Hz, $-OCH_2-$), 6.73 (4H, m, ArH). Found: C, 74.0; H, 6.1%. Calcd for $C_{10}H_{10}O_2$: C, 74.07; H, 6.17%.

Preparation of Alkenyl Sulfoxides (2a—g). The alkenyl sulfoxides **2a**,[8] **2e**,[8] **2f**,[8] and **2g**,[2] have been prepared by us and described elsewhere.

3-(4-Chlorophenoxy)-2-phenylsulfinyl-1-propene (2b). Thermolysis of 1-cyano-2-(phenylsulfinyl)ethane (4.0 g, 22.3 mmol) in the acetylene **1b** (15 g, 90 mmol) for 3 h under N_2 at 110 °C in a toluene vapor jacket gave an oily residue, after distillation to remove excess **1b**, which was purified by column chromatography [(a) (1 : 1) ether–petroleum ether (40 : 60) (b) ether] to give **2** (5.8 g, 89%) as an oil which solidified on keeping. Recrystallization [acetone–petroleum ether (40 : 60)] yielded pure **2b** as a white powder, mp 92—95 °C; IR (KBr) 1040 (>S=O) cm^{-1}; ^{1}H NMR δ=4.33 (1H, d, J=13.5 Hz, diastereotopic allylic proton), 4.70 (1H, d, J=13.5 Hz, diastereotopic allylic proton), 5.93 (1H, s, olefinic proton *trans* to –SOPh), 6.25 (1H, s, olefinic proton *cis* to –SOPh), 6.65 (2H, d, J=8 Hz, ArH *ortho* to oxygen), 7.16 (2H, d, J=8 Hz, ArH *ortho* to Cl), 7.36—7.93 (5H, m, –SOPh); MS m/z 293 (M$^+$), 277, 167, 126. Found: C, 61.3; H, 4.3%. Calcd for $C_{15}H_{13}O_2SCl$: C, 61.54; H, 4.44%.

3-(*p*-Tolyloxy)-2-phenylsulfinyl-1-propene (2c). Thermolysis of 1-cyano-2-(phenylsulfinyl)ethane (2.0 g, 11.1 mmol) in **1c** (11 g, 75.3 mmol) in the above manner gave pure **2c** (2.8 g, 93%) as an oil which solidified on keeping. Recrystallization [acetone–petroleum ether (40 : 60)] yielded a white powder, mp 48—50 °C; IR (KBr) 1040 (>S=O) cm^{-1}; ^{1}H NMR δ=2.25 (3H, s, $-CH_3$), 4.30 (1H, d, J=13.5 Hz, diastereotopic allylic proton), 4.68 (1H, d, J=13.5 Hz, diastereiotopic allyl proton), 5.93 (1H, s, olefinic proton *trans* to –SOPh), 6.20 (1H, s, olefinic proton *cis* to –SOPh), 6.63 (2H, d, J=8 Hz, ArH *ortho* to oxygen), 7.0 (2H, d, J=8 Hz, ArH *ortho* CH_3), 7.36—7.75 (5H, m, –SOPhH); MS m/z 272. Found: C, 70.4; H, 5.8%. Calcd for $C_{16}H_{16}O_2S$: C, 70.59; H, 5.88%.

3-(4-Methoxyphenoxy)-2-phenylsulfinyl-1-propene (2d). Thermolysis of 1-cyano-2-(phenylsulfinyl)ethane (7.0 g, 39.1 mmol) in **1d** (33 g, 6.204 mol) in the above manner yielded pure **2d** (9.6 g, 85%) as a thick brown oil which solidified after prolonged keeping. Recrystallization (as above) yielded a white powder, mp 90—94 °C; IR (KBr) 1050 (>S=O) cm^{-1}; ^{1}H NMR δ=3.70 (3H, s, $-OCH_3$), 4.33 (1H, d, J=14.5 Hz, –OCH–), 4.65 (1H, d, J=14.5 Hz, –OCH–), 5.95 (1H, s, olefinic H *trans* to –SOPh), 6.23 (1H, s, olefinic H *cis* to –SOPh), 6.66 (2H, d, J=7.5 Hz, ArH *ortho* to oxygen), 6.75 (2H, d, J=7.5 Hz, ArH *ortho* to OCH_3), 7.43—7.53 (5H, m, SOPh); MS m/z 288 (M$^+$), 195, 162, 141, 77 (100%). Found: C, 66.5; H, 5.4%. Calcd for $C_{16}H_{16}O_3S$: C, 66.67; H, 5.55%.

Claisen Rearrangement of the Sulfoxides (2a—e). The following procedure illustrated for **2a** was typical. A solution of the sulfoxide **2a** (1.9 g, 7.36 mmol) in dry mesitylene (19 ml) was heated under N_2 in an oil bath maintained at 180 °C for 20—24 h. After removal of the solvent under reduced pressure an oily residue was obtained which was chromatographed [(a) (1 : 1) ether–petroleum ether (40 : 60) (b) ether] to yield mesitylene followed by unchanged **2a** (480 mg, 25%), and finally 2-(2-phenylsulfinyl-2-propenyl)phenol **3a** (1.33 g, 70%) as a pale yellow oil which solidified on keeping. Recrystallization [(CH_2Cl_2–petroleum ether (40 : 60)] afforded pure **3a** as a white powder, mp 94—95 °C; IR (KBr) 3200 (OH, broad), 1020 (>S=O) cm^{-1}; ^{1}H NMR δ=3.10 (d, J=16 Hz, 1H, diastereotopic allylic –OCH–), 3.50 (d, J=16 Hz, 1H, diastereotopic allylic –OCH–), 5.65 (s, 1H, olefinic H *trans* to –SOPh), 6.00 (s, 1H, olefinic H *cis* to SOPh), 6.6—7.20 (m, 4H, ArH), 7.25—7.90 (m, 3H, –SOPh); MS m/z 258 (M$^+$), 218, 131 (100%). Found: C, 69.6; H, 5.3; S, 12.3%. Calcd for $C_{15}H_{14}O_2S$: C, 69.77; H, 5.43; S, 12.40%. Rearrangement of **2a** in 1,2-dichlorobenzene (DCB) gave in **3a** in a higher yield (86%).

4-Chloro-2-(2-phenylsulfinyl-2-propenyl)phenol (3b). Similar to above the sulfoxide **2b** (550 mg, 1.88 mmol) in mesitylene (6 ml) yielded upon heating **3b** (281 mg, 51%) together with unchanged **2b** (260 mg, 47%). The pale yellow oily phenol **3b** solidified upon keeping. Recrystallization (as above) afforded **3b** as a white powder, mp 130—131 °C; IR (KBr) 3195 (OH, broad), 1025, 1030 (>S=O) cm^{-1}; ^{1}H NMR δ=3.05 (d, J=15 Hz, 1H, –OCH–), 3.45 (d, J=15 Hz, 1H, –OCH–), 5.63 (s, 1H, olfefinic H *trans* to SOPh), 6.00 (s, 1H, olefinic H *cis* to SOPh), 6.5—7.15 (m, 3H, ArH), 7.3—7.7 (m, 5H, –SOPh); MS m/z 292 (M$^+$), 277, 165 (100%), 126. Found: C, 61.4; H, 4.3; S, 11.0%. Calcd for $C_{15}H_{13}O_2SCl$: C, 61.54; H, 4.44; S, 10.94%. Rearrangement of **2b** in DCB gave **3b** in 80% yield.

4-Methyl-2-(2-phenylsulfinyl-2-propenyl)phenol (3c). Thermal rearrangement of **2c** (550 mg, 2.02 mmol) in mesitylene (6 ml) in the above manner afforded **3c** (440 mg, 80%) as an oil which solidified on keeping. Recrystallization (as above) yielded **3c** as a white powder, mp 128—130 °C; IR (KBr) 3195 (OH, broad), 1030, 1040 (>S=O) cm^{-1}; ^{1}H NMR δ=2.15 (d, J<2 Hz, 3H, CH_3), 3.12 (d, J=15 Hz, 1H, –OCH–), 3.53 (d, J=15 Hz, 1H, –OCH–), 5.70 (s, 1H, olefinic H *trans* to SOPh), 6.05 (s, 1H, olefinic H *cis* to –SOPh), 6.65—7.05 (m, 3H, ArH), 7.4—7.7 (m, 5H, –SOPh); MS m/z 272 (M$^+$). Found: C, 70.5; H, 5.7; S, 11.6%. Calcd for $C_{16}H_{16}O_2S$: C, 70.59; S, 11.76%. Rearrangement of **2c** in DCB yielded **3c** in higher yield (95%).

4-Methoxy-2-(2-phenylsulfinyl-2-propenyl)phenol (3d). The thermal rearrangement of **2d** (3.0 g, 16.4 mmol) in mesitylene (30 ml) in the above manner produced **3d** (2.55 g, 85%) as a thick dark brown oil; IR (neat) 3190 (OH, broad), 1035 (>S=O) cm^{-1}; ^{1}H NMR δ=3.13 (d, J=16 Hz, 1H, –OCH–), 3.45 (d, J=16 Hz, 1H, –OCH–), 3.67 (s, 3H, $-OCH_3$), 5.67 (s, 1H, olefinic H *trans* to –SOPh), 6.07 (s, 1H, olfefinic H *cis* to –SOPh), 6.50 (d, J=2 Hz, 1H, H-3), 6.65 (dd, J=2 Hz and 8 Hz, 1H, H-5), 6.77 (d, J=8 Hz, 1H, H-6), 7.4—7.55 (m, 3H, –SOPh), 7.55—7.70 (m, 2H, –SOPh); MS m/z 288 (M$^+$), 162 (100%). Found: C, 66.6; H, 6.5; S, 11.0%. Calcd for

$C_{16}H_{16}O_3S$: C, 66.67; H, 5.55; S, 11.11%. Rearrangement of **2d** in DCB afforded **3d** in higher yield (95%).

2-Methylbenzothiophene (4). Thermal rearrangement of **2e** (210 mg, 7.66 mmol) in mesitylene (3 ml) gave **4** (135 mg, 64%), as a pale brown solid; mp 50—52 °C (lit,[4] mp 51—52 °C). The compound had identical ^{1}H NMR with that reported in the literature. The other product obtained from column chromatography of reaction mixture was *S*-phenyl benzenethiosulfinates (PhSSOPh).

The Michael Reactions of the Alkenyl Sulfoxides (3a—d). 2-[4,4-Bis(ethoxycarbonyl)-2-(phenylsulfinyl)butyl]phenol (5a). A solution of **3a** (1.0 g, 3.87 mmol) in absolute EtOH (1 ml) was added to a solution of diethyl sodiomalonate (1.24 g, 7.75 mmol) in absolute EtOH (2.5 ml) and the mixture heated under N_2 in EtOH vapor jacket (ca. 80 °C) for 14 h. The EtOH was evaporated and the residue, after acidification with H_2SO_4 (2 M), was extracted with CH_2Cl_2 (60 ml) and washed with H_2O once. After drying ($MgSO_4$) the organic layer, the solvent was evaporated to yield an oily residue which crystallized upon addition of ether. Recrystallization [CH_2Cl_2–petroleum ether (40 : 60)] yielded pure **5a** (955 mg, 59%) as a cream colored powder that was racemic modification; mp 127—130 °C; IR (KBr) 3240 (OH, broad), 1735 (>S=O, broad, W. 1/2 1.5 cm), 1030 (>S=O) cm^{-1}; ^{1}H NMR δ=0.9—1.40 (m, 6H, 2×CH_3), 2.0—2.30 (m, 2H, H_2C–$C(CO_2Et)_2$), 2.7—3.2 (m, 3H, $-CH_2CHSOPh$), 3.3—3.7 (m, 1H, $-CH(CO_2Et)_2$), 3.9—4.4 (m, 4H, 2×$-OCH_2-$), 6.4—7.30 (m, 4H, ArH), 7.35—7.80 (m, 6H, –SOPh and OH); MS *m/z* 292 (M−PhSOH). Found: C, 63.1; H, 6.1; S, 7.5%. Calcd for $C_{22}H_{26}O_6S$: C, 63.16; H, 6.22; S, 7.65%.

2-[3-[2-(Ethoxycarbonyl)ethylamino]-2-(phenylsulfinyl)propyl]phenol (5b). A solution of **3a** (1.13 g, 4.38 mmol) in absolute EtOH (2 ml) was added to a solution of 2-(ethoxycarbonyl)ethylammonium chloride (700 mg, 4.56 mmol) in absolute EtOH (13 mmol) containing triethylamine (0.7 ml, 1 equiv). The reaction was conducted in an analogous manner to above to yield crude oily product which was purified by column chromatography [(a) ether (b) ether–EtOH (2 : 1)] to give **5b** (1.07 g, 65%) as a pale brown oil; IR (neat) 3440 (NH), 3300 (OH) , 1730 (>S=O) cm^{-1}; ^{1}H NMR δ=1.23 (t, *J*=7 Hz, 3H, CH_3), 2.3—2.8 (m, 5H, $-CH_2CHSOPh-$ and $-CH_2CO_2Et$), 2.8—3.2 (m, 4H, $-CH_2-N-CH_2-$), 4.10 (q, *J*=7 Hz, 2H, $-OCH_2-$), 6.7—7.3 (m, 5H, ArH and OH), 7.33—7.76 (m, 5H, –SOPh). Found: C, 63.8; H, 6.6; N, 3.6; S, 8.5%. Calcd for $C_{20}H_{25}NO_4S$: C, 64.00; H, 6.67; N, 3.78; S, 8.53%.

2-[3-[Ethoxycarbonyl)methylthio]-2-(phenylsulfinyl)-propyl]phenol (5c). In a similar manner to above the alkenyl sulfoxide **3a** (620 mg, 2.40 mmol), sodium ethoxide (2.4 mmol) and ethyl mercaptoacetate (0.6 ml, an excess) in EtOH (1.5 ml) yielded an oily mixture which was chromatographed [(a) (1 : 1) ether–petroleum ether (40 : 60) (b) ether] to yield **5c** (745 mg, 82%) as a light brown oil; IR (neat) 3400 (OH, broad), 1740 (>C=O), 1025 (>S=O) cm^{-1}; ^{1}H NMR δ=1.26 (t, *J*=7 Hz, 3H, CH_3), 2.2—2.5 (m, 2H, $-CH_2S-$), 2.66—3.30 (m, 3H, $ArCH_2CHSO$), 3.45 (s, 2H, $-SCH_2CO_2Et$), 4.13 (q, *J*=7 Hz, 2H, $-OCH_2-$), 6.6—7.3 (m, 4H, ArH), 7.3—7.6 (m, 5H, –SOPh), 7.9 (s, 1H, OH). Found: C, 60.2 H, 5.6; S, 16.8%. Calcd for $C_{19}H_{22}O_4S_2$: C, 60.32; H, 5.82; S, 16.93%.

2-[3-Ethoxy-2-(phenylsulfinyl)propyl]-4-methoxyphenol (5d). This was obtained in a similar manner from **3d** (630 mg, 20.19 mmol) and sodium ethoxide (2.2 mmol) in EtOH (16 ml) as an oil (548 mg, 75%) after column chromatography [ether]; IR (neat) 3320 (OH), 1030 (>S=O) cm^{-1}; ^{1}H NMR δ=1.27 (m, 3H, CH_3), 2.3—2.8 (m, 3H, $-OCH_2CHSO$), 3.76, (s, 3H, $-OCH_3$), 6.4—7.0 (m, 3H, PhH), 7.3—7.6 (m, 6H, –SOPh and OH); MS *m/z* 334 (M$^+$). Found: C, 64.6; H, 6.4; S, 9.4%. Calcd for $C_{18}H_{22}O_4S$: C, 64.67; H, 6.59; S, 9.59%.

2-Bromo-2-propenyl-4-methoxy-2-(2-phenylsulfinyl-2-propenyl)phenyl Ether (6a). This was made by the Williamson synthesis from **3c** (1.35 g, 4.69 mmol), 2,3-dibromo-1-propene (1.1 g, 5.5 mmol) and sodium ethoxide (4.69 mmol) in EtOH (25 ml) to give, after chromatography [ether], **6a** (1.24 g, 68%) as a dark gum; IR (neat) 1040 cm^{-1}; ^{1}H NMR δ=3.25 (d, *J*=17 Hz, 1H, diastereotopic –OCH–), 3.45 (d, *J*=17 Hz, 1H, diastereotopic –OCH–), 3.70 (s, 3H, $-OCH_3$), 4.45 (s, 2H, $-OCH_2-$), 5.36 (s, 1H, –C=CH *trans* to Br), 5.60 (s, 1H, C=CH *cis* to Br), 5.80 (s, 1H, –C=CH *trans* to –SOPh), 6.10, (s, 1H, –C=CH *cis* to SOPh), 6.56 (s, 1H, ArH-3), 6.70 (s, 2H ArH-5,6), 7.50 (m, 3H, –SOPh), 7.66 (m, 2H, *ortho* SOPh); MS *m/z* 408 (M+1, 4%), 280 (58), 161 (1). Found: C, 55.8; H, 4.5; S, 7.6%. Calcd for $C_{19}H_{19}O_3SBr$: C, 56.02; H, 4.67; S, 7.86%.

4-Methoxy-2-(2-phenylsulfinyl-2-propenyl)phenyl 2-Phenylsulfinyl-2-propyl Ether (6b). 3-Bromo-2-phenylsulfinyl-1-propene (650 mg, 2.6 mmol) was reacted in a similar manner to above with a solution of **3c** (730 mg, 2.53 mmol) and sodium ethoxide (2.53 mmol) in EtOH (15 ml) to give, after chromatographic purification [(a) ether (b) ether : : MeOH (2 : 1 : 1)], **6b** (1.03 g, 90%) as a thick dark oil; IR (neat) 1030 (>S=O) cm^{-1}; ^{1}H NMR δ=3.08 (d, *J*=15 Hz, 1H, diastereotopic –CH–), 3.40, (d, *J*=15 Hz, 1H, diastereotopic –CH–), 3.66 (s, 3H, $-OCH_3$), 4.15 (d, *J*=16 Hz, 1H, diastereotopic –OCH–), 4.56 (d, *J*=16 Hz, 1H, diastereotopic –OCH–), 5.27 (fine t, *J*=2 Hz, 1H, –C=CH *trans* to SOPh in allylic group), 5.77 (fine t, *J*=2 Hz, 1H, –C=CH *trans* to SOPh in allyloxy group), 6.05 (s, 1H, –C=CH *cis* to SOPh in allyloxy group), 6.13 (s, 1H, –C=CH, *cis* to SOPh in allyloxy group), 6.4—6.75 (m, 3H, ArH-3,5,6), 7.35—7.75 (m, 10H, –SOPh); MS *m/z* 452 (M$^+$, 12%), 327 (42), 200 (100). Found: C, 66.1; H, 5.1; S, 13.9%. Calcd for $C_{25}H_{24}O_4S_2$: C, 66.38; H, 5.31; S, 14.16%.

The Claisen Rearragement Reactions of 6a and 6b. 2-(2-Bromo-2-propenyl)-4-methoxy-6-(2-phenylsulfinyl-2-propenyl)phenol (7a). A solution of **6a** (1.0 g, 2.46 mmol) in mesitylene (15 ml) was rearranged in the previously mentioned manner to yield, after chromatography [ether], **7a** (650 mg, 65%) as dark brown oil; IR (neat) 3240 (OH, broad), 1040 (>S=O) cm^{-1}; ^{1}H NMR δ=3.12 (d, *J*=17 Hz, 1H, –CH–CSOPh), 3.45 (d, *J*=17 Hz, 1H, –CH–CSOPh), 3.6—3.8 (m, 5H, $-CH_2-CBr=C$ and OCH_3), 5.45 (s, 1H, *trans* –CBr=CH), 5.52 (s, 1H, *cis* –CBr=CH), 5.74 (s, 1H, *trans* –OSPhC=CH), 6.02 (s, 1H, *cis* –OSPhC=CH), 6.47 (m, 1H, ArH-3), 6.65 (m, 1H, ArH-5), 7.25 (s, 1H, OH), 7.44 (m, 3H, –SOPh), 7.55 (m, 2H, *ortho* –SOPh). Found: C, 55.7; H, 4.5; S, 7.6%. Calcd for $C_{19}H_{19}O_3SBr$: C, 56.02; H, 4.67; S, 7.86%.

7-(2-Bromo-2-propenyl)-5-methoxy-2-methylbenzofuran (8a). Repeating the above reaction for **6a** (1.0 g) in the presence of SiO_2 (Fluka 60H) (ca. 1 g) in the reaction mixture gave **8a** (476 mg, 69%); IR (neat) 1620 (s), 1595 (m), 1490 (s), 1440 (s), 1225, 1215 (s) cm^{-1}; ^{1}H NMR δ=2.25 (s, 3H, CH_3), 3.70 (s, 3H, $-OCH_3$), 3.83—4.15 (m, 2H, $-CH_2-CBr=C$), 5.47 (s, 1H, *trans* –CBr=CH), 5.54 (s, 1H, *cis* –CBr=CH), 6.37 (s, 1H, ArH-3), 6.60—6.93 (m, 2H, ArH-4,6). MS *m/z* 281 (M$^+$, 100%), 200 (8), 185 (13). Found: C, 55.3; H, 4.3%. Calcd for $C_{13}H_{13}O_2Br$: C, 55.5; H, 4.63%.

4-Methoxy-2,6-bis(2-phenylsulfinyl-2-propenyl)phenol (7b). A solution of **6b** (100 mg, 0.22 mmol) in mesitylene (2 ml) was

rearranged as above to give, after chromatography [(a) ether, (b) ether–MeOH (3 : 1)], **7b** (72 mg, 72%) as a thick dark oil; ^{1}H NMR δ=2.30 (s, 1H, -OH), 3.15 (d, J=16 Hz, 2H, -CH-CSOPh), 3.45 (d, J=16 Hz, 2H, -CH-CSOPh), 3.70 (s, 3H, OCH_3), 5.63 (s, 2H, *trans* -SOPhC=CH), 6.08 (s, 2H, *cis* -SOPhC=CH), 6.45 (s, 2H, ArH-3,5), 7.4—7.9 (m, 10H, -SOPh); MS m/z 452 (M^+, 6%), 327 (M—SOPh, 44), 202 (13), 201 (55), 200 (100), 185 (30). Found m/z (M^+) 452.5852. Calcd for $C_{25}H_{24}O_4S_2$: M, 452.5822. Rearrangement of **6b** in DCB yielded an oily residue which upon addition of ether partially crystallized to yield an unidentifiable dark brown solid as flakes, mp 170—172 °C (decomp); IR (KBr) 3450, 2925, 1650 (s), 1510 (s), 1490 (s), 1260 (s), 1110 (s), 830 (m), 770 (m) cm^{-1}. The solid was soluble in $CHCl_3$; ^{1}H NMR δ=1.55 (s), 3.2—4.0 (broad peak), 7.2—7.5 (broad peak); ^{13}C NMR δ=8.58, 15.24, 28.14, 45.96, 55.63, 55.86, 114.82, 120.8, 124.74, 129.20, 131.08. MS proved difficult to measure.

5-Methoxy-2-methyl-7-(2-phenylsulfinyl-2-propenyl)-benzofuran (8b). Rearrangement of **6b** (100 mg) in mesitylene (2 ml) in the presence of SiO_2 (Fluka 60H) (ca. 50 mg) yielded **8b** (37 mg, 51%) after chromatography [(a) petroleum ether (40 : 60), (b) ether], as a brown oil; ^{1}H NMR δ=2.50 (d, J=2 Hz, 3H, CH_3-2), 3.10 (d, J=16 Hz, 1H, CH-7), 3.45 (d, J=16 Hz, 1H, -CH'-7), 3.65 (s, 3H, -OCH_3), 5.65 (s, 1H, *trans* -SOPhC=CH), 6.10 (s, 1H, *cis* -SOPhC=CH), 6.40 (q, J=2 Hz, 1H, H-3), 6.75—7.0 (m, 2H, H-4,6), 7.4—7.8 (m, 5H, -SOPh); MS m/z 326 (M^+; 12) , 200 (100). Found: m/z 326.4118. Cacld for $C_{19}H_{18}O_3S$: M, 326.4094.

References

1) a) R. P. Lutz, *Chem. Rev.*, **84**, 205 (1984); b) F. E. Ziegler, *Chem. Rev.*, **88**, 1423 (1988); C. J. Moody, *Adv. Heterocycl. Chem.*, **42**, 203 (1987).

2) M. A. Khan, B. Al-Saleh, *J. Chem. Res., Miniprint,* **1989**, 319, and Refs. 1—7 cited therein.

3) R. Bell, P. D. Cottam, J. Davies, and D. N. Jones, *J. Chem. Soc., Perkin Trans. 1,* **1981**, 2106.

4) W. K. Anderson, E. J. Lavoie, and J. C. Bottaro, *J. Chem. Soc., Perkin Trans. 1,* **1976**, 1.

5) K. Kaneko, H. Katayama, Y. Saito, N. Fujita, and A. Kato, *J. Chem. Soc., Chem. Commun.,* **1986**, 1308.

6) D. H. R. Barton and W. D. Ollis, "Comprehensive Organic Chemistry," ed by J. F. Stoddart, Pergamon (1979), p. 707; b) R. W. Rickards in "Chemistry of Natural Phenolic Compounds," ed by W. D. Ollis, Pergamon, Oxford (1961), p. 1.

7) P. Cagniant and D. Cagniant, *Adv. Heterocycl. Chem.,* **18**, 337 (1975).

8) M. A. Khan, *J. Chem. Res., Synop.,* **1991**, 62; *J. Chem. Res., Miniprint,* **1991**, 601.

 © 1991 The Chemical Society of Japan Bull. Chem. Soc. Jpn., 64, 3687—3689 (1991)

Enhanced Production of Formic Acid by *Halobacterium halobium* MMT_{22} by Reduction of Hydrogencarbonate in Aqueous Solution

Mirza Mohammad Taqui KHAN* and Jayshree BHATT
Central Salt and Marine Chemicals Research Institute, Bhavnagar 364002, India
(Received April 9, 1991)

Enhanced production of formic acid was observed by reduction of hydrogencarbonate in aqueous solution by *Halobacterium halobium* MMT_{22}. A one and half fold increase in the production of formic acid was observed in the presence of ascorbic acid as electron donor and $[Ru(Bipy)_3]^{2+}$ as photosensitizer.

Since 1970's there has been a considerable research effort directed toward harnessing photochemical reactions for solar energy conversion and storage.

Fixation of carbon dioxide has bee extensively studied[1] because of its importance in photosynthesis as a source of C_1 chemicals.[2] Moreover the catalytic, reduction of CO_2 to organic molecules may be fundamentally important to cope with the rapid increase of the concentration of carbon dioxide in the atmosphere as a pollutant resulting from the combustion of fossil fuels.[3-6]

In a previous paper[7] we have reported photobiological as well as photoelectrochemical conversion of CO_2 to formic acid by *Halobacterium halobium* MMT_{22}. As the hydrogencarbonate ion in solution can act as a source of CO_2 in solution where concentrations can be studied over a wide range we report in this paper its reduction to formic acid by *H. halobium* MMT_{22}. The yield of formic acid obtained was 0.42 M (mg cells)$^{-1}$ h^{-1} which increasrs to 0.532 M (mg cells)$^{-1}$ h^{-1} in presence of ascorbic acid and to 0.646 M (mg cells)$^{-1}$ h^{-1} in the presence of ascorbic acid and $[Ru(Bipy)_3]^{2+}$ (1 M=1 mol dm^{-3}).

Experimental

$[Ru(Bipy)_3]^{2+}$ was prepared by literature procedure.[8] All the other chemicals used were of analytical grade.

The extreme halophile, *H. halobium* MMT_{22} was isolated from the brine obtained from the salt farm of CSMCRI in a nutrient medium at pH 7.0. Incubation was carried out at 40 °C under illumination.

Photocatalytic experiments were carried out in a double walled Pyrex glass cylindrical reaction vessel (40 ml) with a flattened surface positioned perpendicular to the incident light (exposed area 10 cm^2, 250 W Xe lamp from Applied Photo Physics).

For the optimization of reaction conditions, different sets of experiments were carried out. In a typical photocatalytic experiment an aqueous system containing 25 ml 25% NaCl; *H. halobium* MMT_{22} as biocatalyst (1—5 mg wet weight); $NaHCO_3$ as a source of CO_2 (0.2—2.0 M) was irradiated with a monochromatic excitation spectral line (420—480 nm). Water at (10—50 °C) was continuously circulated through a water jacketed cell containing the reaction mixture to maintain the desired temperature within ±0.2 °C.

In other sets of experiments investigations were carried out to study the effect of electron donor and photosensitizer on formic acid production.

In a similar experimental system containing 25.0 ml 25% NaCl, 1 mg *H. halobium* MMT_{22}, 1.0 M $NaHCO_3$; with $[Ru(Bipy)_3]^{2+}$ as photosensitizer (10^{-4} M) and ascorbic acid as electron donor (10^{-1}, 10^{-2}, 10^{-3} M) was irradiated with a monochromatic excitation spectral line (460 nm). Water at 40 °C was continuously circulated through a water jacketed cell containing the reaction mixture.

Samples were taken out at various time intervals and made free of bacterial cells. The product analysis was done by HPLC.

Results and Discussion

Under strictly anaerobic conditions on illumination, each bacteriorhodopsin cycling in the purple membrane of *H. halobium*, release 2—3 protons which are released on the exterior of the cells. Simultaneously carbon uptake is greatly increased as CO_2 is fixed through the reductive pathways and NADH is produced during illumination by reversal of electron transport. Thus NADH functions as electron donor in the system.[9-11]

In our previous paper we have reported photobiological as well as photoelectrochemical conversion of CO_2 to formic acid by *H. halobium* MMT_{22}. The yield of formic acid increased considerably by regenerating NADH by cathodic reduction at −0.60 V or in the

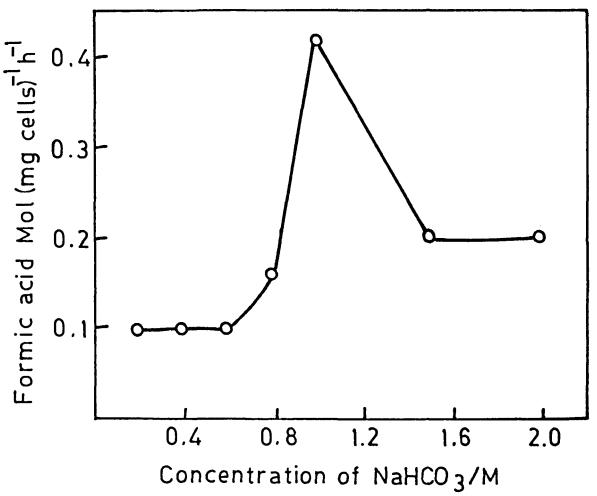

Fig. 1. Formic acid production at different substrate concentration.

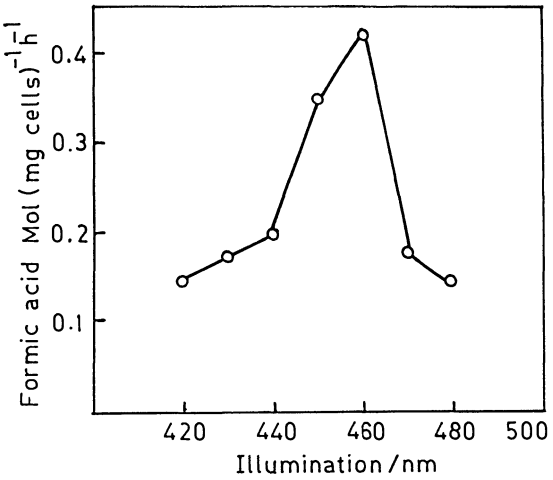

Fig. 2. Formic acid production at different wavelengths when $NaHCO_3$ was used as a source of CO_2.

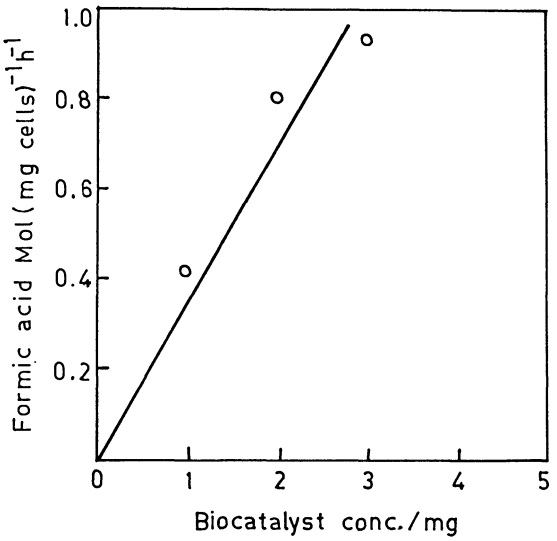

Fig. 3. Formic acid production at different biocatalyst concentrations.

presence of the two electron donor ascorbic acid. Under photoelectrochemical reduction, a maximum yield of 0.2 mol of HCOOH (mg cells)$^{-1}$ h^{-1} was obtained.[7]

In our present studies $NaHCO_3$ was used as a substrate for formic acid production. Optimization of the reaction conditions revealed the following results. 1 M $NaHCO_3$ concentration (Fig. 1), monochromatic excitation spectral line at 460 nm at 40 °C (Fig. 2) were found to be optimum conditions for formic acid production. An increase in the biocatalyst concentration causes a linear increase in formic acid production (Fig. 3).

Tris(bipyridyl)ruthenium complexes $[Ru(Bipy)_3]^{2+}$ have been intensively tested as sensitizers for photochemical water splitting using visible light.[12] There are many reports which describe application of such com-

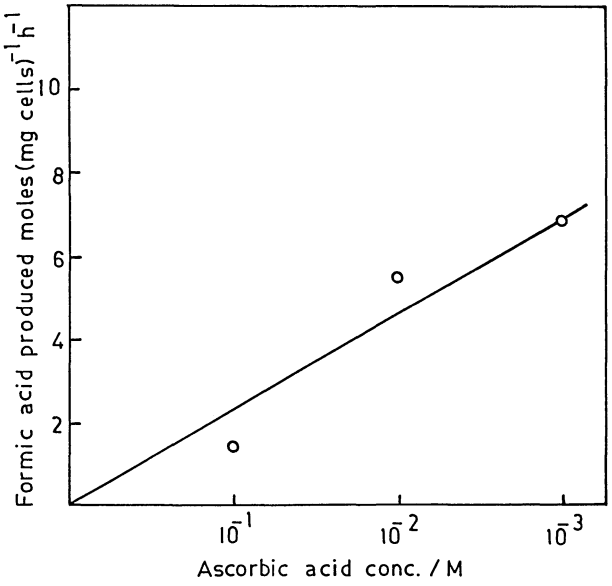

Fig. 4. Effect of ascorbic acid on formic acid production.

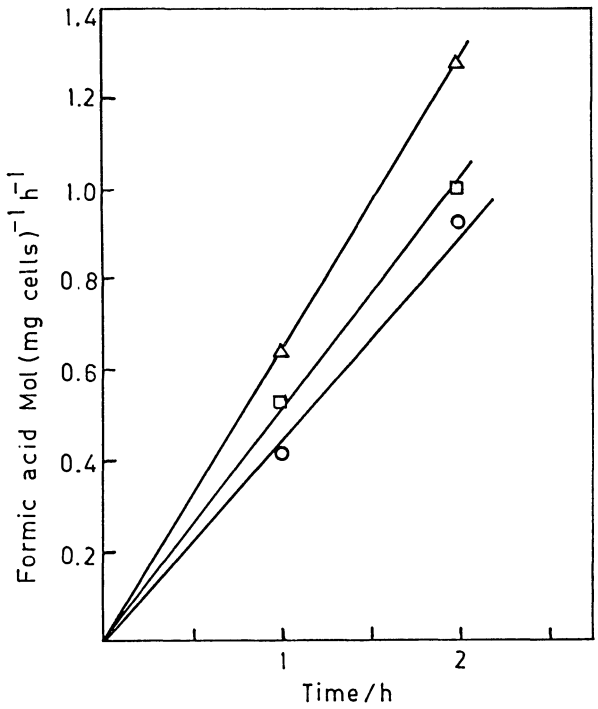

Fig. 5. Formic acid production by *Halobacterium halobium* MMT_{22} in presence of electron donor and photosensitizer.

plexes to CO_2 fixation.[12] Using $[Ru(Bipy)_3]^{2+}$ as a photosensitizer in visible light and ascorbic acid as a sacrificial electron donor and *H. halobium* as the biocatalyst, formic acid was found to be the sole organic product in our present investigations.

In the earlier report[7] *H. halobium* MMT_{22} showed continuous production of HCOOH at the rate of 0.2 M (mg cells)$^{-1}$ h^{-1}. In the present studies using hydro-

Table 1. Reduction of Hydrogencarbonate in Aqueous Solution to Formic Acid by *Halobacterium halobium* MMT_{22}

Time / h	Formic acid produced / M h^{-1} (mg cells)$^{-1}$		
	Conditions		
	H. halobium MMT_{22} in hydrogencarbonate solution	*H. halobium* MMT_{22} +ascorbic acid	*H. halobium* MMT_{22} +accorbic acid+ $[Ru(Bipy)_3]^{2+}$
0	0.0	0.0	0.0
1	0.42	0.532	0.646
2	0.81	1.042	1.30

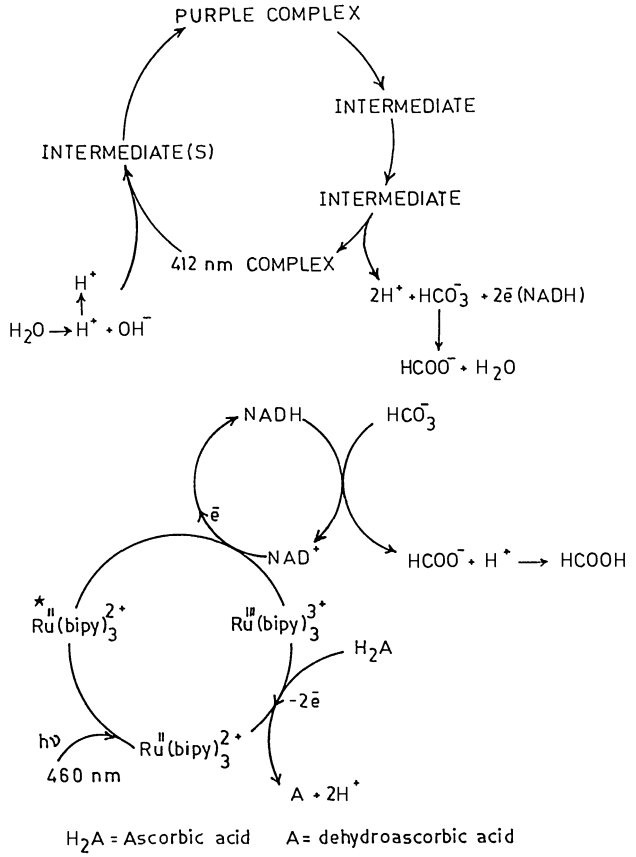

Scheme 1.

gencarbonate in solution an enhanced production of formic acid was observed in aqueous solution. The rate of formation of formic acid is 0.45 M h^{-1}. Figure 4 shows the effect of ascorbic acid concentration on formic acid production. In presence of ascorbic acid the rate increases to 0.55 M h^{-1}. Here ascorbic acid serves as two electron donor which enhances the rate of CO_2 reduction by maintaining the NADH/NAD^+ cycle. In presence of $[Ru(Bipy)_3]^{2+}$ formic acid production was found to be maximum with a rate of 0.66 M h^{-1}. Figure 5 and Table 1 compares the rates of formic acid production when ascorbic acid and $[Ru(Bipy)_3]^{2+}$ were used for the investigations. A 1.5 times increase in formic acid production was observed when $[Ru(Bipy)_3]^{2+}$ was used as a photosensitizer. The mechanism of the reaction is shown in Scheme 1.

References

1) S. Inove, A. Sato, and H. Matsuda, "Yuki Shingen No Kagaku," Kagakuzokan 90, Kagaku-Dojin, Kyoto (1981); Y. Kitano, M. Ichikawa, T. Osa, S. Inova, and K. Asada "Tan San Gasu No Kagaku," Kyoritu Kagaku Library, Kyoritushuppan, Tokyo (1976); S. Inove, *Chem. Tech.*, **1976**, 588.

2) J. R. Bolton and D. O. Hall, *Annu. Rev. Energy*, **4**, 353 (1979).

3) M. Halmann, "Photochemical Fixation of Carbon Dioxide," in "Energy Resources through Photochemistry and Catalysis," ed by Michael Gratzel, Academic Press, London (1983), pp. 507—534, and references therein.

4) I. J. Hawecker, J. M. Lehn, and R. Ziesell, *J. Chem. Soc., Chem. Commun.*, **1984**, 328.

5) M. Tezuka, T. Yajima, A. Tsuchiya, Y. Matsumoto, Y. Uchida, and M. Hidai, *J. Am. Chem. Soc.*, **104**, 6834 (1982).

6) K. Hiratsuka, K. Takahashi, H. Sasaki, and S. Toshima, *Chem. Lett.*, **1977**, 113.

7) Mirza Mohammad Taqui Khan and Jayshree Bhatt, *Bull. Chem. Soc. Jpn.*, **63**, 2393 (1990), and references therein.

8) C. F. Liu, N. C. Liu, and J. C. Bailar, Jr., *Inorg. Chem.*, **3**, 1086 (1964).

9) D. Arlette and U. W. Stoeckenius, *Proc. Natl. Acad. Sci., U.S.A.*, **71**, 1234 (1974).

10) A. Danon and S. R. Kaplan, *FEBS Lett.*, **74**, 255 (1977).

11) D. I. Arnon, "Bioorganic Chemistry IV," ed by E. E. van Tamelen, Academic Press, New York (1978), p. 4.

12) J. Kiwi, K. K. Sundaram, and M. Gratzel, *Struct. Bonding (Berlin)*, **49**, 37 (1982).

Structural Study of the Two Phases of Tetrakis(methylseleno)-tetrathiafulvalene ($TSeC_1$-TTF)

Chikako NAKANO,*,†† Ping WANG, Takehiko MORI, Yusei MARUYAMA, Hiroo INOKUCHI, Hideki YAMOCHI,† and Gunzi SAITO†

Institute for Molecular Science, Myodaiji, Okazaki 444

†Department of Chemistry, Faculty of Science, Kyoto University, Sakyo-ku, Kyoto 606

(Received March 20, 1991)

The crystal structure of the low-melting point phase (L-phase) of a single component organic semiconductor, $TSeC_1$-TTF, is determined and compared with that of the high-melting point phase (H-phase). The intracolumnar overlap mode and the calculated intermolecular overlap integrals are slightly larger in the L-phase, to which is ascribed the low resistivity of the L-phase. The L-phase, however, does not have two-dimensional networks of intercolumnar Se···Se contacts, which exist in the H-phase. This may be associated with the difference of the melting points.

Tetrakis(alkylthio)tetrathiafulvalenes(TTC_n-TTFs) are very unique semiconductors with fairly low resistivity as single component organic compounds. This character is derived from the short intermolecular distance between the adjacent central π systems, because a bundal of long alkyl chains assemble TTC_n-TTF molecules in a fashion that the central π-systems can pile up one after the other very tightly (Fastener Effect).[1,2] $TTeC_n$-TTFs and $TSeC_n$-TTFs, in which the outer sulfur atoms of TTC_n-TTF are replaced by Te and Se atoms respectively, were designed in order to increase the intermolecular interactions. We have found that $TTeC_1$-TTF reveals noticeably low resistivity of 8.1×10^4 (Ω cm) although alkyl chains are too short to attain the Fastener Effect.

The $TTeC_1$-TTF crystal has very unique packing and intercolumnar zigzag Te···Te interactions along the stacking axis.[3] The title compound, $TSeC_1$-TTF, (Fig. 1) crystallizes in two phases, of which electrical conductivities are different by two orders.[4,5] We have reported the structure of the H-phase crystal, $TSeC_1$-TTF(H), in the previous paper.[6] In order to discuss the differences of electrical and thermal properties between these two phases, here, we report the structure of the L-phase crystal, $TSeC_1$-TTF(L) and compare the intermolecular overlap integrals with those of $TSeC_1$-TTF(H).

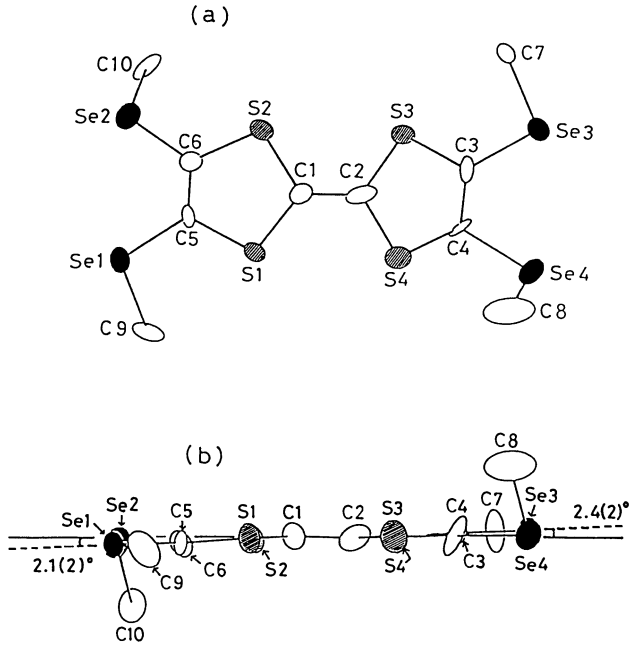

Fig. 1. The molecular structure of $TSeC_1$-TTF(L).
(a) The numbering scheme,
(b) Side view.

†† Toyota research fellow.

Experimental

The synthesis of the $TSeC_1$-TTF compound was reported in the preceding paper.[4] Two kinds of single crystals were prepared by recrystallization from different solvents. Red needle crystals ($TSeC_1$-TTF(L)) were obtained from the mixture of hexane and benzene. On the other hand, dark red plate crystals ($TSeC_1$-TTF(H)) were obtained from pure hexane solution, sometimes together with red needle crystals.

Intensity data of X-ray diffraction were measured on a Rigaku automated four-circle X-ray diffractometer AFC-5R by the θ-2θ scan technique with graphite monochromatized Mo $K\alpha$ radiation ($2\theta<60°$). Crystal data ($TSeC_1$-TTF(L)): $C_{10}H_{12}S_4Se_4$, F.W.=576.28, orthorhombic, space group $Pca2_1$, =18.534(5), b=5.284(1), c=17.533(4) Å, V=1717.0(7) Å^3, Z=4, D_x=2.23 g cm^{-3} and μ(Mo $K\alpha$)=89.12 cm^{-3}, crystal size: 0.02×0.6×0.04 mm^3. The intensity variation of the three standard reflections during the measurement was less than 5%. 2925 unique reflections were measured. The intensity data were corrected for absorption effects using a Gaussian integration procedure. The crystal structure was solved by the Patterson method and refined by the block-diagonal least squares procedure by using 1145 independent reflections ($|F_o|>3\sigma(|F_o|)$). The final R=0.072, R_w=0.068 $\{w=[\sigma^2+(0.015\,F_o)^2]^{-1}\}$ and $(\Delta/\sigma)_{max}$=0.89. Thermal parameters were anisotropic for all the non-hydrogen atoms and isotropic for hydrogen atoms. In the final difference Fourier map, the residual electron density corresponds to |1.7| e Å^{-3} near Se1 atom. Although we assumed the space group was *Pcam* first, in this case we found difficulty in analyzing the structure.

The atomic scattering factors were taken from the International Tables for X-ray Crystallography.[7] All the calculations were carried out on a HITAC M-680H computer with the UNICS III program system.[8]

Results and Discussion

Final atomic coordinates of TSeC1–TTF(L) are shown in Table 1.[9] The molecule is noncentrosymmetric, while the TSeC1–TTF(H) molecule is centrosymmetric,[6] and the terminal parts are slightly twisted because of the large atomic radius of Se atom as compared with those of the S and C atoms (Fig. 1). The dihedral angles between the central C_2S_4 part and terminal $C_2S_2Se_2$ are 2.4(2)° and 2.1(2)°, respectively (TSeC1–TTF(H): 2.72(5)°).

TSeC1–TTF(L) molecules are stacked along the *b*-axis (corresponds to the needle axis) and the overlapping mode is shown in Fig. 2. Although the shortest intracolumnar S ··· S distance is a little longer than that of TSeC1–TTF(H), the overlap along the stacking axis is a little larger. The shortest intracolumnar S ··· S distance is 3.73(1) Å and Se ··· S distances are 3.856(8) Å and 3.885(8) Å. There is no short Se ··· Se contact within a column in both two phases. The distance between the two least squares planes of the central

Table 1. Positional Parameters ($\times 10^4$) and Equivalent Isotropic Thermal Parameters of the TSeC1–TTF (L)

$$B_{eq}=\frac{4}{3}(\sum_i\sum_j B_{ij}\boldsymbol{a}_i\boldsymbol{a}_j)$$

Atom	*x*	*y*	*z*	B_{eq}/Å^2
Se1	5599(2)	9560(6)	3372(2)	2.9
Se2	5085(2)	7588(6)	5188(2)	3.9
Se3	1902(2)	−4586(5)	3030(2)	2.8
Se4	2431(2)	−2783(6)	1239(2)	3.8
S1	4483(4)	5445(15)	2825(4)	2.6
S2	4065(4)	3735(14)	4363(4)	2.8
S3	3023(4)	−476(15)	3626(4)	3.0
S4	3420(5)	1194(15)	2071(4)	3.5
C1	3945(14)	3418(50)	3355(14)	2.5
C2	3517(16)	1533(50)	3052(14)	3.0
C3	2599(14)	−1920(43)	2858(14)	2.2
C4	2852(18)	−1106(49)	2147(14)	3.7
C5	4926(13)	6931(43)	3603(14)	2.0
C6	4751(14)	6154(52)	4294(14)	2.5
C7	1933(18)	−4517(57)	4170(14)	4.0
C8	2019(22)	371(76)	821(18)	6.5
C9	5646(16)	9420(65)	2301(16)	4.1
C10	5424(18)	4588(60)	5739(15)	3.9

Table 2. Differences between the Two Phases of TSeC1–TTF

Phase	L	H
Solvent	Hexane and benzene	Hexane
Color	Red	Dark red
Crystal shape	Needle	Plate
Melting point/ °C[4]	92.5	106.3
Electrical resistivity along the stacking axis/Ω cm[4]	1.0×10^6	2.7×10^8
Activation energy/eV[4]	0.26	0.58
Density/g cm^{-3}[6]	2.23	2.22
Distance between the least square planes/Å	3.568(4)	3.570(1)
The shortest intracolumnar distance/Å		
S ··· S	3.73(1)	3.663(3)
Se ··· S	3.858(9)	3.890(2)
The shortest intercolumnar distance/Å		
Se ··· Se	3.620(5) 3.639(5)	3.670(1)

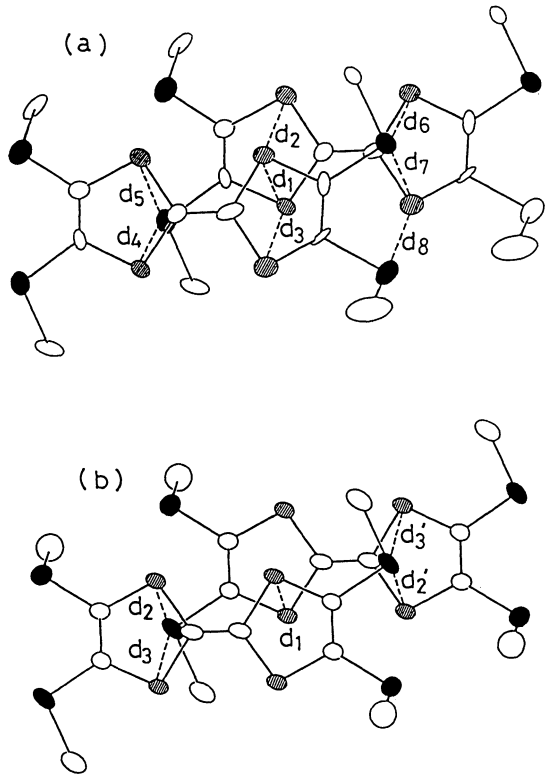

Fig. 2. Comparison of overlapping mode between the two phases.
(a) TSeC1–TTF(L). Intracolumnar distances (<4Å): d_1(S1*···S3**)=3.73(1), d_2(S2*···S3**)=3.84(1), d_3(S1*···S4**)=3.85(1), d_4(Se1*···S1**)=3.856(8), d_5(Se1*···S2**)=3.997(8), d_6(S3*···Se3**)=3.885(8), d_7(S4*···Se3**)=3.964(9), d_8(S4*···Se4**)=3.952(9) Å.
Symmetry operations: *(*x*, *y*, *z*), **(*x*, 1+*y*, *z*).
(b) TSeC1–TTF(H). Intracolumnar distances (<4 Å): d_1(S1*···S1***)=3.663(3), d_2(Se1*···S2**)=3.890(2), d_3(Se1*···S1**)=3.969(2) Å.
Symmetry operations: *(*x*, *y*, *z*), **(*x*, *y*, 1+*z*), ***(−*x*, −*y*, 2−*z*).

$C_6S_4Se_4$ skeletons is 3.568(4) Å and is nearly the same as that of $TSeC_1$–TTF(H) (3.570(1) Å). The densities of these two crystals are also nearly the same (Table 2).

Crystal structure of $TSeC_1$–TTF(L) is shown in Fig. 3. There exist intercolumnar short Se1 ··· Se3 contacts (3.620(5) and 3.639(5) Å), which are much shorter than the sum of the van der Waals radii (4.00 Å). These Se atoms form zigzag chains between neighboring columns along the stacking axis (Fig. 3(b)). These Se ··· Se chains are important to extend the molecular overlapping along the *b*-axis. However, these zigzag chains are formed by Se1 and Se3 atoms, and the other Se2 and Se4 atoms do not have strong intercolumnar interaction (only with the terminal methyl groups with the van der Waals contacts along the stacking axis). There are no short Se ··· Se contact along the *c*-axis. On the other hand, in the case of $TSeC_1$–TTF(H), short intercolumnar Se ··· Se contacts exist in nearly $a+b$ and $a-b$ directions (Fig. 4(b)). The H-phase has two-dimensional array of the short Se ··· Se contacts, whereas the L-phase has short Se ··· Se contacts only along one direction. It could be one of the reasons that melting point of $TSeC_1$–TTF(L) (92.5 °C) is lower than that of $TSeC_1$–TTF(H) (106.3 °C).

We tried to estimate the intermolecular overlap integrals to understand the cause of the difference of the electrical conductivities between these two phases. The overlap integrals calculated by the extended Hückel molecular orbitals between HOMOs for these two crystals are shown in Table 3. The overlap of $TSeC_1$–TTF(L) along the stacking axis (direction *s*) is a little larger than that of $TSeC_1$–TTF(H) (direction *s*). Moreover, in the $TSeC_1$–TTF(L) crystal, one molecule can have intermo-

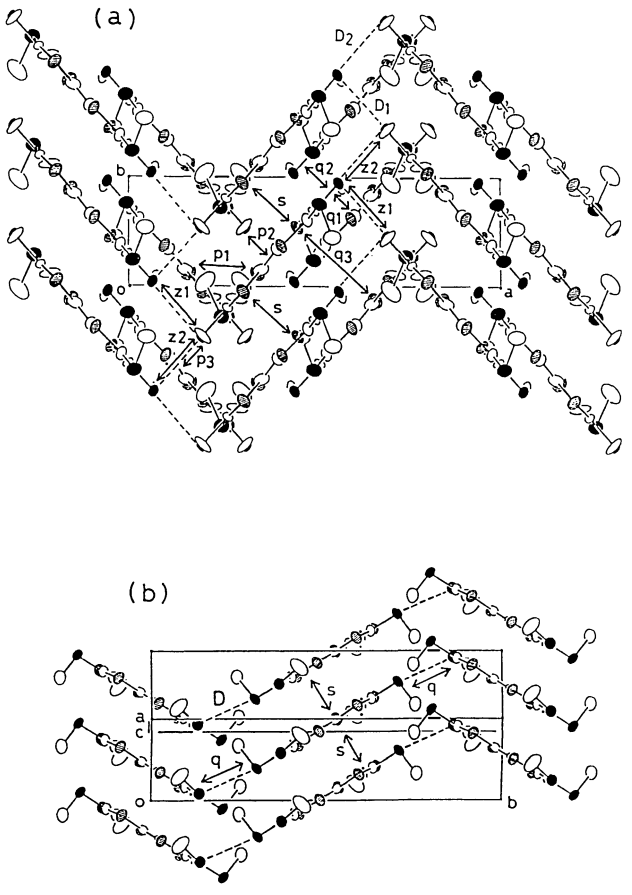

Fig. 3. Crystal structure of $TSeC_1$–TTF viewed nearly along the molecular short axis. The allows and the characters (s, p, q, z) indicate the directions of intermolecular interactions shown in Table 3.
(a) $TSeC_1$–TTF(L) (projected along the *c*-axis)
Dotted lines mean intercolumnar Se···Se distances: D_1=3.620(5), D_2=3.639(5)Å.
(b) $TSeC_1$–TTF(H)
Dotted lines mean intercolumnar Se···Se distances: D=3.670(1) Å.

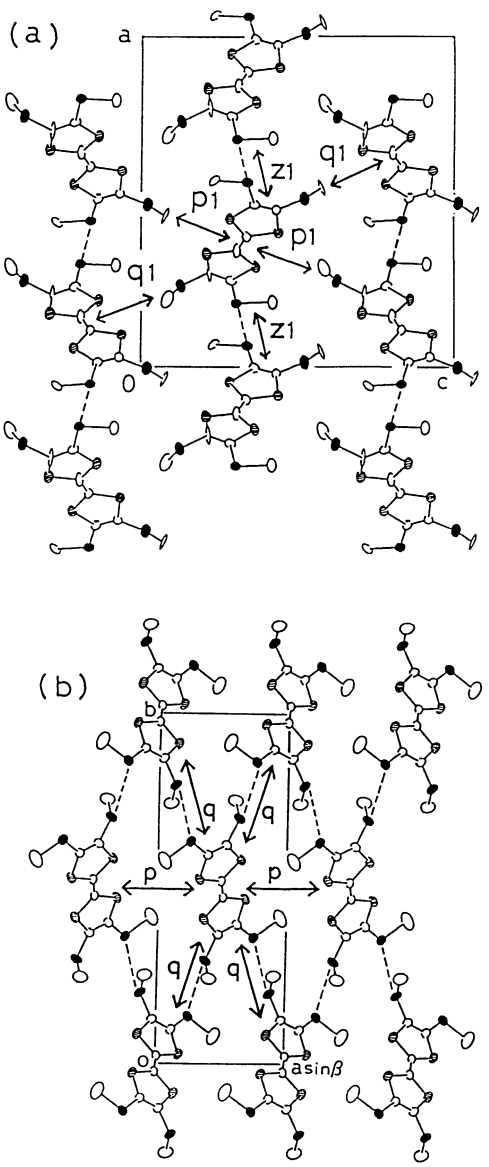

Fig. 4. Crystal structure of $TSeC_1$–TTF viewed nearly along the stacking axis. The arrows and the characters (p, q, s, z) mean the intermolecular interactions shown in Table 3.
(a) $TSeC_1$–TTF(L) (projected along the *b*-axis),
(b) $TSeC_1$–TTF(H) (projected along the *c*-axis).

Table 3. Overlap Integrals ($\times 10^3$) of the HOMOs for $TSeC_1$-TTF(L) and $TSeC_1$-TTF(H). (The symbols are directions of interactions shown in Figs. 3 and 4.)

$TSeC_1$-TTF(L)		$TSeC_1$-TTF(H)	
s	−3.69	s	−3.20
z1	−0.107	p	0.371
z2	0.00569	q	−0.036
p1	−0.223		
p2	0.100		
p3	0.100		
q1	0.0765		
q2	−0.0114		
q3	−0.0114		

lecular interactions with many neighboring molecules (Fig. 3(a) and (b)) and has larger overlap integrals in many directions than the case of $TSeC_1$-TTF(H). These facts are compatible with the result that the electrical resistivity and activation energy for conduction of $TSeC_1$-TTF(L) are lower than those of $TSeC_1$-TTF(H) (Table 2).

In summary, the $TSeC_1$-TTF(L) crystal has better overlap mode along the stacking axis and has larger intermolecular overlap integrals. This may be related to the low resistivity of the L-phase. On the contrary, these Se ··· Se contacts are only along the *b*-axis and do not form network like in $TSeC_1$-TTF(H). This two-dimensional Se ··· Se network may be associated with the higher melting point of the H-phase.

We thank Dr. T. Inabe (Institute for Molecular Science) and Professor T. Enoki (Tokyo Institute of Technology) for their valuable discussion.

References

1) H. Inokuchi, G. Saito, P. Wu, K. Seki, T. B. Tang, T. Mori, K. Imaeda, T. Enoki, Y. Higuchi, K. Inaka, and N. Yasuoka, *Chem. Lett.*, **1986**, 1263.

2) K. Imaeda, T. Enoki, Z. Shi, P. Wu, N. Okada, H. Yamochi, G. Saito, and H. Inokuchi, *Bull. Chem. Soc. Jpn.*, **60**, 3163 (1987).

3) H. Inokuchi, K. Imaeda, T. Enoki, T. Mori, Y. Maruyama, G. Saito, N. Okada, H. Yamochi, K. Seki, Y. Higuchi, and N. Yasuoka, *Nature*, **329**, 39 (1987).

4) H. Yamochi, N. Iwasawa, H. Urayama, and G. Saito, *Chem. Lett.*, **1987**, 2265.

5) P. Wang, T. Enoki, K. Imaeda, N. Iwasawa, H. Yamochi, H. Urayama, G. Saito, and H. Inokuchi, *J. Phys. Chem.*, **93**, 5947 (1989).

6) P. Wang, T. Inabe, C. Nakano, Y. Maruyama, H. Inokuchi, N. Iwasawa, and G. Saito, *Bull. Chem. Soc. Jpn.*, **62**, 2252 (1989).

7) "International Tables for X-Ray Crystallography," Kynoch Press, Birmingham (1974), Vol. IV.

8) T. Sakurai and K. Kobayashi, *Rep. Inst. Phys. Chem. Res.*, **55**, 69 (1979).

9) Tables of atomic parameters of H-atoms, anisotripic thermal parameters, and list of structure factors are deposited as Document No. 8973 at the Office of the Editor of Bull. Chem. Soc. Jpn.

Deuterium Isotope Effects on Aromatic Carbon-13 Chemical Shifts. III. One-, Two-, and Three-Bond Isotope Effects on the ^{13}C Chemical Shifts of 3-Substituted Pyridines

Yasuki NAKASHIMA,† Sadanori BAN, Satoru ITOH, and Kensuke TAKAHASHI*
Department of Applied Chemistry, Nagoya Institute of Technology, Gokiso-cho, Showa-ku, Nagoya 466
†Research and Development Department, Menicon Co., Ltd., Biwajima, Nishi-ku, Nagoya 451
(Received May 14, 1991)

The one-, two-, and three-bond deuterium isotope effects ($^1\Delta$, $^2\Delta$, and $^3\Delta$) on the ^{13}C chemical shifts of 3-substituted pyridines are reported. $^1\Delta$, $^2\Delta$, and $^3\Delta$ are correlated with the ^{13}C chemical shifts of the observed carbons. $^1\Delta$ show a linear correlation with the ^{13}C chemical shifts with a positive slope. On the other hand, $^2\Delta$ and $^3\Delta$ show linear correlations with the negative slopes. They can thus be interpreted in terms of the π-electron density change by the substituent and the electron release effects by carbons one and two bonds apart from deuterium, respectively.

Even though the deuterium isotope effects on the NMR chemical shifts ($^n\Delta$, where n is the number of intervening bonds) have been known for a long time,[1] the true cause for $^n\Delta$ is still unclear. Since experimental data for $^n\Delta$ in π-systems are scarce, it is difficult to discuss them systematically.[2] Especially, only a few studies concerning the $^n\Delta$ of heteroaromatics have been reported.[2,3] Further studies are desired. We have shown that $^1\Delta$ and $^2\Delta$ for substituted benzenes are correlated with the π- and σ-electron densities, respectively.[4] In this study, we chose 3-substituted pyridines and here discuss their $^1\Delta$, $^2\Delta$, and $^3\Delta$. One of the reasons for our selection was that pyridine is an analogue of benzene. Additionally, the interaction between the nitrogen atom and the substituent seems to be small in a 3-substituted pyridine system.[5] It is therefore possible to estimate simply the substituent effect on the isotope shifts. In the present system,$^1\Delta$ were observed at the C_2, C_4, and C_6 positions, and $^2\Delta$ were observed at the C_3 and C_5 positions. The former values enable us to consider the mesomeric effects of the substituent. The latter values enable us to consider the inductive effects. Both $^1\Delta$ and $^2\Delta$ are correlated linearly with the ^{13}C chemical shifts of the observed carbons. The slope of a correlation line for $^1\Delta$ has a positive value. On the other hand, that for $^2\Delta$ is negative. This fact can be explained in terms of the π-electron density changes by the substituents and the electron-release effects due to the α-carbons (D-labelled carbons), respectively. In addition, $^3\Delta$ can be observed on alkyl side-chain carbons; they also show a linear correlation with δ_c. This can be explained in terms of electron release effects due to the β-carbons (*C–C–D).

Experimental

The samples were selected for ten 3-substituted pyridines and the unsubstituted pyridine. The substituents were 3-Me, 3-Et, 3-Bu^n, 3-Cl, 3-NH_2, 3-CH_2NH_2, 3-OH, 3-CH_2OH, 3,5-Me_2, and 3,5-Cl_2. Deuterium-labelled compounds were prepared with base-catalyzed proton–deuteron exchange reactions of the selected pyridines in either D_2O or 5—10 wt% NaOH–D_2O solutions. The starting materials used were commercially available and were used without further purification. The reaction vessels were Pyrex ampoules. A suitable amount of the starting material and a catalyst solution were sealed into an ampoule, and kept at 200—230 °C in an autoclave. H/D exchange reactions occurred at the 2-, 4-, and 6-positions of the pyridines. Therefore, $^1\Delta$ were observed at the C_2, C_4, and C_6 atoms, while $^2\Delta$ were observed at the C_3 and C_5 atoms. Although $^3\Delta$ could be observed on the carbons in the alkyl side chains, the long-range isotope shifts via more than three bonds were not observed on the ring carbons. Pyridine-4-*d* was prepared by a previously reported method.[6] The hydroxyl and amino hydrogens of the substituents exchanged with those in water, and could not be separately observed on the NMR time scale. Then, labelled substituents such as OD, NHD, or ND_2 showed no isotope effect on the ^{13}C chemical shifts. The NMR spectra were measured with a Varian XL-200 FT-NMR spectrometer at 50.3 MHz and a temperature of about 22 °C. The NMR samples were neat for liquid samples. For solid samples, they were dissolved in solvents having high solubility (see Tables 1 and 2). Peak assignments were carried out on the basis of their intensity changes occurring along with H/D exchange reactions, or on

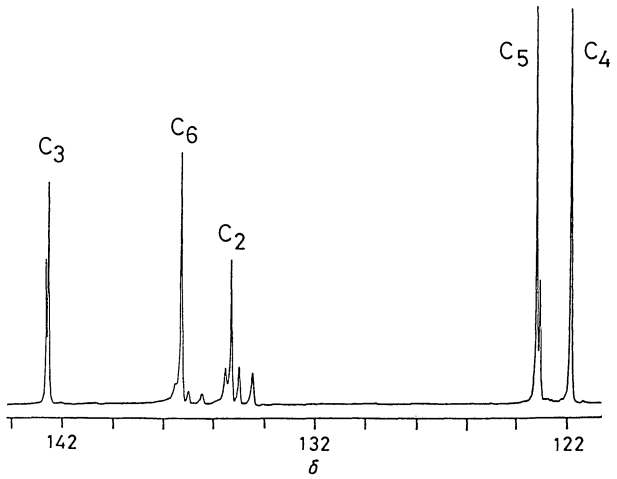

Fig. 1. ^{13}C NMR spectrum of 3-aminopyridine (a mixture of 2-D, 6-D, 2,6-D_2, and nondeuterated compounds).

the basis of splittings and/or broadenings by C–D couplings. An example of the ^{13}C spectra is shown in Fig. 1. In this figure two additional triplets at the C_2 and C_6 carbons are assigned to the signals coming from the deuterated species. The extent of deuteration proceeded fast at C_2, and slow at C_6. No triplet could be observed at C_4.

The isotope effects were evaluated from comparisons of the expanded spectra of these mixed species in the same sample tube, as described previously.[7] MNDO MO calculations were carried out using an NEC PC-9801 RA 32-bit personal computer with a "PASOCON MOPAC/386" program, which is based on the MOPAC (V3.1 QCPE No. 516) by Toray Systems Center.

Results and Discussion

All of the observed $^1\Delta$, $^2\Delta$, and $^3\Delta$ are listed in Tables 1, 2, and 3, respectively. The $^1\Delta$ are in a range from 252 to 363 ppb, while $^2\Delta$ are from 45 to 137 ppb. Their magnitudes are similar to those of the substituted benzenes.[4,7] All of the observed $^1\Delta$, $^2\Delta$, and $^3\Delta$ were toward the high field. The signs, however, are neglected in the tables. The substituents introduced to the pyridine ring usually decreased both $^1\Delta$ and $^2\Delta$. Particularly, large changes were observed at the ipso-positions of the substituents. $^3\Delta$ on alkyl side chains varied from 27 to 52 ppb. Correlations between isotope shifts and the chemical shifts have been reported in several articles.[7,8] We thus investigated them in the present system.

Table 1. α-Deuterium Isotope Shifts($^1\Delta$) of Pyridines in ppb[a]

Substituent	Solvent	Observed carbon		
		C_2	C_4	C_6
—	Neat	351[b]	296	351[b]
3-Me	NaOH–D_2O[c]	351	—[d]	325
3-Et	Acetone-d_6	355[b]	—	316
3-Bu^n	Neat	363	—	330
3-NH_2	D_2O	311	—	299
3-OH	CH_3OH	312[b]	252[b]	294[b]
3-CH_2OH	NaOH–D_2O	316[b]	308[b]	339[b]
3-CH_2NH_2	NaOH–D_2O	362	—	327
3-Cl	Neat	328	278	—
3,5-Cl_2	1,4-Dioxane	323	279	323
3,5-Me_2	Acetone-d_6	351[b]	—	351[b]

a) Errors are estimated to be within 4 ppb. b) With large errors (8 ppb). c) Neutralized after reaction. d) Not available.

Table 2. β-Deuterium Isotope Shifts($^2\Delta$) of Pyridines in ppb[a]

Substituent	Solvent	Observed carbon			
		From 4-D		From 2-D or 6-D	
		C_3	C_5	C_3	C_5
—	Neat	106	106	129	129
3-Me	NaOH–D_2O[b]	—[c]	—	114	135
3-Et	Acetone-d_6	—	—	116	129
3-Bu^n	Neat	—	—	108	136
3-NH_2	D_2O	—	—	85	134
3-OH	CH_3OH	45	98	70	137
3-CH_2OH	NaOH–D_2O	—	106[d]	—	136[d]
3-CH_2NH_2	NaOH–D_2O	78[d]	100	102	134
3-Cl	Neat	81	97	111	—
3,5-Cl_2	1,4-Dioxane	81	81	106	106
3,5-Me_2	Neat	—	—	110	110

a) Errors are estimated to be within 4 ppb. b) Neutralized after reaction. c) Not available. d) With large error (8 ppb).

Table 3. γ-Deuterium Isotope Shifts ($^3\Delta$) on Alkyl Side-Chain Carbons from 2-D in ppb[a]

Substituent	Solvent	$^3\Delta$	δ/ppm
3-Me	NaOH–D_2O[b]	49	18.34[c]
3,5-Me_2	Acetone-d_6	52	18.19
3-Et	Acetone-d_6	43	26.90
3-Bu^n	Neat	40	32.17
3-CH_2OH	NaOH–D_2O	27	62.21

a) Errors are estimated to be within 3 ppb. b) Neutralized after reaction. c) Ref. 13.

$^1\Delta$ vs. δ_c. A linear correlation is found between the $^1\Delta$ and ^{13}C chemical shifts of the observed carbons, as shown in Fig. 2. $^1\Delta$ in ppb can be expressed as

$$^1\Delta\,(\text{ppb}) = 3.70\,\delta_c(\text{ppm}) - 211 \qquad (1)$$

The slope of the least-square line is positive and similar to that of para-substituted benzenes (D–C_6H_4–X), which was previously reported by Berger and Diehl.[8] For further discussions, the π-electron charges (Δq_π) of pyridine ring carbons were evaluated by an MNDO MO

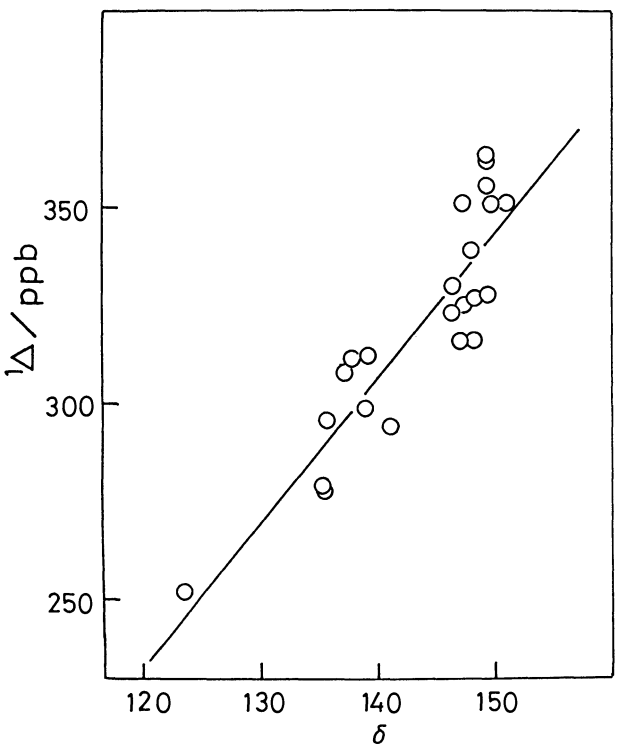

Fig. 2. Correlation between $^1\Delta$ (ordinate in ppb) and δ_c (abscissa in ppm) for 3-substituted pyridines with r=0.895 and a standard deviation of 13 ppb.

calculation. They are listed in Table 4. Plots between Δq_π and $^1\Delta$ are shown in Fig. 3. As can be seen, a linear correlation exists. The slope of the line is 642 ppb/electron unit, close to that of substituted benzenes (517 ppb/electron unit).[4] Recent theoretical findings have established the isotope shifts' origin as discussed below.[2c] The difference in the anharmonicities between the C–H and C–D bonds produce averaged bond-length changes in the NMR time-scale. Therefore, the time-averaged position of the C–D bonding electron should be different from that of the C–H bonding electron. The former will be nearer to the carbon atom than the latter. The D-labelled carbon would therefore be more shielded than the unlabelled carbon. Thus, upfield shifts $^1\Delta$ are observed. If we assume that the contribution of anharmonicity in shorter, stronger C–H bonds is small, the anharmonicity change on going from C–H to C–D is small. Therefore, in such a case, shielding changes of the carbon nuclei will be small. Thus, $^1\Delta$ will be diminished. We recently obtained several experimental results which strongly support this isotope shifts model. One is a correlation between $^1\Delta$ and ν_{CH} in the IR region for monosubstituted methane derivatives.[11] The other is a correlation between $^1\Delta$ and the C–H bond lengths optimized by MNDO MO calculations for several aromatic compounds.[12] From this information, a correlation between Δq_π and $^1\Delta$ is found to exist in the present system, and can be interpreted as discussed below. Electron release effects by substituents increase the π-electron densities at the ortho- and para carbons. For a sp^2 carbon, if it has a high π-electron density, its s-character increases. Its C–H bond length thus becomes shorter, and a smaller $^1\Delta$ is observed. Comparing $^1\Delta$ with the C–H bond lengths optimized by MNDO MO calculations (Table 5), increasing the C–H bond length roughly tends to increased $^1\Delta$.

Table 4. Calculated π-Electron Charges(Δq_π) of Pyridines[a]

Substituent	C_2	C_4	C_6
—	0.091	0.058	0.091
3-Me	0.099	0.064	0.095
3-NH_2	0.041	0.001	0.060
3-OH	0.047	−0.041	0.050
3-Cl	0.103	0.067	0.104
3,5-Me_2	0.103	0.070	0.103

a) Calculated by the MNDO MO method.

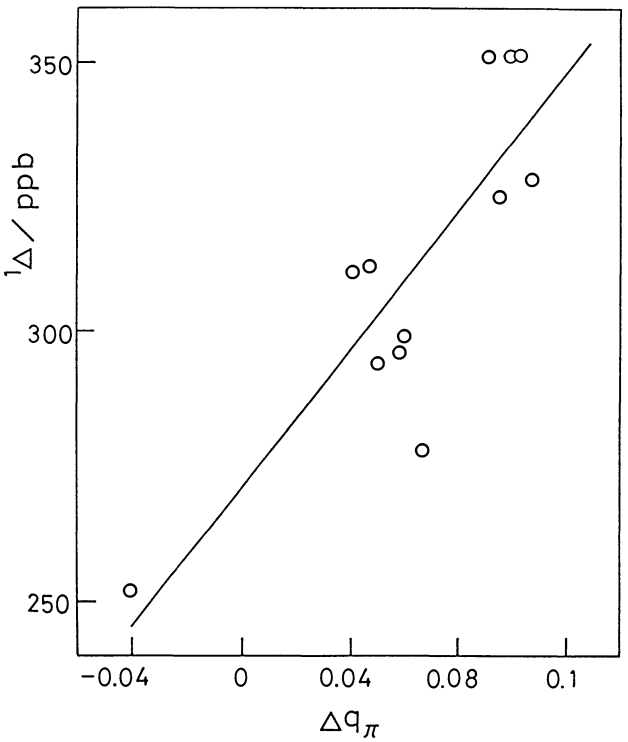

Fig. 3. Correlation between $^1\Delta$ and Δq_π. A correlated straight line is expressed as $^1\Delta$=642 Δq_π+271 with r=0.842.

$^2\Delta$ vs. δ_C. Correlations between the $^2\Delta$ and ^{13}C chemical shifts were also investigated. Different $^2\Delta$ values were obtained for the same carbons in the isotopomers; one was from the 2-D or 6-D isotopomer, and the other was from the 4-D isotopomer, as shown in Scheme 1. Typical expanded ^{13}C NMR spectra of C_3 and C_5 of the products obtained from an H/D exchange reaction of the 3-pyridinol are shown in Fig. 4. Since the reaction occurred at the 2-, 4-, and 6-positions, $^2\Delta$ are observed at C_3 and C_5. In the C_3 signals, the peaks can be assigned from left to right as follows: (a) 2-H, 4-H, (b) 2-H, 4-D, (c) 2-D, 4-H, (d) 2-D, 4-D isotopomers. From signal b, $^2\Delta$ was determined to be 45 ppb, and from signal c, 70 ppb. The value from signal d is consistent with the sum of 45 and 70 ppb. In each isotopomer, two kinds of $^2\Delta$ were differentiated as follows: $^2\Delta$ from 2-D or 6-D is always larger than that from 4-D for the isotopomers.

Table 5. Optimized C–H Bond Lengths of 3-Substituted Pyridines by the MNDO MO Method in Å

Substituent	C_2–H_2	C_4–H_4	C_6–H_6
—	1.095	1.090	1.095
3-Me	1.096	1.091	1.095
3-NH_2	1.096	1.091	1.094
3-OH	1.095	1.090	1.093
3-Cl	1.095	1.090	1.095
3,5-Me_2	1.096	1.092	1.096

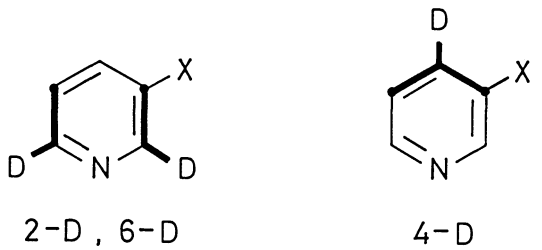

2-D, 6-D 4-D

Scheme 1.

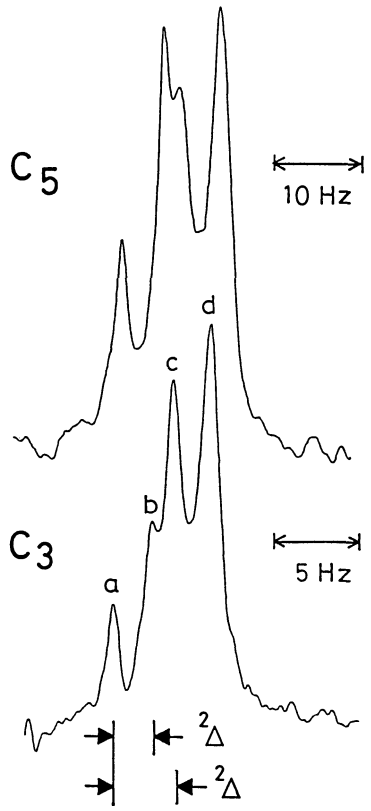

Fig. 4. ^{13}C NMR spectra of C_3 and C_5 of the products obtained from an H/D exchange reaction of 3-pyridinol. See text.

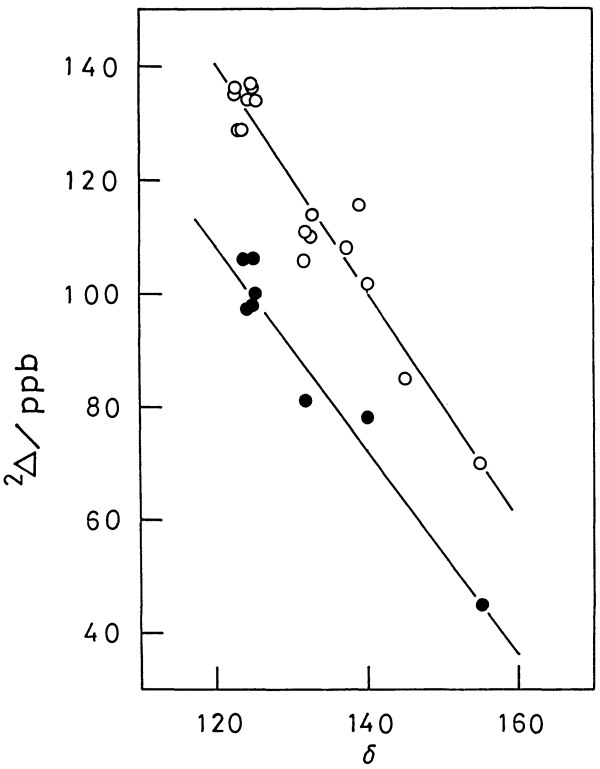

Fig. 5. Correlations between $^2\Delta$ (ordinate in ppb) and δ_c (abscissa in ppm) for 3-substituted pyridines. The white circles are for the 2-D or 6-D isotopomers. The black filled circles are for the 4-D isotopomers.

Since the difference between the two values is nearly constant, two good linear correlations between the $^2\Delta$ and ^{13}C chemical shifts of the observed carbons are obtained (Fig. 5). The two correlation lines have almost a parallel relationship with each other, and their slopes are very close to that of the substituted phenols.[7] These facts suggest that $^2\Delta$ can be explained in terms of electron release effects from the α-carbons (deuterium-labelled carbons).

It is well known that there are linear correlations between the electron densities and the NMR chemical shifts. We therefore evaluated the electron densities on $^2\Delta$-observed carbons by MNDO MO calculations. The calculated net atomic charges are given in Table 6. As shown in Fig. 6, plots between $^2\Delta$ and the net atomic charges (Δq_t) gave two parallel linear correlations. In our previous report, which is concerned with substituted benzenes, we proposed that there is a linear correlation between the $^2\Delta$ and σ-electron charges (Δq_σ).[4] In the present system, however, there are two better correlations between $^2\Delta$ and the total electron charges ($\Delta q_t = \Delta q_\sigma + \Delta q_\pi$) than $^2\Delta$ and Δq_σ, as shown in Fig. 6. The mean proportional coefficient of the two correlated lines is -372 ppb per unit charge. That for substituted benzenes is -355 ppb, which is calculated only for the ipso- and meta-carbons from previously reported data.[4] The present system is therefore similar to the substituted benzenes regarding the behavior of $^2\Delta$ and the charge densities.

In our previous report, we proposed a mechanism to explain $^2\Delta$.[4] The shielding of a D-labelled carbon, which directly reflects $^1\Delta$, is inductively transmitted to its adjacent carbon, whose $^2\Delta$ is dependent upon its net atomic charge (Δq_t) as shown in Fig. 6. However, $^2\Delta$ are not apparently correlated with $^1\Delta$.

As shown in Fig. 6, the almost constant difference between the two parallel correlated lines can be considered to be a part of $^2\Delta$ which is independent of the substituent. Therefore, $^2\Delta$ will be separated into two. One component is dependent on the substitutent and the other is independent of the substituent. The difference

Table 6. Calculated Electron Charges Δq_t (Δq_σ) of Pyridines[a]

Substituent	C_3	C_5
—	−0.124	−0.124
	(−0.081	−0.081)
3-Me	−0.162	−0.128
	(−0.102	−0.081)
3-NH_2	−0.019	−0.098
	(0.003	−0.077)
3-OH	0.047	−0.084
	(0.050	−0.071)
3-Cl	−0.071	−0.122
	(0.033	−0.081)
3,5-Me_2	−0.166	−0.166
	(−0.103	−0.103)

a) Calculated by the MNDO MO method.

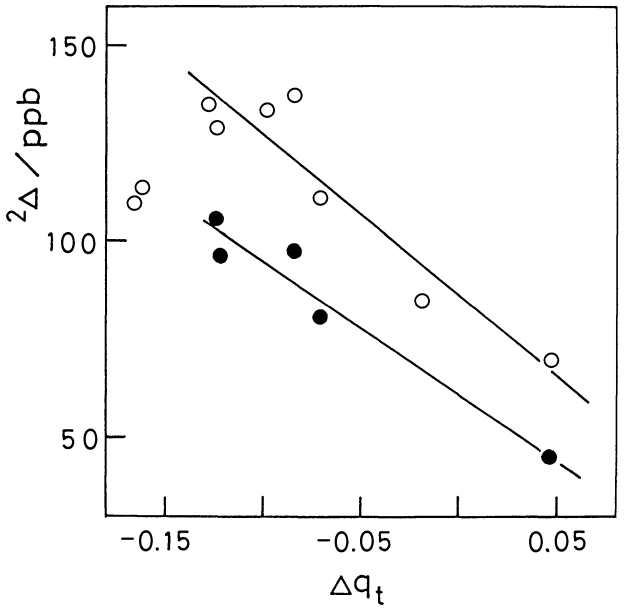

Fig. 6. Correlations between $^2\Delta$ and Δq_t. The white circles are for the 2-D or 6-D isotopomers. The black filled circles are for the 4-D isotopomers. The two correlated straight lines are expressed as $^2\Delta$=−405 Δq_t+87 and $^2\Delta$=−339 Δq_t+61, respectively, except for two points for 2-methyl- (and 3,5-dimethylpyridines.

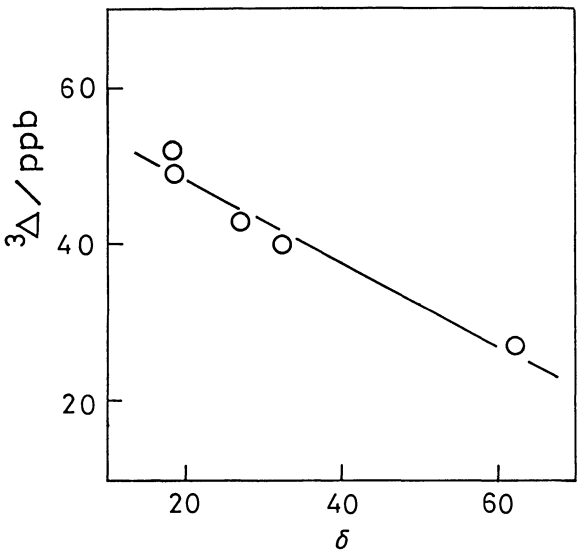

Fig. 7. Correlation between $^3\Delta$ (ordinate in ppb) on the alkyl side-chain carbons and δ_c (abscissa in ppm) for 3-substituted pyridines with r=0.980 and the standard deviation of 2.2 ppb.

mentioned before reflects the latter component. Therefore, $^2\Delta$ from 2-D or 6-D is always larger than that from 4-D for carbons in the isotopomers. In a sense, $^1\Delta$ of the D-labelled carbon will be transmitted to the adjacent $^2\Delta$-observed carbon. Then, $^2\Delta$ would be expected to reflect $^1\Delta$. This shows that $^1\Delta$ induced by 2-D or 6-D are always larger than $^1\Delta$ induced by 4-D for carbons in the isotopomers. These appear exactly in Table 1. However, $^2\Delta$ are strongly dependent upon the electron densities in the observed carbons.

It is considered that the magnitude of electron release effect from D-labelled carbon is controlled by the electron densities on the $^2\Delta$-observed carbon. A comparison of the data between the pyridine-4-*d* and the 4-(methyl-d_3)pyridine[10] (Scheme 2) is also of interest in that two compounds with very large $^1\Delta$ and small $^1\Delta$ give almost similar $^2\Delta$. The transmitting route of the former case is C(sp^2)–C(sp^2); the latter one is C(sp^3)–C(sp^2). Thus, for $^2\Delta$, the transmitting route of the shielding change of the D-labelled carbon may play an important role. For $^2\Delta$ in the present system, however, all routes are similar in C(sp^2)–C(sp^2). Therefore, $^2\Delta$ will be mainly dominated by the electron densities in the $^2\Delta$-observed carbon.

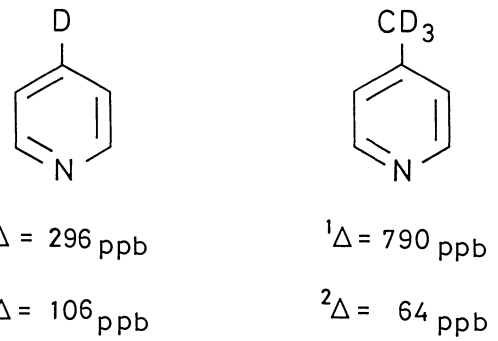

Scheme 2.

$^3\Delta$ vs. δ_c. $^3\Delta$ on the ring carbons could not be observed. They can therefore be considered to be negligibly small. In contrast, $^3\Delta$ on the alkyl side-chain carbons could be observed, as shown in Table 3. Plots of $^3\Delta$ on the alkyl side-chain carbons and δ_c of the observed carbons give a linear correlation, such as in the cases of $^2\Delta$, as shown in Fig. 7. Since the least-square line has a negative slope, we can propose that $^3\Delta$ originates from the transmitted shielding change of the β-carbon ($^2\Delta$-observed carbon). That is to say, $^3\Delta$ is generated by an electron-release effect from the β-carbon. This mechanism is similar to that of $^2\Delta$.

Conclusion

$^1\Delta$ observed on the pyridine ring carbons are dependent upon the π-electron density changes originating from the substituents on the observed carbons. $^2\Delta$ arise as a result of transmitted shielding changes of the α-carbons. The transmitted shielding changes are controlled by the electron density changes in the observed carbons. $^3\Delta$ is generated by a mechanism similar to that for $^2\Delta$.

References

1) A. Bernheim, *Prog. Nucl. Magn. Reson. Spectrosc.*, **3**, 63 (1963).

2) a) P. E. Hansen, *Annu. Rep. NMR Spectrosc.*, **15**, 105 (1983). b) D. A. Forsyth, "Isotopes in Organic Chemistry," ed by E. Buncell and C. C. Lee, Elsevier, New York (1984), Vol. 6, Chap. 1. c) C. J. Jameson and H. J. Osten, *Annu. Rep. NMR Spectrosc.*, **17**, 1 (1985). d) S. Berger, "Isotope Effects in NMR Spectroscopy," ed by H. Günther, Springer, Berlin (1990), Vol. 22, p. 1.

3) E. Breitmaier, G. Jung, W. Voelter, and L. Pohl, *Tetrahedron*, **29**, 2485 (1973).

4) Y. Nakashima, H. Nakane, S. Ban, and K. Takahashi, *Bull. Chem. Soc. Jpn.*, **63**, 2025 (1990).

5) H. L. Retcofsky and R. A. Friedel, *J. Phys. Chem.* **72**, 290 (1968).

6) G. Miyajima, K. Takahashi, and H. Sugiyama, *Org. Magn. Reson.*, **6**, 181 (1974).

7) Y. Nakashima, A. Yoshino, and K. Takahashi, *Bull. Chem. Soc. Jpn.*, **62**, 1401 (1989).

8) S. Berger and B. W. K. Diehl, *Tetrahedron Lett.*, **28**, 1243 (1987).

9) H. Spiesecke and W. G. Schneider, *Tetrahedron Lett.*, **468** (1961).

10) 4-(Methyl-d_3)pyridine was prepared from 4-methylpyridine by repeating H/D exchange reactions. $^1\Delta$ were measured in the neat solutions. $^2\Delta$ were measured in methanol-*d* solutions. Experimental errors for $^1\Delta$ and $^2\Delta$ are estimated to be within 3 ppb and 8 ppb, respectively.

11) Y. Nakashima and K. Takahashi, *Bull. Chem. Soc. Jpn.*, **64**, 3168 (1991).

12) Y. Nakashima, H. Kanada, M. Fukunaga, and K. Takahashi, under preparation.

13) R. J. Cushley, D. Naugler, and C. Ortiz, *Can. J. Chem.*, **53**, 3419 (1975).

On the Splittings of J-Aggregate Band in Pseudoisocyanine

Hirotoshi Ito,* Masaru Agatsuma, and Y. J. I'Haya
Department of Applied Physics and Chemistry, The University of Electro-Communications, 1-5-1, Chofugaoka, Chofu, Tokyo 182
(Received June 3, 1991)

The observation of J-band splittings in the Fano–DeVoe type calculations of pseudoisocyanine aggregates is reported. Based upon the monoclinic structure of pseudoisocyanine iodide crystal, we build four models which respectively assume the lattice constants of the crystal structure. The one-dimensional (1D-) single polymer model is selected along a particular direction from the crystal structure. As we diminish the lattice constants uniformly, the 1D-single-polymer model comes to reproduce single J-bands, while two kinds of 2D-two-inter-polymer interaction models resolve the single J-bands into doublet through multiplet structures for the corresponding parameters. The 3D-four-inter-polymer interaction model brings about doubly split J-bands, but the shortening of the parameters resolves the doublet J-bands into quartet through multiplet structures. However, a single J-band is obtained by the assumption of an orthorhombic 3D-four-inter-polymer model which has the same parameters as those of the monoclinic iodide crystal except for the angle. The shapes calculated are found to be extremely sensitive to the geometrical values as well as the monomer spectroscopic parameters. The cause of the J-band splittings is ascribable to the excitonic interactions between at least two column polymers.

Aqueous solutions of pseudoisocyanine dyes (1,1′-diethyl-2,2′-cyanine, PIC dyes) at high concentrations show extraordinarily narrow, intense *single* bands.[1,2] Similar kinds of bands observed in various cyanine dye aggregates are called J-bands after the discover Jelley,[1] and such aggregates are called J-aggregates or sometimes Scheibe-aggregates. Cooper[3,4] first observed that in a transparent ethylene glycol–water (EGW) matrix at 77 K, such a single J-band of PIC bromide is split into two extremely sharp bands of almost equal intensity separated by 151 cm^{-1}. Also in EGW solution at 77 K, a weak doublet structure of the J-band of PIC iodide was found by Tanaka et al.[5] as a shoulder at shorter wavelength side of the main peak. Perhaps due to the excess amount of iodide ions,[5] Marchetti et al.[6] did not observe the split J-band of PIC iodide in the same EGW solution with 0.1 M KI at 77 K (1 M=1 mol dm^{-3}). Furthermore, Yu et al.[8] observed that the intensities of split J-spectra of PIC bromide in EGW solution become stronger gradually as temperature is reduced below 210 K down to 80 K. It has recently been reported that the relative intensity of split J-bands of PIC bromide changes with the cooling procedure of the glassy solution.[9,10] However also in Ref. 10, Murata has found that the peak appeared at shorter wavelength side of the single J-band of PIC iodide is always weaker than the peak appeared at longer wavelength side, as was reported before.[5] These phenomena lends qualitative supports for the present assumption that J-aggregate models in solutions are similar to the structures of microcrystals of PIC halides.

Any theoretical work has not been done to elucidate the cause of J-band splittings. Cooper[3,4] suggested that the split J-transitions are assigned to two energy levels respectively for the mixed J_1 and J_2 aggregates consisting two different configurations of PIC dye to the axis of PIC polymer chosen in a particular direction. However, he also referred to the excitonic nature of the split J-band, and from Refs. 3 and 4, we cannot deny in a broad meaning such a scheme that the coupling between at least two linear (1D-) J-aggregates of different geometrical orientations gives rise to Davydov splitting.

Our calculations to elucidate this are based upon the Fano–DeVoe theory and its versions,[11–16] which have provided an excellent tool for predicting bandshapes of various polymer systems. First, Briggs and Herzenberg[13,14] beautifully predicted the *single* J-bandshape for the most simplified PIC aggregate model in terms of their coherent exciton scattering theory equivalent to the Fano–DeVoe one. Also, Sumi[15] carried out a coherent potential approximation (CPA) calculation, which gives a single J-like band. Later on, to a rather real model than before, Knapp et al.[16] have applied a simplified version of the CPA theory.[15] They have been able to reproduce a single J-band for the cyclic 1D-aggregate model consisting of 11 PIC molecules by making use of model parameters determined for the PIC monomer and dimer spectra.[17] This treatment is based upon the assumption that the structure of dimer is almost similar to those of dimer units in the longer as well as wider spread J-aggregates. Scherer and Fischer[18] have also followed this treatment for the linear J-aggregates. Thus in their calculations, equi-magnitudes of inter-(sub)molecular interactions have been taken into account as geometrical factors. However, the interaction potentials of J-aggregates are supposed to be not only of short-range forces, but also of long-range forces. Tanaka et al.[5] suggested that such interactions have highly direction dependences for specific neighboring PIC molecules, that is, such interactions are highly anisotropic. Therefore first of all, for a better understanding of J-bands, it is important and necessary to take into account the *explicit geometries* of models which are derived from the crystal structure of the PIC molecule,[29] so that we can involve all the possible

inter(sub)molecular interactions.

Polymer Polarizability Tensor

The *extended* Fano–DeVoe model Hamiltonian of the polymer (N-mer) is assumed to be[19]

$$H=\sum_{f}^{\text{levels}}\sum_{m}^{N}\sum_{g}^{\text{levels}}\sum_{n}^{N}|\psi_m^f\prod_{k\neq m}^{N}\psi_k^0\rangle\langle\psi_m^f\prod_{k\neq m}^{N}\psi_k^0|\,\mathcal{H}|\psi_n^g\prod_{k\neq n}^{N}\psi_k^0\rangle\langle\psi_n^g\prod_{k\neq n}^{N}\psi_k^0|$$

$$-\langle\prod_{k=1}^{N}\psi_k^0|\,\mathcal{H}|\prod_{k=1}^{N}\psi_k^0\rangle\equiv\sum_{f,g}^{\text{levels}}\sum_{m,n}^{\text{sites}}|fm\rangle\langle fm|\,\mathcal{H}|gn\rangle\langle gn|$$

$$-\langle 0|\,\mathcal{H}|\,0\rangle$$

$$=\sum_{f\neq 0}^{\text{level}}\sum_{m}^{\text{sites}}E_{fm,0}|fm\rangle\langle fm|+\sum_{f,g\neq 0}^{\text{levels}}\sum_{m,n}^{\text{sites}}|fm\rangle\langle fm|\mathcal{V}_{mn}|gn\rangle\langle gn|$$

$$\equiv H_0+V, \tag{1}$$

with

$$\mathcal{H}=\sum_{m=0}^{\text{sites}}\mathcal{H}_{\text{m}}^{0}+\sum_{m>n}^{\text{sites}}\sum^{\text{sites}}\mathcal{V}_{mn},\qquad(\mathcal{V}_{mn}\approx\boldsymbol{\mu}_m\cdot\boldsymbol{U}_{mn}\cdot\boldsymbol{\mu}_n) \tag{2}$$

and with the unit dipole–dipole interaction tensor

$$\boldsymbol{U}_{mn}=\frac{1}{|\boldsymbol{R}_{mn}|^5}\{|\boldsymbol{R}_{mn}|^2\mathbb{1}-3\,\boldsymbol{R}_{mn}\boldsymbol{R}_{mn}\},\qquad\boldsymbol{R}_{mn}=\boldsymbol{R}_n-\boldsymbol{R}_m. \tag{3}$$

In the present calculations however, the lowest excited level only is taken in account for simplicity, so that we put actually $f=g$ in the second term of Eq. 1. Note that for the *original* Fano–DeVoe approximation, we must drop the electrostatic term $\langle fm|V|gm\rangle$ involved in Eq. 1. In Eqs. 1 and 2, $\mathcal{H}_m^0$ is the electronic Hamiltonian for the mth submolecule, $\mathcal{V}_{mn}$ the inter(sub)molecular interaction operator, and $\boldsymbol{\mu}_m$ the mth electric dipole moment operator. The eigen-functions ψ_m^0 *and* ψ_m^f for the monomer Hamiltonian $\mathcal{H}_m^0$, respectively, denote the *ground* and the fth *locally excited* states associated with the eigen-values E_0^m and E_f^m, their difference being put to be $E_{fm,0}$. For simplicity, we do not consider the electrostatic shift of $E_{fm,0}$ due to neighboring PIC cations and their counter anions, although we can theoretically make an allowance for such effects, for instance on the basis of Refs. 17—19 and Ref. 24. In Eq. 3, we assume the validity of the dipole–dipole approximation, since it was shown by Tanaka et al.[5] that the distances of neighboring molecules in PIC crystals are larger than the overlapping size of pi-electron clouds from the calculations of overlap integrals.

For the *crude* and *true* Green's operators G_o(E) and $G(E)$ defined by Eq. 1, we have the sum of the mth monomer polarizability tensor $\boldsymbol{\alpha}_{mm}(E)$

$$-\langle 0|\boldsymbol{\mu}G_o(E)\boldsymbol{\mu}|0\rangle=-\langle|\boldsymbol{\mu}(E-H_o+i\eta)^{-1}\boldsymbol{\mu}|0\rangle$$

$$=-\sum_{m}^{N}\sum_{f\neq 0}^{\text{levels}}\frac{\boldsymbol{\mu}_{0f}^{(m)}\boldsymbol{\mu}_{f0}^{(m)}}{E-E_{fm,0}+i\eta_{fm}}\equiv\sum_{m}^{N}\boldsymbol{\alpha}_{mm}(E), \tag{4}$$

where the matrix element of the total electric dipole operator is given by

$$\boldsymbol{\mu}_{0f}^{(m)}=\langle 0|\boldsymbol{\mu}|fm\rangle\equiv\langle 0|\sum_{m}^{N}\boldsymbol{\mu}_m|fm\rangle$$

$$=\langle 0|\sum_{m}^{N}\{\sum_{i\in m}^{\text{elec}}e\boldsymbol{r}_{mi}-\sum_{J\in m}^{\text{nuc}}eZ_J\boldsymbol{r}_{mJ}\}|fm\rangle,\qquad(\boldsymbol{r}_{mi}=\boldsymbol{r}_i-\boldsymbol{r}_m) \tag{5}$$

The m,n-element of the polymer polarizability tensor ${}^p\boldsymbol{\alpha}_{mn}(E)$ is then reduced to

$$-\langle 0|\boldsymbol{\mu}G(E)\boldsymbol{\mu}|0\rangle=-\langle 0|\boldsymbol{\mu}(E-H+i\eta)^{-1}\boldsymbol{\mu}|0\rangle$$

$$=-\langle 0|\boldsymbol{\mu}\{G_o(E)+G_o(E)VG_o(E)+\cdots\}\boldsymbol{\mu}|0\rangle$$

$$\equiv\sum_{m=1}^{N}\sum_{n=1}^{N}{}^p\boldsymbol{\alpha}_{mn}(E) \tag{6}$$

Inserting the resolution of identities ($\sum\sum|fm\rangle\langle fm|=1$) with use of the relationships such as $\langle fm|\mathcal{V}_{mn}|gn\rangle\approx\boldsymbol{\mu}_{f0}^{(m)}\cdot\boldsymbol{U}_{mn}\cdot\boldsymbol{\mu}_{0g}^{(n)}$, we can derive

$${}^p\boldsymbol{\alpha}_{mn}(E)=\{\mathbb{1}+\mathfrak{A}(E)\cdot\mathbb{U}\}_{mn}^{-1}\cdot\boldsymbol{\alpha}_{nn}(E),\qquad m,n=1,2....,N \tag{7}$$

where the suffices m,n of $\mathbb{1}$, $\mathfrak{A}(E)$, and $\mathbb{U}$ denote the elements of the corresponding $3N\times3N$ matrices.

Vibronic Description of Monomer Polarizability Tensor

The purely electronic scheme in the previous section can be extended to the vibronic problem. In the adiabatic approximation, the ground and fth excited states of the mth monomer appearing in Eq. 1 are replaced by the products:

$$\psi_m^f\rightarrow\psi_m^f(\boldsymbol{r},\boldsymbol{Q})\chi_m^{f,v}(\boldsymbol{Q})=\psi_m^f(\boldsymbol{r},\boldsymbol{Q})\prod_{k}^{3N-6}X_m^{f,v_k}(\boldsymbol{Q}_k),\qquad(f=0,f) \tag{8}$$

where the $\boldsymbol{r},\boldsymbol{Q}$ represent collective coordinates for electrons and nuclei. $\chi_m^{f,v}$ represents the total vibrational eigenstate associated with the eigenvalue $E_{f,v}^{m,\text{vib}}$, where v denotes a set of vibrational quantum numbers, i.e., $v\equiv(v_1,v_2,v_3,\cdots v_k\cdots v_{3N-6})$ for the $3N-6$ harmonic-oscillator wavefunctions. In the adiabatic approximation, the mth monomer Hamiltonian for the fixed nuclei is expressed by

$$H_m^0=\sum_{f=f,0}^{\text{levels}}E_f^m(\boldsymbol{Q})|\psi_m^f(\boldsymbol{r},\boldsymbol{Q})\rangle\langle\psi_m^f(\boldsymbol{r},\boldsymbol{Q})|.\qquad(\text{in }H^0=\sum_{m}^{\text{sites}}H_m^0) \tag{9}$$

Now, $E_f^m(\boldsymbol{Q})$ becomes the effective adiabatic potential for the nuclear motion. The nonadiabatic (NA) Hamiltonian of the mth monomer is then represented by

$$H_m^0\rightarrow H_m^0=\sum_{f=f,0}\sum_{v}(E_f^m+E_{f,v}^{m,\text{vib}})|\psi_m^f\rangle|\chi_m^{f,v}\rangle\langle\chi_m^{f,v}|\langle\psi_m^f|$$

$$+\sum_{f\neq g}\sum\sum_{v}\sum_{v'}\sum_{k}^{\text{vib. mode}}|\psi_m^f\rangle|\chi_m^{f,v}\rangle\mathcal{V}_{m,\text{NA}}^{(\text{f,k,g})}\langle\chi_m^{g,v'}|\langle\psi_m^g|, \tag{10}$$

where the off-diagonal term is the *intra*(sub)molecular vibronic coupling (NA) operator.[22] However, to simplify the problem, we do not take such a coupling operator into account. After all, modification of Eq. 1 in terms of Eq. 8 needs the replacement of $E_{fm,0}$ with $E_{\text{fm},0}^{(v)}$ that denotes the vth vibrational state on the fth electronic excited state of an mth monomer. Namely, a vibronically excited level relative to the zero-temperature ground state, leaving the other vibrational

states in the ground state, is written down

$$E_{fm,0} \rightarrow E^{(v)}_{fm,0} = E_{fm,0} + [E_{fm,v} - E_{0m,0}] \equiv E_{fm,0} + E_{fm,0;v0}$$
$$= E_{fm,0} + vE_{fm,0;10} = hc\tilde{\nu}^{(v)}_{fm,0} = h\nu(\tilde{\nu}_{fm,0} + v\,\tilde{\nu}_{fm,0;10}), \quad (11)$$

where $E_{fm,0;10}$ becomes a fundamental vibrational energy on the fth electronic level. The purely electronic transition moment $\boldsymbol{\mu}^{(m)}_{0f}$ is also replaced with the vibronic moment multiplied by the Franck–Condon overlap integral, so that the inter(sub)molecular interaction becomes

$$\langle fm|\boldsymbol{\mathcal{V}}_{mn}|gn\rangle \approx \boldsymbol{\mu}^{(m)}_{f0} \cdot \boldsymbol{U}_{mn} \cdot \boldsymbol{\mu}^{(n)}_{0g}$$
$$\rightarrow \boldsymbol{\mu}^{(m)}_{0f} \langle \chi^{0,0}_m | \chi^{f,v}_m \rangle \cdot \boldsymbol{U}_{mn} \cdot \boldsymbol{\mu}^{(n)}_{0g} \langle \chi^{0,0}_n | \chi^{g,v}_n \rangle. \quad (12)$$

The imaginary part of the usual type of monomer polarizability tensor(in units of cm^3) is given by

$$\mathrm{Im}\ \boldsymbol{\alpha}_{nn}(\tilde{\nu}) = \sum_{g\neq 0} \sum_{v} \frac{+e^2}{hc} \{\boldsymbol{\mu}^{(n)}_{0g}/e\}\{\boldsymbol{\mu}^{(n)}_{g0}/e\} \times$$
$$|\langle \chi^{0,0}_n | \chi^{g,v}_n \rangle|^2 \pi\delta[\tilde{\nu} - \tilde{\nu}^{(v)}_{gn,0}], \quad (e^2/hc = 1.16138 \times 10^{-3}), \quad (13)$$

which corresponds to the treatment made by Hemenger.[23] Actually, the lowest excited sate alone is taken into account for the gth states in Eq. 13, so that we put $f=g$ in Eq. 12.

The δ function in Fq. 13 are usually approximated by both the *Gaussian* and *Lorentzian* type functions. By many investigators,[13,14,16,20] it has been revealed that use of Gaussian type monomer functions can predict J-bands, whichever monomer function we may choose of vibronic and purely electronic polarizabilities. However, Lorentzian type functions were found to require the *vibronic* type monomer polarizability in order to reproduce J-bands.[20,21] We also replace Eq. 13 by the Gaussian function as follows:

$$\mathrm{Im}\ \boldsymbol{\alpha}_{nn}(\tilde{\nu}) = \sum_{g\neq 0} \sum_{v} \frac{+e^2}{hc} \{\boldsymbol{\mu}^{(n)}_{0g}/e\}\{\boldsymbol{\mu}^{(n)}_{g0}/e\} |\langle \chi^{0,0}_n | \chi^{g,v}_n \rangle|^2 \times$$
$$\left(\frac{\sqrt{\pi}}{\tilde{\Delta}^{(v)}_{gn}}\right) \exp\left\{-\left(\frac{\tilde{\nu} - \tilde{\nu}^{(v)}_{gn,0}}{\tilde{\Delta}^{(v)}_{gn}}\right)^2\right\} \equiv \sum_{g\neq 0} \sum_{v} \mathrm{F}[(\tilde{\nu} - \tilde{\nu}^{(v)}_{gn,0})/\tilde{\Delta}^{(v)}_{gn}], \quad (14)$$

where the bandwidth (FWHM in cm^{-1}) has a relationship such as $\tilde{\Gamma}^{(v)}_{gn} = 2\sqrt{\ln 2}\,\tilde{\Delta}^{(v)}_{gn}$ for the normalized Gaussian, and $\tilde{\Delta}^{(v)}_{gn}$ is the half-width at $1/e$ of the peak. Then, we determine the magnitude of $\tilde{\Gamma}^{(v)}_{gn}$ related with $\tilde{\Delta}^{(v)}_{gn}$ so as to adjust $\tilde{\Gamma}^{(v)}_{gn}$ to the observed monomer bandshape, i.e., so as to satisfy the following relationship,[24]

$$f_{gn} = 4.59663 \times 10^{-9} \sum_{v}^{\mathrm{M}} \varepsilon(\tilde{\nu}^{(v)}_{gn,0})\,\tilde{\Gamma}^{(v)}_{gn}, \quad (15)$$

where we assume the *same* bandwidth for each vibrational peak. Thus using the observed oscillator strength[6] and the corresponding molar extinction coefficient[30] in Eq. 15, the FWHM for the vth vibrational level on the gth (=lowest) electronic level is calculated to be $\tilde{\Gamma}^{(v)}_{gn} = 1119.7$ cm^{-1}. In Eq. 11, the values $\tilde{\nu}_{gn,0} = 1915$ cm^{-1} and $\tilde{\nu}^{(v)}_{gn,0;10} = 1368$ cm^{-1} are chosen for the *three* vibrational levels (v=0,1,2) on the gth electronic level from Ref. 17. For the Franck–Condon factor, we assume Poisson's distribution,[14,17]

$$|\langle \chi^{0,0}_n | \chi^{g,v}_n \rangle|^2 = \exp(-a^2/2)\frac{(a^2/2)^v}{v!}, \quad (a=1.2) \quad (16)$$

where an adjustable parameter a=1.2 well reproduces the monomer bandshape.

The Kronig–Kramers transform of Eq. 14 gives rise to its real part:[26]

$$\mathrm{Re}\ \boldsymbol{\alpha}_{nn}(\tilde{\nu}) \sum_{g\neq 0} \sum_{v} \frac{P}{\pi} \int_{-\infty}^{\infty} \mathrm{d}X \frac{F(X)}{X - (\tilde{\nu} - \tilde{\nu}^{(v)}_{gn,0})/\tilde{\Delta}^{(v)}_{gn}}$$
$$= \sum_{g\neq 0} \sum_{v} \frac{P}{\pi} \int_{-\infty}^{\infty} \mathrm{d}X \frac{\mathrm{Im}\ \boldsymbol{\alpha}_{nn}(\tilde{\nu})}{X - (\tilde{\nu} - \tilde{\nu}^{(v)}_{gn,0})/\tilde{\Delta}^{(v)}_{gn}}$$
$$= \sum_{g\neq 0} \sum_{v} \frac{+e^2}{hc} \{\boldsymbol{\mu}^{(n)}_{0g}/e\}\{\boldsymbol{\mu}^{(n)}_{g0}/e\} |\langle \chi^{0,0}_n | \chi^{g,v}_n \rangle|^2$$
$$\times \left(\frac{2}{\sqrt{\pi}}\right)\left(\frac{\sqrt{\pi}}{\tilde{\Delta}^{(v)}_{gn}}\right) \exp\{-[(\tilde{\nu} - \tilde{\nu}^{(v)}_{gn,0})/\tilde{\Delta}^{(v)}_{gn}]^2\}$$
$$\times \int_0^{(\tilde{\nu}^{(v)}_{gn,0} - \tilde{\nu})/\tilde{\Delta}^{(v)}_{gn}} \exp(X^2)\mathrm{d}X, \quad (17)$$

which we have numerically calculated. We must report that instead of Eq. 17, use of the simple formula of asymptotic function[24,26] derived from Eq. 17 has not reproduced the J-band.

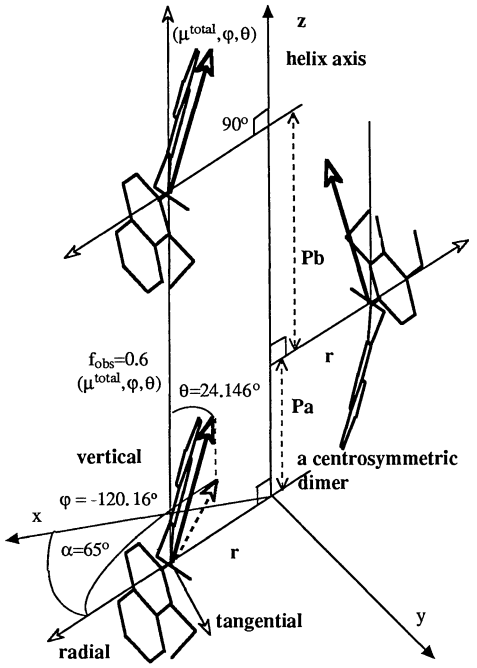

Fig. 1. Schematic illustrations of a quasi 1D-J-aggregate model of PIC which consists of centrosymmetric dimer pairs of PIC's, whose structure is the same as the columns shown on the bottom of Fig. 2. The definitions of the parameter *Pa*, *Pb*, α, r, μ, φ, and θ are given. The direction of the transition moment μ is defined by the angle φ and θ which have been calculated by the CNDO/S method in the Cartesian coordinates used here. We use α=−65.24°, θ=−120.16°, φ=24.16°.

Polymer Bandshape Function J-Aggregate Models

The molar extinction coefficient of the electronic absorption of a polymer system per monomer unit is calculated by

$$^{p}\varepsilon(\tilde{\nu}) = (8\pi^2 N_A/2301.6)\tilde{\nu}\frac{1}{N}\sum_{m}^{N}\sum_{n}^{N}\mathrm{Im}\left[\frac{1}{3}\mathrm{Tr}\,{}^{p}\boldsymbol{\alpha}_{mn}(\tilde{\nu})\right], \quad (1\ \mathrm{mol}^{-1}\,\mathrm{cm}^{-1}). \quad (18)$$

In Fig. 1, we give schematic illustrations of 1D-J-aggregate model with defintion of parameters. The model consists of a helical array of the transition moments $\boldsymbol{\mu}_{g0}^{(n)}$ of propeller-like molecule PIC. As mentioned before, the magnitudes of $|\boldsymbol{\mu}_{g0}^{(n)}|$, $\tilde{T}_{gn}^{(\nu)}$ and $\tilde{A}_{gn}^{(\nu)}$ are estimated from the observed oscillator strength f_{gn}=0.6[6] and its molar extinction coefficient.[30] However, we have no knowledge about the direction of the transition moment. So on the bottom in Fig. 1, we have shown the results of CI calculation of the direction (φ=24.146° and θ=−120.16°) of the total transition moment $\boldsymbol{\mu}_{g0}^{(n)}$ of the lowest electronic excited level for the Cartesian coordinate system given here. Clearly, the transition has the $\pi\pi^*$-character. The 40×40 singly excited CI calculation, whose configurations are chosen from the 8 higher occupied MO's involving HOMO and the 5 low-lying vacant MO's involving LUMO, has been carried out by the CNDO/S method[31] using the geometry of PIC chloride.[27] Also, other X-ray data of PIC halides gave almost similar results. The values of $\tilde{\nu}_{gn,0}$ and f_{gn} for the lowest level are respectively calculated to be 19544 cm^{-1} and 1.07, which are compared with the observed values 19150 cm^{-1} and 0.6. Similarities of J-aggregate models in solutions to the microcrystals of PIC halides were discussed by several authors.[6,29,30] In Fig. 2, we depict a rather simplified 3D-column model picked out along the[101]-direction from the crystal structure of PIC iodide reported by Nakatsu et al.[29] They indicated that the crystal structure is similar to the stair case orientation of dyes of the slipped-deck-of-card type[33] and also to the A1 of the brickstone model.[30] In Fig. 2, each column consists of quasi-1D-sequences of centrosymmetric dimer pairs, so that each column (A,B,A′,B′) constitutes the 1D-polymer model (*1D-J-aggregate*) for which we here assume 10-mer. *Two*-column interactions between A and A′ and/or between B and B′ define the 2D-polymer model (*2D-J1-aggregate*), while *two*-column interactions between A and B and/or between A′ and B constitute the 2D-polymer model (*2D-J2-aggregate*) which is slightly different from the 2D-J1-aggregate model. Here, we do not consider 2D-polymer models such as (A,B′) as well as (A′,B) models. The 3D-polymer model (*3D-J-aggregate*) is defined from *four*-column interactions among A,B,A′, and B′.

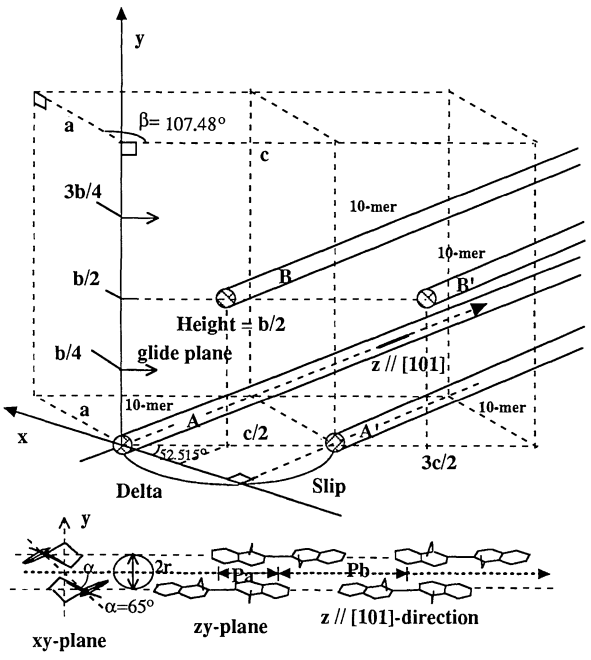

Fig. 2. The 3D-continuation of columns consisting of quasi-1D sequence of centrosymmetric dimer pairs,[29] which are produced by the operations of the *c* glide planes and specified with three parameters such as Delta, Slip, and Height. Each column contains the polymer of PIC's as shown on the bottom. As mentioned in the text, we can defined *four* J-aggregate models such as 1D-J-aggregate, 2D-J1-aggregate, 2D-J2-aggregate, and 3D-J-aggregate.

Results and Discussion

In the calculations, we plot the absorptions of PIC aggregates in the ordinate against the wavelengths with the increment 0.5 nm in the abscissa. In Eq. 18, the summation over large number N is expected to give sufficiently good convergence of bandshapes for any model, but for the 1D-J-aggregate model, all the inter-(sub)molecular interactions between 10-mer give a good convergence. It becomes another reasonable criterion for justifying the 10-mer unit model the fact that the aggregate size of our 10-mer falls into the range within such a molecular size (the values 120 Å $\leqslant$length $\leqslant$500 Å) estimated by Kuhn's energy transfer model of a 1D J-aggregate,[34] so that the range of interactions to be considered may be sufficient. Consequently, the results obtained by considering sufficient chain length effect may be not so different from the present results. In Eqs. 14 and 17, we only take the lowest level over the index g. We have not introduced an isotropic dielectric constant for Eq. 3, although it has often been introduced. This is simply because the introduction of this parameter leads to totally different features of bandshapes for the PIC aggregates. For instance, when we introduce the isotropic dielectric constant 2.0 which is often used in DNA's systems,[12,24] we need to diminish the mutual distances of PIC molecules inappropriately in more compact forms than in the present J-aggregate models in order for reproducing J-bandshapes.

In order to show the dependence of the aggregate

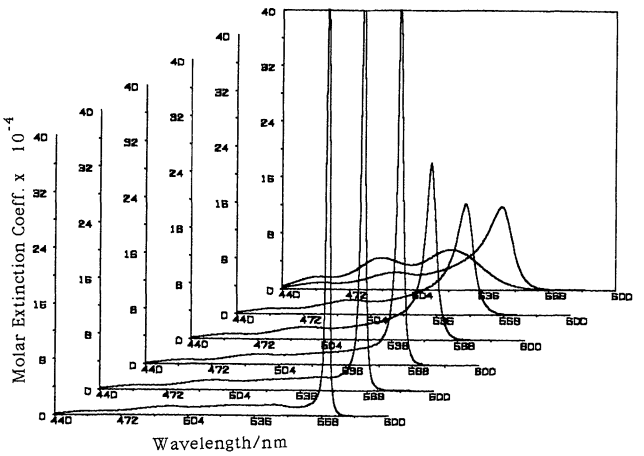

Fig. 3. The absorption spectra for 1D-J-aggregates (*1D-10-mer*). In the L-shaped frames from the left-side to the right-side, each bandshape plotted is calculated by uniformly shortening the parameter (Pa, Pb, Delta, and Slip) of the 1D-J-aggregate crystal model, respectively by the factor 0.6, 0.65, 0.7, 0.8, 0.9, 1.0, but with making the radius r=2.136 Å be constant. In the unscaled model made from Nakatsu's crystal data, we put a=10.787, b=11.626, c=16.484 Å, *Pa*=8.386 Å, *Pb*=1.093 *Pa*, Delta=10.028 Å, Slip=13.080 Å, Height=b/2 in Fig. 2. In the most backward frame, the approximate monomer band is plotted.

models upon their geometries, the bandshapes are plotted in Fig. 3 for the small changes of the 1D-J-aggregate crystal model (*1D-10-mer*). Namely, each band shown is calculated by uniformly shortening the lattice constants a, b, c as well as related parameters (Pa, Pb, Slip, and Delta) of the PIC iodide crystal,[29] respectively by the factor 0.6, 0.65, 0.7, 0.8, 0.9, 1.0, but with making the radius r=2.136 Å be constant. These scalings of geometrical parameters are based merely upon the assumption that the structures of J-aggregates in liquids are given by small modifications of PIC crystal structures. The observed peak position 571 nm of the J-band is reproduced by the scaling factor 0.65, while the unsealed 1D-J-aggregate model does show a sharp J-band.

In the *first four* frames of Fig. 4 from the forward one, each bandshape given is calculated respectively by uniformly scaling down the 2D-J2-aggregate crystal model (*2D-20-mer*) by the factor 0.6, 0.7, 0.8, 0.9, and further in the *last four* frames of Fig. 4, each bandshape is respectively plotted by scaling down the 2D-J1 aggregate crystal model (*2D-20-mer*) by the factor 0.6, 0.7, 0.8, 0.9.

In the first four frames of Fig. 5, we plot bandshapes for the 3D-J-aggregate crystal model (*3D-40-mer*), each of which is calculated respectively by uniformly shorten-

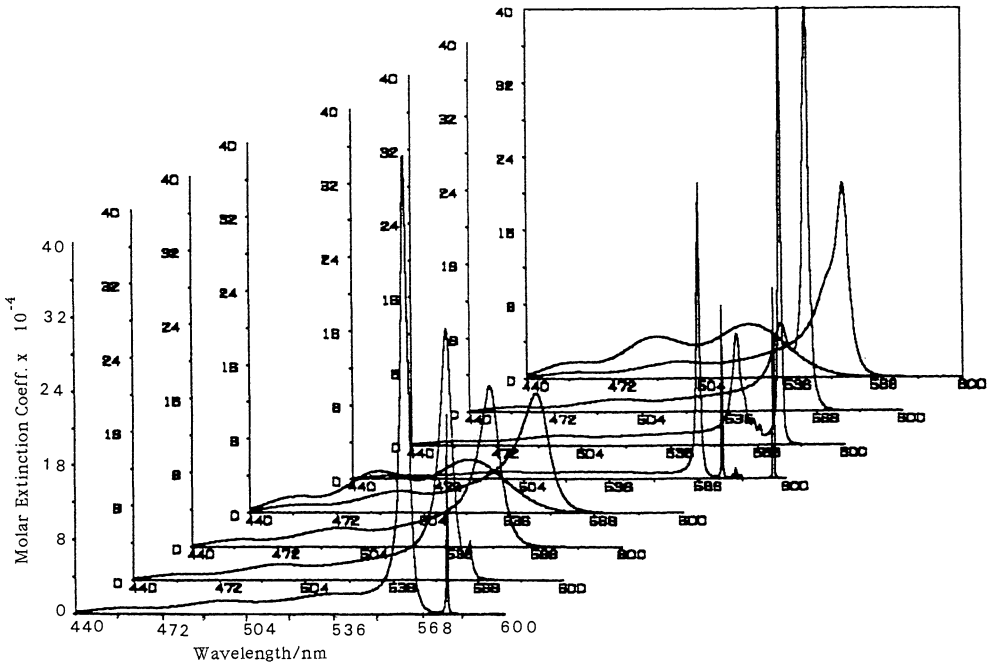

Fig. 4. The absorption spectra for the 2D-J1- and 2D-J2-aggregates. In the L-shaped frames from the left-side to the right-side, each bandshape plotted is calculated by uniformly scaling down the lattice constant (*a, b, c*) as well as the related parameters (*Pa, Pb,* Delta, and Slip) of the 2D-J2-aggregate crystal mode (*2P-20-mer*) respectively by the factor 0.6, 0.7, 0.8, 0.9, and also by uniformly scaling down the 2D-J1-aggregate crystal model (*2D-20-mer*) respectively by the factor 0.6, 0.7, 0.8, 0.9, but with making the radius r=2.136 Å be constant for the both cases. All the parameters used for the unscaled model are the same as those used in Fig. 3.

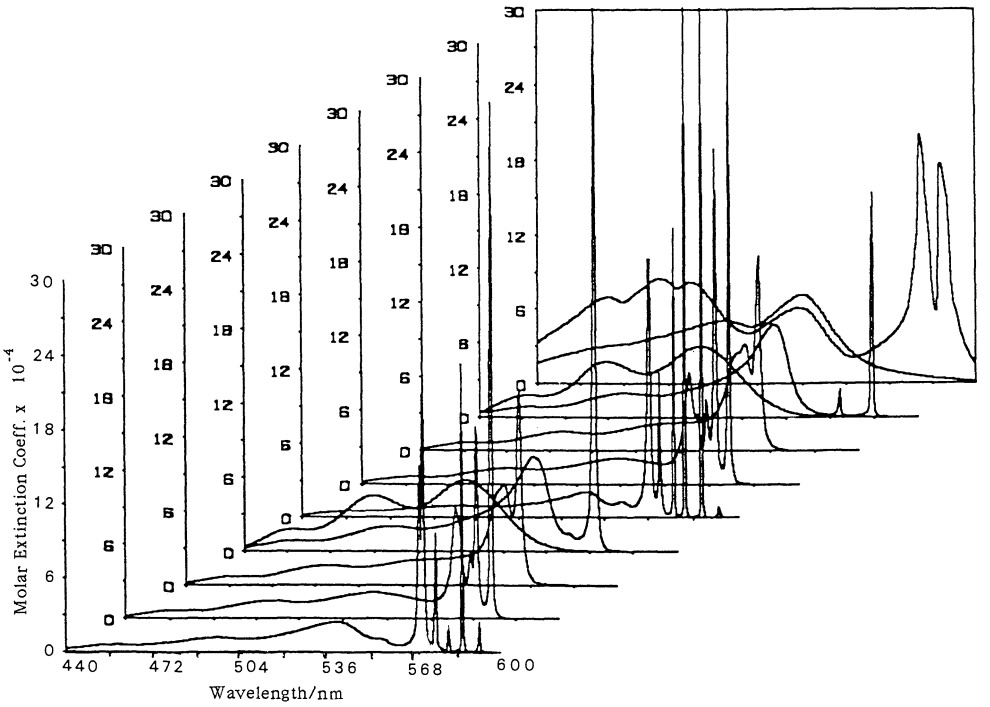

Fig. 5. The absorption spectra for the 3D-J-aggregates. In the *first four* frames, each bandshape shown is calculated by uniformly shortening, respectively by the factor 0.6, 0.7, 0.8, 1.0, the 3D-J-aggregate orthorhombic model (*3D-40-mer*), i.e., β=90° and Delta=Slip=11.656 Å with other parameters being same as those of monoclinic model. In the *last four* frames, each bandshape is calculated respectively by uniformly scaling down, by the factor 0.6, 0.7, 0.8, 1.0, the 3D-J-aggregate monoclinic model [(*3D-40-mer*) with Delta=10.028 Å, Slip=13.080 Å. In the *first* and *eighth* frames, the same monomer bands of PIC molecule are plotted. In the backward frame, the monomer band and the J-split band of the PIC bromide are plotted from Ref. 8.

ing, by the factor 0.6, 0.7, 0.8, 1.0, the crystal model which is modified to be orthorhombic, i.e., β=90° and Delta=Slip=11.656 Å with other parameters being same. However, in the last four frames of Fig. 5, we plot the absorption bandshapes calculated respectively by scaling down the 3D-J-aggregate monoclinic crystal model (*3D-40-mer*) with Delta=10.028 Å, Slip=13.080 Å,[29] that is, by uniformly shortening the crystal structure by the factor 0.6, 0.7, 0.8, 1.0.

As seen in the three Figures, the *split* J-bands are not observed for the 1D-J-aggregate model. In Fig. 4, the 2D-J1- and 2D-J2-models with the shorter lattice constants, respectively, give rise to the *doubly* and/or *multiply* split J-bands. When we look at the most backward frame of Fig. 4, the 2D-J1-model scaled by the factor 0.9 appears to give the bandshape similar to the weak doublet J-band of PIC iodide observed,[5] while in the most forward frame, the 2D-J2-model scaled by the factor 0.6 seems to give the feature of the J-split band observed in the PIC bromide aggregate.[3,4,8] However, the peak positions (563 and 572 nm) of J-split band by the factor 0.6 are insufficient to give a good agreement with the experimental values (571 and 577 nm). These doublet and/or multiplet structures obtained may be assigned to the Davydov splitting of J-band due to the interaction among 1D-J-aggregates, as suggested tacitly by Cooper.[3,4]

On the other hand, the unscaled orthorhombic 3D-J-model gives the single J-band as shown in the fourth frame of Fig. 5, but the orthorhombic model scaled by the factor 0.6 as shown in the most forward frame appears to give the split J-band with main two peaks (570 and 586 nm) separated by 430 cm^{-1}, which is compared with the split J-band of PIC bromide plotted in the most backward frame. However, we must note that the present orthorhombic model scaled by the factor 0.6 is not equal to the orthorhombic crystal model of PIC bromide.[27] It is noticed that as shown in the *eigth* frame of Fig. 5, the *unscaled monoclinic* crystal model PIC iodide is calculated to give the split J-band, i.e., the weak peak at 571 nm and the strong peak at 583 nm with a separation 360 cm^{-1}, which has a feature of J-split aggregate of PIC iodide.[5] It is to be noted that contrary to the unscaled orthorhombic 3D-J-model, the unscaled 1D-J-aggregate model which has the same geometrical parameters those of the crystal does not show a sharp J-band, as mentioned above.

From the monomer and the dimer spectra of PIC

molecule, Kopainsky el al.[17] estimated the essential parameters required also in the present calculations, for an example, the nearest neighbor electronic interaction which Knapp et al.[16] have applied to the bandshape calculations of linear J-aggregates ignoring non-nearest neighbor interactions. Different from Refs. 16 and 17 however, the calculations obtained indicate that the J-aggregate models assumed from the crystal structure do not necessarily have the same structure of essential dimer unit as Knapp et al. have assumed, in each process of aggregation in solution such as monomer→dimer→H-aggregate→J-aggregate.[10,29,30,32] The present calculations have revealed that the bandshapes are extremely sensitive to the geometrical values as well as the monomer spectroscopic parameters used. In case when the polymerization energy shift[16-18] appeared as Stokes shift is tentatively considered by changing $E_{fm,0}$ in Eqs. 1 and 4, the banshapes obtained are found to fall into the range of the present results. So before going a step further to consider the more exact formalism in order for cultivating a better understanding of unusual features of PIC aggregates, it is rather necessary to accumulate the numerical experiences about the geometries of PIC aggregate models, of course by making use of appropriate monomer spectroscopic data of PIC halides, in the belief that the real aggregate model in either solution or glassy solution is quite similar to the crystal structure. We need further studies to get a goal for predicting the whole feature of J-split bands, although the monoclinic 3D-J-four-inter-polymer model of PIC iodide leads to the qualitative feature of the doublet J-band as shown in the the *eighth* frame. For instance, the prediction for the two bands appeared at the shorter wavelength side of the split J-band in the *eighth* frame is failed. However, tentative calculations in the present formulation have been found to give some qualitative features in this region by increasingly piling up the PIC dimers and the columns of PIC's along the *y*-direction (*b*-axis) as shown in Fig. 2. Studies on such models are now in progress.

References

1) E. E. Jelley, *Nature,* **138**, 1009 (1936), *ibid.,* **139**, 631 (1937).
2) G. Scheibe, *Angew. Chem.,* **49**, 563 (1936).
3) W. Cooper, *Chem. Phys. Lett.,* **7**, 73 (1970).
4) W. Cooper, *Photogr. Sci. Eng.,* **17**, 217 (1973).
5) J. Tanaka, M. Tanaka, and M. Hayakawa, *Bull. Chem. Soc. Jpn.,* **53**, 3109 (1980).
6) A. P. Marchetti, C. D. Salzberg, and E. I. P. Walker, *Photogr. Sci. Eng.,* **20**, 107 (1976).
7) A. P. Marchetti, C. D. Salzberg, and E. I. P. Walker, *J. Chem. Phys.,* **64**, 4693 (1976).
8) Z. X. YU, P. Y. Lu, and R. R. Affano, *Chem. Phys.,* **79**, 289 (1983).
9) R. Hirschmann, W. Koler, J. Friedrich, and E. Daltrozzo, *Chem. Phys. Lett.,* **151**, 60 (1988).
10) M. Murata, *J. Soc. Photogr. Sci. Technol. Jpn.,* **52**, 24 (1989).
11) A. Herzenberg and A. Modinos, *Proc. R. Soc.,* **87**, 597 (1966).
12) H. Ito and Y. J. I'Haya, *J. Chem. Phys.,* **77**, 6270 (1982).
13) J. S. Briggs and A. Herzenberg, *Mol. Phys.,* **21**, 865 (1971).
14) J. S. Briggs and A. Herzenberg, *Mol. Phys.,* **23**, 203 (1972).
15) H. Sumi, *J. Phys. Soc. Jpn.,* **38**, 825 (1975).
16) E. W. Knapp, P. O. J. Scherer, and S. F. Fischer, *Chem. Phys. Lett.,* **111**, 481 (1981).
17) B. Kopainsky, J. K. Hallermeier, and W. Kaiser, *Chem. Phys. Lett.,* **83**, 498 (1981).
18) P. O. J. Scherer and S. F. Fischer, *Chem. Phys.,* **86**, 269 (1984).
19) H. Ito and Y. J. I'Haya, *Bull. Chem. Soc. Jpn.,* **60**, 2791 (1987).
20) H. Ito, T. Eri, and Y. J. I'Haya, *Chem. Phys.,* **8**, 68 (1975); *ibid.,* **10**, 49715 (1975).
21) A. V. Lukashin and M. D. Frank-Kamenetskii, *Chem. Phys. Lett.,* **45**, 36 (1977).
22) F. K. Fong, "Radiationless Processes in Molecules and Condensed Phases," Springer-Verlag, Berlin (1976), p. 4.
23) R. P. Hemenger, *J. Chem. Phys.,* **67**, 262 (1977).
24) H. Ito and Y. J. I'Haya, *Chem. Phys. Lett.,* **142**, 25 (1987).
25) A. V. Lukashin and M. D. Frank-Kamenetskii, *Chem. Phys. Lett.,* **45**, 36 (1977).
26) B. J. Caldwell and H. Eyring, "The Theory of Optical Activity," Wiley-Interscience, New York (1971), p. 77.
27) V. B. Dammeier and W. Hoppe, *Acta Crystallogr., Sect. B,* **27**, 2364 (1971).
28) H. Yoshioka and K. Nakatsu, *Chem. Phys. Lett.,* **11**, 255 (1971).
29) K. Nakatsu, H. Yoshioka, and H. Morishita, *Acta Crystallogr., Sect. B,* **33**, 2181 (1977).
30) E. Daltrozzo, G. Scheibe, K. Gschwind, and F. Haimerl, *Photogr. Sci. Eng.,* **18**, 441 (1974).
31) R. L. Ellis, G. Kuehnlenz, and H. H. Jaffe', *Theor. Chim. Acta (Berlin),* **26**, 131 (1972).
32) A. H. Hertz, *Photogr. Sci. Eng.,* **18**, 323 (1974).
33) D. L. Smith, *Photogr. Sci. Eng.,* **18**, 309 (1974).
34) H. Kuhn, *J. Chem. Phys.,* **53**, 101 (1970).

 © 1991 The Chemical Society of Japan Bull. Chem. Soc. Jpn., 64, 3707—3712 (1991)

The Energy Aspect of Oil/Water Partition and Its Application to the Analysis of Quantitative Structure-Activity Relationships. Aliphatic Alcohols in the Liposome/Water Partition System

Hideaki FUJIWARA,* Yong-Zhong DA, Katsuhiko ITO, Tatsuya TAKAGI, and Yukako NISHIOKA
Faculty of Pharmaceutical Sciences, Osaka University, 1-6 Yamada-Oka, Suita, Osaka 565
(Received July 5, 1991)

The energy aspect of oil/water partition has been examined for several solutes in different partition systems by determining the thermodynamic parameters of the partition. The thermodynamic parameters changed systematically, depending on the polarity of the nonaqueous phase of the partition. To further investigate the partition system dependency of the QSAR (quantitative structure-activity relationships) treatments the thermodynamic properties have been determined for various aliphatic alcohols in a liposome/water system; the results are discussed with regard to the previous ones obtained in a 1-octanol/water system, while paying special attention to applicability in the QSAR analysis. The following trends were observed in common with the two partition systems of liposome/water and 1-octanol/water: 1. The enthalpy term (ΔH_p°) can well reproduce the toxicity data for halogenated and nonhalogenated alcohols collectively, whereas the conventional log P (partition coefficient) term can be applied only for the two types of alcohols separately; 2. The entropy term (ΔS_p°) adds a discernible contribution to the refinement of the regression analysis. A distinctive characteristic is also discussed from a statistical method of analysis for the thermodynamic properties obtained in the two partition systems.

Hitherto, oil/water partition coefficients have been studied extensively in relation to the quantitative structure-activity relationships (QSAR) for compounds with biological activity.[1,2] The coefficients reflect the Gibbs free energy change of solutes upon going from a water to an oil medium when the logarithm is taken. Hence, an energy consideration of the partition phenomena will be of great importance in discussing partition phenomena. Most frequently, the partition coefficients have been measured regarding a 1-octanol/water system.[2] It has, however, yet to be debated whether this system can well simulate the partition phenomena which occur in the biophase. Even though studies with a few different partition systems have proved that a linear relation is observed when a partition system is changed from one to another, there exist instances in which such a relation is not followed exactly, or even deviates extremely, for some of the solutes tested. As for the latter cases, dissimilar solute-solvent interactions, such as hydrogen bonding, can be pointed out as a cause. These facts indicate that different partition systems need to be tested before deducing a definite conclusion concerning characteristic aspects of partition for any solute. In a previous paper,[4] the authors attempted to separate the logarithm of the partition coefficient, which corresponds to the Gibbs free energy term, into its components of enthalpy and entropy. The results have disclosed the potential importance of the enthalpy term in the QSAR analysis for alcohol toxicities.

In the present study, different kinds of partition systems are first tested regarding the thermodynamic properties of partition using some typical solutes. The characteristic aspects of partition and its importance in QSAR analyses are then examined for aliphatic alcohols using a liposome/water partition system.

Experimental

Commercially available egg lecithin (Merck) and sodium dodecyl sulfate (Tokyo Kasei Co.) were used without further purification. The lecithin was ascertained to give only a single spot on a silica gel 60 plate in thin-layer chromatography. All other chemicals were distilled in a glass vessel.

Titration calorimetry was performed, following a previous study.[4] Liposome was prepared according to a reversed-phase evaporation method.[5] The concentration of lecithin in the suspension was determined by phosphorus colorimetry.[6] The concentration was typically around 10 mg ml^{-1}.

Determination of Partition Coefficients as Well as Enthalpies and Entropies of Partition. Measurement of partition coefficients was achieved as follows. Each alcohol was first dissolved in water; this aqueous phase was then mixed with a lecithin solution (5 ml) and shaken for 12—18 h in a constant-temperature bath. The bath temperature was regulated within an error of ±0.2 °C. The mixed solution was then separated by ultracentrifuge equipment (Beckman L8-80M). The supernatant aqueous solution was analyzed by gas chromatography using an internal reference, and the alcohol concentration was determined. The initial aqueous phase was also analyzed using the same method. The partition coefficient (K_p) was calculated according to

$$K_p=\left(\frac{A_0-A}{w/d}\right)\Big/\left(\frac{A}{V_s-w/d}\right), \quad (1)$$

where A_0 and A are the relative peak intensities in the gas chromatogram for the brank (initial aqueous phase diluted with 5 ml water) and separated solutions, respectively; w and d are the weight and density of lecithin in the liposome solution, and V_s is the total volume of the solution. The density was cited from a reference.[7] These experiments were repeated several times and the obtained K_p values were averaged so as to give the means and standard deviations. The partition equilibrium was also achieved several times at temperatures near 25 or 40 °C; the resulting K_p values were used to derive

the enthalpy (ΔH_p°) and entropy (ΔS_p°) of the partition:[8]

$$\ln K_p = -\frac{\Delta H_p^\circ}{R}\cdot\frac{1}{T}+\frac{\Delta S_p^\circ}{R}. \quad (2)$$

Since the partition coefficient was defined as the ratio in mol dm^{-3}, the standard state of the derived thermodynamic properties corresponds to unit mol dm^{-3} at 25 °C in solution. Although the symbol K_p is used for the partition coefficient in Eq. 2, in the QSAR analysis below P is also used for this parameter, appearing as log P.

Results and Discussion

Partition System Dependency of the Partition Properties of Some Typical Solutes. The thermodynamic parameters of the partition change depending on the partition system adopted. Such a dependency has hitherto been studied in some different partition systems for the partition coefficient, the logarithm of which corresponds to the Gibbs free energy term, as evidenced by the equation $\Delta G_p^\circ = -RT\cdot\ln K_p$. However, a detailed discussion of the full dependency of the thermodynamic parameters, including the enthalpy and entropy terms, has been prevented because of the necessary extra work in experiments and the limited number of available experimental data. Such data are obtained from titration calorimetry for a few solutes in some partition systems, such as SDS micelle, 1-octanol, tetralin, and 2,2,4-trimethylpentane/water. The resulting data are compiled in Table 1 together with data from different sources. The free energy term (ΔG_p°) is seen to change monotonously, depending on the partition system: it decreases in the order of the nonaqueous phase of 2,2,4-trimethylpentane(saturated hydrocarbon), tetralin(aromatic hydrocarbon), 1-octanol(hydroxy compounds), and micelle(organic salt) or liposome (phospholipid). This order is consistent with the decreasing order in ΔH_p° and with the increasing order in the polarity of a nonaqueous medium. This fact supports the idea that solute–nonaqueous solvent interactions including electrostatic and hydrogen bonding parts stabilize the solutes in the nonaqueous phase, while decreasing the enthalpy (ΔH_p°) and increasing the partition coefficient. Since the entropy (ΔS_p°) changes parallel to the enthalpy (ΔH_p°), it contributes inversely to the free energy (ΔG_p°) as judged from a relation $\Delta G_p^\circ = \Delta H_p^\circ - T\cdot\Delta S_p^\circ$. It is, therefore, concluded that the enthalpy-entropy compensation relation holds and that the ΔH_p° term is the factor governing the partition system dependency regarding the thermodynamic properties. Since the enthalpy and entropy terms cancell each other, at least partly to yield the free energy, the partition system dependency becomes much larger when the free energy is separated into the two components of enthalpy and entropy. This is a merit of studying partition phenomena from a thermodynamic standpoint.

Model membrane (liposome) or micelle systems afford a lower ΔG_p° and a higher partition coefficient than does the widely used 1-octanol system. Since the former systems can better simulate the organized structure of a biophase medium, liposome or micelle systems may be recommended for the purpose of QSAR treat-

Table 1. Partition Properties of a Few Solute Molecules in Various Partition Systems[a]

Solute	Partition System[b]	log K_p	ΔG_p°	ΔH_p°	$T\Delta S_p^\circ$	Ref.
Phenol	SDS micelle/W	1.89±0.05	−10.8 ±0.4	−5.9 ±0.3	5.0 ±0.3	This work
	SDS micelle/W	1.72	−11	−13	−2.3	10)
	1-Octanol/W	1.45±0.01	−8.27±0.05	−7.7 ±0.3	0.56±0.06	This work
	1-Octanol/W	1.54	−8.7	−8.3	0.42	11)
	Tetralin/W	0.27±0.03	−1.6 ±0.1	1.5 ±0.1	3.1 ±0.1	This work
	Isooctane/W	−0.91±0.05	5.2 ±1.0	19.4 ±1.7	14.2 ±0.1	This work
	Isooctane/W		5.48±0.04	19.4 ±0.4	13.92	12)
	Isooctane/W		−0.57	16.4	16.95	13)
4-Methylphenol	DMPC liposome/W		−13.51	−31.5	−18.01	14)
	Isooctane/W		−2.26±0.14	−18.85±0.17	−16.59	12)
1-Pentanol	Liposome/W	1.29±0.01	−7.35±0.06	4.46±1.47	11.81±1.44	This work
	SDS micelle/W	1.67±0.09	−9.6 ±0.2	4.83±0.03	14.3 ±0.2	This work
	1-Octanol/W	1.41±0.06	−8.1 ±0.2	8.4 ±0.1	16.5 ±0.2	This work
	Tetralin/W	0.76±0.01	−4.32±0.03	24.0 ±0.1	28.3 ±0.1	This work
	Isooctane/W		0.89	29.56	28.67	12)
Hexane	Lecithin/W		−27.8	−9.2	18.5	9)
	DOPC liposome/W		−25.9 ±0.2	−7.1	18.7	9)
	SDS micelle/W		−27.4	−8.8	18.7	9)
	1-Octanol/W		−22.7			9)
	Hexane/W		−32.4	0	32.4	9)

a) ΔG, ΔH, and $T\Delta S$ are given in the unit of kJ mol^{-1}. Experimenental values are obtained from the titration calorimetry under constant temperature (this work),[12] and from the temperature dependence of partition coefficient (van't Hoff plot).[9,11,13,14] b) SDS: Sodium dodecyl sulfate. DMPC: Dimyristoyl phosphatidylcholine. DOPC: Dioleoyl phosphatidylcholine. Lecithin: Liposome made from egg york lecithin. W: Water. Isooctane: 2,2,4-Trimethylpentane.

Table 2. Partition Properties of Alcohols in the Liposome/Water System[a)]

	Solute	K_p	ΔG_p°	ΔH_p°	ΔS_p°
1:	Methanol	0.211±0.008	3.86±0.10	17.9±2.1	47.2±7.0
2:	Ethanol	0.460±0.009	1.93±0.05	13.2±1.3	37.9±4.1
3:	1-Propanol	1.26 ±0.02	−0.57±0.05	9.4±1.2	33.5±4.0
4:	1-Butanol	4.25 ±0.09	−3.59±0.05	6.6±1.3	34.2±4.3
5:	1-Pentanol	19.43 ±0.48	−7.35±0.06	4.5±1.5	39.6±4.8
6:	1-Hexanol	47.52 ±1.20	−9.57±0.06	3.5±1.7	43.9±5.5
7:	1-Heptanol	171.4 ±4.5	−12.75±0.06	4.2±1.8	57.0±6.0
8:	2-Propanol	0.92 ±0.01	0.21±0.03	11.6±0.7	38.2±2.3
9:	2-Butanol	2.78 ±0.06	−2.54±0.06	10.5±1.4	43.8±4.6
10:	2-Pentanol	4.87 ±0.09	−3.93±0.05	7.8±1.2	39.5±4.1
11:	2-Hexanol	29.71 ±0.83	−8.41±0.07	3.7±1.9	40.4±6.4
12:	2-Heptanol	88.73 ±2.16	−11.12±0.06	5.2±1.5	54.7±5.0
13:	2-Methyl-1-propanol	3.38 ±0.06	−3.02±0.05	8.3±1.3	38.0±4.3
14:	2-Methyl-2-propanol	1.13 ±0.01	−0.30±0.02	8.7±0.8	30.3±2.7
15:	3-Methyl-1-butanol	5.88 ±0.11	−4.39±0.05	5.8±1.2	34.1±4.0
16:	2-Methyl-2-butanol	4.05 ±0.09	−3.47±0.05	6.6±1.2	33.8±4.0
17:	3-Methyl-2-butanol	17.77 ±0.41	−7.13±0.06	7.7±1.3	49.7±4.3
18:	2,2-Dimethyl-1-propanol	23.86 ±0.56	−7.86±0.06	6.0±1.5	46.6±4.8
19:	3,3-Dimethyl-2-butanol	27.36 ±0.54	−8.20±0.05	4.8±1.2	43.7±4.0
20:	2-Fluoroethanol	0.109±0.003	5.49±0.07	7.8±1.5	7.8±4.9
21:	2-Chloroethanol	0.61 ±0.01	1.24±0.05	6.5±1.2	17.6±4.0
22:	2,2-Dichloroethanol	2.94 ±0.07	−2.67±0.06	2.8±1.4	18.2±4.6
23:	2,2,2-Trichloroethanol	19.76 ±0.37	−7.40±0.05	1.4±1.2	29.5±3.9
24:	2-Bromoethanol	1.75 ±0.04	−1.39±0.06	2.6±1.5	13.4±5.0

a) K_p and ΔG_p° are given at 25 °C. ΔG_p° and ΔH_p° are in the unit of kJ mol^{-1}, and ΔS_p° is in the unit of J K^{-1} mol^{-1}.

ment. In following sections of this paper, the partition properties of aliphatic alcohols (which the authors studied in the 1-octanol/water system[4)]) are examined in the liposome/water system and compared with previous results.

Partition Properties of Aliphatic Alcohols in the Liposome/Water System. The data regarding K_p (at 25 °C), ΔH_p°, and ΔS_p° obtained in the present study are summarized in Table 2. The thermodynamic parameters (ΔG_p°, ΔH_p°, and ΔS_p°) change linearly with the molar volume (V_m) of alcohols (Figs. 1 to 3) when halogenated and nonhalogenated alcohols are veiwed separately. The molar volume dependency of ΔH_p° is parallel for the halogenated and nonhalogenated alcohols (Fig. 2); that of ΔS_p°, however, differs in

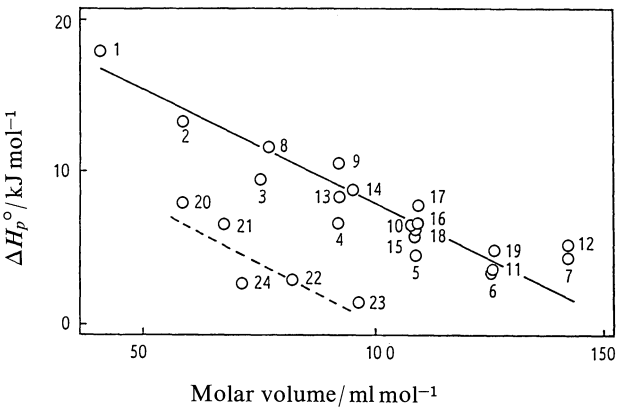

Fig. 2. Plots of ΔH_p° against the molar volume of solutes.

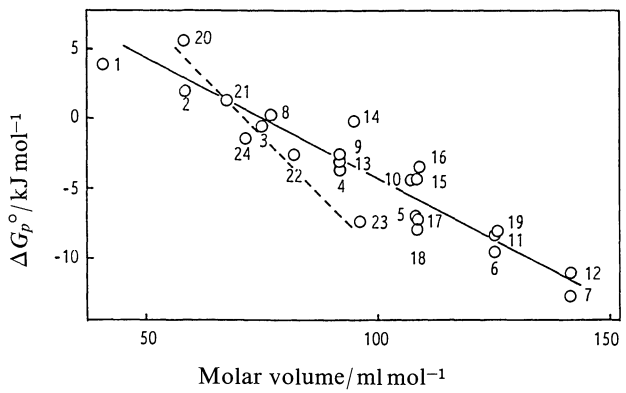

Fig. 1. Plots of ΔG_p° against the molar volume of solutes.

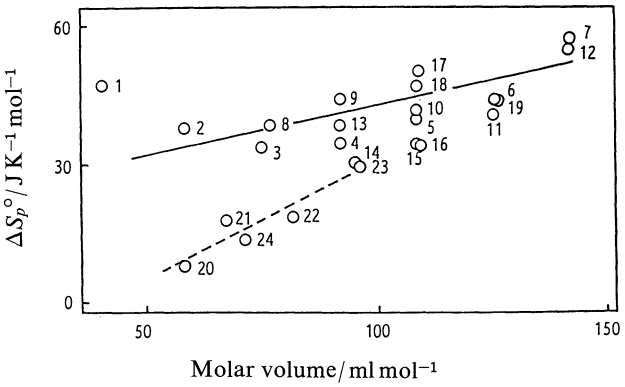

Fig. 3. Plots of ΔS_p° against the molar volume of solutes.

its slope between the two types of alcohols (Fig. 3). The latter difference is responsible for the difference in the slope shown in Fig. 1 for the halogenated and nonhalogenated alcohols. This result offers a rather clear contrast with that reached in the 1-octanol/water partition system:[4] in the latter system, the enthalpy (ΔH_p°; not the entropy) is responsible for the different slope of the molar volume dependency in ΔG_p°. When ΔG_p° and $\log K_p$ at 25 °C, as well as ΔH_p° and ΔS_p°, are interrelated between the partition systems of 1-octanol/water and liposome/water, linear relations are successfully obtained in regression analyses (Table 3). It is seen from the regression coefficients (smaller than 1.0 in Table 3) that the variations in the values of $\log K_p$, ΔG_p°, ΔH_p°, and ΔS_p° are smaller in the liposome/water system than those in the 1-octanol/water system when the solute alcohols are changed. The results listed in Tables 1 and 3 show a trend in that ΔH_p° and ΔS_p° are larger when observed using a more polar (ionic) nonaqueous phase. This trend, however, is inversed with respect to the free energy term. That is, ΔG_p° is increased, being decreased in absolute value, for the aliphatic alcohols in the liposome/water system, compared to that in the 1-octanol/water system (see 1-pentanol in Table 1 and also Table 3). This means that, for the aliphatic alcohols, ΔH_p° does not decrease very much in the liposome system compared to the data observed in other systems; this situation is reversed for ΔS_p°. This is equivalent to saying that the ratio of the enthalpy/entropy changes and the contribution of the enthalpy term is increased in the liposome/water system.

QSAR Analyses of the Biological Activities of Alcohols. Among the alcohols treated in the present study the biological activities are reported for twelve nonhalogenated alcohols,[15] as well as eight nonhalogenated and five halogenated alcohols.[16] The data concerning nonhalogenated alchohols,[15] which include LD_{50} (the concentration causing death in 50% of female white mice from i.v. injection), H (the concentration causing instantaneous hemolysis of erythrocytes), WI (the concentration causing inhibition of all the Tubifex worm movement within 2 min after immersion in a solution of alcohols), and FI (the dose that all fish assumed a side position or inverted position after 9—10 min of exposure to alcohols), were analyzed by means of the molecular connectivity index ($^1\chi$). The data, however, were also found to be quite successfully correlated with $\log P$ (Table 4).[17] Here, the $\log P$ data may be taken from either the liposome/water or the 1-octanol/water system, since the data from these two systems exhibit a high mutual colinearity, especially within the nonhalogenated alcohols (Table 2).

The toxicity data of alcohols, including halogenated ones,[16] are analyzed in Table 5. These data include the product of intrinsic toxicity, T_i (the slope of the dose-response curve in tissue culture), the tissue culture toxicity, ID_{50} (the concentration required to produce 50% inhibition of growth), the hemolytic activity, H_{50} (the concentration required to produce 50% hemolysis in saline at 37 °C), and the acute in vivo toxicity, LD_{50} (the single intraperitoneal dose required to kill 50% of the mice in 7 d). For the sake of a comparison the previous analyses using the partition properties in the 1-octanol/

Table 3. Interrelations of ΔG_p° (at 25 °C), $\log K_p$ (at 25 °C), ΔH_p°, and ΔS_p° Determined in the Partition Systems of Liposome/Water and 1-Octanol/Water[a]

Equations	r[b]	F[c]	SD[d]
$\log K_p$(liposome/W)=0.920(0.081)$\log K_p$(1-octanol/W)−0.132(0.095)	0.989	605	0.128
ΔG_p°(liposome/W)=0.918(0.026)ΔG_p°(1-octanol/W)+0.770(0.176)	0.989	600	0.736
ΔH_p°(liposome/W)=0.750(0.198)ΔH_p°(1-octanol/W)+0.227(1.870)	0.915	67	1.474
ΔS_p°(liposome/W)=0.813(0.163)ΔS_p°(1-octanol/W)−1.983(7.507)	0.948	116	4.493

a) Values in parentheses correspond to 95% confidence intervals. b) Multiple correlation coefficient. c) Variance ratio. d) Standard deviation.

Table 4. Linear Regression Analyses of the Biological Activities of Nonhalogenated Alcohols Based on $\log P$ in the Liposome/Water System and on the Molecular Connectivity Index $^1\chi$

Equations[a]	n[b]	r[c]	F[d]	SD[e]
$-\log LD_{50}$ =0.944(0.135)$\log P$−1.420(0.102)	12	0.980	244	0.132
$-\log H$ =0.885(0.155)$\log P$−0.166(0.117)	12	0.971	163	0.151
$-\log WI$ =1.180(0.135)$\log P$+0.274(0.102)	12	0.987	382	0.132
$-\log FI$ =1.380(0.152)$\log P$+0.458(0.089)	8	0.994	490	0.098
$-\log LD_{50}$ =0.922(0.132)$^1\chi$−3.030(0.309)	12	0.979	236	0.133
$-\log H$ =0.889(0.100)$^1\chi$−0.177(0.232)	12	0.987	389	0.100
$-\log WI$ =1.170(0.130)$^1\chi$−1.820(0.301)	12	0.987	400	0.129
$-\log FI$ =1.410(0.141)$^1\chi$−2.040(0.284)	8	0.995	601	0.089

a) 95% confidence intervals are depicted in parentheses. b) Number of the data. c) Correlation coefficient. d) Variance ratio. e) Standard deviation.

water system are also included in Table 5. The in vivo datum (LD_{50}) is excluded for 2-fluoroethanol in Table 5, since this alcohol is metabolized to a more active intermediate in vivo.[18] All other available data are included in Table 5.

Trends in the analysis of the toxicity data are summarized as follows:

1. All of the data can be correlated well with ΔH_p°.
2. The data exhibit no high correlation with ΔS_p°, but the regression analyses are improved when ΔS_p° is incorporated besides the ΔH_p° term.
3. The data can be correlated with log P only when the halogenated and the nonhalogenated alcohols are treated separately.
4. A slightly higher correlation is observed against ΔS_p° when in vivo toxicity data (LD_{50}) are concerned.

These trends are all in common with the two partition systems of liposome/water and 1-octanol/water. In order to examine more closely the difference of using the data of the two partition systems, a bootstrap method[19] is applied for statistical tests of the regression co-

Table 5. Regression Analyses of the Biological Activities of Alcohols Based on the Partition Properties Obtained in the Liposome/Water and 1-Octanol/Water Systems

Equations[a]	n[b]	r[c]	F[d]	SD[e]
Liposome/water system				
$-\log H_{50} = 0.765(0.570)\log P + 0.250(0.504)$	10	0.736	9.5	0.529
$-\log H_{50} = 0.716(0.190)\log P + 0.005(0.175)$[f]	7	0.974	93.9	0.133
$-\log H_{50} = 1.180(4.690)\log P + 0.709(3.620)$[g]	3	0.955	10.3	0.405
$-\log H_{50} = -0.186(0.057)\Delta H_p^\circ + 2.010(0.455)$	10	0.936	56.4	0.276
$-\log H_{50} = -0.009(0.050)\Delta S_p^\circ + 0.984(1.840)$	10	0.139	0.2	0.775
$-\log H_{50} = -0.204(0.052)\Delta H_p^\circ + 0.015(0.016)\Delta S_p^\circ + 1.610(0.570)$	10	0.963	44.9	0.225
$-\log LD_{50} = 0.095(0.471)\log P + 2.460(0.388)$	12	0.140	0.20	0.451
$-\log LD_{50} = 0.114(0.219)\log P + 2.170(0.192)$[f]	8	0.460	1.61	0.162
$-\log LD_{50} = 0.313(0.317)\log P + 2.910(0.225)$[g]	4	0.949	18.0	0.081
$-\log LD_{50} = -0.102(0.039)\Delta H_p^\circ + 3.230(0.309)$	12	0.878	33.7	0.218
$-\log LD_{50} = -0.028(0.016)\Delta S_p^\circ + 3.450(0.582)$	12	0.770	14.5	0.291
$-\log LD_{50} = -0.076(0.029)\Delta H_p^\circ - 0.016(0.009)\Delta S_p^\circ + 3.590(0.288)$	12	0.957	48.9	0.139
$-\log(1/T_i) = 0.598(0.506)\log P + 3.310(0.422)$	13	0.617	6.77	0.593
$-\log(1/T_i) = 0.854(0.249)\log P + 2.790(0.218)$[f]	8	0.960	70.7	0.184
$-\log(1/T_i) = 0.744(0.884)\log P + 3.860(0.677)$[g]	5	0.840	7.17	0.464
$-\log(1/T_i) = -0.188(0.047)\Delta H_p^\circ + 4.900(0.374)$	13	0.935	76.7	0.267
$-\log(1/T_i) = -0.010(0.034)\Delta S_p^\circ + 3.870(1.190)$	13	0.181	0.37	0.741
$-\log(1/T_i) = -0.205(0.045)\Delta H_p^\circ + 0.012(0.012)\Delta S_p^\circ + 4.650(0.411)$	13	0.957	54.3	0.230
$-\log ID_{50} = 0.546(0.478)\log P + 1.580(0.399)$	13	0.604	6.32	0.560
$-\log ID_{50} = 0.760(0.255)\log P + 1.100(0.223)$[f]	8	0.948	53.4	0.189
$-\log ID_{50} = 0.733(0.640)\log P + 2.120(0.490)$[g]	5	0.903	13.3	0.336
$-\log ID_{50} = -0.180(0.035)\Delta H_p^\circ + 3.100(0.273)$	13	0.961	132	0.195
$-\log ID_{50} = -0.011(0.032)\Delta S_p^\circ + 2.160(1.110)$	13	0.217	0.54	0.686
$-\log ID_{50} = -0.194(0.031)\Delta H_p^\circ + 0.009(0.008)\Delta S_p^\circ + 2.900(0.286)$	13	0.976	102	0.159
1-Octanol/water system				
$-\log H_{50} = 1.010(0.721)\log P + 0.119(0.567)$	8	0.813	11.7	0.513
$-\log H_{50} = 0.814(0.193)\log P - 0.104(0.132)$[f]	5	0.992	179.9	0.073
$-\log H_{50} = 1.010(5.310)\log P + 0.622(4.960)$[g]	3	0.924	5.86	0.519
$-\log H_{50} = -0.155(0.081)\Delta H_p^\circ + 2.030(0.816)$	8	0.887	22.1	0.407
$-\log H_{50} = -0.016(0.057)\Delta S_p^\circ + 1.240(2.400)$	8	0.264	0.45	0.848
$-\log H_{50} = -0.212(0.064)\Delta H_p^\circ - 0.030(0.022)\Delta S_p^\circ + 1.330(0.700)$	8	0.970	39.5	0.235
$-\log LD_{50} = 0.333(0.612)\log P + 2.390(0.468)$	10	0.405	1.57	0.446
$-\log LD_{50} = 0.172(0.439)\log P + 2.140(0.296)$[f]	6	0.478	1.18	0.191
$-\log LD_{50} = 0.277(0.438)\log P + 2.890(0.387)$[g]	4	0.887	7.41	0.127
$-\log LD_{50} = -0.092(0.021)\Delta H_p^\circ + 3.380(0.212)$	10	0.963	102	0.134
$-\log LD_{50} = -0.025(0.017)\Delta S_p^\circ + 3.560(0.729)$	10	0.762	11.1	0.330
$-\log LD_{50} = -0.087(0.035)\Delta H_p^\circ - 0.003(0.012)\Delta S_p^\circ + 3.470(0.326)$	10	0.965	47.4	0.143

Table 5. (Continued)

Equations[a]	n[b]	r[c]	F[d]	SD[e]
$-\log(1/T_i)=-0.679(0.680)\log P-1.810(0.515)$	11	0.599	5.04	0.631
$-\log(1/T_i)=0.876(0.241)\log P+2.670(0.163)$[f]	6	0.981	101	0.105
$-\log(1/T_i)=0.317(1.320)\log P+4.010(1.120)$[g]	5	0.402	0.58	0.711
$-\log(1/T_i)=-0.142(0.058)\Delta H_p^\circ-0.244(0.580)$	11	0.880	30.9	0.374
$-\log(1/T_i)=-0.019(0.034)\Delta S_p^\circ-0.790(1.380)$	11	0.396	1.67	0.724
$-\log(1/T_i)=-0.178(0.071)\Delta H_p^\circ+0.016(0.021)\Delta S_p^\circ-0.545(0.658)$	11	0.916	20.8	0.336
$-\log ID_{50}=0.677(0.615)\log P+1.475(0.466)$	11	0.639	6.20	0.571
$-\log ID_{50}=0.775(0.226)\log P+0.994(0.152)$[f]	6	0.979	90.5	0.099
$-\log ID_{50}=0.712(0.649)\log p+1.990(0.549)$[g]	5	0.896	12.2	0.348
$-\log ID_{50}=-0.137(0.048)\Delta H_p^\circ+3.000(0.482)$	11	0.908	42.2	0.311
$-\log ID_{50}=-0.018(0.032)\Delta S_p^\circ+2.440(1.300)$	11	0.391	1.63	0.683
$-\log ID_{50}=-0.176(0.060)\Delta H_p^\circ-0.017(0.018)\Delta S_p^\circ+2.680(0.558)$	11	0.951	38.0	0.243

a) 95% confidence intervals are depicted in parentheses. b) Number of the data. c) Multiple correlation coefficient. d) Variance ratio. e) Standard deviation. f) For only the nonhalogenated alcohols. f) For only the halogenated alcohols.

Table 6. The 95% Confidence Intervals of the Regression Coefficients Analyzed by the Bootstrap Method

	Liposome/water system	1-Octanol/water system
ΔH_p°	−0.080—−0.022	−0.103—0.006
ΔS_p°	−0.033—−0.012	−0.032—0.002
Constant	3.456— 4.167	3.334—4.175
r[a]	0.892— 0.984	0.763—0.989

a) Multiple regression coefficient.

efficients (Table 6). The results indicate that within the 95% confidence intervals the coefficients of ΔH_p° and ΔS_p° are not reduced to zero in the liposome/water system, whereas they are reduced in the 1-octanol/water system. This supports the superiority of data obtained in the liposome/water system for the QSAR analysis.

We would like to express our sincere gratitude to Professor (Emeritus) Yoshio Sasaki, Osaka University, for his continuous interest and invaluable suggestions.

References

1) R. Franke, "Theoretical Drug Design Methods," Pharmaco-Chemistry Library, ed by W. Th. Nauta and R. F. Rekker, Elsevier, Tokyo (1984), Vol. 7.
2) C. Hansch and A. Leo, "Substituent Constants for Correlation Analysis in Chemistry and Biology," John Wiley, New York (1979).
3) See Ref. 1, Chap. 4.
4) H. Fujiwara, H. Yoshikawa, S. Murata, and Y. Sasaki, *Chem. Pharm. Bull.*, **39**, 1095 (1991).
5) F. Szoka, Jr. and D. Papahadjopoulos, *Proc. Natl. Acad. Sci., USA*, **75**, 4194 (1978).
6) I. Shibuya, H. Honda, and B. Maruo, *Agr. Biol. Chem.*, **31**, 111 (1967).
7) G. C. Newman and C.-H. Huang, *Biochemistry*, **14**, 3363 (1975).
8) The van't Hoff plot was ascertained to be linear between 0 and 50 °C,[9] and the linearity was not tested in the present study to avoid tremendous work in experiment.
9) S. A. Simon, W. L. Stone, and P. Busto-Latorre, *Biochim. Biophys. Acta*, **468**, 378 (1977).
10) S. Terabe, K. Otuka, and T. Ando, *Anal. Chem.*, **57**, 834 (1985).
11) J. A. Rogers and A. Wong, *Int. J. Pharm.*, **6**, 339 (1980).
12) W. Riebesehl, E. Tomlinson, and H. J. M. Gruenbauer, *J. Phys. Chem.*, **88**, 4775 (1984).
13) J. F. M. Kinkel, E. Tomlinson, and P. Smit, *Int. J. Pharm.*, **9**, 121 (1981).
14) J. A. Rogers and S. S. Davis, *Biochim. Biophys. Acta*, **598**, 392 (1980).
15) L. B. Kier and L. H. Hall, *Bull. Environ. Contam. Toxicol.*, **29**, 121 (1982).
16) E. O. Dillingham, R. W. Mast, G. E. Bass, and J. Autian, *J. Pharm. Sci.*, **62**, 22 (1973).
17) log P=log K_p: the symbol log P is used instead of log K_p as conventionally done in the field of QSAR.
18) D. H. Treble, *Biochem. J.*, **82**, 129 (1962).
19) B. Efron and R. Tibshirani, *Statist. Sci.*, **1**, 54 (1986).

Kinetic Studies on the Chemical and Electrochemical Reduction of Some 4-Arylidene-5-pyrazolone Compounds

Mahmoud A. ABDEL-RAHMAN, Refat ABDEL-HAMID,* Mostafa K. RABIA, and Mohamed M. EL-DESSOUKI
Department of Chemistry, Faculty of Science, Sohag, Egypt
(Received March 11, 1991)

Kinetics of chemical and electrochemical reduction of some 4-arylidene-5-pyrazolones were studied. The chemical reduction was performed using aluminum hydride. The electrochemical reduction in 0.1 mol dm^{-3} TEAP/DMF was studied by cyclic and convolution potential sweep voltammetry at HDME. The title compounds exhibit two diffusion-controlled irreversible mono electronic cv waves. Both waves follow EC kinetics and they are attributed to the reduction of the pyrazolin carbonyl group. The kinetics of the chemical and electrochemical reduction were proposed and discussed in terms of the molecular structure of the subject arylidenes.

Though many investigations have been reported concerning the synthesis of arylidenes,[1] dyes[2,3] and electronic absorption spectra of arylidenepyrazolones,[4] scarcely attention has been paid to chemical and electrochemical reduction of such compounds.[5] It was found that the polarographic half-wave potentials of some 4-(4-substituted arylidene)-5-pyrazolones correlate with the Hammett's constant. Kinetics of the chemical and electrochemical reduction of the title compounds were not yet studied.

In continuation of our work[6] an investigation of the chemical and electrochemical reduction mechanism of a series of 4-(4-substituted arylidene)-5-pyrazolones is carried out. Herein, chemical and cyclic and convolution potential sweep voltammetric results are reported and discussed in terms of the molecular structure of the subject arylidenepyrazolones.

Experimental

a) Synthesis of 4-Arylidene-5-pyrazolones. 1-Phenyl-3-methyl-4-arylidene-5-pyrazolones were synthesized and purified as described before.[7] The subject compounds are:

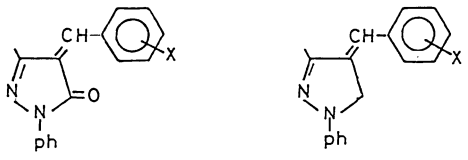

$\mathbf{a}_{1-3}$ $\mathbf{b}_{1-3}$
1, X=H, **2**, X=OCH_3, **3**, X=Br

Stock solution (1.0×10^{-2} mol dm^{-3}) of arylidenepyrazolone was prepared in the supporting electrolyte (0.1 mol dm^{-3} TEAP/DMF).

b) Synthesis of Aluminum Hydride (alane). To a cooled stirring solution of lithium aluminum hydride, $LiAlH_4$, 0.12g (3.0 mmol) in 20.0 ml dry ether was added, 0.12 g (1.0 mmol) of anhydrous aluminum chloride, $AlCl_3$, in portions to give stoichiometrically required amount of AlH_3. The mixture was stirred at room temperature until $AlCl_3$ dissolved and LiCl was completely precipitated.

$$3\ LiAlH_4 + AlCl_3 \rightarrow 3\ LiCl + 4\ AlH_3 \quad (1)$$

c) Selective Reduction of Arylidenepyrazolones with alane. (General Procedure). 20.0 ml etheral solution of AlH_3[8] was added to a stirring solution of the pyrazolone derivative (2.0 mmol) in dry ether. The reaction mixture was refluxed under dry conditions (6—7 h). The excess hydride was decomposed by addition of dilute HCl then the reductive product was extracted with ether and dried over anhydrous $MgSO_4$. Evaporation of the solvent under reduced pressure gave a viscous residue which after grunding with petroleum ether solidifies as colored solid. The products were crystallized from acetone. The arylidenepyrazolones subjected for the selective chemical reduction are: **2a**, **3a**, and 1-phenyl-3,4,4-trimethyl-5-pyrazolone (**4a**). Experimental data of all the isolated products were summarized in Table 1.

Tetraethylammonium perchlorate, TEAP, (Fluka), and *N,N*-dimethylformamide (A.R. grade DMF) were purified as described earlier.[6,9]

d) Controlled Potential Coulometric Measurements. Controlled potential coulometric electrolyses were performed at the peak current potential of the two cv waves. Coulometric measurements were conducted in 1.0×10^{-3} mol dm^{-3} solu-

Table 1. Experimental Data for the Reductive Arylidenepyrazolone Products

Comp No.	Formula	Reaction time h	Yield %	Mp °C	Analysis (calcd/found) C%	H%	N%
2b	$C_{18}H_{18}N_2O$	6.5	50	118	77.69	6.47	10.07
					77.49	6.52	9.80
3b	$C_{17}H_{15}N_2Br$	6.0	84	135	59.82	4.39	8.21
					59.98	4.55	8.13
4b	$C_{12}H_{16}N_2$	7.0	22	140	76.95	8.51	14.89
					76.50	8.70	14.75

tions. The cell was continuously flushed with nitrogen and the analysis was continued until the current had decayed to the background level. Completion of the electrolysis was confirmed by cv measurements.

e) Instrumentations. An EG&G PAR model SMDE 303 mercury drop system of small hanging-drop mode was used as HDME working electrode at 298 K. The electrode area was 1.83×10^{-3} cm^2. The counter electrode was platinum wire. Silver/silver ion (0.01 mol dm^{-3} $AgNO_3$ in 0.1 mol dm^{-3} TEAP/DMF) electrode was used as a reference electrode throughout. All solutions were purged with pure nitrogen.

An EG&G PAR model 173 Potentiostat/Galvanostat with positive feedback IR compensation and EG&G PAR model 175 Universal programmer function generator were used for the cyclic voltammetric measurements. The cyclic voltammograms were recorded on PAR model RE 0091 X-Y recorder.

Controlled potential coulometry was carried out with EG&G PAR model 179 Digital Coulometer and PAR model 337A Coulometric cell system.

Electrochemical data were performed using an AMSTRAD personal computer PC 1512.

Spectrophotometric measurements (IR and ^{1}H NMR spectra) were performed on a Perkin-Elmer 137 IR Spectrophotometer in KBr and Varian A-60 ^{1}H NMR Spectrophotometer at 60 MHz.

Results and Discussion

i) Cyclic Voltammetry. Two cyclic voltammetric reduction waves are observed for all the 1-phenyl-3-methyl-4-arylidene-2-pyrazolin-5-ones (4.98×10^{-4} mol dm^{-3}) in 0.1 mol dm^{-3} tetraethylammonium perchlorate/dimethylformamide (TEAP/DMF) at hanging dropping mercury electrode. The cyclic voltammetric data obtained are given in Table 2. The cv waves appear to be irreversible, their anodic counterparts are lacking at all scan rates explored.

The potential width measured by ($E_p-E_{p/2}$) for the two cv waves are larger than the values expected for a mono-electronic charge-transfer reversible processes (56.5/n mV at 298 K) (c.f. Table 2).[10,11] The peak potential of the two cv waves does shift to more negative potentials on increasing the scan rate, to the extent of 30.0±0.3 and 35±0.2 mV for the tenfold increase in scan rate for the first and second cv waves, respectively. This reveals that, the cv waves are due to a reversible one electron-transfer process coupled with an irreversible first-order follow-up chemical reaction. The chemical reaction is suggested to be protonation.

The peak current, i_p of both cv waves correlates significantly with $\nu^{1/2}$, (r=0.998) and concentration of the depolarizer as well (r=0.999). This evidences that the two cv waves are diffusion-controlled[10] with no adsorption complications.

On comparing i_p–$\nu^{1/2}$ relations with the diagnostic criteria for EC mechanism presented earlier,[10] the diffusion coefficient, D, for the subject arylidenepyrazolones are computed. The data obtained are collected in Table 2.

According to Nicholson and Shain,[10] an excellent agreement between the experimental and calculated peak width ($E_p-E_{p/2}$) is seen. This provides completing evidence that the cv waves follow solely the $E_{rev}C_{irr}$ mechanism. Furthermore, the first-order rate constants of the follow-up irreversible protonation reaction, k_c, are estimated. Moreover, the polarographic half-wave and the formal electrode potentials, if one considers that $D_R=D_O$ (the diffusion coefficients of the reduced and oxidized forms, respectively) are determined using Eqs. 2 and 3.[10]

$$E_p = E_{1/2} - 0.780\,(RT/nF) + RT/2nF \ln\lambda, \quad (2)$$

where $\lambda=k_c(RT/nF)\nu$.

$$E_{1/2} = E^\circ + (RT/nF) \ln\sqrt{(D_R/D_O)}. \quad (3)$$

The computed values of E° and k_c are depicted in Table 2.

Table 2. Cyclic Voltammetric Data for 4.98×10^{-3} mol dm^{-3} 4-Arylidene-5-pyrazolones in 0.1 mol dm^{-3} TEAP/DMF (1st wave)

No.	Scan rate / mV s^{-1}	$-E_p$[a]	$E_p-E_{p/2}$ / mV	$i_p/\nu^{1/2}$ / b)	10^7D[c] / cm^2 s^{-1}	$-E^\circ/E_{1/2}$[d] / V	k_c[e] / s^{-1}
2a	20	1.600	55	6.220	5.45	1.423	0.196
	50	1.615	57	6.44			
	100	1.625	60	6.32			
	200	1.633	61	6.13			
	500	1.640	60	5.71			
1a	20	1.480	60	7.14	6.89	1.310	0.248
	50	1.495	60	7.42			
	100	1.505	65	7.21			
	200	1.515	67	6.79			
	500	1.523	66	6.65			
3a	20	1.400	60	6.79	6.36	1.228	0.229
	50	1.410	60	6.44			
	100	1.420	60	6.76			
	200	1.430	57	6.71			
	500	1.440	63	6.28			

a) ±2.1%. b) in $\mu A(V^{-1}s)^{-1/2}$. c) ±3.2%. d) ±2.5%. e) ±3.5%.

On the other hand, a further verification that the substrate reduces electrochemically via an $E_{rev}C_{irr}$ mechanism is revealed from the slightly decrease in the current function with increasing the scan rate (c.f. Table 2).

The number of electrons involved along the two cv waves is determined on controlling the potential at their peak current potentials. It is found that 1.1 and 0.9 moles of electrons per mole of the arylidenepyrazolone are consumed for electrochemical reduction of the first and second cv waves, respectively. Thus, the number of electrons transferred is one for both cv waves. Similar behavior is seen with the other arylidenepyrazolones under investigation.

ii) Convolution Sweep Voltammetry. Analysis of cyclic voltammetric data has a disadvantage that the potential dependent rate law must be selected before the treatment of data. However, convolution technique allows this disadvantage to be overcome. This is made by convolution of the current with the function $(\pi t)^{1/2}$ and data are processed in terms of both current and convoluted current. It is no longer necessary, under this conditions, to (a priori) state the charge transfer rate law which is instead obtained as a result of the treatment of data[12–16].

Examination of the cyclic voltammetric convoluted data for the 4-arylidenepyrazolones in the scan rate range of 20—500 mV s^{-1} reveals that they electrochemically reduce irreversibly. This is established from the feature of the cyclic convoluted current voltammogram, since the convoluted current, I, neither returns to its initial (zero) value nor superimposes during the reverse half of the sweep with I on the forward sweep regardless of the scan rate. Figure 1 illustrates the cyclic original and convoluted voltammograms for the first cv wave for **1a** at scan rate of 200 mV s^{-1} as a representative example.

The logarithmic analysis of the convoluted data is used to established the mechanism of the electrochemical reduction process. The analysis is tested for the various reaction mechanisms (E_{rev}, E_{irr}, *CE*, *ECE*, ...etc).

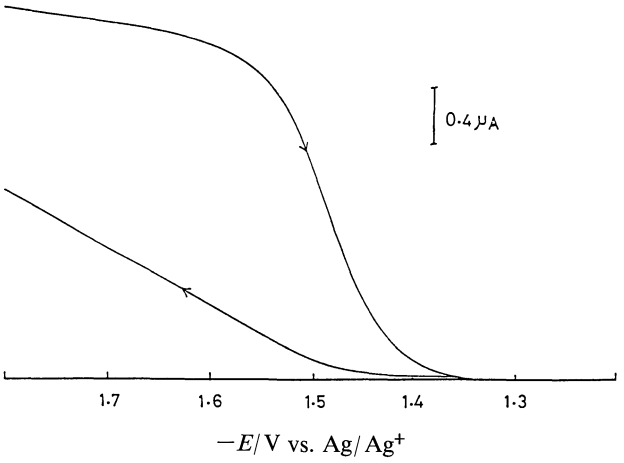

Fig. 1. Convolution voltammogram for the first cv wave of the reduction of 4-arylidenepyrazolone, **1a**, at scan rate of 200 mV s^{-1}.

In the entire range of scan rate, the data fit satisfactorily the following equation for all the subject pyrazolones:

$$E = E^\circ + (RT/2nF)\ln k_c + (RT/nF)\ln[(I_l - I)/i], \quad (4)$$

where I is the convoluted current, i is the original current, $I_l = nFAC_0D^{1/2}$ is the limit of I as E approaches infinity and the remaining symbols have their usual significances. They give rise straight lines with slope values close to the theoretical value ($59.1/n$ mV at 298 K for decimal logarithm) for an $E_{rev}C_{irr}$ mechanism. The regression line obtained for the first cv wave of **1a** as a representative example can be represented by Eq. 5. The linearity and the location of the obtained straight line on the potential axis do not depend on the sweep rate. This behavior verifies the above conclusion that the electrochemical reduction of the subject pyrazolones take place via an $E_{rev}C_{irr}$ kinetics.

$$E = -(1.445 \pm 0.005) + (61.1 \pm 1.1) \times 10^{-3} \log[(I_l - I)/i] \quad r = 0.998 \quad (5)$$

From Eqs. 4 and 5 the formal electrode potential, E°, for the subject arylidenepyrazolones are computed. The results obtained depicted in Table 1. It is clear that these values are in good agreement, within the experimental error limits, with those obtained from the above cyclic voltammetric data.

iii) Chemical Reduction: Special attention is paid to the selective reduction suitable for the reduction of the carbonyl group without reduction of the arylidene group of the subject arylidenepyrazolones.

The most common reducing agents are the metal hydrides and hydrogenation catalysts. The reagents used in the reduction by hydride transfer (metal hydrides)[17] are two types. They are nucleophilic substances such as lithium aluminum hydride (LAH) and sodium borohydride, as well as the electrophilic species diborane, aluminum hydride (alane) and derivative thereof.[18,19]

Lithium aluminum hydride often reduces the α,β-unsaturated ketones.[20,21] The double bond reduction is avoided by the use of aluminum hydride, which selectively reduces the carbonyl group only.

The selective reduction of **2a**—**4a** is carried out using aluminum hydride. The reduction process was followed by ^{1}H NMR spectra, which show a shift in the vinylic proton resonance to a higher magnetic field.

Table 3. IR Spectroscopic Data (KBr, cm^{-1})

Compd	νC=O	νC=N	νC=C Exocyclic
2a	1670	1630	1610
2b	—	1625	1610
3a	1670	1630	1610
3b	—	1630	1590
4a	1685	1620	—
4b	—	1625	—

Table 4. ^{1}H NMR Spectra δ (DMSO)/ppm

Compd	=CH	Arom. proton	OCH_3	$-CH_2$	$-CH_3$
2a	8.8 (s, 1H)	7.1—8.2 (m, 9H)	3.9 (s, 3H)	—	2.4 (s, 3H)
2b	8.3 (br, 1H)	6.8—8.2 (m, 9H)	3.8 (s, 3H)	3.6 (s, 2H)	2.3 (s, 3H)
3a	8.3 (s, 1H)	7.1—8.0 (m, 9H)	—	—	2.2 (s, 3H)
3b	8.1 (br, 1H)	6.7—7.9 (m, 9H)	—	3.9 (s, 2H)	2.2 (s, 3H)
4a	—	7.8—7.2 (m, 9H)	—	—	2.6 (s, 3H); 2.45 (s, 6H)
4b	—	7.8—7.4 (m, 9H)	—	4.2 (br, 2H)	2.2 (s, 3H); 1.2 (d, 3H); 1.2 (s, 3H)

This is attributed to the disappearance of deshielding effect of the carbonyl group. Moreover, new singlet signals are developed due to the appearance of methylene group. The structure of the isolated products are assigned on the basis of elemental and spectral analyses.

A comparison between IR spectra of the reduced products, **2b**—**4b**, and those of the starting materials, **2a**—**4a**, (c.f. Table 3) gives conclusive evidence of the nature of the reaction, since the products show a lack of the C=O bond. ^{1}H NMR spectra (Table 4) are in agreement with the suggested structures.

The mechanism of the reduction by alane differs somewhat from that of complex hydride (LAH). The main difference is in the entirely different chemical nature of the two types (alane and complex hydride). Whereas complex hydride anion is a strong nucleophile which attacks centers of lowest electron density, alane is electrophile and combines with that part of the organic molecule which has a free electron pair.[22]

Thus, the following reaction mechanism of the chemical reduction of **2a**—**4a** with alane (Scheme 1) is suggested.

Coordination is first assumed to occur between the carbonyl oxygen atom and alane. Intramolecular hydride transfer is possible in the complex and intermediate (**I**) still contains hydrogen atom directly attached to the aluminum atom. The intermediate heterolyses by loosing an aluminate ion, a good leaving group, to give carbonium ions which are reduced to methylene group leading to the final product.

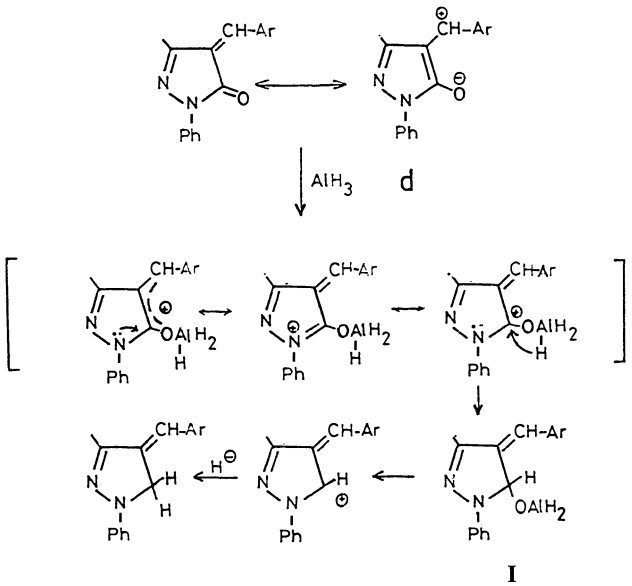

Scheme 1.

From the foregoing results it can be deduced that:

1) $AlCl_3$ is added to reduce the reduction tendency power of $LiAlH_4$ and consequently produces a reagent more specific for the particular reaction as described by elsewhere.[18]

2) The arylidene substituents play a role in the stabilization of the dipolar form **d** (Scheme 1). Introduction of an electron-withdrawing group in the *p*-position of the arylidene moiety increases the facility of the reduction.

Kinetics of the Electrochemical Reduction. Electrochemical reduction kinetics of 1-phenyl-3-methyl-4-arylidene-2-pyrazolin-5-ones in 0.1 TEAP/DMF at 298 K, the electrode reaction mechanism are discussed on the basis of the above results. They are electrochemically reduced via two irreversible diffusion-controlled single-electronic cv waves. These cv waves follow an $E_{rev}C_{irr}$ kinetics.

The subject arylidenepyrazolones have three possible reduction sites, the azomethine, -CH=N, of the pyrazolone nucleus, the cyclic carbonyl, C=O, and the exocyclic arylidene =CH-Ar, groups. The endocyclic -CH=N- group requires high energy for reduction. Therefore, the two other sites are susceptible for reduction.

To establish the site of reduction in the subject substrates, they are subjected to selective chemical reduction for the carbonyl group and then are tested voltammetrically. The reduced products show no cv waves. This is ascribed to the lacking of their 5-carbonyl group. Thus, the electrochemical reduction site is most likely the 5-carbonyl group, while the arylidene group is electroinactive at such circumstances.

The kinetics of the electrochemical reduction of the 4-arylidene-5-pyrazolones is proposed and discussed as follows:

The first irreversible mono-electronic reduction wave is due to reversible addition of an electron to the pyrazo-

lone molecule and can be represented by reaction (6). Simple charge-transfer reaction (6) does not, however, justify the irreversibility of the first wave and other step must be invoked to rationalize the data obtained. Taking into account that the first cv wave proceeds via an $E_{rev}C_{irr}$ mechanism and the reduction of carbonyl group consumes at least two electrons and two protons, an irreversible first-order protonation reaction (7) is assumed to be taken place. At more negative potentials, further electron is reversibly added to the radical ArpyH$^{\cdot}$, according to reaction (8). Another irreversible first-order proton addition, reaction (9), to the ArpyH^{-} anion takes place to the final product. Occurrence of reactions (7) and (9) can justify the irreversibility of the two cv waves.

$$\mathrm{Arpy} + \mathrm{e} \rightleftneq \mathrm{Arpy}^{\cdot-} \quad (6)$$

$$\mathrm{Arpy}^{\cdot-} + \mathrm{H}^{+} \xrightarrow{k_c} \mathrm{ArpH}^{\cdot} \quad (7)$$

$$\mathrm{Arpy}^{\cdot} + \mathrm{e} \rightleftneq \mathrm{ArpyH}^{-} \quad (8)$$

$$\mathrm{ArpyH}^{\cdot-} + \mathrm{H}^{+} \xrightarrow{k_c} \mathrm{ArpH_2} \quad (9)$$

Structural Effects. From the examination of the data obtained (cf. Table 2), it is evident that the influence of the para substituents in the 4-arylidene moiety on the electrochemical reduction (expressed in the values of the peak current potential, E_p) is as expected. The *p*-methoxy substituted derivative exhibits the most negative shift of E_p, whereas the *p*-bromo one shows a positive shift compared to the parent unsubstituted arylidenepyrazolone **1a**. This is explained as follows. On introduction of electron-donating group (methoxyl group) in the arylidene phenyl moiety, an increase in the electron density of the carbonyl group is expected. Consequently, the electrochemical reduction of the carbonyl group becomes more difficult. This appears as a shift in E_p to more negative potentials. On the other hand, introduction of electron-withdrawing group (bromo) reduces the electron density on the carbonyl center. This in turn makes the electrochemical reduction easier and appears as a positive shift in E_p.

The substituent effect is expressed quantitatively by the relation between the peak current potential of the arylidenepyrazolones and the Hammett's substituent constants, σ_p^-. It is evident that, the peak potentials for the first cv wave correlate with the σ_p^- Hammett constants. The best linear least-square line obtained is represented as follows:

$$E_p = (0.218 \pm 0.002)\,\sigma_p^- - (1.463 \pm 0.013) \quad r = 0.983(10) \quad (10)$$

This confirms that the electrochemical reduction of the subject arylidenepyrazolones follow the same mechanism for all the compounds under investigation. On the other hand, the reaction constant ρ obtained is 218 mV comparable to those of substituted benzaldehyde (310 mV), benzophenone oximes (300 mV) and azomethine (300 mV) etc.[23] These are interpreted on the basis as the arylidene moiety becomes a structure completely coplanar with the rest of the molecular plane. Also, this verifies strongly that the electrochemical reduction center is the α,β-unsaturated 5-carbonyl group.

References

1) A. S. Mitra and M. K. Rout, *J. Indian Chem. Soc.*, **38**, 893 (1962).

2) J. Dvorak and A. Beranova, Czech Patent 177547 (Cl Co 98 23/04). 15 Mar. 1979, Appl. 74/6, 467, 20 Sep. 1974, 2pp.

3) A. M. Osman, M. S. K. Youssef, and Kh. M. Hassan, *J. Prakt. Chem.*, **320**, 857 (1978).

4) M. R. Mahmoud, H. S. El-Kashef, and R. Abdel-Hamid, *Spectrochim. Acta, Part A*, **37**, 519 (1981).

5) V. Reganti, M. S. Pecchiarello, P. P. Righetti, and G. Tacconi, *Gaz. Ghim. Ital.*, **110**, 105 (1980).

6) R. Abdel-Hamid, M. A. Abdel-Rahman, F. A. Rashwan, and M. M. El-Dessouki, *Bull. Soc. Chim. Fr.*, **1991**, 128.

7) G. Desimoni, A. Gamba, P. P. Righetti, and G. Tacconi, *Gaz. Chim. Ital.*, **104**, 491 (1972).

8) M. M. Rerick and E. L. Eliel, *J. Am. Chem. Soc.*, **84**, 2356 (1962).

9) a) O. Hammerich and V. D. Parker, *Electrochim. Acta*, **18**, 537 (1973); b) B. S. Jensen and V. D. Parker, *J. Chem. Soc., Chem. Commun.*, **1974**, 367; c) V. D. Parker, *J. Am. Chem. Soc.*, **97**, 5211 (1975); d) R. Lines, B. S. Jensen, and V. D. Parker, *Acta Chem. Scand. Ser. B*, **32**, 510 (1978).

10) R. S. Nicholson and I. Shain, *Anal. Chem.*, **36**, 706 (1964).

11) A. J. Bard and L. R. Faulkner, "Electrochemical Methods: Fundamental and Applications," John Wiley & Sons, New York (1980).

12) M. Grenness and K. B. Oldham, *Anal. Chem.*, **44**, 1121 (1972).

13) J. C. Imbeaux and J. M. Savean, *J. Electroanal. Chem.*, **44**, 169 (1973).

14) L. Nadjo, J. M. Saveant, and D. Tessier, *J. Electroanal. Chem.*, **52**, 403 (1974).

15) J. M. Saveant and D. Tessier, *J. Electroanal. Chem.*, **61**, 251 (1975).

16) J. M. Saveant and D. Tessier, *J. Electroanal. Chem.*, **65**, 57 (1975).

17) a) N. G. Gaylord, "Reduction with Complex Metal Hydride," Wiley, New York (1956); b) H. C. Brown and G. Zweifel, *Org. React.*, **13**, 1 (1963); d) H. O. Hause, in "Modern Synthetic Reaction," Benjamin, New York (1965), pp. 23—49; d) R. E. Lyle and Ander Sem, "P. S. Advances in Heterocyclic Chemistry," Academic Press, New York (1966), Vol. 6, p. 46.

18) E. L. Eliel, *Rec. Chem. Prog.*, **22**, 129 (1961).

19) M. N. Rerick and E. L. Eliel, *J. Am. Chem. Soc.*, **84**, 2356 (1962).

20) H. C. Brown and H. M. Hess, *J. Org. Chem.*, **34**, 2206 (1969).

21) M. J. Jorgenson, *Tetrahedron Lett.*, **1962**, 559.

22) C. F. Lane, *Chem. Rev.*, **76**, 773 (1976).

23) M. Uehara and J. Nakaya, *Bull. Chem. Soc. Jpn.*, **43**, 3136 (1970).

Conductivity of *N*-Methylpyridinium Iodide and Its Methyl Substituted Derivatives in Water-Ethanol Mixture

Ranjan Kumar Swain and B. Behera*
Department of Chemistry, Sambalpur University,
Jyotivihar, Sambalpur 768019, India
(Received April 4, 1991)

The conductivity of *N*-methylpyridinium iodide (NMPI) and its methyl substituted derivatives at 2-, 3-, and 4-positions in water–ethanol solvent mixtures is reported at 25 °C. The conductivity data are analyzed by the Shedlovsky method to get both Λ_0 and K_A, the association constant, simultaneously. The Λ_0 values decrease or increase with increase or decrease of the viscosity of the solvent mixtures. The values of Λ_0 and K are in the order of H>3->4->2-. The Walden product $\Lambda_0\eta$ for these iodide salts behaves in a manner as is expected for highly hydrogen bonded water–alcohol mixtures. A mole fraction of 0.15 to 0.2 in ethanol indicates maximum interaction between water and ethanol. The values of Λ_0 and K_A indicate greater solvation and hence less ion–ion interaction in case of NMPI and 3-CH_3 salts than 2- and 4-CH_3 salts.

N-Methylpyridinium iodide (NMPI) and its methyl substituted derivatives are formed from reaction of pyridine and picolines with methyl iodide in the form of ionic compounds. Kosower,[1] Roy,[2] Hemmes,[3] Jong-Gi Lee,[4] Bagchi[5] and co-workers have reported spectral, kinetic, and thermodynamic studies on NMPI in 90% and 100% ethanol and acetone solvent mixtures. All these studies point out to formation of solvent shared ion-pairs which is represented as:

$$\underset{\text{Contact ion pair}}{CH_3Py^+I^-} \rightleftarrows \underset{\text{Solvent shared ion pairs}}{CH_3Py^+, I^-} \rightleftarrows \underset{\text{Solvent separated ion pair}}{CH_3Py^+ + I^-} \quad (1)$$

Recently we have carried out the viscosity, apparent molar volume[6] in water at various temperatures and conductance[7] studies in water–methanol mixtures in the entire solvent composition range at 25 °C. All these studies indicate existence of solvent shared ion-pair. A mole fraction of 0.27 in methanol has indicated greater interaction between water and methanol. These studies also indicate difference in the solvation of ions and ion–ion interaction in this solvent system.

Conductance[3] studies of NMPI is only reported in 100% and 90% ethanol–water mixture at 25 °C. The entire solvent composition range has not been studied. In this paper we report conductance measurements of iodide salts of *N*-methylpyridinium ($NMPR^+I^-$) and its methyl substituted derivatives (**I**) in the entire water–ethanol composition range at 25 °C.

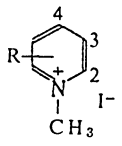

I

$NMPR^+I^-$: R=H, CH_3 at 2-, 3-, 4-positions.
When R=H the salt is NMPI.
Short abbreviations for the salts are H, 2-, 3- and 4-.

Experimental

The iodide salts (**I**) were prepared as already described.[6,7] The purity of the salts was checked by gravimetric estimation of iodide as silver iodide.[8] Ethanol was purified by refluxing over calcium oxide. Conductivity water having specific conductivity of 1.2×10^{-6} $\Omega^{-1}cm^{-1}$ was used. All the solvent mixtures of various composition were prepared by weight at 25 °C. Conductivity measurewments, in triplicate, were carried out as described earlier.[9] The conductivity measurements in the concentration range of 10^{-2} to 10^{-4} M(1 M=1 mol dm^{-3}) of the iodide salts were carried out at 25 °C.

Results and Discussion

NMPI ionizes in solution as

$$CH_3Py^+I^- \rightleftarrows CH_3Py^+ + I^- \quad (2)$$

and the ionization constant K is given by

$$K=\frac{\alpha^2 c}{1-\alpha}f_\pm^2. \quad (3)$$

The symbols have got their usual meaning. By analyzing the conductivity data by the Shedlovsky method[10] we employed

$$\alpha=\frac{\Lambda S(Z)}{\Lambda_0}$$

$$S(Z)=\left[\frac{Z}{2}+\left\{1+\left(\frac{Z}{2}\right)^2\right\}^{1/2}\right]^2 \quad (4)$$

$$Z=S\Lambda_0^{-1.5}(c\Lambda)^{1/2}$$

and

$$S=B_1\Lambda_0+B_2.$$

Both K and Λ_0 were obtained by least-square analysis of Eqs. 5 and 6.

$$\frac{1}{\Lambda S(Z)}=\frac{1}{K\Lambda_0^2}\Lambda C f_\pm^2 S(Z)+\frac{1}{\Lambda_0}, \quad (5)$$

$$\mathrm{Log}f_\pm=-\frac{A\sqrt{I}}{1+\sqrt{I}}, \quad (6)$$

where $I=\alpha C$ and A, B_1, and B_2 are Debye–Hückel and Onsager constants. The values of the physical constants of water–ethanol system[11] are set out in Table 1. In all the calculations the correlation coefficient was found to lie between 0.99 and 1 and the error of estimate

Table 1. Physical Constants[a] of Water+Ethanol Mixture at 25 °C

% Ethanol w/w	ε	η CP	B_1 $mol^{-1/2}\,dm^{3/2}$	B_2 $mol^{-3/2}\,\Omega\,cm^2\,dm^{3/2}$	A
0	78.3	0.8904	0.2299	60.57	0.51108
10	72.8	1.323	0.2564	42.28	0.57008
20	67.0	1.815	0.2904	32.12	0.64569
30	61.1	2.180	0.3335	28.00	0.74143
40	55.0	2.350	0.3905	27.38	0.86814
50	49.0	2.400	0.46437	28.41	1.03238
60	43.4	2.240	0.55902	32.34	1.23851
70	38.0	2.037	0.67996	38	1.51168
80	32.8	1.748	0.84791	47.67	1.88505
90	28.1	1.424	1.06931	63.22	2.37725
100	24.3	1.096	1.32970	88.33	2.95614

a) Data from Ref. 11.

Table 2. Values of Λ_0 of Compounds I in Water+Ethanol Mixture at 25 °C

% Ethanol	Λ_0/ $Ohm^{-1}\,cm^2\,mol^{-1}$			
w/w	H	2-	3-	4-
0	174.91	153.85	160.53	158.11
10	125.47	104.61	111.77	108.57
20	95.76	77.70	82.99	80.93
30	80.05	65.83	71.96	68.82
40	72.12	59.60	66.30	62.55
50	65.76	54.62	63.76	58.67
60	66.62	53.44	62.50	57.53
70	67.33	54.24	65.36	59.07
80	71.53	57.27	66.77	61.59
90	78.49	61.38	73.84	67.78
100	84.41 (62.6)[a]	68.05	80.58	72.60

Error of estimate is 0.02% and r lies between 0.99 and 1.
a) Data from Ref. 3.

Table 3. Values of K_A of Compounds I in Water+Ethanol Mixture at 25 °C

% Ethanol	K_A/ $dm^3\,mol^{-1}$			
w/w	H	2-	3-	4-
0	1.12	5.44	1.80	3.76
10	5.03	12.29	5.69	9.77
20	10.73	16.19	12.14	13.61
30	14.40	20.17	15.78	17.85
40	19.24	25.15	20.58	22.96
50	23.39	30.59	25.79	28.49
60	30.85	38.40	32.27	36.76
70	35.42	46.15	39.48	44.37
80	49.98	61.27	52.50	57.22
90	69.67 (41.7)[a]	86.1	73.07	79.02
100	98.49 (107)[a]	122.14	105.65	112.74

Error of estimate is 0.02% and r lies between 0.99 and 1.
a) Data from Ref. 3.

was 0.02%. The initial value of Λ_0 needed for calculation was obtained from the plot of Λ against $\sqrt{C}$. The results of such calculations are set out in Tables 2 and 3.

The variation of Λ_0 of these compounds and the η of the solvent mixtures with the mole fraction of ethanol are shown in Fig. 1. The viscosity of water-ethanol

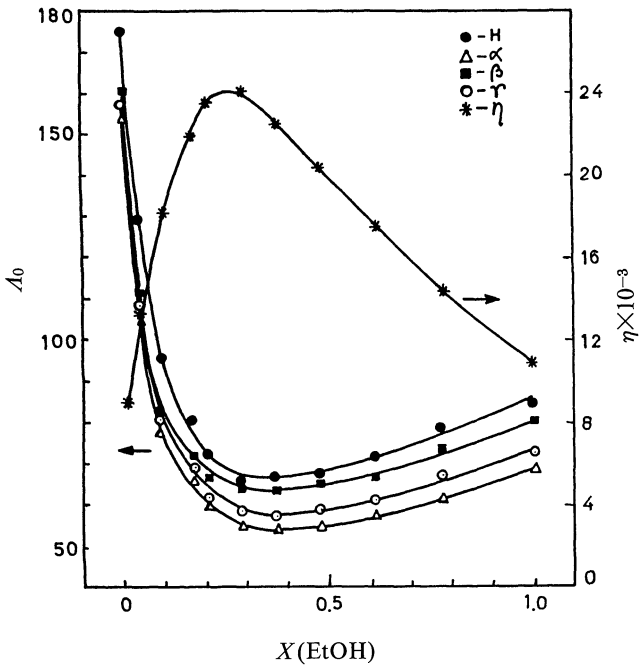

Fig. 1. Variation of Λ_0 and η against mole fraction of ethanol.

mixtures increases up to a mole fraction of 0.31 and then gradually decreases. The Λ_0 values of these iodide salts decrease up to this mole fraction and then increase in ethanol-rich region, showing opposite behavior to the viscosity of the medium. The association constant, K_A, of these salts gradually increases with increase in ethanol composition (Fig. 2). The association constants are in the order H<3-<4-<2-. The Λ_0 values are in the order H>3->4->2-. These results indicate that the viscosity of the medium plays an important role on the mobility of ions in solution.

Fuoss[12] has pointed out that the plot of $\log K_A$ vs. $1/\varepsilon$ should be linear in the vicinity of the dielectric constant, lying below 40. This prediction by Fuoss is obeyed by NMPI and its methyl substituted derivatives in alcohol-rich region where the dielectric constant lies

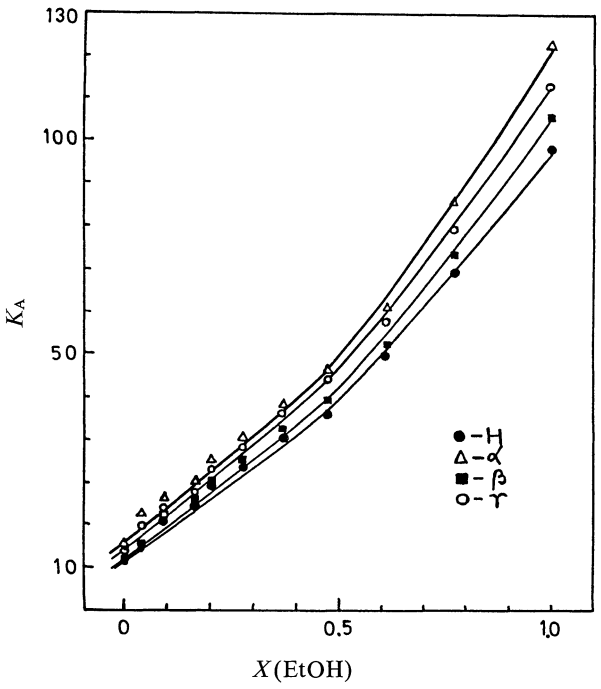

Fig. 2. Variation of K_A with mole fraction of ethanol.

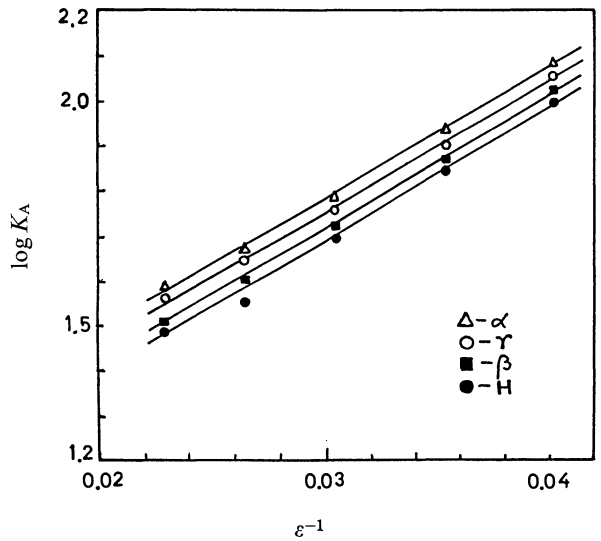

Fig. 3. Variation of log K_A with $1/\varepsilon$.

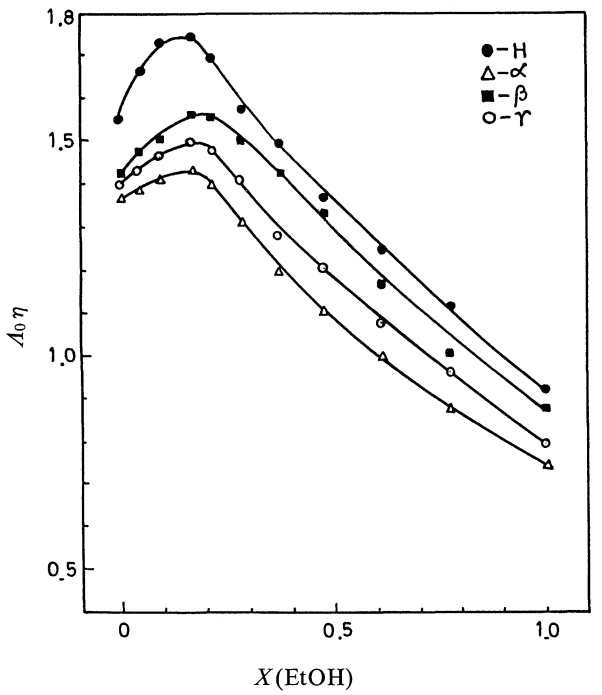

Fig. 4. Variation of Walden product with mole fraction of ethanol.

Table 4. Values of $\Lambda_0\eta$ of Compounds **I** in Water+Ethanol Mixture at 25 °C

% Ethanol	$\Lambda_0\eta$			
w/w	H	2-	3-	4-
0	1.557	1.370	1.429	1.408
10	1.660	1.384	1.479	1.436
20	1.738	1.410	1.506	1.469
30	1.745	1.435	1.569	1.500
40	1.695	1.401	1.558	1.470
50	1.578	1.311	1.500	1.408
60	1.492	1.197	1.424	1.289
70	1.372	1.105	1.331	1.203
80	1.250	1.001	1.167	1.077
90	1.118	0.874	1.051	0.965
100	0.925	0.746	0.883	0.796

below 40 (Fig. 3).

The Walden product $\Lambda_0\eta$ for the entire solvent range for these salts is given in Table 4 and shown in Fig. 4 as a function of mole fraction of ethanol. The Walden product passes through a maximum which lies between 0.15 and 0.2 in ethanol mole fraction and then decreases at higher ethanol content. It has been pointed out[13] that the Walden product of water–alcohol mixtures passes through a maximum and the values are quite high as expected for highly hydrogen-bonded solvents. Both cation $NMPR^+$ and anion I^- can move through the solutions overcoming the viscous forces in the solvent system. The structure of water determines the Walden product in water–ethanol mixtures. The trend in the Walden product of these salts in water–ethanol solvent mixtures clearly indicates strong interaction between water and ethanol.

The Λ_0 and K values indicate that NMPI and 3-CH_3 salts are more close to each other than 2- and 4-salts. The ion–ion interaction takes place between $NMPR^+$ and I^- to form ion-pairs through preferential solvation of these ions in both water-rich and ethanol-rich regions. The electron donating capacity of methyl group at 2- and 4-positions partially neutralizes the positive charge in the pyridinium ion. Such partial neutralization is not possible in NMPI and 3-CH_3 salts. Therefore the 2- and 4-salts are less solvated than NMPI and 3-CH_3 salts. This results in greater ion–ion interaction between $NMPR^+$ and I^- ions of 2- and 4-salts is

reflected in the low values of Λ_0 and high values of K_A than the corresponding values of NMPI and 3-CH_3 salts. All these data favor the existence of solvent shared ion-pairs of these salts in water–ethanol solvent mixtures.

Financial assistance by Council of Scientific and Industrial Research, New Delhi for this piece of work is highly acknowledged.

References

1) E. M. Kosower, D. Hofman, and K. Wallenfels, *J. Am. Chem. Soc.*, **84**, 2755 (1962).
2) A. Roy, *J. Am. Chem. Soc.*, **93**, 7178 (1971).
3) P. Hemmes, J. N. Constanzo, and F. Jordan, *J. Phys. Chem.*, **82**, 387 (1978).
4) Jong-Gi Jee, Young-Hwa Lee, Eui-Ha Woo, and Kyung-Hee Lee, *Bull. Korean Chem. Soc.*, **4**, 115 (1983).
5) M. Pal and S. Bagchi, *Indian J. Chem., Sect. A*, **23**, 800 (1984); M. Pal, K. Medda, and S. Bagchi, *ibid.*, **26**, 458 (1987); K. Medda, M. Pal, and S. Bagchi, *J. Chem. Soc., Faraday Trans. 1*, **84**, 1501 (1988).
6) R. K. Swain, L. K. Tiwary, and B. Behera, *Bull. Chem. Soc. Jpn.*, **63**, 1503 (1990).
7) R. K. Swain, S. C. Das, and B. Behera, *J. Electrochem. Soc. India*, **39**, 89 (1990).
8) A. I. Vogel, "A Textbook of Quantitative Inorganic Analysis," 4th ed, ELBS and Longmans, London (1978), p. 496.
9) K. Behera, B. Sahu, S. Pradhan, and B. Behera, *Indian J. Chem., Sect. A*, **22**, 20 (1983); S. Rath and B. Behera, *J. Electrochem. Soc. India*, **37**, 207 (1988).
10) T. Shedlovsky, *J. Franklin Inst.*, **225**, 661 (1933); R. M. Fuoss and T. Shedlovsky, *J. Am. Chem. Soc.*, **71**, 1496 (1949).
11) E. M: Wooley, D. G. Hurkot, and L. G. Hepler, *J. Phys. Chem.*, **74**, 3908 (1970); H. S. Harned and B. B. Owen, "The Physical Chemistry of Electrolyte Solutions," Reinhold, New York (1958), p. 161.
12) R. M. Fuoss, *J. Am. Chem. Soc.*, **80**, 509 (1958).
13) J. F. Coetzee and C. D. Ritchie, "Solute–Solvent Interactions," Marcel Dekker Inc., New York (1978), Vol. 2, p. 174.

Thermospray Ionization Mass Spectrometry of Polydimethylsiloxane Antifoams

Toshihide NISHIMURA,* Yukimi AOKI, Yukio HIYAMA, and Akio SONODA
Control Research and Development, Upjohn Pharmaceuticals Ltd., 23 Wadai, Tsukuba, Ibaraki 300-42
(Received June 28, 1991)

Mass Spectrometric characterization of several polydimethylsiloxane (PDSI) antifoams has been studied using a thermospray (TSP) ionization technique. The PDSI antifoams dissolved into an eluent were flow-injected to a TSP interface without column separation. A selective formation of PDSI ammonium adduct ions directly reflecting their molecular weight distributions was observed in the mass region up to 3500 daltons. Both cyclic PDSIs and fatty acid esters were detected for a water-dilutable antifoam and their relative abundances and species were characteristic to a particular formulation of antifoam emulsion. Thus TSP mass spectrometric technique seems suitable and useful for analysis of an aqueous antifoam sample to identify both its molecular weight distribution of PDSIs and a type of antifoam formulations used in various fields such as food and pharmaceutical industries.

Since silicone oils are offen used to eliminate foam that has already formed (defoam) and to prevent the formation of foam (antifoam). There are mainly two types of silicone antifoams: One is the antifoam emulsion which is a water-dilutable formulation containing fatty acid esters as emulsifiers, and another is so called the antifoam oil which is a formulation without a water-dilutable emulsifier.

Very few mass spectrometric studies of PDSI polymers have been reported so far. Appeared in the literature were the electron ionization (EI)[1] and fast atom bombardment (FAB)[2] techniques which provided mass spectra covering only the range less than 500 daltons, and their interpretations were limited to fragment ions because of such a hard ionization. Mass spectra reported, therefore, suffer from lack of PDSI molecular weight distribution which is highly important to characterize and/or to identify a formulation of antifoam in a sample to be analyzed.

Field desorption and laser desorption mass spectrometries may be applicable to measure molecular weight distributions of PDSI polymers. There has been a recent publication of mass spectra of quasi-molecular ions obtained by a laser microprobe.[3] However, thermospray (TSP) ionization mass spectrometry[4] is another soft ionization technique to produce mainly quasi-molecular ions, and is directly applicable to an aqueous sample. Here reported is a study on measurement of PDSI molecular weight distributions over a high mass range up to 3500 daltons using TSP ionization mass spectrometry.

Experimental

Instruments. TSP mass spectra were obtained on a Finnigan MAT-90 double-focusing magnetic sector mass spectrometer equipped with a TSP interface and a DEC PDP 11/73 data primary processor system. Voltages applied to an ion source and extraction lens were adjusted to optimize both the intensity and peak shape of m/z 141 ions which are the acetonitrile cluster ions, $(CH_3CN)_3NH_4^+$. All experiments were carried out under mass resolution of ca. 5500 (at 10% valley) at this mass and with the vaporizer and ion source temperatures of about 160 and 230 °C, respectively. The eluents for antifoam emulsions and antifoam oils were a mixture of 30% acetonitrile and 70% reagent water containing 0.1 M (M=mol dm^{-3}) ammonium acetate and that of 30% acetone and 70% 0.1 M ammonium acetate, respectively. The former eluent was chosen since emulsion antifoams are soluble to an aqueous solution but oil antifoams are not. The latter eluent was used for oil antifoams since those such as the KF-96 series partially dissolve into acetone and also acetone itself has a good solubility to water. The eluents were degassed by a continuous purge with helium at about 30 ml min^{-1} to maintain very low levels of dissolved air. The eluents were introduced into a thermospray vaporizer at a flow rate of 1.2 ml min^{-1} using a Waters MS-600 HPLC pump and were effectively pumped out from the ion source by a Bulzers UNO-016B rotary pump with volume flow rate of 16 m^3 h^{-1}. PDSI samples were prepared to be in a concentration of 100—1000 ppm level by an eluent, and were flow-injected directly to a TSP interface by a 100 μl Rheodyne 7125 loop injector without column separation.

Materials. Anti-foaming silicone oils were obtained commercially: Two typical oil antifoams, KF-96-10CS (lot 908646) and KF-96-100CS (lot 906524), and two typical water-dilutable emulsions, KM-72A (lot 909609) and KM-82F (lot 904228). These were all obtained from the Shin Etsu Silicone Corp. Acetonitrile and acetone were of the super special grade (Wako Pure Chemical Industries, LTD.), and reagent water was obtained from a Milli-Q (Millipore Corp.) water purification system. Ammonium acetate was of the JIS super grade (Wako Pure Chemical Industries, LTD.).

Results and Discussion

Molecular Weight Distribution of Polydimethylsiloxanes. TSP ionization of a molecule (A) using ammonium acetate solution results mainly in formation of both molecular protonated ions (AH^+) (Reaction 1) and ammonium adduct ions (ANH_4^+) (Reaction 2), although generally other ions (Reaction 3—5) could be produced. A schematic picture of ion formation could be given briefly as follows:

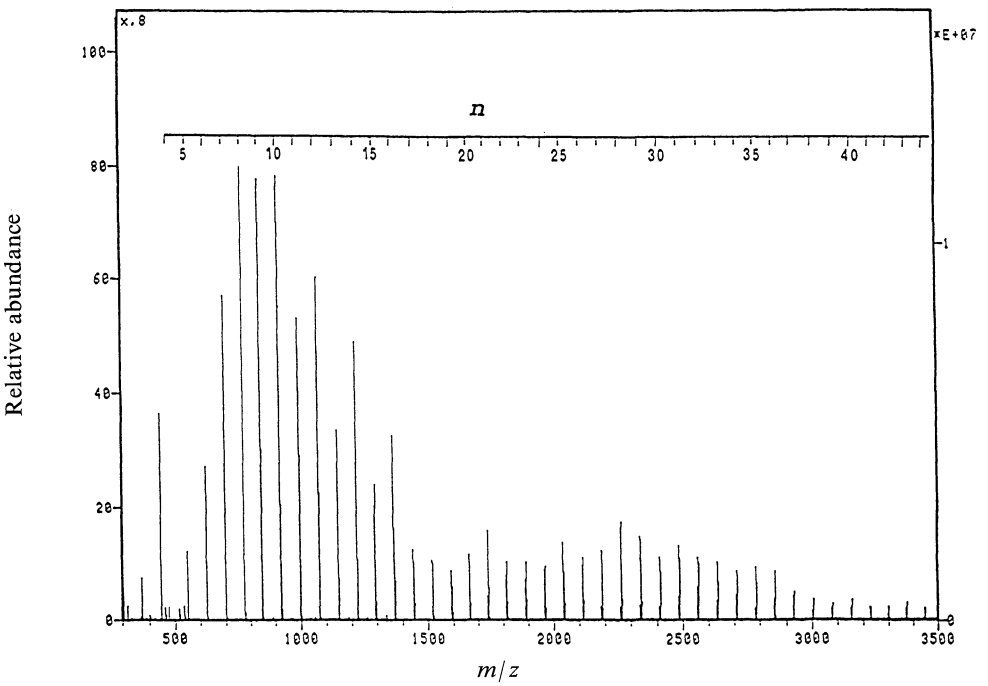

Fig. 1. A TSP mass spectrum of a medium size silicone oil antifoam (Shin Etsu KF-96-10CS).

$$A + (CH_3CN)_3NH_4^+ \longrightarrow AH^+ + 3\ CH_3CN + NH_3 \quad (1)$$

$$\longrightarrow ANH_4^+ + 3\ CH_3CN \quad (2)$$

$$\longrightarrow A(CH_3CN)NH_4^+ + 2\ CH_3CN \quad (3)$$

$$\longrightarrow A(CH_3CN)_2NH_4^+ + CH_3CN \quad (4)$$

$$\longrightarrow A(CH_3CN)_3NH_4^+ \quad (5)$$

when $(CH_3CN)_3NH_4^+$ is a reactant ion, which is one of reagent ions observed commonly in TSP mass spectra obtained using the eluent of ammonium acetate-acetonitrile, while their exact mechanisms of formation have not been known. Abundances of product ions may depend entirely on chemical nature such as proton affinities etc. of both a sample molecule A and a conjugate base of reactant ion. The formation of PDSIs ammonium adduct ions (Reaction 2) took place selectively. The chemical formula of both linear and cyclic PDSIs are respectively:

$$[(CH_3)_3Si\text{-}O\text{-}\{(CH_3)_2Si\text{-}O\text{-}\}_n\ Si(CH_3)_3 + NH_4^+] \quad (6)$$

$$[\{\text{-}(CH_3)_2Si\text{-}O\text{-}\}_{l+2} + NH_4^+] \quad (7)$$

Herein n and l correspond to the size of linear and cyclic PDSIs. Figire 1 shows a typical TSP mass spectrum obtained for the linear silicones (KF-96-10CS) in which individual peaks correspond to quasi-molecular ions formed via ammonium addition to PDSIs of their different sizes. This silicone oil has two maxima in its molecular weight distribution: One is located around n=9 and another is around n=27.

A high natural abundances of Si isotopes results in broad isotope distributions which vary drastically with increasing the size of PDSI, n (Fig. 2). The isotope ratio of $[P_{M+1}]/[P_M]$ for the linear silicones can be

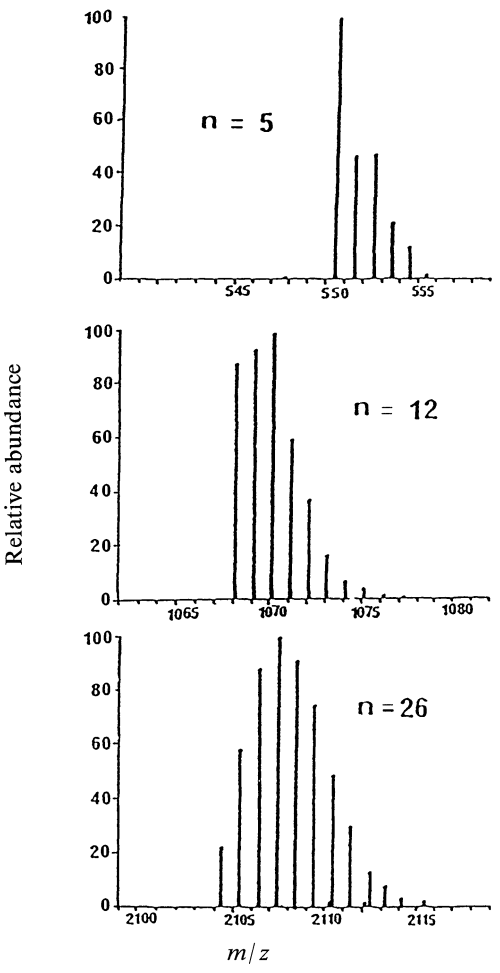

Fig. 2. Typical isotope distributions of several large linear PDSIs (Shin Etsu KF-96-10CS).

approximately expressed by[5]

$$[P_{M+1}]/[P_M]=0.07438n+0.17593 \quad (8)$$

using both the chemical formula of M= $C_{2n+6}H_{6n+22}O_{n+1}Si_{n+2}N_1$, which is the ammonium adduct quasi-molecular ions of linear PDSIs, and the natural isotope abundances for the individual component atoms known in the literature.[6]

Experimental ratios of $[P_{M+1}]/[P_M]$ observed were compared to those calculated by Eq. 8 in Fig. 3, and showed a reasonably good agreement with the calculation. Scattered points for $n>20$ in the figure may be due to low signal-to-noise ratio of the [M] and [M+1] signals observed for a large size silicone. This result may support validity of our estimation of molecular sizes. Detection of very large PDSIs and their quantification will encounter difficulties because of their low solubility to the eluents currently used.

Figure 4 shows a TSP mass spectrum of quasi-molecular ions of PDSI contained in the KF-96-100CS

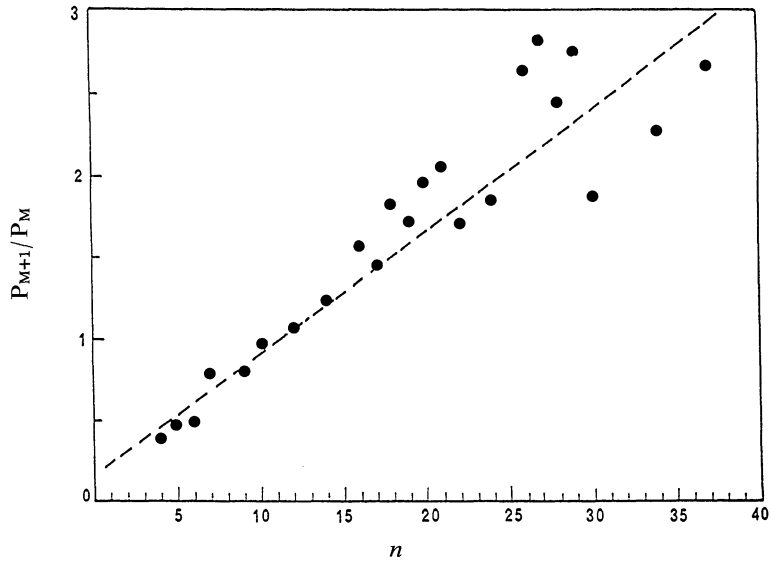

Fig. 3. Experimental isotope ratios $[P_{M+1}/P_M]$ (closed circles) together with theoretical calculations (dashed line).

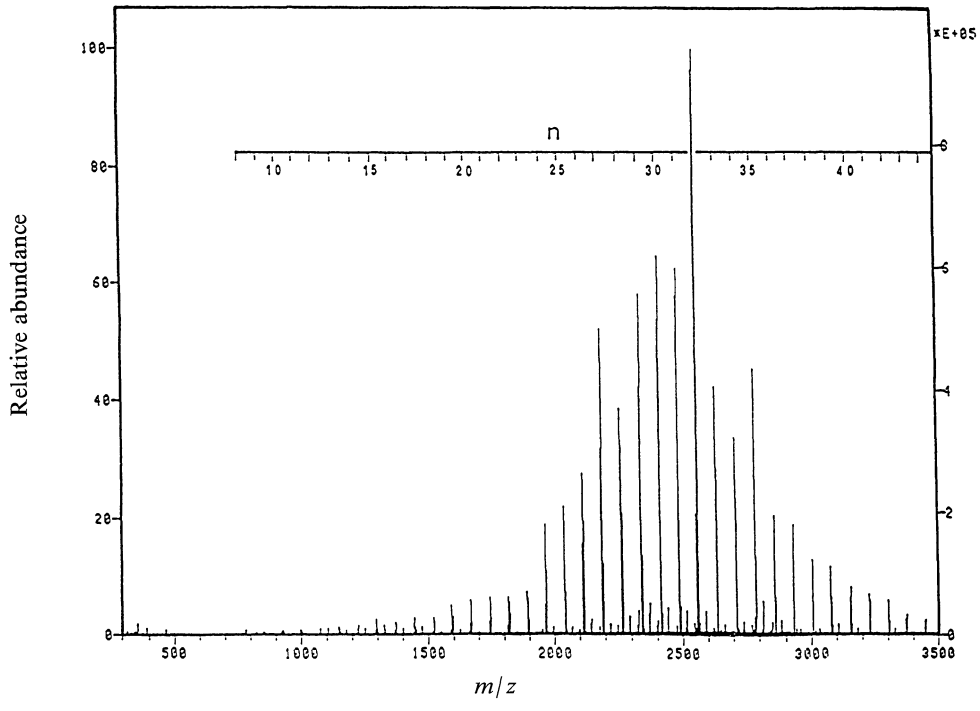

Fig. 4. A TSP mass spectrum of a large size silicone oil antifoam (Shin Etsu KF-96-100CS).

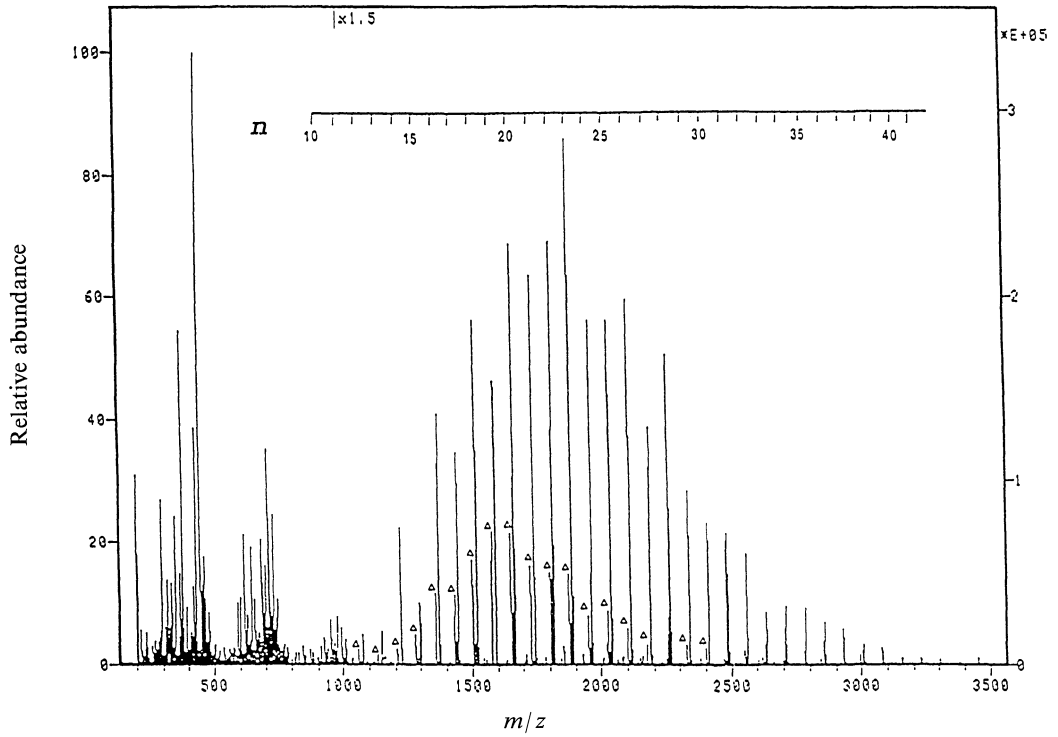

Fig. 5. A TSP mass spectrum of the antifoam emulsion formulation (Shin Estu KM-72A).

silicone oil. Its distribution maximum lay around n=30, and the mass spectrum showed the size of PDSI much larger than those in the KF-96-10CS formulation.

Figure 5 is a typical TSP mass spectrum of the KM-72A water-dilutable antifoam. Its distribution of PDSI quasi-molecular ions spreads from n=12 to n=44, and has a distribution center around n=22 to n=25. Additionally, a considerable amount of cyclic PDSIs

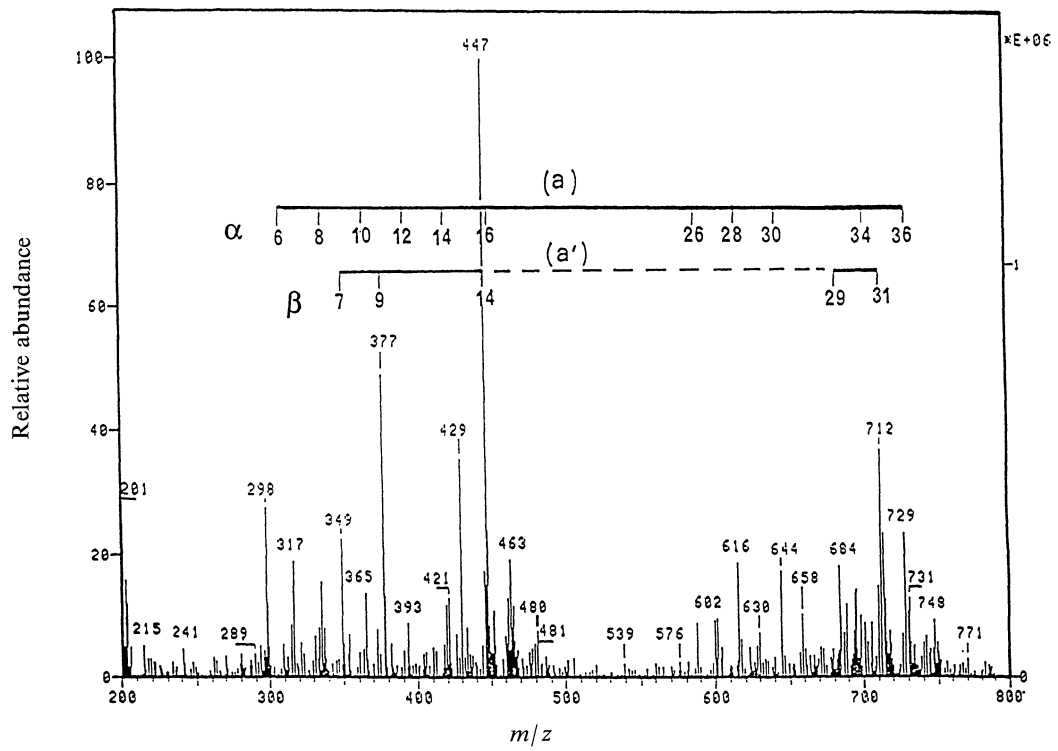

Fig. 6. A mass spectrum of fatty acid esters contained in the antifoam emulsion (Shin Etsu KM-72A): (a) and (a′) denote saturated and unsaturated fatty acid esters with sorbitol, respectively.

(indicated by open triangles) were also observed together with those of linear PDSIs in its mass spectrum.

For the KM-82F, which is another example of antifoam emulsions, its distribution of PDSIs lies from n=7 to n=38, indicating the size of PDSIs slightly smaller than those in the KM-72 formulation. Its distribution center of PDSIs is located around n=20, and the amount of cyclic PDSIs contained is considerably lower than that in the KM-72A formulation.

Fatty Acid Esters in Antifoam Emulsions. Commercial antifoam emulsions (oil-in-water emulsion) contain fatty acid esters as emulsifiers. Species and amounts of these emulsifiers are specific to a type of antifoam emulsion. Their quasi-molecular ions were observed in the mass regime less than 1000 daltons. The TSP mass spectra obtained were characterized by series of molecular protonated ions with the separation of m/z 28 or 14 due to size difference of fatty acid chains.

Typical emulsifiers are esters of fatty acids

Saturated fatty acids

$$CH_3(CH_2)_\alpha COOH \tag{9}$$

Unsaturated fatty acids

$$CH_3(CH_2)_a CH=CH(CH_2)_b COOH$$
$$\beta = a + b \tag{10}$$

with sorbitan, glycerol and sucrose. TSP mass spectra obtained for commercial antifoam emulsions containing sorbitan fatty acid esters often showed quasi-molecular ions of sorbitol fatty acid esters. These sorbitol fatty acid esters seems to be formed via elimination of a water molecule from a sorbitan ester under TSP ionization conditions.

TSP mass spectra of the KM-72A formulation (Fig. 6) showed an inclusion of both sorbitol saturated fatty acid esters (α=6, 8, 10, 12, 14, 16, 26, 28, 30, 34, and 36) and sorbitol unsaturated fatty acids (β=9, 11, 16, 31, and 33) in the region less than 800 daltons. The base ion peak was ascribed to the sorbitol ester with an unsaturated fatty acid, that is sorbitol oleate (MH^+= m/z 477).

In contrast with the KM-72A formulation, both glycerol saturated fatty acids (α=14, 16, and 21) and sucrose saturated fatty acid esters (α=12, 14, and 16), were observed in a TSP mass spectrum of the KM-82F antifoam formulation. The base peak corresponds to the glycerol stearate (m/z 360).

Conclusion

The TSP ionization technique provided mass spectra reflecting molecular weight distribution of polydimethylsiloxane polymers and fatty acid esters contained in emulsion formulations. Both cyclic PDSIs and fatty acid esters observed were found to be characteristic to individual water-dilutable formulations. TSP mass spectrometric analysis of PDSI antifoams thus seems useful to identify a particular type of antifoams contained in aqueous samples.

References

1) J. C. Cleaver and P. N. Fiveash, Vacuum, **20**, 49 (1970).
2) R. B. Freas and J. E. Campana, *Anal. Chem.*, **58**, 2434 (1986).
3) R. Holm, M. Karas, and H. Vogt, *Anal. Chem.*, **59**, 371 (1987).
4) C. R. Blakley, J. J. Carmody, and M. L. Vestal, *J. Am. Chem. Soc.*, **102**, 5933 (1980).
5) K. Biemann, "Mass Spectrometry, Organic Chemical Applications," McGraw-Hill Inc., New York (1962).
6) Natural isotope abundance: "CRC Handbook of Chemistry and Physics," 65th ed, 1984—1985, B236—B239.

Reaction of α-Oxo Ketene Dithioacetals with Glycine

Naoaki FUKADA* and Masato YUZAWA
Department of Chemistry, Faculty of Science, Chiba University, Yayoicho, Chiba 260
(Received April 8, 1991)

Synopsis. 3-Carboxymethylamino-3-methylthio-1-phenyl-2-propen-1-ones were synthesized by the reaction of 3,3-bis(methylthio)-1-phenyl-2-propen-1-ones with glycine in the presence of sodium hydroxide.

We were interested in studying the polarized α-oxo ketene *N,S*- and *N,N*-acetals, a new class of vinylogous amides, which are versatile synthons used for the synthesis of various heterocyclic compounds.[1] Many displacement reactions of α-oxo ketene dithioacetals[2,3] with nucleophiles have been reported, but there have been few reactions with amino acids mentioned in the literature. Gante et al. described the synthesis of glycine ester derivatives (**1**; R^1=CN, R^2=CN or $COOC_2H_5$) from the bis(methylthio)methylene compounds and glycine ethyl ester.[4] Also, Junjappa et al. reported that the reaction of methyl 2-benzoyldithioacetate with glycine ethyl ester gave *N*-ethoxycarbonylmethyl-2-benzoylthioacetamide, which was converted by methylation into 3-ethoxycarbonylmethylamino-3-methylthio-1-phenyl-2-propen-1-one(**1**; R^1=C_6H_5CO, R^2=H).[5]

In this note we report on a new synthesis of 3-carboxymethylamino-3-methylthio-1-phenyl-2-propen-1-ones (**3**) by a reaction of 3, 3-bis (methylthio)-1-phenyl-2-propen-1-ones (**2**)[6–8] with glycine. The starting materials **2**, including new compounds **2b** and **2e**, were prepared from acetophenones, carbon disulfide, and methyl iodide in the presence of sodium hydride.

The reaction of **2** with glycine was conducted in ethanol–water (10 : 1) in the presence of sodium hydroxide under reflux for 20 h. Double molar quantities of glycine and sodium hydroxide were used; yellow or orange products **3** were obtained in moderate to good

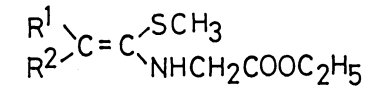

1

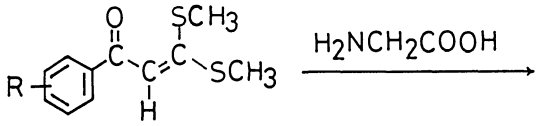

2

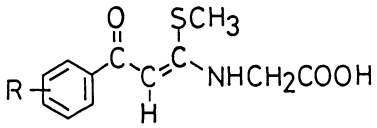

3

a : R=H b : R=3-CH_3
c : R=4-CH_3 d : R=4-CH_3O
e : R=3-NO_2 f : R=4-NO_2

Table 1. Physical Properties and Spectral Data

Compd	Yield[a] %	Mp[b] θ_m/°C (Solvent)	IR spectra in KBr (cm^{-1})	UV spectra in EtOH (nm) (log ε)	Molecular formula	Found (Calcd) (%) C	H	N
3a	63 (22)	154—155 (EtOH)	3030—2880 (s) 1730 (vs) 1590 (vs)	248 (4.00), 346 (4.32)	$C_{12}H_{13}NO_3S$	57.52 (57.35)	5.21 (5.21)	5.59 (5.57)
3b	49 (31)	149—150 (EtOH)	3020—2840 (s) 1725 (vs) 1590sh (m)	251 (4.07), 345 (4.34)	$C_{13}H_{15}NO_3S$	58.93 (58.85)	5.70 (5.70)	5.24 (5.28)
3c	50 (29)	158—160 (EtOH)	3020—2840 (s) 1730 (vs) 1608 (s)	254 (4.14), 345 (4.47)	$C_{13}H_{15}NO_3S$	58.83 (58.85)	5.64 (5.70)	5.20 (5.28)
3d	45 (32)	149—150 (EtOH)	3000—2830 (s) 1735 (vs) 1600 (s)	218 (3.99), 223 (3.99), 265 (3.96), 348 (4.50)	$C_{13}H_{15}NO_4S$	55.65 (55.50)	5.33 (5.37)	4.90 (4.98)
3e	74 (6)	171—172 (AcOH)	3060—2880 (s) 1725 (vs) 1608 (s)	230 (4.09), 247sh (3.99), 350 (4.22)	$C_{12}H_{12}N_2O_5S$	48.57 (48.64)	4.13 (4.08)	9.19 (9.45)
3f	81 (0)	193—195 (AcOH)	2950—2800 (s) 1725 (vs) 1600sh (m)	259 (4.18), 295sh (4.01), 374 (4.20)	$C_{12}H_{12}N_2O_5S$	48.64 (48.64)	4.05 (4.08)	9.26 (9.45)

a) The yield in parenthesis refers to that of the recovered starting material **2**. b) Decomposition.

yields. A larger excess of the base resulted in a lower yield and often gave the corresponding acetophenone in a decomposed form. In the absence of sodium hydroxide the yield was only about 3%, and in the case of using triethylamine or sodium acetate used as a base, the reaction hardly proceeded. A reflux time of 20 h was set in order to make comparisons with the substituent effect of the phenyl groups. Nitro derivatives **2e** and **2f** afforded the desired products, **3e** and **3f**, in good yields; from methyl and methoxy compounds **2b—d**, however, the glycine derivatives **3b—d** were obtained in lower yields and about 30% of the corresponding unreacted starting materials were recovered (Table 1).

The IR spectra of **3** showed a carbonyl absorption of the free carboxyl group at 1725—1735 cm^{-1} as those of other *N*-substituted glycines, *N*-phenylglycine (1720 cm^{-1}) and hippuric acid (1750 cm^{-1}). From the ^1H NMR spectrum of **3a** a single structure of *Z*-isomer was derived, which had the same geometry as its ethyl ester **1** ($R^1=C_6H_5CO$, $R^2=H$).[5] The spectrum showed a single methyl absorption at $\delta=2.55$ and a triplet assigned to NH at a higher field ($\delta=1.70$). This was due to a non-hydrogen-bonding NH proton to the carbonyl oxygen. The reactions of α-oxo ketene dithioacetals with nucleophiles, just as with organocopper reagents, appear to proceed in a stereoselective fashion, and also to involve an addition-elimination sequence.[2,9] In general, the α-oxo ketene *S,S*-acetals arising from alkyl and aryl ketones react with amines to afford *E*- and *Z*-isomers of the α-oxo ketene *N,S*-acetals, respectively.[2] Thus, our reaction probably led to more stable *Z*-isomers.

Attempts to prepare doubly displaced derivatives using a large excess of glycine were unsuccessful.

Experimental

α-Oxo Ketene Dithioacetals (2) were prepared by the reaction of the corresponding acetophenone (0.057 mol) with carbon disulfide (4.5 g, 0.059 mol) and methyl iodide(18 g, 0.13 mol) in the presence of sodium hydride (5 g; 60% dispersion in oil; 0.13 mol) in tetrahydrofuran (80 ml) with 3 h cooling in ice.

3,3-Bis(methylthio)-1-(*m*-tolyl)-2-propen-1-one(2b): Yellow crystals; yield 83%; mp 82—84 °C (CCl_4–hexane); IR(KBr) 1608s cm^{-1} (C=O); UV(EtOH) λ_{max} 225sh (log ε 3.77), 270sh (3.94), 277sh (3.94), and 345 nm (4.28). Found: C, 60.53;H, 5.94%. Calcd for $C_{12}H_{14}OS_2$: C, 60.47; H, 5.92%.

3,3-Bis(methylthio)-1-(*m*-nitrophenyl)-2-propen-1-one(2e): Yellow crystals; yield 84%; mp 130—131 °C (acetone); IR(KBr) 1615vs cm^{-1} (C=O); UV(EtOH) λ_{max} 240 (log ε 4.21), 287 (3.91), and 353 nm (4.26). Found: C, 49.08; H, 4.10; N, 5.17%. Calcd for $C_{11}H_{11}NO_3S_2$: C, 49.05; H, 4.12; N, 5.20%.

3-Carboxymethylamino-3-methylthio-1-phenyl-2-propen-1-ones (3). General Procedure. A solution of glycine (0.3 g, 0.004 mol) and sodium hydroxide (0.16 g, 0.004 mol) in ethanol (20 ml) and water (2 ml) was refluxed for 1 h. The α-oxo ketene dithioacetal **2** (0.002 mol) was added and the mixture was refluxed for 20 h. After the solvents were evaporated, 10 ml of water was added to the residue, and the mixture was stirred for 30 min. An insoluble solid, **2**, was collected, washed with water, and dried. To the filtrate was added a large excess of dilute hydrochloric acid; the mixture was kept overnight. The yellow or orange precipitate, **3** was collected, washed with water, dried, and recrystallized. In the case of **3e** or **3f**, 20 ml of water was added to the residue described above, and the mixture was stirred with warming. The collected **2e** was washed with hot water. Compound **2f** was not recovered.

^1H NMR (DMSO-d_6) of **3a** $\delta=1.70$ (t, 1H, NH), 2.55 (s, 3H, CH_3), 4.17 (d, 2H, CH_2), 5.79 (s, 1H, HC=), 7.32—7.49 (m, 3H, 3′, 4′, 5′-H), and 7.87—7.91 (m, 2H, 2′, 6′-H); ^{13}C NMR (DMSO-d_6) of **3a** $\delta=13.79$ (CH_3), 44.86 (CH_2), 86.50 (CH=), 126.75 (4′-C), 128.20 (3′, 5′-C), 130.58 (2′, 6′-C), 139.94 (1′-C), 168.62 (=CS(N)), 169.94 (COOH), and 183.88 (C=O).

References

1) Z.-T. Huang and X. Shi, *Synthesis,* **1990**, 162; R. T. Chakrasali, H. Ila, and H. Junjappa, *ibid.*, **1988**, 87, 851; A. Datta, H. Ila, and H. Junjappa, *ibid.*, **1988**, 248; A. K. Gupta, H. Ila, and H. Junjappa, *ibid.*, **1988**, 284; W.-D. Rudorf, *ibid.*, **1983**, 926, 928.

2) R. K. Dieter, *Tetrahedron,* **42**, 3029 (1986).

3) M. Kolb, *Synthesis,* **1990**, 171.

4) J. Gante and G. Mohr, *Chem. Ber.*, **108**, 174 (1975).

5) A. Rahman, H. Ila, and H. Junjappa, *Synthesis,* **1984**, 250.

6) C. Kelber, *Ber.*, **43**, 1252 (1910).

7) A. Thuillier and J. Vialle, *Bull. Soc. Chim. Fr.*, **1959**, 1398.

8) R. Spitzner, M. Menzel, and W. Schroth, *Synthesis,* **1982**, 206.

9) R. K. Dieter, L. A. Silks, III, J. R. Fishpaugh, and M. E. Kastner, *J. Am. Chem. Soc.*, **107**, 4679 (1985).

Asymmetric Transformation of (*RS*)-1,2,3,4-Tetrahydro-3-isoquinolinecarboxylic Acid via Salt Formation with (1*S*)-10-Camphorsulfonic Acid

Tadashi SHIRAIWA,* Tsuyoshi FURUKAWA, Tamotsu TSUCHIDA, Shinji SAKATA, Michio SUNAMI, and Hidemoto KUROKAWA
Faculty of Engineering, Kansai University, Yamate-cho, Suita, Osaka 564
(Received June 4, 1991)

Synopsis. Asymmetric transformation of (*RS*)-1,2,3,4-tetrahydro-3-isoquinolinecarboxylic acid [(*RS*)-TIC] by use of (1*S*)-10-camphorsulfonic acid [(*S*)-CS] as a resolving agent gave a salt of (*S*)-TIC with (*S*)-CS with 90% optical purity in hexanoic acid. The TIC obtained from the salt was purified to give optically pure (*S*)-TIC in 80% yield based on the starting (*RS*)-TIC.

(*S*)-1,2,3,4-Tetrahydro-3-isoquinolinecarboxylic acid [abbreviated as (*S*)-TIC] is a useful intermadiate for synthesizing antihypertensive agents such as (*S*)-2-(3-mercapt-1-oxopropyl)-1,2,3,4-tetrahydro-3-isoquinolinecarboxylic acid derivatives.[1—3] Although (*S*)-TIC has been obtained by condensation of L-phenylalanine [L-Phe] with formaldehyde in concentrated hydrochloric acid,[4,5] this reaction gives partially racemized (*S*)-TIC. Acquisition of optically pure (*S*)-TIC, therefore, seems to require a tedious procedure.[4,5]

We found that optically active TIC was apt to racemize only on heating in carboxylic acids and that optical resolution of (*RS*)-TIC by use of (1*S*)-10-camphorsulfonic acid [(*S*)-CS] as a resolving agent gave a salt of (*S*)-TIC with (*S*)-CS as the less soluble diastereomeric salt. In view of this, an asymmetric transformation of (*RS*)-TIC was attempted here via salt formation with (*S*)-CS on heating in a carboxylic acid to convert (*RS*)-TIC efficiently into (*S*)-TIC, as illustrated in Scheme 1.

In what follows, (*S*)·(*S*) salt denotes the salt of (*S*)-TIC with (*S*)-CS, (*R*)·(*S*) salt that of (*R*)-TIC with (*S*)-CS, and (*S*)·(*R*) salt that of (*S*)-TIC with (*R*)-CS.

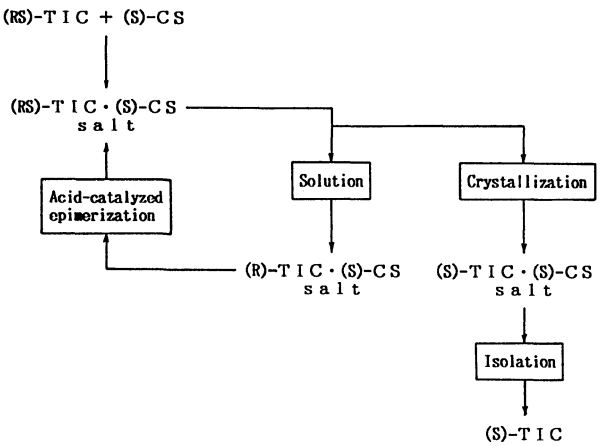

Scheme. 1. Illustration of asymmetric transformation of (*RS*)-1,2,3,4-tetrahydro-3-isoquinolinecarboxylic acid.
TIC: 1,2,3,4-Tetrahydro-3-isoquinolinecarboxylic acid.
(S)-CS: (1*S*)-10-Camphorsulfonic acid.

Experimental

Materials. L-Phe was purchased from Kokusan Chemical Works, Ltd., DL-Phe from Sigma Chemicals Co., and (*S*)- and (*RS*)-CS and (*R*)-CS monohydrate from Wako Pure Chemicals Ind.

(*RS*)- and (*S*)-TIC were prepared by a reaction of the corresponding Phe with formaldehyde in concentrated hydrohchloric acid.[4,5] (*RS*)-TIC was obtained in 69% yield and (*S*)-TIC ($[\alpha]_D^{20}$ −143° (*c* 1.00, 1 mol dm^{-3} aqueous sodium hydroxide)) in 78% yield. (*S*)-TIC was purified via formation of a salt with (*S*)-CS as described below.

Preparation of Standard Salts. (*S*)-TIC (4.43 g, 25.0 mmol) was added to a 10 cm^3 methanol solution containing 25.0 mmol of (*S*)-CS (5.81 g) or (*R*)-CS monohydrate (6.26 g). After stirring for 30 min in an ice bath, the mixture was allowed to stand overnight at 5 °C. The precipitated salt was collected by filtration, washed with diethyl ether, and dried. (*S*)·(*S*) salt: Mp 268—269 °C; $[\alpha]_D^{20}$ −41.3° (*c* 1.00, methanol). Found: C, 58.54; H, 6.58; N, 3.45%. Calcd for $C_{20}H_{27}NO_6S$: C, 58.66; H, 6.65; N, 3.42%). (*S*)·(*R*) salt: Mp 249—250 °C; $[\alpha]_D^{20}$ −85.1° (*c* 1.00, methanol). Found: C, 58.61; H, 6.62; N, 3.33%.

Asymmetric Transformation. A mixture of 1.77 g (10.0 mmol) of (*RS*)-TIC and 2.09 g (9.00 mmol) of (*S*)-CS in 15 cm^3 of butanoic acid or hexanoic acid was stirred for 2—25 h at 120 °C. After further addition of 0.23 g (1.0 mmol) of (*S*)-CS, the mixture was stirred for 5 min and then for 0.5 h in an ice bath. The (*S*)·(*S*) salt formed was collected by filtration, thoroughly washed with diethyl ether, and dried; the optical purity of the salt obtained was determined on the basis of the specific rotations of the standard salts.

After adding an equivalent of triethylamine to a solution of the salt obtained in methanol (25 cm^3 g^{-1}), the mixture was stirred for 1 h in an ice bath. The precipitated (*S*)-TIC was collected by filtration, washed with methanol, and dried. The optical purity was determined on the basis of the specific rotation of (*S*)-TIC; lit,[5] $[\alpha]_D^{19}$ −177.4° (*c* 1.00, 1 mol dm^{-3} aqueous sodium hydroxide).

The (*S*)-TIC (2.00 g) obtained by reaction for 12 h in butanoic acid and those for 20 and 25 h in hexanoic acid were added to a solution containing an equivalent of (*S*)-CS in 17 cm^3 of methanol. After stirring the mixture for 20 min at 20 °C, the (*S*)·(*S*) salt formed was collected by filtration, washed with diethyl ether, and dried. The (*S*)·(*S*) salt was treated with triethylamine in methanol to give optically pure (*S*)-TIC.

Optical Resolution. (*RS*)-TIC (1.77 g, 10.0 mmol) was added to a solution of 2.32 g (10.0 mmol) of (*S*)-CS in 10 cm^3 of methanol. After stirring the mixture for 0.5 h at 20 °C, the formed (*S*)·(*S*) salt of 74.7% optical purity was collected by filtration, washed with diethyl ether, and dried; yield, 40.6% (1.66 g) based on 4.09 g of the salt; $[\alpha]_D^{20}$ −25.3° (*c* 1.00, methanol). The filtrate was dried under reduced pressure to give the (*R*)·(*S*) salt of 57.3% optical purity in 51.1% (2.10 g) yield; $[\alpha]_D^{20}$ +58.1° (*c* 1.00, methanol). The (*S*)·(*S*) and

(*R*)·(*S*) salts obtained were treated with triethylamine in methanol to give (*S*)- and (*R*)-TIC; (*R*)-TIC of 56.1% optical purity was obtained in 49.0% (0.867 g) yield; $[\alpha]_D^{20}$ +99.6° (*c* 1.00, 1 mol dm^{-3} aqueous sodium hydroxide). The (*S*)-TIC obtained was purified via salt formation with (*S*)-CS to obtain (*S*)-TIC of 99.2% optical purity in 33.3% (0.590 g) yield; $[\alpha]_D^{20}$ −176° (*c* 1.00, 1 mol dm^{-3} aqueous sodium hydroxide).

Rate Constant for Racemization. (*S*)-TIC (1.00 mmol) and 0.900, 0.950, or 1.00 mmol of (*RS*)-CS were immediately dissolved in 50 cm^3 of acetic acid, propanoic acid, or butanoic acid at 120 °C, respectively. Portions of the solution were pipetted out at appropriate time intervals and the optical rotation at 589 nm was measured with a Union Giken PM-101 digital polarimeter equipped with a quartz cell of 0.500 dm path length. The rate constant for racemization (k_R/s^{-1}) was calculated by least-squares fitting to the equation

$$\ln \alpha_0/\alpha_t = k_R \cdot t, \quad (1)$$

where α_t is the optical rotation at time t and α_0 that extrapolated to zero time.

Results and Discussion

Racemization of (*S*)-1,2,3,4-Tetrahydro-3-isoquinolinecarboxylic Acid. The racemization of (*S*)-TIC could be regarded as a pseudo first-order reaction because a linear relationship was found between $\ln \alpha_0/\alpha_t$ and time t. The rate constant (k_R/s^{-1}) and half-life period ($t_{1/2}$/s) are listed in Table 1.

The racemization of (*S*)-TIC seems to start with the protonation to the carbonyl oxygen atom by the carboxylic acid used as solvent, followed by the formation of an enol and the concomitant α-proton abstraction by the resulting carboxylate anion, and hence should be influenced by the acidity of the carboxylic acid.[6,7] The acidity constant (pK_a) of acetic acid, propanoic acid, and butanoic acid at 120 °C were estimated from the data at 0—60 °C[8] to be 5.07, 5.21, and 5.27, respectively. Since the k_R value paralells the pK_a value, the rate-determining step seems to be the enol formation.[7] In addition, the k_R value increased with a decrease in the amount of (*RS*)-CS, as seen in Table 1.

Asymmetric Transformation of (*RS*)-1,2,3,4,-Tetrahydro-3-isoquinolinecarboxylic Acid. In the optical resolution by use of (*S*)-CS, the (*S*)·(*S*) salt was obtained as the less soluble diastereomeric salt, as mentioned in the Experimental section. The asymmetric transformation, based on the results of the optical resolution and racemization, gave the (*S*)·(*S*) salt of 75—79% optical purity in 87—90% yield by reaction for 10—14 h in butanoic acid at 120 °C, as shown in Table 2. The (*S*)-TIC obtained from the (*S*)·(*S*) salt of 79% optical purity was purified to give (*S*)-TIC of 98% optical purity in 74% yield, based on the starting (*RS*)-TIC.

The epimerized salt seems to have a relatively high solubility in butanoic acid at 120 °C, and hence cooling of the reaction mixture would lower the optical purity of the resulting (*S*)·(*S*) salt. The (*S*)·(*S*) and (*R*)·(*S*) salts seem to be less soluble in higher carboxylic acids. Although the rates of racemization in the higher carboxylic acids could not be measured because of a poor solubility of (*S*)-TIC, the estimated pK_a value (5.26)[9] of hexanoic acid at 120 °C would suggest that the rate in hexanoic acid is approximately equal to that in butanoic acid. The asymmetric transformation, therefore, was carried out in hexanoic acid and gave the (*S*)·(*S*) salt of 90% optical purity in 86% yield by reaction for 20 and 25 h. Optically pure (*S*)-TIC was obtained in 80% yield by purification of the (*S*)-TIC obtained from these salts.

To summarize, the present results demonstrate that

Table 1. Rate Constant and Half-Life Period for Racemization[a]

Conditions		k_R[c]	$t_{1/2}$[d]
Carboxylic acid	(*RS*)-CS[b] mmol	10^{-4} s^{-1}	10^3 s
AcA[e]	0.900	4.19	1.65
PrA[f]	0.900	4.82	1.44
BuA[g]	0.900	7.75	0.894
	0.950	5.71	1.21
	1.00	2.77	2.50

a) (*S*)-1,2,3,4-Tetrahydro-3-isoquinolinecarboxylic acid 1.00 mmol; carboxylic acid 50 cm^3; temperature 120 °C. b) (*RS*)-CS: (1*RS*,4*SR*)-10-Camphorsulfonic acid. c) k_R: Rate constant for racemization. d) $t_{1/2}$: Half-life period. e) Acetic acid. f) Propanoic acid. g) Butanoic acid.

Table 2. Asymmetric Transformation of (*RS*)-1,2,3,4-Tetrahydro-3-isoquinolinecarboxylic Acid[a]

Carboxylic acid	Reaction time	(*S*)·(*S*) Salt[b] Yield	(*S*)·(*S*) Salt[b] Optical purity	(*S*)-TIC Yield[d]	(*S*)-TIC Optical purity
	h	g [%[c]]	%	%	%
BuA[e]	2	3.79 [92.7]	22.7	89.2	21.6
	4	3.73 [91.2]	42.5	87.0	36.9
	6	3.71 [90.7]	56.9	87.5	55.1
	8	3.68 [90.0]	64.8	84.5	65.9
	10	3.58 [87.5]	74.9	83.2	74.4
	12	3.60 [88.0]	78.7	86.1	76.6
				73.6[g]	98.0
	14	3.56 [87.0]	76.6	85.6	75.6
HxA[f]	2	3.79 [92.7]	11.7	89.6	10.1
	4	3.69 [90.2]	16.4	88.0	14.2
	6	3.56 [87.0]	42.4	84.7	42.3
	8	3.55 [86.8]	55.8	85.1	54.7
	10	3.75 [91.7]	65.2	88.6	63.1
	15	3.57 [87.3]	80.4	83.3	80.8
	20	3.59 [87.8]	90.1	86.5	90.2
				80.0[g]	100
	25	3.57 [87.3]	89.9	86.1	90.0
				79.4[g]	100

a) Conditions: (*RS*)-1,2,3,4-Tetrahydro-3-isoquinolinecarboxylic acid [(*RS*)-TIC] 10.0 mmol; (1*S*)-10-camphorsulfonic acid [(*S*)-CS] 9.00 mmol; carboxylic acid 15 cm^3; temperature 120 °C. b) (*S*)·(*S*) Salt: Salt of (*S*)-TIC with (*S*)-CS. c) The yield was calculated on the basis of 4.09 g (10.0 mmol) of the (*S*)·(*S*) salt. d) The yield was calculated on the basis of 1.77 g (10.0 mmol) of (*S*)-TIC. e) Butanoic acid. f) Hexanoic acid. g) The (*S*)-TIC obtained was purified by formation of a salt with (*S*)-CS.

the asymmetric transformation of (*RS*)-TIC is an efficient means to obtain optically pure (*S*)-TIC.

References

1) D. E. Portlock, Ger. Offen. 3018545 (1980); *Chem. Abstr.*, **94**, 208725p (1981).
2) Y. Oka and K. Nishikawa, Eur. Patent Appl. 18104 (1980); *Chem. Abstr.*, **95**, 42934z (1981).
3) K. Hayashi, J. Kato, T. Uchida, and N. Yoneda, U.S. Patent 4256751 (1981); *Chem. Abstr.*, **95**, 42937c (1981).
4) F. M. Hershenson, *J. Org. Chem.*, **40**, 1260 (1975).
5) K. Hayashi, Y. Ozaki, K. Nunami, and N. Yoneda, *Chem. Pharm. Bull.*, **31**, 312 (1983).
6) M. Bodanszky, "Peptide Chemistry," Springer-Verlag, Berlin, Heidelberg, New York, London, Paris, and Tokyo (1988), pp. 115—116.
7) T. Shiraiwa, S. Sakata, K. Fujishima, and H. Kurokawa, *Bull. Chem. Soc. Jpn.*, **64**, 191 (1991).
8) H. Ohtaki, "Youeki Kagaku," Shoukabou, Tokyo (1985), pp. 184—186.
9) R. P. Bell, "Proton in Chemistry," Cornell University Press (1959), p. 65.

Preparation of *N*-(Substituted formyl) dialkylamino(thioxo)-methanesulfenamides

Katsumi YONEMOTO,* Isao SHIBUYA, Masahiko YASUMOTO,
Yoichi TAGUCHI, and Tohru TSUCHIYA
National Chemical Laboratory for Industry, Higashi, Tsukuba, Ibaraki 305
(Received June 5, 1991)

Synopsis. *N*-(Substituted formyl)dialkylamino(thioxo)-methanesulfenamides ($R_2NCSSNHCOR'$, **2**), anti-foggants for silver halide photographic materials as well as potential precursors for 1,4,2-dithiazolium salts, were prepared in good yields in two "one-pot" procedures. Various amide-type compounds ($R'CONH_2$, **1**) were treated successively with NaH and I_2 and then condensed with dialkyldithiocarbamates (Method A); or **1** were reacted with tetraalkylthiuram disulfides after treatment with NaH (Method B). These methods allowed a wide variation of substituents R′ in **2**: R′=H, dialkylamino, alkoxy, aryl, alkyl, and heterocyclic substituent.

The syntheses of 1,4,2-dithiazolium salts (**3**) were recently established by three research groups independently. 3-Aryl-5-methylthio,[1a] 3-aryl-5-dialkylamino,[1b,c,e] 3,5-diaryl,[1d,g] and 3,5-bis(dialkylamino)[1e] derivatives and parent ring systems[1f] have been prepared so far. Systematic studies on the reactivity of **3** have also been performed.[2]

Our approach for preparation of 1,4,2-dithiazolium salts have been the cyclization of *S*-dialkylthiocarbamoyl and *S*-thioaroyl-*N*-acylsulfenamides with dehydration in strong acidic media.[1b] As an extension of this strategy, we used amide-type compounds (**1**) ($R'CONH_2$: R′=H, dialkylamino, alkoxy, aryl, alkyl, heterocyclic substiluent) as starting materials to prepare various *N*-(substituted formyl)dialkyl(thioxo)methanesulfenamides (**2**), the potential precursors for **3**.

Recently we found that both the sulfenamides (**2**) and the 1,4,2-dithiazolium salts were new types of lead compounds with high fog restraining ability for silver halide photographic materials, e.g., commercial color films.[3] In particular, several derivatives among **2** have been found to show far superior efficacy to the conventional ones only with a little amount of addition.

We now report two alternative methods for successful preparation of **2**, by means of direct formation of S–N bond in the sulfenamide moiety, the methods of which allow a wide variation of substituents R′ in **2**.

Results and Discussion

Our initial approach for preparation of *N*-acyl or *N*-

Table 1. Preparation of Sulfenamides **2**

Entry	Product			Method[a]	Yield[b]
	No.	R′	R_2N		%
1	**2a**	*t*-Bu	Et_2N	A(Ag)	41
2	**2a**	*t*-Bu	Et_2N	B	80
3	**2b**	*t*-Bu	Me_2N	B	84
4	**2c**	*t*-Bu	Piperidino	B	69
5	**2d**	Me	Morpholino	A(Na)	22
6	**2e**	Et_2N	Me_2N	A(Ag)	16
7	**2e**	Et_2N	Me_2N	B	80
8	**2f**	Et_2N	Et_2N	A(Ag)	8
9	**2g**	Me_2N	Et_2N	B	81
10	**2h**	MeO	Et_2N	A(Ag)	89
11	**2i**	MeO	Me_2N	A(Na)	67
12	**2j**	MeO	Piperidino	A(Na)	85
13	**2k**	*i*-PrO	Et_2N	A(Na)	75
14	**2k**	*i*-PrO	Et_2N	B	60
15	**2l**	4-MeOC_6H_4	Et_2N	A(Ag)	39
16	**2m**	4-MeC_6H_4	Et_2N	B	65
17	**2n**	4-ClC_6H_4	Et_2N	A(Ag)	7
18	**2n**	4-ClC_6H_4	Et_2N	B	88
19	**2o**	3-Pyridyl	Et_2N	A(Ag)	37
20	**2p**	3-Pyridyl	Me_2N	B	21
21	**2q**	2-Thienyl	Et_2N	A(Ag)	26
22	**2r**	2-Thienyl	Me_2N	B	81
23	**2s**	H	Piperidino	B	76
24	**2t**	PhCH=CH	Me_2N	B	64

a) Atomic symbols "Ag" and "Na" in parentheses correspond to "M" in $R_2NCSS^-M^+$. b) Isolated yields based on dialkyldithiocarbamates and **1** for Methods A and B, respectively.

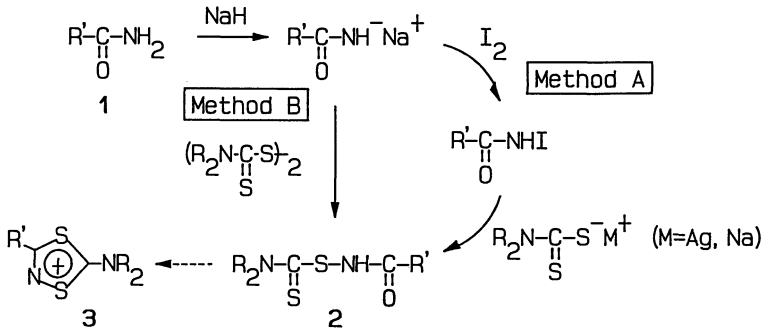

Scheme.

aroyldialkylamino(thioxo)methanesulfenamides (**2**) was the acylation or aroylation of the corresponding *N*-unsubstituted sulfenamides by treating with the corresponding acyl or aroyl chlorides, respectively.[1b] As far as this method was employed, however, variation of substituents R′ in **2** was limited to alkyl (including hydrogen) and aryl groups because of limited availability or poor reactivity of R′COCl (or $(R'CO)_2O$ as substitute) bearing other substituents R′.

In order to extend the variation of the substituents in **2**, we chose the amide-type compounds **1** as starting materials because of a wide variation of substituents R′ in **1**. Consequently, our alternative strategy for preparation of **2** was the introduction of dialkylthiocarbamoylthio group on N-atom in **1** to form a sulfenamide S–N bond directly.[4]

When dialkyldithiocarbamates are used as a substrate, the reaction requires involvement of umpolung of amino reactivity. From this standpoint, we carried out the following "one-pot" procedure including an oxidative process, denoted "Method A" for convenience. After treatment with NaH, **1** were iodinated by I_2-oxidation leading to *N*-iodoamide-type intermediates, which subsequently reacted with dialkyldithiocarbamates to afford **2**. As shown in Table 1, good yields were obtained only when alkyl carbamates were employed (Entries 10—14). The lower yields obtained in many cases are attributable to the formation of considerable amounts of tetraalkylthiuram disulfides as a side reaction. It is most likely that $(R_2NCSS)_2$ is formed by condensation of unreacted $R_2NCSS^-M^+$ with R_2NCSSI which temporarily arises from $R_2NCSS^-M^+$ by oxida-

Table 2. Characterization Data of Sulfenamides **2**

Compd	Mp (solv.) °C	^{1}H NMR[a]	^{13}C NMR[a] C=S, C=O	IR[b]/cm^{-1} NH, C=O	MS (rel intensity) *m/z*
2a	145.5—146.5 (Benzene)	1.3 (6H, br. t), 1.33 (9H, s), 3.4—4.3 (4H, br.), 7.1 (NH, br. s)	196.09 179.63	3296 1674	250 (M^+, 0.4) 116 (100)
2b	119.0—120.0 (Benzene-Hexane)	1.32 (9H, s), 3.2—3.6 (6H, br. s), 7.2 (NH, br. s)	197.34 179.41	3264 1696	220 (M^+, 4) 88 (100)
2c	146.0—147.0 (CH_2Cl_2-Pentane)	1.33 (9H, s), 1.6—1.8 (6H, br.), 3.8—4.2 (4H, br.), 7.2 (NH, br. s)	196.07 179.44	3248 1696	260 (M^+, 3) 128 (100)
2d	156.0—157.0 (CH_2Cl_2-Pentane)	2.27 (3H, br. s), 3.7—3.9 (4H, m), 3.9—4.1 (4H, m), 7.3 (NH, br. s)	198.10 172.23	3248 1681	220 (M^+, 8) 130 (90)
2e	99.0—100.0 (CH_2Cl_2-Pentane)	1.23 (6H, t, *J*=7.2 Hz), 3.44 (4H, q, *J*=7.2 Hz), 3.2—3.6 (6H, br. s), 6.3 (NH, br. s)	200.13 155.54	3296 1668	235 (M^+, 3) 88 (100)
2f	132.5—133.5 (CH_2Cl_2-Pentane)	1.25 (6H, t, *J*=7.2 Hz), 1.3 (6H, br. t), 3.45 (4H, q, *J*=7.2 Hz), 3.4—4.3 (4H, br.), 6.0 (NH, br. s)	199.25 156.10	3220 1645	263 (M^+, 4) 116 (100)
2g	152.0—153.5 (CH_2Cl_2-Hexane)	1.3 (6H, br. t), 3.10 (6H, s), 3.5—4.2 (4H, br.), 6.1 (NH, br. s)	198.96 157.35	3228 1651	235 (M^+, 6) 116 (88)
2h	66.0— 67.0 (Ether-Pentane)	1.3 (6H, br. t), 3.4—4.3 (4H, br.), 3.80 (3H, s), 6.4 (NH, br. s)	197.07 157.22	3228 1735	222 (M^+, 13) 116 (100)
2i	150.5—151.5 (CH_2Cl_2-Hexane)	3.2—3.6 (6H, br, s), 3.78 (3H, s), 6.1 (NH, br. s)	198.51 157.17	3176 1717	194 (M^+, 8) 88 (100)
2j	115.0—116.0 (CH_2Cl_2-Pentane)	1.6—1.8 (6H, br.), 3.80 (3H, s), 3.8—4.2 (4H, br.), 6.1 (NH, br. s)	197.25 157.32	3212 1721	234 (M^+, 8) 128 (100)
2k	90.0— 90.5 (CH_2Cl_2-Pentane)	1.28 (6H, d, *J*=6 Hz), 1.3 (6H, br. t), 3.4—4.3 (4H, br.), 5.00 (1H, m), 6.4 (NH, br. s)	197.07 156.09	3216 1703	250 (M^+, 4) 116 (100)
2o	134.0—135.0 (CH_2Cl_2-Hexane)	1.3 (6H, br. t), 3.5—4.2 (4H, br.), 7.35—7.5 (1H, m), 8.25—8.4 (1H, m and NH), 8.7—8.85 (1H, m), 9.2—9.3 (1H, m)	195.36 167.41	—[c] 1691	269 (M^+, 2) 116 (100)
2p	127.0—127.5 (CH_2Cl_2-Pentane)	3.3—3.6 (6H, br. s), 7.3—7.5 (1H, m), 8.2—8.4 (1H, m and NH), 8.7—8.85 (1H, m), 9.2—9.3 (1H, m)	—[d]	3444 1662	241 (M^+, 5) 88 (100)
2q	116.0—117.0 (Benzene)	1.3 (6H, br. t), 3.5—4.2 (4H, br. t), 7.1—7.2 (1H, m), 7.55—7.65 (1H, m and NH), 7.8—7.9 (1H, m)	195.93 162.91	3268 1658	274 (M^+, 4) 116 (100)
2r	92.0— 93.5 (CH_2Cl_2-Pentane)	3.3—3.6 (6H, br. s), 7.1—7.2 (1H, m), 7.4 (NH, br. s), 7.55—7.65 (1H, m), 7.8—7.9 (1H, m)	—[d]	3212 1646	246 (M^+, 4) 88 (100)
2t	127.0—127.5 (MeCN-Ether)	3.3—3.6 (6H, br. s), 6.76 (1H, d, *J*=16 Hz), 7.1 (NH, br. s), 7.3—7.45 (3H, m), 7.5—7.6 (2H, m), 7.79 (1H, d, *J*=16 Hz)	—[d]	3128 1666	103 (38) 88 (100)

a) In $CDCl_3$, ppm from TMS. No *J* values were often given because the resonances were unresolved. b) Using KBr disks. c) No distinct N–H band was observed. d) Low solubility in ordinary deuterated solvents.

tion with the *N*-iodoamide as a competing pathway.

It is well-known that thiuram disulfides are liable to suffer from cleavage of the S–S bond homolytically[5a] and heterolytically.[5b] Therefore an umpolung synthon R_2NCSS^+ is expected to be produced from $(R_2NCSS)_2$ by the attack of a nucleophile. On the other hand, a convenient method for synthesis of sulfenamides from disulfides and lithium amides has been reported.[6] From this viewpoint, we examined another method, "Method B", using tetraalkylthiuram disulfides as substrates instead of dialkyldithiocarbamates. When **1** were treated with NaH followed by the reaction with $(R_2NCSS)_2$, successful formation of **2** was observed. As seen in Table 1, for R′=alkyl (Entries 1—5), dialkylamino (Entries 6—9), and aryl groups (Entries 15—18), Method B gave far better results than Method A. Furthermore, for R′=heterocyclic substitutent, hydrogen, and PhCH=CH, **2** were also prepared by Method B in moderate to good yields.

Davis et al. have developed a one-step synthesis of sulfenamides from disulfides and amines in the presence of silver salts.[7] The mechanism is believed to involve the complexation of Ag^+ with one of the disulfide sulfurs, followed by nucleophilic attack on the other sulfur by the amine. We attempted some application of this method to our system; but no satisfactory results were obtained. It may be attributable to the lower nucleophilicity of **1** and the instability of products **2** in the presence of Ag^+.

Some attempts to convert **2** into **3** were also carried out according to the same procedure as described in our previous report.[1b] When 40% tetrafluoroboric acid was added dropwise to an acetic anhydride solution of **2b**, **e**, and **r**, respectively, a pale yellow precipitate was immediately deposited in each case. It was found that the three precipitated products were not the corresponding 1,4,2-dithiazolium salts but identical with one another, by means of IR, ^1H NMR, and elemental analysis. The common product was identified with 3,5-bis(dimethyliminio)-1,2,4-trithiolane bis(tetrafluoroborate) by direct comparison with the authentic one which was prepared by the treatment of tetramethylthiuram monosulfide with mCPBA in HBF_4/Ac_2O.[8] Further attempts to prepare **3**, for instance by use of other strong acids or Lewis acids, are currently under way.

Experimental

All melting points were uncorrected. ^1H and ^{13}C NMR spectra were recorded on a Hitachi R-40 and a JEOL FX-90A spectrometer. Mass spectra were taken on a Hewlett Packard 5995A spectrometer by electron impact ionizing technique at 70 eV. IR spectra were measured on a JASCO A-302 spectrometer. The substrates, i.e., dialkyldithiocarbamates,[9] tetraalkylthiuram disulfides,[10] and the amide-type compounds, are readily obtainable according to literatures or commercially.

Preparation of Sulfenamides 2: Method A: General Procedure. Sodium hydride (ca. 60% in oil) (60 mg; 1.5 mmol) was added to a dry THF solution (10 ml) of the amide-type compounds **1** (2 mmol). The reaction mixture was stirred for ca. 15 min at room temperature or, if necessary, by short heating at 60 °C. After the evolution of hydrogen ceased, iodine (254 mg; 1 mmol) was added to the cooled suspension, which was stirred for ca. 15 min at room temperature. Finally, sodium or silver dialkyldithiocarbamates (often hydrated) (1 mmol) were added to the dark red suspension. After the initial dark red color faded, the resulting pale yellow solution was stirred for 1 h. The crude product was extracted with dichloromethane after addition of an aqueous sodium hydrogencarbonate. After the solvent was removed in vacuo, the residue was purified by column chromatography on silica gel and/or recrystallized from appropriate solvents.

Method B: General Procedure. After the amide-type compounds **1** were treated with NaH in the same manner as Method A, tetraalkylthiuram disulfides were added to the reaction suspension, which was stirred for 1 h at room temperature. It should be noted that prolonged standing on the reaction mixture is apt to decrease the yields of **2**. Subsequent work-up and purification were accomplished by a procedure similar to Method A.

The yields of sulfenamides **2** are presented in Table 1, and their melting points and spectral data are listed in Table 2. Characterization of **2l**, **m**, **n**,[1b] and **2r**[1f] have been reported in the literatures. The results of elemental analyses of several representative sulfenamides, i.e., **2b** (R′=alkyl), **2g** (R′=dialkylamino), **2h** (R′=alkoxy), **2p**, **q** (R′=heterocyclic), and **2t** (R′=PhCH=CH), are shown below.

2b: Found: C, 43.50; H, 7.12; N, 12.58%. Calcd for $C_8H_{16}N_2S_2O$: C, 43.61; H, 7.32; N, 12.71%.

2g: Found: C, 40.97; H, 7.14; N, 17.95%. Calcd for $C_8H_{17}N_3S_2O$: C, 40.82; H, 7.28; N,17.85%.

2h: Found: C, 37.82; H, 6.27; N, 12.50; S, 28.73%. Calcd for $C_7H_{14}N_2S_2O_2$: C, 37.82; H, 6.35; N, 12.60; S, 28.85%.

2p: Found: C, 44.48; H, 4.43; N, 17.18; S, 26.57%. Calcd for $C_9H_{11}N_3S_2O$: C, 44.79; H, 4.59; N, 17.41; S, 26.64%.

2q: Found: C, 43.72; H, 5.07; N, 10.12; S, 34.72%. Calcd for $C_{10}H_{14}N_2S_3O$: C, 43.77; H, 5.14; N, 10.21; S, 35.05%.

2t: Found: C, 53.84; H, 5.32; N, 10.85; S, 24.07%. Calcd for $C_{12}H_{14}N_2S_2O$: C, 54.11; H, 5.30; N, 10.52; S, 23.84%.

References

1) a) D. J. Greig, M. McPherson, R. M. Paton, and J. Crosby, *J. Chem. Soc., Chem. Commun.*, **1985**, 696. b) I. Shibuya and K. Yonemoto, *Bull. Chem. Soc. Jpn.*, **59**, 2017 (1986). c) F. S. Y. Chan and M. P. Sammes, *J. Chem. Soc., Chem. Commun.*, **1985**, 1641. d) K-F. Wai and M. P. Sammes, *ibid.*, **1988**, 852. e) F. S. Y. Chan, M. P. Sammes, and R. L. Harlow, *J. Chem. Soc., Perkin Trans. 1*, **1988**, 899. f) K-F. Wai and M. P. Sammes, *ibid.*, **1990**, 808. g) K. Yonemoto, I. Shibuya, T. Tsuchiya, M. Yasumoto, and Y. Taguchi, *Bull. Chem. Soc. Jpn.*, **63**, 2933 (1990).

2) K. Yonemoto and I. Shibuya, *Bull. Chem. Soc. Jpn.*, **61**, 4043 (1988); K. Yonemoto, I. Shibuya, and K. Honda, *ibid.*, **62**, 1086 (1989).

3) I. Shibuya, K. Yonemoto, Y. Kaneko, S. Hirabayashi, Y. Taguchi, T. Tsuchiya, and M. Yasumoto, *Nippon Shashin Gakkai Shi*, **54**, 341 (1991).

4) A recent review on sulfenamides: L. Craine and M. Raban, *Chem. Rev.*, **89**, 689 (1989).

5) a) R. E. Davis and C. Perrin, *J. Am. Chem. Soc.*, **82**. 1590 (1960). b) S. Kato and M. Mizuta, *Int. J. Sulfur Chem., Part A*, **2**, 275 (1972).

6) H. Ikehira and S. Tanimoto, *Synthesis*, **1983**, 716.

7) F. A. Davis, A. J. Friedman, E. W. Kluger, E. B. Skibo, E. R. Fretz, A. P. Milicia, and W. C. LeMasters, *J. Org. Chem.*, **42**, 967 (1977).

8) H. H. Carbacho and L. L. Victorano, *J. Inorg. Nucl. Chem.*, **37**, 1327 (1975). Details will be reported in a separate paper.

9) M. Yokoyama and T. Imamoto, *Synthesis*, **1984**, 797.

10) J. Braun, *Ber.*, **35**, 817 (1902).

Novel Transformation of Formyl Groups into Hydroxyl Groups Utilizing Deformylative Autoxidation of Aldehydes

Hideo KIGOSHI, Yoshifumi IMAMURA, Akihiko SAWADA, Haruki NIWA, and Kiyoyuki YAMADA*
Department of Chemistry, Faculty of Science, Nagoya University, Chikusa, Nagoya 464
(Received June 24, 1991)

Synopsis. Structural requirements that cause deformylative autoxidation of aliphatic aldehydes are investigated. Decarbonylation of acyl radicals proceeds smoothly when the alkyl radicals that are formed can be stabilized by allylic conjugation. Further conjugation of the double bond in the allyl radical with a carbonyl or a cyclopropyl group allows position-selective peroxidation of the alkyl radical.

In the course of the synthetic study on ptaquilosin (**2**), the aglycone of ptaquiloside (**1**) which is a bracken carcinogen, we encountered a necessity to convert an angular formyl group into the hydroxyl group efficiently. After unsuccessful trials, we found that autoxidation of **3** smoothly proceeded with deformylation to give hydroperoxide **4a**, reduction of which gave the desired alcohol **4b** in very high yield (Eq. 1). This novel transformation was applied to aldehydes **5** and **7**, culminating in the total synthesis of racemic ptaquilosin (**2**)[1] and (+)-ptaquilosin (**8b**) (the enantiomer of **2**)[2] via **6a** and **8a**, respectively (Eq. 2, 3). Herein we disclose the experimental details of deformylative hydroxylation of the aldehydes as well as the study on structural requirements causing deformylative autoxidation of aldehydes.

We have chosen aldehydes **9**, **10**, and **11** as the substrates suitable for the study on deformylative autoxidation (Table 1). Autoxidation of **3**, **5**, **7**, **9**, **10**, and **11** was performed in a concentrated ethyl acetate solution under oxygen (1 atm) at 40—65 °C. The resulting peroxides were reduced with Ph_3P and the crude products were purified chromatographically. The results are summarized in Table 1.

In general, autoxidation of aldehydes provides carboxylic acids through peroxidation of acyl radical intermediates. However, acyl radicals are also known to fragment with loss of carbon monoxide to generate alkyl radicals (Scheme 1).[3] If the rate of decarbonylation of

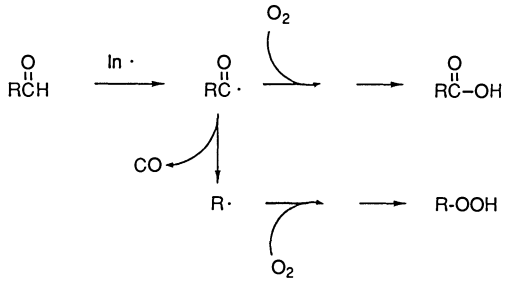

Scheme 1. Autoxidation of aldehydes.

Table 1. Deformylative Hydroxylation of Aldehydes

Entry	Substrate	Conditions temp (°C)/time (h)	Product (%)[a]
1	**3**	40/5	**4b** (92)
2	**5**	45/3.5	**6b** (89)
3	**7**[b]	50/18	**8b** (37)
4	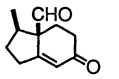 **9**[b]	65/23	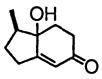 **12**[c] (17) 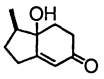 **13**[c] (20)
5	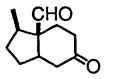 **10**[b]	65/23	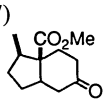 **14**[d] (25)
6	**11**[b]	65/23	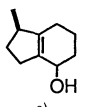 **15**[e] (5) 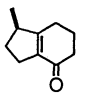 **16** (5) 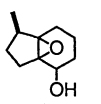 **17**[e] (4) 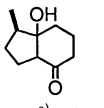 **18**[c] (4)

a) Isolated yields after treatment with Ph_3P. b) This substrate afforded a complex mixture in this reaction, and ill-defined polar compounds were obtained as the major products. c) Stereochemistry of this compound was not determined. d) The carboxylic acid was isolated as methyl ester **14**. e) A mixture of diastereomers.

acyl radicals is faster than that of peroxidation of those, deformylative peroxidation becomes a predominant process in autoxidation of aldehydes. The ease of decarbonylation of acyl radicals may depend on stability of the alkyl radicals that are formed. In autoxidation of **3**, **5**, **7**, **9**, and **11** the facile decarbonylation occurs, being attributable to stabilization of the fragmented alkyl radical by allylic conjugation with the adjacent double bond (Entries 1—4 and 6). Autoxidation of **10**, which lacks structural features stabilizing the fragmented alkyl radical, proceeds without fragmentation to give the corresponding carboxylic acid (Entry 5). Peroxidation of the alkyl radicals generated from **3**, **5**, **7**, and **9**, proceeded in the position-selective manners, while peroxidation of the alkyl radical derived from **11** is nonselective.

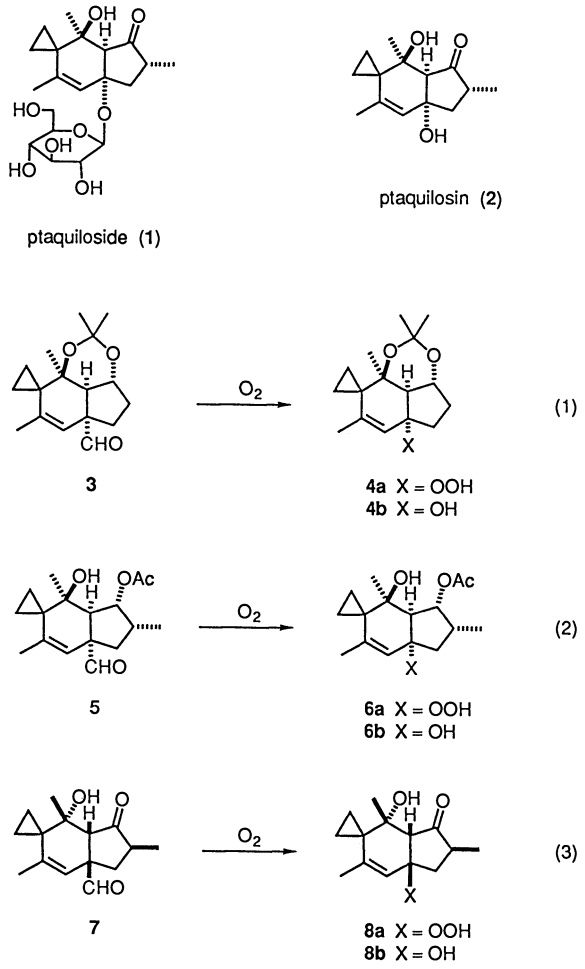

Experimental

Melting points are uncorrected. Optical rotations were measured on a JASCO DIP-181 polarimeter. Infrared (IR) spectra were obtained on a JASCO Model IR-810 spectrophotometer. Proton nuclear magnetic resonance (^{1}H NMR) spectra were recorded on a JEOL JNM-C675 (270 MHz) spectrometer in $CDCl_3$ or C_6D_6 using tetramethylsilane (TMS) as an internal standard. Chemical shifts are expressed in parts per million (ppm) downfield from TMS (δ=0.0) and coupling constants in Hz. The low-resolution (EIMS) and high-resolution (HREIMS) mass spectra were recorded on a JEOL JMS-LG2000 instrument. Fuji-Davison silica gel BW-820MH was used for column chromatography. Merck precoated silica gel 60 F_{254} plates, 0.25 mm thickness, were used for analytical and preparative thin-layer chromatography (TLC).

Preparation of (3′*R,3′a*R**,4′*S**,7′a*R**)-1′,2′,3′,3′a,4′,7′a-Hexahydro-3′,4′-dihydroxy-4′,6′-dimethyl-spiro[cyclopropane-1,5′-[5*H*]indene]-7′a-carbaldehyde Acetonide (3).** Compound **3** was prepared from compound **A**[1] by a three-step sequence [(1) CH_2=C(OCH_3)CH_3, H^+, benzene; (2) Bu_4NF, THF; (3) $CrO_3 \cdot 2Py$, CH_2Cl_2].

3: Colorless solids; IR (CCl_4) 2810, 2710, and 1725 cm^{-1}; ^{1}H NMR (C_6D_6, 270 MHz) δ=0.30—0.37 (1H, m), 0.62—0.77 (2H, m), 1.02—1.15 (1H, m), 1.20 (3H, d, *J*=1.7 Hz), 1.30 (3H, s), 1.31—1.38 (1H, m), 1.40 (3H, s), 1.53 (3H, d, *J*=0.7 Hz) 1.55—1.63 (1H, m), 1.79—1.91 (2H, m), 2.84 (1H, d, *J*=11.2 Hz), 4.12 (1H, ddd, *J*=11.2, 11.2, 5.6 Hz), 5.10 (1H, br s), and 9.23 (1H, s); EIMS *m/z* (rel intensity) 276 (M^+, 3), 218 (20), and 189 (100). HREIMS. Found: *m/z* 276.1752. Calcd for $C_{17}H_{24}O_3$: M, 276.1725.

Autoxidation of 3. A solution of **3** (3.9 mg, 0.014 mmol) in EtOAc (0.05 ml) was stirred under oxygen (1 atm) at 40 °C for 5 h. After the reaction mixture was diluted with ether (0.2 ml), Ph_3P (18 mg, 0.069 mmol) was added. The mixture was stirred at room temperature for 1 h and concentrated under reduced pressure. The residue was purified by column chromatography on silica gel [1 g, hexane–ether (5 : 1→1 : 1)] to give **4b** (3.4 mg, 92%) as colorless crystals: Mp 166.0—167.5 °C (hexane); IR (KBr) 3400, 3200, and 1660 cm^{-1}; ^{1}H NMR (C_6D_6, 270 MHz) δ=0.29—0.40 (2H, m), 0.66—0.80 (2H, m), 1.21 (3H, d, *J*=1.5 Hz), 1.41 (6H, s), 1.49 (3H, d, *J*=0.7 Hz), 1.51—1.63 (2H, m), 1.77—1.93 (3H, m), 2.54 (1H, d, *J*=11.6 Hz), 3.97 (1H, ddd, *J*=11.6, 10.1, 5.6 Hz), and 5.32 (1H, br s); EIMS *m/z* (rel intensity) 264 (M^+, 0.1), 246 (8), 231 (14), 206 (96), 191 (47), and 177 (100). HREIMS. Found: *m/z* 264.1745. Calcd for $C_{16}H_{24}O_3$: M, 264.1726.

Autoxidation of (2′*R,3′*R**,3′a*R**,4′*S**,7′a*R**)-3′-(Acetoxy)-1′,2′,3′,3′a,4′,7′a-hexahydro-4′-hydroxy-2′,4′,6′-trimethyl-spiro[cyclopropane-1,5′-[5*H*]indene]-7′a-carbaldehyde (5).** Autoxidation of **5**[1] (4.0 mg, 0.014 mmol) at 45 °C for 3.5 h and subsequent treatment with Ph_3P were performed as described above. The crude product was purified by column chromatography on silica gel [1 g, hexane–EtOAc (2 : 1)] to give racemic **6b** (3.5 mg, 89%) as a colorless oil. HREIMS. Found: *m/z* 280.1681. Calcd for $C_{16}H_{24}O_4$: M, 280.1675. Spectral properties of racemic **6b** were identical with those of authentic **6b**[4] derived from natural ptaquiloside (**1**), in all respects.

Autoxidation of (2′*S*,3′a*R*,4′*R*,7′a*S*)-1′,2′,3′,3′a,4′,7′a-Hexahydro-4′-hydroxy-2′,4′,6′-trimethyl-3′-oxo-spiro[cyclopropane-1,5′-[5*H*]indene]-7′a-carbaldehyde (7). Autoxidation of **7**[2] (8.3 mg, 0.033 mmol) at 50 °C for 18 h and subsequent treatment with Ph_3P were performed as described above. The crude product was purified by column chromatography on silica gel [1.5 g, hexane–ether (2 : 1→1 : 1)] to give (+)-ptaquilosin (**8b**) [2.9 mg, 37%, $[\alpha]_D^{20}$ +232° (*c* 0.17, $CHCl_3$) as a colorless oil. HREIMS. Found: *m/z* 236.1418. Calcd for $C_{14}H_{28}O_3$: M, 236.1412. Spectral properties of (+)-**8b** were identical with those of authentic (−)-ptaquilosin (**2**)[4] [$[\alpha]_D^{20}$ −246° (*c* 0.824, $CHCl_3$)] derived from natural ptaquiloside (**1**), in all respects.

Preparation of (3*R*,3a*R*)-1,2,3,4,5,6-Hexahydro-3-methyl-6-oxo-3a*H*-indene-3a-carbaldehyde (9), (3*R*,3a*R*,7a*S*)-Octahydro-3-methyl-6-oxo-3a*H*-indene-3a-carbaldehyde (10), and (3*R*,3a*R*)-1,2,3,4,5,6-Hexahydro-3-methyl-3a*H*-indene-3a-carbaldehyde (11). Compounds **9**, **10**, and **11** were prepared from compound **B**[5] as follows: (i) a two-step sequence for **9** [(1) $LiAlH_4$, THF; (2) PCC, CH_2Cl_2]: (ii) a three-step sequence for **10** [(1) H_2/Pd–C, EtOH; (2) $LiAlH_4$, THF; (3) Swern oxidation]: (iii) a four-step sequence for **11** [(1) $HSCH_2CH_2$-

SH, $BF_3 \cdot OEt_2$; (2) Raney-Ni (W-2), EtOH; (3) $LiAlH_4$; (4) Swern oxidation].

9: A colorless oil; IR ($CHCl_3$) 2830, 2740, 1715, and 1660 cm^{-1}; ^1H NMR ($CDCl_3$, 270 MHz) δ=1.15 (3H, d, J=7.9 Hz), 1.59—1.79 (2H, m), 1.89—2.18 (2H, m), 2.30 (1H, ddd, J=17.8, 13.5, 5.0 Hz), 2.41 (1H, ddd, J=17.8, 5.6, 2.3 Hz), 2.59—2.68 (1H, m), 2.70—2.78 (1H, m), 2.89 (1H, dddd, J=20.1, 10.6, 2.3, 2.3 Hz), 6.01 (1H, dd, J=2.3, 1.3 Hz), and 9.73 (1H, s); EIMS m/z (rel intensity) 178 (M^+, 77) and 149 (100). HREIMS. Found: m/z 178.0990. Calcd for $C_{11}H_{14}O_2$: M, 178.0994.

10: A colorless oil; IR ($CHCl_3$) 2820, 2720, and 1715 cm^{-1}; ^1H NMR ($CDCl_3$, 270 MHz) δ=1.06 (3H, d, J=7.4 Hz), 1.26—1.48 (2H, m), 1.72—1.83 (1H, m), 1.88—2.41 (7H, m), 2.48 (1H, dd, J=15.5, 5.9 Hz), 2.78—2.89 (1H, m), and 9.68 (1H, s); EIMS m/z (rel intensity) 180 (M^+, 100), 165 (7), 151 (35), and 133 (72). HREIMS. Found: m/z 180.1130. Calcd for $C_{11}H_{16}O_2$: M, 180.1150.

11: A colorless oil; IR ($CHCl_3$) 2830, 2720, and 1710 cm^{-1}; ^1H NMR ($CDCl_3$, 270 MHz) δ=0.92—1.11 (1H, m), 1.06 (3H, d, J=7.3 Hz), 1.26—1.58 (2H, m), 1.68—1.83 (2H, m), 1.89—2.07 (3H, m), 2.25—2.48 (1H, m), 2.48 (1H, ddd, J=12.9, 3.4, 3.4 Hz), 2.56—2.71 (1H, m), 5.61—5.66 (1H, m), and 9.63 (1H, s); EIMS m/z (rel intensity) 164 (M^+, 14), 149 (1), and 135 (100). HREIMS. Found: m/z 164.1207. Calcd for $C_{11}H_{16}O$: M, 164.1201.

Autoxidation of 9. Autoxidation of **9** (51.1 mg, 0.287 mmol) at 65 °C for 23 h and subsequent treatment with Ph_3P were performed as described above. The crude product was purified by column chromatography on silica gel [16 g, hexane–EtOAc (2 : 1→1 : 1→1 : 2)] to give a mixture of **12** and **13**. Further separation of this mixture by preparative TLC [hexane–EtOAc (1 : 3)] provided pure **12** (7.9 mg, 17%) and **13** (9.5 mg, 20%) as a colorless oil, respectively.

12 (the less polar compound): IR ($CHCl_3$) 3600, 3430, 1660, and 930 cm^{-1}; ^1H NMR ($CDCl_3$, 270 MHz) δ=1.08 (3H, d, J=6.3 Hz), 1.61—1.78 (2H, m), 1.76 (1H, br s, -OH), 1.82—1.96 (2H, m), 2.22 (1H, ddd, J=13.9, 5.3, 2.0 Hz), 2.34—2.54 (2H, m), 2.67—2.82 (2H, m), and 5.85 (1H, dd, J=2.0, 1.0 Hz); EIMS m/z (rel intensity) 166 (M^+, 100), 148 (2), 138 (79), 124 (81), and 96 (87). HREIMS. Found: m/z 166.0996. Calcd for $C_{10}H_{14}O_2$: M, 166.0994.

13 (the more polar compound): IR ($CHCl_3$) 3600, 3420, 1660, and 935 cm^{-1}; ^1H NMR ($CDCl_3$, 270 MHz) δ=0.87 (3H, d, J=7.3 Hz), 1.49 (1H, dddd, J=12.5, 8.2, 3.0, 1.3 Hz), 1.95 (1H, br s, -OH), 1.97—2.15 (2H, m), 2.17—2.45 (3H, m), 2.55 (1H, dddd, J=19.5, 8.2, 8.2, 2.0 Hz), 2.71 (1H, dddd, J=19.5, 9.5, 3.0, 1.0 Hz), 2.78 (1H, ddd, J=17.5, 12.2, 6.3 Hz), and 5.91 (1H, dd, J=2.0, 1.0 Hz); EIMS m/z (rel intensity) 166 (M^+, 48), 148 (3), 138 (100), 124 (98), and 96 (98). HREIMS. Found: m/z 166.1004. Calcd for $C_{10}H_{14}O_2$: M, 166.0994.

Autoxidation of 10. Autoxidation of **10** (58.5 mg, 0.325 mmol) at 65 °C for 23 h and subsequent treatment with Ph_3P were performed as described above. Treatment of the crude product with excess CH_2N_2 and subsequent separation by column chromatography on silica gel [18 g, hexane–EtOAc (5 : 1→5 : 2→1 : 1)] gave **14** (17.4 mg, 25%) as a colorless oil, along with the recovered **10** (7.2 mg, 12%).

14: IR ($CHCl_3$) 1715, 1225, and 1195 cm^{-1}; ^1H NMR ($CDCl_3$, 270 MHz) δ=0.91 (3H, d, J=6.9 Hz), 1.22—1.50 (2H, m), 1.76—2.08 (4H, m), 2.13—2.63 (5H, m), 2.92—3.05 (1H, m), and 3.74 (3H, s); EIMS m/z (rel intensity) 210 (M^+, 42), 178 (100), and 150 (96). HREIMS. Found: m/z 210.1228. Calcd for $C_{12}H_{18}O_3$: M, 210.1256.

Autoxidation of 11. Autoxidation of **11** (88.4 mg, 0.539 mmol) at 65 °C for 23 h and subsequent treatment with Ph_3P were performed as described above. The crude product was subjected to separation by column chromatography on silica gel [30 g, hexane–ether (2 : 1→1 : 1→0 : 1)] to give a mixture of **15** and **16**, crude **17**, and crude **18**. Further purification by preparative TLC [$CHCl_3$–acetone (20 : 1) for the mixture of **15** and **16**; benzene–acetone (5 : 1) for **17**; benzene–acetone (7 : 1) for **18**] provided **15** (4.3 mg, 5%; a 1 : 1 mixture of diastereomers), **16** (4.1 mg, 5%), **17** (3.9 mg, 4%; a 1 : 1 : 2 : 2 mixture of diastereomers), and **18** (4.0 mg, 4%; a 1 : 1 mixture of diastereomers) as a colorless oil, respectively.

15: IR ($CHCl_3$) 3600, and 3450 cm^{-1}; ^1H NMR ($CDCl_3$, 270 MHz) δ=0.98 (1.5H, d, J=6.9 Hz), 1.00 (1.5H, d, J=6.6 Hz), 1.20—1.43 (2H, m), 1.57—2.32 (8H, m), 2.35—2.62 (2H, m), and 4.12—4.21 (1H, m); EIMS m/z (rel intensity) 152 (M^+, 100), 137 (18), and 134 (16). HREIMS. Found: m/z 152.1229. Calcd for $C_{10}H_{16}O$: M, 152.1201.

16: IR ($CHCl_3$) 1655 and 1630 cm^{-1}; ^1H NMR ($CDCl_3$, 270 MHz) δ=1.11 (3H, d, J=7.3 Hz), 1.37—1.51 (1H, m), 1.98—2.62 (9H, m), and 2.76—2.92 (1H, m); EIMS m/z (rel intensity) 150 (M^+, 81), 135 (19), and 122 (100). HREIMS. Found: m/z 150.1047. Calcd for $C_{10}H_{14}O$: M, 150.1044.

17: IR ($CHCl_3$) 3600, and 3450 cm^{-1}; ^1H NMR ($CDCl_3$, 270 MHz) δ=0.91—2.57 (15H, m), and 3.93—4.28 (1H, m); EIMS m/z (rel intensity) 168 (M^+, 13), 153 (16), 150 (11), and 111 (100). HREIMS. Found: m/z 168.1154. Calcd for $C_{10}H_{16}O_2$: M, 168.1150.

18: IR ($CHCl_3$) 3600, 3460, and 1715 cm^{-1}; ^1H NMR ($CDCl_3$, 270 MHz) δ=0.91—1.36 (2H, m), 1.18 (3H, d, J=7.3 Hz), 1.51—2.52 (10H, m), and 2.66—2.75 (1H, m); EIMS m/z (rel intensity) 168 (M^+, 43), 153 (5), 150 (13), 126 (100), and 84 (91). HREIMS. Found: m/z 168.1125. Calcd for $C_{10}H_{16}O_2$: M, 168.1150.

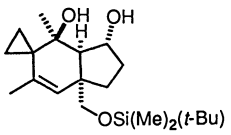

A

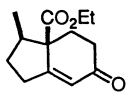

B

References

1) H. Kigoshi, A. Sawada, Y. Nakayama, H. Niwa, and K. Yamada, *Tetrahedron Lett.*, **30**, 1983 (1989).

2) H. Kigoshi, Y. Imamura, H. Niwa, and K. Yamada, *J. Am. Chem. Soc.*, **111**, 2302 (1989).

3) F. A. Carey and R. J. Sundberg, "Advanced Organic Chemistry, Part A," Plenum, New York (1990), Chap. 12.

4) H. Kigoshi, A. Sawada, Y. Imamura, H. Niwa, and K. Yamada, *Tetrahedron*, **45**, 2551 (1989).

5) P. R. Vettel and R. M. Coates, *J. Org. Chem.*, **45**, 5430 (1980).

Fixation of Carbon Dioxide with Diphenylcarbodiimide as a Model of Biotin Enzyme Active Site and a Weak Base: The Carboxylation of Fluorene under Mild Conditions

Koji CHIBA,* Hideyuki TAGAYA,* Masa KARASU, Tsuyoyuki ONO, Masaru SAITO, and Atsushi ASHIKAGAYA
Department of Materials Science and Engineering, Faculty of Engineering, Yamagata University, Jonan, Yonezawa 992
(Received June 28, 1991)

Synopsis. Carbon dioxide was directly fixed into fluorene in the presence of diphenylcarbodiimide (DPC) as a model of a biotin enzyme active site and potassium hydrogencarbonate. It was considered that not only carbon dioxide but also the hydrogencarbonate ion were the carbon source in the presence of DPC. Weak bases such as potassium acetate, potassium propionate, and potassium formate were also effective for carboxylation.

The chemical fixation of carbon dioxide has been widely studied,[1-5] since carbon dioxide is an abundant natural source of carbon. Photosynthesis is known to be the most efficient system for carbon dioxide fixation. However, enzymatic carboxylation without the aid of photoenergy was also known in which biotin enzyme plays an important role.[6,7] It is well known that the active site of biotin is a urea derivative.

We have already reported that active methylene compounds were effectively carboxylated by employing a reagent system, carbon dioxide, diphenylurea or diphenylcarbodiimide (DPC) as a model of biotin active site and potassium carbonate.[8]

In the case of DPC, the reaction occurred even in the presence of water, surprisingly.[8a] The carbonate ion reacts with water to give the hydrogencarbonate ion. Since the hydrogencarbonate ion is a weak base, it is ineffective for a conventional carboxylation reaction. Actually, no carboxylation reaction occurred when potassium hydrogencarbonate was added with diphenylurea. We have found that active methylene compounds can be carboxylated using such weak bases as alkalin metal hydrogencarbonate and DPC. Furthermore, instead of potassium hydrogencarbonate, weak bases such as potassium acetate, potassium propionate, and potassium formate were also effective.

Results and Discussion

It is well known that a strong base, like 1,8-diazabicyclo[5.4.0]undec-7-ene, abstracts a proton from an active methylene compound, producing its carboxylated compound in the presence of carbon dioxide.[9] Since potassium hydrogencarbonate is a weak base, no carboxylation occurred when only potassium hydrogencarbonate was reacted with fluorene under a carbon dioxide atmosphere in DMSO (Table 1). In carboxylation using diphenylurea, a strong base is required since it is believed that the first step is an imine proton abstraction by a strong base. Actually, no carboxylation reaction occurred when a weak base, potassium hydrogencarbonate, was added to diphenylurea. However, when potassium hydrogencarbonate was used with DPC, fluorene was carboxylated and the yield of 9-FLC was as high as 44—47% (Table 1). Sodium hydrogencarbonate was also an effective base.

Table 1. Carboxylation of Fluorene Using a Model of the Biotin Enzyme Active Site[a] and Base under a Carbon Dioxide Atmosphere

Model of the biotin enzyme active site	Base	Water added /mmol	Yield of 9-FLC/%[b]
None	$KHCO_3$	0	0.0
Diphenylurea	$KHCO_3$	0	0.0
Diphenylcarbodiimide	None	0	0.0
Diphenylcarbodiimide	$KHCO_3$	0	43.9, 46.9
Diphenylcarbodiimide[c]	$KHCO_3$	0	49.1
Diphenylcarbodiimide[d]	$KHCO_3$	0	48.5
Diphenylcarbodiimide	$KHCO_3$	10	18.0
Diphenylcarbodiimide	$NaHCO_3$	0	3.7
Diphenylcarbodiimide	$NaHCO_3$	10	11.2

a) Fluorene, 5 mmol; imine, 16.8 mmol; base, 60 mmol; DMSO, 25 ml; reaction temp., 20 °C; reaction time, 2 h. b) The yields were calculated on the basis of fluorene used. c) Under a nitrogen atmosphere. d) Under an air atmosphere.

Table 2. The Solubility of Base

Base	Solubility A[a] H_2O	Solubility B[b] H_2O	The amounts of CO_2 absorption[c] H_2O
	0 (10 mmol)	0 (10 mmol)	0 (10 mmol)
None			16.0 (17.3)
K_2CO_3	0.1 (0.2)	3.7 (8.8)	15.1 (20.0)
$KHCO_3$	0.2 (0.2)	41.0 (19.2)	3.6 (13.0)
$NaHCO_3$	0.2 (0.2)	2.3 (3.3)	17.6 (16.4)
HCOOK	3.6	14.0	31.0
CH_3COOK	3.5	6.8	48.3
C_2H_5COOK	2.1	4.5	52.6

a) Solubility of base in DMSO 100 ml. b) Solubility of base in DPC (67.2 mmol) and DMSO 100 ml. c) The amount of CO_2 absorption (mmol) in the solution of base (240 mmol or 120 mmol), DPC (67.2 mmol), and DMSO 100 ml.

Although the solubilities of carbonate and hydrogencarbonates in DMSO were small, they increased upon the addition of DPC, as shown in Table 2. Especially, the solubility of potassium hydrogencarbonate in DMSO with DPC was as large as 41 mmol/100 ml DMSO, suggesting a reaction of DPC with the base to produce an active intermediate. Upon the addition of water, although the solubilities of potassium carbonate

and sodium hydrogencarbonate increased, the solubility of potassium hydrogencarbonate decreased. The effects of the water addition on the solubility had the same tendency as did the effects of water on carboxylation (Table 1).

In the case of DPC and potassium carbonate, fluorene was carboxylated even in the absence of carbon dioxide, indicating that the carbonate ion was the carbon source. However, the yield of 9-FLC was as low as 6.6%.[8a] In the case of DPC and potassium hydrogencarbonate, the yield of 9-FLC under a nitrogen atmosphere was 49%; the yield under an air atmosphere was also 49%. These values were nearly equal to those under a carbon dioxide atmosphere, clearly indicating that the hydrogencarbonate ion was a carbon source. It was considered that a hydrogencarbonate ion attacked an imine carbon to give anionic intermediates which could transfer carbon dioxide to fluorene.

In biological carboxylation catalyzed by a biotin enzyme, the hydrogencarbonate ion is a carbon source and carboxylation occurs through the activation of a hydrogencarbonate ion. We believe that our result is the first example of a model reaction of biotin enzymatic carboxylation using the hydrogencarbonate ion.

Active methylene compounds other than fluorene were also carboxylated by using a reagent system, DPC, potassium hydrogencarbonate and carbon dioxide. They include indene, indanone, acetophenone, cyclohexanone, 1-tetralone, phenylacetonitrile, and *p*-methoxyacetophenone (Table 3). Higher yields than those using potassium carbonate were obtained in the cases of fluorene, phenylacetonitrile, 1-tetralone, and *p*-methoxyacetophenone. There was no correlation between the pK_a of an active methylene compound and the yield.

Similarly to potassium hydrogencarbonate, potassium acetate, being a weak base, was not an effective base for carboxylation if DPC was not used. However, high yields of more than 50% were obtained by employing a reagent system, carbon dioxide, DPC, and potassium acetate (Table 4). Potassium formate and potassium propionate were also effective, even though the yields were about one half those using potassium acetate. Lithium acetate was not effective.

No carboxylation occurred under a nitrogen atmosphere in the case of potassium acetate, indicating that the acetate ion was not a carbon source, and that only atmospheric carbon dioxide was a carbon source. The amounts of carbon dioxide absorption in the case of potassium acetate are also shown in Table 2. The value (48.3) was fairly larger than 15.1 in the case of potassium carbonate. It is considered that the acetate ion attacks an imine carbon, and that the resulting intermediate easily reacts with carbon dioxide to give carbon dioxide donors.

We have already reported that *o*-substitutions in the phenyl moieties of DPC and diphenylurea were harmful for carboxylation using potassium carbonate. The same result was obtained in the case of potassium hydrogencarbonate, as shown in Table 4. The amounts of carbon dioxide adsorption were not affected by the *o*-substitutions, suggesting that the reaction of carbon dioxide with imine was not blocked by the *o*-substitutions. We considered that *o*-substitutions inhibited the reaction of fluorene with an intermediate including carbon dioxide. However, potassium acetate and potassium propionate were effective bases, even in the case of the *o*-substitution of DPC. We could not clarify any mechanism, however, but speculate two reaction routes. At first, acetate and propionate moieties having a larger space than does the hydrogencarbonate

Table 3. Carboxylation of Active Methylene Compounds Using Potassium Hydrogencarbonate in Carbon Dioxide Atmosphere[a]

Substrate	Yield of carboxylic acid/%[b] (using potassium carbonate)
Indene	21.1 (53.8)
Indanone	44.3 (45.5)
Fluorene	43.9 (35.2)
Acetophenone	4.2 (28.7)
Cyclohexanone	3.6 (14.0)
1-Tetralone	35.9 (21.5)
Phenylacetonitrile	51.5 (29.2)
p-Methoxyacetophenone	20.7 (14.4)

a) Substrate, 5 mmol; diphenylcarbodiimide, 16.8 mmol; $KHCO_3$ 60 mmol or K_2CO_3, 30 mmol; DMSO, 25 ml; reaction temp, 20 °C; reaction time, 2 h. b) The yields of carboxylic acid were calculated on the basis of substrate used. The products were monocarboxylic acids. They were identified by comparision of IR spectra with those of the authentic samples, after esterification with diazomethane, if necessary.

Table 4. Carboxylation of Fluorene Using a Biotin Model and a Weak Base under a Carbon Dioxide Atmosphere[a]

Model of the biotin enzyme active site	Base (Reaction time (h))	Yield of 9-FLC[b] %
None	CH_3COOK (2)	0.0
Diphenylcarbodiimide	CH_3COOK (1)	37.3
Diphenylcarbodiimide	CH_3COOK (2)	52.2, 50.8
Diphenylcarbodiimide	CH_3COOK (3)	52.7, 53.1
Diphenylcarbodiimide	CH_3COOK (5)	52.8
Diphenylcarbodiimide	CH_3COOK (7)	49.6
Diphenylcarbodiimide[c]	CH_3COOK (2)	0.0
Diphenylcarbodiimide	CH_3COOLi (2)	0.0
Diphenylcarbodiimide	CH_3COONa (2)	30.5
Diphenylcarbodiimide	HCOOK (2)	26.5
Diphenylcarbodiimide[c]	HCOOK (2)	8.5
Diphenylcarbodiimide	C_2H_5COOK (2)	27.6, 23.0
Diphenylcarbodiimide[c]	C_2H_5COOK (2)	0.0
Diphenylcarbodiimide	C_6H_5COOK (2)	0.0
o-Cl-DPC[d]	$KHCO_3$ (2)	0.0
o-CH_3-DPC[e]	$KHCO_3$ (2)	0.0
o-Cl-DPC[d]	HCOOK (2)	2.3
o-Cl-DPC[d]	CH_3COOK (2)	48.8, 49.8
o-CH_3-DPC[e]	CH_3COOK (2)	16.9
o-Cl-DPC[d]	C_2H_5COOK (2)	35.8
o-Cl-DPC[d]	C_6H_5COOK (2)	0.0

a) Substrate, 5 mmol; diphenylcarbodiimide, 16.8 mmol; base, 60 mmol; DMSO, 25 ml; reaction temp, 20 °C; reaction time, 2 h. b) The yields of carboxylic acid were calculated on the basis of substrate used. c) Under a nitrogen atmosphere. d) Bis(*o*-chlorophenyl)carbodiimide. e) Bis(*o*-methylphenyl)carbodiimide.

ion may remove the blocking of *o*-substitutions. The second is that the acetate and propionate moieties may activate carbon dioxide.

In any case, we first indicated that weak bases, such as potassium acetate and potassium propionate, are also effective in the case that diphenylcarbodiimide is used as a biotin enzyme active site.

Experimental

DPC and substituted DPC were synthesized according to a method of Campbell et al.[10] Fluorene and DPC were dissolved in DMSO (25 ml); to this solution was added powdered alkali carbonate or alkali hydrogencarbonate. Dry carbon dioxide was then passed into the mixture. The reaction mixture was worked up in the same manner as described previously.[8] The yield of 9-FLC was measured gravimetrically. A reaction under pressure was carried out using a 100 ml magnet-driven autoclave and was treated in the same manner as mentioned above. The solubilities of alkali hydrogencarbonates were determined by titration using aquous HCl (0.01 or 0.001 mol dm^{-3}) after filtration.

The amounts of carbon dioxide absorption in a DMSO solution containing DPC were determined by measuring the weights both before and after carbon dioxide bubbling.

References

1) a) A. Behr, *Angew. Chem., Int. Ed. Engl.*, **27**, 661 (1988). b) P. Braunstein, D. Matt, and D. Nobel, *Chem. Rev.*, **88**, 747 (1988).

2) a) H. Tagaya, M. Onuki, Y. Tomioka, Y. Wada, M. Karasu, and K. Chiba, *Bull. Chem. Soc. Jpn.*, **63**, 3233 (1990). b) S. Tazuke and H. Ozawa, *J. Chem. Soc., Chem. Commun.*, **1975**, 237.

3) M. Aresta and G. Forti, "Carbon Dioxide as a Source of Carbon. Biochemical and Chemical Uses," Kluwer Academic Publishers, Hague (1987).

4) W. M. Ayers, "Catalytic Activation of Carbon Dioxide," ACS Symposium Series 363 (1988).

5) S. Inoue and N. Yamazaki, "Organic and Bioorganic Chemistry of Carbon Dioxide," Kodansha, Tokyo (1982).

6) M. Aresta and J. V. Schloss, "Enzymatic and Model Carboxylation and Reduction Reactions for Carbon Dioxide Utilization," Kluwer Academic Publishers, Hague (1990).

7) a) H. Kohn, *J. Am. Chem. Soc.*, **98**, 3690 (1976). b) R. Kluger and P. D. Adawadkar, *J. Am. Chem. Soc.*, **98**, 3741 (1976). c) D. C. Fry, T. L. Fox, M. D. Lane, and A. S. Mildvan, *J. Am. Chem. Soc.*, **107**, 7659 (1985). d) G. R. J. Thatcher, R. Poirier, and R. Kluger, *J. Am. Chem. Soc.*, **108**, 2699 (1986).

8) a) K. Chiba, H. Tagaya, M. Karasu, T. Ono, K. Hashimoto, and Y. Moriwaki, *Bull. Chem. Soc. Jpn.*, **64**, 966 (1991). b) K. Chiba, H. Tagaya, M. Karasu, T. Ono, and M. Kugiya, *Chem. Lett.*, **1990**, 39. c) K. Chiba, T. Akama, K. Sakakibara, and K. Horie, *Chem. Lett.*, **1978**, 1387. d) K. Chiba, K. Sakakibara, and A. Ohta, *Nippon Kagaku Kaishi*, **1983**, 118.

9) a) E. Haruki, M. Arakawa, N. Matsumura, Y. Otsuji, and E. Imoto, *Chem. Lett.*, **1974**, 427. b) E. J. Corey and R. H. K. Chen, *J. Org. Chem.*, **38**, 4086 (1973).

10) T. W. Campbell, J. J. Monagle, and V. S. Foldi, *J. Am. Chem. Soc.*, **84**, 3673 (1962).

Facile Production of D-Histidine by Asymmetric Transformation of L-Histidine

Tadashi SHIRAIWA,* Kazuyuki SHINJO, Yoko MASUI, Atsushi OHTA, Hisashi NATSUYAMA, Hideya MIYAZAKI, and Hidemoto KUROKAWA
Faculty of Engineering, Kansai University, Yamate-cho, Suita, Osaka 564
(Received July 3, 1991)

Synopsis. An asymmetric transformation from L-histidine [L-His] to D-His was achieved by using salicylaldehyde as a catalyst for epimerization, and (2*R*, 3*R*)-tartaric acid as a resolving agent, in acetic acid. Treatment of the obtained salt with triethylamine in methanol gave D-His with 100% optical purity in 95% yield based on the starting L-His.

Both D- and L-amino acids are useful as chiral reagents in asymmetric syntheses. L-Amino acids are obtained as natural products, whereas D-amino acids are difficult to obtain in large quantities. Although an optical resolution of synthetic DL-amino acid gives both D- and L-amino acids, DL-histidine [abbreviated as DL-His] has not been synthesized on an industrial scale because there is no efficient procedure for preparation of its imidazole ring. L-His, therefore, is inexpensive but D-His is significantly costly. The optical resolution of DL-His by using (2*R*, 3*R*)-tartaric acid [(*R*)-TA], as a resolving agent, gives a salt of D-His with (*R*)-TA as a less soluble diastereomeric salt.[1] In addition, an optically active amino acid is racemized easily by using aldehydes as a catalyst in a carboxylic acid.[2,3] We therefore attempted an efficient production of D-His by the asymmetric transformation of L-His.

Experimental

Materials. L-His ($[\alpha]_D^{20}$+12.2° (*c* 3.00, 6 mol dm^{-3} HCl)) and (*R*)-TA ($[\alpha]_D^{20}$+13.2° (*c* 2.00, water)) were purchased from Kokusan Chemical Works, Ltd. and Wako Pure Chemicals Ind., respectively.

Asymmetric Transformation. A mixture of 3.10 g (20.0 mmol) of L-His, 3.00 g (20.0 mmol) of fine powdery (*R*)-TA, and 2.00 or 10.0 mmol of salicylaldehyde or butanal in 20 cm^3 of acetic acid was stirred for 0.5—7 h at 80 or 90 °C, and subsequently for 0. 5 h in an ice bath. The salt formed (5.7—6.1 g) was collected by filtration, washed thoroughly with diethyl ether, and dried.[4] The D-His·(*R*)-TA salt thus obtained was of 100% optical purity: $[\alpha]_D^{20}$+13.3° (*c* 2.00, water). Found: C, 39.32; H, 4.98; N, 13.52%. Calcd for $C_{10}H_{15}N_3O_8$: C, 39.35; H, 4.95; N, 13.77%. After suspending the obtained salt in 70 cm^3 of methanol, followed by adding 2 molar equivalents of triethylamine for the salt, the mixture was stirred for 1 h in an ice bath. Insoluble D-His was collected by filtration, washed with methanol, and dried. The optical purity of the obtained D-His was estimated on the basis of the specific rotation ($[\alpha]_D$+12.43° (6 mol dm^{-3} HCl))[5] of L-His. The D-His obtained was of 100% optical purity. Found: C, 46.11; H, 5.84; N, 27.13%. Calcd for $C_6H_9N_3O_2$: C, 46.45; H, 5.85; N, 27.08%; $[\alpha]_D^{20}$−12.5° (*c* 3.00, 6 mol dm^{-3} HCl). The degrees of crystallization of D- and L-His ($DC_{(D)}$ and $DC_{(L)}$/%) were calculated from the formulae

$$DC_{(L)}/\% = (1/2)\,[\text{Yield}/\% \times (100 - \text{Optical purity}/\%)]/100, \quad (1)$$

$$DC_{(D)}/\% = \text{Yield}/\% - DC_{(L)}/\%, \quad (2)$$

where the yield was calculated on the basis of 20.0 mmol (3.10 g) of His and, when L-His was obtained, the subscripts D and L in Eqs. 1 and 2 were exchanged with each other.

Rate Constant for Racemization. L-His (40.0 mmol) was dissolved in 50 cm^3 of formic acid, acetic acid, or propanoic acid at 40, 70, or 90 °C. After adding 4.00 mmol of salicylaldehyde or butanal, the solution was stirred at each temperature. A 5-cm^3 aliquot of the solution was pipetted out at appropriate time intervals, cooled rapidly, and diluted to 10 cm^3 with water. The optical rotation of the solution was measured at 589 nm with a Union Giken PM-101 digital polarimeter equipped with a quartz cell of 5.00 cm path length. The rate constant for racemization (k_R/s^{-1}) was calculated by the least-squares method from

$$\ln \alpha_0/\alpha_t = k_R \cdot t, \quad (3)$$

where α_t is the optical rotation at time t and α_0 that extrapolated to zero time. The half-life period ($t_{1/2}$/s) was calculated by using the k_R value from Eq. 3.

Results and Discussion

Racemization of L-Histidine. Racemization of L-His was regarded as a first-order reaction because a linear relationship was found between ln α_0/α_t and time t. The rate constant (k_R/s^{-1}) and half-life period ($t_{1/2}$/s) are summarized in Table 1.

The racemization of L-His was accelerated by using salicylaldehyde as a catalyst rather than butanal. We reported that, in racemization of L-proline [L-Pro] and (*R*)-2-piperidinecarboxylic acid [(*R*)-Pia], the rate of racemization by use of butanal increased with a decrease in acidities of the carboxylic acids used as solvents.[6] An alternative result has been reported that the rates of racemization of optically active amino acids may be largest in acetic acid.[2] As seen in Table 1, the rate of racemization of L-His is largest in acetic acid and the tendency differs from those of L-Pro and (*R*)-Pia.[6] In the racemization of L-His, after forming the Schiff base by reaction of L-His with an aldehyde, the racemization seems to proceed by protonation on its nitrogen atom by the carboxylic acid, followed by α-proton abstraction

Table 1. Kinetic Data for Racemization of L-Histidine[a]

Aldehyde	Carboxylic acid	Temperature / °C	k_R[b] / 10^{-4} s^{-1}	$t_{1/2}$[c] / 10^3 s
SA[d]	AcA[e]	40	3.42	2.03
Butanal	FrA[f]	90	0.114	60.8
	AcA[e]	70	3.06	2.27
		90	34.2	0.203
	PrA[g]	90	10.4	0.666

a) Conditions: L-His 40.0 mmol; aldehyde 4.00 mmol; carboxylic acid 50 cm^3. b) k_R: Rate constant for racemizaion. c) $t_{1/2}$: Half-life period. d) Salicylaldehyde. e) Acetic acid. f) Formic acid. g) Propanoic acid.

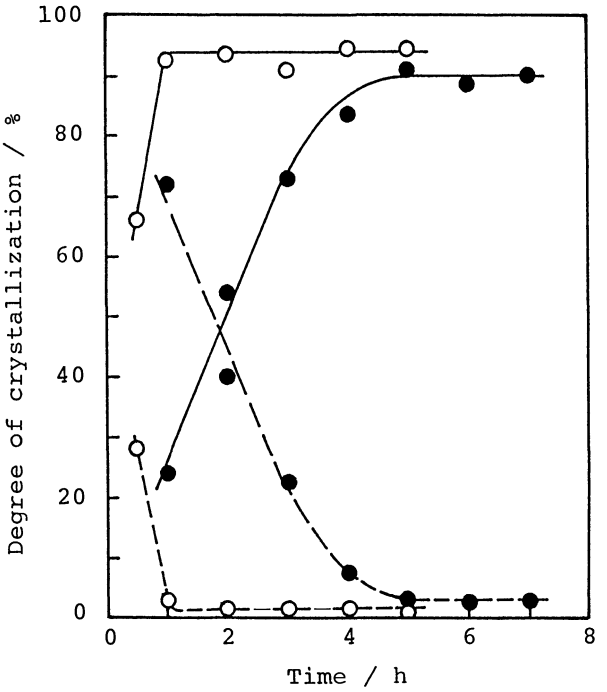

Fig. 1. Comparison of asymmetric transformation by use of salicylaldehyde and butanal as catalyst for epimerization.
Conditions: L-His 20.0 mmol; (*R*)-TA 20.0 mmol; aldehyde 10.0 mmol; acetic acid 20 cm^3; temperature 90 °C. Aldehyde: ○ Salicylaldehyde; ● butanal.
Degree of crystallization: —— $DC_{(D)}$; — — $DC_{(L)}$.

by its carboxylate anion.[2,3] On the other hand, the racemization of L-Pro or (*R*)-Pia proceeds by formation of the Schiff base with concomitant protonation by the carboxylic acid, followed by α-proton abstraction by the resulted carboxylate anion.[2] Since the formation of the Schiff bases seems to be extremely rapid, the rates of racemization of L-Pro and (*R*)-Pia are determined by the process of α-proton abstraction, as described in our previous paper,[6] and that of L-His by both processes of protonation and α-proton abstraction. An order of protonation at 90 °C is estimated from the acidity constant[7] at 90 °C to be formic acid > acetic acid > propanoic acid and that of proton abstraction to be formate anion < acetate anion < propanoate anion. The rate of racemization of L-His, therefore, is estimated to be most rapid in acetic acid, as summarized in Table 1.

Asymmetric Transformation from L-Histidine to D-Histidine. The asymmetric transformation from L-His to D-His was tried by using half molar equivalent of salicylaldehyde or butanal for L-His in acetic acid (Fig. 1); D-His with 15% optical purity was obtained by using 0.1 molar equivalent of butanal at 5 h. Figure 1 suggests that the rate of epimerization of the L-His·(*R*)-TA salt by use of salicylaldehyde as the catalyst is larger than that by butanal, as predicted from the racemization of L-His. The asymmetric transformation was also successfully achieved by using 0.1 molar equivalent of salicylaldehyde for L-His in acetic acid (Table 2). The asymmetric transformation gave efficiently D-His with 100% optical purity in 95% yield, based on the starting L-His, by reacting for 6—7 h at 80 °C and for 3—4 h at 90 °C, respectively.

Table 2. Asymmetric Transformation from L-Histidine to D-Histidine[a]

Temperature	Stirring time	Yield of salt	D-Histidine	
			Yield[c]	Optical purity
°C	h	g [%[b]]	%	%
80	0.5	6.05 [99.2]	93.2[d]	55.0
	1	6.03 [98.9]	92.9[d]	27.0
	2	6.03 [98.9]	92.3	87.3
	3	6.07 [99.5]	96.5	90.1
	4	6.07 [99.5]	97.5	94.1
	5	6.05 [99.2]	95.4	95.7
	6	6.03 [98.9]	95.1	100
	7	6.05 [99.2]	96.6	100
90	1	6.01 [98.5]	95.4	92.5
	2	6.04 [99.0]	95.8	95.7
	3	6.06 [99.3]	95.4	100
	4	6.05 [99.2]	94.6	100

a) Conditions: L-His 20.0 mmol; (*R*)-TA 20.0 mmol; salicylaldehyde 2.00 mmol; acetic acid 20 cm^3. b) The yield was calculated on the basis of 20.0 mmol (6.10 g) of the salt of His with (*R*)-TA. c) The yield was calculated on the basis of the starting L-His (20.0 mmol, 3.10 g). d) Partially racemized L-His.

References

1) F. L. Pyman, *J. Chem. Soc.*, **99**, 1386 (1911).
2) S. Yamada, C. Hongo, R. Yoshioka, and I. Chibata, *J. Org. Chem.*, **48**, 843 (1983).
3) R. Grigg and H. Q. N. Gunaratne, *Tetrahedron Lett.*, **24**, 4457 (1983).
4) Since the absolute value of a difference in the specific rotation between the D-His·(*R*)-TA and L-His·(*R*)-TA salts is extremely small, an estimation of the optical purity of the obtained salt from their specific rotations may result in a large error; lit,[1] of the D-His·(*R*)-TA salt, $[\alpha]_D$+13.3° (*c* 3.69, water); lit,[1] of the L-His·(*R*)-TA salt, $[\alpha]_D$+16.4° (*c* 5.47, water). The optical purity of the obtained salt, therefore, was not estimated from their specific rotations.
5) "Kagaku Daijiten," ed by Kagaku Daijiten Henshu Iinkai, Kyoritsu Shuppan, Tokyo (1971), Vol. 7, p. 376.
6) T. Shiraiwa, K. Shinjo, and H. Kurokawa, *Bull. Chem. Soc. Jpn.*, **64**, 3251 (1991).
7) H. Ohtaki, "Youeki Kagaku," Shoukabou, Tokyo (1985), pp. 184—186.

Asymmetric Hydrocyanation of Benzaldehydes Catalyzed by (5*R*)-5-(4-Imidazolylmethyl)-2,4-imidazolidinedione

Hidenori DANDA
Takarazuka Research Center, Sumitomo Chemical Co., Ltd.,
2-1, 4-Chome, Takatsukasa, Takarazuka, Hyogo 665
(Received July 5, 1991)

Synopsis. The catalytic activity of (5*R*)-5-(4-imidazolylmethyl)-2,4-imidazolidinedione (**3**) was examined in the asymmetric hydrocyanation of 3-phenoxybenzaldehyde (**1a**) to (*S*)-2-hydroxy-2-(3-phenoxyphenyl)acetonitrile ((*S*)-**2a**), an important alcohol moiety of optically active pyrethroid insecticides. Among the catalysts, 3-benzyl derivative (**3d**) exhibited moderate enantioselectivities for **1a** and other benzaldehydes.

(*S*)-2-Hydroxy-2-(3-phenoxyphenyl)acetonimle ((*S*)-**2a**) is an important alcohol moiety of optically active pyrethroid insecticides.[1] With regard to the asymmetric synthesis of optically active cyanohydrins, there have been many reports concerning the enantioselective hydrocyanation or silylcyanation in the presence of a chiral catalyst.[2] Recently, Inoue et al. have reported that the chiral cyclic dipeptides containing an (*S*)-histidine residue, such as *cyclo*[(*S*)-phenylalanyl-(*S*)-histidyl], exhibit high enantioselectivities in the asymmetric hydrocyanation of aldehydes.[3] In conjunction with this finding, our interest has been focussed on the design and screening of catalysts containing the (*R*)-histidine residue to prepare (*S*)-**2a** in high optical yield. We thus prepared various kinds of (5*R*)-5-(4-imidazolylmethyl)-2,4-imidazolidinedione (**3**), which have a structural similar to that of *cyclo*[(*S*)-phenylalanyl-(*S*)-histidyl], and investigated their catalytic activities in the enantioselective addition of hydrogen cyanide to 3-phenoxybenzaldehyde (**1a**) as well as other benzaldehydes (**1b**—**d**) (Scheme 1). Herein, we report on the results concerning asymmetric hydrocyanation catalyzed by **3**.

Results and Discussion

The preparation of the catalyst (**3**) was carried out as illustrated in Scheme 2. The urea (**6**) was prepared by coupling of (*R*)-histidine monohydrochloride hydrate

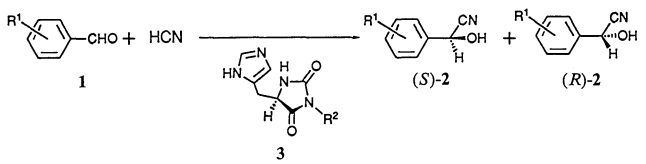

1a, (*S*)-**2a**, (*R*)-**2a**: R¹=m-OPh
1b, (*S*)-**2b**, (*R*)-**2b**: R¹=H
1c, (*S*)-**2c**, (*R*)-**2c**: R¹=p-OMe
1d, (*S*)-**2d**, (*R*)-**2d**: R¹=p-AcOMe

3 : R²=H
3a: R²=R²=C₆H₅
3b: R²=p-ClC₆H₄
3c: R²=p-MeC₆H₄
3d: R²=C₆H₅CH₂
3e: R²=c-C₆h₁₁
3f: R²=

3g: R²=
3h: R²=
3i: R²=
3j: R²=

Scheme 1.

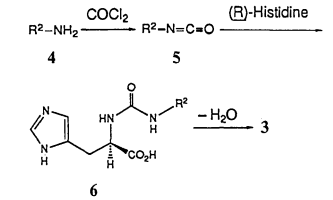

Scheme 2.

with the isocyanate (**5**) which was obtained by a reaction of the corresponding amine (**4**) with phosgene. The urea (**6**) was dehydrated under acidic conditions to give **3** in reasonable yields. The asymmetric hydrocyanation was carried out by using 2.2—5 mol% of the catalyst (**3**) (based on the aldehyde (**1**)). The optical yield (ee) of (*S*)-**2** was determined by HPLC analysis (Sumipax OA-4100).[4]

The asymmetric hydrocyanation of the aldehyde (**1a**) catalyzed by **3** was examined; the results are summarized in Table 1. In all of the catalysts, except for **3f**, (*S*)-cyanohydrin ((*S*)-**2a**) was preferentially obtained, while **3f** gave the opposite enantiomer ((*R*)-**2a**) as a major product (Entry 8). Among the catalysts (**3**), **3d** and **3e** gave (*S*)-**2a** in moderate optical yields (37% ee and 18% ee, Entries 4 and 6). Extending the reaction time decreased the optical yield, which may be due to a racemization of the products (Entry 5). The use of DMF as a solvent decreased the optical yield, even

Table 1. Asymmetric Hydrocyanation of **1a** Catalyzed by **3**[a]

Entry	Catalyst	Sovent	Time/h	Conv. of **1a**/%[b]	Optical yield of **2a**/% ee (confign.)[c]
1	**3a**	Neat	6	90	2 (*S*)
2	**3b**	Neat	4	88	1 (*S*)
3	**3c**	Neat	4	89	10 (*S*)
4	**3d**	Neat	1	90	37 (*S*)
5	**3d**	Neat	4	99	13 (*S*)
6	**3e**	Neat	4	22	18 (*S*)
7	**3e**	DMF	1	69	12 (*S*)
8	**3f**	DMF	4	91	6 (*S*)
9	**3g**	Neat	4	94	6 (*S*)
10	**3h**	Neat	4	97	2 (*S*)
11	**3i**	Neat	4	82	7 (*S*)
12	**3j**	Neat	4	73	1 (*S*)

a) The reactions were carried out at 10 °C by using 1.1 mmol of the catalyst (**3**), 99 mmol of hydrogen cyanide and 50 mmol of the aldehyde (**1a**). In Entries 7 and 8, 40 mL of DMF was used as a solvent because of a poor solubility of **3e** and **3f**. b) Determined by HPLC (LiChrosorb SI-60). Any by-product was not observed on HPLC. c) Determined by HPLC (Sumipax OA-4100).

Table 2. Asymmetric Hydrocyanation of **1a** Catalyzed by **3d**[a)]

Entry	Solvent	Amount of **3d** /mol vs. **1a**	Temp/°C	Time/h	Conv. of **1a**/%[b)]	Optical yield of (*S*)-**2a**/%ee[c)]
1	Toluene	2.2	10	4	No reaction[d)]	—
2	Cyclohexane	2.2	10	4	No reaction[d)]	—
3	CH_3CN	2.2	10	1	89	17
4	CH_2Cl_2	2.2	10	4	No reaction[d)]	—
5	DMF	2.2	10	1	92	11
6	Neat	2.2	0	3	91	40
7	Neat	5	0	1	90	41

a) The reactions were casrried out by using 99 mmol of hydrogen cyanide and 50 mmol of **1a**. 40 mL of solvent was used in Entries 1—5. b) Determined by HPLC (LiChrosorb SI-60). Any by-product was not observed on HPLC. c) Determined by (Sumipax OA-4100). d) **3d** is insoluble.

Table 3. Asymmetric Hydrocyanation of Aldehydes Catalyzed by **3d**[a)]

Entry	Aldehyde	Solvent	Time/h	Conv. of **1**/%[b)]	Optical yield of (*S*)-**2**/%ee[c)]
1	**1b**	Neat	1	90	33
2	**1c**	DMF	3	67	20
3	**1d**	DMF	1	93	16

a) The reactions were carried out at 0 °C by using 1.1 mmol of **3d**, 99 mmol of hydrogen cyanide and 50 mmol of aldehyde. 40 mL of DMF was used in Entries 2 and 3. b) Determined by HPLC (LiChrosorb SI-60). Any by-product was not observed on HPLC. c) Determined by HPLC (Sumipax OA-4100).

though the conversion of **1a** increased (compare Entry 7 with Entry 6). And even though the 3-substituent of **3d** was replaced by chiral benzyl groups, using **3g**—**j**, the optical yield was not improved (Entries 9—12).

Next, the optimal conditions were investigated in the asymmetric hydrocyanation of **1a** catalyzed by **3d**. The results are summarized in Table 2. No reaction was observed when toluene, cyclohexane or CH_2Cl_2 was used as a solvent, because of the poor solubility of **3d** in these solvents. The use of CH_3CN or DMF as a solvent decreased the optical yields. When the reaction temperature was lowered to 0 °C, the optical yield of (*S*)-**2a** was improved (40% ee, Entry 6), whereas it was not improved so much by increasing **3d** (41% ee, Entry 7).

The asymmetric hydrocyanation of benzaldehydes (**1b**—**d**) catalyzed by **3d** was examined. The results are exemplified in Table 3. In all cases, (*S*)-cyanohydrin ((*S*)-**2**) was obtained preferentially, ranging from 16% ee to 33% ee.[4)] However, racemic cyanohydrin was obtained when isobutyraldehyde was employed for the reaction under the same reaction condition as Entry 1 (90% conv. at 1 h).

Thus, **3d** exhibited moderate enantioselectivities in the asymmetric hydrocyanation of benzaldehydes (**1**), particularly atfording (*S*)-**2a** with a maximum optical yield of 41% ee.

We can discuss the mechanism of the enantioselective hydrocyanation catalyzed by **3d**, based on the mechanism which Inoue et al. postulated for the enantioselective hydrocyanation catalyzed by *cyclo*[(*S*)-phenylalanyl-(*S*)-histidyl].[3b)] The carbonyl oxygen of the aldehyde (**1**) is considered to coordinate to the catalyst (**3d**) by a hydrogen bond with the NH group of the histidine residue, and hydrogen cyanide interacts with the imidazolyl moiety of the histidine residue to form a cyanide ion which attacks the *re*-face of the activated carbonyl group, while the *si*-face is blocked by the aromatic ring of benzyl isocyanate residue. However, the blocking by the aromatic ring would be too loose to afford a satisfying enantioselectivity.

A further study dedicated to improving the enantioselectivity is in progress.

Experimental

General. The melting points are uncorrected. Optical rotations were taken on a JASCO DIP-140 digital polarimeter. ^1H NMR spectra were obtained at 200 MHz on a Varian XL-200, except for those of **3**, which were obtained at 90 MHz on a Hitachi R-40; ^{13}C NMR spectra were obtained at 50.3 MHz on a Varian XL-200. IR spectra were obtained on a Hitachi 260-10. HPLC were recorded on a Shimadzu LC-6A, LiChrosorb SI-60 and Sumipax OA-4100 being used as columns for determination of the conversion of **1** and the optical yield of the resulting cyanohydrins ((*S*)-**2**: (*R*)-**2**), respectively. Toluene and xylene were distilled from sodium benzophenone ketyl. DMF and CH_3CN were distilled immediately prior to use. Hydrogen cyanide was provided by Ehime Factory. All other solvents and chemicals were used without further purification.

Preparation of (5*R*)-5-(4-Imidazolylmethyl)-2,4-imidazolidinedione (3). (5*R*)-3-Benzyl-5-(4-imidazolylmethyl)-2,4-imidazolidinedione (3d). To a solution of 7.49 g (70 mmol) of benzylamine in 50 mL of xylene was added at 120 °C over 100 min 27.7 g (280 mmol) of phosgene. After removing the solvent and excess phosgene in vacuo, the crude isocyanate was subjected to the following procedure.

To a solution of 15.7 g (75 mmol) of (*R*)-histidine monohydrochloride hydrate in 180 mL of water was added 2 equiv NaOH until the solution showed pH 9. After the addition of the crude isocyanate obtained above, the reaction mixture was kept at 40 °C for 1 h, adjusted to pH 1 with 35% aqueous HCl, and kept under reflux for 1 h. After being cooled to 5 °C and neutralized to pH 5 with 2 equiv NaOH, the reaction mixture was allowed to stand at 5 °C overnight. The precipitate was filtered, washed with cold water and recrystallized from aqueous ethanol to give 15.2 g (85%) of **3d** as white crystals: Mp 219 °C; $[\alpha]_D^{25}$ 10.6° (*c* 0.87, DMSO); IR (KBr) 3300, 1760, 1710, 1455, 1430 cm^{-1}; ^1H NMR (DMSO-d_6) δ=2.95 (d, *J*=5.2 Hz, 2H), 4.36 (*t*, *J*=5.2 Hz, 1H), 4.47 (s, 2H), 6.80 (s, 1H), 6.9—7.4 (m, 5H), 7.52 (s, 1H), 8.17 (br.s, 1H). Found: C, 65.41; H,

5.49; N, 16.23%. Calcd for $C_{14}H_{14}N_3O_2$: C, 65.61; H, 5.51; N, 16.40%.

(5*R*)-5-(4-Imidazolylmethyl)-3-phenyl-2,4-imidazolidione (3a). The procedure given for **3d** was carried out on the same scale using aniline to give 14.0 g (83%) of **3a** as white crystals: Mp 192—194 °C; $[\alpha]_D^{25}$ 151.1° (*c* 1.02, methanol); IR (KBr) 3200, 1760, 1700, 1430, 1190 cm^{-1}; ^1H NMR (DMSO-d_6) δ=3.08 (d, *J*=6.0 Hz, 2H), 4.44 (t, *J*=6.0 Hz, 1H), 6.90 (s, 1H), 7.2—7.5 (m, 5H), 7.60 (s, 1H), 8.20 (br.s, 1H). Found: C, 64.39; H, 4.87; N, 17.22%. Calcd for $C_{13}H_{12}N_3O_2$: C, 64.45; H, 4.99; N, 17.35%.

(5*R*)-3-(4-Chlorophenyl)-5-(4-imidazolylmethyl)-2,4-imidazolidinedione (3b). The procedure given for **3d** was carried out on the same scale using 4-chloroaniline to give 14.3 g (74%) of **3b** as white crystals: Mp 220—221 °C; $[\alpha]_D^{25}$ 14.5 °C (*c* 0.86, DMSO); IR (KBr) 3300,1710, 1660, 1570, 1400, 1190 cm^{-1}; ^1H NMR (DMSO-d_6) δ=3.01 (d, *J*=5.8 Hz, 2H), 4.45 (t, *J*=5.8 Hz, 1H), 6.89 (s, 1H), 7.1—7.7 (m, 4H), 7.73 (s, 1H), 9.00 (br.s, 1H). Found: C, 56.27; H, 3.89; N, 14.93%. Calcd for $C_{13}H_{11}N_3O_2Cl$: C, 56.43; H, 4.01; N, 15.19%.

(5*R*)-5-(4-Imidazolylmethyl)-3-(4-methylphenyl)-2,4-imidazolidinedione (3c). The procedure given for **3d** was carried out on the same scale using *p*-toluidine to give 13.8 g (77%) of **3c** as white crystals: Mp 243 °C; $[\alpha]_D^{25}$ 113.7° (*c* 0.872, DMSO); IR (KBr) 3200, 3000, 1760, 1705, 1600, 1520, 1430, 1190 cm^{-1}; ^1H NMR (DMSO-d_6) δ=2.30 (s, 3H), 3.02 (d, *J*=5.8 Hz, 2H), 4.42 (t, *J*=5.8 Hz, 1H), 6.86 (s, 1H), 7.0—7.4 (m, 4H), 7.56 (s, 1H), 8.27 (br.s, 1H). Found: C, 65.59; H, 5.35; N, 16.17%. Calcd for $C_{14}H_{14}N_3O_2$: C, 65.61; H, 5.51; N, 16.40%.

(5*R*)-3-Cyclohexyl-5-(4-imidazolylmethyl)-2,4-imidazolidinedione (3e). The procedure given **3d** was carried out on the same scale using cyclohexylamine to give 13.9 g (80%) of **3e** as white crystals: Mp 172—174 °C; $[\alpha]_D^{25}$ 15.6° (*c* 0.87, H_2O); IR (KBr) 3300, 2950, 1620, 1580, 1400 cm^{-1}; ^1H NMR (DMSO-d_6) δ=0.8—0.9 (m, 11H), 2.90 (d, *J*=6.0 Hz, 2H), 4.33 (t, *J*=6.0 Hz, 1H), 6.93 (s, 1H), 7.90 (s, 1H). Found: C, 62.71; H, 7.19; N, 16.84%. Calcd for $C_{13}H_{18}N_3O_2$: C, 62.88; H, 7.31; N, 16.92%.

(5*R*)-5-(4-Imidazolylmethyl)-3-(1-naphtyl)-2,4-imidazolidinedione (3f). The procedure given for **3d** was carried out on the same scale using 1-aminonaphthalene to give 16.6 (81%) of **3f** as white crystals: Mp 205—206 °C; $[\alpha]_D^{25}$ −39.4° (*c* 0.76, DMSO); ^1H NMR (DMSO-d_6) δ=3.07 (d, *J*=6.2 Hz, 2H), 4.53 (t, *J*=6.2 Hz, 1H), 6.97 (s, 1H), 7.3—7.7 (m, 4H), 7.8—8.3 (m, 4H), 8.80 (br.s, 1H). Found: C, 69.76; H, 4.64; N, 14.25%. Calcd for $C_{17}H_{14}N_3O_2$: C, 69.85; H, 4.83; N, 14.38%.

(5*R*)-5-(4-Imidazolylmethyl)-3-[(*R*)-1-phenylethyl]-2,4-imidazolidinedione (3g). The procedure given for **3d** was carried out on the same scale using (*R*)-α-methylbenzylamine to give 12.3 g (65%) of **3g** as white crystals: $[\alpha]_D^{25}$ −20.1° (*c* 1.00, DMSO); IR (KBr) 3300, 1755, 1630, 1550 cm^{-1}; ^1H NMR (DMSO-d_6) δ=1.33 (d, *J*=6.5 Hz, 3H), 2.88 (d, *J*=6.0 Hz, 2H), 4.36 (t, *J*=6.0 Hz, 1H), 4.73 (q, *J*=6.5 Hz, 1H), 6.82 (s, 1H), 7.15—7.4 (m, 5H), 7.65 (s, 1H). Found: C, 66.41; H, 5.80; N, 15.39%. Calcd for $C_{15}H_{16}N_3O_2$: C, 66.65; H, 5.97; N, 15.55%.

(5*R*)-5-(4-Imidazolylmethyl)-3-[(*S*)-1-phenylethyl]-2,4-imidazolidinedione (3h). The procedure given for **3d** was carried out on the same scale using (*S*)-α-methylhenzylamine to give 11.5 g (61%) of **3h** as white crystals: $[\alpha]_D^{25}$ −36.8° (*c* 0.40, DMSO); IR (KBr) 3300, 1760, 1630, 1560 cm^{-1}; ^1H NMR (DMSO-d_6) δ=1.30 (d, *J*=6.5 Hz, 3H), 2.88 (d, *J*=6.0 Hz, 2H), 4.30 (t, *J*=6.0 Hz, 1H), 4.71 (q, *J*=6.5 Hz. 1H), 6.83 (s, 1H), 7.13—7.43 (m, 5H), 7.65 (s, 1H). Found: C, 66.60; H, 5.92; N, 15.47%. Calcd for $C_{15}H_{16}N_3O_2$: C, 66.65; H, 5.97; N, 15.55%.

(5*R*)-5-(4-Imidazolylmethyl)-3-[(*R*)-1,2-diphenylethyl]-2,4-imidazolidinedione (3i). The procedure given for **3d** was carried out on the same scale using (*R*)-1,2-diphenylethylamine to give 13.2 g (55%) of **3i** as white crystals: $[\alpha]_D^{25}$ −15.1° (*c* 1.01, DMSO); IR (KBr) 3340, 1630, 1550, 1510, 1260 cm^{-1}; ^1H NMR (DMSO-d_6) δ=2.85 (d, *J*=6.5 Hz, 2H), 2.88 (d, *J*=6.5 Hz, 2H), 4.27 (t, *J*=6.0 Hz, 1H), 4.80 (t, *J*=6.5 Hz. 1H), 6.80 (s, 1H), 6.9—7.5 (m, 10H), 7.68 (s, 1H). Found: C, 72.68; H, 5.70; N, 11.99%. Calcd for $C_{21}H_{20}N_3O_2$: C, 72.81; H, 5.82; N, 12.13%.

(5*R*)-5-(4-Imidazolylmethyl)-3-[(*S*)-1,2-diphenylethyl]-2,4-imidazolidinedione (3j). The procedure given for **3d** was carried out on the same scale using (*S*)-1,2-diphenylethylamine to give 12.9 g (53%) of **3j** as white crystals: $[\alpha]_D^{25}$ −37.0° (*c* 1.01, DMSO); IR (KBr) 3350, 1630, 1560, 1520, 1260 cm^{-1}; ^1H NMR (DMSO-d_6) δ=2.83 (d, *J*=6.5 Hz, 2H), 2.90 (d, *J*=6.0 Hz, 2H), 4.25 (t, *J*=6.0 Hz, 1H), 4.82 (t, *J*=6.5 Hz, 1H), 6.80 (s, 1H), 7.0—7.6 (m, 10H), 7.68 (s, 1H). Found: C, 72.77; H, 5.71; N, 11.95%. Calcd for $C_{21}H_{20}N_3O_2$: C, 72.81; H, 5.82; N, 12.13%.

General Procedure for Asymmetric Addition of Hydrogen Cyanide to Benzaldehyde (1) Catalyzed by 3. To a mixture of 1.1 mmol of the catalyst (**3**) and 50 mmol of the aldehyde (**1**) (if necessary, 40 mL of an appropriate solvent was used) at 5 °C was added dropwise 3.8 mL (2.67 g, 99 mmol) of hydrogen cyanide under nitrogen; stirring was continued at 0 °C (or 10 °C) for an appropriate period. The reaction mixture was quenched with 0.5% aqueous HCl, and the crude cyanohydrin was extracted twice with toluene. The combined organic layers were dried over Na_2SO_4 and concentrated in vacuo, producing a brown oil which was chromatographed on silica gel to give the pure cyanohydrin. The ^1H NMR and IR spectra were found to be identical with those of an authentic sample. The optical yield of the resulting cyanohydrin ((*S*)-**2**: (*R*)-**2**) was determined by HPLC analysis (column, Sumipax OA-4100; eluent, hexane/1,2-dichloroethane/ethanol/ethyl acetate=800/200/10/1; flow rate, 1.0 mL min^{-1}: detection, 254 nm light). The conversion of **1** was also determined by HPLC analysis (column, LiChrosorb SI-60; eluent, hexane/ethyl acetate/acetic acid=500/60/3; flow rate, 1.0 mL min^{-1}; detection, 254 nm light).

References

1) a) T. Matsuo, T. Nishioka, M. Hirano, Y. Suzuki, K. Tsushima, N. Itaya, and H. Yoshioka, *Pestic. Sci.*, **11**, 202 (1980). b) K. Aketa, N. Ohno, and H. Yoshioka, *Agric. Biol. Chem.*, **42**, 895 (1978).

2) a) J. Oku and S. Inoue, *J. Chem. Soc., Chem. Commun.*, **1981**, 229. b) J. D. Elliott, V. M. F. Choi, and W. S. Johnson, *J. Org. Chem.*, **48**, 2294 (1983). c) M. T. Reetz, F. Kunishi, and P. Heitman, *Tetrahedron Lett.*, **39**, 4721 (1986). d) Y. Kobayashi, S. Asada, I. Watanabe, H. Hayashi, Y. Motoo, and S. Inoue, *Bull. Chem. Soc. Jpn.*, **59**, 983 (1986). e) H. Minamikawa, S. Hayakawa, S. Yamada, N. Iwasawa, and K. Narasaka, *Bull. Chem. Soc. Jpn.*, **61**, 4379 (1988). f) M. Hayashi, T. Matsuda, and N. Oguni, *J. Chem. Soc., Chem. Commun.*, **1990**, 1364.

3) a) A. Mori, Y. Ikeda, K. Kinoshita, and S. Inoue, *Chem. Lett.*, **1989**, 2119. b) K. Tanaka, A. Mori, and S. Inoue, *J. Org. Chem.*, **55**, 181 (1990).

4) The ^1H NMR and IR spectra were found to be identical with those of the authentic sample. The absolute configuration of the resulting cyanohydrins ((*S*)-**2** and (*R*)-**2**) has already been determined.[1b,3b]

3-Aryl-3-butenoic Acids and Their Esters: Practical Synthesis from Diketene by the Palladium-Catalyzed Grignard Coupling Reaction and Application as Monomers for the Radical Copolymerization with Styrene

Kenji ITOH,* Tatsumi HARADA, and Hideo NAGASHIMA
Department of Materials Science, Toyohashi University of Technology, Toyohashi, Aichi 441
(Received July 30, 1991)

Synopsis. Treatment of arylmagnesium bromide with an equimolar amount of zinc chloride followed by the reaction with diketene in the presence of a catalytic amount of $PdCl_2(PPh_3)_2$ provided an improved synthetic method for 3-aryl-3-butenoic acids in a large scale. Application as a monomer for the substituted polystyrenes is exemplified by the copolymerization of methyl 3-phenyl-3-butenoate with styrene.

It is well-known that the reactions of diketene with nucleophiles proceed via the cleavage of its carbonyl–oxygen bond, providing general synthetic methods for acetoacetic acid derivatives.[1] Nonetheless, little has been explored on the nucleophilic reactions via the cleavage of its vinyl–oxygen bond. In 1977, we have reported the first nucleophilic substitution of the carboxylate moiety on the vinyl group in diketene by trimethylsilylmethyl moiety of Me_3SiCH_2MgCl with the aid of simple nickel catalysts, which provides a novel synthetic method for 3-(trimethylsilylmethyl)-3-butenoic acid.[2] Although attempted reactions of diketene with other Grignard reagents under similar conditions only resulted in the formation of intractable materials, improved procedures by Fujisawa[3] and Kato[4] provided preparative routes to 3-(alkyl,[3] aryl,[4] benzyl,[4] ethynyl,[4] and vinyl)-3-butenoic acids[4] by judicious choice of either the transition metal catalysts or organometallic nucleophiles.

We are interested in potential utility of 3-aryl-3-butenoic acids and their derivatives as a novel monomer for the polymerization. Since at least several to several ten grams of the monomer are required for the polymerization studies, the preparative process from diketene by Kato,[4] in which diketene is coupled with arylzinc reagents in situ prepared by aryllithium and zinc chloride, is attractive as a potential large scale synthesis for the monomer. However, there are several problems on the manipulation which should be improved in Kato's process; for example, use of rather expensive organolithium reagents and complicated catalyst system consisting of $PdCl_2(PPh_3)_2$ and diisobutylaluminium hydride (DIBAH). In this paper, we describe a modified process for the synthesis of 3-aryl-3-butenoic acids using rather inexpensive and easily available Grignard reagents as the precursor, acid-catalyzed esterification of the resulting 3-aryl-3-butenoic acids, and application of one of the esters to copolymerization with styrene (Scheme 1). After we started this project, Yamamoto and coworkers briefly reported modification of Kato's process to produce 3-phenyl-3-butenoic acid in their studies of asymmetric hydrogenation of 3-aryl-3-butenoic acids.[5] They used rather complicated procedure than the present method, in which the reaction was undertaken in THF with air-sensitive $Pd(PPh_3)_4$ as the catalyst.[5]

Modification of Kato's procedure was made by successive treatment of an ethereal solution of arylmagnesium bromide with $PdCl_2(PPh_3)_2$ (0.5—1 mol%), $ZnCl_2$, and diketene, providing the desired 3-aryl-3-butenoic acids in 50—80% isolated yields. As shown in Table 1, this procedure can be applied to the synthesis of various 3-aryl-3-butenoic acids. Advantages of this improved process are focussed on the use of less expensive Grignard reagents than aryl lithium compounds and of a catalytic amount of $PdCl_2(PPh_3)_2$ without the aluminium co-catalyst. Furthermore, the following two points are useful for the large scale synthesis. First, a sequence of reactions including synthesis of the Grignard reagents from aryl bromides and magnesium,

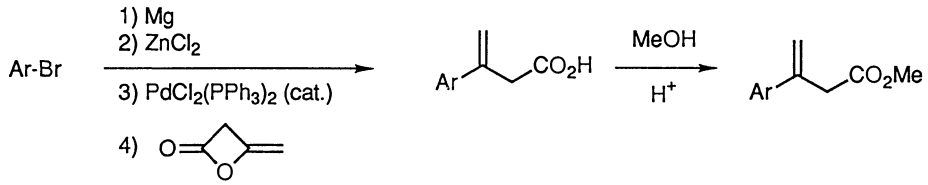

Ar = Phenyl, 1-Naphthyl, o-Tolyl, p-Tolyl, p-Methoxyphenyl, 2-Thienyl

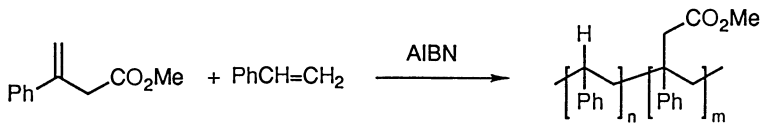

Scheme 1.

Table 1. Palladium-Catalyzed Coupling Reactions of Diketene with Aryl Grignard Reagents

Ar	Cat/%	Time/min	Yield[a]/%
	0.5	30	92 (78)
	1.0	40	94 (79)
	1.0	40	74 (62)
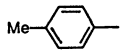	1.0	40	80 (67)
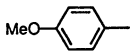	1.0	45	63 (42)
	1.0	30	71 (53)

a) Figures in parenthesis are isolated yields after recrystallization.

transmetallation of the resulting Grignard reagents to aryl zinc reagents by the reaction with $ZnCl_2$, and the palladium-catalyzed coupling reactions with diketene can be carried out in one reaction vessel. Second, 3-aryl-3-butenoic acids are generally solids sparingly soluble in hexane, and hence, pure products were obtained only by extraction of the crude acids by hot hexane. In a typical example, 19 g of 3-phenyl-3-butenoic acid was easily obtained from 7.3 g of bromobenzene and 16 ml of diketene.

Addition of Zn(II) salts (one molar equivalent to the Grignard reagents) is crucially important, and an intractable mixtures of the products were formed in their absence. Use of THF instead of ether also caused serious decrease of the yields. Screening of the reaction conditions revealed that other transition metal salts or complexes such as CoI_2, and $NiCl_2(PPh_3)_2$ also gave the acid but in very low yields. Stoichiometric amounts of Ph_2CuLi in ether reacted with diketene to give 3-phenyl-3-butenoic acid in 40—60% isolated yields. However, attempted reactions of PhMgBr in the presence of catalytic amounts of copper salts only resulted in the formation of intractable products.

Esterification of the 3-aryl-3-butenoic acids involves potential formation of 3-aryl-2-butenoates as the by-product because of facile olefin migration. To avoid the olefin isomerization, Yamamoto and coworkers used diazomethane as the reagent for the esterification.[5] However, we found that the acid-catalyzed esterification of 3-phenyl-3-butenoic acid, 3-(*p*-tolyl)-3-butenoic acid, and 3-(1-naphthyl)-3-butenoic acid was made in MeOH in the presence of H_2SO_4 in 60—80% yields. In the case of 3-(*p*-methoxyphenyl)-3-butenoic acid, 3-(2-thienyl)-3-butenoic acid under the same conditions gave a mixture of isomers due to the isomerization of the olefinic bond from the β,γ- to α,β-position.

Radical polymerization studies were made by methyl 3-phenyl-3-butenoate using α,α'-azobis(isobutyronitrile) (AIBN) as the initiator at 60 °C. Since α-substituted

Table 2. Radical Copolymerization of Methyl 3-Phenyl-3-Butenoate with Styrene at 60 °C

Monomer ratio[a]	Copolymer composition	Time	Conversion	M_n[b]	M_w/M_n[b]
		h	%	$\times10^{-4}$	
1:1	1:5	12	2.5	1.4	1.5
		48	9.5	1.3	1.5
1:5	1:12	12	9.6	2.0	1.5
		48	37.2	2.5	1.7
		96	52.9	2.9	2.0
1:10	1:24	12	18.0	2.9	1.6
		48	50.0	3.5	1.8
1:20	1:35	12	25.9	3.6	1.7
		48	79.1	6.1	1.8
1:40	1:73	12	33.8	4.6	1.7
		48	91.5	7.5	2.2

a) Molar ratios of methyl 3-phenyl-3-butenoate to styrene. b) Determined by GPC based on polystyrene.

styrenes are in general less reactive toward the radical polymerization than styrene, it is reasonable that attempted polymerization of methyl 3-phenyl-3-butenoate itself was in failure. However, copolymerization with styrene successfully produced new polystyrenes including methoxycarbonylmethyl group as the side chain. As shown in Table 2, average molecular weights of the formed polymers were from 13000 to 75000. With higher molar ratios of styrene monomer to methyl 3-phenyl-3-butenoate, copolymers including lower ratios of the ester component with relatively higher molecular weights were formed in high yields. In contrast, with lower molar ratios of styrene monomer to methyl 3-phenyl-3-butenoate were formed copolymers including relatively higher ratios of the ester component but in low yields. Reactivity of styrene (M_1) to methyl 3-phenyl-3-butenoate (M_2) at 60 °C in the copolymerization was estimated by the curve-fitting method as $r_1=6.3$ and $r_2=0.02$.

In conclusion, a simple and versatile synthetic preparative procedure for 3-aryl-3-butenoic acids and their esters suitable to large scale synthesis was established. Furthermore, utility of these compounds as monomer was exemplified by copolymerization of styrene with methyl 3-phenyl-3-butenoate to produce new polystyrenes including polar methoxycarbonylmethyl appendages in their side chain.

Experimental

All manipulations were carried out under nitrogen atmosphere with dry solvents. Reagents were distilled before use. NMR spectra were measured in $CDCl_3$ by a JEOL GX-270 spectrometer (^1H; 270 MHz, ^{13}C; 67.8 MHz) and their δ-values (ppm from TMS) are listed below. IR spectra were measured by a Jasco IR A-3 spectrometer and recorded with the wavenumber. Elemental analysis was made by a Yanaco CHN meter. Mass spectra were measured by a Hitachi M-80B spectrometer. The Grignard reagents described below were prepared from the corresponding aryl bromide and magnesium, which can be stored in a refrigerator as a stock solution. Use of either the freshly prepared Grignard reagents or the stock solution provided similar yields of the desired acids.

General Procedure for the Preparation of 3-Aryl-3-butenoic Acid from Diketene and Arylmagnesium Bromide: The Grignard reagent prepared from Mg turnings (7.3 g, 0.3 mol),

aryl bromide (0.285 mol), and ether (200 ml) was diluted with additional ether (100 ml). Anhydrous $ZnCl_2$ (35 g, 0.257 mmol) was gradually added to the solution and stirred for 45 min to give suspension of white solids in brown solution. Then, $PdCl_2(PPh_3)_2$ (0.726 g, 0.001 mol, 0.5 mol%) and a solution of diketene (16 ml, 0.207 mol) in ether (400 ml) were added dropwise and the mixture was stirred for 30 min. The reaction mixture was poured into a cold 2 equiv HCl aq, and the mixture was extracted with ether. The acid was extracted from the organic layer by 3 equiv NaOH aq. The aqueous layer was acidified by 6 equiv HCl and extracted with ether. The extracts were combined and dried over $MgSO_4$. Removal of the solvents afforded crude 3-aryl-3-butenoic acid (60—80%). This crude acid contained no organic impurities detectable by ^1H NMR spectrum, and can be used for the esterification without further purification. Most of the acids can be purified by recrystalization from hot hexane.

3-Phenyl-3-butenoic Acid: White crystals. Mp 46—47 °C [lit, 46—47 °C].[4,5] ^1H NMR δ=3.54 (2H, s, CH_2CO), 5.26, 5.58 (s, 1H, each, olefin), 7.28—7.45 (m, 5H, Ph). ^{13}C NMR δ=40.8, 116.8, 125.8, 128.0, 128.5, 139.4, 140.2, 177.2. IR (KBr) 1700. Found: C, 74.06; H, 6.21%. Calcd for $C_{10}H_{10}O_2$: C, 74.01; H, 6.25%.

3-(1-Naphthyl)-3-butenoic Acid: White solids. Mp 74.5 °C. ^1H NMR δ=3.56 (s, 2H, CH_2CO), 5.35, 5.62 (s, 1H each, olefin), 7.34—8.03 (m, 7H, aromatic). ^{13}C NMR δ=43.3, 120.3, 125.2, 125.3, 125.4, 125.8, 126.1, 127.8, 128.4, 130.9, 133.7, 139.5, 140.3, 177.1. IR (KBr) 1710. Found: C,79.30; H, 5.76%. Calcd for $C_{14}H_{12}O_2$: C, 79.23; H, 5.70%.

3-(*o*-Tolyl)-3-butenoic Acid: Extraction of the crude acid by hot hexane (100 ml×3) followed by the concentration of the combined extracts gave the pure acid as a yellow oil; ^1H NMR δ=2.32 (s, 3H, Me), 3.39 (s, 2H, CH_2CO), 5.13, 5.41 (s, 1H each, olefin), 7.14—7.18 (m, 4H, aromatic). ^{13}C NMR δ=19.4, 42.5, 118.7, 125.2, 127.0, 128.0, 129.9, 134.5, 140.8, 141.0, 176.6. IR (neat) 1715. Found: C, 74.86; H, 6.95%. Calcd for $C_{11}H_{12}O_2$: C, 74.98; H, 6.86%.

3-(*p*-Tolyl)-3-butenoic Acid: White solids. Mp 106—107 °C [lit, 113—114 °C].[4] ^1H NMR δ=2.34 (s, 3H, Me), 3.52 (s, 2H, CH_2CO), 5.20, 5.54 (s, 1H each, olefin), 7.13, 7.32 (d, J=8.3 Hz, 2H each, aromatic). ^{13}C NMR δ=20.6, 40.5, 115.4, 125.1, 128.6, 136.0, 137.2, 139.4, 176.8. IR (KBr) 1700. Found: C, 74.93; H, 6.84%. Calcd for $C_{11}H_{12}O_2$: C, 74.98; H, 6.86%.

3-(*p*-Methoxyphenyl)-3-butenoic Acid: Yellow solids. ^1H NMR δ=3.52 (s, 2H, CH_2CO), 3.81 (s, 3H, OMe), 5.16, 5.50 (s, 1H each, olefin), 6.86, 7.38 (d, J=8.8 Hz, 2H each, aromatic). ^{13}C NMR δ=40.6, 54.9, 113.3, 114.6, 126.4, 131.4, 139.0, 158.9, 176.0. IR (KBr) 1700. Found: C, 68.76; H, 6.28%. Calcd for $C_{11}H_{12}O_3$: C, 68.74; H, 6.29%.

3-(2-Thienyl)-3-butenoic Acid: Pale yellow solids; yield: 2.52 g (53%); mp 65—66 °C. ^1H NMR δ=3.51 (s, 2H, CH_2CO), 5.14 and 5.61 (s, 1H each, olefin), 6.96 (dd, J=3.4, 5.4 Hz, 1H, 4-H on the thiophene ring), 7.04 (d, J=3.4 Hz, 1H, 5-H on the thiophene ring), 7.18 (d, J=5.4 Hz, 3-H on the thiophene ring). ^{13}C NMR δ=40.8, 114.9, 123.9, 124.6, 127.1, 133.5, 143.2, 176.0. IR (KBr) 1680. Found: C, 57.13; H, 4.86. Calcd for $C_8H_8O_2S$: C, 57.12; H, 4.79%.

Preparation of Methyl Esters: General Procedure: A mixture of the acid (0.13 mol), H_2SO_4 (3 ml, 56 mmol), and methanol (100 ml) was heated under reflux for 30 min. After cooling, H_2SO_4 was neutralized with aqueous $NaHCO_3$ (9.5 g in 100 ml water). Methanol was removed under a reduced pressure and the residue was extracted with CH_2Cl_2. The combined extracts were dried over $MgSO_4$, concentrated, and purified by distillation.

Methyl 3-Phenyl-3-butenoate: Colorless oil; yield 76%; bp 98—106 °C/4 mmHg. ^1H NMR δ=3.51 (s, 2H, CH_2CO), 3.62 (s, 3H, OMe), 5.22, 5.54 (s, 1H each, olefin), 7.25—7.44 (m, 5H, aromatic). ^{13}C NMR δ=40.5, 51.4, 115.7, 125.2, 127.3, 127.9, 139.1, 140.2, 171.1. IR (neat) 1740. HAMS; Found: m/z 176.0836. Calcd for $C_{11}H_{12}O_2$: M, 176.0837.

Methyl 3-(*p*-Tolyl)-3-butenoate: Colorless oil; yield 77%; bp 110—120 °C/4 mmHg. ^1H NMR δ=2.33 (s, 3H, Me), 3.50 (s, 2H, CH_2CO), 3.65 (s, 3H, OMe), 5.18, 5.51 (s, 1H each, olefin), 7.13, 1.32 (d, J=8.3 Hz, 2H each, aromatic). ^{13}C NMR δ=20.7, 40.7, 51.6, 115.0., 125.3, 128.7, 136.4, 137.2, 140.2, 171.4. IR (neat) 1740. HAMS; Found: m/z 190.0994. Calcd for $C_{12}H_{14}O_2$: M, 190.0992.

Methyl 3-(1-Naphthyl)-3-butenoate: Pale yellow oil; yield: 65%; bp 153—156 °C/5 mmHg. ^1H NMR δ=3.54 (s, 2H, CH_2CO), 3.59 (s, 3H, OMe), 5.31, 5.59 (s, 1H each, olefin), 7.33—8.06 (m, 7H, aromatic). ^{13}C NMR δ=43.6, 51.7, 119.7, 125.2, 125.3, 125.4, 125.7, 126.0, 127.7, 128.3, 131.0, 133.7, 139.7, 140.9, 171.3. IR (neat) 1740. Found: C, 79.62; H, 6.28%. Calcd for $C_{15}H_{14}O_2$: C, 79.62; H, 6.24%.

General Procedure of Copolymerization of Methyl 3-Phenyl-3-butenoate with Styrene: A representative experiment was given below. A mixture of methyl 3-phenyl-3-butenoate (2.3 g, 13 mmol), styrene (1.5 ml, 13 mmol), and AIBN (17 mg, 0.1 mmol) was freezed and degassed in a pyrex tube. The tube was sealed under vacuum, and then the mixture was heated at 60 °C for 12 h. The resulting solution was poured into methanol. The formed precipitates were separated by filtration, washed with methanol, and dried under vacuum. The crude polymer was dissolved in benzene and poured into methanol. The precipitates were filtered, washed with methanol, and dried under vacuum to give the copolymer as white solids (92 mg). ^1H NMR δ=0.9—2.7 (br, methylene, methine), 2.8—3.05 (br, CH_2CO), 3.1—3.4 (br, CH_2CO), 6.0—7.3 (br, aromatic ring).

The authors are grateful to Dr. Tsutomu Takeichi and Mr. Seigou Kawaguchi of Toyohashi University of Technology for their helpful discussion on the copolymerization of methyl 3-phenyl-3-butenoate with styrene. One of the authors (K. I.) is grateful to the Ministry of Education, Science and Culture for Grant-in-Aid for The Scientific Research No. 63470073.

References

1) For reviews; T Kato, *Acc. Chem. Res.*, **7**, 265 (1974). R. J. Clemens, *Chem. Rev.*, **86**, 241 (1986).

2) K. Itoh, M. Fukui, and Y. Kurachi, *J. Chem. Soc., Chem. Commun.*, **1977**, 500. K. Itoh, T. Yogo, and Y. Ishii, *Chem. Lett.*, **1977**, 103.

3) T. Fujisawa, T. Sato, Y. Gotoh, M. Kawashima, and T. Kawara, *Bull. Chem. Soc. Jpn.*, **55**, 3555 (1982).

4) Y. Abe, M. Sato, M., H. Goto, R. Sugawara, E. Takahashi, and T. Kato, *Chem. Pharm. Bull.*, **31**, 4346 (1983).

5) K. Yamamoto, K. Ikeda, and L. K. Yin, *J. Organomet. Chem.*, **370**, 319 (1989).

Reaction of Dichlorotriphenylphosphorane with Bis(trimethylsilyl) Peroxide. A New Method for the Formation of Electrophilic Chlorine Source

Kazusato SHIBATA, Yukinori ITOH, Norihiro TOKITOH, Renji OKAZAKI,* and Naoki INAMOTO
Department of Chemistry, Faculty of Science, The University of Tokyo, Hongo, Tokyo 113
(Received August 23, 1991)

Synopsis. Reactions of dichlorotriphenylphosphorane with bis(trimethylsilyl) peroxide in the presence of some organic compounds have been found to give chlorinated products. Aromatic hydrocarbons bearing electron-donating substituents give the corresponding monochloroarenes, while an enol silyl ether is converted into α-chloro ketone. The mechanism is briefly discussed.

In the course of our study on silicon-Polonovski reactions,[1] we became interested in a reagent which was capable of transferring "Me_3SiO^+" species. We thought that the reaction of dichlorotriphenylphosphorane (DCTP) with bis(trimethylsilyl) peroxide (BSPO) would afford a peroxide **1** which might act as a "Me_3SiO^+" source (Scheme 1).

We have found that the reaction of DCTP with BSPO does not produce **1** but it provides a new source for electrophilic chlorine. Reported and discussed are the results observed for chlorination of some organic substrates using this DCTP-BSPO system.

When the reaction of DCTP (2 equiv) (generated in situ from triphenylphosphine and hexachloroethane[2]) with BSPO (1 equiv) in acetonitrile at room temperature was monitored by ^{31}P NMR, a new, single signal (δ_P=30.4) appeared while the signal of DCTP (δ_P=49.0) disappeared completely. When a similar reaction was carried out using 4 equiv of DCTP and 1 equiv of BSPO, two signals were observed roughly in a 1 : 1 ratio; one was the same as the above-mentioned signal while the other is a signal due to remaining DCTP. These facts clearly indicate that DCTP and BSPO react in a 2 : 1 ratio. Furthermore, ^1H, ^{13}C, and ^{29}Si NMR of the solution resulting from the reaction of 2 equiv of DCTP with 1 equiv of BSPO showed the presence of chlorotrimethylsilane (δ_H=0.00, δ_C=2.3, δ_{Si}=31.65) as a sole compound having a trimethylsilyl group; under identical conditions in acetonitrile an authentic sample of chlorotrimethylsilane showed δ_H=0.00, δ_C=1.92, and δ_{Si}=31.61 while that of BSPO exhibited δ_H=−0.29, δ_C=−2.65, and δ_{Si}=26.57. This observation is also in keeping with the above conclusion that DCTP and BSPO react in a 2 : 1 ratio.

When the reaction of DCTP (2 equiv) with BSPO (1 equiv) was conducted at room temperature in the presence of 1,3,5-tri-*t*-butylbenzene (**2**) (1 equiv), 1,3,5-tri-*t*-butyl-2-chlorobenzene (**3**) was obtained in 86% along with triphenylphosphine oxide (95%) and phenyl diphenylphosphinate (**4**, 5%). A similar reaction using DCTP, BSPO, and **2** in a molar ratio of 4 : 2 : 1 gave **3** in 95% in addition to triphenylphosphine oxide (73%) and the phosphinate **4** (13%).

The formation of **3** is suggestive of the generation of electrophilic chlorine in the reaction of DCTP with BSPO. A plausible mechanism for the reaction is shown in Scheme 2.

A combination of a chloride anion with some organic peroxides such as benzoyl peroxide[3] and nitrobenzenesulfonyl peroxides[4] has been known to act as a chlorinating reagent in electrophilic aromatic substitutions and the corresponding acyl or sulfonyl hypochlorites have been proposed as a species responsible for the chlorination. Although a hypohalite like **6** has not been known in the literature, it can be a chlorinating agent. It is not clear at present, however, whether the real reactive species is **6**, phosphine oxide–chlorine complex **7** or molecular chlorine. It has been reported that phosphine oxides including triphenylphosphine oxide form a complex with halogen.[5] Since the only one ^{31}P NMR signal (δ=30.4) was observed in the reaction mixture from DCTP (2 equiv) and BSPO (1 equiv) as

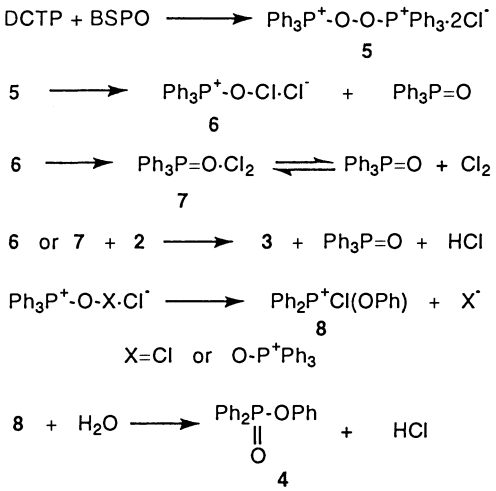

Scheme 2.

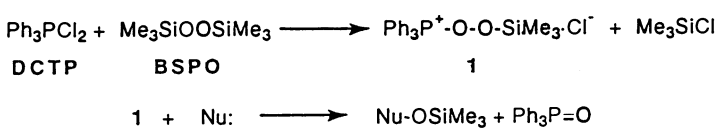

Scheme 1.

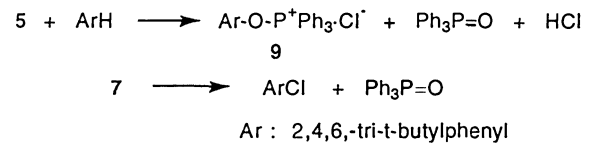

Scheme 3.

Table 1. Chlorination with Dichlorotriphenylphosphorane (DCTP)–Bis(trimethylsilyl) Peroxide (BSPO) System[a]

Substrate	Reaction time	Product	Yield/%[b]
ArH[c]	6 h	ArCl[c]	86 (95)[d]
Mesitylene	6 h	MesCl[e]	44
Anisole	1 h	*p*-chloroanisole	61 (71)[d]
		o-chloroanisole	7 (9)[d]
	4.5 h	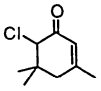	44
10		11	
Ph_2S	2.5 d	Ph_2S=O	12[f]
$(PhCH_2)_3N$	6 d	$(PhCH_2)_2NH \cdot HCl$	20[g]

a) Reactions were carried out in acetonitrile at room temperature using 1 equiv of the substrate, 2 equiv of DCTP and 1 equiv of BSPO. b) Isolated yield except for chloroanisoles where the yields were determined by gas chromatography. c) Ar denotes 2,4,6-tri-*t*-butylphenyl. d) Values in parentheses are yields for the reactions where DCTP(4 equiv) and BSPO(2 equiv) were used. e) Mes denotes mesityl (2,4,6-trimethylphenyl). f) Ph_2S was recovered in 88% yield. g) $(PhCH_2)_3N$ was recovered in 77% yield.

mentioned above, the exchange reaction between **6** and triphenylphosphine oxide as well as the equilibrium between **7** and triphenylphosphine oxide/molecular chlorine is considered to be fast on NMR time scale at room temperature.

Although a mechanism involving an oxygenation followed by a displacement with a chloride anion as shown in Scheme 3 is also conceivable, this possibility can be ruled out by the fact that **9** prepared in a separate experiment from 2,4,6-tri-*t*-butylphenol and DCTP was intact under the reaction conditions even in the presence of chlorotrimethylsilane which might act as Lewis acid by coordination toward the phenolic oxygen to promote an nucleophilic attack by a chloride anion. The formation of the phosphinate **4** can be explained by the shift of a phenyl group in **5** and/or **6** onto the adjacent oxygen atom followed by hydrolysis as shown in Scheme 2. Similar rearrangement of a phenyl group from phosphorus to oxygen has been reported for bis(diphenylphosphinyl) peroxide, $[Ph_2P(=O)O]_2$,[6] suggesting the validity of the involvement of **5** and **6** in the present reaction.

In order to study the scope and limitation of the present chlorinating system (DCTP–BSPO system), some other substrates were submitted to chlorination, the results being summarized in Table 1. Activated arenes such as mesitylene and anisole were also chlorinated, but less reactive substrates like toluene, benzene, and chlorobenzene did not react under similar conditions even when the prolonged reaction time (2 d) was used. This result suggests that the DCTP–BSPO system is less reactive than arenesulfonyl peroxide-chloride system[4] where benzene and toluene are reportedly chlorinated at room temperature. Enol silyl ether **10** was also chlorinated to give α-chloro ketone **11** in a moderate yield, thus providing a new approach to α-chloro ketones. Oxidation of a sulfide to a sulfoxide[6] and dealkylation of a tertiary amine[7] by positive halogen reagents are known processes.

Experimental

Melting points are uncorrected. ^1H (89.60 MHz), ^{13}C (22.53 MHz), ^{29}Si (17.80 MHz), and ^{31}P NMR (36.27 MHz) spectra were measured with JEOL FX-90Q and Brucker AM-500 spectrometers using tetramethylsilane as an internal or external standard for ^1H, ^{13}C, and ^{29}Si NMR, and 85% phosphoric acid as an external standard for ^{31}P NMR. Mass spectra were obtained with a JEOL D-300 mass spectrometer. Gas chromatographic analyses were performed with Shimadzu GC-7A. All reactions were carried out under an argon atmosphere.

Material. Bis(trimethylsilyl) peroxide (BSPO),[9] 1,3,5-tri-*t*-butylbenzene (**2**),[10] and 4,6,6-trimethyl-2-trimethylsilyloxy-1,3-cyclohexadiene (**10**)[11] were prepared by the reported method. Dichlorotriphenylphosphorane (DCTP) was prepared in situ in acetonitrile at room temperature by the method of Appel[2] and used for reactions with BSPO without isolation.

Reaction of 1,3,5-Tri-*t*-butylbenzene (2) with DCTP–BSPO System. An acetonitrile solution of the phosphorane DCTP was prepared[2] by stirring triphenylphosphine (253 mg, 0.966 mmol) and hexachloroethane (229 mg, 0.966 mmol) in acetonitrile (0.4 ml) for 30 min at room temperature. To this solution was added the peroxide BSPO (103 µl, 0.483 mmol) by a syringe (exothermic reaction). After stirring for 30 min an acetonitrile solution (1.4 ml) of **2** was added and the mixture was stirred at room temperature for 6 h during which time white precipitates were formed gradually. The solvent was evaporated to give 520 mg of crude products, which were separated by dry column chromatography (DCC) (silica gel, hexane) to give a mixture of **2** and 1,3,5-tri-*t*-butyl-2-chlorobenzene (**3**) (129 mg), phenyl diphenylphosphinate (**4**) (30 mg, 5%), and triphenylphosphine oxide (257 mg, 95%). The yields of **2** (10%) and **3**[12] (86%) were determined by gas chromatography (column, OV-1; column temperature, 150 °C) by comparing the authentic samples. **3**: ^1H NMR ($CDCl_3$) δ=1.31 (s, 9H), 1.53 (s, 18H), and 7.38 (s, 2H); ^{13}C NMR ($CDCl_3$) δ=30.63, 31.49, 34.96, 37.29, 123.16, 131.36, 147.13, and 147.83.

The phosphinate **4**[13] was identified by NMR and mass spectra; ^1H NMR ($CDCl_3$) δ=6.65—7.54 (m, 5H), and 7.54—8.06 (m, 10H); ^{13}C NMR ($CDCl_3$) δ=120.56, 120.77, 124.62, 127.57, 128.28, 128.87, 129.58, 131.47, 131.96, 132.42, 132.53, and 133.72; ^{31}P NMR δ=28.8 (CH_3CN); δ=30.4 ($CDCl_3$); MS *m/z* (rel intensity) 294 (M^+, 52), 293 (53), 20 (100), 77 (71), 65 (25), and 51 (44).

Reactions of Other Substrates with DCTP–BSPO System. Reactions with other substrates were carried out in a similar way to that described for **2**.

(a) Reaction with mesitylene (112 mg, 0.935 mmol), after separation by preparative TLC, gave 2-chloro-1,3,5-trimethylbenzene[14] (63 mg, 44%), phosphinate **4** (55 mg, 9%), and triphenylphosphine oxide (483 mg, 87%) along with recovered mesitylene (11%). 2-Chloro-1,3,5-trimethylbenzene: ^1H NMR ($CDCl_3$) δ=2.19 (s, 3H), 2.28 (s, 6H), and 6.78 (s, 2H); ^{13}C NMR ($CDCl_3$) δ=20.48, 20.61, 129.18, 131.59, 135.49, and 135.81.

(b) In the reaction with anisole (100 µl, 0.92 mmol), the products, chloroanisoles, were analyzed by gas chromatog-

raphy (column, Carbowax 20M; column temperature, 130 °C). The yields thus obtained are listed in Table 1. The yields of **4** and triphenylphosphine oxide were not determined.

(c) Reaction products with enol silyl ether **10** (0.23 ml, 0.973 mmol) were purified by DCC (silca gel, hexane : ether=2 : 1—1 : 2) to give 6-chloro-3,5,5-trimethyl-2-cyclohexen-1-one (**11**) (74 mg, 44%),[15] phosphinate **4** (18 mg, 3%), triphenylphosphine oxide (544 mg, 97%), and 3,5,5-trimethyl-2-cyclohexen-1-one (isophorone) (23 mg, 17%) which was identified by comparison with an authentic sample. **11**: ^{1}H NMR ($CDCl_3$) δ=0.84—1.35 (m, 6H), 1.80—2.15 (m, 3H), 2.15—2.50 (m, 2H), 3.99 (s, 1H), and 5.85 (br s 1H); ^{13}C NMR ($CDCl_3$) δ=23.78, 24.27, 26.30, 27.95, 38.17, 43.12, 69.26, 123.08, 160.22, and 191.85; MS *m/z* (rel intensity) 172 (M^+, 16), 118 (11), 116 (29), 82 (100), 77 (11), 54 (11), 53 (12), and 52 (16).

(d) Reaction of tribenzylamine (159 mg, 0.553 mmol) gave white precipitates (tribenzylamine hydrochloride, 115 mg, 64 %) after 2.5 d. DCC (alumina, ether) of the filtrate afforded tribenzylamine (20 mg, 13%), dibenzylamine hydrochloride (26 mg, 20%), **4** (56 mg, 34%), and triphenylphosphine oxide (71 mg, 47%).

(e) Reaction of diphenyl sulfide (0.14 ml, 0.84 mmol) afforded, after DCC (silica gel, hexane–ether), diphenyl sulfoxide (21 mg, 12%) and triphenylphosphine oxide (468 mg, 96%) along with recovered diphenyl sulfide (88%). Diphenyl sulfoxide was identified by comparison with an authentic sample prepared by oxidation of diphenyl sulfide with *m*-chloroperbenzoic acid.

The authors thank Shin-etsu Chemical Co., Ltd. and Tosoh Akzo for the generous gift of chlorosilanes and alkyllithiums, respectively.

References

1) R. Okazaki and N. Tokitoh, *J. Chem. Soc., Chem. Commun.*, **1984**, 192; N. Tokitoh and R. Okazaki, *Tetrahedron Lett.*, **25**, 4677 (1984); *idem., Chem. Lett.*, **1984**, 1937; **1985**, 241; *idem., Bull. Chem. Soc. Jpn.*, **60**, 3291 (1987); **61**, 735 (1988).

2) R. Appel and H. Schöler, *Chem. Ber.*, **110**, 2382 (1977).

3) J. K. Kochi, B. M. Graybill, and M. Kurz, *J. Am. Chem. Soc.*, **86**, 5257 (1964); N. J. Bunce and D. D. Tanner, *ibid.*, **91**, 6096 (1969).

4) M. Yoshida, H. Mochizuki, and N. Kamigata, *Chem. Lett.*, **1988**, 2017.

5) For example, R. A. Zingaro and R. M. Hedges, *J. Phys. Chem.*, **65**, 1132 (1961); C. Laurence, M. Queignec-Cabanetos, and B. Wojtkowiak, *J. Chem. Soc., Perkin Trans. 2*, **1982**, 1605.

6) R. L. Dannley, R. L. Waller, R. V. Hoffman, and R. F. Hudson, *J. Org. Chem.*, **37**, 418 (1972).

7) G. C. Barret, "Comprehensive Organic Chemistry," ed by D. N. Jones, Pergamon Press, New York (1979), Vol. 3, Part 11. 3.

8) E. H. White and D. J. Woodcock, "The Chemistry of the Amino Group," ed by S. Patai, Interscience Publishers, New York (1968), Chap. 8.

9) S. Matsubara, T. Okazoe, K. Oshima, K. Takai, and H. Nozaki, *Bull. Chem. Soc. Jpn.*, **58**, 844 (1985).

10) D. E. Pearson and C. A. Buehler, *Synthesis*, **1971**, 455.

11) G. M. Rubottom, J. M. Gruber, H. D. Jave, Jr., and D. A. Charleson, *Org. Synth.*, Coll. Vol. 7, 282 (1990).

12) M. Yoshifuji, S. Tanaka, and N. Inamoto, *Bull. Chem. Soc. Jpn.*, **48**, 2607 (1975).

13) S. Bradamante and G. A. Pagani, *J. Org. Chem.*, **45**, 114 (1980); S. Hoz, E. J. Dunn, E. Buncel, R. A. B. Bannard, and J. Purdon, *Phosphorus Sulfur*, **24**, 321 (1985).

14) G. Häfelinger, F. Hack, and G. Westermeyer, *Chem. Ber.*, **109**, 833 (1976).

15) E. M. Kosower and G.-S. Wu, *J. Org. Chem.*, **28**, 633 (1963).

A Convenient Synthesis of Sulfones by the Oxone Oxidation of Sulfides in an Aprotic Solvent in the Presence of Clay Minerals

Masao HIRANO, Jun-ichirou TOMARU, and Takashi MORIMOTO*
Department of Applied Chemistry, Faculty of Technology, Tokyo University of Agriculture and Technology, Koganei, Tokyo 184
(Received June 28, 1991)

Synopsis. The title oxidation in dichloromethane in the presence of "wet"-montmorillonite and -kaolin afforded the corresponding sulfones in excellent to almost quantitative yield under neutral and mild conditions.

Sulfones are an important intermediate in organic synthesis and, thus, a large number of types of reactions have been developed.[1] Among these, oxidative procedures have been readily accessible and there have been ample methods for this objective.[2] However, there is still a need for effective, inexpensive, and manipulatively secure and simple methods that are performable under mild conditions.

Recently, Oxone[3] has attracted considerable interest because of its versatility as an oxygen-donor for Baeyer–Villiger-type lactonization,[4] the epoxidation of olefins,[5] and the oxidation of sulfides to sulfoxides[6] and sulfones.[4,7] However, Oxone chemistry in a water-free solvent has been hardly explored compared with routine oxidation under aqueous conditions.[4–7] In the course of studies on Oxone oxidation in non-aqueous media,[8] we have disclosed that a montmorillonite clay serves as a highly reactive site for Oxone in the oxidation of sulfides to the sulfones,[8c] which prompted us to search for an initiative and extensive application of various clay minerals for organic synthesis. This paper describes the oxidation of sulfides with Oxone in an aprotic solvent in the presence of such clay minerals as montmorillonite and kaolin, since the reaction offers a facile synthesis of sulfones, the results of which are comparable to chemoselective oxidation under aqueous conditions.[7]

Results and Discussion

The oxidation of sulfides with Oxone in an aprotic solvent was carried out in an inert atmosphere in order to avoid autoxidation. A product study by GLC showed that in addition to a sulfoxide as an incipient product, the sulfone was concomitantly formed, even during the early stage of the reaction. It has been generally accepted that the priority of the formation of a sulfoxide or a sulfone depends on the concentration of the oxidant, as is typically observed in peroxy acid oxidations.[2] In view of an analogous property of Oxone to peroxy acids,[4] the effect of the concentration of Oxone on the selectivity of the products, **2** and **3**, in the oxidation of methyl phenyl sulfide (**1**) was examined. Upon treatment of **1** with one equiv of Oxone in dichloromethane (DM) at room temperature for 24 h, a mixture of **2** (40%) and **3** (18%) was formed, even

$$\underset{\mathbf{1}}{\mathrm{PhSMe}} \xrightarrow{\text{Step 1}} \underset{\mathbf{2}}{\mathrm{PhSOMe}} \xrightarrow{\text{Step 2}} \underset{\mathbf{3}}{\mathrm{PhSO_2Me}}$$

though a considerable amount of **1** (42%; by GLC) still remained. The failure of the selective formation of **2** can be explained in terms of a relatively high susceptibility of **2** to a further oxidation to **3**; this phenomenon is distinctly in contrast with peroxy acid and periodate oxidations,[2] where step 2 is much slower than step 1. Consequently, our interest has been focused on a selective and facile synthesis of the sulfones. To determine favorable conditions for the formation of a sulfone, the effects of the reaction variables on the reactivity of a sulfide, as well as on the selectivity and the yield of the sulfone, were initially investigated.

In the absence or presence of a commercial "dry"-clay mineral, the oxidation of a sulfide was considerably slow, giving a mixture of the sulfoxide and the sulfone. Indeed, the oxidation of **1** ([Oxone]/[**1**]=2.5; mole ratio) in DM at room temperature for 24 h in the absence or presence of a commercial montmorillonite gave 50 or 44% of **2** and 27 or 56% of **3**, respectively (by GLC); 23% of **1** remained in the former case. Whilst in the presence of "wet"-montmorillonite (see Experimental) **1** was completely consumed, even within 2 h under comparable conditions, solely giving **3**. These results indicate that "wet"-montmorillonite plays an important role in facilitating the oxidation. The use of a greater or less amount of "wet"-montmorillonite and of a reagent with a greater or smaller water content than that indicated in the Experimental section resulted in an inferior yield of the sulfone.

The effect of solvents was then examined in the presence of "wet"-montmorillonite. The reactivity of a sulfide was not so affected by the solvents, but the product distribution was strongly dependent on the solvents. For example, upon the oxidation of **1** in benzene, DM, and tetrahydrofuran at room temperature for 2 h ([Oxone]/[**1**]=2.5), **3** was selectively formed; **3** could be isolated in 92, 98, and 95% yields, respectively. Mixtures of **2** and **3**, however, were formed in other solvents in varying ratios: viz., in hexane, $CHCl_3$, CCl_4, ether, AcOEt, MeCN, and acetone, 88, 61, 90, 87, 89, 75, and 94% of **3**, along with 12, 39, 10, 13, 11, 25, and 6% of **2** were formed (by GLC), respectively.

The electronic effect of a ring substituent on the reactivity of a sulfide was also examined in the oxidation of the methyl phenyl sulfides. The time dependence of the product distribution in the oxidation of **1**, and the consumption curves of **1** and the *p*-MeO (**4**) and *p*-NO_2 derivatives, are illustrated in Fig. 1. The apparent reactivity order of the sulfides could be related to the electron-donating property of *para*-substituents, viz. MeO>H>NO_2, as observed in peroxy acid oxidations.[2b] The conversion of sulfoxide (**5**) to the sulfone (**6**) was also faster than that of **7** to **8**; the reaction of

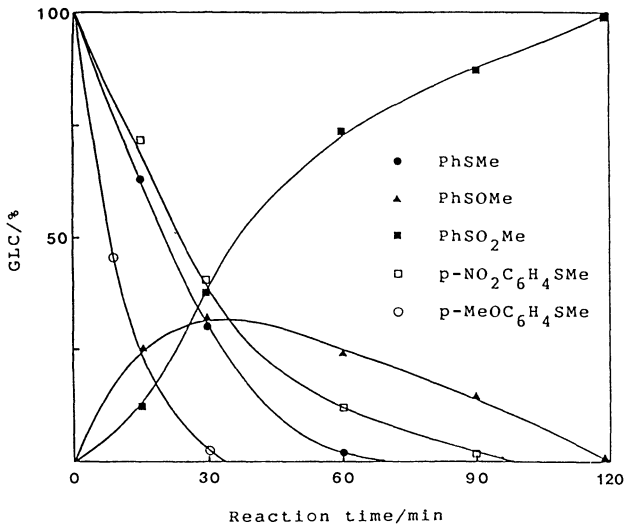

Fig. 1. Conversions and products distribution vs. reaction time in the oxidation of the methyl phenyl sulfides; reaction conditions are identical to those indicated in the oxidation procedure (see the Experimental section).

Table 1. Oxidation of Sulfides with an Oxone–"Wet"-Kaolin System[a]

Entry No.	Sulfides	Time h	Eluents	Sulfones[b] %
1	PhSMe	4	CH_2Cl_2	97
2	*p*-$MeOC_6H_4SMe$	3	AcOEt	99
3	*p*-MeC_6H_4SMe	4	AcOEt	99
4	*p*-BrC_6H_4SMe	5	CH_2Cl_2	98
5	*p*-$NO_2C_6H_4SMe$	4	AcOEt	96
6[c]	PhSPh	24	AcOEt	75
7[c,d]		3	AcOEt	90
8[c]	$(PhCH_2)_2S$	10	AcOEt	96
9	$(Allyl)_2S$	3	CH_2Cl_2	99
10[c]	$(Octyl)_2S$	10	CH_2Cl_2	99
11	(Octyl)SMe	5	CH_2Cl_2	99
12	$(Hexyl)_2S$	5.5	CH_2Cl_2	99
13	BuSBu	5	CH_2Cl_2	97
14	(*s*-$Bu)_2S$	5	CH_2Cl_2	98
15	(*t*-$Bu)_2S$	3	CH_2Cl_2	95
16	PrSPr	4	CH_2Cl_2	98
17	$(Isopropyl)_2S$	4	CH_2Cl_2	97
18	Tetrahydrothiophene	1	$CHCl_3$	97

a) Under argon and under reflux; 1 mmol of sulfide, 1.2 g of "wet"-kaolin, 7 cm^3 of CH_2Cl_2, and ca. 100 cm^3 of an eluent were used in every run; [Oxone]/[Sulfide]=2.5 (mole ratio). b) Isolated yields. c) [Oxone]/[Sulfide] =3.0 (mole ratio). d) In benzene (6 cm^3) at 333 K.

p-$MeOC_6H_4SOMe$ (**5**) *p*-$MeOC_6H_4SO_2Me$ (**6**)

p-$NO_2C_6H_4SOMe$ (**7**) *p*-$NO_2C_6H_4SO_2Me$ (**8**)

4 was thus completed in a shorter period.

Based on the data described above, a synthetic reaction of sulfones was performed at room to reflux temperature in DM in the presence of "wet"-montmorillonite. Using 2.5 moles of Oxone per mole of a sulfide is recommended, since the reaction with two equiv or with a slightly greater amount of Oxone is rather slow. It should be noted that efficient stirring is essential to ensure a smooth oxidation and also to obtain a reproducible result. Under these conditions, the reactions were completed in one to several hours and there was no detectable amount of by-products, giving pure sulfones in usually better than 90% yields.[8c] In order to obtain a high yield of the sulfones, an appropriate choice of an eluent is necessary (see also the forth column in Table 1), since the yield of a sulfone strongly depends on the eluent used. Indeed, **8** was isolated in 70, 60, 67, 96, and 91% yields when DM, ether, $CHCl_3$, AcOEt, and acetone were used as eluents, respectively.

The oxidation of sulfides was also carried out in the presence of "wet"-kaolin in DM in a manner similar to that with an Oxone–"wet"-montmorillonite system, except that the reaction was conducted at an elevated temperature (reflux) and for a longer period, since the efficiency of kaolin is slightly inferior to that using montmorillonite. The results are presented in Table 1. The aromatic-ring (Entries 1—8) and the heterocyclic-ring (Entry 18), as well as the allylic double bond (Entry 9) were found to be intact, leading to a selective formation of the sulfones in excellent yields. The electronic effect of the substituents on the benzene-ring regarding the yield of the sulfones was small (Entries 1—5); they afforded almost quantitative yields of the sulfones. In all instances, some differences in the concentration of Oxone and the reaction times could be mainly ascribed to a difference in the reactivity of the sulfides. Although diphenyl sulfide showed an exceptionally low reactivity in DM (Entry 6), which gave only 75% of the sulfone (**9**), along with 22% of the sulfoxide, the reaction in benzene at 333 K for 3 h exclusively yielded **9** in 90% yield (Entry 7).

The present system is closely related to a conventional clay-supported reagent[9] in the sense that the reaction should be considered to occur on an external surface and/or in an interlayer of a clay mineral, because of the negligible solubility of Oxone in organic solvents, although a relative significance of the phases is obscure. Since the present purpose was synthetic, clear information concerning the observed effects of water and solvents on the reactivity of the sulfides and of the eluents on the yield of sulfones has not yet been obtained. It is well known[9,10] that in addition to water, inorganic as well as organic molecules are adsorbed on a clay surface, and the resultant swelling of the clay, complexation of the clay with these species etc. exert a modified activity of the clay and/or a specific product selectivity. The present reaction may be affected by diverse combinations of possible interactions of a clay with Oxone, a sulfide and/or a sulfone, as well as a solvent (or an eluent), the elucidation of which would provide a satisfactory explanation for the results.

In summary, the oxidation of sulfides with Oxone–"wet"-clay mineral systems in dichloromethane efficiently afforded sulfones in excellent yields. All of the reagents used are inexpensive and safe to handle, and the reaction is fairly clean. The system can be treated just like a clay-supported reagent and, thus, the procedures for isolating the sulfones are facile; it can be emphasized, however, that the reaction is performable instantly without any preparation of a supported re-

agent. The present system thus constitutes an improved version not only of a clay-supported reagent, but of the previous method under aqueous conditions,[7] owing to there being no need to buffer the reaction medium or to carry out tedious work-up procedures. An estimation of the scope and limitations of the systems for organic synthesis is now being undertaken.

Experimental

^{1}H NMR spectra were measured with a JEOL PMX-60 spectrometer for solutions in carbon tetrachloride or deuteriochloroform. IR spectra were recorded for thin films (neat) or KBr disks on a JASCO A-100 spectrophotometer. GLC was carried out on a Shimadzu GC-4CM instrument with a 2 m column packed with Silicone OV-17 on Shimalite WAW-DMCS, with temperature programming.

Starting Materials. All sulfides are commercially available and were used without purification. Oxone and clay minerals are also commercially available. The solvents were rigorously dried and distilled. The "wet"-clay mineral was prepared by adding distilled water (2 g) in eight portions to a commercial clay mineral (10 g) and by vigorous shaking of the mixture upon every addition for a few minutes until a free-flowing powder was obtained.

Oxidation Procedure. The typical procedure is as follows. To a cloudy slurry of "wet"-montmorillonite (1.2 g) and Oxone (2.5 moles of a sulfide) in dichloromethane (6 cm^3; 7 cm^3 of the solvent was used in the case of "wet"-kaolin) in a round-bottommed flask was added methyl phenyl sulfide (1 mmol) in a portion. The flask was flushed with dry argon and then capped with either a glass stopper or a silicon-rubber septum, through which the supernatant was withdrawn by a microsyringe at intervals in order to follow the progress of the reaction. After magnetic stirring for 2 h at room temperature, the whole mixture was transferred onto a Pyrex Buchner funnel with a fritted glass disk; the product was thoroughly eluted with dichloromethane (required ca. 100 cm^3). Rotary evaporation of the combined clear solvent in vacuo left pure (100% by GLC) methyl phenyl sulfone.

The sulfones, thus prepared, had satisfactory purities (over 98%) and were identified by their NMR and IR spectra, as well as the GLC retention times with those of authentic samples.

The partial financial support from Nippon Silica Industrial Co., Ltd. and Daicel Chemical Industries, Ltd. is gratefully acknowledged.

References

1) "Shin-Jikken Kagaku Kouza," Vol. 14- III, p. 1759.

2) a) M. Hudlicky, "Oxidations in Organic Chemistry," Am. Chem. Soc., Washington, DC (1990), p. 250; b) S. O-ae, "Yuki Ioo Kagaku," Kagaku Dojin, Kyoto (1982), Hanno Kiko-hen, p. 318 [*Chem. Abstr.*, **98**, 4051p (1983)].

3) Recent development in Oxone chemistry is conveniently reviewable: R. W. Murray, *Chem. Rev.*, **89**, 1187 (1989); W. Adam, R. Curci, and J. O. Edwards, *Acc. Chem. Res.*, **22**, 205 (1989).

4) R. J. Kennedy and A. M. Stock, *J. Org. Chem.*, **25**, 1901 (1960).

5) R. Bloch, J. Abecassis, and D. Hassan, *J. Org. Chem.*, **50**, 1544 (1985); R. Curci, M. Fiorentino, L. Troisi, J. O. Edwards, and R. H. Peter, *ibid.*, **45**, 4758 (1980); G. Cicala, R. Curci, M. Fiorentino, L. Troisi, and O. Laricchiuta, *ibid.*, **47**, 2670 (1982); P. F. Corey and F. E. Ward, *ibid.*, **51**, 1925, (1986).

6) F. A. Davis, S. G. Lal, and H. D. Durst, *J. Org. Chem.*, **53**, 5004 (1988).

7) B. M. Trost and D. P. Curran, *Tetrahedron Lett.*, **22**, 1287 (1981).

8) a) M. Hirano, M. Oose, and T. Morimoto, *Bull. Chem. Soc. Jpn.*, **64**, 1046 (1991); b) M. Hirano, M. Oose, and T. Morimoto, *Chem. Lett.*, **1991**, 331; c) M. Hirano, J. Tomaru, and T. Morimoto, *ibid.*, **1991**, 523.

9) "Preparative Chemistry Using Supported Reagents," ed by P. Laszlo, Academic Press, San Diego (1987), p. 455.

10) Y. Soma and M. Soma, *Environ. Health Perspect.*, **83**, 205 (1989).

Selective Hydroxymethylation of Emodin

Tarasankar PAL* and Anjali PAL
Department of Chemistry,
Indian Institute of Technology, Kharagpur 721302, India
(Received March 30, 1991)

Synopsis. Electrochemical oxidation of 1,3,8-trihydroxy-6-methylanthraquinone, emodin, in dry alkaline methanol under a constant current of 0.05 A for 10 h under an applied potential difference of 15 V at room temperature resulted, for the first time, in an efficient and selective hydroxymethylation at C-2. The structure of the product was established from the detailed spectral analyses of its trimethyl ether and tetraacetylated derivative.

The field of electrochemistry, so far added many incredible routes to various electroorganic syntheses. Oxidative phenol coupling reaction has also enjoyed its applicabilities when tried with a number of simple substituted phenols,[1-4] though in some cases they ended with usual oxidation products,[5,6] The electrooxidative coupling of phenols has also been extended towards the synthesis of the alkaloidal skeletons.[7-9] Compared with other oxidation routes, electrooxidation appears to be more sensitive to steric factors and the tendency towards the specific formation of the single isomer on electrooxidation is rationalized as arising from a surface reaction, presumably on or near the electrode surface. In spite of the synthetic utility of such an oxidation procedure phenolic polyaromatic quinones, however, remained totally unexplored, though many of them can be used as dyes,[10] and bear clinically important antitumor activities, [11] and indicator properties.[12]

Our primary target was therefore to dimerize 1,3,8-trihydroxy-6-methylanthraquinone, emodin (**1**) an uniquely functionalized phenolic anthraquinone by electrochemical means simulating its chemical transformation.[13,14]

In this report, we wish to present our findings on the electrochemical reaction on emodin (**1**) in dry alkaline methanolic solution, which resulted in the isolation of the hydroxymethylated emodin (**2**) as the sole product (ca. 38%). Anodic oxidation of phenols in methanol has been reported to be a viable route to methoxylation

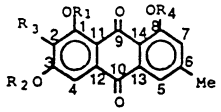

1: $R_1=R_2=R_3=R_4=H$
2: $R_1=R_2=R_4=H$; $R_3=CH_2OH$
3: $R_1=R_2=R_4=Me$; $R_3=CH_2OH$
4: $R_1=R_2=R_4=Ac$; $R_3=CH_2OAc$
5: $R_1=R_2=R_4=Me$; $R_3=H$
6: $R_1=R_2=R_4=Ac$; $R_3=H$

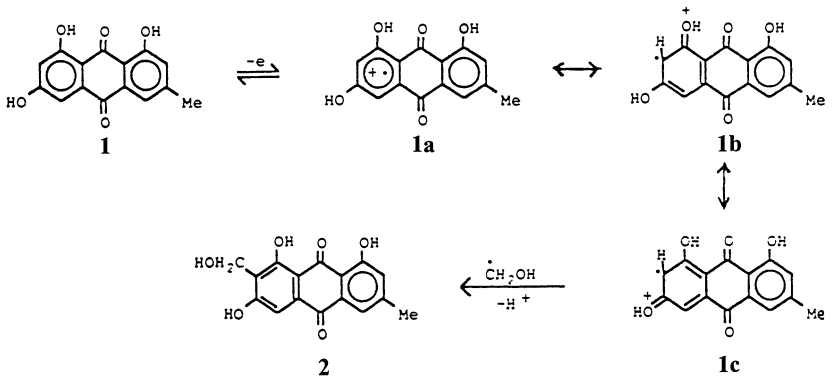

$$\mathbf{1a} + MeOH \longrightarrow \mathbf{1} + MeOH^{+\cdot}$$

$$MeOH^{+\cdot} \xrightarrow{-H^+} \dot{C}H_2OH$$

Scheme 1.

* Present address: Health and Safety Research Division, Oak Ridge National Laboratory, Oak Ridge, Tennessee 37831-6101, U.S.A.

in many cases.[15–18] However, here a hydroxymethylated product was isolated from this type of reaction. The most interesting feature of the product isolated from the reaction in methanol involved the incorporation of the solvent and that too through the formation of a C–C bond, instead of a C–O bond. So this type of hydroxymethylation reaction may have a potential to be used for the synthesis of several important naturally occurring anthraquinonoid compounds like ferruginol,[19] lucidin,[20] tritisporin,[21] asperthecin[22] etc.

The reaction apparently seems to proceed through the formation of a radical cation (**1a**—**c**) followed by the solvent incorporated addition via hydrogen abstraction (Scheme 1). Such type of hydroxymethylation is well known in photochemistry.[23] However, generation of carboxymethyl[24] or nitromethyl[25] radicals by electrolysis of acetic acid and nitromethane in presence of some inorganic or organic mediators are possible, which speaks in favor of the formation of hydroxymethyl radical from methanol. Thus the introduction of hydroxymethyl group in the product isolated seems to be rather unusual though not improbable. The formation of the sole product is the outcome of the balance of the steric and stereoelectronic factors of the radical cation. The other way, the reaction can be rationalized as a hydroxymethylation caused by formaldehyde in-cell generated from the oxidation of methanol in presence of alkali. Such an electrooxidation of methanol to formaldehyde is well documented during the industrial preparation of glycol.[26] In that case also the selective orientation of hydroxymethyl group, as reflected in the product **2**, occurs most efficiently. In this context it is worthwhile to mention that when emodin was allowed to react with formaldehyde in presence of alkali at room temperature, it gave three products, the minor one isolated being authenticated as **2**.

Conversion of emodin (**1**) into **2** was accomplished by carrying out the electrolysis of a dry alkaline methanolic solution of emodin with Pt electrodes for 10 h. The product was established unambiguously to be 2-(hydroxymethyl)emodin (**2**) by a detailed comparative study of the ^{1}H NMR spectral data of the trimethyl ether (**3**) and the tetraacetylated derivative (**4**) of the product with those of the emodin trimethyl ether (**5**)[13] and emodintriacetate (**6**)[27] respectively.

Thus the absence in the ^{1}H NMR spectrum ($CDCl_3$) of **3** of a one proton signal at δ=6.72 corresponding the readily identifiable most upfield aromatic proton signal for H-2 in **5** and the appearance of the proton signal at δ=7.50 as a very sharp singlet, which can be attributed to H-4 of **3** in analogy with H-4 (δ=7.30) of emodin trimethyl ether (**5**), clearly indicates the hydroxymethylation has taken place at C-2. The remaining two aromatic protons appear as two separate doublets at δ=7.10 and 7.67 and can be recognized as H-7 and H-5 respectively when compared with H-7 (δ=7.02) and H-5 (δ=7.57) of trimethyl ether (**5**) of emodin. The coupling (2.0 Hz), however, while lower than is typical for *meta*-standing protons, is not outside the range of some examples, e.g., phthalic acid (0.5 Hz), isophthalic acid (1.6 Hz) and catechol (1.3 Hz). The three aromatic methoxyls in **3** resonated at expected positions (δ=4.0, 3H, s and 4.07, 6H, s). The aromatic methyl appeared at δ=2.50 (3H, s). The presence of two benzylic protons adjacent to a hydroxyl group in **3** is revealed by the appearance of a two proton singlet at δ=4.8.

Table 1. Carbon-13 NMR Spectral Data of Emodin Trimethyl Ether (**5**) and the Trimethylated Derivative of the Product (**3**)

Carbon atoms	Chemical shifts (δ values)	
	5	**3**
C-1	159.76 (s)[a]	161.67 (s)[a]
C-3	161.67 (s)[a]	160.04 (s)[a]
C-8	163.67 (s)[a]	159.88 (s)[a]
C-2	105.26 (d)	129.93 (s)
C-5	118.97 (d)	118.96 (d)
C-6	144.58 (s)	145.13 (s)
C-7	119.56 (d)	119.75 (d)
C-9	181.70 (s)[a]	181.46 (s)[a]
C-10	184.34 (s)[a]	183.70 (s)[a]
C-12	136.39 (s)[b]	135.33 (s)[c]
C-13	134.4 (s)[b]	134.47 (s)[c]
C-4	101.87 (d)	104.28 (d)
C-11	118.39 (s)	122.22 (s)[d]
C-14	121.52 (s)	121.12 (s)[d]
6-Me	22.04 (q)	22.07 (q)
0-Me	55.81 (q)[a]	56.53 (q)[a]
	56.43 (q)[a]	56.25 (q)[a]
	56.45 (q)[a]	54.85 (q)[a]
Ar-CH_2OH	—	63.23 (t)

a) In the absence of adequate data of appropriate model compounds definite assignments were not made. b)—d) Values are interchangeable.

A very interesting feature of the ^{1}H NMR spectrum of the tetraacetyl derivative of **2** is the extraordinary upfield shift of one of the acetoxymethyl groups (δ=2.03) and the other three appeared at δ=2.40, 2.46, and 2.53, which clearly indicates the presence of one aliphatic and three aromatic acetoxyl groups. The benzylic protons appeared at δ=5.30 (2H, s). The aromatic protons resonated at δ=7.35 (1H, d, J=2 Hz; H-7) and δ=8.15 (2H, d, J=2 Hz; H-5) [the signal of H-4 was embedded in the signal of H-5] could also be rationalized when compared with the ^{1}H NMR spectrum[27] of emodintriacetate (**6**).

The most convincing evidence in support of the structure **2** for the product was provided by a comparison of the ^{13}C NMR spectral data of its trimethyl ether (**3**) with those of trimethyl ether (**5**) of emodin[13] (Table 1). The noise-decoupled spectrum of **3** displays 19 carbon signals. The degree of protonation of each carbon atom of the compound was determined by Attached Proton Test (APT) method[28] and the assignments of the carbon chemical shifts were made on the basis of the reported δ_c values of the appropriate anthraquinone monomers.[29]

Experimental

Mps reported are uncorrected. Silica gel (60—100 mesh) was used for column chromatography. TLC analyses were on silica gel plates with 0.2 mm thickness (E. Merck). In all cases of NMR measurements $CDCl_3$ was used as the solvent and TMS as the internal standard. IR spectra were run on a Beckman 20 spectrophotometer, ^{1}H and ^{13}C NMR spectra on a Varian EM-390 instrument operating at 90 MHz and Varian

LX300 (75 MHz) instrument respectively. MS was recorded in an instrument equipped with a direct inlet system and operating at 70 eV. All analytical samples were routinely dried over P_2O_5 for 24 h in vacuo. Na_2SO_4 was used for drying and petrol used had bp 60—80 °C.

Electrolysis and Product Analysis. Electrolysis of the dry methanolic solution (70 ml) of emodin (**1**, 0.14 g) in alkaline medium (pH 9.0 with respect to NaOH) was carried out at a constant current (0.05 A) for 10 h under an applied potential difference of 15 V at room temperature, using platinum plates with an area of 1 cm^2 as the electrodes. After the electrolysis, the electrolytic solution was acidified with 1 M (M=mol dm^{-3}) HCl and then extracted thrice with 30 ml portions of ether. The combined ether layers were dried over anhydrous Na_2SO_4, the solvent was evaporated and the residue was chromatographed.

Unconverted emodin (**1**, 0.06 g) was obtained from the earlier petrol–EtOAc (5:1) eluate and subsequent elution of the column with petrol–EtOAc (3:1) gave 2-(hydroxymethyl)emodin (**2**, 0.054 g) as an orange-red solid, mp>300 °C (petrol–EtOAc); TLC R_f 0.53 (silica gel, 1:1 petrol–EtOAc); IR (KBr) 3550 (OH) cm^{-1}; MS m/z 300 (M^+). Found: C, 64.30; H, 4.11%. Calcd for $C_{16}H_{12}O_6$: C, 64.00; H, 4.00%.

General Procedure for the Formation of the Trimethyl Ether of 2-(Hydroxymethyl)emodin. A solution of 2-(hydroxymethyl)emodin (**2**, 0.025 g) in dry acetone (100 ml) was heated under reflux with Me_2SO_4 (3 ml) over anhydrous K_2CO_3 (100 g) for 10 h. Usual work up and careful column chromatography of the reaction product yielded, along with the tetramethyl ether as a minor product,[12] the trimethyl ether **3** (0.018 g), mp 215 °C (petrol–EtOAc); TLC R_f 0.16 (silica gel, 1:1 petrol–EtOAc); ^1H NMR δ=2.50 (s, 3H, CH_3), 4.0 (s, 3H, OCH_3), 4.07 (s, 6H, OCH_3), 4.80 (s, 2H, CH_2O), 7.10 (d, 1H, J=2.0 Hz, 7-H), 7.67 (d, 1H, J=2.0 Hz, 5-H), 7.50 (s, 1H, 4-H); IR (KBr) 3500 (aliphatic OH) cm^{-1}; MS m/z 342 (M^+). Found: C, 66.80; H, 5.28%. Calcd for $C_{19}H_{18}O_6$: C, 66.66; H, 5.26%. As the major product in its petrol–EtOAc (5:1) eluate.

General Procedure of the Formation of the Tetraacetylated 2-(Hydroxymethyl)emodin (4). Usual acetylation of **2** (0.02 g) (Ac_2O/Py) yielded a tetraacetate **4** (0.016 g), mp 190 °C (petrol–EtOAc); TLC R_f 0.66 (silica gel, 1:1 petrol–EtOAc); ^1H NMR 2.03 (s, 1H, aliphatic $OCOCH_3$), 2.40 (s, 3H, $ArOCOCH_3$), 2.46 (s, 3H, $ArOCOCH_3$), 2.50 (s, 3H, Ar-Me), 2.53 (s, 3H, $ArOCOCH_3$), 5.30 (s, 2H, CH_2O), 7.35 (d, 1H, J=2 Hz, 7-H), 8.15 (d, 2H, J=2 Hz, 5-H) [the signal of 4-H was embedded in the signal of 5-H]; IR (KBr) 1740 (aliphatic $OCOCH_3$) and 1780 (aromatic $OCOCH_3$) cm^{-1}; MS m/z 468 (M^+). Found: C, 61.70; H, 4.29%. Calcd for $C_{24}H_{20}O_{10}$: C, 61.53; H, 4.27%.

We are grateful to our group leader Dr. Tuan Vo-Dinh of the Oak Ridge National Laboratory, Oak Ridge, Tennessee for his invaluable suggestions and all possible help to complete the work.

References

1) F. Fichter and F. Ackermann, *Helv. Chim. Acta,* **2**, 583 (1919).
2) W. B. Smith and Y. H. Yuh, *Tetrahedron,* **24**, 1163 (1968).
3) R. C. Hallcher, *Chem. Abstr.,* **87**, 108551r (1977).
4) R. R. Ismagilov, I. Y. Logutov, Y. I. Michurov, and V. N. Sergeev, *Chem. Abstr.,* **90**, 86869h (1979).
5) D. K. K. Showa, S. I. Takahashi, and H. Uchida, *Chem. Absrt.,* **105**, 215765a (1986).
6) L. Papouchado, G. Petrie, J. H. Sharp, and R. N. Adams, *J. Am. Chem. Soc.,* **90**, 5620 (1968).
7) A. J. Baggaley and R. Brettle, *J. Chem. Soc. C,* **1968**, 2055.
8) W. J. Koehl, Jr., *J. Org. Chem.,* **32**, 614 (1967).
9) A. I. Scott, P. A. Dodson, F. McCapra, and M. B. Meyers, *J. Am. Chem. Soc.,* **85**, 3702 (1963).
10) H. A. Lubs, "The Chemistry of Synthetic Dyes and Pigments," Reinhold, New York (1955), Chap. 7.
11) R. L. Blankespoor, R. Hsung, and D. L. Schutt, *J. Org. Chem.,* **53**, 2877 (1988).
12) V. H. Powell and M. D. Sutherland, *Aust. J. Chem.,* **20**, 542 (1967).
13) P. L. Majumder, A. Pal, and J. N. Shoolary, *Indian J. Chem., Sect. B,* **24**, 318 (1985).
14) B. Frank, R. Chahin, Hans-Greorg Eckert, R. Langenberg, and V. Radtke, *Angew. Chem.,* **14**, 819 (1975).
15) A. Nilsson, A. Ronlan, and V. D. Parker, *Tetrahedron Lett.,* **1975**, 1107.
16) D. R. Henton, K. Anderson, M. J. Manning, and J. S. Swenton, *J. Org. Chem.,* **45**, 3422 (1980).
17) M. Iguchi, A. Nishiyama, Y. Terada, and S. Yamamura, *Tetrahedron Lett.,* **1977**, 4511.
18) M. Iguchi, A. Nishiyama, Y. Terada, and S. Yamamura, *Chem. Lett.,* **1978**, 451.
19) S. Imre, R. Tules, and I. Sengun, *Tetrahedron Lett.,* **1971**, 4681.
20) L. H. Briggs and G. A. Nicholls, *J. Chem. Soc.,* **1953**, 3068.
21) S. Neelakantan, A. Pocker, and H. Raistrick, *Biochem. J.,* **64**, 464 (1956).
22) B. H. Howard and H. Raistrick, *Biochem. J.,* **59**, 475 (1955).
23) H. Aoyama, H. Hatori, and Y. Omote, *J. Org. Chem.,* **54**, 2359 (1989).
24) E. I. Heiba, R. M. Dessau, and P. G. Rodewald, *J. Am. Chem. Soc.,* **96**, 7977 (1974).
25) M. E. Kurz and T. Y. R. Chen, *J. Org. Chem.,* **43**, 239 (1978).
26) R. L. Cook, *Chem. Abstr.,* **106**, 127957e (1987).
27) P. L. Majumder and A. Chattopadhyay, *J. Indian Chem. Soc.,* **62**, 616 (1985).
28) S. L. Patt and J. N. Shoolary, *J. Magn. Reson.,* **46**, 535 (1982).
29) G. Hofle, *Tetrahedron,* **33**, 1963 (1977).

Absorption and Fluorescence Spectra of 1-Methyl-2(1*H*)-pyridinimines and 2-Methylaminopyridine-Acetic Acid Complex

Akira FUJIMOTO and Kozo INUZUKA*
Department of Applied Science, Faculty of Engineering, Tokyo Denki University, Kanda, Chiyoda-ku, Tokyo 101
(Received July 10, 1991)

Synopsis. Upon the addition of acetic acid to 2-methylaminopyridine in isooctane, weak absorption and fluorescence bands appeared near 350 and 465 nm at the tail of the main bands, respectively. These new bands were attributed, on the basis of the spectral results of 1-methyl-, 1,3-dimethyl-, 1,4-dimethyl-, 1,5-dimethyl-, and 1,6-dimethyl-2(1*H*)-pyridinimines, and 1-methyl-2-methylimino-1,2-dihydropyridine, to have originated from 2(1*H*)-pyridinimine moiety (imino-form tautomer) in the 2-methylaminopyridine-acetic acid complex. In addition, the fluorescence quantum yields of the 1-methyl-2(1*H*)-pyridinimines in isooctane were shown to be very small.

Only a limited number of papers have been written on the amino–imino tautomerizations concerning 2-aminopyridine and its related compounds in the ground state.[1–3] In a previous investigation,[1] the UV absorption spectrum of 2-aminopyridine was measured in an acetic acid and isooctane (2,2,4-trimethylpentane) mixed solvent, and its spectrum showed a shoulder band near 335 nm as the concentration of acetic acid increased. A similar shoulder band had been observed at around 345 nm in the case of the 2,6-diaminopyridine–ethanol system; it was assigned to the π, π^* transition of 6-amino-2(1*H*)-pyridinimine.[2] On the other hand, the fluorescence spectra of the 2-aminopyridine-acetic acid system showed a new emission band at 420 nm, and another peak at 360 nm with an increase in the acetic acid concentration.[3] The latter peak was assigned to the monocation species, that is, the aminopyridinium from the fluorescence spectra of 2-aminopyridine in acidic aqueous solution and from the theoretical consideration by the molecular orbital method.[3] However, the shoulder absorption band near 335 nm and the fluorescence band at 420 nm were not clarified experimentally, though these bands had been theoretically assigned to the π–π^* transition of the 2(1*H*)-pyridinimine moiety in the 2-aminopyridine–acetic acid complex.[1,3]

It was found in the present study that the absorption band at 350 nm and the fluorescence bands at 390 and 465 nm for the 2-methylaminopyridine–acetic acid system correspond to the absorption band at 335 nm, and the corresponding bands at 360 and 420 nm for the same system of 2-aminopyridine,[3] respectively. In order to make these bands of 2-methylaminopyridine experimentally more clear the absorption and fluorescence spectra of 1-methyl-2(1*H*)-pyridinimine and its methyl derivatives were investigated by spectroscopic methods.

Results and Discussion

The UV absorption and fluorescence spectra of 2-methylaminopyridine with acetic acid in isooctane solution are shown in Figs. 1 and 2, respectively. The addition of a small amount of acetic acid to 2-methylaminopyridine in isooctane perturbs the absorption spectrum. The large band-shift to the longer wavelength and the appearance of clear isosbestic points at 257 and 305 nm are attributed to the formation of a hydrogen bonded 1 : 1 complex between 2-methylaminopyridine and acetic acid, as shown in Eq. 1.

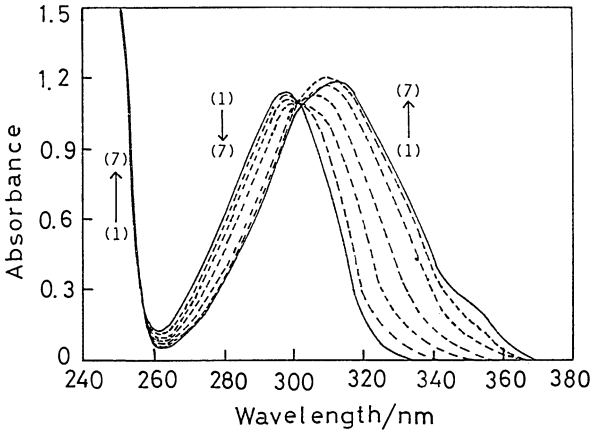

Fig. 1. Absorption spectra of the 2-methylaminopyridine–acetic acid system in isooctane at 20 °C. Concentration of 2-methylaminopyridine: 2×10^{-4} mol dm^{-3}, concentration of acetic acid (mol dm^{-3}): (1) 0, (2) 1×10^{-4}, (3) 5×10^{-3}, (4) 1×10^{-2}, (5) 5×10^{-2}, (6) 1×10^{-1}, (7) 3×10^{-1}.

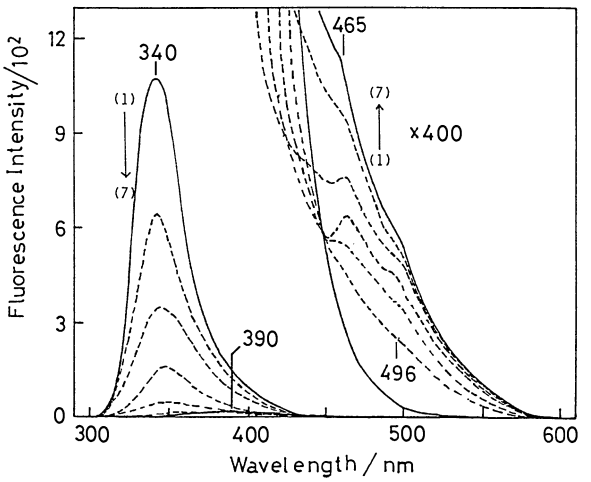

Fig. 2. Fluorescence spectra of the 2-methylaminopyridine–acetic acid system obtained by excitation at 300 nm in isooctane at room temperature. These spectra were measured at the same concentrations as those in Fig. 1.

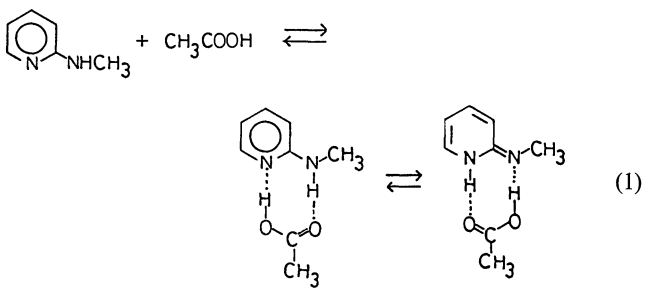

(1)

In a previous paper,[1] similar results had been reported for 2-aminopyridine and its methyl derivatives. In Fig. 1, the absorption band at 315 nm is due primarily to the complex and can be used to determine the equilibrium constant (K) by the method of Benesi and Hildebrand.[4] The enthalpy changes ($-\Delta H$) accompanying hydrogen bond formation can be obtained from knowledge concerning of the variation of K with temperature. In the present experiment the values of K were determined for the methylaminopyridine–acetic acid system at four temperatures within the range from 15 to 40 °C. The values of K, $-\Delta H$, and $-\Delta S$ for 2-methylaminopyridine with acetic acid are 1.8×10^{3} dm^3 mol^{-1} (20 °C), 25.5 kJ mol^{-1}, and 2.5×10^{-2} J K^{-1} mol^{-1}, respectively. The $-\Delta H$ value is smaller than that of 2-aminopyridine with acetic acid (47.3 kJ mol^{-1}).[3] 2-Methylaminopyridine has two conformations with respect to the methylamino group. One of them has a steric hindrance for hydrogen bond formation with acetic acid. The other makes a hydrogen bond without this situation, as shown in Eq. 1. The smaller hydrogen bond energy may be attributed to the above-mentioned two conformations.

Furthermore, upon the addition of acetic acid to 2-methylaminopyridine in isooctane a new, weak shoulder band appeared near 350 nm at the tail of the main band of the hydrogen-bonded complex between 2-methylaminopyridine and acetic acid (Fig 1.). As is shown in Fig. 3, the absorption bands of 1-methyl-2(1H)-pyridinimine[5] and 1-methyl-2-methylimino-1,2-dihydropyridine (as the model of the 2(1H)-pyridinimine moiety (imino-form tautomer) for the 2-methylaminopyridine–acetic acid system) were observed at 345 and 372 nm. These values of 345 and 372 nm are close to the above-mentioned observed value of 350 nm. Therefore, as shown in Eq. 1, it seems reasonable that the shoulder band is due to the 2-methylimino-1,2-dihydropyridine–acetic acid complex formed from the 2-methylaminopyridine–acetic acid complex. The corresponding shoulder bands of the 2-aminopyridine–acetic acid system and the same system of its methyl derivatives had been reported in a previous paper.[1] In Fig. 4, the wavelengthes of the shoulder band of methyl-substituted 2-aminopyridine-acetic acid system and those ones of the absorption band maxima of methyl-substituted 1-methyl-2(1H)-pyridinimine are plotted against the position of the methyl group. Figure 4 shows the existence of a close relationship between the two systems.

On the other hand, the fluorescence spectra of 2-methylaminopyridine in isooctane changes drastically upon the addition of acetic acid (Fig. 2). On the disappearance of the emission at 340 nm with an increase in the acetic acid concentration, a new, very weak emission band appeared at 465 nm; then, with the disappearance of the new, weak emission band, another intense emis-

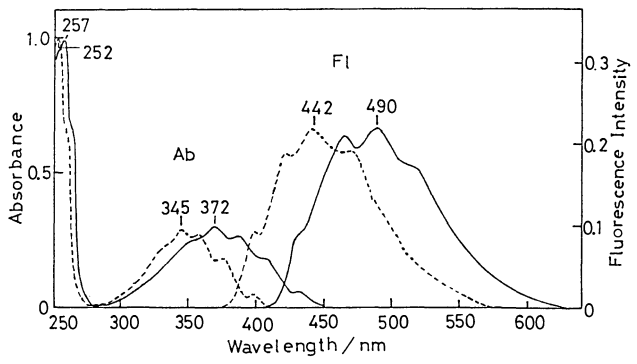

Fig. 3. Absorption (Ab) and fluorescence spectra (Fl) of 1-methyl-2(1H)-pyridinimine (----) and 1-methyl-2-methylimino-1,2-dihydropyridine (——) in isooctane at room temperature. The concentrations of these compounds are 2×10^{-4} mol dm^{-3}.

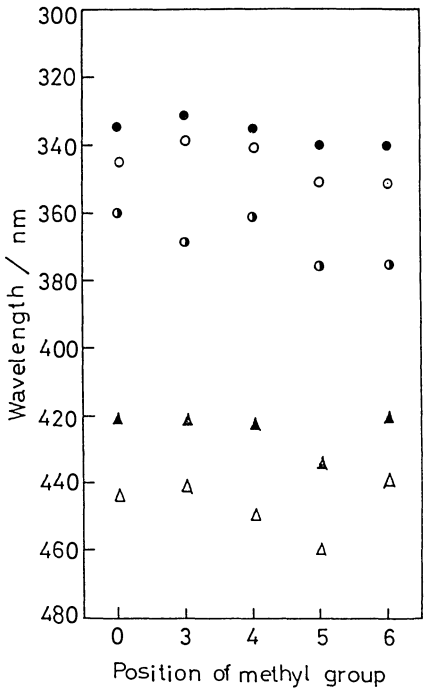

Fig. 4. Plots of the wavelengths of the absorption shoulder bands of the methyl-substituted 2-aminopyridine–acetic acid systems (●), those of the absorption band maxima of methyl-substituted 1-methyl-2(1H)-pyridinimines (○), those of the fluorescence band maxima near 390 nm of the methyl-substituted 2-aminopyridine–acetic acid systems (◑), those of the fluorescence band maxima near 465 nm of the methyl-substituted 2-aminopyridine–acetic acid systems (▲), and those of fluorescence band maxima of methyl-substituted 1-methyl-2(1H)-pyridinimines (△) vs. the position of methyl group. The zero position corresponds to the 2-aminopyridine–acetic acid system or 1-methyl-2(1H)-pyridinimine. The plot ◑ at the zero position is due to the fluorescence band maximum of the pyridinium form of the 2-aminopyridine–acetic acid system.

Table 1. Fluorescence Quantum Yields (ϕ_f) of 2-Methylaminopyridine, 2-Aminopyridine, and Unsubstituted and Monomethyl-Substituted 1-Methyl-2(1*H*)-pyridinimines in Isooctane at Room Temperature

Compound	ϕ_f
2-Methylaminopyridine	$(4.0\pm0.4)\times10^{-2}$
2-Aminopyridine	$(4.3\pm0.4)\times10^{-2}$
1-Methyl-2(1*H*)-pyridinimine	$(3.7\pm0.9)\times10^{-5}$
1-Methyl-2-methylimino-1,2-dihydropyridine	$(3.6\pm0.9)\times10^{-5}$
1,3-Dimethyl-2(1*H*)-pyridinimine	$(1.2\pm0.3)\times10^{-5}$
1,4-Dimethyl-2(1*H*)-pyridinimine	$(7.2\pm1.8)\times10^{-6}$
1,5-Dimethyl-2(1*H*)-pyridinimine	$(9.1\pm2.3)\times10^{-6}$
1,6-Dimethyl-2(1*H*)-pyridinimine	$(9.6\pm2.4)\times10^{-6}$

sion peak was observed at 390 nm, as the acetic acid concentration increased. In Fig. 2, a clear isoemissive point is observed at 448 nm in the fluorescence spectra. The emission near 465 nm has a band progression of ca. 1400 cm^{-1}, while that near 390 nm is a broad band. In order to ascertain an experimental interpretation of the emission bands at 465 and 390 nm, the fluorescence spectra of 1-methy-2(1*H*)-pyridinimine and 1-methyl-2-methylimino-1,2-dihydropyridine as the imino-form model of the 2-methylaminopyridine-acetic acid system were measured. As is shown in Fig. 3, emission peaks having a band progression of ca. 1400 cm^{-1} were observed at 442 and 490 nm, respectively. From the similarity of the band progression and position, the new emission band of the 2-methylaminopyridine-acetic acid system at 465 nm may be considered to correspond to the fluorescence band of the 2-methylimino-1,2-dihydropyridine-acetic acid complex (tautomer) formed through the hydrogen-bond formation of 2-methylaminopyridine with an acetic acid. The fluorescence band of the tautomer at 465 nm can be clearly observed by excitation in the region of the absorption shoulder band near 350 nm.

On the other hand, the fluorescence of 2-methylaminopyridine in 0.1 mol dm^{-3} hydrochloric acid was observed at 388 nm. The observed band of 388 nm of 2-methylaminopyridine in the acidic solution is in fair correspondence with that of 390 nm of the 2-methylaminopyridine–acetic acid system. Accordingly, the fluorescence band at 390 nm may be assigned to the 2-methylaminopyridinium produced from the tautomer in the excited states, as is shown in Eq. 2.

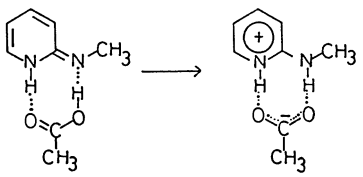

(2)

Both of the emission bands near 465 and 390 nm were observed for the 2-aminopyridine-acetic acid[3] and its methyl derivative–acetic acid systems. The wavelengths of the emission band maxima near 465 nm of the methyl-substituted 2-aminopyridine-acetic acid systems are compared with those ones of the fluorescence band maxima of methyl-substituted 1-methyl-2(1*H*)-pyridinimines, as given in Fig. 4. The former is closely related to the latter. Therefore, the fluorescence band near 465 nm of the methyl derivative–acetic acid systems are due to the imino-forms. On the other hand, the fluorescence bands corresponding to 390 nm for the methyl-substituted derivative–acetic acid systems would be due to the aminopyridinium already described above.

The fluorescence quantum yields (ϕ_f) of 1-methyl-2(1*H*)-pyridinimines in isooctane at room temperature are given in Table 1, with those of 2-methylaminopyridine and 2-aminopyridine. It is noted that the ϕ_f's of the pyridinimines are smaller than those of 2-methylaminopyridine and 2-aminopyridine. This result suggests that the fluorescence quantum yields of imino-form of 2-aminopyridines may be appreciably smaller than those of the amino-forms.

Experimental

Commercial 2-methylaminopyridine (Aldrich) was purified by repeated silica-gel column chromatography using ether as an eluent. 1-Methyl-2(1*H*)-pyridinimine and its methyl substituted derivatives were prepared according to a procedure of Taylar et al.[6] These compounds were purified by alumina column chromatography using isooctane as an eluent. The purification of 2-aminopyridine and its methyl derivatives, isooctane, and acetic acid has been described in the literature.[1,3] The UV absorption and fluorescence spectra were measured with Hitachi model 3410 and F-4010 spectrophotometers, respectively. The fluorescence quantum yields were normalized to a value of 0.006[7] for 1-methyl-2-pyridone in alcohol (ethanol containing 10% methanol) mixture.

This work was supported by grants from Tokyo Denki University Research Institute for Technology.

References

1) K. Inuzuka and A. Fujimoto, *Bull. Chem. Soc. Jpn.*, **63**, 971 (1990).
2) K. Inuzuka and A. Fujimoto, *Bull. Chem. Soc. Jpn.*, **63**, 216 (1990).
3) K. Inuzuka and A. Fujimoto, *Spectrochim. Acta, Part A*, **42**, 929 (1986).
4) H. A. Benesi and J. H. Hildebrand, *J. Am. Chem. Soc.*, **71**, 2703 (1949).
5) This compound has been reported to show the absorption band near 345 nm in cyclohexane. (S. F. Mason, *J. Chem. Soc.*, **1960**, 219.)
6) E. C. Taylor and R. O. Kan, *J. Am. Chem. Soc.*, **85**, 776 (1963).
7) K. Kimura and R. Nagai, *Bull. Chem. Soc. Jpn.*, **49**, 3343 (1976).

Some ^{13}C and ^{15}N NMR Studies on 1,8-Bis (dimethylamino) Naphthalene and Two of Its Salts

E. GRECH,† L. STEFANIAK,†† Isao ANDO,††† Hiroaki YOSHIMIZU,††† and Graham A. WEBB*
Department of Chemistry, University of Surrey, Guildford, Surrey, UK
†Institute of Fundamental Chemistry, Technical University, Szczecin, Poland
††Institute of Organic Chemistry, Polish Academy of Sciences, Warsaw, Poland
†††Department of Polymer Chemistry, Tokyo Institute of Technology, Ookayama, Meguro-ku, Tokyo 152
(Received August 14, 1991)

Synopsis. ^{13}C and ^{15}N NMR data are reported for 1,8-bis(dimethylamino)naphthalene (DMAN) and two of its salts in both the solid state and solutions in CD_3CN. Only the ^{15}N results are sufficiently sensitive to show the presence of the fully protonated form of DMAN in the solid state and of a partially protonated structure in solution.

We have previously reported some ^{13}C and ^{15}N NMR results taken on the solid, and in solution, for 1,8-bis(dimethylamino)naphthalene (DMAN) and its monoprotonated salt with tetrazole.[1] It was found that the ^{13}C chemical shifts were relatively insensitive to salt formation whereas the ^{15}N chemical shifts were very informative regarding differences in structures between the solution and solid states. The present report concerns a similar investigation of a further two salts of DMAN.

Results and Discussion

The results of some ^{13}C and ^{15}N NMR measurements on DMAN and two of its salts at room temperature are presented in Table 1 for both the solid state and for solutions in CD_3CN. The reported assignments of the observed NMR signals are straightforward and in the case of the salts with 1-methyl-1,4-dihydro-5*H*-tetrazole-5-thione (MDTT) the procedures given elsewhere[2] were employed. In general, the ^{13}C chemical shifts for a given compound in Table 1 are very similar for both the solid state and solution cases. Thus not all of the observed ^{13}C chemical shifts are reported in Table 1. In contrast the ^{15}N chemical shifts show some significant differences between the solid state and solution. An exception being the ^{15}N signals for the bis(dimethyl-

Table 1. Some ^{13}C and ^{15}N Solution and Solid State NMR Data for 1,8-Bis(dimethylamino)naphthalene [DMAN] and Two of Its Salts

		Chemical Shifts in a CD_3CN solution[a]	CP MAS chemical shifts[a]
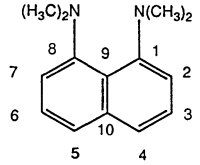 (DMAN)	CH_3	44.7	42.1, 45.2[b]
	N	−338.1	−336.9
	C_1	151.3	150.1
	C_2	113.5	113.2
	C_3	126.0	125.2
	C_4	122.5	121.7
	C_9	121.4	120.9
	C_{10}	138.7	137.3
DMANH$^+$ 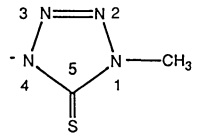	CH_3	45.7	47.3
	N	−345.4	−345.9
	N_1–CH_3	32.4	32.0
	C_5	168.2	169.7
	N_1	−156.7	−153.6
	N_2	−17.1	−15.3
	N_3	3.4	5.5
	N_4	−136.6	−59.3
DMANH$^+$ 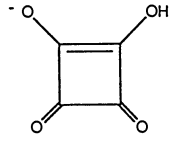	CH_3	47.0	46.0
	N	−347.2	−346.0
	C-ring	198.0	193.7[c]

a) ^{13}C chemical shifts are given with respect to TMS and ^{15}N chemical shifts with respect to neat nitromethane. b) Two methyl ^{13}C signals are observed in the solid state spectrum. These probably are due to packing effects. c) Very broad ^{13}C signal indicating that averaging of the four ring carbon atom environments may not be complete in the solid state.

amino) groups of DMAN. This relative insensitivity of the ^{15}N resonance position to protonation of two dimethylamino groups has been discussed previously.[3]

As noted in the case of the DMAN salt with tetrazole,[1] the N_4 signal of the salt with MDTT shows a large difference between the solid and solution cases. As observed before[1] the solid state ^{15}N signal for N_4 is shielded with respect to that for the solution. In the present case this shielding amounts to about 80 ppm. Comparison of the present ^{15}N chemical shifts for the DMAN salt may be made with those for the free MDTT published previously.[2] For N_4, the position of the signal for the solution of the salt in CD_3CN solution of the salt in CD_3CN solution lies between that of the salt in the solid state and that of the free MDTT in DMSO solution. This suggests that in CD_3CN solution the salt exists in an equilibrium involving the half protonated form of the base as discussed previously.[1]

For the DMAN salt with squaric acid(3,4-dihydroxy-3-cyclobutene-1,2-dione) there are no nitrogen atoms in positions which are sensitive to differences between the solution and solid state cases. However, the averaged position of the ^{13}C signal from the four carbons of the squarate ring shows a small difference between the solution and solid state. Thus ^{13}C NMR is unable to provide information of the type noted above from ^{15}N measurements concerning a possible equilibrium for the salt in solution.

In addition we have some ^{1}H NMR results, for the compounds studied, taken on CD_3CN solutions. We observe that the $N-CH_3$ protons of DMAN are deshielded upon protonation from a chemical shift of 2.7 ppm for DMAN to 3.2 ppm for $DMANH^+Cl^-$, the other salts reported here lie between these values. In the case of $DMANH^+Cl^-$ we have observed $^3J(H-H)$, for the $N-CH_3$ protons and the proton transferred upon salt formation, this is found to be 2.6 Hz in CD_3CN solution. The chemical shift of the transferred proton is observed to be 18.5 ppm, and this proton has a value of 5.1 Hz for $^2J(C-H)$ for its coupling to the carbon atom of the $N-CH_3$ group of DMAN which has a chemical shift of 48.2 ppm in the hydrochloride salt.

The chemical shift of the nitrogen atom in the hydrochloride is -352 ppm which is the most highly shielded of the $N-CH_3$ nitrogens observed in solutions in the present work. Further supporting the conclusion of partial protonation for the other salts studied in solution.

We conclude that nitrogen NMR measurement have again been demonstrated to be the most satisfactory means of investigating the structures studied both in solution and the solid state. Rather less information becomes available for those compounds which do not contain nitrogen atoms in the deprotonated ring.

Experimental

The compounds studied were prepared by published procedures.[4] The solution NMR spectra were taken on a Bruker AM 500 spectrometer operating at 125 and 50.5 MHz for ^{13}C and ^{15}N nuclei, respectively. Solid state NMR measurements were performed on a JEOL GSX 270 instrument operating at 67.5 and 27.3 MHz for the ^{13}C and ^{15}N nuclei respectively. ^{15}N INEPT and inverse gated decoupling measurments were taken on the solutions of the samples.

References

1) E. Grech, L. Stefaniak, I. Ando, H. Yoshimizu, G. A. Webb, and L. Sobczyk, *Bull. Chem. Soc. Jpn.*, **63**, 2716 (1990).

2) E. Bojarska-Olejnik, L. Stefaniak, M. Witanowski, and G. A. Webb, *Bull. Chem. Soc. Jpn.*, **59**, 3263 (1986).

3) M. Witanowski, L. Stefaniak, and G. A. Webb, in "Annual Reports on NMR Spectroscopy," ed by G. A. Webb, Academic Press, London (1986), Vol. 18, p. 251.

4) T. Glowiak, Z. Malarski, L. Sobczyk, and E. Grech, *J. Mol. Struct.*, **157**, 329 (1987).

Studies on Stigmasterol Liquid Membranes

M. L. SRIVASTAVA* and Nikhil K. SHUKLA
Department of Chemistry, University of Gorakhpur, Gorakhpur 273009, U.P. India
(Received December 28, 1990)

Synopsis. Cellulose acetate supported stigmasterol liquid surfactant membrane has been characterized by measuring membrane potentials, using NaCl solutions of different concentrations. Fixed charge density, $\phi\overline{X}$, permselectivity, P_s, have been estimated from ionic transport numbers. Variation of membrane potential with pH and concentration of NaCl solution has also been examined.

Experimental

Cellulose acetate film was prepared as reported elsewhere.[1] The thickness of the film used was 7×10^{-5} m and its cross-sectional area was 1.73×10^{-4} m^2. Water content determined as usual[2,3] was found to be 11.5%.

Results and Discussion

Liquid membranes are formed at every interface encountered by a surfactant solution. Such membranes are of immense importance owing to many of their biological and technological applications.[4-8] The formation of liquid membrane was ascertained by measuring membrane resistance using stigmasterol suspensions of different concentrations. The resistivity changed due to accumulation of stigmasterol in the interfacial region, approaching a constant value after 3—4 h (Fig. 1). Membrane potential was measured using the experimental cell of the type:

Reference Calomel Electrode	Solution	Membrane	Solution	Reference Calomel Electrode

The formation of liquid membrane results in the lowering of membrane potential as it is clear from membrane potential values given in Table 1.

For cellulose acetate which is practically uncharged, the selectivity is considerably low. Permselectivity was estimated using the equation[9]

$$P_s=\frac{\bar{t}_+-t_+}{t_+-(2t_+-1)\,\bar{t}_+}. \quad (1)$$

The transport number on the basis of TMS theory may be given as [10]

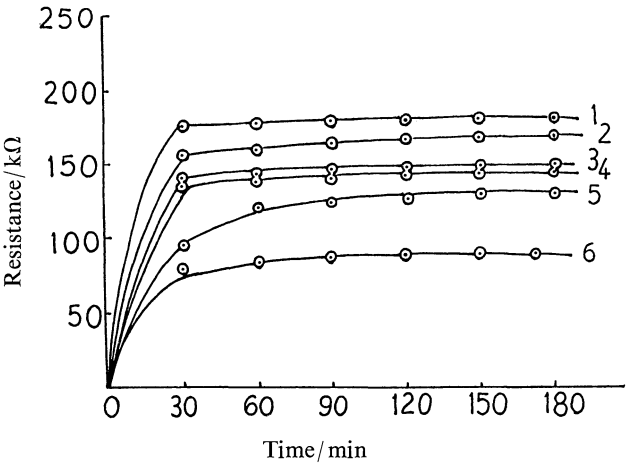

Fig. 1. Variation of resistance with time during liquid membrane formation 1, 30 nM; 2, 25 nM; 3, 20 nM; 4, 15 nM; 5, 10 nM; 6, 5 nM.

Table 1. Membrane Potential Data

Mean concn	C_1	C_2	E/mV	
mol dm^{-3}	mol dm^{-3}	mol dm^{-3}	With Stigmasterol	Without Stigmasterol
0.075	0.10	0.05	6.8	7.3
0.15	0.20	0.10	6.2	6.8
0.30	0.40	0.20	5.7	5.9
0.60	0.80	0.40	4.9	5.1
0.75	1.00	0.50	4.0	4.5

Table 2. Transport Numbers Derived Using Eq. 2

Mean concn	f_1	f_2	E_{max}/mV	Cellulose acetate $\bar{t}_+$		t_+
mol dm^{-3}				Without Stigmasterol	With Stigmasterol	
0.075	0.7730	0.8336	16.13	0.7107	0.7232	0.402
0.15	0.6949	0.7730	15.31	0.7024	0.7219	0.392
0.30	0.5976	0.6949	14.15	0.7013	0.7083	0.388
0.60	0.4828	0.5976	12.52	0.6955	0.7035	0.379
0.75	0.4430	0.5623	11.87	0.6684	0.6895	0.376

$$\bar{t}_+ = \frac{E}{2E_{max}} + 0.5, \quad (2)$$

where the symbols have their usual meaning. A simplification of TMS theory gives:

$$E = \frac{RT}{F}(2\bar{t}_+ - 1)\ln\frac{a'}{a''} \quad (3)$$

and if the membrane is ideally selective,

$$E_{max} = \frac{RT}{F}\ln\frac{a'}{a''}. \quad (4)$$

Permselectivity is related to fixed charge density as[11]

$$\phi\bar{X} = \frac{2\bar{C}P_s}{\sqrt{1-P_s^2}}, \quad (5)$$

where $\bar{C}$ is the mean concentration. Transport numbers derived using Eq. 2 alongwth the values of E_{max} and activity coefficient (f_1 and f_2) using Eq. 4 are given in Table 2. The values of t_+ (solution) have been obtained from Ref. 12. Permselectivity and and fixed charge density values derived using Eqs. 1 and 5 are given in Table 3. It is clear that the fixed charge density increases with increasing mean concentration.

Cellulose acetate is reported[13] to contain a low concentration of weakly ionizable carboxyl group. In Fig. 2 the membrane potential against pH has been plotted, which shows that due to reduction in selectivity of the cellulose acetate, membrane potential increases with decreasing pH values. A steady increase in the values of membrane potential has been observed when cellulose acetate film supports stigmasterol liquid membrane. Table 4 includes the values of permselectivity and fixed charge density at different pH values.

The values for various parameters in the case of stigmasterol liquid membrane supported on cellulose acetate film are larger than those obtained by Singh and Tiwari,[1] showing that it is more effective surfactant than cholesterol. This may be attributed to basic structural difference between stigmasterol and cholesterol. Stigmasterol inspite of having the same skeleton as cholesterol, possesses a double bond in the side chain. The presence of two sp^2 carbons, which essentially have higher electronegativity than sp^3, would be responsible for enhanced surface activity of stigmasterol leading to

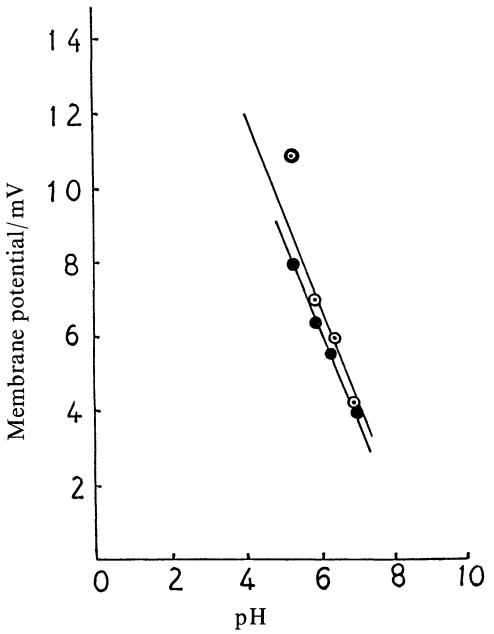

Fig. 2. Variation of membrane potential with pH: ⊙ without stigmasterol, ● with stigmasterol. Mean concentrations of sodium chloride solution used is 0.30 M; C_1=0.40 M; C_2=0.20 M.

Table 3. Permselectivities and Fixed Charge Densities ($\phi\bar{X}$ in mol dm^{-3})

Mean concn	Cellulose acetate			
	P_s		$\phi\bar{X}$	
mol dm^{-3}	Without Stigmasterol	With Stigmasterol	Without Stigmasterol	With Stigmasterol
0.075	0.5866	0.5660	0.1087	0.1030
0.15	0.6021	0.5709	0.2262	0.2541
0.30	0.5859	0.5747	0.4338	0.4214
0.60	0.5908	0.5782	0.8787	0.8506
0.75	0.5732	0.5397	1.0493	0.9617

Table 4. Transport Numbers Permselectivities and Fixed Charge Densities at Different pH Values ($\phi\bar{X}$ in mol dm^{-3})

pH	Cellulose acetate					
	$\bar{t}_+$		P_s		$\phi\bar{X}$	
	Without Stigmasterol	With Stigmasterol	Without Stigmasteral	With Stigmasterol	Without Stigmasterol	With Stigmasterol
6.92	0.6448	0.6342	0.4823	0.4645	0.3303	0.3147
6.45	0.7084	0.6977	0.5860	0.5690	0.4339	0.4152
5.90	0.7434	0.7224	0.6409	0.6082	0.6526	0.4597
5.30	0.8249	0.7780	0.7265	0.6936	0.7078	0.5777

an increase in the values of various parameters.

The authors are thankful to Head, Chemistry Department, University of Gorakhpur, Gorakhpur for providing laboratory facilities and to State Council of Science & Technology, Lucknow, for financial support.

References

1) K. Singh and A. K. Tiwari, *J. Membr. Sci.,* **34**, 155 (1987).
2) K. Singh and A. K. Tiwari, *J. Colloid Interface Sci.,* **116**, 42 (1987).
3) F. Helfferich, "Ion Exchange," McGraw-Hill, New York (1962), p. 232.
4) R. E. Kesting, A. Vincent, and J. Eberlin, *OSW R & D Report,* No. 117, Aug. 1964.
5) R. E. Kesting, Reverse-osmosis Process Using Surfactant Feed Additives, OSW Patent Application SAL 830, Nov. 3, 1965.
6) R. E. Kesting, W. J. Subcasky, and J. D. Paton, *J. Colloid Interface Sci.,* **28**, 156 (1968).
7) R. C. Srivastava and Saroj Yadav, *J. Non-Equilib. Thermodyn.,* **4**, 219 (1979).
8) R. C. Srivastava and R.P.S. Jakhar, *J. Phys. Chem.,* **85**, 1457 (1981).
9) Y. Kobatke and N. Kamo, *Prog. Polym. Sci. Jpn.,* **5**, 257 (1973).
10) N. Lakshminarayanaiah, "Transport Phenomena in Membranes," Academic Press, New York and London (1969), p. 199.
11) K. Singh, R. Shabd, and V. N. Srivastava, *Indian J. Chem.,* **20** (4), 391 (1981).
12) L. Antropov, "Theoretical Electrochemistry," Mir Publication, Moscow (1972).
13) H. K. Lonsdale, in "Desalination by Reverse Osmosis," ed by U. Merten, MIT Press, Cambridge (1966), p. 93.

Partial Oxidation of [Octakis(dodecyloxy)phthalocyaninato]zinc(II) with 2,3-Dichloro-5,6-dicyano-*p*-benzoquinone

Kuninobu KASUGA,* Tadahiro NAKAO, Takuya MIHARA, and Kunihisa SOGABE†
Department of Chemistry, Faculty of Science, Shimane University, Matsue 690
†Department of Chemistry, Faculty of Education, Shimane University, Matsue 690
(Received July 19, 1991)

Synopsis. While an organic oxidant such as 2,3-dichloro-5,6-dicyano-*p*-benzoquinone oxidized [Zn{Pc($OC_{12}H_{25}$)$_8$}] in a chloroform solution, it did not oxidize H_2Pc($OC_{12}H_{25}$)$_8$ and [Cu{Pc($OC_{12}H_{25}$)$_8$}]. Oxidation was confirmed by the electronic and ESR spectra, as well as cyclic voltammograms. The electrical conductivity of the zinc(II) complex increased 10^5 times in partial oxidation.

The partial oxidation of metallophthalocyanines with iodine, bromine or nitrosyl tetrafluoroborate($NOBF_4$) significantly increased their electrical conductivity.[1] The electrochemical oxidation of the complexes was carried out in solution, resulting in single crystals which exhibit metallic conductivity.[2] The conductivity also increased in a partial reduction of the complexes with metallic potassium or sodium dithionite.[3,4] Furtheremore, phthalocyaninatosilicon(IV) polymers bridged by a halogen or an oxygen atom were prepared, and showed good conductivity under partial oxidation.[5]

It was recently reported that metallophthalocyanine complexes with long-chain alkyl or alkoxy substituents were transformed to discotic mesophase.[6,7] It is of interest to prepare the oxidized metallophthalocyanine derivatives which show conductivity in the mesophase.[8] We previously reported the chemical oxidation of tetra-*t*-butylphthalocyanine, H_2Pc(*t*-Bu)$_4$, and its metal(II) complexes with 2,3-dichloro-5,6-dicyano-*p*-benzoquinone (DDQ) to confirm their oxidation behavior by chemical oxidants.[9] This paper describes the chemical oxidation of [octakis(dodecyloxy)phthalocyaninato]-zinc(II), [Zn{Pc($OC_{12}H_{25}$)$_8$}], with DDQ, and its conductivity both in the solid state and in the mesophase.

Experimental

Materials. H_2Pc($OC_{12}H_{25}$)$_8$, [Cu{Pc($OC_{12}H_{25}$)$_8$}], and [Zn{Pc($OC_{12}H_{25}$)$_8$}] were prepared in a similar method described in the literature.[7] Bu_4NBF_4 was prepared and purified using the method shown in a text book.[10] DDQ was recrystallized from benzene under an argon atmosphere.

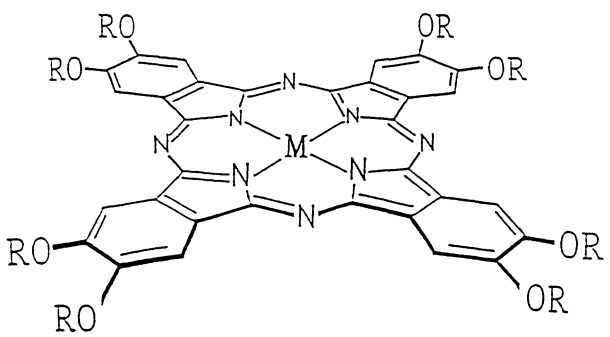

Fig. 1. Schematic representation of the [M{Pc(OR)$_8$}] complex:
OR=$OC_{12}H_{25}$.

Partial Oxidation. The zinc(II) complex was dissolved into a solvent mixture of chloroform and hexane (7 : 3, v/v), to which the chloroform solution of DDQ was added dropwise under a nitrogen atmosphere. The mixture was subsequently stirred at room temperature for several min, and then the dark-black precipitates were obtained upon the concentration of the solution under reduced pressure. The oxidized complex was dried at room temperature under reduced pressure.

Measurements. The electronic spectra in solution were measured on a Hitachi 200-20 spectrophotometer. The ESR spectra were measured with a JEOL-IX spectrometer. Cyclic voltammetric measurements were performed in a chloroform solution containing Bu_4NBF_4 (0.1 mol dm^{-3}) on a Hokuto Denko HA-501 potentiostat with a Hokuto Denko HF-201 function generator.[9] Differential scanning calorimetry experiments were carried out on a Shimadzu DSC-50. Conductivity measurements of pressed pellets were carried out with a two-probe method.

Results and Discussion

By the addition of adequate amounts of DDQ, the green solution of [Zn{Pc($OC_{12}H_{25}$)$_8$}] changed to reddish purple; in the absorption spectrum, the intensity of the Q band at 680 nm decreased, while new bands appeared at 545 and 721 nm. On the other hand, the spectra of the green solution of H_2Pc($OC_{12}H_{25}$)$_8$ or its copper(II) complex did not change upon the addition of DDQ.

When the zinc(II) complex was oxidized with DDQ in a chloroform solution, two ESR signals arising from cationic phthalocyanine ring and anionic DDQ radicals were observed at g=2.002 (line width=7 G) and 2.005 (3 G) at room temperature, respectively. These results show that although the phthalocyanine ring of the zinc(II) complex was oxidized by DDQ, those of H_2Pc($OC_{12}H_{25}$)$_8$ and its copper(II) complex were not oxidized, which is consistent with the oxidation results for H_2Pc(*t*-Bu)$_4$ and its metal(II) complexes.[9]

Cyclic voltammograms of the phthalocyanine derivatives exhibited four redox couples. The half-wave potentials of the first step on the oxidation side are listed in Table 1 to confirm the chemical oxidation. By considering the potential of the first reduction step of DDQ (0.59 V vs. SCE), the zinc(II) complex was only oxidized by DDQ, which is consistent with the results of the absorption and ESR spectra.

H_2Pc($OC_{12}H_{25}$)$_8$ and its copper(II) and zinc(II) complexes showed endothermic peaks at 93, 100, and 107 °C, respectively, indicating their transition to the mesophase.[6,7] The zinc(II) complex doped by DDQ (20 mol %) showed endothermic peaks at 100 °C, and its

Table 1. Electrochemical Results in Chloroform ($E_{1/2}$ (V) vs. SCE)

$H_2Pc(OC_{12}H_{25})_8$	$[Cu\{Pc(OC_{12}H_{25})_8\}]$	$[Zn\{Pc(OC_{12}H_{25})_8\}]$	DDQ
0.86[a]	0.87[a]	0.44[a]	0.59[b]
(0.14)	(0.15)	(0.10)	(0.10)

a) Couple for c^+/c. b) Couple for DDQ/DDQ^-. Parentheses denote ΔE_p (V). Scan rate=100 mV s^{-1}.

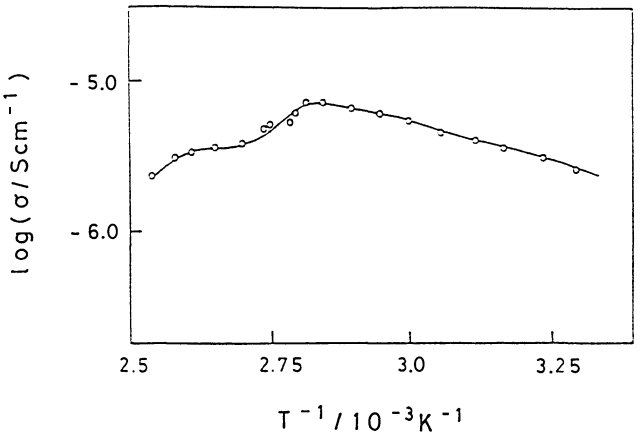

Fig. 2. Specific conductivity (σ/S cm^{-1}) vs. reverse temperature. The concentration of the added DDQ was 20 mol %.

peak reappeared with rising temperature, although the peak shifted to 95 °C with some broadening. Upon the addition of DDQ (more than 20 mol %), the sample did not show the peak.

Although the $[Zn\{Pc(OC_{12}H_{25})_8\}]$ complex was an insulator ($\sigma<10^{-11}$ S cm^{-1} at room temperature) the complex increased its conductivity (2.5×10^{-6} S cm^{-1} at room temperature) in partial oxidation by DDQ (20 mol %) (Fig. 2). In partial oxidation of the complex with $NOBF_4$ (15 mol %), the conductivity was about 10^{-3} times that of the complex doped by DDQ (20 mol %).[11] This may result from the unsuitable position of the tetrafluoroborate anion in the oxidized sample. It was also reported that the conductivity of [bis{octakis(octadecyloxymethyl)phthalocyaninato}lutetium(III)] partially oxidized by phenoxathin hexachloroantimonate (80 mol %) was 1.6×10^{-7} S cm^{-1} at 60 °C.[8] The long paraffinic chains of these phthalocyanine complexes promote the formation of a hexagonal columnar,[12] which might increase the intracolumnar conduction.

The conductivity of the $[Zn\{Pc(OC_{12}H_{25})_8\}]$ complex doped by DDQ increased with rising temperature, but decreased above 80 °C (Fig. 2). The ESR signal arising from the anionic DDQ radical diminished above 80 °C, while that from the cationic phthalocyanine radical remained. The DDQ radical might form an ESR silent dimer upon heating, as shown in the case of cosublimation of [fluoro(phthalocyaninato)aluminium(III)] and DDQ.[13] Although the conductivity seems to decrease with an increase of the temperature in the mesophase, details are presently unknown, because some deformation of the specimen might occur and cause a decrease in the conductivity.

This work was partially supported by a Grant-in-Aid for Scientific Research No. 02453041 from the Ministry of Education, Science and Culture.

References

1) T. J. Marks, *Science,* **227**, 881 (1985), and references cited therein.
2) K. Yakushi, H. Yamakado, M. Yositake, N. Kosugi, H. Kuroda, T. Sugano, M. Kinosita, A. Kawamoto, and J. Tanaka, *Bull. Chem. Soc. Jpn.,* **62**, 687 (1989), and references cited therein.
3) L. Moigne and R. Eren, *J. Chem. Phys.,* **83**, 6472 (1985).
4) K. Kasuga, M. Morisada, M. Handa, and K. Sogabe, *Inorg. Chim. Acta,* **174**, 161 (1990).
5) J. G. Gaudiello, G. E. Kellogg, S. M. Tetrick, and T. J. Marks, *J. Am. Chem. Soc.,* **111**, 5259 (1989).
6) C. Piechocki, J. Simon, A. Skoulios, D. Guillon, and P. Weber, *J. Am. Chem. Soc.,* **104**, 5245 (1982).
7) K. Ohta, L. Jacquemin, C. Sirlin, L. Bosio, and J. Simon, *New. J. Chem.,* **12**, 751 (1988).
8) Z. Belarbi, M. Maitrot, K. Ohta, J. Simon, J. J. André, and P. Petit, *Chem. Phys. Lett.,* **143**, 400 (1988).
9) P. Mu, T. Nakao, M. Handa, K. Sogabe, and K. Kasuga, *Bull. Chem. Soc. Jpn.,* **64**, 3202 (1991).
10) D. T. Sawyer and J. L. Roberts, Jr., "Experimental Electrochemistry for Chemist," Wiley, New York (1974), p. 212.
11) K. Kasuga, T. Mihara, T. Fukumoto, T. Moriguchi, and M. Handa, 39th Symposium on Coordination Chemistry of Japan, Mito, October, 1989, Abstr., 2AP08.
12) C. Piechocki, J. Simon, J. J. André, Guillon, P. Petit, A. Skoulios, and P. Weber, *Chem. Phys. Lett.,* **122**, 124 (1985).
13) I. Hiromitsu, J. Takeuchi, and T. Ito, *J. Phys. Soc. Jpn.,* **59**, 2922 (1990).

Synthesis and Application of 5-Arylazothiophene Derivatives

Ram Wasudeo SABNIS,* Ghadir KAZEMI, and Dinesh Wamanrao RANGNEKAR
Dyes Research Laboratory, Department of Chemical Technology,
University of Bombay, Matunga, Bombay 400019, India
(Received February 21, 1991)

Synopsis. Synthesis of 5-(hetoarylazo or arylazo)thiophene derivatives (**6a—g**) was achieved by diazotization of ethyl 5-amino-2,4-bis(ethoxycarbonyl)-3-thiopheneacetate (**3**) using nitrosyl hydrogensulfate, coupling with suitable heterocyclic hydroxy and *N,N*-dialkyl-substituted arylamines which resulted in thiophene azo dyes. The key intermediate **3**, used as the diazonium component, was synthesized in one pot and in excellent yield from diethyl 3-oxopentanedioate, sulfur and ethyl cyanoacetate following the Gewald Synthesis. The dyes when applied as disperse dyes on polyester fibres gave excellent results.

Several patents[1—6] describe the synthesis and technical importance of azo thiophene disperse dyes. We have recently reported the synthesis of novel heterocyclic dyes and fluorescent brighteners such as benzo[*b*]-thiophenes,[7] thiophenes,[8] 1,2,3-triazoles,[9] pyrimidines,[10] quinoxalines,[11] thiazoles,[12] and their application on synthetic fibres, which gave encouraging results. Thiophene moiety has been extensively studied in the field of medicine[13] and fungicides.[14]

In the present study, we report the synthesis of model compounds of azo dyes derived from novel diazonium component, 5-aminothiophene derivative synthesized by the Gewald Synthesis[15] and their use as disperse dyes for polyester fibres. Azo disperse dyes derived from thiophene have many advantages, such as color deepening effect as an intrinsic property of thiophene ring, small molecular structure leading to better dyeability and heterocyclic structure of thiophene ring resulting in good sublimation fastness of dyed fibres.

Ethyl 5-amino-2,4-bis(ethoxycarbonyl)-3-thiopheneacetate (**3**) is a versatile intermediate in the synthesis of heterocyclic systems. The principle advantages of the key intermediate used here are that the yields are high, time of the reaction is short, the procedure involves only one facile step, the work-up is convenient and thus the starting material can be easily prepared. The presence of diazotizable amino group adjacent to electron-withdrawing groups results in deepening of the dye hues on the polyester fibres.

Results and Discussion

The thiophene intermediate, ethyl 5-amino-2,4-bis-(ethoxycarbonyl)-3-thiopheneacetate (**3**), was synthesized from diethyl 3-oxopentanedioate (**1**), sulfur, and ethyl cyanoacetate (**2**) with diethylamine as a catalyst, using the Gewald Synthesis. Compound **3** was diazotized using nitrosyl hydrogensulfate in the cold and coupled with a variety of heterocyclic hydroxy couplers such as 3-methyl-1-phenyl-1*H*-pyrazol-5-ol (**5a**), 3-cyano-4-methylpyridine-2,6-diol (**5b**), 4-hydroxy-1-methylquinolin-2(1*H*)-one (**5c**), 2,4,6-pyrimidinetriol (barbituric acid) (**5d**), and *N,N*-dialkyl-substituted arylamines such as *N,N*-dimethylaniline (**5e**), *N,N*-bis(2-cyanoethyl)aniline (**5f**), 3-chloro-*N,N*-bis(2-hydroxyethyl)aniline (**5g**) to yield ethyl 5-(hetoarylazo or arylazo)-2,4-bis(ethoxycarbonyl)-3-thiopheneacetate (**6a—g**).

The absorption maxima of these dyes recorded in their DMF solution are shown in Table 1. Their absorption maxima were in the range of 472—588 nm. The absorption maxima of the dyes **6a—d** derived from heterocyclic hydroxy-coupling components, were in the range of 472—502 nm, whereas dyes **6e—g**, derived from *N,N*-dialkylsubstituted arylamines, showed absorption maxima in the range of 576—588 nm.

Dyes **6a—g** were applied on polyester fibres as 1% shade. The hues of the polyester dyed fibres were golden yellow, orange, red, pink, violet, and blue and are shown in Table 1. The pickup values of the dyed polyester fibres varied from two to three, with most of them having a pickup value of three. The light fastness of these dyes varied from three to six, thus the dye **6d** had poor light fastness (three), dyes **6e**, **6g** had fair

Table 1. Absorption Spectra and Dyeing Properties of 5-Arylazothiophene Derivatives

Dye	Color on dyed polyester fibres	Absorption maxima (nm)	log ε	Pick-up	Light fastness	Sublimation fastness
6a	Brilliant golden yellow	472	4.34	3	6	5
6b	Brilliant orange	484	4.39	3	5	4
6c	Brilliant red	498	4.28	3	5	4
6d	Pink	502	4.19	2	3	3
6e	Blue	588	4.64	2	4	4
6f	Blue	582	4.61	3	5	5
6g	Violet	576	4.57	3	4	4

* Present address: North Carolina State University, College of Textiles, P.O.Box 8301, Raleigh, NC 27695-8301, U.S.A.

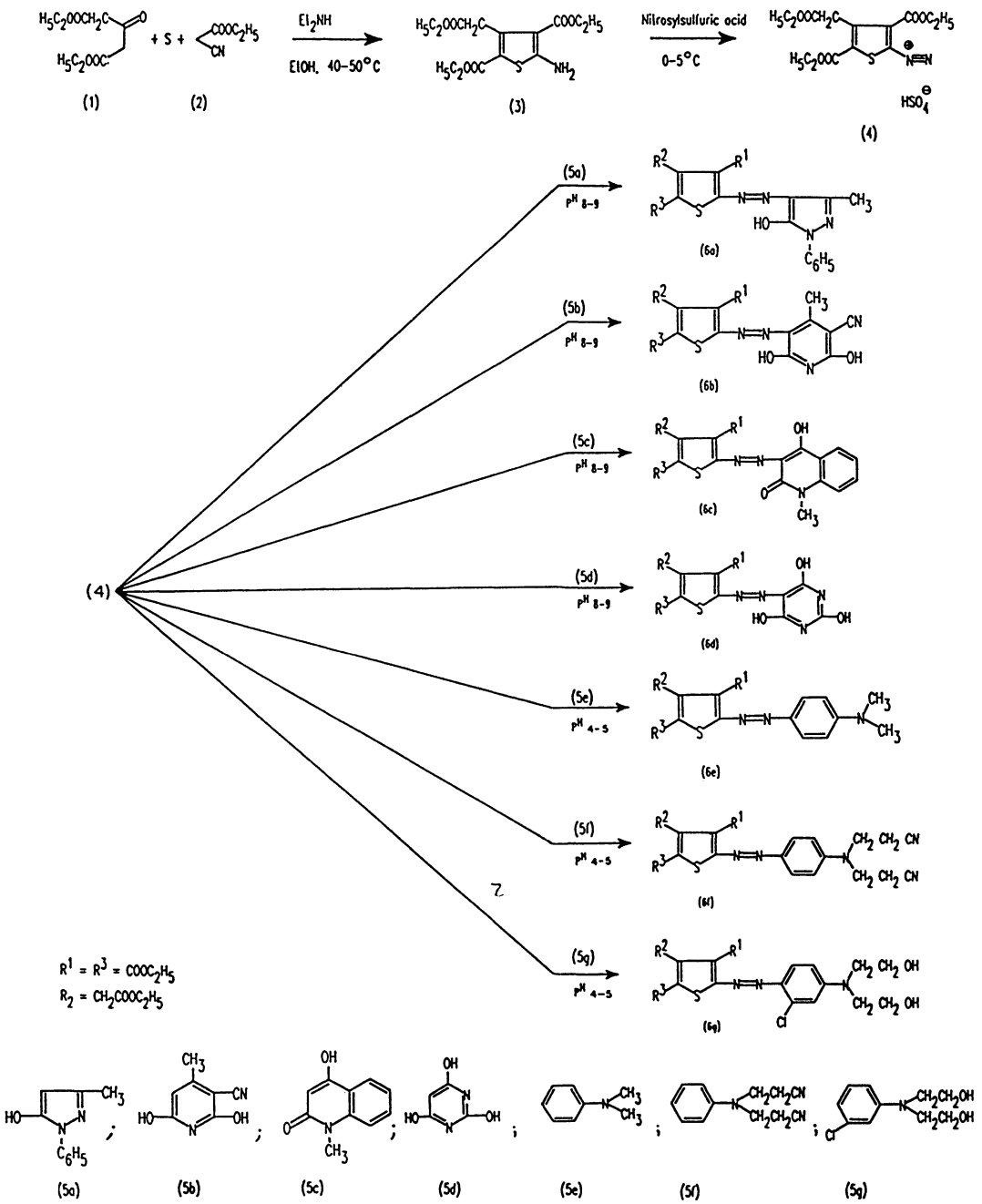

light fastness (four), dyes **6b**, **6c**, **6f** had good light fastness (five) and dye **6a** had very good light fastness (six). The sublimation fastness of these dyes was in the range of three to five, thus the dye **6d** showed good sublimation fastness (three), dyes **6b**, **6c**, **6e**, **6g** showed very good sublimation fastness (four), dyes **6a**, **6f** showed excellent sublimation fastness (five). Dyes **6a**—**c**, **6f**, and **6g** among these dyes thus showed good fastness properties on polyester fibres.

Experimental

All melting points are uncorrected. The IR spectra were recorded on a Perkin-Elmer Model 397 spectrophotometer in Nujol mull. The ^{1}HNMR spectra were recorded on a Varian-60 MHz instrument EM-360L using TMS as internal standard and the chemical shifts are given in ppm. Mass spectra were recorded on a Varian Mat-311 instrument (70 eV). Absorption spectra in DMF solution were recorded on a Beckman Model-25 spectrophotometer.

Ethyl 5-Amino-2,4-bis(ethoxycarbonyl)-3-thiopheneacetate (3). In a 100 ml round bottomed flask, were placed a mixture of diethyl 3-oxopentanedioate (**1**) (20.2 ml, 0.1 mol), sulfur (3.2 g, 0.1 mol), ethyl cyanoacetate (**2**) (11.3 ml, 0.1 mol), ethanol (20 ml), and diethylamine (10 ml). The reaction mixture was stirred on a waterbath for 2 h at 40—50 °C. At the end of the reaction, a reddish brown solid was separated. After cooling to room temperature, the reaction mixture was filtered, washed with cold ethanol and dried. The product was recrystallized from ethanol as shiny white needles. Yield: 87%, mp 179 °C. Anal. Calcd for $C_{14}H_{19}NO_6S$: C, 51.06; H, 5.77; N, 4.25; S, 9.72%. Found: C, 51.11; H, 5.57; N, 4.27; S, 9.74%. IR (Nujol mull) 3330, 3430 (NH_2), 1675 (COOEt), 1720 (CH_2COOEt) cm^{-1}. ^{1}HNMR (DMSO-d_6) δ=1.34 (t, 9H, $3CH_3$), 3.5—4.8 (m, 8H, 4-CH_2)), 5.5—6.1 (s, 2H, NH_2).

MS m/z 329.

Ethyl 5-[(5-Hydroxy-3-methyl-1-phenyl-1*H*-pyrazol-4-yl)-azo]-2,4-bis(ethoxycarbonyl)-3-thiopheneacetate (6a). Ethyl 5-amino-2,4-bis(ethoxycarbonyl)-3-thiopheneacetate (**3**) (1.64 g, 0.005 mol) was added in portions during 1 h to a cooled mixture of nitrosyl hydrogensulfate prepared from sodium nitrite (0.38 g, 0.0055 mol) and concentrated sulfuric acid (10 ml) at 0 °C. The mixture was stirred for an additional 1 h at 0 °C, then added to an ice-water mixture under stirring, excess of nitrous acid was destroyed by the addition of urea (1 g) and the solution was filtered to obtain a clear diazonium salt solution **4**. 3-Methyl-1-phenyl-1*H*-pyrazol-5-ol (**5a**) (0.87 g, 0.005 mol) was dissolved in dilute sodium hydroxide. The solution was cooled by external cooling so that the temperature was at 0—5 °C. To this cooled solution, the prepared diazonium salt **4** was added slowly so that the temperature did not rise above 5 °C. The pH of the reaction mixture was maintained alkaline throughout the coupling period (1 h) by the addition of solid sodium carbonate in portions. After the addition of the diazonium salt was completed, the reaction mixture was stirred for 4 h at 0 °C, when the dye which partially separated was neutralized with dilute hydrochloric acid (5%), filtered, thoroughly washed with water and dried. The product was recrystallized from methanol. Yield: 89%, mp 246 °C. Anal. Calcd for $C_{24}H_{26}N_4O_7S$: C, 56.03; H, 5.05; N, 10.89; S, 6.22%. Found: C, 56.08; H, 5.11; N, 10.82; S, 6.19%. IR (Nujol mull) 3200—3400 (OH), 1680—1700 (COOEt) cm^{-1}.

Ethyl 5-[(2,6-Dihydroxy-5-cyano-4-methyl-3-pyridyl)azo]-2,4-bis(ethoxycarbonyl)-3-thiopheneacetate (6b). the dye was synthesized in the same manner as given for dye **6a**, except that instead of **5a**, 3-cyano-4-methylpyridine-2,6-diol (**5b**) (0.75 g, 0.005 mol) was used. The product was recrystallized from methanol. Yield: 92%, mp 230 °C. Anal. Calcd for $C_{21}H_{22}N_4O_8S$: C, 51.42; H, 4.48; N, 11.42; S, 6.53%. Found: C, 51.39; H, 4.51; N, 11.46; S, 6.58%. IR (Nujol mull) 3380—3440 (OH), 1660—1700 (COOEt), 2210 (CN) cm^{-1}.

Ethyl 5-[(4-Hydroxy-1-methyl-2-oxo-1,2-dihydro-3-quinolyl)azo-2,4-bis(ethoxycarbonyl)-3-thiopheneacetate (6c). The dye was synthesized in the same manner as given for dye **6a** except instead of **5a**, 4-hydroxyl-1-methylquinolin-2(1*H*)-one (**5c**) (0.87 g, 0.005 mol) was used. The product was recrystallized from chloroform. Yield: 81%, mp 144 °C. Calcd for $C_{24}H_{25}N_3O_8S$: C, 55.92; H, 4.85; N, 8.15; S, 6.21%. Found: C, 55.93; H, 4.87; N, 8.18; S, 6.23%. IR (Nujol mull) 3310—3400 (OH), 1675—1720 (COOEt), 1680 (CO) cm^{-1}.

Ethyl 5-[(2,4,6-Trihydroxy-5-pyrimidinyl)azo]-2,4-bis(ethoxycarbonyl)-3-thiopheneacetate (6d). The dye was synthesized in the same manner as given for dye **6a**, except instead of **5a**, 2,4,6-pyrimidinetriol (barbituric acid) (**5d**) (0.64 g, 0.005 mol) was used. The product was recrystallized from ethanol. Yield: 74%, mp 152 °C. Anal. Calcd for $C_{18}H_{20}N_4O_9S$: C, 46.15; H, 4.27; N, 11.96; S, 6.83%. Found: C, 46.08; H, 4.22; N, 11.93; S, 6.81%. IR (Nujol mull) 3200—3400 (OH), 1680—1700 (COOEt) cm^{-1}.

Ethyl 5-[4-(Dimethylamino)phenylazo]-2,4-bis(ethoxycarbonyl)-3-thiopheneacetate (6e). Ethyl 5-amino-2,4-bis(ethoxycarbonyl)-3-thiopheneacetate (**3**) (1.64 g, 0.005 mol) was added in portions during 1 h to a cooled mixture of nitrosyl hydrogensulfate prepared from sodium nitrite (0.38 g, 0.0055 mol) and concentrated sulfuric acid (10 ml) at 0 °C. The mixture was stirred for an additional 1 h at 0 °C, then added to an ice-water mixture under stirring, excess of nitrous acid was destroyed by the addition of urea (1 g) and the solution was filtered to obtain a clear diazonium salt solution **4**. *N,N*-Dimethylaniline (**5e**) (0.60 g, 0.005 mol) was dissolved in acetic acid. The solution was cooled by external cooling so that the temperature was 0—5 °C. To this cooled solution, the prepared diazonium salt **4** was added slowly so that the temperature did not rise above 5 °C. The pH of the reaction mixture was maintained acidic throughout the coupling period (1 h). After the addition of the diazonium salt was completed, the reaction mixture was stirred for 4 h, when the dye which partially separated was neutrallized with sodium carbonate, filtered, thoroughly washed with water and dried. The product was recrystallized from ethyl acetate. Yield: 76%, mp 296 °C. Anal. Calcd for $C_{22}H_{27}N_3O_6S$: C, 57.26; H, 5.85; N, 9.11; S, 6.94%. Found: C, 57.29; H, 5.88; N, 9.16; S, 6.92%. IR (Nujol mull) 1680—1710 (COOEt) cm^{-1}.

Ethyl 5-[4-[Bis(2-cyanoethyl)amino]phenylazo]-2,4-bis-(ethoxycarbonyl)-3-thiopheneacetate (6f). The dye was synthesized in the same manner as given for the dye **6e** except that instead of **5e**, *N,N*-bis(2-cyanoethyl)aniline (**5f**) (0.99 g, 0.005 mol) was used. The product was recrystallized from DMF. Yield: 68%, mp 324 °C. Anal. Calcd for $C_{26}H_{29}N_5O_6S$: C, 57.88; H, 5.38; N, 12.98; S, 5.93%. Found: C, 57.81; H, 5.34; H, 12.92; S, 5.96%. IR (Nujol mull): 1660—1680 (COOEt), 2220 (CN) cm^{-1}.

Ethyl 5-[2-Chloro-4-[bis(2-hydroxyethyl)amino]phenylazo]-2,4-bis(ethoxycarbonyl)-3-thiopheneacetate (6g). The dye was synthesized in the same manner as given for the dye **6e**, except that instead of **5e**, 3-chloro-*N,N*-bis(2-hydroxyethyl)aniline (**5g**) (1.07 g, 0.005 mol) was used. The product was recrystallized from DMF. Yield: 62%, mp >360 °C. Anal. $C_{24}H_{30}ClN_3O_8S$: C, 51.89; H, 5.40; Cl, 6.30; N, 7.56; S, 5.76%. Found: C, 51.81; H, 5.42; Cl, 6.27; N, 7.59; S, 5.72%. IR (Nujol mull) 3320—3400 (OH), 1680—1700 (COOEt) cm^{-1}.

References

1) D. B. Baird, B. R. Fishwick, and R. D. McClelland, (Imperial Chemical Industries Ltd.) Ger. Offen 2333828 (1974); *Chem. Abstr.*, **80**, 146964 (1974).

2) D. B. Baird, B. R. Fishwick, J. S. Campbell, and R. D. McClelland, (Imperial Chemical Industries Ltd.) British Patent 1549184 (1979); *Chem. Abstr.*, **92**, 78079 (1980).

3) U. Bergmann, E. Hahn, G. Hansen, and H. Reichelt, (BASF AG) Ger. Offen DE 3512760 (1986); *Chem. Abstr.*, **106**, 34637 (1987).

4) K. H. Etzbach, G. Hansen, H. Reichelt, and H. Loeffler, (BASF AG) Ger. Offen DE 3639942 (1988); *Chem. Abstr.*, **109**, 192150 (1988).

5) S. Imahori, K. Himeno, and S. Maeda, (Mitsubishi Chem. Ind., Co., Ltd.) Ger. Offen DE 3151114 (1982); *Chem. Abstr.*, **97**, 218025 (1982).

6) W. Groebke, (Sandoz Ltd.) Ger. Offen 2334169 (1974); *Chem. Abstr.*, **81**, 14696 (1974).

7) R. W. Sabnis and D. W. Rangnekar, *Dyes Pigm.*, **10**, 295 (1989).

8) R. W. Sabnis and D. W. Rangnekar, *J. Chem. Technol. Biotechnol.*, **47**, 39 (1990).

9) R. W. Sabnis and D. W. Rangnekar, *J. Heterocycl. Chem.*, **27**, 417 (1990).

10) R. W. Sabnis and D. W. Rangnekar, *Indian J. Tech.*, **28**, 54 (1990).

11) R. C. Phadke and D. W. Rangnekar, *Bull. Chem. Soc. Jpn.*, **59**, 1245 (1986).

12) D. W. Rangnekar and P. Y. Kamat, *Synth. Commun.*, **20**, 2447 (1990).

13) M. Luisetti, P. D. Piccioni, M. Donnini, V. Peona, E. Pozzi, and C. Grassi, *Biochem. Biophys. Res. Commun.*, **165**, 568 (1989).

14) M. Maeda, T. Harada, K. Kitahara, and T. Kono (Daikin Industries Ltd.), Jpn. Kokai Tokkyo Koho JP 01165503 (1989); *Chem. Abstr.*, **112**, 50606 (1990).

15) K. Gewald, E. Schinke, and H. Bottcher, *Chem. Ber.*, **99**, 94 (1966).